A Molecular Orbital Calculation of Chemically Interacting Systems. Interaction between Two Radicals

Tsutomu MINATO, Shinichi YAMABE,* Hiroshi FUJIMOTO, and Kenichi FUKUI
Faculty of Engineering, Kyoto University, Sakyo-ku, Kyoto 606
**Department of Chemistry, Nara University of Education, Takabatake-cho, Nara 630*
(Received April 29, 1977)

The reaction path of radical-radical recombination and disproportionation has been studied by means of a perturbational method with a clear orbital interaction concept, and the mechanism of these reactions has been elucidated theoretically. It has been confirmed that these termination reactions do not have a common transition state. The recombination is found to take the path which gives the maximum interaction between the singly occupied molecular orbitals (SOMO's) of two radical species, whereas the disproportionation is shown to take the route which gives the significant charge transfer interaction from the particular doubly occupied (DO) MO of one radical to the SOMO of the other radical. The DOMO localized at the C–H bond donates electrons to the SOMO to cause the hydrogen abstraction. In the process of disproportionation, one radical which abstracts a hydrogen atom acts as an electron-acceptor and the other radical with the hydrogen atom to be abstracted as an electron-donor. The difference between the mechanism of the recombination and that of the disproportionation is clarified in terms of the mode of the orbital interaction.

When organic free radicals are generated in a reaction, the unpaired-electron species eventually undergo a termination reaction, yielding stable molecules with closed-shell electronic structures through two reaction pathways. One of them is the recombination in Eq. 1 and the other is the disproportionation with the abstraction of a hydrogen atom β to the radical center in Eq. 2.[1]

$$\left.\begin{array}{l} RCH_2CH_2\cdot \\ + \\ R'CH_2CH_2\cdot \end{array}\right\} \begin{array}{l} \xrightarrow{k_c} RCH_2CH_2CH_2CH_2R' \quad (1) \\ \xrightarrow{k_d} RCH_2CH_3 + R'CH{=}CH_2 \quad (2) \end{array}$$

The knowledge of termination modes together with their relative rates is very important in predicting and interpreting the radical chain reactions and their products. For example, a change from recombination to disproportionation can effect a twofold variation in polymer length.

Early pictures of radical-radical reactions assumed a common transition state for the two processes of Eqs. 1 and 2, involving the excited dimer which could either be rearranged to give the disproportionation products or be quenched to give the recombination product.[2] This, however, is ruled out experimentally by a number of observations.[3] Bradley and Rabinovitch suggested an alternative interpretation of the mechanisms of the recombination and disproportionation of alkyl radicals.[4] They rejected the description of the activated complex for the disproportionation as an excited dimer and suggested that different configurations of the composite system may take part involving couplings of the radical species through three-centered hydrogen atom bonds already suggested for the recombination.[5] Consequently, the terms, "head-to-head" and "head-to-tail", used to describe the configuration of the activated complexes are discarded in the Bradley-Rabinovitch model.

$$2CH_3CH_2\cdot \longrightarrow \begin{array}{l} CH_2\cdots H \\ \| \quad \vdots \\ CH_2\cdots CH_2CH_3 \end{array} \begin{array}{l} \longrightarrow CH_3CH_2CH_2CH_3 \\ \longrightarrow CH_3CH_3 + CH_2{=}CH_2 \end{array}$$

Scheme 1.

Benson put forward the argument that both reactions, though quite different from each other, involve loose transition states with a significant ionic character.[3a]

$$2CH_3\cdot \longrightarrow \overset{-}{C}H_3 : \overset{+}{C}H_3 \quad \text{or} \quad \overset{+1/2}{C}H_2\text{-}H\cdots\overset{-1/2}{C}H_3$$
$$\longrightarrow CH_3CH_3$$

Scheme 2a.

$$2CH_3CH_2\cdot \longrightarrow CH_3\overset{-}{C}H_2 : H\text{-}CH_2\overset{+}{C}H_2$$
$$\text{or} \quad CH_3\overset{+}{C}H_2 : \overset{-}{H}\text{-}CH_2CH_2$$
$$\longrightarrow CH_3CH_3 + CH_2{=}CH_2$$

Scheme 2b.

Although it is accepted that the transition states of two radical-radical termination reactions differ, there are two incompatible ways of speculation for these processes as shown in Schemes 1, 2a, and 2b. Since the reaction paths of the recombination and disproportionation are still undetermined, it seems useful to study radical destruction processes theoretically.

Recently, the ΔW method which deals with the radical-radical reacting system in terms of the molecular interaction was developed by the present authors and was applied to the recombination of two methyl radicals.[6] As the result of calculation, the interaction between both the singly occupied molecular orbitals (SOMO's) and the deformation of the methyl radical were found to be of importance for progress of the reaction. The result also demonstrates the applicability of the ΔW method further to larger reacting systems. In the present work, we have made a comparative study on the recombination and disproportionation by the use of the ΔW method. The purpose of this work is to shed light on the disputing point of the mechanism of two reaction pathways. Furthermore, the general aspect of radical-radical reaction is explained conveniently in terms of the shape of MO's of several isolated radical species, since the value of the interaction energy, ΔW, is completely dependent on the overlap of MO's and gap of orbital-energy levels.

Method of Calculation

A system composed of an ethyl radical (ER) and a methyl radical (MR) is selected as a reaction model in the ΔW method. In this reaction system the recombination gives propane and the disproportionation produces methane and ethylene.

In the ΔW method, the wave function (Ψ) of a chemically-interacting system between ER and MR is represented in the configuration interaction (CI) procedure:

$$\Psi = C_0\Psi_0 + \sum_{i=1}^{6}\sum_{l=5}^{7} C_{i\to l}\Psi_{i\to l} + \sum_{k=1}^{3}\sum_{j=8}^{13} C_{k\to j}\Psi_{k\to j} + \sum_{i=1}^{6} C_{i\to o'}\Psi_{i\to o'} + \sum_{k=1}^{3} C_{k\to o}\Psi_{k\to o} + \sum_{l=5}^{7} C_{o\to l}\Psi_{o\to l} + \sum_{j=8}^{13} C_{o'\to j}\Psi_{o'\to j} + C_{o\to o'}\Psi_{o\to o'} + C_{o'\to o}\Psi_{o'\to o}. \quad (3)$$

In order to describe MO's of ER and MR in their isolated states, a semiempirical all-valence-electron SCF-UHF method including overlap integrals is employed.[7] The way of estimating semiempirical parameters to evaluated MO integrals is the same as that used in a previous paper.[8] Without the lowest occupied ls-like MO, ER has six doubly occupied (DO) MO's and MR has three DOMO's. In Eq. 3, Ψ_0 denotes the adiabatically-interacting configuration in which neither electron transfer nor electron excitation takes place as is shown in Fig. 1. The letters "i" and "j" indicate a DOMO and an unoccupied MO, respectively, of ER, and "k" and "l" a DOMO and an unoccuppied MO, respectively, of MR. "o" is the SOMO of the former radical, and "o'" that of the latter. $\Psi_{i\to l}$ denotes a configuration of one-electron shift from the i-th DOMO to the l-th unoccuppied MO. C_0, $C_{i\to l}$, $C_{k\to j}$, $\cdots$, are the CI coefficients obtained by solving the usual CI secular equation. Our attention is focused on the reacting system with the singlet spin state, because in the system with the triplet spin state a radical-radical reaction is far from occurring. In this calculation, no configurations with intramolecular excitations are taken into account in Eq. 3, since it requires much more CPU time to compute the molecular integrals appearing in the CI matrix elements of the above configurations. Also, two reactants are neutral and consequently the excited configurations do not contribute as much as the charge-transferred ones to the stabilization of the reacting systems.[6]

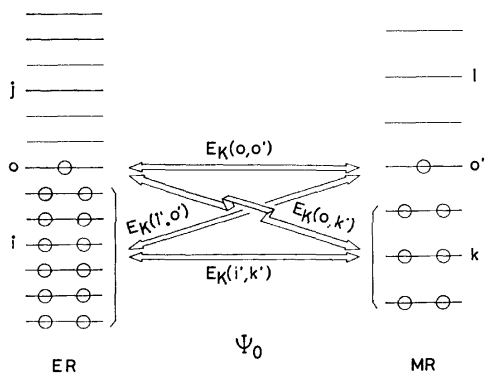

Fig. 1. The adiabatically-interacting configuration (Ψ_0) and the schematic representation of four types of exchange interaction between ethyl (ER) and methyl (MR) radicals. The lowest DOMO of two radicals, *i.e.*, the 1s-type one is omitted in this figure.

When the CI secular equation is expanded perturbationally, the total stabilization energy (ΔW) due to the CI mentioned above can be partitioned into the following three terms, Coulomb (E_Q), exchange (E_K), and delocalization (D).

$$\Delta W = E_Q + E_K - D. \quad (4)$$

E_Q is the classical electronic interaction energy between ER and MR. In both the singlet spin state and the triplet spin state, E_K is found to be the repulsive term (>0) in the system of two radicals of the usual organic-chemical size. E_K can be partitioned approximately into four terms.[6]

$$E_K = E_K(i',k') + E_K(i',o') + E_K(o,k') + E_K(o,o'). \quad (5)$$

In Fig. 1, four components of E_K are shown schematically. D is the stabilization energy due to the mixing-in of the charge transferred configurations with the adiabatically-interacting configuration. D can be represented by the sum of eight components.[6]

$$D = D(i\to l) + D(k\to j) + D(i\to o') + D(k\to o) + D(o\to l) + D(o'\to j) + D(o\to o') + D(o'\to o). \quad (6)$$

In order to visualize the change of electron density along the reaction progress, a contour map of the difference electron density is given. The difference density, $\Delta\rho(1|1)_{E_K}$, of the exchange interaction is partitioned into four terms, each of which corresponds to that of the energy decomposition in Eq. 5.

$$\Delta\rho(1|1)_{E_K} = \Delta\rho(1|1)_{E_K(i',k')} + \Delta\rho(1|1)_{E_K(i',o')} + \Delta\rho(1|1)_{E_K(o,k')} + \Delta\rho(1|1)_{E_K(o,o')}. \quad (7)$$

$\Delta\rho(1|1)_{E_K(i',k')}$, for instance, indicates the difference electron density caused by the exchange interaction between both DOMO's. The difference electron density including the exchange and charge transfer (CT) interactions, $\Delta\rho(1|1)$, is also given.

Figure 2 illustrates the geometry of assumed reaction models. The geometry of the isolated ER comes from Pople's *ab initio* calculation,[9] and that of the isolated MR is referred to Herzberg's book.[10] The length of all C–H bonds and the C_1–C_2 bond of two isolated systems is kept frozen throughout the calculation. Three reaction models (I, II, and III) are shown in Fig. 2. They are distinguished by the position of MR. Models I and II represent a recombination in which MR attacks the radical center (C_2) of ER, MR approaching ER in the *cis*-conformation in I and in the *trans*-conformation in II. Model III represents a disproportionation in which MR attacks a hydrogen atom (H_3) of ER. In this calculation seven geometrical parameters are introduced to indicate various reaction processes. β is the angle between the methylene plane (H–C_2–H) and C_1–C_2 bond axis of ER in Models I, II, and III. R denotes the distance between C_M of MR and C_2 of ER, and α is the angle between $C_M\cdots C_2$ line and the C–H bond of MR in I and II. θ and θ'

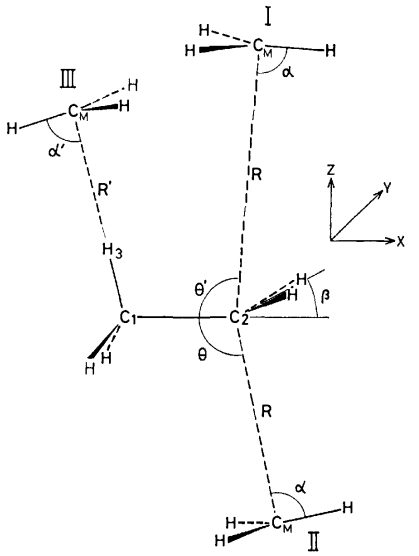

Fig. 2. Three assumed reaction models employed for the calculation of the interaction energy.

stand for the angle between $C_M \cdots C_2$ line and C_1–C_2 bond axis in Models I and II. R' denotes the distance between C_M of MR and H_3 of ER, and α' the angle between $C_M \cdots H_3$ line and the C–H bond of MR in Model III.

Results of Calculation

The interaction energy (ΔW) of Models I and II is given in Table 1. The ΔW of Model I (R=2.7 Å, θ'=100°) is compared with that of Model II (R=2.7 Å, θ=100°). We see that Model II is more favorable for the recombination. The superiority or inferiority of the recombination path is attributable to the two terms of exchange energy, $E_K(i', k')$ and $E_K(i', o')$, (see Fig. 1) and the components originating from o-o' interaction, $E_K(o, o')$, $D(o \rightarrow o')$, and $D(o' \rightarrow o)$. Let us examine the possibility of the three-centered bond exhibited in Scheme 1. If the termination reaction proceeds along Scheme 1, the approach of MR to the C_1–H_3 bond is expected to reduce the ΔW value. In order to see the effect of this geometrical change on each energy, the angle θ' is varied tentatively from 100 to 90° in Model I. This is found to bring about a larger ΔW value, *i.e.*, destabilization of the system (Table 1). In view of the two ΔW's (θ'=100, 90°) of Model I, it is realized that this destabilization comes primarily from the increase of the exchange energy, E_K, and slightly from the decrease of the delocalization energy, D. The analysis of four components of E_K shows that its enlargement is due to the increase of both $E_K(i', k')$ and $E_K(i', o')$ and the decrease of the stabilizing term, $E_K(o, o')$. $D(o \rightarrow o')$ and $D(o' \rightarrow o)$ which are the stabilization energies are reduced by that variation of the geometry. The increase of $E_K(i', k')$ and $E_K(i', o')$ is due to the approach of the electronic cloud of MR to that of the C_1–H_3 bond of ER, whereas the decrease of three stabilizing terms, $E_K(o, o')$, $D(o \rightarrow o')$, and $D(o' \rightarrow o)$ is explained as follows. The SOMO of ER has a node between C_1 and C_2. As MR approaches the C_1–H_3 bond of ER, the out-of-phase overlapping of the SOMO of MR with the lobe of the SOMO of ER localized at C_1 and H_3 becomes larger. The overlap between both the SOMO's becomes small and the stabilization due to $E_K(o, o')$, $D(o \rightarrow o')$, and $D(o' \rightarrow o)$ is reduced by θ'=100→90°.

Table 1. Calculated interaction energies for the recombination and disproportionation of ethyl and methyl radicals

Geometrical parameters, R, R', α, α', β, θ, and θ' are those shown in Fig. 2.

	Model I		Model II		Model III	
R or R' [Å]	2.7	2.7	2.7	2.4	2.4	2.0
α or α' [°]	90	90	90	105	90	105
β [°]	0	0	0	43.2	0	0
θ or θ'[°]	100	90	100	105	—	—
E_Q [eV]	0.020	0.022	0.022	0.069	−0.012	−0.033
$E_K(i', k')$	0.459	0.666	0.394	0.479	0.180	0.452
$E_K(i', o')$	0.190	0.227	0.174	0.338	0.120	0.428
$E_K(o, k')$	0.072	0.057	0.087	0.229	0.010	0.023
$E_K(o, o')$	−0.162	−0.141	−0.178	−0.622	−0.014	−0.047
E_K [eV]	0.559	0.809	0.477	0.424	0.296	0.856
$D(i \rightarrow l)$	0.003	0.007	0.003	0.011	0.001	0.001
$D(k \rightarrow j)$	0.006	0.011	0.004	0.011	0.016	0.030
$D(i \rightarrow o')$	0.072	0.089	0.063	0.108	0.063	0.233
$D(k \rightarrow o)$	0.033	0.030	0.036	0.084	0.001	0.003
$D(o \rightarrow l)$	0.003	0.002	0.003	0.002	0.000	0.000
$D(o' \rightarrow j)$	0.003	0.003	0.003	0.002	0.008	0.019
$D(o \rightarrow o')$	0.103	0.087	0.114	0.377	0.016	0.049
$D(o' \rightarrow o)$	0.110	0.100	0.117	0.372	0.004	0.012
D [eV]	0.333	0.329	0.343	0.967	0.109	0.347
ΔW [eV]	0.246	0.502	0.156	−0.474	0.175	0.476

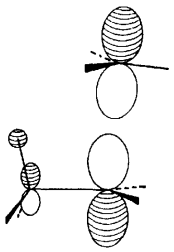
the SOMO of ER

The results show that the process of the radical destruction is not described by Scheme 1 and the recombination takes the route in which MR approaches the radical center, C_2, of ER in the *trans*-conformation to the C_1–H_3 bond of a methyl group of ER.

In Model II (R=2.4 Å, θ=105°), the structural deformation of two radicals is taken into account, *i.e.*, α=90→105° and β=0→43.2°. This deformation operates to reduce the E_K and to increase the absolute value of the stabilization terms, $E_K(o, o')$, $D(o\rightarrow o')$, and $D(o'\rightarrow o)$, making the ΔW negative (Table 1). Thus, the need of the structural deformation of the radical species to promote the reaction is explicable in this MO scheme. The deformation associates the change of the extent of the hybridization ($sp^2\rightarrow sp^3$) of two radical centers, resulting in the growth of the o-o' MO interaction which contributes overwhelmingly to the stabilization of the system. As for Model II (R=2.4 Å), the CI coefficients of Eq. 3 are obtained.

$$\Psi = 0.918\Psi_0 - 0.123\Psi_{o\rightarrow o'} - 0.116\Psi_{o'\rightarrow o} + \cdots. \quad (8)$$

This equation is an alternative expression of the importance of $D(o\rightarrow o')$ and $D(o'\rightarrow o)$ to promote the reaction. From the equation the transition state of the recombination hardly seems to have ionic character due to the almost equal weight of two competing ($o\rightarrow o'$ and $o'\rightarrow o$) CT interactions.

The difference density in the reaction process was investigated with respect to Model II (R=2.4 Å, θ=105°). The density map helps us to visualize the movement of electronic cloud through some types of interactions between ER and MR. Figure 3-a shows the electron redistribution by $\Delta\rho(1|1)_{E_K(i',k')}$ caused by mutual overlap between both the DOMO's. The electron redistribution gives negative contour lines amid the $C_2\cdots C_M$ region, corresponding to the repulsive $E_K(i',k')$. The electron density maps of $\Delta\rho(1|1)_{E_K(i',o')}$ and $\Delta\rho(1|1)_{E_K(o,k')}$ are shown in Figs. 3-b and 3-c. Two terms of the exchange interaction, (i', o') and (o, k'), are seen to reduce the electron density along the $C_2\cdots C_M$ line, reflecting the repulsive character of $E_K(i', o')$ and $E_K(o, k')$. The last component of $\Delta\rho(1|1)_{E_K}$, $\Delta\rho(1|1)_{E_K(o,o')}$, is shown in Fig. 3-d. Since the $E_K(o, o')$ is a considerable stabilization energy (Table 1), $\Delta\rho(1|1)_{E_K(o,o')}$ is expected to give the large bonding density in the middle region between ER and MR. The expectation is confirmed by the central huge build-up of the electron density in this figure. The change of the electron distribution, $\Delta\rho(1|1)$, due to the exchange and CT interactions is shown in Fig. 3-e. It is seen that the addition of CT interaction to the exchange interaction accumulates the electron density significantly in the $C_2\cdots C_M$ region. The electron transfer from ER to MR and the compensating one from MR to ER take place equivalently, the transition state having no ionic character. This result is in line with that pointed out in Eq. 8. The trend of these electron redistributions is similar to that of the recombination of two methyl radicals.[6] From Eq. 8 and Fig. 3, the overlap of two SOMO's, the common origin of $E_K(o, o')$, $D(o\rightarrow o')$, and $D(o'\rightarrow o)$, is shown to contribute remarkably to the new bond formation.

Calculation of the ΔW was carried out with respect to Model III. The results are also given in Table 1. It should be noted that the stabilization components, $E_K(o, o')$, $D(o\rightarrow o')$, and $D(o'\rightarrow o)$, are much smaller (absolute value) in this model than in the two recombination models I and II. The difference is attributable to the fact that the SOMO of ER is localized to a greater extent at the C_2 atom, and the overlap between both two SOMO's in Model III is small. Of the many components of ΔW in Model III, it is $D(i\rightarrow o')$ that gives the greatest stabilization energy to the disproportionation path. Comparing the two geometries of R'=2.4 Å and R'=2.0 Å of Model III, we find that D of R'=2.0 Å is larger than that of R'=2.4 Å, which is mainly due to the increase of its one component, $D(i'\rightarrow o)$, along the decrease of R'. The result shows that the $i\rightarrow o'$ type CT interaction becomes more important with the progress of reaction. In spite of the increase of D, ΔW of R'=2.0 Å is larger that that of R'=2.4 Å (Table 1). The global destabilization of Model III (R'=2.0 Å) is attributable to the increase of the repulsive term, E_K. In this calculation, the extension of the C_1–H_3 bond of ER in the course of disproportionation is not taken into account. In the realistic reaction model with the elongated C_1–H_3 bond, however, E_K would become small because of the separation of MR from ethylene fragment of ER and accordingly its ΔW would be much smaller than the ΔW of Model III which has the constant C_1–H_3 bond length regardless of R'.

In order to find the charge-transferred configuration which contributes most to the stabilization of the reacting system, the CI coefficients are obtained with respect to Model III (R'=2.0 Å).

$$\Psi = 0.955\Psi_0 - 0.120\Psi_{i_4\rightarrow o'} + 0.054\Psi_{o\rightarrow o'} + 0.035\Psi_{i_5\rightarrow o'} + 0.034\Psi_{i_2\rightarrow o'} + 0.024\Psi_{o'\rightarrow o} + \cdots. \quad (9)$$

Terms, i_2, i_4, and i_5, denote the DOMO's of ER and suffix attached to "i" stands for the numbering order counted from the lowest DOMO (see Fig. 1). Equation 9 shows that the CT interaction from i_4 (a') to o' (a_1) is the most important.[11] a' denotes the MO of ER within the X-Z plane belonging to the C_s point group and a_1 the MO of MR along the $C_M\cdots H_3$ line belonging to the C_{3v} point group. The i_4 is localized substantially at the C_1–H_3 bond and is the highest occupied (HO) MO of the C–H bond cleaved by disproportionation.

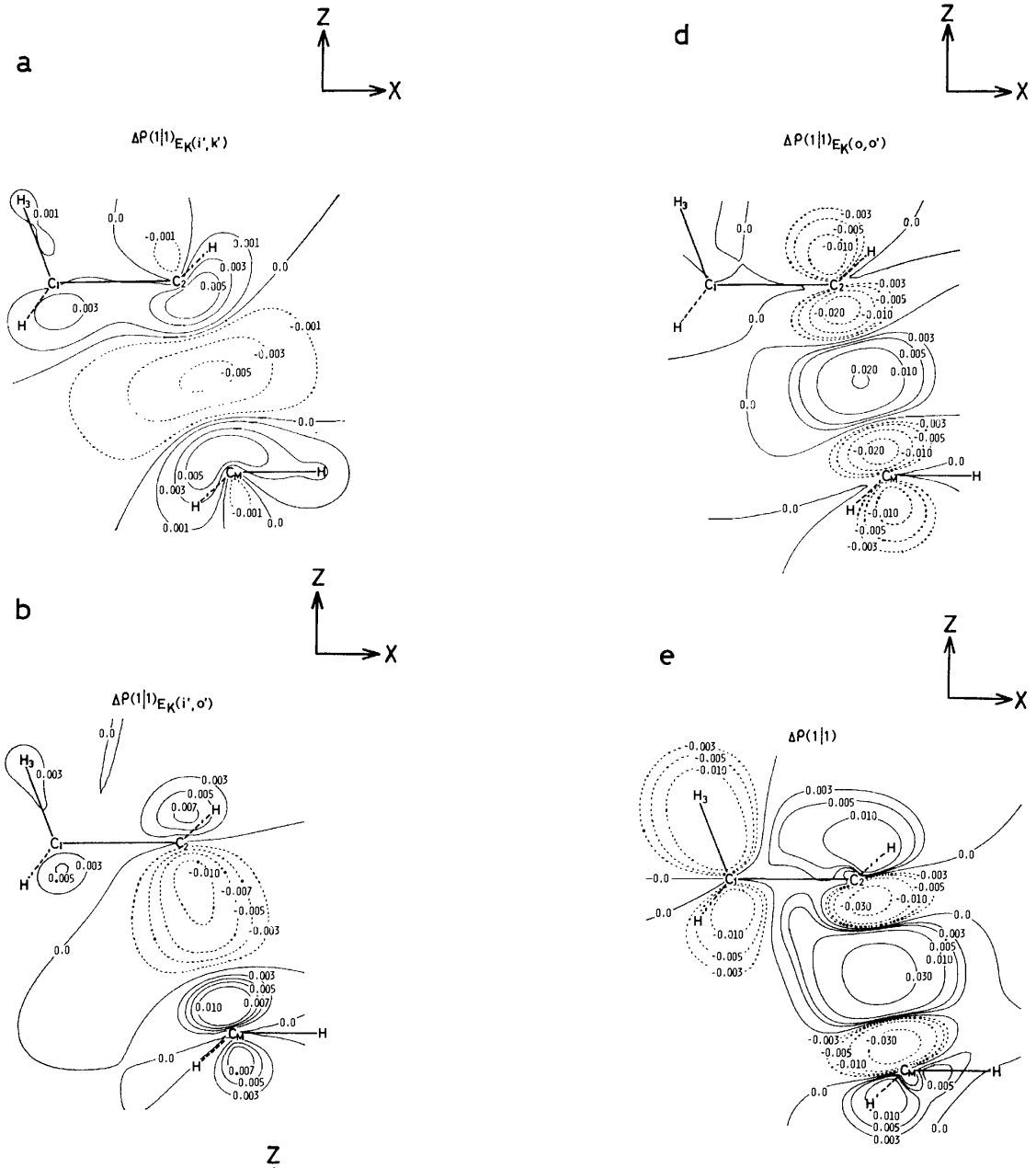

Fig. 3. The difference electron density maps of the recombination between ER and MR in Model II. The number attached to each contour line is in e/Å^3.

a The difference density map of $\Delta\rho(1|1)_{E_K(i',k')}$.
b The difference density map of $\Delta\rho(1|1)_{E_K(i',o')}$.
c The difference density map of $\Delta\rho(1|1)_{E_K(o,k')}$.
d The difference density map of $\Delta\rho(1|1)_{E_K(o,o')}$.
e The difference density map of $\Delta\rho(1|1)$.

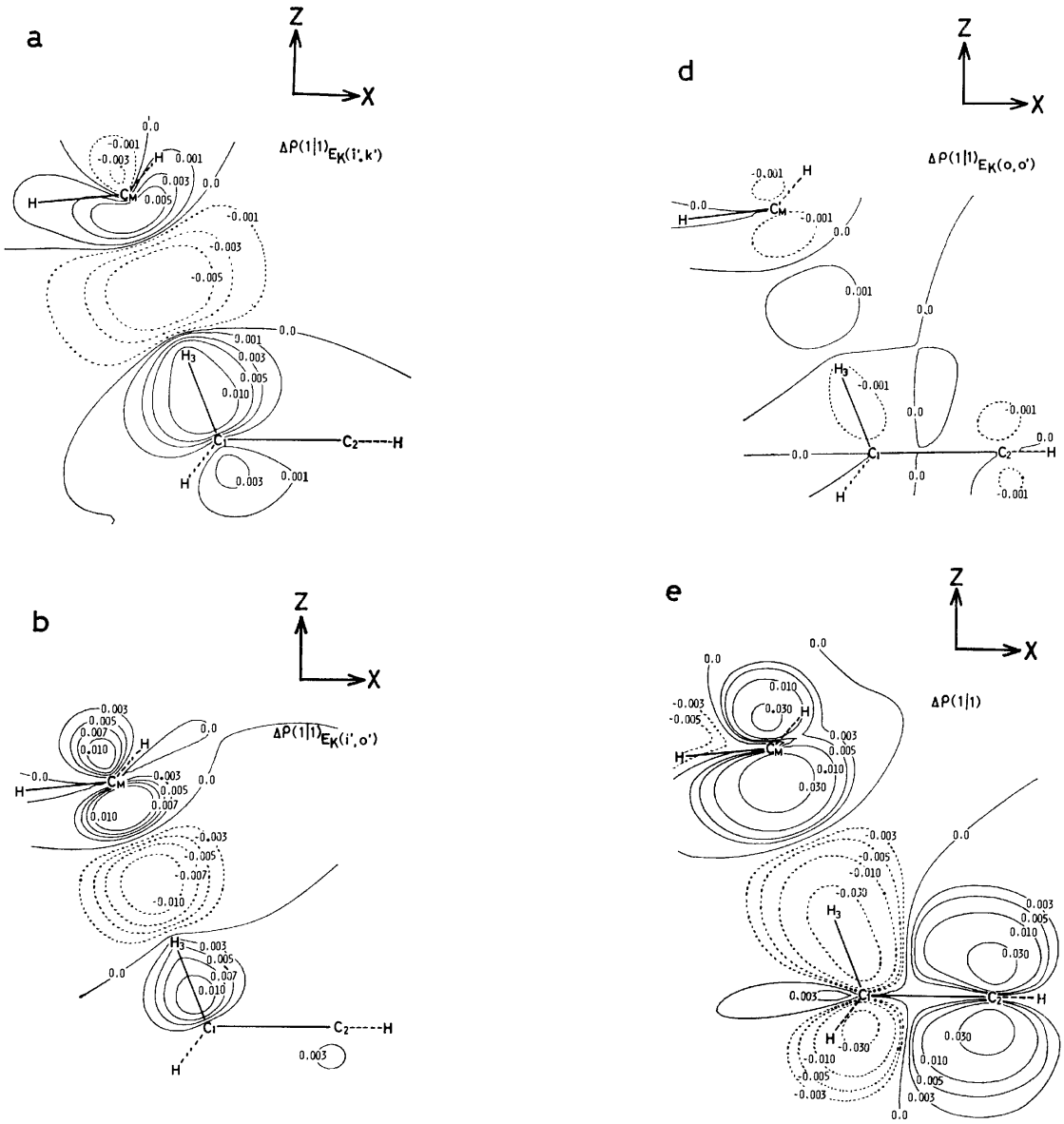

Fig. 4. The difference electron density maps of the disproportionation between ER and MR in Model III. The number attached to each contour line is also in e/Å^3.

a The difference density map of $\Delta\rho(1|1)_{E_K(i',k')}$.
b The difference density map of $\Delta\rho(1|1)_{E_K(i',o')}$.
c The difference density map of $\Delta\rho(1|1)_{E_K(o,k')}$.
d The difference density map of $\Delta\rho(1|1)_{E_K(o,o')}$.
e The difference density map of $\Delta\rho(1|1)$.

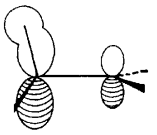

the i_4 MO of ER

The MO of this type is hereafter called the "C–H HOMO." In Model III representing disproportionation, this particular CT interaction plays an important role to weaken the C_1–H_3 bond through the loss of electron density of the i_4, forming a new $C_M \cdots H_3$ bond. From Eq. 9, MR is found to be an electron acceptor and ER to be an electron donor during the course of reaction. This donor-acceptor relation was also observed in a previous work dealing with the hydrogen abstraction reaction of a methane by a methyl radical.[12]

The electron redistribution in disproportionation is evaluated in the same way as in the recombination. Four components of $\Delta\rho(1|1)_{E_K}$ in Eq. 7 are shown separately in Fig. 4. They exhibit the same trend of electron movement as is observed in Fig. 3 of the recombination. $\Delta\rho(1|1)_{E_K(i',k')}$ (Fig. 4-a) show the large amount of the decreased density in the $C_M \cdots H_3$ region. The electron density, running away from this region, is piled up around C_M and the C_1–H_3 bond. The electron density around C_M resembles that of the recombination (Fig. 3-a). The density redistribution, $\Delta\rho(1|1)_{E_K(i',o')}$ (Fig. 4-b) is found to give the decreased density in the $C_M \cdots H_3$ line. Since the overlap between the SOMO of ER and any DOMO of MR is small, the change of the electron arrangement brought about by $\Delta\rho(1|1)_{E_K(o,k')}$ is expected to be minor (Fig. 4-c). The three difference densities, $\Delta\rho(1|1)_{E_K(i',k')}$, $\Delta\rho(1|1)_{E_K(i',o')}$, and $\rho\Delta(1|1)_{E_K(o,k')}$, corresponding to three repulsive energy terms of E_K in Eq. 4 do not contribute to the formation of a new C_M–H_3 bond. The contour map of the electron density of $\Delta\rho(1|1)_{E_K(o,o')}$ is shown in Fig. 4-d. Since the overlap between both SOMO's is smaller in Model III than that in Model II, the density redistribution through $\Delta\rho(1|1)_{E_K(o,o')}$ is not so noticeable in the former model. Figure 4-e shows $\Delta\rho(1|1)$, representing the electron redistribution due to the exchange and CT interactions. The considerable accumulation of the electron density around C_M of MR and C_2 of ER is observed. The diminution of the electron density appears at the C_1–H_3 bond of ER. The electron redistribution shows that the exchange and CT interactions, especially the $i_4 \rightarrow o'$ CT interaction, make electrons of ER flow into MR and that the C_1–H_3 bond is weakened by the loss of bonding electrons. The accumulated electron density around C_M operates to pull the H_3 atom, resulting in the formation of the new C_M–H_3 bond.

The change of atomic charges in Model III ($R'=$ 2.0 Å) is shown in Table 2. We see that the exchange and CT interactions make the charge on the C_M atom of MR more negative and that on the H_3 atom of ER more positive. This indicates that the C_M atom of MR has a negative charge and the H_3 atom of ER has a positive charge at the transition state of disproportionation. The tendency is almost similar to that suggested in the case of the disproportionation of alkoxy radicals. The result showing that the transition state of disproportionation has the ionic character is in agreement with Benson's scheme (Scheme 2b), while that of the recombination has no ionic character as shown with respect to Model II.

Table 2. Change of net charges by the exchange and CT interactions in Model III
A more negative value indicates a larger electron population.

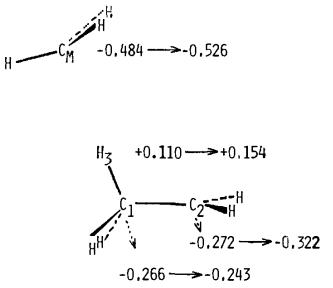

No formation of the π bond between C_1 and C_2 of ER is observed in Fig. 4-e. The absence of the bonding component which is the origin of the π bond in ethylene is attributable to the neglect of the excited configurations in the wave function Ψ of Eq. 3. The process of the π bond formation can be predicted qualitatively, even if the polarization effect is not taken into account explicitly. The orbitals which contribute to the π bond formation are considered to be the i_4 and o, since all residual MO's of ER have no large p_z atomic orbital (AO) component, that is, a π bond character. A schematic representation of the π bond formation by the orbital mixing of i_4 with o through o' is illustrated in Fig. 5.[13] The interaction of o' with o and i_4 gives the ψ_1, ψ_2, and ψ_3 MO's. In a DOMO, ψ_2, o, and o' overlap in phase, whereas i_4 and o' overlap

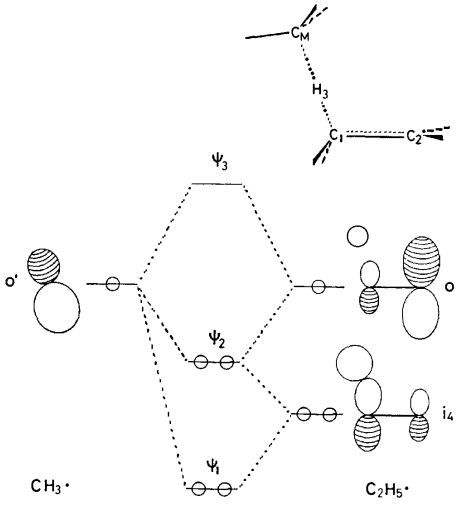

Fig. 5. The schematic representation of the π bond formation of ethyl radical by the orbital mixing of the i_4 and o through the o'. The signs of two MO's (i_4 and o) are chosen so that both of them may have positive overlap integrals with the o'. $\psi_2 = o - i_4 + o'$.

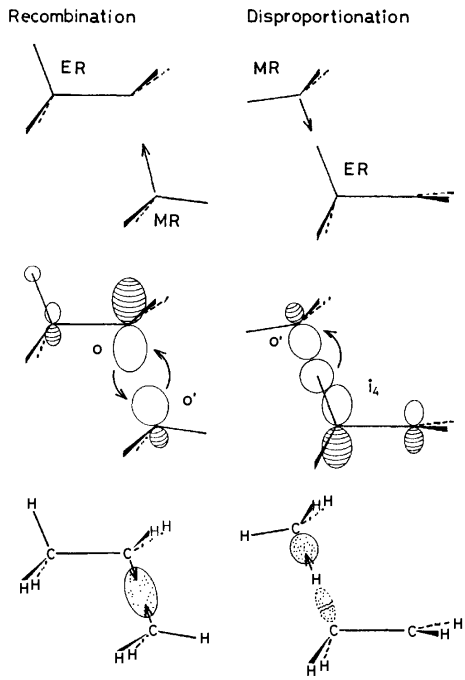

Fig. 6. Schematic representation of the reaction paths of recombination and disproportionation.

out of phase. Consequently in the ϕ_2 orbital the interaction between the lobe at the C_1 atom of i_4 and the lobe at the C_2 atom of o contributes to the π bond formation. Thus, the π bond formation of ER is explained by the orbital mixing of i_4 with o through o'.

Let us summarize our results obtained so far. The reaction pathway of recombination differs a great deal from that of disproportionation, the reactions having no common transition state. This is illustrated schematically in Fig. 6. The SOMO-SOMO interaction is of importance for the progress of the reaction in recombination, whereas the CT interaction from the C–H HOMO (i_4) to the SOMO of one radical directed toward the hydrogen atom of the other is of importance in disproportionation. In the disproportionation, one of radical species which abstracts a hydrogen atom is an electron acceptor and the other radical species which has a hydrogen atom to be abstracted is an electron donor. Consequently the transition state of the disproportionation is expected to have an ionic character. In the recombination, however, this tendency is not observed.

Comparison with Experimental Data

Since the interaction energy, ΔW, is entirely controlled by the extent of the overlap of MO's obtained independently in two radical species, its value can be estimated roughly by analyzing the shape of these MO's. Instead of actual calculation of ΔW, the reactivity of several radical species is conveniently discussed in terms of the shape of some particular MO's. In this section, the theoretical prediction given by such a simple analysis is compared with available experimental data as regards recombination and disproportionation.

Recombination. The simplest way in which odd-electron species are transformed into stable compounds is through the chemical bonding between the radical centers of two such species. However, in a few cases, the recombination takes an unusual path. The dimerization of cyanomethyl radical leads to a ketenimine as well as to the "normal" head-to-head dimer.[14] The former product is an unstable intermediate which rearranges quantitatively to the latter.

$$2R_2\dot{C}\text{—}CN \longrightarrow R_2C\text{—}N{=}C{=}CR_2 + R_2C\text{——}CR_2$$
$$\qquad\qquad\qquad\quad | \qquad\qquad\qquad\qquad\quad | \quad\ |$$
$$\qquad\qquad\qquad\quad CN \qquad\qquad\qquad\qquad CN \quad CN$$

In order to study the reactivity of this radical, the SOMO of cyanomethyl radical is obtained by the extended Hückel (EH) MO method.[15] The shape of the SOMO is as follows.

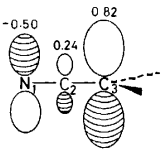

The numbers attached to each lobe denote the coefficients of the AO's of the SOMO. Judging from the shape of the SOMO of cyanomethyl radical, two recombination paths are possible. The first is the formation of the C_3–C_3 bond, giving the latter stable product, the C_3 atom having the largest lobe of the SOMO. The second is the linkage of the N_1 of one radical with the C_3 of the other, giving an abnormal product (ketenimine). The second mode of recombination is probably due to the following. Since N_1 is charged more negatively than C_3, reflecting the difference of electronegativity, the Coulomb long-range force represented by E_Q of Eq. 4 becomes largely attractive by the approach of the $C_3\cdots N_1$. Thus, the second path of recombination is more favorable than the first in the initial stage of reaction. The abnormal recombination product is formed when the carbon radical center of one radical attacks the nitrogen atom of the other.

Disproportionation. Isotopic Effect: The isotopic effect is expected in the disproportionation path shown in Fig. 6. The substitution from H to D on the carbon atom adjacent to the radical center reduces the disproportionation rate constant, k_d, whereas in the recombination path k_c does not seem to be affected so much by this substitution. In Eq. 11, isotopic substitution on the carbon atom adjacent to the radical center has a large effect on the disproportionation, but a small effect on the recombination in Eq. 10 and the disproportionation in Eq. 12. Consequently, the isotopic substitution is expected to reduce k_d/k_c. It is experimentally evident that in the gas, liquid, and solid phases there is a significant kinetic isotopic effect by which the substitution from H to D reduces k_d/k_c.[18] Gibian and Corley measured the k_d/k_c value of $C_6H_5\dot{C}HCH_3$ and $C_6H_5\dot{C}HCD_3$ in the benzene solution, and found the $[k_d/k_c(H)]/[k_d/k_c(D)]$ value to be 1.87.[16] Boddy and Steacie[17] found the k_d/k_c value of $C_2D_5\cdot$ to be 0.0985 in the gase phase, and that of $C_2H_5\cdot$ 0.13,

leading to the ratio $[k_d/k_c(H)]/[k_d/k_c(D)]=1.32$. The data support the reaction paths of recombination and disproportionation assumed throughout the present work.

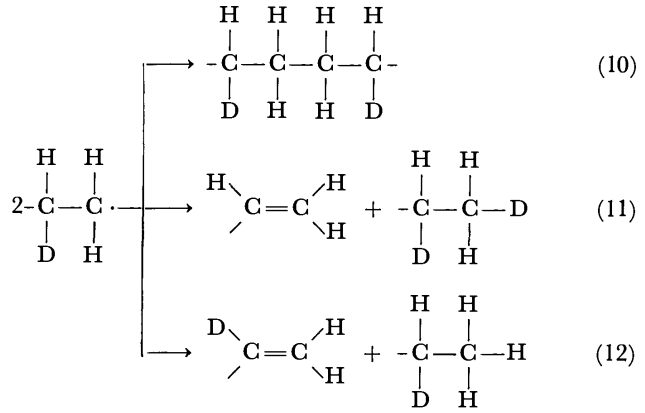

(10)

(11)

(12)

Substitution Effect: The CT interaction from the C–H HOMO of one radical to the SOMO of the other radical is found to be of importance to cause disproportionation. In our calculation of ΔW, the former radical is ER and the latter MR. The result together with $\Delta\rho(1|1)$ of Fig. 4-e leads to the prediction that the disproportionation occurs more easily when the radical receiving an abstracted hydrogen (R) has an electron-accepting group or the radical releasing a hydrogen (R′) has an electron-donating group. Let us examine this substitution effect in more detail. For the sake of convenience, the ratio of the rate constants, k_d/k_c, is denoted by Δ(R, R′). The number of the β-hydrogens of R′ is defined as βH. The large value of Δ(R, R′)/βH indicates the ease of the occurrence of disproportionation.

Table 3 gives the Δ(R, R′) of some small alkyl radical reactions.[1a] The orbital energies of the C–H HOMO of R′ are calculated by the EHMO method. The elevation of the level of the C–H HOMO corresponds to the higher reactivity of the electron-donating radical. The C–H HOMO level of the ethyl radical is found to be raised by the electron donating group. In the disproportionation between the methyl radical and the substituted ethyl radical, the Δ(R, R′)/βH increases as the level of the C–H HOMO of the latter radical rises. This tendency is also observed when the ethyl radical reacts with the substituted ethyl radical (Table 3). This is also understandable from the C–H HOMO level. The inclusion of the electron acceptor group, Cl, to the R′ makes the $\Delta(CCl_3, C_2H_4Cl)/\beta H$ smaller than the $\Delta(CCl_3, C_2H_5)/\beta H$. Although the recombination is assumed to be uninfluenced by the substitution effect, the trend of the above data suggests that the disproportionation rate constant is affected by the energy gap between the SOMO of the radical receiving the hydrogen atom and the C–H HOMO of the radical releasing the hydrogen atom when the height of the SOMO is kept frozen.

Table 3. Ratio of rate constants with the substitution effect

R	R′	Δ(R, R′)	Δ(R, R′)/βH	HOMO level[a] (eV)
$CH_3\cdot$	$CH_3CH_2\cdot$	0.039	0.012	−15.18
	$CH_3CH_2CH_2\cdot$	0.058	0.029	−14.00
	$(CH_3)_2CHCH_2\cdot$	—	—	−13.38
$C_2H_5\cdot$	$CH_3CH_2\cdot$	0.065	0.022	−15.18
	$CH_3CH_2CH_2\cdot$	0.066	0.033	−14.00
	$(CH_3)_2CHCH_2\cdot$	0.04	0.04	−13.38
$CCl_3\cdot$	$CH_3CH_2\cdot$	0.22	0.073	−15.18
	$CH_2ClCH_2\cdot$	0.14	0.070	−15.23

a) The calculated orbital energy of the C-H HOMO (see Text) is indicated.

Solvent Effect: The density map, $\Delta\rho(1|1)$, (Fig. 4-e) shows that the transition state of the disproportionation is polarized in spite of the reaction of two neutral radicals, but not that of recombination. This leads to the expectation that the disproportionation is accelerated in polar solvents, but not recombination. Stefani measured the ratio of the rate constants, k_d/k_c, for the termination reaction of ethyl radicals in various sol-

Table 4. Disproportionation-recombination of ethyl radicals as a function of solvents[a]

	Scavenger	k_d/k_c	δ[b]	Ω	Z[c]	E_T[c]
Gas phase	None	0.14				
Isooctane	None	0.144±0.003	48		60.1	
Isooctane	Styrene	0.145±0.007	48		60.1	
Limonene	None	0.158±0.005	56			
Ethylbenzene	None	0.156±0.001	59			
m-Xylene	None	0.165±0.003	61			
Toluene	None	0.167±0.003	62			33.9
2-Butanol	None	0.168±0.003	68			
2-Propanol	Styrene	0.178±0.001	70		76.3	48.6
1-Propanol	Styrene	0.181±0.003	72		78.3	50.7
Aniline	Styrene	0.195±0.001	75			44.3
Acetonitrile	None	0.200±0.006	83	0.692	71.3	46.0
Acetonitrile	Styrene	0.208±0.006	83	0.692	71.3	46.0
Ethylene glycol	None	0.241±0.003	97		85.1	56.3

a) From Ref. 18. b) Estimated from Fig. 1 of Ref. 18. c) *Cf.*, M. Seno and T. Arai, "Yukikagakuhanno Ni Okeru Yobaikoka," ed by T. Asahara, Sangyotosho, Tokyo (1970).

vents.[18] He found that $\log(k_d/k_c)$ is a linear function of $\sqrt{\delta}$ where δ is the Hildebrand solubility parameter, expressing the internal pressure of the solvent.[19] Herbrandson and Neufeld proposed[20] that δ correlated with various polarity parameters such as Y,[21] Ω,[22] Z,[23] and E_T.[24] The values of k_d/k_c, δ, and these four polarity parameters are given in Table 4. The larger the values of the parameters, the larger the solvent polarity. The transition state of disproportionation is expected to have a polar character to be stabilized by the solvent. This is in line with our proposal of the different ionic characters of recombination and disproportionation.

Alkoxy radicals are known to give very high fractions of disproportionation in comparison with alkyl radicals.[1a] It is suggested that this phenomenon is attributable to the increased polar conditions by an electronegative oxygen atom at the transition state.[25]

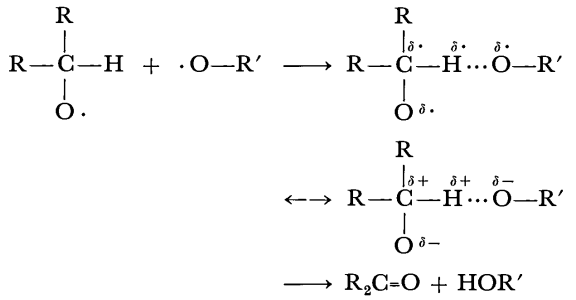

The suggestion that the transition state of the disproportionation of alkoxy radicals has an ionic character supports our view of the transition state of the disproportionation of alkyl radicals.

Conclusion

Recombination, one of two termination reactions, takes a reaction path differing from that of the other termination reaction, disproportionation. These two reactions are shown to have no common transition state. The recombination path is the route by which two radicals approach in such a direction that the overlap between both SOMO's may become maximum. It is suggested that the transition state of recombination is not much polarized. The disproportionation path is the route by which one radical receiving a hydrogen atom attacks the β hydrogen atom of the other radical. The CT interaction from the C–H HOMO of one radical to the SOMO of the other abstracting a hydrogen atom plays an important role to cause disproportionation. The radical receiving a hydrogen atom is found to be an electron acceptor and the radical with the C–H bond broken in the disproportionation an electron donor. The transition state of disproportionation is shown to have a polar character.

We would like to express our gratitude to the staff of the Data Processing Center, Kyoto University, for permission to use the FACOM 230-75 computer. The MO calculation was carried out with financial support of the Ministry of Education (Grant-in-Aid 139012).

References

1) (a) M. J. Gibian and R. C. Corley, *Chem. Rev.*, **73**, 441 (1973); (b) J. A. Kerr, "Free Radicals," Vol. 1, ed by J. K. Kochi, John Wiley & Sons, New York, N. Y. (1973).
2) J. A. Kerr and A. F. Trotman-Dickenson, *Prog. React. Kinet.*, **1**, 107 (1961).
3) (a) S. W. Benson, *Adv. Photochem.*, **2**, 1 (1964); (b) H. A. Gillis, *Can. J. Chem.*, **49**, 2861 (1971).
4) J. N. Bradley and B. S. Rabinovitch, *J. Chem. Phys.*, **36**, 3498 (1962).
5) O. K. Rice, *J. Phys. Chem.*, **65**, 1588 (1961).
6) S. Yamabe, T. Minato, H. Fujimoto, and K. Fukui, unpublished result (1977).
7) T. Yonezawa, K. Yamaguchi, and H. Kato, *Bull. Chem. Soc. Jpn.*, **40**, 536 (1967).
8) K. Fukui, H. Fujimoto, and S. Yamabe, *J. Phys. Chem.*, **76**, 232 (1972).
9) W. A. Lathan, W. J. Hehre, and J. A. Pople, *J. Am. Chem. Soc.*, **93**, 808 (1971).
10) G. Herzberg, "Molecular Spectra and Structure," D. Van Nostrand Co., New York (1966).
11) It should be noted that when a radical receiving a hydrogen atom has a high-lying SOMO, or a radical giving a hydrogen atom has the lowest unoccupied (LU) MO with a very low energy localized at the C–H bond, the CT interaction from the SOMO to the LUMO could be more important than that from the particular DOMO to the SOMO.
12) H. Fujimoto, S. Yamabe, T. Minato, and K. Fukui, *J. Am. Chem. Soc.*, **94**, 9205 (1972).
13) S. Inagaki, H. Fujimoto, and K. Fukui, *J. Am. Chem. Soc.*, **98**, 4054 (1976).
14) (a) C. G. Hammond, O. D. Trapp, R. T. Keys, and D. L. Neff, *J. Am. Chem. Soc.*, **81**, 4878 (1959); (b) G. Ayrey, K. L. Evans, and D. J. D. Wong, *Eur. Polym. J.*, **9**, 1347 (1973).
15) R. Hoffmann, *J. Chem. Phys.*, **39**, 1397 (1963).
16) M. J. Gibian and R. C. Corley, *J. Am. Chem. Soc.*, **94**, 4178 (1972).
17) P. J. Boddy and E. W. Steacie, *Can. J. Chem.*, **38**, 1576 (1960).
18) A. P. Stefani, *J. Am. Chem. Soc.*, **90**, 1694 (1968).
19) J. H. Hildebrand and R. L. Scott, "Regular Solutions," Prentice-Hall, Inc., Englewood Cliffs, N. J. (1962).
20) H. F. Herbrandson and F. R. Neufeld, *J. Org. Chem.*, **31**, 1140 (1966).
21) A. H. Fainberg and S. Winstein, *J. Am. Chem. Soc.*, **78**, 2770 (1956).
22) J. A. Berson, Z. Hamlet, and W. A. Mueller, *J. Am. Chem. Soc.*, **84**, 297 (1962).
23) E. M. Kosower, *J. Am. Chem. Soc.*, **80**, 3253 (1958).
24) K. Dimroth, C. Reichardt, T. Siepmann, and F. Bohlmann, *Ann. Chem.*, **661**, 1 (1963).
25) D. F. Dever and J. G. Calvert, *J. Am. Chem. Soc.*, **84**, 1362 (1962).

The Electronic Structure and Homolytic Dissociation of Dibenzoyl Peroxide

Osamu KIKUCHI, Akihisa HIYAMA, Hiroshi YOSHIDA, and Keizo SUZUKI

Institute of Chemistry, The University of Tsukuba, Sakura-mura, Ibaraki 300-31

(Received May 12, 1977)

The conformations and electronic structures of dibenzoyl peroxide (BPO) and the benzoyloxyl radical (PhCOO) were elucidated by means of closed-shell and restricted open-shell SCF MINDO/3 calculations. The dihedral angle of BPO between the two PhCOO planes was predicted to be 115°, and the barrier to the *trans* form of BPO was estimated to be very small. The ground state of the PhCOO radical was predicted to be of the Σ-type. The non-planar conformation of PhCOO was more stable (2 kcal/mol) than the planar one. The variation in the radical-pair property of the lowest state of acetyl peroxide during the homolytic dissociation process was estimated by the analysis of the two-configuration wavefunctions. The substituent effect on the rate of the homolytic dissociation of BPO was discussed in terms of the electronic structures of substituted BPO.

Dibenzoyl peroxide (BPO) undergoes a variety of reactions because of its weak peroxy O–O bond. A typical process is the simple homolytic cleavage of the O–O bond to form benzoyloxyl radicals:

$$C_6H_5\text{-}\overset{\overset{O}{\|}}{C}\text{-}O\text{-}O\text{-}\overset{\overset{O}{\|}}{C}\text{-}C_6H_5 \longrightarrow 2C_6H_5\text{-}\overset{\overset{O}{\|}}{C}\text{-}O\cdot \qquad (1)$$

Numerous investigations[1] have been experimentally performed on the mechanism of (1) and of the successive reactions. The substituent effect[2] on Reaction (1) has been observed; the rate constant correlates with the Hammet σ constant with $\rho=-0.38$. This substituent effect was explained in terms of the electrostatic repulsion between the two peroxy oxygen atoms[2] or that between the two carbonyl oxygen atoms.[3] These explanations are qualitative ones, and no MO-theoretical studies have been reported on the electronic structures of BPO and the benzoyloxyl radical[4] in connection with the dissociation process of BPO. The purposes of this paper are (i) to examine the electronic structures of BPO, substituted BPO, and the benzoyloxyl radical; (ii) to explain the substituent effect on the rate of the O–O cleavage in terms of the electronic structure of BPO, and (iii) to consider the variation in the electronic structure of BPO during its homolytic dissociation process. The results obtained here will be useful for the understanding of a variety of reactions involving BPO and the benzoyloxyl radical.

Method

The MINDO/3 method[5] was employed to determine the most favorable conformation of BPO. Since a large number of geometrical parameters are involved in BPO, the geometry of diacetyl peroxide (APO) was first optimized; the parameters obtained for the COO groups in APO were then employed in the calculations of BPO. The bond lengths and bond angles of the phenyl groups (CC=1.397 Å, CH=1.087 Å, CCC=CCH=120°)[6] were not optimized. Only two parameters, the peroxy O–O bond length and the dihedral angle between the two PhCOO planes, were optimized. The total energy of BPO was partitioned into atomic energies and atom-atom energies in order to elucidate the electronic factors affecting the conformation of BPO. According to Fischer and Kollmar,[7] the total energy of a molecule can be partitioned into one-center and two-center terms:

$$E_{\text{total}} = \sum_{A} E_A + \sum_{A>B} E_{A,B}, \qquad (2)$$

where the two-center energy between the A and B atoms can be written in the form:[7]

$$E_{A,B} = E^{R}_{A,B} + E^{K}_{A,B} + (E^{J}_{A,B} + E^{V}_{A,B} + E^{N}_{A,B}). \qquad (3)$$

$E^{R}_{A,B}$ is the contribution of the resonance integrals to $E_{A,B}$, $E^{K}_{A,B}$ is the corresponding term of the electronic exchange interaction, and the third term in parentheses is the electrostatic interaction energy between the A and B atoms.

The conformation and electronic structure of the benzoyloxyl radical (PhCOO) were discussed on the basis of the interactions between the MO's of the phenyl radical and those of the bent COO fragment. These discussions were supported by the restricted open-shell SCF calculations with the MINDO/3 approximation. The open-shell SCF method employed was the approximate one proposed by Longuet-Higgins and Pople.[8] The general SCF theory,[9] which gives correct variational solutions for the open-shell problems, was also used to confirm the results obtained by the approximate open-shell SCF calculations.

The small configuration interation (CI) calculations, in which only two configurations related to the σ and σ^* MO's of the peroxy O–O bond were taken into account, were carried out to obtain the qualitative potential curves during the dissociation process (1). As may be seen from Fig. 1, the energy difference between the σ and σ^* orbitals of the peroxy O–O bond becomes small when the O–O distance, R_{OO}, increases.

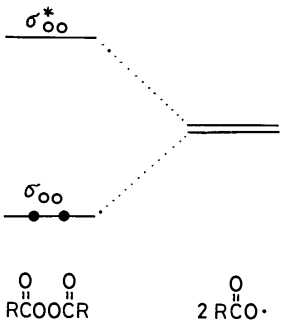

Fig. 1. The correlation diagram for the peroxy O–O σ orbitals along the dissociation process.

Therefore, reliable potential curves of acyl peroxide along the O–O bond cleavage cannot be obtained by the single-configuration wavefunction:[10]

$$\Psi_g = |\cdots\sigma^2\sigma^{*0}|, \quad (4)$$

$$\sigma = \frac{1}{\sqrt{2}}(\chi_a + \chi_b), \quad (5)$$

$$\sigma^* = \frac{1}{\sqrt{2}}(\chi_a - \chi_b), \quad (6)$$

where χ_a and χ_b are the AO's of the two peroxy oxygen atoms, whose directions are parallel to the O–O bond. Near the equilibrium O–O distance, the ground state of acyl peroxide can well be described by Ψ_g, and the mixing of Ψ_g with the excited configuration:

$$\Psi'' = |\cdots\sigma^0\sigma^{*2}|, \quad (7)$$

is very small. When R_{OO} increases, the mixing between Ψ_g and Ψ'' becomes very large and a linear combination of them must be used for the wavefunction of the lowest state. The potential curves were thus calculated by the CI calculations in which Ψ_g and Ψ'' were included. The two-configuration wavefunctions were then analyzed, and the radical-pair property of the RCOO–OOCR system was estimated during the dissociation process of (1).

Results and Discussion

Conformation of BPO. The most stable conformation of BPO predicted by MINDO/3 is shown in Fig. 2. The predicted O–O distance, 1.41 Å, is smaller than the observed value[11] by 0.05 Å, and the dihedral angle, 115°, is slightly larger than the observed value ($\simeq$90°)[11] of BPO. It is interesting that these values are identical with those predicted for APO, despite the large difference in the substituents of BPO and APO. Figure 3 shows the energy variations of BPO and APO with respect to the rotation angle about the peroxy O–O bond. The barrier to a *cis* form was very large($\approx$40 kcal/mol), while that to a *trans* form was very small (1 kcal/mol).

Three factors may be important in analyzing the favorable conformation of BPO: (i) Electron delocalization over both the COO groups through the peroxy O–O bond; (ii) electro-static repulsion between the two carbonyl oxygen atoms, which makes the dihedral angle large, and (iii) the interaction between the lone-pair electrons of the peroxy O–O atoms, which is sensitive to the dihedral angle. These factors were examined on the basis of the partitioned energies. The large dependence upon the dihedral angle, θ, was recognized in the two-center energies between two peroxy oxygen atoms and in those between two carbonyl groups. In Fig. 4, the two-center energy between the two peroxy oxygen atoms, $E_{1,5}$, and that between two carbonyl oxygens, $E_{3,7}$, are plotted. The electrostatic repulsion between two peroxy oxygens, $E^J_{1,5}+E^V_{1,5}+E^N_{1,5}$, was almost constant at any value of θ, because the atomic electron densities of the peroxy oxygen atoms were almost constant to the rotation angle. The lowering of $E_{1,5}$ in the region of θ=60—90° comes from the stabilization of the O–O bond due to the resonance energy:

$$E^R_{1,5} = 2\sum_{r,s} P_{rs}H^{core}_{rs}, \quad (8)$$

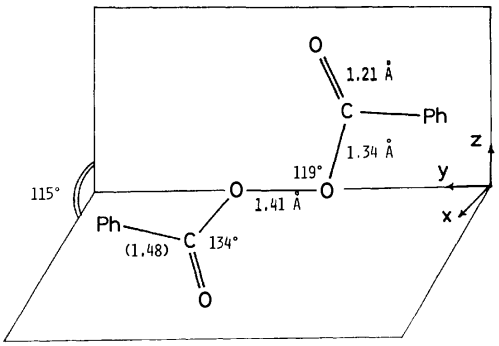

Fig. 2. The predicted geometry of BPO.

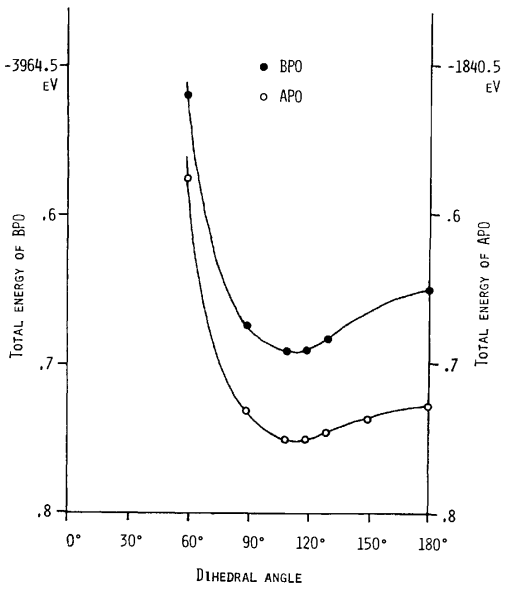

Fig. 3. Dependence of total energies of BPO and APO upon the dihedral angle between two RCOO planes.

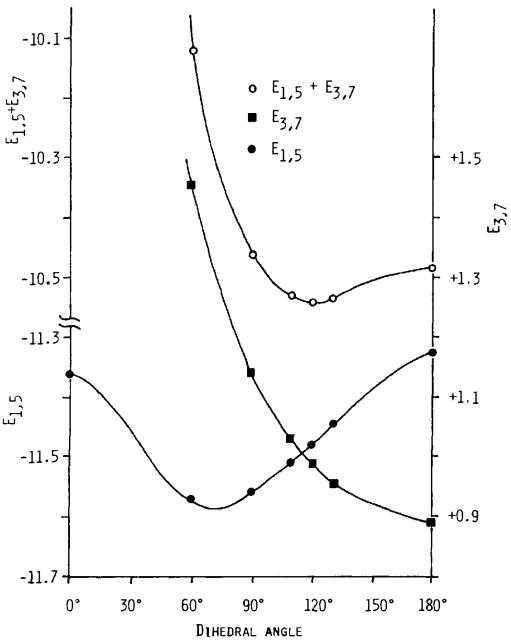

Fig. 4. Dependence of two-center energies of BPO upon the dihedral angle between two PhCOO planes.

Table 1. Electron densities on the COO groups and bond orders between the peroxy oxygen atoms in substituted BPO[a)]

R_1	R_2	Atomic electron density[b)]						Bond order[c)]	
		O1	O5	C2	C6	O3	O7	$P_{1y,5y}$	$P_{1x,5x}+P_{1z,5z}$
OCH_3	OCH_3	6.270	6.270	3.207	3.207	6.570	6.570	0.8933	0.1695
OCH_3	H	6.269	6.267	3.206	3.215	6.570	6.565	0.8932	0.1701
CH_3	CH_3	6.267	6.267	3.215	3.215	6.564	6.564	0.8932	0.1708
CH_3	H	6.267	6.266	3.215	3.215	6.564	6.564	0.8932	0.1708
H	H	6.268	6.268	3.215	3.215	6.562	6.562	0.8932	0.1705
CN	H	6.266	6.266	3.217	3.217	6.559	6.561	0.8932	0.1710
CN	CN	6.266	6.266	3.217	3.217	6.558	6.558	0.8933	0.1711
NO_2	H	6.267	6.264	3.221	3.216	6.548	6.558	0.8931	0.1716
NO_2	NO_2	6.263	6.263	3.219	3.219	6.547	6.547	0.8932	0.1723
OCH_3	NO_2	6.267	6.267	3.208	3.221	6.565	6.549	0.8930	0.1710

a) The geometry of unsubstituted BPO predicted in this paper was employed in the calculations.

b) 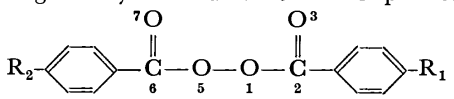

c) The axes, x, y, and z, are shown in Fig. 1. The positive values correspond to the bonding character.

where P_{rs} and H_{rs}^{core} have the usual meanings. The resonance energy between peroxy oxygens decreases (becomes more stable) as a result of the mixing of the lone-pair electrons with the π-electrons of the adjacent carbonyl group.

The electrostatic repulsion energy between two carbonyl oxygens decreases rapidly with increase in θ, because the distance between two carbonyl oxygens increases with θ. This electrostatic energy is dominant in $E_{3,7}$. The angular dependence of $E_{1,5}+E_{3,7}$ shown in Fig. 4 resembles that of the total energy of BPO shown in Fig. 3 The dihedral angle of BPO can thus be interpreted in terms of two factors, the electrostatic repulsion energy between two carbonyl oxygens and the resonance energy between two peroxy oxygens.

Electron Distribution in BPO. Since the rate of the dissociation of BPO depends on the substituents introduced in the phenyl group,[2)] it is worthwhile examining the electronic structures of substituted BPO. Nine substituted BPO were calculated using the conformation of unsubstituted BPO shown in Fig. 2. The electron densities on the carbonyl and peroxy groups and the bond orders between the peroxy oxygen atoms are listed in Table 1. The electron densities appear to reflect gently the characters of the substituents; the electron-withdrawing group, for example, reduces the electron densities on both the peroxy and carbonyl oxygen atoms. The bond order between AO's whose directions are perpendicular to the O–O bond also reflects the characters of the substituents. The effect of CH_3 groups on the electron distribution is very small, perhaps because the $(COO)_2$ group itself has an electron-donating character.

Electronic Structure of the Benzoyloxyl Radical. The energy levels and qualitative pictures of the MO's of the C_∞ CO_2 molecule and those of the bent C_{2v} COO fragment are shown in Fig. 5. A reduction of the symmetry property of CO_2 from C_∞ to C_{2v} causes (i) a rise in the orbital energies of π° and $\bar{\pi}^\circ$ orbitals because of the anti-bonding interaction between the terminal p orbitals, and (ii) a lowering of the 5σ orbital due to the strong mixing of this orbital with the $\bar{\pi}^*$ orbital. Since the instabilization of the $\bar{\pi}^\circ$ orbital is larger than that of the π° orbital, an inversion of the MO levels of $4a_1$ and $3b_2$ is expected for the small OCO angle ($<120°$).

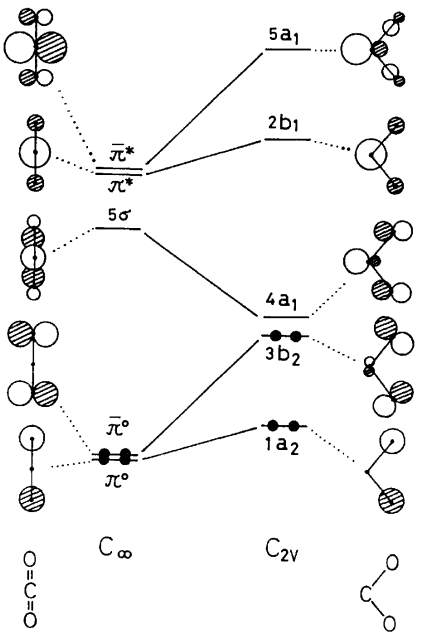

Fig. 5. Energy levels and qualitative pictures of some higher-occupied and lower-unoccupied MO's of the C_∞ CO_2 molecule and the bent CO_2 fragment.

The stability of the PhCOO radical can be elucidated by the interaction between the bent COO fragment and the phenyl radical. The half-occupied MO of the phenyl radical interacts with the unoccupied $4a_1$ MO of COO to form the Ph–COO bond. Since only one electron occupies the newly formed PhCOO bond, the $^2A_1$ state of PhCOO can be expected to break its Ph–COO bond easily to produce the phenyl radical

and CO_2. One-electron migration from the doubly-occupied $3b_2$ orbital to the half-occupied $4a_1$ orbital of the PhCOO radical makes the Ph–COO bond strong. Thus, the stable $^2B_2$ state of the PhCOO radical is expected for the small OCO angle. Since a larger energy is required for the electron migration from la_2 (π) to $4a_1$, the $^2A_2$ state (π-radical) of PhCOO can be expected to be more unstable than the $^2B_2$ state.

The above qualitative discussions were supported by open-shell SCF calculations. Calculations were performed by restricting the COO geometry of PhCOO to C_{2v}. When the OCO angle is 100—120°, the lowest state of PhCOO was predicted to be the $^2B_2$ state (the σ-radical whose unpaired electron occupies the $3b_2$ orbital shown in Fig. 5). When the OCO angle is larger than 130°, the lowest state was $^2A_1$ (σ-radical) and the Ph–COO bond length becomes long. This indicates that the lowest state for OCO>130° is the intermediate stage in the decarboxylation process of PhCOO. The π-state was higher than the σ-state for the entire range of OCO angles. Recently, the σ-ground state of the acyloxyl radical was predicted by semi-empirical NDDO calculations of HCOO and CH_3-COO[12] and by *ab initio* STO-3G calculations of H-COO.[13] However, the σ-ground state predicted in these studies is a distorted one (C_s symmetry), in which the two C–O bond lengths differ from one another. In the present MINDO/3 calculations, the energy lowering caused by the distortion of the OCO geometry was not observed even if the general SCF theory was employed.

The energy dependence of the lowest $^2B_2$ state of PhCOO upon the dihedral angle between the phenyl and COO planes was calculated. The non-planar conformations were more stable than the planar one. When the two planes were perpendicular to each other, the PhCOO radical was the most stable. However, the barrier to the rotation about the Ph–COO bond was very small (2 kcal/mol). The spin delocalization from the COO group into the phenyl group was very small (less than 0.5%) for both the planar and non-planar PhCOO radicals.

Potential Curves and Radical-pair Property during the Homolytic Dissociation. Variations in the electronic properties of APO during the homolytic dissociation process were examined by two-configuration CI calculations in which Ψ_g and Ψ'' were included. The potential curves obtained are shown in Fig. 6, while the wavefunctions of the lowest state are listed in Table 2. It may be seen from Table 2 that the lowest wavefunction at $R_{OO}=\infty$ is

$$\Phi_\infty = \frac{1}{\sqrt{2}}\{\Psi_g - \Psi''\}. \quad (9)$$

This state can be analyzed by expressing the wavefunction in terms of the orbitals of two separate fragments:[14]

$$\Phi_\infty = |\cdots\chi_a^1| \times |\cdots\chi_b^1|, \quad (10)$$

using Eqs. 4—7. It is clear that this wavefunction corresponds to the two-radical, or the radical-pair, state, and that the ground state of acyl peroxide correlates with a pair of acyloxyl radicals at $R_{OO}=\infty$.

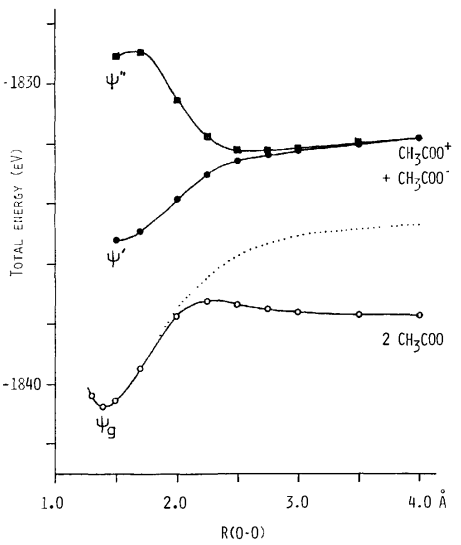

Fig. 6. Potential curves for APO obtained by 2-configuration CI calculations. The dotted line indicates the energy of the single-configuration wavefunction. The Ψ' line corresponds to the electron configuration of $(\cdots\sigma^1\sigma^{*1})$.

TABLE 2. VARIATION IN THE LOWEST WAVEFUNCTION OF APO DURING THE DISSOCIATION OF THE PEROXY O-O BOND

R_{OO} (Å)	Total energy (eV)	Coeffeicients of Ψ_g	Coeffeicients of Ψ''	Radical-pair property (%)
1.30	−1840.378	0.9997	−0.0239	2.5
1.41	−1840.739	0.9996	−0.0285	2.9
1.50	−1840.551	0.9994	−0.0357	3.7
1.70	−1839.469	0.9978	−0.0671	7.2
2.00	−1837.761	0.9857	−0.1685	19.5
2.25	−1837.253	0.9239	−0.3827	50.0
2.50	−1837.342	0.8339	−0.5520	76.5
2.75	−1837.513	0.7723	−0.6353	89.4
3.00	−1837.625	0.7403	−0.6723	95.0
4.00	−1837.750	0.7105	−0.7037	99.5

Similar treatment is possible for the degcnerate states at $R_{OO}=\infty$. They correspond to the ionic states: $RCOO^+$ plus $RCOO^-$ and $RCOO^-$ plus $RCOO^+$.

Since the wavefunction of APO at $R_{OO}=\infty$, $(\Psi_g-\Psi'')/\sqrt{2}$, represents the pure radical-pair, the contribution of this term to the lowest state may be a measure of the radical-pair property of the RCOO–OOCR system. In this sense, the radical-pair property involved in the lowest state of APO was analyzed during the dissociation process. The wavefunction at an arbitrary R_{OO} is expressed by:

$$\Phi \equiv c\Psi_g - d\Psi'' = (c-d)\Psi_g + \sqrt{2}d\left\{\frac{1}{\sqrt{2}}(\Psi_g-\Psi'')\right\}, \quad (11)$$

with $c^2+d^2=1$. The radical-pair property of Φ is thus expressed by:

$$(\sqrt{2}d)^2\left\langle \frac{1}{\sqrt{2}}(\Psi_g-\Psi'')\middle|\frac{1}{\sqrt{2}}(\Psi_g-\Psi'')\right\rangle + (c-d)\sqrt{2}d\left\langle \Psi_g\middle|\frac{1}{\sqrt{2}}(\Psi_g-\Psi'')\right\rangle = d^2+cd, \quad (12)$$

and the covalent-bond property is similarily expressed by c^2-cd. The calculated radical-pair properties of APO during the homolytic dissociation process are listed in Table 2. When $R_{OO}>2.25$ Å, the RCOO–OOCR system can be considered to be a weakly interacting radical pair, while for $R_{OO}<2.25$ Å the covalent-bond property of RCOO–OOCR increases rapidly.

The dissociation energy and the activation energy calculated for the O–O bond cleavage of APO is considerably larger than the observed value ($\simeq$30 kcal/mol).[1,2] In Fig. 6, a large activation energy is predicted for the recombination process of the active acetyloxyl radical. These results may come from the method of calculation employed here where (i) only small configurations were taken into account; (ii) the geometrical parameters involved were not optimized during the dissociation process, and (iii) the inaccuracy inherently involved in the MINDO/3 approximation was not estimated. Thus, any quantitative discussion about the reaction energies may be risky.

Substituent Effect on the Dissociation of BPO. Swain *et al.*[2a] studied the dissociation process of many substituted BPO and found that the electron-withdrawing substituents reduced the rate of the dissociation, while the electron-donating substituents increased the rate. This effect was explained[2a] in terms of the electrostatic repulsion between the two peroxy oxygen atoms, which is reduced by the electron-withdrawing group and which is increased by the electron-donating group. The calculated results (Table 1) reflect the substituent effect pointed out by Swain *et al.* However, the effect is very small. The importance of the electrostatic repulsion between the carbonyl oxygen atoms was pointed out by Imoto.[3] The calculated results show that the electron-donating group increases the repulsion energy between carbonyl oxygens. However, as may be seen from Fig. 3, the barrier to the *trans* form of BPO is expected to be very small, and the increased repulsion between carbonyl oxygens is compensated for by increasing of the dihedral angle, θ.

The bond order between peroxy oxygen atoms, $P_{1y,5y}$, shown in Table 1 is almost constant and fails to explain the substituent effect on the dissociation rate.

Another explanation is more reasonable. When the electron-donating group is introduced to the phenyl group, the electron densities on the carbonyl oxygen atoms increase (Table 1) and the electrostatic repulsion between the oxygen atoms increases. This makes the dihedral angle, θ, large without any appreciable loss of energy, since the barrier to the *trans* form is very small (Fig. 3). The resonance energy between the O–O atoms increases (becomes more unstable) with the increase in the dihedral angle (Fig. 4). As a result, the introduction of the electron-donating group into the phenyl group makes the peroxy bond weak and makes the dissociation of the O–O bond easy.

The radical-pair property defined here may be a measure of the weakness of the O–O bond of BPO. A substituted BPO, in which a large radical-pair property is inherently involved, can be expected to have a low activation energy. The calculated radical-pair properties of *p,p'*-dinitro-BPO (1.5%), unsubstituted BPO (2.1%), *p,p'*-dimethoxy-BPO (2.2%), and APO (2.9%) agreed with the trend of the experimental rates of the dissociation.

One of the authors, O. K., wishes to express his thanks to Professor Katsumi Tokumaru and to Dr. Ken Fujimori for their useful suggestions.

References

1) T. Koenig, "Free Radicals I," ed by J. K. Kochi, John Wiley & Sons, New York (1973), p. 113; Y. Ogata, "Chemistry of Organic Peroxides," Nankodo, Tokyo (1971), p. 170.

2) (a) C. G. Swain, W. H. Stockmayer, and J. T. Clarke, *J. Am. Chem. Soc.*, **72**, 5426 (1950) ; (b) A. T. Blomquist and A. J. Buselli, *J. Am. Chem. Soc.*, **73**, 3883 (1951).

3) M. Imoto, "Theory of Organic Reactions," Kyoritsu Shuppan, Tokyo (1961), p. 430.

4) INDO calculations of BPO were reported by N. J. Karch, E. T. Koh, B. L. Whitsel, and J. M. McBride, *J. Am. Chem. Soc.*, **97**, 6729(1975).

5) R. C. Bingham, M. J. S. Dewar, and D. H. Lo, *J. Am. Chem. Soc.*, **97**, 1285, 1294, 1302, 1307 (1975).

6) E. Sutton, "Tables of Interatomic Distances," Special Publications No. 11, The Chemical Society, London (1958).

7) H. Fischer and H. Kollmar, *Theor. Chim. Acta*, **16**, 163(1970).

8) H. C. Longuet-Higgins and J. A. Pople, *Proc. Phys. Soc.*, **68**, 591(1955).

9) K. Hirao and H. Nakatsuji, *J. Chem. Phys.*, **59**, 1457 (1973).

10) O. Kikuchi and K. Aoki, *Bull. Chem. Soc. Jpn.*, **47**, 2915 (1974).

11) M. Sax and R.K. McMullan, *Acta Crystallogr.*, **22**, 281 (1967); W. Lobunez, J. R. Rittenhouse, and J. G. Miller, *J. Am. Chem. Soc.*, **80**, 3505 (1958).

12) O. Kikuchi, K. Utsumi, and K. Suzuki, *Bull. Chem. Soc. Jpn.*, **50**, 1399(1977).

13) O. Kikuchi, *Tetrahedron Lett.*, **1977**, 2421.

14) O. Kikuchi, *Chem. Lett.*, **1972**, 1121.

MINDO/3 Study of 7-Norbornyl, 7-Norbornenyl, and 7-Norbornadienyl Cations

Akio FURUSAKI and Takeshi MATSUMOTO

Department of Chemistry, Faculty of Science, Hokkaido University, Kita-ku, Sapporo 060

(Received June 9, 1977)

The geometries, charge distributions, and heats of formation for 7-norbornyl, 7-norbornenyl, and 7-norbornadienyl cations have been calculated by the use of the semi-empirical MINDO/3 SCF MO method. Each of these cations is symmetrical with respect to the plane which contains the C(7)–H(7) bond and bisects the C(1)–C(7)–C(4) angle. Both the 7-norbornenyl and the 7-norbornadienyl cations take the nonclassical bridge-structure: the C(2)–C(3) and C(2)–C(7) distances are about 1.43 and 1.67 Å respectively, and the C(2)–C(1)–C(4)–C(7) dihedral angle is about 75°. The classical 7-norbornyl cation also is quite unsymmetrical with regard to the C(1)–C(7)–C(4) plane: the C(2)–C(1)–C(4)–C(7) and C(7)–C(1)–C(4)–C(5) dihedral angles are 94° and 144°, respectively. The calculated barriers to the bridge flipping in the 7-norbornyl and 7-norbornadienyl cations are 3.2 and 33.0 kcal/mol respectively. Although the latter is much higher than its observed value of 19.6 kcal/mol, it seems possible that solvation considerably lowers the barrier height. The present article also touches upon the solvolyses of derivatives of these carbocations.

The chemical behavior of the 7-norbornenyl and 7-norbornadienyl cations, known as unusually stable nonclassical ions, has been closely examined through kinetic, stereochemical, and spectroscopic experiments.[1-4] On the other hand, the theoretical studies which have hitherto been made on these carbonium ions do not necessarily afford enough information to explain their chemical properties.[5-7] For example, the geometries of the cations have not yet been calculated without any assumptions. In order to obtain detailed information about these interesting carbonium ions, we have begun to study them by the MINDO/3 self-consistent-field molecular-orbital method.[8] The present paper will give the calculated geometries, charge distributions, and heats of formation for 7-norbornyl (**1**), 7-norbornenyl (**2**), and 7-norbornadienyl (**3**) cations, and will discuss the stability of these carbocations and the solvent effect on it.

Method of Calculation

The calculations reported here were performed using the MINDO/3 parameters listed in Ref. 8, on a FACOM 230-75 computer at the Computing Center of Hokkaido University. Geometries of carbocations were obtained by minimizing their total energies with respect to all atomic coordinates, using a program written by the present authors. For any cation or molecule, the optimization procedure was repeated until a change in its total energy became less than 0.001 kcal/mol. Transition states were distinguished from other stationary points by two conditions: (a) they have only one negative eigenvalue of the force constant matrix and (b) their transition vector corresponds to the vibration which transforms the reactants into the products.[9]

A difference in solvation energy of two carbocations was estimated by the use of the following equation:

$$\Delta E_s = \Delta[-(1-1/D)(\sum_i q_i^2/2r_i + \sum_{i<j} q_iq_j/r_{ij})], \qquad (1)$$

where D denotes the dielectric constant of the solvent, q_i and q_j represent the net charges of the i-th and j-th atoms in each cation respectively, r_i designates the ionic radius of the i-th atom, and r_{ij} stands for the distance between the i-th and j-th atoms.[10] In this study, the ionic radii of carbon and hydrogen atoms were approximated by their usual van der Waals radii, 1.70* and 1.20 Å, respectively. In applying Eq. 1 to carbocations, we made the following modification: when the interatomic distance, d_{ij}, was less than the sum of the ionic radii, r_i+r_j, the latter was used as r_{ij}; otherwise, as usual, d_{ij} was adopted as r_{ij}. This means that it was assumed that the solvent neither assisted nor prevented the approach of the i-th and j-th atoms from their van der Waals distance to their bond distance. The following example shows that using bond distances as r_{ij}'s may lead to serious errors in the calculation of solvation energies for carbocations.

Let us consider a monoatomic system, A, with an ionic radius of R and a net charge of q and a diatomic system, B, where two atoms with ionic radii of R and net charges of $q/2$ are separated by a bond distance of d. From Eq. 1, the solvation energy for B, relative to that for A, is given by $\Delta E_s=-(1-1/D)(1/d-1/R)q^2/4$, which is negative because usually d is less than R. On the other hand, since B can be well approximated by a monoatomic system with a radius of R' (greater than R) and a net charge of q, the magnitude of the solvation energy for B should be smaller than that for A by $-(1-1/D)(1/R'-1/R)q^2/2$, *i.e.*, ΔE_s should be positive. Such a conflict probably comes mainly from overestimation of solvent effects in the process of forming the covalent bond. For this reason, we made the above-mentioned modification in Eq. 1 as a first approximation. However, it must be kept in mind that, in any way, ΔE_s gives only a rough estimate of a difference in solvation energy.

Results and Discussion

Geometries. Figure 1 shows the calculated geometries for the carbocations **1**, **2**, and **3**. Though no assumption was made about their symmetries, each of these cations has, within the limits of the computational errors, a plane of symmetry which contains the C(7)-H(7) bond and bisects the C(1)–C(7)–C(4) angle. The

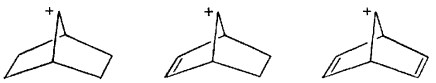

1 **2** **3**

* One-half the thickness of benzene rings in crystals.

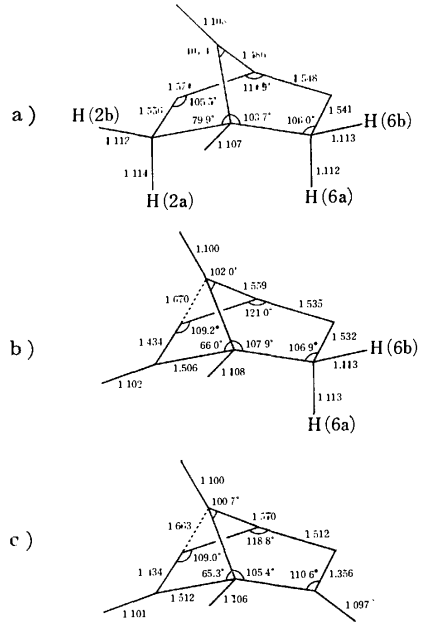

Fig. 1. The calculated geometries (bond lengths in Å) for (a) **1**, (b) **2**, and (c) **3**.

conformations of **1**, **2**, and **3** viewed along the C(1)–C(4) directions are given in Fig. 2. It should be noted here that not only the nonclassical ions **2** and **3**, but also the classical ion **1** is unsymmetrical with respect to the C(1)–C(7)–C(4) plane. As will be shown by an appreciable lengthening of the C(1)–C(2) and C(3)–C(4) bonds, this deformation probably occurs so as to help delocalization of the C(1)–C(2) and C(3)–C(4) σ-bonding electrons into the vacant C(7) 2p-orbital.

The degree of unsymmetry of **2** and **3** is much greater than that of **1**. Both the remarkable lengthening of the C(2)–C(3), C(1)–C(7), and C(4)–C(7) bonds and the close approach of the C(7) atom to the C(2) and C(3) atoms clearly indicate that the vacant C(7) 2p-orbital

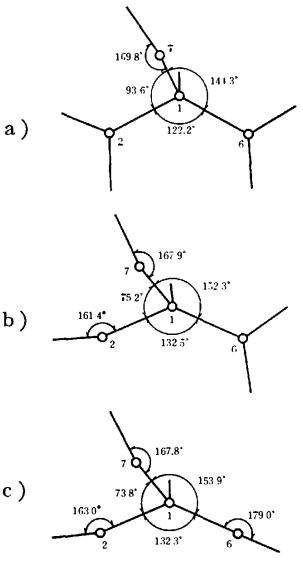

Fig. 2. The conformations viewed along the C(1)-C(4) directions: (a) **1**, (b) **2**, and (c) **3**.

and the C(2)–C(3) π-bonding orbital interact strongly with each other to form a kind of bridged ion. It may be useful for an understanding of this orbital interaction to examine how the two overlapping orbitals in **2** and **3** differ from isolated 2p- and π-orbitals. First, it is found that the C(7)–H(7) bond deviates from the C(1)–C(7)–C(4) plane onto the side opposite to the C(2)–C(3) bond. This will make the C(7) 2p-orbital expand toward the C(2)–C(3) π-bonding orbital, resulting in an increase in the overlapping. On the other hand, both C(2)–H(2) and C(3)–H(3) bonds deviate from the C(1)–C(2)–C(3)–C(4) plane onto the same side as the C(7) atom. Considered simply from the viewpoint of expansion of the π-bonding orbital, such deviations of the two C–H bonds would be unfavorable to the p-π overlapping under consideration, but nevertheless they appear to strengthen this overlapping by directing the C(2) and C(3) 2p atomic orbitals, of which the C(2)–C(3) π-bonding orbital consists, more effectively toward the C(7) 2p-orbital (see Fig. 3).

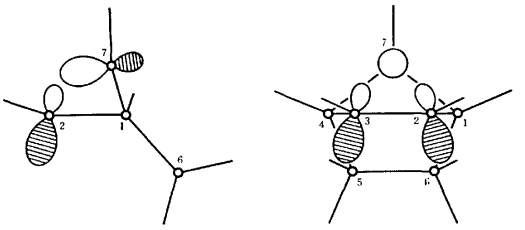

Fig. 3. The overlapping of the C(2) and C(3) p-orbitals with the C(7) vacant orbital in **2**.

Table 1. The distributions of net charges (in units of the electronic charge)

Atom	**1**	**1**[a)]	**2**	**3**	**3**[b)]
C(1), C(4)	−0.011	−0.030	0.062	0.087	0.032
C(2), C(3)	0.045	0.048	0.106	0.106	0.004
C(5), C(6)	0.040	0.048	0.038	−0.013	0.004
C(7)	0.352	0.425	0.086	0.084	0.398
H(1), H(4)	0.073	0.065	0.060	0.058	0.061
H(2a), H(3a)	0.054	0.039	0.081	0.086	0.094
H(2b), H(3b)	0.037	0.028			
H(5a), H(6a)	0.031	0.039	0.031	0.091	0.094
H(5b), H(6b)	0.031	0.028	0.035		
H(7)	0.048	0.044	0.086	0.083	0.025

a), b) The transition states for the bridge flipping in **1** and **3** respectively.

Distributions of Net Charges. The distributions of net charges, which are listed in Table 1, show that the C(2)–C(3) π-bonding electrons in **2** and **3** are so remarkably delocalized that the C(2) and C(3) atoms carry greater net charges than the C(7) atom. This result is consistent with the experimental observation that, in the ^{13}C NMR spectra of **2** and **3**, the absorption of the C(2) and C(3) atoms occurs at lower fields than that of the C(7) atom.[4] Although, in both **2** and **3**, the C(2) and C(3) atoms bear the greatest net charge of $+0.106e$, even this does not reach one-third of the net charge ($+0.352e$) on the cationic center in **1**. Thus,

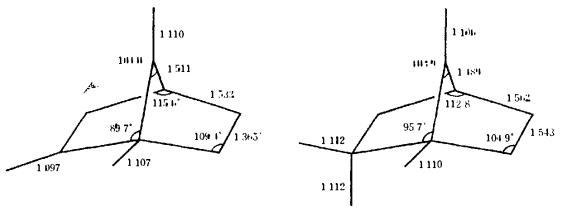

(a) (b)

Fig. 4. The calculated transition state geometries for the bridge flipping in (a) **3** and (b) **1**.

the positive charge of **2** and **3** can be regarded as being spread over almost the whole cation. It is interesting that, in spite of such a pronounced dispersal of the positive charge, the C(5) and C(6) atoms in **3** still bear slight negative net charges ($-0.013e$).**

Bridge Flipping. Figure 4(a) shows the calculated geometry of **3** in the transition state for the bridge flipping. This geometry was calculated on the assumption of C_{2v} symmetry, which was later verified by testing whether the geometry obtained satisfied the two conditions of transition states or not (see the section on Method of Calculation). In the case of the neutral norbornadiene molecule, MINDO/3 optimization affords a length of 1.356 Å to the C(2)–C(3) bond and a value of 121.8° to the C(2)–C(1)–C(4)–C(7) dihedral angle, while the corresponding values of **3** in the transition state are 1.365 Å and 116.2° respectively. This structural variation, caused by extraction of a hydride ion, seems to support the presence of such an interaction between the vacant C(7) 2p-orbital and the C(2)–C(3) or C(5)–C(6) π-bonding orbital, as is shown in **4**. The distribution of net charges, given in the last column of Table 1, also indicates that an appreciable amount of the π-bonding electrons flows into the C(7) 2p-orbital; the C(2), C(3), C(5), and C(6) atoms carry slight positive net charges ($+0.004e$).

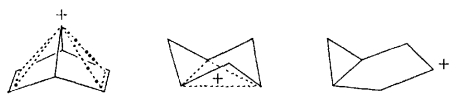

4 **5** **6**

The barrier to the bridge flipping in **3** was estimated to be 33.0 kcal/mol by our MINDO/3 calculation. Since its observed value at 45 °C is 19.6 kcal/mol or more,[11] the calculated barrier seems to be somewhat too high. The difference may be ascribed in part to the MINDO/3 approximation and in part to the solvent effects. As will be seen in Table 1, the C(7) atom bears much more net charge in the transition state than in the stable form. Hence, **3** can acquire more stabilization energy due to solvation in the former. This difference in solvation energy was estimated at 5.7 kcal/mol for $D=\infty$ by using Eq. 1. Jorgensen has recently shown that the presence of one molecule of hydrogen chloride can reduce the difference in energy between the more stable cation, **5**, and the less stable one, **6**, by more than 9 kcal/mol.[12,13] This suggests that solvation may facilitate the bridge flipping in **3** to a considerable extent.***

The calculated barrier to the bridge flipping in **1** was only 3.2 kcal/mol. Moreover, the calculation of solvation energy showed that this barrier might be lowered in solvents with $D=\infty$ by 2.0 kcal/mol. Therefore, it seems difficult to observe the bridge flipping of **1** in solution. The calculated geometry and distribution of net charges of **1** in the transition state for the bridge flipping are given in Fig. 4(b) and in the third column of Table 1 respectively. The C(7) atom of **1** in the transition state carries more net charge than that of **3** in the transition state, which is probably due to the absence of π-bonding electrons to delocalize directly into the ionizing center.

TABLE 2. THE CALCULATED HEATS OF FORMATION (IN kcal/mol)

RX	RH	RCl	R^+	$\Delta\Delta H^{a)}$	$\Delta\Delta H^{b)}$	$\Delta E^{c)}$
9	7.0	−0.1	210.9	34.2	33.1	15.2
10	44.8	36.6	214.5	(0)	(0)	(0)
11	84.0	75.5	249.7	−4.0	−3.7	−3.9
12	91.6	83.2	253.7	−7.6	−7.4	
13	127.8	119.4	290.2	−7.3	−7.1	−4
14						−4.4
15						−4.3

a), b) The calculated relative enthalpies of the gas reactions $RH \rightarrow R^+ + H^-$ and $RCl \rightarrow R^+ + Cl^-$, respectively. c) The relative activation energies estimated from the observed rate constants for the solvolyses of RX. See Refs. 15—19.

Heats of Formation. The calculated heats of formation of **1**—**3** and **7**—**13** are summarized in Table 2. Since MINDO/3 is known to overestimate the heats of formation of **9** and **11** with X=H by about 21 and 25 kcal/mol respectively,[14] the other heats of formation also should be taken as being overestimated to approximately the same extent as those of the two hydrocarbons. Table 2 further contains the calculated enthalpies of the gas reactions,

$$R\text{-}X \longrightarrow R^+ + X^-. \qquad (2)$$

These enthalpy changes seem not to include such large

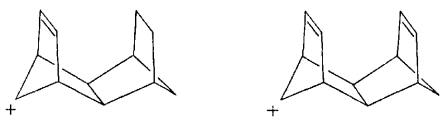

7 **8**

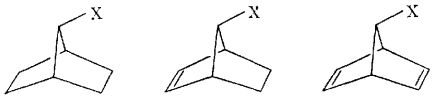

9 **10** **11**

** MINDO/3 gives net charges of $-0.040e$ to the C(5) and C(6) atoms in norbornadiene.

*** The effect of the entropy term on this bridge flipping seems not to be very important, since it is estimated at 2—3 kcal/mol(25 °C) from the entropies of activation for the acetolyses of **9** and **10**.

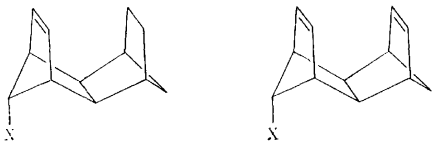

12 **13**

errors as the heats of formation themselves, because the errors of the latter are probably to a marked degree canceled out in deriving the former from the latter. In fact, it has been shown that MINDO/3 brings about an error of only 4 kcal/mol with respect to the heat of hydrogenation of norbornadiene into norbornane.[14] Since, as will be seen in Table 2, the relative enthalpy of Reaction 2 does not change substantially according to whether the reactant is a hydrocarbon or an alkyl chloride, the results with the chlorides will hereinafter be discussed.

The relative activation energies observed for solvolyses of the compounds of interest are given in the last column of Table 2.[15-19] The calculated enthalpies of the **11**→**3** and **13**→**8** reactions are in good agreement with their corresponding activation energies. This suggests that the formation of **3** and **8** should receive nearly as great solvent-assistance as that of **2**. It has recently been found that the relative energies of nonresonant, isomeric secondary and tertiary carbocations are similar in the gas phase and in solution.[20-22] The cationic portion of **8**, not to mention that of **3**, is quite analogous in charge distribution to that of **2**, as will be seen in Table 3. Accordingly, although these three carbocations are neither nonresonant nor isomeric, it is possible that solvent effects on them may be similar.

As to the **9**→**1** reaction, the case is considerably different. The difference between the enthalpies of the **9**→**1** and **10**→**2** gas reactions was estimated at 33.1 kcal/mol by our MINDO/3 calculation, while the solvolysis experiments have shown that the activation energy for **9** is higher than that for **10** by 15.2 kcal/mol.

Table 3. The distributions of net charges (in units of the electronic charge) in **8** and **13** (X=H)

Atom	**8**	**13**
C(1), C(4)	0.067	0.073
C(2), C(3)	0.100	−0.038
C(5), C(6)	0.011	0.019
C(7)	0.087	0.058
C(8), C(11)	0.070	0.073
C(9), C(10)	−0.044	−0.038
C(12)	0.052	0.058
H(1), H(4)	0.050	−0.034
H(2), H(3)	0.074	0.014
H(5), H(6)	0.007	−0.038
H(7a)	0.078	−0.039
H(7b)		−0.033
H(8), H(11)	0.006	−0.034
H(9), H(10)	0.047	0.014
H(12a)	−0.011	−0.039
H(12b)	0.017	−0.033

The difference between these calculated and observed values, 17.9 kcal/mol, seems too large to be regarded as due merely to the usual electrostatic effects of the solvent; for example, from Eq. 1, it was shown that **1** might be only 4.8 kcal/mol more stabilized by solvents with $D=\infty$ than **2**. In order to explain this remarkable discrepancy between the gas reactions and the solvolyses, it is necessary to consider different mechanisms for the solvolyses of **9** and **10**. Although **10** presumably solvolyzes through the free, stable carbonium ion, **2**, the solvolysis of **9** may involve rate-determining formation of solvent-separated ion-pairs, as has been found for the 2-adamantyl derivative.[23] The change of **9** into the solvent-separated ion-pair will not require as much energy as the ionization of **9** into the free carbonium ion, **1**. Consequently, the activation energy for the solvolysis of **9** may actually be much lower than could be expected from the mechanism which involves the free cation, **1**.

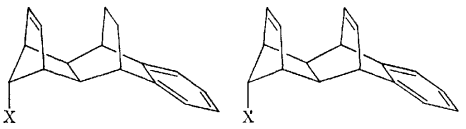

14 **15**

It is known experimentally that **13** solvolyzes about 10^3 times as fast as **10**.[24] Fukui *et al.* have recently tried to explain this additional acceleration by applying their three-system interaction theory to the carbonium ion, **8**.[25] On the other hand, it has been found that the solvolysis rate for **15** is slightly lower than that for **14**.[19] Our calculations with **12** and **13** also show that, if both of their solvolyses proceed through free carbonium ions, **13** will solvolyze somewhat more slowly than **12**. These results suggest that the solvolytic rate enhancement of **13** and **15** may not necessarily be ascribed to additional stabilization of the intermediate carbonium ions, *i.e.*, anchimeric assistance by the double bond more distant from the cationic center, because **12** and **14** without such anchimeric assistance are more reactive than **13** and **15**. The calculated geometries of **8** and **13** are shown in Fig. 5. The two double bonds in **8** appear too remote from each other to have an effective orbital interaction; the distance between the C(2) and C(10) atoms was estimated at 3.51 Å. Further, no weakening of the C(9)–C(10) double bond in **8** can be detected in Fig. 5. The comparison between the charge distributions for **8** and **13** is given in Table 3, which also shows clearly the absence of detectable flow of the C(9)–C(10) π-electrons into the C(2)–C(3) π-orbital. Thus, it may be said that **8** is not appreciably stabilized

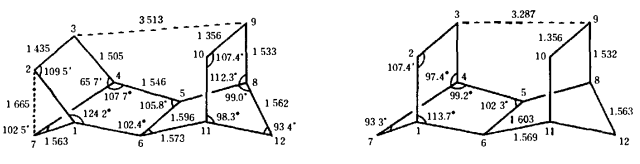

(a) (b)

Fig. 5. The calculated geometries for (a) **8** and (b) **13** (X=H).

by the presence of the C(9)–C(10) double bond. It should thus be concluded that the additional acceleration of the solvolyses of **13** and **15** is due mainly to the relief of steric repulsion between the two adjacent double bonds in the reactants.

The authors wish to thank the Matsunaga Foundation for financial support.

References

1) S. Winstein, *Quart. Rev. (London)*, **23**, 141 (1969), and references therein.
2) P. G. Gassman and D. S. Patton, *J. Am. Chem. Soc.*, **91**, 2160 (1969).
3) R. K. Lustgarten, M. Brookhart, S. Winstein, P. G. Gassman, D. S. Patton, H. G. Richey, Jr., and J. D. Nichols, *Tetrahedron Lett.*, **1970**, 1699.
4) G. A. Olah, A. M. White, J. R. DeMember, A. Commeyras, and Ch. Y. Lui, *J. Am. Chem. Soc.*, **92**, 4627 (1970), and references therein.
5) W. G. Woods, R. A. Carboni, and J. D. Roberts, *J. Am. Chem. Soc.*, **78**, 5653 (1956).
6) R. Hoffmann, *J. Am. Chem. Soc.*, **86**, 1259 (1964).
7) S. Yoneda, Z. Yoshida, and S. Winstein, *Tetrahedron*, **28**, 2395 (1972).
8) R. C. Bingham, M. J. S. Dewar, and D. H. Lo, *J. Am. Chem. Soc.*, **97**, 1285 (1975).
9) J. W. McIver, Jr., and A. Komornicki, *J. Am. Chem. Soc.*, **94**, 2625 (1972).
10) G. J. Hoijtink, E. de Boer, P. H. Van der Meij, and W. P. Weijland, *Rec. Trav. Chim. Pays-Bas*, **75**, 487 (1956).
11) M. Brookhart, R. K. Lustgarten, and S. Winstein, *J. Am. Chem. Soc.*, **89**, 6352, 6354 (1967).
12) W. L. Jorgensen, *Tetrahedron Lett.*, **1976**, 3029.
13) W. L. Jorgensen, *J. Am. Chem. Soc.*, **99**, 280 (1977).
14) R. C. Bingham, M. J. S. Dewar, and D. H. Lo, *J. Am. Chem. Soc.*, **97**, 1294 (1975).
15) S. Winstein, M. Shatavsky, C. Norton, and R. B. Woodward, *J. Am. Chem. Soc.*, **77**, 4183 (1955).
16) S. Winstein, F. Gadient, E. T. Stafford, and P. E. Klinedinst, Jr., *J. Am. Chem. Soc.*, **80**, 5895 (1958).
17) S. Winstein, A. H. Lewin, and K. C. Pande, *J. Am. Chem. Soc.*, **85**, 2324 (1963).
18) S. Winstein and C. Ordronneau, *J. Am. Chem. Soc.*, **82**, 2084 (1960).
19) L. A. Paquette and I. R. Dunkin, *J. Am. Chem. Soc.*, **96**, 1220 (1974).
20) J. L. Fry, J. M. Harris, R. C. Bingham, and P. v. R. Schleyer, *J. Am. Chem. Soc.*, **92**, 2540 (1970), and references therein.
21) J. F. Wolf, P. G. Harch, and R. W. Taft, *J. Am. Chem. Soc.*, **97**, 2904 (1975).
22) E. W. Bittner, E. M. Arnett, and M. Saunders, *J. Am. Chem. Soc.*, **98**, 3734 (1976).
23) J. M. Harris, "Progress in Physical Organic Chemistry," Vol. 11, ed by A. Streitwieser, Jr. and R. W. Taft, John Wiley & Sons, New York (1974), p. 142.
24) E. L. Allred and J. C. Hinshaw, *Tetrahedron Lett.*, **1968**, 1293.
25) S. Inagaki, H. Fujimoto, and K. Fukui, *J. Am. Chem. Soc.*, **98**, 4693 (1976).

Selective Dimerization of Ethylene Catalyzed by Halogenotris-(triphenylphosphine)cobalt(I) Complex-Lewis Acid

Kiyoshi KAWAKAMI, Tsutomu MIZOROKI, and Atsumu OZAKI

Research Laboratory of Resources Utilization, Tokyo Institute of Technology, Ohokayama, Meguro-ku, Tokyo 152

(Received June 16, 1977)

Dimerization of ethylene is highly selectively catalyzed by $CoX(PPh_3)_3$ (X=Cl, Br, and I) in the presence of Lewis acid in halobenzene under mild conditions. The catalytic activity is significantly affected by the solvent, bromobenzene being the most effective. The role of $BF_3 \cdot OEt_2$ seems to be formation of a one-to-one complex of Co(I) and BF_3, since the rate of ethylene dimerization attains a plateau on addition of equimolar amount of $BF_3 \cdot OEt_2$. The isomerization of 1-pentene is enhanced by addition of molecular hydrogen or ethylene to the catalyst system. The isotopic scrambling between C_2H_4 and C_2D_4 takes place faster than dimerization. The results are in line with hydridocobalt intermediate formed by the oxidative addition of ethylene to Co(I) complex.

Many papers have appeared on the ethylene dimerization catalyzed by nickel catalysts,[1] but fewer examples are known of cobalt catalysts for the same reaction: *i.e.*, cobalt oxide–charcoal[2] as a heterogeneous catalyst, homogeneously soluble hydridodinitrogentris(triphenylphosphine)cobalt(I) complex,[3] and cobalt(II) compounds[4] activated with alkylaluminium compounds as the reducing agent.

During a study of the role of Lewis acid in the activation of olefin with cobalt complexes, it was found that halogenotris(triphenylphosphine)cobalt(I) is also fairly active and selective in giving ethylene dimer in the presence of Lewis acid such as $BF_3 \cdot OEt_2$ or $AlCl_3$ in halobenzene at ambient temperature and pressure,[5] but it has no activity at all for propylene dimerization, a unique feature of this catalyst system.

This paper reports the properties of this catalyst system in detail.

Experimental

Materials. Halogenotris(triphenylphosphine)cobalt(I) complexes and bromotris(diphenylmethylphosphine)cobalt(I) complex were synthesized according to the method of Sacco.[6] The complexes were also obtained by another method. $AlEt_2(OEt)$ (16 ml) was added to the ether solution (200 ml) of $Co(acac)_2$ (39 mmol) and PPh_3 (156 mmol) under nitrogen atmosphere at 0 °C, followed by addition of halobenzene. A green precipitate was formed in a few minutes. The precipitate dried in a vacuum was identified to be halogenotris-(triphenylphosphine)cobalt(I) complex by elemental analysis, IR, magenetic susceptibility, and several chemical reactions. The result of elemental analysis of cobalt(I) complex is shown in Table 1.

Trace amounts of water and air in ethylene gas were excluded by vacuum distillation. Solvents were dried by P_2O_5 (halobenzene) or metallic sodium(benzene and ether), and distilled under nitrogen atmosphere. $BF_3 \cdot OEt_2$ was also purified by distillation. $AlCl_3$ was purified by sublimation at 200 °C in nitrogen atmosphere. Other commercial Lewis acids, such as $AlBr_3$, $SnCl_2$, $SnCl_4$, and $TiCl_4$ were used, without purification. Hydrogen gas was deoxidized by passing through a $Pd–Al_2O_3$ pellet at 90 °C and dried with a liquid nitrogen trap.

Procedure. To one of the cobalt(I) complexes placed in a two necked flask(50 ml), were added solvent and $BF_3 \cdot OEt_2$ with stirring under nitrogen atomosphere. The nitrogen gas in the flask was evacuated at liquid nitrogen temperature, before ethylene was introduced. The rate of ethylene absorption was measured at constant temperature and pressure by means of a gas burette. The reaction was terminated by addition of an aqueous solution of NaOH, the products being analyzed by GLC.

Isotopic exchange of $C_2H_4–C_2D_4$, dimerization of C_2D_4, and isomerization of 1-alkene were performed by analogous procedures. Isotopic mixtures of butenes and ethylene were analyzed by mass spectrometry with an ionization potential of 10 eV.

Results and Discussions

Effect of Solvent on Catalytic Activity. The catalytic activity of $CoX(PPh_3)_3–BF_3 \cdot OEt_2$ for ethylene dimerization was determined in various solvents (Table 2). Ethylene was absorbed readily in halobenzene solvents, whereas no absorption was observed in other solvents including benzene, anisole, tetrahydrofran, benzonitrile, ethyl bromide, propyl bromide, benzyl bromide, and dichloromethane. Bromobenzene was the most effective solvent among halobenzenes and the rate of ethylene absorption decreased in the order, bromobenzene > iodobenzene > *o*-dichlorobenzene > chlorobenzene > *o*-chlorotoluene. The color of halobenzene solutions of bromotris(triphenylphosphine)cobalt(I) turned

Table 1. Elemental analysis

	Found[a]			Found[b]			Calcd		
	C (%)	H (%)	X (%)	C (%)	H (%)	X (%)	C (%)	H (%)	X (%)
$CoCl(PPh_3)_3$	72.7	5.7	4.2	72.1	5.2	3.9	73.6	5.2	4.0
$CoBr(PPh_3)_3$	69.6	5.5	8.6	70.4	5.2	9.9	70.1	4.9	8.6
$CoI(PPh_3)_3$	66.2	5.2	12.7				66.7	4.7	13.1
$CoBr(PPh_2Me)_3$	63.3	5.5	10.6				63.3	5.3	10.8

a) The method of Sacco. b) The method described herein.

TABLE 2. DIMERIZATION OF ETHYLENE CATALYZED BY $CoX(PPh_3)_3$

$CoX(PPh_3)_3$ 0.1 mmol, $BF_3 \cdot OEt_2$ 0.48 mmol, Solvent 10 ml, Temp 0 °C, and Time 30 min.

Cat. X	Solvent (ml)	Rate of C_2' absorption (ml/min)	Amount of C_2' absorbed (mmol)	C_4' Distribution		
				1-C_4' (%)	t-2-C_4' (%)	c-2-C_4' (%)
Cl	C_6H_5Cl	0.87	1.4	78	10	11
Cl	C_6H_5Br	15	16	12	46	42
Cl	C_6H_5I	8.1	10	20	39	41
Cl	o-$C_6H_4Cl_2$	1.9	2.1	47	23	31
Cl	o-$CH_3C_6H_4Cl$	0.18	0.78[a]	85	6.4	8.3
Br	C_6H_5Cl	0.55	0.56	90	4.9	5.5
Br	C_6H_5Br	12	12	14	46	40
Br	C_6H_5I	2.1	2.8	53	22	26
Br	o-$C_6H_4Cl_2$	1.8	1.9	50	21	29
Br	o-$CH_3C_6H_4Cl$	0.07	0.35[b]	90	4.6	5.6
I	C_6H_5Cl	0.31	0.40	81	6.1	13
I	C_6H_5Br	12	11	21	41	38
I	C_6H_5I	0	0	—	—	—
I	o-$C_6H_4Cl_2$	2.1	2.7	42	22	36
I	o-$CH_3C_6H_4Cl$	0.25	0.50	70	7.9	22
Br[c]	C_6H_5Br	1.5	1.7	4.9	62	33

a) Time 60 min. b) Time 120 min. c) $CoBr(PPh_2Me)_3$ was used.

from pale green to deep green on addition of $BF_3 \cdot OEt_2$. In benzene or anisole, however, the color of the solution turned gradually to greenish blue with a black precipitate. The following disproportionation seems to take place readily in benzene or anisole.

$$2CoBr(PPh_3)_3 \longrightarrow CoBr_2(PPh_3)_2 + 4PPh_3 + Co$$

On the other hand, $CoBr(PPh_3)_3$ reacts with alkyl halides to give Co(II) complex and quaternary phosphonium salts. Accordingly the $CoX(PPh_3)_3$ activated with $BF_3 \cdot OEt_2$ could act as a catalyst only in halobenzene for the ethylene dimerization.

When ethylene gas was introduced immediately after the addition of $BF_3 \cdot OEt_2$, a high rate of ethylene dimerization was attained. However, when the $CoBr(PPh_3)_3$–$BF_3 \cdot OEt_2$ mixture was left standing for 40 min without introducing ethylene, a trace amount of black precipitate was formed, resulting in complete deactivation of the catalyst for ethylene dimerization. It seems likely that the activated form of the catalyst is stabilized by the presence of ethylene as well as halobenzene.

Effects of Lewis Acid and Cobalt(I) Complex Concentration. As shown in Fig. 1, the rate increases linearly with increase in $BF_3 \cdot OEt_2$ concentration up to $BF_3 \cdot OEt_2/CoBr(PPh_3)_3 = 1$, where it attains a plateau value, while in the case of σ-arylNiBr$(PPh_3)_2$ the rate increases until the ratio $BF_3 \cdot OEt_2/\sigma$-arylNiBr$(PPh_3)_2$ exceeds unity.[7] The result suggests that there is a strong one-to-one interaction between $CoBr(PPh_3)_3$ and $BF_3 \cdot OEt_2$ such as $CoBr(PPh_3)_3 + BF_3 \cdot OEt_2 \rightarrow [Co(PPh_3)_3]^+[BF_3Br]^-$.

The rate of ethylene dimerization is proportional to the $CoBr(PPh_3)_3$ concentration with a constant ratio of $BF_3 \cdot OEt_2$ to $CoBr(PPh_3)_3$ as shown in Fig. 2. When $AlCl_3$ was used as a Lewis acid, an induction time

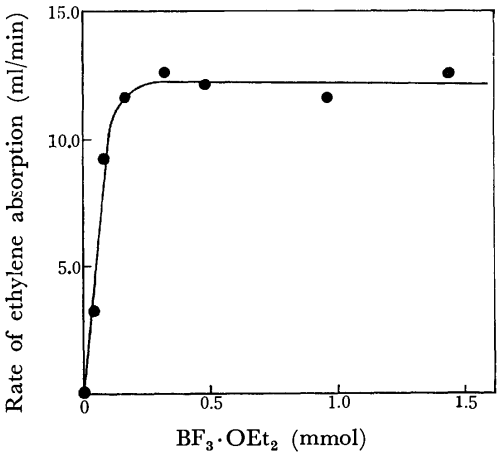

Fig. 1. Rate of ethylene absorption *vs.* the amount of $BF_3 \cdot OEt_2$ added.
$CoBr(PPh_3)_3$ 0.1 mmol, PhBr 10 ml, $P_{C_2'}$ 734 mmHg, and 0 °C.

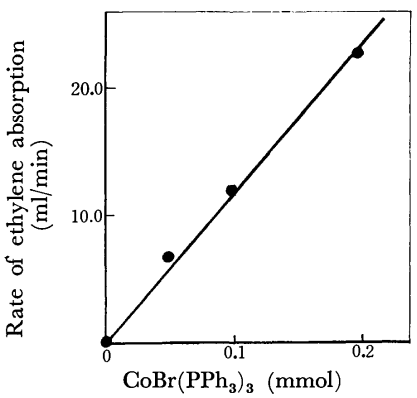

Fig. 2. Rate of ethylene absorption *vs.* the amount of catalyst.
$CoBr(PPh_3)_3/BF_3 \cdot OEt_2$ 1/4.8 (mole ratio), PhBr 10 ml, $P_{C_2'}$ 734 mmHg and 0 °C.

(about 30 min) was observed, which disappeared by pretreatment of $CoBr(PPh_3)_3$ with $AlCl_3$ for 40 min at 0 °C. Since the solubility of $AlCl_3$ is considerably lower than that of $BF_3 \cdot OEt_2$, the induction time can be regarded as the time necessary to activate the Co(I)-complex with $AlCl_3$. No ethylene dimerization was found with the use of other Lewis acids such as $SnCl_2$, $SnCl_4$ and $TiCl_4$.

The addition of PPh_3(PPh_3/$CoBr(PPh_3)_3$=3) to a $CoBr(PPh_3)_3$–$BF_3 \cdot OEt_2$ (1 : 4.8) catalyst system was found to stop the dimerization almost completely. Water was also found to be a strong inhibitor to cause complete deactivation by addition of equimolar amount of water. $CoBr_2(PPh_3)_2$, $ZnBr_2$, or metallic zinc, which might be a contaminant of $CoBr(PPh_3)_3$ in a trace amount, had no effect on the ethylene dimerization.

Isomerization and Isotopic Scrambling of Olefins. Isomerization of 1-alkene was investigated to elucidate why the present catalyst system is highly specific for ethylene dimerization. As shown in Table 3, neither 1-butene, nor 1-pentene is isomerized. The isomerization of 1-pentene, however, is enhanced in the presence of molecular hydrogen or ethylene. The addition of $BF_3 \cdot OEt_2$ is also essential for the isomerization. The rate of 1-pentene isomerization increases with increase in the amount of ethylene. It seems likely that the active species of the catalyst is a hydridocobalt complex to which the hydrogen is supplied from ethylene or molecular hydrogen, but scarcely from the other olefins. It is evident that ethylene is specifically activated by the present catalyst system.

The formation of hydridocobalt species during the course of ethylene dimerization is in line with the result for isotopic scrambling in C_2H_4 and C_2D_4 (Table 4). Since the deuterium distribution in the unreacted ethylene attains a value very close to the equilibrium within 13 min, during which the conversion of ethylene to butenes is only 12%, the hydrogen exchange should proceed much faster than ethylene dimerization. The result for the dimerization of C_2D_4, in which the atomic fraction of hydrogen (f_H) is 0.006, indicates that no hydrogen is supplied from any substance other than ethylene, since no appreciable increase in f_H is observed for the unreacted ethylene as well as for the butenes formed (Table 4). The H–D exchange run between C_2D_4 and C_3H_6 shows that the f_H of propylene considerably decrease, while those of produced butenes and unreacted ethylene decrease, indicating that propylene can react with the hydridocobalt species, while it can not be dimerised.

Possible Processes of Formation of Hydridocobalt Species. Olefin dimerization with transition metal complex catalysts is mostly interpreted in terms of transient hydro- and alkyl-complexes. The isomerization of 1-alkene catalyzed by the present catalyst system in the presence of ethylene or hydrogen (Table 3) and isotopic scrambling in ethylene molecules (Table 4) are also explained by hydridocobalt species, for which the hydrogen is supplied from ethylene.

Since the dimerization proceeds specifically in halobenzene solvents, it may be supposed that halobenzene is oxidatively added to the cobalt(I) complex to give a σ-phenylcobalt(III) complex. Ethylene may, then, be inserted into the σ-phenylcobalt(III) complex, followed by elimination of the β-hydrogen to give H–Co(III) species and styrene. This process, however, seems to be unlikely, since neither styrene, its codimer with ethylene, nor benzene was detected. A more likely process is an oxidative addition of ethylene to give H–Co–CH=CH_2. Oxidative addition of vinyl compounds such as alkyl methacrylate is verified with ruthenium complex.[8] No increase in f_H of butenes and the residual ethylene in the dimerization using deuterioethylene (Table 4) supports this process for the formation of hydridocobalt species, although we have

Table 3. Isomerization of 1-Pentene

$CoCl(PPh_3)_3$ 0.1 mmol, $BF_3 \cdot OEt_2$ 0.48 mmol, PhBr 10 ml, 1-C_5' 0.5 ml, 0 °C, and 20 min.

Additives (ml STP)	1-C_5' (%)	*t*-2-C_5' (%)	*c*-2-C_5' (%)
—	99.6	0.1	0.3
C_2' (10)	97.3	1.1	1.6
C_2' (30)	41.5	27.6	30.9
C_2' (100)	18.9	45.0	36.1
H_2 (63)	22.2	23.0	54.8
H_2[a] (80)	99.3	0.6	0.1

a) No $BF_3 \cdot OEt_2$ was added.

Table 4. Isotopic exchange reaction

$CoCl(PPh_3)_3$ 0.1 mmol, $BF_3 \cdot OEt_2$ 0.48 mmol, PhBr 10 ml, and 0 °C.

C_2D_4 (mmol)	C_2H_4 (mmol)	Time (min)	Sample	D distribution (%) d_0	d_1	d_2	d_3	d_4	d_5	d_6	d_7	d_8	Con. (%)	f_H
0.35	0.65		C_2' (int.)	62	0.8	1.4	4.1	32						0.64
0.35	0.65	5	C_2' (resid.)	28	29	27	9	7.1					0	0.65
0.35	0.65	13	C_2' (resid.)	19 (18)	35 (38)	32 (31)	11 (11)	2.0 (2)*					12	0.65
1.0	0		C_2' (init.)	0	0	0	2.5	97.5						0.006
1.0	0	10	C_2' (resid.)	0	0	0	3.8	96.2						0.009
1.0	0	180	C_4' (prod.)	0	0	0	0	0	0	0.7	5.0	94.3	100	0.008
1.0	C_3H_6 1.0	20	C_4' (prod.)	0.6	3.0	9.2	18	24	23	14	6.6	1.6	64	0.46
			C_3' (resid.)	13	26	27	19	10	5.4					0.66
			C_2' (resid.)	23	31	13	14	9						0.61

( )* Equilibrium value.

no direct evidence.

References

1) P. W. Jolly and G. Wilke, "The Organic Chemistry of Nickel," Academic Press, New York, San Francisco, and London (1975).
2) C. Schuster, *Z. Electrochem.*, **38**, 614 (1932).
3) L. S. Pu, A. Yamamoto, and S. Ikeda, *J. Am. Chem. Soc.*, **90**, 7170 (1968).
4) G. Hata, *Chem. Ind.*, **1965**, 223.
5) K. Kawakami, T. Mizoroki, and A. Ozaki, *Chem. Lett.*, **1975**, 903.
6) M. Aresta, M. Rossi, and A. Sacco, *Inorg. Chim. Acta*, **3**, 227 (1969).
7) K. Maruya, T. Mizoroki, and A. Ozaki, *Bull. Chem. Soc. Jpn.*, **45**, 2255 (1972).
8) S. Komiya, T. Ito, M. Cowie, A. Yamamoto, and J. A. Ibers, *J. Am. Chem. Soc.*, **98**, 3874 (1976); S. Komiya and A. Yamamoto, *Bull. Chem. Soc. Jpn.*, **49**, 2553 (1976).

Raman Studies of Complex Ions in $ThCl_4$–KCl Melt Using Raman Bands Shifts

Susumu YOSHIDA, Ryozo OYAMADA,* and Kazutaka KAWAMURA

Research Laboratory for Nuclear Reactors, Tokyo Institute of Technology, O-okayama, Meguro-ku, Tokyo 152

**Faculty of Education, Nagasaki University, Bunkyo-cho, Nagasaki 852*

(Received August 5, 1976)

Raman spectra of solid and molten $ThCl_4$–KCl system were observed and the structure change of $ThCl_4$ on melting from the octa-coordinate body-centered tetragonal type, D_{4h}, to the tetra-coordinate tetrahedron type, T_d, was studied. The decrease in frequency of the symmetric stretching vibration ν_1 with decrasing $ThCl_4$ concentration for molten $ThCl_4$–KCl is interpreted as due to the presence of $ThCl_4$, $ThCl_5^-$, and $ThCl_7^{3-}$ complexes in the molten $ThCl_4$–KCl mixture. Such a compositional dependence for ν_1 appears to support the idea that, for a decrease in the $ThCl_4$ concentration in molten $ThCl_4$–KCl mixtures, the bond strength between the thorium and chloride ions decreases and the number of chloride ions around the thorium ion increases from 4 to 7.

Various physical properties, such as electromotive force,[1] density,[2] equivalent conductivity,[2] and viscosity[3] for the $ThCl_4$– KCl system, have been measured as fundamentally important data for the electrolytic preparation of thorium metal. In the variation of these physical isothermal properties with $ThCl_4$ concentration, deviations from the additivity line have been attributed to the existence of a complex ion, since the concentration giving the maximum deviation corresponds to that of a congruently melting compound.

In this paper, the formation and structure of complex ions in the $ThCl_4$–KCl system are discussed on the basis of the variation of the Raman bands of solid and molten $ThCl_4$–KCl systems with concentration.

Experimental

Samples. *Thorium Tetrachloride*: As described in a previous report,[4] thorium(IV) chloride was refined by vacuum fractional distillation.

Potassium Chloride: Potassium chloride of special reagent grade was melted, bubbled with dry hydrogen chloride, and the retained HCl was purged by purified argon. The melt was evacuated using a rotary pump for one hour to remove the argon.

Samples: Weighed amounts of thorium and potassium chlorides were melted and mixed in a quartz cell in an HCl atmosphere, and then the mixture was poured into the measuring cell *in vacuo*. The thorium concentration of these samples was corrected by chemical analysis after measuring the spectra.

Apparatus. Raman spectra were recorded with a Spex Model 1401 Ramalog 4 spectrometer. A Coherent Radiation Model 52 488-nm argon-ion laser was used. The furnace temperature for the molten salts was controlled to within ±0.5 °C.

Results and Discussion

Raman Spectra of Pure Thorium Chloride. The Raman spectra of rapidly quenched solid and molten thorium chloride were recorded from 50 to 2000 cm^{-1} at room temperature and at 800 °C, respectively. The Raman bands of solid thorium chloride were found at 296, 182, and 259 cm^{-1} and those of molten thorium chloride at 334, 132, and 270 cm^{-1}, as listed in Table 1.

The crystal structure of thorium(IV) chloride has been reported to be a body-centered tetragonal structure (D_{4h}) as shown in Fig. 1.[5] The number of chloride ion around the thorium(IV) ion is eight. The four Cl^- ions are close to the Th^{4+} ion (2.718 Å) and form a square planar configuration. The remaining four Cl^- ions are far from the Th^{4+} ion (2.903 Å) and form a distorted tetrahedron. Each Th^{4+} ion is dodecahedrally coordinated in a crystal lattice. In the quenched state, pure thorium chloride does not have a stable crystalline form, but is a tetrahedron with a slightly deformed body-centered tetragonal framework resulting from the strong mutual interaction between the four Cl^- ions and the near Th^{4+} ion.[6] Thus, the structure of pure $ThCl_4$ may change from an octa-coordinate body-centered tetragonal structure, D_{4h}, to a tetra-coordinate tetrahedron structure, T_d, upon melting. The Raman band at 334 cm^{-1} for pure molten $ThCl_4$ can be assigned to a symmetric stretching vibration of T_d symmetry, and the other bands at 132 and 270 cm^{-1} to bending vibrations of

Table 1. Raman bands for pure $ThCl_4$

Band (cm^{-1}) for $ThCl_4$		Assignment
solid	melt	
296	334	$\nu_1(A_1)$
182	132	$\nu_2(E)$
—	—	$\nu_3(F_2)$
259	270	$\nu_4(F_2)$

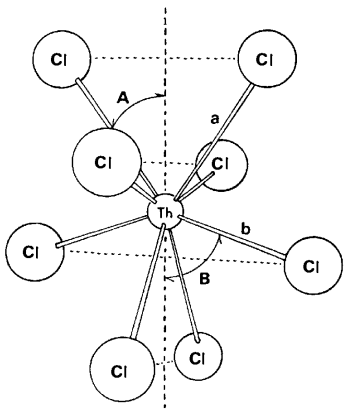

Fig. 1. Coordination about the Th atom in the $ThCl_4$ (D_{4h}) structure.
A: 33.1°, B: 78.0°, a: 2.903 Å, and b: 2.718 Å.

T_d symmetry.[7] The assignments of bands for pure solid $ThCl_4$ listed in Table 1 are in analogy to the assignments for molten $ThCl_4$.

Table 1 shows the band shifts to higher frequencies upon melting. These shifts can be explained if four Cl^- ions far from Th^{4+} ion become free, and the four Cl^- ions near Th^{4+} ion are strongly attracted to the Th^{4+} ion by the strong polarization force. In other words, the strong interaction between the Th^{4+} and Cl^- ions resulting from a decrease in the interionic distance can explain the shifts of the Raman bands toward higher frequencies upon melting.

The Raman bands for ThO_2 which have been reported at 460 cm^{-1} [8] were not observed. No evidence for the existence of $ThOCl_2$ in pure solid $ThCl_4$ was obtained. These facts are also supported by failure to detect any ThO_2 or $ThOCl_2$ upon chemical analysis.

Raman Spectra of the Solid $ThCl_4$–KCl System. Raman spectra of the solid $ThCl_4$–KCl system were obtained over the range from 50—2000 cm^{-1} at room temperature (Fig. 2 and Table 2).

The frequencies for the solid $ThCl_4$–KCl system with 1.0—0.10 molar fractions of thorium chloride remain almost constant. The Raman bands at 250 cm^{-1} and near 280 cm^{-1}, which are obtained for $ThCl_4$ molar fractions of 0.34—0.62, are also observed in the solid form containing $ThCl_4$ molar fractions above 0.62 and below 0.34, respectively. Moreover, the discontinuous variation of Raman bands near 300 cm^{-1} with $ThCl_4$ concentration is illustrated in the phase diagram for $ThCl_4$ and KCl, as shown in Fig. 3. This spectral variation with concentration appears to support the presence of a $ThCl_4$ compound with a molar fraction from 1.0—0.62, of a congruently melting compound $KThCl_5$ with a molar fraction of 0.62—0.34, and K_3ThCl_7 with a molar fraction of 0.34—0.10 of $ThCl_4$. Aside from the existence of K^+ ions, it may be assumed by analogy with $KThF_5$[9] and K_3UF_7,[10] that the $ThCl_5^-$ and $ThCl_7^{3-}$ species have trigonal bipyramidal and pentagonal bipyramidal structures, respectively. The symmetric stretching vibration, ν_1, are easily assigned for the $ThCl_4$, $ThCl_5^-$, and $ThCl_7^{3-}$ species, but the assignments of other modes of vibration are quite difficult due to the structural complexities of the above species. Table 2 shows that the frequency of the ν_1 vibration decreases with the $ThCl_4$ concentration from 1.0 to 0.1 molar fraction, suggesting the presence of two congruently melting compounds.

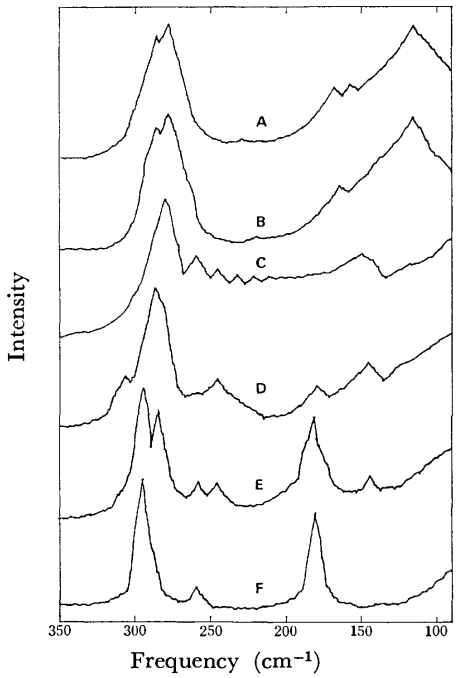

Fig. 2. Raman spectra of the solid $ThCl_4$–KCl system. $ThCl_4$ concentrations (mole fraction): A: 0.10, B: 0.25, C: 0.34, D: 0.50, E: 0.62, and F: 1.00.

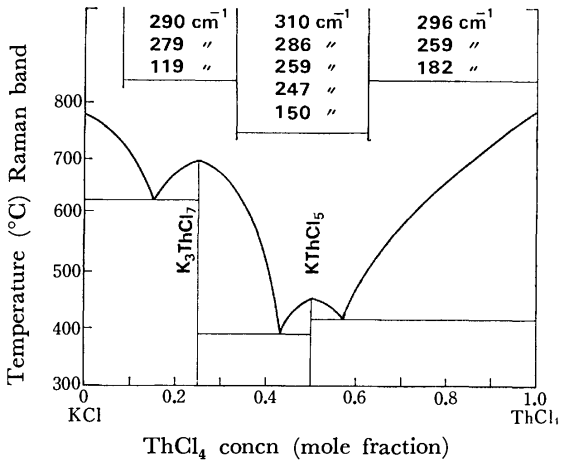

Fig. 3. The relation between Raman bands and the phase diagram for the $ThCl_4$–KCl system.

Raman Spectra of the Molten $ThCl_4$–KCl System. Raman spectra of the molten $ThCl_4$–KCl system were observed over the range 50—2000 cm^{-1} at 800 °C. The spectra for melts containing 1.00—0.25 molar fractions of $ThCl_4$ are shown in Fig. 4 and Table 3. The second column in Table 3 lists also the polarization of each band. While the bands for a 0.5 molar

Table 2. Raman bands for the solid $ThCl_4$-KCl system

$ThCl_4$ concn (mol frac.)	Raman band in cm^{-1} ($\pm 1.0\ cm^{-1}$)							
1.0	—	296(ν_1)	—	259	—	182	—	—
0.6	310	296(ν_1)	285	259	247	182	149	—
0.50	310	—	286(ν_1)	259	247	—	150	—
0.34	310	—	280(ν_1)	259	247	—	150	—
0.25	—	290	279(ν_1)	—	—	—	—	119
0.10	—	289	279(ν_1)	—	—	—	—	119

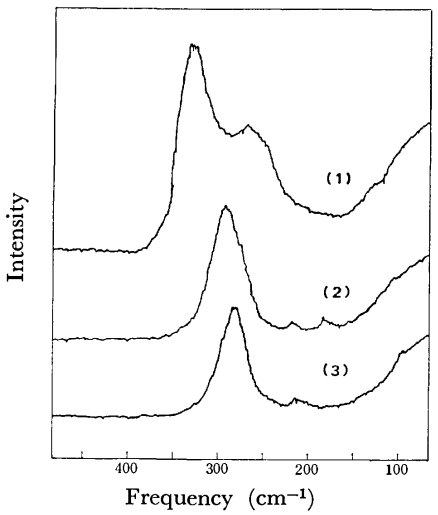

Fig. 4. Raman spectra of molten $ThCl_4$–KCl system at 800 °C with $ThCl_4$ concn compositions (mole fraction): (1): 1.0, (2): 0.50, and (3); 0.25.

TABLE 3. RAMAN BANDS FOR THE MOLTEN $ThCl_4$-KCl

$ThCl_4$ concn (mol frac.)	Raman band (cm^{-1})	Polarization	Assignment
1.00	334	polar	$\nu_1(A_1)$
($ThCl_4$)	132	depol	$\nu_2(E)$
	—	depol	$\nu_3(F_2)$
	270	depol	$\nu_4(F_2)$
0.50	293	polar	$\nu_1(A')$
($ThCl_5^-$)	—	polar	$\nu_2(A_1')$
	213	depol	$\nu_5(E')$
	187	depol	$\nu_7(E')$
	113	depol	$\nu_8(E'')$
0.25	283	polar	$\nu_1(A')$
($ThCl_7^{3-}$)	—	polar	$\nu_2(A')$
	98	depol	$\nu_8(E_2')$
	—	depol	$\nu_9(E_2')$
	219	depol	$\nu_{10}(E_1'')$

fraction of $ThCl_4$ are observed at 293, 219, 187, and 113 cm^{-1}, the bands for a 0.25 molar fraction are observed at 285, 219, and 98 cm^{-1}. As shown in Fig. 3, these compositions of 0.5 and 0.25 molar fractions correspond to those of congruently melting compounds. It should be noted that the wave numbers of Raman bands for a certain concentration range (0.1—0.3 molar frac.) near each congruently melting compound remain almost constant. The above fact suggests the presence of $ThCl_5^-$ and $ThCl_7^{3-}$ complex ions for the melts containing 0.5 and 0.25 molar fractions of $ThCl_4$, respectively. Since the complex ions $ThCl_5^-$ and $ThCl_7^{3-}$ are assumed to have trigonal bipyramidal and pentagonal bipyramidal structures, respectively, the

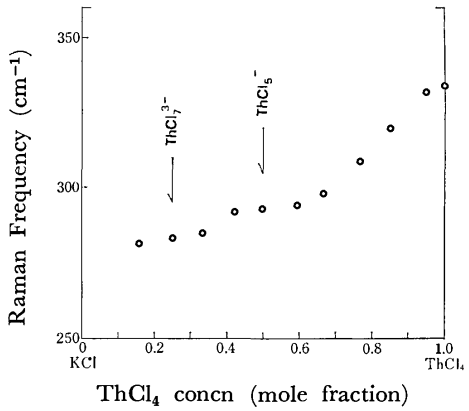

Fig. 5. Frequency shifts of ν_1 band with $ThCl_4$ concentration change in a molten $ThCl_4$–KCl system.

assignments based on these structures are listed in Table 3. From the compositional dependence of the stretching vibration, ν_1, shown in Fig. 5, it is indicated that ν_1 decreases with $ThCl_4$ concentration. Such a compositional dependence of ν_1 appears to support the idea that for decreasing $ThCl_4$ concentration the bond strength between the thorium(IV) ion and chloride ion decreases and the coordination state for thorium-(IV) varies from four, to five and seven coordinations. In these binary mixtures with a common anion, the variations of bond strength and thorium coordination number can be ascribed to a change in the polarization force.

References

1) S. Yoshida and T. Kuroda, *Denki Kagaku*, **41**, 217 (1973).
2) S. Yoshida, T. Ayano, and T. Kuroda, *Denki Kagaku*, **41**, 427 (1973).
3) S. Yoshida, S. Kaji, and K. Kawamura, *Denki Kagaku*, **43**, 195 (1975).
4) S. Yoshida, R. Oyamada, and T. Kuroda, *Denki Kagaku*, **36**, 295 (1968).
5) K. Mucker, G. S. Smith, Q. Johnson, and R. E. Elson, *Acta Crystallogr., Sect. B*, **25**, 2362 (1969).
6) Pauling has reported that for the Th^{4+}–Cl^- ionic distance, the Th^{4+} and Cl^- ion radii are 2.95 and 1.81 Å, respectively, so that the Th^{4+}–Cl^- bond may be considered strong with significant overlapping of the electron clouds. Hence, it is reasonable that this structure be assumed to be of tetrahedron type to a first approximation. See, for example, L. Pauling, "The Nature of the Chemical Bond," Cornell Univ. Press, New York (1960), p. 518.
7) B. Gilbert, K. W. Fung, and G. Mamantov, *J. Inorg. Nucl. Chem.*, **37**, 921 (1975).
8) V. G. Keramidas and W. B. White, *J. Chem. Phys.*, **59**, 1561 (1973).
9) W. H. Zachariasen, *J. Am. Chem. Soc.*, **70**, 2147 (1948).
10) W. H. Zachariasen, *Acta Crystallogr.*, **7**, 792 (1954).

A Finite Element Approach to the Two-dimensional Vibrational Schrödinger Equation and Its Application to the Hydrogen Bond

Isao KANESAKA, Hideyuki ARAI,* and Kiyoyasu KAWAI
Department of Chemistry, Faculty of Science, Toyama University, Gofuku, Toyama 930
(Received November 8, 1976)

The finite element method was examined in relation to the two-dimensional vibrational Schrödinger equation. Some boundary conditions were used because of the symmetry of the potential, resulting in a higher precision in the case of the symmetrical potential, where the harmonic oscillators and the symmetrical hydrogen bond without anharmonicity were examined satisfactorily. An application was made to the symmetrical hydrogen bond with anharmonicity, where the precision was less for the higher levels. By a comparison of the calculated with the observed infrared spectra, the anharmonic potential constants for the assumed potential function were estimated.

A finite element approach has been successfully applied to a one-dimensional vibrational Schrödinger equation[1] with a harmonic or Lennard-Jones potential. Our purpose in this study is to examine the adaptability of the method to a two-dimensional vibrational Schrödinger equation, which is given by:

$$\frac{\hbar^2}{2m}\frac{\partial^2\Psi}{\partial S_1^2}+\frac{\hbar^2}{2M}\frac{\partial^2\Psi}{\partial S_2^2}+(E-V)\Psi=0, \tag{1}$$

where S_1 and S_2 are the symmetry coordinates of the vibrations with the effective masses of m and M respectively; Ψ, a wave function; E, an energy, and V, a potential with a potential surface expressed by a rectangular coordinate system due to S_1 and S_2, as is shown in Figs. 1—3.

In the harmonic oscillators, V is given by:

$$V=\frac{1}{2}kS_1^2+\frac{1}{2}KS_2^2, \tag{2}$$

where k or K is a force constant. In the symmetric hydrogen bond, which is of interest to us, V is assumed to be:[2,3]

$$V=\frac{1}{2}(FS_1^4-fS_1^2)+\frac{1}{2}KS_2^2+V', \tag{3}$$

where V' is assumed to be:

$$V'=\frac{1}{2}(F'S_1^4-f'S_1^2)S_2. \tag{4}$$

The potential constants in Eqs. 3 and 4 may be estimated reliably for the system of the $[X\text{–}H\text{–}X]^+$ ion, where X is a pyridine derivative.

Finite Element Formulation and Boundary Conditions

The functional of Eq. 1 is found to be:

$$\chi=\frac{1}{2}\int_{-\infty}^{+\infty}\int_{-\infty}^{+\infty}\left\{\frac{\hbar^2}{2m}\left(\frac{\partial\Psi}{\partial S_1}\right)^2+\frac{\hbar^2}{2M}\left(\frac{\partial\Psi}{\partial S_2}\right)^2-(E-V)\Psi^2\right\}dS_1dS_2, \tag{5}$$

where the integration is limited in a numerical calculation over the region considered. A trial function is assumed to be:

$$\Psi=\alpha_1+\alpha_2S_1+\alpha_3S_2+\alpha_4S_1^2+\alpha_5S_1S_2+\alpha_6S_2^2=\boldsymbol{N\alpha}. \tag{6}$$

That is, six nodes are used for a triangular element; they are shown in Figs. 1—3. By using the same nota-

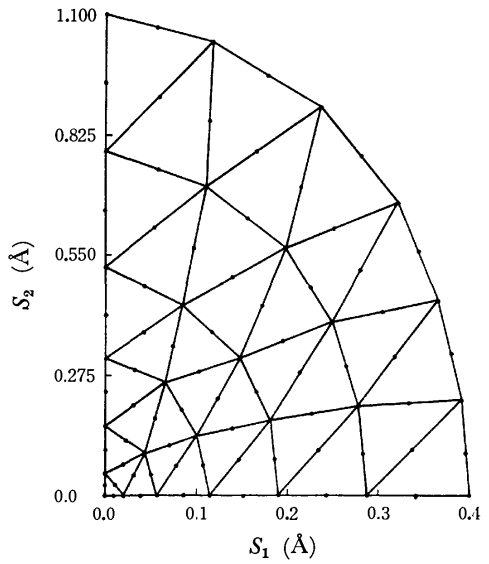

Fig. 1. The triangular elements and the nodes (·) used for harmonic oscillators.

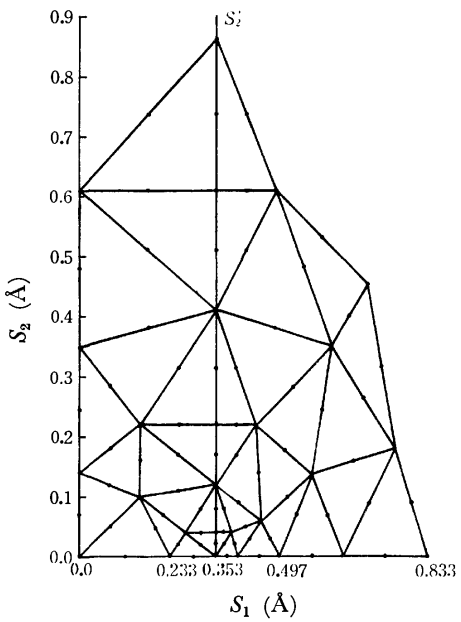

Fig. 2. The triangular elements and the nodes (·) used for the hydrogen bond with $V'=0$.

* *Faculty of Engineering, Toyama University, Nakagawa, Takaoka 933.*

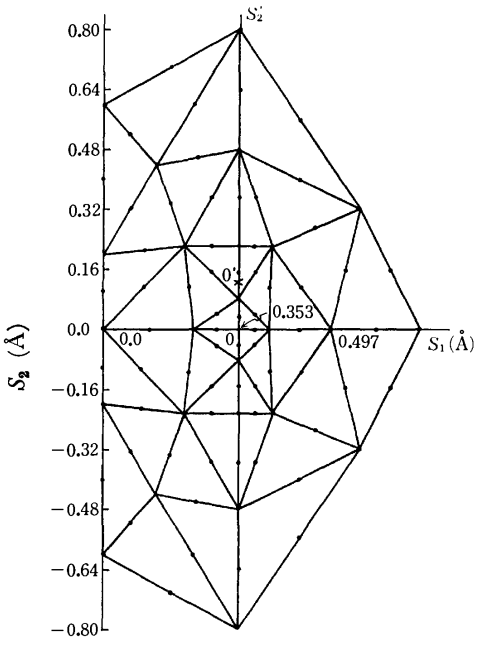

Fig. 3. The triangular elements and the nodes (·) used for the hydrogen bond (H) with $V' \neq 0$. This figure is symmetrical.

as the previous paper,[1] the functional for an element is expressed by:

$$\chi^{(e)} = \frac{1}{2}\boldsymbol{\Psi}^{(e)\mathrm{T}}(\boldsymbol{C}^{(e)-1})^{\mathrm{T}}(\boldsymbol{P}^{(e)} - \boldsymbol{E}\boldsymbol{R}^{(e)})\boldsymbol{C}^{(e)-1}\boldsymbol{\Psi}^{(e)}, \tag{7}$$

where $\boldsymbol{E}$ is the eigenvalue diagonal matrix and where

$$\boldsymbol{P}^{(e)} = \frac{\hbar^2}{2m}\iint \frac{\partial \boldsymbol{N}^{\mathrm{T}}}{\partial S_1}\frac{\partial \boldsymbol{N}}{\partial S_1}\mathrm{d}S_1\mathrm{d}S_2 + \frac{\hbar^2}{2M}\iint \frac{\partial \boldsymbol{N}^{\mathrm{T}}}{\partial S_2}\frac{\partial \boldsymbol{N}}{\partial S_2}\mathrm{d}S_1\mathrm{d}S_2 + \iint V\boldsymbol{N}^{\mathrm{T}}\boldsymbol{N}\mathrm{d}S_1\mathrm{d}S_2, \tag{8}$$

$$\boldsymbol{R}^{(e)} = \iint \boldsymbol{N}^{\mathrm{T}}\boldsymbol{N}\mathrm{d}S_1\mathrm{d}S_2, \tag{9}$$

where the integration is taken over the element. From the procedure given in Appendix I, we obtain:

$$\frac{\mathrm{d}\chi^{(e)}}{\mathrm{d}\boldsymbol{\Psi}^{(e)}} = (\boldsymbol{C}^{(e)-1})^{\mathrm{T}}\boldsymbol{P}^{(e)}\boldsymbol{C}^{(e)-1}\boldsymbol{\Psi}^{(e)} - \boldsymbol{E}(\boldsymbol{C}^{(e)-1})\boldsymbol{R}^{\mathrm{T}(e)}\boldsymbol{C}^{(e)-1}\boldsymbol{\Psi}^{(e)} = 0 \tag{10}$$

The eigenvalues and the eigenfunctions are calculated by interconnecting Eq. 10 over all the elements.

The boundary condition[4] additional to the normal one, which is omitted here, is applied because of the symmetry property of the potential function. In the harmonic oscillators, where the vibrational quantum number for S_1 or S_2 is denoted by v or v' respectively, there are four cases orthogonal to each other;

v, v': even	Non-boundary condition
v: even; v': odd	Zero on the S_1 axis
v: odd; v': even	Zero on the S_2 axis
v, v': odd	Zero on the S_1 and S_2 axes.

They are calculated separately under the boundary conditions, which reduce the matrix of the eigenvalue problem, by using a quarter of the whole region, as is shown in Figs. 1 and 2. If the potential function is symmetric for only one axis, a half of the whole region is necessary, as is shown in Fig. 3. It is clear from Eq. 5 that these treatments give precision to the numerical calculation.

Symmetrical Potential

Harmonic Oscillators. A computational precision of the finite element approach will be examined here by a comparison of the eigenvalues calculated by this method with those obtained analytically.

Since the area of an element greatly affects the calculated eigenvalues, one has to set the elements out carefully in the region considered. We set out the 36 elements with 91 nodes in the elliptical region required by the normal boundary condition, as is shown in Fig. 1. This condition is equal to setting out 144 elements with 337 nodes in the whole region. The i-th element from the origin has the length of id along the coordinate axis, where d is the size of the first element, as has been

Table 1. The eigenvalues (cm^{-1}) of the harmonic oscillators with 3000 and 300 cm^{-1} frequencies and the hydrogen bond with $V'=0$

	Harmonic oscillators		Hydrogen bond			
			H		D	
v v'	Anal.	Calcd	Anal.	Calcd	Anal.	Calcd
0—0	1650	1650.0	−2300.0	−2290.2	−2662.0	−2646.7
0—1	1950	1953.8	−2142.8	−2128.8	−2504.8	−2481.5
0—2	2250	2262.9	−1985.6	−1971.9	−2347.6	−2321.6
1—0	4650	4653.6	−2283.1	−2273.4	−2661.0	−2645.7
1—1	4950	4964.8	−2125.9	−2112.2	−2503.8	−2480.5
1—2	5250	5285.4	−1968.7	−1956.6	−2346.6	−2320.6
2—0	7650	7661.2	−224.4	−217.8	−921.9	−894.3
2—1	7950	7986.6	−67.2	−53.4	−764.7	−720.5
2—2	8250	8271.1	90.0	119.5	−607.5	−604.5
3—0	10650	10651	226.6	233.4	−863.0	−832.5
3—1	10950	10949	383.8	408.2	−705.8	−655.3
3—2	11250	11211	541.0	608.9	−548.6	−602.6

established previously for the one-dimensional problem.[1)]

As we will treat later a problem involving two modes separated extremely in the ir frequencies, ν_1 and ν_2, the higher one is set at 3000 cm^{-1}, and the lower one, at 300 cm^{-1}. Under the conditions shown in Fig. 1, the calculated eigenvalues for small numbers of v and v' are given in Table 1; they are compared with the values obtained analytically.

As is shown in Table 1, the agreement between the calculated and the analytical values is regarded to be satisfactory as an approach made computationally. The manners of variation of the eigenvectors are the same as expected.

Hydrogen Bond with $V'=0$. In the case of a double-minimum potential, it is not easy to divide the region into the elements. By means of a trial-and-error method we set out the elements and nodes as is shown in Fig. 2, where the axis of S_2' is drawn through a bottom of the potential minimas. The S_1 coordinate is defined here by the displacement coordinate of the H atom from the center of the X···X bond as the one-dimensional expression.[5)] The potential constants for the vibration of S_1 are set as $F=9.5$[6)] (mdyn/Å^3) and $f=2.37$[6)] (mdyn/Å); they give the potential minimum of -3721 cm^{-1} at ± 0.353 Å. The value of m of H(D) is assumed to be 0.984 (1.938) amu. The normal frequency of the S_2 mode, which is the X···X stretching vibration, is assumed to be 157 cm^{-1}.

The calculated eigenvalues for the small numbers of v and v' under the conditions shown in Fig. 2 are given in Table 1, along with those obtained *analytically* by the method shown in Appendix II. The agreement between the calculated and the *analytical* values may be satisfactory by making allowance for the fact that there is a certain limit in the way of dividing the region into the elements, as is shown in Fig. 2.

From Table 1 we can find the difference between the precisions for the H and the D systems. The result for the D system is less satisfactory than that for the H system, but may be improved by the adjustment of the nodal values, as will be shown later.

Application

In most hydrogen-bond systems, the anharmonicity is particularly large; thus, it is hard to use an ordinary method of vibrational analysis. The finite element method described here is, then, useful in examining the vibration of those systems. We make an application of this method to a problem for the symmetrical hydrogen bond. In this sort of system, however, it is inevitable that, because the boundary condition for one axis can not be used, the precision of calculation is more or less lowered, and so is the convergence of the eigenvectors.

The elements and nodes are set out in the symmetrical potential with $V'=0$, as is shown in Fig. 3. The calculated eigenvalues for the H system under these conditions are given in Table 2 ($F'=0.0$). The calculated eigenvalues for the D system under these conditions are less satisfactory than those for the H system, but they can be improved by adjusting the area of elements to make it somewhat smaller. The

Table 2. The eigenvalues (cm^{-1}) of the H system with $V'\neq 0$

v v'	$F'=0.0$	$F'=1.0$	$F'=2.0$	$F'=4.0$
0—0	−2292.6	−2300.2	−2324.1	−2420.8
0—1	−2118.2	−2123.9	−2146.6	−2241.7
0—2	−1970.0	−1970.7	−1988.8	−2074.8
1—0	−2275.7	−2283.6	−2308.0	−2407.0
1—1	−2101.3	−2107.0	−2130.3	−2227.5
1—2	−1956.1	−1956.5	−1974.5	−2061.2
2—0	−214.5	−215.2	−218.4	−238.4
2—1	−22.6	−27.0	−44.4	−85.0
2—2	121.0	126.9	128.0	113.4
3—0	241.3	238.8	230.5	194.3
3—1	441.8	437.7	413.0	353.6
3—2	561.5	574.5	587.4	(628.2)

Table 3. The eigenvalues (cm^{-1}) of the D system with $V'\neq 0$

v v'	$F'=0.0$	$F'=1.0$	$F'=2.0$	$F'=4.0$
0—0	−2650.0	−2651.9	−2686.1	−2797.9
0—1	−2482.0	−2483.7	−2513.8	−2622.3
0—2	−2327.4	−2324.8	−2342.1	−2443.7
1—0	−2649.0	−2650.9	−2685.2	−2797.2
1—1	−2481.1	−2482.8	−2513.0	−2621.7
1—2	−2326.7	−2324.0	−2341.3	−2442.9
2—0	−890.9	−887.6	−904.3	−939.9
2—1	−729.4	−727.9	−680.1	−748.9
2—2	−560.9	−555.4	−555.1	−601.3
3—0	−830.4	−826.8	−846.1	−892.9
3—1	−669.5	−668.9	(−624.2)	−690.4
3—2	−500.8	−520.2	(−486.9)	−533.6

results for the D system are given in Table 3 ($F'=0.0$). The agreement between the calculated values given in Table 2 or 3 with the analytical ones for the H or the D system in Table 1 is, as the whole, less than that between them in Table 1. However, the results given in Tables 2 and 3 can be useful in the estimation of the anharmonic potential constants or in the assignment of the observed spectra.

The intensity is calculated by means of this expression:[7)]

$$I_{ij} = \nu_{ij}[\exp\{-(\nu_i-\nu_0)/kT\} - \exp\{-(\nu_j-\nu_0)/kT\}]M_{ij}^2, \quad (11)$$

where ν_{ij} is the transition frequency from the i to the j level; ν_i, ν_j, and ν_0 are the eigenvalues of the i, j, and ground levels respectively, k and T have their usual meanings, and M_{ij} is given by:

$$M_{ij} = \iint \Psi_i S_1 \Psi_j \mathrm{d}S_1 \mathrm{d}S_2, \quad (12)$$

where the integration is carried out in the region considered[3)] by using the normalized function.

The relative intensities, I_{ij}, calculated under the conditions described above for the H and the D systems are shown schematically in Fig. 4-a, in which the observed spectra[8,9)] for the pyridine–H(D)–pyridine system are also given to make a comparison. As is shown in Fig. 4-a, the ν_{ij} values calculated for the H system are

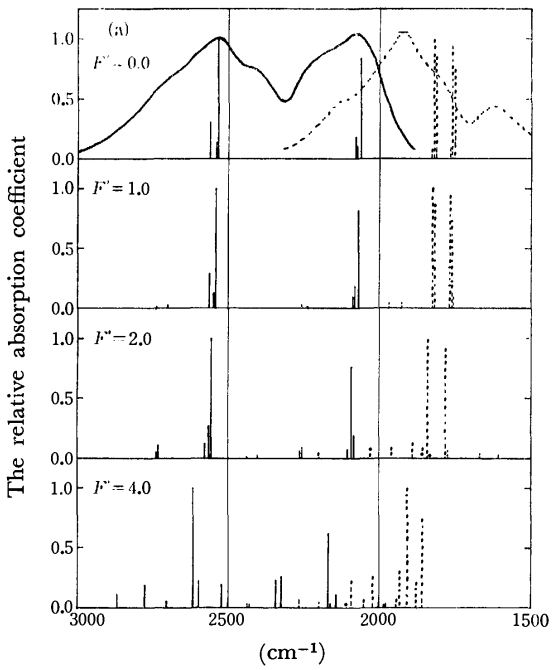

Fig. 4. Variation of the spectra with F'.

in accordance with the observed ones, but those for the D system are not. This disagreement may be attributed mainly to the inadaptability of the potential function assumed for those systems. An other type of potential function, such as the Lippincott-Schroeder potential,[5,10] may be appropriate, though others were not examined here.

In the case with $V' \neq 0$, the force constant, f', in Eq. 4 is assumed to be:

$$f' = 2F'S_e^2, \tag{13}$$

where S_e is the distance between the origin and the potential minimum with $V'=0$ on the S_1 axis. Under the assumption of Eq. 13, the potential minimum is displaced to the point, 0', on the S_2' axis in Fig. 3; the potential is now asymmetric with respect to the abscissa through 0'. Since the more the elements are put on the vicinity of the potential well, the more the result is refined, all elements are transferred parallel with the S_2' axis by a distance between two points, 0 and 0'. Further, the elements above the abscissa are so adjusted that their areas are smaller than those taken under the condition with $V'=0$. On the other hand, the elements below the abscissa remain as they were taken in a good condition with $V'=0$.

The variation in the eigenvalues with F', whose value is set as 1.0, 2.0, or 4.0 (mdyn/Å^3), is given in Tables 2 and 3 for the H and D systems respectively. One notices from those tables that the eigenvalues with a lower quantum number, v, are lowered greatly with an increase in the value of F', while those with a higher v number are lowered only slightly. The eigenvalues in brackets are abnormal and are regarded as being perturbed by a Fermi resonance, since other levels, which are not assigned and which are omitted from the discussion here, appear near those eigenvalues.

The variation in the spectra with the F' is shown schematically in Fig. 4. The spectral feature observed for the H system can be interpreted approximately by I_{ij} calculated with $F'=4.0$; that is, some of the shoulders observed can be assigned satisfactorily to the combination bands. Two places where the observed intensity is higher than the calculated one are seen at about 2100 cm^{-1} in the H system and 1650 cm^{-1} in the D system. This may result from the overlap with the other bands, which may be assigned to a combination band not considered here. When $F=9.0$ and $F'=4.0$ (mdyn/Å^3), the I_{ij} calculated for the H system accords quite well with the observed spectra, but the values, ν_{ij}, calculated for the D system are dislocated much as may be seen in Fig. 4-a.

In the H system, the overtone of the S_1 mode has been observed at 5218 cm^{-1} [8] with a shoulder at 5050 cm^{-1}; it is evaluated *analytically* to be 5211.6 cm^{-1}. When $F'=4.0$ (mdyne/Å^3), it is given as 5178.8 cm^{-1} with the intensity of 0.23 of the maximum given in Fig. 4; this intensity seems to be a little higher than that expected, taking into account the fact that the eigenvectors of the 5-0 level do not converge completely. The transition to the 4-0 level is omitted because of the less convergence of the eigenvectors. On the other hand, in the D system, the eigenvectors of these levels with $F'=4.0$ (mdyn/Å^3) converge well and the calculated intensities are quite weak, in good accordance with the observation.

A very weak band has been observed near 140 cm^{-1} in both systems; it has been assigned to an overlap of such transitions as 0-0→1-1.[3] The calculated intensities in both systems are about 1/1000 of the maximum given in Fig. 4 and nearly half of the observed values.[3,8] This shows that the quadratic term of the transition moment may be quite important, as has been discussed by Singh and Wood.[3] The region near 550 cm^{-1} could not be examined here because of the less convergence of the eigenvectors of the higher v' levels.

Conclusion

The finite element method was examined for the two-dimensional vibrational Schrödinger equation with a high precision in the case of the symmetrical potentials. Thus, even further precision might be obtained if this method were applied to such a symmetrical system as a three-fold potential. On the other hand, though the method is obviously useful for a system with anharmonicity, it would only be adaptable for a system with a large anharmonicity, such as has been examined here, if the eigenvalues of the higher levels are necessary.

The numerical calculation was carried out by using the computer, FACOM 230-45S, of Toyama University.

Appendix

I. Stationary Value in Eq. 5 and the Finite Element Method. We will justify here Eq. 10 by a procedure employing a calculus of variation.[11-13] First, we assume a functional as follows:

$$\chi = \int_{-\infty}^{+\infty}\int_{-\infty}^{+\infty} f(\Psi, p, q, S_1, S_2)\mathrm{d}S_1\mathrm{d}S_2, \tag{A-1}$$

where $p=\partial\Psi/\partial S_1$ and $q=\partial\Psi/\partial S_2$. According to Euler's condition, a characteristic equation is as follows:

$$\frac{\partial}{\partial S_1}\left(\frac{\partial f}{\partial p}\right)+\frac{\partial}{\partial S_2}\left(\frac{\partial f}{\partial q}\right)-\frac{\partial f}{\partial \Psi}=0. \tag{A-2}$$

If we take f as follows:

$$f=\frac{1}{2}\left\{\frac{\hbar^2}{2m}\left(\frac{\partial \Psi}{\partial S_1}\right)^2+\frac{\hbar^2}{2M}\left(\frac{\partial \Psi}{\partial S_2}\right)^2-(E-V)\Psi^2\right\}, \tag{A-3}$$

we find that Eq. A-2 is equal to Eq. 1. Thus, χ, which is called the associated variational functional with Eq. 1, has a stationary value.

Second, we resolve Eq. 5 directly by using a Rayleigh-Ritz approximation, where Ψ is assumed by:

$$\Psi=\sum_i \alpha_i S_1^{m_i} S_2^{n_i}=\boldsymbol{N\alpha}, \tag{A-4}$$

where the summation should be done generally for a very large number of terms. On the other hand, in a finite element method, Eq. A-4 is assumed for an element. To justify this assumption, we introduce a square matrix, $\underline{\boldsymbol{C}}^{(e)}$, which is defined by:

$$\boldsymbol{\Psi}^{(e)}=\underline{\boldsymbol{C}}^{(e)}\boldsymbol{\alpha}, \tag{A-5}$$

and which is determined by the coordinate values. From Eqs. A-4 and A-5, we obtain:

$$\Psi^{(e)}=\boldsymbol{N}\boldsymbol{C}^{(e)-1}\boldsymbol{\Psi}^{(e)}, \tag{A-6}$$

where it should be noticed that $\Psi^{(e)}$ is defined at any point in the element through the matrix $\boldsymbol{N}$ and $\boldsymbol{\Psi}^{(e)}$ for six nodal points.

Finally, since χ in Eq. A-1 is expressed by the integration of the whole region, this is expressed by the summation of the integration of each element:

$$\chi=\sum_i^{\text{all}} \chi_i^{(e)}, \tag{A-7}$$

where $\chi_i^{(e)}$ is obtained by using Eq. A-6 and is given by Eq. 7. Now, χ is expressed by the nodal value Ψ_k. From the first condition, we obtain:

$$\frac{d\chi}{d\Psi_k}=0 \qquad (k=1, 2, \cdots \text{ all nodes}), \tag{A-8a}$$

or:

$$\frac{d\chi^{(e)}}{d\Psi_i^{(e)}}=0 \qquad (i=1, 2, \cdots \text{ all elements}), \tag{A-8b}$$

or:

$$\frac{d\chi}{d\boldsymbol{\Psi}}=0, \tag{A-8c}$$

where $\boldsymbol{\Psi}$ is a column vector consisting of all nodal values. The resultant total equation has a form:

$$(\boldsymbol{A}-\boldsymbol{EB})\boldsymbol{\Psi}=0. \tag{A-9}$$

The eigenvalues and the eigenvectors are calculated from Eq. A-9.

II. Eigenvalues for a One-dimensional Hydrogen Bond.

There is no analytical method to obtain the eigenvalues for the double-minimum potential. Thus, to estimate them we used a finite element method previously reported,[1] because it is clear that the one-dimensional approach is more precise than the two-dimensional one, as may be found from Eq. 5. If the second term in Eq. 1 is neglected and m is replaced by μ, Eq. 1 is equal to Eq. 1 in Ref. 1. The eigenvalues are calculated by using the same potential as used here. The *analytical* values in Table 1 are obtained by the sum of these values and the eigenvalues of the S_2 mode.

References

1) H. Arai, I. Kanesaka, and Y. Kagawa, *Bull. Chem. Soc. Jpn.*, **49**, 1785 (1976).
2) R. L. Somorjai and D. F. Hornig, *J. Chem. Phys.*, **36**, 1980 (1962).
3) T. R. Singh and J. L. Wood, *J. Chem. Phys.*, **48**, 4567 (1968).
4) J. R. Whiteman, "The Mathematics of Finite Elements and Applications," Academic Press, London (1972), p. 351.
5) G. R. Anderson and E. R. Lippincott, *J. Chem. Phys.*, **55**, 4077 (1971).
6) J. L. Wood, *J. Mol. Struct.*, **12**, 283 (1972).
7) E. B. Wilson, J. C. Decius, and P. C. Cross, "Molecular Vibrations," McGraw-Hill, New York (1955), Chap. 7.
8) R. Clements and J. L. Wood, *J. Mol. Struct.*, **17**, 265 (1973).
9) R. Clements and J. L. Wood, *J. Mol. Struct.*, **17**, 283 (1973).
10) E. R. Lippincott and R. Schroeder, *J. Chem. Phys.*, **23**, 1099 (1955).
11) C. S. Desai and J. F. Abel, "Introduction to the Finite Element Method," Van Nostrand, New York (1972).
12) J. W. Craggs, "Calculus of Variations," George Allen and Unwin, London (1973).
13) I. Oshida, "Butsuri Sūgaku," Shokabo, Tokyo (1974), p. 221.

Radiation Chemical Reactions in Carbon Dioxide–Propane System. II. Reoxidation of Carbon Monoxide at Low Propane Concentration

Yasumasa IKEZOE and Shoichi SATO

Japan Atomic Energy Research Institute, Tokai-mura, Ibaraki 319-11

(Received April 18, 1977)

In the γ-radiolysis of carbon dioxide, the back reaction or reoxidation of carbon monoxide, proceeds at a moderate rate with propane concentration less than 0.5%, reducing the apparent G(CO) value. Concerning the total pressure and dose rate dependence of the G(CO) value with such small propane addition, it was found that the back reaction was accelerated by raising the total pressure and by lowering the dose rate. The following reactions of clustered negative ions are considered to explain the pressure and dose rate effects:

$$X^- + CO \rightarrow CO_2 + Y^- + Z_1,$$
$$X^- + C_3H_8 \rightarrow Y^- + Z_2,$$
$$X^- + X^+ \rightarrow mCO_2 + Z_3,$$

where X^- stands for a clustered negative ion.

Radiolysis of carbon dioxide has been studied extensively,[1-3] since Harteck and Dondes[4] irradiated the gas with radon α-rays and reactor radiations in 1955 and 1957. Apparent stability towards ionizing radiation at moderate dose rates ($\approx 10^{16}$ eV/g s) was attributed to a rapid reoxidation reaction, by which carbon monoxide formed is reoxidized to carbon dioxide. However, the detailed mechanism of the reoxidation, or back reaction still remains unclarified. The oxidizing species has not yet been identified, in spite of many species, such as O, O_3, O^+, O_2^+, O^-, O_2^-, CO_3^-, and CO_4^- being proposed. Recently, Parkes[5] suggested that highly clustered ions might be involved in the back reaction.

In this study, we attempted to clarifiy the nature of the back reaction when a small amount of propane is added to carbon dioxide. A controlled amount of propane was added to make the back reaction proceed at a moderate rate, under such conditions, the relation between the apparent G(CO) value and the rate of the back reaction being expected to be connected.

Experimental

Carbon dioxide (Takachiho Chemical, pure gas, stated 99.99% up) and propane (Takachiho Chemical, research grade, stated 99.7% up) were used after removing uncondensable gas with a liquid nitrogen trap. Pyrex glass ampoules (64 ml and 160 ml) were thoroughly washed with distilled water and evacuated to a vacuum of 1×10^{-4} Torr while being heated with a gas burner. The reactant gases were then, introduced into the ampoules, their pressures being measured by a stainless steel Bourdon gage. The total pressure was in the range 0.5—3.2 atm.

The ampoules were irradiated by ^{60}Co γ-rays in the exposure rates in the range 0.32—4.2 MR/h. The absorbed dose was determined by the decomposition of ethylene ($G(H_2) \equiv 1.3$) in the same ampoules as those used for sample irradiation, with a correction for the stopping power ratios of the gases to the secondary electrons.

The uncondensable products (CO, H_2, CH_4) were measured volumetrically by using a Toepler pump. The composition of the products was determined by mass spectrometry and confirmed by gas chromatography. Details were the same as described previously.[3]

Results

Propane Addition and the Back Reaction. In the preceding paper,[3] 1% propane was found sufficient to suppress the back reaction. In this study the propane concentration at which maximum G(CO) value could be obtained was first surveyed. Reactions were carried out at slightly smaller propane concentration, when the back reaction might be expected to proceed at a moderate rate.

The G(CO) value is shown in Fig. 1 as a function of the initial propane concentration. G(CO) values were determined at a constant dose (6.7 Mrad). After irradiation the propane added was consumed to some extent, *e.g.*, 0.55 to 0.39% and 0.27 to 0.18%. The maximum 4.5 was obtained at 0.55% propane concentration. This maximum is greater than the one previously obtained (3.6) by γ and $(n+\gamma)$ rays, but smaller than the one (6.7) by fission fragments.[3]

The gradual decrease in G(CO) with propane concentration higher than 0.55% is the same as our previous results.[3] The effect could be related to the suppression of the formation of carbon monoxide from cationic species by propane.

The gradual decrease in G(CO) with the less than 0.55% decrease in propane concentration is attributable

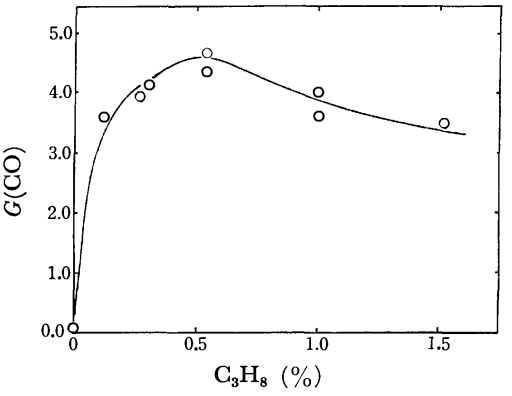

Fig. 1. Effect of propane addition on G(CO). 160-ml glass ampoule, CO_2; 1 atm, γ-rays; 0.95 MR/h, absorbed dose; 6.7 Mrad.

to the back reaction. The lower the concentration of propane, the more pronounced will be the effect of the back reaction. However, when the initial concentration of propane is extremely low (less than 0.1%), the total amount of reaction products, mainly, butane, isobutane, ethane, 2-propanol, and acetone, becomes greater than that of propane at a very small dose.

The radiolysis was carried out mainly at a propane concentration of 0.27%, the middle point between 0.55 % (at which the back reaction became apparent) and 0% (at which the complete back reaction took place). At this propane concentration, dynamic balance was expected between the back reaction and its suppression, no significant interference from the reaction products taking place with the reaction course at the absorbed dose employed. Under these conditions, the quantity of carbon monoxide formed was found to be the same order of magnitude as that of propane present in the reaction system during most of the radiolysis.

Pressure Effect. The pressure dependence of G(CO) at propane concentration less than 0.5% is of special interest, since it may be related to the mechanism of the back reaction.

The pressure dependence of G(CO) at propane concentrations of 0.27, 1.1, and 1.6% is shown in Fig. 2. The pressure dependence of G(CO) at 0.27% clearly differs from that at 1.1 and at 1.6%. The G(CO) value at 0.27% propane decreases from 4.1 to 3.6 with a total pressure rise from 0.4 to 3.2 atm, while the other G(CO) values remain constant (4.0 and 3.6).

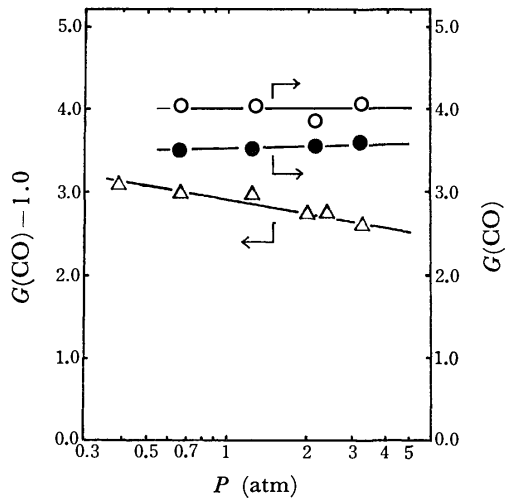

Fig. 2. Pressure dependence of G(CO). 64- and 160-ml glass ampoule, γ-rays; 0.95 MR/h, 6.7 Mrad. ●; C_3H_8 1.6%, ○; C_3H_8 1.1%, △; C_3H_8 0.27%.

This result indicates that higher pressure is favorable for the back reaction. This pressure dependence of the back reaction does not necessarily contradict the result by Yoshimura *et al.*[2] who found that the back reaction is suppressed at much higher density (0.5 g/ml), since there is a large difference between our density of the reaction system (1.8×10^{-3} g/ml) and theirs and a quite different mechanism can be considered as regards the back reaction.

Dose Rate Effect. The dose rate dependence of

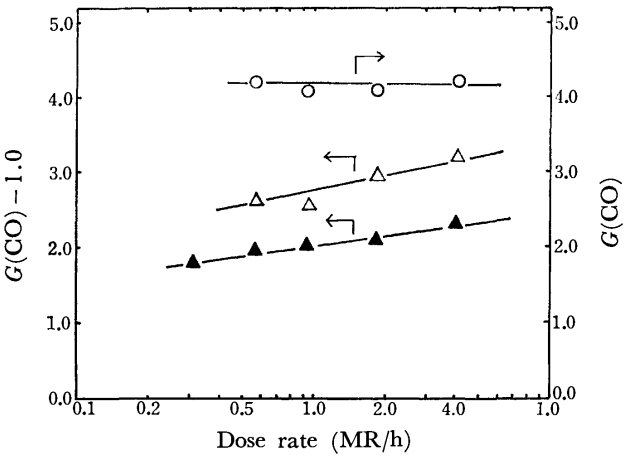

Fig. 3. Dose rate dependence of G(CO). 64-ml glass ampoule, 3.2 atm, 6.7 Mrad. ○; C_3H_8 0.82%, △; C_3H_8 0.27%, ▲; C_3H_8 0.06%.

G(CO) is shown in Fig. 3 at the low propane concentration. At 0.82% propane, where the back reaction can be assumed to be quenched, the G(CO) value is independent of the dose rate. On the other hand, the G(CO) value at 0.27% propane increases from 3.6 to 4.2 with the dose rate increase from 0.57 to 4.2×10^6 R/h. The G(CO) at 0.06% propane shows a similar dependence on the dose rate. The dose rate dependence of G(CO) obtained here is in agreement with that by Anderson and Best.[7] They found that the G(CO) value increased with the dose rate when 0.05% SF_6 was added to carbon dioxide, but remained constant when 1% SF_6 was added.

With respect to the dose rate dependence of the radiolysis of carbon dioxide, it was further found that the steady state concentration of carbon monoxide is proportional to the square root of the dose rate,[8] and that at extremely high dose rate (2×10^{27} eV/g s) carbon dioxide is decomposed with a high G(CO) value (7.8).[9]

All these effects of dose rate indicate that the back reaction becomes less effective at high dose rate.

Discussion

Oxidizing Species. Three kinds of active species, *i.e.*, neutral atomic oxygen, positive and negative ions containing an oxygen atom or molecule,[5] are conceivable as the oxidizing species responsible for the back reaction in the radiolysis of carbon dioxide. Since propane added can scavenge all of them,[2,10] the fact that the back reaction is suppressed by propane affords no information on the nature of the oxidizing species. However, the finding that the back reaction and its suppression is balanced even at 0.27% propane (Fig. 1) indicates that the oxidizing species responsible should have a reactivity of the same order of magnitude for reactions with propane and with carbon monoxide as well.

Of the three kinds of oxidizing species, atomic oxygen is much more reactive with propane than with carbon monoxide.[1] Positive ions containing an oxygen atom or molecule are also more reactive with propane than with carbon monoxide, because the ionization potential

of an oxygen atom (13.6 eV) or of oxygen (12.1 eV) is higher than that of propane (11.1 eV) and lower than that of carbon monoxide (14.0 eV). If two species were the oxidizing species, the balancing between the back reaction and its suppression should have taken place at much lower propane concentration.

On the other hand, negative ions seem to have a similar reactivity both with propane and with carbon monoxide.[11] Negative ions are known to be clustered in carbon dioxide at atmospheric pressure and ambient temperature.[12] Thus, the clustered negative ion containing an oxygen atom or molecule is presumed to be the most probable species responsible for the reoxidation of carbon monoxide in this system.

Parkes[5] has suggested that the following reactions of clustered ions may be responsible for the reoxidation of carbon monoxide.

$$O_2^{\pm}(CO_2)_n + CO \rightarrow O^{\pm}(CO_2)_n + CO_2, \quad (1)$$

$$O^{\pm}(CO_2)_n + CO \rightarrow (CO_2)_n^{\pm} + CO_2. \quad (2)$$

Simple negative ions,[7,8] such as O^-, O_2^-, CO_3^-, and CO_4^-, were found not to be responsible for the rapid back reaction.

Mechanism of the Back Reaction. From the results (Figs. 2 and 3), it is obvious that the back reaction is accelerated by raising the pressure and by lowering the dose rate. The following reactions seem plausible to account for the experimental results:

$$X^- + CO \xrightarrow{k_3} CO_2 + Y^- + Z_1, \quad (3)$$

$$X^- + C_3H_8 \xrightarrow{k_4} Y^- + Z_2, \quad (4)$$

$$X^- + X^+ \xrightarrow{k_5} mCO_2 + Z_3, \quad (5)$$

$$Y^- + X^+ \xrightarrow{k_5} nCO_2 + Z_4. \quad (5')$$

In these reactions, X^- denotes a clustered negative ion containing an oxygen atom or molecule, Y^- an electron or a negative ion other than X^-, X^+ any possible positive ion, and Z neutral reaction products. Reaction 3 is the back reaction, Reaction 4 the scavenging of X^- by propane, and Reaction 5 and 5′ the neutralization of ionic species.

The ratio, R, of the rate of Reaction 3 to that of all reactions of X^-, becomes

$$R = \frac{k_3[CO]}{k_3[CO]+k_4[C_3H_8]+k_5[X^+]} = \frac{1}{1+K_1[C_3H_8]/[CO]+K_2[X^+]/[CO]}, \quad (6)$$

where $K_1=k_4/k_3$ and $K_2=k_5/k_3$.

The concentrations of propane and carbon monoxide are proportional to the total pressure at a constant dose. The concentration of X^+ is proportional to the square root of pressure and dose rate, since it is determined by the balance between the ionization of carbon dioxide by radiations and the neutralization of ionic species.[13] Accordingly, the dependence of R on dose rate and pressure is

$$R = \frac{1}{A+B\cdot I^{1/2}\cdot P^{-1/2}}, \quad (7)$$

where I is the dose rate, P the total pressure, and A and B are constants. R increases with the rise of pressure and with the lowering of dose rate, in qualitative agreement with the dependence of the back reaction on dose rate and pressure.

Pressure and Dose Rate. R can be approximated by the ratio between the reduction in $G(CO)$ due to the back reaction and the ideal $G(CO)$ value, G_0, which would be obtained when no back reaction occurred.

$$R = \frac{G_0-G(CO)}{G_0}. \quad (8)$$

From Eqs. 7 and 8, we have

$$\frac{G_0}{G_0-G(CO)} = A + B\cdot I^{1/2}\cdot P^{-1/2}. \quad (9)$$

The ratio, $G_0/(G_0-G(CO))$, should be linearly dependent on $(I^{1/2}P^{-1/2})$, from the mechanism of the back reaction proposed.

The values of $G_0/(G_0-G(CO))$ are plotted as a function of $(I^{1/2}P^{-1/2})$ in Fig. 4, where $G(CO)$ is taken from the experimental values at 0.27% propane addition (Figs. 2 and 3), and G_0 is estimated to be 5.6 from the primary yields of carbon monoxide obtained by Willis and Boyd.[15,16] It seems possible to draw a straight line in Fig. 4, despite a little scatter at low pressure and high dose rate.

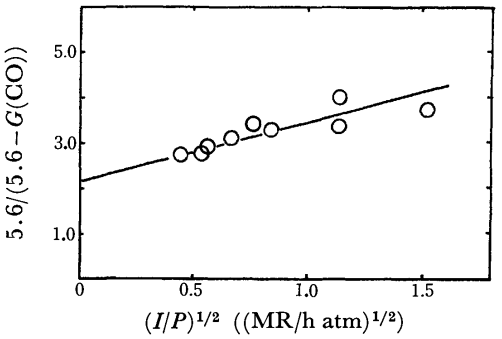

Fig. 4. $G_0/(G_0-G(CO))$ *vs.* $(I/P)^{1/2}$.

From the intercept and the slope of the straight line in Fig. 4, the ratios of the rate constants can be estimated to be $k_4/k_3=1/3$, $k_5/k_3=6.2\times10^7$, using the experimentally determined concentrations of carbon monoxide and propane. k_3 and k_4 become 1.6×10^{-13} and 0.5×10^{-13} $cm^3\,molecule^{-1}\,s^{-1}$, respectively, if we adopt 10×10^{-6} $cm^3\,molecule^{-1}\,s^{-1}$ for the value of k_5.[15] Because of the scatter in Fig. 4 and the approximation included in the above discussion, no accuracy is claimed in these values, though their orders of magnitude seem reasonable when we compare them with those of analogous reactions of a simple negative ion.[17] Clustered ions will have somewhat lower reactivity to the same reactant than ions not clustered.

References

1) A. R. Anderson and D. A. Dominey, *Radiat. Res. Rev.*, **1**, 269 (1968).
2) M. Yoshimura, M. Chosa, Y. Soma, and M. Nishikawa, *J. Chem. Phys.*, **57**, 1626 (1972).
3) Y. Ikezoe and S. Sato, *J. Nucl. Sci. Technol.*, **13**, 503

(1976).
4) P. Harteck and S. Dondes, *J. Chem. Phys.*, **23**, 902 (1955); *ibid.*, **26**, 1727 (1957).
5) D. A. Parkes, *J. Chem. Soc., Faraday Trans. 1*, **69**, 198 (1973).
6) D. A. Parkes, *J. Chem. Soc., Faraday Trans. 1*, **68**, 627 (1972).
7) A. R. Anderson and J. F. V. Best, *Adv. Chem. Ser.*, **82**, 321 (1968).
8) A. R. Anderson and J. F. V. Best, *Trans. Faraday Soc.*, **62**, 610 (1966).
9) C. Willis, A. W. Boyd, and P. E. Binder, *Can. J. Chem.*, **48**, 1951 (1970).
10) D. A. Parkes, *J. Chem. Soc., Faraday Trans. 1*, **68**, 613 (1973).
11) For example, O^- ion reacts with ethylene ($k=6\times10^{-10}$ cm^3 $molecule^{-1}$ s^{-1})[10] and with carbon monoxide ($k=7\times10^{-10}$ cm^3 $molecule^{-1}$ s^{-1})[6] with the rate constants of the same order of magnitude.
12) H. W. Ellis, R. Y. Pai, I. R. Gatland, and E. W. McDaniel, *J. Chem. Phys.*, **64**, 3935 (1976).
13) The concentration of X^+ can be estimated as follows. When the exposure rate is $I\times10^6$ R/h, the pressure of carbon dioxide P atm, and the G value of ionization 3, the rate of ion formation per unit volume, F is
$F=(I\times10^6\ \mathrm{R/h})\ (2.41\times10^{15}\ \mathrm{eV/R\ mol\ CO_2})\ (3\ \mathrm{molecule/100\ eV})\times(P\ \mathrm{atm})/(3600\ \mathrm{s/h})/(2.45\times10^4\ \mathrm{atm\ cm^3/mol\text{-}CO_2})=0.82\times10^{12}PI\ (\mathrm{molecule/cm^3\ s})$.
The rate of disappearance of the ions, D is
$D=k_5[X^+][X^-+Y^-]=k_5[X^+]^2\ (\mathrm{molecule/cm^3\ s})$.
The equilibrium concentration of X^+ is obtained by putting $D=F$. If we use 10×10^{-6} cm^3 $molecule^{-1}$ s^{-1} for the value of k_5, the concentration of X^+, $[X^+]$ is
$[X^+]=2.8\times10^8P^{1/2}I^{1/2}\ (\mathrm{molecule/cm^3})$.
14) H. N. Maier and R. W. Fessenden, *J. Chem. Phys.*, **62**, 4790 (1975).
15) C. Willis and A. W. Boyd, *Int. J. Radiat. Phys. Chem.*, **8**, 71 (1976).
16) G_0 is determined from the equation
$G_0=g(CO)+g(CO^+)+2g(C^+)+g(O^+)=4.72+0.51+0.14+0.21=5.6$
17) $O^-+CO\rightarrow CO_2+e^-$ ($k=6\times10^{-10}$ cm^3 $molecule^{-1}$ s^{-1})[6]
$O^-+C_2H_6\rightarrow C_2H_6O+e^-$ ($k=0.2\times10^{-10}$ cm^3 $molecule^{-1}$ s^{-1}).[18]
18) T. O. Tiernan, "Interaction between Ions and Molecules," ed by P. Ausloos, Plenum Press, New York (1974), p. 382.

Determination of Absolute Configuration of Epishamixanthone, a Metabolite of *Aspergillus rugulosus*, by Anomalous Scattering of Light Atoms

Keiichi FUKUYAMA, Kensaku HAMADA, Tomitake TSUKIHARA, and Yukiteru KATSUBE
Faculty of Engineering, Tottori University, Koyama, Tottori 680

(Received April 30, 1977)

The absolute configuration of epishamixanthone has been determined from the Bijvoet differences by anomalous scattering of light atoms for Cu $K\alpha$ radiation. To verify the determination, the absolute configuration of sterigmatocystin which was already determined has been examined by the same procedure. The reliability of the Bijvoet differences calculated from the structure has been estimated by means of the probability method. The errors in the measured values of the Bijvoet differences have been analysed by the normal probability plot. The accuracy of the measurement may be affected considerably by the habit of crystal. The present analysis has established that the configurations of two asymmetric carbon atoms in epishamixanthone are both *R*.

Many natural products are isolated as optically active substances, and the determinations of their structures, including the absolute configurations, are of interest in connection with the study of stereospecificity in biological systems. Although the X-ray method for the determination of the absolute configuration seems to be more direct and more reliable than the spectroscopic[1] and chemical methods,[2] until recently the application of the X-ray method was confined to a crystal containing heavy atoms. The developments of the isolation technique of minor products and the direct method of the X-ray structure analysis have enhanced the need for a reliable method for the determination of the absolute configuration without further chemical modification. Recently, some authors described the determinations of the absolute configurations by using anomalous scattering of light atoms.[3,4] In the present investigation, the absolute configuration of epishamixanthone **1**, a metabolite of *Aspergillus rugulosus*, has been determined by the method described by Engel.[4] In addition, the reliability of this method has been examined by using sterigmatocystin **2**, whose absolute configuration had already been known from its bromo derivative.[5]

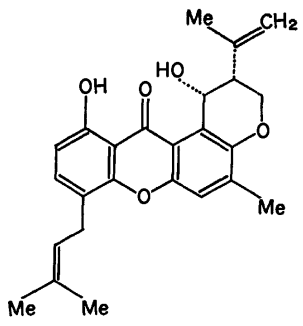

1

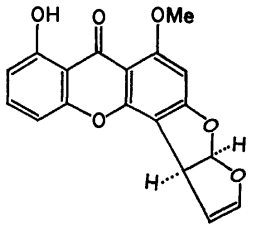

2

Structure Determination

The isolation technique, spectral data, and relative structure of epishamixanthone have been published previously.[6]

Crystallographic Measurement of Epishamixanthone. The crystals of epishamixanthone were grown as greenish-yellow needles elongated along the b axis. The cell constants were obtained by least-squares fits of the θ values for 49 reflections measured by a four-circle diffractometer. Two sets of intensity data were collected to analyze the errors in the calculated Bijvoet differences: the first data-set was collected by the stationary-crystal stationary-counter method and the second set was by the θ-2θ scan method. The experimental conditions for each set are summarized in Table 1(a) together with the crystal data. The intensities were corrected only for the Lorentz and polarization factors.

Structure Determination of Epishamixanthone. The initial structure was determined by using the first data-set. The orientation and location of the xanthone skeleton were determined by application of vector-search method.[7] The location of the remaining non-hydrogen atoms were successively determined by Fourier syntheses. The coordinates and temperature factors were initially refined by the block-diagonal least-squares method by using the carbon scattering factor. The atomic species were determined by inspection of the temperature factors as well as chemical information. The positions of hydrogen atoms were assigned from a difference Fourier synthesis. Including the hydrogen atoms, the refinement reduced the *R* value to 0.081 for 1452 reflections, where the following weighting scheme was adopted: $w=0.63$ for $F_o=0$, $w=1.0$ for $0<F_o\leqq 10$, and $w=1.0/(1.0+0.71(F_o-10))$ for $10<F_o$.

Further refinement was made using the second data-set and the block-diagonal least-squares method. The four strongest reflections, 001, 210, −201, and −311, were rejected from the subsequent calculations. The methyl hydrogen atoms attached to the C(25) atom could not be located; this is probably due to a large thermal motion of the group. Some of the hydrogen atoms obtained from the first set were found to be mislocated. A weighting scheme, $w=0.25$ for $F_o=0$, $w=1.0$ for $0<F_o\leqq 8$, and $w=1.0/(1.0+0.5(F_o-8))$ for $8<F_o$, was used in the final calculation. The final *R* value was 0.058 for 1719 reflections ($R=0.055$ for non-zero reflections). The final atomic parameters refined by the second set are given in Tables 2(a) and 3(a).

Structure Refinement of Sterigmatocystin. The intensity measurement and structure analysis of sterigmatocystin have been described.[8] In order to estimate the effect of error in the atomic parameters on B_{th}*,

TABLE 1. CRYSTAL DATA AND EXPERIMENTAL CONDITIONS

(a) Epishamixanthone
(i) Crystal data
$C_{25}H_{26}O_5$, $M=406.5$
monoclinic, space group $P2_1$
$a=15.038(6)$, $b=6.251(4)$, $c=11.595(5)$ Å
$\beta=105.14(4)°$, $V=1052.1$ Å^3
$D_o=1.28$ g/cm^3
$D_x=1.28$ g/cm^3 (for $Z=2$)
μ(for Cu $K\alpha$) $=7.3$ cm^{-1}
$N_o/N_e=0.20$
(ii) First intensity data-set
Ni-filtered Cu $K\alpha$ radiation
Toshiba four-circle diffractometer
stationary-crystal stationary-counter
peak counting time: 30 s
background: function of 2θ
$\sin\theta/\lambda<0.53$
independent reflections: 1452
(iii) Second intensity data-set
Ni-filtered Cu $K\alpha$ radiation
Rigaku four-circle diffractometer
θ-2θ scan mode
scan range: $\Delta\theta=1.2°+0.15°\tan\theta$
scan speed: 2°/min(θ)
background counting time: 8 s
$\sin\theta/\lambda<0.562$
independent reflections: 1723
(b) Sterigmatocystin
(i) Crystal data
$C_{18}H_{12}O_6$, $M=324.3$
monoclinic, space group $P2_1$
$a=16.056(4)$, $b=4.324(2)$, $c=11.218(3)$ Å
$\beta=113.13(5)°$, $V=716.2$ Å^3
$N_o/N_e=0.33$
(ii) Second intensity data-set
Ni-filtered Cu $K\alpha$ radiation
Rigaku four-circle diffractometer
θ-2θ scan mode
scan range: $\Delta\theta=1.0°+0.15°\tan\theta$
scan speed: 2°/min(θ)
background counting time: 8 s
$\sin\theta/\lambda<0.562$
independent reflections: 1227

intensities were remeasured in different conditions. (The intensity data collected in the condition described in the previous paper is noted as the first set.) The cell constants were remeasured before data collection. The experimental condition for the second set is summarized in Table 1(b) together with refined cell constants. The intensities were corrected only for the Lorentz and polarization factors.

The structure was refined by the block-diagonal least-squares method with the second set. The five strongest reflections, -111, -201, -211, 201, and -312, were omitted from the calculations. The weighting scheme used in the final cycle of the refinement was: $w=0.2$ for $F_o=0$, $w=1.0$ for $0<F_o\leqq14$, and $w=1.0/(1.0+0.6(F_o-14))$ for $14<F_o$. The final R value was 0.039 for 1222 reflections ($R=0.036$ for non-zero reflections). Since the final atomic parameters obtained from the second set seem to be more accurate than those from the first set, they are documented in Tables 2(b) and 3(b). A list of the observed and calculated structure factors is deposited at the office of the Chemical Society of Japan (Document No. 7802).

Determination of Absolute Configuration

Measurement of Bijvoet Differences. The sets of Bijvoet and reference reflections with large BA_{th}* and with relatively large intensity were chosen by hand. Unless otherwise stated, the calculations of the structure factors were executed with $\Delta f_o''=0.02$ and $\Delta f_c''=\Delta f_H''=0.0$. The Bijvoet differences of both compounds were measured under the same experimental condition. A crystal was mounted with its b axis parallel to the ϕ axis of a Rigaku off-line four-circle diffractometer. The θ-2θ scan technique was adopted using Ni-filtered Cu $K\alpha$ radiation with a scan speed of 0.5°/min (θ) and a scan width of 0.8° (θ). Backgrounds were counted for 26 s at both sides of the scan range. In this experimental condition, the intensities of the Bijvoet pair (h_1 k_1 l_1 and h_1 $\bar{k}_1$ l_1) and its reference pair (h_2 k_2 l_2 and h_2 $\bar{k}_2$ l_2) were measured alternately 10 times. To diagnose the error of measurement, the intensities of equivalent reflections ($\bar{h}_1$ k_1 $\bar{l}_1$, $\bar{h}_1$ $\bar{k}_1$ $\bar{l}_1$, $\bar{h}_2$ k_2 $\bar{l}_2$, and $\bar{h}_2$ $\bar{k}_2$ $\bar{l}_2$) were also measured in the same way. The results of the measurements for each compound are summarized in Table 4. The standard deviation of mean value calculated from 10 individual BA's, $\sigma(BA_e)$, is not significantly large compared with that expected from counting statistics, $\sigma(BA_c)$. The signs of DELA for sterigmatocystin are minus through all reflections, while for epishamixanthone a few exceptions are found.

Effect of Error in Atomic Parameters on B_{th}. The magnitude of B_{th} for the enantiomer-sensitive reflection in a light atom structure is fairly small. It is inferred, however, that this fact does not mean that very accurate atomic parameters are necessary to evaluate the B_{th}. The effect of the error in atomic parameters has been quantitatively estimated as listed in Table 5, which shows that each of the $\sigma(B_{th})$ is small enough to hold the sign of the B_{th} invariable. Further, the estimation of the $\sigma(B_{th})$ has been assessed by means of a half-normal probability plot[9] (Fig. 1). These plots show that the $\sigma(B_{th})$'s have been correctly estimated. It should be noted that B_{th} is insensitive to overall thermal parameters; even though the overall thermal parameters obtained from the second data-set for sterigmatocystin are significantly smaller than those from the first set, the slope for sterigmatocystin is approximately 1.0. For the enantiomer-sensitive reflections, all of the signs of the B_{th} calculated at the

* The notations are same as those in Engel's paper.[4] DEL$=B_{ex}/B_{th}$, $B=(Q_{H1}-1)/(1/2)(Q_{H1}+1)$, DELA$=BA_{ex}/BA_{th}$, $BA=(Q_{H1}/Q_{H2}-1)/(1/2)(Q_{H1}/Q_{H2}+1)$, $Q_{Hi}=F_{Hi}/F_{\bar{H}i}$; H1: Bijvoet reflection; H2: reference reflection.

TABLE 2. FINAL ATOMIC PARAMETERS[a] ($\times 10^4$) OF NON-HYDROGEN ATOMS, WITH ESTIMATED STANDARD DEVIATIONS IN PARENTHESES

(a) Epishamixanthone									
	x	y	z	β_{11}	β_{22}	β_{33}	β_{12}	β_{13}	β_{23}
C (1)	3477 (3)	4671 (8)	4593 (4)	48 (2)	242 (12)	121 (4)	6 (9)	42 (5)	−7 (13)
C (2)	3239 (3)	3298 (7)	5403 (4)	44 (2)	226 (13)	106 (4)	16 (8)	44 (4)	6 (11)
C (3)	2601 (2)	1615 (7)	4948 (3)	41 (2)	241 (12)	102 (4)	34 (8)	38 (4)	18 (11)
C (4)	2297 (3)	46 (7)	5689 (4)	44 (2)	249 (13)	105 (4)	37 (9)	37 (4)	39 (12)
C (5)	1657 (3)	−1562 (7)	5081 (4)	40 (2)	216 (12)	122 (4)	−10 (8)	41 (4)	9 (12)
C (6)	1340 (3)	−3233 (8)	5721 (4)	48 (2)	273 (13)	125 (4)	19 (9)	51 (5)	50 (13)
C (7)	744 (3)	−4772 (9)	5105 (5)	52 (2)	288 (15)	161 (5)	−39 (10)	69 (5)	−5 (15)
C (8)	453 (3)	−4718 (10)	3878 (5)	59 (2)	358 (18)	154 (5)	−96 (11)	87 (6)	−93 (16)
C (9)	731 (3)	−3118 (10)	3204 (4)	53 (2)	447 (20)	132 (5)	−76 (12)	58 (5)	−76 (17)
C (10)	1340 (3)	−1589 (8)	3837 (4)	47 (2)	316 (16)	122 (4)	−29 (10)	58 (5)	−41 (14)
C (11)	2232 (3)	1491 (8)	3723 (4)	44 (2)	321 (15)	113 (4)	−23 (10)	39 (4)	8 (14)
C (12)	2452 (3)	2951 (9)	2923 (4)	49 (2)	330 (15)	113 (4)	−23 (10)	36 (5)	29 (14)
C (13)	3065 (3)	4546 (8)	3345 (4)	50 (2)	311 (15)	123 (4)	18 (10)	61 (5)	57 (14)
C (14)	3333 (3)	6137 (10)	2521 (4)	75 (3)	352 (17)	138 (5)	−24 (13)	59 (6)	130 (17)
C (15)	4700 (3)	6109 (10)	6092 (4)	55 (2)	367 (18)	133 (5)	−76 (12)	32 (5)	19 (16)
C (16)	4137 (3)	5779 (8)	6978 (4)	54 (2)	253 (13)	113 (4)	−2 (9)	30 (5)	−5 (13)
C (17)	4671 (3)	6024 (9)	8272 (4)	78 (3)	281 (15)	123 (5)	−23 (12)	20 (6)	−23 (15)
C (18)	4119 (4)	6099 (18)	9146 (5)	81 (3)	911 (44)	129 (5)	−33 (22)	59 (7)	−133 (29)
C (19)	5592 (4)	6129 (13)	8621 (5)	67 (3)	570 (27)	147 (5)	−46 (16)	−8 (6)	−85 (23)
C (20)	3652 (3)	3638 (8)	6733 (4)	44 (2)	217 (11)	117 (4)	19 (8)	28 (4)	17 (12)
C (21)	441 (4)	−3061 (14)	1855 (5)	84 (3)	659 (31)	140 (6)	−212 (19)	46 (7)	−118 (23)
C (22)	−302 (4)	−4582 (14)	1254 (6)	87 (3)	560 (29)	165 (6)	−120 (18)	56 (8)	−124 (23)
C (23)	−1186 (3)	−4135 (11)	857 (4)	71 (3)	490 (21)	95 (4)	−77 (14)	28 (5)	−27 (17)
C (24)	−1820 (5)	−5913 (16)	271 (5)	121 (5)	685 (35)	140 (6)	−163 (25)	62 (9)	−95 (26)
C (25)	−1669 (8)	−2153 (17)	907 (7)	236 (10)	574 (34)	190 (9)	239 (34)	112 (15)	−69 (31)
O (1)	4300 (2)	1997 (6)	7228 (3)	61 (2)	271 (9)	142 (3)	29 (7)	8 (4)	52 (10)
O (2)	2575 (2)	51 (6)	6806 (3)	71 (2)	321 (10)	102 (3)	−51 (8)	26 (3)	53 (9)
O (3)	1610 (2)	−3305 (6)	6922 (3)	74 (2)	335 (11)	129 (3)	−35 (8)	37 (4)	106 (11)
O (4)	1614 (2)	−70 (6)	3170 (3)	56 (1)	369 (11)	108 (3)	−94 (7)	34 (3)	−20 (10)
O (5)	4101 (2)	6280 (6)	4912 (3)	69 (2)	305 (10)	128 (3)	−76 (8)	42 (4)	53 (10)
(b) Sterigmatocystin									
	x	y	z	β_{11}	β_{22}	β_{33}	β_{12}	β_{13}	β_{23}
C (1)	4391 (2)	886 (8)	2594 (2)	32 (1)	487 (20)	67 (2)	13 (9)	20 (3)	−9 (13)
C (2)	3993 (2)	1958 (8)	1334 (2)	33 (1)	414 (18)	69 (2)	14 (8)	39 (3)	−20 (12)
C (3)	3091 (2)	1098 (7)	496 (2)	30 (1)	389 (17)	63 (2)	29 (8)	26 (3)	−27 (12)
C (4)	2631 (2)	2145 (8)	−838 (2)	36 (1)	461 (18)	66 (2)	64 (9)	38 (3)	−11 (12)
C (5)	1722 (2)	938 (8)	−1546 (2)	33 (1)	402 (18)	65 (2)	44 (8)	28 (3)	−48 (12)
C (6)	1218 (2)	1685 (8)	−2862 (2)	41 (1)	481 (20)	65 (2)	70 (10)	26 (3)	−34 (13)
C (7)	355 (2)	562 (9)	−3500 (3)	49 (2)	528 (21)	69 (3)	51 (11)	−9 (3)	−41 (14)
C (8)	−22 (2)	−1343 (9)	−2861 (3)	40 (1)	533 (23)	100 (3)	31 (11)	−7 (3)	−46 (16)
C (9)	446 (2)	−2168 (9)	−1569 (3)	36 (1)	517 (22)	93 (3)	−5 (10)	9 (3)	−21 (15)
C (10)	1311 (2)	−1002 (8)	−947 (2)	34 (1)	425 (18)	70 (3)	34 (9)	14 (3)	−36 (13)
C (11)	2628 (2)	−904 (7)	1012 (2)	30 (1)	386 (17)	61 (2)	7 (8)	28 (3)	−48 (12)
C (12)	3013 (2)	−1987 (7)	2256 (2)	34 (1)	359 (17)	62 (2)	24 (8)	22 (3)	−13 (11)
C (13)	3881 (2)	−1072 (8)	3013 (2)	37 (1)	404 (18)	53 (2)	46 (9)	18 (3)	4 (12)
C (14)	3496 (2)	−4173 (8)	4351 (3)	53 (2)	478 (20)	64 (2)	21 (10)	30 (3)	24 (13)
C (15)	2378 (2)	−1750 (10)	4732 (3)	74 (2)	657 (27)	128 (4)	−12 (14)	127 (5)	−20 (19)
C (16)	1996 (2)	−2285 (9)	3486 (3)	55 (2)	523 (22)	98 (3)	19 (11)	74 (4)	67 (15)
C (17)	2655 (2)	−3943 (7)	3061 (2)	44 (1)	375 (18)	69 (3)	−15 (9)	37 (3)	25 (12)
C (18)	5371 (2)	4504 (10)	1569 (3)	32 (1)	753 (27)	110 (3)	−50 (11)	35 (3)	51 (18)
O (1)	4422 (1)	3884 (6)	821 (2)	32 (1)	589 (15)	82 (2)	−31 (7)	32 (4)	28 (10)
O (2)	2968 (1)	3968 (6)	−1387 (2)	42 (1)	723 (18)	83 (2)	−24 (8)	39 (2)	135 (11)
O (3)	1579 (1)	3531 (7)	−3504 (2)	52 (1)	770 (18)	72 (2)	37 (8)	33 (2)	97 (11)
O (4)	1756 (1)	−1901 (5)	326 (2)	32 (1)	505 (13)	67 (2)	−29 (6)	10 (2)	39 (9)
O (5)	4193 (1)	−2260 (6)	4239 (2)	44 (1)	534 (14)	61 (2)	−23 (7)	5 (2)	48 (9)
O (6)	3248 (2)	−2931 (8)	5335 (2)	72 (1)	915 (21)	72 (2)	−9 (10)	61 (3)	−68 (12)

a) Anisotropic temperature factors are in the form: $\exp[-(\beta_{11}h^2+\beta_{22}k^2+\beta_{33}l^2+\beta_{12}hk+\beta_{13}hl+\beta_{23}kl)]$.

TABLE 3. FINAL ATOMIC COORDINATES ($\times 10^3$) AND ISOTROPIC TEMPERATURE FACTORS ($\times 10$) OF HYDROGEN ATOMS, WITH ESTIMATED STANDARD DEVIATIONS IN PARENTHESES

(a) Epishamixanthone

	x	y	z	B/Å^2
H (C 7)	56 (4)	−568 (11)	560 (5)	64 (15)
H (C 8)	9 (3)	−568 (11)	343 (4)	55 (14)
H (C 12)	209 (3)	284 (10)	200 (4)	44 (12)
H (C 14)	309 (4)	574 (14)	154 (5)	81 (17)
H (C 14)	316 (4)	753 (13)	274 (5)	69 (16)
H (C 14)	399 (3)	586 (11)	261 (4)	48 (12)
H (C 15)	507 (4)	719 (13)	615 (5)	67 (16)
H (C 15)	511 (3)	487 (10)	617 (4)	40 (12)
H (C 16)	362 (3)	674 (10)	674 (4)	45 (12)
H (C 18)	359 (5)	484 (14)	890 (6)	94 (20)
H (C 18)	371 (5)	748 (17)	912 (6)	105 (22)
H (C 18)	434 (4)	679 (12)	999 (5)	66 (15)
H (C 19)	585 (4)	627 (12)	942 (5)	63 (14)
H (C 19)	603 (4)	618 (11)	789 (5)	62 (14)
H (C 20)	308 (3)	355 (9)	718 (4)	30 (10)
H (O 1)	380 (5)	107 (14)	723 (6)	92 (18)
H (O 3)	193 (4)	−206 (13)	719 (6)	80 (18)
H (C 21)	100 (4)	−288 (13)	157 (5)	69 (16)
H (C 21)	9 (5)	−165 (16)	165 (6)	97 (21)
H (C 22)	−5 (4)	−639 (16)	117 (6)	93 (20)
H (C 24)	−230 (4)	−537 (12)	77 (5)	73 (17)
H (C 24)	−165 (4)	−786 (15)	22 (5)	84 (18)
H (C 24)	−210 (4)	−570 (14)	−69 (6)	89 (19)

(b) Sterigmatocystin

	x	y	z	B/Å^2
H (C 1)	502 (2)	146 (10)	319 (3)	31 (8)
H (O 3)	217 (3)	366 (13)	−303 (4)	57 (11)
H (C 7)	1 (2)	118 (10)	−446 (3)	37 (9)
H (C 8)	−65 (2)	−225 (11)	−333 (3)	36 (8)
H (C 9)	15 (2)	−346 (12)	−117 (3)	49 (10)
H (C 14)	379 (2)	−628 (10)	467 (3)	34 (8)
H (C 15)	212 (2)	−78 (12)	529 (4)	52 (10)
H (C 16)	140 (2)	−146 (12)	285 (4)	53 (10)
H (C 17)	244 (2)	−614 (10)	266 (3)	34 (8)
H (C 18)	570 (2)	265 (12)	175 (3)	49 (10)
H (C 18)	548 (3)	540 (15)	257 (4)	70 (12)
H (C 18)	556 (2)	594 (13)	114 (4)	55 (11)

early stage of the refinement were equal to those at the final stage. Therefore, it is not necessary to refine the structure extremely for application of the method described by Engel,[4] if the structure is correctly solved. The other reflections with smaller Bijvoet differences may have a larger value of $\sigma(B_{\rm th})/|B_{\rm th}|$. Average $\sigma(\Delta|F_{\rm c}|)$ value was discussed by Parthasarathy.[10]

Two kinds of $B_{\rm th}$ were calculated: $B_{\rm th}(1)$ with $\Delta f_{\rm o}''=0.032$, $\Delta f_{\rm c}''=0.009$, and $\Delta f_{\rm H}''=0.0$,[11] and $B_{\rm th}(2)$ with $\Delta f_{\rm o}''=0.018$ and $\Delta f_{\rm c}''=\Delta f_{\rm H}''=0.0$. In the $B_{\rm th}(2)$, the $\Delta f_{\rm o}''$ corresponds to the effective anomalous scattering factor of oxygen atom defined by Engel,[4] and the contribution of hydrogen atoms is neglected. For the reflections in Table 5, the values given by $\Sigma|B_{\rm th}(1)-B_{\rm th}(2)|/\Sigma(1/2)(|B_{\rm th}(1)|+|B_{\rm th}(2)|)$ are

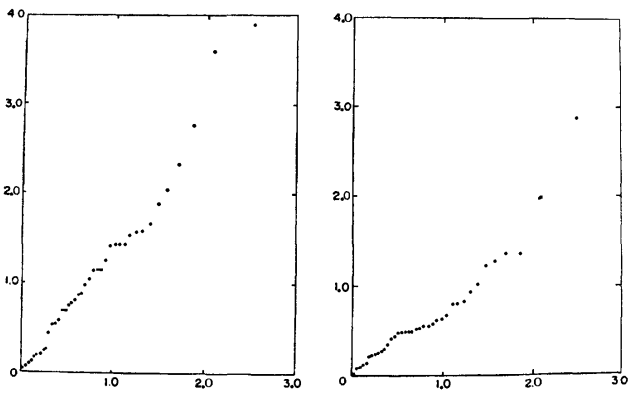

(a) Epishamixanthone (b) Sterigmatocystin

Fig. 1. Half-normal probability plot: the vertical axis is statistic $\delta p_{\rm l}$; the horizontal axis is the expected $\delta p_{\rm l}$.
$\delta p_{\rm l}=||B_{\rm th}(1)_{\rm l}|-|B_{\rm th}(2)_{\rm l}||/\{\sigma^2(B_{\rm th}(1))_{\rm l}+\sigma^2(B_{\rm th}(2))_{\rm l}\}^{1/2}$,
where $B_{\rm th}(1)_{\rm l}$, $B_{\rm th}(2)_{\rm l}$, $\sigma(B_{\rm th}(1))_{\rm l}$, and $\sigma(B_{\rm th}(2))_{\rm l}$ are calculated from two sets of atomic parameters and their estimated standard deviations obtained from independent structure refinement.

0.105 and 0.051 for epishamixanthone and sterigmatocystin respectively.

Error in Intensity Measurement. Various kinds of experimental errors in the detection of the small intensity difference of Bijvoet pair have been eliminated appreciably by the use of the reference reflection; for epishamixanthone mean DEL and DELA are −1.04 ±0.22 and −1.14±0.15 respectively, and for sterigmatocystin the corresponding values are −1.26±0.12 and −0.98±0.07. However, the standard deviation of mean DELA for each compound calculated from individual DELA's is still larger than the corresponding value expected from $\sigma(BA_{\rm c})$'s or $\sigma(BA_{\rm o})$'s. This fact is visualized in the normal probability plot[9] (Fig. 2),

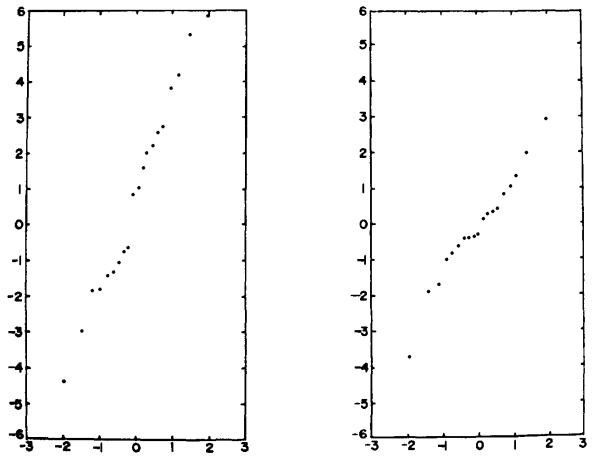

(a) Epishamixanthone (b) Sterigmatocystin

Fig. 2. Normal probability plot: the vertical axis is statistic $\delta m_{\rm l}$; the horizontal axis is the expected $\delta m_{\rm l}$.
$\delta m_{\rm l}=\{(\mathrm{DELA}_{hkl})_{\rm l}-(\mathrm{DELA}_{\bar{h}\bar{k}\bar{l}})_{\rm l}\}/\{\sigma^2(\mathrm{DELA}_{hkl})_{\rm l}+\sigma^2(\mathrm{DELA}_{\bar{h}\bar{k}\bar{l}})_{\rm l}\}^{1/2}$,
where the $\sigma(\mathrm{DELA}_{hkl})_{\rm l}$ and $\sigma(\mathrm{DELA}_{\bar{h}\bar{k}\bar{l}})_{\rm l}$ are calculated from 10 individual DELA's. The plot is independent of $BA_{\rm th}$.

TABLE 4. RESULTS OF THE BIJVOET MEASUREMENTS

BA_{ex} is the mean values of 10 individual BA's. $\sigma(BA_c)$ and $\sigma(BA_e)$ are standard deviations of the mean expected from counting statistics and that calculated from 10 individual BA's respectively. BA_{th}, BA_{ex}, $\sigma(BA_c)$, and $\sigma(BA_e)$ are given in %.

(a) Epishamixanthone										
h_1	k_1	l_1	h_2	k_2	l_2	BA_{th}	BA_{ex}	$\sigma(BA_c)$	$\sigma(BA_e)$	DELA
4	2	0	4	2	1	0.99	−1.38	0.23	0.20	−1.40
							−1.09	0.24	0.34	−1.11
−7	2	1	−8	2	2	0.55	0.02	0.15	0.17	0.04
							−0.57	0.15	0.15	−1.04
6	1	1	7	1	1	−1.09	0.31	0.20	0.25	−0.28
							0.81	0.20	0.20	−0.74
2	1	3	1	1	3	1.03	−0.19	0.21	0.20	−0.19
							−1.66	0.21	0.19	−1.61
−3	2	1	−4	2	1	1.10	−1.88	0.32	0.41	−1.71
							−0.87	0.32	0.39	−0.79
1	2	1	0	2	1	1.79	−2.13	0.47	0.83	−1.19
							−7.81	0.47	0.51	−4.37
1	1	5	2	1	5	−0.72	−0.22	0.31	0.48	0.31
							1.17	0.31	0.44	−1.64
−5	1	2	−6	1	1	−1.01	0.51	0.49	0.54	−0.51
							2.68	0.48	0.53	−2.65
−2	3	2	−1	3	2	1.06	−1.61	0.36	0.41	−1.51
							−0.80	0.36	0.40	−0.75
−5	2	4	−5	2	5	1.65	−2.29	0.35	0.53	−1.39
							−1.39	0.35	0.44	−0.84
3	1	4	3	1	5	−0.72	−0.20	0.30	0.62	0.28
							0.63	0.30	0.47	−0.87
0	2	4	0	2	3	1.17	−2.53	0.27	0.45	−2.15
							−0.11	0.27	0.33	−0.09
6	1	4	5	1	4	−1.37	−0.75	0.49	0.51	0.54
							2.26	0.50	0.60	−1.65
−4	2	6	−4	2	5	1.56	−0.97	0.49	0.29	−0.62
							−2.99	0.48	0.68	−1.92
2	3	0	1	3	0	0.72	−1.31	0.34	0.25	−1.83
							−0.15	0.34	0.59	−0.21
3	1	2	2	1	2	1.45	−1.78	0.53	0.62	−1.23
							−0.94	0.53	0.52	−0.65
−4	2	2	−3	2	2	−0.75	2.36	0.31	0.37	−3.13
							1.02	0.29	0.25	−1.36
−8	1	3	−6	1	3	0.97	−0.22	0.49	0.77	−0.23
							−2.58	0.49	0.86	−2.67
−2	1	2	−2	1	3	−0.97	0.82	0.13	0.21	−0.84
							1.04	0.13	0.14	−1.07
8	2	3	7	2	4	−1.18	1.74	0.61	0.76	−1.47
							1.01	0.62	0.76	−0.85
(b) Sterigmatocystin										
h_1	k_1	l_1	h_2	k_2	l_2	BA_{th}	BA_{ex}	$\sigma(BA_c)$	$\sigma(BA_e)$	DELA
2	1	1	1	1	1	−1.25	1.52	0.11	0.23	−1.21
							1.68	0.11	0.11	−1.35
2	2	2	3	2	2	2.23	−2.35	0.38	0.31	−1.05
							−2.17	0.38	0.45	−0.97
−7	1	2	−6	1	3	−1.77	1.03	0.22	0.32	−0.58
							1.19	0.22	0.23	−0.68
−5	1	5	−4	1	5	−1.44	1.16	0.33	0.31	−0.80
							1.39	0.33	0.52	−0.97
6	1	1	5	1	1	−1.27	0.25	0.16	0.12	−0.19
							0.73	0.16	0.23	−0.58
−11	1	3	−11	1	2	0.81	−0.96	0.29	0.45	−1.19
							−1.23	0.29	0.42	−1.51
−3	2	1	−3	2	0	−1.66	1.85	0.34	0.25	−1.12
							0.97	0.34	0.38	−0.59

TABLE 4. (Continued)

(b) Sterigmatocystin										
h_1	k_1	l_1	h_2	k_2	l_2	BA_{th}	BA_{ex}	$\sigma(BA_c)$	$\sigma(BA_e)$	DELA
4	2	2	5	2	2	−0.54	0.25	0.18	0.18	−0.46
							1.17	0.18	0.17	−2.17
8	2	0	7	2	0	−1.96	3.99	0.56	0.61	−2.04
							2.87	0.56	0.57	−1.46
−4	1	7	−3	1	7	1.00	−0.98	0.21	0.42	−0.98
							−0.58	0.21	0.26	−0.58
−9	1	2	−10	1	2	−1.65	1.55	0.40	0.32	−0.94
							1.46	0.40	0.68	−0.88
5	1	6	6	1	6	−1.09	1.24	0.24	0.20	−1.14
							0.46	0.24	0.18	−0.43
3	2	4	2	2	4	−1.06	1.90	0.51	0.76	−1.79
							1.55	0.50	0.43	−1.46
−7	2	5	−7	2	4	−1.63	0.97	0.65	0.66	−0.60
							0.72	0.67	0.61	−0.44
7	1	0	6	1	0	1.73	−1.29	0.48	0.49	−0.75
							−2.02	0.46	0.52	−1.17
0	1	5	−1	1	6	−1.77	1.42	0.43	0.43	−0.80
							2.52	0.43	0.48	−1.42
4	1	5	5	1	5	−1.27	1.06	0.35	0.43	−0.84
							0.53	0.35	0.26	−0.42
−1	2	6	−1	2	5	−1.73	1.72	0.33	0.40	−1.00
							1.95	0.33	0.51	−1.13
8	1	4	9	1	4	−0.74	0.52	0.28	0.40	−0.70
							0.90	0.28	0.22	−1.21

TABLE 5. EFFECT OF ERROR IN ATOMIC PARAMETERS ON $B_{th}(\%)$[a]

(a) Epishamixanthone				(b) Sterigmatocystin			
h	k	l	B_{th}	h	k	l	B_{th}
8	2	3	−0.99(3)	2	1	1	−1.14(2)
−2	1	2	−0.77(2)	2	2	2	1.54(6)
−8	1	3	1.08(5)	−7	1	2	−1.25(4)
−4	2	2	−0.72(3)	−5	1	5	−0.92(4)
3	1	2	1.50(10)	6	1	1	−1.37(2)
2	3	0	0.63(5)	−11	1	3	0.89(2)
−4	2	6	1.24(5)	−3	2	1	−1.48(5)
6	1	4	−1.38(5)	4	2	2	−0.80(1)
0	2	4	0.71(2)	8	2	0	−1.86(7)
3	1	4	−0.80(3)	−4	1	7	1.13(2)
−5	2	4	1.24(6)	−9	1	2	−0.92(3)
−2	3	2	0.95(4)	5	1	6	−0.67(1)
−5	1	2	−0.59(11)	3	2	4	−1.11(4)
1	1	5	−0.56(1)	−7	2	5	−1.63(7)
1	2	1	1.07(18)	7	1	0	1.22(5)
−3	2	1	1.18(11)	0	1	5	−1.47(6)
2	1	3	0.60(2)	4	1	5	−0.94(2)
6	1	1	−0.90(2)	−1	2	6	−1.06(2)
−7	2	1	0.31(1)	8	1	4	−0.78(1)
4	2	0	0.72(3)				

a) $\sigma(B_{th})$ is given in parentheses with respect to the least significant digit. $\sigma(B_{th})$ has been calculated by the formula: $\sigma^2(B_{th})=\sum_i\{\partial B_{th}/\partial P_i\}^2(\sigma P_i)^2$, where P_i and σP_i are the i-th parameter and estimated standard deviation, respectively, obtained from a block-diagonal least-squares calculation. The parameters and estimated standard deviations in the most refined stage (Tables 2 and 3) have been used in this calculation.

although the number of samples is small. The slopes, especially for epishamixanthone, are larger than 1.0. This indicates the existence of some errors due to geomery of the instrument and/or habit of crystal which were not fully eliminated by the method. This is partly explained by the fact that the width of the peak-profile of epishamixanthone changes more drastically, as the direction of the X-ray beam changes, than that of sterigmatocystin.

The errors exist to a great extent in experimental measurements of Bijvoet difference. Since the method described by Engel is insensitive to experimental errors such as the instability and geometrical error of an instrument, the method may generally give a more significant enantiomer-indication than the R method. Various sources of error were discussed by Engel.[4]

The absolute configuration of epishamixanthone is correctly represented by the parameters in Tables 2(a) and 3(a), if the left-handed coordinate system is adopted. The absolute configuration of sterigmatocystin determined by the present analysis agrees with that determined by its bromo derivative.[5] For each of the present compounds, the probability that the selected absolute configuration is wrong is estimated to be far less than 0.01%, assuming a t-distribution of DELA values.

Crystal and Molecular Structure

The crystal and molecular structure of epishamixanthone is shown in Fig. 3, together with the numbering scheme of atoms used in this paper. The figure is drawn with correct absolute configuration. The bond

Table 6. Bond lengths and angles for epishamixanthone

(a) Bond length (Å)			
C (1) - C (2)	1.386 (7)	C (10) - O (4)	1.355 (6)
C (1) - C (13)	1.420 (7)	C (11) - C (12)	1.402 (7)
C (1) - O (5)	1.358 (6)	C (11) - O (4)	1.384 (6)
C (2) - C (3)	1.429 (6)	C (12) - C (13)	1.359 (7)
C (2) - C (20)	1.520 (7)	C (13) - C (14)	1.505 (8)
C (3) - C (4)	1.454 (6)	C (15) - C (16)	1.508 (8)
C (3) - C (11)	1.385 (7)	C (15) - O (5)	1.432 (7)
C (4) - C (5)	1.442 (6)	C (16) - C (17)	1.513 (8)
C (4) - O (2)	1.253 (6)	C (16) - C (20)	1.515 (7)
C (5) - C (6)	1.433 (7)	C (17) - C (18)	1.469 (13)
C (5) - C (10)	1.396 (7)	C (17) - C (19)	1.339 (10)
C (6) - C (7)	1.380 (7)	C (20) - O (1)	1.428 (6)
C (6) - O (3)	1.346 (6)	C (21) - C (22)	1.494 (12)
C (7) - C (8)	1.375 (8)	C (22) - C (23)	1.317 (11)
C (8) - C (9)	1.399 (9)	C (23) - C (24)	1.506 (12)
C (9) - C (10)	1.393 (8)	C (23) - C (25)	1.445 (14)
C (9) - C (21)	1.510 (11)		
(b) Bond angles (°)			
C (2) - C (1) - C (13)	122.3 (5)	C (9) - C (10) - O (4)	115.8 (5)
C (2) - C (1) - O (5)	123.8 (4)	C (3) - C (11) - C (12)	122.8 (5)
C (13) - C (1) - O (5)	113.9 (4)	C (3) - C (11) - O (4)	123.8 (5)
C (1) - C (2) - C (3)	118.2 (4)	C (12) - C (11) - O (4)	113.5 (5)
C (1) - C (2) - C (20)	119.4 (4)	C (11) - C (12) - C (13)	119.6 (5)
C (3) - C (2) - C (20)	122.4 (4)	C (1) - C (13) - C (12)	118.8 (5)
C (2) - C (3) - C (4)	124.2 (4)	C (1) - C (13) - C (14)	119.5 (5)
C (2) - C (3) - C (11)	118.1 (4)	C (12) - C (13) - C (14)	121.7 (5)
C (4) - C (3) - C (11)	117.7 (4)	C (16) - C (15) - O (5)	109.6 (5)
C (3) - C (4) - C (5)	117.0 (4)	C (15) - C (16) - C (17)	114.5 (5)
C (3) - C (4) - O (2)	122.6 (4)	C (15) - C (16) - C (20)	108.8 (4)
C (5) - C (4) - O (2)	120.4 (4)	C (17) - C (16) - C (20)	112.4 (4)
C (4) - C (5) - C (6)	121.7 (4)	C (16) - C (17) - C (18)	115.9 (6)
C (4) - C (5) - C (10)	121.2 (4)	C (16) - C (17) - C (19)	123.0 (6)
C (6) - C (5) - C (10)	117.1 (4)	C (18) - C (17) - C (19)	121.1 (7)
C (5) - C (6) - C (7)	120.0 (5)	C (2) - C (20) - C (16)	111.3 (4)
C (5) - C (6) - O (3)	120.6 (4)	C (2) - C (20) - O (1)	111.2 (4)
C (7) - C (6) - O (3)	119.5 (5)	C (16) - C (20) - O (1)	108.4 (4)
C (6) - C (7) - C (8)	120.4 (5)	C (9) - C (21) - C (22)	116.5 (7)
C (7) - C (8) - C (9)	122.4 (6)	C (21) - C (22) - C (23)	126.3 (8)
C (8) - C (9) - C (10)	116.6 (6)	C (22) - C (23) - C (24)	117.6 (7)
C (8) - C (9) - C (21)	123.2 (6)	C (22) - C (23) - C (25)	129.8 (8)
C (10) - C (9) - C (21)	120.1 (6)	C (24) - C (23) - C (25)	112.7 (8)
C (5) - C (10) - C (9)	123.6 (5)	C (10) - O (4) - C (11)	119.8 (4)
C (5) - C (10) - O (4)	120.6 (4)	C (1) - O (5) - C (15)	115.0 (4)

lengths and angles for non-hydrogen atoms are shown in Table 6. The configurations of the C(16) and C(20) atoms are both *R*. The absolute configuration of shamixanthone has been assigned by Chexal *et al.* by application of the Horeau asymmetric synthesis.[12] Thus the configuration of C(20) in epishamixanthone is the same as that of the corresponding atom in shamixanthone, while that of C(16) is opposite. From the biosynthetic study,[13,14] it was shown that both the carbon atoms are incorporated from the methyl carbon of acetate, and was suggested that the dihydropyran ring is formed by cyclization between 3-methyl-2-butenyloxy and aldehyde groups in the precursor. Chexal *et al.*[14] discussed the mechanism of the formation of substituted dihydropyran rings. Although epishamixanthone is one of epimers of shamixanthone, it is unlikely, from the absolute configurations of these metabolites, that the metabolites arise through ene-reaction with transition states differing to each other only in the conformation of aldehyde group in the precursor.

The equations of the least-squares planes and the deviations of atoms from each plane are given in Table 7. The ring composed of C(1), C(2), C(20), C(16), C(15), and O(5) forms a half-chair conformation. The torsion angles of C(15)–C(16)–C(17)–C(19) and

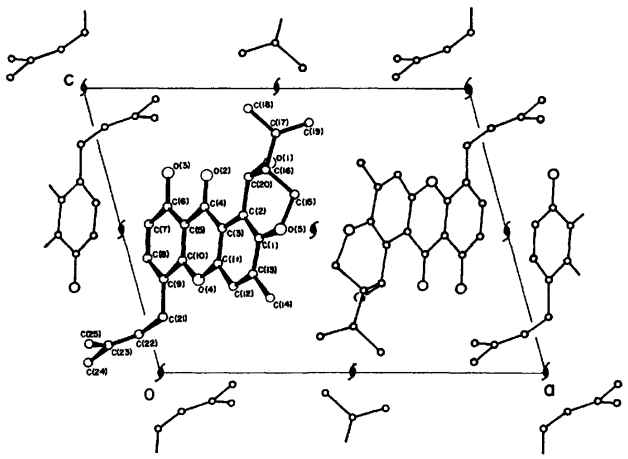

Fig. 3. The crystal and molecular structure of epishamixanthone viewed along the b-axis.

TABLE 7. DEVIATIONS (Å) OF ATOMS FROM LEAST-SQUARES PLANES

In the equations of the plane, X, Y, and Z are $ax+cz\cos\beta$, by, and $cz\sin\beta$ respectively.

Plane: C(1)—C(13), O(2), O(4)

$0.809X-0.584Y-0.058Z=1.036$

[C(1) −0.066, C(2) −0.027, C(3) −0.006, C(4) 0.021, C(5) 0.024, C(6) −0.002, C(7) −0.030, C(8) −0.036, C(9) 0.001, C(10) 0.014, C(11) 0.019, C(12) 0.036, C(13) 0.003, O(2) 0.030, O(4) 0.029, C(21) −0.044 C(14) 0.003, O(5) −0.138, C(20) 0.008, O(1) −1.227, O(3) 0.015]

Plane: C(1), C(2), C(20), O(5)

$0.784X-0.620Y-0.037Z=1.024$

[C(1) 0.015, C(2) −0.011, C(20) 0.005, O(5) −0.008, C(15) −0.452, C(16) 0.331]

Plane: C(16)—C(19)

$0.030X-0.995Y+0.091Z=-2.766$

[C(16) 0.002, C(17) −0.007, C(18) 0.002, C(19) 0.002]

Plane: C(21)—C(25)

$0.380X+0.262Y-0.887Z=-2.308$

[C(21) 0.002, C(22) −0.005, C(23) 0.004, C(24) 0.001, C(25) −0.002]

C(10)-C(9)-C(21)-C(22) are −11.8 and −172.5° respectively. There are two intramolecular hydrogen bonds, O(1)-H(O1)···O(2) and O(3)-H(O3)···O(2). The distances of O(2)···H(O1) and O(2)···H(O3) are 1.89 and 1.76 Å respectively. The angles of O(1)-H(O1)···O(2), O(3)-H(O3)···O(2), H(O1)···O(2)-C(4), and H(O3)···O(2)-C(4) are 157, 144, 108, and 102° respectively. The interplanar distance of xanthone skeletons stacking along the b axis is about 3.65 Å. The intermolecular distances less than 3.8 Å are listed in Table 8. There are neither intermolecular hydrogen bonds nor abnormally short contacts: the crystal is composed of molecules held by van der Waals forces.

The atomic scattering factors were taken from International Tables for X-ray Crystallography.[15] Most of calculations were performed on a TOSBAC-3400 computer at the Tottori University Computing Center by the use of programs written by the authors. The block-diagonal least-squares refinement and the vector-search calculation were executed on a NEAC-2200 N700 computer at the Computation Center of Osaka University using programs written by T. Ashida and I. Tanaka respectively.

TABLE 8. INTERMOLECULAR CONTACTS LESS THAN 3.8 Å EXCLUDING HYDROGEN ATOMS

The superscripts refer to the following equivalent positions: I x, $1+y$, z; II $-x$, $1/2+y$, $1-z$; III $1-x$, $1/2+y$, $1-z$.

C (1)···C (5^{I})	3.763	C (20)···O (3^{I})	3.671
C (2)···C (6^{I})	3.680	C (5)···C (7^{II})	3.733
C (3)···C (7^{I})	3.633	C (6)···C (7^{II})	3.722
C (11)···C (8^{I})	3.613	C (6)···C (8^{II})	3.602
C (12)···C (8^{I})	3.758	C (25)···O (3^{II})	3.467
C (12)···C (9^{I})	3.644	O (2)···C (25^{II})	3.720
C (13)···C (9^{I})	3.765	O (3)···C (8^{II})	3.744
C (13)···C (10^{I})	3.696	O (3)···C (24^{II})	3.521
C (14)···O (4^{I})	3.726	C (14)···O (1^{III})	3.537
C (16)···O (2^{I})	3.527	C (15)···C (1^{III})	3.773

The authors wish to thank the staff of the Institute for Protein Research of Osaka University for the measurement of second data-sets of both compounds by use of Rigaku computer-controlled four-circle diffractometer. They are also grateful to Professor Tamaichi Ashida and Mr. Isao Tanaka of Nagoya University for permission to use their computer programs.

References

1) N. Harada, S. Suzuki, H. Uda, and K. Nakanishi, *J. Am. Chem. Soc.*, **93**, 5577 (1971).
2) A. Horeau and H. B. Kagan, *Tetrahedron*, **20**, 2431 (1964).
3) W. E. Thiessen and H. Hope, *Acta. Crystallogr., Sect. B*, **26**, 554 (1970); H. Hope and U. de la Camp, *ibid., Sect. A*, **28**, 201 (1972); J. B. Wetherington, S. S. Ament, and J.W. Moncrief, *ibid., Sect. B*, **30**, 568 (1974); R. Karlsson, *ibid., Sect. B*, **32**, 2609 (1976).
4) D. W. Engel, *Acta Crystallogr., Sect. B*, **28**, 1496 (1972).
5) K. Fukuyama, T. Tsukihara, Y. Katsube, N. Tanaka, T. Hamasaki, and Y. Hatsuda, *Bull. Chem. Soc. Jpn.*, **48**, 1980 (1975).
6) M. Ishida, T. Hamasaki, Y. Hatsuda, K. Fukuyama, T. Tsukihara, and Y. Katsube, *Agric. Biol. Chem.*, **40**, 1051 (1976).
7) R. Huber, in "Crystallographic Computing," ed by F. R. Ahmed, Munksgaard, Copenhagen (1970).
8) K. Fukuyama, K. Hamada, T. Tsukihara, Y. Katsube, T. Hamasaki, and Y. Hatsuda, *Bull. Chem. Soc. Jpn.*, **49**, 1153 (1976).
9) S. C. Abrahams and E. T. Keve, *Acta Crystallogr., Sect. A*, **27**, 157 (1971).
10) R. Parthasarathy, *Acta Crystallogr.*, **15**, 855 (1962).
11) D. T. Cromer and D. Liberman, *J. Chem. Phys.*, **52**, 1891 (1970).
12) K. K. Chexal, C. Fouweather, J. S. E. Holker, T. J. Simpson, and K. Young, *J. Chem. Soc., Perkin Trans. 1*, **1974**, 1584.
13) J. S. E. Holker, R. D. Lapper, and T. J. Simpson, *J. Chem. Soc., Perkin Trans. 1*, **1974**, 2135.
14) K. K. Chexal, J. S. E. Holker, T. J. Simpson, and K. Young, *J. Chem. Soc., Perkin Trans. 1*, **1975**, 543.
15) "International Tables for X-Ray Crystallography," Vol. III, Kynoch Press, Birmingham (1962), p.202.

Effect of the Trap Density on Switching in Naphthacene Thin Films

Yoshihiko SADAOKA and Yoshiro SAKAI

Department of Industrial Chemistry, Faculty of Engineering, Ehime University, Matsuyama 790

(Received May 19, 1977)

Switching phenomena were observed in Au(+)–naphthacene (crystalline-state)–Al(−). The threshold voltage was found to be expressable as $V_{th} \propto (\text{thickness})^2$; in amorphous films no reproducible switching phenomena were observed within the same region of the field strength. The differences between them were discussed in terms of the trap density, which is closely related to the crystallinity of the evaporated films.

Szymanski *et al.*[1] reported bistable switching in naphthacene thin films with Au and Al electrodes, but the conditions required were not reproducible, while reproducible switching in aromatic hydrocarbon films was observed by Kevorkian *et al.*[2] when a mobile electrode material was used. Although some authors have proposed the *turn-on* to be due to either metallic filament formation, or the formation of carbonized materials,[3] Kasica *et al.*[4] have proposed that the reproducibility of the switching curves is strongly affected by the surrounding conditions and that the switching is interpretable in terms of the double injection mechanism.

This paper deals with the influence of the trap density on the bulk-limited switching characteristics in naphthacene films, because the state of the naphthacene film can be easily controlled by varying the substrate temperature during the evaporation and the bulk-type high field conduction is expected in Au–naphthacene–Al cell. Also, since the heat of sublimation is larger and the melting point of this material is much higher than that of anthracene, the reproducibility of switching should be much better in naphthacene than in anthracene.

Experimental

The geometry of the cell was of the sandwich type, where naphthacene was deposited over a glass substrate on which thirty strips of gold electrodes of 1 mm in width and 1 mm in separation had been evaporated through an etched stainless steel mask. The upper electrodes(Al) were deposited by the same method. The temperature of the substrate was controlled in the range of −120 to 110 °C. The film thickness of naphthacene was measured with the aid of an interferometer. D.c. conductivities and/or switching curves were measured by means of the circuit described in the previous paper.[5] The load(protective) resistor in the circuit can be varied in the range of 10^3—10^8 Ω to control the current which flows in the high conductivity state. All the electrical measurements were carried out in vacuum.

The state of the films was examined using a scanning electron microscope and a polarizing microscope. Polycrystalline structure was observed for the film prepared by the deposition onto the glass substrate kept at a high temperature (≈100 °C). However, an amorphous film was obtained when the glass substrate was kept at a low temperature(≤−100 °C) during evaporation. The scanning electron microscopic views of the films are shown in Fig.1. In addition, the absorption spectra of the film deposited on the quartz substrate also indicated that a crystalline state was obtained when a substrate was held at a high temperature and an amorphous state when a substrate was held at a low temperature(≤−100 °C) at the time of evaporation. These results are consistent with that reported by Maruyama and Iwasaki.[6] In some cases the substrates were kept at room temperature during evaporation. These films were found to be partly crystallized.

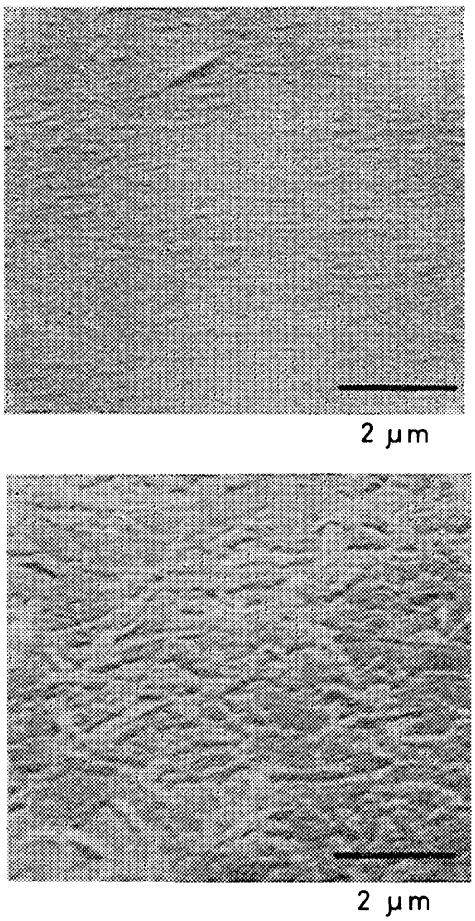

Fig. 1. Scanning electron microscope pictures of film.
a) Low-temperature-evaporated amorphous films,
b) high-temperature-evaporated crystalline film.

Results and Discussion

A typical current-voltage characteristic in the low-conductivity state is shown in Fig. 2 for an Au–naphthacene–Al cell. This curve is typical for a rectifying contact, *i.e.*, the current increases non-linearly with applied voltage. Similar asymmetry in its characteristic has been reported by Ghosh and Feng.[7] Under the forward-bias condition, the V^n dependence of current on voltage due to an exponential trap distribution was found for all samples prepared in various conditions. Rectification ratios as high as 10^4 was observed in the high-field region.

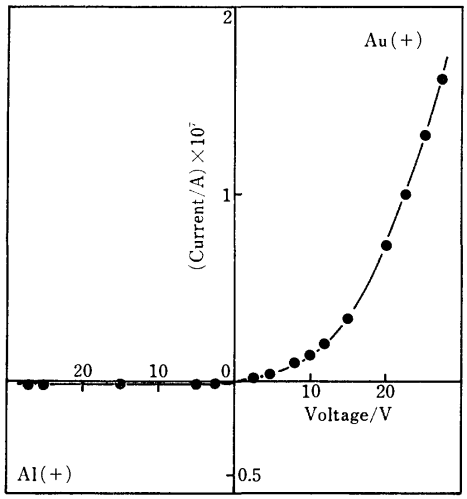

Fig. 2. A typical *I-V* characteristic in the Au–naphthacene–Al cell.

More than 600 films were used for the electrical measurements under the forward-bias conditions in order to clarify the influence of the trap-density on the threshold voltage for the bulk type switching phenomena. Although no switching phenomena were observed in the low-temperature-evaporated films, the switching without any structural changes were observed in the high-temperature-evaporated crystalline-state films in most of the samples. The observed switching characteristics are shown in Fig. 3. When the applied voltage exceeded a critical value (V_{th}) which is poorly dependent on the value of the load resistor R_L, the current abruptly increased, and simultaneously the field dropped (negative resistance region), so that a new high-conductivity state was formed. Since the conductance of this new state is strongly influenced by the value of the load resistor and this dependence on the load resistor cannot be explained by the usual non-linear-conduction mechanisms, this state should be formed in a filamentary way *i.e.* the effective area of this state increases upon decreasing the value of the load resistor.

In addition, the holding voltage (*turn-off* voltage) was observed in the switching characteristics when the load resister R_L was $10^8\ \Omega$, while the memory effect was observed when R_L was $10^5\ \Omega$. After the applied voltage had been taken off, the state with its memory effect quenched off in *ca.* 3 h or more and the initial low-conductivity state was recovered. Such a high-conductivity state with a memory effect may be related to the density of deep trapping levels, and not be caused by any structural changes.

In the low-conductivity state for the crystalline films the current increased rapidly in proportion to V^n with $n \approx 4$. This characteristic is interpretable in terms of the space-charge-limited current (SCLC). According to Mark and Helfrich[8] the SCLC for exponential distribution of traps with energy should follow the equation

$$J = N_0 \mu e^{1-l} \left\{ \frac{\varepsilon \varepsilon_0 l}{H(l+1)} \right\}^l \left(\frac{2l+1}{l+1} \right)^{l+1} \frac{V^{l+1}}{d^{2l+1}}, \quad (1)$$

where N_0 is the effective density of states in the valence band, μ is the hole mobility, ε is the dielectric constant, ε_0 is the vacuum permittivity, e is the electron charge, H is the total hole trap density, d is the film thickness, and $l = T_c/T$. The parameter T_c characterizes the trap distribution. Furthermore, one can obtain an expression for the position dependence of the quasi-Fermi level for holes. It is

$$E_F = kT_c \ln \left[\frac{(l+1)^2}{l(2l+1)} \frac{eHd^2}{\varepsilon \varepsilon_0 V} \left(\frac{x}{d} \right)^{1/l+1} \right], \quad (2)$$

where x is the distance from the injecting electrode (anode). The measurement of the temperature dependence of SCLC yields the value of $E_F(x=d)$, while the density of free carriers, which is proportional to the current, is given by the relation $n \propto \exp(-E_F/kT)$. In Fig. 4, the relation between the activation energy and the value of $\log(d^2/V)$ is shown. From the results in Fig. 4 the total hole trap density was estimated to be $1—2 \times 10^{16}\ \mathrm{cm^{-3}}$ for thicker films(line I) and $1—2 \times$

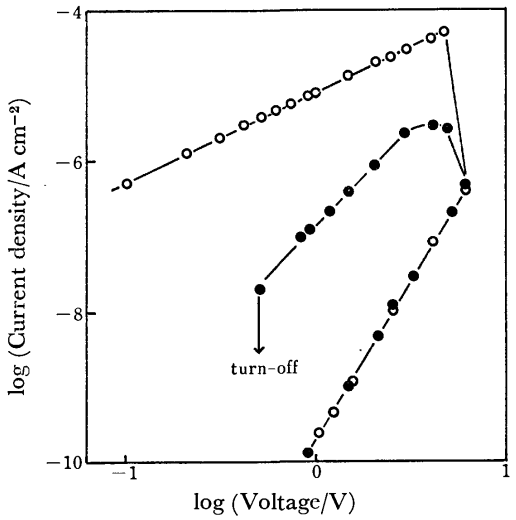

Fig. 3. Current-Voltage characteristic in switching.
(○) with $R_L(10^5\ \Omega)$, (●) with $R_L(10^8\ \Omega)$,
film thickness: 3.5×10^{-5} cm.

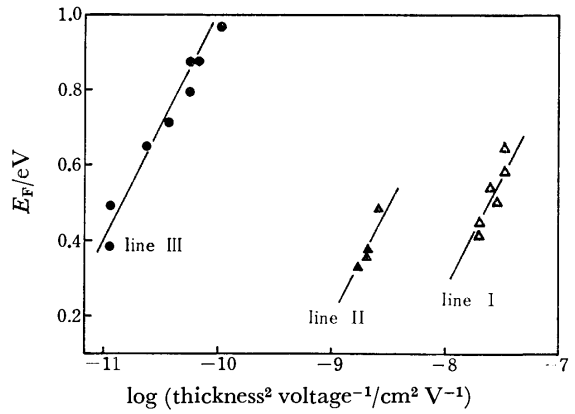

Fig. 4. Plot of E_F against log (d^2/V) relationship.
(●) Low-temperature-evaporated amorphous film,
(▲) high-temperature-evaporated crystalline film,
film thickness: 5.0×10^{-5} cm,
(△) high-temperature-evaporated crystalline film,
film thickness: 1.0×10^{-4} cm.

10^{17} cm^{-3} for thinner films(line II), respectively, by substituting $\varepsilon=3.8$ and, $x=d$. The values of l obtained from the slope of the lines in Fig. 4 are consistent with those obtained from the current-voltage curves. The values of H for the crystalline films are reasonable ones, although they are somewhat higher than that for single crystals grown by sublimation in nitrogen ($H=3\times10^{15}$ cm^{-3}).[9] The fact that the value of H for a thinner film is somewhat larger than that for a thicker film suggests that the traps caused by residual gas molecules and/or defects are located in the surface regions close to the electrode. In addition, in the case of the amorphous films prepared by low-temperature deposition, similar current-voltage characteristics ($l\approx8$) caused by SCLC for an exponential distribution of traps with energy was obtained and a linear relation (line III) between E_F and $\log(d^2/V)$ was also found. The total hole trap density was estimated to be 4×10^{18} cm^{-3}. Since it is well known that lowering the substrate temperature increases structural disorder, the structural irregularity must be the cause of such trapping-levels rather than the chemical impurities because the low- and high-temperature-evaporated films were deposited from the same evaporation source.

On the other hand, the measurement of the thickness dependence of the threshold voltage(V_{th}) was carried out for the high-temperature-evaporated crystalline films in order to determine whether the *turn-on* is based on the thermal effect or the electronic effect, since such a measurement is a very powerful method[10] to distinguish one from the other. As shown in Fig. 5, the threshold voltage is proportional to the square of the thickness (line I), though other line II different from line I was obtained from the films thinner than *ca.* 3×10^{-5} cm. This relation indicates that the *turn-on* is caused by an electronic mechanism such as the space charge overlap model[11] or the one carrier SCLC model[12] in which the concentration of the injected carriers is sufficient to exceed the critical concentration (N_{th}). And this interpretation is confirmed by the fact that the *turn-on* does not occur in the amorphous films at the conditions under which the *turn-on* occurs in the crystalline films. In the space charge overlap model, it is expected that the current-voltage characteristic in the *pre*-switching state is caused by the double injection and the *turn-on* is achieved by the formation of the space charge overlap region. However, in the one carrier SCLC model the *turn-on* may be expected when the space charge density caused by injected holes in the *pre*-switching state reaches a critical value and the injection of electrons begins.[4,12] Since in the *pre*-switching state the current-voltage curve in Au(+)–naphthacene–Al(−) is similar to that in Au–naphthacene–Au, the electric conduction in the *pre*-switching state is most likely due to one carrier SCLC with traps. This current in the high resistivity state may entirely consist of the holes injected from the Au electrode into naphthacene, as was suggested by Ghosh and Feng.[7] Consequently, the *turn-on* is interpretable in terms of the one carrier SCLC model rather than the space charge overlap model based on the double injection in the *pre*-switching state.

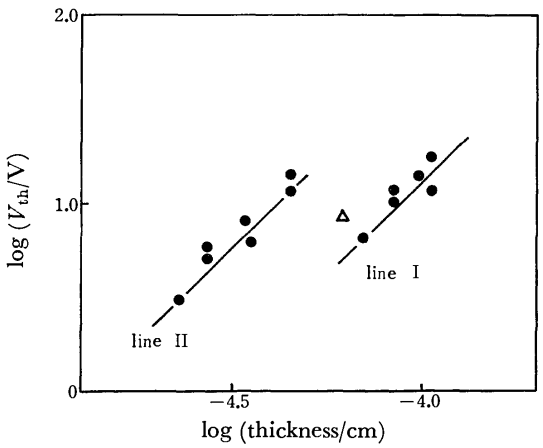

Fig. 5. Thickness dependence of V_{th}.
(●) Observed values, (△) result reported by Szymanski *et al.*[1]

If Q_{th} represents the space charge density formed by the injected holes, the potential distribution in the bulk can be expressed as Eq. 3:

$$V(x)=\frac{Q_{th}}{2\varepsilon\varepsilon_0}x^2. \tag{3}$$

Consequently, the threshold voltage may be introduced as Eq. 4 by substituting $x=d$:

$$V_{th}=\frac{Q_{th}\cdot d^2}{2\varepsilon\varepsilon_0}. \tag{4}$$

The corresponding values of N_{th} and Q_{th} were estimated to be 6×10^{15} cm^{-3} and 9.7×10^{-4} C/cm^{-3} for line I and 2×10^{16} cm^{-3} and 3×10^{-3} C/cm^{-3} for line II, respectively. Since no switching phenomena were observed in the amorphous films and the values of N_{th} obtained by using Eq. 5 for the crystalline films are roughly in agreement with the values of total hole trap density, the *turn-on* can occur when the traps are filled by the injected holes and under such conditions the Al electrode will become an electron-injecting contact. In this case Eq. 4 can be replaced by Eq. 5:

$$V_{th}=\frac{eHd^2}{2\varepsilon\varepsilon_0}. \tag{5}$$

The same relation between the threshold voltage and the trap density was reported in the previous works for poly(*N*-vinylcarbazole)[5] and anthracene.[13]

From the results thus obtained it is concluded that the lack of switching phenomena for the amorphous film is caused by the fact that the number of the trap density is much larger than that in the crystalline films; in these circumstances, the thermal breakdown caused by Joule-heating may occur before the trap-filled state is achieved, since the threshold voltage for the amorphous film of 5×10^{-5} cm in thickness is estimated to be *ca.* 2×10^3 V and the value of l is much larger than that for the crystalline films ($l=4$).

One of us (Y. Sadaoka) thanks the Sakkokai Foundation for a grant.

References

1) A. Szymanski, D. C. Larson, and M. M. Labes, *Appl. Phys. Lett.*, **14**, 88 (1969).

2) J. Kevorkian, M. M. Labes, D. C. Larson, and D. C. Wu, *Discuss. Faraday Soc.*, **51**, 139 (1971).
3) L. F. Pender and R. J. Fleming, *J. Appl. Phys.*, **46**, 3426 (1975).
4) H. Kasica, W. Wlodarski, H. Kurczewska, and A. Szymanski, *Thin Solid Films*, **30**, 325 (1975).
5) Y. Sadaoka and Y. Sakai, *J. Chem. Soc., Faraday Trans. 2*, **72**, 1911 (1976).
6) Y. Maruyama and N. Iwasaki, *J. Non-Cryst. Solids*, **16**, 399 (1974).
7) A. K. Ghosh and T. Feng, *J. Appl. Phys.*, **44**, 2781 (1973).
8) P. Mark and W. Helfrich, *J. Appl. Phys.*, **33**, 205 (1962).
9) H. Baessler, G. Herrmann, N. Riehl, and G. Vaubel, *J. Phys. Chem. Solids*, **30**, 1579 (1969).
10) B. T. Kolomiets, E. A. Lebedev, and I. A. Taksami, *Soviet Phys.-Semiconductors*, **3**, 267 (1969).
11) H. K. Henisch, E. A. Fagen, and S. R. Ovshinsky, *J. Non-Cryst. Solids*, **4**, 538 (1970).
12) T. Shiraishi, T. Kurosu, and M. Iida, *Oyo Butsuri*, **46**, 36 (1977).
13) Y. Sadaoka and Y. Sakai, *Bull. Chem. Soc. Jpn.*, **50**, 2239 (1977).

Ion-Molecule Reactions in the Binary Mixture of Acetaldehyde and Trioxane. I. Hydrogen Atom and Proton Transfer Reactions

Minoru KUMAKURA, Kazuo ARAKAWA, and Toshio SUGIURA*

Takasaki Radiation Chemistry Research Establishment, Japan Atomic Energy Research Institute, Takasaki, Gunma 370-12

** Japan Atomic Energy Research Institute, Shinbashi, Minato-ku, Tokyo 105*

(Received May 19, 1977)

The formation reactions of protonated molecular ions in acetaldehyde–trioxane mixtures have been studied with a modified time-of-flight mass spectrometer. From the analysis of the fine structure of the ionization efficiency curves of fragment and product ions obtained by means of the retarding potential differential technique using acetaldehyde-d_4, the precursors of the product ions were determined. Protonated acetaldehyde is formed by the hydrogen atom transfer reaction of acetaldehyde molecular ion with trioxane, and protonated trioxane by the proton transfer reaction of CHO^+ generated from acetaldehyde with trioxane. The rate constants of the formation reactions of the product ions in acetaldehyde (or acetaldehyde-d_4)–trioxane mixtures were determined and isotope effect was observed. The CHO^+ generated from acetaldehyde participated predominantly in the proton transfer reaction as compared with that generated from trioxane. From the proton transfer reaction involving thermal ion CHO^+ generated from acetaldehyde it was found that the proton affinity of trioxane is smaller than that of acetaldehyde.

In studies on the ion-molecule reactions in the binary mixture of ethylene oxide and trioxane (1,3,5-trioxane) it was found that protonated ethylene oxide and trioxane are formed by cross-reaction.[1] In the ion-molecule reactions of ethylene oxide[2] and acetaldehyde,[3] the CHO^+ plays an important role in the formation of protonated molecular ions. The ion-molecule reactions in acetaldehyde have been studied by several workers.[4-8] However, the ion-molecule reaction of acetaldehyde in the mixture involving cyclic ether molecule of a large member ring such as trioxane does not seem to have been reported. In the present work, the ion-molecule reactions in the binary mixture of acetaldehyde and trioxane were studied in order to clarify the formation mechanism of protonated molecular ions. Highly strained three member ring molecule such as ethylene oxide could be isomerized under appropriate conditions into more stable isomer (acetaldehyde). A relative abundance pattern of the fragment ions from acetaldehyde in electron impact fragmentation resembles that from ethylene oxide.[3] Some oxygen-containing fragment ions of a similar structure were also produced from acetaldehyde, ethylene oxide, and trioxane. A study of the ion-molecule reactions involving the structural isomer ions in acetaldehyde–trioxane mixtures is important in connection with elementary process in radiation and ion chemistry.

Experimental

A Bendix Model 12-101 time-of-flight mass spectrometer modified with a closed ionization chamber was used.[2] Substituted ion source permitted operation under elevated pressures at long delay times. The pulse electronic circuits of the apparatus were also modified. The variable delay time circuit permitted a variation of time between the end of the ionizing pulse and the onset of the ion withdrawal pulse.[1] During the delay time the entire ionization chamber is field-free, ion-molecule reactions occurring during the time interval thus being under purely thermal conditions. The retarding potential differential technique (RPD)[9] was adopted for appearance potential and ionization efficiency curve measurement. Measurement of the ionization efficiency curves of two ions (reactant and product ion) was simultaneously performed by the two-channel ion detection technique. The gas-sample inlet-system consisting of a dual-leak and dual-reservoir was used. Two kinds of samples were introduced separately into the ionization chamber through two separate leaks from separate reservoirs. The partial pressure of the two samples was indirectly measured with an MKS Baratron 90-X RP-2 capacitance manometer, the pressure being calibrated by known rate constant (1.11×10^{-9} cm^3 molecule^{-1} s^{-1}) of CH_5^+ in the ion-molecule reaction of methane.[2]

The following reagents were used: trioxane (Celanese Chemical), acetaldehyde, and acetaldehyde-d_4 (Merck Sharp and Dohme of Canada). The samples were used after vacuum distillation several times.

Results and Discussion

Delay Time Dependence. The delay time dependence of major fragment ions in a 1 : 1 mixture of acetaldehyde and trioxane at pressure of 1.67×10^{13} molecules cm^{-3} and electron energy of 70 eV is shown in Fig. 1. The *m/e* 44 (CH_3CHO^+), 43 (CH_3CO^+), 29 (CHO^+) are fragment ions from acetaldehyde, while *m/e* 89 ($C_3H_5O_3^+$), 61 ($C_2H_5O_2^+$), 31 (CH_3O^+), and a part of *m/e* 29 are those from trioxane. The molecular ion from trioxane was relatively less abundant, its ion intensity being comparable with the ion intensity of ^{13}C atom of *m/e* 89.[9] The variation of ion intensity of the fragment ions with delay time was investigated. The ion intensity of the fragment ions of low mass numbers decreased markedly with increasing delay time as compared with that of high mass numbers. The decrease was mainly due to a mass discrimination effect though a part of the ions was lost by ion-molecule reactions. It is presumed that the CHO^+ ions play an important role in proton transfer reactions.

The delay time dependence of product ions is shown in Fig. 2. The formation of protonated acetaldehyde (CH_3CHOH^+) is remarkable as compared with that of protonated trioxane ($C_3H_6O_3H^+$). The ion intensity ratio of protonated acetaldehyde to protonated trioxane is *ca.* 7 at delay time 1.0 μs. Protonated molecular ions are formed in acetaldehyde as well as in trioxane,[2,10] but further formation of these ions was observed in the mixture. This suggests that the protonat-

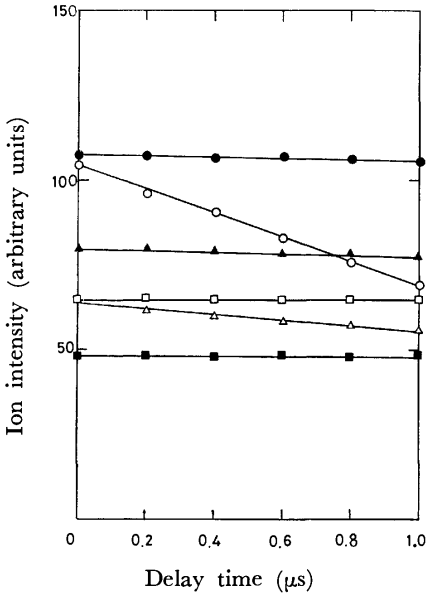

Fig. 1. Delay time dependence of fragment ions in acetaldehyde–trioxane mixtures.
▲: CH_3CHO^+, ■: CH_3CO^+, ○: CHO^+ (X1/5), □: $C_3H_5O_3^+$, ●: $C_2H_5O_2^+$, △: CH_3O^+(X1/5).

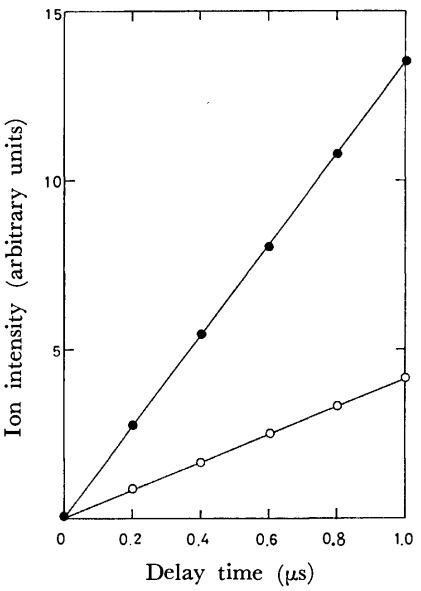

Fig. 2. Delay time dependence of protonated molecular ions in acetaldehyde–trioxane mixtures.
●: CH_3CHOH^+, ○: $C_3H_6O_3H^+$ (X2).

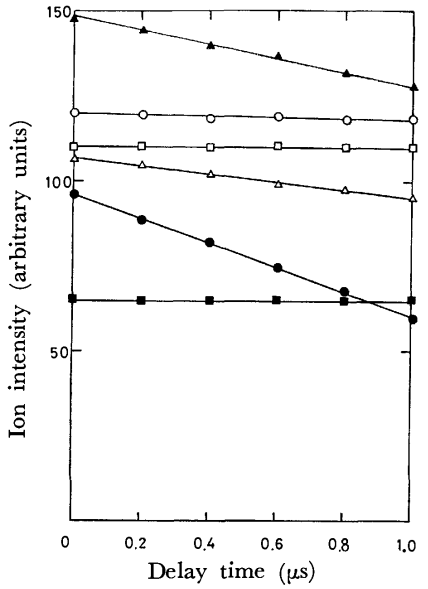

Fig. 3. Delay time dependence of fragment ions in acetaldehyde-d_4–trioxane mixtures.
○: CD_3CDO^+, ■: CD_3CO^+, ▲: CDO^+, □: $C_3H_5O_3^+$, △: CH_3O^+ (X1/5), ●: CHO^+ (X1/2).

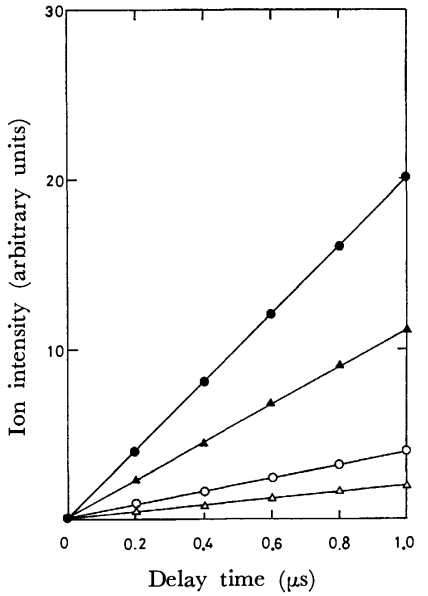

Fig. 4. Delay time dependence of protonated and deuteronated molecular ions in acetaldehyde-d_4–trioxane mixtures.
●: CD_3CDOH^+, ▲: CD_3CDOD^+, ○: $C_3H_6O_3H^+$. △: $C_3H_6O_3D^+$ (X5).

ed molecular ions are formed by cross-reactions. Studies in the mixture using deuterated acetaldehyde were carried out to elucidate the formation mechanism of the protonated molecular ions under the same conditions as unlabeled acetaldehyde mixture. The delay time dependence of major fragment and product ions in acetaldehyde-d_4–trioxane mixtures is shown in Figs. 3 and 4. The CHO^+ ions from both molecule were separated into CHO^+ and CDO^+. The isotopic distribution of product ions is given in Fig. 4. The *m/e* 49 (CD_3CDOH^+) and 50 (CD_3CDOD^+) are protonated and deuteronated acetaldehyde-d_4, and *m/e* 91 ($C_3H_6O_3H^+$) and 92 ($C_3H_6O_3D^+$) protonated and deuteronated trioxane, respectively. The CD_3CDOH^+ and $C_3H_6O_3D^+$ are cross-reaction product ions in acetaldehyde-d_4–trioxane mixtures. The ion intensity ratio of CD_3CDOH^+ to CD_3CDOD^+ and $C_3H_6O_3D^+$ to $C_3H_6O_3H^+$ were *ca.* 2 and 0.1 at delay time of 1.0 μs. It is suggested that the cross-reaction of proton or hydrogen atom transfer occurs in the mixture. These observations give important information on the reactivity of ionic and neutral reactants in the mixture.

Pressure Dependence. The ion intensity variation of the product ions with pressure in each molecule was

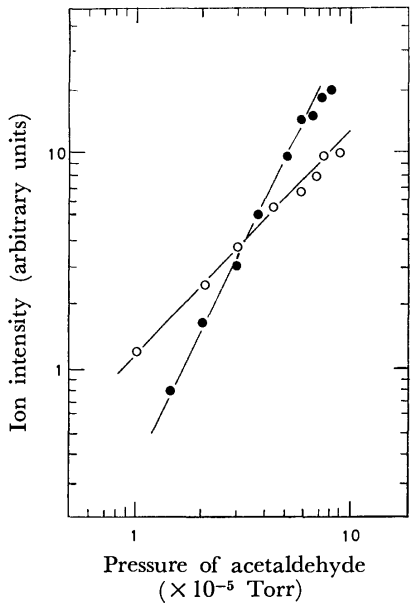

Fig. 5. Dependence of protonated molecular ions on pressure of acetaldehyde.
●: CH_3CHOH^+, ○: $C_3H_6O_3H^+$.

examined in order to clarify the contribution of acetaldehyde and trioxane. The pressure dependence of the protonated molecular ions on acetaldehyde (Fig. 5) was obtained by pressure variation of acetaldehyde using the dual leak at a fixed pressure (8.2×10^{12} molecules cm^{-3}) of trioxane and delay time of 1.0 μs. Protonated acetaldehyde shows a dependence of second order on the pressure of acetaldehyde, protonated trioxane showing one of first order. This suggests that the formation of protonated trioxane is correlated with acetaldehyde. The pressure dependence of protonated molecular ions on trioxane at a fixed pressure (8.2×10^{12} molecules cm^{-3}) of acetaldehyde is shown in Fig. 6. Protonated trioxane and acetaldehyde show

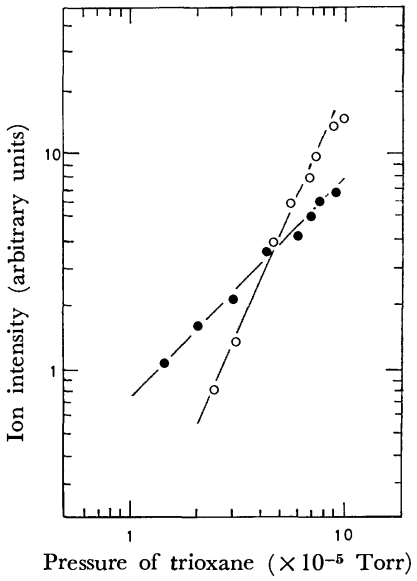

Fig. 6. Dependence of protonated molecular ions on pressure of trioxane.
●: CH_3CHOH^+, ○: $C_3H_6O_3H^+$.

a dependence of second and first order, respectively, on trioxane pressure.

Ionization Efficiency Curves. The ionization efficiency curves of major fragment and product ions in acetaldehyde-d_4–trioxane mixtures were obtained in order to determine the precursors of the product ions at delay time of 1.0 μs. The ionization efficiency curves of CD_3CDOH^+, CD_3CDO^+, and $C_3H_5O_3^+$ are shown in Fig. 7 and those of $C_3H_6O_3D^+$, CD_3CO^+, CDO^+, and CD_3^+ in Fig. 8. The ionization potential of acetaldehyde and the appearance potential of $C_3H_5O_3^+$ from trioxane are 10.32±0.05 and 10.59±0.05 eV, respectively.[9]

The onset and fine structures of the ionization efficiency curves of both CD_3CDOH^+ and CD_3CDO^+ agree. The onset of the ionization efficiency curve of CD_3CDOH^+ approaches that of $C_3H_5O_3^+$, no agreement being observed in the fine structures of the curves of both ions. In fact, the second appearance potentials of CD_3CDOH^+ and $C_3H_5O_3^+$ did not agree, the second and third appearance potential of CD_3CDOH^+ showing a good agreement with those of CD_3CDO^+ in Fig. 7. The appearance potentials (*m/e* 61: 10.79±0.05, 31: 11.49±0.05, and 29: 13.59±0.05 eV) of other fragment ions (*m/e* 61, 31, and 29) from trioxane were higher than that of CD_3CDOH^+, the break points of

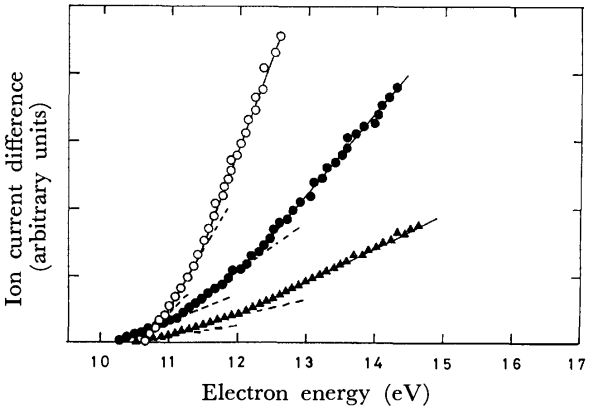

Fig. 7. Ionization efficiency curves of CD_3CDO^+ (●), CD_3CDOH^+ (▲), and $C_3H_5O_3^+$ (○) in acetaldehyde-d_4–trioxane mixtures.

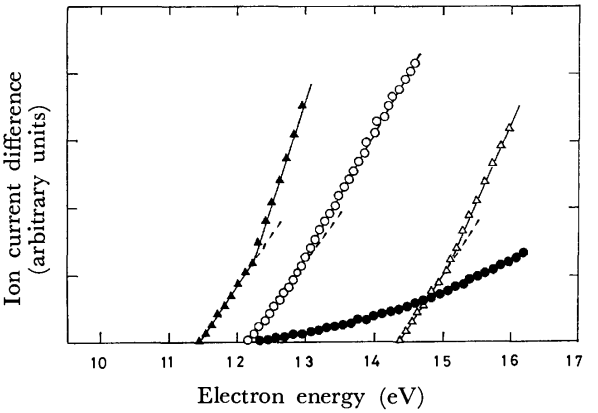

Fig. 8. Ionization efficiency curves of CD_3^+ (△), CDO^+ (○), CD_3CO^+ (▲), and $C_3H_6O_3D^+$ (●) in acetaldehyde-d_4–trioxane mixtures.

the ionization efficiency curve of CD_3CDOH^+ and these fragment ions not agreeing. Thus, it was concluded that CD_3CDO^+ is the sole precursor of CD_3CDOH^+. The onset of the ionization efficiency curve of $C_3H_6O_3D^+$ agreed with that of CDO^+. The appearance potentials of CD_3CO^+ and CD_3^+ which are abundant fragment ions from acetaldehyde-d_4 were 11.42±0.05 and 14.32±0.05 eV, respectively, deviating considerably from the onset of the ionization efficiency curve of $C_3H_6O_3D^+$. The onset of the ionization efficiency curves of both $C_3H_6O_3D^+$ and CD_3CDO^+ did not agree either. It was thus found that the precursor of $C_3H_6O_3D^+$ is CDO^+ from acetaldehyde-d_4.

Reaction Mechanism. The product ions resulting from the reactions in pure acetaldehyde were observed also in acetaldehyde (or acetaldehyde-d_4)–trioxane mixtures.

$$CH_3CHO^+ + CH_3CHO \longrightarrow CH_3CHOH^+ + CH_3CO, \quad (1)$$

$$CHO^+ + CH_3CHO \longrightarrow CH_3CHOH^+ + CO, \quad (2)$$

$$CD_3CDO^+ + CD_3CDO \longrightarrow CD_3CDOD^+ + CD_3CO, \quad (3)$$

$$CDO^+ + CD_3CDO \longrightarrow CD_3CDOD^+ + CO. \quad (4)$$

It is evident from the ionization efficiency curve measurements that CD_3CDOH^+ in acetaldehyde-d_4–trioxane mixtures is formed by hydrogen atom transfer reaction as follows:

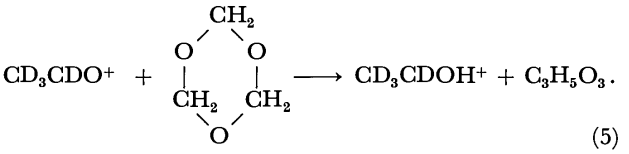

$$CD_3CDO^+ + \text{trioxane} \longrightarrow CD_3CDOH^+ + C_3H_5O_3. \quad (5)$$

Similarly, CH_3CHOH^+ in acetaldehyde–trioxane mixtures is mainly formed by the following reaction:

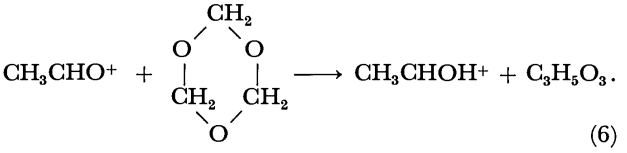

$$CH_3CHO^+ + \text{trioxane} \longrightarrow CH_3CHOH^+ + C_3H_5O_3. \quad (6)$$

On the other hand, protonated trioxane shows a dependence of the second order on the pressure of trioxane. Thus the formation of protonated trioxane occurs in the mixture as follows.

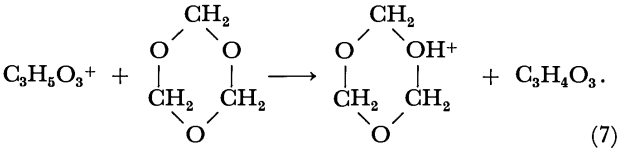

$$C_3H_5O_3^+ + \text{trioxane} \longrightarrow \text{protonated trioxane} + C_3H_4O_3. \quad (7)$$

A slight increase in the ion intensity of $C_3H_6O_3D^+$ with delay time was observed (Fig. 4). The results in the ionization efficiency curve measurements confirm the view that $C_3H_6O_3D^+$ in acetaldehyde-d_4–trioxane mixtures is formed by deuteron transfer from CDO^+ to trioxane.

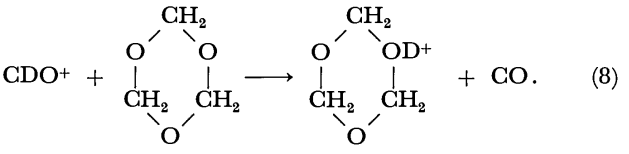

$$CDO^+ + \text{trioxane} \longrightarrow \text{protonated trioxane} + CO. \quad (8)$$

The contribution of other fragment ions from acetaldehyde for the formation of $C_3H_6O_3D^+$ is negligible since the onset and the fine structures of the ionization efficiency curves of these ions and $C_3H_6O_3D^+$ did not agree with each other. Since the ion intensity of trioxane molecular ion is very low, this ion could not be considered as the main precursor. Protonated trioxane in acetaldehyde–trioxane mixtures results mainly from the following reaction:

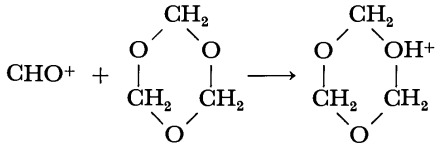

$$CHO^+ + \text{trioxane} \longrightarrow \text{protonated trioxane} + CO. \quad (9)$$

Rate Constants and Reactivity. Protonated acetaldehyde in acetaldehyde–trioxane mixtures was formed by Reactions 1, 2, and 6. Thus the rate constant of Reaction 6 is obtained by subtracting the contribution of Reactions 1 and 2. The rate constant of Reaction 9 is obtained in the same way as for k_6. The rate constants of Reactions 3 and 4 which are concurrent are obtained with a ratio plot technique.[2,3] The rate constants obtained are summarized in Table 1. The rate constant ratio k_4/k_3 is 1.68 which is nearly equal to that of k_2/k_1. The ratios k_1/k_3, k_2/k_4, and k_9/k_8 are 1.23, 1.24, and 1.14, respectively. Thus appreciable isotope effect was observed. The striking feature in the mixture is a predominant hydrogen atom transfer reaction (Reactions 5 and 6). The rate constant of Reaction 6 is smaller than that in ethylene oxide–trioxane mixtures by a factor of 1.2, suggesting that ability of hydrogen atom abstraction of acetaldehyde is lower than one of ethylene oxide. The rate constant of hydrogen atom transfer depends on the proton affinity and/or the hydrogen affinity of neutral molecule. Here, the proton affinity of acetaldehyde is 183±2[11] and 182[12] kcal mol^{-1}, and that of ethylene oxide 183 kcal mol^{-1},[11,13] the proton affinity of both molecules thus being almost equal. It is suggested that the hydrogen affinity of acetaldehyde is smaller than that of ethylene oxide.

TABLE 1. RATE CONSTANTS

Acetaldehyde-Trioxane		Acetaldehyde-d_4-Trioxane	
Reaction	$k\times10^9$ cm^3 molecule^{-1} s^{-1}	Reaction	$k\times10^9$ cm^3 molecule^{-1} s^{-1}
1	1.80[a]	3	1.46
2	3.04[a]	4	2.45
6	3.47	5	3.35
7	1.15[a]		
9	0.137	8	0.120

a) Ref. 3.

The rate constant of Reaction 2 is considerably larger than that of Reaction 9, indicating that the proton affinity of trioxane is smaller than that of acetaldehyde. CHO^+ belongs to proton donor ion among oxygen-containing ions. However, CHO^+ from trioxane did not contribute to the formation reaction of protonated molecular ions as major reactant ion in

acetaldehyde–trioxane mixtures. The effect of the translational and internal energy of reactant ions on ion-molecule reactions is important. In the measurement of translational energies of oxygen-containing ions, it was demonstrated that the energy of CHO^+ from trioxane is considerably higher than that of acetaldehyde.[14] Futrell *et al.*[15] report that the internal energy of CHO^+ depends on the source molecule and that CHO^+ from acetaldehyde has lowest internal energy among the CHO^+ ions from various oxygen-containing molecules. The difference in reactivity of the CHO^+ ions from acetaldehyde and trioxane observed in this work could be explained by an energy effect of reactant ion for proton transfer reaction.

The authors express cordial thanks to Dr. I. Kuriyama for helpful advice and encouragement during the course of the work.

References

1) M. Kumakura and T. Sugiura, *Bull. Chem. Soc. Jpn.*, **50**, 2046 (1977).
2) M. Kumakura, A. Ito, and T. Sugiura, *Mass Spectrosc.*, **22**, 61 (1974).
3) M. Kumakura, K. Arakawa, and T. Sugiura, *Int. J. Mass Spectrom. Ion Phys.*, in press.
4) H. Pritchard and A. G. Harisson, *J. Chem. Phys.*, **48**, 5623 (1968).
5) M. S. B. Munson, *J. Am. Chem. Soc.*, **87**, 5313 (1965).
6) A. S. Blair and A. G. Harrison, *Can. J. Chem.*, **51**, 703 (1973).
7) S.Okada, A.Matsumoto, T.Dohmaru, S.Taniguchi, and T. Hayakawa, *Mass Spectrosc.*, **20**, 311 (1972).
8) M. T. Bowers and P. R. Kemper, *J. Am. Chem. Soc.*, **93**, 5352 (1971).
9) M. Kumakura, T. Sugiura, and S. Okamura, *Mass Spectrosc.*, **16**, 16 (1968).
10) M. Kumakura and T. Sugiura, in "Recent Developments in Mass Spectroscopy," ed by K. Ogata and T. Hayakawa, Univ. of Tokyo Press, Tokyo (1970), p. 988.
11) J. L. Beauchamp and R. C. Dunbar, *J. Am. Chem. Soc.*, **92**, 1477 (1970).
12) M. S. B. Munson and J. L. Franklin, *J. Phys. Chem.*, **68**, 3191 (1964).
13) B. M. A. Haney and J. L. Franklin, *Trans. Faraday Soc.*, **65**, 1794 (1968).
14) M. Kumakura, K. Arakawa, and T. Sugiura, to be published.
15) J. H. Futrell, F. P. Abramson, A. K. Bhattacharya, and T. O. Tiernan, *J. Chem. Phys.*, **52**, 3655 (1970).

Ion-Molecule Reactions in the Binary Mixture of Ethylene Oxide and Trioxane. II. Mechanism for Reaction of Ethylene Oxide Molecular Ion with Trioxane

Minoru KUMAKURA, Kazuo ARAKAWA, and Toshio SUGIURA*

Takasaki Radiation Chemistry Research Establishment, Japan Atomic Energy Research Institute, Takasaki, Gunma 370-12

** Japan Atomic Energy Research Institute, Shinbashi, Minato-ku, Tokyo 105*

(Received May 23, 1977)

The ion-molecule reactions in the binary mixture of ethylene oxide and trioxane have been studied with use of a modified time-of-flight mass spectrometer. As cross-reaction product ions, $C_3H_5O_2^+$, $C_3H_6O_2^+$, and $C_3H_7O_2^+$ were observed under the conditions of long delay times and elevated pressure. It was found that these ions are formed by the dissociation of unstable intermediate-complex resulting from the reaction of ethylene oxide molecular ion with trioxane. It was proposed that the complex is of cyclic structure in which positive charge is delocalized. From the consideration of isotopic distribution of the prodoct ions in ethylene-d_4 oxide–trioxane mixtures, the skeletal structures of the product ions were investigated. The rate constants of the formation reactions of $C_3H_5O_2^+$, $C_3H_6O_2^+$, and $C_3H_7O_2^+$ in ethylene oxide–trioxane mixtures were found to be 2.20×10^{-10}, 2.61×10^{-10}, and 1.74×10^{-10} cm^3 molecule^{-1} s^{-1}, respectively.

As part of our program dealing with radiation and ion chemistry of oxygen-containing molecules, studies were carried out on the ion-molecule reactions in ethylene oxide, trioxane (1,3,5-trioxane), and acetaldehyde.[1-3] The consecutive association reactions leading to the formation of the cluster ions were observed in trioxane and a study of the kinetics of the reactions was made. The ion-molecule reactions in oxygen-containing organic compounds are sensitive to the nature of the functional groups and the molecular structure of the ionic and neutral reactions.[1,4,5] The reaction pathway of oxygenated ions with cyclic oxygen-containing molecules seems to be of interest. So far the ion-molecule reaction in the mixture system of cyclic oxygen-containing molecules involving large member rings has not been studied, although a number of studies in the pure system of cyclic hydrocarbons have been made.[6-10] Since the formation mechanism of only protonated molecular ions by cross-reactions in the binary mixture of ethylene oxide and trioxane has been studied,[11] the present work deals with the formation of other product ions in the binary mixture under long delay times and elevated pressures. Various product ions were formed by the reaction of ethylene oxide molecular ion with trioxane. The present work was carried out in order to obtain mechanistic information on the ion-molecule reactions involving cyclic ion and neutral molecules.

Experimental

A Bendix Model 12-101 time-of-flight mass spectrometer was used. The ion source of the spectrometer was modified in order to permit operation under elevated pressures.[2] Some pulse electronic circuits of the apparatus were also modified.[11] A variable delay time circuit permitted a variation of time between the end of the ionizing pulse and the onset of the ion withdrawal pulse. During the delay time, the entire ionization chamber is field-free, so that ion-molecule reactions occurring during the time interval are under thermal conditions. The retarding potential differential technique (RPD)[12] was adopted for appearance potential and ionization efficiency curve measurement. Measurement of the ionization efficiency curves of two ions was simultaneously performed by a two-channel ion detection method. The gas-sample inlet-system consisting of dual-leak and dual-reservoir was used. Two kinds of samples are introduced individually into the ionization chamber through two separate leaks from separate reservoirs. The partial pressure of the two samples was indirectly measured with an MKS Baratron 90-X RP-2 capacitance manometer, the pressure being calibrated by the rate constant (1.11×10^{-9} cm^3 molecule^{-1} s^{-1}) of CH_5^+ in the ion-molecule reaction of methane.[13]

The following reagents were used: trioxane (Celanese Chemical), ethylene oxide (Nisso Yuka Industry Co., Ltd.), and ethylene-d_4 oxide (Merck Sharp and Dohme of Canada, deuterium atom purity, 98%). The samples were used after being subjected to vacuum distillation several times.

Results and Discussion

Delay Time Dependence. The delay time dependence of fragment and product ions in a 1 : 1 mixture of ethylene oxide and trioxane at 2.61×10^{13} molecules cm^3 is shown in Figs. 1 and 2. In Fig. 1, *m/e* 44 ($C_2H_4O^+$), 43 ($C_2H_3O^+$), and 29 (CHO^+) are

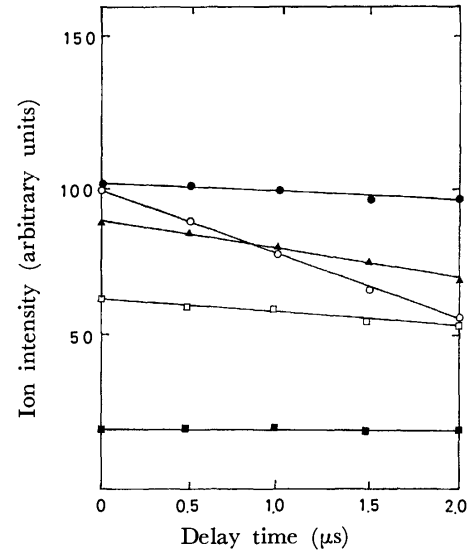

Fig. 1. Delay time dependence of fragment ions in ethylene oxide–trioxane mixtures.
▲: *m/e* 44, ■: *m/e* 43, ○: *m/e* 29 (×1/2), □: *m/e* 89, ●: *m/e* 61.

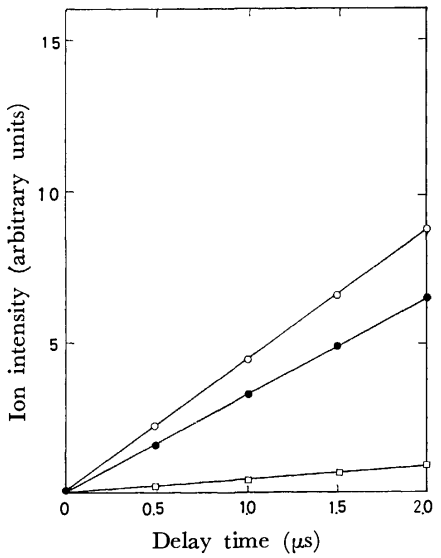

Fig. 2. Delay time dependence of product ions in ethylene oxide–trioxane mixtures.
○: *m/e* 73, □: *m/e* 74, ●: *m/e* 75.

major fragment ions from ethylene oxide, and *m/e* 89 ($C_3H_5O_3^+$), 61 ($C_2H_5O_2^+$), and a part of *m/e* 29 (CHO^+) are those from trioxane. Trioxane molecular ion is relatively less abundant, its ion intensity being comparable with the ion intensity of ^{13}C isotope of *m/e* 89.[12] The *m/e* 73, 74, and 75 were observed as new product ions in the mixture system as shown in Fig. 2. The plots of these ions are not shown, since the behavior of the protonated molecular ions and product ions formed in individual system has been described.[1,2,11] In order to elucidate the formation mechanism of the product ions in the mixture system, the ion-molecule reactions in ethylene-d_4 oxide–trioxane mixtures were studied under the same conditions as for ethylene oxide–trioxane mixtures. The delay time dependence of product ions is shown in Fig. 3. The isotopic product ions (*m/e* 73—79) correspond to the product ions (*m/e* 73—75) formed in ethylene oxide–trioxane mixtures.

The pressure dependence of the product ions on each molecule was examined in order to determine the contribution of ethylene oxide and trioxane at delay time of 1.0 μs. The pressure dependence of the product ions in ethylene oxide–trioxane mixtures is shown in Figs. 4 and 5. The product ions show a dependence of the first order on the pressure of ethylene oxide and trioxane. The results indicate that the product ions are formed by cross-reactions.

Ionization Efficiency Curves and Reaction Mechanism. In order to identify the reactions with each of the prod-

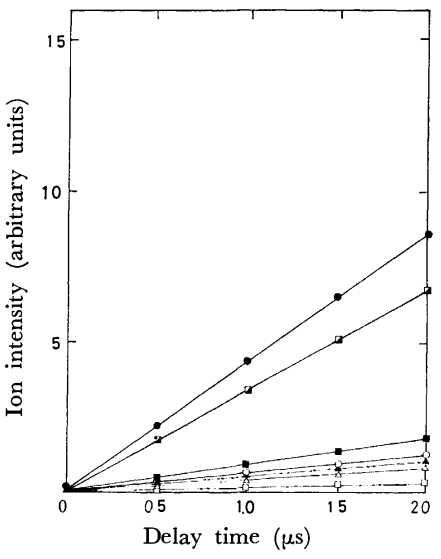

Fig. 3. Delay time dependence of product ions in ethylene-d_4 oxide–trioxane mixtures.
□: *m/e* 73, ▲: *m/e* 74, △: *m/e* 75, ◪: *m/e* 76, ■: *m/e* 77, ○: *m/e* 78, ●: *m/e* 79.

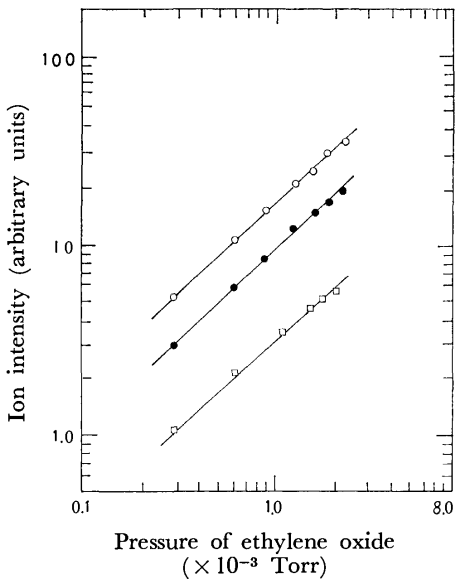

Fig. 4. Pressure dependence of product ions to ethylene oxide at 1.0 μs.
○: *m/e* 73, □: *m/e* 74, ●: *m/e* 75.

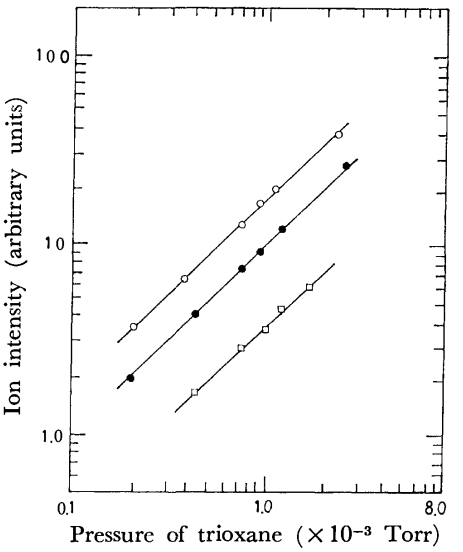

Fig. 5. Pressure dependence of product ions to trioxane at 1.0 μs.
○: *m/e* 73, □: *m/e* 74, ●: *m/e* 75.

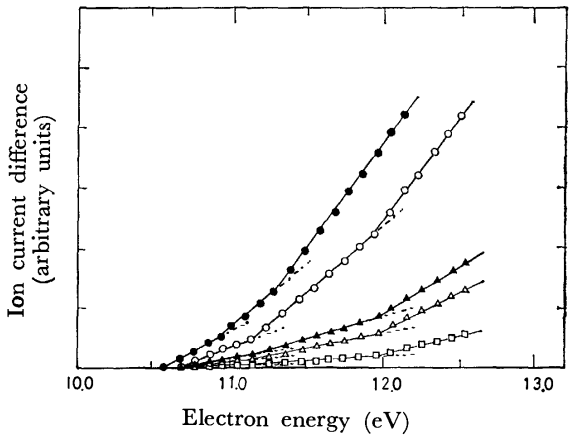

Fig. 6. Ionization efficiency curves of major fragment and product ions in ethylene oxide–trioxane mixtures. ○: *m/e* 44, ●: *m/e* 89, ▲: *m/e* 73, □: *m/e* 74, △: *m/e* 75.

uct ions, we measured the appearance potentials and the ionization efficiency curves of the product ions for comparison with those of the possible reactionts. The fragment ion whose appearance potential lies closest to that of product ion is taken to be the reactant ion (precursor), provided the reaction is energetically possible. If more than one fragment ion is responsible for the formation of a given product ion, a change in the slope of the ionization efficiency curve will often denote the onset of the reaction involving a different reactant ion.

The ionization efficiency curves of major fragment and product ions in ethylene oxide–trioxane mixtures are shown in Fig. 6. All the ionization efficiency curves of the product ions coincide in onset as well as shape. This suggests that the product ions are formed through a common precursor. The onset of the ionization efficiency curves of the product ions agrees with the ionization potential (10.64±0.1 eV) of ethylene oxide. The onset and fine structures in the ionization efficiency curves of the product ions do not agree with those of *m/e* 89 (trioxane). Furthermore, the appearance potentials, *m/e* 61 (10.79±0.05), 31 (11.49±0.05), 43 (12.06 ±0.1 eV),[2,12] of other abundant fragment ions (*m/e* 61, 31, and 43) from both trioxane and ethylene oxide are higher than those of the product ions. An agreement of the break points in the ionization efficiency curves between the product and the fragment ions was not observed. From the results of the ionization efficiency curve measurements of the fragment and the product ions, it is concluded that ethylene oxide molecular ion is the precursor of the product ions. Thus, it is suggested that the product ions result from the dissociation of unstable intermediate-complex.

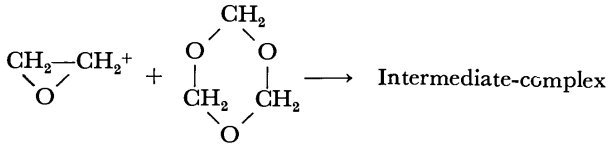

$$\longrightarrow \text{Product ions} + \text{Neutral fragments.} \quad (1)$$

The intermediate-complex resulting from the association reaction of ethylene oxide molecular ion with trioxane is very unstable. The ring opening of ethylene oxide and trioxane molecule would occur after the association of ethylene oxide molecular ion with trioxane. The ring strain energy of ethylene oxide is large (13 kcal mol^{-1}).[14] Furthermore, it is known that the bond dissociation energy of the C–O bond is lower than that of the C–C bond in ethylene oxide.[15]

Rate Constants and Ion Structures. Since the product ions in the mixture system are formed by a complex reaction mechanism, their rate constants are obtained by steady state treatment. The product ions are formed *via* certain dissociation channels of the intermediate-complex as in the following:

$$P_i^+ + M \xrightarrow{k_{1i}} P_iM^{+*}$$

$$P_iM^{+*} \xrightarrow{k_{2ij}} S_{ij}^+ + N_{ij},$$

where M, P^+, S^+, and P_iM^{+*} denote the concentration of neutral molecule and reactant, secondary product ion, and intermediate-complex, respectively. (P_iM^{+*}) and (P_i^+) are expressed by

$$(P_iM^{+*}) = \frac{k_{1i}(P_i^+)(M)}{\sum_j k_{2ij}}, \quad (2)$$

$$(P_i^+) = (P_i^+)_0 \exp[-k_{1i}(M)t], \quad (3)$$

where t is delay time and $(P_i^+)_0$ is the concentration of (P_i^+) at $t=0$. (S_{ij}^+) is determined by the equation

$$\frac{d(S_{ij}^+)}{dt} = k_{2ij}(P_iM^{+*}). \quad (4)$$

Integrating (4) and applying the condition $(S_{ij}^+)=0$ at $t=0$, we get

$$(S_{ij}^+) = \frac{k_{2ij}(P_i^+)_0}{\sum_j k_{2ij}}\{1-\exp[-k_{1i}(M)t]\}. \quad (5)$$

Assuming that the collection efficiencies are the same for both reactant and product ions, and expanding the exponential term, we have

$$\frac{I_{(S_{ij}^+)}}{I_{(P_i^+)_0}} = \frac{k_{2ij}k_{1i}(M)t}{\sum_j k_{2ij}}. \quad (6)$$

$I_{(P_i^+)_0}$ can be written as

$$I_{(P_i^+)_0} = I_{(P_i^+)} + \sum_i I_{(S_{ij}^+)} + I_{(P_iM^{+*})}. \quad (7)$$

Since $I_{(P_iM^{+*})} \approx 0$, Eq. 6 is simplified to

$$\frac{I_{(S_{ij}^+)}}{I_{(P_i^+)} + \sum_j I_{(S_{ij}^+)}} = \frac{k_{1i}k_{2ij}(M)t}{\sum_j k_{2ij}}. \quad (8)$$

Thus $k_{1i}k_{2ij}/\sum_j k_{2ij}$ is readily obtained by using Eq. 8.

The rate constants obtained in ethylene oxide–trioxane and ethylene-d_4 oxide–trioxane mixtures are summarized in Table 1. The sum of the rate constants for the product ions (*m/e* 73—77) in ethylene-d_4 oxide–trioxane mixtures is nearly equal to that of the product ion (*m/e* 73) in ethylene oxide–trioxane mixtures. Similarly, the rate constants for *m/e* 78 and 79 in ethylene-d_4 oxide–trioxane mixtures are respectively comparable with those for *m/e* 74 and 75 in ethylene oxide–trioxane mixtures. The structures of the product ions proposed from the stoichiometric consideration for the product ions in both mixture systems are shown in Table 2.

Table 1. Rate constants

Ethylene oxide-Trioxane		Ethylene-d_4 oxide-Trioxane	
Product ion m/e	$k \times 10^{10}$ cm^3 molecule^{-1} s^{-1}	Product ion m/e	$k \times 10^{10}$ cm^3 molecule^{-1} s^{-1}
		73	0.052
		74	0.195
73	2.20	75	0.260
		76	1.13
		77	0.364
74	0.261	73	0.294
75	1.74	79	1.43

Table 2. Possible structures of products ions

Product ion[a] m/e	Structure	Product ion[b] m/e
73	CH_2-O-CH_2-O-CH$^+$	
74	CX-O-CH_2-O-CH_2^+	
75	CX_2-O-CH_2-O-CH$^+$	73
76	CX-CX_2-O-CH_2-O$^+$	
77	CX_2-CX_2-O-CH-O$^+$	
78	CX_2-CX_2-O-CH_2-O$^+$	74
79	CX_2-CX_2-O-CH_2-OH$^+$	75

a) Etylene-d_4 oxide-trioxane mixtures. b) Ethylene oxide-trioxane mixtures. X denotes H or D atom.

The skeletal structures of the product ions (m/e 74—79) consist of fragment molecules from ethylene oxide and trioxane, while the product ion at m/e 73 consists of fragment molecules derived only from trioxane. This indicates that positive charge is delocalized in the intermediate-complex having cyclic structure as shown in Fig. 7. From the structures of the product ions (Table 2), it is presumed that extensive scrambling in the complex does not occur.

The authors wish to express appreciation to Prof. K. Hayashi, Osaka Univ., and Dr. A. Ito for helpful discussions on the chemical system.

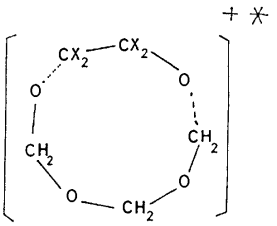

Fig. 7. Possible structure of intermediate-complex. X denotes H or D atom.

References

1) M. Kumakura and T. Sugiura, in "Recent Developments in Mass Spectroscopy," ed by K. Ogata and T. Hayakawa, Univ. of Park Press, London (1970), p. 988.
2) M. Kumakura, A. Ito, and T. Sugiura, *Mass Spectrosc.*, **22**, 16 (1974).
3) M. Kumakura, K. Arakawa, and T. Sugiura, to be published.
4) M. S. B. Munson, *J. Am. Chem. Soc.*, **87**, 5313 (1965).
5) J. L. Beauchamp, M. C. Caserio, and T. B. McMahon, *J. Am. Chem. Soc.*, **96**, 6243 (1974).
6) S. W. Wexler and L. G. Pobo, *J. Phys. Chem.*, **74**, 257 (1970).
7) S. W. Wexler and R. P. Clow, *J. Am. Chem. Soc.*, **90**, 3940 (1968).
8) R. Lesllaux, S. Searles, L. W. Sieck, and P. Ausloos, *J. Chem. Phys.*, **54**, 3411 (1971).
9) I. Koyano, N. Nakayama, and I. Tanaka, *J. Chem. Phys.*, **54**, 2384 (1971).
10) V. Aquilanti, A. Galii, A. Giardini-Guidoni, and G. G. Volpi, *Trans. Faraday Soc.*, **64**, 124 (1968).
11) M. Kumakura and T. Sugiura, *Bull. Chem. Soc. Jpn.*, **50**, 2046 (1977).
12) M. Kumakura, T. Sugiura, and S. Okamura, *Mass Spectrosc.*, **16**, 16 (1968).
13) G. W. Hand and H. Weyssenhoff, *Can. J. Chem.*, **42**, 195 (1964).
14) R. E. Parker and N. S. Isaacs, *Chem. Rev.*, **59**, 737 (1959).
15) J. L. Franklin, *J. Chem. Phys.*, **21**, 2029 (1953).

NvT- and *NpT*-ensemble Monte Carlo Simulations of Ionized Matter. I. *NvT*-ensemble Study on Calcium Oxide Near Normal Melting Point

Akio YAMAMOTO and Hiromu MURATA

Department of Chemistry, Faculty of Science, Hiroshima University, Higashisenda-machi, Hiroshima 730

(Received May 19, 1977)

With special attention to calcium oxide, values obtained by *NvT*-ensemble Monte Carlo calculations are reported for the internal energy, pressure, heat capacity, thermal pressure coefficient, Grüneisen's γ, and component radial distribution functions of ionized matter in the condensed phases. The calculations cover 14 vT points: seven points lying on one isochore at the X-ray density and eight on one isotherm at the normal melting point. Both thermodynamic quantities and structural properties in the vicinity of the melting point are indicative of the fluid-solid phase change. A brief comparison of the Monte Carlo results with the experimental data is also made.

Since the stimulating work by Metropolis *et al.*,[1] considerable work has been carried out on the application of Monte Carlo (MC) techniques to the calculation of the equilibrium properties of a wide variety of physical systems. The success of the method rests primarily on the fact that a model containing a relatively small number of particles is in general found to be sufficient to simulate the behavior of a macroscopic system. In addition, computer experiments on Coulomb systems[2] have in recent years provided much valuable information on the thermodynamic, structural, and transport properties of molten salts or plasmas. The purpose of the present paper is to describe the preliminary application of the isothermal-isochoric or *NvT* method to the study of neutral systems of classical charged particles before going into a detailed study of some intricate ionized matter; the present results are quite suggestive in exploring the question of whether the melting transition of a simple ionic system can be satisfactorily simulated by the simple interionic potential.

Calcium oxide has the simple rocksalt crystal structure[3] as do most alkali halides; it also has ionic crystals, but with the doubly charged ions. It appears that the computer simulations of the thermodynamic properties of the oxide and a detailed comparison of the results with both experiments and theories would lead to a better understanding of the material and perhaps aid in understanding the physical and chemical properties of the presumably better understood alkali halides.

Pair potentials derived from the cohesive energy of the solid[4] are used in the computations of the thermodynamic and structural properties in the condensed phases. Since the intermolecular potentials are well identified, the term-by-term contributions of the Coulomb and non-Coulomb energies to the total energy can be calculated explicitly. The values obtained by the MC method, such as pressure or Grüneisen's γ, involve no approximation other than that of the MC method:[5] the MC method is ideal for two- or three-digit accuracy, which is far more accurate than the results from approximate theories except in very special circumstances. Consequently, because we know the explicit form of the intermolecular potentials, it is in retrospect possible to select the theories from among the many suggested which successfully reproduce the machine results.

The principle of the method, furthermore, is equally applicable to other ensembles as well. We will describe in the next paper an application to ionic systems in the isothermal-isobaric or *NpT* ensemble.[6] The use of the *NpT*-MC method allows direct comparisons with experimental data, because the relevant experimental measurements have been usually made only at atmospheric pressure.

Monte Carlo Procedure

Of the many realistic potentials which could be chosen, we have picked an inverse power potential of the form

$$\phi_{ij}(r) = z_i z_j/r + R_{ij}/r^9 - A_{ij}/r^6,$$

where z_i is the ionic charge of the i-th kind of atom. The values of the coefficients, A_{ij} and R_{ij}, are calculated from the solid state properties of calcium oxide:[4]

A_{ij}	Ca	O	R_{ij}	Ca	O
Ca	35.5	63.6	Ca	7.55	32.5
O	63.6	135	O	32.5	113.5

in units of 10^{-60} erg·cm^6 and 10^{-82} erg·cm^9 respectively. No orientational dependence of the potential is specified, meaning that rotational and intramolecular vibrational modes of motion of molecules are supposed to be independent of density. Then the total energy, Φ, and the total virial, Ψ, of a configuration can be estimated as the sums of pair contributions.

All the results reported in this paper were obtained with a system of $N=64$ particles. With periodic boundary conditions,[7] an infinite system was set up by replicas of the basic parent cube of side L translated by a positive or negative multiple of L along its edge. Unlike non-ionic systems, the estimation of the potential energy is complicated here by the presence of long-range Coulomb forces. No methodological difficulties are, however, encountered when the Coulomb energy is evaluated by the Ewald method.[8] Since there happen to be ions around $r=0.5L$, short-range interactions between particles separated by a distance less than $r_c=0.6L$ were included explicitly and the remaining interactions were combined into the integrals[7]

$$\Phi_c = 2\pi N/v \int_{r_c}^{\infty} r^2 \Phi \mathrm{d}r$$

and

$$\Psi_c = 2\pi N/v \int_{r_c}^{\infty} r^3 \{\mathrm{d}\Phi/\mathrm{d}r\} \mathrm{d}r,$$

by assuming that the particle density is uniform: here

$v=L^3$ denotes the MC-cell volume.

Configurations are generated by the method of Metropolis,[1,7] and hence they are accepted or rejected according to a criterion which ensures that a given configuration occurs with a probability proportional to the Boltzmann factor for that configuration. The rate of convergence of the overall averages as a function of the displacement parameter has not been studied systematically. In application of the NvT method a rule-of-thumb[7] used empirically by workers in this field is to assign to the parameter a value such that approximately one-half of the MC moves generate successful new configurations: the present data were accumulated by the use of such a rule. The pseudo-random numbers used here were obtained by the multiplicative congruential method:[9] the generator operates "modulo 2^{32}."

The basic MC data include ensemble averages (indicated by angular brackets) of

1. the potential energy $\langle\Phi\rangle$,
2. the virial $\langle\Psi\rangle=\langle\sum_{1}^{N}{}_{(k)}r_k(\mathrm{d}\Phi/\mathrm{d}r_k)\rangle$,
3. the variance and covariance $\langle\Phi^2\rangle-\langle\Phi\rangle^2$ and $\langle\Phi\Psi\rangle-\langle\Phi\rangle\langle\Psi\rangle$,

and 4. the component pair radial distribution functions obtained by compiling pair distance histograms with intervals of 0.05 Å at randomly sampled MC steps.

When a computation for a vT point started from the NaCl-type lattice configuration, the first 30000—50000 steps were rejected on account of large fluctuations. The numbers of configurations used to estimate the ensemble averages were rather small (approximately $M=70000$ for each point), and the procedure adopted to calculate the effects of distant particles has since been found to introduce small but systematic errors.

According to the coarsed-grain statistics,[5] the probable error in the MC data is given by

$$\Delta X = 0.6745[\sum_{1}^{m}{}_{(t)}(\langle X_t\rangle-\langle X\rangle)^2/m(m-1)]^{1/2},$$

where ΔX is the estimated probable error in the overall MC average, $\langle X\rangle$, calculated from m subaverages, $\langle X_t\rangle$, over successive groups of M/m configurations: $M/m=5000$ in this work. Of the subaverages, $\langle X_t\rangle$, those which deviate seriously from the overall average, $\langle X\rangle$, were omitted by the visual inspection of the control charts.

The calculations were performed on a HITAC 8700 electronic computer at the Computing Center of Hiroshima University.

Results

Thermodynamic Quantity. The present calculations cover 14 vT points: seven points lying on one isochore at the X-ray density,[3] $\rho=3.346$ g/cm^3, and eight on one isotherm at the normal melting point, $t_m=2572$ °C.[10] The temperature range extends from the room temperature to just below the normal boiling point, $t_b=2850$ °C, while the volume ratio is in the range between 0.90 and 1.10. The numerical results of the computer experiments described in this paper are summarized in Table 1.

Thermodynamic quantities were calculated from the appropriate ensemble averages; some important relations for the NvT-ensemble are recalled here for the sake of easy reference.

The *total energy*, U, of the system is obtained from the mean potential energy by

$$U/NkT = \langle\Phi\rangle/NkT + 3/2,$$

where N is the number of particles in the MC cell and where k is the Boltzmann constant. In Table 1, the potential energy is further divided into the Coulomb and non-Coulomb contributions, the relative contributions being more dependent on the volume change than on the temperature. The *Madelung constant*, M, of the equilibrium configurations is also given in Table 1.

The mean virial determines the *pressure* according to[7]

$$pv/NkT = 1 - \langle\Psi\rangle/3NkT.$$

Table 1. Numerical results for the thermodynamic quantities

°C	v[a]	State	BE[b]	NC[c]	M[d]	Δ	p[e]	Δ	C_v/Nk	Δ	$v\beta/Nk$	Δ	γ[f]	Δ
35	16.8	solid	879.19	8.62	3.4962	0.0003	−59.46	0.23	2.69	0.06	4.16	0.20	1.55	0.06
1400	16.8	solid	864.18	9.24	3.4922	0.0003	8.6	0.5	2.56	0.06	3.34	0.16	1.32	0.06
2322	16.8	solid	854.13	9.62	3.4858	0.0004	50.8	0.8	2.623	0.045	3.98	0.16	1.529	0.044
2472	16.8	solid	851.73	9.79	3.4871	0.0007	61.2	1.2	2.46	0.05	3.81	0.16	1.548	0.040
2572	15.2	solid	848.38	12.88	3.4822	0.0010	355.2	1.8	2.39	0.06	3.38	0.24	1.39	0.06
2572	16.0	solid	850.93	11.18	3.4830	0.0009	185.3	0.8	2.68	0.05	3.78	0.16	1.420	0.037
2572	16.0	liquid					(343)							
2572	16.8	solid	850.89	9.80	3.4856	0.0010	63.6	1.1	2.66	0.07	3.98	0.16	1.496	0.044
2572	16.8	liquid					(188)							
2572	17.6	solid	848.19	8.66	3.4937	0.0007	−15.2	1.3	2.42	0.07	3.45	0.22	1.45	0.06
2572	18.0	liquid					(45)							
2572	18.4	solid	845.45	7.85	3.5033	0.0012	−80.5	1.1	2.308	0.036	3.53	0.09	1.533	0.037
2672	16.8	solid	849.87	9.80	3.4854	0.0003	68.4	1.4	2.46	0.06	3.20	0.13	1.294	0.037
2772	16.8	solid	848.55	9.81	3.4844	0.0008	73.9	1.0	2.50	0.06	3.49	0.14	1.391	0.041

a) Molar volume in cm^3/mol. b) Binding energy in kcal/mol. c) % contribution of non-Coulomb energy to Coulomb energy in magnitude. d) Madelung constant referred to lattice parameter. e) Pressure in kbar. f) Grüneisen's γ. The symbol Δ represents probable errors of the preceding columns.

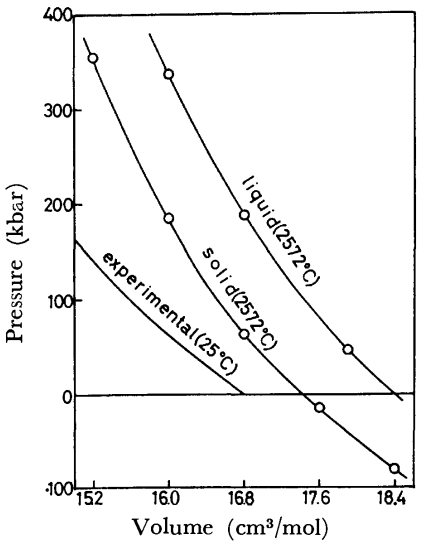

Fig. 1. The p, v-isotherms at the normal melting point.

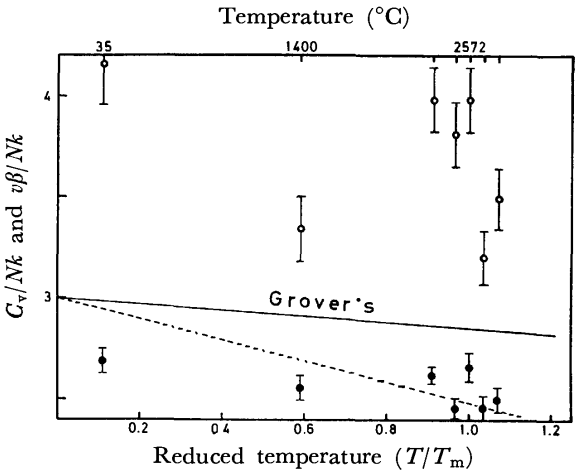

Fig. 2. Isochoric specific heat, C_v/Nk, and thermal pressure coefficient, $v\beta/Nk$, at the X-ray density.
○ $v\beta/Nk$, ● C_v/Nk.
Error bars and T_m represent the probable errors and the normal melting temperature respectively.

The p, v-isotherms at the normal melting point are shown in Fig. 1; no fluctuations indicative of a phase change were observed. The probable errors in the pressure are within 1 kbar. The preliminary data for the liquid branch are also included in Fig. 1. As has been pointed out by Woodcock and Singer,[11] the isotherms obtained from liquid runs are always higher than the solid-branch curve. The molar volume at zero pressure is estimated by interpolation to be approximately 17.4 cm³/mol at the melting point. As is summarized in Table 1, the calculated pressure at constant volume increases roughly linearly with temperature, and at the X-ray density the zero pressure is found to be attained around 1400 °C. The computed change of volume on fusion is 1.0—1.2 cm³/mol at the normal pressure.

The *specific heat* at constant volume, C_v, is determined by fluctuations about the mean as[12]

$$C_v/Nk = 3/2 + N(\langle\Phi^2\rangle - \langle\Phi\rangle^2)/(NkT)^2.$$

As can be seen from Table 1, the specific heat decreases with increasing temperature along isochores and changes little along isotherms. The specific heat on the X-ray density isochores (Fig. 2) shows a tendency to increase near the melting transition.

The *thermal pressure coefficient*, $\beta=(\partial p/\partial T)_v$, can be calculated from the covariance of the potential energy and the virial:[13]

$$v\beta/Nk = 1 + N\langle(\Phi-\langle\Phi\rangle)(\Psi-\langle\Psi\rangle)\rangle/(NkT)^2.$$

Since the coefficient, β, is evaluated as a covariance of two fluctuating quantities, the results are subject to large statistical errors. The calculated values listed in Table 1 show that β decreases with increasing volume along isotherms and that the rate of decrease also decreases in magnitude. The coefficient decreases slowly with increasing temperature along isochores; on fusion β decreases by about 20%. The sudden drop of the coefficient in the vicinity of the normal melting point, both along isotherms and isochores, is certainly indicative of the solid-fluid phase change.

The *Grüneisen's* γ, defined as $\gamma=v(\partial p/\partial T)_v/C_v$, is an extremely useful quantity in high-pressure physics. This parameter, given in the last two columns of Table 1, allows the extraction of a maximum of information from a minimum of data, which is a special virtue for experimental conditions where data are often difficult to obtain.

Radial Distribution Function. The angle-averaged component pair distribution functions, $g_{++}(r)$, $g_{--}(r)$, and $g_{+-}(r)$, are defined by[14]

$$g_{\alpha\beta}(r) = [\Delta n_{\alpha\beta}/\Delta r]/4\pi r^2,$$

where $\Delta n_{\alpha\beta}$ is the number of particles of kind β at a distance between r and $(r+\Delta r)$ from a reference particle of kind α; the mean radial distribution function is given by[15]

$$g_m(r) = [g_{+-}(r)+g_{-+}(r)]/4 + [g_{++}(r)+g_{--}(r)]/4.$$

These functions have been computed as appropriate averages over a total of about 300 randomly-sampled configurations at thermal equilibrium. All the curves are from a 64-particle system, so that beyond $r/L=1/2$ they are directly influenced by the periodicity imposed upon the system; therefore, only the first and second peaks are illustrated in Fig. 3. Furthermore, since the radial distribution functions of like ions are found to be very similar, the averaged function, $g_1(r)=[g_{++}(r)+g_{--}(r)]/2$, is shown in Fig. 3 for the systems on X-ray density isochores. Let us remark that the unambiguous resolution of the component radial distribution functions by X-ray or neutron diffraction is in general difficult, if not impossible. The calculated curves shown in Fig. 3 make it clear that there is some penetration (a few percent) by like ions into the apparent first coordination shell. The appearance of the functions changes gradually with temperature; the well-separated steep peaks at lower temperatures become broad and flat with increasing temperature, and the peaks become connected with each other before 1400 °C. The positions of the first peak also shift slightly from the crystallographic peak position centered at $r=2.405$ Å. In particular, the functions near the melting point exhibit some unexpected features which appear to antici-

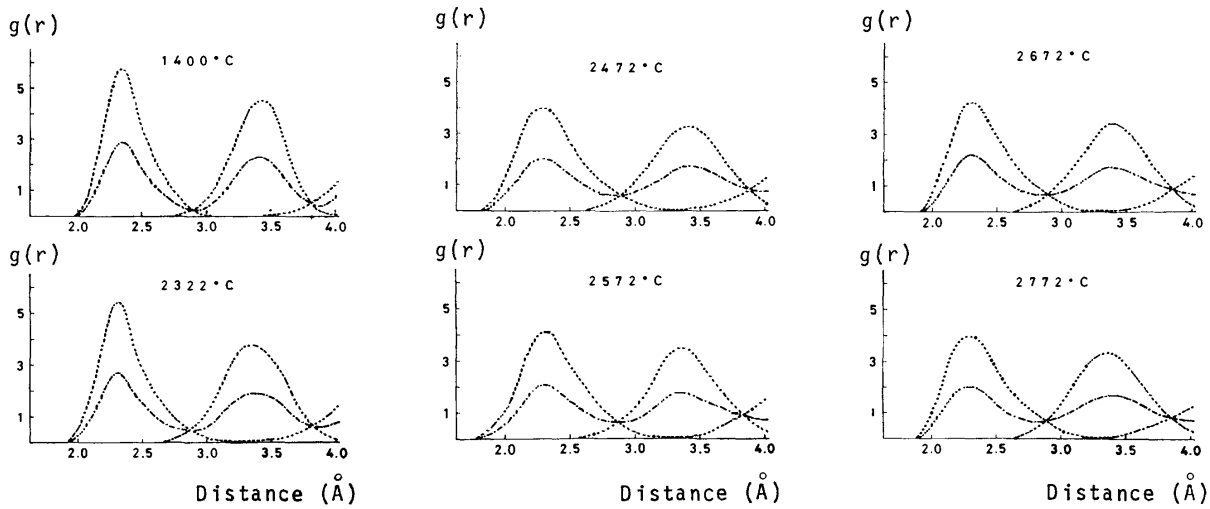

Fig. 3. Radial distribution functions on the X-ray density isochores.
(----) $g_l(r)$ or $g_u(r)$, (—·—) $g_m(r)$.
$g_l(r)=[g_{++}(r)+g_{--}(r)]/2$, $g_u(r)=[g_{+-}(r)+g_{-+}(r)]/2$, and $g_m(r)=[g_l(r)+g_u(r)]/2$.

pate the change on fusion: those below 2322 °C and above 2472 °C differ strikingly from one another.

Discussion

Possible Error. The number dependence of a finite system can be theoretically studied in certain simple situations,[16] whereas similar studies in the "experimental" situations can only be done empirically by using a system with different sizes. So far, this sort of study[17] has yielded the information that differences between the equation-of-state data of the finite system and the corresponding thermodynamically infinite system are not larger than $1/N$, if the system under observation is in the one phase region. Accordingly, the differences are believed to be within two percent except near the phase-transition region: the discrepancies found were seemingly not larger than would be expected from the following MC fluctuations. Another type of error concerns the statistical errors, which can be derived by using the coarsed-grain techniques. The probable errors, listed in Table 1, display a moderately consistent pattern, amounting to approximately a few percent or less in C_v/Nk and $v\beta/Nk$.

Potential Form. The effects on the thermodynamic and structural properties which result from changes in the intermolecular potentials have been studied by many investigators.[18] From the theoretical considerations, the exponential form of the potentials is known to be a better representation of repulsive interactions between close atoms than is the inverse power form. Nevertheless, because of its mathematical simplicity and its apparent adequacy near the minimum of the interaction curve, the inverse power potential is still the most widely used potential of practical importance. Except in the very high density region, effects of deviations from the inverse power potential and from additivity of pair potentials are seen to be fairly small. For instance, the experimental p, v-isotherms at room temperature[19] suggest that CaO is largely ionic at pressures below 160 kbar, but that, as the interionic distance is reduced, new interactions come into play which are not appropriately considered in the pair potential. From an analysis of a considerable amount of shock data,[13] it is also known that Grüneisen's γ varies more rapidly with compression than that calculated by using the Lennard-Jones potential, and consequently infers that even the inverse-12th-power potential is inappropriate for highly compressed materials. At the highest compression, where only the repulsive forces are important, the value becomes $\gamma=[n/6+1/3]=1.88$: such a compressed condition cannot be attained in the present calculations. We have not yet been able to relate these apparent discrepancies to the parameters used in the pair potential. Moreover, the validity of the approximate theories can be best appreciated by comparing with the MC results rather than with the experimental data, since the potential form of the real systems is not fully specified. At present theoretical data does not exist which would enable us to make such a comparison.

The potential parameters used here were prepared so as to be compatible with the properties of the static lattices.[7] Any refinement of the potential parameters[20] was, however, impracticable on account of the heavy demand of computing time.

Polarizability. The effects of ionic polarization in ionic salts[21] are found to be small and negligible except for the excess properties of liquid mixtures.[22] For typical alkali halides, the net contributions to the total energy are estimated to be small (less than few percent in magnitude);[15] this suggests that the polarization is not a factor which significantly affects the structural and thermodynamic properties. Although the introduction of the polarization effects to the present rigid-ion potential appears to be straightforward,[15,23] we have chosen to leave these factors out entirely, in view of the fact that a satisfactory short-range interaction potential is in itself an incompletely understood quantity for the present material.

Thermodynamic Quantity. A preliminary comparison of the MC results with the experimental data

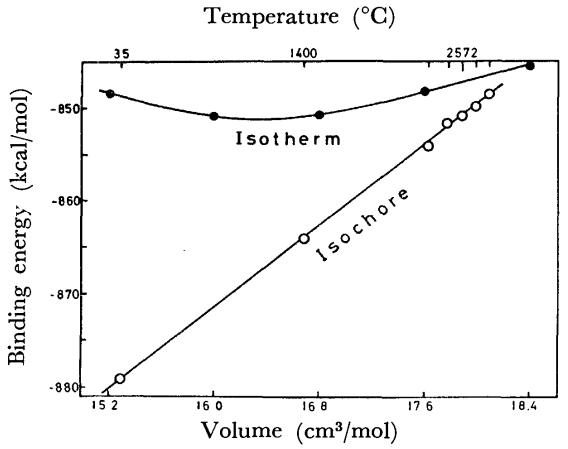

Fig. 4. Binding energy of calcium oxide.
○ Isochores at the X-ray density.
● Isotherms at the normal melting point.

of the real systems is in order, since the available data for CaO are unfortunately too scanty to permit detailed comparison of calculated with measured quantities over a sufficiently wide vT range. First, the *binding energy*, shown in Fig. 4, can give direct information about the temperature- and volume-dependence of the energy at any temperature of practical importance, while the corresponding energy estimated theoretically is exclusively concerned with the perfect crystal in the limit of 0 K. The binding energy of the static lattice is calculated to be 882.5 kcal/mol, which is the largest of the theoretical values reported so far: the thermochemical binding energy is 842 kcal/mol.[24,25] As is illustrated in Fig. 4, the binding energy at the finite temperature decreases linearly with increasing temperature, suggesting that the crystal lattice is destabilized by the thermal motion. On the other hand, the isothermal energy calculated varies only slowly with volume: the most stable molar volume at the normal melting point is energetically found to be around 16.5 cm³/mol. In the sixth column of Table 1 is given the *Madelung constant*, M,[9] of the equilibrium configurations, which, referred to the nearest-neighbor distance, can be said to present an effective number of nearest neighbors. The values listed are those referred to the lattice parameter, and hence they must be halved to obtain the nearest-neighbor values. The MC results indicate that the constant decreases roughly linearly with increasing temperature at constant volume: this points to an increasing cancellation of the potential as a result of an increase of thermal motion. On the contrary, the isothermal values of M vary gradually with volume: a value greater than that for the solid lattice ($M=3.4951$) shows a less complete cancellation of the negative and positive potential due to ion-pair formation. The presence of these pairs has often been pointed out in the molten salts;[26] the shape of the first peak of the radial distribution illustrates well this situation. The measurement of volume as a function of *pressure* can be accomplished in number of ways;[27] however, the data obtained from X-ray diffraction studies at room temperature are the only ones available at present. The experimental p, v-isotherms are included in Fig. 1, showing that the MC curves are similar in the dependence on the volume to the experimental facts. Next, the observed *specific heat* at constant pressure, C_p, can be modified by using the relation,[28]

$$C_v/Nk = C_p/Nk - \alpha^2 vT/\kappa(Nk),$$

to give the experimental specific heat, C_v: here α, κ, and v are the thermal volume expansivity, the compressibility, and the MC-cell volume respectively. The specific heat, C_v/Nk, at room temperature was thus calculated to be 2.3—2.7:[29-32] the MC results lie within the range of rather widely scattered experimental results. The MC calculations also indicate that the simulation fails entirely to account for the very rapid rise in specific heat that is observed near the critical temperature.[33] In the MC method the small value of N and the periodic boundary conditions are considered to suppress all large fluctuations, and the estimated specific heat is, therefore, very much too low in such a region. Aside from these restrictions, the pronounced maxima (Figs. 2 and 5) in the vicinity of the experimentally known melting point[26,34,35] are indicative of large fluctuations in the molecular arrangement. Despite these increases at near-critical temperatures, the calculated values of C_v/Nk decrease nearly linearly with increasing temperature: the data obey Grover's rule that $C_v/Nk=3(1-\delta\tau)$, where $\delta=0.15$ and τ is the temperature divided by the melting temperature, $T_m=2845$ K. The present value of δ is three times as large as that determined experimentally by Grover[36] for several metals, although the uncertainty in the computer-generated specific heat is quite large. The *Grüneisen parameter*, γ, can be thermodynamically derived from the ratio of the thermal pressure coefficient to the specific heat. As for KCl, the parameter is found to be essentially constant in the temperature range from 0 to 750 °C.[37,38] Figure 6 shows that the isothermal values of γ are substantially constant, while the values on the isochores vary but slowly with tem-

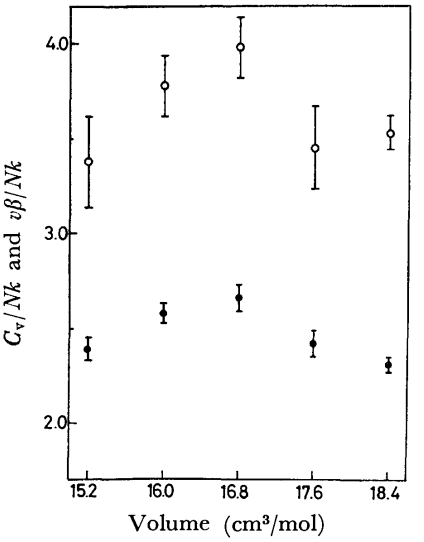

Fig. 5. Pronounced maxima in the isothermal specific heat(●), C_v/Nk, and the thermal pressure coefficient (○), $v\beta/Nk$, at the normal melting point. Error bars represent the probable errors.

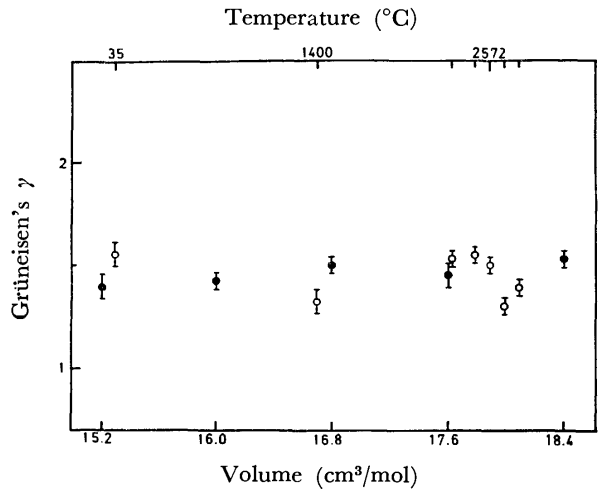

Fig. 6. Isothermal (●) and isochoric (○) Grüneisen parameters of calcium oxide.

perature. The constant-volume data can only be obtained by means of lattice dynamics: the value of 1.76 was assigned to it by Sirdesmukh and Rao.[39]

As the relevant experimental measurements have been made only at effectively constant pressure, we have found it more convenient to work in an isothermal-isobaric ensemble; furthermore, a strict test of the calculation model would involve a comparison of the results with ideal systems having some well-defined intermolecular potentials. Work along these lines is now in progress, and the detailed interpretation of the results and comparison with both experiments and theories will be discussed in a future publication.

Melting Transition. In systems of finite size, especially the small ones which can be treated on a computer, both the region over which metastable phases can occur, and the time for which they persist can be large. Precisely, these difficulties have complicated the search for the phase transitions in small systems. Even in the largest three dimensional systems investigated so far,[5] the particles are found to be either all in the fluid phase or all in the crystalline phase. Most runs were started from a perfect crystal, obviously unstable at low enough density and at high pressure: they would melt spontaneously. Thus the solid phase was extended from high density where it was at least metastable into the low density where it was seemingly unstable thermodynamically. Due to the irregular nature of a fluid structure it is not easy to invent an unbiased initial condition for a fluid run.[40] We plan a more detailed study of the liquid portion of the phase diagram in the near future, and the comparison of two disconnected branches overlapping in the density of the transition will yield some useful information on phase changes. As to the "computer-generated" solid branch, both large fluctuations of the total energy and the abrupt drop of the thermal pressure coefficient in the close vicinity of the experimentally known solid-fluid transition are certainly suggestive of the existence of the transition; the structural properties also indicate such a transition.

References

1) N. Metropolis, A. W. Rosenbluth, M. N. Rosenbluth, A. H. Teller, and E. Teller, *J. Chem. Phys.*, **21**, 1087 (1953).
2) F. H. Ree, in "Physical Chemistry—An Advanced Treatise," ed by D. Henderson, Vol. VIIIA, Academic Press, New York (1971), Chap. 3.
3) R. W. G. Wyckoff, "Crystal Structures," 2nd ed, Vol. 1, Interscience Publ., New York (1963).
4) R. H. Fowler, "Statistical Mechanics," Cambridge University Press, London (1936).
5) W. W. Wood, in "Physics of Simple Liquids," ed by J. S. Rowlinson and G. S. Rushbrooke, North-Holland Publ., Amsterdam (1968), Chap. 5.
6) W. W. Wood, *J. Chem. Phys.*, **48**, 415 (1968).
7) W. W. Wood and F. R. Parker, *J. Chem. Phys.*, **27**, 720 (1957).
8) C. Kittel, "Introduction to Solid State Physics," 2nd ed, John Wiley & Sons Inc., New York (1956), Chap. 3 and Appendix A.
9) D. H. Lehmer, *Ann. Compt. Lab. Harvard Univ.*, **26**, 141 (1951).
10) "Gmelins Handbuch der Anorganischen Chemie," 8th ed, Vol. 28, Verlag Chemie, GMBH, Weinheim (1961).
11) L. V. Woodcock and K. Singer, *Trans. Faraday Soc.*, **67**, 12 (1971).
12) T. L. Hill, "Statistical Mechanics," McGraw-Hill Inc., New York (1956), Chap. 4.
13) A. C. Holt and M. Ross, *Phys. Rev. B*, **6**, 2700 (1970).
14) I. R. McDonald and K. Singer, *Quart. Rev. Chem. Soc.*, **24**, 238 (1970).
15) J. W. E. Lewis, K. Singer, and L. V. Woodcock, *J. Chem. Soc., Faraday Trans. 2*, **71**, 301 (1975).
16) J. L. Lebowitz and J. K. Percus, *Phys. Rev.*, **124**, 1673 (1961).
17) W. G. Hoover, S. G. Gray, and K. W. Johnson, *J. Chem. Phys.*, **55**, 1128 (1971).
18) M. P. Tosi, *Solid State Phys.*, **16**, 1 (1965).
19) E. A. Perez-Albuerne and H. G. Drickamer, *J. Chem. Phys.*, **43**, 1381 (1965).
20) See, for example, I. R. McDonald and K. Singer, *J. Chem. Phys.*, **50**, 2308 (1969).
21) G. Jacucci, I. R. McDonald, and A. Rahman, *Phys. Rev. A*, **13**, 1581 (1976).
22) F. H. Stillinger, in "Molten Salts Chemistry," ed by M. Blander, Interscience Publ., New York (1964).
23) S. Romano and C. Margheritis, *Physica*, **77**, 557 (1974).
24) M. L. Huggins and Y. Sakamoto, *J. Phys. Soc. Jpn.*, **12**, 241 (1957).
25) M. F. C. Ladd and W. H. Lee, *Prog. Solid. State Chem.*, **1**, 37 (1964).
26) F. Lantelme and P. Turq, *J. Inorg. Nucl. Chem.*, **33**, 4025 (1971).
27) P. W. Bridgman, "The Physics of High Pressure," G. Bell & Sons, London (1931).
28) F. Seitz, "The Modern Theory of Solids," McGraw-Hill Inc., New York (1940).
29) E. Gmelin, *Z. Naturforsch., Teil A*, **24**, 1794 (1969).
30) "Landolt-Börnstein Zahlenwerte und Funktionen," Springer Verlag, Berlin (1960).
31) P. R. Son and R. A. Bartels, *J. Phys. Chem. Solids*, **33**, 819 (1972).
32) C. E. Weir, *J. Res. Natl Bur. Stand.*, **56**, 187 (1956).
33) See, for example, H. E. Stanley, "Introduction to Phase Transitions and Critical Phenomena," Clarendon Press, Oxford (1971).
34) W. G. Hoover, M. Ross, K. W. Johnson, D.

Henderson, J. A. Barker, and B. C. Brown, *J. Chem. Phys.*, **52**, 4931 (1970).
35) A. F. Ball, *J. Res. Natl. Bur. Stand.*, **45**, 23 (1950).
36) R. Grover, *Bull. Am. Phys. Soc.*, **13**, 1647 (1968).
37) D. E. Schüle and C. S. Smith, *J. Phys. Chem. Solids*, **25**, 801 (1964).
38) R. A. Bartels and D. E. Schüle, *J. Phys. Chem. Solids*, **26**, 537 (1965).
39) D. B. Sirdeshmukh and B. K. Rao, *J. Phys. Chem. Solids*, **36**, 355 (1975).
40) W. G. Hoover and F. H. Ree, *J. Chem. Phys.*, **49**, 3609 (1968).

Microwave Spectrum, Structure, and Quadrupole Coupling Constant of *o*-Chlorophenol

Masao ONDA, Yoshitomo OSHIMA, and Ichiro YAMAGUCHI

Department of Chemistry, Faculty of Science and Technology, Sophia University, Tokyo 102

(Received May 20, 1977)

The microwave spectrum of *o*-chlorophenol has been observed in the frequency range 10—34 GHz. The rotational and centrifugal distortion constants were obtained for two isotopic species, $^{35}ClC_6H_4OH$ and $^{37}ClC_6H_4OH$. The analysis of the hyperfine structure gives the following nuclear quadrupole coupling constants for ^{35}Cl species: $\chi_{aa}=-67.6$, $\chi_{bb}=33.3$, and $\chi_{cc}=34.3$ (MHz). The spectrum assigned has been attributed to the *cis*-form (intramolecularly hydrogen bonded between Cl and HO) from a brief consideration of the relative intensity of the a- and b- type transitions. No significant effect of the intramolecular hydrogen bonding on the nuclear quadrupole coupling was observed.

Many studies on the molecular structure of *o*-chlorophenol, mainly by means of infrared spectroscopy, have been reported by a number of authors in the last four decades.[1,2] According to these studies, *o*-chlorophenol exists as a mixture of two isomers, the *cis*- and *trans*-forms, in the gas and liquid phases and in solutions (the *trans*-form is the conformer with the hydroxyl hydrogen pointed away from the chlorine, and the *cis*-form with the hydroxyl hydrogen pointed toward to the chlorine), and the *cis*-form is known to form intramolecular hydrogen bonding between the chlorine atom and the hydroxyl group. Carlson *et al.*[2] estimated the population of the *trans*-form as 6.5% at room temperature from the analysis of the torsional frequencies of the hydroxyl group and concluded that the *cis*-form was more stable than the *trans*-form in the gas phase. Two benzene derivatives which have the intramolecular hydrogen bonding have so far been studied by the microwave spectroscopy: salicylaldehyde[3] and *o*-nitrophenol.[4] It is interesting to study the structure of the *o*-chlorophenol molecule in the gas phase by means of microwave spectroscopy, because this molecule is one of those which have the possibility of forming the intramolecular hydrogen bonding.

Azrak and Wilson[5] studied in detail the influence of the hydrogen bonding on the quadrupole coupling constants for 2-chloroethanol, but they observed no significant effect.

The purposes of the present investigation of *o*-chlorophenol are to find out whether the dominant conformation is *cis*- or *trans*-form in the gas phase and to what extent the nuclear quadrupole coupling constants of chlorine are affected by the intramolecular hydrogen bonding in the *cis*-form.

Experimental

The sample used was obtained commercially and was distilled *in vacuo*. The purity of the sample was checked through its NMR and IR spectra. The microwave spectrum was measured with a conventional spectrometer in the frequency range of 10—34 GHz. A square wave of 100 kHz was used for the Stark modulation. Measurements were made at room temperature with sample pressures of 1.3—5.3 Pa. The absorption lines were displayed on a recorder. Frequency measurements were made with a Hewlett-Packard 5245L electronic counter. The accuracy of the measured frequency was better than 0.2 MHz for most lines and it was better than 0.5 MHz for the broadened lines and for the lines which had a strong line nearby.

Results and Discussion

Analysis of the Spectrum. The observed spectrum consisted of very many lines in the observed region. This complexity of the spectrum comes from the existence of two chlorine isotopic species in the vibra tional ground state as well as in their low frequency vibrational excited states. A molecular model of a planar structure was constructed from the structural parameters of chlorobenzenes[6] and phenols.[8] The model calculation for either *cis*- or *trans*-form, where the Ray's asymmetry parameters for both are $\kappa\approx-0.46$, indicated that the transitions of the a- and b-types will appear in the observed frequency region. The initial step of the assignment was for both a- and b-type R-branch transitions. Clear quartets were observed for $J=9\leftarrow8$, $10\leftarrow9$, and $11\leftarrow10$ transitions with $K_{-1}=0$ and 1, and the separations between the two inner lines of the quartets were 12, 5, and 2 MHz, respectively. The assignments were confirmed by comparing the observed hyperfine structures with the predicted ones for the b-type Q-branch transitions with high-J values. The prediction was made using the nuclear quadrupole coupling constants of chlorobenzene[6] and with the planar molecular models of the *cis*- and *trans*- forms.

Many transitions were observed as doublets with separations of a few MHz due to the nuclear quadrupole coupling of chlorine. The center of the doublet was taken as the unperturbed frequency and was used for the least-squares fitting to obtain the rotational and centrifugal distortion constants. The assigned transitions are given in Tables 1 and 2 for both $^{35}ClC_6H_4OH$ and $^{37}ClC_6H_4OH$ species. The spectrum of $^{35}ClC_6H_4OH$ was fitted by the following seven variables: the three rotational and the four centrifugal distortion constants. For the $^{37}ClC_6H_4OH$ species, only six parameters (three rotational and three centrifugal distortion constants) were obtained because only a small number of high-J transitions were observed and the *hfs* were not well resolved. Table 3 gives the parameters thus obtained. The errors attached are the standard deviations obtained from the least-squares fits. The magnitudes of the centrifugal distortion constants τ obtained were small, as expected from several aromatic molecules.[7]

TABLE 1. OBSERVED FREQUENCIES OF R-BRANCH TRANSITIONS (MHz)

Transition	o-$^{35}ClC_6H_4OH$		o-$^{37}ClC_6H_4OH$	
	Observed	$\Delta\nu$[a]	Observed	$\Delta\nu$[a]
$8_{0,8}$—$7_{1,7}$	17329.85	−0.06		
$8_{1,8}$—$7_{1,7}$	17339.42	0.01		
$8_{0,8}$—$7_{0,7}$	17354.38	0.09		
$8_{1,8}$—$7_{0,7}$	17363.93	0.13		
$9_{0,9}$—$8_{1,8}$	19379.76	0.07	19035.22	−0.03
$9_{1,9}$—$8_{1,8}$	19383.31	0.00	19039.73	−0.21
$9_{0,9}$—$8_{0,8}$	19389.28	0.08	19047.11	−0.09
$9_{1,9}$—$8_{0,8}$	19392.80	−0.01	19051.91	0.03
$10_{0,10}$—$9_{1,9}$	21423.55	0.03	21044.14	0.21
$10_{1,10}$—$9_{1,9}$	21424.87	0.01	21046.09	0.36
$10_{0,10}$—$9_{0,9}$	21427.13	−0.00	21048.46	−0.15
$10_{1,10}$—$9_{0,9}$	21428.57	0.10	21050.53	0.11
$9_{1,8}$—$8_{2,7}$	21250.81	0.33		
$9_{2,8}$—$8_{2,7}$	21381.35	−0.02		
$9_{1,8}$—$8_{1,7}$	21539.16	−0.10		
$9_{2,8}$—$8_{1,7}$	21670.09	−0.06		
$11_{0,11}$—$10_{1,10}$	23465.10	0.09	23049.85	0.10
$11_{1,11}$—$10_{1,10}$	23465.54	0.04	23050.57	0.14
$11_{0,11}$—$10_{0,10}$	23466.40	0.04	23051.71	0.16
$11_{1,11}$—$10_{0,10}$	23466.97	0.12	23052.31	0.08
$10_{1,9}$—$9_{2,8}$	23397.50	0.24		
$10_{2,9}$—$9_{2,8}$	23453.77	−0.04		
$10_{1,9}$—$9_{1,8}$	23527.95	−0.21		
$10_{2,9}$—$9_{1,8}$	23584.59	−0.11		
$12_{0,12}$—$11_{1,11}$	25505.89	0.25	25054.54	0.07
$12_{1,12}$—$11_{1,11}$	25505.89	0.07	25054.54	−0.18
$12_{0,12}$—$11_{0,11}$	25505.89	−0.24	25055.11	−0.04
$12_{1,12}$—$11_{0,11}$	25505.89	−0.42	25055.11	−0.29
$13_{0,13}$—$12_{1,12}$	27546.00	0.02	27058.66	−0.12
$13_{1,13}$—$12_{1,12}$	27546.00	−0.04	27058.66	−0.21
$13_{0,13}$—$12_{0,12}$	27546.00	−0.15	27058.66	−0.37
$13_{1,13}$—$12_{0,12}$	27546.00	−0.22	27058.66	−0.47
$14_{0,14}$—$13_{1,13}$	29586.25	0.03	29063.02	0.06
$14_{1,14}$—$13_{1,13}$	29586.25	0.01	29063.02	0.02
$14_{0,14}$—$13_{0,13}$	29586.25	−0.03	29063.02	−0.04
$14_{1,14}$—$13_{0,13}$	29586.25	−0.05	29063.02	−0.07
$15_{0,15}$—$14_{1,14}$	31626.47	0.03	31067.16	0.05
$15_{1,15}$—$14_{1,14}$	31626.47	0.03	31067.16	0.04
$15_{0,15}$—$14_{0,14}$	31626.47	0.01	31067.16	0.02
$15_{1,15}$—$14_{0,14}$	31626.47	0.00	31067.16	0.01
$16_{0,16}$—$15_{1,15}$	33666.68	0.03	33071.47	0.22
$16_{1,16}$—$15_{1,15}$	33666.68	0.02	33071.47	0.22
$16_{0,16}$—$15_{0,15}$	33666.68	0.02	33071.47	0.21
$16_{1,16}$—$15_{0,15}$	33666.68	0.02	33071.47	0.21

a) $\Delta\nu=\nu_{obsd}-\nu_{calcd}$.

TABLE 2. OBSERVED FREQUENCIES OF Q-BRANCH TRANSITIONS (MHz)

Transition	o-$^{35}ClC_6H_4OH$		o-$^{37}ClC_6H_4OH$	
	Observed	$\Delta\nu$[a]	Observed	$\Delta\nu$[a]
$22_{7,15}$—$22_{6,16}$	20473.57	0.05		
$23_{7,16}$—$23_{6,17}$	23759.24	0.08	22101.71	0.17
$17_{8,9}$—$17_{7,10}$	21300.12	0.30		
$18_{8,10}$—$18_{7,11}$	19727.84	0.14		
$19_{8,11}$—$19_{7,12}$	18012.45	−0.00	19087.63	0.04
$20_{8,12}$—$20_{7,13}$	16549.19	−0.02	17467.32	0.00
$21_{8,13}$—$21_{7,14}$	15773.54	−0.03	16301.36	0.05
$22_{8,14}$—$22_{7,15}$	16004.27	0.05		
$23_{8,15}$—$23_{7,16}$	17368.53	0.05	16664.15	0.05
$24_{8,16}$—$24_{7,17}$	19775.88	−0.12	18448.38	0.02
$25_{8,17}$—$25_{7,18}$	22918.62	0.06	21141.52	−0.01
$15_{8,8}$—$15_{7,9}$	23877.24	−0.36	24294.01	−0.38
$16_{8,9}$—$16_{7,10}$	23622.19	−0.14	24029.53	−0.08
$17_{8,10}$—$17_{7,11}$	23449.88	−0.11	23818.53	0.01
$18_{8,11}$—$18_{7,12}$	23436.71	−0.02	23727.29	0.00
$19_{8,12}$—$19_{7,13}$	23661.39	0.01	23830.32	0.14
$20_{8,13}$—$20_{7,14}$	24189.20	0.00	24195.98	0.00
$19_{9,10}$—$19_{8,11}$	24912.29	0.00		
$20_{9,11}$—$20_{8,12}$	23475.68	0.09	24570.23	−0.03
$21_{9,12}$—$21_{8,13}$	21689.74	−0.01	22971.35	−0.20
$22_{9,13}$—$22_{8,14}$	19810.38	−0.07	21125.06	−0.06
$23_{9,14}$—$23_{8,15}$	18270.08	−0.04	19359.16	−0.16
$24_{9,15}$—$24_{8,16}$	17518.30	−0.00	18108.21	0.03
$25_{9,16}$—$25_{8,17}$	17865.68	−0.03	17754.04	0.11
$26_{9,17}$—$26_{8,18}$	19414.25	0.04	18517.38	0.06
$27_{9,18}$—$27_{8,19}$	22032.67	0.08	20417.99	0.00
$28_{9,19}$—$28_{8,20}$	25369.39	0.13	23259.18	−0.28
$24_{10,14}$—$24_{9,15}$	23565.60	0.07	25127.58	0.05
$25_{10,15}$—$25_{9,16}$	21541.67	0.09	23107.64	−0.12
$26_{10,16}$—$26_{9,17}$	19947.93	−0.02	21207.67	0.09
$27_{10,17}$—$27_{9,18}$	19243.65	−0.05	19882.63	0.05
$28_{10,18}$—$28_{9,19}$	19727.06	−0.08	19525.32	−0.02
$29_{10,19}$—$29_{9,20}$	21471.47	−0.04	20354.47	−0.02
$30_{10,20}$—$30_{9,21}$	24302.80	−0.10	22374.73	0.27
$28_{11,17}$—$28_{10,18}$	23215.10	−0.03	25041.91	−0.06
$29_{11,18}$—$29_{10,19}$	21591.15	0.06	23017.48	0.05
$30_{11,19}$—$30_{10,20}$	20956.58	0.08	21628.78	−0.04
$31_{11,20}$—$31_{10,21}$	21593.98	0.06	21277.37	−0.12
$32_{11,21}$—$32_{10,22}$	23544.00	−0.09	22178.43	−0.17
$32_{12,20}$—$32_{11,21}$	23206.81	0.03	24793.15	0.02
$33_{12,21}$—$33_{11,22}$	22662.87	−0.18	23350.44	0.08
$34_{12,22}$—$34_{11,23}$	23470.61	0.01	23013.35	0.15
$35_{13,22}$—$35_{12,23}$	24801.26	−0.10		
$36_{13,23}$—$36_{12,24}$	24368.65	0.10	25050.05	−0.04

a) $\Delta\nu=\nu_{obsd}-\nu_{calcd}$.

This spectrum is assigned to the *cis*-form as described in the later sections. A search for lines arising from the *trans*-form has failed, probably because their intensities are weaker than those of the vibrational excited states of the *cis*-form.

Molecular Structure. A small value of the inertia defect, as given in Table 3, is a strong indication of the planar configuration of this molecule. The positive inertia defect indicates that the effect of the out-of-plane vibrational motion, probably the hydroxyl group torsion, is not dominant. This is in contrast to the small negative value for phenol (−0.03 amu Å^2).[8] The value for *o*-chlorophenol is comparable to that for chlorobenzene and therefore the vibrational amplitude of the OH-torsion is considered to be smaller than for phenol. This reflects that the OH group in

Table 3. Rotational constants (MHz), centrifugal distortion constants (kHz), and inertia defect (amu Å^2) of o-chlorophenol

	$^{35}ClC_6H_4OH$	$^{37}ClC_6H_4OH$
A	2985.454±0.008	2976.812±0.011
B	1549.861±0.003	1510.810±0.004
C	1020.195±0.002	1002.147±0.001
τ_{aaaa}	−1.9 ±0.3	−1.7 ±0.3
τ_{bbbb}	−0.36 ±0.04	−0.29 ±0.03
τ_{aabb}	−0.1 ±0.2	0.0[a]
τ_{abab}	−0.48 ±0.07	−0.50 ±0.02
$I_c-I_a-I_b$	0.014±0.002	0.015±0.002
N[b]	88	67
σ[c]	0.014	0.019

a) Assumed. b) Number of transitions used for the least-squares fitting. c) Standard deviation (MHz) of lines fitted.

Table 4. Principal axis coordinates of Cl (Å)[a]

	$\|a\|$	$\|b\|$
Observed	2.0671±0.0001	0.5132±0.0004
Predicted		
cis model	2.042	0.566
trans model	2.086	0.504

a) $|c|=0$ assumed.

o-chlorophenol is more restricted in the molecular plane than in phenol, suggesting that the molecule is of the *cis*-form, having an intramolecular hydrogen bond between the hydroxyl group and the chlorine atom.

Kraitchman's equation was used to calculate the chlorine atom coordinates in the planar structure. The values obtained using the rotational constants A and B for both species are given in Table 4. The error limits given came from the errors in the moment of inertia. The predicted coordinates of the chlorine atom, with the regular hexagonal benzene ring, are included in Table 4. Comparing these results with the coordinates in the model structures, one cannot decide whether the set of coordinates determined corresponds to the *cis* or *trans* conformation.

To solve the problem of the conformation the relative intensity of the a- and b-type transitions was considered. Each of the lines of a quartet, consisting of the transitions $9_{0,9}\leftarrow 8_{1,8}$, $9_{1,9}\leftarrow 8_{1,8}$, $9_{0,9}\leftarrow 8_{0,8}$, and $9_{1,9}\leftarrow 8_{0,8}$, was observed with comparable intensities. The predicted line strengths of these a- and b-type transitions are almost the same for both of the conformations because they have almost the same asymmetric parameter, $\kappa\approx -0.46$. From the vector sum of the values for chlorobenzene[6] and phenol[8] the components of the electric dipole moment were predicted as given in Table 5. The ambiguity of the calculated intensity comes solely from the model structure and the interaction between two group moments, μ_{C-Cl} and μ_{OH}, but the distinction between *cis*- and *trans*-forms is clear. For the *cis*-form the intensities for the a- and b-type transitions should be almost the same, while for the *trans*-form the intensity for the a-type transitions should be larger than for the b-type transitions. Other similar sets of transitions: $J_{0,J}\leftarrow J-1_{1,J-1}$, $J_{1,J}\leftarrow J-1_{1,J-1}$, $J_{0,J}\leftarrow J-1_{0,J-1}$, and $J_{1,J}\leftarrow J-1_{0,J-1}$, with $J=10$ and 11 for ^{35}Cl and ^{37}Cl species, were also observed with comparable intensities. These results imply that the assigned spectrum came from the molecule which has a dipole moment with comparable magnitudes of the a- and b-components: the *cis* form.

Table 5. Predicted dipole moments (debye)[a]

	cis form	*trans* form
μ_a[b]	1.2	2.3
μ_b	1.2	1.2

a) Calculated from the following values: $\mu_a=1.782$ for chlorobenzene[6] and $\mu_a=0.13$ and $\mu_b=1.27$ for phenol.[8] b) a- and b-axes refer to model structure.

Assuming the rigid planar structure, only two moments of inertia are independent. From the results for the two isotopic species, four structural parameters can therefore be determined, while other parameters are assumed. The parameters derived for the *cis*-form were the bond lengths C–Cl and C–O and the angles ∠C(2)–O–H and ∠C(1)–C(2)–O. Assumptions for the other parameters were as follows: the benzene skeleton is regular hexagonal and the C–C bond length is 1.399 Å; all the C–H bonds and the C–Cl bond are located on the ∠C–C–C bisectors; the C–H bond length is 1.084 Å and the O–H bond length is 1.040 Å. A plausible set of parameters obtained on these assumptions is shown in Table 6. The calculated moments of inertia using these parameters coincide with the observed values within 0.1 amu Å^2. For the distorted benzene skeleton, which is the same as for chlorobenzene,[9] the parameters given in Table 6 were obtained. From two different assumptions about the skeleton structure, the same magnitudes of the C–Cl bond length as in chlorobenzene, and the same angle ∠C–C–O, extended by 2° from 120°, have been obtained.

Quadrupole Coupling Constants. The apparent splitting in the doublet was measured for high-J b-type Q-branch transitions as listed in Table 7. The hyperfine patterns were analyzed based on the first-order quadrupole correction computation using the

Table 6. Structural parameters

	r_{C-Cl} (Å)	r_{C-O} (Å)	∠COH (°)	∠C_1C_2O (°)
Regular hexagon				
o-ClC_6H_4OH[a]	1.713	1.350	120.4	121.9
C_6H_5Cl[b]	1.712	—	—	—
C_6H_5OH[c]	—	1.364	109.0	122.2
Distorted hexagon[d]				
o-ClC_6H_4OH[a]	1.725	1.350	111.	122.
C_6H_5Cl	1.7248	—	—	—

a) This work. b) Ref. 6. c) Ref. 8. d) Benzene ring structure is that obtained from the r_s-coordinates for chlorobenzene, see Ref. 9.

TABLE 7. QUADRUPOLE SPLITTING OF Q-BRANCH TRANSITIONS (MHz)

Transition	*o*-$^{35}ClC_6H_4OH$		*o*-$^{37}ClC_6H_4OH$	
	Obsd	$\Delta\nu$[a]	Obsd	$\Delta\nu$[a]
$22_{7,15}$—$22_{6,16}$	0.76	0.00		
$23_{7,16}$—$23_{6,17}$	0.57[b]	−0.10		
$17_{8,9}$ —$17_{7,10}$	3.15	−0.09		
$18_{8,10}$—$18_{7,11}$	3.14	0.11		
$19_{8,11}$—$19_{7,12}$	2.69	0.05	2.10	−0.06
$20_{8,12}$—$20_{7,13}$	2.07	0.05	1.79	0.00
$21_{8,13}$—$21_{7,14}$	1.28	0.02	1.20	−0.08
$22_{8,14}$—$22_{7,15}$	0.51	0.01		
$23_{8,15}$—$23_{7,16}$	c)		c)	
$24_{8,16}$—$24_{7,17}$	0.46	−0.14	0.31[b]	0.02
$25_{8,17}$—$25_{7,18}$	0.75	−0.01	0.62[b]	−0.09
$15_{8,8}$ —$15_{7,9}$	3.29	0.01	2.64	−0.06
$16_{8,9}$ —$16_{7,10}$	2.73	−0.11		
$17_{8,10}$—$17_{7,11}$	2.48	0.05	1.74[b]	−0.22
$18_{8,11}$—$18_{7,12}$	2.03	0.00	1.86	0.12
$19_{8,12}$—$19_{7,13}$	1.63	−0.02	1.50	0.05
$20_{8,13}$—$20_{7,14}$	1.35	0.05	1.10	−0.08
$19_{9,10}$—$19_{8,11}$	3.00	0.13		
$20_{9,11}$—$20_{8,12}$	3.06[b]	0.25	2.39[b]	−0.24
$21_{9,12}$—$21_{8,13}$	2.68	0.02	2.15	0.06
$22_{9,13}$—$22_{8,14}$	2.21	−0.10	2.09	0.17
$23_{9,14}$—$23_{8,15}$	1.78	0.04	1.57	−0.01
$24_{9,15}$—$24_{8,16}$	1.07	0.03	1.23	0.11
$25_{9,16}$—$25_{8,17}$	0.5[b]	0.16	0.62	0.00
$26_{9,17}$—$26_{8,18}$	0.3[b]	−0.04	c)	
$27_{9,18}$—$27_{8,19}$	0.67	0.02	c)	
$28_{9,19}$—$28_{8,20}$	0.69	−0.09	0.5[b]	−0.05
$24_{10,14}$—$24_{9,15}$	2.33	−0.05	1.86	−0.01
$25_{10,15}$—$25_{9,16}$	1.99	−0.06	1.68	−0.03
$26_{10,16}$—$26_{9,17}$	1.48	−0.04	1.44	0.02
$27_{10,17}$—$27_{9,18}$	0.95	0.08	0.98	−0.02
$28_{10,18}$—$28_{8,19}$	c)		0.55	0.02
$29_{10,19}$—$29_{9,20}$	0.3[b]	−0.01	c)	
$30_{10,20}$—$30_{9,21}$	0.67	−0.01	c)	
$28_{11,17}$—$28_{10,18}$	1.82	−0.02	1.60	0.03
$29_{11,18}$—$29_{10,19}$	1.44	0.11	1.32	0.02
$30_{11,19}$—$30_{10,20}$	0.71	0.00	1.03	0.13
$31_{11,20}$—$31_{10,21}$	c)		0.5[b]	0.06
$32_{11,21}$—$32_{10,22}$	0.3[b]	−0.10	c)	
$32_{12,20}$—$32_{11,21}$	1.17	0.00	1.26	0.07
$33_{12,21}$—$33_{11,22}$	0.62	0.04	0.79	−0.03
$34_{12,22}$—$34_{11,23}$	c)		0.3[b]	−0.07
$35_{13,22}$—$35_{12,23}$	0.95	−0.09		
$36_{13,23}$—$36_{12,24}$	0.45	−0.02	0.75	0.00

a) $\Delta\nu$=observed−calculated. b) Not included in the least-squares fitting. c) Not resolved.

rotational constants in Table 3. The quadrupole coupling constants in the principal inertial axis system, χ_{aa}, χ_{bb}, and χ_{cc}, were obtained using the least-squares method, as shown in Table 8. In this procedure, the inverse of the squared uncertainty, the standard deviation in the measurements of the splitting, was taken as the weight for each line frequency. The

TABLE 8. QUADRUPOLE COUPLING CONSTANTS OF CHLORINE (MHz)[a]

	$^{35}ClC_6H_4OH$	$^{37}ClC_6H_4OH$
χ_{aa}	−67.6±0.3	−55.9±2.0
χ_{bb}	33.3±0.1	26.5±0.3
χ_{cc}	34.3±0.4	29.4±2.3
θ_{za}[b]	5.69°	4.97°
χ_{zz}[c]	−68.6±1.3[e]	−56.5±4.5[e]
χ_{yy}	34.3±0.9[e]	27.1±1.1[e]
χ_{xx}[d]	34.3±0.4	29.4±2.3

a) a, b, and c are the principal inertial axes. b) θ_{za} is the angle between the principal inertial axis a and the principal z axis. c) χ_{zz} is the component along the C–Cl bond. d) χ_{xx} is the component perpendicular to the molecular plane and χ_{yy} is the in-plane component. e) The uncertainties in the χ-values are estimated from the ambiguity in the angle of θ_{za}, ±1°.

TABLE 9. PRINCIPAL QUADRUPOLE COUPLING CONSTANTS OF ^{35}Cl FOR SEVERAL SUBSTITUTED CHLOROBENZENES (MHz)[a]

	χ_{zz}	χ_{yy}	χ_{xx}	η[b]
o-ClC_6H_4OH[c]	−68.6	34.3	34.3	0.00
C_6H_5Cl[d]	−71.10	—	—	—
o-$C_6H_4Cl_2$[e]	−63.3	32.4	30.9	0.02
m-$C_6H_4Cl_2$[f]	−70.2	37.4	32.8	0.06

a) z-Axis is along the C-Cl bond and y-axis is in the molecular plane. b) $\eta=(\chi_{xx}-\chi_{yy})/\chi_{zz}$. c) This work. d) Ref. 6. e) Ref. 10. f) Ref. 11.

uncertainties in Table 8 were calculated from the estimated error in the frequency measurements of the unresolved *F* components. Assuming that the principal z-axis of the χ-tensor lies on the C–Cl bond, the values of χ_{zz} and χ_{yy} are obtained for the *cis*-form, as given in Table 8. The value of χ_{xx}, the component perpendicular to the molecular plane, is the same as χ_{cc}.

The principal values for several substituted chlorobenzenes are listed in Table 9. The value of χ_{zz} in *o*-chlorophenol is apparently smaller than in monochlorobenzene and *m*-dichlorobenzene. The χ_{zz} values, however, depend on the uncertainty of the transformation angle θ_{za}, ±1° as estimated from the ambiguity in the structure model, so that the differences in the values among these compounds are not very significant. The value around −70 MHz for χ_{zz} is considered to be normal for a chlorine atom which has hydrogen atoms nearby at the ortho position.[11] It seems that the hydrogen-halogen interaction does not have a significant effect on the electronic charge distribution about the chlorine nucleus in this molecule. The same conclusion had been obtained for 2-chloroethanol[5] through its microwave spectrum, where the conformation (*gauche-gauche* form) is favorable for the intramolecular hydrogen bond formation. Although the non-bonded distance between chlorine and hydrogen (2.609 Å for 2-chloroethanol and 2.53 Å for *o*-chlorophenol) is shorter than the sum of the van der Waals radii of chlorine and hydrogen (3.0 Å),

no significant effect on the quadrupole coupling constants of chlorine nucleus was observed for o-chlorophenol or for 2-chloroethanol.

The authors wish to express their thanks to Dr. O. Ohashi for his valuable discussions.

References

1) See, for example, the following papers: L. Pauling, *J. Am. Chem. Soc.*, **58**, 94; (1936); D. A. K. Jones and J. G. Watkinson, *Chem. Ind.*, **1960**, 661; E. A. Allan and L. W. Reeves, *J. Phys. Chem.*, **66**, 613 (1962); A. W. Baker and A. T. Shulgin, *Can. J. Chem.*, **43**, 650 (1965); Tien-Sung Lin and E. Fishman, *Spectrochim. Acta, Part A*, **23**, 49 (1967).

2) G. L. Carlson, W. G. Fateley, A. S. Manocha, and F. F. Bentley, *J. Phys. Chem.*, **76**, 1553 (1972).

3) H. Jones and R. F. Curl, Jr., *J. Mol. Spectrosc.*, **42**, 65 (1972).

4) S. Leavell and R. F. Curl, Jr., *J. Mol. Spectrosc.*, **45**, 428 (1973).

5) R. G. Azrak and E. B. Wilson, *J. Chem. Phys.*, **52**, 5299 (1970).

6) R. Poynter, *J. Chem. Phys.*, **39**, 1962 (1963).

7) L. Nygaard, E. R. Hansen, R. L. Hansen, J. Rastrup-Andersen, and G. O. Sørensen, *Spectrochim. Acta, Part A*, **23**, 2813 (1967).

8) T. Pedersen, N. W. Larsen, and L. Nygaard, *J. Mol. Struct.*, **4**, 59 (1969).

9) G. Roussy and F. Michel, *J. Mol. Struct.*, **30**, 399 (1976); F. Michel, H. Nery, P. Nosberger, and G. Roussy, *J. Mol. Struct.*, **30**, 409 (1976).

10) M. Onda and I. Yamaguchi, *J. Mol. Struct.*, **34**, 1 (1976).

11) M. Onda and I. Yamaguchi, *J. Mol. Struct.*, **36**, 158 (1977).

The Crystal Structure of the A-super Form of Lauric Acid

Midori GOTO and Eiichi ASADA

National Chemical Laboratory for Industry, Hon-cho, Shibuya-ku, Tokyo 151

(Received June 4, 1977)

The crystal structure of the A-super form of lauric acid has been determined. The structural parameters were refined by the block-diagonal least-squares method, and the final R value was 0.094. Two types of molecular conformations of a lauric acid exist in the crystal; one is the ordinary type, as seen in the C-form or the A_1-form of the lauric acid, while the other is that rotating the carboxyl group about the C1–C2 bond. This unusual structure was explained by the oxygen-oxygen distance of the adjacent molecule.

Even-numbered fatty acids are known by powder X-ray diffractions to exist in three crystalline forms, named A, B, and C.[1] In the case of lauric acid, the crystal structure of the C-form has been determined by Vand, Morley and Lomer.[2] This has an orthorhombic subcell of the hydrocarbon chain. Another crystal form, belonging to A, was studied by von Sydow[3] in only one projection. He showed that it has the triclinic subcell of the hydrocarbon chains. He named it the A-super form, because it could be regarded as a sixfold superstructure from the chain packing. Later, another crystal form, A_1, belonging to the A form, has been completely determined by Lomer.[4]

Three-dimensional results are required in order to discuss thoroughly the relations among polymorphic forms. We could obtain a single crystal of the A-super form of a sufficient size and studied its structure from a three-dimensional approach.

Experimental

Lauric acid was purified according to the procedure described by Tsuchiya.[5] At first it crystallized in the C-form in an isooctane solution. After it had stood in the solution for about two weeks at room temperature, the C-form was gradually transformed into the A-super form with colorless, triclinic needle-like crystals elongated along the a-axis. The crystal data are listed in Table 1. The intensity data were collected by means of a Rigaku-Denki four-circle diffractometer by using graphite monochromated Cu $K\alpha$ radiation. Reflections with 2θ values up to 60° were collected. The total number of observed reflections was 679.

Structure Determination

The y and z co-ordinates of the atoms were assumed to be those given by von Sydow, and the approximate x co-ordinates were obtained by taking into account three-dimensional Patterson maps and the packing of the molecules.

The hydrogen atoms were placed at the calculated positions assuming the C–H length of 1.10 Å and a tetrahedral arrangement about the carbon atom. The hydrogen atoms of the end were assumed to be at the *gauche* position. The hydrogen atom of the carboxyl group was neglected. Refinements were carried out by the block-diagonal least-squares method using HBLS program (Ashida),[6] with anisotropic temperature factors for non-hydrogen atoms. The parameters of the hydrogen atoms were not refined. The R value was reduced to 0.094.

The final atomic parameters are listed in Table 2.* The y and z co-ordinates did not differ significantly from those given by von Sydow.[3]

Table 1. Crystal data

Lauric acid A-super form	
Molecular weight	200.3
Melting point	44.0 °C
The unit cell was chosen as that of von Sydow.	
Triclinic; $A\bar{1}$	
$Z=12$	
$a=5.415(2)$Å	$\alpha=69.82°(4)$
$b=25.964(11)$Å	$\beta=113.14°(4)$
$c=35.183(13)$Å	$\gamma=121.15°(3)$
$U=3829.9$ Å^3	
$D_x=1.04$ g/cm^3	

Results and Discussion

The bond lengths, bond angles, and internal rotation angles are listed in Table 3. The arrangement of the molecules in the crystal is shown in Fig. 1. The chains are packed in a triclinic subcell with dimensions of $a=4.33$ Å, $b=5.42$ Å, $c=2.52$ Å, $\alpha=75.9°$, $\beta=108.9°$. $\gamma=122.1°$. Both carboxyl and methyl end groups appear in the same molecular layer.

An ORTEP (Johnson)[7] drawing of the three crystallographically independent molecules (I, II, and III) is shown in Fig. 2. The conformation of Molecule (III) is roughly equivalent to that of (II). There are two types of molecular conformations of lauric acid in an asymmetric unit; one type is (I), and the other, (II) and (III).

The carbon atoms in each molecule are nearly coplanar, as is shown in Table 4. The dihedral angle between the plane of the carboxyl group and that of the carbon chain is 83° in Molecule (I), 10° in (II) and 25° in (III) respectively. The plane of the carboxyl group in Molecule (I) is almost perpendicular to the carbon chain, while in (II) and (III) the two planes are roughly parallel, as is found in the A_1 form of lauric acid. The conformation as found in Molecule (I) was also reported in the structure of *dl*-2-hydroxytetradecanoic acid,[8] which has a large substituent near the carboxyl group.

It is rare for two types of molecular conformation

* The table of the observed and calculated structure factors has been submitted and is kept by the Office of the Chemical Society of Japan, 1-5, Kanda-Surugadai, Chiyoda-ku, Tokyo 101 (Document No 7804).

TABLE 2(a). ATOMIC CO-ORDINATES ($\times 10^4$) AND ANISOTROPIC TEMPERATURE FACTORS ($\times 10^4$ Å^2) FOR C AND O ATOMS

The temperature factors are of the form:

$$T=\exp[-(B_{11}h^2+B_{22}k^2+B_{33}l^2+2B_{12}hk+2B_{13}hl+2B_{23}kl)].$$

	x	y	z	B_{11}	B_{22}	B_{33}	B_{12}	B_{13}	B_{23}
C1	3357	−100	483	835	45	3	160	23	11
C2	5870	−247	803	590	37	14	184	−62	−2
C3	6427	28	1213	918	12	13	68	25	−10
C4	9072	−161	1540	913	10	13	121	27	−2
C5	9600	72	1935	63	26	18	1	−35	−9
C6	12036	−120	2289	266	29	10	20	36	−3
C7	12930	118	2699	926	20	4	71	−6	−12
C8	15516	−62	3057	879	12	7	56	7	−6
C9	16250	207	3463	801	22	16	67	65	5
C10	18566	−10	3801	648	7	18	65	60	−1
C11	19358	257	4202	488	34	16	77	−41	−13
C12	21828	64	4542	1058	50	7	119	−91	−26
C13	1552	1552	459	958	6	26	28	92	9
C14	4129	1402	814	685	31	15	118	15	4
C15	4812	1679	1208	937	39	9	119	8	−4
C16	7252	1462	1554	419	40	13	126	−29	−15
C17	8162	1746	1958	301	15	21	−11	35	2
C18	10510	1560	2293	664	2	8	73	53	7
C19	11195	1776	2696	791	26	9	88	24	3
C20	13702	1609	3058	906	19	12	79	16	−2
C21	14513	1871	3468	570	51	20	170	35	−4
C22	17046	1677	3800	849	32	25	46	85	1
C23	17552	1878	4196	999	54	21	183	54	4
C24	20195	1689	4548	1194	26	12	71	0	−13
C25	4368	−1888	507	2069	10	47	165	280	36
C26	7028	−2022	827	1253	17	22	131	112	4
C27	7765	−1682	1219	611	25	11	102	−3	−6
C28	10512	−1850	1559	699	15	10	46	12	−6
C29	11336	−1608	1958	870	28	12	78	45	0
C30	13751	−1806	2311	276	25	21	70	23	−2
C31	14743	−1510	2708	592	28	21	120	−11	−10
C32	17094	−1720	3044	823	25	14	86	48	−4
C33	17994	−1450	3452	334	27	16	42	36	−1
C34	20300	−1730	3806	519	27	18	36	39	−8
C35	21090	−1405	4197	308	16	22	39	−4	−11
C36	23593	−1583	4540	1175	63	14	206	22	7
O1	3469	−1546	490	522	15	8	32	−55	−10
O2	744	1234	150	1187	26	22	101	13	−19
O3	3818	382	185	684	39	15	116	−24	5
O4	557	−443	467	830	69	13	153	35	0
O5	3530	−2123	174	962	40	11	137	−14	−1
O6	715	1849	445	909	47	10	121	−40	−16

The average standard deviations are as follows:

$sx=200$, $sy=40$, $sz=30$, $sB_{11}=720$, $sB_{22}=40$, $sB_{33}=20$, $sB_{12}=160$, $sB_{13}=90$, $sB_{23}=20$, ($\times 10^4$).

TABLE 2(b). ATOMIC CO-ORDINATES ($\times 10^3$) FOR H ATOMS

The temperature factors are isotropic. $B=6.0$ Å^2

	x	y	z		x	y	z
H2	788	2	68	H20	1573	183	295
H'2	509	−74	88	H'20	1286	111	314
H3	733	53	113	H21	1252	164	359
H'3	442	−24	133	H'21	1545	237	339
H4	1110	11	143	H22	1907	193	368

Table 2(b). (Continued)

	x	y	z		x	y	z
H'4	821	−66	161	H'22	1611	117	386
H5	752	−17	203	H23	1553	162	430
H'5	1053	58	187	H'23	1842	238	413
H6	1404	7	218	H24	1942	119	460
H'6	1112	−62	236	H'24	2078	182	485
H7	1094	−9	281	H''24	2223	193	443
H'7	1378	62	263	H26	893	−178	69
H8	1752	16	295	H'26	625	−252	94
H'8	1462	−56	314	H27	582	−192	135
H9	1422	0	357	H'27	864	−119	111
H'9	1730	71	339	H28	968	−235	164
H10	1753	−51	388	H'28	1244	−162	143
H'10	2060	20	369	H29	934	−180	207
H11	1734	4	431	H'29	1230	−110	188
H'11	2029	76	412	H30	1571	−163	219
H12	2092	−44	461	H'30	1275	−231	239
H'12	2250	23	483	H31	1279	−169	282
H''12	2380	26	443	H'31	1578	−101	262
H14	618	164	70	H32	1905	−154	293
H'14	346	91	91	H'32	1604	−223	312
H15	275	146	131	H33	1600	−162	356
H'15	582	218	113	H'33	1914	−95	338
H16	922	166	143	H34	2234	−151	370
H'16	623	96	163	H'34	1915	−220	389
H17	914	225	188	H35	1910	−162	431
H'17	618	155	208	H'35	2203	−91	411
H18	1255	177	219	H36	2427	−141	482
H'18	957	105	236	H'36	2268	−209	462
H19	916	157	280	H''36	2552	−140	442
H'19	1203	228	262				

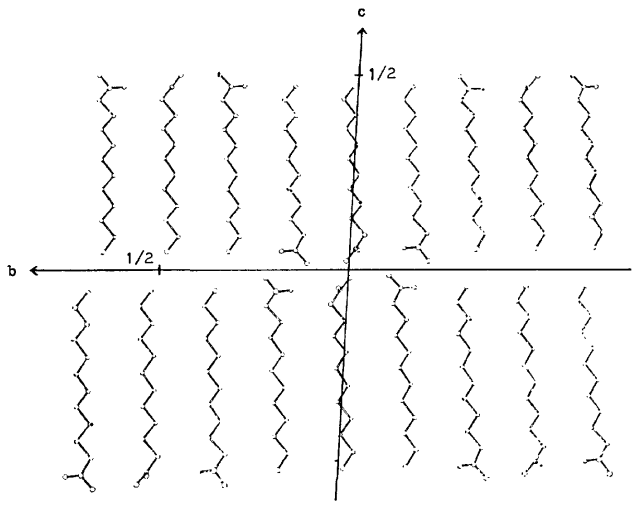

1) A perspective view along the $\mathbf{b}\times(\mathbf{b}\times\bar{\mathbf{a}})$ direction drawn by ORTEP.[7]

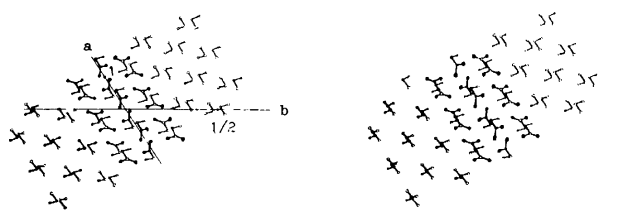

2) Stereoscopic view along the $\mathbf{b}\times(\mathbf{b}\times\bar{\mathbf{c}})$ direction drawn by ORTEP.

Fig. 1. Drawings of the crystal structure.

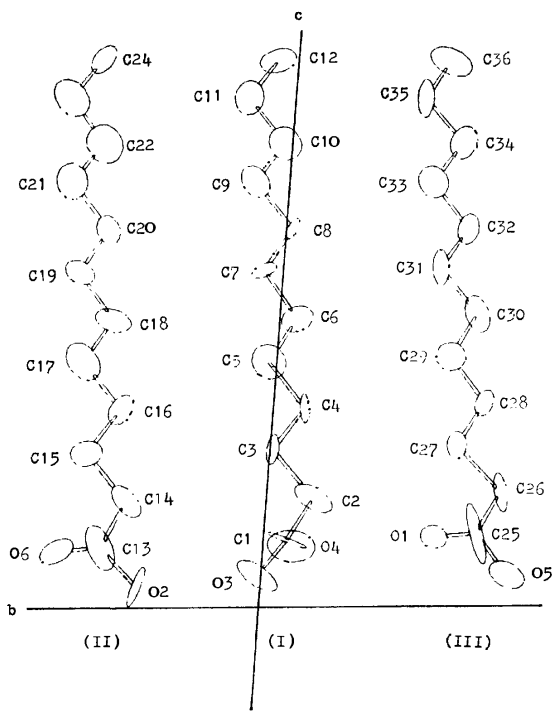

Fig. 2. Three molecules in an asymmetric unit. The atoms are drawn with ellipsoids of thermal vibration of 50% probability.

Table 3. Structural parameter

(a) Interatomic distances[a] (Å)					
C1-C2	1.52	C13-C14	1.54	C25-C26	1.52
C2-C3	1.69	C14-C15	1.61	C26-C27	1.70
C3-C4	1.63	C15-C16	1.61	C27-C28	1.65
C4-C5	1.58	C16-C17	1.63	C28-C29	1.55
C5-C6	1.59	C17-C18	1.53	C29-C30	1.58
C6-C7	1.57	C18-C19	1.56	C30-C31	1.60
C7-C8	1.63	C19-C20	1.59	C31-C32	1.55
C8-C9	1.62	C20-C21	1.62	C32-C33	1.56
C9-C10	1.55	C21-C22	1.59	C33-C34	1.61
C10-C11	1.58	C22-C73	1.53	C34-C35	1.60
C11-C12	1.59	C23-C24	1.66	C35-C36	1.57
O3-C1	1.31	O2-C13	1.34	O5-C25	1.32
O4-C1	1.29	O6-C13	1.14	O1-C25	1.20
(b) Bond angles[b] (°)					
O3-C1-O4	117	O6-C13-O2	123	O1-C25-O5	121
C2-C1-O3	121	C14-C13-O2	110	C26-C25-O5	108
C3-C2-C1	101	C15-C14-C13	107	C27-C26-C25	101
C4-C3-C2	98	C16-C15-C14	101	C28-C27-C26	99
C5-C4-C3	100	C17-C16-C15	105	C29-C28-C27	106
C6-C5-C4	104	C18-C17-C16	106	C30-C29-C28	108
C7-C6-C5	109	C19-C18-C17	106	C31-C30-C29	107
C8-C7-C6	110	C20-C19-C18	109	C32-C31-C30	106
C9-C8-C7	106	C21-C20-C19	109	C33-C32-C31	106
C10-C9-C8	104	C22-C21-C20	104	C34-C33-C32	106
C11-C10-C9	105	C23-C22-C21	103	C35-C34-C33	102
C12-C11-C10	105	C24-C23-C22	104	C36-C35-C34	104
(c) Internal rotation angles (°)					
C3-C2-C1-O3	99	C15-C14-C13-O2	−178	C27-C26-C25-O5	179
C4-C3-C2-C1	178	C16-C15-C14-C13	175	C28-C27-C26-C25	178
C5-C4-C3-C2	−179	C17-C16-C15-C14	178	C29-C28-C27-C26	−177
C6-C5-C4-C3	177	C18-C17-C16-C15	−180	C30-C29-C28-C27	175
C7-C6-C5-C4	177	C19-C18-C17-C16	−176	C31-C30-C29-C28	177
C8-C7-C6-C5	−178	C20-C19-C18-C17	−179	C32-C31-C30-C29	179
C9-C8-C7-C6	180	C21-C20-C19-C18	178	C33-C32-C31-C30	−178
C10-C9-C8-C7	177	C22-C21-C20-C19	−179	C34-C33-C32-C31	177
C11-C10-C9-C8	180	C23-C22-C21-C20	−176	C35-C34-C33-C32	−180
C12-C11-C10-C9	−178	C24-C23-C22-C21	−179	C36-C35-C34-C33	−175

a) The average of the values of the standard deviation is 0.14 Å. b) The average of the standard deviation is 7.

Table 4. Atomic displacements from the least-squares planes of hydrocarbon chains

The equation expressed in the orthogonal Cartesian system:

Z//**c**, X//**a***, Y//**c**×**a*** in Å unit.

C1-C12 $0.362X+0.870Y-0.336Z=0.210$

C13-C24 $0.365X+0.867Y-0.340Z=1.756$

C25-C36 $0.380X+0.843Y-0.380Z=-1.390$

C1	−0.06	C13	−0.09	C25	−0.18
C2	0.02	C14	0.00	C26	−0.03
C3	0.01	C15	0.03	C27	0.01
C4	0.06	C16	−0.02	C28	0.12
C5	0.01	C17	0.07	C29	0.07
C6	−0.03	C18	0.04	C30	0.03
C7	0.00	C19	−0.01	C31	0.09
C8	0.00	C20	0.00	C32	0.05
C9	0.03	C21	0.03	C33	0.04
C10	−0.04	C22	0.04	C34	−0.10
C11	0.00	C23	−0.06	C35	−0.07
C12	−0.01	C24	−0.04	C36	−0.05
O3	1.00	O2	−0.27	O5	−0.21
O4	−1.16	O6	0.11	O1	−0.02

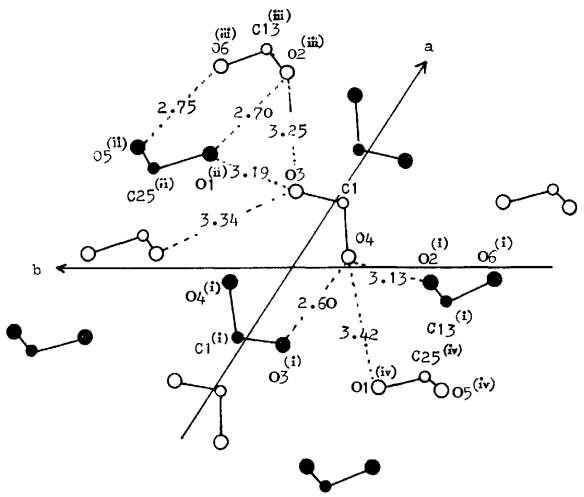

Fig. 3. A projection along the c*-axis.
○: Upper layer atoms, ●: lower layer atoms.
Symmetry code (i) −x, −y, −z, (ii) −x+1, −y, −z, (iii) x+1, y, z, (iv) x−1, y, z.

to appear in a crystal of the simple fatty acid. The larger thermal parameters of the atoms in the carboxyl group, listed in Table 2, might be due to this unusual arrangement of molecules.

The arrangement of the end groups is shown in Fig. 3. As is commonly found in fatty acids, the molecules are bound together to form dimers through hydrogen bonds between the carboxyl groups. The hydrogen-bond lengths are 2.60 Å between O3–O4$^{(i)}$, 2.70 Å between O2$^{(iii)}$–O1$^{(ii)}$, and 2.75 Å between O6$^{(iii)}$–O5$^{(ii)}$.

If Molecule (I) took the same conformation as (II), the O4–O2$^{(i)}$ distance would be 2.34 Å, too close to form a hydrogen bond between the molecules. This short contact is relieved by rotating the carboxyl group about the C1–C2 bond, resulting in a particular conformation of Molecule (I).

In the C-form of lauric acid, carboxyl groups appear in the same layer, but in the A-form, both the A-super form and the A_1-form, they do not. In the A_1-form the carboxyl group is adjacent to the methyl group of the neighboring molecule, and the short contact mentioned above is relieved.

The structure in which the carboxyl groups of the same conformation appear in the same layer, as is seen in the C-form, might be unfavorable in the A-form of lauric acid.

We wish to thank Professor Y. Iitaka of The University of Tokyo for his encouragement and helpful discussions.

References

1) F. Francis and S. H. Piper, *J. Am. Chem. Soc.*, **61**, 577 (1939).
2) V. Vand, W. H. Morley, and T. R. Lomer, *Acta Crystallogr.*, **4**, 324 (1951).
3) E. von Sydow, *Acta Chem. Scand.*, **10**, 1 (1956).
4) T. R. Lomer, *Acta Crystallogr.*, **16**, 984 (1963).
5) T. Tsuchiya, Jitsuyo Yushi Kagaku Binran, Sangyo, Tosho, Tokyo (1946).
6) T. Ashida, HBLS (IV), The Universal Crystallographic Computing System (I), The Crystallographic Society of Japan (1967), p. 65.
7) C. K. Johnson, Oak Ridge National Laboratory Report ORNL-3794.
8) B. Dahién, B. M. Lundén, and I. Pascher, *Acta Crystallogr., Sect. B*, **32**, 2059 (1976).

Measurements of the Solubility Coefficients of Gases and Vapors in Natural Rubber by Gas Chromatographic Technique

Mitsuyasu KAWAKAMI and Shuichi KAGAWA

Department of Industrial Chemistry, Faculty of Engineering, Nagasaki University, Nagasaki 852

(Received June 8, 1977)

The solubility coefficients of hydrocarbons in unvulcanized natural rubber at 25 °C were determined by gas-liquid chromatography. Natural rubber was used as a stationary liquid and nine kinds of lower olefins and paraffins as solutes. The retention volume for all the solutes did not vary with sample size. It was found that the correction for gas phase imperfection is negligible. Thus the solubility coefficient was readily obtained from the specific retention volume without any correction. The values obtained were in fairly good agreement with those determined by the volumetric method given in other works. Modified equations expressing the relationships between the solubility coefficient and the boiling temperature, the critical temperature, and the Lenard-Jones force constant, which might be applicable to a more extensive range of gaseous compounds, were presented.

Recently gas-liquid chromatography (GLC) has attracted attention as a means for determining thermodynamic properties of a solution consisting of stationary liquid and solute gas. Many investigations have been made since Porter *et al.*[1] measured the partition coefficient and the heat of solution by GLC in 1956. The method is especially effective for a system of polymer and organic compounds. For example, the volatility of solvents in polymer coatings was measured by Newman and Prausnitz,[2] and the solubility parameter of polyethylene glycol by Takamiya *et al.*[3] and by Kawakami *et al.*[4] In the present work GLC was employed to determine the solubility coefficients of some lower olefins and paraffins in unvulcanized natural rubber at 25 °C. The values obtained were in fairly good agreement with those determined by van Amerongen[5] and Michaels and Bixler[6] by means of the volumetric method. Modified empirical formulas were proposed on the relation between the solubility coefficient and other physicochemical properties of gases.

Theoretical

When the Henry law holds between stationary liquid and solute gas and the gas phase imperfection can be neglected, the net retention volume V_N is related to the partition coefficient K by[7]

$$V_N = KV_L. \tag{1}$$

Here K is defined by

$$K = \frac{n_L/V_L}{n_G/V_G}, \tag{2}$$

where n_L and n_G are the numbers of moles of solute in the liquid phase and the gas phase with volumes of V_L and V_G, respectively.

The solubility coefficient S, on the other hand, is defined by

$$c = Sp, \tag{3}$$

where c is the concentration expressed in m^3(STP) of solute gas dissolved per m^3 of solvent and p is the equilibrium partial pressure of solute gas. Using the ideal gas equation, the concentrations in the liquid phase and the gas phase are respectively given by $n_L/V_L = cp^\circ/RT^\circ$ (p°=1 atm=101325 Pa, T°=273.2 K) and $n_G/V_G = p/RT$ where T is the column temperature. Thus the partition coefficient is expressed by

$$K = \frac{T}{T^\circ}\frac{p^\circ}{p}c = \frac{T}{T^\circ}p^\circ S, \tag{4}$$

and

$$S = \frac{T^\circ}{T}\frac{1}{p^\circ}\frac{V_N}{V_L}. \tag{5}$$

The simplified expression is obtained by using the specific retention volume V_g which denotes the net retention volume per unit weight of stationary liquid converted into 0 °C. We thus have

$$V_g = \frac{V_N}{w_L}\frac{T^\circ}{T}, \tag{6}$$

where w_L is the weight of stationary liquid. Substitution of Eq. 6 into Eq. 5 gives

$$S = \frac{1}{p^\circ}\rho_L V_g, \tag{7}$$

where ρ_L is the density of stationary liquid. The solubility coefficient can thus be calculated from the specific retention volume. The value of V_g can be obtained experimentally by the equation

$$V_g = \frac{t_R F}{w_L}\frac{T^\circ}{T_r}J_2^3, \tag{8}$$

where t_R is the peak maximum retention time, F is the flow rate of carrier gas at room temperature T_r.

$$J_n^m = \frac{n}{m}\left\{\frac{(p/p_o)^m - 1}{(p_i/p_o)^n - 1}\right\}, \tag{9}$$

where p_i and p_o are the column inlet and outlet pressures, respectively.

Correction is necessary when gas phase imperfection is not negligible.[8] It was first proposed by Everett and Stoddart,[9] and improved by Cruickshank *et al.*[10] According to the latter, the net retention volume is related to the partition coefficient at zero total pressure K_0 by

$$V_N = K_0 V_L \exp(\beta p_o J_3^4). \tag{10}$$

Here

$$\beta = \frac{2B_m - v^\infty}{RT}, \tag{11}$$

where B_m is the second mixed virial coefficient between solute gas and carrier gas, and v^∞ the partial molar volume of solute at infinite dilution. The solubility coefficient at zero pressure S_0 is related to K_0 by Eq. 4. Thus

$$S_0 = \frac{1}{p^\circ}\rho_L V_g \exp(-\beta p_o J_3^4), \quad (12)$$

S_0 can be obtained when the values of B_m and v^∞ are known.

Experimental

Preparation of Column. A certain volume of 1 wt% benzene solution of the stationary liquid, unvulcanized natural rubber (smoked sheet) was added with stirring to a weighed amount of solid support, Uniport B (Gasukuro Kogyo Co.), and then air-dried. For each impregnation operation, the amount of benzene solution equal to the pore volume of solid support was used. The operation was repeated five times to reach the desired coverage ratio of the stationary liquid and finally dried in a vacuum. The coverage ratio measured with a Soxhlet extractor was 8.2 wt%. Since particles adhered to each other with increase in coverage ratio, it was impossible to increase it further. The coated support was packed into a copper tube of 3 mm i.d. and 3 m in length. The density of natural rubber was measured by the floatation method and found to be 910 kg/m^3.

Solute. Nine kinds of commercial lower olefins and paraffins were used.

Apparatus and Procedure. A KOR-70 gas chromatograph (Gasukuro Kogyo Co.) was used. The mercury manometer was attached to the inlet of the column. Helium was used as a carrier gas, the flow rate of which being kept at 10^{-5} m^3/min. The column temperature differed with sample gases in the range -10—25 °C. A solute gas was injected with a micrometer syringe in the range $(2—5)\times10^{-9}$ m^3 as a vapor.

Usually a gas hold-up can be determined from the retention volume of an inert gas. Nitrogen was used as the inert gas. The retention volume of nitrogen, however, has to be corrected, because of its slight solubility in natural rubber. The solubility coefficient of nitrogen determined by Michaels and Bixler[6] was used for the correction.

When the separation of solute gas and air brought within the sample is not sufficient due to lower solubility of the solute gas, the column temperature falls. In such a case the retention volume at 25 °C was estimated by interpolation using a linear relationship between log V_g and $1/T$.

Results and Discussion

Effect of Sample Size on Retention Volume. The retention volume did not vary with sample size. Thus the partition isotherms of all solute gases examined can be regarded as rectilinear under the experimetal conditions.

Correction for Gas Phase Imperfection. The magnitude of the correction term for gas phase imperfection was examined. v^∞ was taken to be equal to the molar volume of pure liquid v°. A negligible error will result from this approximation. The values of B_m, v° and the correction term at 25 °C are given in Table 1. The second mixed virial coefficient was estimated from the McGlashan-Porter reduced equation[11] using Hudson-McCoubrey's combining rule.[12] The molar volume of pure liquid was estimated from the density using the expansion factor proposed by Watson.[13] It is clear from Table 1 that the contribution of the term of $\exp(-\beta p_o J_3^4)$ to the specific retention volume is insignificant. A considerable error may be incurred by the estimation of physical properties such as B_m and v°. Thus it is more reasonable to ignore this term than to make an uncertain correction.

Comparison with Other Works.[14] The results obtained by neglecting gas phase imperfection are given in Table 1. It can be seen that the solubility coefficient of propane is in good agreement with those obtained independently by van Amerongen[5] and Michaels and Bixler,[6] by means of the volumetric method. For propylene, on the other hand, the value obtained seems to differ somewhat from that presented by Michaels and Bixler. Although it is not clear which is accurate, both values do not differ too greatly from the correlations between the solubility coefficient and the physicochemical properties of gases, as described below.

From the assumption that the dissolution process involves condensation and mixing process, the solubility coefficient can be written as[15]

$$2.303\log S = \frac{L_b}{RT_b}\left(\frac{T_b}{T}-1\right)+2.303 \times \log\frac{22.4\times10^{-3}}{v^\circ} - 1 - \chi,$$

where L_b is the molar latent heat of condensation at boiling temperature T_b, and χ is the interaction parameter. When χ can be taken as constant, a linear relationship is valid between log S and T_b. Moreover,

TABLE 1. SECOND MIXED VIRIAL COEFFICIENTS, LIQUID MOLAR VOLUMES, CORRECTION TERMS, AND SOLUBILITY COEFFICIENTS AT 25 °C

	$10^6 B_m$ / m^3 mol^{-1}	$10^6 v^\circ$ / m^3 mol^{-1}	$\exp(-\beta p_o J_3^4)$	$10^5 S$/m^3 (STP)m^{-3} Pa^{-1}	
				This work[a]	Other works
Ethylene	28	129	1.0038	0.93	
Ethane	30	97	1.0019	1.55	
Propylene	34	83	1.0008	6.01	5.2[b]
Propane	36	90	1.0009	6.19	6.1[b]
					6.4[c]
1-Butene	40	96	1.0008	19.3	
trans-2-Butene	40	94	1.0008	24.2	
cis-2-Butene	39	94	1.0008	28.1	
1-Pentene		110		56.1	
Pentane	46	116	1.0012	61.2	

a) Obtained by neglecting gas phase imperfection. b) A. S. Michaels and H. J. Bixler.[6] c) G. J. van Amerongen.[5]

by applying the Guldberg rule, $T_b/T_c \approx 2/3$, a similar relationship between log S and critical temperature T_c can be derived. For solubility coefficients of gases in vulcanized natural rubber Barrer and Skirrow[16] proposed

$$\log S = -7.0 + 0.007\, T_c \text{ (at 50 °C)};$$

van Amerongen[5] proposed

$$\log S = -7.1 + 0.0074\, T_c \text{ (at 25 °C)}$$

and

$$\log S = -7.1 + 0.0123 T_b \text{ (at 25° C)}.$$

The results obtained are shown in Figs. 1 and 2 together with those by van Amerongen and Michaels and Bixler, the relation of van Amerongen being shown by broken lines. Although there exists a fairly good correlation between log S and T_c or T_b, a slight deviation from the broken lines is found when T_c ot T_b becomes higher. Therefore the relationships may be expressed better by the equations

$$\log S = -7.0 + 0.0030\, T_c^{1.15}$$

and

$$\log S = -7.0 + 0.0071\, T_b^{1.10},$$

which were calculated by least-squares treatment with all data in the figures, where the correlation coefficients are 0.994 and 0.992, respectively. These relations are shown in Figs. 1 and 2 by solid lines.

Michaels and Bixler,[6] on the other hand, proposed the use of the Lenard-Jones force constant ε/k instead of T_c or T_b. The plot is shown in Fig. 3. In this study ε/k determined from viscosity[17] was used.[18] The straight line was calculated by least-squares treatment with all data in the figure:

$$\log S = -7.05 + 0.0105\ (\varepsilon/k),$$

where the correlation coefficient is 0.970.

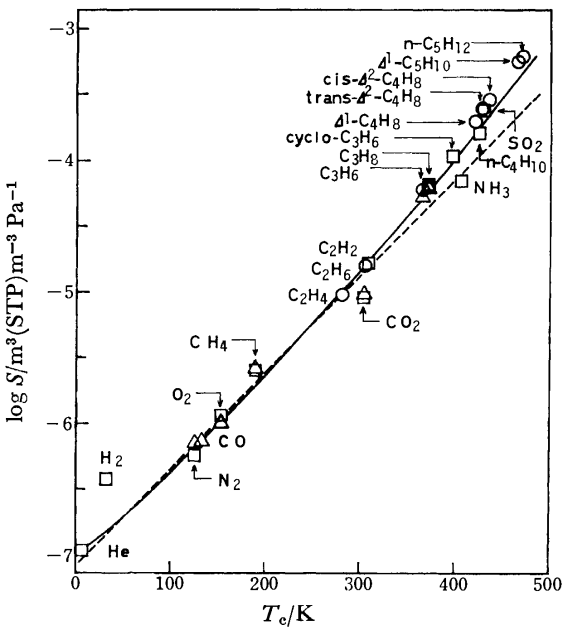

Fig. 1. The relationship between solubility coefficients and critical temperatures.
○: This work, □: Van Amerongen, △: Michaels and Bixler.

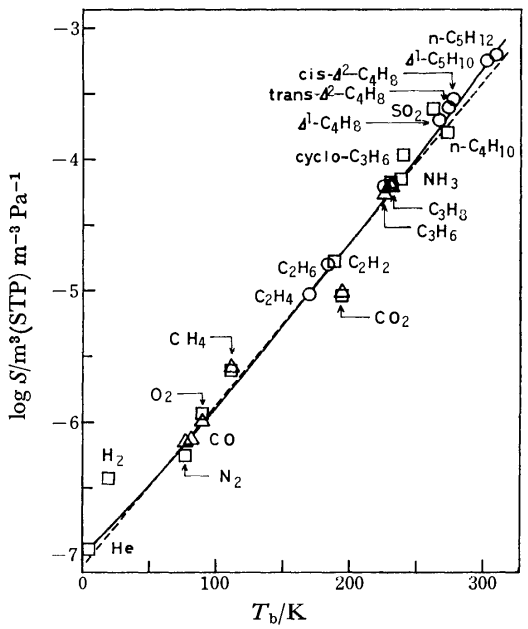

Fig. 2. The relationship between solubility coefficients and boiling temperatures.
○: This work, □: Van Amerongen, △: Michaels and Bixler.

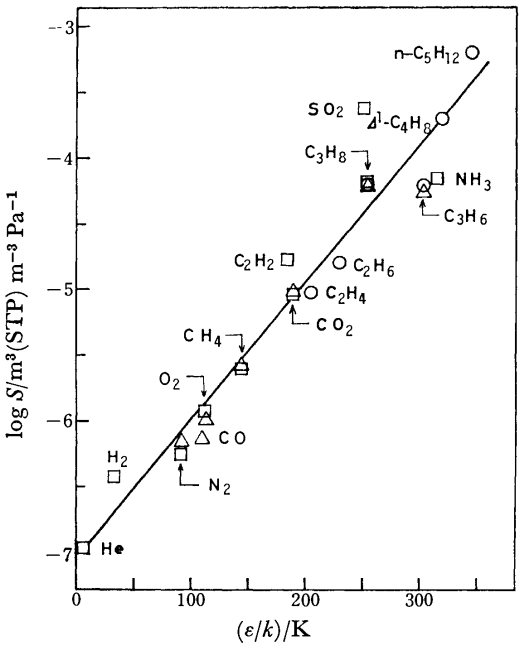

Fig. 3. The relationship between solubility coefficients and Lenard-Jones force constants.
○: This work, □: Van Amerongen, △: Michaels and Bixler.

Thus the values obtained here seem to be reasonable and the relationships are confirmed between log S and T_c, T_b or ε/k.

The solubility coefficients have been measured by the volumetric or gravimetric method. The gas chromatographic technique could be an alternative method, simpler and taking less time than the conventional ones.

References

1) P. E. Porter, C. H. Deal, and F. H. Stross, *J. Am. Chem. Soc.*, **78**, 2999 (1956).
2) R. D. Newman and J. M. Prausnitz, *J. Paint Technol.*, **45**, 33 (1973).
3) N. Takamiya, J. Kojima, and Y. Tomari, *Kogyo Kagaku Zasshi*, **62**, 1371 (1959).
4) M. Kawakami, M. Egashira, and S. Kagawa, *Bull. Chem. Soc. Jpn.*, **49**, 3449 (1976).
5) G. J. van Amerongen, *Rubber Chem. Technol.*, **37**, 1065 (1964).
6) A. S. Michaels and H. J. Bixler, *J. Polym. Sci.*, **50**, 393 (1961).
7) A. I. M. Keulemans, "Gas Chromatography," Reinhold, New York (1962).
8) C. L. Young, *Chromatogr. Rev.*, **10**, 129 (1968).
9) D. H. Everett nad C. T. H. Stoddart, *Trans. Faraday Soc.*, **57**, 746 (1961).
10) A. J. B. Cruickshank, M. L. Windsor, and C. L. Young, *Proc. R. Soc. London, Ser. A*, **295**, 259 (1966).
11) M. L. McGlashan and D. J. B. Porter, *Proc. R. Soc. London, Ser. A*, **267**, 478 (1962).
12) G. H. Hudson and J. C. McCoubrey, *Trans. Faraday Soc.*, **56**, 761 (1960).
13) K. M. Watson, *Ind. Eng. Chem.*, **35**, 398 (1943).
14) The value of the solubility coefficient was converted into SI unit by the authors.
15) G. Gee, *Quart. Rev. Chem. Soc.*, **1**, 265 (1947).
16) R. M. Barrer and G. Skirrow, *J. Polym. Sci.*, **3**, 564 (1948).
17) "Bussei Jyosu 2," ed by The Society of Chemical Engineers, Japan, Maruzen (1964).
18) Michaels and Bixler used ε/k determined from second virial coefficient or by an empirical equation such as $\varepsilon/k = T_c/1.3$.

Emission Spectra of the Vinyl Polymers with Pendant Benzocarbazolyl Groups

Akira ITAYA, Ken-ichi OKAMOTO, and Shigekazu KUSABAYASHI

Department of Chemical Engineering, Faculty of Engineering, Yamaguchi University, Tokiwadai, Ube 755

(Received June 13, 1977)

The emission spectra of poly(*N*-vinyl-5*H*-benzo[*b*]carbazole) (PV5BCz) and poly(*N*-vinyl-7*H*-benzo[*c*]-carbazole) (PV7BCz), which are prepared by radical and cationic polymerization, and their monomeric model compounds were investigated in solutions. In the case of PV7BCz, the fluorescence spectra were composed of a second excimer fluorescence at the shorter wavelength and a sandwich-like excimer fluorescence at the longer wavelength. The difference in the spectra between the radical and cationic polymers was quite similar to that of the poly(*N*-vinylcarbazole) (PVCz) system. The intensity of the sandwich-like excimer fluorescence was independent of the polymerization methods, but the intensity of the second excimer fluorescence increased with an increase in the content of the syndiotactic sequence. In the case of PV5BCz, the behavior of the fluorescence spectra of the radical polymers was similar to that of the PVCz and PV7BCz systems. On the other hand, the fluorescence spectra of the cationic polymers differed markedly from those of the above-mentioned polymers. The cationic polymers did not show the second excimer fluorescence, but a monomer-like structured fluorescence, at the shorter wavelength, although it did show the sandwich-like excimer fluorescence at the longer wavelength. This significant difference in the fluorescence spectra between the radical and cationic polymers is attributable to the difference between their tacticities. On the basis of these results, the characteristics of the second excimer site were further clarified.

In recent years there has been a growing interest in the emission spectra of aromatic vinyl polymers. It is known that aromatic vinyl polymers show excimer fluorescence in dilute solutions. Considerable data on the emission properties of poly(*N*-vinylcarbazole) (PVCz) have been accumulated because of an interest in high photoconductive polymers.[1-8] The monomeric model compound, *N*-ethylcarbazole (ECz), shows no excimer fluorescence in either a concentrated solution or a solid state.[5] The PVCz, both in solution and in film, shows one broad fluorescence, which is composed of not only one component, but of two components. The broad emission at the longer wavelength (ν_{max}; *ca.* 23900 cm^{-1}) is assigned to the sandwich-like excimer fluorescence. On the other hand, the assignment of the broad emission in the shorter-wavelength region (ν_{max}; *ca.* 27000 cm^{-1}) is controversial because of both the absence of the structure and the large Stokes-shift. David *et al.*[3] and Yokoyama *et al.*[5] have assigned this shorter-wavelength band to the monomer fluorescence for PVCz in solution. P. C. Johnson and Offen,[2] and Powell and Venikouas[6] have assigned it to the emission from a dimer trap site for PVCz films. On the other hand G. E. Johnson[4] has recently assigned it to the second excimer fluorescence for PVCz in solution. Klöpffer and Bauser[8] have also assigned it to the second, more weakly bound excimer fluorescence for PVCz films.

We have reported, on the basis of the NMR spectra and glass transition temperature of PVCz, that the samples prepared by the radical polymerization have higher syndiotacticities than the samples prepared by the cationic one.[9] We have also reported that this difference in tacticity between the radical and cationic polymers is reflected in the fluorescence spectra both in solution and in film, and that the broad emission at the shorter wavelength should be assigned to the second excimer fluorescence,[7] as has been proposed by Johnson and Klöpffer.[4,8] It has also been suggested that the second excimer site, where only one benzene ring in each of the neighboring carbazolyl chromophores overlaps with another, is formed only in the syndiotactic sequence.[7]

Spectroscopic studies of vinyl polymers with aromatic chromophores, which are more bulky than a carbazolyl chromophore, make the above-mentioned suggestion clearer. We have synthesized poly(*N*-vinyl-5*H*-benzo-[*b*]carbazole) (PV5BCz), poly(*N*-vinyl-7*H*-benzo[*c*]-carbazole) (PV7BCz). From the NMR spectra, the glass transition temperatures, and the solubility of the polymers, it has already been found that the stereoregularity of these polymers depends on the polymerization method, as is the case in PVCz.[9]

Concerning the vinyl polymers with small aromatic chromophores, the relation between the tacticity of the polymer chain and the fluorescence spectrum has been reported on in several investigations. For polystyrene (PS),[10-12] poly(α-methylstyrene),[13] and poly(*p*-methylstyrene),[14] it has been reported that the ratio of the sandwich-like excimer to the monomer fluorescence intensity, I_E/I_M, for the isotactic polymer is larger than that for the atactic polymer, although an opposite experimental result for PS has also been reported.[10] Y.-C. Wang and H. Morawetz have found, from the NMR and fluorescence spectra of polyacenaphthylene, that the polymers prepared by cationic and radical polymerizations have different configurations, and that this is reflected in the ease with which they form excimers.[15] However, to the knowledge of the present authors, such a relation has never hitherto been studied for the vinyl polymers with large and bulky aromatic chromophores such as benzocarbazole.

In the present investigation, we have investigated the spectroscopic behavior of PV5BCz, PV7BCz, and their monomeric model compounds (*N*-ethyl-5*H*-benzo[*b*]-carbazole(E5BCz) and *N*-ethyl-7*H*-benzo[*c*]carbazole (E7BCz)) and discussed the relation between the tacticity of the polymer chain and the emission spectra.

Experimental

The vinyl polymers (PV5BCz and PV7BCz) were prepared by the methods described previously.[9] The model compounds

(E5BCz and E7BCz) were obtained by the alkylation of benzocarbazole with diethyl sulfate. The E5BCz was recrystallized twice from ethanol and subsequently sublimed *in vacuo* (mp; 149—150 °C). The E7BCz was isolated by column chromatography (silica gel, benzene : hexane=1 : 2) and was recrystallized twice from methanol (78.5—80.0 °C). All of the solvents used were purified by the usual methods.

The solutions were completely degassed by freeze-pump-thaw cycles if necessary.

The emission spectra and fluorescence-decay times were measured with the apparatus described in a previous paper.[7]

Results and Discussion

The materials used for the present investigation are listed in Table 1. The $I_{H/L}$ value in Table 1 is a measure of the amount of the isotactic sequence relative to the syndiotactic one of the polymer, as is described in Ref. 9. The PV7BCz(c)-III has the largest isotactic sequence, and the free-radical polymer, the smallest.

TABLE 1. CHARACTERIZATION OF MATERIALS USED

Sample	Polymerization[a] temp/°C	Degree of polymerization[b]	$I_{H/L}$[c]
E7BCz	—	—	—
PV7BCz(r)	+75	58	0.32
PV7BCz(c)-I	−78	103	0.51
PV7BCz(c)-II	−40	82	0.68
PV7BCz(c)-III	+10	36	0.92
E5BCz	—	—	—
PV5BCz(r)-I	+100	49	—
PV5BCz(r)-II	+80	13	—
PV5BCz(c)	−78	8	—

a) Initiator; (r): AIBN, (c): BF_3OEt_2. Solvent; none for PV5BCz(r)-I, and toluene for the others. b) The polymer molecular weights were determined by means of a vapor-pressure osmometer. c) The $I_{H/L}$ value is the intensity ratio of the higher-field peak to the lower-field one for the methine proton in the NMR spectra. This value for PV5BCz cannot be obtained because of the highly unresolved NMR spectra.

Absorption Spectra. The absorption spectra in 1,2-dichloroethane solutions are shown in Fig. 1. The absorption bands of the polymers are shifted to frequencies higher by *ca.* 200 cm^{-1} as compared with those of the model compounds. This higher-frequency shift is characteristic for polymers of *N*-vinyl compounds with large π-electronic chromophores. Both the decrease in the intensity (or hypochromism) and the spectral change in the ^1B_b and ^1B_a bands of the polymers, as compared with the spectra of the corresponding monomeric model compounds, are similar to what has been observed for PVCz.[16] The degree of the hypochromism is in the order of PV5BCz(r)-I≈PVCz >PV7BCz(r)>PV5BCz(c).

Fluorescence Spectra of E7BCz and PV7BCz. The fluorescence spectra of E7BCz and PV7BCz are shown in Fig. 2. The E7BCz shows no excimer fluorescence even in concentrated solutions up to 0.1 M, as is the case of ECz. The polymers show one broad fluorescence

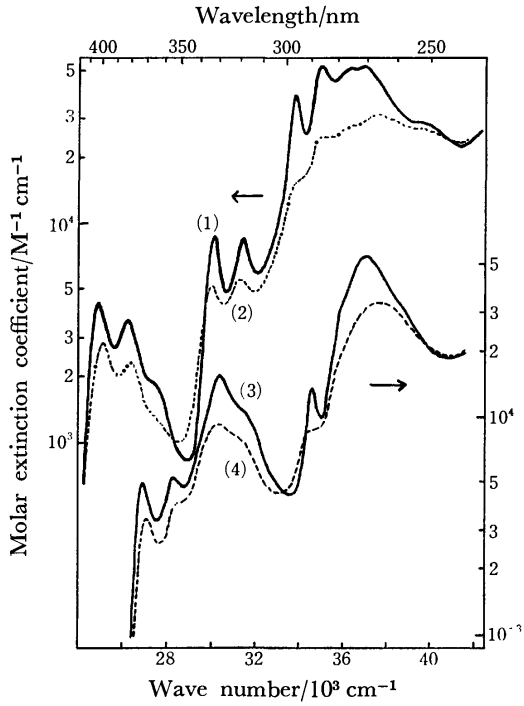

Fig. 1. Absorption spectra of (1) E5BCz, (2) PV5BCz-(r)-I, (3) E7BCz, and (4) PV7BCz(r) in 1,2-dichroloethane solutions at room temperature.

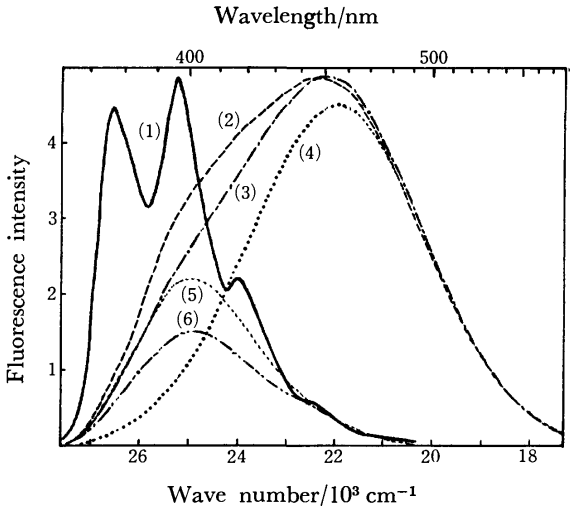

Fig. 2. Fluorescence spectra and their resolution spectra of E7BCz, PV7BCz(r), and PV7BCz(c)-I in MTHF-THF degassed solutions at room temperature. Optical densities of both the polymers at excitation wavelength (350 nm) are 0.249. Fluorescence spectra: (1)——: E7BCz, (2)——, PV7BCz(r), and (3)———: PV7BCz-(c)-I. Resolution spectra: (4)……: the component of the sandwich-like excimer fluorescence of PV7BCz(r) and PV7BCz(c)-I. (5)----, and (6)———: the component of the second excimer fluorescence of PV7BCz-(r) and PV7BCz(c)-I, respectively.

which is composed of two components, as in the case of PVCz. That is, the spectra were successfully resolved into two broad spectral bands with peaks of 21950 and 24900 cm^{-1} on the assumption that the location of the longer-wavelength band in solution was the same as that in film. The energy differences be-

tween the peaks of these two bands and the 0-0 fluorescence band (26560 cm^{-1}) of the E7BCz are 4610 and 1660 cm^{-1}. These are almost the same as the corresponding energy differences between PVCz and ECz (4630 and 1630 cm^{-1}). The fluorescence excitation spectra of the polymers, obtained by monitoring at several wavelengths (390—500 nm), duplicate the absorption spectra of these solutions exactly. By analogy with the fluorescence spectrum of PVCz, the fluorescence bands at the longer wavelength and at the shorter one can be assigned to the sandwich-like excimer fluorescence and the second excimer one respectively. Figure 2 shows that the concentrations of the sandwich-like excimer site are nearly equal between the radical and cationic polymers, and that the concentration of the second excimer site is larger for the radical polymer than for the cationic polymer by a fac tor of about 1.4. That is, the difference in the fluorescence spectra between these two polymers seems to be attributable to the difference in the concentration of the second excimer site.

The $I_{H/L}$ and $\overline{DP}$ of the cationic polymers vary remarkably with the polymerization temperature (Table 1).[9] This result is different from that for PVCz.[9] Thus, the fluorescence spectra of PV7BCz samples in aerated solutions (5.9×10^{-5} M) at room temperature were compared with one another in Fig. 3. The second excimer fluorescence intensities are in the order of (r)> (c)-I>(c)-II>(c)-III. This order is not correlated to the molecular weight of the polymers, but to the decrease in the $I_{H/L}$ value. That is, the concentration of the second excimer site increases with an increase in the syndiotactic sequence.

The sandwich-like excimer fluorescence of each PV7BCz sample has a constant intensity at temperatures from *ca.* −110 to 20 °C, as is shown in Fig. 4. At temperatures above *ca.* 20 °C, the intensity of the sandwich-like excimer fluorescence decreases and the intensity of the second excimer fluorescence increases with

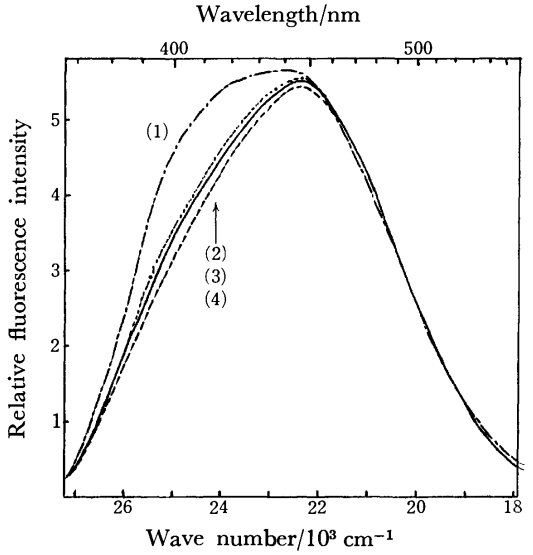

Fig. 3. Fluorescence spectra of (1) PV7BCz(r), (2) PV7-BCz(c)-I, (3) PV7BCz(c)-II, and (4) PV7BCz(c)-III in MTHF-THF aerated solutions at room temperature. Excitation wavelength; 350 nm.

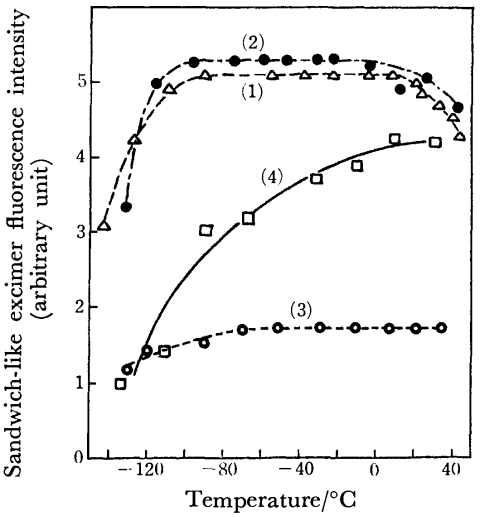

Fig. 4. Temperature dependence of the sandwich-like excimer fluorescence intensity. (1)-△-: PV7BCz(r), (2)-●-: PV7BCz(c)-I, (3)-○--: PV5BCz(r)-II, and (4)-□-: PV5BCz(c).

an increase in the temperature. This phenomenon is also observed for PVCz.[4] This behavior and the presence of the long-lived component decay at the shorter wavelength (*vide infra*) indicate the presence of sandwich-like excimer dissociation to give back the second excimer.

The above-mentioned results with regard to the concentrations of the sandwich-like excimer site and the second excimer one may be qualitatively explained as follows. If we consider only a part of the syndiotactic sequence in the polymer chain, both the concentration of the second excimer site and that of the sandwich-like excimer site are larger for the radical polymers than for the cationic polymers, because a photodynamic equilibrium between the second excimer and the sandwich-like excimer is established. However, the concentration of the sandwich-like excimer site formed in the isotactic sequence, which cannot form the second excimer site, is larger for the cationic polymers than for the radical polymers. Therefore, a clear difference in the concentrations of the second excimer sites between the radical and cationic polymers is observed, although no clear difference in the concentrations of the sandwich-like excimer sites is observed.

The presence of two kinds of emitting species in the fluorescence was also clarified by measuring the fluorescence-decay times of the polymers. The fluorescence-decay curves of the polymers at room temperature are multi-component in the shorter-wavelength region (36±2 ns and initial fast decay), while they are one-component (36±2 ns) in the longer-wavelength region. The long-lived component corresponds to the sandwich-like excimer fluorescence.

The spectral band of the polymers in rigid glass solutions at 77 K is shifted to a lower frequency and broadened as compared with that of E7BCz, as is shown in Fig. 5. This deviation from the monomer-like fluorescence band shape seems to be attributable to a large contribution of the second excimer fluorescence. In the case of the PVCz samples,[7] the cationic

TABLE 2. FLUORESCENCE LIFETIME[a)]

Sample	Monomer[b)]	Monomer-like[c)]	Second excimer[c)]	Sandwich-like excimer[d)]
i-PCz	17±2	—	—	—
PVCz(c)	—	19±2	—	45±1
PVCz(r)	—	17±2	17±2	45±1
E7BCz	13±1	—	—	—
PV7BCz(c)	—	(13)[e)]	25±3	36±2
PV7BCz(r)	—	(13)[e)]	25±1	36±2
E5BCz	24±1	—	—	—
PV5BCz(c)	—	23±2	—	57±3
PV5BCz(r)	—	26[e)]	65—75	57±3

a) Unit; ns. Solvent: MTHF-THF degassed solution. b) At room temperature and 77 K. c) At 77 K. d) At room temperature. e) See text.

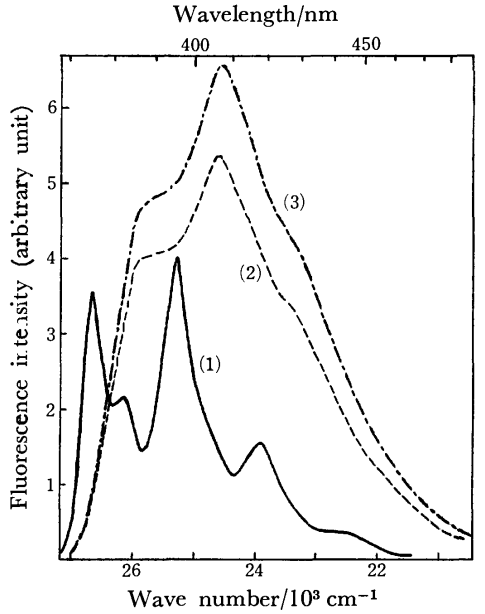

Fig. 5. Fluorescence spectra of (1) E7BCz, (2) PV7BCz-(r), and (3) PV7BCz(c)-I in MTHF-THF rigid glasses at 77 K. Excitation wavelength; 350 nm.

polymer shows a monomer-like structured fluorescence, while the radical polymers shows mainly the second excimer fluorescence. The fluorescence decay times of both the PVCz samples (λ_{obsd}=355—390 nm) are approximately the same as that measured for *N*-isopropylcarbazole (17±2 ns), although a slight departure from a strict first-order decay is observed (Table 2). This fact indicates that the lifetime of the second excimer fluorescence seems to be nearly equal to that of the monomer-like fluorescence. In the case of the PV7BCz samples, the fluorescence decay times of both the polymers at 380 nm are *ca.* 18 ns, while those at the longer wavelength (λ>400 nm) are 25±2 ns. The decay curves are roughly single-exponential. This lifetime (25 ns) is not in agreement with those of the monomeric fluorescence of the model compound (13 ns) and the sandwich-like excimer fluorescence (36 ns). When (at 77 K) the formation of the sandwich-like excimer site from the second excimer site is impossible, this lifetime may correspond to that of the second excimer fluorescence. The decay time (18 ns) at 380 nm seems to be an apparent value due to an overlap of the monomer-like fluorescence and the second excimer one.

Fluorescence Spectra of E5BCz and PV5BCz. The fluorescence spectra of E5BCz and PV5BCz are shown in Fig. 6. The E5BCz shows no excimer fluorescence even in concentrated solutions up to 0.1 M, as is also the case with ECz and E7BCz. The radical polymers show one broad fluorescence, the spectra of which were successfully resolved into two broad bands, with peaks of 20350 and 22550 cm^{-1}, in a manner similar to that in PV7BCz. The energy differences between the peaks of these two bands and the 0-0 fluorescence band (24330 cm^{-1}) of E5BCz are 3980 and 1780 cm^{-1} respectively. The fluorescence excitation spectra of the polymers duplicate exactly the absorption of these solutions. Therefore, the fluorescence bands at the longer and shorter wavelengths can be assigned to the sandwich-like excimer fluorescence and the second excimer one respectively.

The temperature dependence of the fluorescence spectrum of the PV5BCz(r)-II sample is shown in Fig. 7. As may be seen, there is no evidence for the formation of an isoemissive point. The sandwich-like excimer fluorescence has a constant intensity over the temperature range from *ca.* —70 to 40 °C, as is shown in Fig. 4. These phenomena observed for the radical polymers are quite similar to those observed for the PVCz and PV7BCz.

On the other hand, the fluorescence spectrum of the cationic polymer differes markedly from those of the

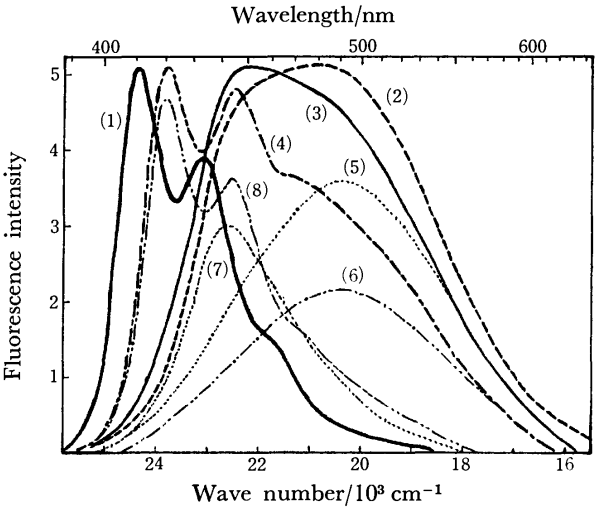

Fig. 6. Normalized fluorescence spectra and their resolution spectra of E5BCz, PV5BCz(r)-I, PV5BCz(r)-II, and PV5BCz(c) in MTHF-THF degassed solutions at room temperature. Excitation wavelength; 350 nm. Fluorescence spectra: (1)——: E5BCz, (2)----; PV5BCz(r)-I, (3)——; PV5BCz(r)-II, and (4)——; PV5BCz(c). Resolution spectra: (5)·····, and (6) ——: the component of the sandwich-like excimer fluorescence of PV5BCz(r)-II and PV5BCz(c), respectively. (7)·····: the component of the second excimer fluorescence of PV5BCz(r)-II, and (8)——; the component of the monomeric fluorescence of PV5BCz-(c).

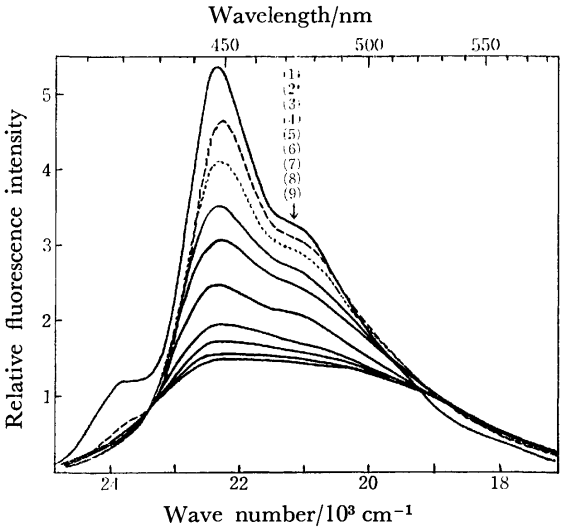

Fig. 7. Temperature dependence of the fluorescence spectra of PV5BCz(r)-II in MTHF-THF degassed solution. Excitation wavelength; 350 nm. (1) 143.5 K, (2) 163 K, (3) 203.5 K, (4) 222 K, (5) 244 K, (6) 263 K, (7) 281 K, (8) 294.5 K, and (9) 308 K.

above-mentioned polymers: (1) The monomer-like structured fluorescence (0-0; 23800 cm^{-1}) in the shorter-wavelength region is observed clearly even at room temperature, while the second excimer fluorescence is not observed, as is shown in Fig. 6. (2) An isoemissive point is clearly observed, as is shown in Fig. 8. (3) The intensity of the sandwich-like excimer fluorescence in the longer-wavelength region increases with an increase in the temperature up to *ca.* 20 °C, as is also shown in Fig. 4.

A dilute fluid solution of a *N*-vinylcarbazole oligomer ($\overline{DP}=10$) at room temperature does not show any structured fluorescence at the shorter wavelength, but a broad fluorescence which is composed of two excimer fluorescences. Therefore, these three significant differences in the fluorescence spectra between the radical and cationic polymers seem not to be attributable to any difference in the molecular weight, but to the difference in their tacticities. This explanation seems also to be supported by the polymerization results: the cationic polymer is considered to be composed of only an isotactic sequence, judging from the fact that only low-molecular-weight polymers are obtained almost quantitatively in high yields. The radical polymers are composed of stereoblock arrangements of the isotactic and syndiotactic helixes.[9] Therefore, the above-mentioned discussion supports the idea that the second excimer site is not formed within the isotactic sequence, but only within the syndiotactic sequence.

The fluorescence-decay curves of both the radical and cationic polymers at room temperature are multicomponent in the shorter-wavelength region (57±3 ns and an initial fast decay), while there is only one component with a long lifetime (57±3 ns) in the longer-wavelength region. The long-lived component corresponds to the sandwich-like excimer fluorescence.

Figure 9 shows the fluorescence spectra of PV5BCz and E5BCz in rigid glass solutions at 77 K. The fluorescence spectra of the cationic polymer is mainly composed of a monomer-like fluorescence, the lifetime of which at 420 nm was 23±2 ns. This is the same value as the decay time of E5BCz. On the other hand, the fluorescence spectra of the radical polymers are markedly broadened as compared with that of the cationic polymer. This fluorescence is mainly emitted from the excited monomer state and the second excimer site, although the fluorescence from the sandwich-like excimer site is slightly involved. The fluorescence lifetime at 410 nm, a wavelength where the fluorescence was mainly emitted from the excited monomer state,

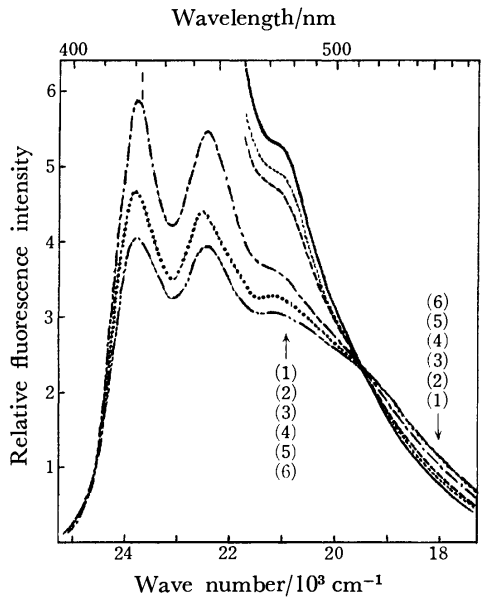

Fig. 8. Temperature dependence of the fluorescence spectra of PV5BCz(c) in MTHF-THF degassed solution. Excitation wavelength; 350 nm. (1) 183.5 K, (2) 202.5 K, (3) 221 K, (4) 262.5 K, (5) 282 K, and (6) 304 K.

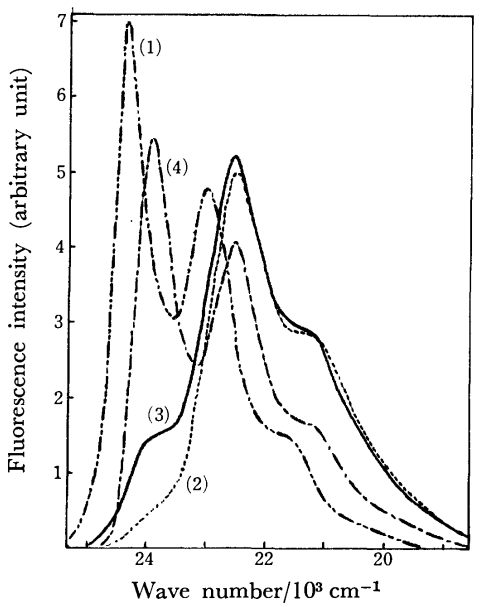

Fig. 9. Fluorescence spectra of (1) E5BCz, (2) PV5BCz-(r)-I, (3) PV5BCz(r)-II, and (4) PV5BCz(c) in MTHF-THF rigid glasses at 77 K. Excitation wavelength; 350 nm.

is *ca.* 26 ns, which is nearly equal to that of E5BCz. The fluorescence decay curves show a departure from the strict exponential decay, with an initial fast component followed by a long tail whose decay constant was 65—75 ns. The ratio of the short-lived component to the long-lived one in the shorter-wavelength region is larger than that in the longer-wavelength region. Therefore, this long-lived component decay may correspond to the lifetime of the second excimer fluorescence of PV5BCz (Table 2).

When we compare the fluorescence spectrum of the PV5BCz(r)-II sample in a polycrystalline 1,2-dichloroethane (fp: −36 °C) matrix at 77 K with the spectrum in a MTHF–THF fluid solution at −29 °C, the concentration of the second excimer site in the matrix turns out to be larger than that in the fluid solution, as is shown in Fig. 10. This is attributable to be impossibility of rotational motion from the second excimer site to the sandwich-like excimer site in the polycrystalline matrix. On the other hand, the cationic sample does not form the second excimer site even under such favorable conditions as the polycrystalline 1,2-dichloroethane matrix. Thus, it may be suggested that the second excimer site is not formed within the isotactic sequence, even under favorable conditions.

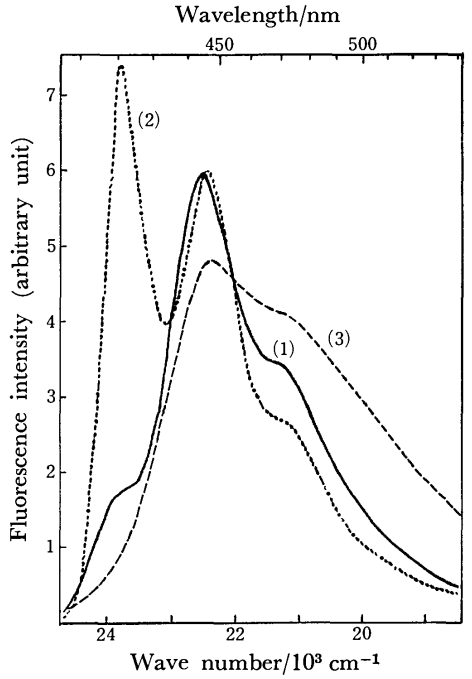

Fig. 10. Fluorescence spectra of (1) PV5BCz(r)-II and (2) PV5BCz(c) in polycrystalline 1,2-dichloroethane matrixes at 77 K. The fluorescence spectra of (3) PV5BCz(r)-II in MTHF-THF fluid solution at −29 °C was also given for comparison.

From the above-mentioned results and discussion, it has further been clarified that the second excimer site is formed only within the syndiotactic sequence. That is, the second excimer site is formed in the conformational state with the lowest energy and the shortest distance between neighboring chromophores in the syndiotactic sequence. Its structure seems to be the overlap of only one benzene ring between the neighboring chromophores, as has been suggested for PVCz.[7]

The present work was partially supported by a Grant-in-Aid for Scientific Research from the Ministry of Education.

References

1) W. Klöpffer, *J. Chem. Phys.*, **50**, 2337 (1969).
2) P. C. Johnson and H. W. Offen, *J. Chem. Phys.*, **55**, 2945 (1971).
3) C. David, M. Piens, and G. Geuskens, *Eur. Polym. J.*, **8**, 1291 (1972).
4) G. E. Johnson, *J. Chem. Phys.*, **62**, 4697 (1975).
5) M. Yokoyama, T. Tamamura, M. Atsumi, M. Yoshimura, Y. Shirota, and H. Mikawa, *Macromolecules*, **8**, 101 (1975).
6) G. W. Venikouas and P. C. Powell, *Chem. Phys. Lett.*, **34**, 601 (1975).
7) A. Itaya, K. Okamoto, and S. Kusabayashi, *Bull. Chem. Soc. Jpn.*, **49**, 2082 (1976); *ibid.*, **50**, 22 (1977).
8) W. Klöpffer and H. Bauser, *Z. Phys. Chem. N. F.*, **101**, 25 (1976).
9) K. Okamoto, M. Yamada, A. Itaya, T. Kimura, and S. Kusabayashi, *Macromolecules*, **9**, 645 (1976).
10) M. T. Vala, J. Haebig, and S. R. Rice, *J. Chem. Phys.*, **43**, 886 (1965).
11) J. W. Longworth, *Biopolymers*, **4**, 1131 (1966).
12) T. Ishii, H. Matsushita, and H. Handa, *Kobunshi Ronbunshu*, **32**, 311 (1975).
13) H. Odani, *Bull. Inst. Chem. Res. Kyoto Univ.*, **51**, 351 (1973).
14) T. Ishii, H. Matsushita, and H. Handa, *Makromol. Chem.*, **177**, 283 (1976).
15) Y. -C. Wang and H. Morawetz, *Makromol. Chem. Suppl.*, **1**, 283 (1975).
16) K. Okamoto, A. Itaya, and S. Kusabayashi, *Chem. Lett.*, **1974**, 1167.

Analysis of Thermal Desorption Curves for Heterogeneous Surfaces. I. A Linear Variation of the Activation Energy of Desorption

Yasuo Tokoro, Makoto Misono, Toshio Uchijima, and Yukio Yoneda

Department of Synthetic Chemistry, Faculty of Engineering, The University of Tokyo, Hongo, Bunkyo-ku, Tokyo 113

(Received June 17, 1977)

This paper deals with the analysis of the desorption curves for heterogeneous surfaces, where the activation energy of desorption, E_d, linearly depends on surface coverage, θ, *i.e.*, $E_d = E_d^0 + \alpha(1-\theta)$. Computer simulation resulted in a characteristic change of curve shapes corresponding to the variation of desorption rate parameters, E_d^0, A, and α. By means of empirical parameters characterizing the peak shapes such as peak temperature, half width and symmetry factor, we were able to obtain a set convenient and valid equations for estimating the rate parameters. The curve fitting method was also investigated and found to be more precise, the equations obtained being very useful for giving an initial set of values for this method. The two methods were applied to the thermal desorption curves of CO_2 on TiO_2, and found to be useful and reliable.

The thermal desorption technique, employing a continuous rise of temperature, has been widely used for studies of chemisorbed states on metal surfaces. Thermal desorption curves have been discussed in terms of the reaction order and the activation energy of desorption from the different surface sites or crystal planes.

The technique has been getting familiar in the field of catalysis on oxides and others. The variations of temperature, area and number of the thermal desorption peaks before and after certain treatments and/or chemical reactions were studied, and discussed qualitatively in relation to the nature of reaction sites and the reaction mechanism. Halpern and Germain[1] have reported interesting results in which the values of activation energy obtained from the thermal desorption curves of oxygen on transition metal oxides are correlated to the catalytic activities for oxidation on the oxides. Although their method for analysis is not so reliable, this kind of application is of interest from the viewpoint of characterization of catalysts.

The thermal desorption curves usually show some multiple peaks and complicated shapes, which is supposed to be due to surface heterogeneity, induced or intrinsic. The surface heterogeneity is expected to play an important role in catalysis. It is desirable to express the desorption energy as a function of surface coverage by quantitative analysis of the thermal desorption curves.

The analyses for homogeneous surface have been reported by Redhead,[2] Cvetanović, and Amenomiya[3] and Lord and Kittelberger.[4] An accurate method, discussed in detail by Cvetanović, is to compare the shifts of the peak maximum temperatures, T_m, of the thermal desorption curves with widely differing heating rates, β, where the slope of $\ln(T_m^2/\beta)$ against T_m gives the activation energy of desorption E_d for the first order desorption.

There are a few reports on the analysis of thermal desorption curves for heterogeneous surface. Hobert and Knappe[5] simulated the desorption curves in the case where E_d changes linearly with coverage. Dawson and Peng[6] assumed the same kind of heterogeneity for the λ state nitrogen on tungsten surface, and determined the rate parameters by the curve fitting method, but there remains a problem about the uniqueness of their solution.

We have investigated how the shapes of the desorption curves change by varying the rate parameters widely and systematically in the heterogeneous case where E_d decreases linearly with coverage. The variation of rate parameters leads to the characteristic change of the curve shapes. In turn, the empirical curve parameters can be correlated well with the rate parameters. The relation gives convenient equations to estimate the rate parameters from experimental desorption curves. The curve fitting method was also examined to determine the rate parameters on the heterogeneous surface with the linear variation of the activation energy of desorption. The analyses were verified to be useful and reliable by applying them to the thermal desorption curves of carbon dioxide on titanium dioxide.

Calculations

In the case where a single adsorbed state exists and no readsorption occurs, the desorption rate is expressed by

$$-d\theta/dT = (A(\theta)/\beta)\cdot\theta^n\cdot\exp(-E_d(\theta)/RT), \quad (1)$$

where β is the heating rate ($T = T_0 + \beta t$), θ the surface coverage, *i.e.*, the fraction of the adsorbed species remaining on the surface, n the order of desorption, $A(\theta)$ the frequency factor and $E_d(\theta)$ the activation energy of desorption. In a flow system for thermal desorption, the left side term of Eq. 1 is equivalent to the partial pressure or concentration of desorbed molecules normalized by the experimental constants such as the saturated amount of adsorption, the catalyst volume and the carrier gas flow rate.[3]

In the present paper, we deal with the simple case in which desorption follows the first order kinetics and surface heterogeneity is reflected only in the activation energy of desorption, *i.e.*, $A(\theta)$ is independent of θ, and $E_d(\theta)$ changes with θ as follows:

$$E_d = E_d^0 + \alpha(1-\theta). \quad (2)$$

This indicates that the activation energy of desorption has a value of E_d^0 at saturation coverage and increases with desorption in proportion to $(1-\theta)$. Equation 1, in which $E_d(\theta)$ is given by Eq. 2, is an ordinary differential equation, which can be solved numerically for different sets of values of A/β, E_d^0 and α. Though β is an experimental parameter independent of A, the reciprocal of β makes an essentially equivalent contribu-

tion in Eq. 1. Thus A/β is treated as an independent parameter. Calculations were carried out to simulate the thermal desorption curve with A/β from 10^8 to 10^{16} K^{-1} at 10^2 K^{-1} intervals, E_d^0 from 10 to 45 kcal*/mol in increments of 5 kcal/mol and α from 0 to 20 kcal/mol in increments of 5 kcal/mol. The starting values of T and θ in the calculation were usually 100 K and 1.0, respectively. The value of A is expected to be close to $h/kT \approx 10^{13}$ s^{-1} according to the simple rate theory, but it was changed in the wide range above, the reported values of A for desorption being scattered in the range 10^4—10^{16} s^{-1}.[3] Calculations were made on a HITAC 8700/8800 computer. The simulated curves, $-d\theta/dT$ *vs.* T, will be shown in the later section.

Experimental

The thermal desorption curves were obtained by linear temperature increase of the sample using a thermal conductivity cell as a detector. The sample was titanium dioxide (Junsei Kagaku Co.), which had been calcined for 5 h at 500 °C in the air. The pre-adsorption was carried out by letting low pressure carbon dioxide in He flow through the sample bed at room temperature. The gases desorbed from the sample into the carrier gas stream were confirmed to consist of only carbon dioxide with a quadrupole mass spectrometer.

Results and Discussion

Estimation of Rate Parameters. Some simulated curves with a wide range of values of A/β, E_d^0, and α are shown in Fig. 1. The effect of A/β on the curves when E_d^0 and α remain constant is given in Fig. 1(a); as the value of A/β decreases, peak temperature shifts to a higher one, and peak width becomes broader. As the value of E_d^0 increases when A/β and α are constant, the peak shifts to higher temperature, and its width becomes slightly broader (Fig. 1(b)). The effect of α on the curves when A/β and E_d^0 are kept constant is given in Fig. 1(c). With increase in the value of α, the peak temperature does not change so much but its shape changes remarkably into a broad and flat one. The behavior is in accord with the results of Hobert and Knappe.[5]

The temperature and shape of the peak are characteristic of a set of values of A/β, E_d^0 and α. This, in turn, affords the possibility that the rate parameters A/β, E_d^0, and α can be determined from the experimental desorption curves, if we choose adequate empirical parameters which characterize their peak shapes.

The peak maximum temperature T_m, the half width D and the symmetry factor γ were chosen as the parameters. The parameter γ is defined as the ratio of the area after and before the peak maximum, and is equivalent to $\theta_m/(1-\theta_m)$, where θ_m is the surface coverage at the peak maximum temperature.

Thermal desorption curves can take almost the same value of T_m with multiple sets of different values of A/β, E_d^0 and α as shown in Table 1. The rate parameters A/β, E_d^0, and α can not be analytically determined by only one empirical parameter, *e.g.* T_m. The effect of the rate parameters on the curves leads to the following results.

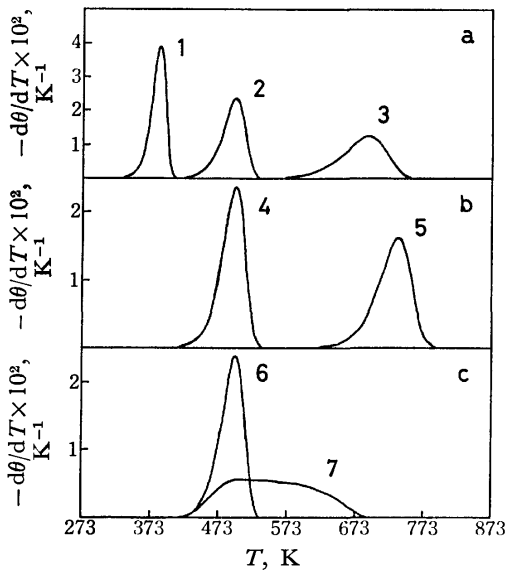

Fig. 1. Simulated thermal desorption curves with various rate parameters. Desorption was treated with the first order kinetics. Numbers in the figures correspond to the rate parameters listed below.

Curve	No.	$\log(A/\beta)$[a]	E_d^0[b]	α[c]
a	1	16	30	0
	2	12	30	0
	3	8	30	0
b	4	12	30	0
	5	12	45	0
c	6	12	30	0
	7	12	30	10

a) A/β, K^{-1}. b) kcal/mol. c) kcal/mol.

Table 1. Comparison of calculated peak maximum temperatures with different sets of rate parameters

T_m[a]	E_d^0[b]	α[c]	$\log(A/\beta)$[d]
601	40.0	20.0	14.0
601	31.1	5.0	9.9
601	25.0	10.0	8.1
600	35.1	15.1	12.1

a) K. b) kcal/mol. c) kcal/mol. d) A/β, K^{-1}.

T_m changes approximately in proportion to the value of E_d^0 and in inverse proportion to that of $\log(A/\beta)$. The plot, T_m *vs.* $E_d^0/\log(A/\beta)$ gives a roughly linear relation. In the same way, D can be related proportionally to $\alpha/\log(A/\beta)$, and γ to $\alpha\log(A/\beta)/E_d^0$.

These relations hold only roughly with a wide range of values of the rate parameters, and should be refined by introducing other rate parameters and constants. For this, we take the following equations:

$$T_m = (a_1E_d^0 + a_2\alpha + a_3)/\log(A/\beta) + a_4, \quad (3)$$

$$D' = (D/T_m^{0.1})^{1.2} = (b_1E_d^0 + b_2\alpha + b_3)/\log(A/\beta) + b_4, \quad (4)$$

$$\gamma = (c_1\alpha\log(A/\beta) + c_2\alpha + c_3)/E_d^0 + c_4. \quad (5)$$

* 1 cal_{th}=4.184J.

Equation 3 and 4 have the same from, but the coefficients of E_d^0 and α differ a great deal from each other. D' in Eq. 4 is used instead of D for correcting the regular deviation from the linear relation in the range of higher T_m. The coefficients of these equations were determined by the least square method. Their values are given in Table 2.

T_m, D', and γ are plotted in Figs. 2, 3, and 4, respectively, against the right side terms of Eqs. 3, 4, and 5 calculated by use of the coefficients in Table 2. The figures show satisfactory straight lines in the range of the given values of the rate parameters. This indicates that the equations are a good approximation to connect the rate parameters with the empirical ones of the desorption curves.

Table 2. Coefficients in Eqs. 3, 4, and 5

Coefficients in Eq. 3	a_1 191.2	a_2 10.8	a_3 −811.9	a_4 92.2
Coefficients in Eq. 4	b_1 2.2	b_2 308.5	b_3 −85.4	b_4 3.6
Coefficients in Eq. 5	c_1 0.2405	c_2 1.4666	c_3 −1.7301	c_4 0.6524

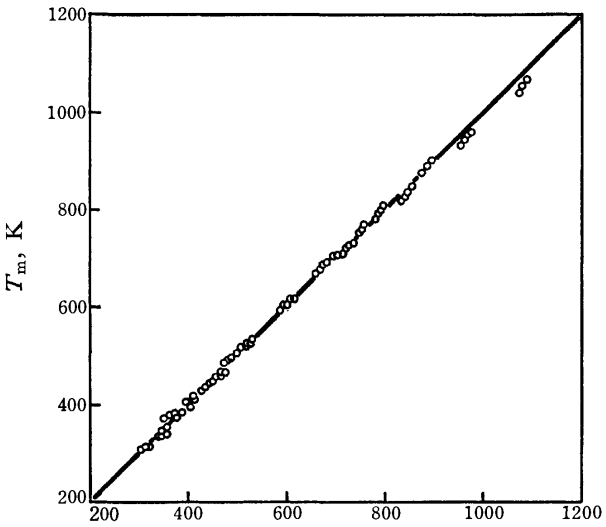

Fig. 2. Correlation of T_m with the right side terms of Eq. 3.

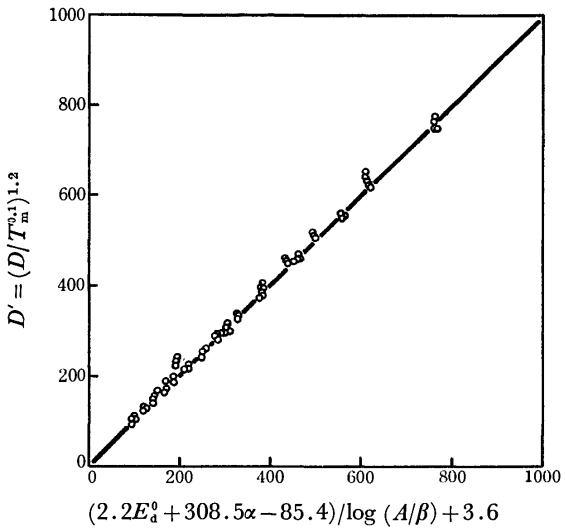

Fig. 3. Correlation of D' with the right side terms of Eq. 4.

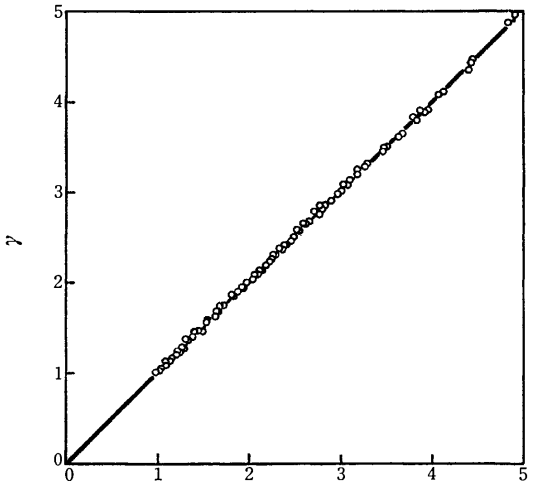

Fig. 4. Correlation of γ with the right side terms of Eq. 5.

The rate parameters should be explicilty expressed by solving these equations. Equations 3, 4, and 5 lead to the relation

$$[\log(A/\beta)]^2 + d_1\log(A/\beta) + d_2 = 0, \quad (6)$$

where d_1 and d_2 are given by Eqs. 7 and 8, respectively,

$$d_1 = (308.5\gamma' T_m' - 10.8\gamma' D'' + 3.2T_m' - 280.4D'' - 3502.8)/(0.522T_m' - 45.98D''), \quad (7)$$

$$d_2 = (249500\gamma' - 80640)/(0.522T_m' - 45.98D''). \quad (8)$$

The terms γ', T_m', and D'' are defined as $\gamma'=\gamma-0.652$, $T_m'=T_m-92.2$, and $D''=D'-3.6$. In the range of values of the rate parameters used for the simulations, the following relations hold. $300<T_m<1100$, $100<D'<800$, $1<\gamma<6$, $d_1>0$, and $d_2<0$. Consequently, the rate parameters can be estimated by Eqs. 9—11 using the empirical parameters T_m, D', and γ.

$$\log(A/\beta) = (-d_1+\sqrt{d_1^2-4d_2})/2 \quad (9)$$

$$E_d^0 = (5.232\times10^{-3}T_m'+1.84\times10^{-4}D'')\log(A/\beta) + 3.97, \quad (10)$$

$$\alpha = (-3.68\times10^{-5}T_m'+3.243\times10^{-3}D'')\log(A/\beta) + 0.25. \quad (11)$$

The values of the rate parameters thus estimated are compared with the true ones used for the simulations. Some examples are given in Table 3. The deviations of the estimated values from the true ones are less than 10%. Thus, Eqs. 9—11 afford a convenient and reliable method for the estimation of the rate parameters from a single desorption curve.

Two restrictions should be pointed out concerning the applicability of the equations. (1) The equations were derived on the basis of first order desorption of a

Table 3. Comparison of the true values of the rate parameters with those estimated by Eqs. 9—11

True values						
E_d^0 [a]	15.0	20.0	25.0	30.0	35.0	40.0
α [b]	10.0	15.0	10.0	20.0	15.0	10.0
$\log(A/\beta)$ [c]	10.0	12.0	16.0	14.0	8.0	12.0
Empirical parameters						
T_m [d]	313	353	336	457	831	679
D [e]	207	259	141	302	280	196
γ	3.12	3.88	2.77	3.78	1.59	1.69
Estimated values						
E_d^0 [a]	16.5	21.1	25.4	30.4	37.1	42.1
α [b]	10.2	15.0	9.9	19.5	15.1	10.1
$\log(A/\beta)$ [c]	10.4	11.9	16.4	13.3	8.3	12.2
Percentage error						
E_d^0, %	+10.0	+5.5	+1.6	+1.3	+6.0	+5.3
α, %	+2.0	0.0	−1.0	−2.5	+0.7	+1.0
$\log(A/\beta)$, %	+4.0	−0.8	+2.5	−5.0	+3.8	+1.7

a) kcal/mol. b) kcal/mol. c) A/β, K^{-1}. d) K. e) K.

single adsorbed state from the heterogeneous surface with the linear variation of the activation energy of desorption. (2) The values of the rate parameters were examined in such range as $10<E_d^0<45$ kcal/mol, $5<\alpha<20$ kcal/mol and $10^8<A/\beta<10^{16}$ K^{-1}.

When the thermal desorption curve has multiple peaks, high resolution between peaks is required for the application of this analysis. It is possible to resolve peaks to a certain extent by large increase of β, although some practical difficulties are encountered.

The desorption order can be determined by the symmetry of the peak in the case of a homogeneous surface, but there are no such means in the case of a heterogeneous one. It is necessary to confirm the desorption order by other measurements.

Curve Fitting Method. The curve fitting method was also investigated for obtaining a more accurate solution. We used the Powell method in order to solve a number of simultaneous equations derived after integration of the differential Eq. 1, the convergence being judged by the summation of squares of differences between the observed and calculated curves.

Even if the summation reaches a minimum in such a nonlinear least square method, it does not always mean the global minimum. In order to get the real solution, a global minimum should be found by widely changing the initial values of the rate parameters. This is the case for thermal desorption, since nearly the same curve could be sometimes reproduced with multiple sets of different values of the rate parameters.

The estimated values would be useful as the initial input values for the application of the curve fitting method, since they are very close to the true values. The curve fitting method was applied to several simulated curves with the result that the values of the rate parameters obtained agreed satisfactorily with the true ones. When the estimated values were used as initial inputs, the calculated result converged more easily to the global minimum. This demonstrates that Eqs. 9—11 are effective not only as a simple method for estimation but also as a method giving good initial input values for the curve fitting calculation.

Application to the Desorption of Carbon Dioxide on Titanium Dioxide. The thermal desorption curve of carbon dioxide from titanium dioxide is shown in Fig. 5. Desorption of carbon dioxide should follow first order kinetics since its dissociative adsorption is very unlikely. The first order thermal desorption from a homogeneous surface is known to give an unsymmetrically shaped curve, but the observed curve has a nearly symmetrical shape. This indicates that the desorption should be treated as one from the heterogeneous surface. The above two methods were applied to this case. The values of the rate parameters obtained by the analysis are compared in Table 4. The two methods give almost the same results, and the calculated curves using the above values reproduce the observed one as shown in Fig. 5.

As a result, the two methods were verified to be effective for getting reliable values of the rate parameters by analyzing a single desorption curve.

There are many complicated cases which can not be treated as such simple heterogeneity. The methods should be extended to analyze a more general heterogeneous surface.

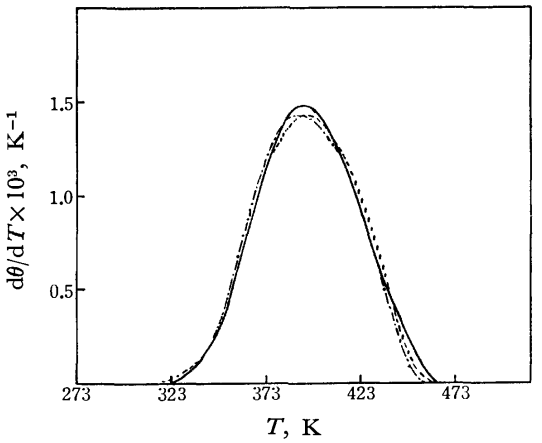

Fig. 5. Observed and calculated thermal desorption curves of carbon dioxide on titanium dioxide: (——) observed; (—·—) calculated using estimated values; (---) calculated by curve fitting method.

Table 4. Rate parameters obtained from the thermal desorption curve of carbon dioxide on titanium dioxide ($\beta=0.3$ °C/s) by Eqs. 9—11 and the curve fitting method

	Estimated values	Curve fitting method
E_d^0 [a]	24.4	22.4
α [b]	3.2	2.7
$\log A$ [c]	12.4	11.1

The observed values of T_m, D, and γ are 393 K, 66 K, and 1.128, respectively. a) kcal/mol. b) kcal/mol. c) A, 1/s.

Financial support in part by the Kawakami Foundation is gratefully acknowledged.

References

1) B. Halpern and J. E. Germain, *J. Catal.*, **37**, 44 (1975).
2) P. A. Redhead, *Vacuum*, **12**, 203 (1962).
3) R. J. Cvetanović and Y. Amenomiya, *Adv. Catal.*, **17**, 103 (1967).
4) F. M. Lord and J. S. Kittelberger, *Surf. Sci.*, **43**, 173 (1974).
5) H. Hobert and B. Knappe, *Kinet. Katal.*, **13**, 1060 (1972).
6) P. T. Dawson and Y. K. Peng, *Surf. Sci.*, **33**, 565 (1972).

Isomorphism in the High-temperature Forms of the Pyrene Complexes with Five Polynitro Aromatic Compounds

Nobuaki INOUE* and Yoshio MATSUNAGA**

Department of Chemistry, Faculty of Science, Hokkaido University, Sapporo 060

(Received June 28, 1977)

Crystalline pyrene complexes with 2,4-dinitrofluorobenzene, 2,4-dinitrochlorobenzene, 2,4-dinitrotoluene, 2,4-dinitrophenol, and picryl chloride exhibit polymorphic transitions. Their temperatures and associated enthalpies are presented. The high-temperature forms show essentially identical X-ray diffraction patterns, losing the special natures of the substituents on the acceptor molecules. Isomorphism is supported by the formation of complete solid solutions demonstrated for combinations of these forms. The enthalpy and entropy of melting of the present complexes are characterized by rather small values, 4—6 kcal mol^{-1} and 12—14 cal deg^{-1} mol^{-1} respectively, indicative of anomalously high thermal motion or disorder in the high-temperature forms. Marked changes in the spectral and electrical properties by the transitions are noted in some cases.

The discovery of polymorphic forms has been reported for a number of electron-donor-acceptor complexes; however, little attention has been paid to their structure or to the properties expected to vary with the transitions.[1-12] In order to understand the significance of polymorphism, systematic studies of this phenomenon and of the change in physical properties by the transitions seemed to be highly desirable. For such studies, polymorphism should be observed with complexes consisting of component compounds structurally related to each other. Our preliminary survey indicated that pyrene complexes with polynitro aromatic compounds suit this purpose well. Especially, the five complexes studied here were found to be of considerable interest because of the isomorphism observed with the high-temperature forms.

Experimental

Materials. The pyrene, Eastman yellow label, was boiled with a large excess of maleic anhydride in xylene to remove the tetracene and other reactive impurities.[13] Then, the hydrocarbon was purified by chromatography on a column of activated alumina and finally zone-refined. The acceptors employed were 2,4-dinitrofluorobenzene (hereafter abbreviated as DNF), 2,4-dinitrochlorobenzene (DNC), 2,4-dinitrotoluene (DNT), 2,4-dinitrophenol (DNP), and picryl chloride (2,4,6-trinitrochlorobenzene) (TNC). They were obtained from commercial sources. The complexes were crystallized from benzene or chloroform solutions containing equimolar amounts of the component compounds. The melting points, listed in Table 1, are in fair agreement with the values reported by Shinomiya when available.[14]

Measurements. Calorimetric curves up to the melting points were recorded on a Rigaku Denki differential scanning calorimeter, Model 8001 SL/C, at a heating rate of 3 °C min^{-1}. The enthalpies of transition and of melting were estimated by comparing the peak areas with the enthalpy of the melting of naphthalene, 4.536 kcal mol^{-1},[15] and also with the enthalpy of transition in hexamethylbenzene, 0.422 kcal mol^{-1}.[16] X-Ray measurements on powdered samples were made with a Toshiba recording diffractometer, Model ADG 301, using filtered copper radiation. The sample was mounted on a aluminum plate with a 20-W heater attached to the other side. The temperature of this plate was monitored by means of a copper-constantan thermocouple and was kept constant with the aid of a Chino temperature-indicating controller, Type E 500.

For spectroscopic measurements, the complexes were melted between two quartz plates. Thin polycrystalline films were obtained by the repeated rubbing of two plates over one another, yielding an optical density of less than 1.0 throughout the visible region. The spectra were recorded on a Beckman DK 2A spectrophotometer at various temperatures between 20 and 80 °C with the aid of a temperature-regulated cell holder. Electrical resistivity measurements were performed on pressed pellets by the two-probe method, as has been described in a paper by Koizumi and Matsunaga.[8]

Results and Discussion

The transition temperature, enthalpy, and entropy are collected in Table 1. Fortunately, the transitions in these complexes occur at reasonably low temperatures and are well separated from the melting points. These conditions make our studies of the high-temperature forms considerably easy. The enthalpy of transition is about 3 kcal mol^{-1} or more in all the complexes but that with DNC. When the high-temperature forms of the DNF, DNT, and DNP complexes are quickly cooled, the metastable phases may be obtained, as evidenced by new transitions appearing at 53, 33, and 39 °C respectively.

The X-ray diffraction patterns observed at room temperature are complicated and distinctly different from each other, reflecting the special natures of the substituents. However, the patterns are drastically simplified upon the transition and become almost identical in all five. As is schematically illustrated in Fig. 1, only four diffraction lines can be seen in the range examined: a strong one appearing between 11 and 12°, two weak ones near 20 and 23°, and a strong one between 26 and 27°. If these high-temperature forms really have the same space group and number of molecules per unit cell, a combination of any two should give a continuous solid solution.[17] Moreover, the combinations examined so far consist of molecular complexes sharing the same acceptor compound.[8,18-20] On the other hand, all the present complexes share the same donor compound, pyrene. Consequently, we decided to look into phase diagrams for several selected pairs by means of differential scanning calorimetry. In addition, the phase boundaries at

* Present address: Fuji Photofilm Co., Minami-ashigara, Kanagawa.

** To whom inquiries may be addressed.

Table 1. Thermodynamic data of pyrene complexes with polynitro aromatic compounds

Acceptor	Transition			Melting		
	t/°C	ΔH/kcal mol^{-1}	ΔS/e. u.	t/°C	ΔH/kcal mol^{-1}	ΔS/e. u.
2,4-Dinitrofluorobenzene	76.5	4.3	12	119	5.0	13
2,4-Dinitrochlorobenzene	41	0.57	1.8	87	4.2	12
2,4-Dinitrotoluene	53.5	2.9	8.9	92.5[a]	4.8	13
2,4-Dinitrophenol	53	3.1	9.5	144[b]	5.9	14
Picryl chloride	79[c]	3.2	9.1	154.5[d]	5.2	12

a) 92.5 °C by Shinomiya (Ref. 14). b) 146.3 °C (Ref. 14). c) 81 °C by Bando and Matsunaga (Ref. 12). d) 154 °C (Ref. 14).

room temperature were checked by the examination of the X-ray diffraction patterns. For example, the diagrams for the following three systems are presented in Fig. 2: pyrene–(DNP,DNC), pyrene–(DNC,DNT), and pyrene–(DNT,DNP). The composition is quoted

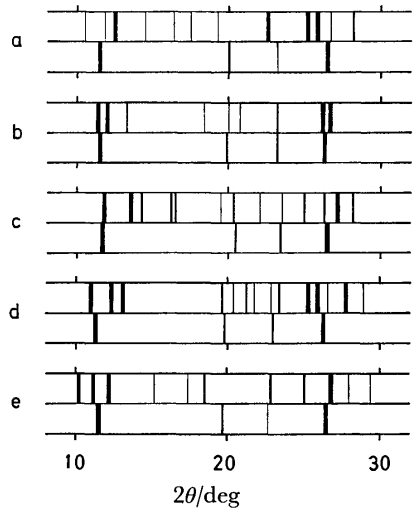

Fig. 1. X-Ray diffraction patterns of the pyrene complexes with a) DNF, b) DNC, c) DNT, d) DNP, and e) TNC. The upper pattern for each complex was recorded at room temperature, and the lower one above the transition temperature.

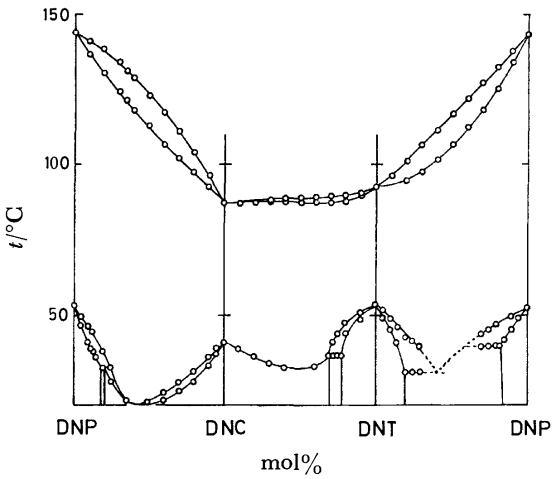

Figs. 2. Phase diagrams for the pyrene–(DNP, DNC), pyrene–(DNC, DNT), and pyrene–(DNT, DNP) systems.

in the mole percentage of the acceptor. The solid-liquid equilibria are of the I type in the Roozeboom classification and clearly indicate the formation of a continuous solid solution within the temperature limits of the diagrams.[21] Similar equilibria have also been noted in pyrene–(DNC,DNF), pyrene–(DNF,DNT), and pyrene–(DNT,TNC). Thus, isomorphism in the high-temperature forms of the five complexes is firmly established.

The solubility characteristics of the low-temperature forms in pyrene–(DNP,DNC) and pyrene–(DNC, DNT) bear a similarity to each other. They are all peritectoid systems. The formation of substitutional solid solutions based on the parent complex lattices occurs over a wide range of stoichiometry. Both the transition temperatures are appreciably lowered by the formation of solid solutions. It is interesting to note that the solubility of the DNP complex into the DNC complex lattice is as much as 80 mol%. Therefore, a miscibility gap with a width as narrow as 2 mol% appears in this system. Similarly, the DNC complex can dissolve the DNT complex to an extent of 70 mol%. The width of the miscibility gap in pyrene–(DNC, DNT) is about 8 mol%.

The diagram for pyrene–(DNT,DNP) could be only partially determined because samples in the range from 30 to 70 mol% of DNP were found not in equilibrium even after standing over two years at room temperature. Nevertheless, the presence of two singular points may be easily noted. As is shown in Fig. 2, one of them may be a eutectoid at about 40 mol% and at 31 °C, while the other may be a peritectoid at about 60 mol% and at 40 °C. If this assignment is correct, and if the equilibrium is achieved, the appearance of a ternary complex dissolving adjacent phases to some extent, and hence of a variable composition, may be expected. This phase may cover a range as wide as 20 mol% of DNP. The formation of two ternary complexes has been known in the (phenanthrene, anthracene)–picric acid system studied by us.[8] They may be supposed to be deposited from mixtures containing liquid phases. In the case of pyrene–(DNT, DNP), the ternary complex must be formed from a solid solution. In other words, an extensive rearrangement of the component molecules must occur in the solid state for the appearance of the new phase. Such a process undoubtedly takes a long time to be accomplished. The other, but less likely, possibility is that the above-mentioned singular points are both eutec-

toids. If so, the miscibility gap for the high-temperature forms is closed at these points, while that for the low-temperature forms covers the whole range from 20 to 84 mol% of DNP.

Although our knowledge of the structural relationship among various molecular complexes is still scanty, several isomorphous pairs are already known. For example, the trinitrobenzene and picric acid complexes of naphthalene, fluoranthene, and pyrene have each been shown to be strictly isomorphous by Herbstein and Kaftory.[9] This relationship has been established for the crystals stable at room temperature. Our results strongly suggest that, if high-temperature forms are examined, isomorphism in molecular complexes may be observed more commonly than has been supposed.

When the interaction between the hydrocarbon molecule and the substituent on the acceptor molecule is specific or localized, the lattice may be rather rigid. The disappearance of this specific interaction above the transition temperature may be due to the onset of an anomalously great thermal motion of the component molecules. This motion appears so great that the interaction is dynamically averaged and becomes nonspecific. Such a thermal motion is expected to contribute significantly to the melting mechanism of the complexes. This speculation is supported by our observation that the enthalpy and entropy of melting of the present complexes are only 4—6 kcal mol^{-1} and 12—14 cal deg^{-1} mol^{-1} respectively (see Table 1). These values are definitely small if compared with the data for the eleven polycyclic aromatic hydrocarbon-trinitrobenzene complexes given by Casellato *et al.*[11] The enthalpy ranges from 6.5 kcal mol^{-1} for the phenanthrene complex to 14.5 kcal mol^{-1} for the dibenzoanthracene complex. The corresponding entropies are 14.9 and 28.5 cal deg^{-1} mol^{-1} respectively. The former complex is known to exhibit a polymorphic transition at 148 °C with an enthalpy value of about 3 kcal mol^{-1}. Apart from this, only the pyrene complex has an entropy value below 20 cal deg^{-1} mol^{-1}. The observed entropies can probably be divided unevenly among the donor and acceptor lattices. On the basis of the wide-line NMR measurements, the reorientation of the donor species in a number of molecular complexes has been suggested by Fyfe and others. It may be added that pyrene and its complexes are notable of this examples.[22-24] The present complexes are now being examined by this technique in our laboratory. The second moments are reduced to 1—2 G^2 at the transition temperatures in all the complexes.

Not only the mode of interaction between the donor and acceptor molecules, but also that between like molecules in a complex may be modified by the structural change upon the polymorphic transition. The charge-transfer absorption has a direct bearing upon the former interaction, and the electrical resistivity, upon the latter. Their temperature dependences may each show anomalies at the transition temperature; however, the magnitudes may be quite different. Consequently, studies of these two properties in parallel may be fruitful. As the only discernible change in the charge-transfer absorption was the intensification

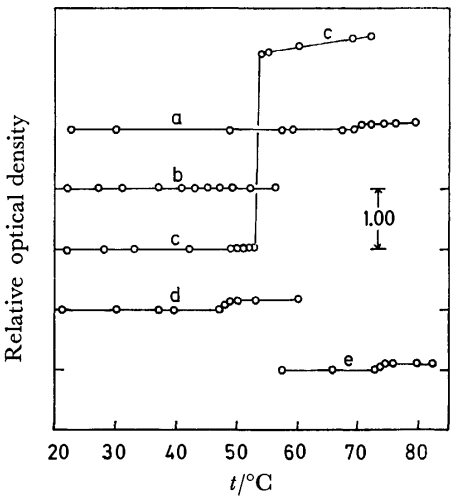

Fig. 3. Temperature dependence of the relative optical density of charge-transfer absorption in the pyrene complexes with a) DNF (at 390 nm), b) DNC (at 400 nm), c) DNT (at 413 nm), d) DNP (at 440 nm), and e) TNC (at 425 nm).

upon the transition, the optical density at the absorption maximum is plotted against the temperature in Fig. 3. The value of the low-temperature form was arbitrarily taken as 1.00 in this figure. The most pronounced change is found with the DNT complex. The optical density at 413 nm after the transition is as much as 4.25 times that before. After the transition, the optical density increases linearly with the temperature, the value at 74 °C being 4.80. The other extreme is observed with the DNC complex, which is known to show the smallest enthalpy of transition. The optical density remains constant throughout the transition. Although the other three complexes show large enthalpy changes upon the polymorphic transition, the increase in the optical density is only about 10% or less.

In Fig. 4, the variation in the electrical resistivity recorded at ascending temperatures is presented. The magnitude of resistivity varies greatly among the members of the series. Thus, the DNF complex is more conducting than TNC complex by a factor of 10^3. All the complexes exhibit abrupt decreases in the resistivities at the transition temperatures. Here again, the change observed with the DNT complex is the largest. Therefore, one may postulate that the donor-donor and/or acceptor-acceptor overlaps are considerably improved by the structural change, as is the overlap between the hydrocarbon and DNT molecules. The DNP complex shows a decrease in the resistivity by almost the same factor. In this case, like molecules presumably gain better overlaps by the transition, without any appreciable effect on the donor-acceptor interaction. It is interesting to point out that, in spite of having the largest enthalpy of transition, the DNF complex exhibits a decrease by merely a factor of five, and that this factor can be well compared with that observed with the DNC complex. The latter is the one with the smallest enthalpy of transition among the complexes studied here. However, we must be aware of a large difference in the magnitude of resis-

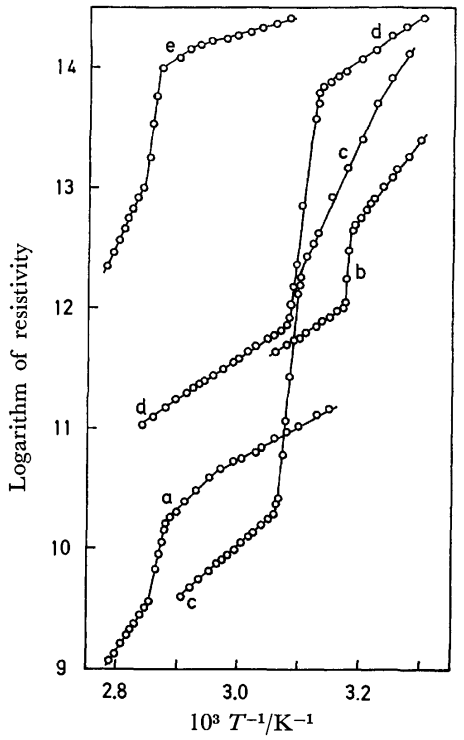

Fig. 4. Electrical resistivities of the pyrene complexes with a) DNF, b) DNC, c) DNT, d) DNP, and e) TNC.

tivity between these two. Since the DNF complex has a relatively low resistivity, the improvement of the overlap between like molecules in this complex cannot be compared with that of the DNC complex by such a factor. If one refers to the magnitude, it is certain that the resistivity change is particularly large for the DNF complex. The acceptor, TNC, is undoubtedly the strongest employed here; nevertheless, its pyrene complex is the least conducting one. The crowded substituents on this acceptor molecule seem to prevent good overlaps between like molecules in this complex. At descending temperatures, large hystereses were observed in all the cases because of a considerable delay in the transition in the reverse direction.

The authors wish to express their thanks to Professor Toshio Yokokawa for letting them use the X-ray diffractometer.

References

1) A. Kofler, *Z. Elektrochem.*, **50**, 200 (1944).
2) D. E. Laskowski, D. G. Grabar, and W. C. McCrone, *Anal. Chem.*, **25**, 1400 (1953).
3) H. Matsuda, K. Osaki, and I. Nitta, *Bull. Chem. Soc. Jpn.*, **31**, 611 (1958).
4) T. Sakurai, *Acta Crystallogr.*, **19**, 320 (1965).
5) Y. Matsunaga, *Nature*, **211**, 183 (1966).
6) Y. Matsunaga, *Bull. Chem. Soc. Jpn.*, **44**, 2868 (1971).
7) F. Pelizza, F. Casellato, and A. Girelli, *Thermochim. Acta*, **4**, 135 (1972).
8) S. Koizumi and Y. Matsunaga, *Bull. Chem. Soc. Jpn.*, **47**, 9 (1974).
9) F. M. Herbstein and M. Kaftory, *Acta Crystallogr., Sect. B*, **31**, 60 (1975).
10) Y. Matsunaga, E. Osawa, and R. Osawa, *Bull. Chem. Soc. Jpn.*, **48**, 37 (1975).
11) F. Casellato, C. Vecchi, and A. Girelli, *Thermochim. Acta*, **13**, 37 (1975).
12) M. Bando and Y. Matsunaga, *Bull. Chem. Soc. Jpn.*, **49**, 3345 (1976).
13) E. Clar, *Ber.*, **69**, 1683 (1936).
14) C. Shinomiya, *Bull. Chem. Soc. Jpn.*, **15**, 259 (1940).
15) J. P. McCullough, H. L. Finke, J. F. Messerly, S. S. Todd, T. C. Kincheloe, and G. Waddington, *J. Phys. Chem.*, **61**, 1105 (1957).
16) M. E. Spaght, S. B. Thomas, and G. S. Parks, *J. Phys. Chem.*, **36**, 882 (1932).
17) A. I. Kitaigorodskii, "Organic Chemical Crystallography," Consultants Bureau, New York (1961), p. 231.
18) H. Rheinboldt and P. Senise, *Bols. faculdade filosofia, cienc. letras. Univ. São Paulo*, **14**, *Quimica* No. 1, 3 (1942), as cited in *Chem. Abstr.*, **40**, 2049 (1946).
19) S. K. Lower, *Mol. Cryst. Liq. Cryst.*, **5**, 363 (1969).
20) S. Koizumi and Y. Matsunaga, *Bull. Chem. Soc. Jpn.*, **46**, 1875 (1973).
21) H. W. B. Roozeboom, *Z. Phys. Chem.*, **30**, 385 (1899).
22) C. A. Fyfe, D. F. R. Gilson, and K. H. Thompson, *Chem. Phys. Lett.*, **5**, 215 (1970).
23) C. A. Fyfe, *J. Chem. Soc. Faraday Trans. 2*, **70**, 1633 (1974).
24) C. A. Fyfe, D. Harold-Smith, and J. Ripmeester, *J. Chem. Soc. Faraday Trans. 2*, **72**, 2269 (1976).

MO Calculations of the Rydberg Transitions of the Methane Molecule

Susumu KOHDA-SUDOH and Shigeyoshi KATAGIRI

Department of Chemistry, Faculty of Science, Hirosaki University, Hirosaki 036

(Received May 30, 1977)

The vertical transition energies of both the Rydberg and valence-shell type transitions of CH_4 were calculated by the use of the *ab initio* SC-LCAO-MO method. We used Slater-type AO's as the basis AO's and added the extra-valence AO's (3s, 3p, 4s, and 4p) of a carbon atom to the minimal-basis set in order to express the Rydberg MO's. From the limited CI calculations, the mixing expressed in terms of the orthogonalized AO's between the Rydberg and valence-shell transitions was shown to be little. The lowest two absorption bands near 9.7 and 11.7 eV were identified as a 3s-like Rydberg transition with a 3p-like one and a 4s-like Rydberg transition with a 4p-like one respectively. The total energy and Mulliken population analysis were also calculated and compared with the results of the minimal-basis calculations.

The studies of the molecular Rydberg states, though not many, have been done continuously for a long time from both experimental and theoretical points of view.[1-15] Recently the Rydberg states of the methane molecule, as well as of water[5,9,15,16] and ethylene[12,16,17] molecules, have been studied in detail because of its simple molecular form. Methane has a diffuse but entirely structureless band system, with a maximum at 9.7 eV in its far ultra-violet absorption spectra.[8] Mulliken[1] identified this band as a $1t_2 \rightarrow 3s$ (Rydberg orbital) transition, using the united atom model. However, another assignment of the valence-shell transition, $1t_2 \rightarrow 2t_2$, is possible. Katagiri and Sandorfy,[18] in fact, carried out P-P-P-type semi-empirical calculations and obtained reasonable values of the transition energies for several *n*-alkanes. Ohmichi *et al.*[19] made modified CNDO calculations of several saturated compounds. They identified the absorption spectra of methane as being due to the valence-shell transitions, in agreement with the Katagiri and Sandorfy results. In 1971 Salahub and Sandorfy[13] carried out CNDO-type calculations with an extended-basis set (RCNDO), in which they used these extra-valence atomic orbitals: 3s and 3p AO's, for a carbon atom and 2s and 2p AO's for a hydrogen atom. The results show that the contribution of the Rydberg orbital to the first excited state of CH_4 is very low. From these semi-empirical calculations, it seems likely that the first band of CH_4 can be explained as the valence-shell transition. Pauzat *et al.*,[20] on the other hand, carried out non-empirical GTO-basis calculations of the ionization and transition energies of this molecule. They used a diffuse molecular orbital (Rydberg MO), as Salahub and Sandorfy did in their RCNDO calculations. The result for the first excited state gave features different from those of Salahub and Sandorfy in its Rydberg character. Williams and Poppinger also carried out non-empirical calculations of CH_4 and H_2O by means of the Equations of Motion and the configuration interaction (CI) method; they obtained a good agreement with the Pauzat *et al.* calculations.

From the experiments on the electron-impact spectra, Harshbager *et al.*[23] assigned the first band to the $1t_2 \rightarrow 3a_1$ (carbon 3s-like MO) Rydberg transition, which is split by Jahn-Teller distortion into two peaks, 9.7 eV and 10.3 eV. Furtheremore, they discussed the band near 11.7 eV and assigned it to the Rydberg transition from $1t_2$ to the carbon 4s-like MO. In our work we used, in order to clarify the nature of the excited states of CH_4, the extra-valence AO's, 3s, 3p, 4s, and 4p AO's of a carbon atom in addition to the minimal-basis set. The Slater-type AO's were used for these AO's. All the following orbital exponents of the STO's except the hydrogen 1s AO's are obtained from Slater's rules: $\delta_{1s}=5.7$, $\delta_{2s}=\delta_{2p}=1.625$, $\delta_{3s}=\delta_{3p}=0.4833$, and $\delta_{4s}=\delta_{4p}=0.3625$ for the carbon atom, and $\delta_{1s}=1.2$ for the hydrogen atom. The symmetry of the molecule is assumed to be T_d, and the nuclear distance is fixed as $R(\text{C–H})=2.05$ a.u.

Calculation and Discussion

The ordinary SC-LCAO-MO calculations are performed for the ground state by the use of the extended-basis set (minimal-basis set plus the extra-valence 3s, 3p, 4s, and 4p AO's of a carbon atom). All the molecular integrals are calculated by using the library program of the University of Tokyo Computer Centre (Y4/TC/ADO5), where the molecular integrals are calculated over the composite GTO's, so we expanded all s-type STO's by 8-terms of the GTO's and the 2p, 3p, and 4p STO's by 6, 6, and 4-terms of GTO's respectively.[27]

The orbital exponents of used AO's are not optimized; *i.e.*, they are fixed as Slater's values. Hosoya[25] calculated the orbital exponents of the carbon Rydberg AO's, *i.e.*, 3s, 3p, and 3d, by optimizing the one-electron energy. He expanded the Rydberg orbitals in terms of several STO's and thus obtained the values of 0.55 and 0.465 for 3s and 3p STO's respectively, which contribute mainly to the optimized Rydberg orbitals. These values are not very different from Slater's values. This shows that, for the orbital exponents of the extra-valence AO's we may use the values obtained from Slater's rules as the first approximation. The calculated SC-LCAO-MO's, both occupied and unoccupied, are shown in Table 1, along with the orbital and total energies. The predicted total energy of the ground state is lower than that of our previous minimal-basis calculations by only 0.0154 a.u.[21] This shows that the employment of the extended-basis set does not affect the total energy greatly. The resulting virtual MO's, however, turn out to be useful in the calculations of the transition energies, as will be shown below.

The gross atomic and bond populations found by Mulliken population analysis are as follows:

Table 1. The MO's and total energy of CH_4

Orbital energy and MO ε_i (a.u.)	1s	2s	3s	4s	2p	3p	4p	H
$-11.2869\,(1a_1)$	0.9953	0.0277	0.0000	0.0002	0.	0.	0.	−0.0058
$-0.9460\,(2a_1)$	−0.2050	0.6817	−0.0576	0.0355	0.	0.	0.	0.1588
$-0.5547\,(1t_2)$	0.	0.	0.	0.	0.5863	0.0372	−0.0193	0.2841
$0.0095\,(3a_1)$	0.0097	−0.0484	0.0002	0.9997	0.	0.	0.	0.0054
$0.0181\,(2t_2)$	0.	0.	0.	0.	−0.0135	−0.1878	1.1321	0.0022
$0.0608\,(4a_1)$	0.0584	−0.2422	1.5605	−1.1581	0.	0.	0.	−0.0212
$0.1049\,(3t_2)$	0.	0.	0.	0.	−0.2099	1.5695	−1.0389	0.1027
$0.6382\,(4t_2)$	0.	0.	0.	0.	1.1242	0.2167	−0.1202	0.6723
$0.8347\,(5a_1)$	0.1928	−1.7567	−0.5338	0.3168	0.	0.	0.	0.7704
Total energy				−40.1284 a.u.				

$n(\mathrm{C})=6.553$, $n(\mathrm{H})=0.862$, $n(\mathrm{C\text{-}H})=0.784$,

and

$n(\mathrm{H\text{-}H})=-0.042$.

Our previous minimal-basis calculations, on the other hand, gave the following results:

$n(\mathrm{C})=6.539$, $n(\mathrm{H})=0.865$, $n(\mathrm{C\text{-}H})=0.784$,

and

$n(\mathrm{H\text{-}H})=-0.042$.

There is little difference. The extra-valence AO's of the carbon atom seem to have no effect in the C–H binding. If we use the extra-valence AO's of the hydrogen atom also, an increase in the bond population may be expected.

The vertical transition energies are calculated by means of Eq. 1, using the virtual orbital approximation

$$\Delta E^{1,3}(i\rightarrow j) = \varepsilon_j - \varepsilon_i - (J_{ij}-K_{ij}) \pm K_{ij}, \qquad (1)$$

where ε_i, J_{ij} and K_{ij} are the orbital energies and the Coulombic and exchange integrals respectively, and where the plus sign of the last term holds for the singlet, and the minus sign for the triplet. The results are shown in Table 2, along with those of other calculations. In the case of the minimal-basis set, the vertical transition energy of the lowest excited state is calculated to be about twice the experimental value. Moreover, this value is higher than the ionization potential. These are common in other *ab initio* minimal-basis calculations.[20,22] The symmetry of the calculated lowest-excited-state is T_1, which is electronically forbidden. On the other hand, the extended-basis calculations bring in another profile of the predicted transition energies. The lowest value for the singlet state appears at 11.61 and 12.37 eV above the ground state with and without CI respectively; this agrees with the experiments fairly well. The symmetry of this state is T_2, which is an allowed transition. The excited states considered to be due to the valence-shell transitions are found at almost the same positions as in the minimal-basis calculations. The relative ordering of the predicted excited states is not necessarily the same in all types of methods and basis sets, but so long as we use the extended-basis set the lowest excited state can be calculated to be T_2 symmetry.[26] Pauzat *et al.*[20] calculated the vertical transition energies by taking into account the Rydberg orbitals, which were constructed by orthogonalizing them to the inner SCF-MO's by the Schmidt procedure. We have already used the carbon 3s, 3p, 4s, and 4p Rydberg AO's as the starting-basis ones, along with the minimal-basis set, in the calculations of the ground state. Therefore, the Rydberg orbitals are assumed to be the virtual SC-LCAO-MO's, and then they are automatically orthonormalized to the inner MO's. It is interesting that the virtual $3a_1$

Table 2. Vertical transition energies (eV)

Symmetry[d]	Minimal	Extended	CI	Pauzat[a]	Klessinger[b]
T_2		12.37 (12.20)[c]	11.61 (11.40)	10.87 (10.53)	
A_1		13.29 (13.27)	12.27 (12.27)	12.18 (11.45)	
T_2		13.30 (13.30)	12.57 (12.43)	11.86 (11.70)	
E		13.32 (13.32)	12.01 (11.87)	11.93 (11.65)	
T_1		13.33 (13.33)	12.66 (12.66)	11.96 (11.70)	
T_2		12.88 (12.87)	13.56 (13.51)		
T_2		13.32 (13.08)	13.95 (13.86)		
E		13.44 (13.23)	14.70 (14.58)		
T_1		13.88 (13.37)	13.98 (13.98)		
A_1		14.04 (13.35)	14.92 (14.92)		
T_1	21.50 (21.28)	21.55 (21.23)	21.61 (21.29)	22.43 (20.21)	
E	21.93 (20.78)	22.32 (21.23)	22.37 (21.33)	23.21 (22.15)	
T_2	23.78 (21.65)	28.38 (25.83)	28.38 (25.99)	27.41 (25.33)	
T_2	24.08 (18.80)	23.73 (18.70)	23.84 (18.80)	25.62 (20.21)	21.11
A_1	27.65 (17.03)	27.58 (17.44)	27.72 (17.62)	28.46 (17.15)	28.11

a) From Table 5 in Ref. 20. b) Ref. 22. c) The parentheses in this table indicate the transition energies of the triplet states. d) The transitions are classified into three types of transitions; the first five transitions are from $1t_2$ to $3a_1$ or $2t_2$ MO's; the second five ones are from $1t_2$ to $4a_1$ or $3t_2$ MO's, and the remaining transitions are from $1t_2$ to $5a_1$ or $4t_2$ MO's.

MO has a strong resemblance to the 4s′ AO which is orthogonalized to the carbon inner 1s and 2s AO's, while the $4a_1$ MO is also like the 3s′ AO which is orthogonalized to the 4s′ AO as follows:

$$3s' = 1.553(3s) - 1.155(4s) - 0.286(2s) + 0.063(1s)$$

$$4a_1 = 1.561(3s) - 1.158(4s) - 0.242(2s) + 0.058(1s)$$

and

$$4s' = 1.014(4s) - 0.028(2s) + 0.006(1s)$$

$$3a_1 = 1.000(4s) - 0.048(2s) + 0.010(1s)$$

These correspondences hold between the $2t_2$ MO and the 4p′ AO, and the $3t_2$ MO and the 3p′ AO respectively: the 3p′ and 4p′ AO's are the orthonormalized AO's, like the above-mentioned 3s′ and 4s′ AO's. The other two virtual MO's, $4t_2$ and $5a_1$, are mainly constructed from the hydrogen 1s and carbon valence AO's.

The results of the CI calculations shown in Table 2 are obtained by means of a limited single-excitation CI. The lowering of the lowest excitation energy is considerable, and the mixing among the excited states seems to be large. Here let us examine six electronically allowed transitions in detail. Three of them (φ_1, φ_2, and φ_3) are one-electron transitions from the $1t_2$ to the $3a_1$, $4a_1$, and $5a_1$ MO's, while the others (φ_4, φ_5, and φ_6) are the transitions from the $1t_2$ to the $2t_2$, $3t_2$, and $4t_2$ MO's respectively. The CI results exhibit the following configuration mixings and transition energies:

$$^1\Psi_1 = 0.588\varphi_1 + 0.807\varphi_2 + 0.058\varphi_3 \quad \Delta E = 11.61\ \text{eV}$$

$$^1\Psi_2 = 0.809\varphi_1 - 0.586\varphi_2 - 0.043\varphi_3 \quad \Delta E = 13.56\ \text{eV}$$

$$^1\Psi_3 = 0.003\varphi_1 - 0.072\varphi_2 + 0.997\varphi_3 \quad \Delta E = 28.38\ \text{eV}$$

$$^1\Psi_4 = 0.683\varphi_4 + 0.726\varphi_5 - 0.075\varphi_6 \quad \Delta E = 12.57\ \text{eV}$$

$$^1\Psi_5 = 0.730\varphi_4 - 0.679\varphi_5 + 0.104\varphi_6 \quad \Delta E = 13.95\ \text{eV}$$

$$^1\Psi_6 = 0.075\varphi_4 + 0.073\varphi_5 - 0.995\varphi_6 \quad \Delta E = 23.84\ \text{eV}$$

for the singlet excited states. We showed previously that there was a likeness between the virtual MO's and the orthogonalized carbon extra-valence AO's, so we can estimate the Rydberg character of the above excited states in terms of the 3s′, 3p′, 4s′, and 4p′ orthogonalized AO's. The contribution of these AO's to each state is calculated approximately as follows:

$$^1\Psi_1 \approx 0.947(3s') - 0.226(4s')$$

$$^1\Psi_2 \approx 0.237(3s') + 0.965(4s')$$

$$^1\Psi_4 \approx 1.010(3p') + 0.012(4p')$$

$$^1\Psi_5 \approx 0.031(3p') - 1.008(4p')$$

From these coefficients of the orthogonalized AO's, four states, $^1\Psi_1$, $^1\Psi_2$, $^1\Psi_4$, and $^1\Psi_5$, are considered to be mainly constructed by the transitions of a $1t_2$ electron to 3s′, 4s′, 3p′, and 4p′, that is the Rydberg MO's, respectively. The remaining two states, $^1\Psi_3$ and $^1\Psi_6$, may be understood as valence-shell types (2s and 2p). We can say, from the above CI results and discussion, that the configuration mixing between the valence-shell and Rydberg transitions does not occur in these excited states of the methane molecule. For the six triplet states which correspond to the above six singlet excited states, the similar configuration mixings given below are obtained:

$$^3\Psi_1 = 0.547\varphi_1' + 0.832\varphi_2' + 0.093\varphi_3' \quad \Delta E = 11.42\ \text{eV}$$

$$^3\Psi_2 = 0.837\varphi_1' - 0.544\varphi_2' - 0.058\varphi_3' \quad \Delta E = 13.51\ \text{eV}$$

$$^3\Psi_3 = 0.002\varphi_1' + 0.109\varphi_2' - 0.994\varphi_3' \quad \Delta E = 25.99\ \text{eV}$$

$$^3\Psi_4 = 0.624\varphi_4' + 0.775\varphi_5' - 0.097\varphi_6' \quad \Delta E = 12.43\ \text{eV}$$

$$^3\Psi_5 = 0.781\varphi_4' - 0.619\varphi_5' + 0.087\varphi_6' \quad \Delta E = 13.86\ \text{eV}$$

$$^3\Psi_6 = 0.008\varphi_4' - 0.130\varphi_5' - 0.991\varphi_6' \quad \Delta E = 18.80\ \text{eV}$$

where the triplet functions, φ_i', are used instead of φ_i. The nature of each triplet state is almost the same as that of the corresponding singlet excited states.

With respect to these transition energies, it is found that the calculated singlet-triplet separation is very small for the Rydberg transitions, but it is quite large for the valence-shell transitions. The experimental values of the singlet-triplet separation are about 1 eV.[24] In order to explain the experimental values, we may need moderate diffuse orbitals for the triplet excited states.

TABLE 3. COMPARISON WITH EXPERIMENTS (eV)

State	Transition type	Calcd	Exptl[a]
$^1\Psi_1$	$1t_2 \longrightarrow 3s'$	11.61	9.7, 10.3
$^1\Psi_4$	$1t_2 \longrightarrow 3p'$	12.57	
$^1\Psi_2$	$1t_2 \longrightarrow 4s'$	13.56	11.7
$^1\Psi_5$	$1t_2 \longrightarrow 4p'$	13.95	

a) Ref. 23.

The vertical transition energies of the four lowest allowed-transitions are summarized in Table 3, along with the experimental values. We may assign the band at 9.7 eV to the $1t_2 \rightarrow 3s'$ Rydberg transition ($^1\Psi_1$): this conflicts with the semi-empirical calculations, but agrees with other extended basis non-empirical calculations. Similarly the band at 11.7 eV is assigned to the $1t_2 \rightarrow 4s'$ Rydberg transition ($^1\Psi_2$) by a comparison with the experimental and calculated energy separation. Two states, $^1\Psi_4$ and $^1\Psi_5$, will overlap with the above two bands respectively. No discussions of the oscillator strength for each allowed transition and the vibronic interactions of the forbidden transitions is given here, so the above assignments of the absorption bands of CH_4 are somewhat qualitative, but they do confirm Hashbarger and Lassetre electron-impact experiments.[23]

The calculations were carried out on the HITAC 8700/8800 Computer at the University of Tokyo Computer Centre. The authors are very grateful to Professor Hiroshi Taketa for his helpful communications about the use of the program (Y4/TC/ADO5: Molecular Integrals over CGTO).

References

1) R. S. Mulliken, *J. Chem. Phys.*, **3**, 518 (1935).
2) A. D. Walsh, *J. Phys. Radium*, **15**, 501 (1954).
3) A. D. Liehr, *Z. Naturforsh., Teil A*, **11**, 752 (1956).
4) S. R. Lapaglia, *J. Mol. Spectrosc.*, **10**, 240 (1963).
5) S. R. Lapaglia, *J. Chem. Phys.*, **41**, 1427 (1964),
6) R. S. Mulliken, *J. Am. Chem. Soc.*, **86**, 3183 (1964).
7) M. B. Robin, R. R. Hart, and N. A. Kuebler, *J. Chem. Phys.*, **44**, 1803 (1966).
8) B. A. Lombos, P. Sauvageau, and C. Sandorfy, *Chem. Phys. Lett.*, **1**, 42 (1967); J. W. Raymonda and W. T. Simpson,

J. Chem. Phys., **47**, 430 (1967).
9) W. J. Hunt and W. A. Goddard, III, *Chem. Phys. Lett.*, **3**, 414 (1969).
10) M. B. Robin, *Int. J. Quantum Chem.*, **6**, 257 (1972).
11) M. B. Robin and N. A. Kuebler, *J. Mol. Spectrosc.*, **33**, 274 (1970).
12) R. J. Buenker, S. D. Peyerimhoff, and W. E. Kammer, *J. Chem. Phys.*, **55**, 814 (1971).
13) D. R. Salahub and C. Sandorfy, *Theor. Chim. Acta*, **20**, 227 (1971).
14) F. H. Watson, A. T. Armstrong Jr., and S. P. McGlynn, *Theor. Chim. Acta*, **16**, 75 (1970).
15) G. R. J. Williams and P. Poppinger, *Mol Phys.*, **30**, 1005 (1975).
16) N. W. Winter, W. A. Goddard, III, and F. W. Bobrowicz, *J. Chem. Phys.*, **62**, 4325 (1975).
17) I. Fischer-Hjalmars and J. Kowalewski, *Theor. Chim. Acta*, **29**, 345 (1973).
18) S. Katagiri and C. Sandorfy, *Theor. Chim. Acta*, **4**, 203 (1966).
19) N. Ohmichi, A. Tajiri, and T. Nakajima, *Bull. Chem. Soc. Jpn.*, **45**, 3026 (1972).
20) F. Pauzat, J. Ridard, and B. Levy, *Mol. Phys.*, **23**, 1163 (1972).
21) S. Kohda and S. Katagiri, *Bull. Chem. Soc. Jpn.*, **45**, 2737 (1972).
22) M. Klessinger and R. McWeeny, *J. Chem. Phys.*, **42**, 3343 (1965).
23) W. R. Harshbarger and E. N. Lassetre, *J. Chem. Phys.*, **58**, 1505 (1973).
24) H. H. Brongersma and L. J. Oosterhoff, *Chem. Phys. Lett.*, **3**, 437 (1969).
25) H. Hosoya, *J. Chem. Phys.*, **48**, 1380 (1968).
26) Bond-orbital calculations by the present authors appear elsewhere.
27) K. O-ohata, H. Taketa, and S. Huzinaga, *J. Phys. Soc. Jpn.*, **21**, 2306 (1966); O. Matsuoka and N. Fuchikami, *Rep. Computer Center, Univ. Tokyo*, **3**, 1 (1970).

A Molecular Orbital Study of the Partial Reactivity of the Hydrogen of Aliphatic Compounds in the Hydrogen-abstraction Reaction by the Hydroxyl Radical

Hiroyuki SHINOHARA, Akira IMAMURA*, Takahiro MASUDA, and Masaharu KONDO

Department of Chemistry, Faculty of Science, Tokyo Metropolitan University, Fukasawa, Setagaya-ku, Tokyo 158

** Shiga University of Medical Science, Seta, Otsu, Shiga 520-21*

(Received June 13, 1977)

The energy required to stretch a C–H bond of alkanes by 0.5 Å from an equilibrium bond length was calculated by the INDO method, and it was found that this energy has a relation with the delocalizability, D_r^R, of hydrogen atoms in alkanes, and with the activation energy for the hydrogen-abstraction reaction of the methyl radical from alkanes. The reactivities of hydrogen atoms in aliphatic alcohols and carboxylate ions, as defined by this energy were found to correlate with the partial reactivities of hydrogen atoms, just as was proposed by Anbar *et al.*, *i.e.*, the rate constants for the hydrogen-abstraction reaction of aliphatic compounds with hydroxyl radicals can be well explained by a summation of the partial reactivities assigned to primary, secondary, and tertiary hydrogen atoms bound to α- or β- (for γ-CH and δ-CH the same value as for β-CH was used) carbon atoms.

It is well established that a hydroxyl radical abstracts a hydrogen atom from C–H bonds of aliphatic alcohols and carboxylate ions. Furthermore, it is well known that the reactivity of an aliphatic compound toward the hydroxyl radical increases with an increase in the number of C–H bonds in a molecule.

Anbar *et al.*[1] determined the rate constants for the reactions of a large number of aliphatic compounds with hydroxyl radicals, and pointed out that the reactivities of long-chain compounds could be calculated by a summation of the assigned partial reactivities of the hydrogen atoms in the molecule. They proposed the following partial reactivities for the hydrogen atoms of carboxylate ions, by the best fit of simultaneous equations derived from the experimental rate constants: (a) the partial reactivities of the hydrogen atoms in the α-position to the carboxyl group are estimated to be 0.235, 2.94, and 8.90×10^8 l mol^{-1} s^{-1} per H atom for the primary ($CH_3CO_2^-$), the secondary ($RCH_2CO_2^-$), and the tertiary ($R_2CHCO_2^-$) hydrogens respectively; (b) the partial reactivities of the hydrogen atoms in the positions other than α are also estimated to be 0.606, 5.05, and 14.1×10^8 l mol^{-1} s^{-1} per H atom for the primary, secondary, and tertiary hydrogens respectively. The originally reported values are corrected by a factor of 1.68, because the rate constant for the reaction of the hydroxyl radical with ethyl alcohol, which was used as a reference substance in their determination of the rate constants, has recently been revised from 1.1×10^9 to 1.85×10^9 l mol^{-1} s^{-1}.[2]

The rate constants calculated from these partial reactivities have been proved to interpret the experimental values successfully. Therefore, it is helpful to investigate the theoretical basis of the assigned partial reactivities from the viewpoint of the molecular orbital method.

In chemical reactions, the delocalization of electrons between reactant and reagent is recognized as the major factor in determining the reactivity.[3,4] Therefore, a hydroxyl radical as well as a reactant should be included in the calculation of the reactivity of the hydrogen atom in order to take the delocalization of electrons into account. However, the total energy of the system including a hydroxyl radical and a reactant can not always be obtained because of the divergent behavior in SCF calculation. In a previous paper,[5] we showed that the reactivity of the hydrogen atom (ΔE), defined as the energy required to stretch a C–H bond by 0.5 Å from the equilibrium bond length, has a close relation with the energy for the hydrogen-abstraction reaction (ΔE_{OH}), calculated from the system including a hydroxyl radical and an amino acid. Therefore, it can be expected that ΔE gives a measure of the reactivity of the hydrogen atom in alcohols and carboxylate ions toward the hydroxyl radical in the present hydrogen-abstraction reaction.

Actually the present results show that ΔE is related to the natural logarithm of the partial reactivities of the primary, secondary, and tertiary hydrogen atoms bound to the α- and β- carbon atoms which were proposed by Anber *et al.*[1]

Method

The total energies were calculated by the INDO method proposed by Pople *et al.*[6]

Results and Discussion

Methyl alcohol, ethyl alcohol, propyl alcohol, isopropyl alcohol, and isobutyl alcohol were taken as a series of alcohols, and acetate, propionate, butyrate, isobutyrate, and isovalerate ions were taken as a series of carboxylate ions. The geometries of these compounds used for the calculation are indicated in Fig. 1. The reactivity of the hydrogen atom expressed by ΔE is calculated by means of Eq. 1;

$$\Delta E = E(\text{C-H } 1.60) - E(\text{C-H } 1.10) \quad (1)$$

where E(C–H 1.60) is the total energy calculated by stretching the C–H bond by 0.5 Å in its singlet state, and E(C–H 1.10) is that at the equilibrium C–H distance in alcohols and carboxylate ions (assumed to be 1.10 Å). In order to examine the validity of ΔE for expressing the reactivity of the hydrogen atom in the hydrogen-abstraction reaction, we compared the ΔE of hydrogen atoms of alkanes with the activation energy for the hydrogen-abstraction reaction of the methyl radical and alkanes. As is shown in Table 1, the order of reactivity for primary, secondary, and tertiary hydrogen atoms is well explained by ΔE, and Fig. 2 shows

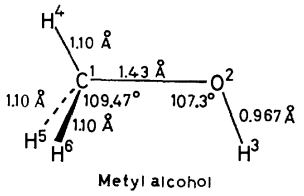

Metyl alcohol

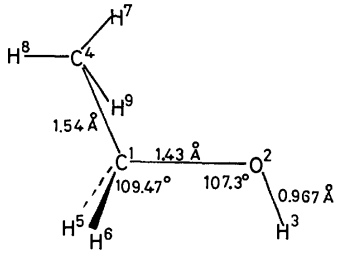

Ethyl alcohol

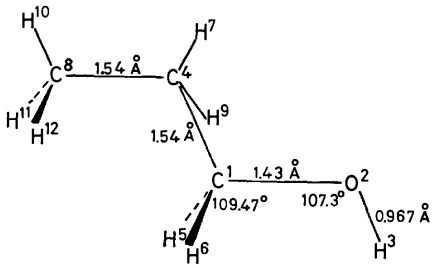

propyl alcohol

Fig. 1-1.

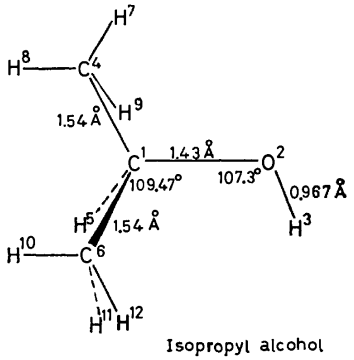

Isopropyl alcohol

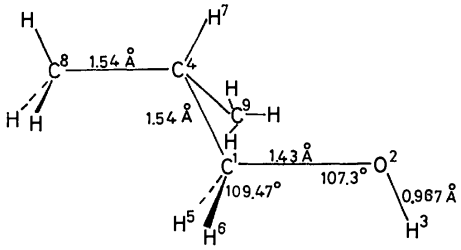

Isobutyl alcohol

Fig. 1-2.

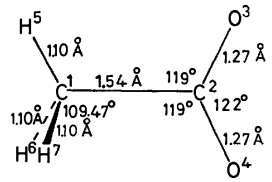

Acetate ion

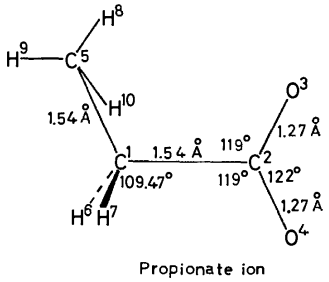

Propionate ion

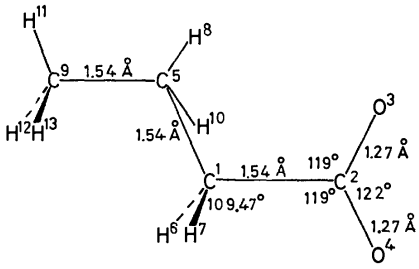

butyrate ion

Fig. 1-3.

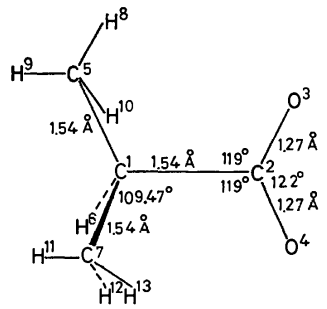

Isobutyrate ion

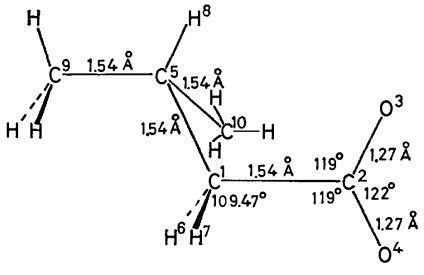

Isovalerate ion

Fig. 1-4.

Fig. 1. The geometries of alcohols and carboxylate ions used for the calculation of ΔE.

TABLE 1. COMPARISON OF ΔE WITH THE EXPERIMENTALLY DETERMINED ACTIVATION ENERGY FOR THE HYDROGEN ABSTRACTION REACTION OF THE METHYL RADICAL AND ALKANES

Alkane (R-H)	ΔE (kcal/mol)	$D_r^R(H)$[a]	E (kcal/mol)[b]
CH_3-H	105.8218	0.9926	11.5
CH_3CH_2-H	101.3681	1.0029	10.0
$CH_3CH_2CH_2$-H	100.3018	1.0037	9.5
$CH_3CH_2CH_2CH_2$-H	100.0508	1.0040	9.3
$(CH_3)_2CHCH_2$-H	100.1136	1.0049	—
$(CH_3)_2CH$-H	97.2281	1.014	8.7
$CH_3CH_2CH(CH_3)$-H	97.0399	1.015	8.2
$(CH_3)_3C$-H	93.3390	1.027	7.7
$(CH_3)_2CH(CH_3)_2C$-H	92.8998	1.029	7.8

a) Ref. 8. b) N. N. Tkhomirova and V. V. Voevodskii, *Dokl. Akad. Nauk SSSR.*, **79**, 993 (1951). These values were cited in Ref. 8.

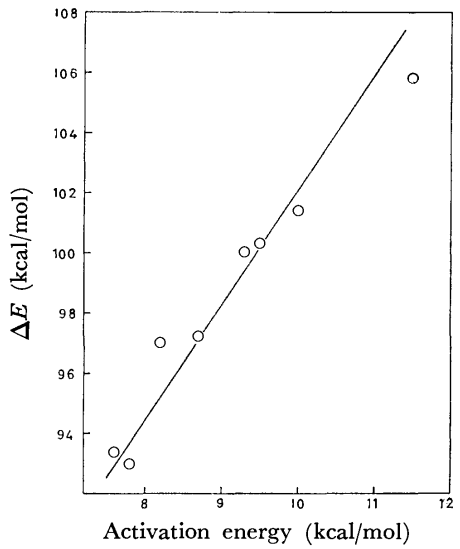

Fig. 2. The linear relationship between ΔE and activation energy for hydrogen abstraction reaction of methyl radical from alkanes.

a linear relationship between ΔE and the activation energy.

It is well known that the delocalizability, D_r^R, reprsented by Fukui *et al.*[7,8] has successfully been used to interpret the reactivity of saturated compounds toward several radicals.[7,8] As is shown in Table 1 and Fig. 3 for alkanes, ΔE is found to have a close relation with the D_r^R calculated by Kato *et al.*[8] Although the correlation shown in Table 1 cannot be taken as direct evidence for ΔE as a measure of the reactivity, the present result and the observed correlation between ΔE and ΔE_{OH} calculated for the partial reactivities of hydrogen atoms in amino acids[5] may support the validity of ΔE for the present purposes. The reactivities of hydrogen atoms in alcohols defined by ΔE are shown in Table 2, while Table 3 shows the result for carboxylate ions. It was suggested that hydrogen atoms bound to the identical carbon atom have different reactivities, depending on the orientation in the molecule;[9] a similar tendency is observed in the

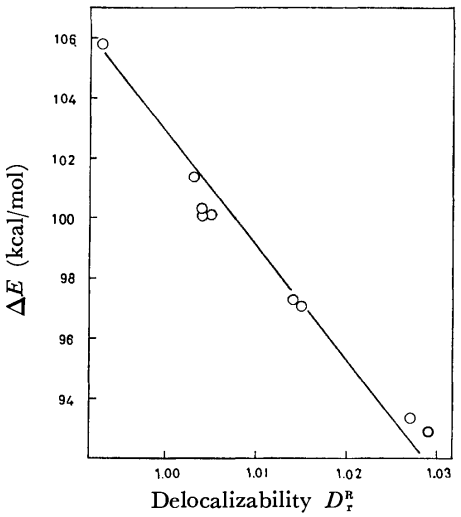

Fig. 3. The linear relationship between ΔE and Delocalizability D_r^R for alkanes.

TABLE 2. THE REACTIVITIES OF HYDROGEN ATOMS OF ALCOHOLS DEFINED BY ΔE

Alcohol	Type of C-H bond		ΔE (au)
CH_3OH	H^4	α-primary	0.1623
	H^5	α-primary	0.1584
C_2H_5OH	H^5	α-secondary	0.1516
	H^7	β-primary	0.1622
	H^8	β-primary	0.1637
$CH_3CH_2CH_2OH$	H^5	α-secondary	0.1513
	H^7	β-secondary	0.1558
	H^{10}	γ-primary	0.1605
	H^{11}	γ-primary	0.1614
$(CH_3)_2CHOH$	H^5	α-tertiary	0.1449
	H^7	β-primary	0.1605
	H^8	β-primary	0.1636
	H^9	β-primary	0.1619
	H^{10}	β-primary	0.1629
	H^{11}	β-primary	0.1599
	H^{12}	β-primary	0.1619
$(CH_3)_2CHCH_2OH$	H^5	α-secondary	0.1499
	H^6	α-secondary	0.1510
	H^7	β-tertiary	0.1498

cases of both alcohols and carboxylate ions. As the β-primary H^7 and H^8 atoms of ethyl alcohol (also the α-primary H^4 and H^5 atoms of methyl alcohol) have different reactivities, we approximate the reactivity of the β-primary hydrogen atom to the average reactivity of H^7 and H^8 atoms by the assuming Maxwell-Boltzmann distribution in order to compare ΔE with the partial reactivities; Table 4 shows the results. The same approximation was used for carboxylate ions. It is well known that, in hydrogen-abstraction reactions of radicals from alkanes, the reactivities of hydrogen atoms increase in this order; primary<secondary<tertiary, and that a similar tendency is observed for hydrogen atoms in the α-position and β-position of alcohols, as is shown in Table 4. The results for carboxylate ions are shown in Table 5 and Fig. 5. Although

Table 3. The reactivities of hydrogen atoms of carboxylate ions defined by ΔE

Carboxylate ion		Type of C-H bond	ΔE (au)
CH_3COO^-	H^5	α-primary	0.1565
	H^6	α-primary	0.1569
$CH_3CH_2COO^-$	H^6	α-secondary	0.1503
	H^8	β-primary	0.1588
	H^9	β-primary	0.1506
$CH_3CH_2CH_2COO^-$	H^6	α-secondary	0.1500
	H^8	β-secondary	0.1527
	H^{11}	γ-primary	0.1545
	H^{12}	γ-primary	0.1596
$(CH_3)_2CHCOO^-$	H^6	α-tertiary	0.1445
	H^8	β-primary	0.1572
	H^9	β-primary	0.1508
	H^{10}	β-primary	0.1588
	H^{11}	β-primary	0.1512
	H^{12}	β-primary	0.1571
	H^{13}	β-primary	0.1597
$(CH_3)_2CHCH_2COO^-$	H^6	α-secondary	0.1486
	H^7	α-secondary	0.1501
	H^8	β-tertiary	0.1467

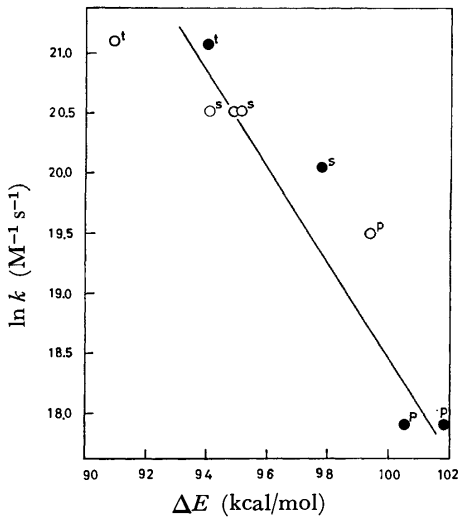

Fig. 4. The relation between ΔE and the partial reactivities of hydrogen atoms in alcohols. ○: α-, ●: β-, p: primary, s: secondary.

points are scattered, a fairly good correlation was found as a whole.

Asmus *et al.*[10] investigated the reaction site of aliphatic alcohols in the reaction with the hydroxyl radical by means of pulse radiolysis, and found that the main reaction is the abstraction of the hydrogen atom from the α-position, but hydrogen abstraction also occurs at β-, γ-, ··· positions with an increase in the number of carbon atoms. Moreover, they determined the relative probabilities of hydrogen abstraction from the α-positions of various alcohols. For example, 84.3, 53.4, 85.5, and 41.0% are obtained for C_2H_5OH, n-C_3H_5OH, $(CH_3)_2CHOH$, and n-C_4H_9OH respectively. The probabilities can be evaluated from the partial reactivities proposed by Anbar *et al.* to be 90.2, 58.5, 80.3, and 43.4% for the above alcohols respectively.

Table 4. Comparison of ΔE with the partial reactivities assigned to every C-H bond of alcohols

Type of C-H bond	Partial reactivity[a] $M^{-1}\,s^{-1}$	ΔE (kcal/mol)
α-Primary	3.02×10^8	99.3813
α-Secondary	8.40×10^8	95.0953[b]
		94.9072[c]
		94.0573[d]
α-Tertiary	1.48×10^9	90.8926
β-Primary	6.06×10^7	101.8342[e]
		100.6491[f]
β-Secondary	5.05×10^8	97.7299
β-Tertiary	1.41×10^9	93.9662
γ-Primary	6.06×10^7	100.8378

a) Ref. 1. b) Estimated from C_2H_5OH. c) From $CH_3CH_2CH_2OH$. d) From $(CH_3)_2CHCH_2OH$. e) From C_2H_5OH. f) From $(CH_3)_2CHOH$.

Table 5. Comparison of ΔE with the partial reactivities assigned to every C-H bond of carboxylate ions

Type of C-H bond	Partial reactivity[a] $M^{-1}\,s^{-1}$	ΔE (kcal/mol)
α-Primary	2.35×10^7	98.2299
α-Secondary	2.94×10^8	94.2799[b]
		94.0917[c]
		93.3752[d]
α-Tertiary	8.90×10^8	90.6417
β-Primary	6.06×10^7	94.4686[e]
		94.6931[f]
β-Secondary	5.05×10^8	95.7854
β-Tertiary	1.41×10^9	92.0217
γ-Primary	6.06×10^7	96.9299

a) Ref. 1. b) Estimated from $CH_3CH_2COO^-$. c) From $CH_3CH_2CH_2COO^-$. d) From $(CH_3)_2CHCH_2COO^-$. e) From $CH_3CH_2COO^-$. f) From $(CH_3)_2CHCOO^-$.

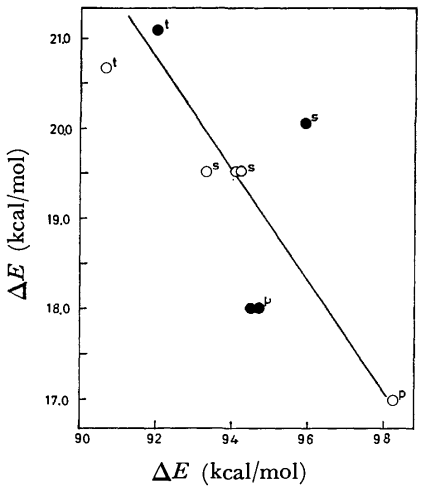

Fig. 5. The relation between ΔE and the partial reactivities of hydrogen atoms in carboxylate ions. ○: α-, ●: β-, p: primary, s: secondary.

This correlation between the observed and the estimated relative probabilities may support the idea that the reactivity of a molecule can be divided into partial reactivities. Furthermore, as is shown in Table 4, the value of ΔE calculated for the α-secondary hydrogen atom of ethyl alcohol is nearly equal to that for the α-secondary hydrogen atom of propyl alcohol or isobutyl alcohol. Similarly, the ΔE for the β-primary hydrogen atom of ethyl alcohol is approximately equal to that for the β-primary hydrogen atom of isopropyl alcohol. For hydrogen atoms in the γ-, δ-, $\cdots$ positions, the same partial reactivities as those for the β-positions are used in the paper of Anber *et al.* The values of ΔE calculated for the β-primary and γ-primary hydrogens may confirm this assignment (Table 4). A similar argument is possible for carboxylate ions (Table 5), although there remains a discrepancy between β-primary and γ-primary hydrogens.

Consequently, the present work, which takes the orientation of hydrogen atoms into consideration, supports the idea that, in hydrogen-abstraction reaction of the hydroxyl radical, the whole reactivity of a molecule can be understood in terms of the partial reactivities assigned to each site of the reaction in the molecule.

The calculations were carried out on the FACOM 230-75 computer of the Computer Center of Kyoto University. The research was supported, in part, by Scientific Grants (139012 and 038012) from the Ministry of Education, Culture and Sciences.

References

1) M. Anbar, D. Meyerstein, and P. Neta, *J. Chem. Soc., B.*, **1966**, 742.
2) R. L. Willson, C. L. Greenstock, G. E. Adams, R. Wageman, and L. M. Dorfman, *Int. J. Radiat. Phys. Chem.*, **3**, 211 (1971).
3) K. Fukui, T. Yonezawa, and H. Shingu, *J. Chem. Phys.*, **20**, 722 (1952); K. Fukui, T. Yonezawa, and H. Shingu, *ibid.*, **22**, 1433 (1954).
4) K. Fukui, T. Yonezawa, and C. Nagata, *Bull. Chem. Soc. Jpn.*, **27**, 423 (1954); K. Fukui, T. Yonezawa, and C. Nagata, *J. Chem. Phys.*, **27**, 1247 (1957).
5) H. Shinohara, A. Imamura, T. Masuda, and M. Kondo, submitted to *Bull. Chem. Soc. Jpn.*
6) J. A. Pople and D. L. Beveridge, "Approximate Molecular Orbital Theory," McGraw-Hill, New York (1970).
7) K. Fukui, H. Kato, and T. Yonezawa, *Bull. Chem. Soc. Jpn.*, **34**, 442 (1961).
8) K, Fukui, H. Kato, and T. Yonezawa, *Bull. Chem. Soc. Jpn.*, **34**, 1111 (1961).
9) K. Shimizu, K. Miyamichi, H. Kato, and T. Yonezawa, *Nippon Kagaku Zasshi*, **90**, 1206 (1969).
10) K-D. Asmus, H. Möclkel, and A. Henglein, *J. Phys. Chem.*, **77**, 1218 (1973).

Far Infrared Reflection Spectra and Lattice Vibrations of $CsNiCl_3$ Crystal

Kenji AKIYAMA, Yoshiyuki MORIOKA, and Ichiro NAKAGAWA

Department of Chemistry, Faculty of Science, Tohoku University, Aoba, Aramaki, Sendai 980

(Received July 7, 1977)

The frequencies of the transverse (TO) and longitudinal (LO) modes of the infrared active vibrations of the crystal $CsNiCl_3$ were obtained from the polarized far infrared reflection spectra. The polarized Raman spectra were also measured. The calculation of the TO and LO frequencies near the center of the Brillouin zone was made on the basis of a rigid ion model which includes effective ionic charges and interionic repulsive force constants. A set of potential constants and effective ionic charges were determined from the observed values of the TO and LO frequencies and Raman frequencies using the least-squares method. The short-range force constant associated with the nickel ion to the chlorine ion indicates that some amount of covalent character is included in this bond.

Cesium nickel trichloride, $CsNiCl_3$, is a so-called ionic crystal which has a hexagonal perovskite-like structure. A large number of double salts of the AMX_3 type (where A is a large univalent cation, M a divalent metal ion and X a halogen ion) are isomorphous to $CsNiCl_3$. The infrared spectra of these crystals reported, however, have been restricted to the transmission spectra of powder samples.[1] McPherson and Chang reported the infrared transmission spectra of powder sample of $CsNiCl_3$.[1] Adams and Smardzewski studied the polarized far infrared transmission spectra of a thin film of $(CH_3)_4NMnCl_3$,[2] the structure of which is closely related to that of $CsNiCl_3$.

Each of the transverse(TO) and the longitudinal (LO) frequencies of the infrared active modes can be determined by the infrared reflection spectra. In the present study we have measured the polarized far infrared reflection spectra and polarized Raman spectra of $CsNiCl_3$. Using the observed frequencies of the normal modes, the short-range potential constants and the effective ionic charges were obtained by means of the normal coordinate analysis for the optically active lattice vibrations.

The crystal structure of $CsNiCl_3$ as shown in Fig. 1 belongs to hexagonal system with the space group D^4_{6h} ($P6_3/mmc$).[3] Bravais unit cell consists of two formula units of $CsNiCl_3$. In this hexagonal structure, the nickel ions are located in the center of octahedra formed by chlorine ions and the chains of slightly compressed $NiCl_3$ octahedra sharing opposite faces run along the c axis of the crystal. The cesium ions are on the planes formed by three chlorine ions. The result of the factor group analysis on the basis of this structure is summarized in Table 1.

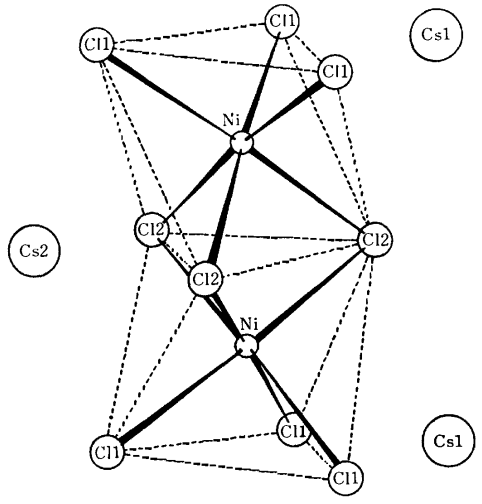

Fig. 1. Crystal structure of $CsNiCl_3$.

TABLE 1. FACTOR GROUP ANALYSIS FOR $CsNiCl_3$

D_{6h}	N[a]	T[b]	$N-T$[c]	Activity
A_{1g}	1	0	1	(xx+yy, zz)
A_{2g}	1	0	1	
B_{1g}	2	0	2	
B_{2g}	0	0	0	
E_{1g}	1	0	1	(yz, zx)
E_{2g}	3	0	3	(xx−yy, xy)
A_{1u}	0	0	0	
A_{2u}	3	1	2	z
B_{1u}	1	0	1	
B_{2u}	2	0	2	
E_{1u}	4	1	3	x, y
E_{2u}	2	0	2	

a) Total freedom. b) Acoustic modes. c) Optical active modes.

Experimental

Sample Preparation. The powder sample of $CsNiCl_3$ was crystallized by evaporation from the hot concentrated aqueous solution of CsCl and $NiCl_2$ in a 1 : 1 mole ratio, and was heated in vacuum for several hours. Completely dehydrated salt was molten in vacuum, filtered through quartz wool and sealed into quartz ampoule. The single crystal was grown from the molten salt by the Bridgman method. Crystal cleaves readily along the (110) plane and this cleavage plane was used for reflection measurement without polishing. For the Raman measurement, the single crystal was polished to a cube, three planes of which were parallel to (100), (001) and (010) planes, respectively.

Spectral Measurement. Polarized far infrared reflection spectra were recorded using a Hitachi 070 far infrared interferometer equipped with a wire-grid polarizer. The reflectivities for the lights polarized perpendicular and parallel to the c axis were measured. The incident angle was fixed at about 20°. The infrared transmission spectrum of the Nujol mull of powder sample was also measured. The polarized Raman spectra of the single crystal were measured by a Narumi double monochromator with a 632.8 nm line

of a He–Ne laser as a source.

Results

Figures 2a and 3a show the observed reflectivities for the lights polarized perpendicular and parallel to the c axis, respectively. The refractive index n, the absorption index k, and the real and imaginary parts of the dielectric constant, ε' and ε'', were obtained from the observed reflectivities using the Kramers-Kronig relation assuming the normal incidence.[4] The obtained results are shown in Figs. 2 and 3 together with the observed reflectivities. The TO frequencies are given by the maxima of the imaginary part of the dielectric constant and the corresponding LO frequencies are given by the frequencies where the real part of the dielectric constant becomes zero in changing from negative to positive values.[5] However, in the frequency region 270—100 cm^{-1} of Fig. 2c the real part of the dielectric constant does not become zero, and the OL frequency 180 cm^{-1} for ν_9(LO) was obtained by the frequency where Im$(-1/\varepsilon)$ has maximum value.[6]

It is clear that the TO and LO frequencies obtained from the reflectivities for the lights polarized perpendicular and parallel to the c axis correspond to the E_{1u} and A_{2u} modes of the factor group D_{6h}, respectively. The all infrared active vibrational modes predicted from the factor group analysis shown in Table 1 have been observed. The assignment of the five observed TO frequencies to the symmetry species is consistent with that of $(CH_3)_4NMnCl_3$ by Adams and Smardzewski, although the structures of $CsNiCl_3$ and $(CH_3)_4N$-

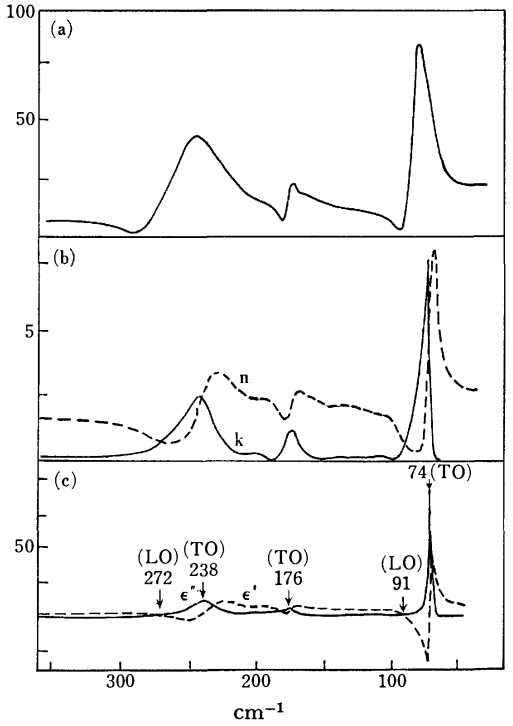

Fig. 2. (a) Percent reflectivity, (b) refractive index n, and absorption index k, and (c) real and imaginary parts of the dielectric constant, ε' and ε'', of $CsNiCl_3$ for the light polarized perpendicular to the c axis.

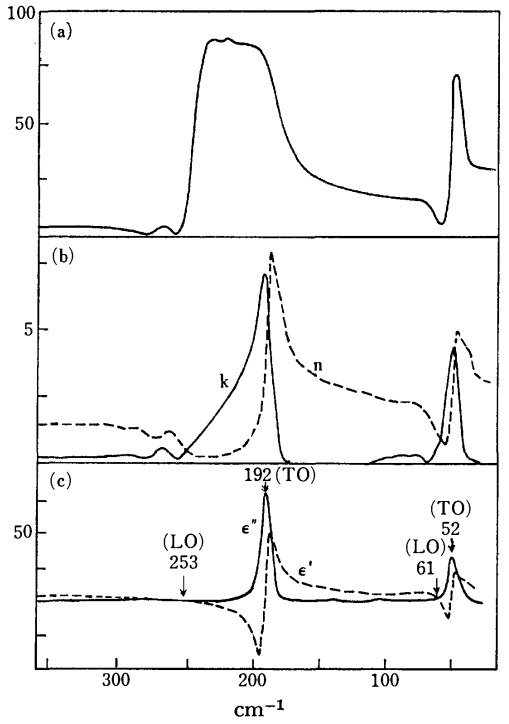

Fig. 3. (a) Percent reflectivity, (b) refractive index n and absorption index k, and (c) real and imaginary parts of the dielectric constant, ε' and ε'', of $CsNiCl_3$ for the light polarized parallel to the c axis.

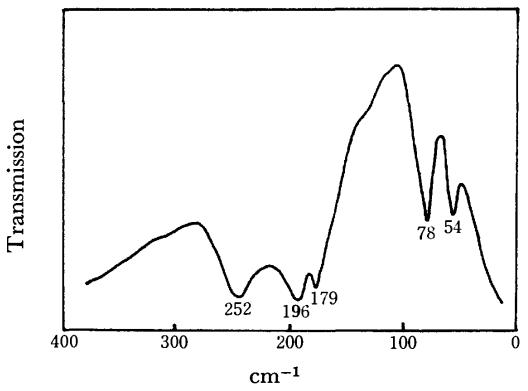

Fig. 4. Transmission spectrum of the powder sample of $CsNiCl_3$.

$MnCl_3$ are not exactly the same.

A short comment should be made on the transmission spectrum of the powder sample. Our result of the powder sample shown in Fig. 4 is in agreement with the spectrum by McPherson and Chang. The maximum absorption frequencies are slightly higher than the TO frequencies determined from the reflection spectra, which may be attributable to the crystal size effect.[7]

Figure 5 shows the observed Raman spectra in which the notations by Damen *et al.*[8] are indicated. On the basis of the Raman tensors of D_{6h} symmetry shown in Table 1 the bands at 264 and 140 cm^{-1} are assigned to the A_{1g} and E_{1g} modes, respectivery, and the bands at 190 and 52 cm^{-1} are assigned to the E_{2g} modes. Observed frequencies and vibrational

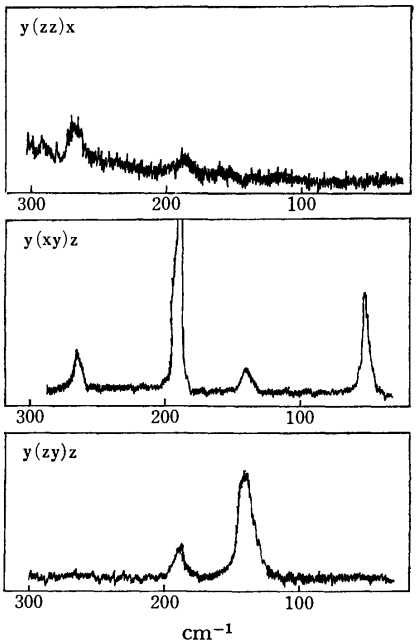

Fig. 5. Polarized Raman spectra of $CsNiCl_3$. Experimental z axis is coincident with the c axis of the crystal.

Table 2. Observed and calculated frequencies of infrared and raman active vibrations in $CsNiCl_3$

		Obsd (cm^{-1})	Calcd Case I (cm^{-1})	Calcd Case II (cm^{-1})
A_{1g}	ν_1	264	241	247
E_{1g}	ν_2	140	167	164
E_{2g}	ν_3	190	199	204
	ν_4		166	163
	ν_5	52	64	64
A_{2u}	ν_6(TO)	192	199	199
	ν_7(TO)	52	47	48
	ν_6(LO)	253	257	257
	ν_7(LO)	61	63	63
E_{1u}	ν_8(TO)	238	227	225
	ν_9(TO)	176	164	167
	ν_{10}(TO)	74	75	72
	ν_8(LO)	272	268	267
	ν_9(LO)	180	182	184
	ν_{10}(LO)	91	86	84

assignments are summarized in Table 2.

Normal Coordinate Analysis

Optically active vibrational frequencies are calculated according to the method of Shimanouchi, Tsuboi and Miyazawa.[9] Equations of motion for a rigid ion model are written in terms of the Cartesian displacement coordinates of component ions of a whole crystal;

$$4\pi^2\nu^2\boldsymbol{MX} = (\boldsymbol{F}_x^R + \boldsymbol{F}_x^C)\boldsymbol{X}, \quad (1)$$

$$\boldsymbol{F}_x^C = \boldsymbol{ZCZ}, \quad (2)$$

where $\boldsymbol{X}$ is column matrix corresponding to the Cartesian displacement coordinates and $\boldsymbol{M}$ and $\boldsymbol{Z}$ are the diagonal matrices specifying the masses and ionic charges. $\boldsymbol{F}_x^R$ and $\boldsymbol{F}_x^C$ (or $\boldsymbol{C}$) denote the short-range repulsive potential and the long-range Coulomb potential, respectively. The secular equation

$$|\boldsymbol{M}^{-1}(\boldsymbol{F}_x^R + \boldsymbol{F}_x^C) - \boldsymbol{E}\lambda| = 0 \quad (\lambda = 4\pi^2\nu^2), \quad (3)$$

is set up and the TO and LO frequencies of crystal are calculated.

Since the TO-LO splittings for the infrared active modes arise from the macroscopic electric field, the effective ionic charges are estimated by using the TO-LO splitting. The relation between the effective ionic charges and the TO-LO splittings is derived as[10]

$$8\pi\left(\frac{e_{Ni}^2}{m_{Ni}} + \frac{e_{Cs}^2}{m_{Cs}} + \frac{3e_{Cl}^2}{m_{Cl}}\right)\Big/ v_a = \sum_i \lambda_i^2(\mathrm{LO}) - \sum_i \lambda_i^2(\mathrm{TO}), \quad (4)$$

where m_{Ni}, m_{Cs}, and m_{Cl} are atomic masses, e_{Ni}, e_{Cs}, and e_{Cl} are effective ionic charges, v_a is the volume of the Bravais unit cell and λ_i is the frequency parameter ($\lambda_i = 4\pi^2\nu_i^2$) of the i-th vibration. For a condition of the electrical neutrality of a crystal as a whole, the effective ionic charges must satisfy the relation

$$Z_{Cs} + Z_{Ni} + 3Z_{Cl} = 0, \quad (5)$$

where $Z_i e = e_i$ (i=Ni, Cs, and Cl). From Eqs. 4 and 5, the relation among Z_{Ni}, Z_{Cs}, and Z_{Cl} is determined and therefore only one Z_i of the three becomes independent.

The long-range Coulomb part $\boldsymbol{F}_x^C$ is calculated from the effective ionic charges and the $\boldsymbol{C}$ matrix, which is obtained using Ewald's transformation according to the method derived by Kellerman.[11]

As for the short-range part $\boldsymbol{F}_x^R$, two different model force fields have been applied.

Case I; The central force type potential was assumed for all the interionic interactions.

Case II; The valence force type potential for the $NiCl_6$ structure and the central force type potential for the ion pairs, for which the nonbonded repulsions or the ionic interactions are expected to be appreciable, were assumed.

In case I, the potential energy of the crystal is given as

$$V = \frac{1}{2}\sum_{lk}\sum_{l'k'}{}' \varphi_{kk'}(r(lk:l'k')), \quad (6)$$

where $\varphi_{kk'}$ is the interaction potential between the k-th and k'-th ions and $r(lk:l'k')$ is the instantaneous distance between the k-th ion in the l-th unit cell and the k'-th ion in the l'-th unit cell. The short-range potential $\varphi_{kk'}$ is a function of only the distance between the two ions. The matrix elements of the short range part $\boldsymbol{F}_x^R$ are given as;

$$F_x^R(k\alpha,k'\beta) = -\sum_{l'}\left\{\frac{x_\alpha x_\beta}{r^2}\left[\varphi''_{kk'}(r) - \frac{1}{r}\varphi'_{kk'}(r)\right] + \frac{\delta_{\alpha\beta}}{r}\varphi'_{kk'}(r)\right\}\Big|_{r=r_0(lk:l'k')}$$

$$F_x^R(k\alpha,k\beta) = \sum_{k'(\neq k)}{}' F_x^R(k\alpha,k'\beta), \quad (7)$$

where $r_0(lk:l'k')$ denotes $r(lk:l'k')$ in the equilibrium arrangement and x_α is the α-Cartesian component

(α=x, y, and z) of $r_0(lk:l'k')$.

The ion pairs within a distance of 4.0 Å were taken into account, since the short-range repulsive force may become significant in this interionic distance. The following ten potential constants were taken;

$$K_1 = [\varphi''(\text{Ni-Cl})(r)]_{r=r_0(\text{Ni-Cl})},$$

$$k_1 = \left[\frac{1}{r}\varphi'(\text{Ni-Cl})(r)\right]_{r=r_0(\text{Ni-Cl})},$$

$$K_2 = [\varphi''(\text{Cs-Cl})_{\text{I}}(r)]_{r=r_0(\text{Cs-Cl})_{\text{I}}},$$

$$k_2 = \left[\frac{1}{r}\varphi'(\text{Cs-Cl})_{\text{I}}(r)\right]_{r=r_0(\text{Cs-Cl})_{\text{I}}},$$

$$K_3 = [\varphi''(\text{Cs-Cl})_{\text{II}}(r)]_{r=r_0(\text{Cs-Cl})_{\text{II}}},$$

$$k_3 = \left[\frac{1}{r}\varphi'(\text{Cs-Cl})_{\text{II}}(r)\right]_{r=r_0(\text{Cs-Cl})_{\text{II}}},$$

$$K_4 = [\varphi''(\text{Cl-Cl})_{\text{I}}(r)]_{r=r_0(\text{Cl-Cl})_{\text{I}}},$$

$$k_4 = \left[\frac{1}{r}\varphi'(\text{Cl-Cl})_{\text{I}}(r)\right]_{r=r_0(\text{Cl-Cl})_{\text{I}}},$$

$$K_5 = [\varphi''(\text{Cl-Cl})_{\text{II}}(r)]_{r=r_0(\text{Cl-Cl})_{\text{II}}},$$

$$k_5 = \left[\frac{1}{r}\varphi'(\text{Cl-Cl})_{\text{II}}(r)\right]_{r=r_0(\text{Cl-Cl})_{\text{II}}},$$

where subscripts I and II denote the inter-layer and intralayer ion pairs, respectively. (According to the numbering of the atoms in Fig. 1, the inter-layer ion-pairs include those of Cs_1–Cl_1, Cs_2–Cl_2, Cl_1–Cl_1, and Cl_2–Cl_2, and the intralayer ion pairs include those of Cs_1–Cl_2, Cs_2–Cl_1, and Cl_1–Cl_2). The interionic distances in the equilibrium arrangement are listed in Table 3.

There are 11 parameters to be determined; ten are the short-range repulsive force constants and one is the effective ionic charge. In the actual procedure, K_4, K_5, k_4, and k_5 were estimated from the nonbonded chlorine-chlorine interaction potential of Lennard-Jones 6—12 type,[12] and k_2 and k_3 were fixed -0.01 mdyn/Å and -0.006 mdyn/Å, respectively, which correspond to the values for -0.1 K_2 and -0.1 K_3*.

The long-range Coulomb part was calculated from various sets of Z_i's and in each case the short-range repulsive force constants were determined by the least squares method using the observed vibrational frequencies. It was found that among the various sets of Z_i's only those for $Z_{\text{Cl}}=-0.6$——-0.7 are physically significant. For the value of Z_{Cl} larger than -0.6 the effective ionic charge of cesium ion becomes negative and for the value smaller than -0.7, no physically significant frequencies are obtained for the low-frequency vibrational modes.

The set of the effective ionic charges shown in Table 3 gives a most satisfactory result. (The sum of the square deviations of the calculated frequencies from the observed ones becomes minimum for this set of Z_i's when Z_{Cl} is varied from -0.6 to -0.7). The calculated frequencies and the obtained short-range repulsive force constants are shown in Tables 2 and 3 as case I, respectively.

In case II, the short-range potential function is given as:

$$V = \frac{1}{2}\sum K_1(\Delta r^i_{\text{Ni-Cl}})^2 + \frac{1}{2}\sum H_1(r^\circ_{\text{Ni-Cl}}\Delta\alpha^i(\text{Cl}_1\text{-Ni-Cl}_1))^2 + \frac{1}{2}\sum H_2(r^\circ_{\text{Ni-Cl}}\Delta\alpha^i(\text{Cl}_1\text{-Ni-Cl}_2))^2 + \frac{1}{2}\sum K_2(\Delta r^i_{(\text{Cs-Cl})_{\text{I}}})^2 + \frac{1}{2}\sum K_3(\Delta r^i_{(\text{Cs-Cl})_{\text{II}}})^2 + \frac{1}{2}\sum K_4(\Delta r^i_{(\text{Cl-Cl})_{\text{I}}})^2 + \frac{1}{2}\sum K_5(\Delta r^i_{(\text{Cl-Cl})_{\text{II}}})^2, \quad (8)$$

where K_1 is the Ni–Cl bond stretching force constant, K_2 and K_3 are those for the interaction between the cesium and chlorine ions, K_4 and K_5 are the repulsive force constants between two chlorine ions and H_1 and H_2 are the Cl_1–Ni–Cl_1 and Cl_1–Ni–Cl_2 bending force constants. The calculated frequencies and the force constants obtained by the least-squares method are shown in Tables 2 and 3 as case II, respectively.

In the procedure of the force constant calculation mentioned above, 4 force constants in case I and 5 force constants in case II were determined by the least-squares method using 14 observed frequencies. The standard deviations are given for these force constants in Table 3.

TABLE 3. DETERMINED SHORT-RANGE FORCE CONSTANTS AND EFFECTIVE IONIC CHARGES

Short range force constants				Corresponding interionic distances (Å)
Case I (mdyn/Å)		Case II (mdyn/Å)		
K_1	0.764(±0.043)	K_1	0.739(±0.048)	2.44
K_2	0.096(±0.022)	K_2	0.085(±0.020)	3.57
K_3	0.064(±0.011)	K_3	0.059(±0.010)	3.70
K_4	0.062	K_4	0.062	3.34
K_5	0.020	K_5	0.020	3.55
k_1	0.082(±0.061)	H_1	0.015(±0.013)	
k_2	−0.010	H_2	0.036(±0.024)	
k_3	−0.006			
k_4	−0.003			
k_5	−0.000			
Effective ionic charges				
$Z_{\text{Cl}}=-0.660$				
$Z_{\text{Ni}}=1.462$				
$Z_{\text{Cs}}=0.518$				

Throughout this paper 1Å=0.1 nm, 1 mdyn/Å=10^2N/m.
The values in parentheses denote standard deviations.

Discussion

The spectrum consisting of the five TO vibrations (two A_{2u} and three E_{1u} modes) as shown in Figs. 2, 3, and 4 reveals a typical feature characteristic of the two-layer type of the AMX_3 perovskite structure. The powder transmission spectrum of $CsNiF_3$ which has the same structure is similar to that of $CsNiCl_3$, although the lowest band was not observed for $CsNiF_3$ due to the limitation of the utilized spectrometer.[14]

The observed infrared and Raman frequencies are well explained by the model used in the calculation.

* The values of k_2 and k_3 do not affect the calculated frequencies significantly. Here, the same assumption as in the case of CdX_2 was made.[13]

This model is simple but it includes both the short-range potential and the long-range Coulomb potential in terms of effective ionic charges and explains quantitatively the splittings of the TO and LO frequencies.

In Table 2 the calculated frequencies by the converged set of force constants are not very different in both cases. The short-range potential of the type in case II has been often used for the complex salts such as K_2PtCl_6 and it has been found that this type of the potential is quite satisfactory to interpret the lattice vibrations due to the interaction between the complex ion and the outer ion as well as the intra-ligand vibrations. However, in the case of more ionic crystals like $CsNiCl_3$, the central force type potential may be more adequate for the analysis of the interionic vibrations. In this type of the potential the first derivatives of the interionic potential $\varphi'_{kk'}$ cannot be neglected. In $CsNiCl_3$, k_1, which corresponds to the first derivative of the interaction potential between the Ni and Cl ions, amounts to a significant value as shown in Table 3. A physically significant K_1 value (the second derivative of the Ni–Cl interaction potential) may be obtained, by taking k_1 into consideration. The neglect of the first derivatives in the central force potential cannot explain both Raman and infrared observed frequencies simultaneously, as in the case of CdX_2.[13]

The value of the Ni–Cl stretching force constant K_1 is obtained as 0.764 mdyn/Å in case I and 0.739 mdyn/Å in case II. These values are definitely smaller than the value 1.8 mdyn/Å of the Ni–C stretching force constant in $Ni(CO)_4$[15] but are comparable to the value 0.977 mdyn/Å for the Ni–F stretching force constant in $KNiF_3$,[16] indicating that some amount of covalent character is included in the Ni–Cl bond.

The ionic displacements for each vibration are shown in Fig. 6 on the basis of the eigenvectors L_x for the secular equation (3). The $\nu_5(E_{2g})$, $\nu_7(A_{2u})$, and ν_{10} (E_{1u}) are the translational lattice modes, and the others are the vibrations of the $NiCl_6$-octahedra. The Ni–Cl stretching and Cl–Ni–Cl bending vibrations are not clearly distinguished unlike those for the cubic perovskite fluorides. However, the $\nu_6(A_{2u})$ and $\nu_8(E_{1u})$ modes may have the nature of the Ni–Cl stretching vibration considering the potential energy distribution.

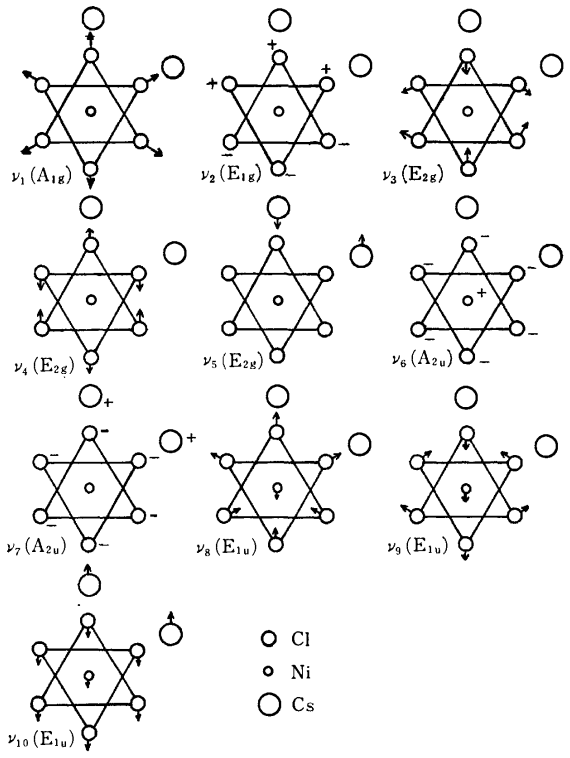

Fig. 6. Displacement of ions for infrared and Raman active vibrations of $CsNiCl_3$ crystal. Projection on the (001) plane.

The authors wish to express their thanks to Professor Mitsuo Ito of Tohoku University for permitting us to use the Raman spectrometer in his laboratory.

References

1) G. L. McPherson and Jin Rong Chang, *Inorg. Chem.*, **12**, 1196 (1973).
2) D. M. Adams and R. R. Smardzewski, *Inorg. Chem.*, **10**, 1127 (1971).
3) G. N. Tischenko, *Jr. Inst. Kristallogr. Akad. Nauk. SSSR.*, **11**, 93 (1955).
4) D. M. Roesller, *Brit. J. Appl. Phys.*, **16**, 1119 (1965). *ibid.*, **17**, 1313 (1966).
5) I. Nakagawa, *Bull. Chem. Soc. Jpn.*, **44**, 3014 (1971).
6) "Far-Infrared Properties of solids," ed by S. S. Mitra and S. Nudelman, Plenum Press New York, London (1970), p. 262.
7) M. Ishii, J. Hiraishi, and H. Takahashi, *Kagaku No Ryoiki*, **27**, 1005 (1973).
8) T. C. Damen, S. P. S. Porto, and B. Tell, *Phys. Rev.*, **142**, 570 (1966).
9) T. Shimanouchi, M. Tsuboi, and T. Miyazawa, *J. Chem. Phys.*, **35**, 1597 (1961).
10) J. Hiraishi, *Bull. Chem. Soc. Jpn.*, **46**, 1334 (1973).
11) E. W. Kellermann, *Phil. Trans. Roy. Soc.*, **238**, 513 (1940).
12) T. Shimanouchi, I. Nakagawa, J. Hiraishi, and M. Ishii, *J. Mol. Spectrosc.*, **19**, 78 (1966).
13) Y. Morioka and I. Nakagawa, *Spectrochim. Acta*, to be published.
14) K. Kohn and I. Nakagawa, *Bull. Chem. Soc. Jpn.*, **43**, 3780 (1970)
15) R. L. Dekock, *Inorg. Chem.*, **10**, 1205 (1971).
16) I. Nakagawa, *Spectrochim. Acta, Part A*, **29**, 1451 (1973).

Vibrational Spectra of Hydantoin and Its *C*- and *N,N'*-Deuterated Compounds

Yutaka SAITO and Katsunosuke MACHIDA*

Faculty of Pharmaceutical Sciences, Okayama University, Tsushima-Naka, Okayama 700

** Faculty of Pharmaceutical Sciences, Kyoto University, Sakyo-ku, Kyoto 606*

(Received August 18, 1977)

Infrared and Raman spectra of hydantoin and its *C*- and *N,N'*-deuterated derivatives in the solid state have been recorded. The fundamental frequencies were assigned by referring to isotopic frequency shifts and vibrational spectra of related compounds. Normal coordinate analysis was carried out by using a planar C_s molecular model. A simple Urey-Bradley force field was used for the stretching and the bending coordinates and a valence force field for the out-of-plane deformation and the torsional coordinates. The force constants were refined by the least squares method to reproduce the observed frequencies

We investigated vibrational spectra and force constants of ethyleneurea, $\boxed{-CH_2CH_2NHCONH-}$, regarding it as a basic compound of ring urea derivatives.[1] Since then we have carried out a detailed vibrational analysis of hydantoin (2,4-imidazolidinedione), $\boxed{-CH_2CONHCONH-}$, which is of biological interest because of its structural analogy to nucleic bases and the anticonvulsive activity of a number of its derivatives.

Infrared and Raman spectra of hydantoin, H-d_0, *C*-deuterated hydantoin, HC-d_2, *N,N'*-deuterated hydantoin, HN-d_2, and perdeuterated hydantoin, H-d_4, were recorded and a normal coordinate analysis based on a modified Urey-Bradley force field was carried out for the four isotopic hydantoins. The force constants fitting the observed frequencies reflect the structural difference between hydantoin and ethyleneurea.

Experimental

Reagent grade H-d_0 (Tokyo Kasei Co.) was recrystallized four times from water. For the preparation of HC-d_2, a mixture of purified H-d_0 (5 g) and 30% D_2SO_4 in D_2O (Merck AG., 10 ml) was warmed at 80 °C in a sealed ampoule for 8 h. The solution was cooled on an ice bath, and the resulting solid was filtered quickly, washed with heavy water and dried under reduced pressure. The procedure was repeated four times until the infrared absorptions due to the CH_2 bending and wagging vibrations became hardly detectable. The yellowish crude product was purified by recrystallization from water: yield 1 g. The *N,N'*-deuteration of H-d_0 and HC-d_2 was carried out by the exchange reaction with heavy water.

The infrared spectra were recorded on a JASCO A-2 and a Hitachi FIS-3 grating spectrophotometers for the samples in Nujol and hexachlorobutadiene mulls. The frequencies were calibrated by the standard absorptions of polystyrene, indene and ammonia. The Raman spectra were recorded on a JEOL S-1 laser Raman spectrophotometer by using the 514.5 nm line of a Coherent 52G Ar^+ laser as the excitation incidence (30 mW at the sample position). The samples were sealed in 1 mm unheparinized haematocrit tubes. The spectra obtained are shown in Figs. 1—3.

Vibrational Assignments

The infrared bands due to the NH stretching modes of H-d_0 and HC-d_2 and the ND stretching modes of HN-d_2 and H-d_4 split into three or four peaks arising certainly from Fermi resonance with the summation tones involving the C=O stretching and the NH (or ND) in plane deformation vibrations. The infrared bands due to the CH_2 and the CD_2 stretching modes are very weak but the corresponding bands in the Raman spectra are observed clearly at 2980 and 2950 cm^{-1} for the *C*-undeuterated compounds H-d_0 and HN-d_2, and at 2240 and 2170 cm^{-1} for the *C*-deuterated compounds HC-d_2 and H-d_4. The *N,N'*-undeuterated compounds, H-d_0 and HC-d_2, show two strong infrared bands near 1775 and 1700 cm^{-1} assignable straightway to the C=O stretching vibrations. The shift of these bands on the *N,N'*-deuteration is much smaller than those reported for methylurea[2] and ethyleneurea.[1]

H-d_0 shows three infrared bands at 1430, 1403, and 1382 cm^{-1} in the region 1500—1350 cm^{-1}. The assignment of the 1430 cm^{-1} band to the CH_2 bending vibration is obvious from its disappearance on *C*-deutera-

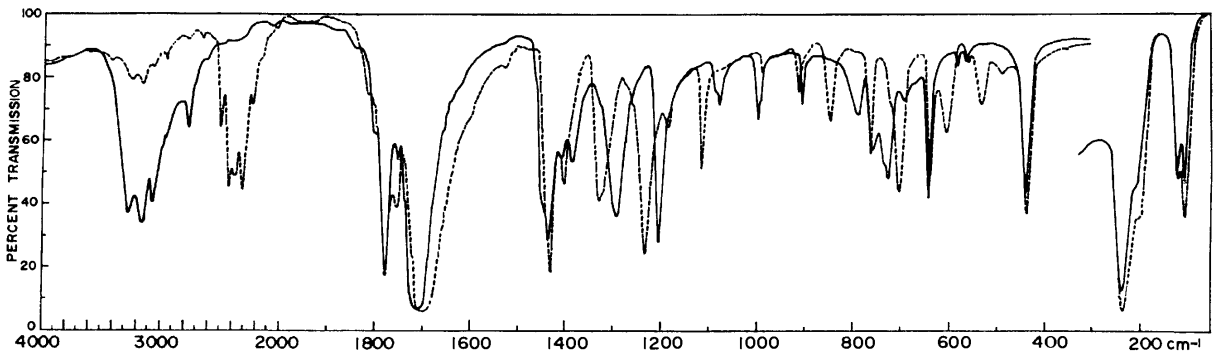

Fig. 1. Infrared spectra of hydantoin (——) and HN-d_2 (----).

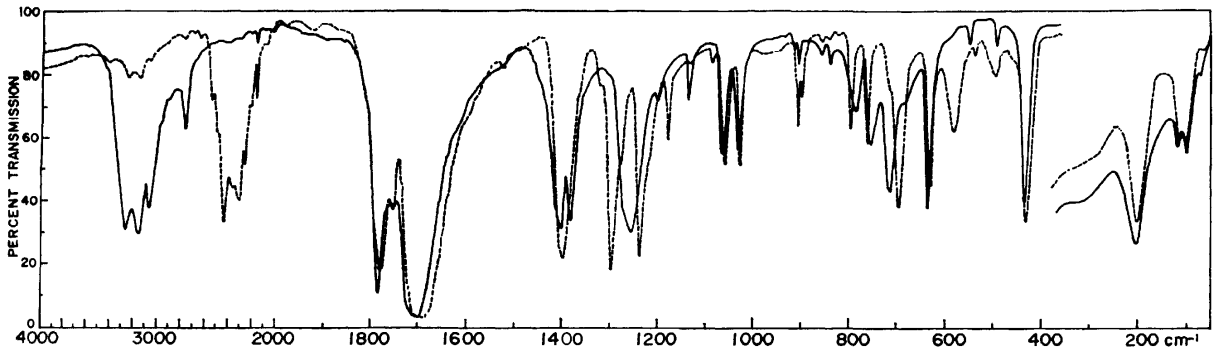

Fig. 2. Infrared spectra of HC-d_2(——) and H-d_4 (---).

Table 1. Observed infrared frequencies and assignments for hydantoin and N,N'-deuterated hydantoin

Hydantoin IR[a]	Calcd	Assignment[b]	N,N'-Deuterated hydantoin IR[a]	Calcd	Assignment[b]
3255 s	3206	νNH+νN'H(a')	2958 vw	2953	ν_sCH$_2$(a')
3143 s	3204	νN'H+νNH(a')		2952	ν_aCH$_2$(a'')
3060 s	—	1706+1382=3088(A')	2486 m	—	1231×2=2462(A')
2762 m	—	1382×2=2764(A')	2420 m	2362	νN'D+νND(a')
2958 vw	2953	ν_sCH$_2$(a'')	2308 m	2354	νND+νN'D(a')
	2952	ν_aCH$_2$(a')	2231 w	—	1114×2=2228(A')
1775 s	1777	νCO+νCN(a')	1773 s	1771	νCO(a')
1706 vs	1698	νC''O+νC''N(a')	1692 vs	1692	νC''O(a')
1440 sh	1439	δN'H+νskel+βCH$_2$(a')	1424 s	1427	βCH$_2$(a')
1430 s	1423	βCH$_2$(a')	1399 m	1396	νCN+νCN'+δskel(a')
1403 m	1405	νskel+δN'H(a')	1320 m	1306	νC''N(a')
1382 m	1373	δNH(a')	—	1260	tCH$_2$(a'')
1289 m	1275	νC''N+δC''O(a')	1231 s	1244	νskel+δND+δN'D(a')
—	1260	tCH$_2$(a'')	1183 w	1191	νC'N+ωCH$_2$(a')
1202 s	1194	ωCH$_2$+νC'N(a')	1114 m	1128	δN'D+ωCH$_2$(a')
1075 w	1079	νC'N+δNH(a')	976 vw	953	νskel+δND(a')
995 w	1006	νCN'+νCN(a')	915 w	894	νC'C''+δND+νCN(a')
906 w	922	νC'C''+νCN(a')	900 sh	879	ρCH$_2$(a'')?
—	882	ρCH$_2$(a'')	842 w	840	δN'D+δND+νCN'(a')
788 m	802	torsion+πCO+πNH(a'')	760 m	755	πCO(a'')
755 m	744	πCO+torsion(a'')	700 m	703	δskel+νskel(a')
723 s	717	δCNC'+δNCN'+νC'N(a')	636 m	633	δCO+νCN(a')
683 m	662	πNH+τCN+πCO(a'')	598 w	581	torsion+πC''O+πN'D(a'')
639 m	652	δCO(a')	554 vw	564	δC'C''N'+νC'C''+δC''O(a')
574 vw	573	δC'C''N'+νC'C''(a')	525 w	532	πC''O+τC''N(a'')
558 vw	537	πC''O(a'')	478 vw	496	πND+τCN(a'')
435 m	432	δC''O+δCO(a')	432 m	430	δC''O+δCO(a')
235 s	233	πNH+torsion(a'')	232 s	230	torsion+πND(a'')
120 m	120	πN'H+torsion(a'')	118 m	119	πN'D+torsion(a'')
104 m	—	lattice vibration	103 m	—	lattice vibration

a) vs, very strong; s, strong; m, medium; w, weak; vw, very weak; sh, shoulder. b) ν, stretching; β, bending; ω, wagging; t, twisting; ρ, rocking; δ, in-plane deformation; π, out-of-plane deformation; τ, torsion.

tion. The 1403 cm^{-1} and the 1382 cm^{-1} bands are assigned to a skeletal stretching vibration and one of the two NH in-plane deformation vibrations, respectively, since the former persists on both the C- and the N,N'-deuteration without large frequency shifts, while the latter disappears on N,N'-deuteration. According to normal coordinate analysis, the other NH in-plane deformation vibration of H-d_0 seems to contribute to the shoulder band at 1440 cm^{-1} which shifts to 1415 cm^{-1} on C-deuteration.

The infrared absorption bands observed in the region 1350—800 cm^{-1} show complicated isotopic shifts, but are given reasonable assignments by taking account of four skeletal vibrations of all the isotopes, a CH$_2$ wagging vibration of H-d_0 and NH-d_2, two ND in-plane deformation vibrations of HN-d_2 and H-d_4, and a CD$_2$ bending and a CD$_2$ wagging vibrations of HC-d_2 and H-d_4. Some of the infrared bands around 900 cm^{-1} are very weak, but can be recognized as fundamentals by virtue of their strong Raman counterparts.

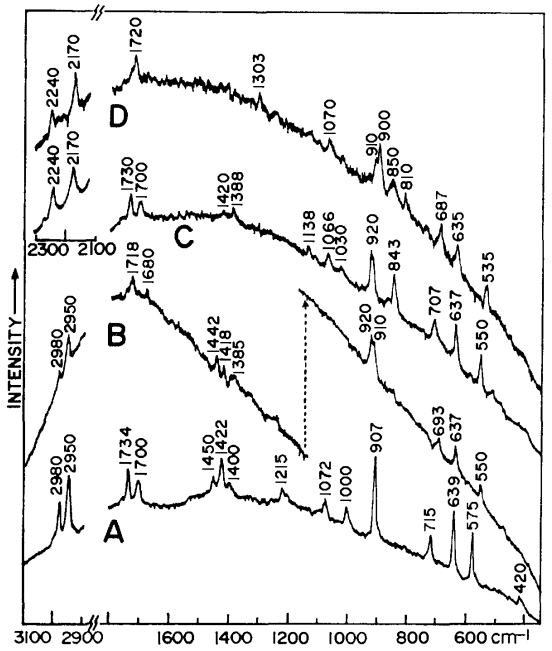

Fig. 3. Raman spectra and the observed frequencies of hydantoin (A), HN-d_2(B), HC-d_2(C), and H-d_4 (D).

As in the case of ethyleneurea,[1] the skeletal in-plane deformation frequencies in the region 800—400 cm^{-1} are easily recognized since they appear strongly in the Raman spectra. The NH and the ND out-of-plane deformation frequencies in the same region were identified from the change of the infrared spectra on *N,N'*-deuteration.

The assigned fundamental frequencies in the a' species of the four isotopic hydantoins were confirmed to be consistent with the product[3] and the sum[4] rules as seen in Table 3. The a" frequencies could not be checked by the isotopic rules because of the lack of data for the CH_2 twisting and the CH_2 and the CD_2 rocking frequencies.

Normal Coordinate Analysis

Taking account of the results of the X-ray analysis of diphenylhydantoin[5] and thiohydantoin,[6] we have assumed a planar C_s conformation of hydantoin. According to this structure, the normal vibrations of hydantoin are classified into 18 a' and 9a" vibrations. On calculating the ***G*** matrices, the C=O bondlength was transferred from diphenylhydantoin[5] and the other structural parameters from thiohydantoin.[6] The out-

Table 2. Observed infrared frequencies and assignments for *C*-deuterated hydantoin and per-deuterated hydantoin

C-Deuterated hydantoin			Per-deuterated hydantoin		
IR[a]	Calcd	Assignment[b]	IR[a]	Calcd	Assignment[b]
3255 s	3206	νNH+νN'H(a')	2532 w	—	1298+1235=2533(A')
3143 s	3203	νN'H+νNH(a')	2434 s	2362	νND+νN'D(a')
3060 s	—	1700+1380=3080(A')	2303 m	2355	νN'D+νND(a')
2760 m	—	1380×2=2760(A')	2262 m	—	1235+1023=2258(A')
2165 vw	2176 2156	ν_aCD$_2$(a") ν_sCD$_2$(a')	2163 w	2176 2154	ν_aCD$_2$(a") ν_sCD$_2$(a')
1774 vs	1776	νCO+νCN(a')	1700 vs	1771	νCO+νCN(a')
1700 vs	1696	νC"O+νC"N(a')	1682 vs	1690	νC"O+νC"N(a')
1415 sh	1430	δN'H+νskel(a')	1392 s	1390	νCN+νCN'+δCO(a')
1395 s	1398	νskel+δN'H+δNH(a')	1298 s	1306	νC"N+δN'D(a')
1380 s	1376	δNH(a')	1235 s	1227	νC'N+νCN+δND(a')
1256 s	1274	νC"N'+νC'C"+δC"O(a')	1174 m	1166	νC'N+νC'C"+δN'D(a')
1135 m	1136	νC'N+ωCD$_2$(a')	1055 m	1062	βCD$_2$(a')
1064 m	1064	βCD$_2$+νC'N(a')	1023 m	1031	δN'D+δND+ωCD$_2$(a')
1034 m	1027	νCN'+νCN(a')	905 w	915	tCD$_2$(a")
914 vw	913	νC'C"+ωCD$_2$+βCD$_2$(a')	898 w	894	νC'C"+νCN+βCD$_2$(a')
905 w	918	tCD$_2$(a")	841 vw	837	δND+δN'D(a')
840 vw	834	ωCD$_2$+δC"O(a')	795 m	788	ωCD$_2$(a')
785 m	799	τCN'+τC"N+πN'H+πCO(a")	758 s	760	πCO(a")
750 m	773	πCO+πNH+ρCD$_2$(a")	—	734	ρCD$_2$+πCO(a")
715 m	709	δskel+νC'N(a')	693 m	696	δNCN'+δCNC'+νC'N(a')
—	712	ρCD$_2$+τCN'+πCO(a")	627 m	625	δCO+δC'C"N'+νCN'(a')
680 sh	659	πNH+τCN+πCO(a")	580 m	571	τCN'+τC"N'+πN'D(a")
637 m	636	δCO+δC'C"N'+νCN'(a')	540 vw	542	δC'C"N'+δC'C"+δCO(a')
550 w	548	δC'C"N'+δCO+νC'C"(a')	495 w	500	πC"O+ρCD$_2$(a")
493 w	501	πC"O(a")		494	πND+τCN(a")
433 m	427	δC"O+δCO(a')	429 m	426	δC"O+δCO(a')
204 s	214	πNH+τCN+τC"N(a")	202 s	211	τCN+πND(a")
120 m	119	πN'H+torsion(a")	115 m	117	πN'D+torsion(a")
102 m	—	lattice vibration	102 m	—	lattice vibration

a) See footnote a), Table 1. b) See footnote b), Table 1.

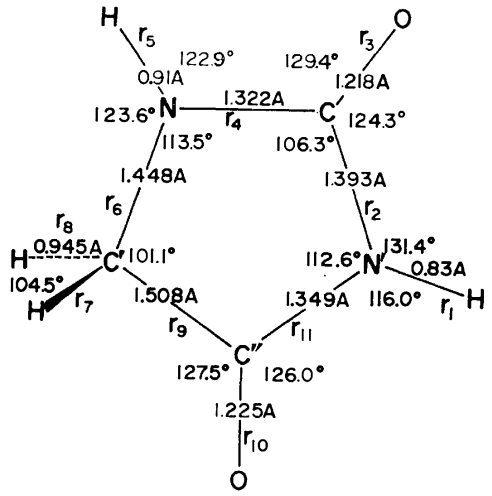

Fig. 4. Structural parameters.

of-plane symmetry coordinates are given in Table 4, where the subscripts for $\Delta\tau$ and $\Delta\pi$ denote the bond indices shown in Fig. 4.

A simple Urey-Bradley force field including 28 force constants was employed for the a′ vibrations. The values of the force constants were transferred initially from ethyleneurea,[1] except that the stretching constants K(C″N′) and K(CN) were taken to be the same as each other on the basis of the similarity in the bond-lengths. After a little adjustment with reference to the $\boldsymbol{J}$ matrix elements, the force constants were refined by the method of least squares to fit the infrared frequencies. The converged set of force constants is given in Table 5. The a″ frequencies were calculated by using a simple Urey-Bradley force field for the CH_2 group and a valence force field for the remaining coordinates. The Urey-Bradley constants were fixed at the final values for the a′ vibrations. The values of the valence type diagonal constants, $f(\pi\text{NH}, \pi\text{NH})$, $f(\tau\text{CN}, \tau\text{CN})$, $f(\pi\text{CO}, \pi\text{CO})$ and $f(\tau\text{C'N}, \tau\text{C'N})$ were taken initially from ethyleneurea,[1] $f(\tau\text{C'C''}, \tau\text{C'C''})$ and $f(\pi\text{C''O}, \pi\text{C''O})$ being estimated by referring to the observed frequencies and the $\boldsymbol{G}$ matrix elements of H-d_0. In order to improve the frequency fit, the off-diagonal constants, $f(\pi\text{NH}, \tau\text{CN})$, $f(\pi\text{CO}, \tau\text{CN})$, $f(\pi\text{CO}, \pi\text{NH})$, and $f(\pi\text{NH}, \tau\text{C'N})$ were added with initial values zero, and the diagonal and the off-diagonal constants were refined alternately by the method of least squares. The final values of the force constants are given in Table 5, and the calculated frequencies in Tables 1 and 2.

Table 3. Product and sum rules for the a′ vibrations

Product rule	H-d_0/HN-d_2	H-d_0/HC-d_2	H-d_0/H-d_4
Obsd	3.741	2.664	10.274
Theor.[a]	3.861	2.731	10.550
Sum rule	$\sum\{\nu^2(\text{H-}d_0)+\nu^2(\text{H-}d_4)\}$		$\sum\{\nu^2(\text{HN-}d_2)+\nu^2(\text{HC-}d_2)\}$
	8.485×10^7 $(\text{cm}^{-1})^2$		8.479×10^7 $(\text{cm}^{-1})^2$

a) Theoretical ratios were obtained from the calculated frequencies.

Table 4. Internal symmetry coordinates for the torsional and out-of-plane deformation vibrations

Coordinate	Description[a]
$S_1=\sum_{i=1,11}\sum_{j=3,4}\Delta\tau_{12j}/4$	τCN′
$S_2=\sum_{i=2,3}\sum_{j=5,6}\Delta\tau_{14j}/4$	τCN
$S_3=\sum_{i=6-8}\sum_{j=10,11}\Delta\tau_{19j}/6$	τC′C″
$S_4=\sum_{i=4,5}\sum_{j=7-9}\Delta\tau_{16j}/6$	τC′N
$S_5=\sum_{i=9,10}\sum_{j=1,2}\Delta\tau_{111j}/4$	τC″N′
$S_6=\Delta\pi_1$[b]	πN′H
$S_7=\Delta\pi_3$[b]	πCO
$S_8=\Delta\pi_5$[b]	πNH
$S_9=\Delta\pi_{10}$[b]	πC″O

a) See footnote b), Table 1. b) The out-of-plane deformation coordinates were defined to be positive when the end atoms (O for S_7 and S_9, and H for S_6 and S_8) move toward the observer from the plane of Fig. 4.

Table 5. Force constants

Urey-Bradley type constants (in mdyn/Å)							
K(NH)	5.360	K(CH)	4.380	K(CO)[a]	$9.449_5(0.121_0)$[b]	K(CN′)	$3.392_5(0.380_8)$
K(CN)[c]	$4.157_9(0.294_3)$	K(C′N)	$2.837_1(0.193_6)$	K(C′C″)	$2.146_3(0.345_2)$	H(CNH)	$0.228_7(0.009_9)$
H(NCO)	$0.323_9(0.089_8)$	H(C′C″O)	$0.461_9(0.159_7)$	H(CNC)	$1.246_2(0.215_6)$	H(NCN′)	$0.309_1(0.162_5)$
H(C″C′N)	$0.183_1(0.136_4)$	H(NC′H)	$0.198_5(0.029_4)$	H(C″C′H)	$0.323_8(0.041_8)$	H(HC′H)	$0.365_1(0.009_5)$
H(C′C″N′)	0.050	F(CNH)	$0.264_1(0.034_8)$	F(NCO)	$1.406_1(0.214_5)$	F(C′C″O)	$0.432_9(0.204_4)$
F(CNC)	0.229	F(NCN′)	$0.661_2(0.264_7)$	F(C″C′N)	0.098	F(NC′H)	$0.613_3(0.064_9)$
F(C″C′H)	$0.100_1(0.084_6)$	F(HC′H)	0.120	F(C′C″N′)	$1.597_3(0.197_1)$	κ	−0.1 mdyn·Å
Valence type constants (in mdyn Å/rad²)[d]							
$f(\tau\text{CN}, \tau\text{CN})$[e]	0.387_5	$f(\tau\text{C'N}, \tau\text{C'N})$	0.032_0	$f(\tau\text{C'C''}, \tau\text{C'C''})$	0.060	$f(\pi\text{N'H}, \pi\text{N'H})$	0.041_5
$f(\pi\text{NH}, \pi\text{NH})$	0.127_4	$f(\pi\text{CO}, \pi\text{CO})$	0.743_7	$f(\pi\text{C''O}, \pi\text{C''O})$	0.473_5	$f(\pi\text{NH}, \tau\text{CN})$	0.040
$f(\pi\text{NH}, \tau\text{C'N})$	-0.025_0	$f(\pi\text{CO}, \tau\text{CN})$	−0.040	$f(\pi\text{NH}, \pi\text{CO})$	0.023		

a) Constants for both the CO and the C′O bonds. b) ( ); dispersion. c) Constants for both the CN and the C″N′ bonds. d) The relevant internal coordinates are shown in parantheses, see also footnote a), Table 1. e) Diagonal constants for τCN, τCN′ and τC″N′.

The magnitudes of the three CN stretching constants, K(CN), K(CN′) and K(C′N) in the final set are well correlated with the adopted bondlengths. The CO stretching constant of the –NHCONH– group of hydantoin is much larger than that of ethyleneurea[1] and is comparable with those of diacetamide[7,8] and diketopiperazine.[9] This result may be related to the increase of the CO bond order caused by the decrease of the N–C–N angle on replacement of the CH_2 group of ethyleneurea by a CO group.

We are grateful to Prof. T. Takenaka and Prof. S. Hayashi for use of FIS-3. The calculation was performed on a FACOM 230-60 computer at the Data Processing Center, Kyoto University, and on a NEAC 2200/500 computer at Okayama University Computer Center.

References

1) Y. Saito and K. Machida, *Bull. Chem. Soc. Jpn.*, **50**, 359 (1977).
2) Y. Saito, K. Machida, and T. Uno, *Spectrochim. Acta*, **31A**, 1237 (1975).
3) O. Redlich, *Z. Phys. Chem.*, (**B**)**28**, 371 (1935).
4) J. C. Decius and E. B. Wilson Jr., *J. Chem. Phys.*, **19**, 1409 (1951).
5) A. Carmerman and N. Carmerman, *Acta Crystallogr.*, **B27**, 2205 (1971).
6) L. A. Walter, K. Folting, and L. L. Merritte Jr., *Acta Crystallogr.*, **B25**, 88 (1969).
7) Y. Kuroda, Y. Saito, K. Machida, and T. Uno, *Spectrochim. Acta*, **27A**, 1481 (1971).
8) Y. Kuroda, Y. Saito, K. Machida, and T. Uno, *Bull. Chem. Soc. Jpn.*, **45**, 2413 (1972).
9) M. Asai, K. Noda, and A. Sadô, *Spectrochim. Acta*, **30A** 1147 (1974).

Derivatographic Studies on Transition Metal Complexes. XIX.[1] Thermal Isomerization of *trans*-$[CrCl_2(en)_2](H_5O_2)Cl_2$ and *trans*-$[CrCl_2(pn)_2]Cl \cdot 1.5H_2O$ in Solid Phase[2]

Tadatsugu YOSHIKUNI, Ryokichi TSUCHIYA, Akira UEHARA, and Eishin KYUNO*

Department of Chemistry, Faculty of Science, Kanazawa University, Kanazawa 920

** Department of Pharmaceutical Science, School of Pharmacy, Hokuriku University, Kanazawa 920*

(Received January 17, 1977)

Thermal *trans*-to-*cis* isomerization of $[CrCl_2(en)_2](H_5O_2)Cl_2$ and $[CrCl_2(pn)_2]Cl \cdot 1.5H_2O$ was studied in the solid phase by derivatographic and isothermal measurements. The former complex was found to isomerize in anhydrous state after the complete elimination of hydrogen chloride and water, the latter in the temperature range for dehydration. The activation energies for the isomerization of these two complexes were isothermally estimated to be 202 and 193 kJ mol^{-1}, respectively. The same type of isomerization mechanism is suggested for these complexes, differing from that for the corresponding cobalt(III) complexes in which lattice waters participate.

Few papers have been given on the *cis*↔*trans* isomerization of $[MX_2(a\text{-}a)_2]X$ in solid phase, where M= Co(III) or Cr(III), X=halide ion and a-a=diamine. The *trans*-to-*cis* isomerization is known to take place in *trans*-$[CoCl_2(pn)_2](H_5O_2)Cl_2$[3,4] and *trans*-$[CoBr_2(pn)_2](H_5O_2)Br_2$,[5] but not in *trans*-$[CoCl_2(en)_2](H_5O_2)Cl_2$. The isomerization of the former two always proceeds at the elimination step of hydrogen halide and water, for which "aquation-anation mechanism" has been proposed.[3,4] In contrast, *trans*-$[CrBr_2(pn)_2]Br \cdot H_2O$ isomerizes in the anhydrous state; the presence of lattice waters has no effect on the isomerization.[6] Thus, another mechanism seems to play an important role in the isomerization of the chromium(III) complexes.

The present study was undertaken (1) to investigate derivatographically and isothermally the *trans*-to-*cis* isomerization of $[CrCl_2(en)_2](H_5O_2)Cl_2$ and $[CrCl_2(pn)_2]Cl \cdot 1.5H_2O$, and (2) to find what differences can be produced by changing ethylenediamine with propylenediamine.

Experimental

Preparation of Complexes. *trans*-$[CrCl_2(en)_2](H_5O_2)Cl_2$ (I),[7] *cis*-$[CrCl_2(en)_2]Cl$(II),[8] *trans*-$[CrCl_2(pn)_2]Cl \cdot 1.5H_2O$ (III),[9] and *cis*-$[CrCl_2(pn)_2]Cl$ (IV)[10] were prepared by modification of the usual methods.

The chemical formulas of these complexes were confirmed by elemental analyses, spectrophotometric measurements and Karl Fischer's method of water determination.

Derivatography. The derivatograms for the complexes were obtained with a MOM Typ-OD-102 Derivatograph. The operating conditions are the same as those reported previously.[1]

Isothermal Measurements. The rates of hydrogen chloride elimination and dehydration were measured with a CHYO 100L thermobalance at 92, 105, 119, and 126 °C for complex I and at 160, 172, 178, and 184 °C for complex III. The rates of isomerization were followed by measuring the change in the absorbancies of a 0.1 M $HClO_4$ solution of each sample heated in an Abderhalden apparatus at 249, 260, 269, 279, or 288 °C for complex I, and at 154, 160, 166, or 172 °C for complex III, and by the use of the following simultaneous equations:

$$\left.\begin{aligned} D_{400} &= 32.3X + 71.1Y \\ D_{520} &= 7.6X + 73.1Y \end{aligned}\right\} \quad \text{for complex I}$$

$$\left.\begin{aligned} D_{400} &= 35.8X + 74.6Y \\ D_{530} &= 10.4X + 74.4Y \end{aligned}\right\} \quad \text{for complex III}$$

where X and Y are the molar concentrations of *trans*- and *cis*-isomers, respectively, contained in a 0.1 M $HClO_4$ solution of each sample, the numerical factors are the molar extinction coefficients of pure *trans*- and *cis*-isomers at two wavelengths 400 and 520 or 530 nm for each complex and D is the absorbancy measured. Figure 1 shows the electronic spectra of *trans*- and *cis*-complexes. The isomerization ratios are, therefore, given by $Y/(X+Y)$.

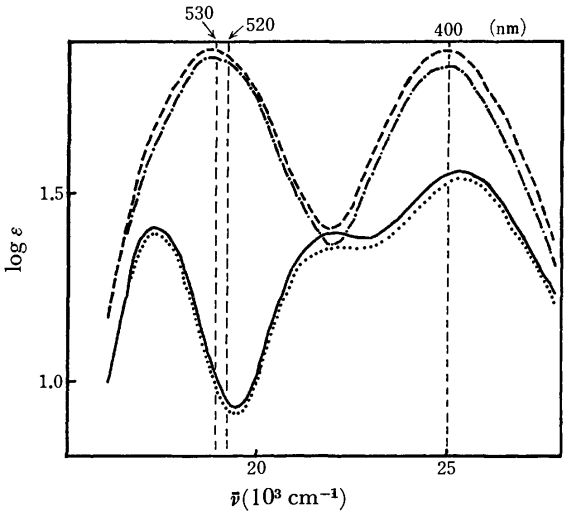

Fig. 1. Electronic spectra of complexes I (·····), II (—·—), III(——) and IV(----).

Results and Discussion

Derivatography. Figure 2 shows the derivatograms of *trans*-$[CrCl_2(en)_2](H_5O_2)Cl_2$ (I) and *trans*-$[CrCl_2(pn)_2]Cl \cdot 1.5H_2O$(III). The TG curve of complex I shows that the complex evolves one mole of hydrogen chloride and two moles of water at 25—120 °C (step I) and then remains unchanged up to 290 °C, above which the decomposition begins. In the DTA curve, an endothermic peak appears at step I and another endothermic peak at 250 °C; a small but clear exothermic peak can be seen just before the second endothermic peak. This is due to the *trans*-to-*cis* isomerization, which was visually confirmed by the color change of the sample from

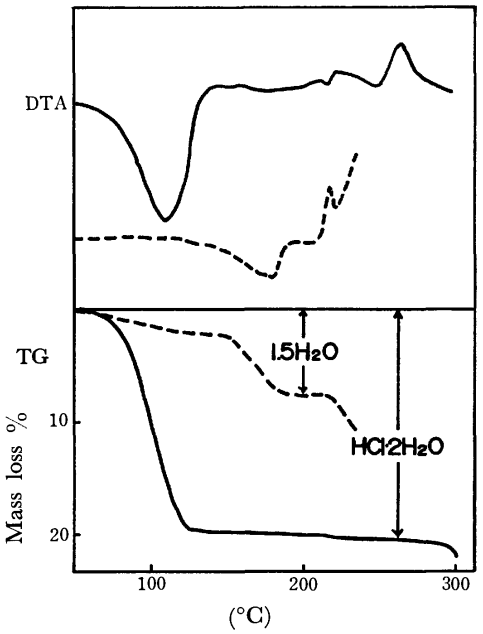

Fig. 2. Derivatograms of complexes I (——) and III (----).

green to violet. The enthalpy change, ΔH, for step I was estimated to be 55 kJ mol^{-1} from analysis of the endothermic curve in the derivatogram.

On the other hand, as seen from the TG curve of complex III, the complex loses 1.5 mol of water at 45—180 °C and decomposes above 215 °C. In the DTA curve, an endothermic peak appears at the dehydration step, and then a clear exothermic peak appears at 210 °C just before the decomposition starts. The complete *trans*-to-*cis* isomerization was also visually confirmed at the end of dehydration.

The isomerization of complex I takes place in an anhydrous state in a manner similar to that of *trans*-$[CrBr_2(pn)_2]Br \cdot H_2O$[6] and *cis*-$[CrCl_2(tn)_2]Cl \cdot 0.5H_2O$.[1] On the other hand, complex III undergoes isomerization with dehydration as mentioned above.

It seems, however, that the presence of lattice water is not always required for the isomerization to occur, if the value of the activation energy obtained by the isothermal measurements is taken into account.

Rate of Step I. The rate of step I was measured with a thermobalance from the weight loss with time. The results for complex I are shown in Fig. 3 in the same way as that reported,[1,6] *viz.*, $\log\{a/(a-x)\}$ is plotted against time, assuming the reaction to proceed in the first order, where a is the initial amount of the starting complex, and x the amount of the hydrated complex which has lost hydrogen chloride or of the anhydrous complex. A curve having a point of inflection was obtained at each temperature. The part below the point of inflection is due to the evolution of hydrogen chloride, and the part above it to dehydration. This was confirmed by chemical analysis of the evolved gas.

The rate constants of step I are given in Table 1 together with those of isomerization. The activation energies for the loss of hydrogen chloride and the dehydration were calculated to be 118 kJ mol^{-1} and 42 kJ mol^{-1}, respectively, from the Arrhenius plots.

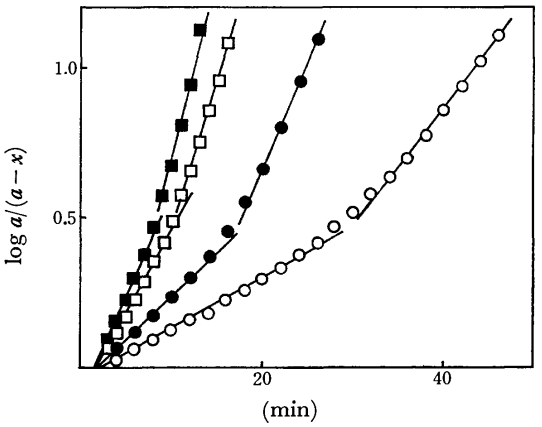

Fig. 3. Plots of $\log\{a/(a-x)\}$ *vs.* time for the hydrogen chloride elimination and dehydration of complex I.
○ 92, ● 105, □ 119, ■ 126 °C.

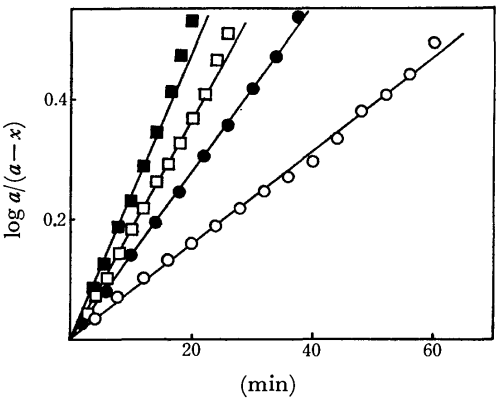

Fig. 4. Plots of $\log\{a/(a-x)\}$ *vs.* time for the dehydration of complex III.
○ 160, ● 172, □ 178, ■ 184 °C.

The relationship of $\log\{a/(a-x)\}$ *vs.* time for the dehydration of complex III is shown in Fig. 4. The rate constants of dehydration are given in Table 2 together with those of isomerization. The activation energy was estimated to be 76 kJ mol^{-1} from the Arrhenius plots of the rate constant.

Rate of Isomerization. The rate of isomerization of complex I measured spectrophotometrically is shown in Fig. 5. It is assumed that the reaction proceeds in

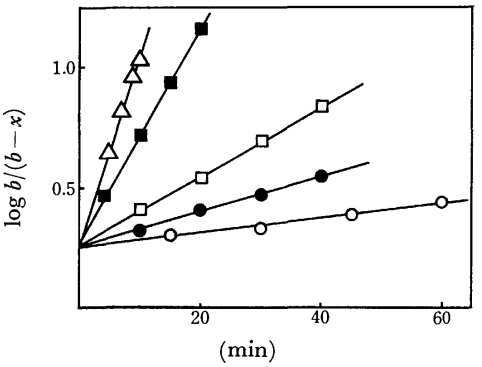

Fig. 5. Plots of $\log\{b/(b-y)\}$ *vs.* time for the isomerization of complex I.
○ 249, ● 260, □ 269, ■ 279, △ 288 °C.

Table 1. Rate constants of hydrogen chloride elimination, dehydration and isomerization of complex I

Temp/°C	92.0	105.0	119.3	125.5	249	260	269	279	288
$k_d(HCl)\times10^{-3}/s^{-1}$	0.642	1.075	2.084	2.572					
$k_d(H_2O)\times10^{-3}/s^{-1}$	1.574	2.764	3.964	4.798					
$k_i\times10^{-4}/s^{-1}$					1.151	2.955	5.245	16.79	29.17

Table 2. Rate constants of dehyration and isomerization of complex III

Temp/°C	154	160	166	172	178	184
$k_d\times10^{-4}/s^{-1}$		3.009		5.322	7.043	9.135
$k_i\times10^{-2}/s^{-1}$	1.490	3.133	6.821	13.083		

the first order. The plots converge to *ca.* 0.26 in the coordinate $\log\{b/(b-y)\}$, where b is the initial amount of the complex I and y that of the *cis*-complex formed during time t. The point to which the plots converge corresponds to 45% isomerization of the complex. Taking the dehydration temperature range under the isothermal heating into account (Fig. 3), the point suggests that 45% of the complex isomerizes very rapidly accompanied by dehydration at least above 249 °C, the residual 55% isomerizing in anhydrous state in the first order.

The rate constants of isomerization for complex I in anhydrous state are summarized in Table 1. From the Arrhenius plots of the rate constants, the activation energy for the isomerization was evaluated to be 202 kJ mol^{-1}.

The rate of isomerization of complex III is shown in Fig. 6 by plotting the isomerization ratio (%) *versus* time. All the plotted lines are linear, indicating that the reaction proceeds in the zeroth order. The rate constants of isomerization for complex III are given in Table 2. The activation energy for the isomerization is calculated to be 193 kJ mol^{-1}.

Complex I isomerizes similarly to *trans*-$[CrBr_2(pn)_2]Br\cdot H_2O$ and *cis*-$[CrCl_2(tn)_2]Cl\cdot 0.5H_2O$, though the last complex undergoes *cis*-to-*trans* isomerization, indicating that the reaction occurs in an anhydrous state with a remarkably large activation energy as compared with cobalt(III) complexes.[4,5] In these complexes, a mechanism differing from "aquation-anation" in the cobalt(III) complexes should be considered.

On the other hand, in complex III, the *trans*-to-*cis* isomerization is completed before dehydration is over. The activation energy is, however, relatively large as compared with the values for the isomerization in cobalt(III) complexes. This suggests that the process of isomerization is independent of the presence of lattice water in these chromium(III) complexes.

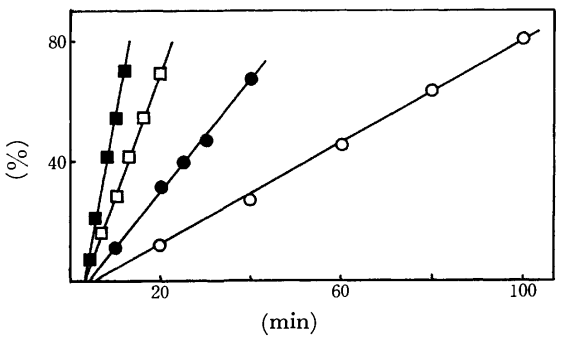

Fig. 6. Plots of isomerization ratio (%) *vs.* time for the isomerization of complex III.
○ 154, ● 160, □ 166, ■ 172 °C.

Thermochemical Reaction Scheme. On the basis of the data presented, the thermochemical reaction schemes for the isomerization of the complexes I and III are illustrated as follows:

In the temperature range 92—126 °C:

trans-$[CrCl_2(en)_2](H_5O_2)Cl_2$

$\downarrow$ $E_d(HCl)=118$ kJ mol^{-1} (28 kcal mol^{-1})
$\downarrow$ $E_d(H_2O)=42$ kJ mol^{-1} (10 kcal mol^{-1})

trans-$[CrCl_2(en)_2]Cl$

At 249—288 °C:

trans-$[CrCl_2(en)_2](H_5O_2)Cl_2$ $\xrightarrow{45\%}$ *cis*-$[CrCl_2(en)_2]Cl$

$\downarrow$ 55%

trans-$[CrCl_2(en)_2]Cl$ $\longrightarrow$ *cis*-$[CrCl_2(en)_2]Cl$

$E_i\simeq 202$ kJ mol^{-1} (48 kcal mol^{-1})

At 154—184 °C:

trans-$[CrCl_2(pn)_2]Cl\cdot 1.5H_2O$: $\xrightarrow[E_i=193\text{ kJ mol}^{-1}\ (46\text{ kcal mol}^{-1})]{}$ *cis*-$[CrCl_2(pn)_2]Cl$

$\downarrow$ $E_d=76$ kJ mol^{-1} (18 kcal mo^{-1})

$[CrCl_2(pn)_2]Cl$

References

1) Part XVIII: T. Yoshikuni, R. Tsuchiya, A. Uehara, and E. Kyuno, *Bull. Chem. Soc. Jpn.*, **50**, 883 (1977).
2) Presented at the 26 th Symposium on Coordination Chemistry, Hokkaido, August, 1976.
3) H. E. LeMay, Jr., *Inorg. Chem.*, **7**, 2531 (1968).
4) R. Tsuchiya, K. Murai, A. Uehara, and E. Kyuno, *Bull. Chem. Soc. Jpn.*, **43**, 1383 (1970).
5) R. Tsuchiya, Y. Natsume, A. Uehara, and E. Kyuno, *Thermochim. Acta*, **12**, 147 (1975).
6) R. Tsuchiya, T. Ohki, A. Uehara, and E. Kyuno, *Thermochim. Acta*, **12**, 413 (1975).
7) E. Pedersen, *Acta Chem. Scand.*, **24**, 3362 (1970); C. L. Rollinson, and J. C. Bailar, Jr., *J. Am. Chem. Soc.*, **65**, 250 (1943); P. Pfeiffer, *Ber.*, **37**, 4255 (1903).
8) C. L. Rollinson and J. C. Bailer, Jr., *J. Am. Chem. Soc.*, **66**, 641 (1944).
9) J. W. Vaughn, O. J. Stvan, Jr., and V. E. Magnuson, *Inorg. Chem.*, **7**, 736 (1968).
10) J. A. Maclean, Jr., and N. A. Maes, *Inorg. Nucl. Chem. Lett.*, **8**, 147 (1972); M. Esparza and C. S. Garner, *J. Inorg. Nucl. Chem.*, **29**, 2377 (1967).

Gel Chromatography of β-Diketones and Their Metal Complexes. IV. The Partition Concept in Gel Chromatography

Koichi SAITOH and Nobuo SUZUKI

Department of Chemistry, Faculty of Science, Tohoku University, Sendai 980

(Received February 3, 1977)

A new theoretical treatment of the solute distribution in gel chromatography is proposed. Practical gel chromatography can be regarded as one based on a combined function of the molecular sieve effect and the partition effect. Introducing the concept of a regular solution to the column system of gel chromatography, the contribution of the partition effect can be estimated from the data on the physical properties of the solute, the solvent, and the gel matrix. The argument being proposed is supported by the experimental data on the gel chromatography of metal (II, III) chelates with acetylacetone and normal alkanes previously obtained in the systems of a poly(vinyl acetate) gel and various eluting solvents.

In the previous work of this series, the solvent dependence of the gel-chromatographic behavior of some metal (II, III) chelates with acetylacetone (2,4-pentanedione: Hacac) on a cross-linked poly(vinyl acetate) gel (Merckogel OR-2000) was examined.[1] The experimental results showed that the distribution coefficients of a chelate were strongly dependent on the eluting solvent used. The effective molar volume, V_{eff}, for every chelate obtained by the use of the calibration charts prepared on the basis of the elution data for normal alkanes also depended on the solvents; the volmes were different from the expectation derived from the literature values of the molar volume, V_m, for the chelate. On the basis of these facts, it seems reasonable to assume that the solute distribution in a given column system is governed not only by the molecular sieve effect related to the molecular dimensions of the solute, but also by some secondary effects related to interactions among the solute, the solvent, and the gel.

In order to explain the separation mechanism in gel chromatography, various theories, such as steric exclusion,[2] restricted diffusion,[3] and thermodynamic equilibrium,[4] have been proposed. In these theories, the dominant factor governing the solute distribution in a given column system is considered to be the radius of the solute molecule, and the contributions of the secondary effects are not taken into account. Some anomalies were occasionally observed, however, such as the reversal of the predicted elution order of the solutes and the unexpectedly large values of the elution volume.[5,6] These facts could not be explained simply in term of the molecular sieve effect. The importance of the secondary effect was stressed in such a case, therefore. It has thus far been generally agreed that the secondary effect is due to the solute-gel matrix adsorption,[7,8] but this adsorption has not been argued quantitatively in terms of the physical properties inherent in the solute, solvent, and gel materials.

In the course of our previous study, we felt it necessary to understand fully the essence of the secondary effect and the solvent effect in gel chromatography. The present paper thus deals with this problem theoretically. The theoretical investigation of the solute distribution in a column system is developed by assuming that gel chromatography is essentially based on the combined function of the molecular sieve effect and the partition effect. This investigation has been undertaken to explain the gel-chromatographic behavior of metal chelates with Hacac previously observed.

Theoretical

Overall Distribution Coefficient. When a substance is chromatographed in a column system consisting of a liquid phase with the volume of V_o (void volume) and a gel phase with the volume of V_x, the elution volume, V_e, of the substance is expressed by the following general equation:

$$V_e = V_o + K_{av}V_x, \tag{1}$$

where K_{av} is the distribution coefficient characterizing the solute distribution in the column system. When the solute distribution is governed not only by the molecular sieve effect, but also by some other effects, K_{av} is essentially a combined function of all the effects.

When the concept of the theoretical plate is applied to the gel-chromatographic-column system, the solute distribution in a theoretical plate is as will be discussed below.

The column system in the theoretical plate consists essentially of a solvent phase (hereafter abbreviated as the O phase) with the volume of v_o and a gel phase (hereafter abbreviated as the X phase) with the volume of v_x. The former and the latter phases correspond to the moving and the stationary phases in this chromatographic system respectively. A solute material, S, introduced in this system equilibrates between these two phases. Only a certain fraction, K_{size}, of the latter phase is, however, available for S, because of the molecular sieve effect. This leads to the following relation:

$$v_p = K_{size}v_x, \tag{2}$$

where v_p is the volume of the available part (hereafter designated as the P phase) for S. According to the theories proposed by Ogston[9] and Laurent and Killander[10], K_{size} is expressed by the equation:

$$K_{size} = \exp\left[-\pi L(r_r + r_s)^2\right], \tag{3}$$

where r_s is the radius of the solute molecule, r_r is the radius of the polymer chain of the gel matrix, and L is the concentration of the polymer chains in the gel phase. Both L and r_r are constant in a combination of the gel matrix and a solvent. The v_p value in a given column system, therefore, varies according only to the size of the solute molecule.

Considering that S is distributed strictly between the O phase and the P phase, and also that these two phases are not always equilivalent with respect to the interaction with S, it is reasonable to assume that, in general, the concentration of S in P phase, C_p, is different from that in the O phase, C_o. When the P phase can be assumed to be such a medium as a mixture of a solvent and a polymer of gel matrix, into which S can be incorporated, the O and P phases can be regarded as constituting a system of partition chromatography. Thus, the K_{part} given by Eq. 4 corresponds with the partition coefficient of S in this system:

$$K_{part} = C_p/C_o \tag{4}$$

The effective plate volume, v_e, in this partition chromatographic system is expressed by this equation:

$$\begin{aligned} v_e &= v_o + K_{part}v_p \\ &= v_o + K_{part}K_{size}v_x \end{aligned} \tag{5}$$

When the number of the theoretical plates in the total column system, N, is sufficiently larger than unity, Eq. 6 can be derived:

$$V_e = Nv_e = V_o + K_{part}K_{size}V_x \tag{6}$$

From Eqs. 1 and 6, one arrives at:

$$K_{av} = K_{part}K_{size} \tag{7}$$

According to Eq. 6, gel chromatography can be regarded as a special case of partition chromatography, in which the volume of the stationary phase varies with the molecular size of the solute substance introduced. It is reasonable to term K_{av} the overall distribution coefficient.

Partition Concept and the Physical Properties of the Solute, the Solvent, and the Gel. When the partition constant of the solute, S, $K^x_{part,s}$, is given by Eq. 8, the overall distribution coefficient, K_{av}, can be expressed by Eq. 9, provided both C_o and C_p are small:

$$K^x_{part,s} = X_{s,p}/X_{s,o} \tag{8}$$

where $X_{s,p}$ and $X_{s,o}$ are the mole fractions of S in the P phase and the O phase respectively.

$$K_{av} = K^x_{part,s}(\overline{V}_{m,o}/\overline{V}_{m,p})K_{size} \tag{9}$$

where $\overline{V}_{m,o}$ and $\overline{V}_{m,p}$ are the average molar volume of the O phase and the P phase respectively.

According to the regular solution theory,[11] the activity of Component 2, a_2, in a binary mixture of Components 1 and 2 is expressed as a function of the mole fraction, X; the molar volume, V_m; the volume fraction, ϕ, and the solubility parameter, δ, by means of the following equation:

$$\ln a_2 = \ln X_2 + V_{m,2}\phi_1^2(\delta_1-\delta_2)^2/RT \tag{10}$$

where R and T are the gas constant and the temperature respectively, and where the subscripts 1 and 2 distinguish the components of the mixture. When the number of moles of a component is denoted by the symbol n, X_2 and ϕ_1 are, respectively, given by these two equations: $X_2=n_2/(n_1+n_2)$ and $\phi_1=n_1V_{m,1}/(n_1V_{m,1}+n_2V_{m,2})$. The solubility parameter is defined as the square root of the cohesive energy density, *e.g.*, of the energy of vaporization, ΔE^v, per unit of volume ($\delta=(\Delta E^v/V_m)^{1/2}$). The regular solution theory can be successfully applied to discussing the solute distribution in solvent extraction.[12-14]

It is expected that the concept of a regular solution can be applied to discussing the solute distribution between the O phase and the P phase when the following two assumptions are accepted: i) the P phase can be regarded as a homogeneous mixture of a solvent and a gel matrix polymer, and ii) specific interactions among the solute, the solvent, and the polymer, such as hydrogen bonding, are absent in the system. In our earlier work, the solvent dependence of gel swelling could be successfully explained quantitatively by introducing the concept of regular solution into the solvent-gel matrix binary system.[15]

The activities of the solute, S, in the O phase, $a_{s,o}$, and in the P phase, $a_{s,p}$, are expressed by Eqs. 11 and 12:

$$\ln a_{s,o} = \ln X_{s,o} + V_{m,s}\phi_o^2(\delta_o-\delta_s)^2/RT \tag{11}$$

$$\ln a_{s,p} = \ln X_{s,p} + V_{m,s}\phi_p^2(\delta_p-\delta_s)^2/RT \tag{12}$$

The subscripts s, o, and p distinguish the components in these systems. When the partition equilibrium of S is achieved between these two phases ($a_{s,o}=a_{s,p}$), the following relation is derived:

$$\ln K^x_{part,s} = V_{m,s}[(\delta_o-\delta_s)^2-(\delta_p-\delta_s)^2]/RT, \tag{13}$$

provided that the concentration of S is so small that both ϕ_o and ϕ_p can be equated with unity. The solubility parameter, δ_p, is approximately expressed by Eq. 14:

$$\delta_p = \phi_g\delta_g + (1-\phi_g)\delta_o, \tag{14}$$

where ϕ_g is the volume fraction of the gel-matrix polymer in the P phase, δ_g is the solubility parameter of the polymer, and δ_o is, of course, the solubility parameter of the solvent. Then, Eq. 13 is modified to:

$$\ln K^x_{part,s} = V_{m,s}[2(\delta_s-\delta_o)(\delta_g-\delta_o)\phi_g-(\delta_g-\delta_o)^2\phi_g^2]/RT \tag{15}$$

This equation reveals the quantitative relationship between the partition effect in gel chromatography and the physical properties of the solute, the eluting solvent, and the packing material (gel). It is quite an important and interesting suggestion that ($\ln K^x_{part,s}$) is equal to zero under such a condition as $\delta_o=\delta_g$.

It is well known that the molar volume can be used as an effective size parameter for low-molecular-weight compounds in gel chromatography.[16-18] We assume here, for the sake of simplification, that various compounds with a equal molar volume have K_{size} values identical to each other in a given column system. When two different substances, S and S′, are chromatographed in a column system, the K_{av} values of these substances are expected by the $K_{av,s}=K^x_{part,s}K_{size,s}$ and $K_{av,s'}=K^x_{part,s'}K_{size,s'}$ equations. When the V_m values of S and S′ are equal to each other, $K_{size,s}=K_{size,s'}$. Then the following equation can be written:

$$R_{s/s'} = K_{av,s}/K_{av,s'} = K_{part,s}/K_{part,s'} \tag{16}$$

According to Eq. 15, the above equation is modified to give:

$$\ln R_{s/s'} = 2V_{m,s}(\delta_s-\delta_{s'})(\delta_g-\delta_o)\phi_g/RT \tag{17}$$

This equation predicts that the $R_{s/s'}$ value is always constant at unity under the condition $\delta_o=\delta_g$. In usual

column systems, $K_{av,s}$ are not always equal to $K_{av,s'}$, even if $V_{m,s}=V_{m,s'}$. It is stressed that the choice of eluting solvent is quite important in gel chromatography. Ideal gel-chromatographic separation based only on the molecular sieve effect is carried out by the use of an eluting solvent in which the solubility parameter of the solvent is equal to that of the gel matrix; then one can estimate the size of a solute molecule by the use of a calibration chart prepared on the basis of the elution data for other compounds.

Discussion

In order to examine the validity of the above arguments, the theory is then applied to the experimental data already obtained. The elution data for normal alkanes,[19] bis(acetylacetonato) beryllium(II) and tris-(acetylacetonato)chromium(III) (hereafter abbreviated as $Be(acac)_2$ and $Cr(acac)_3$ respectively),[1,20] in column systems consisting of Merckogel OR-2000 and various organic solvents are taken. The data on gel swelling[15] are also available.

Equation 15 shows that the solvent dependence of the partition effect can be discussed quantitatively in terms of the solubility parameters of the solvents. However, it is not easy to evaluate K^x_{part} experimentally. Only K_{av} values can be obtained by means of usual chromatographic techniques. When the K_{av} values of two different compounds with equal V_m values are available, the validity of Eq. 15 must be examined indirectly by discussing Eq. 17.

We suppose here two hypothetical normal alkanes: one (hereafter designated by r(Be)) whose V_m value is equal to that of $Be(acac)_2$, and the other (hereafter designated by r(Cr)) whose V_m value is equal to that of $Cr(acac)_3$. An equation analogous to Eq. 17 can be written for the solute pair of $Be(acac)_2$ and r(Be):

$$\ln R_{Be/r(Be)} = \ln (K_{av,Be}/K_{av,r(Be)}) = 2V_{m,Be}(\delta_{Be}-\delta_{r(Be)})(\delta_g-\delta_o)\phi_g/RT, \quad (18)$$

where the subscript Be denotes $Be(acac)_2$. Introducing the degree of swelling for gel, Q, defined as $Q=1/\phi_g$, into the above equation, one can write Eq. 19:

$$Q \ln R_{Be/r(Be)} = [-2V_{m,Be}(\delta_{Be}-\delta_{r(Be)})/RT](\delta_o-\delta_g) \quad (19)$$

It is expected that $(Q \ln R_{Be/r(Be)})$ shows a linear relationship to δ_o with a slope of $[-2V_{m,Be}(\delta_{Be}-\delta_{r(Be)})/RT]$. The $V_{m,Be}$ value was estimated to be 184 $cm^3\,mol^{-1}$.[1] The $K_{av,r(Be)}$ values in the column systems of Merckogel OR-2000 and various eluting solvents can be estimated by introducing the $V_{m,Be}$ value into the K_{av} *versus* V_m relationship for normal alkanes observed in the column systems (see Fig. 2 in Ref. 1). The δ_{Be} value has not been reported. Considering that the solubility parameters of metal chelates with the same ligand are approximately independent of the metals,[14] we estimate δ_{Be} to be at 9.7 $cal^{1/2}\,cm^{-3/2}$. This value is equal to the reportd value of δ_{Cr}.[21] The $\delta_{r(Be)}$ value is estimated to be 7.7 $cal^{1/2}\,cm^{-3/2}$ from the δ *versus* V_m relationship for normal alkanes shown in Fig. 1. According to these values, it can be predicted that the slope of the $(Q \ln R_{Be/r(Be)})$ *versus* δ_o plot is about -1.2 at 25 °C. The relation of $(Q \ln R_{Be/r(Be)})$ plotted against δ_o, prepared based on the data summarized in Table 1, is shown in Fig. 2. All the plots, except for chloroform (1), fall approximately on a line. According to the regression analysis, the slope of this line is $(-0.92\pm$

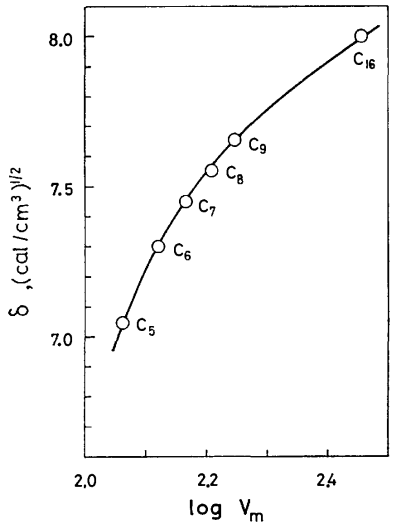

Fig. 1. Relationship between solubility parameter and molar volume for normal alkanes.
C_5, C_6, C_7, C_8, C_9, and C_{16} denote pentane, hexane, heptane, octane, nonane, and hexadecane, respectively
1 cal=4.1840 J.

TABLE 1. VALUES OF δ_o, Q K_{av}, AND R IN THE SYSTEMS OF MERCKOGEL OR-2000 AND AN ORGANIC SOLVENT AT 25 °C

Solvent No.	Solvent Name	δ_o[a]	Q[15]	$K_{av,Be}$[1]	$K_{av,r(Be)}$	$K_{Be/r(Be)}$	$K_{av,Cr}$[1]	$K_{av,r(Cr)}$	$R_{Cr/r(Cr)}$
1	Chloroform	9.3[24]	4.10	0.271	0.385	0.704	0.218	0.268	0.813
2	Benzene	9.15[24]	3.12	0.816	0.373	1.45	0.342	0.255	1.34
3	Toluene	8.9[24]	2.26	0.653	0.319	2.05	0.400	0.207	1.93
4	1,4-Dioxane	10.0[24]	3.32	0.570	0.513	1.11	0.436	0.383	1.14
5	Tetrahydrofuran	9.32[b]	3.18	0.620	0.398	1.56	0.517	0.281	1.84
6	Ethyl acetate	9.05[25]	2.99	0.702	0.468	1.50	0.609	0.360	1.69
7	Acetone	9.89[26]	3.15	0.660	0.532	1.24	0.622	0.439	1.42
8	Ethyl methyl ketone	9.3[26]	2.98	0.653	0.462	1.41	0.628	0.351	1.79
9	Butyl acetate	8.55[25]	2.43	0.828	0.399	2.08	0.790	0.284	2.78

a) In $cal^{1/2}\,cm^{-3/2}$. b) Calculated from the value of the heat of vaporization (7.65 kcal/mol).[27]

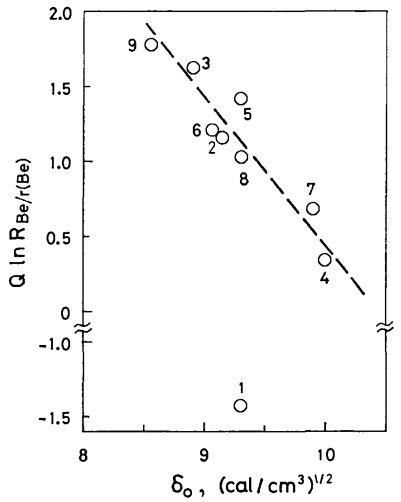

Fig. 2. The $Q \ln R_{Be/r(Be)}$ *versus* δ_0 relationship in the systems of Merckogel OR-2000 and various eluting solvents at 25 °C. Figures 1—9 denote solvents as in Table 1. Dashed line shows the regression line.

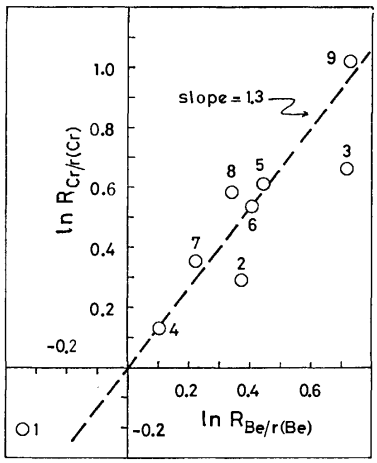

Fig. 3. Correlation between $\ln R_{Cr/r(Cr)}$ and $\ln R_{Be/r(Be)}$. Figures 1—9 denote solvents as in Table 1.

0.12) at a level of significance of 5%. This value is close to the expected one ($=-1.2$). The δ_0-axis intercept of the line, which corresponds with the δ_g value of Merckogel OR-2000, is observed to be (10.4±0.2). This value is near to the δ_g value estimated from the gel-swelling data ($\delta_g=9.7$).[15]

It is shown in Fig. 2 that the relationship expressed by Eq. 17 can be approximately accepted in practice, even in various types of solvents, including both polar and nonpolar ones. Some deviation of the plots from the linearity can still be found. It has not been clarified whether the deviation results from the uncertainty of the original data or from the disregard for the specific interactions among solute, solvent, and gel. Considering that many metal chelates with Hacac form the solvated species in chloroform.[22,23] the remarkable deviation of the plot for chloroform found in Fig. 2 may be referred to the solvation. The concept of the regular solution can be accepted on the assumption that the specific interaction between the solute and the solvent is absent.[11]

One can modify Eq. 17 to give the relation between $Cr(acac)_3$ (designated by the subscript Cr) and r(Cr). Thus,

$$\ln R_{Cr/r(Cr)} = \ln (K_{av,Cr}/K_{av,r(Cr)}) = 2V_{m,Cr}(\delta_{Cr}-\delta_{r(Cr)})(\delta_g-\delta_0)\phi_g/RT \quad (20)$$

From Eqs. 18 and 20, the following equation is derived:

$$\ln R_{Cr/r(Cr)}/\ln R_{Be/r(Be)} = (V_{m,Cr}/V_{m,Be})(\delta_{Cr}-\delta_{r(Cr)})/(\delta_{Be}-\delta_{r(Be)}) \quad (21)$$

It can be expected that ($\ln R_{Cr/r(Cr)}$) is in direct proportion to ($\ln R_{Be/r(Be)}$). The proportional coefficient should be independent of the solvent used, and we should be able to predict it from the physical properties of the solutes. Taking the value of $V_{m,Cr}$ as 267 $cm^3\ mol^{-1}$,[21] $\delta_{r(Cr)}$ is estimated to be 7.9 $cal^{1/2}\ cm^{-3/2}$ from Fig. 1. The δ_{Cr} value has been reported to be *ca.* 9.7 $cal^{1/2}\ cm^{-3/2}$.[21] Then, the proportional coefficient can be predicted to be 1.3.

The values of $K_{av,r(Cr)}$ and $R_{Cr/r(Cr)}$ are estimated in a manner analogous to that used in the case of the $Be(acac)_2$-r(Be) pair and are exhibited in Table 1. When these values are taken, the relationship of ($\ln R_{Cr/r(Cr)}$) plotted against ($\ln R_{Be/r(Be)}$) is as shown in Fig. 3. The dashed line in the figure shows the slope 1.3. It is quite interesting that the plots for many solvents lie close to the prediction. However, benzene (2) and toluene (3) give plots somewhat deviating from the expected line. We have, to data, no clear-cut evidence to explain this deviation.

The facts shown graphically in Figs. 2 and 3 lend some support to the theoretical treatment of the solute distribution in gel chromatography proposed in this paper. The solvent dependence of the gel-chromatographic behavior of metal chelates with Hacac previously observed can be appreciablly explained in terms of the partition effect. The contribution of the partition effect to the overall solute distribution in gel chromatography may be predicted quantitatively in terms of the molar volumes and the solubility parameters of the solute and the solvent. Equation 15 predicts that the partition effect in gel chromatography is not remarkable, provided that the δ value of the eluting solvent is close to that of the gel matrix.

In view of the above arguments, the most reasonable conclusion to be drawn from the available data is that 1,4-dioxane is the nearest to the ideal eluting solvent for the column system including Merckogel OR-2000 as a column packing material, while butyl acetate is farthest from the ideal.

The introduction of the partition concept may give a powerful approach to elucidate the so-called secondary effect in gel chromatography.

References

1) Part 3 in this series: N. Suzuki and K. Saitoh, *Bull. Chem. Soc. Jpn.*, **50**, 2907 (1977).
2) J. Porath, *Pure Appl. Chem.*, **6**, 233 (1963).
3) G. K. Ackers, *Biochemistry*, **3**, 723 (1964).
4) E. F. Casassa, *Separ. Sci.*, **6**, 305 (1971).
5) M. Milk, J. Rochlitz, and H. Bende, *J. Chromatogr.*, **24**, 414 (1966).
6) J. G. Bergmann, L. J. Duffy, and R. B. Stevenson,

Anal. Chem., **43**, 131 (1971).
7) C. A. Streuli, *J. Chromatogr.*, **56**, 219 (1971).
8) S. Mori and T. Takeuchi, *J. Chromatogr.*, **50**, 419 (1970).
9) A. G. Ogston, *Trans. Faraday Soc.*, **54**, 1754 (1958).
10) T. C. Laurent and J. Killander, *J. Chromatogr.*, **14**, 317 (1964).
11) J. H. Hildebrand and R. S. Scott, "The Solubility of Nonelectrolytes," Dover, New York (1964).
12) T. Wakahayashi, S. Oki, T. Omori, and N. Suzuki, *J. Inorg. Nucl. Chem.*, **26**, 2255 (1964).
13) N. Suzuki and K. Akiba, *J. Inorg. Nucl. Chem.*, **33**, 1897 (1971).
14) M. Tanaka, "Proceedings of International Solvent Extraction Conference, ISEC '77," Soc, Chem. Ind., London (1971), p. 18.
15) K. Saitoh, T. Ozawa, and N. Suzuki, *J. Chromatogr.*, **124**, 231 (1976).
16) W. B. Smith and A. Kollmansberger, *J. Phys. Chem.*, **69**, 4157 (1965).
17) G. D. Edward and Q. Y. Ng, *J. Polym. Sci.*, **C21**, 105 (1968).
18) A. Lambert, *Anal. Chim. Acta*, **51**, 63 (1971).
19) K. Saitoh and N. Suzuki, *J. Chromatogr.*, **111**, 29 (1975).
20) K. Saitoh and N. Suzuki, *J. Chromatogr.*, **109**, 333 (1975).
21) H. M. N. H. Irving, "Ion Exchange and Solvent Extraction," Vol. 6, ed by J. A. Marinsky and Y. Marcus, Dekker, New York (1970), p. 139.
22) J. F. Steinbach and J. H. Burns, *J. Am. Chem. Soc.*, **80**, 1839 (1958).
23) F. R. Clark, J. F. Steinbach, and W. F. Wagner, *J. Inorg. Nucl. Chem.*, **26**, 1311 (1964).
24) Ref. 11, p. 435.
25) D. Mangaraj, S. Petra· and S. B. Rath. *Macromol. Chem.*, **67**, 84 (1963).
26) M. Magat, *J. Chim. Phys.*, **46**, 344 (1949).
27) J. A. Riddick and W. B. Bunger, "Organic Solvents," 3rd ed, Wiley-Interscience, New York (1970), p. 220.

The Thermal Decomposition Process of Calcium Sulfite

Ryoko MATSUZAKI, Hagio MASUMIZU, Nagisa MURAKAMI, and Yuzo SAEKI

Research Laboratory of Resources Utilization, Tokyo Institute of Technology, 4259, Nagatsuta-cho, Midori-ku, Yokohama 227

(Received April 27, 1977)

The thermal decomposition of calcium sulfite at temperatures below 880 °C in an argon stream was examined. Also, the reaction between calcium sulfate and calcium sulfide, which were formed during the decomposition process of calcium sulfite, was examined. The thermal decomposition process of calcium sulfite can be represented as follows: on heating calcium sulfite, the reaction, $CaSO_3 \rightarrow CaO + SO_2$, occurs above about 600 °C. Above about 680 °C, the reaction, $4CaSO_3 \rightarrow 3CaSO_4 + CaS$, occurs besides the above reaction. Furthermore, the reaction between calcium sulfate and calcium sulfide which are formed during the decomposition process of calcium sulfite, $3CaSO_4 + CaS \rightarrow 4CaO + 4SO_2$, occurs above about 780 °C.

As regards the thermal decomposition process of calcium sulfite, Foerster and Kubel[1] have reported that the reaction, $4CaSO_3 \rightarrow 3CaSO_4 + CaS$, occurs above about 600 °C, and that the reaction, $CaSO_3 \rightarrow CaO + SO_2$, occurs besides the above reaction above about 650 °C in a nitrogen stream. Zawadzki[2] has briefly reported that the reaction, $4CaSO_3 \rightarrow 3CaSO_4 + CaS$, occurs above about 600 °C, and that the reaction, $3CaSO_4 + CaS \rightarrow 4CaO + 4SO_2$, occurs above about 800 °C. On the other hand, Ketov and Nichkovskii[3] have reported that the reactions, $CaSO_3 \rightarrow CaO + SO_2$, $4CaSO_3 + 2SO_2 \rightarrow 4CaSO_4 + S_2$, and $4CaO + 3S_2 \rightarrow 4CaS + 2SO_2$, take place successively over the temperature range of 600—800 °C in a nitrogen atmosphere.

In this report, the thermal decomposition process of calcium sulfite at temperatures below 880 °C will be described.

Experimental

A sample of $CaSO_3$ was prepared by dehydrating $CaSO_3 \cdot 1/2H_2O$ at 330 °C in an argon stream. The $CaSO_3 \cdot 1/2H_2O$ was prepared from a guaranteed reagent, $CaCO_3$, by the method based on the report of Kelly and Moore.[4]

The results of the chemical analysis of the $CaSO_3$ obtained were Ca 33.3$_8$, SO_3 66.4% (Calcd for $CaSO_3$: Ca 33.36, SO_3 66.64%). The Ca content in the $CaSO_3$ was determined by complexometric titration[5] after the $CaSO_3$ had been dissolved in dilute hydrochloric acid. The SO_3 content in the $CaSO_3$ was determined by decomposing the $CaSO_3$ with hydrochloric acid to convert the SO_3 to SO_2 gas in an argon atmosphere. The amount of SO_2 gas evolved was determined by volumetric iodometry.[6]

The X-ray analysis of the sample was performed with an X-ray powder diffractometer, equipped with a proportional counter, using Ni filtered Cu radiation. The X-ray diffraction data of the $CaSO_3$ are shown in Table 1. The data reported by Matthews and McIntosh,[7] which are cited in the ASTM X-ray diffraction data file, are also shown in Table 1.

The thermogravimetry(TG) and differential thermal analysis (DTA) were performed in an argon stream. A heating rate of 2.5 °C/min was employed. The sensitivity of the quartz helix used for TG was about 0.14 mg/0.01 mm. α-Al_2O_3 was used as a reference for DTA.

Table 1. X-RAY DIFFRACTION DATA OF $CaSO_3$

This work				ASTM card			
d(Å)	I/I_1	d(Å)	I/I_1	d(Å)	I/I_1	d(Å)	I/I_1
5.61	5	2.468	10	5.50	2	1.63	2
4.93	5	2.417	20	3.80	5	1.57	5
3.66	10	2.362	10	3.49	5	1.47	15
3.51	15	2.338	10	3.12	100	1.40	2
3.24	55	2.259	10	2.90	60	1.28	15
3.07	100	2.151	25	2.79	5		
2.98	60	2.006	20	2.71	5		
2.92	25	1.824	20	2.61	5		
2.805	55	1.791	10	2.53	80		
2.747	55	1.647	5	2.34	20		
2.644	60	1.585	5	2.11	40		
2.592	25	1.388	5	1.93	15		
2.536	75			1.82	15		

Results and Discussion

The TG and DTA curves of $CaSO_3$ on heating are shown in Fig. 1. It was observed that the weight loss on heating $CaSO_3$ was accompanied by the evolution of SO_2 gas. The results of the X-ray analysis[8] of the samples heated up to Points A(800 °C) and B(1000 °C) are also shown in Fig. 1.

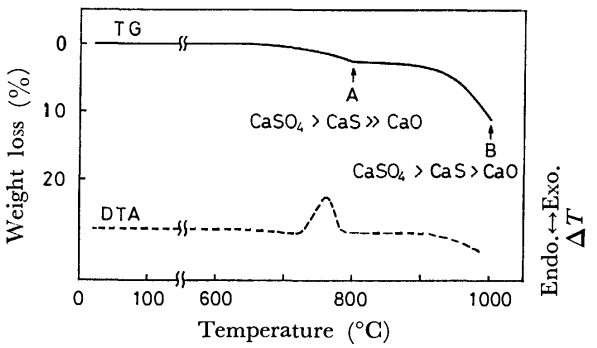

Fig. 1. TG and DTA curves of $CaSO_3$ on heating in an argon stream.

From the facts that CaO was observed in the sample heated up to Point A, and that SO_2 gas was evolved during the weight loss, it was considered that the reaction, $CaSO_3 \rightarrow CaO + SO_2$,[1,3] occurred. Also, an exothermic peak was observed at about 760 °C in the DTA curve, and the formations of $CaSO_4$ and CaS were observed in the sample heated up to Point A. From these facts, it was considered that the reaction, $4CaSO_3 \rightarrow 3CaSO_4 + CaS$,[1,2,9] occurred besides the above reaction.

Furthermore, from the facts that the X-ray diffraction intensity of CaO in the sample heated up to Point B was stronger than that in the sample heated up to Point A, and that the evolution of SO_2 gas was observed during the weight loss from Point A to Point B, it was considered that the reaction, $3CaSO_4+CaS \rightarrow 4CaO+4SO_2$,[2] occurred.

To clarify the thermal decomposition process of $CaSO_3$ in more detail, 1 g of $CaSO_3$ was placed in a quartz boat of 48 mm length, and decomposed in a straight quartz tube (26 mm i. d. and 300 mm heating length) at an argon flow-rate of 100 ml/min for 3 h under isothermal conditions at temperatures below 880 °C. The product obtained in the boat was examined by X-ray analysis. Also, the amount of SO_2 gas formed by the decomposition of $CaSO_3$ was examined. The results are shown in Table 2.

Table 2. Results of heating experiments on $CaSO_3$

Heating temp (°C)	Amount of SO_2 formed (mg)	Sample in the boat
580	—	$CaSO_3$
600	det.	$CaSO_3$
620	3	$CaSO_3$
640	4	$CaSO_3 \gg CaO$
660	10	$CaSO_3 \gg CaO$
680	19	$CaSO_3 > CaSO_4 > CaS \gg CaO$
700	33	$CaSO_4 > CaS \gg CaSO_3 > CaO$
720	31	$CaSO_4 > CaS \gg CaO \fallingdotseq CaSO_3$
740	28	$CaSO_4 > CaS \gg CaO$
760	19	$CaSO_4 > CaS \gg CaO$
780	14	$CaSO_4 > CaS \gg CaO$
800	18	$CaSO_4 > CaS \gg CaO$
840	37	$CaSO_4 > CaS > CaO$
880	83	$CaSO_4 > CaS > CaO$

From the results that the formations of SO_2 gas and CaO were observed at 600—660 °C, it was clarified that the reaction, $CaSO_3 \rightarrow CaO+SO_2$, occurred above about 600 °C. Above 680 °C, the formations of $CaSO_4$ and CaS in addition to CaO were observed; the $CaSO_3$ decreased with the increase in the temperature and was not observed above 740 °C. From these results, it was made clear that the reaction, $4CaSO_3 \rightarrow 3CaSO_4+CaS$, occurred above about 680 °C in addition to the reaction, $CaSO_3 \rightarrow CaO+SO_2$.

Above 800 °C, the amount of SO_2 gas formed was again increased; the X-ray diffraction intensity of the CaO in the product also increased with the increase in the temperature. These facts were considered to indicate a reaction between the $CaSO_4$ and CaS formed during the decomposition process of $CaSO_3$, $3CaSO_4+CaS \rightarrow 4CaO+4SO_2$. Therefore, the reaction between $CaSO_4$ and CaS was examined.

A sample of $CaSO_4$ was prepared by adding an aqueous $CaCl_2$ solution to an aqueous Na_2SO_4 solution.[10] Both the salts used were guaranteed reagents. The resulting precipitate was washed with water and dehydrated at 800 °C. A sample of CaS was prepared by heating the CaO formed by the thermal decomposition of a guaranteed reagent, $CaCO_3$, in a stream of H_2S gas at 1000 °C.[11]

One g of a mixture of $CaSO_4$ and CaS (in a molar ratio of $CaSO_4$: CaS=3 : 1) was heated at a specified temperature below 880 °C for 3 h in an argon stream. The product obtained in the boat and the amount of SO_2 gas formed were examined. The results are shown in Table 3.

Table 3. Results of heating experiments on $(3CaSO_4+CaS)$

Heating temp (°C)	Amount of SO_2 formed (mg)	Sample in the boat
760	—	$CaSO_4 > CaS$
780	3	$CaSO_4 > CaS \gg CaO$
800	9	$CaSO_4 > CaS \gg CaO$
840	21	$CaSO_4 > CaS \gg CaO$
880	71	$CaSO_4 > CaS > CaO$

The formations of SO_2 gas and CaO were observed above 780 °C, and the amount of SO_2 gas formed increased appreciably with the increase in the temperature. Also, the X-ray diffraction intensity of CaO in the product increased with the temperature. These results made it clear that the reaction, $3CaSO_4+CaS \rightarrow 4CaO+4SO_2$, occurred above about 780 °C.

From the above-mentioned experimental results, the thermal decomposition process of calcium sulfite can be represented as follows: on the heating of calcium sulfite, the reaction, $CaSO_3 \rightarrow CaO+SO_2$, occurs above about 600 °C. Above about 680 °C, the reaction, $4CaSO_3 \rightarrow 3CaSO_4+CaS$, also occurs. Furthermore, the reaction between calcium sulfate and calcium sulfide which are formed during the decomposition process of calcium sulfite, $3CaSO_4+CaS \rightarrow 4CaO+4SO_2$, occurs above about 780 °C. The thermal decomposition process of calcium sulfite revealed in this work differs from the previously reported processes mentioned above.[1-3]

References

1) F. Foerster and K. Kubel, *Z. Anorg. Allg. Chem.*, **139**, 261 (1924).
2) J. Zawadzki, *Z. Anorg. Allg. Chem.*, **205**, 180 (1932).
3) A. N. Ketov and V. V. Nichkovskiĭ, *Nauch, Doklady Vysshei Shkoly, Khim. i. Khim. Tekhnol.*, **1958**, 667; *Chem. Abstr.*, **53**, 5840 (1959).
4) K. K. Kelly and G. E. Moore, *J. Am. Chem. Soc.*, **66**, 293 (1944).
5) G. Schwarzenbach, "Complexometric Titrations," Interscience Publishers (1957), p. 63.
6) "Scott's Standard Methods of Chemical Analysis," 5th ed, D. Nostrand Co. (1939), p. 926.
7) F. W. Matthews and A. O. McIntosh, *Can. J. Res.*, **26 B**, 747 (1948); ASTM card 4-599.
8) ASTM cards 4-777, 8-464, 6-226.
9) K. Schwitzgebel and P. S. Lowell, *Environ. Sci. Technol.*, **7**, 1147 (1973).
10) M. Copisarow, *J. Chem. Soc.*, **123**, 796 (1923).
11) J. Zawadzki, K. Kossak, and H. Narbut, *Przemysl. Chem.*, **5**, 225 (1921); *Chem. Abstr.*, **17**, 1692 (1923).

Transition-metal Complexes of Pyrrole Pigments. XV. Coordination of Pyridine Bases to the Axial Sites of Cobalt Corroles†

Yukito MURAKAMI,* Sunao YAMADA, Yoshihisa MATSUDA, and Kazunori SAKATA**

Department of Organic Synthesis, Faculty of Engineering, Kyushu University, Hakozaki, Higashi-ku, Fukuoka 812

(Received May 30, 1977)

Cobalt(III) corroles exist predominantly as polymeric species in a concentration range above 5×10^{-3} M in chloroform at room temperature as confirmed by NMR measurements. The coordination behavior of pyridine bases at the axial sites of cobalt(III) corroles, in a concentration range where they are present exclusively in the monomeric species, has been investigated by measuring electronic spectra in acetone at 25.0±0.1 °C. Penta- and hexa-coordination processes were found to take place, and the stepwise formation constants were interpreted by means of the equations $\log K_i = a\cdot pK_a + b$ and $\log K_i/K_i^0 = \rho\sigma$. When the cobalt corrole was reduced at the nuclear cobalt from trivalent to bivalent state, only one pyridine molecule was coordinated at its axial sites, hexa-coordination being no longer possible as confirmed by ESR measurements. The axial ligation behavior of cobalt corroles is quite analogous in nature to that of cobalt corrinoid.

Axial-ligation equilibria for the corrinoid complexes have been studied rather extensively[1] in order to clarify the metabolic functions of vitamin B_{12} systems. It is important, however, to characterize the corrinoid skeleton by referring to the axial ligation behavior of the cobalt complexes of analogous macrocyclic tetrapyrroles involving different numbers of π-electrons in their skeletons, in view of the increasing interest in the chemistry of vitamin B_{12}. The interaction of various organic bases with 8,12-diethyl-1,2,3,7,13,17,18,19-octamethyltetradehydrocorrinatocobalt(II) perchlorate (Co(II)–TDHC) has been investigated.[2] The cobalt(II) complex of 1,19-disubstituted tetradehydrocorrin was found to take up one amine base in its axial position, but unable to yield the corresponding hexa-coordinated complex in which both axial positions were occupied by amines.

We have shown in this work that the axial coordination sites of cobalt(III) corroles are entirely occupied stepwise by amine bases. The equatorial ligand effect, exerted by the corrole skeleton on the axial coordination behavior, is effectively discussed in the light of vitamin B_{12} chemistry.

Experimental

Electronic spectra were taken on a Union Giken SM-401 high sensitive spectrophotometer. Acetone as a solvent for spectroscopic measurements was prepared by fractional distillation after being refluxed with potassium carbonate and kept over a molecular sieve (3A, 1/16; Ishizu Pharmaceutical Co., Ltd.). A Bruker WH-90 FT spectrometer was used to obtain NMR spectra in chloroform-*d* (>99.5%; E, Merck, Darmstadt) at room temperature. Chemical shifts are given in ppm from internal TMS and calibrated with a chloroform signal as the secondary external reference. ESR spectra were recorded on a JEOL JES-ME-3 X-band spectrometer equipped with a 100 kHz field modulation unit. The anionic cobalt(II) complex was prepared by reduction of the corresponding cobalt(III) corrole with sodium tetrahydroborate in *N,N*-dimethylformamide, and measured in the same solvent at 77 K, concentrations being maintained in the 10^{-2}—10^{-3} M range. The manganese ion diffused thermally into magnesium oxide was used to obtain the standard reference signals for measurements.

Commercial liquid amines (pyridine, 2-methyl-, 3-methyl-, 4-methyl-, and 3-acetylpyridine) were refluxed with potassium hydroxide and fractionally distilled. Commercial 4-cyanopyridine was recrystallized from aqueous ethanol. 4-Aminopyridine was prepared by ammonolysis of (4-pyridinio)-pyridinium dichloride[3] and recrystallized twice from benzene. 3-Hydroxypyridine was obtained from ammonium pyridine-3-sulfonate by treatment with potassium hydroxide at elevated temperature,[4] and purified by sublimation *in vacuo*.

2-Acetoxymethyl-3,4-diethyl-5-ethoxycarbonylpyrrole. Into a solution of 2-methyl-3,4-diethyl-5-ethoxycarbonylpyrrole[5-7] (2.5 g) in dry acetic acid (60 ml) was added lead tetraacetate (5.3 g) in small portions at 15-min intervals with stirring at room temperature. The reaction mixture was further stirred at room temperature for 3 h, evaporated *in vacuo*, and the residue was poured into cold water (120 ml). The resulting orange precipitates were recovered by filtration and washed thoroughly with water. Recrystallization from acetone–water gave colorless plates; yield 2.5 g (78%), mp 88.2—89.0 °C. IR (Nujol mull): 3314 (N–H str.), 1741 (acetoxy C=O str.), and 1668 cm^{-1} (ester C=O str.). NMR (CCl_4, TMS): δ 1.19 (9H, overlapping t J=7.0 Hz, 3- and 4-$CH_2\underline{CH_3}$, and 5-$CO_2CH_2\underline{CH_3}$), 1.99 (3H, s, 2-$CH_2OCO\underline{CH_3}$), 2.54 (4H, overlapping q J=7.0 Hz, 3- and 4-$\underline{CH_2}CH_3$), 4.25 (2H, q J=7.0 Hz, 5-$CO_2\underline{CH_2}CH_3$), 4.96 (2H, s, 2-$\underline{CH_2}OCOCH_3$), and 9.80 (1H, broad s, NH).

3,3',4,4'-Tetraethyl-5,5'-diethoxycarbonyldipyrromethane. A solution of 2-acetoxymethyl-3,4-diethyl-5-ethoxycarbonylpyrrole (3.5 g) in ethanol (70 ml) containing hydrochloric acid (37%, 2.6 ml) was refluxed for 5 h with stirring. The solution was concentrated gradually *in vacuo* until a small amount of crystalline precipitates started to appear. After being allowed to stand overnight in a refrigerator, the crystalline solid was recovered by filtration to give colorless prisms; yield 2.5 g (94%), mp 93.0—96.1 °C. IR (Nujol mull): 3320 (N–H str.), 1696 (free ester C=O str.), and 1657 cm^{-1} (bound ester C=O str.). NMR (CCl_4, TMS): δ 1.09 (18H, overlapping t J=7.0 Hz, 3,3'-$CH_2\underline{CH_3}$, 4,4'-$CH_2\underline{CH_3}$, and 5,5'-$CO_2CH_2\underline{CH_3}$), 2.51 (8H, overlapping q J=7.0 Hz, 3,3'-$\underline{CH_2}CH_3$ and 4,4'-$\underline{CH_2}CH_3$), 3.87 (2H, s, bridging CH_2), 4.16 (4H, q J=7.0 Hz, 5,5'-$CO_2\underline{CH_2}CH_3$), and 10.04 (2H, broad s, NH).

† Contribution No. 439 from this Department. Part XIV: Y. Matsuda and Y. Murakami, *Bull. Chem. Soc. Jpn.*, **50**, 2321 (1977).

* To whom correspondence should be addressed.

** Present address: Kyushu Institute of Technology, Tobata-ku, Kitakyushu 804.

3,3',4,4'-Tetraethyldipyrromethane-5,5'-dicarboxylic Acid. A mixture of 3,3',4,4'-tetraethyl-5,5'-diethoxycarbonyldipyrromethane (2.0 g) and ethanol (35 ml) was refluxed with stirring for a short period. After addition of sodium hydroxide (1.0 g) dissolved in water (10 ml), the reaction mixture was refluxed for 2 h with stirring. A large portion of ethanol was removed *in vacuo* from the mixture, and water (50 ml) was then added to it. Acetic acid was added to adjust the pH of the solution to 4—5. White precipitates were recovered by filtration, washed thoroughly with water, and dried *in vacuo* to give white powder; yield 1.8 g (100%), mp 135—145 °C (dec). On being left to stand the color of the product gradually turned violet particularly when slightly wet. IR (Nujol mull): 3300 (N–H str.), 3210 (O–H str.), and 1661 cm^{-1} (C=O str.).

1,19-Dideoxy-2,3,7,8,12,13,17,18-octaethylbiladiene-ac Dihydrobromide (1). A mixture of 3,3',4,4'-tetraethyldipyrromethane-5,5'-dicarboxylic acid (2.7 g), 2-formyl-3,4-diethylpyrrole[7,8] (2.3 g), and ethanol (80 ml) was heated at 60 °C with occasional shaking. Vigorous reaction took place upon addition of 47% aqueous hydrobromic acid (16 ml) at one time to the hot reaction mixture. The mixture was refluxed for 3 min and allowed to stand overnight in a refrigerator. The glittering red crystals were recovered by filtration, washed with ethyl ether, and recrystallized from chloroform–methanol to give reddish brown prisms; yield 4.0 g (79%). λ_{max} ($CHCl_3$): 374, 433, 460, and 526 nm. IR (KBr disk): 1605 cm^{-1} (biladiene skeletal str.). NMR (CF_3CO_2H, TMS): δ 1.26 (24H, overlapping t J=7.0 Hz, $CH_2\underline{CH_3}$), 2.74 (16H, overlapping q J=7.0 Hz, $\underline{CH_2}CH_3$), 4.60 (2H, s, bridging $-CH_2-$), 7.55 (2H, s, bridging –CH=), and 7.77 (2H, d J= 3.5 Hz, 1,19-H). Found: C, 61.13; H, 7.28; N, 7.90%. Calcd for $C_{35}H_{50}Br_2N_4$: C, 61.21; H, 7.35; N, 8.16%.

1,19-Dideoxy-2,3,17,18-tetramethyl-7,8,12,13-tetraethylbiladiene-ac Dihydrobromide (2). This was prepared from 3,3',4,4'-tetraethyldipyrromethane-5,5'-dicarboxylic acid (1.7 g) and 2-formyl-3,4-dimethylpyrrole[9] (1.05 g) in methanol (50 ml) and aqueous hydrobromic acid (47%, 9 ml) in the same manner as described above; reddish brown prisms, yield 2.4 g (73%). IR (KBr disk): 1608 cm^{-1} (biladiene skeletal str.).

2,3,7,8,12,13,17,18-Octaethylcorrolatocobalt(III) (3). To a mixture of biladiene-ac dihydrobromide **1** (200 mg) and *N,N*-dimethylformamide (25 ml) was added cobalt(II) acetate tetrahydrate (160 mg) dissolved in *N,N*-dimethylformamide (5 ml) with stirring. The reaction mixture was heated at 50 °C for 30 min with stirring and subsequently allowed to cool at 0 °C for 1 h. Recovered crystalline solid was recrystallized from chloroform–methanol as dark brown prisms; yield 90 mg (53%). The osmometric determination of molecular weight in carbon tetrachloride: 1125—1300 in the concentration range 2—4$\times 10^{-3}$ M; calcd mol wt for $C_{35}H_{43}CoN_4$ (monomer) 578.68. This result indicates the existence of monomer-polymer equilibrium in concentrated solutions. Found: C, 72.67; H, 7.46; N, 9.69%. Calcd for $C_{35}H_{43}CoN_4$: C, 72.63; H, 7.50; N, 9.68%.

Pyridine(2,3,17,18-tetramethyl-7,8,12,13-tetraethylcorrolato)cobalt(III) (4). A mixture of cobalt(II) acetate tetrahydrate (800 mg) and pyridine (20 ml) was heated on an oil bath until it turned into a clear solution. Biladiene-ac dihydrobromide **2** (1.0 g) was added to the reaction mixture, which was subsequently heated at 70—75 °C for 20 min with stirring. After addition of hot methanol (70 ml), the mixture was allowed to stand in a refrigerator for 2 h. The crystalline solid was recovered by filtration, and recrystallized from chloroform–methanol–pyridine (3 : 1 : 1) to give glittering purple prisms; yield 720 mg (76%). IR (Nujol mull): 1602 cm^{-1} (pyridine skeletal str.). Found: C, 72.07; H, 6.56; N, 12.48 %. Calcd for $C_{36}H_{40}CoN_5$: C, 71.85; H, 6.71; N, 11.64%.

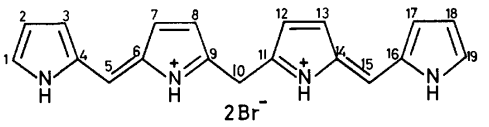

1: $R_2=R_3=R_7=R_8=R_{12}=R_{13}=R_{17}=R_{18}=C_2H_5$
2: $R_2=R_3=R_{17}=R_{18}=CH_3$; $R_7=R_8=R_{12}=R_{13}=C_2H_5$

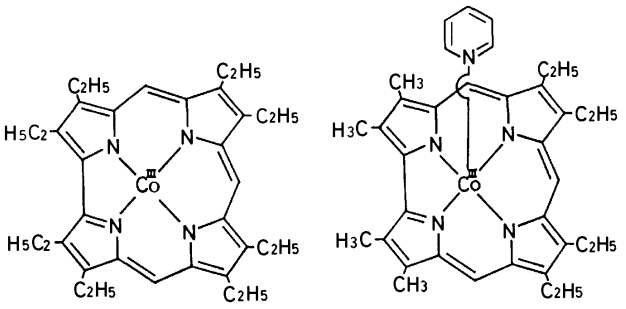

3 **4**

Results

NMR Behavior of Cobalt(III) Corrole. The NMR spectra of cobalt(III) corrole **3** were measured for the 10^{-2}—10^{-4} M concentration range in chloroform-*d* at room temperature. The intensity of proton signals appearing in the −5—+3 ppm region highly depends on concentration of the cobalt chelate as shown in Fig. 1. Particular attention should be paid to proton signals due to methylenes of the ethyl groups placed at the peripheral positions. The intensity of the meth-

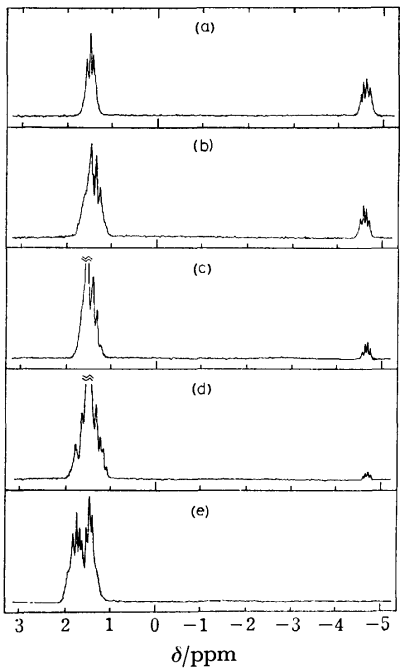

Fig. 1. NMR spectra of cobalt corrole **3** for the −5—+3 ppm range in chloroform-*d* at room temperature at various concentrations: (a), 3.04$\times 10^{-2}$ M; (b), 8.64$\times 10^{-3}$ M; (c), 2.94$\times 10^{-3}$ M; (d), 8.64$\times 10^{-4}$ M; (e), 8.64$\times 10^{-3}$ M (pyridine was added, 1.40$\times 10^{-2}$M).

ylene-proton signal observed at −4.6 ppm in a relatively high concentration range (Fig. 1 (a)) diminishes with decrease in the concentration of the complex. The intensity decrease is counterbalanced with the intensity increase for signals appearing in the 1.5—2.0 ppm range. The high-field signal (−4.6 ppm) disappeared completely, and the new signals were observed in the 1.5—2.0 ppm range upon addition of a 1.5-fold amount of pyridine to the cobalt corrole in 8.64×10^{-3} M (Fig. 1 (e)). The spectral change indicates that the cobalt corrole which exists in polymeric species (D and P in Scheme 2) in a relatively high concentration range dissociates into the monomer form upon coordination of pyridine at the axial sites.

The NMR behavior of the cobalt corrole is in line with the osmometric data which indicate the presence of monomer–dimer–polymer equilibria in a relatively high concentration range. From these measurements, cobalt(III) corrole **3** can exist predominantly in a monomeric species in a concentration range below 10^{-4} M. Since some minor impurity involved in chloroform-*d* showed a proton signal at 1.5 ppm, we were not able to evaluate the equilibrium constant for dimer formation.

Interaction between Cobalt(III) Corrole and Pyridine Bases. The electronic spectra for cobalt corrole **3** were measured by changing the concentration of pyridine bases in a wider range (0.5—10^4-fold amounts relative to **3**), while the concentration of **3** was maintained constant ($\approx7\times10^{-6}$ M). The spectral changes upon addition of pyridine are shown in Fig. 2, where isosbestic points are observed at 373, 400, 450, and 520 nm for the lower pyridine concentrations, and at 393, 460, and 532 nm for the higher concentrations (10^{-3}—10^{-1} M), while no distinct isosbestic points are present for the intermediate concentration range (10^{-4}—10^{-3} M). For the concentration range 10^{-1}—1 M, the electronic spectrum remains practically unchanged. This indicates that the axial sites of **3** are entirely occupied by

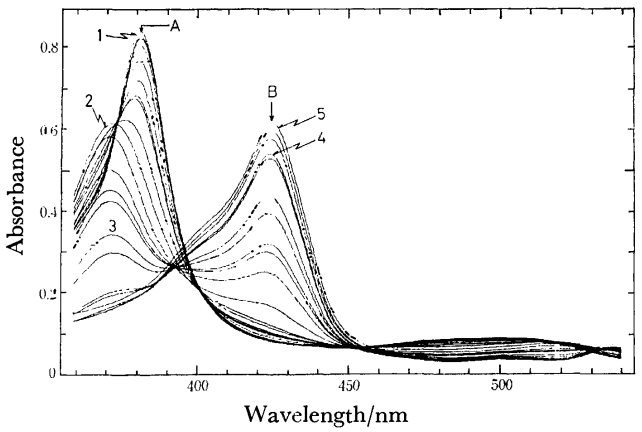

Fig. 2. Electronic spectra of cobalt corrole **3** (7.19×10^{-6} M) in acetone at 25.0±0.1 °C in the presence of pyridine at various concentrations (0—3.47 M): the absorption intensity in A-range decreases as pyridine concentration increases from 0 to higher, while that in B-range increases as pyridine concentration is raised. Pyridine concentrations: 1, 0 M; 2, 4.94×10^{-4} M; 3, 4.94×10^{-2} M; 4, 2.47×10^{-1} M; 5, 3.47 M.

pyridine molecules in this base-concentration range. As the pyridine concentration rises still higher, the spectral curves do not pass the isosbestic points most plausibly due to some solvent effect.

The spectral behavior is in line with the following equilibria.

Penta-coordination: $\mathrm{CoL} + \mathrm{B} \rightleftharpoons \mathrm{CoLB}$

$$K_1 = \frac{[\mathrm{CoLB}]}{[\mathrm{CoL}][\mathrm{B}]} \quad (1)$$

Hexa-coordination: $\mathrm{CoLB} + \mathrm{B} \rightleftharpoons \mathrm{CoLB_2}$

$$K_2 = \frac{[\mathrm{CoLB_2}]}{[\mathrm{CoLB}][\mathrm{B}]} \quad (2)$$

where CoL and B stand for cobalt corrole **3** and a pyridine base, respectively. At relatively low levels of the base concentration where the first set of isosbestic points are observed, the following stoichiometric relations hold.

$$[\mathrm{CoL}]_\mathrm{T} = [\mathrm{CoL}] + [\mathrm{CoLB}] + [\mathrm{CoLB_2}] \quad (3)$$

$$[\mathrm{B}]_\mathrm{T} = [\mathrm{B}] + [\mathrm{CoLB}] + 2[\mathrm{CoLB_2}] \quad (4)$$

where $[\mathrm{CoL}]_\mathrm{T}$ and $[\mathrm{B}]_\mathrm{T}$ represent total concentrations of cobalt corrole **3** and a pyridine base, respectively. Since no hexa-coordinated complex exists in any significant concentration, the last term of each equation can be neglected. The equilibrium constant (K_1) for the first axial coordination is given by

$$K_1 = \frac{[\mathrm{CoLB}]}{([\mathrm{CoL}]_\mathrm{T}-[\mathrm{CoLB}])([\mathrm{B}]_\mathrm{T}-[\mathrm{CoLB}])} \quad (5)$$

We employ here notations ε_i and A_i to represent molar extinction coefficient and optical density, respectively, for a cobalt corrole complex of coordination number i (i=4, 5, and 6), and A_obsd for observed optical density at various base concentrations while the concentration of cobalt complex was maintained constant. The following equation is derived for the first equilibrium step:

$$A_4 - A_\mathrm{obsd} = (\varepsilon_4-\varepsilon_5)[\mathrm{CoLB}]l = \Delta\varepsilon_\mathrm{I}[\mathrm{CoLB}]l \quad (6)$$

where l represents the length of light path.

For the higher base-concentration range where the second set of isosbestic points are observed, Eqs. 3 and 4 can be simplified as follows:

$$[\mathrm{CoL}]_\mathrm{T} = [\mathrm{CoLB}] + [\mathrm{CoLB_2}] \quad (7)$$

$$[\mathrm{B}]_\mathrm{T} = [\mathrm{B}] \quad (8)$$

Since a pyridine base was present in a large excess relative to the cobalt complex, the contribution of [CoLB] and $[\mathrm{CoLB_2}]$ to $[\mathrm{B}]_\mathrm{T}$ can be neglected. The corresponding equilibrium constant (K_2) is

$$K_2 = \frac{[\mathrm{CoLB_2}]}{([\mathrm{CoL}]_\mathrm{T}-[\mathrm{CoLB_2}])[\mathrm{B}]} \quad (9)$$

and

$$A_\mathrm{obsd} - A_6 = (\varepsilon_5-\varepsilon_6)[\mathrm{CoLB}]l = \Delta\varepsilon_\mathrm{II}[\mathrm{CoLB}]l \quad (10)$$

Combination of Eqs. 7 through 10 gives

$$A_\mathrm{obsd} = \frac{\Delta\varepsilon_\mathrm{II}[\mathrm{CoL}]_\mathrm{T}}{1+K_2[\mathrm{B}]_\mathrm{T}}l + A_6 \quad (11)$$

or

$$\frac{[\mathrm{CoL}]_\mathrm{T}l}{A_\mathrm{obsd}-A_6} = \frac{1}{\Delta\varepsilon_\mathrm{II}} + \frac{K_2}{\Delta\varepsilon_\mathrm{II}}[\mathrm{B}]_\mathrm{T} \quad (12)$$

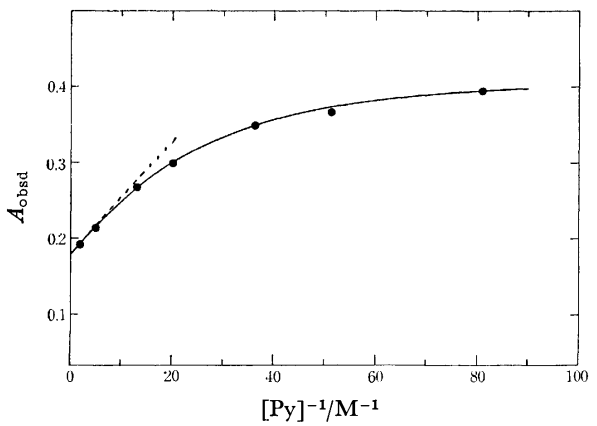

Fig. 3. Correlation of absorbance (at 380 nm) wtih pyridine concentration ([Py]) for the cobalt corrole (**3**)-pyridine system: $[\mathbf{3}]=7.19\times10^{-6}$ M in acetone at 25.0±0.1 °C.

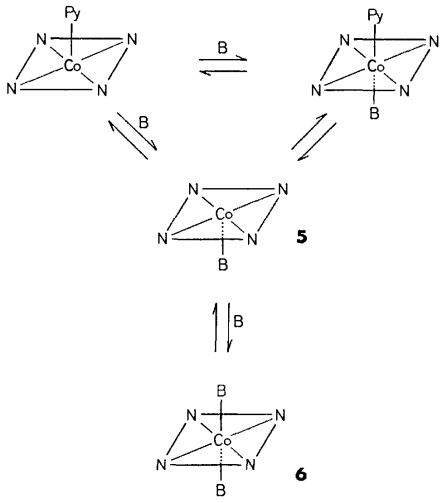

Scheme 1.

The subsequent mathematical treatments were performed by referring to the absorption intensities observed at 380 nm. The A_6-values were evaluated by extrapolation of the A_{obsd}—[Pyridine base]$^{-1}$ correlation curve to [Pyridine base]$^{-1}\rightarrow0$ on the basis of Eq. 11, as exemplified for the **3**–pyridine system in Fig. 3. Since all the cobalt species exist in the hexa-coordinated form at the pyridine-base concentrations of 0.1—1 M as judged from the corresponding spectral behavior (refer to Fig. 2), A_6-values can be evaluated directly from the corresponding spectra. The agreement between graphically and directly determined A_6-values was quite satisfactory; *e.g.*, 0.182 and 0.179, respectively, with pyridine at 7.19×10^{-6} M of **3**. The graphically determined A_6-values were used, however, for further computations for the sake of reliability. K_2 and $\Delta\varepsilon_{II}$ values were obtained by means of Eq. 12, as exemplified for the **3**–pyridine system in Fig. 4. From the analysis of spectral data for the second equilibrium step, ε_5 and ε_6 values were evaluated, which can be used for the analysis of the first equilibrium step by means of Eqs. 5 and 6.

The axial coordination behavior of penta-coordinated cobalt corrole **4** was also investigated in the presence of large excess of pyridine bases and the corresponding K_2-values were evaluated in the same way as described above. The equilibrium step for the **4**–pyridine base systems under investigation can be referred to process **5**⇌**6** shown in Scheme 1. We confirmed this by preparing the penta-coordinated 4-aminopyridine and 4-methylpyridine adducts of (tetramethyltetraethylcorrolato)cobalt(III) independently. In the presence of the same pyridine bases as used for the formation of these base adducts, the corresponding equilibrium constants were evaluated by means of Eq. 12. The values are in good agreement with those evaluated for the **4**–pyridine base systems within an experimental error. All the formation constants obtained in this work are listed in Table 1.

Interaction between Cobalt(II) Corrole Anion and Pyridine. The ESR spectra for the anionic cobalt(II)–corrole complex were not observed at room temperature probably due to short spin-lattice relaxation time. The (2,3,17,18-tetramethyl-7,8,12,13-tetraethylcorrolato)-cobaltate(II) ion shows an ESR spectrum at 77 K with three g-values (g_1, g_2, and g_3) as shown in Fig. 5. Eight hyperfine splitting lines through interaction with ^{59}Co

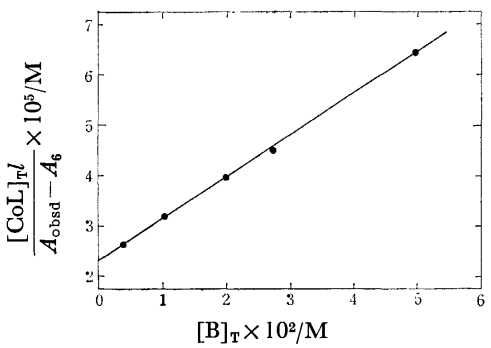

Fig. 4. Determination of K_2 and $\Delta\varepsilon_{II}$ values for the cobalt corrole (**3**)-pyridine (B) system on the basis of Eq. 12: $[\mathbf{3}]=7.19\times10^{-6}$ M in acetone at 25.0± 0.1 °C.

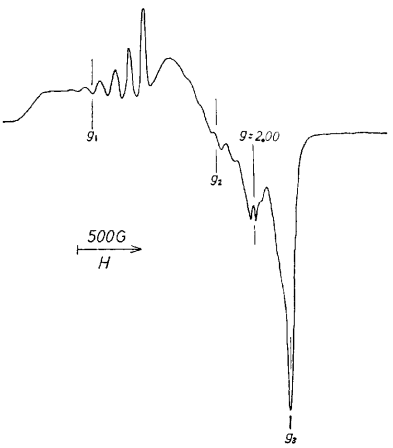

Fig. 5. ESR spectrum of the (2,3,17,18-teramethyl-7,8,12,13-tetraethylcorrolato)cobaltate(II) ion in *N*,*N*-dimethylformamide at 77 K. Thecobalt(III) corrole (**4**) was reduced with $NaBH_4$ in *N*,*N*-dimethylformamide.

Table 1. Formation constants for the pyridine complexes of cobalt(III) corroles[a)]

Pyridine base[b)]	$pK_a(BH^+)$[c)]	3		4
		K_1/M^{-1}	K_2/M^{-1}	K_2/M^{-1}
4-CNPy	1.90	$(1.95\pm0.05)\times10^3$	6.56	1.03×10
Py	5.19	$(1.69\pm0.12)\times10^4$	3.79×10	4.40×10
4-CH_3Py	6.02	$(6.58\pm0.19)\times10^4$	9.82×10	1.21×10^2
4-NH_2Py	9.11	$(7.78\pm0.29)\times10^5$	4.51×10^2	5.52×10^2
3-AcPy	3.18	$(1.07\pm0.09)\times10^5$	1.15×10^2	1.89×10^2
3-HOPy	4.86	$(1.83\pm0.13)\times10^4$	1.35×10	3.50×10
3-CH_3Py	5.68	$(3.50\pm0.16)\times10^4$	5.65×10	7.62×10
2-CH_3Py	5.97	$(1.09\pm0.16)\times10^2$	1.10×10^{-1}	1.67×10^{-1}

a) Measured in acetone at 25.0±0.1 °C. b) Py, pyridine; 4-CNPy, 4-cyanopyridine; 4-CH_3Py, 4-methylpyridine; 4-NH_2Py, 4-aminopyridine; 3-AcPy, 3-acetylpyridine; 3-HOPy, 3-hydroxypyridine; 3-CH_3Py, 3-methylpyridine; 2-CH_3Py, 2-methylpyridine. c) Cited from "Handbook of Biochemistry and Molecular Biology. Physical and Chemical Data," Vol. 1, 3rd ed, ed by G. D. Fasman, CRC Press, Inc., Cleveland, Ohio (1976).

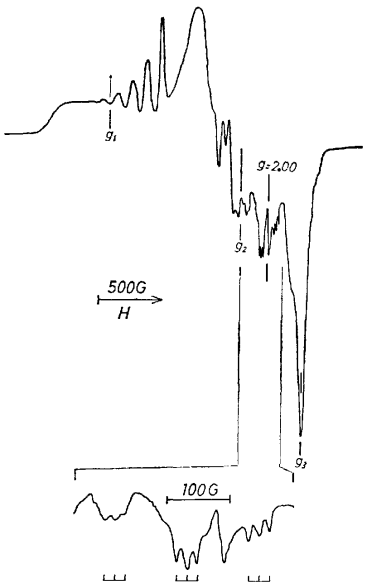

Fig. 6. ESR spectrum of the (2,3,17,18-tetramethyl-7,8,-12,13-tetraethylcorrolato)cobaltate(II) ion in *N,N*-dimethylformamide-pyridine (3 : 1 by volume) at 77 K. The g_2 component is expanded as shown in the lower part; triplet superhyperfine structure is observed.

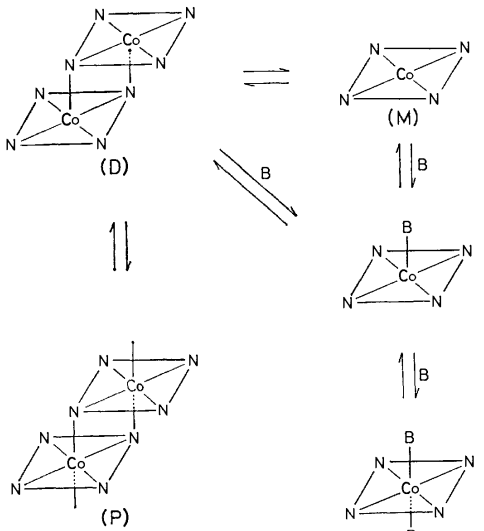

Scheme 2.

nucleus (I=7/2) are also observed in the g_1 and g_2 ranges, indicating that the central cobalt is in a low spin state (S=1/2). Upon addition of pyridine, a triplet superhyperfine structure can be seen on the hyperfine lines of the g_2 component as shown in Fig. 6. This may be caused by the interaction between nitrogen nucleus of the axially coordinated pyridine molecule and electron occupying the d_{z^2} obrital of the nuclear cobalt. Further spectral change was not observed by increasing the pyridine content. Consequently, only one pyridine molecule can be coordinated to the anionic cobalt(II)-corrole complex.

Discussion

The solution equilibria for the cobalt(III) corrole in the presence of amine bases can be illustrated by Scheme 2. The cobalt(III) corrole forms polymeric species in an organic solvent most plausibly through metal–nitrogen bonding in a manner as suggested for the copper(II) complex of phthalocyanine.[10)] The presence of such polymeric species is significant in a concentration range above 5×10^{-3} M as detected by the accumulative NMR measurements. The first equilibrium constants (K_1) for the formation of pyridine adducts of **3** are larger by one order of magnitude than those for the cobalt(II) complex of 1,19-disubstituted tetradehydrocorrin.[2)] This is attributed to the greater electrophilicity of nuclear cobalt in trivalent state. The second equilibrium constants (K_2) are much smaller than the K_1-values by an order of 10^2—10^3 due to the so-called *trans effect* in a manner as observed for the axial ligation of pyridine to tetrakis(4-*N*-methylpyridyl)porphincobalt(III).[11)] The equilibrium constant (K_i, $i=1$ or 2) can be correlated with the basicity of pyridine bases (pK_a) by Eq. 13 for the axial coordination of pyridine bases to the cobalt corroles except for 2-methyl- and 3-acetylpyridine, as shown in Fig. 7.

$$\log K_i = a\cdot pK_a + b \qquad (13)$$

The *a*- and *b*-parameters thus evaluated are listed in

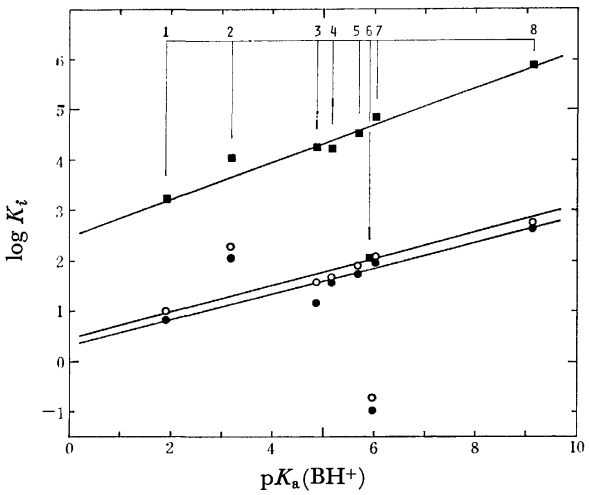

Fig. 7. Correlations between formation constant (K_i) and amine basicity: ■, K_1 for the **3**-amine system; ●, K_2 for the **3**-amine system; ○, K_2 for the **4**-amine system. Amines: 1, 4-CNPy; 2, 3-AcPy; 3, 3-HOPy; 4, Py; 5, 3-CH_3Py; 6, 2-CH_3Py; 7, 4-CH_3Py; 8, 4-NH_2Py (see Table 1 for abbreviations).

Table 2. Lower coordination ability of 2-methylpyridine with respect to the correlation line given by Eq. 13 is attributed to the steric hindrance effect due to the interaction between the corrole skeleton and the 2-methyl group of the pyridine base. The free energy loss by the steric effect is estimated to be 3.5 kcal/mol (25 °C) for the penta-coordination step, while 3.8 kcal/mol (25 °C) for the hexa-coordination process. That the free energy loss for the latter coordination process is comparable to that for the former is quite reasonable because no extra steric effect would be expected for the latter. On the other hand, 3-acetylpyridine shows a greater formation constant for its pK_a-value. The $d\pi$-$p\pi$ interaction betweeen the nuclear cobalt and the pyridine nitrogen, which is facilitated by the 3-acetyl group, would be responsible for such apparent increase in formation constant.

The equilibrium data for the present set of pyridine bases can be referred to the Hammett equation for which the coordination equilibrium with pyridine (K_i^0) is taken as a reference and suffix i stands for either 1 or 2.

$$\log K_i/K_i^0 = \rho\sigma . \quad (14)$$

The evaluated ρ values are listed in Table 2 along with other reference data of relevant cobalt(II) complexes.

It must be noted that both a and $-\rho$ values for the present cobalt(III)–corrole systems are considerably larger than the corresponding values for cobalt(II) complexes of protoporphyrin[12] and tetrakis(*p*-methoxyphenyl)porphyrin.[13] The values for the first coordination step of **3** is even larger than those for Co(II)–TDHC in spite of the fact that TDHC and corrole are anionic ligands with charges of −1 and −3, respectively. The a and ρ values suggest that the nuclear cobalt in cobalt(III) corrole is more electronegative than those in cobalt(II) complexes listed in Table 2, even though the total electric charges at the coordination site of corrole and porphyrin complexes are neutral and that of TDHC complex is positive (+1). It should be pointed out, however, that the a and $-\rho$ values for cobalt(III) corroles in the second coordination process are more or less comparable to those for Co(II)–TDHC. This seems to indicate that the extent of σ- and π-bonding characters of the coordinate bond formed in the final coordination step of cobalt(III) corroles is nearly the same as that of Co(II)–TDHC, since the former complexes secure the trans effect of the initially coordinated pyridine bases.

When the cobalt corrole is reduced at the nuclear cobalt from trivalent to bivalent state, only one pyridine molecule can be coordinated at its axial sites and hexacoordination is no longer possible as confirmed by ESR measurements. Cobalt(III) corrinoid forms the hexacoordinated complexes with amine bases at its axial positions but cobalt(II) corrinoid yields the bis(pyridine) complex only at a very high pyridine concentration, whereas bis(dimethylglyoximato)cobalt(II) takes on two pyridine ligands readily.[14] In this respect, the present tetrapyrrolic ligand gives out an equatorial ligand effect on the nuclear cobalt in a manner analogous to that observed for corrinoid. In other words, the axial ligation behavior of cobalt corrinoid is more or less analogous to that of cobalt corrole and differs a great deal from that of cobaloxime.

This work was supported in part by a Scientific Research Grant (No. 185193) from the Ministry of Education.

References

1) J. M. Pratt, "Inorganic Chemistry of Vitamin B_{12}," Academic Press, London (1972), Chap. 8.
2) Y. Murakami and Y. Aoyama, *Bull. Chem. Soc. Jpn.*, **49**, 683 (1976).
3) A. Albert, *J. Chem. Soc.*, **1951**, 1376.

Table 2. Brønsted[a] and Hammett[b] parameters for the coordination of pyridine bases

Coordination equilibrium	Co-Chelate system[c]	a	b	$-\rho$	Ref.
CoL + B ⇌ CoLB	Co(III) corrole (**3**)	0.37	2.5	2.0	This work
	Co(II)-TDHC	0.24	2.1	1.6	2
	Co(II)-PP(IX)DME	0.06	—	0.6	12
	Co(II)-*p*-MeOTPP	0.19	1.7	1.0	13
CoLB + B ⇌ $CoLB_2$	Co(III) corrole (**3**)	0.26	0.32	1.3	This work
	Co(III) corrole (**4**)	0.27	0.42	1.4	This work

a) Refer to Eq. 13. b) Refer to Eq. 14. c) Ligand abbreviations: TDHC, 8,12-diethyl-1,2,3,7,13,17,18,19-octamethyltetradehydrocorrin; PP(IX)DME, protoporphyrin IX dimethyl ester; *p*-MeOTPP, 5,10,15,20-tetrakis(*p*-methoxyphenyl)porphyrin.

4) H. Weidel and E. Murmann, *Monatsh. Chem.*, **16**, 749 (1895).
5) G. W. Anderson, I. F. Halverstadt, H. W. Miller, and K. O. Robbin, *J. Am. Chem. Soc.*, **67**, 2197 (1945).
6) H. W. Whitlock and R. Hanauer, *J. Org. Chem.*, **33**, 2169 (1968).
7) U. Eisner, A. Lichtarowicz, and R. P. Linstead, *J. Chem. Soc.*, **1957**, 733.
8) A. W. Johnson and I. T. Kay, *J. Chem. Soc.*, **1965**, 1620.
9) G. M. Badger, R. L. N. Harris, and R. A. Jones, *Aust. J. Chem.*, **17**, 1022 (1964).
10) S. E. Harrison and J. M. Assour, *J. Chem. Phys.*, **40**, 365 (1964).
11) R. F. Pasternack, M. A. Cobb, and N. Sutin, *Inorg. Chem.*, **14**, 866 (1975).
12) D. V. Stynes, H. C. Stynes, B. R. James, and J. A. Ibers, *J. Am. Chem. Soc.*, **95**, 1796 (1973).
13) F. A. Walker, *J. Am. Chem. Soc.*, **95**, 1150 (1973).
14) H. A. O. Hill, "Inorganic Biochemistry," Vol. 2, ed by G. L. Eichhorn, Elsevier Scientific Publishing Co., Amsterdam (1973), Chap. 30.

Synergistic Effect of Pyridine and Ammonia in the Extraction of Copper(II) Fixed on the Ion Exchange Resin with 2-Thenoyltrifluoroacetone

Kunio OHZEKI, Katsunori NOZAWA, and Tomihito KAMBARA

Department of Chemistry, Faculty of Science, Hokkaido University, Sapporo 060

(Received May 31, 1977)

The composition of hydrated copper(II), copper-pyridine, and -ammine species fixed on the cation exchange resin was determined by chemical and thermogravimetric analyses. Provided that all the water and bases were coordinated to copper(II) ion, the species on the resin were estimated to be $[Cu(H_2O)_5]^{2+}$, $[Cu(py)(H_2O)_3]^{2+}$, and $[Cu(NH_3)_3(H_2O)_3]^{2+}$, respectively. The removal of copper(II) ion from the resin with 2-thenoyltrifluoroacetone (Htta) was studied in various organic solvents. The rate of reaction was accelerated with the replacement of water molecules coordinated to the metal ion with pyridine or ammonia.

The reaction of metal ion fixed on the ion exchange resin with β-diketone in the organic phase has been investigated.[1-3] The quantitative removal of copper(II) ion fixed on Amberlyst 15 by acetylacetone was first achieved by the addition of a small amount of pyridine.[2] The effect of pyridine in the above system is considered to be similar to that observed in the solvent extraction system, *i.e.*, the rate-promoting synergistic effect.[4,5] Akaiwa *et al.* investigated the kinetics of synergistic extraction with nickel(II)– and cobalt(II)–Htta–pyridine base systems, and reported that the formation of the mono(tta) complex is accelerated by the pyridine base, which seemingly facilitates the release of a water molecule bound to metal ion.[5]

In the present work, it is shown that the reaction of copper(II) ion fixed on the resin with Htta is increased by replacement of some of the coordinated water molecules by unidentate neutral ligands, such as pyridine and ammonia.

Experimental

Apparatus and Reagents. Thermogravimetric curves were recorded with a Shimadzu thermal micro-balance TGA-20 with 5 mg sample at a heating rate 5 °C min^{-1} in the air. A Hitachi 508 atomic absorption spectrometer was used for the determination of copper and for the flame photometric determination of sodium. Visible absorption spectra were measured with a Hitachi 356 two-wavelength double beam spectrophotometer. 2-Thenoyltrifluoroacetone (Wako Pure Chemicals, Inc.) was used without further purification. Chloroform was purified by distillation after washing. Copper(II) sulfate and the other materials used were of guaranteed grade.

Preparation of Copper(II) Form Resin. Macroreticular resin Amberlyst 15 (Rohm and Haas Co.) was used. The dry resin was sized into the 60—80 mesh range, washed with ethanol, cleaned and recycled several times between hydrogen and sodium forms, ending in the latter. It was converted, in a column, into the copper-ammine form with 1.0 M (M=mol dm^{-3}) aqueous ammonia solution containing a total copper(II) concentration of 1.0×10^{-2} M, and washed with a dilute ammonia solution until the effluent became colorless. The copper-py form resin was also prepared using the copper(II) solution containing a large excess of pyridine. The copper(II)-aqua form resin was prepared as usual. The resins were air- and oven-dried at 105 °C for 3 h to purge free base and moisture, and then stored in a desiccator over silica gel for six months. The resin has a characteristic color; namely, Cu-ammine form light blue, Cu-py form grayish green, and Cu-aq form grey, respectively.

Chemical Analysis of the Species on the Resin. The column packed with a known amount of each form of resin was prepared, and the metal ion on the resin was eluted with 2 M hydrochloric acid, and then the column was washed free from the acid with water. The content of hydrogen ion in the resulting resin was determined by titration and the exchange capacity of the resin was evaluated. The analysis of the eluate was carried out as follows. The copper(II) content was determined by EDTA titration. Sodium was determined by flame photometry and the ion exchange sites which have not been displaced by copper(II) were found. Ammonia was determined by back titration; namely, after masking the copper(II) ion with EDTA, a known excess of a standard sodium tetraphenylborate was added to the sample solution, the resulting precipitate was filtered, and then the unreacted precipitant was determined with a standard solution of zephiramine (benzyldimethyltetradecylammonium chloride). The pyridine content was successfully determined spectrophotometrically with potassium thiocyanate-1-phenyl-3-methyl-5-pyrazolone.[6] It was found from the preliminary experiments carried out with synthetic samples that the interference by copper(II) ion could easily avoided with EDTA.

Results and Discussion

Chemical Analysis. The analytical data are given in Table 1. Provided that all the bases found on the resin were coordinated to copper(II), the mole ratio of copper to ammine and that of copper to py in the complexes are 1 : 3 and 1 : 1, respectively. The proportion of the ion exchange sites occupied by the copper(II) species to the exchange capacity was found to be as follows: Cu-aq form resin 100%, Cu-ammine 86%, and Cu-py 66%. The total amounts of copper(II) and sodium ions were less than the exchange capacity in the case of Cu-ammine and Cu-py form resins. Remaining sites on the resins may be occupied by hydrogen ions as a result of the probable decomposition of formerly adsorbed ammonium or pyridinium ions during the course of oven drying.

Thermogravimetric Analysis. It was found from preliminary experiments that a considerable amount of water had been adsorbed on the resin during six months' storage over silica gel in a desiccator. The thermogravimetric analysis was applied to the determination of water content in the resin. The resin matrix begins to decompose at around 300 °C as shown in Fig. 1. Upon further heating, it decomposes rapidly leaving a black residue. Only one step was found on the thermogravimetric curve of the Cu-aq form resin

Table 1. Results of analysis the species on the resin

Complex on the resin	Weight of resin taken (mg)	Cu found (μmol)	Base found (μmol)	Na found (μmol)	H^+ found after conversion to H-form (μmol)	Water found [a] (μmol)
$[Cu(H_2O)_5]^{2+}$	504.5	914			1832	
	5.0	9.1				45
$[Cu(NH_3)_3(H_2O)_3]^{2+}$	492.0	742	2273		1799	
	504.3	789	2312		1847	
	496.5	784		7.0	1824	
	5.0	7.8	23.6			23.6
$[Cu(py)(H_2O)_3]^{2+}$	511.7	608	646		1822	
	502.7	592		478.3	1793	
	5.0	5.9	5.8			19.4

a) Results of thermogravimetric analysis.

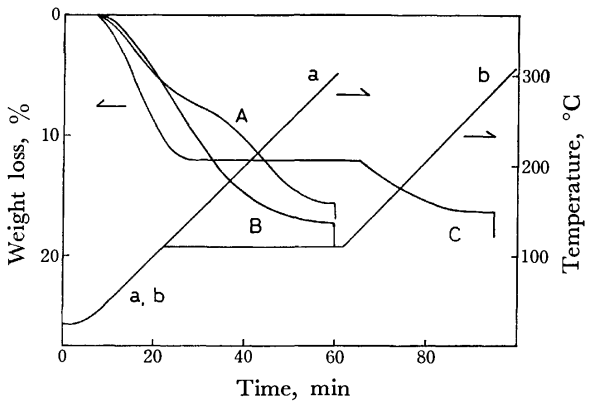

Fig. 1. Thermogravimetric curves of (A) copper-py, (B) copper-ammine, and (C) copper-aq form resin. The curves a and b indicate the heating rate.

at the constant heating rate of 5 °C min^{-1}. The mole ratio of water to copper content on the resin was found to be 5 : 1. On keeping the temperature at 110 °C, the Cu-aq form resin was found to show a constant weight after losing 4 molecules of water (curve C, Fig. 1). Thus, the copper species on the resin at 110 °C was expected to be $[Cu(H_2O)]^{2+}$, which agrees with the result of previous investigation.[2] The copper-py form resin gave two steps before 300 °C. The first step in the temperature range 40—110 °C was assumed to be due to the loss of water, and the second in the range 110—300 °C due to the loss of pyridine. The ratio of pyridine to copper content was found to be 1 : 1, which is consistent with the result of chemical analysis (Table 1), the ratio of water to copper content being 3 : 1. On keeping the temperature at 110 °C, the weight loss reached a constant and definite value, the resulting copper species being found to be $[Cu(py)]^{2+}$. The copper-ammine form resin decomposed in one step before decomposition of the resin matrix. The water content was calculated from the weight loss and analytical data of resin, the weight loss being assumed to be caused by the loss of water and ammonia. The ratio of water to copper content on the resin was found to be 3 : 1.

Copper Species on the Resin. Provided that all the water and base molecules determined by chemical and thermogravimetric analysis are bound to copper(II), the composition of copper species on the resin was found to be $[Cu(H_2O)_5]^{2+}$, $[Cu(py)(H_2O)_3]^{2+}$, and $[Cu(NH_3)_3(H_2O)_3]^{2+}$.

Reaction of Copper Species on the Resin with Htta. A weighed portion of the resin containing 2 mg of copper(II) was taken into an eggplant type flask and a 10-ml portion of 0.1 M Htta solution was added. After mechanical shaking for a certain time at room temperature, the resin was separated by filtration, washed with a small amount of ethanol, and then with water. Copper(II) ions remaining on the resin were eluted with 2 M hydrochloric acid solution and determined by atomic absorption spectrometry. The feasibility of extraction of copper(II) from the resin into Htta-benzene and Htta-chloroform solution increased in the order: Cu-aq, Cu-py, and Cu-ammine (Figs. 2 and 3).

More than 99% of copper(II) was removed from Cu-ammine form resin after a 15-min shaking, while *ca.* 50% of copper(II) was extracted from Cu-aq form resin. The mole ratio of copper to Htta in the complex was confirmed to be 1 : 2. However, the formation of an adduct, such as $[Cu(tta)_2py]$, was not found spectrophotometrically. In carbon tetrachloride

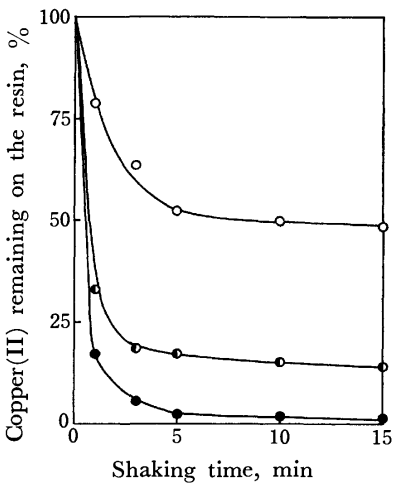

Fig. 2. Effect of shaking time on the removal of copper(II) from the resin into 0.1 M Htta solution in benzene. ○: Copper-aq, ◐: copper-py, ●: copper-ammine form resin.

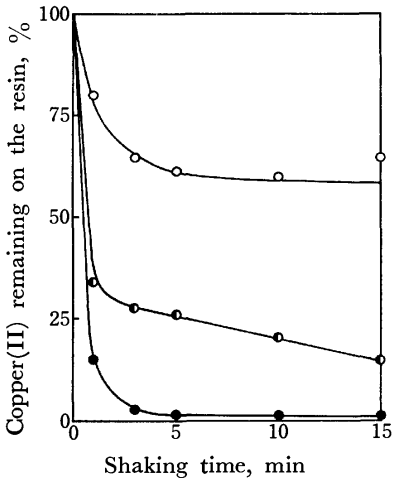

Fig. 3. Effect of shaking time on the removal of copper-(II) from the resin into 0.1 M Htta solution in chloro form. The symbols on each curve are the same as in Fig. 2.

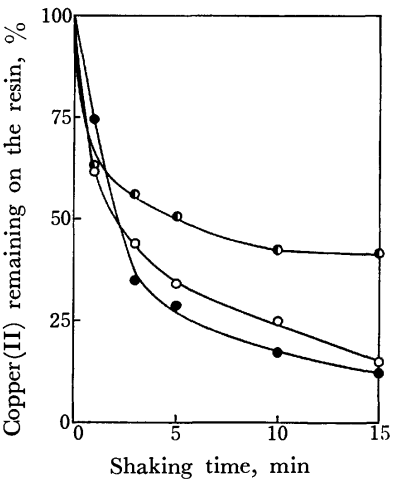

Fig. 5. Effect of shaking time on the removal of copper-(II) from the resin into 0.1 M Htta solution in ethanol. The symbols on each curve are the same as in Fig. 2.

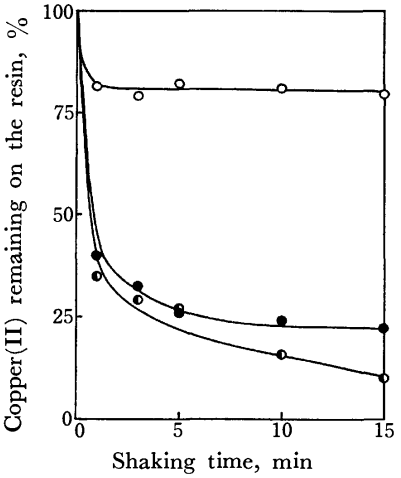

Fig. 4. Effect of shaking time on the removal of copper-(II) from the resin into 0.1 M Htta solution in carbon tetrachloride. The symbols on each curve are the same as in Fig. 2.

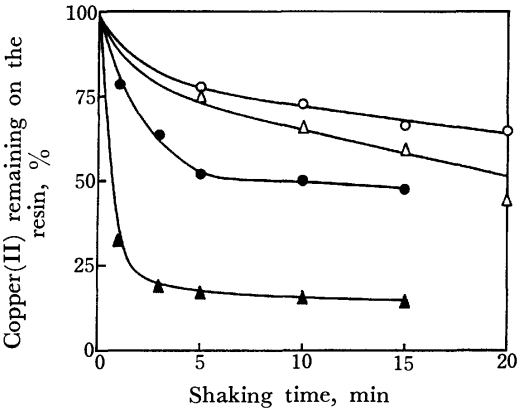

Fig. 6. Effect of water contents on the removal of copper-(II) into 0.1 M Htta solution in benzene. Air-dried resin; ●: copper-aq, ▲; copper-py form. Oven-dried resin; ○: copper-aq, △: copper-py form.

solution, Cu-py species was most easily expelled by Htta, whereas Cu-aq species persistently remained on the resin (Fig. 4). In ethanol solution, the rate of conversion of Cu-aq species on the resin into the tta complex was highly increased in comparison with the other solvent systems (Fig. 5). The color of the resulting solution was light green. The absorption maximum at 670 nm suggests the adduct formation between $[Cu(tta)_2]$ and ethanol. Since the phenomenon was characteristic to the aquacopper(II) ion, the first step of the reaction might be assumed to be the displacement of water molecules associated to copper(II) on the resin with ethanol.

Effect of Water. The Cu-aq and Cu-py form resins were dried at 110 °C and cooled for 3 h over silica gel in a desiccator. The copper species on the resin were estimated to be $[Cu(H_2O)]^{2+}$ and $[Cu(py)]^{2+}$, respectively. Evidence for the binding of pyridine to copper(II) was revealed by the light blue color of the resin phase. The results of the removal of copper(II) by Htta in benzene are given in Fig. 6. For the sake of comparison, the results of $[Cu(H_2O)_5]^{2+}$ and $[Cu(py)(H_2O)_3]^{2+}$ in the Htta-benzene system are also illustrated. The reactivity decreases with the removal of some or all water molecules around copper(II).

It can be assumed that the reaction of copper(II) with Htta is accelerated when the coordination sites around the copper(II) ion on the resin are simultaneously occupied by both water and pyridine. The pyridine probably facilitates the release of a water molecule bound to the copper(II) ion when Htta attacks the metal ion to form the mono(tta) complex, and with the progress of complexation the adsorption sites of the resin are competitively occupied by pyridinium and hydrogen ions. The synergistic effect might also hold in the case of the reaction of the copper–ammine complex with Htta and that of aquacopper(II) species with Htta in ethanol.

References

1) K. Ohzeki, M. Ikeuchi, and T. Kambara, *Bull. Chem. Soc. Jpn.*, **48**, 67 (1975).
2) T. Okamura, K. Ohzeki, and T. Kambara, *Bull. Chem. Soc. Jpn.*, **48**, 469 (1975).
3) K. Ohzeki, T. Tamura, and T. Kambara, *Bull. Chem. Soc. Jpn.*, **48**, 2829 (1975).
4) H. L. Finston and Y. Inoue, *J. Inorg. Nucl. Chem.*, **29**, 2431 (1967).
5) H. Akaiwa, H. Kawamoto, and T. Ishii, *J. Inorg. Nucl. Chem.*, **36**, 2077 (1974).
6) K. Ishii, *Bunseki Kagaku*, **24**, 385 (1975).

The Formation of Manganese and Cobalt Ferrites by the Air Oxidation of Aqueous Suspensions and Their Properties

Masao KIYAMA

Institute for Chemical Research, Kyoto University, Uji, Kyoto 611

(Received June 3, 1977)

Manganese and cobalt ferrites were prepared by the air oxidation of aqueous suspension of $Fe(OH)_2$ and either $Mn(OH)_2$ or $Co(OH)_2$ at 50—80 °C. In alkaline suspensions, all the metal ions are transformed into spinel ferrites, $M_xFe_{3-x}O_4$ (M=Mn or Co), by a suitable combination of the oxidation temperature and the concentration of the excess NaOH. Both manganese and cobalt ferrites consist of ferromagnetic particles (ferrite(A)) when x is smaller than 1.3, nonferromagnetic particles (ferrite(B)) when x is larger than 2, and mixtures of the two in the intervening range. The contents of Mn or Co, both in a solid solution of hydroxides, $M_{x/3}Fe_{1-x/3}(OH)_2$, and in ferrite, increase with the progress of the formation of the ferrite(A) caused by oxidation. The formation of the ferrite(B) begins when x in the solid solution reaches 2. Each particle in the ferrite(A) is less homogeneous in comparison with that in the ferrite prepared by a solid-state reaction, although with the same composition. The difference in the homogeneity causes the essential difference in magnetic properties.

Spinel ferrites with the general formula of $M_xFe_{3-x}O_4$(M being a bivalent metal ion, such as Mn^{2+}, Co^{2+}, Ni^{2+}, or Mg^{2+}), polycrystalline compounds prepared by a solid-state reaction between the constituent oxides, MO and Fe_2O_3, have been thoroughly investigated as regards their properties[1-3] and the conditions needed for their formation.[4] An alternative method of formation, precipitating spinel ferrites from aqueous suspensions containing $M(OH)_2$ and $Fe(OH)_3$ at the boiling point, was worked out by Schuele and Deetscreek.[5] The precipitates thus prepared consist of superparamagnetic particles of MFe_2O_4.

The appropriate conditions of oxidation have been found for the preparation of Fe_3O_4 from a $Fe(OH)_2$ suspension.[6] Since all the spinel ferrites have the same crystal structure as that of Fe_3O_4, it seemed to the present author that it would be possible to prepare the spinel ferrites under conditions similar to those used for the formation of Fe_3O_4, provided that $Fe(OH)_2$ and $M(OH)_2$ coexist in the starting suspension. The formation of a few kinds of spinel ferrites has been achieved from suspensions.[7-9] It was found that the composition of manganese and cobalt ferrites can be optionally varied in the $0 \leq x \leq 3$ range by selecting appropriate oxidation conditions.

This paper will give an account of the conditions and mechanisms for the formation of $Co_xFe_{3-x}O_4$ and $Mn_xFe_{3-x}O_4$ as well as of their properties.

Experimental

The starting suspension containing $Fe(OH)_2$ and either $Mn(OH)_2$ or $Co(OH)_2$ was prepared as follows. The required amounts of $FeSO_4 \cdot 7H_2O$, $MnSO_4 \cdot 5H_2O$ or $CoSO_4 \cdot 7H_2O$ (analytical grade) were dissolved in 1 l water, the resulting solution being acidic. To this NaOH was then added in the required amounts. Each suspension was diluted with water to 3 l. A number of suspensions were thus prepared, varying in the mole ratio of $2OH^-/SO_4^{2-}$ ($=R$) and in the metal concentration. The oxidation of the suspensions was carried out by bubbling air into them at a constant rate of 300 l/h for a period of 20 h. The details of the procedure of oxidation were previously reported.[6] A series of suspensions were prepared by adding excess aqueous ammonia to the solution. Air containing NH_3, bubbled through 0.5 M aqueous ammonia in a separate vessel, was used for oxidation.

The oxidation products were separated from each solution by filtration, washed with water, treated with acetone, and then dried at 50 °C under reduced pressure. The products, found by X-ray analysis to consist of only ferrites, were subjected to electronmicroscopic observation, and BET surface area and magnetic measurements. The mean particle size, $r(\mu m)$, of each product was estimated from the BET surface area by assuming that each particle was cubic.

The contents of Fe, Mn, and Co ions in the products were determined by the usual chemical analysis, combined with either X-ray-fluorescence or atomic-absorption spectrometry. The results agreed to within 0.01 in x; that is, $M_{1.00}Fe_{2.00}O_4$ has $x=1.00(\pm 0.01)$.

The excess oxygen content, δ, in a powdery sample of $MnFe_2O_{4+\delta}$ was determined by means of a reaction between the sample and the Fe^{2+} ion in an acidic solution. After the sample had been dissolved in a mixture of 0.05 M $FeSO_4$ and a dilute solution of H_2SO_4 and H_3PO_4 by heating in a nitrogen atmosphere, the amount of the Fe^{2+} ion remaining in the mixture was titrated with $KMnO_4$.

Results and Discussion

Conditions for the Formation of Ferrites. When a solution of NaOH was added to an acidic solution containing 0.72M $FeSO_4$ and either 0.36M $MnSO_4$ or 0.36M $CoSO_4$, a whitish precipitate was formed. When NaOH was added to the acidic solution in the $0.1<R<1$ range, a whitish precipitate appeared in a neutral or slightly alkaline suspension. The precipitate was found to be amorphous by X-ray analysis. When $R>1$, X-ray analysis showed that the precipitate had a CdI_2-type crystal structure. Through oxidation, the ferromagnetic precipitate was formed indirectly via a dark green intermediate oxidation product, or directly from a whitish precipitate, provided that a suitable oxidation temperature was chosen.

When $R<1$, a dark green precipitate(which is nonferromagnetic at room temperature) appeared upon oxidation. During oxidation, the concentration of the dissolved metal ions in the suspension medium decreased. The dark green precipitate was found by microscopic and X-ray diffraction examinations to consist of hexagonal, plate-like particles with the same crystal structure (a_0 3.17 and c_0 10.7 Å) as that of green rust II.[10] In view of the composition of green rust II, the precipitate is inferred to be a basic sulfate, one-half containing bivalent, and the other half, trivalent

metal ions. The dark green precipitate was gradually transformed into a brownish black and ferromagnetic precipitate during oxidation, provided that the temperature of suspension was kept higher than that at which a yellowish brown precipitate, which is non-ferromagnetic at room temperature, would occur. The intermediate oxidation product was eventually transformed into the brownish black and ferromagnetic precipitate by oxidation, with an abrupt drop of the pH value to 6 or a little lower, and with the cessation of the occurrence of the ferromagnetic precipitate. At the same time, the concentration of the Mn^{2+} or Co^{2+} ion increased to the concentration in the starting suspension medium. Further oxidation merely caused a very slight dissolution of the Mn^{2+} or Co^{2+} ion contained in the ferromagnetic particles.

When $1<R\leq3$, the metal ions were precipitated almost entirely as hydroxides of Fe^{2+} and Mn^{2+} or Co^{2+} in the form of a solid solution of $M_{x/3}Fe_{1-x/3}(OH)_2$ (M=Mn or Co). With a decrease in the amount of the solid solution during oxidation, the amount of the black ferromagnetic precipitate increased in the suspension when a suitable oxidation temperature was selected.

Microscopic and X-ray diffraction examinations showed that the ferromagnetic products consist of cubic or spherical particles of the cubic spinel ferrite, whereas the yellowish brown products consist of needle-like particles with the same crystal structure as that of α-FeO(OH).[11] It was found from these experiments that the temperature at which ferrites were formed was lowered with a decrease in the concentration of excess NaOH or a metal sulfate and that the R range suitable for ferrite formation became wider with an increase in the oxidation temperature beyond 50 °C. The composition of the products obtained at 70 °C by varying the R is given in Table 1, together with the change in pH before and after oxidation. The x value of the $Co_xFe_{3-x}O_4$ samples prepared in the presence of aqueous ammonia is 1.00 or less, depending on the concentration of aqueous ammonia present, as a result of the formation of ammine complexes of Co^{2+} in the suspension medium. When $0.6<R<3$, the needlelike particles besides the ferrite particles were formed at 70 °C.

The sample of ferrite prepared at 70 °C from a suspension containing an excess of aqueous ammonia

Table 1. Composition, x, of ferrites $M_xFe_{3-x}O_4$ (M=Co or Mn) prepared by the oxidation at 70°C of suspensions with various R values

R	$Co_xFe_{3-x}O_4$		$Mn_xFe_{3-x}O_4$	
	pH	x	pH	x
0.70	7.3→3.2	0.44	7.5→3.3	0.14
0.90	7.4→5.2	0.76	8.2→6.0	0.76
1.0	9.5→6.0	0.99	8.9→6.7	0.98
1.06	11.6→10.5	1.00	11.3→10.4	1.00
2.0	12	1.00	12	1.00
>1.0[a)]	9.5	≤1.00	9.5	1.00

a) Excess aqueous ammonia used as a precipitant.

or no excess NaOH ($R<1$) consisted of a mixture of very fine particles(size, 0.01 μm) and spherical particles(size, 0.1—0.2 μm), their mean particle size, r, being less than 0.1 μm. The r value increased as the concentration of excess NaOH in the alkaline suspension was increased.

Properties of Manganese Ferrites. $MnFe_2O_{4+\delta}$ samples were prepared at 50—80 °C from each of the alkaline suspensions with $R=1.1$—3.0 containing 0.36 mol/l of $Mn_{1/3}Fe_{2/3}(OH)_2$. Table 2 demonstrates that an increasing T and/or R increases r and slightly decreases the lattice constant, a_0, and the excess oxygen content, δ. A Mn NMR spectral pattern of the $MnFe_2O_4$ precipitate prepared from a suspension exhibits two peaks, at 551 and 524 MHz, at room temperature, with the higher peak corresponding to the Mn ions at the A sites in the spinel-crystal structure.[8] The patterns of the samples obtained showed that the higher peak becomes higher and steeper with an increasing R and T, but the ratio of peak heights remains almost constant, the Curie temperatures estimated from the patterns all being 500 °C.

Samples of $Mn_xFe_{3-x}O_4$ were prepared by subjecting suspensions containing 0.36 mol/l of $Mn_{x/3}Fe_{1-x/3}(OH)_2$ with various x and one of 0.072, 0.72 or 1.44 M excess NaOH(=1.1, 2.0, and 3.0 in R, respectively) to oxidation at 70 °C. The samples with $0\leq x\leq1.3$ were found to consist only of the cubic spinel ferrite. In the $1.4\leq x\leq1.8$ range, a small amount of tetragonally deformed spinel ferrite coexisted with the cubic spinel

Table 2. Properties of $MnFe_2O_{4+\delta}$ formed at various oxidation temperatures, T, and R values

R	T(°C)	r(μm)	a_0(Å)	δ
1.1	70	0.17	8.464	0.025
1.5	70	0.32	8.462	0.006
3.0	70	0.35	8.456	0.000
1.5	50	0.17	8.477	0.024
1.5	80	0.30	8.462	0.004

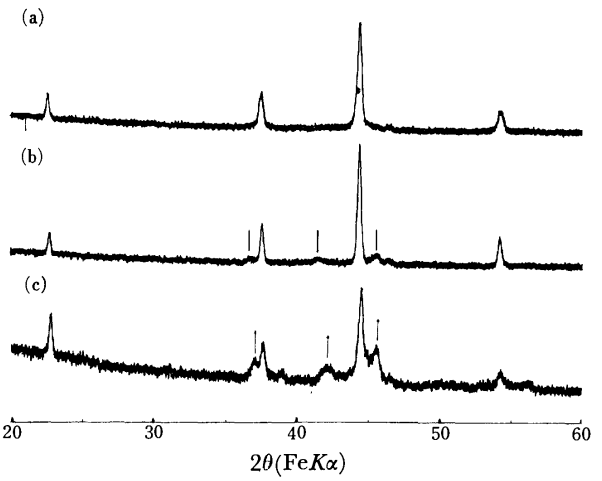

Fig. 1. X-Ray diffraction patterns of $Mn_xFe_{3-x}O_4$ precipitates, (a) $x=1.5$, $R=1.1$, (b) $x=1.5$, $R=2.0$, and (c) $x=2.0$, $R=1.1$. Arrows indicate the peaks caused by the presence of a tetragonal ferrite.

ferrite. As the concentration of excess NaOH increases, the content of the tetragonal ferrite in the mixture slightly increases for a given value of x((a) and (b) in Fig. 1). The content began to increase remarkably at $x=2$ (c) and reached 100% for $x\geq 2.6$. The shape and size of both kinds of ferrite particles with $x\leq 1.3$ and $x\geq 2.6$, prepared at given concentrations of excess NaOH, were found by microscopic examination to be similar. When $x<1$, the a_0 of the cubic spinel ferrites increases with x, regardless of the concentration of excess NaOH(Fig. 2). It approaches 8.5 Å with a further increase in x, depending on the concentrations of excess NaOH. The Mn NMR spectral patterns of these cubic spinel ferrites showed that an increase in x shifts the higher peak to the lower frequency side as a result of lowering the Curie temperature(447 °C for $x=1.3$). Heating the samples of $Mn_xFe_{3-x}O_4$ *in vacuo* at 450 °C decreased the Curie temperature and increased a_0(to the value of the dotted curve shown in Fig. 2), both the values approaching those of a manganese ferrite with the same composition prepared by a solid-state reaction. It was found by electron-microscopic examination that the particle shape and size in each sample with $x\leq 1.3$ remain almost unchanged in spite of heat treatment at 450 °C.

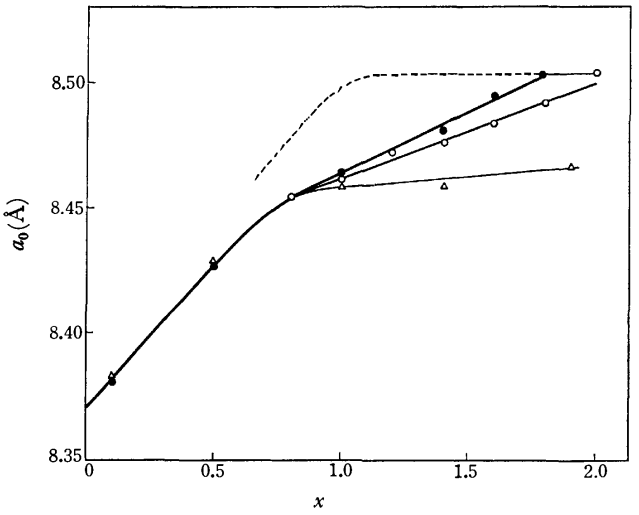

Fig. 2. Lattice constant a_0 of cubic spinel ferrite as a function of x in $Mn_xFe_{3-x}O_4$ preicpitates prepared from the suspensions with $R=1.1$(●), 2.0(○), and 3.0(△) by oxidation at 70 °C.

Properties of Cobalt Ferrites. Samples of $Co_xFe_{3-x}O_4$ were prepared by oxidizing at 70 °C suspensions containing 0.36 mol/l of $Co_{x/3}Fe_{1-x/3}(OH)_2$ with various x and 0.075 M excess NaOH. Figures 3 and 4 show, respectively, electron-micrographs and X-ray diffraction patterns of some typical samples. The black and ferromagnetic samples with $0\leq x\leq 1.3$ consisted of cubic particles (for $0\leq x\leq 0.6$), or spherical particles (for $0.9\leq x\leq 1.3$), and had lattice constants which were nearly constant at 8.38 Å. When $x\geq 1.4$, very fine particles of another kind of ferrite with a_0 8.34—8.31 Å coexist with the spherical particles((a) and (b) in Figs. 3 and 4).

Increasing the x caused a retardation of the rate of transformation of the solid solution of hydroxides, $Co_{x/3}Fe_{1-x/3}(OH)_2$, into ferrites. In the $2\leq x\leq 3$ range, the solid solution was not completely transformed into ferrites in 20 h(Fig. 4(c)), so that the oxidation was carried out for 50 h. The resulting sample with $x=2.4$ was nonferromagnetic because of its Curie temperature, lower than room temperature,[12] consisting of very fine particles (Fig. 3(c)). Incidentally, the nonferromagnetic samples with $2.7\leq x\leq 3.0$ had the same crystal structure as that of $CoHO_2$(=CoO(OH)).[13]

Similar experiments were conducted with $Co_xFe_{3-x}O_4$ by varying the excess NaOH concentration in the 0.1—1.5 M range. The results indicated that increasing the concentration of excess NaOH accelerates the particle growth of $Co_xFe_{3-x}O_4$ with $0\leq x\leq 1.3$ and causes a slight decrease in the content of the nonferromagnetic ferrite for a given value of x(the inset in Fig. 4(b)). In the absence of excess NaOH($0.9\leq R\leq 0.95$), the oxidation products obtained at 70 °C, corresponding to $Co_xFe_{3-x}O_4$ with $2.2\leq x\leq 3.0$, were nonferromagnetic

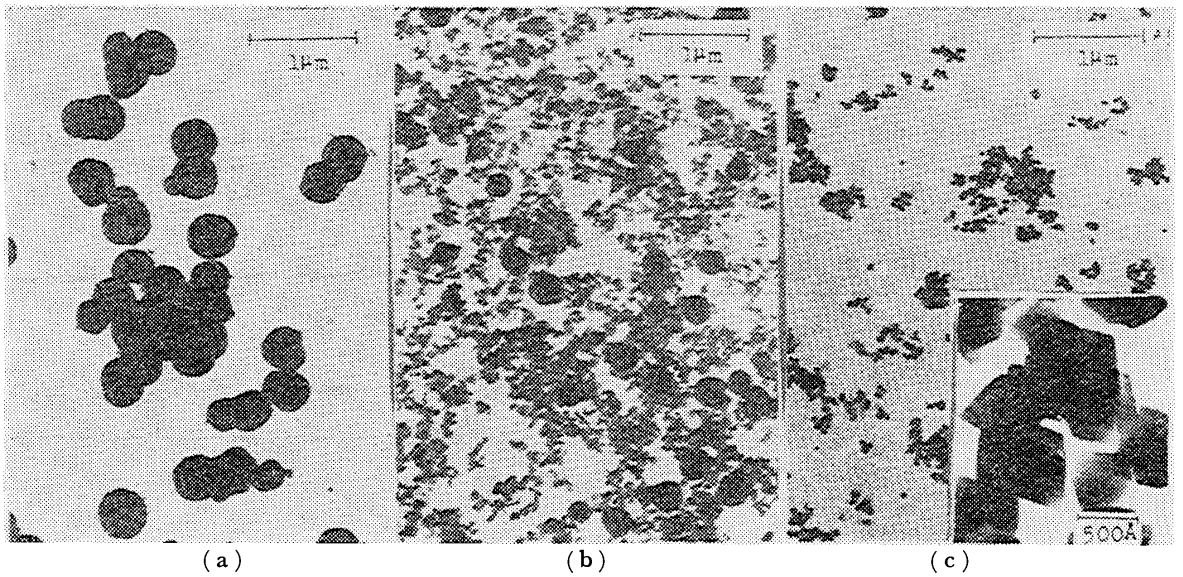

(a) (b) (c)

Fig. 3. Electronmicrographs of $Co_xFe_{3-x}O_4$ precipitates with $x=1.4$(a), 1.7(b), and 2.4(c).

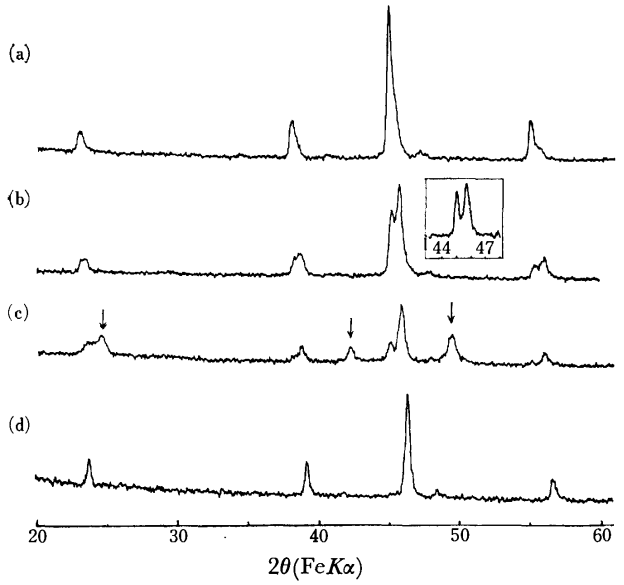

Fig. 4. X-Ray diffraction patterns of $Co_xFe_{3-x}O_4$ precipitates with $x=1.4$(a), 1.7(b), 2.0(c), and 2.4(d) prepared at $R=1.1$. The inset denotes a pattern of a ferrite with $x=1.7$ prepared from the suspension with $R=2.0$. Arrows in (c) indicate the peaks caused by the presence of a solid solution of hydroxides.

at room temperature. The nonferromanetic products with $2.2\leq x\leq 2.5$ were amorphous, and the products with $x\geq 2.6$ had the same crystal structure as that of Co_3O_4.[14]

$Co_xFe_{3-x}O_4$ samples with 0.1—0.2 μm in r were chosen from the products prepared from the alkaline suspensions, and their demagnetization curves at room temperature were obtained after their saturation magnetization, σ_s, had been measured as has been described previously.[15] The increase in x from 0 to 0.8 caused a slight decrease in σ_s. A further increase in x from 1.4 caused a remarkable decrease in σ_s. The coercive force, ${}_iH_c$, increases with x and reaches 1.3 kOe for

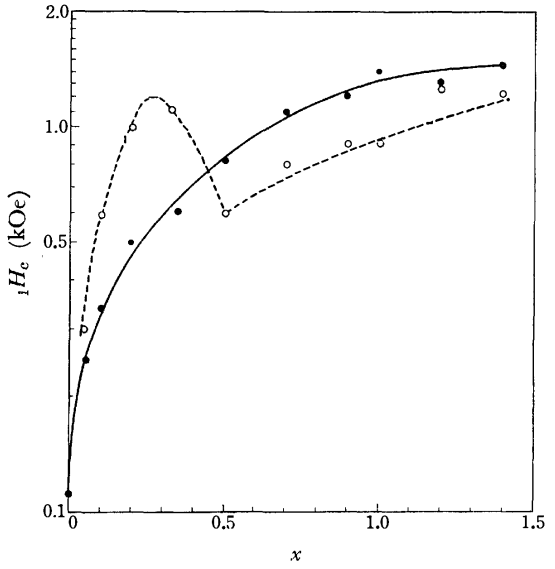

Fig. 5. Coercive force ${}_iH_c$ plotted against x in $Co_xFe_{3-x}O_4$ precipitates before (●) and after(○) heat treatment at 350 °C *in vacuo*.

$x\geq 1.2$(Fig. 5). The magnetic properties of each sample which had been subjected to heating *in vacuo* at 350 °C for 5 h were measured. The shape and size of particles in the sample were found by microscopic examination to remain almost unchanged in spite of the heat treatment. The difference in the magnetic properties before and after the heat treatment is dependent on x (Fig. 5). The change in the magnetic properties by heat treatment must be caused by the diffusion of the metal ions within each particle in the $Co_xFe_{3-x}O_4$ samples as well as in the $Mn_xFe_{3-x}O_4$ samples.

Mechanism of Ferrite Formation. As has been mentioned above, the solid solution, $M_{x/3}Fe_{1-x/3}(OH)_2$ (M=Mn or Co), with $1.4\leq x\leq 2.4$ in the starting suspension was transformed into a mixture of two kinds of ferrites, the content of each in the final oxidation product for a given value of x depending on the excess NaOH concentration. After the ferromagnetic ferrite(A), corresponding to $x\leq 1.3$, had been formed, the transformation of the remaining solid solution, $M_{x/3}Fe_{1-x/3}(OH)_2$(M=Mn or Co), into the other ferrite(B) took place and proceeded gradually. It can be deduced from this finding that the content of the Mn or Co ion in the remaining solid solution increases with the progress of the formation of ferrite(A) caused by oxidation.

As has been generally known, the dissolution rate of ferrite into an acidic solution is extremely small as compared with that of the solid solution of hydroxides. By making use of this fact, the changes in the composition of ferrite and the solid solution with the time lapse of oxidation were studied. Several suspensions, each containing 0.36 mol/l of $M_{x/3}Fe_{1-x/3}(OH)_2$(M=Mn or Co) and either 0.11 or 0.95 M excess NaOH($R=1.1$ or 2.3), were subjected to oxidation at 70 °C for 20 h. In the course of oxidation, 200-ml samples of each suspension were taken out after 2, 5, 8, and 20 h. The particle size of ferrite(A) was found by microscopic examination to become greater with the progress of the formation of ferrite(A) by oxidation. The precipitate in each 200-ml suspension, separated from the alkaline solution by filtration, was added to acetic acid (10 wt%). The alkaline filtrate was found to contain a trace of the metal ions. The acidic suspension with pH=4 containing acetic acid was left standing at room temperature for 10—30 min with occasional stirring. The remaining precipitate was separated from the acidic solution with pH=4 by filtration. The precipitate treated with acetic acid was found by X-ray analysis to consist of ferrites with no hydroxides.

The contents of Mn or Co in the remaining solid solution and in the ferrite formed were estimated from the amounts of the metal ions in the acidic filtrate and in the precipitate obtained by treatment with acetic acid respectively. These results are given in Table 3. The Mn or Co content, both in the solid solution and in ferrite (A), becomes greater as the formation of ferrite (A) proceeds by oxidation, and the formation of ferrite (B) begins when x in the solid solution becomes greater than 2. An increase in the concentration of excess NaOH accelerates the particle growth of ferrite (A) and retards the rate of increase in x in both the

TABLE 3. RELATIVE CHANGE IN THE COMPOSITION(x) OF THE REMAINING SOLID SOLUTION, $M_{x/3}Fe_{1-x/3}(OH)_2$ (M=Mn or Co), AND OF THE FERRITE, $M_xFe_{3-x}O_4$, IN THE COURSE OF OXIDATION AT 70 °C

R	Oxidation time (h)								
	0	2	5	8	20	2	5	8	20
	$Mn_{x/3}Fe_{1-x/3}(OH)_2$					$Mn_xFe_{3-x}O_4$			
1.1	1.04	1.30	1.53	—	—	0.66	0.89	1.05	1.05
1.1	1.50	1.96	2.32	—	—	1.30	1.39	1.46	1.46
1.1	2.08	—	2.45	2.50	—	—	1.66[a]	1.91[a]	2.05[a]
2.3	1.50	1.71	1.99	2.57	—	1.03	1.31	1.45	1.46[a]
	$Co_{x/3}Fe_{1-x/3}(OH)_2$					$Co_xFe_{3-x}O_4$			
1.1	1.56	1.91	1.94	2.13	—	1.36	1.38	1.44	1.56[a]
2.3	1.56	—	1.73	1.78	2.62	—	1.37	1.43	1.57[a]

a) Consisting of a mixture of ferrites (A) and (B).

solid solution and ferrite (A) in the course of oxidation.

The change in the size and shape of the particles before and after the transformation into ferrites suggests that the transformation takes place in the suspension medium by the same mechanism as that described for the formation of Fe_3O_4.[6] The suspension medium is saturated with respect to the solid solution of $M_{x/3}Fe_{1-x/3}(OH)_2$(M=Mn or Co). When the suspension is subjected to oxidation with air, the bivalent metal ions (probably hydroxo complexes) in the suspension medium react with the dissolved oxygen. The relative redox potential of each metal ion between bivalent and trivalent states in the suspension medium has been known to decrease in the order of Co>Mn>Fe.[16] This probably causes the predominant formation of an iron(III) hydroxo complex(probably polynuclear). It is considered that the polynuclear complex reacts with the hydroxo complexes of bivalent metal ions of Fe^{2+} and Mn^{2+} or Co^{2+} to form the nuclei of ferrite (A). The hydroxo complexes consumed by the ferrite formation may be incessantly replenished by the dissolution of the particles of the solid solution into the suspension medium.

The nuclei of ferrite(A) might, therefore, grow on epitaxially by the slow coprecipitation of the hydroxo complexes of bivalent metal ions with the polynuclear complex formed by oxidation. As the growth of the particles of ferrite(A) proceeds, x in the remaining solid solution becomes greater and x in each particle of ferrite(A) increases until the epitaxial reaction of its surface with the complexes has been stopped. Thus, the rate of the increase in x of each particle of ferrite(A) during the growth period, which is influenced by the oxidation conditions, will determine the inhomogeneity in the composition of each particle in the samples with $x \leq 1.3$.

Table 2 indicates that, in spite of the decrease in cation vacancies, the a_0 of the samples of manganese ferrite decreases only slightly with an increase in the r. It can be inferred from these results that the Mn concentration increases continuously from the central to the sub-surface portion of each particle, and that both the difference in the concentration between the two portions and the concentration gradient within the particle depend on the r of the sample with a given value of x. The inhomogeneity in the composition of the individual Mn ferrite particles described above will hold true of the particles in the samples of $Co_xFe_{3-x}O_4$ with $x \leq 1.3$.

In conclusion, the anomalous magnetic behavior of the ferrite(A) prepared from the suspension by oxidation must inevitably be associated with its unique structural properties, differing from those of ferrite with the same composition prepared by the solid-state reaction.

The author is indebted to Professors T. Takada and N. Bando, and to Dr. T. Shinjo (of this Institute) for their valuable advice, and Dr. H. Yasuoka (the University of Tokyo) for his NMR measurements and helpful comments. He also wishes to thank Messrs T. Akita, T. Akiyama, and I. Sugano for their assistance in the experiments and the Sumitomo Special Metal Co., Ltd., for the magnetic measurements with cobalt ferrites.

References

1) J. Smit and H. P. J. Wijn, "Ferrites," International Ed, Tokyo Electrical Enginering College Press, Tokyo (1965), p. 136.
2) J. E. Burke, "Progress in Ceramic Science," 4, Pergamon press Ltd., Oxford (1966), p. 165.
3) D. H. Martin, "Magnetism in Solids," M. I. T. Press, Cambridge, Massachusetts (1967), pp. 38, 241.
4) G. C. Kuczynski, *Ferrites, Proc. Intern. Conf.*, Univ. of Tokyo Press (1971), p. 87.
5) W. J. Schuele and V. D. Deetscreek, *J. Appl. Phys.*, **32**, 235S (1961).
6) M. Kiyama, *Bull. Chem. Soc. Jpn.*, **47**, 1646 (1974).
7) A. Hamamura, M. Kiyama, Y. Bando, and T. Takada, *Jpn. J. Appl. Phys.*, **5**, 1246 (1966).
8) H. Yasuoka, A. Hirai, T. Shinjo, M. Kiyama, Y. Bando, and T. Takada, *J. Phys. Soc. Jpn.*, **22**, 174 (1967).
9) T. Takada, M. Kiyama, Y. Bando, and T. Shinjo, *Bull. Inst. Chem. Res., Kyoto Univ.*, **47**, 298 (1969).
10) J. D. Bernal, E. R. Dasgupta, and A. L. Mackay, *Clay min. Bull.*, **4**, 15 (1959).
11) X-Ray powder data, Card 17—532, A. S. T. M.
12) M. Takahashi and M. E. Fine, *J. Appl. Phys.*, **43**, 4205 (1972).
13) X-Ray powder data, Card 7—169, A. S. T. M.
14) X-Ray powder data, Card 9—418.
15) M. Kiyama, *Bull. Chem. Soc. Jpn.*, **49**, 1855 (1976).
16) W. M. Latimer, "Encyclopedia of Chemical Technology," ed. by R. E. Kirk and D. F. Othmer (Japanese Reprint Edition), Maruzen Co., Ltd., Vol. 9, Tokyo (1960), p. 681.

Magnetic and Spectral Properties of Copper(II) Chloride Complexes of Tridentate Salicylideneamines with ONN Set of Donors

Yoneichiro MUTO and Tadashi TOKII

Department of Chemistry, Faculty of Science and Engineering, Saga University, Saga 840

(Received June 20, 1977)

Four complexes with the general formula of Cu[sal·$(CH_2)_n$·N(R)R′]Cl (sal= ·$\overset{2}{O}$·C_6H_4·$\overset{1}{C}$H=N·; n=2 and 3; R=H and CH_3; R′=CH_3) were characterized by elemental analyses, IR and visible reflectance spectra, ESR spectra, and magnetic susceptibilities. The complexes where n=2, Cu[sal·$(CH_2)_2$·$NHCH_3$]Cl and Cu[sal·$(CH_2)_2$·$N(CH_3)_2$]Cl, showed normal paramagnetic behavior. The Cu[sal·$(CH_2)_3$·$N(CH_3)_2$]Cl complex was obtained in two forms, one red-violet and the other green. The red-violet form showed the usual magnetic behavior expected for a mononuclear copper(II) complex, whereas the green one exhibited the antiferromagnetic behavior typical of binuclear copper(II) complexes. The magnetic properties of these complexes are discussed in terms of structural considerations. The characterization of the Cu[sal·$(CH_2)_3$·$N(CH_3)_2$]Br complex is also reported.

The results of synthetic and characterization studies on copper(II) chloride complexes of *N*-(hydroxyalkyl)-salicylideneamines with ONO set of donors were reported in previous papers.[1,2] In the course of our studies, we found that the antiferromagnetic interaction in dimeric copper(II) chloride complex with *N*-(2-hydroxyethyl)salicylideneamine, $[Cu(sal\cdot en\cdot OH)Cl]_2$, is much weaker than that in the corresponding *N*-(3-hydroxypropyl) complex, $[Cu(sal\cdot pr\cdot OH)Cl]_2$. This observation prompted us to investigate the analogous complexes with ONN tridentate salicylideneaminato ligands of the general formula

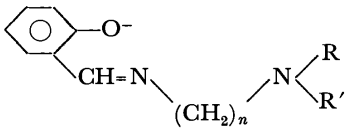

abbreviation

sal·en·N(H)Me; n=2, R=H, R′=CH_3
sal·en·NMe_2; n=2, R=R′=CH_3
sal·pr·NMe_2; n=3, R=R′=CH_3

The complexes Cu[sal·en·N(H)Me]Cl, **1**, and Cu(sal·en·NMe_2)Cl, **2**, were originally synthesized and investigated by Sacconi *et al.*[3] The complex Cu(sal·pr·NMe_2)Cl has been obtained in two forms, one red-violet, **3**, and the other green, **4**; the corresponding bromide complex Cu(sal·pr·NMe_2)Br, **5**, only in a green form. In addition, the interconversion between **3** and **4** has been observed as follows: **3** is converted to **4** by recrystallizing **3** from methanol or chloroform while the reverse conversion is carried out by heating **4** in ethanol. One object of the present work is to elucidate the structure difference between **3** and **4**.

We report here the results of magnetic and spectral studies on these complexes **1**—**5** and discuss their magnetic properties in terms of structural considerations.

Experimental

Syntheses. Compounds **1** and **2** were prepared by methods which were slightly modified from those of Sacconi *et al.*,[3] as follows: *Compound* ***1****, Cu[sal·en·N(H)Me]Cl*: A solution of copper(II) chloride (10 mmol) in ethanol (50 ml) was added to a mixture of bis(salicylaldehydato)copper(II) (10 mmol) and *N*-methylethylenediamine (20 mmol) in ethanol (30 ml). The solution was stirred at *ca.* 70 °C for 1/2 h and then concentrated to one-fourth of its volume. After the solution had been allowed to stand overnight at *ca.* 5 °C in a freezer, the separated green crystals were collected and recrystallized from chloroform. Found: Cu, 23.02%. Calcd for $C_{10}H_{13}N_2OClCu$: Cu, 23.00%. *Compound* ***2****, Cu(sal·en·NMe_2)Cl*: A mixture of Cu(sal·en·NMe_2)$_2$ (10 mmol) and copper(II) chloride (10 mmol) in ethanol (30 ml) was stirred on a hot plate for 1/2 h. The green crystals thus precipitated were collected and recrystallized from chloroform. Found: Cu, 21.64%. Calcd for $C_{11}H_{15}N_2OClCu$: Cu, 21.89%.

Compound ***3****, the Red-violet Form of Cu(sal·pr·NMe_2)Cl*: This was prepared by the reaction of Cu(sal·pr·NMe_2)$_2$ and copper(II) chloride according to the procedure described above (Compound **2**). The purification was made by recrystallization from ethanol. This was also obtained by heating Compound **4** in ethanol. Found: C, 47.29; H, 5.67; N, 9.19; Cu, 20.80%. Calcd for $C_{12}H_{17}N_2OClCu$: C, 47.37; H, 5.63; N, 9.21; Cu, 20.88%.

Compound ***4****, the Green Form of Cu(sal·pr·NMe_2)Cl*: A solution of copper(II) chloride (10 mmol) in methanol (30 ml) was added to a solution of Cu(sal·pr·NMe_2)$_2$ (10 mmol) in methanol (20 ml). The mixture was stirred at *ca.* 40 °C for 1/2 h. The green crystals which precipitated were collected and washed with methanol and dried. This was also obtained by recrystallizing Compound **3** from methanol or chloroform. Found: C, 47.14; H, 5.65; N, 9.10; Cu, 21.05%. Calcd for $C_{12}H_{17}N_2OClCu$: C, 47.37; H, 5.63; N, 9.21; Cu, 20.88%.

Compound ***5****, Cu(sal·pr·NMe_2)Br*: The synthetic procedure is similar to that for Compound **3** except for the use of copper(II) bromide instead of copper(II) chloride. The green crystals collected were recrystallized from ethanol. Found: C, 41.26; H, 4.89; N, 7.99; Cu, 18.10%. Calcd for $C_{12}H_{17}N_2OBrCu$: C, 41.33; H, 4.92; N, 8.03; Cu, 18.22%.

Physical Measurements. The magnetic susceptibilities were determined by the Gouy method in the range from the temperature of liquid nitrogen to room temperature. The effective magnetic moments per copper ion at room temperature were calculated from the equation:

$$\mu_{eff} = 2.83\sqrt{(\chi_A - N\alpha)\cdot T} \quad (1)$$

where χ_A is the molar magnetic susceptibility corrected for the diamagnetism of the constituted atoms using Pascal's constant[4] and $N\alpha$ is the temperature-independent paramagnetism per gram-ion of copper(II). The $N\alpha$ was assumed to be 60×10^{-6} cgs emu.[5] The results are given in Table 1. The ESR (X-band) spectra of polycrystalline samples were recorded with a JEOL ESR-apparatus, model JES-ME-1X, at room temperature. The IR spectral measurements were made with a Hitachi EPI-G2 IR spectrophotometer in the 400—4000 cm^{-1} region on Nujol mulls. The reflectance

Table 1. Magnetic data

	Compound	μ_{eff}/B. M. (T/K)	θ/K	$-2J$/cm^{-1}	g[a]
1.	Cu[sal·en·N(H)Me]Cl	1.81 (295)	0		
2.	Cu(sal·en·NMe_2)Cl	1.81 (293)	0		
3.	Cu(sal·pr·NMe_2)Cl (red-violet form)	1.80 (293)	0		
4.	Cu(sal·pr·NMe_2)Cl (green form)	1.44 (298)		248	2.10 (2.10)
5.	Cu(sal·pr·NMe_2)Br	1.42 (295)		260	2.10 (2.09)

a) The data in parentheses were determined by ESR measurements on the polycrystalline samples.

spectra were recorded with a Hitachi EPS-3T recording spectrophotometer.

Results and Discussion

Magnetic Data. The results of the magnetic susceptibility measurements are shown in Fig. 1.

The susceptibility data of Compounds **1** and **2** follow the Curie law down to liquid nitrogen temperature, indicating that they are magnetically diluted in crystals. Hence they are considered to be mononuclear. The red-violet complex **3** also showed the usual magnetic behavior expected for a mononuclear copper(II) complex; a plot of $(\chi_A - N\alpha)^{-1}$ as a function of temperature gives a Weiss constant θ of almost 0 K (Fig. 1). Their X-band ESR spectra provide further evidence for their monomeric nature: the spectra show a strong signal at *ca.* 3100 G due to a copper(II) ion with $S=1/2$. In contrast to **3**, the green complex **4** and the analogous bromide complex **5** show subnormal magnetic moments at room temperature (*cf.* Table 1), and their magnetic susceptibility data fit the Bleaney-Bowers equation[6]

$$\chi_A = \frac{Ng^2\beta^2}{3kT}\left[1+\frac{1}{3}\exp\left(\frac{-2J}{kT}\right)\right]^{-1} + N\alpha \qquad (2)$$

where each symbol has the general meaning. The J and g values listed in Table 1 were evaluated from the best fit of the cryomagnetic data to Eq. 2, assuming $N\alpha = 60\times10^{-6}$ cgs emu.[5] The negative values of J indicate the presence of antiferromagnetic interaction in these complexes, and the g values are in good agreement with the average g values obtained from ESR measurements (*cf.* Table 1). The close agreement between the experimental and theoretical $\chi_A - T$ curves is a powerful argument for a binuclear structure in these complexes.

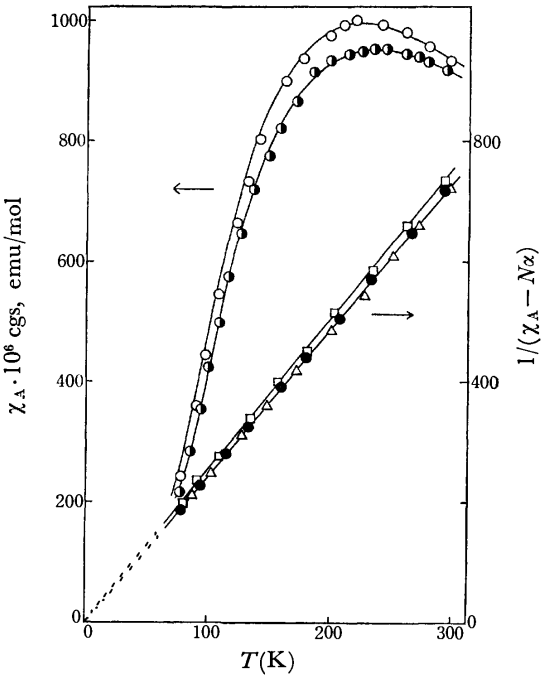

Fig. 1. Variation of magnetic susceptibilities with temperature. (△) Cu[sal·en·N(H)Me]Cl, (●) Cu(sal·en·NMe_2)Cl, (□) Cu(sal·pr·NMe_2)Cl (red-violet form), (○) Cu(sal·pr·NMe_2)Cl (green form), (◑) Cu(sal·pr·NMe_2)Br.

These magnetic data clearly indicate that the two forms of Cu(sal·pr·NMe_2)Cl, red-violet and green in color, are monomer-dimer type isomers of each other.

IR Spectra. The wave number of the intense band near 1540 cm^{-1} observed for the present complexes **1**—**5** and the parent bis-complexes, Cu(sal·en·NMe_2)$_2$ and Cu(sal·pr·NMe_2)$_2$, are listed in Table 2. The IR spectra of mononuclear complexes of salicylaldehyde Schiff bases display a sharp band at *ca.* 1530 cm^{-1}, whereas the band in the spectra of polynuclear salicylideneamine complexes with phenolic oxygen-bridges between metal ions appears in the range 1545—1550 cm^{-1}.[7] This band shift toward higher frequencies is now taken as an umambiguous criterion for the formation of a phenolic oxygen-bridging in polymeric salicylideneamine complexes.[1,2,7-11]

As is shown in Table 2, the band shift was observed for Compounds **4** and **5**. This indicates the presence

Table 2. IR and reflectance spectral data

	Compound	IR absorption band maximum near 1540 cm^{-1} ν/cm^{-1}	Ligand field band maximum[a] $\nu/10^3$ cm^{-1}
1.	Cu[sal·en·N(H)Me]Cl	1531	15.9
2.	Cu(sal·en·NMe_2)Cl	1534	16.7 sh, 15.1
	Cu(sal·en·NMe_2)$_2$	1526	16.7 sh, 14.3
3.	Cu(sal·pr·NMe_2)Cl (red-violet form)	1529	19.0, 14.1, 11.1 sh
4.	Cu(sal·pr·NMe_2)Cl (green form)	1549	11.2, 9.6 sh
5.	Cu(sal·pr·NMe_2)Br	1549	12.5, 11.1 sh
	Cu(sal·pr·NMe_2)$_2$	1534	16.7 sh, 14.1

a) sh = shoulder.

of phenolic oxygen-bridges between copper(II) ions in these complexes. On the other hand, no significant band shift was observed for Compounds **2** and **3**, indicating that, in these complexes, no phenolic oxygen-bridge exists. The strong band at 1531 cm^{-1} for Compound **1** indicates the non-existence of any bridging phenolic oxygen in this complex.

Diffuse Reflectance Spectra. The present complexes give rise to several bands in the 5000—25000 cm^{-1} region in the diffuse reflectance spectra. The wave numbers of the band maxima are collected in Table 2 and their spectral curves are shown in Fig. 2.

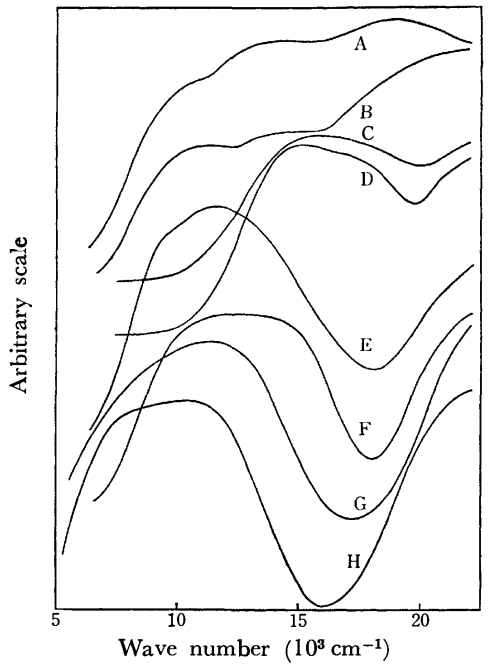

Fig. 2. Reflectance spectra of Cu(sal·pr·NMe_2)Cl (red-violet form) (A), [Cu(sal·*i*-C_3H_7)Cl]$_2$ (B), Cu[sal·en·N(H)Me]Cl (C), Cu(sal·en·NMe_2)Cl (D), Cu(sal·pr·NMe_2)Cl (green form) (E), Cu(sal·pr·NMe_2)Br (F), [$CuCl_2$(pyo)$_2$]$_2$ (G), and [$CuBr_2$(pyo)$_2$]$_2$ (H).

The spectral feature of Compounds **1** and **2** is apparently of a square planar type (Fig. 2), as pointed out by Sacconi *et al.*[3] Compound **3** gave rise to three ligand-field bands in the 5000—25000 cm^{-1} range. This spectral feature indicates a pseudo-tetrahedral geometry around the metal ion.[8,12] For comparison the reflectance spectral curve of [Cu(sal·*i*-C_3H_7)Cl]$_2$ complex with a pseudo-tetrahedral copper(II) geometry[13] is given in Fig. 2. The spectral features of Compounds **4** and **5** apparently indicate that these have a five-coordinated copper(II) geometry, square-pyramid or trigonal-bipyramid. However, unambiguous structural assignments for these complexes could not be drawn from their spectra, since the differences in spectra among a square-pyramidal, a distorted square-pyramidal, a distorted trigonal-bipyramidal, and a trigonal-bipyramidal structure are not always clear. In Fig. 2, for comparison, are given the reflectance spectral curves of the dimeric 1 : 2 complex of copper(II) chloride with pyridine *N*-oxide, [$CuCl_2$(pyo)$_2$]$_2$, in which the geometry around the copper(II) ion is a tetragonal-pyramid,[14] and the analogous bromide complex, [$CuBr_2$(pyo)$_2$]$_2$, which has a distorted trigonal-bipyramidal copper(II) geometry.[15]

Structure and Magnetic Property. The monomeric four-coordinated planar structure shown schematically in Fig. 3A had been proposed for both Compounds **1** and **2** by Sacconi *et al.*[3] on the basis of their electronic reflectance spectra. Our magnetic and spectral data for these complexes have substantiated their structural assignment.

The structure should be compared with that of Cu(sal·en·OH)Cl, which displays a dimer type of antiferromagnetism.[1,2] In previous papers we assigned a chloride-bridging binuclear structure shown in Fig. 3B for Cu(sal·en·OH)Cl on the basis of its magnetic and spectral properties.[1,2] This assignment is further supported by the fact that the J value of -60 cm^{-1} determined for the complex[1] is practically identical with those of -50——-70 cm^{-1} reported for dimeric copper(II) chloride complexes with dithiocarbamates in which a pair of copper(II) ions is bridged by two chloride ions in a similar manner to that shown in Fig. 3B.[16] Since an alcohol group has usually a poorer coordinating ability than does an amine group, it is concluded that the absence of coordination of the OH group in Cu(sal·en·OH)Cl (Fig. 3B) leads to the formation of the chloride-bridged dimer, whereas the coordination of the terminal amine group in Compound **1** or **2** (Fig. 3A) hinders the dimer formation.

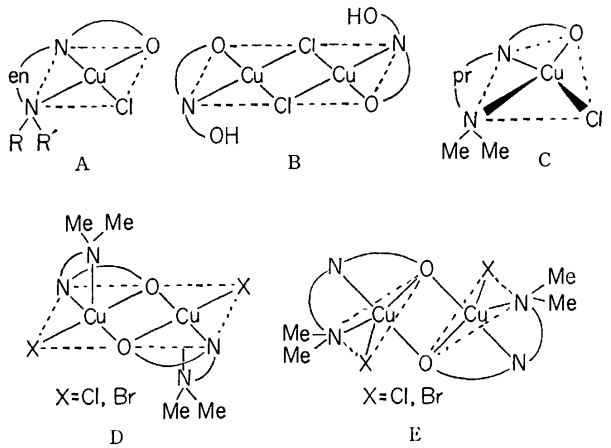

Fig. 3. Schematic representations of possible structure. (A)Cu[sal·en·N(H)Me]Cl and Cu(sal·en·NMe_2)Cl, (B) Cu(sal·en·OH)Cl, (C) Cu(sal·pr·NMe_2)Cl (red-violet form), (D) and (E) Cu(sal·pr·NMe_2)Cl (green form) and Cu(sal·pr·NMe_2)Br.

The monomeric pseudo-tetrahedral structure of the C type shown in Fig. 3 should be assigned to Compound **3** on the basis of its magnetic and spectral data. The magnetic and spectral data for Compounds **4** and **5** showed that these complexes have a phenolic oxygen-bridged binuclear structure with a five-coordinated copper(II) geometry. Molecular models show that two types of five-coordinated metal dimers, one with square-pyramidal and the other trigonal-bipyramidal coordination (Fig. 3D and E), can be produced from sal·pr·NMe_2. This is apparently due to the greater

flexibility of the diamine part in sal·pr·NMe_2 as compared with that in sal·en·NMe_2. Thus, in a similar manner to the case of binuclear four-coordinated copper(II) complexes of the type $[Cu(sal\cdot R)X]_2$, where R=alkyl or aryl and X=Cl, [7,8] Br[9] or NO_3,[10,11] the antiferromagnetism observed in these complexes may be interpreted in terms of superexchange interaction through the bridging phenolic oxygen atoms. It has been well established that the strength of antiferromagnetic interaction in $[Cu(sal\cdot R)X]_2$ complexes decreases as the distortion of copper(II) geometry from planar toward tetrahedral increases.[8,13,17,18] With five-coordinated copper(II) complexes, two metal geometries, trigonal-bipyramid and tetragonal-pyramid, are usually encountered, and a continuous structural variation may take place, through structural deformation, between the two regular geometries depending upon the environments of metal coordination. At present, for five-coordinated copper(II) dimers, the correlation of the structure with the detected degree of antiferromagnetic interaction is not apparent.[8] However, comparison of the J values of Compounds **4** and **5** with those of five-coordinated copper(II) dimers found in the literature seems to suggest a conclusion about the metal geometry of these complexes: The $|J|$ values of Compounds **4** and **5** are about one-half of $[Cu(sal\cdot pr\cdot OH)Cl]_2$ ($J=-252$ cm^{-1},[1] distorted trigonal-bipyramidal)[19] and of $[Cu(sal\cdot R)X\cdot DMF]_2$ ($J=-200$ —-250 cm^{-1},[8,20] DMF=*N*,*N*-dimethylformamide) to which a square-pyramidal copper(II) geometry was previously assigned.[8,20] The J value of $[CuBr_2(pyo)_2]_2$ (distorted trigonal-bipyramidal) is -121 cm^{-1} [21] and this is approximately one-fourth of that of the corresponding chloride complex, $[CuCl_2(pyo)_2]_2$ ($J=-440$ cm^{-1},[21] tetragonal-pyramidal). The J value of $[Cu(sal\cdot t\text{-}C_4H_9)(hfa)]_2$ (hfa=hexafluoroacetylacetonato, slightly distorted trigonal-bipyramidal)[22], -105 cm^{-1},[23] is small and comparable with those of Compounds **4** and **5**. Thus, copper(II) dimers with trigonal-bipyramidal metal coordination happened to give rise to a large $|J|$ value in $[Cu(sal\cdot pr\cdot OH)Cl]_2$, but in the other cases they have shown small values for the exchange integral. On the other hand, the $|J|$ values of copper(II) dimers with tetragonal-pyramidal metal geometry have appeared to be fairly large for the cases so far investigated.[20,21] These facts strongly suggest that the present complexes **4** and **5** take essentially a trigonal-bipyramidal metal coordination. For five-coordinated copper(II) dimers with the same type of ligands, the $|J|$ value is considered to be lowered progressively according as the copper(II) geometry is distorted from regular tetragonal-pyramid toward trigonal-bipyramid; we are now attempting to prepare more copper(II) dimers of the required types in order to clarify this point.

References

1) T. Tokii, Y. Muto, M. Kato, K. Imai, and H. B. Jonassen, *J. Inorg. Nucl. Chem.*, **34**, 3377 (1972).
2) T. Tokii, Y. Muto, M. Kato, K. Imai, and H. B. Jonassen, *J. Inorg. Nucl. Chem.*, **35**, 1539 (1973).
3) L. Sacconi and I. Bertini, *Inorg. Chem.*, **5**, 1520 (1966).
4) P. W. Selwood, "Magnetochemistry," Interscience Publishers, New York (1956), pp. 78, 91.
5) B. N. Figgis and R. L. Martin, *J. Chem. Soc.*, **1956**, 3837.
6) B. Bleaney and K. D. Bowers, *Proc. R. Soc. London, Ser. A*, **214**, 451 (1952).
7) E. Sinn and C. M. Harris, *Coord. Chem. Rev.*, **4**, 391 (1969).
8) M. Kato, K. Imai, Y. Muto, T. Tokii, and H. B. Jonassen, *J. Inorg. Nucl. Chem.*, **35**, 109 (1973).
9) C. M. Harris, J. M. James, P. J. Milham, and E. Sinn, *Inorg. Chim. Acta*, **3**, 81 (1969).
10) M. Kato, Y. Muto, H. B. Jonassen, K. Imai, M. Kondo, K. Katsuki, and S. Ikegami, *Bull. Chem. Soc. Jpn.*, **42**, 3039 (1969).
11) J. O. Miners, E. Sinn, R. B. Coles, and C. M. Harris, *J. Chem. Soc. Dalton Trans.*, **1972**, 1149.
12) L. Sacconi and M. Ciampolini, *J. Chem. Soc.*, **1964**, 276.
13) R. J. Butcher and E. Sinn, *Inorg. Chem.*, **15**, 1604 (1976).
14) J. C. Morrow, *J. Cryst. Mol. Struct.*, **4**, 243 (1974).
15) A. D. Mighell, C. W. Reimann, and A. Santro, *Acta Crystallogr., Sect. B*, **28**, 126 (1972).
16) R. H. Furneaux and E. Sinn, *Inorg. Nucl. Chem. Lett.*, **12**, 501 (1976).
17) R. M. Countryman, W. T. Robinson, and E. Sinn, *Inorg. Chem.*, **13**, 2013 (1974).
18) E. Sinn, *Inorg. Chem.*, **15**, 366 (1976).
19) J. A. Bertrand, J. A. Kelley, and J. L. Breece, *Inorg. Chim. Acta*, **4**, 247 (1970).
20) T. Tokii and Y. Muto, *Bull. Chem. Soc. Jpn.*, **49**, 1849 (1976).
21) S. J. Gruber, C. M. Harris, E. Kokot, S. L. Lenzer, T. N. Lockyer, and E. Sinn, *Aust. J. Chem.*, **20**, 2403 (1967).
22) E. Sinn, *Inorg. Chem.*, **15**, 2698 (1976).
23) H. Yokoi and M. Chikira, *J. Am. Chem. Soc.*, **97**, 3975 (1975).

Ground States of the Square Planar Low-Spin Cobalt(II) Complexes[1)]

Yuzo NISHIDA and Sigeo KIDA

Department of Chemistry, Faculty of Science, Kyushu University, Fukuoka, 812

(Received June 30, 1977)

In order to investigate the ground state configuration of some square planar cobalt(II) complexes such as Schiff base complexes of the *cis*-[CoN_2O_2] type, whose ESR spectra are quite different from those of cobalt(II) phthalocyanine and porphyrins, the spin-orbit matrix based on the four zero-order wave functions, $(yz)^1$, $(xz)^1$,$(z^2)^1$, and $(xy)^{1,2)}$ were diagonalized on assuming reasonable values for necessary parameters. The result has clearly shown that an unpaired electron is localized in d_{yz} orbital in the ground state for these complexes. ESR spectra of a series of cobalt(II) complexes with N_4-macrocyclic ligands were measured and interpreted in terms of the conclusion obtained here.

In recent years the electronic states of low-spin cobalt(II) complexes have attracted attention because of their close relation to Vitamin B_{12} and biological oxygen carriers. As the consequence of studies on ESR and magnetism, it was established that the electronic configuration of the ground state is $(d_{xy})^2(d_{xz})^2(d_{yz})^2(d_{z^2})^1$, (denoted by $(z^2)^{1,2)}$) for cobalt(II) phthalocyanine[3,4)] and porphyrins,[5)] where x, y, and z axes were adopted as shown in Fig. 1-a. This is referred to as Type I. On the other hand, there is another type(Type II) of low-spin cobalt(II) complexes whose ESR spectra show a quite different pattern from that of the former group, as shown in Table 1. They include Schiff base complexes such as [Co(salen)] and [Co(acen)], where H_2salen and H_2acen denote *N,N'*-disalicylideneethylenediamine and *N,N'*-bis(1-acetonylethylidene)ethylenediamine, respectively. Their ESR spectra differ a great deal from those of the Type I group in (1) the large separation between g_x and g_y (whereas the porphyrin group shows axial symmetry of *g*-tensors) and (2) the very small $|A_z|$ and $|A_y|$ values as compared with those of the Type I group. For the ground state configuration of the Type II compounds, three possibilities which have given rise to much argument can be considered.[6—13)] Recently the correct values of *g*- and *A*-tensors for [Co(acen)][11)] and [Co(amben)][13)] were determined in the single crystals of the corresponding nickel(II) complexes, where H_2amben denotes *N,N'*-bis(*o*-aminobenzylidene)ethylenediamine. In their attempt to interpret the result by use of perturbation calculation, Cariati *et al.*[11)] could not give an unambiguous assignment of the ground state configuration. They suggested the mixing of the two configurations for the ground state. However, their conclusion is unsatisfactory, since 1) they employed a positive value (0.28) for the Fermi hyperfine coulpling constant to fit A_1[14)] values with the experimental ones in the case of the $(z^2)^1$ configuration, which is not compatible with the generally accepted view that the Fermi hyperfine coulpling constant assumes a negative value in the case of the $(z^2)^1$ configuration as the consequence of the coupling with the $(4s)^{1,2)}$ configuration, and 2) in order to fit g_1[14)] values with the experimental ones, the energy separation between d_{xz} and d_{yz} orbitals was assumed to be $6—7\times10^3$ cm^{-1} in the case of both $(z^2)^1$ and $(yz)^1$ electronic configuration. Similar results have also been reported.[13,15,16)] However, there appears no reasonable evidence to assume such a large separation between d_{xz} and d_{yz} orbitals for the complexes of the planar *cis*-[CoN_2O_2] and [CoN_4] types.

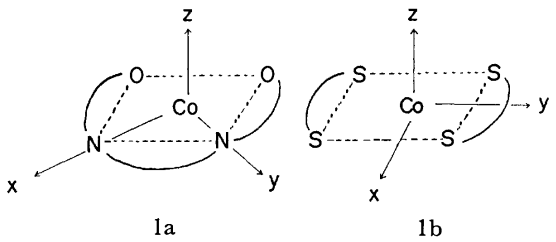

Fig. 1. x, y, and z axis in the square planer complexes.

This unsatisfactory result seems to be due to the inadequate application of the perturbation theory to the present system. Calculation of *g*- and *A*-values for these systems have so far been carried out by use of the well-known formula of the first order perturbation theory for a nondegenerate ground state.[17)]

$$|\psi_g> = N\left[|\psi_g^0> - \sum \frac{\langle\psi_e^0|\lambda\hat{l}\cdot\hat{S}|\psi_g^0\rangle}{\Delta_e}|\psi_e^0\rangle\right] \quad (1)$$

However, application of equation (1) is valid only when $\Delta_e \gg \lambda$. In our system there is a sufficient probability for some of d_{xy}, d_{xz}, d_{yz}, and d_{z^2} orbitals to be

TABLE 1. ESR PARAMETERS OF SQUARE PLANAR COBALT(II) COMPLEXES

Type	Complexes[a)]	g_z	g_x	g_y	$\|A_z\|$	$\|A_x\|$ (10^{-4} cm^{-1})	$\|A_y\|$	Ref.
I	[Co(pc)]	1.91	2.92	2.89	160	270	260	3
	[Co(tpp)]	1.798	3.322	3.322	197	315	315	5
II	[Co(acen)]	2.00	3.26	1.88	34	116	38	11
	[Co(salen)]	1.74	3.805	1.66	30	291	50	8
	[Co(sac)$_2$]	1.899	3.280	1.904	35	105	35	27

a) H_2pc: phthalocyanine, H_2tpp: $\alpha,\beta,\gamma,\delta$-tetraphenylporphyrin, H_2acen: *N,N'*-bis(1-acetonylethylidene)ethylenediamine, H_2salen: *N,N'*-bis(salicylidene)ethylenediamine, Hsac: dithioacetylacetone.

energetically close to each other. Thus, in diagonalizing the 4×4 spin-orbit matrix based on the $(xy)^1$,$(xz)^1$, $(yz)^1$ and $(z^2)^1$ states,[18] we have calculated g_i- and A_i-values as the function of various parameters and compared the results with the experimental values in order to elucidate the ground state of the Type II complexes. In order to examine the conclusion thus reached, we have measured the ESR spectra of a series of cobalt(II) complexes with N_4-macrocyclic ligands.

Calculation

In performing the perturbation calculation for the spin-orbit interaction, we have adopted the eight zero-order wave functions, $(\chi)^{+\text{or}-}$, where $(\chi)^+$ denotes an antisymmetrized determinatal function, $|(\overset{+}{d_{x^2-y^2}})(\overset{-}{d_{x^2-y^2}})(\overset{+}{\chi})|$ ($\chi=d_{xz}$, d_{yz}, d_{xy}, and d_{z^2}) based on the three electron hole formalism. Hence the wave functions for the system were formulated according to the Kramers theorem[19] as follows.

$$\Psi^+ = c_1\overset{+}{(yz)^1} + ic_2\overset{+}{(xz)^1} - ic_3\overset{-}{(z^2)^1} + c_4\overset{-}{(xy)^1} \quad (2)$$

$$\Psi^- = c_1\overset{-}{(yz)^1} - ic_2\overset{-}{(xz)^1} - ic_3\overset{+}{(z^2)^1} - c_4\overset{+}{(xy)^1} \quad (3)$$

The coefficients c_1, c_2, c_3, and c_4 were determined by diagonalizing the following 4×4 matrix,

$\overset{+}{(yz)^1}$	$\overset{+}{(xz)^1}$	$\overset{-}{(z^2)^1}$	$\overset{-}{(xy)^1}$
Δ_4	$i\frac{\lambda}{2}$	$-i\frac{\sqrt{3}}{2}\lambda$	$-\frac{\lambda}{2}$
$-\frac{i}{2}\lambda$	Δ_1	$\frac{\sqrt{3}}{2}\lambda$	$\frac{i}{2}\lambda$
$i\frac{\sqrt{3}}{2}\lambda$	$\frac{\sqrt{3}}{2}\lambda$	Δ_2	0
$-\frac{\lambda}{2}$	$-i\frac{\lambda}{2}$	0	Δ_3

where λ denotes the spin-orbit coupling constant for the system, $\lambda=-k\zeta_{3d}$, ζ_{3d} being the free ion value for Co^{2+}(-515 cm^{-1}), and k is the orbital reduction factor evaluated at 1.0, 0.9, 0.8 and 0.7. The diagonal elements, Δ_1, Δ_2, Δ_3, and Δ_4 are functions of ligand field and interelectronic repulsion.

Based on Eqs. 2 and 3, g_i- and A_i-values can be expressed in terms of k, c_1, c_2, c_3, and c_4 (and κ in the case of A_i/P), where P and κ denote $2g_N\beta_e\beta_N\langle r^{-3}\rangle_{3d}$[20] and Fermi hyperfine coupling energy in units of P, respectively.

$$g_z = 2[c_1^2+c_2^2-c_3^2-c_4^2-2kc_1c_2] \quad (4)$$

$$g_x = 2[c_1^2-c_2^2+c_3^2-c_4^2-2\sqrt{3}kc_1c_3-2kc_2c_4] \quad (5)$$

$$g_y = 2[c_1^2-c_2^2-c_3^2+c_4^2+2\sqrt{3}kc_2c_3-2kc_1c_4] \quad (6)$$

$$A_z/P = 2[-2c_1c_2-\frac{\kappa}{2}(c_1^2+c_2^2-c_3^2-c_4^2) + \frac{1}{7}(c_1^2+c_2^2-2c_3^2+2c_4^2+3c_1c_4 - \sqrt{3}c_1c_3-3c_2c_4-\sqrt{3}c_2c_3)] \quad (7)$$

$$A_x/P = 2[-2\sqrt{3}c_1c_3-2c_2c_4-\frac{\kappa}{2}(c_1^2-c_2^2+c_3^2-c_4^2) + \frac{1}{7}(-2c_1^2+c_2^2-c_3^2-c_4^2-3c_1c_2-3c_1c_4 - \sqrt{3}c_2c_3-2\sqrt{3}c_3c_4)] \quad (8)$$

$$A_y/P = 2[2\sqrt{3}c_2c_3-2c_1c_4-\frac{\kappa}{2}(c_1^2-c_2^2-c_3^2+c_4^2) + \frac{1}{7}(c_1^2+2c_2^2+c_3^2+c_4^2+3c_1c_2 + \sqrt{3}c_1c_3-3c_2c_4-2\sqrt{3}c_3c_4)] \quad (9)$$

Throughout the calculation $P=0.020$ cm^{-1} was adopted (free ion value for P is 0.025 cm^{-1},[21]).

Results and Discussion

After several preliminary calculations we have become convinced that the small $|A_z|$ and $|A_y|$ values of Type II complexes can not be accounted for on the basis of $(z^2)^1$ ground state, where a negative value is to be assigned to the Fermi hyperfine coupling constant, κ.[4,22,23] The $(xy)^1$ ground state is also improbable, because 1) the d_{xy} orbital is practically nonbonding in the Schiff base complexes, and 2) the interelectronic repulsion in the $(xy)^1$ state is higher (at least 6000 cm^{-1}) than that in both the $(z^2)^1$ and $(yz)^1$ states.[24] Recently McGarvey[12] investigated the contributions from the spin-quartet states and the mixing of d_{z^2} and d_{xy}[25] orbitals to the ESR parameters of low-spin cobalt(II) complexes. He showed that the contributions from the spin-quartet states are very important for 5- and 6-coordinated complexes, but can be neglected for 4-coordinated planar complexes. This can be explained as follows. The energy separation between d_{z^2} and $d_{x^2-y^2}$ orbitals in the square planar complexes is larger than that in 5- and 6-coordinated complexes, so that the energy gap between the ground doublet state, $|(\overset{+}{d_{x^2-y^2}})(\overset{-}{d_{x^2-y^2}})(\overset{+}{d_{z^2}})|$ and the excited quartet states such as $|(\overset{+}{d_{x^2-y^2}})(\overset{+}{d_{z^2}})(\overset{+}{d_{yz}})|$ *etc.* is larger than in the former complexes.

McGarvey also took a sizeable mixing of d_{z^2} and d_{xy}[25] into consideration in order to explain the ESR parameters of $[Co(sac)_2]$ and $[Co(mnt)_2]^{2-}$ on the basis of $(z^2)^1$ ground state, these complexes being classified as Type II complexes in this paper. However, his interpretation appears to be imcompatible with our experimental results. Accordingly, we considered here only the $(yz)^1$ configuration for the ground state of the Type II compounds throughout the calculation, assuming the contribution from the spin-quartet states to be negligibly small. This means that we have set Δ_4 to be zero in the 4×4 matrix, therefore Δ_1, Δ_2, and Δ_3 are the energy separation from the ground $(yz)^1$ state for $(xz)^1$, $(z^2)^1$, and $(xy)^1$, respectively.

It has been known that a sharp absorption band is always observed around 8000 cm^{-1} in the complexes with quadridentate Schiff bases of the *cis*-$[CoN_2O_2]$ type.[26] Judging from its intensity ($\log\varepsilon\approx1.5$), this is undoubtedly a spin-allowed d-d transition. This band is most probably assigned to the $(yz)^1\rightarrow(xy)^1$ transition, since the interelectronic repulsion energy in $(xy)^1$ state is much larger than that in $(yz)^1$ and $(z^2)^1$ states, and there seems to be no particular reason to separate

the $(xz)^1$ and $(z^2)^1$ states from the $(yz)^1$ state in such a high energy as 8000 cm^{-1}. Furthermore, it has been revealed in the course of calculation that the large g_x values, 3.2—3.9 (Table 1), can be accounted for in terms of the orbital contribution from the $(xy)^1$ and $(z^2)^1$ states, only when these states are separated from the ground state by less than 3000 cm^{-1}. Thus, Δ_3 was fixed at 8000 cm^{-1} throughout the calculation.

In Figs. 2—9, g_i and A_i values are plotted as functions of Δ_1 and Δ_2. The g_z, g_x, and g_y values vary sensitively with Δ_1 and Δ_2, as seen in Figs. 4, 5 and 6. respectively. It should be noted that g_z(Fig. 4) can be fitted to the

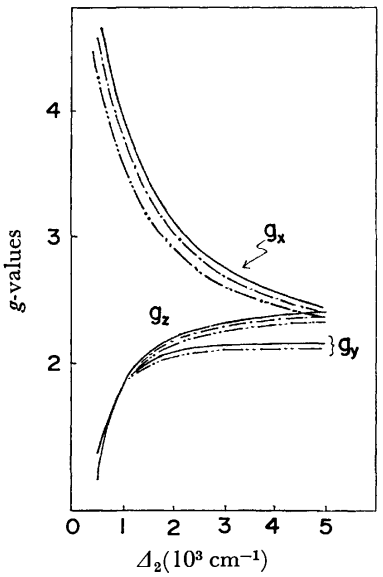

Fig. 2. The variation of g_i-values(i=x, y, z,) *versus* Δ_2, with $k=1.0$(——), $k=0.9$(—·—) and $k=0.8$(—··—). Other parameters, Δ_1 and λ are fixed to be 2000 and -450 cm^{-1}, respectively.

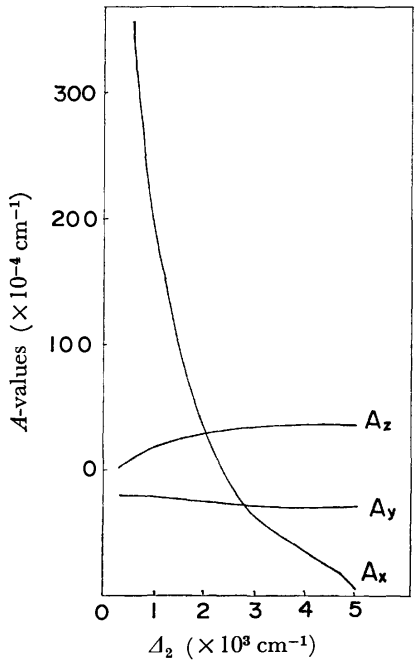

Fig. 3. The variation of A_i-values(i=x, y, z) *versus* Δ_2 with $\Delta_1=2000$ cm^{-1}, $\lambda=-450$ cm^{-1} and $\kappa=0.5$.

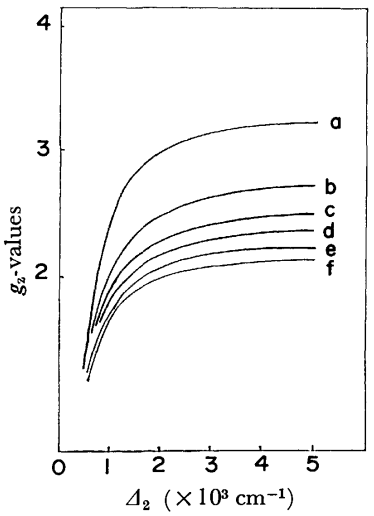

Fig. 4. The variation of g_z as a function of Δ_2. Δ_1 are (a) 500 cm^{-1}, (b) 1000 cm^{-1}, (c) 1500 cm^{-1}, (d) 2000 cm^{-1}, (e) 3000 cm^{-1} and (f) 5000 cm^{-1}. In all cases, k and λ are fixed to be 1.0 and -450 cm^{-1}, respectively.

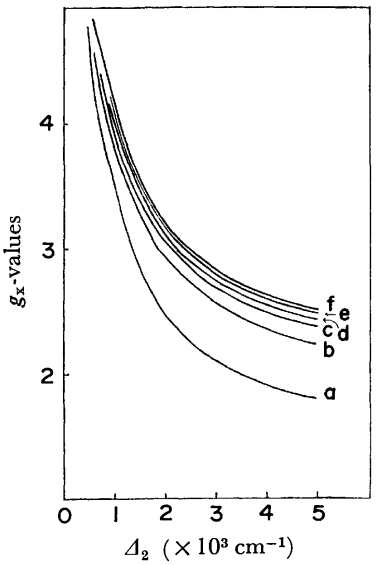

Fig. 5. The variation of g_x as a function of Δ_2. Δ_1 are (a) 500 cm^{-1}, (b) 1000 cm^{-1}, (c) 1500 cm^{-1}, (d) 2000 cm^{-1} (e) 3000 cm^{-1}, and (f) 5000 cm^{-1}. Other parameters, k and λ are fixed to be 1.0 and -450 cm^{-1}, respectively.

experimental value (*e.g.*, 2.00 for [Co(acen)]) by assuming a reasonable d_{xz}-d_{yz} separation, *i.e.*, 0—3000 cm^{-1}, whereas in the case of the calculation based on Eq. 1, an unreasonably large separation ($\geq$5000 cm^{-1}) has to be assumed in order to fit the calculated g_z value to the experimental one.[13,15,16]

The g_x value(Fig. 5) sharply increases with the decrease of Δ_2, the effect of Δ_1 being minor compared with that of Δ_2. Accordingly, Δ_2 can be estimated as 900—1500 cm^{-1} for [Co(acen)] from Fig. 5 and experimental g_x value (3.26).[11] The A_x value (Fig. 8) highly dependent on Δ_2, and suffers little effect from the variation of Δ_1, thereby enabling us to estimate the Δ_2 value for [Co(acen)] at 1300—1600 cm^{-1} from the

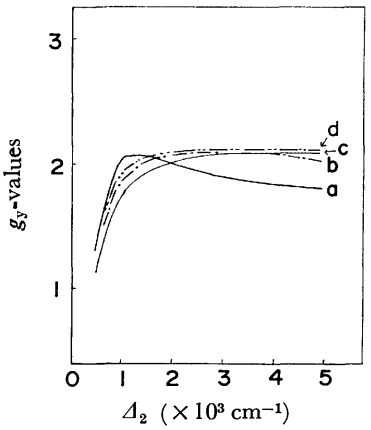

Fig. 6. The variation of g_y as a function of Δ_2. Δ_1 are (a) 500 cm^{-1}, (b) 1000 cm^{-1}, (c) 1500 cm^{-1}, and (d) 5000 cm^{-1}. In all cases, k and λ are fixed to be 1.0 and -450 cm^{-1}, respectively.

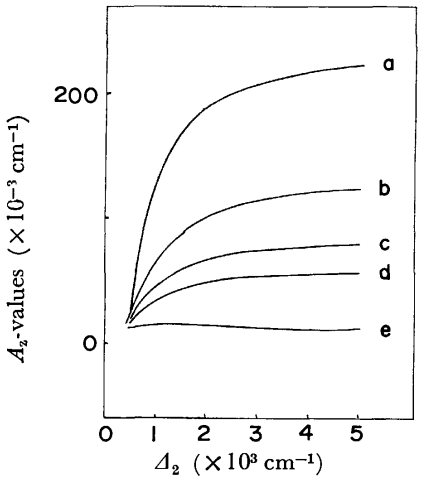

Fig. 7. The variation of A_z as a function of Δ_2. Δ_1 are (a) 500 cm^{-1}, (b) 1000 cm^{-1}, (c) 1500 cm^{-1}, (d) 2000 cm^{-1}, (e) 5000 cm^{-1}. Other parameters, κ and λ are fixed to be 0.4 and -450 cm^{-1}, respedtively.

experimental value of $|A_x|$ (115.8×10^{-4} cm^{-1}).[11] This is compatible with the value, 900—1500 cm^{-1}, estimated from g_x according to the diagram in Fig. 5.

On the basis of the above discussion, assuming reasonable values for the necessary parameters, we obtained satisfactory agreement between calculated and experimental g_1 and A_1 values in the case of the two examples of Type II complexes, as shown in Table 2, where both ESR spectra were measured on single crystals. From the c_1, c_2, c_3 and c_4 values listed in Table 2, it can be concluded that an unpaired electron is localized in the d_{yz} orbital, *i.e.*, mixing of the $(z^2)^1$ is very small.

It is well known that the ESR spectrum of [Co(mnt)$_2$]$^{2-}$, (where H_2mnt denotes 2,3-dimercaptomaleonitrile) shows[20] a pattern similar to that of both [Co(acen)] and [Co(salen)], undoubtedly belonging to Type II. However, analysis of the ESR spectra on single crystals revealed that the directions of principal axes of g-tensors are, as depicted in Fig. 1-b,[20] different from those of [Co(acen)]. Thus, on the basis of the

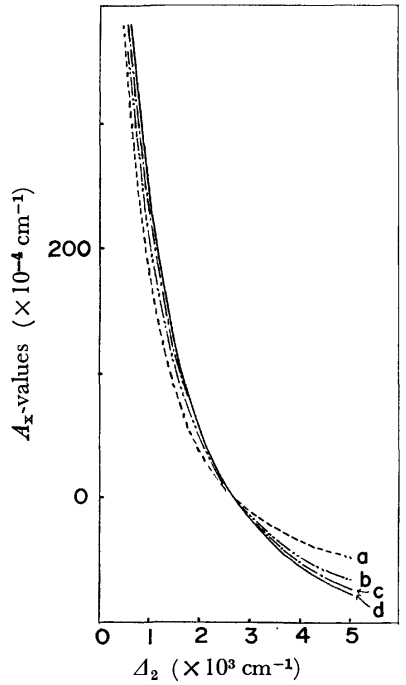

Fig. 8. The variation of A_x as a function of Δ_2. Δ_1 are (a) 500 cm^{-1}, (b) 1000 cm^{-1}, (c) 1500 cm^{-1}, and (d) 3000 cm^{-1}. Other parameters, κ and λ are fixed to be 0.4 and -450 cm^{-1}, respectively.

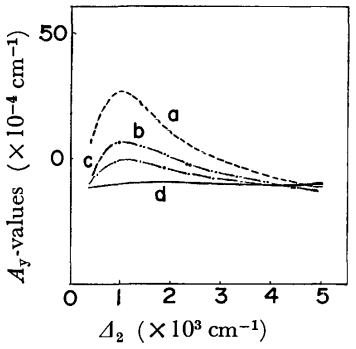

Fig. 9. The variation of A_y as a function of Δ_2. Δ_1 are (a) 500 cm^{-1}, (b) 1000 cm^{-1}, (c) 1500 cm^{-1}, and (d) 3000 cm^{-1}. Other parameters, κ and λ are fixed to be 0.4 and -450 cm^{-1}, respectively.

new x, y, and z axes we formulated equations similar to Eqs. 2—9 according to the same principle. The results was very similar to that obtained in the case of the coordinated system in Fig. 1-a. For example, a similarity of results of the calculation based on the different coordinate systems can be seen, if we compare Figs. 10, 11 and Table 3 (based on the coordinate system in Fig. 1-b) with Figs. 2,3 and Table 2 (based on the coordinate system in Fig. 1-a), respectively. It was confirmed by repeated examination that the choice of the x and y axes does not bring about any significant effect on the calculated values.

From the above discussion, we can conclude that in Type II complexes an unpaired electron is localized in the d_{yz} orbital in the ground state. It should be emphasized that in this approach we could interpret the ESR parameters of the compounds on the assump-

Table 2. Calculated values of g_i, A_i(i=x, y, z) and c_j(j=1, 2, 3, 4) for the coordinate system of Fig. 1-a Experimentally obtained values are given in parentheses.

	[Co(acen)][a]	[Co(salen)][b]
g_z	2.00(2.00)	1.79(1.74)
g_x	3.36(3.26)	3.84(3.805)
g_y	1.94(1.88)	1.80(1.66)
$\|A_z\|$ ($\times 10^{-4}$ cm^{-1})	23(34)	14(30)
$\|A_x\|$ ($\times 10^{-4}$ cm^{-1})	114(116)	250(291)
$\|A_y\|$ ($\times 10^{-4}$ cm^{-1})	22(38)	22(50)
c_1	0.9699	0.9322
c_2	−0.0632	−0.0344
c_3	−0.2332	−0.3617
c_4	−0.0292	−0.0269

a) Assumed values: Δ_1=2000 cm^{-1}, Δ_2=1400 cm^{-1}, Δ_3=8000 cm^{-1}, λ=−450 cm^{-1}, k=0.9 and κ=0.5. b) Assumed values: Δ_1=2000 cm^{-1}, Δ_2=800 cm^{-1}, Δ_3=8000 cm^{-1}, λ=−450 cm^{-1}, k=0.8, and κ=0.5.

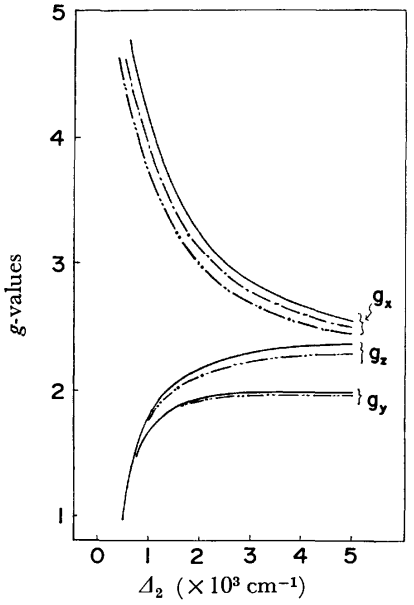

Fig. 10. The variation of g_i-values (i=x, y, z) *versus* Δ_2 in the case of the coordinate system of Fig. 1-b, with k=1.0 (——), k=0.9 (—·—), and k=0.8 (—··—). Other parameters Δ_1, λ, and Δ_3 (in this case, this means the energy separation between $(yz)^1$ and $(x^2-y^2)^1$) are fixed to be 2000, −450, and 8000 cm^{-1}, respectively.

tion of reasonably small energy separation for the d_{xz} and d_{yz} orbitals, for which in the previous calculations[13,15,16] a large separation had to be assumed in order to fit the calculated values to the experimental ones. The present result has enabled us to analyze the ground state configuration of low-spin square planar cobalt(II) complexes from their ESR spectra (even spectra of powder samples), where the magnitude of hyperfine coupling energy of the peaks around the g=2.0 is most characteristic (*cf.* Table 1).

The presently obtained experimental results support the above conclusion. The powder ESR spectra of diluted cobalt(II) complexes with the N_4-macrocyclic ligands, **L-a**, **L-b**, and **L-c** (Fig. 13) are shown in Fig.

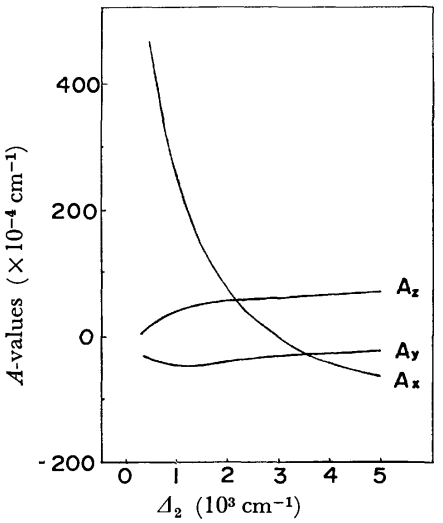

Fig. 11. The variation of A_i-values (i=x, y, z) *versus* Δ_2 in the case of the coordinate system of Fig. 1-b. Other parameters, Δ_1, λ, Δ_3, and κ are fixed to be 2000, −450, 8000 cm^{-1} and 0.4, respectively.

Table 3. Calculated values of g_i, A_i (i=x, y, z), and c_j(j=1, 2, 3, 4) for the coordinate system of Fig. 1-b Experimentally obtained values are given in parentheses.

	[Co(acen)][a]	[Co(salen)][b]
g_z	2.02(2.00)	1.78(1.74)
g_x	3.40(3.26)	3.90(3.805)
g_y	1.86(1.88)	1.68(1.66)
$\|A_z\|$ ($\times 10^{-4}$ cm^{-1})	42(34)	40(30)
$\|A_x\|$ ($\times 10^{-4}$ cm^{-1})	130(116)	254(291)
$\|A_y\|$ ($\times 10^{-4}$ cm^{-1})	53(38)	42(50)
c_1	0.9729	0.9499
c_2	−0.0663	−0.0466
c_3	−0.2195	−0.3077
c_4	−0.0294	−0.0279

a) Assumed values: Δ_1=2000 cm^{-1}, Δ_2=1500 cm^{-1}, Δ_3=8000 cm^{-1}, λ=−450 cm^{-1}, k=0.9, and κ=0.45. b) Assumed values: Δ_1=2000 cm^{-1}, Δ_2=1000 cm^{-1}, Δ_3=8000 cm^{-1}, λ=−450 cm^{-1}, k=0.9, and κ=0.5.

12. It is evident that the ESR pattern of [Co(**L-a**)]$^{2+}$ entirely differs from that of both [Co(**L-b**)] and [Co(**L-c**)]. According to our criterion, [Co(**L-a**)]$^{2+}$ belongs to Type I complexes because of the hyperfine splitting ($|A_3|=138\times10^{-4}$ cm^{-1}) of the highest field absorption (g_3=2.00). On the other hand, two absotptions (g_2, g_3) were observed around g=2.0 for [Co(**L-b**)] and [Co(**L-c**)], their hyperfine splittings being very small ($|A_2|$, $|A_3|<50\times10^{-4}$ cm^{-1}). The features of [Co(**L-b**)] and [Co(**L-c**)] are very similar to those of [Co(amben)] and [Co(acen)], respectively. It should be noted that the hyperfine splitting at the lowest fields aborption of [Co(**L-c**)], (g_1=3.153, $|A_1|=126\times10^{-4}$ cm^{-1}), is much larger than that of [Co(**L-b**)], (g_1=2.636, $|A_1|\cong0$). This can be readily elucidated in terms of our calculated results based on the $(yz)^1$ ground state configuration. One absorption band is observed in the range 10000—12000 cm^{-1} for [Co(amben)][29] and [Co(**L-b**)]. For these cases, we have calculated g_i and A_i

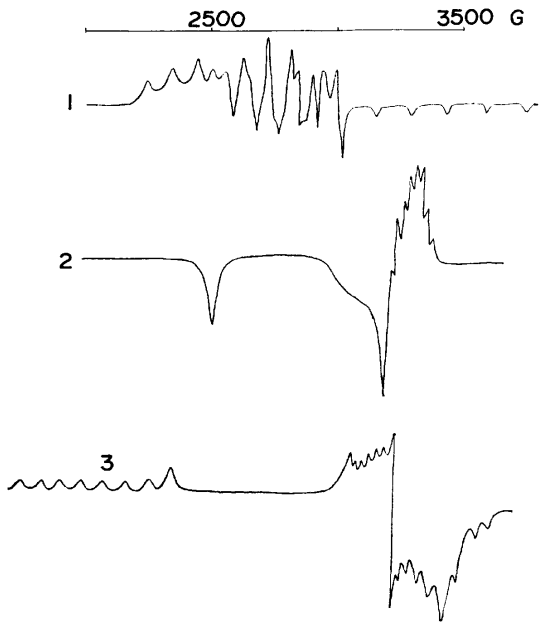

Fig. 12. ESR spectra of some square planar cobalt(II) complexes (obtained at 77 K, and $G=10^{-4}$ T). 1; [Co(**L-a**)]$^{2+}$ 2; [Co(**L-b**)] 3; [Co(**L-c**)].

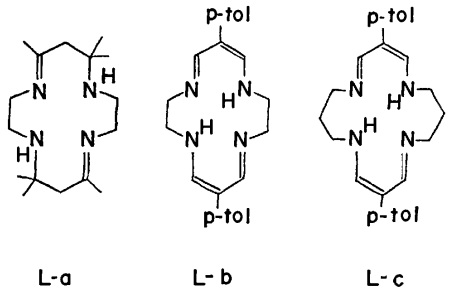

Fig. 13. Some N_4-macrocyclic ligands used in this paper, where *p*-tol represents *p*-tolyl.

values, assuming Δ_3 to be 10000—12000 cm^{-1}. As a result, it was found that the variation of Δ_3 in the range 8000—12000 cm^{-1} brings about no significant effect on the calculated values, shown in Figs. 2—9. As shown in Figs. 8 and 3, A_x is very sensitive to the energy separation between $(yz)^1$ and $(z^2)^1$. As this energy separation increases from 1400 to 2500 cm^{-1}, g_x varies from 3.2, to 2.7, and A_x, from 140×10^{-4} cm^{-1} to zero. Thus, we can elucidate the ESR parameters of [Co(amben)], [Co(**L-b**)] and [Co(**L-c**)] in tersm of our calculated results based on the $(yz)^1$ ground state configuration.

McGarvey took a sizeable mixing of d_{z^2} and d_{xy} orbitals into consideration in order to explain the ESR parameters of $[Co(sac)_2]$ and $[Co(mnt)_2]^{2-}$. According to his discussion, there should be a large difference in the mixing of d_{z^2} and d_{xy} orbitals in [Co(**L-a**)]$^{2+}$, [Co(**L-b**)] and [Co(**L-c**)]. However, this is naturally unrealistic since all these complexes have effective D_{2h} symmetry and such a large difference can not be expected.

Experimental

Preparation. The perchlorate of 5,5,7,12,12,14-hexamethyl-1,4,8,11-tetraazacycotetradeca-1,7-diene, **L-a**, and the tetraphenylborate of [Ni(**L-a**)]$^{2+}$ were prepared according to the methods of Curtis.[30] The ligands, **L-b** and **L-c**, 6,13-di-*p*-tolyl-1,4,8,11-tetraazacyclotetradeca-4,6,11,13-tetraene, and 3,11-di-*p*-tolyl-1,5,9,13-tetraazacyclohexadeca-1,3,9,11-tetraene, were obtained from the reaction mixtures of 4-*p*-tolyl-1,2-dithiolium hydrogensulfate and ethylenediamine or 1,3-propanediamine, according to methods similar to those described by Tang *et al.*[31] Low-spin square planar nickel(II) and cobalt(II) complexes with **L-b** and **L-c** were also prepared according to the methods of Tang *et al.*[31]

Measurements. For the ESR measurements, all the cobalt(II) complexes were diluted in the corresponding nickel(II) complexes. ESR spectra were obtained with a JEOL ESR apparatus model JES-3X-ME using an X-band. DPPH was used as a standard marker.

The calculations were performed on the Facom 230–75 computer at the Computer Center of Kyushu University. Secular determinants were solved by program HERMTS.

References

1) Part V of the series, "Investigation on Low-spin Cobalt(II) Complexes."
2) The electronic configurations of low-spin cobalt(II) complexes such as $(d_{xy})^2(d_{xz})^2(d_{yz})^2(d_{z^2})^1$, $(d_{xy})^2(d_{xz})^2(d_{z^2})^2(d_{yz})^1$, $(d_{xz})^2(d_{yz})^2(d_{z^2})^2(d_{xy})^1$, and $(d_{xz})^2(d_{yz})^2(d_{xy})^2(4s)^1$ are denoted by $(z^2)^1$, $(yz)^1$, $(xy)^1$, and $(4s)^1$, respectively, in this paper.
3) J. F. Gibson, D. J. E. Ingram, and D. Schonland, *Discuss. Faraday Soc.*, **26**, 72 (1958).
4) J. S. Griffith, *Discuss. Faraday Soc.*, **26**, 81 (1958).
5) J. M. Assour, *J. Chem. Phys.*, **43**, 2477 (1965).
6) L. M. Engelhardt, J. D. Duncan, and M. Green, *Inorg. Nucl. Chem. Lett.*, **8**, 725 (1972).
7) Y. Nishida and S. Kida, *Chem. Lett.*, **1973**, 57.
8) A. Zelewsky and H. Fierz, *Helv. Chim. Acta*, **56**, 977 (1973).
9) C. Busetto, F. Cariati, A. Fusi, M. Gullotti, F. Morazzoni, A. Pasini, and R. Ugo, *J. Chem. Soc. Dalton Trans.*, **1973**, 754.
10) K. Migita, M. Iwaizumi, and T. Isobe, *J. Am. Chem. Soc.*, **97**, 4228 (1975).
11) F. Cariati, F. Morazzoni, C. Busetto, E. D. Piero, and A. Zaetta, *J. Chem. Soc. Dalton Trans.*, **1976**, 342.
12) B. R. McGarvey, *Can. J. Chem.*, **53**, 2498 (1975).
13) V. Malatesta and B. R. McGarvey, *Can. J. Chem.*, **53**, 3791 (1975).
14) The subscript i in g_i and A_i denotes three principal axes of each tensor, *i.e.*, i=x, y, or z.
15) C. Busetto, F. Cariati, P. C. Funtucci, D. Galizzioli, and F. Morazzoni, *Inorg. Nucl. Chem. Lett.*, **9**, 313 (1973) and Ref. 6.
16) For the $(yz)^1$ ground state, *cf.* our unpublished work and T. Kawakita, K. Migita, M. Chikira, M. Iwaizumi, and T. Isobe, presented at the 24th symposium on the coordination chemistry, Kanazawa, 1974.
17) For example, R. B. Bentley, F. E. Mabbs, W. R. Smail, M. Gerloch, and J. Lewis, *J. Chem. Soc., A*, **1970**, 3003.
18) For the sake of simplicity, we made allowance only for the contribution from the states where $d_{x^2-y^2}$ is vacant, since in the present system we can assume that energy separation between $d_{x^2-y^2}$ orbital and any of the other d-orbitals is sufficiently large. In this system, the quartet terms were also neglected, since according to McGarvey[12] they are neglible for the square planar cobalt(II) complexes.
19) J. S. Griffith, "The Theory of Transition Metal Ions,"

Cambridge University Press, London (1961), pp. 205—209.
20) A. H. Maki, N. Edelstein, A. Davidson, and R. H. Holm, *J. Am. Chem. Soc.*, **86**, 4580 (1964).
21) B. R. McGarvey, *J. Phys. Chem.*, **71**, 51 (1967).
22) P. A. Narayana and K. V. L. N. Sastry, *J. Chem. Phys.*, **57**, 3266 (1972), and *ibid.*, **58**, 4381 (1973).
23) H. Kon and N. Kataoka, "Electron Spin Resonance of Metal Complexes," ed by T. F. Yen, Plenum Press, New York (1969), pp. 59—69.
24) Y. Nishida and S. Kida, *Bull. Chem. Soc. Jpn.*, **45**, 461 (1972).
25) Our choice of x, y axis differs from that of McGarvey,[12] so that the d_{xy} in this paper corresponds to the $d_{x^2-y^2}$ in McGarvey's paper.
26) H. Nishikawa and S Yamada, *Bull. Chem. Soc. Jpn.*, **37**, 8 (1964).
27) A. K. Gregson, R. L. Martin, and S. Mitra, *Chem. Phys. Lett.*, **5**, 310 (1970).
28) J. M. Assour and W. K. Kohn, *J. Am. Chem. Soc.*, **87**, 207 (1965).
29) M. Green and P. A. Tasker, *Inorg. Chim. Acta*, **5**, 65 (1971).
30) N. F. Curtis, *Coord. Chem. Rev.*, **3**, 3 (1968).
31) S. C. Tang, S. Koch, G. N. Weinstein, R. W. Lane, and R. H. Holm, *Inorg. Chem.*, **12**, 2589 (1973).

The Study of Thermochemical Hydrogen Preparation. VI.[1] A Hydrogen-evolving Step through the H_2S–CO Cycle

Masayuki DOKIYA, Kenzo FUKUDA, Harumi YOKOKAWA, and Tetsuya KAMEYAMA

National Chemical Laboratory for Industry, 2-19-19 Mita, Meguro-ku, Tokyo 153

(Received August 5, 1977)

A two-step decomposition process of hydrogen sulfide was studied. The process is constituted from a hydrogen-evolution step ($CO+H_2S \xrightarrow{ca.\,200\,^\circ C} H_2+COS$) and a carbonyl sulfide-decomposition step ($COS \xrightarrow{ca.\,830\,^\circ C} CO+1/x\cdot S_x$). Almost an equilibrium amount of hydrogen could be produced in the first reaction (*ca.* 40%, 200 °C, 1 atm, $CO/H_2S=2.2$) with a cobalt sulfide or nickel sulfide catalyst. In the second reaction, an almost equilibrium amount of carbonyl sulfide (45%) could also be decomposed into carbon monoxide and elementary sulfur at 830 °C under 1 atm with a sufficient reaction rate and selectivity without using any catalysts. Carbon dioxide was formed as a by-product in the second reaction: however, its yield was only 5% of the carbon monoxide produced. From these results, it may be concluded that this two-step decomposition process of hydrogen sulfide can produce more hydrogen than that produced by the direct decomposition of hydrogen sulfide. In the second reaction, however, the recombination of carbon monoxide with elementary sulfur can not be neglected. Thus, a rapid separation of sulfur from carbon monoxide is required.

The recovery of hydrogen form hydrogen sulfide is of industrial importance in relation to the thermochemical splitting of water[2] and to the desulfurization of oil and coal.[3] It has been found by the present authors that molybdenum(IV) sulfide and tungsten(IV) sulfide effectively decompose hydrogen sulfide into hydrogen and elementary sulfur at 500—800 °C:[4]

$$H_2S \longrightarrow H_2 + 1/x\cdot S_x. \quad (1)$$

The yield of hydrogen was, however, thermochemically limited, and only 5.5% of hydrogen could be produced even at 1000 K under 1 atm.

There have been many investigations undertaken in an attempt to overcome such a thermochemical disadvantage by using the external energies—for example, by α-ray,[5] by γ-ray,[5] by electron beam,[6] by UV irradiation,[7] by electric discharge,[8] or by electrolysis.[9] Besides these methods, it has been proved that the hydrogen can be separated selectively from hydrogen sulfide in the reaction zone by using a micro porous Vycor-type glass as an effusion barrier.[10] Such a process makes possible the production of more hydrogen than the equilibrium amount of Reaction 1.

Besides these single-step methods, several two-step cycles[11] and multi-step open cycles[12] have been proposed.

The present authors have previously reported a method for the production of hydrogen and carbonyl sulfide from hydrogen sulfide and carbon monoxide according to Reaction 2.[13] A closed cycle could be set up for the production of hydrogen and elementary sulfur from hydrogen sulfide if carbonyl sulfide could be decomposed selectively into carbon monoxide and sulfur:

$$H_2S + CO \longrightarrow H_2 + COS, \quad (2)$$

$$COS \longrightarrow CO + 1/x\cdot S_x, \quad (3)$$

$$H_2S \longrightarrow H_2 + 1/x\cdot S_x. \quad (1)$$

In this study, experiments were performed on Reaction 2, 3, and 4 in order to examine the possibility of this cycle:

$$CO + S \longrightarrow COS \quad (4)$$

Experimental

Reaction 2. The apparatus employed in this study was made of Pyrex glass and was a flow reactor under atmospheric pressure, as is shown in Fig. 1. The catalyst was placed in the reactor, A. A mixture of hydrogen sulfide and carbon monoxide ($CO/H_2S=2.2$) was introduced into the reactor, A, at two different constant rates (Table 1). The reactor was then kept at certain given temperatures between 170—380 °C (Table 1). The effluent gas from the reactor was cooled at the trap, E, where the produced sulfur was condensed out; then it was introduced into the two-stage gas chromatograph in order to determine the composition of the reaction mixture. The first stage of the gas chromatograph was equipped with a Deactigel column (Applied Science Co.) in order to separate the mixture of hydrogen and carbon monoxide from the carbonyl sulfide and hydrogen sulfide, while a molecular-sieve column was used in the second stage for the separation of the hydrogen from the carbon monoxide.

Catalyst. The catalysts employed in Reaction 2 were as same as those employed in a previous work.[13]

Reaction 3. This reaction was a non-catalytic thermal decomposition reaction. The apparatus shown in Fig. 1 was used again except that the A reactor was changed to a quartz reactor, B. The carbonyl sulfide gas was introduced

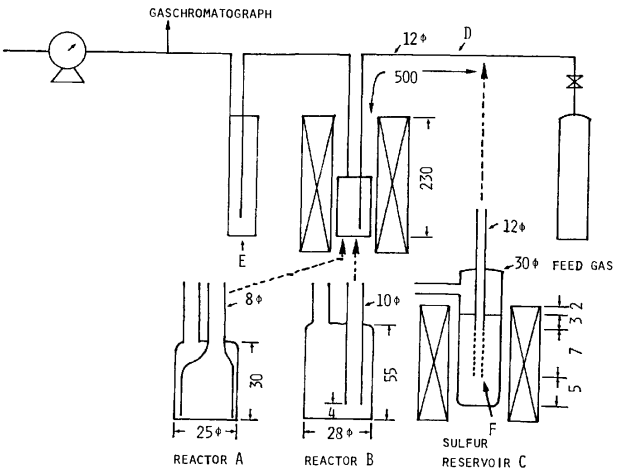

Fig. 1. Apparatus.

Table 1. Results of reaction 2

Catalyst	Weight g	Surface area m^2	Reaction temp °C	Flow rate ml/min	H_2 concn %	H_2S conversion %	Reaction[b] ratio %
NiS	1.60	4.9	350	11.6	9.5	28.8	73.3
	1.60	4.9	250	11.6	5.0	15.8	37.3
Co_9S_8	2.94	93.1	300	14.2	12.1	38.7	94.4
	2.94	93.1	260	14.2	13.0	41.8	99.5
	2.94	93.1	220	14.2	13.3	42.9	97.7
	2.94	93.1	170	14.2	12.7	39.8	87.6
V_3S_4	3.00	12.0	350	14.2	7.5	24.0	61.1
	3.00	12.0	250	14.2	2.2	7.0	16.6
FeS	3.23	25.2	380	14.2	10.5	32.7	84.9
(FeS_2[a])	3.23	25.2	300	14.2	8.3	26.5	60.4
	3.23	25.2	250	14.2	3.3	10.7	25.2
Cr_2S_3	3.00	28.2	330	14.2	10.7	34.5	86.5
	3.00	28.2	280	14.2	6.5	20.8	50.2
MoS_2	4.24	14.0	380	14.2	11.8	37.6	97.7
	4.24	14.0	300	14.2	6.8	21.7	52.9
Ti_5S_4	3.22	349.0	350	14.2	8.4	26.9	68.4
	3.22	349.0	250	14.2	1.5	4.8	11.3

a) Minor component. b) (experimental conversion)/(equilibrium conversion).

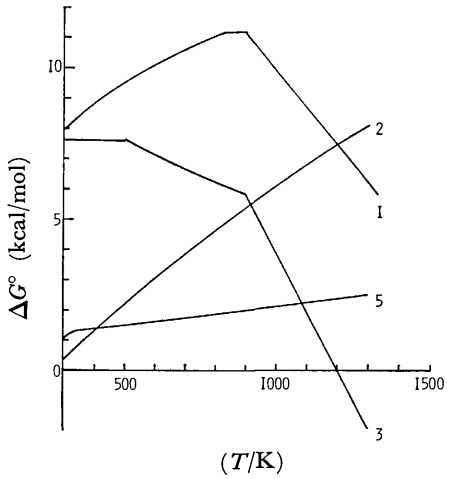

Fig. 2. Temperature dependence of ΔG° of Reactions 1,2 , 3, and 5. Reaction 1: $H_2S \rightarrow H_2 + 1/x \cdot S_x$, Reaction 2: $H_2S + CO \rightarrow COS + H_2$, Reaction 3: $COS \rightarrow CO + 1/x \cdot S_x$, Reaction 5: $COS \rightarrow 1/2 \cdot CO_2 + 1/2 \cdot CS_2$.

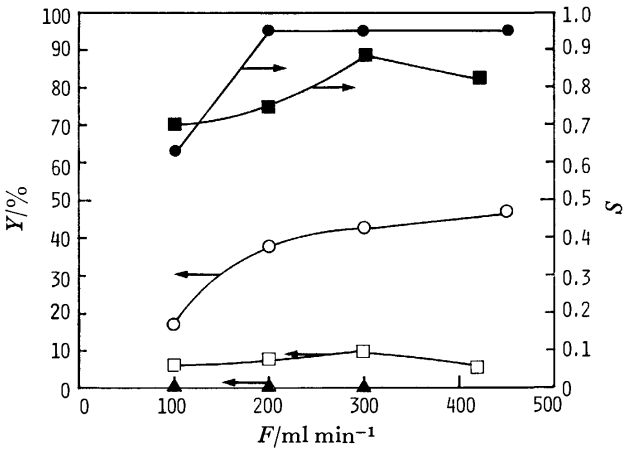

Fig. 3. Yields and selectivity against flow rate in Reaction 3. F: Flow rate, S: selectivity=(CO)/(CO $+2CO_2$), Y: yield=(CO)/(COS). ●, ○: 830 °C, ■, □: 630 °C, ▲: 430 °C.

at the given flow rates (Fig. 3). The reactor, B, was kept at 630, 730, and 830 °C. The composition of the each reaction mixture was determined by the same two-stage gas chromatograph.

Reaction 4. Reaction 4 was also performed in the same apparatus as Reaction 3, but now a sulfur reservoir, C, was attached to the apparatus shown in Fig. 1. The glass pipe, D, between the reactor, B, and the sulfur reservoir, C, was kept at 250 °C to prevent the condensation of the sulfur. The sulfur reservoir and the reactor were kept at the given temperatures (Figs. 4 and 5). In some cases, the inner pipe, F, of the sulfur reservoir was elongated (broken line in Fig. 1) in order to check the effect of the sulfur reservoir on Reaction 4. The carbon monoxide was introduced into the apparatus at certain given flow rates (Figs. 4 and 5). The carbon monoxide was made to react with sulfur in the sulfur reservoir, C, in the pipe, D, and in the reactor, B. The composition of the reaction mixture was determined by the two-state gas chromatograph.

Reagents. The purities of hydrogen sulfide, carbon monoxide, carbonyl sulfide, and sulfur were 99.99, 99.9, 99.9, and 99.5% respectively.

Results and Discussion

Table 1 represents the data for the various metal sulfide catalysts of Reaction 2 obtained at the reaction temperature of 170—380 °C and with the CO/H_2S ratio of 2.2 in the mixture of reactants. The results for Cu_2S, ZnS, and MnS were excluded from the table because the reactions on these catalysts did not proceed with a measurable velocity at 170—380 °C. As can be seen from Table 1, hydrogen and carbonyl sulfide can generally be obtained from hydrogen sulfide and carbon monoxide by using transition metal sulfides as catalysts at 170—380 °C. In the case of cobalt sulfide,

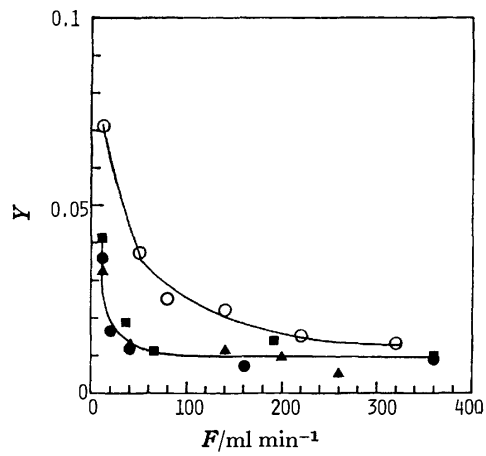

Fig. 4. Yield of Reaction 4 against flow rate (1). F: Flow rate, Y: yield=(COS)/(CO). Temperature of reactor: ○ 500 °C, ■ 450 °C, ● 400 °C, ▲ 300 °C. Temperature of sulfur reservoir: 200 °C.

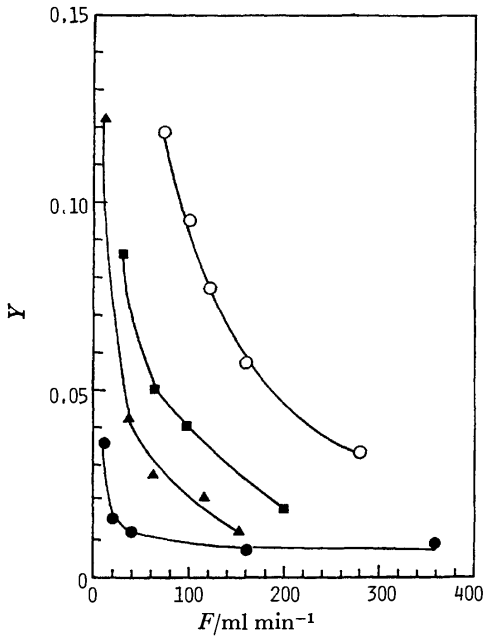

Fig. 5. Yield of Reaction 4 against flow rate (2). F: Flow rate, Y: yield=(COS)/(CO). Temperature of reactor: 400 °C. Temperature of sulfur reservoir: ○ 400 °C, ■ 300 °C, ▲ 200 °C, ● 200 °C.

hydrogen can be obtained in an amount as much as the equilibrated amount even at 220 °C. It should be noted that, in spite of the small surface area of the nickel sulfide catalyst, the conversion of hydrogen sulfide significantly high; thus, the reaction can proceed nearly to the equilibrium below 200 °C if a sufficient amount of a catalyst is employed.

Assuming that it is possible to separate each constituent from the produced gas mixture and that the selective decomposition of carbonyl sulfide into carbon monoxide and elementary sulfur can be performed, a two-step closed cycle for the decomposition of hydrogen sulfide can be constructed by the combination of Reactions 2 and 3.

Figure 2 represents the temperature dependence of the free energy changes of Reactions 1, 2, 3, and 5, which were calculated from the published thermochemical data.[14]

Figure 2 shows that the equilibrium conversions of Reactions 2 and 3 are much higher than that of Reaction 1. If Reaction 1 can be divided into Reactions 2 and 3, the additional yield of the two reactions can exceed that of Reaction 1. This is the most important reason to make up a multi-step cycle for the decomposition of hydrogen sulfide.

Unfortunately, carbonyl sulfide undergoes thermal decomposition by two reaction paths; one is the cracking reaction into carbon monoxide and elementary sulfur, as is expressed by Reaction 3, and the other is the disproportionation reaction to form carbon dioxide and carbon disulfide, as is expressed by Reaction 5.[15] Thus, the selectivity of the decomposition of carbonyl sulfide between Reaction 3 and Reaction 5 becomes a serious problem.

$$2COS \longrightarrow CO_2 + CS_2 \qquad (5)$$

Figure 3 shows the results obtained for the thermal decomposition of carbonyl sulfide. As can be seen in Fig. 3, the selectivity of carbon monoxide formation, which is represented by $CO/(CO+2CO_2)$, was as high as 95%, while that of carbon dioxide was as low as 5% at 830 °C when the flow rate of carbonyl sulfide was 420 ml min^{-1}. This selectivity seems to be sufficient to constitute a two-step closed cycle. Moreover, it must be emphasized that the yield and the selectivity of the carbon monoxide formation depended on the flow rate of the reactant carbonyl sulfide at 830 °C. The more carbon monoxide was produced, the faster the flow rate of the carbonyl sulfide. It was possible to obtain an almost equilibrated amount of carbon monoxide (*ca.* 45%) at 830 °C with the flow rate of 420 ml min^{-1}, without using any catalyst. On the other hand, the yield and selectivity of carbon monoxide were low at 630 and 430 °C over a wide range of flow rates.

When the flow rate was 100 ml min^{-1} at 830 °C, the yield and the selectivity of carbon monoxide formation were as low as that at 630 °C. From this fact, it may be concluded that Reaction 3 is very fast in both forward and reverse directions; thus, when the flow rate is slow, the reverse reaction occurs at the cooler part of the reactor, thus reducing the yield of carbon monoxide. The quenching of the gas mixture produced is, therefore, required in order to prevent the reverse reaction (Reaction 4).

In order to elucidate this reverse reaction more precisely, Reaction 4 was studied. In Fig. 4, the yields (COS/CO) of Reaction 4 are plotted against the fow rates of carbon monoxide at various temperatures of the reactor, B (300, 400, 450, and 500 °C). Below 450 °C, the yields were found to be as small as 1% at flow rates higher than 40 ml min^{-1}. At 500 °C, some increase in the yield was observed; however, the yield could be reduced to be less than 2% by raising the flow rate. Thus, Reaction 4 may be made negligible by increasing the flow rate. These results were obtained when the sulfur reservoir was kept at 200 °C and when the inner pipe, F, was dipped into the liquid

sulfur to a depth of *ca.* 3 cm. Then, in order to estimate the effect of the sulfur reservoir more precisely, the inner pipe, F, was elongated to *ca.* 7 cm and the temperature of the reservoir was raised from 200 to 400 °C, while the temperature of the reactor, B, was kept at 400 °C. The results are shown in Fig. 4. The solid circles in Fig. 5 are the same data as those in Fig. 4. The results in Fig. 5 show that the yield of carbonyl sulfide increased when the carbon monoxide was mixed well with the liquid sulfur in the sulfur reservoir and when the temperature of the reservoir was elevated. The yield of carbonyl sulfide, however, depended greatly on the flow rate of the carbon monoxide. Thus, these results show that the recombination of carbon monoxide and liquid sulfur can be eliminated as negligible if the reaction mixture of Reaction 3 can be cooled promptly and if the separation of carbon monoxide from liquid can be carried out rapidly.

This work was done as part of the Sunshine Project of the Ministry of International Trade and Industry of Japan.

References

1) a) Part I; *Int. J. Hydrogen Energy*, **1**, 117 (1976); b) Part II; *Denki Kagaku*, **45**, 139 (1977); c) Part III; *Bull. Chem. Soc. Jpn.*, **50**, 2657 (1977); d) Part IV; *Denki Kagaku*, **45**, 701 (1977); e) Part V; *Int. J. Hydrogen Energy*, to be published.

2) a) M. A. Soliman, R. H. Carty, W. L. Conger, and J. E. Funk, *Can. J. Chem. Eng.*, **53**, 164 (1975); b) R. E. Chao, *Ind. Eng. Chem., Process Res. Dev.*, **14**, 94 (1974); c) E. D. Glandt and S.L. Myers, *ibid.*, **15**, 100 (1976); d) M.G. Bowman "Conference Proceedings of Ist World Hydrogen Energy Conference," Vol. 1, 5A-27, The Univ. of Miami, Coral Gables, Florida (1976); e) Y. Kotera, *Int. J. Hydrogen Energy*, **1**, 219 (1976).

3) M. E. D. Raymont, *Hydrocarbon Process.*, No. 7, 139 (1975).

4) K. Fukuda, M. Dokiya, T. Kameyama, and Y. Kotera, *Ind. Eng. Chem., Fundam.*, to be published.

5) M. Forys and K. Jerieska, *Radiochem. Radioanal. Lett.*, **1**, 237 (1969).

6) A. W. Boyd, C. Wills, and O. A. Miller, *Can. J. Chem.*, **51**, 1288 (1973).

7) G. R. Wooley and R. J. Cvetanovic, *J. Chem. Phys.*, **50**, 4697 (1969).

8) K. Kawamura, Jpn. Patent 40-14413 (1965).

9) R. Lee, U. S. Patent 2839381 (1958).

10) M. Dokiya, T. Kameyama, and K. Fukuda, *Denki Kagaku*, **45**, 701 (1977).

11) a) J. G. Weiner and C.W. Leggett, U.S. Patent 2979384 (1961); b) Y. Nishimoto, Y. Mizumoto, S. Hasegawa, and S. Mitsuoka, *Jpn, Kokai* 75118983 (1975).

12) a) I. G. Nixon, Brit. Patent 1126465 (1965).
b) S. C. Schuman, U. S. Patent 3388971 (1968).

13) a) K. Fukuda, M. Dokiya, T. Kameyama, and Y. Kotera, *J. Catal.*, **49**, 379 (1977); b) K. Fukuda, N. Todo, and Y. Kotera, U. S. Patent 3856925 (1974); c) K. Fukuda, N. Todo, and Y. Kotera, Jpn. Patent 51-10596 (1976).

14) I. Barin and O. Knacke, "Thermochemical Properties of Inorganic Substances," Springer-Verlag, Berlin (1975).

15) a) R. J. Ferm, *Chem. Rev.*, **57**, 621 (1957); b) J. R. Partington and H. H. Neville, *J. Chem. Soc.*, **1951**, 1230; c) A. Stock and P. Seelig, *Ber.*, **52**, 672 (1919); d) A. Stock, W. Siecke, and E. Pohland, *ibid.*, **57**, 719 (1924).

Studies on the Chemical Shifts of Auger Electron Energies for Magnesium and Zinc in Their Compounds

Shunichi NISHIKIDA and Shigero IKEDA

Department of Chemistry, Faculty of Science, Osaka University, Toyonaka, Osaka 560

(Received August 13, 1977)

The energy shifts of X-ray excited Auger electrons and photoelectrons for zinc and magnesium in their metals, oxides, halides, and chelate compounds are analyzed in terms of the relaxation effect. Zn $2p_{3/2}$, 3d photoelectron, Zn $L_3M_{45}M_{45}{}^1G$ Auger electron, Mg ls, 2p photoelectron and Mg $KL_{23}L_{23}{}^1D$ Auger electron peaks were provided for the investigation. The quantitative estimation of the extra-atomic relaxation energies for core electron emission was performed by combining atomic spectral data, XPS and AES data of the compounds. For zinc compounds, extra-atomic relaxation energies increase in the order of $ZnF_2 < ZnCl_2 < ZnBr_2 \approx ZnO < ZnI_2 \approx ZnS < Zn(acac)_2$, whilst the values are not fairly systematic for magnesium compounds. The nearest neighbored atom is found to be the important function for the extra-atomic relaxation energies.

Few investigations on the XPS for inner shell electrons of magnesium or zinc atoms in their compounds have been undertaken[1-3] because of the small chemical shifts in these binding energies. For zinc halides, shifts of zinc 3d bands have been discussed in terms of the ionic character of the zinc–halogen bonds[4] measured in vapor phase in UPS. For zinc, Auger spectra were measured for atom,[5,6] zinc metal, oxide, and fluoride.[7] Kowalczyk[7] *et al.* have given a theoretical interpretation of Auger energies and discussed the shifts of extra-atomic relaxation energies for zinc in metal, oxide, and fluoride. Hoogewijs *et al.*[8,9] have given a similar but improved results for the analysis of Auger electron energies of zinc atom and metal. No data have been explored about the Auger emission of magnesium compounds other than that of magnesium atom,[10] metal, and oxide.[11]

In this paper, we report on the chemical shifts of the core level electron binding energies and Auger electron energies for zinc and magnesium in their metals and compounds. Atomic spectral data for these elements are applied here to elucidate the extra-atomic relaxation energies in Auger electron emission. For oxides, sulfides and halides, extra-atomic relaxation energies were corelated with polarizabilities of ligands. In both elements, common ligands give the same extent of contributions to the extra-atomic relaxation energy shifts of host atoms.

Experimental

Spectra of photoelectrons and Auger electrons were recorded by AEI ES 200 type spectrometer with the Al $K\alpha_{1,2}$ X-ray source. The pressure in the sample chamber was maintained at about 5×10^{-8} Torr (1 Torr = 133.322 Pa) during the measurements.

Magnesium and zinc metal films were provided for the investigation by evaporating them onto the sample holder.

Testing samples for zinc chloride, bromide, and iodide were deposited onto a stainless holder plate by using a platinum filament. The XPS spectra of these halides were free from the background O ls and C ls photoelectron peaks. Original magnesium chloride and magnesium bromide were obtained by pyrolysis of their double salts with ammonium chloride and ammonium bromide. The dehydration of magnesium iodide was carried out with heating in vacuum.

8-Quinolinolate complexes for zinc and magnesium were prepared by the ordinary method[12] and dehydrated by heating at 150 °C for a few hours.

All the other samples were obtained from commercial sources without further purification.

Solid samples other than halides and metals were powdered and pressed onto the cellophane tape placed on the metal holder to provide for the X-ray exposure.

The energy scale of the spectra was calibrated with reference to the photoelectron energies of the following levels of standard materials: Pd $4d_{5/2}$, Au $4f_{7/2}$, Pd $3d_{5/2}$, Ag $3d_{5/2}$, and Ag $3p_{3/2}$ of highly pure metallic palladium, gold, and silver. From a knowledge of the spectrometer constant thus obtained,[13] the measured values of kinetic energies for various levels in samples were corrected. The binding energies of $4f_{7/2}$ photoelectron peak of gold (83.8 eV) deposited onto each sample were measured and used to evaluate the extent of charging of the respective solid.

Results

The binding energies of 1s and 2p photoelectrons and $KL_{23}L_{23}$ Auger electron energies for all of the measured magnesium compounds are summarized in Table 1.

For zinc compounds, the binding energies of $2p_{3/2}$, 3d and $L_3M_{45}M_{45}$ Auger peaks are summarized in Table 2. Each value for the shifts of these energies referred to those of the respective fluorides is also listed in the tables.

In the photoelectron and the Auger electron spectra for magnesium metal film, peaks due to the partially oxidized magnesium are observed, but no such oxidized peaks were observed for zinc metal in both photoelectron and Auger electron spectra. A satellite peak due to the plasmon loss is observed at the 10.8 eV lower kinetic energy side of the main peak in both photoelectron and Auger electron spectra for magnesium metal. The absence of the O 1s peak in zinc halides gives the evidence of the complete dehydration of these samples by the evaporation method.

In spite of the careful preparations, O 1s photoelectron peak was slightly observed in magnesium chloride, bromide and iodide spectra. For a zinc 8-quinolinolate compound, O 1s peak with rather high intensity was observed compared with the intensity of N 1s peak, despite of the heating at 150 °C for a few hours. On the other hand, the spectrum for magnesium 8-quinilinolate showed appropriate intensity of O 1s photoelectron peak to the predicted stoichiometric value for its structure.

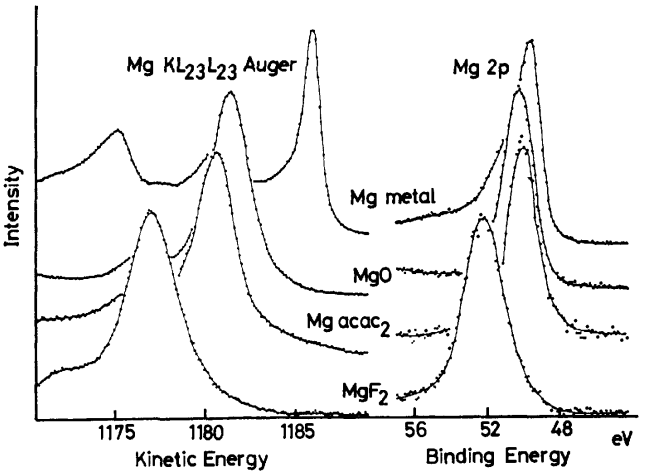

Fig. 1. Magnesium 2p photoelectron and $KL_{23}L_{23}$ Auger electron spectra for various magnesium compounds.

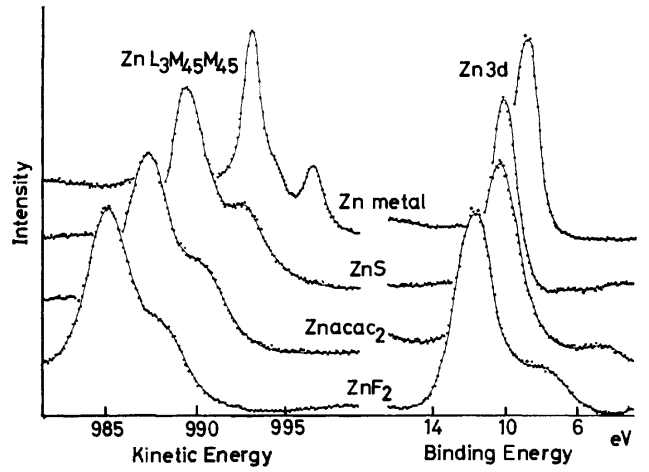

Fig. 2. Zinc 3d photoelectron and $L_3M_{45}M_{45}$ Auger electron spectra for various zinc compounds.

For the other chelate compounds of magnesium and zinc, the intensity ratios in each photoelectron peak give good agreements with the predicted ratios from their structures.

In Fig. 1 the spectra of Mg $KL_{23}L_{23}$ Auger electron and 2p photoelectron for magnesium metal, magnesium oxide, magnesium acetylacetonate, and magnesium fluoride are shown. Also those of Zn $L_3M_{45}M_{45}$ Auger electron and 3d photoelectron for zinc compounds are shown in Fig. 2.

The chemical shifts of Auger lines are larger than those of photoelectrons for both elements in all the compounds.

The magnitudes of the shifts of these lines for each metal referred to their fluorides are the largest of the compounds investigated for both elements. The energy separations of the binding energies between magnesium 1s and 2p photoelectrons are as constant as those between zinc 2p and 3d orbital electrons in all the compounds.

Discussion

As shown in Tables 1 and 2, chemical shifts of Auger electrons are larger than those of photoelectrons. This

Table 1. Chemical shifts of photoelectron binding energies (ΔE_b), Auger electron energies (ΔE_{Auger}) and extra-atomic relaxation energies (R^{ea}) for magnesium compounds

Sample	Mg 2p		Mg $KL_{23}L_{23}(^1D)$		R^{ea}
	E_b	ΔE_b	E_{Auger}	ΔE_{Auger}	
Mg metal	49.7	2.5	1185.9	8.9	15.2
MgF_2	52.2	(0.0)	1177.0	(0.0)	8.8
$MgCl_2$	51.7	0.5	1179.5	2.5	10.8
$MgBr_2$	50.5	1.7	1180.8	3.8	10.9
MgI_2	49.6	2.6	1181.1	4.1	10.3
MgO	50.3	1.9	1181.0	4.0	10.9
[Mg(oxine)[a]$_2$]	49.2	3.0	1182.0	5.0	10.8
[M(acac)[b]$_2$]	50.0	2.2	1180.6	3.6	10.2
Na_2[Mg(edta)]	50.2	2.0	1180.6	3.6	10.4

a) oxine=8-quinolinolate ion. b) acac=acetylacetonate ion=2,4-pentanedionate ion. c) edta=ethylenediaminetetraacetate(4−) ion.

can be interpreted in terms of the larger relaxation energy due to the final state after two-electron ejection in Auger process, as described in the following equation.[7,14–16]

$$E_{Auger}(KLL) = E(K) - 2E(L) + R - F, \quad (1)$$

where $E(K)$ and $E(L)$ are the photoelectron binding energies of 1s and 2p orbitals, respectively, and F is a two-electron interaction term, for which Asaad and Burhop[17] have made a theoretical analysis by taking into account the effect of intermediate coupling in the two-hole final state for KLL Auger transitions. R is a so-called static relaxation energy according to the definition after Shirley.[7] It may be separated into two parts, atomic and extra-atomic static relaxation energies. Static atomic relaxation energy should be twice the dynamic relaxation energy, E_R,[18] accompanied with photoelectron emission. Extra-atomic static relaxation energy, R^{ea}, is the relaxation energy due to surrounding atoms in the electron emission process. Then, Eq. 1 is expressed as follows.

$$E_{Auger}(KLL) = E(K) - 2E(L) + 2E_R + R^{ea} - F. \quad (2)$$

For a free atom, R^{ea} value in Fig. 2 is zero and the following equation will be established.

$$E^A_{Auger}(KLL) = E^A(K) - 2E^A(L) + 2E^A_R - F, \quad (3)$$

where E^A means the energy term for a free atom. The photoelectron binding energy for a free atom is referred to the vacuum level, and the kinetic energy of an Auger electron is independent of the excitation energy. When a measurement is carried out using characteristic X-ray with the energy of $h\nu$, Eq. 3 is expressed as follows.

$$2E_R - F = (E_b(K) - E_b(L)) + (E_{kin}(L) - E_{Auger}(KLL)) - h\nu, \quad (4)$$

where $E_b(K) - E_b(L)$ is equivalent to the value $E_{kin}(L) - E_{kin}(K)$. Then, $2E_R - F$ can be obtained directly from the observed kinetic energies for each peak. Here, the energy level for an Auger electron could be defined with just the same reference as that for photoelectron binding energy.

TABLE 2. CHEMICAL SHIFTS OF PHOTOELECTRON BINDING ENERGIES (ΔE_b), AUGER ELECTRON ENERGIES (ΔE_{Auger}) AND EXTRA-ATOMIC RELAXATION ENERGIES (R^{ea}) FOR ZINC COMPOUNDS

Sample	Zn $2p_{1/2}$		Zn 3d		Zn $L_3M_{45}M_{46}(^1G)$		R^{ea}
	E_b	ΔE_b	E_b	ΔE_b	E_{Auger}	ΔE_{Auger}	
Zn metal	1020.6	2.8	8.9	2.8	993.1	8.1	14.7
ZnF_2	1023.4	(0.0)	11.7	(0.0)	985.1	(0.0)	9.5
$ZnCl_2$	1022.5	0.9	10.8	0.9	987.2	2.1	10.7
$ZnBr_2$	1022.6	0.8	10.9	0.8	987.8	2.7	10.4
ZnI_2	1022.3	1.1	10.6	1.1	989.0	3.9	12.3
ZnO	1022.2	1.2	10.5	1.2	988.0	2.9	11.2
ZnS	1021.9	1.5	10.2	1.5	989.5	4.4	12.4
[Zn(acac)[a]$_2$]	1022.1	1.3	10.4	1.3	987.3	2.2	10.4
[Zn(oxine)[b]$_2$]	1022.5	0.9	10.8	0.9	987.1	2.0	10.6
[Zn(pc)][c]	1021.8	1.6	10.1	1.6	988.6	3.5	11.4

a) acac: acetylacetonate ion (2,4-pentanedionate ion). b) oxine: 8-quinolinolate(2−) ion. c) pc: phthalocyanine.

In a similar fashion for a solid sample, both photoelectron binding energy and Auger electron kinetic energy must be referred to the same level.

Then, the electron energy values can be scaled from the reference level, that is, electrons at the reference level are to be photoejected with the kinetic energy of $h\nu$. In this paper, both photoelectron and Auger electron energies are referred to the Fermi level.

Using Eq. 3 the numerical values of $2E_R^A - F$ term can be estimated for magnesium atom on the basis of the following data; the energy value, 1167.3eV for Mg KL_{23}-$L_{23}{}^1D$ in magnesium atom measured by Breuckmann and Schmidt,[10] the binding energy of 2p orbital electron, 57.64 eV, estimated from the atomic spectral data[19] and 1s orbital binding energy, a sum of the binding energy of 2p orbital and magnesium $K\alpha$ X-ray energy 1256.6 eV[20] being equal to 1311.24 eV. Then the value for $2E_R^A - F$ term is calculated to be −28.66 eV. The result is graphically shown in Fig. 3.

For magnesium, the sum of $2E_R - F$ in Eq. 2 is considered to be equal for all the compounds and then the extra-atomic relaxation energy, R^{ea}, a parameter for the characterization of molecular environment surrounded by a host atom, could be estimated with the following method. As magnesium in its compounds under investigation exists as cation with oxidation number +II, no 3s orbital electrons are assumed to contribute to the atomic relaxation effect. Then, the atomic relaxation of magnesium ion, $2E_R$, was calculated by subtracting the relaxation energy due to 3s orbital electrons and we obtained the value of 3.9 eV by using Slater's orbitals and equivalent core model.[21,22]

$$-F + 2E'_R = -33.02\,\text{eV}$$

where E'_R is dymanic relaxation energy ignoring 3s electrons.

On the other hand, as shown in Fig. 4, the value of $2E_R - F$ can be directly estimated from atomic data[19] for magnesium ion with a similar fashion for magnesium atom. That is, the value can be obtained as a difference between ionization potentials of the spectroscopic MgIII(Mg^{2+}) and MgIV(Mg^{3+}) states, −29.17 eV. As the lowest energy state of $MgV(2s)^2(2p)^4$ is $^3P_2$ in optical term, $-F+2E_R'$ value corresponding to ^1D state can be obtained from a energy difference between $^3P_2$ and ^1D states, 3.8 eV, as follows:

$$-F + 2E'_R = -32.97\,\text{eV}$$

The value is in good agreement with the former results. Utilizing this value with the observed Mg $KL_{23}L_{23}{}^1D$ Auger electron energy, and 1s and 2p photoelectron binding energies, extra-atomic relaxation energy, R^{ea}

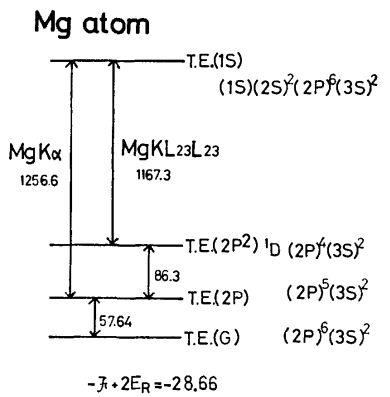

Fig. 3. Total energy (T.E.) level diagram of a free magnesium atom for various core-ionized electron configurations (eV).

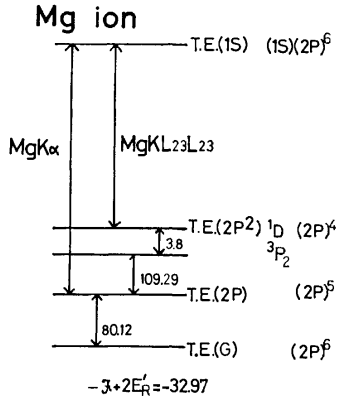

Fig. 4. Total energy (T.E.) level diagram of magnesium ion (+2) for various core-ionized electron configurations (eV).

could be calculated for various magnesium compounds.

For zinc Auger electrons, $L_3M_{45}M_{45}{}^1G$ electron with the highest intensity is adopted to calculate the extra-atomic relaxation. For the fourth ionization potential of zinc atom, the value obtained by Lotz[23] was used and the energy separation between ^1G and $^3F_4$, the lowest energy state of $Zn(Zn^{4+})$ ion ($3d^84s^0$), has the measured value of 3.75 eV for the free zinc atom.[5] The result obtained from these data is graphically shown in Fig. 5.

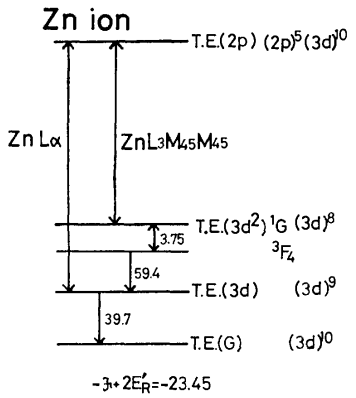

Fig. 5. Total energy (T.E.) level diagram of zinc ion (+2) for various core-ionized electron configuration.

In Tables 1 and 2, the extra-atomic relaxation energies obtained by the above mentioned method (Eq. 2) for various magnesium and zinc compounds are shown, respectively.

The distance between Auger electron and photoelectron peaks is independent of the reference level. The ambiguity of reference level or charging effect can be canceled out. Wagner[24] has also noted this energy difference and defined a parameter for Auger chemical shift. He found out that the shifts of this parameter qualitatively obey the trend of Pearson's concept of soft-hard acid and base character of bonding atoms to host atom. The shift of Auger parameter can be identified with the change of the magnitudes R^{ea}, assuming $E(K)-E(L)$ and $-F+2E_R$ to be constant for all the compounds.

For zinc halides, the electron binding energies of Zn $2p_{3/2}$ are nearly the same for all the compounds but fluoride, whereas the shifts in R^{ea} are clearly progressive and the order of the magnitudes of R^{ea} is quite coordinated with polarizabilities of halide ions. Although the Zn $2p_{3/2}$ binding energies in zinc oxide are the same with that of zinc iodide, R^{ea} in zinc iodide is larger than that in zinc oxide. This corresponds to the fact of the larger polarizability of iodide ion than that of oxygen ion. Sulfide ion with a large polarizability shows a large relaxation energy in zinc sulfide. For three zinc chelate complexes, the order of magnitudes in extra-atomic relaxation energies obeys the donicity of the coordinated atoms, that is, is in the order of O–O, O–N, and N–N.

A plot of the measured relaxation energy *vs.* the product of polarizability[25,26] for a neighbored surrounding atom and the inverse of the nearest neighbor distance[27] for various zinc compounds is shown in Fig. 6. It is seen that the extra-atomic relaxation energies are linearly related to the polarization energies due to nearest neighbored surrounding atoms. A value obtained by extrapolating the line, the intercept of the line with the ordinate, 8.8 eV, means the residual relaxation energies which are commonly contributed to all the compounds. A part of this residual relaxation energies may be due to contributions from all the atoms in crystal except the host and nearest neighbored atoms. The second important contribution may be the participation of 4s orbital electrons. In order to calculate the extra-atomic relaxation energies for zinc compounds, the assumption has been made for 4s orbital electrons to be absent from the host atom, leaving it ideally in Zn^{2+} ion state. Thus, the relaxation energies due to the charge density on zinc atom may be considered as the sum of those localized to the host atom, the values dependent on the bonding character being proportional to the polarizability of surrounding atoms.

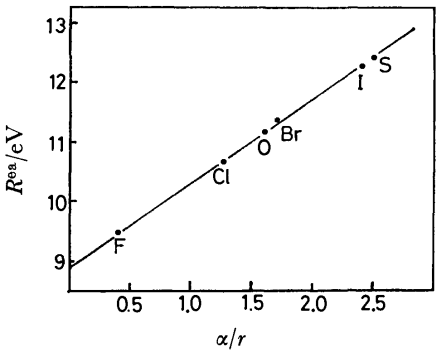

Fig. 6. Corelation between extra-atomic relaxation energies and polarizabilities of neighbor atoms divided by nearest neighbor distance for zinc compounds.

For magnesium halides except for fluorides, the extra-atomic relaxation energies are nearly the same and the order of the magnitude does not correspond to that in zinc halides. Ambiguity exists on the electron emission data sources because of the hydroscopic character of these compounds. For three magnesium chelate compounds investigated, magnesium bonding with nitrogen and oxygen in 8-quinolinol shows the largest relaxation energy. This means that the contribution of nitrogen to relaxation energy may be larger than that of oxygen, like the case of zinc chelate complexes.

The extra-atomic relaxation energies due to the same ligand in both magnesium and zinc compounds are in good agreement with each other except for the bromide and iodide, as shown in Tables 1 and 2.

Reference

1) D. W. Langer and C. J. Vesely, *Phys. Rev. B*, **2**, 4885 (1970).
2) C. J. Vesely and D. W. Langer, *Phys. Rev. B*, **4**, 451 (1971).
3) R. D. Seals, R. Alexander, and L. T. Taylor, *Inorg. Chem.*, **12**, 2485 (1973).
4) B. G. Cocksey, J. H. D. Eland, and C. J. Danby, *J. Chem. Soc., Faraday Trans. 2*, **69**, 1558 (1973).
5) S. Aksela, J. Väyrynen, and H. Aksela, *Phys. Rev. Lett.*, **33**, 999 (1974).
6) S. Aksela and H. Aksela, *Phys. Lett. A*, **48**, 19 (1974).

7) S. P. Kowalczyk, L. Ley, F. R. McFeely, R. A. Pollak, and D. A. Shirley, *Phys. Rev. B*, **9**, 381 (1974).
8) R. Hoogewijs, L. Fiermans, and J. Vennik, *Chem. Phys. Lett.*, **38**, 192. (1976)
9) R. Hoogewijs, L. Fiermans, and J. Vennik, *Chem. Phys. Lett.*, **38**, 471 (1976).
10) B. Breuckmann and V. Schmidt, *Z. Phys.*, **268**, 235 (1974).
11) C. D. Wagner and P. Biloen, *Surf. Sci.*, **35**, 82 (1973).
12) K. Burger, "Organic Reagents in Metal Analysis," International Series of Monographs in Analytical Chemistry, Vol. 54, Pergamon Press (1973), p. 96.
13) G. Johansson, J. Hedman, A. Berndtsson, M. Klasson, and R. Nilsson, *J. Electron Spectrosc.*, **2**, 295 (1973).
14) D. A. Shirley, *Chem. Phys. Lett.*, **17**, 312 (1972).
15) D. A. Shirley, *Phys. Rev. A*, **7**, 1520 (1973).
16) S. P. Kowalczyk, R. A. Pollak, F. R. McFeely, L. Ley, and D. A. Shirley, *Phys. Rev. B*, **8**, 2387 (1973).
17) W. N. Asaad and E. H. S. Burhop, *Proc. Phys. Soc. London*, **71**, 369 (1958).
18) L. Hedin and A. Johnsson, *J. Phys. B*, **2**, 1336 (1969).
19) C. E. Moore, Atomic Energy Levels as Derived from the Analysis of Optical Spectra, NSRDS- NBS **35** (Wasington D. C. Nat. Bur. Std) (1971).
20) J. A. Bearden, *Rev. Mod. Phys.*, **39**, 78 (1967).
21) D. A. Shirley, *Chem. Phys. Lett.*, **16**, 220 (1972).
22) L. C. Snyder, *J. Chem. Phys.*, **55**, 95 (1971).
23) W. Lotz, *J. Opt. Soc. Am.*, **57**, 873 (1967).
24) C. D. Wagner, *Discuss. Faraday Div., Chem. Soc.*, **60**, 291 (1975).
25) J. R. Tessman, A. H. Kahn, and W. Schockley, *Phys. Rev.*, **92**, 890 (1953).
26) K. Fajans and J. Joos, *Z. Phys.*, **23**, 1 (1924).
27) ZnO: Encyclopedia Chimica, Kyoristu Pub. Co., Vol. 3, (1969), p. 890, ZnS: *ibid.*, Vol. 9, p. 645, ZnF_2: *ibid.*, Vol. 7, p. 852, $ZnCl_2(\beta)$, $ZnBr_2$, ZnI_2: *Structure Report*, **24**, 283 (1960), $ZnCl_2(\gamma)$: *ibid.*, **26**, 319 (1961).

Studies of the Metal Complexes of Cyclohexane Derivatives. IV.[1] Copper(II) and Nickel(II) Complexes of 1,2-Cyclohexanediamine Isomers

Reiko SAITO and Yoshinori KIDANI*

Aichi Junior College of Nursing, Kamishidanmi, Moriyama-ku, Nagoya 463

**Faculty of Pharmaceutical Sciences, Nagoya City University, Tanabe-dori, Mizuho-ku, Nagoya 467*

(Received May 9, 1977)

Two types of copper(II) complexes, $Cu(c\text{-chxn})_2X_2\cdot nH_2O$ and $Cu(t\text{-chxn})_2X_2\cdot nH_2O$ ($X=Cl^-$, Br^-, NO_3^-, and ClO_4^-, $n=0$—2), and three types of nickel(II) complexes, $[Ni(c\text{-chxn})_2]X_2$, $[Ni(c\text{-chxn})_3]X_2\cdot nH_2O$ ($X=Cl^-$, Br^-, NO_3^-, and ClO_4^-, $n=0.5$—1.5) and $[Ni(t\text{-chxn})_2(H_2O)_2]X_2$ ($X=Br^-$ and ClO_4^-), were synthesized. Here, *c*-chxn and *t*-chxn stand for *cis*- and *trans*-1,2-cyclohexanediamine respectively. Based upon the analyses of the electronic spectra and magnetic moments, the structures of the copper(II) complexes synthesized were found to be distorted octahedrons. The influence of the steric configurations of the diamine isomers on the structures of the copper(II) complexes is small. The three types of nickel(II) complexes were found to have square planar, octahedral, and distorted octahedral structures respectively. The steric influence of the ligands on the properties of the nickel(II) complexes was also considered.

Although the properties of various metal complexes of *trans*-1,2-cyclohexanediamine (abbreviated as *t*-chxn), but not the 1 : 2 complexes of copper(II) and nickel(II), have been studied so far,[2] no investigation of the metal complexes of *cis*-1,2-cyclohexanediamine (*c*-chxn) has been reported. These ligands may be regarded as C,C′-disubstituted ethylenediamine derivatives, but their steric properties due to the cyclohexane ring are quite different from one another. In the *c*-chxn complexes, the two amino groups are bound to the cyclohexane ring with axial and equatorial orientations simultaneously, so that the cyclohexane ring exists much closer to the chelate ring than in the *t*-chxn complexes. The present authors have prepared copper(II) and nickel(II) complexes of *c*-chxn and *t*-chxn and studied their properties by means of the electronic and infrared spectra, as well as the magnetic moments.

Experimental

Materials. From the Tokyo Kasei Co., Ltd., we purchased 1,2-cyclohexanediamine, which was then separated into *cis*- and *trans*-isomers according to the procedure described in previous paper.[3] The copper(II) and nickel(II) perchlorates were prepared from the corresponding metal basic carbonates and perchloric acid. The other metal salts used were of the highest grade available.

Preparation of Complexes. *$Cu(c\text{-chxn})_2X_2\cdot nH_2O$ and $Cu(t\text{-chxn})_2X_2\cdot nH_2O$ ($X=Cl^-$, Br^-, NO_3^-, and ClO_4^-, $n=0-2$)*: These complexes were synthesized by the reaction of 2 mmol of copper(II) salt and 4 mmol of *c*- or *t*-chxn in methanol. The violet product obtained was recrystallized from methanol–water.

$[Ni(c\text{-chxn})_2]X_2$ ($X=Cl^-$, Br^-, NO_3^-, and ClO_4^-): The syntheses of these complexes were carried out much like those employed for the copper(II) complexes. The yellow crystals obtained were recrystallized from water. In the process of the recrystallization of $[Ni(c\text{-chxn})_2](NO_3)_2$ and $[Ni(c\text{-chxn})_2](ClO_4)_2$, a small amount of the yellow crystals occasionally turned violet. The violet complexes were completely transformed back to the yellow crystals, though, when they were kept in desiccated atmosphere.

$[Ni(t\text{-chxn})_2(H_2O)_2]X_2$ ($X=Br^-$ and ClO_4^-): The bromide complex was obtained by adding 15 ml of a 0.75 M ligand solution in methanol to 15 ml of a 0.5 M aqueous nickel(II) bromide solution. A blue violet precipitate was recrystallized from methanol–water. The perchlorate complex was prepared according to the following procedure. Six mmol of *t*-chxn in 6 ml of methanol were added to a solution of 4 mmol nickel(II) perchlorate in 8 ml of methanol. After removing a small amount of the tris-complex, the solution was heated on a water bath and concentrated until a small amount of product was deposited. The mixture was then allowed to stand at room temperature to give blue violet complex.

$[Ni(c\text{-chxn})_3]X_2\cdot nH_2O$ ($X=Cl^-$, Br^-, NO_3^-, and ClO^-_4, $n=0.5$—1.5): To 3 mmol of *c*-chxn in 2 ml of ethanol we added 1 mmol of nickel(II) halide in 1 ml of water. The violet crystals thus obtained were recrystallized from ethanol–water to give $[Ni(c\text{-chxn})_3]Cl_2\cdot 1.5H_2O\cdot 0.5C_2H_5OH$ and $[Ni(c\text{-chxn})_3]Br_2\cdot H_2O\cdot 0.5C_2H_5OH$. The ethanol was removed by heating at 100 °C in the air for a few hours. $[Ni(c\text{-chxn})_3](NO_3)_2\cdot 0.5H_2O$ and $[Ni(c\text{-chxn})_3](ClO_4)_2\cdot H_2O$ were readily obtained by mixing 3 mmol of the ligand in methanol with 1 mmol of nickel(II) salt in water.

$[Ni(t\text{-chxn})_2(H_2O)_2]X_2$ ($X=Cl^-$ and NO_3^-): These complexes were synthesized according to the methods described in the literature.[4]

Measurements. The magnetic moments were measured with a Shimadzu MB-2 magnetic balance at room temperature. Measurements of the electronic spectra of the copper(II) complexes in solution and the temperature dependence on the ε of the diamagnetic nickel(II) complexes were carried out using a Hitachi 124 spectrophotometer. The absorption and reflectance spectra of the nickel(II) complexes were measured with a Hitachi EPS-3T spectrophotometer. The infrared spectra in the range of 600—4000 cm^{-1} were recorded with a JASCO IRA-2 spectrophotometer by means of the KBr disc method. The far-infrared spectra in the range of 200—600 cm^{-1} were recorded on a JASCO DS-710G spectrophotometer in Nujol mulls.

Results and Discussion

Properties of the Complexes. The results of the elemental analyses, the magnetic moments, and the colors of the complexes newly synthesized in the present study are listed in Table 1. The copper(II) complexes with Cl^- and Br^- have 1—2 moles of water, while those with NO_3^- and ClO_4^- are anhydrous. From the values of the magnetic moments, the copper(II) complexes may be considered to be mononuclear.

The facility of the nickel(II) complex formation depends on the geometrical structure of the ligand, as well

Table 1. Colors, elemental analyses, and magnetic moments of the complexes

Complex	Color[a]	Elemental analyses[b]			μ (B.M.)
		C%	H%	N%	
$Cu(c\text{-chxn})_2Cl_2\cdot H_2O$	V	37.98(37.81)	8.08(7.94)	14.94(14.71)	1.86
$Cu(c\text{-chxn})_2Br_2\cdot H_2O$	V	30.98(30.68)	6.57(6.44)	12.00(11.93)	1.87
$Cu(c\text{-chxn})_2(NO_3)_2$	V	34.75(34.65)	7.11(6.79)	20.55(20.20)	1.84
$Cu(c\text{-chxn})_2(ClO_4)_2$	V	29.11(29.37)	5.57(5.75)	11.26(11.41)	1.88
$Cu(t\text{-chxn})_2Cl_2\cdot 2H_2O$	V	35.93(36.13)	7.75(8.08)	14.35(14.04)	1.88
$Cu(t\text{-chxn})_2Br_2\cdot 2H_2O$	V	30.04(29.54)	6.87(6.61)	11.33(11.49)	1.84
$Cu(t\text{-chxn})_2(NO_3)_2$	V	34.70(34.65)	6.54(6.79)	20.53(20.20)	1.84
$Cu(t\text{-chxn})_2(ClO_4)_2$	V	29.69(29.37)	6.02(5.75)	11.27(11.41)	1.85
$[Ni(c\text{-chxn})_2]Cl_2$	Y	40.06(40.26)	7.93(7.88)	15.73(15.65)	dia
$[Ni(c\text{-chxn})_2]Br_2$	Y	31.83(32.25)	6.08(6.32)	12.53(12.54)	dia
$[Ni(c\text{-chxn})_2](NO_3)_2$	Y	34.87(35.06)	6.77(6.87)	20.59(20.44)	dia
$[Ni(c\text{-chxn})_2](ClO_4)_2$	OY	29.59(29.66)	5.97(5.81)	11.79(11.53)	dia
$[Ni(t\text{-chxn})_2(H_2O)_2]Br_2$	BV	30.15(29.85)	6.92(6.68)	11.40(11.60)	3.23
$[Ni(t\text{-chxn})_2(H_2O)_2](ClO_4)_2$	BV	27.59(27.61)	6.11(6.18)	10.77(10.73)	3.20
$[Ni(c\text{-chxn})_3]Cl_2\cdot 1.5H_2O$	V	43.15(43.30)	8.68(9.09)	16.45(16.83)	3.12
$[Ni(c\text{-chxn})_3]Br_2\cdot H_2O$	V	37.71(37.33)	7.78(7.66)	14.16(14.51)	3.03
$[Ni(c\text{-chxn})_3](NO_3)_2\cdot 0.5H_2O$	V	40.34(40.46)	8.25(8.11)	21.27(20.97)	3.15
$[Ni(c\text{-chxn})_3](ClO_4)_2\cdot H_2O$	V	35.02(34.97)	7.18(7.17)	13.88(13.59)	3.16

a) V=violet, BV=blue violet, Y=yellow, OY=orange yellow. b) Calculated values in parentheses.

as on the counter anion concerned. The diamagnetic nickel(II) complexes of *c*-chxn were preferentially synthesized by the reaction of a 1:2 molar ratio of nickel(II) salt and ligand in a methanol solution. Tsuchida[4] reported the preparation of two types of bis complexes, $[Nichxn_2]X_2$ ($X=Cl^-$, Br^-, and ClO_4^-) and $[Nichxn_2(H_2O)_2]X_2$ ($X=Cl^-$ and NO_3^-), and described the chxn as *t*-chxn. The synthetic method and the electronic and magnetic properties of $[Ni(c\text{-chxn})_2]X_2$ obtained here are almost the same as those of Tsuchida' s$[Nichxn_2]X_2$. Therefore, the $[Nichxn_2]X_2$ obtained by Tsuchida seems to consist of the *c*-chxn complexes formed with a small amount of the *cis* isomer contained in chxn.[3] On the other hand, the *t*-chxn ligand afforded paramagnetic dihydrated bis-complexes. The isolation of $[Ni(t\text{-chxn})_2(H_2O)_2]X_2$ ($X=Br^-$ and ClO_4^-) was a little more difficult than that of the same type of the complexes with Cl^- and NO_3^-, because less soluble $[Ni(t\text{-chxn})_3]X_2\cdot nH_2O$ substances were precipitated during the syntheses of the bis-complexes. The $[Ni(t\text{-chxn})_2(H_2O)_2](ClO_4)_2$ shows a tendency to change to the orange yellow form in the dried atmosphere, losing almost 2 mol of coordinated water, which were, on the contrary, taken up by the complex when it was kept in the air. The $[Ni(c\text{-chxn})_3]Cl_2\cdot 1.5H_2O$ and $[Ni(c\text{-chxn})_3]Br_2\cdot H_2O$ are a little less stable than the corresponding tris-complexes of *t*-chxn and tend to change to yellow complexes when refluxed in methanol. The magnetic moments of all the nickel(II) complexes except for the yellow complexes of the *c*-chxn are around 3.1 B. M., and they indicate octahedral structures.

Electronic Spectra. The electronic spectra of the complexes were studied either in solution or in the solid state. Some typical spectra are shown in Figs. 1—2, and the numerical results, in Tables 2—3. The absorption spectra of the *c*-chxn and *t*-chxn complexes with

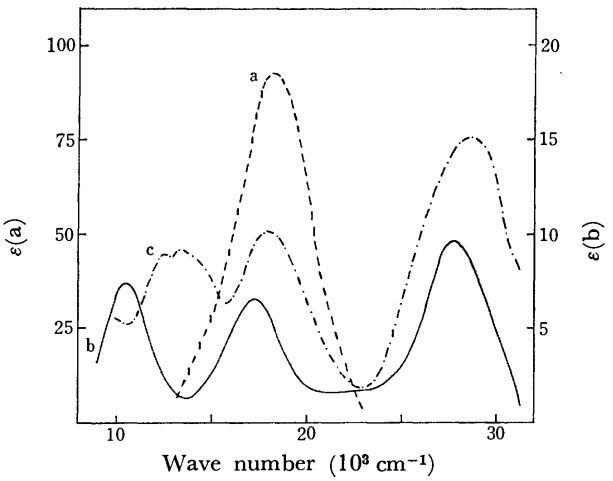

Fig. 1. Electronic spectra of (a) $Cu(t\text{-chxn})_2(ClO_4)_2$ (MeOH soln), (b) $[Ni(t\text{-chxn})_2(H_2O)_2](ClO_4)_2$ (MeOH soln), and (c) $[Ni(t\text{-chxn})_2(H_2O)_2](ClO_4)_2$ (Solid).

copper(II) halides show a d-d transition band at around 17700 cm^{-1}. The corresponding bands of the nitrate and perchlorate complexes appear in a somewhat shorter-wavelength region than those of the halide complexes. The reflectance spectra of the copper(II) complexes show a band in the region of 17900—19400 cm^{-1}. It is generally recognized that the electronic spectra of the copper(II) complexes of ethylenediamine derivatives exhibit a broad d-d band in the region of 14000—22000 cm^{-1}.[5] The structures of the copper(II) complexes obtained are considered to be tetragonally distorted octahedrons, with diamine ligands to form a square planar structure. The degrees of the tetragonal distortion in the structures of the complexes with NO_3^- and ClO_4^- seem to be larger than those of Cl^-

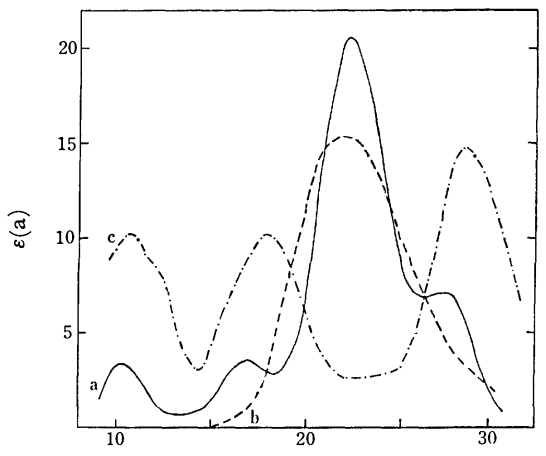

Fig. 2. Electronic spectra of (a) $[Ni(c\text{-chxn})_2](ClO_4)_2$ (H_2O soln), (b) $[Ni(c\text{-chxn})_2](ClO_4)_2$ (Solid), and (c) $[Ni(c\text{-chxn})_3](ClO_4)_2 \cdot H_2O$ (Solid).

and Br^-. The former two polyatomic anions were assumed to coordinate very weakly toward the copper(II) ion, because no appreciable distortion of the free ion was found in their infrared spectra. For the structures of the copper(II) complexes containing both X^- and H_2O, it was difficult to know which ligand, X^- or H_2O, coordinates in the tetragonal positions. The spectral properties suggest, however, that the steric configurations of the ligands have little effect on the coordination tendencies toward copper(II) ions. These results agree with the stability constants of the copper(II) complexes of the chxn isomers, whose values are nearly equal to each other.[6]

The electronic spectra of $[Ni(c\text{-chxn})_2]X_2$ ($X=Cl^-$, Br^-, NO_3^-, and ClO_4^-) in the solid state show a relatively strong band at around 22000 cm^{-1} which is characteristic of a square planar structure. In aqueous solutions of these complexes, three additional bands (Bands I, III, and IV) corresponding to the octahedral structure are observed. These results indicate that $[Ni(c\text{-chxn})_2]^{2+}$ and $[Ni(c\text{-chxn})_2(H_2O)_2]^{2+}$ coexist in water. The $[Ni(c\text{-chxn})_2(H_2O)_2]^{2+}$ cation can be assigned to the *cis* configuration because its spectral features are very similar to those of the $[Ni(en)_2(H_2O)_2]^{2+}$ cation which exists as the *cis* form in solution.[7] Thermochromism is found in aqueous solutions of four $[Ni(c\text{-chxn})_2]X_2$ complexes. As is shown in Fig.3, the intensity of Band V increases with an increase in the temperature. This reveals that the equilibrium between square planar and octahedral structures proceeds toward a dehydration reaction with a rise in the temperature. Similar behavior has been reported for ethylenediamine–nickel(II) complexes.[8]

The structures of the $[Ni(t\text{-chxn})_2(H_2O)_2]X_2$ ($X=Br^-$ and ClO_4^-) complexes in the solid state are regarded as tetragonally distorted octahedrons, with water molecules coordinating in the axial positions, since these spectra show a splitting of Band I, although the peak at the lower wave number has not been measured in the present study, and since the spectra resemble those of $[Ni(en)_2(H_2O)_2]X_2$ ($X=NO_3^-$ and ClO_4^-) and of *t*-chxn complexes of the same type previously

Table 2. Electronic spectra of the copper(II) complexes

Complex	ν 10^3 cm^{-1} (ε)	
	Solid	in Methanol
$Cu(c\text{-chxn})_2Cl_2 \cdot H_2O$	18.7	17.7(119)
$Cu(c\text{-chxn})_2Br_2 \cdot H_2O$	17.9	17.8(122)
$Cu(c\text{-chxn})_2(NO_3)_2$	19.0	18.3(110)
$Cu(c\text{-chxn})_2(ClO_4)_2$	19.4	18.3(107)
$Cu(t\text{-chxn})_2Cl_2 \cdot 2H_2O$	18.4	17.7(108)
$Cu(t\text{-chxn})_2Br_2 \cdot 2H_2O$	17.9	17.8(105)
$Cu(t\text{-chxn})_2(NO_3)_2$	19.2	18.3(91)
$Cu(t\text{-chxn})_2(ClO_4)_2$	18.7	18.3(93)

Table 3. Electronic spectra of the nickel(II) complexes

Complex	State	ν 10^3 cm^{-1} (ε)				
		I	II	III	IV	V
$[Ni(c\text{-chxn})_2]Cl_2$	Solid	—	—	—	—	22.6
	H_2O[a]	10.3(4.9)	—	17.1(4.2)	27.4(7.8)	22.4(21.1)
$[Ni(c\text{-chxn})_2]Br_2$	Solid	—	—	—	—	22.3
	H_2O[a]	10.4(3.3)	—	17.1(3.5)	27.0(7.7)	22.2(21.9)
$[Ni(c\text{-chxn})_2](NO_3)_2$	Solid	—	—	—	—	22.8
	H_2O[a]	10.3(4.6)	—	17.1(4.7)	27.0(9.2)	22.2(22.5)
$[Ni(c\text{-chxn})_2](ClO_4)_2$	Solid	—	—	—	—	21.8
	H_2O[a]	10.4(3.3)	—	16.9(3.6)	27.4(7.1)	22.2(20.7)
$[Ni(t\text{-chxn})_2(H_2O)_2]Br_2$	Solid	13.0	12.2	17.4	28.1	—
$[Ni(t\text{-chxn})_2(H_2O)_2](ClO_4)_2$	Solid	13.3	12.5	18.0	28.6	—
	MeOH	10.5(7.4)	—	17.1(6.6)	27.8(9.7)	—
$[Ni(c\text{-chxn})_3]Cl_2 \cdot 1.5H_2O$	Solid	10.6	12.2[b]	17.7	28.1	—
	MeOH	10.6(7.5)	12.3[b]	17.5(7.9)	28.1(12.1)	—
$[Ni(c\text{-chxn})_3]Br_2 \cdot H_2O$	Solid	10.6	12.2[b]	17.6	28.2	—
$[Ni(c\text{-chxn})_3](NO_3)_2 \cdot 0.5H_2O$	Solid	10.6	12.3[b]	17.8	28.4	—
$[Ni(c\text{-chxn})_3](ClO_4)_2 \cdot H_2O$	Solid	10.9	12.3[b]	17.8	28.4	—

a) The values of ε vary with the temperature. b) Shoulder.

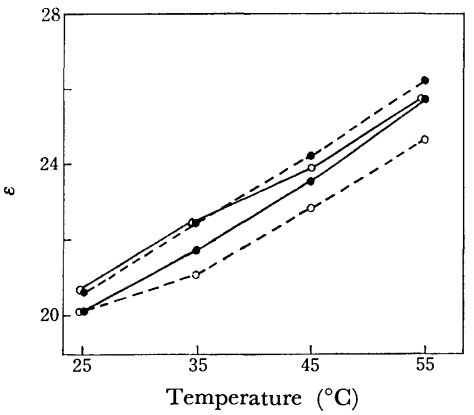

Fig. 3. Temperature dependence of the ε of Band V in the electronic spectra of the nickel(II) complexes (H_2O soln).
●(——): $[Ni(c\text{-chxn})_2]Cl_2$, ●(---): $[Ni(c\text{-chxn})_2]Br_2$, ○(——): $[Ni(c\text{-chxn})_2](ClO_4)_2$, ○(---): $[Ni(c\text{-chxn})_2](NO_3)_2$.

reported.[4,7] In a methanol solution, they are transformed to the *cis* form as well as $[Ni(c\text{-chxn})_2(H_2O)_2]^{2+}$.

The spectra of a series of tris-complexes of *c*-chxn have three main peaks typical of octahedrally coordinated nickel(II). Although these structures are analogous to those of the *t*-chxn and ethylenediamine complexes, the tris-complexes of *c*-chxn are thermodynamically less stable and the successive stability constant, k_3, has not been measured.[6] The instability of the tris-complexes of the *c*-chxn may be ascribable to the configuration of the ligand. The structures of the tris-complexes of *c*-chxn are more puckered due to the axial amino groups than those of the *t*-chxn. Similarly, the fact that hardly no paramagnetic bis-complexes of the *c*-chxn were obtained may also be explained by their unfavorable *cis* form in solution.

Infrared Spectra. All the nickel(II) complexes with the NO_3^- group show a broad strong absorption near 1350 cm^{-1} in their infrared spectra and seem to contain free nitrate ions.[9] Similarly, the $[Ni(c\text{-chxn})_2](ClO_4)_2$, $[Ni(t\text{-chxn})_2(H_2O)_2](ClO_4)_2$, and $[Ni(c\text{-chxn})_3](ClO_4)_2\cdot H_2O$ complexes were assumed to have ionic perchlorate ions on the basis of the ν_{Cl-O} band at around 1080 cm^{-1}.[10] Therefore, in octahedral $[Ni(t\text{-chxn})_2(H_2O)_2](ClO_4)_2$, water molecules were regarded as coordinating to the nickel(II) ion. The ν_{O-H} bands, overlapping the two ν_{N-H} bands, were observed in a lower frequency region than that of water of crystallization. In the spectra of the copper(II) complexes containing NO_3^- and ClO_4^-, hardly any splitting of ν_{N-O} and ν_{Cl-O} was observed.

Table 4 summarizes the infrared frequencies of these complexes. The ν_{N-H} frequencies are found to shift toward higher frequencies in the order of $Cl^- \leqq Br^- < NO_3^- < ClO_4^-$. This shift is considered to arise mainly from the hydrogen bond between the amino group and the anion. The δ_{NH_2} of the bromide complexes shifted to frequencies lower by 2—11 cm^{-1} than those of the corresponding chloride complexes. The deformation frequency may be affected by the strength of the M–N bond and the structural difference of the complexes, in addition to the extent of the hydrogen bond; hence, a systematic trend of band shifts has not been deduced for all the complexes prepared. The rocking modes of the NH_2 groups, which were assigned by means of the deuteration of the representative complexes, are distinctly metal-sensitive as has been described in the literature.[10] Figure 4 illustrates some typical far-infrared spectra of the 1:2 copper(II) and nickel(II) complexes. The assignment of the metal nitrogen stretching bands has been subject to great confusion; however, two bands located at 370—420 and 240—280 cm^{-1} have been found to be fairly metal-sensitive. These bands are illustrated as (A) and (B) in Fig. 4 and are summarized in the last two columns in Table 4. Lever and Mantovani[11] studied the far-infrared spectra of metal complexes of ethylenediamine

Table 4. The main infrared bands of the bis-complexes (cm^{-1})

Complex	ν_{N-H}	δ_{NH_2}	ρ_{rNH_2}	Unassigned
$Cu(c\text{-chxn})_2Cl_2\cdot H_2O$	3210, 3120[a]	1593	—[b]	417 282
$Cu(c\text{-chxn})_2Br_2\cdot H_2O$	3220, 3130[a]	1582	—[b]	417 288
$Cu(c\text{-chxn})_2(NO_3)_2$	3310, 3260, 3170	1602, 1590 sh	730	420 288
$Cu(c\text{-chxn})_2(ClO_4)_2$	3340, 3300	1603, 1592	734	418 285
$Cu(t\text{-chxn})_2Cl_2\cdot 2H_2O$	3270, 3230, 3150[a]	1592	—[b]	418 283
$Cu(t\text{-chxn})_2Br_2\cdot 2H_2O$	3280, 3230, 3150[a]	1592, 1580	—[b]	418 300
$Cu(t\text{-chxn})_2(NO_3)_2$	3340, 3290, 3170	1603	733	420 293
$Cu(t\text{-chxn})_2(ClO_4)_2$	3340, 3290, 3170 sh	1592	711	420 289
$[Ni(c\text{-chxn})_2]Cl_2$	3190, 3090	1605, 1595	665	382 259
$[Ni(c\text{-chxn})_2]Br_2$	3200, 3100	1598, 1588	662	379 251
$[Ni(c\text{-chxn})_2](NO_3)_2$	3260, 3170	1602	660	378 245
$[Ni(c\text{-chxn})_2](ClO_4)_2$	3330, 3180	1600	664	371 240
$[Ni(t\text{-chxn})_2(H_2O)_2]Cl_2$	3340, 3260, 3180[a]	1605	669 sh, 661	408 278
$[Ni(t\text{-chxn})_2(H_2O)_2]Br_2$	3330, 3270, 3170[a]	1603	668 sh, 661	409 276
$[Ni(t\text{-chxn})_2(H_2O)_2](NO_3)_2$	3350, 3290, 3200 sh[a]	1598	692, 670 sh	412 280
$[Ni(t\text{-chxn})_2(H_2O)_2](ClO_4)_2$	3360, 3300, 3180 sh[a]	1596	660	412 276

sh = shoulder. a) These bands seem to be overlapped with the neighboring ν_{O-H} bands. b) 1—2 bands were observed assignable to ρ_{rNH_2} or ρ_{rH_2O} in the 650—750 cm^{-1} region.

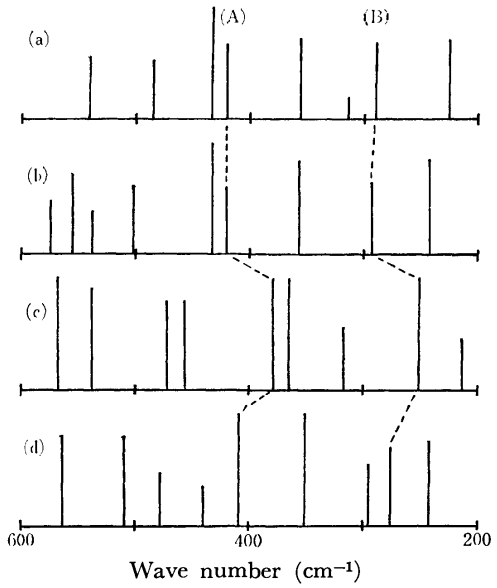

Fig. 4. Observed bands in the infrared spectra in the region between 200 and 600 cm^{-1}. (a): $Cu(c\text{-chxn})_2(NO_3)_2$, (b): $Cu(t\text{-chxn})_2(NO_3)_2$, (c): $[Ni(c\text{-chxn})_2]Br_2$, (d): $[Ni(t\text{-chxn})_2(H_2O)_2]Br_2$.

and its derivatives extensively and assigned the peaks in the regions of 403—421 and 309—331 cm^{-1} to ν_{Cu-N}, while the peaks in the region of 275—395 cm^{-1} were assigned to ν_{Ni-N}. Omura *et al.*[12] assigned the two bands at 412 and 472 cm^{-1} to the ν_{Cu-N} of $[Cu(en)_2]^{2+}$. Therefore, the bands observed around 370—420 cm^{-1} may be regarded one consisting dominantly of the ν_{M-N} band. The other lower metal-sensitive bands are supposed to be characteristic of the δ_{NMN} vibration, considering the values of the same type of complex. It is of interest that the frequency order of the metal-sensitive bands is $Cu(t\text{-chxn})_2X_2 > Cu(c\text{-chxn})_2X_2 > [Ni(t\text{-chxn})_2(H_2O)_2]X_2 > [Ni(c\text{-chxn})_2]X_2$, which is consistent with the order of the stability constants.

The authors would like to thank Dr. Noboru Nakayama of the Goverment Industrial Institute, Nagoya, for the use of a Shimadzu MB-2 magnetic balance, and Dr. Kenji Yoshimoto of the Aichi Environmental Research Center, for the use of a JASCO DS-710G infrared spectrophotometer. Thanks are also due to Misses Masae Ishiguro and Shizuko Iwauchi of the Analytical Center of the Nagoya City University for their elemental analyses.

References

1) Part III of this series: R. Saito and Y. Kidani, *Nippon Kagaku Kaishi*, **1975**, 1734.
2) For example (a) F. S. Treptow, *Inorg. Chem.*, **5**, 1593 (1966); (b) H. Ito, J. Fujita, and K. Saito, *Bull. Chem. Soc. Jpn.*, **40**, 2584 (1967); (c) E. Pedersen, *Acta Chem. Scand.*, **24**, 3362 (1970); (c) M. J. Harding, S. F. Mason, and B. J. Peart, *J. Chem. Soc., Dalton Trans.*, **1973**, 955.
3) R. Saito and Y. Kidani, *Chem. Lett.*, **1976**, 123.
4) M. Tsuchida, *Natural Science Report Ochanomizu Univ.*, **24**, 13 (1972).
5) I. M. Procter, B. J. Hathaway, and P. Nicholls, *J. Chem. Soc., A*, **1968**, 1678.
6) C. R. Bertsch, W. C. Fernelius, and B. P. Block, *J. Phy. Chem.*, **62**, 445 (1958).
7) M. E. Farago, J. M. James, and V. C. G. Trew, *J. Chem. Soc., A*, **1967**, 820.
8) K. Sone and M. Kato, *Z. Anorg. Allg. Chem.*, **301**, 277 (1959).
9) N. F. Curtis and Y. M. Curtis, *Inorg. Chem.*, **4**, 804 (1965).
10) K. Nakamoto, "Infrared Spectra of Inorganic and Coordination Compounds," 2nd ed, Wiley-Interscience, New York (1970).
11) B. P. Lever and E. Mantovani, *Inorg. Chem.*, **10**, 817 (1971).
12) Y. Omura, I. Nakagawa, and T. Shimanouchi, *Spectrochim. Acta, Part A*, **27**, 2227 (1970).

Determination of Micro Amounts of Polythionates. X. Spectrophotometric Determination of Micro Amounts of Pentathionate in Mixtures with Thiosulfate and Sulfite by Means of Its Sulfitolysis

Tomozo Koh, Kazuo Taniguchi, and Iwaji Iwasaki*

Department of Chemistry, Faculty of Science, Tokai University, Hiratsuka, Kanagawa 259-12

**Department of Chemistry, Faculty of Science, Toho University, Funabashi, Chiba 274*

(Received June 2, 1977)

An accurate method has been proposed for the determination of pentathionate in mixtures with thiosulfate and sulfite. The method is based on the formation of thiosulfate equivalent to the pentathionate, and the spectrophotometric determination of excess iodine for the reaction with the thiosulfate formed. The conditions for pentathionate to be quantitatively converted into thiosulfate were established by varying pH, reaction time, and amounts of sulfite. The method can be successfully applied to the determination of pentathionate, thiosulfate, and sulfite when they are mixed in various ratios, giving a relative standard deviation of 0.82% at the 0.5 μmol level of pentathionate in a 10.0 cm^3 sample solution in the presence of 0.5 μmol of thiosulfate and 0.25 μmol of sulfite.

When polythionates are formed in nature like hot springs, or in Wackenroder's solution obtained when hydrogen sulfide is passed into a solution of sulfite, various sulfur species, such as sulfite, thiosulfate, sulfide, sulfate, and free sulfur, can be simultaneously present with polythionates.[1] Renewed interest has arisen in the procedure for determination of micro amounts of polythionates in mixtures with other sulfur compounds, for the clarification of the chemical behavior of sulfur compounds in hot springs or in Wackenroder's solutions. Chapman and Beard have proposed a procedure[2] for the separation and determination of the polythionates in Wackenroder's solution by high-speed liquid chromatography, and Blasius and Münch a coulometric method[3] for polythionates. The reactions of polythionates (tri-, tetra-, penta-, and hexathionate) with cyanide, sulfite, sulfide, and hydroxide should be studied in detail for determining a specific polythionate in the presence of other polythionates.[4]

In regard to the cyanolysis of polythionates, various investigations have been made, the methods for the determination of trithionate,[5-8] tetrathionate,[7-12] pentathionate,[12,13] and hexathionate,[12,14] based on the formation of thiocyanate, being proposed. As a result of these investigations, a method[15] for the determination of polythionates in mixtures with each other was developed, based on the photometric determination of different amounts of thiocyanate formed by the cyanolysis of polythionate in the presence or in the absence of copper(II) ions. A method for determining total amounts of polythionates in mixtures,[16] based on the spectrophotometric measurement of excess iodine for thiosulfate formed by the cyanolysis of polythionates, was also devised.

With respect to the sulfitolysis of polythionates, methods have been described for the determination of tetrathionate[17] and hexathionate,[4] based on the consumption of iodine by the thiosulfate formed. However, no consideration has been given to the spectrophotometric determination of pentathionate by means of its sulfitolysis. The reaction

$$S_5O_6^{2-} + 2SO_3^{2-} = 2S_2O_3^{2-} + S_3O_6^{2-} \quad (1)$$

was investigated in detail and the conditions under which pentathionate is completely converted into thiosulfate were established. Simultaneous sulfitolysis of both pentathionate and hexathionate could be quantitative only under strict conditions. The present method is based on the formation of thiosulfate equivalent to pentathionate, and on the spectrophotometric measurement of excess iodine for the thiosulfate. A procedure for the analysis of mixtures of pentathionate, thiosulfate and sulfite is also described.

Experimental

Apparatus. Spectrophotometric measurements were carried out with a Shimadzu Model QV-50 spectrophotometer with 10-mm quartz cells. pH Measurements were made with a Hitachi-Horiba Model M-7 pH meter.

Reagents. All chemicals except for pentathionate, were of analytical grade and used without further purification.

Potassium Pentathionate was prepared as described by Goehring and Feldmann.[18] The pentathionate obtained was recrystallized twice in an acid medium of 0.5 M (M=mol/dm^3) hydrochloric acid, and then dried at room temperature before storage at -10 ± 2 °C. The water content was estimated by Karl Fischer method to be 10.48% including the water of crystallization. The pentathionate was confirmed to be pure enough for the present purpose; its purity was estimated by determining the total potassium and sulfur contents.[13]

Standard Pentathionate Solution of 1.0×10^{-3} M was prepared by dissolving 186.8 mg of the potassium pentathionate (water content 10.48%) in redistilled water, and then diluting it to 500 cm^3. The standard pentathionate solution was stored at 5 ± 2 °C.

Standard Sulfite Solution was prepared by dissolving sodium hydrogensulfite in freshly boiled and cooled redistilled water, and standardized by iodimetry. Working standards were obtained by appropriate dilution. The sulfite solution (0.15 M), which was not standardized, proved useful for the sulfitolysis of pentathionate 2 weeks after its preparation.

Standard Thiosulfate Solution was prepared by dissolving sodium thiosulfate pentahydrate in freshly boiled and cooled redistilled water containing a small amount of sodium carbonate as a stabilizer, and standardized by iodimetry a week after preparation. Working solutions were prepared by suitable dilution. These standards were used to confirm stoichiometry and completion of the reaction of pentathionate with sulfite.

Standard Iodate-Iodide Solution was prepared by adding 50.0 cm^3 of 1.67×10^{-3} M standard iodate to a solution containing 0.2 g of sodium carbonate and 72.2 g of potassium iodide,

and diluted to 500 cm³ to give 1.67×10^{-4} M iodate in a 0.87 M iodide solution.

Iodide Solution of 0.87 M was prepared by dissolving 72.2 g of potassium iodide in redistilled water containing 0.2 g of sodium carbonate, and then diluting it to 500 cm³.

Buffer Solution series are as follows: acetic acid (0.1, 0.5, or 1 M) and sodium acetate (0.1, 0.5, or 1 M), sodium dihydrogenphosphate (0.2 M) and sodium hydroxide (0.2 M), sodium hydrogencarbonate (0.1, 0.3, or 0.5 M) and sodium carbonate (0.05, 0.3, or 0.5 M), and sodium monohydrogenphosphate (0.5 M) and sodium hydroxide (0.5 M). The buffer solutions (pH 9.9 and 3.5) used in Procedures A and B were prepared by mixing 50 cm³ of 0.3 M sodium carbonate with 50 cm³ of 0.3 M sodium hydrogencarbonate, and by mixing 80 cm³ of 0.5 M acetic acid with 5 cm³ of 0.5 M sodium acetate, respectively.

Acetic Acid Solution was prepared by diluting glacial acetic acid as required.

Formaldehyde Solution was prepared by suitable dilution of formalin.

Procedure A for the Amount of Pentathionate Alone. 1.8 cm³ of a carbonate buffer solution (pH 9.9), 2.0 cm³ of 0.15 M sulfite, and 10.0 cm³ of a sample solution containing pentathionate were placed in a 25-cm³ volumetric flask, the pH of the solution becoming 8.0. The mixture was allowed to stand at room temperature for 10 min, to convert pentathionate completely into thiosulfate, Then, 1.5 cm³ of an acetate buffer solution (pH 3.5) and 2.0 cm³ of 0.5 M formaldehyde were added to the reaction mixture. The pH of the solution was kept at 5.8. The mixture was then allowed to stand for 5 min to mask excess sulfite with formaldehyde completely. To this mixture were added 2.0 cm³ of 15 M acetic acid and 2.4 cm³ of 1.67×10^{-4} M standard iodate in a 0.87 M iodide solution, and the flask was filled to the mark with redistilled water. The contents were mixed well, and the absorbance of the solution of iodine-iodide complex was measured against distilled water at 350 nm within 10 min after the addition of the standard iodate-iodide solution.

An iodate-free reagent blank was prepared by addition of 2.4 cm³ of 0.87 M iodide in place of 2.4 cm³ of 1.67×10^{-4} M standard iodate in a 0.87 M iodide solution and by the same treatment as in the above procedure. The absorbance of this blank was subtracted from all the absorbances obtained.

Procedure B for Mixtures of Pentathionate, Thiosulfate, and Sulfite. Three reaction mixtures were prepared in 25-cm³ volumetric flasks as follows.

Procedure B-I for Total Amount of Pentathionate and Thiosulfate in the Mixtures: A 10.0-cm³ aliquot of the sample solution containing pentathionate, thiosulfate, and sulfite was treated as in Procedure A, in order to convert the pentathionate completely into thiosulfate. 1.5 cm³ of an acetate buffer solution (pH 3.5) and 2.0 cm³ of 0.5 M formaldehyde were then added to the reaction mixture, which was allowed to stand for 5 min to mask the sulfite completely.

Procedure B-II for the Amount of Thiosulfate in the Mixtures: 1.8 cm³ of a carbonate buffer solution (pH 9.9), a 10.0-cm³ aliquot of the sample solution, 1.5 cm³ of an acetate buffer solution (pH 3.5), and 2.0 cm³ of 0.5 M formaldehyde were placed in a 25-cm³ volumetric flask, and the resulting mixture was allowed to stand for 5 min.

Procedure B-III for Total Amount of Thiosulfate and Sulfite in the Mixtures: A 10.0-cm³ aliquot of the sample solution and 1.5 cm³ of an acetate buffer solution (pH 3.5) were placed in a 25-cm³ volumetric flask.

Finally, 2.0 cm³ of 15 M acetic acid and 2.4 cm³ of 1.67×10^{-4} M standard iodate in a 0.87 M iodide solution were added to each mixture. The three flasks were then filled to the mark with redistilled water. The contents were mixed thoroughly and the absorbance of the solution of iodine-iodide complex was measured against distilled water at 350 nm.

Results and Discussion

Calibration Plots. A series of standard solutions of pentathionate and thiosulfate were treated as in Procedure A. The resulting graphs are shown in Fig. 1. According to Eq. 1, when 1 mol of pentathionate undergoes sulfitolysis, 2 mol of thiosulfate are formed. Thus, if pentathionate is completely converted into thiosulfate stoichiometrically, the calibration plot of pentathionate should coincide with that of thiosulfate when the molar concentration scale for thiosulfate is drawn to one second of the scale for pentathionate concentration. Figure 1 shows that pentathionate is quantitatively converted into thiosulfate according to Eq. 1.

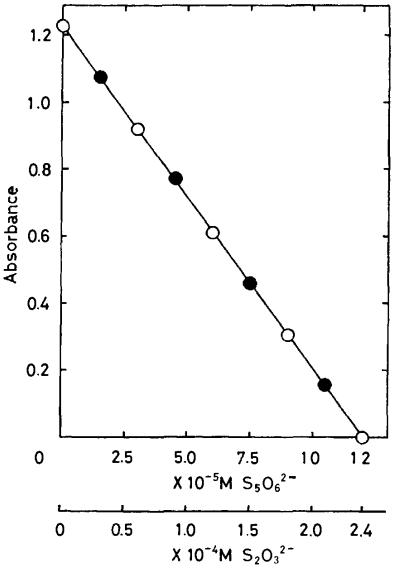

Fig. 1. Calibration plots for pentathionate and thiosulfate.
○: $S_5O_6^{2-}$; ●: $S_2O_3^{2-}$.

Rate of Sulfitolysis of Pentathionate. The rate was studied at both 5 °C and room temperature. The results are given in Tables 1 and 2. At pH 6.5, 8.0, and 8.2, the absorbance which was in complete agreement with the expected value was reached in 20 min at both 5 °C and room temperature, in 4 min at 5 °C and in 3 min at room temperature, and in 3 min at both 5 °C and room temperature, respectively, and then remained constant over different intervals of time. Higher absorbances then ensued as a result of the reaction of thiosulfate formed with the excess sulfite as shown in Eq. 2:

$$S_2O_3^{2-} + 4SO_3^{2-} + 6H^+ = 2S_3O_6^{2-} + 3H_2O \quad (2)$$

deviating from the expected value. The rate of sulfitolysis of pentathionate was little affected by temperature. Thus, pentathionate was allowed to react with sulfite at room temperature.

Table 1. Rate of sulfitolysis of pentathionate at 5°C

t / min	Absorbance pH 6.5 7.5×10^{-5} M $S_5O_6^{2-}$	pH 8.0 7.5×10^{-5} M $S_5O_6^{2-}$	pH 8.2 7.5×10^{-5} M $S_5O_6^{2-}$
	0.456[a)]	0.454[a)]	0.456[a)]
1	0.737	0.546	0.504
3	0.653	0.478	0.459
4	0.612	0.460	0.456
5	0.584	0.455	0.455
10	0.469	0.456	0.455
20	0.455	0.454	0.454
30	0.456	0.456	0.455
40	0.455	0.455	0.456
50	0.457	0.458	0.455
60	0.458	0.460	0.458
70	0.458	0.462	0.460
80	0.466	0.467	0.465
90	0.480	0.470	0.469

a) Absorbance for 1.5×10^{-4} M $S_2O_3^{2-}$.

Table 2. Rate of sulfitolysis of pentathionate at room temperature

t / min	Absorbance pH 6.5 7.5×10^{-5} M $S_5O_6^{2-}$	pH 8.0 7.5×10^{-5} M $S_5O_6^{2-}$	pH 8.2 7.5×10^{-5} M $S_5O_6^{2-}$
	0.454[a)]	0.455[a)]	0.455[a)]
1	0.636	0.490	0.482
3	0.536	0.460	0.457
4	0.524	0.457	0.456
5	0.503	0.455	0.454
10	0.465	0.455	0.455
20	0.455	0.455	0.455
30	0.455	0.455	0.455
40	0.458	0.456	0.455
50	0.460	0.459	0.460
60	0.461	0.460	0.460
70	0.468	0.466	0.465
80	0.474	0.473	0.466
90	0.486	0.480	0.475

a) Absorbance for 1.5×10^{-4} M $S_2O_3^{2-}$.

Effect of pH. In measuring the effect of pH on the sulfitolysis of pentathionate, the reaction was carried out for 10 min at various pH values. Figure 2 shows that pentathionate was quantitatively converted into thiosulfate in the pH range 6.9—8.2. A decrease in absorbance at higher pH levels was thought to be caused by the alkaline decomposition of pentathionate,[19] in addition to its sulfitolysis, as follows.

$$2S_5O_6^{2-} + 6OH^- = 5S_2O_3^{2-} + 3H_2O \quad (3)$$

The optimal pH range could be extended to a lower pH value by lengthening the sulfitolysis time; for instance, it was in the pH range 6.5—8.2 when sulfitolyzed for 20 min. However, the sulfitolysis time cannot be made any longer at the lower pH value, since the

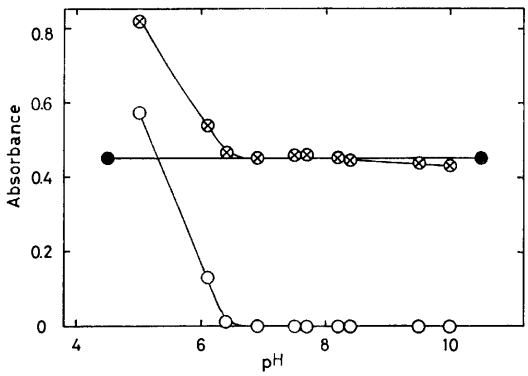

Fig. 2. Effect of pH on the sulfitolysis of pentathionate.
●: 1.5×10^{-4} M $S_2O_3^{2-}$; ⊗: 7.5×10^{-5} M $S_5O_6^{2-}$; ○: 1.2×10^{-4} M $S_5O_6^{2-}$.

lower the pH of the solution, the faster the reaction rate of thiosulfate formed with the sulfite.

The conditions under which sulfitolysis of polythionates goes to stoichiometric completion must be established to determine specific polythionate in mixtures of the polythionates. An optimal pH for the sulfitolysis of hexathionate was found to be in the range 7.5—9.5[4] when sulfitolyzed for 10 min. Therefore, in so far as the pH of the reaction solution is kept in the range 7.5—8.2, the sulfitolysis of both penta- and hexathionate will be quantitative. In fact, the calibration plots for penta- and hexathionate were, respectively, in exact accordance with that for thiosulfate when plotted in terms of equivalent concentrations, demonstrating the fact that sulfitolysis of both the polythionates attained stoichiometric completion.

Effect of Amount of Sulfite. The extent of sulfitolysis of pentathionate can be affected by the concentra-

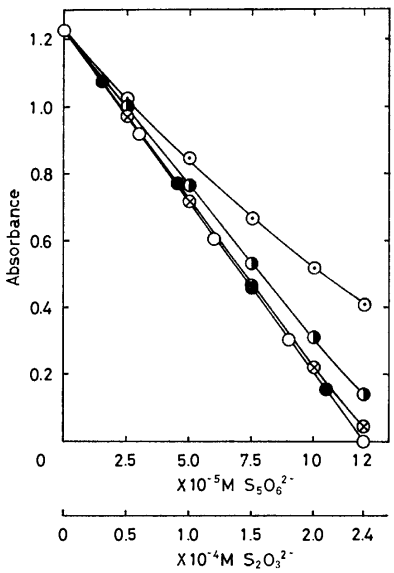

Fig. 3. Effect of amount of sulfite on the sulfitolysis of pentathionate.
⊙: $S_5O_6^{2-}$ with 2.0 cm³ of 0.01 M SO_3^{2-}; ◑: $S_5O_6^{2-}$ with 2.0 cm³ of 0.02 M SO_3^{2-}; ⊗: $S_5O_6^{2-}$ with 2.0 cm³ of 0.03 M SO_3^{2-}; ○: $S_5O_6^{2-}$ with 2.0 cm³ of 0.07, 0.1, or 0.15 M SO_3^{2-}; ●: $S_2O_3^{2-}$ with 2.0 cm³ of 0.15 M SO_3^{2-}.

tion of sulfite. In measuring the effect of the amount of sulfite on the conversion of pentathionate into thiosulfate, 2.0 cm^3 of 0.01, 0.02, 0.03, 0.07, 0.1, and 0.15 M sodium hydrogensulfite were employed, respectively. In all cases, the solutions were kept at pH 6.9—8.2, which is the optimal range for the sulfitolysis of pentathionate when sulfitolyzed for 10 min. As can be seen in Fig. 3, the sulfitolysis of pentathionate was incomplete with 2.0 cm^3 of 0.01, 0.02, or 0.3 M sulfite, because of an insufficient amount of sulfite. However, when 2.0 cm^3 of 0.07, 0.1, or 0.15 M was used, the calibration graph of pentathionate was linear and coincided exactly with that of standard thiosulfate. 2.0 cm^3 of 0.15 M sulfite was therefore used.

The sulfite used for the sulfitolysis consumed iodine completely, as a result of its reaction with iodine. However, it was confirmed that the excess sulfite was completely masked in the pH range 4.0—9.1, when 2.0 cm^3 of 0.5 M formaldehyde was added and the mixture solution was allowed to stand for 5 min. It is desirable to carry out spectrophotometric measurements within at least 10 min after the addition of standard iodate–iodide solution, because the reaction of iodine–iodide complex with the adduct formed ensued slowly.[4]

Analysis of Mixtures of Pentathionate, Thiosulfate, and Sulfite. The three sulfur compounds in mixtures give the following equivalents in three procedures:

Procedure B-I $\triangleq 2S_5O_6^{2-} + S_2O_3^{2-}$

Procedure B-II $\triangleq S_2O_3^{2-}$

Procedure B-III $\triangleq S_2O_3^{2-} + 2SO_3^{2-}$

The absorbance obtained by Procedure B-I corresponds to the sum of twice the pentathionate (see Eq. 1) and the thiosulfate in the mixtures, because sulfite is masked by the formaldehyde added for the removal of excess sulfite. The absorbance obtained by Procedure B-II, in which no sulfitolysis of pentathionate was carried out, corresponds to only the amount of thiosulfate in the mixtures. The absorbance obtained by Procedure B-III corresponds to the sum of the thiosulfate and twice the sulfite in the mixture solution.

Table 3. Analysis of pentathionate, thiosulfate, and sulfite in 10.0 cm^3

Taken (μmol)			Found (μmol)		
$S_5O_6^{2-}$	$S_2O_3^{2-}$	SO_3^{2-}	$S_5O_6^{2-}$	$S_2O_3^{2-}$	SO_3^{2-}
0.10	0.30	0.75	0.11	0.30	0.75
0.35	0.50	0.50	0.35	0.51	0.50
0.75	0.40	0.10	0.76	0.40	0.10
0.30	1.00	0.15	0.30	1.02	0.14
0.45	0.50	0.25	0.45	0.51	0.25
0.50	0.50	0.25	0.50	0.51	0.25

Table 4. Effect of diverse ions

Ion	Added as	Concn (ppm)	Absorbance	
			Reagent blank	6.0×10^{-5} M $S_5O_6^{2-}$
None		0	1.224	0.610
Na^+	Na_2SO_4	1000	1.224	0.609
K^+	K_2SO_4	1000	1.223	0.608
NH_4^+	$(NH_4)_2SO_4$	1000	1.224	0.613
Cu^{2+}	$CuSO_4\cdot5H_2O$	10	1.415	0.801
Mg^{2+}	$MgSO_4\cdot5H_2O$	1000	1.224	0.607
Ca^{2+}	$CaCO_3$	1000	1.234	0.615
Zn^{2+}	$ZnSO_4\cdot7H_2O$	1000	1.225	0.610
Cd^{2+}	$Cd(CH_3COO)_2\cdot2H_2O$	1000	1.224	0.610
Mn^{2+}	$MnSO_4\cdot5H_2O$	1000	1.223	0.612
Pb^{2+}	$Pb(CH_3COO)_2\cdot3H_2O$	10	1.264	0.652
Fe^{2+}	$Fe(NH_4)_2(SO_4)_2\cdot6H_2O$	50	1.654	0.936
Fe^{3+}	$Fe(NH_4)(SO_4)_2\cdot12H_2O$	10	1.341	0.747
		1	1.251	0.640
Al^{3+}	$Al_2(SO_4)_3\cdot18H_2O$	500	1.237	0.631
F^-	NaF	1000	1.224	0.611
Ci^-	NaCl	1000	1.224	0.608
Br^-	KBr	1000	1.225	0.608
I^-	KI	1000	1.223	0.609
NO_3^-	KNO_3	1000	1.246	0.631
NO_2^-	KNO_2	1	1.424	0.755
S^{2-}	$Na_2S\cdot9H_2O$	0.5	1.062	0.462
SO_4^{2-}	Na_2SO_4	1000	1.223	0.607
SO_3^{2-}	$NaHSO_3$	1000	1.223	0.610
$HAsO_4^{2-}$	$Na_2HAsO_4\cdot7H_2O$	1000	1.223	0.606
PO_4^{3-}	$Na_3PO_4\cdot12H_2O$	1000	1.224	0.608
Borate	H_3BO_3	1000	1.225	0.613
Silicate	(as SiO_2)	500	1.230	0.614

Moreover, the calibration graphs for pentathionate, thiosulfate, and sulfite were in full agreement with one another when plotted in terms of equivalent concentrations. Thus, the following equations can be obtained: $(S_5O_6^{2-})=(I-II)/2$, $(S_2O_3^{2-})=II$, and $(SO_3^{2-})=(III-II)/2$, where I, II, and III denote the molar concentration which was determined from the calibration graph for thiosulfate in Fig. 1 using the absorbance obtained by Procedures B-I, B-II, and B-III, respectively. Table 3 shows that the above technique can be successfully applied to the determination of a mixture of pentathionate, thiosulfate, and sulfite at various ratios.

The precision was estimated from six results for three 10.0-cm^3 aliquots of sample solutions containing 0.5 μmol of pentathionate, 0.5 μmol of thiosulfate, and 0.25 μmol of sulfite. The method gave a mean value of 0.498 μmol with a standard deviation of 0.0041, and a ralative standard deviation of 0.82% for pentathionate, 0.503 μmol with 0.0052 and 1.0% for thiosulfate, and 0.257 μmol with 0.0052 and 2.0% for sulfite.

Effect of Diverse Ions. The interference of various ions was checked under the conditions of Procedure A, both in the presence of pentathionate (6.0×10^{-5} M) and in its absence. The results are given in Table 4.

The present method is based on the spectrophotometric measurement of excess iodine such as triiodide for the thiosulfate formed by the sulfitolysis of pentathionate. Therefore, iron(III), copper(II), nitrite, or sulfide which can oxidize iodide or reduce iodine, interferes seriously with the determination of pentathionate. In the case of both lead(II) and iron(II), the positive error in absorbance may be attributed to the formation of lead–iodide complex which exhibits its absorption at 350 nm, and to the oxidation of iodide by the iron(III) ion produced by the air-oxidation of iron(II). Approximately 1000 ppm of almost all the other ions listed in Table 4 is allowable.

References

1) J. H. Karchmer, Ed., "The Analytical Chemistry of Sulfur and Its Compounds," Wiley Interscience, New York (1970), Part I, p. 238.
2) J. N. Chapman and H. R. Beard, *Anal. Chem.*, **45**, 2268 (1973).
3) E. Blasius and J. Münch, *Z. Anal. Chem.*, **261**, 198 (1972).
4) T. Koh and K. Taniguchi, *Anal. Chem.*, **46**, 1679 (1974).
5) P. J. Urban, *Z. Anal. Chem.*, **179**, 422 (1961).
6) T. Koh, A. Wagai, and Y. Miura, *Anal. Chim. Acta*, **71**, 367 (1974).
7) D. P. Kelly, L. A. Chambers, and P. A. Trudinger, *Anal. Chem.*, **41**, 898 (1969).
8) T. Mizoguchi and T. Okabe, *Bull. Chem. Soc. Jpn.*, **48**, 1799 (1975).
9) O. A. Nietzel and M. A. DeSesa, *Anal. Chem.*, **27**, 1839 (1955).
10) P. J. Urban, *Z. Anal. Chem.*, **180**, 110 (1961).
11) T. Koh and I. Iwasaki, *Bull. Chem. Soc. Jpn.*, **39**, 352 (1966).
12) T. Koh, N. Saito, and I. Iwasaki, *Anal. Chim. Acta*, **61**, 449 (1972).
13) T. Koh, *Bull. Chem. Soc. Jpn.*, **38**, 1510 (1965).
14) T. Koh and I. Iwasaki, *Bull. Chem. Soc. Jpn.*, **38**, 2135 (1965).
15) T. Koh and I. Iwasaki, *Bull. Chem. Soc. Jpn.*, **39**, 703 (1966).
16) T. Koh and K. Taniguchi, *Anal. Chem.*, **45**, 2018 (1973).
17) I. Iwasaki and S. Suzuki, *Bull. Chem. Soc. Jpn.*, **39**, 576 (1966).
18) M. Goehring and U. Feldmann, *Z. Anorg. Chem.*, **257**, 223 (1948).
19) M. Goehring, W. Helbing, and I. Appel, *Z. Anorg. Chem.*, **254**, 185 (1947).

Synthesis of Ylide Complexes of Cobalt and the Crystal Structure of [Benzoyl(1-pyridinio)methanide]chlorobis(dimethylglyoximato)cobalt(III) Toluene Solvate

Taro SAITO

Department of Chemistry, Faculty of Science, The University of Tokyo, Hongo, Bunkyo-ku, Tokyo 113

(Received July 4, 1977)

Bis(dimethylglyoximato)halogenocobalt(III) complexes of benzoyl(1-pyridinio)methanide were synthesized by a new kind of oxidative addition reaction of *N*-phenacylpyridinium halides to diaquabis(dimethylglyoximato)cobalt-(II) in air. The crystal structure of the [benzoyl(1-pyridinio)methanide]chlorobis(dimethylglyoximato)cobalt(III) toluene solvate was solved by single-crystal X-ray diffraction techniques. The crystals are monoclinic (space group $P2_1/c$), with cell dimensions of $a=11.41(1)$, $b=10.28(1)$, $c=27.50(3)$ Å, $\beta=116.3(1)°$, and $Z=4$. The final R was 0.068. The ylide ligand coordinates to cobalt through the ylide carbon, with a Co–C distance of 2.07(1) Å, and the chlorine atom is bonded to cobalt with a Co–Cl distance of 2.285(4) Å and with a C(ylide)–Co–Cl bond angle of 175.5(3)°. The dimethylglyoxime ligands and cobalt atom are co-planar to within 0.04 Å.

We have long been interested in the nature of ylide as ligands,[1] and we reported recently the synthesis of chelating ylide ligands and their palladium and platinum complexes.[2] Ylides are formally similar to such neutral ligands as amines or phosphines, but in another respect the ylide carbon-metal bonding formed upon coordination resembles the metal-carbon bond of metal alkyls. Because of this dual function, it seemed intriguing to synthesize ylide complexes of cobaloxime, which is known to form a wide variety of ER_3 (E=N or P) as well as alkyl (E=C) complexes,[3] and to gain insight into the nature of the ylide carbon-metal bonding. Thus, we have succeeded in the preparation of benzoyl-(1-pyridinio)methanide complexes of cobaloxime by a new type of oxidative addition reaction starting from the corresponding *N*-phenacylpyridinium halides; the structures were inferred from the infrared and ^1H NMR spectra.[4] In the present study, the crystal structure of the [benzoyl(1-pyridinio)methanide]chlorobis(dimethylglyoximato)cobalt(III) toluene solvate was determined by X-ray diffraction techniques, and the bonding of the ylide carbon to cobalt was confirmed.

Experimental

Synthesis. $[Co(dmgH)_2(H_2O)_2]$ (dmgH=dimethylglyoxime mono anion)[5] (6.5 g) and *N*-phenacylpyridinium chloride (4.2 g) were suspended in 99% ethanol (50 ml), and air was bubbled into the suspension for 30 min at 10 °C. The mixture became homogeneous, and then a brown solid was precipitated. The product was filtered, washed with ethanol (30 ml) and diethyl ether (30 ml), and dried *in vacuo*, (4.5 g). The infrared spectrum of the crude product indicated that it contained about 20% of $[pyCH_2COC_6H_5]^+[CoCl_2(dmgH)_2]^-$ (ν(CO) 1690 cm^{-1}) (py=pyridine). The product was dissolved in CH_2Cl_2 (250 ml), and diethyl ether (100 ml) was added very slowly to produce very fine crystals of $[CoCl(dmgH)_2(pyCHCOC_6H_5)]$, (2.5 g). $[CoBr(dmgH)_2(pyCHCOC_6H_5)]$ and $[CoI(dmgH)_2(pyCHCOC_6H_5)]$ were prepared in a similar fashion. The properties of these complexes are given in Table 1.

Preparation of the Crystal. $[CoCl(dmgH)_2(pyCHCOC_6H_5)]$ (0.5 g) was dissolved in warm CH_2Cl_2 (50 ml), and then toluene (30 ml) was slowly added and then filtered out. The solution was kept overnight at 5 °C, and the black crystals thus precipitated were filtered, washed with diethyl ether (10 ml), and dried. The ^1H NMR spectrum indicated that the crystals contained one mole toluene per mole of the complex.

Found: C, 54.7; H, 5.6; N, 11.4; Cl, 6.2%. Calcd for $C_{28}H_{33}ClCoN_5O_5$: C, 54.8; H, 5.4, N, 11.4; Cl, 5.8%.

Crystal Data. A single crystal with dimensions of *ca.* $0.45\times0.25\times0.15$ mm was used for the measurements of the diffraction intensities and unit-cell dimensions on a Rigaku automated four-circle diffractometer, by the use of graphite-monochromatized Mo $K\alpha$ radiation. The unit-cell constants were obtained by a least-squares refinement of the angular measurements of 25 reflections, but the results were not always satisfactory because of the weak intensities of the high-angle reflections.

$C_{21}H_{25}ClCoN_5O_5\cdot C_7H_8$, M=613.7, monoclinic, space group $P2_1/c$ from systematic absences: $h0l$, $l=2n+1$, $0k0$, $k=2n+1$. $a=11.14(1)$, $b=10.28(1)$, $c=27.50(3)$ Å, $\beta=116.3(1)°$, $V=2825$ Å^3, $Z=4$, $D_m=1.44$ g cm^{-3}, $D_x=1.44$ g cm^{-3}, $\mu=7.74$ cm^{-1} (Mo $K\alpha$), Mo $K\alpha$ radiation $\lambda=0.7107$ Å.

Data Collection. The intensity data were recorded by the ω-2θ scan technique, with a scan speed of 2° min^{-1}; background counts over 10 s were taken at each end of the scan. The intensities of 3 standard reflections measured every 50 reflections during the data collection did not vary by more than 4%. The intensities were measured up to 2θ 60°, and 1997 independent reflections with $F_o>3\sigma$ were used for the structure analysis. The data were corrected for Lorentz and polarization effects, but not for absorption.

Solution and Refinement of the Structure. The structure

Table 1. Elemental analysis, infrared, and ^1H NMR spectral properties of $[CoX(dmgH)_2(pyCHCOC_6H_5)]$

X	Elemental analysis Found (Calcd)%				IR(KBr) ν(CO) cm^{-1}	^1H NMR(CH_3CN) δ(CH) ppm
	C	H	N	X		
Cl	48.5(48.3)	4.9(4.8)	13.3(13.4)	6.6(6.8)	1654	5.62
Br	44.3(44.5)	4.4(4.5)	12.4(12.4)	14.9(14.1)	1641	5.55
I	40.5(41.1)	4.4(4.1)	11.5(11.4)		1640	5.60

was solved by the usual heavy-atom method. The position of the cobalt atom was determined from a Patterson synthesis, and all the non-hydrogen atoms were located by the subsequent Fourier syntheses. The positions of the atoms were refined by the block-diagonal least-squares method with anisotropic temperature factors. A difference-Fourier synthesis at the stage of $R=0.083$ revealed the positions of the ylide methine hydrogen, 13 aromatic hydrogens, and one hydrogen for each of the methyl groups of the dimethylglyoxime ligands, but no hydrogen atom was located for the methyl group of the toluene molecule or for the oxime groups. Further refinements including the calculated positions (l(C–H) 1.08 Å, $B=3$ Å^2) of the remaining aromatic hydrogen atoms and the methyl hydrogen atoms of the dimethylglyoxime ligands, using isotropic temperature factors for the hydrogen and anisotropic temperature factors for non-hydrogen atoms, reduced the final R factor to 0.068. The H–C–H and C–C–H bond angles were normal within the estimated standard deviations.

Atomic scattering factors were taken from Ref. 6, those of cobalt and chlorine being corrected for the real and imaginary parts of anomalous dispersion, using values from Ref. 7. A weighting scheme with $w=1$ for $|F_o|\geq 21.80$ on an absolute scale and $w=0.5$ in other cases was employed.

The calculations were performed on the HITAC 8700/8800 computer at the Computer Center of the University of Tokyo, using a local version of the UNICS programs.[8]

Results and Discussion

The present ylide complexes of cobaloxime are formed in the presence of air by the replacement of the two H_2O ligands in $[Co^{II}(dmgH)_2(H_2O)_2]$ with halogen and benzoyl(1-pyridinio)methanide. The reaciton seems to proceed according to the following scheme, although the reaction mechanism is not clear:

$$[Co^{II}(dmgH)_2(H_2O)_2] + [pyCH_2COC_6H_5]^+X^- + 1/4O_2 \longrightarrow [Co^{III}X(dmgH)_2(pyCHCOC_6H_5)] + 5/2H_2O.$$

The addition of halogen and the ylide ligands, which is accompanied by the oxidation of Co(II) to Co(III), may be described as a kind of oxidative addition reaction. This reaction, however, is somewhat different from the ordinary oxidative addition of X–Y molecules to Co(II), which results in the formation of two Co(III) species, such that [Co(II)]+X–Y→[Co(III)X]+[Co(III)Y].[9] The synthesis of ylide complexes directly from onium salts is advantageous because these salts are generally much more stable than the corresponding free ylides, and some palladium ylide complexes from phosphonium salts have been reported.[10] The present synthesis provides another example of the *in situ* synthesis of ylide complexes starting from onium salts.

The infrared spectra of the ylide complexes show ν(CO) at lower wave numbers than the corresponding *N*-phenacylpyridinium halides (*cf.* $[pyCH_2COC_6H_5]^+X^-$: 1693 cm^{-1} (X=Cl), 1695 cm^{-1} (X=Br), 1698 cm^{-1} (X=I), KBr disk); the lowering of ν(CO) is considered to indicate the bonding of the ylide carbon to the metal in keto-stabilized ylide complexes.[2] It has been reported that a platinum pyridinium propylide complex, $[PtCl_2(py)(pyCHCH_2CH_3)]$[11] shows an ylide methine proton signal at δ 5.67 in $CDCl_3$, which is near the positions of the signals of the present cobalt complexes. The methyl-proton signals of the dimethylglyoxime ligands at δ 1.9 are split into two absorptions in an intensity ratio of 1 : 1. This splitting may presumably be ascribed to the different magnetic environments of the methyl groups due to the presence of the asymmetric ylide carbon.[10]

Molecular and Crystal Structure. The numbering scheme employed in this paper is shown in Fig. 1. Figure 2 is a stereoview of the unit cell drawn by ORTEP. The final atomic parameters and their standard deviations are listed in Tables 2 and 3. Table 4 gives the bond distances, and Table 5, the bond angles within the molecule. The least-squares planes, dihedral angles, and vector-plane angles are given in Table 6.*

The results of the structure determination of the [benzoyl(1-pyridinio)methanide]chlorobis(dimethylgly-

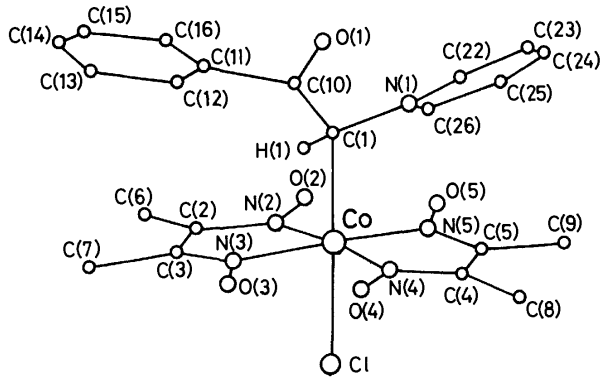

Fig. 1. Molecular structure of $[CoCl(dmgH)_2(pyCHCOC_6H_5)]$ and numbering scheme of atoms. The carbon atoms of toluene are not shown and they are numbered from C(31) to C(37).

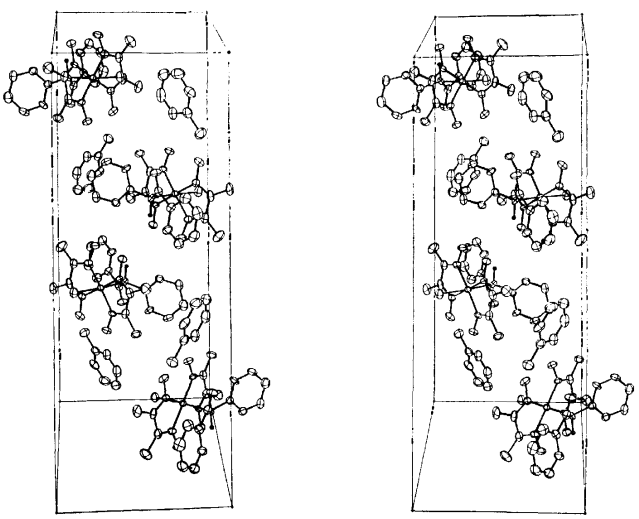

Fig. 2. Stereoview of a unit cell of $[CoCl(dmgH)_2(pyCHCOC_6H_5)]$. The b axis is horizontal to the right, the c axis is vertical, and the a axis is perpendicular coming toward the reader. The thermal ellipsoids are drawn at the 30% probability level (ORTEP).

* The observed and calculated structure factors are held by the office of the Chemical Society of Japan as Document No. 7805.

TABLE 2. ATOMIC COORDINATES ($\times 10^4$) AND ANISOTROPIC THERMAL PARAMETERS ($\times 10^3$) OF THE NON-HYDROGEN ATOMS, WITH THEIR ESTIMATED STANDARD DEVIATIONS IN PARENTHESES

The U_{ij}'s are defined by: $\exp[-2\pi^2(h^2a^{*2}U_{11}+k^2b^{*2}U_{22}+l^2c^{*2}U_{33}+2hka^*b^*U_{12}+2hla^*c^*U_{13}+2klb^*c^*U_{23})]$.

	x	y	z	U_{11}	U_{22}	U_{33}	U_{12}	U_{13}	U_{23}
Co	4703(1)	2699(1)	3838(1)	32(1)	34(1)	37(1)	0(1)	18(1)	−1(1)
Cl	6252(3)	1075(3)	4044(1)	46(2)	45(2)	84(2)	6(2)	36(2)	4(2)
N (1)	3848(8)	5487(9)	3589(4)	45(5)	41(6)	55(6)	3(5)	29(5)	−1(5)
N (2)	3396(8)	1535(8)	3377(4)	41(5)	40(5)	53(6)	3(5)	30(5)	2(5)
N (3)	4182(8)	1943(9)	4354(4)	41(5)	52(6)	53(6)	−1(5)	33(5)	0(5)
N (4)	6044(8)	3795(8)	4308(3)	46(5)	38(5)	28(5)	4(5)	19(4)	9(4)
N (5)	5271(8)	3379(8)	3333(3)	44(5)	44(6)	42(6)	2(4)	30(5)	−7(4)
O (1)	1547(7)	4119(8)	2842(3)	57(5)	86(7)	34(5)	−7(5)	16(4)	4(5)
O (2)	3069(7)	1377(8)	2842(3)	54(5)	65(6)	58(5)	−9(5)	26(4)	−28(5)
O (3)	4714(7)	2350(9)	4871(3)	78(5)	75(6)	42(5)	19(5)	36(4)	13(5)
O (4)	6319(7)	3969(7)	4832(3)	56(5)	56(5)	37(5)	−4(4)	14(4)	−7(4)
O (5)	4676(7)	3027(7)	2814(3)	67(5)	64(6)	43(5)	0(0)	32(4)	−12(4)
C (1)	3393(10)	4230(10)	3710(4)	34(6)	35(7)	40(7)	−1(5)	15(5)	15(5)
C (2)	2871(11)	739(11)	3603(5)	36(6)	33(7)	93(10)	3(5)	32(7)	−7(7)
C (3)	3347(10)	1026(11)	4188(5)	43(7)	39(7)	86(10)	9(6)	39(7)	5(7)
C (4)	6771(10)	4392(11)	4116(5)	29(6)	39(7)	76(9)	−5(5)	20(6)	−10(6)
C (5)	6271(10)	4139(10)	3534(5)	34(6)	39(7)	77(9)	−1(5)	29(6)	4(7)
C (6)	1863(12)	−282(12)	3290(6)	59(8)	45(8)	114(12)	−33(7)	45(8)	−19(8)
C (7)	2885(13)	266(15)	4528(6)	66(9)	89(11)	112(13)	3(9)	60(9)	33(10)
C (8)	7896(13)	5292(14)	4436(6)	66(9)	74(10)	89(11)	−19(8)	35(9)	−11(9)
C (9)	6885(12)	4742(13)	3185(5)	68(8)	71(9)	58(8)	−8(8)	42(7)	6(7)
C (10)	2021(11)	3898(11)	3345(5)	47(7)	42(7)	64(8)	−3(6)	25(7)	−9(7)
C (11)	1131(10)	3264(11)	3557(5)	30(6)	49(7)	57(8)	0(5)	21(6)	9(6)
C (12)	1338(11)	3463(12)	4091(5)	57(8)	63(8)	60(8)	7(7)	35(7)	11(7)
C (13)	390(12)	2893(13)	4223(5)	73(8)	65(9)	96(11)	−14(8)	58(8)	−6(8)
C (14)	−638(12)	2130(14)	3886(6)	64(8)	70(9)	97(10)	−1(8)	51(8)	12(9)
C (15)	−826(11)	1945(13)	3367(6)	40(7)	74(10)	104(11)	−25(7)	24(7)	−19(9)
C (16)	67(11)	2521(14)	3187(5)	60(7)	77(10)	67(8)	19(8)	21(7)	8(9)
C (22)	3721(11)	5742(11)	3079(5)	51(7)	57(8)	51(7)	6(6)	33(6)	22(6)
C (23)	4139(11)	6912(12)	2974(5)	61(7)	77(10)	51(8)	27(7)	36(7)	29(7)
C (24)	4701(12)	7820(13)	3384(6)	65(8)	58(8)	98(11)	9(8)	42(8)	4(9)
C (25)	4819(12)	7547(11)	3901(6)	63(7)	41(8)	87(9)	8(7)	34(7)	−1(8)
C (26)	4402(11)	6359(12)	3975(4)	50(7)	52(8)	50(8)	−1(6)	27(6)	−4(6)
C (31)	177(11)	2340(12)	1329(5)	59(7)	57(8)	74(8)	12(8)	38(7)	−6(8)
C (32)	−691(11)	2279(14)	779(5)	47(7)	76(9)	66(8)	18(8)	13(6)	−21(8)
C (33)	−442(16)	2962(16)	406(6)	131(13)	101(13)	75(10)	55(11)	54(10)	14(10)
C (34)	694(16)	3674(15)	553(6)	140(15)	76(11)	98(13)	38(11)	76(12)	21(10)
C (35)	1559(14)	3737(14)	1111(7)	87(11)	52(9)	144(15)	−8(8)	68(11)	−9(10)
C (36)	1333(13)	3078(12)	1489(6)	67(8)	46(8)	93(11)	−8(7)	34(8)	−7(7)
C (37)	−109(15)	1645(15)	1739(6)	114(13)	77(11)	100(13)	4(10)	73(11)	13(9)

oximato)cobalt(III) toluene solvate have proved that the complex is an ylide complex in which the ylide carbon coordinates to cobalt. The Co–C(1) bond length, 2.07 (1) Å, is close to the bond length of Co–C, 2.04 Å, in carbomethoxymethylbis(dimethylglyoximato)(pyridine)-cobalt(III),[12] one of the few alkyl cobaloxime complexes whose crystal structures have been described in the literature.[13] The alkyl moiety, CH_2COOCH_3, is comparable to benzoyl(1-pyridinio)methanide in that both have a carbonyl group adjacent to the carbon which is bonded to cobalt.

The ylide carbon C(1) is bonded to the N(1) of pyridine, the C(10) of the carbonyl group, and H(1) as well as cobalt, and the bond angles, Co–C(1)–N(1) 114.6(8)°, Co–C(1)–C(10) 112.7(7)° and N(1)–C(1)–C(10) 114.4(8)°, are a little larger than the normal tetrahedral angle of 109°28′; the deviation of C(1) from the plane (4) formed by N(1), C(10), and Co is 0.41 Å. The ylide methine hydrogen atom H(1) is clearly evident in the difference-Fourier map.

The cobalt atom and the four nitrogen atoms of the dimethylglyoxime ligands are planar to within 0.04 Å, The Co–N bond distances range from 1.86(1) to 1.92(1) Å, but we are not certain whether the difference of 0.06 Å, about six times the standard deviation, actually reflects the non-equivalence of the Co–N bonds. The Co–Cl bond distance is 2.285(4) Å, and the Cl···Co vector is almost perpendicular (89.2°) to the plane(1)

TABLE 3. ATOMIC COORDINATES ($\times 10^3$) AND ISOTROPIC THERMAL PARAMETERS OF THE HYDROGEN ATOMS, WITH THEIR ESTIMATED STANDARD DEVIATIONS IN PARENTHESES

	x	y	z	B(Å^2)
H (1)	351 (9)	432 (9)	413 (4)	1 (2)
H (12)	221 (12)	391 (13)	434 (5)	6 (3)
H (13)	53 (9)	324 (10)	450 (4)	2 (2)
H (14)	−130 (12)	174 (13)	407 (5)	6 (4)
H (15)	−148 (9)	134 (9)	304 (4)	1 (2)
H (16)	−11 (13)	263 (15)	286 (5)	8 (4)
H (22)	334 (9)	499 (10)	284 (4)	2 (3)
H (23)	400 (8)	703 (9)	266 (3)	1 (2)
H (24)	504 (11)	874 (12)	340 (4)	5 (3)
H (25)	527 (8)	821 (8)	413 (3)	0 (2)
H (26)	461 (8)	611 (9)	437 (3)	0 (2)
H (32)	−159 (10)	178 (11)	67 (4)	4 (3)
H (33)	−136 (15)	283 (17)	−5 (6)	11 (5)
H (36)	179 (10)	320 (10)	186 (4)	3 (3)
H (61)	159 (12)	−38 (13)	285 (5)	6 (4)
H (71)	221 (13)	−17 (14)	440 (5)	7 (4)
H (81)	801 (9)	558 (10)	475 (4)	2 (3)
H (91)	614 (12)	490 (13)	282 (5)	5 (4)

a) H(mn) is the hydrogen atom bonded to C(mn), while H(61), H(71), H(81), and H(91) are the methyl hydrogen atoms of the dimethylglyoxime ligands.

of the dimethylglyoxime ligands. The C(1)···Co vector is a little out of the perpendicular (85.6°), making the C(1)–Co–Cl bond angle 175.5(3)°. There is no indication that the carbonyl oxygen O(1) forms any significant hydrogen bonding with an oxime hydrogen atom of the dimethylglyoxime ligand, which in [CoCH-$(CH_3)COCH_3(dmgH)_2(py)$] was suspected to account for the lowering of the ν(CO) of the infrared spectra.[14] The C(10)–O(1) bond distance of 1.26 Å indicates an essentially double bond, but the lowering of the ν(CO) of 39 cm^{-1} in the ylide complex compared with that

TABLE 4. BOND LENGTHS (l/Å), WITH THEIR ESTIMATED STANDARD DEVIATIONS IN PARENTHESES

Co-Cl	2.285 (4)	C (10) - C (11)	1.50 (2)
Co-C (1)	2.07 (1)	C (11) - C (12)	1.40 (2)
Co-N (2)	1.88 (1)	C (12) - C (13)	1.39 (2)
Co-N (3)	1.92 (1)	C (13) - C (14)	1.36 (2)
Co-N (4)	1.86 (1)	C (14) - C (15)	1.36 (2)
Co-N (5)	1.90 (1)	C (15) - C (16)	1.42 (2)
N (2) - O (2)	1.36 (1)	C (16) - C (11)	1.40 (2)
N (3) - O (3)	1.34 (1)	C (31) - C (32)	1.39 (2)
N (4) - O (4)	1.35 (1)	C (32) - C (33)	1.37 (2)
N (5) - O (5)	1.33 (1)	C (33) - C (34)	1.36 (2)
N (2) - C (2)	1.31 (2)	C (34) - C (35)	1.41 (2)
N (3) - C (3)	1.26 (1)	C (35) - C (36)	1.35 (3)
N (4) - C (4)	1.30 (2)	C (36) - C (31)	1.39 (2)
N (5) - C (5)	1.27 (1)	C (31) - C (37)	1.49 (2)
C (2) - C (6)	1.50 (2)	C (12) - H (12)	1.0 (1)
C (3) - C (7)	1.48 (2)	C (13) - H (13)	0.8 (1)
C (4) - C (8)	1.49 (2)	C (14) - H (14)	1.1 (2)
C (5) - C (9)	1.54 (2)	C (15) - H (15)	1.1 (1)
C (2) - C (3)	1.48 (2)	C (16) - H (16)	0.8 (2)
C (4) - C (5)	1.47 (2)	C (22) - H (22)	1.0 (1)
C (1) - C (10)	1.45 (1)	C (23) - H (23)	0.8 (1)
C (1) - H (1)	1.1 (1)	C (24) - H (24)	1.0 (1)
O (2) - O (5) [a]	2.49 (1)	C (25) - H (25)	0.9 (1)
O (3) - O (4) [a]	2.48 (1)	C (26) - H (26)	1.0 (1)
C (10) - O (1)	1.26 (1)	C (32) - H (32)	1.0 (1)
C (1) - N (1)	1.48 (2)	C (33) - H (33)	1.2 (1)
N (1) - C (22)	1.37 (2)	C (36) - H (36)	0.9 (1)
C (22) - C (23)	1.37 (2)	C (6) - H (61)	1.1 (1)
C (23) - C (24)	1.38 (2)	C (7) - H (71)	0.8 (1)
C (24) - C (25)	1.40 (2)	C (8) - H (81)	0.9 (1)
C (25) - C (26)	1.35 (2)	C (9) - H (91)	1.0 (1)
C (26) - N (1)	1.32 (1)		

a) The oxygen atoms are probably bonded through an oxime hydrogen atom.

TABLE 5. BOND ANGLES (ϕ/°), WITH THEIR ESTIMATED STANDARD DEVIATIONS IN PARENTHESES

C (1) - Co - Cl	175.5 (3)	C (1) - C (10) - C (11)	120 (1)
N (2) - Co - N (3)	80.9 (4)	C (12) - C (11) - C (16)	122 (1)
N (3) - Co - N (4)	98.3 (4)	C (22) - N (1) - C (26)	120 (1)
N (4) - Co - N (5)	81.9 (4)	C (32) - C (31) - C (36)	118 (1)
N (5) - Co - N (2)	98.8 (4)	O (2) - N (2) - C (2)	118 (1)
Co - N (2) - C (2)	117.0 (9)	O (3) - N (3) - C (3)	122 (1)
Co - N (3) - C (3)	117.0 (9)	O (4) - N (4) - C (4)	119 (1)
Co - N (4) - C (4)	117.1 (9)	O (5) - N (5) - C (5)	124 (1)
Co - N (5) - C (5)	115.0 (9)	N (2) - C (2) - C (3)	112 (1)
Co - N (2) - O (2)	124.2 (7)	N (3) - C (3) - C (2)	113 (1)
Co - N (3) - O (3)	121.4 (7)	N (4) - C (4) - C (5)	111 (1)
Co - N (4) - O (4)	123.8 (7)	N (5) - C (5) - C (4)	115 (1)
Co - N (5) - O (5)	121.0 (7)	C (3) - C (2) - C (6)	125 (1)
Co - C (1) - N (1)	114.6 (8)	C (2) - C (3) - C (7)	122 (1)
Co - C (1) - C (10)	112.7 (7)	C (5) - C (4) - C (8)	125 (1)
Co - C (1) - H (1)	98 (6)	C (4) - C (5) - C (9)	123 (1)
N (1) - C (1) - C (10)	114.4 (8)	N (2) - C (2) - C (6)	123 (1)
H (1) - C (1) - N (1)	106 (6)	N (3) - C (3) - C (7)	125 (1)
H (1) - C (1) - C (10)	110 (6)	N (4) - C (4) - C (8)	124 (1)
C (1) - C (10) - O (1)	121 (1)	N (5) - C (5) - C (9)	122 (1)
O (1) - C (10) - C (11)	118 (1)		

Table 6.

(a) Displacements (l/Å) of relevant atoms from least-squares planes[a)]

Plane (1) [N(2), N(3), N(4), N(5)]
$-0.655X + 0.724Y - 0.216Z + 0.434 = 0$
Co 0.04, N(2) 0.00, N(3) 0.00, N(4) 0.00, N(5) 0.00, O(2) −0.02, O(3) 0.05, O(4) 0.07, O(5) 0.03, C(2) −0.15, C(3) −0.12, C(4) −0.13, C(5) −0.11, C(6) −0.25, C(7) −0.26, C(8) −0.20, C(9) −0.21

Plane (2) [N(1), C(22), C(23), C(24), C(25), C(26)]
$0.888X - 0.388Y + 0.249Z + 0.060 = 0$
N(1) −0.01, C(22) 0.01, C(23) 0.00, C(24) 0.00, C(25) −0.01, C(26) 0.01, C(1) −0.01

Plane (3) [C(11), C(12), C(13), C(14), C(15), C(16)]
$0.497X - 0.816Y + 0.293Z + 1.705 = 0$
C(11) 0.00, C(12) 0.01, C(13) −0.02, C(14) 0.01, C(15) 0.00, C(16) −0.01, C(10) −0.06

Plane (4) [N(1), C(10), Co]
$0.409X - 0.101Y - 0.907Z + 8.631 = 0$
C(1) −0.41

(b) Dihedral angles (ϕ/°) between planes
(1)-(2) 23.7, (1)-(3) 11.4

(c) Vector-plane angles (ϕ/°)
Co···Cl-(1) 89.2, Co···C(1)-(1) 85.6

a) The X, Y, and Z coordinates in Å are referred to the crystallographic axes.

of the N-phenacylpyridinium chloride may be associated with the small reduction of the CO bond order in the ylide complex.[15)]

The stereoview of a unit-cell (Fig. 2) shows a crystal packing of the complex with toluene molecules filling the voids enclosed by the molecules of the complex. The toluene molecules probably make a minor contribution to the lattice forces, since the crystals used in the present X-ray analysis were very brittle.

The author is most grateful to Dr. Akiko Kobayashi for her assistance and helpful discussions during the X-ray study.

References

1) H. Schmidbaur, *Acc. Chem. Res.*, **8**, 62 (1975).
2) Y. Oosawa, H. Urabe, T. Saito, and Y. Sasaki, *J. Organomet. Chem.*, **122**, 113 (1976).
3) "Gmelins Handbuch der anorganischen Chemie," Band 5, Teil 1, Verlag Chemie, Weinheim (1973), pp. 3—23.
4) K. Masuno, T. Saito, and Y. Sasaki, Abstr. No. 4N 03, 26th Sakuen Kagaku Toronkai, Sapporo, 1976.
5) G. N. Schrauzer, *Inorg. Synth.*, **11**, 64 (1968).
6) "International Tables for X-Ray Crystallography," Vol. IV, Kynoch Press, Birmingham (1974), pp. 72—98.
7) Ref. 6, p. 149.
8) "The Universal Crystallographic Computation Program System," Crystallographic Society of Japan (1969).
9) J. Halpern, *Acc. Chem. Res.*, **3**, 386 (1970).
10) H. Nishiyama, K. Itoh, and Y. Ishii, *J. Organomet. Chem.*, **87**, 129 (1975).
11) R. D. Gillard, M. Keeton, R. Mason, M. F. Pilbrow, and D. R. Russell, *J. Organomet. Chem.*, **33**, 247 (1971): M. Keeton, R. Mason, and D. R. Russell, *ibid.*, **33**, 259 (1971).
12) P. G. Lenhert, *J. Chem. Soc., Chem. Commun.*, **1967**, 980.
13) A. Chakravorty, *Coord. Chem. Rev.*, **13**, 1 (1974).
14) G. N. Schrauzer and R. J. Windgassen, *J. Am. Chem. Soc.*, **89**, 1999 (1967).
15) H. Koezuka, G. Matsubayashi, and T. Tanaka, *Inorg. Chem.*, **15**, 417 (1976).

Aluminum Chloride Catalyzed Friedel-Crafts Reaction of Anisole with Epoxide Accompanying Isomerization[1)]

Masashi INOUE, Toshio SUGITA, and Katsuhiko ICHIKAWA*

Department of Hydrocarbon Chemistry, Faculty of Engineering, Kyoto University, Yoshida, Kyoto 606

(Received February 24, 1977)

The reaction of anisole with propylene oxide by aluminum chloride has been studied in various kinds of solvents. While the normal Friedel-Crafts reaction yielded 2-(methoxyphenyl)-1-propanols, 1,1-bis(methoxyphenyl)-propanes were also formed in this reaction; these were not obtained by the subsequent reaction of mono(methoxyphenyl) products with another anisole. The yields of 1,1-bis(methoxyphenyl)propanes increased by increasing the basicity of solvents. The mechanism of the formation of 1,1-bis(methoxyphenyl)propanes can be explained by the isomerization of epoxide to aldehyde and the subsequent condensation with anisole. Various kinds of epoxides also gave 1,1-bis(methoxyphenyl)alkanes in nitromethane.

It is generally believed that Friedel-Crafts reactions of aromatic substrates with epoxides produce β-hydroxyarylalkanes which react further with aromatics to give 1,2-diarylalkanes.[2)]

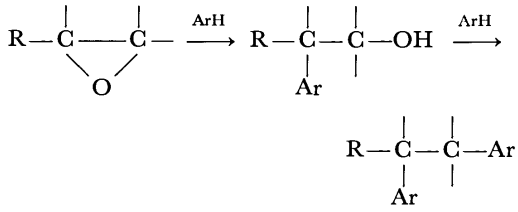

During the course of the study of solvent effects on the ring-opening reaction of epoxide with aluminum chloride,[3)] we found, however, that the reaction of propylene oxide with anisole by aluminum chloride yielded 1,1-bis(methoxyphenyl)propanes (**1**) without any contamination of the 1,2-isomers (**2**). In order to clarify the mechanism, the reaction of various epoxides with anisole has been studied in various solvents.

The reaction of propylene oxide and anisole without solvent at 0—2 °C gave a complex mixture containing at least eight compounds: 2-chloro-1-propanol (**3**, 24 %), 1-chloro-2-propanol (**4**, 8%), 2-(*o*- and *p*-methoxyphenyl)-1-propanols (**5**, 17%), 1-phenoxy-2-propanol (**6**, 4%), and three isomers (*o,o*-, *o,p*-, and *p,p*-) of 1,1-bis(methoxyphenyl)propanes (**1**, 24%). The first two are the ring-opening products of the epoxide; their isomer distribution and stereochemistry have been discussed previously.[3)] The mechanism of the formation of **5**, a normal Friedel-Crafts reaction product of propylene oxide, is considered to be of the S_N2 type analogous to the reported case of benzene.[4)] In this paper, however, we are concerned mainly with the formation of **1**.

Table 1 shows the results of the reaction of propylene oxide with anisole in various solvents. For experimental convenience, the yields of the products which did not include methoxyphenyl moiety were not determined. The other products were chloropropanols, oligomers of the epoxide, and high boiling tarry matter. The characteristic features of the results are as follows. When 1,2-dichloroethane was used as a solvent, changes in the reaction conditions resulted in only minor changes in the product distributions. The formation of **2** was not observed in any experiments except one at a higher temperature (32—34 °C). The yield of **1** increased in the following order of the solvents: hexane<chloroform<1,2-dichloroethane<anisole<nitromethane.

Table 1. Effects of the solvent on the reaction of propylene oxide with anisole[a)]

Solvent	Yield of **5** %	Yield of **1** %	Isomer distribution in **1**		
			o,o- %	*o,p*- %	*p,p*- %
$ClCH_2CH_2Cl$[b)]	8.3	11.3	1.3	24.4	74.3
$ClCH_2CH_2Cl$	5.8	13.4	1.2	24.1	74.5
$ClCH_2CH_2Cl$[c)]	7.4	13.0	0.6	26.5	72.9
$ClCH_2CH_2Cl$[d)]	5.5	11.7	1.0	24.0	75.0
$ClCH_2CH_2Cl$[e)]	10.9	19.3	1.5	27.5	71.0
$ClCH_2CH_2Cl$[f)]	6.1	8.4	0.5	20.0	79.5
$ClCH_2CH_2Cl$[g)]	7.2	14.7	1.0	22.3	76.7
$ClCH_2CH_2Cl$[h)]	4.1	16.2	1.0	26.4	72.6
$ClCH_2CH_2Cl$[i)]	2.5	14.9	(mixture of **1** and **2** (20%))		(80%)
$CHCl_3$	3.2	6.4	1.1	22.7	76.2
$CH_3(CH_2)_4CH_3$	1.3	0.6	1.8	13.2	85.0
CH_3NO_2	0.0	25.8	0.7	12.3	87.0

a) Unless otherwise mentioned, 40 ml of solvent, 20 mmol of epoxide, 40 mmol of anisole, and 20 mmol of aluminum chloride were used. Reaction temperature and time were 0—2 °C and 3.5 h, respectively. b) Reaction time, 1.0 h. c) Reaction time, 6 h. d) Anisole, 20 mmol. e) Anisole, 200 mmol. f) Aluminum chloride, 10 mmol. g) Aluminum chloride, 40 mmol. h) Aluminum chloride, 60 mmol. i) Reaction temperature, 32—34 °C.

In nitromethane, **1** was obtained in a good yield but no mono(methoxyphenyl) products were detected. This result forms a striking contrast to the fact that benzene does not react with propylene oxide in this solvent.[4)] Therefore, the reaction of various epoxides with anisole was examined. Results are summarized in Table 2.

One of the possible routes to **1** is the successive reaction of **5** with another anisole. The literature contains a number of papers on the Friedel-Crafts type alkylation of aromatics with 1,2-difunctional propanes including propylene oxide which gave 1,2-diarylpropanes,[5)] while a few papers have reported the formation of 1,1-diarylpropanes as by-products.[6)] Masuda *et al.* explained the formation of 1,1-diphenylpropane (minor product) in the reaction of 1-phenyl-2-chloropropane and 2-phenyl-1-chloropropane with benzene in terms of an isomerization from a phenonium ion type inter-

Table 2. Products of the reaction of various epoxides with anisole (AnH) by aluminum chloride in nitromethane[a)]

	Epoxide	Product	Isomer distribution in bis(methoxyphenyl) derivatives[b)]		
			o,o-	*o,p*-	*p,p*-
1	MeCH—CH_2 (O)	$EtCH(An)_2$ (**1**, 28%)	1.4	24.8	73.8
2	EtCH—CH_2 (O)	$PrCH(An)_2$ (**9**, 33%)	1.7	24.8	73.5
3	*n*-BuCH—CH_2[d)] (O)	$CH_3(CH_2)_4CH(An)_2$ (**10**, 32%)	2.5	23.3	74.2
4	$ClCH_2CH_2$—CH_2 (O)	None			
5	PhCH—CH_2 (O)	$PhCH_2CH(An)_2$ (**11**, 46%)	2.6	25.0	72.4
6	Ph, Me C—CH_2[e)] (O)	Ph, Me $CHCH(An)_2$ (**12**, 76%)	0.7	22.2	77.1
7	Et_2C—CH_2[f)] (O)	$Et_2CHCH(An)_2$ (**13**, 40%)	2.3	18.2	79.5
8	PhCH—CHPh[g)] (O)	$Ph_2CHCH(An)_2$ (**14**, 56%)[c)] $PhCH_2CH$<Ph, An (**15**, 11%) Ph, An $C{=}CHAn$ (**16**, 10%)	2.2	24.7	73.1
9		$-CH(An)_2$ (**17**, 17%) CH_2An, An (**18**, 8%)	0.7	23.0	76.3
10	Me[h)]	$CH(An)_2$, Me (**19**, 5%)	0.9	22.6	76.5

a) Reactions were conducted with anisole (100 mmol) and $AlCl_3$ (40 mmol) in nitromethane (40 ml), and the epoxide (20 mmol) in nitromethane (20 ml) at 0—2 °C, the mixtures were homogeneous. Isolated yields given in parentheses were calculated on the basis of the epoxides used. b) Calcd from GLPC. c) The possibility of contamination of 1,2-bis(methoxyphenyl)-1,2-diphenylethane cannot be excluded. d) bp 117—118 °C (lit,[15a)] bp 116—119 °C). e) bp 98—100 °C/33 mmHg (lit,[15b)] bp 71 °C/10 mmHg). f) bp 105—106 °C (lit,[15c)] bp 105—107 °C). g) mp 68—69 °C (lit,[15d)] mp 68.5—69 °C). h) bp 72—74 °C/105 mmHg (lit,[15e)] bp 137—138 °C).

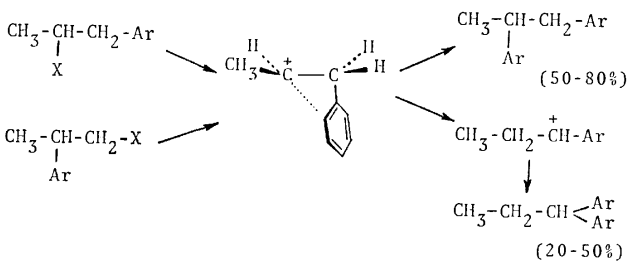

Scheme 1.

mediate to 1-phenyl-1-propyl cation on the basis of stereochemical results.[7,8)]

To examine this reaction sequence, **5** was subjected to react with excess anisole in the presence of aluminum chloride at 0—2 °C. The predominant product was **2** (80%), and **1** was only a minor one (20%). Although the data may not reflect exactly the path of the reaction of propylene oxide with anisole, since hydrogen chloride is produced in the reaction of **5** with aluminum chloride to form the assumed precursor, dichloroaluminum 2-(methoxyphenyl)propoxide, it can be concluded that the main route to **1** is different from this reaction sequence, since the hydride shift from the phenonium type ion to 1-aryl-1-propyl cation is not affected by the leaving groups of the precursors of the carbonium ion.[8)]

Possible routes for the formation of **1** are shown in Scheme 2, in which R is methyl and Ar is methoxyphenyl or phenyl. Isomerization from epoxide to aldehyde, followed by condensation with anisole, leads to **1**. The isomerization competes with the normal Friedel-Crafts reaction and the aldehyde condensation with anisole competes with the formation of tarry matter *via* aldol condensation, Tischenko reaction, and so on.

It is well known that epoxide forms aldehyde under the catalysis of magnesium bromide, zinc chloride, and boron trifluoride–ether complex.[10)] These catalysts are weak Lewis acid as compared with aluminum chloride. The acidity of aluminum chloride dissolved in nitromethane is lower than those in the other usual solvents for Friedel-Crafts reactions, since nitromethane is a

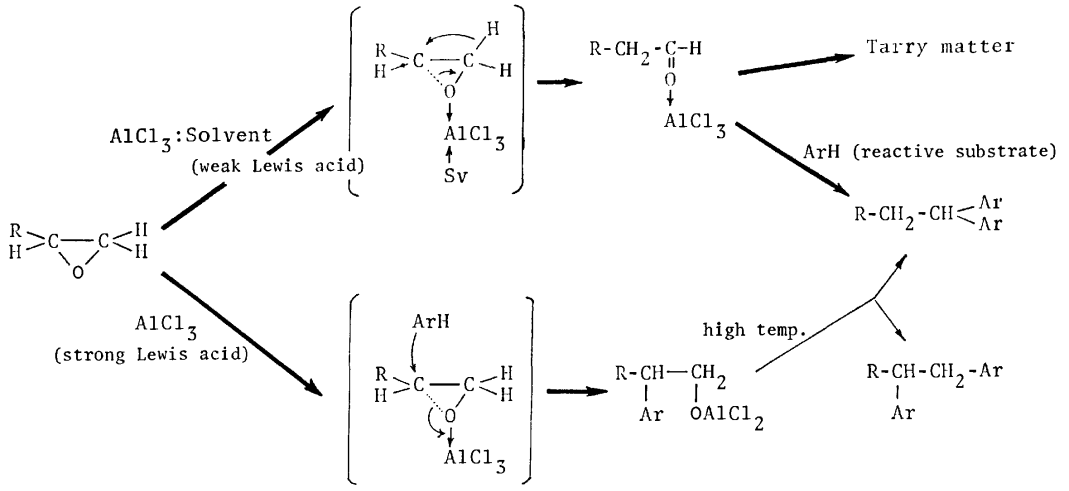

Scheme 2.

stronger base than the other solvents. The activity of the catalyst becomes low, and benzene does not react with propylene oxide in this solvent. When more reactive anisole was used as a substrate, the isomerized aldehyde condenses with anisole to form **1**. As the basicity of the solvents increases in the order mentioned above, the solvent effects on the formation of **1** can be explained along the same line.

Although the condensation of aldehyde with aromatics is well known,[11] no detailed study of the reaction with aluminum chloride catalyst has appeared to our knowledge. The reaction of propionaldehyde with anisole in 1,2-dichloroethane at 0—2 °C in the presence of aluminum chloride gave **1** as a main product (59%), accompanied with 1,1-bis(methoxyphenyl)propenes (**7**, 13%) and 1-methoxyphenylpropanes (**8**, 20%). The formation of the latter two products shows that hydrogen transfer took place, this will be discussed in a separate paper.

The results shown in Table 2 are also well consistent with the mechanistic paths mentioned in Scheme 2. The products in runs 8, 9, and 10 indicate that phenyl and alkyl migrations took place instead of hydrogen migration. The products which are not expected from the reaction sequence mentioned above are suggestive for the study of the nature of aluminum chloride catalysis. The formations of **15** and **16** appear to indicate that the splitting of the phenyl or methoxyphenyl group, isomerization, and a hydride attack to an intermediate carbonium ion occurred. The compound **18** is an isomerization product of **17**.

In a Grignard reaction and a metal hydride (weak nucleophile, *e. g.*, AlH_3 and AlH_2Cl) reduction of epoxides, it is well known that rearrangement to a carbonyl intermediate followed by nucleophilic addition competes with direct nucleophilic ring-opening of epoxide.[12,13] The result presented in this paper is the first example of a Friedel-Crafts type reaction in which the rearrangement to aldehyde followed by condensation has been shown to be the main reaction path.

Experimental

NMR and IR spectra were recorded on a JEOL PMX-60 or a Varian HR-220, and a Hitachi EPI-G2 spectrometers, respectively.

Propylene oxide, 1,2-epoxybutane, and styrene oxide were dried over sodium carbonate and distilled before use. Commercial cyclohexene oxide was used without further purification. Other epoxides were prepared by *m*-chloroperbenzoic acid oxidation of the corresponding olefins. Commercial aluminum chloride (GR grade) was used without further purification. Anisole and nitromethane were dried over sodium hydroxide and phosphorous pentoxide respectively, and distilled before use.

Reaction of Propylene Oxide with Excess Anisole in 1,2-Dichloroethane in the Presence of Aluminum Chloride. To a stirred and cooled (ice bath) solution of 108 g (1.0 mol) of anisole and 14 g (0.11 mol) of aluminum chloride in 200 ml of 1,2-dichloroethane, a mixture of propylene oxide (5.8 g, 0.1 mol) and anisole (54 g, 0.5 mol) was added dropwise during the course of 1.5 h. After 2.0 h, reaction was quenched with 300 ml of water and the organic layer was washed with 100

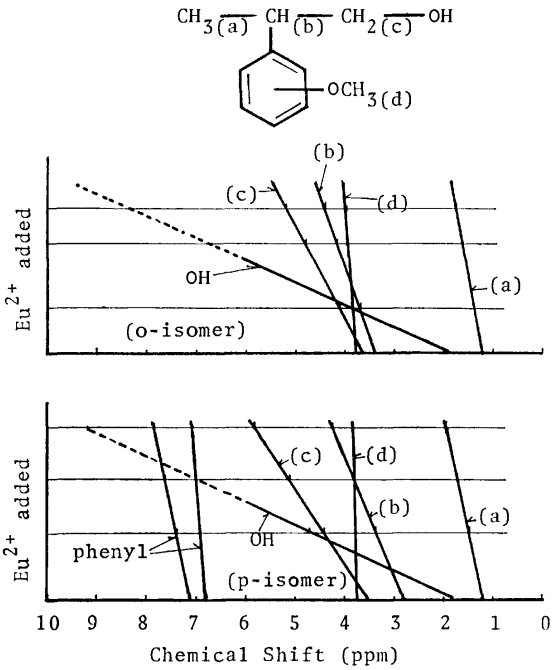

Fig. 1. Paramagnetic shift experiment.

ml of water three times. The combined water layers were extracted with 200 ml of ether three times. The combined organic layers were dried over magnesium sulfate. After removal of the solvents, the product was distilled under reduced pressure: 1st fraction, 70—82 °C/15 mmHg, **3**, **4**, and recovered anisole; 2nd fraction, 0.2 g, 42 °C/5.7 mmHg, phenol; 3rd fraction, 0.7 g, 98 °C/5.0 mmHg, **6**; 4th fraction, 107—111 °C/4.8 mmHg, **5**; 5th fraction, 6.0 g, 140—169 °C/3.2 mmHg, **1**. GLPC analysis showed that the 4th fraction contained 57% and 43% of *o*- and *p*-isomers of **5** respectively together with small amounts of **1** and **6**. To confirm the structure of **5**, a paramagnetic shift experiment in the NMR spectra was carried out using tris(2,2-dimethyl-6,6,7,7,8,8,8-pentafluoro-3,5-octanedionato)europium(III). Results are shown in Fig. 1.

Reaction of Methoxyphenylpropanols with Anisole in the Presence of Aluminum Chloride. In an ice bath, **5** (10 mmol, 70% of *o*-isomer and 30% of *p*-isomer) was treated with anisole (11 g) in the presence of aluminum chloride (20 mmol) for 2 h. After the usual treatments, the reaction mixture was distilled. The yield of a mixture of **1** and **2** (146—172 °C/3.3 mmHg) was 53%. NMR analysis showed that the product contained 20% of **1** and 80% of **2**.

Reaction of Propionaldehyde with Anisole in the Presence of Aluminum Chloride. Propionaldehyde (0.1 mol) was added to anisole (0.2 mol) in 1,2-dichloroethane (300 ml) in the presence of aluminum chloride (0.1 mol) at room temperature for 3.5 h. After the usual work up, 31.7 g of a residual product was obtained. GLPC analysis showed that **1** was formed as a main product, along with many others. Products were separated by column chromatography on silica gel using 30% benzene–hexane.

Reaction of Propylene Oxide with Anisole in the Presence of Aluminum Chloride—Effects of Reaction Conditions. The following example shows a typical experimental procedure. To a solution of anisole (4.33 g) and aluminum chloride (2.7 g) in 1,2-dichloroethane (40 ml) was added 1.33 g of propylene oxide over a period of 2 h at ice-bath temperature. The reaction mixture was stirred at that temperature for an additional 1.5 h. Then the reaction was quenched with a mixture of ice water (50 ml) and concd hydrochloric acid (5 ml). The organic layer was washed with 20 ml of water. The combined water layers were extracted twice with 50 ml of ether and twice with 30 ml. The combined organic layers were dried over magnesium sulfate and distilled to remove the solvent. GLPC analysis of the residual products using dibutyl phthalate as an internal standard showed 785 mg of **1** was formed in this reaction.

Reaction of 1,2-Epoxybutane with Anisole in the Presence of Aluminum Chloride in Nitromethane Solvent. To a mixture of anisole (100 mmol), aluminum chloride (40 mmol), and nitromethane (40 ml) was added a mixture of 1,2-epoxybutane (20 mmol) and nitromethane (20 ml) during the course of 45 min in an ice bath. After an additional 2.5 h, the reaction was quenched as mentioned above. After removal of the solvents, the residual product was purified by chromatography with silica gel, using benzene as an elutant. Distillation of the crude product by a ball-oven apparatus yielded 1.79 g (33.0%) of **9**, bp 169—172 °C/2.5 mmHg. Isomers of the products could be separated by further chromatography using

Table 3. Analytical data

Compound		Bp or mp °C	Formula	Calcd		Found		NMR (δ)		
				C%	H%	C%	H%	CH_3O-		-CH(An)$_2$
1	-*p*,*p*[a]	bp 166—172/3.2 mmHg	$C_{17}H_{20}O_2$	79.65	7.86	79.90	8.13	3.73		3.72
1	-*o*,*p*[a]					79.86	7.60	3.76	3.74	4.24
2	-*p*,*p*	mp 66.5—68	$C_{17}H_{20}O_2$	79.65	7.86	79.35	7.91	3.74	3.75	
2	-*o*,*p*					79.51	8.03			
2	-*o*,*o*					79.66	8.04			
8	-*p*,*p*	mp 93—95[b]	$C_{17}H_{18}O_2$	80.26	7.13	79.98	7.39	3.77	3.82	
9	-*p*,*p*[a]		$C_{18}H_{22}O_2$	79.96	8.20	79.84	8.10	3.7^2		3.7^7
9	-*o*,*p*[a]					80.19	8.01	3.7^4	3.7^5	4.3^7
10	mixt		$C_{20}H_{26}O_2$	80.49	8.78	80.19	8.75			3.8 (*p*,*p*-), 4.3^5 (*o*,*p*-)
11	-*p*,*p*	mp 97.5—98.5[c]	$C_{22}H_{22}O_2$	82.98	6.96	82.71	7.05	3.7^2		3.2^7 (*o*,*p*-; 4.7^0)
12	-*p*,*p*		$C_{23}H_{24}O_2$	83.10	7.28	82.79	7.49	3.6^8	3.4^5	3.9^3
12	-*o*,*p*							3.7^6	3.4^6	4.6^0
13	mixt		$C_{20}H_{26}O_2$	80.49	8.78	80.52	8.87			3.5^8 (*p*,*p*-), 4.2^2 (*o*,*p*-)
14	mixt	mp 196—199								4.6^5 (*p*,*p*-), 4.7^7 (*o*,*p*-)
15	-*p*	mp 84—85[d]	$C_{21}H_{20}O$	87.46	6.99	87.52	7.06	3.6^8		(3.2^8, d, 1; 4.1^7, t, 2, J=8 Hz)
15	-*o*					87.34	6.78	3.5^8		(3.2^8, d, 1; 4.7^2, t, 2, J=8 Hz)
16	-*p*,*p*[e]	mp 89—91[f]	$C_{22}H_{20}O_2$	83.51	6.37	83.49	6.65			
17	-*p*,*p*		$C_{20}H_{24}O_2$	81.04	8.16	81.27	8.12	3.7^5		3.5^0
17	-*o*,*p*					81.25	8.46	3.7^5	3.7^6	4.1^0
18	-*p*,*p*		$C_{20}H_{24}O_2$	81.04	8.16	81.15	7.86	3.7^0		(2.7^1, s, 2, -CH_2An)

a) These products were mentioned by V. A. Topchii, S. V. Zavgorodnii, A. I. Bazaeva, and Ya. I. Yashin, *Izv. Vyssh. Uchebn. Zavend., Khim. Khim. Tekhnol.*, **13**, 1755 (1970), from *Chem. Abstr.*, **75**, 76327f (1971). b) Lit, mp 105 °C, F. v. Wessely, E. Kerschbaum, and A. Kleedorfer, *Monatsh.* **73**, 127 (1940), from *Chem. Abstr.*, **35**, 1781^2 (1941). c) Lit, mp 96—97 °C, K. Sisido, K. Okano, and H. Nozaki, *J. Am. Chem. Soc.*, **77**, 4604 (1955). d) Lit, mp 84—85 °C (*p*-isomer) mp 62—64 °C (*o*-isomer), G. Capozzi, G. Melloni, and G. Modena, *J. Chem. Soc., C*, **1970**, 2621. e) This product may be a mixture of *cis* and *trans* isomers. f) Lit, mp 93—94 °C for *cis* isomer, mp 104.5—105.5 °C for *trans* isomer, Z. Rappoport and Y. Apeloig, *J. Am. Chem. Soc.*, **91**, 6743 (1969).

benzene–hexane (1 : 10) as an elutant. Elemental analyses and NMR spectra are shown in Table 3. The mass spectrum of di-*p*-isomer of **9** was: *m/e* (rel intensity); 270 (M^+, 18), 227 (100), 121 (45).

This work was partially supported by a Grant-in-Aid for Scientific Research from the Ministry of Education, Japan No. 911503.

References

1) A prelimary report of this work was presented at the 30th National Meeting of the Chemical Society of Japan, Higashi-Osaka, April 1974.

2) A. Rosowsky, "Heterocyclic Compounds with Three- and Four-Membered Rings," ed by A. Weissberger, Interscience, New York (1964), Part I, p. 432; A. Schriesheim, "Friedel-Crafts and Related Reactions," Vol. II, Chap. 18, ed by G. A. Olah, Interscience Publishers, New York (1964), p. 543.

3) M. Inoue, T. Sugita, Y. Kiso, and K. Ichikawa, *Bull. Chem. Soc. Jpn.*, **49**, 1063 (1976).

4) T. Nakajima, S. Suga, T. Sugita, and K. Ichikawa, *Tetrahedron*, **25**, 1807 (1969).

5) See, for example, C. D. Nenitzescu and D. A. Isacescu, *Chem. Ber.*, **66**, 1100 (1933).

6) D. L. Ransley, *J. Org. Chem.*, **31**, 3595 (1966); Y. Butsugan, K. Kawase, K. Saheki, M. Muto, and T. Bito, *Nippon Kagaku Kaishi*, **1973**, 2338.

7) S. Masuda, T. Nakajima, and S. Suga, *J. Chem. Soc., Chem. Commun.*, **1974**, 954.

8) Our own results for the reactions of phenylpropanols, which correspond to the phenylchloropropanes reported by Masuda *et al.*,[7] also showed the formation of 1,1-diphenylpropane as a minor component (6%) of the complex products containing 1,2-diphenylpropane (57%), propylbenzene (10%), and 1,1-diphenylpropene (5%). Acetates of the phenylpropanols, corresponding bromides, and allylbenzene gave similar results.[9]

9) M. Inoue, N. Umaki, T. Sugita, and K. Ichikawa, unpublished results.

10) R. E. Parker and N. S. Isaacs, *Chem. Rev.*, **59**, 768 (1959).

11) J. E. Hofmann and A. Schriesheim, "Friedel-Crafts and Related Reactions," Vol. II, ed by G. A. Olah, Interscience Publishers, New York (1964), Chap. 19.

12) M. S. Kharasch and O. Reinmuth, "Grignard Reactions of Nonmetallic Substances," Prentice-Hall, New York (1954), p. 961.

13) M. N. Rerick, "Reduction," ed by R. L. Augustine, Marcel Dekker, New York (1968), Chap. 1.

14) Recently Sekiguchi *et al.* proposed a similar reaction sequence for the reaction of styrene oxide with benzene in the presence of aluminum chloride. K. Kimura, Y. Hayami, K. Matsui, and S. Sekiguchi, Abstr. No. 2D18, 32th National Meeting of the Chemical Society of Japan, Tokyo, April 1975.

15) a) D. J. Pasto and C. C. Cumbo, *J. Org. Chem.*, **30**, 1271 (1965); b) R. E. Parker and B. W. Rockett, *J. Chem. Soc., B*, **1966**, 681; c) B. Rickborn and R. M. Gerkin, *J. Am. Chem. Soc.*, **93**, 1693 (1971); d) D. E. Bissing and A. J. Speziale, *ibid.*, **87**, 2683 (1965); e) D. K. Murphy, R. L. Alumbaugh, and B. Rickborn, *ibid.*, **91**, 2649 (1969).

Reactions of 4*H*-Pyran-4-thiones with Ammonia, Hydrazine, and Guanidine

Hiromichi Besso,* Kimiaki Imafuku,† and Hisashi Matsumura

Department of Chemistry, Faculty of Science, Kumamoto University, Kurokami, Kumamoto 860

(Received March 22, 1977)

The reaction of 4*H*-pyran-4-thiones with ammonia gave 4(1*H*)-pyridinethiones or bis(4-pyridyl) disulfide, while that of 3-methoxy-2-methyl-4*H*-pyran-4-thione with guanidine gave the 1,3-thiazine derivative. 4*H*-Pyran-4-thiones reacted with hydrazine to afford pyridazines, pyrazoles, and 1-amino-4(1*H*)-pyridinethiones. 4*H*-Pyran-4-thiones having the hydroxyl group in the β-position gave the pyridazine derivatives.

Elkaschef and Nosseir[1] obtained 4(1*H*)-pyridinethiones by the reaction of 4*H*-pyran-4-thiones with ammonia. Ainsworth and Jones[2] reported that the reaction of 4-pyrones with hydrazine gives the pyrazole derivatives. Kotani and Tatsumi[3] obtained the 1,4-dihydropyridazine derivative and the pyrazole derivatives by the reaction of kojic acid with hydrazine. However, little is known about the reaction of 4*H*-pyran-4-thiones with hydrazine.[4] We wish to report the reactions of several 4*H*-pyran-4-thiones with ammonia, hydrazine, and guanidine.

Results and Discussion

Reaction of 4H-Pyran-4-thiones with Ammonia. The reaction of 3-methoxy-4*H*-pyran-4-thione (Ia) and 5-methoxy-2-methyl-4*H*-pyran-4-thione (Ib) with ammonia gave respectively 3-methoxy-4(1*H*)-pyridinethione (IIa) and 5-methoxy-2-methyl-4(1*H*)-pyridinethione (IIb), while that of 5-methoxy-2-methoxymethyl-4*H*-pyran-4-thione (Ic) with ammonia gave bis(5-methoxy-2-methoxymethyl-4-pyridyl) disulfide (III) but no 4(1*H*)-pyridinethione. It is thought that the disulfide is produced by further oxidation of 5-methoxy-2-methoxymethyl-4(1*H*)-pyridinethione which might be obtained by the mechanism proposed by Elkaschef and Nosseir.[1] The presence of sulfur in the three products (IIa, IIb, and III) was confirmed by Sugiyama's method.[5]

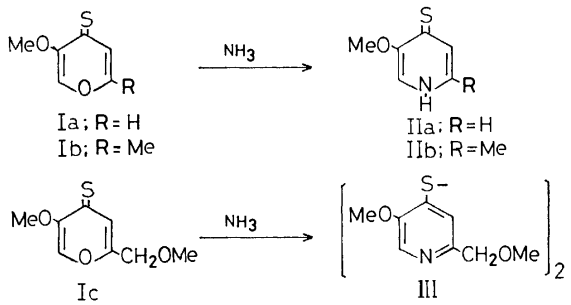

Scheme 1.

Reaction of 4H-Pyran-4-thiones with Hydrazine. The reaction of 5-hydroxy-2-methyl-4*H*-pyran-4-thione (Id) with hydrazine hydrate gave 6-methyl-3-pyridazinecarbaldehyde hydrazone (IVa), and that of 3-hydroxy-2-methyl-4*H*-pyran-4-thione (Ie) with hydrazine hydrate gave 3-acetylpyridazine hydrazone (IVb) and 1-amino-3-hydroxy-2-methyl-4(1*H*)-pyridinethione (Va), respectively.

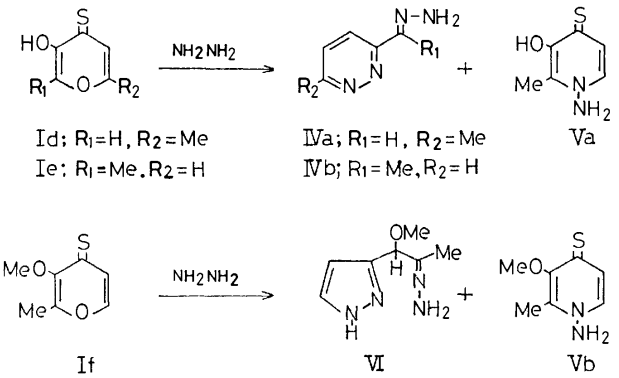

Scheme 2.

Ichimoto[6,7] reported that the attack of hydrazine occurs on the 2- and 6-positions of 3-hydroxy-2-methyl 4-pyrone. It seems that hydrazine attacks on the 6-position of 3-hydroxy-2-methyl-4*H*-pyran-4-thione (Ie) and the 2-position of 5-hydroxy-2-methyl-4*H*-pyran-4-thione (Id), the adducts formed giving the pyridazine derivatives (IVa) and (IVb) according to Scheme 3. The elimination of hydrogen sulfide was confirmed by its conversion into copper(II) sulfide.

The reaction of 3-methoxy-2-methyl-4*H*-pyran-4-thione (If) with hydrazine hydrate is of some interest because of lack of hydroxyl group in the β-position. Actually, the reaction gave the pyrazole derivative but no pyridazine derivative. The products were α-(3-pyrazolyl)-α-methoxyacetone hydrazone (Vb) and 1-amino-3-methoxy-2-methyl-4(1*H*)-pyridinethione (Vb). It was impossible to obtain the 6-membered ring as pyridazines because of the methoxyl group in the β-position, as shown in Scheme 3.

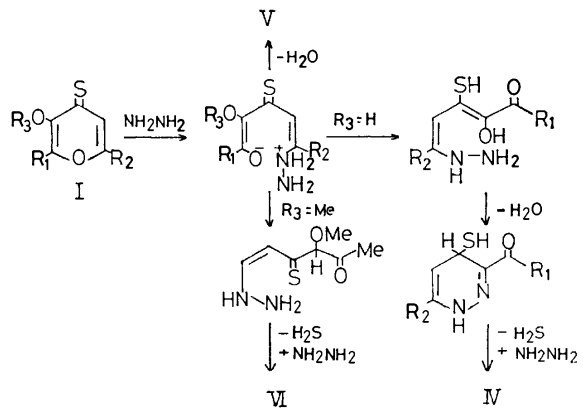

Scheme 3.

* Present address: Wakunage Pharmaceutical Co., Ltd., Koda-machi, Takata-gun, Hiroshima 729-64.

† To whom correspondence should be addressed.

It was found that hydrazine attacks on the 2-position of 5-hydroxy-2-methyl-4*H*-pyran-4-thione (Id) and on the 6-position of 3-hydroxy-2-methyl-4*H*-pyran-4-thione (Ie), and pyridazine (IVa) and (IVb), respectively, are produced by the elimination of water and hydrogen sulfide. However, 4*H*-pyran-4-thiones having no hydroxyl group in the β-position gave the pyrazole derivatives by the elimination of hydrogen sulfide.[4]

Reaction of 3-Methoxy-2-methyl-4H-pyran-4-thione (If) with Guanidine. When 3-methoxy-2-methyl-4*H*-pyran-4-thione (If) was treated with guanidine, the 1,3-thiazine derivative (VII) was obtained in 8.2% yield. The structure was confirmed by the spectral and analytical data. The NMR spectrum in CF_3COOH shows peaks at 2.41 for C–CH_3, 3.84 for O–CH_3, 8.8—8.3 for NH, and 7.01 and 9.65 for -CH=CH-. The IR spectrum shows bands at 3200, 1690, and 1610 cm^{-1}. The mass spectrum shows peak at *m/e* 198 for parent. The fragmentation of VII is shown in Scheme 5. The presence of sulfur was also confirmed as mentioned above.

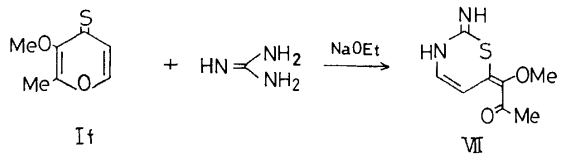

Scheme 4.

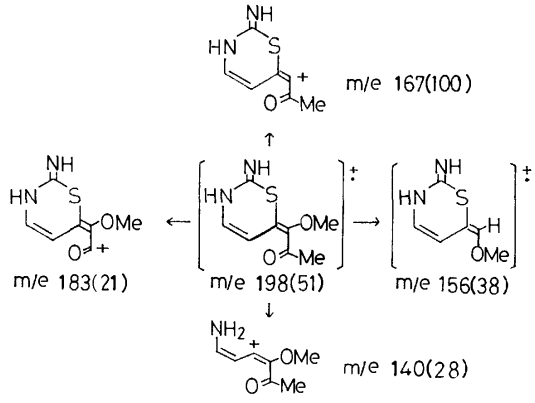

Scheme 5.

We postulate a mechanism in which the amino group of guanidine attacks on the 6-position of 3-methoxy-2-methyl-4*H*-pyran-4-thione (If), and the 1,3-thiazine derivative is formed by the elimination of ammonia from the adduct yielded (Scheme 6).

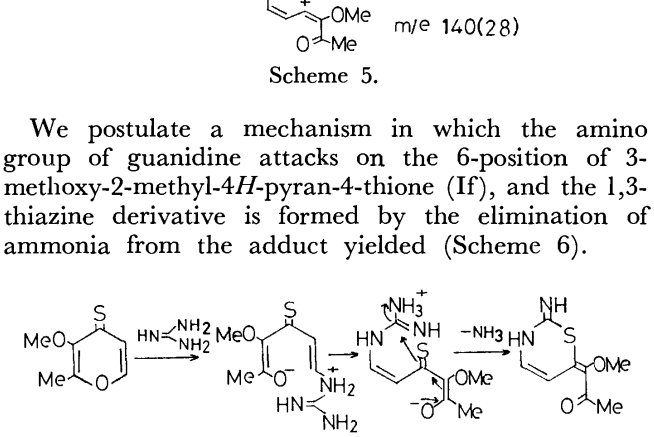

Scheme 6.

Experimental

The melting points were determined with a Yanagimoto micro-melting point apparatus and are uncorrected. All the ^1H NMR spectra were recorded with a Hitachi-Perkin-Elmer R-24 spectrometer (60 MHz), with tetramethylsilane as an internal reference. The IR spectra were taken on a JASCO IRA-1 spectrophotometer, and the UV spectra on a Hitachi EPS-3T spectrophotometer. The mass spectra were taken on a JMS-01 SG-2 mass spectrometer.

Materials. All the 4*H*-pyran-4-thiones were prepared by the reaction of the corresponding 4-pyrones with phosphorus pentasulfide in dry benzene: 5-hydroxy-2-methyl-4*H*-pyran-4-thione (Id); mp 99.5—100.5 °C (lit,[6] 100—101 °C). 3-Hydroxy-2-methyl-4*H*-pyran-4-thione (Ie): mp 78—79 °C (lit,[8] 81—82 °C). 3-Methoxy-4*H*-pyran-4-thione (Ia); mp 110—114 °C (from carbon tetrachloride); Yield, 36%; IR(KBr) 1604 cm^{-1}; NMR($CDCl_3$) δ: 7.45(d, 1H, J=4.7 Hz), 7.45(s, 1H), 7.26(d, 1H, J=4.7 Hz), 3.83(s, 3H). Found: C, 50.49; H, 4.26%. Calcd for $C_6H_6O_2S$: C, 50.71; H, 4.26%. 5-Methoxy-2-methyl-4*H*-pyran-4-thione (Ib); mp 98.5—100 °C (from carbon tetrachloride); Yield, 40%; IR(KBr) 1615 cm^{-1}; NMR($CDCl_3$) δ: 7.43(s, 1H), 7.22(s, 1H), 3.82(s, 3H), 2.24(s, 3H). Found: C, 53.55; H, 5.06%. Calcd for $C_7H_8O_2S$: C, 53.84; H, 5.16%. 5-Methoxy-2-methoxymethyl-4*H*-pyran-4-thione (Ic); mp 56—56.5 °C (from benzene-petroleum ether); Yield, 37%; IR(KBr) 1635 cm^{-1}; NMR($CDCl_3$) δ: 7.47(s, 1H), 7.36(s, 1H), 4.24(s, 2H), 3.86(s, 3H), 3.46(s, 3H). Found: C, 51.48; H, 5.33%. Calcd for $C_8H_{10}O_3S$: C, 51.59; H, 5.42%. 3-Methoxy-2-methyl-4*H*-pyran-4-thione (If); mp 61—63 °C (from petroleum ether); Yield, 47%; IR(KBr) 1625 cm^{-1}; NMR ($CDCl_3$) δ: 7.39 (d, 1H, J=5.0 Hz), 7.16(d, 1H, J=5.0 Hz), 3.85(s, 3H), 2.36(s, 3H). Found: C, 53.58; H, 5.14%. Calcd for $C_7H_8O_2S$: C, 53.84; H, 5.16%.

Reaction of 4H-Pyran-4-thiones with Ammonia. *a) 3-Methoxy-4(1H)-pyridinethione (IIa)*: A mixture of 3-methoxy-4*H*-pyran-4-thione (Ia) (104 mg) and 28% aqueous ammonia solution (0.8 ml) was heated in a sealed tube at 60 °C for 5 min. Ammomia and water were evaporated off, and the residue was recrystallized from methanol to afford IIa, yellow-ochre prisms. Yield 46 mg (44%); mp 149—152 °C; IR (KBr) 3160, 2800, 1602 cm^{-1}; NMR(CF_3COOH) δ: 8.3—7.7(m, 3H), 4.20(s, 3H). Found: C, 50.80; H, 5.02; N, 9.94%. Calcd for C_6H_7NOS: C, 51.06; H, 5.02; N, 9.95%.

b) 5-Methoxy-2-methyl-4(1H)-pyridinethione (IIb): A mixture of 5-methoxy-2-methyl-4*H*-pyran-4-thione (Ib) (187 mg) and 28% aqueous ammonia solution (1.5 ml) was heated in a sealed tube at 60 °C for 10 min. Ammonia and water were evaporated off, and the residue was recrystallized from ethyl acetate to afford IIb, yellow micro-crystals. Yield 123 mg (66%); mp 156—158 °C; IR(KBr) 3245, 2800, 1615 cm^{-1}; NMR(CF_3COOH) δ: 7.9—7.5(m, 2H), 4.15(s, 3H), 2.69(s, 3H). Found: C, 54.04; H, 5.78; N, 8.90%. Calcd for C_7H_9NOS: C, 54.19; H, 5.81; N, 9.03%.

c) Bis(5-methoxy-2-methoxymethyl-4-pyridyl) Disulfide (III): A mixture of 5-methoxy-2-methoxymethyl-4*H*-pyran-4-thione (Ic) (164 mg) and 28% aqueous ammonia solution (0.4 ml) was heated in a sealed tube at 60 °C for 10 min. Ammonia and water were evaporated off, and the residue was recrystallized from methanol to afford III, pale yellow needles. Yield, 46 mg (28%); mp 123—123.5 °C; IR (KBr) 1565 cm^{-1}; NMR($CDCl_3$) δ: 8.07(s, 1H), 7.45(s, 1H), 4.44 (s, 2H), 4.00(s, 3H), 3.29(s, 3H); *m/e* 368 (parent). Found: C, 52.03; H, 5.47; N, 7.64%. Calcd for $C_{10}H_{20}N_2O_4S_2$: C, 52.13; H, 5.47; N, 7.60%.

Reaction of 5-Hydroxy-2-methyl-4H-pyran-4-thione (Id) with Hydrazine Hydrate: A mixture of 5-hydroxy-2-methyl-4*H*-pyran-4-thione (Id) (203 mg, 1.4 mmol) and 80% hydrazine hydrate (280 mg, 3 mmol) in methanol (10 ml) was refluxed for 30 min. After methanol had been evaporated off, the residue was recrystallized from benzene to give 6-methyl-3-

pyridazinecarbaldehyde hydrazone (IVa), yellow plates. Yield, 85 mg (44%); mp 180—182 °C; IR(KBr) 3350, 3200, 1635, 1585 cm^{-1}; NMR($CDCl_3$) δ: 9.03(dd, 1H, J=4.5 and 1.5 Hz), 8.06(s, 1H), 7.95(dd, 1H, J=1.5 and 8.0 Hz), 7.41 (dd, 1H, J=4.5 and 8.0 Hz), 6.5—5.5(br, 2H), 2.67(s, 3H); UV λ_{max}(MeOH) nm(log ε) 230(3.74), 291(4.28). Found: C, 52.85; H, 5.91; N, 41.28%. Calcd for $C_6H_8H_4$: C, 52.92; H, 5.92; N, 41.15%.

*Reaction of 3-Hydroxy-2-methyl-4*H*-pyran-4-thione (Ie) with Hydrazine Hydrate.* A mixture of 3-hydroxy-2-methyl-4*H*-pyran-4-thione (Ie) (434 mg, 3 mmol) and 80% hydrazine hydrate (550 mg, 6 mmol) in methanol (10 ml) was refluxed for 1.5 h. After methanol had been evaporated off, the residue was filtered and recrystallized from methanol to give 1-amino-3-hydroxy-2-methyl-4(1*H*)-pyridinethione (Va), yellow needles. Yield, 91 mg (19%); mp 165 °C (dec); IR(KBr) 3250, 1615 cm^{-1}; NMR(CF_3COOH) δ: 8.09(d, 1H, J=8.0 Hz), 7.50(d, 1H, J=8.0 Hz), 2.81(s, 3H); UV λ_{max}(MeOH) nm(log ε) 254(3.98), 275(3.36), 348(4.27). Found: C, 45.36; H, 5.03; N, 17.71%. Calcd for $C_6H_8N_2OS$: C, 46.15; H, 5.16; N, 17.94%. The filtrate was evaporated off to dryness, and the residue was recrystallized from carbon tetrachloride to give 3-acetylpyridazine hydrazone (IVb), yellow micro-crystals. Yield, 145 mg (35%); mp 67—69 °C; IR(KBr) 3350, 3210, 1645, 1570 cm^{-1}; NMR($CDCl_3$) δ: 9.03(dd, 1H, J=1.5 and 4.5 Hz), 8.06(dd, 1H, J=1.5 and 8.0 Hz), 7.34(dd, 1H, J=4.5 and 8.0 Hz), 6.2—5.4(br, 2H), 2.37(s, 3H); UV λ_{max}(MeOH) nm(log ε) 224(3.69), 288 (4.06); *m/e* 136 (parent). Found: C, 52.72; H, 5.89; N, 41.18%. Calcd for $C_6H_8N_4$: C, 52.92; H, 5.92; N, 41.15%.

*Reaction of 3-Methoxy-2-methyl-4*H*-pyran-4-thione (If) with Hydrazine Hydrate.* A mixture of 3-methoxy-2-methyl-4*H*-pyran-4-thione (If) (404 mg, 2.5 mmol) and 80% hydrazine hydrate (510 mg, 5.5 mmol) in methanol (10 ml) was allowed to stand at roon temperature for 1 h. After methanol had been evaporated off, the residue was filtered and recrystallized from methanol to afford 1-amino-3-methoxy-2-methyl-4(1*H*)-pyridinethione (Vb), yellow plates. Yield, 116 mg (27%); mp 150—152 °C(dec); IR(KBr) 3200, 3150, 1620, 1590 cm^{-1}; NMR(CF_3COOH): 8.25(d, 1H, J= 7.9 Hz), 7.64(d, 1H, J=7.9 Hz), 4.00(s, 3H), 2.85(s, 3H); UV λ_{max}(MeOH) nm(log ε) 252(3.89), 285(3.21), 349(4.33). Found: C, 49.29; H, 5.86; N, 16.40%. Calcd for $C_7H_{10}N_2OS$: C, 49.40; H, 5.92; N, 16.46%. The solvent was evaporated off from the filtrate, and the residue was extracted with chloroform. After chloroform had been evaporated off, an oily product was obtained and confirmed to be α-(3-pyrazolyl)-α-methoxyacetone hydrazone (VI). Yield, 255 mg (58%); IR($CHCl_3$) 3200, 1620 cm^{-1}; NMR($CDCl_3$) δ: 7.53(d, 1H. J=2.2 Hz), 6.24(d, 1H, J=2.2 Hz), 4.94(s, 1H), 3.35(s, 3H), 1.72(s, 3H). This hydrazone decomposed within one day, not forming picrate.

*Reaction of 3-Methoxy-2-methyl-4*H*-pyran-4-thione (If) with Guanidine.* To a sodium ethoxide solution, prepared from sodium (180 mg, 8 mmol) and absolute ethanol (8 ml), were added guanidine hydrochloride (700 mg, 8 mmol) and 3-methoxy-2-methyl-4*H*-pyran-4-thione (If) (244 mg, 1.5 mmol) and the mixture was stirred at room temperature for 5 min. The reaction mixture was poured into water and extracted with chloroform. Chloroform was evaporated off, and the residue was recrystallized from ethyl acetate to give 1,3-thiazine derivative (VII), yellow plates. Yield, 25 mg (8.2%); mp 212 °C (dec); IR (KBr) 3200, 1690, 1610 cm^{-1}; NMR(CF_3COOH) δ: 9.65(d, 1H, J=2.0 Hz), 8.8—8.3(br, 2H), 7.01(d, 1H, J=2.0 Hz), 3.84(s, 3H), 2.41(s, 3H); *m/e* 198(parent). Found: C, 48.43; H, 5.14; N, 14.04%. Calcd for $C_8H_{10}N_2O_2S$: C, 48.48; H, 5.09; N, 14.14%.

The authors wish to thank Dr. Kazu Kurosawa of Kumamoto University for valuable discussions and Mr. Shuichi Ueda of Taiho Pharmaceutical Co., Ltd. for the measurement of mass spectra.

References

1) M. A.-F. Elkaschef and M. H. Nosseir, *J. Am. Chem. Soc.*, **82**, 4344 (1960).
2) C. Ainsworth and R. G. Jones, *J. Am. Chem. Soc.*, **76**, 3172 (1954).
3) R. Kotani and C. Tatsumi, *Bull. Univ. Osaka Pref., B*, **10**, 33 (1960).
4) I. E.-S. El-Kholy, F. K. Refra, and G. Soliman, *J. Chem. Soc.*, **1962**, 1857.
5) N. Sugiyama, "Yuki-kagobutsu no Biryo Kakunin-ho," Baifukan, Tokyo (1957), p. 135.
6) I. Ichimoto, *Bull. Univ. Osaka Pref., B*, **22**, 209 (1970).
7) I. Ichimoto, Y. Kitaoka, and C. Tatsumi, *Tetrahedron*, **22**, 841 (1966).
8) K. Blazevic, K. Jakopcic, and V. Hahn, *Bull. Sci. Cons. Acad. Sci. Arts RSF Yougoslavie, A*, **14**, 1 (1969); *Chem. Abstr.*, **71**, 61124f (1969).

The Hydrolysis of Carbohydrates in the Presence of a Reversed Micelle. II. The Hydrolysis of Sucrose in Benzene

Kenichiro Arai and Yoshitaka Ogiwara

Faculty of Engineering, Gunma University, Kiryu, Gunma 376

(Received March 28, 1977)

The formation of a reversed micelle by dodecylbenzenesulfonic acid in benzene containing a certain amount of water was examined by means of the absorption spectra of the Methylene Blue added to the system. The hydrolysis of the sucrose secondary-solubilized in the system was then investigated. The maximum rate enhancement of 400-fold was obtained in the presence of the micelle on the basis of the reaction in an aqueous solution in the presence of hydrochloric acid, whereas the addition of ethanesulfonic acid to the system showed only a little effect on the reaction rate. The reaction rates were found to show behavior similar to that of the stability of the micelle with respect to changes in the substrate concentration and in the amount of solubilized water. From these results, the greater part of the rate enhancement obtained in the present system might be concluded to result from some effects due to the formation of the reversed micelle.

Numerous studies have been made of new catalysis systems in the presence of a polymer catalyst[1] or a micelle[2] showing interactions with the substrate. However, there is only a little information on the system for the hydrolysis of such carbohydrates as cellulose, starch, and their low-molecular-weight analogues. Although some attempts have been made to employ a polymeric acid[3-9] or a reversed micelle[10] as catalysts for the hydrolysis, the rate enhancements thus obtained were small.

In a previous paper,[10] the hydrolysis of sucrose in the presence of a dodecylbenzenesulfonic acid (DBSH)-reversed micelle in dioxane–water mixed solvents was investigated; rate enhancements up to 21-fold were observed on the basis of the reaction in an aqueous solution. The rate enhancement, however, had been inferred to result from the solvent effect of dioxane, related to the structuredness of water (*ca.* 10-fold), which was also effective in the catalysis in the presence of sulfuric acid, and from the substrate-binding effect by the reversed micelle (*ca.* 2.1-fold).

In the present experiment, the formation of a reversed micelle by DBSH in benzene containing a certain amount of water is examined, and then the hydrolysis of sucrose secondary-solubilized in the system is investigated.

Experimental

Materials. Reagent-grade sucrose, benzene, ethanesulfonic acid, and hydrochloric acid were used. De-ionized and distilled water was used. Commercially available sodium dodecylbenzenesulfonate (Tokyo Chemical Co., Tokyo) was passed through a cation-exchange column in order to obtain a free acidic surfactant.

UV Spectrum. The UV spectra were obtained with a Hitachi Spectrophotometer 124 (Hitachi Seisakusho Co., Tokyo) at various concentrations of DBSH in benzene containing a certain amount of water and a very small amount of Methylene Blue (cationic dye); the shifts of an absorbance peak in the range of 660—690 nm were measured.

Maximum Amount of Solubilized Water. Water was added, drop by drop with a bulet into the DBSH benzene solution, and the amount of water just before turbidity appeared was estimated as the maximum amount of solubilized water.

Measurement of the Reaction Rate. DBSH was dissolved in benzene, and a sucrose aqueous solution was added. The resulting reaction mixture was then quickly poured into a cell and the optical rotatory powers were measured at intervals at 20 °C by means of a polarimeter (Polax, Atago Kogaku Co., Tokyo). The logarithm of the difference in the optical rotatory powers between that at a reaction time t (m_t) and that at infinity (m_∞) (practically, the optical rotatory power of the corresponding 1:1 mixture of glucose and fructose, because the precise value of m_∞ cannot be obtain in an organic solvent) was plotted against the reaction time, and the pseudo-first-order rate constant was estimated from the slope of the straight line thus obtained.

Results and Discussion

The absorption spectra of Methylene Blue added to a DBSH benzene solution containing a certain amount of water were investigated at various concentrations of DBSH, water, and sucrose. Figure 1 shows typical changes in the spectrum with the concentration of DBSH. Two absorbance peaks are observed in the figure, and one of them, on the left-hand side, is found to shift to a longer wave length with an increase in the concentration of DBSH. This sort of red shift is well known as methachromasis and may suggest the forma-

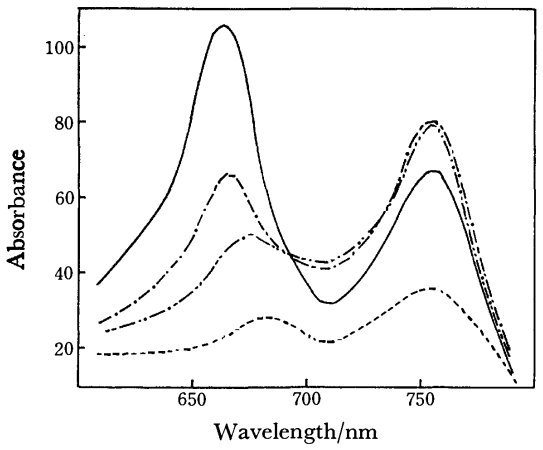

Fig. 1. Typical changes in absorption spectrum of Methylene Blue added to DBSH benzene solution with changing concentration of DBSH. Solubility water, 5 vol%. DBSH concn, N: ——; 0.03, ——; 0.45, ——; 0.50, ----; 0.70.

tion of a micelle. In general, the micelle formed in an apolar solvent such as benzene is known to be a reversed micelle,[11] so the micelle formed in the present system is inferred also to be a reversed one. Figure 2 shows typical changes in the wavelength corresponding to the peak in the spectrum with the concentration of DBSH. A sigmoidal curve is obtained, and the inflection point of the curve is presumed to be a critical micelle concentration of DBSH (CMC).

The maximum amounts of solubilized water in the DBSH benzene solution were measured at various concentrations of DBSH. Figure 3 shows the plots of the maximum amount of water against the concentration of DBSH; the amount of water is found to increase proportionally with the increase in the concentration of DBSH. The slope of the straight line obtained corresponding to 9.3 mol of water/mol of DBSH, which is comparable to the water-solubilizability of Aerosol OT.[12]

The hydrolysis of sucrose secondary-solubilized in the reversed micelle system containing a certain amount of water was investigated at various concentrations of acid, water, and sucrose. Figure 4 shows some typical

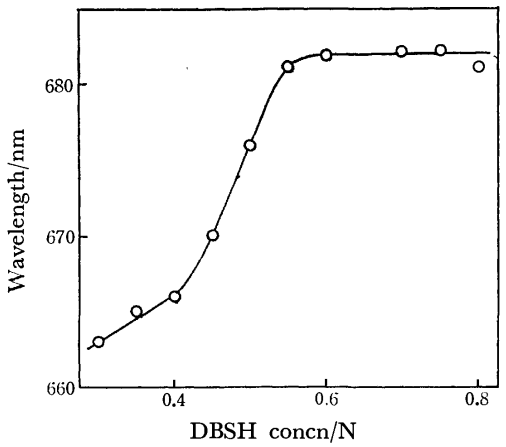

Fig. 2. Typical changes in wavelength corresponding to the peak in absorption spectrum of Methylene Blue added to DBSH benzene solution with changing concentration of DBSH. Solubilized water, 5 vol%.

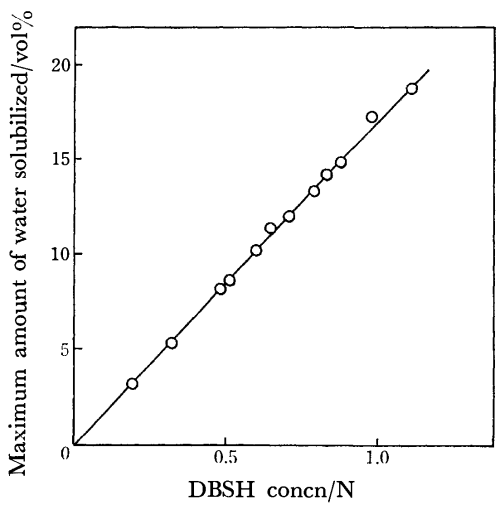

Fig. 3. Plot of maximum amount of water solubilized in DBSH benzene solution against concentration of DBSH.

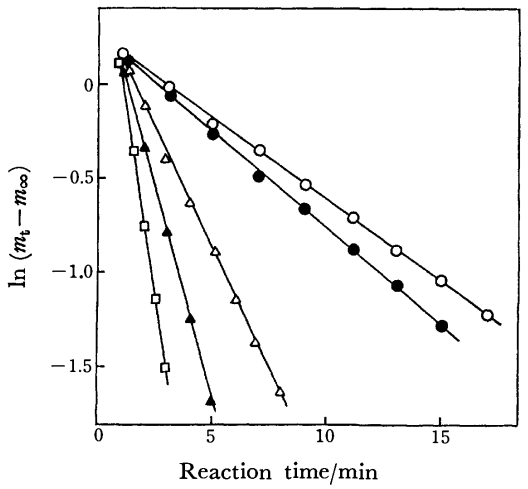

Fig. 4. Typical first-order plots of the changes in the optical rotatory power of sucrose at 20 °C. m_t and m_∞ are the optical rotatory powers at a reaction time t and infinity. Sucrose concn, 32 mM. DBSH concn, N: ○; 0.55, ●; 0.61, △; 0.68, ▲; 0.77, □; 0.86. Solubilized water, 7.5 vol%.

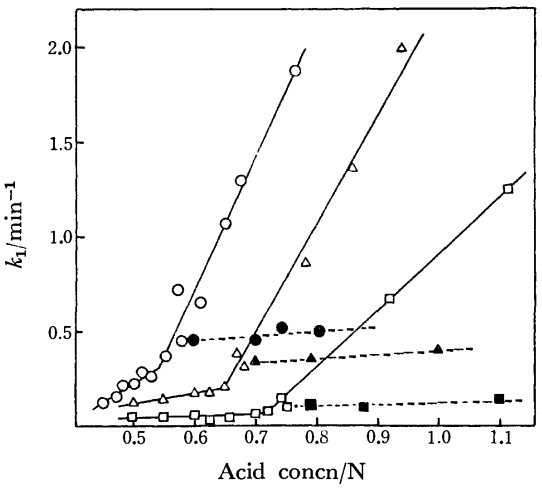

Fig. 5. Plots of pseudo-first-order rate constant, k_1, of sucrose hydrolysis against acid concentration. Sucrose concn, 32 mM. Solubilized water, vol%: ○, ●; 5.0, △, ▲; 7.5, □, ■; 10.0. Acid: ——; DBSH only, ----; ethanesulfonic acid added to DBSH.

first-order plots of the changes in the optical rotatory power of sucrose at 20 °C. A fairly good straight line is obtained for each plot. A pseudo-first-order rate constant, k_1, was estimated from the slope of the straight line. Figure 5 shows the plots of the k_1 against the concentration of acid. the total concentration of DBSH and ethanesulfonic acid. The plots shown with a solid line are those of the k_1 in the presence of DBSH alone; a straight line is obtained for each plot in the concentration range of DBSH higher than a certain concentration, which is nearly in accord with the corresponding CMC presumed from the changes in the absorption spectrum. The slope of the straight line gives an apparent second-order rate constant, k_{2obsd}, when the amount of solubilized water is not considered. The k_{2obsd}'s are far larger than that of the reaction in water

in the presence of hydrochloric acid (the plot is omitted in the figure to avoid complexity, and the second-order rate constant, k_{2HCl}, is 0.016 $l\,mol^{-1}\,min^{-1}$) and is found to decrease with an increase in the amount of solubilized water. The plots shown with dotted line are those of the k_1 in the presence of the ethanesulfonic acid added to the system after DBSH formed the micelle. Ethanesulfonic acid is presumed not to form any micelle, and in fact, CMC was not influenced by the addition of ethanesulfonic acid to the system. In the figure the slopes of the dotted straight lines are found to be far smaller than those in the presence of DBSH alone in a higher concentration range at the same acid concentration.

Figure 6 shows the plots of CMC presumed from the absorption spectrum and of the ratio of the sucrose hydrolysis rates with the DBSH micelle to those with hydrochloric acid, k_{2obsd}/k_{2HCl}, against the concentration of sucrose. Again, for each reaction with different concentrations of sucrose, the DBSH concentration at the break point of the plots of k_1 against the DBSH concentration were nearly in accord with the corresponding CMC. It can be seen in Fig. 6 that CMC decreases with an increase in the concentration of sucrose and that k_{2obsd}/k_{2HCl} also increases in the concentration range higher than 40 mM. It may be explained qualitatively that the more stable the micelle is, the larger k_{2obsd}/k_{2HCl} is given, although the larger values of k_{2obsd}/k_{2HCl} in a concentration range lower than 40 mM cannot be explained at the present time. Figure 7 shows the plots of the CMC and k_{2obsd}/k_{2HCl} against the amount of solubilized water. It is found that the CMC increases proportionally with the amount of solubilized water and that the k_{2obsd}/k_{2HCl} decreases. Again, from these plots it may be possible to explain qualitatively that the more stable the micelle is, the larger k_{2obsd}/k_{2HCl} is given.

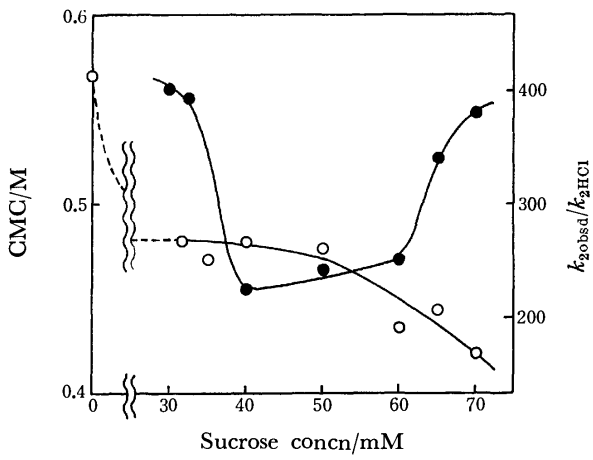

Fig. 6. Plots of CMC (○) and the ratio of sucrose hydrolysis rates with the DBSH micelle to those with hydrochloric acid, k_{2obsd}/k_{2HCl} (●), against sucrose concentration. Solubilized water, 5 vol%.

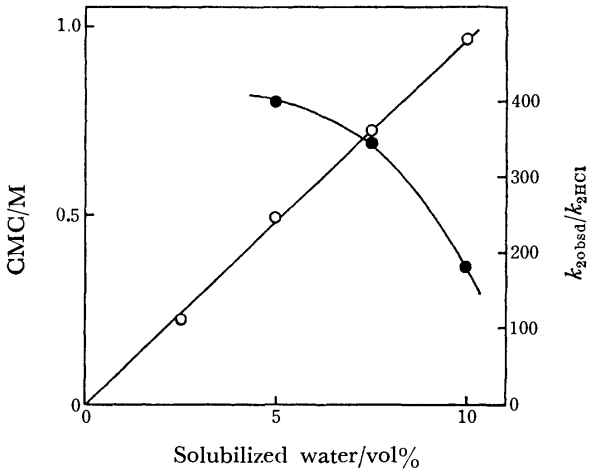

Fig. 7. Plots of CMC (○) and the ratio of sucrose hydrolysis rates with the DBSH micelle to with hydrochloric acid, k_{2obsd}/k_{2HCl} (●), against the amount of solubilized water. Sucrose concn, 32 mM.

Conclusion

The hydrolysis of sucrose secondary-solubilized in a DBSH benzene solution containing a certain amount of water was investigated, and rate enhancements up to 400-fold were obtained on the basis of the reaction in an aqueous solution in the presence of hydrochloric acid. Some facts observed in the present investigation, which show the existence of a close relationship between the changes in the reaction rate and the micelle formation, suggest that the greater part of the rate enhancement is related to the formation of the reversed micelle; in contrast to the corresponding reaction in a dioxane–water mixed solvent,[10] the micelle effect may be far larger than the solvent effect. The micelle effects obtained in the present system are supposed to arise from a substrate-binding effect into the micelle, from the increase in the activities of the water molecules and hydronium ions, from a more suitable conformation of transition state for the reaction, and from other factors. At the present time, however, the details are not apparent.

References

1) For example: I. Sakurada, *Pure Appl. Chem.*, **16**, 263 (1968); C. Overberger, *Acc. Chem. Res.*, **2**, 217 (1969); H. Morawetz, *Acc. Chem. Res.*, **3**, 354 (1970); N. Ise, *Adv. Polym. Soc.*, **7**, 536 (1971).

2) For example: J. Albrizzio, J. Archila, T. Rudulfo, and E. H. Cordes, *J. Org. Chem.*, **37**, 871 (1972); J. R. Cho and H. Morawetz, *J. Am. Chem. Soc.*, **94**, 345 (1972); J. H. Fendler and R. R. Liechti, *J. Chem. Soc., Chem. Commun.*, **1972**, 1041; S. Friberg and S. I. Ahmad, *J. Am. Chem. Soc.*, **94**, 5196 (1972).

3) W. Kern, W. Herold, and B. Scherhag, *Makromol. Chem.*, **17**, 231 (1955).

4) T. J. Painter and W. T. J. Morgan, *Chem. Ind. (London)*, **1961**, 437.

5) N. Hartler and K. Hyllengren, *J. Polym. Sci.*, **55**, 779 (1975).

6) K. Arai and N. Ise, *Makromol. Chem.*, **176**, 37 (1975).

7) K. Arai and Y. Ogiwara, *Makromol. Chem.*, **176**, 2491, 2501 (1975); **177**, 367 (1976).

8) K. Arai, Y. Ogiwara, and N. Ise, *Makromol. Chem.*, **176**, 2871 (1976).

9) K. Arai and Y. Ogiwara, *J. Appl. Polym. Sci.*, **20**, 1989 (1976).

10) K. Arai and Y. Ogiwara, *Bull. Chem. Soc. Jpn.*, **49**, 1059 (1976).

11) A. Kitahara, T. Kobayashi, and T. Tachibana, *J. Phys. Chem.*, **66**, 363 (1962).

12) A. Kitahara, *Yukagaku*, **9**, 169 (1960).

Sensitized Photooxygenation of 9-Vinylphenanthrenes

Masakatsu MATSUMOTO, Satoshi DOBASHI, and Kiyosi KONDO

Sagami Chemical Reserch Center, Nishi-Ohnuma, Sagamihara, Kanagawa 229

(Received April 20, 1977)

The sensitized photooxygenation of several 9-vinylphenanthrenes in carbon tetrachloride was investigated. In the cases of 9-vinyl- and 9-(β-substituted vinyl)phenanthrenes, the 1,4-cycloaddition of singlet oxygen to a conjugated system composed of the side chain and 9,10-double bond of the ring surpassed other oxidation modes, *i.e.*, the "ene" reaction and 1,2-cycloaddition of singlet oxygen, to give the 1,2-dioxatriphenylene-type peroxides. On the other hand, the sensitized photooxygenation of 9-isopropenylphenanthrene gave a hydroperoxide due to the "ene" reaction.

Anthracenes are known to easily undergo photooxygenation to give 9,10-epidioxides, while phenanthrenes have scarcely been reported to react with singlet oxygen.[1] Recently, an aromatic double bond in conjugation with extranuclear unsaturation has observed to produce an active diene system capable of undergoing the 1,4-cycloaddition of singlet oxygen for certain 1,1-diphenylethylenes,[2] cyclic styrene derivatives,[3] vinylnaphthalenes,[4] and some vinyl-substituted heteroaromatics.[5] These facts promted us to investigate the sensitized photooxygenation of 9-vinylphenanthrenes. 9-Vinyl- and 9-(β-substituted vinyl)phenanthrenes, **1a**—**d**, underwent the 1,4-cycloaddition of singlet oxygen to give 1,2-dioxatriphenylene-type peroxides, **2a**—**d**, while 9-(α-substituted vinyl-) such as 9-isopropenylphenanthrene (**1e**) did not, although the "ene" reaction did occur.

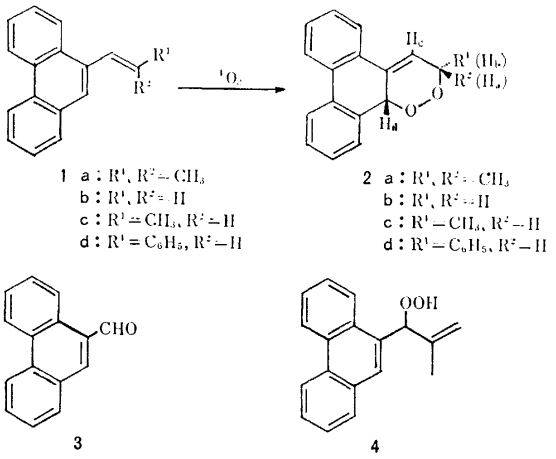

Fig. 1.

Results and Discussion

Preparation of 9-Vinylphenanthrenes. Phenanthrenes having 9-vinyl- (**1b**), 9-isopropenyl- (**1e**), and *trans*-9-styryl- (**1d**) substituents were prepared from 9-formylphenanthrene or 9-acetylphenanthrene using a Wittig reaction. The other phenanthrene, 9-(2-methyl-1-propenyl)- (**1a**) and *trans*-9-(1-propenyl)-phenanthrene (**1c**) were synthesized by dehydration of the corresponding alcohols prepared by a Grignard reaction of 9-bromophenanthrene. The preparations of these vinylphenanthrenes are described in detail in the experimental section.

Photooxygenation of 9-Vinylphenanthrene. First the sensitized photooxygenation of 9-(2-methyl-1-propenyl)-phenanthrene (**1a**) was examined, since **1a** is expected to be most favorable for the 1,4-cycloaddition of singlet oxygen of the phenanthrene **1a**—**e** in accord with the results of the sensitized photooxygenation of 1-vinylnaphthalenes.[5] A solution of **1a** and tetraphenylporphine (TPP) as a sensitizer in carbon tetrachloride was irradiated externally with eight low-pressure sodium vapor lamps in an oxygen atmosphere at 5 °C. When the photolysate was chromatographed on silica gel, a peroxide, **2a**, was obtained in an 80% yield. The structure of **2a** was assigned on the basis of spectral evidence and combustion analysis. In this run, both 9-formylphenanthrene (**3**) and 9-(1-hydroperoxy-2-methyl-2-propenyl)phenanthrene (**4**) were scarcely detected. The former would be formed through the 1,2-addition of singlet oxygen to the side chain of **1a**, and the latter through "ene" reaction of **1a**. Similarly, irradiation of **1b** gave the corresponding endo peroxide, **2b** in a 40% yield. In this case, during the irradiation, a considerable amount of **1b** appeared to be polymerized.

Similar irradiation of *trans*-9-(1-propenyl)phenanthrene (**1c**) gave the corresponding endo peroxides, **2c**, in a 94% yield. The peroxide, **2c**, was one of two obtainable stereoisomers and its configuration was assigned by comparing the NMR spectra of **2a** and **2c** with those of the endo peroxides, **5**, derived from 1-(2-methyl-1-propenyl)-, *trans*-(1-propenyl)-, and *cis*-(1-propenyl)naphthalene.[5] In the NMR spectra of peroxide **2**, the peak of the methyl attached to the carbon atom adjacent to the oxygen atom are situated at 1.29 and 1.42 ppm for **2a**, and at 1.39 ppm for **2c**, as shown in Table 1. On the other hand, in the cases of **5**, the corresponding quasi-axial and quasi-equatorial methyl peaks are located at 1.21—1.25 and 1.51 ppm, respectively.[5] From these facts, **2c** was assigned to have the quasi-equatorial methyl. The sensitized photooxygenation of *trans*-9-styrylphenanthrene (**1d**) gave one of two possible isomeric 1,4-endo peroxides, **2d**, in a 63% yield. The structure of **2d** was also assigned by comparing its NMR spectrum with that

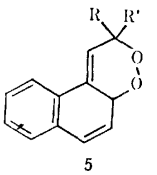

Fig. 2.

TABLE 1. NMR SPECTRAL DATA OF ENDO PEROXIDES **2**[a]

	Chemical shifts (δ ppm)					
	H_a	H_b	H_c	H_d	R^1	R^2
2a	—	—	5.88	5.88	1.42[b]	1.29[b]
2b	5.12	5.37	5.99	5.99	—	—
2c	4.68	—	5.85	6.01	1.39[b]	
2d	5.46	—	6.00	6.17	c)	—
	Coupling constants (Hz)					
	J_{ab}	J_{ac}	J_{ad}	J_{bc}	J_{bd}	J_{cd}
2a	—	—	—	—	—	2.5
2b	17.0	3.0	3.5	3.0	3.0	?
2c	—	2.0	2.5	—	—	2.5
2d	—	3.5	3.5	—	—	2.5

a) Measured in CCl_4. b) R^1 and/or R^2=methyl. c) R^2=phenyl: 7.00—7.50 ppm.

of the endo peroxide of *trans*-1-styrylnaphthalene.[5] Thus, the 1,4-cycloaddition of singlet oxygen to 9-vinylphenanthrenes **1** was confirmed to be stereospecific and the attack of singlet oxygen on the diene system may occur suprafacially. All the endo peroxides **2** obtained in this work were thermally stable and exhibited complex NMR spectra, which were analyzed using the spin-decoupling technique, as shown in Table 1.

For the sensitized photooxygenation of 1-vinylnaphthalenes, the α-substituent on the side chain was found to inhibit the 1,4-cycloaddition of singlet oxygen to the aromatic-extranuclear unsaturation system. This tendency was observed in the reaction of 9-vinylphenanthrene; when 9-isopropenylphenanthrene (**1e**) was oxygenated in a manner similar to that described above, no corresponding endo peroxide, **2**, but instead 9-(3-hydroperoxy-1-propen-2-yl)phenanthrene, (**6**), was formed. This result is in contradiction to the Diels-Alder reaction of maleic anhydride with **2e** in boiling xylene.[6] One of the reasons for this phenomenon may be the steric repulsion between the α-methyl and a hydrogen atom at the 8-position of the aromatic ring, which may be overcome at high temperature.

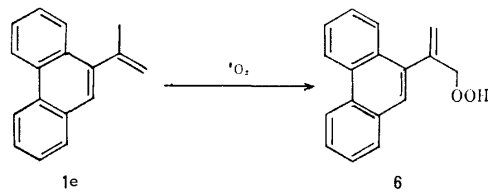

Fig. 3.

In conclusion, it was clarified that, for 9-vinylphenanthrenes excepting aromatics having α-substituted vinyl, such as **2e**, the 9,10-double bond, which is only slightly active itself to singlet oxygen, produces, in conjugation with a 9-ethylenic substituent, an active diene system capable of undergoing the 1,4-cycloaddition of singlet oxygen.

Experimental

All melting points are uncorrected. NMR spectra were recorded on a Varian HA-100 spectrometer with TMS as an internal standard. Mass spectra were obtained with a Hitachi RMU-6E spectrometer. The light source consisted of eight 60-W low-pressure sodium vapor lamps (National SOI-60). The yields are based on reacted starting materials.

*Preparation of 9-(2-Methyl-1-propenyl)phenanthrene (**1a**).* To a solution of 9-phenanthrylmagnesium bromide (prepared from 0.023 mol of 9-bromophenanthrene and 0.023 mol of magnesium) in 50 ml of tetrahydrofuran (THF) a THF solution (10 ml) of isobutylaldehyde (0.024 mol) was added at room temperature. After the usual work-up, crude 1-(9-phenanthryl)-2-methyl-1-propanol was dehydrated with phosphorous pentaoxide in hot benzene (80 ml) for 3 h. A benzene solution containing the crude product was washed with a $NaHCO_3$ aqueous solution and dried over $MgSO_4$. The benzene was evaporated and the residual solid was crystallized from ethanol. Thus, **1a** was obtained as colorless granules, mp 66—67 °C, in 57% yield (3.03 g); IR (KBr): 3050, 2920, 1450, 895, 762, 748, 723 cm^{-1}; NMR ($CDCl_3$): δ 1.73 (s, 3H), 2.00 (s, 3H), 6.58 (m, 1H), 7.4—8.7 (m, 9H) ppm; MS *m/e*: 232 (M^+, 41), 217 (48), 116 (31), 108 (93), 101 (100).

*Preparation of 9-Vinylphenanthrene (**1b**).* To a solution of methylenetriphenylphosphorane (prepared from 0.009 mol of methyltriphenylphosphonium bromide and an equimolar amount of butyllithium) in THF (50 ml) was added 9-formylphenanthrene (0.009 mol) at ambient temperature. After 2 h, the reaction mixture was poured into water and extracted with hexane. The hexane solution was dried over $MgSO_4$ and condensed. The residue was chromatographed on silica gel (Wakogel C-200) and eluted with hexane. Thus, **1b** was obtained as a colorless viscous oil in a 60% yield; IR (liquid film): 3070, 1493, 1450, 990, 771, 751, 730 cm^{-1}; NMR (CCl_4): δ 5.47 (d with fine coupling, J=5.5 Hz, 1H), 5.70 (d with fine coupling, J=16 Hz, 1H), 7.2—8.6 (m, 10H).

Preparation of trans-*9-(1-Propenyl)phenanthrene (**1c**).* The olefin, **1c**, was prepared from 9-bromophenanthrene and allyl bromide according to a procedure in the literature.[6] **1c** was obtained as colorless needles, mp 99—99.5 °C, from hexane (55%) (lit,[6] bp 157 °C/1.25 Torr); NMR (CCl_4): δ 1.95 (d, J=7.0 and 2.0 Hz, 3H), 6.12 (d of q, J=16.0 and 7.0 Hz, 1H), 6.96 (d with fine couping, J=16.0 Hz, 1H), 7.3—8.6 (m, 9H); MS *m/e* :218 (M^+, 80), 217 (37), 203 (100).

Preparation of trans-*9-Styrylphenanthrene (**1d**).* To a solution of benzylidenetriphenylphosphorane (prepared from 0.0049 mol of benzyltriphenylphosphonium bromide and an equimolar amount of butyllithium) in THF (30 ml) was added 0.0049 mol of 9-formylphenanthrene with stirring for 30 min at room temperature. The reaction mixture was treated as in the case of **1b**. Recrystallization of crude **1d** from ethanol gave colorless granules, mp 118 °C (lit,[6] 118 °C) (69%); IR (KBr): 3045, 1597, 1495, 960, 746, 740, 692 cm^{-1}; NMR (CCl_4): δ 6.7—8.7 (m, 16H); MS *m/e*: 280 (M^+, 100), 202 (16), 138 (11).

*Preparation of 9-Isopropenylphenanthrene (**1e**).* To a solution of methylenetriphenylphosphorane (prepared from 0.0086 mol of methyltriphenylphosphonium bromide and an equimolar amount of butyllithium) in 50 ml of THF was added 9-acetylphenanthrene (0.0086 mol). Treatment of the crude product similar to the case of **1b** gave colorless crystals, mp 51 °C (lit,[6] 51 °C) in a 63% yield; IR (KBr): 3060, 1450, 892 cm^{-1}; NMR (CCl_4): δ 2.22 (broad s, 3H), 5.10 (m, 1H), 5.35 (m, 1H), 7.2—8.7 (m, 9H).

*Photooxygenation of 9-(2-Methyl-1-propenyl)phenanthrene (**1a**).* A solution of 0.53 g of **1a** and 5 mg of TPP in 70 ml of CCl_4 was irradiated in an oxygen atmosphere at 5 °C. After 2 h, 53 ml of oxygen was consumed. The photolysate was condensed at room temperature *in vacuo* and the residue was

subjected to chromatography on silica gel. Elution with a hexane–CH_2Cl_2 (3 : 1) mixture gave 0.48 g of peroxide **2a** as colorless granules (mp 94—95 °C, from methanol) (80% yield): IR (KBr): 3050, 2975, 1480, 1445, 1060, 1048, 757, 750, 730 cm^{-1}; MS *m/e* :264 (M^+, 24), 246 (49), 232 (59), 221 (41), 205 (42), 202 (42), 178 (93), 176 (49), 165 (68), 43 (100).

Found: C, 81.15; H, 6.08%. Calcd for $C_{18}H_{16}O_2$: C, 81.79; H, 6.10%.

*Photooxygenation of 9-Vinylphenanthrene (**1b**).* A solution of 1.15 g of **1b** and 5 mg of TPP in 70 ml of CCl_4 was irradiated in an oxygen atmosphere at 5 °C for 5.5 h. The CCl_4 solution was condensed and subjected to chromatography on silica gel. Elution with a hexane-CH_2Cl_2 (3 : 1) mixture gave unreacted **1b** (200 mg) and successively 440 mg of peroxide **2b** (oil): IR (liquid film): 3050, 1450, 1072, 1045, 787, 760, 750 cm^{-1}; MS *m/e*: 237 (M^++1, 33), 205 (100), 179 (47).

Photooxygenation of trans-*9-(1-Propenyl)phenanthrene (**1c**).* Olefin **1c** (0.50 g) and TPP (5 mg) was irradiated in an oxygen atmosphere in 70 ml of CCl_4 for 40 min (O_2 uptake= 54 ml). The CCl_4 was removed from the photolysate under reduced pressure and the residue was purified by chromatography on silica gel in a hexane–CH_2Cl_2 (3 : 1) mixture. Thus, peroxide **2c** (0.54 g) was obtained as colorless granules (from methanol), mp 85—87 °C, in a 94% yield; IR (KBr): 3065, 2975, 1600, 1498, 1450, 1090, 1070, 765, 760, 752, 740 cm^{-1}; MS *m/e*: 250 (M^+, 18), 232 (100), 207 (38), 202 (31), 179 (36), 101 (18).

Found: C, 81.64; H, 5.64%. Calcd for $C_{17}H_{14}O_2$: C, 81.58; H, 5.64%.

Photooxygenation of trans-*9-Stryylphenanthrene (**1d**).* A solution of 0.95 g of **1d** and TPP (5 mg) in CCl_4 (70 ml) was irradiated for 2 h. After the removal of the CCl_4, the crude product was subjected to chromatography on silica gel and eluted with a hexane-CH_2Cl_2 (3 : 1) mixture. As the first fraction, unreacted **1d** (0.43 g) was recovered and successively peroxide **2d** (0.37 g) was obtained as colorless granules, mp 126—127 °C (from hexane); IR (KBr): 3030, 1450, 1085, 1042, 762, 752, 742, 702 cm^{-1}; MS *m/e*: 312 (M^+, 20), 294 (62), 280 (100), 178 (32).

Found: C, 84.09; H, 5.07%. Calcd for $C_{22}H_{16}O_2$: C, 84.59; H, 5.16%.

*Photooxygenation of 9-Isopropenylphenanthrene (**1e**).* A solution of 0.44 g of **1e** and TPP (5 mg) in CCl_4 (50 ml) was irradiated in an oxygen atomosphere at 5 °C, until the sensitizer faded (6 h, O_2 uptake=21 ml). The photolysate was filtered and condensed *in vacuo* at room temperature. The NMR spectrum (in CCl_4) of the crude photolysate showed the existence of 9-(3-hydroperoxy-1-propen-2-yl)phenanthrene (**6**) [δ 4.70 (m, 2H, $-CH_2OO-$), 5.39 (m, 1H, olefinic) ppm] together with unreacted **1e**. No formation of other compounds, such as endo peroxide **2** and 9-formylphenanthrene, was observed. The chromatographic purification of hydroperoxide **6** on silica gel or alumina was unsuccessful. A KI test (for peroxide) of the crude photolysate was positive.

References

1) For a review, see R. W. Denny and A. Nickon, "Organic Reactions," Vol. 20, John Wiley & Sons, New York (1973), p. 133.

2) a) C. S. Foote, S. Mazur, P. A. Burns, and D. Lerdal, *J. Am. Chem. Soc.*, **95**, 586 (1973); b) G. Rio, D. Bricout, and L. Lacomb, *Tetrahedron*, **29**, 3553 (1973).

3) a) P. A. Burns, C. S. Foote, and S. Mazur, *J. Org. Chem.*, **41**, 899 (1976); b) P. A. Burns and C. S. Foote, *ibid.*, **41**, 908 (1976).

4) M. Matsumoto and K. Kondo, *Tetrahedron Lett.*, **1975**, 3935.

5) a) M. Matsumoto, S. Dobashi, and K. Kondo, *Tetrahedron Lett.*, **1975**, 4471; b) M. Matsumoto and K. Kondo, *J. Am. Chem. Soc.*, **99**, 2393 (1977).

6) E. Bergmann and F. Bergmann, *J. Am. Chem. Soc.*, **59**, 1443 (1937).

Autoxidation Reactions of Hydrocarbons Catalyzed by Co(II) Tetra(*p*-tolyl)porphyrin

Yasukazu OHKATSU and Teiji TSURUTA

Department of Synthetic Chemistry, Faculty of Engineering, University of Tokyo, Hongo, Bunkyo-ku, Tokyo 113

(Received April 25, 1977)

Autoxidation reactions of saturated and unsaturated hydrocarbons were carried out using Co(II) tetra(*p*-tolyl)porphyrin as the catalyst in ethyl acetate at 30 °C. The Co(II) complex activated the oxygen molecule to the superoxide ion, which abstracted a hydrogen atom from a saturated hydrocarbon or added to the double bond of an unsaturated hydrocarbon, to initiate autoxidation. The reactivity of the activated oxygen molecule was found at the site of the free radical rather than that of the anion thereof. The reactivities were compared with those of superoxide ions derived from other origins.

The superoxide ion is known to be formed by several different methods: the electroreduction of molecular oxygen,[1,2] the activation of molecular oxygen on some organometallic complexes.[3] and the complexation of the potassium cation of KO_2 with crown ethers.[4]

The superoxide ion is considered to have dual characteristics as a free radical and also as an anion. For example, the electrogenerated free superoxide ion is known[1] to oxidize organic substrates according to the two mechanisms mentioned above. The superoxide ion originating from KO_2, on the other hand, behaves as an anion, as may be seen in the nucleophilic oxidation of alkyl halide to form dialkyl peroxide.[5] Little information, however, has been available on the nature of the molecular oxygen which is activated on a metal complex, especially on a metal porphyrin, though the metal complex is known to catalyze the autoxidation reaction of aldehydes.[6,7]

The purpose of this paper is to elucidate the reactivity of molecular oxygen activated on Co(II) tetra(*p*-tolyl)porphyrin in autoxidation reactions of several hydrocarbons, and to compare the reactivity with that of superoxide ions resulting from other sources.

Experimental

Materials. Co(II) tetra(*p*-tolyl)porphyrin (reffered to as CoTPP) was prepared, according to the method described by Rothemund *et al.*,[8] from pyrrole, *p*-tolualdehyde, and cobalt(II) acetate.

The hydrocarbons, such as tetralin, cumene, 2-norbornene, *dl*-limonene, cyclopentene, cyclohexene, 1-methylcyclohexene, 4-methylcyclohexene, 1,3-dihydrohexadiene, cycloheptene, cyclooctene, and cyclodecene, were purified by conventional methods using activated alumina. The furan, 2,5-dihydrofuran, and 2,3-dihydropyran were used after simple distillations.

The ethyl acetate used as a solvent and the 1,1′-azobiscyclohexanecarbonitrile used as an initiator were purified by usual methods.

Procedure. The autoxidation of a hydrocarbon was carreid out as has been described in a previous paper.[6] The $k_p/(2k_t)^{1/2}$ value was determined with 1,1′-azo-biscyclohexanecarbonitrile under the irradiation of a high-voltage mercury lamp. The rates of chain initiation were determined by the usual induction-period method, using 2,6-di-*t*-butyl-4-methylphenol as the inhibitor. The oxidation products for the two hydrocarbons were analyzed by means of GLC method (column: Silicone SE-1, column temperature: 100 °C) using authentic samples.

Results and Discussion

Autoxidation of Hydrocarbons. It is widely accepted that the autoxidation reactions of organic compounds proceed through the following steps:

$$\mathrm{RH} \longrightarrow \mathrm{R}\cdot \text{ (or } \dot{\mathrm{R}}\mathrm{H}\text{) rate: } R_i, \quad (1)$$

$$\mathrm{R}\cdot + \mathrm{O_2} \longrightarrow \mathrm{RO_2}\cdot \text{ (or } \dot{\mathrm{R}}\mathrm{H} + \mathrm{O_2} \longrightarrow \mathrm{HROO}\cdot), \quad (2)$$

$$\mathrm{RH} + \mathrm{RO_2}\cdot \xrightarrow{k_p} \mathrm{RO_2H} + \mathrm{R}\cdot$$

$$\text{(or } \mathrm{RH} + \mathrm{HROO}\cdot \xrightarrow{k_p} \mathrm{HROO}\dot{\mathrm{R}}\mathrm{H}\text{)}, \quad (3)$$

$$2(\text{peroxyl radical}) \xrightarrow{k_t} \text{inert compounds}, \quad (4)$$

provided that the chain length is sufficiently long and the partial pressure of oxygen is high. The rate of oxidation is expressed[9] as

$$R = -\frac{\mathrm{d}[\mathrm{O_2}]}{\mathrm{d}t} = \{k_p/(2k_t)^{1/2}\}[\mathrm{RH}]R_i^{1/2}. \quad (5)$$

Cobalt(II) tetra(*p*-tolyl)porphyrin was recently shown[6] to behave as a catalyst which initiates the autoxidation of acetaldehyde by activating molecular oxygen into the superoxide type; the rate of initiation reaction was expressed as

$$R_i = k_i[\mathrm{CH_3CHO}][\mathrm{CoTPP}][\mathrm{O_2}]. \quad (6)$$

The present study has revealed that hydrocarbons also undergo the autoxidation reaction with the aid of Co(II) tetra(*p*-tolyl)porphyrin as a catalyst. Tables 1 and 2 show the results of the autoxidation reactions of the two representatitave hydrocarbons, cyclohexene, and 2,3-dihydrofuran respectively. The data in Tables 1 and 2 can satisfactorily be expressed by

$$-\mathrm{d}[\mathrm{O_2}]/\mathrm{d}t = \mathrm{const}[\mathrm{RH}]^{3/2}[\mathrm{CoTPP}]^{1/2}[\mathrm{O}]_2^{1/2}. \quad (7)*$$

By comparing Eq. 7 with Eq. 5, it may be seen that the rate of initiation possesses the formula,

$$R_i = (2k_t)\left(\frac{\mathrm{const}}{k_t}\right)^2[\mathrm{RH}][\mathrm{CoTPP}][\mathrm{O_2}]. \quad (8)$$

Eq. 8 is exactly the same type as that found in the autoxidation of acetaldehyde catalyzed by the same catalyst.[6] The kinetic results are compatible with the concept that the autoxidations of cyclohexene and

* The term "const" in Eq. 7 means $k_p\left\{\frac{2k_t}{k_iK_1}\right\}^{1/2}$, which corresponds to a terms calculated from Eqs. 7, 8, and 11.

Table 1. Oxidation of cyclohexene with Co(II) tetra(*p*-tolyl)porphyrin in ethyl acetate at 30 °C

Cyclohexene (M)	CoTPP Complex ($\times 10^3$ M)	O_2 ($\times 10^3$ M)	$-d[O_2]/dt$ ($\times 10^7$ M)	$\frac{-d[O_2]/dt}{[\text{Cyclohexene}]^{3/2}[\text{CoTPP}]^{1/2}[O_2]^{1/2}}$ ($\times 10^4$ $M^{-3/2}$ s^{-1})
0.5	5.0	2.34[a]	2.0	1.70
0.8	5.0	2.34[a]	4.3	1.76
1.0	5.0	2.34[a]	6.2	1.81
2.0	5.0	2.34[a]	16.6	1.73
1.0	1.0	2.34[a]	2.4	1.58
1.0	2.5	2.34[a]	4.0	1.65
1.0	10	2.34[a]	8.9	1.84
1.0	5.0	1.54[b]	4.8	1.74
1.0	5.0	0.92[c]	3.9	1.60

a) The value at 760 mmHg and at 30 °C. b) The value at 500 mmHg and at 30 °C. c) The value at 300 mmHg and at 30 °C.

Table 2. Oxidation of 2,5-dihydrofuran with Co(II) tetra(*p*-tolyl)porphyrin in ethyl acetate at 30 °C

2,5-Dihydrofuran (M)	CoTPP Complex ($\times 10^3$ M)	O_2 ($\times 10^3$ M)	$-d[O_2]/dt$ ($\times 10^6$ M)	$\frac{-d[O_2]/dt}{[\text{2,5-dihydrofuran}]^{3/2}[\text{CoTPP}]^{1/2}[O_2]^{1/2}}$ ($\times 10^3$ $M^{-3/2}$ s^{-1})
0.5	5.0	2.34	2.7	2.29
1.0	5.0	2.34	8.5	2.48
2.0	5.0	2.34	23.9	2.50
5.0	5.0	2.34	90.8	2.37
1.0	1.0	2.34	3.5	2.31
1.0	2.5	2.34	5.9	2.45
1.0	10	2.34	12.2	2.53
1.0	5.0	1.54	6.3	2.30
1.0	5.0	0.92	5.3	2.22

2,5-dihydrofuran are initiated by molecular oxygen activated on Co(II) tetra(*p*-tolyl)porphyrin (superoxide ion) in a way similar to the autoxidation of acetaldehyde.[6,7]

$$\text{Co(II)TPP} + O_2 \overset{K_1}{\rightleftharpoons} \text{Co(II)TPP-}O_2, \quad (9)$$

$$\text{Co(III)TPP-}O_2 + \text{RH} \xrightarrow{k_1} \text{Co(III)TPP-}O_2\text{H} + \text{R}\cdot, \quad (10)$$

$$\text{or Co(III)TPP-}O_2\dot{\text{R}}\text{H}. \quad (11)$$

Table 3 shows the rates of oxygen absorbed for several hydrocarbons (1 M), using Co(II) tetra(*p*-tolyl)porphyrin (5×10^{-3} M) in ethyl acetate at 30 °C. Significant differences in the rates were observable in response to the kind of hydrocarbons. It is, however, a general trend that Co(II) tetra(*p*-tolyl)porphyrin exhibits a higher reactivity toward hydrocarbons which can undergo both oxidation reactions *via* hydrogen abstraction and addition to double bonds.

Among the cyclic compounds with double bonds, monoenes were generally oxidized more easily than dienes, as exemplified by the comparison of cyclohexene with 1,3-cyclohexadiene, and by that of dihydrofuran with furan.

The oxidation products of both cyclohexene and 2,5-dihydrofuran were representatively analyzed. The former substrate gave cyclohexen-2-one (80%), cyclohexan-2-ol (6%), and cyclohexene oxide (13%); this result forms a contrast with the result[10] obtained by the use of a similar catalyst, Ni(II) phthalocyanine, where 17, 6, and 4% of the above-cited products were obtained respectively. The latter substrate, 2,5-dihydrofuran, on the other hand, formed 2-hydrofuran-5-

Table 3, Oxidation of hydrocarbons with Co(II) tetra(*p*-tolyl)porphyrin

Substrate	$-\frac{d[O_2]}{dt}$,[a] $\times 10^{-7}$ M/s	Modes of oxidation[b]
Tetralin	0	a
Cumene	0	a
2-Norbornene	≈0	b[c]
dl-Limonene	≈0	b[c]
Cyclopentene	6.1	b
Cyclohexene	6.2	b
1-Methylcyclohexene	49	b
4-Methylcyclohexene	8.3	b
1,3-Cyclohexadiene	2.2	b
Cycloheptene	0.9	b
Cyclooctene	49	b
Furan	0.17	c
2,5-Dihydrofuran	85	b[c]
2,3-Dihydrofuran	9.3	b[c]

a) [Hydrocarbon]: 1 M, [Co(II) tetra(*p*-tolyl)porphyrin]: 5×10^{-3} M, Solvent: ethyl acetate, 30 °C. b) a: hydrogen abstraction, b: hydrogen abstraction + addition to double bond(s), c: addition to double bond(s). c) Estimated.

one and 2-hydrofuran-5-ol (79%) and 2,3,5-trihydrofuran-4-one (15%).

The products mentioned above, as is well known,[9] are presumably derived from a hydrogen abstraction reaction

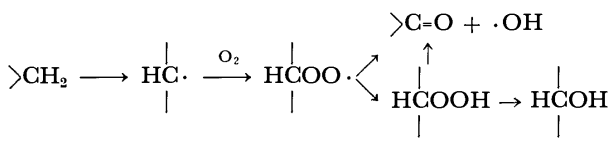

and an addition to double bonds

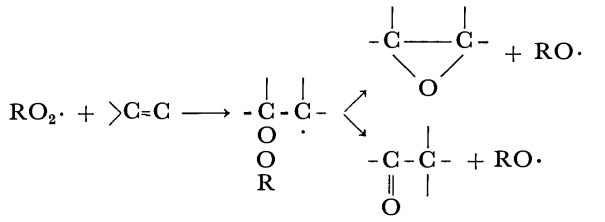

The distribution of these products may suggest the reactivities of the oxygen molecules activated on Co(II) tetra(*p*-tolyl)porphyrin toward hydrocarbons in terms of reaction routes *via* hydrogen abstraction and/or addition to double bonds. This suggestion, however, is apt to be somewhat obscure, because we can observe only overlapped spectra for the distribution of the products which should be derived from peroxyl radicals as well as Co(III)TPP–O_2^-.

*Reactivity of the Oxygen Molecule Activated on Co(II) Tetra(*p*-tolyl)porphyrin.* As shown in Table 3, the modes of the oxidation reactions of hydrocarbons can be classified into those *via* hydrogen abstractions and those *via* additions to double bonds.[11]

The ease of hydrogen abstraction from hydrocarbons is known to be related with the bond dissociation energy between the carbon and hydrogen of the relevant hydrocarbons.[12] Therefore, the hydrogen-abstracting ability of the molecular oxygen, activated on Co(II) tetra(*p*-tolyl)porphyrin, as a free radical can be evaluated by means of the bond-dissociation energy of hydrocarbon, which enters the autoxidation reaction after its initiation by hydrogen abstraction in the presence of the cobalt porphyrin.

The chemical behavior of three types of superoxide ions was compared in terms of the reactivities toward hydrocarbons, which undergo oxidation reactions only *via* hydrogen abstractions. Co(II) tetra(*p*-tolyl)porphyrin and π-allyl $Fe(CO)_3Br$[13] were found to form less reactive superoxide ion than the electrogenerated one. The latter superoxide ion could catalyze, for instance, the autoxidation reactions at 30 °C of 9,10-dihydroanthracene (71 kcal/mol), cumene (79 kcal/mol), tetralin (82 kcal/mol), and cyclohexene (95 kcal/mol), where the numerals in parentheses are the respective C–H bond dissociation energies (D_{C-H}). The former two metal complexes failed to catalyze at 30 °C the autoxidation reaction of cumene and tetralin, which have D_{C-H} values above 79 kcal/mol.

In considering the reactivity of Co(II) tetra(*p*-tolyl)-porphyrin toward the cyclic olefins listed in Table 3, it may necessary first to solve the question of which reaction mode, double-bond addition or hydrogen abstraction, is predominant in the autoxidation reaction. In order to determine such a mode of reaction by the molecular oxygen activated on the cobalt–porpyrin catalyst, the rates of initiation for several cyclohexene derivatives were measured.

The rate of initiation, R_i, was determined by measuring the induction period in autoxidation reactions of cyclohexenes with Co(II) tetra(*p*-tolyl)porphyrin in the presence of 2,6-di-*t*-butyl-4-methylphenol at 30 °C. The values for the rate constant were calculated using

$$R_i = k_i K_1[RH][CoTPP][O_2], \quad (12)$$

which can be derived by assuming Reactions 9—11. Table 4 shows the observed values for the rate of initiation, together with the calculated rate constant, k_iK_1, of Reaction 12 at 30 °C.

The calculated rate constants of the initiation reactions were found to have a good correlation with the $\nu_{C=C}$ of cyclohexenes as is shown in Fig. 1. It should be noted that the oxygen molecule activated on Co(II) tetra(*p*-tolyl)porphyrin cannot abstract the hydrogen atom from 1-methylcyclohexene, 4-methylcyclohexene, and cyclohexene, because the D_{C-H} values of the cyclic olefins are estimated to be about 82 kcal/mol.[10] 1,3-Cyclohexadiene is also considered to enter the autoxi-

Table 4. Determination of rate constants (k_i) of the initiation reaction in the autoxidation of cyclohexene derivatives with Co(II) tetra(*p*-tolyl)porphyrin

Substrates	Temp (°C)	$k_p/(2k_t)^{1/2}$ $M^{-1/2}s^{-1/2}$	R $M\,s^{-1}$	R_i $M\,s^{-1}$	k_iK_i $M^{-2}s^{-1}$
1-Methylcyclohexene	15[a]	1.56×10^{-3}	4.9×10^{-6}	1.58×10^{-6}	1.4×10^{-1}
	30[b]	3.90×10^{-3}			
	40[a]	5.93×10^{-3}			
4-Methylcyclohexene	15[a]	2.78×10^{-3}	8.3×10^{-7}	4.65×10^{-8}	3.97×10^{-3}
	30[b]	3.85×10^{-3}			
Cyclohexene	15[a]	0.6×10^{-3}	6.2×10^{-7}	8.97×10^{-8}	7.67×10^{-3}
	30[b]	2.07×10^{-3}			
	40[a]	2.93×10^{-3}			
1,3-Cyclohexadiene	30[a]	1.0×10^{-9}	2.2×10^{-7}	4.8×10^{-12}	4.14×10^{-5}

a) From Ref. 9. b) This work. Reaction conditions: [cyclohexene derivative]: 1 M, [Co(II) tetra(*p*-tolyl)porphyrin]: 5×10^{-3} M, [O_2]: 2.34×10^{-3} M, in ethyl acetate at 30 °C.

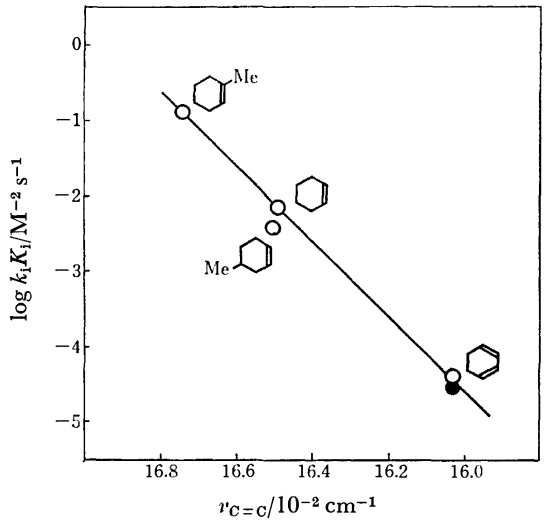

Fig. 1. Correlation of rate constants (k_i) of initiation reaction with $\nu_{C=C}$ of cyclohexene derivatives in autoxidations of the derivatives (1 M) with Co(II) tetra(*p*-tolyl)porphyrin (5×10^{-3} M) under one atom of oxygen at 30 °C.
●: The value calculated by assuming that 73% of 1,3-cyclohexadiene is oxidized through addition reaction.[14]

dation reaction under the initiation through the addition to the double bond, in light of the previous report[14] that about 73% of the autoxidation reaction proceeded through the addition reaction, though the D_{C-H} of 1,3-cyclohexadiene is only 71 kcal/mol.[10]

Therefore, the oxygen molecule activated on Co(II) (*p*-tolyl)porphyrin can be said to react with the double bonds according to an electrophilic addition mechanism, since the value of $\nu_{C=C}$ is regarded as a measure of the electron density of double bonds. From these results and discussion, the reactivity of the activated oxygen molecules can be presumed to be based on the site of the radical.

According to ESR measurement,** the *g*-value of the oxygen molecule activated on Co(II) tetra(*p*-tolyl)-porphyrin was 2.012,[6] which is rather close to that of a peroxy radical (g=2.015),[15] in contrast with the *g*-value of the electrogenerated superoxide ion (2.006).[6] These results suggest the following structure for the activated oxygen molecule:†

$$\text{Co(II)TPP} + O_2 \rightleftharpoons \text{Co(III)TPP}^{-}\text{-OO}\cdot \qquad (13)$$

The Co(III)TPP^{-}-OO· structure can explain the results shown in Fig. 1 in terms of its radical character. The electrophilic reactivity of the oxygen molecule activated on Co(II) tetra(*p*-tolyl)porphyrin should be noticed as a counterpart to the nucleophilic reactivity of other superoxide ions, which are originated, for example, from KO_2.

** The *g*-values for Co(II)TPP-O_2^- and the electrogenerated superoxide ion were measured at −196 °C in the absence of any substrates to be oxidized.[6]

† The transfer of the spin density from Co(II) to O_2 on complex formation is reported to be about 90% for Co(II)(acacen) and 100% for Co(II)(Schiff base)(base). Such oxygen complexes are formally described as Co(III)-O_2^-. The formal description can be also applied to the cobalt(II) protoporphyrin IX dimethyl ester (see Ref. 16).

References

1) R. Dietz, M. E. Peover, and P. Rothbaum, *Chem.-Ing.-Tech.*, **42**, 185 (1970).
2) T. Osa, Y. Ohkatsu, and M. Tezuka, *J. Fac. Eng., Univ. Tokyo*, **A-10**, 1 (1972).
3) T. Hara, Y. Ohkatsu, and T. Osa, *Bull. Chem. Soc. Jpn.*, **48**, 85 (1975).
4) J. S. Valentine and A. B. Curtis, *J. Am. Chem. Soc.*, **97**, 224 (1975).
5) R. A. Johnson and E. G. Nidy, *J. Org. Chem.*, **40**, 1680 (1975).
6) M. Tezuka, O. Sekiguchi, Y. Ohkatsu, and T. Osa, *Bull. Chem. Soc. Jpn.*, **49**, 2769 (1976).
7) Y. Ohkatsu and T. Osa, *Bull. Chem. Soc. Jpn.*, **50**, 2945 (1977).
8) P. Rothemund and A. R. Menotti, *J. Am. Chem. Soc.*, **70**, 1808 (1948).
9) N. M. Emanuel, "Liquid-Phase Oxidation of Hydrocarbon," Plenum Press, New York (1976).
10) C. Paquot, *Bull. Soc. Chim. Fr.*, **1941**, 695.
11) P. E. Van Sickle, F. R. Mayo, R. M. Arluck, and M. G. Syz, *J. Am. Chem. Soc.*, **89**, 967 (1967); *ibid.*, **89**, 977 (1967).
12) S. Korcek, J. H. B. Chenier, J. A. Howard, and K. U. Ingold, *Can. J. Chem.*, **50**, 2285 (1972).
13) Y. Ohkatsu, T. Okuyama, and T. Osa, *Yukagaku*, in press.
14) H. Hock and M. Siebert, *Ber.*, **87**, 554 (1954).
15) M. Bersohn, *J. Am. Chem. Soc.*, **86**, 959 (1964).
16) F. Basolo, B. M. Hoffman, and J. A. Ibers, *Acc. Chem. Res.*, **8**, 384 (1975).

A-Substituted 5β-Steroids. VIII. Synthesis and Bromination of 3-Alkyl-5β-cholestan-2-one

J. Yasuo SATOH, C. Akira HORIUCHI, and Akira HAGITANI

Department of Chemistry, Rikkyo (St. Paul's) University, Nishi-Ikebukuro, Toshima-ku, Tokyo 171

(Received April 26, 1977)

3α-Alkyl-5β-cholestan-2-one (R=CH_3, C_2H_5, and $CH_3CH_2CH_2$) was prepared by the direct alkylation of 5β-cholestan-2-one with alkyl iodide and potassium *t*-butoxide in a reflux of *t*-butyl alcohol-benzene. The 3α-benzyl ketone was prepared from 5β-cholestan-2-one by aldol condensation with benzaldehyde in the presence of potassium hydroxide, followed by hydrogenation of the condensation product. The bromination of these 3α-alkyl ketones gave 3β-bromo-3α-alkyl-5β-cholestan-2-ones.

The alkylation of the steroids which have an oxo group in ring A has been investigated.[1-4] In addition, the preparation and use of hydroxymethylene derivatives of 5β-stigmast-22-en-3-one[5] and pregn-4-ene-3,20-dione[6] have been described.

Recently, as a part of our studies on the A-substituted 5β-steroids, we reported the halogenation[7] of 5β-cholestan-2-one and some reactions[7] of their halo ketones. In the present paper, the direct alkylation of 5β-cholestan-2-one with alkyl iodide (RI; R=CH_3, C_2H_5, or $CH_3CH_2CH_2$) and potassium *t*-butoxide is described, together with the synthesis of α-benzyl ketone of 5β-cholestan-2-one. The bromination of these alkyl derivatives is also described.

Results and Discussion

The reaction of 5β-cholestan-2-one (**1**) with alkyl iodide (RI; R=CH_3, C_2H_5, and $CH_3CH_2CH_2$) and potassium *t*-butoxide yielded the corresponding alkylated ketones (**2a**, **2b**, and **2c**). Each alkylated ketone showed a weak negative Cotton effect in the CD spectrum compared with that of 5β-cholestan-2-one (**1**). Compound **2a** was identical with the hydrogenation product of a hydroxymethylene derivative (**4**), which was obtained by the condensation of 5β-cholestan-2-one with ethyl formate. To determine the position of the hydroxymethylene group in compound **4**, it was brominated with NBS and sodium acetate to yield 3β-bromo-5β-cholestan-2-one.[7] Thus compound **4** was confirmed to be 3-hydroxymethylene-5β-cholestan-2-one.

In order to determine the configuration of **2a** and **2b**, the synthesis of their epimers was attempted. Spencer *et al.*[8] reported that the methylation of the α-bromo ketone with zinc powder–methyl iodide in benzene–dimethyl sulfoxide (10 : 1) in a nitrogen atmosphere gave the α-methyl ketone which retained the configuration at the original site of the bromine. The reaction of 3β-bromo-5β-cholestan-2-one (**5**) with methyl iodide and with ethyl iodide in the presence of zinc powder according to the procedures described above by Spencer *et al.*[8] yielded compounds **6a** and **6b**, respectively. These products (**6a** and **6b**) were isomerized by treatment with concd sulfuric acid in ethanol to give the stable compounds **2a** and **2b**. The structures of the two compounds were confirmed to be 3β-methyl- (**6a**) and 3β-ethyl-5β-cholestan-2-one (**6b**). This was also supported by the CD spectra.

The reaction of 5β-cholestan-2-one (**1**) with benzaldehyde in the presence of base yielded benzylidene ketone (**11**). Hydrogenation of **11** gave a benzyl ketone (**2d**). By comparison with the CD spectra of 3α-alkyl ketones (**2a**, **2b**, and **2c**), the structure of the benzyl ketone (**2d**) was presumed to be 3α-benzyl-5β-cholestan-2-one (**2d**).

The bromination of the alkylated ketones (**2a**, **2b**, **2c**, and **2d**) gave the bromo derivative (**3a**, **3b**, **3c**, or **3d**).

On the basis of the CD, ORD, IR, and NMR spectral data for **3a**, **3b**, **3c**, and **3d**, the structures of these bromo derivatives were determined to be 3α-bromo-3α-alkyl-5β-cholestan-2-ones. This received support from the following evidence. The bromo derivatives (**3a**, **3b**, and **3d**) were reduced with sodium borohydride to give the bromohydrins (**7a**, **7b**, and **7d**), which were converted to the bromohydrin acetates (**8a**, **8b**, and **8d**). The NMR spectra of these bromohydrin acetates showed a quartet at δ 4.24 ppm (J=4.5 and 11.5 Hz) assignable to the 2α-H of an axial character. Therefore, **8a**, **8b**, and **8d** were presumed to be 2β-acetoxy-3β-bromo-3α-alkyl-5β-cholestane. By treating these bromohydrins with potassium hydroxide, the corresponding 3α-alkyl ketone (**2a**, **2b**, or **2d**) was obtained. From these results, a hydroxyl group and a bromine atom of the bromohydrins (**7a**, **7b**, and **7d**) were shown to be *cis*; this led to a 3β-bromo-3α-alkyl-2β-hydroxy-5β-cholestane structure for these bromohydrins.

It was found that the enolisation of the alkylated ketones (**2a** and **2b**) with 60% perchloric acid–acetic anhydride occurred in the direction of a carbon atom possessing an alkyl group, as shown by the NMR spectra. The bromination of the enolisation product (**10a**) of one (**2a**) of the alkylated ketones yielded the 3β-bromo-3α-methyl ketone (**3a**).

From these results, it is suggested that the enolisation of the alkylated ketone occurs at the C_2–C_3 position. The bromination of the 3α-alkyl ketone occurs at a carbon atom having an alkyl group, namely, the C_3β-bond, as has been reported for the bromination of the alkylated ketone.[2]

The reaction of 3β-bromo-3α-methyl ketone (**3a**) with lithium chloride gave the α,β-unsaturated ketone (**9a**), which showed absorptions at 1670 and 1632 cm^{-1} in its IR spectrum. It was determined to be 3-methyl-5β-cholest-3-en-2-one (**9a**) by means of its NMR spectrum, which showed a signal at δ 1.72 ppm due to the olefinic methyl proton. Hydrogenation of **9a** in the presence of 10% palladium charcoal gave the 3α-methyl ketone (**2a**). These facts indicate that the direct alkylation of 5β-cholestan-2-one occurs at the C_3 position.

The reaction of 5β-cholestan-2-one (**1**) with excess methyl iodide yielded the dimethylated ketone (**12**) and 3α-methyl ketone (**2a**).

The bromination product of the dimethylated ketone (**12**) was presumed to be 1β-bromo-3,3-dimethyl ketone (**13**) from the sign of the Cotton effect, the Δ[A]-, and the $\Delta\lambda_1$-values [+141 (+11,200) and +24 nm, as compared with the corresponding values for the dimethylated ketone (**12**)] in the ORD (CD) spectrum, the shift of the C=O stretching band (1703 cm^{-1}) in the IR spectrum, and from the signal (δ 4.29 ppm, singlet) due to the C_1HBr in the NMR spectrum. From these spectral data, it can be considered that the conformation in the A ring of **13** is a distorted form due to the 1 : 3-interaction between the C_1β–Br bond and the C_3β–Me bond.

The bromo ketone (**13**) was then converted to the dimethylated bromohydrin (**14**) by reduction with sodium borohydride, as described above. By treatment of **14** with potassium hydroxide in 2-propanol under reflexing conditions, the dimethylated ketone (**12**) was obtained. From these results, the dimethylated bromohydrin (**14**) was identified as 1β-bromo-2β-hydroxy-3,3-dimethyl-5β-cholestane.

Thus, on the basis of all of the foregoing results, it was concluded that the α-alkylation and the aldol condensation of 5β-cholestan-2-one (**1**) occur at the C_3 position, in contrast with the case of the enolisation and the halogenation of 5β-cholestan-2-one (**1**). It was further concluded that the enolisation of the alkylated ketone occurs in the direction of C_3, and that the bromination of these alkylated ketones forms the 3β-bromo-3α-alkyl ketones.

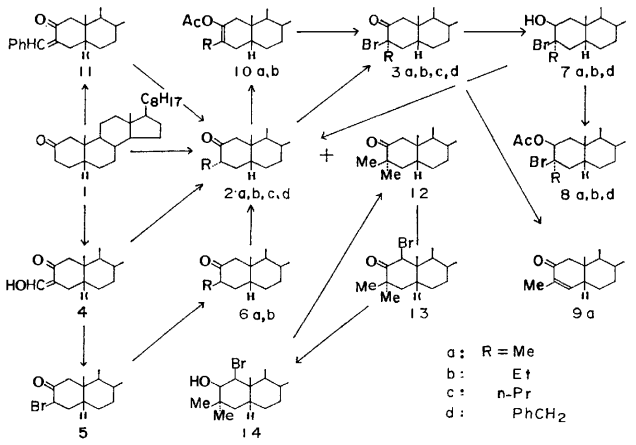

Experimental

All the melting points are uncorrected. The IR, ORD, and CD spectra were measured using a Hitachi model 215 grating infrared spectrophotometer and a model J-20 spectropolarimeter. The NMR spectra were measured in carbon tetrachloride, with TMS as the internal standard, using a nuclear magnetic resonance spectrometer, Hitachi-Perkin Elmer R-20A.

*3α-Methyl-5β-cholestan-2-one (**2a**)* A mixture of **1** (500 mg), methyl iodide (1.0 ml), and potassium *t*-butoxide (200 mg) in *t*-butyl alcohol-dry benzene (1 : 1) (10 ml) was refluxed under stirring in a nitrogen atmosphere for 2 h. The reaction was then removed under reduced pressure; the residue was poured into water and extracted with ether. The ethereal solution was washed with water, dried, and evaporated under reduced pressure. The resultant oil (510 mg) was chromatographed on silica gel (20 g). Elution with benzene–petroleum ether (1:5) (540 ml) gave plates of **2a** (55 mg), from methanol–acetone, mp 102.5—105.5 °C, IR (KBr): 1706 cm^{-1}; ORD (*c*, 0.980, Di) at 27 °C: $[\alpha]_D$ +36.7°, $[\alpha]_{400}$ +78.1°, $[\alpha]_{324}$ 0°, $[\alpha]_{316}$ −99.3° (trough), $[\alpha]_{311}$ 0°, $[\alpha]_{306}$ +49.0° (shoulder), $[\alpha]_{283}$ +410.7° (peak); CD (*c*, 0.980, Di) at 27 °C: $[\theta]_{311}$ −850° (shoulder), $[\theta]_{302}$ −1218° (trough), and $[\theta]_{294}$ −1019° (shoulder).

Found: C, 84.11; H, 11.84%. Calcd for $C_{28}H_{48}O$: C, 83.93; H, 12.08%.

The next fraction, eluted by the same solvent (360 ml) on crystallization from ethanol, gave plates of **1** (95 mg), mp 82—84.5 °C.

*3α-Ethyl-5β-cholestan-2-one (**2b**).* A mixture of **1** (3.0 g), potassium *t*-butoxide (3.02 g), and ethyl iodide (4.0 ml) in *t*-butyl alcohol-benzene was treated according to the procedure described for the methylation of **1**. After the usual work-up, the resultant oil was chromatographed on silica gel (100 g). Elution with hexane (800 ml) and hexane–benzene (10 : 1) (500 ml) gave plates of **2b** (601 mg) from ethanol, mp 92—93 °C, IR (KBr): 1706 cm^{-1}; ORD (*c*, 0.066, Di) at 20 °C: $[\alpha]_D$ +24.2°, $[\alpha]_{400}$ +54.5°, $[\alpha]_{335}$ +60.6°, $[\alpha]_{320}$ +24.2° (trough), and $[\alpha]_{292}$ +29.4° (peak); CD (*c*, 0.567, Di) at 19 °C: $[\theta]_{312}$ −453.6°, $[\theta]_{309}$ −434.3° (shoulder), $[\theta]_{304}$ −499.4° (trough), and $[\theta]_{275}$ +168.9° (peak).

Found: C, 84.14; H, 12.32%. Calcd for $C_{29}H_{50}O$: C, 83.99; H, 12.15%.

*3α-Propyl-5β-cholestan-2-one (**2c**).* A mixture of **1** (4.0 g), potassium *t*-butoxide (4.0 g), and propyl iodide (6.0 ml) in *t*-butyl alcohol-benzene (1 : 1) was treated according to the procedure described for the methylation of **1**. After the usual work-up, the resultant oil (4.1 g) was chromatographed on silica gel (100 g). Elution with hexane (1200 ml) gave plates of **2c** (282 mg) from ethanol–acetone, mp 74—74.5 °C, IR (KBr): 1706 cm^{-1}; ORD (*c*, 0.171, Di) at 21 °C: $[\alpha]_D$ +35.2°, $[\alpha]_{400}$ +117.3°, $[\alpha]_{328}$ +105.6° (trough), and $[\alpha]_{292}$ +263.9° (peak); CD (*c*, 0.572, Di) at 19 °C: $[\theta]_{310}$ −341.5°, $[\theta]_{303}$ −353.9° (trough), and $[\theta]_{273}$ +163.3° (peak).

Found: C, 84.34; H, 12.41%. Calcd for $C_{30}H_{52}O$: C, 84.04; H, 12.23%.

The next fraction was eluted with benzene (800 ml) and on crystallization from ethanol gave 5β-cholestan-2-one (**1**) (1.472 g), mp 86—88 °C.

*3-Hydroxymethylene-5β-cholestan-2-one (**4**).* The ketone (**1**) (753 mg) in dry benzene (10 ml) was treated with ethyl formate (763 mg) and sodium methoxide (131 mg) in a nitrogen atmosphere for 4 h at room temperature. The reaction mixture was then taken up in ether, and the ether extracts were washed with dilute hydrogen chloride and water, dried, and evaporated. The crystallization of the residue from methanol–ether gave plates of **4** (531 mg), mp 128—130 °C, IR (KBr): 1646 and 1593 cm^{-1}; UV (EtOH) λ_{max} 281 nm: (log 4.13).

Found: C, 80.88; H, 11.54%. Calcd for $C_{28}H_{46}O_2$: C, 81.10; H, 11.18%.

*3β-Methyl-5β-cholestan-2-one (**6a**).* The bromo ketone (**5**) (200 mg) in benzene–dimethyl sulfoxide (10 : 1) (11 ml) was stirred with zinc powder (500 mg) and methyl iodide (2.5 ml) in a nitrogen atmosphere at 40—45 °C for 4 h. After the usual work-up, the resultant oil (144 mg) was chromatographed on silica gel (30 g). Elution with hexane (100 ml) gave needles of **6a** (19 mg) from ethanol, mp 120—121 °C, IR (KBr): 1708 cm^{-1}; ORD (*c*, 0.6815, Di) at 22 °C: $[\alpha]_D$ −1.47°, $[\alpha]_{400}$ −5.87°, $[\alpha]_{320}$ −89.5° (trough), $[\alpha]_{312}$ −55.8°

(peak), $[\alpha]_{310}$ −60.2° (trough), and $[\alpha]_{274}$ +105.6° (peak); CD (*c*, 0.6815, Di) at 22 °C: $[\theta]_{316}$ −346.9° (shoulder), $[\theta]_{305}$ −570.3° (trough), $[\theta]_{301}$ −517.4° (peak), and $[\theta]_{296}$ −558.6° (trough).

Found: *m/e* 400.3718. Calcd for $C_{28}H_{48}O$: M, 400.6866.

The next fraction was eluted with hexane-benzene (1 : 1) (150 ml) and on crystallization from ethanol gave 5β-cholestan-2-one (**1**) (52 mg), mp 85—88 °C.

*3β-Ethyl-5β-cholestan-2-one (**6b**).* A mixture of **5** (320 mg), zinc powder (800 mg), and ethyl iodide (4.0 ml) in benzene-dimethyl sulfoxide (10 : 1) (17.6 ml) was treated according to the procedure described for the methylation of **5**. After the usual work-up, the resultant oil (295 mg) was chromatographed on silica gel (20 g). Elution with hexane-benzene (1 : 1) (250 ml) gave needles of **6b** (5 mg) from ethanol, mp 107—108 °C, IR (KBr): 1700 cm^{-1}; ORD (*c*, 0.336, Di) at 24 °C; $[\alpha]_D$ +68.4°, $[\alpha]_{400}$ +181.3°, $[\alpha]_{319}$ +633.2° (peak), $[\alpha]_{314}$ +591.6° (trough), $[\alpha]_{308}$ +633.2° (peak), $[\alpha]_{299}$ +401.3° (shoulder), and $[\alpha]_{273}$ +11.89° (trough); CD (*c*, 0.336, Di) at 24 °C: $[\theta]_{315}$ +1158.9° (shoulder), $[\theta]_{304}$ +2305.4° (peak), $[\theta]_{300}$ +2256.1° (trough), $[\theta]_{294}$ +2551.9° (peak), and $[\theta]_{287}$ +2157° (shoulder).

Found: *m/e* 414.3850. Calcd for $C_{29}H_{50}O$: M, 414.7134.

The next fraction was eluted with the same solvent (150 ml) and on crystallization from ethanol gave 5β-cholestan-2-one (**1**) (119 mg), mp 83—86 °C.

*Isomerization of 3β-Methyl- (**6a**) and 3β-Ethyl-5β-cholestan-2-one (**6b**).* 3β-Methyl (**6a**) and 3β-ethyl ketone (**6b**) (12 mg) in ethanol (10 ml) was treated with a few drops of concd sulfuric acid under refluxing for 2 h. After the usual work-up, crystallization from ethanol afforded plates of **2a** (7 mg) (mp 101—105 °C) and **2b** (5 mg) (mp 89—92 °C), respectively.

*Hydrogenation of 3-Hydroxymethylene-5β-cholestan-2-one (**4**).* The hydroxymethylene ketone (**4**) (200 mg) was hydrogenated in the usual method over 10% palladium charcoal in ethanol-ether (4 : 1) (25 ml). After the usual work-up, crystallization from ethanol afforded plates of **2a** (97 mg), mp 101—103 °C.

*3β-Bromo-5β-cholestan-2-one (**5**).* A mixture of **4** (100 mg), sodium acetate (132 mg) in acetic acid (0.12 ml), and *N*-bromosuccinimide (44.6 mg) in dioxane-water (10 : 1) (11 ml) was stirred overnight at room temperature. After the usual work-up, crystallization of the residue from ethanol gave plates of **5** (67 mg), mp 139—142 °C.

*3β-Bromo-3α-methyl-5β-cholestan-2-one (**3a**).* The methylated ketone (**2a**) (500 mg) in acetic acid (20 ml) was treated with bromine (219 mg) in acetic acid (1.5 ml) containing a few drops of 48% hydrobromic acid at room temperature for 15 min. The reaction mixture was taken up in ether, and the ethereal extracts were washed with a sodium hydrogencarbonate solution and water, dried, and evaporated. The crystallization of the residue from ethanol gave needles of **3a** (364 mg), mp 126—128 °C, IR (KBr): 1712 cm^{-1}; ORD (*c*, 0.794, Di) at 24 °C: $[\alpha]_D$ −94.4°, $[\alpha]_{400}$ −582.4°, $[\alpha]_{337}$ +3085° (trough), and $[\alpha]_{290}$ +3728° (peak); CD (*c*, 0.794, Di) at 24 °C: $[\theta]_{314}$ −25710° (trough).

Found: C, 69.47; H, 9.56%. Calcd for $C_{28}H_{47}OBr$: C, 70.11; H, 9.88%.

*3β-Bromo-3α-ethyl-5β-cholestan-2-one (**3b**).* The bromination of **2b** (50 mg) was carried out using the technique described for the synthesis of 3β-bromo-3α-methyl-5β-cholestan-2-one. After the usual work-up, the resultant oil, on crystallization from methanol, gave needles of **3b** (25 mg), mp 85—86 °C, IR (KBr): 1709 cm^{-1}; ORD (*c*, 0.220, Di) at 22 °C: $[\alpha]_D$ −43.1°, $[\alpha]_{400}$ −272.3°, $[\alpha]_{339}$ −1234° (trough), and $[\alpha]_{290}$ +1688° (peak); CD (*c*, 0.220, Di) at 22 °C: $[\theta]_{318}$ −11469° (trough) and $[\theta]_{290}$ +1688° (peak).

Found: C, 70.12; H, 10.33%. Calcd for $C_{29}H_{49}OBr$: C, 70.57; H, 10.01%.

*3β-Bromo-3α-propyl-5β-cholestan-2-one (**3c**).* The bromination of **2c** (290 mg) was carried out using the technique described for the synthesis of 3β-bromo-3α-methyl-5β-cholestan-2-one. After the usual work-up, the resultant oil, on crystallization from methanol-acetone, gave needles of **3c** (136 mg), mp 83—84 °C, IR (KBr): 1709 cm^{-1}; ORD (*c*, 0.287, Di) at 23 °C: $[\alpha]_D$ −65.4°, $[\alpha]_{400}$ −505.8°, $[\alpha]_{338}$ −2591.6° (trough), $[\alpha]_{318}$ 0°, and $[\alpha]_{289}$ +3261° (peak); CD (*c*, 0.287, Di) at 23 °C: $[\theta]_{318}$ −22753° (trough).

Found: C, 71.06; H, 10.21%. Calcd for $C_{30}H_{51}OBr$: C, 70.98; H, 10.13%.

*3-Benzylidene-5β-cholestan-2-one (**11**).* The ketone (**1**) (256 mg) in methanol (50 ml) was refluxed under stirring with benzaldehyde (7.8 ml) and sodium hydroxide (1.4 g) for 2.5 h. The reaction mixture was then removed under reduced pressure; the residue was poured into water, and extracted with ether. The ethereal solution was washed with sodium bisulfite solution and water, dried, and evaporated. The crystallization of the residue from methanol gave plates of **11** (270 mg), mp 140—141 °C, IR (KBr): 1675, 1587, and 1569 cm^{-1}.

Found: C, 86.04; H, 10.90%, Calcd for $C_{34}H_{50}O$: C, 86.02; H, 10.61%.

*3α-Benzyl-5β-cholestan-2-one (**2d**).* The benzylidene ketone (**11**) (2.10 g) was hydrogenated in the usual way over 10% palladium charcoal in ethanol-ether (10 : 1) (150 ml). After 4 h, the filtrate from catalyst was evaporated under reduced pressure. The crystallization of the residue from ethanol gave needles of **2d** (1.751 g), mp 134—135 °C, IR (KBr): 1709 and 1600 cm^{-1}; ORD (*c*, 0.381, Di) at 22 °C: $[\alpha]_D$ +99.7°, $[\alpha]_{400}$ +251.9°, $[\alpha]_{316}$ +426.4° (trough), and $[\alpha]_{284}$ +911.8° (peak); CD (*c*, 0.238, Di) at 21 °C: $[\theta]_{312}$ −800.7° (trough), $[\theta]_{308}$ −688.1° (peak), and $[\theta]_{303}$ −738.1° (trough).

Found: C, 85.96; H, 11.12%. Calcd for $C_{34}H_{52}O$: C, 85.65; H, 10.99%.

*3β-Bromo-3α-benzyl-5β-cholestan-2-one (**3d**).* A mixture of **2d** (959 mg), bromine (354 mg) in acetic acid (3.1 ml) containing a few drops of 48% hydrobromic acid, and acetic acid (40 ml) was allowed to react according to the procedure described for the synthesis of the 3β-bromo-3α-methyl ketone. After the usual work-up, the resultant oil, on crystallization from ethanol, gave needles of **3d** (604 mg), mp 109—111 °C, IR (KBr): 1712 cm^{-1}; ORD (*c*, 0.333, Di) at 22 °C: $[\alpha]_D$ +21.0°, $[\alpha]_{460}$ 0°, $[\alpha]_{400}$ −24.0°, $[\alpha]_{238}$ −1005.7° (trough), $[\alpha]_{321}$ 0°, and $[\alpha]_{290}$ +2176.5° (peak); CD (*c*, 0.333, Di) at 22 °C: $[\theta]_{318}$ −13212° (trough).

Found: C, 73.61; H, 9.30%. Calcd for $C_{34}H_{51}OBr$: C, 73.49; H, 9.25%.

*3-Methyl-5β-cholest-3-en-2-one (**9a**).* A mixture of **3a** (115 mg), lithium chloride (250 mg), and *N*,*N*-dimethylformamide (10 ml) was refluxed under stirring for 40 min. The reaction mixture was then taken up in ether, and the ether extracts were washed with dilute hydrochloric acid and water, dried, and evaporated. The crystallization of the residue from methanol-ether gave plates of **9a** (55 mg), mp 114—115.5 °C, IR (KBr): 1670 cm^{-1}; NMR (CCl_4) δ=6.18 (1H, m) and 1.72 (3H, m); ORD (*c*, 0.346, Di) at 30 °C: $[\alpha]_D$ −15.9°, $[\alpha]_{400}$ −216.8°, $[\alpha]_{373}$ −439.4° (trough), $[\alpha]_{367}$ −427.9° (peak), $[\alpha]_{358}$ −508.8° (trough), $[\alpha]_{346}$ −263.1° (peak), $[\alpha]_{343}$ −268.9° (trough), $[\alpha]_{335}$ 0°, $[\alpha]_{331}$ +57.8° (peak), $[\alpha]_{329}$ +52.0° (trough), $[\alpha]_{320}$ +196.6° (peak), $[\alpha]_{315}$ +161.9° (trough), $[\alpha]_{311}$ +170.6° (peak), $[\alpha]_{296}$ 0°, $[\alpha]_{255}$ −2205.9° (trough), $[\alpha]_{242}$ 0°, and $[\alpha]_{222}$ +5392.2° (peak); CD (*c*, 0.346,

Di) at 30 °C: $[\theta]_{347}$ −2091° (trough), $[\theta]_{342}$ −2054° (peak), $[\theta]_{335}$ −2529° (trough), $[\theta]_{328}$ −2054° (shoulder), $[\theta]_{280}$ −209.2° (peak), $[\theta]_{241}$ −14182° (trough), $[\theta]_{224}$ 0°, and $[\theta]_{214}$ +60168° (peak).

Found: C, 84.18; H, 11.86%. Calcd for $C_{28}H_{46}O$: C, 84.35; H, 11.63%.

*Hydrogenation of 3-Methyl-5β-cholest-3-en-2-one (**9a**).* A mixture of **9a** (50 mg), 10% palladium charcoal, and hydrogen in ethanol was treated according to the procedure described for the hydrogenation of **4**. After the usual work-up, the resultant oil, on crystallization from ethanol, gave plates of **2a** (19 mg), mp 101—103 °C.

*3,3-Dimethyl-5β-cholestan-2-one (**12**).* The ketone (**1**) (1.0 g) in *t*-butyl alcohol-dry benzene (1 : 1) (25 ml) was treated with methyl iodide (11.0 ml) and potassium *t*-butoxide (3.0 g) under refluxing in a nitrogen atmosphere for 6 h. After the usual work-up, the resultant oil (1.065 g) was chromatographed on silica gel (100 g). Elution with benzene-petroleum ether (1 : 5) (720 ml) gave plates of **12** (365 mg) from acetone, mp 100—101.5 °C, IR (KBr): 1706 cm^{-1}, ORD (*c*, 1.132, Di) at 22 °C: $[\alpha]_D$ +1.77°, $[\alpha]_{400}$ −53.5°, $[\alpha]_{319}$ −954.4° (trough), $[\alpha]_{311}$ −600.9° (peak), $[\alpha]_{309}$ −636.3° (trough), $[\alpha]_{303}$ 0°, and $[\alpha]_{275}$ +1113.4° (peak); CD (*c*, 1.132, Di) at 22 °C: $[\theta]_{313}$ −3870° (shoulder), $[\theta]_{303}$ −6289° (trough), $[\theta]_{298}$ −6047° (peak), and $[\theta]_{294}$ −6168° (trough).

Found: C, 84.53; H, 12.17%. Calcd for $C_{29}H_{50}O$: C, 83.99; H, 12.15%.

The next fraction, eluted with the same solvent (570 ml), on crystallization from methanol-acetone gave 3α-methyl-5β-cholestan-2-one (**2a**) (147 mg), mp 97—104 °C.

*1β-Bromo-3,3-dimethyl-5β-cholestan-2-one (**13**).* The bromination of **12** (300 mg) was carried out using the technique described for the synthesis of **3a**. After the usual work-up, the resultant oil, on crystallization from acetone, gave needles of **13** (200 mg), mp 138—141 °C, IR (KBr): 1703 cm^{-1}; NMR (CCl_4) δ=4.29 (1H, s); ORD (*c*, 0.365, Di) at 30 °C: $[\alpha]_D$ +30.1°, $[\alpha]_{400}$ +123.2°, $[\alpha]_{343}$ +533.8° (peak), $[\alpha]_{320}$ 0°, and $[\alpha]_{280}$ −588.5° (trough); CD (*c*, 0.365, Di) at 30 °C: $[\theta]_{321}$ +4906° (peak), $[\theta]_{317}$ +3746° (trough), $[\theta]_{312}$ +3836° (peak), and $[\theta]_{230}$ −3479° (trough).

Found: C, 70.38; H, 10.27%. Calcd for $C_{29}H_{49}OBr$: C, 70.57; H, 10.01%.

*The Enolisation of 3α-Methyl-5β-cholestan-2-one (**2a**).* This enolisation was treated according to the method of the enolisation described for 5β-cholestan-2-one.[7] The reaction product gave plates of 2-acetoxy-3-methyl-5β-cholest-2-ene (**10a**) from ethanol, mp 78—79 °C, IR (KBr): 1750 and 1739 cm^{-1}; NMR ($CDCl_3$) δ=2.11 (3H, s). A mixture of **10a** (20 mg), bromine (7.9 mg) in tetrachloromethane, and tetrachloromethane (10 ml) containing a few drops of epichlorohydrin was carried out according to the directions of Djerassi *et al.* described for 2-acetoxy-5α-cholest-2-ene.[9] After the usual work-up, the resultant oil, on crystallization from ethanol, gave needles of **3a** (15 mg), mp 126—128 °C.

*Confirmation of the Configuration of 3β-Bromo-3α-methyl-5β-cholestan-2-one (**3a**) by Using Chemical Reactions.* The bromo derivative (**3a**) (60 mg) in methanol-ether (1 : 2) (15 ml) was treated with sodium borohydride (20 mg) at room temperature. After 45 min, water was added and the mixture was extracted with ether. The ethereal solution was washed with water, dried, and evaporated under reduced pressure. Attempts to crystallize the resultant oil (**7a**) were unsuccessful, and the product was used for the next step without purification [IR (NaCl): 3444 cm^{-1}]. A mixture of the methyl bromohydrin (**7a**) (15 mg), acetic anhydride (3 ml), and pyridine (3 ml) was allowed to stand at room temperature overnight. After the usual work-up, attempts to crystallize the resultant oil (**8a**) were unsuccessful. The methylated bromohydrin (**7a**) (35 mg) in 2-propanol (5 ml) was treated with a solution of potassium hydroxide (20 mg) in the same solvent (3 ml), and the mixture was refluxed for 30 min. 2-Propanol was then removed under reduced pressure; the residue was diluted with water, and extracted with ether. The ethereal solution was washed with water, dried, and evaporated under reduced pressure. Crystallization of the residue from methanol gave plates of **2a** (13 mg), mp 101—104 °C.

*Confirmation of the Configuration of 1β-Bromo-3,3-dimethyl-5β-cholestan-2-one (**13**) by Using Chemical Reactions.* The dimethylated bromo ketone (**13**) (150 mg) in methanol-ether (1 : 2) (30 ml) was treated with sodium borohydride (50 mg) at room temperature. After the usual work-up, the resultant oil, on crystallization from ethanol-ether, gave needles of dimethylated bromohydrin (**14**) (97 mg), mp 118—119 °C, IR (KBr): 3575 cm^{-1}; NMR (CCl_4) δ=4.75 (1H, d, J=3.6 Hz). A mixture of **14** (57 mg) and potassium hydroxide (46 mg) in 2-propanol (10 ml) was allowed to react according to the procedure described for the synthesis of 3α-methyl ketone (**2a**) from 3-methyl bromohydrin (**7a**). After the usual work-up, the resultant oil, on crystallization from acetone, gave plates of **12** (17 mg), mp 100—101.5 °C.

The authors are indebted to Mr. Takashi Takakuwa, Applied Research Laboratory of the Japan Spectroscopic Co., Ltd., for the measurement of ORD and CD spectra, and to Mr. Isao Yoshino for collaboration in the experimental work. This research was supported in part by a Matsunaga Research Grant from the Matsunaga Science Foundation.

References

1) R. B. Woodward, A. A. Patchett, D. H. R. Barton, D. A. J. Ives, and R. B. Kelly, *J. Am. Chem. Soc.*, **76**, 2852 (1954).

2) Y. Mazur and F. Sondheimer, *J. Am. Chem. Soc.*, **80**, 5220 (1958).

3) P. Morand, J. M. Lyall, and H. Stollar, *J. Chem. Soc.*, **1970**, 2117.

4) F. Sondheimer, Y. Klinbansky, Y. M. Y. Haddad, G. H. R. Summer, and W. Klyne, *J. Chem. Soc.*, **1961**, 767.

5) R. O. Clinton, R. L. Clarke, F. W. Stonner, A. J. Manson, K. F. Jennings, and D. K. Phillips, *J. Org. Chem.*, **27**, 2800 (1962).

6) K. Tsuda and S. Nozoe, *Chem. Pharm. Bull.*, **7**, 232 (1959).

7) J. Y. Satoh, C. A. Horiuchi, T. Matsukura, and A. Hagitani, *Bull. Chem. Soc. Jpn.*, **41**, 3032 (1968); J. Y. Satoh, C. A. Horiuchi, and A. Hagitani, *ibid.*, **43**, 491 (1970); J. Y. Satoh, C. A. Horiuchi, and A. Hagitani, *Chem. Lett.*, **1972**, 995; C. A. Horiuchi, *St. Paul's Rev. Sci.*, **3**, 73 (1973); J. Y. Satoh, C. A. Horiuchi, and A. Hagitani, *Bull. Chem. Soc. Jpn.*, **48**, 1282 (1975).

8) T. A. Spencer, R. W. Britton, and D. S. Watt, *J. Am. Chem. Soc.*, **89**, 5727 (1967).

9) C. Djerassi and T. Nakano, *Chem. Ind.*, **1960**, 1385; T. Nakano, M. Hasegawa, and C. Djerassi, *Chem. Pharm. Bull.*, **11**, 465 (1962).

An Anion Radical Precursor in the Nucleophilic Substitution of *p*-Dinitrobenzene

Takehiro ABE and Yusaku IKEGAMI*

College of General Education, Tohoku University, Kawauchi, Sendai 980

** Chemical Research Institute of Non-Aqueous Solutions, Tohoku University, Katahira-2-chome, Sendai 980*

(Received May 4, 1977)

Appearance of *p*-dinitrobenzene anion radical has been demonstrated by visible and ESR spectroscopy in the replacement of the one nitro group of *p*-dinitrobenzene by hydroxide ion in aqueous dimethyl sulfoxide. The formation of the anion radical seems to be due to the direct electron transfer from hydroxide ion to *p*-dinitrobenzene. The results of kinetic studies suggest that the anion radical is a precursor in the substitution reaction.

It has been strongly postulated that an *o*-dinitrobenzene anion radical is a precursor in the substitution reaction of the one nitro group of *o*-dinitrobenzene (*o*-DNB) by hydroxide ion in aqueous dimethyl sulfoxide (DMSO).[1] The anion-radical precursor mechanism[2] essentially differs from the widely-accepted conventional one, in which the nucleophilic aromatic substitution should proceed only *via* the Meisenheimer-type intermediate.

In order to pursue the anion-radical precursor mechanism, the following investigations have been made on a similar substitution reaction of *p*-dinitrobenzene (*p*-DNB).[3] (1) Demonstration of the appearance of *p*-DNB$^{\cdot-}$ (the *p*-dinitrobenzene anion radical) by visible and ESR spectroscopy. (2) Discussion on the possibility of the direct electron-transfer from the nucleophilic reagent to *p*-DNB. (3) Kinetic studies for confirmation of the view that the anion radical is the precursor in the replacement of the one nitro group of *p*-DNB by hydroxide ion in aqueous DMSO. Comparison of the results with those for *o*-DNB is made.

Experimental

Commerical *p*-DNB was purified by recrystallization from benzene. DMSO was kept in contact with barium oxide for a week and fractionated twice under reduced pressure.

Unless otherwise stated, the mixing of degassed DMSO solutions of *p*-DNB with degassed DMSO solutions of sodium hydroxide was carried out in sealed cells for the measurements of electronic and ESR spectra. Before degassing, the cells in which the DMSO solutions had been placed were sealed by flame after blowing dry argon through the cells, since DMSO considerably takes up carbon dioxide. Unless argon is blown, the hydroxide ion in the DMSO solution placed in the cell is considerably consumed. Path lengths of 0.1—3 cm were available for the measurements of electronic spectra. Electronic-spectral changes were recorded with a Cary 14 recording spectrophotometer equipped with a thermostated cell compartment. ESR spectra were recorded with a Varian E-4 EPR spectrometer.

Results and Discussion

When a DMSO solution of *p*-DNB was mixed with an aqueous DMSO solution of sodium hydroxide, the resulting reaction system showed absorption spectral changes shown in Figs. 1 and 2. All the absorption curves in Fig. 1 are corrected for the absorption of DMSO, since DMSO absorbs above 700 nm.[1] The reaction system shows characteristic bands in the region

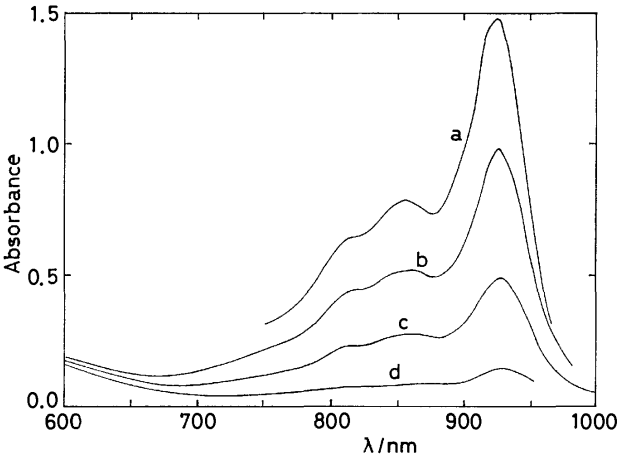

Fig. 1. Spectral change of the DMSO solution containing *p*-dinitrobenzene (3.34×10^{-4} M), sodium hydroxide (1.00×10^{-2} M), and 4%(v/v) water (25 °C). Starting time of scanning at 2.5 nm/s from longer wavelengths after mixing: a, 0.6 min; b, 2.4 min; c, 6 min; d, 11.4 min. Path length was 3.06 cm. All the curves are corrected for the absorption of DMSO.

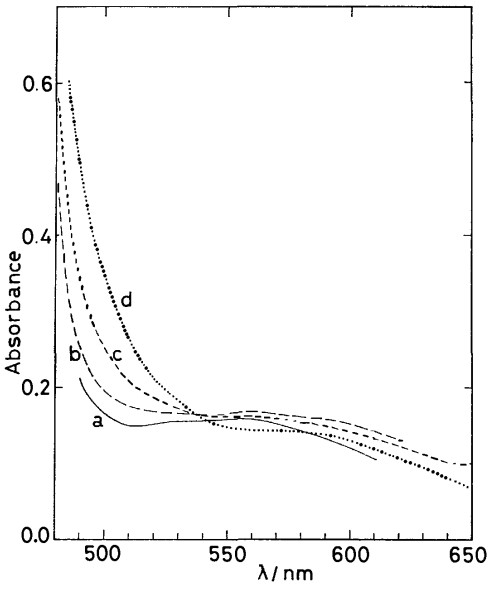

Fig. 2. Spectral change of the DMSO solution containing *p*-dinitrobenzene (3.42×10^{-4} M), sodium hydroxide (9.5×10^{-3} M), and 4%(v/v) water (25 °C). Starting time of scanning at 2.5 nm/s from longer wavelengths after mixing: a, 0.3 min; b, 1.3 min; c, 7.2 min; d, 60 min. Path length was 2.93 cm.

800—1000 nm and a weak band around 555 nm. The weak absorption shoulder is observed at *ca.* 580 nm in the final spectrum (curve d, Fig. 2). The shoulder is probably due to a small amount of a by-product. The bands in the region 800—1000 nm are similar to those of *p*-$DNB^{\cdot-}$ in a rigid solution in 2-methyltetrahydrofuran at 77 K,[4] and are assigned to *p*-$DNB^{\cdot-}$. The weak band around 555 nm is assumed to be the weak 475 nm band of *p*-$DNB^{\cdot-}$ in the rigid solution.[4] This was justified by calculating the absorption coefficient change at 560 nm. According to Shida and Iwata,[4] *p*-$DNB^{\cdot-}$ shows an intense band with vibrational structure in the range 380—430 nm. We were unsuccessful in scanning the spectral change in the range 400—500 nm when the reaction system was degassed, since an intense band rapidly developed at 430 nm. In the case of a similar reaction system open to the air, the initial band with a vibrational structure was observed at *ca.* 440 nm at 32 ms after mixing with a Hitachi rapid scan spectrophotometer RSP-2.[3] The time dependence of absorption-coefficient at 930, 560, and 430 nm is shown in Figs. 3 and 4. Curve b in Fig. 3 indicates that the entire absorption at 430 nm is not due to one species, since the increase in the coefficient slows down at *ca.* 1 min after mixing. We thus infer that the band assigned to *p*-$DNB^{\cdot-}$ initially appears in the range 400—500 nm.

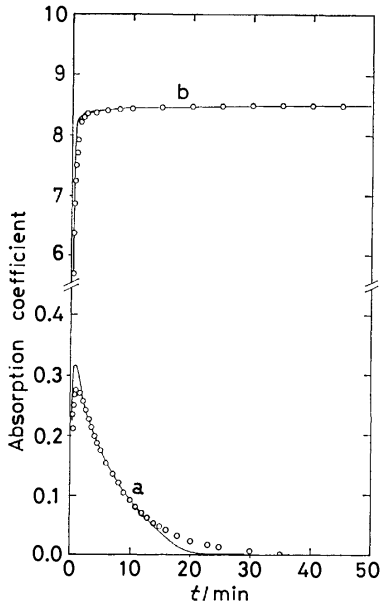

Fig. 3. Time courses (full lines) of absorption coefficient of the same solution as in Fig. 1 (25.0 °C). a, 930 nm; b, 430 nm. Circles show the values calculated according to Eqs. 1—4.

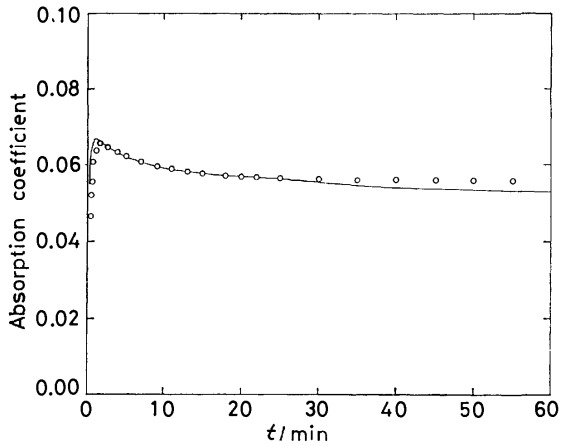

Fig. 4. Time course (full line) of 560-nm absorption coefficient of the same solution as in Fig. 1 (25.0 °C). Circles show the values calculated according to Eqs. 2 and 4.

The reaction system finally showed the 430 nm band identical with that of a similar solution of *p*-nitrophenol in the peak position and shape. A yellow substance was obtained by evaporating the solvent from the final reaction system under reduced pressure at *ca.* 60 °C. Treatment of the substance with aqueous hydrochloric acid gave *p*-nitrophenol. Thus, the final species showing the 430 nm band was identified as *p*-nitrophenoxide ion. The formation of *p*-nitrophenoxide ion in the reaction of *p*-DNB with hydroxide ion in aqueous DMSO open to the air has also been identified spectroscopically by Bowden and Cook.[5] The yield of *p*-nitrophenoxide ion based on spectroscopic estimation was over 90%. Thin-layer chromatography also showed *p*-nitrophenol as the major product. The production of nitrite ion was confirmed by the brown ring test.

The formation of the labile *p*-$DNB^{\cdot-}$ in the reaction system was confirmed by ESR spectroscopy. The generation of *p*-$DNB^{\cdot-}$ in a similar reaction system has been reported by Bilkis and Shein.[6] The reaction system under study showed a strong ESR signal. The hyperfine structure of the ESR spectrum (Fig. 5) is in line with that of the *p*-$DNB^{\cdot-}$ having two equivalent nitrogen atoms. The splitting constants, $a_N = 1.68$ and $a_H = 1.12$ G, agree with the reference values.[7] The time dependence of relative ESR-signal intensity of *p*-$DNB^{\cdot-}$ in the reaction system at *ca.* 24 °C resembles that of the absorption coefficient change at 930 nm in Fig. 3. No other radical species was found in the ESR spectrum of the reaction system. The result eliminates all the schemes in which other free radicals produced reversibly should live together for a length of time with *p*-$DNB^{\cdot-}$, and which do not give the pseudo-first order decomposition of *p*-$DNB^{\cdot-}$, because the decomposition of *p*-$DNB^{\cdot-}$ obeys the pseudo-first order kinetics.[1] Thus *p*-$DNB^{\cdot-}$ is not produced from a Meisenheimer-type complex.

The formation of *p*-$DNB^{\cdot-}$ in DMSO is not due to the electron transfer from methylsulfinylmethanide[8]

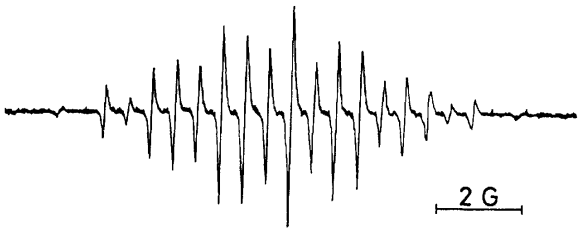

Fig. 5. ESR Spectrum of the same solution as in Fig. 1 (*ca.* 24 °C).

to *p*-DNB, since the mixture obtained by mixing an aqueous solution of sodium hydroxide with an *N,N*-dimethylformamide solution of *p*-DNB showed the same characteristic bands in the region 800—1000 nm as in Fig. 1.

The DMSO solution containing *p*-DNB (5.89×10^{-4} M), *p*-nitrophenol (2.56×10^{-3} M), sodium *p*-nitrophenoxide (1.25×10^{-3} M), and 4%(v/v) water showed no characteristic band in the region above 600 nm. The formation of *p*-$DNB^{\cdot-}$ is, therefore, not ascribed to electron transfer to *p*-DNB from the *p*-nitrophenol or *p*-nitrophenoxide ion produced by the conventional mechanism.

In a similar reaction system of *p*-DNB and hydroxide ion in aqueous DMSO solution, the production of the short-lived hydroxyl radical has been confirmed by Bilkis and Shein by means of spin-trapping with 2-nitroso-2-methylpropane.[6]

Thus, the formation of *p*-$DNB^{\cdot-}$ is probably due to the direct electron transfer from hydroxide ion to *p*-DNB. According to the electron transfer theory proposed by Nagakura and Tanaka,[9,10] nucleophilic aromatic substitution should proceed *via* the anion radical resulting from the one-electron transfer from the highest occupied orbital of a nucleophilic reagent to the lowest vacant orbital of an aromatic molecule. The energy level of the highest occupied orbital should be higher than that of the lowest vacant orbital. The lowest-vacant energy level of *p*-DNB can be estimated to be −6.14 eV from the values[11] of the lowest π-π^* transition energy (4.22 eV) and ionization potential (10.36 eV) of *p*-DNB. The energy level is sufficiently lower by 4.04 eV than the occupied energy level of OH^- (−2.1 eV[9]). The energy level difference of 4.04 eV would not be small in the DMSO solution owing to the poor solubility of OH^- in DMSO.[12] *p*-$DNB^{\cdot-}$ can be formed as a result of the direct electron transfer from hydroxide ion to *p*-DNB.

The plot of logarithmic absorption coefficient ($\log a$) at 930 nm *vs.* time *t* is shown in Fig. 6. We see that the decomposition of *p*-$DNB^{\cdot-}$ obeys the pseudo-first order kinetics from 2.5 min. The absorption coefficient

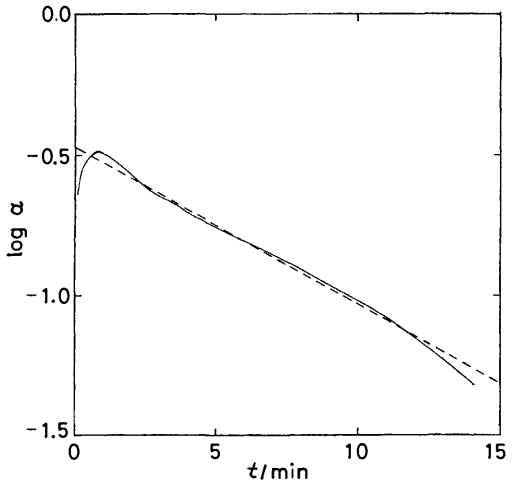

Fig. 6. Plot of logarithmic 930-nm absorption coefficient *vs.* time for curve a in Fig. 3.

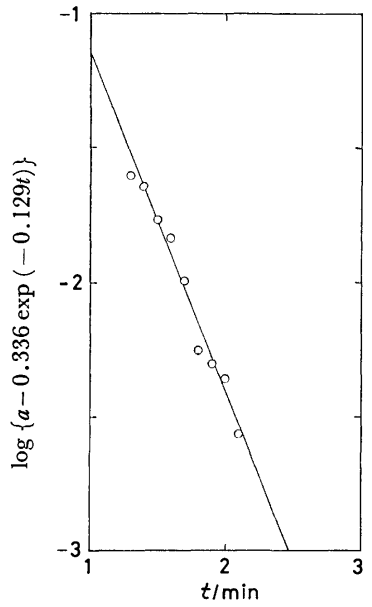

Fig. 7. Plot of $\log\{a-0.336\times\exp(-0.129t)\}$ *vs.* time. Here the values of *a* are those of curve a in Fig. 3.

is expressed by $0.336\times\exp(-0.129t)$ from 2.5 min. From 0.5 min to 2.5 min the $\log a$ values lie over a straight line, though all the $\log a$ values lie on or below the corresponding line in the case of *o*-DNB.[1] This indicates that at the initial stage the decomposition of *p*-$DNB^{\cdot-}$ consists of two kinds of parallel reactions. One of the reactions is probably the same as that where *o*-$DNB^{\cdot-}$ decomposes through the whole reaction course.[1] The degree of the overlying of $\log a$ (Fig. 6) varies to some extent in each measurement. Thus the other reaction, apparently observed at the initial stage, is very sensitive to the experimental conditions. As shown in Fig. 7, the plot of $\log\{a-0.336\times\exp(-0.129t)\}$ *vs.* *t* is linear. This indicates that the reaction of *p*-$DNB^{\cdot-}$ is of the pseudo-first order. The other may therefore be the rapid reaction of *p*-$DNB^{\cdot-}$ with a slight amount of the unknown intermediate appearing in a steady state at the initial stage.

We denote the initial concentrations of *p*-DNB and sodium hydroxide by $[p\text{-DNB}]_0$ and $[NaOH]_0$, respectively. Figure 8 shows that the decomposition of *p*-$DNB^{\cdot-}$ is relatively fast and of the first order in the case of $[NaOH]_0/[p\text{-DNB}]_0\geq3$, and that the decomposition is extremely slow in the case of $[NaOH]_0/[p\text{-DNB}]_0<3$. The slow decomposition is not due to the irradiation of the 930 nm light, since the decomposition proceeded in the absence of the light. It is indicated that the fast decomposition of *p*-$DNB^{\cdot-}$ requires hydroxide ion, and that the conditions of $[NaOH]_0\geq3[p\text{-DNB}]_0$ are necessary for the production of *p*-nitrophenoxide ion. Thus, the present reaction does not proceed by the $S_{RN}1$ mechanism,[13,14] which is characterized by the unimolecular decomposition of the anion radical. The hydroxide ion equivalent to $[p\text{-DNB}]_0$ will be consumed for ionizing *p*-nitrophenol, because *p*-nitrophenol scarcely dissociates in the DMSO solution containing 4%(v/v) water in the absence of sodium hydroxide. Thus, in analogy with the case of *o*-DNB,[1] the two

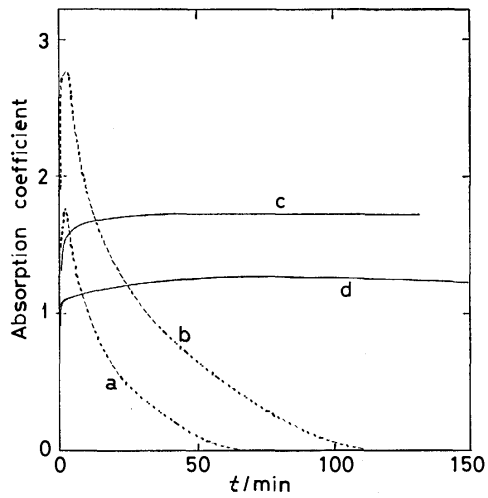

Fig. 8. Time courses of 930-nm absorption coefficient of the following DMSO solution containing 4% (v/v) water (25.0 °C).

	[*p*-DNB]$_0$ $\times 10^3$, M	[NaOH]$_0$ $\times 10^2$, M	[NaOH]$_0$/[*p*-DNB]$_0$
a	2.47	1.00	4.05
b	3.34	1.00	2.99
c	3.36	0.69	2.1
d	3.34	0.33	1.0

possible schemes for the present reaction may be written as shown in Scheme 1 where k_i denotes the rate constant for the ith step, and both k_1 and k_2 contain [NaOH]$_0$. Of course, k_3 is of the pseudo-first order and is negligible after 2.5 min. Since no band of intermediates other than that of *p*-DNB$^{\cdot-}$ is found in Figs. 1 and 2, we make the steady state treatment for the concentrations of **1** and **4**.

According to Scheme 1(a), the absorption coefficient

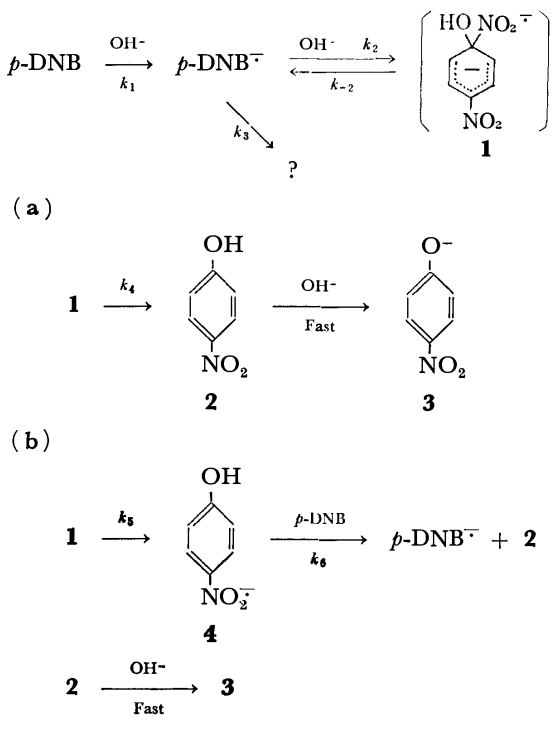

Scheme 1.

changes at 930 and 430 nm with time are expressed below under the conditions of [*p*-DNB]$_0 \ll$ [NaOH]$_0$.

$t<2.5$ min:

$$a(930\text{ nm}) = \frac{k_1\varepsilon_R[p\text{-DNB}]_0}{k_1-k_2'-k_3} \times [\exp\{-(k_2'+k_3)t\} - \exp(-k_1t)] \quad (1)$$

$$a(430\text{ nm}) = \frac{k_2'\varepsilon_3[p\text{-DNB}]_0}{k_2'+k_3} - \frac{k_1[p\text{-DNB}]_0}{k_1-k_2'-k_3} \times \left(\frac{k_2'\varepsilon_3}{k_2'+k_3}-\varepsilon_R'\right)\exp\{-(k_2'+k_3)t\} - \frac{[p\text{-DNB}]_0}{k_1-k_2'-k_3} \times (k_1\varepsilon_R'-k_2'\varepsilon_3) \times \exp(-k_1t) \quad (2)$$

$t\geq 2.5$ min:

$$a(930\text{ nm}) = \frac{k_1\varepsilon_R[p\text{-DNB}]_0}{k_1-k_2'} \times \exp(-k_2't) \quad (3)$$

$$a(430\text{ nm}) = \varepsilon_3[p\text{-DNB}]_0 - \frac{k_1[p\text{-DNB}]_0}{k_1-k_2'} \times (\varepsilon_3-\varepsilon_R') \times \exp(-k_2't) \quad (4)$$

Here $k_2'=k_2k_4/(k_{-2}+k_4)$, and ε_R and ε_3 are molar absorption coefficients of *p*-DNB$^{\cdot-}$ and **3**, respectively. Equations 3 and 4 are similar to the corresponding equations for the case of *o*-DNB,[1] in which the terms including $\exp(-k_1t)$ are neglected. The values calculated according to Eqs. 1—4 are plotted in Fig. 3 by assuming the following values; $k_1=2.88$ min^{-1}, $k_2'=0.129$ min^{-1}, $k_3=0.002$ min^{-1}, $\varepsilon_R(930\text{ nm})=9.61\times10^2$, $\varepsilon_R'(430\text{ nm})=2.49\times10^4$, and $\varepsilon_3(430\text{ nm})=2.54\times10^4$. As compared with the corresponding rate constants of $k_1=0.638$ min^{-1} and $k_2'=0.0519$ min^{-1} for the case of *o*-DNB,[1] *p*-DNB$^{\cdot-}$ has formation and decomposition rates greater than those of *o*-DNB$^{\cdot-}$.

Equations 2 and 4 can be applied to the absorption coefficient change at 560 nm. The result obtained by assuming $\varepsilon_R''(560\text{ nm})=205$ and $\varepsilon_3'(560\text{ nm})=168$ is shown in Fig. 4. Figures 3 and 4 show that the calculated values of absorption coefficients at 930, 560, and 430 nm fairly agree with those observed. The value of $\varepsilon_R'(430\text{ nm})$ is considerably larger than that (*ca.* 1.6×10^4) of the 420 nm band of *p*-DNB$^{\cdot-}$ in the rigid solution at 77 K.[4] The value of $\varepsilon_3(430\text{ nm})$ is smaller than that of 3.17×10^4 for *p*-nitrophenoxide ion in a similar solution. This difference seems to be due mainly to the initial rapid reaction of *p*-DNB$^{\cdot-}$. The value of 3.34×10^{-4} M is calculated for the maximum concentration of *p*-DNB$^{\cdot-}$ by dividing the observed maximum absorption coefficient (0.321) at 930 nm (Fig. 3) by $\varepsilon_R(930\text{ nm})=9.61\times10^2$. The calculation shows that *p*-DNB was almost converted into *p*-DNB$^{\cdot-}$ within 0.7 min. The anion radical is, therefore, probably formed in the main reaction path.

The relation of $k_1=22.3\ k_2'$ and $k_2'=64.5\ k_3$ is obtained from the values assumed above for the case of Scheme 1(a). Under the conditions $k_1\gg k_2'\gg k_3$, Scheme 1(b) gives approximate expressions similar to those to which Eqs. 1—4 can be reduced. Accordingly, Scheme 1(b) is also possible in addition to Scheme 1(a). The mechanisms including the reaction to re-

produce *p*-DNB instead of the reaction step denoted by k_3 in Scheme 1 are also considered. Under the conditions $k_1 \gg k_2' \gg k_3$, however, the mechanisms give approximate expressions which cannot explain the appearance of the initial overlying of $\log a$ and are probably impossible. In conclusion, the kinetic results strongly suggest that *p*-$DNB^{\cdot-}$ is the precursor in the reaction, though we do not know which to select, Scheme 1 (a) or (b).

From the studies on the photosubstitution of 3,5-dinitroanisole[15,16] and on the reaction between DMSO and hydroxyl radical[17] the generation of *p*-$DNB^{\cdot-}$ may be accounted for by the following mechanism as in the case of *o*-$DNB^{\cdot-}$:[1]

$$p\text{-DNB} + OH^- \rightleftharpoons \underset{\mathbf{5}}{[p\text{-}DNB^{\cdot-}\cdots\dot{O}H]}$$

$$\mathbf{5} + CH_3SOCH_3 \longrightarrow p\text{-}DNB^{\cdot-} + \dot{C}H_3 + CH_3S(=O)\text{-}OH$$

The reaction between **5** and DMSO may be extremely rapid, because the rate constant for the reaction of hydroxyl radical with DMSO in aqueous solution is 5×10^9 $M^{-1}\,s^{-1}$ at 25 °C.[17] The methyl radical would undergo a rapid reaction. Thus, only *p*-$DNB^{\cdot-}$ may survive in the present reaction system. The production of short-lived hydroxyl radical[6] supports the formation of **5**.

References

1) T. Abe and Y. Ikegami, *Bull. Chem. Soc. Jpn.*, **49**, 3227 (1976).
2) All the references suggesting anion-radical precursors in the nucleophilic aromatic substitution were cited in Ref. 1.
3) T. Abe, *Chem. Lett.*, **1973**, 1339.
4) T. Shida and S. Iwata, *J. Phys. Chem.*, **75**, 2591 (1971).
5) K. Bowden and R. S. Cook, *J. Chem. Soc., B*, **1971**, 1765.
6) I. I. Bilkis and S. M. Shein, *Tetrahedron*, **31**, 969 (1975).
7) P. H. Rieger and G. K. Fraenkel, *J. Chem. Phys.*, **39**, 609 (1963).
8) G. A. Russell, E. G. Janzen, and E. T. Strom, *J. Am. Chem. Soc.*, **86**, 1807 (1964).
9) S. Nagakura and J. Tanaka, *Bull. Chem. Soc. Jpn.*, **32**, 734 (1959).
10) S. Nagakura, *Tetrahedron*, **19**, Suppl. 2, 361 (1963).
11) M. D. Gordon and J. F. Neumer, *J. Phys. Chem.*, **78**, 1868 (1974).
12) A. J. Parker, *Quart. Rev.*, **16**, 163 (1962).
13) J. K. Kim and J. F. Bunnett, *J. Am. Chem. Soc.*, **92**, 7463, 7464 (1970).
14) J. F. Bunnett, *Acc. Chem. Res.*, **5**, 139 (1972).
15) G. P. de Gunst and E. Havinga, *Tetrahedron*, **29**, 2167 (1973).
16) W. G. Dauben, L. Salem, and N. J. Turro, *Acc. Chem. Res.*, **8**, 41 (1975).
17) B. C. Gilbert, R. O. C. Norman, and R. C. Sealy, *J. Chem. Soc., Perkin Trans. 2*, **1975**, 303.

Optical Activation of 2-Phenylpropionaldehyde *via* Some 2-Substituted Pyrrolidine Enamines

Hajime MATSUSHITA, Yasuko TSUJINO, Masao NOGUCHI, Masahiko SABURI,* and Sadao YOSHIKAWA*

Central Research Institute, The Japan Tabacco and Salt Public Corporation, Umegaoka, Midori-ku, Yokohama, Kanagawa 227

Department of Synthetic Chemistry, Faculty of Engineering, The University of Tokyo, Hongo, Bunkyo-ku, Tokyo 113

(Received May 6, 1977)

Optical activation of 2-phenylpropionaldehyde (PPA) *via* enamines using L-proline derivatives as amine components was studied. *S*(+)-PPA was obtained when *R*(−)-2-methylpyrrolidine and *S*(−)-2-ethoxycarbonylpyrrolidine were used, while *R*(−)-PPA was obtained when *S*(−)-prolinamide, *N*-(L-prolyl)pyrrolidine, *N*-(L-prolyl)piperidine, *S*(+)-2-(1-pyrrolidinylmethyl)pyrrolidine, and *S*(+)-2-(piperidinomethyl)pyrrolidine were used. This suggests that there are two mechanisms for optical activation.

The syntheses of optically active carbonyl compounds have been studied by many workers.[1] The optical activation *via* enamines has been studied in our laboratories.[2-4] Formation of an enamine causes deprotonation from the α-carbon of a racemic α-substituted carbonyl compound, the transformation of the enamine into the iminium salt causing protonation at the carbon. In an asymmetrical circumstance, it is possible that stereospecific protonation to the enamine takes place in the formation of the salt.

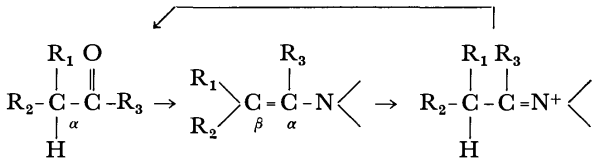

Carbonyl compound Enamine Iminium salt

In the case of optical activation of 2-methylcyclohexanone *via* optically active 2-methylpiperidine enamine, the chirality of the ketone obtained is determined by the stability of the iminium salt. The stability was affected by an interaction between the substituent in amine component and the residue of the enamine.

We have extended the study to the optical activation of PPA *via* enamine using amines derived from L-proline without inversion at the asymmetric carbon, and found that the chirality of the PPA obtained *via* enamines, **3**—**7** is *R*, and that *via* enamines, **1** and **2**, is *S*. This suggests that two reactions may participate in the induction of optical activity.

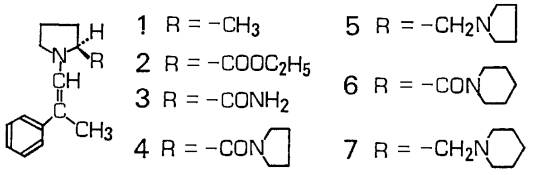

Experimental

Optical rotations were determined with a JASCO Digital Automatic Polarimeter Model DIP 181. Gas chromatographic analyses were carried out using a 2 m column of 20% Carbowax 20 M on Chromosorb W and of 20% SE-30 on Chromosorb W with a Hitachi Gas Chromatograph Model K53. Nuclear magnetic resonance spectra were measured with a JNM-PS-100 Spectrometer using tetramethylsilane or sodium 2,2-dimethyl-2-silapentane-5-sulfonate as an internal standard. Chemical shifts are given in δ values. Infrared spectra were obtained with a JASCO Model IR-G and mass spectra with a Hitachi GC-MS RM-50 (column: 10% SE-30 on Chromosorb W, 3 mm × 1 m).

Preparation of Amines. *S(−)-2-Ethoxycarbonylpyrrolidine*: Esterification of L-proline was carried out in the usual way.

S(−)-Prolinamide: A solution of *N*-benzyloxycarbonyl-L-proline (37.7 g, 0.15 mol) and triethylamine (15.3 g, 0.15 mol) in chloroform was cooled in an ice bath. Ethyl chloroformate (16.4 g, 0.15 mol) was added to the solution at 5—10 °C during a period of 10 min with stirring, the reaction being continued at 5—10 °C for 30 min. Aqueous ammonia (28 %, 40 ml) was then added dropwise to the reaction mixture with vigorous stirring under cooling. The pasty reaction mixture was stirred at 5—10 °C for 1 h. After removal of the aqueous layer, the chloroform layer was washed with an aqueous $NaHCO_3$ solution (5%) and water, and dried over Na_2SO_4. Chloroform was removed *in vacuo*, the residual oil (37.2 g) being crystallized from ethyl acetate. Recrystallization from ethyl acetate gave 29.4 g (78.4%) of *N*-benzyloxycarbonyl-L-prolinamide as mp 91—93.5 °C. IR (Nujol) 3180, 3370, 1670 cm^{-1}; NMR ($CDCl_3$) δ=7.36 (5H, s), 5.9—6.3 (2H, broad), 5.18 (2H, s) 4.2—4.44 (1H, broad), 3.4—3.7 (2H, broad), 1.7—2.4 (4H, m); $[\alpha]_D^{23}$ −34.0° (*c*=2.2, EtOH).

Hydrogenolysis of *N*-benzyloxycarbonyl-L-prolinamide (29.4 g) in ethanol was carried out with 5% Pd-C (1.8 g) in an atmosphere of hydrogen, L-prolinamide (5.7 g, 42.2%) being obtained as very fine white needles. Mp 104.0 °C; IR (Nujol) 3390, 3200, 1645 cm^{-1}; NMR (D_2O) δ=3.8 (1H, t), 3.0 (2H, t), 1.6—2.4 (4H, m); MS 114 (M^+), 70 (base), 43, 44; $[\alpha]_D^{23}$ −106.9° (*c*=0.90, EtOH).

N-(L-Prolyl)pyrrolidine: This was prepared according to the method reported by Otani and Yamada.[5]

S(+)-2-(1-Pyrrolidinylmethyl)pyrrolidine: This was prepared according to the method reported by Sone *et al.*[6]

N-(L-Prolyl)piperidine: The method employed was virtually identical with that for *N*-(L-prolyl)pyrrolidine except that pyrrolidine was replaced by piperidine. *N*-benzyloxycarbonyl-L-proline (43.8 g) gave *N*-(benzyloxycarbonyl-L-prolyl)-piperidine (19.0 g) as white needles from ether-ethyl acetate (4 : 1). Yield 34.3%; mp 93.5—94.5 °C; IR (Nujol) 1635 cm^{-1}; NMR ($CDCl_3$) δ=7.20 (5H), 4.75 (1H, t), 3.2—3.8 (6H, broad), 1.2—2.4 (10H, broad); $[\alpha]_D^{23}$ −14.5° (*c*=1.0, benzene).

Hydrogenolysis of *N*-(benzyloxycarbonyl-L-prolyl)piperi-

dine (18.8 g) in ethanol was carried out with 5% Pd-C (1.0 g) in an atmosphere of hydrogen, *N*-(L-prolyl)piperidine (8.0 g, 74%) being obtained. Bp 128 °C (2 mmHg); IR 3450, 1635 cm^{-1}; NMR ($CDCl_3$) δ=3.9 (1H, t), 3.4—3.7 (4H, broad), 3.06 (1H, s), 2.7—3.3 (2H, m), 1.3—2.4 (10H, broad); $[\alpha]_D^{23}$ −65.1° (c=2.0, benzene).

S(+)-2-(Piperidinomethyl)pyrrolidine: The method used here was virtually identical with that described for *S*(+)-2-(1-pyrrolidinylmethyl)pyrrolidine except that pyrrolidine was replaced by piperidine. Bp 72.0 °C (1.5 mmHg); IR 3300 cm^{-1}; NMR ($CDCl_3$) δ=1.2—2.0 (10H, broad), 2.2—2.7 (7H, broad), 2.7—3.2 (2H, m), 3.4 (1H, s); $[\alpha]_D^{23}$ +1.58° (c=2.2, benzene).

R*(−)-2-Methylpiperidine*: *dl*-2-Methylpiperidine (99 g) was treated with *d*-10-camphorsulfonic acid (125 g) in benzene. Recrystallization of the resulting salt was repeated seven times. The free base was isolated from the salt by the general method. Yield 4.1 g; bp 116—120 °C; $[\alpha]_D^{23}$ −16.4° (c=1.1, hexane).

Preparation of Enamines. Enamines were prepared by the usual azeotropic procedure using benzene as the solvent.

2: IR 1665 cm^{-1} ($\nu_{C=C}$); NMR ($CDCl_3$) mixture of two geometrical isomers in a 22 : 5 ratio at room temperature; major isomer δ=2.09 (C=C–CH_3, s), 6.30 (N–CH=C, s), minor isomer δ=1.96 (C=C–CH_3, s), 6.00 (N–CH=C, s); $[\alpha]_D^{23}$ +0.34° (c=33, benzene).

3: This could not be distilled because of its high boiling point and viscosity. Analysis was carried out using GC-MS. *m/e* 186, 125 (base), 117, 105, 97, 77, 70; $[\alpha]_D^{23}$ +24° (calculated for 100% yield).

4: Bp 175 °C (1.5 mmHg); IR 1638 cm^{-1} ($\nu_{C=C}$); NMR ($CDCl_3$) mixture of two geometrical isomers in a 25 : 7 ratio at room temperature; major isomer δ=2.15 (C=C–CH_3, s), 6.42 (N–CH=C, s), minor isomer δ=2.01 (C=C–CH_3, s), 6.13 (N–CH=C, s).

5: Bp 154 °C (3 mmHg); IR 1630 cm^{-1} ($\nu_{C=C}$); NMR ($CDCl_3$) mixture of two geometrical isomers in a 4 : 1 ratio at room temperature; major isomer δ=2.13 (C=C–CH_3, s), 6.55 (N–CH=C, s), minor isomer δ=2.05 (C=C–CH_3, s), 6.21 (N–CH=C, s); $[\alpha]_D^{23}$ +326.4° (c=1.0, benzene).

6: Bp 189 °C (2 mmHg); IR 1640 cm^{-1} ($\nu_{C=C}$); NMR ($CDCl_3$) mixture of two geometrical isomers in a 16 : 7 ratio at room temperature; major isomer δ=2.12 (C=C–CH_3, s), 6.34 (N–CH=C, s), minor isomer δ=2.00 (C=C–CH_3, s), 6.05 (N–CH=C, s); $[\alpha]_D^{23}$ −2.3° (c=9.0, benzene)

7: Bp 139 °C (1.5 mmHg); IR 1630 cm^{-1} ($\nu_{C=C}$); NMR ($CDCl_3$) mixture of two geometrical isomers in a 39 : 7 ratio at room temperature; major isomer δ=2.12 (C=C–CH_3, s), 6.54 (N–CH=C, s), minor isomer δ=2.03 (C=C–CH_3, s), 6.18 (N–CH=C, s); $[\alpha]_D^{23}$ +265.2° (c=1.7, benzene).

8: Physical data except for specific rotation were reported.[3] $[\alpha]_D^{23}$ −400° (neat).

Hydrolysis of Enamines. *Procedure A*: An equivalent aqueous HCl was added to a benzene solution of enamine in an ice bath with vigorous stirring for 30 min. The aqueous layer was removed and the benzene layer was washed with water several times, dried over Na_2SO_4 and the optical rotation was measured. The concentration of the solution was determined gas-chromatographically.

Procedure B: Dry HCl gas was bubbled into the anhydrous benzene solution of enamines to give the salts. The solution was heated up to 50 °C immediately and the temperature was maintained at 50—60 °C for 30 min. Water was added to the solution with vigorous stirring at 0 °C. Subsequent procedure was identical to that described above.

Oxidation of PPA. *R*(+)-2-Methylpiperidine enamine[3] of PPA (14.6 g) was hydrolyzed by procedure A, optically active PPA (7.06 g, 77.6%) being obtained. $[\alpha]_D^{23}$ +8.58° (c=8.8, benzene). The aldehyde was suspended in water (10 ml), and aqueous $KMnO_4$ (4.5 g in 100 ml) was added dropwise to the suspension.

The precipitated MnO_2 was filtered off, and the aqueous solution was made basic with NaOH pellets. After being washed with ether to remove PPA, the aqueous layer was acidified with HCl, and extracted with $CHCl_3$. The chloroform layer was dried over Na_2SO_4, and concentrated.

The residual oil was distilled to yield 4.1 g (52%). $[\alpha]_D^{23}$ +1.97° (c=6.3, benzene). This was identified as 2-phenylpropionic acid by IR and NMR.

Results and Discussion

Determination of the Absolute Configuration of PPA. In order to elucidate the optical activation mechanism, it is necessary to know the relationship between the direction of optical rotation and the absolute configuration of PPA. The problem was solved by oxidation of (+)-PPA into (+)-2-phenylpropionic acid which is known to have *S*-configuration.

Optical Activation of PPA via *Chiral Enamines.* Enamines were hydrolyzed according to procedure A. The results of the optical activation of PPA *via* enamines of L-proline derivatives and of *R*(−)-2-methylpiperidine are given in Table 1. The direction of optical rotation of PPA obtained is seen to be dependent on the amine components of enamines. Enamines, **1**, **2**, and **8**,[3] gave *S*(+)-PPA. On the other hand, enamines **3**—**7** gave *R*(−)-PPA. The substituents of the amine components in **4**—**7** are bulkier than those of **1**, **2**, and **8**. However, the bulkiness does not seem to determine the chirality of PPA obtained, since the bulkiness of the substituent of the amine component in enamine **3** which gave the same *R*(−)-PPA as **4**—**7** is not so large as that of **2**. The electronic effect of CH_2–N< and CO–N< in the substituents of amine components probably controls the mechanism of the optical activation as well as their steric effect.

It was difficult to isolate the enamines **2**, **3**, and **6**, because their boiling points and viscosities are high and they are unstable at a high temperature. The result of the optical activation *via* **4** suggests that a certain racemization of the enamines takes place during the course of distillation. The extent of racemization was not estimated, so the data in Table 1 cannot be compared except for the directions of the optical rotation.

Mechanism of Optical Activation. Since all the amine components except for *R*(−)-2-methylpiperidine were derived from L-proline, enamines **1**—**7** and their salts seem to have the same stereochemical configuration as regards their asymmetric carbon adjacent to nitrogen atom. With respect to the stereochemistry, **8** and its salts are also identical with **1** and its salts. However, the direction of the optical rotation of PPA obtained from **1**, **2**, and **8** differs from that from **3**—**7**. This suggests that there are two optical activation mechanisms. In a previous paper,[4] the optical activation mechanism of 2-methylcyclohexanone *via* its optically active 2-methylpiperidine enamine was accounted for by the thermodynamical stability of the correspond-

Table 1. Optical activation of PPA *via* enamines

Amine component		Enamine	Obtained ($[\alpha]_D^{25}$)	PPA[a]	Lit
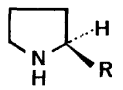	R=-CH_3	**1**	+51.6 (c=8.1)	*S*	3
	-$COOC_2H_5$	**2**	+0.34(c=33.2)[b]	*S*	
	-$CONH_2$	**3**	−3.10(c=9.1)[b]	*R*	
	-CON⟨ ⟩	**4**	−4.39(c=0.9) −18.6 (c=5.1)[b]	*R*	
	-CH_2N⟨ ⟩	**5**	−12.9 (c=3.0)	*R*	
	-CON⟨ ⟩	**6**	−2.30(c=9.0)[b]	*R*	
	-CH_2N⟨ ⟩	**7**	−9.72(c=2.2)	*R*	
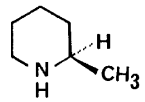		**8**	+80.8 (c=25.0)	*R*	3

a) Enamines hydrolyzed according to procedure A. b) No enamine isolated.

ing iminium salt. The mechanism seems to apply to the optical activation of PPA *via* enamines, **1**, **2**, and **8**. As shown in Scheme 1, the iminium salts would exist as an equilibrium mixture of diastereomeric isomers. The enamine can be considered to be an intermediate of these isomers in the solution. Displacement of the balance in the interconversion reaction in favor of one diastereomeric isomer results in the optically active aldehyde. The thermodynamical stability of the iminium salt determines the direction of the optical rotation of the aldehyde. The existence of the isomers (C) and (D) in the solution seems to be inappreciable in consideration of the steric interaction between substituent *R* and the substituents attached to β-carbon atom using Stuart and Dreiding models.[3] The structure shown in Fig. 1 is considered to be the most stable iminium salt. In this case, *S*(+)-PPA can be obtained from the hydrolyzate of this salt.

On the other hand, the reaction which gave *R*(−)-

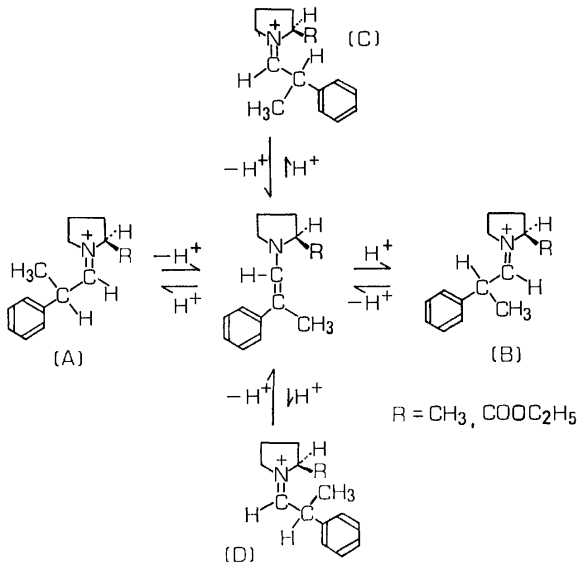

Scheme 1.

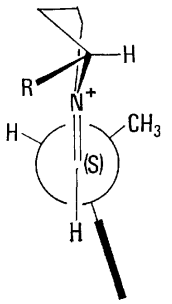

Fig. 1. The most stable structure of the iminium salt.

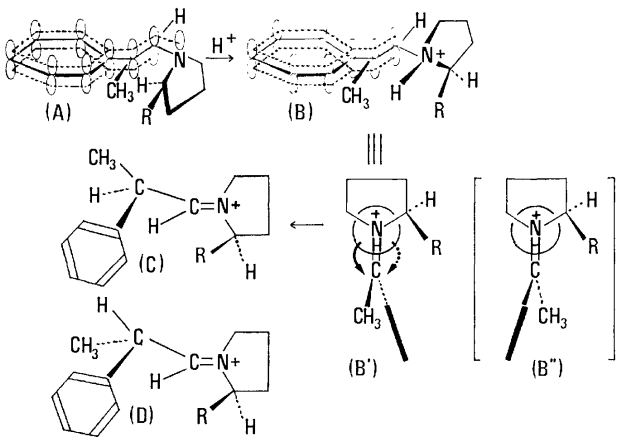

Fig. 2.

PPA is likely to proceed by a different mechanism from that mentioned above. This can be accounted for kinetically in the step of rearrangement from enammonium salt to iminium salt. It is known that protonation of enamines takes place on nitrogen and is followed by transfer of the proton to the β-carbon atom.[7] The electrostereochemical structures of the enamine and its salts are shown in Fig. 2. The enamine is characterized by the overlap of the nitrogen lone pair with the electrons of the double bond and the benzene ring

(Fig. 2(A)). The conversion from enamine into the corresponding enammonium salt implies the disappearance of the lone pair. Consequently, the amine moiety twists out of the coplanality of the olefinic group and the benzene ring (Fig. 2(B)). The geometrical isomer, structure (B″), would not exist because of the steric interaction between pyrrolidine ring moiety and C_β–CH_3. Thus, the predominant conformation of the enammonium salt would be structure (B′) in Fig. 2.

Rearrangement of the enammonium salt to the iminium salt implies the migration of the proton on the nitrogen atom to the β-carbon atom. The migration should take place following the path shown by the arrow(←) in Fig. 2-(B′) because the substituent **R** interferes in the migration in the opposite direction (←···). If hydrolysis of this iminium salt is rapid enough to neglect the contribution of the thermodynamical interconversion between C and D, it would predominantly give *R*(−)-PPA.

In the case of the methyl or ethoxycarbonyl group as a substituent of amine component, the thermodynamical equilibrium between the iminium salts is key step of the optical activation which gives *S*(+)-PPA.

On the other hand, when amine components have groups CH_2–N< or CO–N< as 2-substituents, the rearrangement from enammonium salt to iminium salt seems to be the key step of activation. The substituents probably stabilize the enammonium structure by the hydrogen bond between nitrogen or oxygen lone pair of these substituents and the *N*-coordinated hydrogen atom.

The isolation of the enammonium salt and its easy rearrangement to the corresponding iminium salt by heating were reported.[8] Enamines **3** and **6** which gave *R*(−)-PPA by the hydrolysis procedure A, were hydrolyzed according to procedure B. Application of heat before the addition of water promotes the rearrangement, and the thermodynamical equilibrium of the resulting iminium salts is reached. The results are shown in Table 2. *S*(+)-PPA was obtained according to procedure B, which supports the optical activation mechanism mentioned above.

TABLE 2. OPTICAL ACTIVATION OF PPA *via* ENAMINES
(Hydrolysis by procedure B)

Amine component	Enamine	Obtained PPA($[\alpha]_D^{23}$)
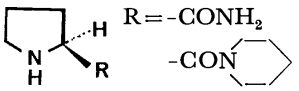 R=-$CONH_2$	**3**	+26.24 (c=0.2)
-CON<	**6**	+34.07 (c=3.1)
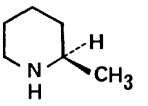	**8**	+71.5 (c=20.8)

There are two optical activation mechanisms of PPA *via* enamines which can be applied to the optical activation of other α-substituted carbonyl compounds. It is necessary to control these two mechanisms in order to obtain the higher or desirable optically active compounds.

References

1) K. Hiroi and S. Yamada, *Chem. Pharm. Bull.*, **23**, 1103 (1975); J. W. Scott, R. Borer, and G. Saucy, *J. Org. Chem.*, **37**, 1659 (1972); L. M. Kogan, V. E. Gulaya, and I. V. Torgov, *Tetrahedron Lett.*, **1967**, 4673; G, Bredig and K. Gajas, *Ber.*, **41**, 752 (1908); R. Kuhn, H. E. Driesen, and H. J. Maas, *Ann.*, **718**, 78 (1968); N. Marckwald and A. Mckenzie, *Ber.*, **32**, 2120 (1899).

2) H. Matsushita, M. Noguchi, M. Saburi, and S. Yoshikawa, *Bull. Chem. Soc. Jpn.*, **48**, 3715 (1975).

3) H. Matsushita, M. Noguchi, and S. Yoshikawa, *Bull. Chem. Soc. Jpn.*, **49**, 1928 (1976).

4) H. Matsushita, Y. Tsujino, M. Noguchi, and S. Yoshikawa, *Bull. Chem. Soc. Jpn.*, **49**, 3629 (1976).

5) G. Otani and S. Yamada, *Chem. Pharm. Bull.*, **21**, 2112 (1973).

6) T. Sone, K. Hiroi, and S. Yamada, *Chem. Pharm. Bull.*, **21**, 2331 (1973).

7) A. G. Cook, "Enamines," Marcel Dekker, Inc., New York and London (1969), p. 117.

8) H. Matsushita, Y. Tsujino, M. Noguchi, and S. Yoshikawa, *Bull. Chem. Soc. Jpn.*, **50**, 1513 (1977).

Regeneration to the Native Form of Hen Egg-White Lysozyme from Its Protected Derivatives

Saburo AIMOTO and Yasutsugu SHIMONISHI

Institute for Protein Research, Osaka University, Yamada-kami, Suita, Osaka 565

(Received May 11, 1977)

The following derivatives of hen egg-white lysozyme were prepared from native hen egg-white lysozyme, 2-chlorobenzyloxycarbonyl-lysozyme, *S*-(4-methylbenzyl)-reduced-lysozyme, and 2-chlorobenzyloxycarbonyl-*S*-(4-methylbenzyl)-reduced-lysozyme. Treatment of these derivatives with anhydrous liquid hydrogen fluoride for 90 min at 0 °C yielded fully active lysozyme with recoveries, in order, of 23, 12, and 7.4%. The properties of the lysozyme recovered were identical with those of native hen egg-white lysozyme, and crystals of this material were indistinguishable from those of native enzyme.

Previously we[1,2] reported the effect of treatment of hen egg-white lysozyme (HEL) with anhydrous liquid hydrogen fluoride (HF) under the usual conditions for peptide synthesis. We recovered fully active enzyme in a crystalline state from HF-solutions of the native and reduced forms of HEL. As a further step in our studies on the chemical synthesis of HEL, this paper describes the preparation of various protected derivatives of HEL from native HEL and the regeneration of active enzyme from them. The protected derivatives synthesized were similar to protected polypeptides covering the entire sequence of HEL, that must be synthesized to obtain the complete lysozyme molecule. Studies were made on the introduction of protecting groups into HEL using the reagents *t*-butoxycarbonyl azide (Boc-N_3), benzyl 2,5-dioxo-1-pyrrolidinyl carbonate (Z-ONSu) and its derivatives with the aromatic ring chlorinated for the amino groups of native HEL, and the reagents 4-methoxybenzyl and 4-methylbenzyl chlorides for the mercapto groups of reduced HEL. These reactions were performed to find suitable protected derivatives of HEL that could be regenerated to the original enzyme by treatment with HF under appropriate conditions for peptide synthesis. The results showed that 2-chlorobenzyloxycarbonyl and 4-methylbenzyl substituents are extremely suitable for protecting amino and mercapto groups, respectively, and that fully active enzyme can be regenerated from derivatives of HEL that are blocked with these protecting groups.

Materials and Methods

Hen egg-white lysozyme (6 × crystallized Lot. E5201 and spray-dried cells of *Micrococcus lysodeikticus* (Lot. No. 21-88-778) were purchased from Seikagaku Fine Biochemicals (Tokyo). Sephadex was purchased from Pharmacia Co. (Uppsala). Hydrogen fluoride was a product of Daikin Industrial Co. (Osaka). Urea of reagent grade was recrystallized from ethanol before use. Chlorinated benzoic acids of extra pure reagent grade were purchased from Nakarai Chemicals Ltd. (Kyoto). All other chemicals used were of analytical grade. Melting points were measured by the capillary method and are given as uncorrected values. HEL derivatives were hydrolyzed in 6 M hydrochloric acid with phenol in sealed tubes for 48 h at 105 °C, and amino acids in the hydrolysates were examined in a Hitachi KLA-5 analyzer by the method of Moore *et al.*[3] The abbreviations used in this text are those recommended by IUPAC-IUB: *J. Biol. Chem.*, **247**, 977 (1972).

Synthesis of Benzyl 2,5-Dioxo-1-pyrrolidinyl Carbonate(Z-ONSu). Benzyloxycarbonyl chloride (17.1 g, 100 mmol) and *N*-hydroxysuccinimide (11.5 g, 100 mmol) were dissolved in dioxane (200 ml). Pyridine (9.5 g, 120 mmol) was added dropwise to the solution at 8—10 °C with stirring, and then the mixture was stirred at room temperature for an hour. The mixture was concentrated *in vacuo*, and the residue was dissolved in ethyl acetate. The solution was washed with water and dried over anhydrous sodium sulfate. The dried solution was concentrated to a crystalline residue *in vacuo*, and the material was recrystallized from ethyl acetate and hexane; wt 16.0 g (64.3%); mp 79.5—81.5 °C.

Found: C, 57.74; H, 4.55; N, 5.80%. Calcd for $C_{12}H_{11}O_5N$: C, 57.83; H, 4.45; N, 5.62%.

Synthesis of Benzyl 2,5-Dioxo-1-pyrrolidinyl Carbonate with the Aromatic Ring Chlorinated. 2-Chlorobenzoic acid was reduced with $LiAlH_4$ in dried ether to give the corresponding alcohol, 2-chlorobenzyl alcohol, in about 90% yield. This 2-chlorobenzyl alcohol (10.0 g, 70 mmol) was added to an ethereal solution (200 ml) of phosgene (25 g). The solution was kept for 20 h at room temperature in a closed vessel. The excess phosgene was removed by passing a stream of dry nitrogen gas through the solution, and the solvent was evaporated off under reduced pressure. The residual oil (2-chlorobenzyloxycarbonyl chloride) was dissolved in dioxane (160 ml) with *N*-hydroxysuccinimide (9.2 g, 80 mmol) and pyridine (7.19 g, 100 mmol) at 8—10 °C. The solution was treated in the similar way to that of the benzyl derivative. 2-Chlorobenzyl 2,5-dioxo-1-pyrrolidinyl carbonate [Z(2-Cl)-ONSu] was obtained in 62% yield; mp 103 °C.

Found: C, 50.63; H, 3.51; N, 4.99; Cl, 12.59%. Calcd for $C_{12}H_{10}O_5NCl$: C, 50.81; H, 3.55; N, 4.94; Cl, 12.50%.

The following derivatives were prepared in a similar way.

3-Chlorobenzyl 2,5-Dioxo-1-pyrrolidinyl Carbonate [Z(3-Cl)-ONSu]: Mp 129.5—130.5 °C. Found: C, 50.74; H, 3.51; N, 5.04; Cl, 12.52%. Calcd for $C_{12}H_{10}O_5NCl$: C, 50.81; H, 3.55; N, 4.94; Cl, 12.50%.

4-Chlorobenzyl 2,5-Dioxo-1-pyrrolidinyl Carbonate [Z(4-Cl)-ONSu]: Mp 125 °C. Found: C, 50.64; H, 3.52; N, 5.05; Cl, 12.58%. Calcd for $C_{12}H_{10}O_5NCl$: C, 50.81; H, 3.55; N, 4.94; Cl, 12.50%.

2,4-Dichlorobenzyl 2,5-Dioxo-1-pyrrolidinyl Carbonate [Z(2,4-Cl_2)-ONSu]: Mp 92—93 °C. Found: C, 45.15; H, 2.82; N, 4.52; Cl, 22.30%. Calcd for $C_{12}H_9O_5NCl_2$: C, 45.31; H, 2.85; N, 4.40; Cl, 22.29%.

3,4-Dichlorobenzyl 2,5-Dioxo-1-pyrrolidinyl Carbonate [Z(3,4-Cl_2)-ONSu]: Mp 118—119 °C. Found: C, 45.08; H, 2.79; N, 4.54; Cl, 22.34%. Calcd for $C_{12}H_9O_5NCl_2$: C, 45.31; H, 2.85; N, 4.40; Cl, 22.29%.

2,6-Dichlorobenzyl 2,5-Dioxo-1-pyrrolidinyl Carbonate [Z(2,6-Cl_2)-ONSu]: Mp 127—128 °C. Found: C, 45.29; H, 2.84; N, 4.54; Cl, 22.03%. Calcd for $C_{12}H_9O_5NCl_2$: C, 45.31; H, 2.85; N, 4.40; Cl, 22.29%.

Reaction of Native HEL with t-Butoxycarbonyl Azide. A solution of native HEL (100 mg) in distilled water (1.4 ml) was mixed with pyridine (0.6 ml) and then *t*-butoxycarbonyl azide (Boc-N_3) (0.428 g, *ca.* 3 mmol) in dimethyl sulfoxide (4 ml). The mixture was gently stirred until it became homogeneous, and then kept for 48 h at 38 °C without stirring. It was concentrated under reduced pressure and the residue was mixed with a large volume of ethyl acetate. The precipitate formed was collected by centrifugation, dissolved in dimethyl sulfoxide and reprecipitated by adding ethyl acetate. The precipitate was again collected by centrifugation and reprecipitated in the same way several times. Finally, the precipitate was dissolved in dimethyl sulfoxide and dialyzed against dilute aqueous acetic acid and then distilled water. The dialyzed solution was lyophilized and the powder was dried over diphosphorus pentaoxide *in vacuo*. This material is denoted as Boc-HEL.

Reaction of Native HEL with Benzyl 2,5-Dioxo-1-pyrrolidinyl Carbonate and Its Derivatives. Native HEL was allowed to react with benzyl 2,5-dioxo-1-pyrrolidinyl carbonate (Z-ONSu) or its derivatives [Z(X)-ONSu] under the same conditions as those used with Boc-N_3. These materials are denoted as Z-HEL and Z(X)-HELs.

Determination of Free Amino Groups in Proteins. The free amino groups in proteins were measured by a modification of the method of Moore and Stein[4] using ninhydrin solution. The reagent was prepared in the following way: tin(II) chloride (0.8 g) was dissolved in 0.2 M citrate buffer (500 ml) at pH 5.0. The solution was mixed with a solution of ninhydrin (20 g) in methyl cellosolve (500 ml), and the mixture was saturated with nitrogen gas and kept in a closed vessel in a refrigerator. Protein was dissolved in 3% aqueous sodium dodecyl sulfate and the solution was mixed with the above stocked solution (1 ml), heated for 20 min in a vigorously boiling water bath, cooled rapidly to room temperature and mixed with 50% aqueous 2-propanol (5 ml). Then within 15 min, the absorbance of the solution at 570 nm was measured. Protein contents of 3% aqueous sodium dodecyl sulfate solutions were determined by measuring the absorbance at 290 nm. The percentage of free amino groups (F%) in a protein was calculated as a ratio to free amino groups of native HEL using the following equation:

$$F = \frac{\dfrac{A_{570}\ \text{sample}}{A_{290}\ \text{sample}}}{\dfrac{A_{570}\ \text{native}}{A_{290}\ \text{native}}} \times 100$$

where A_{570} sample and A_{570} native mean the absorbances at 570 nm of the sample protein and native HEL solutions after treatment with ninhydrin solution, and A_{290} sample and A_{290} native mean the absorbances at 290 nm of solutions of sample protein and native HEL in 3% aqueous sodium dodecyl sulfate.

Treatment of Boc-HEL with Formic Acid. Lyophilized powder (*ca.* 30 mg) of Boc-HEL was dissolved in 99% formic acid (10 ml). The solution was stood for 24 h at 15 °C and then lyophilized. The resulting powder was dissolved in buffer solution (7.9 ml), consisting of 0.2 M tris (3 ml) at pH 8.6, 5% EDTA·2Na (0.3 ml), urea (3.61 g) and 2-mercaptoethanol (0.5 ml), under a nitrogen atmosphere, and stirred overnight at room temperature. Then the solution was acidified to below pH 4 with glacial acetic acid and charged on a column of Sephadex G-10 (3×60 cm). The eluate containing the protein was added to 0.08 M tris buffer solution at pH 8 (1 liter) containing 5.4×10^{-3} M L-cysteine and 4.8×10^{-4} M L-cystine.[5] The pH of the solution was adjusted to 8.0 with glacial acetic acid or concentrated ammonia. Then, the solution was kept for over 5 h at 37 °C, and the pH of the solution was adjusted to 4.5—5 with glacial acetic acid. The solution was applied to a CM-cellulose column (2×30 cm, carboxylic acid cycle). The adsorbed protein was eluted with 0.3 M sodium phosphate buffer at pH 8.0. The eluate containing the protein was acidified with glacial acetic acid and lypohilized. The lyophilized material was desalted by passage through a column of Sephadex G-10 (3.2×60 cm) in 1 M acetic acid and fractions containing the protein were collected and lyophilized.

Treatment of Native HEL and Derivatives of HEL with HF. Lyophilized powder (*ca.* 30 mg) of native HEL or its derivatives was weighed with 1,4-butanedithiol (0.5 ml) and anisole (1.0 ml) in the Daiflon cylinder of an HF-reaction apparatus.[6] The cylinder containing the protein was cooled to −78 °C in a Dry Ice-methanol bath and HF (10 ml) was distilled into it. The reaction was started by transferring the sample from the bath at −78 °C to a bath at 0 °C. The resulting solution was stirred at 0 °C for a certain period and then the HF was rapidly evaporated off as completely as possible from the reaction mixture under reduced pressure. The residue was washed repeatedly with hexane and the amorphous powder obtained was treated in the way used for Boc-HEL.

Reductive Alkylations of Native HEL with Benzyl, 4-Methoxybenzyl and 4-Methylbenzyl Groups in Liquid Ammonia. Native HEL was reduced with dithiothreitol in liquid ammonia at its boiling temperature for 3 h by the method of Meienhofer *et al.*[7] Then an alkylating reagent was added and the solution was refluxed for 3 h. The ammonia was evaporated off from the reaction mixture through a water aspirator.

When benzyl chloride was used as an alkylating reagent, the residue was kept overnight over concentrated sulfuric acid *in vacuo*, and then washed successively with ether, ethyl acetate and methanol. The crude material obtained was dissolved in a buffer containing 1 M acetic acid and 5 M urea, and chromatographed on Sephadex G-75 (3×60 cm) in the same buffer. The fractions containing protein were collected, dialyzed against distilled water and lyophilized. The material obtained is denoted as HEL(*S*-Bzl).

When 4-methoxybenzyl and 4-methylbenzyl chlorides were used as alkylating reagents, the residues were dissolved in dimethyl sulfoxide, and ethyl acetate was added to the solutions. The insoluble material formed was collected by centrifugation, washed repeatedly with ethyl acetate, and then dissolved in dimethyl sulfoxide. The resulting solutions were dialyzed against aqueous acetic acid and then distilled water. The dialyzed solutions were lyophilized and these materials are denoted as HEL(*S*-Bzl(OMe)) and HEL(*S*-Bzl(Me)), respectively.

Reductive Alkylations of Z(2-Cl)-HEL with 4-Methoxybenzyl and 4-Methylbenzyl Groups in Liquid Ammonia. Z(2-Cl)-HEL was reduced with dithiothreitol in liquid ammonia and allowed to react with 4-methoxybenzyl or 4-methylbenzyl chloride under similar conditions to those used with native HEL. The crude products were purified by a similar procedure to that used in the preparations of HEL(*S*-Bzl(OMe)) and HEL(*S*-Bzl(Me)). The purified products are denoted as Z(2-Cl)-HEL(*S*-Bzl(OMe)) and Z(2-Cl)-HEL(*S*-Bzl(Me)), respectively.

Determination of Remaining Thiols in Proteins. The amount of thiols in HEL(*S*-Bzl) that remained to be alkylated was calculated from the amount of *S*-benzylcysteine in the acid hydrolysate of the protein, determined by amino acid analysis. On the other hand, the amounts of thiols that remained to be alkylated in HEL(*S*-Bzl(OMe)), HEL(*S*-Bzl(Me)), Z(2-Cl)-HEL(*S*-Bzl(OMe)) and Z(2-Cl)-HEL(*S*-Bzl(Me)) were calculated from the amount of *S*-(carboxy-

methyl)cysteine measured as follows: Lyophilized powder (*ca.* 15 mg) of the proteins was dissolved in buffer solution consisting of 0.2 M tris (1.2 ml) at pH 8.6, 5% EDTA·2Na (0.12 ml) and guanidine hydrochloride (2.87 g). The solution was diluted with 0.2 M tris (1.5 ml) at pH 8.6 and 5% EDTA·2Na (0.15 ml), mixed with dithiothreitol (24.6 mg) and stirred overnight at room temperature under a nitrogen atmosphere. Then iodoacetic acid (270 mg) in 1 M NaOH (1 ml) was added. The mixture was stirred for 15 min in a dark room, acidified with formic acid and dialyzed against distilled water, and the dialyzed solution was lyophilized. The resulting powder was hydrolyzed with 6 M hydrochloric acid, and the ratios of the amount of *S*-(carboxymethyl)cysteine to the average amounts of glycine and alanine in the hydrolysate were determined by amino acid analysis.

Treatments of the Reduced and Alkylated Derivatives of HEL with HF. Reductively alkylated derivatives of HEL were treated with HF as described above.

Gel-filtration and Ion-exchange Chromatography. Gel-filtration and ion-exchange chromatography were used to isolate fully active HEL from the derivatives of HEL treated with HF, as described in the preceding paper.[1] Materials were detected by measuring the absorption of the eluate at 280 nm.

Enzyme Assays. The specific activity of HEL was determined by measuring the initial rate of lysis of *Micrococcus lysodeikticus* cell walls spectrophotometrically at 540 nm by the method described in the preceding paper,[1] with native HEL as a standard.

Ultraviolet Absorption Spectra. UV-absorption spectra were measured using a Hitachi spectrophotometer type-124, equipped with a recording attachment.

Crystallization of HEL. Crystallization was carried out by the method of Berthou and Jolles[8] with the modification described in the preceding paper.[1]

Results

Reaction of Native HEL with Boc-N_3. When native HEL was treated with Boc-N_3 in the presence of pyridine in a mixture of dimethyl sulfoxide and water, only 76% of its amino groups were acylated with Boc groups, as estimated by the ninhydrin reaction. However, when the partially acylated native HEL was treated with Boc-N_3 repeatedly under the same conditions, but without water, 98% of its amino groups could be acylated.

Reactions of Native HEL with Z-ONSu and Z(X)-ONSu. Native HEL was treated with Z-ONSu in ratios of 1.3 to 65 equivalents of the reagent to one amino group of native HEL, then the product was isolated and its acylated amino groups were estimated by the ninhydrin color reaction. The relation between the ratio of Z-ONSu to amino group of native HEL and the percentage of amino groups acylated with Z groups is summarized in Table 1. Native HEL was also treated with the derivatives of Z-ONSu [Z(X)-ONSu] using a ratio of 6.5 equivalents of the reagents to one amino group of native HEL. Measurements with ninhydrin showed that these derivatives cause almost complete acylation of the amino groups with Z(X) groups, as seen in Table 2.

Table 1. Effect of the ratio of equivalents of Z-ONSu to amino groups of native HEL on the percentage of amino groups acylated

	A	B	C	D	E	F
Z-ONSu (equivalents)	1.3	2.6	6.5	13.0	26.0	65.0
Acylated amino groups (%)	95.5	96.6	98.0	99.0	98.4	98.3

Table 2. Percentages of acylated amino groups in Z(X)-HELs

X in Z(X)-ONSu	Acylated amino groups (%)
2-Cl	98.0
3-Cl	98.0
4-Cl	98.0
2,4-Cl_2	97.0
3,4-Cl_2	97.0
2,6-Cl_2	97.0

Removal of Z Groups from Z-HEL by Treatment with HF. Z-HEL was treated with HF at 0 °C for periods of 0 to 120 min, and then the reaction was stopped by evaporating the HF off completely. The residue was dissolved in 3% aqueous sodium dodecyl sulfate. The protein concentration in the solution was determined by measuring the optical density at 290 nm and free amino groups in the protein regenerated by HF-treatment were determined by the ninhydrin method. The recovery of regenerated amino groups was calculated from the equation given in the methods, and the results are shown in Fig. 1.

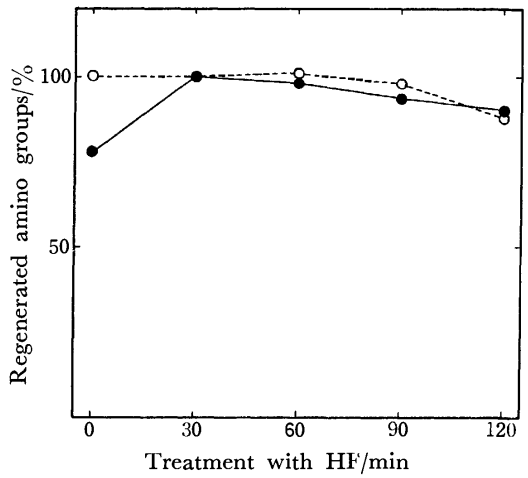

Fig. 1. Removal of Z groups from Z-HEL by HF-treatment.
—●—: Z-HEL, —○—: native HEL.

Table 3. Percentages of free amino groups recovered from Z(X)-HELs by HF-treatment

Z(X)-HEL	HF-treatment at 0 °C (min)				
	0	30	60	90	120
2-Cl	21	96	98	94	83
3-Cl	18	62	97	89	92
4-Cl	74	94	92	90	75
2,4-Cl_2	18	94	95	83	82
3,4-Cl_2	13	58	99	92	75
2,6-Cl_2	18	60	93	90	92

Removal of Z(X) Groups from Z(X)-HELs by Treatment with HF. Z(X)-HELs were treated with HF at 0 °C for periods of 0 to 120 min, and the free amino groups of the proteins recovered were estimated. The results are shown in Table 3.

Regeneration to Native HEL from Boc-HEL. Treatment of Boc-HEL with formic acid for 24 h at 15 °C or with HF for 90 min at 0 °C gave fully active HEL in yields of 46 and 25%, respectively. After treatment of native HEL under the same conditions as Boc-HEL, fully active HEL was recovered in yields of 72 and 50%, respectively.

Regeneration to Native HEL from Z-HEL. Z-HEL, prepared under conditions C in Table 1, was treated with HF at 0 °C for periods of 30 to 90 min. Then the residues of HF-treated Z-HEL were reduced and reoxidized, as described in the methods and the resultant protein fraction was chromatographed on Sephadex G-50 using buffer solution containing 1 M acetic acid and 5 M urea. The fraction eluted in the same position as native HEL was fully active. After treatment of Z-HEL with HF for 30 min at 0 °C the recovery of this fraction was 41%. The recovery of fully active HEL decreased with increase in the period of HF-treatment and after periods of 60 and 90 min the yields of fully active HEL were 28 and 23%, respectively When the Z-HELs prepared under the various conditions described in Table 1 were treated with HF for 30 min at 0 °C, the recoveries of fully active HEL varied depending on the conditions used for preparation of the Z-HELs. The relation between the recoveries of fully active HELs and the conditions used for preparation of Z-HEL are shown in Fig. 2.

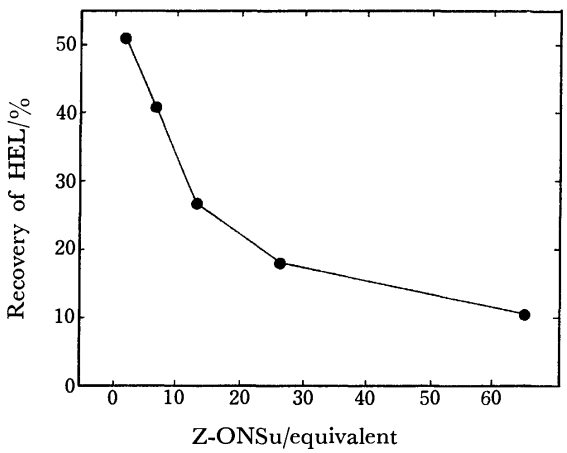

Fig. 2. Effect of the ratio of equivalent of Z-ONSu to amino groups of native HEL used in the synthesis of Z-HEL on the recovery of fully active HEL from Z-HEL by HF-treatment.

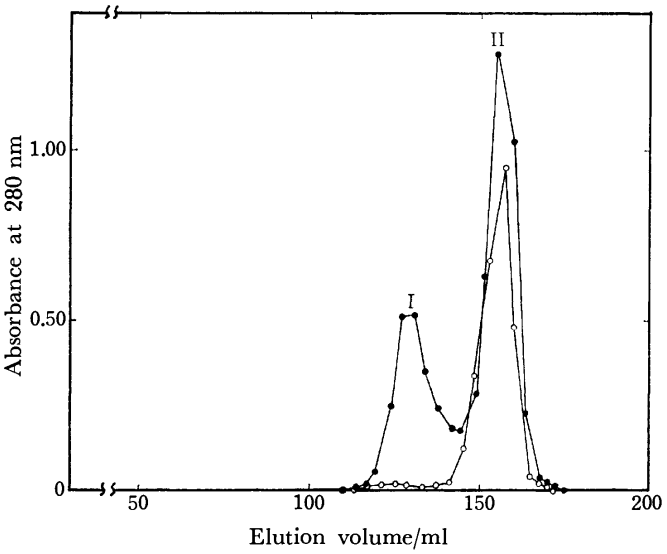

Fig. 3. Gel-filtration of Z(2-Cl)-HEL treated with HF for 60 min at 0 °C (—●—) and native HEL (—○—) on Sephadex G-50 (2×95 cm) using buffer containing 1 M acetic acid and 5 M urea.

Regeneration to Native HEL from Z(X)-HELs. Z(X)-HEL was treated with HF for 60 and 90 min at 0 °C. Then the HF-treated Z(X)-HEL was reduced, reoxidized and chromatographed on Sephadex G-50, as described in the methods. Two fractions (I and II) were eluted from the column: the first (I) had less enzymatic activity than native HEL, whereas the second (II), eluted in the same position as standard native HEL, had full enzymatic activity. A chromatogram of the protein fraction recovered after HF-treatment of Z(2-Cl)-HEL for 60 min at 0 °C is shown in Fig. 3. The recoveries of fraction II's from Z(X)-HELs are summarized in Table 4.

Purification and Crystallization of Fully Active HEL Regenerated from Z(2-Cl)-HEL. Fraction II in Fig. 3 was desalted by passage through Sephadex G-10, and the eluate containing protein was lyophilized. Then the powder was subjected to chromatography on Bio-rex 70 in 0.2 M sodium phosphate buffer solution, pH 7.18, as shown in Fig. 4. In this way four fractions (IIa, IIb, IIc, and IId) were separated. Fraction IId was eluted in the same position as the main fraction of native HEL. The lytic activities of the four fractions, IIa, IIb, IIc, and IId, were 65, 96, 101, and 101%, respectively, of that of native HEL in M/15 sodium phosphate buffer solution containing 0.1% sodium chloride, and 18, 29, 48, and 100%, respectively, of that of native HEL in the same buffer solution containing 1% sodium chloride. The UV absorption spectrum of fraction IId is shown in Fig. 5. Fraction

Table 4. Recoveries of fully active HEL from Z(X)-HELs by HF-treatment

Conditions for HF-treatment	Native HEL	Z-HEL	Z(X)-HEL					
			2-Cl	3-Cl	4-Cl	2,4-Cl_2	3,4-Cl_2	2,6-Cl_2
0 °C, 60 min	59	28	22	10	20	16	7.3	16
0 °C, 90 min	50	23	23	18	26	14	9.5	16

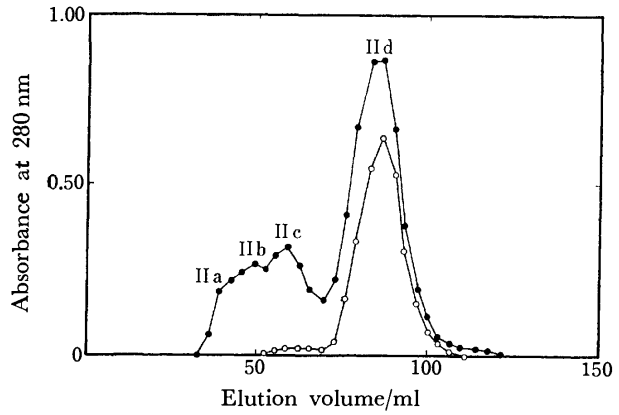

Fig. 4. Ion-exchange chromatogram of fractionII of Fig. 3 (—●—) and native HEL(—○—) on Bio-rex 70 (1.5×33 cm) in 0.2 M sodium phosphate buffer solution (pH 7.18).

IId was desalted by passage through Sephadex G-10, and the eluate containing protein was collected and lyophilized. When the lyophilized material was stood under conditions inducing crystallization, it formed crystals identical with those of native HEL.

Reductive Alkylations of Native HEL with Benzyl, 4-Methoxybenzyl, and 4-Methylbenzyl Groups in Liquid Ammomia. Native HEL was reduced and alkylated under the conditions described for Table 5. The degree of alkylation with benzyl groups was estimated from the ratio of the amounts of *S*-benzylcysteine to the average amounts of glycine and alanine, determined by amino acid analysis of the acid hydrolysate of the alkylated product, as shown in Table 5. It was difficult to estimate the degrees of alkylation with 4-methoxybenzyl and 4-methylbenzyl groups by measuring *S*-(4-methoxybenzyl)cysteine and *S*-(4-methylbenzyl)cysteine in acid hydrolysates of the alkylated products by amino acid analysis, because these *S*-(4-methoxybenzyl)- and *S*-(4-methylbenzyl)cysteine residues are destroyed during acid hydrolysis. Therefore, they were estimated by analysis of the amount of thiols in the protein that remained unalkylated; namely the reduced and alkylated derivatives of HEL were carboxymethylated, and the amounts of *S*-(carboxymethyl)cysteine residues in the carboxymethylated proteins were determined by measuring the amounts of amino acids in their acid hydrolysates with an amino acid analyzer. The results are summarized in Table 5.

Treatment of HEL(S-Bzl) with HF. HEL(*S*-Bzl) was treated with HF under various conditions, the resultant material was hydrolyzed with 6 M hydrochloric acid, and *S*-benzylcysteine in the acid hydrolysate was measured by amino acid analysis. Table 6 shows the percentages of *S*-benzyl groups cleaved by treatment of HEL(*S*-Bzl) with HF under various conditions. The products of the reactions were treated under similar conditions to those used to isolate enzymatically active HEL from the products of Z-HEL. However, no enzymatically active material was recovered under any of the conditions examined.

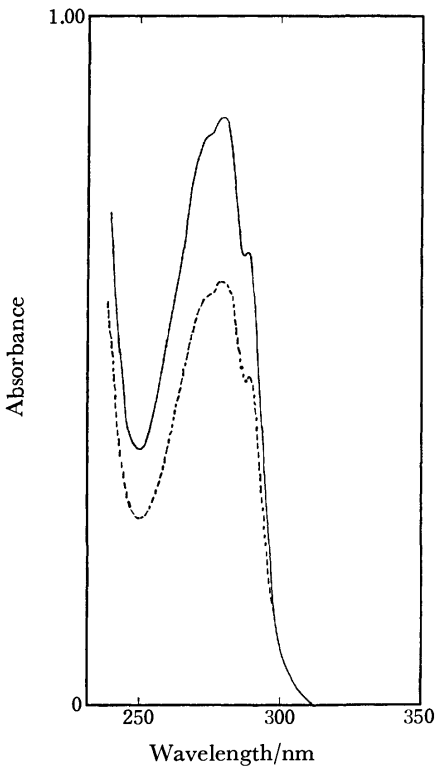

Fig. 5. Ultraviolet absorption spectra of fraction IId of Fig. 4 (——) and native HEL (----). Solvent: 0.2 M sodium phosphate buffer (pH 7.18).

Treatments of S-(4-Methoxybenzyl) and S-(4-Methylbenzyl) Derivatives of Native HEL and Z(2-Cl)-HEL with HF. The derivatives of HEL were treated with HF at 0 °C for 60 and 90 min, and the materials isolated from their HF-solutions were treated under similar conditions to those described above. The percentages of fully active HEL recovered from them are shown in Table 7.

Table 5. Reductive alkylations of native HEL and Z(2-Cl)-HEL

Product	Starting material	(mg)	(μmol)	Liq.NH_3 (liter)	DTT[a] (mmol)	Alkylating reagent	(mmol)	Alkylated SH groups (residue mol)
HEL(*S*-Bzl)	Native HEL	1000	67	2.0	5.3	Bzl-Cl	26.4	8.16
HEL(*S*-Bzl(OMe))	Native HEL	300	20	2.0	2.0	Bzl(OMe)-Cl	20.0	6.80(85.0%)[b]
HEL(*S*-Bzl(Me))	Native HEL	200	13	1.0	1.1	Bzl(Me)-Cl	11.0	7.12(89.0%)[b]
Z(2-Cl)-HEL(*S*-Bzl(OMe))	Z(2-Cl)-HEL	120	8	1.0	1.0	Bzl(OMe)-Cl	10.0	7.36(92.0%)[b]
Z(2-Cl)-HEL(*S*-Bzl(Me))	Z(2-Cl)-HEL	240	16	1.8	2.0	Bzl(Me)-Cl	19.0	7.36(92.0%)[b]

a) DTT: Dithiothreitol. b) Values in parentheses show the ratios of the amount of alkylated mercapto groups to the theoretical value (100%).

Table 6. Percentages of *S*-benzyl groups cleaved by HF-treatment of HEL(*S*-Bzl)

	90 min	120 min	150 min
−75 °C	10	1	2
−25—−15 °C	4	2	5
0 °C	20	32	35

Table 7. Recoveries of fully active HEL from HEL(*S*-Bzl(OMe)), HEL(*S*-Bzl(Me)), Z(2-Cl)-HEL(*S*-Bzl(OMe)), and Z(2-Cl)-HEL(*S*-Bzl(Me)) by HF-treatments

Material	HF-treatment (%)	
	0 °C, 60 min	0 °C, 90 min
HEL(*S*-Bzl(OMe))	0	1.6
HEL(*S*-Bzl(Me))	19	12
Z(2-Cl)-HEL(SH)	20	15
Z(2-Cl)-HEL(*S*-Bzl(OMe))	0	0.5
Z(2-Cl)-HEL(*S*-Bzl(Me))	8.3	7.4

Purification and Crystallization of Fully Active HEL Regenerated from Z(2-Cl)-HEL(S-Bzl(Me)). The material obtained from Z(2-Cl)-HEL(*S*-Bzl(Me)) by HF-treatment for 60 min at 0 °C was reduced, and reoxidized under similar conditions to those used for Z(2-Cl)-HEL. The reoxidized material was chromatographed on Sephadex G-50 using buffer containing 1 M acetic acid and 5 M urea, as shown in Fig. 6. Fraction II, eluted in the same position as native HEL, was fully active. The yield of fraction II was 8.3% on the basis of the protein content of the Z(2-Cl)-HEL(*S*-Bzl(Me)) preparation used, as shown in Table 7. Lyophilized material was obtained from fraction II by desalting and chromatographed on a Bio-rex 70 column using 0.2 M sodium phosphate buffer solution at pH 7.18. Fraction II was separated into four fractions

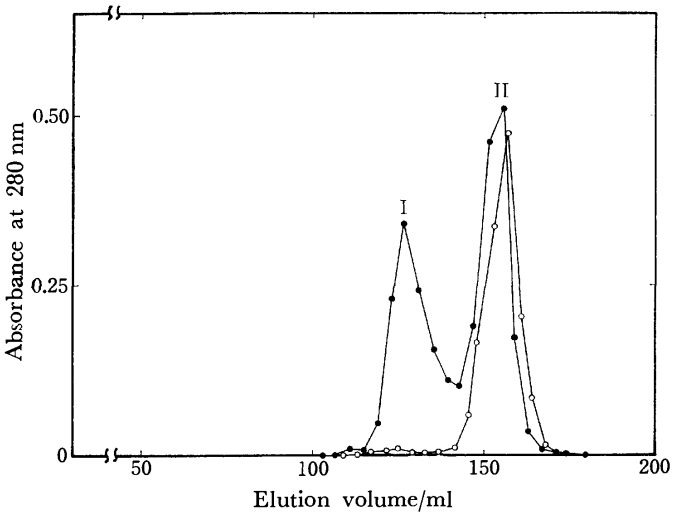

Fig. 6. Gel-filtration of Z(2-Cl)-HEL(*S*-Bzl(Me)) treated with HF for 60 min at 0 °C (—●—) and native HEL (—○—) on Sephadex G-50 (2×95 cm) in buffer containing 1 M acetic acid and 5 M urea.

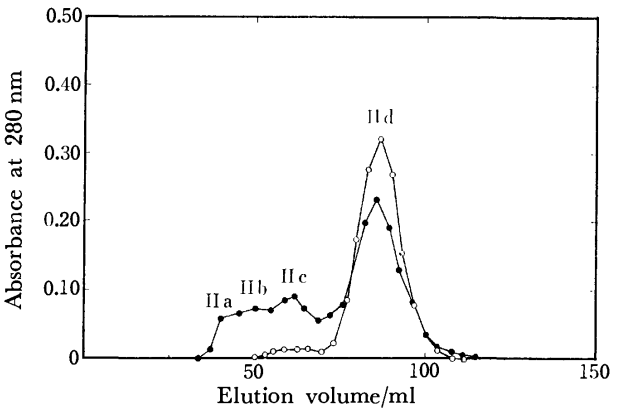

Fig. 7. Ion-exchange chromatogram of fraction II of Fig. 6 (—●—) and native HEL (—○—) on Bio-rex 70 (1.5×33 cm) in 0.2 M sodium phosphate buffer solution (pH 7.18).

(IIa, IIb, IIc, and IId), as shown in Fig. 7. Fraction IId was eluted in the same position as the main fraction of native HEL. These four fractions, IIa, IIb, IIc, and IId, had 79, 99, 101, and 102%, respectively, of the lytic activity of native HEL in buffer containing 0.1% sodium chloride, and 13, 30, 39, and 102% of the latter in buffer containing 1% sodium chloride. The UV absorption spectrum of fraction IId is shown in Fig. 8. When the lyophilized powder obtained from fraction IId (Fig. 7) after desalting was stood under conditions inducing crystallization, it yielded similar crystals to those of native HEL, as shown in Fig. 9.

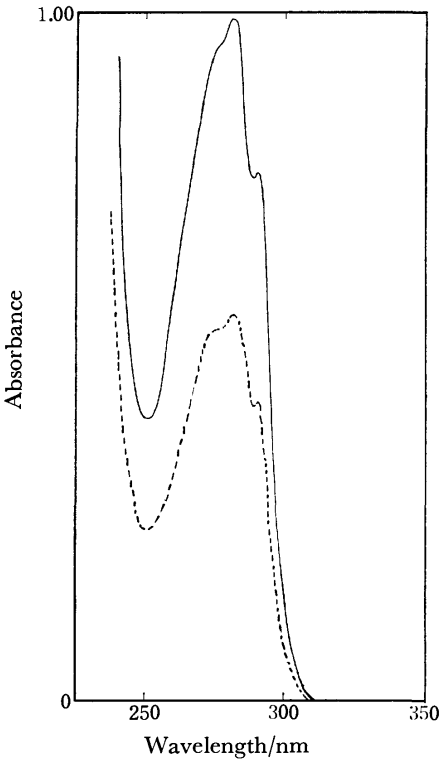

Fig. 8. Ultraviolet absorption spectra of fraction IId of Fig. 7 (——) and native HEL (----). Solvent: 0.2 M sodium phosphate buffer (pH 7.18).

Fig. 9. Microphotograph of crystals of the material from fraction IId of Fig. 7.

Discussion

In this work we first prepared derivatives of native HEL in which the amino groups were combined with *t*-butoxycarbonyl (Boc) or benzyloxycarbonyl (Z) groups or derivatives of the latter, [Z(X)]. These derivatives were prepared by treating the enzyme with Boc-N_3 or Z-ONSu or derivatives of the latter [Z(X)-ONSu]. The first reagent was not very reactive so that repeated treatment was required to achieve complete acylation of the amino groups of native HEL. Then, we tested Z-ONSu, which can easily be prepared by the reaction of benzyloxycarbonyl chloride (Z-Cl) with *N*-hydroxysuccinimide (HONSu), and found that Z groups could be introduced almost quantitatively onto the amino groups of native HEL in a single reaction. We also found that the reaction was complete using a ratio of at least 6.5 equivalents of the reagent to one amino group of native HEL, as shown in Table 1; derivatives of the Z group in which the aromatic ring was chlorinated could be introduced onto the amino groups of native HEL almost completely using 6.5 equivalents of the reagents to one amino group of native HEL.

Next, we examined to regenerate enzymatically active HEL from the derivatives of HEL. Treatments of Boc-HEL with formic acid for 24 h at 15 °C and with HF for 90 min at 0 °C gave fully active HEL in yields of 46 and 25%, respectively, and treatment of native HEL with formic acid and HF under the same conditions gave recoveries of 72 and 50%, respectively, of the active enzyme. Namely, the recovery of fully active HEL from Boc-HEL was about one half of that from native HEL. These results suggest that some side-reactions occur during the treatment of Boc-HEL with formic acid or HF, or that some side-reactions occur during introduction of the Boc group onto native HEL using Boc-N_3 and are not reversed by formic acid- or HF-treatment, whereas these reactions were not examined in this work. However, these results show that enzymatically active material can be recovered in fair yields from Boc-HEL under the conditions described above. We next tested to regenerate enzymatically active HEL from Z-HEL and Z(X)-HELs. We first determined free amino groups regenerated by the treatment of Z-HEL and Z(X)-HELs, in which the amino groups are completely protected, with HF under various conditions. When Z-HEL was treated with HF at 0 °C for 0 and 30 min, the regenerated free amino groups were estimated as 78 and 100% of those of native HEL, respectively. These results indicate that Z groups could be removed from Z-HEL as easily as from oligopeptides by HF-treatment. Then, HELs, substituted with monochloro- or dichloro-Z group, were treated with HF. The free amino groups of the original enzyme could be regenerated almost quantitatively with HF, by 30 min-treatment of Z(2-Cl)-, Z(4-Cl)- and Z(2,4-Cl_2)-HELs and by 60 min-treatment of Z(3-Cl)-, Z(3,4-Cl_2)- and Z(2,6-Cl_2)-HELs. Thus the relative stabilities of these groups on HF-treatment are proportional to their relative stabilities on acidolysis in 50% trifluoracetic acid, in methylene chloride reported by Merrifield *et al.*[9] The results show that the free amino groups of HEL can be regenerated quantitatively from all the derivatives of HEL examined by HF-treatment for up to 60 min at 0 °C. Then, we tried to isolate fully active HEL from the products obtained by HF-treatment of derivatives of HEL. We found that on HF-treatment for 30 min at 0 °C fully active HEL could be recovered in 41% yield from Z-HEL, in which the amino groups had been acylated almost completely under conditions C in Table 1. However, the recovery decreased on increasing the period of HF-treatment. These findings are in accordance with results on HF-treatment of native HEL, described in the preceding paper[1]. When Z-HELs prepared by the reaction of native HEL with Z-ONSu under conditions D, E, and F in Table 1 were treated with HF for 30 min at 0 °C, the recoveries of fully active HELs decreased in order; namely with increase in the ratio of equivalents of the reagent, Z-ONSu, to amino groups of native HEL, the recovery of fully active HEL decreased. Since fully active HEL could be recovered in 69% yield from native HEL on HF-treatment under the same conditions, the results suggest that the acylation of native HEL with Z-ONSu did not cause an irreversible change in the molecule of native HEL, but caused some side-reactions of the molecule or that HF-treatment of Z-HEL caused some modification of the HEL molecule. Therefore, it is essential to use only the minimal amount of the reagent necessary to achieve complete acylation of the amino groups of native HEL. In studies on the recovery of HEL from Z(X)-HELs by HF-treatments at 0 °C for 60 and 90 min, fully active HEL was recovered from Z(2-Cl)- and Z(4-Cl)-HELs in approximately the same yield as from Z-HEL. It has been described[9] that use of Z(2-Cl) group for ε-amino protection of lysine reduces branching at the amino acid residue in peptide synthesis, whereas Z and Z(4-Cl) groups are sufficiently labile in acidic conditions that peptide chains undergo branching at the side chain of lysine residue during peptide synthesis if either group is used for ε-amino protection. This and our results suggest the usefulness of Z(2-Cl) group for ε-amino protection of lysine residue in our studies on the chemical synthesis of HEL. Therefore, HEL substituted with Z(2-Cl) groups was examined further in detail. On the other hand, the recoveries of HEL from other Z(X)-HELs were lowered, as shown in Table 4. These results seem inconsistent with the

fact that all the Z(X) groups could be completely removed from Z(X)-HELs under the same conditions, as described already, because if this is so fully active HEL should be recovered in the same yield from all the derivatives of HEL examined. This inconsistency remains to be explained. It may be due to various extents of side-reactions during preparation of Z(X)-HELs and their treatments with HF.

We also investigated the reductive alkylations of native HEL and Z(2-Cl)-HEL and the regeneration of enzymatically active HEL from reduced and alkylated enzymes by HF-treatment. Meienhofer *et al.*[7] reported that native HEL can be reduced by dithiothreitol in liquid ammonia, and that the resulting mercapto groups can be almost completely alkylated by benzyl chloride. Accordingly native HEL and Z(2-Cl)-HEL were reduced and alkylated by benzyl, 4-methoxybenzyl and 4-methylbenzyl chlorides by their method. Amino acid analyses of acid hydrolysates of the products showed that native HEL and Z(2-Cl)-HEL were reduced and alkylated almost completely by benzyl groups, but partially by 4-methoxybenzyl and 4-methylbenzyl groups, as seen in Table 5. When these derivatives of HEL were treated with HF to regenerate enzymatically active HEL, it was found that the *S*-benzyl substituents were too stable to be cleaved from HEL(*S*-Bzl) under the mild conditions used for peptide synthesis, as presented in Table 6. Moreover, HEL would be destroyed under the stronger conditions necessary for complete cleavage of the *S*-benzyl group from HEL(*S*-Bzl), as described in the preceding paper.[1] Thus, fully active HEL could not be recovered from the HEL(*S*-Bzl) by HF-treatment. It seemed probable that the *S*-4-methoxybenzyl substituent should be removed from HEL(*S*-Bzl(OMe)) and Z(2-Cl)-HEL(*S*-Bzl(OMe)) under appropriate conditions for HF-treatment, because it is known that the *S*-4-methoxybenzyl group can be almost completely removed from oligopeptides containing the *S*-(4-methoxybenzyl)cysteine residue(s) by HF-treatment for 60 min at 0 °C, and completely removed by treatment for 90 min at 0 °C. However, only traces of fully active HEL could be recovered from either HEL(*S*-Bzl(OMe)) or Z(2-Cl)-HEL(*S*-Bzl(OMe)) by HF-treatment for 90 min at 0 °C, and no fully active enzyme could be recovered by treatment for 60 min at 0 °C. These low recoveries of fully active enzyme seemed to be due to use of unsuitable reaction conditions for preparing HEL(*S*-Bzl(OMe)) and Z(2-Cl)-HEL(*S*-Bzl(OMe)), because these derivatives of HEL were always obtained as pale yellow materials. Next, HEL(*S*-Bzl(Me)) and Z(2-Cl)-HEL (*S*-Bzl(Me)) were treated with HF. Erickson and Merrifield[10] reported that *S*-4-methylbenzyl group can be completely removed from *S*-(4-methylbenzyl)cysteine by HF-treatment at 0 °C for 60 min. However, we observed that trace amounts of the group remain in *S*-(4-methylbenzyl)cysteine after treatment with HF under the same conditions, whereas the group is completely removed by HF-treatment for 90 min at 0 °C. Therefore, we treated the above materials with HF at 0 °C for 60 and 90 min. Fully active HEL was recovered in 19 and 12% yield from HEL(*S*-Bzl(Me)) by HF-treatment at 0 °C for 60 and 90 min, respectively. Table 5 shows that about 89% of the mercapto groups were alkylated in the HEL(*S*-Bzl(Me)) preparation; namely, about 11% of the mercapto groups remained unalkylated. Assuming that 11% of the mercapto groups were exclusively constituted by the reduced form of HEL, and that no active enzyme could be recovered from completely alkylated HEL(*S*-Bzl(Me)), we can deduce that fully active HEL could be recovered in only 3—5% yield from the HEL(*S*-Bzl(Me)) preparation by HF-treatment for 60 min at 0 °C, from simple calculation ($0.11 \times 0.33 \times 100\% = 3.63\%$), since the reduced form of HEL gave fully active HEL with 33% yield under the same conditions.[2] Therefore, the 19% yield of fully active HEL was probably mainly derived from *S*-4-methylbenzylated HEL. Next, Z(2-Cl)-HEL (*S*-Bzl(Me)) was treated with HF at 0 °C; fully active enzyme was recovered in yields of 8.3 and 7.4% after treatment with HF for 60 and 90 min, respectively. On the other hand, fully active HEL could be recovered in 20% yield from the reduced form of Z(2-Cl)-HEL, in which not all the mercapto groups were alkylated, by HF-treatment for 60 min at 0 °C. These findings indicate that fully active enzyme was mainly obtained by cleavage of Z(2-Cl) and Bzl(Me) groups from Z(2-Cl)-HEL(*S*-Bzl(Me)) with HF, although 8% of the mercapto groups remained to be alkylated in the Z(2-Cl)-HEL(*S*-Bzl(Me)) preparation.

The fully active HELs recovered by HF-treatment of Z(2-Cl)-HEL and Z(2-Cl)-HEL(*S*-Bzl(Me)) were purified by chromatography on a Bio-rex 70 column. The main fraction, eluted in the position of native HEL, had the same activity on *Micrococcus lysodeikticus* cells as native HEL also purified on Bio-rex 70. The fractions eluted before the main fraction had similar activity to native HEL in buffer containing 0.1% sodium chloride, but had very low enzymatic activity in buffer containing 1% sodium chloride. They may represent deaminated derivatives of HEL formed during the chemical treatments. The main fraction eluted from the Bio-rex 70 column had the same UV-spectra as native HEL, as shown in Figs. 5 and 8. Furthermore, when the protein in this fraction was treated under appropriate conditions, it gave crystals that were identical with those of native HEL, as shown in Fig. 9.

As a further step in the chemical synthesis of hen egg-white lysozyme we prepared Z(2-Cl)-HEL(*S*-Bzl-(Me)) as a model, since it closely resembles the protected polypeptide covering the whole sequence of the lysozyme molecule required to synthesize the whole molecule. The present work showing that fully active HEL can be regenerated in fair yield and in a crystalline state from Z(2-Cl)-HEL(*S*-Bzl(Me)) by treatment with HF is an encouraging indication that chemical synthesis of this enzyme should be possible.

References

1) S. Aimoto and Y. Shimonishi, *Bull. Chem. Soc. Jpn.*, **48**, 3293 (1975).

2) S. Aimoto and Y. Shimonishi, *Bull. Chem. Soc. Jpn.*, **49**, 317 (1976).

3) S. Moore, D. H. Spackman, and W. H. Stein, *Anal. Chem.*, **30**, 1185 (1958).

4) S. Moore and W. H. Stein, *J. Biol. Chem.*, **176**, 367 (1948).
5) V. P. Saxena and D. B. Wetlaufer, *Biochemistry*, **9**, 5015 (1970).
6) S. Sakakibara, Y. Shimonishi, Y. Kishida, M. Okada, and H. Sugihara, *Bull. Chem. Soc. Jpn.*, **40**, 2164 (1967).
7) J. Meienhofer, J. Czombos, and H. Maeda, *J. Am. Chem. Soc.*, **93**, 3080 (1971).
8) J. Berthou and P. Jolles, *FEBS Lett.*, **31**, 189 (1973).
9) B. W. Erickson and R. B. Merrifield, *J. Am. Chem. Soc.*, **95**, 3757 (1973).
10) B. W. Erickson and R. B. Merrifield, *J. Am. Chem. Soc.*, **95**, 3750 (1973).

Nuclear Magnetic Resonance Study of Exchanging Systems. X.[1] Rotational Barriers to *trans-cis* Isomerization in Esters

Hiroshi NAKANISHI, Hitoshi FUJITA, and Osamu YAMAMOTO
National Chemical Laboratory for Industry, Honmachi, Shibuya-ku, Tokyo 151
(Received May 11, 1977)

The ^{13}C NMR spectra of *t*-butyl formate (**1**), 1,1-diethylpropyl formate (**2**), and 2,6-dimethylphenyl formate (**3**) were measured at various temperatures. It was found that the signals of the *trans* and *cis* isomers in **1** and **2** are separated at very low temperatures, and that the signal of **3** only shows a slight line broadening. The complete line shape analyses of these temperature-dependent spectra were performed. The activation energies $E_a(t\text{-}c)$ of the isomerization from the *trans* isomer to the *cis* were determined to be 10.9 kcal/mol for **1** and 7.2 kcal/mol for **2**.

It is well known from a number of dynamic NMR spectroscopic studies[2] that the rotation about the amide C–N bond is sufficiently slow at room temperature, for the C–N bond has a partial double-bond character. In secondary amides, therefore, there is a possibility for two isomers (*trans* and *cis*) to exist. Indeed, in monosubstituted formamides, both *trans* and *cis* isomers exist in the solution state,[3] and the isomerization barrier between the two isomers in formanilide has been reported to be 20 kcal/mol.[4]

In contrast with the case of amides, however, the conformation of the ester, which is a compound structurally analogous to the amide, is reported to be *s-trans* only from the dipole moment and from NMR, IR, and microwave spectroscopic studies,[5] although it is also known[6] that the ester C–O bond has a partial double bond character due to the delocalization of electrons, as is shown below:

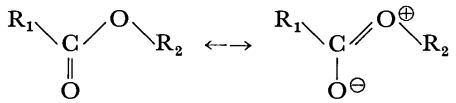

It has also been reported from ultrasonic absorption studies concerning various esters that the population of the *cis* isomer is small.[7-14]

However, in *t*-butyl formate (**1**) and other formates with a very bulky alcohol part, we previously found[15] from the results of studies using the dipole moment and the NMR, UV, and IR methods, that the *cis* isomer exists to a considerable extent. Similarly, the existence of the *cis* isomer was proved in several ester analogues (carbamates,[16] carbonates,[17] thiocarbonates,[18] and chloroformates[19]). Rotational barriers to the isomerization between the *trans* and the *cis* isomers have hardly been investigated at all except for the ultrasonic relaxation and IR investigation. The ΔH^* of the isomerization of methyl formate has been reported to be 7.8 kcal/mol from the ultrasonic relaxation analyses,[11,14,20] while Miyazawa supposed its potential barrier to be 13 kcal/mol in his analysis of the C–O out-of-plane vibrations of its infrared spectrum.[21] The discrepancy between these data is rather large, and so it is necessary to study in more detail the thermodynamic and kinetic parameters of the isomerization between the *trans* and *cis* conformers of the esters in other methods. In this connection, an NMR line-shape analysis is the most appropriate method.

In this paper, we will present the accurate isomerization parameters of formates, including both *trans* and *cis* isomers, on the basis of the complete line-shape analyses of their ^{13}C NMR spectra. In addition, we will discuss the influence of the bulkiness of the alkyl and aryl groups on the rotational barriers in the formates.

Experimental

Materials. *t*-Butyl formate (**1**), 1,1-diethylpropyl formate (**2**), and 2,6-dimethylphenyl formate (**3**) were prepared from the mixed anhydride of formic and acetic acids and the corresponding alcohols and phenol according to Stevens' method.[22] Methyl formate (**4**), ethyl formate (**5**), and isopropyl formate (**6**) were prepared from formic acid and the corresponding alcohols in the presence of a trace of sulfuric acid.

NMR Measurements. The ^{13}C NMR spectra of the esters were recorded on NEVA NV-14 (15.087 MHz) and Varian XL-100-15 (25.16 MHz) spectrometers. The pulsed FT method was made by a Varian 620/L computer (16k). Acetone-d_6 was used for the deuterium lock. The solvents and sample concentrations were as follows: 80 vol% in acetone and acetone-d_6 (5 vol%) for **1**, 30 vol% in dimethyl ether and acetone-d_6 (5 vol%) for **2**, and 10 vol% in dimethyl ether, carbon disulfide (25 vol%), acetone-d_6 (5 vol%) for **3**. The temperature was read by means of a calibrated copper-constantan thermocouple.

Spectral Calculations. The calculations of the theoretical spectra in the computer simulation were made by means of a FACOM 270/30 computer.

Results and Discussion

Previously we found[15] in an ^1H NMR spectral study of *t*-butyl formate (**1**) in DMF, that the line width of the formyl proton signal, which is only a singlet at room temperature, becomes broader as the temperature is lowered, and finally two separate peaks, which were assigned to the *cis* and *trans* isomers, appear at −94.0 °C. It was also found that the two signals of the *trans* and *cis* formyl protons show very complex line shapes at such a conformationally frozen temperature as −99 °C. This occurs because they couple with the methyl protons of the *t*-butyl group through five chemical bonds, and the line shapes show that the long-range spin-spin coupling constant in the *trans* isomer ($^5J_{trans}$) is different from that in the *cis* isomer ($^5J_{cis}$). A complete line-shape analysis of these very complex ^1H NMR spectra of $AX_9 \rightleftarrows A'X'_9$ spin system must be made using the density matrix method.[23,24] The calculation for this multi-spin system is quite hard. Moreover, the population change in the isomers at different tempera-

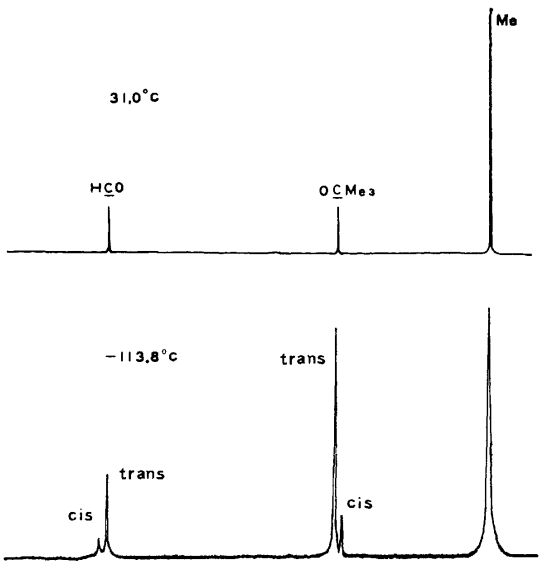

Fig. 1. ^{13}C NMR spectra of **1** at 31.0 and −113.8 °C.

tures makes the line-shape analysis very complex and difficult. Drakenberg *et al.* analyzed the ^{1}H NMR spectra of **1** using a rather approximate method.[25]

On the other hand, it is known that an ^{1}H-decoupled ^{13}C NMR spectral pattern is much simper than that of the ^{1}H NMR spectrum. Therefore, the line-shape analysis can be made much easily in the ^{13}C NMR spectra.[26-28]

Temperature-dependent ^{13}C NMR Line Shape. The ^{13}C NMR spectrum of **1** at an ambient temperature (Fig. 1) shows that the signals of the formyl, alkoxy ($OC(CH_3)_3$), and methyl carbons are sharp singlets. This means that the rate of the isomerization between the *trans* and *cis* isomers is very rapid at that temperature. As the temperature is lowered, the line widths become broader. The signals of the formyl and alkoxy carbons begin to separate into two peaks at about −96 °C (see Fig. 2); the minor peaks were assigned to the *cis* isomer of the ester, because other spectroscopic data show that the population of the *cis* isomer is smaller than that of the *trans* in **1**.[15] In contrast with this, the signal of the methyl groups is not divided into two peaks, even at temperature as low as −113.8 °C, although the line width becomes larger to some extent with the temperature decrease.* This may mean that the difference between the chemical shifts of the methyl

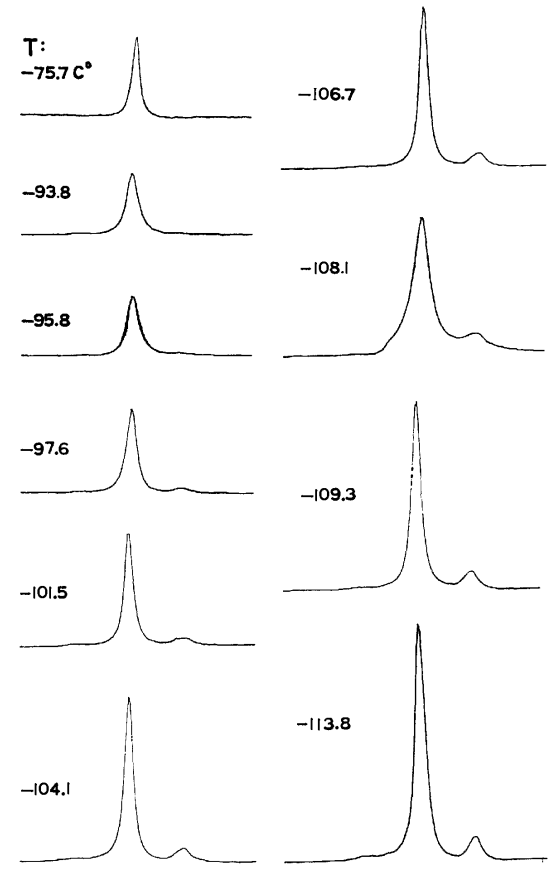

Fig. 2. The temperature-dependent ^{13}C NMR spectra of ethereal carbons in the *trans* and *cis* isomers of **1**.

groups in the two isomers is considerably smaller than those of the formyl and alkoxy carbon signals.

In a previous paper concerning the conformations of esters,[15] it has been discussed that the steric bulkiness of the R group (HCO_2R) severely affects the stabilization of the *trans* and *cis* isomers. This reasonably leads us to consider that the barrier to the rotation about the ester C–O bond must also be influenced by the bulkiness of the R group. Thus, the ester **2** and **3**, whose R groups are bulkier than the *t*-butyl group, were prepared and their ^{13}C NMR spectra were measured at low temperatures. The change in the line shape of **2** with the temperature decrease was almost the same as that of **1**, although the temperature had to be lowered to about −130 °C in order to freeze the isomerization reaction in **2**. In the case of **3**, however, no peak sepa-

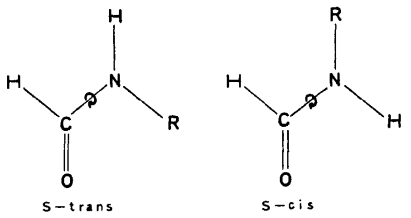

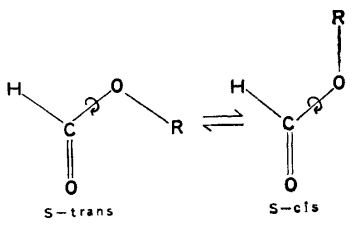

1: R=C(CH3)3

2: R=C(C2H5)3

3: R=

* At temperatures below −110 °C, the broad line shape of the methyl carbon becomes unsymmetrical and a small shoulder signal appears at the lower field of the main peak, although it does not separate into peaks even at −120.3 °C.

TABLE 1. ^{13}C CHEMICAL SHIFTS AND CHEMICAL-SHIFT DIFFERENCES OF THE *cis* AND *trans* ISOMERS IN **1**—**3** (ppm from TMS)

Signal	Isomer	**1**	**2**	**3**
HCO	*cis*	169.4	168.2	162.6
	trans	166.7	165.8	
	$\Delta\delta$	2.7	2.4	
OCR$_3$	*cis*	84.8	90.8	151.2
	trans	86.0	93.5	
	$\Delta\delta$	−1.2	−2.7	
CH$_3$		32.6[a]	12.1	20.0
CH$_2$CH$_3$		—	30.9	—
ortho		—	—	133.8
meta		—	—	132.6
para		—	—	130.1
Temperature (°C)		−113.8	−130.1	−133.0

a) Probably δ of the signal of the *trans* isomer.

rations in the formyl, aryloxy, and methyl carbon signals were found even at temperatures as low as −133 °C, although the line-shape broadening in the formyl carbon signal is quite large.

*^{13}C NMR Chemical Shifts of **1**—**3**.* The chemical shifts and chemical-shift differences of the two isomers in **1**—**3** are given in Table 1. It is worthwhile pointing out that in the carbonyl region of **1** and **2**, the chemical shift of the *cis* isomer is at a lower field than that of the *trans*, while in the alkoxy carbon region, the reverse is the case. This interesting chemical-shift tendency in the carbonyl and alkoxy carbon regions of the *trans* and *cis* isomers in these esters was also found in a structually analogous compound, *N*-*t*-butylformamide (HCONH-^{t}Bu) (**7**).[29] Table 1 shows that the chemical-shift difference ($\Delta\delta$) of the carbonyl carbon signals of the two isomers in **1** is almost the same as that in **2**, while in the alkoxy-carbon region the difference, $\Delta\delta$, in **2** is considerably larger than that in **1**. This result may be explained by considering that there is a very severe steric compression between the carbonyl and the 1,1-diethylpropyl groups in the *trans* isomer of **2**, and that the chemical shift moves to a lower field due to the steric compression effect,[30] while in the *cis* isomer the compression can be expected to be greatly reduced because the counter group for the repulsion is the smallest formyl hydrogen atom.

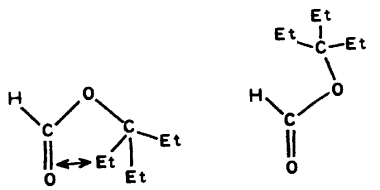

Populations of the Two Isomers. The populations of the *trans* and *cis* isomers change as the temperature is lowered. The determination of the populations was made using a computer simulation by the trial-and-error method in the conformationally frozen temperature range. This method was considered to be the most accurate for determining the populations, making it possible to dispense with the troublesome determination of the base line of the signals. This determination was made independently for the carbonyl and alkoxy carbon signals. The populations obtained in these two regions are in good agreement with each other. The population of the *cis* isomer in **1** is 9% at −113.8 °C, and that in **2** is 7% at −130.1 °C. The thermodynamic static parameters of the ester isomerization ($\Delta G°$, $\Delta H°$, and $\Delta S°$) were determined from these populations at different temperatures and their Arrhenius plots. The results are shown in Table 2.

Isomerization Barriers. The computer simulation of the temperature-dependent spectra of **1** and **2** was performed using the modified Bloch equation method in order to obtain the activation parameters of the isomerization. The computer program is EXNMR1.** The simulation in the line-shape analyses was made by

TABLE 2. THERMODYNAMIC PARAMETERS OF THE ISOMERIZATION BETWEEN THE *trans* AND *cis* ISOMERS IN FORMATES HCO$_2$R AT −100.0 °C AND 25.0 °C
The values in parentheses are those at 25.0 °C.

R	^{t}Bu		C(Et)$_3$	
Process	*t*→*c*	*c*→*t*	*t*→*c*	*c*→*t*
E_a (kcal/mol)	10.9±0.5 (10.9±0.5)	10.3±0.5 (10.3±0.5)	7.2±0.3 (7.2±0.3)	5.9±0.3 (5.9±0.3)
ΔG^* (kcal/mol)	9.3±0.02 (8.5±0.3)	8.6±0.02 (8.1±0.3)	8.4±0.03 (9.5±0.4)	7.6±0.09 (9.2±0.4)
ΔH^* (kcal/mol)	10.6±0.5 (10.3±0.5)	10.0±0.5 (9.7±0.5)	6.9±0.3 (6.6±0.3)	5.6±0.3 (5.3±0.3)
ΔS^* (e. u.)	4.4±1.7 (6.0±1.7)	4.7±1.7 (5.4±1.7)	−5.0±1.0 (−7.7±1.3)	−6.7±1.0 (−13.1±1.3)
$\Delta G°$ (kcal/mol)	0.69±0.05 (0.30±0.07)		0.74±0.08 (0.71±0.08)	
$\Delta H°$ (kcal/mol)	1.22±0.09 (1.22±0.09)		0.76±0.09 (0.76±0.09)	
$\Delta S°$ (e. u.)	1.8 ±0.3 (3.1 ±0.3)		0.1 ±0.3 (0.2 ±0.3)	

** A modified version of EXNMR0.[31]

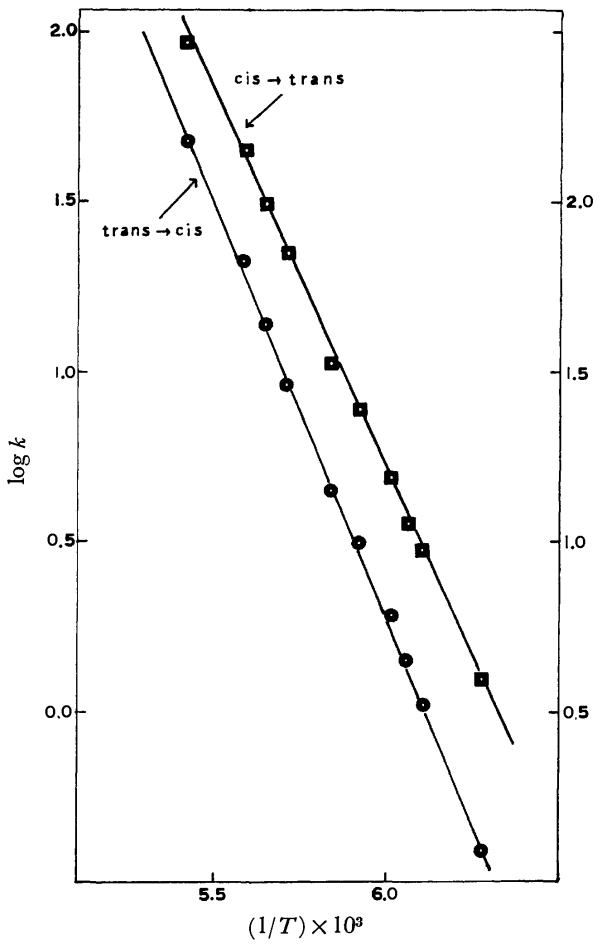

Fig. 3. The Arrhenius plots of log k *versus* $1/T$ in the two isomerization processes of **1**. The square dots □ are for the isomerization process from the *cis* to the *trans*, and the circular dots ○ are for that from the *trans* to the *cis*. The scale in the right hand is for the former process, and that the left hand is for the latter.

independently changing two parameters, the isomerization rate k_1 and the populations p_1, at each temperature. The line-shape analyses were performed in the two regions. The activation parameters of the ester isomerization were obtained from the Arrhenius plots of the k's and from Eyring's equation (Fig. 3). The results are shown in Table 2.*** The activation energy of the isomerization in **1** is considerably larger than in **2**. This may be accounted for by the destabilization of the energy level of the *trans* isomer in **2** at the ground state in comparison with the case of **1** because of the severe steric repulsion between the carbonyl and 1,1-diethylpropyl groups. This steric interaction in the *trans* isomer of **2** is revealed in the steric-compression lower-field shift of the alkoxy carbon signal described before. The activation entropy (ΔS^*) of **2** is much smaller than that of **1**. The reason for the smaller Δ^*S of **2** is not clear at the present time, but it is certain that it causes the activation free energy (ΔG^*) of **2** to increase. Thus, the ΔG^* of **2** is quite near to the ΔG^* of **1** ($\Delta\Delta G^*=0.9$—1.0 kcal/mol), although the difference between the activation energies (E_a) of **1** and **2** is remarkably large ($\Delta E_a=3.7$—4.4 kcal/mol).

In the case of **3**, the line broadening at low temperatures show the coexistence of the *trans* and *cis* isomers, which was also proved by the IR spectroscopic data.[15] However, we cannot determine the activation parameters of the isomerization in **3** because the signal of **3** does not separate into two peaks even at temperatures as low as −133 °C; therefore, we cannot know the chemical shifts and the populations of the two isomers. Assuming the chemical shift difference in the formyl carbon signals of the *trans* and *cis* isomers in **3** similar to those in **1** and **2**, however, it may be supposed that the activation energy in **3** is considerably smaller than those in **1** and **2**. The lower rotational barrier about the ester C–O bond in **3** may be explained by two factors: the destabilization of the *trans* isomer by the repulsion between the carbonyl and aryl groups, and the effect of the resonance between the ester and aryl groups. The latter effect may have a considerable influence, because, if the former factor is predominant, the activation energy in **3** must be larger than that in **2**, for the steric compression between the 2,6-xylyl and carbonyl groups in **3** is smaller than that between the 1,1-diethylpropyl and carbonyl groups in **2**. Concerning the latter factor, a full discussion cannot be made, but it is worthwhile pointing out that, if the resonance form, for example, **3c**, contributes to some extent, the single-bond character in the ester C–O bond may increase and the rotational barrier may be reduced.

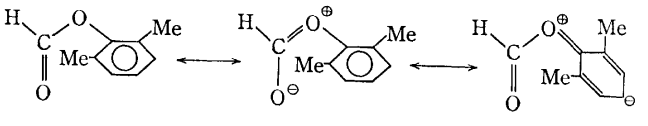

3a **3b** **3c**

Therefore, as it was made clear that the steric bulkiness of the R group in HCO_2R strongly influences the rotational barrier about the ester C–O bond, we measured the ^{13}C spectra of methyl formate (**4**), ethyl formate (**5**), and isopropyl formate (**6**). However, they show little line broadening†, even at the temperatures below −100 °C. This result indicates two possibilities concerning the rotational barriers of these esters. The rotational barriers of these esters are so low that we cannot obtain information about them on the NMR time scale, even at these low temperatures. The second possibility is that, although the barriers of **4**—**6** are higher than those of **1** and **2**, the chemical-shift differences between the two isomers are so small, and/or the population of the *cis* (less stable) isomer is so small, that the line shapes hardly change with the temperature decrease. Since it has been reported[8] that the popu-

*** The activation parameters obtained in this study are somewhat different from those obtained in an ^1H NMR investigation by Drakenberg *et al.*[25] For example, ΔH_{t-c} in **1** at −90 °C is reported to be 9.5 kcal/mol. This small discrepancy may be explained partly by the solvent or concentration effect on the activation parameters and partly by the systematic errors of their approximate method.

† The very slight line broadening is probably caused by the high viscosity effect at low temperature.

lation of the *cis* isomer in **5** is only a few percent at room temperature, it may be negligibly small for the NMR detection at such a low temperature as −100 °C. Thus, at present, unfortunately we cannot conclude which is the true case. Since the rotational barriers of **4** obtained from the ultrasonic relaxation and IR studies are considerably different from each other, as has been described before, more detailed investigation using other techniques should be made in the future.

References

1) Part IX: H. Nakanishi and O. Yamamoto, *Bull. Chem. Soc. Jpn.*, **50**, 3018 (1977).
2) W. E. Stewart and T. H. Siddall, *Chem. Rev.*, **70**, 517 (1970), and references cited therein.
3) L. A. LaPlanche and M. T. Rogers, *J. Am. Chem. Soc.*, **86**, 337 (1964).
4) H. Nakanishi and O. Yamamoto, *Chem. Lett.*, **1974**, 521.
5) G. I. L. Jones and N. L. Owen, *J. Mol. Struct.*, **18**, 1 (1973), and references cited therein.
6) G. W. Wheland, "Resonance in Organic Chemistry," Wiley, New York (1955).
7) J. Karpovich, *J. Chem. Phys.*, **22**, 1767 (1954).
8) D. Tabuchi, *J. Chem. Phys.*, **28**, 1014 (1958).
9) D. N. Hall and J. Lamb, *Trans. Faraday Soc.*, **55**, 784 (1959).
10) W. E. Slie and T. A. Litovitz, *J. Chem. Phys.*, **39**, 1538 (1963).
11) S. V. Subrahmanyam and J. E. Piercy, *J. Acoust. Soc. Am.*, **37**, 340 (1965).
12) J. E. Piercy and S. V. Subrahmanyam, *J. Chem. Phys.*, **42**, 1475 (1965).
13) K. M. Burundukov and Y. F. Yakovley, *Russ. J. Chem.*, **42**, 1141 (1968).
14) J. Barley and A. M. North, *Trans. Faraday Soc.*, **64**, 1499 (1968).
15) M. Ōki and H. Nakanishi, *Bull. Chem. Soc. Jpn.*, **43**, 2558 (1970).
16) M. Ōki and H. Nakanishi, *Bull. Chem. Soc. Jpn.*, **44**, 3148 (1971).
17) M. Ōki and H. Nakanishi, *Bull. Chem. Soc. Jpn.*, **44**, 3419 (1971).
18) M. Ōki and H. Nakanishi, *Bull. Chem. Soc. Jpn.*, **45**, 1993 (1972).
19) M. Ōki and H. Nakanishi, *Bull. Chem. Soc. Jpn.*, **45**, 1552 (1972).
20) K. M. Burundukov and V. F. Jakovlev, *J. Fiz. Chem.*, **42**, 2149 (1968).
21) T. Miyazawa, *Bull. Chem. Soc. Jpn.*, **34**, 691 (1961).
22) W. Stevens and A. van Es, *Recl. Trav. Chim. Pays-Bas.* **83**, 1287 (1964).
23) C. S. Johnson, Jr., "Advances in Magnetic Resonance," Vol. 1, Academic Press, New York (1956), p. 33.
24) O. Yamamoto and H. Nakanishi, *Tetrahedron*, **29**, 781 (1973).
25) T. Drakenberg and S. Forsen, *J. Phys. Chem.*, **76**, 3582 (1972).
26) H. Nakanishi and O. Yamamoto, *Tetrahedron Lett.*, **1974**, 1803.
27) H. Nakanishi and O. Yamamoto, *Chem. Lett.*, **1974**, 521.
28) H. Nakanishi and O. Yamamoto, *Chem. Lett.*, **1975**, 513.
29) H. Nakanishi, unpublished work.
30) G. J. Martin, M. L. Martin, and S. Odiot, *Org. Magn. Reson.*, **7**, 2 (1975).
31) O. Yamamoto, K. Hayamizu, H. Nakanishi, and M. Yanagisawa, *J. Nat. Chem. Lab. Ind. (Tokyo)*, **69**, 14 (1974).

Neighboring Group Participation in Solvolysis. VII. Trifluoroacetolysis of ω-Phenylalkyl 6-Methyl-2-naphthalenesulfonates*

Takashi Ando, Junko Yamawaki, and Yoshimasa Saito

The Institute of Scientific and Industrial Research, Osaka University, Yamadakami, Suita, Osaka 565

(Received May 12, 1977)

The title compounds, $Ph(CH_2)_nOMns$ (n=2—6), were solvolyzed in buffered trifluoroacetic acid in order to elucidate the effect of a phenyl group at a remote position on the reactivity and the course of the reaction. The reactivities varied remarkably with the length of the alkyl chain(n); $2 \gg 3 \ll 4 > 5 > 6$. The rate enhancement was attributed to anchimeric assistance by a remote phenyl group, and the rate depression to the electron-withdrawing inductive effect of a phenyl group. Studies on reaction products revealed that in trifluoroacetolysis of 4-phenylbutyl menasylate (n=4) the only pathway to take place is the one with δ-phenyl participation, and that even for 5-phenylpentyl menasylate (n=5) 12% of the reaction proceeds *via* ε-phenyl participation.

Participation of remote aryl groups in solvolysis has been investigated by Winstein and collaborators with ω-arylalkyl *p*-bromobenzenesulfonates in acetic acid and formic acid.[1] Rate enhancements and formation of cyclic products, however, are not remarkable except when the aryl groups are activated with suitable substituents. Formolysis of 4-phenylbutyl *p*-bromobenzenesulfonate, *e.g.*, proceeded with a comparable rate as that of butyl *p*-bromobenzenesulfonate, and gave only a 17% yield of 1,2,3,4-tetrahydronaphthalene (tetralin). On the other hand, solvents with low-nucleophilicity and high-ionizing power such as trifluoroacetic acid are known to enhance the solvolysis with anchimeric assistance.[2] Recently, Mason reported that a considerable rate enhancement by δ-phenyl participation was detected in trifluoroacetolysis of a series of 1-methyl-ω-phenylalkyl tosylates.[3] He observed a 93% yield of 1-methyltetralin in trifluoroacetolysis of 1-methyl-4-phenylbutyl tosylate. In the case of the secondary tosylates, however, a quantitative discussion is difficult because it can not be denied that the methyltetralin may be produced from the first-formed ion or ion-pair. The present investigation on trifluoroacetolysis of ω-phenylalkyl 6-methyl-2-naphthalenesulfonates was undertaken in order to elucidate quantitatively the effect of a remote phenyl group on the reactivity and the course of the reaction. In this case of the primary esters in the low-nucleophilic solvent, anchimeric assistance must be pronounced and a rate-product correlation must be valid.

Results

By use of a newly-developed leaving group, 6-methyl-2-naphthalenesulfonate (menasylate; Mns), trifluoroacetolysis can be followed easily and accurately by the spectrophotometric method.[4] At the standard substrate concentration (0.05 M) in the presence of 0.125 M of sodium trifluoroacetate, the reaction rates of butyl (**1**) and ω-phenylalkyl menasylates (**2**—**6**) were determined by following decrease in absorption at 326 nm.

$CH_3(CH_2)_3OMns$	$C_6H_5(CH_2)_nOMns$
1	**2** (n=2), **3** (3), **4** (4), **5** (5), and **6** (6)

The observed rate constants together with the corresponding activation parameters are given in Table 1. Each reported rate constant is the average value of duplicate or triplicate runs. The individual runs have correlation coefficients greater than 0.9995 over two half-lives for all compounds except 3-phenylpropyl menasylate (**3**). In the case of **3**, discoloration of the solution was observed as the reaction proceeded. The rate constants were thus calculated from absorbances observed at the earlier stage of the reaction (up to 50—65%) and those at infinity estimated therefrom.

Reaction products were analyzed by gas chromatography after more than seven half-lives under the same conditions as those for the kinetic runs. Reaction solutions containing dodecane or hexadecane as internal standards were injected directly into a gas chromatograph. The yields of the products corrected with their respective sensitivities are summarized in Table 2. All the products were separated by preparative gas chromatography and identified by comparison with authentic samples or by spectroscopic methods. Control experiments showed that primary trifluoroacetates (**7**, **10**, **12**, and **15**) and hydrocarbons (**9**, **11**, and **14**) were stable under the reaction conditions but a secondary trifluoroacetate (**8**) was unstable under the present reaction conditions.

Discussion

It is evident from Table 1 that the chain length has a decisive influence on the trifluoroacetolysis rates of ω-phenylalkyl menasylates. The phenomenon is more clearly demonstrated in Fig. 1, in which logarithms of the relative rate constants (k_{rel}) of ω-phenylalkyl menasylates to the reference compound, butyl menasylate (**1**), are plotted against the number of the alkyl chain. Similar plots for acetolysis and formolysis of ω-phenylalkyl brosylates are also shown in Fig. 1 for comparison.[1]

Large rate enhancements for **2** and **4**, and a distinct rate depression for **3** both in trifluoroacetolysis are apparent in Fig. 1. With respect to the solvent effect, the order of rate increase observed for **2** is exactly the same order of rate decrease for **3**, *i.e.*, $CF_3CO_2H > HCO_2H > CH_3CO_2H$. Thus a solvent of low-nucleophilicity and high-ionizing power is effective for both the rate enhancement and the rate depression. The rate enhancement must be the result of anchimeric

* A preliminary report of this work was presented at the 32nd National Meeting of the Chemical Society of Japan, Tokyo, April 1975.

Table 1. Trifluoroacetolysis rates of ω-phenylalkyl menasylates

Substrate	t/°C	$k_t \times 10^5$/s^{-1}	k_{rel}[a]	ΔH^*/kcal mol^{-1} [b]	ΔS^*/e. u.[c]
$CH_3(CH_2)_3OMns$ (**1**)	100	3.82±0.03	1.00	23.1	−17.2
	110	8.85±0.03			
$C_6H_5(CH_2)_2OMns$ (**2**)	40	2.84±0.01		20.1	−15.1
	50	8.08±0.01			
	60	21.1 ±0.1			
	100	620[d]	162		
$C_6H_5(CH_2)_3OMns$ (**3**)	100	0.99[e]	0.26	24	−18
	110	2.3[e]			
$C_6H_5(CH_2)_4OMns$ (**4**)	60	2.90±0.01		21.2	−15.7
	70	7.46±0.02			
	80	18.9 ±0.1			
	100	100[d]	26.2		
$C_6H_5(CH_2)_5OMns$ (**5**)	100	4.52±0.01	1.18	23.0	−17.3
	110	10.2 ±0.1			
	120	23.2 ±0.2			
$C_6H_5(CH_2)_6OMns$ (**6**)	100	3.99±0.02	1.04	22.5	−18.8
	110	9.05±0.04			

a) Relative rates to that of **1** at 100 °C. b) 1 kcal mol^{-1} = 4.184 kJ mol^{-1}. c) 1 e. u. = 4.184 J K^{-1} mol^{-1}. d) Calculated from data at other temperatures. e) Calculated using absorbances at 50—65% completion of reaction and those at "infinity" estimated therefrom. Data of single runs were used.

Table 2. Trifluoroacetolysis products of ω-phenylalkyl menasylates

Substrate	Product	Yield (%)
3	$C_6H_5(CH_2)_3OCOCF_3$ (**7**)	35
	$C_6H_5CH_2CH(OCOCF_3)CH_3$ (**8**)	0[a]
	Indan (**9**)	0
4	$C_6H_5(CH_2)_4OCOCF_3$ (**10**)	0
	Tetralin (**11**)	100
5	$C_6H_5(CH_2)_5OCOCF_3$ (**12**)	12.3
	1-Methyltetralin (**13**)	65.2
	Benzocycloheptene (**14**)	12.0
6	$C_6H_5(CH_2)_6OCOCF_3$ (**15**)	14.8
	1-Ethyltetralin (**16**)	75.0

a) Decomposition was observed in the control experiment. At 75% completion of reaction, a 1 : 1 mixture of **7** and **8** was detected.

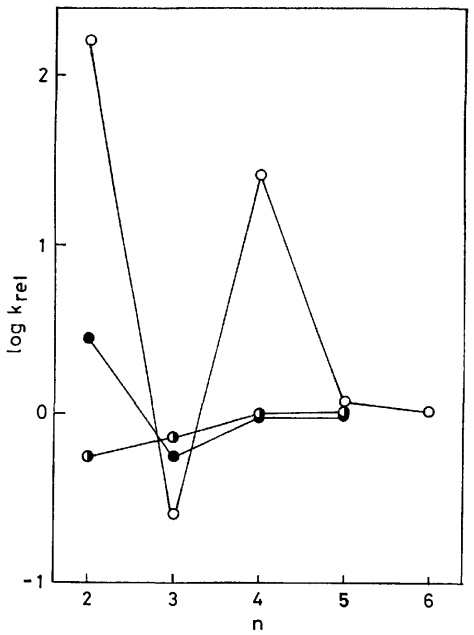

Fig. 1. Plots for logarithms of the relative rate constants of ω-phenylalkyl to butyl arenesulfonates *vs.* numbers of methylene groups.
○: Trifluoroacetolysis of menasylates at 100 °C, ●: formolysis of brosylates at 75 °C, ◑: acetolysis of brosylates at 75 °C.

assistance by a phenyl group, and the rate depression is attributable to the electron-withdrawing inductive effect of a phenyl group.

There have been many kinds of evidence that solvolysis of phenethyl esters is accelerated by anchimeric assistance of the neighboring phenyl group.[5] The fact that anchimeric assistance is usually pronounced in trifluoroacetic acid is also well-known.[2] On the other hand, evidence for anchimeric assistance by a phenyl group at delta to the reaction center has been very limited.[1,3,6-8] A rate enhancement with a factor of 26.2 indicates clearly the existance of such assistance. Another evidence was obtained from the study on the reaction products. In trifluoroacetolysis of **4**, the yield of tetralin (**11**) was quantitative and no other product was detected. As 4-phenylbutyl trifluoroacetate (**10**), a possible product of the solvent-assisted (k_s) pathway from **4**, was stable under the reaction conditions and did not give **11**, trifluoroacetolysis of **4** proceeds exclusively *via* the phenyl-assisted (k_Δ) pathway.

It is interesting to compare the rate enhancement factor of the δ-phenyl participation in the primary menasylates with that in the secondary tosylates. However, it is difficult to calculate the latter one because the reference tosylate was not solvolyzed under the same

conditions. A rate ratio of 1-methyl-4-phenylbutyl tosylate to 1-methyl-5-phenylpentyl tosylate (6.6) is a good estimation for the enhancement. A corresponding ratio in the primary esters, **4** to **5**, is 22.1. A ratio of **4** to **6**, 25.2, may be a better estimation because the trifluoroacetolysis rate of **5** can not be considered as a standard (*vide infra*). The larger rate enhancement factor for the primary esters is quite reasonable as the electron demand in the form of anchimeric assistance is more pronounced in the primary solvolysis with a less stabilized reaction center than in the secondary solvolysis. The mechanism of trifluoroacetolysis of **4** is summarized in Scheme 1.

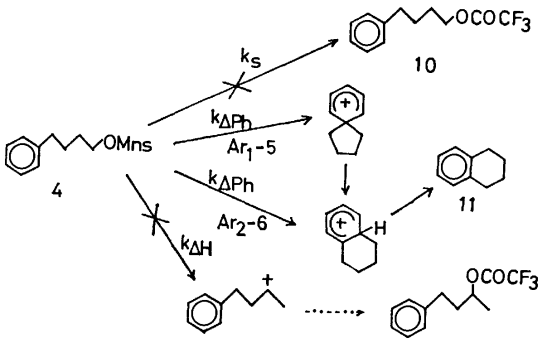

Scheme 1.

No new information was obtained from this study concerning the relative importance of the two possible modes of δ-phenyl participation, Ar_1-5 and Ar_2-6, proposed by Winstein.[1] It will be discussed in detail in a forthcoming paper.[9]

A small rate enhancement (18%) was also observed in trifluoroacetolysis of **5**. Inspection of the reaction products revealed that a 12.0% yield of 6,7,8,9-tetrahydro-5*H*-benzocycloheptene (**14**) was produced in the solvolysis. This is the first case of the production of a seven-membered ring compound through the k_Δ pathway by a carbon atom. By analogy to δ-phenyl participation, two modes of the reaction are possible in ε-phenyl participation; Ar_1-6 and Ar_2-7 (Scheme 2). In order to obtain information on the mechanism of this participation, 5-(*m*- and *p*-methoxyphenyl)pentyl menasylates (**17** and **18**) as well as **5** were solvolyzed under the same conditions. The rate constants and the reaction products were compared with each other (Table 3).

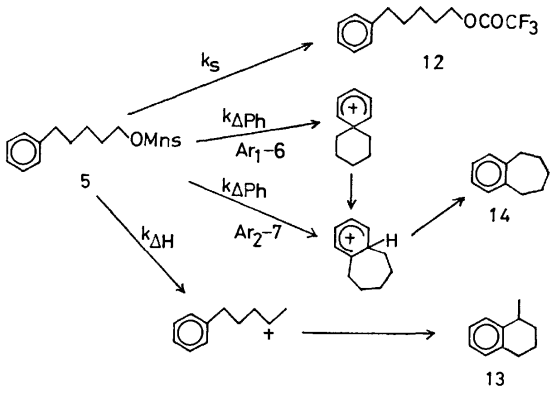

Scheme 2.

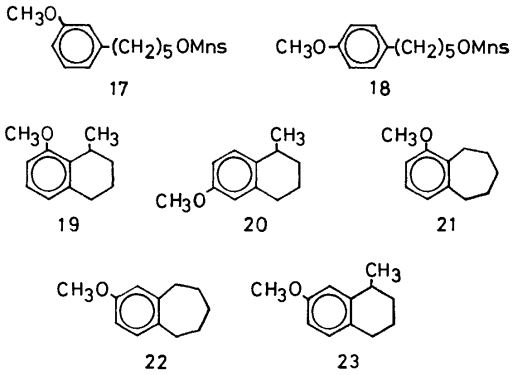

Since a methoxyl group is considered to activate its ortho and para positions and deactivate its meta positions, it was anticipated that introduction of a methoxyl group should have differentiated the two modes of participation. Unfortunately, however, introduction of a methoxyl group also caused the reactants and/or the products unstable under the reaction conditions. Because of faint discoloration of the reaction solutions at "infinity," the rate constants obtained involve much uncertainties. The yield of solvolysis products were also low especially in the case of the *m*-isomer (**17**). Nevertheless, a higher yield (16.8%) of 2-methoxy-6,7,8,9-tetrahydro-5*H*-benzocycloheptene (**22**) from **18** than that of **14** (12.0%) from **5** indicates that activation of the ipso position by the *p*-methoxyl group contributes to an increase of the fraction of the k_Δ pathway. The result clearly verifies the importance of the Ar_1-6 pathway in ε-phenyl participation. Although no definite conclusion can be drawn concerning the Ar_2-7 pathway from a comparable yield (12.5%) of 1- and 2-methoxy-6,7,8,9-tetrahydro-5*H*-benzocycloheptene (**21** and **22**) from **17**, we feel that the Ar_2-7 pathway also operates because deactivation of the ipso position by the *m*-methoxyl group does not decrease the fraction of the k_Δ pathway. A contribution from the Ar_2-7 pathway may compensate the ipso deactivation.

Table 3. Trifluoroacetolysis rates and products of 5-arylpentyl menasylates at 110 °C

Aryl	Rate $k_t \times 10^4/s^{-1}$	Product yield (%)		
		Prim. trifluoroacetate	1-Methyltetralin	Benzocycloheptene
C_6H_5 (**5**)	1.04±0.03	12.3	65.2	12.0
m-$CH_3OC_6H_4$ (**17**)	0.95[a]	12.6	28.2[b]	12.5[c]
p-$CH_3OC_6H_4$ (**18**)	0.99±0.06	14.0	50.4[d]	16.8[e]

a) The rate constant of a single run. b) The sum of yields of **19** (8.9%) and **20** (19.3%). c) The sum of yields of **21** (5.9%) and **22** (6.6%). d) A yield of **23**. e) A yield of **22**.

Formation of a large amount of 1-methyltetralin without a trace of a secondary trifluoroacetate from **5** is noteworthy. As it is well known that even a hydrogen next to the reaction center can participate in the solvolysis in trifluoroacetic acid, **5** must give 1-methyl-4-phenylbutyl cation or ion-pair at first.[10] The rate constant of this pathway should be designated as $k_{\Delta H}$ in contrast to that of the competitive pathway of phenyl participation as $k_{\Delta Ph}$. The cation must cyclize easily to give a 6-membered ring. A secondary trifluoroacetate (**6**) was found to be unstable in trifluoroacetic acid at a high temperature, although it was said stable at 29 °C.[3] Absence of secondary trifluoroacetates in the products from **3**, **5**, and **6** is attributed to their instability.

A phenyl ring at a more remote position than ε seems not to participate to the reaction center. The menasylate **6** was solvolyzed at a comparable rate with **1**. A small quantity (1.2%) of an unknown compound was detected by gas chromatography but its structure could not be identified as 5,6,7,8,9,10-hexahydrobenzocyclooctene. Hydrogen participation followed by hydrogen migration and cyclization is a possible route to 1-ethyltetralin (Scheme 3).

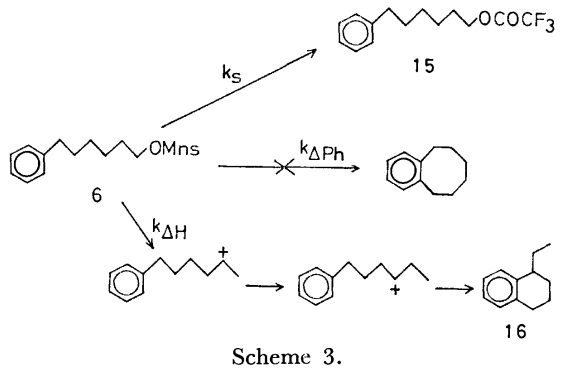

Scheme 3.

Inductive effects are considered to be transmitted to a more remote position in trifluoroacetic acid than in usual solvolysis solvents.[11] A distinct rate depression in **3** (k_{rel}=0.26) is clearly attributable to the electron-withdrawing inductive effect of a remote phenyl group. Indan, a possible product of the phenyl-assisted pathway, was not detected in the reaction mixture. In order to enhance the possibility of the Ar_2-5 pathway, the nucleophilicity of the ortho positions to the alkyl chain was increased by introduction of a methoxyl group at the meta position. Trifluoroacetolysis of 3-(*m*-methoxyphenyl)propyl menasylate (**24**), however, did not give methoxyindan at all. The rate constant for **24** was measured at 110 °C and similar to that of **3**. Accurate rate data could not be obtained because of discoloration of the reaction solutions. Reaction products from both of **3** and **24** were determined at the several stages of the reactions. About 1 : 1 mixtures of the primary and secondary trifluoroacetates were detected at the early stages of the reactions, but the latters decreased gradually and disappeared finally. Thus, the reaction of **3** is summarized in Scheme 4. The disadvantage of the Ar_2-5 pathway appears to be curious since indan is a stable and strain-free compound.

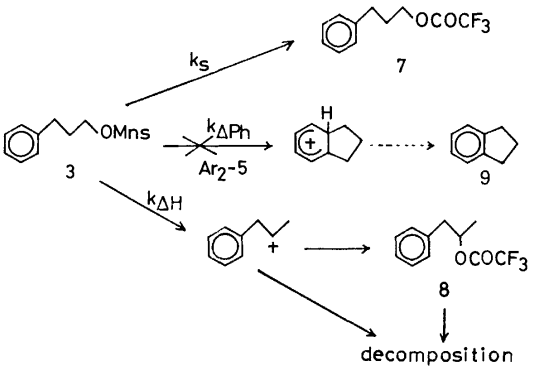

Scheme 4.

In the transition state of the phenyl-assisted pathway, however, the phenyl ring must approach to the reaction center from its perpendicular direction in order to ensure the p-σ overlap. The geometry is apparently a very unfavorable one for the Ar_2-5 pathway.[12]

Although the quantitative discussion on the activated parameters is difficult when the reaction includes composite pathways, useful information on the reaction is sometimes obtained from these parameters as they vary with the composition of the reaction. Relatively high entropies of activation have been considered a good criterion for anchimeric assistance besides rate enhancements and stereochemistry of reaction products.[13] In contrast to $\Delta S^{\ddagger}$ of *ca.* −17——18 e. u. (1 e. u.=4.184 J K^{-1} mol^{-1}) for the solvent-assisted (k_s) solvolysis, $\Delta S^{\ddagger}$ of *ca.* −7 e. u. for Ar_1-3 and *ca.* −10 e. u. for Ar_1-5 have been reported in ethanol, acetic acid, and formic acid.[1,13] Less negative $\Delta S^{\ddagger}$ for the anchimerically assisted (k_Δ) solvolysis can be attributed to a consequence of unimportance of nucleophilic involvement of the solvent in the transition state of the reaction. On the contrary, fairly constant and low $\Delta S^{\ddagger}$ were observed in trifluoroacetolysis throughout the series of ω-phenylalkyl menasylates; −15——16 e.u. for solvolysis with β and δ phenyl participation and −17——19 e.u. for others. As described above, most of the reactions in trifluoroacetic acid proceed *via* the k_Δ pathway in a sense; $k_{\Delta Ph}$ or $k_{\Delta H}$. Relatively constant $\Delta S^{\ddagger}$ can reasonably be expected in these cases. The low values of $\Delta S^{\ddagger}$ for the k_Δ pathway observed in this series are not anomalous in trifluoroacetic acid. $\Delta S^{\ddagger}$ for trifluoroacetolysis of ethyl tosylate, the pure k_s pathway, was −27 e.u. and much more negative than those in other solvents, *ca.* −17 e.u.[10] The differences of *ca.* 10 e.u. between $\Delta S^{\ddagger}$ in trifluoroacetic acid and those in other solvents observed in both of the k_Δ and k_s pathways suggest that electrophilic rather than nucleophilic solvation is important in trifluoroacetic acid and becomes a driving force of the reaction.

The effect of the concentration of sodium trifluoroacetate on the rates and the products was not studied in this series of solvolysis. It should be mentioned, however, that in trifluoroacetolysis of 4-phenylbutyl-1,1-d_2 menasylate (**4**-d_2) in the presence or absence of sodium trifluoroacetate, no deuterium scrambling was detected in the recovered menasylate. The cyclic intermediates of Ar_1-5 and/or Ar_2-6 pathways must afford tetralin without ion-pair return.

Experimental

General. All melting points were measured on a hot stage and not corrected. NMR spectra were recorded with Hitachi R-20 and R-24 spectrometers with tetramethylsilane as an internal standard.

Starting Alcohols. 1-Butanol and 3-phenyl-1-propanol were commercially available and used after purification. Other alcohols were prepared as follows.

4-Phenyl-1-butanol: This alcohol was prepared in a quantitative yield by lithium aluminum hydride reduction of 4-phenylbutanoic acid: bp 99—110 °C/4 Torr (lit,[14] 140 °C/14 Torr).

5-Phenyl-1-pentanol: This material was prepared by the Friedel-Crafts reaction of benzene with glutaric anhydride and aluminum chloride,[15] followed by the Wolff-Kishner reduction, esterification, and lithium aluminum hydride reduction, successively: bp 127 °C/5.5 Torr (lit,[14] 155 °C/20 Torr).

6-Phenyl-1-hexanol: This material was prepared by the Friedel-Crafts reaction of benzene with adipic anhydride polymer and aluminum chloride,[16] followed by the Wolff-Kishner reduction, esterification, and lithium aluminum hydride reduction, successively: bp 124 °C/3.5 Torr (lit,[14] 160—161 °C/13 Torr).

3-(m-Methoxyphenyl)-1-propanol: This alcohol was prepared by the Knoevenagel reaction of *m*-methoxybenzaldehyde with malonic acid,[17] followed by esterification and lithium aluminum hydride reduction: bp 137—138 °C/5.5 Torr (lit,[1] 135—140 °C/3.5 Torr).

5-(m-Methoxyphenyl)-1-pentanol: 3-(*m*-Methoxyphenyl)-1-propanol was converted to the chloride,[18] cyanide,[19] acid, ethyl ester, and 4-(*m*-methoxyphenyl)-1-butanol, successively. Application of the same series of reactions to the butanol gave the pentanol: bp 144—146 °C/3.5 Torr.

5-(p-Methoxyphenyl)-1-pentanol: This alcohol was prepared from 4-(*p*-methoxyphenyl)-1-butanol by the same sequence of reactions as described in the meta series: bp 147—148 °C/3 Torr (lit,[20] 144—145 °C/2 Torr).

4-Phenyl-1-butan-1,1-d_2-ol: This alcohol was prepared from ethyl 4-phenylbutanoate by reduction with lithium aluminum deuteride: bp 119.5 °C/6.5 Torr; deuterium content better than 99% (by ^{1}H NMR). Found: C, 78.91; H(D), 9.48% Calcd for $C_{10}H_{12}D_2O$: C, 78.90; H, 7.95; D, 1.32%.

Preparation of Menasylates. Menasylates were prepared by standard procedures from menasyl chloride and alcohols at 0°C in pyridine as a solvent.[4]

*Butyl Menasylate (**1**)*: Bp 177 °C/0.4 Torr, mp 33.7—34.7 °C. Found: C, 64.66; H, 6.48; S, 16.80%. Calcd for $C_{15}H_{18}O_3S$: C, 64.72; H, 6.52: S, 17.24%.

*Phenethyl Menasylate (**2**)*: Mp 104.3—105.0 °C (lit,[4] 101.9—102.5 °C).

*3-Phenylpropyl Menasylate (**3**)*: Mp 75.0—75.5 °C (from petroleum ether-ether). Found: C, 70.71; H, 5.75; S, 9.20%. Calcd for $C_{20}H_{20}O_3S$: C, 70.56; H, 5.92; S, 9.42%.

*4-Phenylbutyl Menasylate (**4**)*: Mp 104.9—105.0 °C (from hexane-benzene). Found: C, 71.36; H, 6.11; S, 9.17%. Calcd for $C_{21}H_{22}O_3S$: C, 71.16; H, 6.26; S, 9.06%.

*5-Phenylpentyl Menasylate (**5**)*: Mp 63.0—63.4°C (from cyclohexane). Found: C, 71.53; H, 6.27; S, 8.61%. Calcd for $C_{22}H_{24}O_3S$: C, 71.71; H, 6.57; S, 8.70%.

*6-Phenylhexyl Menasylate (**6**)*: Mp 52.0—52.8 °C (from petroleum ether-ether). Found: C, 72.08; H, 6.72; S, 8.33%. Calcd for $C_{23}H_{26}O_3S$: C, 72.22; H, 6.85; S, 8.38%.

*5-(m-Methoxyphenyl)pentyl Menasylate (**17**)*: This menasylate was obtained as an oil at a room-temperature and purified by recrystallization at a low temperature from petroleum ether-ether. Found: C, 69.21; H, 6.45; S, 8.15%. Calcd for $C_{23}H_{26}O_4S$: C, 69.32; H, 6.58; S, 8.05%.

*5-(p-Methoxyphenyl)pentyl Menasylate (**18**)*: Mp 57.7—58.3 °C (from petroleum ether-ether). Found: C, 69.11; H, 6.55; S, 8.15%. Calcd for $C_{23}H_{26}O_4S$: C, 69.32; H, 6.58; S, 8.05%.

*3-(m-Methoxyphenyl)propyl Menasylate (**24**)*: Mp 46.0—47.0 °C (from petroleum ether-ether). Found: C, 67.81; H, 5.71; S, 8.70%. Calcd for $C_{21}H_{22}O_4S$: C, 68.08; H, 5.99; S, 8.65%.

*4-Phenylbutyl-1,1-d_2 Menasylate (**4**-d_2)*: Mp 104.5—105.0 °C (from ligroin); deuterium content better than 99% (by ^{1}H NMR). Found: C, 70.69; H(D), 6.13; S, 9.12%. Calcd for $C_{21}H_{20}D_2O_3S$: C, 70.76; H, 5.66; D, 0.56; S, 8.99%.

Preparation of Trifluoroacetates and Other Solvolysis Products. Authentic samples of trifluoroacetates were prepared from alcohols and three molar equivalents of trifluoroacetic anhydride at 0 °C. Excess of the anhydride was removed under reduced pressure and the residual esters were distilled. Indan (**9**) and tetralin (**11**) were purchased and purified.

*3-Phenylpropyl Trifluoroacetate (**7**)*: Bp 83—90 °C/5.5 Torr. Found: C, 56.98; H, 4.97; F, 24.21%. Calcd for $C_{11}H_{11}F_3O_2$: C, 56.90; H, 4.78; F, 24.55%.

*1-Methyl-2-phenylethyl Trifluoroacetate (**8**)*: Bp 67 °C/6 Torr (lit,[2a] 70—71 °C/5 Torr).

*4-Phenylbutyl Trifluoroacetate (**10**)*: Bp 91.1—92.0 °C/4 Torr. Found: C, 57.75; H, 5.32; F, 23.97%. Calcd for $C_{12}H_{13}F_3O_2$: C, 57.83; H, 5.26; F, 24.07%.

*5-Phenylpentyl Trifluoroacetate (**12**)*: Bp 77—78 °C/2 Torr. Found: C, 59.80; H, 5.95; F, 21.60%. Calcd for $C_{13}H_{15}F_3O_2$: C, 60.00; H, 5.81: F, 21.90%.

*6-Phenylhexyl Trifluoroacetate (**15**)*: Bp 96 °C/6 Torr. Found: C, 61.25; H, 6.44%. Calcd for $C_{14}H_{17}F_3O_2$: C, 61.31; H, 6.25%.

*6,7,8,9-Tetrahydro-5H-benzocycloheptene (**14**)*: This material was prepared by the Wolff-Kishner reduction of 6,7,8,9-tetrahydro-5*H*-benzocyclohepten-5-one: bp 96.5-97.0 °C/13 Torr (lit,[21] 108—109 °C/22 Torr).

Trifluoroacetolysis Media. Trifluoroacetic acid containing 1 wt% of trifluoroacetic anhydride and 0.125 M of sodium trifluoroacetate was prepared according to the procedure described before.[4]

Kinetic Procedures. The usaul ampoule technique described before was employed.[4] Absorbances after more than ten half-lives were used as those at "infinity" except in the cases of **3**, **17**, and **18**. In these cases absorbances at infinity (A_∞) were calculated so as to make plots of $\log(A-A_\infty)$ *vs.* time linear. Absorbances were measured with a Hitachi Perkin-Elmer 139 UV-visible spectrophotometer.

Product Analyses. Reaction solutions containing 0.01 M of dodecane after more than seven half-lives were directly injected into a Varian Aerograph Model 2850-30 gas chromatograph with a flame ionization detector and a Hewlett-Packard 3370B digital integrator. A column packed with Silicon DC550 on Celite 545 was used. For the product analysis of **17**, PEG 20M on Celite 545 as a packing of a column and hexadecane as a standard were used. Sensitivities were determined using authentic samples for primary trifluoroacetates (**7**, **12**, and **15**), a secondary trifluoroacetate (**8**), tetralin (**11**), and 6,7,8,9-tetrahydro-5*H*-benzocycloheptene (**14**). For other compounds sensitivities were calculated by the method described by Sternberg *et al.*[22] Accuracy of calculated sensitivities were established for related compounds.

Identification of Solvolysis Products. All the reaction

products were separated by preparative gas chromatography and identified by comparison with authentic samples when available. Identification of following compounds were performed by spectroscopic analysis. NMR data in carbon tetrachloride are summarized below.

*1-Methyltetralin (**13**)*: δ=1.28 (3H, d, J=7.5 Hz, CH_3), 1.80 (4H, m), 2.80 (3H, m), and 7.07 (4H, m, Ar).

*1-Ethyltetralin (**16**)*: δ=0.95 (3H, t, J=7.5 Hz, CH_3), 1.80 (6H, m) 2.70 (3H, m), and 6.95 (4H, m, Ar).

*1-Methyl-8-methoxytetralin (**19**)*: δ=1.15 (3H, d, J=6.0 Hz, CH_3), 1.75 (4H, m), 2.73 (2H, m), 3.17 (1H, m), 3.77 (3H, s, OCH_3), and 6.42—7.00 (3H, m, Ar).

*1-Methyl-6-methoxytetralin (**20**)*: δ=1.18 (3H, d, J=8.0 Hz, CH_3), 1.67 (4H, m), 2.67 (3H, m), 3.59 (3H, s, OCH_3), and 6.40—7.05 (3H, m, Ar).

*1-Methoxy-6,7,8,9-tetrahydro-5H-benzocycloheptene (**21**)*: δ= 1.68 (6H, m), 2.72 (4H, m), 3.63 (3H, s, OCH_3), and 6.35 —6.92 (3H, m).

*2-Methoxy-6,7,8,9-tetrahydro-5H-benzocycloheptene (**22**)*: δ= 1.71 (6H, m), 2.70 (4H, m), 3.69 (3H, s, OCH_3), and 6.33— 6.92 (3H, m).

*1-Methyl-7-methoxytetralin (**23**)*: δ=1.22 (3H, d, J=7.5 Hz, CH_3), 1.75 (4H, m), 2.65 (3H, m), 3.60 (3H, s, OCH_3), and 6.30—6.85 (3H, m, Ar).

*Trifluoroacetolysis of 4-Phenylbutyl-1,1-d_2 Menasylate (**4**-d_2)*. A reaction solution of 0.05 M of **4**-d_2 in the same media as that for kinetic runs was allowed to react one half-life at 70.0 °C. The solvent was removed under reduced pressure and the residue was poured into ice-water. Precipitates were recovered by filtration and purified by recrystallization. No scrambling of the deuterium in the recovered **4**-d_2 was indicated by the absence of any signal at δ 4.06 (t, CH_2OMns).

A similar experiment in the absence of sodium trifluoroacetate also showed no scrambling of the deuterium in the recovered menasylate.

We thank Dr. Yasuhide Yukawa, Professor Emeritus of Osaka University, for his helpful discussion. The present work was partially supported by a Grant-in-Aid (No. 964097) for Scientific Research from Minitstry of Education.

References

1) R. Heck and S. Winstein, *J. Am. Chem. Soc.*, **79**, 3105, 3114 (1957).
2) See for example; a) J. E. Nordlander and W. G. Deadman, *J. Am. Chem. Soc.*, **90**, 1590 (1968); b) T. Ando, N. Shimizu, S.-G. Kim, Y. Tsuno, and Y. Yukawa, *Tetrahedron Lett.*, **1973**, 117.
3) T. J. Mason, *J. Chem. Soc., Perkin Trans. 2*, **1975**, 1664.
4) T. Ando, Y. Saito, J. Yamawaki, H. Morisaki, M. Sawada, and Y. Yukawa, *J. Org. Chem.*, **39**, 2465 (1974).
5) For the general discussion of this topic, see C. J. Lancelot, D. J. Cram, and P. v. R. Schleyer in "Carbonium Ions," Vol. 3, ed by G. A. Olah and P. v. R. Schleyer, Wiley-Interscience, New York (1972), Chap. 27.
6) R. J. Ouellette, R. Papa, M. Attea, and C. Levin, *J. Am. Chem. Soc.*, **92**, 4893 (1970).
7) L. M. Jackman and V. R. Haddon, *J. Am. Chem. Soc.*, **96**, 5130 (1974).
8) M. Gates, D. L. Frank, and W. C. v. Felten, *J. Am. Chem. Soc.*, **96**, 5138 (1974).
9) T. Ando, Y. Saito, and J. Yamawaki, to be published.
10) I. L. Reich, A. Diaz, and S. Winstein, *J. Am. Chem. Soc.*, **91**, 5635 (1969).
11) P. E. Peterson and D. M. Chevli, *J. Org. Chem.*, **39**, 3684 (1974).
12) B. Capon, *Quart. Rev.*, **18**, 45 (1964).
13) S. Winstein and R. Heck, *J. Am. Chem. Soc.*, **78**, 4801 (1956).
14) J. v. Braun, *Ber.*, **44**, 2867 (1911).
15) L. F. Somerville and C. F. H. Allen, *Org. Synth.*, Coll. Vol. II, 81 (1943).
16) J. W. Hill, *J. Am. Chem. Soc.*, **54**, 4105 (1932).
17) J. Koo, M. S. Fish, G. N. Walker, and J. Blake, *Org. Synth.*, Coll. Vol. IV, 327 (1963).
18) H. Rapoport and J. E. Campion, *J. Am. Chem. Soc.*, **73**, 2239 (1951).
19) L. Friedman and H. Schechter, *J. Org. Chem.*, **25**, 877 (1960).
20) J. M. van der Zanden, *Recl. Trav. Chim. Pays-Bas*, **60**, 291 (1941).
21) W. G. Dauben and J. B. Rogan, *J. Am. Chem. Soc.*, **79**, 5002 (1957).
22) J. C. Sternberg, W. S. Gallaway, and D. T. L. Jones, *Gas Chromatogr. Intern. Symp., 1961*, **3**, 231 (1962).

Branched-chain Sugars. II. Synthesis of Methyl 5-Deoxy-3-*C*-hydroxymethyl-2,3-*O*-isopropylidene-β-DL-*lyxo*-furanoside (Dihydrostreptose) and Ribofuranoside Derivatives

Takamasa KINOSHITA and Toshio MIWA

Faculty of Science, Osaka City University, Sumiyoshi-ku, Osaka 558

(Received May 14, 1977)

The title compounds, methyl 5-deoxy-3-*C*-hydroxymethyl-2,3-*O*-isopropylidene-β-DL-*lyxo*-furanoside, and ribofuranoside derivatives were conveniently synthesized *via* the Birch reduction of 2-methyl-3-furoic acid, and the latter was identified with the sample prepared from D-xylose.

In a previous paper,[1] we reported the synthesis of DL-apiose from 2-methoxy-4-(methoxycarbonyl)tetrahydrofuran which had been prepared *via* the Birch reduction of 3-furoic acid.[2] This paper will describe the synthesis of 5-deoxy-3-*C*-branched-DL-*lyxo*- and ribofuranoses of Type A[3] as an application of the method to the total synthesis of 3-*C*-branched-chain sugars from substituted 3-furoic acids.

Results and Discussion

The Birch reduction of 2-methyl-3-furoic acid (**1**) gave 2-methyl-2,3-dihydro-3-furoic acid, which, after esterification with diazomethane, followed by the acid-catalyzed addition of methanol, was isolated as a methoxy methyl ester (**2**) in a 95% yield. This compound was shown by gas chromatography (GLC) to be a mixture of four diastereoisomers with respect to each functional group, but the constituents could not be separated. The bromination of **2** by pyridinium tribromide in tetrahydrofuran at room temperature afforded a bromo compound (**3**) in a 75% yield. On the treatment of the isomeric mixture **3** with DBU (1,8-diazabicyclo[5.4.0]undec-7-ene) in benzene at room temperature for one minute, 5-methyl-2-methoxy-4-(methoxycarbonyl)-2,5-dihydrofuran (**4**), a mixture of (**4a**) and (**4b**) with the expected spectroscopic data, was obtained in a 75% yield. The oxidation of **4** with osmium tetraoxide–sodium chlorate[4] in aqueous tetrahydrofuran yielded diol in a 95% yield; it was subsequently isolated as an isomeric mixture of isopropylidene compounds, (**5a**), (**5b**), and (**5c**). These were separated by GLC in a ratio of 1.0: 1.5 : 1.7.

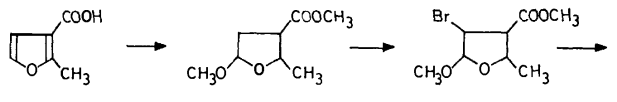

1 2 3

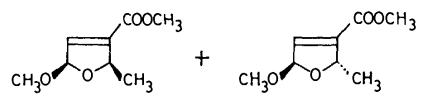

4a 4b

The structures of the compounds were assigned on the basis of the PMR spectrum. No coupling was observed between H-1 and H-2 in **5a** and **5c**, indicating that the methoxyl group is *trans*-disposed[5] to the 2,3-*O*-isopropylidene group. On the other hand, the doublets ($J_{1,2}$=4.6 Hz) for H-1 and H-2 in **5b** indicate these protons to be *cis* on the furanoid ring.[1] Although the exact orientation of the methyl group on carbon-4 was assigned by independent synthesis (see below), the signals of the methyl group in **5c** and that of the anomeric methoxyl group in **5b** appeared at the lowest field as a result of deshielding by the dioxolan ring. At this point, some comments may be added regarding the hydroxylation of **4**. In the oxidation of **4** with osmium tetraoxide, *cis*-**4a** gave exclusively **5a**, while *trans*-**4b** gave **5b** and **5c** in approximately equal quantities; this means that the steric bulkiness towards hydroxylation is almost the same in the methyl and methoxyl group.

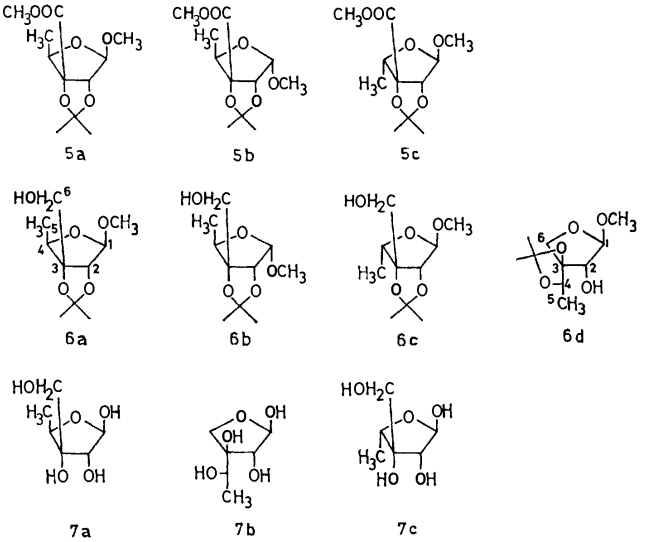

5a 5b 5c

6a 6b 6c 6d

7a 7b 7c

The acid-catalyzed hydrolysis of **5a**, followed by reglycosidation in methanol and acetonation , yielded **5a** and **5b** in a ratio of 2 : 7 (by GLC). This fact shows that **5b**, being an α-anomer, is more stable than **5a**. The methyl esters, **5a**—**c**, were reduced quantitatively to the corresponding alcohols (**6a**—**c**). The assignment of the configuration of (**6**) was based on its PMR spectral data and on the individual conversion of **5** to **6**. The chemical shifts and coupling constants were assigned as is shown in the Table. The fact that the methyl signal in **6a** appeared at the lowest may be explained by the deshielding effect being by the hydroxymethyl group rather than by the dioxolan ring.

A mixture of **6a** and **6b** was converted to a 1,2-*O*-isopropylidene derivative (**8**) *via* the following sequence of reactions: benzylation[6] in DMSO (37%), acid-catalyzed hydrolysis (85%), and acetonation (15%).[7]

Hydrogenation on Pd–charcoal of **8** gave a crystalline 5-deoxy-3-*C*-hydroxymethyl-1,2-*O*-isopropylidene-α-DL-ribofuranose (**9**) (mp 128—129 °C[8]) in a 90% yield. Compound **9** was synthesized in three steps from 5-deoxy-1,2-*O*-isopropylidene-α-D-*erythro*-pentofuranos-3-ulose (**10**),[9] which had been prepared from D-xylose. The reaction of **10** with 2-lithio-1,3-dithiane gave the branched-chain sugar, 5-deoxy-3-*C*-formyl-1,2-*O*-isopropylidene-α-D-ribofuranose trimethylene dithioacetal (**11**). Mercury(II) oxide and boron trifluoride etherate hydrolyzed **11** to 5-deoxy-3-*C*-formyl-1,2-*O*-isopropylidene-α-D-ribofuranose, which was then reduced with sodium borohydride to give **9**. The resulting compound was identified by comparing its PMR and mass spectra with those of the sample derived from 2-methyl-3-furoic acid.

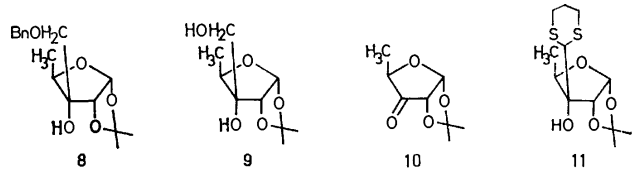

8 9 10 11

The acid-catalyzed hydrolysis of the alcohol **6c** with hydrochloric acid gave dihydrostreptose (**7c**), while that of **6a** or **6b** gave (**7a**). The hydrolysis of **6b**, followed by reglycosidation in methanol and acetonation, gave (**6d**) and **6a** in a ratio of 1 : 5. These substances were separated by GLC. **6a** was identified by comparing its GLC, MS, and PMR. The structure of **6d** was established by spin-decoupling studies. In the PMR spectrum of **6d**, the irradiation of C-5 methyl protons (δ, 1.28) collapsed the H-4 methin proton (δ, 4.20, quartet) to a singlet. The irradiation of H-2 (δ, 3.76) changed the H-1 (δ, 4.78, doublet) and the hydroxyl signals (δ, 2.60, doublet) both into singlets. A small H-1, H-2 coupling constant (1.2 Hz) could be taken as an indication of the *trans* arrangement of the protons. From the above data, **6d** was concluded to be a methyl 3-*C*-(1-hydroxyethyl)-3,3′-*O*-isopropylidene-β-DL-*threo*-furanoside.

Accordingly, in the production of **6d** it may be assumed that **7a** comprised an isomer (**7b**). In the PMR spectrum of **7c**, the methyl signals (doublet, J=6.5) appeared at δ 1.24 (75%, β-anomer) and δ 1.29 (25%, α-anomer), as had been reported by Dyer.[10] The predominance of the β-anomer, contrasted with methyl glycoside, is apparently due to the hydrogen bonding with the 3-*C*-hydroxymethyl group. Although the PMR spectrum of **7a** could not be assigned because of the concomitance of isomeric **7b**, the same situation was observed with the 4-epimer **7a**, which showed the methyl signals at δ 1.20 (25%, α-anomer) and δ 1.24 (75%, β-anomer) in a lower field than those of **7c**.

Experimental

Melting points were determined on a micro hot stage and are uncorrected. GLC was performed on a Varian Aerograph Model 90-P instrument equipped with a 4 mm × 1 mm column of Poly(ethylene glycol) (20% on Chromosorb W-AW, DMCS). The column temperature was 180 °C, and the flow rate was 60 ml of helium/min. IR spectra were taken on a JASCO Model IR-E. PMR spectra were recorded in chloroform-*d* solution at 100 MHz with a JEOLCO PS-100 spectrometer. Mass spectra were recorded with a HITACHI M-52 mass spectrometer at 70 eV. Elemental analyses were carried out on a Perkin Elmer Model 240 elemental analyzer.

*2-Methyl-3-furoic Acid (**1**)* (mp 102 °C) was prepared from ethyl 2-methyl-3-furoate; bp 87—95 °C/25 mmHg (lit,[11] bp 81—84 °C/18 mmHg).

The Birch Reduction of 2-Methyl-3-furoic Acid. To a mixture of 2-methyl-3-furoic acid (5.68 g) and anhydrous methanol (20 ml) in liquid ammonia (150 ml) was added sodium metal (5.2 g) little by little with constant stirring under reflux. The mixture was then stirred for an additional hour and ammonium chloride (11 g) was added. After evaporation of the liquid ammonia at room temperature, the residue was dissolved in water (100 ml). The aqueous solution was acidified with hydrochloric acid to pH 2 and extracted continuously with ether for 15 h. The ether extract was esterified with diazomethane, and, after the evaporation of the solvent, the residue was distilled to give **2**; 7.38 g (95%); bp 99—101 °C/20 mmHg; IR cm^{-1} 2830 (OCH_3), 1735 (C=O) Found: C, 55.09; H, 8.22%. Calcd for **2** ($C_8H_{14}O_4$): C, 55.16; H, 8.10%.

Bromination of 2. To a stirred solution of **2** (1.74 g)

TABLE 1. PMR-SPECTRA OF 5-DEOXY SUGARS (IN $CDCl_3$). CHEMICAL SHIFTS (δ VALUES) AND COUPLING CONSTANTS (Hz)

	5a	**5b**	**5c**	**6a**	**6b**	**6c**	**6d**
H_1	5.00, s	5.03, d	4.84, s	4.93, s	4.86, d	4.85, s	4.78, d
H_2	4.93, s	4.97, d	4.78, s	4.40, s	4.62, d	4.36, s	3.76, bs
H_4	4.42, q	4.30, q	4.35, q	4.38, q	4.20, q	3.98, q	4.20, q
H_6				3.80, s	3.77, q	3.71, s	4.04, q
$COOCH_3$	3.83	3.84	3.80				
OCH_3	3.38	3.48	3.37	3.37	3.50	3.37	3.37
OH				2.05	1.90	1.90	2.60, d
$(CH_3)_2$	1.53	1.60	1.52	1.53	1.60	1.53	1.55
	1.28	1.33	1.37	1.45	1.45	1.45	1.43
CH_3-	1.23, d	1.20, d	1.30, d	1.30, d	1.22, d	1.29, d	1.28, d
		$J_{1,2}$=4.6			$J_{1,2}$=4.5		$J_{1,2}$=1.2
	$J_{4,5}$=7	$J_{4,5}$=7	$J_{4,5}$=7	$J_{4,5}$=7	$J_{4,5}$=7	$J_{4,5}$=7	$J_{4,5}$=6.8
					$J_{6,6'}$=13		$J_{6,6'}$=9.5
							$J_{2,OH}$=2.0

in dry THF (20 ml) was added pyridinium tribromide (3.1 g). The reddish solution was stirred at room temperature. After 12 h, a white precipitate appeared and the color disappeared. The precipitate was filtered off and the filtrate was concentrated to a light-brown oil, which was then purified by chromatography on silica gel (80 g) with benzene to give a colorless liquid (**3**) (1.92 g, 75%); IR cm^{-1} 2830 (OCH_3), 1735(C=O). MS *m/e* (%) 254 (1) (M^+), 252(1) (M^+), 223 (50), 221(49), 191(25), 189 (22), 141 (78), 130 (75), 113(100), 83 (70).

*Dehydrobromination of **3** with DBU.* To a vigorously stirred solution of **3** (1.2 g) in dry benzene (25 ml) was added DBU (1.52 g) at room temperature. There immediately appeared a white precipitate of DBU-hydrobromide. Water (20 ml) was added to the reaction mixture and the organic layer was separated, washed with water, dried over sodium sulfate, and evaporated to give a 2,5-dihydrofuran derivative (**4**) as a colorless liquid (650 mg, 75%); IR cm^{-1} 3080, 2830, 1723, 1645; PMR δ1.47 (3H, d, J=6, CH_3), 3.40 (3H, s, OCH_3), 3.75 (3H, s, $COOCH_3$), 5.10—4.85 (1H, m, H-5), 5.70 (1H, s, H-2), 6.58 (1H, s, H-3).

*Methyl 5-Deoxy-3-*C*-methoxycarbonyl-2,3-*O*-isopropylidene-β- and α-*DL*-Ribofuranoside, **5a** and **5b**,* and *Methyl 5-Deoxy-3-*C*-methoxycarbonyl-2,3-*O*-isopropylidene-β-*DL*-lyxo-furanoside, **5c**.* To a stirred solution of the dihydro compound **4** (4.71 g) and osmium tetraoxide (80 mg) in THF (25 ml) was added a solution of sodium chlorate (3.82 g) in water (25 ml) at room temperature. After stirring for 24 h, the light-yellow solution was decomposed by passing hydrogen sulfide gas through it. Black precipitates were removed by filtration through Celite, and the colorless solution was concentrated to a volume of about 20 ml. The aqueous solution was extracted continuously with ether for 15 h to give a diol as a syrup; crude yield, 4.86 g (91%). IR cm^{-1} 3450, 2830, 1730.

The diol (2.06 g) was acetonated by treatment with dry acetone (150 ml), anhydrous copper(II) sulfate (15 g), and a catalytic amount of sulfuric acid at room temperature for 24 h to afford an oil, a mixture of **5a**, **5b**, and **5c**, after purification by column chromatography on silica gel; yield, 2.24 g (91%). The mixture was separated by GLC in a ratio of 1.0 : 1.5 : 1.7. The retention times: **5a**, 9.5 min; **5b**, 12.0 min; **5c**, 7.2 min. Found for **5a**: C, 53.51; H, 7.33%. Found for **5b**: C, 53.53; H, 7.44%. Found for **5c**: C, 53.50; H, 7.34%. Calcd for ($C_{11}H_{18}O_6$): C, 53.65; H, 7.37%.

*Chemical Conversion of **5a** to **5b**.* Compound **5a** (50 mg) in water-methanol (5 ml; 4 : 1) was hydrolyzed in the presence of a catalytic amount of *p*-toluenesulfonic acid at reflux for 2 h. After the disappearance of the anomeric methoxyl and isopropylidene groups has been ascertained by an estimation of the PMR spectrum in deuterium oxide, the syrup was boiled in dry methanol-dry acetone (20 ml; 10 ml) in the presence of *p*-toluenesulfornic acid for 6 h. The resulting compound (35 mg) was identified by comparing its GLC (**5a** : **5b**=2 : 7) with those of the sample.

*Methyl 5-Deoxy-3-*C*-hydroxymethyl-2,3-*O*-isopropylidene-β- and α-*DL*-Ribofuranoside, **6a** and **6b**, and Methyl 5-Deoxy-3-*C*-hydroxymethyl-2,3-*O*-isopropylidene-β-*DL*-lyxo-furanoside, **6c**.* Those substances were obtained quantitatively by the lithium aluminium hydride reduction in boiling ether for 3 h of **5a**, **5b**, and **5c** respectively. MS *m/e* (%) for **6a**: M^+ (absent), 203(12), 187(16), 171(9), 143(52), 119(20), 100(48), 85(96), 82(88), 73(100), 71(60). **6b**: M^+(absent), 203(4), 187(12), 171(9), 143(32), 119(16), 100(20). 85(35), 82(55), 73(100), 71(80). **6c**: M^+(absent), 203(3), 187(10), 171(5), 143(25), 119(15), 100(25), 85(40), 82(55), 73(100), 71(75). *p*-Nitrobenzoate of **6a**: syrup; **6b**, mp 109—110 °C; **6c**, mp 130—130.5 °C. Found for **6b**: C, 55.86; H, 5.80; N, 3.87%. Found for **6c**: C, 55.54; H, 5.80; N, 3.77%. Calcd for *p*-nitrobenzoate ($C_{17}H_{21}O_8N$): C, 55.58; H, 5.76; N, 3.81%.

*Chemical Conversion of **6b** to **6a** and **6d**.* Compound (**6b**) (70 mg) in water (5 ml) was hydrolyzed in the presence of two drops of concentrated hydrochloric acid at reflux for 10 min. After the evaporation of the solvent, the syrup was boiled in dry methanol-dry acetone (20 ml; 10 ml) in the presence of ion-exchange resin (Dowex 50X8, 500 mg) for 20 h to afford an oil (crude; 85 mg) as a mixture of the two compounds. The mixture was separated by GLC (at 200 °C) in the ratio of 1 : 5. The retention times: 6.2 min (**6d**); 7.5 min (**6a**).

*α,β-DL-Dihydrostreptose, **7c**, and Its 4-Epimer, **7a**.* Compound (**6c**) (300 mg) in water (5 ml) was hydrolyzed in the presence of a catalytic amount of concentrated hydrochloric acid at room temperature for 15 h. The evaporation of the solvent under diminished pressure below 40 °C gave a syrup of **7c** (220 mg, 95%). The PMR spectrum in deuterium oxide showed the absorptions of two isomers. The β-anomer comprised 75% of the mixture and showed absorptions at δ1.24 (3H, d, J=6.5, CH_3–), 3.60 (2H, s, H-6), 4.09 (1H, d, J=4.0, H-2), 4.35 (1H, q, J=6.5, H-4), 5.26 (1H, d, J=4.0, H-1). The α-anomer: δ1.29 (3H, d, J=6.5), 3.60 (2H, s), 4.10 (1H, q, J=6.5), 4.17 (1H, d, J=5.0), 5.23 (1H, d, J=5.0).

By the same procedure, **7a** was also obtained from **6a** or **6b**. δ1.20 (3H, d, J=6.5); α-anomer, 25%. δ1.24 (3H, d, J=6.5); β-anomer, 75%.

*5-Deoxy-3-*C*-hydroxymethyl-1,2-*O*-isopropylidene-α-*DL*-ribofuranose, **9**.* The benzylation of a mixture of **6a** and **6b** (1.0 g) was performed in accordance with Iwashige's method[6] to afford the benzyl ether in a 37% yield. The ether (200 mg) dissolved in dioxane-water (10 ml) was hydrolyzed at reflux for 2 h in the presence of concentrated hydrochloric acid to give a syrup (140 mg), which was then acetonated by the procedure described above to give 1,2-*O*-isopropylidene benzyl ether, **8**; 25 mg (15%); PMR δ5.60 (1H, d, $J_{1,2}$=4, H-1), 4.48 (1H, d, H-2), 3.91 (1H, q, $J_{4,5}$=6, H-4), 3.42(2H, q, $J_{6,6'}$=10, H-6), 2.66 (OH), 1.55 (3H, s), 1.35 (3H, s), 1.17 (3H, d, H-5), 4.52 (2H, q, J=12, benzyl), 7.27 (5H, s, arom.).

The hydrogenation of the benzyl ether **8** (25 mg) over 10% Pd-C in methanol for 5 h afforded a crystalline **9** (15 mg, 90%): mp 128—129 °C; PMR δ5.75 (1H, d, $J_{1,2}$=4, H-1), 4.55 (1H, d, H-2), 3.92 (1H, q, $J_{4,5}$=6.2, H-4), 3.75 (2H, d, $J_{6,6'}$=12, H-6), 2.73 (OH), 3.36 (OH), 1.56 (3H, s), 1.37 (3H, s), 1.18 (3H, d, CH_3–). MS *m/e* (%) M^+ (absent), 189 (14), 129(40), 99(36), 88(25), 71(89), 59(100). Found: C, 52.60; H, 7.86%. Calcd for **9** ($C_9H_{16}O_5$): C, 52.93; H, 7.92%.

*5-Deoxy-3-*C*-formyl-1,2-*O*-isopropylidene-α-*D*-ribofuranose Trimethylene Dithioacetal, **11**.* To a stirred solution of 1,3-dithiane (200 mg) in dry THF (4 ml) was added butyllithium (1.5 ml, 1.2 M in hexane) at −78 °C under a nitrogen atmosphere. After stirring at that temperature for 2 h, the ulose, **10** (170 mg) in dry THF (2 ml) was added and the reaction mixture was stirred for 3 h at room temperature. Water (10 ml) was then added and subsequently extracted with dichloromethane (20 ml×3). After an usual work-up and preparative thin-layer chromatography (0.75 mm silica gel on plate) (benzene-ether, 8 : 2), dithioacetal, **11** (270 mg, 92%), was obtained; mp 123—124 °C; $[\alpha]_D^{26}$ +5° (c=1, in acetone). PMR δ5.86 (1H, d, $J_{1,2}$=4, H-1), 4.74 (1H, d, H-2), 4.43 (1H, s, S–CH–S), 4.02 (1H, q, $J_{4,5}$=7, H-4), 3.00 (1H, s, OH), 2.80—3.00 (4H, m, $-CH_2-S-$), 2.05 (2H, bs, $-CH_2-$), 1.57 (3H, s,), 1.39 (3H, s), 1.45 (3H, d, H-5). MS *m/e* (%) 292 (6) (M^+), 277(1), 217(2), 190(1), 175(5), 146(3), 127(2), 119(100). Found C, 49.31; H, 6.89%. Calcd for

$C_{12}H_{20}O_4S_2$: C, 49.31; H, 6.90%.

5-Deoxy-3-C-hydroxymethyl-1,2-O-isopropylidene-α-D-ribofuranose **9**. To a suspension of red mercury(II) oxide (650 mg) and boron trifluoride etherate (365 mg) in 5 ml of 80% aqueous acetone was added, drop by drop, dithioacetal **11** (250 mg) in THF (2 ml) under a nitrogen atmosphere. After the mixture had been stirred overnight, the color disappeared. Water (2 ml) and acetone (6 ml) were then added, and the mixture was neutralized with a sodium hydroxide solution. The precipitate was filtered off, and the filtrate was concentrated to dryness under diminished pressure below 40 °C, extracted with chloroform, washed with water, and dried over sodium sulfate. The resulting syrup was reduced with sodium borohydride in 70% aqueous methanol (15 ml) to give an oil (120 mg). The residue was chromatographed on silica gel (5 g) (CH_2Cl_2–ether, 10 : 1); fractions were collected every 15 ml. Fraction 4—6 (30 mg) **9**, mp 112—113 °C. The PMR and mass spectra were identified with DL-**9**.

The authors are greately indebted to Dr. Kozo Shibata for the recording and analyses of the mass spectra and to Mr. Junichi Gōda for the elemental analyses. The authors also wish to thank Dr. Yoichi Kawashima for his skillful technical assistance.

References

1) T. Kinoshita and T. Miwa, *Carbohydr. Res.*, **28**, 175 (1973).

2) T. Kinoshita, K. Miyano, and T. Miwa, *Bull. Chem. Soc. Jpn.*, **48**, 1865 (1975).

3) L. Hough and A. C. Richardson, in "Rodd's Chemistry of Carbon Compounds," ed by S. Coffey, IF (1967), p. 529.

4) K. Wiesner and J. Santroch, *Tetrahedron Lett.*, **1966**, 5939.

5) a) J. D. Stevens and H. G. Fletcher, Jr., *J. Org. Chem.*, **33**, 1799 (1968); b) D. H. Ball, F. A. Carey, I. L. Klundt, and L. Long Jr., *Carbohydr. Res.*, **17**, 165 (1971).

6) T. Iwashige and H. Saeki, *Chem. Pharm. Bull.*, **15**, 1803 (1967).

7) The reason for the low yield of **8** is that the acetonation of the ribose-type compound gives, predominantly, the 2,3-*O*-isopropylidene derivative. a) M. Haga, M. Takano, and S. Tejima, *Carbohydr. Res.*, **14**, 237 (1970); b) H. Paulsen, V. Sinwell, and P. Stadler, *Chem. Ber.*, **105**, 1978 (1972).

8) The melting point of 1,2-*O*-isopropylidene-α-D-dihydrostreptose, that is, 5-deoxy-3-*C*-hydroxymethyl-1,2-*O*-isopropylidene-α-D-*lyxo*-furanose, is given as 104—105 °C in Ref. 10.

9) J. M. J. Tronchet, R. Graf, and R. Gurny, *Helv. Chim. Acta*, **55**, 613 (1972).

10) J. R. Dyer, W. E. McGonigal, and K. C. Rice, *J. Am. Chem. Soc.*, **87**, 654 (1965).

11) H. E. Winsberg, F. S. Fawcett, W. E. Mochel, and C. W. Theobald, *J. Am. Chem. Soc.*, **82** 1428 (1960).

Azafulvenes 8.[1] Cycloaddition Reaction of 8-Azaheptafulvene to Sulfene

Takahiko IWASAKI, Shoji KAJIGAESHI, and Shuji KANEMASA

Department of Industrial Chemistry, Faculty of Engineering, Yamaguchi University, Tokiwadai, Ube 755

(Received May 19, 1977)

Peri- and stereoselective cycloadducts were obtained from the reactions of 8-aryl-8-azaheptafulvenes with some sulfenes. 8-Aryl-8-azaheptafulvenes reacted with phenylsulfene to give *cis* [8+2] cycloadducts as the sole products which would have resulted either from the endo approach or *via* the endo intermediate of the two reagents. On the other hand, with benzoylsulfene *trans* [8+2] cycloadducts were isolated. The formation of the latter products was rationalized by considering epimerization of the initially formed *cis* adducts. The *cis* [8+2] cycloadducts to vinylsulfene did not give the *trans* isomers but the hydrogen migrated derivatives under the influence of bases. The mechanism of the above reactions is also discussed.

Thermal [8+2] cycloaddition reaction is, as well known, allowed to proceed in a concerted manner.[2] Nevertheless, this type of reaction concerned with a straight polyene has not been reported hitherto because a [4+2] cycloaddition reaction, which is also thermally allowed and known as the Diels-Alder reaction, would compete with an [8+2] cycloaddition reaction and defeat it. Not a [4+2] but an [8+2] cycloaddition, however, is possible to go on well when both the ends of a conjugate system with eight electrons are sterically fixed at the place where a convenient formation of new bonds is possible to occur. A cross-conjugated or peripherally conjugated 8 pi electrons system serves such an example. Thus, heptafulvene,[3] tropone,[4] tropothione,[5] and pentalene[6] have afforded the corresponding [8+2] cycloadducts. In addition, and 8 pi conjugate system along the perimeter (except for one pair of n-electrons on the condensed nitrogen atom) of indolizine[7] and mesoionic polyazapentalene[8] has combined with electron-deficient olefins and acetylenes to give the tricyclic [8+2] cycloadducts.

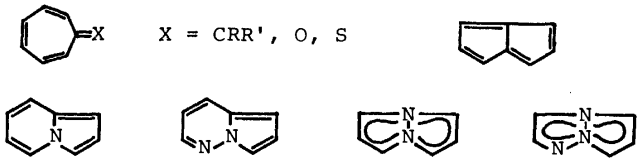

The reactions of 8-azaheptafulvene[9] with isocyanate, isothiocyanate, and ketone showed not only the high reactivity but also the excellent periselectivity of 8-azaheptafulvene toward these heterocumulenes.[10,11] In all of above reactions, 8-azaheptafulvane exclusively behaved only as an 8 pi addend to give the corresponding [8+2] cycloadducts in high yields.

Now, we would like to describe the cycloaddition reaction of 8-aryl-8-azaheptafulvene to some sulfenes. As for tropone, Ciabatonni and his coworker[12] have communicated the reactions with methanesulfonyl or mesylmethanesulfonyl chloride in the presence of triethylamine, both of which yielded the same product that was identified to be the [8+2] cycloadduct of tropone to mesylsulfene. They postulated a stepwise mechanism *via* dipolar intermediate for its formation. Stereoselective [8+2] cycloaddition reactions of tropone to asymmetrically substituted sulfenes have also been reported by Truce and Lin.[13]

Results and Discussion

The reaction of 8-(*p*-methoxyphenyl)-8-azaheptafulvene (**1a**) with phenylsulfene (**2**), generated *in situ* from the corresponding azaheptafulvenium salt and sulfonyl chloride, respectively, afforded the 1 : 1 adduct **3a**. The similarity in the PMR spectrum of **3a** to that of the [8+2] cycloadducts of 8-azaheptafulvenes to some heterocumulenes,[10,11] particularly in spectral patterns for the protons on the seven-membered ring, indicates **3a** to be the [8+2] cycloadduct of **1a** to **2**. Double resonance experiments provided the confirmable assignment for each proton and evidence for the structure of **3a**. The coupling constant between the two methine hydrogens at the 3- and 3a-position was measured to be 8.4 Hz. No difference in the PMR spectra before and after purification shows that the product **3a** is not the mixture of *cis* and *trans* isomer but either of them.

Similarly 8-(*p*-methylphenyl)- (**1b**) and 8-(*p*-chlorophenyl)-8-azaheptafulvene (**1c**) gave the corresponding [8+2] cycloadducts **3b** and **3c** with the same stereochemistry as **3a**.

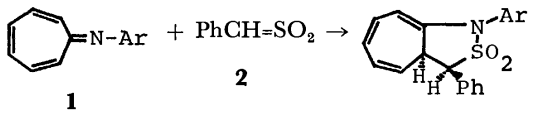

1 **2** **3**

a: Ar=*p*-$CH_3OC_6H_4$
b: Ar=*p*-$CH_3C_6H_4$
c: Ar=*p*-ClC_6H_4

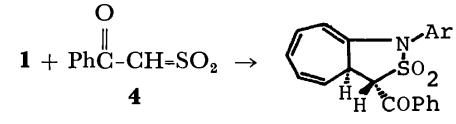

4 **5**

a: Ar=*p*-$CH_3OC_6H_4$
c: Ar=*p*-ClC_6H_4

The reactions of benzoylsulfene (**4**) with **1a** and **1c** gave the 1 : 1 adducts **5a** and **5c**, respectively. In these reactions it had been expected that the [8+4] cycloadducts would be formed besides the [8+2] cycloadducts.[10] Contrary to our expectation, the former products could not be even detected by spectroscopy. The IR spectrum of **5a** revealed the carbonyl stretching vibrations at 1685 cm^{-1} and the absorption bands at

1330 and 1160 cm^{-1} characteristic of sulfonyl group. The coupling constant of 4.2 Hz between the two methine hydrogens at the 3- and 3a-position in **5c** indicates that the structure of **5c** may differ from that of **3** in stereochemistry. It is very difficult to estimate the stereochemistry of the cyclic compound which involves sulfonyl group as one member only on the basis of the coupling constant between the two vicinal hydrogens. Therefore the epimerization reactions of both cycloadducts **3** and **5** were investigated using some bases in order to confirm the above anticipation.

The compound **3a** was recovered unchanged on being refluxed in benzene with triethylamine. But **3a** was converted into the isomer **6** when refluxed either with a catalytic amount of sodium ethoxide in ethanol or 1,5-diazabicyclo[5.4.0]undec-5-ene (DBU) in benzene. The spectral data of **6** are very similar to those of the starting **3a**. The methine proton at the 3-position was observed as doublet with a coupling constant of 7.6 Hz. The above results show that the sole product **3a** from **1a** with **2** was a thermodynamically less stable *cis* isomer which underwent the epimerization into a more stable *trans* isomer **6** *via* the carboanionic intermediate.

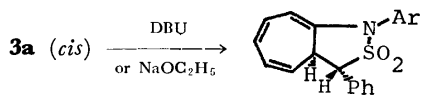

6 (*trans*)

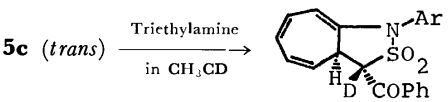

7 (*trans*)

Ar = *p*-ClC_6H_4

On the other hand, the [8+2] cycloadduct **5c** to **4** did not change its stereochemistry even if it was treated with DBU in benzene. An inversion should take place more easily at the 3-position in **5c** than the corresponding position in **3a** because the former contains a more acidic hydrogen atom at 3-position and possibly forms itself into an enolic form. Unchangeableness of **5c** on the treatment with DBU indicates that **5c** is a thermodynamically stable *trans* isomer.

The formation of monodeuterio derivative **7**, which was also a *trans* isomer, from the reaction of **5c** with triethylamine in methanol-*d* at room temperature led us to presume that the reaction of 8-aryl-8-azaheptafulvene (**1**) with **4** would have given the *cis* [8+2] cycloadduct as an initial product and been followed by the epimerization into the isolated *trans* product **5**. The reaction in which the diluted solution of triethylamine in dichloromethane was slowly added to the mixture of **1c** and benzoylmethanesulfonyl chloride in the same solvent at −50 °C, or in which **1c** was trated with the previously generated **4** in dichloromethane at −50 °C failed to form the *cis* [8+2] cycloadduct.

Vinylsulfene (**8**) reacted with **1** affording the 1 : 1 adduct **9** which was also found to be the [8+2] cycloadduct on the basis of the spectral data as well as the chemical conversion. The IR spectrum of **9a** showed the out of plane bending vibration bands at 960 cm^{-1}. The existence of a vinyl group was also confirmed from the PMR spectrum which exhibited the two terminal protons of vinyl group at 5.71 and 5.74 ppm (J_{cis}= 10.0 and J_{trans}=17.8 Hz), and whose spectral patterns were very similar to those of **3** and **5**. The coupling constant between the 3- and 3a-H (8.6 Hz) could not determine whether **9** was the *cis* or *trans* [8+2] cycloadduct.

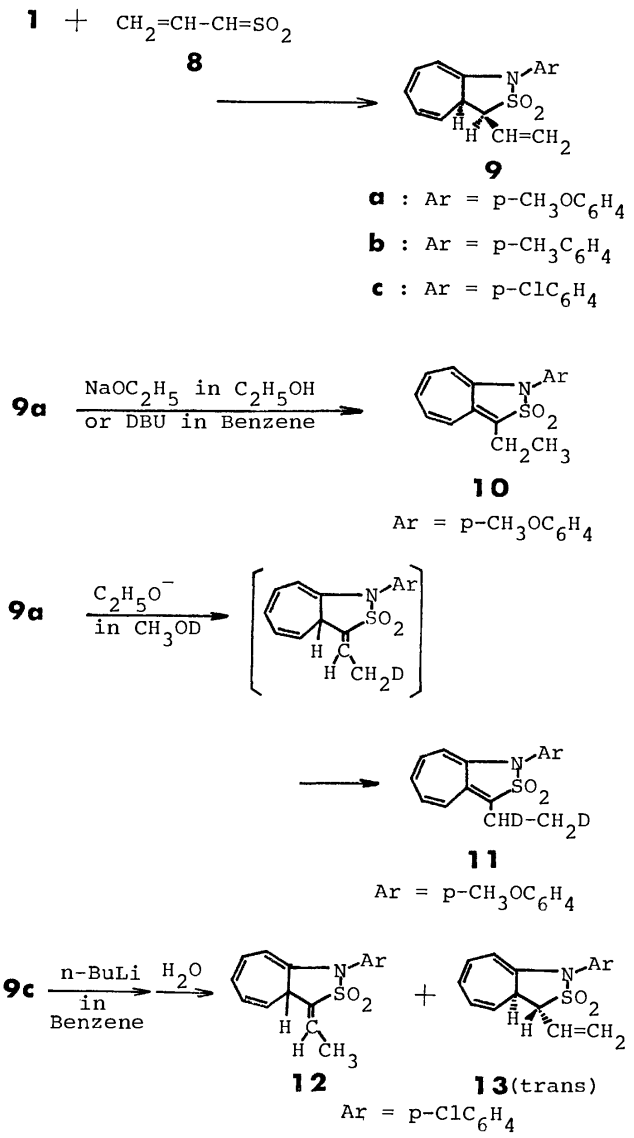

The compound **9a** was recovered unchanged when refluxed with triethylamine in benzene, whereas its treatment with sodium ethoxide in ethanol gave the isomeric **10**. By means of PMR spectroscopy, this product **10** was assigned to the isomer which was derived not from the inversion at carbon atom of the 3-position in **9a** but through the migration of vinyl double bond to a position of conjugation with the seven-membered ring. The mechanism for the double bond migration was confirmed by use of methanol-*d* in the above reaction.

The formation of **10** seemed to be caused by the fact that the allyl anionic intermediate from **9a** by deprotonation readily incorporated a proton from the solvent. Therefore, **9a** was reacted with DBU in dry benzene

at room temperature, but unexpectedly gave the same product **10**. These above results could not determine the stereochemistry of the [8+2] cycloadducts of **1** to **8**.

On the other hand, the reaction of **9c** with butyllithium in dry benzene under nitrogen gave an unseparable mixture of two products **12** and **13** whose structures were decided on the basis of the PMR spectrum of the mixture. The PMR spectrum showed the doublet (1.90, $C\underline{H}_3CH$=), quartet (6.82, $CH_3C\underline{H}$=), and multiplet (3.30 ppm, 3a-H) for the major product **12**, and the complex signals (5.45—5.87, $C\underline{H}_2$=CH– and 4-H), triplet (4.14, 3-H, $J_{3\text{-}3a}$=3.0 Hz), and multiplet (2.89 ppm, 3a-H) for the minor one **13**. The former corresponds to an intermediate involved in the course of isomerization of **9a** to **11**. The latter was assigned to be a thermodynamically stable *trans* [8+2] cycloadduct, whose formation indicated that the reaction of **1** with **8** had afforded the *cis* [8+2] cycloadduct as a sole product. The assignment of stereochemistry of **9** is compatible with the fact that although the treatment with DBU and butyllithium allowed the isomerization into **10**, **12**, and **13**, triethylamine did not change the stereochemistry of **9**.

As mentioned above, the reactions of **1** with **2**, **4**, and **8** gave the corresponding *cis* [8+2] cycloadducts as the isolated and initially formed products. Two mechanisms are possible for these reactions as depicted below: a concerted mechanism and stepwise one. The *cis* [8+2] cycloadduct would have been formed *via* endo approach between the two reagents in a concerted manner or *via* endo zwitterionic intermediate in a stepwise manner. As for the latter mechanism, it has been reported[13] that the reactions of tropone with some sulfenes might proceed stepwise *via* endo zwitterionic intermediates in which Coulombic attractions between the tropylium cation and the negatively charged group would facilitate the formation of thermodynamically unstable *cis* [8+2] cycloadducts.

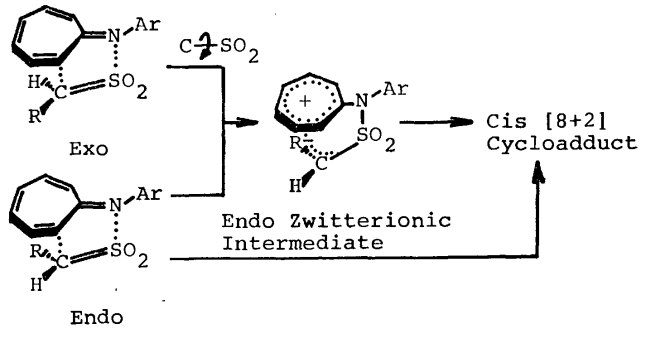

The similar stepwise reactions of **1** with isocyanates and isothiocyanates have given the [8+2] cycloadducts in general cases but the [8+4] cycloadducts in some cases.[10] Furthermore only the *trans* [8+2] cycloadducts have been obtained from the reactions of **1** with phenylketene.[11]

The [8+4] cycloadducts to benzoyl- or vinylsulfene and the *trans* [8+2] cycloadduct to phenylsulfene should be formed when the reaction of **1** with sulfene proceeds in a stepwise mechanism. The above reactions will have taken place, but not conclusively, in a concerted manner *via* the endo approach between 8-azaheptafulvenes and sulfenes. Further investigation has to be made for the clarification of the reaction mechanism.

Experimental

General. Melting and boiling points are all uncorrected. IR spectra were taken in KBr disks with a Japan Spectroscopic Co. IRA-1 spectrometer. PMR spectra were obtained at 100 MHz using a JEOL JNM-MH-100 spectrometer with tetramethylsilane as an internal standard. Mass spectra were determined with a JEOL JMS-D 100 mass spectrometer equipped with a direct inlet and at an ionization energy of 70 eV.

Materials. (8-*p*-Methoxy-, 8-*p*-methyl-, and 8-*p*-chlorophenyl)-8-azaheptafulvenium fluoroborate were prepared from tropylium fluoroborate and the corresponding anilines according to the method mentioned in the literature.[9] Phenylmethane-: mp 92—93 °C (lit,[14] mp 92—93 °C), benzoylmethane-: mp 87—88 °C (lit,[15] mp 87.5—88.2 °C) and 2-propenesulfonyl chloride: bp 76 °C/15 mmHg (lit,[16] bp 74—75 °C/15 mmHg) were synthesized from the reactions between the corresponding sodium sulfonates and phosphorus pentachloride. Triethylamine and dichloromethane were purified by simple distillation and dried with potassium hydroxide and calcium chloride, respectively.

*1-p-Methoxyphenyl-3-phenyl-3,3a-dihydro-1H-cyclohept[c]isothiazole 2,2-Dioxide (**3a**).* To a solution of 8-*p*-methoxyphenyl-8-azaheptafulvenium fluoroborate (0.30 g) and phenylmethanesulfonyl chloride (0.20 g) in dry dichloromethane (10 ml) was added dropwise a solution of triethyl amine (0.25 g) in dry dichloromethane (3 ml) at −50 °C. The reaction mixture was strired at the same temperature for 1 h and at room temperature overnight, and then evaporated *in vacuo* to dryness. The residue was extracted with hot benzene and the extract was evaporated again to give an oily product. The crude, but almost pure, product was filtered through a short column packed with alumina using benzene as eluent, giving pale yellow prisms of **3a** (0.37 g, 99%) which were purified by recrystallization from methanol; mp 123—124 °C. IR(KBr, cm^{-1}): 1615 (C=C), 1325 and 1140 (SO_2); PMR ($CDCl_3$, δ ppm): 3.34 (m, 1H, 3a-H), 3.77 (s, 3H, OCH_3), 4.97 (d, 1H, $J_{3\text{-}3a}$=8.4 Hz, 3-H), 5.11(dd, 1H, $J_{4\text{-}3a}$=4.5 and $J_{4\text{-}5}$=9.0 Hz, 4-H), 5.29 (br. d, 1H, $J_{8\text{-}7}$= 6.5 Hz, 8-H), 6.02—6.54 (m, 3H, 5-, 6-, and 7-H) and 6.86—7.58 (m, 9H, aromatic protons); MS (*m/e*, relative intensity) : 365 (M^+ 94), 301 (M^+-SO_2, 46), 300 (301^+-H, base peak), and 211 (M^+−phenylsulfene, 89).

Found: C, 68.78; H, 5.10; N, 3.64%. Calcd for $C_{21}H_{19}NO_3S$: C, 69.02; H, 5.24; N, 3.83 %.

*1-p-Methylphenyl-3-phenyl-3,3a-dihydro-1H-cyclohept[c]isothiazole 2,2-Dioxide (**3b**).* The reaction of 8-*p*-methylphenyl-8-azaheptafulvenium fluoroborate (0.57 g), phenylmethanesulfonyl chloride (0.40 g) and triethylamine (0.50 g), in a similar way described above, gave colorless prisms of **3b** (0.56 g, 80 %) which were purified by recrystallization from methanol; mp 136—138 °C. IR (KBr, cm^{-1}): 1620 (C=C), 1330 and 1145 (SO_2); PMR ($CDCl_3$, δ ppm): 2.34 (s, 3H, CH_3), 3.33 (m, 1H, 3a-H), 4.96 (d, 1H, $J_{3\text{-}3a}$=8.4 Hz, 3-H), 5.05 (dd, 1H, $J_{4\text{-}3a}$=5.0 and $J_{4\text{-}5}$=9.0 Hz, 4-H), 5.29 (br. d, 1H, $J_{8\text{-}7}$=5.5 Hz, 8-H), 6.01—6.50 (m, 3H, 5-, 6-, and 7-H) and 7.12—7.60 (m, 9H, aromatic protons); MS (*m/e*, relative intensity): 349 (M^+, 57), 285 (M^+-SO_2, 63), 284 (285^+-H, base peak) and 195 (M^+−phenylsulfene, 75).

Found: C, 71.73; H, 5.37; N, 3.84%. Calcd for $C_{21}H_{19}NO_2S$: C, 72.18; H, 5.48; N, 4.01%.

1-p-Chlorophenyl-3-phenyl-3,3a-dihydro-1H-cyclohept[c]*isothiazole 2,2-Dioxide (**3c**).* In a similar way as that of **3a**, the reaction of 8-*p*-chlorophenyl-8-azaheptafulvenium fluoroborate (0.61 g), phenylmethanesulfonyl chloride (0.40 g) and triethylamine (0.50 g) gave colorless prisms of **3c** (0.50 g, 69%) which were purified by recrystallization from methanol; mp 135.5—137 °C. IR (KBr, cm^{-1}): 1615 (C=C), 1330 and 1140 (SO_2); PMR ($CDCl_3$, δ ppm): 3.35 (m, 1H, 3a-H), 5.00 (d, 1H, J_{3-3a}=8.4 Hz, 3-H), 5.08 (dd, 1H, J_{4-3a}=5.0 and J_{4-5}=9.5 Hz, 4-H), 5.31 (br. d, 1H, J_{8-7}=5.5 Hz, 8-H), 6.08—6.60 (m, 3H, 5-, 6-, and 7-H) and 7.19—7.67 (m, 9H, aromatic protons); MS (*m/e*, relative intensity): 369, 371 (M^+, 43, 15), 305, 307 (M^+-SO_2, 73, 24), 304, 306 (305^+-H, base peak, 307^+-H, 32) and 215, 217 (M^+-phenylsulfene, 71, 24).

Found: C, 65.03; H, 4.32; N, 3.79%. Calcd for $C_{20}H_{16}NO_2SCl$: C, 64.95; H, 4.36; N, 3.79%.

3-Benzoyl-1-p-methoxyphenyl-3,3a-dihydro-1H-cyclohept[c]*isothiazole 2,2-Dioxide (**5a**).* To a solution of 8-*p*-methoxyphenyl-8-azaheptafulvenium fluoroborate (0.30 g) and benzoylemthanesulfonyl chloride (0.22 g) in dry dichloromethane (10 ml) was added drowpise a solution of triethylamine (0.20 g) in dry dichloromethane (3 ml) at −50 °C. The reaction mixture was stirred at the same temperature for 1 h and at room temperature overnight, and then evaporated *in vacuo* to dryness. The residue was extracted with hot benzene and the benzene solution was evaporated to give pale yellow prisms of **5a** (0.35 g, 89 %) which were purified by recrystallization from 2-propanol using charcoal; mp 171—173 °C. IR (KBr, cm^{-1}): 1685 (C=O), 1620 (C=C), 1330 and 1160 (SO_2); PMR ($CDCl_3$, δ ppm): 3.66 (m, 1H, 3a-H), 3.77 (s, 3H, OCH_3), 5.16 (dd, 1H, 4-H), 5.21 (br. d, 1H, J_{8-7}=5.5 Hz, 8-H), 5.39 (d, 1H, J_{3-3a}=4.2 Hz, 3-H), 6.06—6.60 (m, 3H, 5-, 6- and 7-H), 6.87, 7.22 (each d, 4H, *p*-methoxyphenyl protons) and 7.52, 8.09 (m, 5H, benzoyl protons); Mass (*m/e*, relative intensity): 393 (M^+, 4), 208 ($M^+-CH_3OPhNSO_2$, 45) and 207 (208^+-H, base peak).

Found: C, 67.25; H, 4.89; N, 3.77%. Calcd for $C_{22}H_{19}NO_4S$: C, 67.16; H, 4.87; N, 3.56 %.

3-Benzoyl-1-p-chlorophenyl-3,3a-dihydro-1H-cyclohept[c]*isothiazole 2,2-Dioxide (**5c**).* In a similar way described above, the reaction of 8-*p*-chlorophenyl-8-azaheptafulvenium fluoroborate (0.30 g), benzoylmethanesulfonyl chloride (0.22 g) and triethylamine (0.20 g) gave colorless needles of **5c** (0.30 g, 78 %) which were purified by recrystallization from methanol; mp 161—162 °C. IR (KBr, cm^{-1}): 1685 (C=O), 1625 (C=C), 1330 and 1160 (SO_2); PMR ($CDCl_3$, δ ppm): 3.68 (m, 1H, 3a-H), 5.20 (dd, 1H, 4-H), 5.32 (br d, 1H, J_{8-7}=5.5 Hz, 8-H), 5.46 (d, 1H, J_{3-3a}=4.2 Hz, 3-H), 6.18—6.66(m, 3H, 5-, 6-, and 7-H), 7.23—7.66 (m, 7H, aromatic protons) and 8.13 (br d, 2H, *o*-protons of benzoyl); MS (*m/e*, relative intensity): 397, 399 (M^+, 2), 208 ($M^+-ClPhNSO_2$, 48) and 207 (208^+-H, base peak).

Found: C, 63.46; H, 4.02; N, 3.80%. Calcd for $C_{21}H_{16}NO_3SCl$: C, 63.39; H, 4.05; N, 3.52%.

*Epimerization of **3a**.* One drop of 1,5-diazabicyclo-[5.4.0]undec-5-ene (DBU) was added to a solution of **3a** (0.10 g) in dry benzene (5 ml) and the mixture was refluxed for 1 h. Evaporation of benzene *in vacuo* gave pale yellow prisms of **5** (0.08 g, 80 %) which were purified by recrystallization from methanol mp 162—163 °C. IR (KBr, cm^{-1}): 1610 (C=C), 1320 and 1130 (SO_2); PMR ($CDCl_3$, δ ppm): 3.33 (m, 1H, 3a-H), 3.84 (s, 3H, OCH_3), 4.77 (d, 1H, J_{3-3a}= 7.6 Hz, 3-H), 5.25 (dd, 1H, 4-H), 5.35 (br. d, 1H, J_{8-7}=6.0 Hz, 8-H), 6.18—6.49 (m, 3H, 5-, 6-, and 7-H) and 6.89—7.61 (m, 9H, aromatic protons); Mass (*m/e*, relative intensity): 365 (M^+, 43), 301 (M^+-SO_2), 300 (301^+-H, 81) and 211 (M^+-phenyl sulfene, base peak).

The *trans* isomer **5** was also obtained from the following reaction: a solution of **3a** (0.32 g) and sodium ethoxide (0.01 g) in 10 ml of ethanol was refluxed for 1 h and evaporated *in vacuo* to dryness. The residue was dissolved in water and extracted with benzene. The extract was dried over magnesium sulfate and evaporated *in vacuo* to give **5** (0.18 g, 56 %).

*Deuteration of **5c**.* A mixture of **5c** (0.10 g), triethylamine (2 drops), and methanol-*d* (CH_3OD, 98 %, 0.5 g) in benzene (2 ml) was stirred at room temperature overnight and then evaporated *in vacuo* to give colorless crystals of **7** (0.098 g, 98 %) which were purified by recrystallization from methanol. In the PMR spectrum ($CDCl_3$) of **7**, the doublet of 3-H in **5c** which had been observed at 4.97 ppm completely disappeared.

1-p-Methoxyphenyl-3-vinyl-3,3a-dihydro-1H-cyclohept[c]*isothiazole 2,2-Dioxide (**9a**).* To a solution of 8-methoxyphenyl-8-azaheptafulvenium fluoroborate (0.60 g) and 2-propenesulfonyl chloride (0.30 g) in dry dichloromethane (10 ml) was added drowpise a solution of triethylamine (0.50 g) at −50 °C. The reaction mixture was stirred at room temperature overnight and evaporated *in vacuo* to dryness. The residue was extracted with hot benzene and the extract was evaporated again to give an oily product. The crude, but almost pure, product was filtered through a short column packed with alumina using benzene as eluent, giving pale yellow needles of **9a** (0.63 g, 100 %) which were purified by recrystallization from 2-propanol; mp 113.5—115 °C. IR (KBr, cm^{-1}): 1620 (C=C), 1320, 1140 (SO_2) and 960 (CH=CH_2); PMR ($CDCl_3$, δ ppm): 2.92 (m, 1H, 3a-H), 3.83 (s, 3H, OCH_3), 4.40 (t, 1H, $J_{3-3a}=J_{3-4}$=8.6 Hz, 3-H), 5.20 (br. d, 1H, J_{8-7}=5.5 Hz, 8-H), 5.47 (dd, 1H, J_{4-3a}=5.2 and J_{4-5}=8.5 Hz, 4-H), 5.71 (br. d, 1H, J_{trans}=17.8 Hz, =CH_2), 5.74 (br. d, 1H, J_{cis}=10.0 Hz, =CH_2), 6.10—6.55 (m, 4H, 5-, 6-, 7-H and -CH=) and 6.97, 7.30 (each d, 4H, aromatic protons); MS (*m/e*, relative intensity): 315 (M^+, 81), 251 (M^+-SO_2, 42), 250 (251^+-H, 76) and 211 (M^+-vinylsulfene, base peak).

Found: C, 64.65; H, 5.35; N, 4.24%. Calcd for $C_{17}H_{17}NO_3S$: C, 64.74; H, 5.43; N, 4.44%.

1-p-Methylphenyl-3-vinyl-3,3a-dihydro-1H-cyclohept[c]*isothiazole 2,2-Dioxide (**9b**).* The reaction of 8-*p*-methylphenyl-8-azaheptafulvenium fluoroborate (0.57 g), 2-propenesulfony chloride (0.35 g) and triethylamine (0.50 g), in a similar way described above, gave pale yellow plates of **9b** (0.35 g, 58 %) which were purified by recrystallization from cyclohexane; mp 97.5—100 °C. IR (KBr, cm^{-1}): 1620 (C=C), 1325, 1150 (SO_2) and 940 (CH=CH_2); PMR ($CDCl_3$, δ ppm): 2.34 (s, 3H, CH_3), 2.93 (m, 1H, 3a-H), 4.33 (t, 1H, $J_{3-3a}=J_{3-4}$=8.6 Hz, 3-H), 5.14 (br. d, 1H, J_{8-7}=5.5 Hz, 8-H), 5.38 (dd, 1H, J_{4-3a}=5.0 and J_{4-5}= 9.0 Hz, 4-H), 5.58 (br. d, 1H, J_{trans}=16.0 Hz, =CH_2) 5.61 (br d, 1H, J_{cis}=10.0 Hz, =CH_2), 5.95—6.38 (m, 4H, 5-, 6-, 7-H, and -CH=) and 7.13 (s, 5H, aromatic protons); MS (*m/e*, relative intensity): 299 (M^+, 57), 235 (M^+-SO_2, 44), 234 (235^+-H, 71) and 195 (M^+-vinylsulfene, base peak).

Found: C, 68.22; H, 5.63; N, 4.55%. Calcd for $C_{17}H_{17}NO_2S$: C, 68.20; H, 5.72; N, 4.68%.

1-p-Chlorophenyl-3-vinyl-3,3a-dihydro-1H-cyclohept[c]*isothiazole 2,2-Dioxide (**9c**).* In a similar way as that of **9a**, the reaction of 8-*p*-chlorophenyl-8-azaheptafulvenium fluorobotate (0.61 g), 2-propenesulfonyl chloride (0.28 g) and triethylamine (0.40 g) afforded colorless prisms of **9c** (0.41 g, 64 %) which were purified by recrystallization from 2-propanol; mp 112.5—113 °C. IR (KBr, cm^{-1}): 1620 (C=C), 1330, 1140 (SO_2) and 960 (CH=CH_2); PMR ($CDCl_3$, δ

ppm): 2.93 (m, 1H, 3a-H), 4.46 (t, 1H, $J_{3-3a}=J_{3-4}=8.6$ Hz, 3-H), 5.31 (br. d, 1H, $J_{8-7}=5.0$ Hz, 8-H), 5.51 (dd, 1H, $J_{4-3a}=5.5$ and $J_{4-5}=9.5$ Hz, 4-H), 5.72 (br. d, 1H, $J_{trans}=17.0$ Hz, $=CH_2$), 5.77 (br. d, 1H, $J_{cis}=10.0$ Hz, $=CH_2$), 6.06—6.64 (m, 4H, 5-, 6-, 7-H, and $-CH=$) and 7.34, 7.48 (each d, 4H, aromatic protons); MS (*m/e*, relative intensity): 319, 321 (M^+, 52, 18), 355, 357 (M^+-SO_2, 36, 13), 354, 356 (355^+-H, 83, 357^+-H, 29) and 215, 217 (M^+-vinylsulfene, base peak, 30).

Found: C, 60.01; H, 4.57; N, 4.29%. Calcd for $C_{16}H_{14}NO_2SCl$: C, 60.09; H, 4.41; N, 4.38%.

*3-Ethyl-1-*p*-methoxypehenyl-1*H*-cyclohept*[c]*isothiazol 2,2-Dioxide (**10**).* A solution of **9a** (0.20 g) and sodium ethoxide (0.04 g) in dry ethanol (10 ml) was refluxed for 1 h. The residue obtained by evaporation of the soluvent *in vacuo* was dissolved in water and the aquious solution was extracted with benzene. The extract was dried over magnesium sulfate and evaporated to give orange prisms of **10** (0.18 g, 90 %) which were recrystallized from 2-propanol; mp 152—153 °C. IR (KBr, cm^{-1}): 1590 (C=C), 1290 and 1150 (SO_2); PMR ($CDCl_3$, δ ppm): 1.38 (t, 3H, $C\underline{H}_3CH_2$), 2.80 (q, 2H, $CH_3-C\underline{H}_2$), 3.93 (s, 3H, OCH_3), 5.78 (br. d, 1H, $J_{4-5}=8.0$ Hz, 4-H), 6.30—6.84 (m, 4H, 5-, 6-, 7-, and 8-H) and 7.10, 7.48 (each d, 4H, aromatic protons): MS (*m/e*, relative intesity): 315 (M^+, base peak).

Found: C, 64.48; H, 5.26; N, 4.42%. Calcd for $C_{17}H_{17}NO_3S$: C, 64.74; H, 5.43; N, 4.44%.

This compound **10** was also obtained by the following procedure: a mixture of **9a** (0.11 g) and DBU (1 drop) in dry benzene (5 ml) was refluxed for 1 h and the solvent was evaporated *in vacuo* to give **10** (0.083 g, 75%).

3-(Ethyl-1,2-d_2*)-1-*p*-methoxyphenyl-1*H*-cyclohept*[c]*isothioazole 2,2-Dioxide (**11**).* A solution of **9a** (0.20 g) and sodium ethoxide (0.04 g) in emthanol-*d* (CH_3OD, 98%, 1.0 g) and dry benzene (1 ml) was refluxed for 1 h. The same work-up as described above gave orange prisms of **11** (0.10 g, 50%) which were recrystallized from 2-propanol; mp 151—152 °C. PMR ($CDCl_3$, δ ppm): 1.39 (m, 2H, $C\underline{H}_2DCHD$), 2.83 (m, 1H, $CH_2DC\underline{H}D$) and the other signals which were at the same positions as those of **10**; MS (*m/e*, relative intensity): 317 (M^+, base peak).

*The Reaction of **9c** with Butyllithium.* To a solution of **9c** (0.10 g) in dry benzene (10 ml) was added butyllithium (15% in hexane, 1.0 ml) at 0 °C under nitrogen. The solution was stirred for 15 min at the same temperature and poured into water. The organic compound was collected with benzene, dried over magnesium sulfate, and then the solution was evaporated *in vacuo*. The residue was filtered through a short column packed with alumina using benzene as eluent to give an yellow oil (**12** and **13**).

References

1) Part 7 of series: see Ref. 11.

2) R. B. Woodward and R. Hoffman, "The Conservation of Orbital Symmetry," Verlag Chemie-Academic Press (1970), p. 70.

3) W. von E. Doering and D. W. Wiley, *Tetrahedron*, **11**, 183 (1960).

4) J. Ciabattoni and H. W. Anderson, *Tetrahedron Lett.*, **1967**, 3377; R. Gompper, A Studeneer, and W. Elser, *ibid.*, **1968**, 1019.

5) T. Machiguchi, M. Hoshino, S. Ebine, and Y. Kitahara, *J. Chem. Soc., Chem. Commun.*, **1973**, 196.

6) E. Le Goff, *J. Am. Chem. Soc.*, **84**, 3975 (1962).

7) A Galbraith, T. Small, R. A. Barnes, and V. Boekelheide, *J. Am. Chem. Soc.*, **83**, 453 (1961); S. Ikeda, S. Kajigaeshi, and S. Kanemasa, *Chem. Lett.*, **1976**, 357.

8) V. Boekelheide and N. A. Fedruk, *Proc. Natl. Acad. Sci. U.S.A.*, **55**, 1385 (1966); O. Tsuge and H. Samura, *Heterocycles*, **2**, 27 (1974) and references cited therein.

9) K. Sanechika, S. Kajigaeshi, and S. Kanemasa, *Synthesis*, **1977**, 202.

10) K. Yamamoto, S. Kajigaeshi, and S. Kanemasa, *Chem. Lett.*, **1977**, 85.

11) K. Yamamoto, S. Kajigaeshi, and S. Kanemasa, *Chem. Lett.*, **1977**, 91.

12) J. Ciabattoni and M. Cabell, *Tetrahedron Lett.*, **1968**, 2693.

13) W. E. Truce and Cheng-I M. Lin *J. Am. Chem. Soc.*, **95**, 4426 (1973).

14) E. Fromm and J. de S. Palma, *Ber.*, **39**, 3308 (1906).

15) W. E. Truce and C. W. Vriesen, *J. Am. Chem. Soc.*, **75**, 2526 (1953).

16) W. E. Truce and J. R. Norell, *J. Am. Chem. Soc.*, **85**, 3231 (1963).

12,13-Epoxy-*C*-nor-*D*-homosteroids. I.[1] The Synthesis and Stereochemistry of 17α-Acetyl-12,13-epoxyetiojervanes

Akio Murai, Hiroshi Sasamori, and Tadashi Masamune
Department of Chemistry, Faculty of Science, Hokkaido University, Sapporo 060
(Received May 30, 1977)

Several 11-substituted 17α-acetyl-12,13-epoxyetiojervanes were prepared from jervine. Jervine was degraded by a known process into (17*E*)-17-ethyletiojerva-4,12,17(20)-triene-3,11-dione, which on epoxidation followed by acid treatment gave 17α-ethyletiojerva-4,12-diene-3,11,20-trione as the main product. Acetalization of the carbonyl groups, at C_3 and C_{20} of the triketone and subsequent hydride reduction produced two 11-epimeric alcohols, which on hydrolysis afforded 17α-ethyl-11α-hydroxyetiojerva-4,12-diene-3,20-dione and its 11β-hydroxy epimer. These alcohols and their acetates were oxidized with perbenzoic acid and/or *t*-butyl hydroperoxide to give the epoxides. The structure and configuration of these epoxides and the synthetic intermediates were determined on the basis of the chemical and spectral evidence.

A number of papers have appeared on the cleavage of an epoxy ring accompanied by the ring skeletal rearrangement in the field of steroid and other closely related compounds.[2] However, only one example[3] seems to be known for the skeletal transformation of a *C*-nor-*D*-homosteroid (etiojervane), *via* the 12,13-epoxy ring opening, into a normal steroid, although the reverse rearrangement (normal to *C*-nor-*D*-homo) has been investigated extensively.[4] In a series of studies aimed at the preparation of biologically active steroids from jervine and other available alkaloids, we have been working on the synthesis and reaction of 12,13-epoxyetiojervanes. In this paper we describe the synthesis and stereochemistry of 17α-acetyl-12,13-epoxyetiojervanes.

Jervine (**1**) was degraded by a known three-step process [*N*-methylation, boron trifluoride etherate (BF_3) treatment and the Oppenauer oxidation][5] into (17*E*)-17-ethyletiojerva-4,12,17(20)-triene-3,11-dione[6] (**2**) in a 70% yield. Compound **2** was then oxidized with perbenzoic acid to give its 17β,20*S*- (**3**) and 17α, 20*R*-epoxy derivatives (**4**), mp 190—192 °C and 176—178 °C, in 73 and 0.4% yields, respectively. The configurations of these compounds were assigned as shown by formulas **3** and **4** mainly by comparison of the NMR spectra with those of the corresponding Δ^5-3-oxo 3-ethylene acetals (**3a**, 17β, 20*S* and **4a**, 17α, 20*R*):[7] δ for 18-C$\underline{H}_3$, $\underline{H}$ at C_{20}, and 21-C$\underline{H}_3$; **3**, 1.98, 3.36, and 1.38; **3a**, 1.96, 3.35, and 1.37; **4**, 1.95, 3.21, and 1.38; **4a**, 1.93, 3.19, and 1.36. The predominant formation[7] of 17β,20*S*-epoxide **3** is understood to be the result of preferential axial attack of the peracid to the 17,20-double bond.[8]

Treatment of 17β,20*R*-epoxide **3** with a large excess of the Lewis acid (BF_3) produced a 5 : 1 (estimated by NMR) mixture of 17βH- and 17αH-methyl ketones (**5**) and (**6**) and 17β-aldehyde (**7**), mp 145—147 °C, in 60 and 7.5% yields, respectively. The mixture of methyl ketones was further separated by fractional recrystallization to yield **5**, mp 151.5—153.5 °C, and **6**, mp 195—197 °C, in pure state. The same treatment of 17α,20*R*-epoxide (**4**) afforded 17α-aldehyde (**8**), mp 148—150 °C, epimeric at C_{17} for **7**, in a 60% yield along with a 30% yield of a 1 : 1 mixture of **5** and **6**. The planar structures of these compounds (**5**—**8**) were completely consistent with the spectral data (see, Experimental). While the configurations at C_{17} of aldehydes **7** and **8** were assigned only by mechanistic consideration, those of methyl ketones **5** and **6** were deduced from the NMR spectra [17βH (pseudo-axial) in **5**, δ 3.33 (br W_H=20 Hz), and 17αH (pseudo-equatorial) in **6**, δ 3.38 (br W_H=11 Hz)], as well as from the relative amplitude in the ORD curves (**5**, a=+40°, and **6**, a=−20°).[9] In accordance with this assignment, the latter (**6**) with a pseudo-axial 17β-side chain was isomerized to the former (**5**) with *p*-toluenesulfonic acid (*p*-TsOH) in benzene under reflux to give a 2 : 1 equilibrium mixture of **5** and **6**. Each of these methyl ketones (**5**) and (**6**) would be formed by initial cleavage of the 17C–O bond with concomitant hydride shift from C_{20} and/or with subsequent deprotonation at C_{20}. The hydride shift would give only 17αH-methyl ketone (**6**) from 17β-epoxide (**3**) and only 17βH-methyl ketone (**5**) from 17α-epoxide (**4**), while the deprotonation would produce (an) enol intermediate(s), which would then be protonated at C_{17} mainly from the β-side with continued overlap between the p-orbitals of 17-, 13-, and 12-carbon atoms and of the labile donor proton (axial approach), giving 17βH-methyl ketone (**5**) as a major product. The result is explained by assuming

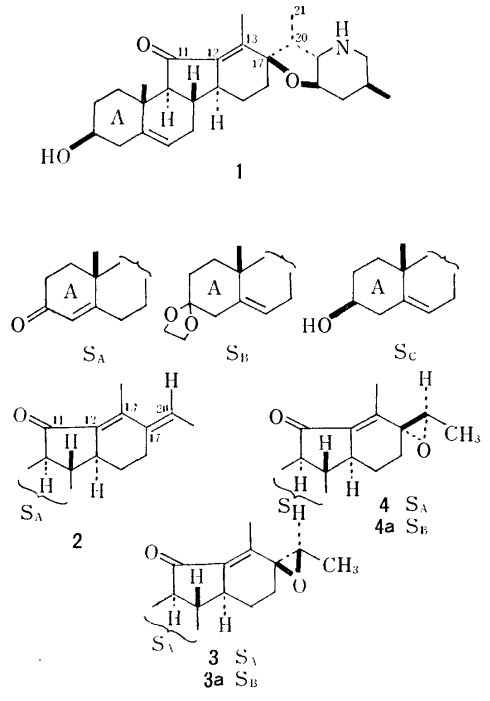

that the β-oriented 17C–O bond (pseudo-axial) in **3** would be cleaved more readily and followed mainly by deprotonation, whereas the corresponding α-bond (pseudo-equatorial) in **4** would require the hydride (and also methanide) shift owing to relatively difficult cleavage of the bond. On the other hand, 17-aldehydes (**7**) and (**8**) would result from the 17C–O bond cleavage accompanied by concurrent methyl migration, most probably from the opposite side against the epoxy group. On this premise, the configurations of 17-aldehydes were assigned as shown in formulas **7** and **8**.

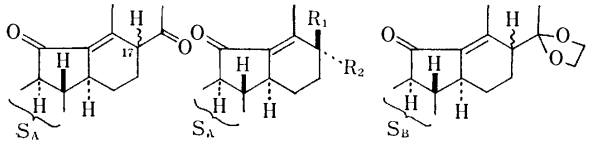

5 17β**H** **7** R_1=CHO, R_2=CH_3 **9** 17β**H**
6 17α**H** **8** R_1=CH_3, R_2=CHO **10** 17α**H**

The 5 : 1 mixture of methyl ketones (**5**) and (**6**) was refluxed with ethylene glycol and acid (*p*-TsOH) in benzene for 6 h to give a mixture of the respective 3,20-di(ethylene acetal)s, from which 17β**H**-3,20-diacetal (**9**), mp 181—183 °C, and 17α**H**-3,20-diacetal (**10**), mp 143.5-144.5 °C, were isolated in 50 and 10% yields, respectively, by fractional recrystallization. The latter (**10**) was epimerized quantitatively to the former (**9**) by the prolonged acid treatment (28 h).

Reduction of 17β**H**-3,20-diacetal (**9**) with aluminium trihydride followed by chromatographic purification gave 11α-alcohol (**11**), mp 135—137 °C, and 11β-alcohol (**12**), mp 163—164 °C, in 80 and 15% yields, respectively. A similar result was obtained by treatment with lithium aluminium hydride (LAH); alcohols **11** and **12** were produced in 73 and 17% yields, respectively. The configuration at C_{11} of each alcohol was assigned as shown in formulas **11** and **12** on the basis of the following evidence. (i) The 19-methyl protons of **12** were observed as a singlet at a lower field (δ 1.24) than those of **11** (δ 1.06), indicating the 1,3-diaxial-like disposition of the hydroxyl and 19-methyl groups in **12**.[10] (ii) Treatment of 11α-alcohol (**11**) with acetic anhydride at room temperature readily produced the corresponding acetate (**11a**), mp 194—196 °C, in a 95% yield, whereas the same treatment of 11β-alcohol (**12**) led to recovery of the starting alcohol; the corresponding acetate (**12a**), mp 143—145 °C, was obtained in a 94% yield by heating with acetic anhydride at 100 °C. The hydride (LAH) reduction of 17α**H**-3,20-diacetal (**10**) afforded a mixture of three compounds, from which 11α-alcohol (**13**), mp 194—196 °C, 11β-alcohol (**14**), mp 139—141 °C, and 12α**H**-11-ketone (**15**), mp 156—157 °C, were isolated in 15, 40, and 22% yields, respectively. The hydroxyl groups at C_{11} of **13** and **14** were assigned α- and β-configurations, respectively, in essentially the same manner as the reduction products of the 17β**H**-epimer (**9**); 19-methyl protons, δ 1.05 for **13**, and δ 1.24 for **14**. Saturated 11-ketone (**15**) was assigned α-hydrogen configuration at C_{12} and C_{13} on the ORD (a negative Cotton effect, a= −86°)[11] and NMR spectral data [19- and 18-methyl protons, δ 1.12 (δ_{calcd} 1.10) and δ 0.88].[10]

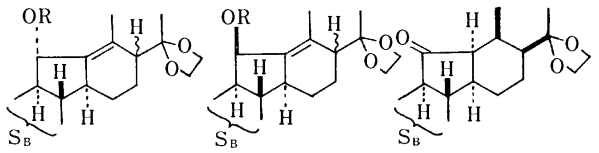

11 17β**H**, R=H **12** 17β**H**, R=H **15**
11a 17β**H**, R=Ac **12a** 17β**H**, R=Ac
13 17α**H**, R=H **14** 17α**H**, R=H

The reduction results for diacetals **9** and **10** deserve the following comments. (i) The hydride reduction of 17α**H**-3,20-diacetal (**10**) yielded 11β-alcohol (**14**) mainly while that of the 17β**H**-epimer (**9**) gave 11α-alcohol (**11**) as a major product irrespective of the reagents.[12] The latter result is remarkable as being the first example of the predominant formation of 11α-alcohol by the hydride reduction of 11-oxoetiojervanes. Compound **9** would take a twist-boat form with the pseudo-axial 17α-side chain rather than a half-chair with the pseudo-equatorial bulky substituent. The conformational change in passing from the ketone (**5**) to the acetal (**9**) would result in decrease of steric interaction between the 18-methyl group and the 17-substituent,[13] leading to more facile attack of the reagent from the less-hindered β-side to the carbonyl carbon at C_{11}, contrary to the approach from the α-side as has been illustrated in many 11-oxoetiojervanes. (ii) While no saturated 11-ketone was isolated from the reduction products of **9**, a considerable amount (22%) of saturated 12α**H**-11-ketone (**15**) was obtained in the reduction of **10**. In view of the slight but definite difference in the absorption maxima [λ_{max} 257 nm (ε 10000) for **9**, and 259 nm (ε 13000) for **10**], it seems that the 12,13-double bond of **9** is conjugated with the carbonyl group at C_{11} to a less extent as compared with that of **10**, suggesting a greater probability of the reduction of the double bond in question in the latter case. It should be emphasized that the 11-ketone (**15**) is the first example of 11-oxo-12α-etiojervanes (13α**H**) formed by the hydride reduction of 11-oxoetiojerv-12-enes. This is rationalized by assuming the preferential attack of the reagent from the less-hindered α-side to the 13-carbon atom and subsequent axial approach of the donor proton from the less-hindered α-side to the 12-carbon atom of the resulting Δ^{11}-11-olate or Δ^{11}-11-ol, since these intermediates would adopt a twist-boat conformation with both the 18-methyl group and the 17-side chain pseudo-equatorial.[11] As expected for 11-oxo-12α-etiojervanes with a bulky 17-substituent,[10] the 11-ketone (**15**) with C/D *cis*-linkage was recovered unchanged by treatment with base under the usual epimerization conditions (see, Experimental), its 12β-epimer (C/D *trans*) being not detected on TLC.

Treatment of 11α-hydroxy 3,20-diacetal (**11**) and its 11-acetate (**11a**) with acid (*p*-TsOH) in aqueous acetone afforded the corresponding 3,20-diketones (**16**) and (**16a**), mp 178—180 °C and 143—145 °C, in 83 and 99% yields, respectively. Likewise, 11β-hydroxy 3,20-diacetal (**12**) and its acetate (**12a**) were converted into the respective 3,20-diketones (**17**) and (**17a**), mp 158—160 °C and 187—190 °C, in 85 and 99% yields. Naturally the two alcohols (**16**) and (**17**) were acetylated

to form the respective acetates (**16a**) and (**17a**) in quantitative yields. It is to be noted that the 12,13-double bond remained unshifted at the original position during the deacetalization, as shown by the UV spectra [λ_{max} 236—238 nm (ε 10,000—11,000) for ketones **16**—**17a**]. 11α-Acetoxy 3,20-diacetal (**11a**) was then submitted to the Birch reduction in ethylamine to give 11-deacetoxy 3,20-diacetal (**18**), mp 139—140 °C in a 90% yield, which was also obtained by the same treatment of 11β-hydroxy 3,20-diacetal (**12**). The diacetal (**18**) underwent deacetalization with acid to give 3,20-diketone (**19**), mp 131—133 °C, in an 80% yield along with a small amount (15%) of 20-oxo 3-acetal (**20**), mp 140—142 °C. The main product (**19**) was also derived in a 70% yield by the Oppenauer oxidation of 3β-hydroxy-17α-ethyletiojerva-5,12-dien-20-one[14] (**21**), a known compound with established configurations. The transformation to correlate compound **11a** with **21** has confirmed the configurations of 17-side chains of a series of the related compounds.

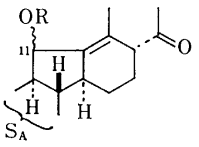

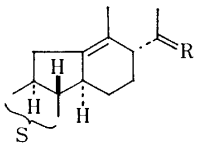

16 11α-OH
16a 11α-OAc
17 11β-OH
17a 11β-OAc

18 R=OCH_2CH_2O-, S=S_B
19 R=O, S=S_A
20 R=O, S=S_B
21 R=O, S=S_C

Epoxidation of 11-alcohols and 11-acetates (**16**—**17a**) with perbenzoic acid proceeded smoothly to give the respective 12,13-epoxides. In general, peracid epoxidation of olefins takes place by an electrophilic attack mainly from a less-hindered side.[8] Hence, the epoxidation of these etiojerv-12-enes is expected to proceed from the rear (α) side of the molecules and result in predominant formation of 12α,13α-epoxides. The oxidation of 11α-alcohol (**16**) gave a single product (**22**), mp 206—208 °C, in a quantitative yield, which was assigned 12α, 13α-epoxy configuration on the basis of the above presumption. Compound **22** on acetylation and the Jones oxidation formed the corresponding 11α-acetate (**22a**), mp 200—203 °C, and 11-ketone (**23**), mp 176.5—178 °C, in good yields. On the other hand, the same treatment of 11β-alcohol (**17**) produced two 12,13-epoxides, one (**24**), mp 204—207 °C, in a 60% yield, and the other (**25**), mp 159.5—160.5 °C, in a 36% yield. These 11β-alcohols (**24**) and (**25**) were converted with acetic anhydride at 100 °C into the respective 11β-acetates (**24a**) and (**25a**), mp 209—211 °C and 165—167 °C, in good yields. Oxidation of the major epoxide (**24**) with the Jones reagent gave the 11-ketone (**23**) in an 80% yield, while that of the minor (**25**) afforded a new 11-ketone (**26**), mp 157—159 °C, in an 87% yield. This indicates that the major epoxide (**24**) is 11β-hydroxy 12α,13α-epoxide with the same epoxy configuration as that of epoxide **22**, and the minor (**25**) 11β-hydroxy 12β,13β-epoxide. Likewise, 11α-acetate (**16a**) was oxidized under almost the same conditions as 11α-alcohol (**16**) to give two epimeric epoxides in 45 and 22% yields along with the recovered 11α-acetate (30%). The main epoxide was identified as 11α-acetoxy 12α,13α-epoxide (**22a**), and the minor (**27**), mp 140—142 °C, as the 12β,13β-epoxy epimer. The same epoxidation of 11β-acetate (**17a**) afforded 11β-acetoxy 12α,13α-epoxide (**24a**) as the only isolable 12,13-oxide in a 27% yield, leaving 41% of the starting 11β-acetate (**17a**) unreacted. The formation of 12β, 13β-epoxide (**27**) on the oxidation of 11α-acetate (**16a**) would result from steric hindrance due to the α-acetoxyl group at C_{11}. Finally, compound **19** having no substituent at C_{11} was oxidized with the peracid. The epoxidation proceeded very rapidly, as compared with that of 11-alcohols and 11-acetates (**16**—**17a**), and one major (**28**), mp 161—163 °C, and two minor products (**29** and **30**), mp 175—177 °C and 202—205 °C, were isolated in 65, 24, and 3.5% yields, respectively. In view of the fact that the major compound was the sole isolable 12,13-epoxide, it was assigned formula **28** with a 12α,13α-epoxy group. Moreover, structures **29** and **30** were assigned tentatively to the minor products on the basis of spectral data (see, Experimental).

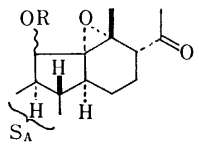

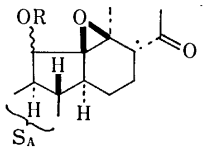

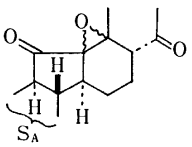

22 11α-OH
22a 11α-OAc
24 11β-OH
24a 11β-OAc

25 11β-OH
25a 11β-OAc
27 11α-OAc

23 12α,13α-O-
26 12β,13β-O-

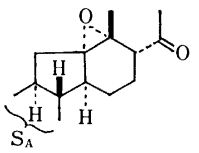

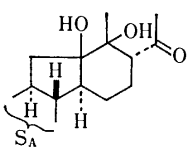

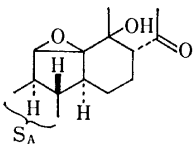

28 **29** **30**

As mentioned in the preceding section, the configurational assignment of compounds **22**—**28** to the 12,13-epoxy groups was deduced from the same ground, the preferential attack of the peracid from the less-hindered rear (α) side. However, the stereoselectivity of epoxidation is also influenced by nearby polar substituents,[15] as has been illustrated by many allyl alcohols,[16] especially in the presence of transition metal catalysts.[17] In good accord with the prediction, 11β-alcohol (**17**) was oxidized with *t*-butyl hydroperoxide in refluxing benzene containing bis(acetylacetonato)oxovanadium(IV) to give 11β-hydroxy 12β,13β-epoxide (**25**) almost quantitatively. Naturally, 11α-alcohol (**16**) yielded the corresponding 12α,13α-epoxide (**22**) quantitatively by the same treatment. The results are in line with the assigned configurations to the 12,13-epoxy groups, supported also by comparison of the chemical shifts of protons at C_{18} and C_{17}: 18-methyl protons, **22** (11α-OH and 13β-CH_3) δ 1.36: **24** (11β-OH and 13β-CH_3) δ 1.47; **25** (11β-OH and 13α-CH_3) δ 1.33: proton at C_{17}, **25**, **25a**, **26**, and **27** (each 12α,13α-epoxy) 3.14 (br W_H=16 Hz), 3.06 (16), 3.16 (16), and 3.04 (16); **22**, **22a**, **23**, **24**, **24a**, and **28** (each 12α,13α-epoxy),

not observed below δ 3.00 as a separated peak.[18]

In a previous paper[10] on the NMR spectra of a number of 12β- and 12α-etiojervanes, it was reported that the effects of many different substituents on the chemical shifts of 19-methyl protons are additive.

Table 1. Contribution ($\Delta\delta$) of functional groups to the chemical shift of the 19-methyl protons of etiojervanes

Groups	A-T[a]	B-T[a]
Reference shifts	0.74[a]	0.79[a]
Functional groups	$\Delta\delta$[b]	$\Delta\delta$[b]
11β-OH, Δ^{12}	0.28	—
11β-OAc, Δ^{12}	0.03	—
11α-OH, Δ^{12}	0.08	—
11α-OAc, Δ^{12}	0.12	—
11β-OH, 12β,13β-O-[c]	0.28	—
11β-OH, 12α,13α-O-[c]	—	0.28
11β-OAc, 12β-13β-O-	0.03	—
11β-OAc, 12α,13α-O-	—	0.03
11α-OH, 12β,13β-O-	0.08	—
11α-OH, 12α,13α-O-	—	0.08
11α-OAc, 12β,13β-O-	0.12	—
11α-OAc, 12α,13α-O-	—	0.12
11=O, 12β,13β-O-	0.11	—
11=O, 12α,13α-O-	—	0.03
12α,13α-O-	—	0.00

a) *Cf.*, Table 2 in Ref. 10. b) "$\Delta\delta$" means deshielding effect. c) Abbreviations "12β,13β-O- and 12α,13α-O-" denote "12β,13β-epoxy and 12α,13α-epoxy," respectively.

Table 2. Chemical shift and spectral pattern of the proton at C_{11} of Δ^{12}- or 12,13-epoxyetiojervan-11-ols and the acetates

Compound No.	C_{11}	Type C_{12}-C_{13}	C_{17}	Chemical shift (δ)	Coupling constant (Hz)	
11	α-OH	Δ[a]	β-H	4.60	d[b]	J=8
11a	α-OAc	Δ	β-H	5.99	br[b]	W_H=12
12	β-OH	Δ	β-H	4.86	br	W_H=12
12a	β-OAc	Δ	β-H	6.18	d	J=4
13	α-OH	Δ	α-H	4.60	d	J=8
14	β-OH	Δ	α-H	4.84	br	W_H=12
16	α-OH	Δ	β-H	4.54	d	J=8
16a	α-OAc	Δ	β-H	5.88	d	J=8
17	β-OH	Δ	β-H	4.89	d	J=4.5
17a	β-OAc	Δ	β-H	6.18	d	J=4
22	α-OH	α-O[a]	β-H	3.85	d	9
22a	α-OAc	α-O	β-H	5.32	d	8
24	β-OH	α-O	β-H	4.25	d	4
24a	β-OAc	α-O	β-H	5.46	d	4
25	β-OH	β-O[a]	β-H	4.33	d	7.5
25a	β-OAc	β-O	β-H	5.68	d	7
27	α-OAc	β-O	β-H	5.34	d	8

a) "Δ, α-O and β-O" denote "double bond, 12α,13α-epoxy, and 12β,13β-epoxy groups," respectively. b) Abbreviations "d and br" denote "doublet and broad."

However, the results for 11-hydroxy, 11-acetoxy and/or 11-oxoetiojervanes with a 12,13-double bond or an 12,13-epoxy group were not given. We now give the contribution of new functional groups (Table 1) in addition to that given previously.[10] The chemical shift and spectral pattern of a proton at C_{11} in these allyl or β,γ-epoxy alcohol and acetate systems are also summarized in Table 2. These data would be valuable for the confirmation of certain stereochemical conclusions as well as the improvement of the structure determination of new derivatives. The summarized results (Tables 1 and 2) are noteworthy in the following points. (i) Each of the 11-hydroxyl and 11-acetoxyl groups with a 12,13-double bond provides the same deshielding effect as the corresponding group with a 12,13-epoxy group, irrespective of the configuration of the epoxy groups (Table 1). (ii) The 11β-protons of etiojerv-12-en-11-ols and their acetates were observed clearly as a doublet with a large coupling constant of *ca.* 8 Hz, while the 11α-protons appeared as broad peaks with small half-width of *ca.* 12 Hz or doublets with a small coupling constant of *ca.* 4 Hz (Table 2). On the other hand, these protons of 12,13-epoxyetiojervan-11-ols and the acetates were observed as doublets with different coupling constants, depending on the configuration of the epoxy groups.

Experimental

All the melting points were uncorrected. The homogeneity of each compound was always checked by TLC on silica gel (Wakogel B-5) with various solvent systems, the spots being developed with cerium(IV) sulfate in dil. sulfuric acid and/or iodine. The optical rotations, ORD curves, UV and IR spectra were measured in chloroform, dioxane, methanol and chloroform, respectively, unless otherwise stated. The NMR spectra were obtained in chloroform-*d* at 60 and/or 100 MHz, and the chemical shifts were given in δ-values, TMS being used as an internal reference. Abbreviations "s, d, q, br, and do" in the NMR spectra denote "singlet, doublet, quartet, broad, and double", respectively.

*(20S)-17,20-Epoxy-17α-ethyletiojerva-4,12-diene-3,11-dione (**3**) and Its 17-Epimer (**4**).* To a solution of (17*E*)-17-ethyletiojerva-4,12,17(20)-triene-4,11-dione[6] (**2**, 20 g) in chloroform (1.2 l) cooled with ice was added perbenzoic acid (10 g, purity, 97.3%) in chloroform (100 ml) under stirring for 10 min. The resulting solution was allowed to stand at room temp for 3 h, and treated with 5% aq sodium thiosulfate to decompose excess of the perbenzoic acid. The chloroform layer was separated, washed with 5% aq sodium hydrogencarbonate and water, dried over anhydrous sodium sulfate, and evaporated to leave an oily residue (21.5 g), which crystallized on trituration with acetone–diisopropyl ether (5 : 1) and was recrystallized from the same solvent mixture to give **3** (14.6 g), mp 190—192 °C; $[\alpha]_D$ +57.0°; MS, *m/e* 326 (M^+); UV, λ_{max} 253 nm (ε 17000) and λ_{max} (dioxane) 254 nm (ε 15000); IR, ν_{max} (Nujol) 1705, 1677, and 1625 cm^{-1}; NMR, δ 1.25 (3H, s, 19-C$\underline{H}_3$), 1.38 (3H, d J=6 Hz, 21-C$\underline{H}_3$), 1.98 (3H, s, 18-C$\underline{H}_3$), 3.36 (1H, q J=6 Hz, $\underline{H}$ at C_{20}), and 5.81 (1H, s, $\underline{H}$ at C_4). Found: C, 77.23; H, 8.03%. Calcd for $C_{21}H_{26}O_3$: C, 77.27; H, 8.03%.

The mother liquors obtained on crystallization of crude **3** were evaporated to give a resinous material, which was crystallized and recrystallized from ethyl acetate–hexane (5 : 1) to yield **4** (80 mg), mp 176—178 °C; $[\alpha]_D$ +203.5 °C; MS,

m/e 326 (M^+), UV, λ_{max} 253 nm (ε 17000) and λ_{max} (dioxane) 257 nm (ε 16000); IR, ν_{max} (Nujol) 1714, 1664, and 1628 cm^{-1}; NMR, δ 1.25 (3H, s, 19-C$\underline{H}_3$), 1.38 (3H, d J=6 Hz, 21-C$\underline{H}_3$), 1.95 (3H, s, 18-C$\underline{H}_3$), 3.21 (1H, q J=6 Hz, $\underline{H}$ at C_{20}), and 5.78 (1H, s, $\underline{H}$ at C_4). Found: C, 77.41; H, 8.04%. Calcd for $C_{21}H_{26}O_3$: C, 77.27; H, 8.03%.

*17α-Ethyletiojerva-4,12-diene-3,11,20-trione (**5**), Its 17β-Epimer (**6**), and 17β-Formyl-17α-methyletiojerva-4,12-diene-3,11-dione (**7**), and Its 17-Epimer (**8**).* (i) A solution of **3** (1.0 g) in benzene (50 ml), dried over sodium and then LAH, was stirred with BF_3 (2.0 ml), freshly distilled over calcium hydride, at room temp for 60 s. The benzene solution was mixed with ether, washed with 5% aq sodium hydrogencarbonate and water, dried and evaporated to leave a resinous substance (1.0 g), which was purified by chromatography over silica gel (Merck, 70—230 mesh, 50 g) with benzene and ether. Eluates with benzene-ether (5 : 1) crystallized on trituration with ether. Recrystallization from ether gave **7** (75 mg), mp 145-147 °C; $[\alpha]_D$ +17°; ORD, $[\Phi]_{338}^{trough}$ −352°, $[\Phi]_{280}^{peak}$ +2280°, a=−26°; MS, *m/e* 326 and 297 (M^+ −CHO); UV, λ_{max} (dioxane) 250 nm (ε 18000); IR, ν_{max} 1717, 1703, and 1658 cm^{-1}; NMR, δ 1.24, 1.30, and 2.12 (each 3H, s, 19-, 17-, and 18- C$\underline{H}_3$), 5.76 and 9.44 (each 1H, s, $\underline{H}$ at C_4 and C$\underline{H}$O).

Eluates with a 3 : 1 mixture of benzene and ether afforded a mixture (600 mg) of **5** and **6**. A part of the mixture was separated by fractional recrystallization to give the respective compounds in pure state. Compound **5**, mp 151.5—153.5 °C (from ether-acetone); $[\alpha]_D$ +95°; ORD, $[\Phi]_{312}^{peak}$ +2710°, $[\Phi]_{298}^{trough}$ −1320°, a=+40°; MS, *m/e* 326 (M^+) and 284 (base); UV, λ_{max} (dioxane) 249 nm (ε 15,000); IR, ν_{max} 1718, 1708, and 1670 cm^{-1}; NMR, δ 1.24, 2.11, and 2.17 (each 3H, s, 19-, 18-, and 21-C$\underline{H}_3$), 3.33 (1H, br W_H=20 Hz, $\underline{H}$ at C_{17}), and 5.76 (1H, s, $\underline{H}$ at C_4). Found: C, 76.95; H, 8.04%. Calcd for $C_{21}H_{26}O_3$: C, 77.27; H, 8.03%. Compound **6**, mp 195—197 °C (from acetone-diisopropyl ether); $[\alpha]_D$ +25°; ORD, $[\Phi]_{314}^{trough}$ −960°, $[\Phi]_{294}^{peak}$ +1080°, a=−20°; MS, *m/e* 326 (M^+) and 284; UV, λ_{max} (dioxane) 251 nm (ε 16000); IR, ν_{max} 1714, 1699, and 1674 cm^{-1}; NMR, δ 1.30, 2.13, and 2.32 (each 3H, s, 19-, 18-, and 21-C$\underline{H}_3$), 3.38 (1H, br W_H=11 Hz, $\underline{H}$ at C_{17}), and 5.08 (1H, s, $\underline{H}$ at C_4). Found: C, 77.24; H, 7.97%. Calcd for $C_{21}H_{26}O_3$: C, 77.27; H, 8.03%.

(ii) 17α,20*R*-Epoxide (**4**, 1.0 g) in dry benzene (50 ml) was treated with dry BF_3 (2.0 ml) at room temp for 60 s and then worked up in the same manner as **3** to give a resinous substance (1.0 g), which was separated by chromatography (silica gel, 50 g). Fractions eluted with benzene-ether (5 : 1) crystallized on trituration with ether and were recrystallized from ether to yield **8** (600 mg), mp 148—150 °C; $[\alpha]_D$ +204°; ORD, $[\Phi]_{328}^{peak}$ +2140°, $[\Phi]_{272}^{trough}$ −3970°; a=+61°; MS, *m/e* 326 (M^+) and 297 (M^+−CHO); UV, λ_{max} (dioxane) 250 nm (ε 18,000); IR, ν_{max} 1725, 1706, and 1668 cm^{-1}; NMR, δ 1.25, 1.32, and 2.08 (each 3H, s, 19-, 17-, and 18-C$\underline{H}_3$), 5.78 and 9.30 (each 1H, s, $\underline{H}$ at C_4 and C$\underline{H}$O). Found; C, 77.24; H, 7.97%. Calcd for $C_{21}H_{26}O_3$: C, 77.27; H, 8.03%. Fractions eluted with a 3 : 1 mixture of benzene and ether afforded a 1 : 1 mixture (300 mg) of **5** and **6** which were isolated by fractional recrystallization as described in part (i).

(iii) A solution of **6** (22 mg) in benzene (4 ml) was stirred with *p*-TsOH (25 mg) under reflux for 2 h. The solution was worked up as mentioned above to leave a crystalline residue, showing a single spot on TLC, which was identified as a 1 : 2 mixture of **6** and **5** on the basis of the NMR spectrum. When compound **5** was submitted to the same treatment, almost the same equilibrium mixture was obtained. However, none of these ketones (**5** and **6**) was isomerized under the conditions (BF_3, room temp, 60 s) as described in parts (i) and (ii).

*17α-Ethyletiojerva-5,12-diene-3,11,20-trione 3,20-Di(ethylene Acetal) (**9**) and Its 17-Epimer (**10**).* The afore-mentioned 5 : 1 mixture (6.0 g) of **5** and **6** was refluxed with ethylene glycol (60 ml) and *p*-TsOH (0.6 g) in benzene (600 ml) for 6 h, water being removed with a Dean-Stark apparatus. After being cooled, the solution was worked up as usual to leave crystalline acetals (7.5 g), which on recrystallization from ether gave **9** (3.3 g), mp 181—183 °C; $[\alpha]_D$ −77°; MS, *m/e* 414 (M^+), 399, 99, and 87; UV, λ_{max} 257 nm (ε 10000); IR, ν_{max} 1710 and 1623 cm^{-1}; NMR, δ 1.09, 1.23, and 2.30 (each 3H, s, 19-, 21-, and 18-C$\underline{H}_3$), 3.97 (8H, s, 2OC$\underline{H}_2$-C$\underline{H}_2$O), and 5.39 (1H, br W_H=10Hz, $\underline{H}$ at C_6). Found: C, 72.04; H, 8.45%. Calcd for $C_{25}H_{34}O_5$: C, 72.43; H, 8.27%.

The mother liquors on recrystallization from ether were evaporated and purified by chromatography over silica gel (80 g). Eluates with benzene gave crystals (1.3 g), which on recrystallization from ether yielded **10** (0.75 g), mp 143.5—144.5 °C; $[\alpha]_D$ −128°; MS, *m/e* 414 (M^+), 399, 99, and 87; UV, λ_{max} 259 nm (ε 13000); IR, ν_{max} 1708 and 1623 cm^{-1}; NMR, δ 1.08, 1.28, and 2.32 (each 3H, s, 19-, 21-, and 18-C$\underline{H}_3$), 3.96 (8H, s, 2OC$\underline{H}_2$C$\underline{H}_2$O), and 5.39 (1H, br W_H=10 Hz, $\underline{H}$ at C_6). Found: C, 72.03; H, 8.04%. Calcd for $C_{25}H_{34}O_5$: C, 72.43; H, 8.27%. Eluates with benzene-ether (10 : : 1) afforded an additional sample of **9** (1.0 g).

17αH-Di(ethylene acetal) (**10**, 30 mg) was treated with ethylene glycol (1 ml) and *p*-TsOH (10 ml) in benzene (10 ml) under reflux for 28 h. The reaction mixture was worked up as usual to leave a crystalline residue (28 mg), showing essentially the same NMR spectrum and TLC spot as those of **9**.

*17α-Ethyl-11α-hydroxyetiojerva-5,12-diene-3,20-dione 3,20-Di(ethylene Acetal) (**11**), Its 11-Acetate (**11a**), and Their 11β-Epimers (**12** and **12a**).* (i) To a solution of **9** (5.2 g) in dry tetrahydrofuran (THF, 260 ml) was added dropwise aluminium trihydride (0.57 g) in dry THF (29 ml) under cooling with ice and stirring in a stream of nitrogen during 20 min, the whole mixture being stirred at room temp for 3 h. After addition of methanol to decompose excess hydride, the mixture was mixed with 6M aq ammonia and then filtered. The filtrate was dried and evaporated to leave an amorphous residue (5.9 g), which was separated by chromatography over silica gel (150 g). Eluates with benzene-ether (3 : 1) were crystallized and recrystallized from ether to give **12** (0.8 g), mp 163—164 °C; $[\alpha]_D$ +32°; MS, *m/e* 416 (M^+); IR, ν_{max} 3580 and 3440 cm^{-1}; NMR, δ 1.18, 1.24, and 1.90 (each 3H, s, 21-, 19-, and 18-C$\underline{H}_3$), 3.88 (8H, s, 2OC$\underline{H}_2$C$\underline{H}_2$O), 4.86 (1H, br W_H=12 Hz, $\underline{H}$ at C_{11}), and 5.24 (1H, br W_H=8 Hz, $\underline{H}$ at C_6). Found: C, 71.77; H, 8.75%. Calcd for $C_{25}H_{36}O_5$: C, 72.08; H, 8.71%.

Eluates with benzene-ether (1 : 2), crystallized on trituration with acetone-diisopropyl ether, were recrystallized from the same solvent mixture to yield **11** (4.2 g), mp 135—137 °C; $[\alpha]_D$ +10°; MS, *m/e* 416 (M^+); IR, ν_{max} 3580 and 3440 cm^{-1}; NMR, δ 1.06, 1.18 and 1.82 (each 3H, s, 19-, 21-, and 18-C$\underline{H}_3$), 3.90 (8H, s, 2OC$\underline{H}_2$C$\underline{H}_2$O), 4.60 (1H, d J=8 Hz, $\underline{H}$ at C_{11}), and 5.36 (1H, br W_H=8 Hz, $\underline{H}$ at C_6). Found: C, 72.00; H, 8.70%. Calcd for $C_{25}H_{36}O_5$: C, 72.08; H, 8.71%.

(ii) 11α-Alcohol (**11**, 200 mg) was stirred with acetic anhydride (Ac_2O, 0.55 ml) in pyridine (Py, 5 ml) at room temp for 24 h. The mixture was worked up as usual to give an amorphous residue, which was crystallized and recrystallized from diisopropyl ether-acetone to give **11a** (210 mg), mp 194—196 °C; $[\alpha]_D$ −6.5°; MS, *m/e* 443 (M^+−CH_3), 398 (M^+ −AcOH), 383, 99, and 87; IR, ν_{max} 1725 cm^{-1}; NMR,

δ 1.11. 1.15, 1.62, and 1.94 (each 3H, s, 19-, 21-, 18-CH$_3$, and OCOCH$_3$), 3.90 (8H, s, 2OCH$_2$CH$_2$O), 5.38 (1H, br W_H=8 Hz, H at C$_6$), and 5.99 (1H, br W_H=12 Hz, H at C$_{11}$). Found: C, 70.62; H, 8.32%. Calcd for $C_{27}H_{38}O_6$: C, 70.71; H, 8.35%.

11β-Alcohol (**12**, 630 mg) was heated with Ac_2O (1.7 ml) in Py (16 ml) at 100 °C for 11h. The mixture, after being worked up as usual, was purified by chlomatography over silica gel (6 g) to give benzene-ether (1 : 1) eluates (650 mg), which crystallized from ether to give **12a**, mp 143—145 °C; $[\alpha]_D$ −6.0°; MS, 443 ($M^+ - CH_3$) and 398 (M^+ −AcOH); IR, ν_{max} 1720 cm^{-1}; NMR, δ 0.98, 1.16, 1.62, and 1.96 (each 3H, s, 19-, 21-, 18-CH$_3$, and OCOCH$_3$), 3.88 (8H, s, 2OCH$_2$-CH$_2$O), 5.28 (1H, br W_H=8 Hz, H at C$_6$), and 6.18 (1H, d J=4 Hz, H at C$_{11}$). Found: C, 70.67; H, 8.30%. Calcd for $C_{27}H_{38}O_6$: C, 70.71; H, 8.35%.

*17β-Ethyl-11α-hydroxyetiojerva-5,12-diene-3,20-dione 3,20-Di(ethylene Acetal) (**13**), Its 11β-Epimer (**14**), and 17β-Ethyl-12α-etiojerv-5-ene-3,11,20-trione 3,20-Di(ethylene Acetal) (**15**).*

(i) A solution of **10** (3.2 g) in THF (162 ml) was treated with aluminium trihydride (0.35 g) in THF (18 ml) at room temp for 5 h in the same manner as **9**. After addition of methanol, the mixture was treated with 6 M aq ammonia and then filtered. The filtrate was dried, evaporated and shaken with water and chloroform repeatedly. The chloroform solutions were combined and worked up as usual to give a resinous material (3.3 g), which was separated by chromatography over silica gel (100 g). Eluates with benzene-ether (8 : 1) gave a crystalline substance, which was recrystallized from diisopropyl ether to yield **15** (690 mg), mp 156—157 °C; $[\alpha]_D$ −56°; ORD, $[\Phi]_{334}^{trough}$ −5200°, $[\Phi]_{300}^{peak}$ +3370°, a=−86°; MS, *m/e* 416 (M^+), 401, 99, and 87; IR, ν_{max} 1730 cm^{-1}; NMR, δ 0.88 (3H, d J=7 Hz, 18-CH$_3$), 1.12 and 1.26 (each 3H, s, 19- and 21-CH$_3$), 3.94 (8H, s, 2OCH$_2$CH$_2$O), and 5.35 (1H, br W_H=8 Hz, H at C$_6$). Found: C, 71.76; H, 8.64%. Calcd for $C_{25}H_{36}O_5$: C, 72.08; H, 8.71%.

Eluates with benzene-ether (5 : 1) gave **14** (1.3 g), mp 139—141 °C (from ether); $[\alpha]_D$ −57°; MS, *m/e* 416 (M^+), 401, and 383; IR, ν_{max} 3608 and 3480 cm^{-1}; MNR, δ 1.24, 1.28, and 1.92 (each 3H, s, 19-, 21-, and 18-CH$_3$), 3.95 (8H, s, 2OCH$_2$-CH$_2$O), 4.84 (1H, br W_H=12 Hz, H at C$_{11}$), 5.24 (1H, br W_H=8 Hz, H at C$_6$). Found: C, 71.80; H, 8.68%. Calcd for $C_{25}H_{36}O_5$: C, 72.08: H, 8.71%.

Eluates with benzene-ether (3 : 1) afforded **13** (0.5 g), mp 194—196 °C (from diisopropyl ether-acetone); $[\alpha]_D$ −53°; MS, *m/e* 416 (M^+), 401, and 383; IR, ν_{max} 3606 and 3480 cm^{-1}; NMR, δ 1.05, 1.22, and 1.91 (each 3H, s, 19-, 21-, and 18-CH$_3$), 3.94 (8H, s, 2OCH$_2$CH$_2$O), 4.60 (1H, d J=8 Hz, H at C$_{11}$), and 5.33 (1H, br W_H=8 Hz, H at C$_6$). Found: C, 71.89; H, 8.70%. Calcd for $C_{25}H_{36}O_5$: C, 72.08; H, 8.71%.

(ii) 11-Ketone (**15**, 100 mg) was refluxed with 5% aq potassium hydroxide in methanol (20 ml) for 7 h under nitrogen. The solution was cooled, neutralized with acetic acid, evaporated, and shaken with water and chloroform. The chloroform solution, after being worked up as usual, gave a crystalline residue (104 mg), showing a single spot on TLC, which displayed the same NMR spectrum as that of the starting ketone and had mp 158—159°C on recrystallization from diisopropyl ether.

*17α-Ethyl-11α-hydroxyetiojerva-4,12-diene-3,20-dione (**16**) and Its 11-Acetate (**16a**).* (i) A solution of **11** (5.1 g) in acetone (1.4 l) and water (220 ml) was refluxed with *p*-TsOH (1.0 g) for 3 h. After being cooled, the solution was evaporated and shaken with water and chloroform, and the chloroform solution was washed with 5% aq sodium hydrogencarbonate and water, dried and evaporated to leave a crystalline residue. The residue was recrystallized from ether to give **16** (3.4 g), mp 178—180 °C; $[\alpha]_D$ +198°; MS *m/e* 328 (M^+); UV, λ_{max} 238 nm (ε 11000); IR, ν_{max} 3447, 1705, and 1660 cm^{-1}; NMR, δ 1.22, 1.71, and 2.14 (each 3H, s, 19-, 18-, and 21-CH$_3$), 3.16 (1H, br W_H=22 Hz, H at C$_{17}$), 4.54 (1H, d J=8 Hz, H at C$_{11}$), and 5.79 (1H, s, H at C$_4$). Found: C, 76.57; H, 8.67%. Calcd for $C_{21}H_{28}O_3$: C, 76.79; H, 8.59%.

(ii) 11α-Acetate (**11a**, 0.5 g) was treated with *p*-TsOH (105 mg) in acetone (140 ml) and water (21 ml) under reflux for 9 h. The reaction mixture was worked up as usual to give a crystalline residue, which was recrystallized from ether to give **16a** (390 mg), mp 143—145 °C; $[\alpha]_D$ +203°; MS, *m/e* 310 (M^+ −AcOH), 295 (310−CH$_3$), and 267 (310 −COCH$_3$); UV, λ_{max} 236 nm (ε 10000); IR, ν_{max} 1724, 1710, and 1660 cm^{-1}; NMR, δ 1.24, 1.50, 2.04, and 1.97 (each 3H, 19-, 18-, 21-CH$_3$, and OCOCH$_3$), 3.10 (1H, br W_H=20 Hz, H at C$_{17}$), and 5.75 (1H, s, H at C$_4$), 5.88 (1H, d J=8 Hz, H at C$_{11}$). Found: C, 74.28; H, 8.02%. Calcd for $C_{23}H_{30}O_4$: C, 74.56; H, 8.16%.

*17α-Ethyl-11β-hydroxyetiojerva-4,12-diene-3,20-dione (**17**) and Its 11-Acetate (**17a**).* (i) 3,20-Di(ethylene acetal) (**12**, 207 mg) was refluxed with *p*-TsOH (60 mg) in acetone (60 ml) and water (9 ml) for 2.5 h. The mixture on the usual work-up gave a crystalline substance, which was recrystallized from ether-acetone to yield **17** (139 mg), mp 158—160 °C; $[\alpha]_D$ +256°; MS, *m/e* 328 (M^+); UV, λ_{max} 238 nm (ε 11000); IR, ν_{max} 3444, 1700, and 1675 cm^{-1}; NMR, δ 1.44, 1.75, and 2.12 (each 3H, s, 19-, 18-, and 21-CH$_3$), 3.20 (1H, br W_H=22 Hz, H at C$_{17}$), 4.89 (1H, d J=4.5 Hz, H at C$_{11}$), and 5.73 (1H, s H at C$_4$). Found: C, 76.57; H, 8.67%. Calcd for $C_{21}H_{28}O_3$: C, 76.79; H, 8.59%.

(ii) 11β-Acetate (**12a**, 0.3 g) was deacetalized in the same manner [*p*-TsOH (63 mg), acetone (84 ml), water (13 ml), reflux, 9 h] as **12** and gave **17a** (230 mg) on recrystallization from ether, mp 187—190 °C; $[\alpha]_D$ +204°; MS, *m/e* 310 (M^+ −AcOH), 295 (310−CH$_3$), and 267 (310−COCH$_3$); UV, λ_{max} 237 nm (ε 10000); IR, ν_{max} 1724, 1710, and 1660 cm^{-1}; NMR, δ 1.20, 1.48, 2.07, and 2.01 (each 3H, s, 19-, 18-, 21-CH$_3$, and OCOCH$_3$), 3.18 (1H, br W_H=20 Hz, H at C$_{17}$), 5.75 (1H, s, H at C$_4$), and 6.18 (1H, d J=4 Hz, H at C$_{11}$). Found: C, 74.28; H, 8.02%. Calcd for $C_{23}H_{30}O_4$: C, 74.56; H, 8.16%.

*17α-Ethyletiojerva-5,12-diene-3,20-dione 3,20-Di(ethylene Acetal) (**18**).* (i) To ethylamine (5 ml), dried over potassium hydroxide, containing lithium lump (20 mg) was added **11a** (100 mg) in THF (4 ml), and the blue-colored mixture was refluxed for 50 min. On addition of ammonium chloride (1 g), the mixture became colorless. It was then evaporated, mixed with water and extracted with chloroform repeatedly. The chloroform solution, after being worked up as usual, left a crystalline residue, which was recrystallized from acetone-diisopropyl ether to yield **18** (78 mg), mp 139—140 °C; $[\alpha]_D$ −12°; MS, *m/e* 400 (M^+), 385, 99, and 87; IR, no absorption maximum near 1700 cm^{-1}; NMR, δ 1.00, 1.22, and 1.71 (each 3H, s, 19-, 21-, and 18-CH$_3$), 4.00 (8H, s, 2OCH$_2$-CH$_2$O), and 5.42 (1H, br W_H=10 Hz, H at C$_6$). Found: C, 74.73; H, 9.02%. Calcd for $C_{25}H_{36}O_4$: C, 74.96; H, 9.06%.

(ii) 11β-Alcohol (**12**, 90 mg) was submitted to the Birch reduction under almost the same conditions [ethylamine (5 ml), lithium (30 mg), THF (4 ml), reflux, 60 min] as **11a**. The mixture was worked up as mentioned above to leave an amorphous residue (92 mg), showing two spots on TLC. The residue was separated by chromatography over silica gel (5 g) into two fractions, one (53 mg) being eluted with benzene-ether (10 : 1) and the other (39 mg) with benzene-

ether (3 : 1). The former with mp 138—140 °C (from acetone–diisopropyl ether) was identified as **18** (TLC, IR and NMR), and the latter with mp 164—166 °C (from acetone–diisopropyl ether) proved to be the starting material (**12**).

*17α-Ethyletiojerva-4,12-diene-3,20-dione (**19**) and 17α-Ethyletiojerva-5,12-diene-3,20-dione 3-Ethylene Acetal (**20**).* (i) 3,20-Di(ethylene acetal) (**18**, 1.95 g) was refluxed with *p*-TsOH (600 mg) in acetone (600 ml) and water (90 ml) for 2 h. The solution, after being worked up as usual, afforded an amorphous substance (1.90 g), which was separated by chromatography over silica gel (40 g). Eluates with benzene–ether (5 : 1) gave **20** (270 mg), mp 140—142 °C (from diisopropyl ether); MS, *m/e* 356 (M^+) and 313 (M^+-COCH_3); IR, ν_{max} 1705 cm^{-1}; NMR, δ 1.01, 1.56, and 2.12 (each 3H, s, 19-, 18-, and 21-C$\underline{H}_3$), 3.10 (1H, br W_H=20 Hz, $\underline{H}$ at C_{17}), 3.98 (4H, s, OC$\underline{H}_2$C$\underline{H}_2$O), and 5.41 (1H, br W_H=10 Hz, $\underline{H}$ at C_6). Found: C, 77.20; H, 9.18%. Calcd for $C_{23}H_{32}O_3$: C, 77.49; H, 9.05%. Eluates with benzene–ether (3 : 1) afforded **19** (1.17 g), mp 131—133 °C (from diisopropyl ether–acetone); $[\alpha]_D$ +198°; MS, *m/e* 312 (M^+) and 269 (M^+-COCH_3); UV, λ_{max} 238 nm (ε 12000); IR, ν_{max} 1700, 1655, and 1603 cm^{-1}; NMR, δ 1.18, 1.57, and 2.13 (each 3H, s, 19-, 18-, and 21-C$\underline{H}_3$), 3.10 (1H, br W_H=20 Hz, $\underline{H}$ at C_{17}), and 5.08 (1H, s, $\underline{H}$ at C_4). Found: C, 80.90; H, 9.15%. Calcd for $C_{21}H_{28}O_2$: C, 80.73; H, 9.03%.

(ii) A solution of 3β-hydroxy-17α-ethyletiojerva-5,12-diene-20-one[14] (**21**, 34 mg) in toluene (20 ml) and dry cyclohexanone (0.5 ml) was heated to distil *ca.* 12 ml of toluene to dry the system by azeotropization. To the stirred solution was added aluminium isopropoxide (34 mg), and the suspended mixture was again heated to distil *ca.* 6 ml of toluene and then refluxed for 2.5 h. After being cooled, the mixture was submitted to distillation with steam, until most of the solvents were removed, and the residue was treated with water and chloroform. The chloroform solution was worked up as usual to leave an amorphous substance, which was purified by preparative TLC to give an α,β-unsaturated ketone (14 mg), mp 126—128 °C (from diisopropyl ether). This was found to be identical with **19** (TLC, IR, NMR, and mixed mp).

*12α,13α-Epoxy-17α-ethyl-11α-hydroxyetiojerv-4-ene-3,20-dione (**22**) and Its 11-Acetate (**22a**).* (i) To a chloroform solution (4 ml) of **16** (25 mg) was added perbenzoic acid (15 mg, purity, 84%) in chloroform (1.2 ml), and the whole solution was allowed to stand at room temp for 24 h. After addition of 5% aq sodium thiosulfate (5 ml) to decompose excess peracid, the solution was washed with 5% aq sodium hydrogencarbonate and water, dried, and evaporated to leave a crystalline residue. The residue was recrystallized from diisopropyl ether–acetone to yield **22** (24 mg), mp 206—208 °C; $[\alpha]_D$ +192°; MS, *m/e* 344; UV, λ_{max} 239 nm (ε 11000); IR, ν_{max} 3400, 1708, and 1663 cm^{-1}; NMR δ 1.28, 1.36, 2.24 (each 3H, s, 19-, 18-, and 21-C$\underline{H}_3$), 3.85 (1H, d J=9 Hz, $\underline{H}$ at C_{11}), and 5.78 (1H, s, $\underline{H}$ at C_4). Found: C, 73.44; H, 8.38%. Calcd for $C_{21}H_{28}O_4$: C, 73.22; H, 8.19%.

(ii) Compound **22** (460 mg) was treated Ac_2O (4.6 ml) and Py (9.2 ml) at room temp for 25 h under stirring. The mixture was worked up as usual to give an amorphous residue (530 mg), which was separated by chromatography over silica gel (11 g). Eluates with benzene–ether (3 : 1) afforded **22a** (430 mg), mp 200—203 °C (from ether); $[\alpha]_D$ +189°; MS, *m/e* 386 (M^+); UV, λ_{max} (EtOH) 238 nm (ε 10,000); IR, ν_{max} 1734, 1706, and 1674 cm^{-1}; NMR, δ 1.24, 1.29, 2.20, and 2.07 (19-, 18-, 21-C$\underline{H}_3$, and COC$\underline{H}_3$), 5.32 (1H, d J=8 Hz, $\underline{H}$ at C_{11}), and 5.78 (1H, s, $\underline{H}$ at C_4). Found: C, 71.10; H, 7.84%. Calcd for $C_{23}H_{30}O_5$: C, 71.48; H, 7.82%. Eluates with ether gave the starting alcohol (**22**, 50 mg), mp 204—206 °C.

(iii) To a refluxing greenish solution of **16** (100 mg) in dry benzene (3 ml) containing bis(acetylacetonato)oxovanadium (IV) [$VO(acac)_2$] (1.35 mg) was added rapidly *t*-butyl hydroperoxide (0.06 ml), when the solution became red-colored. The solution was further refluxed for 30 min and cooled. The resulting yellow mixture was washed with 5% aq sodium thiosulfate, 5% aq sodium hydrogencarbonate, water, dried and evaporated to give a crystalline residue, which on recrystallization from diisopropyl ether–acetone to give **22** (94 mg), mp 204—206 °C, identical with the sample (**22**) in part (i).

*12α,13α-Epoxy-17α-ethyl-11β-hydroxyetiojerv-4-ene-3,20-dione (**24**), Its 12β,13β-Epoxy Epimer (**25**), and Their 11-Acetates (**24a** and **25a**).* (i) A chloroform solution (29.5 ml) of **17** (118 mg) was treated with perbenzoic acid (65 mg, purity, 84%) at room temp for 21 h. The solution was worked up as usual to give an amorphous residue (138 mg), which was separated by chromatography over silica gel (3.5 g). Eluates with benzene–ether (5 : 1) gave **25** (44 mg), mp 159.5—160.5 °C (from ether); $[\alpha]_D$ +118°; MS, *m/e* 344 (M^+); UV, λ_{max} 238 nm (ε 8000); IR, ν_{max} 3500, 1718, and 1673 cm^{-1}; NMR, δ 1.33, 1.44, and 2.22 (18-, 19-, and 21-C$\underline{H}_3$), 3.14 (1H, br W_H=16 Hz, $\underline{H}$ at C_{17}), and 4.33 (1H, d J=7.5 Hz, $\underline{H}$ at C_{11}), and 5.70 (1H, s, $\underline{H}$ at C_4). Found: C, 73.28; H, 8.24%. Calcd for $C_{21}H_{28}O_4$: C, 73.22; H, 8.19%.

Eluates with benzene–ether (2 : 1) gave **24** (74 mg), mp 204—207 °C (from ether–acetone); $[\alpha]_D$ +174°; MS, *m/e* 344 (M^+); IR, ν_{max} 3470, 1695, and 1675 cm^{-1}; NMR, δ 1.45 and 1.47 (each 3H, s, 19- and 18-C$\underline{H}_3$ or *vice versa*), 2.20 (3H, s, 21-C$\underline{H}_3$), 4.25 (1H, d J=4 Hz, $\underline{H}$ at C_{11}), and 5.75 (1H, s, $\underline{H}$ at C_4). Found: C, 73.24; H, 8.10%. Calcd for $C_{21}H_{28}O_4$: C, 73.22; H, 8.19%.

(ii) Compound **24** (33 mg) was heated with Ac_2O and Py at 100 °C for 4 h. The reaction mixture was worked up as usual to yield an amorphous residue, which was purified by preparative TLC followed by recrystallization from ether to give **24a** (18 mg), mp 209—211 °C; $[\alpha]_D$ +140°; MS, *m/e* 386 (M^+) and 326 (M^+-AcOH); UV, λ_{max} (EtOH) 237 nm (ε 14500); IR, ν_{max} 1733, 1713, 1673, and 1613 cm^{-1}; NMR, δ 1.22 (6H, s, 19- and 18-C$\underline{H}_3$), 2.07 and 2.00 (each 3H, s, OCOC$\underline{H}_3$ and 21-C$\underline{H}_3$), 5.46 (1H, d J=4 Hz, $\underline{H}$ at C_{11}). Found: C, 71.10; H, 7.84%. Calcd for $C_{23}H_{30}O_5$: C, 71.48; H, 7.82%. The starting alcohol (**24**, 7 mg) was also recovered unchanged by preparative TLC.

Compound **25** (50 mg) was acetylated under the same conditions as **24** to give an amorphous residue (48 mg), showing a single spot, which was crystallized and recrystallized from ether to yield **25a** (22 mg), mp 165—167 °C; $[\alpha]_D$ +131°; MS, *m/e* 386 (M^+), 344, and 326; UV, λ_{max} (EtOH) 237 nm (ε 12000); IR, ν_{max} 1737, 1715, 1667, 1616, and 1242 cm^{-1}; NMR, δ 1.32, 1.36, 2.20, and 2.10 (each 3H, s, 19-, 18-, 21-C$\underline{H}_3$, and OCOC$\underline{H}_3$), 3.06 (1H, br W_H=16 Hz, $\underline{H}$ at C_{17}), 5.68 (1H, d J=7 Hz, $\underline{H}$ at C_{11}), and 5.72 (1H, s, $\underline{H}$ at C_4).

(iii) A benzene solution (3 ml) of **17** (100 mg) was refluxed with *t*-butyl hydroperoxide (0.06 ml) in the presence of $VO(acac)_2$ (1.35 mg) for 30 min. The reaction mixture was worked up in the same manner as that of **16** to give a crystalline residue (110 mg) showing a single spot, which on recrystallization from ether gave **25** (83 mg), mp 162—164 °C, identical with **25** obtained in part (i).

*12α,13α-Epoxy-17α-ethyletiojerv-4-ene-3,11,20-trione (**23**) and Its 12β,13β-Epimer (**26**).* (i) A solution of **22** (30 mg) in dry acetone (5 ml) was stirred with a few drops of the Jones reagent under cooling with ice for 1 h. After addition of

ethanol to decompose the reagent, the mixture was evaporated and shaken with water and chloroform. The chloroform solution was worked up as usual to leave an amorphous residue (29 mg), which was separated into two fractions by preparative TLC (Wakogel B-5F), ether being used as a solvent. A more mobile fraction gave **23** (10 mg), mp 176.5—178 °C (from diisopropyl ether-acetone); $[\alpha]_D$ +200°; ORD, $[\Phi]_{351}^{trough}$ −1900°; $[\Phi]_{310}^{peak}$ +16100°; $a=-180°$; MS, *m/e* 342 (M^+) and 299 (M^+-COCH_3); UV, λ_{max} (EtOH) 234 nm (ε 13000); IR, ν_{max} 1750, 1710, 1665, and 1618 cm^{-1}; NMR, δ 1.22, 1.55, and 2.21 (each 3H, s, 19-, 18-, and 21-$C\underline{H}_3$), and 5.80 (1H, s, $\underline{H}$ at C_4). Found: C, 73.57; H, 7.65%. Calcd for $C_{21}H_{26}O_4$: C, 73.66; H, 7.66%. A less mobile fraction afforded the starting alcohol (**22**, 12 mg).

Compound **24** (28 mg) was oxidized with the Jones reagent in the same manner as **22** and gave epoxy ketone (22 mg), mp 178—180 °C (from ether), which was identical with the sample (**23**) described above.

(ii) Compound **25** (8 mg) in dry acetone (1 ml) was stirred with one drop of the Jones reagent under ice-cooling for 1 h. The reaction mixture, after addition of ethanol, was worked up as usual to leave a crystalline residue, which was recrystallized from ether to give **26** (7 mg), mp 157—159 °C; $[\alpha]_D$ −25°; ORD, $[\Phi]_{345}^{trough}$ −6900°; $[\Phi]_{305}^{peak}$ +9600°; $a=-165°$; MS, *m/e* 342 (M^+) and 299 (M^+-COCH_3); UV, λ_{max} (EtOH) 233 nm (ε 7000); IR, ν_{max} 1750, 1718, 1665, and 1615 cm^{-1}; NMR, δ 1.26, 1.55, and 2.24 (each 3H, s, 19-, 18-, and 21- $C\underline{H}_3$), 3.16 (1H, br $W_H=16$ Hz, $\underline{H}$ at C_{17}), and 5.82 (1H, s, $\underline{H}$ at C_4). Found: C, 73.31; H, 7.53%. Calcd for $C_{21}H_{26}O_4$: C, 73.66; H, 7.66%.

*Epoxidation of 11α-Acetate (**16a**).* A chloroform solution (30 ml) of **16a** (150 mg) was stirred with perbenzoic acid (75 mg) at room temp for 26 h. The chloroform solution was washed with 5% aq sodium thiosulfate, 5% aq sodium hydrocarbonate and water, dried and evaporated to leave a resinous residue (183 mg), which was separated into three fractions by preparative TLC (Wakogel B-5), a 2 : 1 mixture of benzene and ether being used as solvent. The most mobile fraction (51 mg) was found to be the unchanged starting acetate (**16a**, 51 mg), mp 141—143 °C. A middle fraction was crystallized and recrystallized from ether to yield 12β,13β-epoxy-17α-ethyl-11α-hydroxyetiojerv-4-ene-3,20-dione 11-acetate (**27**, 27 mg), mp 140—142 °C; $[\alpha]_D$ +102°; MS, *m/e* 386 (M^+), 344, and 326; UV, λ_{max} (EtOH) 237 nm (ε 10000); IR, ν_{max} 1734, 1714, 1664, 1612, and 1244 cm^{-1}; NMR, δ 1.24, 1.26, 2.22, and 2.05 (19-, 18-, 21-$C\underline{H}_3$, and $OCOC\underline{H}_3$), 3.04 (1H, br $W_H=16$ Hz, $\underline{H}$ at C_{17}), 5.34 (1H, d $J=8$ Hz, $\underline{H}$ at C_{11}), and 5.76 (1H, s, $\underline{H}$ at C_4). Found: C, 71.74; H, 7.89%. Calcd for $C_{23}H_{30}O_5$: C, 71.48; H, 7.82%.

The least mobile fraction gave crystalline epoxide (71 mg), mp 200—202 °C (from ether), which was identical with the sample (**22a**), obtained by acetylation of **22**.

*Epoxidation of 11β-Acetate (**17a**).* A chloroform solution (20 ml) of **17a** (100 mg) was treated with perbenzoic acid (50 mg) at room temp for 26 h under stirring. The chloroform solution, after being worked up as usual, gave an amorphous residue (122 mg), which was separated into two fractions by preparative TLC (Wakogel B-5), a 2 : 1 mixture of benzene and ether being used as solvent. The starting acetate (**17a**, 41 mg), mp 190—192 °C (from ether) was recovered unchanged from a more mobile fraction. A less mobile fraction yielded epoxy acetate (28 mg), mp 205—207 °C (from ether), which was identified as **24a** described above by comparison of the spectral data.

*Epoxidation of 17α-Ethyletiojerva-4,12-diene-3,20-dione (**19**).* A chloroform solution (192 ml) of **19** (1.04 g) was treated with perbenzoic acid (536 mg) at room temp under stirring. The reaction proceeded rapidly as compared with those of other etiojerv-12-enes and the starting material (**19**) disappeared on TLC after 3 h. The chloroform solution, after being worked up as usual, left a resinous residue (1.15 g), which was separated by chromatography over silica gel (30 g). Eluates with benzene-ether (5 : 1) afforded crystalline epoxide, which on recrystallization from acetone-diisopropyl ether gave **28** (700 mg), mp 161—163 °C; $[\alpha]_D$ +176°; MS, *m/e* 328 (M^+) and 285 (M^+-COCH_3); UV, λ_{max} (EtOH) 237 nm (ε 12000); IR, ν_{max} 1702 and 1663 cm^{-1}; NMR, δ 1.18, 1.28, and 2.21 (each 3H, s, 19-, 18-, and 21-$C\underline{H}_3$), and 5.78 (1H, s, $\underline{H}$ at C_4). Found: C, 76.57; H, 8.59%. Calcd for $C_{21}H_{28}O_3$: C, 76.79; H, 8.59%.

Eluates with benzene-ether (3 : 1) afforded a crystalline substance, which on recrystallization from ether gave **30** (39 mg), mp 202—205 °C; $[\alpha]_D$ +57°; MS, *m/e* 344 (M^+), 326 (M^+-H_2O), 311 ($326-CH_3$), 301 (M^+-COCH_3), and 283 ($326-COCH_3$); UV, λ_{max} 238 nm (ε 15000); IR, ν_{max} (Nujol) 3405, 1705, 1658, and 1611 cm^{-1}; NMR, δ 1.24, 1.33, and 2.32 (each 3H, s, 19-, 18-, 21-$C\underline{H}_3$), 2.66 (1H, s, O$\underline{H}$), 3.68 (1H, br s, $\underline{H}$ at C_{11}), and 5.80 (1H, s, $\underline{H}$ at C_4). Found: C, 73.00; H, 8.25%. Calcd for $C_{21}H_{28}O_4$: C, 73.22; H, 8.19%.

Eluates with benzene-ether (1 : 1) gave a crystalline substance, which was recrystallized from acetone-diisopropyl ether to yield **29** (318 mg), mp 175—177 °C; $[\alpha]_D$ +61°; MS, 346 (M^+), 328 (M^+-H_2O), 310 ($328-H_2O$), 303 (M^+-COCH_3), and 285 ($328-COCH_3$); UV, λ_{max} 239 nm (ε 10000); IR, ν_{max} (Nujol) 3385, 3285, 1693, 1675, and 1612 cm^{-1}; NMR, δ 1.16, 1.26, and 2.33 (each 3H, s, 19-, 18-, and 21- $C\underline{H}_3$), 2.16 and 5.06 (each 1H, s, 2O$\underline{H}$), 3.14 (1H, br $W_H=18$ Hz, $\underline{H}$ at C_{17}), 5.77 (1H, s, $\underline{H}$ at C_4). Found: C, 72.71; H, 8.71%. Calcd for $C_{21}H_{30}O_4$: C, 72.80; H, 8.73%.

References

1) Part XXVII of "*C*-Nor-*D*-homosteroids and Related Alkaloids"; Part XXVI, Ref. 7.

2) a) D. N. Kirk and M. P. Hartshorn, "Steroid Reaction Mechanisms," Elsevier Publishing Comp., New York (1968), P. 353. b) D. Baldwin, J. R. Hanson, and A. M. Holtom, *J. Chem. Soc. Perkin I*, **1973**, 2687, and refs. cited therein.

3) J. M. Coxon, M. P. Hartshorn, and D. N. Kirk, *Tetrahedron*, **21**, 2489 (1965).

4) For a recent review, see, T. Masamune, "International Review of Science, Organic Chemistry Series Two," Vol. 8, ed by W. F. Johns, Butterworth & Co., London (1976), p. 237.

5) S. M. Kupchan and S. D. Levine, *J. Am. Chem. Soc.*, **86**, 701 (1964).

6) S. M. Kupchan, T. Masamune, and G. W. A. Milne, *J. Org. Chem.*, **29**, 755 (1964).

7) A. Murai, H. Sasamori, and T. Masamune, *Chem. Lett.*, **1977**, 669.

8) For a short review of epoxidation with peracids, see, H. O. House, "Modern Synthetic Reactions," W. A. Benjamin Inc., California (1972), p. 302.

9) A. Moscowitz, K. Mislow, M. A. W. Glass, and C. Djerassi. *J, Am. Chem. Soc.*, **84**, 1945 (1962).

10) T. Masamune, A. Murai, K. Nishizakura, T. Orito, S. Numata, and H. Sasamori, *Bull. Chem. Soc. Jpn.*, **49**, 1622 (1976).

11) T. Masamune, A. Murai, K. Orito, S. Numata, and H. Suginome, *Tetrahedron*, **25**, 4853 (1969).

12) *Cf.*, Ref. 8, p. 103.

13) *Cf.*, F. Johnson and S. K. Malhotra, *J. Am. Chem. Soc.*, **87**, 5492 (1965).
14) A. Murai, K. Arita, and T. Masamune, *Bull. Chem. Soc. Jpn.*, **46**, 3536 (1973).
15) S. A. Cerefice and E. K. Fields, *J. Org. Chem.*, **41**, 355 (1976).
16) P. Chamberlain, M. L. Roberts, and G. H. Whitham, *J. Chem. Soc., B*, **1970**, 1374; P. Chamberlain and G. H. Whitham, *ibid.*, **1970**, 1382; H. B. Henbest and R. A. L. Wilson, *J. Chem. Soc.*, **1957**, 1958.
17) K. B. Sharpless and R. C. Michaelson, *J. Am. Chem. Soc.*, **95**, 6136 (1973).
18) *Cf.*, K. Tori, K. Kitahonoki, Y. Takano, H. Tanida, and T. Tsuji, *Tetrahedron Lett.*, **1964**, 559.

The Configuration of 17-Ethyl-3β-hydroxyetiojerva-5,12,17(20)-trien-11-one and Related Compounds[1]

Akio MURAI, Hiroshi SASAMORI, and Tadashi MASAMUNE

Department of Chemistry, Faculty of Science, Hokkaido University, Sapporo 060

(Received May 30, 1977)

The title compound, one of the most important starting materials for the synthesis of *C*-nor-*D*-homosteroid and normal steroid hormones, was determined to possess (*E*)-configuration at the 17,20-double bond on the basis of chemical and spectral evidence.

The title compound (**1**), a simple fragmentation product of jervine (**2**), was first obtained by Fried, Wintersteiner and coworkers[2] as a key substance for the structure elucidation of the jerveratrum alkaloids. The compound and its simple derivatives have since been used extensively as one of the most important starting materials for the synthesis of a number of etiojervanes including *C*-nor-*D*-homosteroid hormones[3] and of normal steroid hormones.[4] However, the configuration of the 17,20-double bond in **1** has not been determined yet, and compounds derived therefrom have often been left undecided stereochemically. In this paper, we present evidence indicating that the double bond in question should be assigned the (*E*)-configuration.[5]

Compound (**1**), prepared in good yields by degradation of *N*-methyljervine (**2a**) with boron trifluoride etherate,[6] forms its 3-acetate[2] (**1a**), and is readily converted into 17-ethyletiojerva-5,12,17(20)-triene-3,11-dione 3-ethylene acetal[7] (**3**) *via* the corresponding Δ^4-3-ketone (**3a**). All these compounds (**1**, **1a**, **3**, and **3a**), which are correlated with each other and exhibit the same NMR signals due to the 20-methine, 18- and 21-methyl protons [δ 6.12—6.14 (1H, q J=6 Hz), 2.29—2.31 (3H, s), and 1.79—1.81 (3H, d J=6 Hz)], have been defined completely with respect to the configurations of all asymmetric carbon atoms. In order to decide the configuration of the 17,20-double bond, we first attempted to prepare its geometrical isomer (**3'**) concerning the double bond by the Wittig reaction of a known 17-ketone, 3β-hydroxyetiojerva-5,12-diene-11, 17-dione 3-acetate[7] (**4**) with triphenylethylidenephosphorane. However, no trienones could be obtained, only a known phenol[2b] (**5**), mp 245—247 °C, being isolated in a 50% yield. Preparation of 20- and/or 17-epimeric 20-alcohols, which might undergo dehydration to yield the desired isomer (**3'**), was then undertaken.

Oxidation of the $\Delta^{5,12,17(20)}$-11-ketone (**3**) with *m*-chloroperbenzoic acid produced a 5:1 (estimated by NMR) mixture of 17,20-monoepoxides in a 50% yield (**3** recovered, 16%), from which major and minor epoxides (**6**) and (**7**), mp 187—189 °C and 160—162 °C, could be separated in pure state by fractional recrystallization. The epoxy groups of **6** and **7** were tentatively assigned β- and α-configurations, respectively, at C_{17} by analogy of the UV spectra [λ_{max} 251 nm (ε 14000) for **6** and 261 nm (ε 11000) for **7**] with those of 17-epimeric 17-hydroxyetiojervanes [λ_{max} 252 nm (ε 14000) for the 17β-hydroxy compound and 261 nm (ε 10300) for the 17α-epimer].[8] The Birch reduction of the mixture of epoxides **6** and **7** followed by chromatography afforded two 20-alcohols (**8**) and (**9**), mp 152—154 °C and 160—162 °C, in 42 and 8% yields, which were naturally obtained from **6** and **7**, respectively, under the same Birch conditions. The 12αH configuration in each of these compounds was deduced from the ORD curves; a=+282° for **8** and a=+300° for **9**.[9] Treatment of **8** with potassium carbonate under mild conditions effected only migration of the 13,17-double bond to give two α,β-unsaturated ketones (**10**) and (**11**), mp 185—187 °C and 175—177 °C, in 66 and 18% yields, respectively. Likewise, compound **9**, when treated under almost the same conditions, was converted into a new α,β-unsaturated ketone (**12**) as an isolable main product (40%). A modification of the Collins oxidation[10] of the 20-alcohols (**10**) and (**11**) gave the corresponding 20-ketones (**13**) and (**14**), mp 160—162 °C and 176—178 °C, in quantitative yields, which were assigned 17αH and 17βH configurations, respectively, on the basis of the ORD and NMR data: **13**, a=−225°,[11] δ 3.33 (1H, br W_H=11 Hz, H at C_{17}); **14**, a=+370°,[11] δ 3.35 (1H, br W_H=20 Hz, H at C_{17}). It is to be noted that the latter (**14**, 17βH) on reduction with lithium aluminium tri-*t*-butoxide hydride formed 20-alcohol **12** as the sole isolable product in a 23% yield (**14** recovered, 61%).

Having available 20- and/or 17-epimeric 20-alcohols (**8**—**11**), we again attempted to prepare the geometrical isomer (**3'**) of **3**. However, 20-epimeric $\Delta^{13(17)}$-20-alcohols (**8**) and (**9**), when treated with tosyl chloride in pyridine (room temp, 22 h), gave rise to only the known trienone (**3**) in good yields. Likewise, 20-alcohol **10** was converted readily into **3** by treatment under the same conditions or with phosphoryl chloride in benzene (room temp, 19 h). Only 20-alcohol **11** formed its tosylate (**11a**), mp 158—160 °C, but attempted base treatment (5% KOH in CH_3OH, reflux, 70 min) of the tosylate led to formation of only **3**, no isomer (**3'**) being detected in the product.

The 20-epimeric Δ^{12}-11-ketones (**11**) and (**12**) were

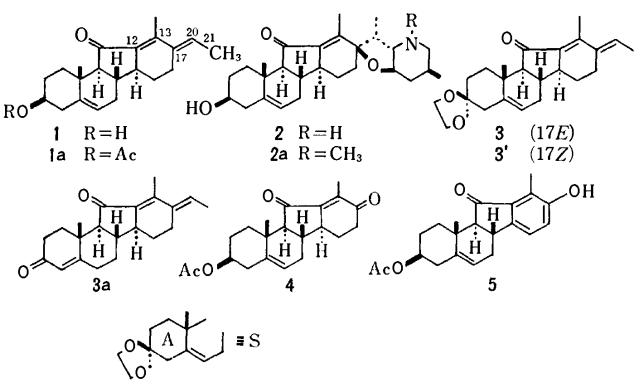

again submitted to the Birch reduction to give the corresponding saturated 11-ketones (**15**) and (**16**), mp 194—196 °C and 182—184 °C, in 76 and 68% yields, respectively. In accordance with the assigned configurations (12βH and 13αH), each of the ketones exhibited the following spectra: **15**, ORD, $a=-145°$,[9] NMR, δ 1.04 (3H, s, 19-C$\underline{H}_3$);[12] **16**, ORD, $a=-145°$,[9] NMR, δ 1.02 (3H, s, 19-C$\underline{H}_3$).[12] Oxidation of **15** under the afore-mentioned conditions[10] produced the corresponding 20-ketone (**17**), mp 184—186 °C, in a quantitative yield, whose ORD curve with a negative Cotton effect ($a=-86°$) confirmed the 17βH configuration; $a_{calcd}=-72°$ for 17βH and $-227°$ for 17αH.[11] The 11,20-diketone (**17**) was also obtained readily by the same oxidation of **16**. All the results indicate that two pairs of the 20-alcohols (**11**, **12**), and (**15**, **16**) possess the same configuration at C_{17} (17βH). They are diastereoisomers differing only at the configuration at C_{20}.

Recently Yamaguchi and co-workers[13] reported a procedure for the determination of the absolute configurations of epimeric secondary alcohols, which involves measurement of the relative magnitude of the lanthanoid induced shift (LIS) by the shift reagent Eu(fod)$_3$ for the NMR signals for the methoxy protons of diastereoisomeric (*R*)-α-methyl-α-trifluoromethyl-α-phenylacetate (MTPA ester) of the epimeric alcohols. The 20-alcohols (**15** and **16**) were then converted by treatment with (*S*)-(+)-α-methoxy-α-trifluoromethyl-α-phenylacetyl chloride[14] (MTPA-Cl) in pyridine into the respective MTPA esters (**15a**) and (**16a**), mp 176—178 °C and 138—140 °C, respectively, in good yields, showing the methoxy protons at δ 3.56 and 3.45 in the respective NMR spectra in chloroform-*d* solutions. Addition of the shift reagent Eu(fod)$_3$ to the solutions caused down-field shift of the relevant protons, and the LIS values for the protons were found to be larger for ester **16a** than for **15a** (Fig. 1 and Table 1). The result indicates that **15** with smaller LIS values has an (*S*)-configuration at C_{20} and its epimer (**16**) with larger LIS values an (*R*)-configuration.[13] This assignment not only confirms the tentatively assigned configurations for epoxides **6** and **7**, but also indicates that all

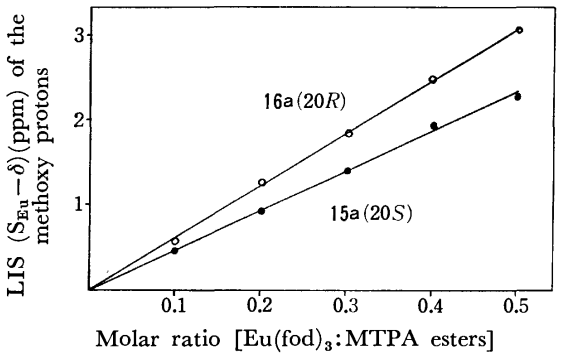

Fig. 1. LIS values of the methoxyprotons of MTPA esters **15a** and **16a**.

Table 1. Chemical shifts (δ, $CDCl_3$) of methoxyl, 19- and 18-methyl, and ethylenedioxy groups of diastereomeric MTPA esters **15a** and **16a** induced by Eu(fod)$_3$

Molar ratio Eu(fod)$_3$/MTPA ester	**15a**				**16a**			
	OCH_3	19-CH_3	18-CH_3	-OCH_2CH_2O-	OCH_3	19-CH_3	18-CH_3	-OCH_2CH_2O-
0.0	3.56	1.05	1.37	3.96	3.47	1.03	1.29	3.93
0.1	4.01	1.06	1.37	3.97	4.03	1.06	1.30	3.96
0.2	4.47	1.09	1.37	3.99	4.70	1.07	1.37	4.00
0.3	4.96	1.09	1.36	4.00	5.31	1.06	1.44	4.01
0.4	5.48	1.12	1.39	4.04	5.94	1.08	1.44	4.04
0.5	5.83	1.14	1.42	4.08	6.52	1.09	1.45	4.07

the other compounds (**8**—**17**) are represented correctly by the respective formulas. On the other hand, hydroboration of the relevant $\Delta^{5,12,17(20)}$-11-ketone (**3**) followed by oxidation resulted in hydration at the 17,20-double bond to give the (20*S*)-alcohol (**11**) as the only isolable product (25%) (**3** recovered, 48%). Since hydroboration usually proceeds in a *cis*-addition manner,[15] the present result leads to the conclusion that the 17,20-double bond in question in **3** and hence in related compounds (**1**, **1a**, and **3a**) should be assigned the (*E*)-configuration. It should be emphasized that the epoxidation and hydroboration of the 17,20-double bond take place preferentially at the β-side (axial approach), suggesting that the hydroxylation with osmium tetraoxide[7] would also lead to formation of (20*R*)-17α,20-glycol (equatorial attack).[16]

Experimental

All the melting points were uncorrected. The homogeneity of each compound was checked by TLC on silica gel (Wakogel B-5) with various solvent systems, the spots being developed with cerium(IV) sulfate in dil sulfuric acid and/or iodine. The optical rotations, ORD curves, UV, IR, and NMR (100 MHz) spectra were measured in chloroform, dioxane, methanol, chloroform, and chloroform-*d*, respectively. Abbreviations "s, d, q, qui, br, and do" in the NMR spectra denote "singlet, doublet, quartet, quintet, broad, and double," respectively.

The Witting Reaction of ***4***. A solution of dry dimethyl sulfoxide (DMSO, 2 ml) containing sodium hydride (157 mg) was heated at 72—80 °C (bath temp) for 20 min and then cooled. To the solution was added ethyltriphenylphosphonium bromide (1.07 g, 2.88 mmol) in dry DMSO (5 ml) and compound **4**[7] (240 mg, 0.71 mmol) in dry tetrahydrofuran (THF, 3 ml) at room temp under stirring. The mixture was stirred at room temp for 20 min and then at 50—56 °C for 15 h. After being cooled, the mixture was poured into ice-water (100 ml) and extracted with dichloromethane. The dichloromethane solution was washed with water, dried over sodium sulfate, and evaporated to leave an amorphous residue (300 mg), which was separated by chromatography over silica gel (Merck, 70—230 mesh, 26 g) with benzene and ether (3 : 1) to give 3β,17-dihydroxyetiojerva-5,12,14,16-tetraen-11-one 3-acetate[2b] (**5**, 120 mg), mp 245—247 °C (from ether) (lit,[2b] 245—247 °C): MS, *m/e* 280 (M^+-AcOH), 265, and 247; NMR, δ 1.22, 2.52, and 2.07 (each 3H, s, 19- and 18-C$\underline{H}_3$, and OCOC$\underline{H}_3$), 4.64 and 5.51 (each 1H, br W_H=22 and 10 Hz, 2$\underline{H}$ at C_3 and C_6), 5.84 (1H, s, O$\underline{H}$), 7.08 and 7.27 (each 1H, ABq J=8 Hz, 2$\underline{H}$ at C_{15} and C_{16}).

*(20S)-17,20-Epoxy-17α-ethyletiojerva-5,12-diene-3,11-dione 3-Ethylene Acetal (****6****) and Its 17,20-Epimer (****7****).* A solution of **3**[7] (14 g) in chloroform (680 ml) was mixed with *m*-chloroperbenzoic acid (9.7 g, 1.2 mol equiv) in chloroform (140 ml) under cooling with stirring, the whole solution being stirred for 20 min under cooling with ice. After addition of 5% aq sodium thiosulfate to decompose excess of the peracid, the chloroform solution was washed with 5% aq sodium hydrogencarbonate and water, dried and evaporated to leave a resinous material (16.5 g), which was separated by chromatography over silica gel (500 g). Eluates with benzene and ether (10 : 1) yielded **3** (2.3 g), mp 130—132 °C, (from diisopropyl ether). Eluates with benzene and ether (5 : 1) afforded a 5 : 1 (estimated by NMR) mixture of **6** and **7**, which on crystallization from diisopropyl ether gave **6** (3.8 g), mp 187—189 °C. The mother liquors were evaporated, crystallized on trituration with acetone to give **7** (340 mg), mp 160—162 °C (from acetone). **6**, $[\alpha]_D$ −154°; MS, *m/e* 370 (M^+); UV, λ_{max} 251 nm (ε 14000); IR, ν_{max} 1708 and 1625 cm^{-1}; NMR, δ 1.09 and 1.95 (each 3H, s, 19- and 18-C$\underline{H}_3$), 1.37 (3H, d J=6 Hz, 21-C$\underline{H}_3$), 3.35 (1H, q J=6 Hz, $\underline{H}$ at C_{20}), 3.97 (4H, s, OC$\underline{H}_2$C$\underline{H}_2$O), and 5.40 (1H, br W_H=10 Hz, $\underline{H}$ at C_6). Found: C, 74.63; H, 8.14%. Calcd for $C_{23}H_{30}O_4$: C, 74.56; H, 8.16%. **7**, $[\alpha]_D$ −28°; MS, *m/e* 370 (M^+); UV, λ_{max} 261 nm (ε 11000); IR, ν_{max} 1707 and 1623 cm^{-1}; NMR, δ 1.08 and 1.93 (each 3H, s, 19- and 18-C$\underline{H}_3$), 1.36 (3H, d J=6 Hz, 21-C$\underline{H}_3$), 3.19 (1H, q J=6 Hz, $\underline{H}$ at C_{20}), 3.95 (4H, s, OC$\underline{H}_2$C$\underline{H}_2$O), and 5.40 (1H, br W_H=10 Hz, $\underline{H}$ at C_6). Found: C, 74.85; H, 8.20%. Calcd for $C_{23}H_{30}O_4$: C, 74.56; H, 8.16%.

*(20S)-17-Ethyl-20-hydroxy-12α-etiojerva-5,13(17)-diene-3,11-dione 3-Ethylene Acetal (****8****), and Its 20-Epimer (****9****).* (i) To liquid ammonia (350 ml), distilled over sodium, containing lithium (880 mg) was added the afore-mentioned mixture (880 mg) of **6** and **7** in dry THF (20 ml), and the mixture was stirred at −70 °C for 15 min. After addition of ammonium chloride (8.8 g), the reaction mixture was stirred for 5 min and evaporated to leave an amorphous material, which was mixed with water (400 ml) and extracted with chloroform repeatedly. The chloroform solution was worked up as usual to give an amorphous residue (925 mg), which was purified by chromatography over silica gel (30 g). Eluates with benzene-ether (3 : 1) gave etiojerva-5,12-diene-3,11-dione 3-ethylene acetal (**18**, 70 mg), mp 177—179 °C (from diisopropyl ether); MS, *m/e* 328 (M^+); NMR, δ 1.08 and 2.15 (each 3H, s, 19- and 18-C$\underline{H}_3$), 3.96 (4H, s, OC$\underline{H}_2$C$\underline{H}_2$O), and 5.42 (1H, br W_H=10 Hz, $\underline{H}$ at C_6). Eluates with benzene-ether (1 : 1) afforded **8** (365 mg), mp 152—154 °C (from diisopropyl ether) and then **9** (65 mg), mp 160—162 °C (from diisopropyl ether). **8**, $[\alpha]_D$ −8.5°; ORD, $[\Phi]_{340}^{peak}$ +11700°, $[\Phi]_{289}^{trough}$ −16500°, a=+282°; MS, *m/e* 372 (M^+) and 354; IR, ν_{max} 3630, 3370, and 1735 cm^{-1}; NMR, δ 1.00 and 1.78 (each 3H, s, 19- and 18-C$\underline{H}_3$), 1.21 (3H, d J=6 Hz, 21-C$\underline{H}_3$), 2.82 (1H, br W_H=10 Hz, $\underline{H}$ at C_{12}), 3.94 (4H, s, OC$\underline{H}_2$C$\underline{H}_2$O), 4.81 (1H, q J=6 Hz, $\underline{H}$ at C_{20}), and 5.38 (1H, br W_H=10 Hz, $\underline{H}$ at C_6). Found: C, 73.99; H, 8.68%. Calcd for $C_{23}H_{32}O_4$: C, 74.16; H, 8.66%. **9**, $[\alpha]_D$ +38°; ORD, $[\Phi]_{340}^{peak}$ +13000°, $[\Phi]_{289}^{trough}$ −17000°, a=+300°; IR, ν_{max} 3630, 3370, and 1735 cm^{-1}; NMR, δ 0.94 and 1.85 (each 3H, s, 19- and 18-C$\underline{H}_3$), 1.17 (3H, d J=6 Hz, 21-C$\underline{H}_3$), 2.83 (1H, br W_H=10 Hz, $\underline{H}$ at C_{12}), 3.95 (4H, s, OC$\underline{H}_2$C$\underline{H}_2$O), 4.87 (1H, q J=6 Hz, $\underline{H}$ at C_{20}), and 5.41 (1H, br W_H=10 Hz, $\underline{H}$ at C_6). Found: C, 73.86; H, 8.42%. Calcd for $C_{23}H_{32}O_4$: C, 74.16; H, 8.66%.

(ii) Compound **6** (300 mg) was reduced under the same Birch conditions as mentioned above to give **8** (125 mg) and **18** (30 mg). Likewise, the same treatment of **7** (300 mg) afforded **8** (113 mg) and **18** (20 mg).

*(20S)-17β-Ethyl-20-hydroxyetiojerva-5,12-diene-3,11-dione 3-Ethylene Acetal (****10****) and Its 17-Epimer (****11****).* A solution of **8** (185 mg) in methanol (48 ml) and water (18 ml), containing potassium carbonate (1.85 g), was stirred at room temp for 30 min under nitrogen. The solution was worked up as usual to give an amorphous residue (195 mg), showing four spots on TLC, which was separated in the order of decreasing R_f value into four fractions by preparative TLC over silica gel (Wakogel B-5F, 20×20 cm^2, 0.75 mm, 10 plates), with benzene and ether (1 : 1), a UV lamp being used as a detector. Compounds **3** (13 mg), mp 128—130 °C, (from acetone-diisopropyl ether), and **18** (11 mg), mp 178—180 °C (from diisopropyl ether), were obtained from the first two fractions. The third fraction (123 mg) was crystallized and recrystallized from diisopropyl ether to yield **10** (77 mg),

mp 185—187 °C; $[\alpha]_D$ −109°; MS, *m/e* 372 (M^+); UV, λ_{max} 258 nm (ε 10000); IR, ν_{max} 3626, 3406, 1706, and 1626 cm^{-1}; NMR, δ 1.10 and 2.27 (each 3H, s, 19- and 18-CH_3), 1.32 (3H, d J=6 Hz, 21-CH_3), 3.97 (4H, s, OCH_2CH_2O), 4.36 (1H, q J=6 Hz, H at C_{20}), and 5.40 (1H, br W_H=10 Hz, H at C_6). Found: C, 74.29; H, 8.51%. Calcd for $C_{23}H_{32}O_4$: C, 74.16; H, 8.66%. The least mobile fraction (34 mg) was recrystallized from diisopropyl ether to give **11** (25 mg), mp 175—177 °C; $[\alpha]_D$ −130°; MS, *m/e* 372 (M^+); UV, λ_{max} 255 nm (ε 16000); IR, ν_{max} 3626, 3406, 1706, and 1626 cm^{-1}; NMR, δ 1.08 and 2,14 (each 3H, s, 19-, and 18-CH_3), 1.04 (3H, d J=6 Hz, 21-CH_3), 3.95 (4H, s, OCH_2CH_2O), 4.39 (1H, q J=6 Hz, H at C_{20}), and 5.38 (1H, br W_H=10 Hz, H at C_6). Found: C, 73.73; H, 8.71%. Calcd for $C_{23}H_{32}O_4$: C, 74.16; H, 8.66%.

(20R)-17α-Ethyl-20-hydroxyetiojerva-5,12-diene-3,11-dione 3-Ethylene Acetal (12). Compound **9** (172 mg) was stirred with potassium carbonate (1.72 g) in methanol (45 ml) and water (35 ml) at room temp for 1.5 h under nitrogen. The solution was worked up as usual to leave an amorphous residue (185 mg), showing two main spots, which was separated into two fractions by preparative TLC over silica gel (10 plates) with benzene and ether (1 : 1). A more polar fraction (68 mg) gave a crystalline substance (68 mg), which was recrystallized from diisopropyl ether to yield **12** (50 mg), mp 148—150 °C; $[\alpha]_D$ −124°; MS, *m/e* 372 (M^+); UV, λ_{max} 255 nm (ε 14000); IR, ν_{max} 3626, 3445, 1705, and 1629 cm^{-1}; NMR, δ 1.10 and 2.24 (each 3H, s, 19- and 18-CH_3), 1.26 (3H, d J=6 Hz, 21-CH_3), 3.94 (4H, s, OCH_2CH_2O), 4.36 (1H, q J=6 Hz, H at C_{20}), and 5.40 (1H, br W_H=10 Hz, H at C_6). Found: C, 74.41; H, 8.60%. Calcd for $C_{23}H_{32}O_4$: C, 74.16; H, 8.66%. A more mobile fraction was found to be a 1 : 1 (estimated by NMR) mixture of a new 17β-ethyl epimer and **9**, but was not further purified.

17β-Ethyletiojerva-5,12-diene-3,11,20-trione 3-Ethylene Acetal (13) and Its 17-Epimer (14). (i) To a stirred suspension of chromium (VI) oxide (33 mg) in dichloromethane (0.81 ml), distilled over phosphorus pentaoxide, and pyridine (0.051 ml), distilled over calcium hydride, was added a solution of **10** (20 mg) in dichloromethane (1 ml). The mixture was stirred at room temp for 15 min and filtered. The resulting ppt was washed with ether. The filtrate and ether washings were combined, washed with 5% aq sodium hydroxide and saturated aq sodium chloride, dried and evaporated to leave a crystalline substance (19 mg), which was recrystallized from diisopropyl ether to yield **13** (15 mg), mp 160—162 °C; $[\alpha]_D$ −198 °; ORD, $[\Phi]_{316}^{trough}$ −6100°, $[\Phi]_{284}^{peak}$ +16400°, a=−225°; MS, *m/e* 370 (M^+); UV, λ_{max} 254 nm (ε 13000); IR, ν_{max} 1714 and 1629 cm^{-1}; NMR, δ 1.10, 2.07, and 2.23 (each 3H, s, 19-, 18-, and 21-CH_3), 3.33 (1H, br W_H=11 Hz, H at C_{17}), and 3.94 (4H, s, OCH_2CH_2O).

(ii) Compound **11** (20 mg) was oxidized in the same way as above to give **14** (17 mg), mp 176—178 °C (from diisopropyl ether); $[\alpha]_D$ −12°; ORD, $[\Phi]_{312}^{peak}$ +14700°, $[\Phi]_{286}^{trough}$ −22300°, a=+370°; MS, *m/e* 370 (M^+); UV, λ_{max} 253 nm (ε 13000); IR, ν_{max} 1713 and 1629 cm^{-1}; NMR, δ 1.12, 2.14, and 2.19 (each 3H, s, 19-, 18-, and 21-CH_3), 3.35 (1H, br W_H=20 Hz, H at C_{17}), and 4.00 (4H, s, OCH_2CH_2O).

Hydride Reduction of 14 to 12. To a stirred solution of **14** (26 mg) in dry THF (6 ml) was added dropwise a suspension of lithium alminium tri-*t*-butoxide hydride (35 mg) in dry THF (5 ml) under cooling with ice. The mixture was stirred at room temp. for 23 h under nitrogen and filtered, after addition of aq ammonium sulfate. The filtrate was evaporated and shaken with water and chloroform. The chloroform extracts were washed with water, dried and evaporated to leave an amorphous residue (25 mg), showing two spots, which was separated into two fractions by preparative TLC over silica gel (one plate) with benzene and ether (1 : 1). While a less polar fraction (16 mg) gave **14**, mp 176—178 °C (from diisopropyl ether), a more polar fraction (8 mg) was crystallized and recrystallized from diisopropyl ether to yield **12** (4 mg), mp 148—150 °C, which was identical with the afore-mentioned sample (MS, IR, NMR, and TLC).

Dehydration of Alcohols 8, 9, 10, and 11. (i) A solution of **8** (20 mg) in pyridine (0.2 ml), distilled over potassium hydroxide, was stirred with tosyl chloride (*p*-TsCl, 25 mg) at room temp for 22 h. The mixture was worked up as usual to leave an amorphous material (18 mg), which was purified by preparative TLC over silica gel (one plate) with benzene and ether (5 : 1) to give **3** (9 mg), mp 130—132 °C.

The same treatment of **9** (20 mg) gave **3** (8 mg), mp 131—133 °C, and that of **10** (20 mg) afforded **3** (8 mg), mp 128—130 °C, and **10** (4 mg), mp 183—186 °C.

(ii) To a stirred and ice-cooled solution of **10** (20 mg) in benzene was added phosphoryl chloride (0.02 ml). The mixture was stirred at room temp. for 19 h, poured into ice-water, and extracted with chloroform. The extracts were washed with 5% aq sodium hydrogencarbonate and water, dried and evaporated to leave a tarry residue (19 mg), which was purified in the same manner as described above to yield **3** (4 mg), mp 130—132 °C, as a sole detectable product.

(iii) Compound **11** (15 mg) was treated with *p*-TsCl (18 mg) in pyridine (0.15 ml) at room temp for 22 h under stirring. The reaction mixture was worked up as usual to yield its tosylate (**11a**, 7 mg), mp 158—160 °C (from diisopropyl ether); $[\alpha]_D$ −102°; MS, *m/e* 354 ($M^+-CH_3C_6H_4SO_3H$); UV, λ_{max} 252 nm (ε 12000) and 228 (13,500); IR, ν_{max} 1708, 1630, 1352, 1170, 1095, 912, and 893 cm^{-1}; NMR, δ 1.05 and 2.03 (each 3H, s, 19- and 18-CH_3), 1.08 (3H, d J=6 Hz, 21-CH_3), 2.46 (3H, s, $CH_3C_6H_4SO_2$), 3.96 (4H, s, OCH_2CH_2O), 5.06 (1H, qui J=6 Hz, H at C_{20}), 5.38 (1H, br W_H=10 Hz, H at C_6), 7.34 and 7.81 (each 2H, ABq J=8 Hz, $CH_3C_6H_4SO_2$). The starting material (**11**; 3 mg), mp 176—178 °C, was recovered.

Compound **11a** (10 mg) was refluxed with 5% potassium hydroxide in methanol (2 ml) for 70 min under nitrogen. The solution was neutralized with 10% acetic acid, evaporated, mixed with water and extracted with chloroform. The chloroform extracts, after being worked up as usual, gave an amorphous residue (8 mg), which was purified by preparative TLC over silica gel (one plate) with benzene and ether (5 : 1) to give **3** (4 mg), mp 131—133 °C, as the sole isolable product.

(20S)-17α-Ethyl-20-hydroxy-12β-etiojerv-5-ene-3,11-dione 3-Ethylene Acetal (15), Its 20-Epimer (16), and Their MTPA Esters (15a and 16a). (i) To liquid ammonia (20 ml), cooled with dry ice-acetone, containing lithium (70 mg), was added **11** (50 mg) in dry THF (1 ml). The mixture was stirred at −78 °C (bath temp) for 30 min, and then worked up as described before to give an amorphous residue (57 mg), which was purified by chromatography over silica gel (5 g) with benzene-ether (1 : 1) to yield **15** (38 mg), mp 194—196 °C (from diisopropyl ether); $[\alpha]_D$ −106°; ORD, $[\Phi]_{334}^{trough}$ −7900°, $[\Phi]_{290}^{peak}$ +6600°, a=−145°; MS, *m/e* 374 (M^+); IR, ν_{max} 3630, 3444, and 1734 cm^{-1}; NMR, δ 1.04 (3H, s, 19-CH_3), 1.06 and 1.26 (each 3H, d J=4 and 6 Hz, 21- and 18-CH_3), 3.94 (4H, s, OCH_2CH_2O), 4.22 (1H, q J=6 Hz, H at C_{20}), and 5.40 (1H, br W_H=8 Hz, H at C_6).

(ii) Compound **12** (50 mg) was reduced under the same Birch conditions as described above to give **16** (34 mg), mp 182—184 °C (from diisopropyl ether); $[\alpha]_D$ −102°; ORD, $[\Phi]_{334}^{trough}$ −7900°, $[\Phi]_{290}^{peak}$ +6600°, a=−145°; MS, *m/e* 374 (M^+); IR, ν_{max} 3630, 3440, and 1734 cm^{-1}; NMR, δ 1.02

(3H, s, 19-C$\underline{H}_3$), 1.16 and 1.28 (each 3H, d J=6 Hz, 21- and 18-C$\underline{H}_3$), 3.91 (4H, s, OC$\underline{H}_2$C$\underline{H}_2$O), 4.18 (1H, q J=6 Hz, $\underline{H}$ at C_{20}), and 5.37 (1H, br W_H=8 Hz, $\underline{H}$ at C_6).

(iii) A solution of **15** (15 mg, 0.04 mmol) in dry pyridine (0.12 ml) and carbon tetrachloride (0.12 ml) was stirred with MTPA-Cl[14] (10.4 μl, 0.056 mmol) at room temp for 6 h.[13] After addition of *N,N*-dimethyl-1,3-propanediamine (9.6 μl), the mixture was allowed to stand for 5 min, diluted with ether, washed with dil hydrochloric acid, saturated aq sodium carbonate and saturated aq sodium chloride, dried and evaporated to leave an amorphous residue, which was passed through a small column packed with silica gel (Merck, 70—230 mesh, 2g) with benzene to yield its crude MTPA ester (22 mg). This was recrystallized from hexane to give **15a** (18 mg), mp 176—178 °C; $[\alpha]_D$ −67°; MS, *m/e* 590 (M^+); IR, ν_{max} 1740, 1170, 710, and 690 cm^{-1}; NMR, δ 1.05 (3H, s, 19-C$\underline{H}_3$), 1.21 (3H, d J=6 Hz, 21-C$\underline{H}_3$), 1.37 (3H, br W_H=6 Hz, 18-C$\underline{H}_3$), 3.56 (3H, s, OC$\underline{H}_3$), 3.96 (4H, s, OC$\underline{H}_2$C$\underline{H}_2$O), 5.38 (1H, br W_H=10 Hz, $\underline{H}$ at C_6), and 5.53 (1H, q J=6 Hz, $\underline{H}$ at C_{20}). Found: C, 67.36; H, 7.17%. Calcd for $C_{33}H_{41}O_6F_3$: C, 67.12; H, 6.95%.

Compound **16** (15 mg) was converted in the same manner as **15** into its MTPA ester (**16a**, 17 mg), mp 138—140 °C (from aq methanol); $[\alpha]_D$ −87°; MS, *m/e* 590 (M^+); IR, ν_{max} 1738, 1175, 710, and 694 cm^{-1}; NMR, δ 1.03 (3H, s, 19-C$\underline{H}_3$), 1.23 and 1.29 (each 3H, d J=6 Hz, 21- and 18-C$\underline{H}_3$), 3.45 (3H, s, OC$\underline{H}_3$), 3.94 (4H, s, OC$\underline{H}_2$C$\underline{H}_2$O), 5.36 (1H, br W_H=10 Hz, $\underline{H}$ at C_6), and 5.42 (1H, q J=6 Hz, $\underline{H}$ at C_{20}). Found: C, 67.38; H, 7.25%. Calcd for $C_{33}H_{41}O_6F_3$: C, 67.12; H, 6.95%.

17α-Ethyl-12β-etiojerv-5-ene-3,11,20-trione 3-Ethylene Acetal (17). To a stirred suspension of chromium(VI) oxide (17 mg) in dry dichloromethane (0.41 ml) and dry pyridine (0.026 ml) was added **15** (11 mg) in dry dichloromethane (0.1 ml). The mixture was stirred at room temp for 15 min and filtered, when ppts formed were washed with ether. The filtrate and ether washings were combined, washed with 5% aq sodium hydroxide and saturated aq sodium chloride, dried and evaporated to leave an amorphous residue, showing a single spot, which crystallized on trituration with diisopropyl ether and was recrystallized from the same solvent to yield **17** (10 mg), mp 184—186 °C; $[\alpha]_D$ −108°; ORD, $[\Phi]_{334}^{trough}$ −3000°, $[\Phi]_{302}^{peak}$ +5600°, a=−86°; MS, *m/e* 372 (M^+); IR, ν_{max} 1735 and 1713 cm^{-1}; NMR, δ 1.07 and 2.17 (each 3H, s, 19- and 21-C$\underline{H}_3$), 1.20 (3H, d J=6 Hz, 18-C$\underline{H}_3$), 3.97 (4H, s, OC$\underline{H}_2$C$\underline{H}_2$O), and 5.41 (1H, br W_H=10 Hz, $\underline{H}$ at C_6).

Compound **16** (14 mg) was oxidized in the same manner as described above to give **17** (13 mg), mp 183—185 °C.

Hydroboration of 3 Followed by Oxidation. To a stirred solution of **3** (2.0 g, 6 mmol) in THF (90 ml) was added diborane in THF (3.6 ml, 2.2 M) under cooling with ice. The solution was stirred at the temp for 50 min under nitrogen. After dropwise addition of water (14.4 ml) to decompose excess of the diborane, the reaction mixture was stirred with 1 M aq sodium hydroxide (43 ml) and 30% aq hydrogen peroxide (29 ml) at room temp for 1 h and then treated with 5% aq sodium thiosulfate (60 ml) under cooling to decompose excess hydrogen peroxide. The THF layer was separated and the aqueous layer was extracted with THF. All the THF solutions were combined, washed with water, dried and evaporated to leave a resinous material (2.4 g), which was separated by chromatography over silica gel (70 g). Eluates with benzene and ether (5 : 1) afforded the starting compound (**3**, 950 mg), mp 130—132 °C. Eluates with benzene and ether (1 : 1) gave a crystalline substance (0.5 g), which on recrystallization from diisopropyl ether afforded **11** (0.44 g), mp 174—176 °C, identical with a sample obtained from **8** (TLC, IR, and NMR).

References

1) Part XXXII of "*C*-Nor-*D*-homosteroids and Related Alkaloids," Part XXXI, Ref. 4a.

2) a) J. Fried, O. Wintersteiner, M. Moore, B. M. Iselin, and A. Klingsberg, *J. Am. Chem. Soc.*, **73**, 2970 (1951); b) J. Fried and A. Klingsberg, *ibid.*, **75**, 4929 (1953).

3) For a recent review, see, T. Masamune, "MTP International Review of Science, Organic Chemistry Series Two," Vol. 8, ed by W. F. Johns, Butterworth & Co., London (1976), p. 237.

4) a) A. Murai, N. Iwasa, and T. Masamune, *Chem. Lett.*, **1977**, 235; b) A. Murai, H. Sasamori, and T. Masamune, *Bull. Chem. Soc. Jpn.*, **50**, 437 (1977).

5)A preliminary communication: A. Murai, H. Sasamori, and T. Masamune, *Chem. Lett.*, **1977**, 669.

6) S. M. Kupchan and S. D. Levine, *J. Am. Chem. Soc.*, **86**, 701 (1964).

7) S. M. Kupchan, T. Masamune, and C. W. A. Milne, *J. Org. Chem.*, **29**, 755 (1964).

8) O. Wintersteiner and M. Moore, *J. Org. Chem.*, **29**, 262 (1964). *Cf.*, S. M. Kupchan and M. I. Suffness, *J. Am. Chem. Soc.*, **90**, 2730 (1968).

9) T. Masamune, A. Murai, K. Orito, H. Ono, S. Numata, and H. Suginome, *Tetrahedron*, **25**, 4853 (1969).

10) R. Ratcliffe and T. Rodehorst, *J. Org. Chem.*, **35**, 4000 (1970).

11) A. Murai, T. Nishimura, and T. Masamune, *Bull. Chem. Soc. Jpn.*, **49**, 1602 (1976). *Cf.*, footnote 15 in Ref. 4b, p. 442.

12) T. Masamune, A. Murai, K. Nishizakura, T. Orito, S. Numata, and H. Sasamori, *Bull. Chem. Soc. Jpn.*, **49**, 1622 (1976).

13) S. Yamaguchi, F. Yasuhara, and K. Kabuto, *Tetrahedron*, **32**, 1363 (1976). The authors wish to express their thanks to Professor Shozo Yamaguchi, Tohoku University, for his kind suggestion on the procedure.

14) J. A. Dale, D. L. Dull, and H. S. Mosher, *J. Org. Chem.*, **34**, 2543 (1969).

15) H. O. House, "Modern Synthetic Reactions," W. A. Benjamin Inc., Menlo Park, California (1972), p. 106.

16) a) H. B. Henbest, *Proc. Chem. Soc.*, **1963**, 159; J. M. Coxon, M. P. Hartshorn, and D. N. Kirk, *Tetrahedron*, **23**, 3511 (1967); J. Bascoul, C. Reliand, A. Guinot, and A. Crastes de Paulet, *Bull. Soc. Chim. Fr.*, **1968**, 4074. The authors wish to express their thanks to the referee for his suggestion on the hydroxylation; b) D. N. Kirk and M. P. Hartshorn, "Steroid Reaction Mechanisms," Elsevier Publ. Comp., Amsterdam (1968), p. 70.

Some Derivatives of Anhydrodiacetyldelcosine (Anhydrodiacetyllucaconine)*[1,2]

Takashi AMIYA, Yoshio KANAIWA, Naomi NAKANO, and Takeo SHIMA**
Hokkaido Institute of Pharmaceutial Sciences, Otaru 047

(Received May 31, 1977)

On the basis of the structure of delcosine (lucaconine), a diterpene alkaloid, the structures of anhydrodiacetyldelcosine and dihydroanhydrodiacetyldelcosine have previously been established. Some reactions of these compounds and their derivatives are described, and the reaction products are shown.

Delcosine (lucaconine) (**1**) ($C_{24}H_{39}O_7N$)[2] is an alkaloid isolated from species of Aconitum and Delphinium.[3] The structure of anhydrodiacetyldelcosine (anhydrodiacetyllucaconine) (**2**) ($C_{28}H_{41}O_8N$) has previously been proposed on the basis of the reactions as it undergoes[3] and the structure of delcosine.[4] The treatment of Compound **1** with acetyl chloride gave Compound **2** by the esterification of the two secondary hydroxyl groups, followed by the loss of one molecule of water between the two vicinal tertiary hydroxyl groups.

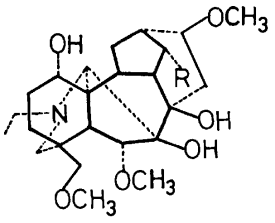

1 R=OH
7 R=H

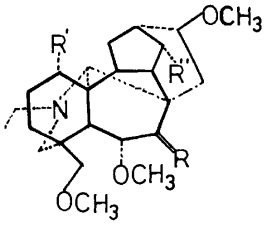

2 R=O R′=R″=OAc
4 R=OH, H R′=R″=OH

Compound **2** absorbs one molecule of hydrogen, giving dihydroanhydrodiacetyldelcosine (anhydrodihydrodiacetyllucaconine) (**3**) ($C_{28}H_{43}O_8N$). The structure and the mechanism of formation of **3** have previously been reported.[3,4]

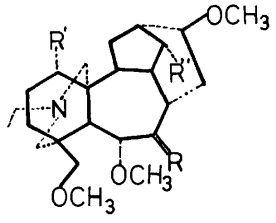

3 R=O, R′=R″=OAc
5 R=O, R′=R″=OH
6 R=OAc, H, R′=R″=OAc
8 R=O, R′=OAc, R″=H

The present paper will deal mainly with some derivatives of Compounds **2** and **3**. The reduction of Compound **2** with lithium aluminium hydride yielded anhydrodelcosinol (anhydrolucaconinol) (**4**) ($C_{24}H_{39}O_6N$). Although the infrared spectrum of Compound **2** showed bands at 1733 and 1721cm^{-1} characteristic of an ester and carbonyl function respectively, Compound **4** showed no carbonyl band. This shows that the carbonyl group in Compound **2** was reduced in Compound **4**. The hydrolysis of Compound **3** gave dihydroanhydrodelcosine (anhydrodihydrolucaconine) (**5**) ($C_{24}H_{39}O_6N$), which showed a band due to a seven-membered cyclic ketone at 1689 cm^{-1} in the infrared spectrum. The reduction of Compound **5** by lithium aluminium hydride, followed by acetylation with acetic anhydride in pyridine, gave dihydroanhydrotriacetyldelcosinol (anhydrodihydrotriacetyllucaconinol) (**6**) ($C_{30}H_{47}O_9N$). This compound showed no carbonyl band near 1689 cm^{-1}, but did show bands due to ester functions in the infrared spectrum. These observations support the reduction of the carbonyl group in Compound **5**. The treatment of deoxy-14-dehydrodelcosine (deoxylucaconinone-I) (**7**) ($C_{24}H_{39}O_6N$)[5] with acetyl chloride, followed by hydrogenation over platinum in acetic acid, gave 1-monoacetyldihydroanhydrodeoxy-14-dehydrodelcosine (anhydrodihydromonoacetyldeoxylucaconine-I) (**8**) ($C_{26}H_{41}O_6N$). Compound **8** showed a seven-membered cyclic carbonyl band at 1686 cm^{-1} and a band due to an ester function at 1730 cm^{-1}. These observations suggest that Compound **8** resulted from **7** by an initial dehydration of **7** to give a cyclic ketone, which was subsequently hydrogenated, just as Compound **3** resulted from Compound **1** *via* **2** in analogous reactions.[3] The oxidation of Compound **3** with the chromium trioxide–pyridine complex, followed by hydrolysis, yielded dihydroanhydrooxodelcosine (**9**) ($C_{24}H_{37}O_7N$).

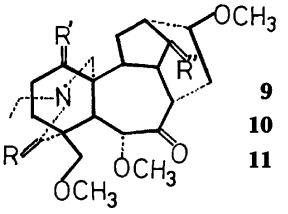

9 R=O, R′=R″=α-OH,H
10 R=R′=R″=O
11 R=H_2, R′=α-OH,H, R″=O

Compound **9** is a monoketo lactam and showed absorption bands at 1689 and 1621 cm^{-1} characteristic of a seven-membered ring ketone and of a lactam respectively. Its ultraviolet absorption spectrum showed a maximum (λ_{max} 307 nm, log ε 1.94) due to a carbonyl group. The oxidation of Compound **5** with the chromium trioxide–pyridine complex gave a neutral product, dihydroanhydro-1,14-didehydrooxodelcosine (**10**) ($C_{24}H_{33}O_7N$), and a base, dihydroanhydro-14-dehydrodelcosine (**11**) ($C_{24}H_{37}O_6N$). Compound **10** is a triketo lactam and showed absorption bands at 1754, 1712, 1681, and 1647 cm^{-1} characteristic of a five-membered ring ketone, a six-membered ring ketone, a seven-membered ring ketone, and a lactam respectively. Its ultraviolet absorption spectrum showed a maximum (λ_{max} 300 nm, log ε 2.11) due to carbonyl groups. Compound **11** is a diketo base.

* A part of this study was carried out in the Department of Chemistry, Faculty of Science, Hokkaido University.

** Central Research Institute, Teijin, Limited, Asahigaoka, Hino-shi, Tokyo 191.

It showed bands at 1751 and 1686 cm^{-1} in the infrared absorption spectrum due to the presence of a five-membered ring ketone and a seven-membered ring ketone respectively.

Experimental

Anhydrodelcosinol (Anhydrolucaconinol) (4). Anhydrodiacetyldelcosine(**2**) (0.5 g) was dissolved in dioxane (10 ml). Lithium aluminium hydride (0.2 g) dissolved in 10 ml ether was then added, and the temperature was raised until the ether evaporated. The mixture was thereafter refluxed for 30 min. Upon cooling, the excess reagent was destroyed by the addition of water, and the aluminium hydroxide formed was removed; the solution was then evaporated *in vacuo*. After the addition of 1 ml of aqueous 10% sodium hydroxide, the residue was extracted with chloroform. The evaporation of the chloroform left a residue (30 mg). The aluminium hydroxide was dissolved in 20 ml of a 10% sodium hydroxide solution and extracted with chloroform five times. A residue (200 mg) was obtained upon the removal of the chloroform. These residues were combined and neutralized with about 5% perchloric acid, and the mixture was allowed to stand to crystallize anhydrodelcosinol perchlorate. The recrystallization of the salt from water gave crystals (150 mg); mp 230 °C. This salt (150 mg) was dissolved in 1 ml of 10% aqueous sodium hydroxide and extracted with chloroform. The removal of the chloroform gave a residue was crystallized from ether. Recrystallization from ethanol gave crystals; mp 185—190 °C. Yield, 0.1 g. The ultraviolet absorption spectrum of this compound in methanol showed an end-absorption and no maximum. The infrared absorption spectrum (in Nujol) showed a hydroxyl absorption (3472 cm^{-1}), but did not show any bands attributable to the presence of an ester or carbonyl group near 1700 cm^{-1}.

Found: C, 66.22; H, 8.47; OCH_3, 20.31%. Calcd for $C_{24}H_{39}O_6N$: C, 65.87; H, 8.98; OCH_3, 21.27%.

Dihydroanhydrodelcosine (Anhydrodihydrolucaconine) (5). Dihydroanhydrodiacetyldelcosine (**3**) (1.5 g) was hydrolyzed under a stream of nitrogen for 1 h by boiling it in methanolic potassium hydroxide. Upon the removal of the methanol, a residue was obtained. Water was added to the residue, and it was extracted with chloroform three times. The residue obtained after the evaporation of the chloroform was crystallized from ethanol. Recrystallization from ethanol afforded crystals; mp 205—210 °C; $[\alpha]_D$ +43.4° (chloroform); pK_a 7.0. The ultraviolet absorption spectrum of this compound in methanol showed an end-absorption and no maximum. The infrared absorption spectrum (in Nujol) showed the presence of hydroxyl groups (3484, 3425, 3356 cm^{-1}) and a carbonyl group (1689 cm^{-1}).

Found: C, 65.98; H, 9.11%. Calcd for $C_{24}H_{39}O_6N$: C, 65.87; H, 8.98%.

Dihydroanhydrotriacetyldelcosinol (Anhydrodihydrotriacetyllucaccninol) (6). A solution of dihydroanhydrodelcosine (**5**) (0.3 g) and lithium aluminium hydride (0.2 g) in tetrahydrofuran was refluxed for 1.5 h. The reaction mixture was allowed to stand overnight, after which the excess reagent was decomposed by the addition of water; after the removal of the aluminium hydroxide formed, the solution was extracted with chloroform. The removal of the chloroform afforded a residue (0.2 g) which was subsequently dissolved in a mixture of acetic anhydride (1 ml) and pyridine (1 ml). The solution was allowed to stand in a sealed tube at room temperature for 3 days. The reaction mixture was poured into 100 ml of water to precipitate the product. Recrystallization from ethanol gave crystals; mp 130—133 °C. Yield, 40 mg. The infrared absorption spectrum (in Nujol) showed the presence of ester groups (1739 and 1727 cm^{-1}).

Found: C, 64.19; H, 8.62; OCH_3, 19.66; $COCH_3$, 20.18%. Calcd for $C_{30}H_{47}O_9N$: C, 63.69; H, 8.38; OCH_3, 16.46;[6] $COCH_3$, 22.83%.

1-Monoacetyldihydroanhydrodeoxy-14-dehydrodelcosine (Anhydrodihydromonoacetyldeoxylucaconine-I) (8). A mixture of 50 mg of deoxy-14-dehydrodelcosine (**7**) and 1 ml of acetyl chloride was allowed to stand in a sealed tube at room temperature for a week. After the removal of the excess acetyl chloride, the residue was treated with water (3 ml) and then with aqueous ammonia to give a precipitate (40 mg). This precipitate was dissolved in 5 ml of glacical acetic acid and hydrogenated with 20 mg of platinum oxide for 1h. After the subsequent removal of the platinum, the solution was evaporated to dryness *in vacuo*. The treatment of the residue with water and then with aqueous ammonia gave a precipitate. Recrystallization from ethanol gave crystals; mp 84—90 °C. Yield, 20 mg. The infrared absorption spectrum (in Nujol) showed the presence of a carbonyl group (1686 cm^{-1}) and an ester function (1730 cm^{-1}).

Found: C, 67.41; H, 9.26; OCH_3, 21.58; $COCH_3$, 10.63%. Calcd for $C_{26}H_{41}O_6N$: C, 67.36; H, 8.91; OCH_3, 20.08; $COCH_3$, 9.28%.

Dihydroanhydrooxodelcosine (9). A mixture of dihydroanhydrodiacetyldelcosine (**3**) (0.5 g) and chromium trioxide (0.5 g) in pyridine (10 ml) that had been allowed to stand overnight at room temperature was evaporated to dryness *in vacuo*. Water (20 ml) was then added to the residue, and the mixture was reduced with sulfur dioxide to remove the excess reagent. The acid solution thus obtained was extracted with chloroform. The evaporation of the chloroform extract gave a residue (0.3 g) which was then hydrolyzed with boiling ethanolic potassium hydroxide for 1 h. After cooling, the solution was evaporated and the residue was extracted with chloroform following the addition of water (10 ml). After the evaporation of the solvent, the residue was crystallized from acetone. The product was recrystallized twice from ethanol to give crystals; 0.2 g; mp 290 °C. The ultraviolet absorption spectrum of this compound in methanol showed λ_{min} 280 nm, log ε 1.71 and λ_{max} 307 nm, log ε 1.94. The infrared absorption spectrum (in Nujol) showed the presence of hydroxyl groups (3497, 3448 cm^{-1}), a carbonyl group (1890 cm^{-1}), and a lactam group (1621 cm^{-1}).

Found: C, 63.23; H, 8.22; N, 2.97; OCH_3, 18.99; (N)-C_2H_5, 4.70%. Calcd for $C_{24}H_{37}O_7N$: C, 63.83; H, 8.26; N, 3.10; OCH_3, 20.62; (N)-C_2H_5, 6.44%.

Dihydroanhydro-1,14-didehydrooxodelcosine (10). A mixture of dihydroanhydrodelcosine (**5**) (0.5 g) and chromium trioxide (1 g) in pyridine (20 ml) that had been allowed to stand overnight at room temperature was evaporated to dryness *in vacuo*. After the addition of water (20 ml), the residue was treated with sulfur dioxide to reduce the excess reagent. The resulting acid solution was extracted with chloroform. A residue (0.3 g) was obtained upon the evaporation of the chloroform. The further oxidation of the residue with the same reagent (0.3 g of chromium trioxide and 6 ml of pyridine), followed by the subsequent treatment mentioned above, gave 0.2 g of a residue. It was dissolved in chloroform (2 ml) and placed in an alumina column (2 g). The column was eluted with chloroform, and then with chloroform containing 1% methanol. From the chloroform eluate, a residue (0.1 g) was obtained. It was crystallized from ethanol. Repeated recrystallizations from ethanol gave a product which melted at 204—207 °C. The ultraviolet absorption spectrum of this compound in methanol

showed λ_{min} 260 nm, log ε 1.75 and λ_{max} 300 nm, log ε 2.11. The infrared absorption spectrum (in Nujol) showed the presence of carbonyl groups (1754, 1712, 1681 cm^{-1}) and a lactam group (1647 cm^{-1}).

Found: C, 64.79; H, 7.91; N, 3.15; OCH_3, 20.15%. Calcd for $C_{24}H_{33}O_7N$: C, 64.41; H, 7.43; N, 3.13; OCH_3, 20.80%.

*Dihydroanhydro-14-dehydrodelcosine (**11**).* The acid solution obtained after the chloroform extraction of Compound **10** in the oxidation of Compound **5** was made alkaline by aqueous ammonia. The chromic hydroxide formed was removed by filtration, and the filtrate was extracted with chloroform. The evaporation of the chloroform gave a residue which was dissolved in chloroform (4 ml) and placed in an alumina column (1.5 g). The column was eluted with chloroform (15 ml), and then with chloroform containing 1% of methanol (30 ml). From the chloroform-methanol eluate a residue was obtained. It was crystallized from acetone. Further recrystallization from ethanol gave crystals which melted at 155 °C. The ultraviolet absorption spectrum of this compound in methanol showed an end-absorption and no maximum. The infrared absorption spectrum (in Nujol) showed the presence of a hydroxyl group (3448 cm^{-1}) and carbonyl groups (1751 and 1686 cm^{-1}).

Found: C, 66.30; H, 8.39; N, 3.08; OCH_3, 20.62%. Calcd for $C_{24}H_{37}O_6N$: C, 66.18; H, 8.56; N, 3.22; OCH_3, 21.38%.

References

1) A preliminary note on part of the contents of this paper appeared in T. Amiya and T. Shima, *Bull. Chem. Soc. Jpn.*, **31**, 1083 (1958).

2) Lucaconine was identical with delcosine.

3) T. Amiya and T. Shima, *Bull. Chem. Soc. Jpn.*, **40** 1597 (1967).

4) S. W. Pelletier and L. H. Keith. "The Alkaloids, Chemistry and Physiology," Vol. XIII, ed by R. H. F. Manske, Academic Press New York (1970), p. 32; S. W. Pelletier and S. W. Page. "MTP Int. Rev. Sci., Org. Chem., Ser. One "Vol. 9, ed by K. Wiesner. Butterworths, London (1973), p. 322.

5) T. Amiya and T. Shima, *Bull. Chem. Soc. Jpn.*, **35**, 740 (1962).

6) The theoretical value in Ref. 1 is revised to this value.

Synthesis Using Pyridinium *N*-Ylides. I. Synthesis and Some Reactions of Substituted 1-(Acetylimino)pyridinium Ylides

Akikazu KAKEHI, Suketaka ITO, Yoshiaki KONNO, and Toshiaki MAEDA

Department of Industrial Chemistry, Faculty of Engineering, Shinshu University, Wakasato, Nagano 380

(Received June 2, 1977)

Pyridinium *N*-imines reacted smoothly with diethyl malonate and ethyl cyanoacetate in ethanol at room temperature to give the corresponding 1-(ethoxycarbonylacetylimino)- and 1-(cyanoacetylimino)pyridinium ylides in 59—87% yields. These ylides were converted to 1-(acetylimino)pyridinium ylide derivatives by the treatment with acetic anhydride. The alkaline treatment of the pyridinium salts which were prepared by the alkylation of the *N*-ylides with alkyl halides, gave the corresponding 3-ethoxycarbonyl- and 3-cyano-1,2-dihydropyrazolo-[1,5-*a*]pyridin-2-one derivatives in 8—51% yields.

In connection with our work in the chemistry of pyridinium *N*-ylides, we became especially interested in the reactions of pyridinium *N*-imines and *N*-methylides with various unsaturated bonds substituted with a leaving group.[1-4] Recently, we found that a certain ester group reacted smoothly with pyridinium *N*-imines to give the corresponding 1-(acetylimino)pyridinium ylides. Since the use of ester compounds such as diethyl malonate and ethyl cyanoacetate in this reaction can lead to the formation of pyridinium *N*-ylides bearing an active methylene group in the substituent at 1-position, we examined the possibility of a new intramolecular coupling reaction between the cationic center of the pyridinium moiety and the anionic center generated at the methylene group.

Kato and Masuda reported recently the preparation of 1-(acetoacetylimino)pyridinium ylide and its conversion to 1,2-dihydropyrazolo[1,5-*a*]pyridin-2-one.[5] In the pyrazolone formation step, a similar coupling reaction of the cationic center with the carbanion was proposed. In this paper we wish to report the new preparations of some 1-(ethoxycarbonylacetylimino)- and 1-(cyanoacetylimino)pyridinium ylides and their reactions which lead to 1-(acetylimino)pyridinium ylide and 1-alkyl-1,2-dihydropyrazolo[1,5-*a*]pyridin-2-one derivatives.

Results and Discussion

*Preparation of 1-(Ethoxycarbonylacetylimino)- **5**—**7** and 1-(Cyanoacetylimino)pyridinium Ylides **9**—**11**.* Syntheses of pyridinium *N*-ylides possessing an active methylene group were achieved by using nucleophilic reactions of pyridinium *N*-imines onto the ester carbonyl carbon of sufficiently active methylene compounds. When 1-aminopyridinium iodides **1**—**3** were treated with diethyl malonate **4** or ethyl cyanoacetate **8** in ethanol in the presence of potassium carbonate at room temperature for 3 days, the expected 1-(ethoxycarbonylacetylimino)-**5**—**7** or 1-(cyanoacetylimino)pyridinium ylides **9**—**11** were obtained in 59—87% yilds (Scheme 1). These *N*-ylides were very stable, colorless hygroscopic substances which solidified gradually on standing, and were not decomposedeven at the refluxing temperature of xylene.

Structural assignments of *N*-ylides **5**—**7** and **9**—**11** were generally accomplished by comparison of their spectra with those of other 1-(acylimino)pyridinium ylides.[6-9] In particular, the IR spectra exhibited a widely shifted absorption band of the carbonyl group conjugated with the imino nitrogen (near 1600 cm^{-1}), and the NMR chemical shifts and their signal patterns due to protons except the methylene protons (δ=3.3—3.5, singlet) are quite similar to those of 1-(ethoxycarbonylimino)-[6-8] and 1-(acetylimino)pyridinium ylides[9] which have already been reported.

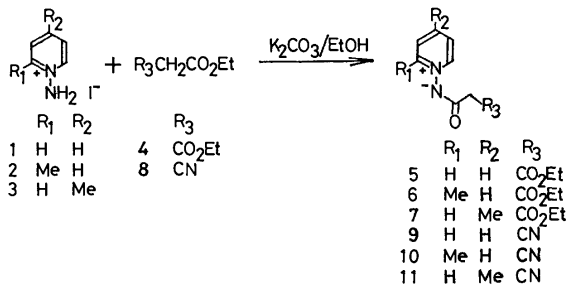

Scheme 1.

Reactions of N-*Ylides **5** and **9** with Acetic Anhydride.* In order to examine the reactivity of the active methylene group of the *N*-ylides prepared above, the reaction with acetic anhydride was first carried out. When *N*-ylide **5** was heated with a large excess of acetic anhydride at ca. 80 °C for 3 h, 1-(acetylimino)pyridinium ylide **12** was obtained in 96% yield as the only isolated product. Similarly, the same *N*-ylide **12** was formed in 65% yield by the reaction of *N*-ylide **9** with acetic anhydride under the same conditions. However, the attempted isolation of the anhydride derivatives **13** and **14** which might be formed in these reactions was unsuccessful. These results are shown in Scheme 2. The structure of *N*-ylide **12** was determined by comparison with the authentic specimen described by Okamoto *et al.*[10]

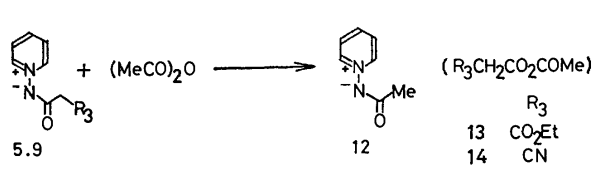

Scheme 2.

*Alkaline Treatment of Pyridinium Salts **15**—**23** and **33**—**41**.* Since the proceeding of transacylation in the above reactions might suggest that the generation of carbanion at the methylene group is unfavorable, we next attempted the formation of a carbanion

by the alkaline treatments of the corresponding 1-(*N*-alkylated imino)pyridinium salts. When pyridinium salts **15**—**23**, readily obtainable from the reactions of *N*-ylides **5**—**7** with methyl iodide, allyl bromide, and benzyl bromide, were treated with excess potassium carbonate in ethanol at room temperature, crystalline products **24**—**32** were formed in 16—51% yields (calculated from *N*-ylide). Similarly, the salts **33**—**41** obtained from *N*-ylides **9**—**11** and the same alkylating agents gave the corresponding products **42**—**45** and **47**—**51** in 8—40% yields. Furthermore, the reaction of the salt **36** also gave the colorless crystalline product **46** in only 4% yield, together with the compound **45** (21%). In the cases of the reactions of pyridinium salts **16**, **19**, **22**, **34**, **37**, and **40** which have a methyl group at 2-position, the yields of products **25**, **28**, **31**, **43**, **47**, and **50** always diminished. These results are shown in Schemes 3 and 4.

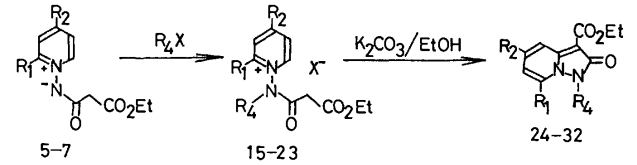

Ylide	R_4X	Salt	Pyrazole	R_1	R_2	R_4	Yield(%. Ylide→Pyrazole)
5	MeI	15	24	H	H	Me	25
6	〃	16	25	Me	H	〃	16
7	〃	17	26	H	Me	〃	22
5	AllylBr	18	27	H	H	Allyl	51
6	〃	19	28	Me	H	〃	19
7	〃	20	29	H	Me	〃	49
5	$PhCH_2Br$	21	30	H	H	$PhCH_2$	34
6	〃	22	31	Me	H	〃	16
7	〃	23	32	H	Me	〃	40

Scheme 3.

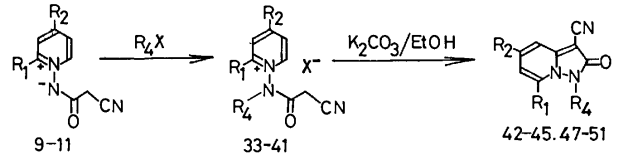

Ylide	R_4X	Salt	Pyrazole	R_1	R_2	R_4	Yield(%. Ylide→Pyrazole)
9	MeI	33	42	H	H	Me	13
10	〃	34	43	Me	H	〃	11
11	〃	35	44	H	Me	〃	40
9	AllylBr	36	45	H	H	Allyl	21
〃	〃	〃	46	H	H	〃	4
10	〃	37	47	Me	H	〃	15
11	〃	38	48	H	Me	〃	37
9	$PhCH_2Br$	39	49	H	H	$PhCH_2$	11
10	〃	40	50	Me	H	〃	8
11	〃	41	51	H	Me	〃	20

Scheme 4.

These products **24**—**32**, **42**—**45**, and **47**—**51** are colorless or pale yellow crystals which are well characterized by their strong fluorescences, their high melting points, and their comparatively low solubilities in common organic solvents. Each IR spectrum showed a characteristic absorption band at 1621—1676 cm^{-1} due to an amide carbonyl group and at 1694—1729 cm^{-1} due to an ester carbonyl group (**24**—**32**) or at 2215—2225 cm^{-1} due to a cyano group (**42**—**45** and **47**—**51**). The NMR spectrum of compound **24**, for example, showed signals at $\delta=6.89$ (1H, br t, $J=7.5$, 7.0 and 2.0 Hz), 7.45 (1H, br t, $J=9.0$, 7.5 and 1.0 Hz), 7.93 (1H, dd, $J=7.0$ and 1.0 Hz), and 8.08 (1H, dd, $J=9.0$ and 2.0 Hz) due to the protons on the pyridine ring and at $\delta=3.65$ (3H, s) due to the methyl protons, together with proton signals at $\delta=1.37$ (3H, t, $J=7.0$ Hz) and 4.33 (2H, q, $J=7.0$ Hz) attributable to the ethoxycarbonyl group (see Table 4). The chemical shifts of the protons of the pyridine ring are intermediate between those in 1-(vinylimino)pyridinium ylides[11] and those in 3,3a-dihydropyrazolo[1,5-*a*]pyridines[11] and are rather similar to those in 1-alkyl-2-allylidene-1,2-dihydropyridines.[12,13] The methyl signals appeared at $\delta=3.65$ indicated that this methyl group is a substituent on a nitrogen atom rather than an oxygen atom. The other chemical shifts of the *N'*-alkyl group derived from alkylating agents were, of course, in good accord with those of known *N*-alkylated compounds,[12-14] and this fact excluded the possibility of the *O*-alkylated compounds, that is, 2-alkoxypyrazolo[1,5-*a*]pyridines, for these products: **24**—**32**, **45**, **47**, **48**, **50**, and **51**. From the above spectral data and an analogous reaction given by Kato and Masuda,[5] these products were assigned to be 1-alkyl-3-ethoxycarbonyl- **24**—**32** and 1-alkyl-3-cyano-1,2-dihydropyrazolo[1,5-*a*]pyridin-2-one derivatives **42**—**45** and **47**—**51**.

On the other hand, the structure of compound **46** was determined to be a 1 : 1 adduct of 1-allyl-3-cyano-1,2-dihydropyrazolopyridine **45** and ethanol by its microanalysis and its NMR spectral inspection. Furthermore, the IR spectrum exhibited absorption bands at 1668 and 3340 cm^{-1} due to an amide carbonyl and a secondary amino group, respectively, but no cyano absorption band was observed. These results suggested clearly that compound **46** is 1-allyl-3-ethoxycarbonimidoyl-1,2-dihydropyrazolo[1,5-*a*]pyridin-2-one.

Mechanism. The transacylations of *N*-ylides **5** and **9** with acetic anhydride may proceed via the formation of *N'*-acetylated intermediate **52**, followed by its decomposition to 1-(acetylimino)pyridinium ylide **12** and anhydride **13** or **14** (Path a). An alternate route (Path b) in which the formation of dehydrogenated compound **53** followed by its decomposition to *N*-ylide **12** and ketene takes place is negligible because the collapse of the intermediate such as **53** should lead to the formation of 2-hydoxypyrazolo[1,5-*a*]pyridine derivative rather than *N*-ylide, as suggested in the alkaline treatment[5] of 1-(acetoacetylimino)pyridinium ylide (Scheme 5).

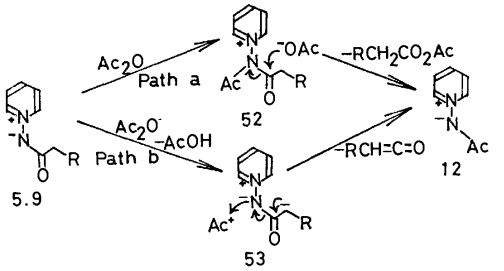

Scheme 5.

On the other hand, the formation of 1,2-dihydropyrazolo[1,5-*a*]pyridin-2-ones **24**—**32**, **42**—**45**, and **47**—**51** seems to proceed via the intramolecular coupling reaction of intermediate **54** formed initially by dehydro-

halogenation of 1-(*N*-alkylated imino)pyridinium salts **15**—**23** and **33**—**41**, followed by the oxidation of the resulting 1,2,3,3a-tetrahydropyrazolopyridine **55** (Scheme 6). This mechanism is the same as that proposed for the alkaline treatment of 1-[*N*-(acetoacetyl)methylamino]pyridinium iodide by Kato and Masuda.[5] Furthermore, imidate **46** must be formed by a base-catalyzed addition of ethanol on the 3-cyano group in 1-allyl-3-cyano-1,2-dihydropyrazolo[1,5-*a*]pyridin-2-one **45**, since the reaction of compound **45** with ethanol did not give the imidate **46** in the absence of alkali even under more drastic conditions, but gave it in the presence of alkali. Similar additions[15] of alcohol to a cyano group have been found often.

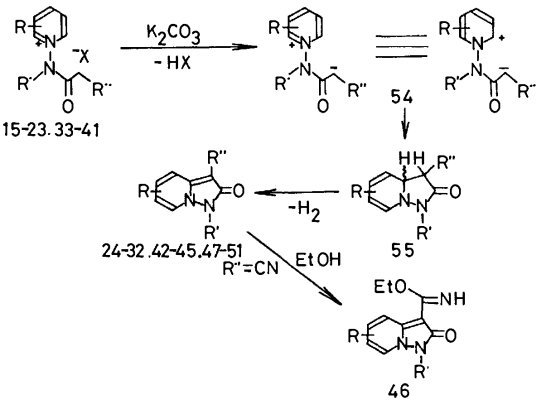

Scheme 6.

Experimental

Melting points were measured with a Yanagimoto micro-melting point apparatus and are uncorrected. Microanalyses were carried out on a Perkin-Elmer 240 Elemental Analyzer. The NMR spectra were determined with a JEOL JNM-100 spectrometer in deuteriochloroform with tetramethylsilane as an internal standard, The chemical shifts are expressed in δ values. The IR spectra were taken with a JASCO DS-301 spectrophotometer.

Preparations of Pyridinium N-*Ylides* ***5***—***7*** *and* ***9***—***11***. *General Method*: A solution of 1-aminopyridinium iodide (3 mmol) and diethyl malonate (4 g, 25 mmol) or ethyl cyanoacetate (4 g, 35 mmol) in 50 ml of ethanol was stirred with potassium carbonate (5 g) at room temperature for 3 days. The reaction mixture was then filtered to remove insoluble inorganic substances and the filtrate was concentrated under reduced pressure. The residue was separated by column chromatography (alumina) using ether and then chloroform as eluents. The pyridinium *N*-ylides **5**—**7** and **9**—**11** thus obtained are colorless substances which solidified gradually on standing. Except for *N*-ylide **11**, recrystallizations of the other *N*-ylides, **5**—**7**, **9**, and **10**, were unsuccessful because of their high hygroscopic properties. Some physical and spectral data of *N*-ylides **5**—**7** and **9**—**11** are summarized in Tables 1 and 2.

Reactions of N-*Ylides* ***5*** *and* ***9*** *with Acetic Anhydride*. A solution of *N*-ylide **5** (208 mg, 1 mmol) in 10 ml of acetic anhydride was heated at *ca.* 80 °C in a water bath for 3 h, and then the reaction mixture was concentrated under reduced pressure. The usual work-up of the residual oil gave 1-(acetylimino)pyridinium ylide **12** (130 mg, 96%) as colorless hygroscopic needless, mp (its picrate) 169—170 °C (lit,[10] 168 °C). The same *N*-ylide **12** was also obtained in 65% yield from the reaction of *N*-ylide **9** and acetic anhydride. However, our attempts to isolate the anhydride **13** or **14** were unsuccessful.

Alkaline Treatments of Pyridinium Salts ***15***—***23*** *and* ***33***—***41***. *General Method*: Pyridinium *N*-ylide (2 mmol) was treated with an alkylating agent (5 ml) without solvent at room temperature for 3—7 days, and then the reaction mixture was concentrated to remove the excess alkylating agent under reduced pressure. The ethanolic solution (50 ml) of the crude pyridinium salt was stirred with potassium carbonate (5 g) at room temperature for 3—5 days. The reaction mixture was filtered and the filtrate was concentrated under reduced pressure. The usual separations of the residues using column chromatography (alumina) gave the corresponding 1-alkyl-3-

Table 1. Some data of pyridinium *N*-ylides

Compd No.	Materials No.		Yield (%)	Mp (°C)	IR (Neat, cm^{-1}) C=O	CN	
5	**1**	**4**	86	125—126[a]	1730	1585	
6	**2**	**4**	64	130—132[a]	1732	1585	
7	**3**	**4**	59	137—138[a]	1728	1585	
9	**1**	**8**	87	154—156[a]		1588	2269
10	**2**	**8**	69	184—186[a]		1590	2275
11	**3**	**8**	74	138—140		1593[b]	2269[b]

Compd No.	Formula	Calcd % C	H	N	Found % C	H	N
5[a]	$C_{16}H_{15}N_5O_{10}$	43.94	3.46	16.02	43.80	3.42	16.13
6[a]	$C_{17}H_{17}N_5O_{10}$	45.24	3.80	15.52	45.17	3.81	15.41
7[a]	$C_{17}H_{17}N_5O_{10}$	45.24	3.80	15.52	45.28	3.76	15.55
9[a]	$C_{14}H_{10}N_6O_8$	43.08	2.58	21.54	42.88	2.46	21.46
10[a]	$C_{15}H_{12}N_6O_8$	44.56	2.99	20.79	44.63	3.04	20.92
11	$C_9H_9N_3O$	61.70	5.18	23.99	61.69	5.17	24.11

a) Its picrate. b) KBr.

Table 2. NMR data of pyridinium *N*-ylides

Compd No	C-2	C-3	C-4	C-5	C-6	CH_2	R_3	
5	8.67	7.64	7.92	7.64	8.67	3.34	4.17	1.28
	br d	br t	br t	br t	br d	s	q	t
	$J_{2,3}=J_{5,6}=7.0$, $J_{3,4}=J_{4,5}=7.5$, $J_{Et}=7.0$ Hz							
6	2.69	7.56	7.92	7.56	8.47	3.40	4.21	1.31
	s	m	br t	m	br d	s	q	t
	$J_{3,4}=J_{4,5}=7.5$, $J_{5,6}=7.0$, $J_{Et}=7.0$ Hz							
7	8.45	7.46	2.52	7.46	8.45	3.33	4.17	1.28
	d	d	s	d	d	s	q	t
	$J_{2,3}=J_{5,6}=7.0$, $J_{Et}=7.0$ Hz							
9	8.65	7.69	7.99	7.69	8.65	3.37		
	br d	br t	br t	br t	br d	s		
	$J_{2,3}=J_{5,6}=7.0$, $J_{3,4}=J_{4,5}=7.5$ Hz							
10	2.61	7.68	8.02	7.68	8.41	3.43		
	s	m	br t	m	br d	s		
	$J_{3,4}=J_{4,5}=7.5$, $J_{5,6}=7.5$ Hz							
11	8.43	7.46	2.53	7.46	8.43	3.32		
	d	d	s	d	d	s		
	$J_{2,3}=J_{5,6}=7.0$ Hz							

Table 3. Some data of 1,2-dihydropyrazolo[1,5-a]pyridin-2-ones

Compd No.	Materials			Yield (%)	Mp (°C)	IR (KBr, cm^{-1})		Appearance	Formula	Calcd %			Found %		
	N-Ylide	Halide	Salt			C=O	CN(NH)			C	H	N	C	H	N
24	**5**	MeI	**15**	25	177—178	1694	1650	Colorless Needles	$C_{11}H_{12}N_2O_3$	59.99	5.49	12.72	59.91	5.53	12.63
25	**6**	MeI	**16**	16	150—151	1680	1656	Colorless Needles	a)	57.13	6.39	11.11	57.28	6.20	10.82
26	**7**	MeI	**17**	22	185—186	1694	1633	Pale Yellow Needles	$C_{12}H_{14}N_2O_3$	61.52	6.02	11.96	61.49	6.00	12.00
27	**5**	AllylBr	**18**	51	138—139	1704	1623	Pale Yellow Needles	$C_{13}H_{14}N_2O_3$	63.40	5.73	11.38	63.21	5.77	11.13
28	**6**	AllylBr	**19**	19	139—140	1709	1621	Pale Yellow Needles	$C_{14}H_{16}N_2O_3$	64.60	6.20	10.76	64.53	6.21	10.78
29	**7**	AllylBr	**20**	49	172—173	1703	1630	Pale Yellow Needles	$C_{14}H_{16}N_2O_3$	64.60	6.20	10.76	64.60	6.21	10.67
30	**5**	$PhCH_2Br$	**21**	34	173—174	1699	1627	Pale Yellow Needles	$C_{17}H_{16}N_2O_3$	68.90	5.44	9.45	68.79	5.49	9.30
31	**6**	$PhCH_2Br$	**22**	16	144—146	1729	1621	Pale Yellow Needles	b)	65.84	6.14	8.53	65.80	5.87	8.83
32	**7**	$PhCH_2Br$	**23**	40	171—172	1698	1630	Pale Yellow Needles	$C_{18}H_{18}N_2O_3$	69.66	5.85	9.03	69.62	5.90	8.97
42	**9**	MeI	**33**	13	271—273	1676	2218	Colorless Needles	$C_9H_7N_3O$	62.42	4.07	24.27	62.14	4.16	24.49
43	**10**	MeI	**34**	11	241—243	1657	2215	Colorless Needles	$C_{10}H_9N_3O$	64.16	4.85	22.45	63.87	4.93	22.59
44	**11**	MeI	**35**	40	277—279	1639	2220	Colorless Needles	$C_{10}H_9N_3O$	64.16	4.85	22.45	64.09	4.89	22.24
45	**9**	AllylBr	**36**	21	143—144	1658	2215	Pale Yellow Needles	$C_{11}H_9N_3O$	66.32	4.55	21.10	66.27	4.54	20.86
46	**9**	AllylBr	**36**	4	96—97	1668	(3340)	Colorless Needles	$C_{13}H_{15}N_3O_2$	63.66	6.16	17.13	63.66	6.17	17.33
47	**10**	AllylBr	**37**	15	158—159	1673	2225	Pale Yellow Needles	$C_{12}H_{11}N_3O$	67.59	5.20	19.71	67.29	5.22	19.42
48	**11**	AllylBr	**38**	37	152—153	1664	2220	Pale Yellow Needles	$C_{12}H_{11}N_3O$	67.59	5.20	19.71	67.60	5.14	19.83
49	**9**	$PhCH_2Br$	**39**	11	206—209	1666	2223	Pale Yellow Needles	$C_{15}H_{11}N_3O$	72.27	4.45	16.86	72.23	4.47	16.88
50	**10**	$PhCH_2Br$	**40**	8	185—186	1671	2220	Yellow Needles	$C_{16}H_{13}N_3O$	72.98	4.98	15.96	72.68	5.01	15.95
51	**11**	$PhCH_2Br$	**41**	20	165—167	1634	2220	Pale Yellow Needles	$C_{16}H_{13}N_3O$	72.98	4.98	15.96	72.04	4.99	16.18

a) $C_{12}H_{14}N_2O_3 \cdot H_2O$. b) $C_{18}H_{18}N_2O_3 \cdot H_2O$.

Table 4. NMR data of 1,2-dihydropyrazolo[1,5-*a*]pyridin-2-ones[a)]

Compd No.	C-4	C-5	C-6	C-7	R_4				R_3[b)]	
24	8.08	7.45	6.89	7.93	3.65				4.33	1.37
	dd	br t	br t	dd	s				q	t
	$J_{4,5}=9.0$, $J_{5,6}=7.5$, $J_{6,7}=7.0$, $J_{4,6}=2.0$, $J_{5,7}=1.0$ Hz									
25	8.03	7.34	6.53	2.72	3.68				4.34	1.38
	dd	q	d	s	s				q	t
	$J_{4,5}=9.0$, $J_{5,6}=7.5$, $J_{4,6}=2.0$ Hz									
26	7.88	2.36	6.67	7.71	3.56				4.33	1.37
	br s	s	dd	d	s				q	t
	$J_{6,7}=7.0$, $J_{4,6}=2.0$ Hz									
27[c)]	8.15	7.47	6.85	7.93	4.86	5.24	5.34	5.80	4.38	1.42
	dd	br t	br t	dd	d	br d	br d	m	q	t
	$J_{4,5}=9.0$, $J_{5,6}=7.5$, $J_{6,7}=7.0$, $J_{4,6}=2.0$, $J_{5,7}=1.0$ Hz									
28	8.07	7.40	6.58	2.68	4.77	4.94	5.02	5.40	4.27	1.41
	dd	q	d	s	d	br d	br d	m	q	t
	$J_{4,5}=9.0$, $J_{5,6}=7.5$, $J_{4,6}=1.5$, $J_{allyl}=5.0$, 10.0, 17.0 Hz									
29	7.93	2.40	6.64	7.78	4.78	5.20	5.28	5.77	4.35	1.40
	br s	s	dd	d	d	br d	br d	m	q	t
	$J_{6,7}=7.0$, $J_{4,6}=2.0$, $J_{allyl}=5.0$, 10.0, 17.0 Hz									
30	8.12	7.40	6.70	7.79	5.40	7.18[d)]			4.38	1.42
	dd	br t	br t	d	s	s			q	t
	$J_{4,5}=9.0$, $J_{5,6}=7.5$, $J_{6,7}=7.0$, $J_{4,6}=1.5$ Hz									
31	7.98	e)	6.39	2.56	5.41	6.8—7.4[d)]			4.35	1.39
	dd		d	s	s	m			q	t
	$J_{4,5}=9.0$, $J_{5,6}=7.5$, $J_{4,6}=2.0$ Hz									
32	7.93	2.35	6.53	7.68	5.37	7.28[d)]			4.39	1.42
	br s	s	dd	d	s	s			q	t
	$J_{6,7}=7.0$, $J_{4,6}=2.0$ Hz									
45	7.3—7.6		6.85	7.93	4.81	5.21	5.33	5.75		
	m		br t	d	d	br d	br d	m		
	$J_{5,6}=7.0$, $J_{6,7}=7.0$, $J_{allyl}=5.0$, 10.0, 17.0 Hz									
46	7.68	7.19	6.65	8.18	4.06	5.12	5.25	6.10	f)	
	dd	br t	br t	d	br t	br d	br d	m		
	$J_{4,5}=9.0$, $J_{5,6}=7.5$, $J_{6,7}=7.0$, $J_{4,6}=1.5$, $J_{allyl}=5.0$, 10.0, 17.0 Hz									
47	7.2—7.5		6.55	2.70	4.86	5.02	5.15	5.50		
	m		br d	s	d	br d	br d	m		
	$J_{5,6}=7.0$, $J_{allyl}=5.0$, 10.0, 17.0 Hz									
48	7.18	2.41	6.66	7.79	4.78	5.20	5.33	5.75		
	br s	s	dd	d	d	br d	br d	m		
	$J_{6,7}=7.0$, $J_{4,6}=1.5$, $J_{allyl}=5.0$, 10.0, 17.0 Hz									
50	e)	e)	6.45	2.63	5.43	6.8—7.5[d)]				
			br d	s	s	m				
	$J_{5,6}=7.0$ Hz									
51	e)	2.36	6.53	7.60	5.33	7.0—7.3[d)]				
		s	dd	d	s	m				
	$J_{6,7}=7.0$, $J_{4,6}=1.5$ Hz									

a) The NMR spectra of compounds **42**—**44** and **49** could not be measured because of their low sulubilities in deuteriochloroform. b) $J_{ethyl}=7.0$ Hz. c) $J_{allyl}=5.0$, 10.0, and 17.0 Hz. d) Phenyl protons. e) Overlapped with the phenyl proton signals. f) The signals due to the ethoxycarbonimidoyl group appeared at $\delta=1.39$ (3H, t, $J=7.0$ Hz), 4.34 (2H, q, $J=7.0$ Hz), and 6.10 (1H, m, NH).

ethoxycarbonyl- **24**—**32** and 1-alkyl-3-cyano-1,2-dihydropyrazolo[1,5-*a*]pyridin-2-one derivatives **42**—**45** and **47**—**51**. In the reaction of salt **36**, imidate **46** was also obtained in only 4% yield, together with compound **45** (21%). These results and some data are shown in Tables 3 and 4.

Furthermore, pyrazolopyridine **45** was converted slowly to the imidate **46** by the reaction with ethanol in the presence of alkali, but not at all in its absence.

References

1) A. Kakehi and S. Ito, *J. Org. Chem.*, **39**, 1542 (1974).
2) A. Kakehi and S. Ito, *Bull. Chem. Soc. Jpn.*, **47**, 938 (1974).
3) A. Kakehi, S. Ito, T. Funahashi, and Y. Ota, *J. Org. Chem.*, **41**, 1570 (1976).
4) A. Kakehi, S. Ito, K. Uchiyama, Y. Konno, and K. Kondo, *J. Org. Chem.*, **42**, 443 (1977).
5) T. Kato and S. Masuda, *Chem. Pharm. Bull.*, **23**, 452 (1975).
6) T. Sasaki, K. Kanematsu, A. Kakehi, I. Ichikawa, and K. Hayakawa, *J. Org. Chem.*, **35**, 426 (1970).
7) A. Balasubramanian, J. M. McIntosh, and V. Snieckus, *J. Org. Chem.*, **35**, 433 (1970).
8) J. Streith, J. P. Luttringer, and M. Nastasi, *J. Org. Chem.*, **36**, 2962 (1971).
9) T. Okamoto, M. Hirobe, and A. Ohsawa, *Chem. Pharm. Bull.*, **14**, 518 (1966).
10) T. Okamoto, M. Hirobe, C. Mizushima, and A. Osawa, *Yakugaku Zasshi*, **83** ,309 (1963).
11) T. Sasaki, K. Kanematsu, and A. Kakehi, *J. Org. Chem.*, **37**, 3106 (1972).
12) A. Kakehi, S. Ito, T. Funahashi, and N. Ogasawara, *Chem. Lett.*, **1975**, 919.
13) A. Kakehi, S. Ito, T. Funahashi, and N. Ogasawara, *Bull. Chem. Soc. Jpn.*, **49**, 2250 (1976).
14) R. M. Acheson and J. Woollard, *J. Chem. Soc., Perkin Trans. 1*, **1975**, 744.
15) F. C. Schaefer and G. A. Peters, *J. Org. Chem.*, **26**, 412 (1961).

The Enantioface-differentiating (Asymmetric) Hydrogenation of the C=O Double Bond with Modified Raney Nickel. XXX. The Temperature Dependency of the Optical Yield

Hiroshi OZAKI

Division of Organic Chemistry, Institute for Protein Research, Osaka University, Suita, Osaka 565

(Received June 4, 1977)

The effect of the reaction temperature upon the optical yield was studied in the liquid-phase enantioface-differentiating hydrogenation of methyl acetoacetate with various modified Raney nickel catalysts (MRNi) under an atmospheric pressure of hydrogen. The results obtained are as follows: 1) the enantiomer produced in excess in the reactions with (*S*)-alanine-, (*S*)-2-aminobutyric acid-, and (*S*)-valine-MRNi, changed from (*S*)-(+) to (*R*)-(−) with the elevation in the reaction temperature (The temperature, T_0, at which the direction of the differentiation changed decreased in the order of alanine-, 2-aminobutyric acid-, and valine-MRNi. The origin of T_0 is expected to be steric and polar effects that act in opposite directions for the differentiation of the enantioface.), and 2) the temperature dependence of the optical yield with (*R*,*R*)-tartaric acid- and (*S*)-lactic acid-MRNi differed from that with other catalysts. The OH group of the modifying reagent is expected to play an important role in enantioface-differentiation by making a hydrogen bond with the substrate.

The Raney nickel catalyst modified with an optically active substance (MRNi) is an intensively studied catalyst for the enantioface-differentiating hydrogenation of the β-keto ester. In a preceeding communication, it has been reported that the interaction of a substrate with a modifying reagent on the catalyst surface was the essential step in the enantioface-differentiation.[1)]

To gain an insight into the origin of the inter-molecular forces participating the enantioface-differentiating process, the effect of reaction temperatures on the optical yield was investigated.

Results and Discussion

The enantioface-differentiating hydrogenation of methyl acetoacetate (MAA) to methyl 3-hydroxybutyrate (MHB) over various MRNi was carried out. As is shown in Fig. 1, each modifying reagent had a characteristic temperature, T_0, at which an optical yield of zero was observed.

The temperature dependence of the ratio of enantiomers produced (C_R/C_S) has generally been discussed based on the following relation:

$$\ln (C_R/C_S) = \Delta\Delta S^*/R - \Delta\Delta H^*/RT.$$

The existence of T_0 may be explained by the contribution of the $\Delta\Delta S^*$ term. If the enantioface-differentiation of MRNi were expressed by the above equation, the linear relationship of $\ln(C_R/C_S)$ toward $1/T$ should be expected. However, none of our results gave a linear relationship between $\ln(C_R/C_S)$ and $1/T$, as is shown in Fig. 2. This fact indicates that it is difficult to explain the result by a simple energetic correlation.

As for the (*S*)-monoamino monocarboxylic acid-MRNi in Fig. 1, the optical yields increase in the direction of an excess of (*R*)-(−)-enantiomer as the reaction temperatures increase. The temperatures, T_0, for valine-, 2-aminobutyric acid-, and alanine-MRNi were at 30—40 °C, 40—50 °C, and 50—60 °C respectively.

Figure 3 shows the temperature dependence of the optical yield in the enantioface-differentiating hydrogenation of methyl acetoacetate and butyl acetoacetate

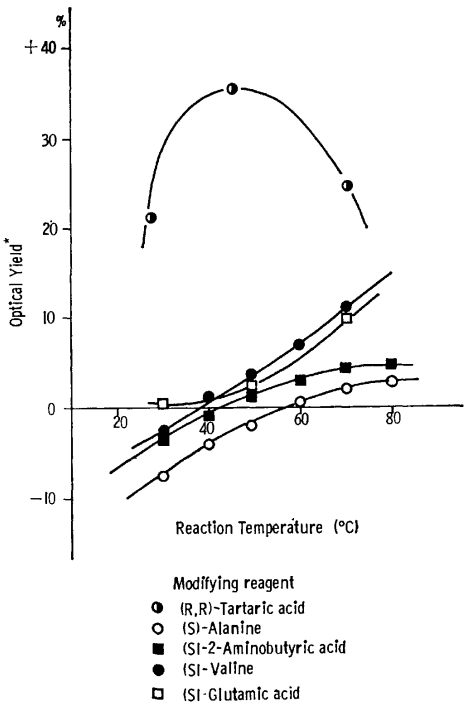

Fig. 1. Effect of modifying reagent on the temperature dependence of optical yield.
*The sign of optical yield is taken as + in the case of an excess of (*R*)-(−)-enantiomer.

with (*S*)-valine-MRNi. T_0 also varies in accordance with the ester moiety of the substrate, and T_0 for methyl acetoacetate is higher than that for butyl acetoacetate. These results show that the temperature, T_0, becomes higher as the chain length of both the alkyl substituent of the modifying reagent and the ester moiety of the substrate decrease.

As the main difference in alkyl substituents is their bulkiness, the above facts may indicate that the steric interaction between a modifying reagent and a substrate is one of the factors in enantioface-differentiation.

As is shown in Fig. 1, the dependence of the optical yield on the reaction temperature for (*R*,*R*)-tartaric acid-MRNi is different from that for amino acid-MRNi.

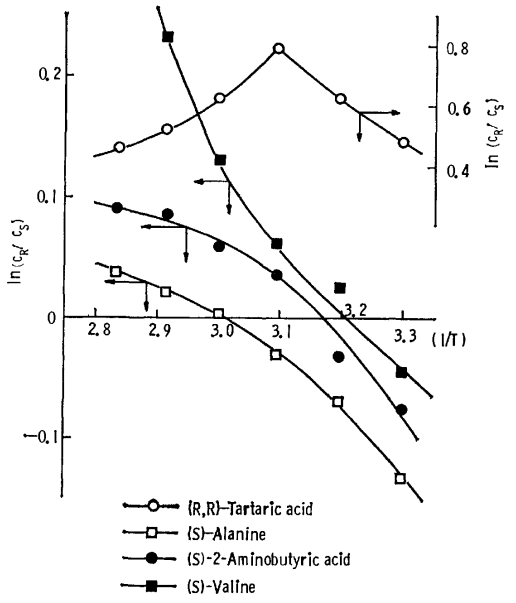

Fig. 2. Plots of $\ln(C_R/C_S)$ against $1/T$.

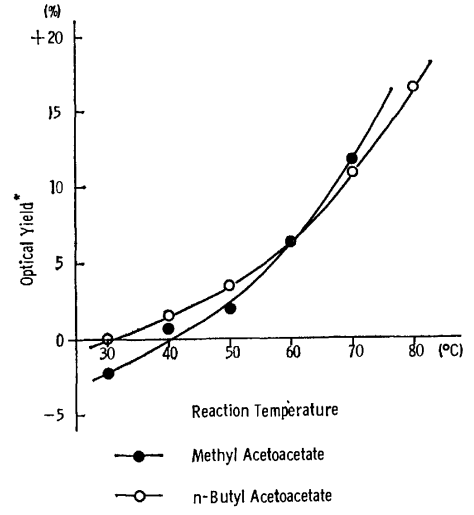

Fig. 3. Effect of ester group in substrate on the temperature dependence of optical yield.
*The sign of optical yield is taken as + in the case of an excess of (*R*)-(−)-enantiomer.

The maximum optical yield is observed at around 50 °C, and the optical yield decreases both above and below this temperature.

Taking into consideration the fact that this temperatue of 50 °C corresponds to the initial temperature of the dissociation of the hydrogen bond, the convex shape of the temperature dependence of the optical yield for (*R*,*R*)-tartaric acid-MRNi can be interpreted by the idea that the OH groups in the modifying reagent participate predominantly in enantioface-differentiation by making a hydrogen bond with the substrate up to the temperature at which the hydrogen bond disappears.

In order to investigate the role of the hydroxy group in α-hydroxy acid-MRNi in enantioface-differentiation, hydrogenations with catalysts modified with α-hydroxy carboxylic acids and their *O*-methyl derivatives were carried out. The results are listed in Table 1. (*S*)-Lactic acid-MRNi tends to afford (*S*)-(+)-enantiomer in excess as the reaction temperature rises.

Table 1. Effect of the modifying reagent on the temperature dependence of the optical yield

Modifying reagent	Reation temperature (°C)	Optical yield[a] (%)
(*S*)-lactic acid	30	0.00
	60	−0.65
	80	−1.08
(*S*)-2-methoxy-propionic acid	60	−0.07
	80	0.33
(*S*)-2-methoxy-3-methylbutyric acid	40	0.00
	60	0.24
	80	1.06

a) The sign of the optical yield is taken as + in the case of an excess of the (*R*)-(−)-enantiomer.

On the other hand, the catalysts modified with (*S*)-α-methoxy carboxylic acids showed the same temperature dependence as (*S*)-α-amino acid-MRNi, in which the amino group has much less capacity of making a hydrogen bond and T_0 decreased with the change in the α-alkyl group from methyl to isopropyl.

These phenomena indicate that the OH group plays an important role in the enantioface-differentiation by its ability of hydrogen bonding and that the function of the OH group in the enantio-differentiation differ from that of the NH_2 or OCH_3 group.

As has been reported, the comparative study of the rate and the optical yield indicates that the role of a modifying reagent can be divided into two independent functions. One is to regulate the rate by occupying a part of the active area of the catalyst, and the other is to differentiate the enantiofaces of the substrate as a reference chiral system.[1]

It is also known that at least two polar groups must attach to a chiral center of a modifying reagent for the stereo-differentiating reaction to take place.[2] When these facts are taken into account, the formation of dipolar interaction or a hydrogen bond between the substrate and modifying reagent could be the essential step in the enantio-differentiating hydrogenation.

Since the mode of the interaction is expected to be determined by the balance of an associative dipolar interaction or hydrogen bond and repulsive steric effect, the origin of T_0 can be explained by the change in the balance of the two effects because of their different temperature dependences.

Thus, T_0 and the feature of the temperature dependence of the optical yield may give a clue to the nature of the stereo-differentiating reaction. In order to understand the origin of T_0 and the temperature dependence of the optical yield in detail, there are still several problems to be solved, such as the temperature effect on the interaction between the modifying reagent and the catalyst and the effect of the minor contaminants of the catalyst, such as the aluminum ion, water, and methanol, on the mode of interaction between the substrate and the modifying reagent.

Further investigation on the origin of T_0 is in progress.

Experimental

The GLC analysis was carried out with a Shimadzu GC-3AH apparatus with a TC detector, using a 300×0.5 cm stainless-steel column packed with PEG 20-M (10%) on Chromosorb W. The optical rotations were measured at the Na-D line with a Perkin-Elmer 241 Polarimeter with a quartz cell (length of light path, 1 dm). All the materials except those listed below were obtained from commercial sources and were used without further purification. Butyl acetoacetate,[3] (*S*)-lactic acid (as Zn salt), $[\alpha]_D$ −7.9 (*c* 2, H_2O),[4] (*S*)-2-methoxy-3-methylbutyric acid,[5] $[\alpha]_D$ −77.6 (neat), and (*S*)-2-methoxypropionic acid,[5] $[\alpha]_D$ +69.1 (neat), were prepared by published procedures.

Preparation of the Catalyst. Into an alkaline solution (52 g of sodium hydroxide in 260 ml of deionized water), which had been cooled to 20 °C on an ice bath, 19.5 g of a well-pulverized Raney alloy (Ni 42%, Al 58%, Kawaken Fine Chemical Co.) was added in portions at such a rate that the temperature of the mixture was maintained at 20± 2 °C with occasional shaking. The resulting suspension of Raney nickel was kept at 75—78 °C for 45 min and then allowed to stand at room temperature for 2 h. After the removal of the alkaline solution by decantation, the Raney nickel was washed four times with 650 ml portions of deionized water. The modification of the catalyst was carried out at 0 °C by a published method.[6] The pH of the modifying solution was adjusted to an isoelectric point for each monoamino monocarboxylic acid and to 5.1 for each hydroxy acid.

Hydrogenation. Into an atmospheric-pressure hydrogenation vessel filled with hydrogen, 0.6 g of a catalyst suspended in 17.5 ml (0.15 mol) of a substrate was introduced. The mixture was then heated at the stated temperature for 3 h under shaking. After the subsequent removal of the catalyst from the reaction mixture by filtration, the filtrate was flash-distilled under reduced pressure. The optical rotation and the concentration of product in the distillate were determined by means of polarimetry at 25 °C and by GLC (90 °C) respectively. The optical purity of the product was determined by means of a calibration chart.

The author wishes to express his thanks to Professor Yoshiharu Izumi, Drs. Akira Tai, and Tadao Harada for their guidance and encouragement.

References

1) H. Ozaki, A. Tai, and Y. Izumi, *Chem. Lett.*, **1974**, 935.
2) Y. Izumi, *Angew. Chem., Int. Ed. Engl.*, **10**, 871 (1971).
3) S. O. Lawesson, S. Gronwall, and R. Sandberg, *Org. Synth.*, Coll. Vol. V, 155 (1973).
4) M. Winitz, L. Bloch-Frankenthal, N. Izumiya, S. M. Birnbaum, C. G. Baker, and J. P. Greenstein, *J. Am. Chem. Soc.*, **78**, 2423 (1956).
5) E. M. Uller, M. Bauer, and W. Runder, *Z. Naturforsch., Teil B*, **14**. 209 (1959).
6) Y. Izumi, T. Harada, T. Tanabe, and K. Okuda, *Bull. Chem. Soc. Jpn.*, **44**, 1418 (1971).

Reactions of Alkyl Diphenylphosphinates and Related Thio Esters with Some Nucleophiles. S_N2 (S) Reaction and Wittig Type Rearrangement

Koshiro GODA, Renji OKAZAKI, Kin-ya AKIBA, and Naoki INAMOTO

Department of Chemistry, Faculty of Science, The University of Tokyo, Hongo, Tokyo 113

(Received June 7, 1977)

Reactions of alkyl diphenylphosphinates $Ph_2P(=X)YCHR^1R^2$ (X, Y=O,S) with organolithiums and Grignard reagents afforded different types of products depending on the combination of X and Y. When Y=O, the reagents (R^3M) mainly attacked the phosphorus atom to give $Ph_2P(=X)R^3$ and $R^1R^2CHO^-$ irrespective of X, while, when X=Y=S, the reaction occurred exclusively at the ester sulfur atom, S_N2(S), to give $R^3SCHR^1R^2$ and $[Ph_2PS]^-$. When the X=O and Y=S, a Wittig type rearrangement of a carbanion $[Ph_2P(=O)SCR^1R^2]^-$ was observed along with attacks on the phosphorus (major) and the sulfur (minor) atoms. Reactions with some other nucleophiles (hydride, amide and alkoxide ions) are also described.

Substitution on the phosphoryl group with Grignard reagents[1] and organolithiums[2] has been used as a synthetic method. However, there seems to be no report on the reaction of alkyl diphenylphosphinates and related thio esters (**1**—**4**) with organolithiums or Grignard reagents.

$Ph_2P(X)-Y-R$ **1**: X=Y=O **3**: X=O, Y=S **2**: X=S, Y=O **4**: X=Y=S

The esters (**1**—**4**) have four reaction centers towards nucleophile, the phosphorus, Y atoms, and the α-carbon and α-hydrogen atoms of the R group. In the course of an investigation on the reactions of the esters (**1**—**4**) with some nucleophiles, we found two types of novel reactions in the case of Y=S (**3** and **4**), *viz.*, Wittig type rearrangement and S_N2 attack on the sulfur atom (S_N2 (S)).[3] This paper gives detailed results of the investigation.

Reactions of **1** *(X=Y=O).* Reactions of diphenylphosphinate esters (**1**) with nucleophiles such as butyl- and phenyllithiums, sodium hydride, and potassium *t*-butoxide were carried out in tetrahydrofuran (THF) under nitrogen. The results are summarized in Table 1.

$$Ph_2P(O)-O-R + R'Li \longrightarrow Ph_2P(O)-R' + ROLi \xrightarrow{H^+} ROH$$

1: **a**: R'=Bu, **b**: R'=Ph → **5**; $\xrightarrow{MeI}$ $ROCH_3$

The formation of (1-methylbutyl)diphenylphosphine oxide (**6**) is attributed to methylation of butyldiphenylphosphine oxide (**5a**) initially formed by methyl iodide in the presence of excess butyllithium.

$$Ph_2P(O)-CH_2CH_2CH_2CH_3 \xrightarrow{BuLi} Ph_2P(O)-\overset{\ominus}{C}HCH_2CH_2CH_3$$

5a

$$\xrightarrow{MeI} Ph_2P(O)-CH(CH_3)CH_2CH_2CH_3$$

6

The formation of bis(diphenylmethyl) ether in the case of diphenylmethyl ester might be due to S_N2 attack on the α-carbon atom by diphenylmethoxide anion produced in the reaction. In the reaction with sodium hydride, benzophenone is considered to be formed in the following ways, $[Ph_2PO]^-$ being isolated as diphenylphosphinic acid because of the easy oxidation during the work-up.

$$Ph_2P(O)-O-CHPh_2 \xrightarrow{B:} Ph_2P(O)-O-\overset{\ominus}{C}Ph_2 \longrightarrow [Ph_2PO]^- + Ph_2CO$$

$$Ph_2P(O)-O-\overset{\ominus}{C}Ph_2 \xrightarrow[\text{rearr.}]{\text{Wittig}} Ph_2P(O)-CPh_2(O^-)$$

The following example of Wittig type rearrangement has been reported.[4]

$$A_2P(O)OCH_2Ph + BuLi \longrightarrow A_2P(O)\overset{\ominus}{O}CHPh \longrightarrow A_2P(O)CHPhO^-$$

A=MeO, EtO, Me_2N

Table 1. Reactions of **1** with nucleophiles (Nu) in THF

R	Nu	Reaction temp (°C)	Reaction time (h)	Product (%)
$PhCH_2$	BuLi[a]	−78	0.5	**6** (60)[b]
Ph_2CH	BuLi[a]	−78	0.5	**6** (59),[b] ROMe (77)[b]
	PhLi	−78	0.5	**5b** (50), ROH (55)
	NaH	r. t.	6.0	$Ph_2P(O)OH$ (51), ROH (trace) Ph_2CO (59)
	t-BuOK[a]	r. t.	0.5	$Ph_2P(O)O$-*t*-Bu (19) ROMe (73),[b] ROR (14)

a) The reaction mixture was treated with methyl iodide. b) Methylated product.

Examples of $S_N2(C)$ reaction has also been reported in the case of phosphate esters with Grignard reagents.[5] However, no reaction of this type was detected in the present system, *i.e.*, diphenylphosphinate esters with organolithiums.

$$(RO)_2P(O)OR + PhMgBr \longrightarrow (RO)_2P(O)O^- + R\text{-}Ph$$

The low yield of *t*-butyl diphenylphosphinates in the reaction with potassium *t*-butoxide is attributed to the easy S_N1 type hydrolysis on silica gel column during the work-up.

Therefore, the main reaction modes in **1** are S_N2 (P) and S_N2(C) reactions.

Reactions of **2** *(X=S, Y=O).* The results of the reaction of *O*-alkyl diphenylphosphinothioates (**2**) with butyllithium are shown in the following scheme.

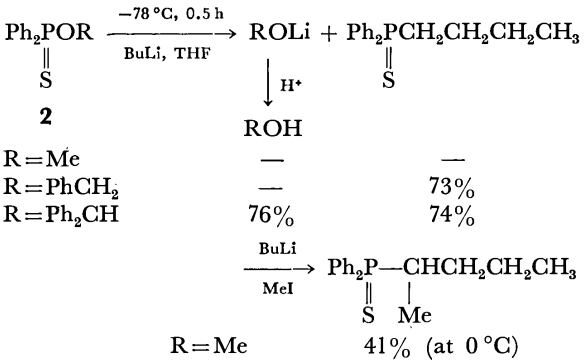

Thus, S_N2(P) pathway occurs mainly.

Reaction of **3** *(X=O, Y=S).* The results are given in Table 2.

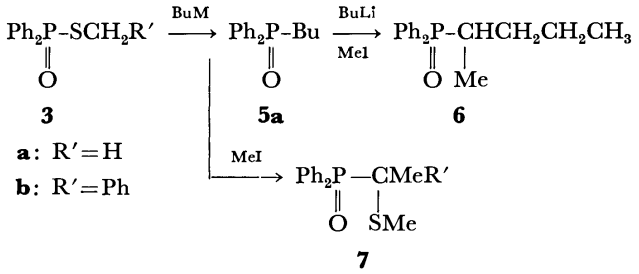

Formation of (α-methylthioalkyl)diphenylphosphine oxide (**7**) is the first example of Wittig type rearrangement in **3**.

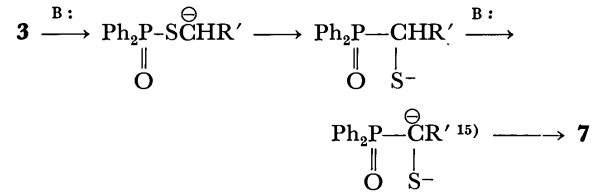

Formation of benzyl methyl sulfide and methyldiphenylphosphine oxide from **3b** is attributed to methylation of α-toluenethiolate anion and $[Ph_2PO]^-$ produced by S_N2(P) and S_N2(S) pathway, respectively. The latter is of the same type as that in the reactions of **4** described below.

Thus, the main pathway is S_N2(P) accompanied by S_N2(S).

Reactions of **4** *(X=Y=S).* Reactions of diphenylphosphinodithioate esters (**4**) with butyllithium or butylmagnesium chloride were carried out in THF at −78 °C or under reflux. The reaction mixture was

Table 2. Reactions of **3** with nucleophiles (Nu) in THF

R′	Nu	Reaction temp (°C)	Reaction time (h)	Product (%)
H	BuMgCl	refl.	0.1	**5a** (93)[b]
	BuLi	−78	0.5	**5a** (48)
	$LiN(c\text{-}C_6H_{11})_2$	−78	0.5	**7a** (12)
Ph	BuLi[a]	−78	0.5	**6** (57), **7b** (11) $Ph_2P(O)Me$ (14), $PhCH_2SMe$ (54)

a) The reaction mixture was treated with methyl iodide. b) Mp 93.0—94.5 °C (lit,[14] 95 °C).

Table 3. Reactions of **4** with butyllithium and butylmagnesium chloride followed by methylation (in THE)

R	M	Reaction temp (°C)	Reaction time (h)	Product (%)[a]
Me	Li	−78	0.5	**10** (100)
	MgCl	refl.	0.5	**10** (47)
Ph	Li	−78	0.5	**10** (94), **9** (95)[b]
	MgCl	refl.	0.5	**10** (35)[b], recovered **4** (48)[b]
$PhCH_2$	Li	−78	0.5	**10** (84), **9** (39)[b]
	MgCl	refl.	0.5	**10** (10),[b] recovered **4** (74)[b]
CH_2=$CHCH_2$	Li	−78	0.5	**10** (62)
t-Bu	Li	−78	1/6	**18** (trace), $Ph_2P(S)CHMe\text{-}n\text{-}C_3H_7$ (main), $Ph_2P(S)SMe$ (minor)

a) Determined by GLC unless noted otherwise. b) Isolated by DCC.

then treated with methyl iodide. The results are summarized in Table 3.

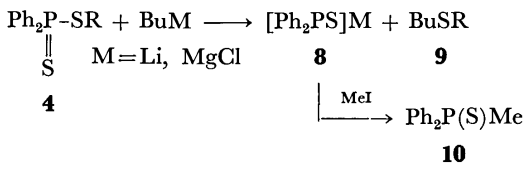

The results show that the reactions of **4** with butyllithium in THF at −78 °C were fast, giving diphenylphosphinothioylide (**8**) and butyl sulfides (**9**) selectively in excellent yields. Thus, the reactions are utilized in preparation of unsymmetrical sulfides.[6]

On the other hand, the reactions with Grignard reagents were very slow. Phenylmagnesium bromide in particular did not react with methyl, phenyl, and benzyl esters to an appreciable extent even in refluxing THF for 3 h.

The reactions are the first example of $S_N2(S)$ reaction in **4**. Since methyl diphenylphosphinodithioate is prepared easily and in a high yield from the Friedel-Crafts reaction of benzene and phosphorus pentasulfide followed by refluxing with methanol,[7] the reaction of methyl diphenylphosphinodithioate with butyllithium is used as a new method for preparation of **8**.

The $S_N2(S)$ reaction did not occur in the case of *t*-butyl ester, because of steric hindrance, the reaction proceeding *via* *E*2 and $S_N2(P)$ pathways as follows:

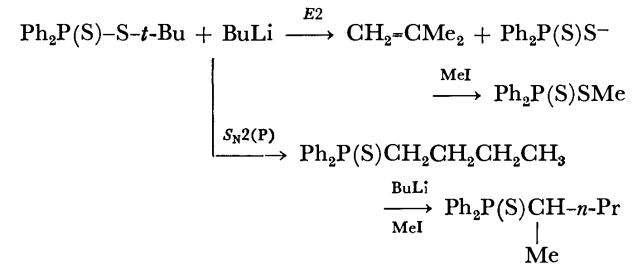

The formation of **8** was also indicated by means of ^{31}P-NMR as shown below.

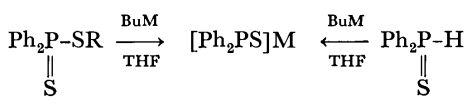

	δ_P		δ_P	δ_P
R=Me	−64.2	M=Li	−20.7	−20.8
Ph	−64.8	MgCl	−14.3	
$PhCH_2$	−62.9			
Et	−62.4			
CH_2=$CHCH_2$	−62.4			

In each case, the signal was observed at the same position, *i.e.*, at −20.7 or −14.3 ppm depending on M=Li or MgCl, respectively.[8]

In the reaction of allyl ester with butylmagnesium chloride, the signal due to $Ph_2P(S)SMgCl$ at −58.6 ppm was detected, indicating the existence of $S_N2(C)$ pathway.

Evidence for $S_N2(S)$ *Mechanism in* **4**. The following three pathways are possible for the formation of **8** and **9**.

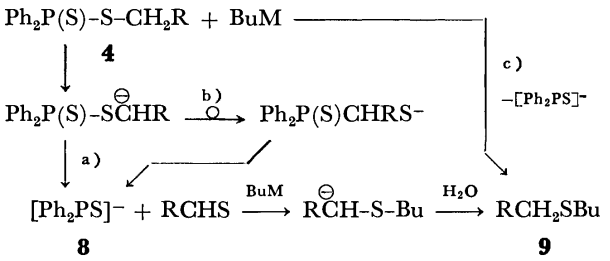

Paths a) and b) involve the formation of the corresponding α-carbanion in the first step, followed by direct elimination of thioaldehyde (path a)) or by the Wittig type rearrangement followed by elimination (path b)). Path c) is a direct attack on the sulfur atom of **4** ($S_N2(S)$ reaction). Paths a) and b) are ruled out in view of the following: 1) the reaction did not require two molar amounts of BuM, the yield of methyldiphenylphosphine sulfide (**10**) being 97 and 100% in the reactions of an equimolar and two molar amounts of butyllithium with methyl ester, respectively, 2) even phenyl ester reacted quantitatively in spite of the absence of α-hydrogen atom, and 3) reaction of benzyl ester with an equimolar amount of butyllithium at −78 °C afforded benzyl butyl sulfide containing no deuterium atom after quenching with D_2O (by MS and NMR).

Thus, it can be concluded that the formation of **8** and **9** takes place through $S_N2(S)$ mechanism (path c)).

Reason for the Differences in Reaction Modes. In the case of **1** and **2** (Y=O), the main path is $S_N2(P)$ reaction. On the other hand, in the case of **4** (X=Y=S), $S_N2(S)$ reaction occurs selectively, and in the case of **3** (X=O, Y=S), the $S_N2(P)$ pathway occurs along with $S_N2(S)$.

The fact that organometalloids R′M attack Y only when Y=S is explained in terms of the possible involvement of **A** as an intermediate (or transition state), since such a structure is impossible in the case of oxygen, $S_N2(P)$ process being considered to occur irrespective of X when Y=O.

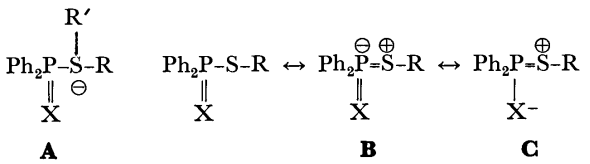

Canonical structures such as **B** and **C** having a positive charge on sulfur may also make some contribution in the ground state of **4**, making the formation of **A** possible.

No $S_N2(S)$ reaction was found to occur in the reaction of butyllithium with *S*-alkyl *O*,*O*-diethyl dithiophosphate, in which the following resonance structures are possible.

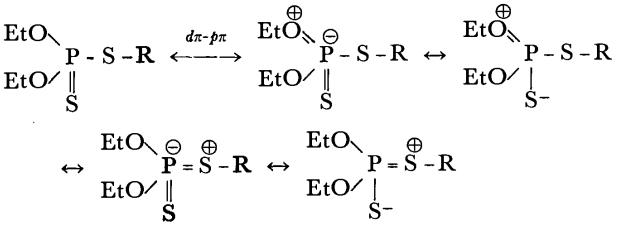

Since the contribution of $d\pi$-$p\pi$ interaction in the S–P bond is considered to be smaller than that in O–P bond, $S_N2(S)$ pathway cannot take place, since the ester sulfur atom does not carry such a positive charge as in **4** to accept organometalloids. The following reaction[9] might support the above interpretation.

$$(EtO)_2P(S)\text{-}Et + EtI \longrightarrow EtO\text{-}P(O)(SEt)_2 + EtI$$

It has been shown that the organolithiums possess a larger thiophilicity than the Grignard reagents, as indicated in the reactions with thioketones[10] and with 2-nitrosoimino-2,3-dihydrobenzothiazoles.[11] The results we obtained are in line with these facts.

The observation that **3** (X=O, Y=S) undergoes both $S_N2(P)$ and $S_N2(S)$ in contrast to the exclusive occurrence of $S_N2(S)$ in **4** (X=Y=S) is easily understandable in view of the well-known greater electrophilic reactivity of phosphinyl group than that of a thiophosphinyl group. For example, diphenylphosphinic chloride undergoes hydrolysis more easily than diphenylphosphinothioic chloride. Similarly, *S*-benzyl diphenylphosphinothioate undergoes hydrolysis more easily than benzyl diphenylphosphinodithioate (see Experimental).

Experimental

^{31}P-NMR spectra were measured with a Hitachi R-20B-R-204 PB spectrometer using 85% phosphoric acid as an external standard.

Materials. *S*-Methyl,[8] *S*-benzyl,[12] *O*-methyl,[12] *O*-benzyl diphenylphosphinothioates,[13] and *t*-butyl diphenylphosphinodithioate[7b] were prepared by the reported methods.

Methyl Diphenylphosphinodithioate. A mixture of sodium hydroxide (20 g, 0.5 mol) and diphenylphosphinodithioic acid (105 g, 0.42 mol) in THF (300 ml) was stirred at room temperature for 1 h. Methyl iodide (60 g, 0.42 mol) was added and the mixture was stirred at room temperature for 1 h. The reaction mixture was washed with water and extracted with benzene. After removal of the solvent from the dried extract, the residue was recrystallized from ethanol, mp 86—87 °C (lit,[7] 82—83 °C), yield 98 g (88%).

Diphenylmethyl Diphenylphosphinate. A mixture of diphenylphosphinic chloride (17.3 g, 73 mmol), diphenylmethanol (22.7 g, 123 mmol) and triethylamine (12 ml) in THF (80 ml) was refluxed for 2 h. The reaction mixture was treated similarly. Mp 138—139 °C (from 2-propanol), yield 20.6 g (73%). NMR ($CDCl_3$): δ 6.60 (d, 1H, J_{POCH}=11 Hz, CH), 7.42 (s, 10H, 2Ph), and 7.30–8.10 (m, 10H, 2P-Ph); ^{31}P-NMR (THF): δ_P −29.5 ppm.

Benzyl Diphenylphosphinate. A mixture of diphenylphosphinic chloride (1.86 g, 79 mmol) and benzyl alcohol (20 ml) in THF (80 ml) was stirred for 1 h. The reaction mixture was washed with 10% aqueous sodium hydrogencarbonate and extracted with benzene. After removal of the solvent from the dried extract, the residue was recrystallized from ether, mp 82.5—83.5 °C, yield 17.1 g (71%). NMR ($CDCl_3$): δ 4.95 (d, 2H, J_{POCH}=7 Hz, OCH_2), 7.22 (s, 5H, Ph), and 7.20—8.00 (m, 10H, 2P-Ph).

Found: C, 74.15; H, 5.65%. Calcd for $C_{19}H_{17}O_2P$: C, 74.02; H, 5.56%.

O-Diphenylmethyl Diphenylphosphinothioate. To a mixture of diphenylmethanol (10 g, 54 mmol) and sodium (1 g, 43 mmol) in THF (40 ml) was added diphenylphosphinothioic chloride (11.0 g, 45 mmol) in THF (50 ml), and the reaction mixture was treated in the usual way, mp 97—98 °C (from ethanol), yield 13.9 g (95%). IR (KBr): 980 (P-O) and 640 cm^{-1} (P=S); NMR ($CDCl_3$): δ 6.75 (d, 1H, J_{POCH}=13 Hz, CH), 7.20 (s, 10H, 2Ph), and 7.10—7.95 (m, 10H, 2P-Ph); ^{31}P-NMR (THF): δ_P −82.1 ppm.

Found: C, 75.06; H, 5.25; S, 8.13%. Calcd for $C_{25}H_{21}OPS$: C, 74.98; H, 5.29; S, 8.01%.

Benzyl Diphenylphosphinodithioate. To a mixture of diphenylphosphinodithioic acid (48 g, 0.19 mol) and sodium (4.6 g, 0.2 mol) in THF (200 ml) was added benzyl bromide (34.2 g, 0.2 mol), and the mixture was stirred for 3 h. After the usual work-up, the reaction mixture was subjected to column chromatography with $CHCl_3$ to give colorless viscous oil, yield 56 g (86%), which could not be distilled. NMR ($CDCl_3$): δ 4.05 (d, 2H, J_{PSCH}=13 Hz, CH_2), 7.05 (s, 5H, Ph), and 7.15—8.05 (m, 10H, 2P-Ph); ^{31}P-NMR (THF): δ_P −62.9 ppm.

Found: C, 66.98; H, 5.06; S, 18.81%. Calcd for $C_{19}H_{17}PS_2$: C, 67.03; H, 5.03; S, 18.84%.

Phenyl Diphenylphosphinodithioate. To a mixture of benzenethiol (10 ml) and sodium (2.5 g, 0.11 mol) in THF (30 ml) was added diphenylphosphinothioic chloride (24 g, 0.095 mol), and the reaction mixture was stirred for 3 h. After the usual work-up, the product was distilled *in vacuo*, bp 229 °C/0.1 mmHg, mp 57—59 °C (from ethanol), yield 24 g (77%). ^{31}P-NMR (THF): δ_P −64.8 ppm.

Found: C, 66.14; H, 4.50; S, 19.57%. Calcd for $C_{18}H_{25}PS_2$: C, 66.23; H, 4.63; S, 19.65%.

Ethyl Diphenylphosphinodithioate. To a mixture of diphenylphosphinodithioic acid (50 g, 0.2 mol) and sodium hydroxide (8 g, 0.2 mol) in THF (150 ml) was added ethyl bromide (15 ml) under stirring at room temperature and the mixture was stirred for 1 h. The usual work-up afforded the ester (46 g, 83%), bp 166 °C/0.2 mmHg (lit,[7b] 166—167 °C/0.3 mmHg).

Allyl Diphenylphosphinodithioate. To a mixture of diphenylphosphinodithioic acid (29 g, 0.12 mol) and sodium hydroxide (6 g, 0.15 mol) in THF (100 ml) was added allyl bromide (10 ml), and the mixture was stirred for 3 h at room temperature. The usual work-up gave the ester (27 g, 80%), bp 160 °C/0.04 mmHg. NMR (CCl_4): δ 3.55 (dd, 2H, J_{PSCH}=13 Hz, CH_2), 4.7—6.0 (m, 3H, $CH{=}CH_2$), and 7.2—8.2 (m, 10H, 2P-Ph); ^{31}P-NMR (THF): δ_P −62.4 ppm.

Found: C, 62.32; H, 4.92%. Calcd for $C_{15}H_{15}PS_2$: C, 62.02; H, 5.21%.

*Reactions of **1** with Nucleophiles.* Only some typical examples are described. Reactions were carried out under nitrogen or argon.

Reaction of Benzyl Diphenylphosphinate with Butyllithium. Butyllithium (3 mmol) in hexane (2 ml) was added to the ester (0.795 g, 2.6 mmol) in THF (30 ml) at −78 °C and the mixture was stirred at this temperature for 0.5 h. After addition of methyl iodide (1 ml), the reaction mixture was warmed to room temperature, washed with water, and extracted with chloroform. After removal of the solvent from the dried extract, the residue was subjected to dry column chromatography (DCC) (SiO_2, $MeCO_2Et$) to give **6** (0.419 g, 60%), mp 86—88 °C (from ether). NMR (CCl_4): δ 0.87 (t, 3H, Me), 1.17 (dd, J_{PCCH}=14 Hz, J_{HH}=7 Hz, 3H, Me), 1.27—1.70 (m, 4H, $2CH_2$), 2.05—2.50 (m, 1H, CH), and 7.20—7.90 (m, 10H, 2P-Ph).

Found: C, 75.22; H, 7.61%. Calcd for $C_{17}H_{21}OP$: C, 74.98; H, 7.71%.

Reaction of Diphenylmethyl Diphenylphosphinate with Sodium Hydride. Sodium hydride (0.157 g, 6.5 mmol) was

added to the ester (0.247 g, 0.64 mmol) in THF (15 ml) at room temperature, and the mixture was stirred for 6 h. After addition of methanol (1 ml), the mixture was acidified with dil. hydrochloric acid and extracted with benzene. Removal of benzene from the extract gave 71 mg (51%) of diphenylphosphinic acid and oily material, the latter being separated with DCC (SiO_2, $CHCl_3$; then SiO_2, hexane) to give benzophenone(69 mg, 59%) and diphenylmethanol (trace) which were identified by IR and NMR.

Reaction of O-*Methyl Diphenylphosphinothioate with Butyllithium.* Butyllithium (10.9 mmol) in hexane (7 ml) was added to a solution of the ester (1.467 g, 5.9 mmol) in THF (30 ml) at 0 °C and the mixture was stirred for 1 h. After addition of methyl iodide (1 ml), the mixture was stirred for 3 h. After the usual work-up, recrystallization of the residue from 2-propanol twice gave 0.699 g (41%) of (1-methylbutyl)diphenylphosphine sulfide, mp 114—115 °C. IR (KBr): 1430, 1105 (P-Ph), and 605 cm^{-1} (P=S); NMR ($CDCl_3$): δ 0.85 (t, 3H, $J_{HH}=7$ Hz, Me), 1.15 (dd, 3H, $J_{PCCH}=19$ Hz, $J_{HH}=7$ Hz, Me), 1.35—1.65 (m, 4H, $2CH_2$), 2.50—2.90 (m, 1H, CH), and 7.35—8.10 (m, 10H, 2P-Ph); MS: *m/e* 288 (M^+, 7%), 218 (Ph_2P^+SH, 100), and 185 (Ph_2P^+, 25).

Found: C, 70.84; H, 7.44; S, 11.12%. Calcd for $C_{17}H_{21}SP$: C, 70.80; H, 7.34; S, 11.12%.

Reaction of S-*Methyl Diphenylphosphinothioate with Lithium Dicyclohexylamide.* Butyllithium (12.5 mmol) in hexane (8 ml) was added to dicyclohexylamine (2.28 g, 12.6 mmol) in THF (25 ml) at −78 °C and the mixture was stirred at this temperature for 0.5 h. *S*-Methyl diphenylphosphinothioate (1.74 g, 7.0 mmol) in THF (25 ml) was then added to the mixture and the mixture was stirred at the same temperature for 0.5 h. After addition of methyl iodide (2 ml), the reaction mixture was warmed to room temperature, washed with aqueous citric acid, and extracted with benzene. The extract was dried, evaporated, and subjected to DCC (SiO_2, AcOEt) to give 0.229 g (12%) of **7a**, mp 185—187 °C (from ether). IR (KBr): 1438, 1120(P-Ph), and 1198 cm^{-1} (P=O); NMR ($CDCl_3$): δ 1.54 (dd, 3H, $J_{PCCH}=14$ Hz, $J_{HH}=7$ Hz, Me), 2.73 (s, 3H, SMe), 3.83 (dq, 1H, $J_{PCH}=14$ Hz, $J_{HH}=7$ Hz, CH-P), and 7.40—8.10 (m, 10H, 2P-Ph); MS: *m/e* 276 (M^+, 7%), 230 (M^+-SCH_2, 100), and 202 (Ph_2P^+OH, 78).

Found: C, 64.93; H, 5.66%. Calcd for $C_{15}H_{17}OPS$: C, 65.20; H, 6.20%.

Reaction of S-*Benzyl Diphenylphosphinothioate with Butyllithium.* Butyllithium (2.0 mmol) in hexane (1.3 ml) was added to the ester (0.354 g, 1.1 mmol) in THF (15 ml) at −78 °C and the mixture was stirred at this temperature for 0.5 h. Methyl iodide (0.5 ml) was added to the mixture at −78 °C. The temperature was then raised to room temperature. The reaction mixture was washed with water and extracted with chloroform. DCC (SiO_2, CCl_4) of the dried extract gave benzyl methyl sulfide (81 mg, 54%), methyldiphenylphosphine oxide (32 mg, 14%), **6** (168 mg, 57%) (by IR and NMR), and oily **7b** (42 mg, 11%).

7b: NMR ($CDCl_3$): δ 1.85 (d, 3H, $J_{PCCH}=14$ Hz, Me), 2.03 (s, 3H, SMe), 7.13 (s, 5H, Ph), and 7.22—8.10 (m, 10H, 2P-Ph).

Found: C, 71.48; H, 6.14; S, 9.03%. Calcd for $C_{21}H_{21}OPS$: C, 71.56; H, 6.01; S, 9.10%.

Reaction of Phenyl Diphenylphosphinodithioate with Butyllithium. Butyllithium (4.5 mmol) in hexane (3 ml) was added to a solution of the ester (0.496 g, 1.5 mmol) in THF (10 ml) at −78 °C and the mixture was stirred at this temperature for 0.5 h. After addition of methyl iodide (0.5 ml) at −78 °C, the mixture was stirred at room temperature for 0.5 h and determined by gas chromatography (GLC, at 210 °C, H 523 column). The yield of **10** was 94%. DCC (SiO_2, CCl_4) of the reaction mixture after the usual work-up gave butyi phenyl sulfide (0.240 g, 95%) (by IR and NMR).

Reaction of Benzyl Diphenylphosphinodithioate with Butyllithium Followed by Treatment with D_2O. A mixture of butyllithium (1.5 mmol) in hexane (1 ml) and the ester (1.06 g, 3.1 mmol) in THF (15 ml) was treated in a similar way to that above and the reaction mixture was quenched with D_2O (0.1 ml). DCC (SiO_2, $CHCl_3$) gave 0.25 g (1.4 mmol) of benzyl butyl sulfide. NMR ($CDCl_3$): $C_6\mathbf{H}_5 : C\mathbf{H}_2$–*n*-Pr= 5.3 : 2.0 (as average value of five measurements). MS: *m/e* 180 (M^+): 181 (M^++1): 182 (M^++2)=100 : 15 : 7 (calcd: 100 : 14 : 5).

Alkaline Hydrolysis. *1) Benzyl Diphenylphosphinodithioate*: The ester (1.295 g, 3.8 mmol) was stirred with 10% aqueous sodium hydroxide (30 ml) at 80 °C for 6 h. The reaction mixture was extracted with chloroform to remove unchanged ester. The extract was acidified with hydrochloric acid and extracted with chloroform. Evaporation of the dried extract gave diphenylphosphinothioic acid (11 mg, 1%), which was identified by IR.

2) S-Benzyl Diphenylphosphinothioate: The ester (0.512 g, 1.6 mmol) was treated in a similar way to that above with 10% aqueous sodium hydroxide (20 ml). The reaction products were diphenylphosphinic acid (0.304 g, 89%) and α-toluenethiol (72 mg, 37%) (by IR and NMR).

References

1) K. D. Berlin and G. B. Butler, *J. Am. Chem. Soc.*, **82**, 2712 (1960); K. D. Berlin and R. U. Pagilagan, *J. Org. Chem.*, **32**, 129 (1967); O. Korpium, R. A. Lewis, J. Chickos, and K. Mislow, *J. Am. Chem. Soc.*, **90**, 4842 (1968).

2) J.L. Willams, *Chem. Ind. (London)*, **1957**, 235.

3) Preliminary report: K. Goda, R. Okazaki, K. Akiba, and N. Inamoto, *Tetrahedron Lett.*, **1976**, 181.

4) G. Sturtz and B. Corbel, *C. R. Acad. Sci., Ser. C*, **276**, 1807 (1973); G. Sturtz and B. Corbel, *ibid.*, **277**, 395 (1973); P. Savignac, M. Dreux, and Y. Leroux, *Tetrahedron Lett.*, **1974**, 2651.

5) K. D. Berlin and M. E. Peterson, *J. Org. Chem.*, **32**, 125 (1967); K. D. Berlin and R. U. Pagilagon, *ibid.*, **32**, 129 (1967).

6) K. Goda and N. Inamoto, *Chem. Lett.*, **1975**, 1009; K. Goda, F. Hanafusa, and N. Inamoto, *Bull. Chem. Soc. Jpn.*, in press.

7) a) W. A. Higgins, P. W. Vogel, and W. G. Craig, *J. Am. Chem. Soc.*, **77**, 1864 (1955); b) T. R. Hopkins and P. W. Vogel, *ibid.*, **78**, 4447 (1956).

8) K. Goda, H. Gomi, M. Yoshifuji, and N. Inamoto, *Bull. Chem. Soc. Jpn.*, **50**, 545 (1977).

9) P. Pistschmuka, *Zh. Fiz. Khim.*, **44**, 1406 (1912); *Chem. Abstr.*, **1**, 1581 (1913).

10) P. Beck and J. W. Worley, *J. Am. Chem. Soc.*, **94**, 597 (1972); E. Schaumann and W. Walter, *Chem. Ber.*, **107**, 3562 (1974).

11) K. Akiba, M. Hisaoka, and N. Inamoto, *Chem. Lett.*, **1974**, 1267; M. Hisaoka, K. Akiba, and N. Inamoto, *Bull. Chem. Soc. Jpn.*, **48**, 3274 (1975).

12) T. A. Mastryukova, T. A. Melent'eva, and M. I. Kabachnik, *Zh. Obshch. Khim.*, **35**, 1197 (1965); *Chem. Abstr.*, **63**, 11605 (1965).

13) K. Issleib and H. Oehme, *Z. Anorg. Allg. Chem.*, **343**, 268 (1966); R. S. Davidson, *J. Chem. Soc., C*, **1967**, 2131.

14) W. Kuchen and H. Buchwald, *Chem. Ber.*, **92**, 227 (1959).

15) Formation of such a dianion ($RR'\overline{C}$-S^-) has been reported in the following papers: D. Seebach and K.-H. Geiss, *Angew. Chem. Int. Ed. Engl.*, **13**, 202 (1974); Y. Minoura and S. Tsuboi, *J. Org. Chem.*, **37**, 2064 (1972).

Synthesis and Absolute Stereochemistry of (+)-7,14-Dihydro-7,14-ethanodibenz[*a*,*h*]anthracene and Its Derivatives

Nobuyuki HARADA, Yuki TAKUMA, and Hisashi UDA

Chemical Research Institute of Nonaqueous Solutions, Tohoku University, Katahira, Sendai 980

(Received June 8, 1977)

(7*R*,14*R*)-(+)-7,14-Dihydro-7,14-ethanodibenz[*a*,*h*]anthracene (**1**), and the 2,9-dimethyl- (**2**) and 2,4,9,11-tetramethyl- (**3**) derivatives were synthesized from (9*R*,10*R*)-(+)-9,10-dihydro-9,10-ethanoanthracene-1,5-dicarbaldehyde (**4**) of known absolute configuration. The CD spectra of **1**, **2**, and **3** clearly exhibit positive first and negative second Cotton effects due to the coupling of the ^1B_b transitions of two naphthalene chromophores: $\Delta\varepsilon_{237.0}=+326.5$, $\Delta\varepsilon_{224.0}=-180.5$, $A=+507.0$, for **1**; $\Delta\varepsilon_{240.6}=+371.5$, $\Delta\varepsilon_{227.0}=-149.4$, $A=+520.9$, for **2**; $\Delta\varepsilon_{242.0}=+340.3$, $\Delta\varepsilon_{225.0}=-88.0$, $A=+428.3$, for **3**. Since the sign of the A values is positive, positive exciton chirality between the two long axes of the naphthalene moieties is assigned. The (7*R*,14*R*) absolute configuration of **1**, **2**, and **3** is established by both CD exciton chirality and X-ray Bijvoet methods.

The circular dichroic exciton chirality method based on chiral exciton coupling between two or more chromophores enables one to determine the absolute stereochemistry of organic compounds in a nonempirical manner.[1,2] We have reported the synthesis and absolute configuration of (+)-6,15-dihydro-6,15-ethanonaphtho[2,3-*c*]pentaphene determined by the exciton chirality method and chemical correlations, providing definite evidence of the consistency between nonempirical CD and X-ray crystallographic methods.[3,4]

This paper describes the synthesis and absolute stereochemistry of (+)-7,14-dihydro-7,14-ethanodibenz[*a*,*h*]anthracene and its derivatives. The CD spectra of these compounds show typical split Cotton effects due to the chiral exciton coupling between two naphthalene chromophores. The absolute configuration determined by the present CD method is in accord with that obtained by the X-ray Bijvoet method, as in the case of (+)-6,15-dihydro-6,15-ethanonaphtho[2,3-*c*]pentaphene.

Results and Discussion

*Synthesis of (7*R*,14*R*)-(+)-7,14-Dihydro-7,14-ethanodibenz*[a,h]*anthracene (**1**) and the 2,9-Dimethyl- (**2**) and 2,4,9,11-Tetramethyl- (**3**) Derivatives.* Compounds **1**, **2**, and **3** were synthesized from (9*R*,10*R*)-(+)-9,10-dihydro-9,10-ethanoanthracene-1,5-dicarbaldehyde (**4**), mp 128.0—129.5 °C, $[\alpha]_D$ +487.3°, the absolute stereochemistry of which has been established by chemical correlations.[3,4]

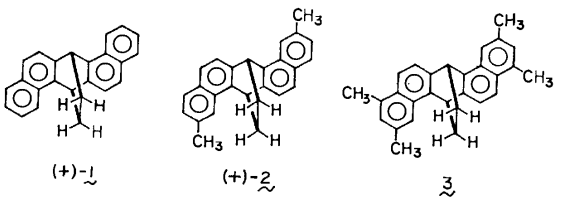

In order to elongate side chains, dialdehyde **4** was subjected to the Wittig reaction with γ-benzyloxypropylenetriphenylphosphorane to afford an isomeric mixture of bisbenzyl ether **5** in an almost quantitative yield (Scheme 1). Catalytic hydrogenation of **5** over palladium on charcoal in acetic acid containing a catalytic amount of sulfuric acid, and successive hydrolysis of the intermediary acetate formed yielded glycol **6**. Oxidation of glycol **6** with Jones reagent, followed by cyclization of the resulting dicarboxylic acid **7** with polyphosphoric acid gave (+)-diketone **8**, $[\alpha]_D$ +184.6°. The Huang-Minlon reduction of **8** afforded hydrocarbon **9**, which was subsequently oxidized with DDQ to yield

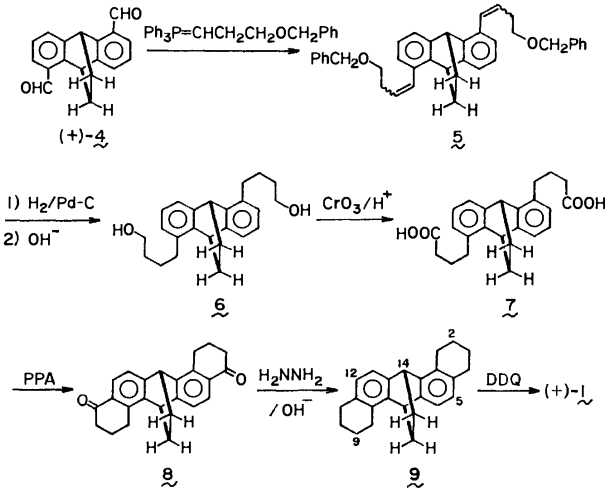

Scheme 1.

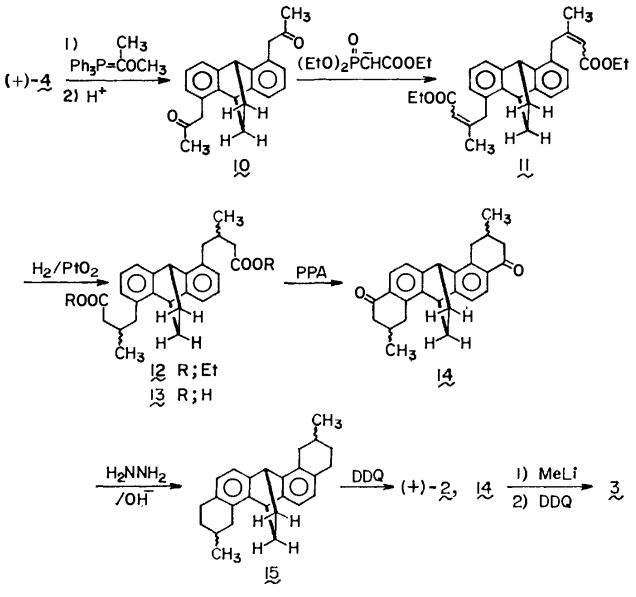

Scheme 2.

the desired hydrocarbon (+)-**1**, mp 234.0—235.5 °C, $[\alpha]_D$ +670.0°.

In the cases of hydrocarbons **2** and **3**, dialdehyde **4** was allowed to react with α-methoxyethylenetriphenylphosphorane to give an isomeric mixture of bisvinyl ether, which was hydrolyzed to diketone **10** (Scheme 2). Diketone **10** was subjected to the second Wittig reaction with triethylphosphonoacetate to yield a *cis,trans* isomeric mixture of diester **11**. Catalytic hydrogenation of the unsaturated diester **11** over platinum oxide and the hydrolysis of ester groups afforded dicarboxylic acid **13**, which was cyclized with polyphosphoric acid yielding diketone **14**. Although the NMR signal of the secondary methyl groups of compound **14** appears as one doublet, diketone **14** could be considered to be a mixture of three possible stereoisomers. Diketone **14** was subjected to the Huang-Minlon reduction giving hydrocarbon **15**, which was oxidized with DDQ to yield the dimethyl derivative (+)-**2**. Methylation of **14** with methyl lithium and successive treatment with DDQ afforded the tetramethyl derivative **3**.

Since the absolute configuration of the ethano-bridge remains unchanged throughout all the reactions, the (7*R*,14*R*) absolute stereochemistry of compounds **1**, **2**, and **3** has been established by the present chemical correlations.

Circular Dichroic Spectra and Absolute Stereochemistry. The linear dichroic properties of electronic transitions of naphthalene chromophore are established as follows. The weak ^1L_b transition around 310 nm (ε 200) and the intense ^1B_b transition around 220 nm (ε 100000) are polarized parallel to the long axis of the chromophore, while the ^1L_a transition of medium intensity around 280 nm (ε 5800) has an electric transition moment along the short axis of the chromophore.[5]

Of these transitions, the allowed ^1B_b transition is ideal for chiral exciton coupling because of its large extinction coefficient value. In fact, hydrocarbon (+)-**1** exhibits strong split Cotton effects due to the exciton coupling between the two ^1B_b transitions: the positive first Cotton effect at 237.0 nm (Δε +326.5) and the negative second one at 224.0 nm (Δε −180.5); $A(\Delta\varepsilon_1 - \Delta\varepsilon_2) = +507.0$ (Fig. 1).[6]

Since the sign of the A value is positive, it is established that the hydrocarbon (+)-**1** has positive exciton chirality between the two long axes of the naphthalene moieties (Fig. 1), which corresponds to the (7*R*,14*R*) absolute configuration in line with the chemical correlation results.

Similarly, compounds (+)-**2** and **3** exhibit strong positive first and negative second Cotton effects in the region of the ^1B_b transition (Figs. 2 and 3). As the number of methyl groups increases, the Cotton effects undergo red shift of 4—5 nm corresponding to that of

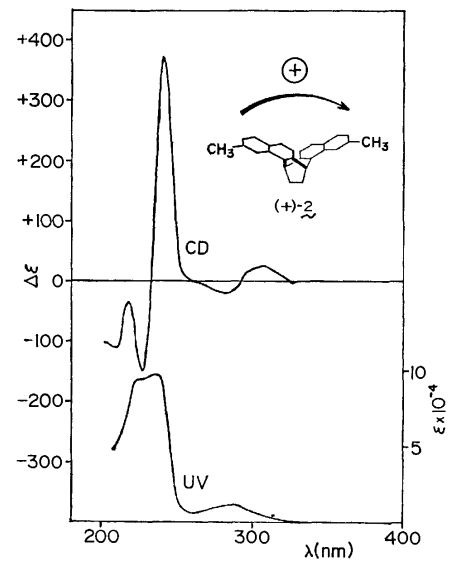

Fig. 2. CD and UV spectra of (7*R*,14*R*)-(+)-7,14-dihydro-2,9-dimethyl-7,14-ethanodibenz[*a*,*h*]anthracene (**2**) (see text for the solvent systems used).

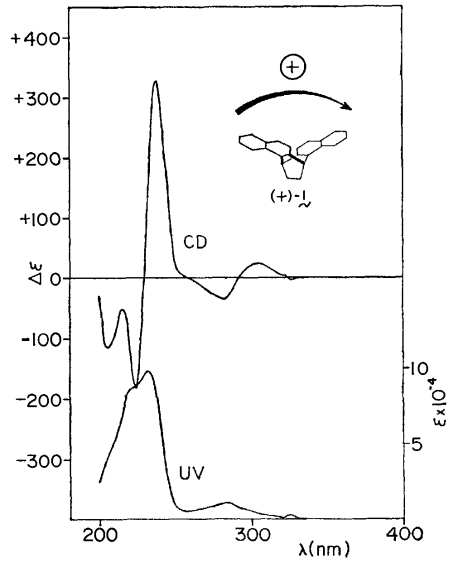

Fig. 1. CD and UV spectra of (7*R*,14*R*)-(+)-7,14-dihydro-7,14-ethanodibenz[*a*,*h*]anthracene (**1**) in ethanol.

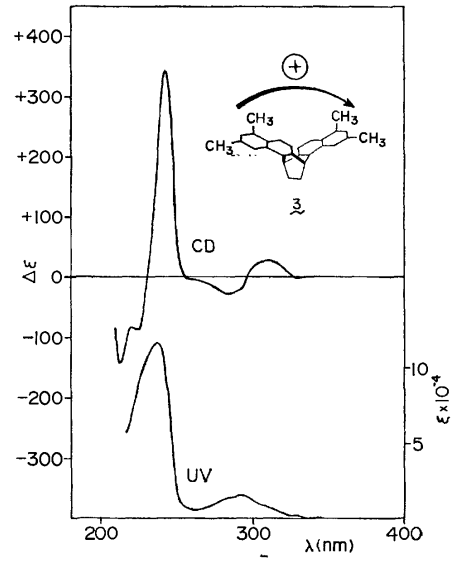

Fig. 3. CD and UV spectra of (7*R*,14*R*)-7,14-dihydro-2,4,9,11-tetramethyl-7,14-ethanodibenz[*a*,*h*]anthracene (**3**) in ethanol.

UV spectrum, the second Cotton effect becoming weaker and the positive first one remaining almost unchanged. On the other hand, the third Cotton effect of negative sign appears around 210 nm, becoming stronger and undergoing red shift as the number of methyl groups increases. In compound **3**, the third and second Cotton effects overlap each other. Although the origin of the third Cotton effect is still unknown, it is obvious that the unsubstituted hydrocarbon **1** is superior to compounds **2** and **3** for observation of exciton split Cotton effects.

In contrast to the case of the intense ^1B_b transition, the Cotton effects due to other weak transitions can not be assigned in a straightforward manner. Compounds **1**, **2**, and **3** show positive first and negative second Cotton effects of medium intensity ($\Delta\varepsilon$ −27) in the region of a ^1L_a transition (around 307 and 283 nm), as if they were based on simple exciton coupling mechanism (Figs. 1, 2, and 3). However, the sequence of the sign of the Cotton effects, *i.e.*, positive and negative from longer wavelength side, is in conflict with the negative exciton chirality predicted by a point dipole approximation method. A similar situation was observed for the weak ^1L_b transition of compound **1** around 325 nm; the sequence of the negative first Cotton effect at 326 nm ($\Delta\varepsilon$ −4.3) and the positive second one at 322 nm ($\Delta\varepsilon$ +5.0) disagrees with the positive exciton chirality between the two long axes of the chromophores. The pattern of the Cotton effects also differs from that of (+)-7,14-dihydro-7,14-ethanodibenz[*a*,*h*]anthracene-15,16-dicarboxylic acid.[7] Thus, the weak ^1L_a and ^1L_b transitions are unsuitable for the exciton chirality method.

The CD spectrum of diketone **8** is of much interest because of its peculiar behavior in the exciton coupling between the two α-tetralone chromophores; the CD spectrum exhibits split Cotton effects of $\Delta\varepsilon_{275.0}=-17.4$ and $\Delta\varepsilon_{252.0}=+24.7$, correospnding to the intramolecular charge transfer transition at 261.0 nm (ε 28300) (Fig. 4).

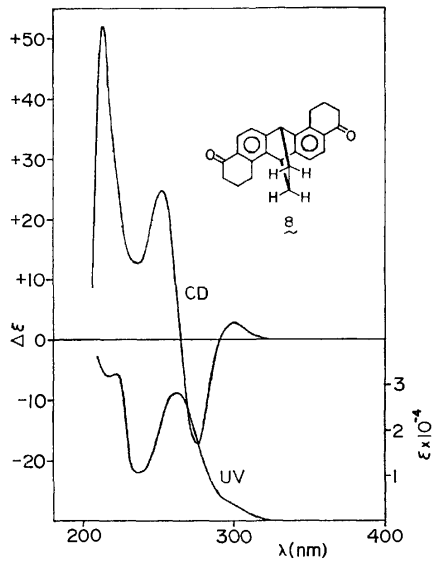

Fig. 4. CD and UV spectra of 1,2,3,7,8,9,10,14-octahydro-7,14-ethanodibenz[*a*,*h*]anthracene-4,11-dione(**8**) in ethanol.

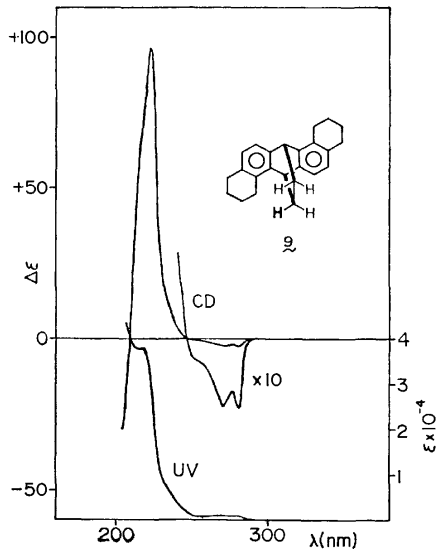

Fig. 5. CD and UV spectra of 1,2,3,4,7,8,9,10,11,14-decahydro-7,14-ethanodibenz[*a*,*h*]anthracene (**9**) in ethanol.

Since the intramolecular charge transfer band has a transition moment along the direction from benzene to carbonyl group,[8] positive exciton chirality is predicted by projection of molecular models. However, the observed sequence of the Cotton effects, *i.e.*, negative and positive, is the reverse of this prediction. A similar case has been reported for (−)-9,10-dihydro-9,10-ethanoanthracene-2,6-diamine.[7] It seems that the homoconjugation effect between the two chromophores makes dominant contribution to the sequence of energy levels.

Hydrocarbon **9** shows a strong positive Cotton effect at 222.5 nm ($\Delta\varepsilon$ +96.4) and a negative one below 209 nm (Fig. 5). Although the extremum of the negative Cotton effect could not be observed, these Cotton effects are presumably due to the exciton coupling of the allowed ^1L_a transition of the benzene chromophores. However, the transition is unsuitable for the exciton chirality method because of the ambiguity of polarization of tetra-alkylated benzene chromophore. Moreover, in the region of a forbidden ^1L_b transition around 280 nm, compound **9** merely exhibits one negative Cotton effect with vibronic structure. It is therefore impossible to determine the absolute configuration of **9** on the basis of these Cotton effects.

For determination of absolute stereochemistries by the circular dichroic method, it is important to chose a suitable electronic transition of suitable chromophores for chiral exciton coupling.

Experimental

General Procedures. Melting points are uncorrected. Spectral data were recorded on the following instruments. NMR: Jeol C-60HL, PMX60, and JNMPS-100 spectrometers; IR: Hitachi EPI-G2 infrared spectrophotometer; MS: Jeol JMS-01 SG-2 mass spectrometer; UV: Hitachi EPS-3T spectrophotometer; CD: Jasco J-20 spectropolarimeter; optical rotations: Jasco DIP-4 spectropolarimeter.

The following CD data are those of the extrema and zero line intersections.

Elemental analyses were carried out in the microanalytical laboratory of our institute.

(3-Benzyloxypropyl)triphenylphosphonium Bromide. To a solution of 2.88 g (11.0 mmol) of triphenylphosphine in 5 ml of dry xylene and 25 ml of ligroine was added 2.29 g (10.0 mmol) of benzyl 3-bromopropyl ether.[9] The reaction mixture was refluxed for 5.5 days under stirring, during which time white crystals deposited. After being cooled to room temp, the crystals were filtered, washed with petroleum ether, and dried *in vacuo*, giving 2.760 g (56%) of the phosphonium salt: IR (KBr) ν_{max} 3025, 2850, 1580, 1480, 1435, 1120, 750, 740, 720, 700 cm^{-1}.

1,5-Bis(4-benzyloxyl-1-butenyl)-9,10-dihydro-9,10-ethanoanthracene (5). To a suspension of 20 g (40.7 mmol) of (3-benzyloxypropyl)triphenylphosphonium bromide in 100 ml of dry THF cooled at −70 °C was added dropwise, over 10 min, 25 ml (1.55 mmol/ml, 38.75 mmol) of a solution of butyl lithium in hexane under nitorgen atmosphere and vigorous stirring. After the dark red reaction mixture had been stirred for 15 min at −70 °C, a solution of 731 mg (2.79 mmol) of (9*R*,10*R*)-(+)-9,10-dihydro-9,10-ethanoanthracene-1,5-dicarbaldehyde (**4**),[4] mp 128.0—129.5 °C, $[\alpha]_D$ +487.3°, in 30 ml of THF was added dropwise. The reaction mixture was stirred overnight, during which time the temperature was allowed to rise to room temp. After addition of water, the mixture was extracted with ethyl acetate and the organic layer was washed with water and brine. Evaporation of the solvent afforded 11.623 g of syrup containing a large amount of triphenylphosphine oxide, which was chromatographed on silica gel giving 1.729 g (*ca.* 100%) of bisbenzyl ether **5**: IR ($CHCl_3$) ν_{max} 3000, 2950, 2850, 1450, 1360, 1100, 700 cm^{-1}; NMR (60 MHz, $CDCl_3$) δ 1.63 (4H, br s, ethane bridge), 2.13—2.80 (4H, m, allylic), 3.33—3.77 (4H, m, α protons of ether), 4.45—4.56 (4H, m, benzylic), 5.43—6.37 (2H, m, bridge head), 6.67—7.46 ppm (20H, m, vinyl and aromatic).

9,10-Dihydro-9,10-ethanoanthracene-1,5-dibutanol (6). A mixture of 1.720 g (3.27 mmol) of bisbenzyl ether **5**, 110 ml of acetic acid, 1.0 ml of concd H_2SO_4, and 1.5 g of 5% palladium on charcoal was magnetically stirred under hydrogen atmosphere at room temp, for 35 h. After removal of the catalyst, the solution was poured into water and extracted with ethyl acetate. The organic layer was washed with water and brine, and evaporated to dryness. To the residue (0.990 g) was added a solution of 2.5 g of KOH in 50 ml of ethanol, and the mixture was gently refluxed for 3 h. After being cooled to room temp, the reaction mixture was poured into water and extracted with ethyl acetate. The organic solution was washed with brine, and evaporated to dryness yielding 0.789 g of syrup, which was subjected to preparative TLC on silica gel ($CHCl_3$–MeOH 20 : 1) giving 315 mg (28%) of glycol **6**: IR ($CHCl_3$) ν_{max} 3600, 3525—3100, 2995, 2920, 2850, 1460, 1425, 1140, 1045 cm^{-1}; NMR (100 MHz, $CDCl_3$) δ 1.68 (14H, m, hydroxyl, ethane bridge, and β and γ protons to hydroxyl group), 2.80 (4H, m, benzylic), 3.68 (4H, m, α protons to hydroxyl group), 4.58 (2H, s, bridge head), 6.82—7.28 ppm (6H, m, aromatic).

9,10-Dihydro-9,10-ethanoanthracene-1,5-dibutyric Acid (7). To a solution of 283 mg (0.807 mmol) of glycol **6** in 35 ml of acetone was added dropwise, under ice-cooling, 2.5 ml (10.03 mmol of oxygen equivalent) of Jones reagent. After being stirred at 0 °C for 3 h, water was added and the mixture was extracted with ethyl acetate. The organic layer was washed with brine, and dried over anhyd Na_2SO_4. Evaporation of the solvent gave 264 mg (86%) of dicarboxylic acid **7** as white solid: IR ($CHCl_3$) ν_{max} 3500—2400, 2930, 1700, 1270, 1140 cm^{-1}; NMR (60 MHz, $CDCl_3$) δ 1.50—2.23 (8H, m, ethane bridge and β protons to carboxyl group), 2.47 (4H, t, J=7.0 Hz, α protons to carboxyl group), 2.83 (4H, t, J=7.0 Hz, benzylic), 4.0 (2H, br s, bridge head), 6.87—7.76 ppm (8H, m, aromatic and carboxyl).

(+)-1,2,3,7,8,9,10,14-Octahydro-7,14-ethanodibenz[a,h]*anthracene-4,11-dione (8).* A mixture of 213 mg (0.563 mmol) of dicarboxylic acid **7** in 3 ml of polyphosphoric acid (prepared by dissolving 10 g of P_2O_5 in 10 ml of 85% H_3PO_4) was heated at 90—100 °C for 3.5 h under stirring. After being cooled to room temp, the reaction mixture was poured into ice-water and extracted with ethyl acetate. The organic layer was washed with brine and dried over anhyd Na_2SO_4. Evaporation of the solvent yielded 178 mg (92%) of diketone **8**: IR ($CHCl_3$) ν_{max} 2950, 1680, 1590, 1330, 1290 cm^{-1}; NMR (100 MHz, $CDCl_3$) δ 1.72 (4H, s, ethane bridge), 2.16 (4H, br quintet, J=7.0 Hz, β protons to carbonyl), 2.62 (4H, dd, J=7.0 and 6.0 Hz, α protons to carbonyl), 3.12 (4H, t, J=6.0 Hz, benzylic), 4.70 (2H, s, bridge head), 7.24 (2H, d, J=7.6 Hz, aromatic meta to carbonyl), 7.88 ppm (2H, d, J=7.6 Hz, aromatic ortho to carbonyl); $[\alpha]_D$ +184.6° (*c* 0.00325, $CHCl_3$); UV (EtOH) λ_{max} 261.0 (ε 28300), λ_{max} 221.5 nm (ε 32700); CD (EtOH) $\Delta\varepsilon_{330.0}$= +0.4, $\Delta\varepsilon_{302.0}$=+2.3 $\Delta\varepsilon_{293.0}$=0.0, $\Delta\varepsilon_{275.0}$=−17.4, $\Delta\varepsilon_{264.5}$= 0.0, $\Delta\varepsilon_{252.0}$=+24.7, $\Delta\varepsilon_{213.5}$=+51.9.

1,2,3,4,7,8,9,10,11,14-Decahydro-7,14-ethanodibenz[a,h]*anthracene (9).* A mixture of 145 mg (0.423 mmol) of diketone **8**, 0.75 ml of hydrazine hydrate, and 5 ml of diethylene glycol was heated at 100 °C for 1 h. Potassium hydroxide (900 mg) was added and the reaction mixture was heated at 200 °C for 2 h, during which time volatile materials were removed by distillation. After being cooled to room temp, the reaction mixture was poured into ice-water, acidified to pH 1 with 2M HCl, and extracted with ethyl acetate. The organic layer was washed with water and brine, and dried over anhyd Na_2SO_4. Evaporation of the solvent afforded 226 mg of syrup, which was chromatographed on silica gel (EtOAc–hexane 1 : 20) giving 35 mg (26%) of hydrocarbon **9**: IR ($CHCl_3$) ν_{max} 2920, 1450, 1430, 1140, 910 cm^{-1}; NMR (60 MHz, $CDCl_3$) δ 1.53—2.03 (12H, m, ethane bridge and methylene), 2.57—3.07 (8H, m, benzylic), 4.51 (2H, s, bridge head), 6.73 and 6.97 ppm (2H each, d, J=7.5 Hz, aromatic): UV (EtOH) λ_{max} 280.0 (ε 900), λ_{max} 270.7 (ε 900), λ_{max} 263.0 (ε 900), λ_{max} 217.5 nm (ε 37900); CD (EtOH) $\Delta\varepsilon_{280.5}$=−2.3, $\Delta\varepsilon_{270.0}$=−2.2, $\Delta\varepsilon_{246.0}$=0.0, $\Delta\varepsilon_{222.5}$= +96.4, $\Delta\varepsilon_{209.0}$=0.0; MS *m/e* 314 ($M^+$).

(+)-7,14-Dihydro-7,14-ethanodibenz[a,h]*anthracene (1).* A solution of 35 mg (0.111 mmol) of hydrocarbon **9** and 300 mg (1.32 mmol) of DDQ in 10 ml of benzene was gently refluxed for 4 h. After being cooled to room temp, excess DDQ and hydroquinone formed were removed by chromatography on silica gel. Evaporation of the solvent gave 29 mg (85%) of compound **1**: mp 234.0—235.5 °C from ethanol; IR (KBr) ν_{max} 3025, 2950, 2850, 1620, 1510 1380, 1170, 1150, 1140, 820, 805, 755, 740, 680, 535, 445 cm^{-1}; NMR (100 MHz, $CDCl_3$) δ 1.82 (4H, s, ethane bridge), 5.34 (2H, s, bridge head), 7.26—7.86 (10 H, m, aromatic), 8.28 ppm (2H, br d, J=8.0 Hz, aromatic); $[\alpha]_D$ +670.0° (*c* 0.02030, $CHCl_3$); UV (EtOH) λ_{max} 325.0 (ε 2500), λ_{max} 283.5 (ε 11100), λ_{max} 232.3 nm (ε 98200); CD (EtOH) $\Delta\varepsilon_{326}$= −4.3, $\Delta\varepsilon_{324}$=0.0, $\Delta\varepsilon_{322}$=+5.0, $\Delta\varepsilon_{304.5}$=+25.5, $\Delta\varepsilon_{291.5}$=0.0, $\Delta\varepsilon_{283.0}$=−35.6, $\Delta\varepsilon_{259.0}$=0.0, $\Delta\varepsilon_{237.0}$=+326.5, $\Delta\varepsilon_{229.5}$=0.0, $\Delta\varepsilon_{224.0}$=−180.5, $\Delta\varepsilon_{205.0}$=−115.0; MS *m/e* (relative intensity) 306 (30, M^+), 278 (100, $M-C_2H_4$).

Found: *m/e* 306.1410. Calcd for $C_{24}H_{18}$: M, 306.1409.

1,1'-(9,10-Dihydro-9,10-ethanoanthracene-1,5-diyl)di-2-propanone (10). To a cooled (−70 °C) suspension of 3.5 g (8.05 mmol) of (1-methoxyethyl)triphenylphosphonium chloride in 30 ml of dry THF was added dropwise, over 10 min,

5.4 ml (1.49 mmol/ml, 8.05 mmol) of a solution of *n*-butyl lithium in hexane under nitrogen with vigorous stirring. After the dark red reaction mixture had been stirred for 20 min at −70 °C, a solution of 175 mg (0.67 mmol) of dialdehyde (+)-**4** in 10 ml of THF was added dropwise. The reaction mixture was stirred for 14 h, during which time the temperature was allowed to rise to room temp. After addition of water, the mixture was extracted with chloroform. The organic layer was washed with water and brine, and evaporated to dryness giving 2.975 g of syrup. The syrup was dissolved in 20 ml of methanol contaning 1 ml of 0.1 M HCl, and the mixture was refluxed for 1 h. After being cooled to room temp, the reaction mixture was poured into water, and extracted with ethyl acetate. The organic layer was washed with water and brine, and evaporated to afford 3.624 g of syrup, which was chromatographed on silica gel in order to remove triphenylphosphine and triphenylphosphine oxide formed. The eluate was evaporated to dryness and the residue was subjected to preparative TLC (EtOAc-hexane, 1 : 4) giving 146 mg (69%) of crystalline diketone **10**: mp 136.5—137.5 °C from ethanol; IR (KBr) ν_{max} 2960, 2950, 1715, 1700, 1360, 1160, 785 cm^{-1}; NMR (100 MHz, $CDCl_3$), δ 1.65 (4H, s, ethane bridge), 2.09 (6H, s, methyl), 3.82 (4H, s, benzylic), 4.49 (2H, s, bridge head), 7.28 (2H, dd, J=7.0 and 2.3 Hz, aromatic), 7.40 (2H, t, J=7.0 Hz, aromatic), 7.55 ppm (2H, dd, J=7.0 and 2.3 Hz, aromatic).

Found: C, 82.99, H, 7.13%. Calcd for $C_{22}H_{22}O_2$: C, 82.98; H, 6.96%.

*Diethyl 9,10-Dihydro-β,β'-dimethyl-9,10-ethanoanthracene-1,5-dicrotonate (**11**).* To a suspension of 331 mg (13.8 mmol) of sodium hydride in dry THF was added dropwise under nitrogen and ice-cooling a solution of 4.65 g (20.7 mmol) of triethylphosphonoacetate in 2 ml of dry THF. After the clear brown reaction mixture had been stirred at room temp for 30 min, a solution of 438 mg (1.38 mmol) of diketone **10** in 1 ml of THF was added dropwise, and the mixture was stirred overnight. After addition of water, the reaction mixture was extracted with ether. The ethereal solution was washed with water and brine, and dried over anhyd Na_2SO_4. Evaporation of the solvent gave 757 mg of syrup, which was chromatographed on silica gel in order to remove excess triethylphosphonoacetate, giving 356 mg (56%) of diester **11** as syrup: IR (neat) ν_{max} 2950, 1733, 1711, 1215, 1145, 1045 cm^{-1}; NMR (60 MHz, $CDCl_3$) δ 1.05—1.45 (6H, m, methyl), 1.50—1.75 (4H, br s, ethane bridge), 1.45—2.30 (6H, m, vinyl methyl), 3.03—3.62 (4H, m, benzylic), 3.90—4.20 (6H, m, bridge head and methylene of ethoxyl group), 5.30—5.85 (1H, m, vinyl), 6.40—7.40 ppm (7H, m, vinyl and aromatic). Thus, the NMR spectrum indicates that diester **11** is a *cis,trans* isomeric mixture.

*Diethyl 9,10-Dihydro-β,β'-dimethyl-9,10-ethanoanthracene-1,5-dibutyrate (**12**).* A mixture of 356 mg (0.778 mmol) of diester **11** and 20 mg of PtO_2 in 20 ml of ethanol was magnetically stirred under hydrogen atmosphere at room temp for 4 h. Removal of the catalyst by filtration, and evaporation of the solvent afforded 348 mg (100%) of an epimeric mixture of diester **12** as syrup: IR (neat) ν_{max} 2950, 1715, 1155, 755 cm^{-1}; NMR (60 MHz, $CDCl_3$) δ 0.70—0.96 (6H, m, methyl), 1.05—1.45 (6H, m, methyl of ethoxy), 1.65 (4H, br s, ethane bridge), 2.10—2.85 (10H, m, methylene and methine) 3.85—4.35 (4H, m, methylene of ethoxy), 4.35—4.70 (2H, br s, bridge head), 6.46—7.28 ppm (6H, m, aromatic).

*9,10-Dihydro-β,β'-dimethyl-9,10-ethanoanthracene-1,5-dibutyric Acid (**13**).* Diester **12** (348 mg, 0.754 mmol) was dissolved in 20 ml of a 5% ethanolic KOH solution and the solution was gently refluxed for 3.5 h. After being cooled to room temp, the reaction mixture was acidified with 2 M HCl under ice-cooling, and extracted with chloroform. The organic layer was washed with water and brine, and dried over anhyd Na_2SO_4. Evaporation of the solvent yielded 314 mg (100%) of dicarboxylic acid **13** as syrup: IR (CCl_4) ν_{max} 3650—2200, 2950, 1705, 1430, 1405, 1290, 1220, 1140, 940 cm^{-1}: NMR (60 MHz, $CDCl_3$) δ 0.60—1.40 (8H, m, methyl and methine), 1.65 (4H, br s, ethane bridge), 1.90—2.95 (8H, m, methylene), 4.55 (2H, br s, bridge head), 6.50—7.30 (6H, m, aromatic), 8.20—8.90 ppm (2H, br s, carboxyl).

1,2,3,7,8,9,10,14-Octahydro-2,9-dimethyl-7,14-ethanodibenz[a,h]*anthracene-4,11-dione (**14**).* A mixture of 275 mg (0.678 mmol) of dicarboxylic acid **13** in 9 ml of polyphosphoric acid (prepared in the same way as described for diketone **8**) was heated at 90 °C for 1 h under stirring. After being cooled to room temp, the reaction mixture was poured into ice-water, and extracted with chloroform. The organic layer was washed with water and brine, and dried over anhyd Na_2SO_4. Evaporation of the solvent gave 281 mg of syrup, which was chromatographed on silica gel to yield 135 mg (50%) of diketone **14** as syrup: IR (CCl_4) ν_{max} 2950, 1685, 1595, 1580, 1285, 1110 cm^{-1}; NMR (100 MHz, $CDCl_3$) δ 1.23 (6H, d, J=6.0 Hz, methyl), 1.72 (4H, s, ethane bridge), 2.19—2.79 (8H, m, methylene and/or methine), 3.12—3.48 (2H, m, methylene or methine), 4.72 (2H, s, bridge head), 7.24 (2H, d, J=7.5 Hz, aromatic meta to carbonyl), 7.85 ppm (2H, d, J=7.5 Hz, aromatic ortho to carbonyl).

1,2,3,4,7,8,9,10,11,14-Decahydro-2,9-dimethyl-7,14-ethanodibenz[a,h]*anthracene (**15**).* A solution of 127 mg (0.342 mmol) of diketone **14** and 5 ml of hydrazine hydrate in 50 ml of diethylene glycol was heated at 100 °C for 30 min. Potassium hydroxide (2.5 g) was added and the reaction mixture was heated at 200 °C for 3 h, during which time volatile substances were distilled. After being cooled to room temp, the reaction mixture was poured into ice-water, acidified with 2 M HCl, and extracted with ether. The ethereal layer was washed with water and brine. Evaporation of the solvent afforded 371 mg of a mixture of yellow crystals and oil, which was recrystallized from methanol giving 68 mg (58%) of hydrocarbon **15**: mp 176.0—177.0 °C; IR (KBr) ν_{max} 2940, 2920, 2360, 1475, 1455, 1435, 825 cm^{-1}; NMR (100 MHz, $CDCl_3$) δ 1.08 (6H, d, J=6.5 Hz, methyl), 1.0—2.0 (6H, m, methylene and methine), 1.62 (4H, s, ethane bridge), 2.31 (2H, dd, J=16.8 and 10.6 Hz, benzylic), 2.73 (4H, m, benzylic), 3.06 (2H, dt, J=16.8 and 4.5 Hz, benzylic), 4.49 (2H, s, bridge head), 6.75 (2H, d, J=7.6 Hz, aromatic), 6.98 ppm (2H, d, J=7.6 Hz, aromatic).

(+)-7,14-Dihydro-2,9-dimethyl-7,14-ethanodibenz[a,h]*anthracene (**2**).* A mixture of 67 mg (0.196 mmol) of hydrocarbon **15** and 426 mg (1.88 mmol) of DDQ in 10 ml of benzene was gently refluxed for 4 h. After being cooled to room temp, excess DDQ and hydroquinone were removed by chromatography on silica gel. The eluate was evaporated and the residue was subjected to preparative TLC (petroleum ether–EtOAc 100 : 3) yielding 47 mg (72%) of hydrocarbon **2**: mp 209.5—211 °C from ethanol; IR (KBr) ν_{max} 3040, 2920, 2850, 1625, 830, 557 cm^{-1}; NMR (100 MHz, $CDCl_3$) δ 1.76 (4H, s, ethane bridge), 2.55 (6H, s, methyl), 5.26 (2H, s, bridge head), 7.15 (2H, dd, J=8.2 and 2.0 Hz, 3-H and 10-H), 7.40 and 7.49 (2H each, d, J=9.0 Hz, 5-H, 6-H, 12-H, and 13-H), 7.64 (2H, d, J=8.2 Hz, 4-H and 11-H), 8.01 ppm (2H, br s, 1-H and 8-H); $[\alpha]_D$ +786° (c 0.01005, 10% dioxane in ethanol); UV (0.18% dioxane in ethanol) λ_{max} 326.3 (ε 1000), λ_{max} 286.5 (ε 11700), λ_{max} 236.8 (ε 98100), λ_{max} 226.0 nm (ε 95300); CD (0.18% dioxane in ethanol) $\Delta\varepsilon_{326.5}=-2.3$, $\Delta\varepsilon_{324.5}=0.0$, $\Delta\varepsilon_{307.0}=+25.1$, $\Delta\varepsilon_{292.0}=0.0$, $\Delta\varepsilon_{281.0}=-18.7$, $\Delta\varepsilon_{261.0}=0.0$, $\Delta\varepsilon_{240.6}=+371.5$, $\Delta\varepsilon_{232.8}=0.0$,

$\Delta\varepsilon_{227.0}=-149.4$, $\Delta\varepsilon_{210.0}=-111.3$; MS *m/e* (relative intensity) 334 (35, M^+), 306 (100, $M-C_2H_4$).

Found: *m/e* 334.1727. Calcd for $C_{26}H_{22}$: M, 334.1720. Found: C, 92.82; H, 6.75%. Calcd for $C_{26}H_{22}$: C, 93.37; H, 6.63%.

7,14-Dihydro-2,4,9,11-tetramethyl-7,14-ethanodibenz[a,h]*anthracene (3).* To a solution of 30 mg (0.0812 mmol) of diketone **14** in 2 ml of dry THF was added dropwise 4 ml of an ethereal solution of methyl lithium (2.0 mmol) under nitrogen and ice-cooling. The reaction mixture was stirred for 2 h. After addition of ice-water, the mixture was extracted with ether. The ethereal layer was washed with water and brine, dried over anhyd Na_2SO_4, and evaporated to dryness giving 24 mg of syrup. The residue was dissolved in 20 ml benzene, to which 82 mg (0.36 mmol) of DDQ was added. The reaction mixture was gently refluxed for 3 h under stirring. After being cooled to room temp, the mixture was poured into water and extracted with ethyl acetate. The organic layer was washed with water, 1% aq KOH, and brine, and dried over anhyd Na_2SO_4. Evaporation of the solvent afforded 39 mg of syrup, which was subjected to preparative TLC on silica gel (EtOAc-hexane 1 : 20) yielding 5.5 mg (19%) of hydrocarbon **3**: mp 124.0—126.0 °C from ethanol; IR (KBr) ν_{max} 2940, 2850, 1620, 1150, 850 cm^{-1}; NMR (100 MHz, $CDCl_3$) δ 1.82 (4H, s, ethane bridge), 2.54 (6H, s, 2-CH_3 and 9-CH_3), 2.61 (6H, s, 4-CH_3 and 11-CH_3), 5.32 (2H, s, bridge head), 7.10 (2H, s, 3-H and 10-H), 7.53 (2H, d, J=8.3 Hz, 6-H and 13-H), 7.73 (2H, d, J=8.3 Hz, 5-H and 12-H), 7.96 ppm (2H, s, 1-H and 8-H); UV (EtOH) λ_{max} 293.0 (ε 16000), λ_{max} 238.0 nm (ε 116200); CD (EtOH) $\Delta\varepsilon_{311.5}=+27.5$, $\Delta\varepsilon_{296.5}=0.0$, $\Delta\varepsilon_{283.0}=-27.1$, $\Delta\varepsilon_{255.5}=0.0$, $\Delta\varepsilon_{242.0}=+340.3$, $\Delta\varepsilon_{230.5}=0.0$, $\Delta\varepsilon_{225.0}=-88.0$, $\Delta\varepsilon_{212.5}=-139.3$.

The authors thank Dr. Hiroshi Hayashi, Asahi Chemicals Industry, Co., for measurements of the mass spectra. The present work was partially supported by a Grant-in-Aid for Scientific Research from the Ministry of Education.

References

1) N. Harada and K. Nakanishi, *Acc. Chem. Res.*, **5**, 257 (1972).

2) N. Harada, S. L. Chen, and K. Nakanishi, *J. Am. Chem. Soc.*, **97**, 5345 (1975) and references cited therein.

3) N. Harada, Y. Takuma, and H. Uda, *J. Am. Chem. Soc.*, **98**, 5408 (1976).

4) N. Harada, Y. Takuma, and H. Uda, *Bull. Chem. Soc. Jpn.*, **50**, 2033 (1977) and references cited therein.

5) H. H. Jaffé and M. Orchin, "Theory and Applications of Ultraviolet Spectroscopy," John Wiley & Sons, Inc., New York (1966), p. 305; see also linear dichroism data, A. Davidson and B. Nordén, *Tetrahedron Lett.*, **1972**, 3093.

6) A similar CD spectrum of ^1B_b transition has been reported for 7,14-dihydro-7,14-ethanodibenz[*a,h*]anthracene-15,16-dicarboxylic acid, the absolute configuration of which was determined by kinetic resolution methods.[7]

7) S. Hagishita and K. Kuriyama, *Tetrahedron*, **28**, 1435 (1972).

8) J. Tanaka, S. Nagakura, and M. Kobayashi, *J. Chem. Phys.*, **24**, 311 (1956) and references cited therein; see also the data of polarized excitation spectrum of phosphorescence, R. Shimada and L. Goodman, *J. Chem. Phys.*, **43**, 2027 (1965).

9) L. I. Smith and J. A. Sprung, *J. Am. Chem. Soc.*, **65**, 1276 (1943).

Peptide Syntheses with Proteinases. Fragment Condensation of ZLeuGlnGlyOH or ZGlnGlyOH with HLeuValNH$_2$ Using Metalloproteinases

Yoshikazu Isowa, Tetsuya Ichikawa, and Muneki Ohmori
Sagami Chemical Research Center, Sagamihara, Kanagawa 229
(Received June 16, 1977)

The crude preparations of microbial metalloproteinase from *Bacillus subtilis var. amyloliquefaciens* (Prolisin) catalyzed the condensation of ZLeuGlnGlyOH or ZGlnGlyOH with HLeuValNH$_2$ in the presence of the serine-proteinase inhibitor from potatoes to give the corresponding Z-penta or tetra-peptide amide in good yields in an aqueous buffer solution. Two other metalloproteinases, from *Bacillus thermoproteoliticus* (Thermolysin or Thermoase) and *Streptomyces caespitosus* (Tacynase N), also catalyzed this reaction; however, they gave poorer results than Prolisin. The yields of the coupling products were affected most by the concentration of the substrates, among the several factors investigated. Addition of a small amount of an organic solvent sometimes promoted the yield for this method.

In previous papers[1] we reported that the peptide linkage is catalytically formed by proteinases from two suitably protected amino acids and peptides and that the catalytic specificities of the enzymes are similar to those in the peptide hydrolysis. Since microbial metalloproteinases hydrolyze specifically the peptide linkage with an amino acid residue carrying a hydrophobic side chain at the amino side of the linkage,[2] they are expected to catalyze the condensation between a C-terminal protected peptide which has this amino acid residue as its N-terminal and an N-terminal protected peptide. Moreover, the proteinases do not usually catalyze the hydrolysis of esters or amides of amino acids or peptides,[2] so that appropriate use of them is very effective for the peptide synthesis.

We investigated their catalytic ability in the peptide bond formation in accordance with their characteristics in hydrolysis. In this article we report that three microbial metalloproteinases catalyze the condensation of ZGlnGlyOH or ZLeuGlnGlyOH with HLeuValNH$_2$ to give ZGlnGlyLeuValNH$_2$ (Secretin 24—27) or ZLeuGlnGlyLeuValNH$_2$ (Secretin 23—27) in good yields. The crude crops from the reaction mixture were almost pure without further purification. Furthermore, it is noticeable that even crude preparations of metalloproteinase were effective in the reaction, under the condition of using serineproteinase inhibitor from potatoes.

Materials and Methods

All amino acids used are of the L configuration. The following abbreviations are used: PU=protease unit; EDTA =ethylenediaminetetraacetic acid; Tris=tris(hydroxymethyl)-methanamine; Z=benzyloxycarbonyl; BOC=*t*-butoxycarbonyl; OSu=*N*-hydroxysuccinimide ester; DCCI=dicyclohexylcarbodiimide; DCU=*N,N'*-dicyclohexylurea; HOBt=1-hydroxybenzotriazole. Thin layer chromatography was performed on precoated TLC plates Silica Gel 60 F254 (from Merck) using the following solvent system: *s*-BuOH-3% aqueous ammonia (8 : 3 by vol). See Ref. 1b for other analytical procedures, execpt that here the UV spectra for the assaying of the protease activity of the proteinases were determined on a Hitachi Recording Spectrophotometer 323.

Serineproteinase Inhibitor from Potatoes. The crude inhibitor (115 g) was obtained by the method of Melville and Ryan[3] from potatoes (60 kg) and used without further purification. This inhibitor will be called potato inhibitor here after in this article.

Proteinases. All proteinases were used without further purification. Protease activity was assayed at pH 7.2 using Hammarsten casein (Merck) by the method of Tsuru *et al.*[4] Thermolysin and Thermoase were dissolved in 0.2 M AcONa–0.2 M Ca(OAc)$_2$ aqueous solution (pH 8.1) and the others in 5×10^{-3} M Ca(OAc)$_2$ aqueous solution. Protease activity was also assayed in the presence of 1/500 M EDTA or of potato inhibitor.

Prolisin:[5] Two lots of Prolisin obtained from *Bacillus subtilis var. amyloliquefaciens* were purchased from Ueda Chemical Co. (Neyagawa, Osaka) and characterized as follows. One of the preparations, which was manufactured May 19, 1976 and stated to have a protease activity of 7.7×10^5 PU/g, was demonstrated to contain metalloproteinase, serineproteinase, amylase, and other proteins and showed the protease activity of 1.9×10^6 PU/g according to Tsuru's method. This specimen of the Prolisin will be called Prolisin A hereafter in this article. The protease activity was 1.45×10^6 PU/g in the presence of potato inhibitor in 10 times the weight of the enzyme (Table 1) and was 5.1×10^5 PU/g in the presence of 1/500 M EDTA. Hence the rough ratio between metallo- and serineproteinase was 14 : 5 PU/PU. The other preparation, which was manufactured on February 8,

Table 1. Protease activity of proteinases in the presence of potato inhibitor

	P.I.: Proteinase wt/wt	Activity PU/g
Prolisin A	0	1.90×10^6
	1:1	1.73
	5:1	1.60
	10:1	1.49
	50:1	1.49
Prolisin B	0	7.2×10^5
	1:2	5.6
	1:1	5.4
	3:2	5.4
Tacynase N	0	2.60×10^5
	1:1	2.47
	3:1	2.37
	5:1	2.33
	10:1	2.30
Thermoase	0	4.0×10^6
	1:1	3.7
	3:1	3.2
	5:1	3.1

1975 and stated to have the activity of 3.0×10^5 PU/g, was found to contain metalloproteinase, serineproteinase, a small amount of amylase, other proteins, and starch as an excipient in about 65% of the weight and exhibited a protease activity of 7.2×10^5 PU/g according to Tsuru's method. This specimen of the Prolisin will be called Prolisin B hereafter in this article. The protease activity was 5.4×10^5 PU/g in the presence of potato inhibitor in equal weight of the enzyme (Table 1) and was 1.6×10^5 PU/g in the presence of 1/500 M EDTA. Hence the rough ratio between metallo- and serineproteinase was 27 : 8 PU/PU.

Tacynase N[6] *(with a Stated Protease Activity of* $\geqslant10^5$ *PU/g)*: This enzyme preparation obtained from *Streptomyces caesptitosus* was purchased from Kyowa Hakko Kogyo Co. (Tokyo, Japan) and found to show a protease activity of 2.6×10^5 PU/g according to Tsuru's method. The enzyme was slightly inhibited by potato inhibitor in 10 times the weight of the enzyme (2.3×10^5 PU/g) (Table 1) and almost completely inhibited by 1/500 M EDTA ($<6\times10^3$ PU/g)

Thermolysin[7] *and Thermoase*: Both enzyme preparations obtained from *Bacillus thermoproteoliticus* were purchased from Daiwa Kasei Co. (Osaka, Japan). Thermoase was an unpurified specimen and its protease activity, which was stated to be 1.6×10^6 PU/g, was found to be 4.0×10^6 PU/g according to Tsuru's method and was reduced to 3.1×10^6 PU/g in the presence of potato inhibitor in 5 times the weight of the enzyme (Table 1) and to 8.5×10^5 PU/g in the presence of 1/500 M EDTA. Thermolysin was the enzyme purified from Thermoase; its protease activity, which was stated to be 8.0×10^6 PU/g, was shown to be 1.8×10^7 PU/g according to Tsuru's method.

Detection and Inhibition of Esterase Action of Crude Proteinase Preparations. The esterase action was detected by observing the drop in pH, on addition of proteinase, of a solution of 0.1 M HPheOEt·HCl (10 ml). The pH had been previously adjusted at 7.0 with 1 M NaOH. The esterase action of Prolisin A,B, and Thermoase were repressed almost completely by the potato inhibitor in 3 times, equal, and equal weight of the enzyme (Table 2); however, that of Tacynase N was not completely inhibited by the potato inhibitor even in 5 times the weight of the enzyme (Table 2). Accordingly, the enzymatic syntheses of peptides with Prolisin A, B, and Thermoase were carried out in the presence of the potato inhibitor in 3 times, equal, and equal weight of the enzyme for 3—17 h, while that with Tacynase N in the presence of the inhibitor in equal weight of the enzyme for 3 h. Thermolysin has scarcely any esterase action, so that the condensation with Thermolysin was carried out in the absence of the potato inhibitor.

Table 2. Inhibitory effect of potato inhibitor on the esterase action of proteinases[a]

	P.I.: Enzyme wt/wt	pH		
		0.5 h	3 h	17 h
Prolisin A	0	4.8	4.1	3.9
	3:1	6.9	6.8	6.4
	5:1	7.0	6.9	6.4
		3/4 h	4 h	20 h
Prolisin B	0	4.6	4.1	4.0
	1:2	6.9	6.8	6.8
	1:1	6.9	6.9	6.9
		1 h	2.5 h	8 h
Tacynase N	0	6.6	5.7	4.8
	1:1	6.7	6.2	5.6
	5:1	6.8	6.5	6.0
		1.5 h	3 h	24 h
Thermoase	0	6.2	5.4	4.1
	1:1	6.9	6.7	6.3
	2:1	6.9	6.8	6.5

a) Amounts of each enzyme used: Prolisin A, 0.035 g; Prolisin B, 0.2 g; Tacynase N, 0.2 g; Thermoase, 0.1 g.

The Enzymatic Syntheses of Peptides (General Procedure). Appropriate amounts of an enzyme and, when necessary, of potato inhibitor were dissolved in an adequate volume of buffer (unless otherwise stated 0.2 M Tris–HCl buffer (pH 8, containing 5×10^{-2} M $Ca(OAc)_2$) was used) and the undissolved materials were filtered off if required. The solution was added to a mixture of a carboxyl and an amine component. Then 4 M NaOH of equimolar quantity with the amine component was added. The mixture was stirred at 38—40 °C for a certain period. The product was collected on a filter by suction, washed thoroughly in succession with 1 M aqueous ammonia, 1 M HCl, and water, and dried *in vacuo* over P_2O_5 at room temperature.

Peptide Syntheses According to the Chemical Methods. Ordinary chemical syntheses were used to prepare some peptides for substrates in the enzymatic synthesis and for the purpose of identification of the products by comparison.

HValNH₂·HCl (I): ZValNH$_2$ (50.0 g, 0.2 mol) was hydrogenated over 10% Pd–C (2 g) in MeOH (300 ml) containing 1 M HCl (21 ml). After filtering the catalyst, the filtrate was evaporated to give a white powder, which was recrystallized from MeOH and ether: yield 29.3 g (96%); mp 281—282 °C (dec); $[\alpha]_D^{24}$ +34.1° (*c* 1, MeOH).

Found: C, 39.52; H, 8.77; N, 18.38; Cl, 23.08%. Calcd for $C_5H_{13}N_2OCl$: C, 39.35; H, 8.58; N, 18.36; Cl, 23.23%.

ZLeuValNH₂ (II): To a cooled solution (−10 °C) of ZLeuOH (103.5 g, 0.39 mol) and HValNH$_2$·HCl (59.3 g, 0.39 mol) in DMF (1500 ml) were added *N*-methylmorpholine (41 g, 0.41 mol), HOBt (58.1 g, 0.43 mol), and DCCI (88.6 g, 0.43 mol) dissolved in DMF; the mixture was stirred at 0 °C for 3 h and at room temperature for 17 h. After filtering DCU, the filtrate was concentrated and water was added. The slightly brownish precipitate obtained was washed successively with 1 M aqueous ammonia, 1 M HCl, and water, air dried, and dried *in vacuo* over P_2O_5 at 60 °C to give a white powder: yield 103.3 g (72.9%); mp 238—239.5 °C; $[\alpha]_D^{20}$ −24.2° (*c* 1, AcOH) (lit,[8] mp 231—232 °C; $[\alpha]_D^{20}$ −24.4±0.5° (*c* 1.8, AcOH)).

HLeuValNH₂·HCl (III): ZLeuValNH$_2$ (17 g, 0.0468 mol) was hydrogenated over 10% Pd–C (2 g) in MeOH (200 ml) containing 1 M HCl (50 ml). After the reaction, the catalyst was removed by filtration and the filtrate was evaporated to give a white powder, which was recrystallized from MeOH and ether: yield 10.8 g (86.9%); mp 153—155 °C; $[\alpha]_D^{26}$ +28.2° (*c* 1, AcOH). Found: C, 49.87; H, 9.05; N, 15.89; Cl 13.15%. Calcd for $C_{11}H_{24}N_3O_2Cl$: C, 49.71; H, 9.10; N, 15.81; Cl, 13.34%.

ZGlnGlyOH (IV): This was obtained from ZGlnGlyOEt (18.3 g, 0.05 mol) according to the procedure described by E. Wünsch *et al.*:[8] yield 15.1 g (90%); mp 185—187 °C; $[\alpha]_D^{28}$ −2.8° (*c* 1, DMF) (lit,[8] mp 183 °C; $[\alpha]_D^{20}$ −3.1±0.5° (*c* 2, DMF)).

ZGlnGlyLeuValNH₂ (V): This was obtained from ZGlnGlyOH (20.4 g, 0.06 mol) and HLeuValNH$_2$·HCl (15.9 g, 0.06 mol) according to the procedure described by E. Wünsch *et al.*:[8] yield 25.5 g (77.5%); mp 243.5—246 °C; $[\alpha]_D^{30}$ −26.0° (*c* 1, AcOH); R_f 0.75. (lit,[8] mp 239.5—240.5 °C; $[\alpha]_D^{20}$ −24.6±0.5° (*c* 1.8, AcOH)). Found: C, 56.91; H, 7.39; N, 15.17%. Calcd for $C_{26}H_{40}N_6O_7$: C, 56.92; H, 7.35; N, 15.32%.

ZLeuGlnGlyOEt (VI): This was obtained according to the procedure described by E. Wünsch *et al.*[8] A solution of HGlnGlyOEt·HCl (0.05 mol equivalent) was obtained by the hydrogenation of ZGlnGlyOEt (18.2 g, 0.05 mol) over 10% Pd-C (2 g) in DMF–H_2O (250 : 70 ml) with 1 M HCl (50 ml) added portionwise to keep the solution at pH 4. After the reaction the catalyst was filtered off and to the filtrate was added DMF (100 ml). To the cooled solution (−10 °C) were added Et_3N (5 g, 0.05 mol), pyridine (3.9 g, 0.05 mol), and ZLeuOSu (18.1 g, 0.05 mol) dissolved in DMF. The mixture was stirred at −10 °C for 2 h and at room temperature for 40 h. The suspension was concentrated to give a white powder, which was washed with water thoroughly, air dried, and dried *in vacuo* over P_2O_5 at 60 °C: yield 23.0 g (96%); mp 214 °C; $[\alpha]_D^{25}$ −14.5° (*c* 1, DMF).

Found: C, 57.88; H, 7.16; N, 11.58%. Calcd for $C_{23}H_{34}N_4O_7$: C, 57.72; H, 7.16; N, 11.71%.

ZLeuGlnGlyOH (VII): A solution of ZLeuGlnGlyOEt (19.5 g, 0.04 mol) in DMF (300 ml) at 50 °C, after addition of MeOH–H_2O (100 : 50 ml), was allowed to cool to room temperature. 1 M NaOH (52 ml) was then added portionwise over 1 h, and the solution was stirred at room temperature for 2 h. After the reaction, water (100 ml) was added and undissolved materials were filtered off. The filtrate was acidified by adding Amberlite CG120 (H form, 3.5 mmol/g, 15 g) and stirring for 10 min, then the resin was filtered off. The filtrate was concentrated to syrup, which was triturated with water. The precipitate which formed was collected by suction, washed with water, air dried, and dried *in vacuo* over P_2O_5 at 60 °C: yield 16.3 g (84%); mp 185—186.5 °C; $[\alpha]_D^{20}$ −13.8° (*c* 1, DMF).

Found: C, 56.13; H, 6.89; N, 12.55%. Calcd for $C_{21}H_{30}N_4O_7$: C, 55.99; H, 6.71; N, 12.44%.

ZLeuGlnGlyLeuValNH$_2$ (VIII): *a) HGlnGlyLeuValNH$_2$·HCl (IX).* This was obtained according to the procedure described by E. Wünsch *et al.*[8] except that DMF–H_2O (3 : 1) was used as the solvent of hydrogenation in place of MeOH–H_2O (3 : 1). ZGlnGlyLeuValNH$_2$ (5.5 g, 0.01 mol) was hydrogenated in DMF–H_2O (3 : 1, 200 ml) over 10% Pd-C (0.5 g) with the addition of two 5 ml portions of 1 M HCl. The catalyst was removed and the filtrate was used immediately in the subsequent step.

b). VIII: To the cooled solution (−10 °C) obtained from the above procedure were added Et_3N (1.0 g, 0.01 mol), pyridine (0.8 g, 0.01 mol), and ZLeuOSu (4.3 g, 0.012 mol) dissolved in DMF (30 ml). The mixture was stirred for 4 h at −10 °C and for 36 h at room temperature. The reaction mixture was concentrated to give a gelatinous mass, which was washed with water three times, air dried, then washed with boiling ethyl acetate (100 ml), air dried, and dried *in vacuo* over P_2O_5 at 60 °C: yield 6.2 g (93.7%); mp 273—275 °C; $[\alpha]_D^{28}$ −33.9 ° (*c* 0.5, AcOH); R_f 0.65.

Found: C, 57.99; H, 7.53; N, 14.58%. Calcd for $C_{32}H_{51}N_7O_8$: C, 58.07; H, 7.77; N, 14.82%.

BOCLeuGlnGlyLeuValNH$_2$ (X): It was synthesized by the same procedure as in the case of the compound VIII. The compound IX obtained from the compound V (2.75 g, 0.005 mol) using 10% Pd-C (0.3 g) and 1 M HCl (5 ml) in DMF–H_2O (3 : 1, 100 ml) was allowed to react with BOCLeuOSu (2 g, 0.006 mol) in the presence of Et_3N (0.5 g) and pyridine (0.4 g): yield 2.7 g (87%); mp 237—238 °C (dec); $[\alpha]_D^{25}$ −18.4° (*c* 0.5, DMF) (lit,[8] mp 234—235 °C (dec); $[\alpha]_D^{20}$ −19.4° (*c* 1, DMF)). Found: C, 55.29; H, 8.52; N, 15.84%. Calcd for $C_{29}H_{53}N_7O_8$: C, 55.48; H, 8.51; N, 15.62%.

Results and Discussion

I. The Influence of the Nature of Buffer Solutions upon the Protease Activity of Metalloproteinase. *Bacillus subtilis* metalloproteinase had been reported to be disadvantageously affected by phosphate ions,[9] so the effect of three buffers (**A** McIlvaine, pH 7; **B** Tris–HCl, pH 7; **C** citrate buffer, pH 6.5) on the protease activity of the metalloproteinase in Prolisin was investigated using varying concentrations in the presence of potato inhibitor to suppress serineproteinase action (Table 3). Tris–HCl buffer solution reduced the activity least among the three and kept about 75% of the initial activity even after 23 h. The other two buffers were inadequate as a medium for the enzymatic synthesis of peptides. Moreover, since metalloproteinases are generally most active in the neutral pH region from 6—9.0 and the pH of the medium slightly fell toward the acidic side during the course of the reaction, it is recommended to use a buffer adjusted to the alkaline side, pH 8 being the best, and in a concentration of 0.2—0.4 M to maintain the correct pH.

Table 3. Influence of three buffers on the protease activity of Prolisin B[a]

	Buffer concn (M)		Activity remaining (%)			
			1 h	4 h	6 h	23 h
	Na_2HPO_4	Citric acid				
A	0.4	0.2	71	37	32	0
	0.2	0.1	74	55	48	0
	0.1	0.05	83	66	58	0
B	0.2		94	89	83	72
	0.1		95	91	83	75
	0.05		95	93	84	79
C	0.1		69	38	25	0
	0.05		88	68	59	21

a) A mixture of Prolisin B (0.1 g) and the potato inhibitor (0.1 g) was incubated in each buffer solution containing 2×10^{-3} M $Ca(OAc)_2$ (10 ml) at 40 °C and the protease activity was assayed at intervals.

II. The Effect of Potato Inhibitor on Commercial Crude Metalloproteinases.[10] The esterase action of crude metalloproteinase preparations probably is due to some serineproteinase which was present in the preparations. Since the serineproteinase, in addition to esterase action, shows amidase action, the crude metalloproteinases in such a condition are inadequate for the present study and must be used in the presence of some suitable serineproteinase inhibitor. Among several serineproteinase inhibitors, the potato inhibitor[11] was chosen and used, for it is attractive to use and not toxic. Consequently, the condensation between ZGlnGlyOH and HLeuValNH$_2$ with Prolisin in the presence of potato inhibitor gave the product in 75% or above of the theoretical yield (see below). On the other hand, the above reaction in the absence of the inhibitor gave a product which showed 3 spots on TLC, one of which corresponded to those of the object matter. Furthermore, though the amount of the product gradually

increased with time and reached a maximum after 3 h, it was far less than that from the reaction in the presence of the potato inhibitor.

III. Fragment Condensation of ZGlnGlyOH or ZLeuGlnGlyOH with HLeuValNH$_2$ by the Aid of Prolisin.

The enzymic condensation between ZGlnGlyOH and HLeuValNH$_2$ (Reaction 1) or ZLeuGlnGlyOH and HLeuValNH$_2$ (Reaction 2) was examined in the search for suitable coupling conditions with respect to the substrate concentration, the enzyme concentration, the reaction period, the reaction temperature, the pH of the buffer, the effect of organic solvent, and the nature of amino-protecting groups, Z or BOC.

1) The Influence of the Substrate Concentration on the Yield: When Reaction 1 was carried out at the substrate concentration of 300 mM in the presence of Prolisin A in 0.2 M Tris-HCl buffer (pH 8), the condensation product was obtained in 71 % of the theoretical yield; however, the reaction at the substrate concentration of 73 mM gave a surprisingly low yield of the product under otherwise the same conditions (Fig. 1). Reaction 2 exhibited results similar to those of Reaction 1 (Fig. 1). These findings indicate that the substrates in higher concentrations will gave better results in these reactions, but that too high a substrate concentration interrupts the progress of the reaction owing to rapid caking of the reaction mixtures.

2) The Influence of the Enzyme Concentration on the Yield: Figure 2 shows the results of Reaction 1 with enzyme concentrations increasing from 0.3—19 mg/ml at 167 (a), 235 (b), and 300 mM (c) substrate concentrations under conditions similar to those described under the heading III-1. It can safely be said that the optimal yield is reached at a rather low concentration of enzyme, *i.e.*, 1.6—3.7 mg/ml.

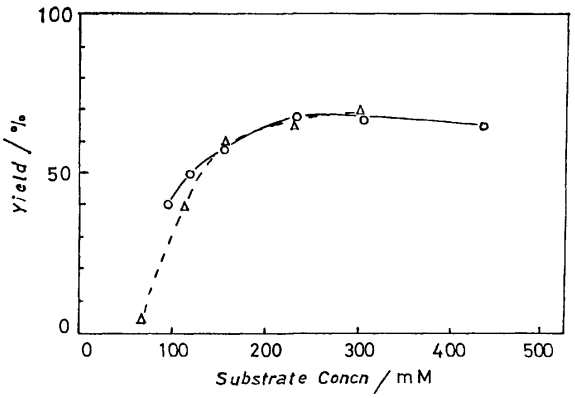

Fig. 1. The influences of substrate concentrations on the syntheses of ZGlnGlyLeuValNH$_2$ with Prolisin A and of ZLeuGlnGlyLeuValNH$_2$ with Prolisin B. Buffer solution used: 0.2 M Tris-HCl (pH 8, containing 5×10^{-2} M Ca(OAc)$_2$). △----△: An equimolar amount of ZGlnGlyOH and HLeuValNH$_2$·HCl (73—300 mM respectively), Prolisin A (4.25 mg/ml), and potato inhibitor (12.5 mg/ml) were used. The reactions were carried out according to the general procedure in the buffer (4 ml) at 40 °C for 3 h. ○——○: An equimolar amount of ZLeuGlnGlyOH and HLeuValNH$_2$·HCl (97.6—444 mM respectively), Prolisin B (24 mg/ml), and potato inhibitor (24 mg/ml) were used. The reactions were carried out according to the general procedure in the buffer at 40 °C for 17 h. Mps and R_f of all products were comparable with those of the products in the investigation III-6 (Table 4 or 5).

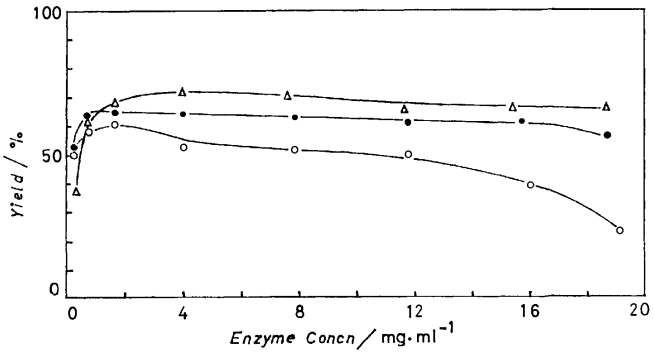

Fig. 2. The effect of enzyme concentration on the yield of ZGlnGlyLeuValNH$_2$. An equimolar amount of ZGlnGlyOH and HLeuValNH$_2$·HCl (167 (○——○), 235 (●——●), and 300 (△——△) mM respectively), Prolisin A (0.3—19 mg/ml), and potato inhibitor(0.9—57 mg/ml, Prolisin A: potato inhibitor=1 : 3 (wt/wt)) were used. The reactions were carried out in 0.2 M Tris-HCl (pH 8, containing 5×10^{-2} M Ca(OAc)$_2$, 4 ml) according to the general procedure at 40 °C for 3 h. Mps and R_f of all products were comparable with those of the products in the investigation III-6 (Table 4).

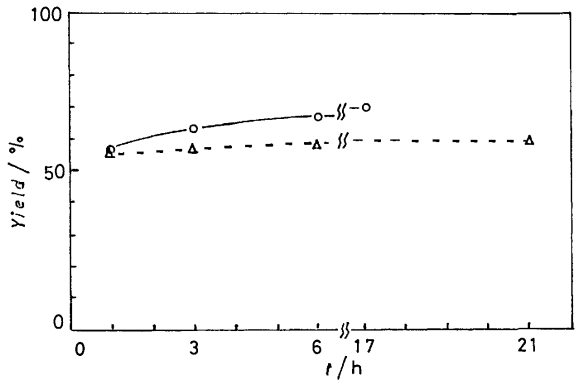

Fig. 3. The influence of the reaction period on the yield of ZGlnGlyLeuValNH$_2$ and ZLeuGlnGlyLeuValNH$_2$ with Prolisin B. The reactions were carried out in 0.2 M Tris-HCl (pH 8, containing 5×10^{-2} M Ca(OAc)$_2$) at 40 °C according to the general procedure. △----△: ZGlnGlyOH and HLeuValNH$_2$·HCl (307 mM respectively), Prolisin B(30.8 mg/ml), potato inhibitor (30.8 mg/ml), and the buffer (3 ml) were used. ○——○: ZLeuGlnGlyOH and HLeuValNH$_2$·HCl (235 mM respectively), Prolisin B (23.5 mg/ml), potato inhibitor (23.5 mg/ml), and the buffer (4 ml) were used. Mps and R_f of all products were comparable with those of the products in the investigation III-6 (Table 4 or 5).

3) The Influence of the Reaction Period on the Yield: Figure 3 illustrates the influence of the reaction period of both condensations (1—21 h) on the yield and the virtual completion of the reactions in 1 or 3 h.

4) The Influence of the Reaction Temperature on the Yield: J. D. McConn *et al.*[9] reported that the activity of *Bacillus subtilis* metalloproteinase has its maximum

at 58 °C in the presence of 5.5×10^{-4} M calcium acetate and was reduced to about 2/3 at 40 °C. However, when Reaction 1 was carried out for 3 h in the presence of Prolisin A under conditions similar to those of III-1 at 20—60 °C, the yield was almost unaffected by variations in temperature.

5) The Influence of the Buffer pH: When Reaction 2 was carried out under conditions similar to those of III-1, the change in the pH of the buffer had no perceptible influence in the range of 6.5—8.5. Therefore, in our examination of other factors influencing the peptide bond formation, the reactions were carried out always in a buffer of pH 8.

6) The Effect of Organic Solvent: Many organic solvents miscible with buffer solutions were examined for their effect on the yield of the product in both condensations under conditions similar to those of III-1 with Prolisin A or B (Tables 4 and 5). The results showed that small amounts (15% of total volume) of dioxane, *n*-BuOH, and MeOH brought about good results in both reactions and acetonitrile in one reaction; however, the addition of more solvent than 32% of the total volume gave unsatisfactory results. It is important to note that these products were generally purer than that from the reaction without organic solvent. It is not understood why better results were brought about by Prolisin A than by Prolisin B in Reaction 2.[12]

7) The Effects of the Amino-protecting Groups: As shown in Table 6, BOC for the amino-protecting group in place of Z brought about unsuccessful results under the same conditions as those of III-1. In this case organic solvents did not give the desired results, in contrast to the former two examples.

IV. Synthesis of ZGlnGlyLeuValNH$_2$ and ZLeuGlnGlyLeuValNH$_2$ with Other Enzymes. Since differences among several microbial metalloproteinases in the rate of hydrolysis of peptide bonds have been reported,[13] the above two reactions were examined further by using Thermolysin (Thermoase) and Tacynase N. The reactions were performed under the conditions most suitable for Prolisin; however, the two enzymes produced poorer results than Prolisin (Table 7). The differences observed with the three enzymes seem to correspond to those in the hydrolysis, though careful examinations will be necessary for each enzyme in view of the fact that the high concentration of Thermolysin brought about good results.

Table 4. The effect of organic solvent on the synthesis of ZGlnGlyLeuValNH$_2$[a]

Substrate (mM)	Prolisin A (mg/ml)	Inhibitor (mg/ml)	Org. solv.	Yield (%)
300	3.9	11.6	None	70.7
254	3.3	9.8	*n*-BuOH	79.4
254	9.8	29.3	*n*-BuOH	78.4
254	3.3	9.8	Dioxane	71.8
254	9.8	29.3	Dioxane	76.7
254	3.3	9.8	CH_3CN	62.4
254	3.3	9.8	THF	68.1
254	3.3	9.8	MeOH	82.9[b]

a) ZGlnGlyOH (0.44 g) and HLeuValNH$_2$·HCl (0.34 g) were allowed to react in a mixed solution of 0.2 M Tris-HCl buffer (pH 8, containing 5×10^{-2} M Ca(OAc)$_2$, 4 ml), organic solvent (0.8 ml), and 4 M NaOH (0.32 ml) at 40 °C for 3 h. b) Mp 245—247 °C; $[\alpha]_D^{30}$ −23.4° (*c* 1, AcOH); R_f 0.75; Found: C, 56.79; H, 7.31; N, 15.42%. Calcd for $C_{26}H_{40}N_6O_7$: C, 56.92; H, 7.35; N, 15.32%. Mps and R_f of all the other products were found comparable with the above data.

Table 5. The effect of organic solvent on the synthesis of ZLeuGlnGlyLeuValNH$_2$ with prolisin A or B[a]

Substrate (mM)	Prolisin (mg/ml)	Inhibitor (mg/ml)	Org. solv. (%)	Total vol. (ml)	Yield (%)
235	B, 23.5	23.5	Done	4.25	68.6
198	B, 19.8	19.8	Dioxane (15.8)	5.05	75.6
160	B, 16.0	16.0	Dioxane (32.0)	6.25	17.5
138	B, 13.8	13.8	Dioxane (41.4)	7.25	0
198	B, 19.8	19.8	THF (15.8)	5.05	70.4
160	B, 16.0	16.0	THF (32.0)	6.25	0
198	B, 19.8	19.8	CH_3CN (15.8)	5.05	74.9
160	B, 16.0	16.0	CH_3CN (32.0)	6.25	0
198	B, 19.8	19.8	CH_3NO_2 (15.8)	5.05	67.4
198	B, 19.8	19.8	$HOCH_2CH_2$-OMe (15.8)	5.05	65.7
198	B, 19.8	19.8	*n*-BuOH (15.8)	5.05	74.9
235	A, 8.0	23.5	None	2.125	70.7
198	A, 6.7	19.8	*n*-BuOH (15.8)	2.525	82.8
198	A, 6.7	19.8	Dioxane (15.8)	2.525	87.3[b]
198	A, 6.7	19.8	MeOH (22.0)	2.725	81.0

a) ZLeuGlnGlyOH and HLeuValNH$_2$·HCl (1 or 0.5 mmol each) were allowed to react in a mixed solution of 0.2 M Tris-HCl (pH 8, containing 5×10^{-2} M Ca(OAc)$_2$), an organic solvent, and 4 M NaOH at 40 °C for 3 h (Prolisin A) or 17 h (Prolisin B). b) Mp 260—262 °C; $[\alpha]_D^{25}$ −30.4° (*c* 0.5, AcOH); R_f 0.65; Found: C, 57.97; H, 7.66; N, 14.86%. Calcd for $C_{32}H_{51}N_7O_8$: C, 58.07; H, 7.77; N, 14.82%. Mps and R_f of all the other products were found comparable with the above data.

Table 6. Synthesis of BOCLeuGlnGlyLeuValNH$_2$ with Prolisin A[a]

Substrate (mM)	Prolisin (mg/ml)	Inhibitor (mg/ml)	Org. solv. (%)	Total vol. (ml)	Yield (%)
444	7.5	22.2	None	2.25	3.0
235	8.0	23.5	None	2.125	19.8[b]
198	6.7	19.8	*n*-BuOH (15.8)	2.525	0
198	6.7	19.8	Dioxane (15.8)	2.525	0

a) BOCLeuGlnGlyOH and HLeuValNH$_2$·HCl (1 or 0.5 mmol each) were allowed to react in a mixed solution of 0.2 M Tris-HCl (pH 8, containing 5×10^{-2} M Ca(OAc)$_2$), organic solvent and 4 M NaOH at 40 °C for 3 h. b) After one recrystallization from MeOH. Mp 230—232 °C; $[\alpha]_D^{25}$ −19.2° (*c* 0.25, DMF); Found: C, 55.54; H, 8.39; N, 15.24%. Calcd for $C_{29}H_{53}N_7O_8$: C, 55.48; H, 8.51; N, 15.62%.

Table 7. Syntheses of ZGlnGlyLeuValNH$_2$ (I) and ZLeuGlnGlyLeuValNH$_2$ (II) with thermolysin (thermoase) or tacynase N[a]

	Subst. (mM)	Protease (mg/ml)	Inhibitor (mg/ml)	Total vol. (ml)	Yield (%)
I	300	Thermoase (2.3)	2.3	4.325	55.5[b]
	300	Tacynase N (46.2)	46.2	4.325	16.4
II	235	Thermolysin	none	4.25	53.6[c]
	444	Thermolysin	none	2.25	63.3
	235	Tacynase N (47.0)	47.0	4.25	36.6

a) A mixture of ZGlnGlyOH and HLeuValNH$_2$·HCl (1.3 mmol each) or ZLeuGlnGlyOH and HLeuValNH$_2$·HCl (1.0 mmol each) was stirred in a combined solution of 0.2 M Tris-HCl (pH 8, containing 5×10^{-2} M Ca(OAc)$_2$) and 4 M NaOH at 40 °C for 17 h (Thermolysin and Thermoase) or 3 h (Tacynase). b) Mp 246—247.5 °C. c) Mp 258.5—259 °C; $[\alpha]_D^{29}$ −33.4° (*c* 0.5 AcOH); Found: C, 57.27; H, 7.74; N, 14.77%. Calcd for $C_{32}H_{51}N_7O_8\cdot1/2H_2O$: C, 57.29; H, 7.81; N, 14.62%.

Conclusions

It was found that ZLeuGlnGlyOH or ZGlnGlyOH is catalytically coupled with HLeuValNH$_2$ by several metalloproteinases to give protected Secretin 23—27 or 24—27 peptide fragments in good yields. Since these reactions are performed in an aqueous solution and the crude products obtained from the reaction mixture are approximately pure in most cases, the after treatments are much easier than with the conventional methods. The lengthening of the peptide chain of a carboxyl component from 2 to 3 seemed to have no influence on the yield. The addition of a small amount of suitable organic solvents usually assisted the enzymatic reaction to give pure products in good yields.

The authors wish to express their deep gratitude to Dr. Yonezo Morino for his constant encouragement throughout the work. Their thanks are also due to Mrs. Tomoko Matsumura and Miss Noriko Shutoh for their technical assistance.

References

1) a) Y. Isowa, M. Ohmori, T. Ichikawa, H. Kurita, M. Satoh, and K. Mori, *Bull. Chem. Soc. Jpn.*, **50**, 2762 (1977); b) Y. Isowa, M. Ohmori, M. Satoh, and K. Mori, *ibid.*, **50**, 2766 (1977). Recently, Morihara and Oka also reported the peptide synthesis using α-chymotrypsin. K. Morihara and T. Oka, *Biochem. J.*, **163**, 531 (1977).

2) H. Matsubara and J. Feder, "The Enzymes," 3rd ed, Vol 3, ed by P. D. Boyer, Academic Press, New York, N. Y. (1971), p. 765.

3) J. C. Melville and C. A. Ryan, *J. Biol. Chem.*, **247**, 3445 (1972).

4) D. Tsuru, T. Yamamoto, and J. Fukumoto, *Agric. Biol. Chem.*, **30**, 651 (1966).

5) a) J. Fukumoto, T. Yamamoto, and K. Ichikawa, *Nippon Nogei Kagaku Kaishi*, **32**, 230 (1958); b) D. Tsuru, J. D. McConn, and K. T. Yasunobu, *Biochem. Biophys. Res. Commun.*, **15**, 367 (1964).

6) a) Y. Yokote, K. Kawasaki, J. Nakajima, and Y. Noguchi, *Nippon Nogei Kogaku Kaishi*, **43**, 125 (1969): b) Y. Yokote and Y. Noguchi, *ibid.*, **43**, 132 (1969).

7) S. Endo, *Hakko Kagaku Zasshi*, **40**, 346 (1962).

8) E. Wünsch, G. Wendleberger, and A. Högel, *Chem. Ber.*, **104**, 2430 (1971).

9) J. D. McConn, D. Tsuru, and K. T. Yasunobu, *J. Biol. Chem.*, **239**, 3706 (1964).

10) See "Methods and Materials,"

11) a) K. Matsushima, *Nippon Nogei Kagaku Kaishi*, **29**, 883 (1955), **31**, 38 (1957); b) J. Fukumoto, T. Yamamoto, and K. Ichikawa, *ibid.*, **33**, 9 (1959); c) D. Tsuru, H. Kira, T. Yamamoto, and J. Fukumoto, *Agric. Biol. Chem.*, **30**, 1261 (1966); d) T. Iwasaki, T. Kiyohara, and M. Yoshikawa, *J. Biochem.*, **70**, 817 (1971); e) T. Kiyohara, T. Iwasaki, and M. Yoshikawa, *ibid.*, **73**, 89 (1973).

12) These results seems to be caused by some differences between Prolisin A and B. Metalloproteinase seems to denature slowly in storage.

13) a) K. Morihara, H. Tsuzuki, and T. Oka, *Arch. Biochem. Biophys.*, **123**, 572 (1968); b) K. Morihara, *Biochem. Biophys. Res. Commun.*, **26**, 656 (1967); c) K. Morihara and H. Tsuzuki, *Arch. Biochem. Biophys.*, **146**, 291 (1971).

The Ullmann Condensation Reaction of Haloanthraquinone Derivatives with Amines in Aprotic Solvents. III. The Formation and Role of Copper(II) Species in the Condensation with 2-Aminoethanol by Copper(I) Catalyst

Sadao ARAI, Mitsuhiko HIDA, and Takamichi YAMAGISHI

Department of Industrial Chemistry, Faculty of Technology, Tokyo Metropolitan University, Fukazawa, Setagaya-ku, Tokyo 158

(Received June 24, 1977)

The ESR spectra of the Ullmann condensation reaction system of 1-bromoanthraquinone-2-aminoethanol-CuBr showed that copper(II) species and 1-bromoanthraquinone radical anion were formed by an electron transfer from copper(I) species to 1-bromoanthraquinone. Although copper(II) species alone had little catalytic activity, the resulting copper(II) species increased the catalytic activity of the copper(I) species, and a pseudo-first order rate constant could be expressed as follows: $k=k_1[Cu^I]+k_2[Cu^I][Cu^{II}]$. According to the magnitude of k_1 and k_2C_0, where C_0 is the initial concentration of copper(I) catalyst, the reaction of haloanthraquinone with 2-aminoethanol by copper(I) catalyst can be classified into three modes. When $k_1<k_2C_0$, an induction period is present. The possible mechanisms of the cooperation between copper(I) and copper(II) species have been proposed. It has been also found that 1-bromoanthraquinone radical anion was responsible for the debromination.

In our preceding papers,[1,2] we reported that copper(II) species was formed in the Ullmann condensation reaction of haloanthraquinones with amines by using a copper(I) salt as a catalyst in aprotic solvents under a nitrogen atmosphere. The reaction rate did not remarkably decrease in spite of the formation of copper(II) species.[1] An induction period was observed in some reaction systems, such as 1-bromoanthraquinone (AQBr)–2-aminoethanol(AE)–CuBr or AQBr–AE–CuI. These results were explained by suggesting that the formation of the copper(II) species increased the catalytic activity of the copper(I) species, though the copper(II) species alone was found to have little catalytic activity for these reactions.[2] Therefore, the formation and catalytic action of the copper(II) species are considered to be a very interesting problem connected with the Ullmann condensation reaction of haloanthraquinones in aprotic media.

In this paper, the formation and role of copper(II) species will be described in more detail and we will propose the reaction mechanism of haloanthraquinones with 2-aminoethanol by copper(I) catalyst in aprotic media under a nitrogen atmosphere.

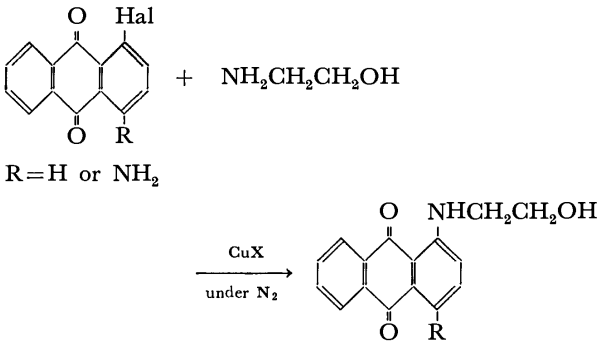

Results and Discussion

The Formation of Copper(II) Species. Previously we described that copper(I) species was oxidized to copper(II) species during the progress of the Ullmann condensation reaction of haloanthraquinones with 2-aminoethanol(AE).[1] The ESR spectra showed that

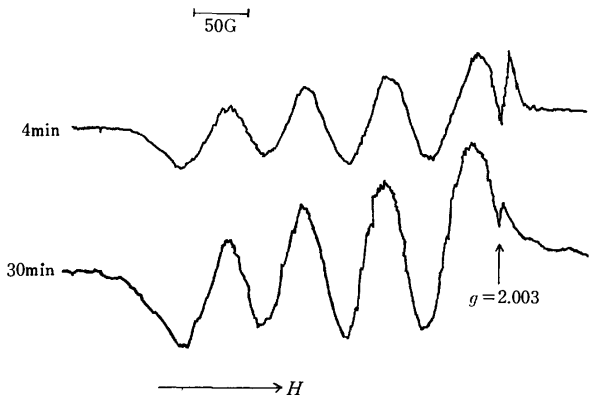

Fig. 1. ESR spectra of the reaction system of 1-bromoanthraquinone–2-aminoethanol–CuBr. $[AQBr]_0=5.00\times10^{-3}$ mol/l, $[AE]_0=0.50$ mol/l, $[CuBr]_0=2.00\times10^{-3}$ mol/l, temp 70 °C, solvent 1,2-dimethoxyethane–methyl cellosolve 4 : 1.

the formation of the copper(II) species was accompanied by an organic paramagnetic species (g value 2.003) (Fig. 1). The spectra seem to reveal that the copper(II) species is mostly present as copper(II) complex containing 2-aminoethanol in the coordination sphere, because the ESR spectra of the copper(II) species in the reaction system are very similar to that of copper(II) bromide in AE solution.

The copper(II) and organic paramagnetic species are considered to be formed by single electron transfer from copper(I) species to 1-bromoanthraquinone (AQBr) or its condensation product [1-(2-hydroxyethylamino)anthraquinone]. A mixture of the condensation product with CuBr–AE, however, gave scarcely any organic paramagnetic species and copper(II) species. The system of AQBr–CuBr–2-(dimethylamino)ethanol, which did not give any amination product, also gave copper(II) and organic paramagnetic species. These results seem to indicate that the organic paramagnetic species cannot be ascribed to a radical anion of the condensation product. Further, the organic paramagnetic species may be a 2-aminoethanol

radical cation, formed by an electron transfer from AE to the resulting copper(II) species.[3] However, this possibility can be ruled out by the finding that the ESR spectra of the system of AQBr–AE–$CuBr_2$ showed only the copper(II) species. The copper(II) species may be possibly formed by the dismutation of the copper(I) species: $2Cu(I) \rightarrow Cu(II) + Cu(0)$.[4] In the absence of 1-bromoanthraquinone, however, no copper(II) and organic paramagnetic species were observed.

Consequently, all of the experimental results indicate that the copper(II) species is not formed by the dismutation of the copper(I) species, but formed by an electron transfer from the copper(I) species to 1-bromoanthraquinone, and that the organic paramagnetic species is a 1-bromoanthraquinone radical anion ($AQBr^{\cdot-}$): $AQBr + Cu(I) \rightarrow AQBr^{\cdot-} + Cu(II)$. Single electron transfer from copper(I) species to aryl halides has been proposed in the halogen-exchange reaction between aryl halides and copper(I) salts[5] and in the Ullmann coupling reaction of *o*-bromonitrobenzene by copper(I) bromide,[6] even though the radical anions of aryl halides have not been directly detected.

In the reaction system of AQBr–AE–CuBr, anthraquinone was produced, along with the condensation product (Fig. 2). This result also seems to support the formation of $AQBr^{\cdot-}$ in the course of the reaction, since $AQBr^{\cdot-}$ can be considered to be debrominated in a similar manner to the dehalogenation of the radical anions of aryl halides: $AQBr^{\cdot-} \rightarrow AQ\cdot \rightarrow AQH$.[7] It is well known that the Ullmann condensation reaction of haloanthraquinones or aryl halides are accompanied by the dehalogenation reaction.[8-14] Although homolytic, heterolytic, or hydride transfer mechanisms have been proposed,[15] our results suggest that the radical anion, formed by an electron transfer from copper(I) species to AQBr, is mainly responsible for the dehalogenation.

After 120 min the yield of anthraquinone was only about 8%, whereas the yield of the copper(II) species was estimated as about 34% on the basis of the ESR signal height for the $CuBr_2$–AE solution. If the radical anion decays out only by its debromination, the yield of anthraquinone should be the same as that of the copper(II) species. Therefore, the 1-bromoanthraquinone radical anion should be considered to decay out only by the debromination, but by other faster decay processes,[16] such as an electron transfer to copper(II) species[17] and/or some other substance, and the dismutation,[18] although the rate of the debromination of the radical anion has remained unknown.

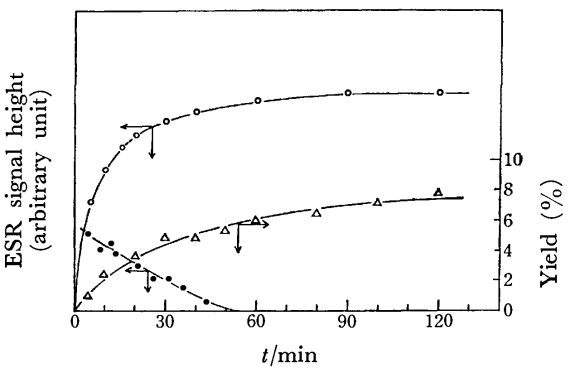

Fig. 2. The time dependence of ESR signal height and the yield of anthraquinone. $[AQBr]_0 = 5.00 \times 10^{-3}$ mol/l, $[AE]_0 = 0.50$ mol/l, $[CuBr]_0 = 2.00 \times 10^{-3}$ mol/l, temp 70 °C, solvent 1,2-dimethoxyethane–methyl cellosolve 4 : 1. ○: Cu(II) species, ●: $AQBr^{\cdot-}$., △: anthraquinone.

The Role of Copper(II) Spceies. In our preceding paper[2] we reported that the copper(II) species increased the catalytic activity of the copper(I) species, since the addition of copper(II) bromide($CuBr_2$) resulted in the vanishing of an induction period in the reaction system of AQBr–AE–CuBr. As is shown in Fig. 3, with the increase of $CuBr_2$ the pseudo-first order rate constant increases, passes through a maximum, and finally falls, when the total concentration of copper species is kept constant. Thus, the addition of copper(II) bromide increases the catalytic activity of the copper catalyst. From Fig. 3 the pseudo-first order rate constant(k_{app}) may be simply expressed by Eq. 1.

$$k_{app} = k_a(1-\alpha) + k_b\alpha(1-\alpha), \quad (1)$$

where α denotes the mole fraction of the copper(II) bromide. However, if k_a and k_b are assumed to be constant, Eq. 1 cannot reproduce the plot in Fig. 3. Because of the addition of copper(II) bromide as copper(II) species, the bromide ions were present in a larger amount than an equivalent to the copper concentration. Thus, the pseudo-first order rate constant seems likely to be affected by the presence of the excess bromide ions.

If k_a is assumed to be unaffected by the presence of the excess bromide ions, it can be estimated from the intercept of the plot of the pseudo-first order rate constant(k_{app}) against α. Then k_b can be given as a function of the concentration of the excess bromide ions by substituting the value of k_a in Eq.1. The rate constant k_b decreases linearly with increasing of the concen-

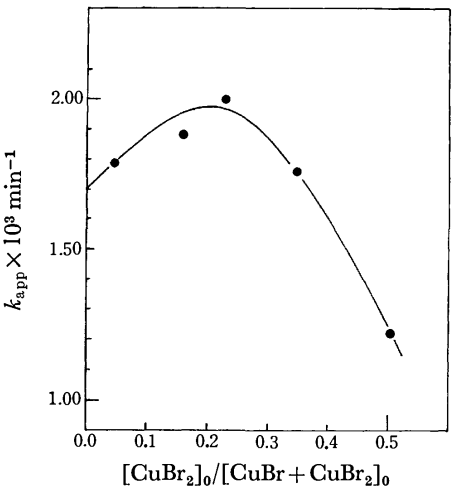

Fig. 3. The effect of the addition of $CuBr_2$ on pseudo-first order rate constant (k_{app}). $[AQBr]_0 = 5.00 \times 10^{-3}$ mol/l, $[AE]_0 = 0.50$ mol/l, $[CuBr + CuBr_2]_0 = 2.00 \times 10^{-3}$ mol/l, temp 70 °C, solvent 1,2-dimethoxyethane–methyl cellosolve 4 : 1. The full circles represent the experimental values. The solid line represents the curve calculated by Eq. 3.

tration of the excess bromide ions (Eq. 2).

$$k_b = k_{bo}(1-\beta), \quad (2)$$

where β is the excess of bromide ions. By combining Eq. 1 with Eq. 2 the pseudo-first order rate constant (k_{app}) is given by Eq. 3:

$$k_{app} = \{k_a + k_{bo}(1-\beta)\alpha\}(1-\alpha). \quad (3)$$

The solid curve in Fig. 3 represents the result calculated according to Eq. 3 by assuming that k_a and k_b are 1.7×10^{-3} and 3.9×10^{-3} min^{-1}, respectively.

In order to confirm the effect of the excess bromide ions, tetraethylammonium bromide was added to the reaction mixture. As shown in Table 1, k_{app} decreased clearly by the addition of tetraethylammonium bromide. The calculated values of k_{app} by using Eq. 3 were close to the observed ones, though the reason for the effect of the excess bromide ions is not yet clearly understood.

Table 1. Effect of the excess bromide ion on pseudo-first order rate constants(k_{app})[a]

$\frac{[CuBr_2]_0}{[CuBr]_0+[CuBr_2]_0}$	k_{app}(min^{-1}) Controlled	Addition of $(C_2H_5)_4N^+Br^-$ [b] Obsd	Calcd[c]
0.063	1.82×10^{-3}	1.71×10^{-3}	1.71×10^{-3}
0.158	1.88×10^{-3}	1.77×10^{-3}	1.70×10^{-3}

a) $[AQBr]_0=5.00\times10^{-3}$ mol/l; $[AE]_0=0.50$ mol/l; $[CuBr]_0+[CuBr_2]_0=2.00\times10^{-3}$ mol/l; temp 70°C; solvent 1,2-dimethoxyethane-methyl cellosolve 4 : 1. b) The excess of bromide is 1.0×10^{-3} mol/l. c) The values calculated by Eq. 3.

These experimental results tell us that the kinetics of the Ullmann condensation reaction cannot be described in terms of the action of copper(I) catalyst alone. Thus, on the basis of the above considerations, the rate law is assumed to be expressable as follows:

$$-\frac{d[AQBr]}{dt} = k_1[Cu^I][AQBr] + k_2[Cu^I][Cu^{II}][AQBr] + k_3[Cu^{II}][AQBr] + k_0[AQBr]. \quad (4)$$

Since k_3 and k_0 are very small compared to k_1 and k_2, both k_3 and k_0 may be neglected. Therefore, the pseudo-first order rate constant can be expressed by Eqs. 5 and 6.

$$k = k_1[Cu^I] + k_2[Cu^I][Cu^{II}], \quad (5)$$

$$k = k_1C_0 + (k_2C_0-k_1)[Cu^{II}] - k_2[Cu^{II}]^2, \quad (6)$$

where C_0 denotes the concentration of total copper or the initial concentration of copper(I) catalyst. Differentiating Eq. 6 by time t, Eq. 7 is derived.

$$\frac{dk}{dt} = (k_2C_0-k_1-2k_2[Cu^{II}])\frac{d[Cu^{II}]}{dt} \quad (7)$$

Since the rate constant has a maximum value, in such a case an induction period is observed:

$$k_2C_0 - k_1 - 2k_2[Cu^{II}] = 0. \quad (8)$$

Thus,

$$[Cu^{II}]_{max} = (k_2C_0-k_1)/2k_2 \quad (9)$$

where $[Cu^{II}]_{max}$ is the concentration of copper(II) species which gives the maximum rate constant(k_{max}). When $k_1<k_2C_0$,

$$k_{max} = \left(C_0-\frac{k_2C_0-k_1}{2k_2}\right)\left(k_1+\frac{k_2C_0-k_1}{2}\right). \quad (10)$$

Therefore,

$$\sqrt{k_{max}} = \frac{\sqrt{k_2}}{2}C_0 + \frac{k_1}{2\sqrt{k_2}}. \quad (11)$$

Consequently, when $k_1<k_2C_0$, the induction period will be present and the rate constant will have a maximum value. If the above assumption is valid, a linear relationship between $\sqrt{k_{max}}$ and C_0 will be obtained. Figure 4 shows that the relationship indicates a good linearity, when C_0 is larger than k_1/k_2 obtained from the intercept on the abscissa axis. This result suggests that the above assumption is valid. The rate constants (k_1 and k_2) are determined from the slope and intercept of the line, as shown in Table 2. By comparing Eq. 3 with Eq. 6, it is obvious that k_1C_0 and $k_2C_0^2$ correspond to k_a and k_{bo} in Eq. 3, respectively. In the reaction system of AQBr–AE–CuBr, the rate constant $k_a(1.7\times10^{-3})$ is nearly equal to the value k_1C_0 (1.778×10^{-3}), while k_{ob} (3.9×10^{-3}) is approximate to $k_2C_0^2$ (3.088×10^{-3}).

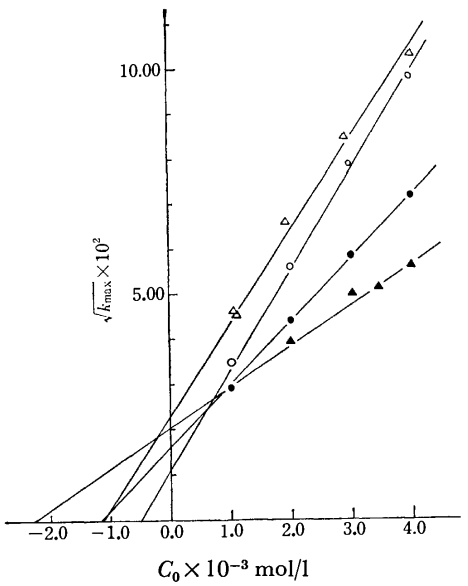

Fig. 4. The relation between $\sqrt{k_{max}}$ and C_0. [haloanthraquinone]$_0=5.00\times10^{-3}$ mol/l, $[AE]_0=0.50$ mol/l, temp 70 °C, solvent 1,2-dimethoxyethane–methyl cellosolve 4 : 1.
△: 1-Amino-4-bromoanthraquinone–AE–CuI,
○: 1-amino-4-bromoanthraquinone–AE–CuBr,
▲: AQBr–AE–CuI, ●: AQBr–AE–CuBr.

Table 2. Rate constants(k_1 and k_2)

Rate constant	AQBr CuBr	AQBr CuI	1-NH_2-4-BrAQ CuBr	1-NH_2-4-BrAQ CuI
k_1(l·mol^{-1}·min^{-1})	0.889	0.737	1.009	1.911
k_2(l^2·mol^{-2}·min^{-1})	772	332	2015	1685

Temp 70°C; solvent 1,2-dimethoxyethane-methyl cellosolve 4 : 1.

The time dependence of the copper(II) species concentration can be well expressed by Eq. 12, if the intensity of ESR signal is proportional to the copper(II) species concentration.

$$[Cu^{II}] = a(1-e^{-\gamma t}) \quad (12)$$

By combining Eq. 6 with Eq. 12 and integrating, Eq. 13 can be derived, if the amount of the debrominated product can be assumed to be negligible.

$$-\ln(1-x) = A(1-e^{-2\gamma t}) + B(1-e^{-\gamma t}) + Ct \quad (13)$$

where x denotes the yield of the aminated product, and where A, B, and C are $-a^2k_2/2\gamma$, $(a/\gamma)\{k_1+k_2\cdot(2a-C_0)\}$, and $(k_1+ak_2)(C_0-a)$, respectively.

At the amine concentration of 0.5 mol·l^{-1} in the reaction system of AQBr–AE–CuBr, k_1, k_2, a, and γ are given as follows: 0.889, 772, 6.8×10^{-4}, and 0.082. Figure 5 shows that the calculated values are in good agreement with the experimental data.

As shown in Table 3, k_1 increases with the increase in the concentration of 2-aminoethanol, but the reverse is found in the value of k_2. When the initial concentration of copper(I) catalyst was kept constant, the induction period was shortened with the increase in the concentration of amine and it was absent at high concentrations of amine, as reported previously.[2] In the reaction system of 1-iodoanthraquinone–AE–copper(I) salt and AQBr–AE–$[Cu(CH_3CN)_4]ClO_4$, the induction period was absent.[2] The presence of the induction period would be ascribed to the catalytic activity of copper(I) species, the reactivities of haloanthraquinones, and the degree of contribution of copper(II) species as a promoter. According to the magnitude of k_1 and k_2C_0, the reaction between haloanthraquinone and 2-aminoethanol by copper(I) catalyst can be classified into three modes, as illustrated in Fig. 6. That is to say, when $k_1<k_2C_0$, an induction period will be present, but when $k_1>k_2C_0$, the reaction rate decreases with the formation of copper(II) species. In the case of the constant concentration of amine, the induction period was shortened with the increase in the concentration of copper(I) catalyst. This result also supports the classification of the reaction mentioned above.

Reaction Mechanism. As described in Table 3, the rate constant k_1 increased with the increase in the concentration of amine. The plot of $1/k_1$ against 1/[AE] gave a good straight line(Fig.7). On the other hand, the rate constant k_2 decreased with the increase in the concentration of amine. The plot of $1/k_2$ against [AE] gave a good straight line (Fig. 8).

All of the results mentioned above can be reasonably explained by assuming the following mechanism.

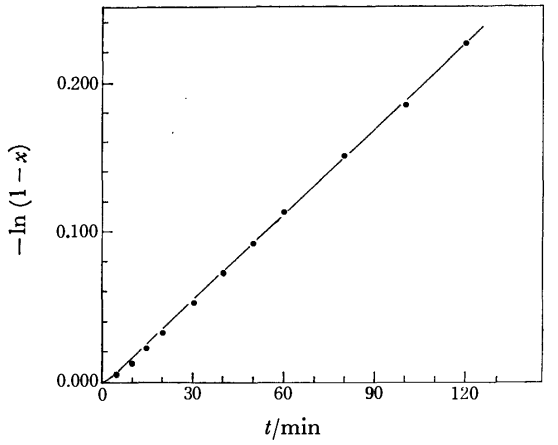

Fig. 5. Pseudo-first order plots for the reaction of 1-bromoanthraquinone with 2-aminoethanol by CuBr catalyst.
$[AQBr]_0=5.00\times10^{-3}$ mol/l, $[AE]_0=0.50$ mol/l, $[CuBr]_0=2.00\times10^{-3}$ mol/l, temp 70 °C, solvent 1,2-dimethoxyethane–methyl cellosolve 4 : 1. The full circles represent the experimetal values. The solid line represents the curve calculated by Eq. 13.

Table 3. Amine concentration dependence of k_1 and k_2 for the reaction of 1-bromoanthraquinone with 2-aminoethanol by CuBr catalyst

$[AE]_0$ mol·l^{-1}	0.25	0.33	0.50	0.76
k_1(l·mol^{-1}·min^{-1})	0.576	0.691	0.889	1.059
k_2(l^2·mol^{-2}·min^{-1})	953	880	772	596

Temp 70 °C; solvent 1,2-dimethoxyethane-methyl cellosolve 4 : 1.

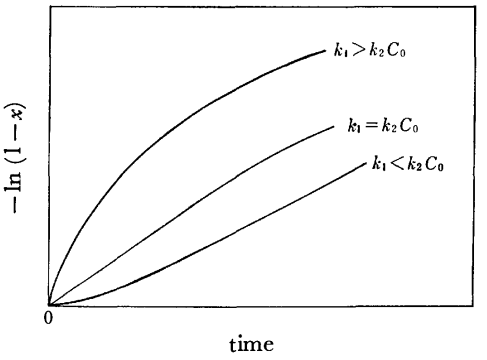

Fig. 6. The modes of pseudo-first order plots for the reaction between haloanthraquinone and 2-aminoethanol by copper(I) catalyst.

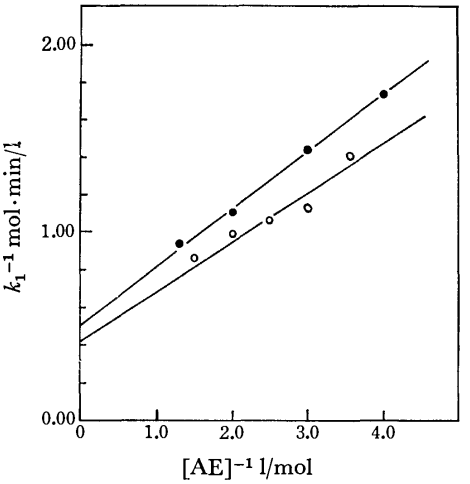

Fig. 7. Plots of $1/k_1$ against 1/[AE]. Temp 70 °C, solvent 1,2-dimethoxyethane–methyl cellosolve 4 : 1. ●: AQBr–AE–CuBr, ○: 1-amino-4-bromoanthraquinone–AE–CuBr.

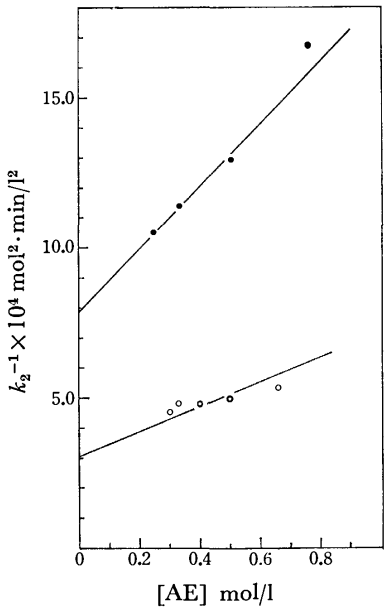

Fig. 8. Plots of $1/k_2$ against [AE]. Temp 70 °C, solvent 1,2-dimethoxyethane–methyl cellosove 4 : 1.
●: AQBr–AE–CuBr, ○: 1-amino-4-bromoanthraquinone–AE–CuBr.

Thus, copper(I) species is supposed to be in equilibrium among Cu^I, Cu^I(AE), and Cu^I(AQBr). The reaction of Cu^I(AQBr) and AE gives an amination product. On the other hand, the copper(II) species formed in the course of the reaction is in equilibrium between Cu^{II} and Cu^{II}(AE). Cu^I(AQBr) reacts with Cu^{II}(AE) to give the product.

$$\left.\begin{array}{l} Cu^I + AE \overset{K_1}{\rightleftharpoons} Cu^I(AE) \\ Cu^I + AQBr \overset{K_2}{\rightleftharpoons} Cu^I(AQBr) \xrightarrow[k_r]{AE} \text{Product} \\ Cu^{II} + AE \overset{K_1'}{\rightleftharpoons} Cu^{II}(AE) \\ Cu^I(AQBr) + Cu^{II}(AE) \xrightarrow[k_r']{} \text{Product} \end{array}\right\} \quad (14)$$

On the basis of this reaction scheme (Eq. 14) the rate constant k_1 is expressed by Eq. 15, while k_2 is expressed by Eq. 16.

$$k_1 = \frac{k_r K_2[AE]}{1+K_1[AE]+K_2[AQBr]} \quad (15)$$

$$k_2 = \frac{k_r' K_2}{1+K_1[AE]+K_2[AQBr]} \cdot \frac{K_1'[AE]}{1+K_1'[AE]} \quad (16)$$

Previously we reported that the pseudo-first order plots were independent of the initial concentration of haloanthraquinone.[2] Therefore, $K_2[AQBr]$ can be supposed to be much smaller than unity: $K_2[AQBr] \ll 1$. In addition, Fig. 9 shows that k_1/k_2 is proportional to the concentration of 2-aminoethanol. This result indicates that $K_1'[AE]$ is much larger than unity: $K_1'[AE] \gg 1$. Thus, Eqs. 15 and 16 can be rewritten as follows:

$$k_1 = \frac{k_r K_2[AE]}{1+K_1[AE]} \quad (17) \quad \text{or} \quad k_1^{-1} = \frac{1}{k_r K_2}\left(\frac{1}{[AE]} + K_1\right), \quad (18)$$

$$k_2 = \frac{k_r' K_2}{1+K_1[AE]} \quad (19) \quad \text{or} \quad k_2^{-1} = \frac{1}{k_r' K_2}(1+K_1[AE]). \quad (20)$$

Therefore,

$$(k_1/k_2) = (k_r/k_r')[AE] \quad (21)$$

Both $k_r K_2$ and K_1 can be evaluated by the slope and the intercept of the straight line in the plot of $1/k_1$ against $1/[AE]$ (Fig. 7), and $k_r' K_2$ and K_1 from the straight line in the plot of $1/k_2$ against [AE] (Fig. 8). The values of K_1 evaluated independently from Eqs. 18 and 20 are nearly equal (Table 4). Since the equilibrium between Cu^I and AE does not include haloanthraquinone, there should not be any difference in the magnitude of K_1 between haloanthraquinones (1-bromoanthraquinone and 1-amino-4-bromoanthraquinone). Table 4 shows that this is the case.

The value of k_r/k_r' given by the ratio between $k_r K_2$ and $k_r' K_2$ agrees with the slops of the linear plot of k_1/k_2 against the concentration of 2-aminoethanol. This result also supports the above mechanism. Table 4 also tells us that both values of $k_r K_2$ and $k_r' K_2$ of 1-amino-4-bromoanthraquinone are greater than those of 1-bromoanthraquinone. We reported previously that the latter was more reactive toward 2-aminoethanol in

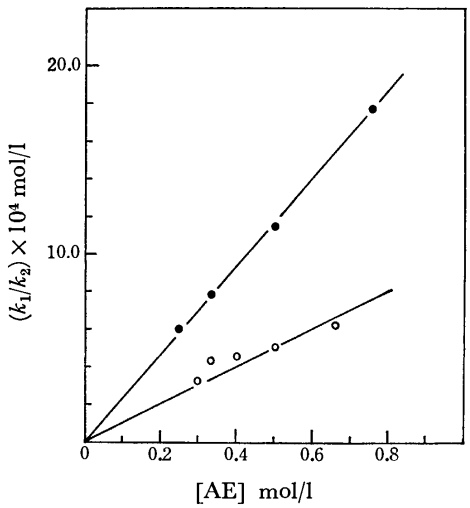

Fig. 9. Plots of k_1/k_2 against [AE]. Temp 70 °C, solvent 1,2-dimethoxyethane–methyl cellosolve 4 : 1.
●: AQBr–AE–CuBr, ○: 1-amino-4-bromoanthraquinone–AE–CuBr.

Table 4. Rate parameters for the reaction with 1-bromoanthraquinone or 1-amino-4-bromoanthraquinone

Rate parameter		AQBr	1-NH_2-4-BrAQ
K_1(l·mol^{-1})	(from Fig. 7)	1.67	1.67
	(from Fig. 8)	1.32	1.32
$k_r K_2$(l^2·mol^{-2}·min^{-1})		3.24	3.85
$k_r' K_2$(l^2·mol^{-2}·min^{-1})		0.127×10^4	0.326×10^4
k_r/k_r'	(from Figs. 7 and 8)	2.55×10^{-3}	1.18×10^{-3}
	(from Fig. 9)	2.33×10^{-3}	1.00×10^{-3}

Temp 70 °C; solvent 1,2-dimethoxyethane–methyl cellosolve 4 : 1.

the absence of copper(I) than the former was, while the reverse was found in the presence of the catalyst.[1] This is mainly caused by the fact that 1-amino-4-bromoanthraquinone possesses larger values of $k_r'K_2$ than 1-bromoanthraquinone does.

Another possible mechanism for the cooperation between copper(I) and copper(II) species can be a complex formation between them. Even if this is the case, however, k_1 can be expressed by Eq. 17, and k_2 by Eq. 19 rewritten by replacing k_r' with $k_r'K_c$, where K_c is the formation constant of the assumed complex between copper(I) and copper(II).

Several variations of the mechanism which satisfy the experimental results could be considered. However, it is difficult to decide which of these mechanisms is valid.

Experimental

The 1-bromoanthraquinone, 1-amino-4-bromoanthraquinone, 1-(2-hydroxyethylamino)anthraquinone, and copper(I) halides were prepared by the methods described in the previous paper.[1] The copper(II) bromide, 2-aminoethanol, and tetraethylammonium bromide were purified according to the usual methods. Commercial guaranteed reagent grade 2-(dimethylamino)ethanol was distilled, and stored under a nitrogen atmosphere. Solvents were dried in the usual manner, distilled, and stored under a nitrogen atmosphere.

The kinetic measurements were the same as those given previously.[1] The anthraquinone formed in the course of the reaction was analyzed by the use of a Shimadzu Du Pont LC-1 high speed liquid chromatograph(column: Zorbax ODS; mobile phase: methanol-water 67 : 33) with 1-methylaminoanthraquinone as the internal standard.

The ESR spectra were measured at 70 °C under a nitrogen atmosphere by the use of a JEOL-PE-3X ESR spectrometer, and the g value was calculated by comparison with a Mn^{2+} marker. Field and modulation width were 3360±500 and 6.3 G, respectively.

References

1) S. Arai, T. Yamagishi, S. Ototake, and M. Hida, *Bull. Chem. Soc. Jpn.*, **50**, 547 (1977).
2) S. Arai, M. Hida, T. Yamagishi, and S. Ototake, *Bull. Chem. Soc. Jpn.*, **50**, 2982 (1977).
3) D. Rehorek and P. Thomas, *Z. Chem.*, **13**, 477 (1973).
4) J. E. B. Randles, *J. Chem. Soc.*, **1941**, 802.
5) G. van Koten, J. T. B. H. Jastrzebski, and J. G. Noltes, *Tetrahedron Lett.*, **1976**, 223.
6) V. V. Litvak and S. M. Shein, *Zh. Org. Khim.*, **11**, 903 (1975); *Chem. Abstr.*, **83**, 8725z (1975).
7) T. Fujinaga, Y. Deguchi, and K. Umemoto, *Bull. Chem. Soc. Jpn.*, **37**, 822 (1964).
8) W. Bradley, E. Leete, and D. S. Stephens, *J. Chem. Soc.*, **1951**, 2147.
9) R. G. R. Bacon and O. J. Stewart, *J. Chem. Soc.*, **1965**, 4953.
10) A. A. Goldberg and W. Kelly, *J. Chem. Soc.*, **1946**., 102.
11) K. Naiki, *Yuki Gosei Kagaku Kyokai Shi*, **12**, 401 (1954).
12) T. N. Kurdyumova, *Org. Poluprod. Krasiteli*, **1969**, 94; *Chem. Abstr.*, **72**, 90134k (1970).
13) G. D. Wood and A. T. Peters, *J. Chem. Soc.*, **1962**, 3373.
14) Y. Takekawa, S. Kato, M. Mabuchi, and T. Kurano, *Kogyo Kagaku Zasshi*, **60**, 595 (1957).
15) R. G. R. Bacon and H. A. O. Hill, *Quart. Rev.*, **19**, 95 (1965).
16) The rate of disappearance of the radical anion was approximate to that of the copper(II) formation, as shown in Fig. 2. This can be understood by the assumption that the rate constant of the disappearance of the radical anion is much greater than that of the formation of copper(II) species.
17) N. K. Bridge and M. Reed, *Trans. Faraday Soc.*, **56**, 1796 (1960).
18) For example, W. Sakai and F. Hori, *Denki Kagaku*, **37**, 623 (1969).

Studies on the Syntheses of Sesquiterpene Lactones. I. Chemical Transformation of α-Santonin into Vulgarin, C_4-Epivulgarin, and Arglanine*

Masayoshi Ando, Atsushi Akahane, and Kahei Takase

Department of Chemistry, Faculty of Science, Tohoku University, Aramaki-aza-Aoba, Sendai 980

(Received July 1, 1977)

Syntheses of vulgarin, C_4-epivulgarin, and arglanine are reported. An efficient conversion of 3-oxo-5αH, 4β,6β, 11βH-eudesm-1-en-6,13-olide into 1-oxo-5αH,4β,6β,11βH-eudesm-2-en-6,13-olide, a key intermediate of these syntheses, was achieved by the Meerwein-Ponndorf reaction and the allylic rearrangement of the resultant 3-hydroxyl derivative followed by the Collins oxidation. Acetalization of 1-oxo-5αH,4β,6β,11βH-eudesm-2-en-6,13-olide and successive isomerization of the double bond gave 1,1-ethylenedioxy-5αH,6β,11βH-eudesm-3-en-6,13-olide regioselectevity. Oxidation of this compound with OsO_4 gave 3α,4α-dihydroxy-1,1-ethylenedioxy-5αH,6β,11βH-eudesman-6,13-olide, 3α,4α-dihydroxy-1-oxo-5αH,6β,11βH-eudesman-6,13-olide and 3β,4β-dihydroxy-1,1-ethylenedioxy-5αH,6β,11βH-eudesman-6,13-olide. Oxidation of 1,1-ethylenedioxy-5αH,6β,11βH-eudesm-3-en-6,13-olide with *m*-chloroperoxybenzoic acid gave 3α,4α-epoxy-1,1-ethylenedioxy-5αH,6β,11βH-eudesm-6,13-olide stereoselectively in a quantitative yield. Treatment of 3α,4α-dihydroxy-1,1-ethylenedioxy-5αH,6β,11βH-eudesman-6,13-olide,3α,4α-dihydroxy-1-oxo-5αH,6β,11βH-eudesman-6,13-olide, and 3α,4α-epoxy-1,1-ethylenedioxy-5αH,6β,11βH-eudesm-6,13-olide with boiling 50% AcOH gave vulgarin. The same treatment of 3β,4β-dihydroxy-1,1-ethylenedioxy-5αH,6β,11βH-eudesman-6,13-olide gave C_4-epivulgarin. Phenylselenenylation of 3α,4α-dihydroxy-1,1-ethylenedioxy-5αH,6β,11βH-eudesman-6,13-olide and successive syn-elimination of the resultant phenylseleno lactone gave 3α,4α-dihydroxy-1,1-ethylenedioxy-5αH,6βH-eudesm-11-en-6,13-olide, which was transformed into arglanine by treatment with boiling 50% AcOH.

The sesquiterpene lactones with α-methylene-γ-lactone moiety fused on various skeletons are a rapidly expanding group of natural products, comprising to date more than 400 varieties.[1] These unsaturated lactones have considerable biological activities as allergenic agents,[2] cytotoxic and antitumor agents,[3] regulators of plant growth and antimitotic activity,[4] and antischistosomal agents.[5] In all these cases, the α-methylene-γ-lactone unit has been assigned a central role in the activity mechanism.

Efficient syntheses of these sesquiterpene lactones are a synthetic challenge which has received much attention during the past few years.[6] For the general syntheses of these sesquiterpene lactones with various skeletons, we envisioned approaches which consisted of the solvolytic rearrangements or the fragmentation reactions of the appropriately functionalized eudesmanolides, such as compounds (**A**), (**B**), and (**C**), as shown in Scheme 1. Solvolytic rearrangements of cis- and trans-decalin derivatives with an equatorial hydroxyl group at C_1 have been applied to the syntheses of guaiane-type sesquiterpenes with rather simple structures, such as bulnesol, bulnesene, and kessane.[7] The fragmentation reaction of alkyl borane derivatives[8] with a partial structure (**D**) is a well-documented reaction and has been applied to the syntheses of hedycaryol. The fragmentation of 1,4a-decalindiol monosulfonates[9] has provided an efficient route to cyclodecenones. But these solvolytic rearrangements or fragmentation reactions have not yet been applied to the syntheses of guaianolides, germacranolides, and elemanolides, probably because of the difficulties of the syntheses of appropriately functionalized eudesmanolides such as **A**, **B**, and **C**. For the syntheses of these compounds, vulgarin

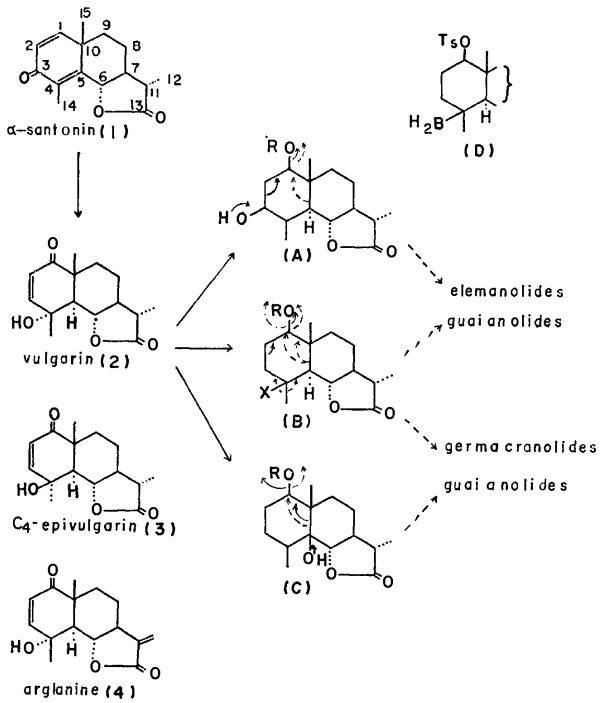

Scheme 1.

(**2**) and the related compounds are considered to be useful materials. Since vulgarin available from a natural source is limited,[10] and no practical synthesis of this compound has so far been reported, we have decided to examine the syntheses of vulgarin and related compounds. In the present paper we wish to report the efficient syntheses of vulgarin (**2**),[11] C_4-epivulgarin (**3**), and arglanine (**4**),[12] from α-santonin (**1**).

Results and Discussion

Synthesis of Vulgarin and C_4-Epivulgarin. Although one synthesis of vulgarin has been reported,[13] its final

* A preliminary report of this work was presented at the 34th Annual Meeting of the Chemical Sciety of Japan, Tokyo, April, 1976.

stages were carried out without the isolation or purification of intermediates and in very poor yield (0.5% in the last two steps). We wish to report the improved syntheses of vulgarin by two different routes starting from the α,β-unsaturated ketone (**5**) which was prepared from α-santonin by the known procedure.[14]

We envisioned an approach which consisted of the transfer of the oxygen function at C_3 of **5** into C_1 (**E**→**F**), protection of the carbonyl group and successive isomerization of the double bond (**F**→**G**), stereoselective oxidation of the double bond (**G**→**H** or **I**), and their transformation into vulgarin by deacetalization and simultaneous dehydration or acid-promoted opening of the epoxide (**H** or **I**→**J**).

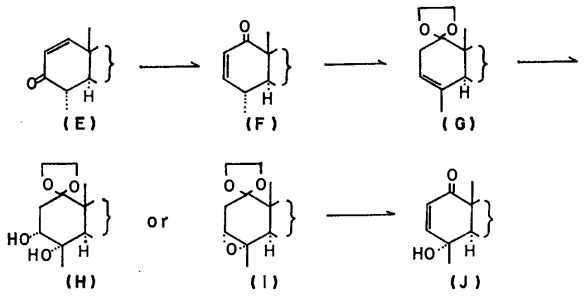

The Wharton rearrangement,[15] which involves the epoxidation of α,β-unsaturated ketone with hydrogen peroxide in alkali solution followed by the reduction of the resultant α,β-epoxy ketone with hydrazine, is a well-known reaction for the purpose of transferring the oxygen function from C_3 into C_1. Application of this method to **5** gave the desired alcohol (**7**) in poor yield (*ca.* 20%) because the γ-lactone moiety was sensitive to the reaction conditions. An efficient conversion of **5** to **7** was achieved by an alternative way. The Meerwein-Ponndorf reaction of **5** gave a 4 : 1 mixture of an allyl alcohol (**6a**) and its C_3-epimer (**6b**) in 98.4% yield.[16] Allylic rearrangement of this mixture by refluxing in THF containing 2 M HCl gave the desired allyl alcohol (**7**) stereoselectively in 78.5% yield, along with the recovery of the starting material (**6**) in 17.8% yield. (The conversion yield of **7** based on the starting material consumed was 95.5%.) The predominant formation of Δ^2-derivative (**7**) in this equilibrium reaction starting from Δ^1-derivative (**6**) is consistent with the fact that in *trans*-decalin series or 5α-steroid series Δ^2-derivatives are thermodynamically more stable than the corresponding Δ^1-derivatives.[17] α(ax)-Configuration of the hydroxyl group at C_1 in **7** was confirmed by the NMR spectrum of its dihydro derivative (**16**), which showed a peak at δ 3.37 (t, J=2.5 Hz, C_1–H) ppm. Oxidation of **7** by the Collins procedure gave an α,β-unsaturated ketone (**8**) in 89.2% yield. In agreement with the structure (**8**) the product exhibited an IR ($CHCl_3$) absorption at 1674 cm^{-1} and the NMR spectrum showed peaks at δ 5.85 (dd, J= 2.5 and 10.0 Hz, C_2–H) and 6.59 (dd, J=2.0 and 10.0 Hz, C_3–H) ppm.

Having completed the conversion of **5** to **8** in a sufficient yield (83.8%), we turned our attention to the problem of the isomerization of the double bond. Acetalization of **8** in a standard condition gave an acetal (**9**) in 71.2% yield.[18] Since it was expected that the acetal (**9**) with disubstituted double bond could be isomerized to the acetal (**10**) with a more stable trisubstituted double bond, the conditions of this isomerization reaction were investigated carefully; the best result was given by the following procedure. The double bond of **9** was isomerized by heating in ethylene glycol in the presence of *p*-toluensulfonic acid at 145 °C for 10 min, yielding **10** in 73.0%. No other double bond isomer of **10** was detected in these conditions.[19] The acetal (**10**) was also prepared in 67.0% overall yield from **8** without isolation of **9**.

Oxidation of the double bond of **10** was carried out by two different procedures and gave different results. Oxidation of **10** with osmium tetraoxide and successive treatment with hydrogen sulfide gave a mixture of an acetal (**11**) (32.3%), a ketone (**12**) (12.3%), and an acetal (**13**) (26.2%). Their stereochemistry was deduced from the coupling constant of C_3–H in their NMR spectra, as well as from the manner of reaction with osmium tetraoxide (cis addition). Since the 1,3-diaxial interaction between the 1α-oxygen of the acetal group and the entering reagent is expected in **10** because of the presence of the acetal group at C_1, the 1 : 1.7 ratio of the β face attack product (**13**) and the α face attack product (**11**+**12**) can be reasonably explained in terms of the competitive steric hindrance of the angular methyl group and the 1α-oxygen of the acetal group to the entering reagent. On the other hand, the epoxidation of **10** with *m*-chloroperoxybenzoic acid in dichloromethane proceeded stereoselectively from the α face to give 3α,4α-epoxide (**14**) in a quantitative yield. The difference of stereoselectivities between the osmylation and the epoxidation of **10** cannot be explained by simple steric factors. Probably the hydrogen-bonding interaction between *m*-chloroperoxybenzoic acid and the 1α-oxygen of the acetal group directs the α face attack of the reagent, as shown below.

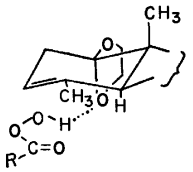

Finally, the syntheses of vulgarin and C_4-epivulgarin have been completed by deacetalization and/or selective dehydration of the C_3-hydroxyl group of **11**, **12** and **13** or deacetalization and simultaneous ring opening of the epoxide (**14**). Deacetalization and selective dehydration of the C_3-hydroxyl group of **11** was accomplished by treatment with boiling 50% aqueous acetic acid for 74 h to give vulgarin in 86.6% yield. The same treatment of **12** gave vulgarin in 68.6% yield by dehydration of the C_3-hydroxyl group. The deacetalization and simultaneous opening of the epoxide ring of **14** to the expected direction was also accomplished by treatment with boiling 50% aqueous acetic acid for 65 h to give vulgarin in 30.3% yield, along with a 36.1% yield of dienone (**15**). The synthetic material was identical with the natural product in its melting point and NMR ($CDCl_3$) and IR ($CHCl_3$) spectra.[11,20] On the other hand, treatment of **13** with

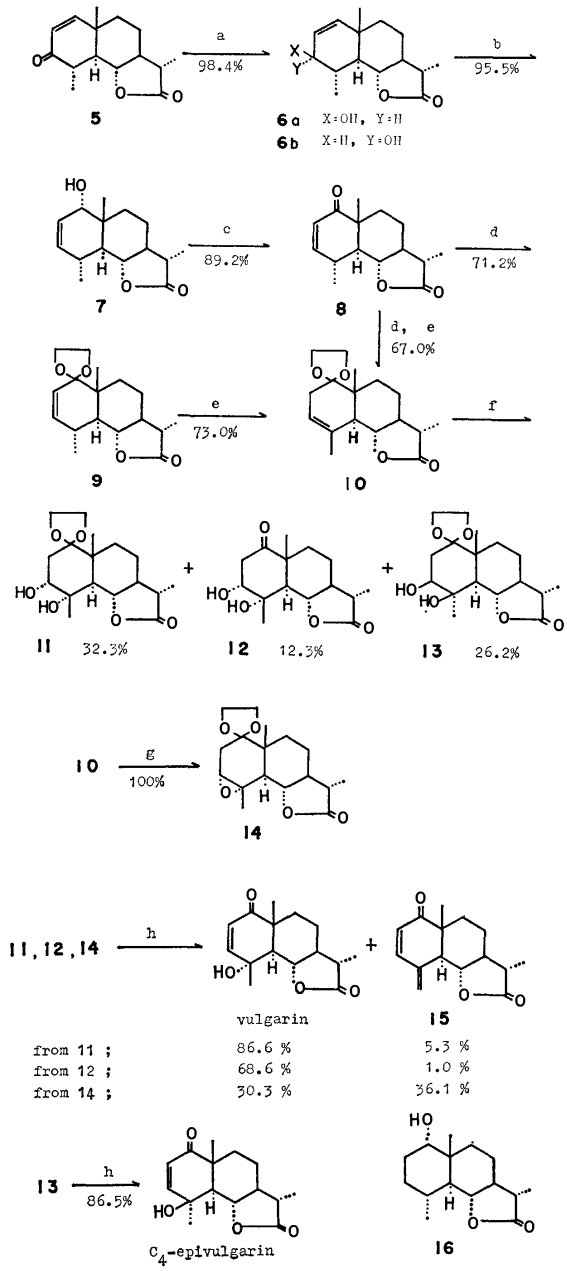

a: $Al(i\text{-}PrO)_3$, *i*-PrOH; b: 2 M HCl, THF; c: $CrO_3 \cdot 2Py$, CH_2Cl_2; d: $HO(CH_2)_2OH$, *p*-TsOH, C_6H_6; e: Δ(145 °C), *p*-TsOH, $HO(CH_2)_2OH$; f: OsO_4, aq Dioxane, H_2S; g: *m*-$ClC_6H_4CO_3H$, CH_2Cl_2; h: 50% aq AcOH.

Scheme 2.

boiling 50% aqueous acetic acid for 72 h gave the C_4-epivulgarin (**3**) in 86.5% yield. The 1,3-diaxial relationship between C_4–OH and C_{10}–Me in this compound was clearly demonstrated in the NMR spectrum, in which the signal of C_{10}–Me appeared at 0.13 ppm lower field than the corresponding signal of vulgarin.[21]

Synthesis of Arglanine. Having completed the synthesis of vulgarin, we turned our attention to the synthesis of arglanine (**4**) with an α-methylene-γ-lactone group. Recently Yamakawa *et al.* reported the chemical transformation of α-santonin into arglanine.[22] We want to report here our independent result of the synthesis of arglanine. The convenient intermediate for this purpose was the compound (**11**) in which the carbonyl group at C_1 was protected as the ethylene acetal. Conversion of α-methyl-γ-lactone group of **11** into α-methylene-γ-lactone group was accomplished by the Grieco's procedure.[23] Thus the phenylselenenylation of **11** with diphenyl diselenide afforded phenylseleno lactone (**17**) in 49.3% yield. Oxidative syn-elimination of **17** with H_2O_2 in THF–HOAc afforded α-methylene-γ-lactone derivative (**18**) in 83.8% yield. Deacetalization and successive dehydration of the C_3-hydroxyl group of **18** was accomplished by treatment with boiling 50% aqueous acetic acid for 71 h to give arglanine in 57.4% yield. The synthetic material was identical with the natural product in IR (KBr) and NMR (60 MHz, $CDCl_3$) spectra.[12]

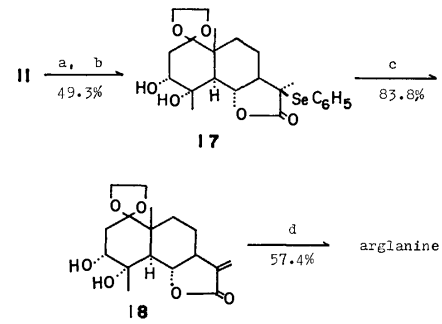

a: $LiN(i\text{-}Pr)_2$, THF; b: $C_6H_5SeSeC_6H_5$, HMPA; c: 30% H_2O_2, AcOH; d: 50% aq AcOH.

Scheme 3.

As the total synthesis of α-santonin has been accomplished,[24] the syntheses of vulgarin, C_4-epivulgarin, and arglanine reported in this paper are the formal total synthesis of these compounds. The investigation of the chemical transformations of vulgarin and related compounds into eudesmane-type α-methylene-γ-lactones,[25] guaiane-type α-methylene-γ-lactones, germacrane-type α-methylene-γ-lactones, and elemane-type α-methylene-γ-lactones are now in progress and will be reported elsewhere.

Experimental

All the melting points were uncorrected. IR spectra were determined on a Shimadzu IRG-I spectrometer. NMR spectra were recorded on Varian A-60 and HA-100 spectrometers in $CDCl_3$ containing TMS as internal standard. Mass spectra were recorded on a Hitachi RMU-6D spectrometer with a direct inlet system operating at 25 eV.

*3-Hydroxy-5αH,4β,6β,11βH-eudesm-1-en-6,13-olide (**6**).* A solution of 3-oxo-5αH,4β,6β,11βH-eudesm-1-en-6,13-olide (**5**, 1.32 g, 5.32 mmol) and $Al(i\text{-}PrO)_3$ (5.00 g, 23.90 mmol) in dry *i*-PrOH (80 ml) was allowed to boil gently in a 200 ml flask fitted with a Vigreux column. The acetone vapor formed was allowed to escape from the reaction mixture. After 4 h *i*-PrOH was distilled and the reaction mixture was reduced to *ca.* a 10 ml volume. Cold 2 M HCl (75 ml) was added, and the resulting acidic solution was extracted with EtOAc. The combined extracts were washed successively with sat $NaHCO_3$ aq and sat NaCl aq, dried (Na_2SO_4), and concentrated *in vacuo* to give 1.31 g (98.4%) of *ca.* 4 : 1

mixture of 3β-hydroxy-5αH,4β,6β,11βH-eudesm-1-en-6,13-olide (**6a**) and 3α-hydroxy-5αH,4β,6β,11βH-eudesm-1-en-6,13-olide (**6b**) as a mixture of plates and needles; mp 159—165 °C. IR (KBr): 3510 and 1750 cm^{-1}. NMR: δ 5.57 (s, 1.6H, C_1- and C_2-H of **6a**) and 5.71 (m, 0.4H, C_1- and C_2-H of **6b**) ppm. Found: C, 71.49; H, 9.26%. Calcd for $C_{15}H_{22}O_3$: C, 71.97; H, 8.86%.

1α-Hydroxy-5αH,4β,6β,11βH-eudesm-2-en-6,13-olide (7). A solution of **6** (1096 mg, 4.25 mmol) in a mixture of THF (95 ml) and 2 M HCl (63 ml) was refluxed under N_2 for 16 h, cooled, and poured into sat NaCl aq (150 ml). The mixture was extracted with $CHCl_3$ (50 ml×3). The combined extracts were washed successively with sat $NaHCO_3$ aq and sat NaCl aq, dried (Na_2SO_4), and concentrated *in vacuo* to give an oily crude product, which was chromatographed over silica gel (Merck, 70—230 mesh, 60 g) and eluated with CCl_4–$CHCl_3$ (2 : 1). The first running gave 40 mg of 1α-chloro-5αH,4β,6β,11βH-eudesm-2-en-6,13-olide, which was recrystallized from $CHCl_3$-ether (1 : 1) to give 20 mg of colorless needles; mp 218—219 °C. IR (KBr); 1770 and 778 cm^{-1}. NMR (100 MHz): δ 1.06 (3H, s, C_{10}–Me), 1.23 (3H, d, J=6.5 Hz, C_4- or C_{11}–Me), 1.24 (3H, d, J=6.5 Hz, C_4- or C_{11}–Me), 3.83 (1H, t, J=10.0 Hz, C_6–H), 4.07 (1H, broad d, J=5.5 Hz, C_1–H), 5.58 (1H, broad d, J=10.0 Hz, C_3–H), and 5.82 (1H, broad q, J=5.5 and 10.0 Hz, C_2–H) ppm. Found: C, 66.68; H, 7.91%. Calcd for $C_{15}H_{21}O_2Cl$: C, 66.97; H, 7.87%. The second running gave 850 mg (78.5%) of **7** as an amorphous substance: mp 138 °C. IR (KBr): 3600, 3400, 1765, and 742 cm^{-1}. NMR; δ 0.90 (3H, s, C_{10}–Me), 1.22 (6H, d, J=6.5 Hz, C_4- and C_{11}-Me), 3.46 (1H, d, J=5.0 Hz, C_1–H), 3.93 (1H, t, J=10.0 Hz, C_6–H), and 5.5—6.1 (2H, m, C_2- and C_3–H) ppm. Found: C, 71.08; H, 9.00%. Calcd for $C_{15}H_{22}O_3$: C, 71.97; H, 8.86%.

The third running gave 195 mg (17.8%) of recovered starting material, which was recrystallized from ether-$CHCl_3$ to give **6a** as colorless prisms; mp 180—181 °C. IR (KBr) 3530, 1758, and 752 cm^{-1}. NMR: δ 1.08 (3H, s, C_{10}–Me), 1.20 (3H, d, J=6.8 Hz, C_{11}–Me), 1.25 (3H, d, J=6.0 Hz, C_4–Me), 2.46 (1H, s, –OH), 3.82 (1H, d, J=8.0 Hz, C_3–H), 3.93 (1H, m, $W_{h/2}$=17.0 Hz, C_6–H), 5.58 (2H, s, C_1- and C_2–H) ppm.

1-Oxo-5αH,4β,6β,11βH-eudesm-2-en-6,13-olide (8). CrO_3 (5.12 g, 51.2 mmol) was added in small portions into a mixture of dry pyridine (10.5 ml, 103 mmol) and dry CH_2Cl_2 (65 ml) at 0 °C and stirred for 10 min. Then **7** (644 mg, 2.57 mmol) dissolved in CH_2Cl_2 (50 ml) was added, and the mixture was stirred at 0 °C for 6 h and filtered. The filtrate was washed successively with sat $NaHCO_3$ aq (30 ml×3), 2 M HCl (30 ml), and sat NaCl aq, dried (Na_2SO_4), and concentrated *in vacuo* to give 586 mg of crystalline material, which was chromatographed over silica gel (Merck, <230 mesh, 27 g) and eluted with CCl_4–$CHCl_3$ (1 : 1) to give 568 mg (89.2%) of **8**. This material (334 mg) was recrystallized from ether to give 206 mg of colorless prisms; mp 110—111 °C. IR (KBr): 1768, 1668, 812, and 738 cm^{-1}. NMR: δ 1.16 (3H, s, C_{10}-Me), 1.33 (6H, d, J=7.5 Hz, C_4- and C_{11}-Me), 4.01 (1H, t, J=10.0 Hz, C_6-H), 5.85 (1H, dd, J=2.5, 10.0 Hz, C_2–H), 6.59 (1H, dd, J=2.0, 10.0 Hz C_3–H) ppm. Found: C, 72.62; H, 8.33%. Calcd for $C_{15}H_{20}O_3$: C, 72.55; H, 8.12%.

1,1-Ethylenedioxy-5αH,4β,6β,11βH-eudesm-2-en-6,13-olide (9). A mixture of **8** (320 mg, 1.28 mmol), ethylene glycol (5 ml), and *p*-toluenesulfonic acid (38 mg) in dry C_6H_6 (60 ml) was refluxed in a flask equipped with a Dean-Stark column packed with molecular sieves for 24 h under N_2. The mixture was cooled and diluted with a mixture of sat NaCl aq and sat $NaHCO_3$ aq and the benzene layer was drawn off. The aqueous layer was further extracted with EtOAc. The combined extracts were washed with sat NaCl aq, dried (Na_2SO_4), and concentrated to give 408 mg of an oil, which was chromatographed over silica gel (Wakogel C-200, 20 g) and eluted with CCl_4–$CHCl_3$ (1 : 2) to give 268 mg (71.2%) of **9**. This material was recrystallized from ether to give a crystal; mp 148—152 °C. IR (KBr): 1777 and 745 cm^{-1}. NMR: δ 1.06 (3H, s, C_{10}–Me), 1.20 (6H, d, J=6.5 Hz, C_4- and C_{11}–Me), 3.5—4.2 (m, 5H, $\langle{}^{-O}_{-O}\rangle$ and C_6–H), 5.52 (2H, m, $W_{h/2}$=2.5 Hz, C_2- and C_3–H) ppm. Found: C, 69.74; H, 8.28%. Calcd for $C_{17}H_{24}O_4$: C, 69.83; H, 8.27%.

1,1-Ethylenedioxy-5αH,6β,11βH-eudesm-3-en-6,13-olide (10) from 9. A mixture of **9** (140 mg), ethylene glycol (8 ml) and *p*-toluenesulfonic acid (17 mg) in dry C_6H_6 was refluxed in a flask equipped with a Dean-Stark column packed with molecular sieves for 1 h under N_2. C_6H_6 was removed and the residue was heated at 145 °C for 10 min under N_2, cooled, diluted with EtOAc, washed with sat NaCl aq, dried (Na_2SO_4) and concentrated to give a crude product which was chromatographed over silica gel (Merck, <230 mesh, 7 g) to give 102 mg (73%) of **10**.

1,1-Ethylenedioxy-5αH,6β,11βH-eudesm-3-en-6,13-olide (10) from 8. A mixture of **8** (438 mg, 1.77 mmol), ethylene glycol (26 ml) and *p*-toluenesulfonic acid (52 mg) in dry C_6H_6 (100 ml) was refluxed in a flask equipped with a Dean-Stark column packed with molecular sieves for 23 h under N_2. C_6H_6 was removed and the residue was heated at 145 °C for 10 min under N_2, cooled, diluted with EtOAc, washed with sat NaCl aq, dried (Na_2SO_4), and concentrated to give an oily crude product (401 mg), which was chromatographed over silica gel (Merck, <230 mesh, 20 g) and eluted with CCl_4–$CHCl_3$ (1 : 1). The first running gave 345 mg (67.0%) of **10**, which was recrystallized from ether to give colorless prisms; 130—131 °C. IR ($CHCl_3$): 1765, 892, 863, and 852 cm^{-1}; NMR: δ 1.03 (3H, s, C_{10}–Me), 1.22 (3H, d, J=6.5 Hz, C_{11}–Me), 1.85 (3H, broad s, C_4–Me), 3.5—4.2 (m, 5H, $\langle{}^{-O}_{-O}\rangle$ and C_6–H), 5.29 (1H, m, $W_{h/2}$=7.0 Hz, C_3–H) ppm. Found: C, 69.70; H, 8.27%. Calcd for $C_{17}H_{24}O_4$: C, 69.83; H, 8.27%. The second running gave 47 mg of recovered **8**.

*Oxidation of **10** with Osmium Tetraoxide; Formation of 3α,4α-Dihydroxy-1,1-ethylenedioxy-5αH,6β,11βH-eudesman-6,13-olide (11), 3α,4α-Dihydroxy-1-oxo-5αH,6β,11βH-eudesman-6,13-olide (12), and 3β,4β-Dihydroxy-1,1-ethylenedioxy-5αH,6β,11βH-eudesman-6,13-olide (13).* To a solution of **10** (885 mg, 3.0 mmol) in dry dioxane (85 ml) was added OsO_4 (800 mg, 3.15 mmol). The mixture was allowed to stand at room temperature for 72 h, then saturated with hydrogen sulfide, and filtered through a layer of celite. The filtrate was poured into sat NaCl aq (250 ml) and extracted with chloroform (100 ml×3). The combined extracts were washed successively with sat $NaHCO_3$ aq (100 ml) and sat NaCl aq (100 ml), dried (Na_2SO_4), and concentrated to give a crude semisolidal product (903 mg) which showed three spots (R_f 0.45, 0.35, and 0.20) on TLC (silica gel GF_{254}, thichness 0.25 mm, EtOAc) and was purified by preparative TLC. The first band gave 256 mg (26.2%) of **13**, which was recrystallized from $CHCl_3$-ether (1 : 1) to give colorless prisms; mp 199—200 °C. IR ($CHCl_3$): 3560, 3460, and 1768 cm^{-1}. NMR: δ 1.17 (3H, d, J=7.0 Hz, C_{11}–Me), 1.27 (3H, s, C_{10}–Me), 1.46 (3H, s, C_4–Me), 2.61 (2H, m, –OH), 3.50 (1H, q, J=6.5, 10.5 Hz, C_3–H), 3.91 (4H, m, $\langle{}^{-O}_{-O}\rangle$), 4.23 (1H, m, $W_{h/2}$=*ca.* 18 Hz,

C_6–H) ppm. Found: C, 63.00; H, 8.28%. Calcd for $C_{17}H_{26}O_6$: C, 62.56; H, 8.08%. The second band gave 104 mg (12.3%) of **12**, which was recrystallized from $CHCl_3$–ether (1 : 1) to give colorless prisms; mp 223 °C. IR (KBr) 3590, 3555, 1775, and 1718 cm^{-1}; NMR: δ 1.22 (3H, s, C_{10}–Me), 1.23 (3H, d, J=6.5 Hz, C_{11}–Me), 1.56 (3H, s, C_4–Me), 2.83—3.65 (2H, m, –OH), 3.92 (1H, t, J=4.0 Hz, C_3–H), 4.14 (1H, t, J=11.0 Hz, C_6–H). MS *m/e*: 282 (M^+). Found: C, 63.43; H, 7.88%. Calcd for $C_{15}H_{22}O_5$: C, 63.81; H, 7.85%. The third band gave 316 mg (32.3%) of **11**, which was recrystallized from $CHCl_3$–ether (1 : 1) to give colorless plates; mp 226—227 °C. IR ($CHCl_3$): 3480, 1782, and 1772 cm^{-1}: NMR: δ 1.14 (3H, s, C_{10}–Me), 1.20 (3H, d, J=6.5 Hz, C_{11}–Me), 1.34 (3H, s, C_4–Me), 3.62 (1H, m, $W_{h/2}$=6.0 Hz, C_3–H), 3.8—4.3 (5H, m, $\langle{}^{-O}_{-O}$ and C_6–H) ppm. After addition of D_2O, the signal at 3.62 ppm was changed to a triplet (J=3.4 Hz). Found: C, 62.53; H, 8.13%. Calcd for $C_{17}H_{26}O_6$: C, 62.56; H, 8.08%.

Vulgarin (Tauremisin) from ***11***. A solution of **11** (225 mg, 0.69 mmol) in 50% AcOH aq (37 ml) was refluxed for 74 h under N_2, cooled, and poured into sat NaCl aq. The mixture was extracted with $CHCl_3$ (20 ml×3). The combined extracts were washed successively with sat $NaHCO_3$ aq (10 ml×2) and sat NaCl aq, dried (Na_2SO_4), and concentrated to give 181 mg of crude crystalline material, which showed two spots (R_f 0.38, minor; R_f 0.10, major) on TLC [silica gel GF_{254}, thickness 0.25 mm, EtOAc–$CHCl_3$ (1 : 9)]. This material was purified by preparative TLC [silica gel GF_{254}, EtOAc–$CHCl_3$ (1 : 9)]. The first band gave 9 mg of 1-oxo-5αH,6β,11βH-eudesm-2,4(14)-dien-6,13-olide (anhydrovulgarin, **15**) as an crystalline material. IR ($CHCl_3$): 1775, 1670, 927, and 840 cm^{-1}. NMR: δ 1.07 (3H, s, C_{10}–Me), 1.24 (3H, d, J=6.7 Hz, C_{11}–Me), 2.83 (1H, dt, J=10.0 and 1.8 Hz, C_5–H), 4.21 (1H, t, J=10.0 Hz, C_6–H), 5.56 and 5.83 (each, 1H, m, $=\langle{}^{H}_{H}$), 5.87 (1H, broad d, J=10.0 Hz, C_2–H), 7.08 (1H, dd, J=0.8 and 10.0 Hz, C_3–H) ppm. UV (MeOH) max: 268 nm. The second band gave 158 mg (86.6%) of vulgarin (Tauremisin), which was recrystallized from ethanol to give fine needles; mp 174—175 °C (lit, 174—175 °C). This material was identical with natural vulgarin in IR ($CHCl_3$) and NMR (60 MHz, $CDCl_3$).

Vulgarin from ***12***. A solution of **12** (56 mg, 0.199 mmol) in 50% AcOH aq (10 ml) was refluxed for 74 h under N_2, cooled, and poured into sat NaCl aq. The mixture was extracted with $CHCl_3$ (10 ml×3). The combined extracts were washed successively with sat $NaHCO_3$ aq, and sat NaCl aq, dried (Na_2SO_4), and concentrated to give 43 mg of crystalline material, which was purified by the combination of preparative TLC [silica gel GF_{254}, EtOAc–$CHCl_3$ (1 : 9)] and recrystallization from ethanol to give 36 mg (68.6%) of vulgarin and 0.5 mg of **15**.

C_4-Epimer of Vulgarin (4β-Hydroxy-1-oxo-5αH,6β,11βH-eudesm-2-en-6,13-olide, ***3***). A solution of **13** (100 mg, 0.307 mmol) in 50% AcOH aq (16 ml) was refluxed 72 h under N_2, cooled, and poured into sat NaCl aq. The mixture was extracted with chloroform (10 ml×3). The combined extracts were washed successively with sat $NaHCO_3$ aq (10 ml×2) and sat NaCl aq, dried (Na_2SO_4), and concentrated to give 95 mg of crystalline material, which was purified by preparative TLC [silica gel GF_{254}, thickness 0.25 mm, EtOAc–$CHCl_3$ (1 : 9), R_f 0.14] to give 70 mg (86.5%) of C_4 epimer of vulgarin (**3**). This material was recrystallized from EtOH to give colorless cubes; mp 185—186 °C. IR (KBr): 3540, 1773, and 1680 cm^{-1}. NMR: δ 1.23 (3H, d, J=6.5 Hz, C_{11}–Me), 1.34 (3H, s, C_{10}–Me), 1.58 (3H, s, C_4–Me), 2.01 (1H, d, J=10.5 Hz, C_5–H), 2.46 (1H, s, –OH), 4.36 (1H, t, J=10.5 Hz, C_6–H), 5.83 (1H, d, J=10.0 Hz, C_2–H), 6.51 (1H, d, J=10.0 Hz, C_3–H) ppm. MS *m/e*: 264 (M^+). Found: C, 67.67; H, 7.83%. Calcd for $C_{15}H_{20}O_4$: C, 68.16; H, 7.63%.

3α,4α-Epoxy-1,1-ethylenedioxy-5αH,6β,11βH-eudesm-6,13-olide (*)*. A mixture of **10** (103 mg, 0.35 mmol) and *m*-chloroperoxybenzoic acid (64 mg, 0.37 mmol) in CH_2Cl_2 (5 ml) was allowed to stand at room temperature for 100 h. The mixture was poured into KI aq and extracted with $CHCl_3$ (10 ml×3). The combined extracts were washed successively with 0.2 M $Na_2S_2O_3$ aq, sat $NaHCO_3$ aq, and sat NaCl aq, dried (Na_2SO_4), and concentrated to give 109 mg (100%) of spectroscopic pure **14**, which was recrystallized from $CHCl_3$–ether (1 : 1) to give colorless needles, mp 257 °C (dec). NMR: δ 1.12 (3H, s, C_{10}–Me), 1.23 (3H, d, J=6.5 Hz, C_{11}–Me), 1.49 (3H, s, C_4–Me), 2.16 (1H, d, J=3.0 Hz, C_2–H), 2.20 (1H, d, J=1.5 Hz, C_2–H), 2.43 (1H, d, J=12.0 Hz, C_5–H), 3.01 (1H, dd, J=1.5 and 3.0 Hz, C_3–H), 3.6—4.1 (5H, m, $\langle{}^{-O}_{-O}$ and C_6–H). Found: C, 66.26; H, 7.89%. Calcd for $C_{17}H_{24}O_5$: C, 66.21; H, 7.85%.

Vulgarin and Anhydrovulgarin from ***14***. A solution of **14** (50 mg, 0.16 mmol) in 50% AcOH aq (5 ml) was refluxed for 65 h. The mixture was poured into sat NaCl aq and extracted with EtOAc (10 ml×2). The combined extracts were washed successively with sat $NaHCO_3$ aq and sat NaCl aq, dried (Na_2SO_4), and concentrated *in vacuo* to give 37 mg of crude product, which was purified by preparative TLC (silica gel GF_{254}, thickness 0.25 mm, EtOAc). The first band gave 20 mg (36.1%) of **15**. The second band gave 18 mg (30.3%) of vulgarin.

3α,4α-Dihydroxy-1,1-ethylenedioxy-11β-phenylseleno-5αH,6βH-eudesman-6,13-olide (*)*. To a dry THF solution of lithium diisopropylamide [prepared from diisopropylamine (77.4 μl, 0.72 mmol), 1.70 M butyllithium in hexane (0.43 ml, 0.72 mmol), and dry THF (1.8 ml) at −78 °C] was added dropwise over a period of 1h, 65 mg (0.2 mmol) of **11** in 2.0 ml of THF. After the solution was stirred at −78 °C for 40 min, diphenyl diselenide (225 mg, 0.72 mmol) in dry THF (1.2 ml) and HMPA (126 μl) was added dropwise at −78 °C. The reaction mixture was stirred at −78 °C for 40 min, then warmed to −40 °C and kept at that temperature for 1 h. The reaction was quenched by the addition of 0.1 M HCl aq (15 ml). The mixture was extracted with EtOAc (10 ml×2). The combined extracts were washed with sat NaCl aq, dried (Na_2SO_4), and concentrated to give 277 mg of product, which was purified by preparative TLC (silica gel GF_{254}, thickness 0.25 mm, EtOAc). The first band (R_f 0.64) gave 177 mg of diphenyl diselenide. The second band (R_f 0.14) gave 57 mg (49.3%) of **17**. NMR: δ 1.10 (3H, s, C_{10}–Me), 1.25 (3H, s, C_4–Me), 1.55 (3H, s, C_{11}–Me), 3.39 (1H, –OH), 3.66 (1H, m, C_3–H), 3.85 (1H, –OH), 3.97 (5H, m, $\langle{}^{-O}_{-O}$ and C_6–H), 7.2—7.8 (5H, m, $-C_6H_5$) ppm.

3α,4α-Dihydroxy-1,1-ethylenedioxy-5αH,6βH-eudesm-11-en-6,13-olide (**). To a solution of **17** (55 mg, 0.114 mmol) in THF (0.6 ml) containing acetic acid (17 μl) cooled to 0 °C was added 30% hydrogen peroxide (81 μl). The mixture was stirred for 30 min at 0 °C, then poured into cold sat $NaHCO_3$ aq and extracted with chloroform (10 ml×3). The combined extracts were washed with sat NaCl aq, dried (Na_2SO_4), and concentrated to give a crystalline material, which was purified by preparative TLC (silica gel GF_{254}, thickness 0.25 mm, EtOAc) to give 31 mg (83.8%) of **18** (R_f 0.20). NMR: δ 1.14 (3H, s, C_{10}–Me), 1.35 (3H, s,

C_4–Me), 3.45 (1H, –OH), 3.64 (1H, m, C_3–H), *ca.* 4.0 (6H, m, –OH, $\langle{}^{-O}_{-O}\rangle$, and C_6–H), 5.42 and 6.09 (each, 1H, d, J=3.0 Hz) ppm.

Arglanine (4). A solution of **18** (30 mg, 0.093 mmol) in 50% AcOH aq was refluxed for 71 h under N_2, cooled, and poured into sat NaCl aq (20 ml). The mixture was extracted with $CHCl_3$ (10 ml×2). The combined extracts were washed with sat $NaHCO_3$ aq (10 ml) and sat NaCl aq (10 ml), dried (Na_2SO_4), and concentrated to give a semi-solidal crude product. This was purified by preparative TLC (silica gel GF_{254}, EtOAc, thickness 0.25 mm) to give 14.0 mg (57.4%) of arglanine (R_f 0.52), which was recrystallized from EtOH to give colorless prisms, mp 190—192 °C. This material was identical with natural arglanine in IR (KBr) and NMR (60 MHz, $CDCl_3$).

The authors wish to thank Prof. V. Herout, Czechoslovak Academy of Sciences, for the generous gift of the IR spectrum of vulgarin. The authors are also grateful to Prof. S. Matsueda, Hirosaki University, for his kindness in supplying the IR and NMR spectra of arglanine.

References

1) T. K. Devon and A. I. Scott, "Handbook of Naturally Occurring Compounds," Vol. 2, Terpenes, Academic Press, New York (1972), pp. 79—175; H. Yoshioka, T. J. Mabry, and B. N. Timmermann, "Sesquiterpene Lactones," University of Tokyo Press, Tokyo (1973).

2) H. Knoche, G. Ourisson, G. W. Perold, J. Foussereau, and J. Maleville, *Science*, **166**, 239 (1969); G, W. Perold, J.-C. Muller, and G. Ourisson, *Tetrahedron*, **28**, 5797 (1972) and references cited therein; J. C. Mitchell, G. Dupuis, and T. A. Geissman, *Brit. J. Dermatol*, **87**, 235 (1972) and references cited therein; Y. Asakawa, G. Ourisson, and T. Aratani, *Tetrahedron Lett.*, **1975**, 3957.

3) S. M. Kupchan, Y. Aynechi, J. M. Cassady, H. K. Schnoes, and A. L. Burlingame, *J. Org. Chem.*, **34**, 3867 (1969); S. M. Kupchan, J. E. Kelsey, M. Maruyama, J. M. Cassady, J. C. Hemingway, and J. R. Knox, *ibid.*, **34**, 3876 (1969); S. M. Kupchan, R. J. Hemingway, D. Werner, and A. Karim, *ibid.*, **34**, 3903, 3908 (1969); S. M. Kupchan, *Trans. N. Y. Acad. Sci.*, **32**, 85 (1970); S. M. Kupchan, M. A. Eakin, and M. A. Thomas, *J. Med. Chem.*, **14**, 1147 (1971) and references cited therein.

4) S. M. Kupchan, *Science*, **161**, 789 (1968); H. Shibaoka, M. Shimokariyama, S. Iriuchijima, and S. Tamura, *Plant Cell Physiol.*, **8**, 297 (1967): H. Morimoto, Y. Sanno, and H. Oshio, *Tetrahedron*, **22**, 3173 (1966); T. Osawa, A. Suzuki, and S. Tamura, *Agric. Biol. Chem.*, **35**, 1966 (1971); T. Osawa, A. Suzuki, S. Tamura, Y. Ohashi, and Y. Sasada, *Tetrahedron Lett.*, **1973**, 5135; T. Osawa, D. Taylor, A. Suzuki, and S. Tamura, *Tetrahedron. Lett.*, **1977**, 1169.

5) P. M. Baker, C. C. Fortes, G. Gazzinelli, B. Gilbert, J. N. C. Lopes, J. Pelligrino, T. C. B. Tamassini, and W. Vichnewski, *J. Pharm. Pharmacol.*, **24**, 853 (1972).

6) E. J. Corey and A. G. Hortmann, *J. Am. Chem. Soc.*, **87**, 5736 (1965); M. Watanabe and A. Yoshikoshi, *J. Chem. Soc., Chem. Commun.*, **1972**, 698; A. E. Greene, J. C. Muller, and G. Ourisson, *J. Org. Chem.*, **39**, 186 (1974); R. B. Miller and E. S. Behare, *J. Am. Chem. Soc.* **96**, 8102 (1974); P. A. Grieco, *Synthesis*, **1975**, 67, and references cited therein; F. Kido, T. Fujishita, K. Tsutsumi, and A. Yoshikoshi, *J. Chem. Soc., Chem. Commun.*, **1975**, 337; K, Yamakawa, K. Nishitani, and T. Tominaga, *Tetrahedron Lett.*, **1975**, 2829; K. Yamakawa, T. Tominaga, and K. Nishitani, *ibid.*, **1975**, 4137; J. A. Marshall and W. R. Snyder, *J. Org. Chem.*, **40**, 1656 (1975); K, Yamakawa, K. Nishitani, and A. Yamamoto, *Chem. Lett.*, **1976**, 177; P. A. Grieco, M. Nishizawa, S. D. Burke, and N. Marinovic, *J. Am. Chem. Soc.*, **98**, 1612 (1976); S. Danishefsky, T. Kitahara, P. F. Schuda, and S. J. Etheredge, *J. Am. Chem. Soc.*, **98**, 3028 (1976); R. A. Kretchmer and W. J. Thompson, *J. Am. Chem. Soc.*, **98**, 3379 (1976); J. A. Marshall and R. H. Ellison, *J. Am. Chem. Soc.*, **98**, 4312 (1976); Y. Fugimoto, T. Shimizu, and T. Tatsuno, *Tetrahedron Lett.*, **1976**, 2041; P. A. Wender and J. C. Lechleiter, *J. Am. Chem. Soc.*, **99**, 267 (1977).

7) C. H. Heathcock and R. Ratcliffe, *J. Am. Chem, Soc.*, **93**, 1746 (1971); M. Kato, H. Kosugi, and A. Yoshikoshi, *J. Chem. Soc., Chem. Commun.*, **1970**, 185, 934.

8) J. A. Marshall and G. L. Bundy, *J. Chem. Soc., Chem. Commun.*, **1967**, 854; P. S. Wharton, C. E. Sundin, D. W. Johnson, and H. C. Kluender, *J. Org. Chem.*, **37**, 34 (1972).

9) P. S. Wharton and G. A. Hiegel, *J. Org. Chem.*, **30**, 3254 (1965); J. A. Marshall, W. F. Huffman, and J. A. Ruth, *J. Am. Chem. Soc.*, **94**, 4691 (1972); C. H. Heathcock and R. A. Badger, *J. Org. Chem.*, **37**, 234 (1972).

10) K. S. Rybalko, A. I. Bankovskij, and M. E. Perelzon, *Medicinskaja Promyšlennost SSSR*, **1960**, No. 10, 21; T. A. Geissman and G. A. Ellestad, *J. Org. Chem.*, **27**, 1855 (1962).

11) K. S. Rybalko and L. Dolejš, *Collect. Czech. Chem. Commun.*, **26**, 2909 (1961); T. A. Geissman and G. A. Ellestad, *J. Org. Chem.*, **27**, 1855 (1962).

12) S. Matsueda and T. A. Geissman, *Tetrahedron Lett.*, **1967**, 2013.

13) V. K. Honwad, E. Siscovic, and A. S. Rao, *Tetrahedron*, **23**, 1273 (1967).

14) E. J. Corey and A. G. Hortmann, *J. Am. Chem. Soc.*, **87**, 5736 (1965).

15) P. S. Wharton and D. H. Bolen, *J. Org. Chem.*, **26**, 3615 (1961).

16) The major product (**6a**) was isolated by the combination of column chromatography over silica gel and recrystallization. β(eq)-Configuration of the hydroxyl group at C_3 in **6a** was deduced from its NMR spectrum, which showed a peak at δ 3.82 (broad d, J=8.0 Hz) ppm, and confirmed by the NMR spectrum of its dihydro derivative (**19**), which showed a peak at δ 3.09 (ddd, J=5.0, 9.5, and 9.5 Hz) ppm.

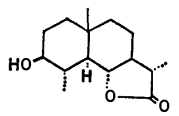

(19)

Although the attempted isolation of the minor product (**6b**) was unsuccessful, **6b** was deduced to be the C_3-epimer of **6a** from the fact that oxidation of the mixture of **6a** and **6b** gave **5** as the sole product.

17) L. F. Fieser, "Steroids," Reinhold Publishing Co. New York (1959), p. 276.

18) In mother liquors a small amount of **10** was observed, but the yield of **10** was not increased by prolonged reaction time under these conditions.

19) The double bond of **10** was further isomerized to the

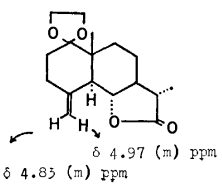

exo double bond under more drastic conditions (higher reaction temperature or prolonged reaction time).

20) H. Yoshioka, T. J. Mabry, and B. N. Timmermann, "Sesquiterpene Lactones," University of Tokyo Press, Tokyo (1973), p. 235.

21) N. S. Bhacca and D. H. Williams, "Applications of NMR Spectroscopy in Organic Chemistry," Holden-Day Inc., San Francisco (1964), p. 29.

22) K. Yamakawa, T. Tominaga, and K. Nishitani, *Tetrahedron Lett.*, **1975**, 4137.

23) P. A. Grieco and M. Miyashita, *J. Org. Chem.*, **39**, 120 (1974),

24) Y. Abe, T. Harukawa, H. Ishikawa, T. Miki, M. Sumi, and T. Toga, *J. Am. Chem. Soc.*, **78**, 1422 (1956).

25) Part II of this series has been published in *Tetrahedron*, **33**, 2785 (1977).

Reduction by a Model of NAD(P)H. XVI. Effect of Magnesium Ion for the Reduction of Thiopivalophenone

Atsuyoshi OHNO, Shinro YASUI, Kaoru NAKAMURA, and Shinzaburo OKA

Institute for Chemical Research, Kyoto University, Uji, Kyoto 611

(Received July 11, 1977)

Magnesium ion retards the reduction of thiopivalophenone with 1-benzyl-1,4-dihydronicotinamide (BNAH) in acetonitrile. Kinetics and other investigation have revealed that the retardation is due to the formation of non-reactive complexes, thiopivalophenone·Mg^{2+} and BNAH·Mg^{2+}.

It has been reported that the reduction of certain substrates, namely those that contain a pyridine moiety, with a derivative of 1,4-dihydronicotinamide is accelerated by a divalent metal ion such as magnesium or zinc ion.[1-4] The acceleration has been interpreted in terms of bidentate chelation of a metal ion onto the substrate to polarize the carbonyl group to be reduced. We reported that magnesium or zinc ion also promotes the reduction of α-keto esters, and the chelation of a metal ion onto a 1,4-dihydronicotinamide derivative was attributed to the promotion of reduction.[5] The polarization of the carbonyl group in an α-keto ester takes place only at the transition state of the reduction.[6]

Hexachloroacetone can be appointed for a third type substrate. The reduction of this compound is decelerated by the addition of a metal ion.[7] These authors proposed that the deceleration is caused by the formation of a complex between a 1,4-dihydronicotinamide derivative and a metal ion.[7]

In order to obtain a universal insight into the role of a metal ion, we studied the reduction of thiopivalophenone (**1**), a substrate in the third type, with 1-benzyl-1,4-dihydronicotinamide (BNAH) in the presence or absence of magnesium ion.

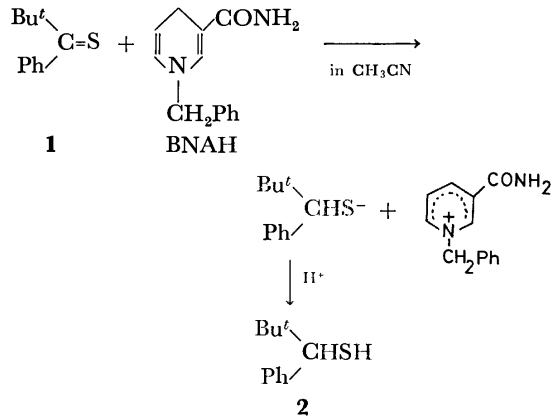

Results

The reaction of **1** with an equivalent molar amount of BNAH in dry acetonitrile at a room temperature afforded 1-phenyl-2,2-dimethyl-1-propanethiol (**2**) in quantitative yield. The direct transfer of a hydrogen at the C_4-position of BNAH onto the C_1-position of the product was confirmed by an experiment with BNAH-4,4-d_2.

As a source of magnesium ion, magnesium nitrate was employed for most reactions. It was confirmed that the substitution of the salt for magnesium perchlorate did not affect the kinetics. Magnesium nitrate contains six molecules of water of crystallization. However, that the water of crystallization did not affect the kinetics was tested with a run with more than equivalent amount of water in the absence of magnesium nitrate.

Kinetics was followed vapor-phase-chromatographically by observing the decrease in the amount of **1**, or,

TABLE 1. RATE CONSTANT FOR THE REACTION OF THIOPIVALOPHENONE (**1**) WITH 1-BENZYL-1,4-DIHYDRONICOTINAMIDE (BNAH) IN ACETONITRILE AT 25 °C

10^3[**1**], M	10^2[BNAH], M	$10^4 k_{obsd}$, s^{-1}	r[a]	$10^3 k_2$, $M^{-1} s^{-1}$ [b]
2.80	5.80	3.37	0.9996	5.82
2.80	5.83	3.38	0.9995	5.79
2.80	2.95	1.73	0.9993	5.86
3.34	3.69	2.13	0.9990	5.77
41.3[c]	0.175	2.18	0.9987	6.05
2.78[d]	5.81	3.25	0.9997	5.59
2.86[e]	5.90	3.93	0.9995	6.66

a) Correlation coefficient. b) $k_2 = k_{obsd}/[BNAH]$. Estimated error in k_2 is ±3%. c) Followed spectrophotometrically. d) The solution contains 2.78×10^{-2} M water. e) The solution contains 1.18×10^{-2} M ammonium perchlorate.

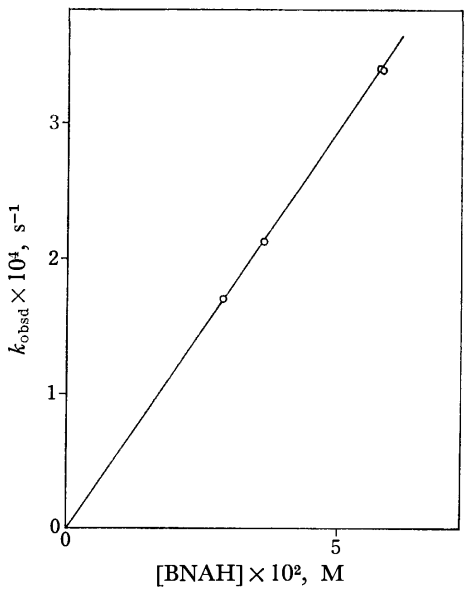

Fig. 1. A linear relationship between observed pseudo-first-order rate constant and the concentration of BNAH, from which the second-order rate constant at 25 °C was calculated.

Table 2. Rate constant for the reaction of thiopivalophenone (**1**) with 1-benzyl-1,4-dihydronicotinamide (BNAH) in the presence of magnesium ion in acetonitrile at 25 °C

10^3[**1**], M	10^2[BNAH], M	10^4[Mg^{2+}], M	$10^4 k_{obsd}$, s^{-1}	r[b]
2.80	5.81	3.76	3.29	0.9998
2.80	5.87	7.57	3.31	0.9996
2.80	5.82	9.44	3.37	0.9997
1.96	5.84	11.27	3.29	0.9995
3.34	2.74	11.90	1.26	0.9994
2.82	4.90	11.93	2.53	0.9998
2.84	6.00	11.93	3.34	0.9997
2.82	13.71	12.00	1.74	0.9998
2.80	2.91	18.80	1.25	0.9998
2.80	5.85	18.86	3.05	0.9995
1.40	2.92	18.92	1.36	0.9997
2.69	5.80	20.44	2.97	0.9993
2.80	5.81	27.55[c]	2.92	0.9999
2.80	5.85	28.28	2.94	0.9999
2.78	2.81	29.76	1.01	0.9992
2.82	4.91	29.84	2.14	0.9994
2.84	6.15	29.84	2.85	0.9996
3.34	3.80	30.00	1.64	0.9993
2.80	5.83	37.83	2.73	0.9997
2.89	5.86	40.01	2.55	0.9999
2.80	5.80	40.87	2.46	0.9998
2.80	5.78	41.77	2.78	0.9997
2.89	5.85	46.95[c]	2.41	0.9995
2.80	5.71	58.48	2.20	0.9996
2·78	2.97	59.51	0.717	0.9994
2.82	4.88	59.67	1.61	0.9992
2.84	6.04	59.67	2.28	0.9998
3.34	3.72	59.98	1.09	0.9996
2.80	5.82	75.47	2.07	0.9992
2.78	4.46	80.34	1.14	0.9998
2.79	3.82	80.34	0.934	0.9994
2.83	5.91	80.34	1.91	0.9996
2.88	8.63	80.34	4.06	0.9996
2.80	5.82	83.46	1.75	0.9993
43.3[d]	0.175	13.10	2.03	0.9989
32.8	0.165	49.90	0.494	0.9983

a) $Mg(NO_3)_2 \cdot 6H_2O$ was used unless otherwise indicated. b) Correlation coefficient. c) $Mg(ClO_4)_2$ was used. d) Followed by spectrophotometry.

in part, spectrophotometrically by observing the decrease in the intensity of absorption at 350 nm (from BNAH). Each run gave a good pseudo-first-order correlation ($r>0.999$). From the result listed in Table 1, the second-order rate constant, k_2, at 25 °C was calculated to be 5.80×10^{-3} M^{-1} s^{-1} (see Fig. 1). Table 2 summarizes kinetic result in the presence of magnesium ion.

Discussion

The fact that two different methods gave the same pseudo-first-order rate constant indicates that the decreases of the concentration of BNAH corresponds directly to that of **1**.[8]

In contrast to the reduction of α-keto esters, the reduction of **1** is retarded by the presence of magnesium ion. On the other hand, ammonium perchlorate results in slight increase in the rate, probably due to a salt effect. In the presence of magnesium ion, the second-order rate constants, k_2, tentatively calculated by dividing k_{obsd} by the concentration of BNAH gave neither a constant value nor a simple dependence on the concentration of magnesium ion. In previous papers we reported that magnesium ion forms a complex with BNAH.[6] However, the complex-formation alone does not explain the present result. That is, one cannot expect the change in the concentration of BNAH.

In analogy with a treatment for kinetics of fully and noncompetitively inhibited enzymic reactions,[9] plots were made for $1/k_{obsd}$ against $1/$[BNAH] for each constant concentration of magnesium ion. The result is illustrated in Fig. 2, from which it is obvious that the substrate, **1**, forms a non-reactive (noncompetitive) complex with magnesium ion. Moreover, the plots give curved lines instead of linear relationships. The result can be interpreted with the following reaction scheme:

$$\mathbf{1} + \mathrm{BNAH} \overset{K_1}{\rightleftharpoons} \mathbf{1}\cdot\mathrm{BNAH} \xrightarrow{k_2} \mathrm{Products}$$

$$\mathbf{1} + Mg^{2+} \overset{K_3}{\rightleftharpoons} \mathbf{1}\cdot Mg^{2+}$$

$$\mathrm{BNAH} + Mg^{2+} \overset{K_4}{\rightleftharpoons} \mathrm{BNAH}\cdot Mg^{2+}$$

$$\mathbf{1}\cdot Mg^{2+} + \mathrm{BNAH} \overset{K_5}{\rightleftharpoons} \mathbf{1}\cdot Mg^{2+}\cdot\mathrm{BNAH}$$

$$\mathrm{BNAH}\cdot Mg^{2+} + \mathbf{1} \overset{K_6}{\rightleftharpoons} \mathbf{1}\cdot Mg^{++}\cdot\mathrm{BNAH}$$

$$\mathbf{1}\cdot\mathrm{BNAH} + Mg^{2+} \overset{K_7}{\rightleftharpoons} \mathbf{1}\cdot Mg^{2+}\cdot\mathrm{BNAH}.$$

Based on the above reaction scheme, the concentrations of free **1** and BNAH are expressed by Eqs. 1 and 2, respectively.[10]

$$[\mathbf{1}] = \frac{[\mathbf{1}]_0}{1+[\mathrm{BNAH}]/K_1+[Mg^{2+}]/K_3+[\mathrm{BNAH}][Mg^{2+}]/K_1K_7}, \tag{1}$$

$$[\mathrm{BNAH}] = \frac{[\mathrm{BNAH}]_0}{1+[\mathbf{1}]/K_1+[Mg^{2+}]/K_4+[\mathbf{1}][Mg^{2+}]/K_1K_7}, \tag{2}$$

where the subscript 0 denotes a stoichiometric concentration. Since

$$v = k_2[\mathbf{1}\cdot\mathrm{BNAH}] = k_2[\mathbf{1}][\mathrm{BNAH}]/K_1, \tag{3}$$

when A, B, C, and D are defined by Eqs. 4—7, the rate expression shown in Eq. 8 is obtained.

$$A = K_1K_7(K_3+[Mg^{2+}])(1+[Mg^{2+}]/K_4), \tag{4}$$

$$B = K_3\,(K_7+[Mg^{2+}]), \tag{5}$$

$$C = (K_3+[Mg^{2+}])(K_7+[Mg^{2+}]), \tag{6}$$

$$D = \frac{1}{2C}(\sqrt{\{A+B([\mathrm{BNAH}]_0-[\mathbf{1}]_0)\}^2+4AB[\mathbf{1}]_0} - \{A+B([\mathrm{BNAH}]_0-[\mathbf{1}]_0)\}), \tag{7}$$

$$\frac{1}{v} = \frac{K_1}{k_2[\mathrm{BNAH}]_0}\left\{\frac{1}{K_1}\left(1+\frac{[Mg^{2+}]}{K_7}\right)+\frac{1}{D}\left(1+\frac{[Mg^{2+}]}{K_4}\right)\right\}. \tag{8}$$

The denominator of the right-hand side in Eq. 8 is composed of the second-, three-halves-, and first-order terms of the stoichiometric concentration of BNAH in accord with the observed result. The result leads to a conclusion that both BNAH-magnesium ion and **1**-magnesium ion complexes are non-reactive, which is a marked contrast with the reaction of α-keto esters. It is known that thioketones form complexes with various metal salts[11] as well as with BNAH.[12]

The validity of the proposed reaction scheme can be tested in several ways. In the range of BNAH-concentrations where the curves in Fig. 2 can be approximated by straight lines, slopes of the lines, m, are expressed by Eq. 9.

$$m = \frac{1}{k_2}\left(1+\frac{[Mg^{2+}]}{K_7}\right). \quad (9)$$

A plot of m against the concentration of magnesium ion indeed gave a straight line as shown in Fig. 3. From the intercept and slope the values of k_2 and K_7 were calculated to be 5.81×10^{-3} M^{-1} s^{-1} and 3.77×10^{-3} M, respectively. Thus, calculated rate constant is identical to the observed one.[13]

The dependence of the rate constants in the presence and absence of magnesium ion on the reaction temperature is listed in Table 3, from which the energy of activations in the presence and absence of magnesium ion were calculated to be identical (8.9±0.5 and 8.0±0.3 kcal/mol for reactions with and without magnesium ion, respectively).[14]

The reduction of **1** with optically active *N*-(α-methylbenzyl)-1-propyl-1,4-dihydronicotinamide (**3**) affords optically active **2**. The reductions with *R*-**3** in the presence and absence of magnesium ion resulted in the formation of **2** of $[\alpha]_D=-5.8$ and -6.2, respectively. Although we do not know the degree of rotation for optically pure **2**, there is no doubt that both reactions gave the identical stereochemical result.

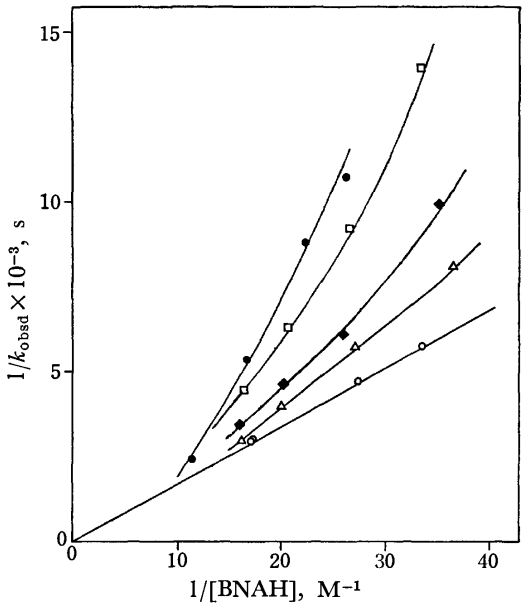

Fig. 2. Correlation of $1/k_{obsd}$ against 1/[BNAH] for constant concentrations of magnesium ion: ○ $[Mg^{2+}]=0$; △ $[Mg^{2+}]=1.2\times10^{-3}$ M; ◆ $[Mg^{2+}]=3.0\times10^{-3}$ M; □ $[Mg^{2+}]=6.0\times10^{-3}$ M; ● $[Mg^{2+}]=8.0\times10^{-3}$ M.

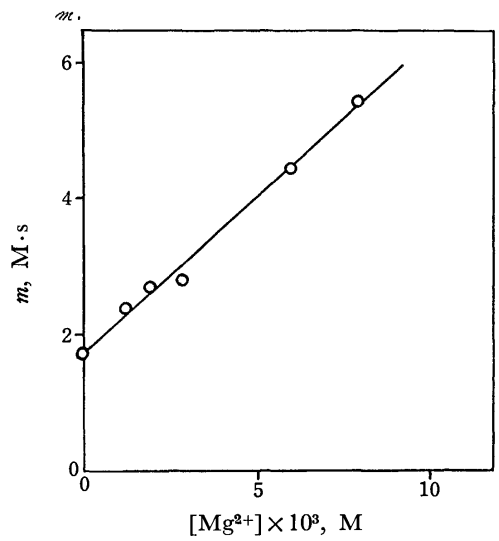

Fig. 3. Dependence of m on the concentration of magnesium ion.

TABLE 3. TEMPERATURE-DEPENDENCE OF RATE CONSTANTS IN PRESENCE AND ABSENCE OF MAGNESIUM ION[a]

$10^3[Mg^{2+}]$, M[b]	Temp, °C[c]	k
6.00	14	0.672[d]
6.00	25	1.09[d]
6.00	30	1.58[d]
0	10	2.83[e]
0	17	3.98[e]
0	25	5.80[e]
0	30	7.12[e]

a) Under the condition of [**1**] $=2.80\times10^{-3}$ M and [BNAH] $=3.72\times10^{-2}$ M. b) $Mg(NO_3)_2\cdot6H_2O$ was used. c) ±0.05 °C. d) 10^4k_{obsd}, s^{-1}. e) 10^3k_2 $(=10^3 k_{obs}/[BNAH])$, M^{-1} s^{-1}.

The final diagnosis was made by kinetic deuterium isotope effect using BNAH-4,4-d_2. The isotope effects, k_H/k_D, for both reactions were found to be identical (5.0±0.2).

All of above results indicate that magnesium ion is not involved in the product-forming process and that the polarization of a substrate does not necessarily result in the acceleration of the reduction. Detailed discussion on the difference in reactivities of **1** and α-keto esters will appear in the following paper.[15]

Partial support in the form of a Scientific Research Grant from the Ministry of Education, Japan, is acknowledged.

Experimental

Materials. Thiopivalophenone[16,17] and 1-benzyl-1,4-dihydronicotinamide[18] were prepared according to literatures. 1-Benzyl-1,4-dihydronicotinamide-4,4-d_2 was prepared from BNA^+Cl^- by three times repetition of D_2O–$Na_2S_2O_4$-reduction—malachite green-oxidation.[18] Magnesium nitrate and perchlorate were commercially available (Wako Chem. Co.) and purified prior to use.[6b] Acetonitrile

was distilled once on phosphorus pentaoxide and kept over molecular sieves 4A.

Procedure. Preparation of solutions for kinetic studies and the method to follow the kinetics by spectrophotometry were described previously.[6] For kinetic observations under the conditions of excess BNAH, 1 ml aliquots were taken out from a 20 ml reaction solution after appropriate time intervals and poured into 5 ml of dilute hydrochloric acid. The organic materials were extracted with 5 ml hexane. The hexane-layer (20 μl) was subjected to VPC (Yanagimoto G-18000, FID, 15% BDS, 1 m, 135 °C). 1,4-Dipropoxybenzene was used as an internal standard. At least 10 points were obtained for a run. The reaction temperatures were kept constant within the accuracy of ±0.05 °C. Least-squares method was employed to evaluate linear relashioships.

Deuterium contents were analyzed on a Varian T-60 NMR Spectrometer and Shimadzu LKB-9000S GC-MS Spectrometer.[19,20] The optical activity of the thiol was measured on a Perkin-Elmer 241 Polarimeter (30 mg/2 ml EtOH).

The method for isolation and identification of 1-phenyl-2,2-dimethyl-1-propanethiol was the same as described previously for the case of 2,2,4,4-tetramethyl-3-pentanethiol.[21]

References

1) D. J. Creighton and D. S. Sigman, *J. Am. Chem. Soc.*, **93**, 6314 (1971).

2) S. Shinkai and T. C. Bruice, *J. Am. Chem. Soc.*, **94**, 8258 (1972).

3) M. Hughes and R. H. Prince, *Chem. Ind.*, **1975**, 648.

4) R. A. Gase, G. Boxhoorn, and U. K. Pandit, *Tetrahedron Lett.*, **1976**, 2889.

5) Y. Ohnishi, M. Kagami, and A. Ohno, *J. Am. Chem. Soc.*, **97**, 4766 (1975).

6) a) A. Ohno, T. Kimura, H. Yamamoto, S. G. Kim, S. Oka, and Y. Ohnishi, *Bull. Chem. Soc. Jpn.*, **50**, 1535 (1977); b) A. Ohno, H. Yamamoto, T. Okamoto, S. Oka, and Y. Ohnishi, *ibid.*, **50**, 2385 (1977).

7) D. C. Dittmer, A. Lombardo, F. H. Batzold, and C. S. Greene, *J. Org. Chem.*, **41**, 2976 (1976).

8) There have been no report which confirms this phenomenon.

9) E. Zeffren and P. L. Hall, "The Study of Enzyme Mechanisms," John Wiley & Sons, Inc., New York, N. Y. (1973), pp. 89—99.

10) K_1's are defined as dissociation constants of complexes.

11) E. Campaigne, *Chem. Rev.*, **39**, 1 (1946).

12) A. Ohno and N. Kito, *Chem. Lett.*, **1972**, 369.

13) K_4 was observed to be 5.56×10^{-4} M. See Ref. 6b.

14) Since the observed rate constant in the presence of magnesium ion is a complex function of the concentration of magnesium ion, the intercept of the line obtained by plotting $\ln k_{obsd}$ against $1/T$ has no physical meaning. From runs without magnesium ion, $\Delta H^*=8.56\pm0.3$ kcal/mol and $\Delta S^*=-56.3\pm2$ eu were calculated. The values are comparable to those of a similar reaction[7] and reasonable for the proposed mechanism.

15) A. Ohno, S. Yasui, H. Yamamoto, S. Oka, and Y. Ohnishi, the succeeding paper.

16) A. Ohno, K. Nakamura, N. Nakazima, and S. Oka, *Bull. Chem. Soc. Jpn.*, **48**, 2403 (1975).

17) J. M. Beiner, D. Lecadet, D. Paquer, A. Thuillier, and J. Vialle, *Bull. Soc. Chim. Fr.*, **1973**, 1979.

18) D. Mauzerall and F. H. Westheimer, *J. Am. Chem. Soc.*, **77**, 2261 (1955).

19) B. J.-S. Wang and E. R. Thornton, *J. Am. Chem. Soc.*, **90**, 1216 (1968).

20) D. J. Creighton, J. Hajdu, and D. S. Sigman, *J. Am. Chem. Soc.*, **98**, 4619 (1976).

21) A. Ohno, K. Nakamura, M. Uohama, S. Oka, T. Yamabe, and S. Nagata, *Bull. Chem. Soc. Jpn.*, **48**, 3718 (1975).

Reduction by a Model of NAD(P)H. XVII. Isotope Effects and Magnesium Ion Catalysis

Atsuyoshi OHNO, Shinro YASUI, Hiroyuki YAMAMOTO, Shinzaburo OKA, and Yutaka OHNISHI*

Institute for Chemical Research, Kyoto University, Uji, Kyoto 611

**Sagami Chemical Research Center, Nishiohnuma, Sagamihara, Kanagawa 229*

(Received July 11, 1977)

The reduction of thiopivalophenone (**1**) with 1-benzyl-1,4-dihydronicotinamide (BNAH) gives the same value for kinetic deuterium isotope effect (k_H/k_D) and isotopic distribution in the product (Y_H/Y_D) regardless of the presence or absence of magnesium ion. The reduction of methyl benzoylformate (**2**) with a BNAH-analog in the presence of magnesium ion also gives similar values for k_H/k_D and Y_H/Y_D. It has been concluded that magnesium ion stabilizes the transition state in the reduction of **2**, whereas an intermediate is stabilized by magnesium ion in the reduction of **1**.

In the preceeding paper, we reported that magnesium ion decelerates the reduction of thiopivalophenone (**1**) with 1-benzyl-1,4-dihydronicotinamide (BNAH).[1] The deceleration was accounted for by the formation of non-reactive complexes, $\mathbf{1}\cdot Mg^{2+}$ and $BNAH\cdot Mg^{2+}$. On the other hand, the reduction of α-keto esters is accelerated by magnesium ion and the acceleration was ascribed to the formation of the reactive complex, $BNAH\cdot Mg^{2+}$.[2]

This paper describes, based on the results from the study on isotope effects, that such an apparently contradictory phenomenon as $BNAH\cdot Mg^{2+}$ being non-reactive in one reaction but reactive in another is not a real contradiction.

Results

All reactions were carried out in acetonitrile at 25 °C. Pseudo-first-roder kinetics for the reduction of methyl benzoylformate (**2**) with *N*-(α-methylbenzyl)-1-propyl-1,4-dihydronicotinamide (PPNAH) was followed spectrophotometrically by observing the decrease in intensity of absorption maximum at 354 nm.[2b] Kinetics for the reduction of **1** with BNAH was followed vapor-phase-chromatographically by observing the decrease in concentration of **1**.[1] It was confirmed that spectrophotometric and vapor-phase-chromatographic methods gave the identical result.[1] It was also confirmed that magnesium nitrate used for the reduction of **1** behaved similarly to magnesium perchlorate.[1] Since the rate of the reduction of **1** is a complex function of the concentration of magnesium ion,[1] the kinetics was followed under a constant concentration of magnesium ion. The rate of the reduction of **2** followed zero-order in magnesium ion under its existence in large excess.[2b] In Tables 1 and 2 are summarized

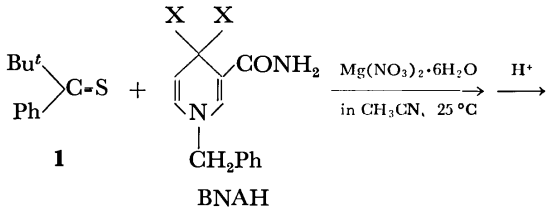

1 BNAH

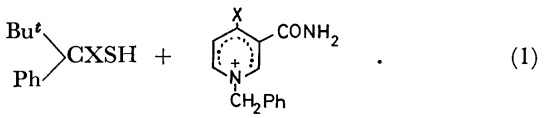

X=H or D (1)

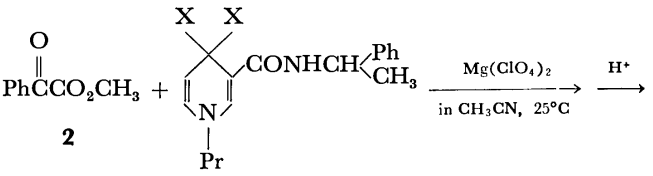

2 PPNAH

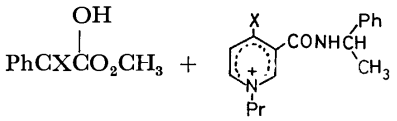

X=H or D (2)

Table 1. Isotope effects in the reduction of thiopivalophenone

Reductant	$10^3[Mg^{2+}]$, M	10^3k_2, $M^{-1}s^{-1}$ a)	k_H/k_D	Y_H/Y_D
BNAH	0	5.80 ±0.18		
BNAH-d_1	0	3.49 ±0.03	4.9±0.2	5.0±0.4
BNAH-d_2	0	1.16 ±0.03	5.0±0.2	
BNAH	6.00	3.74 ±0.11 b)		
BNAH-d_1	6.00	2.22 ±0.07 b)	5.3±0.2	4.9±0.3
BNAH-d_2	6.00	0.779±0.02 b)	4.8±0.2	

a) $k_2=k_{obsd}/[BNAH\text{-}d_x]$. b) Values obtained under the condition of $[\mathbf{1}]=2.73\times10^{-3}$ M and $[BNAH\text{-}d_x]=5.27\times10^{-2}$ M.

Table 2. Isotope effects in the reduction of methyl benzoylformate in the presence of magnesium ion[a)]

Reductant	$10k_2$, $M^{-1}s^{-1}$ b)	k_H/k_D	Y_H/Y_D
PPNAH	1.46 ±0.04		
PPNAH-d_1	0.900±0.03	4.3±0.2	3.7±0.5 c)
PPNAH-d_2	0.340±0.01	4.3±0.2	

a) Under the condition of $[\mathbf{2}]=1.0\times10^{-2}$ M, $[PPNAH\text{-}d_x]=2.0\times10^{-4}$ M, and $[Mg^{2+}]=1.0\times10^{-2}$ M. b) $k_2=k_{obsd}/[\mathbf{2}]$. c) Under the condition of $[\mathbf{2}]=1.0\times10^{-3}$ M, $[PPNAH]=1.0\times10^{-3}$ M, and $[Mg^{2+}]=2.0\times10^{-3}$ M. $Y_H/Y_D=3.1\pm0.3$ was obtained when each 6.8×10^{-2} M of reagent was used.

kinetic results together with isotopic ratio (Y_H/Y_D) in the product, 1-phenyl-2,2-dimethyl-1-propanethiol and methyl mandelate, from the reduction with BNAH-4-*d* and PPNAH-4-*d*, respectively. Kinetic isotope effect (k_H/k_D) was calculated after Steffens and Chipman.[3] The values for k_H/k_D and Y_H/Y_D were corrected for isotopic contents of deuterated BNAH and PPNAH used.

Discussion

Steffens and Chipman suggested elegantly that there is at least one intermediate in the reduction of α,α,α-trifluoroacetophenone with BNAH or its analogs.[3] Their argument based on the fact that kinetic deuterium isotope effect, k_H/k_D, is much smaller than the ratio of the amounts of isotopes incorporated in the product, Y_H/Y_D. Later, Creighton and his coworkers reported similar result in the reduction of 1,10-phenanthroline-2-carbaldehyde.[4] We confirmed that the intermediate proposed by these authors is indeed a charge-transfer-type complex.[5]

The large discrepancy between the values of k_H/k_D and Y_H/Y_D appears only when the free energy of the transition state for k_1-step in Eq. 3 is slightly larger than that for the k_2-step as shown by a solid line in Fig. 1.

$$S+BH \underset{k^{-1}}{\overset{k_1}{\rightleftharpoons}} S\cdot BH \xrightarrow{k_2} SH^- + B^+. \quad (3)$$

The values of k_H/k_D and Y_H/Y_D for the reduction of **1** or hexachloroacetone[6] are equal, respectively, which indicates that the free energy of the transition state for the k_2-step is much larger than that for the k_1-step in this reduction as shown in Fig. 1 by a dotted line. Note that both **1** and hexachloroacetone are substrates that can be reduced without the assistance of metal ion. When metal ion is added to the reaction system, the metal ion may form a stable ternary complex, say, **1**·Mg^{2+}·BNAH.[1] If the free energy of the complex becomes small enough so that the activation energy for the k_2-step becomes larger than that for the k_1-step, the net reduction (more precisely, the transfer of a proton) through the ternary complex becomes difficult to proceed (dashed line in Fig. 1). This argument is partly supported by the following observation:[7] 4,4′-Dichlorobenzil is reduced by BNAH in the presence of magnesium ion in acetonitrile. However, no ESR-signal was detected from the reaction solution. When acetonitrile was substituted by dimethyl sulfoxide, no reduction took place, whereas strong ESR-signal from 4,4′-dichlorobenzil anion radical paired by magnesium ion was recorded. Even in the absence of magnesium ion, weak ESR-signal of the anion radical could be recorded from the mixture in dimethyl sulfoxide. This observation reveals that the charge-transfer intermediate is too unstable in the reacting system to be detected by ESR-spectroscopy. When the solvent is changed to the one which stabilizes the intermediate, the net reduction is prohibited because the k_2-step becomes unfavorable and the intermediate is accumulated. Magnesium ion increases the stability of the intermediate.[8]

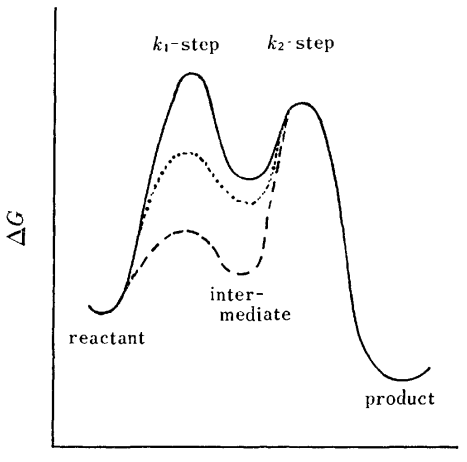

Fig. 1. Schematic energy diagram.

Reduction of **2** in acetonitrile does not take place without magnesium ion. Therefore, there is no doubt that magnesium ion plays a role to reduce the free energy of a transition state for either of k_1- or k_2-step, or both of this reaction. However, it is highly unlikely to expect that the process of electron-transfer is associated with such a large kinetic isotope effect as 4.3, the value which is comparable to that of **1**. This leads to a conclusion that magnesium ion catalyzes the k_1-step, or an electron-transfer process, and the energy diagram for this reaction may be represented by the dotted line in Fig. 1. The similarity in the values of Y_H/Y_D for the reductions of **1** and **2** suggests that the positions of transition states for these reactions may be similar.

It is noteworthy that the ternary complex, **2**·Mg^{2+}·PPNAH, has been proposed to be the transition state,[2] whereas the ternary complex, **1**·Mg^{2+}·BNAH, is in the ground state.[1] The metal ion complex must stabilize the transition state of the reaction in order to assist the reaction effectively, and metal ion complex formation in the ground state depresses the reaction rate. In true catalyses such as enzymic catalysis the strongest coordination must be to the transition state, and not to the reactant or product.[9]

Klinman argued on the transition state of enzymic reductions.[10] Kinetic isotope effects and substituent effects[10,11] reconcile with the energy diagram schematically shown by the dotted line in Fig. 1 provided general-acid catalysis is assumed for the reduction with alcohol dehydrogenases.[12-15] Furthermore, it is interesting to point out that the energy diagrams for the present model reactions with **1** and **2** without magnesium ion correspond fortuitously with those for enzymic reductions of ketones and α-keto esters, respectively. The rate-determining step for the reaction with an alcohol dehydrogenase is the process of a proton-transfer, whereas that with a lactate dehydrogenase is the process that takes place prior to the proton-transfer.[16]

Partial support in the form of a Scientific Research Grant from the Ministry of Education, Japan, is acknowledged.

Experimental

Preparation, purification, and identification of materials were described previously.[1,2,17] Procedures for the kinetics

and the analyses of isotopic contents were also described in previous papers.[1,2b]

The deuterium contents in BNAH-4-*d* or PPNAH-4-*d* were 99.0±1%, and those in BNAH-4,4-d_2 or PPNAH-4,4-d_2 were 91.5±1—94.5±1% depending on the runs of preparation. For the calculation of the purity of dideuterated compound, no contamination of undeuterated compound was assumed.

References

1) A. Ohno, S. Yasui, K. Nakamura, and S. Oka, *Bull. Chem. Soc. Jpn.*, **51**, 290 (1978).

2) a) A. Ohno, T. Kimura, H. Yamamoto, S. G. Kim, S. Oka, and Y. Ohnishi, *Bull. Chem. Soc. Jpn.*, **50**, 1535 (1977); b) A. Ohno, H. Yamamoto, T. Okamoto, S. Oka, and Y. Ohnishi, *ibid.*, in press.

3) J. J. Steffens and D. M. Chipman, *J. Am. Chem. Soc.*, **93**, 6694 (1971).

4) D. J. Creighton, J. Hajdu, and D. S. Sigman, *J. Am. Chem. Soc.*, **98**, 4619 (1976).

5) a) T. Okamoto, A. Ohno, and S. Oka, *J. Chem. Soc., Chem. Commun.*, **1977**, 181; b) A. Ohno and N. Kito, *Chem. Lett.*, **1972**, 369.

6) D. C. Dittmer, A. Lombardo, F. H. Batzold, and C. S. Greene, *J. Org. Chem.*, **41**, 2976 (1976).

7) Y. Ohnishi and A. Ohno, *Chem. Lett.*, **1976**, 697.

8) The reduction of cationic substrate such as malachite green is also retarded by the presence of magnesium ion (preliminary result from our laboratory). There are two pcssibilities for this retardation: one involves a stable ternary complex as an intermediate. The other is due to the ionic repulsion between charges on the substrate and BNAH·Mg^{2+} complex. We have no datum at present to choice the one over the other.

9) M. L. Bender, "Mechanism of Homogeneous Catalysis from Protons to Proteins," Wiley-Interscience, New York (1971), pp. 233 and 235.

10) a) J. P. Klinman, *J. Biol. Chem.*, **247**, 7977 (1972); b) J. P. Klinman, *Biochemistry*, **15** 2018 (1976).

11) L. C. Kurz and C. Frieden, *J. Am. Chem. Soc.*, **97**, 677 (1975).

12) G. J. Hardman, L. F. Blackwell, C. R. Boseell, and P. D. Buckley, *Eur. J. Biochem.*, **50**, 113 (1974).

13) R. H. Abeles, R. F. Hutton, and F. H. Westheimer, *J. Am. Chem. Soc.*, **79**, 712 (1957).

14) *Cf.* also A. Shirra and C. J. Suckling, *J. Chem. Soc., Perkin Trans. 2*, **1977**, 759.

15) The substituent effect on the pre-equilibrium should also be taken into account, because the effect operates oppositely on the electron- and proton-transfer processes.

16) J. J. Holbrook, A. Liljas, S. J. Steindel, and M. G. Rossmann, "Lactate Dehydrogenase," in "The Enzymes," 3rd ed, Vol. XI-A, ed by P. D. Boyer, Academic Press, New York (1975), pp. 284—289.

17) A. Ohno, T. Kimura, S. G. Kim, H. Yamamoto, S. Oka, and Y. Ohnishi, *Bioorg. Chem.*, **6**, 21 (1977).

Studies of Peptide Antibiotics. XXXVII.[1] Synthesis of [1,1',3,3'-L-Alanine]-Gramicidin S

Hideo TAKIGUCHI, Hiroshi NISHIKAWA, Setsuko ANDO, and Nobuo IZUMIYA*

Department of Chemistry, Faculty of Science, Fukuoka University, Nanakuma, Nishi-ku, Fukuoka 814

** Laboratory of Biochemistry, Faculty of Science 33, Kyushu University, Hakozaki, Higashi-ku, Fukuoka 812*

(Received July 29, 1977)

An analog containing alanyl residues in place of valyl and leucyl residues in gramicidin S, namely [1,1',3,3'-L-alanine]-gramicidin S, was synthesized to investigate the influence of the bulky side chains of the amino acid residues for antibacterial activity and conformation. The analog has the small aliphatic side chains of alanyl residues on one side of the ring frame in the gramicidin S-structure. In the experiments of optical rotatory dispersion and circular dichroism, this analog gave curves similar in shape to these of gramicidin S, and thus should have a similar conformation to that of gramicidin S. The analog showed, however, no antibacterial activity. Thus the four methyl side chains of alanyl residues in the analog are not sufficient for the substance to exhibit biological activity.

Various analogs of gramicidin S (GS, Fig. 1) have been studied to investigate the relationship between chemical structure and biological activity. Particularly, some analogs with other amino acid residues in place of either the valyl or leucyl residues have been prepared by Izumiya and his collaborators. Some of them, such as [1,1'-Ala]-[2] and [1,1'-Leu]-GS,[3] exhibited substantial antibacterial activities. On the other hand, very weak or no activity was observed for the other analogs, that is, [1,1'-Gly]-,[2] [3,3'-Gly]-,[4] and [3,3'-Ala]-GS.[4] In Table 1 are listed the antibacterial activities of the 1,1'- or/and 3,3'-position substituted

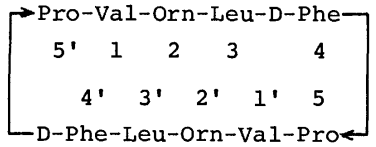

(a) gramicidin S (GS)

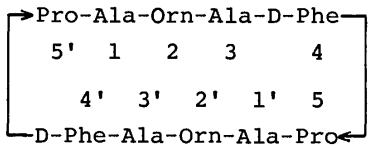

(b) [1,1',3,3'-Ala]-GS

Fig. 1. Structure of GS and [1,1',3,3'-Ala]-GS.

TABLE 1. ANTIBACTERIAL ACTIVITIES OF 1,1'- OR/AND 3,3'-POSITION SUBSTITUTED GS ANALOGS[a]

Substituted residues	*S. aureus*	*B. subtilis*	Reference No.
1,1'-Gly	100	100	2
1,1'-Ala	5	5	2
1,1'-Val (GS)[b]	2—5	2—5	—
1,1'-Leu	5	10	3
3,3'-Gly	>100	>100	4
3,3'-Ala	50	20	4
3,3'-Leu (GS)[b]	2—5	2—5	—
1,1',3,3'-Ala	>100	>100	This work

a) This table shows the minimum inhibitory concentration (μg/ml) with a Bouillon agar medium. b) The natural GS used as the control.

GS analogs. As shown in Table 1, the activity of 3,3'-position substituted GS decreases significantly upon decreasing the bulkiness of the side chains of 3,3'-residues, whereas the bulkiness of the side chains in 1,1'-position substituted GS is not so important for the activity. For the conformation of GS, several models have been proposed. One of them is based on the β-pleated sheet structure shown in Fig. 2, which seems to be the most likely model.[5] In this specific model, the four hydrophobic side chains of valyl and leucyl residues are located on one side of the ring frame consisting of the cyclic peptide chain, while the two hydrophilic side chains of ornithyl residue are placed on the opposite side.

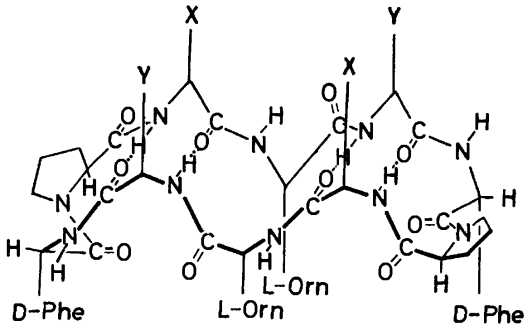

Fig. 2. Possible model of GS (X=Val, Y=Leu) and [1,1',3,3'-Ala]-GS (X, Y=Ala).

For the purpose of investigating the effect of the hydrophobic side chains on the activity, it seemed of interest to synthesize an analog having alanyl residues in place of both the valyl and leucyl residues in GS. The analog has the small aliphatic side chains on one side of the ring frame in the GS-structure. The present paper will describe the synthesis of [1,1',3,3'-L-analine]-gramicidin S ([1,1',3,3'-Ala]-GS) (as shown in Fig. 1), the ORD and CD measurements, and the antibacterial properties.

The synthesis of [1,1',3,3'-Ala]-GS (**10**) is outlined in Fig. 3. Acyldipeptide ester (**1**) was prepared by means of the MA method,[6] and then converted into a hydrazide (**2**). Acyltripeptide ester (**3**) was prepared by stepwise elongation by means of the DCC method as a crystalline solid. It had previously been reported as an oil.[4]

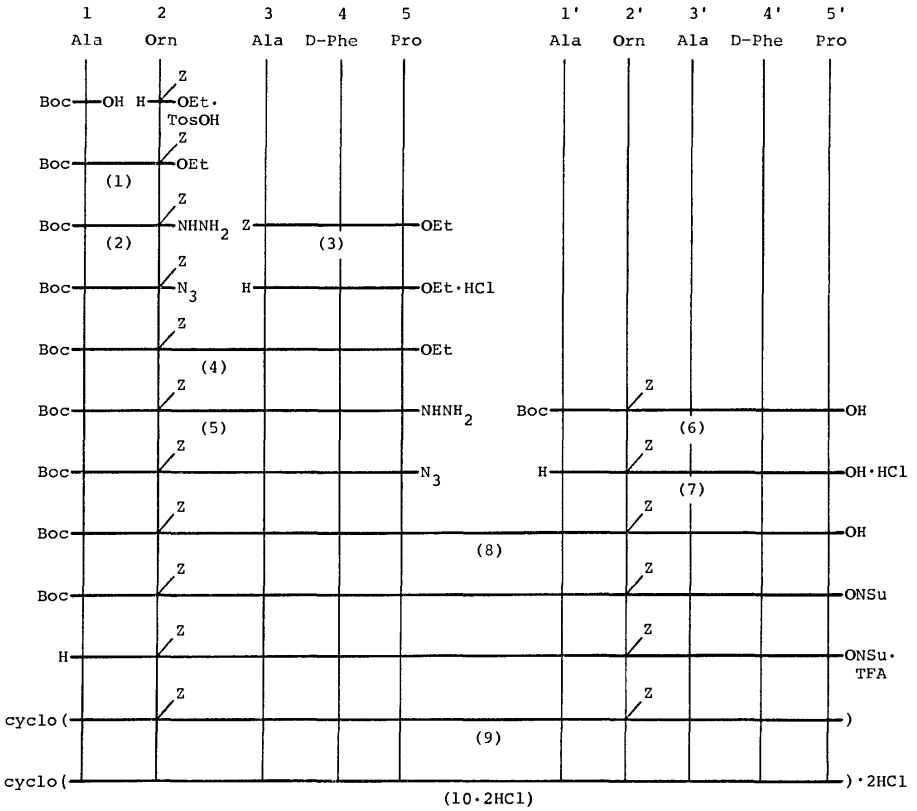

Fig. 3. Synthesis of [1,1',3,3'-Ala]-GS.

Its hydrogenolysis gave a tripeptide ester. Acylpentapeptide ester (**4**) was prepared by condensation of the azide derived from **2** with the tripeptide ester mentioned above. The ester (**4**) was converted into a hydrazide (**5**), while a part of **4** was saponified to afford an acylpentapeptide (**6**). Compound **6** was converted into a pentapeptide (**7**) by treatment with HCl in formic acid. Acyldecapeptide (**8**) was prepared by condensation of the azide derived from **5** with **7**. For its cyclization, the *N*-hydroxysuccinimide ester of **8** was prepared as an active ester, and its Boc-group was removed by the action of TFA at low temperature. The decapeptide active ester was treated with a large amount pyridine, and the resulting Z-substituted cyclic decapeptide (**9**) was purified by passing it through a column of resins. For the synthesis of the final [1,1',3,3'-Ala]-GS, the Z-substituted cyclodecapeptide (**10**) was subjected to hydrogenolysis, and the desired analog was obtained as a crystalline dihydrochloride (**10·2HCl**). The homogeneity of **10** was confirmed by paper and thin-layer chromatography, paper electrophoresis, and elemental analysis.

The ORD curves of the analog (**10**) in ethanol as well as of GS are shown in Fig. 4-a. The analog has a very similar to that which curve with a negative trough at 232 nm, GS possesses. The CD measurements of cyclic and linear peptides relating to GS or its analogs are interesting in connection with the elucidation of antibacterial activities and cyclization reactions. Thus, the CD curves of the analog and GS were measured with methanol as a solvent (Fig. 4-b). The CD curves of both peptides have nearly the same

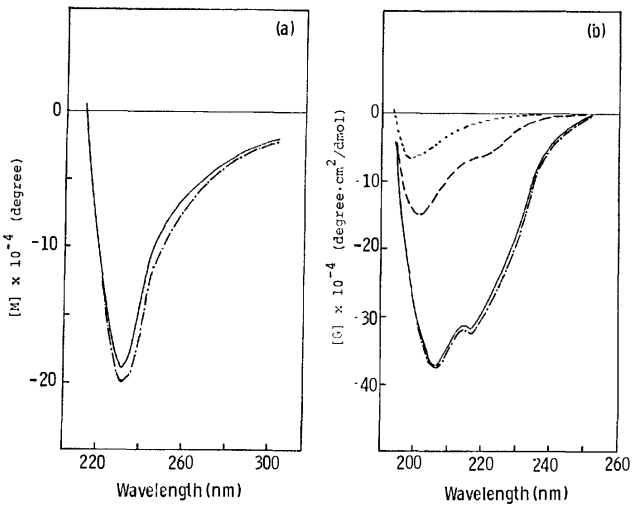

Fig. 4. ORD (a) and CD (b) curves of the cyclic peptides and the Boc-peptides. Solvent: a, ethanol; b, methanol. GS: ——, [1,1',3,3'-Ala]-GS (**10**): ——, Boc-pentapeptide (**6**): ----, Boc-decapeptide (**8**): ———.

pattern, in which the two troughs are at 207 and 217 nm. The CD curves of Boc-peptides (**6** and **8**) were also measured: the trough of the Boc-pentapeptide (**6**) is at 198 nm, whereas that of the Boc-decapeptide (**8**) is at 202 nm. The troughs of the linear peptides (**6** and **8**) are shallower than those of cyclic peptides (GS and **10**).

The results of ORD and CD measurements indicate

that the conformation of the analog (**10**) is similar to that of GS. On the other hand, the CD curve of the Boc-pentapeptide (**6**) shows that **6** has a random structure, and that of the Boc-decapeptide (**8**) indicates that **8** lies in a transition state toward the β-sheet structure such as GS. In a number of experiments, it has been found that a linear decapeptide in the cyclization reaction gives rise to only the cyclic decapeptide, whereas a linear pentapeptide gives a mixture of the cyclic penta- and decapeptides. In the present study, the decapeptide active ester derived from **8** afforded a cyclic monomer in good yield as the sole product; this result can be explained by the suggestion that **8** possesses a spatial conformation resembling that of GS.

At the beginning of this study, we expected that [1,1′3,3′-Ala]-GS (**10**) might possess appreciable antibacterial activity, like [3,3′-Ala]-GS, because [1,1′-Ala]-GS possesses the same strong activity as GS. It seemed that this expectation was supported by the results of the ORD and CD experiments of **10** and GS. Compound **10** showed, however, no activity against any of Gram positive microorganisms even at 100 μg/ml of assay medium. These results indicate that analogs with two methyl side chains in place of either of the two bulky side chains of $Val^{1,1'}$ or $Leu^{3,3'}$ show some activity, but that the analog (**10**) with four methyl side chains loses its activity completely because of its inability to interact with the surface of a Gram positive microorganism.

Experimental

Melting points are uncorrected. TLC was carried out on silica gel G (Merck) with the solvent system: R_f^1, 1-butanol-pyridine-water (4 : 1 : 1 : 2, v/v). Paper chromatography was carried out on Toyo Roshi No. 52 with the above solvent, R_f^3, being used.

*Boc–Ala–Orn(Z)–OEt (**1**).* To a solution of Boc–Ala–OH (3.78 g, 20 mmol) and TEA (2.80 ml, 20 mmol) in THF (40 ml) was added isobutyl chloroformate (2.62 ml, 20 mmol) at −5 °C. After 15 min, a mixture of H–Orn(Z)–OEt TosOH[7] (9.33 g, 20 mmol) and TEA (2.80 ml, 20 mmol) in chloroform (40 ml) was added. The mixture was left to stand overnight at room temperature, evaporated *in vacuo*, and the oily residue was dissolved in ethyl acetate (80 ml). The solution was washed successively with 4% $NaHCO_3$, 10% citric acid, and water, and then dried (Na_2SO_4). The filtrate which separated from the salt was concentrated *in vacuo*. The product which precipitated upon the addition of ether and petroleum ether was collected and washed with the same solvent. It was obtained as very hygroscopic crystals: yield, 5.33 g (57%); mp 49—52 °C; $[\alpha]_D^{29}$ −14.2° (*c* 1, DMF); R_f^1 0.87.

Found: C, 58.81; H, 7.74; N. 8.91%. Calcd for $C_{23}H_{35}O_7N_3 \cdot 1/3H_2O$: C, 58.58; H, 7.62; N, 8.91%.

*Boc–Ala–Orn(Z)–NHNH$_2$ (**2**).* A solution of **1** (5.12 g, 11 mmol) and hydrazine hydrate (10.7 ml, 220 mmol) in DMF (50 ml) was allowed to stand at room temperature for 3 days. The excess hydrazine was evaporated *in vacuo*, and then water (60 ml) was added to the residue. The resulting solid was collected by filtration: yield, 4.18 g (84%); mp 174—175 °C; $[\alpha]_D^{29}$ −27.3° (*c* 1, AcOH).

Found: C, 55.92; H, 7.45; N, 15.48%. Calcd for $C_{21}H_{33}O_6N_5$: C, 55.86; H, 7.37; N, 15.51%.

*Z–Ala–D-Phe–Pro–OEt (**3**).* To a solution of Z–Ala–OH (7.39 g, 33.1 mmol) in chloroform (60 ml) was added DCC (6.83 g, 33.1 mmol) at −5 °C. After several minutes, a solution of H–D-Phe–Pro–OEt·HCl[8] (10.8 g, 33.1 mmol) and TEA (4.63 ml, 33.1 mmol) in chloroform (60 ml) was added to this solution. The mixture was left to stand for 25 h at room temperature, evaporated *in vacuo*, and the oily residue was dissolved in ethyl acetate (150 ml). The solution was washed successively with 4% $NaHCO_3$, 2% HCl, and water, dried (Na_2SO_4), and the filtrate was evaporated. The oily residue solidified upon the addition of ether and petroleum ether. The product was obtained in solid form, though a previous paper[4] had reported it as an oily substance: yield, 10.3 g (63%); mp 93—94 °C; $[\alpha]_D^{20}$ −33° (*c* 1, DMF); R_f^1 0.94.

Found: C, 65.17; H, 6.95; N, 8.44%. Calcd for $C_{27}H_{33}O_6N_3$: C, 65.44; H, 6.71; N, 8.48%.

*Boc–Ala–Orn(Z)–Ala–D-Phe–Pro–OEt (**4**).* A solution of **2** (4.06 g, 9 mmol) dissolved in DMF (50 ml) was cooled to −20 °C. To this solution, 3.70 M HCl in dioxane (4.86 ml) and isopentyl nitrite (1.22 ml, 9 mmol) were added. After 20 min, the solution was neutralized with TEA (2.52 ml, 18 mmol). To this solution was added a chilled solution of H–Ala–D-Phe–Pro–OEt·HCl[4] (3.58 g, 9 mmol) and TEA (1.26 ml, 9 mmol) in DMF (20 ml). The reaction mixture was stirred at 0 °C for 3 days and evaporated. The residual solid was triturated with petroleum ether (30 ml) and water (30 ml), and allowed to stand in a refrigerator. The solid was collected by filtration and washed successively with 4% $NaHCO_3$, 10% citric acid, and water. It was recrystallized from ethanol-ether: yield, 4.92 g (70%); mp 190—192 °C; $[\alpha]_D^{18}$ −27.6° (*c* 1, DMF); R_f^1 0.94.

Found: C, 61.34; H, 7.22; N, 10.89%. Calcd for $C_{40}H_{56}O_{10}N_6$: C, 61.52; H, 7.23; N, 10.76%.

*Boc–Ala–Orn(Z)–Ala–D-Phe–Pro–NHNH$_2$ (**5**).* This hydrazide was obtained from **4** (1.56 g, 2 mmol) as described for the preparation of **2**: yield, 1.44 g (93%); mp 203—206 °C; $[\alpha]_D^{18}$ −75.0° (*c* 1, AcOH).

Found: C, 59.23; H, 7.08; N, 14.21%. Calcd for $C_{38}H_{54}O_9N_8$: C, 59.52; H, 7.10; N, 14.61%.

*Boc–Ala–Orn(Z)–Ala–D-Phe–Pro–OH (**6**).* To a solution of **4** (1.95 g, 2.5 mmol) in a mixture of methanol (10 ml) and DMF (15 ml), 1 M NaOH (3 ml) was added, and the solution was allowed to stand at 5 °C for 1 day. After the addition of 1 M citric acid (5 ml), the solution was evaporated to dryness. The residual oil was dissolved in ethyl acetate and the solution was concentrated *in vacuo*. The product which precipitated upon the addition of ether was collected by filtration: yield, 1.69 g (90%); mp 126—130 °C; $[\alpha]_D^{18}$ −35.6° (*c* 1, DMF); R_f^1 0.74.

Found: C, 60.23; H, 6.92; N, 10.77%. Calcd for $C_{38}H_{52}O_{10}N_6$: C, 60.62; H, 6.96; N, 11.16%.

*H–Ala–Orn(Z)–Ala–D-Phe–Pro–OH·HCl (**7**).* Compound **6** (1.51 g, 2 mmol) was dissolved in 0.164 M HCl in formic acid (15 ml). After being left to stand at room temperature for 20 min, the solution was evaporated to dryness, and the resulting solid was collected by filtration with the aid of ether. The product was a very hygroscopic powder: yield, 1.47 g (107%); mp 131—135 °C; $[\alpha]_D^{18}$ −31.0° (*c* 1, DMF); R_f^1 0.71.

Found: C, 53.27; H, 7.50; N, 11.15%. Calcd for $C_{33}H_{47}O_8N_6Cl \cdot 3H_2O$: C, 53.18; H, 7.17; N, 11.28%.

*Boc–Ala–Orn(Z)–Ala–D-Phe–Pro–Ala–Orn(Z)–Ala–D-Phe–Pro–OH (**8**).* The azide derived from **5** (1.30 g, 1.7 mmol) was coupled with **7** (1.17 g, 1.7 mmol) as described for the preparation of **4**. The product was obtained as a crystalline solid: yield, 2.02 g (93%); mp 134—136 °C;

$[\alpha]_D^{18}$ −39.0° (*c* 1, DMF); R_f^1 0.75.

Found: C, 59.02; H, 6.78; N, 11.30%. Calcd for $C_{71}H_{94}O_{17}N_{12}\cdot 3H_2O$: C, 59.15; H, 6.99; N, 11.66%.

cyclo-[*Ala–Orn(Z)–Ala–*D*-Phe–Pro–*]$_2$ (**9**). To a solution of **8** (770 mg, 0.555 mmol) in ethyl acetate (25 ml), DCC (124 mg, 0.66 mmol) and HONSu (69 mg, 0.66 mmol) were added at 0 °C. After being left to stand at 0 °C for 3 h, the dicyclohexylurea which precipitated was filtered off, and the filtrate was evaporated *in vacuo* at 0 °C. The residual solid was washed with ether by decantation and dried. To this acyldecapeptide *N*-hydroxysuccinimide ester, anisole (0.6 ml) and trifluoroacetic acid (6 ml) were added at −5 °C. After being left to stand for 25 min, the solution was evaporated *in vacuo* at 0 °C, and the residual oil was dissolved in DMF (15 ml). The solution was added dropwise into pyridine (300 ml) at room temperature for 2 h; the stirring was continued for an additional 2 h. After the solvent was removed, the residue was dissolved in a mixture of dioxane, methanol, and water (250 ml, 2 : 1 : 1, v/v). The solution was passed through the columns of Dowex 1 (OH^- form) and 50 (H^+ form). The columns were washed with the same solvent (300 ml), and the effluent was evaporated to dryness. The residual solid was collected by filtration with the aid of water. It was recrystallized from ethanol–dioxane–petroleum ether: yield, 246 mg (35%); mp 288—292 °C (dec); $[\alpha]_D^{24}$ −243° (*c* 0.3, DMF); R_f^1 0.95.

Found: C, 59.63; H, 6.76; N, 12.72%; mol wt 1290.[9] Calcd for $C_{66}H_{84}O_{14}N_{12}\cdot 3H_2O$: C, 59.85; H, 6.85; N, 12.69%; mol wt 1325.

cyclo-*(Ala–Orn–Ala–*D*-Phe–Pro–)*$_2$*·2HCl ([1,1′,3,3′-Ala]-GS·2HCl) (**10·2HCl**).* A solution of **9** (127 mg, 0.1 mmol) in 0.102 M HCl in ethanol (2.35 ml) was hydrogenated in the presence of Pd black. After removal of the catalyst, the filtrate was evaporated, and the resulting crystals were collected by filtration with the aid of ether. It was recrystallized from methanol–ether; yield, 90 mg (84%); mp 246—249 °C (dec); $[\alpha]_D^{24}$ −365° (*c* 0.2, MeOH); R_f^1 0.70, R_f^2 0.87.

Found: C, 52.80; H, 7.14; N, 14.42%. Calcd for $C_{50}H_{74}O_{10}N_{12}Cl_2\cdot 4H_2O$: C, 52.40; H, 7.20; N, 14.66%.

Electrophoresis. Electrophoresis on Toyo Roshi No. 52 paper was carried out with the solvent system: formic acid–acetic acid–methanol–water (1 : 3 : 6 : 10, v/v; pH 1.8) for 3 h at 600 V/30 cm. The mobility of **10** was comparable with that of GS; the ratio of the mobility of **10** *vs.* GS was 1.04.

ORD and CD Measurements. The measurements of ORD and CD were performed with Jasco Models J-20 and J-40, respectively. In Fig. 4-a are shown the ORD curves of **10** and GS, and in Fig. 4-b are shown the CD curves of Boc-pentapeptide (**6**), Boc-decapeptide (**8**), **10**, and GS.

Microbiological Assays. The microorganisms employed were *Escherichia coli*, *Staphylococcus aureus*, *Proteus vulgaris*, and *Bacillus subtilis*. The minimum amount of the compounds necessary for the complete inhibition of growth was determined by a dilution method in nutrient agar medium. GS was examined as a reference compound. Compound **10** exhibited no antibacterial activity against the microorganisms tested even at 100 μg/ml, whereas the minimum concentration of GS for inhibition were 2—5 μg/ml on *S. aureus* and 1—2 μg/ml on *B. subtilis*.

The authors wish to express their thanks to the staff members of Takeda Chemical Industries, Ltd., for the microbiological assays.

References

1) Part XXXVI of this series: O. Abe, Y. Utsumi, and N. Izumiya, *Bull. Chem. Soc. Jpn.*, in press.

2) M. Kondo and N. Izumiya, *Bull. Chem. Soc. Jpn.*, **40**, 1975 (1967).

3) M. Kondo and N. Izumiya, *Bull. Chem. Soc. Jpn.*, **43**, 1850 (1970).

4) O. Abe and N. Izumiya, *Bull. Chem. Soc. Jpn.*, **43**, 1202 (1970).

5) D. C. Hodgkin and B. M. Oughton, *Biochem. J.*, **65**, 752 (1957).

6) Abbreviations: Z, benzyloxycarbonyl; Boc, *t*-butoxycarbonyl; HONSu, *N*-hydroxysuccinimide; MA, mixed anhydride method; DCC, dicyclohexylcarbodiimide; TosOH, *p*-toluenesulfonic acid; TEA, triethylamine; TFA, trifluoroacetic acid; DMF, *N*,*N*-dimethylformamide. Amino acid symbols, except D-Phe, denote the L-configuration.

7) N. Izumiya, T. Kato, Y. Fujita, M. Ohno, and M. Kondo, *Bull. Chem. Soc. Jpn.*, **37**, 1809 (1964).

8) M. Ohno, T. Kato, S. Makisumi, and N. Izumiya, *Bull. Chem. Soc. Jpn.*, **39**, 1738 (1966).

9) Molecular weight was determined by a Hitachi Osmometer, type 115, using methanol as a solvent.

Cycloaddition Reactions of Thioacylketene Thioacetals and *N*-Thioacyldithioimidocarbonates

Masaharu O-OKA, Akihide KITAMURA, Renji OKAZAKI, and Naoki INAMOTO
Department of Chemistry, Faculty of Science, The University of Tokyo, Hongo, Tokyo 113
(Received August 10, 1977)

Thioacylketene thioacetals (**7**) and *N*-Thioacyldithioimidocarbonates (**8**) undergo 1,4-cycloaddition reactions with active acetylenes and olefins to give six-membered heterocycles. Tetracyanoethylene behaves in a different way to afford conjugated dienes. In the reactions with diphenylketene and diazo compounds, **7** and **8** undergo different types of reactions; **7** gave products derived from 1,2-cycloaddition to the C=S bond, while **8** afforded 1,4-cycloadducts. Compound **7** was found to be more reactive than **8**. The reactivity difference between **7** and **8** is discussed.

Conjugated dienes and their heteroanalogues (*i.e.*, heterodienes) (**1**) have been thoroughly investigated in organic chemistry.[1-5] However, investigations on heterodienes having a thiocarbonyl group (**1**, W and/or Z=S), are relatively scarce.[6-9]

W=X—Y=Z

1 W, X, Y, Z=C, O, N, S *etc.*

The finding[10] that the photoreactions of 1,2,4-dithiazole-3-thione (**2**) and 1,2-dithiole-3-thione (**3**) with olefins (**4**) provide a facile and efficient route to conjugated thiones such as 2-thioacylimino- (**5**) and 2-thioacylmethylene-1,3-dithiolanes (**6**) has aroused interest in the reactivity of these conjugated heterodienes containing a thiocarbonyl group.

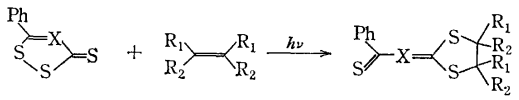

2: X=N
3: X=CH, CPh

4

5: X=N
6: X=CH, CPh

Compounds **5** and **6** undergo 1,2- and 1,4-cycloaddition reactions with some types of reagents.[11,12] This paper gives a detailed account of these cycloaddition reactions.

Reactions with Electron-Deficient Acetylenes. Reactions of **7** and **8** with dibenzoylacetylene or dimethyl acetylenedicarboxylate afforded 1,4-cycloadducts (**9**, **10**, or **11**) in good yields.

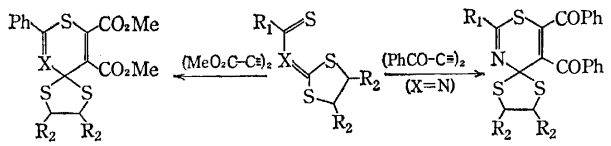

10: X=CH, $R_2R_2=(CH_2)_4$
11: X=N, R_2=H

7: X=CH, R_1=Ph, $R_2R_2=(CH_2)_4$
8a: X=N, R_1=Ph, $R_2R_2=(CH_2)_4$
8b: X=N, R_1=Ph, R_2=H
8c: X=N, R_1=Me, R_2=H

9a—c

The possibility of a 1,2-cycloadducts such as **12** or **13** was excluded for the following reasons: (i) the UV spectra of **9** and **11** show no absorption due to a thiocarbonyl or thioamide group in the visible region, (ii) the NMR signals of four methylene protons in **9b** and **9c** appear as an A_2B_2 multiplet at δ 3.5, while **8b** and **8c**, which have an iminodithiolane ring, show their methylene protons as a singlet at δ 3.5, and (iii) thiete[13] is unstable in contrast to the high thermal stability of **9**—**11** obtained here.

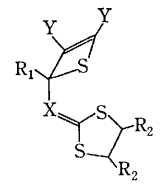

12

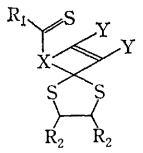

13

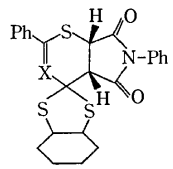

14: X=CH
15: X=N

Reactions with Electron-Deficient Olefins. Reactions of **7** and **8** with *N*-phenylmaleimide in refluxing benzene afforded 1,4-cycloadducts **14** and **15** in 67 and 70% yields, respectively. The NMR signals of the two methine protons at 5- and 6-positions appear as an AB quartet (J=10 Hz for **14** and J=9 Hz for **15**) at about δ 4.4. The value of this coupling constant indicates their *cis* configuration.

Reactions of **7**, **8a**, and **8b** with acrylamide in refluxing xylene afforded 1,4-cycloaddition products **16**, **17a**, and **17b**, respectively. In the case of **8a** and **8b**, the cycloadditions were carried out using acrylonitrile, methyl vinyl ketone, methyl and ethyl acrylates, and acrylaldehyde. The yields of the products and the reaction conditions are summarized in Table 1.

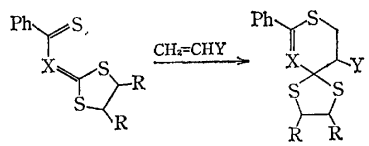

7: X=CH, RR=$(CH_2)_4$
8a: X=N, RR=$(CH_2)_4$
8b: X=N, R=H

16: X=CH, RR=$(CH_2)_4$, Y=$CONH_2$
17: X=N, Y=$CONH_2$
18: X=N, Y=CN
19: X=N, Y=$COCH_3$
20: X=N, Y=CO_2CH_3
21: X=N, Y=CHO
22: X=N, Y=$CO_2C_2H_5$

Compound **17a** consists of two isomers (**17a**α and **17a**β), both of which can be isolated by chromatography. Very similar spectral characteristics of the two isomers (see Experimental) indicate that they are isomeric with respect to the direction of the cyclohexane ring, although no assignment has been made. Hereafter such isomers are denoted by α and β. As regards compound **17b**,

Table 1. Yields and conditions of reactions of **8** with monosubstituted olefins

8	Olefin	Solvent	Temp (°C)	Time (h)	Product (%)
8a	$Y=CONH_2$	Xylene	140	24	**17a** (52)
8b	$Y=CONH_2$	Xylene	140	8	**17b** (22)
8a	Y=CN	Xylene[a)]	140	24	**18a** (73)
8a	$Y=COCH_3$	Xylene[a)]	140	24	**19a** (80)
8a	$Y=CO_2CH_3$	Xylene[a)]	140	24	**20a** (40)
8b	Y=CHO	Benzene[a)]	90	9	**21b** (74)
8b	$Y=CO_2C_2H_5$	DMF[a)]	154	12	**22b** (44)

a) In a sealed tube.

a single product and no isomer was obtained, in line with the above argument.

The orientation of addition in these reactions was established by acid-catalyzed hydrolysis of **19a**, affording **23**.

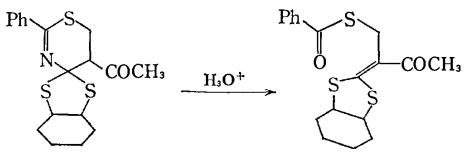

19a **23**

Since the other adducts (**17**—**22**) show similar spectral features to those of **19**, they would have a similar orientation to that in **19**, suggesting that the addition reaction takes place in a regioselective manner.

The reactions of **7** and **8a** with dimethyl fumarate, dimethyl maleate, and crotononitrile were carried out in order to examine the stereospecificity of the 1,4-cycloaddition reactions. However, they did not occur under the same conditions.

Reaction of **7** with tetracyanoethylene (TCNE) in refluxing acetonitrile afforded **24** (57%), while **8a** gave **25** (10%) and **26** (18%).

The formation of **24**—**26** can be explained in terms of the intermediacy of the zwitterion **27**; 1,2-addition followed by the elimination of $(NC)_2C{=}S$[14] would give **24** and **25** and hydrolysis by adventitious water in the solvent would lead to **26**.

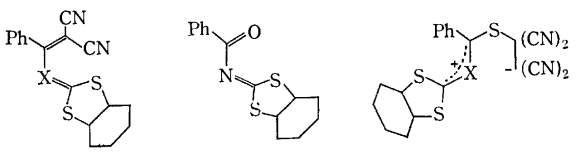

24: X=CH **26** **27**
25: X=N

Reaction with Diphenylketene. Reactions of **7** and **8a** with diphenylketene in *N,N*-dimethylformamide (DMF) at room temperature afforded diene **28** and 1,4-cycloadduct **29** in 88 and 80% yields, respectively. The NMR spectrum of **29** shows two methine protons as multiplets centered at δ 2.60 and 3.25 with equal intensity, suggesting the presence of two isomers (α and β forms). Compound **28** is identical with the compound obtained by desulfurization of episulfide **35** (*vide infra*).

The mass spectrum of **29** shows a weak metastable ion peak corresponding to the loss of COS from the molecular ion, but no molecular ion peak. The IR spectrum shows the presence of a carbonyl group at 1700 cm^{-1}, typical of an ester of alkanethioic *S*-acid.[15]

Formation of vinylketene thioacetal (**28**) is explicable by 1,2-cycloaddition to the thiocarbonyl bond followed by elimination of COS, in contrast to the formation of 1,4-cycloadduct (**29**) from **8a**.

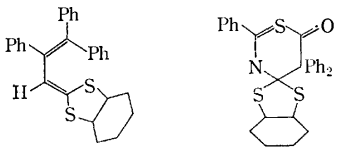

28 **29**

Reactions with Diazo Compounds. Reactions of **8a** and **8b** with diazomethane in ether at room temperature afforded 1,4-adducts **30a** (90%) and **30b** (90%), respectively, while **7** gave no tractable product.

Compound **30a** consists of two stereoisomers (**30a**α and **30a**β), both of which are isolable by chromatography. The fact that the UV spectrum of **30a** has an absorption maximum at 247.5 nm, which is similar to that of the above-mentioned [4+2] adducts with olefins, strongly supports the structure **30** having Ph–C(=N–)S– unit.

A strong peak at *m/e* 121 ($PhCS^+$) in its mass spectrum is compatible with **30**, but not with isomeric structure **31**.

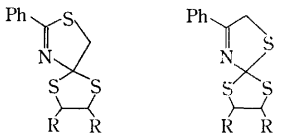

30a: RR=$(CH_2)_4$ **31**
b: R=H

Acid hydrolysis of **30a** yielded **32**. The UV spectrum shows absorption maxima at 254.5 (ε 15700) and 308 nm (7310), which are much higher than those reported[16] for **33** [238 (ε 18000) and 268 nm (12200)], a structure similar to that obtained from **31**.

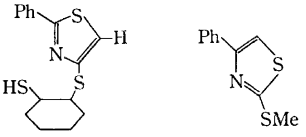

32 **33**

The possibility of episulfide (**34**) as an alternative structure of **30** is excluded by the fact that **30** was not desulfurized by triphenylphosphine. Episulfide **35** underwent desulfurization by triphenylphosphine to give diene **28**.

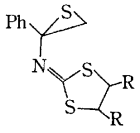

34

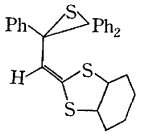

35

Compound **7** reacted with diphenyldiazomethane in ether at room temperature to give episulfide **35** in 47% yield, whereas **8a** (in benzene) afforded **36** (51%), **37** (16%), and **38** (7%).

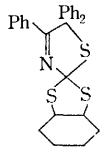

36

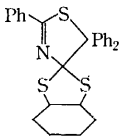

37

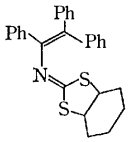

38

Compound **36** also consists of two chromatographically isolable stereoisomers (**36**α and **36**β). The fragmentation pattern of the mass spectrum of **36** is similar to that of **38**, but not to that of **37**. Compound **36** has strong peaks at *m/e* 427 (M^+—S), 287 ($PhCPh_2CS^+$), and 255 ($PhCCPh_2^+$), whereas these peaks are negligible in the case of **37**. Although both **36** and **37** have an absorption maximum near 253 nm, they differ in pattern, that of **37** being very similar to the pattern of [4+2] adducts obtained from olefins. Further support for the structure **36** comes from conversion (treatment with trimethyloxonium tetrafluoroborate and subsequent hydrolysis) of the thioacetal into the carbonyl group to give **39**, which has a different melting point from that reported for **40**.[17]

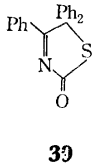

39

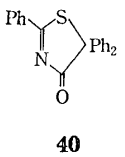

40

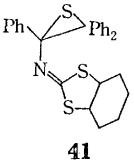

41

The possibility of episulfide **41** as an alternative to **36** or **37** is excluded also in this case; the compounds (**36** and **37**) undergo no desulfurization by triphenylphosphine.

Reaction of **7** with phenyldiazomethane in ether led to diene **42** (61%) instead of the corresponding episulfide like **35**.

Thione **43** also reacted with diphenyl- or phenyldiazomethane to give **44** (93%), or **45** (7%), and **47** (67%), respectively. Episulfide **44** gave **46** by triphenylphosphine.

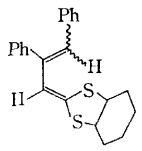

42

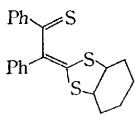

43

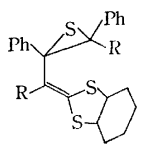

44: R=Ph **45**: R=H

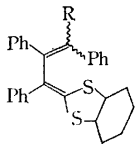

46: R=Ph **47**: R=H

Reaction with Sulfene. Sulfene generated *in situ* from methanesulfonyl chloride and triethylamine at 5 °C in benzene reacted with **7** to afford 1,4-cycloadduct **48** (57%). Under comparable conditions **8a** did not react with sulfene.

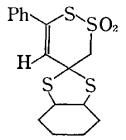

48

Comparison of the Reactivities of Thioacylketene Thioacetal (7) and N-Thioacyldithioimidocarbonate (8). A comparison of the reaction conditions of **7** with those of **8** in some reactions is given in Table 2.

Table 2. Comparison of the reactions of **7** and **8**

Reagents	**7**	**8**
MeO_2C-C≡C-CO_2Me	in CH_2Cl_2, r.t. 10 h	in benzene, r.t. 7 days
N-Phenylmaleimide	in benzene, reflux, 4 h	in benzene, reflux, 58 h
Acrylamide	in xylene, reflux, 2 h	in xylene, reflux, 24 h
TCNE	in CH_3CN, reflux, 2 h	in CH_3CN, reflux, 28 h
Ph_2CN_2	in ether, r.t. 15 h	in ether, r.t. 3 days
Sulfene[a]	in benzene, 5 °C, 1 h	no reaction

a) Generated from methanesulfonyl chloride and triethylamine.

We see that **8** requires severer conditions than **7**, indicating that the reactivity of **8** is lower than that of **7**. This is in line with the known fact[2] that the reactivity of dienes decreases upon replacement of its component carbon by nitrogen, which is due to the lowering of HOMO level of the diene part.

The reactions of **8** with diphenylketene and diazo compounds give rise to 1,4-cycloadducts, while those of **7** afford products *via* 1,2-addition. The preference of 1,4-addition over 1,2-addition in the reactions of **8** presumably reflects an importance of the lone pair electrons of nitrogen in these reactions.

The reaction with diphenylketene most likely proceeds *via* zwitterionic intermediate (**49**). This is strongly supported by the observation that the reaction of **7** with the ketene is greatly accelerated by use of a polar solvent; the reaction requires refluxing for 2 days in benzene whereas in DMF it was complete after 12 h at room temperature.

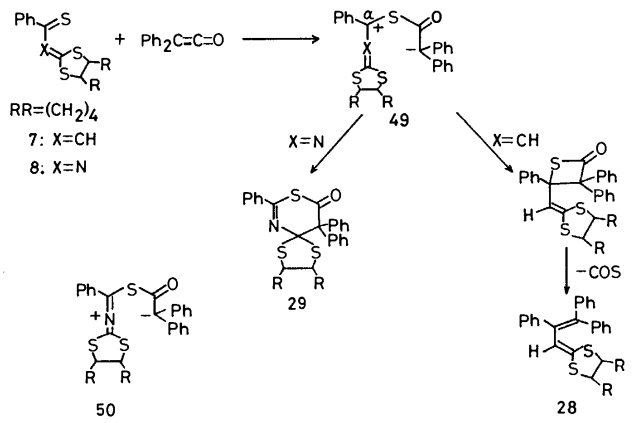

In the case of **8**, the possible contribution of canonical structure (**50**) would reduce reactivity of C_α, thus leading to 1,4-adduct. It is noteworthy that the reaction pattern of **7** and **8** with the ketene differs from that of thiobenzophenone, a typical thioketone, which gives 3-oxothietane (**51**).[18]

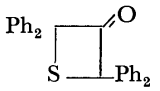

51

The fact[19] that the reaction product of a thioketone with diphenyldiazomethane is always an episulfide shows that **35** is the expected product in the reaction of **7** with diphenyldiazomethane.

The instability of **52** as compared with **35** is most probably due to the additional assistance of the heterolytic cleavage by the nitrogen lone pair electrons other than by the N=C double bond as depicted below. The preferable cleavage *via* path *a* over *via* path *b* is presumably due to the higher lability of the C–S bond in heterolytic cleavage and also to the stability of thiolate anion thus formed.

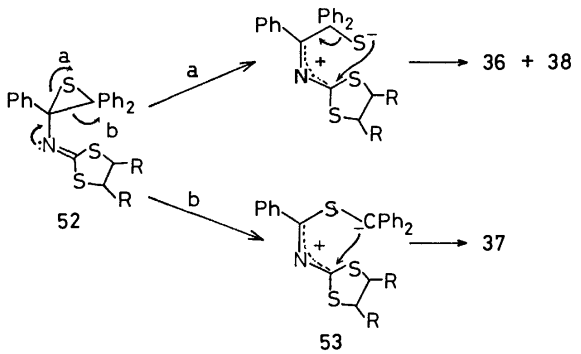

For the formation of **37**, however, the possibility that **53** or its diradical counterpart is formed directly from the two substrates can not be excluded.

Experimental

IR and UV spectra were recorded on Hitachi EPI-G2 and ESP-3 spectrophotometers, respectively. The NMR spectra were obtained in deuteriochloroform solution, unless otherwise noted, at 60 MHz with a Hitachi R-24 spectrometer using tetramethylsilane as an internal standard. The mass spectra were measured with a Hitachi RMU-6 spectrometer (beam energy 70 eV). All the reactions were carried out under nitrogen or argon.

*Preparation of 2-Thiobenzoylimino-1,3-dithiolane (**8b**).* To a solution of 2-benzoylimino-1,3-dithiolane[20] (0.5 g, 2.2 mmol) in benzene (20 ml) was added phosphorus pentasulfide (2 g, 4 mmol) and pyridine (1 ml). The mixture was refluxed for 4.5 h under stirring. The phosphorus pentasulfide was filtered off and the filtrate was washed with water until the aqueous layer became neutral. The benzene layer was dried ($MgSO_4$) and evaporated under reduced pressure. The residue was subjected to dry column chromatography (DCC) (silica gel, ether-hexane (1 : 2)) to give 246 mg (46%) of **8b** as a purple oil. The oil was crystallized from ether at Dry Ice temperature as thin purple crystals, mp 49—50 °C; NMR: δ 3.4 (s, 4H), 7.2—7.6 (m, 3H), and 8.2—8.5 (m, 2H); UV: λ_{max} (CH_2Cl_2) 239 (ε 13400), 327 (25500), 370 sh (10100), and 560 nm (161).

*Preparation of 2-Thioacetylimino-1,3-dithiolane (**8c**).* A mixture of 2-acetylimino-1,3-dithiolane[20] (1 g, 6.2 mmol), phosphorus pentasulfide (3 g, 6 mmol) and pyridine (1 ml) in benzene (40 ml) was heated at 70 °C for 1 h under stirring. After the usual work-up, the residue was subjected to DCC (silica gel, CH_2Cl_2) to give 0.5 g (46%) of **8c** as a red oil, which could not be crystallized. NMR: δ 2.75 (s, 3H) and 3.55 (s, 4H).

*Reaction of **7** with Dimethyl Acetylenedicarboxylate.* A solution of **7**[10] (140 mg, 0.48 mmol) and the ester (91 mg, 0.64 mmol) in dichloromethane (3 ml) was left to stand at room temperature for 10 h. After evaporation of the solvent, the residue was recrystallized from methanol to give **10** (173 mg, 83%); mp 128—129 °C; IR (KBr): 1735 cm^{-1}; NMR: δ 1.3—2.2 (m, 8H), 3.85 (s, 6H), 3.9—4.2 (m, 2H), 6.30 (s, 1H), and 7.30—7.65 (m, 5H).

Found: C, 58.32; H, 5.08; S, 21.87%. Calcd for $C_{21}H_{22}O_4S_3$: C, 58.04; H, 5.10; S, 22.13%.

*Reaction of **8a** with Dibenzoylacetylene.* A solution of **8a**[10] (293 mg, 1 mmol) and the acetylene (281 mg, 1.2 mmol) in benzene (30 ml) was refluxed for 9.5 h. The solvent was evaporated *in vacuo* and the residue was subjected to DCC (silica gel, CH_2Cl_2–CCl_4 (1 : 1)) to give **9a** (320 mg, 61%) as colorless crystals; mp 148—149 °C (dec) (from cyclohexane); IR (KBr): 1660 cm^{-1}; NMR: δ 1.1—2.5 (m, 8H), 3.7—4.0 (m, 2H), and 7.1—8.1 (m, 15H); UV: λ_{max} (CH_2Cl_2) 257 nm (ε 35400); MS: *m/e* 104 (30%) and 103 (100).

Found: C, 68.19; H, 4.65; N, 2.48; S, 18.11%. Calcd for $C_{30}H_{25}NO_2S_3$: C, 68.28; H, 4.77; N, 2.65; S, 18.23%.

*Reaction of **8b** with Dibenzoylacetylene.* A solution of **8b** (102 mg, 0.4 mmol) and the acetylene (100 mg, 0.4 mmol) in benzene (20 ml) was stirred at room temperature for 4 days. A similar treatment to that in the reaction of **8a** gave 168 mg (84%) of **9b**; mp 170—170.5 °C (dec) (from CH_2Cl_2–MeOH); IR (KBr): 1660 and 1590 cm^{-1}; NMR: δ 3.5 (m, 4H) and 7.1—8.1 (m, 15H).

Found: C, 66.01; H, 3.90; N, 3.01; S, 20.33%. Calcd for $C_{26}H_{19}NO_2S_3$: C, 65.93; H, 4.04; N, 2.96; S, 20.31%.

*Reaction of **8b** with Dimethyl Acetylenedicarboxylate.* A mixture of **8b** (156 mg, 0.65 mmol) and the ester (*ca.* 0.3 ml) in benzene (20 ml) was stirred at room temperature for 7 days. The benzene was evaporated and the residue was chromatographed (DCC, silica gel) with CH_2Cl_2 to give 196 mg (79%) of **11**; mp 171—172 °C (from CH_2Cl_2–MeOH); IR (KBr): 1730 cm^{-1}; NMR: δ 3.65 (m, 4H), 3.92 (s, 3H), 3.95 (s, 3H), 7.3—7.6 (m, 3H), and 7.7—8.1 (m, 2H); UV: λ_{max}

(CH_2Cl_2) 254.5 nm (ε 22000); MS: *m/e* 381 (M^+, 9%) and 353 (100).

Found: C, 50.32; H, 3.80; N, 3.72; S, 25.04%. Calcd for $C_{16}H_{15}NO_4S_3$: C, 50.37; H, 3.96; N, 3.67; S, 25.21%.

Reaction of ***8c*** *with Dibenzoylacetylene.* A solution of **8c** (231 mg, 1.4 mmol) and the acetylene (332 mg, 1.4 mmol) in chloroform (10 ml) was stirred at room temperature for 4 days. After removal of chloroform, the residue was chromatographed with CH_2Cl_2–CCl_4 (2 : 1) to give 460 mg (80%) of **9c**; mp 62—63 °C (CH_2Cl_2–MeOH); IR (KBr): 1660 cm^{-1}; NMR: δ 2.4 (s, 3H), 3.4 (m, 4H), and 7.1—8.0 (m, 10H); UV: λ_{max} (CH_2Cl_2) 259.5 nm (ε 29800); MS: *m/e* 411 (M^+, trace) and 47 (100%).

Reaction of ***7*** *with* N-*Phenylmaleimide.* A mixture of **7** (144 mg, 0.50 mmol) and the imide (110 mg, 0.63 mmol) in benzene (4 ml) was refluxed for 4 h. The residue obtained after removal of benzene was recrystallized from ethanol to afford **14** (122 mg, 67%); mp 179.5—181.0 °C; IR (KBr): 1720 cm^{-1}; NMR: δ 1.1—2.2 (m, 8H), 3.6—4.2 (m, 2H), 4.35 (ABq, 2H, J=10 Hz, $\Delta\delta$=0.29), 6.97 (s, 1H), and 7.1—7.7 (m, 10H).

Found: C, 59.30; H, 6.48; N, 3.55; S, 26.00%. Calcd for $C_{25}H_{23}NO_2S_3$: C, 59.14; H, 6.34; N, 3.83; S, 26.31%.

Reaction of ***8a*** *with* N-*Phenylmaleimide.* A solution of **8a** (293 mg, 1 mmol) and the imide (208 mg, 1.2 mmol) in benzene (30 ml) was refluxed for 58 h. The solvent was evaporated and the residue was subjected to preparative TLC (silica gel, CH_2Cl_2–hexane (1 : 1)) to give **15** (326 mg, 70%) as colorless crystals; mp 208—209 °C (from EtOH); IR (KBr): 1720 cm^{-1}; NMR: δ 1.0—2.7 (m, 8H), 3.6—4.1 (m, 2H), 4.1 (d, 1H, J=9 Hz), 4.7 (d, 1H, J=9 Hz), and 7.0—8.2 (m, 10H); UV: λ_{max} (EtOH) 249 (ε 19800) and 309 nm (3690); MS: *m/e* 466 (M^+, 19%), and 104 (100).

Found: C, 61.98; H, 4.76; N, 5.96; S, 20.41%. Calcd for $C_{24}H_{22}N_2O_2S_3$: C, 61.77; H, 4.75; N, 6.00; S, 20.61%.

Reaction of ***7*** *with Acrylamide.* A suspension of **7** (146 mg, 0.50 mmol), acrylamide (351 mg, 5.0 mmol) and a trace of hydroquinone in xylene (4 ml) was refluxed for 2 h. After cooling, excess acrylamide was filtered off and the filtrate was washed thoroughly with water to remove acrylamide. After removal of the solvent, the residue was recrystallized from methylcyclohexane to give **16** (127 mg, 70%); mp 190—191 °C; IR (KBr): 3450 and 1670 cm^{-1}; NMR: δ 0.9—2.3 (m, 8H), 3.32 (bs, 3H), 3.7—4.1 (m, 2H), 6.28 (s, 1H), 6.1—6.6 (m, 2H), and 7.1—7.7 (m, 5H).

Found: C, 59.78; H, 5.90; N, 3.75; S, 26.18%. Calcd for $C_{18}H_{21}NOS_3$: C, 59.47; H, 5.82; N, 3.85; S, 26.46%.

Reaction of ***8a*** *with Acrylamide.* A mixture of **8a** (293 mg, 1 mmol), acrylamide (710 mg, 10 mmol) and a small amount of hydroquinone in xylene (10 ml) was refluxed for 24 h. After similar work-up to that in the reaction of **7**, the reaction mixture was subjected to DCC (silica gel, ether). The column was divided into four fractions. The second fraction was recrystallized from methanol to afford 76 mg (21%) of **17a**α; mp 194—194.5 °C; IR (KBr): 3460, 3420, and 1660 cm^{-1}; NMR: δ 1.0—2.5 (m, 8H), 3.35 (m, 1H), 3.4—3.7 (m, 2H), 3.9—4.4 (m, 2H), 5.8—6.9 (bd, 2H), 7.2—7.6 (m, 3H), and 7.7—8.0 (m, 2H); UV: λ_{max} (EtOH) 246 nm (ε 13400); MS: *m/e* 364 (M^+, trace) and 121 (100%).

Found: C, 56.27; H, 5.56; N, 7.39; S, 26.27%. Calcd for $C_{17}H_{20}N_2OS_3$: C, 56.01; H, 5.53; N, 7.68; S, 26.39%.

The third fraction was also recrystallized from methanol to give 112 mg (31%) of **17a**β; mp 192—192.5 °C; IR (KBr): 3450 and 1665 cm^{-1}; NMR: δ 1.2—2.6 (m, 8H), 3.15 (m, 1H), 3.4—3.7 (m, 2H), 3.7—4.1 (m, 2H), 6.2—7.0 (bd, 2H), 7.25—7.65 (m, 3H), and 7.65—8.0 (m, 2H); UV: λ_{max} (EtOH) 246 nm (ε 13400); MS: *m/e* 364 (M^+, trace) and 121 (100%).

Found: C, 55.99; H, 5.55; N, 7.77; S, 26.10%. Calcd for $C_{17}H_{20}N_2OS_3$: C, 56.01; H, 5.53; N, 7.68; S, 26.39%.

Reaction of ***8b*** *with Acrylamide.* A solution of **8b** (359 mg, 1.5 mmol), acrylamide (727 mg, 10 mmol), and a small amount of hydroquinone in xylene (15 ml) was refluxed for 8 h. After the same treatment as described above, the residue was subjected to preparative TLC on silica gel with chloroform-ethyl acetate (1 : 1) to give 69 mg (22%) of **17b**; mp 179—180 °C (from MeOH); IR (KBr): 3460 and 1685 cm^{-1}; NMR: δ 3.2—3.9 (m, 7H), 6.1—6.9 (bd, 2H), 7.2—7.6 (m, 3H), and 7.6—8.0 (m, 2H).

Found: C, 50.10; H, 4.49; N, 8.98; S, 30.70%. Calcd for $C_{13}H_{14}N_2OS_3$: C, 50.29; H, 4.55; N, 9.02; S, 30.98%.

Reaction of ***8b*** *with Ethyl Acrylate.* A solution of **8b** (239 mg, 1 mmol), the ester (1 g, 10 mmol), and a small amount of hydroquinone in DMF (20 ml) was heated at 154 °C for 14 h in a sealed tube. The DMF solution was poured into water and extracted with CH_2Cl_2. The extracts were washed with water, dried ($MgSO_4$) and evaporated. The residue was subjected to preparative TLC (silica gel, CH_2Cl_2) to give 149 mg (44%) of **22b** as a yellow oil; IR (neat): 1730 cm^{-1}; NMR: δ 1.23 (t, 3H, J=7 Hz), 3.2—3.9 (m, 7H), 4.2 (q, 2H, J=7 Hz), 7.2—7.6 (m, 3H), and 7.6—8.0 (m, 2H).

Reaction of ***8a*** *with Acrylonitrile.* A mixture of **8a** (293 mg, 1 mmol), acrylonitrile (530 mg, 10 mmol) and a small amount of hydroquinone in xylene (1 ml) was heated in a sealed tube at 140 °C for 1 day. After removal of the solvent *in vacuo*, the residue was subjected to DCC (silica gel, CH_2Cl_2) to give 252 mg (73%) of **18a** as colorless crystals; mp 134—135 °C (from MeOH); IR (KBr): 2240 cm^{-1}; NMR: δ 1.0—2.1 (m, 8H), 3.45 (bs, 3H), 3.85—4.3 (m, 2H), 7.2—7.65 (m, 3H), and 7.65—7.9 (m, 2H); UV: λ_{max} (EtOH) 248 nm (ε 18100); MS: *m/e* 346 (M^+, 2%) and 121 (100).

Found: C, 59.19; H, 5.30; N, 7.92; S, 27.47%. Calcd for $C_{17}H_{18}N_2S_3$: C, 58.92, H, 5.24; N, 8.08; S, 27.76%.

Reaction of ***8a*** *with Methyl Vinyl Ketone.* The reaction was carried out in the same scale and under the same conditions as those in the reaction with acrylonitrile. The same work-up gave 291 mg (80%) of **19a**; mp 175—176 °C (from MeOH); IR (KBr): 1710 cm^{-1}; NMR: δ 1.0—2.4 (m, 8H), 2.35 (s, 3H), 3.5 (bs, 3H), 3.7—4.0 (m, 1H), 4.0—4.35 (m, 1H), 7.2—7.6 (m, 3H), and 7.6—8.1 (m, 2H); UV: λ_{max} (EtOH) 247 nm (ε 16900); MS: *m/e* 363 (M^+, trace) and 121 (100%).

Found: C, 59.29; H, 5.75; N, 3.81; S, 26.42%. Calcd for $C_{18}H_{21}NOS_3$: C, 59.47; H, 5.82; N, 3.85; S, 26.46%.

Acid-catalyzed Hydrolysis of ***19a***. A mixture of **19a** (530 mg, 1.46 mmol) and 1 M sulfuric acid (3 ml) in ethanol (10 ml) was refluxed for about 10 h. After removal of ethanol 100 ml of water was added and the solution was extracted with CH_2Cl_2. The dried extract was evaporated and the residue was subjected to DCC (silica gel, CH_2Cl_2) gave 177 mg (33%) of **23**; mp 127—128 °C (from MeOH); IR (KBr): 1650 and 1630 cm^{-1}; NMR: δ 1.05—2.30 (m, 8H), 2.30 (s, 3H), 3.47—3.96 (m, 2H), 4.25 (s, 2H), 7.0—7.46 (m, 3H), and 7.5—8.17 (m, 2H); UV: λ_{max} (EtOH) 238 (ε 12600), 273 (11100), and 330 nm (14700); MS: *m/e* 364 (M^+, 5%) and 227 (100).

Found: C, 59.22; H, 5.42; S, 26.36%. Calcd for $C_{18}H_{20}O_2S_3$: C, 59.31; H, 5.53; S, 26.39%.

Reaction of ***8a*** *with Methyl Acrylate.* The reaction was also carried out in the same way as that in the reaction with acrylonitrile to give **20a** (154 mg, 40%); mp 132.5—133 °C

(from MeOH); IR (KBr): 1740 cm^{-1}; NMR: δ 1.0—2.6 (m, 8H), 3.4—3.75 (m, 3H), 3.72 (s, 3H), 3.75—4.1 (m, 2H), 7.15—7.5 (m, 3H), and 7.6—7.9 (m, 2H); UV: λ_{max} (EtOH) 247 nm (ε 14000); MS: *m/e* 379 (M^+, trace) and 121 (100%).

Found: C, 57.16; H, 5.54; N, 3.65; S, 25.11%. Calcd for $C_{18}H_{21}NO_2S_3$: C, 56.96; H, 5.58; N, 3.69; S, 25.34%.

Reaction of ***8b*** *with Acrylaldehyde.* A solution of **8b** (239 mg, 1 mmol), acrylaldehyde (168 mg, 3 mmol), and a small amount of hydroquinone in benzene (3 ml), was heated at 90 °C for 9 h in a sealed tube. After evaporation of the solvent, the residue was chromatographed with ether-hexane (4 : 1) to give 219 mg (74%) of **21b** as a yellow oil; IR (KBr): 1720 cm^{-1}; NMR: δ 2.8—4.0 (m, 7H), 7.2—7.6 (m, 3H), 7.6—7.9 (m, 2H), and 9.9 (s, 1H).

Reaction of ***7*** *with TCNE.* A solution of TCNE (144 mg, 1.12 mmol) and **7** (290 mg, 1.0 mmol) in acetonitrile (5 ml) was refluxed for 2 h. After the usual work-up, the reaction mixture was subjected to DCC (silica gel, $CHCl_3$) to give yellow crystals **24** (212 mg, 57%); mp 146.5—148 °C (from MeOH); IR (KBr): 2200 (C≡N) and 1495 cm^{-1} (conj. C=C); NMR: δ 1.1—2.0 (m, 8H), 3.6—4.0 (m, 2H), 6.98 (s, 1H), and 7.1—7.6 (m, 5H); MS: *m/e* 324 (M^+, 33%) and 81 (100).

Found: C, 66.75; H, 5.02; N, 8.77; S, 19.55%. Calcd for $C_{18}H_{16}N_2S_2$: C, 66.63; H, 4.97; N, 8.63; S, 19.76%.

Reaction of ***8a*** *with TCNE.* A solution of **8a** (293 mg, 1 mmol) and TCNE (153 mg, 1.2 mmol) in acetonitrile (50 ml) was refluxed for 28 h. Purification by DCC (silica gel, CH_2Cl_2-CCl_4 (2 : 1)) and preparative TLC (silica gel, CH_2Cl_2-hexane (2 : 1)) gave 32 mg (10%) of **25** (a yellow oil); IR (neat): 2220 cm^{-1}; NMR: δ 1.2—2.4 (m, 8H), 3.9—4.4 (m, 2H), and 7.2—7.9 (m, 5H); UV: λ_{max} (CH_2Cl_2) 230 (ε 13500), 277 (17200), 314 (19600), and 324 nm (18400); MS: *m/e* 325 (M^+, 2%) and 81 (100); and 51 mg (18%) of **26** (colorless crystals); mp 110.5—111 °C (from EtOH); IR (KBr): 1625 cm^{-1}; NMR: δ 1.2—2.4 (m, 8H), 3.7—4.2 (m, 2H), 7.25—7.65 (m, 3H), and 8.15—8.45 (m, 2H); MS: *m/e* 277 (M^+, 3%) and 105 (100).

Found: C, 60.85; H, 5.40; N, 4.85; S, 23.09%. Calcd for $C_{14}H_{15}NOS_2$: C, 60.62; H, 5.45; N, 5.05; S, 23.12%. Compound **25** was not purified so as to give an analytically pure specimen.

Reaction of ***7*** *with Diphenylketene.* A DMF solution (10 ml) of **7** (292 mg, 1 mmol) and the ketene[21] (1.0 g, 5.2 mmol) was stirred at room temperature for 10 h. Addition of water, extraction with ether and then DCC (hexane-ether (9 : 1)) afforded **28** (376 mg, 88%) as yellow crystals. A similar reaction in refluxing benzene for 47 h also gave **28** (85%), which was identical with the desulfurization product of **35** by triphenylphosphine (*vide infra*).

Reaction of ***8a*** *with Diphenylketene.* A solution of **8a** (293 mg, 1 mmol) and the ketene (1.07 g, 5.5 mmol) in DMF (10 ml) was stirred at room temperature for 2 days. After similar work-up to that described above, DCC (silica gel, CH_2Cl_2-hexane (2 : 1)) of the residue afforded 389 mg (80%) of **29**. It was thermally unstable, undergoing fragmentation to **8a** upon refluxing in ethanol. Mp 122—125 °C (dec) (from CH_2Cl_2-MeOH). IR (KBr): 1700 cm^{-1}; NMR: δ 0.7—2.5 (m, 8H), 2.4—2.8 (m, 1H), 3.05—3.45 (m, 1H), and 6.9—7.85 (m, 15H); UV: λ_{max} (CH_2Cl_2)229 (ε 17400) and 251 nm (18200); MS: *m/e* 427 (0.3%) and 165 (100).

Found: C, 68.68; H, 5.11; N, 2.86; S, 19.49%. Calcd for $C_{28}H_{25}NOS_3$: C, 68.96; H, 5.17; N, 2.87; S, 19.72%.

Reaction of ***8a*** *with Diazomethane.* A solution of **8a** (293 mg, 1 mmol) and a large excess of diazomethane[22] in ether (150 ml) was stirred for 1 h. The ether was evaporated and the residue was subjected to preparative TLC (silica gel, benzene) to give 129 mg (41%) of **30a**α and 154 mg (50%) of **30a**β. **30a**α: mp 90—91 °C (from EtOH); NMR: δ 1.1—2.7 (m, 8H), 4.07 (s, 2H), 3.8—4.3 (m, 2H), 7.3–7.7 (m, 3H), and 7.8—8.2 (m, 2H); UV: λ_{max} (EtOH) 247.5 (ε 17800) and 285 sh nm (6340); MS: *m/e* 307 (M^+, 12%), 274 (10), 225 (100), and 121 (22).

Found: C, 58.69; H, 5.61; N, 4.63; S, 31.01%. Calcd for $C_{15}H_{17}NS_3$: C, 58.59; H, 5.56; N, 4.56; S, 31.28%.

30aβ: mp 92—93 °C (from EtOH); NMR: δ 1.1—2.7 (m, 8H), 4.07 (s, 2H), 3.9—4.4 (m, 2H), 7.3—7.7 (m, 3H), and 7.8—8.2 (m, 2H); UV: λ_{max} (EtOH) 247.5 (ε 17800) and 285 sh nm (6340); MS: *m/e* 307 (M^+, 5%), 274 (4), 225 (27), 193 (100), and 121 (10).

Found: C, 58.83; H, 5.55; N, 4.80; S, 30.96%. Calcd for $C_{15}H_{17}NS_3$: C, 58.59; H, 5.56; N, 4.56; S, 31.28%.

Acid-Catalyzed Hydrolysis of ***30a***α. An ethanol solution (25 ml) of **30a**α (192 mg, 0.63 mmol) and 3/2M sulfuric acid (2 ml) was refluxed for 15 h. After removal of ethanol, 50 ml of water was added and the solution was extracted with CH_2Cl_2, the extract being dried over $MgSO_4$, and the solvent evaporated. The residue subjected to preparative TLC (silica gel, hexane-ether (4 : 1)) gave 108 mg (56%) of **32** as a colorless oil; IR (neat): 2550 cm^{-1}; NMR: δ 0.8—2.1 (m, 8H), 2.04 (d, 1H, J=6.5 Hz), 3.5 (m, 1H), 3.86 (m, 1H), 7.18 (s, 1H), 7.25—7.6 (m, 3H), and 7.7—8.15 (m, 2H); MS: *m/e* 307 (M^+, 4%) and 193 (100); and 21 mg (11%) of **30a**β.

Reaction of ***8b*** *with Diazomethane.* A solution of **8b** (239 mg, 1 mmol) and a large excess of diazomethane in ether (200 ml) was stirred at room temperature for 1 h. The solvent was evaporated and the residue was chromatographed (DCC, silica gel) with CH_2Cl_2–CCl_4 (1 : 1) to give 228 mg (90%) of **30b**; mp 104—105 °C (from EtOH); NMR: δ 3.52 (m, 4H), 3.95 (s, 2H), 7.2—7.6 (m, 3H), and 7.6—8.0 (m, 2H); MS: *m/e* 253 (M^+, 28%), 193 (100), and 121 (29).

Found: C, 52.26; H, 4.21; N, 5.43; S, 37.86%. Calcd for $C_{11}H_{11}NS_3$: C, 52.14; H, 4.34; N, 5.53; S, 37.96%.

Reaction of ***7*** *with Diphenyldiazomethane.* A mixture of **7** (876 mg, 3.0 mmol) and the diazomethane[23] (873 mg, 4.5 mmol) in ether (70 ml) was stirred at room temperature for 17 h. Colorless precipitates **35** (651 mg, 47%) were collected and recrystallized from benzene-ether; mp 147—148 °C; NMR: δ 0.9—2.0 (m, 8H), 3.5—3.75 (m, 2H), 5.85 (s, 1H), and 6.8—7.7 (m, 15H); MS: *m/e* 458 (M^+, trace), 426 (70%), and 344 (100).

Found: C, 73.41; H, 5.86; S, 20.67%. Calcd for $C_{28}H_{26}S_3$: C, 73.31; H, 5.72; S, 20.97%.

Reaction of ***8a*** *with Diphenyldiazomethane.* A solution of **8a** (879 mg, 3 mmol) and the diazomethane (679 mg, 3.5 mmol) in benzene (30 ml) was stirred for 5 days. The solvent was evaporated *in vacuo* and the residue was subjected to preparative TLC (silica gel, benzene-CCl_4 (1 : 1)) to give 592 mg (43%) of **36**α, 109 mg (8%) of **36**β, 219 mg (16%) of **37**α, and 93 mg (7%) of **38** as pale yellow crystals. **36**α: mp 158.5—159 °C (from CH_2Cl_2–MeOH); NMR: δ 1.0—2.5 (m, 8H), 3.8—4.15 (m, 2H), and 6.9—7.9 (m, 15H); UV: λ_{max} (EtOH) 253 (ε 12900) and 281 nm (9180); MS: *m/e* 459 (M^+, 2%), 427 (100), 345 (56), 313 (42), 287 (39), and 255 (42).

Found: C, 70.32; H, 5.37; N, 3.22; S, 20.93%. Calcd for $C_{27}H_{25}NS_3$: C, 70.55; H, 5.48; N, 3.05; S, 20.92%.

36β: mp 171—172 °C (from CH_2Cl_2–MeOH); NMR: δ 1.0—2.5 (m, 8H), 3.9—4.3 (m, 2H), and 6.8—7.8 (m, 15H); UV: λ_{max} (EtOH) 253 (ε 12900) and 281 nm (9180); MS: *m/e* 459 (M^+, 8%), 427 (87), 345 (35), 313 (45), 287 (26), 255 (38), and 81 (100).

Found: C, 70.49; H, 5.38; N, 3.17; S, 20.99%. Calcd for $C_{27}H_{25}NS_3$: C, 70.55; H, 5.48; N, 3.05; S, 20.92%.

37α: mp 185—186 °C (from CH_2Cl_2–MeOH); NMR: δ 1.0—2.5 (m, 8H), 3.1—3.5 (m, 2H), and 6.9—8.0 (m, 15H); UV: λ_{max} (EtOH) 253 (ε 16100) and 310 nm (3350); MS: *m/e* 459 (M^+, 11%), 427 (3), 345 (8), 313 (54), 261 (41), and 121 (100).

Found: C, 70.82; H, 5.47; N, 3.23; S, 20.84%. Calcd for $C_{27}H_{25}NS_3$: C, 70.55; H, 5.48; N, 3.05; S, 20.92%.

38: mp 92—93 °C (from hexane); NMR: δ 1.0—2.0 (m, 8H), 3.6—4.1 (m, 2H), and 7.0—7.6 (m, 15H); UV: λ_{max} (EtOH) 236 (ε 14200) and 305 nm (8110); MS: *m/e* 427 (M^+, 100%), 345 (38), 313 (13), 287 (30), and 255 (33).

A similar experiment was carried out in ether using 293 mg (1 mmol) of **8a** and 241 mg (1.2 mmol) of diphenyldiazomethane, 144 mg (31%) of **36α**, 62 mg (13%) of **36β**, 57 mg (12%) of **37α**, 73 mg (16%) of **37β** and 101 mg (24%) of **38** being obtained. **37β**: mp 231—232 °C (from CH_2Cl_2–MeOH); NMR: δ 1.0—2.0 (m, 8H), 3.8—4.2 (m, 2H), and 6.9—7.9 (m, 15H); UV: λ_{max} (EtOH) 253 (ε 16100) and 305 nm (3350); MS: *m/e* 459 (M^+, 8%), 427 (4), 345 (24), 313 (49), 261 (36), and 121 (100).

Found: C, 70.54; H, 5.44; N, 3.42; S, 20.40%. Calcd for $C_{27}H_{25}NS_3$: C, 70.55; H, 5.48; N, 3.05; S, 20.92%.

*Conversion of **36α** into **39**.* A solution of **36α** (100 mg, 0.22 mmol) and trimethyloxonium tetrafluoroborate (66 mg, 0.46 mmol) in CH_2Cl_2 (20 ml) was refluxed for 10 h. The reaction mixture was subjected to preparative TLC (silica gel, benzene) to give 27 mg (27%) of unchanged **36α**, 48 mg (48%) of **36β**, and 15 mg (27%) of **39**, mp 166—167 °C; IR (KBr): 1705 cm^{-1}; NMR: δ 7.3—7.8 (m, 13H) and 7.8—8.15 (m, 2H); MS: *m/e* 329 (M^+, 21%) and 198 (100).

*Reaction of **7** with Phenyldiazomethane.* An ethereal solution (40 ml) of **7** (205 mg, 0.7 mmol) and excess phenyldiazomethane[24] was stirred at room temperature for 2 h. TLC purification afforded **42** (176 mg, 61%) as a yellow oil. NMR: δ 1.0—2.1 (m, 8H), 3.5—3.85 (m, 2H), 6.50 (s, 1H), 7.10 (s, 1H), and 6.9—7.5 (m, 10H); MS: *m/e* 350 (M^+, 14%) and 278 (100).

Found: C, 75.16; H, 6.07%. Calcd for $C_{22}H_{22}S_2$: C, 75.37; H, 6.34%.

*Reaction of **43** with Diphenyldiazomethane.* A benzene solution (35 ml) of **43**[10] (368 mg, 1 mmol) and diphenyldiazomethane (388 mg, 2 mmol) was stirred at room temperature for 15 h. After the usual work-up, **44** (447 mg, 93%) was obtained as colorless crystals. No analytically pure sample could be obtained. Mp 157—158.5 °C (dec) (from hexane-ether); NMR: δ 0.8—2.1 (m, 8H), 3.2—3.6 (m, 2H), and 6.8—7.6 (m, 20H); MS: *m/e* 534 (M^+, trace), 502 (trace), and 78 (100%).

*Reaction of **43** with Phenyldiazomethane.* A benzene solution (25 ml) of **43** (204 mg, 0.55 mmol) and excess phenyldiazomethane was stirred at room temperature for 2 h. DCC (SiO_2, hexane-benzene(1 : 1)) gave yellow crystals (201 mg), recrystallization of which from ether gave **45** (18 mg, 7.1%) as colorless crystals, the filtrate affording **47** (157 mg, 67%) as pale yellow crystals. **45**: mp 159—160.2 °C (dec); NMR: δ 0.9—1.55 (m, 8H), 3.2—3.75 (m, 2H), 4.45 (s, 1H), and 6.9—7.6 (m, 15H); MS: *m/e* 458 (M^+, trace), 426 (8%), and 344 (100). **47**: mp 64—65 °C; NMR: δ 0.8—1.9 (m, 8H), 3.3—3.85 (m, 2H), and 6.9—7.6 (m, 16H); MS: *m/e* 426 (M^+, 13%) and 344 (100). No analytically pure sample could be obtained.

*Desulfurization of Episulfides **35** and **44**.* a) A benzene solution (10 ml) of **35** (46 mg, 0.1 mmol) and triphenylphosphine (29 mg, 0.11 mmol) was left to stand at room temperature for 5 days. The usual work-up afforded **28** (43 mg) quantitatively as yellow crystals. Mp 144—145.5 °C (from EtOH); NMR: δ 0.9—1.9 (m, 8H), 3.4—3.7 (m, 2H), 6.25 (s, 1H), and 6.7—7.35 (m, 15H); MS: *m/e* 426 (M^+, 71%) and 344 (100).

Found: C, 78.55; H, 5.88; S, 14.90%. Calcd for $C_{28}H_{26}S_2$: C, 78.82; H, 6.15; S, 15.03%.

Desulfurization was also effected by refluxing benzene solution (24 h) of **35** without triphenylphosphine.

b) A benzene solution (10 ml) of **44** (54 mg, 0.1 mmol) and triphenylphosphine (29 mg, 0.11 mmol) was refluxed for 4 h. TLC purification gave 46 mg (91%) of **46** as yellow crystals; mp 164.5—165.5 °C (from EtOH); NMR: δ 1.0—2.0 (m, 8H), 3.5—3.8 (m, 2H), and 6.9—7.8 (m, 20H); MS: *m/e* 502 (M^+, 52%), 420 (76), and 344 (100).

Found: C, 81.43; H, 6.01; S, 17.55%. Calcd for $C_{34}H_{30}S_2$: C, 81.24; H, 6.02; S, 17.75%.

*Reaction of **7** with Sulfene.* To a benzene solution (5 ml) of **7** (292 mg, 1.0 mmol) and methanesulfonyl chloride (296 mg, 2.58 mmol) was added dropwise triethylamine (290 mg, 2.87 mmol) in benzene at 5 °C. After 1 h, insoluble material was filtered off, the filtrate being washed with water and dried over anhydrous magnesium sulfate. The solvent was evaporated to give brown solid (0.356 g), which was purified by TLC (silica gel, $CHCl_3$: CCl_4 = 1 : 2) to afford **48** (211 mg, 57%); mp 149—150 °C (from MeOH); IR (KBr): 1450 and 1320 cm^{-1} (SO_2); NMR: δ 1.2—2.3 (m, 8H), 4.0—4.4 (m, 2H), 4.51 (s, 2H), 6.02 (s, 1H), and 7.2—7.6 (m, 5H); MS: *m/e* 306 (M^+–SO_2, 16%) and 64 (100).

Found: C, 51.57; H, 4.95; S, 34.28%. Calcd for $C_{16}H_{18}O_2S_4$: C, 51.86; H, 4.90; S, 34.61%.

References

1) S. B. Needleman and M. C. C. Kno, *Chem. Rev.*, **62**, 405 (1962).
2) J. Hamer, "1,4-Cycloaddition Reactions," Academic Press, New York, N. Y. (1967), p. 217.
3) J. Sauer, *Angew. Chem. Int. Ed. Engl.*, **5**, 211 (1966).
4) R. Huisgen, R. Grashey, and J. Sauer, "The Chemistry of Alkenes," ed by S. Patai, John Wiley & Sons, New York, N. Y. (1964), Chap. 11.
5) G. Desimoni and G. Tacconi, *Chem. Rev.*, **75**, 651 (1975).
6) W. Kusters and P. de Mayo, *J. Am. Chem. Soc.*, **96**, 3502 (1974).
7) G. Lang and J. Vialle, *Bull. Soc. Chim. Fr.*, **1967**, 2865; M. Ahmed, J. M. Buchshriber, and D. M. McKinnon, *Can. J. Chem.*, **48**, 1991 (1970); D. B. J. Easton, D. Leaver, and T. J. Rawlings, *J. Chem. Soc., Perkin Trans. 1*, **1972**, 41.
8) K. Burger, J. Albanbauer, and W. Foag, *Angew. Chem. Int. Ed. Engl.*, **14**, 767 (1975).
9) J. C. Meslin and H. Quinou, *Tetrahedron*, **31**, 3055 (1975).
10) R. Okazaki, F. Ishii, K. Ozawa, and N. Inamoto, *J. Chem. Soc., Perkin Trans. 1*, **1975**, 270.
11) R. Okazaki, A. Kitamura, and N. Inamoto, *J. Chem. Soc., Chem. Commun.*, **1975**, 257.
12) R. Okazaki, M. O-oka, and N. Inamoto, *J. Chem. Soc., Chem. Commun.*, **1976**, 562.
13) D. C. Dittmer, P. L.-F. Chang, F. A. Davis, M. Iwanami, I. K. Stamos, and K. Takahashi, *J. Org. Chem.*, **37**, 1111 (1972).
14) *Cf.* A. Ronessac and J. Vialle, *Bull. Soc. Chim. Fr.*, **1968**, 2054.
15) A. W. Baker and G. H. Harris, *J. Am. Chem. Soc.*, **82**, 1923 (1960).
16) G. Kjellin and J. Sandstrom, *Acta Chem. Scand.*, **23**,

2888 (1969).
17) J. Goerdeler and R. Schimpf, *Chem. Ber.*, **106**, 1496 (1973).
18) H. Staudinger and H. Freudenberger, *Ber.*, **61**, 1576 (1928).
19) M. Fukuyama and A. Ohno, *Kagaku No Ryoiki*, **22**, 1091 (1968).
20) J. Burkhardt, R. Feinauer, E. Gulbins, and K. Hamann, *Chem. Ber.*, **99**, 1912 (1966).
21) E. C. Taylor, A. McKillop, and G. H. Hawks, *Org. Synth.*, **52**, 36 (1972).
22) T. J. Boer and H. J. Baker, *Org. Synth.*, Coll. Vol. 4, 250 (1963).
23) L. I. Smith and K. L. Howard, *Org. Synth.*, Coll. Vol. 3, 351 (1954).
24) C. G. Overberger and J. P. Anselme, *J. Org. Chem.*, **28**, 592 (1963).

Reactions of Thioacylketene Thioacetals and *o*-Thioquinone Methides with Enamines

Renji Okazaki, Fumio Ishii, and Naoki Inamoto

Department of Chemistry, Faculty of Science, The University of Tokyo, Hongo, Tokyo 113

(Received August 10, 1977)

o-Thioquinone methide reacted with enamines to give [4+2] cycloadduct in good yield. In the case of morpholinoenamine, 1 : 2 adduct was obtained. Thiobenzoylketene thioacetals underwent dimerization accompanied by concomitant desulfurization upon reaction with 1-(1-pyrrolidinyl)cyclohexene. The reaction mechanism of these reactions were discussed. Some other reactions of thioacylketene thioacetals with enamines were also described.

1,2-Dithiole-3-thiones (**1**) and (**2**) photochemically react with olefins to give α-thioacylketene thioacetals (**3**) and (**4**) respectively in good yields, the latter thioacylketene thioacetal (**4**) (*i. e.*, *o*-thioquinone methide) existing as an equilibrium mixture with the dimer in solution.[1,2]

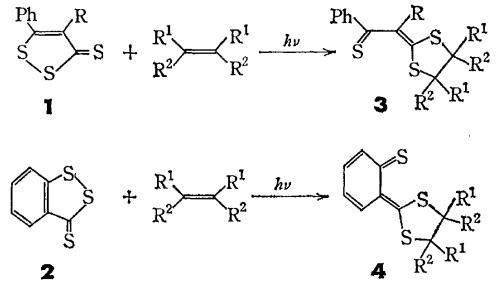

We became interested in the reactivities of these conjugated thioacetals because very few reactions have been reported on compounds of this type inspite of recent intensive studies on vinylketene (**6**)[3] and α-keto ketene thioacetals (**7**).[4]

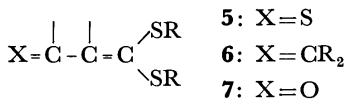

5: X=S
6: X=CR_2
7: X=O

Reactions of **3** and **4** with some electron-deficient olefins and acetylenes have been reported.[2,5] This paper gives a full account of the reactions of **3** and **4** with an electron-rich olefin, enamine.[6]

Results and Discussion

Reactions with o-*Thioquinone Methides.* *o*-Thioquinone methide (**8**) reacted with excess enamines (**9a—c**) in refluxing acetonitrile to give 1:1 adducts (**10**). Of two possible structures for the cycloadduct, **11** was eliminated by the fact that desulfurization of **10c** with Raney-nickel resulted in the formation of 2-methyl-1-phenyl-3-(1-pyrrolidinyl)propane.

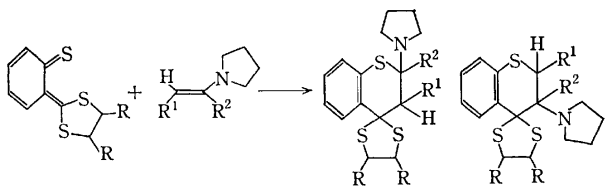

8 **9** **10** **11**

RR=$(CH_2)_4$

10a: $R^1R^2=(CH_2)_3$ 77%
10b: $R^1R^2=(CH_2)_4$ 47%
10c: R^1=Me, R^2=H 62%

It is reasonably assumed that the orientation in the cycloaddition of **9a** and **9b** is the same as that of **9c**; the products from them would thus be **10a** and **10b**, respectively.

The reaction probably proceeds *via* a zwitterionic intermediate **12** followed by cyclization.

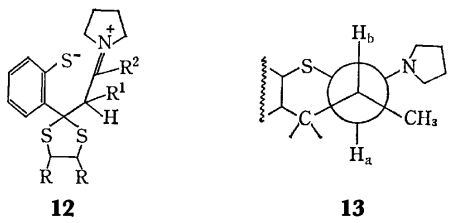

12 **13**

The NMR spectrum of **10c** shows a doublet (J= 10.0 Hz) at δ 4.66 attributable to H_a (see **13**). The large J value is compatible only with the configuration **13**. The formation of **13** can be explained by the cyclization of the intermediate **12** to **10** with the most stable configuration.

Enamine (**9d**) reacted with **8** in a different way from **9a—c** to afford a 1 : 2 adduct(40%), the orientation of which is presumably as shown in **14** by analogy with that of **10**. Enamine (**14**) was hydrolyzed to give ketone (**15**) upon chromatographic purification.

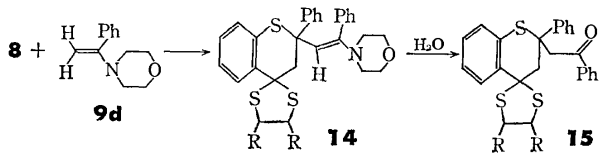

9d **14** **15**

The formation of **14** can be explained as depicted in Scheme 1.

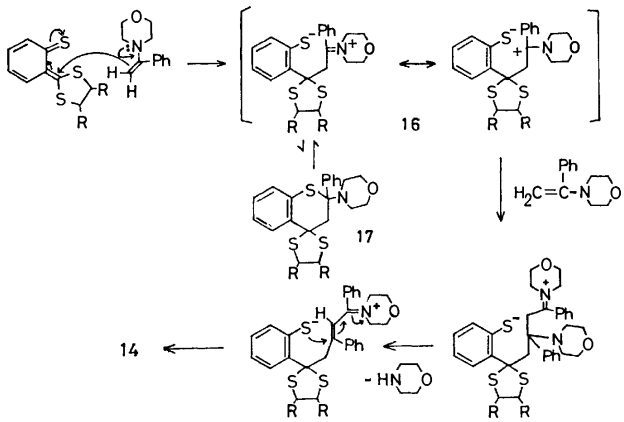

Scheme 1.

The formation of the 1:2 adduct only in the case of **9d** would be due to the enhanced stabilization of the carbocation center of **16** caused by the phenyl group. Since 1:1 adduct **17** could be subjected to cleavage because of the stabilization, **16** could be attacked by another enamine followed by the elimination of morpholine and cyclization to give **14**.

Reactions with Thioacylketene Thioacetals. Thiobenzoylketene thioacetals (**3a—c**) reacted with 1-(1-pyrrolidinyl)cyclohexene (**9b**) to give 2,3-diphenylbutane derivatives (**18**) (in refluxing acetonitrile for 10—20 h).

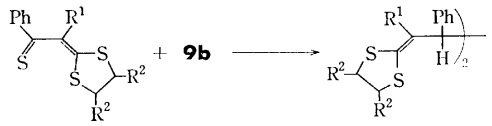

3a: R^1=Ph, R^2R^2=$(CH_2)_4$ **18a**: 48%
3b: R^1=H, R^2R^2=$(CH_2)_4$ **18b**: 24%
3c: R^1=CH_3, R^2=H **18c**: 4%

The structure of **18** was determined by spectral data and elemental analyses. Although mass spectra of the products show a weak or no parent peak, a very strong peak of half the parent peak always appears, suggesting a symmetric structure such as **18**. An intensive peak due to $[PhCH\text{-}C(R)=C=S]^+$ was also observed in each compound. The NMR spectra also support the structure **18**.

In the case of the reaction of **3b** with **9b**, two isomeric products **18b** (18%, mp 160—161 °C) and **18b'** (6%, mp 217—238 °C) were obtained. They show the same fragmentation pattern in the mass spectra, their IR spectra being nearly the same. It was impossible to measure the NMR spectrum of the isomer with a higher melting point because of poor solubility. These observations suggest that they are *meso*- and *dl*-compounds. In view of the fact that the *dl*-isomer has a lower melting point and higher solubility,[7] **18b** with a lower melting point and higher solubility was tentatively assigned to a *dl*-isomer and hence **18b'** with a higher melting point and lower solubility to a *meso*-isomer.

In this reaction thioamide **19** (4%) was also obtained in addition to **18b** and **18b'**. Since **19** was produced from **3b** and pyrrolidine under similar conditions, **19** obtained in the enamine reaction seems to be formed as a by-product from the reaction of **3b** with pyrrolidine derived from enamine.

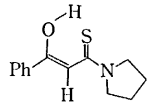

19

The formation of **18** could be explained by an attack of an enamine on the sulfur atom of thiocarbonyl group (Scheme 2). The zwitterionic intermediate **20** thus formed would undergo fragmentation to form carbene **21** stabilized by the phenyl group which subsequently abstracts a hydrogen atom, dimerizing to give the final product **18**.

The ground state of vinylcarbene is triplet and capable of abstracting hydrogen atom of allylic position,[8] supporting the mechanism in Scheme 2.

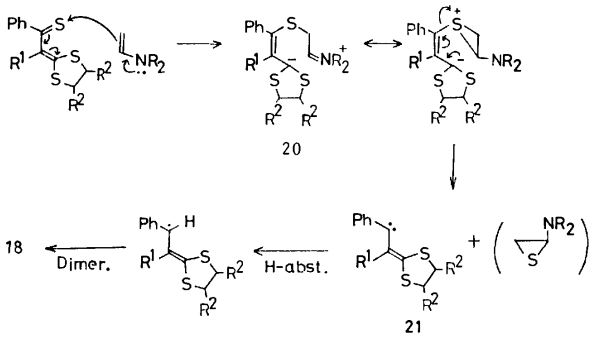

Scheme 2.

This is the first observation that an enamine can attack the sulfur atom of a thiocarbonyl group (*i.e.*, "thiophilic reaction") as in the case of organolithium compounds or Grignard reagents.[9-12] Phenyllithium attacks diphenyl trithiocarbonate to produce bis(phenylthio)carbene.[9,10] Carbene **21** can be regarded as a vinylog of dithiocarbene of type **22**, similarity between these two reactions being noteworthy.

$$(PhS)_2C{=}S + PhLi \longrightarrow (PhS)_3C^-Li^+ \rightleftarrows PhSLi + (PhS)_2C:$$

22

Thioacylketene thioacetal (**23**) reacted with **9b** to give conjugated thione (**24**) in 10% yield. The structure of **24** was established by its NMR and mass

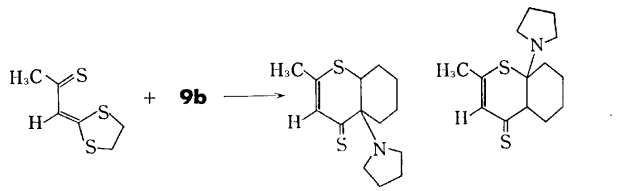

23 **24** **25**

spectra and elemental analysis. The chemical shift (δ 3.20—3.80) of a broad doublet assignable to four α-protons of the pyrrolidine ring is considerably lower than that of **10a** (δ 2.5—2.9), **10b** (δ 2.4—2.9), and **10c** (δ 2.5—3.0). The lower chemical shift of **24** could be explained in terms of magnetic anisotropy of the thiocarbonyl group, suggesting structure **24** rather than **25**. The demonstrated thiophilicity described above of **3a—c** is also evidence for **24**.

The formation of **24** can be accounted for by Scheme 3. The heterolytic cleavage of the C–S bond in **26**

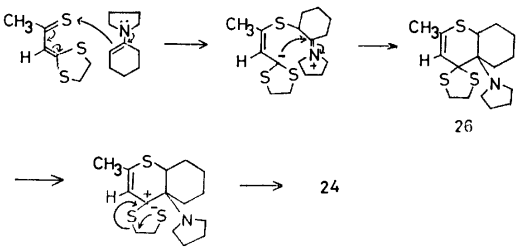

Scheme 3.

might be supported by such factors as stability of the carbocation formed, participation of α-nitrogen, and high polarity of the solvent.

No reaction of 2-(1,3-dithiolan-2-ylidene)cyclopentanethione (**27**) and enamine **9b** took place in refluxing acetonitrile for 30 h. However, the reaction in *N,N*-dimethylformamide (DMF) at 110—120 °C for 15 h led to the formation of conjugated thione (**28**) (24%).

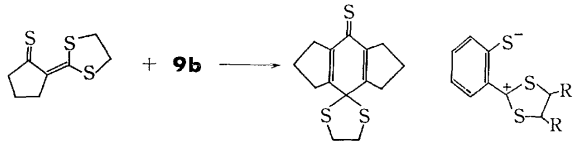

27 **28** **29**

Elemental analysis and the mass spectrum show that the molecular formula of the product is $C_{14}H_{16}S_3$. The NMR spectrum suggests the symmetric nature of the product and the UV spectrum (225 (log ε 4.23), 329 (4.44), 468 (269), and 526 nm (1.22)) reveals the presence of a conjugated thione system. The mechanism of the formation of **28** has not been clarified as yet.

The difference in reactivity in which the attack of an enamine occurs at the sulfur atom of the thiocarbonyl group in **3** but at the β-carbon of the thiocarbonyl group in *o*-thioquinone methide (**8**), can be explained mainly in terms of a greater contribution of an ionic canonical structure **29** in the case of **8**. It would reduce the thionic nature of **8** and enhance the electrophilicity of the β-carbon.

Experimental

All the reactions were carried out under nitrogen. The IR and UV spectra were measured on Hitachi EPI-G2 and EPS-3 spectrophotometers, respectively. The NMR spectra were recorded as $CDCl_3$ solutions with a Hitachi R-24 or R-20B spectrometer, tetramethylsilane being used as an internal standard. Mass spectra were determined on a Hitachi RMU-6L mass spectrometer operating at 70 eV.

Reactions of o-Thioquinone Methides (8) with Enamine (9). Thione **8**(0.662 g, 2.5 mmol)[2] was suspended in dry acetonitrile (30 ml) and two or three molar excess of **9** was added in a small portion over a period of 5 min. The solution was heated to reflux and maintained at this temperature with agitation for 1—2 h. The solution turned colorless from blue. The reaction was monitored by TLC. When the reaction was complete, acetonitrile was removed *in vacuo*. The residue was recrystallized from methanol or ethanol. All the products **10** were colorless crystals.

4,4-(1,2-Cyclohexylenedithio)-2-(1-pyrrolidinyl)-2,3-trimethylenethiochroman (**10a**): 0.78 g (77%); mp 154—155 °C (EtOH); NMR: δ 1.00—2.40 (m, 18H), 2.50—2.90 (m, 4H), 2.95—3.30 (m, 1H), 3.65—4.00 (m, 2H), 7.03—7.44 (m, 3H), and 8.10—8.26 (m, 1H).

Found: C, 65.28; H, 7.38; N, 3.43; S, 23.79%. Calcd for $C_{22}H_{29}NS_3$: C, 65.46; H, 7.24; N, 3.47; S, 23.83%.

4,4-(1,2-Cyclohexylenedithio)-2-(1-pyrrolidinyl)-2,3-tetramethylenethiochroman (**10b**): 0.45 g (47%); mp 71—72 °C (MeOH); NMR: δ 0.90—2.95 (m, 25H), 3.50—4.14 (m, 2H), 6.94—7.46 (m, 3H), and 8.08—8.37 (m, 1H); MS: *m/e* 226 (12%), 184 (24), 151 (45), 105 (100), and 78 (71).

Found: C, 65.98; H, 7.68; N, 3.54; S, 23.07%. Calcd for $C_{23}H_{31}NS_3$: C, 66.14; H, 7.48; N, 3.35; S, 23.03%.

4,4-(1,2-Cyclohexylenedithio)-2-(1-pyrrolidinyl)-3-methylthiochroman (**10c**): 0.584 g (62%); mp 145—146 °C (PhH:EtOH=1:2); NMR: δ 0.86—2.44 (m, 16H), 2.44—2.98 (m, 4H), 3.43—4.15 (m, 2H), 4.66 (d, J=10.0 Hz, 1H), 6.91—7.54 (m, 3H), and 8.08—8.38 (m, 1H).

Found: C, 63.78; H, 7.23; N, 3.64; S, 25.52%. Calcd for $C_{20}H_{27}NS_3$: C, 63.61; H, 7.21; N, 3.70; S, 25.47%.

Desulfurization of 10c with Raney Nickel. To 2.48 g (6.5 mmol) of **10c** was added Raney nickel[13] prepared from 25 g of Al-Ni alloy in 60 ml of ethanol. The solution was heated under reflux for 1 h. After Raney nickel was separated, the filtrate was concentrated, 10 ml of ether was added and the mixture was extracted with 50 ml of 0.1 M aq HCl. The aqueous solution was neutralized with 0.1 M aq KOH, extracted with ether, and dried over anhydrous magnesium sulfate. The solution was concentrated and the residue (0.646 g, 49%) was purified by gas chromatography (JEOL JGC-750, Versamide 900, 1 m, 125 °C) to give 2-methyl-1-phenyl-3-(1-pyrrolidinyl)propane, the structure of which is supported by the following spectral data: NMR: δ 0.88 (d, J=6.0 Hz, 3H), 1.60—3.10 (m, 13H), and 7.21 (s, 5H); MS: *m/e* 203 (M^+, 0.7%), 91 (8), and 84 (100).

Reaction of 8 with 9d. To 0.709 g (2.7 mmol) of **8** in 30 ml of dry acetonitrile was added 1.90 g (10 mmol) of **9d**. The solution was heated under reflux for 6.5 h. Upon cooling, 4,4-(1,2-cyclohexylenedithio)-2-phenyl-2-(β-morpholinostyryl)thiochroman (**14**) was precipitated as colorless crystals and recrystallized from a mixture of benzene and ethanol (1:2), 0.511 g, 34%. Mp 190—191 °C; NMR: δ 1.00—2.90 (m, 14H), 3.35—3.75 (m, 4H), 3.80—4.30 (m, 2H), 4.68 (s, 1H), and 6.60—8.80 (m, 14H); MS: *m/e* 557 (M^+, 0.1%), 291 (59), and 184 (100).

Found: C, 71.20; H, 5.88; N, 2.58; S, 16.91%. Calcd for $C_{33}H_{35}NOS_3$: C, 71.05; H, 6.32; N, 2.51; S, 17.24%.

The filtrate was concentrated and subjected to dry column chromatography on silica gel with dichloromethane. 4,4-(1,2-Cyclohexylenedithio)-2-phenacyl-2-phenylthiochroman (**15**) was precipitated as colorless crystals, and recrystallized from a mixture of benzene and ethanol (1:2), yield 81 mg (6%). Mp 220—221 °C; NMR: δ 1.00—2.70 (m, 10H), 3.40—4.20 (m, 2H), 4.20—4.70 (m, 2H), and 6.90—8.70 (m, 14H); IR(KBr): 1680 cm^{-1} (C=O); MS 488 (M^+, 0.2%) and 184 (100).

Found: C, 71.11; H, 5.88; S, 19.34%. Calcd for $C_{29}H_{28}OS_3$: C, 71.27; H, 5.77; S, 19.68%.

Reaction of 3 with 9b. a) To **3b**[1] (0.83 g, 3.0 mmol) in refluxing acetonitrile (30 ml) was added 2.57 g (17 mmol) of **9b** in a small portion over a period of 10 min. The solution was stirred at this temperature for 12 h. When the reaction was complete, the color of the solution turned red from deep green. Upon cooling, **18b'** (45 mg, 6%) was precipitated as colorless crystals and recrystallized from THF. The filtrate was subjected to dry column chromatography on silica gel with dichloromethane to give 2,3-diphenyl-1,4-bis(4,5-tetramethylene-1,3-dithiolan-2-ylidene)butane **18b** (0.14 g, 18%) and 3-hydroxy-*N,N*-tetramethylenethiocinnamamide **19** (30 mg, 4%), the latter being identical with an authentic sample.[14]

18b: mp 160—161 °C; NMR: δ 1.10—2.20 (m, 16H), 3.50—4.10 (m, 6H), 5.60—5.80 (dd, J=7.6 Hz, J=1.5 Hz, 2H), and 6.90—7.40 (m, 10H); MS: *m/e* 522 (M^+, 7%), 261 ($M^+/2$, 46), and 147 (100).

Found: C, 69.09; H, 6.62; S, 24.20%. Calcd for $C_{30}H_{34}S_4$: C, 68.92; H, 6.55; S, 24.53%.

18b': mp 237—238 °C; MS: *m/e* 522 (M^+, 0.9%), 261 ($M^+/2$, 36), and 147 (100).

Found: C, 68.79; H, 6.68; S, 24.56%. Calcd for $C_{30}H_{34}S_4$: C, 68.92; H, 6.55; S, 24.53%.

b) Reactions of **3a**[1] (0.280 g, 0.76 mmol) and **3c**[15] (1.89 g, 0.75 mmol) with **8b** (2.00 g, 13.2 mmol for **3a** and 3.00 g, 18.7 mmol for **3c**) were carried out in a similar way to that for **3b**.

1,2,3,4-Tetraphenyl-1,4-bis(4,5-tetramethylene-1,3-dithiolan-2-ylidene)butane (**18a**): 0.124 g, 48%; mp 244—245 °C; NMR: δ 1.10—2.40 (m, 16H), 3.50—4.10 (m, 4H), 4.30—4.60 (m, 2H), and 6.90—7.60 (m, 20H); MS: *m/e* 337 ($M^+/2$, 100%) and 223 (70).

Found: C, 74.81; H, 6.26; S, 18.63%. Calcd for $C_{42}H_{42}S_4$: C, 74.73; H, 6.27; S, 18.99%.

3,4-Diphenyl-2,5-bis(1,3-dithiolan-2-ylidene)hexane (**18c**): 60 mg, 4%; mp 260—261 °C; NMR: δ 1.84 (s, 6H), 3.30 (s, 8H), 4.58 (s, 2H), and 7.00—7.50 (m, 10H); MS: *m/e* 442 (M^+, trace), 221 ($M^+/2$, 100), and 161 (33).

Found: C, 65.41; H, 5.87; S, 28.79%. Calcd for $C_{26}H_{24}S_4$: C, 65.11; H, 5.92; S, 28.97%.

*Reaction of **23** with **9b**.* To 0.870 g (5 mmol) of **23**[15] in 30 ml of dry acetonitrile was added 3.00 g (19 mmol) of **9b** in a small portion. The reaction mixture was refluxed for 2 h. After the solvent had been removed, the residue was dissolved in benzene and chromatographed on alumina. 2-Methyl-5,6-tetramethylene-5-(1-pyrrolidinyl)-5,6-dihydro-4*H*-thiopyran-4-thione (**24**) (0.125 g, 10%) was eluted with a mixture of benzene and ethyl acetate (1:1), which was recrystallized from ethanol as yellow crystals, mp 220—221 °C. NMR: δ 1.10—2.50 (m, 12H), 2.72 (s, 3H), 3.20—3.80 (m, 5H), and 6.46 (s, 1H); MS: *m/e* 267 (M^+, 55%), 234 (39), 223 (32), 190 (47), 152 (20), and 41 (100).

Found: C, 62.70; H, 7.87; N, 5.14; S, 24.00%. Calcd for $C_{14}H_{21}NS_2$: C, 62.87; H, 7.92; N, 5.24; S, 23.97%.

*Reaction of **27** with **9b**.* To a DMF solution (30 ml) of **27**[15] (2.32 g, 11 mmol) was added **9b** (4.50 g, 30 mmol) in a small portion. After being refluxed at 110—120 °C for 15 h, the solution was poured into 50 ml of water and extracted with 100 ml of dichloromethane, the extract being dried over anhydrous magnesium sulfate. After removal of the solvent, the residue was dissolved in benzene and subjected to dry column chromatography on silica gel with dichloromethane. 4,4-(Ethylenedithio)-2,3 : 5,6-bis(trimethylene)-2,5-cyclohexadiene-1-thione (**28**) was precipitated as purple crystals, and recrystallized from a mixture of benzene and hexane (1:1), 0.363 g (24%). Mp 133—134 °C; NMR: δ 1.60—2.10 (m, 4H), 2.40—3.20 (m, 8H), and 3.46 (s, 4H); MS: *m/e* 280 (M^+, 98%), 252 (12), 220 (29), and 176 (100); UV: λ_{max} (EtOH) 225 (log ε 4.23), 329 (4.44), and 468 (2.69); λ_{max} (PhH) 526 nm (1.22).

Found: C, 59.82; H, 5.79; S, 34.60%. Calcd for $C_{14}H_{16}S_2$: C, 59.95; H, 5.75; S, 34.30%.

References

1) R. Okazaki, F. Ishii, K. Ozawa, and N. Inamoto, *Chem. Lett.*, **1972**, 9; R. Okazaki, F. Ishii, K. Okawa, and N. Inamoto, *J. Chem. Soc., Perkin Trans. 1*, **1975**, 270.

2) R. Okazaki and N. Inamoto, *Chem. Lett.*, **1974**, 1439. See also P. de Mayo and H. Y. Ng, *J. Chem. Soc., Chem. Commun.*, **1974**, 877.

3) F. A. Carey and A. S. Court, *J. Org. Chem.*, **37**, 4474 (1972); D. Seebach, M. Kolb, and B.-T. Gröbel, *Angew. Chem. Int. Ed. Engl.*, **12**, 69 (1973).

4) E. J. Corey and R. H. K. Chen, *Tetrahedron Lett.*, **1973**, 3817; I. Shahak and Y. Sasson, *ibid.*, **1973**, 4207; R. R. Rastogi, H. Ila, and H. Junjappa, *J. Chem. Soc., Chem. Commun.*, **1975**, 645; S. M. S. Chauhan and H. Junjappa, *Synthesis*, **1975**, 880; Y. Ittah and I. Shahak, *ibid.*, **1976**, 320; A. Kumar, H. Ila, H. Junjappa, and S. Mhatre, *J. Chem. Soc., Chem. Commun.*, **1976**, 592; A. Kumar, H. Ila, and H. Junjappa, *ibid.*, **1976**, 593; S. M. S. Chauhan and H. Junjappa, *Tetrahedron*, **32**, 1911 (1976); A. Kumar, H. Ila, and H. Junjappa, *Synthesis*, **1976**, 324.

5) R. Okazaki, A. Kitamura, and N. Inamoto, *J. Chem. Soc., Chem. Commun.*, **1975**, 257.

6) Preliminary report: F. Ishii, R. Okazaki, and N. Inamoto, *Tetrahedron Lett.*, **1976**, 4283.

7) For example, for $(PhCHCH_2CO_2H)_2$, mp's of the *dl*- and *meso*-forms are 185—186 °C and 270—271 °C respectively. M. P. Oommen and A. I. Vogel, *J. Chem. Soc.*, **1930**, 2148.

8) M. L. Manion and H. D. Roth, *J. Am. Chem. Soc.*, **97**, 6919 (1975); G. E. Palmer, J. R. Bolton, and D. R. Arnold, *ibid.*, **96**, 3708 (1974); R. S. Hutton, M. L. Manion, H. D. Roth, and E. Wasserman, *ibid.*, **96**, 4680 (1974).

9) P. Beak and J.W. Worley, *J. Am. Chem. Soc.*, **94**, 597 (1972).

10) D. Seebach, *Chem. Ber.*, **105**, 487 (1972).

11) D. Paquer, *Bull. Soc. Chim. Fr.*, **1975**, 1439.

12) P. Beak, J. Yamamoto, and C. J. Upton, *J. Org. Chem.*, **40**, 3052 (1975).

13) A. A. Pavlic and H. Adkins, *J. Am. Chem. Soc.*, **68**, 1471 (1946).

14) F. Ishii, M. Stavaux, and N. Lozac'h, *Bull. Soc. Chim. Fr.*, in press.

15) A. Thuillier and J. Vialle, *Bull. Soc. Chim. Fr.*, **1962**, 2182; J. Maignan and J. Vialle, *ibid.*, **1973**, 2388.

NOTES

BULLETIN OF THE CHEMICAL SOCIETY OF JAPAN, VOL. 51 (1), 313—314 (1978)

Environment Effect on the Symmetry of Yang's Biradical

Kazuo MUKAI

Department of Chemistry, Faculty of Science, Ehime University, Matsuyama 790

(Received June 6, 1977)

Synopsis. The ESR spectrum of Yang's biradical, which has a structural three-fold symmetry and degenerate, partially filled levels, has been measured in several solvents at 77 K. The results of the analyses of the ESR spectra have shown that Yang's biradical must lack a three-fold symmetry in frozen solutions. The notable solvent effects observed for the zero-field splitting parameters (D and E) suggest that the asymmetric environment due to frozen-solvent molecules contributes to the molecular distortion found for Yang's biradical.

Yang and Castro have reported the preparation of a fairly stable phenoxyl biradical, which is known as Yang's biradical (I).[1] Yang's biradical is a ground-state triplet molecule which has a structural three-fold symmetry and degenerate, partially filled levels.[2-4] However, recently, the toluene rigid matrix ESR spectrum of Yang's biradical was reported to be a characteristic spectrum of a non-axially symmetrical triplet, with $D=34.1$ and $E=2.3$ G.[5] This result may be explained by assuming that at least one of the twist angles of the three phenyl rings is different from the other two rings in the low-temperature rigid matrix. It is probable that the Jahn-Teller effect induces such molecular

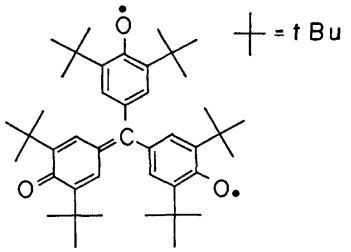

Yang's Biradical (I)

distortion in Yang's biradical, thus splitting the degenerate, partially filled levels. In addition to the above Jahn-Teller distortion, the asymmetric environment due to frozen solvent molecules may contribute to the molecular distortion found for Yang's biradical in the low-temperature rigid matrix. In fact, recent ENDOR studies[6] of phenylgalvinoxyl and some of its derivatives in fluid solutions and ESR studies[7] of *p*- and *m*-phenylenebis(galvinoxyl) biradicals in frozen solutions have given evidence that solvent molecules may play an important role in fixing the conformation and symmetry of the radical in both fluid and frozen solutions.

On the other hand, the fluid-solution ESR spectrum of Yang's biradical shows seven equally spaced lines, due to the six equivalent protons in the biradical.[5] The results of NMR and ENDOR studies[8,9] in solution also indicate that the six ring protons are magnetically equivalent, giving a hyperfine splitting for the six meta-ring protons. The expected inequivalence of the proton splitting was not observed in these measurements.

In the present work, in order to obtain further information on such molecular distortion, we have measured the ESR spectra of Yang's biradical in five solvents— ethanol, toluene, 2-methyltetrahydrofuran (2-MTHF), diethyl ether, and diglyme, and have studied the effect of solvents on the unpaired spin distribution and symmetry of Yang's biradical.

Experimental

Yang's biradical was prepared by the oxidation of the corresponding bisphenol (mp 276—278 °C) (lit, mp 278—279 °C)[1] with alkaline potassium hexacyanoferrate (III) in diethyl ether under a nitrogen atmosphere, with the temperature kept between 5 and 10 °C, according to the method of Yang and Castro.[1] A deep purple crystalline compound with a metallic luster was isolated from the diethyl ether layer. The ESR spectra were obtained at the X band using a JES-ME-3X spectrometer equipped with a Takeda-Riken microwave frequency counter to measure the klystron frequency. The ESR splittings were determined using $(KSO_3)_2NO$ ($a^N=13.05\pm0.03$ G) as a standard. The g-values were measured relative to the value of Li-TCNQ powder, calibrated with $(KSO_3)_2NO$ ($g=2.0054$).[10]

Results and Discussion

When the solution containing the biradical is frozen into a rigid glass (77 K), one can observe some dipolar splittings. The zero-field parameters (D and E) and g-tensor values have been tentatively estimated from the positions of the three pairs of turning points (ZZ', YY', XX'), as performed in a previous paper.[5] Notable solvent dependences of the zero-field splitting parameters were observed in the frozen-solution spectra of the biradical; the results are summarized in Table 1. The observed D and E values are 34.6 and 1.5 G in ethanol, 34.1 and 1.9 G in toluene, 33.1 and 1.9 G in 2-MTHF, 32.7 and 4.7 G in diethyl ether, and 32.1 and 3.6 G in diglyme, respectively. The g-tensor values also appear to be slightly solvent-dependent, while the observed change in the g_{iso} value of the biradical at 20 °C is negligible, as is shown in Table 1.

Since the axial spectra, *i.e.*, the spectra characterized by only one zero-field splitting parameter, D, could not be observed in any of the solvents used, Yang's biradical must lack a three-fold symmetry in these frozen solutions. In a previous paper,[5] it was suggested that both Jahn-Teller distortion and the asymmetric environment due to the frozen-solvent molecules may contribute to such molecular distortion in Yang's biradical. The notable solvent effect observed for the zero-field param-

Table 1. *D*- and *g*-tensor values of Yang's biradical (I) in several solvents at 77 K

	$\|D\|$[a] (G)	$\|E\|$[a] (G)	g_{zz}[b]	g_{yy}	g_{xx}	g_{av}[c]	g_{iso}[d]
Ethanol	34.6	1.5	2.0025	2.0057	—[e]	—	2.00441
Toluene	34.1	1.9	2.0026	2.0054	2.0054	2.0045	2.00451
2-MTHF	33.1	1.9	2.0025	2.0054	2.0058	2.0046	2.00443
Diethyl ether	32.7	4.7	2.0032	2.0060	—	—	2.00446
Diglyme	32.1	3.6	2.0033	2.0061	—	—	2.00442

a) The $|D|$ and $|E|$ values were calculated from the $ZZ'=2D$ and $YY'=D+3E$ separations, because the turning points, X and X', are not obvious as a result of overlapping with the central monoradical signal. The E value thus calculated is smaller than the true value, considering the overlapping of the inner two pairs of lines.[5] The experimental errors in the values of $|D|$ and $|E|$ are ± 0.3 and 0.5 G respectively. b) The experimental errors in the values of g_{zz}, g_{yy}, g_{xx}, and g_{av} are ± 0.0003. c) The average $g_{av}=1/3(g_{zz}+g_{yy}+g_{xx})$. d) The isotropic g_{iso}-values measured at 20 °C. The experimental errors in the values of g_{iso} are ± 0.00003. e) In ethanol, diethyl ether, and diglyme solvents, the g_{xx} values could not be determined because of overlap with the central monoradical signal.

eters of Yang's biradical indicates that solvent molecules may contribute remarkably to a change in the steric structure of the radical molecule. In addition, it is interesting that this solvent effect on the symmetry of Yang's biradical is larger than the effects due to the asymmetric deuterium[5] and tertiary pentyl[11] substitutions. Yang's biradical may be considered to have a propeller configuration, with a twist angle of about 30°. Due to the delocalization of each unpaired electron, the principal Z axis of the *D*-tensor, corresponding to the maximum $2D$ value (ZZ'), is probably parallel to the $2p_z$ orbital of the center triphenylmethyl carbon atom. Therefore, in Yang's biradical with a non-zero E value, at least one of the twist angles of the three phenyl rings is different from the other two rings in the low-temperature rigid matrices. Upon an increase in these twist angles, the D parameter will decrease and, inversely, the E parameter will increase. In fact, it can be seen from Table 1 that the decrease in the D parameter results in the increase in the E parameter.

On the other hand, the fluid solution ESR spectra of Yang's biradical in the above solvents at 20 °C appear to correspond to hyperfine interaction with the six equivalent meta-ring protons. This result can be explained as follows: (i) the biradical apparently shows an equivalent hyperfine splitting due to the rapid exchange between distorted structures, or (ii) the radical molecule retains a three-fold symmetry in fluid solutions, because the asymmetric environment due to frozen solvent molecules disappears in fluid solutions.

We wish to express our gratitude to Mr. Jun Sakamoto for his kind help in preparing Yang's biradical.

References

1) N. C. Yang and A. J. Castro, *J. Am. Chem. Soc.*, **82**, 6208 (1960).
2) D. Kearns and S. Ehrenson, *J. Am. Chem. Soc.*, **84**, 739 (1962).
3) R. Kreilick, *J. Chem. Phys.*, **43**, 308 (1965).
4) K. Mukai, K. Ishizu, and Y. Deguchi, *J. Phys. Soc. Jpn.*, **27**, 783 (1969).
5) K. Mukai, T. Mishina, and K. Ishizu, *J. Chem. Phys.*, **66**, 1680 (1977).
6) K. Mukai, T. Kamata, T. Tamaki, and K. Ishizu, *Bull. Chem. Soc. Jpn.*, **49**, 3376 (1976).
7) K. Mukai and T. Tamaki, *Bull. Chem. Soc. Jpn.*, **50**, 1239 (1977).
8) P. W. Kopf and R. W. Kreilick, *J. Am. Chem. Soc.*, **91**, 6569 (1969).
9) H. V. Willigen, M. Plato, K. Möbius, K. P. Dinse, H. Kurreck, and J. Reusch, *Mol. Phys.*, **30**, 1359 (1975).
10) J. J. Windle and A. K. Wiersma, *J. Chem. Phys.*, **39**, 1139 (1963).
11) K. Mukai, K. Yorimitsu, and T. Mishina, *Bull. Chem. Soc. Jpn.*, **50**, 2471 (1977).

BULLETIN OF THE CHEMICAL SOCIETY OF JAPAN, VOL. 51 (1), 315—316 (1978)

A Molecular Orbital Study of the Conformation and *g*-Factors of the $HSSH^-$ Radical Anion

Osamu KIKUCHI

Department of Chemistry, The University of Tsukuba, Sakura-mura, Ibaraki 300-31

(Received July 22, 1977)

Synopsis. The electronic structure and *g*-factors of the $HSSH^-$ radical anion were calculated by means of a restricted open-shell SCF MO method with the MINDO/3 approximation, and the dependence of the *g*-factors upon the conformation was clarified. The most stable conformation predicted agreed well with the experimentally estimated –S–S– geometry of dialkyl disulfide anions, and its *g*-factors agreed well with the observed values.

Attention has been drawn in recent literature[1,2] to the electronic structures of sulfur-containing radicals and their ESR data. Lin and Lunsford[1] observed the $HSSH^-$ radical anion formed by allowing H_2S to react with trapped electrons on MgO. From the hyperfine splittings and the *g*-factors ($g_\perp=2.015$, $g_{//}=2.003$), they pointed out that the radical earlier identified as H_2S^- by Bennett *et al.*[3] is $HSSH^-$. Since the principal values of the *g*-tensor correlate strongly with the electronic structure of a radical, the theoretical analysis of the *g*-tensor can clarify the electronic structure and conformation of the radical. The purpose of the present note is to investigate the relation between the *g*-factors and the conformation of $HSSH^-$ by means of restricted open-shell SCF calculations.

The MO's of the spin-restricted doublet state were obtained by the approximate SCF version which has been proposed by Longuet-Higgins and Pople[4] for π-radicals and which has since been applied to all-valence-electron systems by the present author.[5] For the evaluation of the electron integrals involved, the MINDO/3 approximation[6] was employed. The geometry of $HSSH^-$ was first optimized with respect to three parameters; the S–S bond length, the HSS angle, ψ, and the dihedral angle, θ, between two planes containing the HSS' or SS'H group. The dependence of the *g*-factors upon ψ and θ was calculated according to Stone's formula,[7] the S–S bond length being fixed at the optimized value, 2.17 Å. A more detailed description of the calculation has been reported elsewhere.[8]

Results and Discussion

The electronic structure and *g*-factors of a typical conformation (shown in Fig. 1) will be discussed first, since the *g*-tensor of this conformation is practically diagonal in terms of the axes, x, y, and z. The ground electron configuration of C_2 symmetry is:

$$\cdots(2a)^2(2b)^2(3a)^2(3b)^2(4a)^2(4b)^1:\ ^2B$$

where 2a and 2b MO's are bonding S–H σ orbitals and where 3a is the bonding S–S $3p\sigma$ orbital directed along the S–S bond. The 3b and 4a orbitals are nearly degenerate and are expressed as $(3p_\alpha(S)+3p_\beta(S'))/\sqrt{2}$ and $(3p_\alpha(S)-3p_\beta(S'))/\sqrt{2}$ respectivley. The half-occupied MO, 4b, is the anti-bonding $3p\sigma^*$ orbital directed along the S–S bond. The contribution of each excited configuration to the principal values of the *g*-tensor is shown in Table 1. The large deviation of g_{xx} from the free-spin value can be understood as resulting from the spin-orbit mixing of the ground state with the 4a→4b excited configuration, and that of g_{zz}, from the mixing with the 3b→4b excited configuration. The contributions of the bonding S–H σ orbitals (2a and 2b) compensate for those of the anti-bonding S–H σ^* orbitals (5a and 5b). The calculated principal values ($g_\perp=2.011$ and $g_{//}=2.002$) are in fair agreement with the observed values.[1]

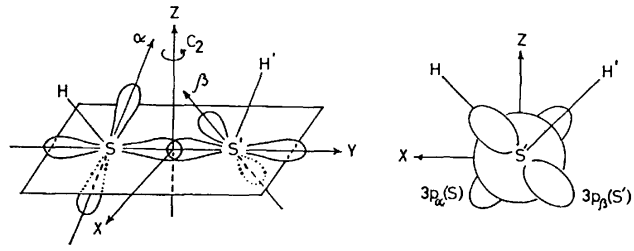

Fig. 1. The coordinate axes and the Newman projection for a typical conformation of $HSSH^-$ viewed in the direction of the S–S bond. The dihedral angle, θ, between two planes containing H–S–S' and S–S'–H' is 90° and the HSS' angle, ψ, is 90°.

TABLE 1. CALCULATED Δg_{ii}[a] VALUES OF THE $HSSH^-$ OF THE C_2 SYMMETRY, WITH $\theta=90°$ AND $\psi=90°$

Excited configuration	ΔE (eV)[b]	Δg_{xx}	Δg_{yy}	Δg_{zz}
1a→4b	16.40	0	0	0
1b→4b	11.46	0	0	2
2a→4b	6.33	77	0	0
2b→4b	6.06	0	0	79
3a→4b	3.98	5	0	0
3b→4b	2.53	0	0	81
4a→4b	2.51	79	0	0
4b→5a	2.26	0	0	−66
4b→5b	2.29	−65	0	0
Total[c]		96	0	96

a) Deviation from the free-spin value. The value of $\Delta g_{ii}\times10^4$ are listed in each column. b) Energy difference between the ground state and an excited configuration. c) The three principal values calculated from these values are: $g_{xx}=2.0119$, $g_{yy}=2.0023$, and $g_{zz}=2.0119$.

The ground state of the $HSSH^-$ with the C_2 symmetry was calculated to be the ^2B state for any value of ψ or θ. Though the half-occupied MO is always expressed as $3p\sigma^*$, its shape depends considerably upon ψ and θ. This is the reason why the *g*-factors of $HSSH^-$ depend largely on the conformation of $HSSH^-$. The dependence of $g_{av}=1/3(g_1+g_2+g_3)$ upon ψ and θ is shown in Fig. 2. It can be seen from Fig. 2 that there are many conformations for a given value of g_{av}. The three principal values, however, vary largely with the

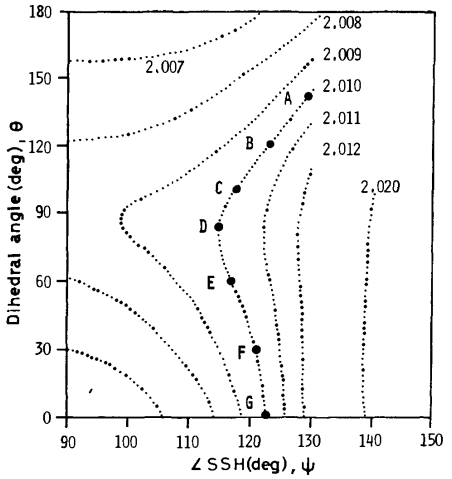

Fig. 2. The conformational dependence of the g_{av} value of $HSSH^-$. The bond lengths shown in Fig. 4 were employed.

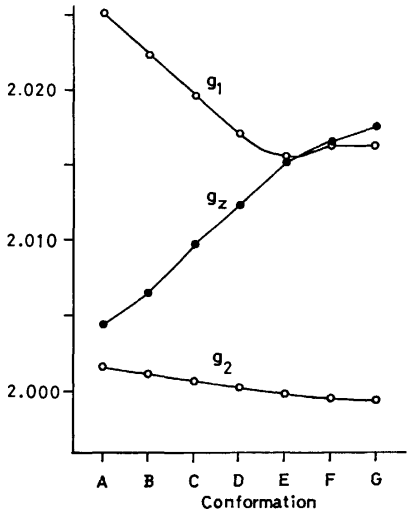

Fig. 3. Variations of three principal values of the g-tensor of $HSSH^-$ along A→G cited in Fig. 2.

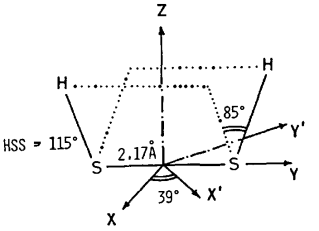

Fig. 4. The most stable conformation of $HSSH^-$ and the principal axes, x', y', and z, of its g-tensor.

conformation of $HSSH^-$. When $g_{av}=2.010$, for example the three principal values of the conformations corresponding to A—G in Fig. 2 vary as is shown in Fig. 3. From a detailed examination of the three principal values, it was found that the conformations whose calculated three principal values agree with the observed ones within ±0.003 have (i) $\theta=90°$ and $90°<\psi<115°$ or (ii) $60°<\theta<90°$ and $105°<\psi<115°$. The g-factors for the D conformation ($\theta=85°$, $\psi=115°$, SS=2.17 Å, SH=1.358 Å (ass.)) cited in Fig. 4 are worth listing, since this conformation is most stable in the present calculations and closely resembles the estimated –S–S– geometry of dialkyl disulfide anions.[9] The g-factors calculated ($g_{x'x'}=2.0172$, $g_{y'y'}=2.0003$, $g_{zz}=2.0124$, $g_{av}=2.0010$) agree well with the observed values.[1]

The radicals which have been attributed to $R_2S_2^-$ are RCH_2–S–S–CH_2R^- ($g_\perp=2.018$, $g_{//}=2.002$),[9] the n-amyl disulfide anion ($g_\perp=2.022$, $g_{//}=2.003$),[10] and the dibenzoyldisulfide anion ($g_1=2.014$, $g_2=2.010$, $g_3=2.004$).[11] In spite of the large substituents in these radicals, their g-factors have the same features as those of $HSSH^-$. This indicates that the dependence of the conformation of $R_2S_2^-$ and of the electronic structure of the –S–S– group upon the substituent is relatively small, and that the present analysis of the g-factors gives information not only about $HSSH^-$, but also about $RSSR^-$.

The spin distribution of $HSSH^-$ is worth discussing since the identification of $HSSH^-$ has thus far rested on the ^1H and ^{33}S hyperfine coupling constants. The small ^1H coupling constants[1] suggest that the primary interaction in ^1H coupling is due to spin polarization by an unpaired electron on the sulfur atom. The spin densities were thus calculated by means of the unrestricted SCF version[12] with the MINDO/3 approximation. The spin density on the 3s(S) AO is almost constant (0.06—0.07) for all the above conformations (i) and (ii). The spin density on the 1s(H) AO depends largely on the HSS angle (−0.050(90°), −0.040(100°), −0.009 (115°), +0.001(120°), with the constant value of $\theta=90°$), while its dependence on θ is small. The calculated spin distribution[13] and observed ^1H coupling constants (6—9 G)[1] predict that the HSS angle will be 105°—115°.

The author wishes to express his thanks to Dr. Tatsuo Numata for his helpful discussions.

References

1) M. J. Lin and J. H. Lunsford, *J. Phys. Chem.*, **80**, 2015 (1976).
2) M. R. S. Symons, *J. Chem. Soc., Perkin Trans. 2*, **1974**, 1618; B. C. Gilbert, D. K. C. Hodgeman, and R. O. C. Norman, *ibid.*, **1973**, 1738; W. K. Musker and T. L. Wolford, *J. Am. Chem. Soc.*, **98**, 3955 (1976).
3) J. E. Bennett, B. Mile, and A. Thomas, *Chem. Commun.*, **1966**, 182.
4) H. C. Longet-Higgins and J. A. Pople, *Proc. Phys. Soc.*, **68**, 591 (1955).
5) O. Kikuchi, *Bull. Chem. Soc. Jpn.*, **42**, 47 (1969).
6) R. C. Bingham, M. J. S. Dewer, and D. H. Lo, *J. Am. Chem. Soc.*, **97**, 1285 (1975). It was uncertain whether or not MINDO/3 correctly predicts the conformation of a molecule with vicinal lone pairs. The calculations for the neutral HSSH molecule were, therefore, carried out. The dihedral angle was correctly predicted (85°; obsd: 90.5°; G. Winnewisser, M. Winnewisser, and W. Gordy, *J. Chem. Phys.*, **49**, 3465 (1968)).
7) A. J. Stone, *Proc. R. Soc. London. Ser, A*, **271**, 424 (1963). The value of 382 cm^{-1} was used for the spin-orbit coupling constant for the 3p AO of the sulfur atom: A. Carrington and A. D. McLachlan, "Introduction to Magnetic Resonance," Harper & Row, New York (1967), p. 138.
8) O. Kikuchi, *Bull. Chem. Soc. Jpn.*, **42**, 1187 (1969); T. Morikawa, O. Kikuchi, and K. Someno, *Theoret. Chim. Acta*, **22**, 224 (1971).
9) K. Akasaka, S. Ohnishi, T. Suita, and I. Nitta, *J. Chem. Phys.*, **40**, 3110 (1964).
10) F. K. Truby, *J. Chem. Phys.*, **40**, 2768 (1964).
11) H. C. Box, H. G. Freund, K. T. Lilga, and E. E. Budzinski, *J. Phys. Chem.*, **74**, 40 (1970).
12) A. Brickstock and J. A. Pople, *Trans. Faraday Soc.*, **50**, 901 (1954).
13) The isotropic hyperfine coupling constant, a_H, of the proton was estimated from the spin density, ρ_H, on the hydrogen 1s orbital by the use of $a_H=507\rho_H$; J. R. Morton, *Chem. Rev.*, **64**, 453 (1964).

BULLETIN OF THE CHEMICAL SOCIETY OF JAPAN, VOL. 51 (1), 317—318 (1978)

The Gas Chromatographic Analysis of Bis(chloromethyl) Ether in Air

Yoshio BABA and Toshiyuki TANAKA

National Research Institute for Pollution & Resources, Kawaguchi, Saitama 332

(Received June 10, 1977)

Synopsis. Bis(chloromethyl) ether was converted into bis(ethylthiomethyl) ether by a reaction with sodium ethanethiolate in a hexane solution; the latter sulfur-containing compound was then analyzed by means of a gas chromatograph equipped with a flame photometric detector.

Bis(chloromethyl) ether (BCME) is known to be one of the impurities present in chloromethyl methyl ether, which is a commercial chloromethylating reagent widely used in the production of anion-exchange resins, membranes, and other aromatic products.

Because of its strong carcinogenicity at the 100 ppb level concentration in air, possible industrial exposure to BCME has been of great concern, and so several analytical techniques for monitoring the ppb level of BCME in air have been developed. These analytical methods include gas chromatography and high-resolution mass spectroscopy.[1-5]

BCME is known to be unstable in humid air, and a recent kinetic study of its hydrolysis in an aqueous solution showed that BCME was hydrolyzed very fast, with a half-life of the order of 10 s;[6] this unstability of BCME has presented difficulty in the process of concentrating the air sample in the preparation of the analytical sample used in the analysis described above.

Collier[5] used an enriching column packed with Porapak Q resin, which retains only the organic material, to concentrate the ppb level of BCME in air, and Solomon[2] used the 2,4,6-trichlorophenyl ether derivative of BCME ($2,4,6\text{-}Cl_3C_6H_2\text{-}OCH_2OCH_2OCH_3$) in the analysis by means of a gas chromatograph equipped with an electron-capture detector.

In this study, BCME was converted into bis(ethylthiomethyl) ether (BETME), and the latter sulfur-containing derivative was detected by means of a flame photometric detector (FPD). FPD's selective and sensitive detectability of the sulfur compounds permits the selective detection of the sulfur-containing derivative of BCME in a contaminated sample obtained by the concentration of an air sample containing foreign compounds other than BCME.

BETME can be prepared simply by the reaction of BCME and sodium ethanethiolate (NaSEt) in a hexane solution; this sulfur compound is not only stable to the hydrolysis, but also the presence of water in the reaction mixture does not interfere with the BETME formation reaction.

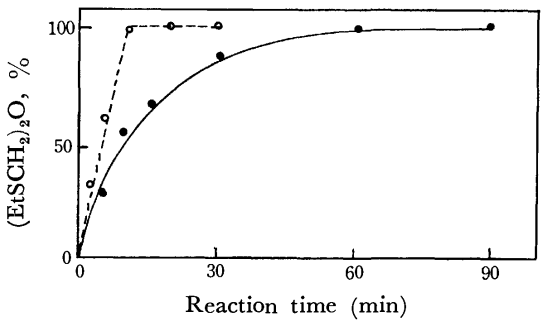

Fig. 1. Reaction rate of the $(EtSCH_2)_2O$ formation reaction.
——: At room temp,
----: at reflux temp of hexane solution.

As is shown in Fig. 1, the reaction of BCME with sodium ethanethiolate proceeds in the course of 1 h at room temperature. The reaction rate can be accelerated with a higher reaction temperature; at the reflux temperature of the hexane solution the reaction can be completed within 10 min. No side reactions have been observed in either reaction. However, the use of freshly prepared sodium ethanethiolate is recommended to keep the reaction rate rapid. The sodium ethanethiolate, even when kept in a desiccator, gradually loses its reactivity in the reaction with BCME, and after one month's storage a large depression of its reactivity was observed.

The presence of water does not change the course of the reaction, as is shown in Table 1, but it decreases the rate of the reaction. In the presence of 960% of water to BCME (mole ratio), 3 h stirring at room temperature was required to complete the reaction. However, no side reaction was observed in this case.

Excellent linearity and reproducibility were observed

Table 1. The effect of water in the BCME/NaSEt reaction

Run	NaSEt	BCME	H_2O added		H_2O/BCME %	H_2O/NaSEt %	$(EtSCH_2)_2O$/IS[a]
			μl	mol × 10^{-5}			
1	100×10^{-5} mol	23×10^{-5} mol	0	—	—	—	2.40
2			1	5.5	24	5.5	2.42
3			2	11	48	11	2.36
4			10	55	240	55	2.39
5			20	110	480	110	2.37
6			40	220	960	220	2.41

a) $n\text{-}Pr_2S$ was used as an internal standard.

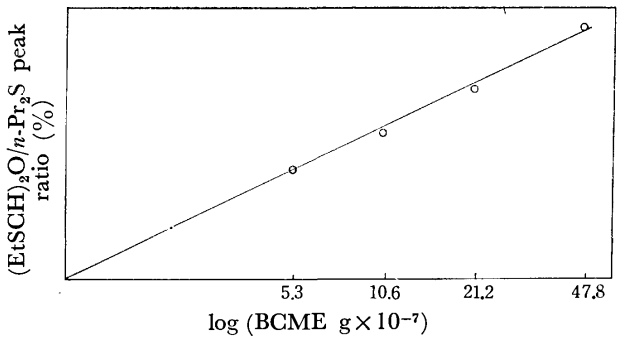

Fig. 2. Calibration curve of bis(ethylthiomethyl) ether.

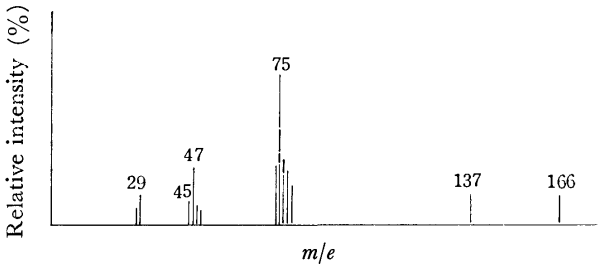

Fig. 3. Mass spectrum of bis(ethylthiomethyl) ether.

in the preparation of the calibration curve (Fig. 2); this fact indicates this analytical method can be applied practically. The mass spectra of the product obtained by the BCME/NaSEt reaction have been shown to be consistent with the assignment of bis(ethylthiomethyl) ether (Fig. 3).

Experimental

Bis(ethylthiomethyl) Ether. A solution of sodium methoxide in methanol (10%) was mixed with a slightly excessive molar amount of ethanethiol. The solution was stirred for 10 min and then evaporated to dryness under a vacuum. The solid residue was pulverized, and a solution of BCME in hexane was added (mole ratio of NaSEt/BCME=2.5). The reaction mixture was stirred for 1 h at room temperature, or refluxed for 10 min.

Gas Chromatography. Micro Tek Instruments Corp. A Model 160 gas chromatograph equipped with a flame photometric detector was used. The analytical column was 1 m× 3 mm i.d. Teflon column packed with 25% 1,2,3-tris(2-cyanoethoxy)propane on Chromosorb W AW(60—80 mesh). The column oven was kept at 150 °C (isothermal). The carrier gas was a chromatographic grade nitrogen at a flow rate of 60 ml/min.

Mass Spectrometry. The mass spectra of bis(ethylthiomethyl) ether were obtained using a JMS-Q 10 Gas Chromatograph-Mass Spectrometer operated at an ionizing potential of 70 eV.

References

1) L. S. Frankel and R. F. Black, *Anal. Chem.*, **48**, 732 (1976).
2) R. A. Solomon and G. J. Kallos, *Anal. Chem.*, **47**, 955 (1975).
3) J. C. Tou and G. J. Kallos, *Anal. Chem.*, **46**, 1866 (1974).
4) L. S. Frankel, K. S. McCallum, and L. Collier, *Environ. Sci. Technol.*, **8**, 356 (1974).
5) L. Collier, *Environ. Sci. Technol.*, **6**, 930 (1972).
6) J. C. Tou and L. B. Westover, *J. Phys. Chem.*, **78**, 1096 (1974).

BULLETIN OF THE CHEMICAL SOCIETY OF JAPAN, VOL. 51 (1), 319—320 (1978)

The Esterification of Thujopsene with Bismuth(III) Sulfate in Carboxylic Acids

Kazuo Abe and Masaaki Ito

Chemistry Laboratory, Department of General Education, Higashi Nippon Gakuen University, Onbetsu, Hokkaido 088-01

(Received March 7, 1977)

Synopsis. The catalytic interaction of *cis*-(−)-thujopsene with a series of organic acids from acetic to octanoic in the presence of bismuth(III) sulfate afforded the corresponding esters in 20—34% yields, accompanied by skeletal rearrangement. The follow-up of the reaction, an investigation of the reaction conditions, and the effects of catalysts are described.

In organic acids, the autoxidation of some olefins occurs in the presence of bismuth(III) sulfate.[1] Valkanas[2] has recently found that the interaction of *d*-α-pinene with a series of organic acids from acetic to octanoic, over a wide range of olefin-to-acid ratios, yields esteric and rearrangement products. We have obtained some findings on the esterification of thujopsene **1** with a series of organic acids from acetic to octanoic in the presence of bismuth(III) sulfate. Thus, it may be seen that the esterification proceeds through a skeletal conversion to give a bicyclic ester as the major product, without any autoxidation reaction occurring.

The esterification of thujopsene was carried out using organic acid in a ratio of 20 parts of thujopsene to 0.25 parts of bismuth(III) sulfate at 70 °C for 40 h. The results are summarized in Tables 1 and 2, including the spectral data of the reaction products. The reactions all afforded the same reaction products, regardless of the carboxylic acid used. The amounts of esterification are shown to increase from 20 to 34% between acetic acid and valeric acid, and to decrease from 34 to 29% between valeric acid and octanoic acid. The structures of the esters were confirmed by means of the analytical and spectral data, and also by the fact that the hydrolysis of the esters afforded 2β-hydroxymethyl-2α,8,8,4aβ-tetramethyl-1(8a)-octalin (*cis*-neopentyl-type alcohol)[3] evenly, in disregard of the partial structures from carboxylic acids. The isomeric α-type neopentyl ester has already been reported by us.[4]

The rise-and-fall ratio of intermediates or products in the reaction path was observed by GLC (Fig.1): in a reaction time of 2 min, Peak **a** (thujopsene) is shown to isomerize into the other hydrocarbons of Peaks **b**, **c**, and **d**: in 15 min, Peak **a** decreases strikingly to give a hydrocarbon (Peak **c**) and Peak **e**: in 40 h, Peak **e** reaches a suitable amount and a new peak, **f**, appears. Peaks **c** and **f** were identified, by comparisons of the spectral (IR and NMR) data and the GLC retention times with those of authentic samples, as 1,4,11,11-tetramethylbicyclo[5.4.0]undeca-3,7-diene,[5] **3**, and 2,2,3,7-tetramethyltricyclo[5.2.2.0^{1,6}]undec-3-ene,[5] **4**, respectively.

Then, the suitable conditions of the esterification were determined by experiments using propionic acid. To obtain a high yield of the ester, the reaction must be carried out at the reaction temperature of 70 °C, for a reaction time of 40 h, and using carboxylic acid in a ratio of 20 parts of thujopsene to 0.25 parts of the

Table 1. Analytical data of the esters

	Ester	Yield %	Ester value Found(Calcd)	Found (Calcd) % C	H	IR (CCl_4) cm^{-1} $\nu_{C=O}$	ν_{C-O}
1	Acetic	20	16.24(16.28)	76.95(77.22)	10.51(10.67)	1740	1225
2	Propionic	24	20.45(20.50)	77.43(77.65)	10.66(10.86)	1738	1178
3	Butyric	28	24.24(24.31)	77.86(78.03)	10.92(11.03)	1738	1178
4	Valeric	34	27.72(27.78)	78.23(78.38)	11.05(11.18)	1737	1166
5	Hexanoic	31	30.85(30.94)	78.59(78.70)	11.17(11.32)	1737	1164
6	Heptanoic	30	33.75(33.83)	78.71(78.99)	11.36(11.45)	1737	1162
7	Octanoic	29	36.41(36.49)	79.08(79.25)	11.45(11.57)	1735	1160

Table 2. NMR spectra of the esters

Ester	ppm Value in chloroform-*d*
1	0.97(s, CH_3), 1.05(s, $2CH_3$), 1.16(s, CH_3), 2.03(s, $OCOCH_3$), 3.80(m, 2H), 5.07(s, 1H, olefinic)
2	0.98(s, CH_3), 1.04(s, $2CH_3$), 1.08(s, CH_3), 1.15(s, CH_3), 2.33(q, 2H), 3.80(q, 2H), 5.08(s, 1H, olefinic)
3	0.97(s, CH_3), 1.05(s, $3CH_3$), 1.15(s, CH_3), 2.28(t, 2H), 3.79(q, 2H), 5.08(s, 1H, olefinic)
4	0.98(s, CH_3), 1.04(s, $2CH_3$), 1.09(s, CH_3), 1.17(s, CH_3), 2.31(t, 2H), 3.80(q, 2H), 5.09(s, 1H, olefinic)
5	0.98(s, CH_3), 1.06(m, $3CH_3$), 1.16(s, CH_3), 2.30(t, 2H), 3.38(q, 2H), 5.09(s, 1H, olefinic)
6	0.98(s, CH_3), 1.04(d, $3CH_3$), 1.16(s, CH_3), 2.32(t, 2H), 3.80(q, 2H), 5.09(s, 1H, olefinic)
7	0.98(s, CH_3), 1.04(d, $3CH_3$), 1.15(s, CH_3), 2.30(t, 2H), 3.80(q, 2H), 5.08(s, 1H, olefinic)

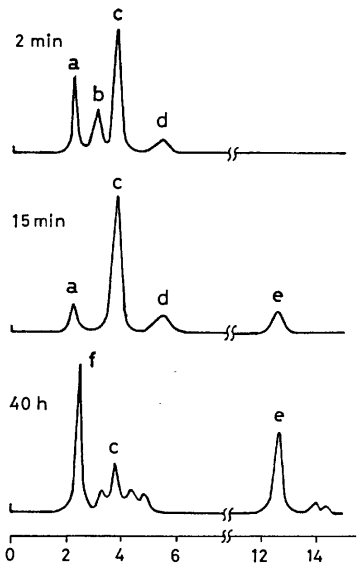

Fig. 1. Follow-up of the reaction path by GLC at the esterification of thujopsene using C_2H_5COOH and $Bi_2(SO_4)_3$.

catalyst.

In the presence of bismuth(III) sulfate, this esterification reaction proceeded most readily under mild conditions, accompanied by rearranged products of thujopsene. In this system, however, no ester or rearranged products could be found in a blank reaction at temperatures lower than 70 °C for 40 h or more. Also, tin(II) sulfate and antimony(III) sulfate showed a catalytic effect, affording the same products. In view of these results, and with reference to the reaction mechanisms using other reagents presented by Dauben and Friedrich[5] and by Hochstetler and Kitchens,[6] the esterification to give the β-type bicyclic ester as the major product, accompanied by the tricyclic hydrocarbon, **4**, may be explained as is shown in Scheme 1. By considering the results for the follow-up of the reaction shown in Fig. 1, the protonation of (−)-thujopsene leads to the **1b** cation the subsequent attack of the carboxylate anion as **1b** would lead to the bicyclic ester, **2**, *via* Path A. Path B would afford the tricyclic hydrocarbon, **4**, *via* the **3a** cation by the pathway reported by Dauben and Friedrich.[5]

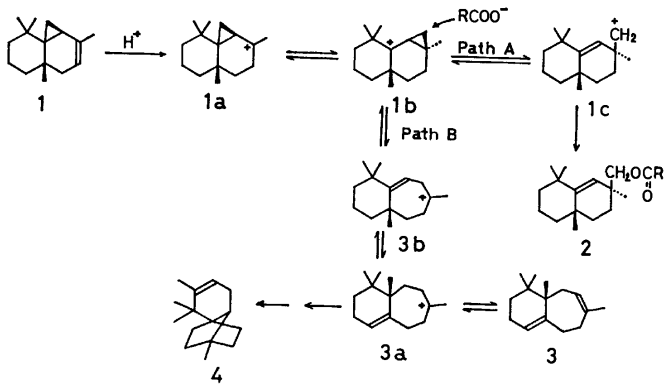

Scheme 1.

Experimental

The spectra were recorded on a JEOL JNM-PMX 60 NMR spectrometer, using TMS as the internal standard, and a Shimadzu IR-400 IR spectrometer. The elemental analyses were performed by a Hitachi 026 CHN analyzer. The analytical GLC were performed on a Shimadzu GC-4B apparatus with a 1.5 m glass column packed with 15% OV-17, at 10 °C/min 150—250 °C. For the preparative GLC, a JEOL JGC-1100 apparatus was employed with 15% OV-17 at 240 °C.

The thujopsene used was purified by the careful distillation of Cedar H oil (Takasago Perfumery Co., Ltd.) through a concentric column; bp 120 °C/10 mmHg. The inorganic salts used for the catalyst and organic acids were commercial, extra-pure reagents.

Esterification of Thujopsene. A mixture of 3.07 g (15 mmol) of thujopsene, 0.3 mol of organic acid, and 2.65 g (3.75 mmol) of bismuth(III) sulfate was stirred in a thermostated bath at 70 °C for 40 h. After the organic acid had been removed under reduced pressure, the resulting residue was poured into a cold mixture of petroleum ether and 5% aqueous sodium hydroxide while standing. The petroleum layer was further washed with a sodium hydrogencarbonate solution and dried over anhydrous sodium sulfate, and then the solvent was removed. The residue was analyzed by GLC. The analytical sample was chromatographed on a silica gel column and further purified by preparative GLC to yield material of a 97—98% purity. The saponification value was determined using a 2-h boiling in a 90% aqueous ethanolic solution of 0.3 M potassium hydroxide.

Follow-up of the Reaction Path by GLC. A mixture of 1.54 g (7.5 mmol) of thujopsene, 11.1 g (0.15 mol) of propionic acid, and 1.33 g (1.88 mmol) of bismuth(III) sulfate was stirred at 70 °C in the manner described above. The reaction product was analyzed by GLC, using sample aliquots at appropriate time intervals after the reaction mixture had been worked-up as described above.

References

1) S. Suzuki, Y. Moro-oka, and T. Ikawa, *Chem. Lett.*, **1976**, 29.
2) G. N. Valkanas, *J. Org. Chem.*, **41**, 1179 (1976).
3) W. G. Dauben and L. E. Friedrich, *Tetrahedron Lett.*, **1967**, 1735.
4) M. Ito, K. Abe, and H. Takeshita, *Bull. Chem. Soc. Jpn.*, **45**, 1913 (1972).
5) W. G. Dauben and L. E. Friedrich, *J. Org. Chem.*, **37**, 241 (1972).
6) A. R. Hochstetler and G. C. Kichens, *J. Org. Chem.*, **37**, 2750 (1972).

BULLETIN OF THE CHEMICAL SOCIETY OF JAPAN, VOL. 51 (1), 321—322 (1978)

The Micellar Acceleration of the Reduction of Nitroblue Tetrazolium by Superoxide Anion Radicals during the Autoxidation of Polyphenols

Teruhiro TAKABE, Masako MIYAKAWA, and Sueki NIKAI

Department of Chemistry, Faculty of Science and Technology, Meijo University, Tenpaku, Nagoya 468

(Received April 25, 1977)

Synopsis. The rates of the reduction of Nitroblue Tetrazolium by O_2^- during the autoxidation of pyrogallol, epinephrine, and catechol were increased 110, 55, and 37-fold respectively in the presence of hexadecyltrimethylammonium bromide. A nonionic micelle of polyoxyethylene dodecyl ether also accelerated these reactions. The microenvironment effects on the electron-transfer from O_2^- to Nitroblue Tetrazolium were discussed.

The superoxide anion radical (O_2^-) is known to be produced by a number of biologically significant oxidations and is probably generated, to some degree, in all oxygen-metabolizing cells.[1] Recently, O_2^- has also been shown to be generated during the autoxidation of some phenols[2,3] and thiols.[4] Many other autoxidizable compounds may be found to generate O_2^- during autoxidation. Therefore, it is useful to develop easy and sensitive methods to detect O_2^-. The detection of O_2^- has been carried out by using direct kinetics techniques, such as EPR, or pulse radiolysis, and using inhibition by superoxide dismutase (SOD).[1] Nitroblue Tetrazolium (NBT) has been used for the detection of small amounts of such reducing agents as O_2^-, S^{2-}, and $S_2O_4^{2-}$.[5] Since it has been reported that the nucleophilic reactivity of the hydroxide ion and thiol are affected by the cationic micellar environment,[6] one may anticipate that the reaction rate between O_2^- and NBT is also accelerated by the micellar systems. In this study, we will report that the rate of electron transfer from O_2^- to NBT is accelerated by the surface-active cation hexadecyltrimethylammonium bromide (CTAB) and by nonionic micelles of polyoxyethylene dodecyl ether (Brij 35), and that NBT in micellar systems may be used in an easy and sensitive method to detect O_2^- during autoxidation.

Experimental

The pyrogallol was purified by sublimation. The epinephrine (Merck A. G.) and catechol (Katayama Chem. Co.) were used without further purification. Sodium dodecyl sulfate (NaLS) and CTAB were recrystallized from methanol and water respectively. Brij 35 (Katayama Chem. Co.), NBT (Sigma Chem. Co.), and bovin Cu–Zn SOD (Sigma Chem. Co.) were used without further purification. The water was deionized and distilled.

The spectroscopic measurements were made with a Shimadzu UV-200S recording spectrometer at 25 °C. The rates of the autoxidation of polyphenols were taken from the increase in the absorbance at 420 nm for pyrogallol[2] and at 480 nm for epinephrine[3] and catechol. The reduction of NBT was measured from the increase in the absorbance at 560 nm due to the accumulation of blue formazan. In all cases, reactions were started by adding an aliquot of an acidic (pH 2.0) stock solution of polyphenol to the buffered reaction mixture.

Results and Discussion

Since it has been shown that the autoxidations of pyrogallol, epinephrine, and catechol all involve O_2^-,[2,3] these polyphenols can transfer electrons to NBT *via* oxygen under aerobic conditions. Therefore, we investigated the reduction of NBT by O_2^- in micellar systems. As the mixing of NaLS and NBT resulted in precipitation, we used CTAB and Brij 35 for the experiment. The initial rates of the aerobic reduction of NBT during the autoxidation of pyrogallol were linear functions of the NBT concentration in either the absence or presence of a detergent, as is shown in Fig. 1. This result indicates that the rates of the reduction of NBT were accelerated by both CTAB and Brij 35. We show in Fig. 2 the effects of the concentrations of CTAB and Brij 35 on the reduction of NBT by O_2^- during the autoxidation of pyrogallol at pH 8.0. The reduction rate of NBT was markedly accelerated above 1×10^{-3} M CTAB (the critical micelle concentration is 0.92×10^{-3} M[6]) and tended to be saturated beyond 7×10^{-3} M CTAB. The rate was also accelerated by Brij 35 and saturated above the detergent concentration of 2×10^{-3} M. 5×10^{-3} M of CTAB and Brij 35 increased the rates by factors of 110 and 13-fold respectively. Similar results were obtained for the autoxidations of epinephrine and catechol, as is shown in Table 1. We can see that 5×10^{-3} M CTAB accelerated the reduction of NBT during the autoxidations of epinephrine and catechol by factors 55 and 37-fold respectively. 5×10^{-3} M Brij 35 also accelerated these reactions by factors of 7 and 5-fold respectively. The drastic acceleration in micellar systems described above raises the question whether these micelles accelerate the rate of autoxidation or electron-transfer from O_2^- to NBT. In order to clarify this point, we examined the micellar effects on the rates of the autoxidation of polyphenols by the methods described in the experimental section. We found that CTAB, Brij 35, and NaLS had almost no effect on the rates of autoxidation of these polyphenols with the

TABLE 1. MICELLAR EFFECT ON THE REDUCTION OF NBT DURING THE AUTOXIDATION OF EPINEPHRINE AND CATECHOL

The reaction mixture contained 2.5×10^{-4} M of polyphenol, 8.3×10^{-5} M of NBT, 5×10^{-3} M of the surfactant, and 1×10^{-4} M of EDTA in 0.1 M Tris-HCl at pH 9.0.

	Δ Absorbance at 560 nm/min		
	Non-surfactant	CTAB	Brij 35
Epinephrine	0.011	0.590	0.079
Catechol	0.007	0.260	0.033

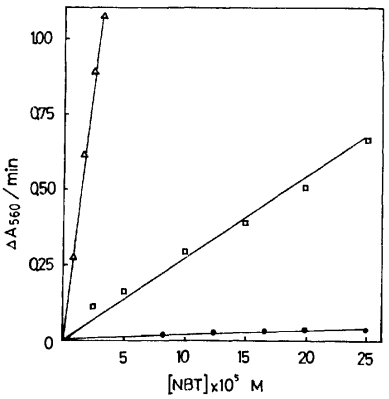

Fig. 1. The initial reduction rate of NBT as a function of NBT concentration. 2.5×10^{-4} M pyrogallol was added to the reaction mixture containing indicated concentration of NBT, 5×10^{-3} M surfactant, 1×10^{-4} M EDTA, and 0.1 M Tris-HCl at pH 8.0. ●; No surfactant, △; CTAB, □; Brij 35.

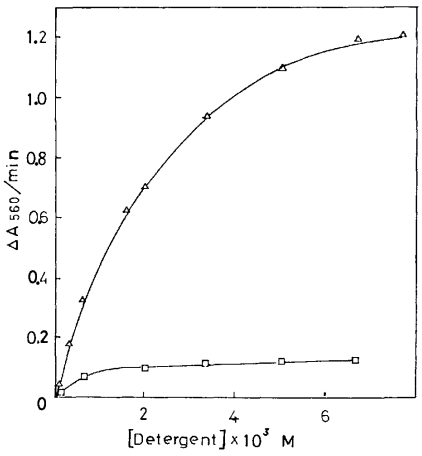

Fig. 2. Plots of the observed pseudo-first-order rate constant against the surfactant concentration for the reduction of NBT during the autoxidation of pyrogallol. Reaction-mixture contained 2.5×10^{-4} M pyrogallol, 3.3×10^{-5} M NBT, 0.1 M Tris-HCl at pH 8.0, and the indicated concentration of CTAB (△) and Brij 35 (□).

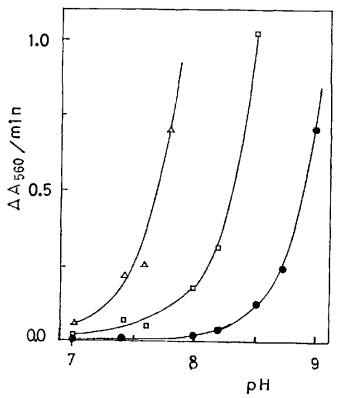

Fig. 3. Effect of pH on the reduction rate of NBT during the autoxidation of pyrogallol. Reaction mixture contanied 2.5×10^{-4} M pyrogallol, 8.3×10^{-5} M NBT, 5×10^{-3} M detergent, and 1×10^{-4} M EDTA in the following buffer systems; pH 7.0 and 7.4, 0.1 M potassium phosphate; other pH, 0.1 M Tris-HCl. ●; No surfactant, △; CTAB, □; Brij 35.

exception of the autoxidation of pyrogallol in the presence of CTAB. 5×10^{-3} M CTAB accelerated the autoxidation of pyrogallol 11-fold. However, its value is quite small in comparison with that for the reduction of NBT (110-fold). Therefore, these results indicate that CTAB and Brij 35 accelerated the rate of electron-transfer from O_2^- to NBT.

Since it has been shown that polyphenols are autoxidized rapidly in an aqueous alkaline solution,[2,3] we investigated the pH effects on the reduction of NBT. As is shown in Fig. 3, the reduction of NBT was accelerated by both CTAB and Brij 35 over the whole pH range of 7.0—9.0. This indicates that even a small amount of O_2^- generated during the autoxidation at a neutral pH is detectable by NBT in the micellar systems. From these result, it seems likely that the catalytic functions of both CTAB and Brij 35 are due to binding organic substrates to the micellar phase, giving more favorable environment for the O_2^- attack on NBT (the orientation effect[6]). Both Fig. 3 and Table 1 indicate that CTAB accelerates the reduction of NBT about 8 times more than does that Brij 35. Therefore, for the rate-enhancement effect by CTAB, besides the orientation effect, electrostatic interactions between the cationic micelle and O_2^- might be important. When KO_2 was directly added to the NBT solution, the rate of the reduction of NBT was accelerated only 30 percent by CTAB and Brij 35 compared with that in the non-micellar system. Therefore, the generation of O_2^- in the micellar phase may be important for the rapid reduction of NBT.

In order to determine whether or not O_2^-, which is generated during the autoxidation of polyphenols, practically reduces NBT in these micellar systems, we examined the effect of SOD on the reduction of NBT. As is shown in Fig. 4, the reduction of NBT during the autoxidation of pyrogallol was inhibited by SOD in either the absence or the presence of a surfactant. The

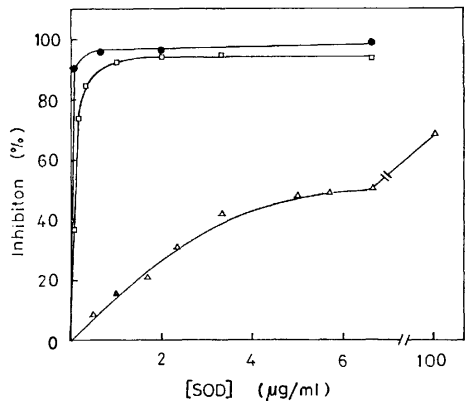

Fig. 4. Inhibition of the reduction of NBT during the autoxidation of pyrogallol by SOD. Cuvets contained 2.5×10^{-5} M NBT, 5×10^{-5} M pyrogallol, 5×10^{-3} M surfactant, 1×10^{-4} M EDTA, and 0.1 M Tris-HCl at pH 8.0. ●; No surfactant, △: CTAB, □; Brij 35.

reductions of NBT during the autoxidation of epinephrine and catechol were also inhibited by SOD in a manner similar to that is the case of pyrogallol. Quite similar micellar effects were also observed in the cases of the autoxidations of anthrone and such thiols as dithiothreitol, 2-mercaptoethanol, glutathione, and *l*-cysteine, all involving O_2^-. Therefore, NBT in the micellar systems might be useful as an easy and sensitive method to detect O_2^- during autoxidation.

References

1) I. Fridovich, *Ann. Rev. Biochem.*, **44**, 147 (1975).
2) S. Markund and G. Markund, *Eur. J. Biochem.*, **47**, 469 (1974).
3) H. P. Misra and I. Fridovich, *J. Biol. Chem.*, **247**, 3170 (1972).
4) H. P. Misra, *J. Biol. Chem.*, **249**, 2151 (1974).
5) A. W. Nineham, *Chem. Rev.*, **55**, 355 (1955).
6) J. H. Fendler and E. J. Fendler, "Catalysis in Micellar and Macromolecular Systems," Academic Press, New York (1975).

BULLETIN OF THE CHEMICAL SOCIETY OF JAPAN, VOL. 51 (1), 323—324 (1978)

Steric Effects on Carbon-13 Chemical Shifts in 3-Aryl-1,2,3-oxathiazolidine 2-Oxides

Tomihiro NISHIYAMA, Takashi MIZUNO, and Fukiko YAMADA

Department of Applied Chemistry, Faculty of Engineering, Kansai University, Senriyama, Suita, Osaka 564

(Received May 11, 1977)

Synopsis. The carbon-13 NMR spectra of 3-aryl-1,2,3-oxathiazolidine 2-oxides were obtained and discussed. Some of the carbon shifts are greatly influenced by the conformation of the oxathiazolidine ring.

In a previous paper,[1] we reported the conformations of a series of 3-aryl-1,2,3-oxathiazolidine 2-oxides (**1**) as determined by means of their ^{1}H-NMR spectra. In continuation of our studies concerning the steric structure of **1**, this paper will describe the relationships between their carbon-13 NMR spectra and the conformational structures of the oxathiazolidines.[1]

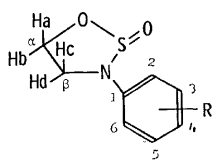

1

I, R=H
IIa, R=*o*-CH_3
IIb, R=*m*-CH_3
IIc, R=*p*-CH_3
IIIa, R=*o*-OCH_3
IIIc, R=*p*-OCH_3
IV, R=*p*-Br
Va, R=*o*-Cl
Vb, R=*m*-Cl
Vc, R=*p*-Cl

Experimental

Measurements. The ^{13}C-NMR spectra were obtained using a JNM-PS-100/EC-100 spectrometer equipped with a Fourier transform recorder at 25.15 MHz under a complete proton decoupling. The pulse width and repetition time were 10.2 μs and 6 s respectively. The spectral width and data points were 6250 Hz and 8191 respectively. The chemical shifts were reported in ppm downfield from the internal TMS, using deuteriochloroform.

Compounds. The preparations and the physical properties of **1** were reported in a previous paper by the present authors,[2,3]

Results and Discussion

Carbon-13 NMR measurements were made on the above 10 compounds. The carbons in the oxathiazolidine ring are represented by the notations of C-α and C-β respectively, and those in the benzene ring, by C-1—C-6, as is shown in the above diagram. The assignments of the carbons were made on the basis of (1) the relative signal intensity, (2) the off-resonance decoupling technique, and (3) the predicted chemical shifts obtained by the aid of the additivity rule.[4]

As can be seen in Table 1, the C-α signals appeared at around 70 ppm, whereas the C-β appeared at 46—49 ppm. The observed shifts from C-1 to C-6 were in close agreement with the predicted values for the compounds with an *m*- or *p*-substituent except for the case of IIIc. On the other hand, the shifts of C-1, C-2, and C-6 for the compounds with an *o*-substituent deviated from the predicted ones. In IIIa, the C-3 signal is shifted upfield compared with the predicted one (−3.1 ppm). This fact is considered to be a steric shift caused by the preferred conformation of the terminal CH_3 of the OCH_3 group being turned away from the C-1 and being now close to C-3.[5]

Table 2 shows the values obtained by subtracting the substituent parameters (S.P.) from the observed

TABLE 1. ^{13}C CHEMICAL SHIFTS (ppm) OF 3-ARYL-1,2,3-OXATHIAZOLIDINE 2-OXIDES

Compd No.	C-α	C-β	C-1	C-2	C-3	C-4	C-5	C-6	CH_3 or OCH_3
I	70.9	45.9	140.7	116.5	129.8	122.7	129.8	116.5	—
IIa	70.9	48.2	137.2 (141.4)	135.3 (125.4)	131.0 (130.5)	126.7 (122.6)	126.7 (126.9)	125.0 (116.4)[a]	18.2
IIb	70.6	46.1	140.2 (140.6)	117.5 (117.2)	139.7 (138.7)	123.8 (123.4)	129.5 (129.7)	113.9 (113.6)	21.5
IIc	70.4	46.1	137.7 (137.8)	117.2 (116.4)	129.9 (130.5)	132.3 (131.6)	129.9 (130.5)	117.2 (116.4)	20.4
IIIa	69.5	45.8	130.0 (126.1)	150.4 (147.7)	112.0 (115.1)	124.3 (123.4)	121.4 (121.8)	119.6 (117.3)	55.7
IIIc	71.0	46.9	132.9 (133.0)	120.4 (117.5)	114.9 (115.4)	156.4 (154.1)	114.9 (115.4)	120.4 (117.5)	55.5
IV	71.1	46.4	140.0 (139.1)	118.3 (118.2)	132.7 (133.2)	115.3 (117.2)	132.7 (133.2)	118.3 (118.2)	—
Va	71.4	47.4	143.5 (141.2)	136.7 (122.7)	130.6 (130.2)	127.5 (124.0)	128.0 (127.9)	125.8 (117.7)	—
Vb	70.9	46.1	141.9 (142.0)	116.1 (116.9)	135.2 (136.0)	122.4 (123.2)	130.8 (131.2)	114.5 (114.6)	—
Vc	71.1	46.4	139.5 (138.8)	118.0 (117.8)	129.7 (130.2)	127.9 (128.9)	129.7 (130.2)	118.0 (117.8)	—

a) Calcd value.

Table 2. Chemical shifts differences $\Delta=\delta_{obsd}-S.P.$

Compd No.	C-1	C-2	C-3	C-4	C-5	C-6	Torsion[a] angle θ
I	140.7	116.5	129.8	122.7	129.8	116.5	15
IIa	136.5	126.4	130.3	126.8	129.6	125.1	−11
IIb	140.3	116.8	130.8	123.1	129.6	116.8	12
IIc	140.6	117.3	129.2	123.4	129.2	117.3	11
IIIa	144.4	119.0	126.4	123.3	129.1	118.6	−5
IIIc	140.6	119.4	129.3	125.0	129.3	119.4	4
IV	141.6	116.6	129.3	120.8	129.3	116.6	14
Va	143.1	130.5	130.2	126.2	129.9	124.5	−11
Vb	140.6	115.7	129.0	122.0	129.5	116.4	15
Vc	141.4	116.7	129.3	121.7	129.3	116.7	12

a) These values are taken from Ref. 1.

values. Consequently, these values show mainly the effects of the oxathiazolidine ring on the shifts of the benzene-ring carbons. From the data of I, the substituent parameters of the oxathiazolidine ring can be obtained as follows: +12.2 for C-1, −12.0 for *ortho*, +1.3 for *meta*, and −4.8 for *para* carbons. In the compounds with an *m*- or *p*-substituent, the individual carbon shifts come close to those of I, and the electronic effects of the substituent may contribute greatly to the shifts of benzene carbons. In these cases, there is no steric hindrance between either benzene or oxathiazolidine rings. In IIa, IIIa, and Va, the shifts of C-1, C-2, and C-6 deviate greatly from those of I.

In a previous paper,[1] we reported that the oxathiazolidine rings tend to form twist-envelope conformations, that their torsion angles with both the position and the nature of the ring substituent, and that the distortions of the oxathiazolidine ring of the compounds with *m*- and *p*-substituents are in the direction of the **2** projection, while those with an *o*-substituent cause a distortion toward the **3** projection, as can be seen in the following diagram. The values of the torsion angles are listed in Table 2.

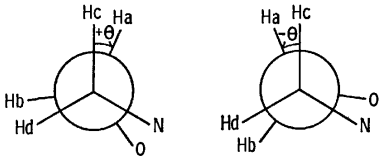

2 **3**

θ: Torsion angle

In order to obtain further information about the conformational influence of the oxathiazolidine ring on the shifts of benzene-ring carbons, an attempt was made to plot the shifts of the ring carbons against their torsion angles.

As can be seen in Fig. 1, all the shifts of C-1 in the cases of the *m*- and *p*-substituents appeared at about 141 ppm, regardless of the torsion angle, while that of IIa appeared upfield about 4.5 ppm, and those of IIIa and Va shifted downfield about 3.4 and 2.1 ppm respectively. In IIa, the preferred comformation of the oxathiazolidine ring may be considered, from the evidence of the upfield shifts for both C-1 and methyl carbon (Table 1), that in which the lone pair of electrons on nitrogen is located close to the *o*-substituted methyl group. In the case of IIIa or Va, the lone pair of nitrogen was turned away from the *o*-substituent. On the other hand, two kinds of good linear correlations are obtained in the cases of C-2 and C-6. The

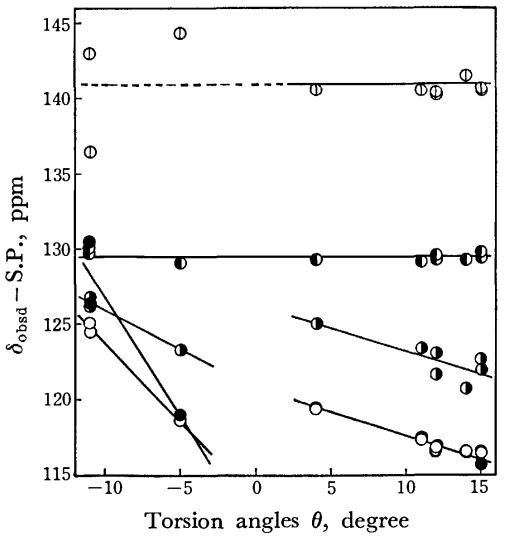

Fig. 1. Plots of the chemical shifts of benzene ring carbons *vs.* torsion angles.
◐: C-1, ●: C-2, ◐: C-3, C-5, ◑: C-4, ○: C-6.

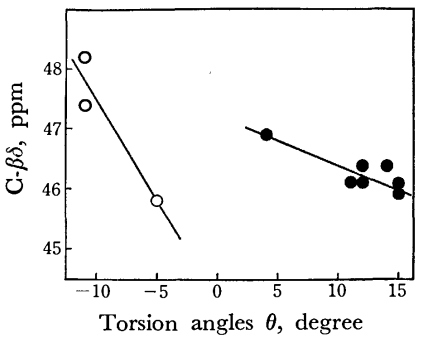

Fig. 2. Plots of the chemical shifts of C-β *vs.* torsion angles.
○: The compound bearing an *o*-substituent,
●: *m*-, or *p*-substituent.

left line is due to the data of the compounds bearing an *o*-substituent (Projection **3**), while the right line is due to those bearing an *m*- or *p*-substituent (Projection **2**). From the slopes of these lines, the effects on the chemical shifts of the *o*-substituent are larger than those of the other conformation.

The correlation of the chemical shifts of C-β *versus* their torsion angles is shown in Fig. 2. The effects on the chemical shifts of the *o*-substituent are shown to be larger than that of the *m*- or *p*-substituent, just as in Fig. 1.

References

1) F. Yamada, T. Nishiyama, and H. Samukawa, *Bull. Chem. Soc. Jpn.*, **48**, 1878 (1975).
2) T. Nishiyama and F. Yamada, *Bull. Chem. Soc. Jpn.*, **44**, 3037 (1971).
3) F. Yamada, T. Nishiyama, M. Kinugasa, and M. Nakatani, *Bull. Chem. Soc. Jpn.*, **43**, 3611 (1970).
4) P. C. Lauterbur, *J. Am. Chem. Soc.*, **83**, 1846 (1961); G. C. Levy and G. L. Nelson, "Carbon-13 Nuclear Magnetic Resonance for Organic Chemists," Wiley-Interscience, New York, N. Y. (1972), p. 81.
5) K. S. Dhami and J. B. Stothers, *Can. J. Chem.*, **44**, 2855 (1966).

BULLETIN OF THE CHEMICAL SOCIETY OF JAPAN, VOL. 51 (1), 325—326 (1978)

Syntheses of Heliparvifoline and *O*-Demethylpteleine

Tetsuya SEKIBA

Faculty of Chemical Engineering, Toyama Technical College, Hongo, Toyama 930

(Received May 13, 1977)

Synopsis. 2,3-Dihydroheliparvifoline (Va) was obtained from 4-methoxy-3-benzyloxyaniline by condensation with diethyl (2-benzyloxyethyl)-malonate, and by subsequent methylation, debenzylation, and then cyclodehydration. Benzyl ether of Va was dehydrogenated and then treated with hydrochloric acid to give heliparvifoline.

Recently, heliparvifoline was isolated from the leaves and twigs of *Helietta parvifolia* Benth (Rutaceae).[1] Its structure was proposed to be 4,6-dimethoxy-7-hydroxyfuro[2,3-*b*]quinoline (Ia) on the basis of the spectral data. However, the synthesis of Ia has not yet been reported. Although *O*-demethylpteleine (Ib) has not yet been found in any natural source, it is considered valuable to synthesize this substance, because it may be expected to occur in nature and to be an intermediate in medicosmine synthesis.[2] Govindachari and his co-workers attempted to synthesize Ib, but they merely obtained benzyl ether of Ib.[3] In previous papers,[4,5] the present author reported the syntheses of some furoquinoline alkaloids through the corresponding dihydrofuroquinolines as key intermediates.

The present paper will describe convenient syntheses of Ia and Ib from 3-benzyloxy-4-methoxyaniline. The condensation of an aniline derivative and diethyl (2-benzyloxyethyl)-malonate without a solvent gave the 4-hydroxy-2-quinolone derivatives (IIa, b), which were methylated with diazomethane into 4-methoxy compounds (IIIa, b). The catalytic debenzylation of IIIa and IIIb using 5% Pd–C gave 3-(2-hydroxyethyl)-4-methoxy-2-quinolone derivatives (IVa, b). The IR spectra of IVa and IVb indicated the presence of a hydroxyl group (*ca.* 3500 cm^{-1}), and the NMR spectra of IVa and IVb indicated the complate debenzylation and exhibited a signal for one proton of the hydroxyl group which easily disappeared upon deuterium exchange. The cyclodehydration of IVa and IVb with polyphosphate ester yielded 2,3-dihydrofuro[2,3-*b*]quinoline derivatives (Va, b). The structures of Va and Vb were assigned on the basis of their NMR spectra, which showed signals at δ *ca.* 3.42(t) and 4.58(t) ppm attributable to two methylene protons of a dihydrofuran-ring system. Since the dehydrogenation of Va and Vb with DDQ (2,3-dichloro-5,6-dicyanobenzoquinone) was unsuccessful, Va and Vb were treated with benzyl chloride to give benzyl ether (VIa,b), whose IR spectra indicated the absence of the hydroxyl group, and their NMR spectra showed signals characteristic of a benzyl group. VIa and VIb were then treated with DDQ in dry toluene to give the corresponding dehydro compounds (VIIa,b). The structures of VIIa and VIIb were assigned on the basis of their NMR spectra, which showed signals at δ 7.04 (d) and 7.62 (d) ppm attributable to the 2,3-protons of a furan-ring system. The debenzylation of VIIa and VIIb with ethanol-hydrochloric acid gave furo[2,3-*b*]quinoline derivatives (Ia; heliparvifoline and Ib; *O*-demethylpteleine). The synthetic heliparvifoline (Ia) was shown to be identical with a natural specimen by a mixed-melting-point determination and by a comparison of the IR, UV, and NMR spectra.

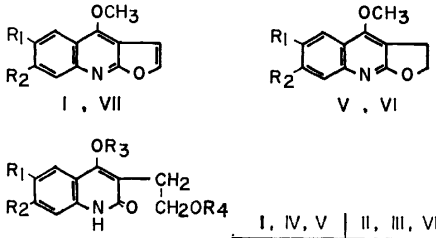

II, R_3=H, R_4=CH_2Ph
III, R_3=CH_3, R_4=CH_2Ph
IV, R_3=CH_3, R_4=H

	I, IV, V		II, III, VI, VII	
	R_1	R_2	R_1	R_2
a	OCH_3	OH	OCH_3	OCH_2Ph
b	OH	H	OCH_2Ph	H

Experimental*

3-(2-Benzyloxyethyl)-4-hydroxy-2-quinolones (IIa, b). A mixture of 3-benzyloxy-4-methoxyaniline (4.2 g) or 4-benzyloxyaniline (3.5 g) and diethyl (2-benzyloxyethyl)-malonate (6.3 g) was heated under reduced pressure (*ca.* 70 mmHg). The temperature was then raised to 180 °C over a period of 30 min, maintained at that temperature for a further 30 min, and then raised and kept at 250 °C for 30 min. The cooled reaction mixture was subsequently dissolved in chloroform. The chloroform solution was treated in a way similar to that described in previous papers.[4,5] IIa: Mp 185—186 °C (pale yellow plates from EtOH) (yield, 58.0%). Found: C, 72.08; H, 5.99; N, 3.21%. Calcd for $C_{26}H_{25}O_5N$: C, 72.37; H, 5.84; N, 3.25%. IR (cm^{-1}, Nujol): 3200, 1650. NMR ($CDCl_3$): δ 3.14, 3.82 ppm (both 2H, t, J=5.0 Hz, CH_2–CH_2), 3.93 (3H, s, OCH_3), 4.66, 5.20 (both 2H, s, CH_2Ph), 6.85 (1H, s, arom-**H**), 7.2—7.5 (11H, m, arom-**H** and 2×CH_2**Ph**), 9.68 (1H, br, O**H**), 12.04 (1H, br, N**H**). IIb: Mp 190.5—191.5 °C (pale yellow needles from ethyl acetate) (yield, 88.5%). Found: C, 74.73; H, 5.72; N, 3.50%. Calcd for $C_{25}H_{23}O_4N$: C, 74.79; H, 5.78; N, 3.49%. IR (Nujol); 3400, 1650. NMR ($CDCl_3$): δ 3.20, 3.90 (both 2H, t, J=5.3 Hz, CH_2–CH_2), 4.67, 5.15 (both 2H, s, CH_2Ph), 7.28, 7.38 (both 5H, s, CH_2**Ph**) 7.2—7.6 (3H, m, arom-**H**), 9.75 (1H, br, O**H**), 12.00 (1H, br, N**H**).

3-(2-Benzyloxyethyl)-4-methoxy-2-quinolones (IIIa, b). Prepared by the usual diazomethane method: IIIa: Mp 175—176 °C (colorless plates from ethyl acetate) (yield, 81.0%). Found: C, 72.52; H, 6.16; N, 3.08%. Calcd for $C_{27}H_{27}O_5N$: C, 72.79; H, 6.11; N, 3.14%. IR (Nujol): 1660. NMR ($CDCl_3$): δ 3.92, 3.94 (both 3H, OCH_3), 3.06, 3.82 (both 2H, t, J=6.8 Hz, CH_2–CH_2), 4.51, 5.18 (both 2H, s, CH_2Ph), 6.8—7.5 (12H, m, arom-**H** and CH_2**Ph**),

* All the melting points are uncorrected.

12.46 (1H, s, NH). IIIb: Mp 163—165 °C (pale yellow needles from EtOH) (yield, 90.5%). Found: C, 75.08; H, 6.01; N, 3.45%. Calcd for $C_{26}H_{25}O_4N$: C, 75.16; H, 6.07; N, 3.37%. IR (Nujol): 1650. NMR ($CDCl_3$): δ 3.87 (3H, s, OCH_3), 3.07, 3.83 (both 2H, t, J=7.2 Hz, CH_2–CH_2), 4.55, 5.12 (both 2H, s, CH_2Ph), 7.24, 7.40 (both 5H, s, CH_2Ph), 7.0—7.5 (3H, m, arom-H), 12.25 (1H, br, NH).

3-(2-Hydroxyethyl)-4-methoxy-2-quinolones (IVa, b). To a hydrogen-saturated solution of Pd-C (5%, 2.0 g) in abs ethanol 100 ml, IIIa or IIIb (5.0 g) was added; the mixture was then stirred for 3 h at *ca.* 60 °C in an atmosphere of hydrogen. After the catalyst had been filtered off, the residue was recrystallized from ethanol to give 1.7 g (62.7%) of IVa or 1.8 g (63.6%) of IVb. IVa: Mp 217—219 °C. Found: C, 58.80; H, 5.69; N, 5.27%. Calcd for $C_{13}H_{15}O_5N$: C, 58.86; H, 5.70; N, 5.28%. IR (Nujol): 3500, 3200, 1650. NMR (DMSO-d_6): δ 3.87, 3.91 (both 3H, s, OCH_3), 2.77, 3.65 (both 2H, t, J=7.0 Hz, CH_2–CH_2), 6.85, 7.06 (both 1H, s, C_8–H and C_5–H), 8.28, 9.80, 11.40 (each 1H, br, OH and NH). IVb: Mp 227—229 °C (colorless needles from EtOH). Found: C, 61.04; H, 5.65; N, 6.24%. Calcd for $C_{12}H_{13}O_4N$: C, 61.27; H, 5.57; N, 5.96%. IR (Nujol): 3600, 3200, 1655. NMR (DMSO-d_6): δ 3.86 (3H, s, OCH_3), 2.70, 3.57 (both 2H, t, J=6.0 Hz, CH_2–CH_2), 4.66 (1H, t, J=5.25 Hz, CH_2OH), 6.8—7.4 (3H, m, arom-H), 9.38 (1H, s, OH), 11.45 (1H, s, NH).

2,3-Dihydrofuro[2,3-b]quinolines (Va, b). A mixture of IVa or IVb (1.0 g) and polyphosphate ester (15 g) was heated at 120—130 °C for 2.5 h. The cooled mixture was then poured into water, and the insoluble materials were filtered off. The aq. solution was neutralized with ammonia. The precipitate was collected, washed with water, and recrystallized to give Va or Vb. Va: Mp 320 °C (dec, pale green needles from EtOH) (yield, 42.2%). Found: C, 63.30; H, 5.29; N, 5.47%. Calcd for $C_{13}H_{13}O_4N$: C, 63.15; H, 5.30; N, 5.67%. IR (Nujol): 3400, 1630, 1490. NMR (DMSO-d_6): δ 3.60, 4.50 (both 2H, t, J=7.8 Hz, CH_2–CH_2), 3.85, 4.18 (both 3H, s, OCH_3), 6.93, 7.23 (both 1H, s, C_8–H and C_5–H), 9.55 (1H, br, OH). Vb: Mp 288—290 °C (colorless needles from EtOH) (yield, 67.7%). Found: C, 66.46; H, 5.07; N, 6.50%. Calcd for $C_{12}H_{11}O_3N$: C, 66.35; H, 5.10; N, 6.45%. IR (Nujol): 3450, 1630, 1520. NMR (DMSO-d_6): δ 3.60, 4.50 (both 2H, t, J=7.5 Hz, CH_2–CH_2), 4.15 (3H, s, OCH_3), 6.95—7.55 (3H, m, arom-H), 9.45 (1H, s, OH).

Benzyl Ether of 2,3-Dihydrofuro[2,3-b]quinolines (VIa, b). To a sodium ethoxide solution prepared from metallic sodium (140 mg) and abs. ethanol (100 ml), Va (1.0 g) or Vb (0.9 g), and benzyl chloride (0.7 g) were added, after which the mixture was refluxed for 8 h in an atmosphere of nitrogen. After the mixture had then been evaporated under a vacuum, the residue was extracted with chloroform. The chloroform solution was washed with a sodium hydroxide solution and water, and then extracted with a 6M hydrochloric acid solution. The acidic solution was neutralized with ammonia and extracted with chloroform. After the solvent had been evaporated, the residue was recrystallized to give VIa or VIb. VIa: Mp 177—179 °C (colorless plates from EtOH) (yield, 60.2%). Found: C, 71.23; H, 5.61; N, 4.05%. Calcd for $C_{20}H_{19}O_4N$: C, 71.20; H, 5.68; N, 4.15%. NMR ($CDCl_3$): δ 3.90, 4.09 (both 3H, s, OCH_3), 3.51, 4.49 (both 2H, t, J=8.8 Hz, CH_2–CH_2), 4.44 (2H, s, CH_2Ph), 7.14 (7H, m, arom-H and CH_2Ph). VIb: Mp 182—184 °C (colorless plates from EtOH) (yield, 63.5%). Found: C, 74.02; H, 5.52; N, 4.40%. Calcd for $C_{19}H_{17}O_3N$: C, 74.25; H, 5.58; N, 4.56%. NMR ($CDCl_3$): δ 4.10 (3H, s, OCH_3), 3.50, 4.50 (both 2H, t, J=8.0 Hz, CH_2–CH_2), 5.07 (2H, s, CH_2Ph), 7.38 (5H, s, CH_2Ph), 7.0—8.0 (3H, m, arom-H).

Benzyl Ether of Furo[2,3-b]quinolines (VIIa, b). To a solution of VIa or VIb (1.0 g) in dry toluene (150 ml), DDQ (2.0 g) was added; the mixture was then stirred under reflux for 16 h in an atmosphere of nitrogen. The mixture was filtered, and the filtrate was washed with water and extracted with 6M hydrochloric acid. After the acidic solution had been neutralized with ammonia, the resulting precipitate was collected and recrystallized to give VIIa or VIIb. The product was purified by means of chromatography on Wako-gel C-200 (10% $CHCl_3$–C_6H_6). VIIa: Mp 186—187 °C (pale yellow needles from EtOH) (yield, 42.4%). Found: C, 71.43; H, 5.25; N, 4.20%. Calcd for $C_{20}H_{17}O_4N$: C, 71.63; H, 5.11; N, 4.18%. NMR ($CDCl_3$): δ 3.97, 4.35 (both 3H, s, OCH_3), 6.96, 7.50 (both 1H, d, J=2.4 Hz, C_3–H and C_2–H), 5.27 (2H, s, CH_2Ph), 7.44 (7H, m, arom-H and CH_2Ph). VIIb: Mp 193—194.5 °C (colorless needles from EtOH) (yield, 32.6%). Found: C, 74.68; H, 5.20; N, 4.79%. Calcd for $C_{19}H_{15}O_3N$: C, 74.74; H, 4.95; N, 4.59%. NMR ($CDCl_3$): δ 4.40 (3H, s, OCH_3), 7.01, 7.57 (both 1H, d, J=3.0 Hz, C_3–H and C_2–H), 5.16 (2H, s, CH_2Ph), 7.95 (1H, d, J=9.0 Hz, arom-H), 7.2—7.6 (7H, m, arom-H and CH_2Ph).

Heliparvifoline (Ia) and O-Demethylpteleine (Ib). A mixture of VIIa or VIIb (0.5 g) and ethanol-hydrochloric acid (1 : 1, 50 ml) was treated by a method similar to that described in previous papers.[4,5] The precipitate was collected and recrystallized to give 4,6-dimethoxy-7-hydroxyfuro[2,3-*b*]-quinoline (heliparvifoline, Ia) and 6-hydroxy-4-methoxyfuro[2,3-*b*]quinoline (*O*-demethylpteleine, Ib). Ia: Mp 243—245 °C (lit,[1] 245—246 °C; a mixed melting point with natural heliparvifoline was not depressed.) (pale yellow cubic from MeOH) (yield, 76.5%). Found: C, 63.55; H, 4.48; N, 5.65%. Calcd for $C_{13}H_{11}O_4N$: C, 63.67; H, 4.42; N, 5.71%. IR (Nujol): 3500, 1630, 1490. NMR (DMSO-d_6): δ 3.94, 4.38 (both 3H, s, OCH_3), 7.06 (1H, d, J=2.4 Hz, C_3–H), 7.52 (1H, d, J=2.4 Hz, C_2–H), 7.20 (1H, s, C_8–H), 7.40 (1H, s, C_5–H), 7.70 (1H, s, OH, disappeared with D_2O). Ib: mp 216—217 °C (pale yellow prisms from EtOH–C_6H_6) (yield, 51.7%). Found: C, 66.75; H, 4.30; N, 6.44%. Calcd for $C_{12}H_9O_3N$: C, 66.97; H, 4.22; N, 6.51%. NMR (DMSO-d_6): δ 4.41 (3H, s, OCH_3), 7.14 (1H, d, J=2.4 Hz, C_3–H), 7.68 (1H, d, J=8.0 Hz, arom-H), 7.90 (1H, d, J=2.4 Hz, C_2–H), 6.7—7.4 (2H, m, arom-H), 9.60 (1H, br, OH, disappeared with D_2O).

The author wishes to express his deep gratitude to Dr. Mitsuru Nakayama, Hiroshima University, for his encouragement throughout the course of this work, and also to Dr. G.A. Cordell, University of Illinois, Chicago, for his gift of a natural specimen of heliparvifoline.

References

1) P. T. O. Chang, G. H. Aynilian, G. A. Cordell, M. Tin-wa, H. H. S. Fong, R. E. Perduer, Jr., and N. R. Farnsworth, *J. Pharm. Sci.*, **65**, 561 (1976).

2) J. A. Lamberton and J. R. Price, *Aust. J. Chem.*, **6**, 173 (1953).

3) T. R. Govindachari, S. Prabhakar, V. N. Ramachandran, and B. P. Pai, *Indian J. Chem.*, **9**, 1031 (1971).

4) T. Sekiba, *Bull. Chem. Soc. Jpn.*, **46**, 577 (1973).

5) T. Sekiba, *J. Sci. Hiroshima Univ., Ser. A*, **40**, 143 (1976).

BULLETIN OF THE CHEMICAL SOCIETY OF JAPAN, VOL. 51 (1), 327—328 (1978)

The Reaction of *N*-(Phenylsulfonyl)benzohydrazonoyl Chloride with Enamines

Suketaka Ito, Yumo Tanaka, Akikazu Kakehi, and Toshiyuki Matsuno

Department of Industrial Chemistry, Faculty of Engineering, Shinshu University, Wakasato, Nagano 380

(Received May 23, 1977)

Synopsis. 3-(Diethylamino)crotonic acid esters and 1-diethylamino-1-cyclohexene react with *N*-(phenylsulfonyl)-benzohydrazonoyl chloride to give substituted pyrazoles in 87—89% and 1.4% yields, respectively, the corresponding morpholine enamines affording no pyrazoles. The pyrazole formation is interpreted in terms of a step-by-step process involving the nucleophilic attack of the enamines on the hydrazonoyl chloride.

N-Phenylbenzohydrazonoyl chloride reacts with benzamidine to give 1,3,5-triphenyl-1*H*-1,2,4-triazole,[1] and with enamines to afford substituted pyrazoles;[2,3] the 1,3-dipolar cycloaddition mechanism has been suggested for these reactions.[2,4]

On the other hand, the reaction of *N*-(phenylsulfonyl)-benzohydrazonoyl chloride(**1**) with benzamidines and benzimidates proceeds through a two-step path involving the nuclephilic attack of amidines or imidates on the imidoyl carbon of the hydrazonoyl chloride, leading also to the formation of 1,2,4-triazoles.[5]

The present study shows a pyrazole-formation by the reaction of **1** with enamines which proceeds through the two-step path involving the nucleophilic process.

When a mixed solution of **1** and one equivalent of ethyl or allyl 3-(diethylamino)crotonate(**2a** or **2b**) in THF was allowed to stand at room temperature, 4-ethoxycarbonyl- or 4-allyloxycarbonyl-5-methyl-3-phenyl-1-phenylsulfonylpyrazole(**3a** or **3b**) was formed in a good yield. Much the same result was obtained when two equivalents of **2** were used. In the reaction with 1-diethylamino-1-cyclohexene(**2c**), however, the corresponding pyrazole(**3c**) was obtained in a low yield, 3,6-diphenyl-1,4-bis(phenylsulfonyl)-1,4-dihydro-1,2,4,5-tetrazine(**4**) being formed together with a small amount of *N*-(phenylsulfonyl)-*N*-[*N*-(phenylsulfonyl)-benzohydrazonoyl]benzohydrazonoyl chloride(**5**)[5] and 3,5-diphenyl-4-phenylsulfonylamino-4*H*-1,2,4-triazole (**6**)(Scheme 1).

In contrast, the corresponding morpholine enamines (**2'a** and **2'c**) afforded no pyrazoles but **4** and/or **5** and **6**. *N*-Phenylsulfonylmorpholine was also obtained along with N^2-(phenylsulfonyl)benzohydrazide[6] in the reaction with ethyl 3-morpholinocrotonate(**2'a**). The results are summarized in Table 1.

Table 1. Reaction of *N*-(phenylsulfonyl)benzohydrazonoyl chloride with enamines

Enamines[a]	Yield(%) of Products[b]			
	3	**4**	**5**	**6**
2a	89(**3a**)	—	—	—
2b	87(**3b**)	—	—	—
2c	1.4(**3c**)	42	2.7	4.0
2'a[c]	—	trace	14	13
2'c	—	48	—	—

a) **2'a**: Me-C(-N O)=CH-COOEt, **2'c**: O N-C_6H_9. b) Yield(isolated) as mole per cent based on **1**. c) Yield of *N*-phenylsulfonylmorpholine: 18%. Yield of N^2-(phenylsulfonyl)benzohydrazide: 24%.

In the hydrazonoyl chloride **1**, the electron-attractive phenylsulfonyl group may enhance the acidity of the amino group and also the electrophilicity of the imidoyl carbon of **1**. Thus, for the formation of **5** and **4**, the following reaction route can be given: (Scheme 2). Actually, **4** was obtained almost quantitatively by the treament of **5** with a base.

The attempted reactions of **1** with a number of dipolarophiles in the presence of a base were unsuccessful, but resulted in the formation of **4** in all cases:[5] the negative charge of the *N*-(phenylsulfonyl)benzohydrazonoyl chloride *N*-anion (**1'**) may be delocalized by the sulfonyl group, so that the anion becomes stable and will not release chloride anion to form the 1,3-dipolar nitrilimine. Furthermore, the 1,3-dipolar cycloaddition mechanism cannot explain the different reactivity of

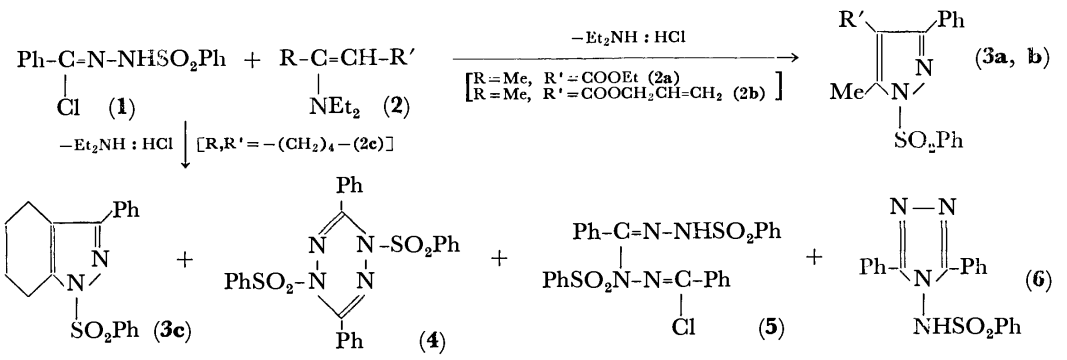

Scheme 1.

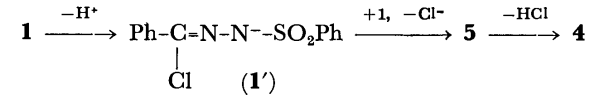

Scheme 2.

enamines in the present pyrazole-formation.

Consequently, it is reasonable to consider that the pyrazole formation may proceed via the nucleophilic attack of **2** on the imidoyl carbon of **1** followed by the intramolecular cyclization of the resulting intermediate (Scheme 3).

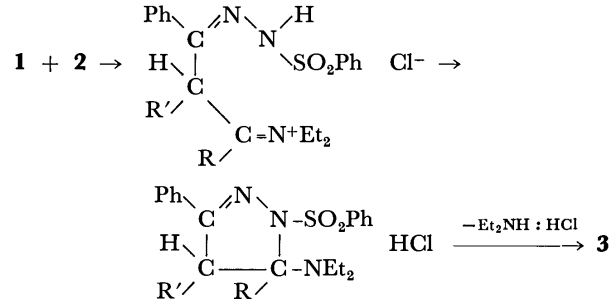

Scheme 3.

Since enamine **2c** is a stronger base than **2a** and **2b**, the proton abstraction from **1** by **2c** takes place predominantly to lead to the formation of **5** and **4**. Owing to the internal strain which arises in the iminium salt structure of morpholine moiety, it may be difficult for the first step of pyrazole-formation to take place in the reaction with the morpholine enamines. These circumstances and the stronger basicity of morpholine enamines probably account for their different behavior.

Compound **5** may be the precursor of the triazole **6**: efforts have been made to verify this postulation, but no experimental evidence could be obtained.

Experimental

Melting points were determined with a Yanagimoto micro-melting point apparatus Model MP-S3 and are uncorrected. The microanalysis was performed on a Perkin-Elmer elemental analyzer Model 240. The IR and NMR spectra were recorded with a JASCO DS-301 spectrometer and a JEOL JNH-4H-100 spectrometer, respectively.

N-(Phenylsulfonyl)benzohydrazonoyl chloride (**1**) was prepared by the method reported.[7] Ethyl and allyl 3-(diethylamino)crotonate (**2a**: bp 150—152 °C/18 mmHg, **2b**: bp 169—170 °C/20 mmHg), and ethyl 3-morpholinocrotonate (**2'a**: bp 172—174 °C/14 mmHg) were prepared according to the procedure of Décombe.[8] 1-Diethylamino-1-cyclohexene (**2c**: bp 66—67 °C/6 mmHg) and 1-morpholino-1-cyclohexene (**2'c**: bp 133—134 °C/17 mmHg) were obtained according to the method of Blanchard[9] and of Hünig *et al.*,[10] respectively.

The products were identified by their analytical and spectral data.

*Reaction of **1** with Enamines (1 : 1 mole ratio). General Procedure*: A solution of **2** (0.01 mol) in THF (20 ml) was mixed with a solution of **1** (0.01 mol) in THF (20 ml) at room temperature. In a few minutes, precipitates began to separate. The reaction mixture was allowed to stand for one day. The separated precipitates (amine hydrochloride) were filtered and washed with THF. The filtrate was concentrated and chromatographed over silica gel (20 g) using benzene as an eluent to give the products shown in Table 1.

*4-Ethoxycarbonyl-5-methyl-3-phenyl-1-phenylsulfonylpyrazole (**3a**).* Mp 111—112 °C (benzene). IR (KBr, cm^{-1}): 1700 (ν_{CO}); 1575, 1543 (ring $\nu_{C=C}$, $\nu_{C=N}$); 1370, 1184 (ν_{SO_2}), NMR ($CDCl_3$, δ): 1.13 ppm (3H t, J=7.5 Hz, CH_3CH_2–); 2.91 ppm (3H s, 5-CH_3); 4.27 ppm (2H q, J=7.5 Hz, CH_3–CH_2–); 7.40—8.00 ppm (8H m, 3-Ph, *m,m'* and *p*-protons of $PhSO_2$–); 8.16—8.35 ppm (2H m, *o,o'*-protons of $PhSO_2$–). Found: C, 61.49; H, 4.88; N, 7.57%. Calcd for $C_{19}H_{18}N_2O_4S$: C, 61.61; H, 4.90; N, 7.56%.

*4-Allyloxycarbonyl-5-methyl-3-phenyl-1-phenylsulfonylpyrazole (**3b**).* Mp 104—105 °C (CCl_4). IR (KBr, cm^{-1}): 1713 (ν_{CO}); 1575, 1532 (ring $\nu_{C=C}$, $\nu_{C=N}$); 1370, 1184 (ν_{SO_2}), NMR ($CDCl_3$, δ): 2.93 ppm (3H s, 5-CH_3); 4.73 ppm (2H brd, J=5.0 Hz, $-OCH_2-CH=CH_2$); 5.21 ppm (1H brd, J=17.5 Hz, $-OCH_2>C=C<\underline{H}$); 5.24 ppm (1H brd, J=10.0 Hz, $-OCH_2>C=C<\underline{H}$); 5.90 ppm (1H m, $-OCH_2-C\underline{H}=CH_2$); 7.45—7.80 ppm (8H m, 3-Ph, *m,m'* and *p*-protons of $PhSO_2$–); 8.15—8.30 ppm (2H m, *o,o'*-protons of $PhSO_2$–). Found: C, 62.75; H, 4.65; N, 7.24%. Calcd for $C_{20}H_{18}N_2O_4S$: C, 62.81; H, 4.73; N, 7.33%

*3-Phenyl-1-phenylsulfonyl-4,5,6,7-tetrahydrobenzo[c]pyrazole (**3c**).* Mp 243—244 °C (acetone). IR (KBr, cm^{-1}): 1580, 1565 (ring $\nu_{C=C}$, $\nu_{C=N}$); 1372, 1183 (ν_{SO_2}), NMR ($CDCl_3$, δ): 1.50—2.00 ppm (4H m, C^5 and C^6–H); 2.66 ppm (2H m, C^4–H); 3.05 ppm (2H m, C^7–H); 7.45—7.95 ppm (8H m, 3-Ph, *m,m'* and *p*-protons of $PhSO_2$–); 8.10—8.30 ppm (2H m, *o,o'*-protons of $PhSO_2$–). Found: C, 67.56; H, 5.16; N, 8.21%. Calcd for $C_{19}H_{18}N_2O_2S$: C, 67.43; H, 5.36; N, 8.28%.

*3,5-Diphenyl-4-phenylsulfonylamino-4H-1,2,4-triazole (**6**).* Mp 312—315 °C (dec) (acetone). IR (KBr, cm^{-1}): 3171 (ν_{NH}); 1580 ($\nu_{C=N}$); 1353, 1165 (ν_{SO_2}); 1276 (triazole ring). Found: C, 63.51; H, 4.29; N, 14.59%. Calcd for $C_{20}H_{16}N_4O_2S$: C, 63.81; H, 4.28; N, 14.88%.

References

1) R. Fusco and C. Musante, *Gazz. Chim. Ital.*, **68**, 147 (1938).

2) M. E. Kuehne, S. J. Weaver, and P. Franz, *J. Org. Chem.*, **29**, 1582 (1964).

3) The reaction of ethyl (phenylhydrazono)chloroacetate with enamines gives also pyrazoles: R. Fusco, G. Bianchetti, and D. Pocar, *Gazz. Chim. Ital.*, **91**, 1233 (1961).

4) J-P. Anselme, in "The Chemistry of the Carbon-Nitrogen Double Bond," ed by S. Patai, Interscience, London (1970), p. 315.

5) S. Ito, Y. Tanaka, A. Kakehi, and H. Miyazawa, *Bull. Chem. Soc. Jpn.*, **50**, 2969 (1977).

6) This compound should be derived from unaltered **1** by hydrolysis on silica gel used in the chromatographic treatment.

7) S. Ito, Y. Tanaka, and A. Kakehi, *Bull. Chem. Soc. Jpn.*, **49**, 762 (1976).

8) J. Décombe, *Ann. Chim.*, **18**, 81 (1932); *Chem. Abstr.*, **27**, 2134 (1933).

9) E. P. Blanchard, Jr., *J. Org. Chem.*, **28**, 1397 (1963).

10) S. Hünig, E. Lücke, and W. Brenninger, *Org. Synth.*, **41**, 65 (1961).

BULLETIN OF THE CHEMICAL SOCIETY OF JAPAN, VOL. 51 (1), 329—330 (1978)

Photochemical Reactions of Aromatic Compounds. XXIX.[1] Photochemical and Thermal Cycloreversions of 1,2,2a,8b-Tetrahydrocyclobuta[*a*]naphthalenes

Chyongjin PAC,* Kazuhiko MIZUNO,** and Hiroshi SAKURAI
The Institute of Scientific and Industrial Research, Osaka University, Suita, Osaka 565

(Received June 18, 1977)

Synopsis. Photochemical and thermal cycloreversions of 1,2,2a,8b-tetrahydrocyclobuta[*a*]naphthalenes were investigated. The cycloreversion in the excited singlet state was completely stereospecific; a concerted mechanism was assigned. The benzophenone-sensitized and thermal decomposition gave a mixture of *cis*- and *trans*-olefins, but favored stereoretention. The mechanisms are discussed in terms of singlet and triplet 1,4-biradicals.

The [2+2] cycloreversions of cyclobutane compounds have been of theoretical and mechanical interest in relation to the Woodward-Hoffmann rule[2] and 1,4-biradical intermediates.[3] We wish to report here on the stereochemical features of photochemical and thermal cycloreversions of 1,2,2a,8b-tetrahydrocyclobuta[*a*]naphthalenes **1a—d**.

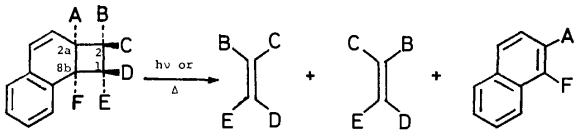

1 2 3 4

	A	B	C	D	E	F
a:	H	H	CH_3	OC_6H_5	H	CN
b:	H	CH_3	H	OC_6H_5	H	CN
c:	CN	H	CH_3	OCH_3	H	H
d:	CN	CH_3	H	OCH_3	H	H

The direct or benzophenone-sensitized photolysis of **1a—d** quantitativlly gave **2a—d**, **3a—d**, and **4**. The results are listed in Table 1. The olefin formation by the direct photolysis of **1a**, **b** occurred with >95% stereospecificities, whereas the cycloreversion in the presence of ferrocene or in neat 1,3-pentadiene was completely stereospecific. Since ferrocene and 1,3-pentadiene are well-known to be good triplet quenchers, the formation of small amounts of **3a**, **b** in the absence of such compounds probably occurs by means of a triplet mechanism. Similarly, the direct photolysis of **1c** or **1d** in the presence of ferrocene gave only **2c** or **2d** each. In the excited singlet state, therefore, the cycloreversions proceed *via* a $_s2_s+_s2_s$ concerted mechanism.

On the other hand, the benzophenone-sensitized decomposition of **1a**, **b** occurred with only a partial stereoretention. In recovered **1a**, **b**, the epimers could not be detected. The results suggest that triplet biradicals, ^{3}**4c** and ^{3}**5t**, undergo the C_1–C_2 bond rotation in competition with the intersystem crossing to singlet biradicals (Scheme 1).[4]

The thermal decomposition of **1a—d** at 300±10 °C gave **2a—d**, **3a—d**, and **4**> in 80% yields, with high stereospecificities. It should be noted that the stereoretention of the *cis* configuration in **1a**, **c**→**2a**, **c** predominanted over that of the *trans* configuration in **1b**, **d**→**2b**,**d**;[6] usually the retention of the *trans* configuration predominates over that of the *cis* configuration in thermolyses of cyclobutane[5a,5c,7] and oxetane[8] compounds. The C_2–C_3 bond cleavage of singlet biradicals is spin-allowed and favored by the aromatization of the dihydronaphthyl residue. Moreover, the sterically crowded nature of ^{1}**4c** reinforces the bond cleavage which overcomes the C_1–C_2 bond rotation, whereas ^{1}**5t** undergoes the bond rotation to a significant extent

TABLE 1. PHOTOCHEMICAL AND THERMAL CYCLOREVERSIONS OF **1a—d**[a]

			1a		**1b**		**1c**		**1d**	
			2a[b]	**3a**[c]	**2b**[c]	**3b**[b]	**2c**[d]	**3c**[e]	**2d**[e]	**3d**[d]
Photolysis	Direct	A[f,g]	95±1	5±1	98±1	2±1	—	—	—	—
		C[f,h]	95±1	5±1	99	1	—	—	—	—
		P[i]	>99	<1	100	0	—	—	—	—
		F[j]	100	0	100	0	100	0	100	0
	Sens[k]	A[f,g]	55±1	45±1	78±1	22±1	—	—	—	—
Thermolysis[l]		300 °C	95±2	5±2	76±2	24±2	90±3	10±3	80±3	20±3
		350 °C	90	10	76	24	—	—	—	—
		480 °C	88	12	75	25	—	—	—	—

a) Averaged for each three runs. b) *cis*-1-Phenoxypropene. c) *trans*-1-Phenoxypropene. d) *cis*-1-Methoxypropene. e) *trans*-1-Methoxypropene. f) Extrapolated at zero-time irradiation. g) Acetonitrile solution. h) Cyclohexane solution. i) In neat 1,3-pentadiene; conversion, <10%. j) Acetonitrile solution in the presence of ferrocene; conversion, <10%. k) Sensitized by benzophenone. l) The thermolyses were carried out in the inlet part of a GC-2C machine.

** Present adress: Department of Applied Chemistry, College of Engineering, University of Osaka Prefecture, Mozu-Umemachi, Sakai 591.

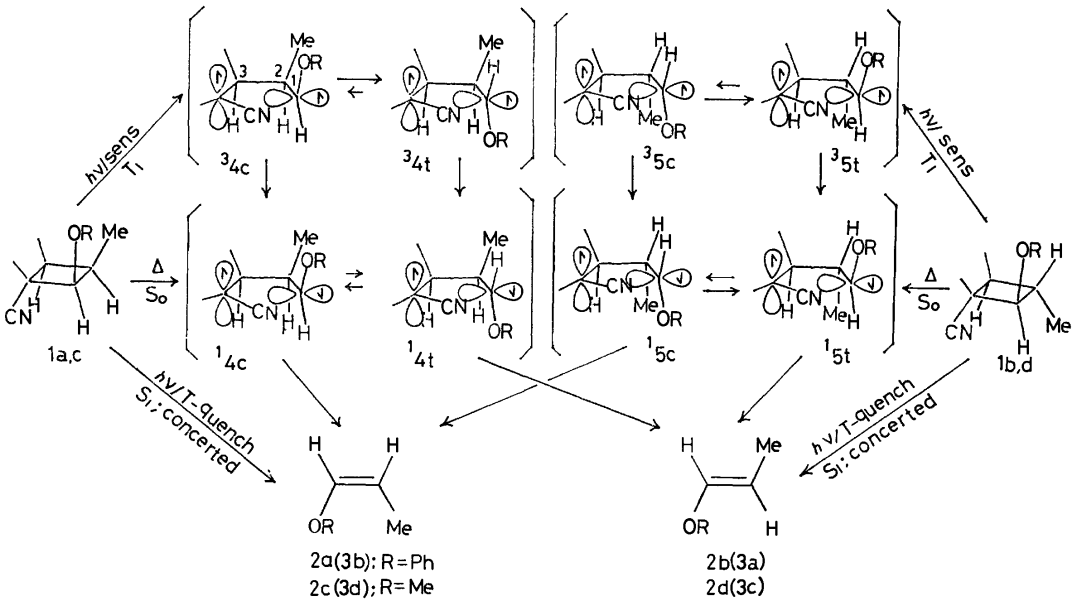

Scheme 1.

because of the smaller steric repulsion. Alternatively, a biradicaloid transition-state mechanism[3b,3f] offers an attractive speculation; a concerted mechanism could contribute more to the cycloreversion of **1a**, **c** than to that of **1b**,**d**.[8b,9]

Experimental

Materials. *cis*- and *trans-endo*-1-Phenoxy-2-methyl-1,2,2a,8b-tetrahydrocyclobuta[*a*]naphthalene-8b-carbonitriles **1a** (mp 138.5—139.5 °C) and **1b** (mp 97.5—98.5 °C) were obtained by the photocycloaddition of *cis*- and *trans*-1-phenoxypropenes to 1-naphthonitrile[10] respectively. Similarly, **1c** (mp 65—66 °C) and **1d** (mp 127.5—129 °C) were prepared according to the method reported previously.[11] These materials, benzophenone, and ferrocene were recrystallized from methanol. The 1,3-pentadiene was distilled from sodium under a nitrogen atmosphere.

Photolyses. Solutions of **1a**—**d** (2 mg/cm³) in cyclohexane, acetonitrile, or 1,3-pentadiene were prepared. Solutions of **1a**—**d** (2 mg/cm³) and ferrocene (2 mg/cm³) or benzophenone (1 mg/cm³) in acetonitrile were also prepared. Each solution (2 cm³) was placed in a Pyrex tube, bubbled with a pure nitrogen stream, and irradiated with a high-pressure mercury arc at 20±2 °C, using a merry-go-round apparatus. In benzophenone-sensitized runs, a hexane solution of naphthalene (13 g/dm³, 1 cm path length) was used as the light filter. During the course of the irradiation, the photolysates were analyzed by VPC at 5-min intervals.

Thermolyses. Pyrex tubes, in which **1a** or **1b** (10—20 mg) was placed, were degassed ($<10^{-3}$ mmHg), sealed, and heated on a metal bath maintained at 300±10 °C for 2—3 h. The decomposition was completed. 1-Naphthonitrile and a mixture of *cis*- and *trans*-1-phenoxypropenes were formed in *ca.* 90 and 80% yields respectively. More conveniently, the thermolyses were carried out by introducing 0.5—1.0 μl portions of acetonitrile solutions of **1a**—**d** into a Shimadzu GC-2C gas chromatograph, the inlet part of which was maintained at a constant temperature (300—480 °C).

References

1) Part XXVIII: C. Pac, A. Nakasone, and H. Sakurai, *J. Am. Chem. Soc.*, **99**, 5806 (1977).

2) R. B. Woodward and R. Hoffmann, "The Conservation of Orbital Symmetry," Verlag Chemie, GmbH, Weinheim/Bergstr. (1970).

3) (a) L. Salem and C. Rowland, *Angew. Chem., Int. Ed. Engl.*, **11**, 92 (1972); (b) R. Hoffmann, S. Swaminathan, B. G. Odell, and R. Gleiter, *J. Am. Chem. Soc.*, **92**, 7091 (1970); (c) L. M. Stephenson and T. A. Gibson, *ibid.*, **94**, 4599 (1972); (d) M. J. S. Dewar, S. Kirschner, H. W. Kollmar, and L. E. Wade, *ibid.*, **96**, 5242, 5246 (1974); (e) R. G. Bergman, in "Free Radicals," ed by J. K. Kochi, John Wiley & Sons, Vol. 1, New York (1973), p. 191; (f) G. Jones, II, *J. Chem. Educ.*, **51**, 175 (1974); (g) L. M. Stephenson and J. I. Brauman, *J. Am. Chem. Soc.*, **93**, 1988 (1971).

4) The **6** biradicals could be alternative intermediates, but are energetically less favorable than **4** and **5**.

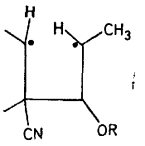

6

5) (a) H. R. Gerberich and W. D. Walters, *J. Am. Chem. Soc.*, **83**, 4884 (1961); (b) L. A. Paquette and G. L. Thompson, *ibid.*, **94**, 7127 (1972); (c) L. M. Stephenson and T. A. Gibson, *ibid.*, **96**, 5624 (1974).

6) Under the conditions of the thermolyses, the isomerization of **2a**—**d** and **3a**—**d** is negligible.

7) (a) A. T. Cocks, H. M. Frey, and I. D. R. Stevens, *J. Chem. Soc., Chem. Commun.*, **1969**, 458; (b) G. Jones, II and M. H. Williamson, Jr., *J. Am. Chem. Soc.*, **96**, 5617 (1974).

8) (a) H. A. J. Carles, *Tetrahedron Lett.*, **1974**, 3425; (b) G. Jones, II and J. C. Staires, *ibid.*, **1974**, 2099.

9) G. Jones, II and V. L. Chow, *J. Org. Chem.*, **39**, 1447 (1974).

10) K. Mizuno, C. Pac, and H. Sakurai, *J. Chem. Soc., Chem. Commun.*, **1974**, 648.

11) K. Mizuno, C. Pac, and H. Sakurai, *J. Org. Chem.*, **42**, 3313 (1977).

BULLETIN OF THE CHEMICAL SOCIETY OF JAPAN, VOL. 51 (1), 331—332 (1978)

The Synthesis of 1,2,3,4-Tetramethyl-5-nitronaphthalene and 1,2,3,4-Tetramethyl-6-nitronaphthalene

Akira Oku and Akira Matsui

Department of Chemistry, Kyoto Institute of Technology, Matsugasaki, Sakyo-ku, Kyoto 606

(Received June 27, 1977)

Synopsis. 1,2,3,4-Tetramethyl-5-nitronaphthalene and 1,2,3,4-tetramethyl-6-nitronaphthalene were prepared by the pyrolysis of 5- and 8-nitro-1,2,3,4,10,10-hexamethyl-1,4-dihydro-1,4-ethanonaphthalen-9-ones and their 6- and 7-nitro-isomers respectively.

Polymethyl-substituted nitronaphthalenes, in which one aromatic ring is fully substituted by four methyl groups and the other ring by a certain number of nitro groups, are of particular interest from the point of view of their electronic structures. Their syntheses, however, have not hitherto reported except in the cases of such homologues as dimethylnitronaphthalenes,[1] because a) the substitution on the α-position of naphthalenes by a bulky group, which causes a severe nonbonded peri-interaction, is difficult and b) the electrophilic nitration of polymethylnaphthalenes usually occurs on the methylated ring and often leads to abnormal reactions that take place on alkyl side chains.[2]

In this report, we wish to present the first syntheses of two tetramethylnitronaphthalenes, *i.e.*, 1,2,3,4-tetramethyl-5-nitro-naphthalene (**8**) and 1,2,3,4-tetramethyl-6-nitronaphthalene (**10**), prepared by a method that does not require the direct introduction of a nitro group on the naphthalene ring. This method is based on a modification of the one that has been used successfully to synthesize a number of polymethylnaphthalenes.[3] The synthetic process is outlined in Scheme 1.

A mixture of Compound **6** and **7**, both of which were obtained from either 4- or 5-nitroanthranilic acid and hexamethyl-2,4-cyclohexadien-1-one (**2**),[4] was used as the precursor of naphthalene **10**, and it was subjected to the following two treatments: A) treatment with the methylsulfinylmethanide anion in dimethyl sulfoxide, and B) pyrolysis. Method A has been known to be an efficient method[3] to prepare a certain number of polymethylnaphthalenes from the methylaryne-adducts of Type **11**. By applying this method to the nitrobenzyne adducts (**6** and **7**) under various conditions, however, only a slight amount of **10** was formed (3%). Thus, Method A was found to be preparatively inadequate. (The same inapplicability was also encountered in the cases of chloro- and dichlorobenzyne-adducts.)

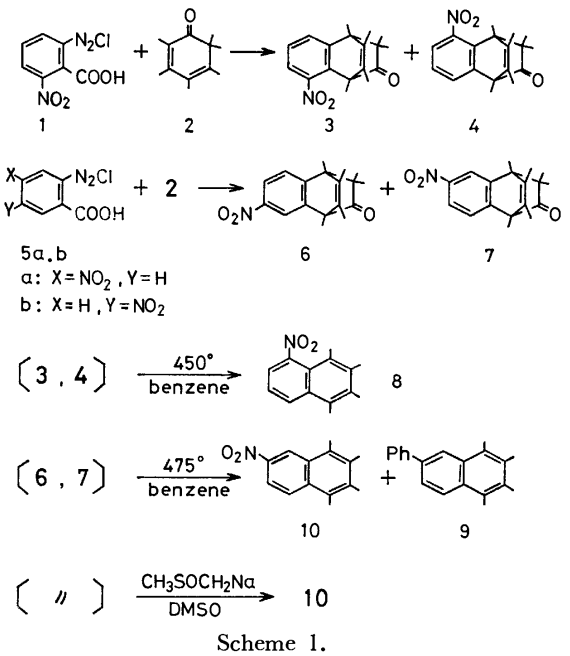

Scheme 1.

On the other hand, Method B proved effective. The pyrolysis of the adduct was carried out by means of a simple pyrolysis apparatus heated at 475±5 °C; it gave naphthalene, **10**, in a 60% yield. This naphthalene is thermally unstable, for the VPC analysis at 250 °C did not give any reliable chromatogram of **10**. Related to this characteristic, when the pyrolysis was carried out at 500 °C and above, 1,2,3,4-tetramethyl-6-phenylnaphthalene (**9**) was formed as the major by-product (>7%). It was apparently formed by the homolysis of **10** in the atmosphere of benzene.[5]

Similarly, nitronaphthalene **8** was obtained (16%) from a mixture of Compounds **3** and **4** by the pyrolysis at 450±5 °C. This nitronaphthalene **8** is also thermally unstable, and its VPC analysis was unsuccessful. Of particular interest is the fact that the mass spectrum of **8** taken while varying the chamber voltage between 80—12 eV showed its major fragment peak at *m/e* 212 (M^+-17). This is fragmentation behavior characteristic of **8**, differentiating it from **10**, and it can be interpreted in terms of the elimination of OH[6] from the peri-position (see **12**), where the 4-methyl and 5-nitro groups are subjected to a severe peri-interaction. This interaction is also illustrated by the ^{1}H-NMR spectra of **8**, in which the 4-methyl proton absorbs at a higher field (δ 2.31) than does the 1-methyl proton (2.61), indicating that the 5-nitro group is twisted perpendicularly to the ring plane.[7]

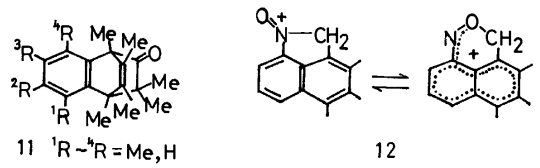

Experimental

Preparation of Nitrobenzyne-adducts ***3***, ***4***, ***6***, *and* ***7***. These compounds were prepared from the corresponding nitrobenzenediazonium-2-carboxylate hydrochlorides[8,9] by means of the reaction with hexamethyl-2,4-cyclohexadien-1-one (**2**)

according to the procedure previously reported.[4]

Pyrolysis Procedure. A vertically held Pyrex tube (15 mm ID × 300 mm length) packed with glass beads (5.5 mm OD) was heated at 450—500 °C under a gentle stream of nitrogen (15 ml/min). A benzene solution of the adduct mixture (6.0 g, 0.02 mol) in 120 ml of benzene was then dropped into this tube from the dropping funnel placed on the top of the tube. The pyrolyzed products were collected through a condenser that was connected to the bottom-end of the tube, and were chromatographed through a silica gel column (developing solvent: cyclohexane for **9**, cyclohexane/benzene=3 for **8**, and benzene for **10**) to give the nitronaphthalenes.

*1,2,3,4-Tetramethyl-6-nitronaphthalene (**10**).* The best yield of this naphthalene was attained by the pyrolysis performed at 475±5 °C; 60%. Mp 155—156 °C (recrystallized from cyclohexane, yellow needles); MS(*m/e*) 229 (M^+); ^{1}H-NMR(δ, CCl_4) 2.59 (6H, bs, α-Me), 2.42 (6H, bs, β-Me), 7.89—8.02 (2H, m, Ar-H at 7- and 8-positions), 8.74 (H, a pair of d, Ar-H at the 5-position); ^{13}C-NMR (δ, $CDCl_3$) Ar-Me at 15.3 (2Me), 17.4, and 17.7, Ar-C at 117.2, 120.8, 125.4, 129.1, 130.9, 133.7, 135.4, 137.8, and 143.9 (C–NO_2); UV(EtOH) max 222(ε 4.3×10^4), 280(2.9×10^4), and 326(8.7×10^3). Found: C, 73.26; H, 6.63; N, 6.21%. Calcd for $C_{14}H_{15}NO_2$: C, 73.34; H, 6.60; N, 6.11%.

When the pyrolysis was carried out at 500 ± 5 °C, 1,2,3,4-tetramethyl-6-phenylnaphthalene (**9**) was isolated from the chromatograph fraction that eluted faster than **10**. Yield, 8%; mp 135—136 °C(pet. ether); MS(*m/e*) 260 (M^+); ^{1}H-NMR(δ, CCl_4) 2.37 (6H, s, β-Me), 2.57 (3H, s, α-Me), 2.61 (3H, s, α-Me), 7.17—8.17 (8H, m, Ar-H); UV(EtOH) max 218 (ε 2.9×10^4), 260 (5.6×10^4), and 300 nm (8.8×10^3). Found: C, 91.99; H, 7.73%. Calcd for $C_{20}H_{20}$: C, 92.30; H, 7.69%.

*1,2,3,4-Tetramethyl-5-nitronaphthalene (**8**).* This naphthalene **8** was obtained in a 16% yield when the pyrolysis was performed at 450±5 °C. Mp 111—113 °C (recrystallized from cyclohexane, orange-yellow needles); MS(*m/e*) 229(M^+), 212(M^+-17, base peak); ^{1}H-NMR(δ, CCl_4) 2.31 (3H, s, 4-Me), 2.41 (6H, bs, 2- and 3-Me), 2.61 (3H, s, 1-Me), 7.17—7.68 (2H, m, Ar-H at 7- and 6-positions), 8.12 (H, a pair of d, J_1=8.2, J_2=1.6 Hz, Ar-H at 8-position); ^{13}C-NMR(δ, $CDCl_3$) Ar-Me at 15.8, 17.5, 17.7, and 18.1, Ar-C at 122.0, 122.4, 123.7, 127.0, 128.8, 129.3, 133.0, 135.2, 138.1, and 149.1 (C–NO_2); UV(cyclohexane) max 233(ε 4.2×10^4) and 260 nm (1.0×10^4). Found: C, 73.41; H, 6.57; N, 6.18%. Calcd for $C_{14}H_{15}NO_2$: C, 73.34; H, 6.60; N, 6.11%.

References

1) a) A. Davies and K. D. Warren, *J. Chem. Soc., B*, **1969**, 873; b) S. R. Robinson and C. H. J. Wells, *Tetrahedron*, **29**, 2203 (1973); c) S. R. Robinson, S. C. Weff, and C. H. J. Wells, *J. Chem. Soc., Perkin Trans. 1*, **1974**, 2239.

2) a) H. Suzuki and K. Nakamura, *Bull. Chem. Soc. Jpn.*, **44**, 303 (1971); b) A. Fischer and A. L. Wilkinson, *Can. J. Chem.*, **50**, 3988 (1972).

3) a) A. Oku, T. Kakihana, and H. Hart, *J. Am. Chem. Soc.*, **89**, 4554 (1967); b) A. Oku and Y. Yuzen, *J. Org. Chem.*, **40**, 3850 (1975); c) H. Hart and A. Oku, *ibid.*, **37**, 4269 (1972).

4) A. Oku and A. Matsui, *Bull. Chem. Soc. Jpn.*, **50**, 3343 (1977).

5) C. W. Hand, *J. Org. Chem.*, **42**, 841 (1977).

6) A similar fragmentation pattern has been reported in the case of *o*-nitrotoluene, see J. H. Beynon, R. A. Saunders, A. Topham, and A. E. Williams, *J. Chem. Soc.*, **1965**, 6403; S. Meyerson, I. Puskas, and E. K. Fields, *J. Am. Chem. Soc.*, **88**, 4974 (1966).

7) J. W. Emsley, J. C. Lindon, S. R. Salman, and D. T. Clark, *J. Chem. Soc., Perkin Trans. 2*, **1973**, 611.

8) Caution should be taken when handling dry nitrobenzenediazonium-2-carboxylates, because they detonate upon heating or hammering. Their hydrochlorides, **1** and **5** can, however, be handled more safely.

9) 3-Nitroanthranilic acid was inadequate as a precursor of nitrobenzyne, because it undergoes the *ipso* substitution of the nitro group during the diazotization.

BULLETIN OF THE CHEMICAL SOCIETY OF JAPAN, VOL. 51 (1), 333—334 (1978)

The Reaction of Dibenzylselenonium Ylides with Various Acids[1)]

Seizo TAMAGAKI, Katsuyuki TAMURA, and Seizi KOZUKA
Department of Applied Chemistry, Faculty of Engineering, Osaka City University, Sugimoto-cho, Sumiyoshi-ku, Osaka 558

(Received July 4, 1977)

Synopsis. Dibenzylselenonium cyano(methoxycarbonyl)methylide and dibenzylselenonium dicyanomethylide react readily with strong acids at room temperature, giving 1,3-diselena compounds and active methylene compounds.

The reactions of stable alkylsulfonium ylides with electrophilic reagents such as acids,[2)] molecular halogens,[3)] and acyl peroxides[4)] have been intensively studied and the reactions are assumed to proceed by a common mechanism in which sulfonium intermediates are first formed, as follows.

$$R_2S{=}CR'_2 \xrightarrow{XY} \left[R{-}S^{\oplus}(R)(CXCR'_2)\ Y^{\ominus} \right] \begin{cases} \rightarrow RY + RSCXR'_2 \\ \rightarrow R'_2CXY + R_2S \end{cases}$$

However, no report seems to have been presented so far for the decomposition of selenonium ylides by electrophilic reagents. We have examined the reaction of dibenzylselenonium ylides with various acids, and found that the reaction involves an α-carbon attack by the counter anions in the initial stage,[5)] similar to the reactions mentioned above, one of the products, however, eventually giving disproportionation products, *i.e.*, 1,3-diselena compounds and active methylene compounds.

Results and Discussion

Dibenzylselenonium cyano(methoxycarbonyl)methylide (Ia) was allowed to react with dried gaseous hydrogen chloride and the equivalent of trifluoroacetic acid in chloroform or with an equimolar amount of aqueous sulfuric and nitric acids in acetonitrile at room temperature. The reaction with hydrogen chloride was followed by thin-layer chromatography. After completion of the reaction, evaporation of the solvent and the subsequent preparative thin-layer chromatographic separation of the residue gave an oily material, the structure of which was identified by its MS, IR, and NMR spectra and elemental analysis as methyl α,α-bis(benzylseleno)-α-cyanoacetate (IIIa). From another part of the TLC plate, the corresponding methylene compound (IVa) was isolated in a good yield. The products and yields are summarized in Table 1.

$$(PhCH_2)_2Se{=}C(CN)(COOMe) \xrightarrow{HCl} PhCH_2Cl$$

$$+\ (PhCH_2Se)_2C(CN)(COOMe) + CH_2(CN)COOMe$$

(IIIa) (IVa)

The NMR and IR spectra of the reaction mixture show that the appearance of some peaks is due to a substance (IIa) not isolable in the pure state and also to benzyl chloride; the former displays the IR band at 2250 and 1759 cm^{-1} due to its cyano and ester carbonyl groups and NMR peaks at 7.3 (Ph), 4.2 (CH_2), 4.03 (CH), 3.75 (OCH_3) ppm with the intensity ratio of 5 : 2 : 1 : 3, respectively; the methylene protons of the latter lie at 4.53 ppm. A similar phenomenon was observed in the reaction with other acids such as tri-

Table 1. Reaction of dibenzylselenonium ylides (I)[a)] with various acids at room temperature

$R_2SeCCNY$, Y	Solvent	Time	HX, X	Mole ratio, HX/I	Products, mol% yield		
					RX	$(RSe)_2CCNY$[b)] or others	CH_2CNY
COOMe	$CHCl_3$	10 min	Cl	c)	(100)	21	40
COOMe	$CHCl_3$	3 h	CF_3COO	1	(100)	33	d)
COOMe	CH_3CN	2 h	HSO_4	1	d)	35	d)
COOMe	CH_3CN	24 h	NO_3	1	(94)	19	31
COOMe	CH_3CN	24 h	HSO_4	10[e)]	d)	$(RSe)_2$, 31	d)
COOMe	CH_3CN	30 min	Br	2	57	$(RSe)_2$, 13 Se, 39	
CN	$CHCl_3$	2 h	CF_3COO	3	(90)	29[f)]	(20)[g)]
CN	$CHCl_3$	22 h	$CHCl_2COO$	3	(80)	$(RSe)_2$, 20	d)
CN	CH_3CN	22 h	NO_3	1	17	RSeCN, 22	d)

a) $R_2Se{=}C(CN)Y$: $R{=}PhCH_2$. b) All the compounds shown were isolated by thin-layer chromatography. c) In a solution saturated with gaseous HCl. d) Yields were not determined. e) Concentrated acid was used. f) In addition, dibenzyl diselenide was obtained in 5% yield. g) Characterization was performed by NMR. Yields determined by NMR are given in parentheses.

fluoroacetic, sulfuric, and nitric acids.

These observations demonstrate that compound (IIa) initially produced is methyl α-(benzylseleno)-α-cyanoacetate which is very stable under acidic conditions but decomposes readily, on a TLC plate, *via* disproportionation to give isolable products. Thus, the following reaction pathway is the most probable.

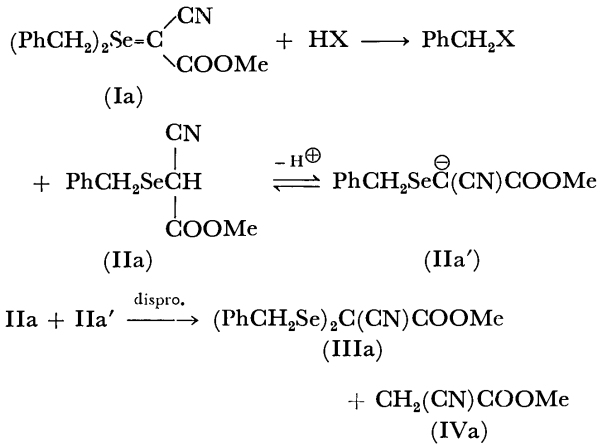

As was the case for Ia, dibenzylselenonium dicyanomethylide (Ib), when subjected to reaction with trifluoroacetic acid, gave benzyl trifluoroacetate almost quantitatively together with, the expected selenide, α-(benzylseleno)malononitrile (IIb) as evidenced by the NMR analysis. However, malononitrile and α,α-bis-(benzylseleno)malononitrile (IIIb) were the products isolated.

$PhCH_2SeCH(CN)_2$ (IIb) $(PhCH_2Se)_2C(CN)_2$ (IIIb)

The latter was unstable and spontaneously decomposed, at room temperature within 2 days, into dibenzyl diselenide in a moderate yield. The reaction of the ylide, Ib, with hydrochloric, sulfuric, and nitric acids is complicated.

Experimental

Typical experimental procedures are as follows:

Reaction of Ia with Trifluoroacetic Acid. A mixture of Ia (1 mmol) and trifluoroacetic acid (1 mmol) was stirred in 20 ml of chloroform at room temperature for 3 h. Evaporation of the solvent and subsequent thin layer chromatography of the residue afforded an oily IIIa. The yields are given in Table 1. The NMR data (IIIa in $CDCl_3$, δ) are as follows: 7.25(10H), 4.25(4H), 3.60(3H) ppm; IR (KBr): 2230 and 1740 cm^{-1}; MS: *m/e* 439 (M^+), 342, 269, 262, 171, and 91; Found: C, 49.48; H, 3.84; N, 2.98 %. Calcd for $C_{18}H_{17}O_2NSe_2$: C, 49.72; H, 4.02; N, 3.11%.

The Reaction of Ib with Trifluoroacetic Acid. Ib (1 mmol) was suspended in a chloroform solution of trifluoroacetic acid (3 mmol). After 2 h, the reaction mixture was concentrated *in vacuo*. Preparative TLC (Kieselgel G, chloroform) afforded an oily IIIb (29%). NMR 7.25 (10H), 4.43(4H) ppm; IR(KBr): 2240 cm^{-1}; MS: *m/e* 406(M^+), 342, 262, 171 and 91; Found: C, 50.79; H, 3.71; N, 7.12%. Calcd for $C_{17}H_{14}N_2Se_2$: C, 50.51; H, 3.50; N, 6.93%.

References

1) S. Tamagaki, K. Tamura, and S. Kozuka, *Chem. Lett.*, **1977**, 725.
2) S. Oae, A. Nakanishi, and N. Tsujimoto, *Tetrahedron*, **28**, 298 (1972).
3) H. Matsuyama, H. Minato, and M. Kobayashi, *Bull. Chem. Soc. Jpn.*, **48**, 3287 (1975).
4) T. Yagihara and S. Oae, *Int. J. Sulfur Chem.*, **A.1**, 159 (1971).
5) L. Hevesi, M. Sevrin, and A. Krief, *Tetrahedron Lett.*, **1976**, 2651.

BULLETIN OF THE CHEMICAL SOCIETY OF JAPAN, VOL. 51 (1), 335—336 (1978)

The Acetoxylation of *p*-Substituted Acetophenones and β-Diketones with (Diacetoxyiodo)benzene

Fujio MIZUKAMI, Moriyasu ANDO, Tatsuo TANAKA, and Juichi IMAMURA
National Chemical Laboratory for Industry, Honmachi, Shibuya-ku, Tokyo 151

(Received July 6, 1977)

Synopsis. The methyl groups of *p*-substituted acetophenones and the methylene groups of β-diketones were acetoxylated with (diacetoxyiodo)benzene. When the substrates were *p*-chloroacetophenone, *p*-nitroacetophenone and 4,4,4-trifluoro-1-phenyl-1,3-butanedione, the corresponding acetoxylated compounds were obtained in high yields.

The oxidations of glycols and alkenes with (diacetoxyiodo)benzene ($PhI(OAc)_2$) are well known to proceed by means of a mechanism[1-3] similar to those with lead tetraacetate, and the acetoxylation of the methylene group adjacent to the carbonyl group with lead tetraacetate has been reported.[4] However, there have been no reports on the acetoxylation of the methyl and methylene groups adjacent to the carbonyl group with $PhI(OAc)_2$. In the present work, we will report that *p*-substituted acetophenones (p-$XC_6H_4COCH_3$) and β-diketones are acetoxylated with $PhI(OAc)_2$.

Results and Discussions

The reactions of p-$XC_6H_4COCH_3$ (X=CH_3O, CH_3, H, Cl, NO_2, CN) and β-diketones with $PhI(OAc)_2$ were carried out at 30 °C in a mixed solvent of acetic acid and acetic anhydride, using sulfulic acid as the catalyst. When X in p-$XC_6H_4COCH_3$ was CH_3, H, Cl, or NO_2, the acetoxylated compounds were obtained; their structures were determined from the spectra (IR and NMR) and elemental analyses, as is shown in Tables 1 and 2. When X in p-$XC_6H_4COCH_3$ was OCH_3, the diaryliodonium salt ($[CH_3O(CH_3CO)$-C_6H_3-I^+-Ph]Br^-) was obtained in a 59.1% yield and the acetoxylated compound occurred in a trace amount. In the reaction of *p*-cyanoacetophenone with $PhI(OAc)_2$, neither the acetoxylated compound nor the diaryliodonium salt could be isolated, although both $PhI(OAc)_2$ and *p*-cyanoacetophenone were easily consumed at 30 °C and a tarry matter was obtained. The yields of the acetoxylated compounds increased in this order: X=Cl>NO_2≫H>CH_3⋙CH_3O. High yields were obtained in the case of the substrates in which the *p*-substituents are electron-attracting, execpt for X=CN.

4,4,4-Trifluoro-1-phenyl-1,3-butanedione (C_6H_5-$COCH_2COCF_3$) was easily acetoxylated with $PhI(OAc)_2$. Acetylacetone and dibenzoylmethane were also confirmed from the NMR spectra to be acetoxylated with $PhI(OAc)_2$, although their acetoxylated compounds gave only an approximate coincidence between found and calculated analytical results. As is shown in Table 1, the acetoxylated compound of $C_6H_5COCH_2COCF_3$ was obtained in a higher yield than those of *p*-substituted acetophenones.

It has been stated that the acetoxylation of the methylene group adjacent to the carbonyl group with lead tetraacetate seems to proceed by means of the following mechanism:[3]

TABLE 1. THE ACETOXYLATION OF *p*-SUBSTITUTED ACETOPHENONES AND β-DIKETONE WITH (DIACETOXYIODO)BENZENE

Substrate	Product: Structure	Yield[a] (%)	Mp (°C)	Found (%) C	Found (%) H	Calcd (%) C	Calcd (%) H
p-$CH_3C_6H_4COCH_3$	p-$CH_3C_6H_4COCH_2OAc$	21.9	84.5	68.56	6.09	68.74	5.42
$C_6H_5COCH_3$	$C_6H_5COCH_2OAc$	25.0	125/5[b]	67.10	5.44	67.41	5.66
p-$ClC_6H_4COCH_3$	p-$ClC_6H_4COCH_2OAc$	56.5	70.3	56.20	4.34	56.49	4.27
p-$NO_2C_6H_4COCH_3$	p-$NO_2C_6H_4COCH_2OAc$[c]	50.4	123.8	53.82	4.06	53.72	4.15
$C_6H_5COCH_2COCF_3$	$C_6H_5COCH(OAc)COCF_3$	62.8	92.0	52.09	3.80	52.56	3.30

a) Based on (diacetoxyiodo)benzene. b) Bp (°C)/mmHg. c) Nitrogen analysis: found, 6.28; calcd, 6.12.

TABLE 2. IR AND ^1H NMR DATA FOR THE ACETOXYLATED COMPOUNDS

Compound	IR[a] (ν_{CO}, cm^{-1})	NMR[b] δ, (ppm)
p-$CH_3C_6H_4COCH_2OAc$	1695, 1740	2.25(OAc), 2.45(-CH_3), 5.34(OCH_2O), 7.2—8.0(C_6H_4)
$C_6H_5COCH_2OAc$	1705, 1750	2.20(OAc), 5.34(OCH_2O), 7.3—8.1(C_6H_5)
p-$ClC_6H_4COCH_2OAc$	1690, 1740	2.21(OAc), 5.26(OCH_2O), 7.3—8.0(C_6H_4)
p-$NO_2C_6H_4COCH_2OAc$	1698, 1742	2.25(OAc), 5.37(OCH_2O), 8.0—8.6(C_6H_4)
$C_6H_5COCH(OAc)COCF_3$	1690[c], 1750	2.10(OAc), 6.20, 6.40(keto and enol COCH), 7.4—8.2(C_6H_5)

a) KBr disk. b) In $CDCl_3$. c) Broad band.

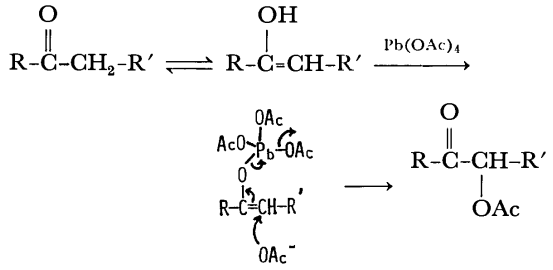

Briody[5] has also reported that, in the presence of sulfuric acid, (diacetoxyiodo)benzene in acetic acid seems to dissociate into ions according to the following equilibria: $PhI^+(OAc)+OAc^- \rightleftharpoons PhI(OAc)_2 \overset{H_2SO_4}{\rightleftharpoons} PhI^+(OAc)+HSO_4^-$.

Accordingly, if the oxidation with $PhI(OAc)_2$ in the present work proceeds by means of a mechanism similar to that with lead tetraacetate, the acetoxylation mechanism may be thought to be as follows:

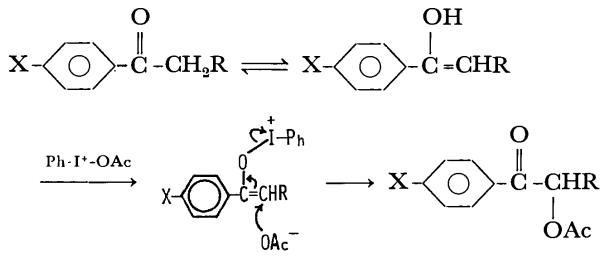

The fact that such substrates *p*-$ClC_6H_4COCH_3$, *p*-NO_2-$C_6H_4COCH_3$, and $C_6H_5COCH_2COCF_3$ produce the acetoxylated compounds in high yields seems to be explained by the above Scheme, because these substrates tend to be converted into enol forms.

Experimental

All the melting points and boiling points are uncorrected. The IR spectra were obtained on Shimadzu 27G and 400 spectrometers. The NMR spectra were obtained on a JEOL C-60-HL spectrometer, using tetramethylsilane as the internal standard. The amount of acetoxylated compound in the reaction mixture was determined by means of a JEOL JGC-1100 chromatograph with a 2 m × 3 mm column packed with Silicone DC550 (20%) coated on Chromosorb AW-DMCS.

Materials. Reagent-grade *p*-substituted acetophenones and *β*-diketones were used without further purification. The (diacetoxyiodo)benzene was synthesized according to the procedure submitted by Sharefkin and Saltzman[6] and was used after recrystallization from 5M acetic acid.

Preparation of Acetoxylated Compounds. The *p*-substituted acetophenone or *β*-diketone (0.06 mol) was dissolved in 55 cm^3 of a mixed solution (AcOH 50 cm^3, Ac_2O 5 cm^3) with stirring at 30 °C. To the vigorously stirred solution, we then added 5 cm^3 of sulfuric acid and then eight 2-g portions of $PhI(OAc)_2$ (total 0.05 mol) at 30-min intervals. The temperature was kept at about 30 °C throughout the additions. The reaction mixture was then stirred at 30 °C for another 6 h.

In the first stage, the reaction mixture was extracted with three 100-cm^3 portions of water and the extract was concentrated. Potassium bromide was then added to the concentrated solution. When diaryliodonium salt was present in the solution, white crystals were deposited.

In the second stage, the above reaction mixture was extracted with three 100-cm^3 portions of chloroform or ether and the extract was concentrated under reduced pressure. When the acetoxylated compound was crystalline, the concentrated solution was cooled to 0 °C. The crystals were filtered off and recrystallized from hexane. When the acetoxylated compound was liquid, the concentrated solution was distilled under reduced pressure.

References

1) R. Griegee and H. Beucker, *Ann.*, **541**, 218 (1938).
2) D. F. Banks, *Chem. Rev.*, **66**, 243 (1966).
3) Y. Ogata, "Yukikagobutsu No Sanka To Kangen," Nankodo, Tokyo and Kyoto (1963), pp. 330, 342.
4) O. Dimroth and R. Schweizer, *Ber.*, **56**, 1375 (1923).
5) J. M. Briody, *J. Chem. Soc., B*, **1968**, 93.
6) J. G. Sharefkin and H. Saltzman, *Org. Synth.*, Coll. Vol. V, 660 (1973).

BULLETIN OF THE CHEMICAL SOCIETY OF JAPAN, VOL. 51 (1), 337—338 (1978)

Formation of Dialkyl α-Siloxybenzylphosphonate *via* 1,2-Anionic Rearrangement of a Silyl Group

Akira SEKIGUCHI, Masayuki IKENO, and Wataru ANDO
Department of Chemistry, The University of Tsukuba, Niiharigun, Ibaraki 300-31
(Received July 8, 1977)

Synopsis. The reactions of silyl phenyl ketones with trialkyl phosphites and dialkyl sodiophosphonates gave dialkyl α-siloxybenzylphosphonates in good yields. The mechanism involves the migration of a silyl group from carbon to anionic oxygen. No deoxygenation of silyl ketone with trialkyl phosphite was observed.

Silylcarbenes have recently been found to be one of the most interesting species for the formation of silicon-carbon double bond. A report was given on the intermolecular and intramolecular reactions of silylcarbenes generated by either photolysis or thermolysis of silyl diazo compounds.[1] On the other hand, trialkyl phosphite is known to deoxygenate or desulfurate to give carbene intermediates.[2] We attempted to generate a silylcarbene by deoxygenation of a silyl phenyl ketone.

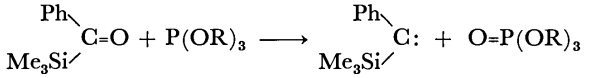

However, we found 1,2-anionic rearrangement of a silyl group in the reaction of silyl phenyl ketone with trialkyl phosphite instead of the formation of silylcarbene.

A mixture of trimethylsilyl phenyl ketone **1a**(5.72 mmol) and triethyl phosphite(60 mmol) was heated at 80 °C with stirring for 12 h. Distillation of the reaction mixture afforded **2a**(1.09 g, 60%, bp 142 °C/2 mmHg), which was found to be diethyl α-trimethylsiloxybenzylphosphonate from analysis of the spectra. The phosphonate **2a** was desilylated by refluxing methanol followed by crystallization from cyclohexane to give diethyl α-hydroxybenzylphosphonate **3** in 86% yield. Phosphonate **3** was also obtained from a variety of other silyl ketones, **1b**, **1c**, and **1d** in 72, 43, and 38% yields, respectively.

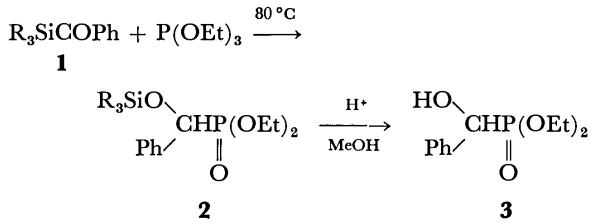

a: $R_3=Me_3$, **b**: $R_3=Et_3$,
c: $R_3=PhMe_2$, **d**: $R_3=Ph_3$.

The low yields of product **3** in the case of **1c** and **1d** may be ascribed to the steric hindrance on the silicon having phenyl groups. The formation of the products may be explained as resulting from the addition of triethyl phosphite to the carbonyl group to give betaine **4**, which may rearrange to triethoxymethylenephosphorane **5** by 1,2-anionic rearrangement of the silyl group.[3] However, no Wittig-type products expected from the reaction of the methylenephosphorane with the starting silyl ketone were observed. An attempt to trap the methylenephosphorane with benzaldehyde was unsuccessful. Thus, the reaction of **1a**(5.76 mmol) with triethyl phosphite(60 mmol) in the presence of benzaldehyde(8.07 mmol) also led to the formation of **2a** in 65% yield under the above conditions.

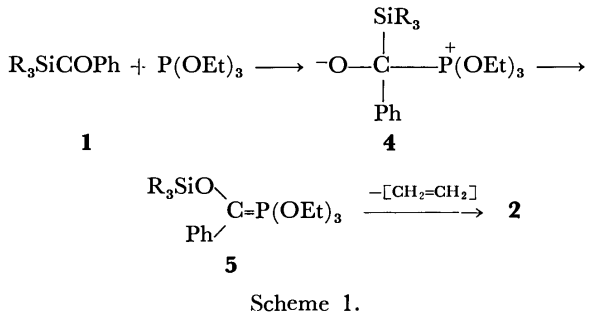

Scheme 1.

Methylenephosphorane **5** also decomposes to phosphonate **2** with cyclic elimination of ethylene under the reaction conditions (Scheme 1). Generation of ethylene was ascertained by trapping with a solution of bromine in 1,2-dibromoethane, but the yield was only 22% based on the silyl ketone **1a**.[4]

Dimethyl α-trimethylsiloxybenzylphosphonate **6** was produced in the reaction of **1a** with an excess trimethyl phosphite under the above conditions, probably with elimination of methylene. However, **1a** did not react with triphenyl phosphite under the same conditions, probably because of the incapability of olefin elimination.

Extended studies on the 1,2-anionic rearrangement of the silyl group were carried out by the reaction of the silyl ketone with dialkyl sodiophosphonate. Diethyl sodiophosphonate reacts with the silyl ketone under mild conditions. Catalytic amount of sodium hydride (1.07 mmol) was added to the mixture of the silyl ketone **1a**(5.91 mmol) and diethyl phosphite(36 mmol) with stirring. An exothermic reaction took place with evolution of hydrogen, phosphonate **2a** being produced in 59% yield. However, **2a** was not formed in the absence of sodium hydride even if a mixture of **1a** and diethyl phosphite was heated at 100 °C for 16 h (Scheme 2). Adduct **7** can be formed initially by the addition of diethyl sodiophosphonate to the silyl ketone **1a** followed by rearrangement to anion **8** which may abstract hydrogen from diethyl phosphite to produce **2a** and diethyl sodiophosphonate. Diethyl sodiophosphonate produced again reacts with the silyl ketone as shown in Scheme 2. The phosphonate **6** was also obtained in 56% yield in the reaction of **1a** with dimethyl phosphite in the presence of catalytic sodium hydride.

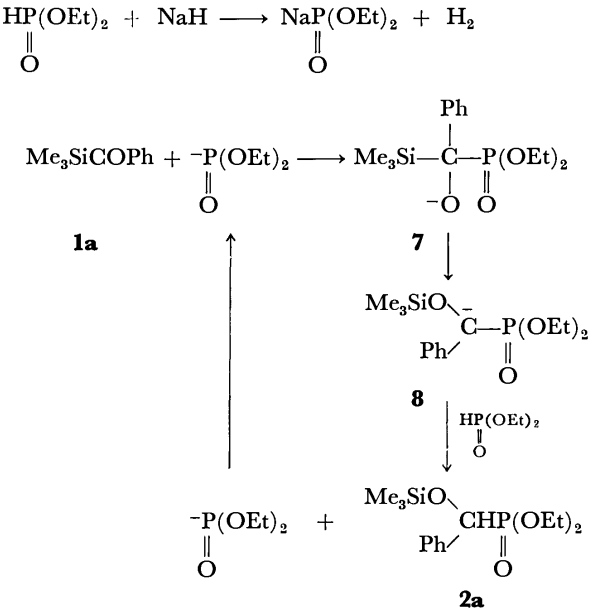

Scheme 2.

Experimental

General. NMR data were obtained on a Varian A-60D spectrometer, IR spectra on a Hitachi EP-1-G3 spectrometer and mass spectra on a Nippon Denshi JMF-07 at 20 eV. All silyl ketones were prepared by the hydrolysis of the corresponding dibromides with silver acetate in water-acetone-ethanol system using the method of Brook.[5] Melting points are uncorrected.

Reaction of ***1a*** *with Triethyl Phosphite.* A mixture of **1a** (5.72 mmol) and triethyl phosphite(60 mmol) was heated at 80 °C for 12 h. After removal of excess triethyl phosphite *in vacuo*, **2a**[6] was obtained by vacuum distillation in 60% yield, bp 142 °C/2mmHg; IR(NaCl) 1250, 1070—1020 cm^{-1}; NMR(CCl_4) δ 0.08(s, 9H, SiMe), 1.20(t, J=7Hz, 6H, $OCCH_3$), 3.6—4.2(m, 4H, OCH_2), 4.80(d, J=14Hz, 1H, POCH), and 7.0—7.6(m, 5H, ArH). Phosphonate **2a** was desilylated in refluxing methanol. Crystallization from cyclohexane after removal of the methanol yielded **3** in 86% yield, mp 83 °C; IR(KBr) 3250, 1230, 1205, 1050, and 1030 cm^{-1}; Mass *m/e*: M^+ 244(rel. int. 39), 138(100), 111(56), and 106(28); NMR($CDCl_3$) δ 1.1—1.4(m, 6H, $OCCH_3$), 3.7—4.3(m, 4H, OCH_2), 4.51(br. s, 1H, OH), 5.01(d, J= 12 Hz, 1H, POCH), and 7.2—7.7(m, 5H, ArH); Found: C, 53.93; H, 7.27%. Calcd for $C_{11}H_{17}O_4P$: C, 54.10; H, 7.02%.

Reaction of Other Silyl Ketones, ***1b****,* ***1c****, and* ***1d*** *with Triethyl Phosphite.* The reactions of **1b**(5.70 mmol), **1c**(6.12 mmol), and **1d**(5.22 mmol) with triethyl phosphite(60 mmol) were performed under the same conditions as described above. Desilylation in refluxing methanol containing one drop of hydrochloric acid yielded **3** in 72, 43, and 38% yields, respectively.

Reaction of ***1a*** *with Trimethyl Phosphite.* A mixture of **1a**(7.08 mmol) and trimethyl phosphite(80 mmol) was heated at 80 °C for 12 h. Phosphonate **6** was obtained in 50% yield, bp 128 °C/2 mmHg; IR(NaCl) 1260, 1060—1020 cm^{-1}; NMR(CCl_4) δ 0.08(s, 9H, SiMe), 3.45(d, J= 10Hz, 6H, POMe), 4.75(d, J=14 Hz, 1H, POCH), and 7.2(m, 5H, ArH). Desilylation of **6** in refluxing methanol gave dimethyl α-hydroxybenzylphosphonate, mp 98—99 °C; IR(KBr) 3620, 1205, 1060, and 1020 cm^{-1}; Mass *m/e*: M^+ 216(12), 111(13), 110(100), 107(19), 106(36), 105(35), and 104(25); NMR($CDCl_3$) δ 3.67(d, J=11 Hz, 3H, POMe), 3.75(d, J=11 Hz, 3H, POMe), 5.07(d, J=11 Hz, 1H, POCH), 5.17(br. s, 1H, OH), and 7.2—7.7(m, 5H, ArH); Found: C, 50.49; H, 6.14%. Calcd for $C_9H_{13}O_4P$: C, 50.01; H, 6.06%.

Reaction of ***1a*** *with Diethyl Phosphite in the Presence of Sodium Hydride.* Sodium hydride(1.07 mmol) was added to a mixture of **1a**(5.91 mmol) and diethyl phosphite(36 mmol) with stirring. Exothermic reaction occurred with evolution of hydrogen. After the reaction ceased, the reaction mixture was distilled under reduced pressure to give **2a** in 59% yield.

Reaction of ***1a*** *with Dimethyl Phosphite in the Presence of Sodium Hydride.* Sodium hydride(1.60 mmol) was added to a mixture of **1a**(9.07 mmol) and dimethyl phosphite(45 mmol) with stirring. Phosphonate **6** was obtained in 56% yield.

References

1) W. Ando, A. Sekiguchi, and T. Migita, *Chem. Lett.*, **1976**, 779, and references cited therein.

2) E. J. Corey and R. A. E. Winter, *J. Am. Chem. Soc.*, **85**, 2677 (1963); F. Ramirez, H. Yamanaka, and O. H. Basedow, *ibid.*, **83**, 173 (1961); F. Ramirez, S. B. Bhatia, and C. P. Smith, *J. Org. Chem.*, **31**, 4105 (1966).

3) A. G. Brook, *Acc. Chem. Res.*, **7**, 77 (1974).

4) 1,2-Dibromoethane was estimated with a NMR spectrometer.

5) A. G. Brook, *J. Am. Chem. Soc.*, **79**, 4373 (1957); A. G. Brook, M. A. Quigley, G. J. D. Peddle, N. V. Schwartz, and C. M. Warner, *ibid.*, **82**, 5102 (1960).

6) A. Hashizume, M. Sekine, and T. Hata, 36th National Meeting of Chemical Society of Japan, Osaka, April 1977.

BULLETIN OF THE CHEMICAL SOCIETY OF JAPAN, VOL. 51 (1), 339—340 (1978)

Electrochemical Reaction of Organoboranes in the Presence of Propenoic Acid Esters. A Convenient Carboxylic Ester Synthesis from Organoboranes

Yuzuru TAKAHASHI, Kazuma YUASA, Masao TOKUDA, the late Mitsuomi ITOH, and Akira SUZUKI*

Faculty of Engineering, Hokkaido University, Sapporo 060

(Received July 28, 1977)

Synopsis. Electrolysis of trialkylboranes using two platinum electrodes in the presence of α,β-unsaturated esters in an acetonitrile solution containing tetraalkylammonium halide as a supporting electrolyte, produces the corresponding alkylated carboxylic acid esters in good yields.

Previously, we have reported that organoborane undergo spontaneous 1,4-addition reactions in the presence of oxygen to numerous α,β-unsaturated carbonyl compounds including methyl vinyl ketone[1] and acetylacetylene,[2] and to α,β-unsaturated oxiranes such as 1,3-butadiene monoxide[3] and 3,4-epoxy-1-butyne,[4] followed by hydrolysis to give corresponding alkylated compounds (Eqs. 1—4). However, it has been shown

$$R_3B + CH_2{=}COCH_3 \xrightarrow{O_2} RCH_2CH{=}C(CH_3)(OBR_2) \xrightarrow{H_2O} RCH_2CH_2{-}COCH_3 \quad (1)$$

$$R_3B + CH{\equiv}C{-}COCH_3 \longrightarrow RCH{=}C{=}C(CH_3)(OBR_2) \longrightarrow RCH{=}CH{-}COCH_3 \quad (2)$$

$$R_3B + CH_2{=}CH{-}\underset{\backslash O /}{CH}{-}CH_2 \longrightarrow RCH_2CH{=}CHCH_2OBR_2 \longrightarrow RCH_2CH{=}CHCH_2OH \quad (3)$$

$$R_3B + CH{\equiv}C{-}\underset{\backslash O /}{CH}{-}CH_2 \longrightarrow RCH{=}C{=}CHCH_2OBR_2 \longrightarrow RCH{=}C{=}CHCH_2OH \quad (4)$$

that neither acrylonitrile nor ethyl acrylate (**1**) reacts with organoboranes under the same conditions. Although we have recently reported that the reaction of acrylonitrile or **1** with copper(I) trialkylmethylborates gives corresponding alkylation products,[5] this procedure has a disadvantage in that there is a difficulty in introducing secondary alkyl groups. On the other hand, the electrochemical reactions of trialkylboranes with compounds containing acidic hydrogens such as acetonitrile,[6] nitromethane,[7] and 1-alkynes[8] have also been reported by us to give the corresponding alkylated products such as cyanoalkanes, nitroalkanes and internal acetylenes, respectively.

In the present paper we wish to report that the electrochemical reaction of trialkylboranes with α,β-unsaturated esters such as **1** or ethyl methacrylate (**2**) in an acetonitrile solution containing tetraalkylammonium halide as a supporting electrolyte produces corresponding saturated carboxylic acid ester in good yields (Eq. 5).

The electrochemical reaction was carried out by means of controlled current electrolysis in an undivided

$$R_3B + CH_2{=}C(R')CO_2Et \xrightarrow[Pt\text{-}Pt,\ CH_3CN]{\text{Electrolysis: } R_4''NX} RCH_2CH(R')CO_2Et \quad (5)$$

1, R′=H; **2**, R′=CH_3 — **3**, R′=H; **4**, R′=CH_3

cell. The results of representative reactions are summarized in Table 1. As shown in the table, in this procedure there appears to be no difficulty in introducing secondary alkyl groups of organoboranes as well as primary alkyl groups. The effect of supporting electrolytes on the yield of **3c** in the reaction of tripropylborane with **1** was as follows: $(C_2H_5)_4NI$, 63; $(C_2H_5)_4NBr$, 17; $(n\text{-}C_4H_9)_4NI$, 77; $(n\text{-}C_4H_9)_4NBr$, 31; $(n\text{-}C_4H_9)_4NClO_4$, 0%. These results indicate that tetraalkylammonium bromide and iodide are effective as the supporting electrolyte in the reaction, whereas electrolysis using tetrabutylammonium perchlorate gives no detectable amount of the corresponding addition product.

Although the detailed reaction mechanism is not clear at present, several points must be noted. (a) The halide ion of a supporting electrolyte seems to play an important role in the reaction. (b) When a mixture of tripentylborane and **1** was electrolyzed in an undivided cell, small amounts of ethyl 2-pentyloctanoate (**6**; R=C_5H_{11}) and ethyl 2-methylheptanoate (**8**; R=C_5H_{11}) were obtained as by-products together with the normal product, ethyl octanoate. (c) When the electrolysis was carried out in a divided cell, the desirable reaction did not occur. By the use of a divided cell, electrolysis of a mixture of trialkylborane and **1** in an acetonitrile solution containing tetraalkylammonium iodide afforded the corresponding alkyl iodide at the anode and the dimer of **1** at the cathode as the main products. (d) Electrolysis of butyl iodide, instead of tributylborane, in the presence of ethyl acrylate under the same conditions described above gave ethyl heptanoate in a 22% yield. (e) The reduction potentials of

TABLE 1. ELECTROCHEMICAL REACTION OF TRIALKYLBORANES WITH **1** OR **2**

Organoborane, R_3B, R	Product	Yield of **3** (%)[a]	Product	Yield of **4** (%)[a]
$n\text{-}C_5H_{11}$	**3a**	86	**4a**	94
$n\text{-}C_4H_9$	**3b**	57	**4b**	64 (60)[b]
$n\text{-}C_3H_7$	**3c**	77	**4c**	85 (73)[b]
$s\text{-}C_4H_9$	**3d**	65 (59)[b]	—	—
$c\text{-}C_5H_9$	**3e**	51	**4e**	51

a) VPC yields based on organoborane used.
b) Isolated yields.

* To whom all correspondence should be addressed.

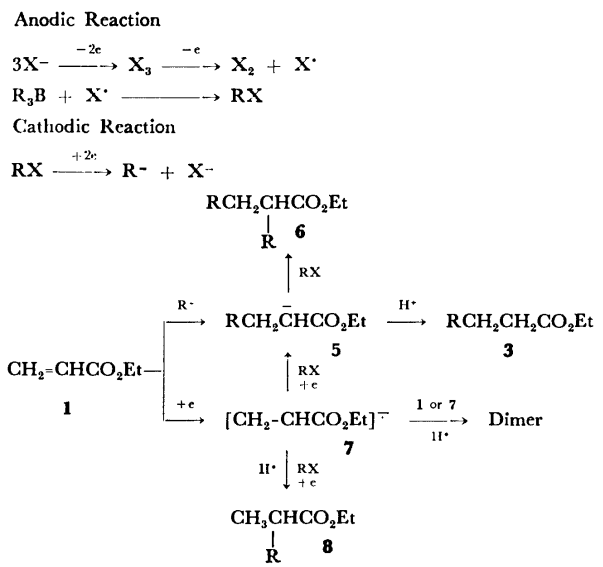

Scheme 1.

1 and **2** were observed at −2.28 and −2.41V *vs.* SCE, respectively, whereas those of alkyl iodide and alkyl bromide were reported to be around −1.63—−2.37V *vs.* SCE.[9,10] From these results the following mechanism involving two independent reaction pathways at the anode and the cathode may be proposed for the reaction of **1** (Scheme 1).

Experimental

Materials. Trialkylboranes were obtained by hydroboration of olefins.[11] Ethyl acrylate (**1**) and ethyl methacrylate (**2**) were distilled before use. Acetonitrile was dried over diphosphorus pentaoxide and distilled.

The IR and NMR spectra were taken on a Hitachi-Perkin-Elmer Model 125 spectrophotometer and a Hitachi R-22 spectrometer at 90 MHz using tetramethylsilane as the internal standard, respectively.

Quantitative analyses were carried out with Hitachi-063 gas chromatograph using a column of 15% Carbowax 20M on Uniport-B. Preparative VPC was done with JEOL JGC-20K gas chromatograph using the same type of column. The electrolyses were carried out with Yanagimoto VE-8.

General Procedure. The following procedure for the preparation of ethyl 2-methylhexanoate (**4c**) is representative. The electrolysis was carried out in the usual undivided cell equipped with two platinum plate electrodes (20×20 mm²), a magnetic stirring bar and a reflux condenser. Tripropylborane (4.9 mmol) and 4.0 ml of **2** are dissolved in 17 ml of acetonitrile containing Bu_4NI (0.5 g, 1.35 mmol). The solution was electrolyzed at a constant current (0.5 A/cm²) for 5 h under nitrogen atmosphere. After the electrolysis, the reaction mixture was oxidized by adding 3N aqueous sodium hydroxide (5.0 ml) and 30% hydrogen peroxide (5.0 ml) for 2 h at room temperature. The products were extracted with ether and dried over sodium sulfate. Distillation of organic layer gave 0.56 g (73%) of ethyl 2-methylhexanoate (**4c**), bp 50—52 °C/16 mmHg.

Identification of the Products. *Ethyl Octanoate (**3a**)*: n_D^{22} 1.4213. Found: C, 69.98; H, 11.88%. Calcd for $C_{10}H_{20}O_2$: C, 69.72; H, 11.70%. MS: *m/e*=172 (M^+). IR (neat): 1730 cm⁻¹. NMR (CCl_4): δ, 0.90 (3H, t, *J*=5.4 Hz), 1.15—1.80 (13H, m), 2.20 (2H, t, *J*=7.0 Hz), 4.08 ppm (2H, q, *J*=7.4 Hz). *Ethyl Heptanoate (**3b**)*: n_D^{22} 1.4137. Found: C, 68.03; H, 11.32%. Calcd for $C_9H_{18}O_2$: C, 68.31; H, 11.47%. MS: *m/e*=158 (M^+). IR (neat): 1735 cm⁻¹. NMR (CCl_4): δ, 0.91 (3H, t, *J*=5.2 Hz), 1.10—1.80 (9H, m), 2.22 (2H, t, *J*=7.4 Hz), 4.09 ppm (2H, q, *J*=7.2 Hz). *Ethyl Hexanoate (**3c**)*: n_D^{22} 1.4055. Found: C, 66.80; H, 11.38%. Calcd for $C_8H_{16}O_2$: C, 66.63; H, 11.18%. MS; *m/e*=144 (M^+). IR (neat): 1735 cm⁻¹. NMR (CCl_4): δ, 0.90 (3H, t, *J*=6.0 Hz), 1.23 (3H, t, *J*=6.4 Hz), 1.20—1.70 (6H, m), 2.21 (2H, t, *J*=7.4 Hz), 4.11 ppm (2H, q, *J*=7.2 Hz). *Ethyl 4-Methylhexanoate (**3d**)*: n_D^{22} 1.4152. Found: C, 68.11; H, 11.29%. Calcd for $C_9H_{18}O_2$: C, 68.31; H, 11.47%. MS; *m/e*=158 (M^+). IR (neat): 1735 cm⁻¹. NMR (CCl_4): δ, 0.92 (6H, m), 1.25 (3H, t, *J*=7.4 Hz), 1.20—1.80 (5H, m), 2.23 (2H, t, *J*=7.8 Hz), 4.05 ppm (2H, q, *J*=7.2 Hz). *Ethyl 3-Cyclopentylpropanoate (**3e**)*: n_D^{23} 1.4072. Found: C, 70.30; H, 10.68%. Calcd for $C_{10}H_{18}O_2$: C, 70.54; H, 10.66%. MS: *m/e*=170 (M^+). IR (neat): 1735 cm⁻¹. NMR (CCl_4): δ, 1.00—1.40 (2H, m), 1.24 (3H, t, *J*=7.4 Hz), 1.40—2.10 (9H, m), 2.24 (2H, t, *J*=7.0 Hz), 4.08 ppm (2H, q, *J*=7.2 Hz). *Ethyl 2-Methyloctanoate (**4a**)*: n_D^{22} 1.4168. Found: C, 70.50; H, 11.60%. Calcd for $C_{11}H_{22}O_2$: C, 70.92; H, 11.90%. MS: *m/e*=186 (M^+). IR (neat): 1735 cm⁻¹. NMR (CCl_4): δ, 0.89 (3H, t, *J*=5.6 Hz), 1.09 (3H, d, *J*=7.4 Hz), 1.10—1.80 (13 H, m), 2.31 (H, m), 4.08 ppm (2H, q, *J*=7.0 Hz). *Ethyl 2-Methylheptanoate (**4b**)*: n_D^{22} 1.4113. Found: C, 69.80; H, 11.77%. Calcd for $C_{10}H_{20}O_2$: C, 69.72; H, 11.70%. MS; *m/e*=172 (M^+). IR (neat): 1735 cm⁻¹. NMR (CCl_4): δ, 0.90 (3H, t, *J*=5.0 Hz), 1.11 (3H, d, *J*=7.0 Hz), 1.25 (3H, t, *J*=7.0 Hz), 1.10—1.80 (8H, m), 2.30 (H, m), 4.09 ppm (2H, q, *J*=6.6 Hz). *Ethyl 2-Methylhexanoate (**4c**)*: n_D^{22} 1.4072. Found: C, 68.55; H, 11.53%. Calcd for $C_9H_{18}O_2$: C, 68.31; H, 11.47%. MS: *m/e*=158 (M^+). IR (neat): 1735 cm⁻¹. NMR (CCl_4): δ, 0.91 (3H, t, *J*=6.0 Hz), 1.11 (3H, d, *J*=6.8 Hz), 1.25 (3H, t, *J*=7.8 Hz), 1.10—1.80 (6H, m), 2.31 (H, m), 4.08 ppm (2H, q, *J*=7.0 Hz). *Ethyl 3-Cyclopentyl-2-methylpropanoate (**4e**)*: n_D^{23} 1.4380. Found: C, 71.97; H, 11.03%. Calcd for $C_{11}H_{20}O_2$: C, 71.69; H, 10.94%. MS: *m/e*=184 (M^+). IR (neat): 1735 cm⁻¹. NMR (CCl_4): δ, 0.80—2.00 (11H, m), 1.11 (3H, d, *J*=7.2 Hz), 1.24 (3H, t, *J*=7.0 Hz), 2.38 (H, m), 4.08 ppm (2H, q, *J*=7.4 Hz).

References

1) A. Suzuki, A. Arase, H. Matsumoto, M. Itoh, H. C. Brown, M. M. Rogić, and M. W. Rathke, *J. Am. Chem. Soc.*, **89**, 5708 (1967).

2) A. Suzuki, S. Nozawa, M. Itoh, H. C. Brown, G. W. Kabalka, and G. W. Holland, *J. Am. Chem. Soc.*, **92**, 3503 (1970).

3) A. Suzuki, N. Miyaura, M. Itoh, H. C. Brown, G. W. Holland, and E. Negishi, *J. Am. Chem. Soc.*, **93**, 2792 (1971).

4) A. Suzuki, N. Miyaura, M. Itoh, H. C. Brown, and P. Jacob, *Synthesis*, **1973**, 305.

5) N. Miyaura, M. Itoh, and A. Suzuki, *Tetrahedron Lett.*, **1976**, 255.

6) Y. Takahashi, M. Tokuda, M. Itoh, and A. Suzuki, *Chem. Lett.*, **1975**, 523.

7) Y. Takahashi, M. Tokuda, M. Itoh, and A. Suzuki, *Synthesis.*, **1976**, 616.

8) Y. Takahashi, M. Tokuda, M. Itoh, and A. Suzuki, *Chem. Lett.*, **1977**, 999.

9) Von M. V. Stakelberg and W. Stark, *J. Electrochem. Soc.*, **53**, 118 (1949).

10) F. Lambert and K. Kobayashi, *J. Am. Chem. Soc.*, **86**, 3154 (1964).

11) H. C. Brown, "Organic Synthesis *via* Boranes," John-Wiley, New York (1975).

BULLETIN OF THE CHEMICAL SOCIETY OF JAPAN, VOL. 51 (1), 341 (1978)

An Additional Discussion of the Micropore-volume Determination of Active Carbon Using Dubinin-Radushkevich Plots

Ryoichi TSUNODA

Industrial Research Institute of Kanagawa Prefecture, Showa-machi, Kanazawa-ku, Yokohama 236

(Received July 20, 1977)

Synopsis. The validity of the recently presented method for determining the micropore volume (V_o) from the distribution curve of the adsorption potential based on the Dubinin-Radushkevich plot is further discussed in terms of the relationship between the V_o and the adsorption volume (V_h) at the beginning of the hysteresis loop on the adsorption isotherm.

In a recent paper,[1] the present author reported that the adsorption volume (V) corresponding to the adsorption potential ($A=RT\ln P_o/P$), at which the plot of $dV/d(-A)$ *vs.* A has its minimum value, is the micropore volume (V_o) when the extrapolation of the Dubinin-Radushkevich plot cannot be applied because of its non-linearity. However, the relationship between the micropore volume (V_o), determined by the new method described above, and the adsorption volume (V_h) at the beginning of the hysteresis loop on the adsorption isotherm was not clarified quantitatively. In this report, this relationship is clarified on the basis of the experimental data on 6 types of active carbons.

The adsorption of methanol on active carbons at 30 °C was measured gravimetrically by means of a conventional quartz spring balance. The active carbons examined were Pittsburgh CAL-, Filtrasorb 100-, SGL-, PCB (5.3% burn-off)-,[1] and PCB (33.3% burn-off)[1]-type activated carbons; for the latter 4 carbons, the experimental data shown in the previous paper[1] were used. The conditions of the experiment were the same as those reported previously.[1]

The effective radius at the beginning of hysteresis is considered to be 15 Å,* and the hysteresis is attributed to the filling of transitional pores by the mechanism of capillary condensation.[2] The point of the beginning of hysteresis is also the boundary point dividing micropores from transitional pores according to the customary classification of pores.[2] Furthermore, this point is the end of the filling of micropores and, at the same time, that of the beginning of the capillary condensation of transitional pores, but monolayers and multilayers exist on the walls of the transitional pores. Moreover, the adsorption volume (V_h) at the hysteresis must be the sum of the micropore volume (V_o) and the volume (V_l) of adsorption layers on the transitional-pore walls.

The surface area (S_{trans}) of the transitional pores can be calculated by means of the equation

$$S_{trans} = \sum 2\Delta V/\bar{r}, \quad (1)$$

from the curve of the pore-volume distrubution,[1] here, $\Delta V=V_i-V_{i-1}$, and $\bar{r}=(r_i+r_{i-1})/2$, and with r_j lying from 15 to 100 Å. (The shapes of the pores are assumed to be cylindrical, and the surface area of the large pores (radii>100 Å) may be neglected compared with that of the small pores (15 Å≦radii≦100 Å).) Moreover, the volume (V_l) of the adsorption layers on the walls of the transitional pores at the beginning of hysteresis is obtained by the multiplication of S_{trans} by the thickness of the adsorption layers, 4.9 Å, corresponding to the radius of 15 Å in the Kelvin equation;[1]

$$V_l = 4.9\times S_{trans}. \quad (2)$$

The values of V_o, V_l, and V_h are shown in Table 1. The sum of the V_o and V_l coincide with V_h. These results show that the adsorption volume at $dV/d(-A)$=minimum on the distribution curve of the adsorption potential corresponds to the micropore volume; the validity of the method for determinimg the micropore volume of active carbon from the adsorption-potential distribution is thus further confirmed.

References

1) R. Tsunoda, *Bull. Chem. Soc. Jpn.*, **50**, 2058 (1977).
2) M. M. Dubinin, "Chemistry and Physics of Carbon," ed by P. L. Walker, Jr., Vol. 2, Mercell Dekker, N. Y. (1966), p. 51.

TABLE 1. RELATIONSHIPS BETWEEN MICROPORE VOLUMES AND ADSORPTION VOLUMES AT THE BEGINNING OF HYSTERESIS

Active carbon	V_o[a] (cm³/g)	$V_{l,ads}$[b] (cm³/g)	$V_{l,des}$[b] (cm³/g)	$V_o+V_{l,ads}$ (cm³/g)	$V_o+V_{l,des}$ (cm³/g)	V_h[c] (cm³/g)
SGL	0.315[d]	0.047	0.055	0.362	0.370	0.360[d]
PCB	0.390[d]	0.012	0.015	0.402	0.405	0.415[d]
PCB (5.3% burn-off)	0.405[d]	0.031	0.039	0.436	0.444	0.430[d]
PCB (33.3% burn-off)	0.480[d]	0.104	0.124	0.584	0.604	0.535[d]
Filtrasorb 100	0.305	0.033	0.039	0.338	0.344	0.340
CAL	0.355	0.048	0.052	0.403	0.407	0.382

a) V_o is the micropore volume corresponding to the adsorption volume at $dV/d(-A)$=minimum on the adsorption-potential distribution. b) V_l is the volume of adsorption layers on the transitional-pore walls at the relative pressure corresponding to the radius of 15 Å in the Kelvin equation.[1] The subscripts, ads and des, indicate the calculation branch on the adsorption isotherm. c) V_h is the adsorption volume at the beginning of hysteresis on the adsorption isotherm. d) Ref. 1.

* Throughout this paper 1 Å=0.1 nm.

BULLETIN OF THE CHEMICAL SOCIETY OF JAPAN, VOL. 51 (1), 342 (1978)

The Chromium(VI) Oxide Oxidation of Epimeric 1,2,3,4-Tetrahydro-1-naphthols

Kaoru HANAYA, Sachio AWANO, and Hideaki KUDO

Department of Chemistry, Faculty of Science, Yamagata University, Koshirakawa-cho, Yamagata 990

(Received July 7, 1977)

Synopsis. The rates of the chromium(VI) oxide oxidation of 2- and 3-substituted 1-tetralols(1,2,3,4-tetrahydro-1-naphthols) have been determined. In the 3-substituted compounds, the rates of *cis*-isomers(eq'-OH) are markedly larger than those of *trans*-isomers(ax'-OH). On the other hand, in the case of 2-substituted compounds, the rates of the *cis*-isomers(ax'-OH) and *trans*-isomers (eq'-OH) are almost equal.

It is well known[1] that the epimeric axial cyclohexanols are oxidized more rapidly by chromium(VI) oxide than the equatorial ones. However, turning to the allylic alcohols, it has been demonstrated that the quasi-equatorial alcohols are oxidized more rapidly than the quasi-axial ones.[2] Although isolated studies of the oxidation rates of allyl alcohols are on record, few systematic studies have been made.

Recently, Yamaguchi *et al.*[3] have studied the chromium(VI) oxide oxidation of 4-chromanols and discussed the effect of conformational and strain factors. 1-Tetralols are considered to have conformations similar to those of the corresponding 4-chromanols.

In order to learn more about the stereochemistry of the chromium(VI) oxide oxidation of the cyclic benzyl alcohols, we have examined the chromium(VI) oxide oxidation of 2- and 3-substituted 1-tetralols. The results are summarized in Table 1.

TABLE 1. OXIDATION RATE OF EPIMERIC 1-TETRALOLS

Compound	Preferred conformation of OH	k(l/mol·s)	k_{cis}/k_{trans}
Ia	eq'	0.296	1.60
Ib	ax'	0.185	
IIa	eq'	0.428	1.80
IIb	ax'	0.238	
IIIa	eq'	0.208	1.03
IIIb	ax'	0.215	
IVa	eq'	0.292	0.91
IVb	ax'	0.267	

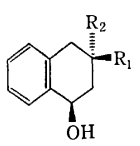

Ia $R_1=C_6H_5$, $R_2=H$
Ib $R_1=H$, $R_2=C_6H_5$
IIa $R_1=CH_3$, $R_2=H$
IIb $R_1=H$, $R_2=CH_3$

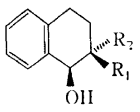

IIIa $R_2=C_6H_5$, $R_1=H$
IIIb $R_2=H$, $R_1=C_6H_5$
IVa $R_2=CH_3$, $R_1=H$
IVb $R_2=H$, $R_1=CH_3$

These results show the rates of *cis*-3-substituted 1-tetralols (eq'-OH) to be markedly larger than those of *trans*-isomers(ax'-OH). In the case of 2-substituted 1-tetralols, on the other hand, the rates of the *cis*-isomers (ax'-OH) and *trans*-isomers(eq'-OH) are almost equal.

In the 3-substituted compounds, it is considered that the greater reactivity of the *cis*-isomer over the *trans*-isomer should be attributed to the relief of strain from the *peri*-interaction—the $A^{1,2}$ strain between the hydroxyl group and the aromatic methin group at Position 8 —when the above 1-tetralols are converted to the ketones. The *peri*-interaction in the *cis*-isomer involving a quasi-equatorial hydroxyl group may be larger than that is the *trans*-isomer; therefore, the former epimer will undergo oxidation more rapidly than the latter.

In the oxidation of *cis*-2-substituted 1-tetralols, the steric effect due to the *gauche* interaction between the hydroxyl group and the adjacent substituent should also be considered. In this case, the steric effect of the *peri*-interaction in the *trans*-isomer and the *gauche* interaction in the *cis*-isomer appear to be almost equal.

Experimental

Materials. 1-Tetralols were prepared by the reduction of the corresponding α-tetralones according to the literature.[4] The conformations of 1-tetralols were examined by means of their NMR[5] and IR[6] spectra.

Kinetic Determinations. The chromium(VI) oxide oxidations were carried out at 25±0.1 °C and were followed spectrophotometrically by measuring the decrease in the optical density of the Cr^{VI} maximum at 380 nm, as has been described in the literature.[3] The medium was 85% acetic acid; the concentrations of alcohol and CrO_3 were 1.75×10^{-3} M and 2.00×10^{-3} M respectively. A Hitachi ESP-3T spectrophotometer and standard 1.00-cm quartz cells were used.

References

1) E. L. Eliel, S. H. Shroeter, T. J. Brett, F. J. Biros, and J. Richer, *J. Am. Chem. Soc.*, **88**, 3327 (1966).

2) S. H. Burstein and H. J. Ringold, *J. Am. Chem. Soc.*, **89**, 4722 (1967).

3) S. Yamaguchi, K. Kabuto, Y. Kikuchi, and N. Inoue, *Bull. Chem. Soc. Jpn.*, **44**, 3487 (1971).

4) K. Hanaya, *Nippon Kagagku Zasshi*, **87**, 745, 991, 995 (1966).

5) S. Mitsui, A. Kasahara, and K. Hanaya, *Bull. Chem. Soc. Jpn.*, **41**, 2526 (1968).

6) H. Iwamura and K. Hanaya, *Bull. Chem. Soc. Jpn.*, **43**, 3901 (1970); K. Hanaya, S. Onodera, and H. Kudo, *ibid.*, **47**, 2607 (1974).

BULLETIN OF THE CHEMICAL SOCIETY OF JAPAN, VOL. 51 (1), 343—344 (1978)

The Photoreaction of 1-Cycloalkenyl Phenethyl Ketone

Masaru TADA, Hiroshi SAIKI, Hidemi MIZUTANI, and Kyo MIURA

Department of Chemistry, School of Science and Engineering, Waseda University, Shinjuku, Tokyo 160

(Received July 18, 1977)

Synopsis. The UV irradiation of 1-cyclopentenyl phenethyl ketone in benzene or methanol gave a cyclobutane derivative. The irradiation of 1-cyclohexenyl phenethyl ketone in methanol or in benzene containing either BF_3–Et_2O or CF_3COOH gave a cycloheptanone derivative. The formation of the cycloheptanone derivative requires an acid catalyst.

In an earlier paper[1] we reported that 1-cycloalkenyl benzyl ketones (I and II) undergo photo-cyclization to give tricyclic ketones (III and IV). In this paper we wish to report on the difference in the photo-reactivity between 1-cyclopentenyl phenethyl ketone (V) and 1-cyclohexenyl phenethyl ketone (VI).

The 1-cycloalkenyl phenethyl ketones (V and VI) were synthesized by the Friedel-Crafts-type acylation[2] of cycloalkene with 3-phenylpropionyl chloride, followed by the base-catalyzed elimination of hydrogen chloride. The UV irradiation of 1-cyclopentenyl phenethyl ketone (V) in benzene containing 0.05 M BF_3–Et_2O gave the product VII in poor yield and recovered most of the starting material. The reaction did not proceed extensively due to the deterioration of the reaction mixture, which turned into a non-transparent, dark brown solution. This deterioration must be due to the interaction between the acid catalyst and the ketene formed by the photolysis of VII, as has been reported by Smith and Agosta[3] for a similar system. The photoreactions of ketone V in methanol or benzene without an acid catalyst were clean and gave the product VII in better yields (30 and 80% respectively). The structure of VII was deduced from the spectral data: an IR absorption at 1780 cm^{-1} is characteristic of cyclobutanone, the NMR signals at 3.73—3.36 ppm (δ) have an ABC pattern, and attempted decoupling by resonating the hydrogens at a higher field (cyclopentane moiety) did not change the signal pattern. This fact demonstrates that these signals are due to three hydrogens on the cyclobutanone moiety isolated from the hydrogens on the cyclopentane moiety.

The irradiation of 1-cyclohexenyl phenethyl ketone (VI) in the presence of BF_3–Et_2O under the same conditions as were used for ketone V afforded a product VIII in 67% yield. The photoreaction of VI in methanol or benzene containing 0.05 M CF_3COOH also gave ketone VIII in a 40% yield. The irradiation of ketone VI in benzene containing no acid catalyst, however, did not give any VIII, but instead a small amount of fragmentation products. The structure of VIII was deduced from the spectral data: an IR absorption at 1690 cm^{-1} is typical of a seven-membered ketone, and an absorption at 762 cm^{-1} is due to an ortho-disubstituted benzene. The NMR signals are complex but the integration showed the signal ratio of four hydrogens at 7.20—6.80 ppm, six hydrogens due to methylenes and methines adjacent to the benzene ring and the carbonyl group at 3.20—2.4 ppm.

There is no difference in the reaction pattern between 1-cyclopentenyl benzyl ketone (I) and 1-cyclohexenyl benzyl ketone (II) and irradiation in the presence of acid catalysts gives tricyclic ketones, III and IV respectively.[1] This feature of 1-cycloalkenyl benzyl ketones (I and II) is in sharp contrast with the photochemical-behavior of 1-cycloalkenyl phenethyl ketones (V and VI) described here. We previously proposed the importance of a π-aryl interaction in the excited state of the BF_3-complexes of 1-cycloalkenyl benzyl ketones for photo-cyclization.[1] The nature of this π-aryl interaction in the ketones V and VI must be a little different from that of ketones I and II due to the extension of the methylene chain. In the case of ketone VI, however, the π-aryl interaction is still effective enough to cause the photocyclization (Eq. 2) in the presence of an acid catalyst or in a protic solvent. Though the π-aryl interaction is still effective, the existence of benzylic hydrogen adequately located in relation to the enone moiety must alter the reactivity of ketone V. β-Carbon of 1-acylcyclopentenones has been reported to have a strong ability to abstract hydrogen intramolecularly.[3] The excited state of non-substituted cyclopentenone has a strong $n\pi^*$ character,[4] and the photo-reactivity of ketone V can be understood by means of the preferential hydrogen abstraction by triplet $n\pi^*$ excited state.[3]

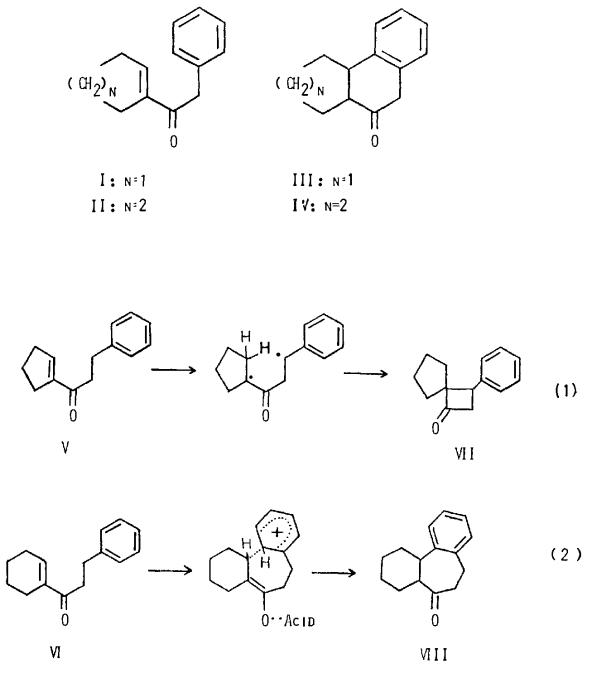

Fig. 1.

Experimental

Preparation of 1-Cyclopentenyl Phenethyl Ketone (V) and 1-Cyclohexenyl Phenethyl Ketone (VI). Stannic chloride (10.4 g, 0.04 mol) in dry dichloromethane (25 ml) was cooled below −70 °C and was then treated, drop by drop, with a mixture of freshly distilled 3-phenylpropionyl chloride (6.6 g, 0.04 mol) and one of the cycloalkenes (0.04 mol) over the period of 3 h. During the reaction the system was maintained below −70 °C and kept in a nitrogen atmosphere. After the completion of the treatment, the reaction mixture was slowly warmed up to 0 °C and poured onto a mixture of ice and concd hydrochloric acid. The dichloromethane layer was separated, and the aqueous layer was extracted with ether. The combined organic layer was washed with water and dried over anhydrous sodium sulfate. The subsequent evaporation of the solvent *in vacuo* gave the crude 2-chloro-1-cycloalkenyl phenethyl ketone. The chloro ketone thus obtained was dissolved in benzene (25 ml) and heated to refluxed in the presence of triethylamine (7 g) for 20 h. After cooling, the reaction mixture was washed with 1M-hydrochloric acid, a saturated sodium hydrogencarbonate solution, and water. The evaporation of the solvent after drying over anhydrous sodium sulfate gave the oily 1-cycloalkenyl phenethyl ketone in a high yield. The ketone V was essentially pure after distillation under reduced pressure, while ketone VI was further purified by chromatography on silica gel eluted by hexane-benzene. V, 129—130 °C/0.7 mmHg. IR(neat): 1655, 1615, 1503, 750, and 695 cm^{-1}. NMR(CCl_4): 7.36(5H), 6.76 (1H, diff. s), 2.94 (4H, s), 2.75—2.33 (4H, m), and 2.12—1.15 ppm (δ) (2H, m). Semicarbazone, mp 124—124.5 °C. Found: C, 69.72: H, 7.25; N, 16.15%. Calcd for $C_{15}H_{19}N_3O$: C, 70.00; H, 7.44; N, 16.33%. VI, 100 °C/0.1 mmHg. IR(neat): 1662, 1613, 1505, 754, and 693 cm^{-1}. NMR(CCl_4): 7.36 (5H, s), 6.97 (1H, diff. s), 2.90 (4H, s), 2.50—2.12 (4H, m), and 1.88—1.60 ppm (δ) (4H, m). Semicarbazone, mp 146—147 °C. Found: C, 70.55; H, 7.81; N, 15.38%. Calcd for $C_{16}H_{21}N_3O$: C, 70.82; H, 7.80; N, 15.49%.

General Procedure for the Photoreaction. Irradiations were carried out externally with a 500-W high-pressure mercury lamp through a Pyrex filter in (a) benzene containing 0.05 M BF_3–Et_2O, (b) benzene containing 0.05 M CF_3COOH, (c) benzene, and (d) methanol under argon or nitrogen. In each run, a 0.1 M solution of the ketone V or VI was irradiated and the progress of the reaction was monitored by means of the IR spectra and by GLC analyses. The reaction mixture was passed through a column of alumina, using benzene as the eluent, to remove the acid catalyst and other polar by-products. The eluates were condensed and further purified by chromatography on silica gel, using hexane-chloroform as the eluent, to give an essentially pure product, VII or VIII. These products, VII and VIII, were further purified by a preparative GLC for spectral measurements. VII, colorless oil. MS: m/e=200 (M^+). IR(neat): 1780, 1505, 765, and 699 cm^{-1} NMR(CCl_4): 7.60 (5H, m), 3.73—3.36 (3H, ABC pattern), and 2.45—1.20 ppm (δ) (8H, m). Semicarbazone, mp 175—176 °C. Found: C, 69.69; H, 7.29; N, 16.09%. Calcd for $C_{15}H_{19}N_3O$: C, 70.00; H, 7.44; N, 16.33%. VIII, colorless oil. Found: C, 84.13; H, 8.53%. Calcd for $C_{15}H_{18}O$: C, 84.07; H, 8.47%. MS: m/e=214 (M^+). IR (neat): 1695, 1502, 762, and 698 cm^{-1}. NMR (CCl_4): 7.20—6.80 (4H, m), 3.20—2.4 (4H, m), and 2.4—0.90 ppm (δ) (8H, m).

References

1) M. Tada, H. Saiki, K. Miura, and H. Shinozaki, *J. Chem. Soc., Chem. Commun.*, **1975**, 55; *Bull. Chem. Soc. Jpn.*, **49**, 1666 (1976).

2) N. Jones and H. T. Taylor, *J. Chem. Soc.*, **1959**, 4017.

3) A. B. Smith, III, and W. C. Agosta, *J. Am. Chem. Soc.*, **95**, 1961 (1973).

4) R. L. Cargill, W. A. Bundy, D. M. Pond, and A. B. Sears, *Mol. Photochem.*, **3**, 123 (1971).

Triplet-Triplet Energy Transfer between Like Molecules

Akinori INOUE, Hiroshi CHUMAN, and Nozomu EBARA

Department of Chemistry, College of General Education, The University of Tokyo, Komaba, Meguro-ku, Tokyo 153

(Received February 5, 1977)

The previously proposed method of studying T-T energy trasfer between like molecules using isotopic mixtures was further improved and applied to an investigation of naphthalene and phenanthrene molecules. Critical transfer distances of 15 and 13 Å were determined for naphthalene and phenanthrene, respectively. The present method has the advantage that it is free from the effect of S-S energy transfer.

Triplet-triplet energy transfer between organic molecules in rigid media has been investigated extensively. Most of the previous works were concerned with energy transfer between unlike molecules. The phosphorescence intensities of donor molecules have been measured as a function of acceptor concentration[1,2] and their time dependences have been analyzed.[3-5] However, not much of the most fundamental information about T-T energy transfer between like molecules is available, possibly due to experimental difficulties. The above methods, which use donor-acceptor systems, are not applicable to this case. The previous studies employed the methods of concentration depolarization[7,8] or magneto-photoselection of phosphorescence.[9] These methods, however, have the fatal drawback that the results are masked by the effect of singlet-singlet energy transfer, whenever it occurs. Studies have been made with several molecules like naphthalene and phenanthrene using these methods;[7,9] in these studies the authors assumed that the singlet-singlet transfer was not efficient. However, as is shown in a later section, the critical transfer distances of these molecules for S-S transfer, estimated from Förster's theory,[10] are comparable to those in the T_1 state. The effect of S-S transfer seems to be large enough in these cases to preclude determination of reliable critical transfer distances in the triplet states, so that the earlier methods should be used only with reservation.

In a previous paper (I),[11] we have developed a new method of studying T-T transfer between like molecules, using isotopic mixtures, and have made an investigation of naphthalene molecules. Phosphorescence decay curves for equal amounts of protonated and perdeuterated naphthalene in poly(methylmethacrylate) were measured as a function of concentration. The new method utilized the fact that the phosphorescence lifetime of a protonated compound (H) and that of a deuterated compound (D) usually differ greatly, while their electronic properties are quite similar.

In (I), however, a somewhat oversimplified model was introduced, which might lead to a rather large value for the critical transfer distance R_0. In the present paper, measurements of phosphorescence decay curves were made again for naphthalene molecules in order to get more accurate data than in (I). The results were analyzed beased on an improved model. The present method was also successfully applied to the investigation of phenanthrene molecules.

Experimental

The methods used for the purification of naphthalene isotopic isomers and for the phosphoresence measurements are the same as in (I). Commercial phenanthrene-d_0 and -d_{10} were sublimed *in vacuo* and then used for the measurements. Plastic specimens including phenanthrene molecules were also prepared by the same method as in (I), *i.e.*, by polymerizing methyl methacrylate solutions at about 80 °C, with no inhibitor being used. Specimens were annealed at about 100 °C for a few hours. The concentration change due to polimerization were taken into account by the use of the specific gravities of methyl methacrylate and its polymer (PMMA). The specific gravity of 1 M naphthalene in PMMA was approximately 1.18, almost identical to that of pure PMMA (1.19). Thus, the change of density for PMMA because of the presence of solute molecules can be ignored.

All the measurements were made at 77 K. The volume contraction of PMMA by cooling from room temperature to 77 K was estimated to be only a few percent. Hence, this effect was also ignored. The fluorescence and absorption spectra were measured for EPA solutions of naphthalene and phenanthrene and their deuterated compounds at 77 K with a hand-made spectrofluorimeter.

Results and Discussion

The previous experiments[11] on naphthalene isotopic mixtures can be summarized as follows:

a) The phosphorescence decay curves could be expressed in terms of two exponential functions in the concentration region studied;

$$f(t) = D_1 \exp(-k_1 t) + D_2 \exp(-k_2 t). \quad (1)$$

b) The decay rate of each component varied little with concentration.

c) The decay rate of the long-lived component (k_2) was similar to that of the phosphorescence of the solution of pure D (β), whereas the short-lived component had a slightly smaller decay rate (k_1) than that of the H molecule (α).

d) The ratio of the pre-exponential factors, the short-lived over the long-lived components, r ($=D_1/D_2$), increased with increasing concentration. The change was drastic at higher concentrations.

e) The phosphorescence spectrum of the isotopic mixture was simply a susperposition of those for H and D, indicating that impurity molecules or triplet excimers or exciplexes are not responsible for the concentration dependence of the phosphorescence decay curves.

Our new results have features similar to the above. The concentration dependences of k_1, α, β, and r are

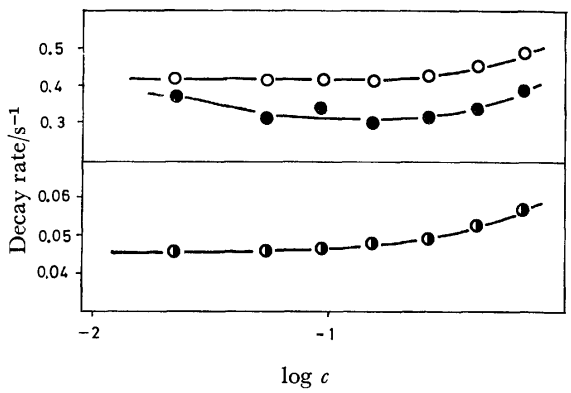

Fig. 1. Concentration dependences of α(○), β(◑), and γ(●) for naphthalene.

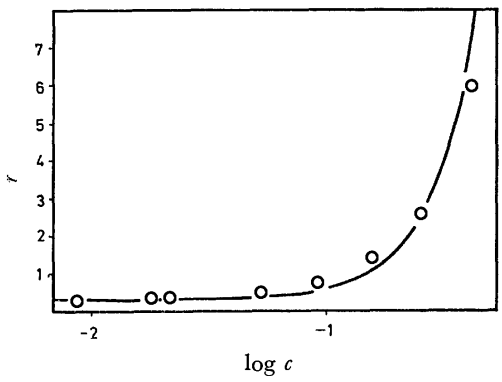

Fig. 2. Concentration dependence of r for naphthalene; -○- experiments; —calculated using Eq. 8.

shown in Figs. 1 and 2.

The previous data were interpreted in terms of triplet-triplet energy transfer between H and D molecules. It was assumed that energy transfer took place only between H-D pairs whose intermolecular separations were smaller than the critical transfer distance R_0. This gave the value of $R_0=17$ Å for naphthalene molecules. This value is relatively large compared with those reported for the energy transfer between unlike molecules.[1-6] The difference of the values may not be due to any intrinsic difference in the transfer mechanism, but may instead be ascribed to the assumptions included in (I). In (I), energy transfer was assumed to take place only between pairs and transfer among more than three molecules was ignored. This assumption may not be valid at higher concentrations.

In the present analysis, we have developed an improved model. The following emitting species were assumed to be present in the rigid solutions: A) isolated H molecules and clusters composed only of H molecules, B) isolated D molecules and clusters composed only of D molecules, and C) clusters containing both H and D molecules. Here, the word "cluster" is used to represent a group of molecules in which no molecules are isolated by distances larger than R_0 from all other members of the group, but they are separated by distances larger than R_0 from all molecules which do not belong to this group. Thus the rate of energy transfer between molecules within a cluster is much faster than the intramolecular decay process, whereas the energy transfer between two clusters can be assumed to be forbidden. The molecules in a cluster can be assumed to retain their individualities.

Phosphorescence decay rates of A and B clusters are identical to those of the isolated molecules, α for H and β for D, respectively, while the phosphorescence from C clusters has various lifetimes, depending on their compositions.

The decay rate of a cluster composed of n_H H molecules and n_D D molecules is

$$\gamma_s = (s\alpha+K\beta)/(s+K), \tag{2}$$

with

$$s = n_H/n_D,$$

where K is the ratio of the rate constants of the T-T transfer processes H→D and D→H.

In a cluster with the same total number of molecules, n, the ratio s shows a binomial distribution. For a C cluster with two molecules, which is certainly the most numerous one when the concentration is not so high, s is exactly unity. Hence, among all C clusters the most numerous clusters are those with the ratio s not much different from unity. Moreover, γ_s is a relatively slowly varying function of s, as can be verified easily ($\gamma_{1/2}=0.25$, $\gamma_1=0.30$, and $\gamma_2=0.34$ when $\alpha=0.40$, $\beta=0.047$ s^{-1}, and $K=0.37$). It can then be shown that the decay rates of C clusters extend from α to β with a very sharp peak at γ_1, so that they can be safely approximated by a single rate constant $\gamma=\gamma_1$.

Each decay curve is thus expected to be composed of three exponential functions:

$$f(t) = A[(k_H^r\rho_H/\alpha)\exp(-\alpha t) + (k_D^r\rho_D/\beta)\exp(-\beta t) + (k_{HD}^r\rho_{HD}/\gamma)\exp(-\gamma t)], \tag{3}$$

where k_H^r and k_D^r are the radiative rate constants for the phosphorescence of A and B clusters, and ρ_H, ρ_D, and ρ_{HD} are the probabilities that molecules belong to the respective clusters, when they are excited. k_{HD}^r is an effective radiative rate constant for C clusters:

$$k_{HD}^r = (k_H^r+Kk_D^r)/(1+K). \tag{4}$$

The singlet absorption cross section and the rate for intersystem crossing are assumed to be the same for H and D molecules. Equation 4 applies to a phosphorescence decay of the mixture after the steady state condition for excitation is established.

The observed phosphorescence decay curves for isotopic mixtures consisted of two exponential functions instead of three over a wide concentration range, as mentioned before. This was because γ is close to α and, in the distribution of decay rates, the peak at α is too low compared with that at γ. That such a distribution of rate constants can be represented by a single rate constant can be shown by a model calculation, so that

$$k_1 = \gamma,$$

and

$$D_1 = A[(k_H^r\rho_H/\alpha)+(k_{HD}^r\rho_{HD}/\gamma)]. \tag{5}$$

The value of K is equal to the ratio of overlap of the phosphorescence and S-T adsorption spectra in the framework of Dexter's theory.[12] Due to the lack of spectroscopic data, the constant was equated in (I) to

the Boltzman factor, 0.13, as is often employed. In this approximation, however, several factors such as the correction for spectral line width cannot be taken into account. Hence, we discard this value. K was estimated to be 0.37 using Eq. 2 and the values of α, β, and γ. This valus was found to be constant for 0.1 to 0.4 M solutions.

The ratio, r, of the pre-exponential factors of the short-lived to long-lived components is then

$$r = [(k_H^r\rho_H/\alpha) + (k_{HD}^r\rho_{HD}/\gamma)]/(k_D^r\rho_D/\beta). \quad (6)$$

Since we are dealing with solutions containing equal amounts of H and D molecules, it is evident that

$$\rho_H = \rho_D,$$

and

$$\rho_{HD} = 1 - (\rho_H + \rho_D) = 1 - 2\rho_D,$$

so that

$$r = p\beta/\alpha - 2(\beta/\gamma)(p+K)/(1+K) + (\beta/\gamma\rho_D)(p+K)/(1+K), \quad (7)$$

where p is the ratio k_H^r/k_D^r. Denoting as w_n the fraction of clusters composed of n molecules altogether, regardless of H or D molecules,

$$\rho_D = \sum_n 2^{-n}w_n.$$

If the concentration is not too high, the terms with large n are expected to be small, since each w_n is small and is accompanied by a factor 2^{-n}. Thus, we can retain only w_1 and w_2 and neglect higher terms. By this approximation only clusters composed of not more than two molecules are considered for A and B clusters. On the other hand, since the factor 2^{-n} is not present for C clusters, all possibilities are taken into account by using $\rho_{HD}=1-2\rho_D$. The present approximation is valid in the concentration range where $w_1>w_2$; otherwise, higher terms must be taken into account for ρ_H and ρ_D. The validity of this condition will be examined below. Equation 7 then leads to

$$r = p\beta/\alpha - 2(\beta/\gamma)(p+K)/(1+K) + (\beta/\gamma)(p+K)/(1+K)[(w_1/2)+(w_2/4)]. \quad (8)$$

w_1 is the probability of a molecule having no neighbors within the active sphere, $v=4\pi R_0^3/3$ (cm^3), so that

$$w_1 = \exp(-Nvc). \quad (9)$$

Here, $N=6.02\times10^{20}$ mol^{-1} and c is the total concentration of H and D together (M). w_2 is given by[13]

$$w_2 = 4\pi Nc \exp(-4\pi R_0^3 Nc/3) \times \int_0^{R_0} R^2 \exp[-\pi Nc(R_0^2R - R^3/12)]dR. \quad (10)$$

Figure 2 depicts the comparison of the concentration dependence of the experimental value of r to that calculated using Eq. 8, with experimentally determined parameters α, β, and γ. The value of p was taken from the paper by Kanamaru.[14] The best fit was obtained with $R_0=15$ Å. This value is smaller than the previous value of 17 Å.

We applied the same method to phenanthrene systems. In this case, decay curves were also found to be consistent with two exponential functions. No anomalous emission which might be ascribed to an impurity or excimer (exciplex) was observed in the phosphorescence spectra. The value of each decay rate, whose concentration dependence is shown in Fig. 3, does not change much with concentration. The ratio r changes greatly with concentration (Fig. 4). The calculated curve based on Eq. 8 with $R_0=13$ Å fitted well with the experiments.

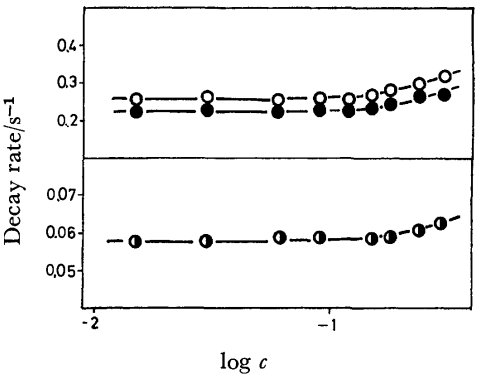

Fig. 3. Concentration dependences of α(○), β(◑), and γ(●) for phenanthrene.

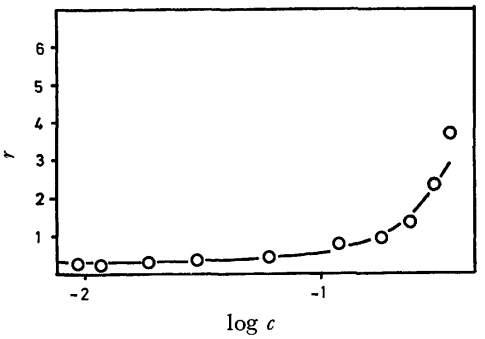

Fig. 4. Concentration dependence of r for phenanthrene;
-○- experiments; — calculated using Eq. 8.

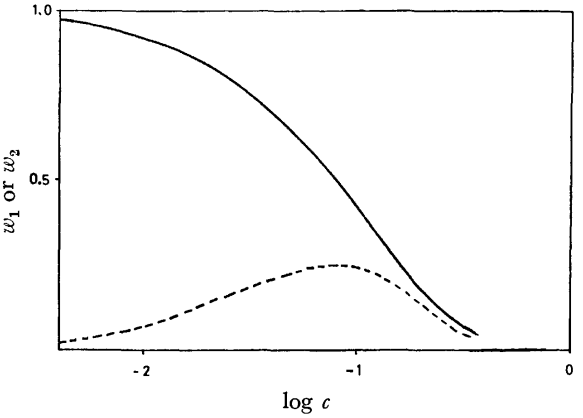

Fig. 5. Calculated w_1 (—) and w_2 (---) with $R_0=15$ Å as a function of concentration.

The concentration dependences of w_1 and w_2 with $R_0=15$ Å are depicted in Fig. 5. The condition $w_1>w_2$ is shown to be obeyed in the concentration range studied, and it is evident that this inequality holds for smaller values of R_0. Thus, neglecting higher terms in w_n is justified in the present case.

In the above approximation, the initial steady state

triplet population in each kind of cluster is assumed to be proportional to its lifetime. This requires that the redistribution of excitation among different kinds of clusters should be forbidden also in the singlet state, or that the initial equilibrium populations in the excited singlet state are the same for all kinds of clusters. We have measured the absorption and fluorescence spectra of H and D molecules at 77 K for naphthalene and phenanthrene, from which the critical concentrations c_{HD} for singlet-singlet energy transfer H→D and c_{DH} for D→H were calculated by the standard method.[10] These were 0.17 and 0.15 M for naphthalene and 0.31 and 0.31 M for phenanthrene. The critical distances for S-S transfer are then 14 Å for naphthalene and 11 Å for phenanthrene. These are close to, but do not exceed the critical distances for T-T transfer, and assure that the transfer between clusters in the singlet state is forbidden.

In quite a few cases the S-S critical transfer distances between like molecules never exceed the T-T transfer distances,[15] so that the present method can very often be used without any correction. In cases where the S-S critical distances R_{0s} is larger than R_0, the following small correction may suffice:

The fractions of A and B clusters which are not isolated in an S-S transfer but are isolated in a T-T transfer are

$$\Delta\rho_H = \Delta\rho_D = \rho_D(R_0) - \rho_D(R_{0s}),$$

in which the probability ρ is considered to be a function of isolation distance. The populations of singlet excitation in these portions are to be modified by $2/(1+q)$ for A clusters and $2q/(1+q)$ for B clusters. Here q is an equilibrium constant and can be derived from Förster's theory:[16]

$$q = (\eta_{HD}/\eta_H)(1-\eta_{DH}/\eta_D)/(\eta_{DH}/\eta_D)(1-\eta_{HD}/\eta_H). \quad (11)$$

η_H and η_D are the fluorescence quantum yields of H and D molecules, respectively, in the absence of S-S transfer to their isotopic isomers and η_{HD} and η_{HD} are those in the presence of the latter. The probabilities ρ_H and ρ_D in Eq. 6 are then to be replaced by $\rho_H + \Delta\rho_H(1-q)/(1+q)$ and $\rho_D - \Delta\rho_D(1-q)/(1+q)$, respectively.

In the present case, no such correction was required, as mentioned above, and the calculation of this value by using Förster's formulae[10]

$$\eta_{HD}/\eta_H = 1 - \sqrt{\pi}x \exp(x^2)[1-2\Phi(\sqrt{2}x)],$$

$$\Phi(y) = (1/\sqrt{2\pi})\int_0^y \exp(-t^2/2)dt,$$

$$x = \sqrt{\pi}c/2c_{HD},$$

shows that q is almost unity within the concentration range studied.

In this way, the present method seems to have wide applicability for investigations of T-T energy transfers, because the effect of S-S transfer is usually ignorable, or, if not, correction for it can be made easily. On the contrary, the conventional methods such as photoselection of phosphorescence cannot be used when even a small amount of S-S transfer manifests itself.

The critical transfer distance for the triplet energy transfer between identical molecules obtained in the present work is of the same order of magnitude as those reported previously for unlike molecules.[1-6] The difference of the values for naphthalene and phenanthrene may not be important when we consider the experimental errors and the precision of approximation employed in the analysis.

References

1) V. L. Ermolaev, *Uspekhi Fiz. Nauk.*, **80**, 3 (1963); Engl. Transl., *Soviet Physics-Uspekhi*, **6**, 333 (1963).
2) J. T. Dubois and F. Wilkinson, *J. Chem. Phys.*, **38**, 2541 (1963).
3) M. Inokuchi and F. Hirayama, *J. Chem. Phys.*, **43**, 1978 (1965).
4) H. Kobashi, T. Morita, and N. Mataga, *Chem. Phys. Lett.*, **20**, 376 (1973).
5) G. B. Strambini and W. C. Galley, *J. Chem. Phys.*, **63**, 3467 (1975).
6) G. B. Strambini and W. C. Galley, *Chem. Phys., Lett.*, **39**, 257 (1976).
7) N. K. Chaudhuri and M. A. El-Sayed, *J. Chem. Phys.*, **42**, 1947 (1965).
8) Y. Gondo, M. Hirai, T. Iwao, T. Kakibaya, T. Kuroi, H. Nagamoto, and T. Kanda, *Chem. Lett.*, **1975**, 463.
9) S. Siegel and L. Goldstein, *J. Chem. Phys.*, **44**, 2780 (1966).
10) Th. Förster, *Ann. Phys.*, **2**, 55 (1948).
11) A. Inoue and N. Ebara, *Chem. Lett.*, **1975**, 1137.
12) D. L. Dexter, *J. Chem. Phys.*, **21**, 836 (1953).
13) R. S. Knox, *Physica*, **39**, 361 (1968).
14) N. Kanamaru, H. R. Bhattachariee, and E. C. Lim, *Chem. Phys. Lett.*, **26**, 174 (1974)
15) I. B. Berlman, "Energy Transfer Parameters of Aromatic Compounds," Academic Press, New York and London (1973).
16) Th. Förster, *Discuss. Faraday Soc.*, **27**, 7 (1959).

The Effect of High Density Excitation on the Phosphorescence Spectra and Decay Times of Several Crystalline Uranyl(VI) Salts

Takayoshi KOBAYASHI

The Institute of Physical and Chemical Research, Wako, Saitama, 351

(Received January 22, 1977)

The effect of high density excitation on the phosphorescence spectra and their decay curves of crystalline uranyl(VI)nitrate hexahydrate, uranyl(VI)acetate dihydrate, and zinc uranyl(VI)acetate heptahydrate was studied using a nitrogen laser as the exciting light source. The relative emission intensity of the spectra in the shorter wavelengths decreased and the vibrational structure became broader at higher density excitations; these changes were attributed to the saturation in excitation and to the temperature increase in the irradiated volume of the sample crystal caused by the heat released in the radiationless decay process. A decrease in the decay time was also observed at high density excitations; this shortening was attributed to bimolecular quenching of triplet excitons in the crystal. The rate constant for this process in crystalline uranyl nitrate hexahydrate was measured at several temperatures between 77 and 295K; it was 2.6×10^{-13} cm^3 s^{-1} at 295K for example. From this rate constant the hopping rate for a triplet exciton in crystalline uranyl nitrate hexahydrate was obtained: 4.3×10^{8} cm^3 s^{-1} at 295K. The activation energy for the exciton migration was found to be 320 cm^{-1}.

Uranyl salts with the simplest monomolecular type of luminescence have been extensively investigated for more than a century.[1,2] Tolstoi *et al.* observed decreases in both the phosphorescence lifetime and the quantum yield at high density excitations.[3,4] They measured the relative quantum yield and the average lifetime at various excitation densities. They determined the bimolecular quenching rate constants in a uranyl(VI)-nitrate hexahydrate crystal by matching the theoretical curves to the experimental points. The bimolecular quenching rate constant obtained by them is erroneous because of the following two reasons: (i) The decay curve is not exponential when both monomolecular and bimolecular decay processes are present, as is shown in the later part of this paper, whereas they assumed it to be exponential, and (ii) the decrease in the phosphorescence yield was assumed to be caused only by biexcitonic quenching; the saturation effect in the excitation and other effects were disregarded.

In the present paper the effect of high density excitation on the phosphorescence decay curves was studied for crystalline uranyl(VI)nitrate hexahydrate ($UO_2(NO_3)_2\cdot6H_2O$), uranyl(VI)acetate dihydrate ($UO_2(CH_3COO)_2 : 2H_2O$), and zinc uranyl(VI)acetate heptahydrate ($Zn(UO_2)_2(CH_3COO)_6\cdot7H_2O$) (hereafter abbreviated as UN, UA, and ZUA, respectively) and the rate constants for bimolecular quenching and hopping of excitons in a UN crystal were obtained as a function of temperature between 77 and 295 K by analyzing the phosphorescence decay curves.[5,6] The critical concentration for bimolecular quenching and the activation energy for the exciton hopping were also obtained.

The effect of high density excitation on the phosphorescence spectra was also studied for the three uranyl salts. The cause of the spectral change at high density excitation is interpreted in terms of the saturation in excitation and the temperature increase in the irradiated volume of the sample crystal which is caused by the heat released in the radiationless decay process.[6]

Experimental

A nitrogen laser described in a previous paper[7] was used as the excitation light source for observing the phosphorescence decay curves and their time-resolved spectra. The laser beam intensity was attenuated by quartz plates with evaporated aluminium. The intensity of the phosphorescence from the crystalline samples was also reduced by appropriate neutral density filters of copper mesh. A Spex 1704 monochromator, an EMI 6256S photomultiplier, and a Hitachi V1000 oscilloscope were used to record the phosphorescence decay curves. The time constant of the detecting system was about 10 μs. A PAR model 160 boxcar integrator was used in order to obtain time resolved phosphorescence spectra and to improve the signal to noise ratio. The aperture time, time base, and time constant of the boxcar integrator were 10 μs, 0.1 ms, and 0.1 ms, respectively. The phosphorescence was detected at right angles to the excitation light beam.

The triplet-triplet ($T_n\leftarrow T_1$) absorption spectrum of UN in acetonitrile solution was measured by a newly developed method which was described in a previous paper.[8]

Reagent grade UN and UA (Wako Pure Chemical Industries) and GR grade ZUA (Kanto Chemical Co., Inc.) were used without further purification. For study of the high density excitation effect, crystalline powder was used. The spectral dependence of the phosphorescence lifetimes was checked for these three crystals at 295, 201, and 77 K. The phosphorescence lifetimes were constant all over the spectral region for the three crystals, UN, UA, and ZUA, at these three temperatures. This shows that the effect of the impurity emission on the phosphorescence spectra of these three crystals of the uranyl salts is negligibly small.[9,10]

The phosphorescence excitation spectrum of the UN crystal was measured on a HITACHI MPF spectrophotofluorometer at Ochanomizu University.

Results and Discussion

Spectral Changes. Phosphorescence spectra of UN, UA, and ZUA within the first 10 μs after the laser excitation were measured at 295 K at high and low excitation densities; the results are shown in Fig. 1(a).

Vibrational bands in the phosphorescence spectra of the three kinds of crystals, UN, UA, and ZUA, are hereafter referred to as bands h, a, b, c, d, and e, as

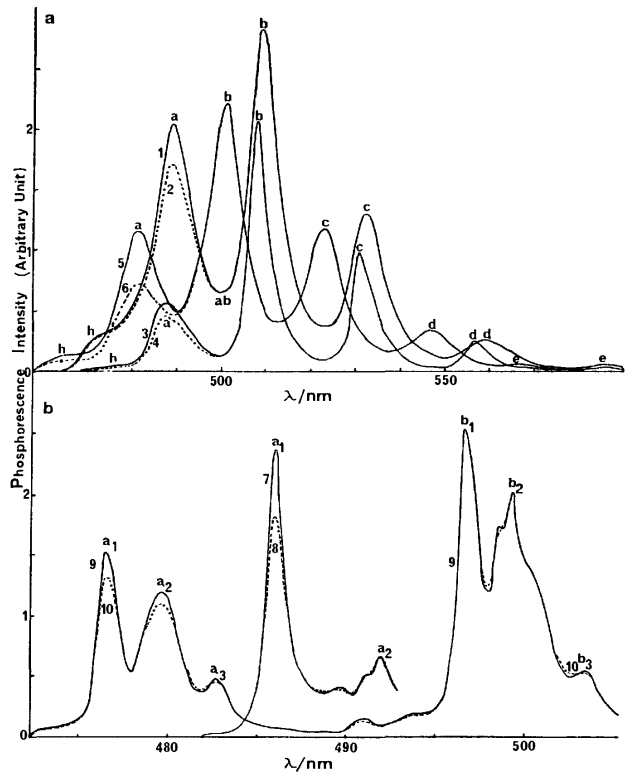

Fig. 1, (a) Time resolved phosphorescence spectra of crystalline UN (curves 1 and 2), UA (curves 3 and 4), and ZUA (curves 5 and 6) just after low (solid curves) and high (broken curves) density excitations at 295 K. Exciting light intensity at high density excitation is about 100 kW per 0.08 cm² (=1.25 MW/cm²).
(b) Time resolved phosphorescence spectra of UA (curves 7 and 8) and ZUA (curves 9 and 10) crystals just after low (solid curves) and high (broken curves) density excitations at 77 K. Only band a and bands a and b are shown in the spectra for UA and ZUA, respectively, since the change is observed only in the regions of those bands.

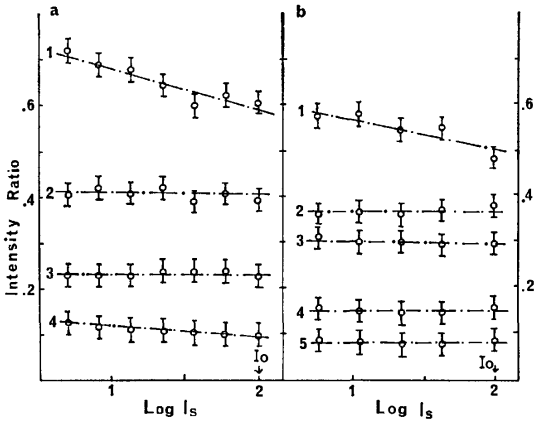

Fig. 2. Phosphorescence intensities of crystalline UN(2a) and UA(2b) at intensity maxima h, a, c, d, and of minima ab and bc relative to that at the maximum b in the time resolved spectrum just after excitation, as functions of logarithmic exciting light intensity (I_s). I_0 is the highest intensity in the present experiment, 100 kW per 0.08 cm². Plotted lines 1, 2, 3, and 4 in Fig. (2a) indicate I_a/I_b, I_c/I_b, I_{ab}/I_b, and I_h/I_b respectively, and those 1, 2, 3, 4, and 5 in Fig. (2b) indicate I_a/I_b, I_c/I_b, I_{ab}/I_b, I_{bc}/I_b, and I_d/I_b, respectively.

indicated in Fig. 1. Band h is a hot band. The intensity minima between the two maxima are referred to as ab, bc, cd, and de, *etc.* (Fig. 1). I_a and I_{ab} represent the emission intensities at the wavelength of band a and at the intensity minimum ab in the spectrum, respectively.

The common change in the phosphorescence spectra of UN, UA, and ZUA crystals with high density excitation at room temperature is the decrease in the intensity relative to that at the peak position of the phosphorescence spectra at shorter wavelengths. The relative intensities of bands h and a are weaker at high density excitation than at low density excitation. This can be shown more clearly from Figs. 2a and 2b, where the ratios of phosphorescence intensities at several wavelengths are shown for various excitation intensities, I_s. We can see that I_h/I_b and I_a/I_b decrease as I_s increases, while I_c/I_b, I_{ab}/I_b, and I_{bc}/I_b remain constant.

The effect of high density excitation on the phosphorescence spectra of UA and ZUA at 77 K is shown in Fig. 1(b). A change in the phosphorescence spectra of UA is observed in the spectral region between 483 and 493 nm, as shown in Fig. 1(b). Vibrational bands in the phosphorescence spectra of UA and ZUA are hereafter referred to as a_1, a_2, and a_3··· and b_1, b_2, and b_3···, as indicated in Fig. 1(b).

The relative intensities of band a in the spectrum of UN,[11] of band a_1 in the spectrum of UA, and of band a_1, a_2, and a_3 of ZUA decrease at high density excitations, as shown in Figs. 1 and 2. The amount of the decrease is in the order of $a_1 > a_2 > a_3$ for the spectrum of ZUA at 77 K.

In the spectra shown in Fig. 1(b) another spectral change can be found for UA and ZUA crystals. This is a vibrational band broadening. The vibrational bands become slightly obscure at the high density excitation in the 489—492 nm region of the UA spectrum, and in the 476—483, 490—493, and 498—500 nm regions of the ZUA spectrum. This broadening is also observed in the 506—509 nm region of the UN spectrum at 77 K.[12] The spectral change caused by high density excitation is observed also at 201 K. The change observed at this temperature is quite similar to that at 295 K.

The changes commonly observed to appear in the spectra of UN, UA, and ZUA crystals at high density excitations are therefore summarized as follows.

(1) The relative intensity of the spectra in the shorter wavelengths decreases at high density excitations.

(2) The vibrational band at 77 K becomes obscure at high density excitation. These spectral changes are reversible. Neither color change nor decomposition of the crystals was observed after exposure to about 10^4 shots. Furthermore, low density excitations before and after the high density excitation at the same spot on the sample crystal gave the same spectral distribution of fluorescence intensity, within 1%. Therefore, the main cause of the spectral change at high density excitation is not an irreversible chemical reaction.[13]

There are four possible interpretations for the observed

reversible spectral change (1):[14] (a) At the high density excitation the temperature in the irradiated volume of the crystal is increased not only by the heat given off in the ordinary linear radiationless decay processes of the molecules whose number increased at the high density excitations but also by the heat released in the nonlinear bimolecular quenching process referred to in a later part of the present paper. This temperature increase causes an increase in the absorbance of the hot band. Therefore, the relative intensity of the spectra at the shorter wavelengths is decreased because of their large overlap with the hot band of the absorption spectra. (b) The ratio of the phosphorescence emitted from the surface of the crystal to that from the inner part decreases at high density excitations because of the saturation effect.[7] Since the phosphorescence was detected at right angles to the excitation light beam, the phosphorescence suffers from the reabsorption because the phosphorescence and $T_1 \leftarrow S_0$ absorption spectra overlap with each other to some extent. The phosphorescence emitted from the inner part is more seriously affected by the reabsorption than that emitted from the surface of the crystal. Therefore the reabsorption effect becomes more prominent at high density excitations. (c) Induced emission appears at high density excitations. (d) The emission spectrum is affected by reabsorptions due to transitions from the lowest excited triplet state (T_1) to higher triplet states (T_n).

Possibility (c) can be excluded since no spectral narrowing, but only broadening, could be found. In order to check possibility (d) we measured the $T_n \leftarrow T_1$ absorption spectrum of a saturated solution of uranyl nitrate in acetonitrile. The result is shown in Fig. 3. The $T_n \leftarrow T_1$ spectrum of UN has maxima at 570 nm.[15] Figure 3 shows $A_a < A_{ab} < A_b < A_c < A_d$, where A_a and A_{ab} are the absorbances of T_1 at the wavelength of band a and of intensity minimum b. Therefore, if possibility (d) is the main cause of spectral change (1), then I_h/I_b and I_a/I_b should increase in the spectrum of UN measured at 295 K with the increase in excitation intensity. However, as is shown in Fig. 2a, the actual spectral change of (1) is in the opposite direction. This implies that possibility (d) is not the main cause of spectral change (1) at high density excitations for UN crystals.

If possibilities (a) and (b) are the main causes of spectral change (1), I_h/I_b and I_a/I_b should increase with high density excitation for all three crystals, since bands a and h suffer from reabsorption less seriously than the other bands. This was what was actually observed for UN, UA, and ZUA crystals; therefore, it is concluded that (a) and (b) are the dominant causes of spectral change (1).

Two tentative explanations for spectral change (2) are as follows: (a) The vibrational structure becomes obscure at high density excitations because of the temperature increase caused by the heat given off by radiationless decay at high density excitations. (b) The new emission which appears is caused by the exciton-exciton interaction.

Possibility (b) is ruled out by the fact that the change in the phosphorescence decay time which accompanies the high density excitation can be completely interpreted in terms of the bimolecular collisional quenching of the triplet exciton, there is no evidence that there appears any new emission originating from some interacted state of two excitons with a possibly different decay time from that of the normal phosphorescence at low density excitation.

In order to check possibility (a), the phosphorescence spectra of a ZUA crystal at low density excitations at several temperatures higher than 77 K by steps of ten degrees were measured (Fig. 4); these were compared with that at the high density excitation at 77 K. From the comparison of Figs. 2 and 4, the ratio $I_{a_2}/I_{a_1a_2}$ at the high density excitation at 77 K is between those at 95 and 103 K with low density excitations. This shows that the temperature increase, ΔT, in the irradiated volume of crystalline ZUA at the high density excitation can be estimated at between 18 and 26 K.

The ratio $I_{a_1}/I_{a_1a_2}$ is much more seriously decreased

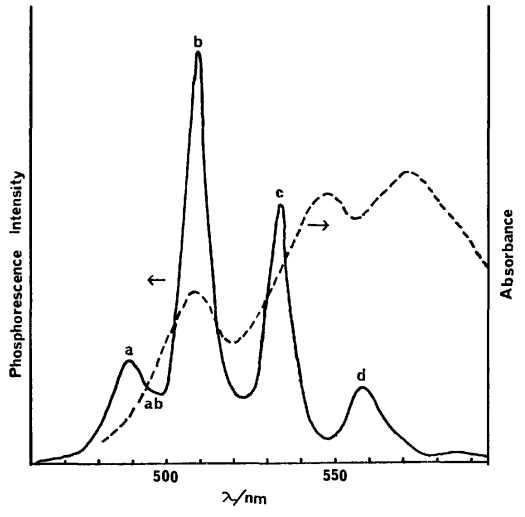

Fig. 3. Time resolved phosphorescence spectrum of UN crystal at 295 K just after low density excitation (curve 1) and the $T_n \leftarrow T_1$ absorption spectrum of a saturated solution of UN in CH_3CN (curve 2).

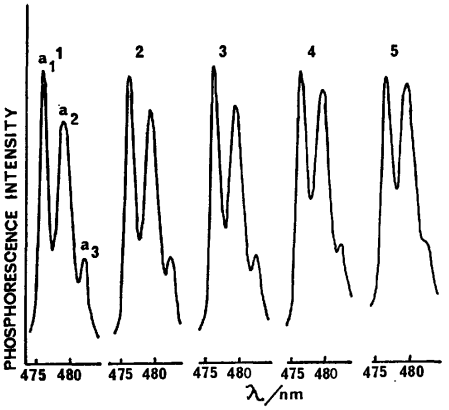

Fig. 4. Time resolved phosphorescence spectra of crystalline ZUA just after low density excitation at different temperature between 77 and 108 K. Figs. 1, 2, 3, 4, and 5 indicate the spectra at 77, 93, 95, 103, and 108 K, respectively.

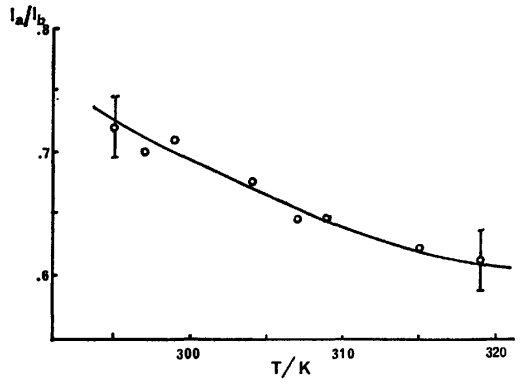

Fig. 5. Temperature dependence of the intensity ratio I_a/I_b between 295 and 319 K in the time-resolved spectrum just after low density excitation of UN.

than $I_{a_2}/I_{a_1a_2}$. This is because the band a_1 is decreased not only by the increase of the reabsorption effect caused by the temperature increase but also by the excitation saturation of the sample crystal already mentioned as possibility (b) for the cause of spectral change (1).

The temperature increase in the irradiated volume in crystalline UN can be also estimated to be ≈25 °C by a comparison with Figs. 3a and 5, which show the intensity ratio I_a/I_b as functions of temperature at low density excitation and of excitation density at 295 K, respectively.

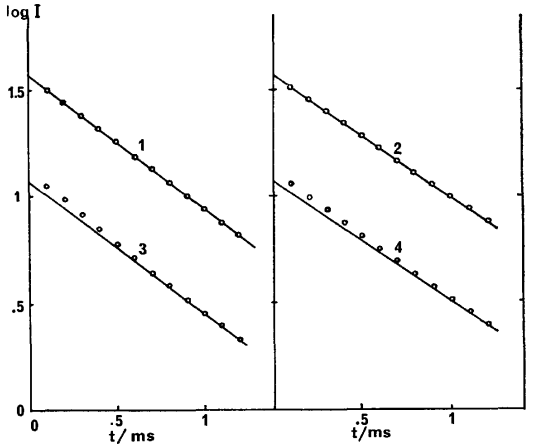

Fig. 6. Semilogarithmic plots of phosphorescence intensities *versus* time after excitation at low (1 and 2) and high (3 and 4) density excitations at 295 (1 and 3) and at 77 K (2 and 4).

Change in Decay Curve. In Fig. 6, the logarithm of the phosphorescence intensity (I) of the UN crystal is plotted against time for high and low density excitations at 295 and 77 K. The phosphorescence lifetimes, τ's, at the low density excitation are 697 μs at 295 K and 764 μs at 77 K. The decay times obtained from the initial slope of the phosphorescence decay curve are 620 μs at 295 K and 690 μs at 77 K at the high density excitation. Therefore, the decreases in the lifetimes τ are 77 μs at 295 K and 74 μs at 77 K. This is contrary to the expected effect of temperature upon τ. From Fig. 7, it can be seen that $\Delta\tau/\Delta T$ is smaller at high

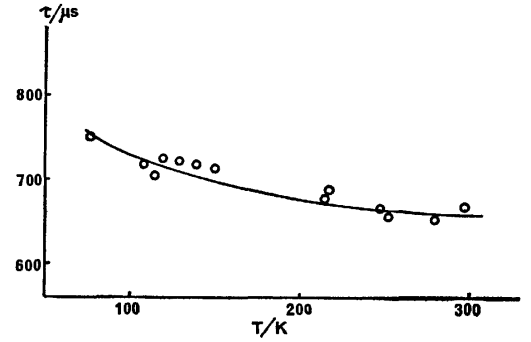

Fig. 7. Temperature dependence of phosphorescence lifetime of crystalline UN.

temperatures, where $\Delta\tau$ and ΔT are the change in lifetime and temperature. The decreases in the phosphorescence lifetimes, $\Delta\tau$, caused by the temperature increase, $\Delta T \cong 25$ °C, estimated above by the spectral change, were calculated to be much less than 10 μs at 295 K and 25 μs at 77 K. These decreases are too small to be the cause of the decrease in the lifetime. Induced emssion has also been ruled out. Therefore, the only possible cause of the lifetime shortening is biexcitonic quenching of triplet excitons in the crystal. When the bimolecular quenching process becomes significant, the time dependence of the exciton density $n(t)$ is given by the following equation:

$$1/n(t) = (1/n_0 + \gamma/\alpha)\exp(\alpha t) - \gamma/\alpha, \quad (1)$$

where n_0 is the initial excitation density and α and γ are the rate constants for the monomolecular and bimolecular decay processes, respectively. As is expected, $1/n(t)$ was found to be linearly proportional to $\exp(\alpha t)$ at several temperatures between 295 and 77 K. From the slopes of the lines, γ was obtained at various temperatures, the results are given in Fig. 8. This figure shows that the plot of $\log\gamma$ *versus* $1/T$ is approximately linear and, therefore, γ can be written in the form

$$\gamma = \gamma_0 \exp(-\Delta E/kT). \quad (2)$$

From the slope of the line in Fig. 8, ΔE was found to be 320 cm^{-1}. The following relation between γ and the exciton hopping rate, λ, has been derived in a previous paper:[6]

$$\gamma = \frac{\lambda\mu}{\lambda+\mu}\frac{z_n V_0}{z_u}(2-A), \quad (3)$$

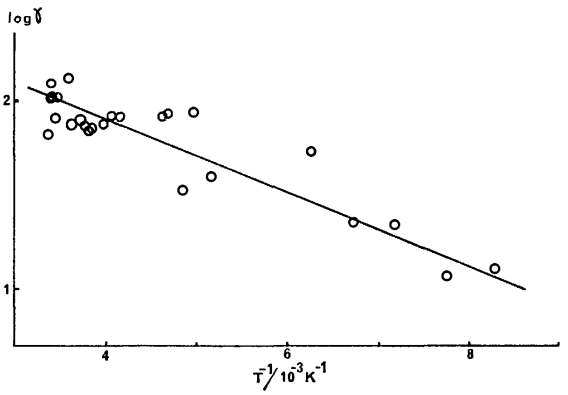

Fig. 8. Temperature dependence of γ of an exciton in crystalline UN. γ is in an arbitrary unit.

where μ, z_n, z_u, V_0, and A have the same meaning as in the previous paper.[6] As is expected for a triplet exciton, if the exciton hopping rate, λ, is much slower than the monomolecular quenching rate constant, μ, of the two neighboring excitons, Eq. 3 may be simplified to

$$\gamma = \lambda \frac{z_n V_0}{z_u}(2-A). \quad (4)$$

By combining Eqs. 2 and 4, we obtain

$$\lambda = \lambda_0 \exp\left(\frac{-\Delta E}{kT}\right), \quad (5a)$$

$$\lambda_0 \equiv \gamma_0 \frac{z_u}{z_n V_0} \frac{1}{2-A}. \quad (5b)$$

We found the activation energy for bimolecular quenching and hence for exciton migration to be 320 cm^{-1}.

The Absolute Values of γ and λ. In order to estimate the absolute values of γ and λ, it is necessary to know the concentration of the triplet excitons. The triplet exciton concentration in the irradiated volume the exciton is estimated from the following equation, since the intersystem crossing yield is nearly equal to unity in uranyl salts because of the heavy atom effect:[1,2]

$$n_0 = LI_0 \frac{0.6321\varepsilon_{3371}c}{\Delta S}, \quad (6)$$

where L is a loss factor of the laser pulse intensity caused by reflections off the surfaces of the lens, the sample tube, and the crystalline sample; ΔS is the area of the focused spot; I_0 is the number of photons per pulse; ε_{3371} is the molar extinction coefficient of the sample at the excitation wavelength; and c is the molar concentration of UN in the crystalline state. I_0 and ΔS were measured experimentally to be 1.0×10^{14} photons per pulse and 0.08 cm^2, respectively. From the crystal structure,[16] c was found to be 5.37 M.

When the laser intensity is greater than 3×10^{14} photons/pulse, the phosphorescence intensity is not proportional to the laser intensity. This saturation effect may be caused by two photon excitations (both simultaneous and stepwise), by reabsorption of the phosphorescence associated with the $T_n \leftarrow T_1$ transitions, and by ground state depletion.

The absorption spectrum of UN in CH_3CN solution and the uncorrected phosphorescence excitation spectrum of a UN crystal were measured at room temperature (295 K), the result is shown in Fig. 9. The vibrational structures of the spectra resemble each other, and the crystal shift is very small; thus, ε_{3371} of UN in the crystalline state is not much different from that in solution. Therefore, ε_{3371} for crystalline UN is assumed to be 9.2 M^{-1} cm^{-1}, the same as the molar extinction coefficient of UN in CH_3CN solution.

By substituting these experimental data in Eq. 6, n_0 was found to be 2.2×10^{18} cm^{-3} s^{-1}.[17] Since it is difficult to determine A experimentally,[6] it is assumed to be zero. This assumption only changes the calculated exciton hopping rate by a factor of two and the error caused by this assumption is smaller than possible experimental errors which accompany the determination of n_0 and, therefore, γ and λ as well.

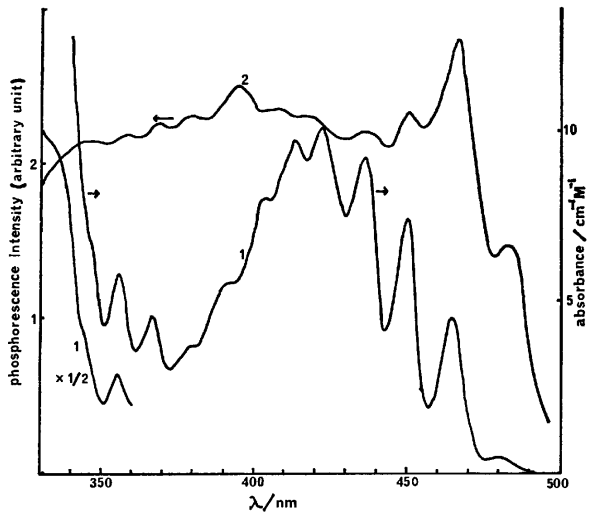

Fig. 9. Absorption spectrum of UN in CH_3CN solution (curve 1) and phosphorescence excitation spectrum of crystalline UN (curve 2) at 295 K.

With this assumption, we obtained 4.3×10^8 s^{-1} for λ at 295 K. This value is reasonable for the migration rate of a triplet exciton. From the values of λ and τ at 295 K, we deduce that the exciton travels over about 3×10^5 sites in crystalline uranyl nitrate during its lifetime.

Table 1. Characteristic data for triplet excitons in crystalline uranyl nitrate hexahydrate at 295 K

τ	697 μs
α	1.43×10^3 s^{-1}
γ	2.6×10^{-13} cm^3 s^{-1}
λ	4.3×10^8 s^{-1}
n_c	5.5×10^{15} cm^{-3}
R_c	352 Å
D	5.5×10^{-6} cm^2 s^{-1}
l	8800 Å
d	7.8×10^5 Å

In the same manner as was used in the preceding work,[6] we determined the critical concentration, n_c, the diffusion coefficient, D, the mean diffusion length, l, and the critical radius, R_c, for bimolecular quenching at room temperature (295 K). The results are shown in Table 1. The relations between these parameters are as follows:

$$n_c\gamma = \alpha, \quad \frac{4\pi}{3}(R_c)^3 n_c = 1, \quad D = 2a^2\lambda, \quad l = (2D\tau)^{1/2}, \quad (7)$$

where $a = V_0^{1/3}$ is the mean distance between neighboring sites and V_0 is the volume of a unit cell. This table shows that the mean diffusion length, l, is much smaller than the absorption depth of the exciting light, d, in crystalline uranyl nitrate, which was found to be $d = 7.8\times10^5$ Å by use of the relation $d = (2.303\varepsilon_{3371}c)^{-1}$. Therefore, almost none of the triplet excitons initially generated by the nitrogen laser pulse escape from the irradiated region during their lifetime. This justifies the neglect of the diffusion term,

$$\sum_{i,j} D_{ij} \frac{\partial^2 n(t,x)}{\partial x_{ij}^2},$$

in the equation determining the behavior of $n(t,x)$, *viz.*,

$$-\frac{dn}{dt} = \alpha n + \gamma n^2 + \sum_{i,j} D_{ij} \frac{\partial^2 n}{\partial x_{ij}^2}. \quad (8)$$

The neglect of the last term on the right hand side of Eq. 8 leads to Eq. 1. The diffusion coefficient of the triplet exciton at room temperature was obtained for anthracene (2×10^{-4} cm^2 s^{-1}),[18] pyrene (($8\pm4)\times10^{-4}$ cm^2 s^{-1}),[19] and *p*-dibromobenzene (($2\pm1)\times10^{-4}$ cm^2 s^{-1}).[20] The diffusion coefficient at room temperature obtained for the UN crystal in the present paper is about 100 times smaller than those in the three aromatic molecular crystals. The difference may be explained in the following way. The magnitude of the diffusion coefficient of the triplet exciton in the crystal is closely related to the exchange interaction between two neighboring molecules. The average distance between two neighboring molecules in the UN crystal is 10.6 Å which is much longer than those of anthracene (6.2 Å), pyrene (6.4 Å), and *p*-dibromobenzene (5.5 Å). Therefore the exchange interaction between two neighboring molecules and therefore the exciton hopping rate in the UN crystal are much smaller than those in anthracene, and *p*-dibromobenzene crystals.

The author wants to express his sincere gratitude to Professor Saburo Nagakura, Tokyo University, for his discussion and encouragement during the research. He also thanks Professor Haruo Hosoya of Ochanomizu University for the use of the HITACHI MPF spectrophotometer, and Dr. Akinori Inoue for the use of a program for obtaining γ. He also wants to express his thanks to Dr. John M. Morris, Melbourne University, for his critical reading.

References

1) E. L. Nichols and H. L. Howes, "Fluorescence of the Uranyl Salt," Carnegie Institution, New York (1919).

2) G. H. Dieke and A. B. F. Duncan, "Spectroscopic Properties of Uranium Compounds," National Nuclear Energy Ser. III-2, McGraw Hill Book Company Inc., New York (1949).

3) N. A. Tolstoi, A. P. Abramov, and I. N. Abramova, *J. Lumin.*, **1**, **2**, 330 (1970).

4) A. P. Abramov, I. N. Abramova, and N. A. Tolstoi, *Sov. Phys. Solid State*, **9**, 1516 (1968).

5) A. Bergman, M. Levine, and J. Jortner, *Phys. Rev. Lett.*, **18**, 593 (1967).

6) T. Kobayashi and S. Nagakura, *Mol. Phys.*, **24**, 695 (1972).

7) T. Kobayashi and S. Nagakura, *Mol. Cryst. Liq. Cryst.*, **26**, 33 (1974).

8) T. Kobayashi and S. Nagakura, *Chem. Lett.*, **1974**, 235.

9) S. Iwashima, T. Kobayashi, and J. Aoki, *Nippon Kagaku Kaishi*, **1972**, 686.

10) T. Kobayashi, S. Iwasima, S. Nagakura, and H. Inokuchi, *Mol. Cryst. Liq. Cryst.*, **18**, 117 (1972).

11) The spectra of UN at high and low density excitations at 77K are not shown, but they are quite similar to that at room temperature except that a slight sharpening of the bands are observed. The changes observed at 77K are quite similar to those at room temperature.

12) The reason why the vibrational band broadening is only observed in the spectra measured at 77K is as follows: The vibrational bands in the spectra measured at 295 and 201K are much broader than those measured at 77K, and the slight change which appears in the vibrational bands is more difficult to be detected for the broad spectra. So it is reasonble to consider that the undetectably slight vibrational band broadening is also occurring in the spectra mesured at higher temeratures.

13) More than 10^4 repetitions of high and low density excitations at the same spot of the crystal caused slight changes in the phosphorescence spectrum of the uranyl nitrate crystal. The following discussion uses only data obtained before the sample showed any irreversible change.

14) T. Kobayashi and S. Nagakura, *Mol. Cryst. Liq. Cryst.*, **25**, 153 (1974).

15) Since the phosphorescence spectra of UN in the crystalline state are quite similar to those in solution, the electronic state of the lowest triplet in the crystalline phase and that in solution are considered to be quite similar to each other. Therefore the absorption spectrum of T_1 shown in Fig. 9 is thought to be quite similar to that in the crystalline phase. From this it is assumed that the $T_n \leftarrow T_1$ absorption in the crystalline phase is the same as that in solution.

16) V. M. Vdovenko, E. V. Stroganov, A. P. Soklov, and V. N. Zandin, *Radiokhimiya*, **2**, 24 (1960).

17) This value is 12 times greater than 1.8×10^{-14} cm^3 s^{-1} the value determined by Tolstoi *et al.*[3]

Their value is erroneous for the following two reasons.

(1) The saturation effect was not taken into account and therfore, the number of excitons was overestimated and, hence, the value for γ was underestimated.

(2) The γ value of Tolstoi *et al.* results from their method of analysis of the experimental data. They determined γ from the initial slope of the phosphorescence decay curve. In practice, γ can not be determined with high enough accuracy by this method, because not enough data can be obtained with small errors in the short interval of time during which the initial slope is measured. In the present paper the exact solution of the equation was applied. To determine γ from the experimental data by using the exact solutions, one makes use of all the data points, not just the ones which are taken during the short time interval. Therefore the slopes can be determined from the experimental data with greater accuracy and, hence, γ can be calculated more accurately than by the method of Tolstoi *et al.*

Study of the Quasi-peaks in the Ion Cyclotron Double Resonance

Katsuyuki AOYAGI[1)]

JEOL Ltd., 1418 Nakagami, Akishima-shi, Tokyo 196

(Received August 16, 1976)

Quasi-peaks which do not correspond to any reactant ion in the ion-molecule reaction were observed in the ion cyclotron double-resonance spectrum. The field-sweep quasi-ICDR spectrum was also observed. Expressions giving the frequencies of the quasi-peaks observed in the ion cyclotron double-resonance spectrum were obtained; the results agreed with those obtained previously. Both the ion mass and ion drift-voltage dependences of the quasi-peaks were shown. A close agreement between the calculated and measured values was obtained. A method to repress the quasi-peaks is discussed.

It has been demonstrated that ion cyclotron double-resonance (ICDR) spectroscopy is useful in elucidating the mechanism of ion-molecule reactions.[2)] In an ion-molecule reaction, $R^+ + M \longrightarrow P^+ + N$, R^+ is the reactant ion, P^+, the product ion, and M and N, the reactant molecule and the neutral product. The signal from the product ion can be continuously monitored while an irradiating rf field is swept through the range of cyclotron frequencies. When the irradiating frequency matches the cyclotron frequency of the reactant ion, the energy from the irradiating rf field is absorbed by the reactant ion and the translational energy of reactant ion is increased. Since most reaction-rate constants are dependent on the ion velocity, the concentration of the product ion will change, and this change is presented as a peak in the ICDR spectrum. If the product ion is observed at its cyclotron frequency of f_1 while the irradiating frequency, f_2, is swept, the signals will be observed for values of f_2 corresponding to the cyclotron-resonance frequencies of the reactant ions which yield the product ion. At a low irradiating-field strength, a change in the monitored ion intensity reflects a change in the reaction rate constant as the kinetic energy of reactant ion is increased.[3)] At a high irradiating-field strength, however, intense peaks which do not correspond to any reactant ion are observed in the ICDR spectrum. These quasi-peaks accompanying a negative response are recorded symmetrically about the irradiating frequency of $f_2=f_1$. These peaks have been recognized as spurious peaks by Freiser, McMahon, and Beauchamp.[4)] However, it is important to recognize the detailed nature of these quasi-peaks in order to avoid an erroneous interpretation of the ICDR spectrum.

The motion of an ion which moves under the simultaneous application of the magnetic and electric fields appropriate for an ICR cell has been described in detail.[5)] The electrostatic trapping field of the same polarity as the ions under investigation is used to prevent ion loss in the direction parallel to the magnetic field. The ions execute an oscillatory motion in the trapping field. The frequency, f_t, of this oscillatory motion is given by[6,7)]

$$f_t = \frac{1}{2\pi}\left[\frac{8e}{m(d_x^2+d_z^2)}\left(V_t - \frac{V_{ud}+V_{ld}}{2}\right)\right]^{1/2}, \qquad (1)$$

where e/m is the charge-to-mass ratio of an ion, d_x, the spacing between the drift plates, d_z, the spacing between the trapping plates, V_t, the trapping voltage, and V_{ud} and V_{ld}, the drift voltages applied to the upper- and lower-drift plate respectively. The quasi-peaks discussed herein were observed using a square-type cell ($d_x=d_z$); the cell has been described in detail previously.[2d)]

In the present paper, we wish to report the features of the quasi-peaks, especially the drift-voltage dependence of their resonant frequencies for the quasi-peaks, and present a method to suppress them.

Experimental

The quasi-ICDR spectra recorded with a JEOL JIC-3B spectrometer have been described in detail.[7)] The ICR cell was of a three-section square type ($2.5\times2.5\times14$ cm) similar to the conventional one.[2a)] Single-resonance spectra of krypton and *t*-butyl alcohol were obtained by fixing the marginal oscillator frequency of 100.00 kHz, while that of 2-methylpropene was obtained by means of a Twin-T bridge detector with the oscillator frequency fixed of 99.986 kHz and sweeping the magnetic field using a field-modulation phase-sensitive detection scheme. The double-resonance experiments were carried out in the pulsed-modulation mode while sweeping the frequency of the irradiating oscillator. The field-sweep quasi-ICDR spectra of 2-methylpropene were obtained by fixing the observing and irradiating frequencies at 99.986 and 118.00 kHz respectively, using a pulsed-modulation mode of the irradiating field. The other experimental conditions were as follows: energy of ionizing electron, 70 eV; modulation frequency, 80 Hz; trapping voltage, +0.25 V; upper analyzer-drift voltage, 0 V, and lower analyzer-drift voltages in the −1.2—0 V range.

Results and Discussion

a) Frequency-sweep Quasi-ICDR Spectra. The quasi-ICDR spectrum of the *m/e* 84 ion of krypton at 2×10^{-5} Torr is shown in Fig. 1. Irradiation at $f_2=120.9$ and 79.6 kHz resulted in a decrease in the intensity of the peak due to the ion with *m/e* 84. The peaks observed with the frequencies of 120.9 and 79.6 kHz correspond to the *m/e* 69.5 and 105.5 ions which were not present in the single-resonance spectrum of krypton. Therefore, these peaks are not the actual double-resonance peaks. The spectrum exhibits the quasi-peaks symmetric about the frequency of the irradiating rf field of $f_2=f_1$.

Figure 2 shows the quasi-icdr spectrum of $(CH_3)_2$-COH^+ (*m/e* 59) of *t*-butyl alcohol obtained at 2.2×10^{-5} Torr. Irradiation at $f_2=124.6$ and 76.0 kHz caused a decrease in the intensity of the peak due to the ion with *m/e* 59. The spectrum indicates the quasi-peaks at the distances of f_1+2f_t and f_1-2f_t respectively from

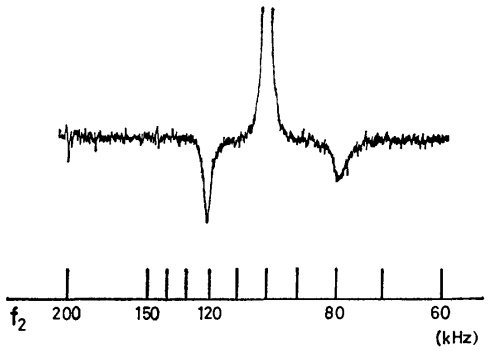

Fig. 1. Frequency-sweep quasi-ICDR spectrum of the *m/e* 84 ion of krypton with the pressure of 2×10^{-5} Torr, the observing rf field of 0.04 V/cm, the irradiating rf field of 0.32 V/cm, the trapping voltage of +0.25 V, and the upper and lower analyzer-drift voltages of 0 and −0.55 V. The large spike appearing at the 100 kHz frequency results from the interaction of the irradiating and observing oscillators, while the small spike at the 200 kHz frequency is due to the irradiating oscillator exciting the first sub-harmonic of the observing frequency.

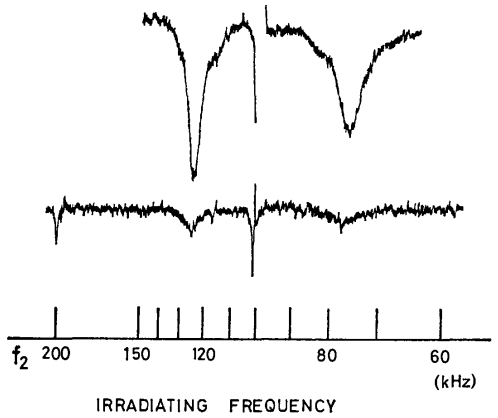

Fig. 2. Frequency-sweep quasi-ICDR spectrum of the $(CH_3)_2COH^+$ (*m/e* 59) of *t*-butyl alcohol with the pressure of 2.2×10^{-5} Torr; the other conditions are identical with those under which Fig. 1 was recorded. The sharp spike appearing at the 100 kHz frequency results from the interaction of the irradiating and observing oscillators, while the small feature at the 200 kHz frequency is due to the irradiating oscillator exciting the first overtone of the marginal oscillator.

the frequency of $f_2=f_1$. The peak observed with the frequency of 124.6 kHz corresponds to the *m/e* 47.3 ion, which was not present in the single-resonance spectrum of *t*-butyl alcohol. The *m/e* 59 ion derived from electron-impact ionization of *t*-butyl alcohol is an α-cleavage product that is, a primary ion.[8] Therefore, these peaks observed with the frequencies of 76.0 and 124.6 kHz corresponding to the *m/e* 47.3 and 77.6 ions are not the actual double-resonance peaks.

When ICDR studies were made of 2-methylpropene, the following results were obtained. In the case of $C_3H_5^+$ (*m/e* 41), irradiation at $f_2=123.7$ and 75.4 kHz resulted in a decrease in the intensity of the peak due

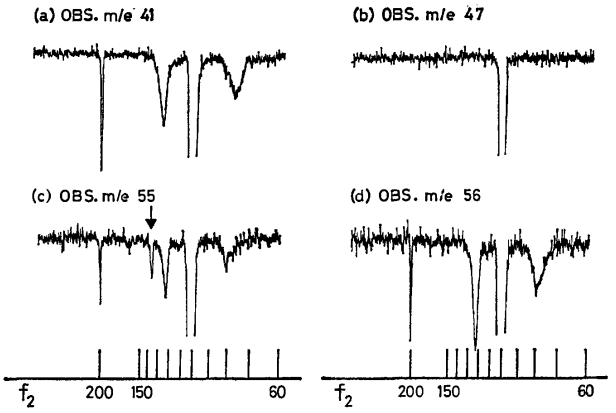

Fig. 3. (a) Frequency-sweep quasi-ICDR spectrum of the $C_3H_5^+$ (*m/e* 41) of 2-methylpropene with the pressure of 3×10^{-5} Torr, the observing rf field of 0.02 V/cm, the irradiating rf field of 0.24 V/cm, the trapping voltage of +0.25 V, and the upper and lower analyzer-drift voltages of 0 and −0.3 V. (b) Frequency-sweep quasi-ICDR spectrum of the *m/e* 47 ion of 2-methylpropene with the conditions are identical with those under which (a) was recorded. The ion corresponding to *m/e* 47 is absent from the single-resonance spectrum of 2-methylpropene; therefore, the quasi-peaks are not observed either. (c) Frequency-sweep quasi-ICDR spectrum of the $C_4H_7^+$ (*m/e* 55) of 2-methylpropene with the conditions are identical with those under which (a) was recorded. The peak at 134.6 kHz (indicated by an arrow) is the actual double-resonance peak corresponding to the reaction producing *m/e* 55. (d) Frequency-sweep quasi-ICDR spectrum of the $C_4H_8^+$ (*m/e* 56) of 2-methylpropene with the conditions are identical with those under which (a) was recorded. In this figure, the large spikes appearing at the 100 kHz frequency result from the interaction of the irradiating and observing oscillators, while the sharp spikes appearing at the 200 kHz frequency are due to the irradiating oscillator exciting the first sub-harmonics of the observing frequency.

to the $C_3H_5^+$, as is shown in Fig. 3a. Irradiation at $f_2=121.3$ and 79.6 kHz give rise to a decrease in the intensity of the peak due to the $C_4H_7^+$ (*m/e* 55), as is shown in Fig. 3c. In another case, that of $C_4H_8^+$ (*m/e* 56), the intensity of the peak due to the $C_4H_8^+$ is decreased by the irradiation at $f_2=121.1$ and 79.2 kHz, as is shown in Fig. 3d. The peaks observed with the frequencies of 123.7 and 75.4 kHz; 121.3, and 121.1 kHz correspond to the *m/e* 33.1 and 54.4; *m/e* 45.3, and 46.2 ions respectively, but these ions were absent from the single-resonance spectra. The quasi-peaks appearing at the frequencies of 79.6 and 79.2 kHz corresponding to the *m/e* 69.1 and 70.7 ions are not associated with any resonable ion-molecule reaction. Therefore, these peaks observed in the double-resonance spectra are also false peaks.

b) Frequencies of Occurrence of the Quasi-peaks.

From the experimental results described above, it follows that the quasi-peaks occur when the difference between the observing and irradiating frequencies is equal to $2f_t$, *i.e.*; $|f_1-f_2|=2f_t$, where f_t is given by

Eq. 1. This result agrees with that of Freiser *et al.*[4]

In the ICR spectrometers,[2a-d] naked electric wires are usually employed as the rf feeders in the vacuum chamber of the icr detector, because the coaxial cable used in a ultra high-vacuum is absent. Similarly, a naked wire is also employed to feed the electrostatic trapping voltage to the icr cell. As a result of the use of the naked wires, the observing and irradiating rf voltages are picked up by the wire for trapping voltage. In the ICR cell, thus, leakage of the rf field results from the rf voltages superimposed on the trapping voltage. Therefore, the generation of quasi-peaks is considered to be caused by the ejection of the ion from the trapping field by the leakage of the rf field. That is, when the observing frequency is fixed and the irradiating frequency is swept, the oscillatory motion of an ion increases in its amplitude in the trapping field at $|f_1-f_2|=2f_t$. Then, the ion is neutralized when it strikes the trapping plate, and the ion is ejected from the trapping field. Therefore, the quasi-peaks are observed with the frequencies of the irradiating rf field which are given by

$$f_2 \doteq f_1 \pm 2f_t, \qquad (2)$$

and the frequency-sweep quasi-ICDR spectrum is recorded as the quasi-peaks accompanying the negative response. Equation 2 has been reported in a slightly different form.[4] Using as practical units V_t, V_{ud}, and V_{ld} in volts, M in atomic mass unit, and f_1, f_2, and f_t in Hz, the frequencies, f_{2q}, of the occurrence of the quasi-peaks observed are given by

$$f_{2q} = f_1 \pm 246\left[\frac{V_t-(V_{ud}+V_{ld})/2}{M}\right]^{1/2} \text{ kHz}. \qquad (3)$$

The frequencies of the occurrence of all the quasi-peaks described in the preceding item are calculated from Eq. 3; they are listed in Table 1. The calculated results agree well with the experimental values.

As predicted by Eq. 3, the frequencies of the occurrence of the quasi-peaks vary with the square root of the ion mass or the difference between the trapping voltage and half of the drift voltage. On the other hand, the frequency of the irradiating rf field of the actual double-resonance peak is independent of the trapping and drift voltage. The variation in the frequency of occurrence of the quasi-peak observed in 2-methylpropene with the square root of the ion mass is shown in Fig. 4. Under these conditions the trapping and drift voltages remain constant; the observation of several ionic species confirms the inverse linear variation in the frequency of the occurrence of the quasi-peaks with the square root of the ion mass, as predicted by Eq. 3. Moreover, the variation in the frequency of the occurrence of the quasi-peak of $C_4H_7^+$ (*m/e* 55) in 2-methylpropene with

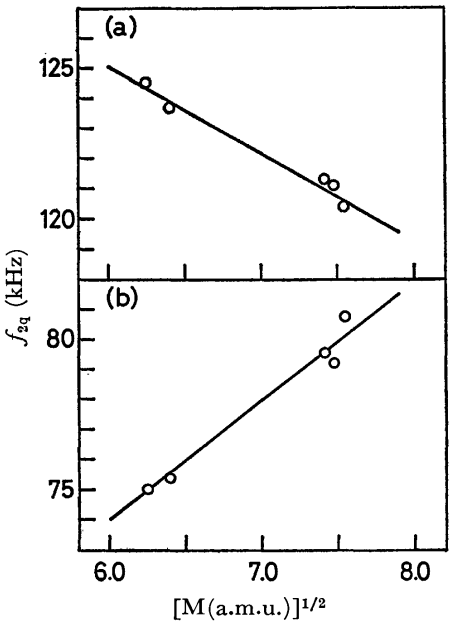

Fig. 4. Linear variation in the frequency of occurrence with the square root of the ion mass for 2-methylpropene. (a) $f_{2q}>f_1$, (b) $f_{2q}<f_1$.

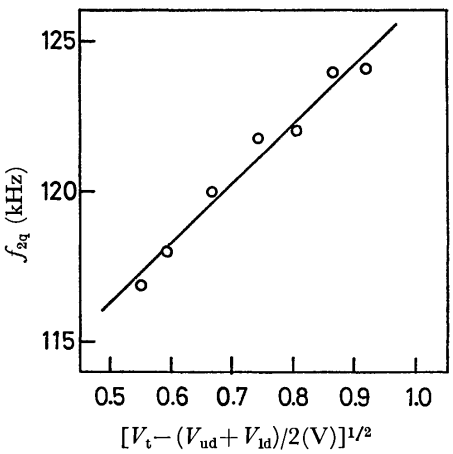

Fig. 5. Linear shift in the frequency of occurrence with the square root of the difference between the trapping voltage and half of the analyzer-drift voltage for $C_4H_7^+$. The trapping voltage is fixed at +0.25 V.

Table 1. Observed and calculated frequencies for some ionic species

Compound	Observed ion *m/e*	Species	Frequencies of occurrence (kHz) Obsd		Calcd	
Krypton	84		120.9	79.6	119.45	80.55
t-Butyl alcohol	59	$(CH_3)_2COH^+$	124.6	76.0	123.21	76.80
2-Methylpropene	39	$C_3H_3^+$	124.5	≈75	124.89	75.07
	41	$C_3H_5^+$	123.7	75.4	124.28	75.69
	55	$C_4H_7^+$	121.3	79.6	120.96	79.01
	56	$C_4H_8^+$	121.1	79.2	120.78	79.20
	57	$C_4H_9^+$	120.4	80.8	120.59	79.38

the square root of the difference between the trapping voltage and half of the drift voltage is illustrated in Fig. 5. When the trapping voltage is fixed, the observation of the quasi-peaks at several drift voltages confirms the linear variation in the frequency of the occurrence of the quasi-peak with the square root of the difference between the trapping voltage and half of the drift voltage.

Compared with the quasi-peaks, the most remarkable feature of the actual double-resonance peak is the constancy of the frequency of the irradiating rf field. The frequencies of the irradiating rf field at which the actual double-resonance peak corresponding to the ion-molecule reaction,

$$C_3H_5^+ + C_4H_8 \longrightarrow C_4H_7^+ + C_3H_6,$$

is observed at several drift voltages, are independent of the drift voltage, as Table 2 shows.

TABLE 2. OBSERVED AND CALCULATED FREQUENCIES AS FUNCTIONS OF THE ANALYZER-DRIFT VOLTAGE FOR THE $C_4H_7^+$ OF 2-METHYLPROPENE

Analyzer-drift voltages (V)		Frequencies of occurrence (kHz)		Irradiating frequencies(kHz) Obsd in $C_4H_7^+$—$[C_3H_5^+]$[a]
Upper	Lower	Obsd	Calcd	
0	−1.2	≈124	124.59	b)
0	−1.0	124.0	123.44	134.30
0	−0.8	122.0	122.24	134.87
0	−0.6	121.85	120.96	134.60
0	−0.4	120.10	119.61	134.60
0	−0.2	118.0	118.15	135.0
0	−0.1	116.9	117.38	134.4
0	−0.0	b)	116.57	b)

a) $C_4H_7^+ - [C_3H_5^+]$ indicated that $C_4H_7^+$ is observed when $C_3H_5^+$ is irradiated.
b) Too weak for the frequency to be determined.

c) Field-sweep Quasi-ICDR Spectrum. If the magnetic field, H, is swept, while the observing and irradiating frequencies described in Eq. 3 are fixed and the trapping and drift voltages are held constant, an oscillatory ion in the trapping field is translationally excited at the field of $H=aM$ (a is the costant); then, the field-sweep quasi-ICDR spectrum is obtained. Figure 6 shows the field-sweep quasi-ICDR spectra of 2-methylpropene obtained by sweeping the magnetic field with $f_2/f_1=118.00/99.986$. The spectrum exhibits the quasi-peaks of each ion which is observed in the single-resonance spectrum, but the relative intensity ratio of the quasi-peaks is not proportional to the ionic concentrations of each ion, because the exact f_2/f_1 ratios are not satisfied for any of them except for the m/e 55 ion. The quasi-peaks intensities decrease with a decrease in the strength of the irradiating rf field. This behavior of the quasi-peak intensity indicates that the generation of quasi-peaks can be minimized by the reduction of the leakage of the rf field. By using the shielded feeders, the quasi-peak intensity decreased by approximately 80 db compared with the previous result. This experimental result reveals that the generation of quasi-peaks is due to the ejection of the ion from the trapping field by the leakage of the rf field.

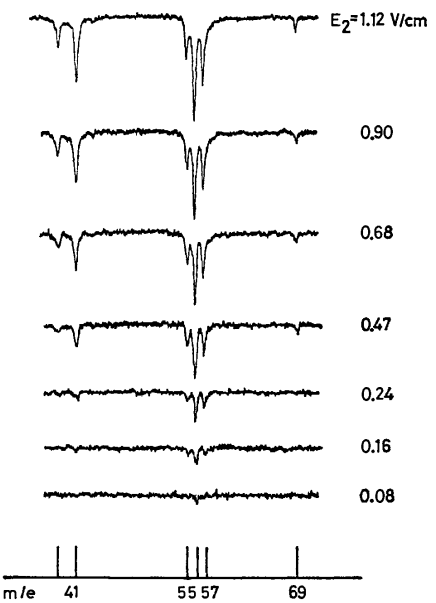

Fig. 6. Field-sweep quasi-ICDR spectra of 2-methylpropene at various irradiating field strengths. f_2/f_1 is fixed in the ratio of 118.00/99.986. The pressure is 3×10^{-5} Torr; trapping voltage, +0.25 V; upper and lower analyzer-drift voltages, 0 and −0.2 V.

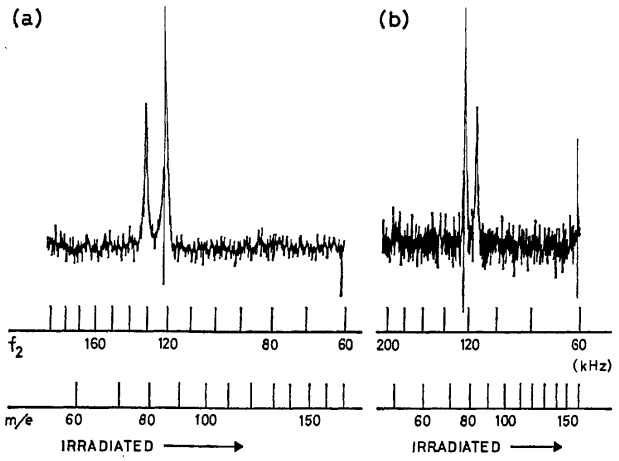

Fig. 7. (a) Double-resonance spectrum of $C_6D_6^+$ in a 1: 1 mixture of benzene and benzene-d_6 with the pressure of 2×10^{-5} Torr, the observing rf field of 0.05 V/cm, the irradiating rf field of 0.24 V/cm, the trapping voltage of +0.25 V, and the upper and lower analyzer-drift voltages of 0 and −0.4 V. (b) Double-resonance spectrum of $C_6H_6^+$ in a 1: 1 mixture of benzene and benzene-d_6 with the conditions are identical with those under which (a) was recorded. In this figure, the large spikes appearing at the 122.8 kHz frequency result from the interaction of the irradiating and observing oscillators, while the sharp spikes at the 61.4 kHz frequency are due to the irradiating oscillator exciting the first sub-harmonics of the observing frequency.

The double-resonance spectra of the $C_6D_6^+$ and $C_6H_6^+$ molecular ions in a mixture of benzene-d_6 and benzene (1: 1 ratio) are shown in Figs. 7a and 7b respectively.

The irradiation of $C_6H_6^+$ caused an increase in the intensity of $C_6D_6^+$, and the intensity of $C_6H_6^+$ was increased when $C_6D_6^+$ was irradiated. These double-resonance responses indicate that the charge-transfer reaction occurs between $C_6D_6^+$ and $C_6H_6^+$ as follows:

$$C_6H_6^+ + C_6D_6 \rightleftharpoons [C_6H_6 \cdot C_6D_6]^+ \rightleftharpoons C_6D_6^+ + C_6H_6.$$

This charge-transfer reaction corresponds to the equilibrium reaction reported by Field, Hamlet, and Libby.[9] The double-resonance spectra were obtained using a strong irradiating rf field (the strength of the irradiating field is 4.8 times as strong as that of the observing field), but the quasi-peaks are not observed in the spectra.

We may conclude from the experimental results described above that the quasi-peaks are caused by the leakage of the rf field, especially by the leakage of the strong irradiating rf field. The suppression of the leakage of the rf fields is important for eliminating the quasi-peaks and thus for the proper interpretation of the double-resonance spectra.

References

1) Present address: Taiatsu Industry Co., Ltd., 3-27-9 Honkomagome, Bunkyo-ku, Tokyo 113.

2) a) J. L. Beauchamp, *Ann. Rev. Phys. Chem.*, **22**, 527 (1971); b) J. H. Futrell, "Dynamic Mass Spectrometry," Vol. 2, ed by D. Price, Heyden and Son, New York (1971); c) H. Hartmann, K. H. Lebert, and K.-P. Wanczek, *Fortscher Chem. Forsh.*, **43**, 57 (1973); d) K. Aoyagi, *Bunseki-kiki*, **10**, 703 (1972), and "Kohbunshi-gohsei to Kiki-bunseki," ed by K. Hayashi, Sankyo-Shuppan, Tokyo (1976), Chap. 6.

3) J. L. Beauchamp and S. E. Buttrill, Jr., *J. Chem. Phys.*, **48**, 1783 (1968).

4) B. S. Freiser, T. B. McMahon, and J. L. Beauchamp, *Int. J. Mass Spectrom. Ion Phys.*, **12**, 249 (1973).

5) K. Aoyagi, *Bull. Chem. Soc. Jpn.*, **47**, 519 (1974).

6) S. Fujiwara, K. Aoyagi, and T. Miyamae, *Bull. Chem. Soc. Jpn.*, **43**, 561 (1970).

7) K. Aoyagi, K. Hayashi, and J. Sohma, *Bull. Fac. Eng. Hokkaido Univ.*, **62**, 65 (1971).

8) J. L. Beauchamp, M. C. Caserio, and T. B. McMahon, *J. Am. Chem. Soc.*, **96**, 6243 (1971).

9) F. H. Field, P. Hamlet, and W. F. Libby, *J. Am. Chem. Soc.*, **89**, 6035 (1967); *ibid.*, **91**, 2839 (1969).

Stark Effect on the Electronic Bands of a Symmetric-top Molecule

Yoshito AMAKO, Yoshi-ichi SATO, and Akiyoshi WATANABE
College of General Education, Tohoku University, Sendai 980

(Received April 4, 1977)

Calculations have been performed on the energy matrix of a rigid symmetric-top molecule, HCHO, in order to determine the transition energies and intensities of the rotational sub-bands of the electronic spectrum under various magnitudes of external electrostatic fields. Though HCHO is an asymmetric-top molecule, the rotational structure of the 3390 Å band of this molecule is close to that of a perpendicular band of a symmetric-top molecule, at least, for not too small values of K. The variation in the band structures with the applied fields can be illustrated by the behavior of several selected bands, ^{p}P, ^{p}Q, ^{r}R, and ^{r}Q. Below 100 kV/cm, the overall Stark splittings have been linearly dependent on the field strength, regardless of the branch types. Over 100 kV/cm, however, a deviation from the linear dependence has been found for a certain branch. Changes in the band shape have appeared at such small values of external fields that no deviation from the linear field dependence of the overall Stark splitting has been observed. Such changes are dependent on the branch types, especially in the cases of branches with small J values and with $K<J$. The intensity enhancement of some forbidden bands has also been observed, the magnitude of which is proportional to the square of the field strength below 100 kV/cm. However, the relation between the intensity enhancement and the electric fields has been found to be complicated at fields over 100 kV/cm, the enhanced intensity being proportional to a coupled sum of E^2 and higher terms. At a fixed electric field, a linear relation has been found between the overall Stark splitting and the various μ values assumed for the excited state. The analysis of the data has enabled us to determine the electric dipole moment of the lowest $n\rightarrow\pi^*$ excited state of HCHO as 1.65 D.

Electric dipole moments in excited electronic states of gaseous molecules have been measured by means of electric-field-induced spectra, or the optical Stark effect.[1] When an electric field is applied to a molecule with a fine rotational structure in the electronic spectrum, some rotational lines may split into their Stark components. The splitting will be a function of the magnitude of the applied field and the dipole moments of the molecule in both states related to the transition. Thus, this method affords an important means for us to obtain some exact structural information on the short-lived excited molecules as well as on the ground-state molecules.

The first-order perturbation theory is usually used for the estimation of the dipole moments of electronic excited states from the Stark splittings of a symmetric-top molecule. However, the value of the splitting calculated on the basis of this theory differs greatly from the one observed at high electric fields, and sometimes gives a significant discrepancy even at low electric fields.

Therefore, in order to improve the calculation, we need to include higher-order terms in the perturbation theory. From this point of view, Shirley[2] has given an extensive treatment of the energy levels for all the rotational states through $J=4$, obtained from the direct diagonalization of the energy matrix of a rigid symmetric-top molecule under an electric field. On the other hand, as for an asymmetric-top molecule, West and Mizushima[3] have calculated the Stark effect of the lower rotational levels of H_2S and SO_2. However, both these calculations have been carried out only for molecules in one electronic state, *i.e.*, the electronic ground state.

Lombardi[4] was the first to make calculations of the Stark splittings and the band shapes of certain selected rotational sub-branches associated with *an electronic transition* of an asymmetric-top molecule under an electric field. In principle, Lombardi's calculation appears to cover all cases, and so it may seem unnecessary to do a similar calculation on a symmetric-top molecule.

However, for asymmetric-top molecules, the Stark effect is essentially of the second order, while it is of the first order for symmetric-top molecules. Moreover, so far there have been no such calculations made on symmetric-top molecules or on asymmetric-top ones whose behavior may be actually considered to be those of symmetric-top ones. For these molecules, it will be necessary to get detailed information about the Stark effect on their electronic transitions, because so far there has been no discussion on how large magnitudes of electric fields can make invalid the results obtained by the first-order perturbation theory, on how the band shapes in various branches may change with the electric fields, and on how the forbidden bands of a symmetric-top molecule in a zero field can get their intensities with electric fields, *etc.*

Moreover, the recent progress of very high resolution spectroscopy[5] free from Doppler broadening, especially the progress of a tunable cw dye laser technique, has attracted much attention. Then, also in the very-high-resolution spectra of the Stark splitting of electronic bands, it would be necessary to know the detailed M structures rather than the overall doublet splitting usually observed in moderately-high-resolution spectra, even though such very-high-resolution spectroscopy has not yet been well established.

In consideration of these circumstances, our calculation has been performed with special interest taken in the details of the intensity variation of each Stark component in different types of transitions with the field strengths and in the limits of the application of the perturbation theory for a symmetric-top molecule under an external electric fields.

Theoretical

The main program of the diagonalization of the energy matrix of a symmetric-top molecule under an external electric field closely parallels Shirley's. However, here we need eigenfunctions for the intensity calculation as well as the eigenvalues of the energy matrices for each set of J, K, and M. Therefore, we must directly diagonalize the fixed dimensions of the energy matrices.

The term values of each rotational state are expressed as

$$F(\mathrm{II}) = B(\mathrm{II}) \times E(\mathrm{II}, J, K, M) + \{A(\mathrm{II}) - B(\mathrm{II})\} \times K^2, \quad (1)$$

where $A(\mathrm{II})$ and $B(\mathrm{II})$ are the rotational constants of the related states and where $E(\mathrm{II},J,K,M)$ are the eigenvalues of the matrix to be mentioned below. The frequencies of the rotational bands associated with an electronic transition are given by

$$\nu = \nu_0 + F(2) - F(1), \quad (2)$$

where ν_0 is the frequency of vibronic origin.

The energy matrix for the determination of $E(\mathrm{II},J,K,M)$ is

$$\begin{vmatrix} a_1-E & \sqrt{b_2} & 0 & \cdot & \cdot \\ \sqrt{b_2} & a_2-E & \sqrt{b_3} & \cdot & \cdot \\ 0 & \sqrt{b_3} & a_3-E & \cdot & \cdot \\ \cdot & \cdot & \cdot & \cdot & \cdot \\ \cdot & \cdot & \cdot & \cdot & \cdot \end{vmatrix} = 0, \quad (3)$$

where

$$a_k = (J_0+k-1)\times(J_0+k) - \frac{R(\mathrm{L},\mathrm{II})\times M\times K}{(J_0+k-1)\times(J_0+k)}, \quad (4)$$

$$b_k = \frac{R(\mathrm{L},\mathrm{II})^2\times\{(J_0+k-1)^2-K^2\}\times\{(J_0+k-1)^2-M^2\}}{(J_0+k-1)^2\times\{4\times(J_0+k-1)^2-1\}}, \quad (5)$$

and

$$R(L,\mathrm{II}) = \mu(\mathrm{II})\times V(L)/B(\mathrm{II}).$$

Throughout these equations, the notation II is used to distinguish the ground state (II=1) or the excited state (II=2). $\mu(\mathrm{II})$ denotes the dipole moment of the ground or excited state, and $V(L)$, various field strengths, with $L=1, 2, 3, \cdots$ J_0 is the lowest J value for the special set of the K and M quantum numbers; it is equal to the larger of the two quantities, $|K|$ and $|M|$. For example, $J_0=5$ for each set of $|K|=0$—5 and $|M|=5$.

The energy matrices are diagonal for the K and M quantum numbers, but not for the J quantum number because the nondiagonal element, b_k, induces the mixing between the rotational states of $\Delta J=\pm1$, $\Delta K=\Delta M=0$. Therefore, the exact energy matrices for each set of K and M are infinite in dimensions. For the purpose of computation they must be truncated. The truncated matrices of definite dimensions are then expanded to give two types of continued fractions, both of which are solved by an iteration method improved by the application of the Newton-Raphson procedure discussed by Swalen and Pierce.[6] A program which has been written for this purpose is available from the authors on request.

Table 1. Comparison of the eigenvalues for the energy matrices of 5×5 and 6×6[a]

II	L	J_0	J	K	M	$K2$	$W(k2)$	$W(k2)$
1	9	5	5	5	5	1	29.24844	29.24844
1	9	5	6	5	5	2	41.46239	41.46239
1	9	5	7	5	5	3	55.59698	55.59698
1	9	5	8	5	5	4	71.68682	71.68682
1	9	5	9	5	5	5	89.75537	89.74968
1	9	5	10	5	5	6		109.8012

a) The first and second columns show those eigenvalues obtained for the ground state (II=1) and under an applied electric field of $V(L=9)=28.1$ kV/cm. The last two columns show the eigenvalues of the energy matrices of 5×5 and 6×6 respectively.

In the present calculation, we truncated all the matrices into 5×5, whose eigenvalues are classified by J_0, J_1, J_2, J_3, and J_4, J_0 being the lowest. However, as is shown in Table 1, the truncation of the matrices into 5×5 will remain a sufficiently good approximation for at least the lower four states from J_0 to J_3 unless extremely high fields are achieved. Table 1 shows the comparison of each eigenvalue of the 5×5 and 6×6 matrices for the states of $J_0=5$, $K=5$, and $M=5$ at an applied field of $V(9)=28$ kV/cm.

Table 2. Rotational sub-states J_{KM} calculated in the present work[a]

J_0	Rotational sub-states
0	0_{00}, 1_{00}, 2_{00}, 3_{00} ;
1	1_{01}, 2_{01}, 3_{01}, 4_{01} ; 1_{11}, 2_{11}, 3_{11}, 4_{11} ; 1_{1-1},2_{1-1},3_{1-1},4_{1-1};
2	2_{02}, 3_{02}, 4_{02}, 5_{02} ; 2_{12}, 3_{12}, 4_{12}, 5_{12} ; 2_{22}, 3_{22}, 4_{22}, 5_{22} ; 2_{1-2},3_{1-2},4_{1-2},5_{1-2}; 2_{2-2},3_{2-2},4_{2-2},5_{2-2};
3	3_{03}, 4_{03}, 5_{03}, 6_{03} ; 3_{13}, 4_{13}, 5_{13}, 6_{13} ; 3_{23}, 4_{23}, 5_{23}, 6_{23} ; 3_{33}, 4_{33}, 5_{33}, 6_{33} ; 3_{1-3},4_{1-3},5_{1-3},6_{1-3}; 3_{2-3},4_{2-3},5_{2-3},6_{2-3}; 3_{3-3},4_{3-3},5_{3-3},6_{3-3};

a) The energy matrices are symmetric for K and M. Therefore, the eigenvalues for $J_{\pm K\pm M}$ and $J_{\pm M\pm K}$ are the same, but the state energies of Eq. 1 are different for $|K| \neq |M|$. In the table the states of $J_{\pm M\pm K}$ and also of higher J_0 values than $J_0=3$ are not written because the space is limited, though we have calculated all the states through $J_0=9$.

In the case of $J_0=5$, the present truncation limits the states of $K=5$ and $M=5$ to the states of $J=5$ to 8. The highest state 9_{55}, (in the notation of J_{KM}), of the 5×5 matrix has been omitted because the approximation obtained is not good enough compared with that for lower states, as is shown in Table 1. Accordingly, if we take the energy matrices to be of definite dimensions, we will inevitably get only limited information for each set of K and M, as is shown in Table 2. Table 2 shows the rotational sub-states of J_{KM} calculated by the present method, but the states of $J_{\pm M\pm K}$ and J_0 values higher than $J_0=3$ are not shown.

The eigenfunctions corresponding to each eigenvalue have been obtained by solving the simultaneous equations derived from Eq. 3 and by using the normalization conditions. In the present approximation, the general form of the eigenfunctions of a symmetric-top molecule

under the Stark effect is written as

$$\Psi(\mathrm{II}, J_0^{KM}) = T(\mathrm{II}, 1, 1)\times\phi(J_0^{KM}) + T(\mathrm{II}, 2, 1)\times\phi(J_1^{KM}) + \cdots + T(\mathrm{II}, 5, 1)\times\phi(J_4^{KM}), \quad (7)$$

where the superscript in J^{KM} denotes a state that has a definite K and M, and $T(\mathrm{II}, \xi+1, \eta+1)$, the coefficients of the symmetric-top bases, $\phi(J_\xi^{KM})$, in $\Psi(\mathrm{II}, J_\eta^{KM})$.

The transition moment, TM, of a rotational sub-band associated with an electronic transition is, then, given by

$$TM = \int\Psi(1, J_{\eta''}^{K''M''})\times\phi_{Fg}\times\Psi(2, J_{\eta'}^{K'M'})\times d\tau = \sum_{\xi'',\xi'} T(1, \xi''+1, \eta''+1)\times T(2, \xi'+1, \eta'+1) \times\int\underline{\phi(J_{\xi''}^{K''M''})\times\phi_{Fg}\times\phi(J_{\xi'}^{K'M'})\times d\tau}, \quad (8)$$

where ϕ_{Fg} are the direction cosines between space-fixed F and molecule-fixed g coordinate axes and where $''$ and $'$ refer to the ground and excited states respectively.

The transition intensity, I, is written as

$$I = |TM|^2\times\exp\{-E(1, J'', K'', M'')/kT\}. \quad (9)$$

In Figs. 1—4 the transition intensities have been calculated with Eqs. 8 and 9, although the matrix element associated with the direction consine, the integral underlined in Eq. 8, is taken from the table given by Allen and Cross.[7]

Results and Discussion

To carry out the numerical calculation with the program stated in the previous section, it is necessary to know the rotational constants of the ground and excited states of a symmetric-top molecule.

In the previous experimental work,[8] we studied the Stark effect on the 3390 Å band of formaldehyde. Several reports[1] have also been given on the same problem of this molecule. In this calculation we shall take the rotational constants of formaldehyde given in Table 3. The following discussion will be mainly concerned with the Stark effect on the spectrum of formaldehyde.

Table 3. Rotational constants of H_2CO[a]

States	a	b	c
$^1A''$	8.7517	1.1245	1.0123
$^1A_1$	9.4053	1.2953	1.1342

a) Taken from "Molecular Spectra and Molecular Structure," III, ed by G. Herzberg, Van Nostrand Reinhold Company (1966), p. 612.

Strictly, formaldehyde is an asymmetric-top molecule, but it is very close to a symmetric-top one, the two larger moments of inertia being nearly equal and much greater than the moment of inertia around the C=O axis. When the value of K is not too small, the rotational structure of the 3390 Å band is almost the same as that of a perpendicular band of a symmetric-top molecule* whose rotational constants are taken as $A=a$, $B=(b+c)/2$ at both states related to the transition, where a, b, and c are those of formaldehyde.

For the perpendicular transition of a symmetric-top, the selection rules are $\Delta K=\pm1$ and $\Delta J=0$ and ±1. The transitions are designated as ^{r}R, ^{r}P, and ^{r}Q for $\Delta K=+1$, and ^{p}R, ^{p}P, and ^{p}Q for $\Delta K=-1$. In the series of sub-bands with $\Delta K=+1$, the ^{r}R branches are much stronger than the ^{r}Q branches, while the ^{r}P branches are too weak to be observed. In the series with $\Delta K=-1$, the situation is reversed, the ^{p}P and ^{p}Q branches being observed, while the ^{p}R branches are absent.

In the present work we have calculated the transition energies and intensities for all possible transitions among the Stark components of the rotational sub-branches shown in Table 2. However, it is impossible to show all of them in our limited space. Thus, it will be more instructive to choose the intense branches in a zero field, such as ^{r}R, ^{r}Q, ^{p}P, and ^{p}Q, and to show how the band splittings and shapes of these branches vary with the increase in the electric field.

The results of our calculation are shown in Figs. 1—4. Figures 1 and 2 show the field dependence of the Stark splittings of the ^{r}R 5(5) and ^{p}P 5(5) sub-branches of

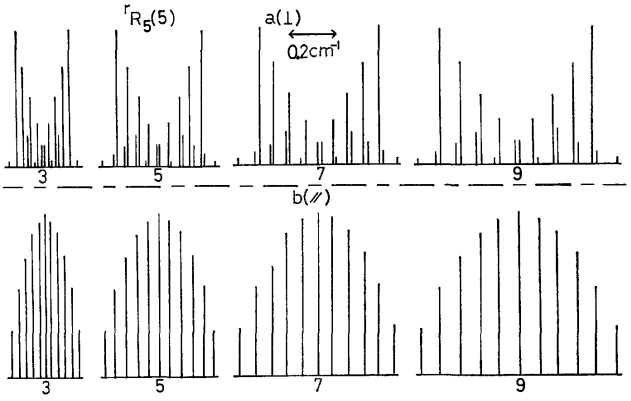

Fig. 1. The Stark splitting of ^{r}R 5(5) branch and its change with field strengths. Throughout Figs. 1 to 4 (a) and (b) correspond to the absorption with perpendicular and parallel polarizations to the direction of the applied field, and $\mu(2)=1.44$ D is assumed. The numbers written under each figure mean the values of the field strength $10\times\mu(1)\times V(L)/B(1)$.

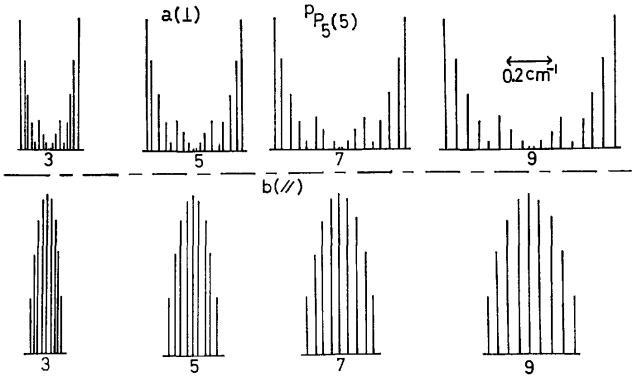

Fig. 2. The Stark splitting of ^{p}P 5(5) branch and its change with field strengths.

* For a slightly asymmetric-top, the asymmetric splitting is, in general, unobservably small for the state with $K>3$.

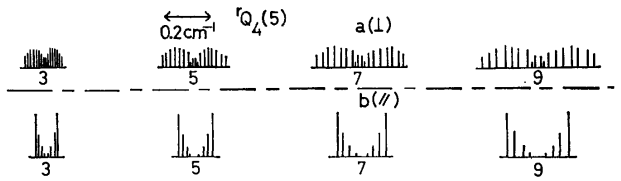

Fig. 3. The Stark splitting of ^{r}Q 4(5) branch and its change with field strengths.

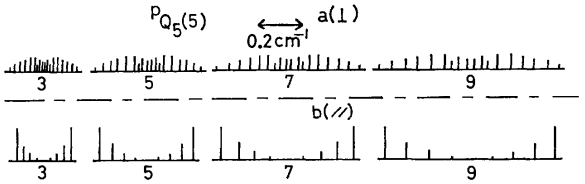

Fig. 4. The Stark splitting of ^{p}Q 5(5) branch and its change with field strengths.

the 3390 Å absorption band for the light polarized perpendicular and parallel respectively to the field direction. Here, to show explicitly the lower-state quantum numbers of the ^{r}R and ^{p}P transitions, the notation $K''(J'')$ has been inserted after the branch notations. Figures 3 and 4 also show the field dependence of the Stark splittings for the ^{r}Q 4(5) and ^{p}Q 5 (5) sub-branches under the same conditions as in Figs. 1 and 2.

Table 4. Intensity criteria of the profiles of incompletely resolved Stark patterns

	$\Delta J=-1$	$\Delta J=0$	$\Delta J=+1$
$\Delta M=0$ (parallel polarization)	broadening	doublet	broadening
$\Delta M=\pm 1$ (perpendicular polarization)	doublet	broadening	doublet

Throughout Figs. 1—4 the general features of each band are in agreement with those suggested by the criteria based on the intensity rule shown in Table 4. Certainly, the envelopes of the ^{r}R and ^{p}P absorption lines in the perpendicular spectra seem to show a doublet splitting, while those for the parallel spectra seem to show line-broadenings. However, it must be noted that the detailed features of these spectra are rather different from those obtained by the usual perturbation theory, especially for the ^{r}Q and ^{p}Q branches in the perpendicular spectra shown in Figs. 3 and 4.

Figure 5 shows how the overall splittings $\Delta\nu$ of the ^{p}P 5(5) branch in the perpendicular spectra vary with the increase in the electric field. There, we can see a linear relation between the overall splittings, $\Delta\nu$, and the field strengths. This linear relation indicates the validity of the usual perturbation theory, which we shall consider in our later discussion of the same problem in other branches.

The calculated spectra shown in Figs. 1—4 are obtained by assuming the dipole moments in the

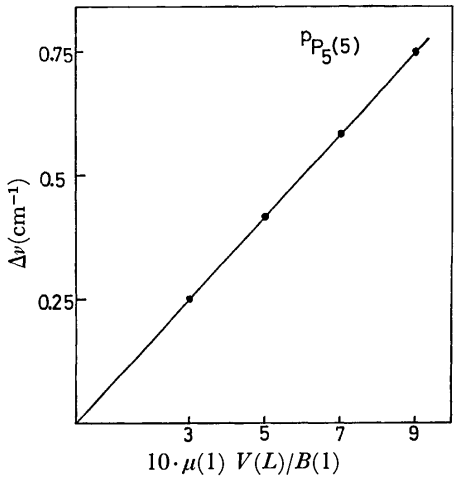

Fig. 5. The linear relation between the overall splittings of ^{p}P 5(5) and the field strengths. $10\times\mu(1)\times V(9)/B(1)=9$ corresponds to a field strength 28.1 kV/cm, and $\mu(2)=1.44$ D is assumed.

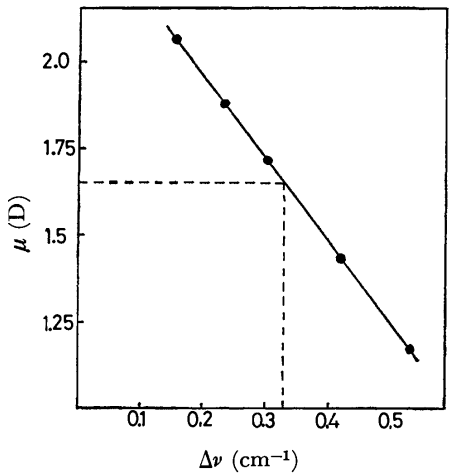

Fig. 6. The change of the overall Stark splitting of ^{p}P 5(5) branch with various assumed dipole moments of the excited state under a constant electric field 15.6 kV/cm. The dotted line is drawn to determine the dipole moment of the excited state corresponding to the observed doublet splitting of HCHO spectrum under the same field strength.

electronic ground and excited states to be 2.34[9] and 1.44 D respectively. Figure 6 shows how the overall splitting, $\Delta\nu$, of ^{p}P 5(5) varies when only the dipole moment of the molecule in the electronic excited state is changed, while other quantities, such as the dipole moment in the ground state and the applied field strength, keep constant. In this figure we see that, as the value of the dipole moment in the excited state becomes smaller compared with that in the ground state, the overall splitting becomes larger.

The dipole moment of the excited state can be determined from Fig. 6 if the overall splittings $\Delta\nu$ have been established experimentally. However, it must be noted that the available data on the overall splittings have been obtained from moderately-high-resolution spectra, that is, from a blended doublet splitting, but

not from well-resolved splittings such as were those in Figs. 1—4.

Before making use of the experimental overall splitting values, it will be useful to know how to get a blended doublet pattern from the resolved splitting, or *vice versa*. For this purpose, we have assumed a Gaussian distribution with a half-band width of 0.1 cm^{-1} for each resolved splitting line.**

Naturally the band shapes obtained through such blending depend not only on the type of branch, but also on the magnitude of the assumed excited state dipole moment and on the applied fields. We have obtained a factor of 1.13 to be multiplied for the transformation from an observed blended doublet to a resolved overall splitting, especially for the case of the ^{P}P 5(5) branch under the same conditions as those of our experiment.

The value on the abscissa shown by a dotted line in Fig. 6 shows the $\Delta\nu$ recalculated from the observed doublet splitting with the above factor. The intersection of the dotted line with the ordinate gives the value of the dipole moment of the excited state obtained by this calculation.

The value of 1.65 D obtained here for the excited-state dipole moment is comparable with the 1.61 D obtained when the first-order perturbation theory (also *cf.* Ref. 1a) is applied to our experimental results. It should be noted that there is a little discrepancy between the dipole moment obtained by the first-order perturbation theory and that obtained in the present work, because the present calculation includes implicitly higher-order perturbation terms together with the usual first-order perturbation theory.

The calculated μ value is, of course, obtained from the experimental correspondence, as has been stated above. The experimental value of the Stark splitting has been obtained from the spectra observed by the use of a newly designed Fabry-Perot interferometer spectroscope,

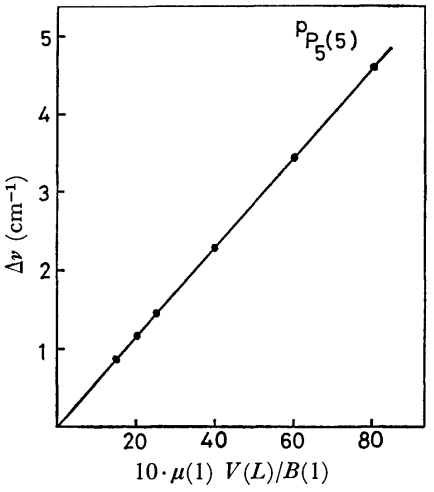

Fig. 7. The linear relation between the overall splittings of ^{P}P 5(5) and the field strengths over 30 kV/cm. The abscissa shows the field strengths $10\times\mu(1)\times V(L)/B(1)$, and $\mu(2)=1.75$ D is assumed.

** The value of 0.1 cm^{-1} was taken from the observation for half-band widths in a field-free spectrum.

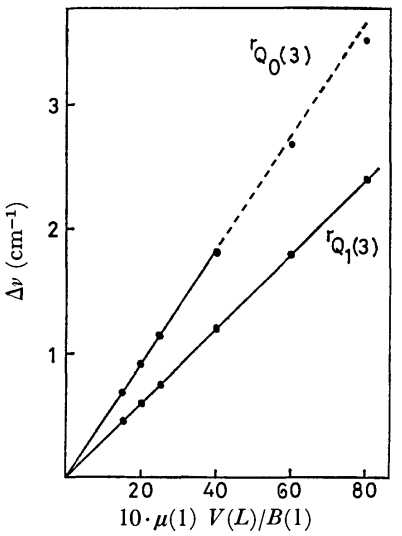

Fig. 8. The change of the overall Stark splittings of ^{r}Q 0(3) and ^{r}Q 1(3) branches with field strengths.

whose details have previously been described.[8,10] The Stark cell is a parallel-plate condenser, the two brass plates (100 cm long, 5 cm wide, 0.7 cm thick) being separated (0.5 cm) by Teflon spacers. The overall errors of our experimental work are within 5%. The value of 1.65 D obtained here for the $n\rightarrow\pi^*$ excited state of formaldehyde is, then, in good agreement with the other data: 1.56 ± 0.1 D,[1a] 1.67 ± 0.15 D (Method I), and 1.4 ± 0.1 D (Method II).[1b]

Let us return to the problem of the linear relation between the overall splitting of ^{P}P 5(5) and the applied field strength observed in Fig. 5, where applied fields are varied below 30 kV/cm. In Fig. 7 it should be noted that the linear relation holds up to such a high field strength as 200 kV/cm or more. Certainly this seems to reflect the validity of the usual first-order perturbation theory in such a high field. However, it is certain that the linear relation is also dependent on the type of branch. In Fig. 8 the same relation is shown for ^{r}Q 0(3) and ^{r}Q 1(3).*** Especially for the ^{r}Q 0(3) branch, we can observe a noticeable departure from the linear relation around 100 kV/cm, while the ^{r}Q 1(3) branch still shows a linear field dependence. However, as for the band shape of the latter branch as well as of the former, the symmetric pattern at low fields changes to an asymmetric one even at rather small field strengths, and presents a quite different appearance around 200 kV/cm, as is shown in Fig. 9.

It may be considered that such characteristic behavior of the ^{r}Q 0(3) and ^{r}Q 1(3) branches clearly shows the existence of higher-order interactions, even at rather low field strengths.

At least under field strengths below 100 kV/cm, and so long as the magnitude of the overall splittings is in question, there seems to be no serious disagreement between the first-order perturbation theory and the

*** These branches with $K<3$ should show a large asymmetric effect in the spectrum of HCHO, and so here they were only chosen as prototypes of such bands in a symmetric-top molecule.

Table 5. The intensity enhancement of the forbidden band $1''_{01}$ to $1'_{01}$ in a zero-field limit[a)]

Field strength	0.1	0.3	0.5	0.7	0.9	1.5	2.0	2.5	4.0	6.0	8.0
Intensity	0.0001	0.0006	0.0017	0.0035	0.0057	0.0181	0.0310	0.0463	0.0999	0.1735	0.2377

a) As the field strength we used the value of $\mu(1)V/B(1)$. The intensities at the field strengths from 0.1 to 0.9 are those obtained under the assumption of $\mu(2)=1.44$ D, but the others were obtained under the assumption of $\mu(2)=1.75$ D.

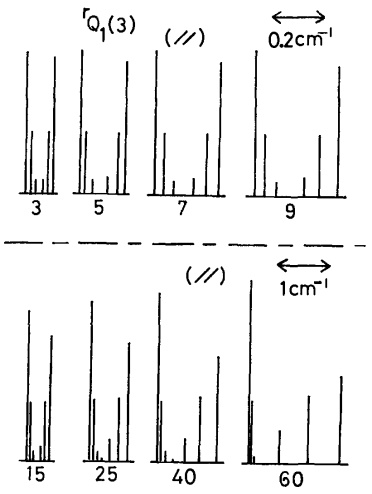

Fig. 9. The Stark splitting of ^{r}Q 1(3) branch and its change with field strengths.

present treatment, regardless of the type of branch. However, as for the band shapes or the band structure, it should be noted that a serious discrepancy may occur depending on types of the branches. This is especially remarkable for the branches with small J values and with $K<J$.

Lastly, we shall discuss the intensity enhancement of the forbidden branches of a symmetric top in a zero field. Table 5 shows the intensities of the transition from the $1''_{01}$ to the $1'_{01}$ rotational sub-branch. This transition is, of course, a forbidden one† due to the selection rule of $\Delta J=\pm 1$ for $K=0$ of a symmetric-top in a zero field. From the table we can see that the intensity of the transition is appreciable at a field strength of 30 kV/cm, and that it increases with a quadratic dependence on the field strengths. With a further increase in the field strengths, the intensity increases more and more, until beyond 100 kV/cm it is no longer distinguishable from that of the allowed transition and also shows an appreciable deviation from the quadratic-field dependence.

Conclusion

By way of conclusion, we may summarize the present work as follows:

(1) By the direct diagonalization of the energy matrices of a symmetric top under an external electric field, we have calculated the Stark splittings and intensities of the rotational sub-branches associated with the 3390 Å band of HCHO. For some selected branches we have given the detailed band structures, which can, it is hoped, be used as model spectra of the Stark splittings in very-high-resolution spectroscopy.

(2) Below 100 kV/cm, the overall Stark splittings are dependent linearly on the field strength, regardless of the branch type. Over 100 kV/cm the deviation from the linear-field dependence becomes appreciable, depending on the branch type.

(3) The change from a symmetric to an asymmetric appearance of the band shapes of a certain band occurs even below 30 kV/cm, and becomes appreciable with a further increase in the field strength. The effects depending on the branch types stated in (2) and (3) are especially remarkable for the branches with small J values and with $K<J$.

(4) Between the assumed dipole moments of the excited state and the overall splitting of the ^{p}P 5(5) branch, there exists a linear relation at field strengths below 100 kV/cm. From this relation, the value of 1.65 D has been determined for the dipole moment of the first excited $n\rightarrow\pi^*$ state of HCHO.

(5) The intensity enhancement of the forbidden bands of a symmetric-top molecule in a zero field shows a quadratic dependence on the applied field strength below 100 kV/cm, but comes to show an appreciable deviation from the quadratic-field dependence over 100 kV/cm.

The numerical calculations have been carried out with an NEAC 2200-700 electronic computer at Tohoku University.

† In this work we carried out the calculations for both parallel- and perpendicular-type bands of a symmetric-top. The transition from $1''_{01}$ to $1'_{01}$ is the forbidden branch ^{q}Q 0(1) of a parallel-type band.

References

1) a) D. E. Freeman and W. Klemperer, *J. Chem. Phys.*, **45**, 52 (1966); D. E. Freeman, J. R. Lombardi, and W. Klemperer, *ibid.*, **45**, 58 (1966); J. R. Lombardi, D. Campbell, and W. Klemperer, *ibid.*, **46**, 3482 (1967); J. R. Lombardi, D. E. Freeman, and W. Klemperer, *ibid.*, **46**, 2746 (1967); J. R. Lombardi, *ibid.*, **48**, 348 (1968); **50**, 3780 (1969). b) N. J. Bridge, D. A. Haner, and D. A. Dows, *ibid.*, **44**, 3128 (1966); **48**, 4196 (1968); A. D. Buckingham and D. A. Ramsay, *ibid.*, **42**, 3720 (1965); D. A. Dows and A. D. Buckingham, *J. Mol. Spectrosc.*, **12**, 189 (1964), *etc.*

2) J. H. Shirley, *J. Chem. Phys.*, **38**, 2896 (1963).

3) B. G. West and M. Mizushima, *J. Chem. Phys.*, **38**, 251 (1963).

4) J. R. Lombardi, *J. Chem. Phys.*, **48**, 348 (1968).

5) "Very High Resolution Spectroscopy," ed by R. A. Smith, Academic Press (1976).

6) J. D. Swalen and L. Pierce, *J. Math. Phys.*, **2**, 736 (1961).
7) H. C. Allen and P. C. Cross, "Molecular Vib-rotors," John Wiley & Sons (1963), p. 102.
8) Y. Sato, A. Watanabe, and Y. Amako, *Jpn. J. Appl. Phys.*, **15**, 703 (1976).
9) J. N. Shoolery and A. H. Sharbaugh, *Phys. Rev.*, **82**, 95 (1951).
10) Y. Sato, A. Watanabe, and Y. Amako, *Jpn. J. Appl. Phys.*, **14**, 1357 (1975).

Isomerization of *cis*-2-Butene Caused by Electronically-excited Sulfur Dioxide ($^3B_1$) Adsorbed on Porous Vycor Glass

Kiyoshi Otsuka, Masaki Fukaya, and Akira Morikawa

Department of Chemical Engineering, Tokyo Institute of Technology, Ookayama, Meguro-ku, Tokyo 152

(Received April 14, 1977)

The *cis-trans* isomerization of *cis*-2-butene caused by electronically-excited sulfur dioxide has been studied at the gas-solid interface of porous Vycor glass. All of the quantum yields for the isomerization obtained gave values larger than ≈30. Infrared studies show that the product on the glass is the polysulfone formed through the copolymerization of sulfur dioxide and *cis*-2-butene. These results and the kinetic data for the isomerization can be explained satisfactorily by the proposed mechanism in which the isomerization occurs through the addition and elimination of 2-butene molecules at the terminal of the polysulfone formed on the glass; the copolymerization is initiated by an electronically-excited SO_2 ($^3B_1$) state.

The photochemistry of sulfur dioxide is of special interest to the scientist who is concerned with the rates and mechanisms for the removal of sulfur dioxide in sunlight-irradiated atmospheres. There is substantial evidence that the harmful effect of sulfur dioxide on health is enhanced when there are significant levels of suspended particulates in polluted atmospheres.[1] This leads to a consideration of the effect of suspended particulates on photochemical reactions involving sulfur dioxide, through excitation due to the absorption of sunlight in the first allowed absorption band ($SO_2(^1B_1) \leftarrow SO_2(\tilde{X}, {}^1A_1)$), which extends from 340 to 240 nm.

The chemical reactions between photochemically-excited sulfur dioxide and olefin hydrocarbons have been studied by a number of investigators.[2-9] All these studies, however, have been limited to homogeneous systems of gas or liquid phase, and there appear to be no published studies on these reactions at the gas-solid interface.

Recently, Otsuka *et al.* have reported that sulfur dioxide adsorbed on porous Vycor glass catalyzes the geometrical isomerization of 2-butenes.[10] The rate of this reaction is enhanced to a great extent by ultraviolet irradiation. Hence, in this report, the isomerization of *cis*-2-butene induced by electronically-excited sulfur dioxide over porous Vycor glass is described in detail. This system can be regarded as a very basic model of the system which involves the atmospheric reaction of sulfur dioxide with olefins over solid particulates in sunlight-irradiated atmospheres. Porous Vycor glass was chosen as the solid adsorbent because of its large surface area and high transparency to ultraviolet radiation down to wavelengths of about 210 nm, which is advantageous for ultraviolet spectral measurements of the adsorbed molecules and for a kinetic investigation of the photo-excited adsorbed molecules.

Experimental

The porous Vycor glass (Corning No. 7930, 30×8×1 mm plate, surface area=149 m^2/g), sulfur dioxide, *cis*-2-butene and apparatus used were described previously.[10]

Procedure. Before each run, the porous Vycor glass (0.50 g) placed in the reactor was calcined at 600 °C in dried oxygen and then degassed for 2 h in a vacuum down to about 8×10^{-5} Torr at the same temperature. Following the introduction of sulfur dioxide into the reactor, which was maintained at a given temperature, the reaction was initiated by irradiating the glass immediately after introducing the *cis*-2-butene and circulating the sulfur dioxide-*cis*-2-butene gas mixture through the reactor. A small amount of the reacting gases was periodically collected for analysis by gas chromatography, and the amount of *trans*-2-butene produced was determined. The ultraviolet light generated by a Toshiba H-400-P medium-pressure mercury lamp was filtered upon passage through 1 cm of water, a Corning 7-54 glass filter and either a Toshiba UV-29 (transparent to 270—410 nm) or a UV-31 (290—410 nm) glass filter. The temperature of the reactor was controlled to within ±0.2 °C using the air or water bath shown in Fig. 1.

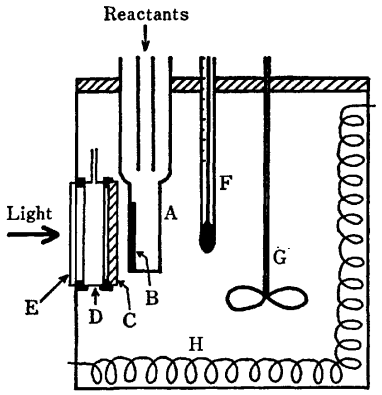

Fig. 1. Schematic diagram of the reaction system. A: Reaction vessel, B: porous Vycor glass, C: glass filters, D: water filter, E: quartz window, F: thermometer, G: stirrer, and H: electric heater.

Estimation of Absorbed Light Intensities and Quantum Yields. The emission intensity distribution of the mercury lamp (from Toshiba Technical Data No. 21-HM-11) and the transmission of the combined filters provided the energy distribution of the incident light, $I_0(\lambda)$. The relative light intensity absorbed by the sulfur dioxide adsorbed on the glass, I_r, was calculated using the equation,

$$I_r = \int_0^\infty I_0(\lambda)\left\{1-\frac{T(\lambda)}{100}\right\}\left\{\frac{D_{SO_2}(\lambda)}{D_{SO_2}(\lambda)+D_G(\lambda)}\right\}d(\lambda),$$

where $D_{SO_2}(\lambda)$ and $D_G(\lambda)$ are the optical densities of the adsorbed sulfur dioxide and of the porous glass, at wavelength λ, respectively,[11] and $T(\lambda)$ is the transmittance of the glass–sulfur dioxide system.

A quantitative determination of the incident light intensity at the cell face was made employing potassium ferrioxalate

actinometry, and the absolute light intensity absorbed by sulfur dioxide, I_a, was calculated using the equation,

$$I_a = I_t I_r \Big/ \int_0^\infty I_0(\lambda)\mathrm{d}(\lambda),$$

where I_t is the incident light intensity at the cell face. The absolute quantum yield of the isomerization of *cis*-2-butene is given by $R_{c\to t}/I_a$, where $R_{c\to t}$ is the rate of geometrical isomerization.

Results

The cis-trans *Isomerization of* cis-*2-Butene.* The light of wavelength longer than 270 nm applied in this study induces no reaction of *cis*-2-butene in the absence of sulfur dioxide. If sulfur dioxide is present on the porous Vycor glass, selective *cis-trans* isomerization occurs thermally.[10] The initial rate of this thermal isomerization, $R^T_{c\to t}$, or the rate of *trans*-2-butene formation, is plotted against the amount of adsorbed sulfur dioxide, V_{SO_2}, in Fig. 2, where the experiments were carried out at 25 °C at an initial pressure of *cis*-2-butene of 150 Torr.

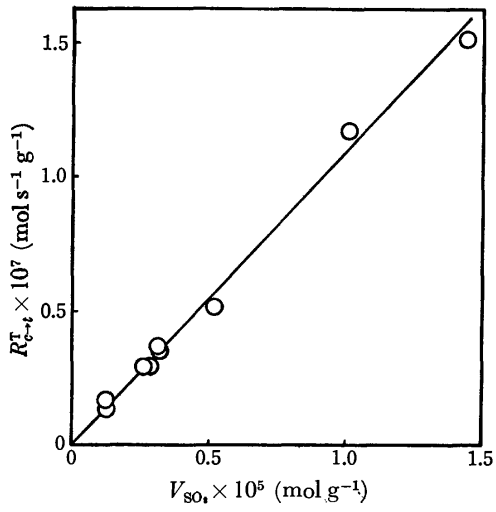

Fig. 2. Plot of the rate of thermal isomerization, $R^T_{c\to t}$, *vs.* the amount of sulfur dioxide adsorbed, V_{SO_2}, at $P_{cis\text{-but}}=105$ Torr; the reactions were carried out at 25 °C.

Ultraviolet irradiation of the glass, onto which sulfur dioxide had been adsorbed, markedly accelerated the rate of isomerization. The rate of photo-induced isomerization, $R^P_{c\to t}$, calculated from the difference between the rate measured under irradiation and $R^T_{c\to t}$, was obtained for various *cis*-2-butene pressures and amounts of adsorbed sulfur dioxide. Figure 3 shows the plot of $R^P_{c\to t}$ as a function of the *cis*-2-butene pressure. $R^P_{c\to t}$ does not depend on the pressure for pressures higher than 100 Torr. The effect of V_{SO_2} on $R^P_{c\to t}$ is indicated in Fig. 4. It has been confirmed in advance that the sulfur dioxide preadsorbed on the glass does not desorb after the addition of *cis*-2-butene for the experimental conditions under which the data in Figs. 3 and 4 were obtained.

The relative quantum yields of isomerization for the data in Fig. 4 are plotted against the amount of adsorbed

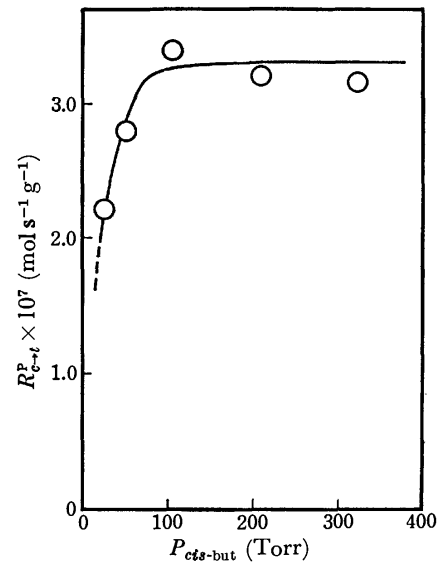

Fig. 3. Plot of the rate of photo-induced isomerization, $R^P_{c\to t}$, *vs.* the pressure of *cis*-2-butene, $P_{cis\text{-but}}$. The filters were Corning 7-54 and UV-31 filters. The amount of sulfur dioxide adsorbed is 2.5×10^{-6} mol/g; the reactions were carried out at 25 °C.

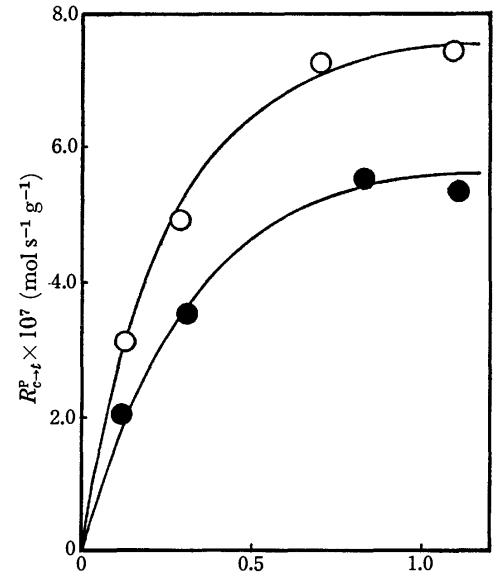

Fig. 4. Plot of $R^P_{c\to t}$ *vs.* V_{SO_2}, at $P_{cis\text{-but}}=105$ Torr and at 25 °C. Filters: (○); Corning 7-54 and UV-29, and (●); Corning 7-54 and UV-31.

sulfur dioxide in Fig. 5. It can be seen that the quantum yield decreases with the amount of sulfur dioxide adsorbed. The estimated absolute quantum yield, $R^P_{c\to t}/I_a$, for the lowest value in Fig. 5 is about 30. This high quantum yield suggests that the reaction proceeds *via* a chain process.

The addition of a small amount of nitric oxide (0.77×10^{-5} mol) to a system of sulfur dioxide (0.55×10^{-5} mol) and *cis*-2-butene (1.44×10^{-3} mol) completely poisons the photo-induced isomerization, suggesting that the reaction intermediate is a radical.

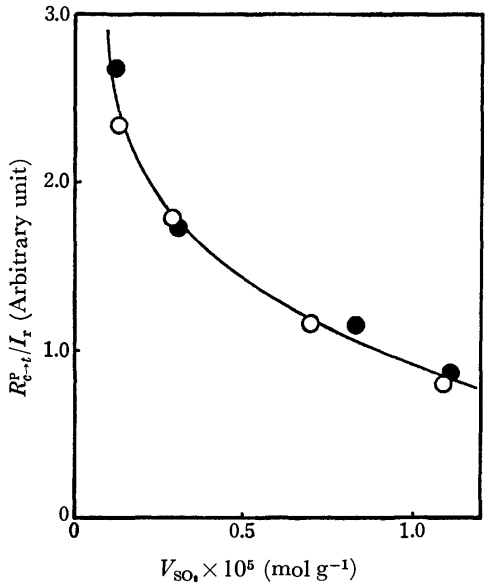

Fig. 5. Plot of the relative quantum yield of the photo-induced isomerization, $R^p_{c\to t}/I_r$, as a function of the amount of adsorbed sulfur dioxide. Filters: (○); Corning 7-54 and UV-29, and (●); Corning 7-54 and UV-31.

The Copolymerization of Sulfur Dioxide with cis-*2-Butene.* All the experiments described in this section were carried out with a sulfur-dioxide concentration (2.1×10^{-3} mol) compared to that applied in the preceding section ($<1.3\times 10^{-5}$ mol).

After a photo-induced geometrical isomerization for 150 min at 0 °C, the product on the glass was extracted with dioxane. The solution was dropped onto a KBr film and the dioxane solvent was evaporated. After several repetitions of this procedure, the infrared spectrum of the film was recorded (Fig. 6). This spectrum exhibits the two characteristic absorption bands of the polysulfone from *cis*-2-butene, one at 1300 cm^{-1} and the other at 1105—1140 cm^{-1} due to the symmetrical and asymmetrical stretching vibrations of the sulfone group, respectively.[12]

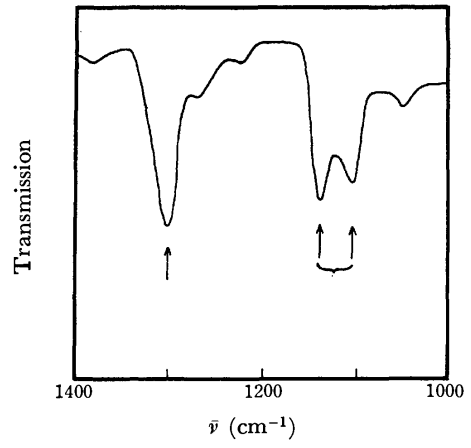

Fig. 6. Infrared spectrum of the polysulfone formed on the glass from *cis*-2-butene and sulfur dioxide under irradiation. The reaction was carried out at 0 °C under initial pressures of *cis*-2-butene and sulfur dioxide of 105 Torr (2.10×10^{-3} mol).

During the progress of the isomerization, the pressure decrease due to the reaction of SO_2 with *cis*-2-butene on the glass was followed by reading a glass Bourdon gauge at different temperatures. After the initial rapid adsorption, no reactants were consummed in the gas phase when the temperature was higher than ≈40 °C. However, a considerable consumption of gas was observed at low temperatures (<20 °C). Without irradiation, no gas consumption was detected after the initial adsorption for all temperatures in the range from 0 to 60 °C. The average rate of gas consumption under irradiation for times of 10—30 min, $\Delta V_g/\Delta t$, and the rate of photo-induced isomerization are plotted as a function of temperature in Fig. 7. The rate of isomerization has a maximum value at just the temperature for which the consumption of reactants becomes negligible (≈30 °C). It was shown that at a low sulfur-dioxide concentration (0.15×10^{-5} mol) the rate of isomerization decreases monotonically with a rise in temperature from 0 to 70 °C.

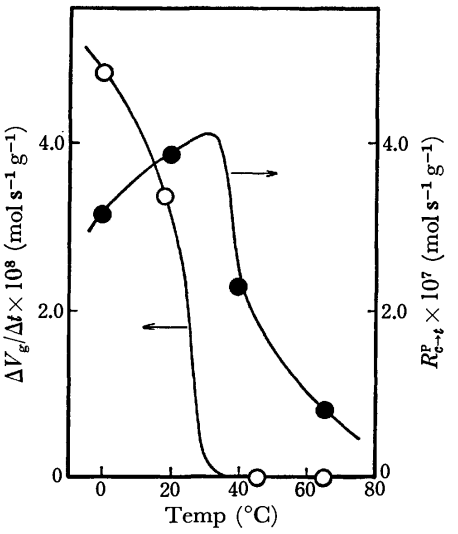

Fig. 7. Temperature effects on the rate of gas consumption, $\Delta V_g/\Delta t$, and on that of photo-induced isomerization, $R^p_{c\to t}$, (○); $\Delta V_g/\Delta t$ and (●); $R^p_{c\to t}$. The initial pressures of *cis*-2-butene and sulfur dioxide were 105 Torr.

Discussion

Many studies of the gas-phase photolysis of sulfur dioxide–olefin hydrocarbon mixtures have suggested that electronically-excited sulfur dioxide sensitizes the geometrical isomerization of the olefins.[4,6–9,13–17] Furthermore, it has been observed that the $^3B_1$ state of sulfur dioxide is the only excited electronic state of sulfur dioxide participating in the geometrical isomerization of 2-butenes,[6,8,9] 1,2-dichloroethylenes,[13] 1,2-difluoroethylenes,[14,15] and 2-pentenes.[16,17] In these gas-phase studies, however, the absolute quantum yield for isomerization never exceeds unity. The high quantum yields (>30) obtained in the present work cannot be explained by means of the mechanism proposed for the photosensitized isomerization in the gas phase.

Bristow and Dainton first observed that irradiated mixtures of *cis*- or *trans*-2-butene in liquid sulfur dioxide result in a fast *cis-trans* isomerization, in addition to the polysulfone formation *via* the copolymerization of SO_2 and 2-butene.[3] The formation of polysulfone over glass confirmed in the present work (Fig. 6) suggests that the isomerization at the gas-solid interface occurs *via* a mechanism similar to that proposed for the reaction in the liquid phase.[3]

Assuming $^3B_1$ is the only electronically-excited state of SO_2 initiating the copolymerization, the following mechanism is proposed:[3,10]

$$SO_2 + h\nu \xrightarrow{I_a} {}^1SO_2(^1B_1),$$

$$^1SO_2(^1B_1) + \textit{cis}\text{-2-butene} \longrightarrow {}^3SO_2(^3B_1) + \textit{cis}\text{-2-butene}, \quad (1)$$

$$\longrightarrow SO_2 + \textit{cis}\text{-2-butene}, \quad (2)$$

$$^3SO_2(^3B_1) + \textit{cis}\text{-2-butene} \longrightarrow P_s + P_b, \quad (3)$$

$$\longrightarrow SO_2 + \textit{trans}\text{- or }\textit{cis}\text{-2-butene}, \quad (4)$$

$$P_s + \textit{cis}\text{-2-butene} \longrightarrow P_b, \quad (5)$$

$$P_b + SO_2 \longrightarrow P_s, \quad (6)$$

$$P_b \longrightarrow P_s + \textit{trans}\text{-2-butene}, \quad (7)$$

$$\longrightarrow P_s + \textit{cis}\text{-2-butene}, \quad (8)$$

$$P_s \longrightarrow P_b + SO_2, \quad (9)$$

$$P_b \longrightarrow \text{stabilized}. \quad (10)$$

$$P_s \longrightarrow \text{stabilized}, \quad (11)$$

where the mechanism is considered for a low isomerization conversion rate and a low sulfur-dioxide concentration compared to those for *cis*-2-butene. All species appearing in the above reactions are in the adsorbed layer. For low sulfur-dioxide concentrations the unimolecular decay of the $^1B_1$ and $^3B_1$ states of sulfur dioxide and the quenching of these states by ground-state sulfur dioxide molecules are unimportant[18,19] and have not been included in the above process. P_s and P_b represent the terminal group of active polysulfone ($P_s \rightarrow \dot{S}O_2CH(CH_3)CH(CH_3)\cdots\cdots SO_2CH(CH_3)\dot{C}H(CH_3) \leftarrow P_b$). The strong poisoning effect of nitric oxide must be due to the quenching of these terminal groups through a reaction with nitric oxide. The selective *cis-trans* isomerization occurs mainly through depropagation Steps 7 or 8 of the copolymerization since the contribution from Reaction 4 can be neglected because of the low quantum yield (<1.0).[8,9,15-17]

If the consumption of reactants during the isomerization is due to polysulfone formation, the results shown in Fig. 7 (open circles) indicate that the copolymerization of sulfur dioxide and *cis*-2-butene on the glass has a ceiling temperature around 30 °C. Above the ceiling temperature, the rates of the depropagation steps exceed those of the propagation steps and, thus, polymerization can no longer occur. The decrease in the rate of isomerization above the ceiling temperature (Fig. 7 closed circles) can reasonably be explained as a consequence of the decrease in the number of long-chain polysulfone sites necessary for the isomerization.

Dainton and Ivin have shown that the ceiling temperature for the polysulfone formation decreases with decreasing concentrations of comonomers.[22] The fact that, at low sulfur-dioxide concentrations, no maximum of the isomerization rate has been observed within the temperature range down to 0 °C, may be due to a shift of the ceiling temperature to a lower value below 0 °C.

According to the Reactions 1—11 indicated above, the rate of photo-induced isomerization can be described by Eq. i:

$$R^p_{c\rightarrow t} = I_a k_7 \left(\frac{k_1}{k_1+k_2}\right)\left(\frac{k_3}{k_3+k_4}\right) \times \left\{\frac{2(k_5[\textit{cis}\text{-2-but}]+k_9)+k_{11}}{k_{10}(k_5[\textit{cis}\text{-2-but}]+k_9+k_{11})+k_{11}(k_6[SO_2]+k_7+k_8)}\right\}, \quad \text{(i)}$$

where the concentrations for *cis*-2-butene and sulfur dioxide are those on the surface, and I_a is the light intensity absorbed by sulfur dioxide on the glass; we have neglected the contribution of photo-sensitized isomerization (Reaction 4). At high *cis*-2-butene pressures (>100 Torr), it has been shown that the rate of isomerization is independent of the pressure (Fig. 3). This must be attributed to saturation of the active site on the glass by the chemically-adsorbed *cis*-2-butene which is involved in propagation Step 5.[23]

We can rearrange Eq. i to Eq. ii in order to observe the effect of the adsorbed sulfur-dioxide concentration, thus,

$$I_a/R^p_{c\rightarrow t} = A + B[SO_2], \quad \text{(ii)}$$

where

$$A = \frac{(k_1+k_2)(k_3+k_4)}{k_1k_3k_7} \times \left\{\frac{k_{10}(k_5[\textit{cis}\text{-2-but}]+k_9+k_{11})+k_{11}(k_7+k_8)}{2(k_5[\textit{cis}\text{-2-but}]+k_9)+k_{11}}\right\}$$

and

$$B = \frac{(k_1+k_2)(k_3+k_4)}{k_1k_3k_7}\left\{\frac{k_6k_{11}}{2(k_5[\textit{cis}\text{-2-but}]+k_9)+k_{11}}\right\}.$$

At high *cis*-2-butene pressures (>100 Torr), A and B can be regarded as constant (Fig. 3). Using the data in

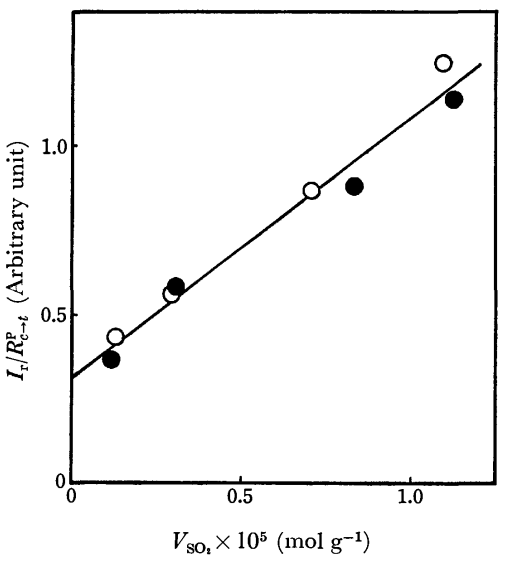

Fig. 8. Plot of $I_r/R^p_{c\rightarrow t}$ *vs.* V_{SO_2}. Filters: (○); Corning 7-54 and UV-29, (●); Corning 7-54 and UV-31.

Fig. 4, which were obtained in experiments carried out at a constant *cis*-2-butene pressure of 105 Torr, $I_r/R^p_{c\to t}$ is plotted against the amount of adsorbed sulfur dioxide in Fig. 8. A reasonably good linear relation between these variables supports the proposed process.

As described above, all the results and the kinetic data obtained in this work can be explained satisfactorily by the reaction mechanism in which the geometrical isomerization of *cis*-2-butene accompanies the copolymerization of sulfur dioxide with *cis*-2-butene, which is initiated by the electronically-excited $^3B_1$ state of sulfur dioxide.

References

1) U. S. Dept. of Health, Education, and Welfare, "Air Quality Criteria for Sulfur Oxides," Public Health Service, Consumer Protection and Environmental Health Service, National Air Protection Control Administration, Washington, D. C. (1969); NAPCA publication No. AP-50.

2) F. S. Dainton and K. J. Ivin, *Trans. Faraday Soc.*, **46**, 374, 382 (1950).

3) G. M. Bristow and F. S. Dainton, *Proc. R. Soc. London, Ser. A*, **229**, 525 (1955).

4) R. B. Cundall and T. F. Palmer, *Trans. Faraday Soc.*, **56**, 1211 (1960).

5) E. Cehelnik, C. W. Spicer, and J. Heicklen, *J. Am. Chem. Soc.*, **93**, 5371 (1971).

6) R. D. Penzhorn and H. Güsten, *Z. Naturforsh.*, **27a**, 1401 (1972).

7) R. A. Cox, *J. Photochem.*, **2**, 1 (1973—1974).

8) K. L. Demerjian, J. G. Calvert, and D. L. Thorsell, *Int. J. Chem. Kinet.*, **6**, 829 (1974).

9) K. L. Demerjian and J. G. Calvert, *Int. J. Chem. Kinet.*, **7**, 45 (1975).

10) K. Otsuka, K. Eshima, and A. Morikawa, *Bull. Chem. Soc. Jpn.*, **50**, 631 (1977).

11) The ultraviolet spectra of the sulfur dioxide-*cis*-2-butene system adsorbed on porous Vycor glass has been studied in detail in a preceding paper.[10] When sulfur dioxide coadsorbs with *cis*-2-butene, the absorbance for the first allowed transition, $SO_2(^1B_1)\leftarrow SO_2(\tilde{X}, {}^1A_1)$, is enhanced in the long wavelength region by the proximity of the π-donating *cis*-2-butene molecules. As a consequence of this, the threshold of the absorption band shifts to a longer wavelength of about 420 nm.

12) R. E. Cook, F. S. Dainton, and K. J. Ivin, *J. Poly. Sci.*, **26**, 351 (1957).

13) F. B. Wampler and J. W. Bonttenheim, *Int. J. Chem. Kinet.*, **8**, 585 (1976).

14) F. B. Wampler, *Int. J. Chem. Kinet.*, **8**, 511 (1976).

15) F. B. Wampler, *Int. J. Chem. Kinet.*, **8**, 519 (1976).

16) F. B. Wampler, *Int. J. Chem. Kinet.*, **8**, 935 (1976).

17) F. B. Wampler, *Int. J. Chem. Kinet.*, **8**, 945 (1976).

18) H. W. Sidebottom, C. C. Badcock, J. G. Calvert, G. W. Reinhardt, B. R. Rabe, and E. K. Damon, *J. Am. Chem. Soc.*, **93**, 2587 (1971).

19) T. N. Rao, S. S. Collier, and J. G. Calvert, *J. Am. Chem. Soc.*, **91**, 1609 (1969).

20) R. D. Snow and F. E. Frey, *J. Am. Chem. Soc.*, **65**, 2417 (1943).

21) F. S. Dainton and G. M. Bristow, *Nature*, **172**, 804 (1953).

22) F. S. Dainton and K. J. Ivin, *Proc. R. Soc. London, Ser. A*, **212**, 207 (1952).

23) Adsorption experiments for *cis*-2-butene on porous Vycor glass have shown that a considerable increase in the amount of adsorption with increasing pressure, even in the range between 100 and 200 Torr. This is natural since most of the *cis*-2-butene on the glass may be physically adsorbed. The chemisorption of *cis*-2-butene occurs presumably at the Al^{3+} site, which is an impurity in the glass.[10]

Reactions of Isomeric Transition-Activated ^{80}Br in the $H^{80m}Br$–CH_4 System

Kenjiro KONDO and Masuo YAGI

Laboratory of Nuclear Science, Faculty of Science, Tohoku University, 1-Kanayama Tomizawa, Sendai 982

(Recieved April 15, 1977)

The reaction of isomeric transition-activated ^{80}Br was studied in the gaseous $H^{80m}Br$–CH_4($HBr/CH_4=0.1\pm 0.01$) system. $CH_3{}^{80}Br$, $CH_2{}^{80}BrBr$ and $CH^{80}BrBr_2$ were identified as the products, and their absolute yields were 1.60, 2.65, and 0.05%, respectively. The effects of Kr and Xe additives show that these products were produced only through kinetic-energy independent (thermal ionic) processes. The results are compared with those obtained in the $^{80m}BrBr$ (or $^{82m}BrBr$)–CH_4 system, in which the C–*Br formation proceeds mainly *via* kinetic-energy dependent processes, and the difference between them is explained on the basis of the cross sections for charge neutralization and capture collision complex formation of bromine ions as a function of the kinetic energies initially acquired by the ^{80}Br and ^{82}Br atoms. The persistent complex ion, $CH_4{}^{80}Br^+$, is considered to be a precursor of the product formations, and the formation of individual products is discussed on the basis of ion-molecule reactions of $CH_4{}^{80}Br^+$ with surrounding molecules. Furthermore, the effect of HCl and $CH_2{=}CH_2$ additives on the yield distribution were examined to elucidate the reaction mechanisms of the product formations.

The chemical effects associated with the nuclear transformations of bromine atoms in gaseous systems have been studied extensively,[1–10] and one of the most interesting subjects is to determine the relative importance of kinetic energy and charge in the recombination reactions involving recoiling bromine atoms.

So far the reactions of (n,γ)[1,2,4] and/or fission[11] activated bromine in gaseous CH_4 have been found to proceed principally through kinetic processes. Similary, it has been reported that the recoiling halogen atoms produced by the $^{19}F(\gamma,n)^{18}F$[12] and $^{40}Ar(\gamma,p)^{39}Cl$[13] reactions enter into organic combinations only through kinetic-energy dependent (hot) reactions as neutral atoms in a gaseous CH_4 system. It is conceivable that these recoiling atoms initially have positive charges. However, these experimental results indicate that the charge neutralization of positively-charged recoiling atoms proceeds fast and is nearly completed before the recoiling atom reaches the energy region causing hot reactions.

On the other hand, in the case of isomeric transitions (IT) of ^{80m}Br and ^{82m}Br, the initial high positive charge on the bromine atom, as a consequence of the Auger process following the isomeric transition, is partially neutralized by intra-molecular electron transfer, resulting in Coulombic repulsion. Therefore, the bromine atom can acquire appreciable kinetic energy. When $^{80m}BrBr$ is used as a source molecule, the kinetic energy of the ^{80}Br is calculated to be 40.3 eV[14] on the average, assuming that the original charge of the ^{80}Br is 8 and is equally divided between the bromine atoms. This value is fairly small compared with those for the other nuclear transformations stated above. It has been reported that, not only the kinetic energy, but also the positive charge plays a very important role in the reactions of ^{80}Br and/or ^{82}Br activated by isomeric transitions for the Br_2–CH_4 system.[3,7,15–17] These results indicate that some of the positively-charged bromine atoms lose their kinetic energies and have the opportunity to undergo ion-molecule reactions leading to C–*Br formation before charge neutralization occurs. The cross sections for charge neutralization and ion-molecule reactions depend largely on the kinetic energy of the ions. Thus, it is very interesting to estimate the organic yields due to the thermal ionic process on the basis of the kinetic energy of the charged bromine atom.

This is the record of an experiment of I.T.-activated ^{80}Br reactions with CH_4 using HBr as the source molecule. In this case, the kinetic energy of the ^{80}Br atoms is 0.75 eV on the average,[5] and therefore, this experiment is considered to be highly suited to evaluating the role of the charge and kinetic energy of the ^{80}Br atom on recombination reactions in the near-thermal energy region. The results were compared with those obtained from (n,γ) and IT experiments using Br_2,[1,2,10] and can be explained in terms of competition between charge-transfer and ion-molecule reactions involving bromine ions.

Furthermore, the formation mechanisms of individual products were examined by adding HCl and $CH_2{=}CH_2$ to the system. These are discussed on the basis of ion-molecule reactions involving the $^{80}Br^+$ ion.

Experimental

Materials. All gaseous reagents were used directly as supplied by Takachiho Chemical Co. without further purification. The nominal purities are 99.95% for Kr and CH_4, 99.9% for Xe, 99.8% for $CH_2{=}CH_2$, and 99.5% for HCl. The purities of all other reagents purchased from the Junsei Chemical Co., Ltd., were extremely high.

Preparation of $H^{80m}Br$. First, the $^{80m}Br_2$ molecules were obtained by the thermal decomposition of palladium bromide irradiated by bremsstrahlung, which was produced by the impact of 40—60 MeV electrons from the linear electron accerelator of Tohoku University on a Pt plate (2 mm thick). The bombardment was carried out for about 2 h at an average electron-beam intensity of 150 μA. The $^{80m}BrBr$ molecules thus obtained were introduced into a vessel containing red phosphorus and a small amount of distilled water. Then, the vessel was closed with a stopcock and the temperature of the vessel was increased to about room temperature. After completion of the Br_2 reaction, the $H^{80m}Br$ thus obtained was further purified by distillation through a P_2O_5 column and a Dry Ice trap for the sake of complete removal of trace amounts of unreacted species.

Sample Preparation. The amount of CH_4, HBr, and other additives required was measured with a mercury manometer, all reaction mixtures were sealed into cylindrical

pyrex glass ampoules with capacities of 50, 100, and 200 ml and fitted to the long neck of a capillary tube.

All these procedures were carried out using a vacuum line incorporating greaseless stopcocks and joints. The ratio of HBr to CH_4 and total pressure were maintained constant at 0.1 ± 0.01 and 660 ± 30 mmHg, respectively, throughout the series of addition experiments.

Extraction Procedures, Activity Measurements, and Yield Determinations. The reaction mixture was allowed to stand for more than 2 h in the dark at 40 °C to permit a ^{80m}Br–^{80}Br parent-daughter equilibrium to be established. Then, the tip of the ampoule was broken, and 4 ml of 0.5 N Na_2SO_3, 1 ml of 0.5 N KBr and 5 ml of CCl_4 were added to the ampoule which was cooled to liquid-nitrogen temperature. Care was taken so that these solutions did not come into direct contact with reactants deposited on the walls during the cooling of the ampoule. Then the temperature was increased to approximately −100 °C to exclude air liquefied in the ampoule. Then, radioactive bromine was extracted into the organic and inorganic layers by vigorous shaking. The organic layer was washed twice with distilled water. After the addition of carriers, such as CH_3Br, CH_2Br_2, CH_2BrCl, *etc.*, a portion of the organic fraction was submitted to gas chromatography and product analysis was carried out using a column (75 cm long, 3 mm in diameter) filled with 60—80 mesh celite 545, which was coated with silicone oil (20% in weight).

A fraction of each product was collected in a glass tube cooled in a Dry Ice–ethanol bath at the outlet of the column. The radioactive emissions from each product were measured with a NaI(Tl) scintillation counter, and the relative yields of the individual products were determined. Also the organic and inorganic fractions in a given quantity were pipetted into test tubes. The inorganic fraction was allowed to stand for more than 1.5 h to establish ^{80m}Br–^{80}Br equilibrium, and only the 0.618 MeV photopeak from ^{80}Br was counted for a period of about eight half-lifes of ^{80m}Br (4.38 h). No other radioactive contamination was observed in the organic fraction. The radioactivity measurements of the organic fractions were usually started about 7 min after extraction. The radioactivity measurements of these fractions was performed with a high-resolution Ge(Li) semiconductor detector (36 ml in volume) connected to a 4096-channel pulse-height analyzer.

The activities of both the inorganic and organic fractions were corrected for the separation time. The organic yields were determined as the percent ratio of the radioactivity of the organic fraction to the total radioactivity, and the individual product yields were obtained by simply multiplying the relative yield of each product by the organic yield. For several runs, the product yields were determined by the radio gas chromatographic technique adopted by Tachikawa and Kahara for the $^{80m}BrBr$–CH_4 system.[3] However, there was no difference in the yields for both methods.

The experimental error resulting from statistical fluctuations in the counting were approximately 7—15%. The experimental error due to inefficiencies in the extraction and collection of the products at the outlet of the gas chromatograph column were almost negligible.

Results

The bromine exchange reactions were first examined in the $H^{82}Br$–CH_3Br and/or CH_2Br_2 (HBr/CH_3Br (or CH_2Br_2) $=0.1\pm0.01$) systems at a constant pressure of 150 mmHg prior to the actual experiment. After storage in the dark for 2 h at 40 °C, the radioactivity of the organic fraction after extraction was less than 0.1% of the total activity. Furthermore, no dependence of the yields on the storage period of the reaction vessels was found for storage periods between 2 and 10 h.

From the radio gas chromatograms of the organic fractions, $CH_3{}^{80}Br$, $CH_2{}^{80}BrBr$, and $CHBr_2{}^{80}Br$ were identified as the products in the $H^{80m}Br$–CH_4 system. However, the $CHBr_3$ yields were very small and in most cases less than 0.1%. On the other hand, $CH_2{}^{80}BrCl$ and $CH_3CH^{80}BrCl$ for the system with the HCl additive and $CH_3CH_2{}^{80}Br$ for that with the $CH_2{=}CH_2$ additive were observed, in addition to $CH_3{}^{80}Br$ and $CH_2{}^{80}BrBr$, respectively.

No pressure dependence of the organic and product yields was observed in the range from 100 to 1400 mmHg at a constant HBr/CH_4 ratio of 0.1 ± 0.01.

In order to differentiate the kinetic-energy dependent from the kinetic-energy independent (thermal ionic) yield for the $H^{80m}Br$–CH_4 system, Kr and Xe were added as moderators for ^{80}Br while the HBr/CH_4 ratio was maintained constant at 0.1 ± 0.01. The results are given in Table 1 and depicted graphically in Fig. 1. The $CH_3{}^{80}Br$ and $CH_2{}^{80}BrBr$ yileds were 1.60 and 2.65% for 0 mf of additives, respectively. The $CH_2{}^{80}BrBr$ yield was much greater than that for $CH_3{}^{80}Br$ over the entire additive concentration range, contrary to the results obtained from the IT-experiments of the $^{80m}Br_2$[1,10] and/or $^{82m}Br_2$[3,15]–CH_4 systems. No change in the yield distribution was observed for additive concentrations less than about 0.6 mf, while the $CH_2{}^{80}BrBr$ yiled showed a tendency to increase gradually at concentrations greater than 0.6 mf, as was observed for

Table 1. Percent ^{80}Br stabilized in organic combinations in a gaseous mixture of an additive and CH_4
($HBr/CH_4=0.1\pm0.01$, Total pressure $=660\pm30$ mmHg)

Molar fraction additive (mf)		CH_3Br (%)	CH_2Br_2 (%)	Organic yield (%)
Kr	Xe			
0	0	1.6±0.2	2.7±0.2	4.3±0.3
0	0	1.6±0.1	2.6±0.3	4.2±0.3
0	0	—	—	4.2±0.3
—	0.10	1.6±0.3	2.6±0.3	4.2±0.5
—	0.10	—	—	4.4±0.3
0.20	—	1.6±0.2	2.6±0.3	4.2±0.3
0.21	—	—	—	4.0±0.2
0.29	—	1.4±0.1	2.5±0.2	3.9±0.4
—	0.30	1.6±0.2	2.4±0.3	4.0±0.3
0.40	—	1.7±0.3	2.5±0.3	4.2±0.3
0.50	—	—	—	4.2±0.5
0.60	—	1.6±0.2	2.5±0.3	4.1±0.4
—	0.61	1.3±0.2	2.8±0.2	4.1±0.4
0.60	—	—	—	4.2±0.5
0.70	—	0.81±0.1	3.2±0.4	4.2±0.3
—	0.70	1.2±0.1	3.2±0.4	4.4±0.4
0.70	—	—	—	4.3±0.4
—	0.75	0.9±0.09	3.4±0.3	4.3±0.5
0.80	—	0.81±0.08	3.8±0.4	4.6±0.4
—	0.80	1.0±0.09	3.7±0.3	4.7±0.4
0.85	—	0.85±0.08	3.7±0.3	4.6±0.5
—	0.85	0.94±0.09	4.0±0.4	4.9±0.4

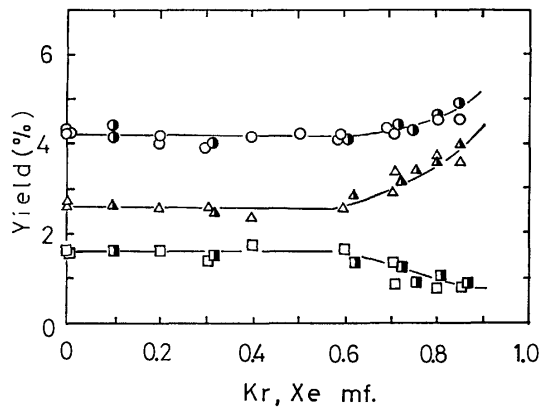

Fig. 1. Effect of Kr and Xe additives on the product yield distribution ($H^{80m}Br/CH_4=0.1\pm0.01$).
Kr additive Xe additive
-○- -◑-: total organic yield
-△- -▲-: $CH_2{}^{80}BrBr$
-□- -◨-: $CH_3{}^{80}Br$

the $H^{82m}Br$–CH_4[18] and $^{80m}BrBr$–CH_4[19] systems. However, the $CH_3{}^{80}Br$ yield decreased slightly at high additive concentrations.

The effect of the HCl additive on the yield distributions is shown in Fig. 2. The organic yield is almost constant for 0—0.6 mf of HCl, and the decrease in the $CH_3{}^{80}Br$ and $CH_2{}^{80}BrBr$ yileds nearly offset the increase in the $CH_2{}^{80}BrCl$ and $CH_3CH^{80}BrCl$ yields.

In addition, the effect of the CH_2=CH_2 additive on the yield distribution is shown in Fig. 3. From preliminary experiments using ^{77}Br-labeled HBr($t_{1/2}$=57 h for ^{77}Br) under the same experimental conditions, no addition reaction of HBr with CH_2=CH_2 was observed and therefore, this indicates that the yields are derived from reactions associated with the isomeric transition of ^{80m}Br. A sharp increase in the $CH_3CH_2{}^{80}Br$ yield was observed upon the addition of a small amount of CH_2=CH_2, and for concentrations above about 0.05 mf, the yield gradually increased. However, the addition of a small quantity of CH_2=CH_2 resulted in a sharp decrease in the $CH_2Br^{80}Br$ yield, and the $CH_3{}^{80}Br$ yields decreased relatively slowly with increasing CH_2=CH_2 concentration.

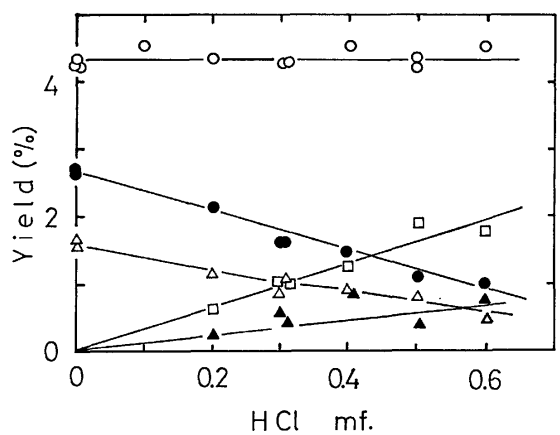

Fig. 2. Effect of HCl additive on the product yield distribution ($H^{80m}Br/CH_4=0.1\pm0.01$).
-○-: Total organic yield, -●-: $CH_2{}^{80}BrBr$, -△-: $CH_3{}^{80}Br$, -□-: $CH_2{}^{80}BrCl$, -▲-: $CH_3CH^{80}BrCl$.

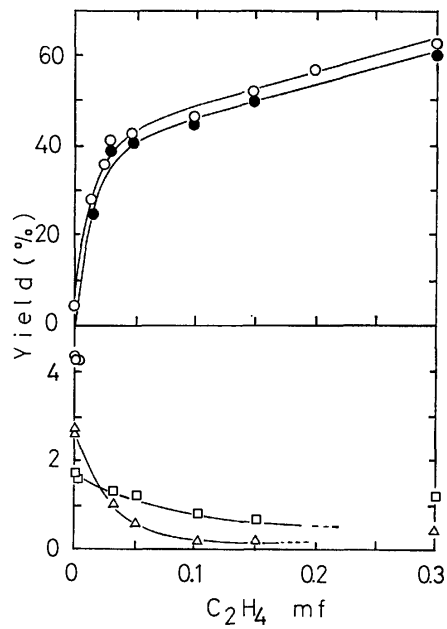

Fig. 3. Effect of CH_2=CH_2 additive on the product yield distribution ($H^{80m}Br/CH_4=0.1\pm0.01$).
-○-: Total organic yield, -△-: $CH_2{}^{80}BrBr$, -●-: $CH_3CH_2{}^{80}Br$, -□-: $CH_3{}^{80}Br$.

Discussion

Evaluation of the Yields via *Kinetic and Thermal Process.* Up to the present time, many investigations have been carried out on the reactions of bromine produced by a variety of nuclear transformations in gaseous systems, especially in order to evaluate the role of the charge and kinetic energy of the bromine atom in the recombination reactions. The most convenient way to differentiate an energetic reaction from a kinetic energy independent (thermal ionic) reaction is by the addition of an inert gas which can serve as an energy sink for the energetic Br atoms. Kr is the most effective moderator since the mass of Kr is almost equal to that of Br, and Kr is also found to have small cross sections for quenching excited species and for undergoing charge transfer with Br^+ ions due to its high ionization potential of 13.99 eV.[15] Therefore, if the yield decreases upon the addition of Kr, it must be due to the removal of the ^{80}Br kinetic energy, and the remainder, which is insensitive to the Kr additive, can be derived from thermal ionic reactions. The high electron affinity of Br^{+n} ($n\geq2$) suggests that the thermal ionic reaction concerns mostly the reaction involing the $^{80}Br^+$ ion.

As Fig. 1 shows, no change in the $CH_3{}^{80}Br$ and $CH_2{}^{80}BrBr$ yields was observed in the range from 0 to 0.6 mf of Kr and Xe. This indicates that both products are formed *via* thermal ionic reactions. These findings are very different from those obtained for the $^{80m}BrBr$-($^{82m}Br_2$)–CH_4[3,15,20] and (n,γ)-activated ^{80}Br–CH_4 systems,[4] for which the organic yields resulted mainly from kinetic-energy dependent reactions. This difference

can be explained on the basis of the kinetic energy acquired initially by the Br atom.

In the case of the isomeric transition of ^{80m}Br, the kinetic energy of ^{80}Br ranges from 0 eV to maxima of 1.3 and 158 eV when HBr and Br_2, respectively, are used as source molecules, with the most probable energies being 0.75 and 37 eV, respectively.[5]

On the other hand, it is known from neutron binding-energy data[21] that the ^{80}Br and $^{82m}Br+^{82}Br$ produced by (n,γ) activation have kinetic energy spectra ranging from 0 to 417 eV, and from 0 to 378 eV, respectively. Wexler has also determined that approximately 18 and 25% of the neutron activation processes resulted in positively-charged ^{80}Br and ^{82}Br, respectively.[8] The present data are compared with those obtained from the IT and (n,γ) experiments in Table 2. Thermal ionic yields increase with decreasing kinetic (recoil) energy, E_{max}, but on the contrary, the kinetic-energy dependent yields tend to increase with increasing E_{max}. It is considered that the thermal ionic yield largely depends on the probability of the bromine ions reaching the thermal energy region upon escaping from the charge neutralization. Therefore, it is very interesting to estimate the cross sections for charge neutralization and ion-molecule reactions as a function of the $^{80}Br^+$ kinetic energy.

Rapp and Francis[22a] have calculated the cross section for resonant charge transfer at intermediate impact velocities (10^5—10^8 cm/s) using the semiclassical impact-parameter method. The values obtained are in good agreement with experimental values in many cases. The cross sections for the resonant charge-transfer reaction of Br^+ with Br, which is the highest of the charge-transfer reactions involving the Br^+ ion, can be obtained by interpolating the resonant charge-transfer cross sections calculated by Rapp and Francis.[22a] Whereas the velocity, v_{max}, for which the asymmetric charge-transfer cross section is maximum, was calculated from

$$v_{max} = \frac{|\Delta E|a}{h}, \quad (1)$$

assuming that the asymmetric charge-transfer cross section is close to that for resonant charge transfer at velocities above v_{max}.[22a] The threshold energy (E_{th})[23] for *endo*-energetic charge-transfer reactions was calculated using the relation

$$E_{th} = \frac{M_{Br^+} + M_{target}}{M_{target}}, \quad (2)$$

where ΔE, h, a, and M are the energy defect, Planck's constant, the adiabatic parameter (7×10^{-8} cm),[24] and the mass, respectively. The values of v_{max} and E_{th} are tabulated in Table 3.

On the other hand, the cross sections for capture collisions between Br^+ and CH_4 were calculated using[22b]

$$\sigma(v) = (2\pi e/v)(\alpha/\mu)^{1/2}, \quad (3)$$

where μ, α, v and e are the reduced mass of the collision pair, the polarizability of CH_4 (2.60×10^{-24} cm^3/mol),[25] the relative velocity of the ion and the charge on the ion, respectively. Pottie *et al.*,[26] Boelrük and Hamill,[27] and Kubose and Hamill[28] have indicated that Eq. 3 is applicable to ions with energies below about 1 eV. The cross sections thus obtained are shown in Fig. 4 as a function of the Br^+ velocity (lower abscissa). The velocity dependence for reactions C and D in Fig. 4 are hypothetical and are drawn on the basis of values of v_{max} and E_{th}. E_{max} for the $^{79}Br(n,\gamma)^{80}Br$ reaction and the isomeric transition of ^{80m}Br in Br_2 and HBr are shown by arrows pointing downward on the upper abscissa of this figure.

This figure indicates that the charge-neutralization reaction is predominant in the high-energy region above about 1 eV, and the formation of a capture collision complex is favorable at energies below 1 eV. Therefore, most Br^+ ions produced by the (n,γ) reaction and IT in Br_2 lose their charges before reaching the energy region in which the collision-complex formation reactions preferentially occur. In the present case, the kinetic energy initially acquired by the ^{80}Br atom is 0.75 eV on the average.[5] Therefore, the formation of the capture collision complex competes with the charge transfer reaction, as is seen in Fig. 4 and occurs with higher probability in the energy region below 1 eV.

Table 2. The percentage yields of organic products due to kinetic and thermal ionic processes in IT and (n,γ) experiments ($HBr(or\ Br_2)/CH_4=0.1\pm0.01$)

		System			
		$H^{80m}Br$–CH_4[a]	$Br^{80m}Br$–CH_4[b]	$Br^{82m}Br$–CH_4[b]	(n,γ)-activated[c]* ^{80m}Br–CH_4
E_{max} (eV)		1.3	158	158	417
Org. Yield (%)		4.25	4.7	6.1	13.8
Kinetic process	CH_3Br (%)	≈0	3.0	4.5	11.4
	CH_2Br_2(%)	≈0	≈0	0	1.0
Thermal ionic process	CH_3Br (%)	1.60	0.5	0.5	0.9
	CH_2Br_2(%)	2.65	1.1	1.1	0.5

a) Present work. b) Ref. 35. c) Ref. 4. * Br_2/CH_4= 0.02—0.03.

Table 3. v_{max} and E_{th} for asymmetric charge-transfer reactions of Br^+ with CH_4, Kr, and Xe

Electronically excited state of Br^+	Excitation energy (eV)	Energy defect ΔE (eV)			E_{th} (eV)			v_{max} (cm/s)		
		CH_4	Kr	Xe	CH_4	Kr	Xe	CH_4	Kr	Xe
$^3P_2$	0	1.11	2.11	0.29	6.65	4.12	0.47	1.88×10^7	3.57×10^7	4.91×10^6
$^3P_1$	0.39	0.72	1.72	0.10	4.31	3.36	—	1.22×10^7	2.91×10^7	1.69×10^6
$^3P_0$	0.48	0.63	1.63	0.19	3.78	3.18	—	1.07×10^7	2.76×10^7	3.22×10^6
$^1D_2$	1.41	0.30	0.70	1.12	—	1.36	—	5.07×10^6	1.19×10^7	1.89×10^7

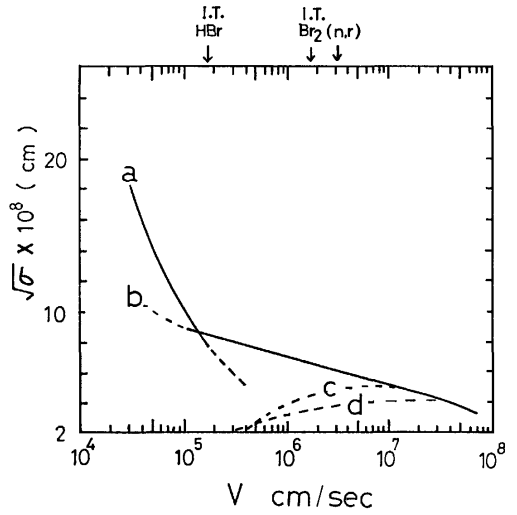

Fig. 4. Relationship between the velocity of Br^+ and cross sections for ion-molecule and charge neutralization reactions.
(a): Capture collision $Br^+ + CH^4 \rightarrow CH_4Br^+$,
(b): resonant charge transfer $Br^+ + Br \rightarrow Br^0 + Br^+$,
(c): $Br^+(^3P_2) + CH_4 \rightarrow Br + CH_4^+$,
(d): $Br^+(^3P_2) + Kr \rightarrow Br + Kr^+$.

Here, the charge transfer reaction of Br^+ with HBr is exothermic by 0.2 eV and is expected to occur efficiently from a consideration of the vibrationally-excited states of HBr. Even if neutralization occurs, the ^{80}Br cannot undergo any kinetic-energy dependent reaction leading to C–^{80}Br bond formation because its kinetic energy is not sufficient for H and/or Br substitution reactions to proceed. Thus, the present data can be explained in terms of competition between the charge neutralization and ion-molecule reactions.

On the other hand, Kazanjian and Libby[14] have studied the reaction of IT-activated ^{80}Br using HBr as the source molecule in a solution of *n*-PrBr with 1% HBr, and found that the type of products and the organic yields are almost the same as those obtained in the (n,γ) experiment for a pure *n*-PrBr system. They explained these results assuming that the IT-activated ^{80}Br can acquire appreciable kinetic energy due to Coulomb repulsion during partial inter-molecular neutralization and then reacts in a manner identical to the hot bromine produced by the (n,γ) reaction.

However, the present experimental results indicate that even if the ^{80}Br atoms acquire kinetic energy to some extent by a similar process, this kinetic energy is not sufficient for hot reactions to occur.

Formation of $CH_2{}^{80}BrBr$ and $CH_3{}^{80}Br$ via *Thermal Ionic Processes.* It was indicated in the previous section that the $CH_2{}^{80}BrBr$ and $CH_3{}^{80}Br$ molecules are formed through thermal ionic reactions involving the $^{80}Br^+$ ion. From the energetics of the reactions, the capture collision complexes, such as $CH_4{}^{80}Br^+$ and $HBr^{80}Br^+$ will be formed first by the reactions

$$^{80}Br^+ + CH_4 \longrightarrow CH_4{}^{80}Br^+ \quad (4)$$

and

$$^{80}Br^+ + HBr \longrightarrow HBr^{80}Br^+, \quad (5)$$

since generally no activation energy is required for these reactions.

Although there is no direct evidence for the presence of these complexes in the present case, the presence of sticky collision complexes of a similar type has been confirmed in various alkyl halide and hydrocarbon systems by mass-spectroscopic studies.[29-31] Henglein and Muccini have pointed out that the complex ion, CH_4I^+, had a lifetime longer than about 10^{-6} s.[32] From a calculation of the lifetime of the $CH_4{}^{80}Br^+$ ion, using the equation proposed by Magee and Burton,[33] it is expected that the $CH_4{}^{80}Br^+$ ion has a relatively long lifetime ($\approx 10^{-2}$ s).[34]

As a possible explanation for the formation of $CH_2{}^{80}BrBr$ *via* thermal ionic processes in IT experiment involving the $^{80m}BrBr$–CH_4 system, Tachikawa[35] has previously suggested that the $CH_4{}^{80}Br^+$ formed by Reaction 4 undergoes charge neutralization following decomposition to fragments, such as $CH_3{}^{80}Br$ and $CH_2{}^{80}Br$, and the $CH_2{}^{80}Br$ radical thus formed can easily be scavenged by Br_2 to form $CH_2{}^{80}BrBr$. If this is the case, the reaction

$$CH_2{}^{80}Br + HBr \longrightarrow CH_3{}^{80}Br + Br, \quad (6)$$

which leads to $CH_3{}^{80}Br$ formation will be more energetically favorable than the reaction

$$CH_2{}^{80}Br + HBr \longrightarrow CH_2{}^{80}BrBr + H, \quad (7)$$

which gives the $CH_2{}^{80}BrBr$ of this experiment using HBr as the source molecule, since Reaction 6 is exothermic by 6.8 kcal/mol, while Reaction 7 is endothermic by 24.9 kcal/mol.[36] However Fig. 1 showed that the $CH_2{}^{80}BrBr$ yield was greater than that of $CH_3{}^{80}Br$ over a whole range of additive concentrations.

Similarly, it is thought that the $CH_2{}^{80}Br$ radical in the HCl-additive system reacts with HCl to form $CH_3{}^{80}Br$ in preference to the formation of $CH_2{}^{80}BrCl$, since the reaction

$$CH_2{}^{80}Br + HCl \longrightarrow CH_3{}^{80}Br + Cl \quad (8)$$

is less endothermic than the reaction

$$CH_2{}^{80}Br + HCl \longrightarrow CH_2{}^{80}BrCl + H. \quad (9)$$

However, both $CH_3{}^{80}Br$ and $CH_2{}^{80}BrBr$ yields decreased almost linearly with increasing HCl concentration, as is seen in Fig. 2, and the $CH_2{}^{80}BrCl$ yield was greater than that of $CH_3{}^{80}Br$ at HCl concentrations above 0.35 mf. Therefore, the assumption that the $CH_2{}^{80}Br$ radical is present in this system as a precursor for $CH_2{}^{80}BrBr$ formation is unacceptable.

On the other hand, if $CH^{80}Br$ (bromocarbene) is present as a precursor, which can be produced through decomposition following the charge neutralization of $CH_4{}^{80}Br^+$ or through some other pathway, it is believed that the $CH^{80}Br$ present reacts readily with HBr and/or HCl to form $CH_2{}^{80}BrBr$ and $CH_2{}^{80}BrCl$, respectively, since these reactions are energetically very efficient.

In order to determine this point, an experiment using a $CH_2{=}CH_2$ additive was conducted. $CH_2{=}CH_2$ reacts instantaneously with $CH^{80}Br$ to form arylbromide or cyclo-bromopropane.[37]

$$CH^{80}Br + CH_2{=}CH_2 \longrightarrow \begin{matrix} CH_2{-}CH_2 \\ \diagdown\ \diagup \\ CH^{80}Br \end{matrix} \text{ or } CH_2{=}CHCH_2{}^{80}Br \text{ or } CH_3CH{=}CH^{80}Br. \quad (10)$$

However, the radio gas chromatogram showed no radioactive peaks at retention times corresponding to

these compounds and, therefore, the above assumption also unacceptable.

In the study of ion-molecule reactions using mass spectrometers, it has been observed that collision complex ions are formed effectively at high pressures and have ample opportunity to react with surrounding molecules during subsequent collisions.[38] Under the present experimental conditions, the possibility exsits that the $CH_4{}^{80}Br^+$ reacts with surrounding molecules giving the individual products.

Although no precise information is available concerning the ion-molecule reactions leading to $CH_3{}^{80}Br$ and $CH_2{}^{80}BrBr$ because of lack of knowledge concerning the chemical behaviour of complex ions at high pressure, the possibility of formation of $CH_3{}^{80}Br$ and $CH_2{}^{80}BrBr$ by ion-molecule reactions of $CH_4{}^{80}Br^+$ with CH_4 and/or HBr were evaluted from a thermodynamic viewpoint.

Loberg *et al.*[39] have studied reactions of thermal $^{123}I^+$ ions, formed by the $^{123}Xe \xrightarrow{EC,\beta^+} {}^{123}I$ process, in gaseous CH_4, and the formation of $CH_3{}^{123}I$ was explained in terms of the H^+-transfer reaction from the complex ion, $CH_4{}^{123}I^+$, to CH_4. Assuming that the intermediate $CH_4{}^{80}Br^+$ is a persistent collision complex rather than a molecular ion, we can estimate the $\Delta H^\circ{}_{298}$ for Reaction 4. The potential energy (V) between $^{80}Br^+$ and CH_4, which is stored in the $CH_4{}^{80}Br^+$ ion as binding energy, is calculated to be 5.5 kcal/mol, using the relation,[40]

$$V = -\frac{1}{2}\cdot\frac{\alpha e^2}{r^4}, \qquad (11)$$

where α is the polarizability of CH_4 (2.69×10^{-24} cm/mol),[25] r is the distance between ^{80}Br and CH_4 (3 Å),[41] and e is the charge. From this calculation, the heat of reaction for the reactions

$$CH_4{}^{80}Br^+ + CH_4 \longrightarrow CH_3{}^{80}Br + CH_5^+, \qquad (12a)$$

and

$$CH_4{}^{80}Br^+ + HBr \longrightarrow CH_3{}^{80}Br + H_2Br^+, \qquad (12b)$$

can be calculated roughly to be exothermic by 47 and 63 kcal/mol for ground-state Br^+, respectively. Therefore, it is conceivable that the H^+-transfer reactions from $CH_4{}^{80}Br^+$ to CH_4 and/or HBr are the principal reactions for the formation of $CH_3{}^{80}Br$.

On the other hand, it appears reasonable to assume that $CH_3{}^{80}Br$, $CH_2{}^{80}BrBr$, $CH_2{}^{80}BrCl$, and $CH_3CH^{80}BrCl$ are formed *via* the same precursor on the basis of the fact that both the $CH_3{}^{80}Br$ and $CH_2{}^{80}BrBr$ yields decrease linearly with increasing HCl concentration, and the decrement in their yields is almost equal to the increment of the $CH_2{}^{80}BrCl$ and $CH_3CH^{80}BrCl$ yields, as is shown in Fig. 2. As far as was observed, no ion-molecule reactions of $CH_4{}^{80}Br^+$ and $HBr^{80}Br^+$ with additives leading directly to the formation of these products are favored because of their high endothermicities. Of the various types of ion-molecule reactions concerning the intermediate ions, the following reactions are all exothermic, and probably one-step, reaction routes leading to the final products:

$$CH_4{}^{80}Br^+ + HBr \longrightarrow CH^{80}BrBr^+ + 2H_2 \quad (\Delta H^\circ = -45 \text{ kcal/mol}), \qquad (13)$$

$$CH_4{}^{80}Br^+ + HCl \longrightarrow CH^{80}BrCl^+ + 2H_2 \quad (\Delta H^\circ = -28 \text{ kcal/mol}), \qquad (14)$$

$$CH_4{}^{80}Br^+ + CH_2{=}CH_2 \longrightarrow CH_4 + CH_2CH_2{}^{80}Br^+ \quad (\Delta H^\circ = -88 \text{ kcal/mol}), \qquad (15)$$

and

$$CH_4{}^{80}Br^+ + CH_2{=}CH_2 \longrightarrow CH_3{}^{80}Br^+ + CH_3CH_2 \quad (\Delta H^\circ = -29 \text{ kcal/mol}). \qquad (16)$$

However, along which pathways the product ions thus formed lose their charges, and result in the end products appears to be rather complicated. If these ions lose their charge through free-electron capture, the high exothermicity resulting from these processes is dissipated in the form of internal energy of the molecule and probably results in the rupture of the C–^{80}Br bond. Therefore, these processes could not lead to the formation of $CH_3{}^{80}Br$, $CH_2{}^{80}BrBr$, and $CH_2{}^{80}BrCl$. Further, charge-transfer reactions of these ions with additives cannot occur because these reactions are also highly endothermic.

However, if these product ions lose their charges through charge-transfer reactions with the impurities present in the system or with the walls of the reaction vessel, and the energy defects (ΔE) for charge transfer are not so large as to lead to C–^{80}Br bond rupture, there is the possibility that the radicals and molecules in somewhat excited states thus formed are stabilized by collisions with their surroundings and undergo H-abstraction to give corresponding products.

Thus, ion-molecule reactions (13—16) may finally lead to the formation of $CH_2{}^{80}BrBr$, $CH_2{}^{80}BrCl$, $CH_3CH_2{}^{80}Br$, and $CH_3{}^{80}Br$, respectively, and the effect of additives on the yield distributions in Figs. 2 and 3 can be explained on the basis of these competitive reactions involving the precursor, $CH_4{}^{80}Br^+$.

Generally, it is known that thermal ions at high pressure form ion clusters containing several molecules held together by the electrostatic force between the ion and the molecules.[42–44] If this is the case, the energy ΔE deposited on the radical or molecule during the neutralization process can be effectively dissipitated to the cluster molecules. Even if the lifetimes of these excited radicals are relatively short, the radicals can be stabilized easily by collisions under liquid-like conditions,[33] and undergo H-abstraction reactions with surrounding molecules to form corresponding products, since the H-abstraction reactions are energetically most favorable. The above discussion is somewhat qualitative, but details of it will be elucidated upon the further accumulation of knowledge concerning ion-molecule reactions involving Br^+ in gases at atmospheric pressure.

The most prominent feature in Fig. 3 is the sharp increase in the $CH_3CH_2{}^{80}Br$ yield for a small amount of $CH_2{=}CH_2$. This can be explained on the basis of the thermal ^{80}Br reaction with $CH_2{=}CH_2$ (Reaction 17), in which ^{80}Br is produced through charge neutralization of $^{80}Br^+$ with HBr, CH_4 and/or $CH_2{=}CH_2$, thus

$$^{80}Br + CH_2{=}CH_2 \longrightarrow CH_2CH_2{}^{80}Br, \qquad (17a)$$

$$CH_2CH_2{}^{80}Br + HBr \longrightarrow CH_3CH_2{}^{80}Br + Br. \qquad (17b)$$

However, the gradual increase in the $CH_3CH_2{}^{80}Br$ yield at concentrations above 0.03 mf is attributable to reactions of ^{80}Br and $^{80}Br^+$ with $CH_2{=}CH_2$ and/or Reaction 15.

As Fig. 1 shows, the marked change in the yield curves is due to the additional formation of $CH_2{}^{80}BrBr$ for Kr and Xe concentrations greater than 0.6 mf. A similar increase in the CH_2BrBr yield was observed for

a highly-moderated system in IT-experiments of the $^{80m}BrBr$[19] and $H^{82m}Br$–CH_4 systems.[18] The collision frequency of $^{80}Br^+$ ions with Kr and Xe atoms increases abruptly for concentrations over 0.6 mf. This additional formation of $CH_2{}^{80}BrBr$ may thereby be explained in terms of (i) the increase in the number of $^{80}Br^+$ ions with lower kinetic energies and of electronically-excited states, since the kinetic energy spectra of $^{80}Br^+$ shifts to lower energies at high concentrations of Kr and Xe, and (ii) ion-molecule reactions involving complex ions containing inert gas molecules. If assumption (i) is valid, a similar increase in the $CH_3{}^{80}Br$ yield will be observed, because $CH_3{}^{80}Br$ formation greatly depends on the number of $^{80}Br^+$ ions. However, no increase in the $CH_3{}^{80}Br$ yield was observed, as can be seen in Fig. 1. Although no information on ion-molecule reactions of Br^+ with inert gases is available, there may be some reaction pathways for the additional formation of $CH_2{}^{80}BrBr$ involving, presumably, the reactions of the $Kr^{80}Br^+$ (or $Xe^{80}Br^+$) ion with the surrounding molecules. However, the details of the reaction pathways leading to the additional formation of $CH_2{}^{80}BrBr$ must await further experiments.

The authors wish to thank the laboratory crew for operating the linear accelerator.

References

1) E. P. Rack and A. A. Gordus, *J. Phys, Chem.*, **65**, 944 (1961).
2) L. D. Spicer and A. A. Gordus "Symposium on Chemical Effects Associated with Nuclear Reactions and Radioactive Transformation," IAEA, Vol. 1, Vienna (1965), p. 185.
3) E. Tachikawa and T. Kahara, *Bull. Chem. Soc. Jpn.*, **43**, 1293 (1970).
4) M. Saeki, K. Numakara, and E. Tachikawa, *Bull. Chem. Soc. Jpn.*, **45**, 1715 (1962).
5) M. E. Berg, W. H. Grauer, R. W. Helton, and E. P. Rack, *J. Phys. Chem.*, **79**, 1327 (1975).
6) Z. B. Alfassi and S. Amiel, *Radiochim. Acta*, **20**, 130 (1973).
7) M. Yagi, K. Kondo, and T. Kobayashi, *Bull. Chem. Soc. Jpn.*, **44**, 580 (1971).
8) S. Wexler and H. Davies, *J. Chem. Phys.*, **20**, 1688 (1952).
9) S. H. Daniel, H. J. Ache, and G. Stöcklin, *J. Phys. Chem.*, **78**, 1043 (1974).
10) S. H. Daniel and H. J. Ache, *Radiochim. Acta*, **19**, 132 (1973).
11) M. D. Silbert and R. H. Tomlison, *Radiochim. Acta*, **5**, 217 (1966).
12) N. Colebourne, J. F. J. Todd, and R. Wolfgang, *J. Phys. Chem.*, **71**, 2875 (1967).
13) L. D. Spicer and R. Wolfgang, *J. Chem. Phys.*, **50**, 3466 (1969).
14) A. R. Kazanjian and W. F. Libby, *J. Chem. Phys.*, **42**, 277 (1965).
15) J. B. Nicholas and E. P. Rack, *J. Chem. Phys.*, **48**, 4085 (1968).
16) E. Tachikawa, *Bull. Chem. Soc. Jpn.*, **42**, 2304 (1970).
17) E. Tachikawa and J. Okamoto, *Radiochim. Acta*, **13**, 159, (1970).
18) M. Yagi, K. Kondo, and T. Kobayashi, unpublished data.
19) K. Numakara, M. Saeki, and E. Tachikawa, *Bull. Chem. Soc. Jpn.*, **46**, 1 (1973).
20) M. Yagi and K. Kondo, *Res. Rep. Lab. Nucl. Sci. Tohoku Univ.*, **3**, 138 (1970).
21) J. H. E. Mattauch and W. Thiele, *Nucl. Phys.*, **67**, 32 (1965).
22) a) D. Rapp and W. E. Francis, *J. Chem. Phys.*, **37**, 2631 (1962); b) G. Gioumousis and D. P. Stevenson, *J. Chem. Phys.*, **29**, 294 (1958).
23) C. F. Giese and W. B. Maier II, *J. Chem. Phys.*, **39**, 197 (1963).
24) D. Seewald and R. Wolfgang, *J. Chem. Phys.*, **47**, 143 (1967).
25) J. O. Hirshfelder, C. F. Curtiss, and R. B. Bird, "Molecular Theory of Gases and Liquids," John Wiley & Sons, Inc., (1954), p. 950.
26) R. F. Pottie, A. J. Lorguet, and W. H. Hamill, *J. Chem. Soc.*, **84**, 529 (1963).
27) N. Boelrijk and W. H. Hamill, *J. Chem. Soc.*, **84**, 730 (1962).
28) D. A. Kubose and W. H. Hamill, *J. Chem. Soc.*, **85**, 125 (1963).
29) R. F. Pottie and W. F. Hamill, *J. Phys. Chem.*, **63**, 877 (1959).
30) C. E. Melton and P. S. Rudolph, *J. Chem. Phys.*, **32**, 1128 (1960).
31) C. D. Wagner, P. A. Wadsworth, and D. P. Stevenson, *J. Chem. Phys.*, **28**, 517 (1958).
32) A. Henglein and G. A. Muccini, *Z. Naturforshg*, **15a**, 584 (1960).
33) J. L. Magee and M. Burton, *J. Chem. Soc.*, **56**, 842 (1952).
34) The lifetime of collision complexes can be expressed by the equation[33]
$$\tau = \nu^{-1}\left(1-\frac{E_\beta}{E}\right)^{1-\alpha}$$
where E is the actual relative energy of the system, E_B is the binding energy of the two entities which form the complex, α is the number of vibrational degrees of freedom of the complex, and ν is a constant having dimensions of frequency and of the order of magnitude of a molecular vibrational frequency. From a rough approximation, $\tau_{CH_4Br^+}$ is calculated to be 2.0×10^{-2} s for $\nu=10^{13}$, $\alpha=12$, $E_B=0.24$ eV, and $E=E_B+kT$. (k is Boltzmann's constant and T is the absolute temperature (298 K)).
35) E. Tachikawa, *Bull. Chem. Soc. Jpn.*, **43**, 63 (1900).
36) The thermodynamic values used for the calculation were taken from the following references: a) J. L. Beauchamp, *Ann. Rev. Phys. Chem.*, **22**, 527 (1971); b) V. I. Vedeneyev, L. V. Gurvich, V. N. Kondratyév, V. A. Medvedev, and Ye. L. Frankevich, "Bond Energies, Ionization Potentials and Electron Affinities," (English translation), Edward Arnold, Ltd., London (1966); c) F. W. Lampe, J. L. Fraklin, and F. H. Field, "Progress in Reaction Kinetics," ed by G. Porter, Pergamon Press, Vol. 1, New York (1961), p. 67.
37) J. M. Rodriguez, J. M. Lo, and C. M. Wai, *Radiochem. Radioanal. Lett.*, **20**, 353 (1975).
38) "Mass Spectrometry of Organic Ions," ed by F. McLafferty, Academic Press, New York (1963), p. 65.
39) M. D. Loberg, K. A. Krohn, and M. J. Welch, *J. Chem. Soc.*, **95**, 5496 (1973).
40) E. W. McDaniel, "Collision Phenomena in Ionized Gases," Wiley, New York (1964), p. 67 and Appendix II.
41) The distance between CH_4 and $^{80}Br^+$ is considered to be close to that for the CH_4–$^{123}I^+$ system (3.18 Å).[39] 3 Å was assumed for r in this calculation.
42) "Ion-Molecule Reactions," ed by J. L. Franklin, Plenum Press, Vol. 1, New York (1972), p. 315.
43) S. Bloom and H. Margenau, *Phys. Rev.*, **85**, 670 (1952).
44) J. L. Magee and L. Funabashi, *Radiation Res.*, **10**, 622 (1959).

Kinetic Studies of Photosensitized Oxygenation by Singlet Oxygen in Aqueous Micellar Solutions

Yoshiharu Usui, Michio Tsukada, and Hiroko Nakamura

Department of Chemistry, Faculty of Science, Ibaraki University, Mito 310

(Received April 28, 1977)

Singlet oxygen produced by the dye-sensitized reaction in an aqueous solution penetrates into the interior of the surfactant micelles of sodium dodecyl sulfate (SDS) and dodecyltrimethylammonium chloride (DTAC), reacting with the solubilized acceptors such as 9,10-dimethylanthracene, 2,5-diphenyloxazole, and 1,3-diphenylisobenzofuran. From the acceptor concentration effect on the photooxygenation quantum yield, the reactivity index (β), the ratio of the rate constant of the spontaneous decay of singlet oxygen to that of the reaction with an acceptor, is obtained in the aqueous micellar solution. It has been shown that the lifetime of singlet oxygen is mainly dependent on the solvent composition in the bulk phase from the kinetic analysis of the mixed solvent effect on the quantum yield in SDS and DTAC micellear solutions and that in a homogeneous solution.

Singlet oxygen is one of the active species for the oxidative process in a biological system as well as supperoxide ion, hydroxyl radical, hydrogen peroxide, ozone, *etc.* Investigation of the dye-sensitized photooxidation by singlet oxygen in a solution in which an acceptor is dissolved in the surfactant micelles affords significant information on their use in the study of photodynamic inactivation of enzyme and cells.[1-5] Since a surfactant micelle serves as both structural and functional models for complex bioaggregates of proteins or biomembrances, kinetic investigations are required to determine the mechanism of the micelles with singlet oxygen produced by the energy transfer from the dye bound on micelles or dissolved in a liquid phase.

Studies on the fluorescence quenching of aromatic compounds within some surfactant micelles by oxygen dissolved in an aqueous solution suggest that an oxygen molecule can undergo unrestricted diffusion into the micelles.[6,7] In the case of singlet oxygen, although such diffusion into the micelles is also expected, its lifetime in the liquid phase which is highly dependent on the type of solvent can be responsible for the reaction efficiency for the micellar system. In order to explain the solvent effect on the lifetime of singlet oxygen an electronic-to-vibrational energy transfer theory (*i.e.*, to the C–H or O–H streching vibrational mode of solvent) was introduced.[8] It seems that singlet oxygen is subjected to deactivation by water and surfactant micelles. However, despite the fact that the lifetime in aqueous solution (2 μs) is the shortest among those observed in a number of solvents, it is of interest that singlet oxygen is scarcely quenched by micelles itself and reacts with the acceptor dissolved in micelles efficiently.[9,10]

In this paper, the reaction mechanism in some micellar systems has been discussed from the concentration effect of singlet oxygen acceptor and the mixed solvent effect upon the quantum yield of the disappearance of the acceptor in micelles as compared with the effects in the homogeneous solutions.

Experimental

Materials. Sodium dodecyl sulfate and dodecyltrimethylammonium chloride (Tokyo Kasei, G. R.) were recrystallized from methanol. 9,10-Dimethylanthracene, 2,5-diphenyloxazole, 2,5-dimethylfuran, tryptophan, histidine (Tokyo Kasei, G. R.), and 1,3-diphenylisobenzofuran (Aldrich Co.) were used without further purification. Methylene blue (MB) and eosine (EOS) were recrystallized twice from 1-butanol and ethanol, respectively. Singlet oxygen acceptors were solubilized in each surfactant (0.1 M) by gentle stirring of the mixture at 50—70 °C in the dark.

Procedures. A fresh sample in a $1\times1\times4$ cm^3 or $0.3\times1\times4$ cm^3 cell was irradiated by a cross-illumination apparatus with a steady light at 25.0 °C. The experimental procedure to determine the quantum yield was similar to that described previously.[11] Flash photolysis experiments were carried out by using a Q-switched ruby laser (NEC, SLG-2007). A suitable cut-off filter and an interferance filter (λ=410 nm) were placed in the analyzing beam from a tungsten lamp in order to avoid the photolysis of singlet oxygen acceptor. The fluorescence spectra were measured with a Shimadzu RF-500 fluorimeter.

Results and Discussion

Acceptor Concentration Dependence on the Quantum Yield in a Homogeneous Solution. The essential reaction scheme and the disappearance quantum yield Φ_{-A} of a singlet oxygen acceptor (A) in solution are expressed as follows:[11-13]

$$^1\mathrm{Sens} \xrightarrow{h\nu} {}^3\mathrm{Sens}^* \qquad \phi_{st} \quad (1)$$

$$^3\mathrm{Sens}^* \longrightarrow {}^1\mathrm{Sens} \qquad k_d \quad (2)$$

$$^3\mathrm{Sens}^* + {}^1\mathrm{Sens} \longrightarrow \mathrm{Sens}^+ \cdots \mathrm{Sens}^-,\ {}^1\mathrm{Sens} + {}^1\mathrm{Sens} \qquad k_D \quad (2')$$

$$^3\mathrm{Sens}^* + {}^3\mathrm{O}_2 \longrightarrow {}^1\mathrm{Sens} + {}^1\mathrm{O}_2 \quad (k^r_{O_2}) \qquad (3)$$

$$\searrow\ {}^1\mathrm{Sens} + {}^3\mathrm{O}_2,\ \mathrm{Sens}^+ \cdots \mathrm{O}_2^- \qquad k^s_{O_2} \quad (4)$$

$$^3\mathrm{Sens}^* + \mathrm{A} \longrightarrow {}^1\mathrm{Sens} + \mathrm{A} \qquad k^s_{TA} \quad (5)$$

$$^1\mathrm{O}_2 \longrightarrow {}^3\mathrm{O}_2 \qquad k'_d \quad (6)$$

$$^1\mathrm{O}_2 + \mathrm{A} \longrightarrow \mathrm{AO}_2 \quad (k'^r_A) \qquad (7)$$

$$\searrow\ \mathrm{A} + {}^3\mathrm{O}_2 \qquad k'^s_A \quad (8)$$

$$\Phi_{-A} = \Phi_{so}\alpha r\frac{[A]}{\beta+[A]} \qquad (9)$$

where $\Phi_{so}=\phi_{st}\gamma_{so}$ (yield of singlet oxygen formation), $r=k'^r_A/k'^s_A$ (reaction probability of A with singlet oxygen), $\beta=k'_d/k'^s_A$ (reactivity index of A with singlet oxygen), γ_{so} stands for the singlet oxygen formation probability ($=k^r_{O_2}/k^s_{O_2}$) from triplet sensitizer (^{3}Sens) *via*

process 3, and α is the reaction probability of AO_2 to its successive processes. If these is no successive reaction following AO_2, the relation of the double reciplocal plot of Φ_{-A}^{-1} *vs.* $[A]^{-1}$ on Eq. 9 would be linear. From the slope and intercept the value of β can be obtained and the k'^{s}_{A} value is estimated by substituting the value of k'_d in the solvent.

The values of k'_d and k'^{s}_{A} are independently determined by means of the laser flash photolysis utilizing the kinetic analysis proposed by Kearns *et al.*,[8] Adams and Wilkinson,[14] and Young *et al.*[15] The reaction parameters obtained by these methods are given in Table 1 including some of the reference data.

Table 1. Rate constants of decay and reactions of singlet oxygen in various solution

Acceptor	Solvent	Sens	$k'_d\ 10^{-3}$ (s^{-1})	$k'^{s}_{A}\ 10^{-8}$ ($M^{-1}\ s^{-1}$)	β (M)
HIS	H_2O	MB	500[a]	54.3	9.2×10^{-5}
HISA	H_2O	MB	500[a]	2.0	2.5×10^{-3}
DMF	H_2O	MB	500[a]	15.6	3.2×10^{-4}
	MeOH	MB	110	3.9	2.8×10^{-4}
	MeOH[13]	MB	—	—	2.8×10^{-4}
	EtOH	MB	83[a]	3.8	2.2×10^{-4}
DMA	EtOH	MB	83[a]	0.39	2.1×10^{-3}
	EtOH	EOS	83[a]	0.44	1.9×10^{-3}
DPO	H_2O/D_2O[b]	MB	258[a]	1.6	1.6×10^{-3}
DPBF	MeOH	MB	110	16.2	6.8×10^{-5}
	MeOH	MB	110	16.4	6.7×10^{-5}(L)
	MeOH[15]	MB	88	13.0	6.7×10^{-5}(L)
	MeOH	ERY	110	15.5	7.1×10^{-5}
	EtOH	EOS	83[a]	12.8	6.5×10^{-5}
	TeCE	MB	8.3	4.4	1.9×10^{-5}(L)
	TeCE	MB	8.3	5.9	1.4×10^{-5}
	DeCE	MB	15	6.0	2.5×10^{-5}(L)
	DeCE	MB	15	10	1.5×10^{-5}
	CH_2Cl_2	MB	16	10.8	1.5×10^{-5}(L)
	CH_2Cl_2	MB	16	16	1.0×10^{-5}
	$CHCl_3$[19]	MB	16.7	6.0	2.8×10^{-5}
	$CHCl_3$	MB	9.0	7.0	1.3×10^{-5}(L)
	$CHCl_3$	MB	9.0	9.0	1.0×10^{-5}
	CCl_4	MB	1.4[a]	1.1	1.2×10^{-5}
	n-BuOH[15]	MB	52	8.0	6.5×10^{-5}(L)
	Dioxane[15]	MB	29	12.1	2.4×10^{-5}(L)
	Pyridine[15]	MB	31	21	1.5×10^{-5}(L)
	Glycol[15]	MB	51	15	3.1×10^{-5}(L)
DMA/DTAC	H_2O	MB	500[a]	7.5	6.6×10^{-4}
	D_2O	MB	50[a]	7.4	6.8×10^{-5}
	H_2O	EOS/DTAC	500[a]	9.1	5.5×10^{-4}
DPO/DTAC	H_2O/D_2O[c]	MB	275[a]	1.6	2.2×10^{-3}
DPBF/SDS	H_2O	MB/SDS	500[a]	47.1	1.1×10^{-4}
	H_2O	EOS	500[a]	42.4	1.2×10^{-4}

a) Data of Kearns *et al.* for k'_d are used in the calculation of k'^{s}_{A} values.[8] b) $\chi_{MeOH}=0.3$, $\chi_{D_2O}=0.5$. c) $\chi_{D_2O}=0.5$. Abbreviations: Histidine (HIS), histamine (HISA), methanol (MeOH), ethanol (EtOH), 1-butanol (*n*-BuOH), 1,1,2,2-tetrachloroethane (TeCE), 1,1-dichloroethane (DeCE), and erythrosine (ERY). L denotes the value obtained by laser flash experiment.

In air-saturated aqueous or ethanol solution, the triplet state of methylene blue reacts predominantly with dissolved oxygen; $k^{s}_{O_2}[O_2] \gg k_d + k_D[MB] + k^{s}_{TA}[A]$. Thus, the value of Φ_{so} would be that of ϕ_{st} ($=0.52$) since γ_{so} is approximately equal to unity.[8] For efficient acceptors such as 9,10-dimethylanthracene (DMA), 1,3-diphenylisobenzofuran (DPBF), and 2,5-dimethylfuran (DMF) which can react without the deactivation reaction of singlet oxygen (Eq. 8, $r\simeq1$), the maxmum value for the reaction quantum yield Φ_A^{max} should be close to ≈0.52 (ϕ_{st} value). However, the observed value of Φ_A^{max} is about twice of ϕ_{st} (≈1.2) as shown in Fig. 1. Although it can be expected that a complex chain reaction is involved to consume a couple of these acceptor molecules, the following results seems to deny the existence of the chain reaction in the case of the photooxygenation of DMF in an aqueous solution.

1) The UV-absorption spectrum of the MB–O_2–DMF system changes with an isobestic point at 233 nm during the course of irradiation.

2) *cis*-3-Hexene-2,5-dione is a main oxidation product from DMF, the concentration of the peroxide produced being smaller than 20% of the initial concentration of DMF at $\approx10^{-4}$ M. From the results it can be proposed that the following successive reaction of A with AO_2 occurs efficiently at higher concentrations of acceptors:[11,16]

$$AO_2 + A \longrightarrow 2AO. \tag{10}$$

If we assume that AO_2 is a certain intermediate such as the collisional adduct or the charge transfer complex between A and $^1O_2$, the quantum yield of Φ_{-A} including the competitive unimolecular decay of AO_2 (rate constant ratio; γ) *via* process 10 is given by

$$\Phi_{-A} = \Phi_{so}\frac{[A]}{\beta+[A]}\left(1+\frac{[A]}{\gamma+[A]}\right), \tag{11}$$

where $1+([A]/(\gamma+[A]))$ corresponds to α in Eq. 9. When Reaction 10 is predominant in the decay of AO_2 ($\gamma \ll [A]$), Eq. 11 approximately becomes

$$\Phi_{-A} = 2\Phi_{so}\frac{[A]}{\beta+[A]}. \tag{12}$$

In the case that AO_2 is an *endo*-peroxide and Reaction 10 is involved, Eq. 12 can similarly be applied. Thus, the maximum value of Φ_{-A} at higher concentrations of A ($\gamma \ll \beta \ll [A]$) tends to be $2\Phi_{so}$ which approaches the value of ≈1.2 as shown in Fig. 1.

By addition of the acceptor in high concentration, Process 5 can compete with Process 3 for the singlet oxygen formation. When the acceptor on a triplet sensitizer causes mostly its deactivation and the decomposition of A is negligible in Process 5, the quantum yield of disappearance of A is given by

$$\Phi_{-A} = \phi_{st}\alpha\frac{k^{r}_{O_2}[O_2]}{k_d + k^{s}_{TA}[A] + k^{s}_{O_2}[O_2]}\frac{r[A]}{\beta+[A]}. \tag{13}$$

Thus, the concentration effect of A on Φ_{-A} has a maximum where the concentration of A is given by $\sqrt{(k_d + k^{s}_{O_2}[O_2])/k^{s}_{TA}}$. In the system of MB–$O_2$–DPBF for example, Φ_{-DPBF} decreases at higher concentration

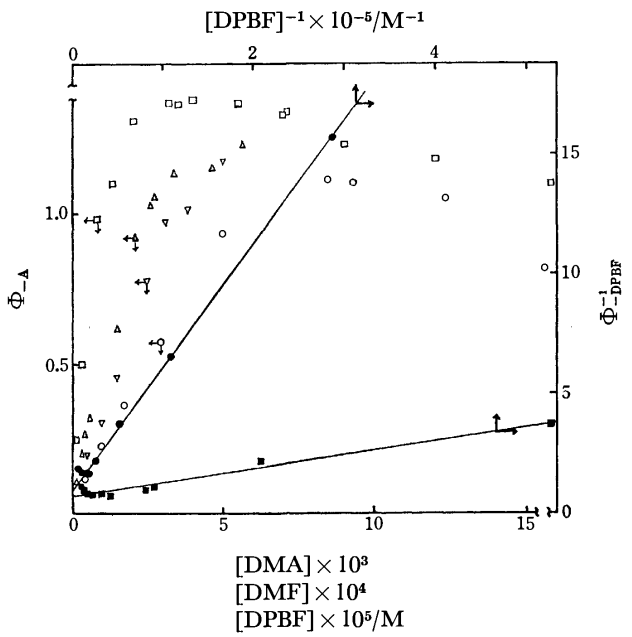

Fig. 1. Effect of [A] on Φ_{-A} and the double reciprocal plots. A: DMF in H_2O (▽), DMA in EtOH (△), DPBF in TeCE (□ and ■), and MeOH (○ and ●). [MB]: 10 μM.

of DPBF as shown in Fig. 1. The rate constant k^s_{TA} for MB and DPBF was estimated to be 2.7×10^9 M^{-1} s^{-1} (in 1,1,2,2-tetrachloroethane, TeCE) and 5.8×10^9 M^{-1} s^{-1} (in methanol, MeOH) by means of the laser flash apparatus. If we use the values of β in Table 1 and those of $(k_d+k^s_0[O_2])$, 1.5×10^6 s^{-1} in TeCE and 4.0×10^6 s^{-1} in MeOH, the calculated concentrations of DPBF give the maximum quantum yield at 9.7×10^{-5} M and 2.1×10^{-4} M for the respective solvents. The coincidence of these values with the results in Fig. 1 shows that Process 5 is appreciable to the concentration of DPBF above $\approx1\times10^{-4}$ M. Thus, when a reactive acceptor is added with a sensitizer it should be noted that the reaction scheme switches from the singlet oxygen reaction (Type II mechanism) to the direct reaction of A with the triplet sensitizer (D–R or D–O mechanism[17]) depending on the concentration of A.

Solvent Effect of the Quantum Yield in a Homogeneous Solution. The lifetime of singlet oxygen ($^1\Delta_g$) depends highly on the type of solvent. Kearns *et al.* ortedrep that the lifetime is related to the optical densities (O.D.) of the solvents at the waven umbers of 7880 and 6280 cm^{-1} corresponding 0-0 and 0-1 components of the $^1O_2(^1\Delta)-{}^3O_2(^3\Sigma)$ transition as follows:[8]

$$k'_d\times10^{-6}\simeq0.5(\text{O.D.})_{7880}+0.05(\text{O.D.})_{6280}\equiv D. \quad (14)$$

Under the conditions $\beta\gg$[A] in Eq. 9, the solvent effect on the value of Φ_{-A} should explicitly reflect the solvent sensitivity of k'_d, k'^s_A, Φ_{so}, and αr. If the maximum quantum yields Φ^{max}_{-A} $(=\Phi_{so}\,\alpha r)$ in two kinds of solvents are equal to each other, the possibility that Φ_{so} and αr afford the large solvent effect on Φ_{-A} can be neglected. Further, since the rate constant k'^s_{-DPBF} does not seem to be so sensitive to solvents as compared with the solvent sensitivity of k'^s_d (Table 1), the large solvent effect on Φ_{-DPBF} could reflect the solvent sensitivity of the lifetime of singlet oxygen to the photooxygenation of DPBF.

In the mixture of solvent 1 and 2 at the mole fractions of χ_1 and χ_2, it can be assumed that Kearns'-type equation for the solvent quenching to singlet oxygen is expressed as

$$k'_d\times10^{-6}\simeq D_{mix}=\chi_1D_1+\chi_2D_2, \quad (15)$$

where D_1 and D_2 stand for the sum of Eq. 14 to solvents 1 and 2, respectively. When the condition $\beta\gg$ [DPBF] holds for the mixed solvent, Φ_{-DPBF} in the mixture would be given by

$$\Phi_{-DPBF}=\Phi_{so}\alpha r(k'_d/k'^s_A)^{-1}[DPBF]. \quad (16)$$

Substituting Eq. 15 into Eq. 16 and neglecting the solvent effects on the values of Φ_{so}, αr, and k'^s_A, we obtain the ratio of $\Phi^{(2)}_{-DPBF}$ in the pure solvent 2 against Φ_{-DPBF} in the mixture in a linear form with respect to χ_1 as follows.

$$\Phi^{(2)}_{-DPBF}/\Phi_{-DPBF}=1-\left(1-\frac{D_1}{D_2}\right)\chi_1. \quad (17)$$

In several mixtures (Fig. 2) where the relation $D_{mix}=\chi_1D_1+\chi_2D_2$ holds, the experimental points of $\Phi^{(2)}_{-DPBF}/\Phi_{-DPBF}$ coincide with the predicted lines from Eq. 17. The relation can be applied to the mixture of water and deuterium oxide too.

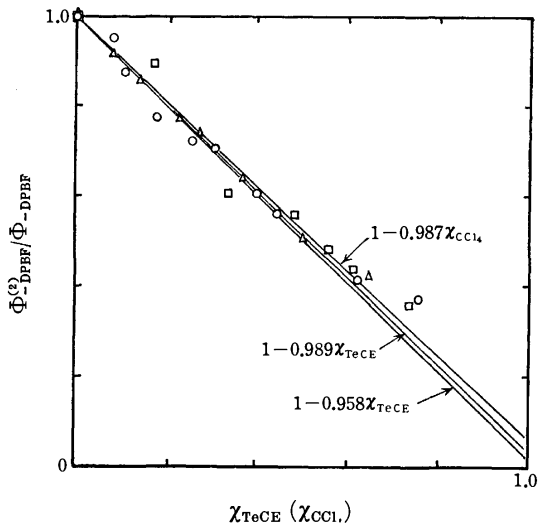

Fig. 2, Effect of mixed solvent on Φ_{-DPBF}. [MB]: 4 μM. [DPBF]: 35 μM. MeOH (solv. 2)-TeCE (solv. 1) (△), Hexane (solv. 2)-TeCE (solv. 1) (○), and Hexane (solv. 2)-CCl_4 (solv. 1) (□).

The relation $D_{mix}=\chi_1D_1+\chi_2D_2$ does not hold for the mixture of water and ethanol. In such case, the k'_d value has to be estimated directly by measuring the values of D_{mix} over each ratio of the mixture. If the value of k'^s_A does not depend on the mole fraction of alcohol, the following equation can be derived in the range $\beta\gg$[A] since Φ^{max}_{-A} equals to $\Phi_{so}\,\alpha r$.

$$\frac{\Phi^{(1)}_{-A}}{\Phi^{max(1)}_{-A}}\Big/\frac{\Phi_{-A}}{\Phi^{max}_{-A}}=\frac{D_{mix}}{D_1}=k'_d/k'^{(1)}_d \quad (18)$$

However, for the systems of MB–O_2–DMF and MB–O_2–DPBF in the water–ethanol or water–methanol mixture,

the quantum yields differ a great deal from what is expected in Eq. 18. The solvent effect on Φ_{-A} shows a maximum around $\chi_{ethanol} \simeq 0.3$, decreasing gradually in the region of $\chi_{ethanol}$ over 0.3. Since Young *et al.* reported the values of k'^{s}_{DPBF} as 1.2—1.3$\times 10^9$ M^{-1} s^{-1} in methanol and 5.1$\times 10^9$ M^{-1} s^{-1} in 1:1 methanol–water mixture, the k'^{s}_{DPBF} value depends on the mole fraction of methanol.[15] Using these values of k'^{s}_{DPBF}, the ratio of the quantum yield (2.3) in the 1:1 mixture of methanol and water to that in methanol is explained by the corrections ($\approx$2.9) for both k'_d and k'^{s}_{DPBF} values.

Sensitized Photooxygenation in Micelles. Acceptor Concentration Dependence on the Quantum Yield: Recently it was reported that DPBF and 2,5-diphenylfuran solubidized in sodium dodecyl sulfate (SDS) micelles can be oxidized by the photosensitized reaction.[9,10] In order to determine the reaction mechanism in other micellar systems for several combinations of the sensitizing dyes, the acceptor and the micelles, kinetic investigations were carried out on the effects of the acceptor concentration, solvent composition, and the surfactant concentration upon the quantum yield.

In the region of 1st CMC of dodecyltrimethylammonium chloride (DTAC) micelles, most of MB does not bind to the micelle but exists in a bulk phase because of an electrostatic repulsion between the cationic DTAC micelle and dye. Thus, DMA or 2,5-diphenyloxazole (DPO) which is dissolved into Hartley's cubic micelles of DTAC, reacts with singlet oxygen produced by energy transfer from dye in the bulk phase.

The concentration effect of DMA/DTAC on $\Phi_{-DMA/DTAC}$ is shown in Fig. 3 and the reciprocal plot of $1/\Phi_{-DMA/DTAC}$ against 1/[DMA/DTAC] exhibits a linear relationship similar to that in a homogeneous solution. The β value obtained from Eq. 19 in a water–micellar solution is about ten times greater than that in a deuterium oxide –micellar solution (Table 1). Since the same value of $\Phi^{max}_{-DMA/DTAC}$ is obtained both in water– and deuterium oxide–micellar solutions it is resposible for the result that the k'_d value in water is just ten times greater than that in deuterium oxide as shown by Kearns *et al.*[8] The $\Phi^{max}_{-DMA/DTAC}$ value $\approx$0.5, which is about a half of that obtained from the concentration effect in ethanol, may be explained as reasonable since photooxygenated DMA in the micelles is hard to react with another DMA molecule, indicating that process 10 is not involved in this system. The deuterium oxide effect on β and $\Phi^{max}_{-DPO/DTAC}$ value was also observed in the case of DPO/DTAC-oxygenation sensitized by MB in the bulk phase. The results suggest that the α value in Eq. 9 is close to unity. The following equation can be written for an aqueous micellar solution.

$$\Phi_{-DMA/DTAC} = \Phi_{so}\frac{k'^{r}_{A}[DMA/DTAC]}{k'_d + k'^{s}_{A}[DMA/DTAC]}. \quad (19)$$

The DMA/DTAC concentration dependence on $\Phi_{-DMA/DTAC}$ was investigated in the photooxygenation sensitized by an anionic dye of eosine (EOS) adsorbed on the micelles. The result also gives a linear relationship between $1/\Phi_{-DMA/DTAC}$ and 1/[DMA/DTAC] ([EOS/DTAC]: 10 μM, [DTAC]: 50 mM, and [DMA/DTAC]: 0.6—18.5$\times 10^{-5}$ M). Referring to the case sensitized

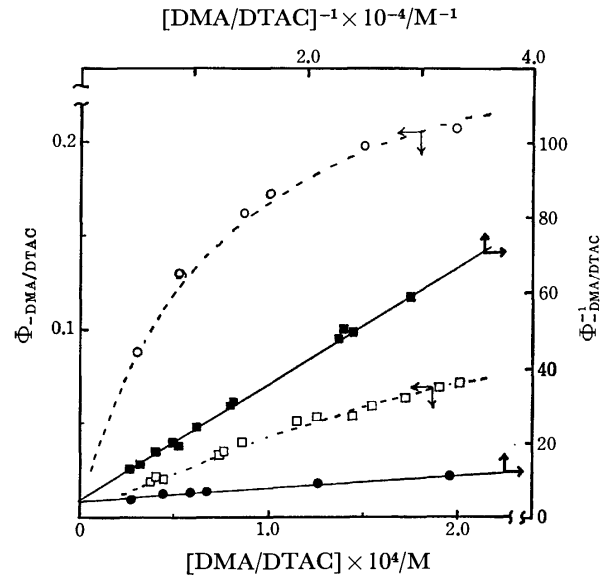

Fig. 3. Effect of [DMA/DTAC] on $\Phi_{-DMA/DTAC}$ in H_2O and in D_2O. [MB]; 10 μM. [DTAC]: 50 mM.

by MB, a similar β value 5.5$\times 10^{-4}$ M is obtained in the water–micellar solution. If we substitute the k'_d value obtained in an aqueous solution for the micellar systems into Eq. 19, the estimated rate constant $k'^{s}_{DMA/DTAC}$ becomes greater than that for DMA in ethanol. Thus, it is confirmed that singlet oxygen readily penetrate into the micellar phase, reacting with DMA efficiency in spite of whether dye is electrostatically bound on the ionic surfactant micelles or not. From the results putting A/micelle instead of A, the schemes (1)—(8) might be accepted.

Solvent Effect on the Quantum Yield in Micellar Solution. From the results mentioned above, the mixed solvent effect on the quantum yield for a micellar system can be

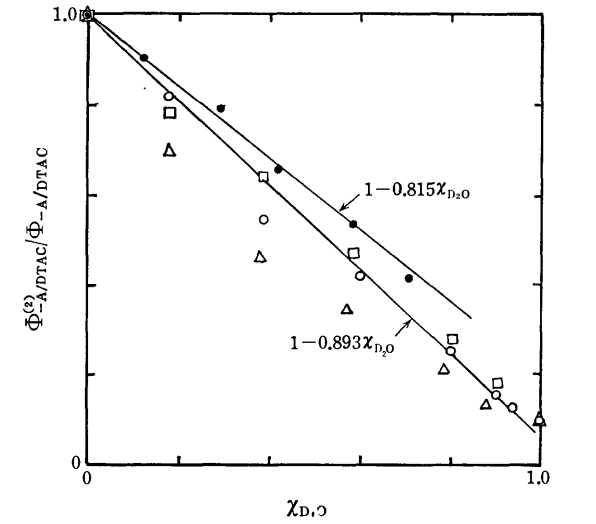

Fig. 4. Effect of mixed solvent of H_2O–D_2O on Φ_{-DMA} in water and $\Phi_{-A/DTAC}$ in DTAC micellar solution (50 mM). ●; [MB]: 10 μM, [DMA]: 1.0$\times 10^{-4}$ M, [DTAC]: 0 M, χ_{EtOH}=0.3. △; [MB]: 10 μM, [DMA/DTAC]: 100 μM. ○; [MB]: 5 μM, [DPO/DTAC]: 25 μM. □; [EOS/DTAC]: 10 μM, [DMA/DTAC]: 37 μM.

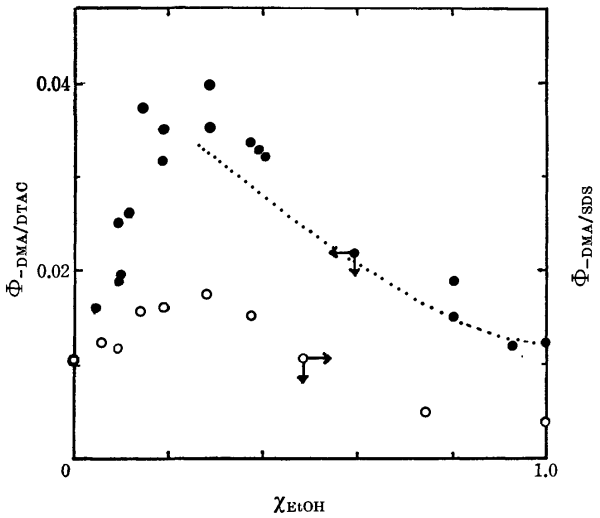

Fig. 5. Effect of mixed solvent of H_2O-EtOH on $\Phi_{-DMA/DTAC}$ and $\Phi_{-DMA/SDS}$. [MB]: 5 μM, [DMA/DTAC]: 26 μM, [DTAC]: 50 mM (●) and [EOS]: 20 μM, [DMA/SDS]: 14 μM, [SDS]: 20 mM (○). Data on the mixture without DTAC (dotted line) are normalized at $\chi_{EtOH}=1$.

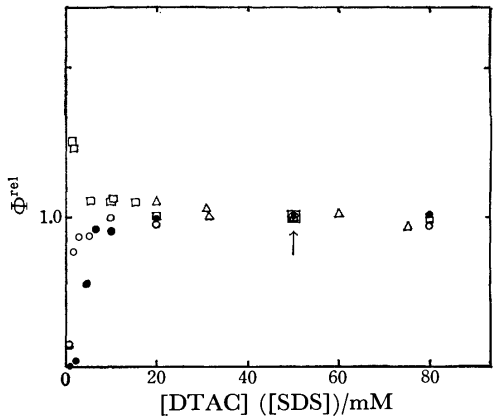

Fig. 6. Surfactant concentration effect on the relative quantum yields normalized at 50 mM. MB–O_2–DMA/DTAC (△), MB–O_2–DPO/DTAC (□), MB/SDS–O_2–DPBF/SDS (●) and EOS–O_2–DPBF/SDS (○).

treated by means of Eq. 17, and specified by the lifetime of singlet oxygen in bulk phase as well as in a homogeneous solution. The effect of deuterium oxide on the $\Phi_{-DMA/DTAC}$ (or $\Phi_{-DPO/DTAC}$) value sensitized by MB or EOS/DTAC can be explained by Eq. 17 as shown in Fig. 4.

In the case of water and ethanol mixture, the results for MB–O_2–DMA/DTAC and EOS–O_2–DMA/SDS systems are anomalous. At the mole fraction of ethanol $\chi_{EtOH}\approx 0.2$, $\Phi_{-DMA/DTAC}$ has a maximum (≈ 0.04 for the system of MB–O_2–DMA/DTAC), decreasing in the χ_{EtOH} region over 0.3 where the degree of decrement coincides with the dotted line in Fig. 5. This seems to be due to the decomposition of DTAC micelles in the region $\chi_{EtOH}>0.3$. On the other hand, the Φ_{so} value could not be affected by the addition of ethanol in the region $\chi_{EtOH}\lesssim 0.3$. The β values at $\chi_{EtOH}=0$ and 0.2, were about 6.6×10^{-4} and 5.2×10^{-4} M, respectively. If DMA/DTAC micelles start to decompose into the homogeneous solution even in the region $\chi_{EtOH}<0.3$, the quantum yield of DMA disappearance would decrease with increasing χ_{EtOH} beyond 0.3, since the β values at $\chi_{EtOH}>0.3$ are greater than that at $\chi_{EtOH}=0$. However as shown in Fig. 5, the effect of ethanol on $\Phi_{-DMA/DTAC}$ shows a reverse tendency. The increment in $\Phi_{-DMA/DTAC}$ may be due to the DMA liberation from the micelles by the swelling effect of ethanol because the existence of free DMA molecules contributes to the disappearance of DMA in the region $\chi_{EtOH}<0.3$ (Eq. 9).

Micelle Concentration Effect on the Quantum Yield. In order to check the deactivation of the excited states of sensitizer and singlet oxygen by micelles, the micelle concentration effect on the quantum yield was tested. As shown in Fig. 6, in the region between 1st and 2nd CMC the quantum yield does not depend on the micelle concentration, the effect being negligible for the systems of MB–O_2–DMA/DTAC, MB–O_2–DPO/DTAC, MB/SDS–O_2–DPBF/SDS, and EOS–O_2–DPBF/SDS. In contrast, under 1st CMC the complex features are shown for each case.

Effect of N_3^- Addition on DPO Fluorescence and the Quantum Yield. Fluorescence quenching of some substances in the micelles by an ionic quencher deviates from the Stern-Volmer plot because of the electrostatic interaction on the Stern layer of charged micelle.[18] In the case of the quenching of DPO in DTAC micelles by azide ion N_3^-, the Stern-Volmer plot deviates from the concentration of N_3^- ion over 80 mM, becoming saturated around 300 mM as shown in Fig. 7. The quenching of DPO fluorescence in the micelles by N_3^- is about ten times greater than that in a 10% EtOH–H_2O solution. Since the Stern-Volmer plot in the solution does not deviate at the concentration of N_3^- around $\approx 10^{-1}$ M, the quenching of DPO in DTAC micelles can occur by N_3^- adsorbed electrostatically on

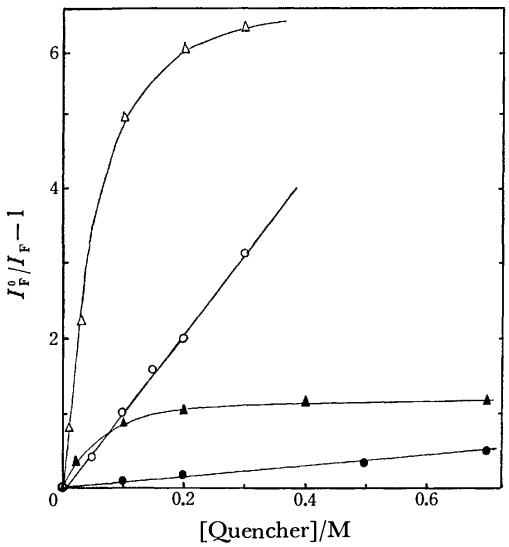

Fig. 7. Stern-Volmer plots for the fluorescence quenching of DPO/DTAC. Quencher; NaN_3 (△; in 50 mM DTAC and ○; in 10% EtOH–H_2O) and NaBr (▲; in 50 mM DTAC and ●; in 10% EtOH–H_2O).

the micelles, simultaneously. A similar feature was observed on NaBr quenching (Fig. 7).

It is well-known that the N_3^- ion is an efficient quencher to singlet oxygen. In the case of photooxygenation of DPO/DTAC the quantum yield $\Phi_{-DPO/DTAC}$ becomes small by the addition of NaN_3 of 50 mM (3.1×10^{-4}, [DPO/DTAC]: 14.4 μM), no deuterium oxide effect being observed on the $\Phi_{-DPO/DTAC}$ value. Singlet oxygen would be predominantly deactivated by N_3^- bound to the micelles and in solution, where DPO/DTAC is protected from the attack by singlet oxygen. Although the effect of N_3^- bound to the DPO/DTAC micelles on the DPO fluorescence seems to be significant at the order of 10^{-1} M (Fig. 7), the degree of N_3^- bound on the micellar periphery is too small to affect the quantum yield in the concentration lower than 1 mM. The binding effect on the singlet oxygen reaction was checked by measurements of $\Phi_{-DMA/DTAC}$ values in the presence of another anion (1 mM NaCl) or the high micelle concentration ([DTAC micelle]: 0.936 mM). Since both effects of the NaCl addition and the micelle concentration are scarcely observed, the contribution of bound N_3^- ion is negligible for the singlet oxygen reaction in such lower concentration of N_3^-.

Table 2. Rate constants of N_3^- ion with singlet oxygen in aqueous and micellar solutions

System (solv. pH)	k_N (M^{-1} s^{-1})
MB-O_2–Tryptophan (H_2O, 8.37)	$1.7\pm0.2\times10^9$
MB-O_2–DPO/DTAC (H_2O, 7.0)	$2.2\pm0.3\times10^9$
MB-O_2–DMA/DTAC (H_2O, 7.0)	$2.3\pm0.3\times10^9$

In order to confirm the results of solvent effect on the quantum yield in a micellar solution which shows that the lifetime of singlet oxygen is restricted by the property or the composition of a solvent mixture in the bulk phase, we studied the effect of N_3^- on $\Phi_{-DPO/DTAC}$ in the range $[N_3^-] < 1$ mM, where the reaction of N_3^- with the excited state of sensitizer is negligible.[20] The quenching rate constant of singlet oxygen by N_3^- (k_N) can be estimated from the slope and intercept in the following equation:

$$1/\Phi_{-DPO/DTAC} = \frac{k_d' + k_A'^s[DPO/DTAC] + k_N[N_3^-]}{\phi_{st}k_A'^r[DPO/DTAC]}. \quad (20)$$

The value of k_N obtained are given in Table 2. The coincidence of k_N values both in micellar solutions and in an aqueous solution within experimental error shows that singlet oxygen is quenched in the bulk phase as in the aqueous solution. There is no specific effect on the surface in the dilute concentration of N_3^-. Therefore, this supports the view that the lifetime and behaviour of singlet oxygen are mainly affected by the condition or the solvent composition in the bulk phase.

The authors wish to express their thanks to Miss Setsuko Kodera, Miss Akiko Sakamoto, and Mrs. Mieko Sakaue for their contribution to this work.

References

1) J. P. Spikes and B. W. Glad, *Photochem. Photobiol.*, **3**, 907 (1969).
2) A. G. Kepka and L. I. Grossweiner, *Photochem. Photobiol.*, **10**, 49 (1973).
3) I. Saito, K. Inoue, and T. Matsuura, *Photochem. Photobiol.*, **21**, 27 (1975).
4) K. Kobayashi and T. Ito, *Photochem. Photobiol.*, **23**, 21 (1976).
5) T. Ito, *Photochem. Photobiol.*, **25**, 47 (1977).
6) M. Chen, M. Graetzel, and J. K. Thomas, *J. Am. Chem. Soc.*, **97**, 2052 (1975).
7) M. Wong, J. K. Thomas, and M. Graezel, *J. Am. Chem. Soc.*, **98**, 2391 (1976).
8) D. R. Kearns, P. B. Merkel, and R. Nilsson, *J. Am. Chem. Soc.*, **94**, 7244 (1972).
9) Y. Usui and S. Kodera, Abstr. No. 3J13, 32nd National Meeting of the Chemical Society of Japan, Tokyo, April 1975.
10) A. A. Gorman, G. Lovering, and M. A. J. Rodgers, *Photochem. Photobiol.*, **23**, 399 (1976).
11) Y. Usui and K. Kamogawa, *Photochem. Photobiol.*, **19**, 245 (1974).
12) C. S. Foote, *Acc. Chem. Res.*, **1**, 104 (1968).
13) R. H. Young, K. Wehry, and R. L. Martin, *J. Am. Chem. Soc.*, **93**, 5774 (1971).
14) D. R. Adams and F. Wilkinson, *J. Chem. Soc., Faraday Trans. 2*, **68**, 586 (1973).
15) R. H. Young, D. Brewer, and R. A. Keller, *J. Am. Chem. Soc.*, **95**, 375 (1973).
16) Y. Usui, *Chem. Lett.*, **1973**, 743.
17) M. Koizumi and Y. Usui, *Mol. Photochem.*, **4**, 57 (1972).
18) M. R. Eftink and C. A. Ghiron, *J. Phys. Chem.*, **80**, 486 (1976).
19) C. A. Long and D. R. Kearns, *J. Am. Chem. Soc.*, **97**, 2018 (1975).
20) C. S. Foote, T. T. Fujimoto, and Y. C. Chang, *Tetrahedron Lett.*, **1972**, 45.

ENDOR Relaxation Study of the Effects of Intramolecular Cation Migration on the Ion-pair System*

Masaharu OKAZAKI and Keiji KUWATA

Department of Chemistry, Faculty of Science, Osaka University, Toyonaka, Osaka 560

(Received June 16, 1977)

The ENDOR spectra of the ion-pair system of the 2,5-di-*t*-butyl-*p*-benzoquinone anion and the alkali metal cation in 1,2-dimethoxyethane were observed. The influence of the intramolecular cation migration on both the linewidth and the intensity of the ENDOR spectra was experimentally examined. The results obtained were discussed theoretically using the Kaplan-Alexander formula. The intramolecular exchange due to the cation migration was shown to be effective in ENDOR.

Many studies of the dynamic processes in the ion-pair system of a radical anion and an alkali cation in solution have been carried out.[1] As an example of these processes, the so-called linewidth alternation in the ESR spectrum due to the intramolecular cation migration among more than two sites is well known.[2] Kinetic study by measuring the changes in the linewidth of the ESR spectrum is difficult when the rate of the process is smaller than the apparent width of the inhomogeneously broadened line.

ENDOR is useful for the study of the dynamic processes with such small rates. The ENDOR intensity is sensitive to the combination and the competition among various relaxation processes including such a dynamic process.[3–5] Moreover, the ENDOR linewidth does not depend on the secular terms of the *g*-anisotropy of electron and the hf-anisotropy of the nucleus whose resonance frequencies are different from that of the pumping NMR transition.[4] The approach using the ENDOR linewidth has been applied to the kinetic study by a few groups.[6–10] Recently Möbius *et al.* have investigated the restricted rotation by analyzing the ENDOR linewidth quantitatively.[8–10] The study with the ENDOR linewidth, however, has the difficulty that the saturation broadening tends to hide the slight changes due to dynamic processes when the ESR and the NMR transitions are saturated to observe the ENDOR.

The investigation with the ENDOR intensity is more reliable in principle for the study of relaxation processes including such dynamic processes. The linewidth alternation of the ESR spectrum in the system of the 2,5-di-*t*-butyl-*p*-benzoquinone anion and the alkali cation in 1,2-dimethoxyethane was first studied by Chippendale *et al.*[11] In the present investigation the ENDOR study of this system was pursued and the observed results for both the ENDOR intensity and the linewidth were well reproduced by the introduction of the intramolecular exchange process into the theoretical calculation. It was confirmed that the intramolecular exchange due to such a dynamic process has large effects on the ENDOR intensity.

Experimental

The purification of 2,5-di-*t*-butyl-*p*-benzoquinone (DBQ) was done by recrystallization from ethanol. 1,2-Dimethoxyethane (DME) was dehydrated by refluxing over Na–K alloy for 10 h. The sample solution of the DBQ anion was prepared by the alkali metal reduction of DBQ in DME. The concentration of the DBQ anion in the sample solution was about 5×10^{-4} mol dm^{-3}.

In the observation of ENDOR the temperature at the sample position was monitored using a copper-constantan thermocouple, and was controlled by varying the flow rate of the chilled nitrogen in the temperature range from 185K to 243K. The ENDOR spectra were taken with a home-made spectrometer.[12] The microwave power was greater by 5 db than the power which gave the maximum amplitude of the ESR signal. The rf-power was kept constant at about 0.5 mT in the rotating frame. The rf-power was roughly estimated from the coherent splitting of the ENDOR spectrum of K^+DBQ^- in isopropyl alcohol according to the procedure of Freed *et al.*[5]

Method of Calculation

By the introduction of the effects of the intramolecular exchange, the equation of motion for the density operator of the spin system can be given as[13–15]

$$d\rho/dt = i[\rho, \mathcal{H}] - \Gamma(\rho-\rho^0) + (\boldsymbol{P}\rho\boldsymbol{P}-\rho)/\tau_{ex}, \qquad (1)$$

where $\boldsymbol{P}$ is an exchange operator[15] which represents the exchange between the two spin states shown in Fig. 1. These states are connected *via* the transition of k. τ_{ex} is the reciprocal of the exchange rate. $\Gamma(\rho-\rho^0)$ represents the relaxation of ρ to its thermal equilibrium state, ρ^0, due to the perturbational Hamiltonian modulated

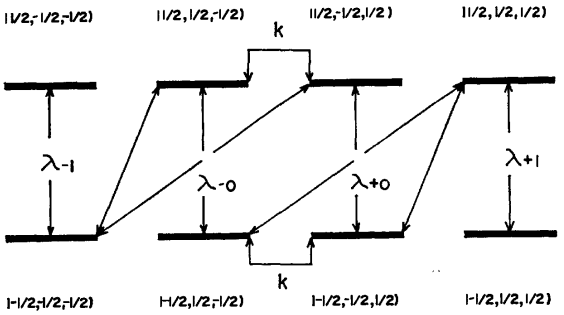

Fig. 1. Energy diagram of the system. Each level is expressed using wave function $|\sigma_e, \sigma_n^1, \sigma_n^2)$. Oblique lines are flip-flip or flop-flop transitions arising from the modulation of the END interaction. Horizontal line with arrow shows the transition corresponding to the intramolecular exchange. $\lambda_{\pm1}$, $\lambda_{\pm0}$ designate the ESR transitions.

* This work was presented at the 15th symposium on ESR Spectroscopy, Kumamoto, Oct. 1976.

by the random molecular motions. $\mathcal{H}$ is the spin Hamiltonian given by

$$\hbar\mathcal{H} = g_e\beta_e B_0 S_z + \sum_i(-\gamma_n\hbar B_0 I_z^i + a_i I_z^i S_z - 2B_2\gamma_n\hbar I_x^i \cos\omega_n t) + 2B_1 g_e\beta_e S_x \cos\omega_e t, \quad (2)$$

where B_1 and B_2 are the strengths of the microwave and the rf-field at the frequencies of ω_e and ω_n respectively, and where g_e and γ_n are the g-factor of the electron and the magnetogyric ratio of the nuclei respectively. B_0 is the strength of the static field, I_z^i and S_z are the z components of the nuclear and electron spin angular momentum, β_e represents the Bohr magneton, and a_i is the isotropic hfsc for the nucleus numbered "i."

The energy levels of the system are shown in Fig. 1, where t-butyl protons are omitted from consideration. Each ESR transition is designated using the sum of the quantum numbers for the ring protons, such as λ_{-1}, λ_{-0}, λ_0, and λ_1. For example, λ_{-0} is the transition between $|1/2, 1/2, -1/2)$ and $|-1/2, 1/2, -1/2)$; here $|\sigma_e, \sigma_n^1, \sigma_n^2)$ represents the spinwave function of the system. The subscripts "e" and "n" indicate electron and nucleus respectively.

The ENDOR intensity observed at the λ_j ESR transition is expressed as E_j. The ENDOR spectra have three peaks, 17.7, 16.2, and 13.8 MHz in the frequency region higher than the free proton frequency of 13.75 MHz. The intensity of the highest frequency peak of 17.7 MHz is expressed as E_j^{high}; it is defined as follows

$$E_j^{high} = (Z''(\lambda_j\text{: rf on}) - Z''(\lambda_j\text{: rf off}))/Z''(\lambda_j\text{: rf off}), \quad (3)$$

where Z'' corresponds to the absorption signal. E_j^{low} and $E_j^{t\text{-butyl}}$ are defined in the same manner as E_j^{high}. RE is defined as

$$RE = E_{-1}/E_{-0}. \quad (4)$$

The ENDOR spectra were calculated according to the theory developed by Freed, using Eqs. 1 and 2 for an eight-level system as is shown in Fig. 1. The coherent effects were omitted for the sake of brevity in the calculation.[5] The matrix elements in Eq. 1 were calculated by the standard procedure.[16] The correlation time was approximated according to the model developed by Debye and Einstein.[17] These results are listed in Tables 1 and 2. The temperature dependence of the reciprocal of the correlation time $(\tau_{ex})^{-1}$ in Eq. 1 was described by means of the Arrhenius equation as

$$k = (\tau_{ex})^{-1} = A\exp(-E_a/RT), \quad (5)$$

where A is the preexponential factor and E_a is the activation energy of the cation migration. The hfsc and the g-factor used in the calculation are listed in Table 3. The viscosity data for DME were taken from the literature.[18] The hydrodynamic radius was tentatively taken as 300 pm** on the basis of the molecular model.

** The radius of the DBQ molecule was estimated using the Stewart model, and the cubic root value was 370 pm. Atherton and Day have employed 350 pm for the 2,6-di-t-butyl-4-methylphenoxy radical; *cf.* N. M. Atherton and B. Day, *Mol. Phys.*, **27**, 145 (1974).

Table 1. Transition probabilities[a)]

$W_e^{g'}$	$10^{-1}\hbar^{-2}(\beta B_0)^2(g'\text{: }g')(\tau_r/1+\omega_e^2\tau_r^2)$
W_e^{sr}	$18^{-1}(\Delta g\text{: }\Delta g)\tau_r^{-1}$
W_n^i	$40^{-1}(A_1'\text{: }A_1')\tau_r$
$W_{x_1}^i$	$60^{-1}(A_1'\text{: }A_1')(\tau_r/1+\omega_e^2\tau_r^2)$
$W_{x_2}^i$	$10^{-1}(A_1'\text{: }A_1')(\tau_r/1+\omega_e^2\tau_r^2)$
Intramolecular exchange	k

a) The contributions of the hf interaction term and its cross terms with g-anisotropy to the electronic transition were disregarded. $W_e^{g'}$ and W_e^{sr} mean the electronic-transition probabilities arising from the modulation of the anisotropic g-tensor and the spin-rotation interaction respectively. W_n^i is the transition probability of the number i nucleus; *i.e.*, W_n^1 is of the nucleus at a low resonance frequency, while W_n^2 is of the nucleus at a high resonance frequency. $W_{x_1}^i$ and $W_{x_2}^i$ are the cross-relaxation probabilities arising from the END interaction of the "i" nucleus. 1 and 2 in the subscripts mean flip-flop and flop-flop or flip-flip transitions respectively. g' and Δg are the traceless part of the g-tensor and the deviation of g from the free-spin value respectively. (X: Y) denotes the inner product of the X and Y tensors.

Table 2. ESR and NMR linewidths[a)]

ESR	$\lambda_{\pm1}$	$7/3(\sum_i W_n^i) + W_e^{g'}(7/3+4/3\omega_e^2\tau_r^2) + W_e^{sr}$
	$\lambda_{\pm0}$	$7/3(\sum_i W_n^i) + W_e^{g'}(7/3+4/3\omega_e^2\tau_r^2) + W_e^{sr} + k$
NMR	high freq.	$7/3W_n^2 + W_e^{g'} + W_e^{sr} + W_n^1 + k$
	low freq.	$7/3W_n^1 + W_e^{g'} + W_e^{sr} W_n^2 + k$

a) These expressions are given by disregarding the contributions from various cross terms, and also the cross relaxations.

Table 3. Input parameters[a)]

Hyperfine tensors	proton 1	$A_{xx}=-0.21$G, $A_{zz}=1.90$G	$A_{yy}=-1.69$G
	proton 2	$A_{xx}=-0.14$G, $A_{zz}=1.24$G	$A_{yy}=-1.11$G
g-Tensor		$g_{xx}=2.0076$, $g_{zz}=2.0024$	$g_{yy}=2.0036$

a) The elements of the hf tensors of Na^+DBQ^- in DME were calculated using McConnell-Strathdee's formula.[27] Here only the contribution of the electron at the adjacent carbon atom was assumed, and Q_{CH} was taken as 2.30 mT.

Results and Discussion

Figures 2 and 3 show the temperature dependencies of E_j^{high}, E_j^{low}, RE^{high}, and RE^{low} for Na^+DBQ^- in DME. At temperatures higher than 220 K, E_{-1} is greater than E_{-0}. This tendency continued throughout the extrapolation of B_1 to infinity. The dependence on the rf-power was not examined for the lack of a reliable way to examine the incident rf-power on the sample, but the theoretical calculations show that RE^{high} and RE^{low} have small dependencies on the rf-power.

In solution, a difference in ENDOR intensity has been found among hf lines with same degeneracy, and

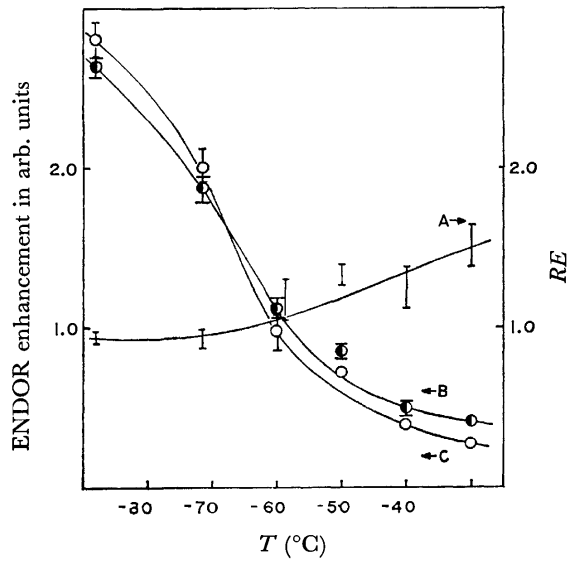

Fig. 2. ENDOR enhancements and the ratio as a function of temperature. B: E_{-1}^{high}; C: E_{-0}^{high}; A: RE^{high}.

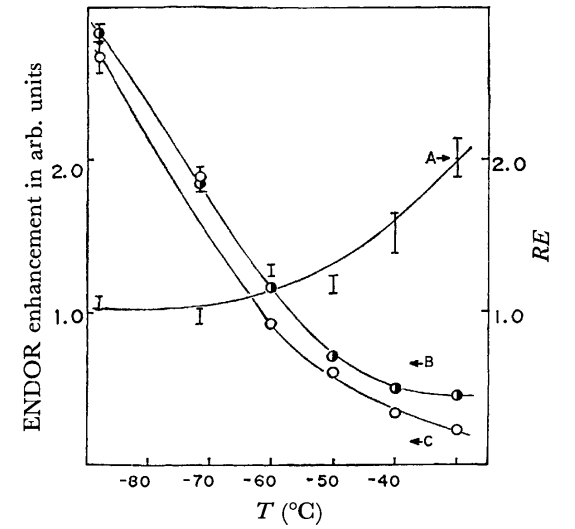

Fig. 3. ENDOR enhancements and the ratio as a function of temperature. B: E_{-1}^{low}; C: E_{-0}^{low}; A: RE^{low}.

this phenomenon has been explained on the basis of the cross relaxations due to the modulation of the isotropic hfc and electron nuclear dipole (END) interactions.[19-22] In the present system, however, the observed results could not be interpreted by the cross relaxations because E_{-1}^{high} and E_{-0}^{high} should be equal in the case of the cross relaxations. As is shown in the calculated results in Fig. 4, the temperature dependencies of RE's can be well interpreted by the introduction of the effect of the cation migration. The parameters used in the calculations in Figs. 4 and 5 were 3.0×10^{10} s^{-1} for A and 6.0 kcal mol^{-1} for E_a in Eq. 5. RE^{low} was larger than RE^{high} in the temperature range of the present experiment and also in the calculated results. Because this difference in the calculation comes from the cross relaxation, flip-flip, or flop-flop relaxation due to the modulation of the END interaction, this W_{x_2} may play an important role in the higher temperature region.

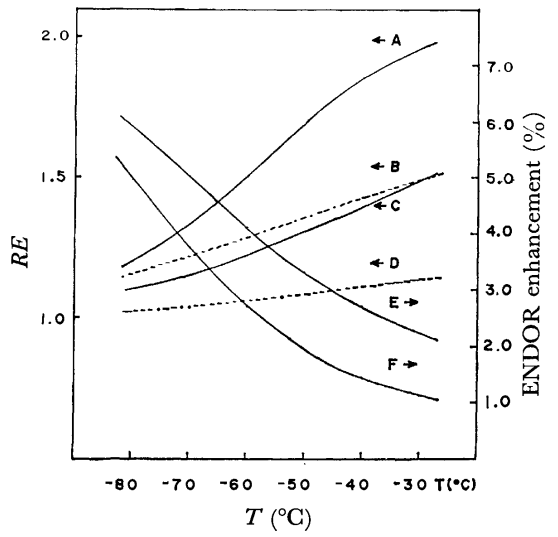

Fig. 4. ENDOR enhancement (calculated) as a function of temperature. A: RE^{low}; B: RE^{low} (without intramolecular exchange); C: RE^{high}; D: RE^{high} (without intramolecular exchange); E: E_{-1}^{low}; F: E_{-0}^{low}. The parameter B_1 was set as, $B_1=\sqrt{1.5}\,(T_1T_2)^{-1/2}(g_e\beta_e)^{-1}\hbar$ for each temperature. The parameter B_2 was set to be 0.5 mT throughout the calculation.

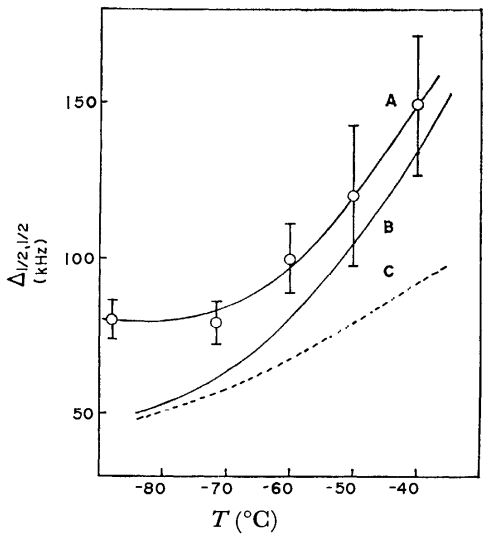

Fig. 5. ENDOR linewidth *vs.* temperature for Na^+-DBQ^- in DME. A: experimental; B: calculated with intramolecular exchange; C: calculated without intramolecular exchange. The parameters were the same as those taken in the calculation demonstrated in Fig. 4. The experimental conditions were shown in the text.

In the present system, all the levels are nondegenerate; thus, Heisenberg spin exchange contributes to all the nuclear transitions to the same extent. Therefore, it can not be the origin of the difference between E_{-1} and E_{-0}.

The ENDOR linewidth is a parameter which reflects the cation migration. The experimental and calculated results for the linewidth are shown together in Fig. 5. No difference was found between linewidths in the ENDOR spectra at the λ_{-1} and λ_{-0} ESR transitions.

The solid line shows the result of the calculation including intramolecular exchange, while the dotted line shows those of the calculation without exchange. The ENDOR linewidth rises steeply with the temperature. It increases by about 70 kHz as the temperature increases from −71.5 to −40 °C. There is no distinct change in the ESR spectra in this temperature range.

The Heisenberg spin exchange is a mechanism, the temperature dependence of whose rate is similar to that of the observed ENDOR linewidth. Leniart *et al.* have obtained the ESR linewidth of semiquinones in DME and have reported the rates of spin exchange at various temperatures.[23] Their results give an increase in the ENDOR linewidth of about 30 kHz in the concentration of about 5×10^{-4} mol dm^{-3} in the temperature range from −71.5 to −40 °C.[24] Thus, the contribution of this mechanism was ignored throughout the present calculation.[24]

Both the experiment and the calculation were carried out under the conditions of partial saturation; the saturation broadening is probably one of the main causes of the linewidth. Though the results obtained under partial saturation are less reliable than the ENDOR linewidth extrapolated to zero microwave and rf-power, it is useful only practically in the study of the systems which give merely a weak ENDOR signal.

In the case of K^+DBQ^-, *RE* departs from 1.0 at a lower temperature than in the case of Na^+DBQ^-. This fact corresponds to the results obtained for the ESR linewidth by Chippendale *et al.*, who have reported that the potassium ion starts its migration between two oxygen atoms at a lower temperature than does the sodium ion.[11]

Figure 6 shows the E_{-1} and E_{-0} of *t*-butyl protons at various temperatures, where superscripts denote the counter ions. A large difference between E_{-1} and E_{-0} was found; it may be considered to be another piece of evidence for the effect of the intramolecular exchange on the ENDOR intensity. The optimum temperatures for E_{-1} and E_{-0} were also different, as was to be expected from the fact that the temperature dependence of the intramolecular exchange is different from that of the other relaxation mechanisms.

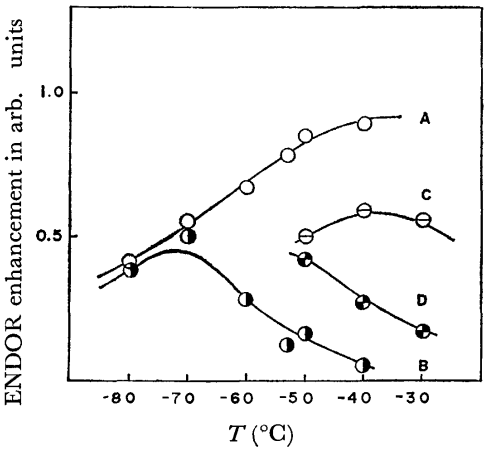

Fig. 6. ENDOR enhancement *vs.* temperature for the *t*-butyl protons of DBQ anion in DME. A: $E_{-1}(K^+)$; B: $E_{-0}(K^+)$; C: $E_{-1}(Na^+)$; D: $E_{-0}(Na^+)$. Counter ions are given in the parentheses.

As the hfsc of the *t*-butyl protons is of the same order as the ESR linewidth of the spin packet, the effect which has been pointed out by Allendoerfer and Maki becomes important.[25] This relationship gives the relative ENDOR intensities as a function of T_2 and hfsc:

$$E = E^0(T_2\Delta\omega)^2/[2.5+(T_2\Delta\omega)^2], \quad (6)$$

where E^0 is the ENDOR enhancement in the case of $T_2\Delta\omega\gg1$ and where $\Delta\omega$ is hfsc expressed in s^{-1}. The observed results, however, can not be described in terms of this effect because: 1) the spin packets of the ESR transitions, λ_{-1} and λ_{-0}, are equally broadened by the intramolecular exchange when the rate is much smaller than the hfsc of the *t*-butyl protons; 2) a tentative calculation using Eq. 6 shows that $RE^{t\text{-butyl}}$ is much smaller than 1.2 at 230 K, even if the value of k is simply added to the linewidth of the λ_{-0} ESR transition. Here 1.0×10^6 s^{-1} and 1.1×10^6 s^{-1} were used for the reciprocals of the spin-spin relaxation time of the λ_{-1} and λ_{-0} ESR transitions respectively.

The effect of the intramolecular cation migration on the ENDOR intensity is also apparent in the case of *t*-butyl protons.

Conclusion

The intramolecular cation migration in the system of the DBQ anion and the Na cation in DME was investigated by means of ENDOR at the smaller exchange rate. The ENDOR intensities of the DBQ anion at λ_{-1} and λ_{-0} ESR transitions were different from each other. The ratio (*RE*) of the ENDOR intensities, E_{-1} and E_{-0}, increased when the temperature was raised, becoming greater than 1.5 at temperatures higher than 240 K. This feature was successfully explained using the Kaplan-Alexander theory.

Besides the various mechanisms which determine the ENDOR intensity,[12,26] a new mechanism, the intramolecular exchange, was shown also to be important in ENDOR.

The fact that RE^{low} is greater than RE^{high} for the ring protons suggests a contribution of the flop-flop or flip-flip relaxation due to the END interaction with the ENDOR intensity[19] at high temperatures. The study of the dynamic process with both the linewidth and the intensity of ENDOR was shown to be more reliable than the study with only the linewidth.

References

1) For example, K. S. Chen and N. Hirota, "Investigation of Rates and Mechanisms of Reactions," Part 2, ed by G. G. Hammes, John Wiley & Sons, New York (1974), Chap. 8.

2) E. de Boer and E. L. Mackor, *J. Am. Chem. Soc.*, **86**, 1513 (1964).

3) J. H. Freed, *J. Chem. Phys.*, **43**, 2312 (1965).

4) J. H. Freed, *J. Phys. Chem.*, **71**, 38 (1967).

5) J. H. Freed, D. S. Leniart, and J. S. Hyde, *J. Chem. Phys.*, **47**, 2762 (1967).

6) J. S. Hyde, R. Breslow, and C. DeBoer, *J. Am. Chem. Soc.*, **88**, 4763 (1966).
7) M. R. Das, H. D. Conner, D. S. Leniart, and J. H. Freed, *J. Am. Chem. Soc.*, **92**, 2258 (1970).
8) C. von Borczyskowski, K. Möbius, and M. Plato, *J. Magn. Reson.*, **17**, 202 (1975).
9) M. Plato, R. Biehl, K. Möbius, and K. P. Dines, *Z. Naturforsch.*, **31a**, 169 (1976).
10) C. von Borczyskowski and K. Möbius, *Chem. Phys.*, **12**, 281 (1976).
11) J. C. Chippendale and E. Warhurst, *Trans. Faraday Soc.*, **64**, 2332 (1964).
12) Y. Kotake and K. Kuwata, *Bull. Chem. Soc. Jpn.*, **47**, 45 (1974).
13) J. I. Kaplan, *J. Chem. Phys.*, **29**, 462 (1958).
14) S. Alexander, *J. Chem. Phys.*, **37**, 967 (1962).
15) Y. Doi and K. Kuwata, Abstr. p. 86, 13th Symposium on ESR Spectroscopy, Nagoya, 1974.
16) For example, A. Carrington and A. D. McLachlan, "Introduction to Magnetic Resonance," Harper and Row, New York (1976), Appendix 1.
17) P. Debye, "Polar Molecules," Dover Publications, New York (1945), Chap. 5.
18) C. Carvajal, K. J. Tolle, J. Smid, and M. Szwarc, *J. Am. Chem. Soc.*, **87**, 5548 (1965).
19) D. S. Leniart, J. C. Vedrine, and J. S. Hyde, *Chem. Phys. Lett.*, **6**, 637 (1970).
20) N. M. Atherton and B. Day, *Chem. Phys. Lett.*, **15**, 428 (1972).
21) H. van Willigen, M. Plato, R. Biehl, K. P. Dinse, and K. Möbius, *Mol. Phys.*, **26**, 793 (1973).
22) N. M. Atherton and B. Day, *J. Chem. Soc., Faraday Trans. 2*, **69**, 1801 (1973).
23) D. S. Leniart, H. D. Conner, and J. H. Freed, *J. Chem. Phys.*, **63**, 165 (1975).
24) Figure 16 in Ref. 23 shows the Heisenberg exchange rate of durosemiquinone in DME. The increase in the rate is about 33 kHz for a 5×10^{-4} mol dm^{-3} solution as the temperature increases from -70 to -40 °C. For a larger DBQ molecule the increase in the rate may be smaller than 25 kHz.
25) R. Allendoerfer and A. H. Maki, *J. Magn. Reson.*, **3**, 396 (1970).
26) J. S. Hyde, *J. Chem. Phys.*, **43**, 1806 (1965).
27) H. M. McConnell and J. Strathdee, *Mol. Phys.*, **2**, 129 (1959).

Cyclohexadienyl Radicals in γ-Irradiated *catena*-μ-Ethylenediaminecadmium(II) *catena*-Tetra-μ-cyanomercurate(II)-Benzene (1/2) and the Analogous Clathrates

Toschitake IWAMOTO, Mamoru KIYOKI, and Niro MATSUURA

Department of Chemistry, College of General Education, The University of Tokyo, Komaba, Meguro, Tokyo 153

(Received June 24, 1977)

Cyclohexadienyl radicals produced by γ-ray irradiation are thermally stable up to 423 K in the mother benzene clathrates $Cd(en)Hg(CN)_4\cdot 2C_6H_6$, $Cd(en)Cd(CN)_4\cdot 2C_6H_6$, $Cd(tn)Hg(CN)_4\cdot 2C_6H_6$, and $Cd(NH_3)_2Hg(CN)_4\cdot 2C_6H_6$. However, no thermally stable $C_6H_7\cdot$ radicals have been observed in $Cd(NH_3)_2Ni(CN)_4\cdot 2C_6H_6$ and $Cd(en)Ni(CN)_4\cdot 2C_6H_6$ even immediately after irradiation. The ESR spectra of $C_6H_7\cdot$ show the hyperfine splitting constants of the methylene, para, ortho, and meta protons 48, 13, 9, and 3 G, respectively.

The cavity for a guest molecule is expected to be a good reservoir of chemically unstable species in the host structure of a clathrate compound when the interaction between the guest and the host is negligibly weak. As has been demonstrated in the crystal structures determined by X-ray diffraction,[1] the guest benzene molecules in Hofmann type and the analogous benzene clathrates are individually imprisoned in the cavities surrounded by three-dimensional bridged metal complex host structures. Each benzene molecule apprears to be an isolated molecule trapped in a container of the volume slightly larger than that of the molecule itself. If a chemically unstable radical is once trapped in the container surrounded by an inactive wall, the radical may survive for a long time even at high temperature. From this point of view the present authors undertook to produce paramagnetic radicals from the guest species by γ-ray irradiation of diamagnetic Hofmann type and the analogous clathrates, and to investigate the stability of the radicals in the mother clathrates. A preliminary communication[2] gave a brief account of the thermal stability of the cyclohexadienyl $C_6H_7\cdot$ radicals up to 423 K which were produced by γ-irradiation of $Cd(en)M(CN)_4\cdot 2C_6H_6$ (M=Cd or Hg) clathrates. This paper reports on detailed experimental results obtained from γ-irradiated $Cd(diam)M(CN)_4\cdot 2C_6H_6$ (diam=en, tn, or $(NH_3)_2$; M=Cd, Hg, or Ni) clathrates, and on the correlation of clathrate structure with stability of the radicals.

Experimental

The benzene clathrates examined are as follows: $Cd(en)Hg(CN)_4\cdot 2C_6H_6$,[3] $Cd(en)Cd(CN)_4\cdot 2C_6H_6$,[3] $Cd(tn)Hg(CN)_4\cdot 2C_6H_6$,[15] $Cd(NH_3)_2Hg(CN)_4\cdot 2C_6H_6$,[4] $Cd(en)Ni(CN)_4\cdot 2C_6H_6$,[5] and $Cd(NH_3)_2Ni(CN)_4\cdot 2C_6H_6$.[6] $Cd(en)Hg(CN)_4\cdot 2C_6D_6$, $Cd(en)Hg(CN)_4\cdot 2C_4H_5N$, and $Cd(en)Hg(CN)_4$ were also irradiated for the sake of comparison.

The polycrystalline specimens were evacuated at 195K and sealed in silica ampoules at 1.3×10^{-3} Pa. The sealed specimens were irradiated with 6.5×10^3 J/kg ^{60}Co γ-rays at liquid nitrogen temperature. The irradiated specimens were kept at liquid nitrogen temperature till their ESR measurements. The ESR spectra were recorded on a JEOL-JES-PE-3X spectrometer with an X-band frequency and a field modulation of 100 kHz in the temperature range 77—423 K.

Results and Discussion

General Features of the ESR Spectra. At liquid nitrogen temperature all the irradiated specimens gave ESR signals due to radicals produced from the host constituents. Also observed were strong signals due to organic radicals centered at $g=2.003$ for the pyrrole and the benzene clathrates except for $Cd(en)Ni(CN)_4\cdot 2C_6H_6$ and $Cd(NH_3)_2Ni(CN)_4\cdot 2C_6H_6$. The signals due to the host constituents are thought to be those of the hot ions Cd(I) and Hg(I),[7] H·, and other unidentified radicals. These signals were observed over a wide (0.2 T) range of magnetic field with intensities far lower than those of the organic radicals as shown in Fig. 1. Their features differ with specimen, depending on host constituent. As the temperature is increased to 200 K, the signals due to the host constituents decay showing their thermal instability. Furthermore, the hyperfine structure in signals centered at $g=2.003$ becomes more clearly resolved with increasing temperature. For the benzene clathrates, the strong absorptions are assigned to cyclohexadienyl $C_6H_7\cdot$ radicals produced from the

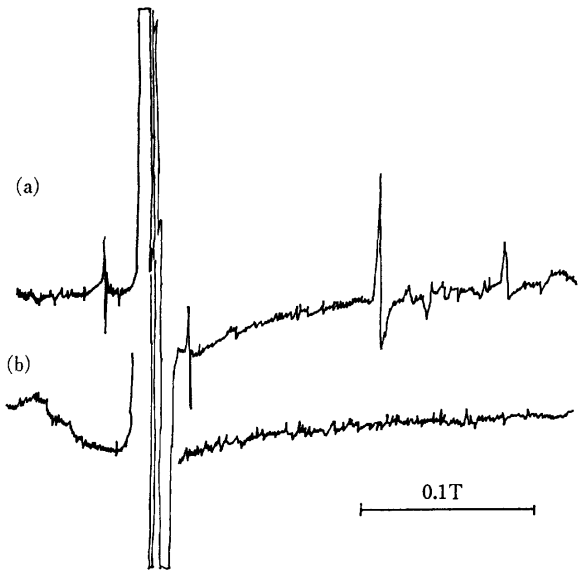

Fig. 1. ESR Spectra of the irradiated $Cd(en)Hg(CN)_4\cdot 2C_6H_6$ measured (a) at 100 K and (b) at 200 K. The strongest absorption centered at $g=2.003$ in due to organic radicals, and it is omitted is (b).

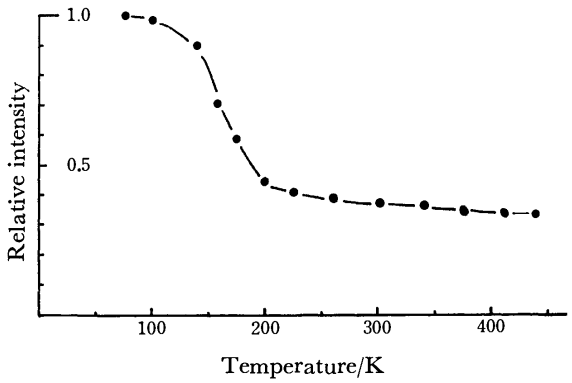

Fig. 2. Temperature dependence of the relative ientensity of the C_6H_7· absorption in the ESR spectrum of the irradiated Cd(en)Hg(CN)$_4$·2C_6H_6. The intensity was measured at each temperature with 1 h interval successively from 77 to 423 K.

enclathrated benzene molecules. The apparent intensity of the C_6H_7· absorption decreases strongly with increasing temperature up to 200 K where it is approximately 40% of that at liquid nitrogen temperature, the decrease becoming more gradual from 200 to 423 K (Fig. 2). The spectral linewidths become narrower with increasing temperature. Except for the two cases mentioned above, the thermal behavior of the C_6H_7· ESR signal is the same for all the irradiated benzene clathrates. Above 423 K the host metal complex begins to decompose thermally in the sealed ampoules.

The irradiated pyrrole clathrate also gave ESR signals due to organic radicals produced from the guest pyrrole. The spectral analysis, however, has not yet been completed.

Spectral Assignment of C_6H_7·. The ESR spectrum assigned to C_6H_7· has a main triplet of the intensity ratio 1:2:1 with about 48 G splitting, where G=10^{-4} T. The 48 G splitting of the triplet has been observed by a number of workers.[8-12] The 1:2:1 intensity ratio excludes significant formation of C_6H_5· observed for irradiated neat benzene.[8] The triplet is due to the hyperfine coupling of the electron spin with two methylene protons. The irradiated benzene-d_6 clathrate Cd(en)Hg(CN)$_4$·2C_6D_6 gave a broad doublet (*ca.* 40 G) structure in its ESR spectrum at low temperature. With increasing temperature the spectra became so complicated that the hyperfine structures except for a doublet (41.5 G) with a triplet (7.2 G) substructure could hardly be interpreted. The doublet may be due to the proton in the methylene position of C_6D_6H· and the triplet to the deuteron in the same position.[10] According to these observations, the formation scheme of C_6H_7· in the irradiated benzene clathrate is suggested as follows:

$$\text{HostH} \xrightarrow{\gamma\text{-rays}} \text{Host}\cdot + \text{H}\cdot$$

$$\text{H}\cdot + C_6H_6 \longrightarrow C_6H_7\cdot$$

The H· may be produced from the diamine or diammine ligand of the host metal complex.

Each component of the 48 G triplet shows a pseudoquartet structure with a 13 G splitting between the inner pair and a 9 G splitting between the outer and the inner components. A third hyperfine splitting (hfs) of a triplet (3 G) becomes clearer in each component of the pseudoquartet with increasing temperature above 200 K owing to the motional narrowing of linewidths. As has been demonstrated by wide-line ^{1}H-NMR of the benzene clathrates,[13] the enclathrated benzene molecules begin to reorientate about the molecular sixfold axis at 125 K and rotate with little hindrance above 160 K. The motional behavior of the C_6H_7· resembles that of the benzene molecule judging from the narrowing of ESR linewidths.

No radicals other than C_6H_7· have been identified, although in some cases broad and very weak signals are observed which overlap with the C_6H_7· absorption up to 323 K.

The Hfs Constants of C_6H_7·. According to the calculations by Shida and Hanazaki,[12] the hfs constants for the *p*-proton and the *o*-protons of C_6H_7· are 11.2 G and 10.6 G, respectively. Morokuma *et al.*[14] reported another set of −11.4 and −11.1 G. However, the

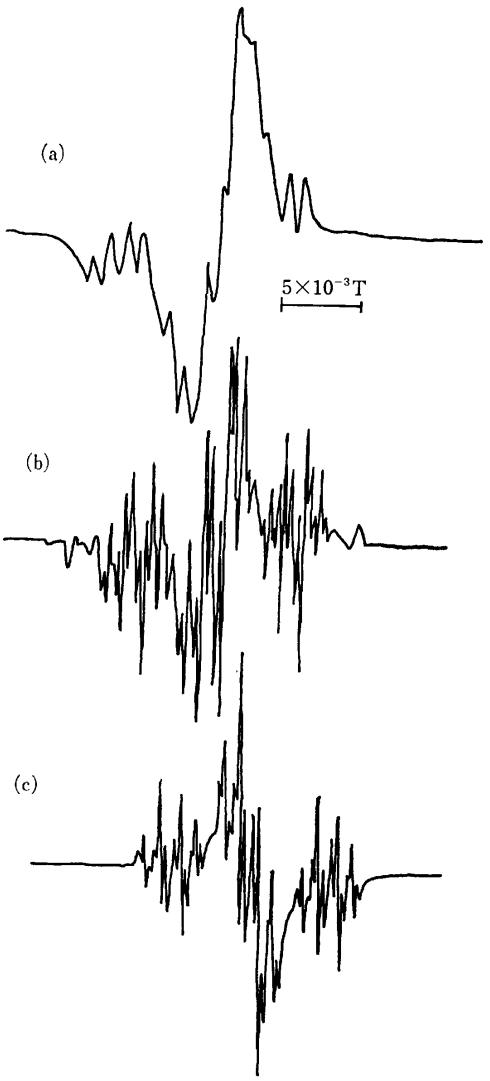

Fig. 3. ESR Spectra of the irradiated Cd(en)Cd(CN)$_4$·2C_6H_6 measured (a) at 77 K and (b) at 293 K, and that of the irradiated Cd(en)Hg(CN)$_4$·2C_6H_6 measured (c) at 373 K.

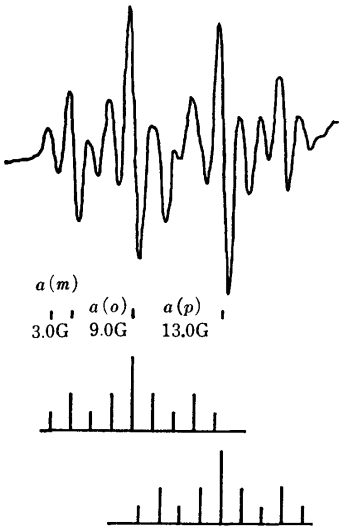

Fig. 4. The ESR hyperfine structure of $C_6H_7\cdot$ in the irradiated $Cd(en)Hg(CN)_4\cdot 2C_6H_6$ observed at 423 K. The lower field side of the 48.3 G main triplet is shown along with Fessenden-Schuler's scheme.[11]

difference between these hfs constants has never been observed for $C_6H_7\cdot$ produced by the irradiation of neat benzene or benzene solutions because of the thermal instability of the $C_6H_7\cdot$ radicals in the matrices used. The previous workers assigned the observed pseudo-quartet to the hfs due to the three protons at the para and ortho positions with nearly the same hfs constants. As shown in Fig. 3 for the present clathrates, it is possible to observe the ESR spectrum of $C_6H_7\cdot$ with a fairly good resolution up to such a high temperature that all of the unstable species collapse and the intermolecular dipole interactions become negligible. Although the resolution is still not high enough to make all the hfs components split clearly, we can discriminate between the hfs constants of the *p*-proton and the *o*-protons (Fig. 4). It is clearly seen that the spectrum of $C_6H_7\cdot$ in the irradiated $Cd(en)Hg(CN)_4\cdot 2C_6H_6$ is composed of a main triplet due to methylene protons (a(methylene)=48.3 G), a doublet due to the *p*-proton ($a(p)$=13.0 G), a triplet due to *o*-protons ($a(o)$=9.0 G), and a triplet due to *m*-protons ($a(m)$=3.0 G). The magnitude of the respective splitting constants is nearly the same for the $C_6H_7\cdot$ radicals in all the irradiated benzene clathrates. These observations do not agree with the previous observations with low resolution spectra for which approximately the same hfs constants were assigned for the *p*-proton and *o*-protons. However, the present results are in good agreement with those of Fessenden and Schuler.[11] They observed the ESR spectrum of liquid 1,4-cyclohexadiene during the course of irradiation with 0.4 μA of 2.8 mV electrons. Although their spectrum was not displayed, 72 resolved lines were assigned to $C_6H_7\cdot$ with a(methylene)=47.71 G, $a(p)$=13.04 G, $a(o)$=8.99 G, and $a(m)$=2.65 G. They observed that the central region of the main triplet splits into two sets of 18 lines owing to the release of degeneracy of the two m=0 states because of the second order effect for the large splitting constant. In the present spectrum of the solid specimen, the 1.5 G linewidth hides the second order splitting (0.69 G), only 13 lines being observed even in the central region. However, the spectrum can be interpreted substantially in terms of the scheme by Fessenden and Schuler.

Clathrates as Chemical Reservoir of Radicals. The $C_6H_7\cdot$ radicals produced in these benzene clathrates are thermally stable up to 423 K and survive for at least a few hours at 423 K. When the irradiated clathrates were kept at liquid nitrogen temperature even after the temperature of the specimen had been raised up to 423 K, the radicals still survived for at least a few weeks. Thus, the host metal complex Cd(diam)$M(CN)_4$ (diam=en, tn, or $(NH_3)_2$; M=Cd or Hg) is an excellent reservoir for the $C_6H_7\cdot$ radicals. However, it should be noted that no ESR spectrum for $C_6H_7\cdot$ was observed for the γ-irradiated $Cd(en)Ni(CN)_4\cdot 2C_6H_6$ and $Cd(NH_3)_2Ni(CN)_4\cdot 2C_6H_6$ even at liquid nitrogen temperature, although signals due to the thermally unstable radicals originating from the host constituents were observed.

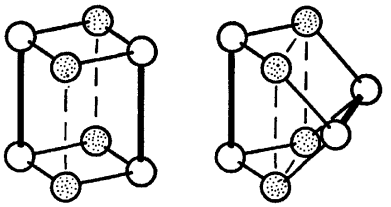

Fig. 5. Two kinds of guest cavities in Cd(diam)$M(CN)_4\cdot 2C_6H_6$ clathrates. (a) Tetragonal or rhombic frame is built up with square-planar $Ni(CN)_4$, or tetrahedral $Cd(CN)_4$ or $Hg(CN)_4$ moieties. (b) Biprismatic frame is possible only with the tetrahedral moieties. Open circle: Cd, dotted circle: M, thick line: diam (en, tn, or $(NH_3)_2$), thin line: CN.

The Hofman type $Cd(NH_3)_2Ni(CN)_4\cdot 2C_6H_6$ and the Hofmann-en type $Cd(en)Ni(CN)_4\cdot 2C_6H_6$ have a host of two-dimensionally extended $CdNi(CN)_4$ sheets containing the square-planar $Ni(CN)_4$ moieties. In the Hofmann type host two ammonia molecules protrude from adjacent sheets at the Cd atoms; in the Hofmann-en type host the protrusions between adjacent sheets are replaced by an ambident en ligand. These hosts have only one kind of guest cavity with a tetragonal or rhombic shape, as is shown in Fig. 5, while the hosts of the other clathrates, which stabilize $C_6H_7\cdot$, have both tetragonally and biprismatically shaped cavities due to the linkages of tetrahedral $Cd(CN)_4$ or $Hg(CN)_4$ moieties.[15] It appears that only the biprismatic cavity is effective in stabilizing $C_6H_7\cdot$. The partial volume of unit cell per benzene molecule was found to be *ca.* 270 Å^3 (Å=10^{-10} m) for the clathrate having biprismatic cavity. It is larger by *ca.* 30 Å^3 for the Hofmann type and Hofmann-en type, which gave no stable $C_6H_7\cdot$. The effective volume of the cavity might also be a critical factor in radical stability.

The authors' thanks are due to Professors Shizuo Fujiwara and Katsumi Tokumaru for their kind

permission to use their ESR spectrometers at the Department of Chemistry, Faculty of Science, this University, in the preliminary stage of this investigation.

References

1) T. Iwamoto and M. Kiyoki, *Bull. Chem. Soc. Jpn.*, **48**, 2414 (1975), and references cited there in.
2) T. Iwamoto, M. Kiyoki, and N. Matsuura, *Chem. Lett.*, **1975**, 847.
3) T. Iwamoto and D. F. Shriver, *Inorg. Chem.*, **11**, 2570 (1972).
4) R. Kuroda, *Inorg. Nucl. Chem. Lett.*, **9**, 13 (1974).
5) M. Miyoshi, T. Iwamoto, and Y. Sasaki, *Inorg. Chim. Acta*, **6**, 59 (1972).
6) Y. Sasaki, *Bull. Chem. Soc. Jpn.*, **42**, 2412 (1969).
7) J. Isoya and S. Fujiwara, *Bull. Chem. Soc. Jpn.*, **45**, 2182 (1972).
8) S. Ohnishi, T. Tanei, and I. Nitta, *J. Chem. Phys.*, **37**, 2402 (1962).
9) H. Fischer, *Kolloid Z. Z. Polym.*, **180**, 64 (1964).
10) J. A. Leone and W. S. Koski, *J. Am. Chem. Soc.*, **88**, 224 (1966).
11) R. W. Fessenden and R. H. Schuler, *J. Chem. Phys.*, **38**, 773 (1963).
12) T. Shida and I. Hanazaki, *Bull. Chem. Soc. Jpn.*, **43**, 646 (1970).
13) T. Miyamoto, T. Iwamoto, and Y. Sasaki, *J. Mol. Spectrosc.*, **35**, 244 (1970).
14) K. Morokuma, S. Ohnishi, T. Masuda, and K. Fukui, *Bull. Chem. Soc. Jpn.*, **36**, 1228 (1963).
15) T. Iwamoto, M. Kiyoki, Y. Ohtsu, and Y. Takeshige-Kato, *Bull. Chem. Soc. Jpn.*, **51**, 488 (1978).

Emission Spectra of Naphthalene Derivatives by Controlled Electron Impact

Teiichiro OGAWA, Nobuaki MIYAMOTO,* and Nobuhiko ISHIBASHI
Faculty of Engineering, Kyushu University, Hakozaki, Fukuoka 812
(Received June 30, 1977)

Naphthalene, 1-methylnaphthalene, 2-methylnaphthalene, 1-naphthol, 1-naphthylamine, 2-chloronaphthalene, 1-bromonaphthalene, 2-bromonaphthalene, and tetralin were excited in a very low pressure by controlled electron beam of 150—400 eV. The molecules, except those with a halogen atom, revealed an intense emission band similar to fluorescence. The band was assigned to the transition from their lowest-excited singlet state to their ground state. It was concluded that the most important process of photoemission is the excitation into a higher excited state in the primary collision and the subsequent non-radiative transfer to the lowest-excited state. The molecules showed photoemission of such excited fragments as H, CH, C_2, $C_4H_2^+$, CN, NH, OH, CO, CO^+, HCl^+, and HBr^+. A two-electron process by way of an intermediate was found to be important for the formation of such fragments as CN from naphthylamine.

The electron impact method has certain advantages for the investigation of the elementary process of molecular excitation, ionization, and dissociation. A comparatively intense photoemission can be obtained in a very low pressure and the excitation energy can be controlled easily in a wide range. The discharge method was used for this purpose; however, the use of a controlled electron beam in a low pressure has made it possible to investigate the elementary process without collision participation. The emission spectra of benzene,[1] its derivatives,[1,2] and naphthalene[3] by this method have been reported and the primary process of their excitation and dissociation has been investigated.[4]

The emission spectra of naphthalene derivatives, noteworthy for a stronger fluorescence than that of benzene derivatives, will be presented in this report. The excitation process of these molecules and the effect of a substituted group on the spectrum will be discussed in reference to the results of the benzene derivatives.

Experimental

The experimental apparatus was essentially the same as the one described previously.[1] The collision chamber was made of glass and was separated into two parts by a brass plate with a hole of 4 mm at its center. The thermal electrons were accelerated and collimated in the upper part, and introduced into the collision region (the lower part) through the hole. The sample was deaerated and introduced into the collision region through a nozzle (0.1—8 mm). When necessary, the sample manipulation line could be heated for the purpose of increasing the vapor pressure of sample. The collision chamber was continuously evacuated with two oil-diffusion pumps, the sample pressure in the collision region being estimated to be 10^{-2}—10^{-3} Torr. The sample vapor revealed photoemission upon collision with the electron beam. The photoemission was observed photoelectrically by use of a Jasco CT-50 monochromator (blazed for 300 nm). The energy of the electron beam was 150—400 eV, and the electron-beam current was 10—200 μA.

The excitation spectrum of fluorescence in a solution was recorded on a Hitachi MPF-4 fluorescence spectrophotometer. The spectral response of this instrument was calibrated down to 250 nm in references to the fluorescence of rhodamine B.

The naphthalene derivatives (Tokyo Kasei Co. and Kishida Chem. Co.) and cyclohexane, the solvent for the measurement of the excitation spectrum (luminasol, Dojindo Chem. Co.), were used.

Results

A typical spectrum of 2-methylnaphthalene is shown in Fig. 1. A diffuse band in the 315—390 nm region was assigned to the transition from the lowest-excited electronic state (S_1) to the ground electronic state (S_0), since its fluorescence spectrum was located in the same region[5] and the similar spectrum was obtained for toluene.[1] Some vibrational structures appeared on the spectrum of toluene[1] and naphthalene.[3] However, the spectrum of 2-methylnaphthalene indicated no definite structures even by measurement with a 2.5 Å resolution. The hydrogen Balmer lines and the bands of CH(A-X) and CH(B-X) were observed in the spectrum. The bands of C_2 and $C_4H_2^+$ were also observed in the longer wavelength region. The spectrum of 1-methylnaphthalene was very similar to that of 2-methylnaphthalene.

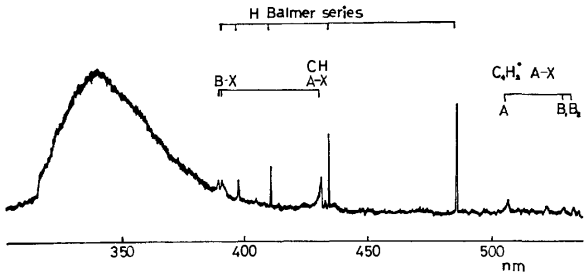

Fig. 1. Emission spectrum of 2-methylnaphthalene by controlled electron impact. Electron energy, 200 eV; electron-beam current, 30 μA.

The spectrum revealed no appreciable alteration with a change in the electron energy (150—400 eV). The intensity of the bands of the parent molecule, $H(H_\beta)$, and CH(A-X) was proportional to the electron-beam current at 200 eV excitation. This indicates that the excitation of the parent molecule and the dissociative excitation of H and CH proceed through one-electron primary processes.

* Present address: Ariake Technical College, Omuta, Fukuoka 836.

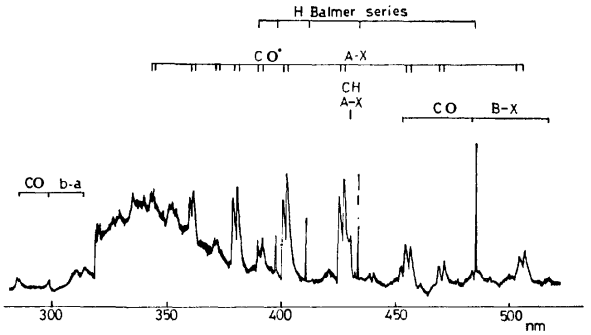

Fig. 2. Emission spectrum of 1-naphthol by controlled electron impact. Electron energy, 200 eV; electron-beam current, 80 μA.

A typical emission spectrum of 1-naphthol is shown in Fig. 2. The band of the S_1-S_0 transition of the parent molecule was diffuse, its peak being located at *ca.* 340 nm. The hydrogen Balmer lines, and the bands of CH(A-X), CO^+(A-X), CO(b-a), and CO(B-A) were also observed. The intensity of the emission of the parent molecule, H, and CH was proportional to the electron-beam current, indicating that these excited species are produced in one-electron primary processes. The intensity of the band of CO^+, however, was found to be proportional to about 1.5 powers of the electron-beam current; its formation should involve some secondary process.

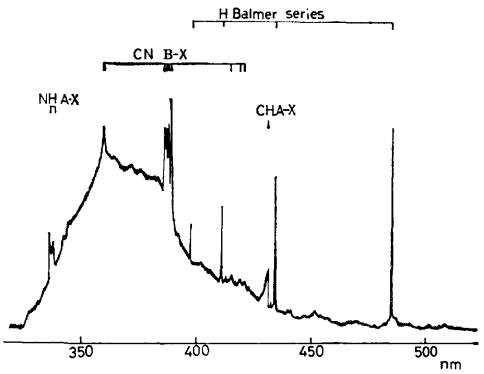

Fig. 3. Emission spectrum of 1-naphthylamine by controlled electron impact. Electron energy, 200 eV; electron-beam current, 20 μA.

A typical emission spectrum of 1-naphthylamine is shown in Fig. 3. The band of the S_1-S_0 transition of the parent molecule was diffuse, its peak being located at *ca.* 370 nm. The bands of NH(A-X), and CN(B-X) were observed in addition to those of H and CH. The intensity relationship of these bands excited at 200 eV is shown in Fig. 4. The intensity of the bands of the parent molecule, H, and CH was proportional to the electron-beam current as in the case of other molecules. However, that of CN was proportional to *ca.* 1.2 powers of the electron-beam current.

The emission spectra of 2-chloronaphthalene and 1- and 2-bromonaphthalene were similar to those of chloro- and bromo-benzene,[2] respectively. In both cases, no features identifiable as the S_1-S_0 transition

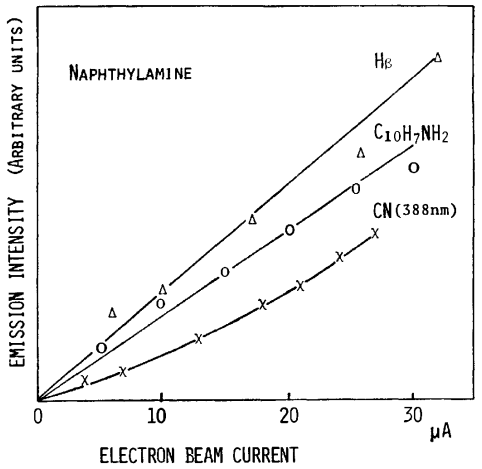

Fig. 4. Dependence of emission intensities on the electron-beam current. Electron energy, 200 eV.

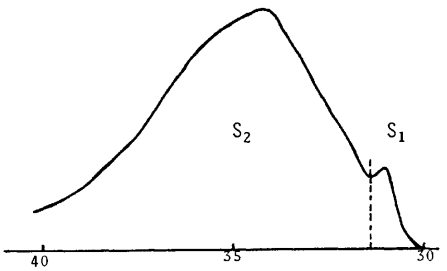

Fig. 5. Excitation spectrum of fluorescence of 1-naphthol in a cyclohexane solution. The spectral response of the spectrophotometer was corrected.

of the parent molecule could be observed, partly because the intense bands of HCl^+(A-X) or HBr^+(A-X) were located in the interesting region. The emission spectrum of tetralin revealed a band in the 270—315 nm region, which could be assigned to the S_1-S_0 transition of the parent molecule, since the location and band shape were similar to those of xylene.[1]

A typical excitation spectrum of fluorescence at 338 nm of 1-naphthol is shown in Fig. 5. Its absorption maxima were reported to be at 31300 and 34100 cm^{-1} for the S_1-S_0 and S_2-S_0 transitions, respectively.[6] The band was divided into two parts in the valley at 31400 cm^{-1} and the relative intensity was determined by the band area. Identical measurements were also carried out for naphthalene and 2-methylnaphthalene and the results are shown as ϕf in Table 1.

Table 1. Relative contribution of the two excitation process

		ϕf	$\phi f/E$
Naphthalene	S_1	1	1
	S_2	45	40
2-Methyl-naphthalene	S_1	1	1
	S_2	34	30
1-Naphthol	S_1	1	1
	S_2	22	20

Discussion

The Spectrum. The results of emission spectra observed in the present study are summarized in Table 2. The bands are classified according to their intensity relation to the electron-beam current.

TABLE 2. EMISSION SPECTRA OF NAPHTHALENE DERIVATIVES BY CONTROLLED ELECTRON IMPACT

Compound	S_1-S_0[a]	H	CH	$C_4H_2^+$	Others[b]
Naphthalene	○	○	○	○	
1-Methylnaphthalene	○	○	○	▽	
2-Methylnaphthalene	○	○	○	▽	
1-Naphthylamine	○	○	▽	▽	CN ●, NH ▽
1-Naphthol	○	○	▽		CO^+●, CO▽
2-Chloronaphthalene	×	▽	▽	▽	HCl^+ ▽
1-Bromonaphthalene	×	▽	▽	▽	HBr^+ ▽
2-Bromonaphthalene	×	▽	▽	▽	HBr^+ ▽
Tetralin	○	○	○	▽	

○: Band observed; intensity proportional to the electron-beam current. ●: Band observed; intensity not proportional to the electron-beam current. ▽: Band observed; intensity not measured. ×: No band observed.
a) Band of the parent molecule from the lowest excited state (S_1) to the ground state (S_0). b) Bands of excited fragment species.

The bands of the S_1-S_0 transition of the naphthalene derivatives are broad, lacking remarkable structures in contrast to their fluorescence spectra in cyclohexane.[5] Although the resonance fluorescence of naphthalene (0.05 Torr) is sharp and has many structures, it becomes broad and diffuse upon irradiation into the second excited state (S_2).[7] Thus, the band shape of the emission spectra by electron impact is similar to that of the resonance fluorescence obtained by the S_2 excitation. This is due to the fact that the excitation into higher excited states (such as S_2) is important in the electron-beam excitation.

The location and intensity of the S_1-S_0 transition of parent molecule depend on the kind of substituted group. The bands of the methyl and hydroxyl derivatives shift a little to the longer wavelength region as compared with that of naphthalene; the band of the amino derivative shifts considerably in the same direction. Although some fluorescence band was observed for the halogen derivatives in the cyclohexane solution, its quantum efficiency was small,[5] and no emission could be identified as their S_1-S_0 transition under electron-impact excitation. Heavy halogen atoms, such as Cl or Br, attached to an aromatic molecule are known to accelerate the rate of intersystem crossing and reduce the quantum efficiency. Furthermore, the C–X bond is susceptible to the bond scission and this can also contribute to the reduction of the emission intensity.

Excitation Process. Most fluorescent molecules, in a vapor phase or in a solution, emit fluorescence radiation mostly from the S_1 state, even when they are excited into a higher state. This is also the case with the emission spectra by controlled electron impact. Since an electron can excite a molecule into various excited states below the electron energy, it is significant to determine which excited state is actually contributing the observed photoemission.

The probability of the excitation of a molecule from the S_0 state to the S_i state is proportional to f_i/E_i, where f_i and E_i denote the oscillator strength and the transition energy of the i-th transition, respectively.[9] The probability of photoemission from the S_i state after the non-radiative transfer from the initially prepared state (S_i) to the S_1 state is represented by the fluorescence quantum yield (ϕ_i). Thus, the intensity of photoemission (I_i), which involves the S_i state in the primary process, is[3]

$$I_i = a\phi_i f_i/E_i, \quad (1)$$

where a is a proportionality constant.

Although the values of ϕ_i, f_i, and E_i measured in a vapor phase should be used to estimate I_i, no such spectroscopic parameters of naphthalene derivatives seem to have been reported. The fluorescence quantum yield of naphthalene was reported to be 0.23 in a cyclohexane solution[5] and 0.4—0.8 in vapor;[8] its f value did not show a large variation in proceeding from vapor to solution.[10] The results indicate that the difference of the optical parameters in vapor and in a solution is not significant and the spectroscopic parameters in a cyclohexane solution may be carried over for a semi-quantitative estimation of the excitation process by use of Eq. 1.

The relative intensity of the excitation spectrum of fluorescence can be set to the relative value of $\phi_i f_i$ in this approximation. The results of $\phi_2 f_2$ relative to $\phi_1 f_1$ are shown in Table 1. The spectrum is similar to the absorption spectrum. This indicates that the quantum yield varies little in this region and the present estimation should be taken as a semi-quantitative one.

There are two excitation processes: The direct excitation process, in which the molecule is excited primarily into the S_1 state and radiates from this state directly, and the indirect excitation process, in which the molecule is excited in the S_2 state primarily, relaxes to the S_1 state non-radiatively and then emits radiation from the S_1 state. As shown in Table 1, the indirect excitation process is more important. Since naphthalene and its derivatives have large f_2 and f_3 and the rate of non-radiative transition to the S_1 state is relatively large, the indirect process gives a larger contribution to the photoemission than the direct process.[3] This is partly due to a larger conjugate system and a smaller difference of the energies between the S_1 state and the S_2 and S_3 states than that of benzene derivatives.[11]

The band of the S_1-S_0 transition of the parent molecules is more diffuse and structureless than that of fluorescence in a solution and shifts to the longer wavelength region. This has much to do with the excitation process. In a solution large intermolecular interaction induces a fast non-radiative transfer of the initially prepared excited state to the ground vibrational level of the S_1 state and the transition from this level reveals some vibrational structures. However, when the collisional deactivation within the lifetime of the radiative excited state is negligible, the initially

prepared highly excited state transfers intramolecularly to the higher vibrational levels of the S_1 state and then the molecule emits radiation. Since high vibrational levels are involved and the naphthalene derivatives have more complicated vibrational levels than the benzene derivatives, the emission band becomes diffuse and structureless and shifts to the red as compared with that in a solution. This is consistent with the fact that the resonance fluorescence becomes broad and structureless with increase in excitation energy.[7]

Dissociative Excitation. The emission spectra excited by controlled electron impact have many bands of excited fragment species as summarized in Table 2. The intensity of bands of H and CH is proportional to the electron-beam current. It can be concluded that these species are produced in one-electron primary processes as in the case of benzene derivatives.[4] The sum of the dissociation energy and the excitation energy in the formation of H* and CH* is larger than the ionization energy of the parent molecules. This may indicate that the formation of H* and CH* proceeds by way of a superexcited state.[12]

The emission intensities of CO^+ from 1-naphthol and of CN* from 1-naphthylamine are not proportional to the electron-beam current as indicated in Fig. 4 and Table 2. The formation of CN* from aniline also exhibits a non-linear relationship,[2] but not that of CO^+ from phenol.[11]

The excited fragment species, the intensity of which was not proportional to the electron-beam current, often have two or more heavy atoms (C, N, O, *etc.*) and are also produced by breaking two or more skeletal bonds of the parent molecule.[13] The formation of such species was elucidated by the scheme in which two dissociative excitation processes contribute to an appreciable extent:[11,13]

$$C_{10}H_7NH_2 + e \longrightarrow CN^* \quad \text{(one-electron process)}$$

$$\left.\begin{array}{l} \searrow\ M \\ M + e \longrightarrow CN^* \end{array}\right\} \text{(two-electron process)}$$

where M stands for an unidentified intermediate species. Although the collision probability of a radiative species is negligible, any fragment species in the metastable or ground electronic states may be affected by collision. The relative importance of these two processses are dependent on the reactivity of the species concerned. In the formation of such species as H* and CH*, the two-electron process is of negligible importance in the region studied.

In brief, the emission spectra of naphthalene derivatives agree qualitatively with those of benzene derivatives; however, there are some quantitative differences.

The authors thank Mr. Masaharu Tsuji of the Research Institute of Industrial Science for his discussion and Mr. Kenyu Kina for his cooperation in the measurement of the excitation spectrum of fluorescence.

References

1) T. Ogawa, M. Tsuji, M. Toyoda, and N. Ishibashi, *Bull. Chem. Soc. Jpn.*, **46**, 2637 (1973).
2) T. Ogawa, M. Tsuji, M. Toyoda, and N. Ishibashi, *Bull. Chem. Soc. Jpn.*, **46**, 1063 (1973); M. Tsuji, T. Ogawa, and N. Ishibashi, *ibid.*, **46**, 3380 (1973).
3) M. Tsuji, T. Ogawa, and N. Ishibashi, *Chem. Phys. Lett.*, **26**, 586 (1974).
4) K. Hirota, M. Hatada, and T. Ogawa, *Int. J. Radiat. Phys. Chem.*, **8**, 205 (1976).
5) I. S. Berlman, "Handbook of Fluorescence Spectra of Aromatic Molecules," Academic Press, N. Y. (1971).
6) A. Nakajima, *Bull. Chem. Soc. Jpn.*, **45**, 1687 (1972).
7) J. M. Blondeau and M. Stockburger, *Chem. Phys. Lett.*, **8**, 436 (1971).
8) J. C. Hsieh, C. S. Huang, and E. C. Lim, *J. Chem. Phys.*, **60**, 4345 (1974).
9) M. Inokuti, *Rev. Mod. Phys.*, **43**, 297 (1971).
10) G. A. George and G. C. Morris, *J. Mol. Spectrosc.*, **26**, 67 (1968).
11) M. Tsuji, T. Ogawa, Y. Nishimura, and N. Ishibashi, *Bull. Chem. Soc. Jpn.*, **50**, 2432 (1977).
12) R. L. Platzman, *Vortex*, **23**, 272 (1962).
13) T. Ogawa, T. Imasaka, M. Toyoda, M. Tsuji, and N. Ishibashi, *Bull. Chem. Soc. Jpn.*, **48**, 645 (1975).

Barrier to Internal Rotation around the Isopropyl-Nitrogen Bond of Some *N,N*-Diisopropyl-1,3-dithia- and 1,3-diselenacycloalkan-2-iminium Salts, $[\overline{X(CH_2)_nXCN(i\text{-}Pr)_2}]^+Y^-$ (X=S, Se; Y=Br, PF_6; n=2,3)

Yu-ichi TAKEDA, Tsuneo MATSUDA, and Toshio TANAKA

Department of Applied Chemistry, Faculty of Engineering, Osaka University, Suita, Osaka 565

(Received July 4, 1977)

Activation parameters for rotation around the isopropyl-nitrogen bond of the title compounds were determined by the line shape analysis of ^1H NMR spectra. The E_a values lie in the ranges of 58—60 kJ/mol for X=S and 52—54 kJ/mol for X=Se. The activation parameters are little influenced by the ring size of the 1,3-diheteracycloalkane moiety and the counter anions.

Internal rotation around the isopropyl-nitrogen bond in metal complexes of diisopropyldichalcogenocarbamate is well known to cause interconversion between two stable equivalent rotamers as follows.[1-3]

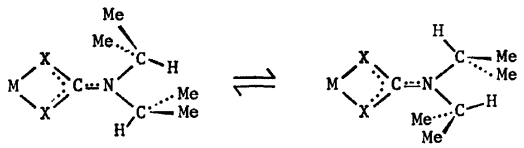

X=S, Se

The barriers (E_a) to rotation of this kind have been reported for some metal complexes of diisopropyldithiocarbamate (dtc) and diisopropyldiselenocarbamate (dsc). The E_a values obtained so far, however, are rather scattered; $Ni(dtc)_2$, 19;[1] $Co(dtc)_3$, 21;[1] $Ti(dtc)_nCl_{4-n}$, 42.3 for n=2 and 41.0 for n=3, 4;[2] $R_2Sn(dtc)_2$, 76.6 for R=Cl and 68.6 for R=Me;[3] and $R_2Sn(dsc)_2$, 69.0 for R=Cl and 58.2 for R=Me[3] (the values in kJ/mol). The values for the Ni(II) and Co(III) complexes were obtained by line shape analysis of the methine proton signal, and those for the other complexes by the same analysis of the isopropyl-methyl proton signal. A similar interconversion between two equivalent rotamers has been proposed for (diisopropylamino)bis(methylthio)methylium perchlorate, $[(MeS)_2CN(i\text{-}Pr)_2]^+ClO_4^-$, only $\Delta G^{\ddagger}$ value being obtained.[4]

This paper reports the results of line shape analysis of the isopropyl-methyl proton signal of *N,N*-diisopropyl-1,3-dithia- and 1,3-diselenacycloalkan-2-iminium bromides and hexafluorophosphates, $[\overline{X(CH_2)_nXCN(i\text{-}Pr)_2}]^+Y^-$ (X=S, Se; Y=Br, PF_6; n=2, 3). The purpose of this work is to elucidate both effects of the hetero atoms in the 1,3-dichalcogenacycloalkane ring and the ring size on the activation parameters for rotation around the isopropyl-nitrogen bond.

Experimental

N,N-Diisopropyl-1,3,-dithiacyclohexane- and -cyclopentan-2-iminium bromides and their diselena analogs, $[\overline{X(CH_2)_nXCN(i\text{-}Pr)_2}]^+Br^-$ (n=3, X=S (**1a**); n=2, X=S (**2a**); n=3, X=Se (**3a**); n=2, X=Se (**4**)), were prepared by the reaction of 1,3-dibromopropane or 1,2-dibromoethane with Na(dtc) or $Me_2Sn(dsc)_2$ according to the method described for the *N,N*-dimethyl derivatives.[5] The corresponding hexafluorophosphates, $[\overline{X(CH_2)_nXCN(i\text{-}Pr)_2}]^+PF_6^-$ (n=3, X=S (**1b**); n=2, X=S (**2b**); n=3, X=Se (**3b**)), were obtained by the addition of an ethanol solution of NH_4PF_6 to the bromide salts in ethanol.

All the compounds were recrystallized from a mixture of CH_2Cl_2 and petroleum ether. The elemental analysis and properties are summarized in Table 1.

Measurement of ^1H NMR spectra in dichloromethane (0.01—0.1 M) and line shape analysis were carried out as described previously.[3] The ^1H chemical shift data of **1a—3a**, **4**, and **1b—3b** are given in Table 2.

Results and Discussion

Figure 1a depicts variable temperature ^1H NMR spectra of **1a** in dichloromethane. At room temperature **1a** exhibits a doublet signal due to the isopropyl-methyl

TABLE 1. PROPERTIES AND ANALYTICAL DATA OF $[\overline{X(CH_2)_nXCN(i\text{-}Pr)_2}]^+Y^-$

Compound	X	Y	n	Mp, °C	Found %			Calcd %			*M.W.*[a]	
					C	H	N	C	H	N	Found	Calcd
1a	S	Br	3	176—177	39.83	6.82	4.71	40.26	6.76	4.70	295	298
2a	S	Br	2	189—191	37.68	6.50	4.92	38.03	6.38	4.93	272	284
3a	Se	Br	3	152—153	30.41	5.09	3.51	30.63	5.14	3.57	394	392
4	Se	Br	2	170—172	28.41	4.74	3.65	28.59	4.80	3.70	386	378
1b	S	PF_6	3	194—195	26.37	4.54	3.17	26.27	4.51	3.06	368	363
2b	S	PF_6	2	196—198	31.64	5.39	4.00	31.44	5.19	4.01	377	349
3b	Se	PF_6	3	200—203	26.73	4.54	3.17	26.27	4.41	3.06	423	457

a) Measured in CH_2Cl_2 at 25 °C by vapor pressure osmometry.

Table 2. Proton chemical shifts (δ) in CH_2Cl_2, 0.05 M

Compound	$\delta(CH_3)$[a]	$\delta(C\text{-}CH_2\text{-}C)$[b]	$\delta(S\text{-}CH_2)$[b]
1a	1.47, 1.67	2.50	3.48
2a	1.48, 1.58	—	4.18
3a	1.47, 1.67	2.49	3.49
4	1.49, 1.60	—	4.31
1b	1.44, 1.64	2.43	3.35
2b	1.48, 1.57	—	3.95
3b	1.48, 1.68	2.45	3.39

a) At −30 °C, $J(CH_3\text{-}CH)=7.2\pm0.2$ Hz. b) At room temperature.

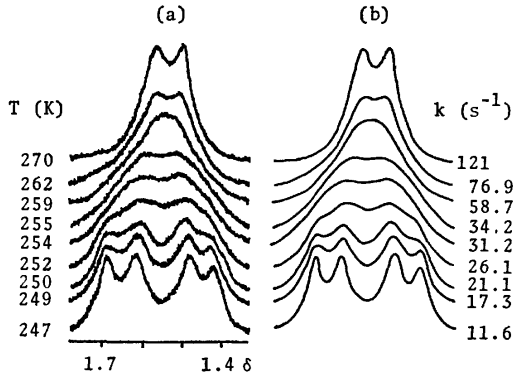

Fig. 1. Observed (a) and calculated (b) spectra of the isopropyl-methyl protons of $[\overset{\frown}{S(CH_2)_3SCN}(i\text{-}Pr)_2]^+Br^-$.

protons (not shown in Fig. 1a). With fall in temperature, the signal coalesces into a broad one, splitting into two broad signals at about −18 °C. On further fall in temperature, the methyl protons appear as two doublets with identical intensities. A similar temperature dependence was also observed in the ^1H NMR spectra of all the other compounds. The spectra show no concentration dependence for solutions in the range 0.1—0.01 M. The spectral patterns of all the compounds in the range from room temperature to −30 °C are very similar to those of some diisopropyldithiocarbamato and -diselenocarbamato complexes of tin(IV), $R_2Sn(dtc)_2$ and $R_2Sn(dsc)_2$ (R=Me and Cl).[3] It is therefore suggested that the rotation around the isopropyl-nitrogen bond is restricted at relatively low temperatures, while that near room temperature occurs rapidly on the NMR time scale, resulting in interconversion between two identical rotamers as shown below.

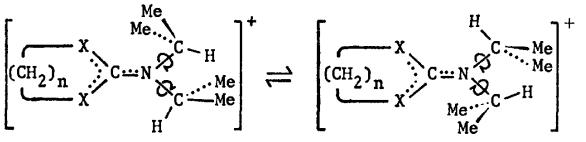

X=S, Se; n=3, 2

The rate constants of the interconversion, k, were determined by line shape analysis of the isopropyl-methyl signal. Figure 1 shows an example of the best fits between the observed and calculated spectra of **1a**. The plots of $\ln k$ *vs.* $1/T$ and $\ln(k/T)$ *vs.* $1/T$ of **1a**, **2a**, **3a**, and **4** are given in Figs. 2 and 3 respectively, from

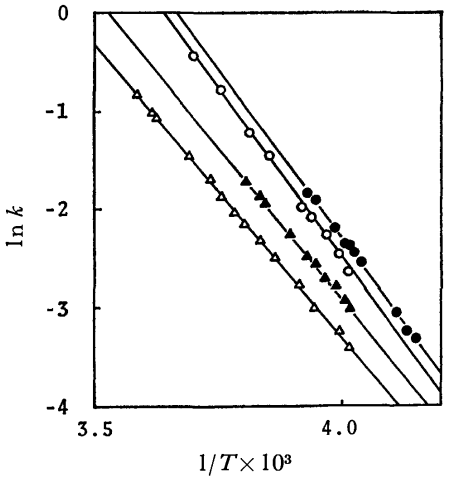

Fig. 2. Arrhenius plots for exchange of the isopropyl-methyl group in $[\overset{\frown}{X(CH_2)_nXCN}(i\text{-}Pr)_2]^+Br^-$: X=S, n=3 (○); X=S, n=2 (●); X=Se, n=3 (△); X=Se, n=2 (▲).

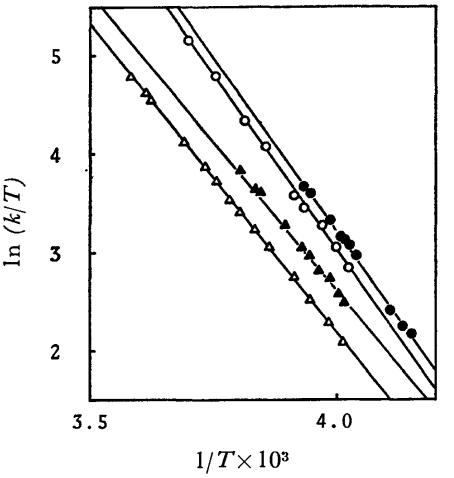

Fig. 3. Eyring plots for exchange of the isopropyl-methyl group in $[\overset{\frown}{X(CH_2)_nXCN}(i\text{-}Pr)_2]^+Br^-$: X=S, n=3 (○); X=S, n=2 (●); X=Se, n=3 (△); X=Se, n=2 (▲).

Table 3. Thermodynamic data[a] for internal rotation around the isopropyl-nitrogen bond

Compound	E_a (kJ/mol)	$\Delta H^{\ddagger}$ (kJ/mol)	$\Delta S^{\ddagger}$ (J/(K mol))	$\Delta G^{\ddagger}_{298}$ (kJ/mol)
1a	59.9±1.7	57.7±1.7	12.4±6.6	54.0±2.6
2a	59.3±1.8	57.3±1.8	12.4±7.5	53.6±2.9
3a	52.2±0.5	50.0±0.5	−25.3±2.1	57.5±0.7
4	53.8±1.4	51.6±1.4	−15.3±5.5	56.2±2.2
1b	58.8±1.3	56.7±1.3	6.3±5.0	54.8±2.0
2b	58.7±2.4	56.6±2.4	7.8±9.8	54.3±3.8
3b	52.1±0.4	49.9±0.4	−27.5±1.7	58.1±0.7

a) Errors were estimated at the 95% confidence level.

which the Arrhenius and Eyring activation parameters, E_a, $\Delta H^{\ddagger}$, and $\Delta S^{\ddagger}$, were calculated by the least-squares method. The results together with the $\Delta G^{\ddagger}$ value are summarized in Table 3.

The barriers to the rotation around the isopropyl-nitrogen bond, E_a (52—60 kJ/mol) are close to those in $PhC(S)N(i\text{-}Pr)_2$ and $PhCH_2C(S)N(i\text{-}Pr)_2$ (51.0 and 59.4 kJ/mol at −25 °C, respectively).[6] This seems to indicate that the 1,3-dichalcogenacycloalkane moiety of the present compounds does not appreciably influence the barrier to rotation around the isopropyl-nitrogen bond. In fact, there is little difference in the E_a value between any of the pairs of cyclohexane and cyclopentane compounds, **1a**—**2a**, **3a**—**4**, and **1b**—**2b**. The E_a values of the bromide salts, **1a**, **2a**, and **3a**, are essentially the same as those of the hexafluorophosphate salts, **1b**, **2b**, and **3b**, respectively (Table 3). On the other hand, the dithia compounds, **1a**—**3a** and **4** give E_a values larger by 5—8 kJ/mol than the diselena analogs, **1b**—**3b**. The difference is compared with that between the E_a values of $R_2Sn(dtc)_2$ and $R_2Sn(dsc)_2$ (7.5 and 10.4 kJ/mol when R=Cl and Me, respectively)[3] where the steric repulsion of the isopropyl group with the sulfur atoms has been suggested to be larger than that with the selenium atom owing to the shorter length of the C–S bond than that of the C–Se bond. The absolute values of ΔS^* obtained are not so large (less than 28 J/(K mol)), suggesting the occurrence of an intramolecular process in solution.

References

1) R. M. Golding, P. C. Healy, P. W. G. Newman, E. Sinn, and A. H. White, *Inorg. Chem.*, **11**, 2435 (1972).

2) A. N. Bhat, R. C. Fay, D. F. Lewis, A. F. Lindmark, and S. H. Strauss, *Inorg. Chem.*, **13**, 886 (1974).

3) Y. Takeda, N. Watanabe, and T. Tanaka, *Spectrochim. Acta, Part A*, **32**, 1553 (1976).

4) A. Lindén, C. Roussel, T. Liljefors, M. Chanon, R. E. Carter, J. Metzger, and J. Sandström, *J. Am. Chem. Soc.*, **98**, 2853 (1976).

5) K. Tanaka and T. Tanaka, *Bull. Chem. Soc. Jpn.*, **45**, 489 (1972).

6) K. C. Ramey, D. J. Louick, P. W. Whitehurst, W. B. Wise, R. Mukherjee, J. F. Rosen, and R. M. Moriarty, *Org. Magn. Reson.*, **3**, 767 (1971).

The Effect of Σ-Π Interaction on the Electronic Structure of Molecules in the Excited States. II. Oscillator Strength

Izumi MAKI, Kazuo KITAURA, and Kichisuke NISHIMOTO

Department of Chemistry, Faculty of Science, Osaka City University, Sumiyoshi-ku, Osaka 558

(Received June 27, 1977)

The effect of Σ-Π interaction on the oscillator strength of π-π^* transition has been investigated in terms of the configuration interaction method considering all singly excited configurations. It has been found that the transition moment associated with π-π^* excitation is modified by σ-electrons. The correction term of the transition moment resulting from the Σ-Π interaction can be expressed by the bond index matrix. The present theory has been applied to the calculation of the oscillator strength of benzene and naphthalene derivatives. Agreement between the calculated values and experimental data is satisfactory. The effect of Σ-Π interaction on the transition moment has been demonstrated pictorially.

In the previous paper,[1] the effective π-electron Hamiltonian for the excited state which includes the Σ-Π interaction was derived using the partitioning technique.[2] The effective electron repulsion integrals were represented in terms of the bond index matrix.

The oscillator strength calculated by the traditional π-electron theory is generally larger than that obtained by experiments.[3] This discrepancy might be caused by neglecting the Σ-Π interaction[4] and the π-electron correlation.[5] In the present paper, we consider the effect of Σ-Π interaction on the oscillator strength of π-π^* transition.

The theoretical procedure is as follows. We consider the wave function including the σ-σ* configurations in the excited state, and represent the transition moment in terms of the bond index matrix. Applying this theory to benzene, naphthalene, pyridine, pyrazine, phenol, aniline, quinoline, and isoquinoline, we show the role of the σ-electrons on the transition moments associated with the π-π^* transitions. We then analyze the effect of induced σ-electron polarization on the π-π^* transition moment, and show that the induced σ-electron polarization can be assigned to the individual localized σ-bonds.

Theoretical

The effective total π-electron Hamiltonian for the excited state is expressed as follows:[1]

$$\tilde{\boldsymbol{H}}(\pi) = \boldsymbol{H}(\pi) - \boldsymbol{V}\boldsymbol{P}\frac{1}{\boldsymbol{H}-\boldsymbol{E}\boldsymbol{I}}\boldsymbol{P}\boldsymbol{V}, \tag{1}$$

where $\boldsymbol{V}$ denotes the electron repulsion interaction between σ and π electrons and $\boldsymbol{P}$ is the projection operator defined by

$$\boldsymbol{P} = \sum_{kr}\left|\begin{matrix}\gamma\\ k\end{matrix}\right\rangle\left\langle\begin{matrix}\gamma\\ k\end{matrix}\right|, \tag{2}$$

where $\left|\begin{matrix}r\\ k\end{matrix}\right\rangle$ is the singly excited configuration associated with the excitation of an electron from the k-th occupied σ-MO to the γ-th unoccupied σ*-MO. In this paper the following notations are used: i,j for the occupied π-MO, α,β for the unoccupied π^*-MO, k,l for the occupied σ-MO, γ,δ for the unoccupied σ*-MO, μ,ν for the π-AO and r,s for the σ-AO. In accordance with the prescribed P-P-P method,[6] the zero differential overlap (ZDO) approximation is also used.

With use of the effective total π-electron Hamiltonian[1] the corresponding excited wave function, $|\Phi\rangle$, expressed by the linear combination of the π-π^* singly excited configurations, can be obtained from the following equation:

$$\tilde{\boldsymbol{H}}(\pi)|\Phi\rangle = \boldsymbol{E}|\Phi\rangle, \tag{3}$$

where

$$|\Phi\rangle = \sum_{i\alpha} C_{i\alpha}\left|\begin{matrix}\alpha\\ i\end{matrix}\right\rangle, \tag{4}$$

$|\Phi\rangle$ is normalized in the subspace associated with π-π^* configurations, and $C_{i\alpha}$ is the variation parameter.

On the other hand, the actual wave function, $|\Psi\rangle$, for the lower excited state is given by the linear combinations of the π-π^* and σ-σ* singly excited configurations as follows:

$$|\Psi\rangle = \frac{1}{\sqrt{N}}\left[\sum_{i\alpha} C_{i\alpha}\left|\begin{matrix}\alpha\\ i\end{matrix}\right\rangle + \sum_{kr} C_{kr}\left|\begin{matrix}\gamma\\ k\end{matrix}\right\rangle\right], \tag{5}$$

where $\sqrt{N}$ is the normalization factor. According to the partitioning technique,[2] C_{kr} in Eq. 5 is written as follows:

$$C_{kr} = -\sum_{i\alpha}[(\boldsymbol{H}-\boldsymbol{E}\boldsymbol{I})_{kr,kr}]^{-1}\left\langle\begin{matrix}\gamma\\ k\end{matrix}\right|\boldsymbol{V}\left|\begin{matrix}\alpha\\ i\end{matrix}\right\rangle C_{i\alpha}. \tag{6}$$

Substituting Eq. 6 into Eq. 5, we obtain

$$|\Psi\rangle = \frac{1}{\sqrt{N}}\left(|\Phi\rangle - \boldsymbol{P}\frac{1}{\boldsymbol{H}-\boldsymbol{E}\boldsymbol{I}}\boldsymbol{P}\boldsymbol{V}|\Phi\rangle\right). \tag{7}$$

The normalization factor is given by

$$N = 1 + \sum_{i\alpha}\sum_{j\beta} C_{i\alpha}C_{j\beta}\sum_{kr}\frac{4V_{ik\alpha r}V_{jk\beta r}}{[(\boldsymbol{H}-\boldsymbol{E}\boldsymbol{I})_{kr,kr}]^2}, \tag{8}$$

where $V_{ik\alpha r}$ means the exchange type MO integral which is defined as follows:

$$V_{ik\alpha r} = \iint i^*(1)k^*(2)v_{12}\alpha(1)\gamma(2)\,d\tau_1 d\tau_2.$$

As we did in the previous paper,[1] the averaged energy parameter is used instead of the denominator in Eq. 8. Then, the normalization factor can be written as

$$N = 1 - \frac{1}{e^2}\sum_{i\alpha}\sum_{j\beta} C_{i\alpha}C_{j\beta}\sum_{\mu\nu}\sum_{AB} d_{i\mu}d_{j\nu}d_{\alpha\mu}d_{\beta\nu}\gamma_{\mu A}\mathbf{B}_{AB}\gamma_{B\nu}, \tag{9}$$

in terms of the bond index matrix $\mathbf{B}$. $d_{i\mu}$ is the coefficient of the μ-th AO of the i-th MO. e is an averaged energy parameter. The bond index matrix element $\mathbf{B}_{AB}$ is defined as follows:[1]

$$\mathbf{B}_{AB} = -\sum_{r}^{A}\sum_{s}^{B}\sum_{k}^{\sigma}\sum_{\gamma}^{\sigma^*} 4d_{kr}d_{ks}d_{\gamma r}d_{\gamma s}.$$

The value of $\sqrt{N}$ calculated by means of Eq. 9 is almost 1.0. Thus $\sqrt{N}$ is put to be 1.0 in the calculation.

The transition moment $\mathbf{m}$ associated with the excitation of an electron from the ground state to an excited singlet state, Ψ, is given by

$$\mathbf{m} = \langle 0|\sum_i \mathbf{r}_i|\Psi\rangle, \tag{10}$$

Substituting Eq. 7 into Eq. 10, we obtain the transition moment including the effect of Σ-Π interaction as follows:

$$\mathbf{m} = \langle 0|\sum_i \mathbf{r}_i|\Phi\rangle - \langle 0|\sum_i \mathbf{r}_i P\frac{1}{\boldsymbol{H}-\boldsymbol{EI}}\boldsymbol{P}\boldsymbol{V}|\Phi\rangle, \tag{11}$$

where $\mathbf{r}_i$ is the position vector of the i-th electron. The first term of Eq. 11 corresponds to the transition moment of the traditional P-P-P scheme, the second term being the correction due to the Σ-Π interaction. According to the usual P-P-P method, the transition moment from the ground state to the excited configuration, $\left|{}^{\beta}_{j}\right\rangle$, can be expanded by means of LCAO coefficients as

$$\langle 0|\sum_i \mathbf{r}_i\left|{}^{\beta}_{j}\right\rangle = \sqrt{2}\sum_\mu d_{j\mu}d_{\beta\mu}\mathbf{r}_\mu, \tag{12}$$

where $\mathbf{r}_\mu$ represents the coordinate of the μ-th atom. Therefore, Eq. 11 becomes

$$\mathbf{m} = \sqrt{2}\sum_{i\alpha}C_{i\alpha}\sum_\mu d_{i\mu}d_{\alpha\mu}\left(\mathbf{r}_\mu + \frac{1}{2e}\sum_{AB}\mathbf{r}_A\mathbf{B}_{AB}\gamma_{B\mu}\right). \tag{13}$$

By means of this equation, the oscillator strength, f, including the Σ-Π interaction is written as follows:

$$f = 0.0875 \times \mathbf{m}^2 \times \Delta E \times G, \tag{14}$$

where ΔE (in eV) is the excitation energy and G is the degree of the degeneracy of the excited state.

Let us further consider the transition moment $\mathbf{m}$. Equation 13 can be rewritten as

$$\mathbf{m} = \mathbf{m}_0 + \Delta\mathbf{m},$$

where $\mathbf{m}_0$ and $\Delta\mathbf{m}$ are given by

$$\mathbf{m}_0 = \sqrt{2}\sum_{i\alpha}\sum_\mu C_{i\alpha}d_{i\mu}d_{\alpha\mu}\mathbf{r}_\mu,$$

$$\Delta\mathbf{m} = \frac{1}{\sqrt{2}\,e}\sum_{i\alpha}\sum_\mu C_{i\alpha}d_{i\mu}d_{\alpha\mu}\sum_{AB}\mathbf{r}_A\mathbf{B}_{AB}\gamma_{B\mu}. \tag{15}$$

$\Delta\mathbf{m}$ is rewritten as

$$\Delta\mathbf{m} = \sum_{AB}\mathbf{r}_A\mathbf{B}_{AB}\mathbf{X}_B, \tag{16}$$

where $\mathbf{X}_B$ is given by

$$\mathbf{X}_B = \frac{1}{\sqrt{2}\,e}\sum_{i\alpha}\sum_\mu C_{i\alpha}d_{i\mu}d_{\alpha\mu}\gamma_{B\mu}.$$

Since $\Sigma\mathbf{B}_{AB}=0$, $\Delta\mathbf{m}$ becomes as follows:

$$\begin{aligned}
\Delta\mathbf{m} &= \frac{1}{2}\sum_A\sum_B(\Delta\mathbf{m}_{AB}+\Delta\mathbf{m}_{BA}) \\
&= \frac{1}{2}[\sum_A\sum_B\mathbf{r}_A\mathbf{B}_{AB}\mathbf{X}_B+\sum_A\sum_B\mathbf{r}_B\mathbf{B}_{BA}\mathbf{X}_A] \\
&= \frac{1}{2}[(\sum_A\sum_B\mathbf{r}_A\mathbf{B}_{AB}\mathbf{X}_B-\sum_B\mathbf{r}_B\mathbf{X}_B\sum_A\mathbf{B}_{AB}) \\
&\quad +(\sum_B\sum_A\mathbf{r}_B\mathbf{B}_{BA}\mathbf{X}_A-\sum_A\mathbf{r}_A\mathbf{X}_A\sum_B\mathbf{B}_{BA})] \\
&= \frac{1}{2}[\sum_A\sum_B(\mathbf{r}_A-\mathbf{r}_B)\mathbf{B}_{AB}\mathbf{X}_B+\sum_B\sum_A(\mathbf{r}_B-\mathbf{r}_A)\mathbf{B}_{BA}\mathbf{X}_A] \\
&= \sum_{A>B}(\mathbf{r}_A-\mathbf{r}_B)\mathbf{B}_{AB}(\mathbf{X}_B-\mathbf{X}_A) \\
&= \sum_{A>B}\Delta\mathbf{M}_{AB},
\end{aligned} \tag{17}$$

where

$$\Delta\mathbf{M}_{AB} = (\mathbf{r}_A-\mathbf{r}_B)\mathbf{B}_{AB}(\mathbf{X}_B-\mathbf{X}_A).$$

Thus, $\Delta\mathbf{m}$ can be decomposed into the contributions of individual σ-bonds. $\Delta\mathbf{M}_{AB}$ is the induced σ-polarization associated with the σ-bond, A–B, caused by the π-π^* transition. The present theory has been applied to the calculation of the oscillator strength of π-π^* transition of some aromatic compounds.

Results and Discussion

The calculated transition moments and oscillator strengths of benzene and naphthalene are summarized in Table 1. The calculated and experimental excitation energies and oscillator strengths of benzene and naphthalene are compared in Fig. 1, where PPP-NM denotes the conventional P-P-P calculation using Nishimoto-Mataga formula[6] for the two center electron repulsion integrals. We see that the calculated results based on the present theory agree with the experimental ones satisfactorily for both the singlet and triplet states. It should be noted that the present theory brings about an appreciated improvement in the oscillator strength. The conventional P-P-P method gives too large values of oscillator strengths. The Σ-Π interaction gives rise,

TABLE 1. CALCULATED TRANSITION MOMENTS AND OSCILLATOR STRENGTHS OF BENZENE AND NAPHTHALENE

	States[a]	Transition moments[b] $\mathbf{m}_0$ x	$\mathbf{m}_0$ y	$\Delta\mathbf{m}$ x	$\Delta\mathbf{m}$ y	$\mathbf{m}$ x	$\mathbf{m}$ y	Oscillator strengths[c] f_0	f	f/f_0
Benzene	$^1B_{2u}$	0.	0.	0.	0.	0.	0.	0.	0.	—
	$^1B_{1u}$	0.	0.	0.	0.	0.	0.	0.	0.	—
	$^1E_{1u}$	0.	1.400	0.	−0.424	0.	0.976	1.201	0.584	0.487
	$^1E_{1u}$	1.400	0.	−0.424	0.	0.976	0.	1.201	0.584	0.487
Naphthalene	$^1B_{3u}$	0.	0.	0.	0.	0.	0.	0.	0.	—
	$^1B_{2u}$	0.	0.755	0.	−0.264	0.	0.491	0.233	0.099	0.421
	^1A_g	0.	0.	0.	0.	0.	0.	0.	0.	—
	$^1B_{3u}$	1.984	0.	−0.423	0.	1.561	0.	1.999	1.237	0.619

a) Singlet state is placed in the order of increasing energy. b) x and y denote the component of the transition moment. c) f_0 and f are calculated by using $\mathbf{m}_0$ and $\mathbf{m}$, respectively.

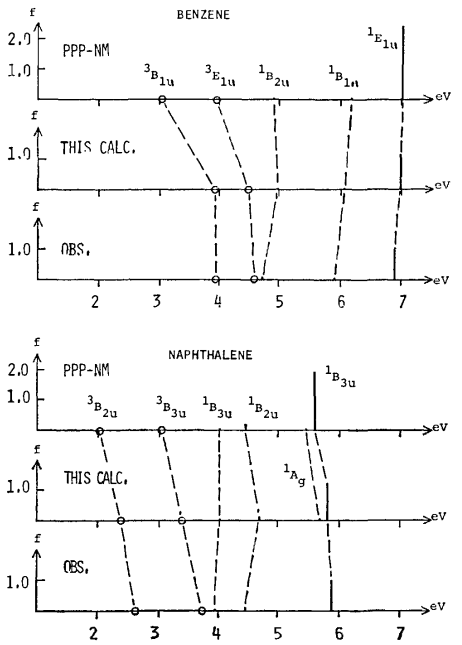

Fig. 1. The calculated experimental (OBS) excitation energies and oscillator strengths of benzene and naphthalene. (The experimental values are taken from Ref. 8.)

therefore, to a substantial reduction in the conventionally calculated oscillator strength. For an example, the calculated f-value (oscillator strength) associated with the $^1A_{1g} \rightarrow {}^1E_{1u}$ transition of benzene varies from 2.40 to 1.17, when the Σ-II interaction is considered (experimental value, 1.0[8]). The f-value of naphthalene corresponding to the transition with a medium intensity ($^1A_g \rightarrow {}^1B_{2u}$) and that with the strongest intensity ($^1A_g \rightarrow {}^1B_{3u}$) also vary from 0.23 and 2.00 to 0.10 and 1.24, respectively. The corresponding experimental values are 0.10 and 1.0,[8] respectively. The reason for this improvement in the oscillator strength is that the π-π^* transition induces the polarization of σ-electrons in the direction opposite to the π-π^* transition moment.

It is convenient to demonstrate the effect of Σ-II interaction on the transition moment pictorially. Figure

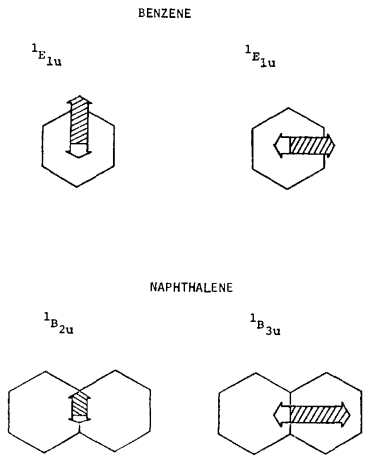

Fig. 2. The transition moments of benzene and naphthalene. $\mathbf{m}_0$ and $\Delta\mathbf{m}$ are represented by a shaded and a hollow arrows, respectively.

2 shows the transition moments of benzene and naphthalene, where $\mathbf{m}_0$ (Eq. 15) is shown by a shaded arrow and induced moment $\Delta\mathbf{m}$ is shown by a hollow arrow. The total transition moment is the sum of these two moments. In the case of the lower $^1B_{2u}$ state of naphthalene, the value of $\mathbf{m}_0$ is 0.76 eÅ (in unit of electron angstrom) and $\Delta\mathbf{m}$ is −0.26 eÅ, so that the sum is to be 0.50 eÅ. Consequently, the oscillator strength is to be reduced to about one-half of its initial value. The value of $\mathbf{m}_0$ of the strongly allowed transition ($^1A_g \rightarrow {}^1B_{3u}$) is 1.98 eÅ and that of induced moment is −0.42 eÅ. Generally speaking, the larger π-π^* transition moment causes the larger induced moment

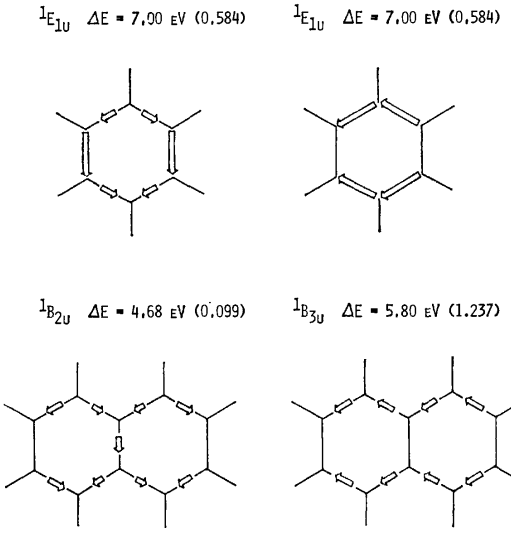

Fig. 3. The divided induced transition moments, $\Delta\mathbf{M}_{AB}$'s, of benzene and naphthalene.

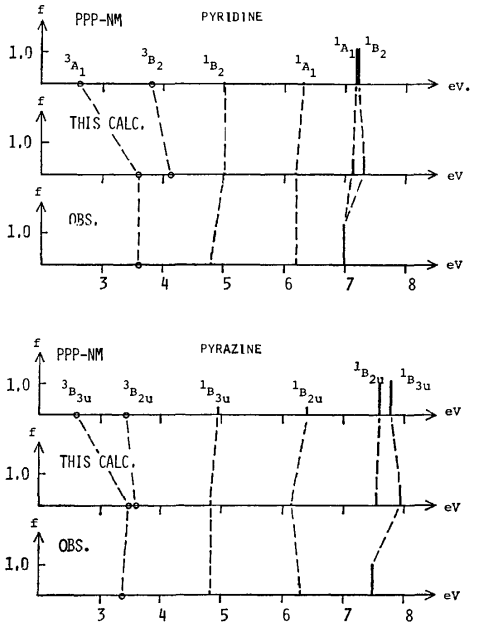

Fig. 4. The calculated and experimental (OBS) excitation energies and oscillator strengths of pyridine and pyrazine. (The experimental values are taken from Refs. 10, 11, and 12.)

TABLE 2. CALCULATED TRANSITION MOMENTS AND OSCILLATOR STRENGTHS OF PYRIDINE, PYRAZINE, ANILINE, PHENOL, QUINOLINE, AND ISOQUINOLINE

	State[a]	Transition moments[b] $\mathbf{m}_0$ x	$\mathbf{m}_0$ y	$\Delta\mathbf{m}$ x	$\Delta\mathbf{m}$ y	$\mathbf{m}$ x	$\mathbf{m}$ y	Oscillator strengths[c] f_0	f	f/f_0
Pyridine	$^1B_2$	0.453	0.	−0.137	0.	0.316	0.	0.090	0.044	0.489
	$^1A_1$	0.	0.284	0.	−0.078	0.	0.206	0.044	0.023	0.523
	$^1A_1$	0.	1.334	0.	−0.440	0.	0.894	1.112	0.499	0.449
	$^1B_2$	1.305	0.	−0.395	0.	0.910	0.	1.088	0.529	0.486
Pyrazine	$^1B_{3u}$	0.784	0.	−0.237	0.	0.547	0.	0.260	0.126	0.485
	$^1B_{2u}$	0.	0.582	0.	−0.175	0.	0.407	0.182	0.089	0.489
	$^1B_{2u}$	0.	1.222	0.	−0.454	0.	0.768	0.988	0.390	0.395
	$^1B_{3u}$	1.214	0.	−0.368	0.	0.847	0.	1.026	0.499	0.486
Aniline	$^1B_2$	0.490	0.	−0.160	0.	0.330	0.	0.089	0.041	0.461
	$^1A_1$	0.	1.050	0.	−0.217	0.	0.832	0.499	0.314	0.629
	$^1A_1$	0.937	0.	−0.303	0.	0.635	0.	0.500	0.229	0.458
	$^1B_2$	0.	1.244	0.	−0.317	0.	0.927	0.908	0.504	0.551
Phenol	$^1B_2$	0.354	0.	−0.107	0.	0.247	0.	0.051	0.025	0.490
	$^1A_1$	0.	0.691	0.	−0.181	0.	0.510	0.236	0.128	0.542
	$^1B_2$	0.	1.384	0.	−0.387	0.	0.996	1.135	0.588	0.518
	$^1A_1$	1.245	0.	−0.377	0.	0.868	0.	0.920	0.447	0.486
Quinoline	S_1	0.430	0.103	−0.091	−0.034	0.339	0.069	0.069	0.042	0.609
	S_2	−0.096	0.699	0.023	−0.256	−0.073	0.444	0.204	0.083	0.407
	S_3	1.177	−0.078	−0.251	0.036	0.925	−0.042	0.678	0.418	0.617
	S_4	1.374	0.111	−0.291	−0.032	1.084	0.079	1.011	0.628	0.622
	S_5	0.342	0.896	−0.076	−0.295	0.266	0.601	0.501	0.236	0.471
Isoquinoline	S_1	0.162	0.427	−0.037	−0.145	0.126	0.281	0.073	0.033	0.452
	S_2	−0.177	0.669	0.037	−0.233	−0.140	0.436	0.199	0.087	0.437
	S_3	0.488	0.294	−0.111	−0.096	0.377	0.198	0.160	0.089	0.556
	S_4	1.779	−0.046	−0.403	0.031	1.375	−0.015	1.610	0.962	0.598
	S_5	0.280	−0.214	−0.063	0.076	0.216	−0.138	0.067	0.036	0.537

a), b), c) See the footnotes of Table 1.

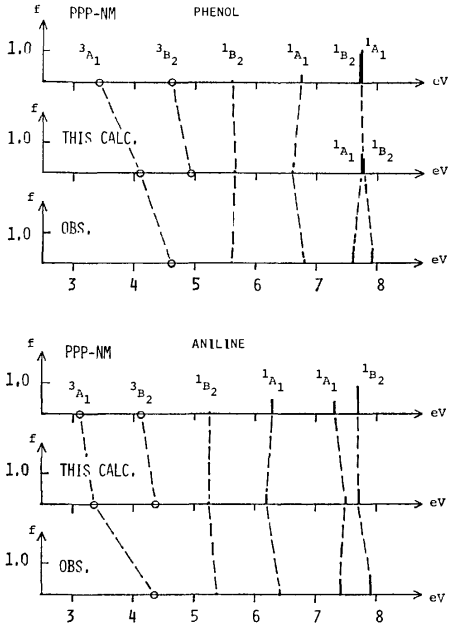

Fig. 5. The calculated and experimental (OBS) excitation energies and oscillator strengths of phenol and aniline. (The experimental values are taken from Refs. 9 and 10.)

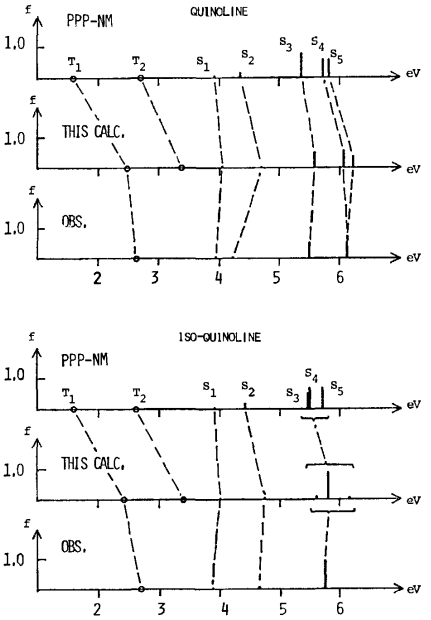

Fig. 6. The calculated and experimental (OBS) excitation energies and oscillator strengths of quinoline and isoquinoline. (The experimental values are taken from Refs. 7 and 8.)

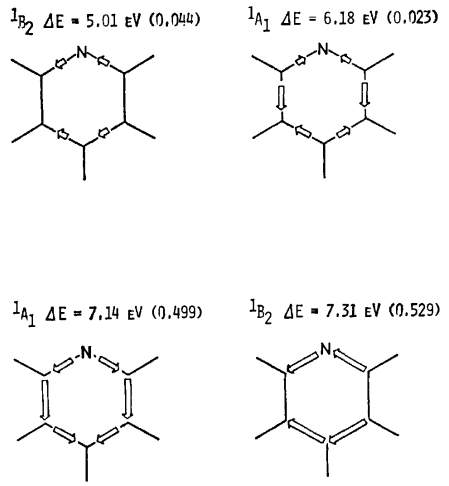

Fig. 7. The divided induced transition moments, $\Delta\mathbf{M}_{AB}$'s, of pyridine.

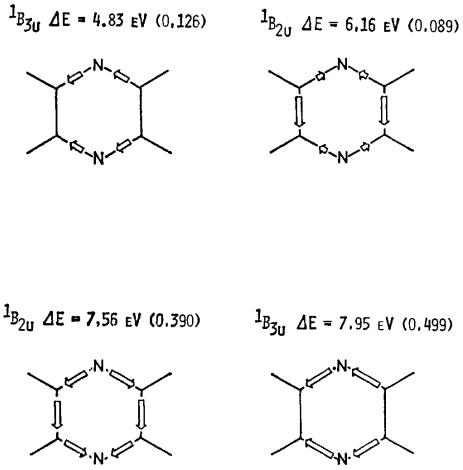

Fig. 8. The divided induced transition moments, $\Delta\mathbf{M}_{AB}$'s, of pyrazine.

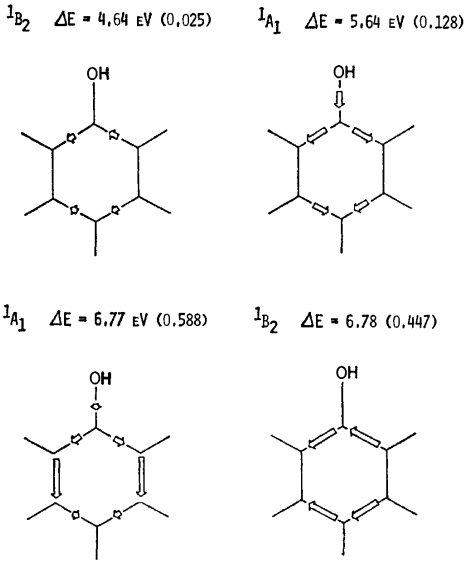

Fig. 9. The divided induced transition moments, $\Delta\mathbf{M}_{AB}$'s, of phenol.

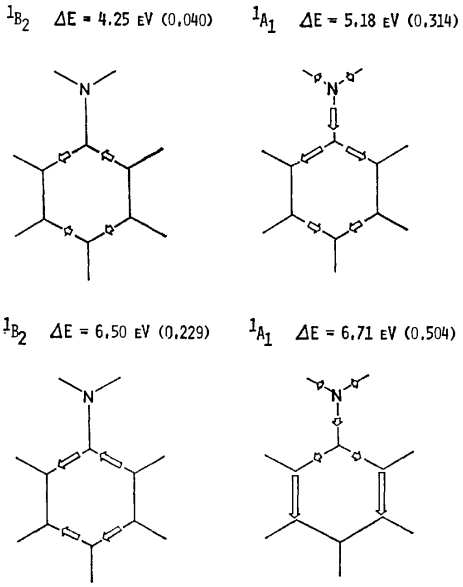

Fig. 10. The divided induced transition moments, $\Delta\mathbf{M}_{AB}$'s, of aniline.

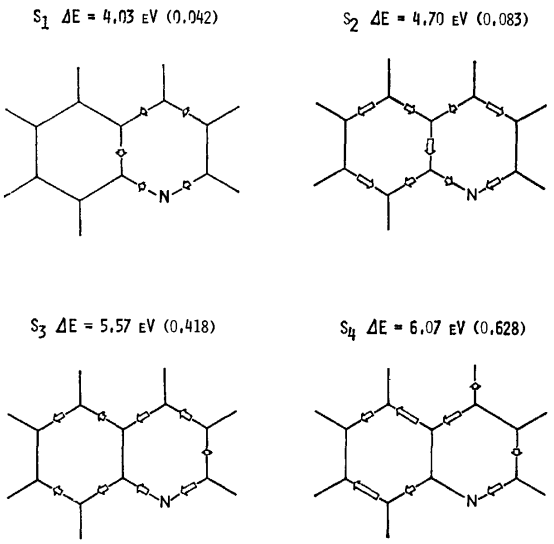

Fig. 11. The divided induced transition moments, $\Delta\mathbf{M}_{AB}$'s, of quinoline.

in the opposite direction. However, there is no quantitative relation between these two moments.

According to Eq. 17, the induced moment, $\Delta\mathbf{m}$, for a given transition can be divided into $\Delta\mathbf{M}_{AB}$ associated with the σ-bond A–B. Figure 3 shows such $\Delta\mathbf{M}_{AB}$ for benzene and naphthalene. The values of ΔE and f in this figure are the calculated transition energy and oscillator strength, respectively.

The calculated transition moment and oscillator strength of pyridine, pyrazine, aniline, phenol, quinoline, and isoquinoline are summarized in Table 2. The calculated and experimental excitation energies and oscillator strengths (f) of these molecules are compared in Figs. 4—6. The divided induced moment, $\Delta\mathbf{M}_{AB}$, associated with each transition of molecules is shown in Figs. 7—12.

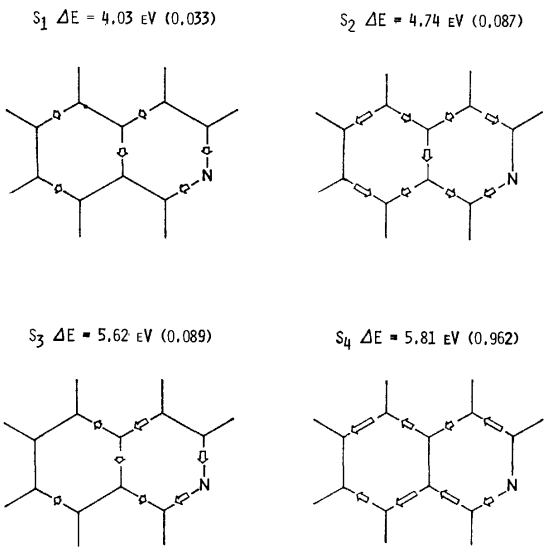

Fig. 12. The divided induced transition moments, $\Delta\mathbf{M}_{AB}$'s, of isoquinoline.

For the molecules considered in the present study, the absolute value of $\Delta\mathbf{m}$ is *ca.* 1/5—1/3 of the corresponding $\mathbf{m}_0$ (Tables 1 and 2). Thus the ratio of f (oscillator strength calculated by $\mathbf{m}$) to f_0 (oscillator strength calculated by $\mathbf{m}_0$) is found to be *ca.* 0.4—0.6. The oscillator strength of π-π^* transition calculated by the conventional P-P-P method is larger by about twice that obtained by experiment.[5,7] For azanaphthalenes, Baba and Yamazaki[7] showed that when the value of the oscillator strength calculated by P-P-P method is multiplied by 0.596, it is in a good agreement with the experimental ones. From Tables 1 and 2, it is found that their prescription is appreciated as a good approximation. In the cases of quinoline and isoquinoline which have no molecular symmetry, the two moments, $\mathbf{m}_0$ and $\Delta\mathbf{m}$, do not lie on a straight line. Thus the π-π^* transition moment is not only reduced but also altered it's direction by means of the Σ-Π interaction. For *N*-heterocycles, the diagonal matrix element of the bond index matrix associated with *N* atom is set to be -2.0, namely the lone pair orbital is treated as completely localized. In spite of this approximation, the results for these molecules are good for both the excitation energies and oscillator strength, (Figs. 4-6). This suggests that the present method is also applicable to *N*-heterocycles.

In the present theory, the electron correlation between π-electrons which reduces the oscillator strength has not been considered. Although Σ-Π interaction is a kind of electron correlation, the effect might be overestimated in the present method. It is obvious that the Σ-Π interaction has a very large effect on the π-π^* excitation energies and oscillator strengths.

We would like to express our gratitude to the Data Processing Center, Kyoto University, for its generous permission to use the FACOM M-190 computer.

References

1) I. Maki, K. Kitaura, and K. Nishimoto, *Bull. Chem. Soc. Jpn.*, **50**, 1720 (1977).
2) P. O. Löwdin, "Perturbation Theory and its Application in Quantum Mechanics," ed by C. H. Wilcox, Wiley, New York (1966).
3) L. Salem, "Molecular Orbital Theory of Conjugated System," Benjamin, Massachusetts (1972), Chap. 7.
4) P. G. Lykos and R. G. Parr, *J. Chem. Phys.*, **24**, 1166 (1956); R. A. Harris, *ibid.*, **47**, 3967 (1967).
5) S. Iwata, *Kagaku No Ryoiki*, **30**, 41 (1976); T. Shibuya, Y. J. I'Haya, and V. McKoy, *Int. J. Quant. Chem.*, **9**, 505 (1975); K. Kitaura and K. Nishimoto, *Theor. Chim. Acta (Berl)*, **31**, 91 (1973); K. Kitaura and K. Nishimoto, *ibid.*, **28**, 111 (1973).
6) K. Nishimoto and N. Mataga, *Z. Phys. Chem. (Frankfurt)*, **12**, 335 (1957).
7) H. Baba and I. Yamazaki, *J. Mol. Spectrosc.*, **44**, 118 (1972); S. Suzuki, T. Fujii, and H. Baba, *ibid.*, **47**, 243 (1973).
8) J. B. Birks, Ed., "Organic Molecular Photophysics," John Wiley & Sons, Vols. 1, 2, New York (1973).
9) K. Kimura and S. Nagakura, *Mol. Phys.*, **9**, 117 (1965).
10) S. L. Murov, "Handbook of Photochemistry," Marcel Dekker, Inc. New York (1973).
11) J. H. Ruch and H. Sponer, *J. Chem. Phys.*, **20**, 1847 (1952); H. P. Stephenson, *ibid.*, **22**, 1077 (1954).
12) B. Bak, L. Hansen-Nyggard, and J. Rastrup-Anderson, *J. Mol. Spectrosc.*, **2**, 361 (1958).

Preparation and Electrical Conductivity of Some Simple and Complex Salts Formed between *N,N*-Dialkyl-1,3-dichalcogenacycloalkan-2-iminium and $TCNQ^{\cdot-}$

Shingo ARAKI, Hiromi ISHIDA, and Toshio TANAKA

Department of Applied Chemistry, Faculty of Engineering, Osaka University, Suita, Osaka 565

(Received July 11, 1977)

Four simple salts and six complex salts of $TCNQ^{\cdot-}$ radical anion with *N,N*-dialkyl-1,3-dichalcogenacycloalkan-2-iminium cations, $(CH_2)_n^{Y}C{=}\overset{+}{N}R_2\cdot TCNQ^{\cdot-}$ and $(CH_2)_n^{Y}C{=}\overset{+}{N}R_2\cdot(TCNQ)_2^{\cdot-}$ (n=2 or 3, Y=S or Se, R=Me or Et) were prepared. The electrical resistivity of $(CH_2)_2^{Se}C{=}\overset{+}{N}Et_2\cdot TCNQ^{\cdot-}$ (1.1×10^4 ohm cm) was more than 10 times lower than other three simple salts ($(6.1-8.7)\times10^5$ ohm cm). Electronic absorption spectra and magnetic susceptibilities suggest that the latter three involve dimeric $(TCNQ)_2^{2-}$, while in the former the interaction between two $TCNQ^{\cdot-}$ radical anions is weak in the solid state. All the complex salts with compaction samples exhibited the resistivity of 2.4—4.0 ohm cm with very low activation energies (0.018—0.087 eV). Electronic spectra and magnetic susceptibilities show that the interaction between two $TCNQ^{\cdot-}$ radical anions decreases owing to the implication of neutral TCNQ.

There has been reported the preparation of various salts of 7,7,8,8-tetracyanoquinodimethane (TCNQ) radical anion with inorganic and organic cations which show a wide range of electrical conductivities, largely depending on the properties of the counter cations. Some of those are known as best electrically conductive organic salts, such as quinolinium-$(TCNQ)_2^{\cdot-}$ [1] and *N*-methylphenazinium-$TCNQ^{\cdot-}$.[2] Charge-transfer complexes between TCNQ and tetrathiafulvalene or its derivatives also were reported to display high electrical conductivities.[3] The cationic moieties of these electrically conductive organic salts or complexes generally not only adopt a planar structure but also involve hetero atoms with large polarizability. Garito and Heeger have mentioned the importance of these two factors for obtaining organic complexes with high electrical conductivities.[4]

Some time ago, one of the authors prepared *N,N*-dimethyl-1,3-dithia- and 1,3-diselenacycloalkan-2-iminium dimethyltin(IV) halides, $(CH_2)_2^{Y}C{=}\overset{+}{N}Me_2\cdot Me_2SnBr_3^-$ (Y=S and Se) and $[(CH_2)_3^{S}C{=}\overset{+}{N}Me_2]_2\cdot Me_2SnBr_4^{2-}$.[5-7] The iminium cations of these salts adopt a planar Y_2CN moiety[6] involving largely polarizable hetero atoms. This fact prompted us to prepare $TCNQ^{\cdot-}$ radical anion salts of these iminium cations. This paper reports the synthesis and the electrical conductivity of several simple and complex salts of $TCNQ^{\cdot-}$ with the iminium cations, $(CH_2)_n^{Y}C{=}\overset{+}{N}R_2\cdot TCNQ^{\cdot-}$ and $(CH_2)_n^{Y}C{=}\overset{+}{N}R_2\cdot(TCNQ)_2^{\cdot-}$ (n=2, 3; Y=S, Se; R=Me, Et; but not all combinations). Electronic spectra and magnetic properties of these salts also are described in terms of interaction between the $TCNQ^{\cdot-}$ radical anions.

Experimental

Materials. *N,N*-Dimethyl-1,3-dithia- and 1,3-diselenacyclopentan-2-iminium dimethyltin(IV) tribromide, $(CH_2)_2^{Y}C{=}\overset{+}{N}Me_2\cdot Me_2SnBr_3^-$ (Y=S, Se), and bis(*N,N*-dimethyl-1,3-dithiacyclohexan-2-iminium) dimethyltin(IV) tetrabromide, $\left[(CH_2)_3^{S}C{=}\overset{+}{N}Me_2\right]_2\cdot Me_2SnBr_4^{2-}$ were prepared as described in the previous papers.[5-7] The corresponding *N,N*-diethyliminium compounds, $(CH_2)_n^{Y}C{=}\overset{+}{N}Et_2\cdot Me_2SnBr_3^-$, mp 97—99 °C for n=2 and Y=S, 130—132 °C for n=3 and Y=S, and 122—124 °C for n=2 and Y=Se, were similarly synthesized by reaction of bis(diethyldithiocarbamato or diethyldiselenocarbamato)dimethyltin(IV), $Me_2Sn(Y_2CNEt_2)_2$ (Y=S, Se), with 1,2-dibromoethane or 1,3-dibromopropane.

*N,N-Dialkyl-1,3-dichalcogenacycloalkan-2-iminium–TCNQ Simple Salts, $(CH_2)_n^{S}C{=}\overset{+}{N}Me_2\cdot TCNQ^{\cdot-}$ (n=2 (**1**), 3 (**2**)) and $(CH_2)_2^{Se}C{=}\overset{+}{N}R_2\cdot TCNQ^{\cdot-}$ (R=Me (**3**), Et (**4**)).*

To a solution of $Li^+TCNQ^{\cdot-}$ (2.8 mmol) in boiling ethanol (40 cm³) was added a hot ethanol (20 cm³) solution of $(CH_2)_2^{S}C{=}\overset{+}{N}Me_2\cdot Me_2SnBr_3^-$ (2.8 mmol). The mixture was allowed to stand at room temperature, giving purple plates of **1**, which were recrystallized from ethanol, 71% yield. Other three simple salts were similarly prepared by reactions of $TCNQ^{\cdot-}$ with the appropriate iminium cations in ethanol, 60—77% yields.

*N,N-Dimethyl-1,3-dithiacycloalkan-2-iminium–TCNQ Complex Salts, $(CH_2)_n^{S}C{=}\overset{+}{N}Me_2\cdot(TCNQ)_2^{\cdot-}$ (n=2 (**5**), 3 (**6**)).*

To a boiling acetonitrile (50 cm³) solution of **1** obtained above (2.0 mmol) was added neutral TCNQ (2.0 mmol) in boiling

Table 1. Properties and analytical data of the TCNQ$^{\cdot}$ salts

No.	Compound		Mp (dec) °C	Found (%) C	H	N	Calcd (%) C	H	N
1	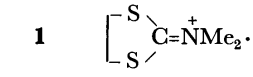	Purple plates	220—223	57.99	3.87	20.05	57.93	4.01	19.87
2	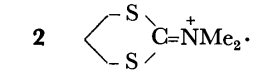	Purple plates	205—209	59.06	4.21	19.09	58.98	4.41	19.11
3	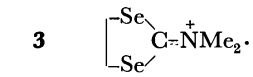	Purple plates	237—239	45.71	2.94	15.75	45.74	3.17	15.70
4	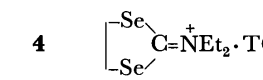	Dark-blue plates	172—175	47.80	3.58	14.76	48.11	3.83	14.77
5	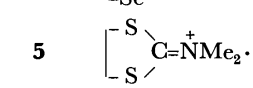	Black needles	245—250	62.55	3.00	22.79	62.56	3.27	22.65
6	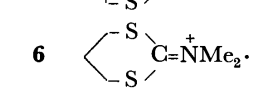	Black needles	227—244	62.67	3.14	22.05	63.13	3.54	22.09
7	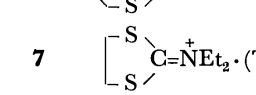	Black needles	240—243	63.80	3.59	21.51	63.68	3.79	21.56
8	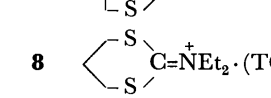	Black needles	217—227	63.98	3.78	21.14	64.18	4.05	21.06
9	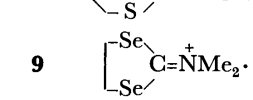	Black needles	278—280	53.35	2.71	19.28	53.55	2.79	19.38
10	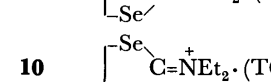	Black needles	198—200	55.00	3.17	18.30	54.88	3.27	18.58

acetonitrile (30 cm^3). After filtration, the mixture was allowed to stand in a refrigerator overnight to afford black needles of **5**, 88% yield. Complex salt **6** was similarly prepared by reaction of **2** with TCNQ at the mole ratio of 1: 1 in acetonitrile, 85% yield.

N,N-*Diethyl-1,3-dithiacycloalkan-2-iminium-TCNQ Complex Salts,* 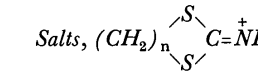 *(n=2 (7), 3 (8)).*

To a boiling ethanol (30 cm^3) solution of Li$^+$TCNQ$^{\cdot}$ (2.2 mmol) was added 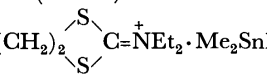 (2.2 mmol) in hot ethanol (20 cm^3). The mixture was allowed to stand in a refrigerator overnight to give black needles of **7**, which were recrystallized from acetonitrile, 62% yield based on Li$^+$TCNQ$^{\cdot}$. A similar reaction of 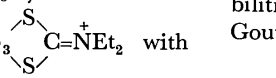 with TCNQ$^{\cdot}$ at the mole ratio of 1: 1 in ethanol afforded **8**, 60% yield based on TCNQ$^{\cdot}$.

N,N-*Dialkyl-1,3-diselenacyclopentan-2-iminium-TCNQ Complex Salts,* 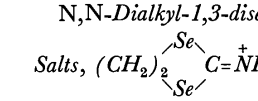 *(R=Me (9), Et (10)).*

These complex salts were prepared by reaction of the appropriate simple salt, **3** or **4** with TCNQ in acetonitrile by the procedure described in **5** and **6**.

Elemental analyses and properties of the simple and complex salts obtained are listed in Table 1.

Physical Measurements. Electrical resistivities were measured by two-probe method in the 20—90 °C range; current measurements were performed with a TOA DEMPA KOGYO PM-18 micro volt-ammeter or a TAKEDA RIKEN-TR-6355 multimeter, and voltage measurements with a NATIONAL VP-653B pen-recorder calibrated by the use of the multimeter. A compaction sample, 20 mm in diameter and about 1 mm thick, for the measurement was prepared by pressing at 270 kg/cm^2, followed by vacuum-evaporating gold metal as electrodes. The resistivities of some complex salts were also measured by four-probe method; the values obtained were very close to those by two-probe method (see Table 2).

Electronic absorption spectra were recorded in Nujol mulls and in acetonitrile (10^{-5} M) on a HITACHI EPS-03 spectrophotometer (3850—16700 cm^{-1}) and a HITACHI 124 spectrophotometer (12500—40000 cm^{-1}). Infrared spectra were measured in hexachlorobutadiene mulls on a HITACHI 215 grating infrared spectrophotometer. Magnetic susceptibilities were measured for micro-crystalline materials by the Gouy method at room temperature.

Results and Discussion

Synthesis. *N,N*-Diethyl-1,3-dithiacycloalkan-2-iminium cations reacted with TCNQ$^{\cdot}$ to give the complex salts, **7** and **8**, whereas the reaction of the remaining iminium cations with TCNQ$^{\cdot}$ afforded the simple salts, **1**—**4**, irrespective of the mole ratio of the reactants. These simple salts further reacted with an equimolar amount of neutral TCNQ to yield the complex salts, **5**, **6**, **9**, and **10**. All the TCNQ$^{\cdot}$ salts obtained here are stable to air in the solid state.

Electrical Properties. Figures 1 and 2 show the electrical resistivity (ρ) of the simple and the complex salts at various temperatures, respectively. The ρ values

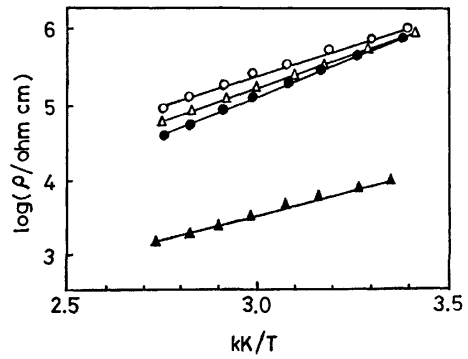

Fig. 1. Temperature dependence of the resistivity of the TCNQ$^{\cdot}$simple salts; **1** (○), **2** (△), **3** (●), and **4** (▲).

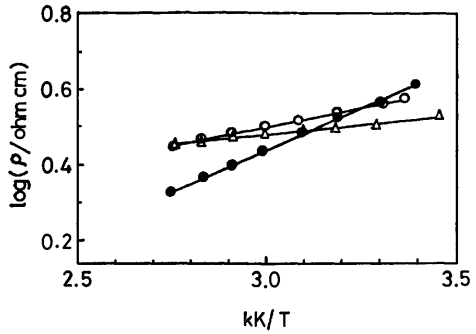

Fig. 2. Temperature dependence of the resistivity of the TCNQ$^{\cdot}$ complex salts; **5** (○), **7** (△), and **9** (●).

Table 2. Electrical resistivity and activation energy of the TCNQ$^{\cdot}$ salts

Compound	$\rho_{25\,°C}$[a] ohm cm	E_a eV
Simple salt		
1	8.7×10^{5}	0.30
2	6.8×10^{5}	0.34
3	6.1×10^{5}	0.37
4	1.1×10^{4}	0.27
Complex salt		
5	3.8	0.041
6	3.5	0.076
7	3.3	0.018
8	2.9(2.6)	0.060
9	4.0(3.4)	0.087
10	2.4	0.046

a) The values in parentheses were obtained by four-probe method.

at 25 °C and the activation energies (E_a) calculated from the equation $\rho=\rho_0\exp(E_a/kT)$ are summarized in Table 2. It is noted that the ρ value of **4** was more than 10 times lower than those of the other simple salts, although the E_a values of the four simple salts were in the same order of magnitude.

The electrical resistivity of TCNQ$^{\cdot}$ complex salts is known to markedly depend on the nature of counter cations. The ρ values of the present complex salts are relatively small compared with those of many TCNQ$^{\cdot}$ complex salts reported so far,[1] but larger by one order of magnitude than that of the highest conductive complex salt with a compaction sample, quinolinium-(TCNQ)$_2^{\cdot}$ (0.5 ohm cm).[1] The E_a values of the complex salts obtained here also are small, in particular that of **7** (0.018 eV) is compared with the activation energy of quinolinium-(TCNQ)$_2^{\cdot}$ (0.013 eV).[1]

Electronic Spectra and Magnetic Properties. An acetonitrile solution of **1** exhibited absorption bands around 12000 and 24000 cm^{-1}. Essentially the same spectra were observed for **2**—**4** in the same solvent, irrespective of the counter iminium cations. The appearance of these spectra also closely resembles that of K$^+$TCNQ$^{\cdot}$[8] and Et$_3$NH$^+$TCNQ$^{\cdot}$[1] in acetonitrile, where they are known to dissociate into monomeric TCNQ$^{\cdot}$ and K$^+$ or Et$_3$NH$^+$.

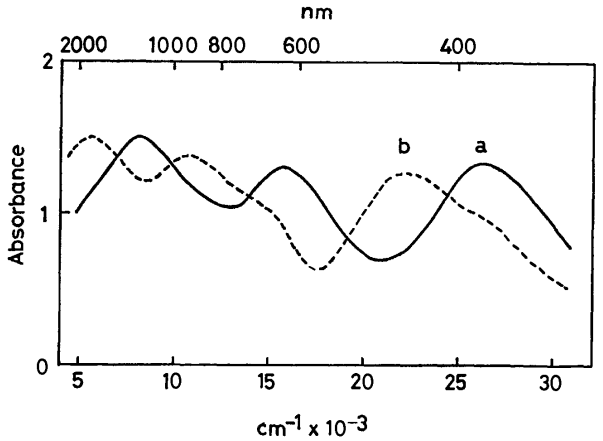

Fig. 3. Absorption spectra of **1** (a) and **4** (b) in Nujol mulls.

Figure 3 illustrates the electronic absorption spectra of two representative simple salts, **1** and **4**, in the solid state. Compound **1** exhibits three absorption maxima, whose wave numbers (see Table 3) are close to those observed in the reflectance spectra of several TCNQ$^{\cdot}$ simple salts such as with Li$^+$, NH$_4^+$, and MePh$_3$P$^+$ (around 9000, 16000, and 27000 cm^{-1}) reported previously; the lowest energy band has been assigned to the charge-transfer (CT) transition between TCNQ$^{\cdot}$ radical anions,[8,9] and the two remaining bands to the (TCNQ)$_2^{2-}$ dimer.[8] The band around 16000 cm^{-1} has also been suggested to be characteristic of the dimer type electron configuration of TCNQ$^{\cdot}$ crystals.[9] It is therefore suggested that **1** consists of the iminium cation and dimeric (TCNQ)$_2^{2-}$ anion in the solid state. The existence of (TCNQ)$_2^{2-}$ is also evidenced from the fact that **1** exhibited a diamagnetic susceptibility of -1.7×10^{-4} emu mol^{-1} at 25 °C, which is in good agreement with the value calculated from Pascal's constants (-1.697×10^{-4} emu mol^{-1}). This diamagnetism indicates that two TCNQ$^{\cdot}$ radical anions may be coupled completely with each other. The same conclusion can be drawn for **2** and **3** on the basis of similarity of their electronic spectra to that of **1**, although the highest energy band of **3** was found at a little low frequency, as shown in Table 3.

The spectrum of **4** in the solid state showed three absorption maxima at 5600, 10800, and 22200 cm^{-1}.

Table 3. Absorption maxima of the electronic spectra of the $TCNQ^{\cdot}$ salts in nujol mulls

Compound	$cm^{-1} \times 10^{-3}$ a)				
1	8.3			15.9	26.3
2	8.3			15.6	27.0
3	8.1			15.2	24.4
4	5.6	10.8		(15)	22.2 (27)
5		10.0	11.4	17	26.7
6		9.9	11.4	17	26.7
7		10.0	11.4	17	27.0
8		9.9	11.2	17	27.0
9		9.9	11.4	17	26.7
10		9.9	11.2	17	27.0

a) Shoulders in parentheses.

The lowest energy band may tentatively be assigned to the CT transition between $TCNQ^{\cdot}$ radical anions, although the wave number is considerably lower than that of **1**—**3** (Fig. 3 and Table 3). On the other hand, the 10800 and 22200 cm^{-1} bands, which are assignable to locally-excited transitions of the $TCNQ^{\cdot}$ moiety, LE_1 and LE_2 respectively,[9] showed no appreciable blue shift compared with the corresponding bands arising from monomeric $TCNQ^{\cdot}$ in acetonitrile. Thus, the absorption spectrum has not revealed the electronic state of $TCNQ^{\cdot}$ in solid **4**. It is, however, noted that the magnetic susceptibility of **4** in the solid state was 1.5×10^{-4} emu mol^{-1} at 25 °C. Such a paramagnetism which is unusual in various simple salts, may be correlated with somewhat higher electrical conductivity of **4** than **1**—**3**.

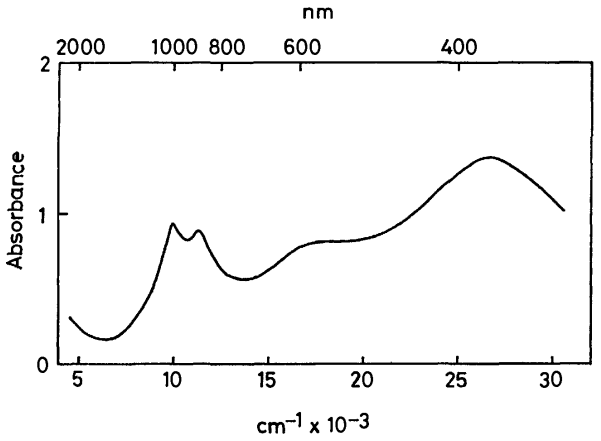

Fig. 4. Absorption spectra of **5** in Nujol mulls.

Complex salt **5** in acetonitrile gave a similar spectrum in appearance to some $TCNQ^{\cdot}$ complex salts, such as with Et_3NH^{+}[1] and $MePh_3P^{+}$,[8] in the same solvent. The solid state spectrum of **5** is illustrated in Fig. 4, which shows three absorption bands around 10000, 17000, and 27000 cm^{-1}. The latter two frequencies are close to those of the two high energy bands observed in solid **1**—**3** (Table 3). The intense absorption around 27000 cm^{-1} may be contributed from both the LE_2 state of $TCNQ^{\cdot}$ and the excited state of neutral TCNQ.[9] The band around 10000 cm^{-1} is due to the $TCNQ^{\cdot}$ monomer, as previously described in the reflectance spectra of some $TCNQ^{\cdot}$ complex salts.[8] More quantitatively, this band is assigned to a transition to the LE_1 state of $TCNQ^{\cdot}$ or the coupled transition of the LE_1 state of $TCNQ^{\cdot}$ and the CT state between $TCNQ^{\cdot}$.[9] The presence of monomeric $TCNQ^{\cdot}$ does not contradict the fact that **5** exhibited a large paramagnetic susceptibility of 6.5×10^{-4} emu mol^{-1} at 25 °C. This magnitude of the paramagnetism is commonly found in many $TCNQ^{\cdot}$ complex salts.[10] Other complex salts **6**—**10** exhibited essentially the same spectra as **5** in the solid state. In addition, all the complex salts displayed a very broad band ranging from 3400 to 2700 cm^{-1}, which was never seen in the spectra of the simple salts. This band is assignable to the charge-transfer transition between $TCNQ^{\cdot}$ and TCNQ.[8] It may therefore be concluded that the interaction between two $TCNQ^{\cdot}$ radical anions in the solid complex salts decreases owing to the implication of neutral TCNQ.

References

1) L. R. Melby, R. J. Harder, W. R. Hertler, W. Mahler, R. E. Benson, and W. E. Mochel, *J. Am. Chem. Soc.*, **84**, 3374 (1962).
2) L. R. Melby, *Can. J. Chem.*, **43**, 1448 (1965).
3) J. Ferraris, D. O. Cowan, V. Walatka, Jr., and J. H. Perlstein, *J. Am. Chem. Soc.*, **95**, 948 (1973); L. B. Coleman, M. J. Cohen, D. J. Sandman, F. G. Yamagishi, A. F. Garito, and A. J. Heeger, *Solid State Commun.*, **12**, 1125 (1973); M. J. Cohen, L. B. Coleman, A. F. Garito, and A. J. Heeger, *Phys. Rev. B*, **10**, 1298 (1974); T. E. Phillips, T. J. Kistenmacher, J. P. Ferraris, and D. O. Cowan, *J. Chem. Soc., Chem. Commun.*, **1973**, 471; A. N. Bloch, D. O. Cowan, K. Bechgaard, R. E. Pyle, R. H. Banks, and T. O. Poehler, *Phys. Rev. Lett.*, **34**, 1561 (1975); R. C. Wheland and J. L. Gillson, *J. Am. Chem. Soc.*, **98**, 3916 (1976).
4) A. F. Garito and A. J. Heeger, *Acc. Chem. Res.*, **7**, 232 (1974).
5) T. Tanaka and T. Abe, *Inorg. Nucl. Chem. Lett.*, **4**, 569 (1968).
6) T. Tanaka, K. Tanaka, and T. Yoshimitsu, *Bull. Chem. Soc. Jpn.*, **44**, 112 (1971).
7) K. Tanaka and T. Tanaka, *Bull. Chem. Soc. Jpn.*, **45**, 489 (1972).
8) Y. Iida, *Bull. Chem. Soc. Jpn.*, **42**, 71, 637 (1969).
9) J. Tanaka, M. Tanaka, T. Kawai, T. Takabe, and O. Maki, *Bull. Chem. Soc. Jpn.*, **49**, 2358 (1976).
10) R. G. Kepler, *J. Chem. Phys.*, **39**, 3528 (1963).

The Construction of an Energy-dispersive X-Ray Diffractometer for Liquids and Its Application to CCl_4

Yoshitada MURATA* and Keiko NISHIKAWA

Department of Chemistry, Faculty of Science, Gakushuin University, Mejiro, Toshima-ku, Tokyo 171

(Received July 15, 1977)

An energy-dispersive X-ray diffractometer using a solid-state detector is constructed for the determination of the liquid structure. It has two merits over the usual angle-dispersive diffractometer, *i.e.*, a higher resolution of the s-value and a wider measurable s-region. The procedure of the data analysis and the results for liquid CCl_4 are described. The absorption correction is important in the reflection method. By taking advantage of the energy-dispersive method, it is shown that liquid CCl_4 has a long-range correlation at room temperature.

The intensity measurement of X-rays by using a solid-state detector (SSD), since it was introduced by Giessen and Gordon,[1] has been used in various experiments on X-ray scattering, for example, the Compton profile,[2] diffractometry for a single crystal[3] or for a powdered sample,[4] and the determination of the anomalous scattering factor at energies near the absorption edge.[5] However, the X-ray diffraction of liquids has scarcely been studied by means of the energy-dispersive method with the SSD.[6]

The energy-dispersive method in X-ray diffraction is carried out by using white X-rays as the primary beam and the SSD for the energy analysis of the scattered X-rays. In other words, a parameter in the diffraction of a liquid, $s=4\pi \sin\theta/\lambda$ (λ: wavelength, 2θ: scattering angle), *i.e.* the scattering vector, is determined mainly by measuring λ, while only θ is changed in the traditional angle-dispersive method.

Energy-dispersive diffractometry has the following merits in comparison with the angle-dispersive one:

(1) A higher resolution of the s-value can be obtained. The resolution of the s-value is determined by two factors, as is shown by the following relation;

$$\Delta s/s = \Delta E/E + \cot\theta \cdot \Delta\theta. \quad (1)$$

The first term on the right side of Eq. 1 indicates the energy resolution, which is determined by that of the SSD and which varies with the energy.[7] The second term, the angular resolution, is determined by the beam divergence in a collimator system. A small beam divergence is achieved without increasing the time of measurement, since the integrated intensity of the white X-ray radiations is much stronger than that of a characteristic X-ray radiation. Though the diffraction pattern of a liquid forms diffuse halos, a high resolution of the s-value is essential if we are to investigate the presence of a long-range correlation.

(2) The fluctuation in the primary beam intensity does not influence the scattering intensity, since scattered photons corresponding to the various s-values are collected simultaneously. This is effective in getting relative-intensity curves with high precision.

(3) It is possible to expand the observable region of the s-values. This diminishes the termination error in the Fourier transformation, since the diffraction intensities can be measured from small to large s-values.

(4) The design of the diffractometer is simple, because no scanning mechanism is necessary. Accessories such as sample holders for high and low temperatures can be mounted easily.

A vertical goniometer is adopted in the present experiment instead of the usual horizontal one, though this selection is not necessarily related to energy-dispersive diffractometry. In the horizontal goniometer, the free surface of a liquid is measured and an X-ray tube and a detector are moved simultaneously on the vertical plane. On the other hand, in the vertical goniometer an X-ray tube or a detector travels on the horizontal plane around the sample; hence, the mechanism of the apparatus is simplified. In addition, the vertical goniometer system makes it possible to measure both reflection and transmission intensities. This expands the measurable region of s, especially to very small s-values.

However, there are some demerits and difficulties in the energy-dispersive method:

(1) When a liquid specimen includes such elements as heavy metal ions, the fluorescent X-ray emissions disturb the intensity curve.

(2) The absorption and Compton corrections may introduce a significant error.

(3) The intensity curves obtained at different scattering angles must be connected adequately.

The difficulties arising from (2) and (3) were resolved as will be described below.

The present paper will describe the construction of an energy-dispersive diffractometer for liquids. The procedure of the data analysis applied to liquid CCl_4 at room temperature will also be described.

Construction of the Apparatus

The experimental arrangement is shown in Fig. 1.

Goniometer. An X-ray tube can be rotated around the vertical axis of a goniometer, which has a θ-2θ scanning system. An SSD with a heavy cryostat is fixed. The movable range of the tube is from -20 to $100°$ in 2θ. When the white X-ray radiations from a tungsten tube are used at the target voltage of 45 kV, the scattering intensity is obtained over the range from $s=0.15$ to $30\ \text{Å}^{-1}$.

X-Ray Source. A fine-focus Phillips tube with a tungsten target is used, because strong white X-rays can be obtained without any disturbance by characteristic X-rays. Although radiations from the tungsten

* Present address: The Institute for Solid State Physics, The University of Tokyo, Roppongi, Minato-ku, Tokyo 106.

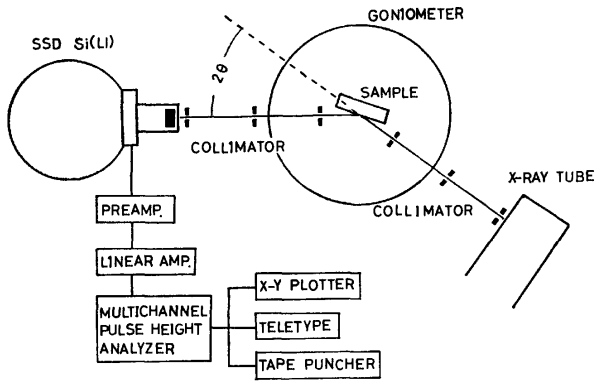

Fig. 1. Shematic diagram of the experimental apparatus. The arrangement for the reflection method is shown.

tube have the L radiations in the 8—11 keV region (λ=1.2—1.4 Å), as shown in Fig. 5, they do not disturb the present measurements. A high-voltage power supply for X-rays of the Rigaku Denki Co. was used. The stability of the high voltage is better than 0.1%. The X-ray tube was usually operated at 45 kV and 20 mA. However, in the energy-dispersive method it is necessary to measure the spectrum of the incident beam by means of the voltage and collimating system used for the measurement of the intensity scattered from the sample. Since the 20 mA beam is too strong for the direct-beam measurement, we modified the power supply system so as to operate it in the microampere region.

Detecting System. The scattered X-rays were analyzed by means of a Si(Li) detector made by the JEOL Co., Tokyo. The energy resolution of the detector ΔE is 200 eV FWHM at 21.99 keV (Ag $K\alpha_2$), and $\Delta E/E$ is less than 1% in the energy region used in this apparatus (E=12—32 keV). It is connected to a linear amplifier (NAIG D-130) and a multichannel pulse-height analyzer (MCA) with 1024 channels (Canberra Model 8100). The gain of the linear amplifier was set so that the energy width per channel of the MCA was about 40 eV.

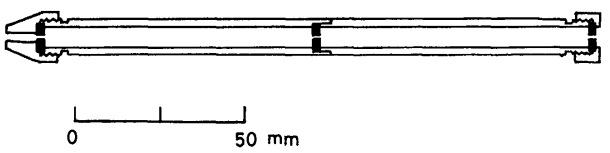

Fig. 2. Collimator. It is 180 mm long and has three apertures with diameter of 1 or 2 mm. Apertures are made of W or Pb.

Collimator. The resolution in the s-value is determined by two factors, as shown by Eq. 1. The second term of Eq. 1, in which $\Delta\theta$ is the beam divergence, is determined by the design of the collimator system. In this respect it is desirable to use a collimator of an appreciable length and a small diameter. However, this induces a decrease in the X-ray intensities. An optimum condition was realized by keeping the first term in Eq. 1 a little smaller than the second term. We made a couple of collimators 180 mm in length and 1 or 2 mm in diameter, as is shown in Fig. 2. Three stages of collimating apertures were effective in getting a well-collimated X-ray beam. If two stages of collimating apertures are used for the measurement; not only is the beam divergence increased, but also a significant error is introduced into the absorption correction in the reflection method, as will be described later. In this system, $\Delta\theta$ is 0.3 or 0.6°. The latter value, 0.6°, is used only at large scattering angles, which correspond to small $\cot\theta$ values.

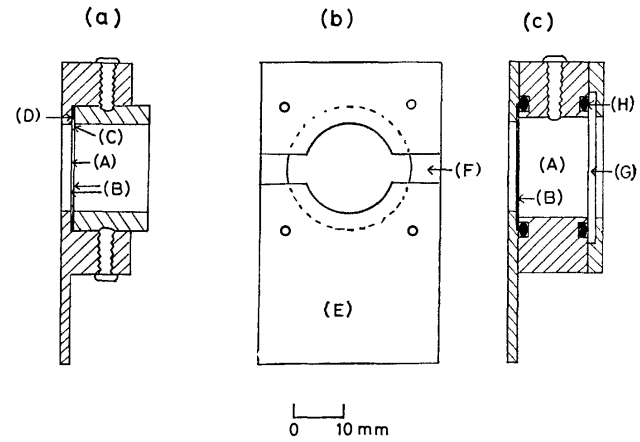

Fig. 3. Sample holder (a) for the transmission method and (b), (c) for the reflection method. (A) sample, (B) Myler film or Be plate, (C) stainless steel ring to determine the thickness of sample (0.5 mm in thickness), (D) rubber ring to seal, (E) stainless steel plate to set the holder to the goniometer, (F) ditch to expand the observable region of the scattering angle, (G) glass plate, (H) O-ring.

Sample Holder. The sample holders are shown in Fig. 3. Figure 3(a) illustrates a sample holder for the transmission method, which is used for the measurements at small scattering angles. Myler films (20 μm thick) or Be thin plates (0.2 mm thick) were used for the window of the sample holder. The window was sealed with epoxide resin, which is not insoluble in the CCl_4 sample. For other organic liquid samples, the window was made by welding the Be plate with a Cu block by diffusion bonding in a vacuum oven. A sample holder for the reflection method is shown in Figs. 3(b) and (c).

Measurements of CCl_4

Carbon tetrachloride is one of the simplest molecules which are liquid at room temperature, and so it has been studied well.[8-11] Therefore, it was selected as a suitable sample for the first experiment with this apparatus. The carbon tetrachloride molecule has a nearly spherical electron cloud and has no heavy atoms to disturb the energy distribution curve by fluorescent X-rays in the energy-dispersive measurements.

In order to obtain the relation of the energy *vs.* the channel number in the MCA, the fluorescent X-rays from Ba, Ag, Mo, and Cu were measured. The results are shown in Fig. 4. The channel numbers of these peaks in the MCA were fitted to the energies of the

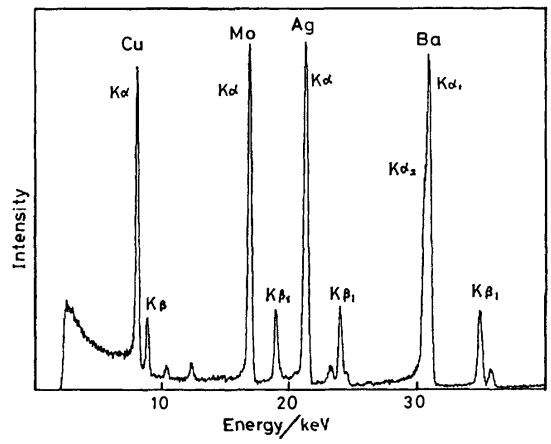

Fig. 4. A spectrum of the fluorescent X-rays from several targets for the calibration of the energy scale in the MCA.

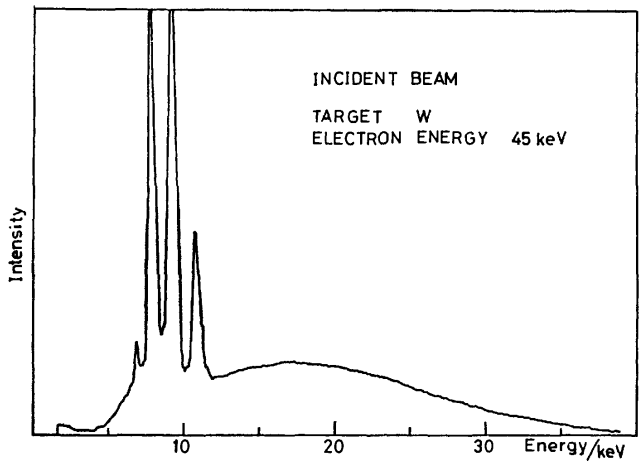

Fig. 5. A tungsten spectrum for the incident white X-rays. The X-ray source was operated at 45 kV and 10 μA.

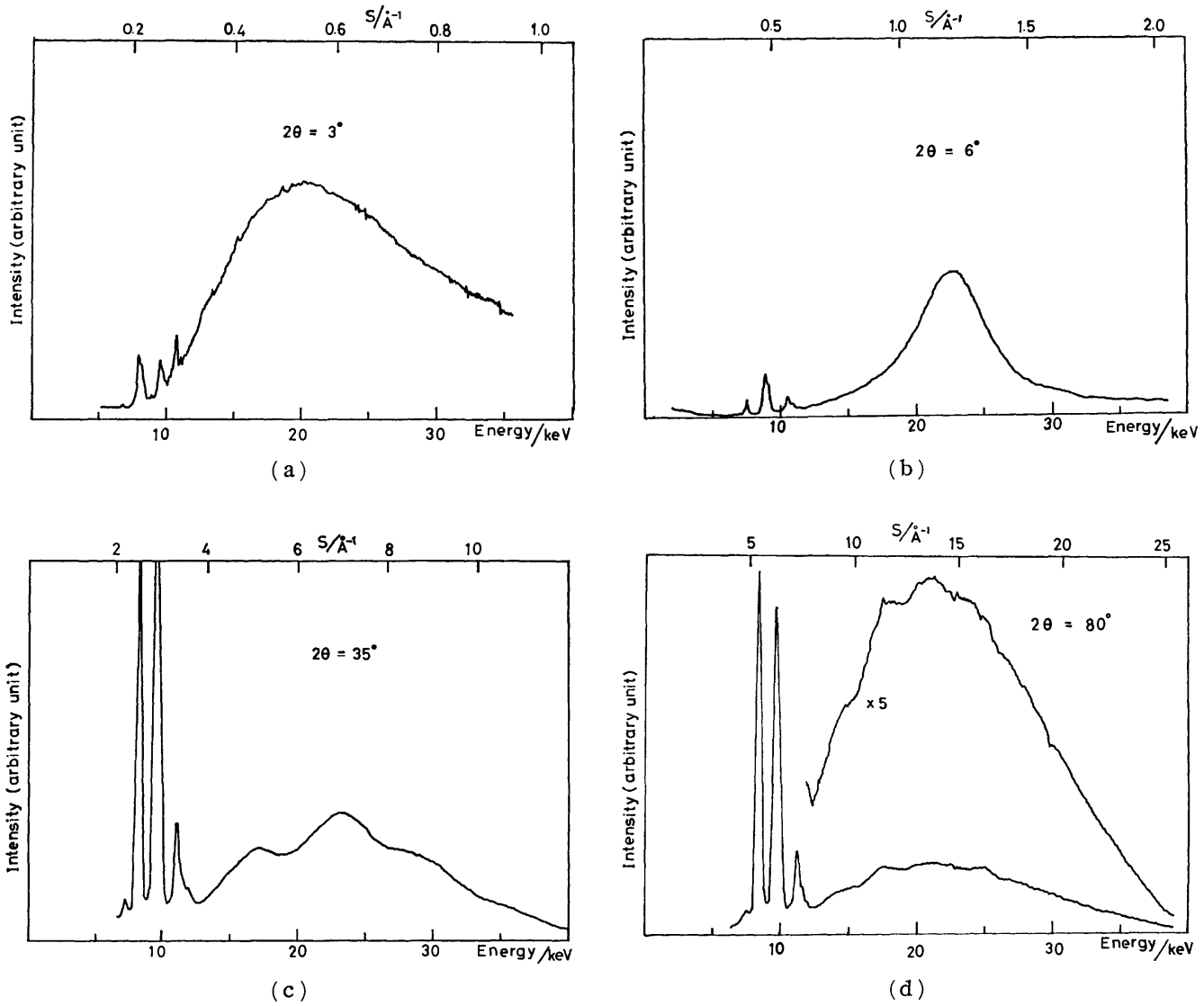

Fig. 6. Scattered intensities from liquid CCl_4 at room temperature. (a) $2\theta=3°$, (b) $2\theta=6°$, (c) $2\theta=35°$, (d) $2\theta=80°$; (a), (b) transmission method, (c), (d) reflection method.

corresponding characteristic X-ray radiations by using a table by Bearden.[12] Since the doublets of Cu $K\alpha$, Mo $K\alpha$, and Ag $K\alpha$ can not be separated by the SSD, the weighted mean energy of $K\alpha_1$ and $K\alpha_2$ was used. The radiations of $K\alpha_1$, $K\beta_1$ in Ba and $K\beta_1$ in Mo and Ag were also used for the calibration. A linear relation between the energy and the channel number was obtained.

The observed energy distribution curve of the incident beam is shown in Fig. 5. This spectrum was obtained from the tungsten target operated at 45 kV and 10 μA.

X-Rays scattered from liquid CCl_4 were collected at the scattering angles of $2\theta=1.5$, 3, 6, 18, 35, 56, and 80°. The specimen was held at room temperature. The data for $2\theta=1.5$, 3, 6, and 18° were measured by means of the transmission method. The reflection method was applied to $2\theta=35$, 56, and 80°. The setting of $2\theta=1.5$, 3, 6, 18, 35, 56, and 80° made it possible to measure $s=0.15$—0.41, 0.30—0.83, 0.56—1.86, 1.75—4.91, 3.78—9.45, 5.90—14.8, and 8.08—23.0 Å^{-1} respectively. The measuring time at each scattering angle was $5\times10^4-10^5$ s, and more than 4000 counts per channel were obtained. The diffraction patterns collected in the MCA are shown in Fig. 6. The $s=0.30$—0.82 Å^{-1} region, $2\theta=3°$, is shown in Fig. 6(a), where no halo due to interference between atoms appears. In Fig. 6(b), $2\theta=6°$, the peak at $s=1.2$ Å^{-1} indicates the first halo due to interference. Figures 6(c) and (d) show the diffraction patterns obtained at $2\theta=$ 35 and 80° respectively; we can see several halos whose amplitudes gradually decrease as the s-value increases.

The scattering from the Myler film or the Be thin plate of the window of the sample holder was also measured. This curve was denoted as I_w. The magnitude of I_w was about 5% of the total scattering intensity from liquid CCl_4.

Data Analysis

Smoothing and Normalization. Smoothing was done by adding the counts collected in each group of five channels, because the resolution of the SSD is about 200 eV and the linear amplifier was so set that the energy width for each channel in the MCA was about 40 eV. The counts at each point after smoothing were more than 2×10^4, which were sufficient to diminish the statistical random error. Each scattering intensity from which the intensity, I_w, was subtracted was divided by the energy distribution curve of the incident beam (normalization).

Absorption Correction. The most important correction in energy-dispersive diffractometry of liquids is the absorption correction, because the linear absorption coefficient, μ, changes with the energy of the X-rays and the effect of the path length in scattering must also be taken into account.

We checked whether or not the calculated values of μ agreed with the observed ones. The value of μ was calculated as follows

$$\mu/\rho = \tau + \sigma, \tag{2}$$

where ρ is the density of the liquid, τ is the photo-electric absorption and σ is the absorption due to the Compton effect. The empirical relation of τ is given by

$$\tau = C\lambda^3 - D\lambda^4, \tag{3}$$

where λ is the X-ray wavelength in Å and where C and D are constants characteristic of atoms. These constants are tabulated in the International Tables. The C's for carbon and chlorine are 1.22 and 33.4 respectively, and the D's are 0.0142 and 3.03 respectively.[13] The absorption due to the Compton effect was given by Klein and Nishina[14] as

$$\sigma = \frac{2\pi e^4}{m^2c^4}\left[\frac{1+\alpha}{\alpha^2}\left\{\frac{2(1+\alpha)}{1+2\alpha}-\frac{1}{\alpha}\ln(1+2\alpha)\right\}+\frac{1}{2\alpha}\ln(1+2\alpha)-\frac{1+3\alpha}{(1+2\alpha)^2}\right], \tag{4}$$

where $\alpha=h/mc\lambda$ and m is the electron rest mass.

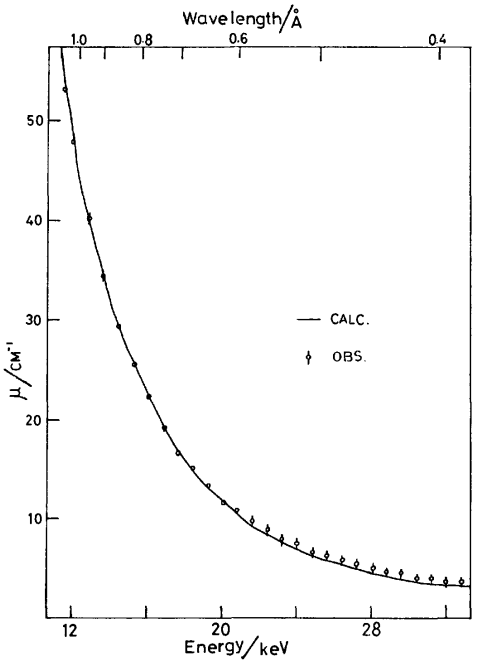

Fig. 7. Calculated and observed linear absorption coefficient, μ, of liquid CCl_4.

The observed values of μ were measured from the trasmittance of the sample at $\theta=0°$. The observed and calculated values are shown in Fig. 7. A good agreement was obtained except in the high-energy region, where the latter values are somewhat smaller than the former. The observed values were used for the data analysis.

The path length in the case of the transmission method can be estimated easily as shown in Fig. 8(a), because the θ-2θ scanning system has been used in this experiment. The path length is given by $t\cdot\sec\theta$, where t is the thickness of the sample. The absorbed intensity, I', is given by

$$I' = I\exp(-\mu t\sec\theta), \tag{5}$$

where I is the intensity without absorption.

In the reflection method, the absorption correction is complicated, because the path length differs depending on the position at which the X-ray is scattered, as shown in Fig. 8(b). The absorbed intensity in the

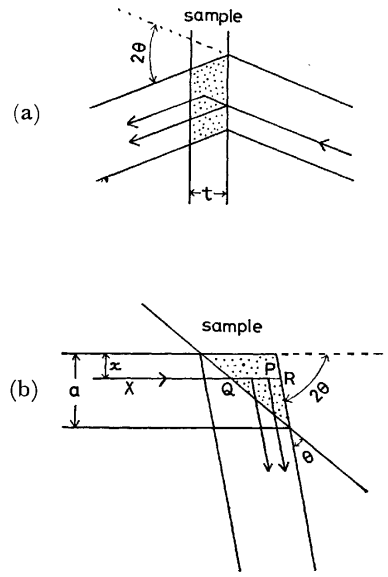

Fig. 8. Path length for the absorption correction. (a) Transmission method. The path length is always t sec θ wherever X-rays are scattered. (b) Reflection method. The path length depends on the position where X-rays are scattered. The X-rays scattered in the dotted area reach the detector.

reflection method is given by

$$I' = I\frac{a^2}{4\mu}\left[\frac{\pi}{2}-\int_{\pi/2}^{3\pi/2}\cos^2\phi\,\exp\{-\mu a(1+\sin\phi)/\sin 2\theta\}\mathrm{d}\phi\right], \quad (6)^{**}$$

where a is the beam diameter on the sample. The derivation of this equation is given in the Appendix.

For the absorption correction, it is important to estimate the effective value of the beam diameter on the sample. A criterion for the estimation of the effective beam diameter is that the background intensity for the observed intensity curve after the Compton correction is proportional to the calculated curve of $\sum_n f_n(s)^2$, where $f_n(s)$ is the atomic scattering factor for a component atom, n, of the molecule. The background intensity means a monotonically decreasing curve corresponding to $\sum_n f_n(s)^2$. The effective beam diameter was 1.2 times as large as the diameter of the aperture at $2\theta=35°$ and grew a little larger as the scattering angle increased. The presence of multiple scattering is probably the reason for the dependence of the effective diameter on the scattering angles. In this apparatus, each collimator has three stages of apertures, as shown in Fig. 2. When each collimator has only two apertures, the effective value of the beam diameter can not be obtained. Figure 9 indicates the importance of the estimation of the effective value of the beam diameter by showing three curves of I'/a^2I in Fig. 6. Curve (a) in Fig. 9 shows the contribution from the first term in the brackets. This is the usual absorption correction in the reflection method for a strong absorption case, in which

** The reflection from the wall of the sample holder is ignored in Eq. 6. This is justified in the present experiment.

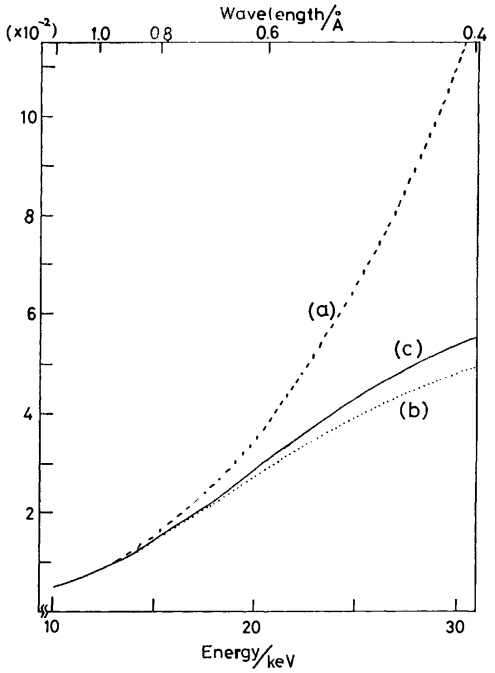

Fig. 9. Curve (a) (broken line) denotes $\pi/8\mu$. Curves (b) (dotted line) and (c) (full line) are

$$\frac{1}{4\mu}\left[\frac{\pi}{2}-\int_{\pi/2}^{3\pi/2}\cos^2\phi\cdot\exp\{-\mu a(1+\sin\phi)/\sin 2\theta\}\mathrm{d}\phi\right]$$

where a is 1.0 mm in (b) and 1.2 mm in (c).

a is much larger than μ^{-1}. Curve (b) shows the result for $a=1$ mm, in which a agrees with the diameter of the apertures. Curve (c) is calculated using the effective beam diameter on the sample in which $a=1.2$ mm. We can recognize from Fig. 9 that the second term in the brackets of Eq. 6 is important for the absorption correction. The second term becomes more significant as the X-ray energy increases (*i.e.* μ decreases) and as a decreases. Therefore, this correction is characteristic of this energy-dispersive method. The curvature of these curves influences the background intensity of the observed intensity curve.

Compton Correction and Absorption Intensity. The scattered intensity, $I(s)$, after the absorption correction is given by

$$I(s) = K[\sum_n f_n(s)^2 + i_1(s) + i_2(s) + kI_C I_0(\lambda)/I_0(\lambda')], \quad (7)$$

where I_C is the intensity of the Compton scattering, k is the recoil factor, and K is the conversion factor from the experimental to absolute intensity (in electron units). $I_0(\lambda)$ and $I_0(\lambda')$ are the intensities of the incident beam at the wavelengths of λ and λ' respectively, and $\lambda'-\lambda$, the Compton shift, is given by $(h/mc)(1-\cos 2\theta)$. The first term in Eq. 7 represents the scattering from individual atoms. The second term is called the molecular term, which is the interference from each atom pair within a molecule. The third term represents the interference from atom pairs between different molecules.

The molecular term for CCl_4 is represented by

$$i_1(s) = 8f_C f_{Cl}\frac{\sin sr_{C-Cl}}{sr_{C-Cl}}\exp\left(-\frac{l^2_{C-Cl}s^2}{2}\right) + 12f^2_{Cl}\frac{\sin sr_{Cl-Cl}}{sr_{Cl-Cl}}\exp\left(-\frac{l^2_{Cl-Cl}s^2}{2}\right), \quad (8)$$

where l_{ij} denotes the root mean-square amplitude due to the vibration of the atom pair around the mean internuclear distance, r_{ij}. Since $i_2(s)$ vanishes at large s-values, the absolute intensities are obtained by adjusting the experimental intensities to the calculated intensities, which are obtained by adding the first, second, and fourth terms of Eq. 7 at large s-values. In the calculation, the r_{C-Cl}, r_{Cl-Cl}, l_{C-Cl}, and l_{Cl-Cl} values obtained by gas electron diffraction of CCl_4[15] were used and the intensities of the Compton scattering calculated by Cromer[16] were employed.

The conversion factor from the experimental to absolute intensity, K, were easily obtained for $2\theta=35$, 56, and 80°; the agreement of the intensity curves in the overlapping region was good. In the cases of $2\theta=$ 1.5, 3, 6, and 18°, an approximation of $i_2(s)=0$ is not so good. Accordingly, each intensity curve was successively connected with that of $2\theta=35°$ after the absorption correction. Then, K was obtained for each intensity curve.

The total coherent intensity

$$I_{co}(s) = \sum_n f_n(s)^2 + i_1(s) + i_2(s), \quad (9)$$

was obtained by subtracting the fourth term in $I(s)/K$ of Eq. 7. The Compton correction was carried out by using the calculated values reported by Cromer.[16] Figure 10 shows the observed coherent intensity of liquid CCl_4 at room temperature, together with the calculated value corresponding to independent atoms of carbon tetrachloride, $\sum_n f_n(s)^2$.

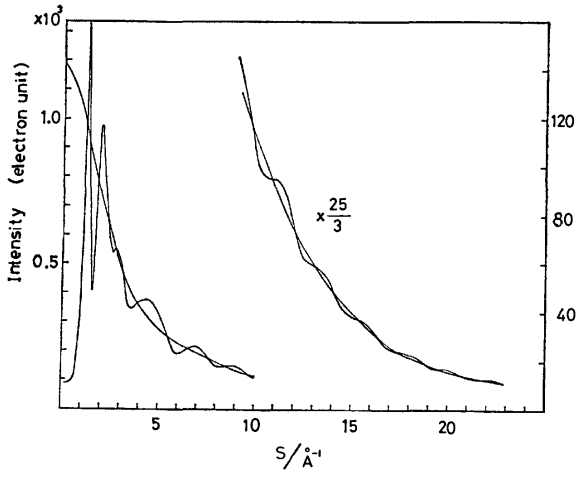

Fig. 10. Observed total coherent intensity I_{co} for liquid CCl_4 at room temperature and calculated one assuming that atoms in CCl_4 are independent.

The weighted structure function, $si(s)$, of liquid CCl_4 is shown in Fig. 11, where $i(s)=i_1(s)+i_2(s)$ is the reduced intensity. An electronic pair correlation function, $g_e(r)$, was defined by the Fourier transformation of $si(s)$;

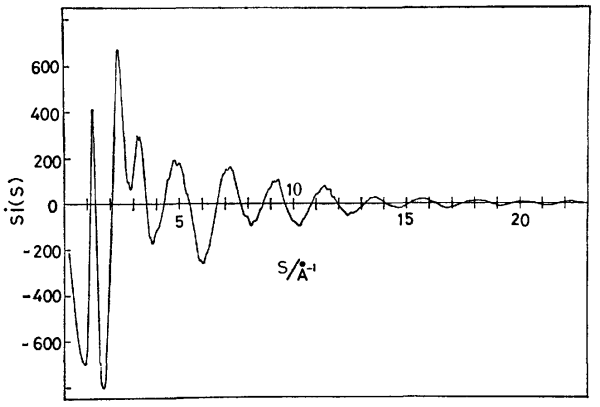

Fig. 11. Weighted structure function $si(s)$ for liquid CCl_4 at room temperature.

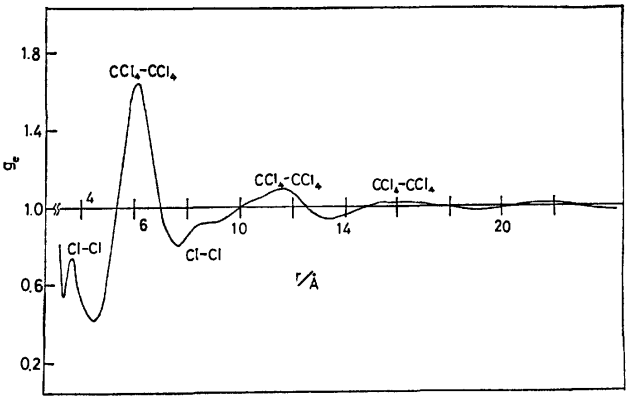

Fig. 12. Electronic pair correlation function $g_e(r)$ for liquid CCl_4 at room temperature.

$$g_e(r) = \frac{1}{2\pi^2 r\rho_0\sum_n Z_n^2}\sum_{s=0}^{s_{max}} si(s)\sin sr\cdot\Delta s + 1, \quad (10)$$

where ρ_0 is the bulk liquid density and Z_n is the atomic number of a component atom n (Fig. 12). In the transformation, only the observed values of $si(s)$ were used throughout the whole region except for $s=0.05$ and 0.10, at which $si(s)$ were extrapolated. This extrapolation can not cause any significant error, since I_{co}'s have a constant value at these positions, as shown in Fig. 10. The $\Delta s=0.05$ Å^{-1} interval and $s_{max}=23.0$ Å^{-1} were used. This range of s is sufficient to eliminate the termination error for Fourier transformation.

The electronic pair correlation function calculated from Eq. 10 is different from the usual pair correlation function, which corresponds to the distribution of the nucleus. The former expresses the distribution of the electron, since, in the present paper, $i(s)$ is $\sum_{i\neq j} f_i f_j(\sin sr/sr)\exp(-l_{ij}^2 s^2/2)$. Therefore, the mean square amplitude obtained directly from Fig. 12 includes the effect of the distribution of the electron cloud. If we try to obtain the usual pair correlation function, $g(r)$, by multiplying $(\sum_n f_n(s)^2)^{-1}$, which is a convenient factor to change from the electron density to the nuclear density, some errors may be introduced by the correction.

Results and Discussion

Figure 12 shows that liquid CCl_4 at room temperature

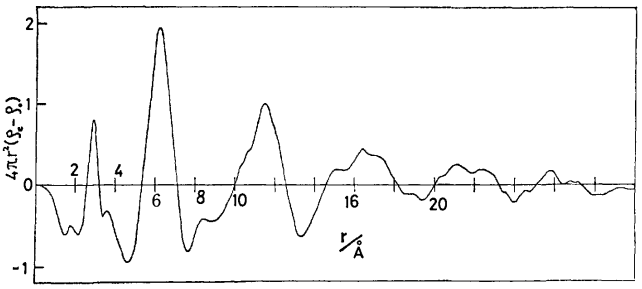

Fig. 13. Electronic radial distribution function from which the bulk density was subtracted, $4\pi r^2(\rho_e-\rho_0)$.

has a long-range correlation. In order to see it more clearly, the electron radial distribution function from which the bulk density was subtracted, $4\pi r^2(\rho_e-\rho_0)$, is shown in Fig. 13. The peak at 6.3 Å corresponds to the first nearest neighbor molecules, while the three other peaks, appearing at 11.4, 16.3, and 21.5 Å, are due to interference between molecules. The interference with the fourth nearest neighbor molecules has a distinct peak in the radial distribution function.

Though information on the long-range order in the liquid is confined mainly to the $s\lesssim 2$ region of the weighted structure function, it is clearly recognized elsewhere. Figure 11 shows that the intensity curve has a fine structure with a short periodicity at small s-values.*** The fine structure near the top and bottom of the halos, such as those at $s=3.2$ and 4.7 Å^{-1}, was reproducible not only in repeated measurements but also in measurements at different scattering angles. The periodicity in this fine structure was 0.2—0.3 Å^{-1}, which was larger than the estimated resolution in the s-value ($\Delta s=0.14$ Å^{-1} at these s-values) in the present experiment. The difference between the collected counts of the top and the bottom of these small waves was about 500 counts, more than the statistical radom error ($\sqrt{n}=170$; $n=3\times10^4$). In the energy-dispersive method, the scattered intensity is scarcely influenced by the fluctuation in the incident-beam intensity. Therefore, the statistical random error given by the square root of the total counts at each position is the main origin of the noise. Though attention has not yet been paid to this fine structure in the liquid structure analysis, the fine structure may indicate that CCl_4 in the liquid phase at room temperature has a long-range order.

The scattering intensities at small s-values contain information about the density fluctuation. The decrease in the total coherent intensity near $s=0$ shown in Fig. 10 is due to the intermolecular correlation. The fluctuation in the number density of a liquid can be estimated from the absolute value of the total coherent intensity at $s=0$, which is obtained by extrapolating the observed intensities. A constant value in the intensity, I_{co}, was obtained at small s-values, as shown in Fig. 10, so that the extrapolation to $s=0$ is easy. According to liquid theory,[17,18] the mean square of the fluctuation in the number density is given by

$$\langle(N_v-\langle N_v\rangle)^2\rangle = \langle N_v\rangle I_{co}(0)/(\sum_n Z_n)^2, \qquad (11)\dagger$$

where N_v is the number of molecules in a small volume v, $\langle N_v\rangle$ means the average value of N_v, $I_{co}(0)$ is the total coherent intensity at $s=0$ in electron units (e.u.), and Z_n is the atomic number. As shown in Fig. 10, $I_{co}(0)$ equals 87 e.u. Hence, $\langle(N_v-\langle N_v\rangle)^2\rangle$ was $9.9_5\times10^{-5}v$ in Å units. This means that $\langle(N_v-\langle N_v\rangle)^2\rangle$ becomes unity when v is 1.00×10^4 Å^3, in which there are 63 molecules, on the average. In other words, there are 63 ± 1 molecules in 1.00×10^4 Å^3 and 252 ± 2 molecules in 4.00×10^4 Å^3. Of cource, this estimation includes some error because the absolute intensity at small s-values was not measured directly, but obtained successively from that observed at $2\theta=35°$. This value is, though, in good agreement with the compressibility of liquid CCl_4 $\kappa=10.34\times10^{-11}$ cm^2 dyn^{-1} (at 20 °C).[19] The details of the results for liquid CCl_4 including the temperature dependence will be reported elsewhere.[20]

Finally, let us compare this apparatus with a usual angle-dispersive diffractometer.[21] The resolution in the s-value is given by Eq. 1. The first term of Eq. 1, $\Delta E/E$ (≈0.01), in this apparatus is much larger than that in the usual one. On the other hand, the $\Delta s/s$ in the usual apparatus is at least twice as large as that in the present one, because $\cot\theta\cdot\Delta\theta\lesssim0.01$ over the range from $s=1.5$ to 30 Å^{-1} in this apparatus, since the collimating system is so designed that the beam divergence, $\Delta\theta$, is 0.3 or 0.6°, in contrast to the usual 2—4°. This difference in $\Delta s/s$ is significant, because the periodicities of the fine structures observed in the scattering intensity value, $si(s)$, $\Delta s=0.2$—0.3 Å^{-1}, are about twice as large as the resolution of this apparatus. Moreover, these fine structures are hardly influenced at all by the intensity fluctuation of the primary beam in the present experimental method.

Diffraction intensities can be obtained over the range from $s=0.15$ to 30 Å^{-1} in the present apparatus by using white X-rays. On the contrary, the intensities in the usual apparatus are taken s-values from 0.4 to 16 Å^{-1}, in which the scattering angle, 2θ, is varied from 4 to 140° if Mo $K\alpha$ ($\lambda=0.7107$ Å) is used. Therefore, the electronic radial distribution function without the termination error in Fourier transformation can be obtained with the present apparatus by using only the observed intensities.

The total time required for collecting the data with this apparatus is comparable to that with the usual one. Nevertheless, a higher resolution in s-value and a wider region of observable intensity can be obtained with this apparatus.

The authors wish to express their thanks to Dr. Teruo Nomura, Rikkyo University, for his collaboration, and

*** The fine structure at large s-values is random noise, because the ratio of the reduced intensity $i(s)$ to the total scattering intensity is small.

† In the above discussions, we have done the calculations considering the atomic distribution, but in the estimation of the density fluctuation we must consider the molecular distribution by taking $(\sum_n Z_n)^2$ instead of $(\sum_n Z_n^2)$ as the denominator.

to Dr. Tomoe Fukamachi and Prof. Sukeaki Hosoya, The Institute for Solid State Physics, for their discussion and for allowing us to do our preliminary experiments in their laboratory. We also would like to thank Prof. Kozo Kuchitsu, The University of Tokyo, for permission to use a computer program for gas electron diffraction and Messrs. Kyozuka, Kimura, Kato, and Yamada, JEOL Co., for making the detector. Thanks are also due to Dr. Masahiro Kotani of Gakushuin University for reading the manuscript. The present work was partially supported by Grants-in-Aid for Scientific Research and a Grant-in-Aid for Developmental Scientific Research from the Ministry of Education.

Appendix

The derivation of Eq. 6 is as follows. In Fig. 8(b), when the beam, X, is scattered at the point P, the contribution of absorption becomes $\exp(-2\mu\overline{PQ})$, where $\overline{PQ}$ means the distance between P and Q. Because P can change from the point Q to R in the case of the X beam, the possible range of $\overline{PQ}$ becomes from 0 to $(a-x)/\sin 2\theta$, where x is as is shown in Fig. 8(b) and varies from 0 to a. The total contribution of absorption in the X beam is given by

$$A_x = \int_0^{(a-x)/\sin 2\theta} \exp(-2\mu y)\mathrm{d}y$$
$$= \{1-\exp(-2\mu(a-x)/\sin 2\theta)\}/2\mu.$$

The absorption correction for incident and scattered parallel beams, the diameters of which are equal to a, is given by

$$A_{\text{total}} = \int_0^a 2\sqrt{\left(\frac{a}{2}\right)^2-\left(\frac{a}{2}-x\right)^2}A_x\mathrm{d}x.$$

If we put $1-2x/a=\sin\phi$, we get

$$A_{\text{total}} = \frac{a^2}{4\mu}\int_{\pi/2}^{3\pi/2}\cos^2\phi\,[1-\exp\{-\mu a(1+\sin\phi)/\sin 2\theta\}]\mathrm{d}\phi$$
$$= \frac{a^2}{4\mu}\left[\frac{\pi}{2}-\int_{\pi/2}^{3\pi/2}\cos^2\phi\,\exp\{-\mu a(1+\sin\phi)/\sin 2\theta\}\mathrm{d}\phi\right].$$

References

1) B. C. Giessen and G. E. Gordon, *Science*, **159**, 973 (1968).
2) T. Fukamachi, S. Hosoya, Y. Hosokawa, and H. Hirota, *Phys. Status Solidi A*, **10**, 437 (1972).
3) B. Buras and J. Stan Olsen, *Acta Crystallogr., Sect. A*, **31**, 327 (1975).
4) B. Buras, J. Chawaszczewska, S. Szarras, and Z. Szmid, (1968), Report 894/II/PS, Institute of Nuclear Research, Warsaw; R. Uno and J. Ishigaki, *J. Appl. Crystallogr.*, **8**, 578 (1975).
5) T. Fukamachi and S. Hosoya, *Acta Crystallogr., Sect. A*, **31**, 215 (1975).
6) J. M. Prober and J. M. Schultz, *J. Appl. Cryst.*, **8**, 405 (1975).
7) T. Fukamachi, S. Hosoya, and O. Terasaki, *J. Appl. Crystallogr.*, **6**, 117 (1973).
8) A. Eisenstein, *Phy. Rev.*, **63**, 304 (1943).
9) R. W. Gruebel and G. T. Clayton, *J. Chem. Phys.*, **46**, 639 (1967).
10) A. H. Narten, M. D. Danford, and H. A. Levy, *J. Chem. Phys.*, **46**, 4875 (1967).
11) A. H. Narten, *J. Chem. Phys.*, **65**, 573 (1976).
12) J. A. Bearden, *Rev. Mod. Phys.*, **39**, 78 (1967).
13) "International Tables for X-Ray Crystallography," Kynoch Press, Vol. III, Birmingham (1962), p. 171.
14) O. Klein and Y. Nishina, *Z. Phys.*, **52**, 853 (1929).
15) Y. Morino, Y. Nakamura, and T. Iijima, *J. Chem. Phys.*, **32**, 643 (1960).
16) D. T. Cromer, *J. Chem. Phys.*, **50**, 4857 (1969).
17) M. Toda, "Ekitairon," Iwanami, Tokyo (1955), p. 38.
18) Y. Murata, *J. Cryst. Soc. Jpn.*, **17**, 36 (1975).
19) R. E. Gibson and O. H. Leoffer, *J. Am. Chem. Soc.*, **63**, 898 (1941).
20) K. Nishikawa and Y. Murata, *Chem. Phys. Lett.*, (to be published).
21) H. A. Levy, M. D. Danford, and A. H. Narten, ORNL Rept. ORNL-3960 (1962).

The Molecular Sieving Action of Ion-exchanged Zeolites A

Tatsuo OHGUSHI, Atsushi YUSA, Kunio KINOSHITA, and Yoshifumi YATSURUGI

Komatsu Electronic Metals Co., 2612 Shinomiya, Hiratsuka 254

(Received July 16, 1977)

K_{12}-A zeolite was ion-exchanged with Mg^{2+}, Mn^{2+}, Co^{2+}, Cd^{2+}, or Pb^{2+}, and molecular sieving properties of the resultant zeolites were studied, mainly for PH_3 and SiH_4. (K, Mg)-A and (K, Mn)-A adsorbed PH_3 but not SiH_4, and hence are usable as a purifier for SiH_4. (K, Co)-A, (K, Cd)-A, and (K, Pb)-A decomposed both PH_3 and SiH_4, and are unsuitable as an adsorption purifier for SiH_4. By using adsorption columns containing (K, Mn)-A or (K, Mg)-A, breakthrough curves were obtained for PH_3 in SiH_4. The breakthroughs of (K, Zn)-A and (K, Ca)-A columns were also measured for comparison. The breakthrough point increased in the order of (K, Ca)-A$<$(K, Mg)-A$<$(K, Mn)-A$<$(K, Zn)-A. The mechanism of the molecular sieving is discussed. It is concluded that introduced bivalent cations increase the Debye-Waller factor of K^+ blocking the windows. A large Debye-Waller factor causes a decrease in the activation energy required for adsorbate molecule to pass through the blocked window.

Zeolite A is synthesized in its sodium form, Na_{12}-$(AlO_2)_{12}(SiO_2)_{12}(NaAlO_2)_\delta \cdot nH_2O$ with $0 \leq \delta \leq 1$, whose twelve Na^+'s are easily ion-exchanged with univalent cation M^I or bivalent cation M^{II}, and $(AlO_2)_{12}(SiO_2)_{12}$ constitutes the zeolite framework. [$(AlO_2)_{12}(SiO_2)_{12}$-$(NaAlO_2)_\delta \cdot nH_2O$ is generally abbreviated as -A.] A large cavity is located at the center of a cubic unit cell. There are three 8-membered oxygen rings per unit cell. The 8-ring is on each of the {100} faces of the unit cube, and constitutes a window to the cavity. In Na_{12}-A and K_{12}-A zeolites, all windows in them are blocked by Na^+ and K^+, respectively. Their molecular sieving properties, classified as 4A and 3A, respectively, are determined by the width of the aperture of the partially blocked window. In other words, the sieving character is directly controlled by the radius of the blocking cation.

Recently, Takaishi *et al.*[1] found another possible control mechanism. In (K,Zn)-A, the Debye-Waller factor of K^+ blocking the window is markedly influenced and increased by Zn^{2+} occupying sites other than window sites.[2] Such K^+ is easily pushed aside by a visiting adsorbate molecule, making way for the visitor.[1] PH_3 having a rather large molecular diameter is not adsorbed with Na_{12}-A, but is with $(K_{7.6}Zn_{2.2})$-A[1] in which the above mechanism operates. This result is of practical importance, being applied to the purification of SiH_4 which contains a small amount of PH_3.

In a subsequent section, the phenomenon of the indirect control is further discussed with respect to (K,Mg)-A, (K,Mn)-A, (K,Co)-A, (K,Cd)-A, and (K,Pb)-A. Their adsorption properties were measured for N_2, Ar, butane, 1-butene, *trans*-2-butene, *cis*-2-butene, PH_3 and SiH_4. The results are discussed from a practical point of view, for instance, which is the best adsorbent for the purification of SiH_4.

Experimental

Materials and Chemical Analysis. The starting material was Shōwa-Unox molecular sieve 4A powder (lot No. 490401). After the standard treatment of the sample, its composition was determined by the usual procedure.[3] The chemical formula was $Na_{11.8}H_{0.2}(AlO_2)_{12} \cdot (SiO_2)_{12}(NaAlO_2)_\delta$ with $0.2 \leq \delta \leq 0.3$. This differs from the stoichoimetric composition $Na_{12}(AlO_2)_{12}(SiO_2)_{12}$.[4,5] The deficiency of sodium may be ascribed to partial hydrolysis, though protons, which had replaced alkaline metal cations, were not analyzed. The value of δ was further examined by the following method. It has been established that $(NaAlO_2)_\delta$ molecule is contained in the β-cage (the sodalite unit) and its Na^+ cannot be exchanged with Ca^{2+}. After fully ion-exchanging Na^+ in the starting zeolite with Ca^{2+}, the residual amount of Na^+ in the resultant zeolite was determined, by activation analysis, to be 0.21 ions per unit cell ($\delta = 0.21$).

A fully ion-exchanged K_{12}-A was obtained by decanting the starting material repeatedly with 1 M KCl solutions, and washing it with distilled water. This zeolite contained 11.4 K^+ per unit cell. $(K_{12-2x}M_x^{II})$-A zeolites were prepared by treating K_{12}-A with solutions of a mixture of KCl and $M^{II}Cl_2$, of 0.2 total metal ion normality, at 80 ± 2 °C. As for (K, Pb)-A, nitrate solution was used instead of chloride. In most cases, the composition of an ion-exchanged zeolite was calculated from that of the ion-exchanging solution and material balance. The composition of the ion-exchanging solution was determined by the titration with ethylenediaminetetraacetic acid. On the other hand, zeolites of high contents of Mg^{2+} and Mn^{2+} were obtained only after repeated treatment with pure solutions of $MgCl_2$ and $MnCl_2$, respectively. In these cases, the composition of the zeolites was directly analyzed by usual methods. Zeolites containing Mg^{2+} or Mn^{2+} in amount more than 5 ions per unit cell could not be prepared.

All chemical reagents used were S.P. grade, and common adsorbate gases contained in glass cylinders (supplied by the Takachiho Chemical Co.) had nominal purities better than 99.9% as determined by mass-spectroscopic analysis. Less common gases, such as SiH_4 and PH_3, were obtained from the Nihon Oxygen Co., and were of special high purities, *i.e.*, semiconductor grade.

Measurements of Adsorbed Amounts of Gases. Adsorption measurements were made with a McBain type quartz spring balance and electrobalance (Chan Instrument Co., Model No. RG2050). The former had a sensitivity of 0.5 m/g and an accuracy of ± 0.5 mg. Prior to adsorption measurements, adsorbents were baked-out at 390 °C for 4 h under a vacuum better than 10^{-5} Torr.

Results

Amounts Adsorbed. *(K,Mg)-A Series*: Adsorptive capacities of (K,Mg)-A zeolite are shown in Fig. 1.

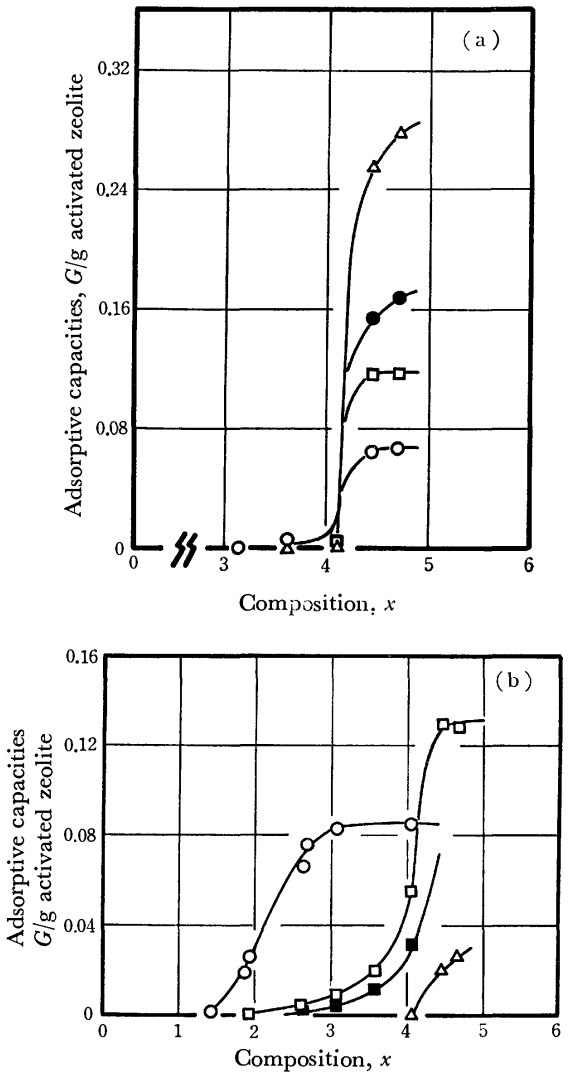

Fig. 1. (a) Adsorption of non-polar gases on $(K_{12-2x}Mg_x)$-A zeolites. (△) argon, 150 Torr, −196 °C; (●) nitrogen, 130 Torr, −196 °C; (□) butane, 160 Torr, 0 °C; (○) SiH_4, 150 Torr, 0 °C.
(b) Adsorption of polar gas and unsaturated hydrocarbons on $(K_{12-2x}Mg_x)$-A zeolites. (○) PH_3, 95 Torr, 0 °C; (□) 1-butene, 160 Torr, 0 °C; (■) *trans*-2-butene, 160 Torr, 0 °C; (△) *cis*-2-butene, 160 Torr, 0 °C.

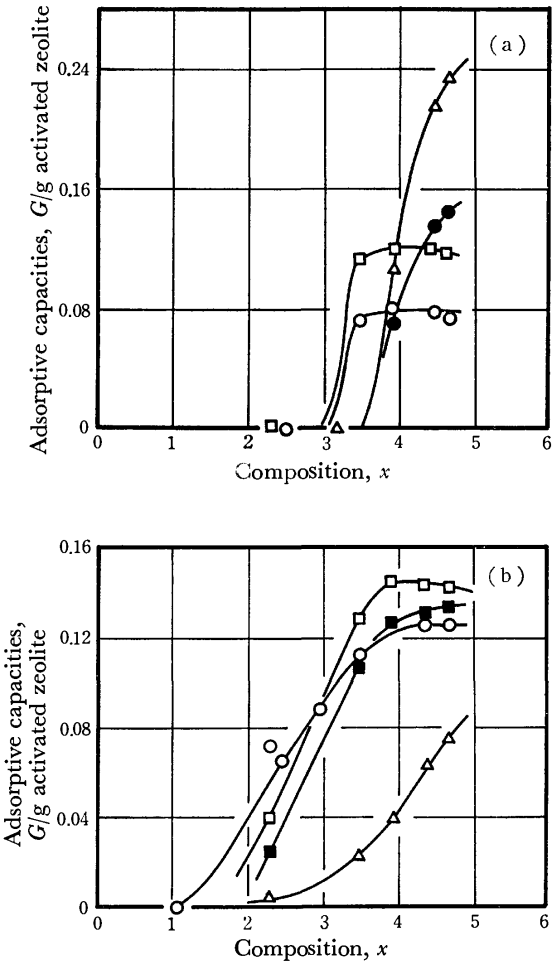

Fig. 2. (a) Adsorption of non-polar gases on $(K_{12-2x}Mn_x)$-A zeolites. (△) argon, 150 Torr, −196 °C; (●) nitrogen, 130 Torr, −196 °C; (□) butane, 160 Torr, 0 °C; (○) SiH_4, 150 Torr, 0 °C.
(b) Adsorption of polar gas and unsaturated hydrocarbons on $(K_{12-2x}Mn_x)$-A zeolites. (○) PH_3, 95 Torr, 0 °C; (□) 1-butene, 160 Torr, 0 °C; (■) *trans*-2-butene, 160 Torr, 0 °C; (△) *cis*-2-butene, 160 Torr, 0 °C.

Curves in Fig. 1(a), which refer to non-polar gases, rise steeply at the same composition, for instance $x=4.1$. On the other hand, curves in Fig. 1(b), which refer to polar gas or unsaturated hydrocarbons, have gentle slopes.

(K,Mn)-A Series: Figures 2(a) and (b) show adsorption properties of (K,Mn)-A series for non-polar molecules, and for polar and unsaturated hydrocarbon molecules, respectively. Slopes of curves in Fig. 2(b) are more gentle than those in Fig. 1(b).

(K,Co)-A, (K,Cd)-A, and (K,Pb)-A Series: These were colored when either PH_3 or SiH_4 was introduced, and yielded a gas uncondensable with liquid nitrogen. The weight of the zeolite sample was irreversibly increased on contact with PH_3 or SiH_4, that is, it was not decreased outgassing at temperatures up to 350 °C. This means that PH_3 or SiH_4 was decomposed and hydrogen was produced. The higher the degree of ion-exchange, the higher the catalytic activity for the decomposition. These features are not suitable for a purifier, since the non-volatile residuals block the zeolite window and degrade the adsorption activity.

Dynamic Characteristics of the Adsorption Column. Another important property of the purifier, the dynamic property of adsorbent, was studied. Breakthrough curves of columns, containing (K,Mg)-A or (K,Mn)-A zeolite of promising compositions, were plotted for PH_3 contained in SiH_4 by the aid of gas-chromatographic techniques. The breakthroughs of (K,Zn)-A and (K,Ca)-A columns were also measured for comparison. A gas mixture of PH_3 and SiH_4 in 5.5: 10^4 volume ratio was passed through the column at a flow rate of 350 ml/min and 0 °C. Results are given in Fig. 3, which shows that the breakthrough point for (K,Zn)-A is longer than others.

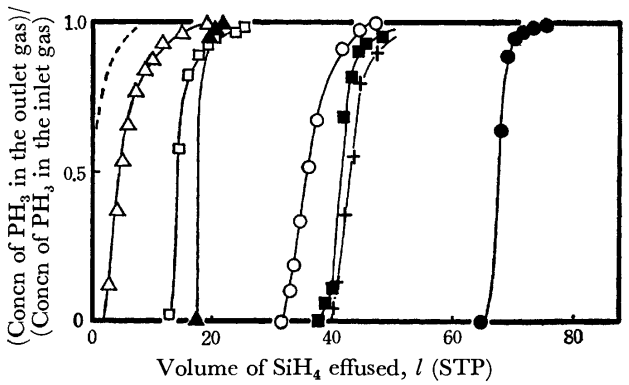

Fig. 3. Breakthrough curves of the adsorption column at 0 °C.
(---) $(K_{7.2}Ca_{2.4})$-A; (×) $(K_{4.8}Ca_{3.6})$-A; (△) $(K_{7.2}Mg_{2.4})$-A; (▲) $(K_{4.8}Mg_{3.6})$-A; (□) $(K_{7.4}Mn_{2.3})$-A; (■) $(K_{5.2}Mn_{3.4})$-A; (○) $(K_{7.4}Zn_{2.3})$-A; (■) $(K_{5.0}Zn_{3.5})$-A.

Discussion

As can be seen from Figs. 1 and 2, the curves for non-polar molecules have forms considerably different from those for polar and unsaturated. The latter two have gentle slopes and the former steep ones. This difference originates from the difference in the sieving mechanism. That is, non-polar molecules are adsorbed into zeolite A by passing through windows whose aperture width is larger than the molecular diameter. The width of the window aperture is simply determined by the ionic radius of a cation occupying the 8-ring site. The present authors have named this mechanism of the control of sieving action the direct control mechanism. In the adsorption of polar molecules, on the other hand, the following additional factor operates. The potential experienced by the ion on the 8-ring site is changed by ion-exchanges. If the change is such that the curvature of the potential surface is reduced and becomes fairly gentle, the amplitude of the oscillation of the ion, or its Debye-Waller factor, is increased. Then, the window-blocking action of the ion concerned becomes incomplete with increasing temperature. Hence, molecules having a diameter slightly larger than the width of the window aperture can be adsorbed, the rate of adsorption depending upon the incompleteness. The former phenomenon is confirmed by Takaishi *et al.*[6] in the systems of (Na,Ca)-A and (K,Ca)-A. This control mechanism of the sieving action has been named the indirect control mechanism. The above change in the potential form is induced by electrostatic forces due to cations, and hence is influenced further by the dipole or quadrupole of a visiting adsorbate. Consequently, the indirect control mechanism markedly operates on the adsorption of a polar molecule. Owing to this mechanism, zeolites having windows blocked by K^+, such as $(K_{12-2x}Mg_x)$-A with $1.5<x<3.5$ and $(K_{12-2y}Mn_y)$-A with $1.1<y<3.0$, can remove PH_3 contained in SiH_4, as well as (K,Zn)-A.[1,7] The degree of the indirect control is delicately affected by the ionicity and location of the bivalent cation, and is of the order of

$$Mn^{2+}, Zn^{2+} > Mg^{2+}, Ca^{2+}.$$[8]

Now, let us compare and discuss breakthrough points of (K,Mg)-A, (K,Mn)-A, (K,Zn)-A, and (K,Ca)-A having the similar content of bivalent cation, say about 2.3 cations per unit cell. In general, the breakthrough point is to be affected by two factors, the capacity and rate of adsorption. Experimental results are recapitulated as follows:
for the capacity

$$(Mn), (Mg) > (Zn) > (Ca),$$[8]

for the rate[7]

$$(Zn), (Mn) \gg (Mg) > (Ca),$$[8]

and for the breakthrough point

$$(Zn) > (Mn) > (Mg) > (Ca),$$

where symbols (Zn), (Mn), (Mg), and (Ca) designate zeolites containing the respective bivalent cations. The order of the breakthrough point is similar to that of the rate of adsorption. Thus, it may be said that the breakthrough point is mainly determined by the rate of adsorption in the present system. However, at composition 3.6 bivalent cations per unit cell, the breakthrough point of (Ca) is larger than that of (Mg). Hence, the point may also be affected by other factors, such as heat of adsorption for PH_3 and for SiH_4, though these values were not measured in the present work. (K,Zn)-A was concluded to be the best purifier among those studied.

Finally, let us discuss the role of the indirect control mechanism in a fine molecular sieving action for other gases. $(K_{12-2x}Mg_x)$-A with $2.4<x<4.0$ and $(K_{12-2y}Zn_y)$-A with $1.5<y<3.6$[1] can sieve 1-butene and *trans*-2-butene from *cis*-2-butene. If the shape of a butene molecule is roughly approximated by a prolate spheroid, the minor axis of *cis*-2-butene is larger than that of 1-butene or *trans*-2-butene. Then, *cis*-2-butene requires, to pass through the window, a larger displacement of the blocking K^+, or a larger activation energy. Thus, the fine separation of these isomers can be realized by the adsorption.

The present authors are deeply grateful to Professor T. Takaishi of Rikkyo University, who kindly read and discussed the manuscript. The authors are also grateful to Professor Gene S. Lehman of Rikkyo University for his language corrections to the manuscript.

References

1) T. Takaishi, Y. Yatsurugi, A. Yusa, and T. Kuratomi, *J. Chem. Soc., Faraday Trans. 1*, **71**, 97 (1975).
2) N. V. Raghavan and Karl Seff, *J. Phys. Chem.*, **80**, 2133 (1976).
3) F. P. Treadwell and W. T. Hall, "Analytical Chemistry," 9th ed, Vol. II, Wiley, New York (1959), p. 409.
4) D. W. Breck, W. G. Eversole, R. M. Milton, T. B. Read, and T. L. Thomas, *J. Am. Chem. Soc.*, **78**, 5963 (1956).
5) R. M. Barrer and W. H. Meier, *Trans. Faraday Soc.*, **54**, 1074 (1958); **55**, 130 (1959).
6) T. Takaishi, A. Yusa, and Y. Kamei, private communication.
7) A. Yusa, Y. Yatsurugi, and T. Takaishi, *J. Electrochem. Soc.*, **122**, 1700 (1975).
8) T. Ohgushi, Y. Yatsurugi, A. Yusa, and K. Kinoshita, unpublished data.

ESR Spectra of Bis(acetylacetonato)oxovanadium(IV) and Related Chelates in Molten *o*-Terphenyl and Some Other Organic Compounds

Yoshio MATSUNAGA

Department of Chemistry, Faculty of Science, Hokkaido University, Sapporo 060

(Received July 18, 1977)

All the patterns from the isotropic ESR spectrum to the anisotropic one of bis(acetylacetonato)oxovanadium-(IV) and related chelates are recorded by employing molten *o*-terphenyl as a solvent and by changing the temperature above and below the melting point. The results are qualitatively explained in terms of the anisotropic molecular motion and are considered to be evidence for the presence of clusters in the melt. Similar observations are made with some derivatives of 2,4,6-trinitrodiphenylamine, but only partially with *m*-terphenyl and the 3′-methoxy and 3′-ethoxy derivatives of 2,4-dinitrodiphenylamine. The implications of the results concerning the structure of the melts are discussed.

The ESR spectra of oxovanadium(IV) chelates are known to be substantially modified by the medium.[1] The isotropic spectra obtainable in liquid solutions consist of eight hyperfine lines arising from the nuclear spin $I=7/2$ of vanadium 51. On the other hand, each of the randomly oriented paramagnetic species immobilized in glasses separately contributes eight transitions to the spectrum; therefore, a superposition of the spectra associated with each orientation, weighted in proportion to the probability of finding the chelate molecules at that particular orientation, may be observed. In several liquid solutions, the appearance of an anisotropic molecular reorientation has been suggested in order to explain a marked deviation from the isotropic spectra.[2] If the viscosity of a solvent varies by many orders of magnitude upon a change in the temperature, one may observe all the patterns from the isotropic spectrum to the entirely anisotropic one. Knowledge of such spectral patterns is expected to be useful in studies of motional behavior in general, not only of liquids but also of solids, since the reorientation of the chelate molecule manifests the motion of the solvent or host molecules. In order to standardize the pattern, we initiated our work with an examination of the ESR spectra of three oxovanadium(IV) chelates dissolved in molten *o*-terphenyl, the viscosity of which has been reported in detail by Ubbelohde and his collaborators and also by Greet and Turnbull.[3–5] Then, attempts were made to study the motional behavior in melts of some derivatives of 2,4-dinitro- and 2,4,6-trinitrodiphenylamines.

Experimental

The bis(acetylacetonato)oxovanadium(IV), hereafter abbreviated $VO(acac)_2$, was commercially obtained. The bis(benzoylacetonato)oxovanadium(IV), $VO(bza)_2$, and bis(dibenzoylmethanato)oxovanadium(IV), $VO(dbm)_2$, were prepared following the procedures reported by Selbin *et al.*[6] The terphenyls were freed from polar impurities by chromatography on a column of activated alumina, using petroleum ether as the elutrient; they were then recrystallized from the same solvent. The melting points of the *o*- and *m*-terphenyls agreed well with the literature values of 55.5 and 87 °C.[3] The derivatives of the 2,4-dinitro- and 2,4,6-trinitro-diphenylamines were obtained by the condensation of appropriate derivatives of aniline with 2,4-dinitro- and 2,4,6-trinitrochlorobenzenes respectively. The concentrations of the paramagnetic probe dissolved in the organic melts were in the order of 10^{-3} M. As our work is not concerned with the linewidth, the solutions were not degassed. The spectra were recorded on a JEOL model JES-ME-3X spectrometer with 100 kHz modulation in the range from room temperature to 160 °C. The magnetic-field scan was calibrated with Mn^{2+}-doped MgO powder (86.9 G).

Results and Discussion

The oxovanadium chelates employed here are known to have approximately axial hyperfine and *g* tensors.[7–9] Their components parallel and perpendicular to the V=O bond direction will be denoted by $A_{\parallel}$ and $A_{\perp}$,[10]

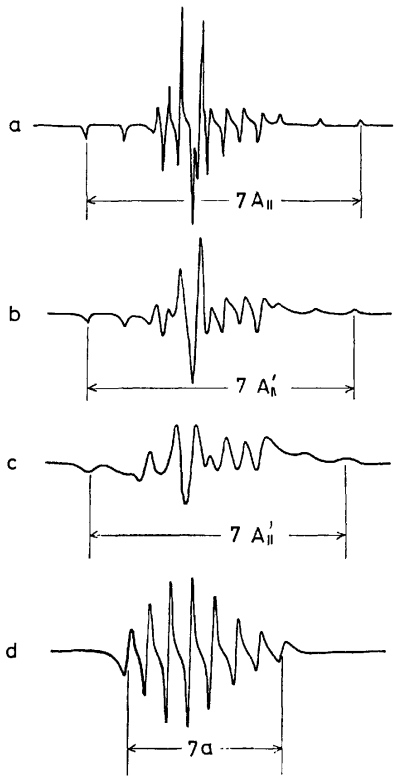

Fig. 1. ESR spectra of bis(acetylacetonato)oxovanadium(IV) in molten *o*-terphenyl at 24 °C (a), 40 °C (b), 50 °C (c), and 100 °C (d).

and by $g_{\parallel}$ and $g_{\perp}$, respectively. However, the rather small anisotropy in the latter will be ignored for the sake of simplicity in the following discussion. Some representative spectra of $VO(acac)_2$ in molten *o*-terphenyl observed at four different temperatures are presented in Fig. 1. At room temperature the supercooled melt exhibits an ESR spectrum typical of glasses. Here, the $VO(acac)_2$ molecules may be supposed to be randomly and rigidly oriented in the space. Although the central portion is complicated by an overlap of the parallel and perpendicular resonance lines, the $M_I=\pm 7/2$ and $\pm 5/2$ parallel resonance lines are well resolved. The values of $7A_{\parallel}$ are given by the distance between the outermost lines corresponding to the $M_I=\pm 7/2$. Thus, $A_{\parallel}$ is estimated to be 189 G.

The spectrum recorded at 40 °C is shown in Fig. 1b. The main feature of the room-temperature spectrum is still noticeable; however, each line has become much broader, and the distance between the outermost lines is markedly diminished, $7A'_{\parallel}$. Although it is not easy to observe, the perpendicular resonance spectrum is expected to be expanded; that is, $A'_{\perp}>A_{\perp}$. These are the spectral characteristics exhibited by a paramagnetic probe undergoing slow motion.[11] The spectrum taken at 50 °C indicates increased molecular motion (see Fig. 1c). If the probe molecules are tumbling rapidly, both $A'_{\parallel}$ and $A'_{\perp}$ are reduced to a, the isotropic hyperfine constant. As is shown in Fig. 1d, the isotropic eight-line pattern normally expected under such conditions is observed at 100 °C. The coupling constant is 107 G; therefore, $A_{\perp}$ may be estimated to be 66 G by the $(A_{\parallel}+2A_{\perp})=3a$ relation. The former value can be well compared with that of 108 G observed in a benzene solution by Stoklosa and Wasson.[9] Some years ago, Luckhurst and Ockwell examined the ESR spectrum of $VO(acac)_2$ in molten *o*-terphenyl.[12] Their measurements were apparently carried out at too high temperatures for the drastic change to be observed.

When the temperature is not high enough to observe the isotropic spectrum, the motion of the present probe molecule may be supposed to be anisotropic. If this motion is rapid, the parameter

$$S = (3\langle\cos^2\theta\rangle - 1)/2 \qquad (1)$$

is known to be equal to

$$(A'_{\parallel}-A'_{\perp})/(A_{\parallel}-A_{\perp}) \text{ or } (A'_{\parallel}-a)/(A_{\parallel}-a), \qquad (2)$$

where the θ angle is that between the V=O bond direction and the magnetic field, and where the average is temporal.[13] Upon a further lowering of the temperature, the anisotropic molecular motion may become so slow in the time scale of ESR spectroscopy that the average must be considered to be spatial. Nevertheless, for the sake of convenience, we will continue to employ the $(A'_{\parallel}-a)/(A_{\parallel}-a)$ ratio, denoted by S, as a measure of molecular motion throughout the temperature range examined. As a matter of fact, the S value can be estimated by means of the above equation only in the range from 1.00 (as the rigid limit) to about 0.55. Beyond the latter value, it is not possible to locate the outermost lines. Therefore, the rapid anisotropic molecular motion model may be not valid at all in the observable temperature range.

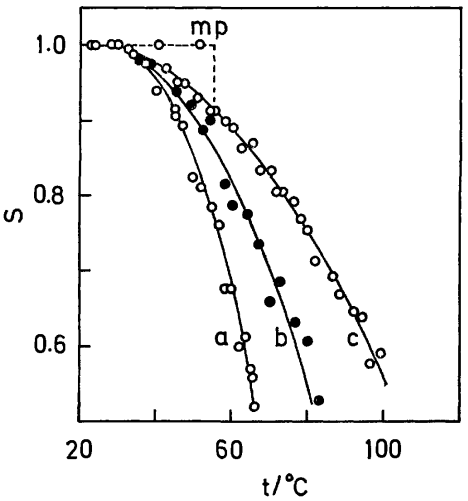

Fig. 2. Temperature dependence of the parameter S for $VO(acac)_2$ (a), $VO(bza)_2$ (b), and $VO(dbm)_2$ (c) in *o*-terphenyl. The horizontal line is for $VO(dbm)_2$ in solidified *o*-terphenyl.

The variation in S with the temperature for $VO(acac)_2$ is plotted in Fig. 2, along with those for $VO(bza)_2$ and $VO(dbm)_2$. At the melting point of pure *o*-terphenyl, the values of S are 0.77 for $VO(acac)_2$, 0.87 for $VO(bza)_2$, and 0.91 for $VO(dbm)_2$. Thus, the larger the chelate molecule, the more difficult the motion round two axes lying in the flat plane of the molecule appears to be. In order to achieve the same value of S, say 0.80, *o*-terphenyl must be heated to 73 °C in the case of $VO(dbm)_2$ compared with 53 °C in the case of $VO(acac)_2$. The agreement in S does not mean that the motional behavior of one chelate is the same as that of the other, since the mode of the molecular motion expressed as a function of θ depends upon the size and shape of the chelate molecule.

As the melting point is approached, molten *o*-terphenyl is known to show a marked departure from the linearity in the plot of the logarithm of the viscosity against $1/T$. On the basis of this departure, the formation of interlocked clusters in molten *o*-terphenyl near and below the melting point has been postulated by Ubbelohde and his collaborators.[3,4] According to them, clusters of a few molecules exist from temperatures of about 195 down to 70 °C. At the latter temperature the volume fraction of the cluster is estimated to be about 0.3. As the motion of the chelate molecule is largely governed by the volume of the solvent to be displaced by it, interlocking to this extent is enough to affect the ESR spectra of $VO(bza)_2$ and $VO(dbm)_2$ markedly. Between 70 °C and the melting point, clusters of a higher order appear to be formed in appreciable concentrations. In this temperature range, the rotation of even the smallest chelate molecule, $VO(acac)_2$, is clearly restricted. When the temperature is lowered still further, the clustering mechanism becomes more complex, eventually leading to the ESR spectra of the immobilized chelate molecule.

Upon a rise in the temperature, the viscosity, η, of the medium and also the kinetic energy of the probe molecule change. The two changes certainly contribute to the decrease in the parameter, S. Therefore, the

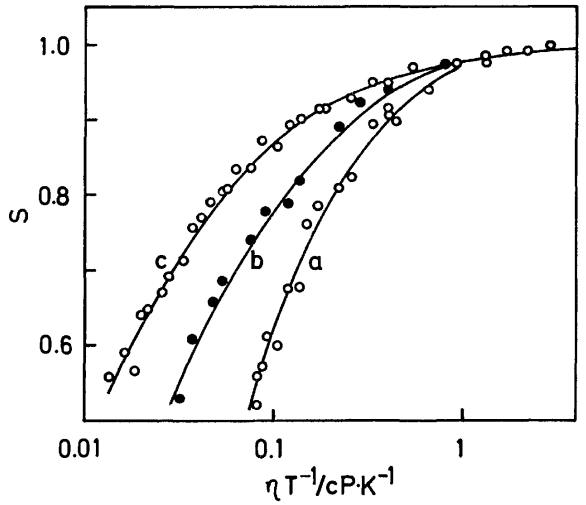

Fig. 3. Variation of the parameter S with η/T for VO(acac)$_2$ (a), VO(bza)$_2$ (b), and VO(dbm)$_2$ (c) in *o*-terphenyl.

variation in S with η/T shown in Fig. 3 may be more useful than the variation in S with t (or T) shown in Fig. 2. The viscosity values of the molten *o*-terphenyl required for the plots were calculated by means of the equation of Greet and Turnbull applicable to the range from -16 to 250 °C.[5] The η/T ratio appears in the well-known equation relating the viscosity of a medium to the Debye correlation time, τ

$$\tau = 4\pi r^3\eta/3kT, \quad (3)$$

where r is the radius of the probe molecule rotating in the medium. As r may not be constant in the slow-motion model, the plots in Fig. 3 may be different from the variation in S with τ.

Now, let us comment on the observation made by Stoklosa *et al.*[2] Their spectra of VO(bza)$_2$ in quinoline and 2-methylbenzoxazole measured at room temperature are well approximated by our spectra in *o*-terphenyl at 80 °C (S=0.61) and 83 °C (S=0.53) respectively. The spectral pattern is so sensitive to the temperature that one can easily differentiate such a small change. The viscosities of quinoline and 2-methylbenzoxazole have been reported by them to be 2.314 and 3.403 cP at 25 °C. The corresponding values of η/T, 0.0078 and 0.011 cP K^{-1}, are markedly smaller than the values of *o*-terphenyl at the above-mentioned temperatures, as can readily be seen by Fig. 3. Therefore, it is apparent that viscosity alone cannot account for the deviations from the isotropic ESR spectra observed by Stoklosa *et al.* It must be added that, in this temperature range, the viscosities calculated by means of the equation of Greet and Turnbull are larger than those of Andrews and Ubbelohde. Fortunately, the choice does not affect the present conclusion. When the size of the probe molecule is larger, the viscosity effect becomes more dominant in the determination of the ESR spectrum. The spectrum of VO(dbm)$_2$ recorded in 2-methylbenzoxazole can well be compared with that observed in *o*-terphenyl at 92 °C (S=0.65), the η/T value being 0.022 cP K^{-1} (Greet and Turnbull) or 0.015 cP K^{-1} (Andrews and Ubbelohde). The latter value agrees almost entirely with the observed one.

When *o*-terphenyl solidifies, VO(acac)$_2$ and VO(bza)$_2$ exhibit single broad absorptions, indicating the segregation of the chelates, but VO(dbm)$_2$ remains dissolved. Although the spectrum of the last-mentioned substance consists of rather broad lines, the pattern is similar to that shown in Fig. 1a. No temperature dependence was observed up to the melting point, as is indicated by the horizontal line in Fig. 2. In sharp contrast to this, VO(dbm)$_2$ has been found to move slowly in some solid charge-transfer complexes. The results of these measurements will be the subject of forthcoming papers.

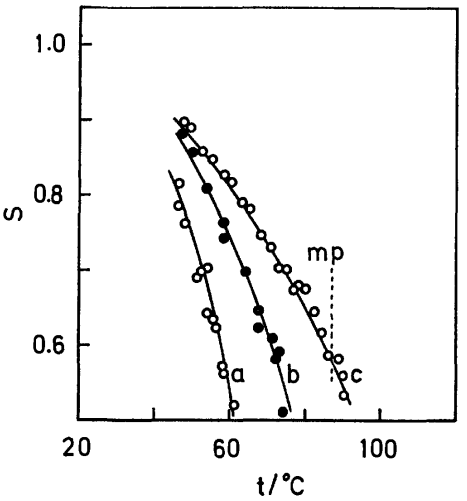

Fig. 4. Temperature dependence of the parameter S for VO(acac)$_2$ (a), VO(bza)$_2$ (b), and VO(dbm)$_2$ (c) in *m*-terphenyl.

m-Terphenyl behaves similarly, but less significantly than *o*-terphenyl, in the transport process.[3] In this terphenyl, too, a dramatic change in the ESR spectra could be recorded. The values of S measured with the three chelates are plotted against the temperature in Fig. 4. As the melts could not be cooled low enough for the anisotropic spectra to be observed, the $A_{\parallel}$ values determined in *o*-terphenyl were applied to these systems. The melting point of *m*-terphenyl is higher by about 30 °C than that of *o*-terphenyl; nevertheless, the temperature ranges shown in Fig. 4 are lower than the corresponding ones in Fig. 2. For example, an S value of 0.58 is found at the melting point in the case of VO(dbm)$_2$. If one assumes that the η/T value of *m*-terphenyl at this temperature is equal to that in *o*-terphenyl at S=0.58, the viscosity may be estimated to be 6.2 cP. This is in fair agreement with the value of 5.4 cP calculated by means of the equation of Andrews and Ubbelohde.[3]

The results presented above strongly suggest that extensive molecular interlocking in organic melts may be detected by measurements of the ESR spectra of dissolved oxovanadium chelates. Furthermore, the viscosity of the medium may be estimated by comparing these spectra with the ESR spectra recorded in molten *o*-terphenyl. As we have seen in the cases of VO(bza)$_2$ dissolved in quinoline and 2-methylbenzoxazole, the apparent viscosity obtained by the ESR technique is

significantly larger than the actual one if some other interactions between the probe and the medium are conceivable. The present author earlier reported that the melts of some derivatives of 2,4,6-trinitrodiphenylamine are colored more deeply than the crystals and that they are readily supercooled without fading.[14] The presence of a strong molecular entanglement, assisted by the charge-transfer interaction between the electron-donating moiety of a molecule and the accepting moiety of the neighboring molecule, was suggested to account for this phenomenon. As will be described in the following paragraphs, the ESR spectra of dissolved $VO(acac)_2$ revealed that the viscosities at their melting points are as large as the corresponding values of molten o-terphenyl. The $A_{\parallel}$ values were found to be essentially the same as that in molten o-terphenyl. On the other hand, the a values could not be measured because of the rapid decomposition of $VO(acac)_2$ at high temperatures. Therefore, the latter was assumed to be 107 G.

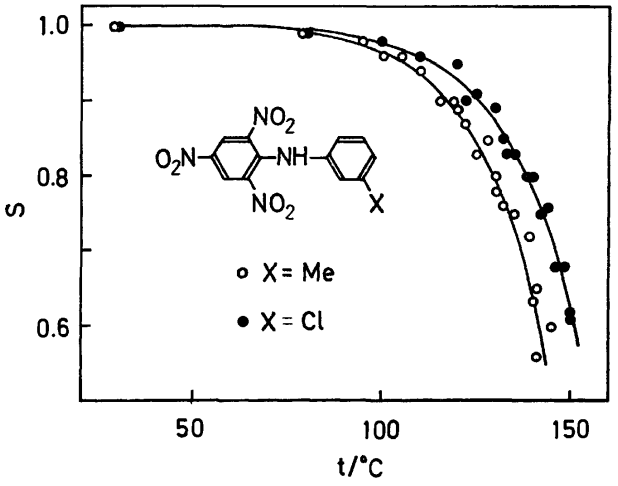

Fig. 5. Temperature dependence of the parameter S for $VO(acac)_2$ in 2,4,6-trinitro-3′-methyldiphenylamine (○) and 2,4,6-trinitro-3′-chlorodiphenylamine (●).

In Fig. 5, the results obtained by the use of the 3′-methyl and 3′-chloro derivatives are presented. The melting point of the former compound is 133 °C (130 °C by Busch and Pungs[15]) and that of the latter, 142—143 °C (137—139 °C by Wedekind[16]). The substituents are similar in size, but the bond moments are very different from each other. The higher melting point of the 3′-chloro derivative may be ascribed to the contribution of the large C–Cl bond moment to the intermolecular forces. The curve for the 3′-chloro derivative in Fig. 5 appears to be shifted to a higher temperature than that for the 3′-methyl derivative by just the difference in the melting point. As is shown by the electronic absorption spectra, the intermolecular charge-transfer interaction in melts is more pronounced in the 3′-methyl derivative than in the 3′-chloro derivative. However, its effect on the S value could not be detected. The S values at the melting points are 0.75 in both cases. The apparent viscosities are 65—67 cP. In these cases, the S values vary more gradually with

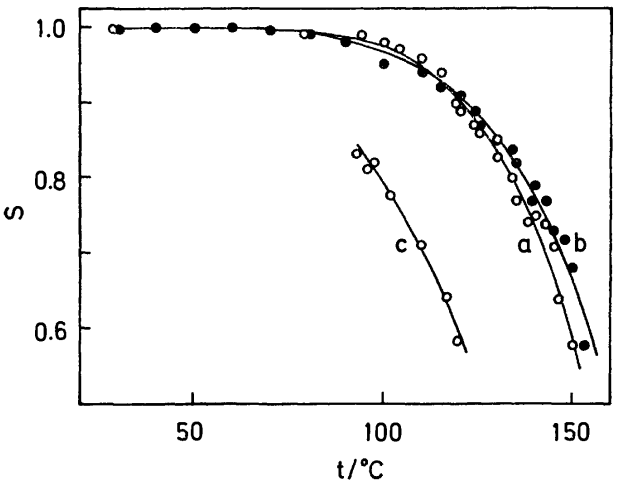

Fig. 6. Temperature dependence of the parameter S for $VO(acac)_2$ in 2,4,6-trinitro-2′-methoxydiphenylamine (a), 2,4,6-trinitro-3′-methoxydiphenylamine (b), and 2,4-dinitro-3′-methoxydiphenylamine (c).

the temperature than that in molten o-terphenyl. In other words, the temperature dependence of the viscosity of the diphenylamines is less than that of o-terphenyl.

The values of S displayed by the 2′- and 3′-methoxy derivatives are plotted against the temperature in Fig. 6. The substituent is more strongly electron-donating and more polar than methyl group. These factors favor a strong intermolecular interaction, but the bulkiness opposes it. As a result, the former compound melts at 148 °C (143 °C by James *et al.*[17]) and the latter, at 123—124 °C. Once melted, the 3′-methoxy derivative is slightly more viscous than the 2′-methoxy derivative in most of the examined temperature range. Two curves are nearly superimposed on the curve for the 3′-chloro derivative given in Fig. 5. The S value at the melting points are 0.63 and 0.89 respectively. Hence, the viscosities are about 44 and 130 cP. One may conclude that the intermolecular interaction in the 3′-methoxy derivative is drastically intensified upon melting.

Before reporting our attempts with 2,4-dinitro-2′-methoxydiphenylamine, it will be interesting to note other information. In the first place, this compound is known to be dimorphic. The unstable orange-yellow form transforms into the bright red form around 145 °C, and then melts at 165.5 °C.[18] The second outstanding feature of interest is that the melting point is markedly higher than that of 2,4,6-trinitro-2′-methoxydiphenylamine. Moreover, the color of the stable form is deeper than that of the trinitro compound. In contrast to the melt of the latter, the melt of the former compound could not be supercooled. The 3′-methoxy derivative is yellow and melts at 141—142 °C. This temperature, too, is higher than the melting point of the corresponding trinitro compound. Nonetheless, the curve for this compound (shown in Fig. 6) is located about 35 °C lower. Besides, the crystallization takes place around 93 °C. It is clear that no extensive formation of clusters occurs near the melting point of this compound. Thus, the absence of the nitro group at the

6 position increases the stability of the crystalline state, but decreases the cluster-forming potential in the melt. The clusters are some form of structural association into groups different from crystal nuclei; therefore, spontaneous crystallization may be prevented by extensive cluster formation. In addition to the stability of the crystalline state, the difficulty in cluster formation helps to explain why the dinitro compounds show a pronounced tendency to crystallize.

The behavior of the 2′- and 3′-ethoxy derivatives of 2,4-dinitro- and 2,4,6-trinitro-diphenylamines resemble that of the corresponding methoxy derivatives. Because of the presence of the bulky ethoxy group, each curve observed with the trinitro compound is located at a temperature about 10 °C lower than that of the methoxy derivative. The melt of 2,4-dinitro-3′-ethoxydiphenylamine could be supercooled to 85 °C, but that of the 2′-ethoxy derivative could not. The curve obtained with the former compound lies at slightly lower temperatures than that obtained with 2,4-dinitro-3′-methoxydiphenylamine. It is clear that the non-ideal viscosity-against-temperature characteristics displayed by these compounds are sensitive to small changes in the molecular shape.

References

1) B. A. Goodman and J. B. Raynor, *Adv. Inorg. Chem. Radiochem.*, **13**, 135 (1970).
2) H. J. Stoklosa, H. L. Huffman, and J. R. Wasson, *J. Inorg. Nucl. Chem.*, **35**, 2584 (1973).
3) J. N. Andrews and A. R. Ubbelohde, *Proc. R. Soc. London, Ser. A*, **228**, 435 (1955).
4) E. McLaughlin and A. R. Ubbelohde, *Trans. Faraday Soc.*, **54**, 1804 (1958).
5) R. J. Greet and D. Turnbull, *J. Chem. Phys.*, **46**, 1243 (1967).
6) J. Selbin, G. Maus, and D. L. Johnson, *J. Inorg. Nucl. Chem.*, **29**, 1735 (1967).
7) S. H. Glarum and J. H. Marshall, *J. Chem. Phys.*, **46**, 55 (1967).
8) G. C. Fryburg and E. Gelerinter, *J. Chem. Phys.*, **52**, 3378 (1970).
9) H. J. Stoklosa and J. R. Wasson, *J. Inorg. Nucl. Chem.*, **38**, 677 (1976).
10) $A_{\parallel}$ and $A_{\perp}$ are known to be negative, but the absolute values are considered here.
11) R. F. Campbell and M. W. Hanna, *J. Phys. Chem.*, **80**, 1892 (1976).
12) G. R. Luckhurst and J. N. Ockwell, *Mol. Phys.*, **16**, 165 (1969).
13) W. L. Hubbell and H. M. McConnell, *J. Am. Chem. Soc.*, **93**, 314 (1971).
14) Y. Matsunaga, *Bull. Chem. Soc. Jpn.*, **49**, 1411 (1976).
15) M. Busch and E. Pungs, *J. Prakt. Chem. 2*, **79**, 546 (1909).
16) E. Wedekind, *Ber.*, **33**, 426 (1900).
17) T. C. James, J. I. M. Jones, and R. I. Lewis, *J. Chem. Soc.*, **117**, 1273 (1920).
18) N. M. Cullinane, O. E. Embrey, and D. R. Davies, *J. Phys. Chem.*, **36**, 1434 (1932).

Flash Photolysis Study on the Addition Reaction of Alkylthiyl Radical to Olefins

Osamu Ito and Minoru Matsuda

Chemical Research Institute of Non-aqueous Solutions, Tohoku University, Katahira, Sendai 980

(Received July 18, 1977)

The transient absorption band appearing at 370 nm by flash photolysis of di-*t*-butyl dusilfide was assigned to the *t*-butylthiyl radical. Photolyses of the disulfide solutions containing olefins such as 1,1-diphenylethylene and styrene gave new transient bands in a wavelength region similar to that of the diphenylmethyl radical and benzyl radical, respectively. These new bands can be attributed to the radicals produced by the addition of the thiyl radical to olefins; $(Ph)_2\dot{C}-CH_2-SR$ and $H(Ph)\dot{C}-CH_2-SR$. Kinetic studies including the addition of the thiyl radical to olefins were performed.

A number of studies have been carried out on the reactivity of free radicals in solution by means of flash photolysis, attention being focused mainly on the recombination and hydrogen abstraction reactions of the radicals.[1-3] Flash kinetic spectroscopy was applied to the triplet anthracene[4] and the diarylcarbenes[5] for the addition reaction to olefins. Addition of the thiyl radical to olefin was followed indirectly in the competition reaction between thiolate anion and olefin.[6] However, no study seems to have been carried out on the detection of the radical produced from the addition of the primary formed radical by flash exposure to olefin. The thiyl radicals are known to react very rapidly with olefins by means of the rotating sector in the mode of anti-Markownikoff addition.[7,8] If this is the case, the absorption spectrum of the radical formed from the addition reaction having the structure $R'(R'')\dot{C}-CH_2-SR$ might be detected.

Experimental

Di-*t*-butyl disulfide, styrene, and 1,1-diphenylethylene were purified by distillation under reduced pressure. Ferrocene was purified by sublimation after recrystallization. All the solvents were of spectrophotometric grade. The solutions were degassed up to 10^{-5} Torr. The flash photolysis apparatus of standard design[9] delivered a flash with an energy of up to 100 J from xenon-filled flash lamps with a half-peak duration of 20 μs. A band pass filter (Toshiba UV-D25) transmitting light between 240 nm and 400 nm was used. The quartz irradiation vessel, length 10 cm and diameter 1 cm, had optically flat quartz window at both ends. The photolysis was carried out at 23 °C.

Results and Discussion

Thiyl radicals are formed by the photolysis of disulfides. The derivatives of diphenyl disulfide give only thiyl radicals which exhibit absorption at around 500 nm.[2,10] Although dialkyl disulfides give the dithio radicals (RSS·) besides a large amount of the thiyl radical under the irradiation of light of a short wavelength such as 195 nm,[11] photolysis with light of a longer wavelength (>240 nm) has not been studied by means of the flash photolysis. Before studying the addition reaction of the alkylthiyl radical to olefin, the absorption spectra of the alkylthiyl radical should be examined.

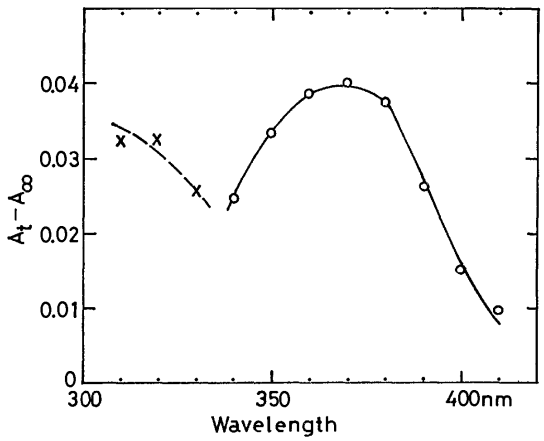

Fig. 1. Transient absorption spectra produced by the flash photolysis of the degassed hexane solution of di-*t*-butyl disulfide (5.0 mM). (a); Immediately after flash (-○-). (b); 500 μs after flash (-×-). A_t-A_∞ is difference of the absorbance at time t and time ∞ after flash.

Flash photolysis of the degassed solution of di-*t*-butyl disulfide gave the transient absorption spectra as shown in Fig. 1. The main band at 370 nm reaches maximum immediately after flash (*ca.* 40 μs) and decays rapidly with a half-life (τ) of 150 μs, a large decrease in the initial intensity being observed in the aerated solution. Another band can be seen in a shorter wavelength region than 330 nm. The band reaches maximum at *ca.* 500 μs after flash, decaying slowly with τ=*ca.* 3 ms, and is insensitive to oxygen. It thus can not be attributed to the free radical formed directly by the flash photolysis of disulfide. The band at 370 nm can not be assigned to the triplet←triplet absorption of disulfide, since its initial intensity and decay rate were not affected by addition of ferrocene which is known to be efficient triplet quencher,[12] and thus, it could be attributed to the *t*-butylthiyl radical. With another disulfide such as dibutyl disulfide, a weak absorption band, observed at 370 nm, is slightly longer as compared with that of HS· in gas phase reported by Norrish and Zeelenberg[13] and that of the thiyl radicals having amino acid group reported by Hoffman and Hayon.[14] $2k_r/\varepsilon$, in which ε is molar extinction coefficient and k_r the second order rate constant, was obtained from the slope of the second order plot at 370 nm. Assuming that ε of the

thiyl radical at absorption maximum is similar to that of the thiyl radical having amino acid group (ε= 300—600 M^{-1} cm^{-1}),[14] 2 k_r was given as 2—4$\times 10^9$ M^{-1} s^{-1} in hexane at 23 °C, suggesting that the thiyl radical decays predominantly with the recombination. Since these values are 4 times greater than those in liquid paraffin (5—10$\times 10^8$ M^{-1} s^{-1}), the rate of recombination is thought to be a diffusion-controlled reaction.

When a mixed solution of 1,1-diphenylethylene and di-*t*-butyl disulfide was subjected to irradiation of flash light a new intense band was observed at 332 nm having a shoulder at 315 nm (Fig. 2). The absorbance at 332 nm was 30 times stronger than that of transient band observed without olefin. The transient spectrum shown in Fig. 2 is very similar to that of the diphenylmethyl radical.[15] Thus, the band could be assigned to the radical having diphenylmethyl radical moiety, which might be formed by the anti-Markownikoff addition of the thiyl radical to 1,1-diphenylethylene, $(Ph)_2\dot{C}$–CH_2–SR, to form a more stable intermediate radical. The mixed solution of disulfide and styrene gave a new sharp band at 322.5 nm (Fig. 3), the absorbance at this region being twice as strong as that of the transient band observed without styrene. A band at 370 nm, assigned to the thiyl radical, was also observed decaying more rapidly than the new band at 322.5 nm. Since the new band at 322.5 nm is very similar to that of the benzyl radical,[15] it can be attributed to the radical having benzyl radical moiety, which might be formed by the anti-Markownikoff addition of the thiyl radical to styrene, $H(Ph)\dot{C}$–CH_2–SR.

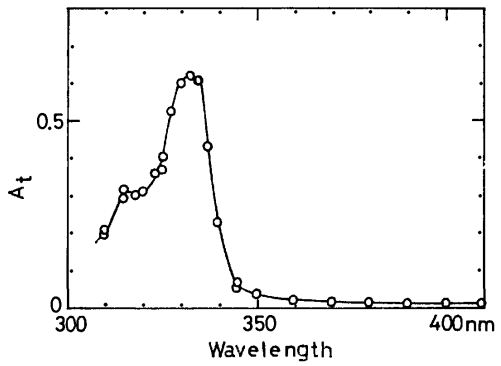

Fig. 2. Transient absorption spectrum produced by the flash photolysis (200 μs after flash) of the degassed hexane solution containing 1,1-diphenylethylene (2.3 mM) and di-*t*-butyl disulfide (2.0 mM).

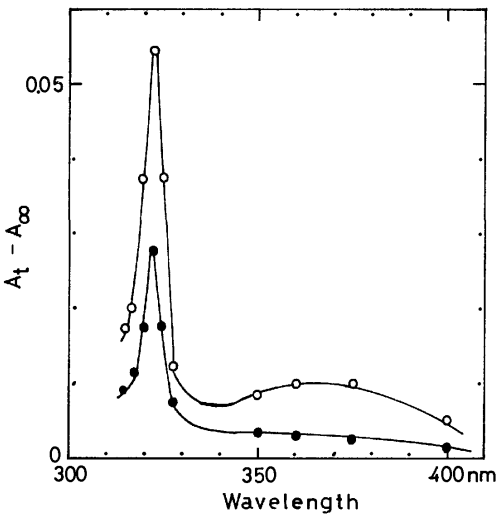

Fig. 3. Transient absorption spectra produced by the flash photolysis of the degassed solution containing styrene (140 mM) and di-*t*-butyl disulfide (4.9 mM). (a); 200 μs after flash (-○-). (b); 500 μs after flash (-●-).

It is most unlikely that these new bands are attributed to the radical ion formation, since no absorption bands due to the radical anions and cations of disulfide[16] and olefins[17] were observed for a mixed solution of disulfide and olefin even in the polar solvent such as dichloromethane. Possibility of the triplet←triplet absorption of olefins also should be examined. Even when 0.9 mM of ferrocene, an efficient triplet quencher, was added to the solution of disulfide and 1,1-diphenylethylene, no difference was observed either in the initial intensity or decay rate. Thus, any process involving the triplet states can not be included.

The new bands reached maximum intensity at 150 μs after flash, indicating that the absorption band related to the addition is attributed to the band at 370 nm rather than the shorter wavelength band than 330 nm band which is observed with flash light irradiation on the di-*t*-butyl disulfide solution without olefin. This is also supported by the effect of oxygen added. The band at 370 nm observed in the absence of olefin was very reactive to oxygen and scarcely observed in aerated solution, while the band at shorter wavelength was insensitive to oxygen. In the system containing olefins, no transient band due to the radicals formed from the addition reaction was observed in the presence of oxygen. The benzyl and diphenylmethyl radicals were reactive to oxygen as indicated by Porter and Windsor,[15] but this might mainly result from the reactivity of the primarily formed thiyl radical assigned to the band at 370 nm. It has been reported that small portion of dithio radical was formed [11,18] by photolysis of disulfide with the short wavelength light. Although no evidence for the formation of the dithio radical was obtained in our flash experiment, the dithio radical is known to be not reactive to olefin.[19] Furthermore, the alkyl radical, which may be formed as a pair of the dithio radical, is also known to add to olefin considerably more slowly (10^2—10^3 M^{-1} s^{-1}) as compared with the thiyl radical.[7,20]

The observed reactions above can be accounted for by the following scheme:

$$RSSR \xrightarrow{h\nu} RSSR^* \quad (1)$$

$$RSSR^* \longrightarrow 2RS\cdot \quad (2)$$

$$2RS\cdot \xrightarrow{k_r} RSSR \quad (3)$$

$$RS\cdot + R'(R'')C{=}CH_2 \xrightarrow{k_a} R'(R'')\dot{C}{-}CH_2{-}SR \quad (4)$$

I

RSSR* may not be the triplet state since the initial yield and decay rate of the thiyl radical was not affected by mixing with ferrocene. Decrease in thiyl radical formation by oxygen should be due to the reactivity of the thiyl radical to oxygen. In Reaction 4, k_a can be estimated from the decay of the thiyl radical. In the case of 1,1-diphenylethylene, however, the tail of the larger absorption band at 332 nm of radical **I** masked the band of the thiyl radical. For styrene, although the initial yield of the thiyl radical decreased with increase in the concentration of styrene, the increase in the decay rate of the band at 370 nm was observed. The decay kinetics fit the first order plottings up to 70% consumption in the styrene concentration range 1—11 mM. Further addition of styrene interfered in the analysis of the decay kinetics because of decrease in the initial yield. Pseudo-first order rate constants were proportional to the concentration of styrene as shown in Fig. 4. From the slope, a value 3.8×10^5 $M^{-1}\,s^{-1}$ ($\pm15\%$) was obtained, which might correspond to the addition rate, if the observed decrease in the initial yield was simply due to the decrease in the light intensity of a flash by the absorption of styrene. The rate constant is 10^2—10^3 times smaller than the value obtained by the rotating sector method.[7,8] We have no criterion more reliable. As regards our flash experiment, there is one disadvantage; we can not completely neglect the possibility that the decrease in the initial yield of the band at 370 nm in the presence of styrene is related to the faster reaction of thiyl radical with styrene. Even if the value estimated by the flash technique may be a lower limit for the addition reaction, this is larger than that of the alkyl radical,[19] and comparable to that of the diarylcarbenes (10^5 $M^{-1}\,s^{-1}$).[5]

The ralative rate of addition reaction can be given, since the initial yield of the band at 332 nm decreased by the addition of styrene to the solution of diphenylethylene and disulfide. The reduction of the absorbance with the system containing an equimolar amount (1.5 mM) of styrene and diphenylethylene was 40% as compared with the absorbance of 3.0 mM of diphenylethylene. Assuming that this decrease was caused by the competitive addition reaction of the thiyl radical to both olefins, the rate of addition to diphenylethylene is 1.3 times greater than that of styrene. The ratio might be comparable to that of methyl radical (ratio=2.0)[21] and diphenylcarbene (ratio=1.0).[5]

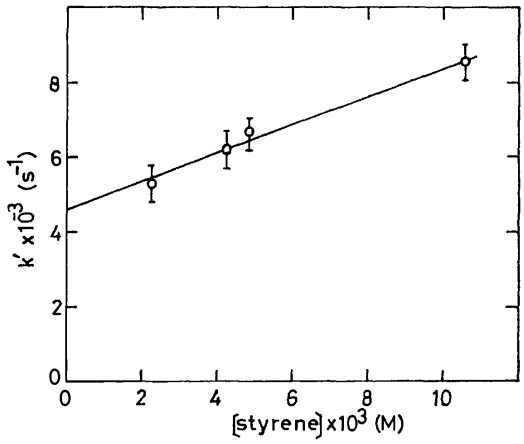

Fig. 4. Pseudo-first order rate constant (k') for the disappearance of the band at 370 nm as a function of styrene concentration.

Concerning the cause of the large absorbance observed for diphenylethylene compared with the case of styrene, the following factors might be mentioned: Large ε value, high addition rate, high efficient selectivity of anti-Markownikoff addition, and /or stability of radical **I** formed. In the absence of oxygen, decay of radical **I** formed can be caused by the recombination of the radicals, hydrogen abstraction from solvent, and addition to the remaining excess olefins. Half-lives of these radicals were 1 ms for diphenylethylene and 500 μs for styrene. In the case of diphenylethylene, a mixed order decay was observed. The decay kinetics of the styrene system at 322.5 nm band obeys the second order plot, giving $k/\varepsilon=5\times10^5$. In this case, ε of radical **I** may be similar to that of the benzyl radical. Choosing $\varepsilon=5500$ of the benzyl radical at absorption maximum as obtained by the pulse radiolysis technique,[22] the rate of the recombination of radical **I** was given to be 2.8×10^9 $M^{-1}\,s^{-1}$. The value is slightly smaller than that of the benzyl radical (3.1×10^9 $M^{-1}\,s^{-1}$).[22] The decay rate of radical **I** was not affected by the addition of styrene, since the rate constant of the propagating step is known to be very small for the polystyryl radical (100 $M^{-1}\,s^{-1}$ at room temperature).[23]

The authors wish to thank Professor H. Kokubun and Dr. K. Kikuchi, Tohoku University, for introduction of the flash photolysis technique and for their useful discussions.

References

1) E. J. Land, "Progress in Reaction Kinetics," ed by G. Porter, Pergamon Press, Vol. III, London (1965), p. 369.
2) T. Miyashita, M. Iino, and M. Matsuda, *Bull. Chem. Soc. Jpn.*, **50**, 317 (1977).
3) H. H. Thoi, O. Ito, M. Iino, and M. Matsuda, *J. Phys. Chem.*, in press.
4) R. G. W. Norrish and J. P. Simons, *Proc. R. Soc. London, Ser. A*, **251**, 4 (1959).
5) G. L. Closs and B. E. Rabinow, *J. Am. Chem. Soc.*, **98**, 8190 (1976).
6) T.-L. Tung and J. A. Stone, *J. Phys. Chem.*, **78**, 1130 (1974).
7) M. Onyszchuk and C. Sivertz, *Can. J. Chem.*, **33**, 1034 (1955).
8) C. Sivertz, *J. Phys. Chem.*, **63**, 34 (1959).
9) G. Porter and M. A. West, "Techniques of Chemistry," ed by A. Weissberger, John Wiley & Sons, Vol. VI, New York (1974), p. 367.
10) F. C. Thyrion, *J. Phys. Chem.*, **77**, 1478 (1973).
11) A. B. Callear and D. R. Dickson, *Trans. Faraday Soc.*, **66**, 1987 (1970).
12) K. Kikuchi, H. Kokubun, and M. Kikuchi, *Bull. Chem. Soc. Jpn.*, **48**, 1378 (1975).
13) R. G. W. Norrish and P. Zeelenberg, *Proc. R. Soc. London, Ser. A*, **240**, 293 (1957).
14) H. Z. Hoffman and E. Hayon, *J. Am. Chem. Soc.*, **94**, 7950 (1972).

15) G. Porter and M. W. Windsor, *Nature*, **180**, 187 (1957).
16) T. Shida, *J. Phys. Chem.*, **72**, 2597 (1968).
17) T. Shida and Hamill, *J. Chem. Phys.*, **44**, 2375 (1966).
18) S. M. Rosenfeld, R. G. Lawler, and H. R. Ward, *J. Am. Chem. Soc.*, **94**, 9255 (1972).
19) I. Kende, T. L. Pickering, and A. V. Tobolsky, *J. Am. Chem. Soc.*, **87**, 5582 (1965).
20) J. A. Kerr, "Free Radical," ed by J. K. Kochi, John Wiley & Sons, Vol. I, New York (1973), p. 22.
21) M. Szwarc, *J. Polym. Sci.*, **16**, 367 (1955).
22) H. C. Christensen, K. Sehested, and E. J. Hart, *J. Phys. Chem.*, **77**, 983 (1973).
23) K. Yokota, M. Kani, and Y. Ishitani, *J. Polym. Sci., Part A*, **6**, 1325 (1968).

Temperature Effects on the Raman Intensity of Liquid Samples and an Averaged Molecular Field

Haruo HATAKEYAMA and Tsunetake FUJIYAMA

Department of Chemistry, Faculty of Science, Tokyo Metropolitan University, Setagaya, Tokyo 158

(Received July 23, 1977)

The relative Raman intensities of the ν_1 line of carbon tetrachloride, the ν_8 line of acetonitrile, and the ν_3 line of chloroform were observed in the liquid phase and at various temperatures. The apparent intensity change due to the temperature were explained in terms of the local field effect, the density change, the statistical distribution effect, and the contribution of transition hyperpolarizability in the presence of a non-zero averaged molecular field.

Raman intensity measurements have a great advantage, in principle, over the intensity measurements of absorption spectra. They are free from the effects of a slit-function,[1] the effects related to anomalous dispersion,[2-6] the effects of multi-reflections inside sample layers,[7-10] the so-called baseline effects,[1,11] and so on, all of which are notorious difficulties in the intensity measurements of liquid samples by infrared absorption methods. Therefore, careful measurements of Raman intensities will afford useful information about intermolecular interactions in the liquid phase.

In our preceding report, the intermolecular interaction of a dipole-dipole type has been shown to be most important in explaining the concentration dependence of the Raman intensities in various binary solutions.[12] If the component molecules in solutions have dipole moments, there exists a non-zero averaged molecular field at a given molecule, and the contribution of the transition hyperpolarizability cannot be neglected in comparison with that of the transition polarizability. As the concentration dependence of the averaged molecular field results from the change in an intermolecular distance due to different concentrations,[13] the averaged molecular field and, therefore, the Raman intensity may be expected to be dependent on the temperature, also.

In the present report, the temperature effects on the Raman intensities were measured for three different liquid systems in order to study the role of the averaged molecular field which was produced by the dipole-dipole interaction. Carbon tetrachloride, acetonitrile, and chloroform were chosen because they were typical examples of a non-polar molecule, a molecule with a large dipole moment, and a molecule with a rather small dipole moment respectively.

Experimental

The spectrometer used for the present work was designed and constructed in our laboratory. The instrument was composed of a He-Ne gas laser source (NEC GLG 105, 15 mW), a grating monochromator (JEOL JSG 125B), a photomultiplier (HTV R374, S-20 response), a lock-in amplifier (NF LI-573), and a recorder.

The temperature of a sample cell ($10\times20\times40$ mm^3) was regulated by means of a thermostating box whose temperature was controlled by changing the electrical current supplied to nichrome heaters. The temperatures of the thermostating box and the sample cell were observed by means of a mercury thermometer and a thermocouple respectively. The temperature drift of the sample was less than ±1 K within the temperature range of 300—370 K.

The stability of the laser out-put during the individual spectral measurements was observed by monitoring the light energy which penetrated through the 100% reflectance mirror of the laser cavity. When the power of the laser source drifted more than 1% during the measurements, the data observed were completely discarded.

All the chemicals used in the present study were commercial products. The carbon tetrachloride and acetonitrile were purified by fractional distillations repeated three times. The chloroform was purified by column chromatography on alumina.

The Raman spectra were observed for the ν_1 line of carbon tetrachloride, the ν_8 line of acetonitrile, and the ν_3 line of chloroform. The Raman intensity was determined from the observed band area by means of the weight method. The observations were repeated four times for each temperature; their averaged values were then taken as the observed intensities. The deviations of the observed band areas from the averaged values were less than 2%.

Results and Discussion

ν_1 Line of Carbon Tetrachloride. The Raman intensities of the ν_1 line of liquid carbon tetrachloride were observed in the temperature range from 291 to 333 K. The observed relative intensity ratios are summarized in Table 1, where the relative intensity at 291 K serves as the standard. The relative intensity decreases about 8% as the temperature changes from 291 to 333 K.

Table 1. ν_1 Line of carbon tetrachloride

T/K	d/d_{291}	s/s_{291}	L/L_{291}	Lsd/Lsd_{291}	I/I_{291}
291	1.000	1.000	1.000	1.000	1.000
315	0.972	1.021	0.961	0.954	0.948
326	0.957	1.033	0.943	0.932	0.929
330	0.952	1.038	0.936	0.925	0.917

The apparent intensity change due to the temperature has been discussed in detail in a previous report,[14] where the effects of the density, the local field, and the statistical distribution of molecules in relation to a vibrational state have been emphasized. These factors are all temperature-dependent and should be taken into account in interpreting the present results.

The density, d, as a function of the temperature may be found in the International Critical Tables.[15] The relative values of the density at various temperatures,

d/d_{291}, are summarized in Table 1, where the density at 291 K is chosen as the standard.

The statistical factors, s, may be expressed as

$$s = \frac{1}{1-\exp(-hc\nu/kT)}, \quad (1)$$

where ν is the frequency displacement of a Raman line from that of the radiating wave; T, the absolute temperature; h, the Planck constant; k, the Boltzmann constant, and c, the velocity of light. The calculated relative values, s/s_{291}, are summarized in Table 1, where the s value at 291 K is taken as the standard.

The local-field correction in the Raman scattering, L, of the Eckhardt type may be expressed as[16]

$$L = \left(\frac{n^2+2}{3}\right)^4, \quad (2)$$

where n is the refractive index at the Stokes frequency. The calculated relative values of the local-field correction factors, L/L_{291}, are summarized in Table 1, where L at 291 K is taken as the standard. In the calculation, the refractive indices for the different temperatures were estimated from the density values found in the International Critical Tables and the empirical Eykman equation:

$$\frac{n^2-1}{n+0.4} = \frac{d}{M} \times C, \quad (3)$$

where C is a constant characteristic for a molecule, M, the molecular weight, and d, the density.[17]

Finally, the products of L, s, and d were calculated. They are summarized in Table 1 (designated as (Lsd)). The relative values, $(Lsd)/(Lsd)_{291}$, are expected to agree with those of the relative intensity, I/I_{291}, if the factors considered here contribute mainly to the apparent intensity change resulting from the change in the temperature. Actually, the agreement between these two sets of values is excellent.

Table 2. ν_8 Line of acetonitrile

T/K	d/d_{290}	s/s_{290}	L/L_{290}	Lsd/Lsd_{290}	I/I_{290}
290	1.000	1.000	1.000	1.000	1.000
301	0.981	1.016	0.980	0.977	0.950
305	0.974	1.022	0.974	0.969	0.929
314	0.963	1.031	0.962	0.955	0.900

ν_8 Line of Acetonitrile. The same procedure was applied to the ν_8 line of liquid acetonitrile in the temperature range from 290 to 314 K. The results are summarized in Table 2. It may be seen from the table that the apparent intensity ratio, I/I_{290}, of this line decreases about 10% as the temperature changes from 290 to 314 K, where the relative intensity at 290 K is chosen as the standard. On the other hand, the calculated correction factor, $(Lsd)/(Lsd)_{290}$, decreases only 5% within the same temperature range. The disagreement between these two sets of values is in good contrast with the excellent agreement found for the ν_1 line of carbon tetrachloride and can be ascribed mostly to the physical property of acetonitrile. Therefore, we will focus our attention on the role of the large dipole moment of acetonitrile in a consideration of the temperature dependence of the apparent intensities.

It has been shown in our previous report[12] that the apparent Raman intensity can be affected by the transition hyperpolarizability in the presence of an averaged molecular field produced by the dipole moments of the surrounding molecules. According to the theory, the Raman scattering cross section corresponding to the ν_8 line of acetonitrile, $\Omega(CH_3CN; \nu_8)$, is expressed as

$$\Omega(CH_3CN; \nu_8) \propto \frac{14}{15}(B + A\langle F_{oz}\rangle_{av}), \quad (4)$$

where

$$A = 2\{{}^{Q_8}(\alpha_1^\circ)_{xy}\,{}^{Q_8}(\beta_1^\circ)_{xyz} + {}^{Q_8}(\alpha_1^\circ)_{yz}\,{}^{Q_8}(\beta_1^\circ)_{yzz}\},$$
$$B = {}^{Q_8}(\alpha_1^\circ)_{xy}^2 + {}^{Q_8}(\alpha_1^\circ)_{yz}^2.$$

In the above equations, ${}^{Q_8}(\alpha_1^\circ)_{ij}$ and ${}^{Q_8}(\beta_1^\circ)_{ijk}$ are the i,j-element of the transition polarizability and the i,j,k-element of the transition hyperpolarizability tensor related with the normal coordinate, Q_8, respectively, and the i, j, and k refer to the molecular fixed Cartesian coordinates, with the molecular axis being chosen as the z-axis. In the case of the ν_8 line of acetonitrile, the A and B of Eq. 4 have been determined experimentally as

$$A = 15.308 \times 10^{-10}\ (\text{Å}^6\,\text{dyn}^{-1}\,\text{esu}),$$
$$B = 1.66 \times 10^{-3}\ (\text{Å}^6),$$

from the observation of the concentration dependence of the Raman intensity. $\langle F_{0z}\rangle_{av}$ is the averaged electric field produced at the position of a molecule by the influence of the surrounding molecules.

There are various types of intermolecular interactions which produce electric fields at the position of a given molecule in a liquid. The simplest and most important of these is the interaction of a dipole-dipole type. A molecule with a dipole moment affects the orientational distribution of surrounding molecules through dipole-dipole interactions. This results in the appearance of a non-zero averaged electric field at the position of the central dipole. For a pure liquid, this averaged electric field has been calculated to be[13]

$$\langle F_{0z}\rangle_{av} = \frac{4\pi^2}{27} N_a^2 \frac{\mu_0^3}{kT} \frac{\rho^2}{W_m^2} + \frac{2\pi^2}{25\times 243} N_a^2 \frac{\mu_0^7}{(kT)^3} \frac{\rho^4}{W_m^4}, \quad (5)$$

where μ_0 is a permanent dipole moment; ρ, the density; W_m, the molecular weight; k, the Boltzmann constant; T, the absolute temperature, and N_a the Avogadro number. Using the permanent dipole moment value of 3.92 D observed for acetonitrile,[18] the $\langle F_{0z}\rangle_{av}$ value is calculated to be of the order of 10^5 dyn esu^{-1}; the detailed results are shown in Table 3. Obviously, the $\langle F_{0z}\rangle_{av}$ value is temperature-dependent. By inserting the numerical values of A, B, and $\langle F_{0z}\rangle_{av}$ into Eq. 4, the relative magnitudes of the scattering cross sections were calculated for the various temperatures. Obviously, the calculated relative scattering cross sections, Ω/Ω_{290}, are temperature-dependent. The products of the calculated relative scattering cross sections, Ω/Ω_{290}, and the relative correction factors, Lsd/Lsd_{290}, are in good agreement with the observed

Table 3. Averaged molecular field and Raman intensity for ν_8 line of acetonitrile

T/K	$\langle F_{0z}\rangle_{av}$ (dyn esu^{-1})	Ω/Ω_{290}	$\frac{\Omega \cdot Lsd}{\Omega_{290} \cdot Lsd_{290}}$	I/I_{290}
290	4.31×10^5	1.000	1.000	1.000
301	3.81×10^5	0.967	0.944	0.950
305	3.66×10^5	0.957	0.927	0.929
314	3.40×10^5	0.940	0.900	0.900

relative intensities, I/I_{290}. This result shows that the transition hyperpolarizability derivative plays an important role in producing the apparent temperature dependence of the Raman intensity under the existence of a considerable magnitude of $\langle F_{0z}\rangle_{av}$.

ν_3 Line of Chloroform. Exactly the same procedures were applied to the ν_3 line of liquid chloroform. The results are summarized in Table 4. It can be seen from the table that the relative intensity of this line decreases about 8% as the temperature changes from 292 to 320 K, while the calculated correction factor, $(Lsd)/(Lsd)_{292}$, decreases about 3%. It is clear that the discrepancy between the observed and the calculated intensity ratios can hardly be explained by the effect of the averaged molecular field, $\langle F_{0z}\rangle_{av}$.

Table 4. ν_3 Line of choroform

T/K	d/d_{292}	s/s_{292}	L/L_{292}	Lsd/Lsd_{292}	I/I_{292}
292	1.000	1.000	1.000	1.000	1.000
305	0.983	1.013	0.977	0.973	0.974
312	0.975	1.022	0.966	0.963	0.950
320	0.964	1.032	0.954	0.950	0.923

The scattering cross section of this line, including the effect of the averaged molecular field, can be expressed as[12]

$$\Omega(CHCl_3;\nu_3) \propto \frac{1}{15}(B+A\langle F_{0z}\rangle_{av}),$$

where

$$\begin{aligned} A &= 18^{Q_3}(\alpha_1^0)_{xx}{}^{Q_3}(\beta_1^0)_{xxz} + 8^{Q_3}(\alpha_1^0)_{zz}{}^{Q_3}(\beta_1^0)_{zzz} \\ &\quad + 2^{Q_3}(\alpha_1^0)_{xx}{}^{Q_3}(\beta_1^0)_{zzz} + 2^{Q_3}(\alpha_1^0)_{zz}{}^{Q_3}(\beta_1^0)_{xxz}, \qquad (6) \\ B &= 9^{Q_3}(\alpha_1^0)_{xx}^2 + 2^{Q_3}(\alpha_1^0)_{xx}{}^{Q_3}(\alpha_1^0)_{zz} + 4^{Q_3}(\alpha_1^0)_{zz}^2. \end{aligned}$$

The magnitude of $\langle F_{0z}\rangle_{av}$ can be calculated from Eq. 5 using the dipole moment value of 1.05 D for chloroform.[19] The $\langle F_{0z}\rangle_{av}$ value of chloroform is of the order of 10^3 dyn esu^{-1}, which is about hundredth of that for acetonitrile. As the magnitude of A for chloroform may be expected to be as large as that for acetonitrile, the effect of $\langle F_{0z}\rangle_{av}$ on the Raman intensity is negligibly small. Therefore, the discrepancy between the observed and the calculated intensity ratios corresponds to the real change in the transition polarizability of this line on passing from 292 to 320 K; this can be explained with respect to the direct intermolecular interactions, such as the break-down of hydrogen bonding between chloroform molecules in the liquid phase on the elevating of the temperature. It is important to add that the relative intensity changes its magnitude about 20% as the temperature changes from 297 to 313 K in the case of the ν_2 line of liquid chloroform, while the correction factor, $(Lsd)/(Lsd)_{297}$ decreases only 6%.[14] This discrepancy may originate from the same type of intermolecular interaction.

Averaged Molecular Field and Conclusions. A few important conclusions can be drawn from the present results. In most cases, the effects of the L, s, and d factors make the observed Raman intensities temperature-dependent. When a component molecule has a large dipole moment, the Raman intensity is temperature-dependent because of the existence of a non-zero averaged molecular field, $\langle F_{0z}\rangle_{av}$, in the liquid phase. If the magnitude of $\langle F_{0z}\rangle_{av}$ is of the order of 10^5 dyn esu^{-1} or more, the Raman intensity is determined not only by the transition polarizabilities (the first term of Eq. 4 or 6) but also by the transition hyperpolarizabilities (the second term of Eq. 4 or 6).

References

1) K. S. Sehardi and R. N. Jones, *Spectrochim. Acta*, **19**, 1013 (1963).
2) P. N. Schatz, *Spectrochim. Acta*, **21**, 617 (1965).
3) S. R. Polo and M. K. Wilson, *J. Chem. Phys.*, **23**, 2376 (1955).
4) H. E. Hallman, "Infrared Spectra and Molecular Structure," Chapt. XII, Elsevier, N.Y. (1963).
5) A. A. Clifford and B. L. Crawford, Jr., *J. Phys. Chem.*, **70**, 1536 (1966).
6) T. Fujiyama and B. L. Crawford, Jr., *J. Phys. Chem.*, **72**, 2174 (1968).
7) M. Yasumi, *Bull. Chem. Soc. Jpn.*, **28**, 489 (1955).
8) S. Maeda and P. N. Schatz, *J. Chem. Phys.*, **35**, 1617 (1961).
9) J. V. White and W. M. Ward, *Anal. Chem.*, **37**, 268 (1965).
10) T. Fujiyama, J. Herrin, and B. L. Crawford, Jr., *Appl. Spectrosc.*, **24**, 9 (1970).
11) W. J. Potts, Jr., "Chemical Infrared Spectroscopy," Vol. 1, John Wiley & Sons, N.Y. (1963).
12) J. Koike, T. Suzuki, and T. Fujiyama, *Bull. Chem. Soc. Jpn.*, **49**, 2724 (1976).
13) M. Kakimoto and T. Fujiyama, *Bull. Chem. Soc. Jpn.*, **48**, 2258; **49**, 3003 (1975).
14) T. Fujiyama, *Bull. Chem. Soc. Jpn.*, **46**, 87 (1973). In this report, one of the present authors (TF) made a serious mistake. In the report, "the 367 cm^{-1} line of liquid chloroform" should be read "the 672 cm^{-1} line of liquid chloroform."
15) International Critical Tables, McGraw-Hill Book Company, Vol. III, N. Y. (1928), pp. 27ff.
16) G. Eckhardt and W. G. Wagner, *J. Mol. Spectrosc.*, **19**, 144 (1968).
17) Weissberger *et al.*, "Organic Solvents, Technique of Organic Chemistry," Interscience Publishers, N. Y. (1955), Vol. VII.
18) S. N. Ghosh, R. Trambarulo, and W. Gordy, *Phys. Rev.*, **87**, 172 (1952); *J. Chem. Phys.*, **21**, 308 (1953).
19) C. P. Smyth and O. S. Morgan, *J. Am. Chem. Soc.*, **50**, 1547 (1928).

Charge-transfer Absorption of Complex TCNQ Anion Radical Salts: $(Cs^+)_2(TCNQ)_3^{\cdot -}$ and $(Morpholinium^+)_2(TCNQ)_3^{\cdot -}$

Yôichi IIDA

Department of Chemistry, Faculty of Science, Hokkaido University, Sapporo 060

(Received July 29, 1977)

The charge-transfer transition between ion radical molecules is known to take place in solid ion radical salts. The present paper describes some spectroscopic features of the charge-transfer absorptions observed in complex anion radical salts of $(Cs^+)_2(TCNQ)_3^{\cdot -}$ and $(Morpholinium^+)_2(TCNQ)_3^{\cdot -}$. A one-dimensional Hubbard model consisting of equivalent sites with less than half-occupied orbitals was applied to those systems in order to explain the transition energy and the line shape of the charge-transfer absorptions.

In a number of solid ion radical salts, the planar ion-radical molecules are known to form, in themselves, a face-to-face stacking into infinite one-dimensional columns so as to make a large overlap between their half-occupied molecular orbitals.[1–11] In this case, since any individual radical molecule interacts through charge-transfer most strongly with two other neighboring radicals, the electronic spectrum of the solid salt differs distinctly from the monomer spectrum of the radical ion in solution but shows a charge-transfer transition between ion radicals in the low-energy region.[8–11]

It is well known that 7,7,8,8-tetracyanoquinodimethane (TCNQ) forms chemically-stable crystalline anion radical salts with various diamagnetic counter cations.[1–9] We can obtain two kinds of TCNQ anion radical salts depending on their chemical composition.[6–9] One belongs to simple anion radical salts where each TCNQ has one unpaired electron. Another is called complex anion radical salts, which include not only TCNQ anion radicals but also formally neutral TCNQ molecules. In a previous paper,[12] we studied the optical properties of the charge-transfer absorption of simple TCNQ anion radical salts. We applied the one-dimensional Hubbard model to the columns of TCNQ anion radicals by assuming equivalent sites with half-occupied orbitals, and investigated the character of the intermolecular charge-transfer absorption by using a Green's function method. On the other hand, in complex TCNQ anion radical salts, each TCNQ species no longer has one unpaired electron because of the existence of formally neutral TCNQ molecules. In the present paper, by the use of an approach similar to our previous work,[12] we examined the spectroscopic features of charge-transfer transition between TCNQ anion radicals for one-dimensional system of sites with less than half-occupied orbitals. The transition energy and the theoretical line shape of the charge-transfer absorption were derived and were compared with those observed in such complex salts as $(Cs^+)_2(TCNQ)_3^{\cdot -}$ and $(Morpholinium^+)_2(TCNQ)_3^{\cdot -}$.[9]

Results

In order to describe a narrow energy band with strong electron correlation in crystalline ion radical salts, we consider a system of electrons expressed by the Hubbard Hamiltonian;[13–15]

$$\mathcal{H} = \sum_{i,j,\sigma} t_{ij} C_{i\sigma}^{+} C_{j\sigma} + I \sum_{i} n_{i\downarrow} n_{i\uparrow}, \qquad (1)$$

where $n_{i\sigma}=C_{i\sigma}^{+}C_{i\sigma}$, and $C_{i\sigma}^{+}$ and $C_{i\sigma}$ are the creation and annihilation operators of an electron with σ-spin at the i-th site, respectively, and where t_{ij} is the transfer matrix element between the i-th and j-th sites, and the intra-site Coulomb repulsive potential, I, appears only when two electrons with up and down spins are on the same site. Hereafter, we confine our system within the framework of the one-particle Green's function given by Hubbard in his first paper (it is often referred to as Hubbard I),[13] and consider one-dimensional stacks of ion radical molecules in the solid state. For the sake of simplicity, we assume a non-alternant linear chain of equivalent sites for which the transfer matrix element is taken only between nearest neighbor sites and is denoted by $T(<0)$, and we only consider the charge-transfer transition between ion radicals. According to the previous paper,[12] the charge-transfer absorption due to the transition of electrons with up spin in such one-dimensional column is given by $\mathrm{Re}\,\sigma_{xx}(\omega) \propto \mathrm{Re}\,\sigma^{+}(\omega) + \mathrm{Re}\,\sigma^{-}(\omega)$;

$$\mathrm{Re}\,\sigma^{\pm}(\omega) = \frac{e^2}{2} \frac{I^2 n_{\downarrow}(1-n_{\downarrow})}{\omega^2 \sqrt{\omega^2 - 4I^2 n_{\downarrow}(1-n_{\downarrow})}} \times \sqrt{4T^2 - \{-(2n_{\downarrow}-1)I \pm \sqrt{\omega^2 - 4I^2 n_{\downarrow}(1-n_{\downarrow})}\}^2}\,\theta_{\pm}(\omega), \qquad (2)$$

where ω is the frequency of electromagnetic wave absorbed by electrons with up spin and $n_{\downarrow}=\langle n_{i\downarrow}\rangle$ is the mean number of electrons with down spin per site, and where $\theta_{\pm}(\omega)$ is the term related to Fermi distribution function. When the intra-site Coulomb repulsion energy is much greater than the observed temperature, we can well put $\theta_{\pm}(\omega)=1$. If we assume paramagnetic state (*i.e.*, $n_{\downarrow}=n_{\uparrow}$) for our system, an expression of the absorption analogous to Eq. 2 is obtained for electrons with down spin. Therefore, we only consider the absorption due to electrons with up spin, as given in Eq. 2.

Let us examine how the optical absorption of Re $\sigma^{+}(\omega)$ and Re $\sigma^{-}(\omega)$ depends on $n_{\downarrow}$. From Eq. 2, if $2|T| \geq (2n_{\downarrow}-1)I$, that is, if $-T/I+1/2 \geq n_{\downarrow} \geq T/I+1/2$, both Re $\sigma^{+}(\omega)$ and Re $\sigma^{-}(\omega)$ make contribution to the charge-transfer absorption of Re $\sigma_{xx}(\omega)$. We can see that both Re $\sigma^{+}(\omega)$ and Re $\sigma^{-}(\omega)$ have a sharp divergent peak at the energy $\omega_0=2I\sqrt{n_{\downarrow}(1-n_{\downarrow})}$, where the spectra have a van Hove singularity in the lower energy side. They have no absorption in the energy region below ω_0, but have absorption in the energy region above ω_0. The absorption intensities of Re $\sigma^{+}(\omega)$ and Re $\sigma^{-}(\omega)$ are the greatest at $\omega=\omega_0$, and decrease

progressively with increasing ω. For Re $\sigma^+(\omega)$, the maximum frequency at which absorption can occur is at $\omega_-=\sqrt{4T^2-4IT(2n_\downarrow-1)+I^2}$ where the intensity becomes zero, and the spectrum has a shoulder in the energy region between ω_0 and ω_-. On the other band, for Re $\sigma^-(\omega)$, the maximum frequency takes place at $\omega_+=\sqrt{4T^2+4IT(2n_\downarrow-1)+I^2}$ where the intensity drops to zero, and the spectrum has a shoulder in the energy region between ω_0 and ω_+. Since Re $\sigma_{xx}(\omega)$ consists of the superposition of Re $\sigma^+(\omega)$ and Re $\sigma^-(\omega)$, the charge-transfer absorption spectrum of our system does not have a simple line shape, but has a structure due to the different line shapes of Re $\sigma^+(\omega)$ and Re $\sigma^-(\omega)$. In the case of $n_\downarrow=1/2$, however, as we can see from Eq. 2, Re $\sigma^+(\omega)$ coincides with Re $\sigma^-(\omega)$, so that the charge-transfer absorption of Re $\sigma_{xx}(\omega)$ can be described by a simple line shape of 2Re $\sigma^+(\omega)$ or 2Re $\sigma^-(\omega)$.

Next, we consider the case of $2|T|<(2n_\downarrow-1)I$, that is, $n_\downarrow>-T/I+1/2$ or $n_\downarrow<T/I+1/2$. In the case of $n_\downarrow>-T/I+1/2$, the charge-transfer absorption of Re $\sigma_{xx}(\omega)$ comes solely from Re $\sigma^+(\omega)$, and there is no contribution of Re $\sigma^-(\omega)$ to Re $\sigma_{xx}(\omega)$. We can easily see from Eq. 2 that, for Re $\sigma^+(\omega)$, the minimum value of ω takes place at $\omega_+=\sqrt{4T^2+4IT(2n_\downarrow-1)+I^2}$, where Re $\sigma^+(\omega)=0$ and no discontinuity exists. As ω increases slightly, Re $\sigma^+(\omega)$ rises very steeply and takes the greatest value of Re $\sigma^+(\omega)$ at the energy just above ω_+. As ω further increases, Re $\sigma^+(\omega)$ decreases progressively and has a shoulder, falling down to zero at $\omega_-=\sqrt{4T^2-4IT(2n_\downarrow-1)+I^2}$. Then, the charge-transfer absorption of Re $\sigma_{xx}(\omega)$ ranges from ω_+ to ω_- with no discontinuity. On the other hand, in the case of $n_\downarrow<T/I+1/2$, the situation is reversed, and the charge-transfer absorption of Re $\sigma_{xx}(\omega)$ comes solely from Re $\sigma^-(\omega)$. The spectrum ranges from $\omega_-=\sqrt{4T^2-4IT(2n_\downarrow-1)+I^2}$ to $\omega_+=\sqrt{4T^2+4IT(2n_\downarrow-1)+I^2}$ with no discontinuity. Re $\sigma^-(\omega)$ has the greatest value at the frequency just above ω_-, and has a shoulder in the region between ω_- and ω_+. It is interesting to note from Eq. 2 that, except for Fermi distribution term, Re $\sigma^-(\omega)$ for $n_\downarrow$ has properties symmetrical to those of Re $\sigma^+(\omega)$ for $1-n_\downarrow$.

In the previous paper,[12] we have already examined the charge-transfer absorption for the system of $n_\downarrow=1/2$. Therefore, in the present paper, we will discuss, as a case of $n_\downarrow\neq1/2$ system, the optical properties of complex TCNQ anion radical salts with composition ratio of (2: 3) such as $(Cs^+)_2(TCNQ)_3^{-}$ or (Morpholinium$^+$)$_2$(TCNQ)$_3^{-}$. In these systems, three TCNQ molecules share two unpaired electrons. According to X-ray analysis data reported by Arthur *et al.*,[2,3] the crystal structure of $(Cs^+)_2(TCNQ)_3^{-}$ belongs to the monoclinic system with space group $P2_1/c$. The crystal structure reported by them is shown in Fig. 1. The structure consists of one-dimensional columns of TCNQ molecules parallel to the b axis with a plane-to-plane stacking. The caesium cations occupy sites between TCNQ columns in such a manner that each Cs^+ ion is surrounded by eight nitrogen atoms at the corners of a distorted cube. In one-dimensional stacking of TCNQ molecules, however, the sites are crystallographically no longer equivalent and TCNQ molecules form a triad; in a unit cell two rather ionic TCNQ anions are at non-centric positions and one rather neutral TCNQ molecule is at centric position.[3] On the other hand, the crystal structure of (Morpholinium$^+$)$_2$(TCNQ)$_3^{-}$ was determined by Sundaresan and Wallwork.[5] The arrangements of TCNQ molecules were found to be very similar to those of the caesium salt. In both of these anion radical salts, the charge distribution of unpaired electrons depends on the sites, but our present model for the charge-transfer absorption given in Re $\sigma_{xx}(\omega)$ and Eq. 2 is based on homogeneous charge distribution of the electrons along one-dimensional column. This point will be further discussed in the following section. In order to examine the applicability of our model and to explain the character of the charge-transfer absorptions observed in those solid salts, we proceed to consider the system of $(Cs^+)_2(TCNQ)_3^{-}$ or (Morpholinium$^+$)$_2$(TCNQ)$_3^{-}$ in terms of one-dimensional column consisting of equivalent TCNQ sites where each TCNQ species carries a formal charge of $-2/3$.

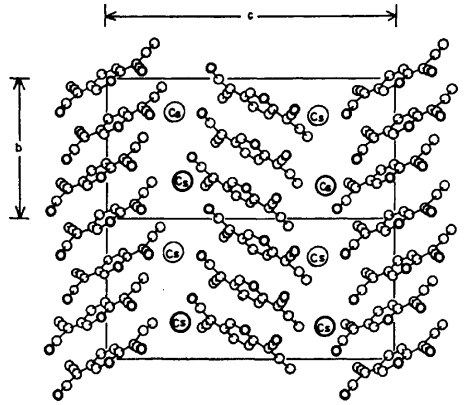

Fig. 1. View of the crystal structure of $(Cs^+)_2(TCNQ)_3^{-}$ reported by Chesnut and Arthur and by Fritchie and Arthur. See Refs. 2 and 3.

On the other hand, neutral TCNQ molecule is almost planar, and has sixteen molecular orbitals for sixteen $2p\pi$ electrons.[16] Then, in the ground state of $TCNQ^{-2/3}$, the molecular orbitals from the lowest to the 8 th are fully occupied, while 2/3 unpaired electron is in the 9 th molecular orbital. The other molecular orbitals are vacant orbitals. In the column of TCNQ molecules, we take only the 9 th molecular orbital with the 2/3 unpaired electron for one site of TCNQ molecule, and assume a model of non-alternant one-dimensional column composed of infinite number of such sites. In this model, each TCNQ molecular site is composed of one identical molecular orbital with equal energy level, and there is 2/3 electron per each site. Then, we have $n_\downarrow=1/3$ if we assume paramagnetic state for our system. Under these situations, we consider the optical absorption (intermolecular charge-transfer absorption) of crystalline $(Cs^+)_2(TCNQ)_3^{-}$ and (Morpholinium$^+$)$_2$(TCNQ)$_3^{-}$ as expressed by Re $\sigma_{xx}(\omega)$ and Eq. 2. At this time, we have two possibilities for the system of $n_\downarrow=1/3$, depending on the magnitudes of I and T. If $|T|\geq(1/6)I$, the charge-transfer absorption will come from the case of $-T/I+1/2\geq n_\downarrow\geq T/I+1/2$. In this case, as has been mentioned, Re $\sigma_{xx}(\omega)$ has two contributions of Re

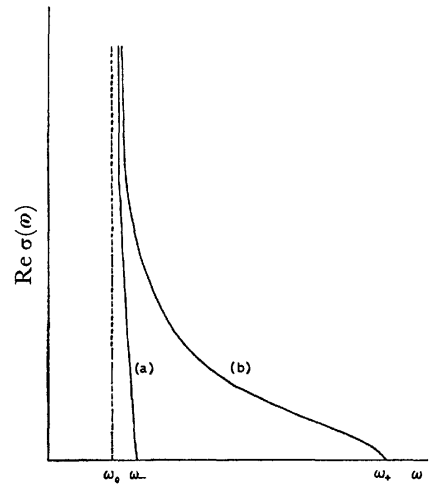

Fig. 2. The intermolecular charge-transfer absorption spectrum Re $\sigma_{xx}(\omega) \propto$ Re $\sigma^+(\omega)$+Re $\sigma^-(\omega)$, as given by Eq. 2 for the $n_\downarrow = 1/3$ system with $|T| \geq (1/6)I$, where (a) Re $\sigma^+(\omega)$, (b) Re $\sigma^-(\omega)$, $\omega_0 = (2/3)\sqrt{2}\,I$, and $\omega_\pm = \sqrt{4T^2 \mp 4IT/3 + I^2}$. See text.

$\sigma^+(\omega)$ and Re $\sigma^-(\omega)$; both of them have a divergent peak at $\omega_0 = 2\sqrt{2}\,I/3$. The Re $\sigma^+(\omega)$ component converges to zero at $\omega_- = \sqrt{4T^2+4IT/3+I^2}$, while the Re $\sigma^-(\omega)$ component, at $\omega_+ = \sqrt{4T^2-4IT/3+I^2}$. Since $T<0$ and $\omega_- < \omega_+$, the band width is determined by $\omega_+ - \omega_0$. Then, the spectrum of the charge-transfer absorption, Re $\sigma_{xx}(\omega)$, is given by the superposition of Re $\sigma^+(\omega)$ and Re $\sigma^-(\omega)$; both of them are shown in Fig. 2. On the other hand, if $|T| < (1/6)I$, the charge-transfer absorption corresponds to the case of $n_\downarrow < T/I + 1/2$. In this case, Re $\sigma_{xx}(\omega)$ comes solely from Re $\sigma^-(\omega)$, which ranges from $\omega_- = \sqrt{4T^2+4IT/3+I^2}$ to $\omega_+ = \sqrt{4T^2-4IT/3+I^2}$ with no discontinuity, and has absorption maximum at the energy just above ω_-. Then, the spectrum of the charge-transfer absorption, Re $\sigma_{xx}(\omega)$, is schematically given in Fig. 3.

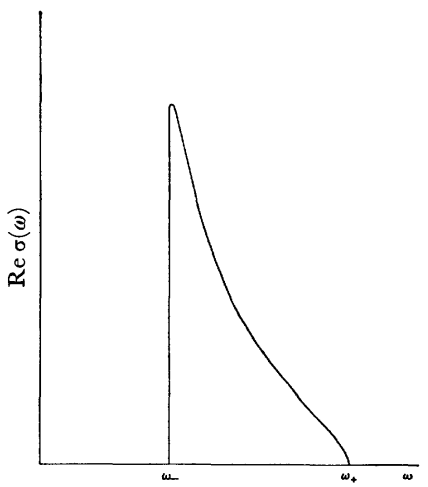

Fig. 3. The intermolecular charge-transfer absorption spectrum Re $\sigma_{xx}(\omega) \propto$ Re $\sigma^-(\omega)$, as given by Eq. 2 for the $n_\downarrow = 1/3$ system with $|T| < (1/6)\,I$, where $\omega_\pm = \sqrt{4T^2 \mp 4IT/3 + I^2}$. See text.

Discussion

Let us compare these theoretical predictions with the experimental electronic spectra of crystalline $(Cs^+)_2(TCNQ)_3^{--}$ and $(Morpholinium^+)_2(TCNQ)_3^{--}$. In a previous paper,[9] we measured those electronic spectra by means of diffuse reflection method. The observed spectra are reproduced in Fig. 4. The Kubelka-Munk function, $f(R) = (1-R)^2/2R$, where R is the reflectance and $f(R)$ is proportional to the absorbance, was plotted *versus* wave number (10^3 cm^{-1} unit).

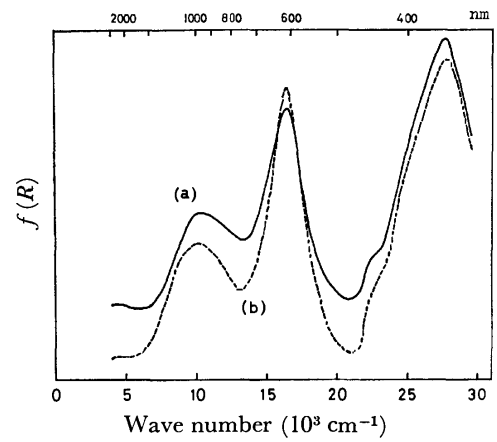

Fig. 4. The experimental results on the diffuse reflection spectra of the solid salts of (a) $(Cs^+)_2(TCNQ)_3^{--}$ and (b) $(Morpholinium^+)_2(TCNQ)_3^{--}$, where the value of Kubelka-Munk function, $f(R) = (1-R)^2/2R$, was plotted *versus* wave number. See Ref. 9.

In the case of $(Cs^+)_2(TCNQ)_3^{--}$, the solid-state spectrum has four absorptions in the energy region from 5000 to 30000 cm^{-1}. The absorptions at 27500 and 16200 cm^{-1} are the shifted bands of the monomer spectrum of the TCNQ anion radical at 22800 and 11900 cm^{-1}, respectively, while the low-energy band at 10100 cm^{-1} characteristic of the solid salt has been assigned to the charge-transfer transition between TCNQ anion radicals in the one-dimensional column.[9] Moreover, the complex salt shows additional weak and broad absorption around the energy region of 4000—6000 cm^{-1}; this band has been assigned to the charge-transfer transition from TCNQ anion radical to the neutral TCNQ.[9] The spectroscopic features of the former three absorptions are very similar to those of simple TCNQ anion radical salts such as K^+TCNQ^-,[8,12] while the absorption around 4000—6000 cm^{-1} is characteristic of the complex salt.

The theoretical approach in the preceding section can solely explain the charge-transfer absorption due to the transition between TCNQ anion radicals, but cannot explain the other electronic transitions. Therefore, the absorption at 10100 cm^{-1} of $(Cs^+)_2(TCNQ)_3^{--}$ is of our main interest. If Re $\sigma_{xx}(\omega)$ with $|T| \geq (1/6)I$ and $-T/I+1/2 \geq n_\downarrow \geq T/I+1/2$ corresponds to this charge-transfer band, the observed peak value of 10100 cm^{-1} should be $\omega_0 = 2\sqrt{2}\,I/3$ thus giving $I = 10700$ cm^{-1}. The absorption band width is related to the $|T|$ value,

which should be larger than $(1/6)I$. If we assume $|T| \approx 0.2\,I$ for example, the theoretical band width is $\omega_+ - \omega_0 \approx 2700\ \mathrm{cm^{-1}}$. This width should only take place in the energy region higher than the absorption peak, and the charge-transfer band shape will have strong asymmetric character with respect to $\omega=\omega_0$. However, as is shown in Fig. 4, the observed charge-transfer absorption at $10100\ \mathrm{cm^{-1}}$ has almost symmetrical line shape with respect to the peak energy axis, although this band overlaps appreciably, in the higher energy region, with the $16200\ \mathrm{cm^{-1}}$ band. Therefore, the case of $|T| \geq (1/6)I$ will not be applicable to the observed charge-transfer absorption.

Next, we examine the case of $|T| < (1/6)I$ and $n_\downarrow < T/I+1/2$. If the $|T|$ value is assumed to be of the order of 0.1 I, the theoretical peak value of the absorption is very close to $\omega_- = 0.954\ I$, which will correspond to the observed peak value of $10100\ \mathrm{cm^{-1}}$. Therefore, $I = 10600\ \mathrm{cm^{-1}}$ and $|T| \approx 1100\ \mathrm{cm^{-1}}$ is estimated for this case. The I and $|T|$ values thus estimated are of quite reasonable magnitudes because of the following explanation. By the use of those I and $|T|$ values, the absorption width, $\omega_+ - \omega_-$, is estimated to be $1300\ \mathrm{cm^{-1}}$, and the absorption line shape is then given by Fig. 3 with $\omega_- = 10100\ \mathrm{cm^{-1}}$ and $\omega_+ = 11400\ \mathrm{cm^{-1}}$. As has been discussed in the previous paper,[12] for many reasons, the actual charge-transfer absorption involves certain width other than the width due to non-zero transfer matrix element, and the actual absorption has a width even in the energy region lower than ω_-. It appears that such a width is of the order of 3500—4000 $\mathrm{cm^{-1}}$ and is much larger than the width of $1300\ \mathrm{cm^{-1}}$ due to transfer matrix element. Then, with respect to the axis of peak energy, the charge-transfer absorption will have a width of 3500—4000 $\mathrm{cm^{-1}}$ in the lower-energy side and a width of 4800—5300 $\mathrm{cm^{-1}}$ in the higher-energy side. The asymmetric character of the line shape of this absorption is so weak that we can well expect almost symmetrical line shape of the charge-transfer absorption with respect to the peak energy axis. This consideration seems to agree well with the observed charge-transfer absorption of $(Cs^+)_2(TCNQ)_3^{--}$ at 10100 $\mathrm{cm^{-1}}$.

The solid-state spectrum (see Fig. 4) of (Morpholinium$^+$)$_2$(TCNQ)$_3^{--}$ has three strong absorptions at 27600, 16300, and 10000 $\mathrm{cm^{-1}}$ and a broad and weak low-energy absorption around 4000—6000 $\mathrm{cm^{-1}}$.[9] These spectroscopic features are very similar to those of the caesium salt. From the peak energy and the line shape of the charge-transfer absorption at $10000\ \mathrm{cm^{-1}}$, the magnitudes of I and $|T|$ of the morpholinium salt were found to be almost the same as the corresponding magnitudes of the caesium salt.

Our theoretical treatment for the charge-transfer absorptions of $(Cs^+)_2(TCNQ)_3^{--}$ and (Morpholinium$^+$)$_2$(TCNQ)$_3^{--}$ assumed a narrow energy band and uniform 2/3-charge distribution in equivalent site systems. This simple model only led to a single charge-transfer transition around $10000\ \mathrm{cm^{-1}}$, which may be interpreted as the transition between $TCNQ^{-2/3}$ molecules. However, another electronic transition from rather ionic TCNQ to rather neutral TCNQ is actually taking place around 4000—6000 $\mathrm{cm^{-1}}$ (see again Fig. 4). This transition thus gives strong evidence for the existence of both rather ionic and neutral TCNQ molecular species in those crystalline complex salts. It is to be noted that one cannot explain such kind of transition as long as one uses uniform charge distribution model. One way of taking those inequivalent TCNQ molecular species into consideration was made by Soos and Klein,[17] who used the modified Hubbard model to include three crystallographic sites per unit cell in one-dimensional column. Their treatment led to three bands of $N/3$ levels, and the two lower-energy bands accomodate the $2N/3$ electrons of the 1/3-filled Hubbard model. The charge-transfer transition between ionic and neutral sites was interpreted as the transition from the occupied band to the unoccupied band. Our problem will then be to find an appropriate theoretical treatment by the Green's function method for one-dimensional system consisting of inequivalent sites and to explain more quantitatively the charge-transfer transitions between ionic and neutral sites as well as those between ionic sites in $(Cs^+)_2(TCNQ)_3^{--}$ and (Morpholinium$^+$)$_2$(TCNQ)$_3^{--}$.

Some Remarks

Finally, we compare some spectroscopic features of the charge-transfer absorption of $n_\downarrow \neq 1/2$ system (complex ion radical salts) with those of $n_\downarrow = 1/2$ system (simple ion radical salts) on the basis of Re $\sigma_{xx}(\omega)$ and Eq. 2. As for the peak energy, the $n_\downarrow = 1/2$ system, where each site has one unpaired electron with paramagnetic state, has a divergent peak at $\omega_0 = I$.[12] On the other hand, the $n_\downarrow \neq 1/2$ system with $-T/I+1/2 \geq n_\downarrow \geq T/I+1/2$ has a divergent absorption peak at $\omega_0 = 2I\sqrt{n_\downarrow(1-n_\downarrow)}$, which is definitely less than the ω_0 value of the $n_\downarrow = 1/2$ system. The $n_\downarrow > -T/I+1/2$ system has absorption peak at the energy close to $\omega_+ = \sqrt{4T^2+4IT(2n_\downarrow-1)+I^2}$, while the $n_\downarrow < T/I+1/2$ system, at the energy close to $\omega_- = \sqrt{4T^2-4IT(2n_\downarrow-1)+I^2}$. For these cases, since $T<0$ and $\omega_\pm < I$, the peak energy is again smaller than the I value. Therefore, the peak energy of the charge-transfer absorption of less than half-occupied or more than half-occupied orbital system is definitely smaller than that of half-occupied orbital system.

Next, we consider the band width, which is related to the magnitudes of $|T|$ and I. Therefore, by using the constant values of $|T|$ and I, we examine how the band width of the charge-transfer absorption depends on $n_\downarrow$. For the $n_\downarrow = 1/2$ system, the band width is given by $\sqrt{I^2+4T^2} - I$.[12] In the system of $n_\downarrow \neq 1/2$, however, the band widths are $|\omega_+ - \omega_-|$ for the case of $n_\downarrow > -T/I+1/2$ or $n_\downarrow < T/I+1/2$, $\omega_- - \omega_0$ for the case of $-T/I+1/2 \geq n_\downarrow > 1/2$, and $\omega_+ - \omega_0$ for the case of $1/2 > n_\downarrow \geq T/I+1/2$. In all cases, the band width for the $n_\downarrow \neq 1/2$ system becomes much broader than the width for the $n_\downarrow = 1/2$ system. The reason is as follows. As has been discussed in the previous paper,[12] in the Hubbard Hamiltonian of Eq. 1, the unperturbed band energy, ε_k, of unpaired electron system splits into two subbands, $E_{k\sigma}^L$ and $E_{k\sigma}^U$, through correlation effect. Here, $E_{k\sigma}^L$

is the energy of an electron with σ-spin which moves about avoiding other electrons with $-\sigma$-spin, while $E_{k\sigma}{}^{U}$ is the energy of an electron which propagates mainly among sites already occupied with electrons with $-\sigma$-spin. The charge-transfer absorption is then composed of elementary transitions from $E_{k\sigma}{}^{L}$ to $E_{k\sigma}{}^{U}$ in the first Brillouin zone by conserving $\boldsymbol{k}$ and σ (*i.e.*, vertical transition). In the $n_{\downarrow}=1/2$ system, however, since the sites occupied by electrons with $-\sigma$-spin and those unoccupied exist with equal probability, the energy spectra of the two subbands have nearly the same shape. Therefore, the charge-transfer absorption of the $n_{\downarrow}=1/2$ system becomes narrow and has a steep peak at the energy $\omega=I$. On the other hand, in the case of $n_{\downarrow}>1/2$, the $E_{k\sigma}{}^{L}$ subband becomes flat but the $E_{k\sigma}{}^{U}$ subband has strong $\boldsymbol{k}$ dependence with considerable width, while in the case of $n_{\downarrow}<1/2$, the situation is reversed. Therefore, in both cases, the charge-transfer absorption spectra become much broader than that of the $n_{\downarrow}=1/2$ system.

The author wishes to express his thanks to Dr. Kenn Kubo of Tokyo Kyoiku University for his valuable discussion regarding this work.

References

1) G. R. Anderson and C. J. Fritchie, Jr., Second National Meeting, Society for Applied Spectroscopy, San Diego, Paper 111 (1963).
2) D. B. Chesnut and P. Arthur, Jr., *J. Chem. Phys.*, **36**, 2969 (1962).
3) C. J. Fritchie, Jr. and P. Arthur, Jr., *Acta Crystallogr.*, **21**, 139 (1966).
4) H. Kobayashi, Y. Ohashi, F. Marumo, and Y. Saito, *Acta Crystallogr., Sect. B*, **26**, 459 (1970), and the references cited therein.
5) T. Sundaresan and S. C. Wallwork, *Acta Crystallogr., Sect. B*, **28**, 491 (1972).
6) L. R. Melby, R. J. Harder, W. R. Hertler, W. Mahler, R. E. Benson, and W. E. Mochel, *J. Am. Chem. Soc.*, **84**, 3374 (1962).
7) W. J. Siemons, P. E. Bierstedt, and R. G. Kepler, *J. Chem. Phys.*, **39**, 3523 (1963); R. G. Kepler, *J. Chem. Phys.*, **39**, 3528 (1963).
8) Y. Iida, *Bull. Chem. Soc. Jpn.*, **42**, 71 (1969).
9) Y. Iida, *Bull. Chem. Soc. Jpn.*, **42**, 637 (1969).
10) Y. Iida, *Bull. Chem. Soc. Jpn.*, **43**, 2772 (1970); **44**, 663, 1777 (1971); **45**, 105, 624 (1972).
11) J. Tanaka, M. Tanaka, T. Kawai, T. Takabe, and O. Maki, *Bull. Chem. Soc. Jpn.*, **49**, 2358 (1976), and the references cited therein.
12) Y. Iida, *Bull. Chem. Soc. Jpn.*, **50**, 1445 (1977).
13) J. Hubbard, *Proc. R. Soc. London, Ser. A*, **276**, 238 (1963).
14) J. Hubbard, *Proc. R. Soc. London, Ser. A*, **281**, 401 (1964).
15) K. Kubo, *J. Phys. Soc. Jpn.*, **31**, 30 (1971).
16) D. A. Lowitz, *J. Chem. Phys.*, **46**, 4698 (1967).
17) Z. G. Soos and D. J. Klein, *J. Chem. Phys.*, **55**, 3284 (1971).

Studies of the Adsorbing Particle Flotation of Fe^{3+} and Cu^{2+}

Koichi KOBAYASHI,* Kenichi NATORI,** Masamizu KAMAYA,† and Tsunetaka SASAKI††

Department of Chemistry, Faculty of Science, Tokyo Metropolitan University, Setagaya, Tokyo 158

(Received July 29, 1977)

The adsorbing particle flotation of Fe^{2+} or Fe^{3+} and Cu^{2+} ions was studied by the combined use of bentonite (Bt) and a cationic surfactant, benzylhexadecyldimethylammonium chloride (BHDAC). Fe^{3+} ions were effectively floated from an aqueous solution by the use of Bt and cationic surfactant in a manner similar to the flotation by the use of sodium silicate and cationic surfactant. Most Fe^{2+} ions were found to be floated as Fe^{3+} ions, when the pH was increased by the addition of sodium hydroxide. The maximum floatability of 98% was obtained for Fe^{3+} under optimum conditions. The pH corresponding to the beginning of flotation of Fe^{3+} was influenced by the manner in which the pH of the solution was controlled. Cu^{2+} ions could also be floated, but less effectively than Fe^{3+} ions. Selective flotation of Fe^{3+} from the mixed solution of Fe^{3+} and Cu^{2+} was attempted and effectively achieved.

A limited number of studies have been reported for Fe^{3+} and Cu^{2+} ion flotation. Rubin and Johnson studied the effect of pH on the precipitation flotation of Fe^{3+} ion using an anionic surfactant, sodium dodecyl sulfate; the results were compared with a calculated precipitation flotation curve.[1] Rubin *et al.* found that Fe^{3+} ions were effectively removed from an aqueous solution by the use of sodium dodecyl sulfate.[1] They also studied the removal of Fe^{3+} and Cu^{2+} ions by octadecylamine as a function of pH.[1] Floatability of Cu^{2+} ions as $Cu_2[Fe(CN)_6]$ or the 8-quinolinol complex has also been reported.[2]

In a previous paper, it was reported that Fe^{3+} ions were effectively removed from an aqueous solution by the ion flotation using sodium silicate and a cationic surfactant, and that the floatability is greatly influenced by the order of addition of these reagents.[3] We have also reported that various kinds of heavy metal ions were more effectively floated by the combined use of bentonite and cationic surfactant than by the use of an anionic surfactant alone.[4]

In this study, therefore, the adsorbing particle flotation of Fe^{2+}, Fe^{3+}, and Cu^{2+} ions has been attempted and the effects of pH, gas-flow time, and the amount of bentonite on the floatability are reported.

Experimental

Materials. Extra-pure grade ammonium iron(II) sulfate and ammonium iron(III) sulfate, obtained from the Wako Pure Chemical Industries, Ltd. were used without further purification. The copper(II) sulfate used was an extra-pure grade $CuSO_4 \cdot 5H_2O$; it was recrystallized from distilled water. The bentonite powder (Bt) used as an ion exchanger was obtained from the Wako Pure Chemical Industries, Ltd.; the fraction passing through a 350-mesh sieve was collected and dried under reduced pressure. The benzylhexadecyldimethylammonium chloride, a product of the Kao Soap Co., Ltd., was recrystallized from acetone and was dried under reduced pressure. All other chemicals used for colorimetric determination were of analytical reagent-grade, except that the carbon tetrachloride and ammonia used were of special grade.

Apparatus and Procedure. The apparatus and method used for flotation measurements were the same as have been described previously.[5] The concentrations of Fe^{2+} and Cu^{2+} ions were determined by colorimetric methods as follows.

Iron:[6] Five cm^3 of the solution after flotation was transferred into a 25 cm^3 flask, 0.2 to 0.5 cm^3 of 0.5 mol/dm^3 H_2SO_4 was added to dissolve iron hydroxide, and 2 cm^3 of acetate buffer solution and 1 cm^3 of a 10% solution of hydroxylammonium chloride were added to insure the complete reduction of Fe^{3+} to Fe^{2+} ions. Further, 1 cm^3 of a 0.2% aqueous solution of 1, 10-phenanthroline solution was added to develop the color. After 30 min, the total volume was increased with water to 25 cm^3. The concentration of Fe^{2+} ions was then determined by the colorimeter, Bausch & Lomb, Spectronic 20, at 510 nm. The errors in the colorimetric method due to the scattering of light by Bt are of the order of $\pm 2\%$; this was taken into account by the blank experiment.

Copper:[7] 2 to 3 cm^3 of sample solution were transferred into a separatory funnel together with a little water. To this solution were added 5 cm^3 of 20% aqueous solution of ammonium citrate and 2—3 drops of Tymol Blue solution. The mixed solution was adjusted to pH 9.0—9.2 with ammonia, and the total volume was then made 50 cm^3 with water. To this solution was added 1 cm^3 of 1% aqueous solution of sodium diethyldithiocarbamate. The concentration of Cu^{2+} ions extracted in carbon tetrachloride solution was determined by using the colorimeter at 440 nm.

A humidified nitrogen gas was bubbled through a sintered glass plate (No. 4) at the gas-flow rate of 10 cm^3/min. The measurements were conducted at the room temperature of about 25 °C. Floatability was expressed as the percentage of the sublate floated.

Results and Discussion

Ion Flotation of Fe. Floatability and Gas-flow Time: Figure 1 shows the effects of gas-flow time on floatability for the solution containing 1.8×10^{-4} mol/dm^3 Fe^{2+} (which floated as Fe^{3+} ions, as will be mentioned later), 5.0×10^{-5} mol/dm^3 BHDAC, and 1.0×10^{-2}% Bt at the optimum floatability of pH=10.7. It can be seen that the floatability attains a steady value after 1.5 min. Accordingly, all subsequent experiments were made at a gas-flow rate of 10 cm^3/min and a gas-flow time of 2 min

* Present address: Laboratory of Chemistry, Musashi Institute of Technology, 1-28-1, Tamatsutsumi, Setagaya, Tokyo 158.

** Present address: Kao Soap Co., Ltd., 1-1, Kayaba-cho, Nihonbashi, Chuo-ku, Tokyo 103.

† Present address: Asahi Kasei Co., Ltd., Yako, Kawasaki-ku, Kawasaki, Kanagawa 210.

†† Present address: Department of Chemistry, Faculty of Science, Tokai University, Hiratsuka, Kanagawa 259-12.

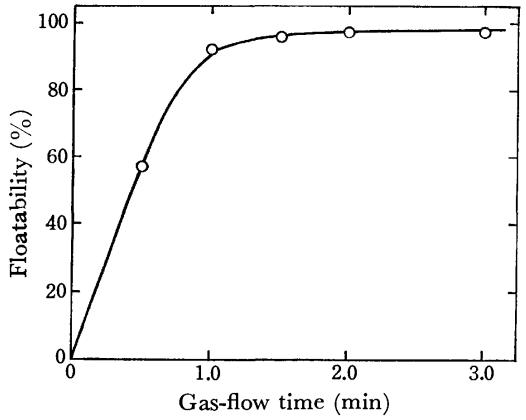

Fig. 1. Effect of gas-flow time on Fe^{3+} floatability.
Fe^{3+}: 1.8×10^{-4} mol/dm^3, BHDAC: 5.0×10^{-5} mol/dm^3, Bt: 1.0×10^{-2}%, pH: 10.7.

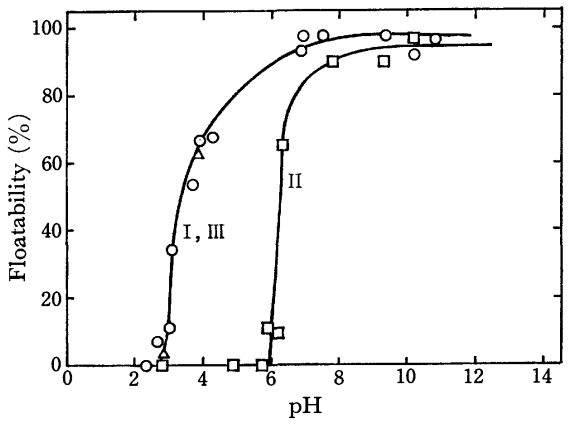

Fig. 2. Effect of pH on Fe^{3+} floatability.
Fe^{2+}: 1.8×10^{-4} mol/dm^3, BHDAC: 5.0×10^{-5} mol/dm^3, Bt: 1.0×10^{-2}%, gas-flow time: 2 min.
I, ○: Aqueous solution prepared by dissolving ammonium iron(II) sulfate in dilute sulfuric acid (pH 2.3) and increasing pH by NaOH.
II, □: Aqueous solution prepared by dissolving ammonium iron(II) sulfate in distilled water (pH 5.7) and increasing pH by NaOH decreasing pH by H_2SO_4.
III, △: Aqueous solution prepared by dissolving ammonium iron(II) sulfate in distilled water(pH 5.7), adjusting pH 2 by H_2SO_4, and raising pH by NaOH.

unless stated otherwise.

Floatability and pH: In order to study the effect of pH on floatability, the flotation was carried out under the conditions of 1.8×10^{-4} mol/dm^3 Fe^{2+}, 5.0×10^{-5} mol/dm^3 BHDAC and 1.0×10^{-2}% Bt. This composition of flotation agents is modeled on the optimum composition of Co^{2+} ion flotation mentioned in a preceding paper.[8] The results are shown in Fig. 2. In Fig. 2, the circles (system I) show the floatability of Fe^{2+} ions from aqueous solutions of varying pH, which were obtained by dissolving ammonium iron(II) sulfate in an aqueous sulfuric acid at pH 2.3 and then increasing the pH by adding sodium hydroxide. The squares (system II) show the floatability of Fe^{2+} ions from an aqueous solution prepared by dissolving ammonium iron(II) sulfate in distilled water of pH 5.7 and adjusting the pH by sodium hydroxide for higher pH and sulfuric acid for lower pH. The triangles (system III) show the floatability of Fe^{2+} ions from an aqueous solution prepared by dissolving ammonium iron(II) sulfate in distilled water of pH 5.7, followed by decreasing the pH to 2 by sulfuric acid and then increasing the pH by the addition of sodium hydroxide.

In the case of systems I and III, the floatabilities increase sharply at pH 3, and reach 95% at pH 6 and above; in the case of system II, the floatability increases sharply by the slight addition of sodium hydroxide only from pH 6 and reaches 95% at pH 8 and above. Generally, metal ions are known to be floated effectively from a solution whose pH value corresponds to the beginning of metal hydroxide formation.[1] However, the present results show that the pH corresponding to the beginning of flotation is influenced by the reagent to be used for the pH control.

In order to clarify the state of the iron ions floated, the amount of Fe^{3+} ions in the sample solution was determined by the chelate titration method using EDTA.[9] The results show that the aqueous solution(I) contains 11% Fe^{3+} ions at pH 2.3, but that the aqueous solution(III), whose pH was decreased below 3 by H_2SO_4 and then increased above 3 by the addition of sodium hydroxide solution, contains 98% Fe^{3+} ions. It was also observed that the precipitate became reddish-brown at pH 3 and above by the addition of sodium hydroxide in the case of systems I and III and above pH 5.7 in the case of system II. In the case of Fe^{3+} solution using ammonium iron(III) sulfate, the floatability curve was the same as that of the systems I and III. Therefore, in the case of systems I and III, Fe^{2+} ions in ammonium iron(II) sulfate solution are considered to be oxidized almost completely to Fe^{3+} ions, as is mentioned in the literature.[10] In the case of system II, the flotation does not occur and the color of the solution does not change to reddish-brown in the pH region of 5.7 and 3. In this pH range for the conditions II, the solution is considered to be in a state of Fe^{2+} ions. Thus the beginning of the flotation and probably the formation of iron(III) hydroxide seems to

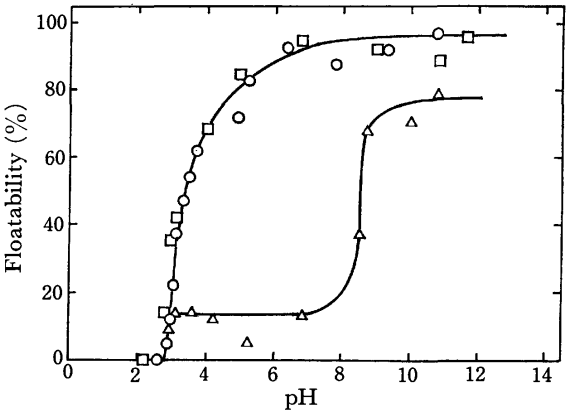

Fig. 3. Effect of pH on Fe^{3+} floatability.
Fe^{3+}: 1.8×10^{-4} mol/dm^3,
△; BHDAC: 5.0×10^{-5} mol/dm^3, gas-flow time: 2 min,
○; BHDAC: 1.0×10^{-4} mol/dm^3, gas-flow time: 7 min,
□; BHDAC: 5.0×10^{-5} mol/dm^3, gas-flow time: 2 min,
Bt: 1.0×10^{-2}%.

be influenced at least by the addition of sodium hydroxide, the reagent used for controlling pH. The reason is not clear at present.

Effect of Bentonite: In order to study the effect of Bt on Fe^{3+} ion flotation, the flotation was carried out at various pH values with and without Bt addition. The results are shown in Fig. 3. As may be seen in Fig. 3, in the system without Bt addition the floatability for the case of gas-flow time of 2 min shows a plateau of 14% in the pH region of 3 to 8, above which it sharply increases. But in the case of the system with Bt addition, as has been shown, the floatability increases sharply at about pH 3; this is shown by the squares in the figure. A marked effect of Bt addition is evident from these curves. Here the Bt acts as a bridge between positively charged iron(III) hydroxide and BHDAC, especially in the relatively low pH region. The rather rapid increase of floatability in a strongly alkaline region in the case of the system without the Bt addition in Fig. 3 may be explained by the interaction between negatively charged iron(III) hydroxide and positive BHDAC ions, as has been reported.[11] It should be mentioned, however, that when the gas-flow time is increased to 7 min, the floatability of the above system without the Bt addition is found to increase and the floatability curve coincides with that of the system I of Fig. 2, as shown by the circles in Fig. 3. The reason for this is not certain, but it is perhaps due to the flotation caused by the weak interaction between similarly charged iron(III) hydroxide and BHDAC, aided by the prolonged gas-flow time.

We have also studied in detail the flotation behavior in the relatively high pH region, and obtained the floatability of Fe^{3+} in a solution of fixed BHDAC concentration at pH 11 as a function of Bt amount added. The results are shown in Fig. 4. In Fig. 4, the floatability decreases for system I with increasing Bt concentration. The decrease of floatability is due to the uptake of BHDAC by Bt, resulting in the decomposition of the Fe hydroxide–BHDAC complex which is effective in

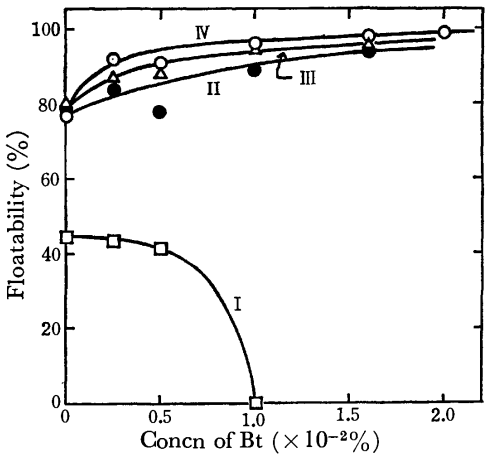

Fig. 4. Effect of Bt on Fe^{3+} floatability.
Fe^{3+}: 1.8×10^{-4} mol/dm^3, gas-flow time: 2 min,
I, □; BHDAC: 2.5×10^{-5} mol/dm^3, pH: 10.9,
II, ●; BHDAC: 5.0×10^{-5} mol/dm^3, pH: 10.9,
III, △; BHDAC: 7.5×10^{-5} mol/dm^3, pH: 10.9,
IV, ○; BHDAC: 1.0×10^{-4} mol/dm^3, pH: 11.7.

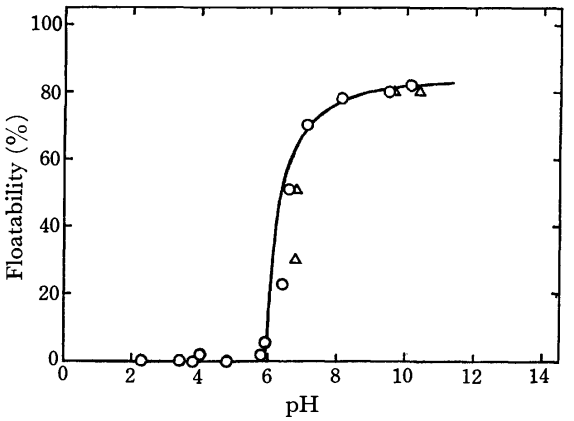

Fig. 5. Effect of pH on Cu^{2+} floatability.
Cu^{2+}: 2.0×10^{-4} mol/dm^3, BHDAC: 5.0×10^{-5} mol/dm^3, gas-flow time: 2 min, ○: 1.0×10^{-2}% Bt, △: 0.5×10^{-2}% Bt.

the flotation process. In the case of systems II, III, and IV, the floatability increases with increasing addition of BHDAC. In these systems, the presence of a sufficient amount of BHDAC ensures the flotation of negatively charged Fe-hydroxide in the presence of Bt by a mechanism similar to the flotation of permanganate anions reported in an earlier paper.[3]

Ion Flotation of Cu. Floatability and pH: The effect of pH on the floatability of Cu^{2+} ions was also measured under conditions of 2.0×10^{-4} mol/dm^3 Cu^{2+}, 5.0×10^{-5} mol/dm^3 BHDAC, and 1.0 or 0.5×10^{-2}% Bt. The results are shown in Fig. 5. It can be seen in this figure that the floatability sharply increases from zero above pH 6; this corresponds to the beginning of $Cu(OH)_2$ precipitation. The increase of the amount of Bt added has little effect, as seen by the comparison of the systems of circles and triangles in the figure. The maximum flotation obtained is not so large as that for the Fe^{3+} ions.

Effect of Bentonite: In order to study the effect of Bt, the flotation was carried out for the system without the addition of Bt and a comparison was made. The results are shown in Fig. 6, together with the system with Bt

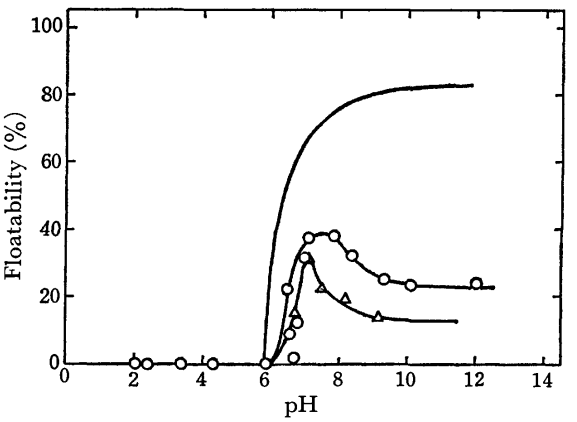

Fig. 6. Effect of pH on Cu^{2+} floatability.
Cu^{2+}: 2.0×10^{-4} mol/dm^3, BHDAC: 5.0×10^{-5} mol/dm^3, gas-flow time (○: 7 min, △: 5 min).
The solid line shows the floatability of Cu^{2+} ions from Fig. 5.

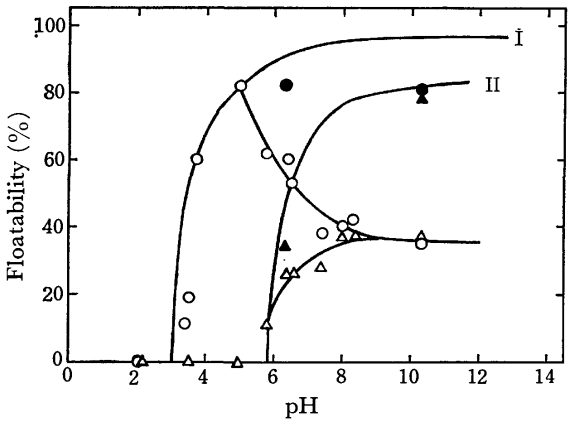

Fig. 7. Selective flotation of Fe^{3+} and Cu^{2+} ions.
Fe^{3+}: 2.0×10^{-4} mol/dm^3, Cu^{2+}: 2.0×10^{-4} mol/dm^3, gas-flow time: 2 min.
BHDAC: 5.0×10^{-5} mol/dm^3, Bt: 1.0×10^{-2}% } Fe^{3+}(○), Cu^{2+}(△)
BHDAC: 1.0×10^{-4} mol/dm^3, Bt: 2.0×10^{-2}% } Fe^{3+}(●), Cu^{2+}(▲)
Solid line I: simple system of Fe^{3+} ions.
Solid line II: simple system of Cu^{2+} ions.

(Fig. 5). It is seen in this figure that the lack of Bt remarkably decreases the floatability of Cu^{2+}, and the increase of gas-flow time from 2 min through 5 to 7 min increases the floatability in a slightly different way from the case of Fe^{3+} flotation. The increase of BHDAC concentration shows no effect. Thus, the addition of Bt is found effective in both the reduction of gas-flow time and the increase of floatability.

Selective Ion Flotation from a Mixed System. The flotation of Cu^{2+} and Fe^{3+} ions from a solution containing 2.0×10^{-4} mol/dm^3 Cu^{2+}, 2.0×10^{-4} mol/dm^3 Fe^{3+}, 1.0×10^{-2}% Bt, and 5.0×10^{-5} mol/dm^3 BHDAC was carried out by controlling pH with NaOH. The results are shown in Fig. 7, as open circles and triangles respectively, together with the results obtained for the separate systems of Cu^{2+} and Fe^{3+} ions, shown as solid lines. In the mixed systems, Fe^{3+} and Cu^{2+} ions are floated above pH 3 and 6 respectively, as in the flotations of the separate systems. Thus, even in the mixed system the flotation begins at the point of the formation of insoluble iron and copper hydroxides. Accordingly, the selective flotation of Fe^{3+} ions was achieved between pH 3 and 6, enabling the separation of Fe^{3+} ions from Cu^{2+} ions. However, in the above system, because of a relatively limited amount of Bt and BHDAC, the floatability of Fe^{3+} ions decreases as soon as the Cu^{2+} ion flotation begins and they both attain a steady value of about 40% at pH values higher than 8. In the case of a sufficient addition of Bt and BHDAC, as shown by the solid curves and triangles in Fig. 7, the flotation of Fe^{3+} and Cu^{2+} ions increases; beyond pH 10, the flotation of both Fe^{3+} and Cu^{2+} attains their steady maximum of about 80%. These conditions are applicable for the non-selective removal of both Fe^{3+} and Cu^{2+}.

References

1) A. J. Rubin and J. D. Johnson, *Anal. Chem.*, **39**, 298 (1967).
2) B. M. Davis and F. Sebba, *J. Appl. Chem.*, **17**, 41 (1967); E. J. Mahne and T. A. Pinhold, *Chem. Ind. (London)*, **30**, 1299 (1966).
3) I. Takayanagi, K. Kobayashi, K. Hachisuka, and T. Sasaki, *Bull. Chem. Soc. Jpn.*, **49**, 2419 (1976).
4) K. Kobayashi, *Bull. Chem. Soc. Jpn.*, **48**, 1750 (1975); K. Kobayashi, H. Sato, K. Kachi, M. Nakamura, and T. Sasaki, *ibid.*, **48**, 3533 (1975); K. Kobayashi, N. Watabe, and T. Sasaki, *ibid.*, **49**, 2701 (1976).
5) K. Kobayashi, *Bull. Chem. Soc. Jpn.*, **48**, 1180 (1975).
6) F. Snell and C. Snell, "Colorimetric Methods of Analysis," C. Van Nostrand Company, New Jersey (1948), p. 314.
7) F. Snell and C. Snell, "Colorimetric Methods of Analysis," D. Van Nostrand Company, New Jersey (1948), p. 111.
8) K. Kobayashi, H. Sato, K. Kachi, M. Nakamura, and T. Sasaki, *Bull. Chem. Soc. Jpn.*, **48**, 3533 (1975).
9) K. Sugahara and T. Michino, "Teiryobunseki," Asakura Co., Tokyo (1962), p. 101.
10) G. Charlot, "L'analyse Qualitative et Les Réactions en Solution," Mason et Cie, Paris (1957).
11) R. B. Grieves and D. Bhattacharyya, *J. Am. Oil Chem. Soc.*, **44**, 498 (1967).

Thermal Decomposition of CF_3CN in Shock Waves

Kazuo OKADA, Okitsugu KAJIMOTO, and Takayuki FUENO

Department of Chemistry, Faculty of Engineering Science, Osaka University, Toyonaka, Osaka 560

(Received August 4, 1977)

The thermal decomposition of CF_3CN diluted to 0.2 and 0.5 mol% in argon was studied behind incident shock waves over the temperature range 2450—3610 K. Mass spectrometry of the reaction mixture revealed that the decomposition products are C_2F_6, C_2N_2, C_2F_4, and a trace of FCN. The course of the primary process of decomposition, $CF_3CN+Ar \rightarrow CF_3+CN+Ar$, was followed by monitoring the CN(0—1) violet absorption centered at 421.5 nm. It was confirmed that the reaction is still in the low-pressure limit under our experimental conditions. The initial slope of absorption gave the bimolecular rate constant, $k=(7.9\pm3.1)\times10^{15}\exp[-(94.0\pm2.8)$ kcal mol$^{-1}/RT]$ cm^3 mol^{-1} s^{-1}. The rate constants obtained are best fitted by the classical collision-theory expression $k=\lambda(Z/n!)(E/RT)^n\exp(-E/RT)$ with $\lambda=0.44$, $n=2$, and $E=D_0(CF_3\text{–}CN)=102.7$ kcal/mol. The mechanism of the overall decomposition was suggested and checked by numerical integrations of the relevant rate equations.

The shock-tube decomposition of simple cyano compounds such as C_2N_2,[1,2] ClCN,[3] BrCN,[4,5] and HCN[6,7] in argon has already been a subject of intensive studies by several groups of workers. It is generally agreed that the primary step of the decomposition is the bimolecular process:

$$XCN + Ar \longrightarrow X + CN + Ar. \quad (1)$$

The present work is an extension of our previous studies on C_2N_2,[2] BrCN,[5] and HCN[7] to the case of trifluoroacetonitrile CF_3CN. Despite the larger number of atoms involved, the primary decomposition step proved to be still in the low-pressure limit under the shock-wave conditions adopted. The bimolecular rate constants for the primary step (1) were obtained from the initial slopes of the CN absorption records.

Product analysis showed that small amounts of C_2F_4 and FCN were formed in addition to the major decomposition products C_2F_6 and C_2N_2. The overall decomposition mechanism is thus somewhat more complex than that already established for simpler cyano compounds.[3–5,7] Presumably, the sources of these minor products are CF_2 and F which have been generated by a further decomposition of CF_3. A possible overall mechanism was inferred on this basis. Adequacy of the assumed mechanism was examined by numerical integrations of the overall kinetic equations. The time-concentration profiles calculated for CN radicals showed an excellent agreement with the observed CN absorption traces.

Experimental

Material. Trifluoroacetonitrile was prepared by heating a mixture of trifluoroacetamide and diphosphorus pentaoxide at 145—150 °C for 2 h,[8] and purified by trap-to-trap distillations. Commercial argon having a purity of 99.999% was used without further purification. Sample gases of 0.2 and 0.5 mol% CF_3CN in Ar were prepared at a total pressure of *ca.* 600 Torr [1 Torr=(101325/760) Pa].

Kinetic Measurements. Decomposition experiments were conducted in a stainless-steel shock tube having an internal diameter of 10.4 cm. The initial total pressure P_1 of gas samples ranged from 8.3 to 34 Torr. Hydrogen was used as driver gas. The diaphragms used were Myler sheets of 0.10 and 0.25 mm in thickness, which gave the driver bursting pressures of 3 and 9 atm (1 atm=101325 Pa), respectively. The temperatures T calculated for the shock-heated gas samples were in the range from 2450 to 3610 K. No temperature correction was made for the reaction heat, inasmuch as the gas samples used were sufficiently dilute to ignore it.

The course of decomposition was followed by monitoring the CN $B^2\Sigma^+$—$X^2\Sigma^+$ (0—1) absorption at 421.50±0.21 nm. To isolate the spectral bandwidth, a Rikotsusho grating monochromator MC-50 was used at the entrance and exit slit width of 0.30 mm. The band selected encompasses the overlapping rotational lines $J=9$—36 of the ground-state CN($X^2\Sigma^+$, $v=1$). The detection devices and procedure used were entirely the same as those described previously.[2] The response time of the optics and its associated electronic circuit was no greater than 2 μs.

Product Analysis. A gas sample, 4 mol% CF_3CN in Ar, was shock-heated for an unspecified time interval at *ca.* 3400 K by using helium as driver gas. The gaseous reaction mixture, which was cooled down to room temperature by the rarefaction, was let pass through a trap immersed in liquid nitrogen. After having been degassed in the trap, the liquefied material was allowed to evaporate at room temperature.

The reactant-product mixture gas thus prepared was subjected to mass-spectrometric analysis. The mass-spectrum obtained had the intensity peaks ascribable to CF_3CN, C_2N_2, C_2F_6, C_2F_4, and FCN. Attempts were made to determine the relative concentrations of these species from the intensity ratios between relevant mass peaks. The standard intensity ratios between such peaks were calibrated beforehand with various equimolar binary mixtures (CF_3CN–C_2N_2, C_2F_6–C_2N_2, C_2F_6–C_2F_4, and C_2F_6–FCN) as references. The results of determination (in mol%) were as follows:

$$CF_3CN : C_2N_2 : C_2F_6 : C_2F_4 : FCN = 85.15 : 5.16 : 8.01 : 1.50 : 0.16.$$

Results

Equilibrium. As has been confirmed by mass-spectrometry, the main products of the CF_3CN decomposition are C_2N_2 and C_2F_6. By the analogy to the mechanism already established for the decompositions of ClCN,[3] BrCN,[4,5] and HCN,[7] the main body of the present decomposition is considered to consist of the following elementary reactions:

$$CF_3CN + Ar \overset{1}{\rightleftarrows} CF_3 + CN + Ar,$$

$$C_2N_4 + Ar \overset{2}{\rightleftarrows} 2CN + Ar,$$

$$C_2F_6 + (Ar) \overset{3}{\rightleftarrows} 2CF_3 + (Ar),$$

$$CN + CF_3CN \overset{4}{\rightleftarrows} C_2N_2 + CF_3,$$

$$CF_3 + CF_3CN \overset{5}{\rightleftarrows} C_2F_6 + CN.$$

The formations of C_2F_4 and FCN as minor products strongly suggest the intermediacies of CF_2 and F. The elementary reactions of importance which involve these transient species are conceivably as follows:

$$CF_3 + Ar \overset{6}{\rightleftarrows} CF_2 + F + Ar,$$

$$C_2F_4 + Ar \overset{7}{\rightleftarrows} 2CF_2 + Ar,$$

$$F_2 + Ar \overset{8}{\rightleftarrows} 2F + Ar,$$

$$FCN + Ar \overset{9}{\rightleftarrows} F + CN + Ar,$$

$$CF_4 + Ar \overset{10}{\rightleftarrows} F + CF_3 + Ar,$$

$$F + CF_3CN \overset{11}{\rightleftarrows} CF_4 + CN.$$

Presumably, both CF_2 and F are generated directly from CF_3 by Reaction 6. Reactions 7 and 8 are the dissociation-homorecombination processes associated with these species. Reactions 9 and 10 concern the associations of F with the primary radicals CN and CF_3, respectively. Reaction 11 is a bimolecular reaction between F and CF_3CN, which is equivalent in type to Reaction 5.

Oscillographic records of the CN absorption showed, in all cases, an initial rapid rise in intensity, followed by a gradual increase up to a steady level. The constancy in absorbance may be taken as an indication that the overall process, Reactions 1 through 11, is in a complete equilibration.

Of the eleven species (except for Ar) present, only nine can take on independent concentrations at any given instance, since the total numbers of CN and F should be conserved all the time. At complete equilibrium, however, the local equilibria 4 and 5 cannot be independent ones either; $K_4=K_1/K_2$ and $K_5=K_1/K_3$. In addition, one may assume complete dissociations of C_2F_6, C_2F_4, and F_2 (*i.e.*, $K_3=K_7=K_8=\infty$) in the temperature range studied.[9] The overall equilibrium problem could thus be solved for six independent concentrations [CF_3CN], [CF_3], [CN], [CF_2], [F], and [FCN] by use of the six equilibrium constants for Reactions 1, 2, 6, 9, 10, and 11. The standard free energy changes ΔG_T° for the various elementary reactions have been taken from the JANAF tables[10] and are listed in Table 1.

The equilibrium concentrations $[CN]_e$ calculated in the above-described manner should be related to the observed absorbance at equilibrium through[1,2,5]

$$\ln (I_0/I)_e = \beta_{01} l F_{ab}(T) [CN]_e \qquad (2)$$

Here, β_{01} is the effective absorption coefficient for the CN radicals in the absorbing levels, l is the optical path length (l=10.4 cm), and $F_{ab}(T)$ is the fractional population of the absorbing $CN(X^2\Sigma^+)$ radicals (v=1, J=9—36). The $F_{ab}(T)$ for the present case is given by

$$F_{ab}(T) = \frac{\sum_{J=9}^{36}(2J+1)\exp\left(-\frac{J(J+1)\varepsilon_r+\varepsilon_v}{kT}\right)}{Q_r Q_v}, \qquad (3)$$

where ε_r and ε_v respectively denote the rotational and vibrational quanta of CN radicals and where Q_r and Q_v are the corresponding partition functions.

The β_{01} values to be obtained for different runs should be least temperature-dependent.[2,5] This was

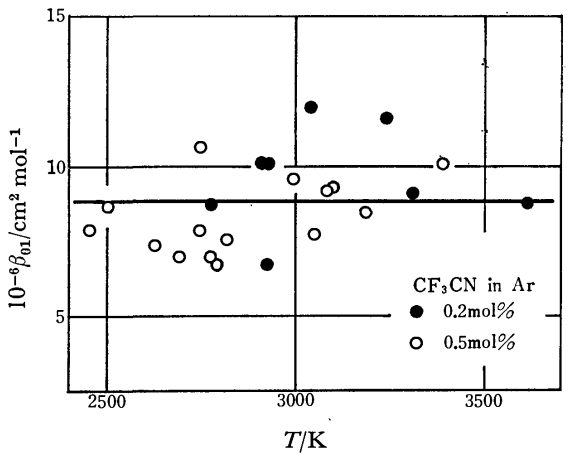

Fig. 1. Constancy of the CN absorption coefficient β_{01} over the temperature range studied.

Table 1. Elementary reactions

	$H_0^{\circ a)}$ kcal mol^{-1}	$G_T^{\circ a)}$ kcal mol^{-1}	Rate constant k_i/cm^3 mol^{-1} s^{-1}	Reference
1	102.7	$-0.03522T+98.3$	$k_1=7.9\times10^{15}\exp(-94.0\text{ kcal mol}^{-1}/RT)$	This work
2	125.6	$-0.03547T+122.2$	$k_2=6.66\times10^{16}\exp(-98.6\text{ kcal mol}^{-1}/RT)$	2
3	91.2	$-0.0383\ T+92.6$	$k_3=(1/[Ar]_0)\ 3.2\times10^{16}\exp(-88.0\text{ kcal mol}^{-1}/RT)$ [b)]	—
4	−22.9	$0.00040T-24.8$	$k_4=1.2\times10^{12}\exp(-8.7\text{ kcal mol}^{-1}/RT)$	Adjusted[c)]
5	11.5	$0.00340T+12.5$	$k_5=1.2\times10^{12}\exp(-11.5\text{ kcal mol}^{-1}/RT)$ [b)]	—
6	89.1	$-0.0338\ T+89.8$	$k_6=1.57\times10^{49}\ T^{-9}\exp(-92.25\text{ kcal mol}^{-1}/RT)$	11
7	72.0	$-0.0373\ T+65.2$	$k_7=5.2\times10^{29}\ T^{-3.5}\exp(-72.0\text{ kcal mol}^{-}/RT)$ [b)]	—
8	36.8	$-0.0310\ T+40.6$	$k_8=3.1\times10^{12}\exp(-27.3\text{ kcal mol}^{-1}/RT)$ [b)]	12
9	111.4	$-0.0331\ T+112.8$	$k_9=1.3\times10^{22}\ T^{-1.5}\exp(-111.0\text{ kcal mol}^{-1}/RT)$	Estimated
10	125.7	$-0.0386\ T+126.8$	$k_{10}=6.15\times10^{34}\ T^{-4.64}\exp(-122.4\text{ kcal mol}^{-1}/RT)$	11
11	−23.0	$0.0030\ T-27.4$	$k_{11}=2.1\times10^{13}\exp(-26.5\text{ kcal mol}^{-1}/RT)$	Adjusted[c)]

a) 1 kcal=4.184 kJ. b) Not used for the computation of the overall kinetics. c) Adjusted by fitting the calculated CN concentration profiles to the observed CN absorption curves.

Table 2. Rate data

m / mol%	P_1 / Torr	U_s [a] / mm/μs	ρ_{21} [b]	T / K	$[Ar]_0$ / 10^{-6} mol/cm^3	$[CN]_e$ / 10^{-9} mol/cm^3	x_e-y_e [c]	k_1 / cm^3 mol^{-1} s^{-1}
0.200	18.9	1.67	3.60	2775	3.66	4.35	0.593	2.47×10^8
0.207	16.8	1.72	3.62	2920	3.29	5.81	0.851	7.03×10^8
0.206	13.5	1.82	3.66	3235	2.66	5.28	0.960	3.21×10^8
0.206	10.1	1.93	3.69	3610	2.02	4.16	0.998	1.44×10^{10}
0.498	30.1	1.56	3.55	2455	5.78	2.93	0.101	2.89×10^7
0.502	29.5	1.62	3.58	2625	5.73	7.69	0.266	8.84×10^7
0.501	12.0	1.69	3.61	2815	2.35	7.18	0.608	3.65×10^8
0.501	9.79	1.78	3.64	3100	1.92	8.92	0.921	1.78×10^9
0.498	9.05	1.80	3.65	3180	1.79	8.57	0.958	3.60×10^9
0.498	8.32	1.86	3.67	3385	1.65	8.12	0.981	5.44×10^9

a) Shock velocity. b) Density ratio across the shock front. c) $[CN]_e/[CF_3CN]_0$, Ref. 5.

substantiated as is shown in Fig. 1. The average value of β_{01} was found to be $(8.85\pm0.95)\times10^6$ cm^2 mol^{-1}, in good agreement with the value $(9.16\pm0.76)\times10^6$ cm^2 mol^{-1} observed previously in the study of the dissociation equilibrium: $C_2N_2\rightleftharpoons2CN$.[2]

Dissociation Rates of CF_3CN. With the β_{01} value at hand, we have determined the bimolecular rate constants k_1 from the initial slope of absorbance

$$r_0 = \{d \ln (I_0/I)/dt\}_0, \quad (4)$$

where t is the particle time. k_1 is obtained as

$$k_1 = r_0/\beta_{01}lF_{ab}(T)[CF_3CN]_0[Ar]_0, \quad (5)$$

where $[CF_3CN]_0$ and $[Ar]_0$ are the concentrations at zero time, *i.e.*, immediately behind the shock front. The values of k_1 obtained for some representative runs are given in Table 2, together with pertinent experimental data.

Figure 2 shows the Arrhenius plots of k_1 obtained for a total of 25 runs. A single straight line is seen to fit the plots, irrespective of the $[CF_3CN]_0/[Ar]_0$ ratio. Although the total gas pressure was not changed independently

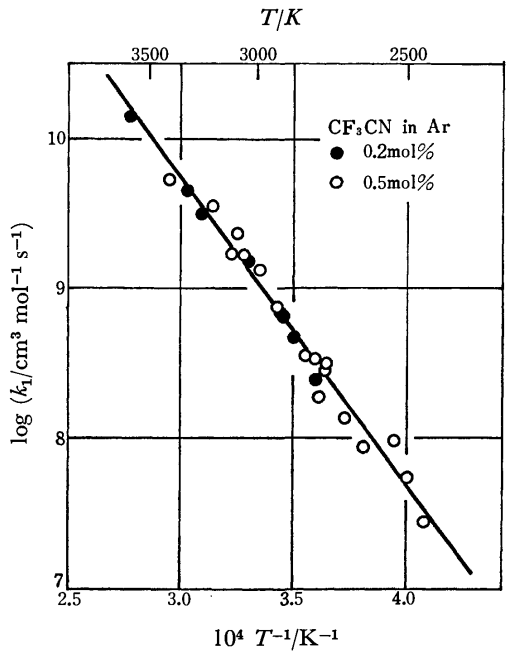

Fig. 2. Arrhenius plots of k_1.
$k_1=7.9\times10^{15}\exp(-94.0$ kcal mol$^{-1}/RT)$ cm^3 mol^{-1} s^{-1}.

of the reaction temperature, it is evident that the dissociation rate is proportional to $[Ar]_0$. Thus the reaction is indeed bimolecular under the experimental conditions adopted in this work. Least-squares treatment of the linearity has led to the Arrhenius expression

$$k_1 = (7.9\pm3.1)\times10^{15} \times \exp[-(94.0\pm2.8) \text{ kcal mol}^{-1}/RT] \text{ cm}^3 \text{ mol}^{-1} \text{ s}^{-1}. \quad (6)$$

Overall Decomposition Kinetics. The rate equations for the entire mechanism comprising Reactions 1—11 were subjected to numerical (Runge-Kutta-Gill) integration on a computer. The rate constants used for computation are listed in Table 1. The forward rate constants for Reactions 1, 2, 6, 8, and 10 were those determined experimentally.[2,11,12] The constant k_3, when multiplied by $[Ar]_0$, was assumed to be equal to the first-order rate constant for the ethane decomposition in the high-pressure limit.[13] The preexponential factors for k_7 and k_9 were estimated from those observed for the dissociations of N_2F_4[14] and BrCN.[5] Entirely indeterminate at this stage are k_4, k_5, and k_{11}. Most likely, the preexponential factor for k_5 would be about the same as that for k_4, and the activation parameter in k_5 would be nearly equal to the endothermicity of Reaction 5. It was decided to estimate k_4 and k_{11} by requiring the best overall fit of the calculated time-concentration profiles of CN radicals to the observed absorption curves. The rate constants for the reverse reactions were all calculated from those for the forward reactions and the equilibrium constants. The time step used for integration was 0.5 μs.

Preliminary calculations showed that the rate constants k_3, k_5, k_7, and k_8 exert virtually no effect on the CN concentration profiles. In what follows, therefore, we will ignore Reactions 3, 5, 7, and 8 throughout. The simplification is in line with the assumption of complete dissociations of C_2F_6, C_2F_4, and F_2 which has been invoked in the equilibrium considerations.

The time histories of the CN radical concentrations calculated for the cases of T=3385 and 2920 K are shown in Fig. 3. The full lines indicate the CN concentrations calculated for the entire mechanism (excluding Reactions 3, 5, 7, and 8), while the dashed lines show the concentrations which CN radicals would have if Reaction 1 were the only reaction to be considered.

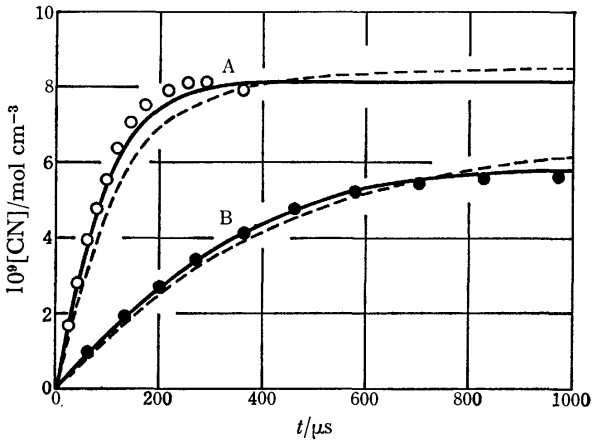

Fig. 3. Comparisons of the computed CN concentration profiles with the observed.
A: T=3385 K, m=0.5 mol%, $[Ar]_0=1.65\times10^{-6}$ mol/cm^3;
B: T=2920 K, m=0.2 mol%, $[Ar]_0=3.29\times10^{-6}$ mol/cm^3.
—: Computed with the rate constants given in Table 1; ---: Reaction 1 alone; ○, ●: experimental; t: particle time.

The experimental values of [CN] read from the absorption records are indicated with circles.

As a whole, the assumed mechanism with the rate constants given in Table 1 seems to be detailed enough to account for the observed time-concentration profiles of CN radicals. It has also been verified that the various reactions following the primary step 1 exert little influence on the initial slope. These results corroborate not only the adequacy of the assumed overall mechanism but also the legitimacy of the initial slope technique used to determine the k_1 values.

Discussion

In the computer tracing of the CN concentration profiles, the rate constants for the abstraction Reactions 4 and 11 were treated as the only adjustable parameters. The values for the Arrhenius A factors obtained for k_4 and k_{11} both appear to be reasonable; the A factors for abstractions by a radical are generally of the order of 10^{12} cm^3 mol^{-1} s^{-1} while those for similar reactions of an atom are usually *ca.* 10^{14} cm^3 mol^{-1} s^{-1}.[15] Not much can be said, however, about the activation energies obtained.

The experimental activation energy E_a=94.0 kcal/mol found for the CF_3CN dissociation is apparently smaller than the bond dissociation energy D_0=102.7 kcal/mol. This can readily be accounted for in terms of the participation of the internal energy of CF_3CN to its dissociation.

The classical collision theory due to Fowler and Guggenhiem[16] provides a semi-quantitative clue for understanding the above-stated situation. According to the theory, the rate constant for a bimolecular reaction is expressed as

$$k_1 = \lambda(Z/n!)(D_0/RT)^n \exp(-D_0/RT), \quad (7)$$

where n is the effective number of the internal degrees of freedom contributing to the activation process and where λ is a correction factor termed the "steric" factor. The temperature variation of the present experimental results, Eq. 6, is best fitted to that of Eq. 7, when n is assigned a value of 2. The least-squares fit of Eq. 7 with n=2 to the experimental k_1 values has led to the expression

$$k_1 = [4.30\times10^{12}/2]T^{1/2}(D_0/RT)^2 \exp(-D_0/RT) \text{ cm}^3 \text{ mol}^{-1} \text{ s}^{-1}. \quad (8)$$

Assuming the CF_3CN-Ar collision diameter to be 0.42 nm, we get λ=0.44, a value which does not appear unreasonable.

The Fowler-Guggenheim expression, Eq. 7 is formally equivalent to the low-pressure-limit form of the RRK theory for unimolecular reactions.[17] The theory permits a rough estimation of the "fall-off pressure"

$$P_{1/2} \simeq \frac{\bar{\nu}}{\lambda Z}\left\{1+\frac{D_0}{(n+1)RT}\right\}^{-n} RT, \quad (9)$$

where $\bar{\nu}$ is a mean frequency of the vibrations participating in the activation process. Taking $\bar{\nu}=10^{13}$ s^{-1}, $P_{1/2}$ for the CF_3CN dissociation was calculated to be 210 and 140 atm at 3000 and 2500 K, respectively. The dissociation in question is thus considered to be in the low-pressure limit under our experimental conditions.

It was not *a priori* obvious that the thermal dissociation of CF_3CN, a six-atom molecule, would exhibit the bimolecular behavior. Perhaps, the C–F bondings are rigid enough for the CF_3 group to be regarded as a pseudoatom. The value n=2 agrees closely with n=1.5 found for the case of BrCN,[5] a triatomic molecule.

The conclusion that the CF_3CN dissociation is bimolecular in the ordinary pressure region is interesting in connection with the results reported by Perettie and Janz.[18] They investigated the thermal decomposition of pure CF_3CN by the flow method in the temperature range 684—809 K. The reaction obeyed a kinetics of second order in CF_3CN

$$2CF_3CN \longrightarrow C_2F_6 + (CN)_2, \quad (10)$$

with the bimolecular rate constant

$$k = 10^{14.7}\exp[-(64.7\pm3.0) \text{ kcal mol}^{-1}/RT] \text{ cm}^3 \text{ mol}^{-1} \text{ s}^{-1}. \quad (11)$$

Although the conclusion that Reaction 10 is a concerted (one-step) process involving a four-centered cyclic activated complex may perhaps be still debatable, the observed kinetics certainly negates a dominance of the unimolecular decomposition of CF_3CN. Even if the concerted Process 10 is involved in our shock-wave kinetics, it is least significant in our reaction system in which CF_3CN was used in an extremely high dilution in argon as environment gas. At 2455 K, the lowest temperature studied, the rate of Reaction 10 should be only one-sixth that of Reaction 1.

This work was supported in part by a Scientific Research Grant from the Ministry of Education, Japan (No. 110301).

References

1) W. Tsang, S. H. Bauer, and M. Cowperthwaite, *J. Chem. Phys.*, **36**, 1768 (1962).
2) T. Fueno, K. Tabayashi, and O. Kajimoto, *J. Phys. Chem.*, **77**, 575 (1973).
3) D. Schofield, W. Tsang, and S. H. Bauer, *J. Chem. Phys.*, **42**, 2132 (1965).
4) P. J. Kayes and B. P. Levitt, *J. Chem. Soc., Faraday Trans. 1*, **69**, 1415 (1973).
5) K. Tabayashi, O. Kajimoto, and T. Fueno, *J. Phys. Chem.*, **79**, 204 (1975).
6) P. Roth and Th. Just, *Ber. Bunsenges. Phys. Chem.*, **79**, 682 (1975).
7) K. Tabayashi, T. Fueno, K. Takasa, O. Kajimoto, and K. Okada, *Bull. Chem. Soc. Jpn.*, **50**, 1754 (1977).
8) H. Gilman and R. G. Jones, *J. Am. Chem. Soc.*, **65**, 1458 (1943).
9) Reactions 3, 7, and 8 are the only reactions for which ΔG_T° take large negative values in the temperature region near 3000 K.
10) D. R. Stull, Ed., "JANAF Thermochemical Tables," Dow Chemical Co., Midland, Mich. (1965).
11) A. P. Modica and S. J. Sillers, *J. Chem. Phys.*, **48**, 3283 (1968).
12) D. J. Seery and D. Britton, *J. Phys. Chem.*, **70**, 4074 (1966).
13) K. J. Laidler, "Theories of Chemical Reaction Rates," McGraw-Hill, New York, N.Y. (1969), p. 150.
14) A. P. Modica and D. F. Hornig, *J. Chem. Phys.*, **49**, 629 (1968).
15) S. W. Benson, "Thermochemical Kinetics," Wiley, New York, N. Y. (1968), p. 99.
16) R. Fowler and E. A. Guggenheim, "Statistical Thermodynamics," Cambridge Univ. Press, Cambridge, Mass. (1952), pp. 495—499.
17) For example, see S. W. Benson, "The Foundations of Chemical Kinetics," McGraw-Hill, New York, N. Y. (1960), Chap. 11.
18) D. J. Perettie and G. J. Janz, *J. Am. Chem. Soc.*, **91**, 6590 (1969).

Ring Transformation of γ-Butyrolactone into γ-Thiobutyrolactone over Alkaline Cation Exchanged Zeolites

Kou HATADA,* Yoichi TAKEYAMA, and Yosho ONO

Department of Chemical Engineering, Tokyo Institute of Technology, Ookayama, Meguro-ku, Tokyo 152

(Received August 6, 1977)

The reaction of γ-butyrolactone and hydrogen sulfide to give γ-thiobutyrolactone over zeolites was studied. Alkaline cation exchanged zeolites have high catalytic activity for the ring conversion, acidic zeolites very low activity. γ-Thiobutyrolactone was obtained in 99% yield with CsY at 330 °C. There is no decay of catalytic activity with time. The reaction kinetics over LiY, NaY, and CsY are expressed by

$$r = \frac{k(a_L P_L)(a_H P_H)}{(1+a_L P_L+a_H P_L)^2},$$

where r is the rate of reaction, P_L and P_H are the partial pressure of γ-butyrolactone and hydrogen sulfide, respectively, and k, a_L, a_H are constants. The activation energies for k are 39, 31, and 26 kcal mol^{-1} with LiY, NaY, and CsY, respectively. Catalytic activity is enhanced by addition of pyridine but almost completely depressed by addition of hydrogen chloride. It is concluded that basic sites play an important role in the ring transformation.

Synthetic zeolites usually act as acidic catalysts, having very high activity for major carbonium ion hydrocarbon transformations such as cracking, alkylation and isomerization. For these reactions, hydrogen-, rare-earth-, and alkaline earth-exchanged zeolites are the most active catalysts. However, the parent Na^+ and K^+-exchanged zeolites are inactive.[1] There are, however, some reactions in which NaY has a catalytic activity comparable with HY, *e.g.* the reactions of γ-butyrolactone with primary amines to form 1-alkyl-2-pyrrolidinone.[2] The mechanism proposed for this reaction involves the activation of primary amines on basic sites.[2] A related reaction, the conversion of γ-butyrolactone in the presence of hydrogen sulfide has been studied by Venuto and Landis.[3]

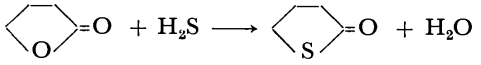

A notable feature of the reaction is that NaX was found to be the most active catalyst among the zeolites studied, HY and ReX having only a meager catalytic activity.[3] The catalytic activity for this reaction does not seem to be associated with Brönsted centers.

The kinetic behavior of the ring transformation of γ-butyrolactone into γ-thiobutyrolactone (tetrahydro-2-thiophenone) was examined over a series of alkaline Y-zeolites in order to find the mechanistic grounds of high activity of alkaline zeolites for the ring conversion reaction.

Experimental

Materials. γ-Butyrolactone (purity>99%) was distilled prior to each run. Commercial hydrogen sulfides, NaX and NaY (Linde Division of Union Carbide Corp.) were used. Various cation forms of Y-zeolites were prepared by means of the conventional cation exchange using salt solution. The cation exchanged zeolites were pelleted without a binder and crushed and made into 9—16 mesh. They were stored in a desiccator containing a saturated aqueous ammonium chloride.

* Present address: Faculty of Education, Saitama University, Urawa, Saitama 338.

Apparatus and Procedure. A continuous flow reactor was used under atmospheric pressure. The reactor was silica tubing (13 mm i.d.) placed in a vertical furnace. Prior to the reaction, the catalyst in the reactor was heated up to the reaction temperature in a nitrogen stream. Hydrogen sulfide was then fed. After 15 min, γ-butyrolactone was pumped into the preheating zone of the reactor containing 10 ml quartz powder. Nitrogen was used as diluent for regulating the initial pressure of reactants. The gaseous materials were fed through flowmeters. Reaction products collected in the receiver were withdrawn at certain intervals during the run and analyzed by gas chromatography.

Result and Discussion

Catalytic Activity of Various Forms of Zeolites. The catalytic activities of various cation forms of zeolites for the reaction of γ-butyrolactone and hydrogen sulfide were compared at 330 °C. The activities and selectivities to γ-thiobutyrolactone production on various zeolites are given in Table 1. We can see the following features of the reaction.

Table 1. Catalytic activity of various zeolites

Catalyst	Exchanged (%)	Conversion (%)	Yield (%)
LiY	58	27	26
NaY	—	52	51
KY	97	45	45
RbY	64	51	51
CsY	64	79	78
NaX	—	99	86
KL	—	23	22
HY	66	4	1
MgY	56	2	2

Reaction conditions; 330 °C, H_2S/lactone=6, W/F=6.26 g h mol^{-1}.

(1) Alkaline forms of zeolites are much more active than acidic zeolites (HY, MgY).

(2) The catalytic activity of alkaline forms of Y-zeolites increases in the following order.

$$LiY < NaY \simeq KY \simeq RbY < CsY$$

(3) NaX is a more active catalyst than NaY, but shows less selectivity.

(4) The selectivity to γ-thiobutyrolactone is essentially 100% over alkaline Y-zeolites.

It should be noted that no decay of activity with time is observed except for the case of MgY.

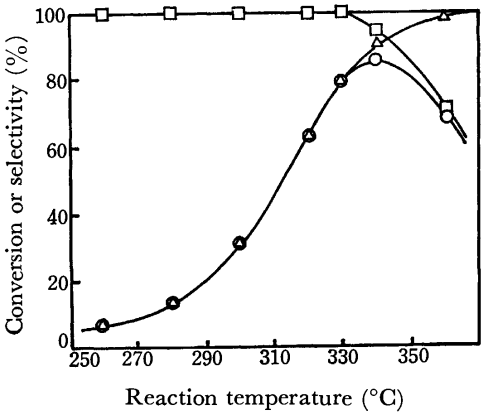

Fig. 1. Variation of the conversion (△), the yield (○) and the selectivity (□) with reaction temperature.
CsY 1.0 g, W/F=6.26 g h mol^{-1}, H_2S/lactone=6.

Influence of Reaction Temperature. The effect of reaction temperature on the yield and the selectivity to γ-thiobutyrolactone was examined with CsY as a catalyst. As shown in Fig. 1, the yield of γ-thiobutyrolactone sharply increases with temperature below 340 °C. Maximum yield is reached at 340 °C. The yield falls at higher temperatures. The selectivity to γ-thiobutyrolactone is 100% up to 330 °C, decreasing at higher temperatures.

Effect of Contact Time. The effect of contact time (W/F) on the yield of γ-thiobutyrolactone was examined at 330 °C. W/F is defined as follows:

$$W/F = \frac{\text{Weight of catalyst (g)}}{\text{Total feed } (H_2S+\text{lactone}+N_2)\ (\text{mol h}^{-1})}.$$

The results are illustrated in Fig. 2. The yield increases with contact time. At W/F=18.8 g h mol^{-1}, a 99% yield can be attained. The selectivity for γ-thiobutyrolactone is always 100% at this temperature.

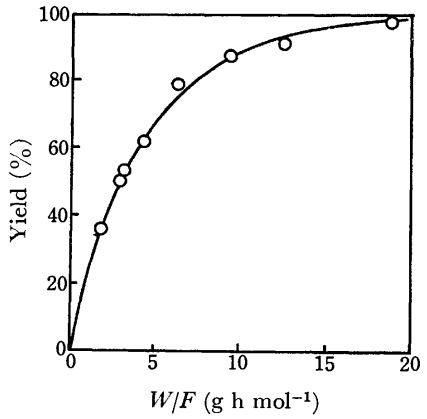

Fig. 2. Effect of contact time on γ-thiobutyrolactone yield.
CsY, 330 °C, H_2S/lactone=6.

Reaction Kinetics. The kinetics of the reaction was studied in a short contact time with LiY, NaY, and CsY as catalyst. The effect of partial pressure of γ-butyrolactone on the reaction rate was examined by keeping the partial pressure of hydrogen sulfide at 0.5 atm. The partial pressure of nitrogen was adjusted to keep the contact time constant. The results for CsY are given in Fig. 3. The rate decreases with increase in lactone partial pressure.

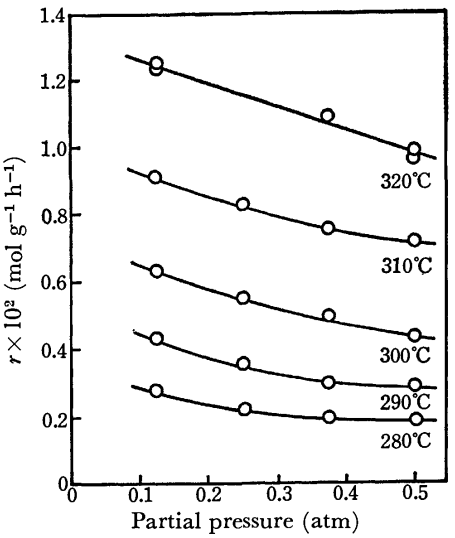

Fig. 3. Dependence of the reaction rate over CsY on the partial pressure of γ-butyrolactone.
CsY 0.5 g, W/F=2.74 g h mol^{-1}, P_H=0.5 atm.

The dependence of reaction rate on the partial pressure of hydrogen sulfide was examined by keeping the lactone partial pressure at 0.125 atm. The results for CsY are given in Fig. 4.

The presence of the reaction products (water and γ-thiobutyrolactone) does not affect the reaction rate, since addition of these substances to the reactant feed does not change the yield of γ-thiobutyrolactone.

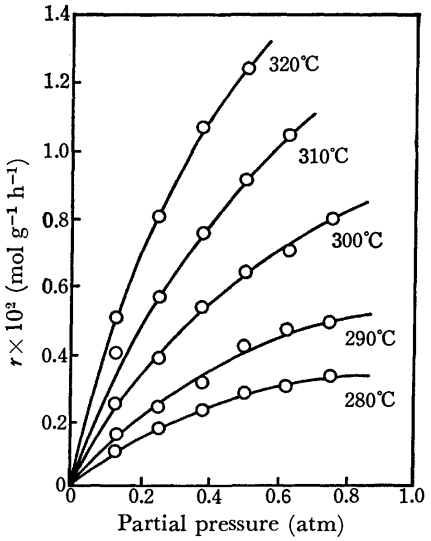

Fig. 4. Dependence of the reaction rate over CsY on the partial pressure of hydrogen sulfide.

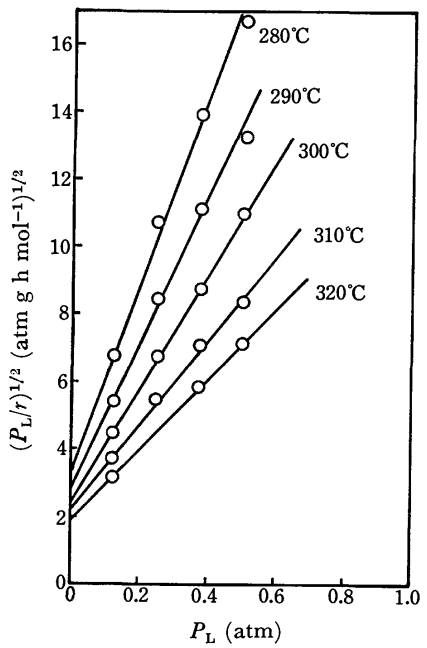

Fig. 5. $(P_L/r)^{1/2}$ *vs.* P_L plot for CsY.

It was found that the rate of the reaction can be expressed by

$$r = \frac{k(a_L P_L)(a_H P_H)}{(1+a_L P_L+a_H P_H)^2}, \quad (1)$$

where r is the rate of reaction, P_L and P_H are the partial pressures of γ-butyrolactone and hydrogen sulfide, respectively, and k, a_L, a_H are constants.

By rearranging Eq. 1, we have

$$\left(\frac{P_L}{r}\right)^{1/2} = \frac{1+a_H P_H}{(k a_L a_H P_H)^{1/2}} + \frac{a_L}{(k a_L a_H P_H)^{1/2}} \cdot P_L, \quad (2)$$

or

$$\left(\frac{P_H}{r}\right)^{1/2} = \frac{1+a_L P_L}{(k a_H a_L P_L)^{1/2}} + \frac{a_H}{(k a_L a_H P_L)^{1/2}} \cdot P_H. \quad (3)$$

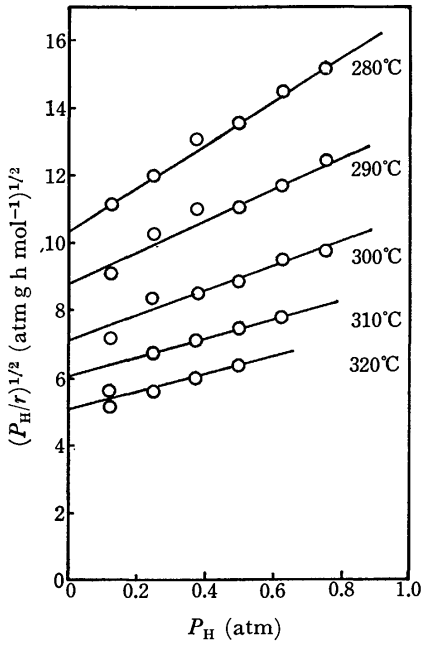

Fig. 6. $(P_H/r)^{1/2}$ *vs.* P_H plot for CsY.

Table 2. Kinetic parameters for the conversion of γ-butyrolactone into γ-thiobutyrolactone over CsY

Temperature (°C)	k (mol g^{-1} h^{-1})	a_L (atm^{-1})	a_H (atm^{-1})
280	2.3×10^{-2}	14	1.8
290	4.1×10^{-2}	13	1.3
300	6.0×10^{-2}	12	1.5
310	8.0×10^{-2}	11	1.8
320	11.7×10^{-2}	10	1.6

Table 3. Kinetic parameters for the conversion of γ-butyrolactone into γ-thiobutyrolactone at 320 °C

Catalyst	k (mol g^{-1} h^{-1})	a_L (atm^{-1})	a_H (atm^{-1})	E_a (kcal mol^{-1})
LiY	4.0×10^{-2}	8	0.5	39
NaY	6.1×10^{-2}	7	0.9	31
CsY	11.7×10^{-2}	10	1.6	26

Straight lines are obtained (Fig. 5) when $(P_L/r)^{1/2}$ is plotted against P_L by using the data given in Fig. 3. Straight lines are obtained (Fig. 6) also when $(P_H/r)^{1/2}$ is plotted against P_H by using the data given in Fig. 4. From the slopes and intercepts of the plots of Figs. 5 and 6, the constants, k, a_L, a_H are determined as given in Table 2. In a similar way, the rate constants and the constants (a_L, a_H) for LiY and NaY were determined. The values at 320 °C are given in Table 3. The rate constant, k, changes with the increasing order LiY$<$NaY$<$CsY. The constant a_H also changes with the increasing order LiY$<$NaY$<$CsY, while the constant a_L does not depend much on the catalyst used. From the temperature dependence of the rate constant, the activation energy for k is determined to be 39, 31, and 26 kcal mol^{-1} for LiY, NaY, and CsY, respectively.

Nature of Active Centers. Acidic zeolites (HY and MgY) have only a limited activity for this ring transformation reaction (Table 1). However, alkaline zeolites are very effective. This clearly indicates that the active centers are not acidic sites.

Yashima *et al.*[4] found that in the alkylation of toluene with methanol or formaldehyde, xylenes were selectively formed over Li zeolite, styrene and ethylbenzene being produced over the other alkaline zeolites. They concluded that the formation of xylenes depends on the solid acidity, the formation of styrene and ethylbenzene depending on the solid basicity. The side-chain alkylation is promoted by added aniline, while the nuclear alkylation is promoted by hydrogen chloride.[4] The presence of basic sites has been further confirmed by the conversion of 2-propanol over alkaline zeolites,[5] since the dehydration and dehydrogenation of alcohols are catalyzed by the acidic and the basic sites, respectively.[6] The order of catalytic activity of alkaline Y-zeolites is as follows.[5]

For dehydration LiY$>$NaY$>$KY$>$RbY$>$CsY,

For dehydrogenation LiY$<$NaY$<$KY$<$RbY$<$CsY.

The order of catalytic activity among alkaline zeolites

for the reaction of γ-butyrolactone and hydrogen sulfide suggests that the active centers for this ring conversion is basic in nature. In order to gain further insight into the active centers, the effects of addition of hydrogen chloride and of pyridine on the catalytic activity were examined.

Effect of Hydrogen Chloride. Matsumoto *et al.*[7] reported that the cracking of cumene over NaY is greatly enhanced by addition of hydrogen chloride to the system. The enhancement of the catalytic activity is ascribed to the formation of Brönsted acid sites by the interaction of hydrogen chloride with NaY.

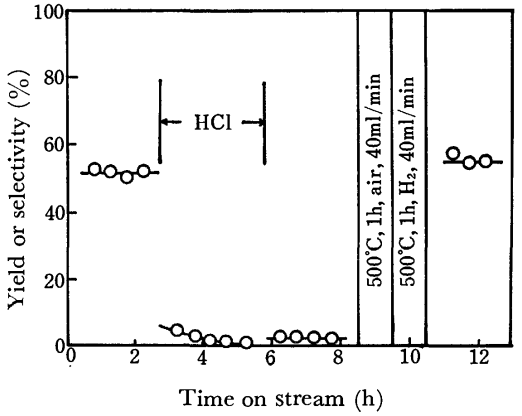

Fig. 7. Effect of hydrogen chloride on the reaction rate.
CsY, 330 °C, W/F=3.13 g h mol^{-1}, H_2S/lactone=6.

Addition of hydrogen chloride was carried out by passing a hydrogen sulfide stream over the concentrated hydrogen chloride aqueous solution. The results are given in Fig. 7. Hydrogen chloride almost completely inhibits the catalytic activity. The effect is irreversible, since the activity does not recover when feeding of hydrogen chloride is interrupted. The activity can be recovered by consecutive treatment of the catalyst with air and hydrogen at 500 °C. This eliminates the possibility of deactivation being caused by the destruction of the zeolite framework. The presence of water vapor does not affect the catalytic activity. Thus, it can be assumed that the deactivation is associated with the poisoning of the active centers, presumably the basic sites, by hydrogen chloride.

Effect of Pyridine. Pyridine is often used to poison acidic center. The effect of addition of pyridine on the ring conversion was examined. The dependence of the rate of γ-thiobutyrolactone on the pyridine partial pressure is given in Fig. 8. We see that pyridine does not poison the catalysis. However, it enhances the catalytic activity; the activity increases 35 and 250% for CsY and LiY, respectively, with pyridine partial pressure$>$0.01 atm.

The effect of hydrogen chloride and pyridine indicates that the acidic sites are not responsible for the catalysis, but the active centers are associated with basic sites. The enhancement of activity by pyridine may be caused by enrichment of the electron density of the oxygen anions in $(AlO_4)^-$ unit by the induced effect of pyridine absorbed close to the basic center. A similar mechanism of the enhancement by adsorbed pyridine

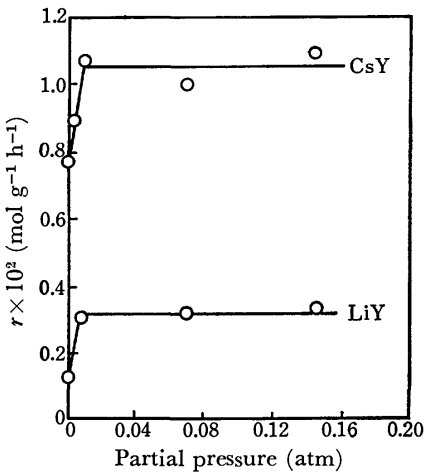

Fig. 8. Effect of pyridine partial pressure on the reaction rate.
CsY, 300 °C, W/F=3.14 g h mol^{-1}, P_H=0.714 atm, P_L=0.143 atm.

has been postulated for the base catalyzed butadiene formation from ethanol over SiO–MgO (75:25) catalyst.[8] Flockhart *et al.* found that the striking increase in reducing power of the decationated zeolites is caused by the addition of electron donors and suggested the existence of a strong interaction between electropositive and electronegative $(AlO_4)^-$ sites.[9]

Catalysis by Silica-Magnesia. Niyama *et al.*[8,10] determined the acidity and basicity of SiO_2–MgO catalysts of various compositions, and found that the basicity per unit area increases with increase in MgO content, the acidity per unit area having maximum at MgO/SiO_2=1. The ring transformation of γ-butyrolactone into γ-thiobutyrolactone was carried out with SiO_2–MgO catalysts. The results are summarized in Table 4. The rate per unit area increases with increasing MgO content. This indicates also that the basic sites, rather than acid sites, are responsible for the ring conversion.

Table 4. Ring conversion of γ-butyrolactone to γ-thiobutyrolactone over SiO_2–MgO catalysts

Catalyst	Yield (%)	Surface area (m^2 g^{-1})	Rate (mol m^{-2} h^{-1})
SiO_2	1	180	1.3
SiO_2–MgO (3:1)	5	170	6.7
SiO_2–MgO (1:1)	7	150	11
SiO_2–MgO (1:3)	10	130	18
MgO	3	23	30

Reaction conditions; 330 °C, H_2S/lactone=6, W/F= 6.16 g h mol^{-1}.

Nature of Basic Sites. All the results suggest that the active centers are basic in nature. A possible candidate for the basic sites in zeolites are oxygen anions bound to aluminum cations $(AlO_4)^-$. A negative charge at the site is neutralized and shielded by an alkaline cation. However, our results suggest that the reactant molecules are accessible to and are adsorbed on the basic oxygen anions at reaction conditions. A recent infrared study by Karge and Raskò[11] has shown

that hydrogen sulfide is dissociatively adsorbed on Na form of faujasite-like zeolites. They suggest that the adsorption sites are cationic sites of low coordination, where the Na^+ cations are weakly bound. The higher the Si/Al ratio, the smaller the population of such sites. This explains why hydrogen sulfide dissociates quite easily over NaX, but not over NaY.[11] Our result showing that NaX has higher catalytic activity for the ring transformation than NaY appears to support the idea. The order of reactivity among Y-zeolites (LiY< NaY<KY<RbY<CsY) may be associated with the ionic radius of the cations. The larger cations are bound more weakly to the basic sites, which, in turn, are more readily attacked by foreign molecules. The observed activation energy values can be understood on this basis. Thus, the activation energy for CsY is much smaller than that for NaY and LiY, which implies that the reactant molecules are more easily activated by the former catalyst.

Mechanism of the Reaction. The above discussion indicates that the active center involves the basic $(AlO_4)^-$ tetrahedron. Thus, hydrogen sulfide may be activated by the following scheme.

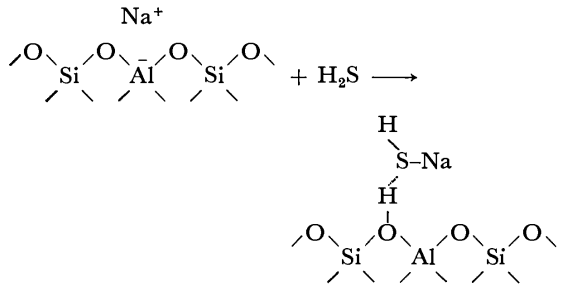

Karge and Raskò[11] showed that hydrogen sulfide dissociates on NaX. They found no evidence of the dissociation of hydrogen sulfide on NaY. It is very plausible, however, that H_2S molecules dissociate at reaction conditions (≈300 °C) on NaY.

γ-Butyrolactone molecules have an easily polarizable carbonyl group and can be activated by the electrostatic field exerted by a Na^+ cation and/or a $(AlO_4)^-$ unit. The reaction may proceed through the reaction between adsorbed hydrogen sulfide and adsorbed γ-butyrolactone, which may compete for the adsorption sites made up of the combination of Na^+-$(AlO_4)^-$ unit.[12] This explains the observed Langmuir-Hinshelwood type kinetics where the adsorption of γ-butyrolactone is much easier than that of hydrogen sulfide ($a_L<a_H$).

The authors are very grateful to Prof. Tominaga Keii for many fruitful discussions.

References

1) M. L. Poustma, in "Zeolite Chemistry and Catalysis," ed by J. A. Rabo, American Chemical Society, Washington (1977), p. 437.
2) K. Hatada and Y. Ono, *Bull. Chem. Soc. Jpn.*, **50**, 2517 (1977).
3) P. B. Venuto and P. S. Landis, *Adv. Catal.*, **18**, 259 (1968).
4) T. Yashima, K. Sata, and N. Hara, *J. Catal.*, **26**, 303 (1972).
5) T. Yashima, H. Suzuki, and N. Hara, *J. Catal.*, **33**, 486 (1974).
6) G. V. Krylov, in "Catalysis by Nonmetals," Academic Press, New York (1970), p. 116.
7) H. Matsumoto, K. Yasui, and Y. Morita, *J. Catal.*, **12**, 84 (1968).
8) H. Niyama, S. Morii, and E. Echigoya, *Bull. Chem. Soc. Jpn.*, **45**, 655 (1972).
9) B. D. Flockhart, M. C. Meggarry, and R. C. Pink, *Adv. Chem. Ser.*, **121**, 509 (1973).
10) H. Niyama and E. Echigoya, *Bull. Chem. Soc. Jpn.*, **45**, 938 (1972); H. Niyama and E. Echigoya, *Bull. Petro. Inst.*, **14**, 83 (1972).
11) H. G. Karge and J. Raskò, private communication.
12) K. Hatada, M. Shimada, Y. Ono, and T. Keii, *J. Catal.*, **37**, 166 (1973).

Conductivities of the Methyl Orange-Dodecyltrimethylammonium Complex in Dioxane-Water Mixtures

Masaru MITSUISHI, Yuzoh YAMAGUCHI, and Naoko ISHII

Faculty of Textile Science and Technology, Shinshu University, Tokida, Ueda 386

(Received August 16, 1977)

The ionic-association reaction of the complex between the Methyl Organic anion and the dodecyltrimethylammonium cation in dioxane–water mixtures has been studied by analyzing the conductivity data. The equivalent conductivities at an infinite dilution and the ionic association constants (K_A) have been determined by means of Shedlovsky's treatment, and they have been compared with those of Methyl Orange (sodium salt). The K_A values have been seen to increase with a rise in the temperature and with an increase in the dioxane content. The Walden products have been essentially constant, and they have been found to be comparable to those of Methyl Orange (sodium salt). The data have been analyzed further by the use of the Denison-Ramsey equation, and the ion-ion distance in an associate has been obtained. The ionic-association reaction have been found to increase the heat content and also the entropy.

In a previous paper,[1] we have concluded, on the basis of the conductivity data, that the sodium salt of an anionic dye such as the sodium salt of 1,5-dihydroxy-4,8-diaminoanthraquinone-2-sulfonic acid exists in the form of an ionic associate in dioxane–water mixtures.

Recently, the formation of a complex between large organic ions of opposite charges in water has been found to be explainable in terms of a twofold interaction mechanism, *i.e.*, Coulombic and hydrophobic interactions.[2,3]

Since there have been few reports on the ionic-association reaction of large organic anions with large organic cations in organic solvent–water mixtures with low dielectric constants, it seems that it would be valuable to examine the conductivity behavior of complexes between large organic ions of opposite charges, such as the Methyl Orange–dodecyltrimethylammonium complex in dioxane–water mixtures, and to compare the ionic-association reaction of the complex with that of Methyl Orange (sodium salt).

In this paper, the conductivity data on this kind of ionic complex were used to determine the equivalent conductivity at an infinite dilution and the ionic association constant by means of Shedlovsky's treatment[4] based on Onsager's theory,[5] and the behavior of the complex in the mixtures was considered.

Experimental

Materials. The Methyl Orange (sodium salt) was prepared by coupling diazotized sulfanilic acid with *N,N*-dimethylaniline in a weakly acetic acid solution, after which the product was recrystallized three times from water.

The dodecyltrimethylammonium bromide was prepared by boiling a mixture of trimethylamine and dodecyl bromide in ethanol for several hours. The product was recrystallized from acetone and benzene after the ethanol has been removed by distillation.

The Methyl Orange–dodecyltrimethylammonium complex (M–D complex) was prepared as follows: 1 dm^3 of 10^{-3} mol/dm^3 Methyl Orange (sodium salt) was added to the same volume of a 10^{-3} mol/dm^3 dodecyltrimethylammonium bromide aqueous solution. The finely dispersed M–D complex was then separated by centrifugation from the solution. The M–D complex was purified by recrystallizing from ethanol. Microelemental analysis gave the following results. Found: C, 64.87; H, 8.93; N, 10.61%. Calcd for $C_{29}H_{48}N_4SO_3$ (1:1 M–D complex): C, 65.41; H, 9.02; N, 10.53%.

The dioxane used in this experiment was purified by the method described in a previous work.[1]

Conductivity Measurements. These measurements were carried out at 15, 25, 35, and 45±0.01 °C using the same apparatus and the same procedures as those described in a previous work.[1]

Results and Discussion

The equivalent conductivities, Λ, of the M–D complex in dioxane–water mixtures at 25 °C are plotted against the square root of the concentration, $C^{1/2}$, as shown in Fig. 1.[6] The Λ values in 45 and 70% dioxane are seen to become larger almost linearly with an increase in the dilution. In 82% dioxane, the Λ value decreases monotonically with an increase in the complex concentration. The dotted lines in Fig. 1 give the limiting slopes of the Onsager equation.[5] The slopes of the experimental curves of the Λ-$C^{1/2}$ plot are seen to be larger than those of the corresponding theoretical

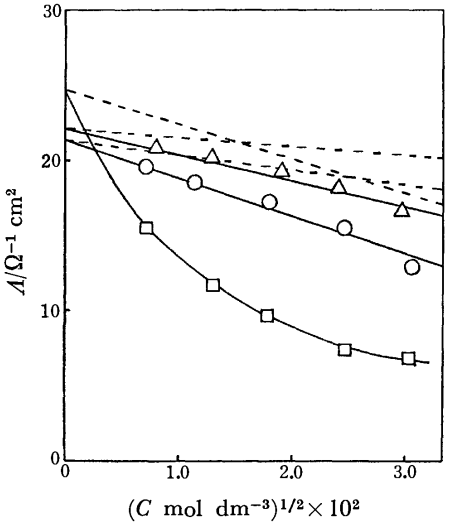

Fig. 1. Equivalent conductivities of Methyl Orange–dodecyltrimethylammonium complex in dioxane–water mixtures at 25 °C.
△: 45% dioxane, ○: 70% dioxane, □: 82% dioxane.

Table 1. Constants for sodium Methyl Orange and Methyl Orange–dodecyltrimethylammonium complexes in dioxane–water mixtures

Solutes	Solvents	t/°C	Λ_0	$\Lambda_0\eta$	K_A
Sodium Methyl Orange	82% dioxane	15	19.97	0.420	6.98×10^3
		25	25.92	0.433	8.97
		35	30.13	0.409	1.05×10^4
M–D Complex	45% dioxane	15	16.21	0.398	3.15×10^2
		25	22.10	0.406	3.64
		35	28.58	0.409	4.90
		45	37.18	0.425	6.31
	70% dioxane	15	15.84	0.393	8.32×10^2
		25	21.47	0.412	9.72
		35	27.30	0.416	1.05×10^3
		45	34.40	0.426	1.19
	82% dioxane	15	18.36	0.387	1.70×10^4
		25	24.72	0.413	1.91
		35	30.73	0.417	2.01
		45	36.14	0.404	2.51

lines. These results suggest that the ionic-association reaction between the Methyl Orange anion and the dodecyltrimethylammonium cation takes place in the mixtures. Similar plots were also obtained at 15, 35, and 45 °C.

From the results of the conductivity measurements, the equivalent conductivities at an infinite dilution, Λ_0, and the ionic-association constants, K_A, were obtained by means of Shedlovsky's treatment,[4] based on Onsager's limiting equation,[5] in a manner similar to that described in the previous work[1] and the results are shown in Table 1. From Table 1 the K_A values of Methyl Orange (sodium salt) and the M–D complex are seen to increase with a rise in the temperature of the solvents at a constant solvent composition, and they also increase with the dioxane content, *i.e.*, with a lowering in the dielectric constant of the solvents. The K_A values of the M–D complex are much larger than those of Methyl Orange (sodium salt) in 82% dioxane. This suggests that the dodecyltrimethylammonium ion contributes strongly to the formation of the ionic associate with the Methyl Orange.

The Walden products,[7] $\Lambda_0\eta$, of the Methyl Orange (sodium salt) and the M–D complex are also shown in Table 1. Their $\Lambda_0\eta$ values are essentially constant. This can be explained most simply by assuming that the ions in the mixtures are selectively hydrated over the entire solvent composition range studied, *i.e.*, the dioxane molecules are excluded from the first coordination sphere of the ions.[8,9] The evidence that the Walden products of the Methyl Orange (sodium salt) in 82% dioxane are almost equal to those of the M–D complex may suggest also that the Stokes's radii of the sodium and dodecyltrimethylammonium ions are equal to each other.

In an attempt to analyze the data further, the relation of K_A to $1/DT$[10] was examined by means of the Denison-Ramsey equation[11] as a first approximation,

$$K_A = \exp(e^2/aDkT). \quad (1)$$

Here, e is the electron charge, a is the center-to-center distance of the ions in an associate, and k is the Boltzmann constant.

According to Eq. 1, the plot of K_A *vs.* $1/DT$ must be linear. As an example, the plot of log K_A *vs.* $1/DT$ for the M–D complex in 82% dioxane is shown in Fig. 2. This plot gives a straight line. From the slope, the a value is obtained. The a values of Methyl Orange (sodium salt) and the M–D complex in the mixtures are shown in Table 2. All the a values are seen to be reasonable except for the one in 45% dioxane, and they are comparable to those of some of the organic and inorganic electrolytes in organic solvent–water mixtures.[1,12–15]

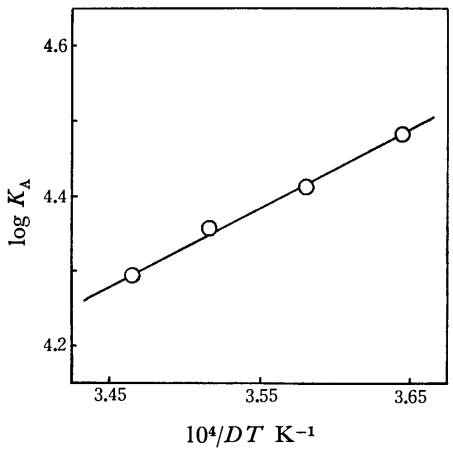

Fig. 2. The relation betweem log K_A and $1/DT$ in 82% dioxane.

The enthalpy changes ($\Delta H°$) and entropy changes ($\Delta S°$) in the ionic-association reactions can be obtained in the usual way; they are also shown in Table 2. Since the $\Delta H°$ values are positive, the reactions are endothermic. The $\Delta H°$ values are comparable to those for the ionic-association reactions of several organic

Table 2. Thermodynamic parameters of ionic-association reactions at 25 °C and center-to-center distance of ions in an associate

Solute	Solvents	K_A	$\Delta H°$ kcal[a] mol^{-1}	$\Delta G°$ kcal mol^{-1}	$\Delta S°$ cal K^{-1} mol	a Å[b]
Sodium Methyl Orange	82% dioxane	8.94×10^3	0.17	−5.39	19	5.0
M–D Complex	45% dioxane	3.64×10^2	6.10	−3.50	32	1.4
	70% dioxane	9.72×10^2	2.05	−4.08	21	6.8
	82% dioxane	1.91×10^4	2.22	−5.84	27	8.2

a) 1 cal=4.814 J. b) 1 Å=1 nm.

salts in water and some of the anionic dyes in dioxane–water mixtures.[1)]

The $\Delta S°$ values for the reactions are also positive. The results can be considered to reflect the fact that the degree of freedom of the system increases, since the solvent molecules are removed from the solvation sphere of the ions when the ionic-association reaction takes place. The $\Delta S°$ values are comparable to those for the reaction of the sodium salt of an acid dye in dioxane–water mixtures, and those for some of the thallium and the calcium salts in water.[16,17)]

References

1) M. Mitsuishi, M. Hashizume, A. Katayama, and N. Kuroki, *Bull. Chem. Soc. Jpn.*, **43**, 955 (1970).
2) M. Mitsuishi and M. Hashizume, *Bull. Chem. Soc. Jpn.*, **46**, 1946 (1973).
3) G. I. Mukhayer and S. S. Davis, *J. Colloid Interface Sci.*, **56**, 350 (1976).
4) T. Shedlovsky, *J. Frankline Inst.*, **225**, 739 (1938).
5) L. Onsager, *Physik. Z.*, **27**, 388 (1926).
6) As the M–D complex was slightly soluble in water and 20% dioxane, no conductivity measurement was made.
7) The symbol "η" represents the solvent viscosity.
8) Some electrolytes, such as LiCl and LiF, are considered to be selectively hydrated in water–ethanol mixtures containing more than 25% ethanol.[9)]
9) G. Wada, *Nippon Kagaku Zasshi*, **77**, 391 (1956).
10) J. T. Denison and J. B. Ramsey, *J. Am. Chem. Soc.*, **77**, 2615 (1955).
11) "D" represents the dielectric constant of the solvent.
12) R. M. Fuoss and G. Atkinson, *J. Am. Chem. Soc.*, **55**, 1019 (1933).
13) C. J. Hallada and G. Atkinson, *J. Am. Chem. Soc.*, **83**, 3759 (1961).
14) G. Atkinson and S. Petrucci, *J. Am. Chem. Soc.*, **86**, 7 (1964).
15) R. W. Kunze and R. M. Fuoss, *J. Phys. Chem.*, **67**, 911 (1963).
16) R. P. Bell and J. H. B. George, *Trans. Faraday Soc.*, **49**, 617 (1953).
17) G. H. Noncolls, *Discuss. Faraday Soc.*, **24**, 108 (1957).

Adsorption of 1,2-Propanediol and Methyl Cellosolve at Mercury–0.10 m KCl aq Interface at 25 °C

M. V. RAMANAMURTI and B. V. APPARAO

Department of Chemistry, Faculty of Science, Banaras Hindu University, Varanasi 221005, India

(Received April 30, 1977)

Adsorption of 1,2-propanediol and methyl cellosolve (isomeric compounds) at Hg–0.10 m KCl (aq) solution interface evaluated through equilibrium double layer capacity measurements indicated congruency of adsorption isotherms with respect to both potential (E) and charge density (σ^M); applicability of Langmuir's adsorption isotherm; quadratic dependence of $\Delta\bar{G}^\circ$ on E and single stable orientation with the hydrocarbon chain facing the electrode and functional group in solution throughout the coverage region, for both the compounds. Surface excess, standard free energy of adsorption and the anodic shift of E_{pzc}, are greater while the charge corresponding to maximum adsorption is more negative, for methyl cellosolve than for the diol.

The differences in the adsorption behaviour of some aromatic isomeric compounds[1] at the mercury-solution interface were attributed to differences in dipole moment and intramolecular hydrogen bonding. However, such studies are scanty in the literature.

Diols have been shown to behave in a different way[2,3] from monohydric alcohols at the mercury-aq solution interface. Adsorption of glycol has been thoroughly studied by electrocapillary[3] and differential capacity measurements.[4] 1,2-Propanediol (methyl glycol) and 2-methoxy ethanol (glycol monomethyl ether also known as methyl cellosolve) are two isomeric compounds with dipole moments 2.25 and 2.04 respectively, the hydrogen bonding of the former with water molecules being relatively higher. The present communication describes their adsorption behaviour at Hg–0.10 m KCl (aq) solution interface through equilibrium double layer capacity measurements.

Experimental

Differential capacities were measured by Grahame's a.c. bridge method[5,6] using a dropping mercury electrode. A variable signal generator (Marconi TF 1370) facilitated variation of a.c. frequency from 200 to 10000 Hz. Observed frequency independent capacity data with Hg–0.10 m KCl aq agreed with Grahame's data.[6] In the presence of the adsorbates, the capacity was frequency dependent and the data reported in this paper are equilibrium double layer capacities (extrapolated zero frequency values). Mercury drops knocked off periodically at a prefixed interval by a locally made electromagnetic drop detacher were perfectly spherical at the instant of bridge balance. Interval of two successive knocks of the detacher was measured accurate to 0.005 s. The bridge was balanced at the instant of the detachment of the drop from the capillary tip. The bridge output signal amplified by a multistage transistor preamplifier (Marconi TM 6591A) was displayed on a Dumont oscillograph (type 274). A large mercury pool electrode and 1 M KCl calomel electrode (NCE) were used as the auxiliary and reference electrodes respectively. The potential between the test electrode and the reference electrode was measured on a portable potentiometer (Pye-Cambridge; accuracy one mV). Differential capacities were measured in the potential range -0.10 to -1.80 V *vs.* NCE. The measurements were carried out in an air thermostat controlled at 25 ± 0.1 °C.

Mercury was purified following Trasatti's method.[3] KCl (BDH-AnalaR) twice recrystallized from conductivity water was used. Methyl cellosolve (Riedel) was treated with lithium hydride until the evolution of hydrogen gas ceased and then distilled twice. 1,2-Propanediol (BDH-AnalaR) was twice distilled under reduced pressure and the middle cut was collected. Solutions at required molalities of the adsorbates in 0.10 m KCl (aq) were deoxygenated with purified and presaturated nitrogen before carrying out the experiments.

The differential capacitance measured was independent of the drop time even at the desorption peaks indicating universal attainment of adsorption equilibrium.

Results and Discussion

The differential capacity-potential curves for both 1,2-propanediol (Fig. 1) and methyl cellosolve (Fig. 2) follow the same shape typical for an aliphatic organic compound. The capacity curves for methyl cellosolve exhibit small cathodic and anodic desorption peaks whereas these peaks are totally absent in the curves for 1,2-propanediol; there is only a characteristic cross-over of the curves at extreme cathodic and anodic polarizations. With the increase in concentration of

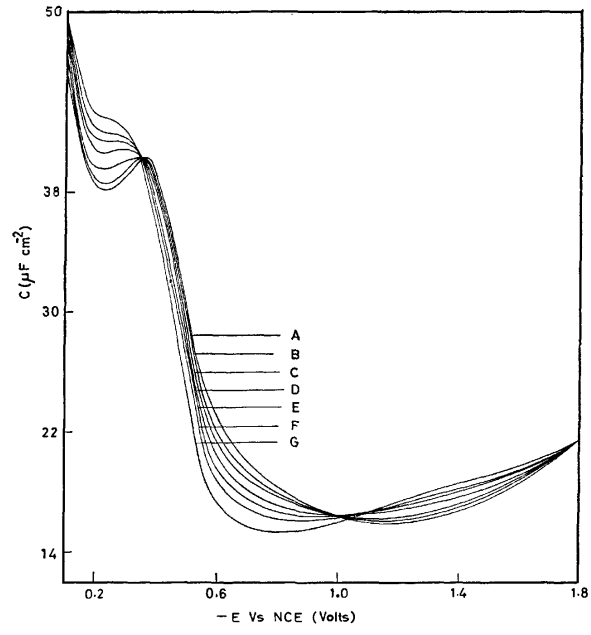

Fig. 1. Differential capacity-potential curves for Hg in 0.10 m KCl solution containing 1,2-propanediol at concentrations: (A) 0, (B) 0.05, (C) 0.10, (D) 0.20, (E) 0.30, (F) 0.40, (G) 0.60 m.

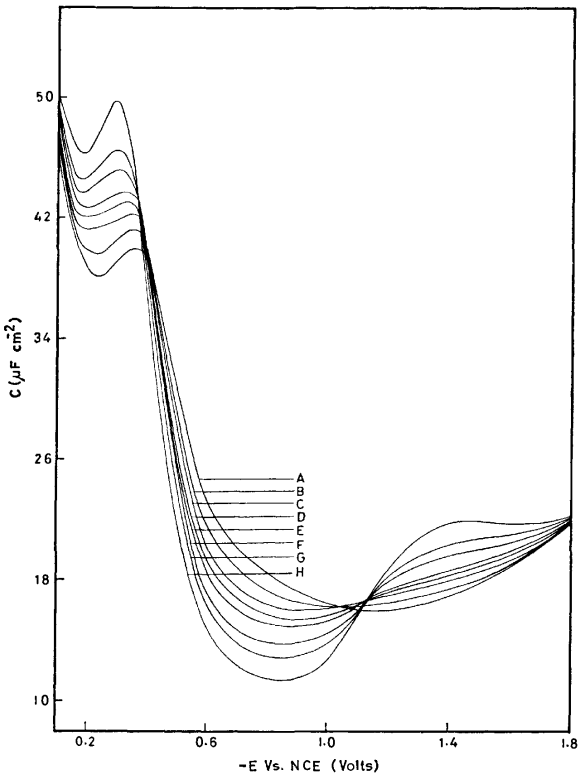

Fig. 2. Differential capacity-potential curves for Hg in 0.10 m KCl solution containing methyl cellosolve at concentrations: (A) 0, (B) 0.05, (C) 0.10, (D) 0.15, (E) 0.20, (F) 0.30, (G) 0.40, (H) 0.60 m.

methyl cellosolve, the cathodic desorption peak shifts towards more cathodic potentials and the anodic peak, towards more anodic potentials.

Evaluation of σ^M *and* Γ_A. Charge density on the electrode surface (σ^M) has been computed according to the equation:

$$\sigma^M = \int C dE + K_1, \qquad (1)$$

and surface excess of the organic adsorbate (Γ_A), with the help of the equation:

$$\Gamma_A = \frac{1}{2.303RT}\left(\frac{\partial \sigma^M}{\partial \log c}\right)_E dE + K_2, \qquad (2)$$

where R and T have their usual thermodynamic meaning.

Both the integrations have been performed numerically at the intervals of 10 mV starting at extreme cathodic potential *viz.*, −1.8 V *vs.* NCE at which the capacity curves at all concentrations of the adsorbates coincided with the corresponding one of the base electrolyte. K_1 was the charge density on the electrode in pure base electrolyte solution (K_2 being equal to zero) at −1.8 V. The differential term in Eq. 2 is obtained from σ^M *vs.* log c plots; these adsorbates are knwon to behave ideally especially in the concentration range studied and hence the activity is replaced by concentration.

Surface Excess of the Organic Adsorbates. The surface excess-potential curves (*cf.* Fig. 3) show complete desorption of both the compounds at extreme cathodic polarizations; desorption is, however, incomplete at

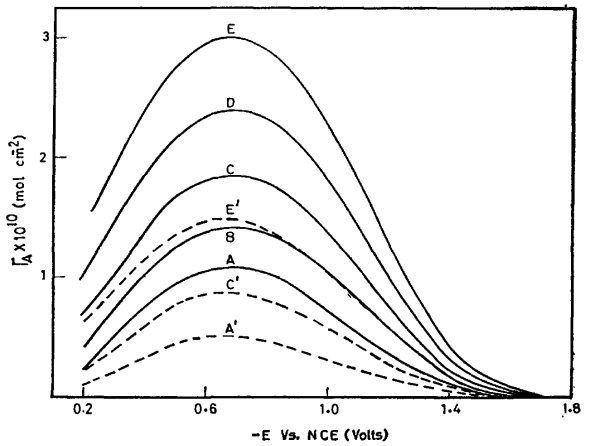

Fig. 3. Surface excess of the adsorbate as a function of electrode potential. (A) 0.10, (B) 0.15, (C) 0.20, (D) 0.30, (E) 0.40 m methyl cellosolve. (A′) 0.10, (C′) 0.20, (E′) 0.40 m 1,2-propanediol.

anodic polarizations in the potential range studied. At a given bulk concentration and potential, the surface excess of methyl cellosolve is found to be more than that of 1,2-propanediol.

Linear plots observed in the variation of (i) electrode charge *vs.* surface excess at constant potential and (ii) electrode potential *vs.* surface excess at constant charge suggest that the adsorption isotherms for both the compounds are congruent with respect to both electrode potential and charge.[7,8] Such plots for methyl cellosolve are shown in Figs. 4a and 4b.

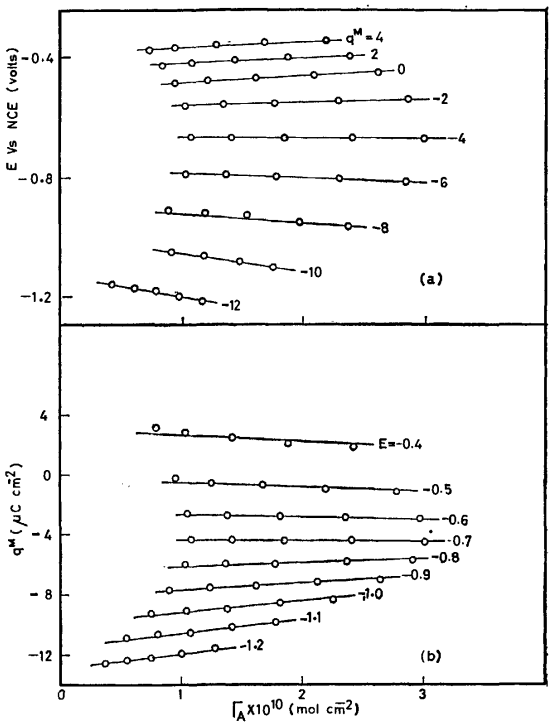

Fig. 4. (a) Electrode potential as a function of surface excess of methyl cellosolve at constant charge. Charge (μC cm^{-2}) indicated on each line.
(b) Electrode charge as a function of surface excess of methyl cellosolve at constant potential. Potential (V *vs.* NCE) indicated on each line.

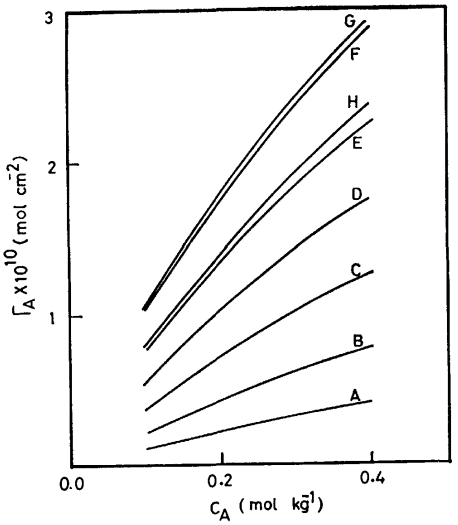

Fig. 5. Surface excess as a function of bulk concentration of methyl cellosolve at constant potential. (A) $E=-1.4$, (B) -1.3, (C) -1.2, (D) -1.1, (E) -1.0, (F) -0.8, (G) -0.6, (H) -0.4 V *vs.* NCE.

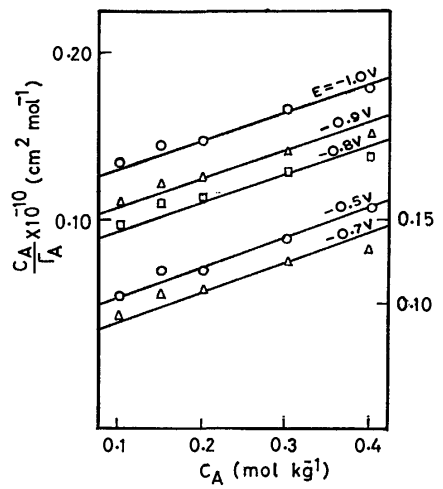

Fig. 6. Test for Langmuir's isotherm for methyl cellosolve at various potentials. Potential (V *vs.* NCE) indicated on each line.

The plots of surface excess *vs.* bulk concentration at constant electrode potential for both the compounds do not yield saturation value of surface excess (Γ_S) within the concentration range studied (*cf.* Fig. 5 for methyl cellosolve). The value of Γ_S is therefore obtained by an indirect method as given below. The plots of c_A/Γ_S *vs.* c_A at constant E are linear and parallel for both the compounds showing thereby that their adsorption behaviour obeys Langmuir's adsorption isotherm with a slope equivalent to $1/\Gamma_S$. These plots for methyl cellosolve are shown in Fig. 6. The values of Γ_S thus obtained are 5.00 and 5.26 for 1,2-propanediol and methyl cellosolve respectively.

Standard Free Energy of Adsorption. The standard free energy of adsorption ($\Delta\bar{G}^\circ$) has been calculated according to the equation given by Conway and Barradas[9] when the adsorption isotherm is of Langmuir's type.

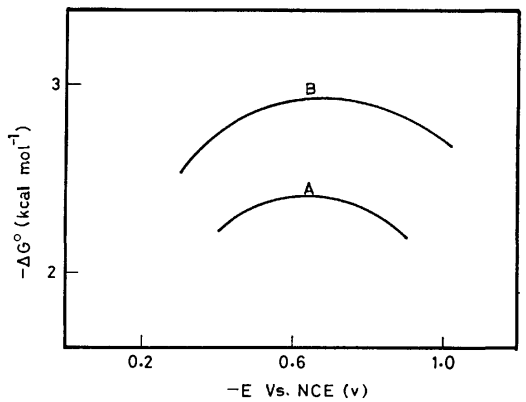

Fig. 7. Standard free energy of adsorption ($\Delta\bar{G}^\circ$) as a function of electrode potential (E). (A) 1,2-propanediol, (B) methyl cellosolve.

$$\ln\left(\frac{55.5}{c_A}\cdot\frac{\theta}{1-\theta}\right)=\frac{-\Delta\bar{G}^\circ}{RT}. \qquad (3)$$

The values of $\Delta\bar{G}^\circ$ have been obtained at constant coverage, $\theta=0.3$ ($\theta=\Gamma_A/\Gamma_S$) and at various electrode potentials. The dependence of $\Delta\bar{G}^\circ$ on E (*cf.* Fig. 7) is found to be quadratic for both the compounds as expected for simple neutral organic substances. The magnitude of $\Delta\bar{G}^\circ$ at any potential is higher for cellosolve than for diol. This can be attributed to the relatively weaker hydrogen bonding of cellosolve molecules with water molecules than that of diol.

E_{pzc} vs. log c_A and θ. Anodic shift of E_{pzc} with the increase in concentration of both the adsorbates

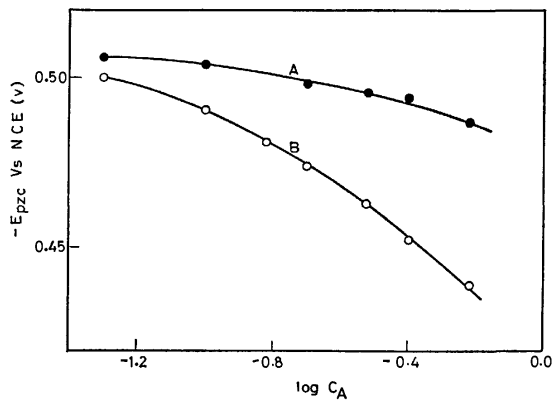

Fig. 8. E_{pzc} as a function of log c_A of the adsorbates. (A) 1,2-propanediol, (B) methyl cellosolve.

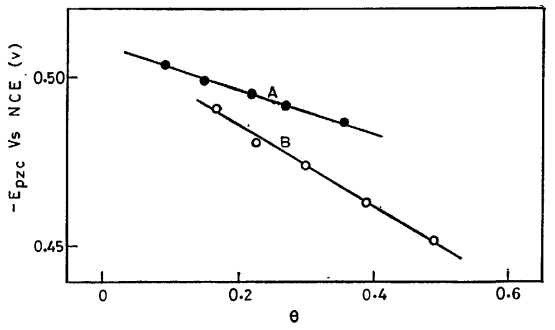

Fig. 9. E_{pzc} as a function of surface coverage of the adsorbates. (A) 1,2-propanediol, (B) methyl cellosolve.

indicates their orientation with the positive end towards the electrode and functional group in solution (*cf.* Fig. 8). Linear shift of E_{pzc} with surface coverage (θ) of the adsorbates (*cf.* Fig. 9) suggests single and stable orientation[10] throughout the coverage region. The magnitude of $(\partial E_{pzc}/\partial\theta)_{\theta\to 0}$ which accounts for the contribution due to normal components of the permanent organic dipoles[11] is greater for methyl cellosolve than for 1,2-propanediol. For equivalent concentrations, the magnitude of ΔE_{pzc} is more for cellosolve than for diol. This can be explained on the basis of (i) the normal component of the cellosolve dipoles being higher than that of diol dipoles and (ii) more number of negatively oriented water dipoles being replaced, due to relatively stronger adsorption of cellosolve dipoles than diol dipoles.

The electrode charge corresponding to maximum adsorption (σ^{M}_{max}) is $-3.2\ \mu C\ cm^{-2}$ for 1,2-propanediol and $-4.2\ \mu C\ cm^{-2}$ for methyl cellosolve. Damaskin and Frumkin[12] have expressed σ^{M}_{max} as

$$\sigma^{M}_{max} = -\left(\frac{\partial E_{pzc}}{\partial\theta}\right)_{\theta\to 0}\left(\frac{C_0^2}{C_0-C_1}\right). \quad (4)$$

The first term on the right hand side accounts for the contribution due to permanent dipoles and the second term, due to induced dipoles where C_0 and C_1 are the capacities at $\theta=0$ and $\theta=1$ respectively. It appears that the contribution due to permanent dipoles (Methyl cellosolve>1,2-propanediol) controls the value of σ^{M}_{max} in these two compounds and hence more negative σ^{M}_{max} for methyl cellosolve.

The authors are grateful to the Head of the Department of Chemistry, Banaras Hindu University for providing the necessary facilities and to the UGC, New Delhi, for the financial assistance to one of them (BVA).

References

1) S. L. Dyatkina and B. B. Damaskin, *Elektrokhimiya*, **5**, 438 (1969).
2) E. Dutkiewicz, J. D. Garnish, and R. Parsons, *J. Electroanal. Chem.*, **16**, 505 (1968).
3) S. Trasatti, *J. Electroanal. Chem.*, **28**, 257 (1970).
4) B. V. Apparao, Ph. D. Thesis, Banaras Hindu University, Varanasi (1977).
5) D. C. Grahame, *J. Am. Chem. Soc.*, **63**, 207 (1941).
6) D. C. Grahame, *J. Am. Chem. Soc.*, **71**, 2975 (1949).
7) A. N. Frumkin, *Z. Physik.*, **35**, 792 (1926).
8) R. Parsons, *Trans. Faraday Soc.*, **55**, 999 (1959).
9) B. E. Conway and R. G. Barradas, *Electrochim. Acta*, **5**, 319 (1961).
10) S. Trasatti, *J. Electroanal. Chem.*, **53**, 335 (1974).
11) B. A. Abd-El-Nabey and S. Trasatti, *J. Chem. Soc., Faraday Trans. 1*, **71**, 2130 (1975).
12) B. B. Damaskin and A, N. Frumkin, *J. Electroanal. Chem.*, **34**, 191 (1972).

Oxidation of Azide by Peroxodisulfate in Aqueous Medium

V. PONNURAJ, M. S. RAMACHANDRAN, T. S. VIVEKANANDAM, and U. CHANDRA SINGH
School of Chemistry, Madurai University, Madurai 652021, India

(Received May 11, 1977)

Results on the oxidation of N_3^- by peroxodisulfate in neutral and acid media are presented. The rate of the reaction is found to be proportional to $[N_3^-]$ and $[S_2O_8^{2-}]$directly. The product of oxidation is found to be pure nitrogen. The stoichiometry of the reaction is

$$S_2O_8^{2-} + 2N_3^- = 2SO_4^{2-} + 3N_2.$$

The reaction shows positive salt effect. Thermodynamic activation parameters ΔH^* and ΔS^* have been calculated for this reaction. It is observed that H^+ ion inhibits the reaction. The mechanism is discussed in terms of the kinetic results.

Peroxodisulfate ion is a powerful two-electron oxidizing agent with a redox potential of −2.01 eV. Oxidations of both inorganic and organic substrates were reviewed by House,[1] by Wilmarth and Haim[2] and recently by Wilson[3] and by Buist.[4] The oxidations of hydroxylamine[5] and hydrazine[6] were studied by Gupta *et al.* and they reported a multi-electron-transfer from the substrate to $S_2O_8^{2-}$. The chemistry of azide has gained impetus in recent years[7,8] because of the powerful complexing properties of this ion. From a survey of the literature it appears that the oxidation of this ion by $S_2O_8^{2-}$ has not been reported so far. The reactions of this ion with triiodide ion[9,10] and carbon disulfide[11] have been studied. The present paper reports the kinetic study of the oxidation of this ion with peroxodisulfate in neutral and acid medium.

The oxidation-reduction stoichiometry of the azide-peroxodisulfate reaction in neutral medium was determined by mixing various non-stoichiometric amounts of the reactants and measuring the amount of the reactant in excess at the completion of the reaction. The results show that the redox stoichiometry of the reaction is accurately represented by

$$S_2O_8^{2-} + 2N_3^- = 2SO_4^{2-} + 3N_2. \quad (1)$$

The product of oxidation was found to be pure nitrogen by gas chromatographic analysis in accordance with the above equation.

Experimental

Potassium peroxodisulfate (E. Merck, GR) was used without further purification. The stock solution was prepared daily and was analyzed quantitatively by cerimetry. Sodium azide (E. Merck, Germany) solution was prepared daily and was estimated by iodometry.[12] Water, deionized by passing through ion exchange resin (Permutit Mark-8) was distilled twice from alkaline permanganate in Corning glass apparatus and was stored in a stoppered polythene bottle. All solutions were prepared using this water.

Because of the high reactivity of azide ion, chemical method was not used to follow the reaction. The rate was followed by measureing the amount of gases produced from the system. The apparatus consisted of a 100 ml flask with ground glass joints. The flask was connected to a horizontal capillary tube of uniform bore of about 120 cm length, with inner diameter of ≈1.5 mm, having a mercury thread. A meter scale was attached to the tube and from the movements of the mercury thread the rate was measured.

The solution containing requisite amount of sodium perchlorate, peroxodisulfate was thermostated in the reaction vessel and was saturated with pure N_2 gas. The azide solution was thermostated separately and after the attainment of thermal equilibrium requisite amount of N_3^- solution was pipetted into the reaction vessel. The total volume of the reaction mixture was 50 ml. Powdered glass were added to avoid supersaturation. When the evolution of gas became steady, the rate was measured. It was observed that the steady state was attained within 5—10 minutes. The method was quite sensitive and the rate constant could be reproduced within 2—3%.

Results and Discussion

The plot of time *vs.* scale reading was perfectly linear (Fig. 1) and from the slope the rate dv/dt ($cm^3\ s^{-1}\ l^{-1}$) was calculated by taking the volume of the tube per cm.

N_3^- Dependence. The effect of N_3^- on rate was studied over a tenfold range of initial N_3^- concentration. The plot of log (dv/dt) *vs.* log $[N_3^-]$ shows that the rate is first order in N_3^- concentration in this range (Fig. 2).

$S_2O_8^{2-}$ Dependence. The concentration of peroxodisulfate was varied from 0.02 to 0.16 M. The plot of log (dv/dt) *vs.* log $[S_2O_8^{2-}]$ yields a slope of ≈1.0

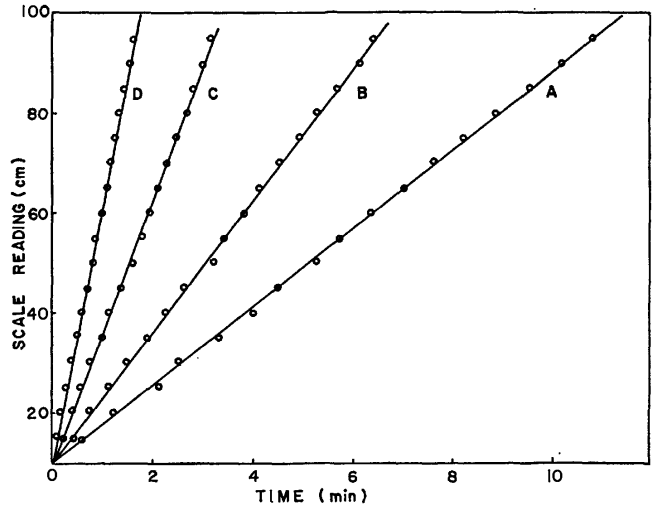

Fig. 1. The scale reading as a function of time under various initial $[N_3^-]$.
$[S_2O_8^{2-}]_0 = 0.04$ M; $\mu = 0.92$ $t = 45.0$ °C; A: 0.06 M, B: 0.10 M, C: 0.20 M, D: 0.40 M.

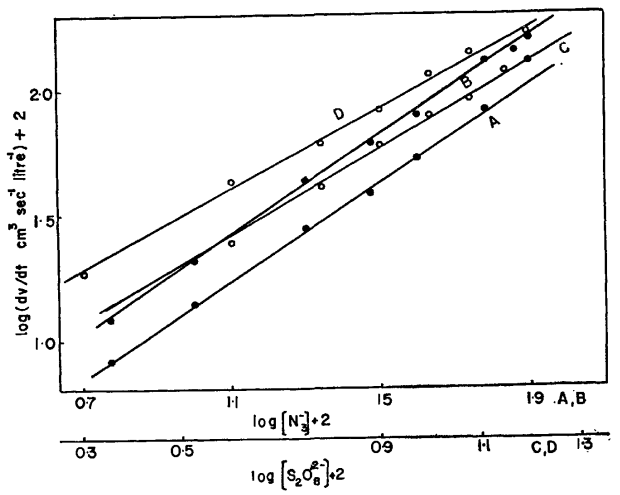

Fig. 2. Dependence of $[N_3^-]$ and $[S_2O_8^{2-}]$ on rate of the reaction.
A, B: N_3^- dependence, A: $[S_2O_8^{2-}]_0=0.04$ M; $\mu=0.92$; $t=45.0$ °C; Slope=1.0. B: $[S_2O_8^{2-}]_0=0.04$ M; $\mu=0.92$, $t=50.0$ °C; Slope=1.0. C, D: $[S_2O_8^{2-}]$ dependence. C: $[N_3^-]_0=0.20$ M; $\mu=0.72$; $t=45.0$ °C, Slope=1.15. D: $[N_3^-]_0=0.20$ M $\mu=0.92$, $t=50$ °C, Slope=1.08.

showing the first order dependence of $S_2O_8^{2-}$ (Fig. 2).

Hydrogen ion Dependence. The rate was found to decrease linearly with the addition of H^+ and almost reached to zero when the concentration of H^+ added was equal to $[N_3^-]_0$ (Fig. 3).

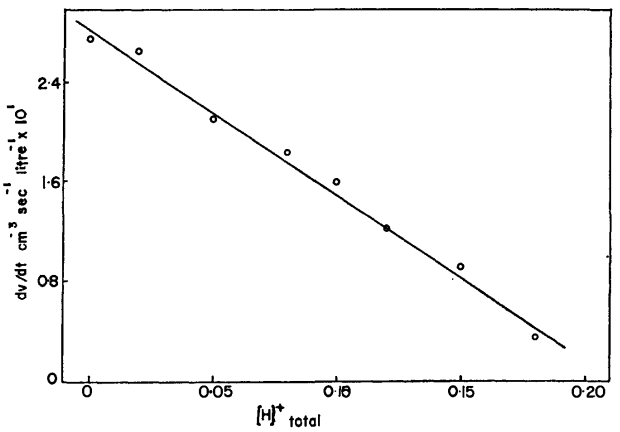

Fig. 3. Effect of H^+ on rate of the reaction. $[S_2O_8^{2-}]_0=0.04$ M; $[N_3^-]_0=0.20$ M. $\mu=0.92$; $t=45.0$ °C.

Evaluation of the Rate Constant. From the first order dependence of N_3^- and $S_2O_8^{2-}$ on rate and the stoichiometry of the reaction, the rate law could be written as

$$\frac{d[N_2]}{dt} = 3k_1[N_3^-][S_2O_8^{2-}]. \quad (2)$$

Applying the gas law Eq. 2 is modified as

$$(dv/dt)\times P/3RT = k_1[N_3^-][S_2O_8^{2-}]. \quad (3)$$

Taking $P\approx 1$ atm, $T=(300\pm0.5)$ K and the initial concentrations of N_3^- and $S_2O_8^{2-}$ the absolute rate constant k_1 was calculated.

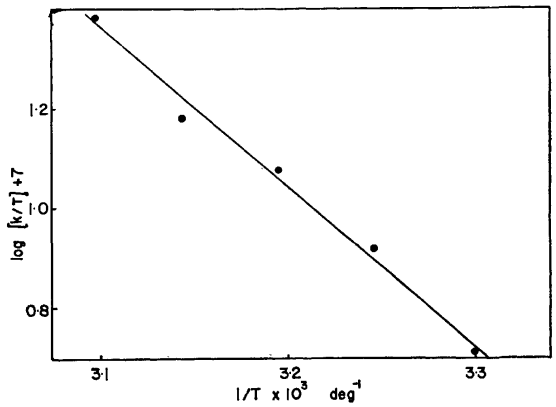

Fig. 4. Temperature dependence of k_1 between 30 and 50 °C.

Temperature Dependence. The kinetic study was made at the temperature range of 30—50°C. The plot of $\log(k/T)$ *vs.* $1/T$ was linear from which thermodynamic activation parameters were computed (Fig. 4). The values are $\Delta H^*=15.0$ kcal M^{-1} and $\Delta S^*=-25$ e.u.

Other Dependence. The rate increased with the increase in the ionic strength of the medium (Table 1). The reaction was not affected by the presence of Cu(II), Co(II), Mn(II), and Fe(III) (Table 1).

We suggest the following mechanism for the reaction in the light of the experimental results.

$$S_2O_8^{2-} + N_3^- \xrightarrow{k_1} N_3 + SO_4^{2-} + SO_4^{\cdot-} \quad (4)$$

Table 1. Rate constant of reaction of peroxodisulfate and azide ions under various conditions

$[S_2O_8^{2-}]_0=0.04$M, $[N_3^-]_0=0.20$M, $t=45.0$ °C.

Exp.	μ	$[Cu^{2+}]\times10^4$M	$[Co^{2+}]\times10^3$M	$k\times10^5$ $M^{-1}s^{-1}$
1	0.32	—	—	25.0
2	0.52	—	—	32.6
3	0.72	—	—	40.6
4	0.92	—	—	45.8
5	0.37	—	—	26.4
6	0.37	1.0	—	27.6
7	0.37	2.0	—	27.0
8	0.37	4.0	—	27.4
9	0.37	10.0	—	27.0
10	0.37	20.0	—	27.6
11	0.37	50.0	—	27.5
12	0.37	—	1.6	26.5
13	0.37	—	6.4	27.0
14	0.37	—	9.6	27.3
15	0.37	—	11.2	26.6
16	0.37	—	16.0	27.0
17	0.37	1[a]	—	27.8
18	0.37	2[a]	—	28.0
19	0.37	5[a]	—	27.5
20	0.37	10[a]	—	26.8
21	0.37	—	10[b]	27.3
22	0.37	—	20[b]	26.7
23	0.37	—	30[b]	28.0

a) $[Mn^{2+}]\times10^3$M. b) $[Fe^{3+}]\times10^5$M.

$$SO_4^{\cdot-} + N_3^- \longrightarrow N_3 + SO_4^{2-} \quad (5)$$

$$N_3 + N_3 \longrightarrow 3N_2 \quad (6)$$

The rate determining step is the one-electron transfer from N_3^- to $S_2O_8^{2-}$ followed by the fast consumption of SO_4^{2-} by N_3^- to form the transient species N_3 which subsequently decompose into molecular nitrogen. The reaction (6) is indeed shown[13] to be very fast ($k = 1.3\times10^{10}\ M^{-1}\ s^{-1}$). The positive salt effect and the highly negative values of ΔS^* lend support for the above mechanism. It can be shown[14] that for a bimolecular reaction between two charged species with charges Z_A and Z_B, ΔS^* would be approximately equal to $-10Z_AZ_B$. The agreement between the calculated value ($\Delta S^* \approx -20$ e.u.) and the experimental value in this investigation is reasonably good. Further, during the course of the reaction the change in the acid concentration is negligible in accordance with the above mechanism (Table 2).

TABLE 2. PRODUCTION OF ACID DURING THE REACTION
$\mu=0.72$, $t=45.0$ °C.

$[S_2O_8^{2-}]_0$	$[N_3^-]_0$	pH	
		Initial	Final
0.04	0.10	7.90	8.20
0.04	0.20	8.00	8.35
0.08	0.20	7.25	7.70
0.08	0.30	6.95	8.00
0.12	0.20	6.80	7.90

In acid medium the following steps may be included along with (3)—(6).

$$N_3^- + H^+ \overset{K_a}{\rightleftharpoons} HN_3 \quad (7)$$

$$HN_3 + S_2O_8^{2-} \overset{k_2}{\longrightarrow} N_3 + HSO_4^- + SO_4^{\cdot-} \quad (8)$$

$$SO_4^{\cdot-} + HN_3 \longrightarrow N_3 + HSO_4^- \quad (9)$$

Surprisingly H^+ acts as an anti-catalyst for the reaction. Hydrazoic acid is a very weak acid[15] ($K_a = 2.1\times10^{-5}$ at 20°C) with high thermal stability.[16] Assuming the complete formation of HN_3 with the addition of H^+ ($[HN_3] \approx [H^+]_t$) the rate equation is given by

$$\frac{d[N_2]}{dt} = 3(k_1[N_3^-]_0 + (k_2-k_1)[H^+]_t)[S_2O_8^{2-}], \quad (10)$$

where $[N_3^-]_0$ represents the total concentration of azide in the solution. The value of k_2 is found to be $\approx 3.0\times10^{-5}\ M^{-1}\ s^{-1}$ which may be compared with k_1 ($45.8\times10^{-5}\ M^{-1}\ s^{-1}$). The result clearly shows that H^+ stabilizes azide ion towards $S_2O_8^{2-}$.

It is a pleasure to acknowledge the kind help and encouragement of Prof. N. R. Subbaratnam, and Dr. K. Venkata Rao, School of Chemistry, Madurai University, India. One of us (M.S.R.) wishes to acknowledge C.S.I.R., India for their financial support as Junior Research Fellowship.

References

1) D. A. House, *Chem. Rev.*, **62**, 185 (1962).
2) W. K. Wilmarth and A. Haim, in "Peroxide Reaction Mechanisms," ed by J. O. Edwards, Interscience, New York (1962), p. 175.
3) I. R. Wilson, in "Comprehensive Chemical Kinetics," Vol. 6, ed by C. H. Bamford and C. F. H. Tipper, Elsevier, New York (1972), p. 271.
4) G. J. Buist, in "Comprehensive Chemical Kinetics," Vol. 6, ed by C. H. Bamford and C. F. H. Tipper, Elsevier, New York (1972), p. 435.
5) R. Waroop and Y. K. Gupta, *J. Inorg. Nucl. Chem.*, **36**, 169 (1974).
6) A. P. Bhargawa, R. Swaroop, and Y. K. Gupta, *J. Chem. Soc., A*, **1970**, 2183.
7) S. Patai, "The Chemistry of the Azido Group," Interscience, New York (1971).
8) Z. Dori and R. F. Ziolo, *Chem. Rev.*, **73**, 247 (1973).
9) N. Hofman-Bang and W. Szybalski, *Acta Chem. Scand.*, **3**, 1418 (1949).
10) P. Senise, *J. Phys. Chem.*, **55**, 1151 (1951).
11) N. Hofman-Bang and B. Holten, *Acta Chem. Scand.*, **5**, 333 (1951).
12) A. Wtorkowska-Zaremba, *Chem. Anal., (Warsaw)*, **14**, 847 (1969).
13) E. Hayon and M. Simic, *J. Am. Chem. Soc.*, **92**, 7486 (1970).
14) K. J. Laidler, "Chemical Kinetics," McGraw-Hill, New York (1965).
15) D. Bunn, F. S. Dainton, and S. Duckworth, *Trans. Faraday Soc.*, **57**, 1131 (1961).
16) G. Peter, *Chem. Soc. Rev.*, **17**, 441 (1963).

The Use of Solvent E_T-values in High Pressure Kinetics

Jörn von JOUANNE, Donald A. PALMER, and Hartwig KELM
Institute for Physical Chemistry, University of Frankfurt, Robert-Mayer-Strasse 11, D-6000 Frankfurt am Main, West Germany

(Received August 1, 1977)

The solvatochromic shift and its pressure dependence of the charge transfer band of 2,4,6-triphenyl-pyridinium-*N*-(3,5-diphenyl-)phenol betaine (E_T-values) have been measured together with partial molar volumes of the betaine in a number of solvents.

Despite the relative success of the Kirkwood theory, considerable effort[1] has been made to replace it by a more general description of the influence of various solvents on chemical equilibria and rate constants. Since the physical forces that govern solute-solvent interactions differ widely in strength and range it seems most unlikely that a comparatively simple theory will exceed the Kirkwood theory. An alternative is to try and replace the theoretical description by an empirical approach. Among the latter, the scale of E_T values, which was originally derived by Dimroth and coworkers[2,3] from the solvatochromic effect on the charge transfer band of 2,4,6-triphenyl-pyridinium-*N*-(3,5-diphenyl-)phenol betaine, has deserved the most interest.[4]

The present study was undertaken in order to investigate whether: 1. the effect of pressure on E_T might be a useful parameter to describe the overall variation of solvent properties with applied pressure; 2. the zwitterionic ground state of the betaine could prove to be a good model for ionic transition states as may be demonstrated by studying the solvent dependence of the partial molar volume of the betaine itself. In view of some recent publications[5–8] the limitations and the reliability of the parameters E_T, dE_T/dp and $\bar{V}$ will be critically discussed.

Experimental

The synthesis of the 2,4,6-triphenyl-pyridinium-*N*-(3,5-diphenyl-)phenol betaine was conducted according to literature procedures[2] and yielded a product with one mole of water of crystallization (formula $C_{41}H_{24}NO \cdot H_2O$, mol wt 563.71). A determination of its molecular weight in solution by the vapor pressure depression method indicated that, even at the highest concentrations (*ca.* 10^{-2} M in CH_2Cl_2), no detectable dimerization takes place. All solvents were purified according to standard procedures.

Precision density measurements of the betaine solutions were carried out using a DMA 02C instrument (Anton Paar K.G.) at 25 °C. The temperature was controlled to within ±0.001 °C and monitored by a Hewlett-Packard 280 A quartz thermometer. Spectrophotometric studies were made with a Zeiss DMR 10 instrument equipped with a high pressure attachment which is described elsewhere.[9]

Results and Discussion

Solvatochromic Shifts. The band maximum, λ_{max}, of the intramolecular charge transfer transition of the betaine shows the most remarkable solvatochromic shift so far known. The values of λ_{max} given in Table 1 agree with the results of a number of previous investigations.[2–4] As has been already discussed by Dimroth[2] and Reichardt,[4] generally the more polar the solvent, the more λ_{max} is blue-shifted. Two distinct classes of solvents have emerged: protic and aprotic.

There are many examples[7,10] in which linear free energy relationships satisfactorily hold for the solvent dependence of rate constants of reactions with polar routes and the E_T values of the pure solvents. The concept to use the E_T values of the betaine as a microprobe monitoring local polarities within a solvent might be of even more interest in mixed solvents than in pure ones. The rate constants of the Menschutkin reaction: 3,5-lutidine+ethyl iodide, have been shown to perfectly follow a $\ln k$ *vs.* E_T relationship in benzene–nitrobenzene mixtures.[7] The E_T values of two mixed systems with widely differing dielectric constants have been measured during this study: water–dioxane and methanol–dichloromethane (Fig. 1). For the system water–dioxane the shape of the $E_T(x)$ (x=mole fraction) function is very different from that of the $q(x) = (D(x)-1)/(2D(x)+1)$ parameter. Kinetic data on the hydrolysis of the 1-chloro-2-nitroethane, chlorodiphenyl-

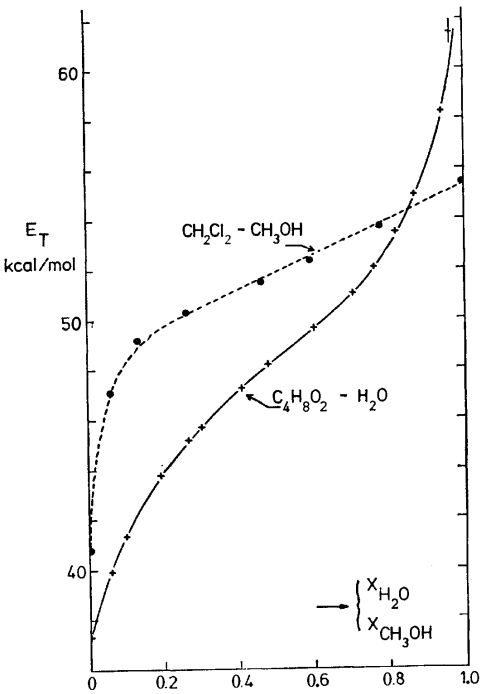

Fig. 1. Variation of solvent E_T parameters in mixed solvents.
——: Dioxane–water, ------: dichloromethane–methanol.

methane, and benzoylchloride[11] show that in water–dioxane mixtures (excluding very high and very low mole fractions) a linear dependence $\ln k \approx E_T$ is found only in the latter case. For the former reactions no preference of E_T above q can be established. In the inorganic field, data of Burgess *et al.*[12,13] show that in water–dioxane either E_T, or Y (Winstein-Grunwald parameter) or q correlate with $\ln k$. The rate constants for the isomerization of *trans*-diaquobis(oxalato)-chromate(III) anions in water–dioxane mixtures[14] closely obey a linear free energy relationship with E_T. Thus the choice of the proper parameter depends crucially on the reacting system in question.

A close inspection of the E_T values in water–dioxane mixtures reveals that E_T is influenced by several effects. The sharp decline of E_T when small amounts of dioxane are added in the water rich region ($1 > x_{H_2O} > 0.8$) is similar to the decline of the dielectric constant, but *not* of q. Thus E_T seems to be sensitive to the rupture of the water structure. The hydrophobic interactions between the phenyl substituents of the betaine and the solvent obviously play a major part in determining E_T. In the dioxane rich region ($x_{dioxane} \geqq 0.8$) the functions $q(x)$ and $E_T(x)$ are very similar. Thus lowering the ground state of the betaine by dipolar interactions is dominant when the dielectric constant of the mixture is increased by adding water. How far specific solvation interactions between the positions of very high charge density within the betaine molecule and the polar water molecules are reflected in E_T is not known. The existance of such a type of interaction can be concluded from the fact that the betaine contains water of crystallization, but is insoluble in pure water. An attempt to gain further insight into these interactions failed because the betaine has no triplet ESR spectrum which could give information about the distribution of electron density within the molecule. Furthermore, the experimental dipole moment of 12 Debye[3] does not agree with a simple $N^+—O^-$ dipole. However, the existence of some preferential solvation by the polar component of a mixture is also evident from the E_T values in dichloromethane–methanol mixtures. Minor amounts of methanol in dichloromethane drastically increase E_T as is shown in Fig. 1.

TABLE 1. ABSORPTION MAXIMUM OF CHARGE TRANSFER BAND, λ_{max}, BLUE-SHIFT OF λ_{max} UNDER PRESSURE AND PARTIAL MOLAR VOLUMES, $\bar{V}$, OF 2,4,6-TRIPHENYLPYRIDINIUM-*N*-(3,5-DI-PHENYL)PHENOL BETAINE IN DIFFERENT SOLVENTS

Solvent	D[a]	q	λ_{max} nm	$d\lambda/dP \cdot 10^3$ nm/atm	$\bar{V}$ ml/mol
$CHCl_3$	4.70	0.356	732	8	455.1±2.7
CH_2Cl_2	8.9	0.420	700	7	451.2±1.4
$(CH_3)_2CO$	20.5	0.464	684	6	417.0±3.6
$(CH_3)_2NCHO$	36.7	0.480	653	4	445.7±2.4
$(CH_3)_2SO$	48.9	0.485	634	4	462.6±3.8
CH_3CN	37.5	0.480	625	5	440.4±3.4
C_2H_5OH	24.3	0.470	550.5	5	426±20
CH_3OH	32.6	0.477	515	6	421±10

a) Ref. 4 and the references quoted therein.

Piezo-Solvatochromic Shifts. Generally, when hydrostatic pressure is applied on a solution of the betaine the charge transfer band is blue-shifted. The total effect at 1000 bar, however, reaches only 4 to 8 nm (Table 1). Considering that the charge transfer band is very broad (width at $\varepsilon_{max}/2$ *ca.* 170 nm in $CHCl_3$ at 25 °C) and unsymmetrical, the accuracy in determining λ_{max} may be expected to be *ca.* ±1 nm at best. Thus within our experimental conditions no definite trend between $\Delta\lambda_{max}/\Delta P$ and the nature of the various solvents could be established. This is despite the varied nature of the solvents employed. Therefore we are convinced that the effect of pressure on the betaine charge transfer band is not a suitable indicator of the sum of all the pressure dependent solvent-solute interactions. In particular, no useful empirical parameter could be derived from $\Delta\lambda_{max}/\Delta P$ of the betaine describing the rearrangement of solvent structure in the vicinity of a dipolar species under various external pressures. The linear dependence of $\ln k(P)$ *vs.* $\Delta\lambda_{max}/\Delta P$ reported for two Menschutkin reactions in two solvents[5,8] seems to be more or less accidental in view of the limited range and accuracy of the $\Delta\lambda_{max}/\Delta P$ parameter. On the contrary, the values of $\Delta\lambda_{max}/\Delta P$ can be explained satisfactorily on the basis of the simple Kirkwood theory taking into account the pressure dependence of the macroscopic dielectric constant (q_p-parameter). Therefore we conclude that under pressure mainly the ground state of the betaine is lowered by dipolar solvent-solute interactions. How far the less polar excited state of the betaine, which according to the Franck Condon principle is not in thermodynamic equilibrium with its solvation shell, is influenced by pressure is not known. An attempt to determine the effect of pressure on the excited state failed because no fluorescence spectrum of the betaine could be found. It is most probable that the solvent structure around an excited nonpolar betaine molecule is very similar to that around the very polar ground state.[8] Only the induced dipole moments of the solvent molecules can follow the optical transition of the betaine. However, interaction with induced dipole moments is known to be comparatively small.

Partial Molar Volumes. The apparent molar volumes, φ_i, were determined according to the equation

$$\varphi_i = M/d_0 - (d_i - d_0) \cdot 1000/c_i \cdot d_0,$$

where M is the molecular weight of the betaine and c_i is its molar concentration, while d_i and d_0 are the densities of the solution and the pure solvent, respectively. Within experimental errors, no concentration dependence of φ_i was observed, which may be expected considering the relatively low concentration range studied, *i.e.*, $c \leqq 0.02$ M. Thus the partial molar volumes $\bar{V}$, of the betaine were merely taken from the average values of φ_i over the entire concentration range.

These values, which are listed in Table 1, certainly show no distinctive trend with solvent polarity parameters such as D, q, or E_T. Thus the effects that govern the solvent dependence of $\bar{V}$ are not solely of a dipolar origin (electrostriction). Therefore, we conclude that with respect to partial molar volumes the dipolar ground

state of the betaine is not a suitable model for ionic transition states in chemical kinetics, *e.g.* in Menschutkin reactions. Of all possible solvent parameters the $\bar{V}$ values of the betaine correlate best with the compressibilities and internal pressures of the different solvents. Following Dack's arguments,[15] such a behaviour is caused by the sum of all solvent-solute interactions as well as "the ability of the solvent to create cavities absorbing the intrinsic volume" of the betaine. Unfortunately, the individual contributions to $\bar{V}$ such as: electrostriction due to charge-dipole and dipole-dipole interactions; hydrogen bonding; hydrophobic and van der Waals interactions, *etc.* cannot be separated. Despite the severe limitations of the Kirkwood theory, so far the $q_p=\frac{\partial}{\partial P}\left(\frac{D-1}{2D+1}\right)$-parameter seems to best describe the large electrostriction effects found when the solvent dependence of activation volumes in polar reactions is studied.

It is obvious from the above arguments that a lot of questions on solute-solvent interactions, which were hoped to be "solved" by introducing empirical parameters, are still open. In view of the many exceptions that exist, both when the Kirkwood theory or the scale of E_T values is used, the choice of a proper description of solvent effects depends on the system studied and perhaps on personal judgement as to whether one prefers an oversimplified but theoretically based physicochemical treatment, or a more overall empirical approach.

The authors wish to thank Drs. M. Geiss and F. K. Fleischmann of their preliminary investigations. The financial assistance of the Deutsche Forschungsgemeinschaft is gratefully appreciated.

References

1) E. S. Amis, "Solvent Effects on Reaction Rates and Mechanisms," Academic Press, New York and London (1966).
2) K. Dimroth, C. Reichardt, T. Siepmann, and F. Bohlmann, *Ann. Chem.*, **661**, 1 (1963).
3) K. Dimroth, C. Reichardt, and A. Schweig, *Ann. Chem.*, **669**, 95 (1963).
4) C. Reichardt, *Angew. Chem.*, **77**, 30 (1965).
5) K. Tamura, Y. Ogo, and T. Imoto, *Chem. Lett.*, **1973**, 625.
6) K. Tamura and T. Imoto, *Chem. Lett.*, **1973**, 1251.
7) K. Tamura, Y. Ogo, and T. Imoto, *Bull. Chem. Soc. Jpn.*, **46**, 2988 (1973).
8) K. Tamura and T. Imoto, *Bull. Chem. Soc. Jpn.*, **48**, 369 (1975).
9) F. K. Fleischmann, E. G. Conze, D. R. Stranks, and H. Kelm, *Rev. Sci. Instrum.*, **45**, 1427 (1974).
10) G. Steiner and R. Huisgen, *J. Am. Chem. Soc.*, **95**, 5055 (1973).
11) D. Büttner and H. Heydtmann, *Ber. Bunsenges. Phys. Chem.*, **73**, 640 (1969).
12) J. Burgess, E. R. Gardner, and F. M. Mekhail, *J. Chem. Soc., Dalton Trans.*, **1972**, 487.
13) J. Burgess, F. M. Mekhail, and E. R. Gardner, *J. Chem. Soc., Dalton Trans.*, **1973**, 1335.
14) H. Kelm, H. Stieger, and G. M. Harris, *Chem. Ber.*, **104**, 2743 (1971).
15) M. R. Dack, *Aust. J. Chem.*, **29**, 779 (1976).

Solid-phase Thermal Syntheses of Binuclear Chromium(III) and Cobalt(III) Complexes Containing *N*-(2-Sulfoethyl)iminodiacetic Acid[1]

Masazo KIMURA, Akira UEHARA, Eishin KYUNO,* and Ryokichi TSUCHIYA

Department of Chemistry, Faculty of Science, Kanazawa University, Kanazawa 920
**Department of Pharmaceutical Science, School of Pharmacy, Hokuriku University, Kanazawa 920*

(Received June 7, 1977)

The following four chromium(III) and cobalt(III) double complexes were prepared and the thermal reactions were investigated both isothermally and non-isothermally in the solid-phase: [(Cr or Co)(H_2O)(NH_3)$_5$][(Cr or Co)(sida)$_2$] where sida denotes *N*-(2-sulfoethyl)iminodiacetate ion. The double complexes were found to be thermally deaquated to form the homo- and hetero-metal binuclear complexes [(NH_3)$_5$(Cr or Co)(sida)(Cr or Co)-(sida)] in which one of *N*-(2-sulfoethyl)iminodiacetate ions functions as the bridging ligand between two metal ions. The complexes thus obtained were purified from a 50% $HClO_4$ or a 1 M $NaClO_4$ solution in the forms of the hydrogen salts [(NH_3)$_5$(Cr or Co)(sida)(Cr or Co)(sidaH)]ClO_4 or the sodium salts [(NH_3)$_5$(Cr or Co)(sida)-(Cr or Co)(sidaNa)]ClO_4.

Only a few complexes are known in which natural or artificial amino acids function as the bridging ligand: the homo-metal binuclear complexes[2] such as [en_2Co(L-asp)Co(H_2O)en_2](ClO_4)$_4$·H_2O[3] and [(NH_3)$_5$Co(edta)-Co(H_2O)](ClO_4)$_2$[4] were recently isolated by means of column chromatography. When the solid-phase bridging[5–7] and ligand-transfer[8] reactions reported previously were applied to the preparation of the amino acid-bridging binuclear complexes, they were obtained easily.

The present study was therefore undertaken to prepare the amino acid-bridging homo- and hetero-metal binuclear complexes[2] by the use of solid-phase thermal reactions. The preparative procedures of the present study are based on the following thermal reactions:

$$[(\text{Cr or Co})(H_2O)(NH_3)_5][(\text{Cr or Co})(\text{sida})_2] \xrightarrow[\Delta]{-H_2O} [(NH_3)_5(\text{Cr or Co})(\text{sida})(\text{Cr or Co})(\text{sida})],$$

where sida denotes *N*-(2-sulfoethyl)iminodiacetate ion.

The thermal syntheses according to the above reaction have the following characteristics: firstly, the hetero-metal binuclear complexes can conveniently be synthesized by selecting the combination of metal ions in the starting double complexes. Secondly, amino acid-bridging binuclear complexes can be obtained with simpler processes. Thirdly, the complexes in which the $-SO_3$ group in sida is coordinated to a metal ion can be isolated, although they have not been isolated previously because of the weak coordination ability of a $-SO_3$ group.[9,10]

Experimental

Preparation of the Starting Complexes for Obtaining Double Complexes. The starting complexes [Cr(H_2O)(NH_3)$_5$](NO_3)$_3$,[11] [Co(H_2O)(NH_3)$_5$](NO_3)$_3$,[12] *trans*(*N*)-K_3[Cr(sida)$_2$]·4H_2O[9] and *trans*(*N*)-K_3[Co(sida)$_2$]·4H_2O[13] were prepared by the same method as that reported in each literature, and they were identified by means of elemental analyses and spectrophotometric measurements.

Preparation of Double Complexes. Aquapentaamminechromium(III) Bis(N-(2-sulfoethyl)iminodiacetato)chromate(III) Dihydrate, [Cr(H_2O)(NH_3)$_5$][Cr(sida)$_2$]·2H_2O (Red) (I). Ten and seven tenth grams (3.2×10^{-2} mol) of [Cr(H_2O)(NH_3)$_5$](NO_3)$_3$ and 15.0 g (3.2×10^{-2} mol) of *trans*(*N*)-K_3[Cr(sida)$_2$]·4H_2O were dissolved separately in about 50 ml of water and then they were mixed together. The mixture was stirred with a glass rod for a few minutes and allowed to stand in a refrigerator overnight, red crystals being obtained. They were collected by filtration, washed with small amounts of water, ethanol and ether, and air-dried. Yield about 16 g.

Found: C, 19.98; H, 5.02; N, 13.27%. Calcd for $C_{12}H_{37}O_{17}N_7S_2Cr_2$: C, 20.03; H, 5.19; N, 13.63%.

Aquapentaamminechromium(III) Bis(N-(2-sulfoethyl)iminodiacetato)cobaltate (III) Dihydrate, [Cr(H_2O)(NH_3)$_5$][Co(sida)$_2$]·2H_2O (Pink) (II). This was prepared in a manner similar to that of complex I except that a solution of 15.3 g (3.2×10^{-2} mol) of *trans*(*N*)-K_3[Co(sida)$_2$]·4H_2O in 50 ml of water was used in place of the solution of *trans*(*N*)-K_3[Cr(sida)$_2$]·4H_2O.

Found: C, 19.78; H, 5.03; N, 13.55%. Calcd for $C_{12}H_{37}O_{17}N_7S_2CrCo$: C, 19.83; H, 5.14; N, 13.50%.

Aquapentaamminecobalt(III) Bis(N-(2-sulfoethyl)iminodiacetato)-chromate(III) Dihydrate, [Co(H_2O)(NH_3)$_5$][Cr(sida)$_2$]·2H_2O (Orange) (III). The complex was also obtained by a method similar to that of complex I except that a solution of 10.9 g (3.2×10^{-2} mol) of [Co(H_2O)(NH_3)$_5$](NO_3)$_3$ in 150 ml of water was used instead of the solution of [Cr(H_2O)(NH_3)$_5$]-(NO_3)$_3$. Yield about 15 g.

Found: C, 19.49; H, 5.07; N, 13.12%. Calcd for $C_{12}H_{37}O_{17}N_7S_2CrCo$: C, 19.83, H, 5.14; N, 13.50%.

Aquapentaamminecobalt(III) Bis(N-(2-sulfoethyl)iminodiacetato)-cobaltate(III) Dihydrate, [Co(H_2O)(NH_3)$_5$][Co(sida)$_2$]·2H_2O (Pale Red) (IV). This was synthesized according to a procedure similar to that of complex I from 10.9 g (3.2×10^{-2} mol) of [Co(H_2O)(NH_3)$_5$](NO_3)$_3$ and 15.3 g (3.2×10^{-2} mol) of *trans*(*N*)-K_3[Co(sida)$_2$]·4H_2O in 150 ml and 50 ml of water, respectively.

Found: C, 19.66; H, 5.06; N, 13.48%. Calcd for $C_{12}H_{37}O_{17}N_7S_2Co_2$: C, 19.65; H, 5.09; N, 13.37%.

Preparation of Binuclear Complexes. μ-N-*(2-Sulfoethyl)iminodiacetatopentaamminechromium(III)(or cobalt(III))hydrogen(or sodium)*-N-*(2-sulfoethyl)iminodiacetatochromium(III)(or cobalt(III)) Perchlorates, [(NH_3)$_5$(Cr or Co)(sida)(Cr or Co)(sidaH or sida-Na)]ClO_4 (Reddish Violet) (V through XII).* For simplification, the procedures for preparing the binuclear complexes are schematically outlined in Fig. 1.

First of all the corresponding double complexes were triturated thoroughly in an agate mortar and were heated at given temperatures for a given period of time. The products [(NH_3)$_5$(Cr or Co)(sida)(Cr or Co)(sida)] were purified in

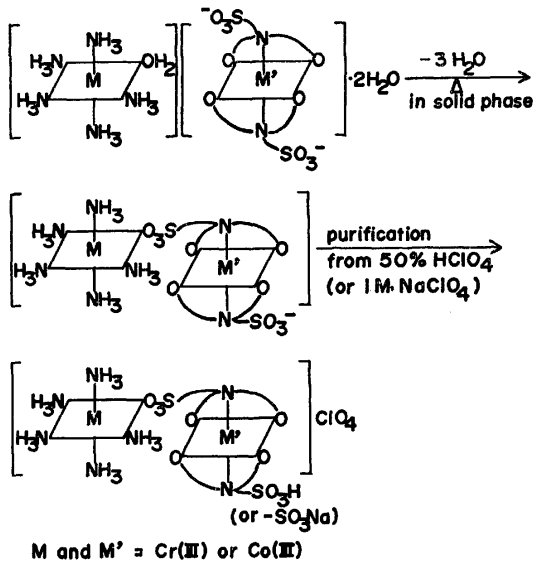

Fig. 1. Procedures for obtaining the binuclear complexes.

the forms of the hydrogen salts $[(NH_3)_5$(Cr or Co)(sida)(Cr or Co)(sidaH)$]ClO_4$ and the sodium salts $[(NH_3)_5$(Cr or Co)-(sida)(Cr or Co)(sidaNa)$]ClO_4$ from a 50% $HClO_4$ solution and a 1 M $NaClO_4$ solution, respectively. The yields of the hydrogen salts and the sodium salts were about 40% and 30% based on the amounts of the double complexes used, respectively.

Table 1 summarizes the binuclear complexes obtained, their analytical data, the starting double complexes, and the heating conditions determined non-isothermally (derivatographically) and/or isothermally.

Derivatographic Measurements. The derivatograms of the samples were recorded on a MOM Derivatograph Typ-OD-102. All the measurements were carried out in a nitrogen stream at the heating rate of 1 °C min^{-1}, 0.4 g of the samples being used in each run.

Isothermal Measurements. For the determination of the heating conditions for obtaining the desired binuclear complexes, isothermal measurements were carried out by using a Shimadzu TM-1A Thermanobalance in a static air at various temperatures.

Spectral Measurements. Visible and ultra-violet, and IR absorption spectra of the samples were measured in aqueous solutions and in KBr disks with Union High-sens. Spectrophotometer SM-401 and with a JASCO A-3 Infrared Spectrophotometer, respectively.

Magnetic Susceptibilities. The magnetic susceptibilities of the samples were measured by Gouy method at room temperatures. The effective magnetic moments were evaluated from the magnetic susceptibilities measured above and corrected by the use of Pascal's constants for each component in the complexes.

Molar Conductivities. Molar conductivities were measured to determine the charges of the binuclear complexes with a YEW Universal Bridge TYPE BU-Z-13A.

Behaviors toward Ion Exchangers. The behaviors of the binuclear complexes toward ion exchangers were examined to find whether they were cationic complex species or not. Dowex 1-X8 (100—200 mesh) and Dowex 50W-X8 (50—100 mesh) were used as anion and cation exchangers, respectively.

Results and Discussion

For convenience, in the following discussion, the double complexes ([Cr or Co)$(H_2O)(NH_3)_5$][(Cr or Co)-$(sida)_2$]) and binuclear complexes ($[NH_3)_5$(Cr or Co)-(sida)(Cr or Co)(sida)]) will be abbreviated as [Cr or Co][Cr or Co] and [(Cr or Co)–(Cr or Co)], and the hydrogen salts ($[(NH_3)_5$(Cr or Co)(sida)(Cr or Co)-(sidaH)$]ClO_4$) and the sodium salts ($[(NH_3)_5$(Cr or Co)-(sida)(Cr or Co)–(sidaNa)$]ClO_4$) will be designated similarly as [(Cr or Co)–(Cr or Co)H] and [(Cr or Co)–(Cr or Co)Na], respectively.

(1) Determination of the Conditions for Thermal Syntheses of Binuclear Complexes. For the determination of preparative conditions (temperature and duration of heating) of the binuclear complexes, the thermal reactions of the corresponding double complexes were observed both derivatographically and isothermally.

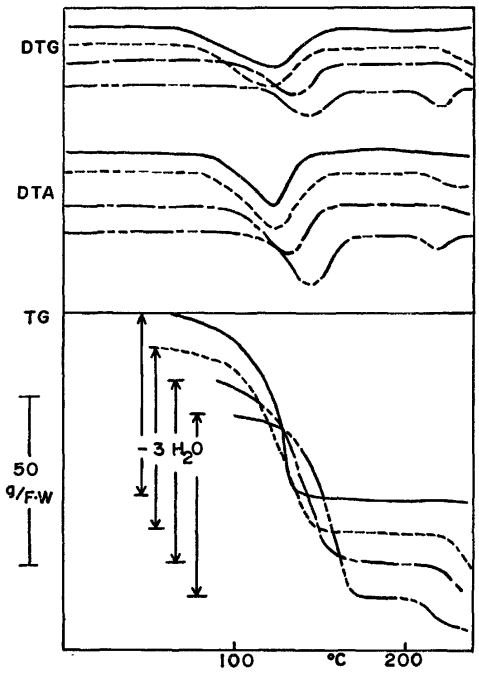

Fig. 2. Derivatograms of $[Cr(H_2O)(NH_3)_5][Cr(sida)_2]\cdot 2H_2O$ (——), $[Cr(H_2O)(NH_3)_5][Co(sida)_2]\cdot 2H_2O$ (·····), $[Co(H_2O)(NH_3)_5][Cr(sida)_2]\cdot 2H_2O$ (·—·), and $[Co(H_2O)(NH_3)_5][Co(sida)_2]\cdot 2H_2O$ (··—··).

Derivatography. The derivatograms of the double complexes are depicted in Fig. 2. The TG curves show that all the double complexes evolve smoothly three moles of water (two moles of lattice water and one mole of coordinated water) in the temperature range of 60—135 °C ([Cr][Cr]), 50—150 °C ([Cr][Co]), 90—160 °C ([Co][Cr]), and 100—170 °C ([Co][Co]), remaining unchanged in weight losses up to 200—220 °C. The [Cr][Cr] complex was stable even at about 220 °C, but the other three ([Cr][Co], [Co][Cr] and [Co][Co]) were decomposed gradually in a complicated way above 200—210 °C with the reduction of Co(III) to Co(II) ions. These double complexes were initially orange or pink in color, but changed to reddish violet at the end of the evolution of three moles of water. The

TABLE 1. BINUCLEAR COMPLEXES OBTAINED, ANALYTICAL DATA, STARTING DOUBLE COMPLEXES, AND HEATING CONDITIONS

Binuclear complex	Analytical data %[a] C	H	N	Starting double complex	Heating conditions[b] Temp (°C)	Time (min)
$[(NH_3)_5CrsidaCrsidaH]ClO_4$ (V)	19.09 (18.81)	4.39 (4.21)	12.53 (12.08)	$[CrH_2O(NH_3)_5]\cdot[Cr(sida)_2]\cdot 2H_2O$	122	120
$[(NH_3)_5CrsidaCrsidaNa]ClO_4$ (VI)	18.47 (18.29)	4.09 (3.97)	12.23 (12.44)			
$[(NH_3)_5CrsidaCosidaH]ClO_4$ (VII)	18.95 (18.64)	4.43 (4.18)	12.69 (12.69)	$[CrH_2O(NH_3)_5]\cdot[Co(sida)_2]\cdot 2H_2O$	122	120
$[(NH_3)_5CrsidaCosidaNa]ClO_4$ (VIII)	18.46 (18.13)	4.16 (3.94)	12.31 (12.34)			
$[(NH_3)_5CosidaCrsidaH]ClO_4$ (IX)	19.02 (18.64)	3.94 (4.18)	12.96 (12.69)	$[CoH_2O(NH_3)_5]\cdot[Cr(sida)_2]\cdot 2H_2O$	130	110
$[(NH_3)_5CosidaCrsidaNa]ClO_4$ (X)	18.25 (18.13)	4.01 (3.94)	12.27 (12.34)			
$[(NH_3)_5CosidaCosidaH]ClO_4$ (XI)	18.80 (18.49)	4.19 (4.14)	12.32 (12.57)	$[CoH_2O(NH_3)_5]\cdot[Co(sida)_2]\cdot 2H_2O$	142	210
$[(NH_3)_5CosidaCosidaNa]ClO_4$ (XII)	18.33 (17.97)	4.07 (3.90)	12.11 (12.23)			

a) The figures in parentheses are calculated values. b) The heating conditions were determined derivatographically and/or isothermally.

color changes are, as will be mentioned later, due to the liberation of the coordinated water in the complex cation ($[(Cr \text{ or } Co)(H_2O)(NH_3)_5]^{3+}$) and the subsequent coordination of the $-SO_3^-$ group in the complex anion ($[Cr \text{ or } Co)(sida)_2]^{3+}$).

The information obtained here implies that all the complexes are highly stable even after the liberation of water and hence the desired binuclear complexes are obtained by the use of the thermal reaction in the solid-phase without controlling conditions.

Isothermal Measurements. On the basis of the above results, preliminary experiments were carried out to determine the effective heating conditions for the thermal syntheses. Figure 3 shows the change in the weight losses of the double complexes with time at the given temperatures.

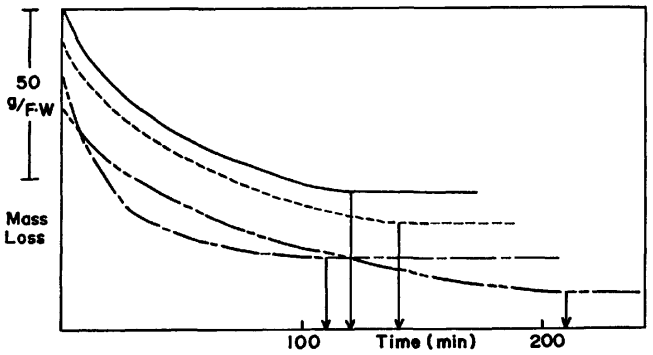

Fig. 3. Changes in weight losses with time of $[Cr(H_2O)(NH_3)_5][Cr(sida)_2]\cdot 2H_2O$ at 122 °C (——), $[Cr(H_2O)(NH_3)_5][Co(sida)_2]\cdot 2H_2O$ at 122 °C (·····), $[Co(H_2O)(NH_3)_5][Cr(sida)_2]\cdot 2H_2O$ at 130 °C (·—·), and $[Co(H_2O)(NH_3)_5][Co(sida)_2]\cdot 2H_2O$ at 142 °C (··—··).

The [Cr][Cr] double complex gradually and monotonously loses the weight of 54 g/*F.W.* (*F.W.*=Formula Weight) which corresponds to 3 mol of water, no further weight change being found even after prolonged heating. From this result, 122 °C and 120 min were selected as the optimal heating temperature and the time duration for the thermal synthesis of the [Cr–Cr] binuclear complex. Similarly, the heating conditions for the other three complexes were determined as specified in Table 1.

(2) Properties of the Binuclear Complexes. Magnetic Susceptibilities: The [Cr][Cr] double complex gave the value of 3.9 B.M. (290 K) per one chromium ion. The values 3.9 B.M. (291 K) and 3.8 B.M. (291 K) were observed for the [Cr][Co] and [Co][Cr] double complexes, respectively. The [Co][Co] double complexes were found to be diamagnetic (291 K).

On the other hand, the values for the binuclear complexes are, in general, slightly smaller as compared with those for the corresponding double complexes: 3.6 B.M. (291 K) for [Cr–CrH], 3.7 B.M. (291 K) for [Cr–CoH] and 3.5 B.M. (291.5 K) for [Co–CrH]. The [Co–CoH] binuclear complex was diamagnetic (292 K). These results suggest that the cobalt and chromium ions are all tervalent in both the double and binuclear complexes.

Molar Conductivities: Table 2 lists the molar conductivities. The binuclear complexes of the hydrogen and

TABLE 2. MOLAR CONDUCTIVITIES (25 °C) OF THE BINUCLEAR COMPLEXES

Complex			Molar Conductivities (mho cm^{-1})[a]
Hydrogen salts	[Cr–CrH]	(V)	432
	[Cr–CoH]	(VII)	321
	[Co–CrH]	(IX)	406
	[Co–CoH]	(XI)	359
Sodium salts	[Cr–CrNa]	(VI)	145
	[Cr–CoNa]	(VIII)	137
	[Co–CrNa]	(X)	142
	[Co–CoNa]	(XII)	133

a) 1.0×10^{-3} mol/l of aqueous solution was used.

Table 3. IR data for the starting double complexes and the hydrogen salts of binuclear complexes obtained (cm^{-1})

Complex			H_2O ν(O–H)	ClO_4^- ν(Cl–O)	R–SO_3^- $\nu(SO_3^-)$
Double complexes	[Cr][Cr]	(I)	3450	—	642, 1035, 1053, 1190
	[Cr][Co]	(II)	3460	—	648, 1040, 1058, 1210
	[Co][Cr]	(III)	3450	—	641, 1035, 1054, 1194
	[Co][Co]	(IV)	3480	—	653, 1042, 1059, 1208
Binuclear complexes	[Cr–CrH]	(V)	—	1095	638, 1030, 1047, 1180
	[Cr–CoH]	(VII)	—	1100	643, 1032, 1049, 1185
	[Co–CrH]	(IX)	—	1095	638, 1032, 1047, 1182
	[Co–CoH]	(XI)	—	1085	648, 1037, 1052, 1189

the sodium salts exhibited 320—430 mho cm^{-1} and 130—145 mho cm^{-1}, respectively. These values may correspond to the conductivities of $HClO_4$ (hydrogen salts) and $NaClO_4$ (sodium salts) in solutions.

Both the hydrogen and sodium salts were adsorbed on neither cation nor anion exchangers at pH 7, but were adsorbed on cation exchanger at pH 3. These results indicate that at pH 7 the complexes are dissociated into $[(NH_3)_5$(Cr or Co)(sida)(Cr or Co)(sida)$]^0+Na^+ + ClO_4^-$, and at pH 3, $[(NH_3)_5$(Cr or Co)(sida)(Cr or Co)-(sidaH)$]^+ + ClO_4^-$.

IR Data. The IR data of the double and binuclear complexes are summarized in Table 3. The characteristic band due to H_2O (3450—3480 cm^{-1}) is seen in the double complexes, but not in the binuclear complexes. The band due to ClO_4^- (1085—1100 cm^{-1}) is detected in the binuclear complexes. The characteristic bands due to the $-SO_3^-$ group of the binuclear complexes appear in the lower wavenumber region as compared with those of the double complexes. The shifts probably result from the coordination of a $-SO_3^-$ group in the cationic moiety of the double complexes.

Table 4. Visible and UV spectral data for the starting double complexes and the hydrogen salts of binuclear complexes obtained

Complex			$\bar{\nu}_1$ 10^{-3} cm^{-1} (log ε_1)	$\bar{\nu}_2$ 10^{-3} cm^{-1} (log ε_2)
Double complexes	[Cr][Cr]	(I)	19.53(2.13)	26.95(2.09)
	[Cr][Co]	(II)	19.34(2.17)	26.60(2.13)
	[Co][Cr]	(III)	19.38(2.15)	26.67(2.11)
	[Co][Co]	(IV)	19.19(2.19)	26.32(2.15)
Binuclear complexes	[Cr–CrH]	(V)	18.02(2.15)	25.38(2.10)
	[Cr–CoH]	(VII)	17.86(2.18)	25.06(2.15)
	[Co–CrH]	(IX)	17.89(2.17)	25.13(2.12)
	[Co–CoH]	(XI)	17.73(2.20)	24.81(2.16)

Electronic Spectra. Table 4 summarizes the absorption maxima in the region of d-d transitions. The absorption bands of the binuclear complexes appear at lower wavenumber regions than those of the corresponding double complexes. The shifts may be due to the fact that the coordinated water in the complex cation ($[$(Cr or Co)$(H_2O)(NH_3)_5]^{3+}$) is expelled and replaced by the $-SO_3^-$ group in the complex anion ($[$(Cr or Co)$(sida)_2]^{3-}$).

When the aqueous solutions of the binuclear complexes were allowed to stand at room temperature overnight, their absorption maxima were shifted to those of the corresponding double complexes. Thus the binuclear complexes are hydrolyzed gradually in aqueous media changing from $[(NH_3)_5$(Cr or Co)(sida)(Cr or Co)-(sida)] into $[$(Cr or Co)$(H_2O)(NH_3)_5]^{3+} + [$(Cr or Co)-$(sida)_2]^{3-}$.

References

1) Presented at the 26th Symposium on Coordination Chemistry, Hokkaido, August, 1976.

2) Throughout this paper, the terms "homo-metal" and "hetero-metal" were used to distinguish the binuclear complexes consisting of the same metal ions from those consisting of the different metal ions.

3) T. Yasui, H. Kawaguchi, Z. Kanda, and T. Ama, *Bull. Chem. Soc. Jpn.*, **47**, 2393 (1974).

4) H. Ogino, K. Tsukahara, and N. Tanaka, *Inorg. Chem.*, **16**, 1215 (1977).

5) R. A. Castelló, C. P. Mac-Coll, N. B. Egen, and A. Haim, *Inorg. Chem.*, **8**, 699 (1969).

6) R. Tsuchiya, S. Nakagawa, A. Uehara, and E. Kyuno, *Bull. Chem. Soc. Jpn.*, **46**, 169 (1973).

7) R. Tsuchiya, A. Uehara, and E. Kyuno, *Bull. Chem. Soc. Jpn.*, **46**, 3737 (1973).

8) In this paper, the term "ligand-transfer" was employed to express multidentate ligand transfer between two metal ions as represented by the following equation $M+M'L \rightleftharpoons M'+ML$, where M and M′ are different metal ions and L is a multidentate ligand such as ethylenediaminetetraacetate (edta) and nitrilotriacetate (nta) ions: see a) R. K. Steinhause and R. L. Swann, *Inorg. Chem.*, **12**, 1855 (1973); b) R. Tsuchiya, A. Uehara, and E. Kyuno, *Chem. Lett.*, **1974**, 595.

9) A. Uehara, E. Kyuno, and R. Tsuchiya, *Bull. Chem. Soc. Jpn.*, **42**, 2835 (1969).

10) G. Schwarzenbach, H. Ackermann, and P. Ruckstull, *Helv. Chim. Acta*, **32**, 1175 (1949).

11) E. Kyuno, M. Kamada, and N. Tanaka, *Bull. Chem. Soc. Jpn.*, **40**, 1848 (1967).

12) S. M. Jörgensen, *Z. Anorg. Chem.*, **17**, 461 (1898); *J. Prakt. Chem.*, **31**, 89 (1885).

13) A. Uehara, E. Kyuno, and R. Tsuchiya, *Bull. Chem. Soc. Jpn.*, **43**, 1397 (1970).

2.5 th Order Differential Electroanalysis

Masashi GOTO, Takafumi HIRANO, and Daido ISHII

Department of Applied Chemistry, Faculty of Engineering, Nagoya University, Chikusa-ku, Nagoya 464

(Received June 8, 1977)

The theory which describes the properties of the 2.5th order derivative of current, e'', *vs.* the electrode potential, E, curves is presented in response to an imposed ramp signal on a stationary electrode. The 2.5th order differential, $e''(t)$, of the current, $i(t)$, is defined by

$$e''(t) \equiv \frac{d^{2.5}}{dt^{2.5}} i(t) = \frac{d^3}{dt^3}\left[\frac{1}{\sqrt{\pi}}\int_0^t \frac{i(\lambda)}{\sqrt{t-\lambda}} d\lambda\right].$$

The predicted dependences of peak height, peak potential, and peak width on concentration, electron number, and scan rate, *etc.* have been confirmed experimentally, using the analogue circuit to monitor the electroreductions of Cd^{2+}, Pb^{2+}, Tl^+, Zn^{2+}, and Ni^{2+} on a hanging mercury electrode. It was proved that the proposed technique adds the advantages of further higher resolution and higher sensitivity to those of semidifferential electroanalysis. At the scan rate of 100 mV/s, the signals observed in this technique were about 50 and 8 times larger than those in linear sweep voltammetry for the reductions of Cd^{2+} and Ni^{2+}, respectively. Sufficient resolution was obtained for the qualitative analyses between Pb^{2+} and Tl^+, between Ni^{2+} and Zn^{2+}, and between Ni^{2+} and H^+ at pH 1.4 in this technique.

Oscillographic polarography with applied voltage or, in other words, linear sweep voltammetry was first introduced by Matheson and Nichols[1] and developed by Randles[2] and Sevcik,[3] and many others[4] in order to reduce the time necessary for a polarographic analysis. In the linear sweep voltammetry, the electrolytic current increases up to a certain maximum value and then decreases rather gradually with increasing applied voltage. The maximum current, measured from the base line, is proportional to the bulk concentration of depolarizer, but it depends upon the potential scan rate and its constancy. The shape of the observed curve renders the determination of two or more depolarizers present very difficult. In 1972 Oldham[5-7] first introduced a new electroanalytical method "semiintegral electroanalysis" that has the merit of being independent of the details of the applied potential signal. The semiintegral, $m(t)$, of the current, $i(t)$, is defined by

$$m(t) \equiv \frac{d^{-0.5}}{dt^{-0.5}} i(t) = \frac{1}{\sqrt{\pi}}\int_0^t \frac{i(\lambda)}{\sqrt{t-\lambda}} d\lambda.$$

The method measures the semiintegral of the current as a function of electrode potential. When a ramp signal is applied, the shape of the observed curve is similar to that of a classical d.c. polarogram. Imbeux and Saveant,[8] and Senda and Ikeda[9] have also proposed, under the heading "convolutive potential sweep voltammetry," and "a new method for recording polarographic curves in oscillographic polarography with applied voltage, in which the surface concentration *vs.* potential curve is recorded," a similar transformation of the current *vs.* potential curve with reference to kinetic analysis of mechanisms and to analytical application, respectively.

By analogy with the relationship between d.c. polarography and a.c. polarography (or between normal pulse polarography and differential pulse polarography), a companion method "semidifferential electroanalysis" for semiintegral electroanalysis was recently announced by the present authors *et al.*[10-12] In this method, the semiderivative of current or the derivative of $m(t)$ is measured as a function of electrode potential, and the method appends the features of higher sensitivity and higher resolution to those of semiintegral electroanalysis as expected. For further higher resolution and higher sensitivity, the present article has proposed a new technique in which the 2.5th order derivative of current is recorded as a function of electrode potential.

Theory

Consider the case of a working electrode immersed in a solution containing, in addition to excess supporting electrolyte, a concentration C of the electroreducible species Ox. This species undergoes the n-electron reduction

$$Ox + ne^- \longrightarrow Rd \qquad (1)$$

to the initially-absent species Rd. A potential ramp,

$$E = E_0 - vt, \qquad (2)$$

is applied to the working electrode, where E is the electrode potential, E_0 is the initial potential, v is the scan rate of potential, and t is the time. E_0 is adjusted at a value at which Ox is virtually not reduced. It will be assumed throughout this article that the transport of Ox to, and of Rd in the reversible case from, the electrode is solely by semiinfinite diffusion.

We use the symbol e to denote the semiderivative[13] (0.5th order derivative) of the current i with respect to t

$$e \equiv \frac{d^{0.5}}{dt^{0.5}} i = \frac{d}{dt}\left[\frac{1}{\sqrt{\pi}}\int_0^t \frac{i(\lambda)}{\sqrt{t-\lambda}} d\lambda\right]. \qquad (3)$$

If Reaction 1 is reversible, the following equations[10]

$$e = \frac{nFv}{4RT} m_d \operatorname{sech}^2(x), \qquad (4)$$

where

$$m_d = nAF\sqrt{DC}\,, \qquad (5)$$

$$x = \frac{nF}{2RT}(E_{1/2} - E), \qquad (6)$$

relate the semiderivative of current to the electrode potential. In these equations, F is the Faraday constant, R is the gas constant, T is the absolute temperature, A is

the electrode area, D is the diffusion coefficient of Ox. and $E_{1/2}$ is the half-wave potential of the d.c. polarogram.

Differentiation of Eq. 4 with respect to t is aided by the chain rule in the form

$$e' \equiv \frac{de}{dt} = \frac{de}{dx} \cdot \frac{dx}{dt}, \tag{7}$$

and yields

$$e' \equiv \frac{d^{1.5}}{dt^{1.5}} i = -\left(\frac{nFv}{2RT}\right)^2 m_d \operatorname{sech}^2(x) \tanh(x), \tag{8}$$

as the expression for the shape of the 1.5th order derivative of current e' *vs.* E curve. On differentiation of Eq. 8, the 2.5th order derivative of current e'' is derived and presented by

$$e'' \equiv \frac{d^{2.5}}{dt^{2.5}} i = -\left(\frac{nFv}{2RT}\right)^3 m_d \{\operatorname{sech}^2(x) - 3\operatorname{sech}^2(x) \tanh^2(x)\}. \tag{9}$$

This equation represents the shape of a reversible e'' *vs.* E curve observed in the proposed method, to which the name "2.5th order differential electroanalysis" is suggested. The curve is symmetrical consisting of a minimum and two maxima as shown by the solid line in Fig. 1. The negative peak height is

$$e''_p = -m_d\left(\frac{nFv}{2RT}\right)^3, \tag{10}$$

and the potential corresponding to the negative peak is simply

$$E_p = E_{1/2}, \tag{11}$$

the polarographic half-wave potential. The width of the negative peak at an ordinate value equal to one-half of the peak height or, in short, the peak width is

$$W_p = \frac{1.56RT}{nF}. \tag{12}$$

Notice that the above peak width is much narrower than that of e *vs.* E curve which is 3.53 RT/nF.[11]

If Reaction 1 is totally irreversible, the following relation applies:[14]

$$e = -\frac{n\alpha Fv}{RT} m_d \sum_{j=1}^{\infty} \frac{(-1)^j j \exp(jz)}{\sqrt{j!}}, \tag{13}$$

where z is defined by

$$z = \frac{n\alpha F}{RT}(E_s - E) + \frac{1}{2}\ln\left(\frac{RTk_s^2}{n\alpha FvD}\right) \equiv \frac{n\alpha F}{RT}(E_* - E). \tag{14}$$

Here α is the transfer coefficient, E_s is the standard potential, k_s is the standard, heterogeneous rate constant, and E_* is a characteristic potential for an irreversible species being defined by Eq. 14. Differentiations of Eq. 13 with respect to t yield

$$e' = -\left(\frac{n\alpha Fv}{RT}\right)^2 m_d \sum_{j=1}^{\infty} \frac{(-1)^j j^2 \exp(jz)}{\sqrt{j!}}, \tag{15}$$

and

$$e'' = -\left(\frac{n\alpha Fv}{RT}\right)^3 m_d \sum_{j=1}^{\infty} \frac{(-1)^j j^3 \exp(jz)}{\sqrt{j!}}, \tag{16}$$

in the same way as for the reversible case. Equation 16 is the expression for the shape of a totally irreversible e'' *vs.* E curve observed in the proposed technique.

Values of the summation term in Eq. 16 for an assortment of small z values are listed in Table 1 together with the values of the hyperboric function term in Eq. 9 for x values. For large z values, sufficient precison of computation could not be retained. These data are also plotted as the dashed line in Fig. 1 for comparison with the corresponding shape of a reversible e'' *vs.* E curve. As expected, the irreversible peak is broader, and is somewhat asymmetric. From Table 1, the minimum value of the summation term is −0.2194, whence it follows that the negative peak height is

Table 1. Values of the function that describes the shapes of e'' *vs.* E curves

x, z	$-\{\operatorname{sech}^2(x) - 3\operatorname{sech}^2(x)\tanh^2(x)\}$	$-\sum_{j=1}^{\infty}(-1)^j j^3 \exp(jz)/(j!)^{1/2}$
−2.50	0.0511	0.0495
−2.06	—	0.0553(b)
−2.00	0.1263	0.0551
−1.50	0.2634	0.0370
−1.15	0.3333(b)	—
−1.00	0.3108	−0.0276
−0.62(d)	—	−0.1097
−0.50	−0.2826	−0.1373
−0.39(c)	−0.5000	—
0.00	−1.0000(a)	−0.2177
0.07	—	−0.2194(a)
0.39(c)	−0.5000	—
0.50	−0.2826	−0.1606
0.67(d)	—	−0.1097
1.00	0.3108	−0.0049
1.15	0.3333(b)	—
1.20	—	0.0757
1.50	0.2634	
2.00	0.1263	
2.50	0.0511	

The entries marked (a) and (b) correspond to the negative and positive peaks of e'' *vs.* E curves, respectively, while those marked (c) and (d) correspond to the negative half-peak potentials of reversible and irreversible curves, respectively.

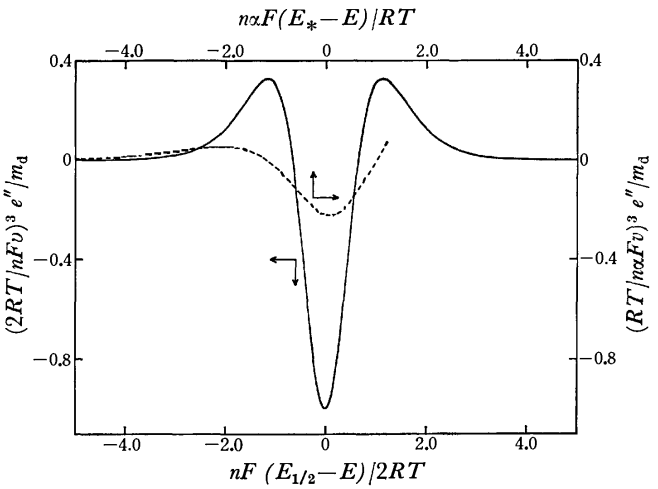

Fig. 1. Shapes of reversible (full line) and irreversible (dashed line) e'' *vs.* E curves.

$$e''_p = -0.219 m_d \left(\frac{n\alpha Fv}{RT}\right)^3. \quad (17)$$

From the fact that the minimum value of the summation occurs when z equals 0.07, if follows that the negative peak potential is

$$E_p = E_* - \frac{0.07RT}{n\alpha F}. \quad (18)$$

Likewise the tabulated data indicate the peak width to be

$$W_p = \frac{1.29RT}{n\alpha F}. \quad (19)$$

Information from Eqs. 10—12, 17—19 has been assembled into Table 2 which for 20 °C, summarizes the features of reversible and irreversible curves observed in the proposed technique.

Table 2. Features of e'' *vs.* E curves at 20 °C

	Reversible	Irreversible
Peak potential, E_p	$E_{1/2}$	$E_* - \frac{(1.77\text{ mV})}{n\alpha}$
Peak height, e''_p	$-\frac{n^4 A\sqrt{D}Cv^3}{(1.33n\ \text{V}^3\ \text{mol/C})}$	$-\frac{n^4\alpha A\sqrt{D}Cv^3}{(0.76n\ \text{V}^3\ \text{mol/C})}$
Peak width, W_p	$\frac{(39.4\text{ mV})}{n}$	$\frac{(32.5\text{ mV})}{n\alpha}$

The peak currents observed in linear sweep polarography[15] are given by

$$i_p = 0.447 m_d \left(\frac{nFv}{RT}\right)^{0.5}, \quad (20)$$

for reversible electrode processes, and

$$i_p = 0.496 m_d \left(\frac{n\alpha Fv}{RT}\right)^{0.5}, \quad (21)$$

for totally irreversible processes. Therefore the ratios of e''_p to i_p for reversible and irreversible processes are represented respectively by the following equations:

$$\frac{e''_p}{i_p} = -0.280 \left(\frac{nFv}{RT}\right)^{2.5}, \quad (22)$$

and

$$\frac{e''_p}{i_p} = -0.442 \left(\frac{n\alpha Fv}{RT}\right)^{2.5}. \quad (23)$$

The actual values of the ratios are listed in Table 3 for different potential scan rates, n and $n\alpha$ values at 20 °C. It is expected from Table 3 that the signals observed in this proposed method are further larger than those in linear sweep voltammetry at higher scan rates in both reversible and irreversible cases.

Table 3. Comparison of theoretical peak heights between e'' *vs.* E and i *vs.* E curves at 20 °C

v(V/s)	$-e''_p/i_p$ ($s^{-2.5}$) Reversible			Irreversible		
	$n=1$	$n=2$	$n=3$	$n\alpha=0.5$	$n\alpha=1$	$n\alpha=1.5$
0.05	1.54	8.74	24.1	0.429	2.44	6.72
0.10	8.74	49.4	136	2.44	13.8	38.0
0.20	49.4	280	770	13.8	78.0	215
0.50	488	2760	7610	136	771	2120
1.00	2760	15600	43100	771	4360	12000

Experimental

Apparatus. The instrument for 2.5th order differential electroanalysis was constructed from a function generator (NF Co., model FG-121B) as the applied potential sweeper, an analogue circuit for 2.5th order differential, and a recorder (Toa Electronics Ltd., model EPR-2TC). The 2.5th order differential circuit is shown in Fig. 2 with the circuit for correction of electrode sphericity effect. The current flowing through an indicator electrode is converted to voltage signal by means of a current follower (A1). The output of the current follower is fed to both a semidifferentiator (A2) and a potentiometer (PT). The potentiometer is adjusted to feed the voltage equivalent to $(\sqrt{D}/r)\ s^{1/2}$ portion of the output of the current follower to an adder (A3), where r is the radius of electrode sphere. The attenuated output of the current follower is subtracted from the output of the semidifferentiator by the adder. The output of the adder is fed to two differentiators (A4 and A5) in turn. When i, e', and e'' are to be recorded, the terminals of T1, T2, and T3 are connected directly to the recorder, respectively. Oldham's paralleling geometric ladder was used with a little modification as shown in Fig. 2 of the literature[16] as the semidifferential element (SE) in Fig. 2.

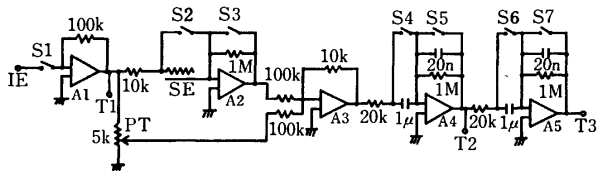

Fig. 2. 2.5th order differential circuit with the circuit for correction of electrode sphericity effect. IE: Indicator electrode, SE: semidifferential element, PT: potentiometer for the correction of electrode sphericity effect, S1: switch for electrolysis, S2—S7: switches for circuit reset, A1—A5: operational amplifiers (Analog Devices Co., model 118A), T1, T2, and T3: terminals for i, e', and e'' measurments, respectively.

A hanging mercury drop (Beckman Instruments Inc., model 39016) was used as a working electrode. A saturated calomel electrode with large surface area was served for both a counter and a reference electrode. A potential ramp signal was applied to the working electrode against the saturated calomel electrode.

Reagents etc. The salts $Cd(NO_3)_2 \cdot 4H_2O$, $Ni(NO_3)_2 \cdot 6H_2O$, $ZnSO_4 \cdot 7H_2O$, $TlNO_3$, and $Pb(NO_3)_2$ were used as solutes in 100 mmol/l KNO_3 plus HNO_3 at various concentrations. Solutions were prepared by direct weighing of the appropriate quantities of reagent grade chemicals, and deoxygenated by passage of N_2 gas. Measurments were made at room temperature (about 20 °C).

Results and Discussion

Figures 3 and 4 show typical e'' *vs.* E curves for Cd^{2+} as an example of reversibly reduced species and for Ni^{2+} as an example of irreversibly reduced ones, respectively, and also show the corresponding i *vs.* E and e' *vs.* E curves. As expected from the theory, a symmetric,

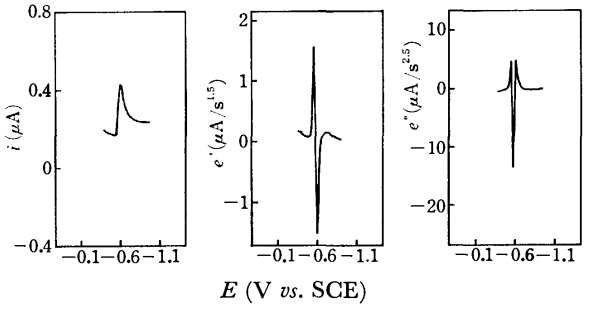

Fig. 3. Comparison of i *vs.* E, e' *vs.* E, and e'' *vs.* E curves of 10.5 μmol/l Cd^{2+} in 100 mmol/l KNO_3. Scan rate: 100 mV/s, electrode area: 4.69 mm^2.

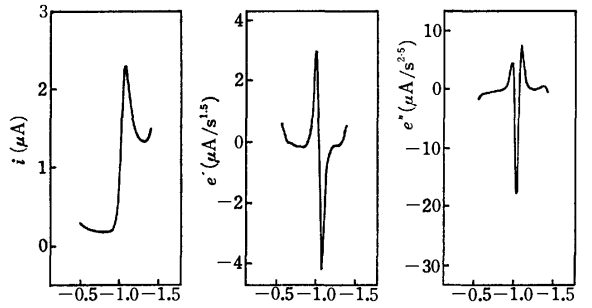

Fig. 4. Comparison of i *vs.* E, e' *vs.* E, and e'' *vs.* E curves of 104 μmol/l Ni^{2+} in 100 mmol/l KNO_3 plus 0.101 mmol/l HNO_3 (pH 4.1). Scan rate and electrode area: as Fig. 3.

sharp peak was observed in the e'' *vs.* E curve of Cd^{2+}, while a somewhat asymmetric, broad peak was observed in that of Ni^{2+}. It is evident from these diagrams that e'' *vs.* E and e' *vs.* E curves have attractive and promising features for both qualitative and quantitative analyses over ordinary i *vs.* E curve.

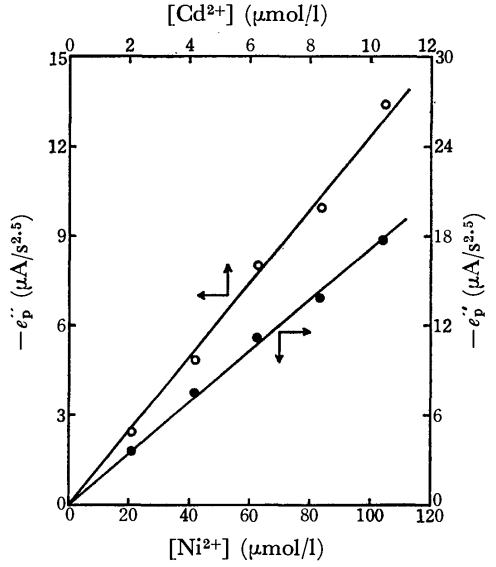

Fig. 5. Relationship between negative peak height of e'' *vs.* E curve and concentration of electroactive solutes. ○: Cd^{2+} in 100 mmol/l KNO_3, ●: Ni^{2+} in 100 mmol/l KNO_3 plus 0.101 mmol/l HNO_3, scan rate and electrode area: as Fig. 3.

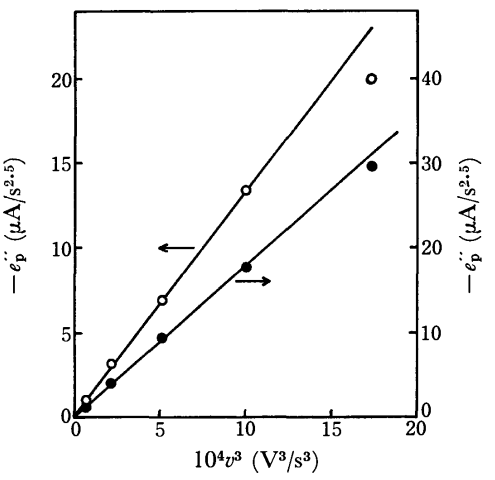

Fig. 6. Relationship between negative peak height of e'' *vs.* E curve and scan rate. ○: 10.5 μmol/l Cd^{2+} in 100 mmol/l KNO_3, ●: 104 μmol/l Ni^{2+} in 100 mmol/l KNO_3 plus 0.101 mmol/l HNO_3, electrode area: 4.69 mm^2.

Equations 5, 10, and 17 predict a linear dependence of negative peak height of e'' *vs.* E curve on the concentration of electroactive species and the cubic power of potential scan rate. These proportionalities are tested in Figs. 5 and 6 for Cd^{2+} and Ni^{2+} reductions, examples comprising both a reversible and an irreversible electrode reaction. In both cases, linearity was satisfactory and the lines passed through the origin. The slope de''_p/dC for Cd^{2+} in Fig. 5 has an experimental value of -1.24 A $s^{-2.5}$ mol^{-1} l, compared with a theoretical value, $-nAF\sqrt{D}(nFv/2RT)^3$, of -1.48 A $s^{-2.5}$ mol^{-1} l, calculated on the basis of a diffusion coefficient[17] of 6.9×10^{-6} cm^2 s^{-1}. Similarly for the Ni^{2+} line, the experimental slope $de''_p/dC=-0.170$ A $s^{-2.5}$ mol^{-1} l compares well with the theoretical value $-0.219nAF\sqrt{D}(n\alpha Fv/RT)^3=-0.166$ A $s^{-2.5}$ mol^{-1} l, based on $D=6.9\times10^{-6}$ cm^2 s^{-1} [18] and $\alpha=0.4$.[19] The slopes of the lines in Fig. 6 also agree approximately with the values predicted by Eqs. 10 and 17.

In Table 4 the experimental peak heights of e'' *vs.* E curves are compared with those of i *vs.* E curves at different concentrations for the Cd^{2+} and Ni^{2+} reductions. Table 4 also shows the corresponding, theoretical

Table 4. Comparison of experimental peak heights between e'' *vs.* E and i *vs.* E curves at the scan rate of 100 mV/s

Species	C (μmol/l)	i_p (μA)	e''_p (μA/$s^{2.5}$)	$-e''_p/i_p$($s^{-2.5}$) Exptl.	Theor.
Cd^{2+}	6.30	0.150	−8.09	53	49
Cd^{2+}	8.40	0.192	−9.96	52	49
Cd^{2+}	10.5	0.260	−13.4	52	49
Ni^{2+}	62.4	1.37	−11.2	8.2	7.9
Ni^{2+}	83.2	1.75	−13.8	7.9	7.9
Ni^{2+}	104	2.09	−17.7	8.5	7.9

Supporting electrolyte: 100 mmol/l KNO_3 for Cd^{2+}, 100 mmol/l KNO_3 plus 0.101 mmol/l HNO_3 for Ni^{2+}, electrode area: 4.69 mm^2.

Table 5. Peak potentials of e'' *vs.* E curves for Cd^{2+} and Ni^{2+} at different concentrations

$[Cd^{2+}]$ (μmol/l)	E_p for Cd^{2+} (mV *vs.* SCE)	$[Ni^{2+}]$ (μmol/l)	E_p for Ni^{2+} (mV *vs.* SCE)
2.10	−575	20.8	−1044
4.20	−586	41.6	−1048
6.30	−583	62.4	−1040
8.40	−587	83.2	−1046
10.5	−575	104	−1037
	Theor. −578[17]		Theor. −1034[18]

Supporting electrolyte, scan rate, and electrode area: as Table 4.

peak ratios of both curves for reference. It is evident from Table 4 that at the scan rate of 100 mV/s, the proposed technique provides about 50 and 8 times larger signals for Cd^{2+} and Ni^{2+} reductions, respectively, than linear sweep voltammetry does.

The peak potentials of e'' *vs.* E curves for the reductions of Cd^{2+} and Ni^{2+} were found to be independent of concentration, as shown in Table 5, and to average respectively −581 and −1043 mV *vs.* SCE (the latter value refers to $v=100$ mV/s). The experimental peak potential for Cd^{2+} is to be compared with the polarographic half-wave potential in the literature[17] of −578 mV *vs.* SCE. That for Ni^{2+} may likewise be compared with the −1034 mV *vs.* SCE value calculated from the half-wave potential of −980 mV *vs.* SCE at the mercury drop time τ of 4.48 s in classical polarography[18] by application of Eq. 18 and the relation[11]

$$E_{1/2} = E_* + \frac{0.30RT}{n\alpha F} + \frac{RT}{2n\alpha F}\ln\left(\frac{n\alpha Fv\tau}{RT}\right). \quad (24)$$

For Ni^{2+} reduction, the peak potential should vary with scan rate in accordance with the relation:

$$E_p = E_s + \frac{RT}{2n\alpha F}\ln\left(\frac{0.869RTk_s^2}{n\alpha FD}\right) - \frac{RT}{2n\alpha F}\ln(v)$$

predicted by Eqs. 14 and 18, while it should be independent of scan rate for Cd^{2+} reduction. Table 6 resorts the experimental data and lists the theoretical values of peak potentials. Agreement is within a few millivolts in all the cases.

Table 7 assesses how well the observed peak widths in the proposed technique agree with theoretical predictions. The data refer to the reduction of Cd^{2+} and Ni^{2+}

Table 6. Scan rate dependence of peak potentials of e'' *vs.* E curves for Cd^{2+} and Ni^{2+}

v (mV/s)	E_p for Cd^{2+} (mV *vs.* SCE)		E_p for Ni^{2+} (mV *vs.* SCE)	
	Exptl.	Theor.	Exptl.	Theor.
20	−576	−578	−1015	−1008
40	−573	−578	−1023	−1019
60	−571	−578	−1028	−1026
80	−572	−578	−1030	−1030
100	−575	−578	−1037	−1034
120	−574	−578	−1041	−1036

Supporting electrolyte and electrode area: as Table 4, electroactive concentration: 10.5 μmol/l for Cd^{2+}, 104 μmol/l for Ni^{2+}.

Table 7. Peak width values of e'' *vs.* E curves for Cd^{2+} and Ni^{2+}

C (μmol/l)	v (mV/s)	W_p for Cd^{2+} (mV)		W_p for Ni^{2+} (mV)	
		Exptl.	Theor.	Exptl.	Theor.
8.40	100	24	20		
10.5	100	22	20		
20.8	100			42	41
41.6	100			39	41
62.4	100			41	41
10.5	20	22	20		
10.5	60	24	20		
10.5	80	23	20		
104	20			41	41
104	60			41	41
104	100			42	41

Supporting electrolyte and electrode area: as Table 4.

as an example of reversible and irreversible processes, respectively. The theoretical predictions are based on Eqs. 12 and 19.

All theoretical predictions concerning 2.5th order differential electroanalysis have been confirmed. Though this entire article is couched in terms of cathodic processes, it is evident that the conclusions are easily widened to embrace electrooxidations.

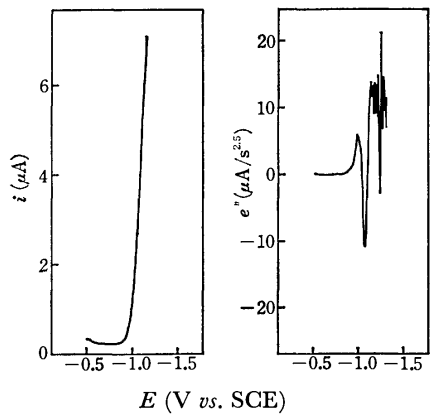

Fig. 7. Comparison of resolution between i *vs.* E and e'' *vs.* E curves for 104 μmol/l Ni^{2+} plus 50.5 mmol/l H^+ in 100 mmol/l KNO_3. Scan rate and electrode area: as Fig. 3.

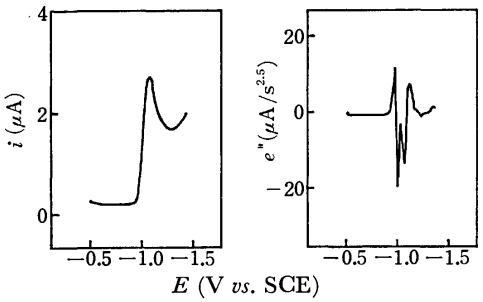

Fig. 8. Comparison of resolution between i *vs.* E and e'' *vs.* E curves for 25.0 μmol/l Zn^{2+} plus 104 μmol/l Ni^{2+} in 100 mmol/l KNO_3 plus 0.101 mmol/l HNO_3. Scan rate and electrode area: as Fig. 3.

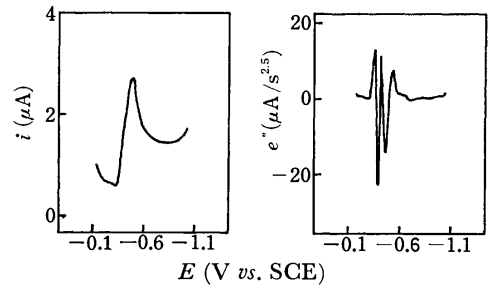

Fig. 9. Comparison of resolution between i *vs.* E and e'' *vs.* E curves for 20.0 μmol/l Pb^{2+} plus 100 μmol/l Tl^{+} in 100 mmol/l KNO_3 plus 10.1 mmol/l HNO_3. Scan rate and electrode area: as Fig. 3.

Figures 7, 8, and 9 demonstrate how clear resolution the proposed technique provides by comparison with ordinary linear sweep voltammetry. It is evident from these diagrams that Ni^{2+} in 100 mmol/l KNO_3 at pH 1.4 can be detected separately from hydrogen wave and simultaneous detections between Zn^{2+} and Ni^{2+}, and between Pb^{2+} and Tl^{+}, whose reduction potentials close together, are possible in the proposed technique.

In conclusion, 2.5th order differential electroanalysis is an attractive, fast method for the identification of many electroactive species coexistent in solution, and may provide quite high sensitivity for the detection of electroactive species at higher scan rates of potential as expected from Table 3. The study of detection limit for various species in this technique is continuing in our laboratory.

The authors are grateful to Dr. T. Matsuzaki and Mr. K. Kitagawa, Nagoya University, for computational assistance.

References

1) L. A. Matheson and N. Nichols, *Trans. Electrochem. Soc.*, **73**, 193 (1938).
2) J. E. B. Randles, *Trans. Faraday Soc.*, **44**, 3241 (1950).
3) A. Sevcik, *Coll. Czech. Chem. Commun.*, **13**, 349 (1948).
4) S. P. Perone, D. O. Jones, and W. F. Gutknecht, *Anal. Chem.*, **41**, 1154 (1969).
5) K. B. Oldham, *Anal. Chem.*, **44**, 196 (1972).
6) M. Grenness and K. B. Oldham, *Anal. Chem.*, **44**, 1121 (1972).
7) M. Goto and K. B. Oldham, *Anal. Chem.*, **45**, 2043 (1973).
8) J. C. Imbeux and J. M. Saveant, *J. Electroanal. Chem.*, **44**, 169 (1973).
9) M. Senda and T. Ikeda, *Rev. Polarogh. (Kyoto)*, **19**, 51 (1973).
10) M. Goto and D. Ishii, *J. Electroanal. Chem.*, **61**, 361 (1975).
11) P. Dalrymple-Alford, M. Goto, and K. B. Oldham, *J. Electroanal. Chem.*, **85**, 1 (1977).
12) P. Dalrymple-Alford, M. Goto, and K. B. Oldham, *Anal. Chem.*, **49**, 1390 (1977).
13) K. B. Oldham and T. Spanier, "The Fractional Calculus," Academic Press, New York (1974), p. 115.
14) M. Goto and K. B. Oldham, *Anal. Chem.*, **48**, 1671 (1976).
15) H. Matsuda and Y. Ayabe, *Z. Elektrochem.*, **59**, 494 (1955).
16) M. Goto, M. Kato, and D. Ishii, *Nippon Kagaku Kaishi*, **1977**, 42.
17) J. Heyrovsky and J. Kuta, "Principles of Polarography," Academic Press, New York (1965), pp. 106, 534.
18) P. Kivalo, K. B. Oldham, and H. A. Laitinen, *J. Am. Chem. Soc.*, **75**, 4148 (1953).
19) N. Tanaka and R. Tamamushi, *Electrochim. Acta*, **9**, 963 (1964).

The Preparation and Some Properties of 3-Substituted 2,4-Pentanedionato Metal(II, III) Complexes

Kuninobu KASUGA, Masao ANAMI, and Yasuo YAMAMOTO

Department of Chemistry, Faculty of Literature and Science, Shimane University, Nishikawatsucho, Matsue 690

(Received June 25, 1977)

In the substitution reactions of phenol, benzenethiol, and their sodium salts on the chelate ring of 3-bromo-2,4-pentanedionato metal complexes (metal=iron(III), aluminium(III), and beryllium(II)), benzenethiol was found to be substituted for bromine, while phenol was not substituted under the same conditions. In the case of sodium salts, both sodium phenoxide and benzenethiolate gave substituted products. The UV and PMR data of tris(3-substituted 2,4-pentanedionato)aluminium(III) complexes gave some information on the substituted groups.

The electrophilic substitution on the chelate ring of acetylacetonato complexes is known to be brought about by various reagents, such as bromine,[1,2] iodine,[1] *N*-halosuccinimides,[1,5] and nitro derivatives,[3,4] while only a few reports have appeared on the further conversion of the substituted chelates.[6,7] It was found by Yoshida *et al.* that the bromine atom on the chelate ring of 3-bromo-2,4-pentanedionatocobalt(III), -chromium(III), or -aluminium(III) is replaced by benzenethiol or its derivatives.[7] On the other hand, we ourselves have previously reported that the bromine atom on the chelate ring of 3-bromo-2,4-pentanedionatoiron(III) is replaced by succinimide or phthalimide in the presence of sodium methoxide.[8] In this paper another nucleophilic substitution reaction will be presented for the bromine atom on the chelate ring of iron(III), aluminium(III), cobalt(III), or beryllium(II) complex by phenol, benzenethiol, or their sodium salts.

Experimental

The 3-position carbons of 2,4-pentanedionato metal(II, III) complexes were halogenated according to the procedure of Collman *et al.*[1]

The Syntheses of 3-Phenoxy-2,4-pentanedionato Metal(II, III) Complexes. From Phenol: A 20-ml dichloromethane solution of phenol (0.02 mol) was added to a solution of 3-bromo-2,4-pentanedionatoiron(III), -aluminium(III), -cobalt(III), -chromium(III), -beryllium(II), or their chloro compounds (0.005 mol) in 50 ml of dichloromethane, after which the mixture was left standing for 5—6 days at room temperature. However, phenol was found not to react with these complexes, and the starting material was recovered in each case.

From Sodium Phenoxide: A mixture of sodium phenoxide (0.02 mol) and tris(3-bromo-2,4-pentanedionato)iron(III) (0.005 mol) in 50 ml of dichloromethane was left to stand, with stirring, for three days at room temperature, after which the precipitates formed were filtered off. The filtrate was washed twice with aqueous sodium hydrogencarbonate and then with water. After the solution had been dried with anhydrous sodium sulfate, the dichloromethane was evaporated under a reduced pressure. The resulting solid was recrystallized from ethanol, yielding the red powder of tris(3-phenoxy-2,4-pentanedionato)iron(III) (abbreviated as Fe(acacOph)$_3$). Yield, 36% (based on Fe(acacBr)$_3$). Found: C, 62.79; H, 5.16%. Calcd for $C_{33}H_{33}O_9Fe$: C, 62.97; H, 5.28%. The other substituted products were also prepared according to the same procedure; their analytical results were as follows: Al(acacOph)$_3$. Yield, 31% (based on Al(acacBr)$_3$). Found: C, 66.18; H, 5.38%. Calcd for $C_{33}H_{33}O_9Al$: C, 66.00; H, 5.54%. Be(acacOph)$_2$. Yield, 22% (based on Be(acacBr)$_2$). Found: C, 67.62; H, 5.18%. Calcd for $C_{22}H_{22}O_6Be$: C, 67.52; H, 5.67%. Also from 3-chloro-2,4-pentanedionato metal(II, III) complexes, the same substituted products were obtained, but the yields were less than those from the bromo compounds. In the case of the chromium(III) complex, sodium phenoxide was not substituted by the same method or by reflux for three days; neither its bromo and chloro complexes gave a substituted product. As to the cobalt(III), both the bromo and chloro complexes were immediately decomposed by the same reaction.

The Syntheses of 3-Phenylthio-2,4-pentanedionato Metal(II, III) Complexes. From Benzenethiol: A solution of benzenethiol (0.03 mol) in 20 ml of dichloromethane was slowly stirred, into a solution of tris(3-bromo-2,4-pentanedionato)iron(III) (0.005 mol) in 50 ml of dichloromethane. After standing for 2 h at room temperature, the solution was washed with aqueous sodium hydrogencarbonate and water, and then dried with anhydrous sodium sulfate. The dichloromethane was removed and the resulting tarry solid was recrystallized from ethanol–water. Yield, 18%(based on Fe(acacBr)$_3$). Found: C, 58.25; H, 5.29%. Calcd for $C_{33}H_{33}O_6S_3Fe$: C, 58.49; H, 4.91%. The other substituted products were also synthesized by the same procedure; the analytical results were as follows: Be(acacSph)$_2$. Yield, 55%(based on Be(acacBr)$_2$). Found: C, 61.98; H, 5.49%. Calcd for $C_{22}H_{22}O_4S_2Be$: C, 62.39; H, 5.24%. The substituted products were not obtained from 3-chloro-2,4-pentanedionatoiron(III) or -beryllium(II) under the same conditions.

From Sodium Benzenethiolate: The substituted products were obtained according to the procedure used for the preparations of 3-phenoxy-2,4-pentanedionato metal(II, III) complexes. The analytical results were as follows: Fe(acacSph)$_3$. Yield, 24%(based on Fe(acacBr)$_3$). Found: C, 57.94; H, 4.93%. Calcd for $C_{33}H_{33}O_6S_3Fe$: C, 58.49; H, 4.91%. Al(acacSph)$_3$. Yield, 43%(based on Al(acacBr)$_3$). Found: C, 61.01; H, 5.30%. Calcd for $C_{33}H_{33}O_6S_3Al$: C, 61.10; H, 5.13%. Be(acacSph)$_2$. Yield, 37%(based on Be(acacBr)$_2$). Found: C, 62.21; H, 5.42%. Calcd for $C_{22}H_{22}O_4S_2Be$: C, 62.39; H, 5.24%.

Measurements. The electronic spectra in solution and the infrared spectra using KBr pellets were measured on a Hitachi 124-type spectrophotometer and a Hitachi 215-type spectrophotometer respectively. The PMR spectra were recorded with a JEOL-MH 100 spectrophotometer at a frequency of 100 MHz. The chemical shifts were determined in ppm, using TMS as the internal standard. The elemental analyses were carried out by means of a Yanagimoto MT 2 CHN Corder.

Table 1. The electronic, infrared, and PMR data of the tris(3-substituted 2,4-pentanedionato)aluminium(III) complexes

Complex	Electronic spectra λ max(nm) in CH_2Cl_2	Infrared spectra cm^{-1} (KBr pellets)		PMR spectra δ values (ppm) in CCl_4	
		C=C[a]	C–H[b]	Methyl group	Phenyl group
$Fe(acacOph)_3$	277, 387, 480	1485	820	—	—
$Al(acacOph)_3$	270[sh], 310	1490	825	2.06	6.80—7.20
$Be(acacOph)_2$	270[sh], 316	1492	824	2.04	6.80—7.19
$Fe(acacSph)_3$	253, 280[sh], 340[sh], 435	1489	805	—	—
$Be(acacSph)_2$	253, 292, 320[sh]	1479	824	2.34	6.80—7.20

sh=shoulder; acacOph=3-phenoxy-2,4-pentanedione anion; acacSph=3-phenythio-2,4-pentanedione anion.
a) The band assigned to the skelton stretching of the phenyl group[2]. b) The C-H -out-of-plane bending of the phenyl group[2].

Results and Discussion

Electronic, Infrared, and PMR Spectra. From the data given in Table 1, we see that the 3-phenoxy derivatives of these metal complexes and phenylthio compounds show the band of the phenoxyl or phenylthio group at around 270 or 253 nm respectively. In the infrared spectra, these substituted compounds show the bands characteristic of a skeletal stretching and a CH-out-of-plane bending of the phenyl group at around 1490 and 820 cm^{-1} respectively.[7] In the PMR spectra, the methyl proton of acetylacetone shows a singlet signal in the range of 1.4—2.4 ppm, while the phenyl proton shows multiplet signals in the range of 6.8—7.4 ppm. The PMR spectrum of the iron(III) complex was not measured because of its paramagnetism.

The UV and PMR Spectral Data of the Tris(3-substituted 2,4-pentanedionato)aluminium(III) Complexes. From the UV data given in Table 2, we can see that the chloro, bromo, and phenoxy complexes show the absorption band due to a π-π^* transition of an acetylacetone ring at around 310 nm, while the acetylacetonato complex and its benzenethiol, succinimide, and phthalimide derivatives show the absorption bands at around 290 nm. It has been known that the absorption band of the π-π^* transition of benzene is shifted to longer wavelengths when the hydrogen of benzene is replaced by such a group as chlorine, bromine, or amine, which has lone-pair electrons taking part in the π system of benzene.[9] Therefore, the oxygen atom of the phenoxyl group in this compound has hybridized sp or sp^2 orbitals and the electrons of the nonhybridized p orbital must participate in the π system of the acetylacetone ring. The sulfur atom of the phenylthio group may have hybridized sp^3 orbitals and no electrons which take part in the π system of an acetylacetone ring; thus, the absorption band of the phenylthio compound shows no shift to longer wavelengths. The succinimido or phthalimido group of this compound is perpendicular to an acetylacetone ring because of the steric hindrance between the carbonyl group of these imides and the methyl group of the acetylacetone ring. Therefore, the absorption band arising from the π-π^* transition of the acetylacetone ring is not shifted. The PMR signals of the methyl protons of the chelated acetylacetone of the 2,4-pentanedionatoaluminium(III) complex, and its 3-bromo and 3-chloro compounds are shifted to lower magnetic fields in the order of their electronegativities. The PMR signal of the phenylthio compound is shifted to a lower magnetic field than that of the phenoxy compound. It can be said that this is caused by the ring-current effect of benzene. From the UV spectra and the fact that the PMR signal of the methyl group is a singlet in these compounds, the oxygen atom of the phenoxyl group can be said to have sp hybridized orbitals, while the sulfur atom of the phenylthio group has sp^3 hybridized orbitals. That is, the benzene ring of phenylthio group is situated nearer to the methyl group than that of the phenoxyl group. Thus, the methyl protons of phenoxy compounds are affected by the ring current of benzene more strongly than that of phenylthio compounds, and the PMR signal of the phenylthio compound is shifted to a lower magnetic field than that of the phenoxy compound. The PMR spectra of the 3-succinimido and 3-phthalimido compounds have also been compared. In spite of the strong electron attraction of a carbonyl group of these imides, the signal of the methyl protons of these compounds appears at nearly the same position as that of

Table 2. The UV and PMR spectral data of the tris(3-substituted 2,4-pentanedionato)-aluminium(III) complexes

$Al(acacX)_3$ X=	UV spectra λ max (nm) in CH_2Cl_2	PMR spectra[a] δ values (ppm) in CCl_4
Succinimido[b]	286	1.92
H	288	1.93
Phthalimido[b]	289	2.04
phS	292	2.36
Cl	308	2.29
Br	309	2.27
phO	310	2.03

a) Signals for the methyl group on the chelate ring.
b) The details of the syntheses of these complexes will be published.

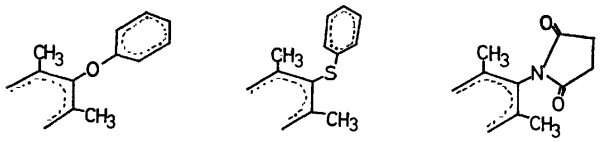

The conformations of the substituted groups.

the 2,4-pentanedionato compound. This may arise from the magnetic anisotropy. The protons of methyl groups of the acetylacetone ring are situated over the π system of O–C–N–C–O, because the plane of cyclic imides and the acetylacetone ring are perpendicular to each other. Thus, the anisotropic effects can shift the PMR signal to a higher magnetic field.

References

1) J. P. Collman, R. A. Moss, H. Malz, and C. C. Heindel, *J. Am. Chem. Soc.*, **83**, 531 (1961).
2) H. Reihlen, R. Ilig, and R. Wittig, *Ber.*, **58**, 12 (1925).
3) C. Djoidjeric, J. Lewis, and R. S. Nyholm, *Chem. Ind., (London)*, **1959**, 122.
4) J. P. Collman, R. A. Moss, S. D. Goldby, and V. S. Tvhanousky, *Chem. Ind. (London)*, **1960**, 1213.
5) R. W. Kluiber, *J. Am. Chem. Soc.*, **82**, 4839 (1960).
6) R. W. Kluiber, *J. Am. Chem. Soc.*, **83**, 3030 (1961).
7) Z. Yoshida, H. Ogoshi, and Y. Shimizu, *Kogyo Kagaku Zasshi*, **72**, 1648 (1969).
8) Y. Yamamoto, K. Kasuga, and A. Sumita, *Bull. Chem. Soc. Jpn.*, **49**, 2021 (1976).
9) L. Doub and J. M. Vandenbelt, *J. Am. Chem. Soc.*, **69**, 2714 (1947).

Studies of the Hydrous Titanium Oxide Ion Exchanger. III. Distribution Coefficients and Some Applications*

Yasushi INOUE and Masamichi TSUJI**

Department of Nuclear Engineering, Faculty of Engineering, Tohoku University, Aramaki, Sendai 980

(Received July 16, 1977)

In order to understand the cation-exchange behavior of hydrous titanium oxide, the distribution coefficients of various cations were measured as a function of the pH and the ionic strength. The order of selectivity for alkali metal ions is $Cs^+ > Rb^+ > K^+ > Na^+$, for alkaline earth metal ions, $Ba^{2+} > Sr^{2+} > Ca^{2+}$, and for bivalent transition metal ions, $Zn^{2+} > Cu^{2+} > Co^{2+}$. From the dependency of the distribution coefficients on the pH, it is concluded that the apparent dissociation constants of the exchanger reported previously are not constant, but gradually decrease with the pH of the medium. By using ammonium chloride and ammonium nitrate solutions as eluents, nearly quantitative separations of ^{137}Cs—^{133}Ba and ^{137}Cs—^{89}Sr were achieved with a relatively small column.

The method of synthesizing hydrous titanium oxide as an ion exchanger proposed by the present authors has the merits of good reproducibility and the large ion-exchange capacity of the product. The adsorption of cations on this material was confirmed, through the measurement of the amount of hydrogen ion released by the uptake of a definite amount of sodium or strontium ions, to occur by cation-exchange reaction. Other important properties of the exchanger, such as its composition, stability against various chemicals, and its ion-exchange properties including ion-exchange capacity and acidity, have also been investigated, as has been described in the foregoing reports.[1,2] The studies of the application of hydrous titanium oxide have been concentrated on the recovery of uranium from seawater,[3] scarcely have been devoted to the chromatographic separations of cations except in a few cases—the separation of ^{134}Cs—^{90}Sr, ^{134}Cs—^{142}Pr,[4] and chromate and phosphate ions.[5]

The purpose of the present investigation is to understand the cation-exchange reaction of the exchanger through the examination of the distribution coefficients of various cations as a function of the pH, and to show the applicability of the exchanger to the chromatographic separation. As examples, the separations of ^{137}Cs—^{133}Ba and ^{137}Cs—^{89}Sr were performed by using ammonium nitrate and ammonium chloride solutions as eluents.

Experimental

Reagents and Apparatus. Hydrous titanium oxide was prepared by a method described previously.[2] The radioactive purity of the radioisotopes employed was confirmed in advance; all the reagents, of the highest grade of purity, were obtained from Wako Pure Chemical Industries, Ltd.

The equipment for the β- and γ-counting was the same as has been described previously.[1,2]

Distribution Coefficients. The distribution coefficients were determined in the following way, except as otherwise noted.

A half gramme of the exchanger of a desired ionic form was placed in contact, in a thermostat at 25 °C, with 50 cm³ of a suitable solution containing 2.0×10^{-4} M (1 M = 1 mol/dm³) of the cation in question until the concentration of the cation in the supernatant solution became constant (about 2 d). After filtration, the pH and the concentration of cations in the solution were measured. The amount of cation employed was less than 1% of the total ion-exchange capacity of the exchanger. The analysis of Na, K, Rb, Cs, Ca, Sr, Ba, Fe, Co, Cu, Zn, Ga, and Y was carried out radiometrically using ^{22}Na, ^{42}K, ^{86}Rb, ^{137}Cs, ^{45}Ca, ^{89}Sr, ^{133}Ba, ^{59}Fe, ^{60}Co, ^{64}Cu, ^{65}Zn, ^{72}Ga, and ^{90}Y respectively as tracers.

The distribution coefficients, K_d, were calculated by means of the following equation:

$$K_d = \frac{I-F}{F} \cdot \frac{V}{m} \quad (\mathrm{cm^3/g}),$$

where I and F are the initial and the final radioactivity concentrations in the solution respectively; V, the volume of the solution in cm³, and m, the weight of the exchanger in g. The distribution coefficients thus obtained were not equilibrium values, as will be described later.

The total concentration of alkali metal ions was determined in the following way. To a 10-cm³ aliquot of the sample solution, an excess amount of a 6 M HCl solution was added. This was then heated to dryness and dissolved in water. Finally the alkali metal ion was indirectly determined by titrating the chloride ion with Fajans' method.

Column Operation. Two grammes of the exchanger in H^+ form (100—200 mesh) were packed in a glass column, 7 mm in inside diameter, and completely converted into the NH_4^+ form by passing through a 3% NH_4OH solution. The flow rate of the effluent was kept nearly constant, 0.08—0.13 cm³/min, throughout a series of elutions. The radioisotopes used were carrier-free except for ^{133}Ba, the specific activity of which was about 2 mCi/mg.

Results and Discussion

Distribution Coeffcients. Figures 1 and 2 show the dependency of the distribution coefficients of the alkali metal and alkaline earth metal ions on the pH. Table 1 presents the distribution coefficients of the other metal ions. The order of selectivity is $Cs^+ > Rb^+ > K^+ > Na^+$ for alkali metal ions and $Ba^{2+} > Sr^{2+} > Ca^{2+}$ for alkaline earth metal ions. These series follow the same pattern as those shown by strongly acidic cation-exchange resin. For bivalent transition metal ions, the series is $Zn^{2+} > Cu^{2+} > Co^{2+}$, assuming that the dependency of the distribution coefficients on the pH is about the same as that for alkaline earth metal ions.

* Thesis submitted by one of the authours (M. T.) to Tohoku University in partial fulfillment of the requirements for the degree of Kogaku-Hakushi (Ph. D).

** Present address: Department of Chemistry, Tokyo Institute of Technology, Ookayama, Meguro-ku, Tokyo 152.

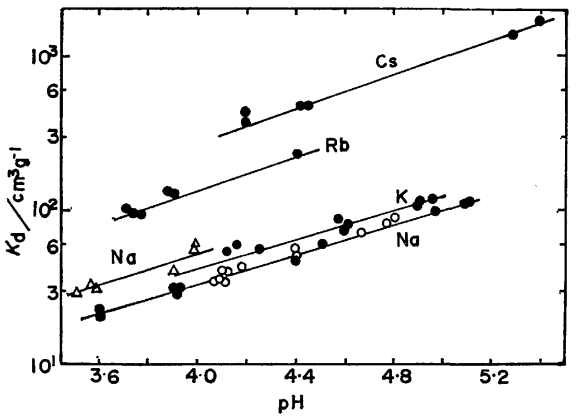

Fig. 1. Distribution coefficients for alkali metal ions ($RH+N^+ \rightarrow H^+ + RN$). Concentration of cations; Na^+, Rb^+, Cs^+: 2.0×10^{-4} M, K^+: 4.2×10^{-4} M. Exchanger; H^+ form. ○: 35—65 mesh, 500 mg, ●: 100—200 mesh, 500 mg, △: 100—200 mesh, 100 mg.

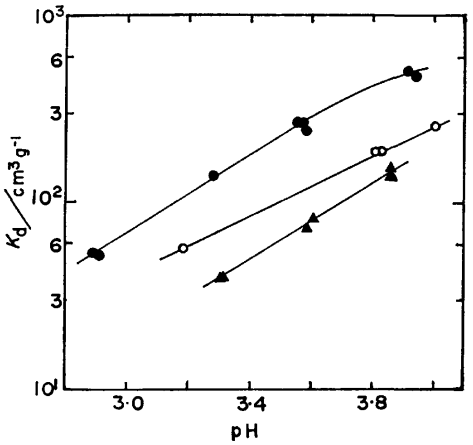

Fig. 2. Distribution coefficients for alkaline earth metal ions ($2RH+N^{2+} \rightarrow 2H^+ + R_2N$).
Concentration of cations; 2.0×10^{-4} M, ●: Ba^{2+}, ○: Sr^{2+}, ▲: Ca^{2+}.
Exchanger; H^+ form 100—200 mesh, 500 mg.

Table 1. Distribution coefficients of some cations

Ion	pH	K_d / cm^3 g^{-1}
Co^{2+}	3.62	$(8.7\pm0.2)\times10$
	3.82	$(1.50\pm0.03)\times10^2$
	3.92	$(2.05\pm0.04)\times10^2$
Cu^{2+}	3.70	$(2.50\pm0.04)\times10^2$
Zn^{2+}	2.19	6.7 ± 2.5
	3.96	$(4.7\pm0.1)\times10^2$
Fe^{2+}	1.30	≈0
	2.43	4.8 ± 0.9
Fe^{3+}	1.08	4.2 ± 2.0
	1.40	$(2.5\pm0.2)\times10$
Ga^{3+}	3.48	$(9.3\pm0.3)\times10$
	3.79	$(4.0\pm0.3)\times10$
Y^{3+}	3.41	$(3.7\pm0.3)\times10$
	3.68	$(1.56\pm0.05)\times10^2$
	3.83	$(3.8\pm0.3)\times10^2$

The selectivity series for alkali metal ions is the same as that found by Heitner-Wirguin *et al.*,[6] but the order for Co^{2+} and Cu^{2+} is reversed. The possible reasons for this conflicting result are as follows: (1) The concentration of the cations adopted by them is 0.01 M, which is considerably higher than that used in the present experiment; (2) Their ion exchanger contains about 4% of oxalate as an impurity; (3) The properties of the exchangers themselves differ from each other as a result of the difference in the synthetic methods. If the oxalate groups contained in their ion exchanger are considered to act as exchanging sites, the improvement in the selectivity for an ion will increase its prominence with the stability of the oxalato-complex. Since the stability constant of oxalato-complex of Cu^{2+} is not larger than that of Co^{2+},[7] the second possibility seems unlikely. As the inversion of the selectivity cannot be considered to occur in such a low concentration as this, the third possibility appears most promising.

Figure 1 also shows that the distribution coefficients of the sodium ion did not depend on the particle size of the ion exchanger. This observation suggests that the exchanging sites are distributed uniformly within the body of the exchanger, which corresponds to the fact that the ion-exchange capacity is independent of the particle size of the ion exchanger, as has been pointed out previously.[1] The distribution coefficients of the sodium ion were affected by the ratio between the volume of the liquid phase and the weight of the exchanger. This means that the curves in Fig. 1 do not show true equilibrium values, although two phases have been in contact with each other until the adsorbed amount of the sodium ion becomes constant.

Figure 3 indicates that a linear relationship held between the logarithms of the distribution coefficients of the cesium ion on the ion exchanger in the Na^+ form and the concentration of the sodium ion at a constant pH. The slope of the line increased with the pH until it reached unity at pH 7. When the solution became more basic than this, essentially the same relation was obtained at any pH. Figure 4 shows the relation at

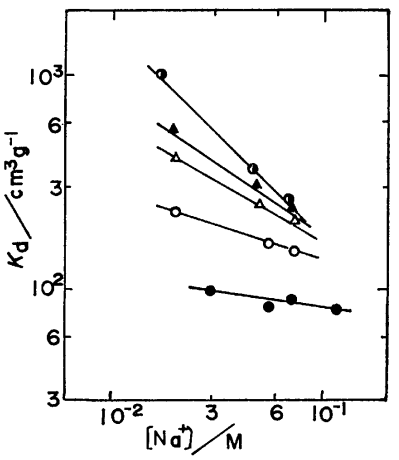

Fig. 3. Dependency of distribution coefficients of Cs^+ on the concentration of Na^+ ($RNa+Cs^+ \rightarrow RCs+Na^+$). Exchanger; Na^+ form, 100—200 mesh, 500 mg. pH; ●: 3, ○: 4, △: 5, ▲: 6, ◑: 7.

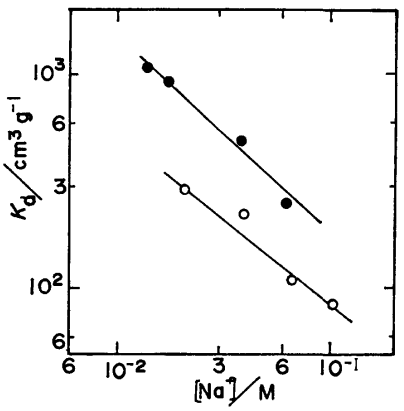

Fig. 4. Dependency of distribution coefficients of Cs^+ on the concentration of Na^+ at pH 8. Exchanger; Na^+ form, 100—200 mesh, 500 mg.
○: Forward reaction ($RNa+Cs^+ \rightarrow RCs+Na^+$),
●: reverse reaction ($RCs+Na^+ \rightarrow RNa+Cs^+$).

pH 8 as an example. The distribution coefficients obtained from the forward- and the reverse reactions did not agree with each other. Therefore, the reaction never reached equilibrium, as in the H^+–Na^+ exchange reaction mentioned above. This introduces the problem that it is difficult to discuss the relation in terms of the theory of chemical equilibrium. However, if the curves determined from the forward- and the reverse reactions run parallel with each other, it is natural to assume that the curve in true equilibrium may be somewhere between, and parallel with, them. Therefore, one can discuss the dependency of the apparent distribution coefficients on various factors from the viewpoint of the chemical equilibrium theory with due regard to the limitation imposed by the assumption.

The ion-exchange reaction between the monovalent cation, M^+, and the n-valent cation, N^{n+}, and the equilibrium constant can be expressed by the following equations:

$$nMR + N^{n+} = NR_n + nM^+, \tag{1}$$

$$K = \frac{a_{NR_n}(a_M)^n}{(a_{MR})^n a_N} = \frac{f_N[NR_n](a_M)^n}{\gamma_N[N^{n+}](a_{MR})^n}, \tag{2}$$

where a denotes the activity, R^-, the matrix anion of the exchanger, [ ], the concentration, f_N, the activity coefficient of the N^{n+} ion in the exchanger, and γ_N, the activity coefficient of the N^{n+} ion in the solution.

The distribution coefficient, K_d, of the N^{n+} ion is expressed by this equation:

$$K_d = \frac{[NR_n]}{[N^{n+}]} \quad (cm^3/g). \tag{3}$$

By combining Eqs. 2 and 3, we obtain

$$K = K_d \frac{f_N(a_M)^n}{\gamma_N(a_{MR})^n}. \tag{4}$$

When the amount of N^{n+} is negligible as compared with that of M^+, a_{MR} and f_N are regarded as constant. Moreover, γ_N is also constant if the ionic strength of the solution is kept constant. Under such conditions, the following equation holds, by taking the logarithm of Eq. 4:

$$\log K_d = \text{const} - n \log a_M. \tag{5}$$

That is, if the logarithm of the distribution coefficients of N^{n+} is plotted against pH, a straight line possessing the slope of n should be obtained.

The results in Figs. 1 and 2 cannot be explained by this argument because the slopes are about a half of the valency of the exchanging cation, N^{n+}. Since the experimental condition satisfies the assumption for deducing Eq. 5, this contradiction compels us to consider that K must depend on the pH.

If the solution is acidic enough to permit the participation of only ion-exchange sites with the lowest apparent pK_a value[2] in the ion-exchange reaction, and if the cations to be exchanged are present as hydrated ions, it can be regarded that the reaction of Eq. 1 on the H^+-form exchanger is a combination of the following two reactions:

$$HR = H^+ + R^-, \qquad K_H = \frac{a_H a_R}{a_{HR}}, \tag{6}$$

$$nR^- + N^{n+} = NR_n, \qquad K_N = \frac{a_{NR_n}}{(a_R)^n a_N}. \tag{7}$$

Accordingly,

$$K = K_H{}^n \cdot K_N. \tag{8}$$

Equation 6 represents the acid dissociation of the exchanger, and Eq. 7, the reaction of the anionic form of the exchanger with the exchanging cation, N^{n+}. As a similar conflict between Eq. 5 and the experimental results was observed for every kind of ion examined, it was considered that the contradiction was attributable to the gradual decrease in the acid dissociation constant, K_H, of the ion exchanger with the pH. Accordingly, it is considered that the pK_i described in the previous paper[2] is not constant, but a certain average value.

If this discussion holds true, the relation of Eq. 5 should hold in the ion-exchange reaction between alkali metal ions in an alkaline medium, where the acid dissociation can be ignored. In the ion-exchange reaction between Na^+ and Cs^+ in a basic medium, the results obeyed Eq. 5 as was expected (Fig. 4).

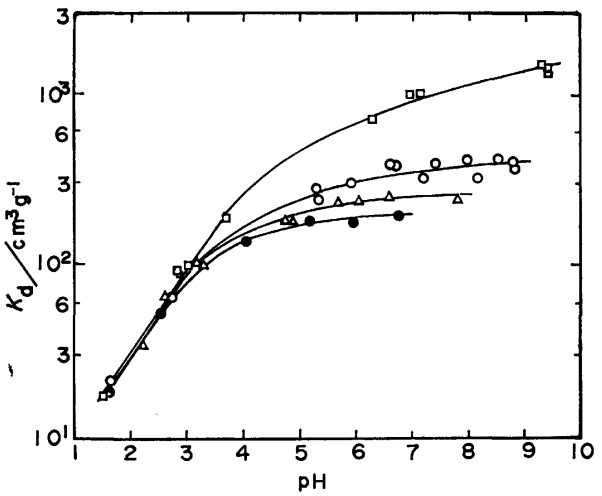

Fig. 5. Dependency of distribution coefficients of Cs^+ on pH ($RNa+Cs^+ \rightarrow RCs+Na^+$).
Exchanger; Na^+ form, 100—200 mesh, 500 mg. I/mol dm^{-3}; □: 0.012—0.029, ○: 0.050—0.062, △: 0.063—0.080, ●: 0.11—0.12.

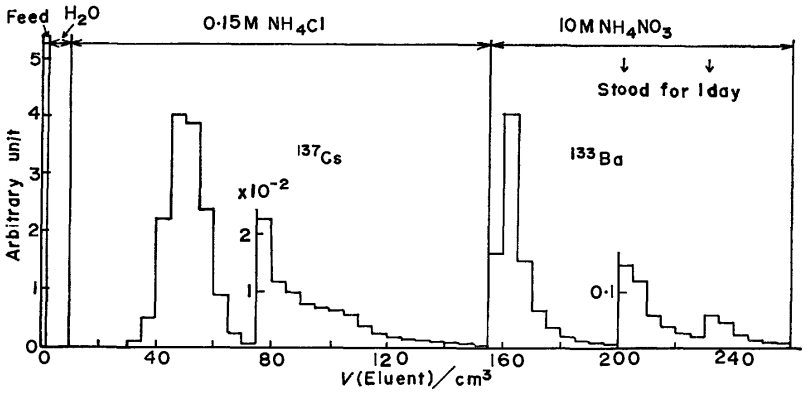

Fig. 6. Separation of ^{137}Cs and ^{133}Ba.
Column: 0.7 cm $\phi \times 3.8$ cm (NH_4^+ form, 100—200 mesh, 2 g).
Flow rate: 0.10—0.13 cm³/min.

The relationship between the distribution coefficient of the cesium ion on the exchanger in the Na^+ form and the pH is compatible with the argument presented above, as is shown in Fig. 5.

Gallium behaved differently; that is, the distribution coefficient decreased with the pH. This unusual behavior is attributable to the hydrolysis of the ion, because the gallium ion hydrolyzes at a pH value above 2.

Separations of ^{137}Cs—^{89}Sr and ^{137}Cs—^{133}Ba. In order to confirm that the hydrous titanium oxide ion exchanger could be used for the chromatographic separation, an attempt was made to separate the long-lived fission products, Cs, Sr, and Ba ions.

The results for the ^{137}Cs—^{133}Ba separation are represented in Fig. 6. Cs^+ and Ba^{2+} were eluted with 0.15 M ammonium chloride and 10 M ammonium nitrate solutions respectively. The sharp elution peaks were followed by slight tailings. ^{137}Cs could be quantitatively recovered by the use of 150 cm³ of the eluent, but the recovery of ^{133}Ba was only 94% even after passing through 160 cm³ of the eluent.

Figure 7 shows the separation of ^{137}Cs—^{89}Sr. After the ^{137}Cs had been eluted by a 0.15 M ammonium chloride solution in a manner similar to that shown in Fig. 6, a 0.3 M ammonium chloride–0.1 M hydrogen chloride solution was passed through. In this case, also, some tailings appeared after the sharp elution peaks. ^{89}Sr, however, could be recovered nearly quantitatively by letting 125 cm³ of this eluent flow through.

Therefore, we can conclude that the complete separation of ^{137}Cs from ^{89}Sr is possible.

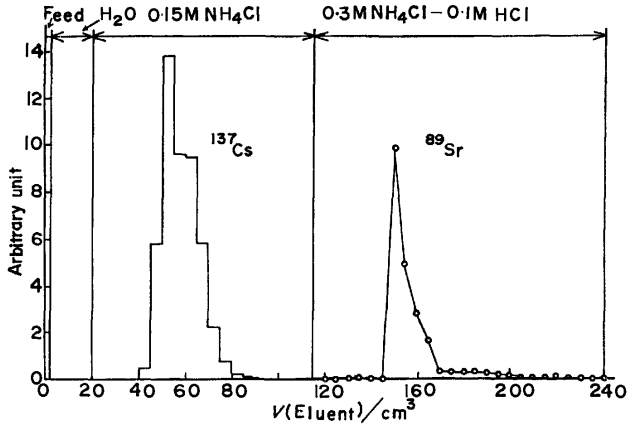

Fig. 7. Separation of ^{137}Cs and ^{89}Sr.
Column: 0.7 cm $\phi \times 3.8$ cm (NH_4^+ form, 100—200 mesh, 2 g). Flow rate: 0.08 cm³/min.

References

1) Y. Inoue and M. Tsuji, *J. Nucl. Sci. Technol.*, **13**, 85 (1976).
2) Y. Inoue and M. Tsuji, *Bull. Chem. Soc. Jpn.*, **49**, 111 (1976).
3) A. V. Kas'yanov, A. A. Bezborodov, V. A. Zhorov, and A. G. Kobylyanskaya, *Radiokhimiya*, **17**, 477 (1975).
4) A. K. Lavrukhina, V. V. Malyshev, and S. S. Rodin, *Zh. Vses. Khim. Obshschest. D. I. M.*, **8**, 227 (1963).
5) K. A. Kraus, H. O. Phillips, T. A. Carlson, and J. S. Johnson, *Proc. 2nd Int. Conf. Peaceful Uses At. Energy, Geneva*, **28**, 3 (1958).
6) C. Heitner-Wirguin and A. Albu-Yaron, *J. Inorg. Nucl. Chem.*, **28**, 2379 (1966).
7) L. G. Sillén and A. E. Martell, "Stability Constants of Metal-ion Complexes, Supplement No. 1," The Chemical Society, London (1964), pp. 14—30.

A Kinetic Study of the Ligand Exchange between Bis(acetylacetonato)-oxovanadium(IV) and Acetylacetone[^{14}C] in Organic Solvents

Masato NISHIZAWA and Kazuo SAITO

Chemistry Department, Faculty of Science, Tohoku University, Aramaki, Aoba, Sendai 980

(Received July 19, 1977)

Square pyramidal [VO(acac)$_2$] (acac, acetylacetonate) undergoes ligand exchange with Hacac[^{14}C] in 1,2-dichloroethane (DCE) without side reactions. The rate is expressed by $R=k_2$[complex][Hacac], where [Hacac] stands for the concentration of free acetylacetone in enol form. The second order rate constant and activation parameters are 0.071 M^{-1} s^{-1} (M=mol dm^{-3}) at −33 °C, $\Delta H^{\ddagger}=(46.7\pm1.7)$ kJ mol^{-1} and $\Delta S^{\ddagger}=(-61.9\pm8.4)$ J·mol^{-1} K^{-1}. The deuterium isotope effect is $k_H/k_D=1.3\pm0.2$. It appears as if the free Hacac first interacts with the complex as unidentate and the chelation of the unidentate accompanied by proton transfer to the leaving $acac^-$ is the rate determining step. On addition of a donor solvent the exchange rate decreases, and the extent is correlated with Gutmann's donor number. The k_2, $\Delta H^{\ddagger}$ and $\Delta S^{\ddagger}$ in 0.06 M dimethyl sulfoxide (DMSO) in DCE are 0.0038 M^{-1} s^{-1} at −33 °C, (71.9±10.0) kJ mol^{-1}, and (−4±40) J mol^{-1} K^{-1}, respectively. The DMSO molecule seems to interact with the intermediate species with a unidentate Hacac and inhibits the associative rate determining step.

Vanadium(IV) gives characteristic square pyramidal complexes with an oxo-anion on the apical position. Interaction of various species including the solvent molecules with the complex has been studied by visible and ultraviolet (UV) absorption spectrometry[1] and correlated with various parameters of the interacting molecule such as donor number.[2] ESR studies in organic solvents disclosed that the interaction at the apical site was a very rapid phenomenon and the rate was mostly diffusion controlled.[3] Reuben and Fiat, and Wüthrich and Connick found two rates for the exchange of water between $[VO(H_2O)_5]^{2+}$ and the solvent by NMR spectroscopy with ^{17}O, and assigned them to the exchanges at the apical ($\approx10^{11}$ s^{-1}) and the basal site (5.2×10^2 s^{-1}).[4] Substitution reactions at the basal site have been studied by absorption and PMR spectrometry by use of bidentate ligands such as glycinate[5] and malonate,[6] and found to be much slower than those at the apical site.

As an extension of our studies of isotopic exchange of various acetylacetonato complexes of main group and transition elements,[7] we have found that the exchange between bis(acetylacetonato)oxovanadium(IV), [VO(acac)$_2$], and acetylacetone[^{14}C] is measurable in 1,2-dichloroethane at a temperature below −20 °C, and the rate decreases on addition of donor solvents. This paper deals with the kinetic studies, and presents a plausible reaction mechanism.

Experimental

Materials. VO(acac)$_2$ was prepared by Rowe and Jones' method[8] and recrystallized from benzene. The purity was examined by elemental analysis of carbon and hydrogen, and visible and ultraviolet absorption spectra. Acetylacetone[^{14}C] was synthesized by the known method.[9]

1,2-Dichloroethane (DCE) was washed with potassium hydroxide solution and water, dried with calcium chloride, fractionally distilled through an effective column, and the distillate dried with Molecular Sieve 4A. Acetonitrile (AN) was dried with calcium chloride and distilled over phosphorus pentoxide. Nitromethane (NM) was distilled, frozen at −40 °C and distilled over Molecular Sieve 4A under a reduced pressure. Dimethyl sulfoxide (DMSO) was dried with activated alumina and distilled under a reduced pressure. *N,N*-Dimethylformamide (DMF) was dried with anhydrous copper(II) sulfate and distilled under a reduced pressure. Methanol was distilled and dried with Molecular Sieve 3A. 1,1,2,2-Tetrachloroethane (TCE) was shaken with several portions of concentrated sulfuric acid until the acid layer remained colorless, washed with water and distilled under a reduced pressure. The purity of the purified solvents was examined by gas chromatography, and the water content determined by Karl-Fischer titration.

Kinetic Runs. The complex solution (≈0.02 M, M=mol dm^{-3}; 5 to 8 cm^3) and acetylacetone (Hacac) labelled with ^{14}C (*ca.* 0.2 μCi) in DCE (10^{-2}—10^{-1} M, 2 to 5 cm^3) were introduced into each of the two bottoms of a co-necked flask with a glass stopper. It was placed in a thermostat, and both solutions were mixed. One cubic centimeter portions were pipetted out at appropriate time intervals, and poured into hexane (10 cm^3) in a test tube chilled at −55 to −58 °C within 8 s. The tubes were shaken and placed in a mixture of dry ice and methanol (−77 °C) to freeze DCE. The curd was filtered with filter paper at room temperature to leave crystalline VO(acac)$_2$, which was washed with hexane and dried *in vacuo*. For kinetic runs at −39.8 °C, 10% TCE (v/v) was added to the DCE solvent to prevent the freezing of DCE. Donor solvents (NM, AN, DMF, and DMSO) were added to DCE prior to the dissolution of the complex. When the reaction mixture contained NM and AN, 10% diethyl ether (v/v) was added to hexane.

The purified DCE contained *ca.* 3×10^{-3} M water, which floated mostly as ice on the surface of the reaction mixture in the thermostat. Hence the water content of the reaction mixture should be much less than 0.03 M but remained unknown.

The separated VO(acac)$_2$ was dissolved in AN (3 cm^3) and the absorption coefficient measured at 394 nm ($\varepsilon_{max}=77$ cm^{-1} M^{-1}). A 1 cm^3 portion was dissolved in toluene containing 0.01% (w/v) 1,4-bis(5-phenyl-2-oxazolyl)benzene (POPOP) and 0.4% (w/v) *p*-terphenyl (14 cm^3) and the counting rate measured by liquid scintillation counting.

Apparatus. The visible and UV absorption spectra were recorded with a Hitachi 323 Spectrometer. The counting rate due to ^{14}C was recorded with a Nuclear Chicago Unilux IIA Counter. A Haake KT 33 Thermostat was used for keeping the temperature the range from −40 to −20 °C (±0.3 °C).

Calculation of the Exchange Rate. The specific counting

rate of the recovered $[VO(acac)_2]$ was known from the recorded counting rate and the weight of $[VO(acac)_2]$, which was calculated from the extinction coefficient of the AN solution. McKay's formula was used to find the rate of exchange.

$$R = -2.3[2ab/(2a+b)][\log(1-F)]/t. \quad (1)$$

Where a and b stand for the concentrations of the complex and the free ligand, respectively. The t is the lapse of time and F is the fraction of reaction expressed by $(x_t-x_0)/(x_\infty-x_0)$. The x's are the specific counting rates at time 0, i, and infinity, respectively. The x_∞ is known by both calculation and experiment. Acetylacetone is in tautomeric equilibrium between keto and enol form, and the interchange rate (*ca.* 10^{-5} s^{-1} at 25 °C[10]) is smaller than the present ligand exchange. The percentages of enol form are 81.4[11] and 80 in itself and in DCE, respectively at 25 °C. Since the Hacac was kept at room temperature for a long time before use, dissolved and cooled immediately before mixing, 0.80 time of the concentration of Hacac was taken as b. (Preferential participation of the enol form in the exchange was also reported for the system $[Ti(acac)_3]^+$ *vs.* Hacac in AN.[12]) The calculated x_∞ value on this basis coincided with the experimental value. Hence the participation of the keto-form in the ligand exchange reaction was not taken into consideration.

Results

Absorption Spectrum. Selbin measured the visible absorption spectrum of $[VO(acac)_2]$ in various solvents, and found that the difference in wave numbers ($\Delta\nu$) between the two absorption peaks in 600—800 nm region was characteristic of the solvents.[1] Gutmann found a good correlation[13] between $\Delta\nu$ and the donor number[2] of the solvent. We have measured the visible absorption spectrum of $VO(acac)_2$ in Hacac and found two peaks at 13980 and 17120 cm^{-1} with ε values 39 and 33 cm^{-1} M^{-1}, respectively. From the difference in wave numbers of these peaks the donor number of Hacac can be calculated to be 20 at room temperature.

Gutmann measured the absorption spectra of $VO(acac)_2$ in dichloromethane containing varying amounts of organic solvents and calculated the formation constants of one to one adducts between $VO(acac)_2$ and the solvent molecules.[14] We have applied this method to the present system and obtained the formation constants of $[VO(acac)_2 \cdot Hacac]$ to be 0.14 and 0.19 M^{-1} at 25 and −33 °C, respectively, the corresponding $\Delta G°$ values being 4.8 and 3.3 kJ mol^{-1}.

In the reaction mixtures additivity law in the UV absorption spectrum was obeyed between $[VO(acac)_2]$ and Hacac. Since the concentrations of both the complex and Hacac were very low, the concentration of the adduct should be too small to be reflected in the absorption spectrum.

Kinetic Data. The visible and UV absorption spectra of the reaction mixture in DCE remained unchanged during the course of the kinetic runs. McKay plots of the runs gave straight lines with very small intercepts, which seemed to be separation-induced. Hence it was verified that the ligand exchange reaction took place exclusively throughout the reaction time. The gradients were determined by the least square method, and the experimental errors in R values calculated on 70% confidence level to be *ca.* 10%. McKay plots were linear in the presence of donor solvents, too.

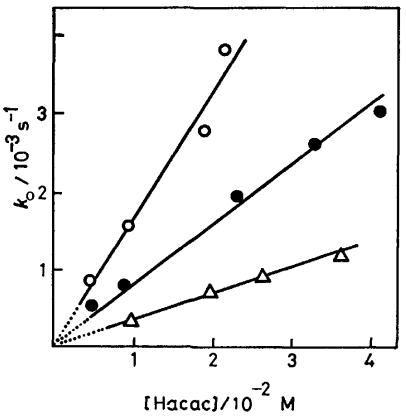

Fig. 1. Dependence of the observed first-order rate constants upon the concentration of free Hacac in enol form in DCE.
-○-: −25.0, -●-: −33.0, -△-: −39.8 °C.

The R was linearly dependent on a in the range between 0.0127 and 0.030 M and the first order rate constant k_0 ($=R/a$) can be the measure of rate of the present ligand exchange. Figure 1 indicates that k_0 increases linearly with increase in b, and the intercept is zero within experimental error. Hence Eq. 2 holds for the range of b from 0.0046 to 0.041 M.

$$R = k_0 a = k_2 ab. \quad (2)$$

The activation parameters obtained from k_2 values at −39.8, −33.0, and −25 °C are listed in Table 1.

Table 1. Rate constants and activation parameters for the substitution reaction of oxovanadium(IV) complexes

System	Method	t/°C	k/s^{-1}	ΔH^*/kJ mol^{-1}	ΔS^*/J $mol^{-1}K^{-1}$
$[VO(H_2O)_5]^{2+}$—H_2O in H_2O[a]	^{17}O NMR	25	520	57.2	−6.3
(same)[b]	^{17}O NMR	25	$\approx 10^{11}$	—	—
$[VO(H_2O)_5]^{2+}$—gly^- in water { formation[c]	Stopped flow	25	1300 M^{-1}	50.2	−16.7
{ dissoc.	Calcd	25	460	54.8	−10.0
$[VO(gly)(H_2O)_4]^+$ in water[d]	T-jump	25	37	—	—
(chelation)	Stopped flow	25	35	—	—
$[VO(acac)_2]$—Hacac* in DCE[e]	Label	−33	0.071 M^{-1}	47.6±1.7	−61.9±8.4
$[VO(acac)_2]$ in DCE+DMSO[f]	Label	−33	0.0038 M^{-1}	71.9±10	−4±40

a) Substitution at the basal site. b) At the apical site; both Ref. 4. c) Ref. 5. d) Ref. 18. e) Present study f) Present study in 0.0643 M DMSO.

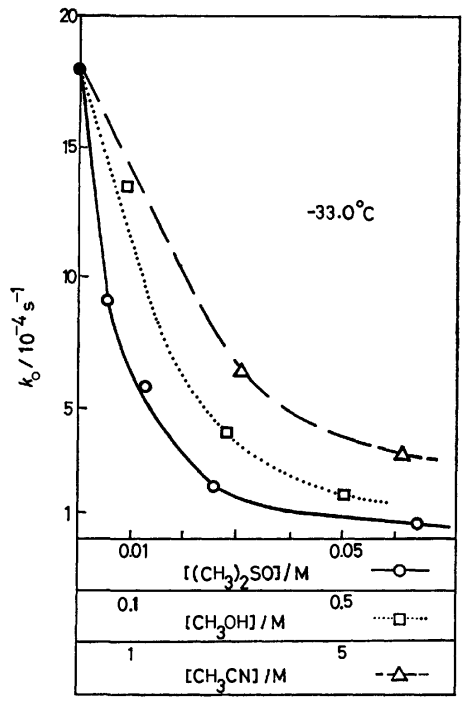

Fig. 2. Decrease in rate of the isotopic exchange on addition of donor solvents to the DCE solution.
—○—: DMSO, ···□···: methanol, ---△—: AN, at −33.0 °C, [Hacac]=0.0222 (—○—, ···□···), 0.0218 M (---△---).

The ligand exchange becomes slower on addition of donor solvents to the DCE solution (Fig. 2). The extent of retardation increases in the following sequence (Eq. 3). (Gutmann's donor numbers are shown in the parentheses).

$$\underset{\text{NM}}{CH_3NO_2} < \underset{\text{AN}}{CH_3CN} < \underset{\text{MeOH}}{CH_3OH} < \underset{\text{DMF}}{HCON(CH_3)_2} < \underset{\text{DMSO}}{(CH_3)_2SO} \qquad (3)$$

$$\underset{(2.7)}{\text{NM}} \quad \underset{(14.1)}{\text{AN}} \quad \underset{(19)}{\text{MeOH}} \quad \underset{(26.6)}{\text{DMF}} \quad \underset{(29.8)}{\text{DMSO}}$$

NM gave only a negligible effect. The extent of retardation by all the other donor solvents increased with increase in their concentrations in DCE. The dependence of k_0 upon b was similar to Eq. 2 in DCE containing DMSO as indicated in Fig. 3. The k_2 and activation parameters in 0.0643 M DMSO in DCE are shown in Table 1.

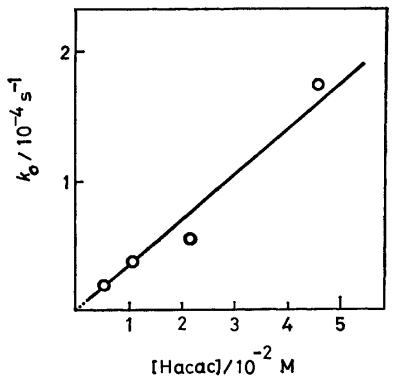

Fig. 3. Dependence of the first-order rate constant upon the concentration of free Hacac in enol form in DCE containing DMSO. At −33.0 °C, [DMSO]=0.0643 M.

Acid and base catalysis were not examined, because trichloroacetic and *m*-toluic acid caused rapid decomposition of [VO(acac)$_2$], and pyridine hindered the separation of the complex in the reaction mixture.

The deuterium isotope effect was measured in a system [VO(acac[^{14}C])$_2$] *vs.* Hacac[^2H] to find the ratio $k_H/k_D=1.3\pm0.2$ at −33 °C in DCE.

Discussion

The basal and the apical site of a square pyramidal structure are not equivalent to each other, and the known rates of substitution at these two sites are different from each other. All the known data support that the substitutions at the apical and the basal site take place with rate constants $>$ *ca.* 10^7,[3,4,15] and 10^2—10^3 s^{-1},[4-6,15,16] respectively.

Since the absorption spectra of the reaction mixtures remained unchanged, no other reactions than isotopic exchange have taken place. The influence of donor solvents is characteristic, and the reaction mechanism is discussed separately in their absence and presence.

In Dichloroethane. We have considered that the interaction between [VO(acac)$_2$] and Hacac reflected in the visible absorption spectra must be due to the addition of the free ligand at the basal position of [VO(acac)$_2$] to give *cis*-[VO(acac)$_2$(Hacac)].[17] The interaction at the basal site can involve either a direct addition or an intramolecular rearrangement, in which the free ligand first associated at the apical site rearranges to the basal site. In either case substitutions at the basal site must proceed much faster than the present isotopic exchange. Hence we consider that the exchange would proceed through the adduct, as shown in Eq. 4.

$$[VO(acac)_2] + Hacac^* \overset{K_L}{\rightleftharpoons} cis[VO(acac)_2(Hacac^*)] \qquad (4)$$

$$cis[VO(acac)_2(Hacac^*)] \overset{k_{ex}}{\longrightarrow} cis[VO(acac^*)_2(Hacac)]. \qquad (5)$$

Thus the observed rate constant k_0 should be expressed by

$$k_0 = R/a = k_2 b = k_{ex}K_L b, \qquad (6)$$

and the k_{ex} values are calculated to be 0.37 and 63 s^{-1} at −33 and 25 °C, respectively.

For the exchange of acac$^-$ to be completed, the reaction of Eq. 5 should involve two steps, *i.e.* transfer of a proton from the incoming Hacac to the coordinated acac$^-$, and the following chelation of the deprotonated unidentate ligand. The calculated k_{ex} (63 s^{-1}) at 25 °C is similar to that of the rate of chelation of unidentate glycinate in water[18] (Table 1). If the proton transfer itself were the rate determining step, isotope effect should be significant between Hacac and Dacac. Experiments gave a ratio $k_H/k_D=1.3\pm0.2$. Decisive conclusion is difficult because of the large experimental error, but the proton transfer does not seem to be an

independent rate determining step. Chelation associated with the proton transfer would be responsible in determining the k_{ex}.

The ΔH^* value for the overall k_2 in DCE is rather small, and the ΔS^* is large in minus. These suggest an associative mechanism at the rate determining step. When the incoming Hacac at the basal site undergoes chelation to eliminate the old ligand, associative attack by the free end upon the old V–O bond, which is in consonance with the proton transfer, would be responsible in determining the rate (Fig. 4).

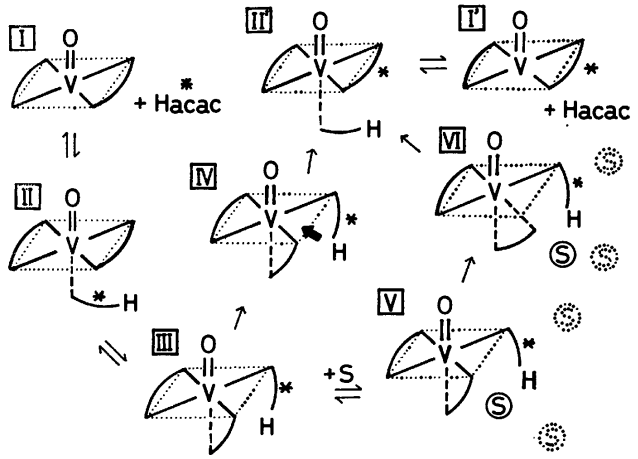

Fig. 4. Plausible reaction mechanism of the ligand exchange in DCE in the absence and the presence of donor solvents. S, donor solvent molecule; arc-like curves, acac$^-$; *, ^{14}C-labelled ligands; thick broken line, weak interaction.

Solvent Effect. In the presence of donor solvents the rate of exchange decreases. The extent is better correlated with Gutmann's donor number than with other parameters such as dielectric constant and dipole moment. Hence a direct interaction between the complex and the donor solvent should be taken into consideration. The kinetics were closely studied with DMSO as a model. The interaction can be understood in two ways: one is to reckon the competition between DMSO and free Hacac towards the coordination site of the complex as responsible, and presumes no difference in the actual route of isotopic exchange; the other is to anticipate a different mechanism in the presence of DMSO.

If the exchange proceeded through the same route as Eqs. 4 and 5, and DMSO molecule behaved as merely a rival of Hacac for the coordination site, the kinetic formula should be modified as Eq. 7, where K_S stands for the formation constant of the adduct [VO(acac)$_2$(DMSO)],

$$k_0 = k_2 b = k_{ex} K_L b/(1+K_S[S]), \qquad (7)$$

where [S] stands for the concentration of donor solvent. If this were valid, the plot of $1/k_2$ *vs.* [S] should give a straight line. However, the diagram is concave upwards. The activation parameters in the presence and the absence of DMSO differ significantly as shown in Table 1. Hence we have to consider that the contribution of competition should be small, not necessarily be ignored, and a different mechanism should be operating in the presence of donor solvent.

The large ΔH^* and almost zero ΔS^* in the presence of DMSO suggest that the exchange would proceed *via* a dissociative mechanism. If DMSO molecules interact with intermediate III in Fig. 4 to give an outer-sphere coordination (V), the nucleophilic attack of the free end of unidentate Hacac upon the V–O bond of the leaving acac$^-$ would be disturbed, so that the associative mechanism would not function any more. Hence a dissociative cleavage of the V–O bond of the leaving acac$^-$, which is accompanied by the proton transfer from the incoming Hacac, would become responsible for the exchange (VI in Fig. 4). (A dissociative mechanism could operate on the adduct [VO(acac)$_2$(DMSO)], but such a route would operate independently of the free Hacac concentration to bring about an intercept on Fig. 3. Absence of intercept on Fig. 3 excludes such a route.) Thus we can conclude that the main role of a donor solvent molecule should be an outer sphere coordination to the intermediate, which hinders the progress of associative rate-determining step of the exchange. Formation of an inactive adduct as [VO(acac)$_2$(DMSO)] would give only a minor contribution, if not necessarily nothing.

Haake and Pfeiffer introduced a new parameter, number of solvent participation, n.[19] This figure indicates the number of solvent molecules which interact with the substrate complex to inhibit the attack of a nucleophilic reagent upon the substrate. The n values were measured in the present system to be 1.6, 0.6, and 1 to 2 (depending on the concentration of methanol), for DMSO, AN and methanol in DCE, respectively. The non-integral figures reflect the complexicity with which the donor solvent molecules interact with the substrate. They may compete with Hacac in the formation of II (Fig. 4), and more than one molecule can interact with III to give V. Hence the n values do not seem to contradict our reaction mechanism.

The authors thank the Ministry of Education for financial support.

References

1) J. Selbin, *Chem. Rev.*, **65**, 153 (1965).
2) V. Gutmann and E. Wychera, *Inorg. Nucl. Chem. Lett.*, **2**, 257 (1966).
3) F. A. Walker, R. L. Carlin, and P. H. Rieger, *J. Chem. Phys.*, **45**, 4181 (1966).
4) J. Reuben and D. Fiat, *Inorg. Chem.*, **6**, 579 (1967); K. Wüthrich and R. E. Connick, *ibid.*, **6**, 583 (1967).
5) H. Tomiyasu, K. Dreyer, and G. Gordon, *Inorg. Chem.*, **11**, 2409 (1972).
6) H. Tomiyasu, S. Ito, and S. Tagami, *Bull. Chem. Soc. Jpn.*, **47**, 2843 (1974).
7) K. Saito, *Pure Appl. Chem.*, **38**, 325 (1974).
8) R. A. Rowe and M. M. Jones, *Inorg. Synth.*, **5**, 115 (1957).
9) K. Saito and K. Masuda, *Bull. Chem. Soc. Jpn.*, **41**, 384 (1968).

10) H. Watarai and N. Suzuki, *J. Inorg. Nucl. Chem.*, **36**, 1815 (1974).
11) R. J. Irving and I. Wadsö, *Acta Chem. Scand.*, **24**, 589 (1970).
12) M. Nishizawa, H. Kido, I. Kinoshita, Y. Soma, and K. Saito, *Bull. Chem. Soc. Jpn.*, **49**, 819 (1976).
13) V. Gutmann, "Coordination Chemistry in Nonaqueous Solution," Springer Verlag, Wien (1968).
14) V. Gutmann and U. Mayer, *Manatsh. Chem.*, **99**, 1383 (1968).
15) K. Wüthrich and R. E. Connick, *Inorg. Chem.*, **7**, 1377 (1968).
16) A. Schlund and H. Wendt, *Ber. Bunsenges. Phys. Chem.*, **72**, 652 (1968).
17) A. Nagasawa, M. Nishizawa, H. Ichiji, and K. Saito, in preparation.
18) H. Tomiyasu and G. Gordon, *Inorg. Chem.*, **15**, 870 (1976).
19) P. Haake and R. M. Pfeiffer, *J. Am. Chem. Soc.*, **92**, 5243 (1970).

The Analogs of Hofmann Type Clathrate Formed between Diammine- or Diaminemetal(II) Tetracyanometallate(II) Host and Aromatic Guest Molecule

Toschitake IWAMOTO, Mamoru KIYOKI, Yutaka OHTSU, and Yasuko TAKESHIGE-KATO

Department of Chemistry, College of General Education, The University of Tokyo, Komaba, Meguro, Tokyo 153

(Received July 29, 1977)

A novel series of clathrates $Cd(tn)M'(CN)_4 \cdot 2G$ ($M'=Cd$ or Hg; $G=C_4H_4S$, C_4H_5N, C_6H_6, or $C_6H_5NH_2$) were prepared as an analogous series of Hofmann type clathrate. Including the novel series, Hofmann type and the analogous clathrates with a general formulation $M(diam)M'(CN)_4 \cdot 2G$ were classified into five groups according to the combination of the host constituents and the resulting host framework structures as follows: Hofmann type $M(NH_3)_2M'(CN)_4 \cdot 2G$ with square-planar $M'(CN)_4$, Hofmann-en type $Cd(en)NM'(CN)_4 \cdot 2G$ with ambident en and square-planar $M'(CN)_4$, Hofmann-Td type $Cd(NH_3)_2M'(CN)_4 \cdot 2G$ with tetrahedral $M'(CN)_4$, en-Td type $Cd(en)M'(CN)_4 \cdot 2G$ with ambident en and tetrahedral $M'(CN)_4$, and tn-Td type $Cd(tn)M'(CN)_4 \cdot 2G$ with ambident tn and tetrahedral $M'(CN)_4$. Their structural features were discussed based on the flexibility of the framework whether it can enclathrate aniline as the largest guest or not.

Among the clathrates formed between metal complex host and aromatic guest molecules, a family can be grouped with a general formulation $M(diam)M'(CN)_4 \cdot 2G$ where M refers to a bivalent metal ion, diam to diammine or diamine ligand, $M'(CN)_4$ to a square-planar or tetrahedral tetracyanometallate(II), and G to an aromatic guest species. This family of the clathrates originates from Hofmann's benzene clathrate $Ni(NH_3)_2Ni(CN)_4 \cdot 2C_6H_6$ first prepared in 1897.[1] The naming "Hofmann type clathrate" was proposed to the clathrates with a general formulation $M(NH_3)_2M'(CN)_4 \cdot 2G$ (M=Mn, Fe, Co, Ni, Cu, Zn, or Cd; M'=Ni, Pd, or Pt; $G=C_4H_4S$, C_4H_5N, C_6H_6, $C_6H_5NH_2$, or $C_{12}H_{10}$),[2-6] in which the host is isostructural to that of the original Hofmann's clathrate.[7-10] Several analogous clathrates have been prepared by replacing $(NH_3)_2$ in Hofmann type by an ambident en ligand,[11-13] or by replacing the square-planar $M'(CN)_4$ by tetrahedral $M'(CN)_4$ (M'=Cd or Hg).[14-16] In this paper, a novel series of $Cd(tn)M'(CN)_4 \cdot 2G$ clathrates will be reported for M'=Cd or Hg and $G=C_4H_4S$, C_4H_5N, C_6H_6, or $C_6H_5NH_2$. Some novel members of the known series will also be described. Their structural features will be discussed on the basis of the flexibility of host framework whether the host can enclathrate aniline as the largest guest or not. According to these features the family of Hofmann type and the analogous clathrates including the present novel one can be classified into five groups.

Experimental

Preparation. *$Cd(tn)M'(CN)_4 \cdot 2G$ ($M'=Cd$ or Hg; $G=C_4H_4S$, C_4H_5N, C_6H_6, or $C_6H_5NH_2$)*: Fifteen millimoles of tn (trimethylenediamine) was added to an aqueous solution of $CdCl_2$ (5 mmol in 50 cm³). A white precipitate once formed did not completely dissolve away by adding the excessive amounts of tn. After the small amounts of undissolved precipitate were filtered off, $K_2[M'(CN)_4]$ (5 mmol in 50 cm³ aq solution) was added to the filtrate in a conical flask. The aqueous phase was kept in contact with the organic phase of the relevant guest species mixed with xylene (1:1) in the flask covered by a stopper for a few weeks in a refrigerator. Colorless crystals grown up on the interface between the aqueous and the organic phases were picked out, washed successively with small amounts of water and ethanol, and dried on a sintered clay plate in a desiccator charged with silica gel desiccator and saturated vapor of neat liquid of the guest species.

$Cd(en)M'(CN)_4 \cdot 2G$ ($M'=Cd$ or Hg; $G=C_4H_4S$ or C_4H_5N): These clathrates were prepared by the methods analogous to those for $Cd(en)Ni(CN)_4 \cdot 2G$[13] and $Cd(en)M'(CN)_4 \cdot 2C_6H_6$[14] using the relevant combination of the potassium tetracyanometallate(II) and the guest species diluted with xylene.

$Cd(NH_3)_2M'(CN)_4 \cdot 2C_6H_5NH_2$ ($M'=Cd$ or Hg): After aniline–xylene mixture (1:1) was shaken with an aqueous solution (*ca.* 100 cm³) containing 5 mmol each of $CdCl_2$ and $K_2[M'(CN)_4]$, and 15 cm³ of concd ammoniacal water at 0 °C, the whole mixture was kept standing in a refrigerator for a few weeks. Colorless crystals were grown up on the interface between the organic and the aqueous phases separated spontaneously. The crystals were treated with the procedure similar to that for $Cd(tn)M'(CN)_4.2C_6H_5NH_2$.

$Cd(NH_3)_2Hg(CN)_4 \cdot 2C_6H_6$:[17] A benzene–xylene (1:1) mixture was placed over an aqueous solution (*ca.* 100 cm³) containing 5 mmol each of $CdCl_2$ and $K_2[Hg(CN)_4]$ and 15 cm³ of concd ammoniacal water in a conical flask. The flask covered with a stopper was kept standing in a refrigerator for a few weeks. Colorless crystals grown up on the interface between the aqueous and the organic phases were treated similarly to the above-mentioned method.

Measurements. The powder X-ray diffraction patterns were recorded on a JEOL diffractometer with Ni-filtered Cu$K\alpha$ radiation and a GM counter. Preliminary single crystal diffraction data were collected with Weissenberg photographs. The infrared spectra were recorded on a JASCO DS403G spectrometer in the 4000—400 cm^{-1} region for the Nujol and the hexachlorobutadiene mulls.

Results and Discussion

Formation and Classification of the Clathrates. The analytical results of the clathrates prepared in the present study are listed in Table 1. It was rather difficult to obtain stoichiometric results for the thiophene clathrates because of the high dissociation pressure and the small dimensions of thiophene molecule. All the clathrates presently prepared as well as those previously reported are generally not stable enough to retain guest species stoichiometrically in an open atmosphere at

Table 1. The analytical results: found (calcd) in %

	C	H	N	Cd	Hg
$Cd(NH_3)_2Cd(CN)_4\cdot 2C_6H_5NH_2$	35.4(35.0)	3.6(3.6)	19.9(20.4)	40.8(41.0)	
$Cd(NH_3)_2Hg(CN)_4\cdot 2C_6H_5NH_2$	30.5(30.2)	2.9(3.1)	17.3(17.6)	18.1(17.7)	32.0(31.5)
$Cd(NH_3)_2Hg(CN)_4\cdot 2C_6H_6$	30.2(31.6)	3.1(3.0)	14.2(13.8)	18.4(18.5)	33.4(33.0)
$Cd(C_2H_8N_2)Cd(CN)_4\cdot 2C_4H_4S$	28.3(30.2)	2.5(2.9)	15.7(15.1)	41.5(40.3)	
$Cd(C_2H_8N_2)Cd(CN)_4\cdot 2C_4H_5N$	34.7(34.1)	4.0(3.5)	21.0(21.4)	43.5(43.0)	
$Cd(C_2H_8N_2)Hg(CN)_4\cdot 2C_4H_4S$	25.1(25.7)	2.2(2.5)	13.4(12.8)	17.5(17.2)	30.6(30.7)
$Cd(C_2H_8N_2)Hg(CN)_4\cdot 2C_4H_5N$	27.2(27.5)	2.7(3.0)	18.6(18.3)	18.5(18.4)	33.4(32.8)
$Cd(C_3H_{10}N_2)Cd(CN)_4\cdot 2C_6H_5NH_2$	38.8(38.7)	3.9(4.1)	18.9(19.1)	38.2(38.1)	
$Cd(C_3H_{10}N_2)Cd(CN)_4\cdot 2C_6H_6$	40.4(40.8)	4.0(4.0)	14.9(15.0)	41.2(40.9)	
$Cd(C_3H_{10}N_2)Cd(CN)_4\cdot 2C_4H_4S$	29.6(31.5)	3.2(3.2)	16.0(14.7)	41.2(39.4)	
$Cd(C_3H_{10}N_2)Hg(CN)_4\cdot 2C_6H_5NH_2$	33.9(33.9)	3.6(3.6)	16.7(16.6)	16.6(16.6)	29.6(29.6)
$Cd(C_3H_{10}N_2)Hg(CN)_4\cdot 2C_6H_6$	34.8(35.3)	3.4(3.4)	13.3(13.0)	17.7(17.4)	30.7(31.0)
$Cd(C_3H_{10}N_2)Hg(CN)_4\cdot 2C_4H_4S$	28.2(27.3)	3.0(2.8)	13.4(12.7)	17.5(17.0)	30.0(30.4)
$Cd(C_3H_{10}N_2)Hg(CN)_4\cdot 2C_4H_5N$	28.6(28.8)	2.9(3.2)	17.6(17.9)	18.5(18.0)	34.2(32.1)

room temperature. There is a tendency that the guest species with lower boiling point of its neat liquid is more easily released from the clathrate. Even in the case of Hofmann type biphenyl clathrate, the decomposition occurs gradually.[6] Therefore, analytical results were often poor for finely crystallized samples owing to the partial decomposition of the products. However, it is again difficult to evacuate the guest completely from the host for those clathrates with ambident diamine ligands and tetrahedral M'(CN)$_4$ in the host framework. For example, it took longer than 24 h to evacuate benzene completely from Cd(tn)Hg(CN)$_4$·2C$_6$H$_6$ under a reduced pressure at 80 °C.

The formation of clathrate is feasibly diagnosed on the infrared spectrum of the product. The characteristic bands are those of the out-of-plane CH bending modes for the aromatic guest, and additionally those of the NH or NH$_2$ vibration modes for pyrrole or aniline guest. Some of the typical results are given in Table 2.

Those clathrates which so far have been prepared with the general formulation M(diam)M'(CN)$_4$·2G are seen in Table 3 with the classification and the tentative namings. The M metal was limited to cadmium(II) for those clathrates other than Hofmann type. Zinc(II) did not give any stable clathrates, and mercury(II) precipitates its cyanide or diaminedicyanomercury(II) complexes under the preparation procedures described in Experimental section. The bivalent metal cations of Mn, Fe, Co, Ni, and Cu which give the host complex of Hofmann type[5] never gave the clathrates with the diamine ligands presumably because of the high stabilities of their en or tn chelated species in solution.

The classification is defined on the combination of host constituents diam and M'(CN)$_4$, the geometrical features of which rule the size and shape of the cavities for guest molecule. The host framework with square-planar M'(CN)$_4$ gives a tetragonal[10,12] or rhombic[18] rectangular box to a guest molecule. There are two

Table 2. The characteristic IR bands of the guests in several host frameworks (in cm^{-1})

Benzene in		Aniline in		Thiophene in		Pyrrole in	
I[a]	III[c]	I	III	II[b]	III	II	III
3076 w	3077 mw	3450 w	3461 m	3138 vw		3470 s	3460 s
3056 w	3057 w	1620 s	1617 s	3091 w	3092 vw	3160 m	3153 mw
3024 w	3024 mw	1603 s	1602 s	1495 mw	1495 m	1532 m	1532 mw
1980 vw		1501 s	1498 s	1253 ms	1254 m	1455 w	1442 w
1966 w	1970 wbr						
1955 vw		1278 m	1280 ms	1081 s	1084 ms	1139 w	1122 m
1842 w	1828 wbr	1176 m	1177 ms	1032 w	1031 w	1087 s	
1823 vw							
		1027 w	1028 m	831 ms	833 m		1077 s
1480 s	1478 s						
		997 w	997 mw	725 vs	738 vs	1047 s	1047 ms
1035 m	1036 ms			713 s	728 s		
		883 m	882 mw			1014 s	1014 s
701 vs	697 s				697 m		
688 vs	687 vs	761 s	766 vs			867 w	867 vw
676 s	677 msh			454 w	467 w		
						741 vs	744 vs
						725 msh	726 msh
						694 wsh	698 wsh

a) I=Cd(NH$_3$)$_2$Hg(CN)$_4$. b) II=Cd(en)Hg(CN)$_4$. c) III=Cd(tn)Hg(CN)$_4$.

TABLE 3. HOFMANN TYPE AND THE ANALOGOUS CLATHRATES: M(diam)M'(CN)$_4$·2G

Naming	M	diam	M'	G
Hofman	a)	$(NH_3)_2$	Ni, Pd, Pt	C_4H_5N, C_4H_4S, C_6H_6, $C_6H_5NH_2$, $C_{12}H_{10}$
Hofmann-en	Cd	en[b]	Ni, Pd	C_4H_5N, C_4H_4S, C_6H_6
Hofmann-Td	Cd	$(NH_3)_2$	Cd, Hg	C_6H_6, $C_6H_5NH_2$
en-Td	Cd	en	Cd, Hg	C_4H_5N, C_4H_4S, C_6H_6
tn-Td	Cd	tn[c]	Cd, Hg	C_4H_5N, C_4H_4S, C_6H_6, $C_6H_5NH_2$

a) M=Mn, Fe, Co, Ni, Cu, Zn, Cd. b) en=ethylenediamine: $C_2H_8N_2$. c) tn=trimethylenediamine: $C_3H_{10}N_2$.

kinds of cavities in the host framework with tetrahedral M'(CN)$_4$. One is similar to the rectangular box in the square-planar framework, and the other is a biprismatic box as has been demonstrated for Cd(en)Cd(CN)$_4$·2C$_6$H$_6$[15] and Cd(NH$_3$)$_2$Hg(CN)$_4$·2C$_6$H$_6$.[16] When diam is $(NH_3)_2$ there is no bridge between two six-coordinate M metals. On the other hand, ambident en or tn bridges two Cd atoms to make the host framework less flexible.

Structural Features of the Classified Clathrates. The host of Hofmann type M(NH$_3$)$_2$M'(CN)$_4$·2G is built of two-dimensional sheets of square-planar M(NC)$_4$ and M'(CN)$_4$ arrays in which the ambident CN ligand bridges adjacent M and M' atoms; the two NH$_3$ ligands coordinate to an M metal up and down from the sheet.[6-10] Among the stacked sheets guest molecules are enclathrated. The larger the dimensions of guest are, the longer becomes the distance between the sheets.[5] The observed distance ranges from 7.97 Å for a pyrrole clathrate to 9.33 Å for an aniline clathrate. An exceptionally long distance 12.65 Å has been observed for a biphenyl clathrate Ni(NH$_3$)$_2$Ni(CN)$_4$·2C$_{12}$H$_{10}$.[6]

Hofmann-en type Cd(en)M'(CN)$_4$·2G (M'=Ni or Pd) is obtained by replacing two NH$_3$ ligands of Hofmann type structure between the adjacent square-planar sheets by an ambident en ligand bridging two Cd atoms in the respective sheets. The resulting three-dimensional host framework gives a limit to the dimensions of guest molecule within the distance between the sheets. Therefore, aniline molecule can no longer be enclathrated in Hofmann-en type host. The longest distance between the sheets has been observed for a benzene clathrate Cd(en)Ni(CN)$_4$·2C$_6$H$_6$ to be 8.06 Å,[12] and the distance decreases to 7.86 Å in the pyrrole clathrate Cd(en)Ni(CN)$_4$·2C$_4$H$_5$N.[18]

Hofmann-Td and en-Td types are derived from Hofmann and Hofmann-en types by replacing the square-planar M'(CN)$_4$ by tetrahedral M'(CN)$_4$. In Hofmann-Td type host Cd(NH$_3$)$_2$M'(CN)$_4$ (M'=Cd or Hg), three-dimensional host framework is built of *catena*-tetra-μ-cyanometallate(II) bridging M' and Cd(NH$_3$)$_2$. This structure resembles PdO structure when the square-planar Pd and tetrahedral O sites are occupied by Cd(NH$_3$)$_2$ and M'(CN)$_4$, respectively, and the PdO linkage is replaced by the Cd–NC–M' linkage.[16] In en-Td type, the six-coordinate Cd atoms are additionally bridged by an ambident en ligand instead of two protrusions of ammine ligands.[15] This additional Cd–en–Cd bridge makes the en-Td host framework less flexible than Hofmann-Td host framework. The former cannot enclathrate aniline molecule but the latter can.

Among the powder diffraction patterns of the novel members of en-Td type clathrates, that of Cd(en)Cd(CN)$_4$·2C$_4$H$_4$S can be interpreted in terms of a tetragonal system as likely to those of Cd(en)Cd(CN)$_4$·2C$_6$H$_6$ and Cd(en)Hg(CN)$_4$·2C$_6$H$_6$.[14,15] The unit cell dimensions a=8.16 Å and c=15.62 Å are shorter in a by 0.1 Å and longer in c by 0.1 Å than those of Cd(en)Cd(CN)$_4$·2C$_6$H$_6$ (a=8.26 Å and c=15.50 Å).[15] Since the a dimension of the latter corresponds to the Cd–en–Cd bridge length in its host framework, the length decreases to 8.16 Å in the thiophene clathrate by assuming that the both framework structures are isostructural to each other. The decrement in a appears to be cancelled by the increment in c to keep the host framework tetragonal. Those diffraction patterns of Cd(en)Cd(CN)$_4$·2C$_4$H$_5$N, Cd(en)Hg(CN)$_4$·2C$_4$H$_4$S, and Cd(en)Hg(CN)$_4$·2C$_4$H$_5$N could not be assigned to any tetragonal system or those systems with higher symmetries. Monoclinic or triclinic distortion may occur in these host frameworks to hold the smaller guest molecules with optimal fitness.

TABLE 4. THE POWDER X-RAY DIFFRACTION OF Cd(tn)Hg(CN)$_4$·2C$_6$H$_6$.

CuKα (λ=1.5418 Å), Ni-filtered, GM-Counter

Cd(C$_3$H$_{10}$N$_2$)Hg(CN)$_4$·2C$_6$H$_6$
tetragonal a=8.67$_4$ and c=14.80$_5$ Å

2θ/°	I	d_{obsd}Å[a]	hkl	d_{calcd}Å
10.17	36	8.70	100	8.67$_4$
11.83	45	7.48	101	7.48$_5$
15.52	19	5.71	111	5.66$_7$
15.84	55	5.60	102	5.63$_2$
18.77	100	4.73	112	4.72$_8$
20.42	94	4.35	200	4.33$_7$
26.00	30	3.43	104	3.41$_1$
30.90	19	2.89	300	2.89$_4$
32.08	20	2.79	204	2.81$_8$
33.76	19	2.66	214	2.68$_0$
34.92	26	2.57	312	2.57$_5$

a) The eleven strong lines are listed.

When the ambident en in Cd–en–Cd bridge in en-Td type is replaced by an ambident tn, the novel host tn-Td type is derived. In tn-Td type, the powder diffraction pattern of Cd(tn)Hg(CN)$_4$·2C$_6$H$_6$ was assigned to a tetragonal system with a=8.67 Å and c=14.81 Å as listed in Table 4. Assuming that the tn-Td benzene clathrate has the structure similar to that of the en-Td type Cd(en)Cd(CN)$_4$·2C$_6$H$_6$ except that the en is replaced by the tn, the a dimension 8.67 Å corre-

sponds to the Cd–tn–Cd bridge length. The 0.4 Å increment in a appears to be cancelled by the 0.7 Å decrement in c from those for Cd(en)Cd(CN)$_4$·2C$_6$H$_6$ so that the volumes per a benzene molecule in the both structures are 278 and 284 Å^3, respectively.

Another fact to be noted is that tn-Td host can enclathrate aniline molecule which is rejected by en-Td host. The Cd–tn–Cd bridge length appears to be 8.80 Å in Cd(tn)Cd(CN)$_4$·2C$_6$H$_5$NH$_2$ structure preliminarily refined using the single crystal diffraction data. The refinement has not been advanced from the present stage with R=0.18 because of disorders in the conformation of tn molecules and in the orientation of aniline molecules in the monoclinic unit cell with dimensions a=11.86 Å, b=13.01 Å, c=15.14 Å, and β=89.01° (Z=4). However, the distance between two Cd atoms linked with a tn molecule can be read on the Fourier projection at the present stage.

Since Baur and Schwarzenbach examined to develop "Hofmann type clathrate" from Hofmann's Ni(NH$_3$)$_2$-Ni(CN)$_4$·2C$_6$H$_6$ by replacing the octahedral Ni by Cu, Zn, and Cd,[19] the present authors and coworkers have developed several types of M(diam)M'(CN)$_4$·2G clathrates. The purpose of these investigations was to materialize an idea to design a host framework of metal complex with an appropriate combination of host constituents in order to enclathrate desired guest molecule. A successful example may be seen in the case of tn-Td type host enclathrating aniline molecule. However, tn-Td host appears not to have a capability to enclathrate styrene molecule.

The authors wish to express their thanks to Professors Niro Matsuura and Yukichi Yoshino for their kind supports and encouragement throughout this work. This work was partially supported by Grants-in-Aid for Scientific Research from the Ministry of Education, Nos. 054070 and 047027.

References

1) K. A. Hofmann and F. Z. Küspert, *Z. Anorg. Chem.* **15**, 204 (1897); K. A. Hofmann and F. Höchtlen, *Ber.*, **36**, 1149 (1903); K. A. Hofmann and H. Arnoldi, *ibid.*, **39**, 339 (1906).
2) T. Iwamoto, T. Miyoshi, T. Miyamoto, Y. Sasaki, and S. Fujiwara, *Bull. Chem. Soc. Jpn.*, **40**, 1174 (1967).
3) T. Nakano, T. Miyoshi, T. Iwamoto, and Y. Sasaki, *Bull. Chem. Soc. Jpn.*, **40**, 1297 (1967).
4) M. Morita, T. Miyoshi, T. Miyamoto, T. Iwamoto, and Y. Sasaki, *Bull. Chem. Soc. Jpn.*, **40**, 1556 (1967).
5) T. Iwamoto, T. Nakano, M. Morita, T. Miyoshi, T. Miyamoto, and Y. Sasaki, *Inorg. Chim. Acta*, **2**, 313 (1968).
6) T. Iwamoto, T. Miyoshi, and Y. Sasaki, *Acta Crystallogr., Sect. B*, **30**, 687 (1974).
7) H. M. Powell and J. H. Rayner, *Nature*, **163**, 566 (1949); J. H. Rayner and H. M. Powell, *J. Chem. Soc.*, **1952**, 319.
8) Y. Sasaki, *Bull. Chem. Soc. Jpn.*, **42**, 2412 (1969).
9) T. Miyoshi, T. Iwamoto, and Y. Sasaki, *Inorg. Chim. Acta*, **7**, 97 (1973).
10) R. Kuroda and Y. Sasaki, *Acta Crystallogr., Sect. B*, **30**, 687 (1974).
11) T. Iwamoto, *Inorg. Chim. Acta*, **2**, 269 (1968).
12) T. Miyoshi, T. Iwamoto, and Y. Sasaki, *Inorg. Nucl. Chem. Lett.*, **6**, 21 (1970); *Inorg. Chim. Acta*, **6**, 59 (1972).
13) T. Iwamoto and Y. Ohtsu, *Chem. Lett.*, **1972**, 463.
14) T. Iwamoto and D. F. Shriver, *Inorg. Chem.*, **11**, 2570 (1972).
15) T. Iwamoto, *Chem. Lett.*, **1973**, 723.
16) R. Kuroda, *Inorg. Nucl. Chem. Lett.*, **9**, 13 (1973).
17) The crystal structure alone has been reported in Ref. 16 without any description of the preparation.
18) T. Iwamoto and M. Kiyoki, *Bull. Chem. Soc. Jpn.*, **48**, 2414 (1975).
19) R. Baur and G. Schwarzenbach, *Helv. Chim. Acta*, **43**, 842 (1960).

The Crystal Structure of Guanidinium Hexamolybdobis(phenylarsonate) Tetrahydrate, $(CN_3H_6)_4[(C_6H_5As)_2Mo_6O_{25}H_2]\cdot 4H_2O$

Kazuko Y. MATSUMOTO

Department of Chemistry, Faculty of Science, The University of Tokyo, Hongo, Bunkyo-ku, Tokyo 113

(Received August 17, 1977)

Two heteropoly anions, $[C_6H_5AsMo_6O_{21}(H_2O)_6]^{2-}$ and $[(C_6H_5As)_2Mo_6O_{25}H_2]^{4-}$, have been synthesized by the reaction of phenylarsonic acid with molybdenum trioxide in an aqueous solution of pH *ca.* 2. The latter anion has been subjected to crystal-structure analysis as a guanidinium salt, $(CN_3H_6)_4[(C_6H_5As)_2Mo_6O_{25}H_2]\cdot 4H_2O$, and a heteropoly anion with a new type of structure has been established. The crystal is monoclinic with the space group of $P2_1$ and cell dimensions of $a=13.754(5)$, $b=15.752(7)$, $c=11.900(5)$ Å, $\beta=115.59(2)°$, $V=2325.3$ Å^3, $D_m=2.25$, $D_x=2.28$ g cm^{-3}, and $Z=2$. The formula of the anion has been proved to be $[(C_6H_5As)_2Mo_6O_{25}H_2]^{4-}$, which is different from the expected formula, $[(C_6H_5As)_2Mo_6O_{24}]^{4-}$, though the latter had previously been proposed on the basis of a ^{17}O NMR study and an independent X-ray investigation of the methyl derivative had confirmed the existence of the $[(CH_3As)_2Mo_6O_{24}]^{4-}$ anion. The present anion, $[(C_6H_5As)_2Mo_6O_{25}H_2]^{4-}$, consists of six MoO_6 octahedra, which form a ring with one face-, two corner- and three edge-sharings, the two $C_6H_5AsO_3$ tetrahedra are attached to the ring from above and below, with their three oxygens shared with molybdenums. The two phenyl groups are oriented upwards and downwards from the ring respectively.

In a previous paper[1] the present author reported the structure of two heteropoly molybdates derived from methylarsonic acid and dimethylarsinic acid. That study suggested the possibility that many other such acids with metal-organic group bonds may act as hetero elements to enter poly anions. Thus, the author has continued this preparative and structural study, extending the hetero parts from methyl derivatives to a phenyl derivative of arsenic acid. In this paper the author will report on the crystal structure of $(CN_3H_6)_4[(C_6H_5As)_2Mo_6O_{25}H_2]\cdot 4H_2O$; a preparative description of this appeared as early as in 1913,[2] but the analytical results seem unsatisfactory and no further study has been undertaken since.

Experimental

Preparation. Two g (0.01 mol) of $C_6H_5AsO_3H_2$ and 0.8 g of NaOH were dissolved in 500 ml of water and then 8.6 g (0.06 mol) of MoO_3 was gradually added while the solution was heated to boiling. After the solution had then been filtered to remove the small amount of unreacted MoO_3, the filtrate was condensed to 75 ml on a water bath and 2 g of CN_3H_6Cl was added. A colorless precipitate which appeared instantly was filtered out. The reaction of the formation of the heteropoly anion may be described as follows:

$$2C_6H_5AsO_3^{2-} + 6MoO_3 + H_2O \longrightarrow [(C_6H_5As)_2Mo_6O_{25}H_2]^{4-}.$$

The results of elemental analyses are: Found: C, 11.99; H, 2.72; N, 10.38%. Calcd for $(CN_3H_6)_4[(C_6H_5As)_2Mo_6O_{25}H_2]\cdot 4H_2O$: C, 12.05; H, 2.79; N, 10.55%.

After the filtrate had stood at room temperature for about a week, colorless, bush-like crystals appeared. Their composition was formulated as $(CN_3H_6)_2[C_6H_5AsMo_6O_{21}(H_2O)_6]\cdot 3H_2O$, and from the IR spectrum the anion was concluded to be analogous to the corresponding methyl derivative reported in a previous paper.[1] The formation reaction may be described as follows:

$$C_6H_5AsO_3^{2-} + 6MoO_3 + 6H_2O \longrightarrow [C_6H_5AsMo_6O_{21}(H_2O)_6]^{2-}.$$

The results of elemental analyses are: Found: C, 7.32; H, 2.65; N, 6.28%. Calcd for $(CN_3H_6)_2[C_6H_5AsMo_6O_{21}(H_2O)_6]\cdot 3H_2O$: C, 7.13; H, 2.63; N, 6.24%.

Crystal Data. The single crystal of $(CN_3H_6)_4[(C_6H_5As)_4Mo_6O_{25}H_2]\cdot 4H_2O$ was obtained by the diffusion method, its approximate dimensions were $0.1\times0.15\times1.0$ mm. Preliminary Weissenberg photographs exhibited a monoclinic symmetry, and the observed systematic absence indicated the space group to be $P2_1/m$ or $P2_1$. However, a satisfactory solution for the Patterson map was achieved only when $P2_1$ was assumed, hence, the space group was determined to be $P2_1$. The crystal data are as follows:

$(CN_3H_6)_4[(C_6H_5As)_2Mo_6O_{25}H_2]\cdot 4H_2O$
monoclinic $P2_1$
$a = 13.754(5)$
$b = 15.752(7)$
$c = 11.900(5)$ Å
$\beta = 115.59(2)°$
$V = 2325.3$ Å^3
$M.W. = 1594.2$
$Z = 2$
$D_m = 2.25$
$D_x = 2.28$ g cm^{-3}
$\mu = 16.6$ cm^{-1} (for Mo $K\alpha$ radiation)

Data Collection. All the intensities were measured on a Philips automatic four-circle diffractometer. Graphite-monochromated Mo $K\alpha$ radiation was used, and the scan mode was ω-2θ, with a scan rate of 2θ 1° min^{-1}. The scan range was calculated for each reflection according to this formula: $\omega=1.4+0.6\tan\theta$, and stationary-crystal, stationary-counter background counts of 20 s were taken at the end of each scan. In order to check the crystal deterioration, three standard reflections were monitored every three hours, but no significant intensity loss was observed throughout the data collection. The data were corrected for the Lorentz and polarization effects. No absorption or extinction corrections were applied. The intensities were collected up to $2\theta=60°$, and 4720 independent reflections with $|F_o|\geq3\sigma(|F_o|)$ were used for further computation.

Solution and Refinement of the Structure. The coordinates of the molybdenum atoms were determined from the Patterson map, while all the remining non-hydrogen atoms were located from the successive Fourier syntheses. After the structure had been refined with isotropic temperature factors by the block-diagonal least-squares method, anisotropic temperature factors were applied to all the atoms. After the refinement had been

TABLE 1. FINAL POSITIONAL PARAMETERS ($\times 10^4$), WITH THEIR ESTIMATED STANDARD DEVIATIONS IN PARENTHESES

$[(C_6H_5As)_2Mo_6O_{25}H_2]^{4-}$ anion	x	y	z
Mo(1)	2421(2)	443(1)	−1169(2)
Mo(2)	642(1)	0(0)	−44(2)
Mo(3)	266(1)	1414(1)	2264(2)
Mo(4)	2646(2)	1870(1)	4406(2)
Mo(5)	4951(1)	1120(1)	3878(2)
Mo(6)	4751(1)	1183(1)	983(2)
As(1)	2386(2)	1811(1)	1213(2)
As(2)	3357(2)	−452(1)	1872(2)
O(1)	3439(11)	1356(8)	−486(12)
O(2)	1455(15)	945(10)	−2419(13)
O(3)	3042(16)	−180(11)	−1835(16)
O(4)	1568(11)	−360(9)	−819(13)
O(5)	1672(11)	1141(8)	42(11)
O(6)	3667(10)	47(8)	773(12)
O(7)	−356(12)	371(10)	−1375(14)
O(8)	2118(12)	−220(8)	1716(13)
O(9)	259(11)	666(8)	1055(13)
O(10)	201(11)	−980(9)	117(16)
O(11)	−494(13)	2227(11)	1395(14)
O(12)	−572(13)	899(13)	2772(17)
O(13)	1130(10)	2047(8)	3780(12)
O(14)	1834(10)	1820(8)	2251(12)
O(15)	1717(11)	509(9)	3555(13)
O(16)	3119(15)	2871(9)	4629(16)
O(17)	2829(14)	1523(9)	5842(13)
O(18)	3799(10)	1252(8)	4316(12)
O(19)	5897(13)	634(9)	5166(15)
O(20)	5398(15)	2153(9)	4092(16)
O(21)	4223(11)	−148(8)	3296(13)
O(22)	5537(10)	838(9)	2696(12)
O(23)	3696(9)	1530(9)	1954(12)
O(24)	5478(13)	599(9)	393(16)
O(25)	5237(13)	2213(9)	1108(16)
C(1)	2240(19)	2913(12)	552(23)
C(2)	1805(19)	3043(15)	−712(24)
C(3)	1769(20)	3968(17)	−1044(24)
C(4)	2087(24)	4568(18)	−276(27)
C(5)	2516(26)	4427(17)	972(31)
C(6)	2611(24)	3589(14)	1432(28)
C(7)	3498(19)	−1635(13)	1757(21)
C(8)	3150(24)	−2011(14)	583(23)
C(9)	3158(28)	−2863(21)	433(34)
C(10)	3666(23)	−3406(18)	1570(28)
C(11)	4302(26)	−2984(19)	2600(28)
C(12)	4254(29)	−2022(21)	2917(32)
Guanidinium cations	x	y	z
C(13)	−1636(20)	170(14)	4744(28)
N(1)	−622(18)	−38(18)	4984(25)
N(2)	−2148(20)	−160(15)	5414(22)
N(3)	−2149(18)	775(14)	3853(21)
C(14)	4469(21)	−763(15)	6491(23)
N(4)	4398(18)	−1244(13)	7311(20)
N(5)	4875(19)	−1051(13)	5770(20)
N(6)	4248(17)	56(12)	6483(20)
C(15)	−1144(22)	2426(16)	−2368(24)
N(7)	−1186(19)	1787(15)	−3047(21)
N(8)	−1374(21)	3226(16)	−2785(23)
N(9)	−782(19)	2236(15)	−1162(20)
C(16)	3946(18)	3433(15)	−1806(22)
N(10)	3783(17)	3977(14)	−2773(20)
N(11)	3599(17)	2623(13)	−2031(18)
N(12)	4384(17)	3753(13)	−652(20)
Water molecules	x	y	z
$H_2O(1)$	234(18)	3791(13)	3019(19)
$H_2O(2)$	1605(14)	−381(12)	5401(16)
$H_2O(3)$	1416(17)	−2005(14)	5239(19)
$H_2O(4)$	441(17)	2210(14)	5642(19)

TABLE 2. FINAL TEMPERATURE FACTORS ($\times 10^4$), WITH THEIR ESTIMATED STANDARD DEVIATIONS

The β_{ij}'s are of the form: $\exp[-(\beta_{11}h^2+\beta_{22}k^2+\beta_{33}l^2+2\beta_{12}hk+2\beta_{13}hl+2\beta_{23}kl)]$.

$[(C_6H_5As)_2Mo_6O_{25}H_2]^{4-}$ anion	β_{11}	β_{22}	β_{33}	β_{12}	β_{13}	β_{23}
Mo(1)	69(1)	22(1)	46(1)	−2(1)	38(1)	−1(1)
Mo(2)	47(1)	15(1)	49(1)	−3(1)	22(1)	−5(1)
Mo(3)	42(1)	23(1)	56(1)	0(1)	28(1)	−6(1)
Mo(4)	53(1)	18(1)	48(1)	2(1)	27(1)	−7(1)
Mo(5)	41(1)	16(1)	52(1)	−1(1)	21(1)	−2(1)
Mo(6)	55(1)	16(1)	62(1)	1(1)	39(1)	4(1)
As(1)	46(1)	12(1)	44(1)	1(1)	26(1)	1(1)
As(2)	44(1)	11(1)	44(1)	−1(1)	25(1)	0(1)
O(1)	55(10)	18(5)	54(12)	0(6)	28(9)	10(7)
O(2)	100(15)	32(7)	35(12)	7(8)	23(11)	12(8)
O(3)	122(18)	37(8)	76(16)	8(10)	71(15)	−10(9)
O(4)	52(10)	26(6)	66(13)	−14(6)	40(10)	−21(8)
O(5)	59(10)	15(4)	38(10)	1(6)	29(8)	3(7)
O(6)	48(9)	16(5)	55(12)	−6(6)	32(9)	−4(7)
O(7)	51(11)	33(7)	62(14)	−6(7)	14(10)	−20(9)
O(8)	72(12)	18(5)	62(13)	0(6)	45(11)	7(7)
O(9)	42(9)	21(5)	64(13)	−9(6)	30(10)	−11(7)
O(10)	44(10)	17(5)	104(17)	−9(6)	41(11)	0(8)
O(11)	58(12)	44(8)	56(14)	15(8)	11(11)	−9(9)
O(12)	54(12)	70(12)	102(19)	−5(10)	53(13)	−6(12)
O(13)	35(8)	16(5)	59(12)	2(5)	29(9)	−5(6)
O(14)	43(9)	12(4)	60(12)	7(5)	30(9)	−6(7)
O(15)	54(10)	22(6)	57(12)	−4(6)	28(10)	−2(7)
O(16)	92(15)	18(6)	91(18)	−10(8)	36(14)	−5(9)
O(17)	97(14)	22(6)	55(13)	1(8)	49(12)	−3(7)
O(18)	45(9)	18(5)	56(12)	−7(6)	33(9)	−14(7)
O(19)	65(12)	17(6)	81(15)	−7(7)	32(11)	−10(8)
O(20)	100(16)	19(6)	93(18)	−10(8)	56(14)	−8(9)
O(21)	45(9)	13(5)	65(13)	−5(5)	29(9)	0(7)
O(22)	33(8)	30(6)	43(11)	20(6)	12(8)	11(7)
O(23)	21(7)	24(5)	47(12)	3(5)	7(8)	1(7)
O(24)	71(12)	26(6)	109(18)	17(7)	69(13)	12(9)
O(25)	67(13)	19(6)	106(18)	−4(7)	41(13)	3(9)
C(1)	68(17)	12(7)	99(24)	4(9)	55(18)	6(11)
C(2)	58(17)	34(10)	99(26)	27(11)	46(18)	24(14)
C(3)	62(18)	38(11)	94(25)	7(11)	41(18)	16(14)
C(4)	112(25)	37(12)	137(31)	24(15)	75(24)	36(17)
C(5)	116(28)	27(11)	146(38)	−16(14)	62(28)	0(17)
C(6)	107(25)	12(8)	124(32)	8(11)	42(24)	20(13)
C(7)	67(17)	20(8)	79(22)	14(10)	46(17)	3(11)
C(8)	119(27)	15(8)	69(23)	20(12)	0(20)	−11(11)

C(9)	113(31)	47(16)	144(40)	−6(18)	45(30)	−15(21)
C(10)	77(21)	35(12)	112(29)	−3(12)	35(21)	2(15)
C(11)	114(27)	45(14)	92(29)	−2(16)	33(24)	3(17)
C(12)	146(33)	46(15)	136(37)	16(18)	82(30)	5(20)

Guanidinium cations

	β_{11}	β_{22}	β_{33}	β_{12}	β_{13}	β_{23}
C(13)	66(18)	22(9)	140(32)	−8(10)	52(21)	−16(14)
N(1)	68(17)	57(12)	140(29)	10(13)	44(19)	10(17)
N(2)	106(20)	39(11)	109(25)	15(12)	65(19)	22(13)
N(3)	70(16)	39(10)	94(22)	−1(10)	30(16)	4(13)
C(14)	82(20)	29(9)	79(23)	5(11)	49(19)	5(12)
N(4)	83(17)	30(9)	91(21)	8(10)	52(16)	12(11)
N(5)	102(20)	31(9)	83(21)	3(11)	51(17)	9(11)
N(6)	88(17)	23(7)	98(22)	5(10)	58(17)	−1(11)
C(15)	83(21)	32(11)	85(25)	3(12)	37(20)	4(14)
N(7)	98(19)	40(10)	102(23)	2(12)	49(18)	−6(14)
N(8)	110(22)	44(11)	110(26)	4(13)	56(20)	1(15)
N(9)	84(18)	47(11)	80(21)	2(12)	35(17)	−4(13)
C(16)	48(15)	30(9)	78(22)	−3(10)	27(16)	4(12)
N(10)	71(16)	35(9)	81(20)	−1(10)	29(15)	6(12)
N(11)	71(16)	32(9)	72(19)	−5(10)	32(15)	−3(11)
N(12)	73(16)	34(9)	88(21)	−8(10)	38(16)	−3(12)

Water molecules

	β_{11}	β_{22}	β_{33}	β_{12}	β_{13}	β_{23}
$H_2O(1)$	121(19)	47(10)	101(21)	2(11)	34(17)	2(12)
$H_2O(2)$	75(14)	47(9)	80(17)	−7(9)	33(13)	1(11)
$H_2O(3)$	114(18)	54(10)	106(22)	−15(12)	49(17)	−10(13)
$H_2O(4)$	109(18)	57(11)	119(23)	5(12)	64(17)	7(13)

continiued several more cycles, the final R value was 0.066 ($R=\sum||F_o|-|F_c||/\sum|F_o|$).

The final atomic coordinates and temperature factors are listed in Tables 1 and 2 respectively. The F_o-F_c table is kept at the office of this Bulletin (Document No. 7801). The atomic scattering factors were based on Ref. 3, and the effects of the anomalous dispersion for molybdenum and arsenic were corrected according to Ref. 4. All the calculations were performed on a HITAC 8700/8800 computer at the Computer Center of the University of Tokyo.

TABLE 3. THE BOND LENGTHS (Å) IN $[(C_6H_5As)_2Mo_6O_{25}H_2]^{4-}$ ANION AND GUANIDINIUM CATIONS, WITH THEIR ESTIMATED STANDARD DEVIATIONS IN PARENTHESES

$[(C_6H_5As)_2Mo_6O_{25}H_2]^{4-}$ anion

Mo(1)...Mo(2)	3.331(4)	Mo(4)...Mo(5)	3.683(4)
Mo(2)...Mo(3)	3.740(4)	Mo(5)...Mo(6)	3.337(4)
Mo(3)...Mo(4)	3.244(4)	Mo(6)...Mo(1)	3.332(4)
Mo(1)—O(1)	1.925(14)	Mo(2)—O(4)	1.948(19)
O(2)	1.701(15)	O(5)	2.263(15)
O(3)	1.700(22)	O(7)	1.691(14)
O(4)	1.884(17)	O(8)	2.224(13)
O(5)	2.372(17)	O(9)	1.920(18)
O(6)	2.291(13)	O(10)	1.691(16)
Mo(3)—O(9)	1.855(17)	Mo(4)—O(13)	1.908(14)
O(11)	1.693(17)	O(14)	2.314(14)
O(12)	1.718(22)	O(15)	2.478(15)
O(13)	1.952(13)	O(16)	1.683(16)
O(14)	2.255(16)	O(17)	1.706(18)
O(15)	2.393(14)	O(18)	1.903(16)
Mo(5)—O(18)	1.881(17)	Mo(6)—O(22)	1.927(14)
O(19)	1.704(14)	O(23)	2.278(17)
O(20)	1.719(16)	O(24)	1.716(20)
O(21)	2.198(13)	O(25)	1.737(16)
O(22)	1.950(18)	O(1)	1.914(12)
O(23)	2.286(12)	O(6)	2.272(15)
As(1)—O(14)	1.707(18)	As(2)—O(8)	1.673(19)
O(5)	1.685(13)	O(6)	1.724(17)
O(23)	1.687(13)	O(21)	1.666(13)
C(1)	1.881(21)	C(7)	1.885(22)
C(1)—C(2)	1.373(37)	O(8)—O(10)	2.770(19)
C(2)—C(3)	1.506(37)	O(15)	2.726(26)
C(3)—C(4)	1.259(37)	O(21)	2.689(19)
C(4)—C(5)	1.360(49)	O(9)—O(10)	2.803(21)
C(5)—C(6)	1.413(37)	O(11)	2.764(24)
C(6)—C(1)	1.424(33)	O(12)	2.762(30)
C(7)—C(8)	1.398(36)	O(14)	2.712(18)
C(8)—C(9)	1.355(41)	O(15)	2.789(19)
C(9)—C(10)	1.495(44)	O(11)—O(12)	2.687(29)
C(10)—C(11)	1.333(38)	O(13)	2.765(18)
C(11)—C(12)	1.569(47)	O(14)	2.979(23)
C(12)—C(7)	1.458(37)	O(26)	3.022(27)
		O(12)—O(13)	2.785(23)
O(1)—O(2)	2.781(19)	O(15)	2.937(25)
O(3)	2.816(23)	O(13)—O(14)	2.429(25)
O(5)	2.780(25)	O(15)	2.604(21)
O(6)	2.487(20)	O(16)	2.794(23)
O(23)	2.782(22)	O(17)	2.685(18)
O(24)	2.801(22)	O(14)—O(15)	2.629(22)
O(25)	2.736(20)	O(16)	3.091(20)
O(2)—O(3)	2.655(27)	O(18)	2.900(16)
O(4)	2.753(24)	O(23)	2.771(22)
O(5)	2.829(23)	O(15)—O(17)	2.950(20)
O(3)—O(4)	2.788(32)	O(18)	2.855(21)
O(6)	2.862(24)	O(16)—O(17)	2.693(25)
O(4)—O(5)	2.547(21)	O(18)	2.796(22)
O(6)	2.757(18)	O(17)—O(18)	2.712(27)
O(7)	2.689(23)	O(18)—O(19)	2.788(22)
O(8)	2.783(23)	O(20)	2.725(27)
O(10)	2.745(27)	O(21)	2.691(21)
O(5)—O(6)	3.032(20)	O(23)	2.787(22)
O(7)	2.834(20)	O(19)—O(20)	2.658(22)
O(8)	2.800(20)	O(21)	2.706(18)
O(9)	2.795(25)	O(22)	2.780(24)
O(14)	2.757(21)	O(20)—O(22)	2.712(24)
O(23)	2.798(16)	O(23)	2.788(19)
O(6)—O(8)	2.834(27)	O(21)—O(22)	2.696(23)
O(21)	2.775(22)	O(23)	3.001(19)
O(22)	2.884(17)	O(22)—O(23)	2.539(19)
O(23)	2.717(20)	O(24)	2.733(26)
O(24)	2.853(27)	O(25)	2.785(23)
O(7)—O(9)	2.680(23)	O(23)—O(25)	2.917(27)
O(10)	2.657(22)	O(24)—O(25)	2.745(23)
O(8)—O(9)	2.709(22)		

Guanidinium cations

C(13)—N(1)	1.337(38)	C(15)—N(7)	1.280(37)
N(2)	1.371(47)	N(8)	1.337(36)
N(3)	1.369(32)	N(9)	1.335(37)
C(14)—N(4)	1.269(37)	C(16)—N(10)	1.370(33)
N(5)	1.291(43)	N(11)	1.352(31)
N(6)	1.319(32)	N(12)	1.336(32)

TABLE 4. THE BOND ANGLES(°) IN $[(C_6H_5As)_2Mo_6O_{25}H_2]^{4-}$ ANION AND GUANIDINIUM CATIONS, WITH THEIR ESTIMATED STANDARD DEVIATIONS IN PARENTHESES

O(1)—Mo(1)—O(2)	99.97(61)	O(18)—Mo(5)—O(23)	83.35(57)
O(3)	101.75(85)	O(19)—Mo(5)—O(20)	101.89(68)
O(4)	144.40(64)	O(21)	86.83(55)
O(5)	79.89(54)	O(22)	98.86(67)
O(6)	71.70(48)	O(23)	168.70(53)
O(2)—Mo(1)—O(3)	102.62(89)	O(20)—Mo(5)—O(21)	170.92(61)
O(4)	100.21(69)	O(22)	95.14(72)
O(5)	86.29(61)	O(23)	87.03(58)
O(6)	165.91(55)	O(21)—Mo(5)—O(22)	84.01(42)
O(3)—Mo(1)—O(4)	102.05(91)	O(23)	80.85(59)
O(5)	170.41(85)	O(22)—Mo(5)—O(23)	73.17(57)
O(6)	90.39(81)	O(22)—Mo(6)—O(23)	73.74(54)
O(4)—Mo(1)—O(5)	72.50(64)	O(22)—Mo(6)—O(24)	97.05(76)
O(6)	82.04(58)	O(25)	98.83(62)
O(5)—Mo(1)—O(6)	81.11(48)	O(1)	151.98(52)
O(4)—Mo(2)—O(5)	74.01(65)	O(6)	86.34(51)
O(7)	95.02(70)	O(23)—Mo(6)—O(24)	161.40(78)
O(8)	83.40(63)	O(25)	92.19(64)
O(9)	155.04(74)	O(1)	82.68(52)
O(10)	97.65(74)	O(6)	73.33(52)
O(5)—Mo(2)—O(7)	90.36(57)	O(24)—Mo(6)—O(25)	105.36(84)
O(8)	77.22(48)	O(1)	100.89(75)
O(9)	83.42(61)	O(6)	90.23(75)
O(10)	164.50(62)	O(25)—Mo(6)—O(1)	96.96(61)
O(7)—Mo(2)—O(8)	167.45(55)	O(6)	162.72(61)
O(9)	95.66(67)	O(1)—Mo(6)—O(6)	72.32(48)
O(10)	103.55(67)	O(5)—As(1)—O(14)	108.75(69)
O(8)—Mo(2)—O(9)	81.30(59)	O(23)	112.18(57)
O(10)	89.00(59)	C(1)	108.24(74)
O(9)—Mo(2)—O(10)	101.67(71)	O(14)—As(1)—O(23)	109.44(68)
O(9)—Mo(3)—O(11)	102.23(72)	C(1)	107.12(84)
O(12)	101.19(89)	O(23)—As(1)—C(1)	110.95(74)
O(13)	146.94(60)	O(6)—As(2)—O(8)	113.02(81)
O(14)	81.94(62)	O(21)	109.87(68)
O(15)	80.99(57)	C(7)	108.85(83)
O(11)—Mo(3)—O(12)	103.92(92)	O(8)—As(2)—O(21)	107.23(74)
O(13)	98.40(64)	C(7)	109.85(88)
O(14)	96.94(66)	O(21)—As(2)—C(7)	107.89(76)
O(15)	165.00(62)		
O(12)—Mo(3)—O(13)	98.52(83)	C(1)—C(2)—C(3)	112.33(216)
O(14)	157.61(84)	C(2)—C(3)—C(4)	125.39(249)
O(15)	89.63(81)	C(3)—C(4)—C(5)	121.14(257)
O(13)—Mo(3)—O(14)	70.09(52)	C(4)—C(5)—C(6)	120.21(268)
O(15)	72.84(47)	C(5)—C(6)—C(1)	118.04(251)
O(14)—Mo(3)—O(15)	68.81(49)	C(6)—C(1)—C(2)	122.89(207)
O(13)—Mo(4)—O(14)	69.47(50)	C(7)—C(8)—C(9)	122.16(246)
O(15)	71.52(51)	C(8)—C(9)—C(10)	118.34(284)
O(16)	102.02(65)	C(9) C(10)—C(11)	114.41(262)
O(17)	95.78(68)	C(10)—C(11)—C(12)	128.35(262)
O(18)	148.18(60)	C(11)—C(12)—C(7)	105.43(238)
O(14)—Mo(4)—O(15)	66.44(45)	C(12)—C(7)—C(8)	124.38(223)
O(16)	100.10(61)		
O(17)	152.93(64)	N(1)—C(13)—N(2)	122.39(251)
O(18)	86.29(55)	N(2)—C(13)—N(3)	119.21(257)
O(15)—Mo(4)—O(16)	166.29(61)	N(3)—C(13)—N(1)	118.25(286)
O(17)	87.64(64)	N(4)—C(14)—N(5)	120.33(251)
O(18)	80.16(55)	N(5)—C(14)—N(6)	119.84(266)
O(16)—Mo(4)—O(17)	105.26(76)	N(6)—C(14)—N(4)	119.31(276)
O(18)	102.31(69)	N(7)—C(15)—N(8)	124.67(267)
O(17)—Mo(4)—O(18)	97.28(71)	N(8)—C(15)—N(9)	122.09(252)
O(18)—Mo(5)—O(19)	101.97(68)	N(9)—C(15)—N(7)	113.13(237)
O(20)	98.29(72)	N(10)—C(16)—N(11)	120.39(208)
O(21)	82.18(59)	N(11)—C(16)—N(12)	121.46(229)
O(22)	152.23(70)	N(12)—C(16)—N(10)	117.97(208)

Description of the Structure and Discussion

The structure of the anion is depicted in Fig. 1, while the interatomic distances and angles within the anion and guanidinium cations are listed in Tables 3 and 4.

Each molybdenum is octahedrally coordinated by six oxygen atoms, and the anion is constituted of six MoO_6 octahedra and two $C_6H_5AsO_3$ tetrahedra. These octahedra are connected with one face-sharing (the shared face is O(13)–O(14)–O(15)), two corner-sharings (the shared corners are O(9) and O(18)), and three edge-sharings (the shared edges are O(4)–O(5), O(1)–O(6), and O(22)–O(23)) to form a ring. The six molybdenum atoms are not coplanar. Each of the two arsenics is tetrahedrally coordinated by three oxygen atoms and a phenyl group, and each joins the ring through sharing the three oxygens with molybdenums, one arsenic atom from above and the other from below the ring. These two arsenics are not, however, equivalent in their bonding manner. As(1) is bonded to O(5), O(14), and O(23), each of which is shared with two molybdenums besides As(1), whereas As(2) is coordinated by O(6), O(8), and O(21), of which each of O(8) and O(21) is bonded to one molybdenum and O(6) is shared with two molybdenums. There is no significant difference observed between the bond lengths and angles in the two $C_6H_5AsO_3$ tetrahedra of the present anion and those of free arsonic acid.[5]

Just before the present structural analysis had been completed, the ^{17}O NMR spectra of a heteropoly molybdate containing phenylarsonic acid was reported.[6] Based on the similarity of its spectral pattern to that of $[TeMo_6O_{24}]^{6-}$, the formula of the anion was concluded to be $[(C_6H_5As)_2Mo_6O_{24}]^{4-}$, which has one less oxygen than the present anion. Then the problem arose of whether these anions are really different anions or whether they are the same but have been considered to be different merely because of an erroneous interpretation of the experimental results. However, subsequent X-ray structural analysis of the analogous methyl derivative, $[(CH_3As)_2Mo_6O_{24}]^{4-}$, confirmed its formula and structure,[7] which is depicted in Fig. 2, and it was concluded that there are two kinds of heteropoly molybdate anions, both of which have a hetero part to the molybdenum atoms in the ratio 2:6, but which are different in the number of their oxygens. The $[(CH_3As)_2Mo_6O_{24}]^{4-}$ anion is synthesized at pH 4—5 and consists of six MoO_6 octahedra, all of which share

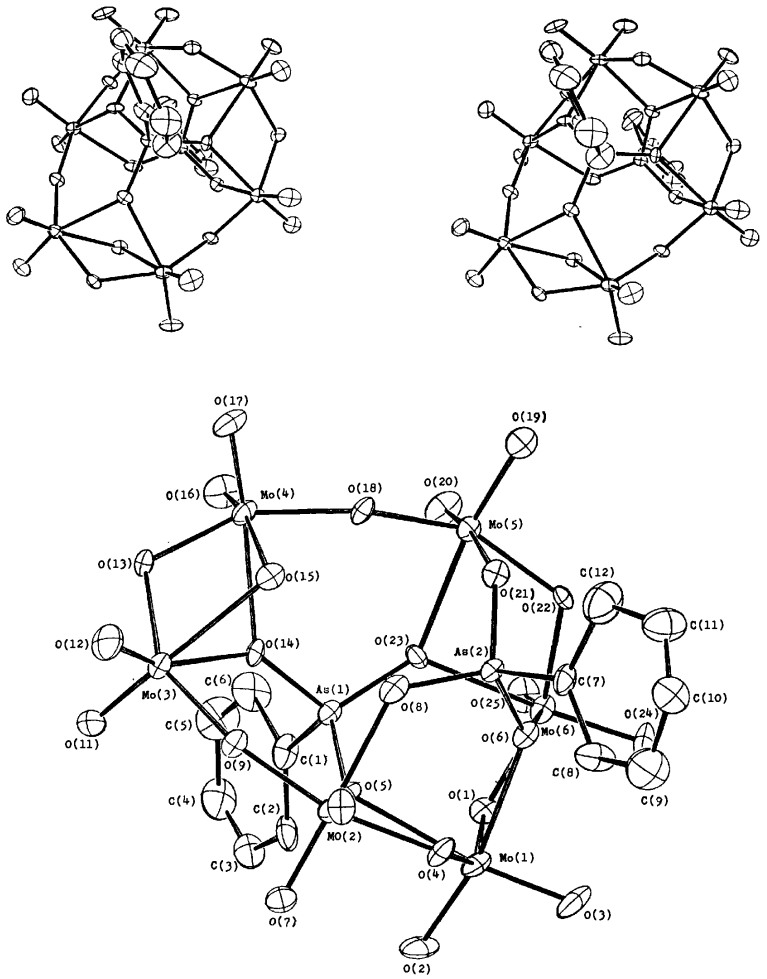

Fig. 1. Stereoscopic view of the $[(C_6H_5As)_2Mo_6O_{25}H_2]^{4-}$ anion, with the vibrational ellipsoids drawn at the 50% probability level (ORTEP, Johnson, 1971).

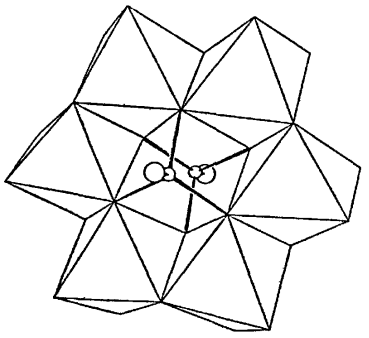

Fig. 2. The structure of the $[(CH_3As)_2Mo_6O_{24}]^{4-}$ anion. All the MoO_6 groups are expressed as octahedra.

edges to form a coplanar ring.

The crystal structure viewed along the b axis is shown in Fig. 3, while the interionic distances are listed in Table 5.

Parallel to the present work, Pope *et al.* have independently studied the same system, consisting of MoO_4^{2-} and $RAsO_3^{2-}$. However, the anions they obtained were $[(RAs)_2Mo_6O_{24}]^{4-}$ and $[(RAs)_4Mo_{12}O_{46}]^{4-}$ (R=CH_3, C_6H_5, and *p*-$NH_2C_6H_4$ for the former and R=CH_3, C_2H_4OH, C_6H_5, and *p*-$NH_2C_6H_4$ for the latter), whose structures have been clarified by the X-ray diffraction technique.[7,8] This system thus exhibits a complicated aspect, giving various heteropolyanions with different ratios of molybdenum to hetero parts depending on the pH of the solution. All these reactions are summarized below, including both the present work and that of Pope *et al.*:

(I) $RAsO_3^{2-} + 6MoO_3 + 6H_2O \xrightarrow{\text{pH 2}} [RAsMo_6O_{21}(H_2O)_6]^{2-}$ [1]

(II) $2RAsO_3^{2-} + 6MoO_3 + H_2O \xrightarrow{\text{pH 2}} [(RAs)_2Mo_6O_{25}H_2]^{4-}$

(III) $4RAsO_3^{2-} + 12MoO_3 + 4H^+ \xrightarrow{\text{pH 2}} [(RAs)_4Mo_{12}O_{46}]^{4-} + 2H_2O$ [8]

(IV) $2RAsO_3^{2-} + 6MoO_3 \xrightarrow{\text{pH 4.5}} [(RAs)_2Mo_6O_{24}]^{4-}$ [8]

Table 5. Interionic distances less than 3.1 Å, with their estimated standard deviations

O(1).....N(11)	2.788(28)
O(7).....N(7)	2.876(28)
O(7).....N(9)	3.028(30)
O(11).....H_2O(1)	3.022(27)
O(11).....N(9)	2.894(32)
O(12).....N(3)	2.968(38)
O(12).....N(1)	3.040(39)
O(13).....H_2O(1)	2.987(25)
O(13).....H_2O(4)	2.772(33)
O(15).....H_2O(2)	2.662(27)
O(17).....N(6)	2.907(27)
O(18).....N(6)	3.035(27)
O(21).....N(5)	3.035(27)
N(1).....H_2O(2)	2.933(34)
H_2O(2).....H_2O(3)	2.570(30)
H_2O(1).....N(1^{i})	2.877(37)
H_2O(1).....N(2^{i})	2.988(31)
H_2O(4).....H_2O(3^{i})	2.620(31)
N(8).....H_2O(3^{ii})	2.917(40)
N(9).....O(10^{ii})	3.045(28)
H_2O(1).....O(4^{ii})	3.034(23)
O(2).....H_2O(4^{iii})	2.909(26)
O(3).....N(4^{iii})	2.922(35)
N(11).....O(17^{iii})	2.867(26)
O(3).....H_2O(2^{iii})	3.034(23)
O(19).....N(2^{iv})	2.859(34)
O(22).....N(3^{iv})	2.873(26)
O(20).....N(5^{v})	2.878(27)
O(25).....N(4^{v})	2.988(28)
O(22).....N(10^{vi})	3.067(26)
O(24).....N(12^{vi})	2.922(26)

Symmetry code

i	$-x$,	$0.5+y$,	$1.0-z$
ii	$-x$,	$0.5+y$,	$-z$
iii	x,	y,	$-1.0+z$
iv	$1.0+x$,	y,	z
v	$-1.0-x$,	$0.5+y$,	$-1.0-z$
vi	$-1.0-x$,	$-0.5+y$,	$-z$

The (III) anion is of the same structural type as $[As_4Mo_{12}O_{50}H_4]^{4-}$, in which R groups are replaced

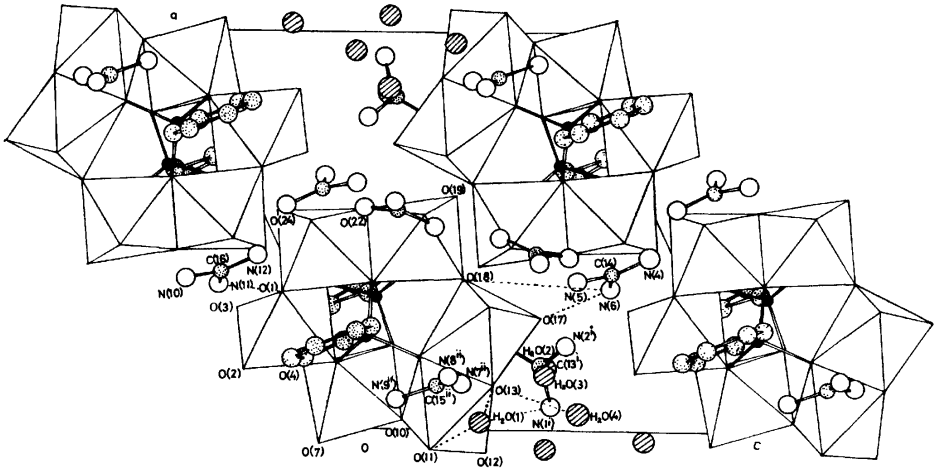

Fig. 3. The crystal structure of $(CN_3H_6)_4[(C_6H_5As)_2Mo_6O_{25}H_2]\cdot 4H_2O$ viewed along b axis.

by hydroxyl groups.[9] The (IV) anion is probably structurally analogous to $[As_2Mo_6O_{26}]^{6-}$.[10]

In such a system where two or more anions may be expected to exist in equilibrium with one another, it is of interest and important to know what species is formed and stable in which pH region and what equilibrium relations exist among them in the solution. Although the study attempting to clarify these points is still in progress and has not been completed, an interesting interconversion through dehydration and rehydration has been proved, with the aid of the Raman, IR, and 90 MHz ^{1}H FT-NMR spectra, to occur between the $[(C_6H_5As)_2Mo_6O_{25}H_2]^{4-}$ and $[(C_6H_5As)_2Mo_6O_{24}]^{4-}$ anions when the CD_3CN solution of $(n\text{-}Bu_4N)_4[(C_6H_5As)_2Mo_6O_{25}H_2]$ is kept at 90 °C and then cooled to room temperature, as is expressed in the following:[11]

$$[(C_6H_5As)_2Mo_6O_{25}H_2]^{4-} \xrightarrow[90^\circ C]{-H_2O} [(C_6H_5As)_2Mo_6O_{24}]^{4-}$$

$$\xrightarrow[r.t.]{H_2O} [(C_6H_5As)_2Mo_6O_{25}H_2]^{4-}$$

It can not said decisively what the two hydrogen atoms in the $[(C_6H_5As)_2Mo_6O_{25}H_2]^{4-}$ anion are bonded to. However, the above-mentioned interconversion caused by hydration and dehydration and the two anomalously long Mo–O bonds to O(15) (Mo(3)–O(15) is 2.393 Å and Mo(4)–O(15) is 2.478 Å; see Fig. 1 and Table 3) suggest that O(15) is a water molecule and is bridging Mo(3) and Mo(4).

The author wishes to express her thanks to Professor M. T. Pope of Georgetown University, who kindly sent her the IR data and some other helpful information on compounds related to those in the present work. The author is also indebted to Professor Yukiyoshi Sasaki of the University of Tokyo for his continual interest in the present work. Thanks are also due to Prefessor Hisao Kuroya and Dr. K. Matsumoto of Osaka City University for the use of a Philips automatic diffractometer.

References

1) K. Y. Matsumoto, *Bull. Chem. Soc. Jpn.*, to be published.
2) A. Rosenheim and R. Bilecki, *Chem. Ber.*, **4**, 543 (1913).
3) "International Tables for X-Ray Crystallography," Kynoch Press, Vol. IV, Birmingham (1974).
4) D. T. Cromer, *Acta Crystallogr.*, **18**, 17 (1965).
5) K. Nakatsu, *Bull. Chem. Soc. Jpn.*, **34**, 639 (1961).
6) M. Filowitz and W. G. Klemperer, *J. Chem. Soc., Chem. Commun.*, **1976**, 233.
7) W. Kwak, L. M. Rajkovic, J. K. Stalik, M. T. Pope, and C. O. Quicksall, *Inorg. Chem.*, **15**, 2778 (1976).
8) M. T. Pope, C. O. Quicksall, W. Kwak, L. M. Rajkovic, J. K. Stalik, K. M. Barkigia, and T. F. Scully, 2nd International Conference on the Chemistry and Use of Molybdenum, Oxford (1976).
9) H. Nishikawa, A. Kobayashi, and Y. Sasaki, *Chem. Lett.*, **1975**, 1185.
10) Y. Sasaki and K. Y. Matsumoto, *Kagaku No Ryoiki*, **29**, 853 (1975).
11) M. T. Pope, private communication.

1-Allylpyrazole as a Ligand. V.*) Preparation and Characterization of Some Iron(0) and Group VI Metal(0) Carbonyls

Kazuo FUKUSHIMA, Takeshi MIYAMOTO, and Yukiyoshi SASAKI

Department of Chemistry, Faculty of Science, The University of Tokyo, Hongo, Tokyo 113

(Received August 25, 1977)

The 1-allylpyrazole complexes of the general formula $Fe(CO)_3L$ (L=substituted 1-allylpyrazoles) have been prepared by the photochemical reaction of $Fe(CO)_5$ in the presence of 1-allylpyrazoles, and characterized by the IR, ^1H-, and ^{13}C-NMR spectroscopies. These complexes show a large decrease of ν(C=C) frequency and ^1H- and ^{13}C-NMR upfield shifts of the olefinic nuclei compared with free ligands. The upfield shifts of olefinic ^1H-NMR spectra are not influenced by the substituent groups on the pyrazole ring, but, so far as the terminal olefinic protons are concerned, the shifts are distinctively decreased on replacement of the allyl by the 2-methylallyl group. The upfield shifts of ^{13}C-NMR spectra substantially parallel those of ^1H-NMR spectra in these complexes. On refluxing $Fe(CO)_3L$ in a hexane solution containing PPh_3, the complex liberates 1-allylpyrazole to give *trans*-$Fe(CO)_3(PPh_3)_2$ in a small yield. Some new complexes of general formula $M(CO)_4L$ (M=Cr, Mo, or W, L= 1-allylpyrazole) have also been prepared for comparison.

In order to rationalize the metal-olefin bond, Dewar, Chatt and Duncanson had postulated a model,[1] which emphasized the dual bonding nature, that is, olefin→metal σ-donation and metal→olefin π-back donation. The properties of some metal–olefin complexes have been well explicated by this model. However, many types of the olefin complexes are now accumulating, and in order to elucidate the particular bonding nature in each type of the complexes, it is important to study systematically closely related complexes.

In previous reports,[2–5] we have already prepared and characterized a large number of the 1-allylpyrazole–transition metal complexes. Thus successful preparation of these chelating-olefin complexes has so far enabled us to obtain much information concerning the particular bonding nature in each metal complex. We have now extended our study to a series of iron(0) complexes $Fe(CO)_3L$ (L=substituted 1-allylpyrazole), and spectroscopically characterized these complexes. Spectroscopic data on the isolated iron complexes are compared with those of other olefin–transition metal complexes. The effects of pyrazole substituents upon the metal–olefin and metal–carbonyl bonds are also discussed on the basis of IR and NMR data.

Experimental

All manipulations were carried out under a nitrogen atmosphere. The solvents were dried over sodium wire or lithium aluminium hydride and were distilled just before use. Metal carbonyls (Strem Chemicals or Pressure Chemicals Co.,) were used without further purification.

The IR and ^1H-NMR spectra were recorded as described previously.[5] The ^{13}C-NMR spectra were recorded on a JEOL-PET-100 Fourier Transform Spectrometer operating at 25.2 MHz with proton noise decoupling. In order to make the assignment clear, some ^{13}C-NMR spectra were obtained without decoupling. Chemical shifts were referred to the internal standard of TMS. Samples were dissolved in $CDCl_3$ as much as possible (about 20 wt%) and sealed up under an argon atmosphere.

Ligands. The ligands were synthesized from the reaction of pyrazole derivatives with allyl halide or 2-methylallyl halide. The vigorous stirring throughout the reaction generally gave a high yield of product. The boiling points and yields of ligands are summarized in Table 1.

Table 1. List of the 1-allylpyrazoles

Abbreviation[a)]	Bp (°C/mmHg)	Yield (%)
ap	90—100/100	66
admp	90—100/30	35
amdmp	55—62 /0.2	35
atmp	85—86 /12	48
amtmp	99—103/12—14	43
admpBr	106—107/14	57
amdmpBr	118—125/14	70
admpNO_2	150—151/12	63

a) ap=1-allylpyrazole, admp=1-allyl-3,5-dimethylpyrazole, amdmp=1-(2-methylallyl)-3,5-dimethylpyrazole, atmp=1-allyl-3,4,5-trimethylpyrazole, amtmp=1-(2-methylallyl)-3,4,5-trimethylpyrazole, admpBr=1-allyl-4-bromo-3,5-dimethylpyrazole, amdmBr=1-(2-methylallyl)-4-bromo-3,5-dimethylpyrazole, amdmpNO_2=1-allyl-3,5-dimethyl-4-nitropyrazole.

Group VI Metal Complexes, $M(CO)_4(ap)$ (M=Cr, Mo, or W, ap=1-allylpyrazole). The group VI metal complexes $M(CO)_4$(ap) were prepared as described already.[5] They were sparingly soluble in hexane and were recrystallized from diethyl ether–hexane.

Tricarbonyl-1-allylpyrazoleiron(0), $Fe(CO)_3(C_6H_8N_2)$. The iron complexes were obtained in a similar manner to the group VI metal complexes. A tetrahydrofuran solution (300 ml) containing both pentacarbonyliron(0) (2.0 g, 0.01 mol) and allylpyrazole (1.1 g. 0.01 mol) was irradiated with a mercury lamp (400 W). The flask(Riko, UVL-400 HA) was equipped with a gas buret to follow the course of the reaction. In 3—4 h, the reaction was completed showing the stoichiometric evolution of CO. The amber-colored solution was evacuated to dryness and the resulting residue was completely extracted with hexane(100 ml) at room temperature. The hexane solution was filtered and condensed to half a volume *in vacuo*. On cooling the solution at −78 °C, yellow fine crystals were deposited in a yield of 80%(2.0 g). The product was purified by the repeated recrystallization from hexane.

Similarly the iron(0) complexes containing substituted 1-allylpyrazole were prepared as listed in Table 2. The complexes are soluble in most organic solvents usually used. In

* Part IV, see Ref. 5.

a crystalline form, they are fairly air-stable, but in a solution they are rapidly decomposed by contact with air.

No solid product was obtained in the reaction of $Fe(CO)_5$ with 1-allyl-3,5-dimethyl-4-nitropyrazole, in spite of the excessive generation of CO gas.

Reaction of $Fe(CO)_3$(ap) with PPh_3. A hexane solution containing $Fe(CO)_3$(ap)(0.3 g, 1.2 mmol) and triphenylphosphine (1.2 g, 4.6 mmol) was refluxed for 5 h. On standing, yellow crystals are formed to give a yield of 0.3 g. The product was identified to be *trans*-$Fe(CO)_3(PPh_3)_2$ by IR and elemental analysis. IR data in $CHCl_3$: 1886(s) [lit,[6] 1887 (s)] cm^{-1}.

Results and Discussion

King and coworkers[7] isolated the complexes $Fe(CO)_3$(ap) and $Fe(CO)_3$(admp) (ap=1-allylpyrazole, admp=1-allyl-3,5-dimethylpyrazole), firstly as by-product of the reaction of (π-allyl)$Fe(CO)_3I$ with potassium monohydridotris(1-pyrazolyl)borate or potassium monohydridotris(3,5-dimethylpyrazolyl)borate, and subsequently as main products of the thermal reaction of $Fe_2(CO)_9$ with the ligands (ap or admp). However, those iron complexes were not fully characterized. In our experiment, the iron complexes have been synthesized quite smoothly by the photochemical reactions of $Fe(CO)_5$ with the 1-allylpyrazole ligands, in the same way as the group VI metal carbonyl complexes.[5]

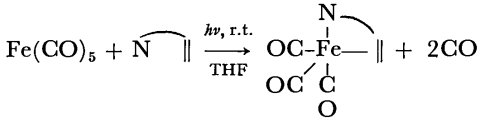

^{1}H-NMR and IR Spectra. Although a great number of iron-olefin complexes have so far been prepared,[8] the infrared spectrum, which is one of the most important criteria of the metal–olefin bond, have been curiously ignored in literatures. The IR band ν(C=C) for the iron complexes $Fe(CO)_3L$ (L=1-allylpyrazole) was tentatively assignable in comparison with the spectra of the chromium(0) analogues $Cr(CO)_4L$ in the region of 1400—1600 cm^{-1}. The lowered shifts $\Delta\nu$(C=C) for the iron complexes were determined to be *ca.* 180 cm^{-1}. This abnormally large shift of ν(C=C) well agreed with the large NMR upfield shifts of the olefinic

Table 2. Elemental analyses and (CO) frequencies

	C	H	N	Mp (°C)	(CO) (cm^{-1})[a]
$Cr(CO)_4$(ap)[b]	44.14(44.13)	3.12(2.96)	10.21(10.29)	97—99	2029, 1950, 1931, 1895
$Mo(CO)_4$(ap)	38.03(37.99)	2.76(2.55)	9.16(8.86)	95—98	2039, 1952, 1939, 1896
$W(CO)_4$(ap)	29.99(29.73)	2.22(2.00)	7.21(6.93)	116—119	2038, 1948, 1935, 1894
$Fe(CO)_3$(ap)	43.84(43.58)	3.38(3.25)	11.65(11.30)	65—66	2039, 1964, 1956
$Fe(CO)_3$(admp)	47.96(47.86)	4.50(4.38)	10.26(10.15)	60—61	2035, 1961, 1950
$Fe(CO)_3$(amdmp)	49.88(49.68)	4.89(4.86)	9.33(9.66)	53—54	2031, 1957, 1948
$Fe(CO)_3$(atmp)	49.93(49.68)	4.54(4.86)	9.78(9.66)	105—106	2032, 1960, 1949
$Fe(CO)_3$(amtmp)	51.67(51.34)	5.49(5.30)	9.12(9.21)	35	2030, 1956, 1947
$Fe(CO)_3$(admpBr)	37.03(37.22)	2.83(3.12)	7.64(7.89)	115—118	2036, 1963, 1954
$Fe(CO)_3$(amdmpBr)	38.88(39.06)	3.70(3.55)	7.30(7.59)	83—85	2033, 1960, 1951

a) Hexane solution. b) Abbreviations are shown in Table 1.

Table 3. ^{1}H-NMR Chemical shifts of the olefinic protons (in ppm)

	$H_f(\Delta H_f)$[a]	$H_g(\Delta H_g)$	$H_h(\Delta H_h)$	$\lvert J_{fg}\rvert$	$\lvert J_{fh}\rvert$	Solv.
ap	5.97	5.18	5.11	10	17	$CDCl_3$
$Cr(CO)_4$(ap)	4.71(−1.26)	3.25(−1.93)	2.74(−2.37)	9	12	CS_2
$Mo(CO)_4$(ap)	4.96(−1.01)	3.51(−1.67)	3.29(−1.82)	9	13	CS_2
$W(CO)_4$(ap)	b)	3.27(−1.91)	2.74(−2.37)	9	12	CS_2
$Fe(CO)_3$(ap)	3.69(−2.28)	2.17(−3.01)	1.27(−3.84)	8	10	CS_2
admpBr	5.96	5.27	5.08	10	18	$CDCl_3$
$Fe(CO)_3$(admpBr)	3.72(−2.24)	2.11(−3.16)	1.28(−3.80)	b)	11	CS_2
admp	5.80	5.01	4.82	10	17	$CDCl_3$
$Fe(CO)_3$(admp)	3.76(−2.04)	2.15(−2.86)	1.31(−3.51)	b)	10.5	CS_2
atmp	5.81	5.03	4.85	10	17	$CDCl_3$
$Fe(CO)_3$(atmp)	3.70(−2.11)	2.07(−2.96)	1.27(−3.58)	7	10	CS_2
amdmpBr	—	4.82	4.49	—	—	$CDCl_3$
$Fe(CO)_3$(amdmpBr)	—	2.18(−2.64)	1.42(−3.07)	—	—	CS_2
amdmp	—	4.80	4.48	—	—	$CDCl_3$
$Fe(CO)_3$(amdmp)	—	2.18(−2.62)	1.44(−3.04)	—	—	CS_2
amtmp	—	4.73	4.49	—	—	$CDCl_3$
$Fe(CO)_3$(amtm)	—	2.14(−2.59)	1.41(−3.08)	—	—	CS_2

a) The symbol ΔH represents the difference in chemical shifts between a proton in an iron complex and one in a free ligand. b) Not measurable by overlapping.

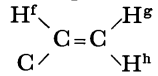

Table 4. ^{13}C-NMR data of some 1-allylpyrazole (ap) complexes
(Solvent; $CDCl_3$, in δ_{ppm} from TMS)

Compound	Ring[a]			Allyl[a]			Carbonyl	$\Delta\nu$(C=C)[b] (cm^{-1})
	C^1	C^2	C^3	C^4	C^5	C^6		
Free ligand	138.7 (184.3)	105.2 (175.8)	128.5 (185.6)	54.1 (138.4)	132.7 (162.3)	117.7 (153.4)		—
$Cr(CO)_4$(ap)	142.6 (185.5)	107.7 (179.9)	130.8 (186.8)	52.0 (142.9)	77.4 (168.5)	64.2 (167.4)	230.7, 224.3, 223.6, 223.5	131
$Mo(CO)_4$(ap)	143.3	107.4	131.0	53.0	81.2	67.2	218.6, 217.9, 210.3, 209.6	119
$W(CO)_4$(ap)	143.3	107.8	130.9	52.3	69.7	56.1	212.8, 208.6, 204.0, 203.0	138
Fe(CO)(ap)	142.0 (189.7)	108.2 (180.5)	130.3 (189.5)	55.0 (137.7)	48.3 (160.6)	36.0 (158.1)	213.1	189

a) $|J_{C-H}|$ in parentheses.
b) Lowered shifts of ν(C=C) measured in KBr disks.

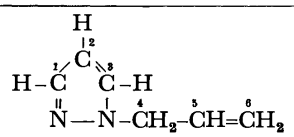

protons. The observed value $\Delta\nu$(C=C) of about 180 cm^{-1}, as well as the value of the upfield shifts $\Delta\delta$H of 2.2—3.8 ppm were much larger than those of the chromium(0) complexes ($\Delta\nu$(C=C): 120 cm^{-1}, $\Delta\delta$H: 1.0—2.4 ppm). Tolman and coworkers[9] tabulated the spectroscopic data on the many ethylene–transition metal complexes. According to the table, it can be clearly shown that the iron(0)-olefin interaction is classified as the largest, and the chromium(0)-olefin one as the medium.

Through a series of the iron complexes, $Fe(CO)_3L$, the increase of the methyl sibstituents on the pyrazole ring caused a substantial decrease of the ν(C=O) frequencies as shown in Table 2, but did not give significant changes in the final chemical shifts for the olefinic protons (Table 3), regardless of the fairly different chemical shifts of the free ligands. These results indicate that the metal-olefin bond in these iron complexes has a lower sensitivity towards the methyl substitution on the pyrazole ring, compared with the metal-carbonyl bond. The increase in the σ-donor ability of the *N*-coordinating site owing to the methyl substituents seems to promote the π-delocalization to the carbonyl moiety, but not to the olefinic group.

^{13}C-NMR Spectra. The ^{13}C-NMR spectral data for the four 1-allylpyrazole (ap) complexes are listed in Table 4 together with the shift data of the stretching frequencies of ν(C=C). The shift difference between the two olefinic carbons decreased as a result of coordination of the olefinic part in ap, compared with free ap; such a case had already been reported by Brown.[10] The ^{13}C-NMR spectra due to the olefinic carbons as a whole shifted towards a higher magnetic field from the position of the free ligands as described in the case of ^{1}H-NMR spectra. Though ^{13}C-NMR spectral data of other group VI metal–olefin complexes are not available, the observation that the ^{13}C-NMR chemical shift of the $M(CO)_4L$, where M=Cr, W, and L=ap move upfield when chromium is replaced by tungsten may be consistent with the stronger olefin–metal bond present in the tungsten complex.

While each group VI metal carbonyl complexes showed the four carbonyl carbon resonances, only one signal was found for three unequivalent carbonyls of the iron complex. As has been reported in detail by several workers,[11] it indicates the high fluctionality of the iron carbonyl complexes. The carbonyl carbon resonance for the group VI metal complexes have the following order of deshielding as: Cr>Mo>W. This is the same order as that observed in the parent hexacarbonyls $M(CO)_6$ and a series of pentacarbonyl complexes, $M(CO)_5L$ (M=Cr, Mo, or W, L=a unidentate ligand).[12]

Displacement Reaction of the Coordinated Ligand. The great tendency to the displacement of the coordinated *N*-allylpyrazole by the strong donor ligands has been the most remarkable feature for the Pt(II), Cr(0), and Mo(0) complexes.[3,5] The iron(0) complex $Fe(CO)_3L$, however, did not react with PPh_3 under mild conditions. Only after refluxing both reagents in a hexane solution for several hours, the complex, *trans*-$Fe(CO)_3(PPh_3)_2$ was obtained in a low yield. The lability of the coordinated ap ligand in the iron complex is obviously lower than that in the chromium complex $Cr(CO)_4$(ap).

Metal–Olefin Bond Strength. The correlation between the NMR upfield shifts and the metal-olefin bond nature has not been confirmed yet.[13] One research group attributed it to the paramagnetic shielding effect induced by the non-bonding partially filled d-orbitals,[14] while the other group to the magnitude of the π-bond order due to the π-back donation.[15] Our results support the latter one, since so far as iron(0) and the group VI metals(0) concerned, the large NMR upfield shifts were always accompanied by the larger decrease in the ν(C=C) frequencies and the lower activity of the displacement of the coordinated olefinic ligand, *i.e.*, in the order of Fe>W>Cr>Mo. This result that iron(0) is more strongly bonded to the olefin than chromium(0) by the larger π-back bonding will support Hoffmann's MO calculations of the metal carbonyl fragments.[16]

The authors gratefully acknowledge Dr. Hideomi Koinuma, the University of Tokyo for ^{13}C-NMR measurements.

References

1) M. J. S. Dewar, *Bull. Soc. Chim. Fr.*, **1951**, C79; J. Chatt and L. A. Duncanson, *J. Chem. Soc.*, **1955**, 293.

2) K. Fukushima, T. Miyamoto, and Y. Sasaki, *Inorg. Chim. Acta*, **15**, 105 (1975).
3) T. Miyamoto, K. Fukushima, T. Saito, and Y. Sasaki, *Bull. Chem. Soc. Jpn.*, **49**, 138 (1976).
4) K. Fukushima, T. Miyamoto, and Y. Sasaki, *Bull. Chem. Soc. Jpn.*, **49**, 143 (1976).
5) K. Fukushima, T. Miyamoto, and Y. Sasaki, *J. Organomet. Chem.*, **107**, 265 (1976).
6) F. A. Cotton and R. V. Parish, *J. Chem. Soc.*, **1960**, 1440.
7) R. B. King and A. Bond, *J. Am. Chem. Soc.*, **96**, 1343 (1974).
8) H. W. Quinn and J. H. Tsai, *Adv. Inorg. Radiochem.*, **12**, 217 (1769).
9) C. A. Tolman, A. D. English, and L. E. Manzer, *Inorg. Chem.*, **14**, 2353 (1975).
10) K. R. Aris, V. Aris, and J. M. Brown, *J. Organomet. Chem.*, **42**, C67 (1972).
11) L. Kruczuski and J. Takats, *J. Chem. Soc.*, **96**, 932 (1974); G. R. Langford, M. Akhtar, P. D. Ellis, A. G. MacDiarmid, and J. D. Odom, *Inorg. Chem.*, **14**, 2937 (1975).
12) L. J. Todd and J. R. Wilkinson, *J. Organomet. Chem.*, **77**, 1 (1974).
13) J. Evans and J. R. Norton, *Inorg. Chem.*, **13**, 3042 (1974).
14) D. Cooper, R. P. Hughes, and J. Powell, *J. Am. Chem. Soc.*, **94**, 9244 (1972).
15) M. H. Chisholm, H. C. Clark, L. E. Manzer, and J. B. Stothers, *J. Am. Chem. Soc.*, **94**, 5087 (1972).
16) M. Elian and R. Hoffmann, *Inorg. Chem.*, **14**, 1058 (1975).

Stereoselective Substitution of *trans*-2-Butene for the *S,S*-2-Butene in Trichloro-*S,S*-2-buteneplatinate(II) in Acetone

Yoshiro TERAI and Kazuo SAITO

Department of Chemistry, Faculty of Science, Tohoku University, Aoba, Aramaki, Sendai 980

(Received September 1, 1977)

A new complex salt $[Ph_4P][PtCl_3(S,S\text{-tbn}[1,3\text{-}^3H])]$ (tbn, *trans*-2-butene) undergoes racemization and ligand isotopic exchange in acetone containing a large excess of tbn without side reactions. Both rates are expressed by the second order rate equations, $R_{(CD)}=k_{2(CD)}[Pt][tbn]$ and $R_{(IE)}=k_{2(IE)}[Pt][tbn]$, the k_2 values being 17.6 and $70.6\times10^{-3}M^{-1}s^{-1}$ at 8.0 °C, respectively (M=mol dm^{-3}). Individual k_2 values for the substitutions without and with inversion of configuration of coordinated tbn are calculated to be 62.0 and $8.7\times10^{-3}M^{-1}s^{-1}$, respectively, the corresponding $\Delta H^{\ddagger}$ and $\Delta S^{\ddagger}$ values being 36.3 ± 3.1 and 37.6 ± 2.7 kJ mol^{-1}, and -138 ± 12 and -149 ± 10 J·mol^{-1} K^{-1}. Source of the stereoselectivity appears to consist in the difference in ease of formation of square pyramidal transition state on the nucleophilic attack of tbn upon the complex.

In a previous paper we have reported the kinetics of ligand isotopic exchange and epimerization of *trans*(*N*, olefin)[PtCl(L-pro)(*S,S*-2-butene)] in acetone in the presence of an excess of *trans*-2-butene (tbn), and found that the coordinated *S,S*-2-butene is replaced by tbn faster with retention than with inversion of configuration by *ca.* 10 times.[1] The substrate complex has two asymmetric sources, the L-prolinate (with two asymmetric centers, the carbon and the coordinated nitrogen) and the *S,S*-2-butene. In order to find the origin of the stereoselectivity, complexes having only one source of asymmetry should be needed. We have found that *trans*(*N*,olefin)[PtCl(L-pro)(*S,S*-2-butene[1,3-^3H])] gives $[PtCl_3(S,S\text{-2-butene}[1,3\text{-}^3H])]^-$ in 6 M hydrochloric acid and crystallizs as tetraphenylphosphonium salt with retention of configuration. This salt enabled us to carry out kinetic studies of the isotopic exchange and racemization in acetone.

Experimental

Materials. Tetraphenylphosphonium trichloro-*S,S*-2-butene[1,3-^3H]platinate(II) was prepared by treating optically active [PtCl(L-pro)(*S,S*-2-butene[1,3-^3H])] (0.2 g, $\Delta\varepsilon$ at 27000 cm^{-1} 1.05) with 6 M hydrochloroic acid (4 cm^3) and tetraphenylphosphonium chloride (0.23 g) for 1 h at room temperature, and cooling in a refrigerator. The precipitated product was filtered off, air dried, and recrystallized from acetone by adding petroleum ether. Yield 0.3 g (85% on platinum). The specific activity was *ca.* 2×10^4 d.p.m. per mg, and $\Delta\varepsilon$ at 23800 cm^{-1} *ca.* 0.7. The purity was examined by the ultraviolet (UV) absorption spectrum. The elemental analysis of carbon and hydrogen was carried out by use of a similarly prepared non-radioactive sample. Found: C, 48.22; H, 4.04%, Calcd C, 48.25; H, 4.05%.

trans-2-Butene of research grade (>99.3%) from Nippon Tokushu Gas Co. was used without further purification. Acetone and acetonitrile were purified by the usual method.

Kinetic Runs. *trans*-2-Butene boils at 0.88 °C under atmosphere and the solutions for kinetic studies should be prepared carefully as follows. *trans*-2-Butene chilled in a mixture of Dry Ice and acetone (0.1 to 2 g) was swiftly added into a stoppered Erlenmeyer flask containing a known amount (30 to 40 cm^3) of acetone, weighed, and preserved in a mixture of Dry Ice and acetone. The complex solution (to produce *ca.* 5 cm^3 of 10^{-4} to 10^{-3} M) was added to 6 to 10 small test tubes kept in a mixture of Dry Ice and acetone, and the tbn solution was added to each tube by use of a pipette wrapped with powdered Dry Ice. The tubes were stoppered and kept in a thermostat at −30 to +8 °C. They were withdrawn at appropriate intervals, placed in a liquid nitrogen bath, and tbn and the solvent evaporated off in a vacuum line at Dry Ice and room temperature, respectively. The residue consisting of pure complex was dissolved in acetonitrile (5 ml), and the UV absorption and CD spectra were recorded. A 1 ml portion of the AN solution was mixed with the liquid scintillation medium (0.108 mg of *p*-bis(5-phenyl-2-oxazolyl)benzene and 4.29 g of terphenyl per 1 dm^3; 14 cm^3) and submitted to the counting of the β-rays. The density of tbn solution in acetone differs significantly at reaction and Dry Ice–acetone temperatures, and due correction was made.

The experimental results of racemization and isotopic exchange were calculated in accordance with the first order kinetic law and the McKay formula, respectively.

Measurements. The UV absorption and CD spectra were recorded with a Hitachi 323 Spectrophotometer, and JASCO J-40 Spectrometer, respectively. The radioactivity was recorded with a Liquid Scintillation Spectrometer from Nuclear Chicago. The electrolytic conductivity was measured with a Conductoscope from Metrohm Co.

Results and Discussion

Synthesis and Spectra. The UV absorption curve (Fig. 1) is very similar to that of Zeise's salt,[2] and remains unchanged for many hours both in the absence and the presence of an excess of tbn in many kinds of solvent. Konya *et al.* gave the CD spectrum of $(+)^{\Delta\varepsilon}_{330}$-*trans*(*N*,olefin)[PtCl(L-pro)(*S,S*-2-butene)] in concentrated hydrochloric acid, and considered that the pattern represented the CD of $[PtCl_3(S,S\text{-butene})]^-$.[3] The CD curve in Fig. 1 is very similar to theirs, and the small difference may be due to the difference in solvent, and to the presence of free L-proline in their solution, which can give outer-sphere perturbation. Since the tetraphenylphosphonium salt of this complex is sparingly soluble in hydrochloric acid, the pure salt must have been precipitated as shown in the Experimental part.

This salt is insoluble in water and methanol, rather readily soluble (to give 0.1 M solution) in acetone, acetonitrile (AN), *N,N*-dimethylformamide (DMF), and dichloromethane, and dissolves in dimethyl sulfoxide with gradual decomposition. The CD pattern changes very slowly in acetone, AN, and DMF. The apparent first order rate constant of the spontaneous racemization

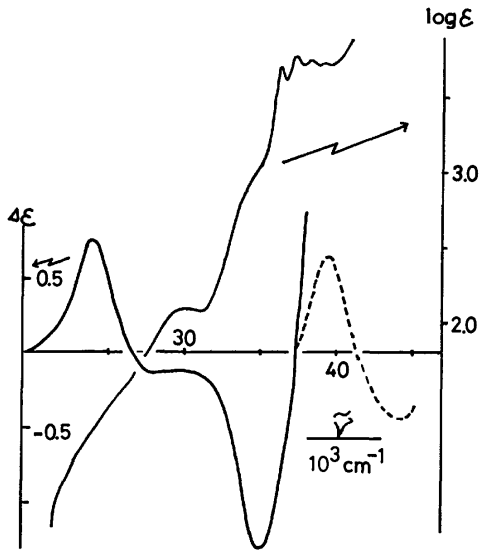

Fig. 1. Ultraviolet (UV) absorption and circular dichroism (CD) spectra of $[(C_6H_5)_4P][PtCl_3(S,S\text{-2-butene})]$ in acetonitrile (AN) at room temperature.

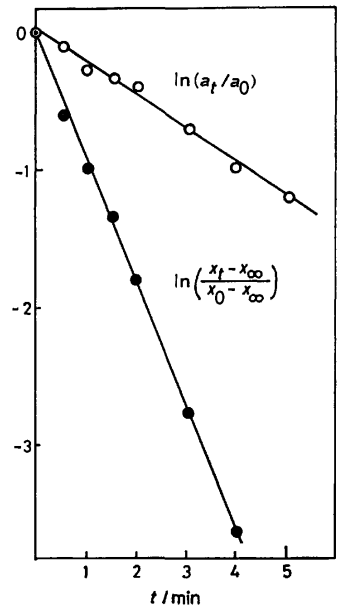

Fig. 2. The first order kinetic plots of the racemization (○) and isotopic exchange (●) of $[PtCl_3(S,S\text{-2-butene-}[^3H])]^-$ in acetone at 8.0 °C. [Complex], 8.61×10^{-4} M, [tbn], 0.218 M

is $<3\times10^{-6}$ s^{-1} at 15 °C in acetone. Addition of water, acetic acid and alcohols enhanced whilst that of chloride retarded the spontaneous racemization. However, under the present experimental conditions, such a CD change can be ignored. Molar conductivity measurement in acetone gave a straight line on the plot *vs.* square root of concentration of this salt for $<1\times10^{-3}$ M. The degree of electrolytic dissociation of a 0.9×10^{-3} M solution (almost equal to the concentration at which the kinetic studies were made) was 0.91 at 8.0 °C.

Kinetic Data. The absorption spectrum of the reaction mixtures was equal to that of the complex and remained unchanged during the course of the kinetic runs. The kinetic measurements were made in the concentration ranges, [complex]=0.0005 to 0.003 M and [*trans*-2-butene]=0.02 to 1.15 M (40 to 1500 times excess to the complex). The CD strength at 23800 cm^{-1} decreased with time to reach zero at infinite time, and the diagram $\ln(a_t/a_0)$ *vs.* t was straight as shown in Fig. 2. (a_t and a_0 stand for the CD strengths at time t and zero, respectively). The observed first order rate constant $k_{o(CD)}$ increased linearly with increase in free tbn concentration, and it did not change on addition of tetraphenylphosphonium chloride (Fig. 3). The decrease in specific β-activity of the recovered complex also decreased in accordance with first order rate law as shown in Fig. 2, where x's denote the specific counting rate at the times indicated by the subscripts. McKay's R was proportional to the concentration of the complex, and the observed first order rate constant $k_{o(IE)}$ increased linearly with increase in concentration of the free tbn as shown in Fig. 3.

Thus the rate constants obtained by both CD and β-activity measurement can be written as Eqs. 1 and 2.

$$k_{o(CD)} = k_{2(CD)}[tbn] \quad (1)$$

$$k_{o(IE)} = k_{2(IE)}[tbn] \quad (2)$$

The k_2 values are shown in Table 1.

The linear diagrams in Fig. 3 give no intercept. The spontaneous racemization was very slow, and the racemization must proceed exclusively *via* a bimolecular mechanism. When the individual second order rate constants of the substitution reaction with retention and inversion of configuration are written as $k_{2[SS]}$ and $k_{2[SR]}$, they are related to the observed k_2's by Eqs. 3 and 4.

$$k_{2(CD)} = 2k_{2[SR]} \quad (3)$$

$$k_{2(IE)} = k_{2[SR]} + k_{2[SS]} \quad (4)$$

TABLE 1. SECOND ORDER RATE CONSTANTS AND ACTIVATION PARAMETERS FOR THE SUBSTITUTION OF *trans*-2-BUTENE FOR $[PtCl_3(S,S\text{-}trans\text{-2-BUTENE}[1,3\text{-}^3H])]^-$ IN ACETONE

Temp / °C	$k_{2(CD)}$ / 10^{-3} M^{-1} s^{-1}	$k_{2(IE)}$ / 10^{-3} M^{-1} s^{-1}	$k_{2[SS]}$ / 10^{-3} M^{-1} s^{-1}	$k_{2[SR]}$ / 10^{-3} M^{-1} s^{-1}	$k_{2[SS]}/k_{2[SR]}$
8.0	17.3	70.6	62.0	8.7	7.2
−5.0	6.74	35.1	31.7	3.4	9.3
−20.0	2.65	11.4	10.1	1.3	7.8
ΔH^* / kJ mol^{-1}			36.3±3.1	37.6±2.7	
ΔS^* / J mol^{-1} K^{-1}			−138±12	−149±10	

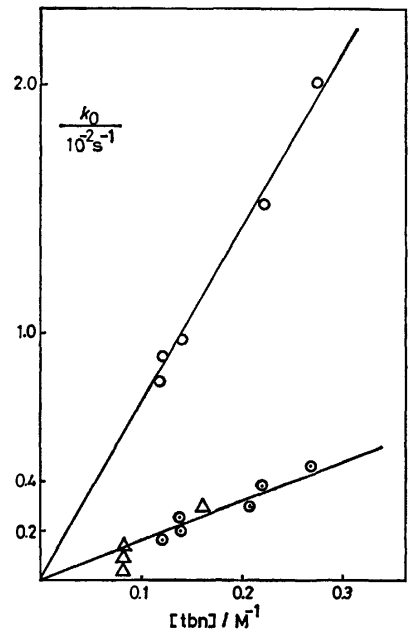

Fig. 3. Dependence of the observed first order rate constants of the racemization (○) and isotopic exchange (●) of $[PtCl_3(S,S\text{-2-butene}[^3H])]^-$ upon the concentration of free tbn in acetone at 8 °C. (△0.0034 M Ph_4PCl added.)

On the basis of the observed k_2's, $k_{2[SR]}$, and $k_{2[SS]}$ were calculated as shown in Table 1. The activation parameters are also included in the same table.

Dynamic Stereoselectivity. The ratio $k_{2[SS]}/k_{2[SR]}$ is *ca.* 8 in the present temperature range. The activation parameters involve rather large experimental errors, but the difference in k_2's must consist in the ΔS^* term. It is generally believed that the substitution of such square planar complexes proceed *via* S_N2 mechanism, and the ease of nucleophilic attack by the incoming ligand is the rate-determining step. The two kinds of substitution with retention and inversion of configuration should have very similar transition states and the approach of tbn resulting in retention of configuration must be slightly easier than that resulting in inversion. Such a difference must be of a steric origin, and very naturally reflected in the ΔS^* rather than in the ΔH^* value.

So far as the substitution reaction proceeds *via* an associative mechanism, the transition state should be either a trigonal bipyramid or a square pyramid. Some

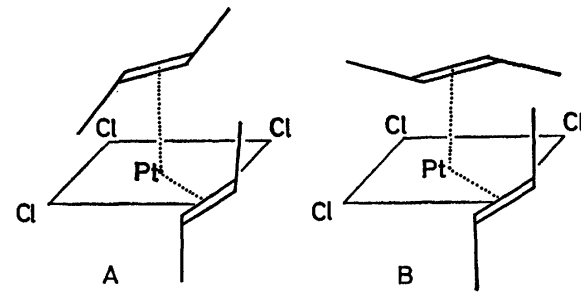

Fig. 4. Plausible transition state on the nucleophilic attack of tbn upon $[PtCl_3(S,S\text{-2-butene})]^-$.

trigonal bipyramidal complexes have been isolated as crystals (*e.g.* $[PtCl_2(C_2H_4)(phen)]$[4] and $[Ir^ICl(C_2H_4)_4]$[5]), and π-accepting ligands are claimed to stabilize trigonal bipyramidal structure.[6] Hence the present substitution reaction may have a square pyramidal transition state (Fig. 4), which undergoes internal rearrangement to give a trigonal bipyramidal intermediate. Even a simple molecular model study discloses that the approach of tbn as shown in Fig. 4A involves less steric hindrance than that as shown in Fig. 4B. The stereoselctivity of the present substitution is slightly smaller than that in the substitution of tbn for *trans*(*N*, olefin)[PtCl(L-pro)(*S,S*-2-butene)], but very near to it. Similar difference to that shown in Fig. 4 may be encountered in the substitution of the L-prolinato complex, and we can conclude that the main source of selectivity in this complex should be in the asymmetrically coordinated *trans*-2-butene.

The authors thank the finantial support given by Takeda Science Foundation.

References

1) Y. Terai, H. Kido, J. Fujita, and K. Saito, *Bull. Chem. Soc. Jpn.*, **48**, 1233 (1975).
2) R. G. Denning, F. R. Hartley, and L. M. Venanzi, *J. Chem. Soc., A*, **1969** 1322.
3) K. Konya, J. Fujita, and K. Nakamoto, *Inorg. Chem.*, **10**, 1699 (1971).
4) L. Maresca, G. Natile, and L. Cattalini, *Inorg. Chim. Acta*, **14**, 79 (1965).
5) A. L. Onderdelinden and A. van der Ent, *Inorg. Chim. Acta*, **6**, 420 (1972).
6) C. H. Langford and H. B. Gray, "Ligand Substitution Processes," W. A. Benjamin Inc., New York (1965).

Non-isothermal Studies of the Dehydration of Double Salt Hydrates and Their Deuterium Oxide Analogues. I

N. RAY CHAUDHURI, M. K. DASGUPTA, S. MITRA, and G. K. PATHAK

Inorganic Chemistry Laboratory, Indian Association for the Cultivation of Science, Calcutta 700032, India

(Received December 10, 1976)

Non-isothermal studies of the dehydration of double salt hydrates of the type $(NH_4)_2AB_4 \cdot M(II)SO_4 \cdot 6H_2O$ and their D_2O analogues in solid state were carried out with a derivatograph, where $AB_4 = BeF_4^{2-}$ or SeO_4^{2-}, M(II)=Mg(II), Mn(II), Co(II), Ni(II), Cu(II), or Zn(II). These salt hydrate molecules lost water/heavy water in single or multiple steps upon heating. Intermediate hydrates were isolated and characterised by elemental analysis and IR spectral measurements. The activation energy for each step of dehydration of the salt hydrate was evaluated from the analysis of TG, DTG, and DTA curves of the respective derivatograms. Enthalpy change was evaluated from the DTA peak area and the order of reaction was found to be unity for each step of dehydration. The nature of dehydration was little affected by deuteration. Thermal parameters for the $(NH_4)_2AB_4 \cdot M(II)SO_4 \cdot 6H_2O$ and their D_2O analogues were compared with the salt hydrates, $K_2AB_4 \cdot M(II)SO_4 \cdot 6H_2O$, $(NH_4)_2SO_4 \cdot M(II)SO_4 \cdot 6H_2O$ and their D_2O analogues.

Non-isothermal studies on the dehydration of double salt hydrates of the type $M(I)_2SO_4 \cdot M(II)SO_4 \cdot 6H_2O$ where M(I)=NH_4(I),[1] K(I),[2] Rb(I),[3] Cs(I),[4] or Tl(I)[5] and M(II)=Mg(II), Mn(II), Co(II), Ni(II), Cu(II), Zn(II), or Cd(II) and their D_2O analogues were carried out. Thermal studies on the dehydration of double salt hydrates of the type $K_2AB_4 \cdot M(II)SO_4 \cdot 6H_2O$, where $AB_4 = BeF_4^{2-}$ or SeO_4^{2-} and their D_2O analogues[6] were also reported. These studies showed that the thermal properties are affected by changes of univalent cation and/or anion contained in the double salt hydrates. The present paper deals with the dehydration of double salt hydrates of the type $(NH_4)_2AB_4 \cdot M(II)SO_4 \cdot 6H_2O$ where $AB_4 = BeF_4^{2-}$ or SeO_4^{2-}, M(II) =Mg(II), Mn(II), Co(II), Ni(II), Cu(II), or Zn(II) and their D_2O analogues, which was carried out in order to see the cation effect with change of K(I) by NH_4 (I) and the anion effect with change of SO_4^{2-} by BeF_4^{2-} or SeO_4^{2-} attached to the univalent cation. The values of activation energies of dehydration processes were evaluated from TG, DTG and DTA curves simultaneously, the order of reaction from TG, enthalpy changes from DTA peak area and the thermal stability from first DTG peak temperature. The effect of deuteration on the thermal properties is described. The role of divalent cation on the thermal properties of dehydration is also discussed.

Experimental

Preparation of $(NH_4)_2BeF_4 \cdot M(II)SO_4 \cdot 6H_2O$ where M(II) =Mg(II), Mn(II), Co(II), Ni(II), Cu(II), or Zn(II). These salts were prepared by the standard procedure.[7-9]

Preparation of $(NH_4)_2SeO_4 \cdot M(II)SO_4 \cdot 6H_2O$, where M(II)=Mg(II), Mn(II), Co(II), Ni(II), Cu(II), or Zn(II). These salts were prepared by crystallization from a mixture of equimolecular proportions of the corresponding single salts in water. D_2O analogues of the salt hydrates were prepared by dissolving the anhydrous single salts required in D_2O (99.5%) and subsequent crystallization. Elemental analysis of all the salt hydrates and their D_2O analogues was carried out before thermal analysis.

A Paulik-Paulik-Erdey type MOM derivatograph was used for the thermal analysis. The particle size of the sample was 150—200 mesh. A platinum crucible was used, the heating rate being maintained at 1.5 °C min^{-1}. The volume of the sample was nearly the same in each case.

The following abbreviations were used for the double salt hydrates of the present two series and also other series given in Results and Discussion.

A: $(NH_4)_2SO_4 \cdot M(II)SO_4 \cdot 6H_2O$
B: $(NH_4)_2BeF_4 \cdot M(II)SO_4 \cdot 6H_2O$
C: $(NH_4)_2SeO_4 \cdot M(II)SO_4 \cdot 6H_2O$
A(K): $K_2SO_4 \cdot M(II)SO_4 \cdot 6H_2O$
B(K): $K_2BeF_4 \cdot M(II)SO_4 \cdot 6H_2O$
C(K): $K_2SeO_4 \cdot M(II)SO_4 \cdot 6H_2O$

The following abbreviations were used for representation of a particular salt of any series.

A-Mg(II): $(NH_4)_2SO_4 \cdot MgSO_4 \cdot 6H_2O$
B-Mn(II): $(NH_4)_2BeF_4 \cdot MnSO_4 \cdot 6H_2O$
C-Co(II): $(NH_4)_2SeO_4 \cdot CoSO_4 \cdot 6H_2O$ *etc.*

Results

The derivatograms of B-Mg(II), B-Mn(II), and B-Co(II) are shown in Fig. 1. B-Mg(II) and B-Co(II) lose water molecules in a single step. The TG curve for the dehydration of B-Mn(II) shows dehydration taking place in a single step. However, the two DTA peaks partially overlap each other and two DTG peaks also partially overlap each other, indicating the existence of a thermally unstable intermediate product. The derivatograms of B-Ni(II), B-Cu(II), and B-Zn(II) are shown in Fig. 2. B-Ni(II) and B-Zn(II) show single step dehydration, whereas B-Cu(II) undergoes dehydration as follows: $(NH_4)_2BeF_4 \cdot CuSO_4 \cdot 6H_2O \rightarrow (NH_4)_2BeF_4 \cdot CuSO_4 \cdot H_2O \rightarrow (NH_4)_2BeF_4 \cdot CuSO_4$. The intermediate hydrate is not stable enough to be isolated. B-Mg(II) and B-Ni(II) start decomposition as soon as the dehydration ceases. The derivatograms C-Mg(II), C-Mn(II), and C-Co(II) are shown in Fig. 3. C-Mg(II) loses water molecules in a single step. C-Mn(II) becomes anhydrous passing through an unstable intermediate *i.e.*, dihydrate. The two DTA peaks and also the two DTG peaks overlap each other. C-Co(II) becomes anhydrous passing through an unstable hemihydrate. The derivatograms of C-Ni(II), C-Cu(II), and C-Zn(II) are shown in Fig. 4. C-Ni(II) and C-Zn(II) show dehydration in a single step, but the latter shows a shoulder in its DTA and DTG curves,

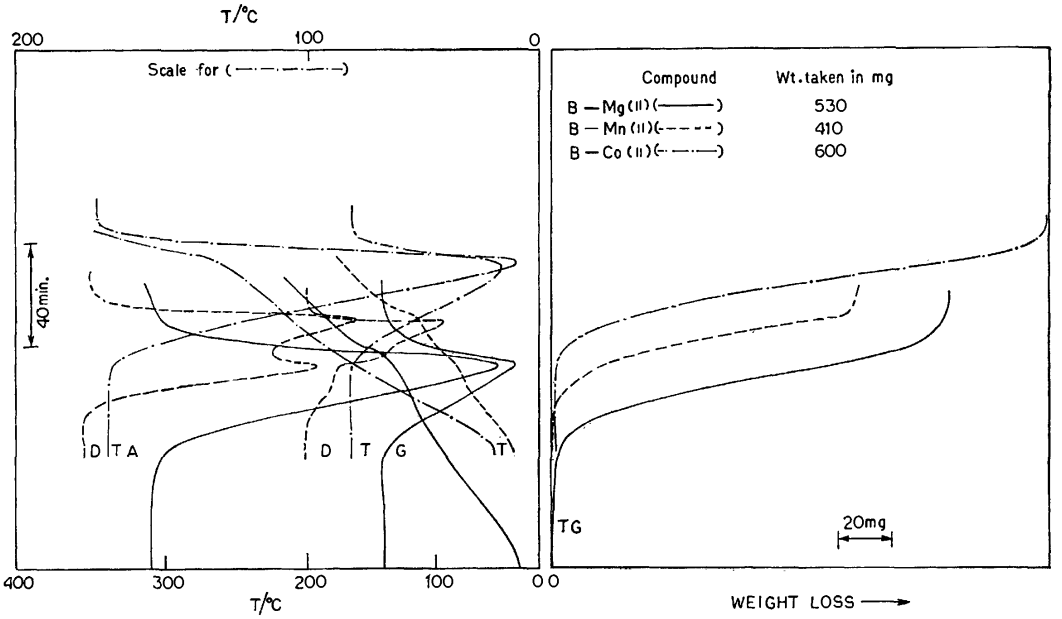

Fig. 1. Derivatograms for $(NH_4)_2BeF_4 \cdot MgSO_4 \cdot 6H_2O$[B-Mg(II) (——)], $(NH_4)_2BeF_4 \cdot MnSO_4 \cdot 6H_2O$[B-Mn(II) (— — —)], and $(NH_4)_2BeF_4 \cdot CoSO_4 \cdot 6H_2O$[B-Co(II) (—·—·—)].

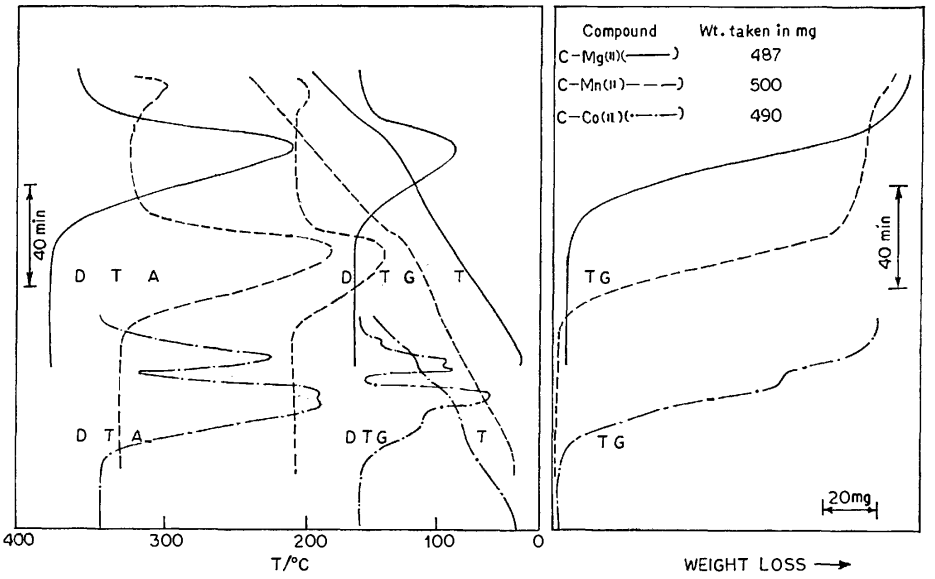

Fig. 3. Derivatograms for $(NH_4)_2SeO_4 \cdot MgSO_4 \cdot 6H_2O$[C-Mg(II) (——)], $(NH_4)_2SeO_4 \cdot MnSO_4 \cdot 6H_2O$[C-Mn(II) (—·—·—)], and $(NH_4)_2SeO_4 \cdot CoSO_4 \cdot 6H_2O$[C-Co(II) (———)].

indicating a very unstable intermediate hydrate. C-Cu(II) dehydrates through an unstable dihydrate. The derivatograms of the deuterated salt hydrates are not given since the nature of dehydration remains unaltered.

DTG peak temperatures and the temperature ranges of dehydration of the double salt hydrates of "B" and "C" and their D_2O analogues are given in Tables 1 and 2, respectively. Enthalpy changes for each step of dehydration of the double salt hydrates and their D_2O analogues were evaluated by the method used by Tsuchiya *et al.*[10] using copper sulfate pentahydrate as a standard. When the peaks are too much overlapped, the values are evaluated from the overall area of the DTA curves. Activation energies for each step of dehydration of the salt hydrates and their D_2O analogues are evaluated from the analysis of TG curves using Freeman and Carroll's equation.[11] The activation energies for each step of dehydration were evaluated from the analysis of DTG curves using the method of Dave and Chopra[12] and also from that of DTA curves using the equation of Brochardt and Daniels[13] for first order reactions. In a few cases the values of activation energy obtained from TG curves appear high in comparison with those determined from the corresponding DTA and DTG curves (Table 2). As a result, we evaluated the activation energy also from TG curves

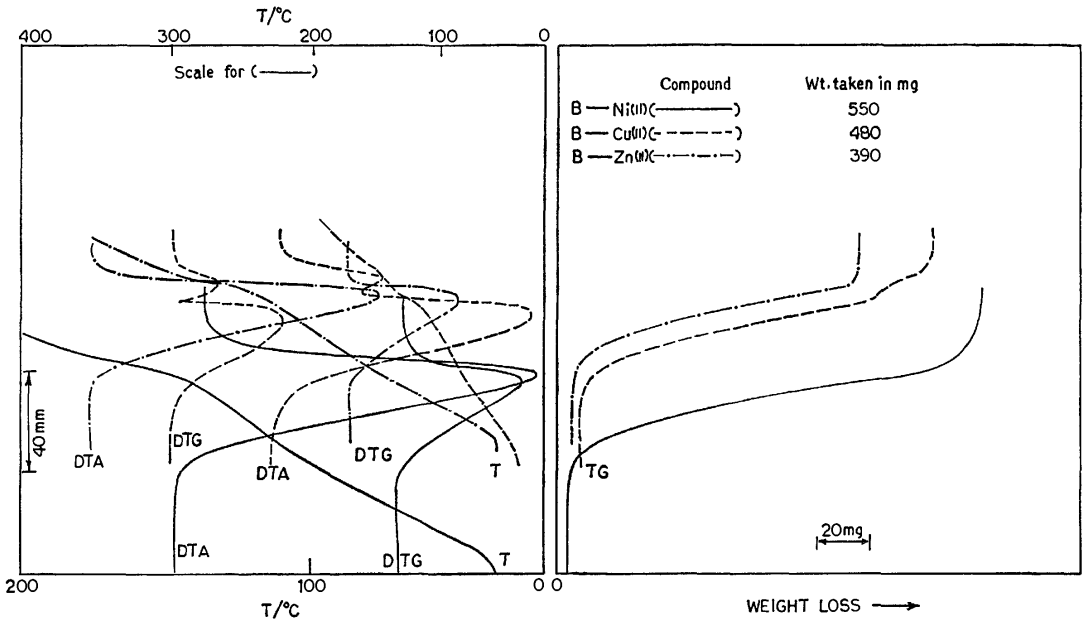

Fig. 2. Derivatograms for $(NH_4)_2BeF_4 \cdot NiSO_4 \cdot 6H_2O$[B-Ni(II) (——)], $(NH_4)_2BeF_4 \cdot CuSO_4 \cdot 6H_2O$ [B-Cu(II) (— — —)], and $(NH_4)_2BeF_4 \cdot ZnSO_4 \cdot 6H_2O$[B-Zn(II) (—·—·—)].

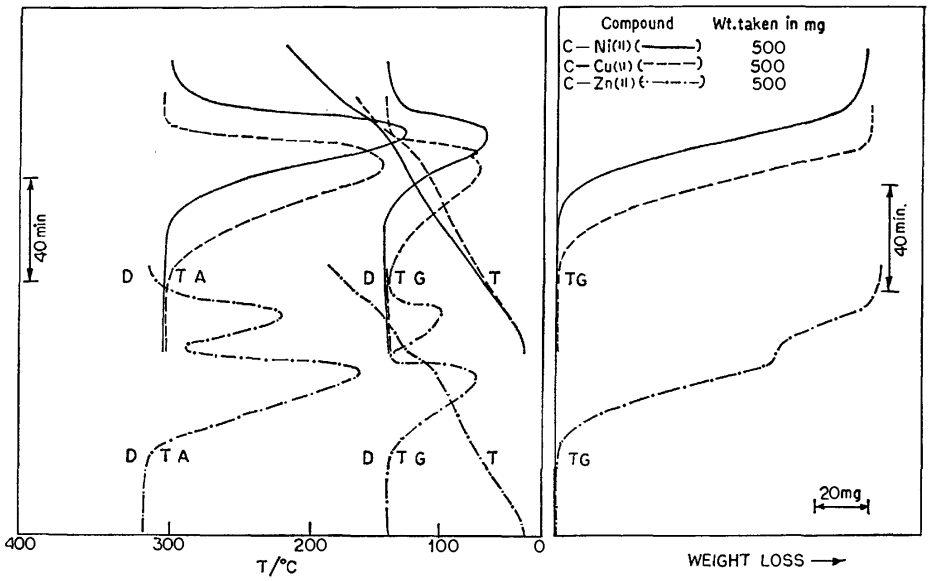

Fig. 4. Derivatograms for $(NH_4)_2SeO_4 \cdot NiSO_4 \cdot 6H_2O$[C-Ni(II) (——)], $(NH_4)_2SeO_4 \cdot CuSO_4 \cdot 6H_2O$[C-Cu(II) (—·—·—)], and $(NH_4)_2SeO_4 \cdot ZnSO_4 \cdot 6H_2O$[C-Zn(II) (———)].

using Horowitz and Metzger's equation[14] and a modified Dharwadkar and Phandnis equation.[15] The results are given in Table 2 within parentheses. The order of reaction is found to be unity for the dehydration of all the double salt hydrates and their D_2O analogues. The IR spectra of the salt hydrates and their D_2O analogues were taken to confirm the fact that the deuteration of the hydrates takes place to the desired extent.

Discussion

The patterns of elimination of water molecules of B-Mg(II) and C-Mg(II) are similar to each other, but differ from that of A-Mg(II). The mode of dehydration of B-Mg(II) does not differ from that of B(K)-Mg(II), but that of C-Mg(II) differs from that of C(K)-Mg(II) where dehydration takes place in double steps. B-Mn(II) differs from C-Mn(II), but shows similarity to A-Mn(II) with respect to the pattern of elimination of water molecules. B-Co(II) shows similarity to A-Co(II), but differs from C-Co(II) with respect to the elimination of water molecules. Our earlier work shows that the patterns of elimination of water molecules for both B-Co(II) and C-Co(II) differ from those of B(K)-Co(II) and C(K)-Co(II). The modes of elimination

Table 1. Thermal parameters of dehydration of salt hydrates (B) and their deuterium oxide analogues

	Decomposition reaction	Temp. range (°C)	DTC peak temp (°C)	Activation energy[a] (kcal mol^{-1}) TG	DTG	DTA	m[b]	Enthalpy change (kcal mol^{-1})
I	$(NH_4)_2BeF_4\cdot MgSO_4\cdot 6H_2O \longrightarrow (NH_4)_2BeF_4\cdot MgSO_4$	75—181	120	29.6	26.5	33.0	30.6	12.5
I′	$(NH_4)_2BeF_4\cdot MgSO_4\cdot 6D_2O \longrightarrow (NH_4)_2BeF_4\cdot MgSO_4$	72—174	117	26.3	30.6	29.9		14.4
II	$(NH_4)_2BeF_4\cdot MnSO_4\cdot 6H_2O \longrightarrow (NH_4)_2BeF_4\cdot MnSO_4$	49—130	112	34.5	—	—		14.7[c]
II′	$(NH_4)_2BeF_4\cdot MnSO_4\cdot 6D_2O \longrightarrow (NH_4)_2BeF_4\cdot MnSO_4$	47—130	107	34.5	—	—		11.1[c]
III	$(NH_4)_2BeF_4\cdot CoSO_4\cdot 6H_2O \longrightarrow (NH_4)_2BeF_4\cdot CoSO_4$	70—164	126	23.4	24.5	23.4	46.0	16.0
III′	$(NH_4)_2BeF_4\cdot CoSO_4\cdot 6D_2O \longrightarrow (NH_4)_2BeF_4\cdot CoSO_4$	68—160	120	23.0	28.7	30.6		15.3
IV	$(NH_4)_2BeF_4\cdot NiSO_4\cdot 6H_2O \longrightarrow (NH_4)_2BeF_4\cdot NiSO_4$	84—200	145	21.2	26.8	22.0	34.1	13.3
IV′	$(NH_4)_2BeF_4\cdot NiSO_4\cdot 6D_2O \longrightarrow (NH_4)_2BeF_4\cdot NiSO_4$	81—195	145	20.8	23.0	21.0		12.7
Va	$(NH_4)_2BeF_4\cdot CuSO_4\cdot 6H_2O \longrightarrow (NH_4)_2BeF_4\cdot CuSO_4\cdot H_2O$	55—120	107	34.5	34.5	—	40.2	13.4[c]
Vb	$(NH_4)_2BeF_4\cdot CuSO_4\cdot H_2O \longrightarrow (NH_4)_2BeF_4\cdot CuSO_4$	120—185	145	133.4	—	—		
V′a	$(NH_4)_2BeF_4\cdot CuSO_4\cdot 6D_2O \longrightarrow (NH_4)_2BeF_4\cdot CuSO_4\cdot D_2O$	53—120	108	32.4	32.4	—		13.9[c]
V′b	$(NH_4)_2BeF_4\cdot CuSO_4\cdot D_2O \longrightarrow (NH_4)_2BeF_4\cdot CuSO_4$	120—181	145	128.8	—	—		
VI	$(NH_4)_2BeF_4\cdot ZnSO_4\cdot 6H_2O \longrightarrow (NH_4)_2BeF_4\cdot ZnSO_4$	59—142	117	20.0	23.0	23.0	25.2	12.5
VI′	$(NH_4)_2BeF_4\cdot ZnSO_4\cdot 6D_2O \longrightarrow (NH_4)_2BeF_4\cdot ZnSO_4$	55—140	115	20.9	24.7	25.1		10.9

a) In some cases thermal parameters could not be calculated due to very poor resolution of the curve. b) Activation energy for the first step of dehydration of B(K). c) Overall enthalpy change where DTA curves overlap too much.

of water molecules of B-Ni(II) and C-Ni(II) are similar to each other and are also similar to A-Ni(II). B-Ni-(II) shows no change in the elimination of water molecules due to the change of cation K by NH_4, but in C-Ni(II) a difference is observed from C(K)-Ni(II) where dehydration takes place in double steps. The patterns of elimination of water molecules of B-Cu(II) and C-Cu(II) differ from each other, and also from A-Cu(II) where dehydration takes place in three steps. Both B-Cu(II) and C-Cu(II) differ in the nature of dehydration from B(K)-Cu(II) and C(K)-Cu(II), respectively. Apparently A-Zn(II), B-Zn(II), and C-Zn-(II) show no difference in the nature of dehydration, but in C-Zn(II) a slight difference is observed. B-Zn-(II) shows similarity to B(K)-Zn(II). C-Zn(II) difffers from C(K)-Zn(II) with respect to the elimination of water molecules.

Salt hydrates of "B" show no dihydrate, whereas our earlier work on the dehydration of the salt hydrates of "B(K)" shows thermally stable dihydrates in the cases of Co(II) and Cu(II). On the other hand, salt hydrates of "C" show the existence of thermally unstable dihydrates in the cases of Mn(II) and Cu(II), and the salt hydrates of "C(K)" show thermally stable dihydrates in the cases of Mg(II), Co(II), Ni(II), and Zn(II).

No noticeable change in the nature of dehydration due to deuteration is observed in the salt hydrates of "A", "B", and "C". In the salt hydrates of "B(K)" a slight deuteration effect was observed in the case of Cu(II) only, whereas appreciable deuteration effect was observed in C(K)-Ni(II) and C(K)-Cu(II).

The first DTG peak temperature of the salt hydrates of "B" shows thermal stability to be in the order: Ni(II)>Co(II)>Mg(II)>Zn(II)>Mn(II)>Cu(II) and that of "C" in the order: Ni(II)>Mg(II)>Co(II)>Zn-(II)>Cu(II)>Mn(II). In both series thermal stability of Ni(II) is appreciably high. This phenomenon is observed in "A" and also in "B(K)" and "C(K)" we reported.

In our works on non-isothermal studies on the dehydration of salt hydrates we evaluated the value of activation energy and order of reaction (n) from TG using Freeman and Carroll's equation,[11] reaction order always being found to be unity. It was observed that the specific rate constant of the reaction at different temperatures can be ascertained from the equation of Dave and Chopra[12] as follows:

$$k = \frac{\left(\frac{A}{N_0}\right)^{n-1}\left(-\frac{dx}{dt}\right)}{(A-a)^n},$$

where k=specific rate constant,
N_0=number of molecules of the sample at the time when DTG peak appears,
A and a=the total peak area and the area swept up till time t,
dx/dt=the displacement of DTG curve from the base line at time t,
and n=the order of reaction.

The values of log k are plotted against the reciprocal of the absolute temperature assuming different values of n, the correct one resulting in a straight line. The slope of the line gives the value of activation energy for the order of reaction. The value of n evaluated by this method is in good agreement with the value determined from Freeman and Carroll's equation. When the value of n becomes greater or less than unity, evaluation of the specific rate constant by means of Brochardt and Daniel's equation becomes very difficult. We did not face this difficulty as we observe unit value of n evaluated from the plot of Freeman and Carroll's equation. As a result we chose Freeman and Carroll's equation instead of other kinetic equations, *e.g.*,

Table 2. Thermal parameters of dehydration of salt hydrates (C) and their deuterium oxide analogues

	Decomposition reaction	Temp range (°C)	DTG peak temp (°C)	Activation energy[a] (kcal mol^{-1}) TG	DTG	DTA	m[b]	Enthalpy change (kcal mol^{-1})
I	$(NH_4)_2SeO_4\cdot MgSO_4\cdot 6H_2O \longrightarrow (NH_4)_2SeO_4\cdot MgSO_4$	85—200	132	28.8, (29.7),[c] (25.5)[d]	30.6	27.6	69.0	10.1
I′	$(NH_4)_2SeO_4\cdot MgSO_4\cdot 6D_2O \longrightarrow (NH_4)_2SeO_4\cdot MgSO_4$	80—195	130	27.6	20.9	24.3		10.8
IIa	$(NH_4)_2SeO_4\cdot MnSO_4\cdot 6H_2O \longrightarrow (NH_4)_2SeO_4\cdot MnSO_4\cdot 2H_2O$	50—90	87	32.8	—	—		12.2[e]
IIb	$(NH_4)_2SeO_4\cdot MnSO_4\cdot 2H_2O \longrightarrow (NH_4)_2SeO_4\cdot MnSO_4$	108—142		64.4	—	—		
II′a	$(NH_4)_2SeO_4\cdot MnSO_4\cdot 6D_2O \longrightarrow (NH_4)_2SeO_4\cdot MnSO_4\cdot 2D_2O$	50—92	88	35.8	—	—		10.6[e]
II′b	$(NH_4)_2SeO_4\cdot MnSO_4\cdot 2D_2O \longrightarrow (NH_4)_2SeO_4\cdot MnSO_4$	92—150	120	43.3	—	—		
IIIa	$(NH_4)_2SeO_4\cdot CoSO_4\cdot 6H_2O \longrightarrow (NH_4)_2SeO_4\cdot CoSO_4\cdot 0.5H_2O$	87—200	121	64.4, (24.5),[c] (25.5)[d]	21.2	24.7	54.4	11.8
IIIb	$(NH_4)_2SeO_4\cdot CoSO_4\cdot 0.5H_2O \longrightarrow (NH_4)_2SeO_4\cdot CoSO_4$	200—245	235	—	—	—		
III′a	$(NH_4)_2SeO_4\cdot CoSO_4\cdot 6D_2O \longrightarrow (NH_4)_2SeO_4\cdot CoSO_4\cdot 0.5D_2O$	87—200	118	69.0, (26.6),[c] (25.3)[d]	28.7	28.3		10.8
III′b	$(NH_4)_2SeO_4\cdot CoSO_4\cdot 0.5D_2O \longrightarrow (NH_4)_2SeO_4\cdot CoSO_4$	200—245	237	—	—	—		
IV	$(NH_4)_2SeO_4\cdot NiSO_4\cdot 6H_2O \longrightarrow (NH_4)_2SeO_4\cdot NiSO_4$	97—200	145	29.0	27.0	33.0	37.1	10.6
IV′	$(NH_4)_2SeO_4\cdot NiSO_4\cdot 6D_2O \longrightarrow (NH_4)_2SeO_4\cdot NiSO_4$	98—200	142	36.1	21.9	25.8		12.3
Va	$(NH_4)_2SeO_4\cdot CuSO_4\cdot 6H_2O \longrightarrow (NH_4)_2SeO_4\cdot CuSO_4\cdot 2H_2O$	60—115	102	28.8	30.6	—	23.0	13.9
Vb	$(NH_4)_2SeO_4\cdot CuSO_4\cdot 2H_2O \longrightarrow (NH_4)_2SeO_4\cdot CuSO_4$	125—165	145	64.4, (46.0),[c] (32.2)[d]	42.4	—		
V′a	$(NH_4)_2SeO_4\cdot CuSO_4\cdot 6D_2O \longrightarrow (NH_4)_2SeO_4\cdot CuSO_4\cdot 2D_2O$	50—120	100	26.3	25.1	—		11.7
V′b	$(NH_4)_2SeO_4\cdot CuSO_4\cdot 2D_2O \longrightarrow (NH_4)_2SeO_4\cdot CuSO_4$	120—180	145	76.6, (40.2),[c] (36.8)[d]	39.4	—		
VI	$(NH_4)_2SeO_4\cdot ZnSO_4\cdot 6H_2O \longrightarrow (NH_4)_2SeO_4\cdot ZnSO_4$	60—140	115	23.0	24.8	23.0	23.0	12.9
VI′	$(NH_4)_2SeO_4\cdot ZnSO_4\cdot 6D_2O \longrightarrow (NH_4)_2SeO_4\cdot ZnSO_4$	70—140	120	26.3	23.0	27.6		14.0

a) In some cases thermal parameters could not be calculated due to very poor resolution of the curve. b) Activation energy for the first step of dehydration of C(K). c) Evaluated by method of Horowitz and Metzger. d) Evaluated by modified method of Dharwadkar and Phadnis. e) Overall ethalpy change.

Horowitz and Metzger,[14] modified Dharwadkar and Phadnis[15] *etc.* for TG curves where the value of n is based on assumption. The value of n obtained by using Freeman and Carroll's equation appears greater or less than one besides the unit value in number of cases observed by different workers.[16–18] However, in our works on salt hydrates[1–6] and the adduct molecules of metallic halides[19–23] with oxo compounds we did not find the order of reaction other than unity, and found a closeness of values of activation energy evaluated using Freeman and Carroll's equation for TG, Dave and Chopra's equation for DTG and Brochardt and Daniel's equation for DTA. This is also observed in most of the cases of the present two series. In a few cases (see Table 2) Freeman and Carroll's equation shows values appreciably high in comparison with the values evaluated from DTA and DTG curves. In such cases on application of two other standard equations, Horowitz and Metzger's equation and modified Dharwadkar and Phadnis equation, to the TG curve, the value of activation energy becomes closer to those obtained from DTA and DTG curve. However, when the value of activation energy obtained by using Freeman and Carroll's equation does not differ much from that evaluated from DTA and DTG curves, application of other two methods to the TG curve gives comparable values. Under such context we have emphasised Freeman and Carroll's equation because of its advantage over the other kinetic equation for TG curve.

The activation energy for the first step of dehydration of salt hydrates of "A" increased with increase in atomic number in the order Mg(II)<Mn(II)<Co(II)<Ni(II), reaching a maximum in Cu(II) and decreasing as Zn(II)>Cd(II). This trend is not observed in both of the present series. The values of activation energy for the first step of dehydration of B-Mg(II), B-Mn(II) and B-Cu(II) are very close and the values of B-Co(II), B-Ni(II), and B-Zn(II) are close to each

other respectively, but the former values are appreciably high (Table 1). The highest value of activation energy is observed in C-Mn(II). The values of activation energies of C-Mg(II), C-Ni(II), and C-Cu(II) are close to each other. Those of C-Co(II) and C-Zn(II) are also close, but the former values are higher than those of latter such as the salt hydrates of "B" (Table 2). B-Ni(II) shows considerably low value of activation energy due to change of K by NH_4, though the pattern of dehydration hardly differs. The difference in the value of activation energy between the salt hydrates of "B" and "C" is not so prominent as was observed for the salt hydrates of "B(K)" and "C(K)" (Tables 1 and 2).

No deuteration effect is observed on the value of activation energy in both the salt hydrates of "B" and "C". It was observed in the salt hydrates of "B(K)" and more clearly in the salt hydrates of "C(K)".

The values of enthalpy changes of dehydration of the salt hydrates of "B" and "C" are $\approx$10—$\approx$16 kcal mol^{-1}. Deuteration causes no marked effect on the value of ΔH.

In the salt hydrates of "A", "B", and "C" for particular divalent cation except Mg(II) and Cu(II) we observed pronounced anion effect with respect to elimination of water molecules, whereas this effect was observed for each divalent cation amongs the salt hydrates of "A(K)", "B(K)", and "C(K)".

References

1) N. Ray Chaudhuri, G. K. Pathak, and S. Mitra, *Proc. 4th Int. Conf. Therm. Anal.*, **1**, 615 (1974).

2) N. Ray Chaudhuri and G. K. Pathak, *Thermochim. Acta*, **12**, 71 (1975).

3) N. Ray Chaudhuri and G. K. Pathak, *Thermochim. Acta*, **12**, 287 (1975).

4) N. Ray Chaudhuri and G. K. Pathak, *Thermochim. Acta*, **12**, 397 (1975).

5) N. Ray Chaudhuri and G. K. Pathak, *Thermochim. Acta*, **13**, 71 (1975).

6) N. Ray Chaudhuri and G. K. Pathak, *Thermochim. Acta*, **13**, 207 (1975).

7) P. C. Ray, *Nature*, **124**, 481 (1939).

8) T. K. Ghosh, T. N. Chakrabarty, and N. N. Ray, *J. Indian Chem. Soc.*, **42**, 847 (1965).

9) N. N. Ray, *Z. Anorg. Chem.*, **206**, 209 (1932).

10) R. Tsuchiya, Y. Kaji, A. Uehara, and E. Kyuno, *Bull. Chem. Soc. Jpn.*, **42**, 1881 (1969).

11) E. S. Freeman and B. Carroll, *J. Phys. Chem.*, **62**, 394 (1958).

12) N. G. Dave and S. K. Chopra, *Z. Phys. Chem.*, **48**, 257 (1966).

13) H. J. Brochardt and F. Daniels, *J. Am. Chem. Soc.*, **79**, 41 (1957).

14) H. H. Horowitz and G. Metzger, *Anal. Chem.*, **35**, 1464 (1963).

15) S. R. Dharwadkar and A. B. Phadnis, *Indian J. Chem.*, **7**, 1032 (1969).

16) K. Nagase, K. Muraishi, K. Sone, and N. Tanaka, *Bull. Chem. Soc. Jpn.*, **48**, 3184 (1975).

17) R. P. Bonomo, S. Gurrieri, S. Musumeci, E. Rizzarelli, and G. Siracusa, *Thermochim. Acta*, **9**, 373 (1974).

18) V. M. Padmanabhan, S. C. Saraiya, and A. K. Sundaram, *J. Inorg. Nucl. Chem.*, **12**, 356 (1950).

19) N. Ray Chaudhuri, S. Mitra, and G. K. Pathak, *Bull. Chem. Soc. Jpn.*, **48**, 2375 (1975).

20) N. Ray Chaudhuri and S. Mitra, *Bull. Chem. Soc. Jpn.*, **49**, 1035 (1976).

21) N. Ray Chaudhuri and S. Mitra, *Bull. Chem. Soc. Jpn.*, **48**, 2837 (1975).

22) N. Ray Chaudhuri and S. Mitra, *Thermochim. Acta*, **13**, 59 (1975).

23) N. Ray Chaudhuri and S. Mitra, *Thermochim. Acta*, **13**, 193 (1975).

Kinetics and Mechanism of Thermal Isomerisation of Aryl Alkanehydrazonates into *N'*,*N'*-Diarylhydrazides. Extension of a Recent Free Radical Analogue of the Chapman Rearrangement

Ahmad Sami SHAWALI, Hamdi Mahmoud HASSANEEN, and Saleh ALMOUSAWI
Department of Chemistry, Faculty of Science, University of Cairo, Giza, Egypt

(Received December 18, 1977)

A series of twelve aryl *N*-(*p*-nitrophenyl)alkanehydrazonates (I) have been prepared and their thermal rearrangement into *N*-acyl-*N'*,*N'*-diarylhydrazines (II) was investigated. The structures of I and II were derived from their elemental analyses and spectral properties. Hydrolysis of II afforded the corresponding *N'*,*N'*-diarylhydrazines. Kinetic experiments have shown that electron withdrawing substituents decrease the rate of the rearrangement whereas electron donating groups increase it. The rate of conversion of I into II was also increased by addition of benzoyl peroxide. A free radical mechanism was proposed to account for the results.

We have been exploring the synthesis and thermal isomerization of several hydrazonates of type I (R= aryl, H_5C_2OOC- or C_6H_5NHCO-).[1-4] In continuation of these studies, we have investigated the synthesis of a number of aryl alkanehydrazonates (I, R=alkyl) and examined the kinetics of their rearrangement into the hydrazides (II, R=alkyl).

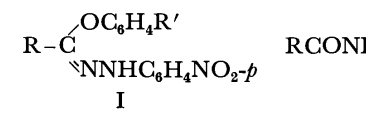

I

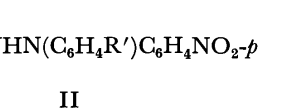

II

a, R=CH_3, R'=H
b, R=CH_3, R'=*p*-CH_3
c, R=CH_3, R'=*p*-Cl
d, R=CH_3, R'=*p*-NO_2
e, R=CH_3CH_2, R'=H
f, R=CH_3CH_2, R'=*p*-CH_3
g, R=CH_3CH_2, R'=*p*-Cl
h, R=CH_3CH_2, R'=*p*-NO_2
i, R=$(CH_3)_2CH$, R'=H
j, R=$(CH_3)_2CH$, R'=*p*-CH_3
k, R=$(CH_3)_2CH$, R'=*p*-Cl
l, R=$(CH_3)_2CH$, R'=*p*-NO_2

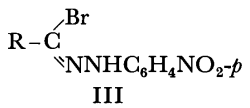

III

IIIa, R=CH_3,; IIIb, R=CH_3CH_2; IIIc, R=$(CH_3)_2CH$

Results and Discussion

Treatment of *N*-(*p*-nitrophenyl)ethanehydrazonoyl bromide (IIIa) with sodium phenoxide in ethanol results in the formation of phenyl *N*-(*p*-nitrophenyl)ethanehydrazonate (Ia). The latter ester was also prepared by treating IIIa with phenol in ethanol in presence of triethylamine at room temperature. These two procedures were found to be general and good yields of the hydrazonate esters, Ib to Il were obtained when other alkanehydrazonoyl bromides and phenols were used. In an attempt to prepare Ia, Ie, and Ii by the reaction of the respective hydrazonoyl bromides with phenol in presence of sodium acetate in ethanol, *N*,*N'*-diacyl-*N*-*p*-nitrophenyl)hydrazines (IVa, IVe, and IVi) were obtained and no hydrazonate was formed (Scheme 1). These results indicate that the formation of I involves the carbonium ion, (V)[5] or the nitrilimine, VI[6] as intermediate. The former ion can be attacked by nucleophilic reagents, namely the phenoxide and acetate

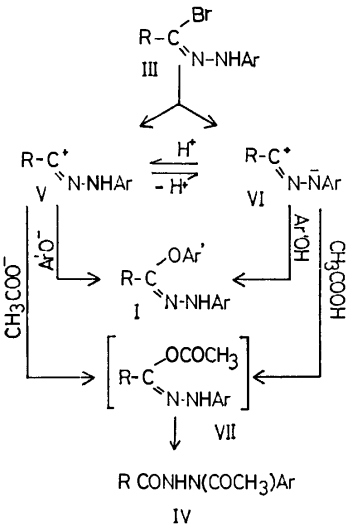

Scheme 1.

ions to form I and the acetate ester VII, respectively. Alternatively, the nitrilimine can add phenol and acetic acid to give I and VII respectively. The acetate ester VII seems to be unstable; it undergoes OAc→NAc rearrangement to form IV as it is formed[7] (Scheme 1).

The structures of the hydrazonates Ia to Il were derived from their elemental analyses and spectral data. Thus, the IR spectra showed, in each case, two characteristic bands at 1264 and 1080 cm^{-1} assignable to an aryl ether linkage. The UV absorption pattern was of typical hydrazones. The data are summarized in Table 1.

On heating the hydrazonates Ia to Il at 125 °C for 60 min in the absence of solvent, rearrangement occurred and the corresponding *N*-acyl-*N'*,*N'*-diarylhydrazines (IIa to IIl) were obtained. The latter products were characterized by strong absorption band near 1680 cm^{-1} assignable to the CONH grouping. The assigned hydrazide structure for the rearranged products was also indicated by the fact that *N*-phenyl-*N*-(*p*-nitrophenyl)hydrazine (VIII) was obtained upon acid hydrolysis of the rearranged products IIa and IIi. Acetylation of VIII with acetic anhydride gave back IIa.

The thermal isomerization of I was also effected by refluxing the esters in xylene for 1—3 h. The hydrazide

Table 1. Aryl N-(p-nitrophenyl)alkanehydrazonates

Compound No.	Mp, °C	Molecular formula	C, % Calcd	C, % Found	H, % Calcd	H, % Found	N, % Calcd	N, % Found	λ_{max}^{EtOH} nm, (log ε)
Ia	114—115	$C_{14}H_{13}N_3O_3$	61.98	61.80	4.83	4.73	15.49	15.34	395(4.349); 250(4.11)
Ib	151—151.5	$C_{15}H_{15}N_3O_3$	63.15	62.99	5.30	5.34	14.73	14.64	392(4.24); 250(4.17)
Ic	175—176	$C_{14}H_{12}ClN_3O_3$	55.00	55.40	3.96	4.06	13.74	13.47	390(4.43); 248(4.17)
Id	174—175	$C_{14}H_{12}N_4O_5$	53.17	53.09	3.82	4.05	17.72	17.99	382(4.45); 225(4.18)
Ie	113—114	$C_{15}H_{15}N_3O_3$	63.15	63.03	3.29	3.18	14.73	14.83	390(4.45); 250(4.18)
If	111—113	$C_{17}H_{17}N_3O_3$	64.20	64.28	5.73	5.81	14.04	14.11	393(4.43); 250(4.18)
Ig	164—165	$C_{15}H_{14}ClN_3O_3$	56.33	56.21	4.41	4.40	13.14	13.00	384(4.32); 355(3.89) sh; 256(3.85) sh
Ih	156.5—158	$C_{15}H_{14}N_4O_5$	54.57	54.21	4.20	4.15	16.97	17.62	390(4.25); 250(4.00)
Ii	134—135	$C_{16}H_{17}N_3O_3$	64.20	64.13	5.73	5.62	14.03	14.07	390(4.45); 250(4.20)
Ij	121—123	$C_{17}H_{19}N_3O_3$	65.16	64.93	6.11	5.79	13.41	13.53	392(4.46); 250(4.20)
Ik	115—116	$C_{16}H_{16}ClN_3O_3$	57.57	57.33	4.82	4.77	12.59	11.96	386(4.28); 250(4.12)
Il	199—201	$C_{16}H_{16}N_4O_5$	55.80	55.91	4.68	4.55	16.27	16.11	383(4.12); 325(3.71) sh; 255(3.66) sh.

Table 2. N-Acyl-N',N'-diarylhydrazines

Compound No.	Mp, °C	Molecular formula	C, % Calcd	C, % Found	H, % Calcd	H, % Found	N, % Calcd	N, % Found	λ_{max}^{EtOH} nm, (log ε)
IIa	197—197.5	$C_{14}H_{13}N_3O_3$	61.98	62.00	4.83	4.96	15.96	15.55	365(4.23); 250(3.85)
IIb	193—194	$C_{15}H_{15}N_3O_3$	63.15	62.98	5.30	5.36	14.73	14.85	366(4.21); 250(3.89)
IIc	233—235	$C_{14}H_{12}ClN_3O_3$	55.00	55.40	3.96	4.13	13.74	13.68	366(4.28); 250(4.02)
IId	239—241	$C_{14}H_{12}N_4O_5$	53.17	52.90	3.82	3.90	17.72	17.61	380(4.31); 325(4.00) sh; 258 (3.92) sh
IIe	176—177	$C_{15}H_{15}N_3O_3$	63.15	63.01	3.29	3.11	14.73	14.66	361(4.21); 250(3.87)sh
IIf	203—204	$C_{16}H_{17}N_3O_3$	64.20	64.30	5.73	5.76	14.04	14.20	366(4.23); 250(3.91)sh
IIg	190—192	$C_{15}H_{14}ClN_3O_3$	56.33	56.20	4.41	4.51	13.14	13.00	361(4.26); 260(3.92)sh
IIh	246—247.5	$C_{15}H_{14}N_4O_5$	54.57	54.32	4.20	4.01	16.97	16.81	382(4.39); 325(3.93) sh; 255(3.89) sh
IIi	183—184	$C_{16}H_{17}N_3O_3$	64.20	64.09	5.73	5.77	14.03	13.98	366(4.22); 250(3.88)
IIj	189.5—190	$C_{17}H_{19}N_3O_3$	65.16	65.23	6.11	6.24	13.41	13.10	368(4.21); 250(3.88)
IIk	191—192	$C_{16}H_{16}ClN_3O_3$	57.57	57.20	4.80	4.60	12.59	12.42	364(4.19); 255(3.86)
III	246—248	$C_{16}H_{16}N_4O_5$	55.80	55.72	4.68	4.52	16.27	16.01	372(4.40); 266(3.90)

obtained from a given ester by this method was identical in all respects with that obtained by the above procedure. The compounds prepared and their physical constants are listed in Table 2.

To shed more light on the mechanism of the rearrangement of I, the kinetics of the rearrangement of the esters Ia to Il were studied in p-xylene spectrophotometrically. In this solvent both the ester and the respective hydrazide have absorption maxima in the region 350—390 nm. However, the molar absorptivity of the ester, at a given wavelength, is higher than that of the hydrazide at the same wavelength. The data are summarized in Table 3. Therefore the absorbance in the region 350—390 nm decreases with the progress of the rearrangement. Accordingly, the rates of the isomerization of I were followed spectrophotometrically at the wavelength where maximum absorbance difference was observed. In case of the p-nitrophenyl esters (Id, Ih, and Il) a tight isosbestic point in the UV spectra was observed. This indicates that the rearrangement occurred without the formation of intermediates which absorb in the same region.

For the rearrangement of all esters, the following first order rate equation was obtained;

$$-\log(A_t - A_\infty) = k_1 t/2.3 - \log(A_0 - A_\infty),$$

where A_0, A_t, and A_∞ are the absorbance values of the reaction mixture at time 0, t, and ∞, respectively. The rate constant was calculated from the slope of the plot

Table 3. UV data of aryl alkanehyrazonates (I) and N',N'-diarylhydrazides (II) in p-xylene and rate constants for conversion of I into II at 110 °C

Ester-I Compound No.	Ester-I λ_{max}	Ester-I ε	Hydrazide-II Compound No.	Hydrazide-II λ_{max}	Hydrazide-II ε	$10^4 k_1$ (s^{-1})
Ia	370	25119	IIa	360	13489	1.67
Ib	373	25119	IIb	360	16982	1.87
Ic	370	23442	IIc	360	11220	1.32
Id	362	20417	IId	384	16218	0.79
Ie	370	24547	IIe	360	14125	0.93
If	371	25119	IIf	360	16982	1.18
Ig	370	23442	IIg	360	11749	0.71
Ih	361	19952	IIh	380	16596	0.37
Ii	376	19952	IIi	360	15135	0.52
Ij	370	25119	IIj	360	15849	0.69
Ik	367	23442	IIk	360	15849	0.30
Il	360	16218	III	380	15135	0.23

of log $(A_t - A_\infty)$ *versus* time using the least squares method. In Table 3 are listed the first-order rate constants obtained for the esters investigated. The values reported are the average of those obtained in duplicate or triplicate experiments. The data indicate that the rate of the rearrangement is influenced by the nature of both the substituent on the phenolic moiety and the C-alkyl group. In a given series of esters, electron withdrawing substituents decrease the reactivity, whereas electron donating ones increase it. The esters having the same OAR group, and different R's, their rates follow the sequence: $CH_3 > CH_3CH_2 > (CH_3)_2CH$.

TABLE 4. RESULTS OF STATISTICAL TREATMENT OF THE KINETIC DATA[a)]

Series	$-\rho \pm s$	$-\log k_H \pm s$	r	n
Ia—d	0.396±0.012	3.79±0.005	0.999	4
Ie—h	0.522±0.009	4.02±0.004	0.994	4
Ii—l	0.497±0.013	4.29±0.053	0.939	4

a) ρ, reaction constant; log k_H, intercept of the Hammett plot; r, correlation coefficient; s, standard deviation; n, number of points.

The values of log k_1 for each series of esters were then correlated with the Hammett substituent constant, σ, as taken from the compilation of Ritchie and Sager.[8)] The results of statistical analysis of the rate data by the least squares method are summarized in Table 4. The rho values obtained are in agreement with a free radical pathway because their absolute value is small, and with an electron deficient transition state because they are negative.

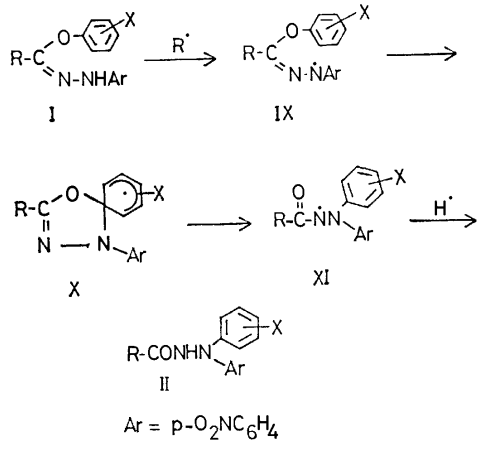

Scheme 2.

The sequence that probably accounts for the foregoing results is presented in Scheme 2. It is assumed that a radical initiator, R·, removes the amino hydrogen atom to give the hydrazonate radical, IX; this then undergoes intramolecular rearrangement possibly *via* the cyclic radical species X to give the more stable hydrazide radical XI. Hydrogen abstraction from the solvent or from another hydrazonate ester then gives the hydrazide II. The intermediacy of hydrazyl radicals has been postulated for several reactions of hydrazones,[9)] and their stability has been examined by Goldschmidt *et al.*[10)]. Under the conditions which we have used to investigate the kinetics of the conversion of I into II, the radical initiator is probably the trace of oxygen[11)] which might be present. This was substantiated by the observation that the rate of the rearrangement was increased by addition of the free radical initiator namely benzoyl peroxide. For example, the rate constant of the isomerization of the ester Ie in xylene at 110 °C in presence of 4.95×10^{-5} M benzoyl peroxide has a value of 2.08×10^{-4} s^{-1}; whereas in the absence of the peroxide the value of the rate constant was 0.93×10^{-4} s^{-1}. The suggested mechanism (Scheme 2) is also consistent with the recent observation by Hegarty *et al.*[9)] that the rate of the rearrangement of the related aryl arenecarbohydrazonates in dioxane–water mixture is accelerated by the addition of oxidizing agents such as manganese dioxide.

Experimental

All melting points are uncorrected and were measured on a Gallenkamp Electrothermal melting point apparatus, model 1A6301. Elemental analysis was performed by Alfred Bernhardt Mikroanalytisches Chemie Laboratorium, West Germany. Infrared and ultraviolet spectra were measured with Unicam SP1000 and SP8000 spectrophotometers respectively. The solvent *p*-xylene was Analar grade and redistilled twice before use in kinetic study.

The alkanehydrazonoyl bromides (III, R=CH_3, CH_3CH_2, and $(CH_3)_2CH$) used in synthesis of I were prepared by literature method, and their constants (mp' s) corresponded to liserature data.[12)]

Aryl Alkanehydrazonates, Ia to Il. Method-A. To an ethanolic sodium ethoxide solution (prepared from sodium (0.11 g, 0.005 g atom) and ethanol (20 ml) was added the appropriate phenol (0.005 mol) followed by the hydrazonoyl bromide (0.005 mol). The mixture was stirred for 5 min and left overnight at room temperature. The crude ester that precipitated was collected, washed with water and finally crystallized from methanol. The results are summarized in Table 1.

Method-B. Equivalent amounts (0.005 mol each) of hydrazonoyl bromide and phenol were stirred in ethanol or acetonitrile (30 ml) containing triethylamine (0.01 mol) at room temperature for 2 h. The product was collected by filtration, washed with water and dried. Crystallization from methanol gave the hydrazonates Ia to Il in 50 to 75% yield. The results are given in Table 1.

Reaction of III with Phenol in Presence of Sodium Acetate. To a suspension of III (R=CH_3) (0.003 mol) in ethanol (20 ml) was added a solution of sodium acetate and phenol (0.003 mol each) in water (5 ml). The reaction mixture was stirred for 5 min and left overnight at room temperature. The solid was collected and crystallization from ethanol gave IVa, mp 184—185 °C, Found: C, 50.60; H, 5.07; N, 18.02%. Calcd for $C_{10}H_{11}N_3O_4$: C, 50.63; H, 4.67; N, 17.70%.

Similar treatment of III (R=CH_3CH_2) and III (R=$(CH_3)_2CH$) with phenol and sodium acetate afforded IVe and IVi respectively. Compound IVe, mp 133.5—134 °C; Found: C, 52.98; H, 5.12; N, 16.50%. Calcd for $C_{11}H_{13}N_3O_4$: C, 52.58; H, 5.21; N, 16.72%. Compound IVi, mp 192 °C, Found: C, 54.10; H, 5.66; N, 15.62%. Calcd for $C_{12}H_{15}N_3O_4$: C, 54.32; H, 5.69; N, 15.84%.

Thermal Rearrangement of Aryl Alkanehydrazonates. Method-A: The hydrazonate (0.5 g) was heated in a test tube

in an oil bath at 120 °C for 1 h. The crude product was extracted with acetone. The solvent was then evaporated and the residue was boiled with benzene (20 ml), cooled, then filtered. Crystallization from methanol–water mixture gave II in 60—70% yield.

Method-B: The hydrazonate (0.5 g) was refluxed in xylene for 3 h. The pale yellow solid that precipitated on cooling was collected (0.45 g). Crystallization from methanol–water mixture gave II (*ca.* 0.4 g). The hydrazides prepared are listed in Table 2 together with their physical constants.

Hydrolysis of IIa and IIi. The hydrazide IIa (0.5 g) was refluxed in 95% ethanol (20 ml) and concentrated hydrochloric acid (20 ml) for 10 h. The reaction mixture was then concentrated to its 1/4 volume and cooled. The solid formed was collected, and washed with dilute solution of sodium acetate. Crystallization from dilute methanol gave *N*-phenyl-*N*-(*p*-nitrophenyl)hydrazine, VIII, yellow needles, mp 100—102 °C, Found: C, 62.42; H, 4.85; N, 17.73%. Calcd for $C_{12}H_{11}N_3O_2$: C, 62.86; H, 4.84; N, 18.33%.

Following the same procedure the hydrazide IIi yielded the hydrazine VIII in 55% yield.

Kinetic Experiments. A stock solution 10^{-4} to 10^{-5} M (suitable for UV analysis) in hydrazonate was prepared in xylene at room temperature. The resulting solution was distributed among ampules (15 at minimum). The ampules were placed in an oil bath at 110 ± 1 °C. At suitable time intervals, the ampule was taken out of the bath, quenched in ice and the UV spectrum of its contents was recorded. The first spectrum was usually taken after 10 min to allow temperature equilibration. Complete spectra taken at the end of each kinetic run corresponded to the spectra of hydrazide solution in xylene of the same concentration. Under these conditions reasonable first order plots of log (A_t-A_∞) *vs.* time, *t*, min were obtained. Each kinetic run was repeated at least twice and the average rate constants are reported. The average deviation was $<\pm8\%$.

References

1) A. S. Shawali and H. M. Hassaneen, *Tetrahedron Lett.*, **1972**, 1299.
2) A. S. Shawali and H. M. Hassaneen, *Tetrahedron*, **28**, 5903 (1972).
3) A. S. Shawali and M. K. Ahmad, *Bull. Chem. Soc. Jpn.*, **46**, 3625 (1973).
4) A. S. Shawali, N. F. Eweiss, H. M. Hassaneen, and M. Sami, *Bull. Chem. Soc. Jpn.*, **48**, 365 (1975).
5) M. S. Gibson, *Tetrahedron*, **18**, 1377 (1962); F. L. Scott, M. P. Cashman, and A. F. Hegarty, *J. Chem. Soc., B*, **1971**, 1607.
6) J. S. Clovis, A. Eckell, R. Huisgen, and R. Sustmann, *Chem. Ber.*, **100**, 60 (1967); *J. Org. Chem.*, **33**, 2291 (1968).
7) A. S. Shawali and A. Osman, *Tetrahedron*, **27**, 2517 (1971), and the references cited therein.
8) C. D. Ritchie and W. F. Sager, "Progress in Physical Organic Chemistry," Vol. 2, Interscience Publishers Inc., New York (1964).
9) A. F. Hegarty, J. A. Kearney, and F. L. Scott, *J. Chem. Soc., Perkin 2*, **1973**, 1422.
10) S. Goldschmidt *et al.*, *Ber.*, **53**, 44 (1920); *ibid.*, **55**, 616, 628 (1922); *ibid.*, **61**, 1858 (1928).
11) E. G. E. Hawkins, *J. Chem. Soc., C*, **1971**, 1474; W. F. Taylor, H. A. Weiss, and T. J. Wallace, *J. Org. Chem.*, **34**, 1759 (1969); A. J. Bellamy and R. D. Guthrie, *J. Chem. Soc.*, **1965**, 2788; H. Yao and P. Resnick, *J. Org. Chem.*, **30**, 2832 (1965).
12) A. F. Hegarty, M. P. Cashman, and F. L. Scott, *J. Chem. Soc., Perkin 2*, **1972**, 1381.

Structural Assignment by NMR Analyses of *N*-(Diacylamino)imide Derivatives. Diels-Alder Adducts of 2,3-Dimethylnaphthalene and 6,6-Diphenylfulvene with Maleic Anhydride

Shiva Mohan VERMA and Ashok Kumar SINGH
Department of Chemistry, Banaras Hindu University, Varanasi 221005, India
(Received October 22, 1976)

The configurations of the Diels-Alder adducts of maleic anhydride with 2,3-dimethylnaphthalene and 6,6-diphenylfulvene have been investigated by NMR spectroscopy. Restricted rotation and non-planar conformations about the N–N bond in the corresponding *N*-aminoimide derivatives of the adducts have been employed in solving the structural problem. While the *N'*,*N'*-diacetyl system has been shown to be a suitable probe for configurational assignment, *N'*-acetyl-*N'*-aroyl-*N*-aminoimide derivatives have been found to be a more diagnostic probe even to simple adducts.

Preferred conformations about N–N bond in the system of type I have been reported with the help of a cage-moiety which is asymmetric about the plane of the succinimydyl ring.[1–3] Hindered rotation and non-planar conformations about N–N bond in *N'*,*N'*-diacylaminoimides of Diels-Alder adducts have been used for their configurational (*endo*/*exo*) assignments. The utility of this NMR technique was first explored with naphthalene maleic anhydride adducts and their reduction products as model compounds. It is shown that *N'*-acetyl-*N'*-aroyl-*N*-aminoimide system can be a versatile probe for direct determination of the configurations of such adducts.[4,5] It is evident that this system enables the assignment of correct configuration to either *endo* or *exo*-adduct without a comparison with the pattern of the corresponding isomer, and therefore, this method offers a distinct advantage over the earlier methods especially when one of the isomers is not formed.

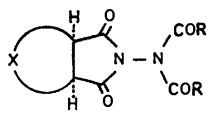

X= Chain of four Carbons

I

In this communication we have demonstrated the configurational assignment of 2,3-dimethylnaphthalene–maleic anhydride and 6,6-diphenylfulvene–maleic anhydride Diels-Alder adduct with the help of NMR spectral studies of their *N*-aminoimide derivatives (IIa—IId, IIIa—IIIf, IVa—IVd, and Va—Vd).

The Diels-Alder reaction of 2,3-dimethylnaphthalene with maleic anhydride was reported by Kloetzel and Herzog[6] to give adducts having the benzobicyclo-[2.2.2]octene system. The configuration of anhydride group of the adduct was studied by these workers with the help of UV absorption and also by chemical methods but the problem remained unsettled. This Diels-Alder reaction has also been carried out in the presence of aluminium chloride and the product was assigned the *exo*-configuration[7] which was later shown to have the *endo*-configuration. The configuration of these adducts has been proposed with the help of their NMR spectra: the one which has deshielded C-2 and C-3 methine protons (δ 3.41) was assigned the *endo*-configuration

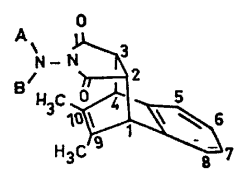

II-*exo**

(IIa) A=B=H
(IIb) A=B=$COCH_3$
(IIc) A=$COCH_3$, B=COC_6H_5
(IId) A=$COCH_3$, B=$COC_6H_4CH_3(p)$

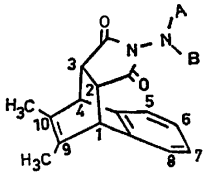

III-*endo**

(IIIa) A=B=H
(IIIb) A=B=$COCH_3$
(IIIc) A=$COCH_3$, B=COC_6H_5
(IIId) A=$COCH_3$, B=$COC_6H_4CH_3(o)$
(IIIe) A=$COCH_3$, B=$COC_6H_4CH_3(m)$
(IIIf) A=$COCH_3$, B=$COC_6H_4CH_3(p)$

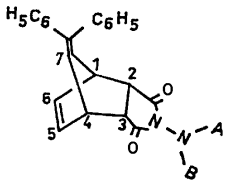

IV-*endo***

(IVa) A=B=H
(IVb) A=B=$COCH_3$
(IVc) A=H, B=COC_6H_5
(IVd) A=$COCH_3$, B=COC_6H_5

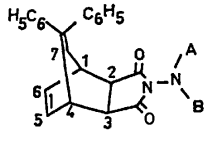

V-*exo***

(Va) A=B=H
(Vb) A=B=$COCH_3$
(Vc) A=H, B=COC_6H_5
(Vd) A=$COCH_3$, B= COC_6H_5

while the other having shielded C-2 and C-3 methine protons (δ 3.28), the *exo*-configuration.[8,9] The *exo*- and *endo*-adducts were also confirmed by lactonization studies: the adduct which formed an iodolactone was assigned an *exo*-configuration, while the other isomer which did not undergo lactone formation but yielded

* The prefixes *endo* and *exo* are used in the sense that substituents on the same side of the bicyclo[2.2.2]octene ring as benzene ring are *endo*, those on the other side are *exo*.

** The prefixes *endo* and *exo* are used in the sense that the isomer with the succinimidyl ring towards the cage olefinic system is *endo* and that with the succinimidyl ring away from the olefinic system is *exo*.

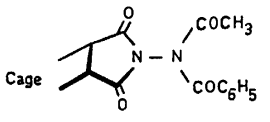

VI

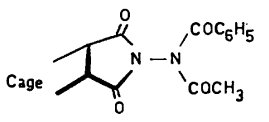

VII

its carboxylic acid was given *endo*-configuration.[9] Based on aromatic solvent induced shift studies in rigid cyclic ketones,[10] the configurations of these adducts have also been reported.[9] These adducts showed a small shift difference for the methyl protons and the configuration of either *exo*- or *endo* can be assigned only when the spectrum of the other corresponding isomer is available.

The configuration of 6,6-diphenylfulvene and maleic anhydride adduct was first studied by the ozonization method and was assigned the *exo*-configuration, no *endo*-isomer being produced.[11] The work was reinvestigated and the *endo* and *exo* configurations were established by chemical methods. The *endo*-adduct on treatment with hypobromous acid formed bromolactone acid which subsequently yielded a dilactone. The *exo*-adduct formed a lactone acid with hypobromous acid.[12]

Results and Discussion

N-(Diacylamino)imide Derivatives (IIb—IId and IIIb—IIIf) The NMR spectra of the isomeric *N*-(diacylamino) imide derivatives (IIb and IIIb) are in accordance with the restricted rotation about N–N bond showing two singlets each for the *N'*-acetyl protons with an internal chemical shift of 10 Hz and 97 Hz, respectively (Table 1). On shielding considerations on one of the *N'*-acetyl groups, IIIb could be assigned the *endo*-configuration and IIb the *exo*-configuration.[5]

The spectra of *N'*-acetyl-*N'*-benzoyl derivatives (IIc and IIIc) exhibit two conformations VI and VII resulting from the restricted rotation about N–N bond. Splitting in the cage-methyl resonances by the *N'*-benzoyl group in the compound IIc confirms the *exo*-configuration of the adduct (Table 1). In the other isomeric product IIIc, the cage-methyl resonances remain unaffected and the splitting in the *N'*-acetyls ($\Delta\nu$=60 Hz) demonstrates the *endo*-configuration of the adduct.

A careful study of the spectra shows the preference for conformation (VII) in both the *endo* and *exo*-isomers, where the *N'*-benzoyl group lies *anti* to the cage-moiety. While the conformational preference (VI) has been reported in the *exo*-derivatives of naphthalene-maleic anhydride adduct,[5] sterically the same conformer is not favoured in the case of IIc. The other *N'*-acetyl-*N'*-aroyl compounds (IId and IIId—IIIf) also support the configurational assignment.

N',N'-Diacetyl Derivatives (IVb and Vb). The NMR spectra of *N',N'*-diacetyl-*N*-amino [2.2.1] bicyclo-5-heptene-7-diphenylmethylene-2,3-*endo/exo*-dicarboximide (IVb) and (Vb) in $CDCl_3$ exhibit a similar pattern (Table 2). These isomeric compounds show two singlets, one each for *N'*-acetyl protons, with an internal chemical shift of 16 and 20 Hz, respectively, along with other proton resonances. These observations suggest that the C-5 and C-6 olefinic protons and 7-diphenylmethylene group exert a similar shielding effect on the *N'*-acetyl protons. In such a system where *N'*-acetyls do not appear to be a diagnostic probe for the configurational study, introduction of a group at the *exo*-cyclic nitrogen, which can strongly influence the resonance of the cage protons, would give useful information. *N'*-Acetyl-*N'*-benzoyl-*N*-amino-

Table 1. 60MHz NMR Spectral data[a] of the compounds IIa—IId and IIIa—IIIf

Compound	δA	δB	δ(1+4)	δ(2+3)	δ(9+10)	δ(5—8)
IIa	4.28 (m, 1H)	4.28 (m, 1H)	4.08 (t, 2H)	2.92 (t, 2H)	1.7 (s, 6H)	7.13 (m, 4H)
IIb	2.28 (ds, 3H), 1: 1; 10 Hz	2.28 (ds, 3H), 1: 1; 10 Hz	4.21 (t, 2H)	3.1 (t, 2H)	1.76 (s, 6H)	7.23 (m, 4H)
IIc	2.44 (ds, 3H), 2: 1; 11 Hz	7.39 (m, 5H)	4.12 (m, 2H)	2.89 (dt, 2H), 1: 2; 23 Hz	1.57 (ds, 6H), 2: 1; 22 Hz	7.39 (m, 4H)
IId	2.47 (ds, 3H), 2: 1; 6 Hz	2.33 (s, 3H) 7.28 (m, 4H)	4.16 (m, 2H)	2.85 (dt, 2H), 1: 2; 19.5 Hz	1.60 (ds, 6H), 2: 1; 20 Hz	7.28 (m, 4H)
IIIa	3.67 (m, 1H)	3.67 (m, 1H)	4.17 (t, 2H)	3.09 (t, 2H)	1.84 (s, 6H)	7.21 (m, 4H)
IIIb	1.67 (ds, 3H), 1: 1; 97 Hz	1.67 (ds, 3H), 1: 1; 97 Hz	4.17 (t, 2H)	3.32 (t, 2H)	1.83 (s, 6H)	7.14 (m, 4H)
IIIc	1.70 (ds, 3H), 1: 7; 60 Hz	7.31 (m, 5H)	4.15 (t, 2H)	3.23 (t, 2H)	1.82 (s, 6H)	7.31 (m, 4H)
IIId	1.71 (ds, 3H), 1: 8; 58 Hz	2.27 (ds, 3H), 8: 1; 5 Hz 7.23 (m, 4H)	4.16 (t, 2H)	3.23 (t, 2H)	1.82 (s, 6H)	7.23 (m, 4H)
IIIe	1.72 (ds, 3H), 1: 10; 60 Hz	2.34 (ds, 3H), 10: 1; 2 Hz 7.30 (m, 4H)	4.19 (t, 2H)	3.27 (t, 2H)	1.86 (s, 6H)	7.30 (m, 4H)
IIIf	1.70 (ds, 3H), 1: 7; 62 Hz	2.35 (s, 3H) 7.25 (m, 4H)	4.15 (t, 2H)	3.24 (t, 2H)	1.82 (s, 6H)	7.25 (m, 4H)

a) The NMR spectra of all the compounds were recorded in $CDCl_3$. The total number of protons and the multiplicity of the bands are indicated brackets. In case of multiplicity due to slow rotation, the ratio of the intensity of downfield to upfield and the separation in Hz are indicated. In case of multiplets the mean δ values are given: s= singlet, t=triplet, m=multiplet, ds=double singlet, dt=double triplet, dm=double multiplet. TMS was used as an internal reference.

Table 2. 60 MHz NMR Spectral data of the compounds IVa—IVd and Va—Vd

Compound	δA	δB	δ(5+6)	δ(1+4)	δ(2+3)	Aromatic Protons
IVa	3.25 (m, 1H)	3.25 (m, 1H)	6.37 (t, 2H)	3.92 (m, 2H)	3.4 (m, 2H)	7.23 (m, 10H)
IVb	2.3 (ds, 3H), 1: 1; 16 Hz	2.3 (ds, 3H), 1: 1; 16 Hz	6.35 (t, 2H)	4.05 (m, 2H)	3.68 (m, 2H)	7.24 (m, 10H)
IVc	2.15 (m, 1H)	7.28 (m, 5H)	6.52 (t, 1H)	3.97 (m, 2H)	3.52 (m, 2H)	7.28 (m, 10H)
IVd	2.53 (ds, 3H), 2: 1; 4 Hz	7.26 (m, 5H)	6.04 (dt, 2H), 1: 2; 57 Hz	3.86 (m, 2H)	3.41 (dm, 2H), 2: 1; 17 Hz	7.26 (m, 10H)
Va	3.81 (m, 1H)	3.81 (m, 1H)	6.51 (t, 2H)	3.73 (m, 2H)	2.92 (s, 2H)	7.16 (m, 10H)
Vb	2.32 (ds, 3H), 1: 1; 20 Hz	2.32 (ds, 3H), 1: 1; 20 Hz	6.62 (t, 2H)	4.03 (m, 2H)	3.03 (s, 2H)	7.2 (m, 10H)
Vc	7.82 (m, 1H)	7.18 (m, 5H)	6.54 (t, 2H)	3.86 (m, 2H)	2.86 (m, 2H)	7.23 (m, 10H)
Vd	2.2 (ds, 3H), 2: 3; 29 Hz	7.21 (m, 5H)	6.50 (t, 2H)	3.82 (m, 2H)	2.81 (m, 2H)	7.21 (m, 10H)

imide system has been found to be suitable for the purpose.

N'-Acetyl-N'-benzoyl Derivatives (IVd and Vd) The NMR spectrum of IVd shows multiplicity for C-5 and C-6 olefinic proton resonances ($\Delta\nu$=57 Hz) as well as for the *N'*-acetyl protons (intensity ratio 2: 1, $\Delta\nu$=4 Hz) with other proton resonance (Table 2) caused by restricted rotation about the N–N bond. The spectral features of the compound IVd are very similar to those of *N'*-acetyl-*N'*-benzoyl derivative of *N*-amino[2.2.1]-bicyclo-5-heptene-2,3-*endo*-dicarboximide. The compound also shows preference for the conformation (VI) where the benzoyl group lies *syn* to the cage-olefinic protons. The multiplicity in the cage-olefinic protons indicates the *endo*-configuration of the adduct. The spectrum of the isomeric compound Vd shows two singlets for *N'*-acetyl protons (intensity ratio 2: 3, $\Delta\nu$= 29 Hz) and a triplet for C-5 and C-6 olefinic protons along with other proton resonance (Table 2). The spectral pattern is in conformity with the restricted rotation about N–N bond, showing the presence of two conformations. The appearance of *N'*-acetyl resonance at the shielded position (δ 1.96) indicates that the conformation (VII), in which the acetyl group lies *syn* to 7-diphenylmethylene, is preferred. Since no multiplicity in the cage-olefinic resonance has been observed, the spectrum indicates it to be an *exo*-adduct. Shielding of the *N'*-acetyl protons by the 7-diphenylmethylene further supports the *exo*-configuration.

Experimental

NMR spectra were recorded on a Varian A-60D spectrometer equipped with a variable temperature controller (Model No. V-6040). IR spectra were recorded for Nujol mulls on Perkin-Elmer-720 spectrophotometer. NMR spectral data are given in Tables 1 and 2, and IR spectral data, melting points and elemental analyses of all the compounds (IIa—IId, IIIa—IIIf, IVa—IVd, and Va—Vd) in Table 3.

Table 3. Mps, elemental analysis and characteristic IR peaks

Compound	Mp, °C	Found		Calcd		IR ν_{max}, cm^{-1}
		C%	H%	C%	H%	
IIa	185—187	71.48	5.89	71.62	6.01	3340m, 3260m, 3185m, 1780m, 1715s, 1620w
IIb	215—217	68.02	5.54	68.17	5.72	1800w, 1750s, 1739s, 1710m
IIc	159—160	72.40	5.29	72.45	5.35	1795w, 1750s, 1735s, 1720m, 1610w
IId	214—215	72.66	5.50	72.88	5.65	1790w, 1740s, 1730s, 1605w
IIIa	193—195	71.52	5.84	71.62	6.01	3350m, 3275w, 1780m, 1715s, 1695s, 1595w
IIIb	180—182	68.32	5.78	68.17	5.72	1795w, 1730s, 1710m
IIIc	204—206	72.15	5.15	72.45	5.35	1790w, 1735s, 1720m, 1605w
IIId	212—214	72.56	5.48	72.88	5.65	1800w, 1735s, 1710m, 1610w
IIIe	175—177	73.03	5.70	72.88	5.65	1795w, 1740s, 1715m, 1605w
IIIf	232—234	72.69	5.52	72.88	5.65	1795w, 1735s, 1710s, 1610m
IVa	150—152	76.92	5.16	77.17	5.30	3325m, 3205w, 1795m, 1705s, 1600w
IVb	204—205	73.01	5.17	73.23	5.20	1800w, 1735s, 1610w
IVc	158—160	79.21	5.04	78.01	4.97	3450m, 3175m, 1800w, 1710s, 1670s, 1635m, 1600w
IVd	199—200	76.11	4.82	76.23	4.92	1795w, 1740s, 1600w
Va	114—116	76.86	5.20	77.17	4.30	3350m, 3280m, 3195w, 1780m, 1710s, 1610m
Vb	128—130	73.44	5.29	73.23	5.20	1795w, 1735s, 1705m, 1605w
Vc	162—164	77.76	4.86	78.01	4.97	3475m, 3250m, 1790w, 1730s, 1710s, 1605w
Vd	145—147	77.19	4.86	76.23	4.92	1790w, 1730s, 1605w

m=medium, s=strong and w=weak

*1,2,3,4-Tetrahydro-9,10-dimethyl-1,4-ethenonaphthalene-2,3-*exo/endo-*dicarboxylic Anhydride.* The *exo* and *endo*-adducts of 2,3-dimethylnaphthalene and maleic anhydride were obtained by the method of Kloetzel and Herzog.[6] A mixture of 2,3-dimethylnaphthalene (1 g) and maleic anhydride (19 g) was heated on an oil bath at 99—100 °C for about 24 h. The hot reaction mixture was poured into water; unreacted maleic anhydride went into the solution leaving behind adduct (*exo/endo*) diacids and 2,3-dimethylnaphthalene. The product was subsequently washed with water and the unreacted 2,3-dimethylnaphthalene was eliminated by converting the *exo/endo*-diacids into water soluble potassium salts by treating the mixture with KOH solution (5%). These acids were liberated by acidification with hydrochloric acid, filtered and then converted into their anhydrides by heating with acetic anhydride on a water bath for about 2 h. A fractional crystallization procedure from carbontetrachloride was developed for the isolation of *exo* (mp 193—195 °C) and *endo* (mp 175—176 °C) adducts. The *exo*-isomer crystallized out first.

[*2.2.1*]*Bicyclo-5-heptane-7-diphenylmethylene-2,3-*endo/exo*dicarboxylic Anhydride.* These isomeric adducts were obtained according to the method of Alder *et al.*[12] The *endo*-isomer was obtained from 6,6-diphenylfulvene and maleic anhydride in benzene solution at room temperature which on recrystallisation from ethylacetate melted at 174 °C. However, the more predominant *exo*-adduct was obtained on boiling the reactants in xylene. The *exo*-adduct was more soluble in ethylacetate (mp 147 °C).

N-*Aminoimide Derivatives (IIa, IIIa, IVa, and Va).* *N*-Aminoimide derivatives of these isomeric adducts were prepared by adding hydrazine hydrate dropwise while stirring, to the equimolar quantities of adducts in ethanol at room temperature. These *N*-amino-imides were characterised by IR, NMR and chemical analyses.

N′,N′-*Diacetyl Derivatives (IIb, IIIb, IVb, and Vb).* *N′,N′*-Diacetyl derivatives were prepared by heating the corresponding *N*-aminoimides with an excess of acetic anhydride. The product was washed with water, dried and recrystallized from ethanol.

N′-*Acetyl*-N′-*aroyl Derivatives (IIc, IId, IIIc—IIIf, IVd, and Vd).* The *N′*-acetyl-*N′*-benzoyl derivatives were prepared in two steps: *N′*-mono benzoyl derivatives were obtained by refluxing equimolar amounts of *N*-aminoimides and benzoyl chloride with a few drops of pyridine in dry benzene for 4 h. After removal of the solvent, the product was washed with water and recrystallized. The mono-benzoyl derivatives thus obtained were acetylated with an excess of acetic anhydride and a few drops of pyridine on a water bath for 3—4 h. The product was washed with water, dried and recrystallized from ethanol. The other aroyl derivatives were obtained in the same way.

We thank the C.S.I.R., India, for the award of a research fellowship (to A. K. Singh).

References

1) a) B. H. Korsch and N. V. Riggs, *Tetrahedron Lett.*, **1966**, 5897; b) N. V. Riggs and S. M. Verma, *Aust. J. Chem.*, **23**, 1913 (1970).

2) S. M. Verma and C. Koteswara Rao, *Tetrahedron*, **28**, 5029 (1972).

3) a) S. M. Verma and R. Prasad, *J. Org. Chem.*, **38**, 1004 (1973); b) S. M. Verma and O. Subba Rao, *Aust. J. Chem.*, **26**, 1963 (1973).

4) S. M. Verma, O. Subba Rao, and C. Koteswara Rao, *Tetrahedron Lett.*, **1973**, 1639.

5) S. M. Verma and O. Subba Rao, *Tetrahedron*, **30**, 2371 (1974).

6) M. C. Kloetzel and H. L. Herzog, *J. Am. Chem. Soc.*, **72**, 1991 (1950).

7) P. Yates and P. Eaton, *J. Am. Chem. Soc.*, **82**, 4436 (1960).

8) A. Oku, Y. Ohnishi, and F. Mashio, *J. Org. Chem.*, **37**, 4264 (1972).

9) J. W. Zuzack, W. J. Hufker, Jr., H. B. Donahue, J. S. Meek, and J. J. Flynn, *J. Org. Chem.*, **37**, 4481 (1972).

10) D. H. Williams, *Excerpta Med. Found. Int. Congr. Ser.*, No. 132, 159 (1966).

11) O. Diels, K. Alder, and P. Pries, *Ber.*, **62**, 2081 (1929).

12) K. Alder, F. W. Chambers, and W. Trimborn, *Ann.*, **566**, 27 (1950).

Structural Assignment by NMR Spectroscopy: Restricted Rotation about Aryl C–N Bond and Configurations of Diels-Alder Adducts

Shiva Mohan VERMA and Nripendra B. SINGH

Department of Chemistry, Banaras Hindu University, Varanasi 221005, India

(Received February 28, 1977)

Restricted rotation and non-planar conformations about the aryl C–N bond in *ortho* substituted arylimides have been studied in order to assign the *endo* and *exo* configurations of Diels-Alder adducts, employing the adducts of maleic anhydride with naphthalene and cyclopentadiene as model compounds. The adducts are readily transformed into their *o*-tolylimide derivatives and the *N*-*o*-tolyl probes satisfactorily into the magnetic environment of the cage moiety. In 1-naphthylimide derivatives, the *naphthyl* group causes splitting in the cage-proton resonances and is found to be more diagnostic for structural assignment.

Recently we reported restricted rotation and non-planar ground state conformations about the aryl C–N bond in a system of type (I).[1] The high energy barrier (ΔG^* 22 kcal/mol) was attributed purely to the steric interaction of the *o*-substituent, the carbonyl groups of the succinimidyl ring which is of similar order as that of the N–N bond in tetracylhydrazines (II) having lone pair electronic interactions at the two nitrogens.[2] With the help of conformational studies about the N–N bond through their *N*-aminoimide derivatives the *endo*/*exo* configuration of Diels-Alder adducts of maleic anhydride with cyclic dienes such as cyclopentadiene,[3] β-naphthol,[4] naphthalene,[5,6] and substituted anthracenes[7] was demonstrated. In this communication the applicability of the N–C bond conformations in the structural assignment of the Diels-Alder adducts is discussed. *o*-Substituted phenylimide(I) is quite diagnostic and effective in the structural elucidation which can easily be obtained from the DA adducts in one step under ordinary experimental conditions. Earlier studies revealed that *o*-CH_3 or 2,3-*benzo* substituents in the *N*-phenyl(I) can be more diagnostic than *o*-OCH_3, *o*-Cl, and *o*-Br substituents in the structural assignments.[1] *o*-Substituted anilides of cyclopentadiene–maleic anhydride and naphthaline–maleic anhydride and their reduced products (III to X) have been prepared and their NMR spectra are discussed in the light of their configurational assignment.

Results and Discussion

Naphthalene–Maleic Anhydride Adducts (endo/exo) *1) o-Toluidide Derivatives (IIIa, IVa)*: The NMR spectrum of the compound IIIa shows two singlets for the *o*-tolyl methyl protons at δ 1.0 and 2.0 and a multiplet of 0.58 H intensity at δ 5.45 along with the other normal proton resonances (Table 1). In the other isomeric derivative (IVa), the *o*-tolyl protons also appear as two singlets at δ 2.10, and 2.13 along with other normal resonances (Table 1). These spectral multiplicities are due to the hindered rotation about aryl C–N bond[1] and the existence of the two conformations XI and XII is indicated.

On the basis of shielding effect on the syn-*o*-tolyl protons by the cage-moiety (XII) a reasonable assignment of the configuration of the adduct is possible. A high degree of shielding on the *o*-methyl protons ($\Delta\nu$= 60 Hz) suggests the *endo* configuration for IIIa while

TABLE 1. 60 MHz NMR SPECTRAL DATA[a] (δ ppm) OF THE COMPOUNDS IIIa, IIIb, IVa, IVb, Va, Vb, VIa, VIb

Compound	R	Ortho (*N*-phenyl)	2+3	1+4	9+10	5—8+*N*-phenyl (m & p)
IIIa	1.0, 2.0 (ds, 2: 3, 3H)	5.45, 7.16 (dm, 3: 2, 1H)	3.23 (t, 2H)	4.5 (m, 2H)	6.65 (q, 2H)	7.16 (m, 7H)
IIIb	7.33 (m, 4H)	5.33, 7.33 (dm, 2: 1, 1H)	3.33 (t, 2H)	4.53 (m, 2H)	6.5 (q, 2H)	7.33 (m, 6H)
IVa	2.10, 2.13 (ds, 6: 7, 3H)	7.18 (m, 1H)	3.13 (t, 2H)	4.48 (m, 2H)	6.65 (q, 2H)	7.18 (m, 7H)
IVb	7.5 (m, 4H)	7.5 (m, 1H)	3.15 (m, 2H)	4.51 (m, 2H)	6.66, 6.83 (dq, 1: 1, 2H)	7.5 (m, 6H)
Va	0.9, 2 (ds, 2: 3, 2H)	5.45, 7.25 (dm, 3: 2, 1H)	3.27 (t, 2H)	4.51 (m, 2H)	1.53 (q, 4H)	7.25 (m, 7H)
Vb	7.43 (m, 4H)	5.3, 7.43 (dm, 2: 1, 1H)	3.33 (t, 2H)	3.73 (m, 2H)	1.66 (q, 4H)	7.43 (m, 6H)
VIa	2.15, 2.31 (ds, 5: 7, 3H)	7.25 (m, 1H)	3.01 (m, 2H)	3.61 (m, 2H)	1.66 (bq, 4H)	7.25 (m, 7H)
VIb	7.43 (m, 4H)	7.43 (m, 1H)	3.12 (m, 2H)	3.81 (m, 2H)	1.68 (m, 4H)	7.43 (m, 6H)

a) The NMR spectra of all the compounds were recorded in $CDCl_3$. The total number of protons and the multiplicity of the bands are indicated in brakets. In the case of multiplicity due to slow rotation, the ratio of the intensity of the upfield to down field signales are indicated. Signals are abbreviated as: s=singlet; t=triplet; ds=double singlet; dt=double triplet; q=quartet; dq=double quartet; bq=broad quartet; dm=double multiplet.

the small shielding value ($\Delta\nu$=2 Hz) suggests the *exo*-configuration for IVa.

The *endo* configuration for IIIa is further demonstrated by the observation of a multiplet at δ 5.45 (0.58 H) which could arise from the shielding of the *ortho*-hydrogen of the *N*-phenyl by the cage benzo ring in the conformer XI.

2) 1-Naphthylimide Derivatives (IIIb, IVb): The spectra of 1-naphthylimide derivatives of the isomeric adducts (*endo*/*exo*) are diagnostic in the configurational assignment of the adducts as the 2,3-benzo group of the 1-naphthylimide strongly influences the resonances of the cage protons providing fruitful results.

The NMR spectrum of VIb shows a double quartet for the C9 and C10 olefinic protons at δ 6.66 and 6.83 ($\Delta\nu$=10 Hz) with other normal proton resonances, while the spectrum of the other isomeric adduct IIIb shows a single quartet for the C9 and C10 olefinic protons at δ 6.5 and a multiplet at δ 5.33 (0.68 H) for the *ortho* proton of the naphthylimide. The appearance of the olefinic protons as a double quartet in IVb indicates the *exo* configuration of the adduct, whereas no multiplicity in the olefinic proton resonances as well as the appearance of the *ortho* naphthyl proton at a shielded postion in IIIb suggest the *endo* configuration.

3) o-Toluidides of Reduced Products (Va, VIa): The NMR spectra of both the isomeric adducts (Va, VIa) show a double singlet each for the tolyl methyl protons with internal chemical shifts of 66 Hz and 10 Hz respectively. The spectrum of Va also shows a multiplet for the *ortho N*-phenyl proton at an upfield position and a quartet for the C9 and C10 methylene protons at δ 1.53, while the spectrum of VIa shows a broad quartet at δ 1.66 for the C9 and C10 methylene protons (Table 1). These observations further support the assignment of the *endo* (Va) and *exo* configurations (VIa).

4) 1-Naphthylimide Derivatives of the Reduced Products (Vb, VIb): The NMR spectra exhibit similar features to those of the unreduced derivatives (IIIb, IVb). The spectrum of Vb shows a quartet for the C9 and C10 protons at δ 1.66, while (VIb) shows a broad multiplet at δ 1.68 for C9 and C10 protons (Table 1). The appearance of the broad multiplet for the C9 and C10 protons is caused by the shielding of the 2,3-*benzo* group and the adduct could be assigned as *exo*, while a quartet in the spectrum of Vb for C9 and C10 indicates the *endo* configuration.

Cyclopentadiene–Maleic Anhydride Adducts.

1) o-Toluidide Derivatives (VIIa, VIIIa): The configuration of the adducts (*endo*/*exo*) could be assigned by comparing the spectra of their *o*-toluidide derivatives. The NMR spectrum of VIIa shows two singlets for the *o*-tolyl methyl protons at δ 2.06 and 2.09 with an internal chemical shift of 2 Hz and an AB quartet for C7 methylene protons at δ 1.53 and δ 1.78, while the other isomer (VIIIa) shows a singlet of 3H intensity at δ 2.16 for the *o*-tolyl protons and a multiplet at δ 1.58 for the C7 methylene proton (Table 2).

The spectral pattern is in conformity with the restricted rotation about N–C bond and the existence of two conformations XI and XII is indicated. The multiplicity in methyl resonances of the *o*-tolyl group indicates the *endo* configuration (VIIa) whereas its appearance as a singlet suggests the *exo* configuration (VIIIa) resulting from the less magnetic interaction of methylene bridge.

2) 1-Naphthylimide Derivatives (VIIb, VIIIb): Compound VIIb shows a double triplet for the C5 and C6 olefinic protons at δ 6.4 and 6.58 ($\Delta\nu$=11 Hz) and an AB quartet for the C7 methylene protons with other normal proton resonances (Table 2). The spectrum of the other isomeric compounds (VIIIb) shows a triplet at δ 6.3 for the olefinic protons along with duplication in the resonances of C7, C2+C3, and C1+C4 protons (Table 2). The multiplicity in the olefinic protons suggests the *endo* configuration for (VIIb), while a single triplet for the olefinic protons as well as the multiplicity in methylene proton resonances indicate the *exo* configuration (VIIIb).

3) o-Toluidide of Reduced Products (IXa, Xa): The spectra of the reduced products (IXa and Xa) also exhibit similar features to those of their unreduced de-

Table 2. 60 MHz NMR spectral[a] data (δ ppm) of the compounds VIIa, VIIb, VIIIa, VIIIb, IXa, IXb, Xa, Xb

Compound	R	2+3	1+4	7 AB	5+6	Aromatic
VIIa	2.06, 2.09 (ds, 7: 8, 3H)	3.4 (s, 2H)	3.4 (s, 2H)	1.53, 1.78 (q, 2H)	6.28 (t, 2H)	7.06 (m, 4H)
VIIb	7.5 (m, 4H)	3.53 (s, 2H)	3.53 (s, 2H)	1.61, 1.85 (q, 2H)	6.40, 6.58 (dt, 6: 4, 2H)	7.5 (m, 3H)
VIIIa	2.16 (s, 3H)	2.88 (s, 2H)	3.43 (m, 2H)	1.58 (bm, 2H)	6.4 (t, 2H)	7.18 (m, 4H)
VIIIb	7.11 (m, 4H)	2.88, 2.93 (ds, 1: 1, 2H)	3.35 (m, 2H)	1.63, 1.8 (dbm, 2H)	6.3 (t, 2H)	7.11 (m, 3H)
IXa	2.11, 2.23 (ds, 7: 8, 3H)	2.93 (m, 2H)	3.26 (m, 2H)	1.66 (m, 2H)	1.66 (m, 4H)	7.2 (m, 4H)
IXb	7.5 (m, 4H)	2.93 (m, 2H)	3.71 (m, 2H)	1.7 (m, 2H)	1.7 (m, 4H)	7.5 (m, 3H)
Xa	2.15 (s, 3H)	2.83 (m, 2H)	2.83 (m, 2H)	1.58 (m, 2H)	1.53 (q, 4H)	7.08 (m, 4H)
Xb	7.55 (m, 4H)	2.81 (ds, 2H)	3.4 (bm, 2H)	1.55 (bm, 2H)	1.55 (bm, 4H)	7.55 (m, 3H)

a) The NMR spectra of all the compounds were recorded in $CDCl_3$. The total number of protons and the multiplicity of the bands are indicated in brackets. In the case of multiplicity due to slow rotation the ratio of the intensity of the upfield to down field signals are indicated. Signals are abbreviated as: s=singlet; t=triplet; m=multiplet; ds=double singlet; dt=double triplet; dm=double multiplet; bm=broad multiplet; dbm=double broad multiplet.

rivatives (VIIa and VIIIa). In IXa, the tolyl methyl protons appear as two singlets at δ 2.11 and 2.23 with an internal chemical shift of 7 Hz and C5 and C6 protons appear as a quartet at δ 1.66, whereas the *o*-methyl protons in Xa appear as a singlet at δ 2.15 and C5 and C6 protons as a multiplet (Table 2). The *endo* configuration can thus be assigned to IXa and *exo* configuration to Xa.

4) 1-Naphthylimide Derivatives of Reduced Products (IXb, Xb): The spectra of these derivatives also provide valuable information regarding the structural elucidation of the adducts. The naphthyl group influences the C5 and C6 cage methylene protons in IXb, indicating the *endo* configuration, while C5 and C6 methylene protons remain unaffected in Xb suggesting the *exo* configuration (Table 2).

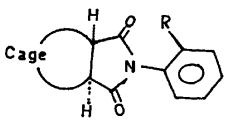

(I)

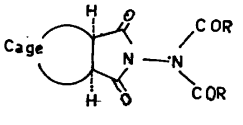

(II)

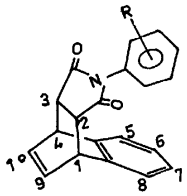

(III) *endo**
(III) a R=*o*-CH_3
b R=2,3-benzo

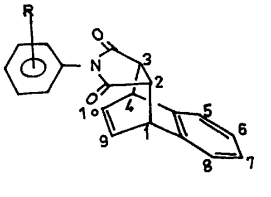

*exo** (IV)
(IV) a R=*o*-CH_3
b R=2,3-benzo

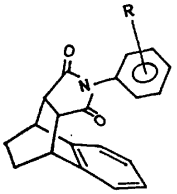

(V) *endo**
(V) a R=*o*-CH_3
b R=2,3-benzo

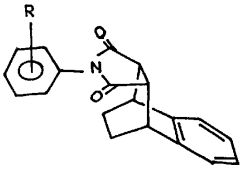

*exo** (VI)
(VI) a R=*o*-CH_3
b R=2,3-benzo

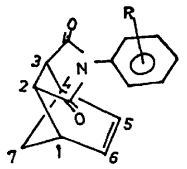

(VII) *endo***
(VII) a R=*o*-CH_3
b R=2,3-benzo

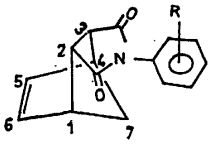

*exo*** (VIII)
(VIII) a R=*o*-CH_3
b R=2,3-benzo

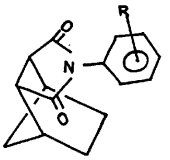

(IX) *endo***
(IX) a R=*o*-CH_3
b R=2,3-benzo

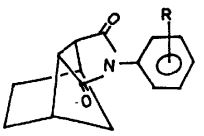

*exo*** (X)
(X) a R=*o*-CH_3
b R=2,3-benzo

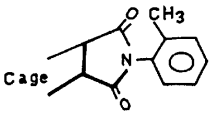

(XI)

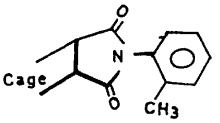

(XII)

* Prefixes *endo* and *exo* are used in the sense that substituents on the same side of the bicyclo[2.2.2]octene ring as benzene ring are *endo*, those on the other side are *exo*.

** Prefixes *endo* and *exo* are used in the sense that substituents on the same side of [2.2.1]bycyclo-5-heptene are *endo* and those on the other side are *exo*.

TABLE 3. MP, ELEMENTAL ANALYSES AND CHARACTERISTIC IR PEAKS

Compound	Mp, °C	Calcd		Found		IR ν_{max}, cm^{-1}
		C%	H%	C%	H%	
IIIa	188—189	79.98	5.43	79.79	5.32	1705s, 1780w, 765m
IIIb	185—186	82.03	4.88	81.98	4.65	1700s, 1780w, 765m
IVa	205—208	79.98	5.43	79.76	5.25	1700s, 1780w, 760m
IVb	210—211	82.03	4.88	82.13	4.66	1705s, 1775w, 765m
Va	214—215	79.47	6.03	79.31	5.98	1700s, 1770w, 780m
Vb	248—251	81.56	5.42	81.38	5.28	1705s, 1780w, 785m
VIa	174—177	79.47	6.03	79.29	6.23	1700s, 1775w, 780m
VIb	200—201	81.56	5.42	81.32	5.35	1700s, 1770w, 770m
VIIa	126—129	75.87	5.97	75.72	5.79	1700s, 1775w, 750m
VIIb	152—153	78.87	5.23	78.69	5.45	1705s, 1780w, 775m
VIIIa	228—229	75.87	5.97	75.69	5.72	1705s, 1775w, 760m
VIIIb	208—211	78.87	5.23	78.69	5.03	1710s, 1780w, 760m
IXa	143—146	75.27	6.71	75.37	6.98	1700s, 1775w, 775m
IXb	193—194	78.33	5.88	78.13	5.62	1705s, 1770w, 765m
Xa	198—199	75.27	6.71	75.37	6.81	1700s, 1770w, 770m
Xb	228—230	78.33	5.88	78.13	5.63	1710s, 1780w, 770m

m=medium, s=strong and w=weak

Experimental

NMR spectra were recorded on a Varian A60D spectrometer at 45 °C. Spectral data of the compounds are given in Tables 1 and 2. Infrared spectra were recorded in Nujol mull on a Perkin Elmer-720 spectrometer. Melting points, chemical analyses and IR bands of the compounds are given in Table 3.

*Naphthalene-Maleic Anhydride Adducts (*endo/exo*) and Their Derivatives (IIIa, IVa, IIIb, IVb, Va, VIa, Vb, VIb).* The *endo* and *exo* adducts of maleic anhydride with naphthalene were obtained according to the method of Takeda *et al.*[8] and separated from ethanol by fractional crystallisation. Adducts were transformed into their toluidide (IIIa and IVa) and naphthylimide derivatives (IIIb and IVb) by heating carefully with equimolar amounts of *o*-toluidine and, 1-naphthylamine respectively in a round bottomed flask fitted with an air condenser at 80 °C for *ca.* 2 h. The products obtained were crystallised from ethanol. The toluidide and naphthylimide derivatives on further refluxing with hydrazinehydrate (slightly excess than 2 mol) in ethanol in the presence of animal charcoal gave the reduced products[9] (Va, VIa, Vb, VIb). These compounds were recrystallised from ethanol.

Cyclopentadiene-Maleic Anhydride Adducts and Their Derivatives (VIIa, VIIIa, VIIb, VIIIb, IXa, Xa, IXb, Xb). [2.2.1] Bycyclo-5-heptene 2,3 *endo/exo* dicarboxalic anhydride were prepared according to the method of Craig.[10]

Toluidide (VIIa and VIIIa) and naphthylimide (VIIb and VIIIb) derivatives were obtained on heating the isomeric adducts with equimolar amounts of *o*-toluidine and 1-naphthylamine, respectively, in a round bottomed flask attached to an air condenser at 100—120 °C for 3 h. The products obtained were crystallised from ethanol. These compounds on further refluxing with hydrazinehydrate (slightly excess than 2 mol) in ethanol in the presence of animal charcoal gave the reduced products[9] (IXa, Xa, IXb, Xb) which were recrystallised from ethanol.

References

1) S. M. Verma and N. B. Singh, *Aust. J. Chem.*, **29**, 295 (1976).
2) a) S. M. Verma and R. M. Singh, *J. Org. Chem.*, **40**, 897 (1975); b) S. M. Verma and C. K. Rao, *Indian J. Chem.*, **13**, 1278 (1975).
3) S. M. Verma and A. K. Singh, *Indian J. Chem.*, **14B**, 834 (1976).
4) S. M. Verma and O. S. Rao, *Aust. J. Chem.*, **26**, 1963 (1973).
5) S. M. Verma, O. Subba Rao, and C. Koteswara Rao, *Tetrahedron Lett.*, **1973**, 1639.
6) S. M. Verma and O. S. Rao, *Tetrahedron*, **30**, 237 (1974).
7) S. M. Verma and R. M. Singh, *Aust. J. Chem.*, **29**, 1215 (1976).
8) K. Takeda, K. Kitachonoki, M. Sugiura, and Y. Takano, *Chem. Ber.*, **95**, 2344 (1962).
9) A. Furst, R. C. Berlo, and S. Hooton, *Chem. Rev.*, **65**, 51 (1965).
10) D. Craig, *J. Am. Chem. Soc.*, **73**, 4889 (1951).

Synthesis and Reactions of Some New 1,3-Dioxa-2-bora Heterocycles Derived from *o*-Hydroxybenzyl Alcohol

G. SRIVASTAVA and P. N. BHARDWAJ

Department of Chemistry, University of Rajasthan, Jaipur 302004, India

(Received March 22, 1977)

2-Isopropoxy-4*H*-1,3,2-benzodioxaborin(I), obtained from isopropyl borate and *o*-hydroxybenzyl alcohol, reacts with a variety of hydroxy compounds (*viz.*, *t*-butyl alcohol, phenol, ethane-1,2-diol, 2-aminoethanol, *o*-amino phenol) and acetic anhydride to give the corresponding 2-substituted heterocycles. Reactions of (I) as well as other 1,3-dioxa-2-bora heterocycles with bases (*viz.*, ammonia, triethylamine, pyridine, dimethylformamide) show that the electrophilicity of boron decreases in the order: 2-alkoxy-1,3,2-benzodioxaborole>2-phenoxy-4*H*-1,3,2-benzodioxaborin>(I)>2-alkoxy-1,3,2-dioxaborinane.

Codisproportionation reaction between bis(4*H*-1,3,2-benzodioxaborin-2-yl)oxide (obtained directly from boric acid and *o*-hydroxybenzyl alcohol) and triorganotin hydroxide or oxide yields 2-triorganostannoxy-4*H*-1,3,2-benzodioxyborin. Cleavage and insertion reactions of these compounds have been studied.

Boron heterocycles containing two oxygen atoms, *e.g.*, 1,3,2-dioxaborolanes,[1] -borinanes[2] and 1,3,2-benzodioxaboroles[3] have been extensively studied. The effect of ring size on the stability[4] as well as the electrophilic nature of boron[5] in such derivatives have also been investigated. The higher reactivity of benzodioxaborole derivatives in comparison to dioxaborinanes and dioxaborolanes can be easily understood in terms of greater electron deficient character of boron in the former class of compounds. Boron heterocycles derived from *o*-hydroxybenzyl alcohol form a mixed system and have been synthesized only recently by the reactions of this ligand with tris(dimethylamino)borane, tris(ethanethiolato)borane and phenylboric acid.[6] Azeotropic removal of water from a mixture of *o*-hydroxybenzyl alcohol, boric acid and an alcohol leads to the formation of the corresponding 2-alkoxy-4*H*-1,3,2-benzodioxaborin. In the present paper we report a detailed study of the synthesis and reactions of various 2-substituted-4*H*-1,3,2-benzodioxaborins. Attempts have also been made to compare the electrophilic nature of boron in these and in other types of 1,3-dioxa-2-bora heterocycles.

Results and Discussion

2-Isopropoxy-4*H*-1,3,2-benzodioxaborin (I) is obtained as a colourless volatile liquid by the interaction of isopropyl borate with *o*-hydroxybenzyl alcohol in refluxing benzene, with azeotropic removal of the liberated isopropanol.

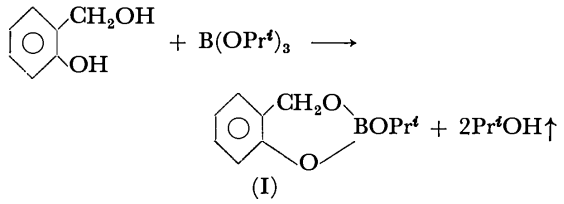

(I)

The isopropoxy group of the boron heterocycle (I) could be easily replaced by other alkoxy and phenoxy groups by simple alcohol interchange technique in benzene. The progress of the reaction could be followed by estimating the amount of isopropanol in azeotrope. It has been observed qualitatively that these reactions are comparatively slower than those of 2-isopropoxy-1,3,2-benzodioxaborole.

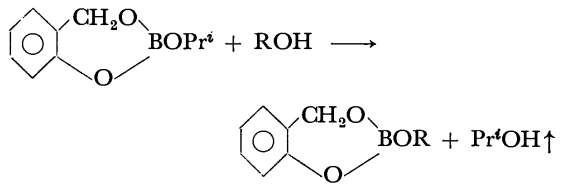

(II), R=Bu^t; (III), R=Ph

Reaction of I with ethylene glycol affords 2,2′-ethylenedioxybis(4*H*-1,3,2-benzodioxaborin) (IV) as a white solid.

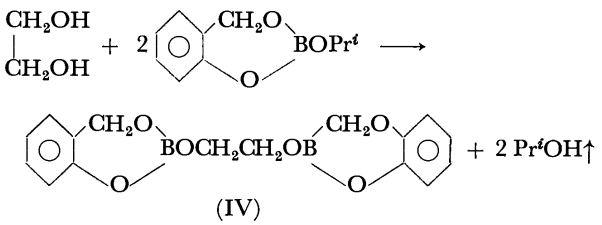

(IV)

It is noteworthy that the reaction of I with *o*-hydroxybenzyl alcohol in 2: 1 molar ratio does not proceed to completion and only half of the calculated amount of isopropanol is obtained in the azeotrope. The resulting semisolid on distillation yields, some unreacted 2-isopropoxyborin (I) and decomposed residue. Similar results are obtained when reaction of isopropyl borate with *o*-hydroxybenzyl alcohol in 2: 3 molar ratio is carried out. It appears that the product in these reactions is an equimolar mixture of I and bis(*o*-benzomethylenedioxy)borate (V). 2,2′-(*o*-Benzomethylenedioxy)bis(4*H*-1,3,2-benzodioxaborin) is not obtained in these reactions even under forcing conditions. This may be due to steric reasons. Molecular models show that two 4*H*-1,3,2-benzodioxaborin-2-yl moieties present on the two oxygen atoms of *o*-benzomethylenedioxy moiety cannot rotate freely.

Compound V is obtained in quantitative yields as a viscous semisolid by the following routes:

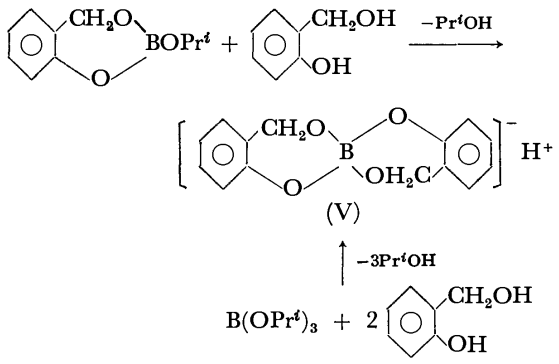

Attempts to synthesize the sodium salt of V by crystallisation from an aqueous solution of boric acid, *o*-hydroxybenzyl alcohol and sodium hydroxide were unsuccessful. The ammonium salt $[(C_7H_6O_2)_2B]^-[NH_4]^+$ (VI), however, is immediately precipitated on passin gammonia to a benzene solution of V.

Reactions of 2-phenoxy- and 2-isopropoxy-4*H*-1,3,2-benzodioxaborin with nitrogen donors have been studied. The phenoxy derivative (III) forms stable 1:1 complexes with triethylamine and pyridine (VII and VIII respectively) exothermally whereas with dimethylformamide, no reaction appears to take place. I also does not give an adduct with dimethylformamide but on mixing with pyridine, heat is evolved and liquid complex (IX) is formed which loses pyridine slowly under high vacuum, leaving behind a highly viscous semisolid, insoluble in benzene and carbon tetrachloride. This semisolid yielded I on distillation under reduced pressure. The structure of the semisolid could not be studied further. Unlike pyridine, ammonia forms a stable 1:1 complex (X) with I. Attempts to prepare a salt of the type $[C_6H_4\langle{}^{O}_{CH_2O}\rangle B(OPr^i)_2]^-[NH_4]^+$ by passing ammonia to an equimolar mixture of I and isopropanol in benzene were unsuccessful. The addition complex (X) was precipitated in these cases also. It may be pointed out in this context that 2-isopropoxy-1,3,2-benzodioxaborole forms addition complexes with various donors including dimethylformamide whereas 2-isopropoxy-4,4,6-trimethyl-1,3,2-dioxaborinane does not show any tendency of complex formation.[7] Thus, the electrophilicity of boron in 1,3-dioxa-2-bora heterocycles appears to decrease in the order: 2-isopropoxy-1,3,2-benzodioxaborole>III>I>2-isopropoxy-4,4,6-trimethyl-1,3,2-dioxaborinane.

Reactions of I with 2-aminoethanol and *o*-aminophenol in refluxing benzene give insoluble solid products XI and XII in which there is internal coordination from nitrogen to boron. In contrast to I and III, the derivatives XI and XII do not show any tendency to form complexes with nitrogen donors.

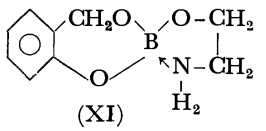

(XI)

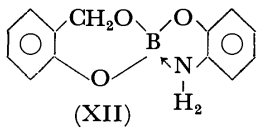

(XII)

Azeotropic removal of water with benzene from an equimolar mixture of boric acid and *o*-hydroxybenzyl alcohol yields bis(4*H*-1,3,2-benzodioxaborin-2-yl)oxide (XIII) which reacts further with bis(tributyltin)oxide and triphenyltin hydroxide giving 2-tributylstannoxy- and 2-triphenylstannoxy-4*H*-1,3,2-benzodioxaborin, XIV and XV, respectively. These are new examples of stannoboroxanes.[8] The facile cleavage of Sn–O–B bond in XV by trimethylchlorogermane and -silane affords the corresponding trimethylgermoxy (XVI) and trimethylsiloxy (XVII) derivatives which are easily separated from triphenyltin chloride by fractional distillation.

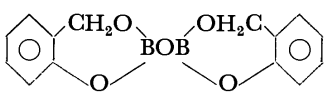

(XIII)

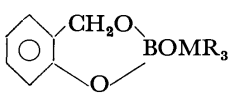

(XIV) $MR_3=SnBu_3$
(XV) $MR_3=SnPh_3$
(XVI) $MR_3=GeMe_3$
(XVII) $MR_3=SiMe_3$

The higher reactivity of Sn–O bond in comparison to B–O bond in stannoboroxanes has been demonstrated previously by the study of their cleavage and insertion reactions.[9] Insertions of unsaturated substrates across Sn–O bond are very facile. On the other hand, the only reported example of insertion across B–O bond appears to be the extremely slow reaction (24% yield in 30 days at room temperature) of 2-butoxy-1,3,2-benzodioxaborole with phenyl isocyanate.[10] The present studies show that whereas I, as expected, does not show any tendency to react with phenyl isocyanate, the corresponding 2-tributylstannoxy derivative (XIV) reacts immediately and exothermally to give the insertion product (XVIII). Aminoethoxy derivative (XI) also reacts with phenyl isocyanate presumably at the amino group and based on earlier studies,[11] the addition compound has been tentatively assigned structure XIX, in which the carbonyl group of the substituted urea moiety coordinates with boron.

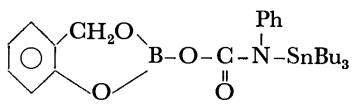

(XVIII)

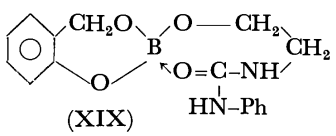

(XIX)

IR and PMR Spectra. The common peaks present in the IR spectra of all the derivatives (I—XIX) are; (i) a sharp and strong peak at 755 cm^{-1} (out of plane aromatic C–H bending); (ii) peaks of medium intensity at 1030, 1115 and 1160 cm^{-1} (inplane C–H bending), (iii) strong intensity peaks at 1080 and 1255 ± 5 cm^{-1} (due to aliphatic and aromatic C–O stretching vibrations respectively) and (iv) a weak intensity band at 3050 ± 10 cm^{-1} (due to aromatic C–H stretching). The region 1300—1500 cm^{-1} shows four to five strong peaks and an attempt to assign ν_{B-O}

Table 1. Reactions of 2-isopropoxy-4*H*-1,3,2-benzodioxaborin (I) with hydroxy compounds

S. No.	Wt of borin (I) (g) (mmol)	Hydroxy compound (g) (mmol)	Pr^iOH in azeotrope (g) Found Calcd	Product molecular formula Nature	Yield (g) (%)	Bp (°C/mmHg) (Mp, °C)	Boron (%) Found Calcd	Nitrogen (%) Found Calcd	PMR (CCl_4) peaks (τ)
1	2.12 (11.0)	*t*-Butyl alcohol 3.0	0.59 0.68	$C_{11}H_{15}BO_3$ Colourless liquid (II)	1.80 (80)	68/0.01 —	5.21 5.34	—	2.8—3.7 (m, 4H, aromatic), 5.16 (s, 2H, CH_2), 8.85 (s, 9H, Bu^t).
2	2.16 (11.3)	Phenol 1.15 (12.2)	0.49 0.69	$C_{13}H_{11}BO_3$ Semisolid (III)	2.20 (87)	135/0.01 —	4.76 4.87	—	2.55—3.6 (m, 9H, aromatic), 4.96 (s, 2H, CH_2).
3	2.36 (12.3)	Ethyleneglycol 0.40 (6.5)	0.65 0.76	$C_{16}H_{16}B_2O_6$ White solid (IV)	2.03 (97)	— (70)	6.57 6.75	—	2.6—3.45[a] (m, 8H, aromatic), 4.95 (s, 4H, CH_2) 5.96 (s, 4H, CH_2CH_2).
4	7.10 (36.4)	Ethanolamine 2.25 (36.8)	2.06 2.16	$C_9H_{12}BNO_3$ White solid (XI)	6.89 (97)	165/4.0 (120)	5.67 5.61	7.10[b] 7.15	
5	1.75 (9.1)	*o*-Aminophenol 1.0 (9.2)	0.46 0.54	$C_{13}H_{12}BNO_3$ Grey solid (XII)	2.20 (100)	— (137)	4.63 4.56	5.67[b] 5.82	

a) In $CDCl_3$. b) Insoluble in CCl_4 and $CDCl_3$.

with any amount of certainty is rather difficult. $\nu_{B-OC(aliphatic)}$ and $\nu_{B-OC(aromatic)}$ will absorb at different positions, the latter being at higher wave number and the two peaks present in 1350—1420 cm^{-1} region may tentatively be assigned to these vibrations.

In the derivative XIV, the presence of tributylstannoxy group[12] is shown by the appearance of $\nu_{as\ SnC_3}$ at 670 and 600 cm^{-1}, $\nu_{s\ SnC_3}$ at 515 cm^{-1} and ν_{B-O-Sn}[9] at 1280 cm^{-1}. Similarly compound (XVII) shows the characteristic peaks[13,14] of B–OSiMe$_3$ group at 840 cm^{-1} ($\rho_{as\ CH_3}$), 660 cm^{-1} ($\nu_{as\ SiC_3}$), 620 cm^{-1} ($\nu_{s\ SiC_3}$) and 1325 cm^{-1} ($\nu_{as\ B-O-Si}$). The corresponding peak positions for BOGeMe$_3$ group in derivative XVI are 830 cm^{-1} ($\rho_{as\ CH_3}$), 615 cm^{-1} ($\nu_{as\ GeC_3}$), 575 cm^{-1} ($\nu_{s\ GeC_3}$) and 1300 cm^{-1} ($\nu_{as\ B-O-Ge}$).[15] The symmetric deformation of Si–CH_3 and Ge–CH_3 groups, generally appearing at 1240—1260 cm^{-1} are masked by the strong ν_{C-O} band.

ν_{N-H} appears as a sharp weak peak at 3180 cm^{-1} in the *o*-aminophenoxy derivative (XII) but in the 2-aminoethoxy derivative (XI) it is present as a broad shoulder at 3100—3200 cm^{-1}. In the insertion product XIX of the latter compound with phenyl isocyanate, the ν_{NH} peak moves to a higher frequency at 3300 cm^{-1} and the $\nu_{C=O}$ peak is present at 1630 cm^{-1}. The $\nu_{C=O}$ peak in the ureido compound (XVIII) appears at 1610 cm^{-1}.

The purity of most of the new heterocycles (I—XIX) was checked by their PMR spectra in CCl_4. The specific peak positions are reported in the experimental section. The common peaks due to *o*-O–C_6H_4–CH_2–O-moiety, present in all the PMR spectra are a complex multiplet at 2.5—3.7 τ due to aromatic protons and a sharp singlet near 5.0 τ due to CH_2 protons. The position of the latter peak appears to be influenced by the coordination number of boron. Thus, the methylene singlet is present at 4.97 and 4.96 τ in 2-isopropoxy and 2-phenoxy-4*H*-1,3,2-benzodioxaborins respectively. In the corresponding 1 : 1 pyridine complexes, this peak shifts to 5.2 and 5.4 τ respectively. This increased shielding of the methylene protons probably reflects decreased p→pπ bonding from oxygen to born when the latter goes from three-coordinate to four-coordinate state.

Experimental

o-Hydroxybenzyl alcohol (Fluka) was used as supplied. Benzene (B.D.H., L.R.) was kept overnight on sodium wire and distilled, and was finally dried azeotropically with ethanol. Molecular weights were determined ebulliometrically in benzene using thermistor sensing.

Boron was estimated by Thomas' method.[16] Isopropanol in the azeotrope was estimated by oxidation method.[17] Infrared spectra were recorded on Perkin-Elmer model 337-grating spectrometer. PMR spectra were recorded on Perkin-Elmer R12B spectrometer.

2-Isopropoxy-4H-1,3,2-benzodioxaborin. Fractionation of a mixture of isopropyl borate (3.55 g, 18.8 mmol) and *o*-hydroxybenzyl alcohol (2.27 g, 18.3 mmol) in benzene (≈60 ml) yielded isopropanol (2.06 g, calcd 2.26 g) in the azeotrope and the desired product (I) (3.03 g, 88%) at 72 °C/0.01 mmHg as a colourless liquid. (Found: B, 5.63; M, 185. Calcd for $C_{10}H_{13}BO_3$: B, 5.73%; M, 192).

PMR (CCl_4): τ 2.7—3.3 (m, 4H, aromatic), 4.97 (S, 2H, CH_2). 5.5 (Septet, 1H, J=6 Hz), 8.83 (d, 6H, CH_3, J=6 Hz).

Bis(o-benzomethylenedioxy)borate and Its Ammonium Salt.

(a) On refluxing isopropyl borate (2.77 g, 14.7 mmol) with *o*-hydroxybenzyl alcohol (3.65 g, 29.4 mmol) in benzene (≈60 ml) for one hour followed by fractionation, isopropanol (2.66 g, calcd 2.71 g) was obtained in the azeotrope. On removing excess of solvent under reduced pressure, the desired product (V) (3.68 g, 99.2%) was obtained as viscous semisolid. (Found: B, 4.18. Calcd for $C_{14}H_{13}BO_4$: B, 4.24%).

PMR (CCl_4): τ 2.9—3.45 (m, 8H, aromatic), 5.2 (s, 4H, CH_2).

(b) A mixture of 2-isopropoxy-4*H*-1,3,2-benzodioxaborin (1.92 g, 10.0 mmol) and *o*-hydroxybenzyl alcohol (1.24 g, 10.0 mmol) in benzene (≈40 ml), on fractionation, gave isopropanol (0.50 g, calcd 0.60 g) in the azeotrope. After removal of excess benzene *in vacuo*, the product (V) (2.55 g,

100%) was obtained as a viscous semisolid (Found: B, 4.15. Calcd for $C_{14}H_{13}BO_4$: B, 4.24%).

By passing ammonia to a solution of V (3.38 g) in benzene (≈60 ml), the ammonium salt was immediately precipitated (VI) (3.48 g, 96.7%) mp 210—213 °C (Found: B, 3.82; N, 4.46. Calcd for $C_{14}H_{16}BNO_4$: B, 3.96; N, 4.83%).

Attempted Preparation of 2,2'-(o-Benzomethylenedioxy)bis(4H-1,3,2-benzodioxaborin). *(a)*: A mixture of isopropyl borate (2.89 g, 15.3 mmol) and *o*-hydroxybenzyl alcohol(2.78 g, 22.4 mmol) in benzene (≈60 ml) was refluxed for 3 h and fractionated (Found: isopropanol 2.20 g, calcd for 46 mmol 2.76 g) Removal of excess benzene under vacuum, yielded a semisolid (3.36 g) which on distillation under reduced pressure gave 2-isopropoxy-4*H*-1,3,2-benzodioxaborin(1.07 g) at 62 °C/0.05 mmHg (authentic IR and PMR spectra) and a light yellow solid (1.36 g) as undistilled residue (Found: B, 5.40%).

(b): Reaction of compound I (2.04 g, 12.5 mmol) and *o*-hydroxybenzyl alcohol (0.66 g, 5.3 mmol) in benzene (≈60 ml) yielded isopropanol (0.30 g, calcd 0.64 g) and a viscous product (2.35 g, calcd 2.06 g) (Found: B, 4.88%).

Reactions of 2-Isopropoxy-4H-1,3,2-benzodioxaborin with Hydroxy Compounds. A mixture of I and the hydroxy compound in benzene was refluxed and fractionated. After complete removal of the liberated isopropanol azeotropically, the solvent was distilled. The product was finally freed of solvent *in vacuo*. The details of these reactions are summarised in Table 1.

Addition Complexes of 2-Isopropoxy-4H-1,3,2-benzodioxaborin.

(a): Heat was evolved on adding pyridine (1.08 g) to 2-isopropoxy-4*H*-1,3,2-benzodioxaborin (1.92 g). Excess of pyridine was removed *in vacuo* leaving 1: 1 complex (2.70 g) as a viscous product. PMR (CCl_4): τ 1,3—3.1 (m, 5H, pyridine), 3.1—3.6 (m, 4H, aromatic), 5.2 (s, 2H, CH_2), 5.75 (Septet, 1H, C*H*Me_2), 8.95 (d, 6H, CH*Me*$_2$). This complex lost pyridine very slowly (20 h/0.01 mmHg) giving a highly viscous semisolid (2.16 g, Found: B, 5.05%). This on distillation gives I (0.78 g) at 82 °C/0.01 mmHg leaving an undistilled residue (1.14 g).

(b): A solid product X (1.44 g, 100%) mp 205—208 °C, was precipitated immediately on passing ammonia to a solution of compound I (1.32 g) in benzene(≈40 ml) (Found: B, 5.25; N, 6.69. Calcd for $C_{10}H_{16}BNO_3$: B, 5.27; N, 6.70%).

The above complex X (0.92 g, mp 205—208 °C) was also precipitated on passing ammonia to a mixture of compound I (0.86 g) and isopropanol (0.42 g) in benzene (≈50 ml). Unreacted isopropanol (0.4 g) was obtained from the filtrate by azeotropic distillation.

Addition Complexes of 2-Phenoxy-4H-1,3,2-benzodioxaborin.

(a): A solid 1: 1 complex (VII) (0.58 g, 90%) mp 135—138 °C was precipitated on adding triethylamine (0.34 g) to a benzene solution of 2-phenoxy-4*H*-1,3,2-benzodioxaborin (0.44 g)(Found: B, 3.36. Calcd for $C_{19}H_{26}BNO_3$: B, 3.46%).

(b): Heat was evolved on adding pyridine (0.20 g) to 2-phenoxy-4*H*-1,3,2-benzodioxaborin (0.40 g). Excess of pyridine was removed *in vacuo*, leaving 1: 1 complex (VIII) (0.54 g, 100%) as a solid, mp 120 °C (Found: B, 3.53. Calcd for $C_{18}H_{16}BNO_3$: B, 3.55%). PMR(CCl_4): τ 1.3—3.1 (m, 5H, pyridine), 3.1—3.7 (m, 9H, aromatic), 5.4 (s, 2H, CH_2).

(c): No reaction appeared to take place on adding dimethylformamide (0.40 g) to the 2-phenoxy derivative (III) (1.12 g); unchanged (III) was obtained on removing dimethylformamide *in vacuo*.

2-Acetoxy-4H-1,3,2-benzodioxaborin. A mixture of acetic anhydride (0.59 g, 5.8 mmol) and 2-isopropoxy-4*H*-1,3,2-benzodioxaborin (0.97 g, 5.1 mmol) was kept at room temperature for several days. The liberated ester was removed *in vacuo* yielding the product (0.97 g, 100%) as viscous semisold (Found: B, 5.81; $OCOCH_3$, 27.53. Calcd for $C_9H_9BO_4$: B, 5.73; $OCOCH_3$, 28.63%).

Bis(4H-1,3,2-benzodioxaborin-2-yl)oxide. On removal of water azeotropically from a mixture of boric acid (1.17 g, 18.9 mmol) and *o*-hydroxybenzyl alcohol (2.34 g, 18.9 mmol) in benzene (≈60 ml), followed by drying the product under reduced pressure, bis(4*H*-1,3,2-benzodioxaborin-2-yl)oxide (XIII) (2.66 g, 100%) was obtained as a viscous semisolid which solidified slowly on keeping at low temperature, (mp 160—164 °C)(Found: B, 7.80. Calcd for $C_{14}H_{12}B_2O_5$: B, 7.64%).

2-Tributylstannoxy-4H-1,3,2-benzodioxaborin. A mixture of bis(4*H*-1,3,2-benzodioxaborin-2-yl)oxide (3.98 g, 14.1 mmol) and bis(tributyltin)oxide (8.41 g, 14.9 mmol) in benzene was refluxed for 2 h. The product was freed from solvent *in vacuo* to yield the desired product (XIV) (11.77 g, 95.3%) as a colourless liquid, bp 178—180 °C/0.9 mmHg. (Found: B, 34; Sn, 26.94; M, 430. Calcd for $C_{19}H_{33}BO_3Sn$; B, 2.37; Sn, 27.06%; M, 439).

PMR (CCl_4): τ 2.65—3.35 (m, 4H, aromatic), 5.0 (s, 2H, CH_2), 7.7—9.5 (m, 27H, Bu_3Sn).

2-Triphenylstannoxy-4H-1,3,2-benzodioxaborin. Water was removed azeotropically from a mixture of bis(4*H*-1,3,2-benzodioxaborin-2-yl)oxide (2.14 g, 7.6 mmol) and triphenyltin hydroxide (5.51 g, 15.0 mmol) in benzene. Removal of excess benzene gave the product (7.49 g, 100%) as a viscous semisolid (XV) (Found: B, 2.18; Sn, 23.60. Calcd for $C_{25}H_{21}BO_3Sn$: B, 2.20; Sn, 23.68%).

2-Trimethylsiloxy-4H-1,3,2-benzodioxaborin. Trimethylchlorosilane (1.53 g, 14.4 mmol) reacted exothermally with 2-triphenylstannoxy-4*H*-1,3,2-benzodioxaborin (7.49 g, 15.0 mmol). Distillation under reduced pressure yielded 2-trimethylsiloxy-4*H*-1,3,2-benzodioxaborin (XVII) (2.50 g, 85.1 %) as a colourless liquid, bp 80 °C/0.8 mmHg. leaving triphenyltinchloride (6.90 g) as an undistilled residue (Found: B, 4.91; Si, 12.40; M, 214. Calcd for $C_{10}H_{15}BO_3Si$: B, 4.95; Si, 12.47%; M, 222).

PMR (CCl_4): τ 2.6—3.45 (m, 4H, aromatic), 5.06 (s, 2H, CH_2), 8.85 (s, 9H, Me_3Si).

2-Trimethylbermoxy-4H-1,3,2-benzodioxaborin. On adding trimethylchlorogermane (2.40 g, 15.7 mmol) to 2-triphenylstannoxy-4*H*-1,3,2-benzodioxaborin (7.49 g, 15.0 mmol) heat was evolved. Distillation yielded the desired compound (XVI) (3.52 g, 88.2%), bp 125 °C/1.0 mmHg as a colourless liquid (Found: B, 4.11%; M, 261. Calcd for $C_{10}H_{15}BGeO_3$: B, 4.12%; M, 267).

PMR (CCl_4): τ 2.9—3.35 (m, 4H, aromatic), 5.0 (s, 2H, CH_2), 9.52 (s, 9H, Me_3Ge).

Reaction between 2-Tributylstannoxy-4H-1,3,2-benzodioxaborin and Phenyl Isocyanate in 1: 1 Molar Ratio. Phenyl isocyanate (0.31 g, 2.6 mmol) reacted exothermally with 2-tributylstannoxy-4*H*-1,3,2-benzodioxaborin (1.14 g, 2.6 mmol) in benzene (≈5 ml) giving the adduct as a light brown viscous liquid (XVIII) (1.45 g, 100%) which showed no free isocyanate peak in the IR spectrum (Found: B, 1.93; Sn, 20.77. Calcd for $C_{26}H_{38}BNO_4Sn$: B, 1.94; Sn, 20.91%). The compound distils with slight decomposition at 210 °C/1.0 mmHg.

PMR (CCl_4): τ 2.5—3.5 (m, 9H, aromatic), 5.0 (s, 2H, CH_2), 7.9—8.5 (m, 27H, Bu_3Sn).

Reaction between 2-(2-Aminoethoxy)-4H-1,3,2-benzodioxaborin and Phenyl Isocyanate in 1: 1 Molar Ratio. To a suspension of 2-aminoethoxy-4*H*-1,3,2-benzodioxaborin (1.52 g, 7.9 mmol) in benzene (≈10 ml), phenyl isocyanate (0.95 g, 7.9 mmol) was added. The mixture was refluxed for 2 h giving a white crystalline solid (XIX) (2.46 g, 100%) (mp 160—165 °C) which was filtered and dried at 30 °C/0.01 mmHg (Found: B, 3.51; N, 7.20%. Calcd for $C_{16}H_{17}BN_2O_4$: B, 3.53; N,

7.26%).

We are grateful to Prof. J. N. Gaur, Head of the Chemistry Department for providing necessary facilities. One of us (PNB) is thankful to CSIR, New Delhi for the award of a Junior Research Fellowship.

References

1) J. A. Blau, W. Gerrard, and M. F. Lappert, *J. Chem. Soc.*, **1957**, 4116; **1960**, 667; R. C. Mehrotra and G. Srivastava, *ibid.*, **1962** 3021; R. H. Cragg, *J. Inorg. Nucl. Chem.*, **30**, 395 (1968); S. H. Rose and S. G. Shore, *Inorg. Chem.*, **1**, 744 (1962).

2) A. Finch, J. C. Lockhart, and J. Pearn, *J. Org. Chem.*, **26**, 3250 (1961); R. C. Mehrotra and G. Srivastava, *J. Chem. Soc.*, **1962**, 1032.

3) W. Gerrard, M. F. Lappert, and B. A. Mountfield, *J. Chem. Soc.*, **1959**, 1529; R. C. Mehrotra and G. Srivastava, *ibid.*, **1961**, 4045; M. F. Lappert, M. K. Majumdar, and B. P. Tilley, *ibid.*, *A*, **1966**, 1590.

4) J. Dale, B. Hargitay, and A. J. Hubert, *J. Chem. Soc.*, **1961**, 910, 922, 931.

5) G. E. MeAchran and S. G. Shore, *Inorg. Chem.*, **5**, 2044 (1966).

6) R. H. Cragg and M. Nazery, *J. Chem. Soc., Dalton Trans.*, **1974**, 162.

7) G. Srivastava and P. N. Bhardwaj, unpublished results.

8) S. K. Mehrotra, G. Srivastava, and R. C. Mehrotra, *J. Organomet. Chem.*, **73**, 277 (1974).

9) S. K. Mehrotra, G. Srivastava, and R. C. Mehrotra, *J. Organomet. Chem.*, **65**, 361, 367 (1974).

10) R. H. Cragg, M. F. Lappert, and B. P. Tilley, *J. Chem. Soc.*, **1964**, 2108.

11) J. S. Hartman and G. J. Schrobilgen, *Can. J. Chem.*, **50**, 713 (1972).

12) T. Tanaka, *Organomet. Chem. Rev. A*, **5**, 1 (1970).

13) H. Bürger, *Organomet. Chem. Rev. A*, **3**, 425 (1968).

14) S. K. Mehrotra, G. Srivastava, and R. C. Mehrotra, *Syn. React. Inorg. Metalorg. Chem.*, **4**(1), 27 (1974).

15) S. K. Mehrotra, G. Srivastava, and R. C. Mehrotra, *J. Organomet. Chem.*, **54**, 139 (1973).

16) L. H. Thomas, *J. Chem. Soc.*, **1946**, 820.

17) D. C. Bradley, F. M. A. Halim, and W. Wardlaw, *J. Chem. Soc.*, **1950**, 3450.

Solvolysis in Carboxamides. II.[4] Solvolytic Elimination of 7β-Methylbicyclo[3.3.1]non-3β-yl Tosylate in Carboxamides†

Seiki SAITO, Tatsumi YABUKI,** Toshio MORIWAKE, and Kunio OKAMOTO*

Department of Synthetics Chemistry, School of Engineering, Okayama University, Tsushima, Okayama 700
**Department of Hydrocarbon Chemistry, Faculty of Engineering, Kyoto University, Sakyo-ku, Kyoto 606*

(Received May 13, 1977)

Solvolysis of 7β-methylbicyclo[3.3.1]non-3β-yl tosylate (**1**) was carried out in a series of carboxamides, *N*-methylformamide (NMF), *N*-methylacetamide (NMA), *N,N*-dimethylformamide (DMF), and *N,N*-dimethylacetamide (DMA), as solvents. The rate (k_1, first-order rate constant) of **1** decreases in the order NMF>NMA>DMF>DMA, a linear free-energy relationship being found between the rates of **1** and those of 1-adamantyl tosylate in acetic acid and 80% ethanol as well as the carboxamides. The products consist of olefin (≥96%) (*exo*-7-methylbicyclo[3.3.1]non-2-ene (**4**) and 3-methylbicyclo[3.3.1]non-2-ene (**5**)) and small amounts of esters (acetates or formates, ≤4%). The content of rearranged olefin **5** is considerably less than that of acetolysis (55%) and ethanolysis (55%), decreasing in the order NMF (34%)>NMA(22%)>DMF(13%)>DMA(9%). A linear reactivity-selectivity relationship holds between log k_1 and log (%**5**/%**4**) for the four carboxamide solvents. The observed kinetic isotope effect ($k_H/k_D=1.01\pm0.03$) for 7α-deuterium-tagged derivative (**1**-7α-*d*) in NMF indicates that the σ(C(7)–H)-assisted ionization process for the solvolysis of **1** in the amides is absent. The results are in line with the stepwise mechanism which involves the formation of an intimate ion-pair intermediate followed by competitive processes such as 1,5-hydride shift, *syn*-E1 reaction, and nucleophilic substitution by the amide molecules. Substitution by the amide molecule leads to the formation of a cationic imidate, the hydrolysis of which affords the carboxylic esters. It is proposed that the *syn*-E1 process *via* an intimate ion-pair intermediate is affected by the tosylate anion reactivity in each amide solvent and suppressed by the hydrogen bonding of the each amide with the tosylate anion.

The occurrence of intramolecular hydride shift in S_N1 solvolysis has been demonstrated in various secondary alkyl or cycloalkyl systems.[1] As regards 7β-methylbicyclo[3.3.1]non-3β-yl tosylate (**1**), Eakin *et al.*[2] observed that acetolysis of **1** is accompanied by significant 1,5-transannular hydride shift (55%). They reported that the hydrogen migration occurs after the rate-determining step, on the basis of the absence of a detectable kinetic isotope effect with regard to 7α-deuterium-tagged substrate (**1**-7α-*d*).

Stéhelin *et al.*[3] observed by use of Taft-Hammett treatment that solvolysis of 7β-substituted (CH_3OCH_2–, CH_3OCO–, and NC–) derivatives and **1** is accelerated when it is accompanied by hydride migration from C(7) to C(3), concluding that there is σ(C(7)–H) participation in the rate-determining step of the ethanolysis. Thus, both the stepwise mechanism, involving the formation of an ion-pair intermediate followed by subsequent processes, and the partially or fully concerted mechanism have been proposed.

In the course of our study on the characteristics of carboxamides as an S_N1 solvolysis solvent, it was shown[4] that the solvolysis of *trans*-4-*t*-butylcyclohexyl tosylate in *N*-methylacetamide (NMA) proceeds with markedly suppressed 1,2-hydride shift as compared with acetolysis[5] and phenolysis,[6] giving exclusively unrearranged olefin. From this finding it has been suggested that intramolecular elimination by the leaving tosylate anion in the intimate ion-pair intermediate is markedly accelerated in NMA solvent.

In the present system **1**, the tosyloxy group is oriented in an equatorial position as in the case of *trans*-4-*t*-butylcyclohexyl system. Thus, it is of interest to examine whether solvolysis of **1** in carboxamide solvents proceeds with suppression of 1,5-hydride shift as compared with acetolysis[2] and ethanolysis.[3] It is also interesting to see whether the solvolysis proceeds with σ(C(7)–H) participation or not. We have studied the solvolysis of **1** in carboxamides, *N*-methylformamide (NMF), *N,N*-dimethylformamide (DMF), and *N,N*-dimethylacetamide (DMA), in addition to NMA.

Results and Discussion

Solvolytic Elimination Rates of 7β-Methylbicyclo[3.3.1]non-3β-yl Tosylate **1**. Solvolysis rates of **1** were determined in four carboxamides (NMF, NMA, DMF, and DMA) at two or three temperatures by the usual titrimetric method. Good first-order behavior was observed for all the kinetic runs over two to three half-lives both in the absence and the presence of pyridine added as a neutralizing agent for the liberated *p*-toluenesulfonic acid. Absence of the effect of added pyridine on the rate indicates that the solvolysis proceeds by the typical S_N1-type mechanism. The rate constants and thermodynamic parameters are given in Table 1. The solvolysis rates for **1** decrease in the sequence NMF>NMA>DMF>DMA in line with the trend observed for 1-adamantyl tosylate.[7]

A good linear relation has been observed in a plot of log k_1 (25 °C) for **1** *vs.* log k_1 (25 °C) for 1-adamantyl tosylate, when the solvolysis rates are compared for a series of solvents, such as 80% ethanol,[3,8] acetic acid,[2,8] NMF,[7] NMA,[7] DMF,[7] and DMA[7] (Fig. 1). The magnitude of the Grunwald-Winstein *m* value[9] (0.53) is comparable to those (0.4—0.7) known for the solvolysis of the usual secondary substrates.[10]

Deuterium Isotope Effects in the Solvolysis of 7α-Deuterium-Tagged Substrate **1**-7α-d *in NMF*. If transannular

† Presented in part at the 29th (Hiroshima, October, 1973) and 32nd (Tokyo, April, 1975) National Meetings of the Chemical Society of Japan.

** Present address: Okayama Industrial Research Institute, Ifuku-cho, Okayama 700.

Table 1. Kinetic data for the solvolysis of 7β-methylbicyclo[3.3.1]non-3β-yl tosylate (**1**) in various carboxamides

Amide	$k_1/(10^{-5}\ s^{-1})$[b]			$\Delta H^{\neq}$[c]	$\Delta S^{\neq}$[c]
	25 °C	35 °C	50 °C	4.184 KJ/mol	4.184 J/(K mol)
DMA	0.114	0.515	3.77	26.2±0.3	2.2±0.8
DMF	0.218	0.949	5.83	24.5±0.7	−2.0±1.7
NMA	1.08	4.24	—	24.4±0.7	0.6±1.7
NMF	3.20	12.4	—	24.1±0.8	1.8±1.9

a) $[ROTs]_0=0.05$ mol/dm³. The rate constants obtained in the presence of equimolar amount of pyridine were essentially the same as those in its absence. b) Mean deviation for k_1 is ±3.6%. c) Probable errors are quoted.

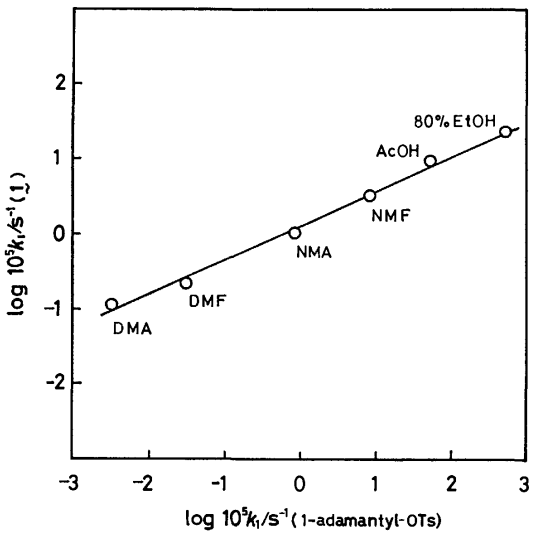

Fig. 1. A linear free-energy relationship between log k_1 (**1**) and log k_1(1-adamantyl tosylate) at 25 °C.

C–H bond breaking (σ-participation) is involved in the rate-determining step, a positive kinetic isotope effect ($k_H/k_D>1$) should be observed upon replacement of the migrating hydrogen atom by a deuterium atom. Thus, the rate of solvolysis of 7α-deuterium-tagged substrate **1**-7α-*d* was determined, using NMF as a solvent. NMF was selected for the reason that a maximal yield of the rearranged olefin (3-methylbicyclo[3.3.1]non-2-ene (**5**)) was observed in the case of NMF as a solvent (*vide infra*). The observed value $k_H/k_D=1.01\pm0.03$, indicates that the solvolysis of **1** proceeds without σ(C(7)–H) participation in NMF.

Elimination Products of the Solvolysis of ***1*** *in the Carboxamides.* In acetic acid[2] and 80% aqueous ethanol[3] the solvolysis product is exclusively a mixture of *exo*-7-methylbicyclo[3.3.1]non-2-ene (**4**) and **5** (**4**: **5**=45: 55). The latter is supposed to be derived from a carbenium ion intermediate (**3**) produced by a transannular C(7)–C(3) hydride shift from the intimate ion-pair intermediate (**2**) of solvolysis (Scheme 1).

It has been accepted that the tosylate **1** has predominantly a twin chair conformation.[11] In this conformation the intermolecular *anti*-elimination is sterically less favored because of the equatorial position of the tosyloxy group, the proton abstraction in this elimination thus being intramolecularly caused by the tosylate anion.

The results of GLC analysis of the solvolysis products

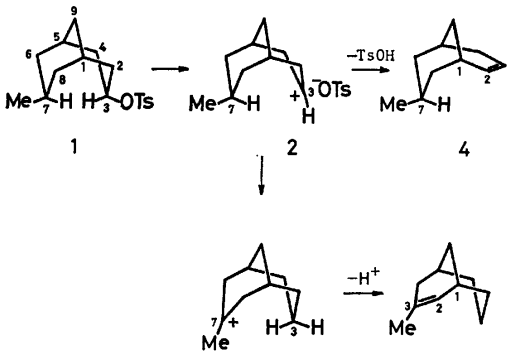

Scheme 1.

indicate that the major product in a series of carboxamide solvolysis is an olefin mixture of **4** and **5**. However, in contrast to the results of acetolysis[2] and ethanolysis,[3] the yield of **5** is much lower and decreases in the order NMF>NMA>DMF>DMA (Table 2). In other words, the hydride shift is suppressed in the carboxamide solvents in the sequence DMA>DMF>NMA>NMF.

Thus, the suppression of hydride shift seems to be a general feature of the carboxamide solvent, since such

Table 2. Products for the solvolysis of 7β-methylbicyclo[3.3.1]non-3β-yl tosylate (**1**) in various carboxamides

Solvent[e]	t/°C	Yield/%[b]				
		Olefin		Ester		ROH[f]
		4	**5**	3α	3β	
DMA	35	90.0	9.3	0.3	0.4	0.1
DMF	35	84.1	13.0	1.5	1.0	0.0[g]
NMA	35	74.3	22.0	1.6	1.5	0.6
NMF	35	66.0	33.6	0.0[g]	0.0[g]	0.5
AcOH[h]	25	44	55	—	1	—
80% EtOH[i]	25	45	55	—	—	0

a) $[\mathbf{1}]_0=0.05$ mol/dm³. [pyridine]=0.0535 mol/dm³. b) Average of two independent experiments. c) Water contents for carboxamides are ≤0.03 mol/dm³. d) Inverted acetate for DMA and NMA, and formate for DMF and NMF. e) Retained acetate for DMA and NMA, and formate for DMF and NMF. f) 7-Methylbicyclo[3.3.1]-nonan-3-ol; isomer compositions were not determined. g) Trace amount of these compounds were detected on GLC. h) Ref. 2. i) Ref. 3.

phenomenon has also been observed in the solvolysis of 4-*t*-butylcyclohexyl tosylate in NMA.[4] Possible causes for such a suppression might be a) specific solvation from the rear side of the carbenium ion **2** by the nucleophilic carboxamide molecule (negative end of dipole) and/or b) the enhancement of the rate of deprotonation in the intimate ion-pair intermediate **2** due to an increase in the basicity of the leaving tosylate anion in such a solvent as carboxamides. However, judging from the steric disadvantage for the carboxamide molecule to achieve such a solvation toward the U-shaped cationic intermediate **2**, cause a) seems less likely.

The basicity of the leaving tosylate anion in the carboxamide solvents would be the reverse of the hydrogen bonding order (NMF>NMA>DMF>DMA),[12] being in line with the observed solvent sequence for the suppression of rearrangement.

The acceleration of intramolecular *syn*-elimination in E1 reaction has been observed in the elimination of 1-methylpropyl-2-*d* tosylate in a dipolar aprotic solvent, *i.e.* nitrobenzene.[13] Kim and Brown[14] proposed that the leaving group anion can in principle attack β-hydrogen in the stage of tight ion-pair formation to give elimination products. The process leading to the unrearranged olefin **4** (**2**→**4** in Scheme 1) in the present study appears to be close to the one they proposed.

A reactivity-selectivity linear relation[15] has been observed between the rates and the composition of olefin **4** and **5**, when log k_1 values in NMF, NMA, DMF, and DMA are plotted against the logarithms of the ratio %**5**: %**4** (Fig. 2), indicating that both elimination products stem from a single intermediate **2** as depicted in Scheme 1.[16]

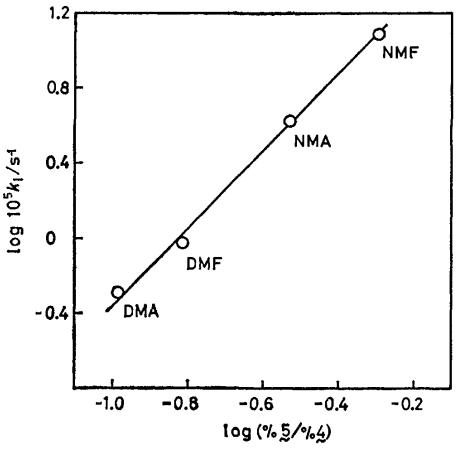

Fig. 2. Linear reactivity-selectivity relationship between log k_1 and log(%**5**/%**4**) for the carboxamide solvent.

Substitution Products of the Solvolysis of ***1*** *in the Carboxamides.* Besides the elimination products, formation of small amounts (≤3%) of ester (acetate or formate) was observed (Table 2). Since the carboxamide solvent used for the solvolysis study is usually contaminated with water (*ca.* 0.003 mol/dm³ or less) even after rigorous purification, the esters seem to be produced by the hydrolysis of an *N*-protonated (as to NMF or NMA) or *N*-methylated (as to DMF or DMA) imidate ester (**6**)[17] which might be derived from the ion-pair intermediate **2** (Scheme 2, *vide infra*). In fact, an examination of the ester yield in DMF with various water contents indicates (Fig. 3, *vide infra*) that no formate is obtained in a completely dried DMF. It is known that a protonated or methylated imidate ester similar to **6** can be rapidly hydrolyzed.[18]

Small amounts of bicyclic alcohol (≤0.7%) are also produced by the hydrolysis of **1** with water contained in the carboxamide solvent.

Effects of Added Water on the Product Distribution in the Solvolysis of ***1*** *in DMF.* GLC product analysis were carried out on the solvolysis of **1** in DMF in the presence of various amounts of water (0.003—0.519 mol/dm³). With an increase in the water content, the yield of the formate increases from zero and reaches a maximum value (7.3%), accompanied by a decrease in the yield of unrearranged olefin **4** from 85.8 to 79.5% (Table 3), whereas the yield of rearranged olefin **5** remains unchanged throughout the whole range of water concentration.

Table 3. Effects of added water on the product distribution for the solvolysis of 7β-methylbicyclo[3.3.1]non-3β-yl tosylate (**1**) in DMF at 35 °C[a]

$[H_2O]$[b] mol/dm³	Yield/% Olefin **4**	Olefin **5**	Ester 3α[c]	Ester 3β[d]	ROH[e]
0.003	85.8	12.8	0.2	0.7	0.5
0.019	84.6	12.5	1.6	1.3	0.0
0.036	83.4	12.9	2.4	1.3	0.0
0.068	82.3	12.6	3.8	1.2	0.0
0.126	80.4	12.7	5.6	1.1	0.2
0.519	79.5	12.7	6.7	0.6	0.5

a) $[ROTs]_0=0.08$ mol/dm³. [pyridine]=0.084 mol/dm³. b) Desired amount of water was added except for the first run, in which the $[H_2O]$ was determined by means of the Karl-Fischer titration. c) Inverted formate. d) Retained formate. e) 3-ol; isomer compositions were not determined.

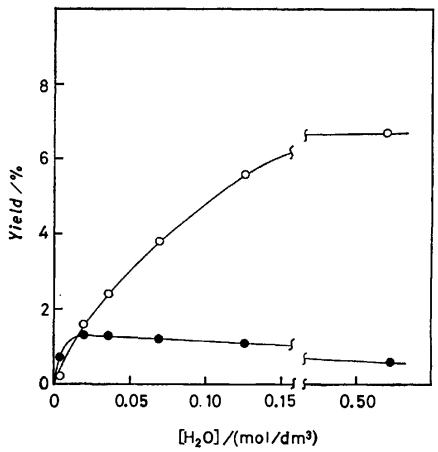

Fig. 3. Effect of added water content in DMF on the formation of 3α- (○) and 3β-formates (●).

The fact that the change in water content affects the yield of unrearranged olefin **4** as well as the yield of the formate suggests that cationic imidate **6** is produced even in the absence of water to form olefin **4**, not returning to the intimate ion-pair intermediate **2**. If such a return course is probable, a decrease in the yield of the olefin **5** would be observed with an increase in the water content. However, this is not the case (Table 3). The probable reaction pathways are shown in Scheme 2.

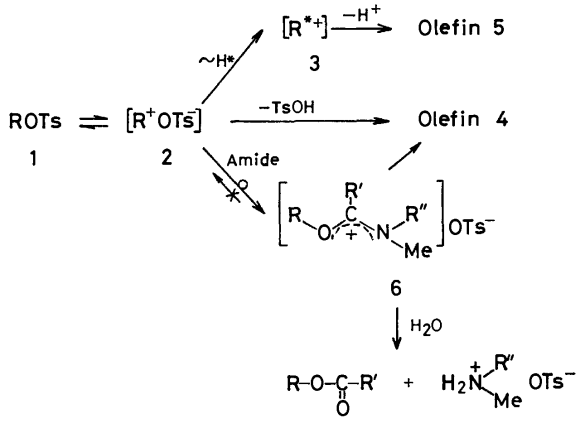

Scheme 2. (R′=H or Me; R″=H or Me)

The yields of the 3β-formate are less than 1.3%, while the yields of 3α-formate continuously increase with an increase in the water content up to 6.7% (Table 3 and Fig. 3). The latter is most probably formed through the usual inversion course in the reaction sequence as shown in Scheme 2. The course of the formation of 3β-formate remains open for further examination, though it is in low yields and might not represent a major feature of the solvolysis.

In conclusion, the solvolysis of **1** in the carboxamide solvents proceeds *via* the initially-formed intimate ion-pair intermediate **2** upon which the transannular 1,5-hydride shift, *syn*-E1 reaction, and nucleophilic displacement by the carboxamide molecule occur competitively (Scheme 2). The mechanism is essentially in line with Graham's conclusion.[2]

Experimental

All the melting points are uncorrected. NMR spectra were measured with a Hitachi R-24 instrument, tetramethylsilane being used as an internal standard, IR spectra with a Hitachi 215 or EPI-S2 spectrometer, only the major absorption being cited, and mass spectra with a Hitachi RMS-4 mass spectrometer at 70 eV, the molecular ion being cited. For GLC analysis, a Hitachi K-53 gas chromatograph fitted with a flame ionization detector was used with a 3 m column (i.d. =3 mm) packed with Carbowax 20M or PEG 6000 on Chromosorb W.

Purification of Carboxamides. All the carboxamides used in this study were purified as follows. A reagent grade material was dried for three days over molecular sieves (Type 4A). It was distilled under reduced pressure in the presence of concd H_2SO_4 and the distillate was allowed to stand over CaO or CaH_2 (except for NMF) for several hours. The liquid was transferred to a distillation flask using a large-bore, double ended needle under a positive pressure of nitrogen and distilled under reduced pressure in a dry nitrogen system. The purified carboxamide was stored in an amber bottle with a septum closure under dry nitrogen. In use, a syringe needle is pushed through the septum to gain access to the carboxamides. Titration with Karl Fischer reagent indicates that the water content of the carboxamide is less than 0.003 mol/dm³.

Synthesis of the Substrate ***1***. The synthesis of **1** was reported by Eakin *et al.*[2,19] without any details of the preparation or properties of the substances.

1-Hydroxy-7β-methylbicyclo[3.3.1]nonan-3-one ***(7)***: The procedure is essentially the same as that of Macrosson *et al.*[20] To a stirred solution of NaOMe in MeOH (Na; 0.4 g, MeOH; 30 cm³) was added a mixture of 5-methyl-2-cyclohexen-1-one[21] (1.9 g) and ethyl acetoacetate (2.7 g). After the solution had been heated under reflux for 72 h, a solution of KOH (2.6 g) in water (7.6 cm³) was added, heating under reflux being continued for 12 h. The methanolic solution was concentrated by rotoevaporation. The organic layer was taken up in CH_2Cl_2 and the organic extracts were washed with 5% aq HCl, saturated aq $NaHCO_3$, and saturated aq NaCl. The CH_2Cl_2 solution was dried (Na_2SO_4), concentrated, and recrystallized from CCl_4–hexane, giving 1.95 g (68%) of the hydroxy ketone **7**: mp 79—80 °C; IR (KBr) 3300 (OH) and 1702 cm⁻¹ (C=O); NMR ($CDCl_3$) δ=0.86 (d, 3H, J=4.4 Hz, CH_3), 1.03—2.23 (m, 12H), and 2.59 ppm (s, 1H, exchangeable with D_2O); MS, *m/e* 168. (Found: C, 71.15; H, 9.41%).

1-Bromo-7β-methylbicyclo[3.3.1]nonan-3-one ***(8)***: To a stirred solution of **7** (1.96 g) in dry ether (15 cm³) was added freshly distilled PBr_3 (1.11 g) and the resulting solution was heated under reflux for 30 min. The ether solution was washed with cold water, dried (Na_2SO_4), concentrated, and recrystallized from hexane, giving 2.38 g (88%) of bromo ketone **8**: mp 64.5—65.4 °C; IR (CCl_4) 1718 cm⁻¹ (C=O); NMR ($CDCl_3$) δ=0.86 (d, 3H, J=3.6 Hz, CH_3), 1.0—2.8 (m, 10H), and 3.06 ppm (s, 2H, C(Br)–CH_2–CO).

7β-Methylbicyclo[3.3.1]nonan-3-one ***(9)***: A mixture of **8** (2.1 g), (*n*-Bu)$_3$SnH (5.48 g), AIBN (2.07 g), and dry toluene (60 cm³) was heated at 60—65 °C for 4 h. After removal of toluene by rotoevaporation, the residue was treated with hexane and filtered. The filtrate was concentrated and distilled (100 °C/67 Pa) to give crude ketone, from which 1.2 g (87%) of ketone **9** was isolated by means of preparative TLC (alumina PF_{254}, Merck) using hexane–CH_2Cl_2 (19: 1, v/v) as a developing agent: mp 54—54.5 °C (lit,[22] mp 57—58 °C); IR (CCl_4) 1710 cm⁻¹ (C=O); NMR ($CDCl_3$) δ=0.83 (d, 3H, J=5 Hz, CH_3) and 1.1—2.7 ppm (m, 13H).

7β-Methylbicyclo[3.3.1]nonan-3β-ol ***(10)***: Lithium (0.334 g) was dissolved in NH_3 (l) (80 cm³) and to this solution was added a solution of **9** (1.5 g) in dry THF (30 cm³). After being stirred for 30 min, dry EtOH (6.8 cm³) was added and the mixture was stirred until the blue color disappeared. The usual work-up afforded 1.27 g (84%) of the alcohol: mp 69—76 °C. It was found convenient to convert the alcohol into the corresponding formate for separation of the 3α- and 3β-epimers. This was done by treatment of the alcohol with large excess of acetic formic anhydride in pyridine (12 h at room temp). The formate was isolated after the usual work-up as a pale yellow oil (1.45 g) which was recrystallized from ether at −78 °C to give 1.38 g (94%) of 3β-formate (**11**): mp 37—38 °C; IR (neat) 1728 (C=O) and 1185 cm⁻¹ (C–O–C); NMR ($CDCl_3$) δ=0.85 (d, 3H, J=5.8 Hz, CH_3), 1.0—2.3 (m, 13H), 5.56 (nine-line m, 1H, C<u>H</u>(OCHO)), and 7.99 ppm (s, 1H, CHO).

Found: C, 72.77; H, 9.73%. Calcd for $C_{11}H_{18}O_2$: C, 72.49; H, 9.95%.

Pure 3β-alcohol **10** was obtained by the hydrogenolysis of

11 with $LiAlH_4$ in 98% yield: mp 76—78.5 °C (lit,[22] mp 72—75 °C); IR (CCl_4) 3620 (OH), 3300 (OH), and 988 cm^{-1} (C–O); NMR ($CDCl_3$) δ=0.84 (d, 3H, J=5 Hz, CH_3), 1.0—2.5 (m, 14H), and 4.34 ppm (nine-line m, 1H, C<u>H</u>(OH)); MS, *m/e* 154.

7β-Methylbicyclo[3.3.1]non-3β-yl Tosylate ***1***: The compound was prepared from **10** following the method of Stéhelin *et al.*[22] Spectroscopic data for **1** were identical with those reported:[3,22] mp 63.5 °C (dec) (lit,[3,22] mp 64 °C (dec)).

7β-Methylbicyclo[3.3.1]nonan-3α-ol (12).[2] To s atirred solution of $NaBH_4$ (1.5 g) in MeOH (20 cm^3) was added a solution of **9** (1.35 g) in MeOH (60 cm^3) and the resulting mixture was stirred for 15 h at room temp. After the usual work-up, sublimation of the residue *in vacuo* afforded 1.2 g (88%) of an alcohol. GLC assay for the corresponding acetate showed that the alcohol consists of **10** and **12** in the ratio 13: 87. 3α-Alcohol **12** was isolated conventionally from the mixture by fractional crystallization from hexane in 26% yield (based on **9**): mp 66.5—68.5 °C; IR (CCl_4) 3620 (OH), 3300 (OH), and 983 cm^{-1} (C–O): NMR ($CDCl_3$) δ=0.85 (d, 3H, J=6.6 Hz, CH_3), 0.6—2.5 (m, 14H), and 3.92 ppm (distorted m, 1H, C<u>H</u>(OH)); MS, *m/e* 154. (Found: C, 77.53; H, 11.54%).

exo-*7-Methylbicyclo[3.3.1]non-2-ene* ***4***.[2,3] Dehydration of **12** with $POCl_3$ and pyridine afforded olefin **4** in 72% yield: bp 80 °C (bath temp)/427 Pa; IR (neat) 3005 (=C–H) and 1650 cm^{-1} (C=C); NMR ($CDCl_3$) δ=0.83 (d, 3H, J=6 Hz, CH_3), 0.9—2.7 (m, 11H), and 5.70 ppm (m, 2H, CH=CH).

3-Methylbicyclo[3.3.1]non-2-ene ***5***.[2,3] The olefin was separated from a mixture of **4** and **5**, obtained by treating **4** with boiling formic acid,[23] by means of preparative GLC, and used as an authentic sample for GLC assay.

*7β-Methylbicyclo[3.3.1]non-3β-yl-7α-*d *Tosylate* ***1-7α-d***.[2] The compound was prepared according to the reported methods.[2,22] 7-Methylenebicyclo[3.3.1]nonan-3-one obtained by fragmentation of 1,3-dibromoadamantane[24] was reduced with $LiAlD_4$ in ether.[25] By chromatography over neutral alumina (Merck Al_2O_3, 90), pure 7-methylenebicyclo[3.3.1]nonan-3β-ol-3α-*d* was obtained as a minor reduced product (15%). The alcohol was treated with concd H_2SO_4 in MeOH (1: 1, v/v) at room temp for 3 min[2] to furnish the ketone (**9**-7α-*d*), from which **1**-7α-*d* was derived by the method described for the preparation of **1** (*vide supra*): mp 63.5 °C (dec); NMR ($CDCl_3$) δ=0.83 (s, 3H, CH_3–C(7)), 1.0—2.3 (m, 12H), 2.43 (s, 3H, aryl CH_3), 5.20 (nine-line m, 1H, CH(OTs)), and 7.53 ppm (m, 4H, aryl H).

The Acetates of ***10*** *and* ***12****, and the Formate of* ***12***. The acetates were prepared by the usual method (acetic anhydride–pyridine) and the formate was prepared by the same method as described above. They were used as authentic sample for GLC assay.

Spectral Data for 3β-Acetate: IR (CCl_4) 1730 (C=O) and 1022 cm^{-1} (C–O); NMR ($CDCl_3$) δ=0.85 (d, 3H, J=5.2 Hz, CH_3–C(7)), 1.0—2.3 (m, 13H), 2.0 (s, 3H, CH_3CO), and 5.43 ppm (nine-line m, 1H, C<u>H</u>(OAc)).

Spectral Data for the 3α-Acetate: IR (CCl_4) 1730 (C=O) and 1029 cm^{-1} (C–O); NMR ($CDCl_3$) δ=0.86 (d, 3H, J=6 Hz, CH_3–C(7)), 0.7—2.5 (m, 13H), 1.98 (s, 3H, CH_3CO), and 4.98 ppm (distorted m, 1H, C<u>H</u>(OAc)).

Spectral Data for the 3α-Formate: IR (CCl_4) 1728 (C=O) and 1180 cm^{-1} (C–O); NMR ($CDCl_3$) δ=0.87 (d, 3H. J=6 Hz, CH_3), 0.7—2.6 (m, 13H), 5.12 (distorted m, 1H, C<u>H</u>(OCHO)), and 8.01 ppm (s, 1H, CHO).

Found: C, 72.48; H, 9.73%. Calcd for $C_{11}H_{18}O_2$: C, 72.49; H, 9.95%.

Kinetic Measurement. Rates in carboxamides for **1** were determined titrimetrically by the usual sealed-ampoule technique. In a typical experiment, 13 ampoules each containing *ca.* 1.1 cm^3 of the solution were prepared. They were sealed after being flashed with nitrogen. An aliquot (1 cm^3) of the reaction mixture was pipetted from each ampoule after quenching thermally and titrated with standardized (n-Bu)$_4$NOH (in 2-propanol–MeOH; 3: 1, v/v) or with KOH (in EtOH) solution, using Thymol Blue or Thymol Blue–phenolphthalein mixed indicator, respectively. The rate constants were calculated by means of a linear least-squares fit of the integrated form of the first-order rate equation. All the rate constants are the average values of at least two independent determinations.

Product Analysis. Tosylate **1** (100 mg) was weighed into an ampoule which was repeatedly evacuated and filled with dry nitrogen. A septum is placed over the opening, and a solvent (*ca.* 6.5 cm^3) was introduced with a dried syringe, followed by addition of pyridine (0.028 cm^3) with a dried micro syringe through the septum. The ampoule was then sealed under nitrogen and kept at the desired temperature for ten half-lives. The mixture was poured into water (50 cm^3) and extracted with ether (15 cm^3, three times). The combined ether solution was washed with water, 5% aq HCl, saturated aq $NaHCO_3$, and saturated aq NaCl. After being dried (Na_2SO_4), the ether solution was carefully concentrated by use of a 30-cm column packed with glass helix to *ca.* 1—2 cm^3. The condensed ether solution was subjected to GLC assay.

The products from the solvolysis of **1** in the carboxamides were identified by their retention times on GLC. Separation was achieved at 70 °C for olefins (**4** and **5**) and at 140 °C for esters (3α- and 3β-acetates or formates).

The authers wish to express their thanks to Mr. Masami Inaba for measurement of the mass spectra, and to Messrs. Eiichiro Amano and Tadashi Hanafusa for the microanalysis.

References

1) G. A. Olah and P. v. R. Schleyer, Ed., "Carbonium Ions," Wiley-Interscience, Vol. 2, New York (1970), pp. 521—571.

2) M. A. Eakin, J. Martin, W. Parker, S. C. Egan (D.H. G.), and S. H. Graham, *J. Chem. Soc., Chem. Commun.*, **1968**, 337.

3) L. Stéhelin, L. Kanellias, and G. Ourisson, *J. Org. Chem.*, **38**, 847 (1973).

4) Part I: S. Saito, T. Yabuki, T. Moriwake, and K. Okamoto, *Bull. Chem. Soc. Jpn.*, **46**, 1795 (1973).

5) a) S. Winstein and N. J. Holness, *J. Am. Chem. Soc.*, **77**, 5562 (1955); b) N. C. G. Campbell, D. M. Muir, R. R. Hill, J. H. Parish, R. M. Southan, and M. C. Whiting, *J. Chem. Soc., B*, **1968**, 355.

6) K. Okamoto, S. Saito, and H. Shingu, *Bull. Chem. Soc. Jpn.*, **42**, 3288 (1969).

7) S. Saito, K. Doihara, T. Moriwake, and K. Okamoto, unpublished observations (submitted for publication in this journal).

8) D. N. Kevill, K. C. Kolwyck, and F. L. Weitl, *J. Am. Chem. Soc.*, **92**, 7300 (1970).

9) E. Grunwald and S. Winstein, *J. Am. Chem. Soc.*, **70**, 846 (1948); Calculated by multiplication of the slope (0.45) of the linear plot (Fig. 1) by the *m* value (1.18) (Ref. 7) for the solvolysis of 1-adamantyl tosylate in the series of carboxamide solvents.

10) A. Streitwieser, Jr., *Chem. Rev.*, **56**, 571 (1956).

11) See footnote 8 cited in Ref. 2.

12) It has been proposed that the ability of a series of carboxamide solvents to donate hydrogen bonding to anion is in the quoted order. The importance of hydrogen bonding order has been demonstrated in the S_N2 reaction between methyl iodide and chloride anion in the series of carboxamides as solvents: V. Gold, Ed., "Advances in Physical Organic Chemistry," Academic Press, Vol. 5, New York (1967), pp. 196—197.

13) P. S. Skell and W. L. Hall, *J. Am. Chem. Soc.*, **85**, 2851 (1963).

14) C. J. Kim and H. C. Brown, *J. Am. Chem. Soc.*, **94**, 5051 (1972).

15) R. A. Sneen, J. V. Carter, and P. S. Kay, *J. Am. Chem. Soc.*, **88**, 2594 (1966).

16) Although the limitations on this linear free-energy relationship (D. J. Raber, J. M. Harris, R. E. Hall, and P. v. R. Schleyer, *J. Am. Chem. Soc.*, **93**, 4821 (1971)) should not be underestimated, the straight line (Fig. 2) provides an evidence for a typical S_N1 nature of solvolysis of **1** in the carboxamide solvents. See also the following references in which it has been reported that the Sneen-Carter-Kay treatment (Ref. 15) is successful: a) J. M. Harris, J. F. Fagan, F. A. Walden, and D. C. Clark, *Tetrahedron Lett.*, **1972**, 3023; b) J. M. Harris, A. Becker, D. C. Clark, J. F. Fagan, and S. L. Kennan, *ibid.*, **1973**, 3813; c) K. Okamoto and T. Kinoshita, *Chem. Lett.*, **1974**, 1037; d) A. Pross and R. Koren, *Tetrahedron Lett.* **1975**, 3613.

17) In this compound, contribution of oxonium structure (a) is considered to be small because of an electron-donating character of the amino moiety: See H. Perst, "Oxonium Ions in Organic Chemistry," Verlag Chemie, London (1971), p. 7.

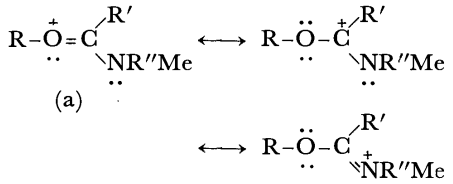

18) a) See the monograph (Ref. 17), p. 132; b) R. K. Chaturvedi and G. L. Schmir, *J. Am. Chem. Soc.*, **90**, 4413 (1968); c) T. C. Pletcher, S. Koehler, and E. H. Cordes, *ibid.*, **90**, 7072 (1968); d) T. Okuyama, T. C. Pletcher, D. J. Sahn, and G. L. Schmir, *ibid.*, **95**, 1253 (1973); e) V. F. Smith, Jr. and G. L. Schmir, *ibid.*, **97**, 3171 (1975).

19) M. A. Eakin, J. Martin, and W. Parker, *Chem. Commun.*, **1968**, 298.

20) W. D. K. Macrosson, J. Martin, W. Parker, and A. B. Penrose, *J. Chem. Soc., C*, **1968**, 2323.

21) J. P. Blanchard and H. L. Goering, *J. Am. Chem. Soc.*, **73**, 5863 (1951).

22) L. Stéhelin, L. Kanellias, and G. Ourisson, *J. Org. Chem.*, **38**, 851 (1973).

23) R. A. Appleton and S. H. Graham, *Chem. Commun.*, **1965**, 297.

24) A. R. Gagneux and R. Meier, *Tetrahedron Lett.*, **1969**, 1365.

25) M. A. Eakin, J. Martin, and W. Parker, *Chem. Commun.*, **1965**, 206.

Chemistry of Nitrosoimines. XVI.[1] A New Method for Facile Preparation of Azamonomethinecyanines *via* Nitrosoimines

Kin-ya AKIBA, Kiyofumi ISHIKAWA, and Naoki INAMOTO

Department of Chemistry, Faculty of Science, The University of Tokyo, Hongo, Tokyo 113

(Received June 10, 1977)

The reaction of 3-substituted 2-nitrosoimino-2,3-dihydrobenzothiazoles (**1**) with Grignard-type reagents of 3-substituted 2-imino-2,3-dihydrobenzothiazoles (**2**) gave azamonomethinecyanines (**3**) in high yields (71—96%). This is a new type of reaction for the preparation of **3**. Hydrolysis of **3** afforded ring-opened disulfides, bis[*o*-{*N*-methyl-*N*-(3-methyl-2,3-dihydrobenzothiazol-2-ylidenecarbamoyl)amino}phenyl] disulfides, in high yields (78—85%). Formation of by-products is explained by the presence of transnitrosation between **1** and **2** and ring-opening equilibrium of Grignard-type reagent of 2-imino-3-phenyl-2,3-dihydrobenzothiazole.

A series of investigations on the reactivity of nitrosoimines has revealed that there are three paths of attack on 3-substituted 2-nitrosoimino-2,3-dihydrobenzothiazoles (**1**) by organometalloids depending on the structure of the latter, *i.e.*, paths a and b by organolithiums[2] and paths b and c by Grignard regents[3] (Scheme 1). The reactivities are recognized by the large contribution of charge separated structures to the ground state of **1** shown by spectroscopic measurements, especially by ESCA.[4]

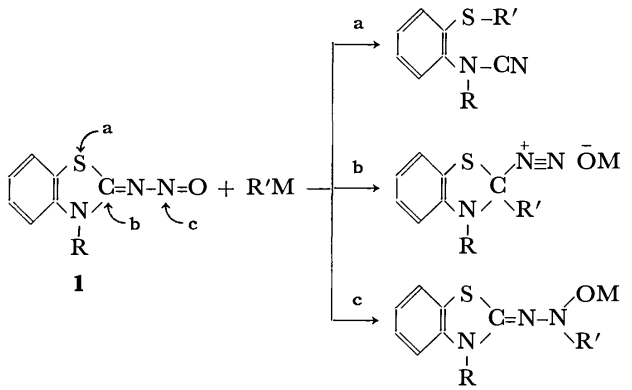

Scheme 1.

In continuation of the research directed to find out conditions under which each path is observed specifically, we report the reaction of **1** with Grignard-type reagents of 3-substituted 2-imino-2,3-dihydrobenzothiazoles (**2**) which followed path b almost exclusively to give the corresponding azamonomethinecyanines (**3**).[5] Concerning the preparation of azamonomethinecyanines, the reaction of 3-methyl-2-phenylsulfonylazobenzothiazolium tetrafluoroborate with sodium azide,[6] that of 2-amino-3-methylbenzothiazolium iodide with 3-methyl-2-methylthiobenzothiazolium iodie,[7] and base-catalyzed decomposition of triazatrimethinecyanine[8] are known.

3-Methyl-2-nitrosoimino-2,3-dihydrobenzothiazole (**1a**) reacted with Grignard-type reagent of 2-imino-3-methyl-2,3-dihydrobenzothiazole (**2a**) in THF at room temperature under nitrogen to give azamonomethinecyanine chloride (**3'a, a**) almost quantitatively, which gave the perchlorate (**3a, a**) in 84.5% yield by treatment with excess perchloric acid.

Evolution of nitrogen was followed for the reaction of **1a** with Grignard-type reagent of **2a** by measuring the increase of the gas volume of the reaction vessel set up as a closed system. Gas was evolved continuously during the course of reaction to yield 87% of the calculated amount (3.5 h, at 27.5 °C). No additional gas evolution was observed by injection of excess acetic acid. The cyanine perchlorate (**3a, a**) was obtained in 83% yield by the usual work-up.

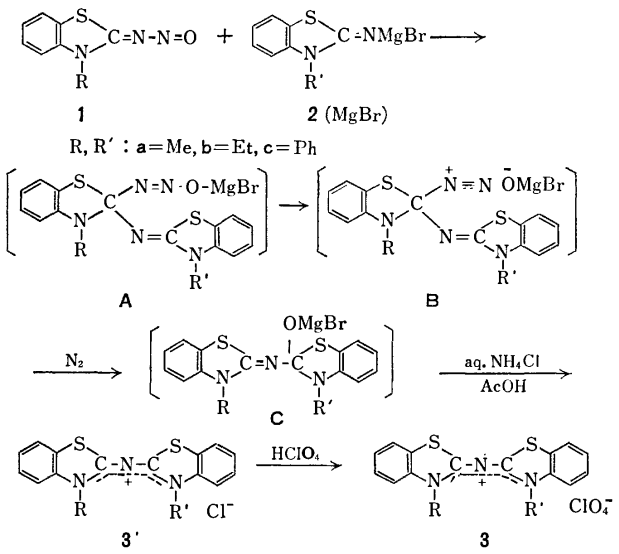

Scheme 2.

Table 1. Yields and melting points of azamonomethinecyanine perchlorates (**3**)

1	2	3	Yield (%)[a]	Mp (°C)	Recovery of **2** (%)[b]
R=Me	R'=Me	a, a	84.5	319.0—320.0 (dec)	29.3
Me	Et	a, b	89.8	276.8—278.0	29.8
Et	Me	b, a	95.8	276.8—278.0	34.7
Et	Et	b, b	89.3	275.0—276.5	28.6
Ph	Me	c, a	70.9	312.0—314.0 (dec)	36.7
Ph	Et	c, b	78.0	253.5—255.0	28.2
Ph	Ph	c, c	80.0[c]	316.0—317.3 (dec)	28.2

a) After recrystallization from ethanol once. b) Based on **2** initially charged. c) The reaction was carried out at 0 °C.

Formation of **3** can be explained as shown in Scheme 2. The Grignard-type reagent of **2** attacks the *C*-2 of benzothiazoline ring of **1** (path b). The resulting diazotate (**A**) is not stable under the reaction conditions releasing nitrogen to give the alcohol (**C**), where contribution of diazonium character (**B**) to the transition state may be significant. The intermediate alcohol (**C**) is converted into a stabilized cation, *i.e.*, azamonomethinecyanine (**3**).

The results are given in Table 1.

Similar reactions of 2-nitrosoimino-3,4-diphenyl-2,3-dihydrothiazole (**4**) with Grignard-type reagents of **2** also gave the corresponding azamonomethinecyanine perchlorate (**5**) in high yields (Table 2).

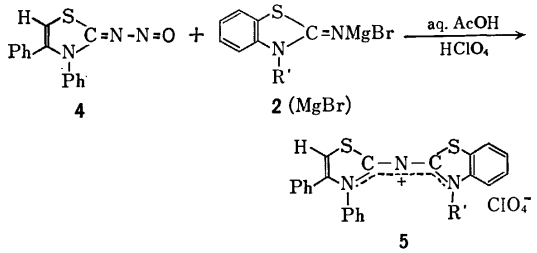

Table 2. Yields and melting points of azamonomethinecyanine perchlorates (**5**)

5	Yield[a] (%)	Mp (°C)	Recovery of 2 (%)[b]
a) R′=Me	80.5	236.8—238.2	33.6
b) R′=Et	74.6	274.2—276.0(dec)	27.7

a) After recrystallization once from ethanol. b) Based on **2** initially charged.

The yield of **3c**, **a** (70.9%) was relatively low. **2c** (18.4%) and 3-methyl-2,3-dihydrobenzothiazol-2-one (**6a**, 13.6%) were obtained from the benzene extract of the reaction mixture along with the recovered **2a** (36.7 %) as shown in Table 1. This can be explained by the attack of Grignard-type reagent on the nitroso group (path c), where the nitroso group is transferred to the imine of stronger basicity.

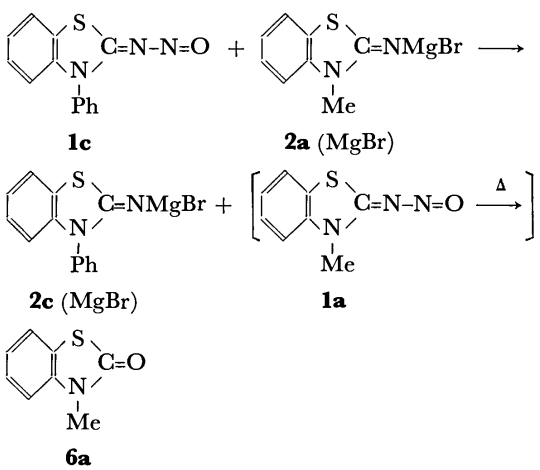

For the preparation of **3c**, **c**, the reaction was carried out at 0 °C instead of at room temperature. When the reaction was carried out at room temperature, **3c**, **c** was obtained in lower yield. Thus the same reaction was carried out at higher temperature (60—80 °C) in order to examine the nature of side reactions. The following products were isolated.

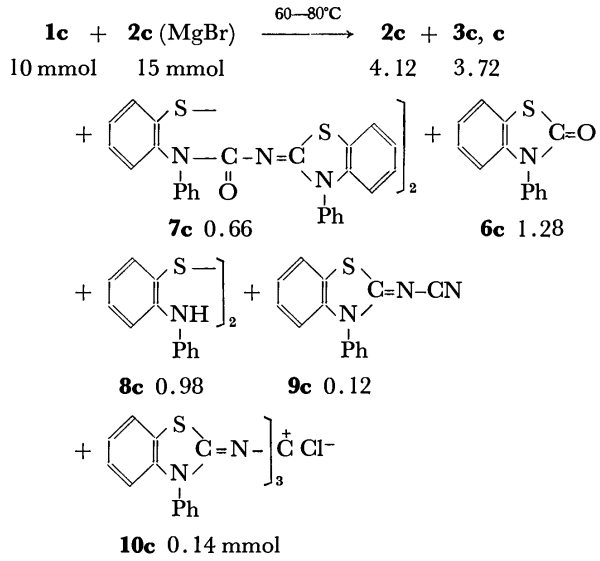

Table 3. Yields and melting points of the disulfides (**7**)

7	Yield (%)	Mp (°C)
a) R=Me	84.0	253.0—253.5
b) R=Et	84.5	119.5—120.5
c) R=Ph	78.0	230.0—231.0

The formation of **8c** and **9c** can be rationalized by assuming the presence of ring-opening equilibrium in Grignard-type reagent of **2c**.[9]

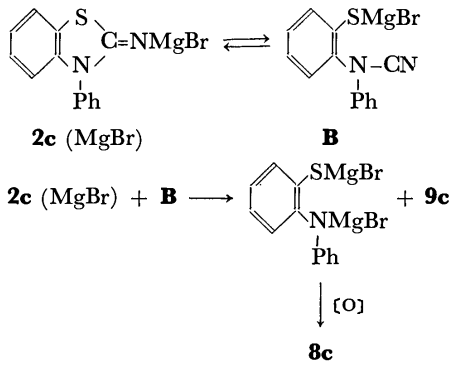

The formation of **10c** can be explained by the following sequence of reactions.

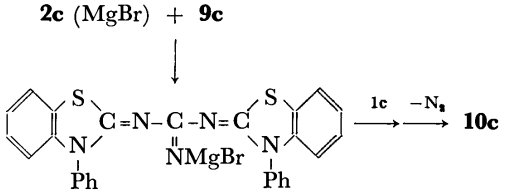

The structure of **10c** is supported by the following reactions where products were obtained almost quantitatively.

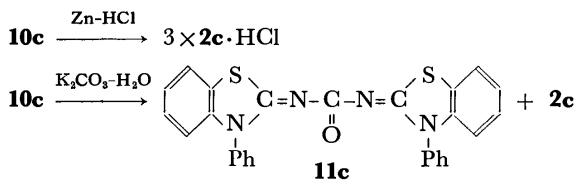

Compound (**10c**) seems to be less stable for alkaline hydrolysis than **3c**, **c**, in spite of the presence of a larger conjugation system for the carbonium ion.

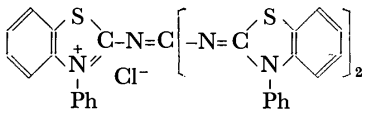

10c

The formation of **7c** is due to the thermal decomposition of the intermediate alcohol (*C*) of **3c**, **c**.

Lithium reagent of **2a** reacted with **1a** in THF at 0 °C under nitrogen to give bis [*o*-{*N*-methyl-*N*-(3-methyl-2,3-dihydrobenzothiazol-2-ylidenecarbamoyl)-amino}phenyl] disulfide (**7a**, 78.3%) as a major product and cyanine chloride (**3'a**, **a**, 10.9%) as a minor product.

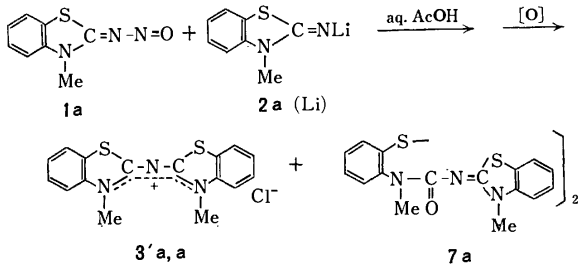

1a **2a** (Li) **3'a, a** **7a**

Formation of **7a** during the course of reaction is understandable by simultaneous ring-opening of lithium alkoxide (*C*) which might be produced after extrusion of nitrogen.

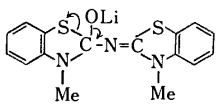

C

For the sake of clarification, symmetrical cyanine chlorides (**3'**) were treated with sodium hydroxide in ethanol which gave the disulfides (**7**) in high yields.

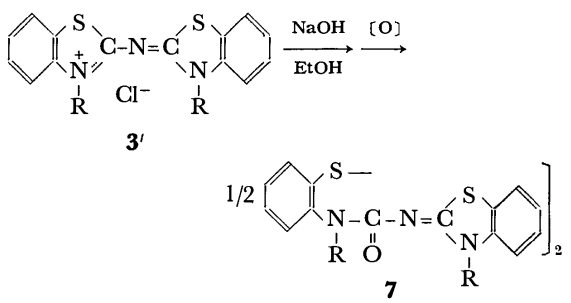

3' **7**

Ring-opening reaction of azamonomethinecyanine (**3'**) by sodium hydroxide is in contrast to the decomposition of triazatrimethinecyanine (**12**).

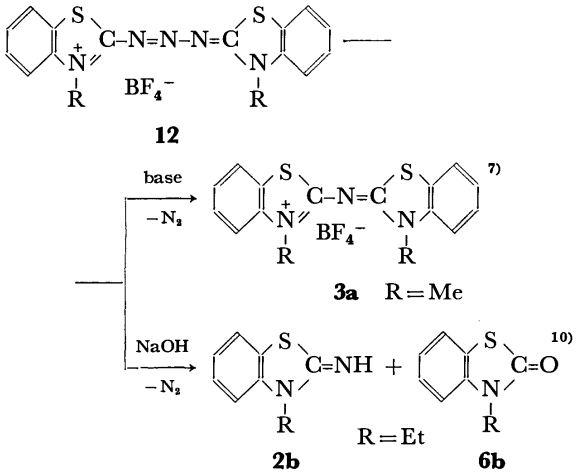

12 **3a** R=Me **2b** **6b** R=Et

Experimental

NMR spectra were recorded with Hitachi R-20 B and R-24 spectrometers (60 MHz) using TMS as an internal standard, IR spectra with a Hitachi EPI-G2 spectrometer and MS with a Hitachi RMU-6L mass spectrometer at 70 eV. All the melting points are uncorrected.

Materials. 2-Imino-3-methyl- (**2a**, mp 122—123 °C),[11] 3-ethyl-2-imino- (**2b**, mp 86—87 °C),[12] and 2-imino-3-phenyl-2,3-dihydrobenzothiazoles (**2c**, mp 73—74 °C)[11,13] were pre pared by reported methods. 3-Methyl-2-nitrosoimino-(**1a**, mp 146—147 °C (dec)),[11] 3-ethyl-2-nitrosoimino(**1b**, mp 147—148 °C (dec))[12] and 2-nitrosoimino-3-phenyl-2,3-dihydrobenzothiazoles (**1c**, mp 139—140 °C (dec))[11,13] were also prepared by reported methods. 2-Imino-3,4-diphenyl-2,3-dihydrothiazole (mp 108—109.5 °C)[14] was nitrosated in acetic acid with an aqueous solution of sodium nitrite to give 2-nitrosoimino-3,4-diphenyl-2,3-dihydrothiazole (**4**), mp 154—155 °C (dec).[15]

All the reactions were carried out under nitrogen except for the alkaline hydrolysis reactions of **3'**.

General Procedure for the Reaction of 3-Substituted 2-Nitrosoimino-2,3-dihydrobenzothiazole (1) with Grignard-type Reagent of 3-Substituted 2-Imino-2,3-dihydrobenzothiazole (2). A THF (50 ml) solution of **2** (7.5 mmol) was added dropwise at room temperature to a stirred solution of Grignard reagent prepared from magnesium (0.18 g, 7.5 mmol) and ethyl bromide (0.82 g, 7.5 mmol) in THF (25 ml) and the resulting solution was stirred for 30 min. **1** (5.0 mmol) was then added portionwise. The reaction took place immediately and precipitation appeared meanwhile. The mixture was stirred for 2 h and the solvent was evaporated under reduced pressure. To the residue were added a saturated aqueous solution of ammonium chloride (50 ml), glacial acetic acid (0.5 ml) and benzene (25 ml), and the mixture was stirred vigorously. After separation of the benzene layer, the remaining precipitates were collected by filtration and washed with 10% aqueous acetic acid (10 ml) and with water (25 ml) and then recrystallized from ethanol to give azamonomethinecyanine chloride (**3'**). The chloride was dissolved in ethanol and an excess of 70% aqueous perchloric acid was added to the solution. The resulting precipitates were collected by filtration after cooling in an ice bath and recrystallized from ethanol to give azamonomethinecyanine perchlorate (**3**).

By evaporation of benzene from the benzene layer under reduced pressure, the resulting residue was recrystallized from benzene–hexane (1: 5) to give recovered **2**.

NMR spectra were recorded for cyanine chlorides (**3'**),

since the solubility of cyanine perchlorates (**3**) in methanol was too small for measurement.

Measurement of Evolved Gas Volume. To a THF (25 ml) solution of Grignard reagent prepared from magnesium (182 mg, 7.5 mmol) and ethyl bromide (0.82 g, 7.5 mmol) was added **2a** (1.230 g, 7.5 mmol) in THF (50 ml) at 0 °C under nitrogen. This was carried out in a three-necked 100 ml round bottomed flask equipped with a rubber septum, a gas outlet tube and a Liebig condenser. A small flask containing **1a** (965 mg, 5.0 mmol) was connected to the top with a rubber tube. After the solution had been stirred at 0 °C for 30 min, **1a** was added in small portions from the top and stirring was continued at 0 °C during the course of reaction. Gas was evolved continuously during 3.5 h up to 108 ml measured at 27.5 °C (r.t.) (87.6% based on added **1a**, 5.0 mmol). No additional gas was evolved by addition of excess acetic acid (0.5 ml).

Reaction of 2-Nitrosoimino-3,4-diphenyl-2,3-dihydrothiazole (4) with Grignard-type Reagent of 2b. **4** (1.41 g, 5 mmol) was added portionwise at room temperature to a stirred solution of Grignard-type reagent of the imine prepared from ethylmagnesium bromide (7.5 mmol) and **2b** (1.36 g, 7.5 mmol) in THF (75 ml) and the resulting mixture was stirred for 2 h. A similar work-up to that above gave cyanine chloride (**5'b**, mp 298.2—299.5 °C (dec), (7.46 mmol, 74.6%). Treatment of the chloride with 70% aqueous perchloric acid gave cyanine perchlorate (**5**).

Residual **2b** (mp 86—87 °C, 368 mg, 27.7%) was recovered from the benzene layer.

Reaction of 1c with Grignard-type Reagent of 2c at Higher Temperature (60—80 °C). **2c** (3.30 g, 15 mmol) in THF (100 ml) was added at room temperature to a stirred solution of ethylmagnesium bromide (15.0 mmol) in THF (50 ml). The solution became turbid because of low solubility of Grignard-type reagent of **2c**. **1c** (2.56 g, 10.0 mmol) was then added to the solution portionwise. The mixture was stirred for 10 min at room temperature, and then refluxed for 17 h. The residue obtained by evaporation of the solvent under reduced pressure was extracted with dichloromethane (50 ml × 5) after addition of saturated aq ammonium chloride (100 ml).

By condensation of the extract, greenish yellow ppt were collected to give **3c,c** (0.84 g, 1.86 mmol) after recrystallization from ethanol. The filtrate was chromatographed on silica gel.

The following products were eluted from silica gel chromatography in the described order with the solvents shown in parentheses: bis(*o*-anilinophenyl) disulfide (**8c**, 0.39 g, 0.98 mmol, benzene),[16] 3-phenyl-2,3-dihydrobenzothiazol-2-one (**6c**, mp 73—74 °C, 0.29 g, 1.28 mmol, benzene),[17] bis[*o*-{*N*-phenyl-*N*-(3-phenyl-2,3-dihydrobenzothiazol-2-ylidenecarbamoyl)amino}-pheyl] disulfide [**7c**, mp 231—232 °C, 0.60 g, 0.66 mmol, benzene-ether (5: 1)], 2-cyanoimino-3-phenyl-2,3-dihydrobenzothiazole [**9c**, mp 190—191.2 °C, 0.03 g, 0.12 mmol, benzene-ether (5: 1)], **2c** [mp 74—75 °C, 0.93 g, 4.12 mmol, ether and ether-acetone (2: 1)],[11] tris(3-phenyl-2,3-dihydrobenzothiazol-2-ylideneamino) carbonium chloride [**10c**, mp>360 °C, 0.10 g, 0.14 mmol, UV: λ_{max}^{EtOH} 401 nm (ε 6.4×10^3): EA of **10c**: Found: C, 62.77: H, 3.75; N, 10.20: S, 12.06%. Calcd for $C_{40}H_{27}N_6ClO_4S_3$: C, 61.02; H, 3.46; N, 10.67; S, 12.22%, acetone and acetone-ethanol (2: 1)], and **3c, c** [mp 301—302 °C, 1.86 mmol, acetone-ethanol(1:2)]. An authentic sample of **9c** was prepared by refluxing of **2c** (2.78 g, 12.3 mmol) in benzene (20 ml) with cyanogen bromide (0.83 g, 7.79 mmol) in benzene (50 ml) for 3 h. The resulting ppt., hydrobromide of **2c** (1.86 g), were filtered off and the filtrate was shaken with aq sodium hydroxide. The product, **9c**, 1.52 g, mp 190—191.2 °C, was obtained by the usual work-up. EA of **9c**: Found: C, 66.97; H, 3.35; N, 16.46%. Calcd for $C_{14}H_9N_3S$: C, 66.91; H, 3.61; N, 16.72%.

Reduction of 10c with Zinc Dust and Hydrochloric Acid. Zinc dust (100 mg) was added with stirring to **10c** (68 mg, 0.097 mmol) dissolved in acetic acid (10 ml) and ethanol (2 ml).

Since the reaction proceeded very slowly, concd HCl (2 ml) was first added, and then zinc dust (200 mg) and concd HCl (3 ml) were added in two portions over a period of 7 h. The precipitates were filtered and washed with ethanol (10 ml). The filtrate and washings were combined and evaporated to dryness. The residue was extracted with dichloromethane (15 ml × 4) after addition of concd HCl (2 ml) and water (20 ml).

Table 4. Elemental analyses and spectral data of the cyanines (**3** and **5**)

Compound **3** and **5**		**3** Found (Calcd) % C	H	N	S	Mp (°C) of the chloride (**3'**)	NMR data of the chloride (**3'**) in CD_3OD
3a, a	$C_{16}H_{14}N_3O_4ClS_2$	46.64 (46.66)	3.26 (3.43)	10.43 (10.20)	15.60[a] (15.57)	278.0—279.0	4.17 (6H, s, N-Me), 7.4—8.3 (8H, m)
3a, b	$C_{17}H_{16}N_3O_4ClS_2$	47.64 (47.94)	3.61 (3.79)	9.77 (9.84)	14.68 (15.05)	253.5—254.5	1.52 (3H, t, J=7), 4.05 (3H, s, N-Me), 4.68 (2H, q, J=7), 7.3—8.1 (8H, m)
3b, b	$C_{18}H_{18}N_3O_4ClS_2$	49.36 (49.14)	3.92 (4.12)	9.33 (9.55)	14.31 (14.58)	272.3—273.2	1.62 (6H, t, J=7), 4.74 (4H, q, J=7) 7.2—8.2 (8H, m)
3c, a	$C_{21}H_{16}N_3O_4ClS_2$	53.48 (53.22)	3.33 (3.40)	8.89 (8.87)	13.20 (13.53)	245.0—246.5	3.74 (3H, s, N-Me), 7.2—8.5 (13H, m)
3c, b	$C_{22}H_{18}N_3O_4ClS_2$	54.14 (54.15)	3.60 (3.72)	8.65 (8.61)	—	262.5—263.8	1.20 (3H, t, J=7), 4.27 (2H, q, J=7), 7.1—8.4 (13H, m)
3c, c	$C_{26}H_{18}N_3O_4ClS_2$	58.13 (58.26)	3.30 (3.38)	7.59 (7.84)	12.20[a] (11.96)	301.0—302.0	7.0—8.5 (18H, m)[b]
5a	$C_{23}H_{18}N_3O_4ClS_2$	55.04 (55.25)	3.53 (3.63)	8.46 (8.40)	—	256.4—257.5	3.65 (3H, s, N-Me)[c] 7.2—8.0 (15H, m)
5b	$C_{24}H_{20}N_3O_4ClS_2$	56.31 (56.08)	3.70 (3.92)	7.87 (8.17)	—	298.2—299.5	1.14 (3H, t, J=7), 4.14 (2H, q, J=7)[c] 7.2—8.1 (15H, m)

a) Chlorine analyzed for **3a,a**, found 8.62 and calcd 8.61; for **3c,c** found 6.77 and calcd 6.61%. b) In $CDCl_3$. c) Perchlorate in (CD_3OD+$CDCl_3$). IR (KBr): A very strong band at 1520—1540 cm^{-1} is common to all **3** and **5**. A band at 750—760 cm^{-1} (m) is common to all **3** and **5**, and a band at 690—695 cm^{-1} (m) appears when there is N-Ph, *i.e.*, **3c,a**; **c,b**, and **c,c** and **5a** and **b**. Bands at 1100 (s) and 620 cm^{-1} (m) are ascribed to ClO_4^-.

Hexane was added to the concetrated extract dried with anhydrous magnesium sulfate in order to precipitate the hydrochloride of **2c** (mp 278—279 °C, 64 mg, 0.244 mmol, 84%). The hydrochloride was nitrosated to give **1c** almost quantitatively.

Hydrolysis of ***10c*** *with Potassium Carbonate.* When a suspension of **10c** (21 mg, 0.03 mmol) in benzene (20 ml) was stirred with potassium carbonate (*ca.* 30 mg) at room temperature, two poducts were obtained: *N,N'*-bis(3-phenyl-2,3-dihydrobenzothiazol-2-ylidene)urea [**11c**, mp 357.5—358.7 °C, 13 mg, 0.027 mmol; MS: *m/e* 478 (M^+, 8%) and 253 (100%): IR (KBr): 1470 cm^{-1} (very strong)] and **2c** (5.4 mg, 0.024 mmol).

An authentic sample of the urea (**11c**) was prepared quantitatively from Grignard-type reagent of **2c** (15 mmol) in THF (100 ml) and ethyl chloroformate (0.48 ml, 5 mmol) by refluxing the solution for 30 min, which showed the same character as above. EA of **11c**: Found: C, 68.98; H, 4.11; N, 12.07%. Calcd for $C_{27}H_{18}N_4OS_2$: C, 67.76; H, 3.80; N, 11.71%.

Reaction of ***1a*** *with Lithium Reagent of* ***2a***. A solution of butyllithium (12.5 mmol) in hexane (8 ml) and THF (25 ml) was added dropwise at 0 °C to a stirred solution of **2a** (2.15 g, 13 mmol) in THF (100 ml). The solution was stirred for 10 min and then **1a** (2.01 g, 10.5 mmol) was added portionwise. After the mixture had been stirred for 1.5 h, the solvents were evaporated under reduced pressure. The residue was extracted with dichloromethane (50 ml×3) after addition of water (100 ml) and the extract was dried over anhydrous magnesium sulfate. After the solvent had been evaporated, the residue was chromatographed on silica gel. Bis[*o*-{*N*-methyl-*N*-(3-methyl-2,3-dihydrobenzothiazol-2-ylidenecarbamoyl)amino}phenyl] disulfide (**7a**, 2.70 g, 78.3%) was eluted with dichloromethane and dichloromethane–ether (1: 1), mp 253.0—253.5 °C (from ether–hexane).

Cyanine chloride (**3'a**, **a**, 0.37 g, 10.9%) was eluted with acetone, mp 278.0—279.0 °C (from ethanol).

A trace amount of 3-methyl-2,3-dihydrobenzothiazol-2-one (**6a**, mp 75—76 °C) was eluted with dichloromethane.

*Alkaline Hydrolysis of Azamonomethinecyanine Chloride (****3'****).* Sodium hydroxide (1 g) in water (1 ml) was added to a solution of **3'** (0.35 mmol) in ethanol (30 ml) at room temperature. After being stirred for 4 h, the solvent was evaporated under reduced pressure. The residue was extracted with dichloromethane (20 ml×3) after addition of water (20 ml).

The extract was dried over anhydrous magnesium sulfate and the solvent was evaporated. The residue was recrystallized from ether–hexane to give disulfide (**7**).

The results are given in Table 3 and elemental analyses and spectral data in Table 5.

Table 5. Elemental analyses and molecular weights of the disulfides (**7**)[a]

Compound **7**	Found(Calcd) (%) C	H	N	S	MW (Rast)
a) $C_{32}H_{28}N_6O_2S_4$	58.20 (58.51)	4.54 (4.30)	12.60 (12.79)	—	624 657
b) $C_{36}H_{36}N_6O_2S_4$	60.48 (60.65)	5.28 (5.09)	11.55 (11.79)	—	—
c) $C_{52}H_{36}N_6O_2S_4$	68.97 (69.00)	3.84 (4.01)	9.05 (9.28)	14.43 14.17	881 905

a) NMR ($CDCl_3$) of **7a**: 3.14 (3H, s), 3.26 (6H, s), 3.34 (3H, s), and 7.1—7.4 (16H, m). IR (KBr): 1620 cm^{-1} (νC=O), common to all **7**. Recrystallization solvent: ether–hexane.

References

1) For part XV: see, K. Akiba, T. Kawamura, M. Ochiumi, and N. Inamoto, *Bull. Chem. Soc. Jpn.*, **49**, 1913 (1976).

2) M. Hisaoka, K. Akiba, and N. Inamoto, *Bull. Chem. Soc. Jpn.*, **48**, 3274 (1975).

3) K. Akiba, T. Kawamura, M. Hisaoka, and N. Inamoto, *Bull. Chem. Soc. Jpn.*, **48**, 3262, 3266, 3270 (1975).

4) K. Akiba, M. Hisaoka, N. Inamoto, T. Ohta, and H. Kuroda, *Chem. Lett.*, **1975**, 347.

5) Preliminary report: K. Akiba, K. Ishikawa, and N. Inamoto, *Heterocycles*, **2**, 555 (1974).

6) S. Huening, H. Geiger, G. Kaupp, and W. Kniese, *Justus Liebigs Ann. Chem.*, **697**, 116 (1966).

7) H. Balli, *Angew. Chem.*, **75**, 673 (1963).

8) a) J. D. Kendall, Brit. Patent 424, 559 (1935); *Chem. Abstr.*, **29**, 4596 (1935); b) Brit. Patent 447, 038 (1936); *Chem. Abstr.*, **30**, 6958 (1936).

9) K. Akiba, K. Ishikawa, and N. Inamoto, *Chem. Lett.*, **1976**, 1111.

10) H. Balli and F. Kersting, *Justus Liebigs Ann. Chem.*, **663**, 96 (1963).

11) E. Besthorn, *Ber.*, **43**, 1519 (1910).

12) W. Gebhart, *Ber.*, **17**, 2088 (1884).

13) H. Passing, *J. Prakt. Chem.*, **153**, 1 (1939).

14) H. Beyer and G. Ruling, *Chem. Ber.*, **89**, 107 (1956).

15) K. Akiba, I. Fukawa, N. Nomura, and N. Inamoto, *Bull. Chem. Soc. Jpn.*, **45**, 1867 (1972).

16) A. I. Kiprianov and I. K. Ushenko, *J. Gen. Chem.*, **17**, 2201 (1947); *Chem. Abstr.*, **42**, 5016 (1948).

17) J. Goerdeler, A. Huppertz, and K. Wember, *Chem. Ber.*, **87**, 68 (1954).

Low Temperature Photolysis of *o*-Benzoquinones. Spectroscopic Detection of Cyclopentadienones and Bis-Ketenes[1)]

Hideo TOMIOKA,* Hiroshi FUKAO, and Yasuji IZAWA

Department of Industrial Chemistry, Faculty of Engineering, Mie University, Tsu, Mie 514

(Received June 10, 1977)

The photodecarbonylation of *o*-benzoquinone to cyclopentadienone at low temperature was monitored by infrared and ultraviolet spectra which showed that the reaction is highly sensitive to substituents. 3,5-Di-*t*-butyl-*o*-benzoquinone undergoes clean decarbonylation to give cyclopentadienone under irradiation at −170 °C. Similar irradiation of 4-*t*-butyl-, 4-methyl-, 3-methyl-, and unsubstituted *o*-benzoquinones also leads to decarbonylation to cyclopentadienones. However, competitive α-cleavage to bis-ketene becomes important in these systems. Direct spectroscopic observation of the elusive cyclopentadienone was unsuccessful because of the overlapping absorption of the by-product. The infrared spectrum of bis-ketene from 4-*t*-butyl-*o*-benzoquinone shows that it exists as a mixture of rotamers, not undergoing thermal interconversion even at −170 °C.

Much attention has been paid to the preparation and properties of cyclopentadienones[2)] because of the theoretical interest in this system. The classic problem concerning their isolation and direct spectroscopic observation as a monomer is their pronounced facility to dimerize in a mode of the Diels-Alder reaction. While relatively many tri- and tetra-substituted derivatives have been isolated as monomer, minimally substituted derivatives thus far isolated were di-*t*-butyl derivatives.[3)] Further, it was not until 1971 that the parent compounds was detected spectroscopically in the pyrolytic decarbonylation of *o*-benzoquinone.[4)] Recently, however, a similar decarbonylation was observed[5)] also in the UV irradiation of 3,5- and 3,6-di-*t*-butyl-*o*-benzoquinones at room temperature to yield the corresponding cyclopentadienones. During the course of studies on the low temperature photochemistry of organic molecules,[1,6)] it was found that the photodecarbonylation of 3,5-di-*t*-butyl-*o*-benzoquinone occurs equally efficiently upon irradiation in infrared cell even at low temperature. Although there have been many reports on the syntheses of cyclopentadienones, only a few examples[7)] exist on the ingenious approaches for the generation of cyclopentadienone and its simply substituted derivatives under the conditions associated with general spectroscopic observation.

The present reaction, thus, might be expected to provide another convenient route which permits the spectroscopic observation of unstable cyclopentadienones as monomer if the reaction could be applied to the other simply substituted *o*-benzoquinones (**1b—d**) as well as the parent. The irradiation of *o*-benzoquinones at low temperature monitored by infrared and ultraviolet spectroscopy revealed that the photodecarbonylation is highly sensitive to the substituents on benzoquinone and the competitive α-fission to give interesting bis-ketene becomes more important in simpler benzoquinones.

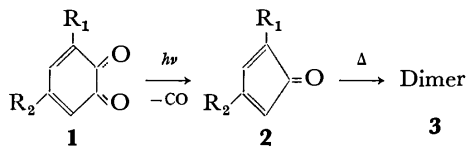

a: $R_1=R_2={}^t$Bu
b: R_1=H, $R_2={}^t$Bu
c: R_1=H, R_2=Me
d: R_1=Me, R_2=H
e: $R_1=R_2$=H

Results and Discussion

A thin film of 3,5-di-*t*-butyl-*o*-benzoquinone (**1a**) as a suspension in Nujol in a liquid nitrogen-cooled infrared cell equipped with a vacuum shroud and dewar was irradiated with a 250 W mercury lamp through a pyrex window and monitored by infrared spectra. As shown in

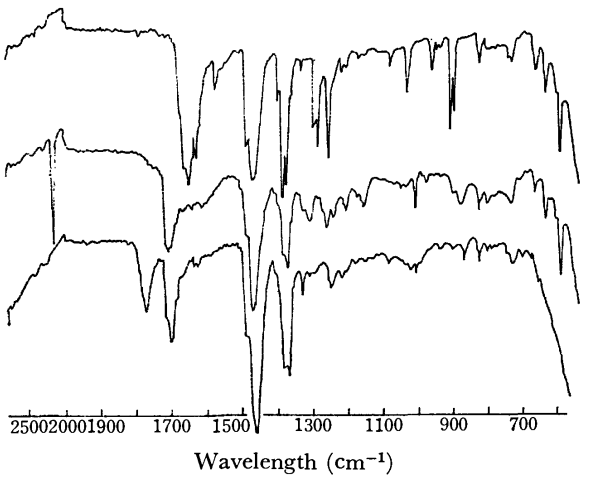

Fig. 1. IR spectra of **1a** in Nujol mulls at −170 °C before irradiation (top), after irradiation for 150 min (center), and after standing at room temperature for 1 day (bottom).

Fig. 1, irradiation led to rapid disappearance of the absorption of the starting material and concurrent appearance of new bands at 2138, 1702, 1320, 1300, 1196, 1145, 1003, 956, and 867 cm^{-1}. A strong and sharp band appearing at 2138 cm^{-1} is easily attributable to carbon monoxide by comparison with the reported value.[8)] The new carbonyl band at 1702 cm^{-1} did not change upon warming the cell slowly to room temperature. After the photomixture had been allowed to stand at room temperature for one day, a new band appeared at 1768 cm^{-1} concomitant with slight shift and change in shape of the original carbonyl band. 2,4-Di-*t*-butylcyclopentadienone (1708 cm^{-1}) is thermally stable at room temperature but slowly dimerizes to

give a single Diels-Alder dimer (1700 and 1765 cm^{-1}) upon standing at the same temperature.[3] TLC analysis of the photomixture within the cell after standing overnight showed the presence of the dimer **3a**. The above results strongly suggest that the photodecarbonylation of **1a** to **2a** occurs within the infrared cell at low temperature.

A similar photolysis of 4-*t*-butyl-*o*-benzoquinone (**1b**) in the infrared cell, however, gave different results. Irradiation caused the starting band to disappear rapidly and the carbon monoxide band to appear along with a broad new absorption at around 1700 cm^{-1} (Fig. 2). Warming the cell to room temperature resulted in the disappearance of the 2138 cm^{-1} band but the broad carbonyl band remained unchanged and no new band appeared even on standing for 2 days. The results exclude the possible assignment of the broad carbonyl band to 3-*t*-butylcyclopentadienone **2b**, since it dimerizes rapidly above −80 °C to give **3b** which has new carbonyl bands at 1790 and 1710 cm^{-1}.[3] Inefficient increase in the intensity of a rather broad band at 2138 cm^{-1} on continued irradiation prompted us to investigate the reaction on a wider scale in the wave number range 2000—2300 cm^{-1}. The results (Fig. 3) revealed that two more new bands at 2125 and 2156 cm^{-1}, probably attributable to bis-ketene arising from the α-cleavage of *o*-benzoquinone, appear along with the carbon monoxide band in this region. Warming in the dark shows that one of the ketene bands at 2125 cm^{-1} rapidly disappears above −90 °C, while the other at 2156 cm^{-1} remains unchanged until −70 °C. This indicates that each band is associated with two different ketenes. Similar irradiation of 4-methyl-(**1c**), 3-methyl-(**1d**), and parent *o*-benzoquinones (**1e**) also resulted in rapid disappearance of the starting materials and concurrent formation of carbon monoxide and bis-ketene. No distinct new carbonyl band was observed in these compounds. Only one ketene band appeared at 2125 cm^{-1}, disappearing upon warming above −90 °C.

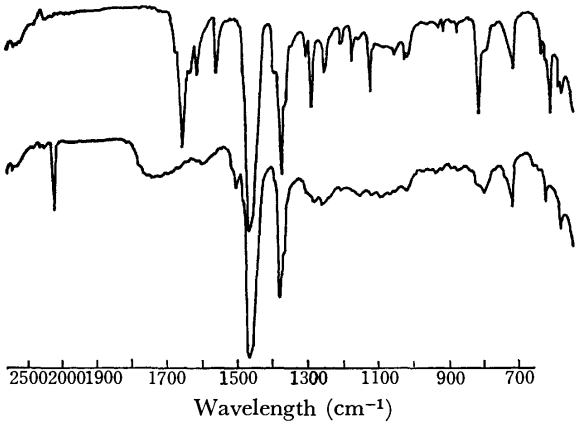

Fig. 2. IR spectra of **1b** in Nujol mulls at −170 °C before irradiation (top), after irradiation for 60 min (bottom).

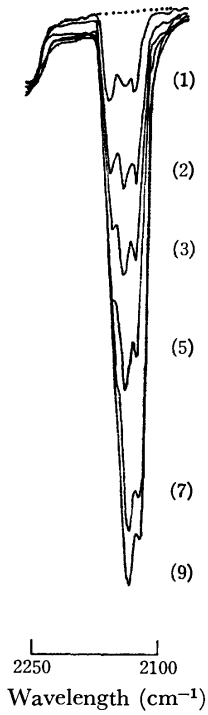

Fig. 3. IR spectra of **1b** in Nujol mulls at −170 °C in the region at 2100—2250 cm^{-1} in expanded scale, ----: before irradiation, ——: after irradiation. Numbers in parentheses refer to irradiation time in min.

Thus, the results show that the photodecarbonylation is quite general for other *o*-benzoquinones, but the photo-α-cleavage to give the bis-ketene occurs concurrently as a relatively important pathway in the photolysis of less substituted *o*-benzoquinones (**1b—e**). However, direct observation of cyclopentadienones was unsuccessful since the broad and thermally stable band[9] in the carbonyl region interferes with the expected carbonyl absorption of cyclopentadienones.

The possibility that carbon monoxide can be formed in the photodecarbonylation[10] of bis-ketene initially formed was excluded, since plots of the intensities of carbon monoxide and ketene absorption as a function of irradiation time indicate that both compounds are the primary photoproduct of *o*-benzoquinones (Fig. 4). Strong chemical evidence of the intervention of cyclopentadienone and bis-ketene were provided by GLPC and TLC analyses of the photomixture obtained in the low temperature irradiation of *o*-benzoquinone (**1e**) in the presence of ethanol. Both analyses show the presence

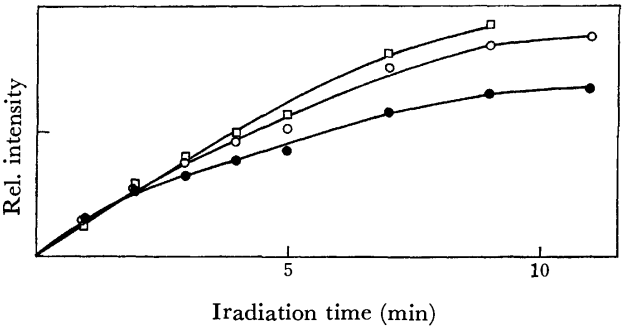

Fig. 4. Plot of relative intensity of bis-ketene and carbon monoxide bands as a function of irradiation time obtained from IR spectra on Fig. 3: -□-, CO (2138 cm^{-1}); -○-, $\nu_{C=O}$ (2125 cm^{-1}) and -●-, $\nu_{C=O}$ (2156 cm^{-1}) of bis-ketene **4b**.

of dicyclopentadienone (**3e**) and diethyl 3-hexenedioate (**5**), a trapped product of bis-ketene by ethanol.

The presence of two ketene bands with different thermal stability in the spectrum of photolyzed **1a** reminds us of the photochemical cleavage[11a-c] of α-pyrone to ketene–aldehyde in Ar matrix at 8 K. Four ketene bands observed at 2022, 2129, 2136, and 2146 cm^{-1} have been attributed to the four possible rotamers available by rotation about C–C single bond. Thus, we assigned the two ketene bands from **1a** to a mixture of bis-ketene rotamers **4A** and **4B**. The band at 2125 cm^{-1} would be associated with bis-ketene **4A**, which is formed first and rapidly rotates photochemically and/or thermally around C–C single bond to the more stable isomer **4B** (2156 cm^{-1}).[12]

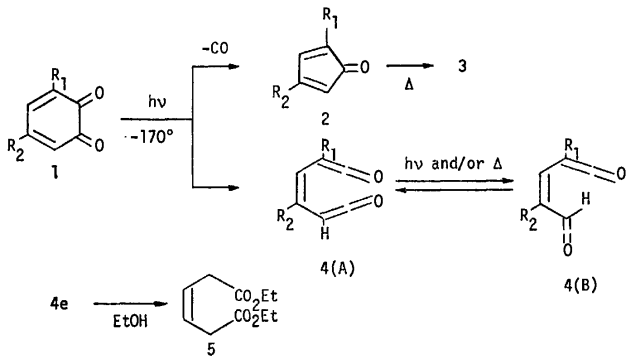

Direct observation of a mixture of rotamers at −170 °C seems to have achieved for the first time. Apparently, the energy barrier to single bond rotation is large with respect to kT at 8 K and the rotamers are essentially different compounds at this temperature. However, the relative intensities of each ketene–aldehyde absorption in the spectrum of photolyzed α-pyrone change remarkably upon warming the sample to 35 K from 8 K in the dark,[11b] suggesting that thermal rotation around C–C single bond occurrs at this low temperature.[13] This, along with the failure to observe a mixture of rotamer in bis-ketene **4c—e** at −170 °C implies that the barrier to the rotation in bis-ketene **4b** is raised by the bulky group to the extent of permitting the observation of each rotamer at this temperature.

Photolysis of **1b—e** in EPA matrix at −196 °C monitored by ultraviolet spectra resulted in rapid decrease in the intensity of original absorption to a very broad and weak absorption at around 380 nm, which disappeared on thawing of the matrix. This might be attributed to either the elusive cyclopentadiene or bis-ketene.[14]

In conclusion we have found that *o*-benzoquinones undergo two important photochemical transformations, *i.e.*, decarbonylation and α-cleavage, depending on the position and bulkiness of the substituent. An interesting bis-ketene has been observed for the first time as a mixture of rotamers at −170 °C.

Experimental

The IR spectra were measured with a JASCO IR-G grating instrument and the UV spectra with a Shimadzu UV-200 spectrophotometer. The GLPC analysis was carried out on a Yanagimoto GC-1800 apparatus equipped with hydrogen-flame detectors using a column consisting of 5% silicone SE-30 on Diasolid L (5.0 mm × 2.0 m).

Materials. *o*-Benzoquinone (**1e**) was prepared[15] by the oxidation of catecohol with silver oxide in anhydrous ether. The fine red crystals of **1e** ($\nu_{C=O}$ 1662 cm^{-1}) turned to black powder upon standing and hence were used immediately. 3-Methyl derivative (**1d**) was similarly prepared immediately before use; IR (Nujol): $\nu_{C=O}$ 1660 cm^{-1}. **1a**, mp 113—114 °C (lit,[5a] mp 114—115 °C); **1b**, mp 67—67.5 °C (lit,[16] mp 68 °C); **1c**, mp 80—81 °C (lit,[16] mp 80—82 °C). Diels-Alder dimer (**3a**) of 2,4-di-*t*-butylcyclopentadienone was prepared by the irradiation[5a] of **1a** in acetonitrile, followed by standing for 2 days at room temperature, mp 152—153 °C (lit,[5a] mp 152.5—153.0 °C). Dicyclopentadienone (**3e**) was prepared[17] by the hydrolysis of the dimer of cyclopentadienone dioxime,[18] mp 101—102 °C (lit,[17] mp 101—101.5 °C). Diethyl *cis*-3-hexendioate (**5**) was prepared by the esterification[19] of the corresponding diacid, bp 125 °C/10 mmHg (lit,[19] bp 125—127 °C/10 mmHg.

Irradiation of 1 Monitored by Infrared Spectra. A thin film of *o*-benzoquinone as a suspension of Nujol was prepared between two polished sodium chloride plates which were mounted in the metal cell holder of the Air Product low temperature infrared spectroscopy unit fitted with a potassium bromide and pyrex windows. The cell was then cooled with liquid nitrogen and at the same time gradually evacuated in order to prevent the condensation of moisture and carbon dioxide. The temperature of the cell was monitored through a copper-constantan thermocouple during the course of the operation as well as irradiation. The infrared spectra of the sample at low temperature was recorded through the potassium bromide windows. A slight increase in intensity of all the peaks in the spectrum was observed upon cooling. The vacuum shroud was then rotated 90° for irradiation through the pyrex window with an Ushio 250 W high-pressure point-source mercury-arc lamp. The spectrum of the sample was recorded periodically until almost all the absorptions of the starting materials disappeared. When irradiation was accomplished, the liquid nitrogen was removed from the cooling unit of the cell and the temperature of the cell was continuously monitored while specific regions (*i.e.*, 2000—2300 and 1500—1850 cm^{-1}) of the spectrum were scanned to observed changes of reactive intermediates upon warming. At the end of warming, the sample was washed from the cell and further characterized by comparison of thin layer and gas chromatographic behavior with that of authentic specimens.

Irradiations of 1 Monitored by Ultraviolet Spectra. Photolysis of **1** in EPA at −196 °C was performed by immersing the reaction cell directly in a transparent quartz Dewar vessel containing liquid nitrogen. A rectangular quartz cell (1 × 0.2 × 5 cm) was used for the reaction.

The authors wish to express their thanks to Professor Jiro Tsuji, Tokyo Institute of Technology, for the supply of *cis*-3-hexenedioic acid and to Prof. Katsumasa Sakanishi, Suzuka College of Techlogy, for that of *o*-benzoquinones.

References

1) a) Low Temperature Photochemistry of Organic Molecules. Part III. Preceding paper: H. Tomioka and Y. Izawa, *J. Am. Chem. Soc.*, **99**, 6128 (1977); b) Presented in part at the 36th National Meeting of the Chemical Society of Japan, Osaka, April 1977.

2) M. A. Ogliaruso, M. G. Romanelli, and E. I. Becker, *Chem. Rev.*, **65**, 261 (1965).

3) E. W. Gabisch, Jr., and R. F. Sprecher, *J. Am. Chem. Soc.*, **88**, 3433, 3434, (1966); **91**, 6785 (1969).

4) O. L. Chapman and C. L. McIntosh, *J. Chem. Soc., Chem. Commun.*, **1971**, 770.

5) a) R. C. DeSelms and W. R. Schleigh, *Synthesis*, **1973**, 614; b) V. B. Voléva, V. V. Ershov, I. S. Belostotskaya, and N. L. Komissarova, *Izv. Akad. Nauk SSSR. Ser. Khim.*, **1974**, 739.

6) H. Tomioka, T. Inagaki, and Y. Izawa, *J. Chem. Soc., Chem. Commun.*, **1976**, 1023.

7) G. Maier and F. Bosslet, *Tetrahedron Lett.*, **1972**, 1025.

8) B. Meyer, "Low Temperature Spectroscopy," American Elsevier Publishing Co., New York, N. Y. (1971), p. 329.

9) Although the origin of this broad band is not clear at present, it might be related to an intractable black polymer formed upon standing of *o*-benzoquinone at room temperature, since the polymer shows similar carbonyl absorption.

10) The photodecarbonylation of ketene to carbene is known; W. Kirmse, "Carbene Chemistry," 2nd ed, Academic press, New York, N. Y. (1971), p. 14.

11) a) C. Y. Lin and A. Kranz, *J. Chem. Soc., Chem. Commun.*, **1972**, 1111; b) O. L. Chapman, C. L. McIntosh, and J. Pacansky, *J. Am. Chem. Soc.*, **95**, 244 (1973); c) R. G. S. Pong and J. S. Shirk, *ibid.*, **95**, 248 (1973); d) L. Barber, O. L. Chapman, and J. Lassila, *ibid.*, **90**, 5933 (1968); e) O. L. Chapman and J. D. Lassila, *ibid.*, **90**, 2449 (1968); f) G. Quinkert, *Angew. Chem. Int. Ed. Engl.*, **14**, 790 (1975).

12) Thermal instability of structure **A** would be related to the thermal electrocyclic closure reaction to *o*-benzoquinone, since **A** is favored over **B** for such closure reaction. Although we could not demonstrate the back reaction spectroscopically, there are examples demonstrating the electrocyclic closure reaction of ketene–aldehyde[11a-c] and diene–ketene,[11d-e] which are closely analogous to the present system.

13) Detection and photochemical interconversions of rotamers in but-3-en-2-one at 20 K have been reported: A. Krantz, T. D. Goldfarb, and C. Y. Lin, *J. Am. Chem. Soc.*, **94**, 4022 (1972).

14) See for example a) V. Dvorák, J. Kolc, and J. Michl *Tetrahedron Lett.*, **1972**, 3443; b) R. Arad-Yellin, B. S. Green, and K. A. Muszkat, *J. Chem. Soc., Chem. Commun.*, **1976**, 14: c) G. Quinkert, *Angew. Chem.*, **84**, 1157 (1972).

15) J. L. E. Erickson and J. M. Dechary, *J. Am. Chem. Soc.*, **74**, 2644 (1952); M. A. Ansell, A. F. Gosden, V. J. Lesile, and R. A. Murray, *J. Chem. Soc., C*, **1971**, 1401.

16) H. J. Teuber and G. Staiger, *Chem. Ber.*, **88**, 802 (1955).

17) C. H. Depuy and B. W. Ponder, *J. Am. Chem. Soc.*, **81**, 4629 (1959).

18) W. von E. Doering and C. H. Depuy, *J. Am. Chem. Soc.*, **75**, 5955 (1953).

19) E. Demole and M. Stoll, *Helv. Chim. Acta*, **45**, 692 (1962).

Formation of 1,3-Di(2-fluorenyl)-1-butene from 2-(1-Bromoethyl)-fluorene with Silver Powder

Masahiro MINABE, Makoto SUZUKI,* Takao OOYA,** and Kazuo SUZUKI

Department of Industrial Chemistry, Faculty of Engineering, Utsunomiya University, Ishiicho, Utsunomiya 321-31

(Received June 20, 1977)

An unexpected compound, 1,3-di(2-fluorenyl)-1-butene, was formed as the major product, accompanied by *meso*- and *dl*-2,3-di(2-fluorenyl)butane as the minor products, in the reaction of 2-(1-bromoethyl)fluorene with silver powder. The structure of the butene was confirmed to be the *E* form by a comparison of the UV spectra of the related compounds.

The Wurtz-Fittig-type reaction of 2-(1-bromoethyl)-fluorene (**1**)[1] afforded the unexpected 1,3-di(2-fluorenyl)-1-butene (**2**) as the major product in addition to the expected diastereomers, *meso*-(**3a**) and *dl*-2,3-di(2-fluorenyl)butane (**3b**),[1] as minor products. The present paper is concerned with the formation, the stepwise synthesis, and the configurational assignment of **2**.

Results and Discussion

The reaction of **1** with silver powder in benzene gave **2** as the main product, and **3a**, **3b**, 2-vinylfluorene (**4**), and 2-ethylfluorene (**5**) as by-products accompanied by a considerable amount of resinous material. An appreciable quantity of hydrogen bromide was produced in this system.

The yield of **2** is higher than that of **3**, which may be formed by the usual Wurtz-Fittig reaction (Scheme 1). This finding is due to the fact that the unstable **1** is decomposed into **4** *via* 1-(2-fluorenyl)ethyl cation instead of 1-(2-fluorenyl)ethanide anion, and presumably to the smaller extent of the ionization of silver compared with that of sodium.

The reactive **1** is cleft easily into the olefin **4**, with elimination of hydrogen bromide, in the presence of the silver ions which are formed. The electrophilic attack of the α-carbon atom on the alkyl group of **1** to the methylidene carbon of **4** would form **2** through 1,3-di(2-fluorenyl)butyl cation.

The compound **2** (17%) was obtained by the reaction[1] of 1-(2-fluorenyl)ethanol (**6**) with potassium hydrogensulfate. Moreover, **2** was isolated by the Friedel-Crafts reaction between **1** and **4** (11%), and by treatment of **6** with polyphosphoric acid (2%).

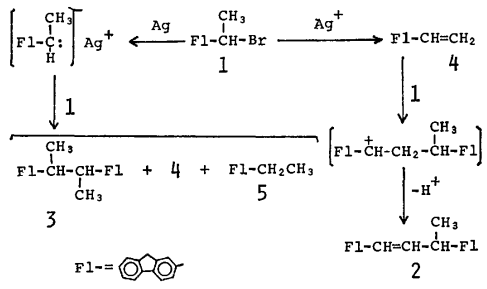

Scheme 1.

Hydrogenation of **2** yielded 1,3-di(2-fluorenyl)butane (**7**) and oxidation of **2** with potassium permanganate gave 2-acetyl-9-fluorenone and 9-oxofluorene-2-carboxylic acid. The structural proof of **2** was established by the independent synthesis using a procedure similar to that of Ela and Cram[2] (Scheme 2).

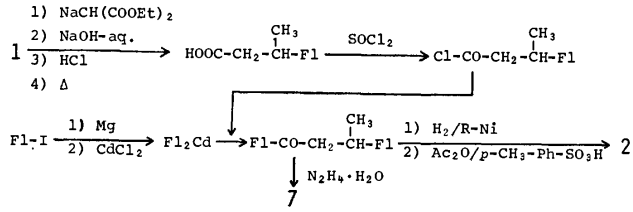

Scheme 2.

Geometrical isomers of **2** can, in principle, exist in analogy with the case of 1,3-diphenyl-1-butene.[2] The UV spectrum of **2** is strikingly similar to that of **4** (I in Fig. 1). A solution of **2** in cyclohexane was irradiated by ultraviolet light and the progress of the isomerization was traced by UV spectra, as shown in Fig. 1. After a short irradiation (for example, 3 min), the absorption maximum shifted to a shorter wavelength and showed some resemblance to that of **7** (II in Fig. 1). The spectrum obtained after a longer period (60 min) irradiation showed a further shift to a shorter wave-

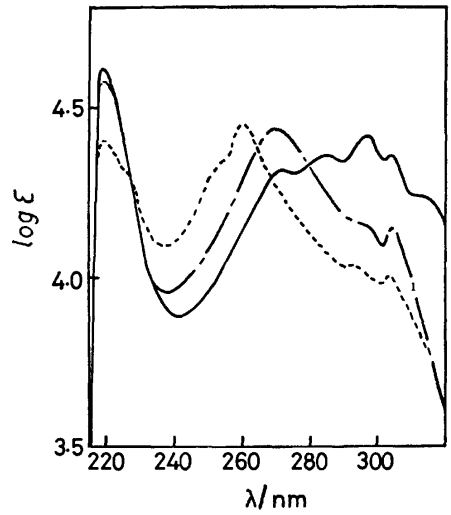

Fig. 1. UV spectra of **2** under ultraviolet irradiation. ——: Original (I), —·—: 3 min (II), ——: 60 min (III).

* Present address: Obu City Office, Obu 474.

** Present address: Institute of Pharmacology, Banyu Pharmaceutical Co., Ltd., Meguro, Tokyo 153.

length and was like that of the parent fluorene (III in Fig. 1).

The consideration of molecular models indicates that the vinylene bond of the *E* configuration in **2** can be situated on the same plane with respect to the adjacent 2-fluorenyl group. The absorption maximum of this conjugated system shifts to a bathochromic region, as in the case of **4**. However, the *Z* form of **2** can not be situated in the same plane as that of the *E* form, due to the steric interference between the two bulky fluorenyl rings at the 1- and 3-positions or between the fluorenyl ring at the 1-position and the methyl group at the 3-position in **2**. Therefore, the vinylene and fluorenyl π-electron systems might exist independently of each other and give spectra similar to that of fluorene. Accordingly, the configuration of the isolated **2** can be assigned to be the *E* form, and the compound having the UV spectrum of III may be the *Z*-isomer.

The compound obtained by a long irradiation (14 h) was first separated by silica gel column chromatography and dried *in vacuo* at 120 °C. The NMR spectrum shows that the resulting mixture consists of *E*- (**2**-*E*) and *Z*-isomers (**2**-*Z*) in a ratio of *ca.* 1 : 1. The UV spectrum of the mixture has a shape similar to that of II. Repeated recrystallization of the mixture afforded only **2**-*E*, whose spectrum was identical with that of I. Consequently, the attempt to isolate pure **2**-*Z* failed. These findings suggest that **2**-*E* can be isomerized to **2**-*Z* by ultraviolet irradiation and that the **2**-*Z* is converted gradually to **2**-*E* upon heating and/or standing in solution.

Experimental[3)]

The instruments used in this experiment were the same as those described elsewhere.[1)] UV spectra were recorded at a scanning speed of 0.76 s/nm in cyclohexane.

*Reaction of **1** with Silver Powder.* A solution of 8.19 g of **1** in 140 ml of dry benzene was refluxed with 3.24 g of silver powder for 40 h. A considerable amount of hydrogen bromide evolved during this period.

After cooling, the precipitate was filtered and extracted with benzene. The combined benzene solution was evaporated to dryness and the residue was distilled with steam. The distillate was recrystallized fractionally from hexane to give 0.005 g (0.09%) of **4**, mp 135—137 °C, and 0.015 g (0.26%) of **5**, mp 99—100 °C. The sticky residue was recrystallized fractionally from ethyl acetate to give 0.18 g (3.3%) of **3a**, mp 306—308 °C, and 0.08 g (1.4%) of **3b**, mp 234—235 °C. The mother liquor was evaporated to dryness and the residual solid was recrystallized from benzene–cyclohexane (1 : 1) to yield 2.20 g (38%) of **2**: mp 176—178 °C; NMR (pyridine-d_5) δ=1.54 (3H, d, J=6.9 Hz), 3.79 (1H, m), 3.83 (4H, s), 6.67 (2H, d, J=2.4 Hz), and 7.18—7.97 (14H, m); MS, *m/e*, 384 (M^+), 369, 353, 339, 218, 203, 192, 179, 165, and 152.

Complex of **2** with 2,4,7-trinitro-9-fluorenone (mole ratio= 1/2): mp 142—143 °C (dec); IR 1732 cm^{-1} (>C=O).

*Photo-irradiation of **2**.* A sample of **2** was prepared with the density of 9.54×10^{-6} mol per 1000 ml solution. The solution (5 ml) was sealed in a quartz cell and irradiated using a 100-W high-pressure mercury lamp. After each time interval, the UV spectrum was recorded immediately without any treatment.

A second irradiation of **2** (0.50 g) in cyclohexane (400 ml) was carried out for 14 h under an atmosphere of nitrogen. The mixture was concentrated to 100 ml and chromatographed on a silica gel column. The colorless eluate was evaporated *in vacuo* at 120 °C during a period of 5 h to leave a powder (0.40 g), which was found to be pure by means of thin layer chromatography and gas chromatography. NMR (benzene-d_6) δ=1.46 (-CH_3 of 2-*Z*, J=7.0 Hz, 45%) and 1.52 (-CH_3 of 2-*E*, J=7.0 Hz, 55%).

The materials gave 0.26 g of **2**-*E*, mp 176—178 °C, by repeated recrystallization from cyclohexane, cyclohexane–hexane, and cyclohexane–benzene.

*Reaction of **6** with Copper Powder and Potassium Hydrogensulfate.* A powdered mixture of 12.6 g of **6**, 2.73 g of potassium hydrogensulfate, and 1.36 g of copper powder was sublimed at 180—200 °C under reduced pressure for 30 min; the sublimate gave 3.61 g of **4**. The residual part was recrystallized from cyclohexane–benzene (1: 1) to yield 2.01 g (17%) of **2**.

*Friedel-Crafts Reaction of **4** with **1**.* A mixture of 1.37 g of **1**, 0.96 g of **4**, and 0.035 g of fused zinc chloride in 60 ml of carbon disulfide was refluxed for 2.5 h to give 0.216 g (11%) of **2**.

*Hydrogenation of **2**.* Butene **2** (1.00 g) was hydrogenated with hydrogen, using 10 g of Raney nickel (W-4) as catalyst in benzene (70 ml); 0.72 g (72%) of **7**, mp 161—163 °C, was obtained. UV_{max} 219 (log ε 4.70), 264 (4.48), 268 (4.50), 293 (4.01), and 304 nm (4.06); NMR (pyridine-d_5) δ=1.35 (3H, d, J=6.9 Hz), 2.07 (2H, t), 2.45—2.93 (3H, m), 3.86 (4H, s), and 7.23—8.05 (14H, m); MS, *m/e*, 386 (M^+).

*Oxidation of **2**.* A mixture of 0.38 g of **2**, 2.0 g of potassium permanganate, and 100 ml of acetone was stirred at room temperature for 2 h; 0.27 g (61%) of 9-oxofluorene-2-carboxylic acid, mp 336 °C (dec), and 0.04 g (18%) of 2-acetyl-9-fluorenone, mp 159—161 °C, were isolated.

3-(2-Fluorenyl)butanoic Acid. Dry ether (10 ml) containing diethyl malonate (6.4 g) was added to an ice-cooled solution of sodium ethoxide (2.7 g) in ether (30 ml) over a 10 min period with stirring under an atmosphere of nitrogen. To this was added a solution of 10.9 g of **1** in 50 ml of dry benzene, and the reaction mixture was stirred for an additional hour. After standing overnight at room temperature, the mixture was refluxed for 5.5 h and filtered, and the filtrate was evaporated to dryness to give diethyl 2-(2-fluorenyl)-1,1-propanedicarboxylate: mp 71—72 °C; IR 1740 and 1714 cm^{-1} (>C=O); NMR (CCl_4) δ=0.95 (3H, t), 1.21 (6H, t), 3.78 (2H, s), 3.43—4.33 (6H, m), and 7.05—7.70 (7H, m); MS, *m/e*, 352 (M^+).

The diester was refluxed with 12.8 g of sodium hydroxide in 100 ml of water for 4 h. After filtration, the filtrate was neutralized with hydrochloric acid to yield dicarboxylic acid: mp 195—196 °C (dec); IR 1723 cm^{-1} (>C=O).

The dibasic acid was heated at 150—160 °C for 1 h and the residue was sublimed *in vacuo* at 180 °C; the sublimate was recrystallized from benzene to give 7.63 g (76% based on **1**) of 3-(2-fluorenyl)butanoic acid: mp 155.5—157.0 °C; IR 2900 (-OH) and 1692 cm^{-1} (>C=O); NMR (benzene-d_6) δ=1.13 (3H, d, J=7.2 Hz), 2.43 (2H, d), 3.15 (1H, sex), 3.45 (2H, s), 6.93—7.73 (7H, m), and 11.55 (1H, s); MS, *m/e*, 252 (M^+).

Acid chloride (92% yield); mp 68—70 °C (dec); IR 1796 cm^{-1} (>C=O).

Methyl ester (93% yield): mp 86.5—87.0 °C; IR 1732 cm^{-1} (>C=O); NMR (CCl_4) δ=1.30 (3H, d), 2.48 (2H, d), 3.26 (1H, sex), 3.53 (3H, s), 3.76 (2H, s), and 6.97—7.68 (7H, m); MS, *m/e*, 266 (M^+).

3-(2-Fluorenyl)-1-butanol. The above methyl ester was reduced to the alcohol (98%): mp 82—83 °C; IR 3326 cm^{-1} (-OH); MS, *m/e*, 238 (M^+).

Corresponding acetate: mp 51.5—52.5 °C; IR 1732 cm^{-1} (>C=O); NMR (benzene-d_6) δ=1.15 (3H, d, J=6.9 Hz), 1.65 (3H, s), 1.77 (2H, q), 2.71 (1H, sex), 3.49 (2H, s), 3.96 (2H, t), and 6.92—7.67 (7H, m); MS, *m/e*, 280 (M^+).

1,3-Di(2-fluorenyl)-1-butanone. To the active magnesium prepared from 2.04 g of anhydrous magnesium chloride according to the literature,[4] there was added 4.38 g of 2-iodofluorene in 70 ml of dry tetrahydrofuran (THF) for 30 min at room temperature, and the reaction mixture was stirred for 1.5 h. Anhydrous cadmium chloride (1.4 g) was added all at once and the mixture was stirred for 2 h. To the solution of difluorenylcadmium, there was added the foregoing butanoyl chloride (prepared from 1.76 g of acid) in 20 ml of THF for 10 min at room temperature. The mixture was refluxed for 1 h and allowed to stand overnight at room temperature. This provided 0.50 g (18%) of 1,3-di(2-fluorenyl)-1-butanone: mp 175—176 °C; IR 1668 cm^{-1} (>C=O); MS, *m/e*, 400 (M^+).

Wolff-Kishner Reduction of 1,3-Di(2-fluorenyl)-1-butanone. A mixture of 0.10 g of the above ketone, 0.03 g of potassium hydroxide, 0.10 ml of hydrazine hydrate (90%), and 20 ml of diethylene glycol was treated in the usual manner to give 0.088 g (91%) of **7**: mp 161—163 °C.

1,3-Di(2-fluorenyl)-1-buthanol. The ketone (0.86 g) was reduced over Raney nickel (3.0 g) under an atmosphere of hydrogen at room temperature to afford 0.70 g (81%) of the alcohol: mp 151—153 °C; IR 3585 cm^{-1} (-OH); MS, *m/e*, 402 (M^+).

Dehydration of 1,3-Di(2-fluorenyl)-1-butanol. A solution of 0.30 g of the alcohol, 0.3 ml of acetic anhydride, 0.03 g of *p*-toluenesulfonic acid monohydrate, and 80 ml of acetic acid was refluxed for 4 h to yield 0.254 g (89%) of **2**: mp 176—178 °C.

References

1) M. Minabe, M. Yoshida, M. Fujimoto, and K. Suzuki, *J. Org. Chem.*, **41**, 1935 (1976).

2) S. W. Ela and D. J. Cram, *J. Am. Chem. Soc.*, **88**, 5777 (1966).

3) All the melting points are uncorrected. All new compounds gave satisfactorily elemental analyses.

4) R. D. Rieke and S. E. Bales, *J. Chem. Soc., Chem. Commun.*, **1973**, 879.

A Modified Synthesis of 2,15-Hexadecanedione, a Precursor of Muscone, from a Butadiene Telomer

Jiro TSUJI, Mitsumasa KAITO, and Takashi TAKAHASHI

Department of Chemical Engineering, Tokyo Institute of Technology, Ookayama, Meguro, Tokyo 152

(Received June 20, 1977)

8-Acetoxy-1,6-octadiene was oxidized with $PdCl_2/CuCl/O_2$ to give 8-acetoxy-6-octen-2-one. Hydrolysis and hydrogenation of the ketone produced 8-hydroxy-2-octanone, which was converted to the tosylate after protection of the ketone. The tosylate was converted into the iodide and bromide. The bromide was converted into the Grignard reagent, and coupled with the iodide by the catalysis of CuI coordinated by 2,2′-bipyridyl to give 2,15-hexadecanedione.

Muscone (3-methylcyclopentadecanone **2**) is a naturally occurring fragrant compound with musk odor. Many synthetic attempts for this unique natural product have been carried out. One method carried out by Stoll is based on the intramolecular aldol condensation of 2,15-hexadecanedione (**1**) to form the 15-membered cyclic ketone.[1]

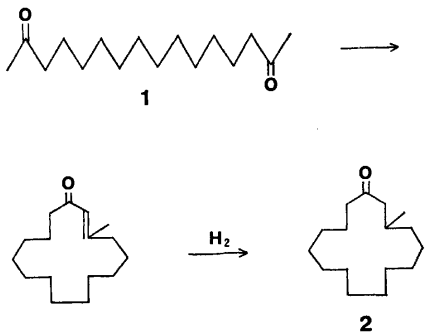

One drawback of the Stoll method is a low yield of the intramolecular aldol condensation, which competes with the intermolecular reaction. In order to make this method more useful and make up for the low yield of the aldol condensation, it is essential to synthesize the diketone **1** as the precursor easily in high yield. Only a few synthetic methods are known for this diketone. For example Stoll synthesized this diketone by the reaction of 1,10-dibromodecane with ethyl acetoacetate, followed by decarboxylation.[2] Another method is the cross Kolbe reaction of 10-oxoundecanoic acid and 6-oxoheptanoic acid.[1] The cross coupling inevitably produced a mixture of coupled products. We have reported the simple synthetic method for this diketone starting from a butadiene telomer easily obtained by the palladium catalyzed telomerization of butadiene with acetic acid.[3] We have carried out further elaboration of the synthesis from the telomer and results of the modification are presented in this paper.

Results and Discussion

Our original synthesis of the diketone **1** was carried out by the following sequence.[4]

In this synthetic method, there are two problems to be improved. The first one is the iron catalyzed coupling of the allylic chlorides **5** and **6**. Although the desired tetraene **7** was obtained as a main product in 55%, the

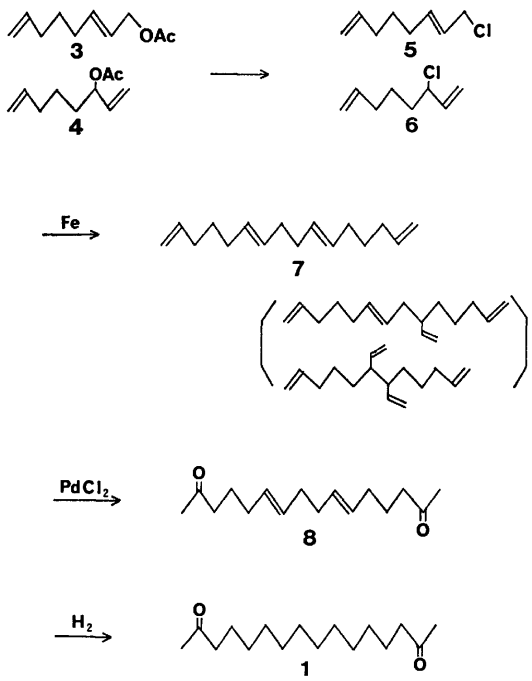

formation of the branched isomers as by-products cannot be avoided. The coupling of even pure 8-chloro-1,6-octadiene (**5**) produced the same mixture as expected for a usual allylic coupling. Another problem is the selective oxidation. The oxidation of the terminal double bonds of the tetraene **7** catalyzed by $PdCl_2/CuCl/O_2$ produced the unsaturated diketone **8**. Usually the oxidation of the internal double bond is very sluggish and the selective formation of **8** is expected. However, the prolonged oxidation of **7** caused the slow oxidation of the internal olefin to form a trione. This is due to the fact that these internal olefins are 1,5-diolefins and can coordinate easily to palladium as bidentate ligand. Therefore, in order to avoid over-oxidation, the oxidation must be stopped before the complete consumption of the tetraene, and hence chromatographic separation of the products is necessary. In order to solve these problems, the present study has been carried out.

The new method starts from 8-acetoxy-1,6-octadiene (**3**)[3] and the synthesis of the diketone **1b** was carried out by the following sequence of reactions.

In this method, the selective oxidation of **3** was carried out at first. Also the formation of by-product in the coupling reaction was avoided by applying a reaction

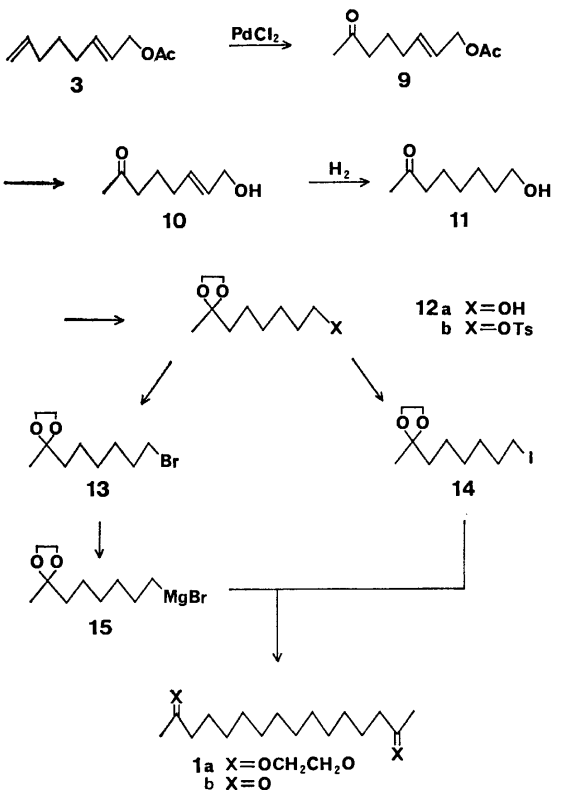

of the saturated Grignard reagent **15** with the saturated iodide **14**. Thus the above mentioned problems of the first method were solved.

The selective oxidation[5] of the terminal olefin of **3** with $PdCl_2/CuCl/O_2$ in aqueous DMF at room temperature proceeded smoothly with high selectivity to form the keto acetate **9** in 82% yield. The hydrolysis of **9** with K_2CO_3 in aqueous ethanol, followed by hydrogenation using Raney nickel catalyst produced the keto alcohol **11** in 87% yield. When the hydrogenation of the allylic acetate **9** was carried out, extensive hydrogenolysis was observed to give 2-octanone. The ketone moiety of **11** was protected as an ethylene acetal and the resulting alcohol **12a** was converted into the tosylate **12b**. The tosylate **12b** was transformed into the bromide **13** and the iodide **14** by treatment with LiBr and NaI in acetone in 72 and 74% overall yields from the alcohol **12a**, respectively. A direct bromination of the alcohol gave **13** in rather poor yield.

The formation of the C_{16} diketone **1b** was carried out by the coupling of the C_8 halide with the corresponding Grignard reagent. In general, a satisfactory coupling of a Grignard reagent with an aryl or vinyl halide proceeds by using transition metal complexes, especially nickel compounds, as catalyst.[6-8] On the other hand, the coupling of alkyl halides is more difficult, although several catalysts are known.[9,10] At first nickel complexes of phosphine or 2,2'-bipyridyl were used, but these complexes did not give satisfactory results. The coupling by the catalysis of $CuCl_2/LiCl$ and CuCl/LiCl[11] was tried without much success. The most satisfactory results were obtained by the use of CuI coordinated by 2,2'-bipyridyl. The reaction of the bromide **13** with the Grignard reagent **15** with this catalyst gave the coupled product in 60% yield. Then the iodide **14** was used for the reaction together with a slight excess of the Gringnard reagent **15** in THF, the yield increased to 83%. The hydrolysis of the acetal under mild conditions produced 2,15-hexadecanedione as colorless crystals, which was identified on the basis of its melting point,[2] spectral data and elemental analysis.

Experimental

Melting points were taken on SHIBATA (No. 297) melting point apparatus. Infrared spectra were determined on a JASCO (IRA-2) spectrophotometer. NMR spectra were determined in CCl_4 solution on a HITACHI (R-24A) spectrometer using tetramethylsilane as an internal standard.

Oxidation of 8-Acetoxy-1,6-octadiene (3). A mixture of $PdCl_2$ (1.60 g, 9.03 mmol), CuCl (8.86 g, 89.5 mmol), *N,N*-dimethylformamide (45 ml) and water (5.4 ml) was placed in a 200 ml glass vessel fitted with a gas inlet tube and shaken under oxygen atmosphere for 1 h, during which time 430 ml of oxygen was absorbed. 8-Acetoxy-1,6-octadiene (14.9 g, 88.4 mmol) was added and the reaction mixture was shaken for 6 h (total absorption was 1080 ml). The reaction was quenched with 3N-hydrochloric acid (50 ml). The mixture was extracted with dichloromethane. The extract was washed with brine and dried over Na_2SO_4. Filtration and concentration of the extract *in vacuo* gave a crude product (15.7 g) as yellow oil, which was distilled (bp 67—85 °C/2.5 Torr) to give 8-acetoxy-6-octen-2-one (**9**) (13.2 g, 72.0 mmol, 81.5%). NMR (CCl_4): δ 5.75 (double d, J=4 and 14 Hz, 1H), 5.40 (double d, J=6 and 14 Hz, 1H) 4.45 (d, J=4 Hz, 2H), 2.40 (t, J=7 Hz, 2H), 2.2—1.8 (m, 2H), 2.05 (s, 3H), 1.95 (s, 3H), and 1.62 (m, 2H). IR (neat): 2950, 1740, 1710, 1670, 1370, 1240, 1165, 1030, 980, and 610 cm^{-1}.

Preparations of 8-Hydroxy-6-octen-2-one (10). A mixture of the keto acetate **9** (10.3 g, 55.9 mmol), 13% aqueous K_2CO_3 (50 ml) and ethanol (100 ml) was stirred for 72 h at room temperature. The reaction mixture was extracted with dichloromethane. The aqueous layer was extracted with dichloromethane several times. The combined extract was washed with brine and dried over Na_2SO_4. Filtration and concentration of the extract *in vacuo* gave a crude product (7.68 g), which was further purified by distillation (bp 78—81 °C/3 Torr) to give 8-hydroxy-6-octen-2-one (6.92 g, 48.7 mmol) 87.2%). NMR (CCl_4): δ 5.2—5.8 (m, 2H), 3.95 (broad, 2H), 3.20 (broad, 1H, -OH), 2.40 (t, J=7.0 Hz, 2H), 2.10 (s, 3H), 1.80—2.10 (broad, 2H), and 1.40—1.70 (broad, 2H). IR (neat): 3600—2950, 2925, 1710, 1360, 1160, 1090, 1000, and 970 cm^{-1}.

Preparation of 8-Hydroxy-2-octanone (11). 8-Hydroxy-6-octen-2-one (3.86 g, 27.2 mmol) in ethanol (20 ml) was hydrogenated with a Raney nickel catalyst (80 mg) under 11.5 atm of hydrogen at 25 °C with stirring for 1.5 h, during which time 650 ml of hydrogen was absorbed. The reaction mixture was filtered through celite and the celite was washed with ethanol. The combined filtrate was evaporated *in vacuo* to give 8-hydroxy-2-octanone (**11**) (3.89 g) which was used without purification. NMR (CCl_4): δ 3.80 (broad, 1H, -OH), 3.60 (t, J=7.0 Hz, 2H), 2.45 (t, J=7.0 Hz, 2H), 2.10 (s, 3H), and 1.10—1.80 (broad, 8H). IR (neat): 3600—2950, 2920, 1710, 1360, 1165, 1055, 720, and 600 cm^{-1}.

Acetalization of 8-Hydroxy-2-octanone. A mixture of the alcohol **11** (2.71 g, 18.8 mmol), ethylene glycol (30 g, 480 mmol), benzene (120 ml) and a catalytic amount of *p*-toluenesulfonic acid was placed in a 200 ml flask, equipped with a

water-separator and a condenser. The reaction mixture was refluxed for 8 h. After the usual work-up, a crude product (3.20 g) was chromatographed on silica gel. Elution with 1% isopropyl alcohol in hexane gave the acetal **12a** (2.96 g, 15.8 mmol, 83.6%). NMR (CCl_4): δ 4.30 (s, 4H), 3.90 (t, J=7.0 Hz, 2H), 3.0 (broad, 1H, -OH), 1.30—1.80 (broad, 10H), and 1.40 (s, 3H). IR (neat): 3600—3100, 2925, 1380, 1250, 1220, 1140, 1060, 950, and 850 cm^{-1}.

Preparation of 6-(2-Methyl-1,3-dioxolan-2-yl)hexyl p-*Toluenesulfonate (**12b**).* A solution of the acetal **12a** (1.08 g, 5.77 mmol) in dry pyridine (10 ml) was treated at 0 °C under nitrogen with freshly recrystallized *p*-toluenesulfonyl chloride (2.0 g, 10.6 mmol) overnight. The reaction mixture was poured into dichloromethane, and the dichloromethane solution was washed with ice-cold 1N-hydrochloric acid (until the aqueous layer reached pH 4). The aqueous layer was extracted with dichloromethane several times, the combined extract was washed with an ice-cold $NaHCO_3$ solution and brine and dried over $MgSO_4$. Filtration and concentration of the extract *in vacuo* gave the tosylate **12b** (1.92 g, 5.60 mmol, 97%), which was used without purification. NMR (CCl_4): δ 7.7 (d, J= 8.0 Hz, 2H), 7.25 (d, J=8.0 Hz, 2H), 3.90 (t, J=6.0 Hz, 2H), 3.80 (s, 4H), 2.4 (s, 3H), 1.1—1.8 (broad, 10H), and 1.20 (s, 3H). IR (neat): 2925, 1600, 1360, 1180, 1100, 955, 920, 810, 660, and 560 cm^{-1}.

*Preparation of 1-Bromo-6-(2-methyl-1,3-dioxolan-2-yl)hexane (**13**).* A mixture of the tosylate **12b** (4.5 g, 13.4 mmol), LiBr (6.71 g, 77.2 mmol) and dry acetone (80 ml) was refluxed for 3 h. Most of acetone was removed *in vacuo* at 25 °C. The residue was diluted with ether, insoluble material was removed by filtration and the ethereal filtrate was washed with water. The aqueous layer was extracted with ether several times and the combined ethereal extract was washed with brine and dried over $MgSO_4$. Filtration and concentration of the extract *in vacuo* gave a crude product (3.08 g), which was chromatographed on silica gel. Elution with 20% ether in hexane gave pure bromide **13** (2.50 g, 9.97 mmol, 72.2% (2 steps) based on **12a**). NMR (CCl_4): δ 3.80 (s, 4H), 3.3 (t, J=6.0 Hz, 2H), 1.2—2.0 (broad, 10H), and 1.20 (s, 3H). IR (neat): 2925, 1380, 1250, 1220, 1060, 950, 870, 730, 650, 560, and 530 cm^{-1}.

*Preparation of 1-Iodo-6-(2-methyl-1,3-dioxolan-2-yl)hexane (**14**).* The iodide **14** was prepared by the same procedure as described above, from the tosylate **12b** (1.48 g, 4.34 mmol) and NaI (3.10 g, 20.7 mmol) in dry acetone (40 ml). Chromatography on silica gel and elution with 20% ether in hexane gave the iodide **14** (0.99 g, 3.32 mmol, 74.2% (2 steps) based on **12a**). NMR (CCl_4): δ 3.75 (s, 4H), 3.10 (t, J=6.0 Hz, 2H), 1.1—2.0 (broad, 10H), and 1.2 (s, 3H). IR (neat): 2925. 1380, 1260, 1220, 1060, 950, 870, 710, 600, and 530 cm^{-1}.

*Preparation of the Grignard Reagent (**15**).* A 25 ml two neck round bottom flask, equipped with a magnetic bar, a condenser, a rubber septum and a gas inlet was flame-dried. Sliced metal magnesium (154 mg, 6.34 mmol) was added to the flask, and nitrogen was introduced into the apparatus, to which a solution of the bromide **13** (1.02 g, 4.05 mmol) in dry tetrahydrofuran (2 ml) was added dropwise with stirring at room temperature over 10 min. A catalytic amount of 1,2-dibromoethane was added as an initiator, and then the reaction mixture was stirred for 1 h at 40 °C. The Grignard reagent was titrated with 0.1N-hydrochloric acid. The normality of the Grignard reagent was 0.24N.

*Coupling of the Grignard Reagent **15** and the Iodide **14**.* A 25 ml two neck round bottom flask equipped with a magnetic bar, a rubber septum and a gas inlet was flame dried. Purified CuI (40.4 mg, 0.2 mmol) and 2,2'-bipyridyl (31.7 mg, 0.2 mmol) were added to the flask, and nitrogen was introduced. Then dry tetrahydrofuran (2 ml) was added to the flask. The mixture was stirred for 30 min at room temperature and cooled to 2 °C to which a solution of the iodide **14** (299 mg, 1.0 mmol) in dry tetrahydrofuran (2 ml) was added at once at 2 °C and the mixture was stirred for 10 min. To this solution a solution of the Grignard reagent **15** in tetrahydrofuran (6.3 ml of 0.24N solution, 1.5 mmol) was added dropwise at 2 °C over 10 min. The reaction mixture was stirred for 2 h at 2 °C and quenched with a saturated NH_4Cl solution. The reaction mixture was extracted with dichloromethane and the organic layer was washed with a saturated NH_4Cl solution (until the aqueous layer remained colorless), brine and dried over $MgSO_4$. Filtration and concentration of the extract *in vacuo* gave colorless oil, which was purified by chromatography on silica gel. The column was eluted with 20% ether in hexane. Concentration of the eluent *in vacuo* gave the coupled product **1a** (269 mg, 0.79 mmol, 79%) as a crystalline material. Further purification by recrystallization from methanol gave pure 1,12-bis(2-methyl-1,3-dioxolan-2-yl)dodecane (**1a**) mp 69.0—70.5 °C). NMR (CCl_4): δ 3.80 (s, 8H), 1.1—1.7 (broad, 24H), and 1.2 (s, 6H). IR (KBr disk): 2965, 2900, 2850, 1465, 1450, 1370, 1250, 1230, 1140, 1070, 1050, 1030, 950, 860, 810, 730 and, 580 cm^{-1}.

*2,15-Hexadecanedione (**1b**) by Deacetalization of **1a**.* The diacetal **1a** (42 mg, 0.12 mmol) and $CuSO_4$ (50 mg) in MeOH (2 ml) and water (0.5 ml) were heated under reflux for 15 min. Undissolved $CuSO_4$ was filtered off, and most of methanol was removed *in vacuo* at room temperature. The residue was dissolved in ether, and the ethereal solution was washed with brine and dried over $MgSO_4$. Filtration and concentration of the solution *in vacuo* gave the diketone **1b** (25.6 mg) as a crystalline material. Further purification by recrystallization from MeOH gave pure 2,15-hexadecanedione **1b** (mp 83.5—84.5 °C. reported mp 83—84 °C[2]). NMR (CCl_4): δ 2.2 (t, J=7.0 Hz, 4H), 1.95 (s, 6H), and 1.0—1.7 (broad, 20H). IR (KBr): 2900, 2830, 1710, 1460, 1160, 800, 720, and 600 cm^{-1}. Found: C, 75.77; H, 11.81, Calcd for $C_{16}H_{30}O_2$: C, 75.54; H, 11.89%.

References

1) M. Stoll and A. Rouvé, *Helv. Chim. Acta*, **30**, 2019 (1947).

2) M. Stoll, *Helv. Chim. Acta.*, **34**, 1817 (1951).

3) S. Takahashi, T. Shibano, and N. Hagihara, *Tetrahedron Lett.*, **1967**, 2451.

4) J. Tsuji, K. Mizutani, I. Shimizu, and K. Yamamoto, *Chem. Lett.*, **1976**, 773.

5) J. Tsuji, I. Shimizu, and K. Yamamoto, *Tetrahedron Lett.*, **1976**, 2975.

6) For review: H. Felkin and G. Swierczewski, *Tetrahedron*, **31**, 2735 (1975).

7) R. J. P. Corriu and J. P. Masse, *J. Chem. Soc., Chem. Commun.*, **1972**, 144.

8) K. Tamao, K. Sumitani, and M. Kumada, *J. Am. Chem. Soc.*, **94**, 4374 (1972).

9) V. G. Fouquent and M. Schlosser, *Angew. Chem.*, **86**, 50, (1974).

10) C. R. Johnson and G. A. Dutra, *J. Am. Chem. Soc.*, **95**, 7777, 7783 (1973).

11) M. Tamura and J. K. Kochi, *J. Organomet. Chem.*, **42**, 205 (1972).

α,β-Unsaturated Carboxylic Acid Derivatives. XIII. The Synthesis and Configuration of Alkyl 2-Acylamino-2-alkenoates and Their Cyclized 2,5-Piperazinedione Derivatives[1)]

Chung-gi SHIN, Masato HAYAKAWA, Takamichi SUZUKI, Akira OHTSUKA,* and Juji YOSHIMURA**

Laboratory of Organic Chemistry, Faculty of Technology, Kanagawa University, Rokkakubashi, Kanagawa-ku, Yokohama 221

***Laboratory of Chemistry for Natural Products, Faculty of Science, Tokyo Institute of Technology, Ookayama, Meguro-ku, Tokyo 152*

(Received June 24, 1977)

It is described that alkyl (*E*)- and (*Z*)-2-halo (Cl, Br, and I)-acetylamino-2-alkenoate (DHA), obtained by the condensation of alkyl 2-oxoalkanoate with chloro- or bromoacetamide and by halogen exchange from the chlorine of DHA to iodine, are cyclized with ammonia or hydroxylamine to give the (*E*)- and (*Z*)-isomers of unsymmetric 3-alkylidene-2,5-piperazinediones and their 1-hydroxy derivatives respectively. Alkyl (*E*)- and (*Z*)-2-iodoacetylamino-2-alkenoates were converted into the corresponding acetylamino- and phthalimidoacetylamino derivatives. The configurations of all the DHA and 2,5-piperazinedione derivatives were determined from the NMR spectra data.

Although there have been many works on the synthesis of 2-acylamino-2-alkenoic acids (α-dehydroamino acids; DHA), only a few papers have been recently reported on the geometric stereochemistry. Especially with regard to the chemical proof for the configurational assignment of the geometric isomers, only one example has been recently reported.[2)] Austel and Steglich distingiushed the configuration of (*Z*)-3-methyl-5,5,5-trifluoro-2-trifluoroacetyl-4-trifluoroacetoxy-2-pentenoic acid by successfully converting it into the corresponding lactone, whereas the (*E*)-isomer did not cyclize. The NMR data of this compound indicated that methyl or methine protons *cis* to the trifluoroacetyl group appeared downfield relative to the occupied *trans* position. More recently, Srinivasan *et al.*[3)] and another workers[4)] have also commented that the low chemical shifts of 3-methyl groups *cis* to the alkoxycarbonyl group of DHA form a more reliable criterion for the assignment of stereochemistry than that of those *trans*.

Previously, Shin *et al.* reported briefly on the possibility of the available chemical determination of alkyl (*E*)- and (*Z*)-2-chloroacetylamino-2-alkenoates (**1**) on the basis of the chemical behavior of 3-alkylidene-2,5-piperazinediones (**6**), cyclization products of **1**, in acetylation.[5,6)]

In this paper, we wish to report in detail an NMR method which can be used for the configurational determination of several DHA's and the stereochemistry of 3-alkylidene-(**6**)- and 3-alkylidene-1-hydroxy-2,5-piperazinediones (**7**), obtained by the cyclization of DHA with ammonia and hydroxylamine respectively.

Results and Discussion

Alkyl 2-Acylamino-2-alkenoates. The alkyl 2-chloroacetyl-(**1**)- and bromoacetylamino-2-alkenoate (**2**) were prepared in one step by the reaction of alkyl 2-oxoalkanoates with chloroacetamide or bromoacetamide in benzene under reflux for *ca.* 15 h, as has been reported previously.[5)] Since the DHA thus obtained was found to be a mixture of (*E*)- and (*Z*)-isomers, the mixture was separated by chromatography on a silica gel column, using benzene as the eluent, to give, first, a colorless syrup and then crystals.

According to a method previously reported,[2-6)] the geometric stereochemistry of the above DHA was readily determined by a comparison of the NH, vinyl, and 3-alkyl protons between (*E*)- and (*Z*)-isomers. The NMR data in Table 2 show that all the chemical shifts of the NH, vinyl, and 3-alkyl protons of **1** and **2** obtained in the oily state resonate at fields lower by 0.51—0.69, 0.26—0.54, and 0.33—0.76 ppm respectively than those of **1** and **2** in the crystalline state, indicating that the former syrup has the (*E*)-configuration, while the latter crystals have the (*Z*)-configuration.

Moreover, the syntheses of both alkyl (*E*)- and (*Z*)-2-iodoacetylamino-2-alkenoates (**3**) were readily achieved and in fairly good yields by the treatment of pure (*E*)- or (*Z*)-**1** with potassium iodide in acetone under reflux for 3 h (Table 1). The NMR spectrum shows a tendency similar to that described above, resonating the chemical shifts of the NH, vinyl, and 3-alkyl protons of the (*E*)-isomer at fields lower by 0.35—0.74, 0.26—0.35, and 0.30—0.68 ppm respectively than that of the (*Z*)-isomer. It is noteworthy that the chemical shifts of not only methylene but also of NH protons in the haloacetylamino groups in both (*E*)- and (*Z*)-isomers in the same series were lower by the order of **1**, **2**, or **3**, indicating that the substituent effect of halogen atoms reaches the nitrogen atom beyond the carbonyl function.

On the other hand, the configuration of one isomer of the alkyl 2-acetylamino-(**4**)- and 2-(phthalimidoacetylamino)-2-alkenoate (**5**),[7,8)] obtained previously by the elimination of alkyl 2-(acetoxyamino)- or 2-(*N,O*-diacetylhydroxyamino)-2-alkenoates with a base, was confirmed unambiguously to have the (*Z*)-geometry by the agreement of the physical constants and spectral data with those derived here by the reaction of (*Z*)-**3** with zinc powder or potassium phthalimide. A similar treatment of (*E*)-**3** gave (*E*)-**4** and **5** in fairly good yields

* Present address: Kokusan Kagaku Co., Ltd., Itabashi-ku, Tokyo 174.

(Table 3). The NMR spectral pattern of **4** is very similar to those of **1**, **2**, and **3**, whereas in the case of **5** the chemical shifts of the NH and 3-alkyl protons of the (*E*)-isomer resonate at fields lower by 0.26—0.35 and 0.19—0.27 ppm respectively than that of the (*Z*)-isomer, while that of the vinyl proton of the (*E*)-isomer appears at field higher by 0.50—0.58 ppm, as has been reported recently.[3]

The evidence regarding the NMR data of DHA mentioned here can also be used to determine the configurations of other alkyl 2-(2-halopropionylamino)- and 2-(ethoxycarbonylamino)-2-alkenoate[1] and 2-azido-2-alkenoate[9] as well as 2-amino-2-alkenoate[10] by a comparison of the NH, vinyl, and 3-alkyl protons. These results will be reported and discussed elsewhere.

In the IR spectral data on **1**—**4** and **5**, the characteristic differences between the (*E*)- and (*Z*)-geometric isomers could not be recognized. The absorption bands of NH in the 3150—3350 cm^{-1} region, the ester carbonyl in the 1720—1735 cm^{-1} region, and the amide carbonyl in the 1645—1690 cm^{-1} region supported these structures, but that of the carbon-carbon double bond overlapped the amide carbonyl region.

The yields, physical constants, and spectral data of **1**—**4** and **5** are summarized in Tables 1, 2, and 3.

Cyclization Reactions. According to the method previously reported by us[5,6,8] and by Cook and Slater,[11] the cyclization reaction of individual (*E*)- and (*Z*)-**1** with ammonia and that of (*E*)- and (*Z*)-**2** and **3** with hydroxylamine were carried out. Pure (*E*)- or (*Z*)-**1** was treated with excess gaseous ammonia in ethanol to convert it into (*E*)- and (*Z*)-**6** respectively in *ca.* 50% yields. Since the cyclization of **1** with hydroxylamine in ethanol did not proceed, a similar treatment of the pure (*E*)- or (*Z*)-**2** with hydroxylamine under reflux in a stream of nitrogen for 18 h gave the expected (*E*)- and (*Z*)-**7** respectively as pinkish crystals, although the yields were low. However, in the case of **3**, it was found that the similar cyclization proceeded to give **7** in a comparatively good yield. The **7** thus obtained turned deep violet upon coloration with ferric chloride in methanol, indicating the presence of a hydroxamic acid structure. This seems to be the first example of the formation of unsymmetric cyclic monohydroxamic acid (**7**). This result offers many useful suggestions for the synthesis of antibiotics mycelianamide,[12] which has a cyclic dihydroxamic acid structure.

The yields, physical constants, and spectral data of **6** and **7** are summarized in Tables 4 and 5.

The NMR data of **6** and **7** may be summarized as follows:

1) Chemical shifts of NH and methylene protons of these cyclic compounds: **6** and **7** are lower, but those of vinyl protons are higher than those of **1**—**4**, reflecting

Table 1. The yields, physical constants, and elemental analyses of **1**, **2**, and **3**

Compound	R		Yield (%)	Bp °C/mmHg (Mp °C)[a]	Formula	Found (Calcd), % C	H	N
1a	CH_3	*E*	12.6	120—122/1				
		Z	37.7	(48—49)				
1b	C_2H_5	*E*	11.1	121—123/1				
		Z	34.9	(53—54)				
1c	*n*-C_3H_7	*E*	10.5	132—133/1				
		Z	31.5	(52—53)				
1d	*i*-C_3H_7[c]	*E*	11.2	133—135/1				
		Z	33.8	(68.5—69)				
1e	C_6H_5	*E*	14.1	178—181/1				
		Z	28.4	(103—104)				
2a	CH_3	*E*	8.5	123—125/1	$C_8H_{12}NO_3Br$	38.53	4.71	5.61
		Z	37.2	(71—73)		(38.42	4.80	5.60)
2b	C_2H_5	*E*	12.3	132—134/1	$C_9H_{14}NO_3Br$	40.81	5.23	5.40
		Z	40.7	(66—68)		(40.92	5.31	5.31)
2c	*n*-C_3H_7	*E*	9.8	139—141/1	$C_{10}H_{16}NO_3Br$	43.21	5.70	4.99
		Z	57.7	(75—76)		(43.20	5.76	5.04)
2d	*i*-C_3H_7[c]	*E*	10.7	125—128/1	$C_9H_{14}NO_3Br$	40.92	5.11	5.42
		Z	35.2	(68—69)		(40.92	5.31	5.31)
2e	C_6H_5	*E*	11.3	160—163/1	$C_{13}H_{14}NO_3Br$	50.11	4.50	4.32
		Z	28.9	(105—107)		(50.02	4.49	4.49)
3a	CH_3	*E*	90.2	(80—81)	$C_8H_{12}NO_3I$	33.76	4.02	4.76
		Z	93.4	(105—106)		(33.33	4.04	4.72)
3b	C_2H_5	*E*	88.5	(87—88)	$C_9H_{14}NO_3I$	34.62	4.44	4.25
		Z	92.7	(107—108)		(34.74	4.05	5.40)
3c	*n*-C_3H_7	*E*	87.9	(79—80)	$C_{10}H_{16}NO_3I$	36.81	4.93	4.17
		Z	81.1	(76—77)		(36.94	4.92	4.31)
3d	*i*-C_3H_7[c]	*E*	91.3	(64—65)	$C_9H_{14}NO_3I$	35.01	4.48	4.49
		Z	94.8	(70—71)		(34.71	4.05	4.50)
3e	C_6H_5	*E*	83.9	syrup	$C_{13}H_{14}NO_3I$	43.44	3.90	3.64
		Z	90.2	(137—138)		(43.43	3.90	3.90)

a) Colorless needles from dibutyl ether. b) Elemental analyses of the mixture of the (*E*)- and (*Z*)-isomers.
c) Methyl ester.

TABLE 2. THE SPECTRAL DATA OF **1**, **2**, AND **3**

Compound	R		IR spectrum, cm^{-1} in KBr			NMR spectrum, δ in $CDCl_3$			
			NH	Ester	NCO C=C	3-Alkyl (Phenyl)	Vinyl (J_{Hz})	-NH-	$-CH_2X$
1a	CH_3	*E*	3340—3260	1720	1678	2.16	7.30(7.5)	8.57	4.12
		Z	3200—3160	1720	1658	1.81	6.90(7.0)	7.88	4.17
1b	C_2H_5	*E*	3340—3260	1720	1665	2.65	7.18(8.0)	8.57	4.14
		Z	3230	1720	1658	2.16	6.64(7.5)	8.06	4.10
1c	*n*-C_3H_7	*E*	3350—3275	1730	1680	2.60	7.12(7.5)	8.54	4.10
		Z	3250	1725	1660	2.16	6.70(7.5)	7.85	4.10
1d	*i*-C_3H_7[a]	*E*	3260	1730	1678	3.40	6.94(10.5)	8.45	4.11
		Z	3250	1740	1690	2.63	6.62(10.5)	7.78	4.15
1e	C_6H_5	*E*	3290	1730	1680	(7.22)[b]	7.89	8.67	4.09
		Z	3240	1730	1670	(7.52—7.20)[c]		8.00	4.10
2a	CH_3	*E*	3300	1730	1680	2.14	7.22(7.5)	8.46	3.96
		Z	3250	1720	1660	1.81	6.91(7.5)	7.81	3.99
2b	C_2H_5	*E*	3300	1735	1690	2.63	7.16(7.5)	8.36	3.91
		Z	3250	1730	1660	2.21	6.74(7.5)	7.77	3.99
2c	*n*-C_3H_7	*E*	3250	1733	1675	2.56	7.03(7.5)	8.49	3.96
		Z	3250	1720	1660	2.15	6.77(7.5)	7.84	3.98
2d	*i*-C_3H_7[a]	*E*	3380	1730	1680	3.34	6.94(10.0)	8.30	3.92
		Z	3250	1730	1670	2.58	6.60(10.5)	7.68	3.96
2e	C_6H_5	*E*	3275	1720	1680	(7.23)[b]	7.94	8.60	3.90
		Z	3225	1728	1670	(7.52—7.20)[c]		7.92	3.90
3a	CH_3	*E*	3250	1718	1660	2.12	7.10(7.5)	7.98	3.77
		Z	3250	1720	1660	1.82	6.83(7.0)	7.60	3.83
3b	C_2H_5	*E*	3250	1730	1662	2.59	7.02(7.5)	7.90	3.77
		Z	3260	1730	1662	2.20	6.67(7.5)	7.55	3.81
3c	*n*-C_3H_7	*E*	3250	1733	1662	2.56	7.04(7.5)	7.93	3.77
		Z	3260	1733	1668	2.17	6.70(7.5)	7.50	3.80
3d	*i*-C_3H_7[a]	*E*	3250	1730	1670	3.32	6.81(10.0)	7.86	3.77
		Z	3250	1735	1645	2.64	6.55(10.0)	7.38	3.77
3e	C_6H_5	*E*	3225	1730	1660	(7.21)[b]	7.68	8.36	3.80
		Z	3225	1728	1662	(7.52—7.20)[c]		7.62	3.76

a) Methyl ester. b) Sharp singlet. c) Multiplet.

TABLE 3. THE YIELDS, PHYSICAL CONSTANTS, AND SPECTRAL DATA OF **4** AND **5**

Compound	R		Yield (%)	Mp °C[a] (Bp °C/mmHg)	IR spectrum, cm^{-1} δ in KBr			NMR spectrum, δ in $CDCl_3$			
					NH	Ester	NCO C=C	3-Alkyl (3-Phenyl)	Vinyl(J_{Hz})	-NH-	$-COCH_3$ $-CH_2-X$
4a	CH_3	*E*	83.9	syrup[b]	3260	1738	1670	2.10	6.99(7.5)	7.76	2.16
		Z	90.2	66—66.5	3260	1740	1672	1.80	6.80(7.0)	7.32	2.14
4b	C_2H_5	*E*	65.0	syrup[b]	3270	1740	1675	2.58	6.93(8.0)	7.56	2.12
		Z	81.0	(115—118/1)	3260	1740	1675	2.19	6.65(7.0)	7.32	2.12
4c	*n*-C_3H_7	*E*	78.5	syrup[b]	3260	1735	1670	2.55	6.96(7.5)	7.96	2.28
		Z	87.3	syrup[b]	3260	1735	1670	2.16	6.66(7.5)	7.45	2.12
4d	*i*-C_3H_7[c]	*E*	80.7	syrup[b]	3260	1738	1670	3.26	6.66(10.0)	7.55	2.10
		Z	84.5	syrup[b]	3250	1738	1670	2.60	6.52(10.0)	7.38	2.19
4e	C_6H_5	*E*	75.3	syrup[b]	3260	1730	1670	(7.55)[d]		8.00	2.12
		Z	82.8	97—98	3248	1725	1665	(7.60—7.24)[e]			2.04
5a	CH_3	*E*	73.4	161—162.5	3260	1740	1680	1.90	6.04(7.5)	9.82	4.32
		Z	74.5	180.5—181.5[f]	3250	1738	1680	1.71	6.57(7.0)	9.56	4.36
5b	C_2H_5	*E*	73.6	158—158.5	3260	1730	1678	2.31	5.94(7.5)	9.83	4.32
		Z	75.8	173—173.5	3250	1740	1680	2.12	6.46(7.5)	9.58	4.36
5c	*n*-C_3H_7	*E*	77.6	160—160.5	3250	1730	1675	2.31	5.95(8.0)	9.77	4.32
		Z	78.3	174—174.5	3250	1735	1675	2.12	6.45(7.5)	9.50	4.36
5d	*i*-C_3H_7[c]	*E*	70.0	181.5—183	3250	1740	1680	2.92	5.80(10.5)	9.87	4.32
		Z	81.1	162—165[i]	3250	1738	1670	2.65	6.31(10.0)	9.52	4.36
5e	C_6H_5	*E*	77.1	190—191.5	3260	1738	1670	(7.30)[k]	6.71	10.35	4.40
		Z	82.5	191—193[j]	3260	1725	1690	(7.80—7.38)[l]	7.29	10.00	4.42

a) **4**; Colorless needles from dibutyl ether, **5**; colorless needles from ethanol. b) Colorless, purified on a silica gel column using benzene as the eluent. c) Methyl ester. d) Sharp singlet (phenyl and vinyl protons). e) Multiplet (phenyl, vinyl, and NH protons). f) Lit,[7] mp 176—179 °C. g) Lit,[7] mp 173—174 °C. h) Lit,[14] mp 196—197 °C. i) Lit,[14] mp 164—165 °C. j) Lit,[7] mp 191—193 °C. k) Sharp singlet (phenyl protons). l) Multiplet (phenyl protons).

Table 4. The yields, physical constants, and spectral data of **6**

Compound	R		Yield (%)	Mp °C[a] (dec)	IR spectrum, cm^{-1} in KBr				NMR spectrum, δ in CF_3COOH				
					NH	NCO		C=C	3α-Alkyl (3α-Phenyl)	Vinyl (J_{Hz})	NH		Methylene
6a	CH_3	*E*	43.8	263—264	3180	1700	1668	1640	2.27	6.11 (7.5)	8.16	9.70	4.42
		Z	55.0	294—295	3190	1710	1685	1640	2.00	6.60 (7.5)	8.40	9.70	4.48
6b	C_2H_5	*E*	45.6	258—259	3185	1700	1660	1632	2.83	6.08 (7.5)	8.24	9.76	4.46
		Z	58.0	275—276	3190	1715	1690	1645	2.41	6.56 (7.5)	8.48	9.78	4.50
6c	*n*-C_3H_7	*E*	43.1	257—258	3190	1700	1668	1635	2.76	6.05 (7.5)	8.18	9.67	4.41
		Z	53.0	270—271	3175	1705	1685	1640	2.38	6.59 (8.0)	8.43	9.79	4.51
6d	*i*-C_3H_7	*E*	47.9	258—259	3200	1700	1680	1640	3.75	5.90 (10.0)	8.26	9.72	4.46
		Z	57.0	269—271	3200	1720		1645	2.84	6.44 (10.8)	8.46	9.78	4.52
6e	C_6H_5	*E*	55.8	270—271	3194	1700	1690	1620	(7.24)[b]	6.96	8.14	9.84	4.46
		Z	65.0	260—262	3220	1700		1635	(7.50)[c]	7.41	8.44	9.31	4.54

a) Colorless prisms from boiling water. b) Broad singlet. c) Sharp singlet.

Table 5. The yields, physical constants, and spectral data of **7**

Compound	R		Yield[a] (%)	Yield[b] (%)	Mp °C	Formula	Found (Calcd), %			IR spectrum[c]		NMR spectrum, δ in DMSO-d_6			
							C	H	N	NH (OH)	NCO (C=C)	NH	Vinyl (J_{Hz})	3α-Alkyl (3α-Phenyl)	CH_2
7a	CH_3	*Z*	19.8	30.5	263—265	$C_6H_8N_2O_3$	46.11 (46.15)	5.23 (5.16)	17.96 (17.94)	3210, (2760)	1680 (1640)	10.00,	5.85 (7.6),	1.66,	4.26
7b	C_2H_5	*Z*	20.5	41.1	237—240	$C_7H_{10}N_2O_3$	49.86 (49.41)	5.93 (5.92)	16.41 (16.46)	3180, (2760)	1690 (1640)	9.94,	5.74 (7.6),	2.18,	4.25
7c	*n*-C_3H_7	*Z*	21.1	42.0	233—235	$C_8H_{12}N_2O_3$	52.12 (52.17)	6.49 (6.57)	15.16 (15.21)	3195, (2760)	1680 (1640)	9.99,	5.80 (8.2),	2.18,	4.27
7d	*i*-C_3H_7	*E*	—	38.9	249—251	$C_8H_{12}N_2O_3$[e]	52.09 (52.17)	6.48 (6.57)	15.05 (15.21)	3060, (2790)	1695 (1620)	10.12,	5.32 (9.5),	3.72,	4.22
		Z	15.9	57.1	250—251					3200, (2760)	1690 (1625)	10.00,	5.67 (10.5),	2.88,	4.29
7e	C_6H_5	*E*	—	46.5	244—245	$C_{11}H_{10}N_2O_3$[e]	60.93 (60.55)	4.57 (4.62)	12.97 (12.84)	3040, (2930)	1670 (1625)	10.47,	6.43,	(7.52—7.16)[d]	4.33
		Z	10.7	80.0	245—247					3050, (2780)	1690 (1630)	9.98,	6.78,	(7.56—7.28)[d]	4.39

a) From Compound **2**. b) From Compound **3**. c) cm^{-1} in KBr. d) Multiplet. e) Elemental analyses of the mixture of the (*E*)- and (*Z*)-isomers.

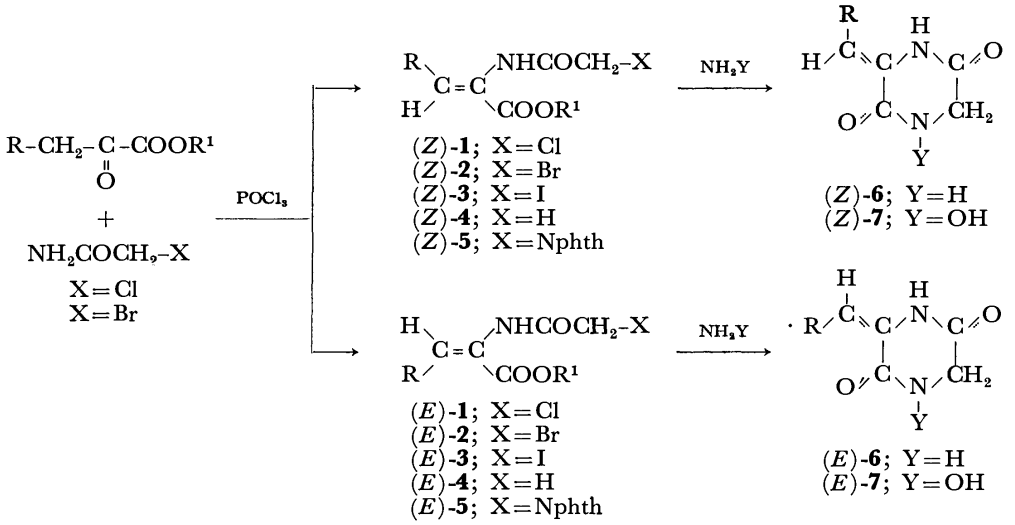

a; R=CH_3, **b**; R=C_2H_5, **c**; R=*n*-C_3H_7, **d**; R=*i*-C_3H_7, **e**; R=C_6H_5
R^1=C_2H_5 (excepting R^1=CH_3 in the case of R=*i*-C_3H_7)

Scheme 1.

the change in the coplanarity of the molecules.

2) The chemical shifts of the methylene, vinyl, and 3α-alkyl protons of **7** are higher than those of **6**, indicating the introduction of an electron-releasing hydroxyl group into **6**.

3) The vinyl and methylene protons of the (*Z*)-isomer of **6** and **7** resonate at a lower magnetic field ($\Delta\delta$ 0.35—0.54 and 0.04—0.10 ppm respectively) compared with that of the (*E*)-isomer, whereas 3α-alkyl protons of (*Z*)-isomer resonate at a higher magnetic field ($\Delta\delta$ 0.27—0.91 ppm). These facts seem to indicate a flattened boat-conformation[13] for these cyclic compounds (**6** and **7**).

The IR spectrum of **7** showed a characteristic absorption band in the 2760—2930 cm^{-1} region due to a hydroxamic acid, supporting the structure of **7**.

Experimental

All the boiling and melting points are uncorrected. The IR spectra were recorded with a Hitachi EPI-G3 Spectrometer. The NMR spectra were measured with a JNM-PS-100 Spectrometer (Japan Electron Optics Laboratory Co., Ltd.), using tetramethylsilane as the internal standard.

Materials. The (*E*)- and (*Z*)-isomers of **1** were prepared by the method previously reported.[5] The mixture of (*E*)- and (*Z*)-isomers thus obtained was separated by chromatography on a silica gel column using benzene; the earlier eluted one was an oil thought to be the (*E*)-isomer, and the latter, crystals thought to consist of the (*Z*)-isomer.

*Preparation of **2**.* According to the above method, when a solution of ethyl or methyl 2-oxoalkanoate (0.10 mol) and bromoacetamide (0.12 mol) in benzene (100 ml) in the presence of phosphoryl chloride (0.02 mol) was refluxed for *ca.* 15 h, a colorless syrup was obtained in *ca.* a 40% yield after the removal of the benzene and the subsequent distillation of the residue under reduced pressure. The mixture syrup of (*E*)- and (*Z*)-isomers thus obtained was similarly worked up to give an oil ((*E*)-isomer) and crystals ((*Z*)-isomer).

*Preparation of **3**.* The purely isolated (*E*)- and (*Z*)-isomers of **1** (0.01 mol) were treated separately with potassium iodide (0.02 mol) in acetone (50 ml) under reflux for 3 h to convert it into the (*E*)- and (*Z*)-isomers of **3** respectively as colorless crystals in an almost quantitative yield, after the removal of the potassium chloride deposited and the acetone.

*Preparation of **4**.* A mixture of the (*E*)- or (*Z*)-isomer of **3** (0.01 mol) and zinc powder (6.54 g, 0.1 mol) in ethanol (50 ml) was stirred at room temperature for 5 h. After the subsequent removal of the zinc and the ethanol, the residue was distilled under reduced pressure to give a colorless oil or crystals ((*E*)- and (*Z*)-isomers of **4** respectively).

*Preparation of **5**.* A solution of the (*E*)- or (*Z*)-isomer of **3** (0.01 mol) and potassium phthalimide (0.01 mol) in dimethyl sulfoxide (30 ml) was stirred at room temperature for 5 h. When the reaction solution was then poured into ice water (100 ml), colorless crystals (**5**) were separated out.

*Preparation of **6**.* According to the method previously reported,[5] the individual (*E*)- and (*Z*)-isomer of **6** was prepared by the reaction of the (*E*)- or (*Z*)-isomer of **1** with ammonia.

*Preparation of **7**.* A solution of the individual (*E*)- and (*Z*)-isomer of **2** or **3** (0.005 mol) and hydroxylamine (made from hydroxylamine hydrochloride (0.02 mol) and sodium (0.02 mol) in dry ethanol (5 ml)) in dry ethanol (50 ml) was refluxed under nitrogen gas for 18 h. The reaction solution was then evaporated to dryness under reduced pressure, the residue obtained was dissolved in water (1000 ml), and the aqueous solution was passed successively through columns of Dowex 50 WX-12 cation-exchange regin and Dowex 1-X8 anion-exchange regin (acetate form). The aqueous fraction thus eluted evaporated under reduced pressure to give faint pinkish crystals (**7**).

References

1) Part XII: C. Shin, Y. Sato, H. Sugiyama, K. Nanjo, and J. Yoshimura, *Bull. Chem. Soc. Jpn.*, **50**, 1786 (1977). This work was presented at the 33rd and the 35th National Meetings of Chemical Society of Japan, Fukuoka, October, 1975; Sapporo, September, 1976.

2) V. Austel and W. Steglich, *Chem. Ber.*, **108**, 2361 (1975).

3) A. Srinivasan, K. D. Richards, and R. K. Olsen, *Tetrahedron Lett.*, **1976**, 891.

4) D. Hoppe and R. Follmann, *Chem. Ber.*, **109**, 3062 (1976).

5) C. Shin, M. Fujii, and J. Yoshimura, *Tetrahedron Lett.*, **1971**, 2499; C. Shin, K. Sato, A. Ohtsuka, K. Mikami, and J. Yoshimura, *Bull. Chem. Soc. Jpn.*, **46**, 3876 (1973).

6) C. Shin, M. Hayakawa, K. Mikami, and J. Yoshimura, *Tetrahedron Lett.*, **1977**, 863.

7) C. Shin, K. Nanjo, E. Ando, and J. Yoshimura, *Bull. Chem. Soc. Jpn.*, **47**, 3109 (1974).

8) C. Shin, K. Nanjo, M. Kato, and J. Yoshimura, *Bull. Chem. Soc. Jpn.*, **48**, 2584 (1975).

9) C. Shin, Y. Yonezawa, and J. Yoshimura, *Chem. Lett.*, **1976**, 1063.

10) C. Shin, Y. Yonezawa, and J. Yoshimura, *Chem. Lett.*, **1976**, 1095.

11) A. H. Cook and C. A. Slater, *J. Chem. Soc., C*, **1956**, 4130.

12) W. K. Anslow and H. Raistrick, *Biochem. J.*, **25**, 39 (1931).

13) J. Yoshimura, Y. Sugiyama, and H. Nakamura, *Bull. Chem. Soc. Jpn.*, **46**, 2850 (1973); J. Yoshimura, H. Nakamura, and K. Matsunari, *ibid.*, **48**, 605 (1975).

14) C. Shin, M. Masaki, and M. Ohta, *Bull. Chem. Soc. Jpn.*, **43**, 3219 (1970).

Chemical Modification of Neamine. 5. Preparation of Amino-deoxyneamines

Shigeru NISHIYAMA, Yasuhide ISHIKAWA, Masahiko YAMAZAKI, and Tetsuo SUAMI*

Department of Applied Chemistry, Faculty of Engineering, Keio University, Hiyoshi, Yokohama 223

(Received July 5, 1977)

An aminocyclitol antibiotic neamine has been modified in its 2-deoxystreptamine moiety by converting the hydroxyl group into an amino group to give three antibiotic amino-deoxyneamines. Their antimicrobial activities were determined against several microorganisms.

In connection with preceding papers[1-3] directed toward a synthesis of a more active antibiotic than the parent neamine, an amino group was introduced to the 2-deoxystreptamine moiety of neamine.

In the present article, we wish to report a preparation of three antibiotic amino-deoxyneamines (**3**, **7**, and **11**).

5-Amino-5-deoxyneamine (3). *O*-Deacetylation of 6,3′,4′-tri-*O*-acetyl-5-chloro-5-deoxy-1,3,2′,6′-tetra-*N*-(ethoxycarbonyl)-5-epineamine[2] (**1**) in methanolic ammonia, followed by azidolysis and acetylation gave 6,3′,4′-tri-*O*-acetyl-5-azido-5-deoxy-1,3,2′,6′-tetra-*N*-(ethoxycarbonyl)neamine (**2**) as crystals in 54% yield.

Catalytic hydrogenation of **2** in the presence of platinum oxide, followed by hydrolysis in aqueous barium hydroxide afforded 5-amino-5-deoxyneamine (**3**) as amorphous powder in 58% yield. *N*-Acetylation of **3** with acetic anhydride in methanol gave 1,3,5,2′,6′-penta-*N*-acetyl-5-amino-5-deoxyneamine (**4**).

The structure of **3** was established by a degradation of **3** in 8.8 M hydrobromic acid. From the degradation mixture, the known 1,3,5-triacetamido-4,6-di-*O*-acetyl-1,2,3,5-tetradeoxy-*scyllo*-inositol[4] was obtained.

6-Amino-6-deoxyneamine (7). When 5,3′,4′-tri-*O*-acetyl-6-chloro-6-deoxy-1,3,2′,6′-tetra-*N*-(ethoxycarbonyl)-6-epineamine[2] (**5**) was *O*-deacetylated and subsequently treated with sodium azide in *N*,*N*-dimethylformamide, 5,3′,4′-tri-*O*-acetyl-6-azido-6-deoxy-1,3,-2′,6′-tetra-*N*-(ethoxycarbonyl)neamine (**6**) was obtained in 30% yield. Catalytic hydrogenation of **6** in the presence of platinum oxide, followed by hydrolysis in aqueous barium hydroxide gave 6-amino-6-deoxyneamine (**7**) as chromatographically homogeneous powder in 71% yield. *N*-Acetylation of **7** with acetic anhydride in methanol gave 1,3,6,2′,6′-penta-*N*-acetyl-6-amino-6-deoxyneamine (**8**).

The structure of **7** was established by the analogous degradation of **3** as described above, where L-1,3,4-triacetamido-5,6-di-*O*-acetyl-1,2,3,4-tetradeoxy-*scyllo*-inositol was obtained as crystals. The compound showed identical IR and ^{1}H NMR spectra with its racemate.[5]

5-Amino-5-deoxy-5,6-diepineamine (11). When 3′,4′-di-*O*-acetyl-5,6-anhydro-1,3,2′,6′-tetra-*N*-(ethoxycarbonyl)-6-epineamine[6] (**9**) was treated with freshly distilled boron trifluoride etherate in acetonitrile, two products (**10a** and **10b**) were obtained in 35 and 28% yield respectively. Considering from the reaction mechanism proposed by Fox *et al.*[7] on the reaction of

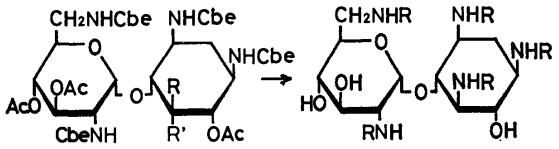

1 R=H, R'=Cl
2 R=N3, R'=H
3 R=H
4 R=Ac

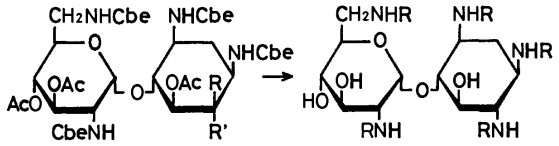

5 R=Cl, R'=H
6 R=H, R'=N3
7 R=H
8 R=Ac

Scheme 1.

nucleoside 2′,3′-epoxide with boron trifluoride etherate in acetonitrile, an introduction of an acetamido group into the 2-deoxystreptamine moiety of neamine might occur on C-5 or C-6. Therefore, compound **10a** and **10b** might be positional isomers, since both compounds gave a correct elemental analysis for the predicted structures.

However, degradation of **10a** or **10b** in 8.8 M hydrobromic acid gave the same compound: L-1,3,5-triacetamido-4,6-di-*O*-acetyl-1,2,3,5-tetradeoxy-*allo*-inositol. Its structure was established by the ^{1}H NMR spectra in comparison with its *O*-trideuterioacetyl derivative. This fact indicated that an introduction of an acetamido group occurred only at the C-5 position in a manner of trans diaxial opening. Therefore, the structures of **10a** and **10b** were comprehensible in terms of a possible migration of an ethoxycarbonyl group between an amino group on C-1 and a hydroxyl group on C-6.

An intact mixture of **10a** and **10b** was hydrolyzed in aqueous barium hydroxide and the hydrolyzate was purified by an ion-exchange resin chromatography to give 5-amino-5-deoxy-5,6-diepineamine (**11**) as amorphous powder.

Also, compound **11** was prepared by an alternative reaction process *via* an azido derivative in the following manner. When compound **9**[6] was heated with sodium

* To whom correspondence should be addressed.

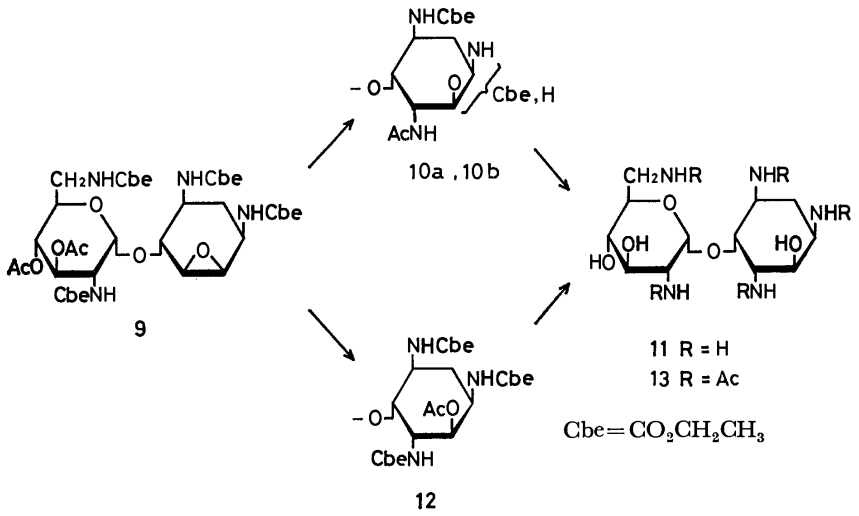

Scheme 2.

TABLE 1. ANTIMICROBIAL ACTIVITY OF 5-AMINO-5-DEOXY- (**3**), 6-AMINO-6-DEOXY- (**7**), 5-AMINO-5-DEOXY-5,6-DIEPI-NEAMINE (**11**), AND NEAMINE

Compound	Diameter of inhibition zone in mm, determined by the paper disk method					
Concentration 1 mg/ml	*Staphylococcus aureus* 6538P	*Bacillus subtilis* ATCC 6633	*Escherichia coli* *D*-12	*Mycobacterium smegmatis* ATCC 607	*Klebsiella*[a] *pneumoniae* 7	*Escherichia*[a] *coli* ML-1629
3	14.5	27.8	26.9	20.8[b]	0	13.8
7	12.8	23.0	21.0	0[b]	0	0
11	0	15.1	16.0	0[b]	0	0
Neamine	18.0	30.5	30.1	27.2[b]	0	0

a) Kanamycin resistant strains. b) Concentration 0.5 mg/ml.

azide and ammonium chloride in 2-methoxyethanol, an azido derivative was obtained. The product was hydrogenated in the presence of Raney nickel and the reduction product was treated with ethyl chloroformate in sodium carbonate solution. After acetylation, the product was purified by column chromatography to give 6,3',4'-tri-*O*-acetyl-5-amino-5-deoxy-1,3,5,2',6'-penta-*N*-(ethoxycarbonyl)-5,6-diepineamine (**12**) in 17% yield. Compound **12** was heated in aqueous barium hydroxide to give **11** as chromatographically homogeneous solid. *N*-Acetylation of **11** gave 1,3,5,2',6'-penta-*N*-acetyl-5-amino-5-deoxy-5,6-diepineamine (**13**).

Compound **3** was slightly less active than neamine, but active against *E. coli* ML-1629 resistant strain. Compounds **7** and **11** showed a considerably lower activity against the microorganisms tested in comparison with neamine (Table 1).

Experimental

General Methods. Melting points were determined in capillary tubes and are uncorrected. Solutions were evaporated under diminished pressure. Optical rotations were measured with a Japan Spectroscopic DIP-SL polarimeter. ^{1}H NMR spectra were recorded at 60 MHz with a Varian A-60D spectrometer in chloroform-*d*, unless otherwise noted, with tetramethylsilane as the internal standard and the peak positions are given in δ values. IR spectra were recorded on potassium bromide disks with a Hitachi-Perkin-Elmer 225 spectrophotometer. Acetylation was performed conventionally with acetic anhydride in pyridine. TLC was performed on Wakogel B-10 (Wako Pure Chemical Co., Ltd.) plates. Silica gel (Wakogel C-300) was employed for column chromatography. Elemental analyses were performed by Mr. Saburo Nakada.

6,3',4'-Tri-O-acetyl-5-azido-5-deoxy-1,3,2',6'-tetra-N-(ethoxycarbonyl)neamine (2). A 402 mg portion of 6,3',4'-tri-*O*-acethyl-5-chloro-5-deoxy-1,3,2',6'-tetra-*N*-(ethoxycarbonyl)-5-epineamine[2] (**1**) was dissolved in methanolic ammonia (7 ml) and the solution was settled in a refrigerator overnight to give 5-chloro-5-deoxy-1,3,2',6'-tetra-*N*-(ethoxycarbonyl)-5-epineamine (310 mg) as precipitates. The deacetylation product was heated with sodium azide (310 mg) in *N*,*N*-dimethylformamide (5 ml) at 100 °C for 19 h under agitation. The mixture was filtered and the filtrate was evaporated. The residue was acetylated and the product was recrystallized from ethanol–ether to give 193 mg of **2**, mp 228—229 °C; $[\alpha]_D^{23}$ +64.9° (*c* 0.97, chloroform). The second crop (24 mg) of the product was obtained from the mother liquor by column chromatography. Total yield was 54%. IR: 2175 cm^{-1} (N_3). ^{1}H NMR: δ 1.10—1.37 (m, 12, 4×$CO_2CH_2C\underline{H}_3$), 2.01 (s, 3, OAc), 2.03 (s, 3, OAc), 2.14 (s, 3, OAc).

Found: C, 47.05; H, 6.16; N, 12.59%. Calcd for $C_{30}H_{47}N_7O_{16}$: C, 47.30; H, 6.22; N, 12.87%.

5-Amino-5-deoxyneamine (3). Compound **2** (611 mg) was hydrogenated in the presence of platinum oxide (50 mg) in methanol (35 ml) under hydrogen atmosphere (3.4 kg/cm^2) for 45 h in a Parr apparatus. The mixture was filtered and the filtrate was evaporated. The residue was heated in water

(10 ml) containing barium hydroxide (7.6 g) for 10 h under reflux. Carbon dioxide was bubbled into the mixture, and the precipitate was filtered off. The filtrate was evaporated and the residue was purified on a column of Amberlite CG-50 (NH_4^+). The column was washed with water, 0.1M, and 0.2M aqueous ammonia and then eluted with 0.3M aqueous ammonia to give 150 mg (58%) of **3**, mp 135 °C (dec); $[\alpha]_D^{21}$ +92.0° (*c* 0.81, water). The product showed a single spot at R_f 0.23 on TLC in 5: 8: 10: 7 (v/v) 28% ammonia–1-butanol–ethanol–water. IR: 1570 cm^{-1} (NH_2). ^1H NMR (D_2O at pD 1): δ 5.86 (d, 1, J=3 Hz, H-1′).

*1,3,5,2′,6′-Penta-*N*-acetyl-5-amino-5-deoxyneamine (**4**).* Compound **3** (17 mg) was acetylated with acetic anhydride (0.5 ml) in methanol (1 ml) to give 24 mg (83%) of **4**, mp 255—260 °C (dec); $[\alpha]_D^{20}$ +71.2° (*c* 0.69, water). IR: 1630 (amide I), 1540 cm^{-1} (amide II). ^1H NMR (D_2O): δ 1.94 (s, 3, NAc), 1.99 (s, 6, 2×NAc), 2.03 (s, 3, NAc), 2.04 (s, 3, NAc), 5.18 (d, 1, J=3.5 Hz, H-1′).

Found: C, 48.25; H, 6.87; N, 12.51%. Calcd for $C_{22}H_{37}N_5O_{10}\cdot H_2O$: C, 48.08; H, 7.15; N, 12.74%.

*Degradation of **3** in 8.8M Hydrobromic Acid.* Compound **3** (72 mg) was heated in 8.8M hydrobromic acid (4 ml) for 43 h under reflux. The solution was diluted with water and neutralized with Dowex 1×2 (OH^-) resin. The solution was evaporated and the residue was purified on a column of Amberlite CG-50 (NH_4^+). After washed with water and 0.1M aqueous ammonia, the column was eluted with 0.3M aqueous ammonia and a ninhydrin positive fraction was collected and evaporated. The residue was acetylated and the product was recrystallized from ethanol–ethyl acetate to give 36 mg (43%) of 1,3,5-triacetamido-4,6-di-*O*-acetyl-1,2,3,5-tetradeoxy-*scyllo*-inositol which was identical with an authentic sample,[4] mp 308—309 °C (dec). (Found: C, 51.92; H, 6.77; N, 11.38%).

*5,3′,4′-Tri-O-acetyl-6-azido-6-deoxy-1,3,2′,6′-tetra-*N*-(ethoxycarbonyl)neamine (**6**).* 5,3′,4′-Tri-*O*-acetyl-6-chloro-6-deoxy-1,3,2′,6′-tetra-*N*-(ethoxycarbonyl)-6-epineamine[2] (**5**, 1.48 g) was dissolved in methanolic ammnia (50 ml) and the solution was settled overnight at ambient temperature. The solution was evaporated and the residue was washed with ether, and then heated with sodium azide (1.28 g) in *N*,*N*-dimethylformamide (15 ml) at 95 °C for 16 h with mechanical agitation. The solution was evaporated and the residue was acetylated. The acetylation product was purified by a column chromatography using 30: 1 (v/v) chloroform–ethanol as eluant. Fractions showing a single spot at R_f 0.30 on TLC in 20: 1 (v/v) chloroform–ethanol were combined and evaporated to give 449 mg (30%) of **6** as amorphous powder, mp 110—117 °C; $[\alpha]_D^{20}$ +54.4° (*c* 1.3, chloroform). IR: 2140 cm^{-1} (N_3). ^1H NMR: δ 1.25 (t, 12, J=7 Hz, 4×$CO_2CH_2C\underline{H}_3$), 1.98 (s, 3, OAc), 2.02 (s, 3, OAc), 2.07 (s, 3, OAc).

Found: C, 47.25; H, 6.05; N, 12.48%. Calcd for $C_{30}H_{47}N_7O_{16}$: C, 47.30; H, 6.22; N, 12.87%.

*6-Amino-6-deoxyneamine (**7**).* Compound **6** (434 mg) was hydrogenated, followed by hydrolysis in barium hydroxide solution as described in the preparation of **3** to give 129 mg (71%) of **7** as amorphous powder, mp 118—121 °C (dec); $[\alpha]_D^{20}$ +81.9° (*c* 1.4, water). The product showed a single spot at R_f 0.32 on TLC in the same solvent as described for **3**. ^1H NMR (D_2O at pD 1): δ 6.09 (d, 1, J=3.5 Hz, H-1′).

*1,3,6,2′,6′-Penta-*N*-acetyl-6-amino-6-deoxyneamine (**8**).* Compound **7** (28 mg) was acetylated with acetic anhydride (0.1 ml) in methanol (1.5 ml) to give 35 mg (73%) of **8** as amorphous powder, mp above 290 °C; $[\alpha]_D^{17}$ +89.1° (*c* 0.9, water). ^1H NMR (D_2O): δ 1.95 (s, 3, NAc), 2.00 (s, 3, NAc), 2.02 (s, 3, NAc), 2.05 (s, 3, NAc), 2.07 (s, 3, NAc), 5.42 (d, 1, J=3 Hz, H-1′).

Found: C, 48.34; H, 7.05; N, 12.53%. Calcd for $C_{22}H_{37}N_5O_{10}\cdot H_2O$: C, 48.08; H, 7.15; N, 12.74%.

*Degradation of **7** in 8.8M Hydrobromic Acid.* Compound **7** (47 mg) was heated in 8.8M hydrobromic acid (2 ml) for 50 h under reflux. The solution was treated analogously as described in the degradation of **3** to give 20 mg (37%) of 1L-1,3,4-triacetamido-5,6-di-*O*-acetyl-1,2,3,4-tetradeoxy-*scyllo*-inositol, mp 298—302 °C (dec); $[\alpha]_D^{21}$ +4.4° (*c* 0.4, methanol). ^1H NMR (DMSO-d_6): δ 1.76 (s, 3, NAc), 1.78 (s, 6, 2×NAc), 1.91 (s, 3, OAc), 1.92 (s, 3, OAc).

Found: C, 51.78; H, 6.77; N, 11.20%. Calcd for $C_{16}H_{25}N_3O_7$: C, 51.74; H, 6.79; N, 11.31%.

*Reaction of Epoxide **9** with Boron Trifluoride Etherate in Acetonitrile.* 3′,4′-Di-*O*-acetyl-5,6-anhydro-1,3,2′,6′-tetra-*N*-(ethoxycarbonyl)-6-epineamine[6] (**9**, 1.19 g) was dissolved in freshly distilled dry acetonitrile (15 ml), and freshly distilled boron trifluoride etherate (2.5 ml) was added gradually to the solution. The mixture was settled at ambient temperature for 20 h. The solution was poured into saturated sodium hydrogencarbonate solution (50 ml) and extracted with chloroform. After dried over anhydrous sodium sulfate, the chloroform solution was evaporated. The residue was purified by a column chromatography using 30: 1 (v/v) chloroform–ethanol.

Fractions showing a single spot at R_f 0.40 on TLC in 20: 1 (v/v) chloroform–ethanol were combined and evaporated. The residue was dissolved in benzene and hexane was added to the solution to give 450 mg (35%) of **10a**, mp 110—121 °C (dec); $[\alpha]_D^{16}$ +100.7° (*c* 1.1, chloroform). ^1H NMR: δ 1.1—1.4 (m, 12, 4×$CO_2CH_2C\underline{H}_3$), 2.00 (s, 3, OAc), 2.03 (s, 3, OAc), 2.12 (s, 3, NAc).

Found: C, 48.76; H, 6.57; N, 9.27%. Calcd for $C_{30}H_{49}N_5O_{16}$: C, 48.97; H, 6.71; N, 9.52%.

Fractions showing a single spot at R_f 0.15 on TLC in the same solvent were combined and evaporated to give 360 mg (28%) of **10b**, mp 149—157 °C (dec); $[\alpha]_D^{20}$ +72.5° (*c* 1.6, chloroform). ^1H NMR: δ 1.1—1.5 (m, 12, 4×$CO_2CH_2C\underline{H}_3$), 1.99 (s, 3, OAc), 2.01 (s, 3, OAc), 2.04 (s, 3, NAc).

Found: C, 48.83; H, 6.51; N, 9.32%. Calcd for $C_{30}H_{49}N_5O_{16}$: C, 48.97; H, 6.71; N, 9.52%.

*Degradation of **10a** and **10b** in 8.8M Hydrobromic Acid.*
a) Compound **10a** (184 mg) was heated in 8.8M hydrobromic acid (5 ml) under reflux for 48 h. The reaction mixture was treated analogously as described in the degradation of **3** to give 47 mg (51%) of 1L-1,3,5-triacetamido-4,6-di-*O*-acetyl-1,2,3,5-tetradeoxy-*allo*-inositol, mp 178—182 °C; $[\alpha]_D^{20}$ +14° (*c* 0.43, methanol). ^1H NMR (DMSO-d_6): δ 1.79 (s, 6, 2×NAc), 1.88 (s, 3, OAc), 1.91 (s, 3, NAc), 2.12 (s, 3, OAc).

Found: C, 51.95; H, 6.73; N, 11.36%. Calcd for $C_{16}H_{25}N_3O_7$: C, 51.74; H, 6.79; N, 11.31%.

b) Compound **10b** (159 mg) was treated with the above procedure to afford the same inosatriamine derivative (24 mg, 30%). (Found: C, 51.87; H, 6.61; N, 11.39%).

5L-1,3,5-triacetamido-1,2,3,5-tetradeoxy-4,6-di-O-trideuterioacetyl-allo-inositol. 1L-1,3,5-triacetamido-4,6-di-*O*-acetyl-1,2,3,5-tetradeoxy-*allo*-inositol (47 mg) was dissolved in 0.02M methanolic hydrogen chloride (2 ml) and the solution was settled overnight. The solution was evaporated and the residue was acylated with acetic anhydride-d_6 (0.3 ml) in pyridine (0.5 ml) to give 32 mg (67%) of crystalline product, mp 189—198 °C (dec); $[\alpha]_D^{20}$ +14° (*c* 0.5, methanol). ^1H NMR (DMSO-d_6): δ 1.79 (s, 6, 2×NAc), 1.91 (s, 3, NAc).

*5-Amino-5-deoxy-5,6-diepineamine (**11**).* a) Compound **9**[6] (800 mg) was treated analogously as described above to give a mixture of **10a** and **10b** (820 mg). The product was hydrolyzed in a mixture of barium hydroxide (9 g) and water (30 ml) at 100 °C for 24 h. The hydrolyzate was purified analogously as described in the preparation of **3** to give 112 mg

(29%) of **11**, mp 165—196 °C (dec); $[\alpha]_D^{20}$ +126° (*c* 1.0, water). ^{1}H NMR (D_2O at pD 1): δ 5.90 (d, 1, J=3.5 Hz, H-1′).

b) Compound **9** (930 mg) was heated with sodium azide (319 mg) and ammonium chloride (270 mg) in 2-methoxyethanol (7 ml) for 20 h under reflux. The mixture was evaporated and the residue was acetylated. The product was dissolved in chloroform and the solution was passed through a short column of activated alumina. The effluent was evaporated to give 923 mg of a syrup. The syrup was dissolved in 0.5M ethanolic sodium ethoxide (10 ml). After overnight, the solution was neutralized with Amberlite IR-120 (H^+) ion-exchange resin and evaporated. The residue was hydrogenated in the presence of Raney nickel in an atmosphere of hydrogen (3.4 kg/cm^2) for 3 h to give 513 mg of a product. The product was dissolved in 1:1 (v/v) aqueous methanol containing sodium carbonate (1.2 g), and ethyl chloroformate (1 ml) was added to the solution under ice cooling. After 48 h, the solution was neutralized with 6M hydrochloric acid and evaporated. The residue was acetylated and subsequently purified by a column chromatography using 30:1 (v/v) chloroform–ethanol as eluant. Fractions showing a single spot at R_f 0.17 on TLC in 20:1 (v/v) chloroform–ethanol were combined and evaporated to give 187 mg of 6,3′,4′-tri-*O*-acetyl-5-amino-5-deoxy-1,3,5,2′,6′-penta-*N*-(ethoxycarbonyl)-5,6-diepineamine (**12**), mp 158—160 °C (dec); $[\alpha]_D^{19}$ +72.5° (*c* 1.0, chloroform). ^{1}H NMR: δ 1.1—1.4 (m, 15, 5×CO_2-$CH_2C\underline{H}_3$), 1.99 (s, 3, OAc), 2.02 (s, 3, OAc), 2.14 (s, 3,OAc).

Found: C, 48.30; H, 6.43; N, 8.29%. Calcd for $C_{33}H_{53}N_5O_9$: C, 48.11; H, 6.48; N, 8.50%.

Compound **12** (179 mg) was hydrolyzed in aqueous barium hydroxide as described in the preparation of **3** to give 27 mg (39%) of **11**.

1,3,5,2′,6′-Penta-N-*acetyl-5-amino-5-deoxy-5,6-diepineamine(**13**)*. Compound **11** (36 mg) was acetylated with acetic anhydride (0.1 ml) in methanol (1 ml) to give 52 mg (83%) of **13**, mp 216 °C (dec); $[\alpha]_D^{16}$ +104.9° (*c* 1.5, water). ^{1}H NMR (D_2O): δ 1.97 (s, 3, NAc), 1.98 (s, 3, NAc), 2.00 (s, 3, NAc), 2.02 (s, 6, 2×NAc), 4.85 (d, 1, J=3.3 Hz, H-1′).

Found: C, 47.50; H, 7.46; N, 12.50%. Calcd for $C_{22}H_{37}N_5O_{10}\cdot 3/2H_2O$: C, 47.30; H, 7.22; N, 12.5%.

We are grateful for financial support of this research by a grant of the Japanese Ministry of Education.

References

1) T. Suami, S. Nishiyama, Y. Ishikawa, and S. Katsura, *Carbohydr. Res.*, **52**, 187 (1976).

2) T. Suami, S. Nishiyama, Y. Ishikawa, and S. Katsura, *Carbohydr. Res.*, **53**, 239 (1977).

3) T. Suami, S. Nishiyama, Y. Ishikawa, and S. Katsura, *Carbohydr. Res.*, **56**, 415 (1977).

4) A. Hasegawa and H. Z. Sable, *Tetrahrdron*, **25**, 3567 (1969): S. Ogawa, T. Ueda, Y. Funaki, Y. Hongo, A. Kasuga, and T. Suami, *J. Org. Chem.*, **42**, 3083 (1977).

5) Unpublished data.

6) S. Nishiyama, Y. Ishikawa, S. Katsura, E. Umemura, T. Tsuchioka, and T. Suami, accepted for publication in *Carbohydr. Res.*, in press.

7) U. Reichman, D. H. Hollenberg, C, K. Chu, K. A. Watanabe, and J. J. Fox, *J. Org. Chem.*, **41**, 2042 (1976).

Synthesis of Carbamic Ester by a Reaction of Carbon Dioxide, Tetrakis(dimethylamido)titanium(IV) and Epoxide

Yasuhiko YOSHIDA and Shohei INOUE

Department of Synthetic Chemistry, Faculty of Engineering, University of Tokyo, Bunkyo-ku, Hongo, Tokyo 113

(Received July 11, 1977)

2-Hydroxycyclohexyl dimethylcarbamate was synthesized quantitatively by a reaction of carbon dioxide, tetrakis(dimethylamido)titanium(IV) and 1,2-epoxycyclohexane.

Carbon dioxide was inserted into the metal-nitrogen bond or the metal-oxygen bond to give metal carbamate or carbonate,[1] and the products were easily decomposed by water to regenerate carbon dioxide.

Since studies by Inoue *et al.*[2] suggested the possibility of the reaction of metal carbamate with epoxide to form carbamic ester resulting in the irreversible fixation of carbon dioxide, the reaction of tetrakis(dimethylamido)titanium(IV) ($Ti(NMe_2)_4$), carbon dioxide (CO_2) and 1,2-epoxycyclohexane was examined.

Results and Discussion

A reaction of $Ti(NMe_2)_4$, CO_2 and 1,2-epoxycyclohexane, followed by hydrolysis of the reaction mixture, was found to give 2-hydroxycyclohexyl dimethylcarbamate (**1**) in a high yield, thus

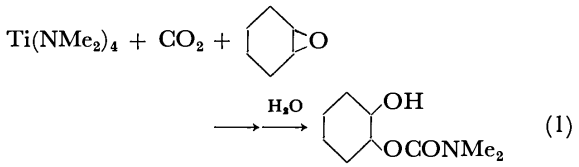

(1)

The carbamic ester (**1**) was confirmed to be in *trans*-form by comparison with an authentic sample prepared by a reaction of *trans*-1,2-cyclohexanediol with dimethylcarbamoyl chloride in the presence of pyridine. The main product of this reaction was carbamic ester (**1**), accompanied by small amounts of CO_2-epoxide copolymer (**2**), cyclic carbonate and a homopolymer of 1,2-epoxycyclohexane, depending upon the reaction conditions.

As shown in Table 1, the reactions were carried out under CO_2 pressure (50 kg/cm^2), since the reaction did not occur at atmospheric pressure at room temperature. The reaction at 80 °C in a large excess of epoxide gave carbamic ester (**1**) in a quantitative yield (Run 7). Reactions carried out in benzene and THF (Runs 4 and 5) gave similar results. However, for the reaction carried out in dichloromethane, the yield of carbamic ester (**1**) was low and the by-products, such as CO_2-epoxide copolymer (**2**), cyclic carbonate and polyether were formed, although in small amounts. At 35 °C (Runs 1 and 2), carbamic ester (**1**) was obtained in a lower yield, but with no by-products. For the reaction of 1,2-epoxypropane, instead of 1,2-epoxycyclohexane, in THF at 80 °C over a period of 160 h, the carbamic ester yield was 58% and the amount of cyclic carbonate formed was 1/3 by weight of carbamic ester.

Since $Ti(NMe_2)_4$ has been reported to react rapidly with CO_2 to form $Ti(OCONMe_2)_4$,[3,4] the formation of carbamic ester is considered to proceed as follows:

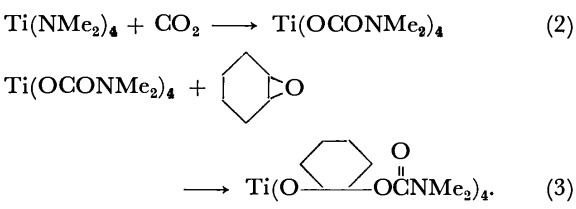

This reaction is the first example of a metal carbamate and epoxide reaction resulting in the fixation of carbon dioxide.

$Ti(NMe_2)_4$ is considered to react preferentially with CO_2 even in the presence of epoxide, since $Ti(NMe_2)_4$ does not react with epoxyethane and 1,2-epoxypropane, as reported previously.[4] It was found that 1,2-epoxycyclohexane did not react with $Ti(NMe_2)_4$ at room temperature, but at 80 °C gave the polymer (poly-

Table 1. Reaction of tetrakis(dimethylamido)titanium, carbon dioxide and 1,2-epoxycyclohexane[a]

Run	$Ti(NMe_2)_4$ (g)	Epoxide (g)	Solvent	Temp (°C)	Time (h)	Product (**1**)[b] (g)	(**1**)[b] (%)[c]	Product (**2**)[d] (g)
1	0.4	9.7	CH_2Cl_2	35	360	0.18	(13)	trace
2	1.0	9.7	THF	35	290	0.17	(5.0)	0
3	1.0	9.7	CH_2Cl_2	80	150	0.07	(2)	0.034
4	1.0	9.7	Benzene	80	210	1.7	(50)	0.027
5	1.0	9.7	THF	80	240	2.5	(74)	0.025
6	1.0	9.7	THF	80	23	0.30	(8.8)	0
7	1.0	39	—	80	220	3.4	(100)	0.007
8	1.8	3.1	THF	80	190	0.94	(15)	0

a) CO_2 50 kg/cm^2. Solvent 40 ml. b) 2-Hydroxycyclohexyl *N,N*-dimethylcarbamate. c) Yield based on four Ti-N bonds. d) Epoxide-CO_2 copolymer.

ether) in a 10% yield after 12 days. In the presence of CO_2, the homopolymerization of 1,2-epoxycyclohexane by $Ti(NMe_2)_4$ was not observed, except for the reaction in dichloromethane (Run 3).

It can be considered that the carbamic ester (**1**) is formed by the reaction of $Ti(NMe_2)_4$ with cyclic carbonate, the latter having been produced from CO_2 and epoxide. This mechanism, however, is believed to be negligible, since, in the reaction of 1,2-epoxycyclohexane under the present conditions, cyclic carbonate was hardly formed. Furthermore, the existence of unchanged $Ti(NMe_2)_4$ is most unlikely because of its extremely high reactivity with CO_2, which gives rise to $Ti(OCONMe_2)_4$.

An alternative mechanism for the formation of **1** would be the reaction of epoxide with carbamic acid, the latter being formed from carbon dioxide and amine which may be present in trace amounts. **1** would then react with titanium carbamate to regenerate carbamic acid. However, such a reaction requires the liberation of a stronger acid (carbamic acid) upon the reaction of the salt with a weaker acid (alcoholic group of **1**).

Concerning the formation of CO_2-epoxide copolymer as a by-product, the following mechanism can be considered, referring to the mechanism proposed for the formation of the CO_2-epoxide copolymer by an organozinc catalyst.[5,6]

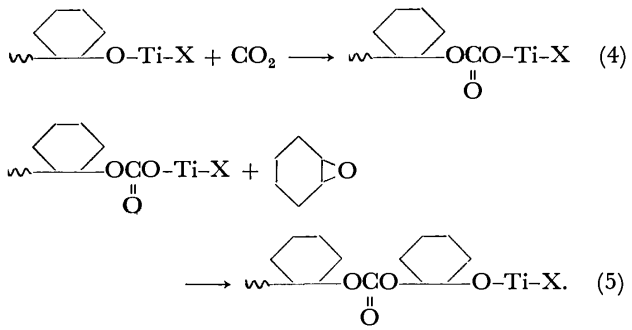

In accord with this mechanism, the reaction of 1,2-epoxycyclohexane and CO_2, with titanium isopropoxide as a catalyst, in THF at 80 °C for 210 h gave the copolymer (**2**), although in a low yield.

Experimental

Materials. Tetrakis(dimethylamido)titanium(IV) was synthesized from lithium dimethylamide and titanium tetrachloride in diethyl ether.[7] After lithium chloride was filtered off and the solvent removed, distillation of the residual liquid afforded a yellow liquid product ($Ti(NMe_2)_4$), bp 75 °C/3 mmHg (lit,[7] bp 44 °C/0.006 mmHg).

Commercially available epoxides, such as 1,2-epoxycyclohexane and 1,2-epoxypropane, and solvents, such as THF, benzene, and dichloromethane, were purified employing usual procedures and stored in a nitrogen atmosphere.

Commerical high-purity carbon dioxide gas was introduced into an autoclave directly from a gas cylinder without further purification.

Procedure. All reactions were carried out in a manner similar to that for Run 4, as follows.

A mixture of $Ti(NMe_2)_4$ (1 g, 4.5 mmol) and 1,2-epoxycyclohexane (10 ml, 99 mmol) in benzene (40 ml) was placed in a 200 ml autoclave and constantly stirred at 80 °C under CO_2 pressure (50 kg/cm^2). After 210 h of reaction, a few drops of water were added to the reaction mixture, the latter was filtered to remove insoluble materials, and the filtrate was concentrated under reduced pressure at room temperature. To the filtrate concentrate was added about 100 ml of petroleum ether with stirring. The mixture was seeded by a small amount of pure crystalline **1** and cooled in a refrigerator overnight, during which time white needles separated out. The crystals were filtered off and dried at room temperature *in vacuo*.

White needle-like crystals, *trans*-2-hydroxycyclohexyl dimethylcarbamate (**1**), mp 52—53 °C, (Found: C, 57.75; H, 9.31; N, 7.52; mol wt, 196 (V. P. O.), Calcd for $C_9H_{17}NO_3$: C, 57.71; H, 9.15; N, 7.48; mol wt, 187), was obtained in a 50% yield (1.7 g). NMR (chloroform-*d*): δ=1.2—2.2 (8H, m, cyclohexane-ring methylenes), 2.92 (6H, s, $N(CH_3)_2$), 3.41 (1H, s, OH), 3.56 (1H, m, hydroxyl-group methine), 4.48 (1H, m, carbamoyloxy-group methine). IR (KBr tablet method): 3500 cm^{-1} (O–H) and 1700 cm^{-1} (C=O).

After separation of the carbamic ester (**1**), the filtrate was concentrated and added to a large amount of methanol to give CO_2-epoxide copolymer, which was identified by IR spectrum,[5] as a methanol insoluble fraction (27 mg).

We are grateful to Professor Teiji Tsuruta for valuable discussions.

References

1) S. Inoue, *Kagaku Zokan*, **63**, 33 (1974).
2) T. Tsuruta, K. Matsuura, and S. Inoue, *Makromol. Chem.*, **83**, 289 (1965); **103**, 118 (1967).
3) M. H. Chisholm and M. W. Extine, *J. Am. Chem. Soc.*, **99**, 782; 792 (1977).
4) G. Chandra, A. D. Jenkins, M. F. Lappert, and R. C. Srivastava, *J. Chem. Soc., A*, **1970**, 2550.
5) S. Inoue, *Prog. Polym. Sci. Jpn.*, **8**, 1 (1975).
6) S. Inoue, *Chemtech.*, **6**, 588 (1976).
7) A. D. Jenkins, M. F. Lappert, and R. C. Srivastava, *Eur. Polym. J.*, **7**, 289 (1971).

Syntheses of Polymerizable Aromatic Mannich Bases by Means of Amine Exchange Reaction

Hiroyoshi KAMOGAWA, Kuniaki KUBOTA, and Masato NANASAWA
Department of Applied Chemistry, Yamanashi University, Takeda, Kofu 400
(Received July 21, 1977)

Amine exchange reactions between *p*-vinyl-*β*-dimethylaminopropiophenone and arylamine hydrochloride provided six novel aromatic Mannich bases bearing a vinyl group which were otherwise hardly accessible. Thus, by refluxing in ethanol–water (1: 1), *p*-vinyl-*β*-(*p*-anisidino)-, *p*-vinyl-*β*-(*p*-toluidino)-, *p*-vinyl-*β*-(*p*-hydroxyanilino)-, *p*-vinyl-*β*-anilino-, *p*-vinyl-*β*-(*p*-carboxyanilino)-, and *p*-vinyl-*β*-(*p*-nitroanilino)-propiophenones were obtained in 62.0, 55.2, 24.5, 32.0, 47.3, and 29.1% yields, respectively. The Mannich bases thus synthesized underwent ready radical polymerizations to afford the corresponding vinyl polymers, bearing aromatic Mannich base units as pendants.

Amine exchange reactions between aliphatic Mannich bases and arylamines[1] are useful for the syntheses of aromatic Mannich bases, since direct syntheses do not usually provide satisfactory results.[2] In the course of our studies of the amine exchange reactions between various Mannich bases and arylamines, we have found that *p*-vinyl-*β*-dimethylaminopropiophenone, a Mannich base with a vinyl group, which possesses the potentiality of a Michael acceptor, brings about amine exchange reactions with arylamines smoothly, keeping the vinyl group intact, thereby affording a novel group of aromatic Mannich bases bearing a vinyl group, which is otherwise hardly accessible.

p-Vinyl-*β*-dimethylaminopropiophenone (**3**) was prepared by the dehydrobromination of *p*-(2-bromoethyl)-*β*-dimethylaminopropiophenone hydrochloride (**2**), which had itself been synthesized by Mannich-base formation from *p*-(2-bromoethyl)acetophenone (**1**).[3,4]

The amine exchange reactions take place as follows:

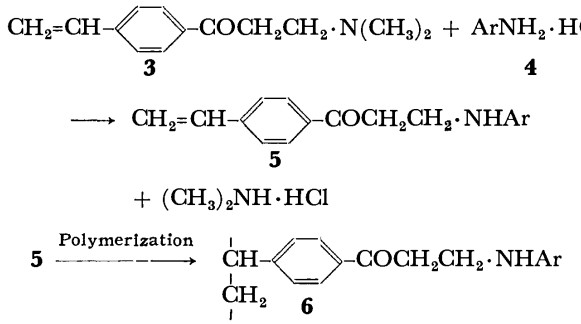

4a, **5a**, **6a**: Ar=*p*-$CH_3OC_6H_4$
4b, **5b**, **6b**: Ar=*p*-$CH_3C_6H_4$
4c, **5c**, **6c**: Ar=*p*-HOC_6H_4
4d, **5d**, **6d**: Ar=C_6H_5
4e, **5e**, **6e**: Ar=*p*-$HOOCC_6H_4$
4f, **5f**, **6f**: Ar=*p*-O_2N-C_6H_4

The novel aromatic Mannich bases synthesized (**5**) underwent radical polymerizations under conventional conditions to afford the corresponding polymers (**6**).

Table 1 summarizes the results obtained in the amine exchange reactions. It can be seen from this table that electron-donating para substituents, such as methoxyl and methyl groups in the starting arylamine hydrochlorides (**4**), provide higher yields than the electron-withdrawing ones, such as the nitro group, in spite of the prolonged reaction times assigned to the latter.

Table 1. Effect of the *p*-substituents on the yields of the aromatic Mannich bases produced in the amine exchange reactions

Product	*p*-Substituent	Reaction time h	Yield %
5a	CH_3O	2	62.0
5b	CH_3	2	55.2
5c	OH	2	24.5 (50.8)[a]
5d	H	2	32.0
5e	COOH	10	47.3
5f	NO_2	25	29.1

a) Under nitrogen.

The fact that the yield for the electron-donating hydroxyl group (**5c**) was low indicates that the starting arylamine (*p*-aminophenol) was very susceptible to air oxidation, thereby affording considerable amounts of oxidation products.

Craig and Moyle[1] proposed three mechanisms for the amine exchange reactions of *β*-diethylaminopropiophenones: S_N1, S_N2, and the Michael addition to the vinyl ketone produced. The step common to all three mechanisms is the nucleophilic attack of the arylamines produced from **4** by the hydrogen chloride exchange with **3**. Accordingly, it appears reasonable that more nucleophilic arylamines bearing more electron-donating para substituents promote the reaction.

Table 2 indicates the polymerization behavior of the **5** monomers. As expected, the **5a** and **5b** monomers, with electron-donating para substituents, provide lower values of $[\eta]$ than do **5e** and **5f**, with electron-withdrawing ones, presumably because of the enhanced radical

Table 2. Polymerization behavior of the **5a**—**f** monomers

Monomer	Conversion %	Appearance of polymer	$[\eta]$dl[a]/g
5a	77	Light yellow powder	0.25
5b	80	Light yellow powder	0.30
5c	84	Light brown powder[b]	0.33
5d	83	Light yellow powder	0.33
5e	93	Light brown powder	0.65
5f	84	Yellow powder	0.41

a) Intrinsic viscosity at 25°C in a *N*,*N*-dimethylformamide solution. b) Insolubilized by air oxidation.

trapping actions of the ArNH– portions in the former.

The synthetic procedure described here leads readily to vinyl polymers with pendant aromatic Mannich base units which are novel and which may be used for various purposes, including the preparation of functional polymers.

Experimental

The IR, ^{1}H-NMR, and mass spectra were obtained with Hitachi EPI-G spectrophotometer, a JNM-PMX 60 spectrometer, and a Hitachi RMU-6 MG spectrometer, respectively, under standard measurement conditions. The elemental analyses were carried out using a Perkin-Elmer 240 instrument.

p-*Vinyl-β-dimethylaminopropiophenone (**3**).* A 5.5-g (17 mmol) portion of **2** in 60 ml of methanol containing 2.4 g (43 mmol) of potassium hydroxide was stirred at room temperature for 24 h in the presence of a small amount of hydroquinone. To the resulting dark solution we then added 2.4 g (43 mmol) of potassium hydroxide, after which stirring was continued for 3 more h. The reaction mixture was then poured into iced water and extracted with ether. The organic layer was washed with water, dried over anhydrous sodium sulfate, and evaporated *in vacuo* at 40 °C to leave a crude product, which was recrystallized from petroleum ether to afford colorless needles of mp 52—55 °C (lit,[3] 54.5—58.5 °C) in a 46.4% yield. The IR, NMR, and mass spectra as well as the CHN analyses identified it as **3**.

General Procedure for Amine Exchange Reactions. A mixture of 8 mmol of **3**, 9 mmol of an arylamine hydrochloride (**4**), a small amount of hydroquinone, and 7 ml of water–ethanol (1 : 1) was refluxed for 2—25 h in an oil bath. The reaction mixture, sometimes with the crystalline precipitates thus produced, was cooled in a refrigerator overnight with or without the addition of water to provide the crude product, which was then purified by repeated recrystallizations.

p-*Vinyl-β-(*p-*anisidino)propiophenone (**5a**).* Recrystallizations of the crude product from ethanol provided lustrous, pale yellow needles with a mp of 140—141 °C. Found: C, 76.72; H, 6.84; N, 5.01%. Calcd for $C_{18}H_{19}NO_2$: C, 76.84; H, 6.81; N, 4.98%. IR(KBr): 1660 (C=O), 990, 930 (vinyl) cm^{-1}. NMR ($CDCl_3$): δ 3.2 (d, 2H, CH_2), 3.5 (d, 2H, CH_2), 3.8 (s, 3H, OCH_3), 5.4 (d, 1H, vinyl), 5.8 (d, 1H, vinyl), 6.5—8.0 (m, 9H, vinyl+ArH) ppm. Mass (*m/e*): 281 (M$^+$, 100).

p-*Vinyl-β-(*p-*toluidino)propiophenone (**5c**).* Lustrous, pale yellow plates (mp 142—143 °C) were isolated from ethanol. Found: C, 81.33; H, 7.33; N, 5.27%. Calcd for $C_{18}H_{19}NO$: C, 81.47; H, 7.22: N, 5.28%. IR(KBr): 1670 (C=O), 990, 910 (vinyl) cm^{-1}. NMR ($CDCl_3$): δ 2.3 (s, 3H, CH_3), 3.2 (t, 2H, CH_2), 3.6 (t, 2H, CH_2), 5.35 (d, 1H, vinyl), 5.7 (d, 1H, vinyl), 6.5—8.0 (m, 9H, vinyl+ArH) ppm. Mass (*m/e*): 265 (M$^+$, 80), 120 (100).

p-*Vinyl-β-(*p-*hydroxyanilino)propiophenone (**5c**).* A yellow, crystalline powder (mp 136—137 °C) was obtained by recrystallization from ethanol. Found: C, 76.72; H, 6.58; N, 4.73%. Calcd for $C_{17}H_{17}NO_2$: C, 76.38; H, 6.41; N, 5.24%. IR(KBr): 3370 (OH), 1660 (C=O), 990, 920 (vinyl) cm^{-1}. NMR (DMSO-d_6+CCl_4): δ 3.1—3.9 (m, 4H, $2CH_2$), 5.4 (d, 1H, vinyl), 5.8 (d, 1H, vinyl), 6.3—8.2 (m, 10H, vinyl+OH+ArH) ppm. Mass (*m/e*): 267 (M$^+$, 63), 131 (100).

p-*Vinyl-β-anilinopropiophenone (**5d**).* Recrystallizations from ethanol afforded a lustrous, yellow, crystalline powder (mp 111—113 °C). Found: C, 81.24; H, 6.76; N, 5.62%. Calcd for $C_{17}H_{17}NO$: C, 81.24; H, 6.82; N, 5.57%. IR(KBr): 1660 (C=O), 990, 910 (vinyl) cm^{-1}. NMR ($CDCl_3$): δ 3.4—3.9 (m, 4H, $2CH_2$), 5.6 (d, 1H, vinyl), 6.0 (d, 1H, vinyl), 6.8—8.1 (m, 10H, vinyl+ArH) ppm. Mass (*m/e*): 251 (M$^+$, 9), 18 (100).

p-*Vinyl-β-(*p-*carboxyanilino)propiophenone (**5e**).* Recrystallizations from *N,N*-dimethylformamide–water afforded a colorless, crystalline powder with a mp of 205—206 °C. Found: C, 73.19; H, 5.95; N, 4.62%. Calcd for $C_{18}H_{17}NO_3$: C, 73.20; H, 5.80; N, 4.72%. IR(KBr): 1660 (C=O), 985, 915 (vinyl) cm^{-1}. NMR (DMSO-d_6+CCl_4): δ 3.0—3.8 (m, 4H, $2CH_2$), 5.4 (d, 1H, vinyl), 5.9 (d, 1H, vinyl), 6.5—8.0 (m, 9H, vinyl+ArH) ppm. Mass (*m/e*): 295 (M$^+$, 20), 131 (100).

p-*Vinyl-β-(*p-*nitroanilino)propiophenone (**5f**).* A yellow crystalline powder (mp 136—137 °C) was isolated from ethanol–water. Found: C, 68.99; H, 5.42; N, 9.32%. Calcd for $C_{18}H_{16}NO_3$: C, 68.91; H, 5.44; N, 9.45%. IR(KBr): 1660 (C=O), 1300 (NO_2), 990, 935 (vinyl) cm^{-1}. NMR (DMSO-d_6+$CDCl_3$): δ 3.4 (d, 2H, CH_2), 3.6 (d, 2H, CH_2), 5.5 (d, 1H, vinyl), 5.9 (d, 1H, vinyl), 6.9—8.2 (m, 9H, vinyl+ArH) ppm. Mass (*m/e*): 296 (M$^+$, 100).

*Polymerization of the **5a**—**f** Monomers.* A solution of 0.3 g of a monomer, 0.003 g of α,α′-azobisisobutyronitrile, and 2 ml of *N,N*-dimethylformamide in a deaerated Pyrex glass ampoule was kept at 70 °C for 48 h. The resulting viscous solution was poured into ethanol to precipitate the polymer. The IR spectra of all the polymers thus synthesized indicated no vinyl absorptions in the 900—930 cm^{-1} region, only strong CH_2 absorptions attributable to the polymer backbone at 1930 and 1860 cm^{-1}, together with characteristic absorptions of the aromatic Mannich bases.

References

1) J. C. Craig and M. Moyle, *J. Org. Chem.*, **29**, 410 (1964).

2) S. R. Sandler and M. Karo, "Organic Functional Group Preparations I," Academic Press, New York (1968), p. 335.

3) S. Tanimoto, J. Horikawa, M. Okano, and R. Oda, *J. Synthetic Org. Chem., Jpn.*, **26**, No. 8, 43 (1968).

4) S. R. Sandler and M. Karo, Ref. 2, p. 178.

5) E. C. Horning, *Org. Synthe.*, Coll. Vol. III, 305 (1955).

Reaction of Nitrile Oxides with *N*-Aryl-*S,S*-dimethylsulfimides

Shinsaku SHIRAISHI, Tadashi SHIGEMOTO, and Shojiro OGAWA

Institute of Industrial Science, The University of Tokyo, Roppongi Minato-ku, Tokyo 106

(Received July 21, 1977)

Both benzimidazole 3-oxides and 1,2,4-benzoxadiazines were formed in reactions of sterically-stabilized benzonitrile oxides with *N*-aryl-*S,S*-dimethylsulfimides, whereas only 1,2,4-benzoxadiazines were produced in reactions of 2,6-unsubstituted benzonitrile oxides. The reactions are thought to proceed *via* the intermediacy of a nitroso compound formed by the nucleophilic attack of sulfimide on the carbon atom of the nitrile oxide and the subsequent release of dimethyl sulfide. The nitrogen or the oxygen atom of the nitroso group of this intermediate can attack the ortho position of the benzene ring originating from sulfimide to form benzimidazole 3-oxide or 1,2,4-benzoxadiazine, respectively, Conjugation of the nitroso group with the *C*-aryl group can be attained in *s-cis* form for the intermediate derived from 2,6-unsubstituted benzonitrile oxide, and thus, exclusive O-attack takes place to afford 1,2,4-benzoxadiazines. On the other hand, conjugation of the nitroso group with the *C*-aryl group cannot be considered for the intermediate derived from 2,6-disubstituted benzonitrile oxide because of the steric hindrance of the substituents. In this case, the intermediate nitroso compound is either in *s-cis* or in *s-trans* form. This causes the formation of both benzimidazole 3-oxide and 1,2,4-benzoxadiazine. Characterization data of benzimidazole 3-oxides are also described.

In the field of heterocyclic chemistry, the 1,3-dipolar cycloaddition reaction represents a very useful synthetic method. Nitrile oxides, which are typical 1,3-dipoles, are known to react with various unsaturated bonds to form heterocycles. Furthermore, many studies have been reported on the reactions of nitrile oxides with ylide compounds.[1] However, very few examples of reactions with N–S unsaturated bonds have been reported.[2–4] This is due to the difficulty of synthesizing compounds having such functional groups, except for *N*-(*p*-tosyl)-sulfimides.[5] *N*-(*p*-Tosyl)sulfimides are very stable and easily synthesized, but do not react with nitrile oxides and nitrones.

Recently, Sharma and his collaborators improved the synthetic method of *N*-arylsulfimides,[6] and Claus *et al.* also synthesized these compounds by a different route.[7] Most are unstable, but *S,S*-dimethyl-*N*-(*p*-nitrophenyl)-sulfimide is stable enough to remain unchanged in a refluxing benzene solution for 10 h. The reactions of nitrile oxides with *N*-arylsulfimides are being investigated in this laboratory in order to elucidate the ionic character of 1,3-dipolar cycloaddition reactions. In the course of the investigation, it was found that both benzimidazole 3-oxides and 1,2,4-benzoxadiazines were formed in the reactions of 2,6-disubstituted benzonitrile oxides with *N*-arylsulfimides, though 1,2,4-benzoxadiazines were the sole products in the reactions of 2,6-unsubstituted benzonitrile oxides.

Gilchrist *et al.* have reported on reactions of nitrile oxides with *N*-aryl-*S,S*-dimethylsulfimides from the viewpoint of 1,2,4-benzoxadiazine synthesis.[8] They used only 2,6-unsubstituted benzonitrile oxides and other aliphatic nitrile oxides, and therefore, paid no attention to the formation of benzimidazole 3-oxides.

Results and Discussion

Sterically-stabilized 2,3,5,6-tetramethylbenzonitrile oxide (DNO), 2,4,6-trimethylbenzonitrile oxide (MNO), and 2,6-dichlorobenzonitrile oxide (DCNO) were allowed to react with some *N*-aryl-*S,S*-dimethylsulfimides (**1**). In almost all cases, two types of products were obtained as main products, benzimidazole 3-oxides (**2**) and 1,2,4-benzoxadiazines (**3**), although the yields were poor. In addition, some minor products formed by the decomposition or isomerization of the starting materials were found. The reaction conditions and yields are shown in Table 1. The reactions of 2,6-unsubstituted benzonitrile oxides with *S,S*-dimethyl-*N*-(*p*-nitrophenyl)sulfimide (**1a**) were also carefully studied, but the formation of benzimidazole 3-oxide was not observed. These results are also shown in Table 1.

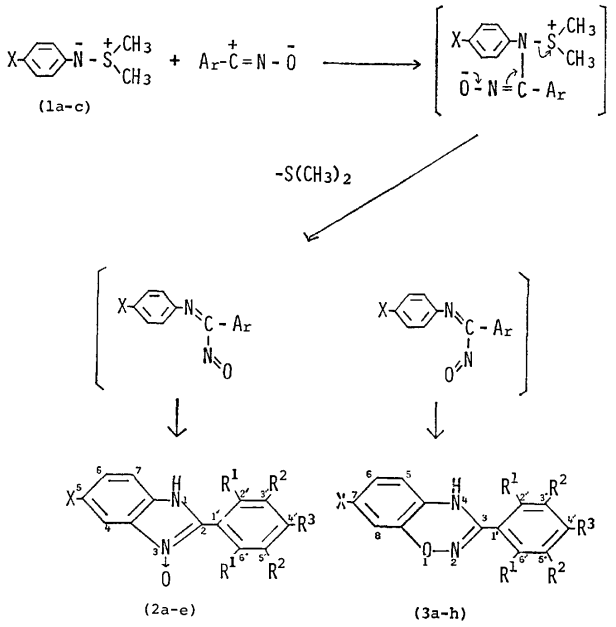

Scheme 1. Reaction route to the benzimidazole 3-oxide and benzoxadiazine.

The formation of benzimidazole 3-oxides in reactions of benzonitrile oxides with *N*-aryl-*S,S*-dimethylsulfimides has not been reported as yet. Characterization data of the benzimidazole 3-oxides are summarized in Table 2. Benzimidazole 3-oxides were formed as fleecy crystals during the reactions. High melting points and poor solubilities in the usual solvents are common to products of this type. Their IR spectra show characteristic broad absorptions in the range from 2100 to 2800 cm^{-1}

Table 1. Reaction conditions and yields of reactions of nitrile oxides with *N*-aryl-*S*,*S*-dimethylsulfimides

Nitrile oxide (Ar)	Sulfimide	Reaction conditions			Yields	
		Solvent	Temp	Time	**2**	**3**
DNO	**1a**	$CHCl_3$	room	190 h	8.3%	14.4%
DNO	**1a**	$CHCl_3$	reflux	10 h	10.7	27.4
DNO	**1a**	PhH	reflux	4 h	11.9	24.7
DNO	**1a**	$PhCH_3$	reflux	2 h	8.5	12.0
DNO	**1a**	Dioxane	reflux	2 h	3.7	trace
DNO	**1a**	THF	reflux	4 h	0.0	6.8
MNO	**1a**	$CHCl_3$	room	18 days	7.6	27.2
MNO	**1a**	PhH	reflux	4 h	7.7	33.8
DCNO	**1a**	$CHCl_3$	room	45 h	14.2	59.5
DCNO	**1a**	$CHCl_3$	reflux	1 h	12.0	65.6
DNO	**1b**	$CHCl_3$	0 °C	a)	16.3	14.3
DNO	**1c**	$CHCl_3$	0 °C	a)	8.1	7.4
Ph-	**1a**	$CHCl_3$	0 °C	a)	0.0	34.6
Ph-	**1a**	THF	0 °C	a)	0.0	61.0
p-ClC_6H_4-	**1a**	$CHCl_3$	0 °C	a)	0.0	37.8
p-ClC_6H_4-	**1a**	THF	0 °C	a)	0.0	68.8
p-$NO_2C_6H_4$-	**1a**	$CHCl_3$	0 °C	a)	0.0	56.3
p-$NO_2C_6H_4$-	**1a**	THF	0 °C	a)	0.0	81.3

a) The reaction mixture was allowed to stand overnight at room temperature.

Table 2. Characterization data of benzimidazole 3-oxides (**2**)

Compd No.	X	R^1	R^2	R^3	Mp (dec) °C (recryst. solvent)		Found	Calcd	NMR, δ (in CF_3COOH)
2a	NO_2	Me	Me	H	334 (DMF)	C:	65.65	65.58	2.12 (s, 6H, Me-2′, 6′), 2.37 (s, 6H, Me-3′, 5′) 7.47 (s, 1H, H-4′), 8.17 (d, 1H, H-7), 8.67 (dd, 1H, H-6), 9.02 (d, 1H, H-4) $J_{4,6}$=2.5 Hz, $J_{6,7}$=10 Hz
						H:	5.45	5.50	
						N:	13.60	13.50	
2b	NO_2	Me	H	Me	306 (DMF)	C:	64.71	64.64	2.24 (s, 6H, Me-2′, 6′), 2.44 (s, 3H, Me-4′), 7.20 (s, 2H, H-3′, 5′), 8.11 (d, 1H, H-7), 8.65 (dd, 1H, H-6), 8.93 (d, 1H, H-4) $J_{4,6}$=1.2 Hz, $J_{6,7}$=8.4 Hz
						H:	5.35	5.09	
						N:	14.22	14.13	
2c	NO_2	Cl	H	H	318 ($DMF+H_2O$)	C:	47.34	48.17	7.69 (s, 3H, H-3′, 4′, 5′), 8.17 (d, 1H, H-7), 8.71 (dd, 1H, H-6), 8.99 (d, 1H, H-4) $J_{4,6}$=1.2 Hz, $J_{6,7}$=9 Hz
						H:	2.34	2.18	
						N:	12.48	12.96	
2d	Cl	Me	Me	H	319 (DMF)	C:	67.44	67.88	2.08 (s, 6H, Me-2′, 6′), 2.36 (s, 6H, Me-3′, 5′) 7.40 (s, 1H, H-4′), 7.76–7.98 (m, 3H, H-4, 6, 7)
						H:	5.62	5.70	
						N:	9.64	9.31	
2e	Br	Me	Me	H	328 (DMF)	C:	59.37	59.14	2.08 (s, 6H, Me-2′, 6′), 2.40 (s, 6H, Me-3′, 5′) 7.39 (s, 1H, H-4′), 7.82–8.13 (m, 3H, H-4, 6, 7)
						H:	5.13	4.96	
						N:	8.20	8.11	

(Fig. 1). Chua *et al.* have attributed the broad absorption in this range to intermolecular hydrogen bonding.[9] Mass spectra also support the structure. All products of this type show similar fragmentation patterns. It should be emphasized that the (M^+-16) fragment ion peak is very characteristic, because the oxygen atom of usual *N*-oxide compounds is thought to be easily stripped off during the ionization process.[10] And the intensity of the (M^++1) ion peak is much stronger than the value calculated from the natural isotope abundance, because of intermolecular hydrogen bonding. The NMR spectra are understandable on the basis of this structure. The signal due to the proton at the 6-position appears in doublet-doublet form, because of interactions with the protons at the 4- and 7-positions. The coupling constant between the protons at 4- and 6-positions is consistent with those of the protons at the meta-positions. The signal due to the proton at the 4-position appears at a field lower than that of the corresponding signal for the 1,2,4-benzoxadiazines. This suggests that the proton is in the neighborhood of and affected by the magnetic anisotropy of the *N*-oxide moiety.

Characterization data of the benzoxadiazines are listed in Table 3. In the mass spectra of the oxadiazines obtained here, the (M^+-15) fragment is very characteristic and this is attributed to NH splitting. This agrees well with the results reported by Gilchrist *et al.*[8] A methanolic solution of 7-nitro-1,2,4-benzoxadiazines produced a color change from yellow to violet, upon addition to an alkaline solution. This color change was

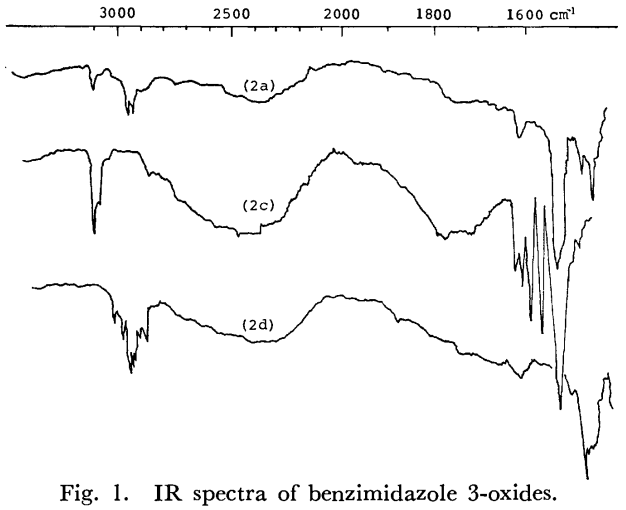

Fig. 1. IR spectra of benzimidazole 3-oxides.

reversible and the violet color returned to its original color upon neutralization.

As seen in Table 1, the reactions of 2,6-disubstituted benzonitrile oxides with *N*-aryl-*S*,*S*-dimethylsulfimides gave both benzimidazole 3-oxides and 1,2,4-benzoxadiazines, whereas 2,6-unsubstituted benzonitrile oxides gave no benzimidazole 3-oxides. The reaction leading to the formation of a benzimidazole 3-oxide or a 1,2,4-benzoxadiazine is considered to proceed by the nucleophilic attack of the nitrogen atom of the sulfimide on the carbon atom of the nitrile oxide followed by the liberation of dimethyl sulfide to form an intermediate nitroso compound. When the nitrogen atom of the nitroso group attacks the ortho-position of the benzene ring, benzimidazole 3-oxide is produced. On the contrary, when the oxygen atom of the nitroso group attacks, 1,2,4-benzoxadiazine is formed (Scheme 1). For the intermediate nitroso compounds, there are two conformational structures, which are *s-cis* and *s-trans* with respect to the –N=C–N=O structure, as shown in Scheme 1. In the *s-trans* form, the lone pair of nitrogen atom faces the *N*-phenyl substituent and, from this structure benzimidazole 3-oxide is produced. In the *s-cis* form, the lone pair faces the opposite side, and nitrogen attack on the *N*-phenyl substituent is inconceivable. Regarding the nitroso intermediate, it is considered to be somewhat more stable when the –N=C–N=O group is in the plane of the aryl group attached to the carbon atom, than when this is not the case. In the case of the reaction of a 2,6-unsubstituted benzonitrile oxide with a sulfimide, the nitroso intermediate can take the more stable *s-cis* form and, therefore, gave only a 1,2,4-benzoxadiazine. However, in the case of the reaction of a 2,6-substituted benzonitrile oxide, coplanarity between the –N=C–N=O and the aryl group attached to the carbon atom is not attained at all due to steric hindrance and thus the intermediate can take either the *s-cis* or the *s-trans* form leading to both 1,2,4-benzoxadiazine and benzimidazole 3-oxide.

When THF was used as the reaction solvent, no benzimidazole 3-oxide formation was observed and the decomposition of the sulfimide to the corresponding

Table 3. Characterization data of 1, 2, 4-benzoxadiazines (**3**)

Compd No.	X	R^1	R^2	R^3	Mp (dec) °C (recryst. solvent)		Found	Calcd	NMR, δ (in DMSO-d_6)
3a	NO_2	Me	Me	H	214—219 (acetone+H_2O)	C:	65.44	65.58	2.21 (s, 12H, Me) 6.75 (d, 1H, H-5) 7.02 (s, 1H, H-4′) 7.46 (d, 1H, H-8) 7.82 (dd, 1H, H-6) $J_{5,6}$= 8.4 Hz, $J_{6,8}$=2.4 Hz
						H:	5.39	5.50	
						N:	13.87	13.50	
3b	NO_2	Me	H	Me	216—220 (acetone+H_2O)	C:	65.18	64.64	2.31 (s, 9H, Me) 6.77 (d, 1H, H-5) 7.02 (s, 2H, H-3′, 5′) 7.46 (d, 1H, H-8) 7.85 (dd, 1H, H-6) $J_{5,6}$=8.4 Hz, $J_{6,8}$=2.4 Hz
						H:	5.34	5.09	
						N:	14.21	14.13	
3c	NO_2	Cl	H	H	183—186 (acetone+H_2O)	C:	48.25	48.17	6.82 (d, 1H, H-5) 7.53 (d, 1H, H-8) 7.69 (s, 3H, H-3′, 4′, 5′) 7.89 (dd, 1H, H-6) $J_{5,6}$=8.4 Hz, $J_{6,8}$=2.4 Hz
						H:	2.93	2.18	
						N:	12.68	12.96	
3d	Cl	Me	Me	H	176—179 ($CHCl_3$+hexane)	C:	67.90	67.88	2.21 (s, 12H, Me) 6.54—7.07 (m, 4H)
						H:	5.85	5.70	
						N:	9.55	9.31	
3e	Br	Me	Me	H	182—183 ($CHCl_3$+hexane)	C:	59.00	59.14	2.20 (s, 12H, Me) 6.52 (d, 1H, H-5) 6.83—7.08 (m, 3H) $J_{5,6}$=8.4 Hz
						H:	5.25	4.96	
						N:	8.33	8.11	
3f	NO_2	H	H	H	179—182[a] ($CHCl_3$)	C:	61.36	61.18	6.93 (d, 1H, H-5) 7.40—7.97 (m, 7H) $J_{5,6}$=8.4 Hz
						H:	3.58	3.55	
						N:	16.57	16.46	
3g[b]	NO_2	H	H	Cl	217—219 ($CHCl_3$)	C:	54.01	53.90	5.99 (d, 1H, H-5) 6.65 (d, 1H, H-8) 7.53 (d, 2H, H-3′, 5′) 7.59 (dd, 1H, H-6) 8.01 (d, 2H, H-2′, 6′) $J_{5,6}$=8.4 Hz, $J_{6,8}$=2.4 Hz, $J_{2',6'}=J_{3',5'}$= 28.8 Hz, $J_{2',3'}=J_{5',6'}$=8.4 Hz
						H:	2.94	2.78	
						N:	14.77	14.51	
3h[b]	NO_2	H	H	NO_2	228—230 (THF)	C:	51.97	52.01	6.15 (d, 1H, H-5) 6.59 (d, 1H, H-8) 7.35 (dd, 1H, H-6) 8.10 (d, 2H, H-2′, 6′) 8.15 (d, 2H, H-3′, 5′) $J_{5,6}$=8.4 Hz $J_{6,8}$=2.4 Hz, $J_{2',6'}=J_{3',5'}$=1.2 Hz, $J_{2',3'}=J_{5'6'}$=3 Hz
						H:	2.82	2.69	
						N:	19.14	18.66	

a) Mp lit,[8] 178 °C. b) In measurements of MNR spectra, 1,5-diazabicyclo[5,4,0]undecene-5 (DBU) was added to enhance the solubility of 1,2,4-benzoxadiazine by proton abstraction at the 4-potition due to its strong basicity.

The intermediate nitroso compound derived from 2,6-unsubstituted benzonitrile oxide.

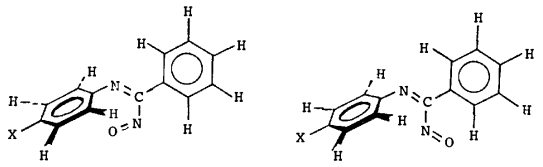

s-cis form *s-trans* form

The intermediate nitroso compound derived from 2,6-substituted benzonitrile oxide.

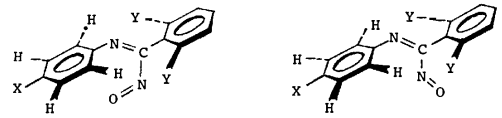

s-cis form *s-trans* form

Fig. 2. Conformational structures of the intermediate nitroso compounds.

aniline was marked. The reason is not clear, but this may be attributed to the solvation of the zwitterionic intermediate which permits annellation only by the attack of anionic oxygen.

Gilchrist and co-workers have reported the formation of 1,2,4-triazolo[1,5-*a*]pyridin 3-oxides in the reactions of nitrile oxides with *S,S*-dimethyl-*N*-(2-pyridyl)sulfimide.[11] In these reactions, the intermediates are also thought to be nitroso compounds, however, the reaction proceeds by attack of the nitrogen atom of the pyridine ring on the nitroso group. If the lone pair of nitrogen atom of the nitroso group attacks, annellation on the carbon atom at another ortho-position of the pyridine must also occur. However, no such product has been reported.

Furthermore, other two reaction products, isocyanate and 2-amino-5-nitrobenzyl methyl sulfide which are isomerization products of each starting material, were isolated in a reaction of a sterically-stabilized nitrile oxide with *S,S*-dimethyl-*N*-(*p*-nitrophenyl)sulfimide. It is well known that sterically-stabilized benzonitrile oxides isomerize to the appropriate isocyanates either thermally or photochemically.[2] However, when the sulfimide alone was subject to the identical and more severe conditions, it remained unchanged. The decomposition of sulfimide to the *p*-nitroaniline is induced also in alcohols. The mechanism is now under investigation.

Experimental

Melting points were measured using a micro-melting-point measuring apparatus (Yazawa Co., Ltd.) and are uncorrected. IR spectra were recorded with a Hitachi infrared spectrometer 215. Mass spectra were recorded with a Hitachi RMU-7M high-resolution mass spectrometer. NMR spectra were recorded with a Hitachi Perkin-Elmer 20R-A high-resolution NMR spectrometer (60 MHz).

Materials. Stable nitrile oxides were synthesized using the method of Grundmann *et al.*[12] 2,6-Unsubstituted benzonitrile oxides were generated *in situ* from the appropriate benzhydroxamoyl chlorides, which were synthesized by the usual methods.[13] *N*-Aryl-*S,S*-dimethylsulfimides were synthesized with DMSO, substituted anilines, and sulfur trioxide.[6]

Reaction of 2,3,5,6-Tetramethylbenzonitrile Oxide (DNO) with S,S-*Dimethyl*-N-*(*p*-nitrophenyl)sulfimide (***1a***).* *a) In Chloroform under Reflux*: A solution of 351 mg (2.00 mmol) of DNO and 377 mg (1.90 mmol) of **1a** in 30 ml of chloroform was heated to reflux with the precipitation of fleecy crystals. After 10 h, the solid product was separated by filtration while the reaction mixture was hot, and was then washed with hot chloroform. The solid product weighed 67 mg (11.3%) and was identified to be 2-duryl-5-nitro-1*H*-benzimidazole 3-oxide (**2a**). The combined filtrate and washing were evaporated giving an oily residue, which was worked up using column chromatography on silica gel (Wacogel C-200) eluted with chloroform. From the elutes, the following were isolated; 199 mg of DNO (56.7% recovery), 19 mg of 2-amino-5-nitrobenzyl methyl sulfide (5.1%), 171 mg of 3-duryl-7-nitro-4*H*-1,2,4-benzoxadiazine (**3a**) (28.9%), and 19 mg of *p*-nitroaniline (7.2%).

b) In Benzene under Reflux: In 50 ml of dry benzene, 877 mg (5.01 mmol) of DNO and 992 mg (5.00 mmol) of **1a** were dissolved and the solution was heated to reflux. Fleecy crystals were deposited during the reaction. After 4 h, the crystals were separated by filtration while hot and washed with hot benzene. They were identified to be **2a**, which weighed 186 mg (11.9%). The combined solution was allowed to stand overnight at room temperature to precipitate the starting ylide, which was removed by filtration (328 mg, 33.1% recovery). The filtrate was evaporated under reduced pressure to give a viscous oil, the trituration of which with a small amount of ether gave a solid. This solid was identified to be **3a** and weighed 286 mg. From the residual ethereal solution, further 48 mg of **3a** was obtained upon trituration with benzene. The residual solution was evaporated and treated on silica-gel column chromatograph with chloroform, and the following substances were isolated: 2,3,5,6-tetramethylphenyl isocyanate (128 mg, 15.7%), DNO (289 mg, 32.9% recovery), 2-amino-5-nitrobenzyl methyl sulfide (109 mg, 11.0%), and **3a** (50 mg). The total amount of **3a** was 384 mg (24.7%).

c) In THF under Refulx: DNO and **1a** (5.00 mmol each) were dissolved in 50 ml of THF and the solution was heated to reflux for 4 h. No crystal formation was observed even upon prolonged heating. The solution was evaporated under reduced pressure. Trituration of the residual oil with cold chloroform gave 144 mg of the starting ylide (14.6% recovery). The chloroform solution was worked up using column chromatography on silica gel (Wacogel C-200) with chloroform. The following substances were isolated: DNO (729 mg, 93.0% recovery), 2-amino-5-nitrobenzyl methyl sulfide (38 mg, 3.8%), **2a** (106 mg, 6.8%), and *p*-nitroaniline (502 mg, 72.6%).

Reaction of p-*Chlorobenzonitrile Oxide with* ***1a***. *In Chloroform*: In a cold solution (below 0 °C) of 496 mg (2.50 mmol) of **1a** in 30 ml of chloroform, 0.40 ml of triethylamine was added with stirring, and then a solution of *p*-chlorobenzhydroxamoyl chloride (475 mg, 2.50 mmol) in 20 ml of chloroform was added dropwise for thirty minutes. After the addition, the cooling bath was removed and the reaction mixture was allowed to stand overnight at ambient temperature. The solvent was removed by evaporation under reduced pressure. The residue was washed with THF to give white crystals of triethylammonium chloride (316 mg, 91.7%). From the THF-soluble part, 274 mg (37.8%) of 3-(*p*-chlorophenyl)-7-nitro-4*H*-1,2,4-benzoxadiazine (**3g**) was obtained upon trituration with chloroform. The residual oil was worked up using column-chromatography on alumina with chloroform to give 260 mg (52.5% recovery) of the starting

ylide (**1a**). No 2-(*p*-chlorophenyl)-5-nitrobenzimidazole 3-oxide was obtained.

Reaction of p-*Nitrobenzonitrile Oxide with* ***1a***. *In Chloroform*: In a cold solution (below 0 °C) of 496 mg (2.50 mmol) of **1a** in 20 ml of chloroform, 0.38 ml of triethylamine was added with stirring, and then a solution of *p*-nitrobenzhydroxamoyl chloride (502 mg, 2.50 mmol) in 30 ml of chloroform was added dropwise for 30 m. During the reaction, a brownish-red precipitate appeared. After the addition, the cooling bath was removed and the reaction mixture was allowed to stand overnight at ambient temperature. The brownish-red precipitate was filtered off and dried, and was identified to be 3-(*p*-nitrophenyl)-7-nitro-4*H*-1,2,4-benzoxadiazine (**3h**). It weighed 396 mg. The filtrate was evaporated under educed pressure to give an oily product. Washing the oily product with THF produced white crystals of triethylammonium chloride (331 mg, 96.2%). The residual THF solution was evaporated and triturated with a small amount of chloroform to give 27 mg of the 3-(*p*-nitrophenyl)-7-nitro-4*H*-1,2,4-benzoxadiazine (**3h**). The total amount of **3h** was 358 mg (56.3%). No 2-(*p*-nitrophenyl)-5-nitrobenzimidazole 3-oxide was found.

Reaction of Benzonitrile Oxide with ***1a***. *In THF*: In a cold solution (below 0 °C) of 496 mg (2.50 mmol) of **1a** in 30 ml of THF, 0.40 ml of triethylamine was added with stirring, and then a solution of benzhydroxamoyl chloride (391 mg, 2.51 mmol) in 20 ml of THF was added for 30 m. After the addition, the cooling bath was removed and the reaction mixture was allowed to stand over-night at ambient temperature. The first drop of benzhydroxamoyl chloride caused the precipitation of triethylammonium chloride. The precipitate was removed by filtration and washed with THF. The solid was almost pure salt and weighed 296 mg (86.0%). The filtrate was evaporated under reduced pressure giving an oil. Trituration of the oil with a small amount of chloroform gave 250 mg of 3-phenyl-7-nitro-4*H*-1,2,4-benzoxadiazine (**3f**). The residue was worked up employing column chromatography on alumina eluted with chloroform. From the elutes, 139 mg of **3f** and 47 mg of **1a** (5.7% recovery) were isolated. The total amount of **3f** was 389 mg (61.0%).

Mass Spectral Data of Benzimidazole 3-Oxides (2). 2-Duryl-5-nitrobenzimidazole 3-oxide (**2a**); *m/e*=312 (M^++1), relative abundance 8; 311.1288 (M^+, calcd for $C_{17}H_{17}N_3O_3$=311.1269), 42; 295 (M^+−16), 15; 294 (M^+−17), 58; 248, 100: 2-Mesityl-5-nitrobenzimidazole 3-oxide (**2b**); 298 (M^++1), 8; 297.1122 (M^+, calcd for $C_{16}H_{15}N_3O_3$=297.1112), 46; 281 (M^+−16), 22; 280 (M^+−17), 41; 234, 100: 2-(2′,6′-Dichlorophenyl)-5-nitrobenzimidazole 3-oxide (**2c**); 326 (M^++3), 3; 325 (M^++2), 23; 324 (M^++1), 4; 322.9868 (M^+, calcd for $C_{13}H_7N_3O_3Cl_2$=322.9864), 33; 309 (M^+−14), 7; 307 (M^+−16), 12; 173, 100; the (M^+−17) ion peak was not observed in this case. 2-Duryl-5-chlorobenzimidazole 3-oxide (**2d**); 303 (M^++3), 4; 302 (M^++2), 13; 301 (M^++1), 10; 300.1014 (M^+, calcd for $C_{17}H_{17}N_2OCl$=300.1028), 38; 286 (M^+−14), 8; 285 (M^+−15), 31; 284 (M^+−16), 22; 283 (M^+−17), 100: 2-Duryl-5-bromobenzimidazole 3-oxide (**2e**); 347 (M^++3), 7; 346 (M^++2), 50; 345 (M^++1), 8; 344.0530 (M^+, calcd for $C_{17}H_{17}N_2OBr$=344.0524), 52; 330 (M^+−14), 22; 329 (M^+−15), 100; 328 (M^+−16), 24; 327 (M^+−17), 100.

References

1) R. Huisgen and J. Wuff, *Chem. Ber.*, **102**, 1833 (1969); *ibid.*, **102**, 1848 (1969).

2) C. Grundmann and P. Grunanger, "The Nitrile Oxides," Springer-Verlag, Berlin (1971), pp. 62, 134.

3) E. S. Levchenko and I. E. Sheinkman, *Zh. Obshch. Kim.*, **36**, 428 and *Chem. Abstr.*, **65**, 643e (1966).

4) P. Rajagopalan and B. G. Advani, *J. Chem. Soc.*, **1965**, 3369.

5) K. Tsujihara, N. Furukawa, K. Oae, and S. Oae, *Bull. Chem. Soc. Jpn.*, **42**, 2631 (1969).

6) A. K. Sharma, T. Ku, A. D. Dawson, and D. Swern, *J. Org. Chem.*, **39**, 3365 (1974); T. E. Varkey, G. F. Whitfield, and D. Swern, *ibid.*, **40**, 2758 (1975).

7) P. K. Claus, W. Reider, and P. Hofbauer, *Tetrahedron*, **31**, 505 (1975).

8) T. L. Gilchrist, C. J. Harris, F. D. King, M. E. Peek, and C. W. Rees, *J. Chem. Soc., Perkin Trans. 1*, **1976**, 2161 and T. L. Gilchrist, C. J. Harris, and C. W. Rees, *J. Chem. Soc., Chem. Commun.*, **1974**, 485.

9) S. O. Chua, M. J. Cook, and A. R. Katritzky, *J. Chem. Soc., B*, **1971**, 2350.

10) K. Volkamer and H. W. Zimmermann, *Chem. Ber.*, **102**, 4177 (1969).

11) T. L. Gilchrist, C. J. Harris, D. G. Hawkins, C. J. Moody, and C. W. Rees, *J. Chem. Soc., Perkin Trans. 1*, **1976**, 2166.

12) C. Grundmann and R. Richter, *J. Org. Chem.*, **33**, 476 (1968); C. Grundmann and J. M. Dean, *ibid.*, **30**, 2809 (1965).

13) M. H. Benn, *Can. J. Chem.*, **42**, 2393 (1964).

Structure and Absolute Configuration of α-Pompene. II. An X-Ray Analysis of the Mono *p*-Bromobenzoate of the Diol Derived from α-Pompene

Hiroshi NOZAKI, Akihiko MATSUO, Mitsuru NAKAYAMA, Yoshihiko KUSHI, Nagao KAMIJO,* and Shûichi HAYASHI**

Department of Chemistry, Faculty of Science, Hiroshima University, Hiroshima 730
**Government Industrial Research Institute, Osaka, Midorigaoka, Ikeda 536*

(Received July 23, 1977)

The mono *p*-bromobenzoate of the diol derived from α-pompene has been studied by X-ray crystal structure analysis and determined to be 9-*p*-bromobenzoxy-8-hydroxy-1,2,6,8-tetramethyltricyclo[5.3.1.$0^{2,6}$]undecane. The crystals are of the orthorhombic space group $P2_12_12_1$, $a=46.53(2)$, $b=12.20(2)$, $c=7.39(2)$ Å, $Z=8$, and hence there are two independent molecules per asymmetric unit. The structure was solved by the heavy-atom methods, and refined by block-diagonal least-squares calculations to a final R value of 0.103 for 2493 observed reflections. The structures of the two independent molecules in the asymmetric unit are quite similar. Both molecules contain a tricyclo[5.3.1.$0^{2,6}$]undecane ring in which three fused rings (cyclohexane, cyclopentane, and cyclopentane) are present. The overall configuration of these three fused rings can be described as a "*cis*" type. The conformation of the cyclohexane ring is of a chair form, and the two cyclopentane rings exhibit envelope forms. Based on the anomalous X-ray dispersion effect of the bromine atoms, the absolute configuration of the title compound was also determined.

(+)-α-Pompene, $C_{15}H_{24}$, is a novel tricyclic sesquiterpene hydrocarbon which was isolated from the extract of a liverwort, *Bazzania pompeana* (Lac.) Mitt. together with (−)-β-pompene. We have previously assigned the structure (I) for (+)-α-pompene on the basis of the chemical and spectral evidence.[1] For the purpose of confirming this structure, α-pompene was converted to a diol. Its mono *p*-bromobenzoate was prepared for examination by X-ray crystallographic analysis. The conclusion was that the structures of (+)-α- and (−)-β-pompene should be represented by 1,2,6,8-tetramethyltricyclo[5.3.1.$0^{2,6}$]undec-8-ene (II) and 1,2,6,8-tetramethyltricyclo[5.3.1.$0^{2,6}$]undec-8(15)-ene (III), respectively.[2] A portion of this result has already been reported briefly, together with the absolute configurations of the hydrocarbons, which were determined by the CD measurement.[3] We report here the detailed results of the X-ray crystal structure analysis of α-pompene diol mono *p*-bromobenzoate.

Experimental

The crystals of mono *p*-bromobenzoate, $C_{22}H_{29}O_3Br$, mp 79—80 °C were recrystallized from a hexane–EtOAc (4: 1) mixture at room temperature.[3] The colorless crystals thus obtained were well-formed needles elongated along the c-axis. Crystal data are as follows: $C_{22}H_{29}O_3Br$, $M=421.4$, Orthorhombic, $a=46.53(2)$, $b=12.20(2)$, $c=7.39(2)$ Å, $U=4195$ Å^3, $D_m=1.31$ (by flotation in $ZnCl_2$ solution), $Z=8$, $D_c=1.33$ g/cm^3, $F(000)=1760$; Ni $K\alpha$ radiation ($\lambda=1.6591$ Å), $\mu=38.2$ cm^{-1}. The space group is shown to be $P2_12_12_1$ (D_2^4) from the following systematic absences: $h00$ when $h=2n+1$, $0k0$ when $k=2n+1$, and $00l$ when $l=2n+1$. The unit-cell dimensions were evaluated from the least-squares refinement of the $hk0$, $h0l$, and $0kl$ reflection data recorded on Weissenberg photographs calibrated with a sodium chloride crystal. The data for the intensity measurements were recorded by equi-inclination multiple-film Weissenberg photographs (Ni $K\alpha$ radiation) of the $hk0$-$hk5$ and $h0l$ reciprocal lattice levels. The intensity data obtained (maximum $\sin\theta/\lambda=0.55$) were estimated visually by the comparison with a calibrated intensity scale. Spot-shape and the usual Lorentz and polarization corrections were applied, and 2840 independent observed structure amplitudes were obtained. No correction was made for absorption ($\mu r=0.5$).

Solution and Refinement of the Structure

The structure was solved by the heavy-atom methods. Initial coordinates for the two independent bromine atoms were derived from the three-dimensional Patterson map. The subsequent electron density syntheses, though complicated in the first step by the false inversion center, finally gave the non-hydrogen atom skeleton of both molecules.

This model was refined by several cycles of the block-diagonal least-squares adjustment of the positional and the isotropic thermal parameters using the HBLS program.[4] Cruickshank's weighting scheme was used, in which $W=1/(A+B|F_o|+C|F_o|^2)$, and $A=5.0$, $B=1.0$, and $C=0.024$.[5] The scattering factors from the "International Table" were used.[6] The final difference electron density map showed no spurious peak. However, it was difficult to estimate the hydrogen-atom positions clearly. Hydrogen atoms, except for methyl groups, were therefore located by assuming the C–H bond length of 1.08 Å and the tetrahedral angle for each carbon atom. Contributions for hydrogen atoms with fixed position and isotropic thermal factor $B=4.5$ were included in further least-squares iterations, during which the non-hydrogen atoms were allowed to assume anisotropic temperature factors. The final R value was 0.103 for 2493 non-zero reflections.

In the final stage of the refinements the absolute configuration of the molecule was determined by the anomalous dispersion method.[7] In order to estimate the differences between $I_o(hkl)$ and $I_o(\bar{h}\bar{k}\bar{l})$ values, both intensities were measured visually from the Weissenberg

** To whom the correspondence should be addressed.

Table 1. Determination of the absolute configuration (Ni $K\alpha$ radiation)

h	k	l	Calcd $F^2(hkl)$	Calcd $F^2(\bar{h}\bar{k}\bar{l})$	Obsd $I(hkl)$	Obsd $I(\bar{h}\bar{k}\bar{l})$
11	2	1	160	230	<	
1	4	1	150	202	≪	
8	4	1	343	259	>	
1	5	1	430	360	>	
7	6	1	213	180	≫	
15	1	2	97	128	<	
18	1	2	88	114	≪	
13	2	2	287	242	>	
1	3	2	14	5	>	
10	1	3	242	288	<	
18	1	3	52	31	≫	
6	3	3	120	93	>	
9	3	3	134	104	>	
3	5	3	132	109	>	
2	1	5	69	53	≫	

photographs rotated around the c-axis, as taken with Ni $K\alpha$ radiation. Structure factors were calculated for all the hkl and $\bar{h}\bar{k}\bar{l}$ reflections, using an atomic scattering factor for the bromine atom of the form $f_{Br}=f_{Br}+\Delta f'_{Br}+i\Delta f''_{Br}$, where $\Delta f'_{Br}=-0.86$ and $\Delta f''_{Br}=1.63$.[8] The results are summarized in Table 1. These results also indicate that the parameters of Table 2 represent the true absolute configuration. The table of observed and calculated structure factors is kept as Document No. 7803 at the Chemical Society of Japan.

Result and Discussion

The final atomic coordinates and anisotropic thermal parameters ($\times 10^4$) are listed in Table 2. The interatomic distances and valency angles, with the estimated standard deviations in parentheses, are also listed in Table 3. The atomic arrangement in the two crystallographically independent molecules of α-pompene diol *p*-bromobenzoate viewed along the c-axis is shown in Fig. 1. The numbering scheme of the atoms in this figure agrees with the conventional chemical sequence employed in the chemical formula (IVb). The two molecules have very similar conformations; the skeleton of each molecule consists of three rings: cyclohexane and the two cyclopentanes. For purposes of comparison, the values for the two molecules of the asymmetric unit are labeled A and B respectively, and those for the latter data are shown in square brackets. From the above results, the structure of α-pompene diol can be shown by the chemical formula 1,2,6,8-tetramethyltricyclo[5.3.1.$0^{2,6}$]undecan-8,9-diol, with the stereochemistry (IVa) and the overall molecular conformation (IVb). Therefore, the structure assigned previously to α-pompene should be revised to be 1,2,6,8-tetramethyltricyclo[5.3.1.$0^{2,6}$]undec-8-ene, while that of β-pompene is 1,2,6,8-tetramethyltricyclo[5.3.1.$0^{2,6}$]undec-8(15)-ene. The absolute configurations of their compounds are presented by stereostructures (II) and (III). The equations of planes and the displacements of the atoms from the mean planes are listed in Table 4.

Table 2. Positional and thermal parameters of atoms (e.s.d.'s in parentheses)

(a) Fractional co-ordinates.

Molecule A	X	Y	Z	Molecule B	X	Y	Z
Br	0.4039(1)	0.5832(3)	0.4267(6)	Br	0.3320(1)	0.8978(3)	0.9478(6)
O(1)	0.2650(3)	0.7473(13)	1.1373(21)	O(1)	0.4828(3)	0.8566(16)	0.3035(24)
O(2)	0.2749(3)	0.7147(12)	0.7900(20)	O(2)	0.4681(3)	0.8406(16)	0.6458(22)
O(3)	0.2611(3)	0.7143(12)	0.5017(22)	O(3)	0.4781(3)	0.8062(14)	0.9398(23)
C(1)	0.2110(5)	0.9000(20)	0.9287(36)	C(1)	0.5445(4)	0.9244(19)	0.5397(35)
C(2)	0.1834(4)	0.8359(17)	0.8714(38)	C(2)	0.5643(4)	0.8313(21)	0.6119(41)
C(3)	0.1812(5)	0.7933(21)	0.6756(43)	C(3)	0.5600(5)	0.7822(24)	0.7925(37)
C(4)	0.1671(6)	0.6765(26)	0.7008(56)	C(4)	0.5644(7)	0.6552(22)	0.7672(53)
C(5)	0.1828(5)	0.6267(23)	0.8600(38)	C(5)	0.5472(7)	0.6297(24)	0.6052(44)
C(6)	0.1845(4)	0.7212(20)	0.9947(35)	C(6)	0.5540(4)	0.7216(22)	0.4724(38)
C(7)	0.2133(5)	0.7425(16)	1.1114(41)	C(7)	0.5321(4)	0.7800(17)	0.3390(35)
C(8)	0.2423(4)	0.7013(17)	1.0325(36)	C(8)	0.4997(4)	0.7811(18)	0.4077(35)
C(9)	0.2449(4)	0.7326(16)	0.8482(27)	C(9)	0.4989(3)	0.8166(16)	0.5998(40)
C(10)	0.2386(4)	0.8582(19)	0.8281(34)	C(10)	0.5151(5)	0.9291(17)	0.6239(33)
C(11)	0.2147(4)	0.8654(19)	1.1274(37)	C(11)	0.5407(5)	0.8987(17)	0.3405(32)
C(12)	0.2095(5)	1.0264(14)	0.9108(44)	C(12)	0.5580(5)	1.0453(19)	0.5750(50)
C(13)	0.1554(5)	0.9053(22)	0.9087(55)	C(13)	0.5975(5)	0.8552(36)	0.5830(60)
C(14)	0.1601(5)	0.7119(21)	1.1333(42)	C(14)	0.5779(5)	0.6779(23)	0.3402(43)
C(15)	0.2455(5)	0.5692(21)	1.0487(44)	C(15)	0.4836(5)	0.6575(26)	0.3982(55)
C(16)	0.2794(4)	0.7024(14)	0.6168(29)	C(16)	0.4615(4)	0.8310(20)	0.8151(34)
C(17)	0.3108(4)	0.6761(17)	0.5690(33)	C(17)	0.4288(5)	0.8434(15)	0.8457(39)
C(18)	0.3195(4)	0.6894(18)	0.4013(34)	C(18)	0.4179(5)	0.8454(19)	1.0211(33)
C(19)	0.3482(4)	0.6600(17)	0.3599(40)	C(19)	0.3890(4)	0.8614(23)	1.0517(41)
C(20)	0.3660(4)	0.6236(21)	0.4827(40)	C(20)	0.3710(5)	0.8760(20)	0.9108(42)
C(21)	0.3574(4)	0.6121(21)	0.6563(41)	C(21)	0.3822(5)	0.8795(29)	0.7321(44)
C(22)	0.3287(4)	0.6404(23)	0.7094(33)	C(22)	0.4115(5)	0.8658(20)	0.6987(39)

(b) Anisotropic temperature factors ($\times 10^4$) expressed in the form $\exp[-(\beta_{11}h^2+\beta_{22}k^2+\beta_{33}l^2+\beta_{12}hk+\beta_{13}hl+\beta_{23}kl)]$.

Molecule A	$\beta^{a)}_{11}$	β_{22}	β_{33}	β_{12}	β_{13}	β_{23}	Molecule B	$\beta^{a)}_{11}$	β_{22}	β_{33}	β_{12}	β_{13}	β_{23}
Br	53(1)	190(4)	471(10)	18(1)	12(2)	61(12)	Br	59(1)	161(3)	534(11)	10(1)	10(2)	−182(11)
O(1)	49(7)	130(15)	175(40)	−9(5)	−14(9)	−27(39)	O(1)	60(8)	160(18)	237(45)	6(7)	6(10)	107(51)
O(2)	45(6)	113(13)	152(36)	0(5)	2(7)	12(38)	O(2)	54(7)	170(19)	168(39)	10(6)	−1(8)	−17(47)
O(3)	41(6)	110(13)	232(41)	12(5)	8(8)	17(40)	O(3)	46(7)	132(15)	206(41)	−4(5)	−18(8)	25(44)
C(1)	56(11)	108(22)	247(67)	6(8)	6(13)	1(70)	C(1)	30(8)	102(20)	321(67)	−3(6)	14(12)	81(67)
C(2)	38(9)	68(17)	364(75)	−2(6)	−4(13)	33(60)	C(2)	34(9)	122(23)	385(82)	1(4)	−5(14)	165(76)
C(3)	75(14)	89(21)	356(84)	15(9)	13(18)	−32(73)	C(3)	76(14)	137(26)	214(70)	−4(10)	−26(16)	−102(77)
C(4)	85(17)	142(30)	559(122)	−26(12)	3(24)	−317(106)	C(4)	121(22)	86(23)	496(112)	−26(11)	−32(26)	175(91)
C(5)	61(12)	140(27)	267(72)	−21(10)	−10(15)	−20(76)	C(5)	120(21)	118(26)	315(86)	11(12)	22(23)	110(86)
C(6)	49(10)	111(22)	236(66)	2(8)	11(13)	107(63)	C(6)	50(10)	137(26)	295(75)	8(8)	−30(13)	−206(77)
C(7)	76(14)	47(16)	318(76)	−2(7)	6(16)	27(56)	C(7)	35(8)	68(16)	302(66)	−4(6)	−6(12)	−10(57)
C(8)	57(11)	61(16)	276(68)	4(7)	4(14)	−84(55)	C(8)	55(10)	99(18)	63(51)	−11(7)	1(10)	−107(50)
C(9)	40(8)	74(16)	104(51)	−4(6)	4(9)	15(45)	C(9)	29(8)	52(15)	460(83)	−4(5)	11(14)	53(63)
C(10)	42(9)	94(20)	263(65)	−11(7)	−2(13)	34(6)	C(10)	72(12)	64(17)	199(60)	5(8)	0(13)	6(54)
C(11)	56(11)	93(20)	262(71)	0(8)	0(13)	15(62)	C(11)	81(13)	60(17)	194(59)	−10(8)	−14(14)	−24(53)
C(12)	92(15)	13(14)	431(88)	−3(7)	−7(19)	71(57)	C(12)	68(13)	73(20)	523(100)	−24(8)	−14(20)	58(84)
C(13)	51(11)	106(24)	651(122)	−1(8)	−3(20)	123(108)	C(13)	30(10)	285(50)	625(129)	−16(11)	−26(19)	112(157)
C(14)	64(12)	96(2)	379(88)	−23(9)	38(17)	−29(72)	C(14)	69(13)	137(27)	333(82)	30(10)	25(17)	−22(80)
C(15)	63(12)	91(21)	432(89)	13(8)	−17(17)	60(79)	C(15)	47(11)	150(29)	598(119)	−14(10)	−1(20)	−170(112)
C(16)	47(9)	44(14)	159(52)	4(6)	−4(10)	23(44)	C(16)	40(9)	125(23)	218(62)	−4(7)	−16(12)	−136(63)
C(17)	44(9)	80(17)	206(58)	6(6)	−16(12)	−39(55)	C(17)	73(12)	27(14)	357(76)	−19(7)	22(16)	−20(55)
C(18)	35(8)	96(19)	241(64)	5(6)	−5(11)	−37(59)	C(18)	75(13)	85(19)	180(63)	−8(8)	13(14)	16(57)
C(19)	43(9)	56(16)	418(83)	−8(6)	9(14)	119(64)	C(19)	44(10)	147(26)	332(79)	−11(9)	15(15)	32(85)
C(20)	48(10)	118(24)	348(79)	9(8)	6(14)	−156(75)	C(20)	63(12)	98(22)	343(78)	11(8)	−1(16)	−37(75)
C(21)	44(10)	115(23)	386(80)	13(8)	−30(15)	20(77)	C(21)	56(13)	185(35)	398(96)	2(10)	−36(18)	−132(97)
C(22)	36(9)	164(27)	176(59)	11(8)	−3(11)	139(67)	C(22)	77(13)	88(20)	260(71)	13(9)	2(16)	9(65)

a) All values for β_{11} are shown in the scale factor $\times 10^5$.

(c) Calculated co-ordinates and the assigned isotropic temperature factor for hydrogen atoms.

Molecule A	X	Y	Z	B	Molecule B	X	Y	Z	B
H(3a)	0.167	0.846	0.593	4.5	H(3a)	0.575	0.818	0.889	4.5
H(3b)	0.202	0.788	0.612	4.5	H(3b)	0.538	0.801	0.842	4.5
H(4a)	0.144	0.678	0.279	4.5	H(4a)	0.587	0.632	0.752	4.5
H(4b)	0.170	0.623	0.581	4.5	H(4b)	0.557	0.607	0.887	4.5
H(5a)	0.171	0.557	0.921	4.5	H(5a)	0.553	0.550	0.544	4.5
H(5b)	0.204	0.597	0.822	4.5	H(5b)	0.524	0.627	0.633	4.5
H(7)	0.211	0.693	1.238	4.5	H(7)	0.533	0.735	0.206	4.5
H(9)	0.230	0.683	0.766	4.5	H(9)	0.510	0.775	0.713	4.5
H(10a)	0.257	0.905	0.873	4.5	H(10a)	0.503	0.995	0.560	4.5
H(10b)	0.236	0.877	0.680	4.5	H(10b)	0.518	0.950	0.767	4.5
H(11a)	0.235	0.895	1.183	4.5	H(11a)	0.524	0.950	0.279	4.5
H(11b)	0.198	0.901	1.125	4.5	H(11b)	0.561	0.913	0.266	4.5
H(18)	0.305	0.720	0.292	4.5	H(18)	0.433	0.831	1.135	4.5
H(19)	0.357	0.672	0.222	4.5	H(19)	0.380	0.869	1.191	4.5
H(21)	0.372	0.581	0.760	4.5	H(21)	0.367	0.893	0.622	4.5
H(22)	0.321	0.630	0.845	4.5	H(22)	0.420	0.868	0.561	4.5

The tricyclo[5.3.1.$0^{2,6}$]undecane framework of the α-pompene derivative has a crowded "*cis*" configuration.[9] In relation to the chemical formula, tricyclo-[5.3.1.$0^{2,6}$]undecane, this new framework is in agreement with that of α-caryophyllene alcohol (Va).[10] However, the configurations of the bicyclo[3.3.0]octane fragment in the two molecules are completely different. The α-caryophyllene alcohol framework has a strain free "*trans*" configuration (Vb).[9]

The cyclohexane ring, (C(7), C(8), C(9), C(10), C(1), and C(11)), in both A and B molecules adopts a chair conformation. As shown in Fig. 1, the two oxygen atoms which belong to the diol groups occupy the axial position for the O(1) atom and the equatorial position

TABLE 3. BOND LENGTHS AND BOND ANGLES (e.s.d.'s IN PARENTHESES)
The values of molecule B are shown in square brackets.

(a) Bond lengths [Å]

Br	– C(20)	1.88(3) [1.85(3)]	O(1)	– C(8)	1.42(3) [1.44(3)]
O(2)	– C(9)	1.48(3) [1.50(4)]	O(2)	– C(16)	1.31(3) [1.29(3)]
O(3)	– C(16)	1.21(3) [1.24(3)]	C(1)	– C(2)	1.56(4) [1.56(4)]
C(1)	– C(10)	1.57(4) [1.51(4)]	C(1)	– C(11)	1.54(4) [1.52(4)]
C(1)	– C(12)	1.55(4) [1.62(5)]	C(2)	– C(3)	1.54(4) [1.48(4)]
C(2)	– C(6)	1.67(4) [1.76(4)]	C(2)	– C(13)	1.58(5) [1.59(5)]
C(3)	– C(4)	1.58(5) [1.57(5)]	C(4)	– C(5)	1.51(5) [1.47(5)]
C(5)	– C(6)	1.53(4) [1.52(4)]	C(6)	– C(7)	1.61(4) [1.59(4)]
C(6)	– C(14)	1.54(4) [1.58(4)]	C(7)	– C(8)	1.56(4) [1.59(3)]
C(7)	– C(11)	1.51(4) [1.50(4)]	C(8)	– C(9)	1.42(3) [1.48(4)]
C(8)	– C(15)	1.62(4) [1.69(5)]	C(9)	– C(10)	1.57(3) [1.58(4)]
C(16)	– C(17)	1.53(3) [1.55(4)]	C(17)	– C(18)	1.31(4) [1.39(4)]
C(17)	– C(22)	1.40(4) [1.38(4)]	C(18)	– C(19)	1.41(4) [1.38(4)]
C(19)	– C(20)	1.31(4) [1.35(4)]	C(20)	– C(21)	1.35(4) [1.40(5)]
C(21)	– C(22)	1.44(4) [1.40(5)]			

(b) Bond angles [°]

C(9)	– O(2) – C(16)	117.0(17) [115.4(21)]	O(1)	– C(8) – C(7)	108.2(21) [110.8(18)]
C(2)	– C(1) – C(10)	112.6(21) [115.1(21)]	O(1)	– C(8) – C(9)	110.7(21) [108.2(20)]
C(2)	– C(1) – C(11)	102.4(21) [104.5(21)]	O(1)	– C(8) – C(15)	106.5(21) [107.9(21)]
C(2)	– C(1) – C(12)	115.8(23) [112.2(20)]	C(7)	– C(8) – C(9)	110.2(22) [109.5(20)]
C(10)	– C(1) – C(11)	105.9(21) [107.8(21)]	C(7)	– C(8) – C(15)	111.8(23) [113.6(21)]
C(10)	– C(1) – C(12)	108.7(22) [104.6(22)]	C(9)	– C(8) – C(15)	109.3(21) [106.8(22)]
C(11)	– C(1) – C(12)	111.0(23) [112.9(22)]	O(2)	– C(9) – C(8)	108.7(18) [107.5(21)]
C(1)	– C(2) – C(3)	118.6(23) [121.7(25)]	O(2)	– C(9) – C(10)	107.1(17) [105.1(21)]
C(1)	– C(2) – C(6)	104.1(21) [101.1(21)]	C(8)	– C(9) – C(10)	109.8(19) [110.4(22)]
C(1)	– C(2) – C(13)	111.4(24) [113.4(26)]	C(1)	– C(10) – C(9)	115.1(20) [110.9(21)]
C(3)	– C(2) – C(6)	103.4(22) [100.7(22)]	C(1)	– C(11) – C(7)	101.1(22) [103.7(20)]
C(3)	– C(2) – C(13)	106.9(25) [109.1(27)]	O(2)	– C(16) – O(3)	124.2(20) [126.2(23)]
C(6)	– C(2) – C(13)	112.4(24) [109.1(25)]	O(2)	– C(16) – C(17)	113.7(18) [111.6(22)]
C(2)	– C(3) – C(4)	102.8(26) [105.9(26)]	O(3)	– C(16) – C(17)	122.0(20) [122.0(22)]
C(3)	– C(4) – C(5)	104.7(29) [103.5(29)]	C(16)	– C(17) – C(18)	119.0(22) [119.8(23)]
C(4)	– C(5) – C(6)	103.2(25) [104.9(27)]	C(16)	– C(17) – C(22)	117.3(21) [118.6(24)]
C(2)	– C(6) – C(5)	106.0(21) [103.8(22)]	C(18)	– C(17) – C(22)	123.6(24) [121.1(25)]
C(2)	– C(6) – C(7)	100.6(20) [101.4(20)]	C(17)	– C(18) – C(19)	117.7(24) [120.8(25)]
C(2)	– C(6) – C(14)	113.7(22) [115.4(22)]	C(18)	– C(19) – C(20)	122.4(27) [119.9(28)]
C(5)	– C(6) – C(7)	120.9(22) [126.8(24)]	Br	– C(20) – C(19)	122.2(23) [120.9(24)]
C(5)	– C(6) – C(14)	109.9(22) [107.3(24)]	Br	– C(20) – C(21)	117.5(22) [119.4(24)]
C(7)	– C(6) – C(14)	105.6(22) [102.8(22)]	C(19)	– C(20) – C(21)	120.3(29) [119.6(29)]
C(6)	– C(7) – C(8)	117.9(23) [114.5(20)]	C(20)	– C(21) – C(22)	120.8(27) [121.2(30)]
C(6)	– C(7) – C(11)	103.8(22) [104.9(21)]	C(17)	– C(22) – C(21)	115.2(25) [117.1(27)]
C(8)	– C(7) – C(11)	108.3(23) [104.0(20)]			

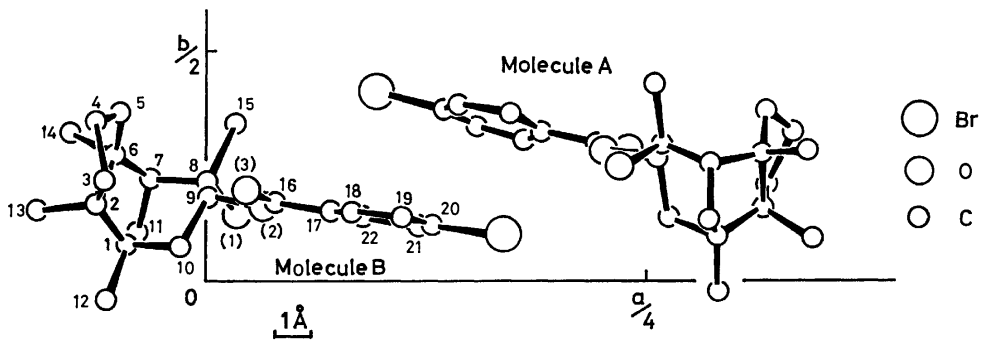

Fig. 1. The atomic arrangement in the crystallographically independent molecules of α-pompene diol mono-*p*-bromobenzoate viewed along the c-axis. (This figure corresponds to the equivalent positions of "1/2−*x*, 1−*y*, 1/2+*z*" relative to the original "*x*, *y*,*z*" coordinates.)

Table 4. Equations of planes and displacements (Å) of the atoms from mean planes
X, Y, Z are orthogonal co-ordinates (Å), values for molecule B in square brackets.

Plane (1): C(1), C(7), C(8), C(10)
$0.5358X + 0.5312Y + 0.6563Z = 15.5556$
$[0.2632X - 0.6758Y + 0.6885Z = 1.7983]$

C(1)	−0.04 [0.01]	C(10)	0.04 [−0.02]	C(12)	−1.16 [1.04]
C(7)	0.04 [−0.02]	C(9)	0.60 [−0.64]	C(15)	−2.84 [2.91]
C(8)	−0.04 [0.03]	C(11)	−0.88 [0.85]		

Plane (2): C(1), C(2), C(6), C(7)
$-0.5314X + 0.4597Y + 0.7115Z = 4.7264$
$[0.7358X + 0.2635Y - 0.1239Z = 19.1385]$

C(1)	0.01 [0.02]	C(7)	−0.02 [−0.02]	C(15)	2.10 [2.29]
C(2)	−0.02 [−0.03]	C(11)	−0.76 [−0.69]		
C(6)	0.02 [0.03]	C(12)	−0.64 [−0.67]		

Plane (3): C(2), C(3), C(5), C(6)
$0.9971X - 0.0083Y - 0.0763Z = 7.9342$
$[0.9538X - 0.3000Y - 0.0168Z = 21.9081]$

C(2)	0.01 [−0.02]	C(6)	−0.01 [0.02]	C(13)	1.33 [−1.41]
C(3)	−0.01 [0.02]	C(4)	0.65 [−0.65]		
C(5)	0.01 [−0.02]	C(14)	1.23 [−1.22]		

Plane (4): C(16), C(17), C(18), C(19)
$0.2691X + 0.9392Y + 0.2131Z = 12.5214$
$[0.1393X + 0.9893Y + 0.0427Z = 13.2438]$

C(16)	0.01 [−0.02]	C(20)	0.02 [−0.03]	O(3)	0.28 [0.12]
C(17)	−0.01 [0.02]	C(21)	−0.01 [−0.09]	Br	0.11 [−0.04]
C(18)	−0.01 [0.02]	C(22)	−0.03 [−0.07]		
C(19)	0.01 [−0.02]	O(2)	−0.35 [−0.12]		

Plane (5): O(2), C(16), O(3)
$0.2273X + 0.9712Y - 0.0708Z = 10.9562$
$[0.1606X + 0.9766Y + 0.1429Z = 14.1791]$

O(2)	−0.01 [0.01]	C(18)	−0.39 [−0.08]	C(21)	0.27 [0.06]
C(16)	0.01 [−0.02]	C(19)	−0.39 [−0.12]	C(22)	0.28 [0.07]
O(3)	−0.01 [0.01]	C(20)	−0.07 [0.00]	Br	−0.00 [0.00]
C(17)	−0.04 [0.04]				

for the O(2) atom in this cyclohexane ring. The atoms C(1), C(7), C(8), and C(10) of this ring are closely coplanar and atoms C(11) and C(9) are displaced by −0.88 [0.85] and 0.60 [−0.64] Å from the plane.

Substituted carbocyclic and heterocyclic bicyclo-[3.2.1]octane moieties are found in a wide variety of natural products. Available X-ray results[10] show that the displacement of the unique bridging atom, C(11), of bicyclo[3.2.1]octane moieties from the plane which is defined by the four carbon atoms (C(1), C(7), C(8), and C(10)) in the cyclohexane ring (−0.88 [0.85] Å in the present α-pompene derivative and 0.80 Å in α-caryophyllene alcohol) exceeds the value of 0.73 Å appropriate to an ideal cyclohexane ring.[11]

The distortion of the cyclohexane ring in α-pompene derivative is also reflected in the valency angles, which are similar to those in α-caryophyllene alcohol.[10] The angle C(1)–C(11)–C(7), 101 [104]°, (α-caryophyllene alcohol 104°) is considerably less than, and the angles C(1)–C(10)–C(9), 115 [111]°, and C(7)–C(8)–C(9), 110 [110]°, (α-caryophyllene alcohol 112 and 112°) are slightly greater than the ideal tetrahedral value. In addition, C(10)–C(1)–C(11), 106 [108], and C(8)–C(7)–C(11), 108 [104]° are also slightly less than the tetrahedral value (α-caryophyllene alcohol 111 and 110°).

The cyclopentane angles in the present α-pompene derivative average 102 [103] in the central ring (C(1), C(2), C(6), C(7), and C(11)) and 104 [103]° in the terminal ring (C(2), C(3), C(4), C(5), and C(6)); these values are consistent with the values which observed in a typical envelope type. Both five-membered rings adopt envelope conformations, in which atoms C(11) and C(4) constitute the flap of the envelopes and have displacements of 0.76 [−0.69] and 0.65 [−0.65] Å, respectively, from the four-atom planes (C(1), C(2), C(6), C(7) and C(2), C(3), C(5), C(6)) of the envelope forms.

The five-membered rings of the bicyclo[3.2.1]octane fragments in α-caryophyllene alcohol derivative[10] and in beyeran-3α-ol derivative[12] exist in envelope conformations. But in a number of other natural product derivatives the conformation of the five-membered ring in the bicyclo[3.2.1]octane fragment is intermediate between the half-chair and envelope forms and closer to the former.[11]

The twin-envelope conformation of the bicyclo[3.3.0]-octane fragment in the present α-pompene derivative has a notable resemblance to the "extended crown" conformation of the eight-membered ring in several cyclooctane derivatives.[13] In contrast to this, the conformation of the bicyclo[3.3.0]octane fragment in

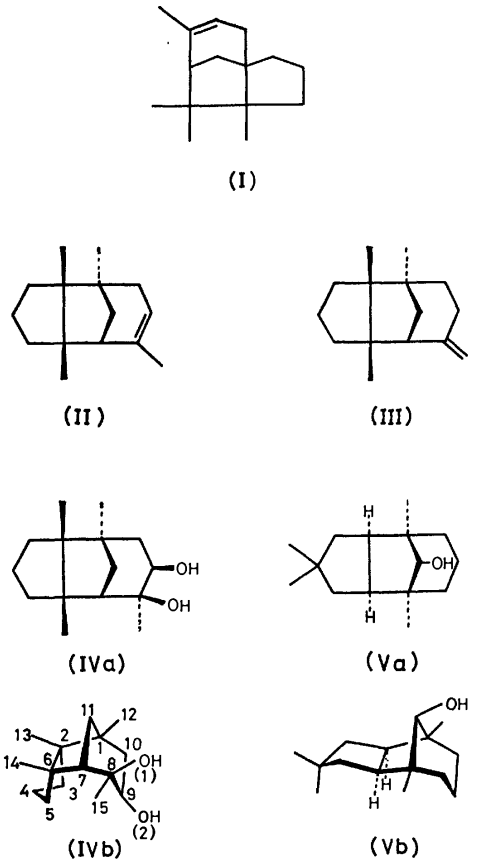

α-caryophyllene alcohol derivative[10] is similar to the "boat-chair" conformation of the eight-membered ring.[13]

The angles C(10)–C(1)–C(2) and C(8)–C(7)–C(6) are both 113 [115] and 118 [115]°, respectively, and the corresponding angles in bicyclo[3.2.1]octane have a mean value of 109°.[11] The bridgehead angles C(1)–C(2)–C(3) and C(7)–C(6)–C(5) of the bicyclo[3.3.0]-octane fragment in the present α-pompene derivative are 119 [112] and 121 [127]° respectively, and are noticeably greater than the ideal tetrahedral value. On the other hand, the mean C(sp^3)–C(sp^3) bond length in the present molecule is 1.56 [1.57] Å, but the C(2)–C(6) length, 1.67 [1.76], and the C(8)–C(15) length, 1.62 [1.69] Å, are appreciably longer than the expected value. These values suggest that the following non-bonded contacts cause greater strain to the α-pompene derivative: C(3)···C(10), 3.01 [3.02], C(3)···C(9), 3.31 [3.21], C(5)···C(15), 3.31 [3.35], C(5)···C(9), 3.17 [3.20], and C(13)···C(14), 2.89 [2.93] Å. The angles C(1)–C(2)–C(13), 111 [113] and C(2)–C(1)–C(12), 116 [112]°, are also significantly greater than the tetrahedral value, because of the repulsion of the two adjacent methyl groups, C(12) and C(13). In order to clarify the presence of such a greater strain, the conformational analysis by Boyd's method[14] of the α-pompene derivative and related compounds is now under investigation.[15]

The bond distances in the *p*-bromobenzoate group are within the expected values: C–C ring system 1.37

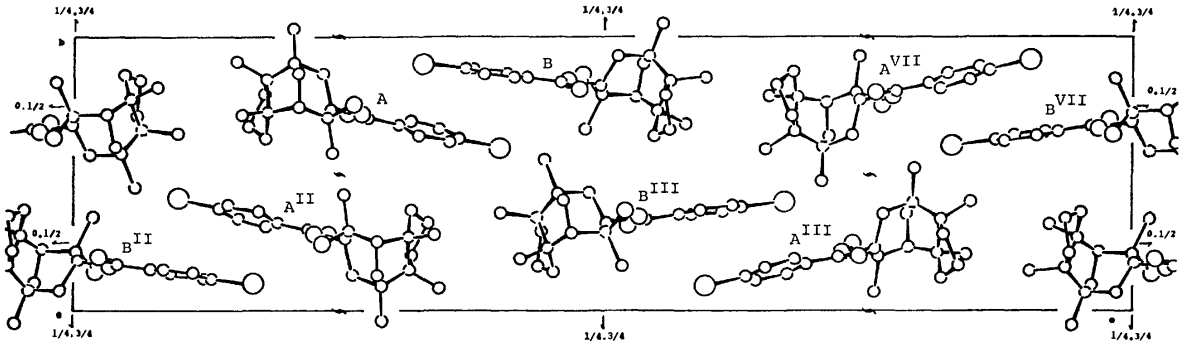

Fig. 2. The molecular arrangement in this crystal viewed along the c-axis.

Table 5. Intermolecular distances (≤3.8 Å)

O(1)A···O(3)A^{I}	2.72	C(15)B···C(11)B^{III}	3.80
O(3)B···O(1)B^{I}	2.77	O(3)B···C(14)B^{IV}	3.61
O(1)A···C(16)A^{I}	3.66	C(5)B···C(17)B^{IV}	3.67
O(1)A···C(18)A^{I}	3.27	C(16)B···C(12)B^{IV}	3.68
O(3)B···C(9)B^{I}	3.64	C(17)B···C(12)B^{IV}	3.70
C(7)A···O(3)A^{I}	3.65	C(13)B···C(14)A^{V}	3.67
C(8)A···O(3)A^{I}	3.57	O(1)A···C(12)A^{VI}	3.61
C(18)B···O(1)B^{I}	3.66	C(12)A···O(3)A^{VI}	3.52
C(15)A···O(3)A^{II}	3.48	C(12)A···C(16)A^{VI}	3.70
C(15)A···C(16)A^{II}	3.53	C(12)A···C(18)A^{VI}	3.72

Roman numerals as superscripts refer to the following equivalent positions relative to the reference molecule at x, y, z:

I	$x, y, z+1$	II	$1/2-x, 1-y, 1/2+z$
III	$1-x, -1/2+y, 1/2-z$	IV	$1-x, -1/2+y, 3/2-z$
V	$1/2+x, 3/2-y, 2-z$	VI	$1/2-x, 2-y, 1/2+z$
VII	$1/2+x, 3/2-y, 1+z$		

[1.38], C–C single bond 1.53 [1.55], C–O 1.31 [1.29], C=O 1.21 [1.24] and C–Br 1.88 [1.85] Å. These distances are in good agreement with those found in other *p*-bromobenzoate groups.[16] The *p*-bromobenzoate ester moieties are not completely planar; the dihedral angle between the plane of C(16)—C(22) and the plane C(16), C(17), O(2), O(3) is 16.6 [5.9]°. The bromine atom (Br–A) is displaced by a small amount from the C(17)—C(20) plane (0.11 Å). This small displacement from coplanarity is probably due to the effects of the non-bonded interaction: Br–A···C(15)B, 3.83; C(21)A···C(21)B, 3.51; and Br–B···C(22)A, 3.61 Å. The molecular arrangement in this crystal viewed along the c-axis is shown in Fig. 2. Selected intermolecular distances were calculated, and the most significant contacts ($\leq$3.80 Å) are summarized in Table 5. The two molecules in an asymmetric unit form a dimeric unit with van der Waals contacts between the *p*-bromobenzoate moieties. Along the c-axis these dimeric unit are connected by the intermolecular hydrogen bonds, O(1)A···O(3)A^{I}, 2.72 and O(3)B···O(1)B^{I}, 2.77 Å; therefore, a linear chain is present parallel to this direction. Moreover, several short contacts are found, as shown in Table 5. The shortest contact except for the hydrogen bond is O(1)A··· C(18)A^{I}, 3.27 Å.

We thank the Hiroshima University Computer Center for a generous allocation of computer time.

References

1) A. Matsuo, T. Maeda, M. Nakayama, and S. Hayashi, *Tetrahedron Lett.*, **1973**, 4131.

2) (−)-*β*-Pompene (III), which contains an *exo* double bond, is an isomer of (+)-*α*-pompene (II), which contains an endo double bond. Since *α*-pompene was coincident with the structure which had been proposed a year before for a sesquiterpene hydrocarbon isolated from another liverwort, *Gymnomitrion obtusum* (J. D. Connolly, A. E. Harding, and I. M. S. Thornton, *Chem. Commun.*, **1972**, 1320; the identity of both hydrocarbons was confirmed using the spectra kindly sent by Dr. J. D. Connolly.).

3) A. Matsuo, H. Nozaki, M. Nakayama, Y. Kushi, S. Hayashi, and N. Kamijo, *Tetrahedron Lett.*, **1975**, 241.

4) All the computations were carried out by means of the HITAC-8700 computer at Hiroshima University. The computer programs used were "UNICS, Crystallographic Society of Japan (1965)," and slightly modified forms.

5) D. W. J. Cruickshank, "Computing Methods and the Phase Problem in X-Ray Crystal Analysis," ed by R. Pepinsky, J. M. Robertson, and J. C. Speakman, Pergamon Press, Oxford (1961), p. 45.

6) "International Tables for X-Ray Crystallography," Vol. III, Kynoch Press, Birmingham (1965), p. 216.

7) J. M. Bijvoet, A. F. Peerdeman, and A. J. van Bommel, *Nature*, **168**, 271 (1951).

8) The values of $\Delta f'$ and $\Delta f''$ for bromine atoms with Ni $K\alpha$ radiation were calculated by interpolation of the values from "International Tables for X-Ray Crystallography," Vol. III, Kynoch Press, Birmingham (1968), pp. 213, 214. The values are: $\Delta f' = -0.86$, $\Delta f'' = 1.63$.

9) We used the name "*cis*" (IVb) and "*trans*" (Vb) in order to distinguish the two different types of the overall configuration of tricyclo[5.3.1.$0^{2,6}$]undecane framework.

10) K. W. Gemmell, W. Parker, J. S. Roberts, J. Monteath Robertson, and G. A. Sim, *J. Chem. Soc., B*, **1970**, 947.

11) P. Coggon and G. A. Sim, *J. Chem. Soc., B*, **1969**, 413.

12) J. R. Hanson, G. M. McLaughlin, and G. A. Sim, *J. Chem. Soc., Perkin Trans. 2*, **1972**, 1124.

13) I. C. Paul and K. T. Go, *J. Chem. Soc., B*, **1969**, 33.

14) R. H. Boyd, *J. Chem. Phys.*, **47**, 3736 (1967).

15) Y. Kushi, unpublished work.

16) J. C. Portheine, C. Romers, and F. W. M. Rutten, *Acta Crystallogr., Sect. B*, **28**, 849 (1972).

Electrophilic Sulfides(II) as a Novel Catalyst. VI.[1] Reaction of Sulfonium Ylides with Arenesulfenyl Thiocyanates

Haruo MATSUYAMA,* Hiroshi MINATO, and Michio KOBAYASHI

Department of Chemistry, Faculty of Science, Tokyo Metropolitan University, Fukazawa, Setagaya, Tokyo 158

(Received July 28, 1977)

Arenesulfenyl thiocyanates (Ar–S–SCN) reacted with sulfonium ylides ($MeR\overset{\oplus}{S}\text{-}\overset{\ominus}{C}(COOMe)_2$) in chloroform at room temperature, forming sulfonium ion, $MeRS^{\oplus}\text{-}C(SAr)(COOMe)_2\ SCN^{\ominus}$, which further reacted. The mechanism of this reaction was discussed.

We have reported that the disulfides containing electron-withdrawing substituents, $\overset{\delta-}{R}\leftarrow\overset{\delta+}{S}\text{—}\overset{\delta+}{S}\rightarrow\overset{\delta-}{R}$ (R= OMe, CN, CF_3, and COPh), react as novel catalysts for several reactions of sulfonium ylides.[2–5] In the presence of these disulfides as catalysts, the following reactions take place smoothly at room temperature.

a) Formation of sulfonium ylides by condensation between alkyl sulfides and diazo esters:[2]

$$\begin{matrix}R^1\\ \quad S\\ R^2\end{matrix} + N_2C(COOMe)_2 \longrightarrow \begin{matrix}R^1\\ \quad \overset{\oplus}{S}\text{-}\overset{\ominus}{C}(COOMe)_2\\ R^2\end{matrix} + N_2$$

b) Transylidation of sulfonium ylides:[3,5]

$$\begin{matrix}Ph\\ \quad \overset{\oplus}{S}\text{-}\overset{\ominus}{C}(COOMe)_2\\ Me\end{matrix} \xrightarrow{CHCl_3}$$

$$\xrightarrow{R^1SR^2} \begin{matrix}R^1\\ \quad \overset{\oplus}{S}\text{-}\overset{\ominus}{C}(COOMe)_2\\ R^2\end{matrix} + PhSMe$$

$$\xrightarrow{X\text{-}C_5H_4N} X\text{-}C_5H_4\overset{\oplus}{N}\text{-}\overset{\ominus}{C}(COOMe)_2 + PhSMe$$

c) Olefin formation:[4]

$$2\ Me_2\overset{\oplus}{S}\text{-}\overset{\ominus}{C}(COOMe)_2 \xrightarrow{CHCl_3} (MeOOC)_2C{=}C(COOMe)_2 + 2Me_2S$$

$$2\ Me_2\overset{\oplus}{S}\text{-}\overset{\ominus}{C}(CN)_2 \xrightarrow{CHCl_3} (NC)_2C{=}C(CN)_2 + 2Me_2S$$

Under the above reaction conditions, these disulfides are not reactants, but catalysts.

Recently, we found that arenesulfenyl thiocyanates (Ar–S–SCN) react with sulfonium ylides $MeR\overset{\oplus}{S}\text{-}\overset{\ominus}{C}(COOMe)_2$. Very little has been published on the reaction of sulfonium ylides with disulfides.[6] The results are described and the mechanism of the reactions are discussed in this paper.

Results and Discussion

As is shown in Table, arenesulfenyl thiocyanates reacted with sulfonium ylides in chloroform at room temperature. In these reactions, alkanesulfenyl thiocyanates R–S–SCN (R=Et, *t*-Bu) did not react with sulfonium ylide **1a**, but arenesulfenyl thiocyanates Ar–S–SCN (Ar=Ph, p-Me–C_6H_4, and 2-$C_{10}H_7$) reacted smoothly with ylides **1a—e**. The above results are probably ascribable to the smaller electron density on the sulfur atoms of arenesulfenyl thiocyanates compared with that of alkanesulfenyl thiocyanates due to the presence of the electron-withdrawing aryl groups.

$$\overset{\delta-}{Ar}\text{—}\leftarrow\overset{\delta+}{S}\text{—}\rightarrow\overset{\delta-}{SCN} \qquad R\text{—}\rightarrow\overset{\delta\delta+}{S}\text{—}\rightarrow\overset{\delta-}{SCN}$$

The S–S bonds of disulfides containing two different substituents are easily cleaved by nucleophilic attacks, compared to those of disulfides containing two equal substituents.[7] As is shown in Table, ylides **1a—e** and arenesulfenyl thiocyanates react, forming sulfonium ions and anion $SCN^{\ominus}$, which further react in three different ways (namely, Me-attack, R-attack, and C(SAr)-

Table 1. Reaction of sulfonium ylides with arenesulfenyl thiocyanates

1	R	Ar	Products (mol %)					
			Me-attack		R-attack		C(SAr)Q_2-attack	
			Me–SCN[a]	RS(ArS)CQ_2[b,c]	R–SCN[d]	MeS(ArS)CQ_2[a,c]	MeSR[a]	ArS(SCN)CQ_2[c,e]
1a	Ph	Et			no reaction			
1a	Ph	*t*-Bu			no reaction			
1a	Ph	Ph	0	0	—	—	84	58
1b	Me	Ph	78	74	—	—	14	(14)
1b	Me	*p*-Me–C_6H_4	80	73	—	—	13	(13)
1b	Me	2-$C_{10}H_7$	76	75	—	—	21	(21)
1c	Et	Ph	50±3	(50±3)	(30±3)	30±3	19±2	(19±2)
1d	*i*-Pr	Ph	20±2	(20±2)	(40±2)	40±2	40±2	(40±2)
1e	$PhCH_2$	Ph	9±2	(9±2)	90±2	90±2	0	0

a) Determined from its methyl singlet absorption. b) The amount of RS(ArS)CQ_2 was estimated by assuming the equimolar formation of Me–SCN and RS(ArS)CQ_2. c) Q=COOMe. d) The amount of $PhCH_2$–SCN was determined from its singlet δ=4.11 ppm. The amounts of other R–SCN's were estimated from the assumption of the equimolar formation of R–SCN and MeS(ArS)CQ_2 (determined from its MeS singlet). e) The amount of ArS(SCN)CQ_2 was estimated by assuming the equimolar formation of MeSR and ArS(SCN)CQ_2.

$(COOMe)_2$-attack).

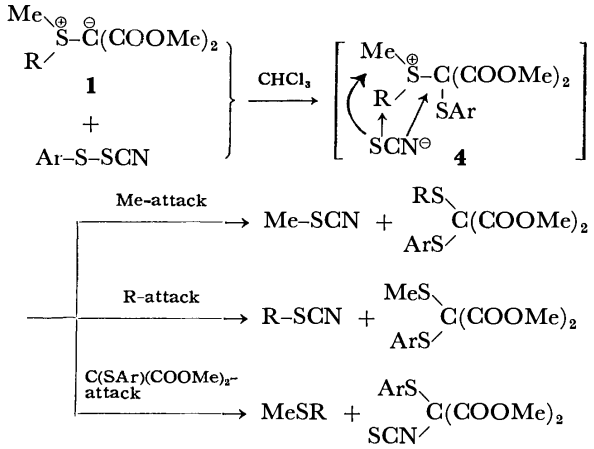

Usually **1** and arenesulfenyl thiocyanates were allowed to react without isolating intermediates **4**. However, when **4′** shown below was separately prepared and allowed to react with ammonium thiocyanate, the results obtained were consistent with those shown in Table.

$$Me_2\overset{\oplus}{S}\text{–}C(COOMe)_2 + NH_4^{\oplus}\,SCN^{\ominus} \longrightarrow$$
$$\underset{\text{4′}}{\overset{|}{\underset{|}{SPh}}\;ClO_4^{\ominus}}$$

$$\text{Me–SCN} + \text{MeS–}\underset{|}{\overset{|}{C}}(COOMe)_2 + Me_2S$$
$$SPh$$

(86%) (60%) (14%)

When R in **4** is an alkyl group, competitive S_N2 attacks on the methyl and alkyl groups are expected. The relative reactivities of alkyl groups on sulfonium ions with anion $SCN^{\ominus}$ (the ratios between the yields of methylated and alkylated products) are $PhCH_2$ 10.0, *i*-Pr 2.0, Me 1.0, and Et 0.60. These results suggest that these reactions involve an S_N1-like process. The order of the reactivity of alkyl groups for the reaction between $MeR\overset{\oplus}{S}\text{–}C(SPh)(COOMe)_2$ and anion $Cl^{\ominus}$ is:[8]

$$PhCH_2\,(\infty) > i\text{-Pr}\,(4.2) > \text{Me}\,(1.0) > \text{Et}\,(0.85)$$

Therefore, the R-attack course of the reactions of **4** is probably expressed as follows.[8]

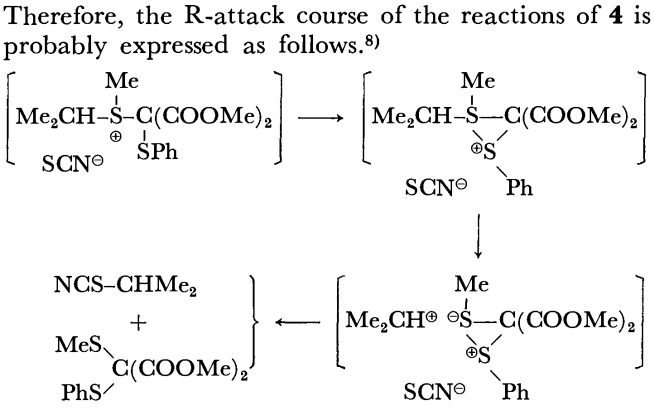

Experimental

Materials. Sulfonium bis(methoxycarbonyl)methylides **1a—e** were prepared by copper sulfate-catalyzed decomposition of dimethyl diazomalonate in large excess sulfides[9] and by transylidation.[3,5] Ethanesulfenyl thiocyanate (bp 40—45 °C/8 mmHg), 2-methyl-2-propanesulfenyl thiocyanate, benzenesulfenyl thiocyanate, *p*-toluenesulfenyl thiocyanate and 2-naphthalenesulfenyl thiocyanate (mp 62.5—63 °C (lit, 61.5—63 °C)) were synthesized by the methods described in the literature.[10] Sulfonium salt **4′** was prepared by the dropwise addition of a CCl_4 solution of benzenesulfenyl chloride (1.45 g) to a nitromethane solution of **1a** (1.94 g) and silver perchlorate (2.07 g) at 0 °C. Yield, 3.6 g (90%); recrystallized from ethanol; mp 105—106 °C; IR (KBr), 1740 cm^{-1} (ν_{CO}); NMR (DMSO-d_6), δ=7.60 (5H, s, PhS), 3.93 (6H, s, COOMe) and 3.20 (6H, s, $Me\overset{\oplus}{S}$). Found: C, 38.76; H, 4.25. Calcd for $C_{13}H_{17}O_8ClS_2$: C, 38.96; H, 4.27.

*Reactions of Ylide **1a** with Alkanesulfenyl Thiocyanates.* a) A $CDCl_3$ solution of **1a** (0.57 mmol) and ethanesulfenyl thiocyanate (0.78 mmol) did not react. After 1 day, ylide **1a** (80%) was recovered. b) A $CDCl_3$ solution of **1a** (0.80 mmol) and 2-methyl-2-propanesulfenyl thiocyanate (0.82 mmol) did not react under the same condition. After 1 day, ylide **1a** (80%) was recovered.

*Reactions of Ylides **1a** and **1b** with Arenesulfenyl Thiocyanates.* a) A chloroform (13 g) solution of **1b** (2.08 g, 10.9 mmol) was mixed with PhS–SCN (2.0 g, 11.9 mmol) at room temperature. After 30 min, the ylide carbonyl absorption (1630 and 1670 cm^{-1}) were replaced by the ester absorption (1730 cm^{-1}). The NMR spectra of the reaction mixture showed the presence of MeSCN (δ=2.56, s; 78%), Me_2S (2.01, s; 14%) and MeS-(PhS)C(COOMe)$_2$ (2.15, s, MeS; 74%). The low-boiling fractions from the mixture were trapped in liquid nitrogen, and the presence of MeSCN was shown by NMR (δ=2.59, s) and IR (ν_{SCN} 2150 cm^{-1}, strong and sharp) spectroscopy. The high-boiling fractions were chromatographed (Florisil), and the white crystals obtained from the benzene eluates were found to be MeS(PhS)C(COOMe)$_2$ (2.30 g, 8.07 mmol; 74%); mp 71—72 °C; IR (KBr), 1730 cm^{-1} (ν_{CO}); NMR (CCl_4), δ=2.15 (3H, s, MeS), 3.64 (6H, s, COOMe) and 7.30 (5H, s, PhS). Found: C, 50.52; H, 4.93%. Calcd for $C_{12}H_{14}O_4S_2$: C, 50.33; H, 4.93%. b) In a similar manner, a mixture of **1b** (3.10 g, 16.2 mmol) and *p*-Me–C_6H_4–S–SCN (3.0 g, 16.6 mmol) in chloroform (23 g) gave MeSCN (δ= 2.55, s; 80%), Me_2S (2.10, s; 13%) and MeS (*p*-Me–C_6H_4S)-C(COOMe)$_2$ (from benzene eluates; 3.54 g, 11.8 mmol; 73%); mp 60—61 °C; IR (KBr), 1740 cm^{-1} (ν_{CO}); NMR (CCl_4), δ=2.15 (3H, s, MeS), 2.33 (3H, s, *p*-Me), 3.67 (6H, s, COOMe) and 7.18 (4H, q, C_6H_4). Found: C, 51.85; H, 5.33%. Calcd for $C_{13}H_{16}O_4S_2$: C, 52.00; H, 5.37%. c) A mixture of a $CHCl_3$ (27 g) solution of **1b** (1.00 g, 5.21 mmol) and 2-$C_{10}H_7$S–SCN (1.09 g, 5.64 mmol) gave MeSCN (δ= 2.51, s; 76%), Me_2S (2.09, s; 21%) and MeS (2-$C_{10}H_7$S)-C(COOMe)$_2$ (from benzene eluates; 1.33 g, 3.96 mmol; 75%); mp 84—85 °C; IR (KBr), 1740 cm^{-1} (ν_{CO}); NMR ($CDCl_3$), δ=2.27 (3H, s, MeS), 3.73 (6H, s, COOMe) and 7.20—8.05 (7H, m, 2-$C_{10}H_7$). Found: C, 57.00; H, 4.82%. Calcd for $C_{16}H_{16}O_4S_2$: C, 57.14; H, 4.80. d) In a similar manner, a mixture of **1a** (1.75 g, 6.87 mmol) and PhS–SCN (1.17 g, 7.0 mmol) in chloroform (9 g) gave MeSPh (from hexane eluates; 0.71 g, 5.75 mmol; 84%) and PhS(S=C=N–)-C(COOMe)$_2$ (oil from benzene eluates; 1.19 g, 4.0 mmol; 58%; IR (neat), 1740 cm^{-1} (ν_{CO}) and 2100 cm^{-1} ($\nu_{N=C=S}$, strong and broad);[11] NMR (CCl_4), δ=3.75 (6H, s, COOMe) and 7.16—7.55 (5H, m, PhS)).

*Reaction of Sulfonium Ion **4′** with Thiocyanate Ion.* A DMSO-d_6 solution of **4′** (1.0 mmol) and ammonium thiocyanate (2.0 mmol) was heated at 50 °C for 5 min. The NMR spectrum of the reaction mixture showed the presence of MeSCN (δ=2.67, s; 86%), MeS(PhS)C(COOMe)$_2$ (2.20, s, MeS; 60%) and Me_2S (2.07, s; 14%).

Reactions of Ylides ***1c—e*** *with Benzenesulfenyl Thiocyanate.* The $CDCl_3$ solution of ylides **1c—e** (0.7—1.0 mmol) and PhS–SCN (0.8—1.1 mmol) containing nitromethane (internal standard, 50 μl, 0.79 mmol) were allowed to react in NMR tubes at 25 °C, and the amounts of the reaction products were determined from their singlet methyl absorption by NMR spectroscopy (see Table); Me–SCN (δ=2.56), Me_2S (2.0—2.10), MeSEt (2.05—2.12), MeSPr-*i* (2.10) and MeS(PhS)-$C(COOMe)_2$ (2.19—2.20).

References

1) Part V of this series: H. Matsuyama, H. Minato, and M. Kobayashi, *Bull. Chem. Soc. Jpn.*, **50**, 3393 (1977).
2) H. Matsuyama, H. Minato, and M. Kobayashi, *Bull. Chem. Soc. Jpn.*, **46**, 1512 (1973). (Part I).
3) H. Matsuyama, H. Minato, and M. Kobayashi, *Bull. Chem. Soc. Jpn.*, **46**, 2845 (1973). (Part II).
4) H. Matsuyama, H. Minato, and M. Kobayashi, *Bull. Chem. Soc. Jpn.*, **46**, 3158 (1973). (Part III).
5) H. Matsuyama, H. Minato, and M. Kobayashi, *Bull. Chem. Soc. Jpn.*, **46**, 3828 (1973). (Part IV).
6) L. Field and H.-K. Chu, *J. Org. Chem.*, **42**, 1768 (1977).
7) A. J. Parker and N. Kharasch, *J. Am. Chem. Soc.*, **82**, 3071 (1960).
8) H. Matsuyama, H. Minato, and M. Kobayashi, *Bull. Chem. Soc. Jpn.*, **48**, 3287 (1975).
9) W. Ando, T. Yagihara, S. Tozune, S. Nakaido, and T. Migita, *Tetrahedron Lett.*, **1969**, 1979.
10) H. Lecher and M. Wittwer, *Ber.*, **55B**, 1474 (1922); R. G. Hiskey and M. A. Harpold, *Tetrahedron*, **23**, 3923 (1967).
11) R. G. Bacon, "Thiocyanates, Thiocyanogen, and Related Compounds," in Chapter 27 of "Organic Sulfur Compounds," Vol. 1, ed by N. Kharasch, Pergamon Press, New York (1961); Thiocyanates exhibit a strong, sharp band, due to the C≡N stretching vibration, at ≈2140 cm^{-1}, while isothiocyanates exhibit a very strong and broad band at≈2040—2180 cm^{-1}. The ease of formation of isothiocyanate increases from primary to secondary to tertiary carbon derivatives, and is favored by the presence of carbonyl groups on the carbon atom at which substitution occurs.

Photoaddition Reaction of *N*-Acetyldiphenylmethyleneamine with Cyclic and Acyclic Olefins. An Example of Heavy Atom Effect in Photoreaction

Naoki Toshima, Shuichiro Asao, and Hidefumi Hirai

Department of Industrial Chemistry, Faculty of Engineering, The University of Tokyo, Hongo, Bunkyo-ku, Tokyo 113

(Received July 29, 1977)

Irradiation of *N*-(diphenylmethylene)acetamide (*N*-acetyldiphenylmethyleneamine, **1**) in cyclopentene gave *N*-[1,1-diphenyl-1-(cyclopenta-2′-enyl)methyl]acetamide, the addition product of cyclopentene to the C=N bond of imine **1**, in 31% yield. The photoreaction of **1** was observed in other cyclic and acyclic olefins. The reactivity of the olefins decreases in the order; cyclopentene>cyclohexene>cyclooctene>2-pentene≃2-hexene. The photoreaction is promoted by the presence of the heavy atom solvent or the sensitizer. The mechanism of photoreaction is discussed in terms of the excited triplet state of the imine.

Increasing attention is being paid to the photochemistry of carbon-nitrogen double bonds.[1] Hydrogen abstraction is the most popular reaction occurring on irradiation of the imine. In 1969 Padwa and co-workers explained the photoreduction of *N*-alkylketimine in terms of chemical sensitization, where the carbonyl compound present in the reactant system as an impurity abstracts a hydrogen atom on irradiation and the ketyl radical produced transfers the hydrogen to the ketimine.[2] They applied a similar mechanism to the photoreduction of *N*-benzoylketimine in 2-propanol.[3] All photochemical hydrogen abstraction reactions of the imine seem to be explained by this chemical sensitization mechanism, the excited state of the imine not taking part. Padwa and co-workers suggested that only the cyclic imine has reactivity, the excited acyclic imine having none, since the acyclic imine easily undergoes syn-anti isomerization by which the excited energy should be consumed.[2]

There are some observations on the photochemistry of the acyclic imines that cannot be explained without taking participation of the excited state of the imine into account. Examples of the photoreaction of the acyclic imine through the excited states contain the deuterium exchange in *ortho*-alkyl derivatives of *N*-(*o*-tolylphenylmethylene)acetamide[4] and the cleavage of the bond between benzylic carbon and imino nitrogen on irradiation of *N*-benzylidenebenzylamine.[5]

Furthermore, even a simple cyclic imine was found to have low reactivity in the photochemical hydrogen abstraction, showing that the low photoreactivity of the imine is not due to the syn-anti isomerization.[6] In fact, the lowest excited states of the imine have been suggested to have the (π,π^*) character rather than the (n,π^*) character.[6,7] The hydrogen abstraction property is characteristic of the $^3(n,\pi^*)$ state rather than of the $^3(\pi,\pi^*)$ state.[8] *N*-(α-Alkylbenzylidene)benzamide has been reported to be reduced photochemically in 2-propanol through the excited triplet state, rather than *via* the chemical sensitization,[9] the mechanism of photochemical hydrogen abstraction thus differing entirely with the reaction system.

In a preliminary communication, a report was given on the photoreaction of *N*-(diphenylmethylene)acetamide (**1**) in cyclohexene.[10] The addition product was the only product isolated, although four kinds of

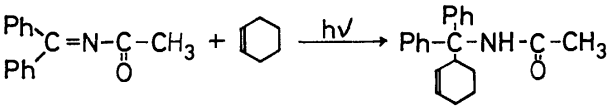

(1) (2b)

products were reported to be obtained in the photoreaction of benzophenone in cyclohexene.[11] This suggests the photoreaction through the excited state of the acyclic imine. Further studies on this system have been carried out including the external heavy atom effect, which has been found to be convenient for demonstrating the participation of the excited state in the light-induced reaction.[12]

Results

Photoreaction of N-*(Diphenylmethylene)acetamide (*N-*Acetyldiphenylmethyleneamine, 1) with Cyclopentene.* Irradiation of cyclopentene solution of *N*-(diphenylmethylene)-acetamide (*N*-acetyldiphenylmethyleneamine, **1**) was carried out in a quartz tube under nitrogen atmosphere with a 500 W high pressure mercury lamp for 100 h. After irradiation, cyclopentene was distilled off and the residues were chromatographed over silica gel. The addition product (**2a**) of the imine **1** to cyclopentene

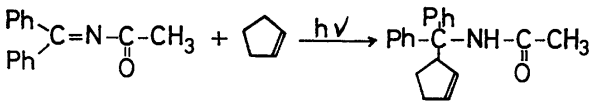

(1) (2a)

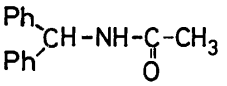

(3)

detected by HLC was obtained almost selectively except for a trace amount of the hydrogenation product, *N*-(diphenylmethyl)acetamide (**3**). The structure of **2a** was inferred from its composition ($C_{20}H_{21}NO$), olefin tests such as the Bayer test and bromine test, and spectral data. The spectral data included mass spectra

(M^+/e=291) and the infrared absorption bands for an amide group (ν_{NH} 3280, ν_{CO} 1658, δ_{NH} 1548 cm^{-1}). The structure of **2a** was confirmed by the NMR spectrum showing acetyl protons (3H, δ 1.90 ppm), methylene protons (4H, δ 2.08—2.20), a methine proton (1H, δ 4.29—4.66), olefin protons (2H, δ 5.71), an NH proton (1H, δ 6.02—6.42), and phenyl protons (10H, δ 6.93—7.51).

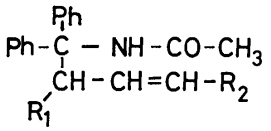

2a	$R_1,R_2=-(CH_2)_2-$
2b	$R_1,R_2=-(CH_2)_3-$
2c	$R_1,R_2=-(CH_2)_5-$
2d	$R_1=R_2=-CH_3$
2e	$R_1=-C_2H_5, R_2=-CH_3$
2e'	$R_1=-CH_3, R_2=-C_2H_5$

Comparison of Photoreactivity of N-*Acetyldiphenylmethyleneamine (1) toward Several Kinds of Olefins.* On irradiation of imine **1** in other cyclic olefins such as cyclohexene and cyclooctene, and in the acylic olefins such as 2-pentene and 2-hexene, the same kind of product (**2**) as the amide **2a** was obtained. Amide **2** is the C–C bond formation product between the iminoyl carbon of imine **1** and the allylic carbon of the olefin. The results of the photoreaction are summarized in

Table 1. Photoreaction of *N*-(diphenylmethylene)-acetamide (**1**) with olefins[a]

1	Amount of 1 (mmol)	Olefin	Amount of olefin (mmol)	Yield[b] (%)
a	4.8	Cyclopentene	72	31
b	5.7	Cyclohexene	54	15
c	5.6	Cyclooctene	48	2
d	16	2-Pentene	37	0.9
e	16	2-Hexene	30	1.1

a) Olefinic solutions (*ca.* 5 ml) of **1** (1—3 g) were irradiated in quartz tubes under nitrogen atmosphere with a 500 W high pressure mercury lamp for 100 h. b) Conversion of the starting imine **1**. See Experimental.

Table 1. Product yields determined by the silica gel column chromatography indicate the conversion of the starting imine under the given conditions, since amide **2** is the only product in this reaction, the yield increasing with irradiation time.

Effect of Additives on Photoreaction of Imine 1 with Cyclohexene. The photoreaction of imine **1** with cyclohexene was carried out in the presence of several kinds of additives (Table 2). A cyclohexene (55 mmol) solution of imine **1** (4.6 mmol) with benzophenone (4.6 mmol) in a quartz tube under nitrogen atmosphere was irradiated for 100 h giving the adduct **2b** in 38% yield. Benzophenone (E_T=68.5 kcal/mol[13]) and acetophenone (E_T=73.6 kcal/mol[13]) acted as good sensitizers, benzil (E_T=53.7 kcal/mol[13]) sensitizing the reaction only slightly. Piperylene quenched the reaction completely. The results are nearly compatible with those of the photoreaction of imine **1** in toluene.[14]

Table 2. Dependence of the photoreaction yield of *N*-acetyldiphenylmethyleneamine (**1**) with cyclohexene in the presence of several kinds of additives[a]

Additive	Amount of additive (mmol)	E_T[b] (kcal/mol)	Product yield[c] (%)
None[d]	—	—	9
Benzophenone	4.6	68.5	38
Acetophenone	6.7	73.6	25
Benzil	4.1	53.7	12
Piperylene[e]	23	*trans* 59.3 *cis* 56.9	0

a) A solution of 4.6 mmol of **1** and 55 mmol of cyclohexene in the presence of the additive in a quartz tube was irradiated with a 500 W high pressure mercury lamp for 100 h. b) Excited triplet energy. See Ref. 13. c) Conversion of the starting imine **1**. See text. d) The starting imine **1** contained a small amount of benzophenone as an impurity (<3%). e) Mixtures of *cis*- and *trans*-piperylene.

Dependence of the Yield of Photoreaction of Imine 1 with Cyclohexene upon the Concentration of Benzophenone. Since benzophenone acts as a sensitizer on the photoreaction of *N*-acetyldiphenylmethyleneamine (**1**) with cyclohexene, the dependence of the reaction yield of **2b** upon the concentration of benzophenone was investigated. The data are plotted in Fig. 1. The starting sample **1** contains a small amount of benzophenone, the hydrolysis product of imine **1** which is easily hydrolyzed. The amount of benzophenone is the sum of that determined by GLPC in the starting imine as an impurity and that added separately. The full line in Fig. 1 indicates the experimental data and the dashed line the extrapolation of the results. The yield of product **2b** increases linearly with the concentration of benzophenone.

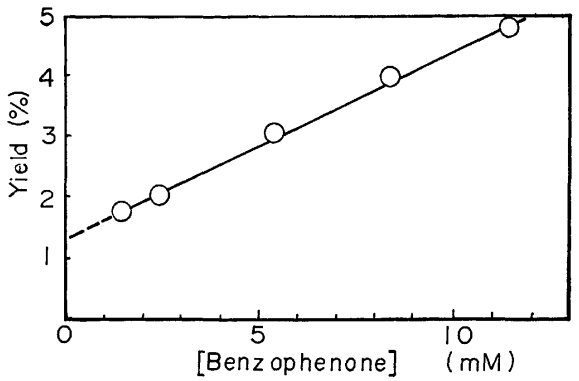

Fig. 1. Dependence of the yields of the photoaddition reaction of *N*-acetyldiphenylmethyleneamine (**1**) with cyclohexene on the concentration of benzophenone: [*N*-Acetyldiphenylmethyleneamine] 0.23 mol/l, [cyclohexene] 10 ml. Irradiation was carried out above 300 nm for 70 h at 25 °C.

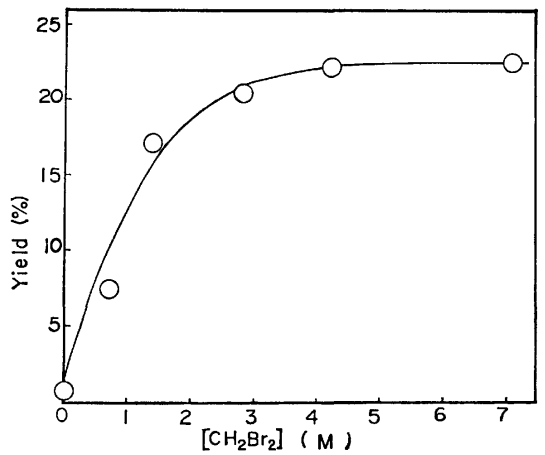

Fig. 2. Dependence of product yield on the concentration of dibromomethane in the photoreaction of *N*-acetyldiphenylmethyleneamine (**1**) in cyclohexene. A solution of **1** (1.22 mmol) and cyclohexene (5 ml) in benzene was irradiated.

Dependence of the Yield of Photoreaction of Imine **1** *with Cyclohexene upon the Concentration of the Heavy Atom Solvent.* The photoaddition product of imine **1** with alkylbenzene increases in yield in the presence of the heavy atom solvent.[14] In the case of the photoreaction of imine **1** with cyclohexene, the yield of **2b** also increases remarkably in the presence of the heavy atom solvent. The photoreaction of imine **1** with cyclohexene was carried out using various concentrations of dibromomethane. The results are shown in Fig. 2. The product yield increases noticeably as the concentration of dibromomethane increases from 0 to 2 M. Further increase in the concentration of heavy atom solvent over 3 M, however, resulted in constant yields.

Discussion

Effect of Additives. The effect of additives on the photoreaction of imine **1** in cyclohexene (Table 2) is in fair agreement with that of the imine in toluene.[14] Benzophenone (E_T=68.5 kcal/mol) and acetophenone (E_T=73.6 kcal/mol) act as sensitizers, and piperylene (*trans*-piperylene, E_T=59.3 kcal/mol; *cis*-piperylene E_T=56.9 kcal/mol) as a quencher. The results suggest that the reaction proceeds *via* a triplet state. However, benzil, whose triplet energy (E_T=53.7 kcal/mol) is lower than that of piperylene, can also sensitize the reaction a little. The curious result indicates that the sensitization concerns the hydrogen transfer *via* "chemical sensitization."[2] The hydrogen abstracting property is a character common to the compounds which sensitize the reaction. As shown in Scheme 1, benzophenone as well as benzil can act as a chemical sensitizer.[2,15]

Dependence of the Yield on the Concentration of Benzophenone. The photoproduct yields increase linearly with the amount of benzophenone (Fig. 1). The usual steady state treatment of Scheme 1 gives the following equation for the product (A_d):[16]

$$\frac{d[A_d]}{dt} = k_r[\text{Olefin}][Ph_2CO^*(T_1)] + k_r'[\text{Olefin}][Ph_2CNAc^*(T_1)]. \quad (1)$$

This shows that the yield should be proportional to the concentration of benzophenone ([Ph_2CO]) since [$Ph_2CO^*(T_1)$] is proportional to [Ph_2CO],[17] and [Olefin] and [$Ph_2CNAc^*(T_1)$] are almost constant.[18] The linear relation between the yield and the concentration of benzophenone (Fig. 1) agrees with the equation.

If imine **1** in excited state cannot abstract a hydrogen atom and the reaction proceeds only by chemical sensitization mechanism (only processes a—e taking place in Scheme 1), the reaction yields should converge to 0% at the point of no benzophenone according to the following equation:

$$\frac{d[A_d]}{dt} = k_r[\text{Olefin}][Ph_2CO^*(T_1)]. \quad (2)$$

Actually, however, Fig. 1 clearly shows the formation of 1.3% of the product without benzophenone. This is exactly the yield derived from the excited state of imine **1** itself, based on the second term of Eq. 1.

Relative Reactivity of Olefins towards N-Acetyldiphenylmethyleneamine (1). The yields in Table 1 show the relative reactivity of olefins toward imine **1**. The yields decrease in the following order depending on the kind of olefin: Cyclopentene>Cyclohexene>Cyclooctene>2-Hexene≃2-Pentene. The results indicate that the reactivity of an olefin is correlated with the stability of the allyl radical derived by hydrogen abstraction from the olefin, and that the lower reactivity of an acyclic olefin than that of a cyclic olefin is due to smaller conjugation of the allyl radical because of the flexibility of the molecule.

Heavy Atom Effect in Photoreaction. The heavy atom effect for increasing the yields in photoreactions

$$Ph_2CO \xrightarrow{h\nu} Ph_2CO^*(S_1) \longrightarrow Ph_2CO^*(T_1) \quad (a)$$

$$Ph_2CO^*(T_1) \xrightarrow{k_d} Ph_2CO \quad (b)$$

$$Ph_2CO^*(T_1) + R_1\text{-}CH{=}CH\text{-}CH_2\text{-}R_2 \xrightarrow{k_r} Ph_2\dot{C}OH + R_1\dot{C}H{\cdots}CH{\cdots}CH\text{-}R_2 \quad (c)$$

$$Ph_2\dot{C}OH + Ph_2C{=}NAc \xrightarrow{k_H} Ph_2\dot{C}NHAc + Ph_2CO \quad (d)$$

$$Ph_2\dot{C}NHAc + R_1\text{-}\dot{C}H{\cdots}CH{\cdots}CH\text{-}R_2 \xrightarrow{k_{cc}} \begin{matrix} Ph_2CNHAc & & Ph_2CNHAc \\ | & \text{and/or} & | \\ R_1\text{-}CH\text{-}CH{=}CH\text{-}R_2 & & R_2\text{-}CH\text{-}CH{=}CH\text{-}R_1 \end{matrix} \quad (e)$$

$$Ph_2CNAc \xrightarrow{h\nu'} Ph_2CNAc^*(S_1) \longrightarrow Ph_2CNAc^*(T_1) \quad (f)$$

$$Ph_2CNAc^*(T_1) \xrightarrow{k_d'} Ph_2CNAc \quad (g)$$

$$Ph_2C{=}NAc^*(T_1) + R_1\text{-}CH{=}CH\text{-}CH_2\text{-}R_2 \xrightarrow{k_r'} Ph_2\dot{C}NHAc + R_1\text{-}\dot{C}H{\cdots}CH{\cdots}CH\text{-}R_2 \quad (h)$$

Scheme 1.

could be of importance for effective utilization of photoenergy. However, only a few examples are known.[12,19] The heavy atom effect in the present photoreaction was investigated in order to clarify the initial step of the photoreaction. The photoreaction of imine **1** with olefins is greatly susceptible to the heavy atom solvent, as observed in the photoreaction of imine **1** with alkylbenzenes.[12] Carbonyl compounds such as benzophenone are known not to be influenced by the heavy atom effect.[20] Thus chemical sensitization by the action of benzophenone would not be influenced by the heavy atom effect, though the excited state of imine **1** might be susceptible. The heavy atom effect is known to increase the probability of the transition between the singlet state and triplet state of a π,π^* character,[21,22] and the reactive state of the imine **1** would be the triplet state with some π,π^* character.[23] The reaction was confirmed to proceed *via* the excited triplet state of imine **1** by the fact that the photoreaction of **1** with cyclohexene was completely quenched by piperylene (Table 2).

The variation of the reaction yield depending on the concentration of dibromomethane shown in Fig. 2 seems to arise from the influence of the heavy atom effect toward the initial step of the excited state of imine **1** as shown in Scheme 2, where D is *N*-acetyldiphenylmethyleneamine (**1**) and the superscript is the multiplicity of the excited state of **1**.

$$D \xrightarrow{h\nu'} {}^1D \qquad (i)$$

$$^1D \xrightarrow{k_{1c}} D \qquad (j)$$

$$^1D \xrightarrow{k_{1s}} {}^3D \qquad (k)$$

$$^3D \xrightarrow{k_d} D \qquad (l)$$

$$D \xrightarrow{h\nu''} {}^3D \qquad (m)$$

Scheme 2.

The main processes influenced by the heavy atom effect are (a) an intersystemcrossing from the lowest singlet state to the triplet state of **1** (Eq. k), and (b) a radiative or radiationless decay from the triplet state to the ground state (Eq. 1). Increase of the yield with concentration of heavy atom solvent demonstrates the importance of Step k in the heavy atom effect. This indicates that the excited triplet state of **1** is mainly produced by the singlet excited state of **1** and not by the energy transfer of benzophenone. The behavior of the excited imine **1** in the reaction with olefins is just the same as that in the reaction with alkylbenzenes.[12]

Experimental

Materials. Cyclopentene, cyclooctene, 2-pentene, 2-hexene, piperylene (Tokyo Chemical Industry), and cyclohexene (Yoneyama Chemical Industry) were dried over sodium by refluxing and distilled. Acetophenone (Yoneyama Chemical Industry) and dibromomethane were dried over magnesium sulfate and distilled. Benzophenone (Yoneyama Chemical Industry) and benzil (Tokyo Chemical Industry) were recrystalized from ethanol. Commercial cyclohexane, benzene, dichloromethane, chloroform, and ethanol were used as eluting solvents for column chromatograpy. The reagent for the bromine test was 2% carbon tetrachloride solution of bromine and that for the Bayer test 0.5% aq solution of potasium permanganate. *N*-Acetyldiphenylmethyleneamine (**1**), bp 168—170 °C/1 mmHg (lit,[24] bp 168—170 °C/1 mmHg), was prepared by the reaction of diphenylketimine[25] with acetic anhydride and distilled repeatedly.

Instrumentations. Irradiation was performed with a 500 W Halos high pressure mercury lamp (Eikosha Ltd.). Most comparative runs were carried out on a merry-go-round type reactor (Rikokagaku Ltd.) with a turntable device holding the rotating pyrex tubes. The turntable also rotates around the lamp in a water cooled quartz immersion well. The turntable and tubes were held in a constant temperature water bath maintained at 25 °C. GLPC analysis was carried out on an Ohkura Rikagaku gas chromatograph with a flame ionization detector employing a 2 m×3 mmϕ stainless steel column packed with 10% Apiezon Grease L on 60—80 mesh Diasolid A. High speed liquid chromatography (HLC) was performed with a Waters ALC-202 high speed liquid chromatograph with a 600 type high pressure pump, a U6K universal injector, and a 660 type solvent programmer equipped with a stainless steel colum packed with Microporasil. Chloroform was used as an eluting solvent. Infrared spectra were taken on a JASCO IR-E spectrometer. NMR spectra were obtained on a JEOL C-60, 4H-100, PS-100 or a Hitachi Perkin-Elmer R-20B spectrometer. Mass spectra were recorded on a Hitachi RMS-4 spectrometer. Melting points were determined on a Yanagimoto micro melting point apparatus, and were uncorrected.

Photoreaction of N-*Acetyldiphenylmethyleneamine (1) and Cyclopentene.* A cyclopentene (72 mmol) solution of *N*-acetyldiphenylmethyleneamine (4.8 mmol) in a quartz tube was degassed in three successive freeze-thaw cycles, and then irradiated under nitrogen with a 500 W high pressure mercury lamp for 100 h. After irradiation cyclopentene was distilled off and the residue was chromatographed over silica gel. The fraction eluted with benzene contained imine **1** and benzophenone, most of which was produced by the hydrolysis of **1** in a column. The product **2a** was eluted with chloroform in 31% yield. The yield represents the conversion percentage of starting imine **1** since **2a** is the only product in the reaction. The product was purified by recrystalization several times from the mixed solvent of cyclohexane and ethanol. The structure of **2a** (mp 147.0—147.8 °C) was inferred from its composition (Found: C, 82.41; H, 7.11; N, 4.76%; mol wt, 291 by mass spectra. Calcd for $C_{20}H_{21}NO$: C, 82.44; H, 7.26; N, 4.81%; mol wt, 291.38), the results of olefin tests, and its spectral data. The bromine test and the Bayer test indicated the presence of a C=C bond in the molecule. Infrared spectra showed an amide absorption (ν_{NH}, 3280; ν_{CO}, 1658; δ_{NH}, 1548 cm^{-1}); NMR spectra (in $CDCl_3$) showed ten phenyl protons (δ 7.51—6.93), an NH proton (δ 6.42—6.02), two olefinic protons (δ 5.71), a methine proton (δ 4.66—4.29), four methylene protons (δ 2.20—2.08), and three acetyl protons (δ 1.90).

Photoreaction of N-*Acetyldiphenylmethyleneamine (1) with Cyclohexene.* A cyclohexene (54 mmol) solution of imine **1** (5.7 mmol) in a qaurtz tube was irradiated in the same way as given above, the photoproduct **2b** being obtained in 15% yield. Its structure was identified as *N*-(1,1-diphenyl-1-cyclohexa-2′-enylmethyl)acetamide: mp 181 °C. Found: C, 82.37; H, 7.32; N, 4.61%; mol wt 305 by mass spectra. Calcd for $C_{21}H_{23}NO$: C, 82.58; H, 7.59; N, 4.59%; mol wt, 305.42. Infrared spectra showed an amide band (ν_{NH}, 3290, ν_{CO}, 1660; δ_{NH}, 1548 cm^{-1}). NMR spectra (in $CDCl_3$) showed ten phenyl protons at δ 7.70—6.99, an NH proton at δ 6.42—6.20, two

olefin protons at δ 5.65, a methine proton at δ 4.00—3.65, six methylene protons at δ 2.08—0.85, and three acetyl protons at δ 1.89. An NH proton was assigned by disappearance in the present of deuteruim oxide. UV spectra gave four peaks of 253.6 nm (ε_{max} 5.12×10^2), 259.4 (5.58×10^2), 265.0 (4.69×10^2), and 270.5 (2.92×10^2).

Photoreaction of N-*Acetyldiphenylmethyleneamine (1) with Cyclooctene.* A cyclooctene (48 mmol) solution of *N*-acetyldiphenylmethyleneamine (5.6 mmol) was irradiated in the same way as above, the product **2c** being obtained in 2% yield. Its structure (mp 233 °C) was determined by mass spectra (mol wt 333) and other spectral analysis: Infrared spectra have an amide group (ν_{NH}, 3310; ν_{CO}, 1667; δ_{NH}, 1525 cm^{-1}), and NMR spectra showed ten phenyl protons (δ 7.58—6.02), an NH proton (δ 6.24), two olefin protons (δ 5.83—5.39, 5.32—4.91), a methine proton (δ 4.40—4.00), three acetyl protons (δ 1.82), and ten methylene protons (δ 2.60—0.52).

Photoreaction of N-*Acetyldiphenylmethyleneamine (1) with 2-Pentene.* A solution of imine **1** (16 mmol) and 2-pentene (37 mmol) was irradiated in the same way as given above, the product **2d** being given in 0.9% yield. Its structure was dentified to be *N*-(1,1-diphenyl-2-methyl-3-pentenyl)acetamide, from its spectral data and the results of the olefin tests. Infrared spectra showed an amide band (ν_{NH}, 3300; ν_{CO}, 1670; δ_{NH}, 1530 cm^{-1}) and molecular weight was observed to be 293 by mass spectra. NMR spectra showed ten phenyl protons (δ 7.50—6.70), an NH proton (δ 6.56—6.24), two olefinic protons (δ 5.62—4.99), a methine proton (δ 4.64—4.16), three acetyl protons (δ 1.79), three methyl protons adjacent to the olefinic carbon (δ 1.51), and three methyl protons adjacent to the methine carbon (δ 0.73).

Photoreaction of N-*Acetyldiphenylmethyleneamine (1) with 2-Hexene.* A solution of imine **1** (16 mmol) and 2-hexene (30 mmol) was irradiated in the same way as described above. The products were eluted with 5% benzene solution of ether in 1.1% yield. They were identified to be two kinds of isomers (**2e** and **2e'**) by the spectral data. Mass spectra showed the molecular weight ($M^+/e=307$); the infrared spectra showed an amide group (ν_{NH}, 3300; ν_{CO}, 1670; δ_{NH}, 1530 cm^{-1}); NMR spectra showed the phenyl protons (δ 8.10—6.72), the NH proton (δ 6.63), the olefinic protons (δ 5.80—4.90), the methine proton (δ 4.59—4.24), the allylic methylene protons (δ 1.94), the allylic methyl protons (δ 1.45), the acetyl protons (δ 1.83), and the methyl protons adjacent to the tertiary carbon (δ 0.95).

Photoreaction of N-*Acetyldiphenylmethyleneamine (1) with Cyclohexene in the Presence of the Additives.* A cyclohexene (55 mmol) solution of imine **1** (4.6 mmol) and the additive was irradiated in a quartz tube under nitrogen atmosphere after being degassed in three freeze-thaw cycles at 15 °C for 100 h. Separation was carried out in the same way as described in the photoreaction of the imine **1** with cyclopentene. No products derived from the additive were detected.

Dependence of Photoreaction of N-*Acetyldiphenylmethyleneamine (1) with Cyclohexene upon the Concentration of Benzophenone.* A cyclohexene (10 ml) solution of imine **1** (0.23 M) in the presence of a fixed amount of the heavy atom solvents in a Pyrex tube was degassed in three successive freeze-thaw cycles and irradiated under nitrogen with a 500 W high pressure mercury lamp at 25 ± 1 °C for 70 h. After irradiation cyclohexene was distilled off and the reaction mixtures were analyzed with a gas chromatograph equipped with a 80 cm×3 mmϕ stainless steel column with 10% Apiezon Greese L on 60—80 mesh Diasolid A. Yields are given in terms of the conversion percentage of the starting imine.

Dependence of Photoreaction of N-*Acetyldiphenylmethyleneamine(1) with Cyclohexene upon the Concentration of Dibromomethane.* A cyclohexene (5 ml) solution of imine **1** (1.2 mmol) in the presence of benzene solutions (5 ml) of varying amounts of dibromomethane in a Pyrex tube was degassed and irradiated under nitrogen with a 500 W high pressure mercury lamp at 25 ± 1 °C for 10 h. After irradiation solvents were distilled off, and the residue was analyzed by high speed liquid chromatography of Microporasil using chloroform as an eluting solvent. Yields are given in terms of the conversion percentage of the starting imine **1**.

The work was partially supported by a Grant-in-Aid for Scientific Research from the Ministry of Education. Financial support from the Kawakami Foundation to one of us (N. T.) is gratefully acknowledged.

References

1) Recent reviews: A. Padwa, *Chem. Rev.*, **77**, 37 (1977); A. C. Pratt, *Chem. Soc. Rev.*, **6**, 63 (1977).
2) A. Padwa, W. Bergmark, and D. Pahayan, *J. Am. Chem. Soc.*, **91**, 2653 (1969).
3) A. Padwa and M. Dharan, *Tetrahedron Lett.*, **1972**, 1053.
4) M. Saeki, N. Toshima, and H. Hirai, *Bull. Chem. Soc. Jpn.*, **48**, 476 (1975).
5) H. Ohta and K. Tokumaru, *Chem. Lett.*, **1974**, 1403.
6) H. Ohta and K. Tokumaru, *Tetrahedron Lett.*, **1974**, 2965; J. M. Hornback, G. S. Proehl, and I. J. Starner, *J. Org. Chem.*, **40**, 1077 (1975).
7) H. Ohta and K. Tokumaru, *Bull. Chem. Soc. Jpn.*, **48**, 1669 (1975); M. Yoshida, H. Sakuragi, T. Nishimura, S. Ishikawa, and K. Tokumaru, *Chem. Lett.*, **1975**, 1125.
8) N. J. Turro, "Molecular Photochemistry," W. A. Benjamin, Inc., New York (1965), Chap. 6.
9) A. Padwa and W. P. Koehn, *J. Org. Chem.*, **40**, 1896 (1975).
10) N. Toshima, S. Asao, K. Takada, and H. Hirai, *Tetrahedron Lett.*, **1970**, 5123.
11) J. S. Bradshaw, *J. Org. Chem.*, **31**, 237 (1966).
12) N. Toshima, S. Asao, and H. Hirai, *Chem. Lett.*, **1975**, 451; S. Asao, N. Toshima, and H. Hirai, *Bull. Chem. Soc. Jpn.*, **49**, 224 (1976).
13) W. G. Herkstroeter, A. A. Lamola, and G. S. Hammond, *J. Am. Chem. Soc.*, **86**, 4537 (1964).
14) S. Asao, N. Toshima, and H. Hirai, *Bull. Chem. Soc. Jpn.*, **48**, 2068 (1975).
15) P. S. Engel and B. M. Monroe, "Advances in Photochemistry," ed by W. A. Noyes, Jr., G. S. Hammond, and J. N. Pitts, Jr., Wiley-Interscience, Vol. 8, New York (1971), p. 245.
16) The possibility of contribution of photochemical hydrolysis of imine **1** to Scheme 1 was pointed out by a referee. However, photochemical hydrolysis of the imine is known only in the presence of oxygen (*cf.* R. L. Furey and R. O. Kan, *Tetrahedron*, **24**, 3085 (1968)) or in ether or methanol probably containing water in the case of a special imine.[7] In the present study, irradiation was carried out in a dry solvent under nitrogen. Lack of photochemical hydrolysis of imine **1** in the present case is further supported by the fact that the product yield increases linearly with irradiation time.
17) The concentration of excited triplet benzophenone is not proportional to the benzophenone concentration, but follows the equation

$$[Ph_2CO^*(T_1)] = Ia/(k_r[\text{Olefin}]+k_d)$$

where, Ia is the rate of light absorption of benzophenone to form triplet state of benzophenone, k_r and k_d are constants. The concentration of olefin ([Olefin]) is very high and con-

sidered to be constant during the course of reaction.

18) $[Ph_2CNAc^*(T_1)]$ is proportional to the concentration of imine **1** ($[Ph_2CNAc]$), which changes with reaction time. In this experiment, however, the change is less than 5% and the concentration of the imine is kept almost constant, since the conversion of the reactant imine is less than 5%.

19) C. W. Jefford and F. Delay, *J. Am. Chem. Soc.*, **97**, 2272 (1975); D. Bryce-Smith, R. R. Deshporde, and A. Gilbert, *Tetrahedron Lett.*, **1975**, 1627; R. Korenstein, K. A. Muszkat, M. A. Slifkin, and E. Fischer, *J. Chem. Soc., Perkin Trans. 2*, **1976**, 438; W. W. Schlomann, Jr. and B. F. Plummer, *J. Am. Chem. Soc.*, **98**, 3254 (1976); and references cited therein.

20) R. F. Borkman and D. R. Kearns, *Chem. Commun.*, **1966**, 446; M. A. El-Sayed, *J. Chem. Phys.*, **41**, 2462 (1964); D. R. Kearns and W. A. Case, *J. Am. Chem. Soc.*, **88**, 5087 (1966); P. J. Wagner, *J. Chem. Phys.*, **45**, 2335 (1966).

21) M. A. El-Sayed, *Acc. Chem. Res.*, **1**, 8 (1968); S. K. Lower and M. A. El-Sayed, *Chem. Rev.*, **66**, 199 (1966).

22) D. S. McClure, *J. Chem. Phys.*, **17**, 905 (1949); M. R. Padhye, S. P. McClynn, and M. Kasha, *ibid.*, **24**, 588 (1956); S. P. McClynn, R. Sunseri, and N. D. Christodouleas, *ibid.*, **37**, 1818 (1962); S. P. McClynn, T. Azumi, and M. Kasha, *ibid.*, **40**, 507 (1964); S. Siegel and H. J. Judeikis, *ibid.*, **42**, 3060 (1965); G. G. Gianchino and D. R. Kearns, *ibid.*, **52**, 2964 (1969).

23) It is difficult to determine whether hydrogen abstraction by the excited *N*-acylimine occurs on the oxygen atom or on the nitrogen atom of the acylimine chromophore. We have suggested the abstraction on the oxygen atom in the photoreduction of *N*-acylimine by the term "intramolecular chemical sensitization" (T. Okada, M. Kawanisi, H. Nozaki, N. Toshima, and H. Hirai, *Tetrahedron Lett.*, **1969**, 927). Padwa and co-workers also made the same suggestion on the basis of the failure of the imine nitrogen to initiate Norrish type II reactions.[9]

24) J. E. Banfield, G. M. Brown, F. H. Davey, W. Davies, and T. H. Ramsay, *Aust. J. Sci. Res.*, **A1**, 330 (1948).

25) P. L. Pickard and T. L. Tolbert, *J. Org. Chem.*, **26**, 4886 (1961).

Cyclic Peptides. IV.[1] Synthesis of Diastereomeric Dihydro-AM-toxin I and Its Analogs[2]

Yasuyuki SHIMOHIGASHI, Sannamu LEE, Tetsuo KATO, and Nobuo IZUMIYA

Laboratory of Biochemistry, Faculty of Science 33, Kyushu University, Higashi-ku, Fukuoka 812

(Received August 1, 1977)

Diastereomeric cyclotetradepsipeptides [L-Ala²]- and [D-Ala²]-AM-toxin I, corresponding to the hydrogenated products of AM-toxin I, were synthesized by the conventional method and their biological activities were tested. [D-Ala²]-AM-toxin I exhibits weak but recognizable necrotic activity (5—10 μg/ml) on apple leaves. [L-Ala²]-AM-toxin I is inactive even in a high concentration of 100 μg/ml. The results of NMR and ORD measurements of [D-Ala²]-AM-toxin I and [L-Tyr(Me)¹, D-Ala²]-AM-toxin indicates the presence of a common conformer. The results on [L-Ala²]-AM-toxin I and [L-Tyr(Me)¹, L-Ala²]-AM-toxin revealed the presence of more than two conformers, the predominant conformation differing from that of D-isomers. Difference in activity between [D-Ala²]- and [L-Ala²]-AM-toxin I can be attributed to the difference in conformation of the diastereomers.

AM-toxins are host-specific phytotoxins produced by *Alternaria mali* causing necrosis on apple leaves.[3] The structures of AM-toxin I (**1a**) and its analog [L-Tyr-(Me)¹]-AM-toxin (**1b**) are shown in Fig. 1.[4] Peptide **1a** and its analogs such as **1b** and di-AM-toxin I (cyclic octadepsipeptide) were synthesized in this laboratory, the minimum toxic activity of **1a**, **1b**, and di-AM-toxin I being determined to be 0.002, 20, and 10—20 μg/ml, respectively.[5]

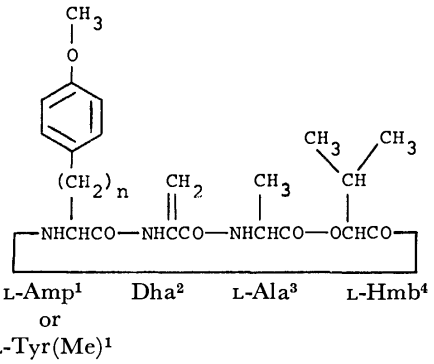

Fig. 1. Structure of AM-toxin I (**1a**) and [L-Tyr(Me)¹]-AM-toxin (**1b**). **1a**, $n=3$; **1b**, $n=1$.

This paper describes studies on the role of a double bond in the Dha² residue in **1a**. Since hydrogenation of natural **1a** produces a mixture of [L-Ala²]- and [D-Ala²]-AM-toxin I (**8a**-L and **8a**-D), pure **8a**-L and **8a**-D were prepared by the conventional method of peptide synthesis. The biological activities of the synthesized peptides were tested. Analogs (**8b**-L and **8b**-D) containing *O*-methyl-L-tyrosine (**2b**) in place of L-2-amino-5-(*p*-methoxyphenyl)pentanoic acid (**2a**) were also synthesized in order to investigate the influence of variation of the side chain in **2a** on necrotic activity and on conformation. When the synthesis of **1a** and **1b** was carried out in a previous study, a mixture of cyclic oligomers was obtained by the cyclization reaction of the corresponding linear tetradepsipeptides. The cyclic oligomers behaved chromatographically in a very similar way to each other, and thus purification with silica gel column was tedious and complete separation difficult.[5] In the present study, effective separation of cyclic oligomers was attained by fractional crystallization

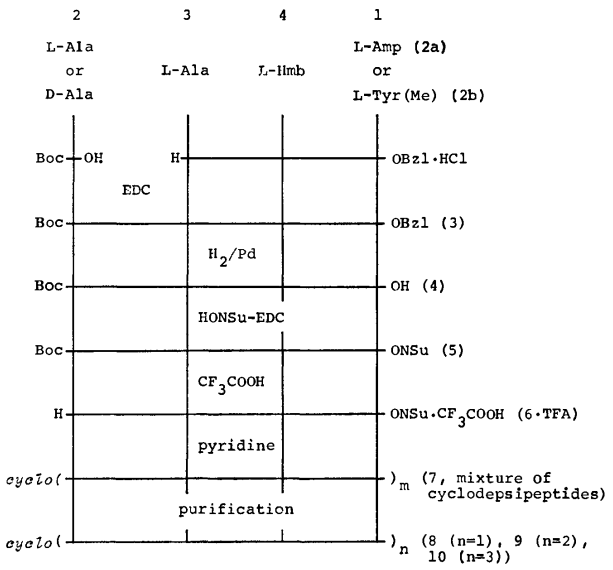

Fig. 2. Synthetic route for dihydro-AM-toxin I (**8a**-L and **8a**-D) an [DL-Tyr(Me)¹]-dihydro-AM-toxin (**8b**-L and **8b**-D).

with use of minute differences in the solubility of the oligomers.

Figure 2 shows the reaction route for the synthesis. L-Amp was prepared by the resolution of Ac-DL-Amp-OH with acylase.[6] Ester H-L-Ala-L-Hmb-L-Amp-OBzl·HCl[1] was coupled with Boc-L- or Boc-D-Ala-OH by the EDC method to give Boc-L- or Boc-D-Ala-L-Ala-L-Hmb-L-Amp-OBzl (**3a**-L or **3a**-D). Ester **3a**-L or **3a**-D was catalytically hydrogenated to give tetradepsipeptide acid (**4a**-L or **4a**-D), the acid being converted into active ester **5a**-L or **5a**-D with the use of HONSu and EDC. The active ester **5a**-L was treated with TFA at 0 °C for 20 min, the salt **6a**-L·TFA obtained was dissolved in DMF, and the solution was subjected to cyclization reaction in pyridine. A mixture (**7a**-L) of cyclodepsipeptides was obtained showing three spots on a thin layer chromatogram corresponding to cyclic monomer (**8a**-L), dimer (**9a**-L), and trimer (**10a**-L). In order to isolate each of the pure products, reprecipitation with dioxane was carried out. Less soluble fraction of **7a**-L was treated with DMF-dioxane to give pure **8a**-L and **10a**-L. Similar precipitation of

more soluble fraction of **7a**-L gave pure dimer **9a**-L. On the other hand, cyclization of **6a**-D gave monomer **8a**-D exclusively. Analogous cyclic depsipeptides containing L-Tyr(Me) (**2b**) were obtained similarly.

When natural **1a** was catalytically hydrogenated in acetic acid, a mixture consisting of **8a**-L and **8a**-D was found on a thin layer chromatogram. In order to determine the ratio of **8a**-L to **8a**-D in the mixture, the procedure of Shimohigashi *et al.*[6] was applied; the hydrogenated residue of the mixture was hydrolyzed in hydrochloric acid and the hydrolyzate was acylated with Z-L-Leu-ONSu in aqueous dioxane. Upon debenzyloxycarbonylation, leucyl dipeptides obtained were applied to an amino acid analyzer. The calculated ratio of L-Leu-L-Ala to L-Leu-D-Ala was 2.21: 1.00. From the result, the ratio of **8a**-L to **8a**-D in the hydrogenated mixture was determined to be 38: 62.

Experimental

All the melting points are uncorrected. TLC was carried out on silica gel G (Merck) with the following solvent systems, the ratio in parentheses being indicated by vol: R_f^1, $CHCl_3$–MeOH (5: 1); R_f^2, $CHCl_3$–MeOH–AcOH (95: 5: 1); R_f^3, $CHCl_3$–MeOH (9: 1). Optical rotations were measured with a Union high sensitivity polarimeter PM-71. Mass spectra were taken on a Hitachi RMS-4 mass spectrometer with a direct inlet system operating at 70 eV, UV spectra on a Hitachi 124 spectrophotometer, and NMR spectra on a JEOL JNM PS-100 spectrometer, tetramethylsilane being used as an internal reference. ORD measurements were carried out with a JASCO ORD/UV-5 spectropolarimeter using a 0.1 cm cell; sample concentration, 0.01%. Amino acid analyses were determined with a Hitachi amino acid analyzer KLA-5. Details of the synthetic procedures are described mainly for [L-Ala²]-AM-toxin I and its derivatives as a representative case. Other compounds were synthesized in a similar way. Physical constants, yields, and the results of elemental analyses are summarized in Table 1.

Boc-L-Ala-L-Ala-L-Hmb-L-Amp-OBzl (3a-L). Boc-L-Ala-OH (0.45 g, 2.37 mmol), H-L-Ala-L-Hmb-L-Amp-OBzl·HCl[1] (1.23 g, 2.37 mmol), and Et_3N (0.33 ml, 2.37 mmol) were dissolved in $CHCl_3$ (15 ml). To the solution was added EDC·HCl (0.50 g, 2.61 mmol) at 0 °C. The mixture was stirred for 2 h at 0 °C and overnight at room temperature, evaporated *in vacuo*, and the residue was treated with a mixture of water and EtOAc. The organic layer was washed with 4% $NaHCO_3$, 10% citric acid and water, dried (Na_2SO_4), and evaporated to leave an oil, which was crystallized by the addition of ether and petroleum ether; yield, 1.39 g. The solid was contaminated with a small amount of by-products and was purified with a silica gel column (3.3×40 cm) using a solvent of $CHCl_3$–EtOAc (1: 1). The fractions (260—380 ml) were collected and evaporated, and the residual solid was recrystallized from EtOAc–ether–petroleum ether; yield, 1.24 g (79%).

Boc-L-Ala-L-Ala-L-Hmb-L-Amp-OH (4a-L). Ester **3a**-L (1.12 g, 1.70 mmol) was dissolved in THF (20 ml) and hydrogenated in the presence of Pd black. The filtrate from the catalyst was evaporated and the residue was crystallized from $CHCl_3$–petroleum ether; yield, 0.89 g (93%).

Boc-L-Ala-L-Ala-L-Hmb-L-Amp-ONSu (5a-L). To a chilled solution of **4a**-L (453 mg, 0.80 mmol) in DMF (5 ml), HONSu (138 mg, 1.20 mmol) and EDC·HCl (184 mg, 0.96 mmol) were added at 0 °C. After 24 h at 0 °C the solution was evaporated, and the residual oil was solidified by the addition of water. Powder obtained was filtered off quickly and dried over P_2O_5; yield, 531 mg (100%); R_f^1 0.87.

A Mixture of Cyclopeptides (7a-L). Ester **5a**-L (531 mg, 0.80 mmol) was dissolved in TFA (5 ml) at 0 °C. After 20 min the solution was evaporated to leave an oil, which was solidified by the addition of ether. The solid (**6a**-L·TFA) obtained was dissolved in DMF (5 ml) and stirred in pyridine (260 ml) at room temperature. After 24 h the solution was evaporated, and the residue was triturated with cold water and 10% citric acid; yield of solid (**7a**-L), 300 mg (84%). TLC of **7a**-L showed three spots by monomer (**8a**-L), dimer (**9a**-L), and trimer (**10a**-L).

Cyclo(-L-Amp-L-Ala-L-Ala-L-Hmb-) ([L-Ala²]-AM-toxin I) (8a-L). Mixture **7a**-L (300 mg) was added to dioxane (20 ml) and the suspension was stirred at room temperature for 1 day. The insoluble solid was collected and washed with hot dioxane (yield of the solid, 180 mg), the filtrate (**7a**-L-**f**)

Table 1. Analytical data of synthetic peptides

Compound	Formula	Yield (%)	Mp(°C)	R_f^1	R_f^2	R_f^3	$[\alpha]^{20}$	Found C(%)	Found H(%)	Found N(%)	Found M⁺	Calcd C(%)	Calcd H(%)	Calcd N(%)	Calcd mol wt
3a-L	$C_{35}H_{49}O_9N_3$	79	119—120	0.70	0.56		−40.8[a]	63.78	7.53	6.42		64.10	7.53	6.41	
3a-D	$C_{35}H_{49}O_9N_3$	77	131—133	0.69	0.57		+2.8[a]	63.86	7.55	6.42		64.10	7.53	6.41	
3b-L	$C_{33}H_{45}O_9N_3$	66	140—141	0.86	0.56		−40.4[a]	63.00	7.22	6.69		63.14	7.23	6.69	
3b-D	$C_{33}H_{45}O_9N_3$	71	119—120	0.81	0.58		−0.2[a]	63.02	7.25	6.63		63.14	7.23	6.69	
4a-L	$C_{28}H_{43}O_9N_3$	93	136—138	0.57	0.42		−29.0[a]	59.32	7.67	7.42		59.45	7.66	7.43	
4a-D	$C_{28}H_{43}O_9N_3$	95	137—139	0.56	0.40		+0.2[a]	59.28	7.64	7.34		59.45	7.66	7.43	
4b-L	$C_{26}H_{39}O_9N_3$	100	138—140	0.29	0.38		−20.4[a]	57.75	7.35	8.12		58.08	7.31	7.82	
4b-D	$C_{26}H_{39}O_9N_3$	99	107—108	0.33	0.43		+8.6[a]	57.48	7.34	7.40		57.13[b]	7.38[b]	7.69[b]	
8a-L	$C_{23}H_{33}O_6N_3$	27	277—278[c]		0.17	0.31	−6500[d]	61.52	7.45	9.37	447	61.72	7.43	9.39	447
8a-D	$C_{23}H_{33}O_6N_3$	72	>300[c]		0.60	0.80	−6800[d]	61.48	7.41	9.32	447	61.72	7.43	9.39	447
8b-L	$C_{21}H_{29}O_6N_3$	36	>300[c]		0.15	0.30	−5700[d]	59.93	6.94	10.14	419	60.13	6.97	10.02	419
8b-D	$C_{21}H_{29}O_6N_3$	50	>300[c]		0.61	0.82	−6800[d]	60.02	6.94	9.96	419	60.13	6.97	10.02	419
9a-L	$C_{46}H_{66}O_{12}N_6$	17	217—219[c]		0.36	0.51	−1600[d]	60.77	7.37	9.30	894	60.50[e]	7.51[e]	9.21[e]	894
9b-L[f]	$C_{42}H_{58}O_{12}N_6$	4	255—256[c]		0.52	0.63	−1900[d]	59.20	6.97	9.71	838	59.49[g]	7.01[g]	9.91[g]	838
10a-L	$C_{69}H_{99}O_{18}N_9$	8	>300[c]		0.41	0.51	−1100[d]	60.71	7.36	9.32	1342	60.90[e]	7.48[e]	9.27[e]	1342

a) $[\alpha]_D$ (*c* 1, $CHCl_3$). b) $1/2H_2O$. c) With decomp. d) $[\alpha]_{250}$ (*c* 0.01, CF_3COOH). e) Monohydrate. f) $[\alpha]_D^{27}$ −83° (*c* 0.3, DMF). g) $1/4H_2O$.

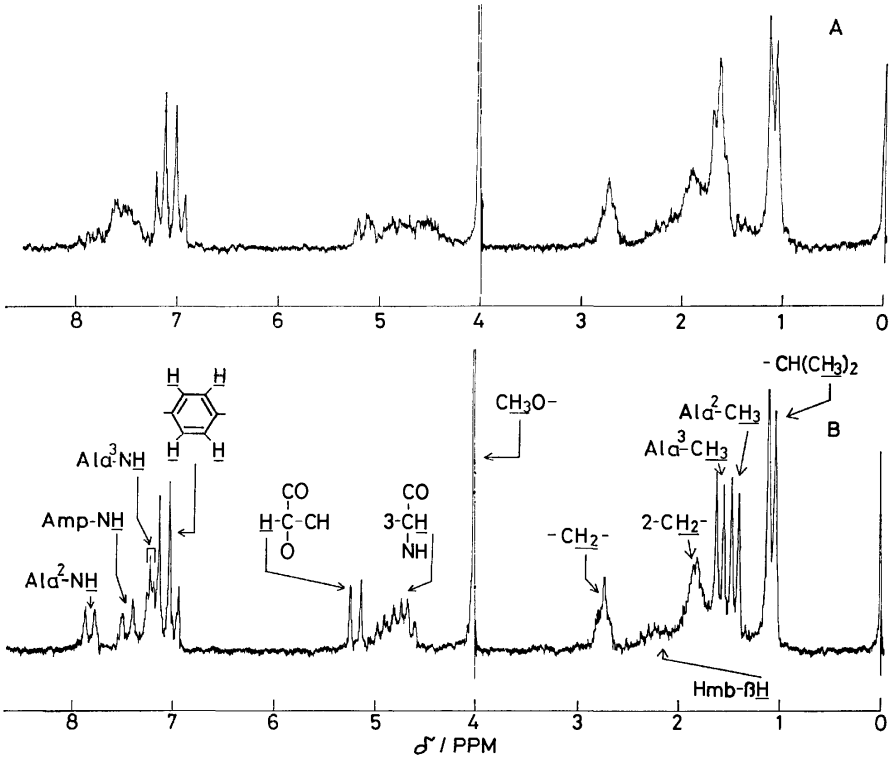

Fig. 3. NMR spectra of dihydro-AM-toxin I in TFA. A, [L-Ala^2]-AM-toxin I (**8a**-L); B, [D-Ala^2]-AM-toxin I (**8a**-D).

being put aside for the isolation of **9a**-L. The solid was dissolved in hot DMF (2 ml) and cooled to room temperature. The resulting precipitate was collected with the aid of dioxane (yield of the precipitate, 34 mg), the precipitate (**7a**-L-**p**) being used for the isolation of **10a**-L. The filtrate was evaporated, and the residue was repeatedly recrystallized from the following solvent systems: DMF–EtOAc, DMF–dioxane, and DMF–EtOAc–ether; yield of **8a**-L, 95 mg (27%).

Cyclo[-(L-*Amp*-L-*Ala*-L-*Ala*-L-*Hmb*)$_2$-] (**9a**-L). The filtrate **7a**-L-**f** mentioned above was evaporated, and the residue (107 mg) was crystallized from dioxane–EtOAc–ether–petroleum ether; yield, 66 mg. Further recrystallization from dioxane–ether–petroleum ether gave 60 mg (17%).

Cyclo[-(L-*Amp*-L-*Ala*-L-*Ala*-L-*Hmb*)$_3$-] (**10a**-L). The precipitate **7a**-L-**p** mentioned above was crystallized from DMF–EtOAc–ether; yield, 29 mg (8%).

Cyclo(-L-*Amp*-D-*Ala*-L-*Ala*-L-*Hmb*-) ([D-*Ala*^{2}]-*AM-toxin I*) (**8a**-D). Ester **5a**-D (332 mg) obtained from **4a**-D (283 mg, 0.50 mmol) was treated with TFA as described for **7a**-L, and **6a**-D·TFA obtained was subjected to cyclization reaction for three days. After evaporation of pyridine the residue was triturated with cold water and filtered off. Recrystallization of the solid from DMF–EtOAc gave 161 mg (72%).

Hydrogenation of Natural AM-toxin I. Natural **1a** (4 mg, 9 μmol) was dissolved in AcOH (5 ml) and hydrogenated in the presence of Pd black. The filtrate from the catalyst was evaporated, and the residue (3.2 mg) showed two spots on TLC corresponding to **8a**-L and **8a**-D. A portion (1.6 mg) of this residue was dissolved in 6 M HCl (1 ml) and hydrolyzed at 110 °C for 24 h. After evaporation the residue was dissolved in a mixture of water (0.5 ml) and dioxane (0.5 ml) and the mixture was neutralized by the addition of Et_3N. To this mixture were added a solution of Z-L-Leu-ONSu (7.8 mg, 21 μmol) in dioxane (0.5 ml) and Et_3N (14 μmol) at 0 °C. The reaction mixture was stirred for 2 h at 0 °C and overnight at room temperature. After evaporation, the residue was dissolved in a mixture (3 ml) of MeOH–AcOH–water (5:1:1) and hydrogenated in the presence of Pd black. The product was evaporated, and an aliquot of the diastereomeric dipeptides obtained was applied to an amino acid analyzer.[6] The molar ratio of L-Leu-L-Ala to L-Leu-D-Ala was determined to be 2.21: 1.00. After the correction of one equivalent of L-alanine present in **1a** as L-Ala^3, the ratio of **8a**-L to **8a**-D in the hydrogenated product was calculated to be 0.38: 0.62. When natural **1a** was hydrogenated in dioxane instead of AcOH, the ratio was 0.41: 0.59.

NMR Spectroscopy. Figure 3 shows the NMR spectra of **8a**-L and **8a**-D in TFA at ambient temperature with sample concentration at 15 mg/0.4 ml. Signals of **8b**-D were assigned as follows: δ=0.92 (3H, d, J=7.0 Hz, HmbCH$_3$), 1.04 (3H, d, J=7.0 Hz, HmbCH$_3$), 1.38 (3H, d, J=7.0 Hz, D-Ala^2-CH$_3$), 1.58 (3H, d, J=7.0 Hz, L-Ala^{3}CH$_3$), 2.2 (1H, m, HmbβH), 3.0—3.4 (2H, ABX, Tyr(Me)CH$_2$), 4.00 (3H, s, OCH$_3$), 4.5—5.0 (3H, m, αH), 5.12 (1H, d, HmbαH), 6.98—7.30 (5H, aromatic H and NH), 7.58 (1H, d, J=10.0 Hz, Tyr(Me)NH), 7.80 (1H, d, J=9.0 Hz, D-Ala^{2}NH). Because of poor solubility of **8a**-D and **8b**-D the use of other solvents was not attempted.

Biological Assay. Biological assay on apple leaves (susceptible cultivar, Indo) was carried out as described previously.[7] The minimum toxic concentrations of **8a**-D and **1a** were 5—10 and 0.002 μg/ml, respectively. **8a**-L, **8b**-L, and **8b**-D showed no activity in high concentration up to 100 μg/ml.

Results and Discussion

Since the results of the bioassay revealed a distinct difference between the activity of **8a**-L and that of **8a**-D, we investigated the conformations of these diastereomeric peptides in order to clarify the structure-activity relationship. The NMR spectra of **8a**-D and **8b**-D

showed well resolved but very similar patterns (one difference between them being the splitting of the Hmb side chain), suggesting the presence of a common and stable conformation for **8a**-D and **8b**-D. On the other hand, **8a**-L and **8b**-L displayed complex spectra indicating that each of these L-peptides is a mixture of at least two conformers. For example, **8a**-L and **8b**-L gave the complex signals of α-CH and NH protons in contrast with the well resolved signals of the corresponding protons of **8a**-D and **8b**-D. Furthermore, **8a**-L revealed weak signals with the same chemical shifts at those obtained in **8a**-D or **8b**-D spectra, such as doublets at 1.40 ppm and at 7.80 ppm.

These observations suggest that predominant conformations of **8a**-L and **8b**-L differ from those of **8a**-D and **8b**-D. Unfortunately, information obtained from the NMR spectra was not sufficient to deduce a definite conformation for **8a**-D and **8b**-D. At least two conformations were in line with the results of NMR study; one with the all-*trans* backbone system[8] and the other with the *cis-trans-cis-trans* backbone.[9] In general the presence of *cis* peptide bond is observed only for α-imino acid such as proline. In case of cyclotetrapeptides, however, the all-*trans* backbone system has to be strained because of steric constraint.[10] Thus, the presence of a conformation containing a *cis* bond can not be excluded. Natural **1a** showed similar NMR spectra to those of **8a**-D. However, rapid decomposition of **1a** in TFA made further study difficult.

The ORD curves of selected synthetic peptides are shown in Figs. 4 and 5. All cyclic tetradepsipeptides show a significant trough, [α]=−6000—−9000°, around 245 nm region in their ORD curves. In contrast, ORD curves of dimers (**9a**-L and **9b**-L) and a trimer(**10a**-L) show a shallow trough around 245 nm, the depth being less than −2500°. The results suggest that peptide

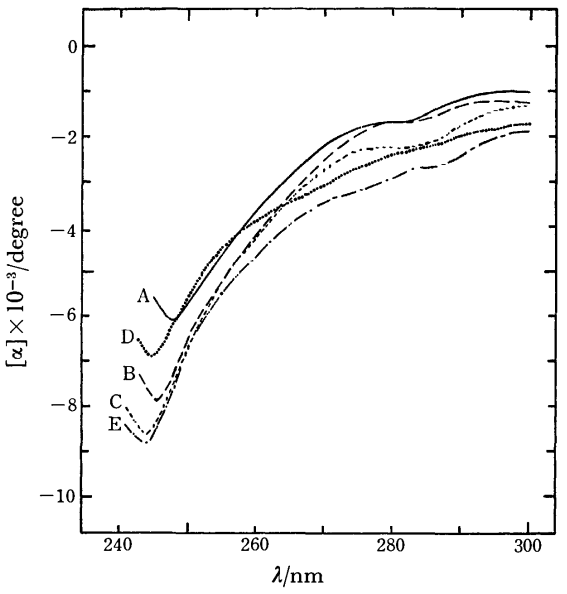

Fig. 4. ORD curves of AM-toxin I and its analogs in TFA. A, natural AM-toxin I (**1a**); B, [L-Ala²]-AM-toxin I (**8a**-L); C, [D-Ala²]-AM-toxin I (**8a**-D); D, [L-Tyr(Me)¹,L-Ala²]-AM-toxin(**8b**-L); E, [L-Tyr(Me)¹, D-Ala²]-AM-toxin (**8b**-D).

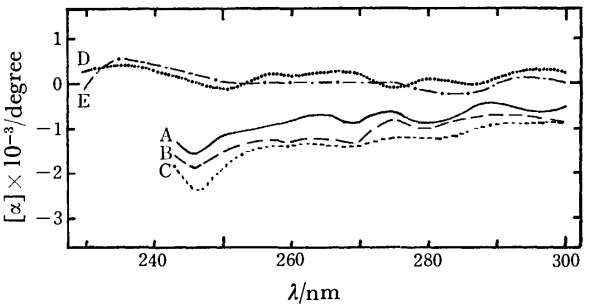

Fig. 5. ORD curves of cyclic polymers (A, B, and C in TFA) and linear peptides (D and E in MeOH). A, cyclo[-(L-Tyr(Me)-L-Ala-L-Ala-L-Hmb)$_2$-]; B, cyclo-[-(L-Amp-L-Amp-L-Ala-L-Ala-L-Hmb)$_2$-]; C, cyclo-[-(L-Amp-L-Ala-L-Ala-L-Hmb)$_3$-]; D, Boc-D-Ala-L-Ala-L-Hmb-L-Amp-OBzl; E, Boc-D-Ala-L-Ala-L-Hmb-L-Amp-OH.

chromophores in cyclic tetradepsipeptides have a certain distinct spatial orientation, but chromophores in peptides with larger ring structure together with linear tetradepsipeptide derivatives have no such definite orientation. In contrast to NMR spectra, there is no

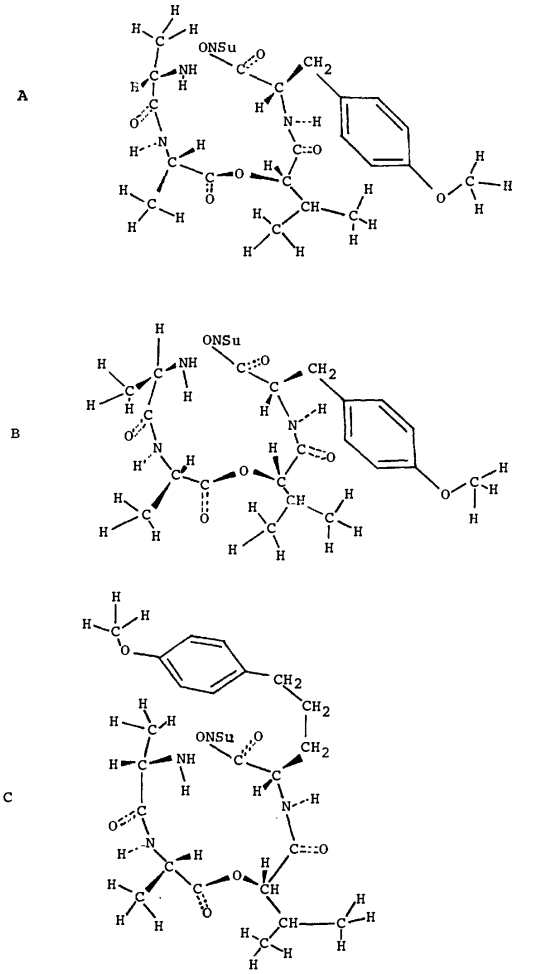

Fig. 6. Supposed conformation of reaction-intermediates in cyclization reaction starting from: A, H-L-Ala-L-Ala-L-Hmb-L-Tyr(Me)-ONSu (**6b**-L); B, H-D-Ala-L-Hmb-L-Tyr(Me)-ONSu (**6b**-D); C, H-L-Ala-L-Ala-L-Hmb-L-Amp-ONSu (**6a**-L).

distinct difference between **8a**-D or **8b**-D and **8a**-L or **8b**-L in their ORD curves. All these cyclotetradepsipeptides should have a similar orientation of chromophores.

Previous results showed that cyclic tetradepsipeptides containing one ester bond are obtained in high yields by cyclization reaction when a hydroxy acid residue occupies the third position from N-terminus in linear precursors.[5] An explanation for this finding has been presented.[7] Results obtained in this study indicate that not only the sequence of linear peptides but also the presence of D-amino acid in the N-terminus is important for giving a cyclic monomer in high yield. Exclusive formation of monomers (**8a**-D and **8b**-D) is of particular interest. This and the corresponding NMR data suggest that monomeric cyclization can readily proceed when a D-amino acid residue is present in a linear precursor. A possible substance of the intermediate having a *cis-trans-cis-trans* backbone is shown in Fig. 6. The methyl group in N-terminal L-Ala may hinder the access of the active ester group in Tyr(Me) (Fig. 6-A). In case of **6b**-D, the methyl group in D-Ala leads to a leftward direction away from the active ester (Fig. 6-B). Not only the active ester but also the bulky side chain in Amp was sterically hindered by the methyl group in L-Ala (Fig. 6-C). The fact that **6a**-L yielded much more dimer and trimer than **6b**-L supports this view. A similar discussion holds for another conformer with all-*trans* backbone.

Rich *et al.* reported that tentoxin, a similar phytotoxic cyclotetrapeptide, loses its activity upon hydrogenation even in high concentrations.[11] Since saturation of the double bond in the Dha^2 residue in **1a** results in about 2000—5000 times lowering in activity, the presence of the double bond in Dha^2 is undoubtedly important. However, while **8a**-D still retains recognizable activity (5—10 μg/ml), **8a**-L is inactive even in 100 μg/ml. This shows that the presence of a double bond is not an exclusive factor for revealing activity and that some other unknown factor seems to play a role in the activity. NMR studies indicate the presence of a common conformer of **8a**-D and **8b**-D. On the other hand, the content of the same conformer of **8a**-L and **8b**-L, if any, must be extremely low. This suggests the specific conformation is related to biological activity.

We thank Dr. H. Aoyagi, Kyushu University, for his skillful technical assistance and valuable discussion. We also thank Prof. H. Fukami and Dr. T. Ueno, Kyoto University, for the supply of natural AM-toxin I.

References

1) Part III of this series: Y. Shimohigashi, S. Lee, H. Aoyagi, T. Kato, and N. Izumiya, *Int. J. Pept. Protein Res.*, **10**, 323 (1977).

2) A part of this paper was briefly communicated: Y. Shimohigashi, S. Lee, T. Kato, N. Izumiya, T. Ueno, and H. Fukami, *Agric. Biol. Chem.*, **41**, 1533 (1977).

3) T. Ueno, T. Nakashima, Y. Hayashi, and H. Fukami, *Agric. Biol. Chem.*, **39**, 1115 (1975).

4) Abbreviations given by the IUPAC-IUB Commission (*J. Biol. Chem.*, **247**, 977 (1972)) have been used throughout. Other abbreviations: Amp, 2-amino-5-(*p*-methoxyphenyl)-pentanoic acid; Dha, dehydroalanine; Hmb, 2-hydroxy-3-methylbutanoic acid; Tyr(Me), *O*-methyltyrosine; EDC, 1-ethyl-3-(3-dimethylaminopropyl)carbodiimide; HONSu, *N*-hydroxysuccinimide; DMF, *N,N*-dimethylformamide; THF, tetrahydrofuran; TFA, trifluoroacetic acid.

5) S. Lee, H. Aoyagi, Y. Shimohigashi, N. Izumiya, T. Ueno, and H. Fukami, *Tetrahedron Lett.*, **1976**, 843.

6) Y. Shimohigashi, S. Lee, and N. Izumiya, *Bull. Chem. Soc. Jpn.*, **49**, 3280 (1976).

7) Y. Shimohigashi, S. Lee, H. Aoyagi, T. Kato, and N. Izumiya, *Int. J. Pept. Protein Res.*, **10**, 197 (1977).

8) J. L. Flippen and I. L. Karle, *Biopolymers*, **15**, 1081 (1976).

9) J. Konnert and I. L. Karle, *J. Am. Chem. Soc.*, **91**, 4888 (1969).

10) N. Go and H. A. Scheraga, *Macromolecules*, **3**, 178 (1970).

11) D. Rich, P. Mathiaparanam, J. A. Grant, and P. Bhatnagar, in "Peptides. Chemistry, Structure and Biology, Proceeding of Fourth American Peptide Symposium," ed by R. Walter and J. Meienhofer, Ann Arbor Science Publishers, Ann Arbor (1975), p. 943.

Dehalogenative Coupling of *gem*-Dihalides and Benzyl Halides by Means of Hexacarbonyltungsten(0) and Related Compounds

Yuzo FUJIWARA* Ryuichi ISHIKAWA, and Shiichiro TERANISHI

Department of Chemical Engineering, Faculty of Engineering Science, Osaka University, Toyonaka, Osaka 560

(Received August 8, 1977)

$W(CO)_6$ and WCl_6–$LiAlH_4$ systems have been found to cause coupling of *gem*-dihalides and benzyl halides giving olefins and bibenzyl derivatives, respectively. The tungsten reagents also cause coupling of some alcohols. The carbene intermediate was suggested from the formation of a cyclopropane derivative.

Dehalogenative coupling of organic halides by transition metal complexes is of importance for the formation of carbon-carbon bond.[1] Transition metal complexes such as iron, nickel, cobalt, and palladium complexes cause coupling of *gem*-dihalides to give olefins or cyclopropane derivatives.[2]

Coffey reported that metal carbonyls such as $Fe(CO)_5$ or $W(CO)_4$(pyridine)$_2$ cause coupling of *gem*-dihalides, but not $W(CO)_6$ probably because of the complete shielding of tungsten atom by carbon monoxide ligands.[3] However, in the course of studies on the reactions with tungsten compounds, we found that $W(CO)_6$ as well as WCl_6–$LiAlH_4$ is highly reactive for the reactions of *gem*-dihalides, benzyl halides, and also alcohols at room temperature. In this paper, we report on the coupling reactions of *gem*-dihalides, benzyl halides and some alcohols by lower valent tungsten compounds to give coupling products, the mechanism also being given.

Results and Discussion

Reaction of gem-*Dihalides.* The reaction of hexacarbonyltungsten(0), $W(CO)_6$, with benzylidene dichloride in THF at room temperature under nitrogen atmosphere gave (*E*)- and (*Z*)-stilbenes in 41 and 7% yields, respectively.[4]

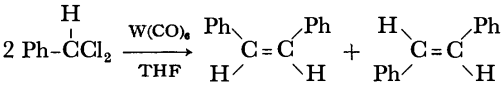

The coupling reactions of benzylidene dichloride by zerovalent tungsten carbonyl complexes, and also tungsten hexachloride, WCl_6, plus lithium aluminum hydride, $LiAlH_4$, are summarized in Table 1. In order to attain good yields, it was important to use a half equivalent amount of *gem*-dihalides to tungsten reagents.

Table 1. Coupling of benzylidene dichloride by tungsten(0) carbonyls

Tungsten carbonyl	Stilbene yield,% [a]	
	E	*Z*
$W(CO)_6$	41	7
$W(CO)_6$–$AlCl_3$ [b]	64	8
$W(CO)_5PPh_3$	56	7
$W(CO)_5NH_2C_6H_{11}$	40	5
WCl_6–$LiAlH_4$ [b]	43	8

a) Based on benzylidene dichloride. b) An amount (0.4 mmol) equivalent to tungsten compounds was added.

Coffey reported that $W(CO)_6$ causes no coupling of *gem*-dihalides in refluxing benzene.[3] On the contrary, $W(CO)_6$ was found to cause readily coupling of the dihalides even at room temperature. Addition of an equivalent amount of $AlCl_3$ to the $W(CO)_6$ system increases the yield. This is probably because $AlCl_3$ eliminates CO ligand from $W(CO)_6$ furnishing the coordinatively unsaturated site. Triphenylphosphine-pentacarbonyltungsten(0) is as reactive as $W(CO)_6$–$AlCl_3$. WCl_6 alone is not reactive for the reaction. However, addition of $LiAlH_4$ causes the reaction. This suggests that WCl_6 is reduced by $LiAlH_4$ to some lower valent tungsten species such as W(II) which is active for the reaction.

The coupling reactions of other *gem*-dihalides by $W(CO)_6$ and WCl_6–$LiAlH_4$ reagents are summarized in Table 2. We see that $W(CO)_6$ is as reactive as WCl_6–$LiAlH_4$ for the coupling reaction. Although the coupling occurs with alkyl dihalides, the yield is lower than that of aromatic halides. Since $W(CO)_6$ is relatively stable against air and easy to handle, this provides a convenient synthetic route for symmetric olefins.

Mechanism. Coffey[3] and Joshi[5] suggested a carbene mechanism for transition metal carbonyl-promoted coupling reaction. Furukawa and Kiji also suggested a carbenoid intermediate in the reaction of $Ni(COD)_2$, $Fe(CO)_5$ or $Co(CO)_8$ with *gem*-dihalides by obtaining cyclopropane derivatives.[2] On the other hand, the reaction with $Co_2(CO)_8$ proceeds step by step by a radical process.[6] In order to investigate the intermediate, we attempted to trap a carbene intermediate. From the reaction of benzylidene dichloride and $W(CO)_6$ in the presence of 1-(2-methyl-1-propenyl)-pyrrolidine (**2**), cyclopropane derivative (**1**) was obtained in 13% yield together with 9% yield of stilbene. This shows that a carbene intermediate is involved during the course of reaction. Similarly cyclopropane (**1**) was formed in 1% yield by the reaction with WCl_6–$LiAlH_4$ system.

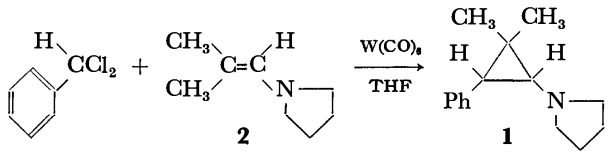

It should be pointed out that $W(CO)_6$ catalyzes the olefin metathesis reaction involving a carbene intermediate.[7] Thus there is another route for the formation of **1**, *viz.*, $W(CO)_6$ and the stilbene formed by the

* Present address: Department of Applied Chemistry, Faculty of Engineering, Kyushu University, Fukuoka 812.

Table 2. Coupling of *gem*-dihalides by $W(CO)_6$ or WCl_6–$LiAlH_4$

gem-Dihalide	Product	Yield, %[a] *E*	Yield, %[a] *Z*	Reagent[b]
CH_3O-C$_6$H$_4$-$CHCl_2$	CH_3O-C$_6$H$_4$-CH=CH-C$_6$H$_4$-OCH_3[c]	34	4	A
		47	8	B
Cl-C$_6$H$_4$-$CHCl_2$	Cl-C$_6$H$_4$-CH=CH-C$_6$H$_4$-Cl[c]	60	4	A
		62	11	B
$PhCHBr_2$	PhCH=CHPh	61	3	A
		60	5	B
Ph_2CCl_2	$Ph_2C=CPh_2$		80	A
			46	B
Ph_2CBr_2	$Ph_2C=CPh_2$		63	A
			37	B
C$_6$H$_4$Cl$_2$	C$_6$H$_4$=C$_6$H$_4$[d]		6	A
			1	B

a) Based on *gem*-dihalides. b) A: WCl_6–$LiAlH_4$, B: $W(CO)_6$. c) D. F. Hoeg and D. I. Lusk, *J. Organomet. Chem.*, **5**, 1 (1966). d) W.D. Emmons, *Org. Synth.*, **47**, 34 (1967).

coupling of benzylidene dichloride, give rise to a carbene complex, $XW{=}C\langle^{Ph}_{H}$ which then would react with olefin **2** to give **1**. However, this possibility could be ruled out from the fact that only 0.5% yield of **1** was obtained when the reaction of stilbene and $W(CO)_6$ was performed under similar reaction conditions. Thus we suggest the following reaction path involving the formation of a carbene-W complex (**3**) from the reaction

$$R_2CCl_2 + W(CO)_6 \longrightarrow \underset{\mathbf{3}}{\left[(CO)_xCl_2W{=}CR_2\right]}$$

$$\mathbf{3} \longrightarrow R_2C{=}CR_2 + WCl_2(CO)_x$$

of *gem*-dihalides and $W(CO)_6$, and subsequent dimerization of the carbene derived from the carbene complex (**3**).

Cross Coupling of Benzylidene Dichloride with Benzaldehyde. Benzaldehyde has been found to react with $W(CO)_6$ or WCl_6–$LiAlH_4$ to give stilbene derivatives in a high yield. Carbene-W complex is thought to be an intermediate of this coupling reaction.[8] It is expected that cross coupling between *gem*-dihalides and benzaldehyde could take place on being treated with $W(CO)_6$ or WCl_6–$LiAlH_4$. We found that from the reaction of benzylidene dichloride and *p*-methoxybenzaldehyde in the presence of WCl_6–$LiAlH_4$, *p*-methoxystilbene (*E* and *Z*) was obtained in 8% yield together with stilbene (*E*, 5%, *Z*, 1%) and *p*,*p*-dimethoxystilbene (*E*, 44%, *Z*, 2%). $W(CO)_6$ similarly brings about the cross coupling.

Table 3. Tungsten-promoted coupling of alcohols and benzyl halides

Substrate	Product	Yield,[a] %	Reagent[b]
C$_6$H$_5$-CH_2OH	C$_6$H$_5$-CH_2-CH_2-C$_6$H$_5$	76	A
		60	B
CH_3O-C$_6$H$_4$-CH_2OH	CH_3O-C$_6$H$_4$-CH_2CH_2-C$_6$H$_4$-OCH_3[c]	41	A
		22	B
Cl-C$_6$H$_4$-CH_2OH	Cl-C$_6$H$_4$-CH_2CH_2-C$_6$H$_4$-Cl[d]	69	A
		13	B
C$_6$H$_5$-OH	C$_6$H$_5$-C$_6$H$_5$[e]	2	A
		0.1	B
C$_6$H$_5$-CH_2Cl	C$_6$H$_5$-CH_2CH_2-C$_6$H$_5$	2	A
		8	B
C$_6$H$_5$-CH_2Br	C$_6$H$_5$-CH_2CH_2-C$_6$H$_5$	29	A
		21	B

a) Based on the starting alcohols or halides. b) A: WCl_6–$LiAlH_4$, B: $W(CO)_6$. c) J. S. Buck and S. S. Jenkins, *J. Am. Chem. Soc.*, **51**, 2163 (1929). d) R. L. Datta and F. V. Fernandes, *J. Am. Chem. Soc.*, **38**, 1812 (1916). e) W. Hückel and D. Neunhoeffer, *Justus Liebigs Ann. Chem.*, **477**, 106 (1930).

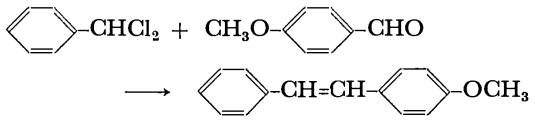

Reaction of Alcohols and Benzyl Halides. The transition metal-promoted dehydroxygenative coupling of alcohols to dimeric compounds is known.[9] In connection with coupling of *gem*-dihalides described above, we carried out reactions of alcohols, and found that $W(CO)_6$ and WCl_6–$LiAlH_4$ are also active for coupling reaction. In this case, reaction gives saturated hydrocarbons but no olefins. The results are summarized in Table 3. Coupling of benzyl alcohols proceeds smoothly to give bibenzyl derivatives. However, alkyl alcohols are far less reactive. Benzyl halides were also found to undergo coupling to give bibenzyl derivatives.

In conclusion it was made clear that zerovalent tungsten carbonyls such as $W(CO)_5L$ (L=CO, $P(Ph)_3$, and $C_6H_{11}NH_2$) and WCl_6–$LiAlH_4$ cause coupling of *gem*-dihalides, benzyl halides, and some alcohols to give olefins or dimeric hydrocarbons.

Experimental

Materials. Benzylidene dibromide,[10] diphenyldibromomethane,[11] *p*-methoxybenzylidene dichloride,[12] *p*-chlorobenzylidene dichloride,[13] and 1-(2-methyl-1-propenyl)pyrrolidine,[14] were prepared according to the reported methods. Other starting materials were of commercial grade. THF was refluxed and distilled from a dark purple solution of sodium benzophenone dianion under nitrogen. WCl_6 was purified by sublimation. $W(CO)_5PPh_3$ was prepared from $W(CO)_6$ and triphenylphosphine according to the literature.[15] Cyclohexylaminepentacarbonyltungsten(0) was prepared from $W(CO)_6$ and cyclohexylamine.[16]

General Procedure for Coupling of gem*-Dihalides by Tungsten Carbonyls.* In a flame-dried, 50-ml centrifuge tube containing a magnetic stirring bar, were placed 10 ml of THF and tungsten carbonyl (0.4 mmol), the tube then being sealed with a No-Air stopper. After the tube had been flushed with nitrogen, 0.2 mmol of *gem*-dihalides was added by means of a syringe. The mixture was stirred for 6 h at room temp under nitrogen atmosphere. The tube was then cooled to −78 °C, and the precipitated tungsten complexes were removed by filtration. The filtrate was poured into ether and the ether layer was washed with water and dried with Na_2SO_4. After evaporation of the solvent, the products were analyzed and isolated by gas chromatography. The products were identified by comparison of melting point, IR, NMR, and retention time with those of authentic samples. The results are summarized in Tables 1 and 2.

General Procedure for Coupling of gem*-Dihalides by WCl_6–$LiAlH_4$.* In a flame-dried, 50-ml centrifuge tube containing a magnetic stirring bar, was placed 10 ml of THF by means of a syringe, and the tube was sealed with a No-Air stopper. After the tube had been flushed with nitrogen, the solvent was cooled to −78 °C, and WCl_6 (0.4 mmol) and $LiAlH_4$ (0.4 mmol) were added under nitrogen atmosphere. The solution turned dark brown from green. Then 0.2 mmol of *gem*-dihalides was added with a syringe. The mixture was stirred for 6 h at room temp under nitrogen atmosphere. The reaction mixtures were quenched with 20% aq NaOH. The organic materials were extracted with ether. The ethereal solution was washed with water and concentrated. The products were analyzed by VPC. The results are summarized in Tables 1 and 2.

Trapping of Carbene Intermediate. In a flame-dried, 50-ml centrifuge tube containing a magnetic stirring bar, were placed 10 ml of THF and 0.4 mmol of $W(CO)_6$ and the tube was sealed with a No-Air stopper. After the tube had been flushed with nitrogen, 0.2 mmol of benzylidene dichloride and excess amounts (10 ml) of 1-(2-methyl-1-propenyl)pyrrolidine (**2**) were added. The mixture was stirred for 6 h at room temp under nitrogen atmosphere. After the same work-up as described above the products were analyzed by VPC to obtain 1-(2,2-dimethyl-3-phenylcyclopropyl)pyrrolidine (**1**) and stilbene in 13 and 9% yields, respectively. These products were identified by comparison with standard samples.

Cross Coupling of Benzyl Chloride with Benzaldehyde. Reaction was carried out using the same procedure as described above charging WCl_6, $LiAlH_4$ (0.8 mmol each), benzylidene dichloride (0.2 mmol), *p*-methoxybenzaldehyde (0.2 mmol), and THF (10 ml). Products analysis was carried out by VPC using authentic samples. The products were *p*-methoxystilbene (*E* and *Z*, 8%), stilbene (*E*, 5%, *Z*, 1%), and *p*,*p*-dimethoxystilbene (*E*, 44%, *Z*, 2%).

Coupling of Alcohols. Reactions were performed as in the coupling of *gem*-dihalides under the same reaction conditions. The results are given in Table 3. The products were identified by comparison with authentic samples.

*Preparation of 1-(2,2-Dimethyl-3-phenylcyclopropyl)pyrrolidine (**1**).* In a 300-ml, three-necked, round-bottomed flask equipped with a magnetic stirring bar, dropping funnel, nitrogen inlet, and a condenser with a bubble counter at the top was placed a solution of 3.5 g of CuCl, 45 ml of 1-(2-methyl-1-propenyl)pyrrolidine (**2**) and 200 ml of abs ether. Then 20 ml of phenyldiazomethane in 50 ml of ether was added dropwise over 2 h under nitrogen. The mixture was stirred for 20 h at room temp and then filtered, ether being evaporated. The residue was distilled to give the starting pyrrolidine (**2**) and colorless oil, bp 103—105 °C/1 Torr (*ca.* 1 g) which was purified by preparative VPC (column OV-17) and assigned to 1-(2,2-dimethyl-3-phenylcyclopropyl)pyrrolidine. IR (neat): 2992, 1445, 1456, 1183, 754, and 703 cm^{-1}. NMR (C_6D_6): δ 7.12(s, 5H), 2.80—2.12(m, 4H), 1.85(d, 1H, J= 6.6 Hz), 1.78—1.48 (m, 4H), 1.41 (s, 3H), 1.12 (d, 1H, J= 6.6 Hz), and 0.84 (s, 3H). MS: *m/e* 215 (M^+). Found: C, 83.92; H, 9.59%. Calcd for $C_{15}H_{21}N$: C, 83.67; H, 9.83%. Infrared spectra were recorded on a Japan Spectroscopic IR-E spectrometer. NMR spectra were obtained with a JEOL C-60HL spectrometer with TMS as an internal standard. Mass spectra were obtained with a Hitachi RMS-4 spectrometer.

References

1) M. F. Semmelhack, *Org. React.*, **19**, 119 (1972).
2) J. Furukawa, A. Matsumura, Y. Matsuoka, and J. Kiji, *Bull. Chem. Soc. Jpn.*, **49**, 829 (1976).
3) C. E. Coffey, *J. Am. Chem. Soc.*, **83**, 1623 (1961).
4) Yields are based on the starting halides or alcohols.
5) K. K. Joshi, *J. Chem. Soc., A*, **1966**, 594.
6) D. Seyferth and M. D. Miller, *J. Organomet. Chem.*, **38**, 373 (1972).
7) J. M. Basset, J. L. Bilhou, R. Mutin, and A. Theolier, *J. Am. Chem. Soc.*, **97**, 7376 (1977). for a review for olefin metathesis, see N. Calderon, E. A. Ofstead, and W. A. Judy, *Angew. Chem. Int. Ed. Engl.*, **15**, 404 (1976).
8) Presented at 35th National Meeting of the Chemical Society of Japan, Sapporo, August 1976.

9) (a) E. E. van Tamelen and M. A. Schwartz, *J. Am. Chem. Soc.*, **87**, 2277 (1965); (b) K. B. Sharpless, R. P. Haznlik, and E. E. van Tamelen, *ibid.*, **90**, 209 (1968), **91**, 1552 (1969); (c) J. E. McMurry, and M. Silvestri, *J. Org. Chem.*, **40**, 2687 (1975).
10) Th. Curtius and E. Quedenfeldt, *J. Prakt. Chem.*, **58**, 369 (1898).
11) S. Friedel, *Bull. Soc. Chim. Fr.*, **33**, 339 (1897).
12) H. Schmidt, *Ber.*, **41**, 2331 (1908).
13) F. Asinger and G. Lock, *Monatsh. Chem.*, **62**, 323 (1933).
14) A. Brossi, *Org. Synth.*, **53**, 48 (1973).
15) T. A. Magee, C. N. Matthews, T. S. Wang, and J. H. Wotiz, *J. Am. Chem. Soc.*, **83**, 3200 (1961).
16) C. S. Kraihanzel and F. A. Cotton, *Inorg. Chem.*, **2**, 533 (1963).

Some Aspects on the Mechanism of Palladium-complex-catalyzed Decomposition of and Cyclopropanation with Ethyl Diazoacetate

Akira NAKAMURA, Teruhisa KOYAMA, and Sei OTSUKA

Department of Chemistry, Faculty of Engineering Science, and Department of Polymer Science, Faculty of Science, Osaka University, Toyonaka, Osaka 560

(Received August 11, 1977)

Carbenoid decomposition of ethyl diazoacetate in the presence of various palladium complexes as catalysts was found to kinetically depend on the identity of halide ligands. The use of several chiral ligands did not induce appreciable enantioselective catalytic cyclopropanation between ethyl diazoacetate and styrene. The active catalyst species is not under the influence of the chiral ligands but under control of halides which are bound more strongly to the metal.

Transition metal-catalyzed cyclopropanation reactions are one of the important organic synthesis.[1] Although (a) various Ag and Cu salts, (b) ligand-modified Cu, Pd, and Rh catalysts and (c) Lewis-acidic metal halides have been known[1-10] to induce homo- or heterogeneously-catalyzed decomposition of diazoalkanes, the mechanism or the nature of active species, however, has remained to be elucidated. Since a variety of ligand-modified palladium complexes act as efficient catalysts, we have examined the Pd-catalyzed reaction in some detail and the results are reported here.

Results and Discussion

Palladium(II) complexes of type, PdX_2L_2 (X= halide, L=neutral ligand), are active for decomposition of ethyl diazoacetate at room temperature in homogeneous solutions. The ligand effect was studied to obtain information on the active species. The catalytic activity can be assesed by rates of nitrogen evolution from the diazo compound (Table 1). An induction period is generally observed. After attaining the maximum rate, the decomposition by $PdCl_2(PPh_3)_2$ and $PdBr_2(PPh_3)_2$ slowed down according to apparent first- to third-order kinetics with respect to concentration of the free diazoacetate. The order also depends on concentration of the catalyst (Table 1). The rate for the corresponding iodide, however, seemed to obey zero- to first-order kinetics depending on the initial concentration of the catalyst. The length of the induction period was proportional to the initial catalyst concentration. The maximum rate attained after the induction period was also roughly proportional to the catalyst concentration but independent of the diazo concentration (*cf.* Table 1). The rate especially at low catalyst concentrations fell rapidly as the reaction proceeds. Apparently this is due to deterioration of the active catalyst. The following reaction scheme is consistent with the kinetics.

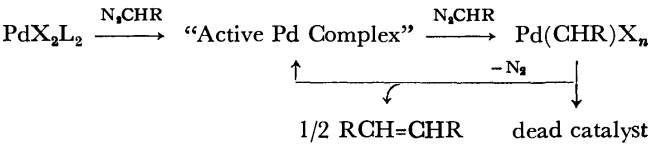

The reaction of the active Pd species with diazo acetate becomes the rate-determining step after the induction period. In the case of the decomposition by $PdI_2(PPh_3)_2$, the subsequent unimolecular decomposition of $Pd(CHR)I_n$ becomes rate-determining. The rate-determining step thus varies depending on the halide ligands.

The palladium-complex-catalyzed carbenoid reaction in neat cyclohexene gave a mixture of carbene dimers and cyclopropanation products (*endo*- and *exo*-norcarane-7-carboxylates) listed in Table 2. The isomeric product ratios obtained by the several palladium complexes catalysts are not critically influenced by the identity of the neutral ligands. By contranst, the length of induction period depends on L when a comparison was made among five $PdCl(\eta^3\text{-}C_3H_5)L$ catalysts; L=Py, 2 min, PPh_3 10 min, P-*n*-Bu_3, 15 min, $P(OPh)_3$ 15 min; P(O-*n*-Bu)$_3$, 2 min. The results contrasts with the catalysis by cobalt(II) dioximato chelates[11,12] which show a dramatic effect by added donor molecules, *e.g.* pyridine. Asymmetric synthesis of ethyl 2-phenylcyclopropanecarboxylate was attempted by reaction of ethyl diazoacetate with styrene in the presence of the following chiral palladium complexes; dichlorobis((*S*)-α-methylbenzylamine) palladium, di-μ-chlorobis(7,1,2-η^3(−)-pinenyl) dipalladium, bis[(−)-hydroxymethylenecamphorato] palladium, di-μ-chlorobis[(*S*)-*N*,*N*-dimethyl-α-methylbenzylamine-2-*C*, *N*]dipalladium,[21] di-μ-chlorobis[(*S*)-*N*,*N*-dimethyl-2-naphthylamine-3-*C*,*N*]palladium,[22] and bis(β-camphorquinone dioximato)palladium.[16] However, the optical yields of the cyclopropane isomers were only 0—2% although

Table 1. Dependence of apparent order of the carbenoid reaction of ethyl diazoacetate and induction periods on concentration of palladium(II) catalysts

Catalyst	Catalyst concentration (mmol/l)	Apparent[a] order with [N_2CHCO_2-Et] concn	Induction periods (min)	Max. rates (N_2 evolved/min) (ml)
$PdCl_2(PPh_3)_2$	4	2.0	33	3.3
	2	2.2	25	2.0
	1	4.0	15	0.9
$PdBr_2(PPh_3)_2$	4	1.5	15	3.2
	2	2.1	14	1.7
	1	2.8	8	0.9
$PdI_2(PPh_3)_2$	4	0	35	0.5
	2	1.0	30	0.7
	1	1.6	30	0.4

a) The order was determined graphically by plotting the rate (ml/min) *vs.* time after the maximum rate is attained.

TABLE 2. RATIOS OF ISOMERIC CARBENOID REACTION PRODUCTS FORMED BY Pd-COMPLEX-CATALYZED REACTION BETWEEN ETHYL DIAZOACETATE AND CYCLOHEXENE[a)]

Catalyst precursor	Temp (°C)	Isomer ratios of products: Diethyl fumarate/diethyl maleate	Isomer ratios of products: *exo/endo* in ethyl norcaranecarboxylate
$PdCl_2(cod)$	60	2.5	4
$PdCl_2(PPh_3)_2$	20	2.5	10
$[PdCl(C,N\text{-phe})]_2$[b)]	60	2	5
$[PdCl(C,N\text{-phe})]_2$[b)]	20	1.3	8
$[PdCl(\eta\text{-}C_3H_5)]_2$	20	5	8
$PdCl(\eta\text{-}C_3H_5)(Py)$	20	6	10
$PdCl(\eta\text{-}C_3H_5)\cdot(PPh_3)$	20	4	10
$PdCl(\eta\text{-}C_3H_5)\cdot[P\text{-}(n\text{-}Bu_3)]$	20	4	10
$PdCl(\eta\text{-}C_3H_5)\cdot[P(OPh)_3]$	20	5	10
$PdCl(\eta\text{-}C_3H_5)\cdot[P(O\text{-}n\text{-}Bu)_3]$	20	4	10

a) Reaction conditions: catalyst concentration; 0.01 mol/l, diazoacetate concentration 2 mol/l in neat cyclohexene. b) C,N-phe=*N,N*-Dimethyl-α-methylbenzylamine-2*C,N*

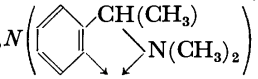

the chemical yields were good (*ca.* 70%). The absence of the appreciable chiral ligand effect implies that the neutral, η^3(C), C,N-, N,N-, or O,O-ligands are mostly eliminated during the formation step of the active species. The elimination of these ligands seems to take place by the reaction of transient reactive carbene-metal moiety generated from diazo compounds. The reaction of coordinated η^3-C_3H_5, phosphines, or isocyanides with diazoalkanes has been known to give CH_2=CH–CH_2=CHR,[15] alkylidenephosphorane (R_3P=CHR)[1] or ketenimine (RCH=C=NR).[1,14] The corresponding reaction with coordinated halides seems to be a very slow process.[13]

Some palladium complexes at the formal oxidation state of one and zero are also examined. A chloro-bridged Pd(I) complex, $[PdCl(t\text{-BuNC})_2]_2$, was found active without an induction period. The catalysis of $[PdCl(\eta^3\text{-}C_3H_5)]_2$ also belongs to this category. Pd-$(PPh_3)_4$ and $Pd_2(t\text{-BuNC})_4$ were weakly active at room temperature, but the catalysis deteriorated readily. These observations indicate formal oxidation state of the metal to be unimportant. The catalysis critically depends on the identity of the metal in a similar ligand environment. Thus, $PtCl_2(PPh_3)_2$ showed only a weak activity even at 60 °C. By contrast $[RhCl(CO)_2]_2$, $[RhCl(C_8H_{12})]_2$, $[RhCl(C_2H_4)_2]_2$, and $RuCl_2(PPh_3)_3$ have very high activity at room temperature. No activity was found for $NiCl_2(PPh_3)_2$ or $CoCl_2(PPh_3)_2$.

The stereochemical paths of the $[PdCl(\eta^3\text{-}C_3H_5)]_2$-catalyzed cyclopropanation was investigated by using *cis*-dideuteriostyrene. As shown in Eq. 1, an almost complete retention of the original stereochemistry at the olefin was observed.

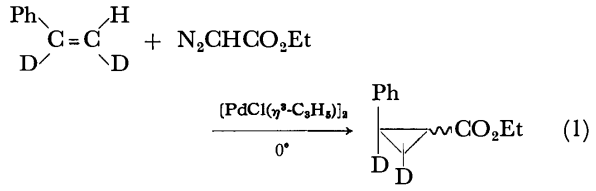

This contrasts to the bis(camphorquinone dioximato)-cobalt-catalysis where a considerable stereochemical inversion (up to 35%) is involved.[16] Thus, the Pd-catalysis is characterized with a stereochemical retention for the olefin component implying a multicentered transition state.

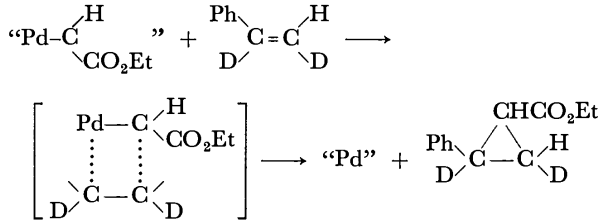

Since free carbenes with CO_2Et substituents are known to be triplet especially in the presence of compounds with heavy atoms, this result suggests the catalytically active species is not the free carbene.

We have a already studied thermal reactions of Pd(0) diazoalkane complexes, $PdL_2(dfl)$: L=PPh_3, *t*-BuNC; dfl=9-diazofluorene, where *N,N*-η^2-coordination of the diazoalkane was established.[14,17] The coordination retards the decomposition with nitrogen evolution and hinders the olefin attack leading to cyclopropanes. The observed low activity of Pd(0) complexes is thus understood. In contrast to the retardation of decomposition by virtue of these metal complexes with high metal electron densities, a Lewis acidic center, *e.g.* $ZnCl_2$, or $FeCl_3$, acts as an effective catalyst site.[1,10] The present palladium or rhodium catalysis does not involve such a strong Lewis acidic site. A different orbital interaction must be postulated for the present catalysis. Clearly, a further study including molecular orbital analysis is required.

Experimental

The following metal complexes were prepared by the methods in literature; $[PdCl(t\text{-BuNC})_2]_2$,[18] $PdCl_2(cod)$,[19] $[PdCl(\eta\text{-}C_3H_5)]_2$,[20] and known chiral Pd complexes[21,22] mentioned in the text. Some new chiral Pd complexes were prepared as follows.

a) Bis(hydroxymethylenecamphorato)palladium(II): An ethanol solution (4 ml) of (−)-hydroxymethylenecamphor (1.8 g) was mixed with an aq suspension of $PdCl_2$(0.6 g, 3.4 mmol) at 80 °C and then with aq KOH (1 M, 1.5 ml). The brown suspension turned into a yellow precipitate in 30 min. which was filtered and dried. Recrystallization from a mixture of hot benzene and hexane gave orange crystals (78% yield, mp 170 °C dec, $[\alpha]_D^{23}$ +153° (c=0.4)).

b) Dichlorobis(α-methylbenzylamine)palladium(II): A methanol solution (5 ml) of K_2PdCl_4 (0.22 g, 0.7 mmol) was mixed with (−)-α-methylbenzylamine (0.29 g, 2.4 mmol) with stirring to give a yellow precipitate which was filtered, dried, and recrystallized from a mixture of benzene and hexane (yield 87%, mp 131—134 °C, $[\alpha]_D^{23}$ −39.0° (c=4.95)).

Kinetics of Catalytic Decomposition of Ethyl Diazoacetate. A palladium complex in question (0.04—0.01 mmol) dissolved in benzene (20 ml) was mixed with a benzene solution (2 ml) of ethyl diazoacetate (0.23 g) under nitrogen in a 50 ml flask connected with gas burettes at 30.0°. The reaction mixture was stirred magnetically in a flask covered with aluminum foil to prevent any photodecomposition of the diazo compound during the catalysis. The amount of evolved gas was followed to measure the decomposition rate. The reaction mixture remained apparently homogeneous throughout the kinetic runs, but after the prolonged standing a small amount of metallic palladium deposited. The products from the catalyzed cyclopropanation in cyclohexene performed under the conditions described in Table 2 were analyzed by GLC (Apiezon Grease L).

Cyclopropanation of cis-*Dideuteriostyrene with Ethyl Diazoacetate by* $[PdCl(\eta\text{-}C_3H_5)]_2$. *cis*-Dideuteriostyrene was prepared by selective hydrogenation of phenylacetylene with deuterium gas in the presence of Lindlar catalyst and found to be stereochemically 86% pure. A solution of ethyl diazoacetate (2.09 g, 18.3 mmol) in the styrene-d_2 (1.3 ml) was added to a solution of $[PdCl(\eta\text{-}C_3H_5)]_2$ (0.21 g, 0.56 mmol) in the styrene-d_2 (2.5 ml) at 0° with stirring. After vigorous nitrogen evolution had ceased, the reaction mixture was distilled (85—87°C/2 Torr) to give ethyl 2,3-dideuterio-*cis*- and -*trans*-2-phenylcyclopropanecarboxylate (0.3 g, 8.6% yield, *trans*/*cis*=1.5). Each isomer of the cyclopropanes was separated by GLC and hydrolyzed to the corresponding acids. Since the ^{1}H-NMR spectra of each isomeric acids had been already assigned, the stereochemical distribution of deuterium was determined by the nmr to find *cis*-d_2/*trans*-d_2=6.1 for the *trans*-phenyl compound and *cis*-d_2/*trans*-d_2=2.6 for the *cis*-phenyl compounds. Corrections due to the stereochemical purity of 86% of the starting styrene were made to find the stereochemical process at the cyclopropanation leading to the *trans*-phenyl compounds to be completely retention.

The authors acknowledge the experimental assistance of Mr. A. Konishi and M. Kudo.

References

1) W. Kirmse, "Carbene Chemistry," 2nd ed, Academic Press, New York-London (1971).
2) H. Nozaki, H. Takaya, S. Moriuti, and R. Noyori, *Tetrahedron*, **24**, 3655 (1968); T. Aratani, Y. Yoneyoshi, and T. Nagase, *Tetrahedron Lett.*, **1975** 1707.
3) W. R. Moser, *J. Am. Chem. Soc.*, **91**, 1135, 1141 (1969).
4) R. K. Armstrong, *J. Org. Chem.*, **31**, 618 (1966).
5) E. T. McBee, G. W. Calundann, and T. Hodgins, *J. Org. Chem.*, **31**, 4260 (1966).
6) D. S. Wulfman, *Tetrahedron*, **32**, 1231 (1976).
7) R. Paulissen, Ph. Moniotte, A. J. Hubert, and Ph. Teyssié, *Tetrahedron Lett.*, **1974**, 3311; R. Paulissen, H. Riemlinger, E. Hayes, A. H. Hubert, and Ph. Teyssié, *Tetrahedron Lett.*, **1973**, 2233; R. Paulissen, E. Hayes, A. H. Hubert and Ph. Teyssié, *Tetrahedron Lett.*, **1974**, 607.
8) Ph. G. Moniotte, A. J. Hubert, and Ph. Teyssié, *J. Organomet. Chem.*, **88**, 115 (1975).
9) R. G. Salomon and J. K. Kochi, *J. Am. Chem. Soc.*, **95**, 3300 (1973).
10) S. H. Goh, L. E. Closs, and G. L. Closs, *J. Org. Chem.*, **34**, 25 (1969).
11) A. Nakamura, A. Konishi, and S. Otsuka, *J. Am. Chem. Soc.*, in press.
12) Y. Tatsuno, A. Konishi, A. Nakamura, and S. Otsuka, *J. Chem. Soc., Chem. Commun.*, **1974**, 588.
13) F. D. Mango and I. Dvoretzky, *J. Am. Chem. Soc.*, **88**, 1654 (1966).
14) S. Otsuka, A. Nakamura, T. Koyama, and Y. Tatsuno, *Justus Liebigs Ann. Chem.*, **1975**, 626, and references cited therein.
15) I. Moritani, Y. Yamamoto, and H. Konishi, *J. Chem. Soc., Chem. Commun.*, **1969**, 1457.
16) A. Nakamura. A. Konishi, R. Tsujitani, and S. Otsuka, *J. Am. Chem. Soc.*, in press.
17) A. Nakamura, T. Yoshida, M. Cowie, S. Otsuka, and J. A. Ibers, *J. Am. Chem. Soc.*, **99**, 2108 (1977).
18) S. Otsuka, Y. Tatsuno, and K. Ataka, *J. Am. Chem. Soc.*, **93**, 6705 (1971).
19) D. Drew and J. R. Doyle, *Inorg. Syn.*, **13**, 52 (1972).
20) W. T. Dent, R. Long, and G. Wilkinson, *J. Chem. Soc.*, **1964**, 1985.
21) S. Otsuka, A. Nakamura, T. Kano, and K. Tani, *J. Am. Chem. Soc.*, **93**, 4301 (1971).
22) K. Tani, L. D. Brown, J. Ahmed, J. A. Ibers, M. Yokota, A. Nakamura, and S. Otsuka, *J. Am. Chem. Soc.*, **99**, 7876 (1977).
23) K. Dunne and F. J. McQuillin, *J. Chem. Soc., C*, **1970**, 2200.

The Substituent Effect. XII. Solvolysis of 3′- and 4′-Substituted 1-(4-Biphenylyl)ethyl Chlorides

Yuho Tsuno,* Wei-Yuen Chong, Yoshihiko Tairaka, Masami Sawada, and Yasuhide Yukawa

The Institute of Scientific and Industrial Research, Osaka University, Suita, Osaka 565
**Department of Chemistry, Faculty of Science, Kyushu University, Hakozaki, Fukuoka 812*

(Received August 13, 1977)

Rate constants of solvolysis of 3′- and 4′-substituted 1-(4-biphenylyl)ethyl chlorides were measured in 80% (v/v) aqueous acetone. The effect of substituents could be correlated excellently with the LArSR relationship.

$$\log k/k_0 = -1.56(\sigma^0+0.84\Delta\bar{\sigma}_R^+)$$

The ρ and r^+ values are smaller than those in the corresponding phenyl system under identical conditions ($\rho=-4.95$, $r^+=1.15$). The difference of the r^+ values is interpreted in terms of twisting of the two phenyls around the pivot bond in biphenyl. The same treatment has been applied successfully to other sets of reactivity data; solvolysis, protodesilylation, alkaline hydrolysis, and piperidinodebromination. The results indicate a consistently reduced effectiveness of *pi*-electronic transmission in biphenylyl relative to phenyl system in all reactions studied.

In our continuing interest in substituent effects, the LArSR relationship, Eq. 1,[1,2] has been investigated in order to apply it to reactivities for the *pi*-systems beyond the phenyl system; extensive rate studies have already been performed in the solvolysis of substituted 1-phenylethyl chlorides.[2]

$$\log k/k_0 = \rho(\sigma^0+r^+\Delta\bar{\sigma}_R^++r^-\Delta\bar{\sigma}_R^-) \quad (1)$$

In the substituted 1-naphthyl system,[3] the substituent effect was successfully separated into a reaction-independent inductive (*I*) effect and a reaction-dependent *pi*-electronic (*Pi*) effect.

To check the general applicability of the LArSR Eq. 1 to substituent effects in the biphenylyl system and to compare the resulting substituent-effect parameters with those of the corresponding phenyl system,[2] we have studied the solvolysis of 3′- and 4′-substituted 1-(4-biphenylyl)ethyl chlorides. The present paper discusses (i) the LArSR treatment for the biphenylyl reactivities, where the different types of electrophilic and nucleophilic reactions available[4a] are included, and (ii) the comparisons of the resulting parameters with those obtained in the phenyl systems under the same conditions. These results must reflect the characteristic features of the intervening biphenylyl *pi*-system between substituents and the reaction center.

Results and Discussion

Rate constants for the solvolysis of nine 3′- and 4′-substituted 1-(4-biphenylyl)ethyl chlorides were determined in 80% (v/v) aqueous acetone at convenient temperatures to give moderate rates which were followed with the usual acid-base titration method. All kinetic runs followed accurately the first-order kinetic law. The reproducibility of the rate constants from repeated runs was within ±1.5%. The 4′-substituted derivatives were confirmed to be of 99—100% purity, based on their infinity readings, while the 3′-halogeno derivatives, which were used for kinetic measurements immediately after the evaporation of solvent and without purification, were estimated to be of *ca.* 97% purity.

The rate constants at various temperatures and the relative rates with respect to substituents are listed in Table 1,[4b] together with the activation parameters. The activation entropies obtained are quite constant at −11.8±1.5 eu (10.7±0.3 log A unit) over the range of substituent, suggesting the operation of a constant mechanism throughout the series.[2] Logarithms of the relative rates at 45 °C are linearly correlated in excellent precision (corr coeff, $r=0.9997$, $s=\pm0.016$) with those at 25 °C, giving a slope of 0.950. The temperature change provides a negligibly small effect on the ρ value with a change of only a few percent. As anticipated from the intervention of the second phenyl group between substituents and the reaction center, apparent substituent effects in the biphenylyl system are much smaller than those in the corresponding phenyl system, for the electronic effects of substituents are transmitted across a longer distance or a larger number of bonds to the reaction center.

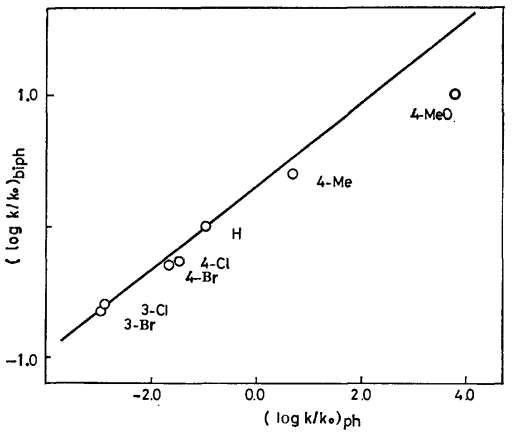

Fig. 1. The log-log plot of biphenylyl *vs.* phenyl system in the present solvolysis.

The log *k*-log *k* plot of the solvolysis rates between the biphenylyl and the phenyl systems under identical conditions does not show a linear relation (Fig. 1). All −*R*(*pi*-donor) 4′-substituted derivatives deviate downward from the line drawn through the 3′-substituted and unsubstituted derivatives, suggesting not only a far smaller ρ value but also a smaller r^+ value for the 4-biphenylyl system than for the phenyl system ($\rho=$

Table 1. Solvolysis rates of 3′- and 4′-substituted 1-(4-biphenylyl)ethyl chlorides in 80% (v/v) aq acetone

Subst.	Temp (°C)	10^5k_1 (s^{-1})	$\log k/k_0$ (45 °C)[4b]	$\log k/k_0$ (25 °C)[4b]	$\Delta H^{\neq}$ (kcal/mol)	$\Delta S^{\neq}$ (eu)
4′-MeO	39.65	47.0				
	30.00	16.0				
	20.00	5.35				
	45.00	79.8[a]	1.024		19.5	−11.4
	25.00	9.41[a]		1.086		
4′-Me	55.00	54.3				
	49.75	30.3				
	39.65	10.7				
	45.00	18.9[a]	0.399		20.8	−10.3
	25.00	1.95[a]		0.402		
H	55.00	20.7				
	49.75	13.0				
	39.65	4.16				
	45.00	7.55[a]	0.000		20.9	−11.9
	25.00	0.772[a]		0.000		
4′-Cl	59.85	20.3				
	49.75	6.58				
	39.65	2.27				
	45.00	4.08[a]	−0.263		21.8	−10.3
	25.00	0.378[a]		−0.310		
4′-Br	59.85	17.6				
	49.75	6.05				
	39.65	2.10				
	45.00	3.74[a]	−0.305		21.1	−12.5
	25.00	0.372[a]		−0.317		
3′-Cl	59.85	9.48				
	49.75	3.11				
	39.65	1.02				
	45.00	1.87[a]	−0.606		22.2	−10.5
	25.00	0.166[a]		−0.668		
3′-Br	59.85	7.94				
	49.75	2.66				
	39.65	0.904				
	45.00	1.63[a]	−0.666		21.6	−12.6
	25.00	0.154[a]		−0.700		
4′-CN	81.75	26.8				
	75.00	14.5				
	65.00	5.48				
	45.00	0.664[a]	−1.056		21.9	−13.4
	25.00	0.0608[a]		−1.104		
4′-NO_2	81.75	19.6				
	75.00	10.3				
	65.00	3.92				
	45.00	0.461[a]	−1.214		22.2	−13.3
	25.00	0.0409[a]		−1.276		

a) Extrapolated or interpolated from other temperatures.

−4.95, $r^+=1.15$).[2]

A plot of the biphenylyl data at 45 °C against Brown's σ^+ [5,8] appears to give a good linear relation with a ρ^+ value of −1.46 ($r=0.9988$, $s=\pm0.037$, $n=9$); the dotted line in Fig. 2. An unfavorable deviation is seen for the unsubstituted point; this amounts to 0.08 log-unit, which corresponds to a 20% change in the rate constant obtained. Such an error should not be expected for the rate measurements.

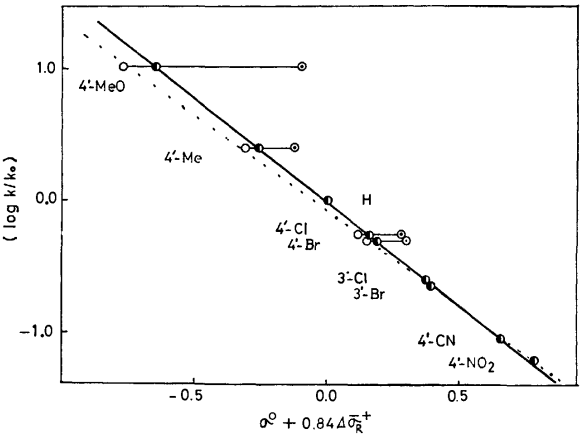

Fig. 2. The LArSR plot for the solvolysis of 1-(4-biphenylyl)ethyl chlorides at 45 °C (◐). A dotted line shows Brown's σ^+ correlation; ○ and ⊙ indicate σ^+ and σ° plots for $-R$ substituents, respectively.

The application of Eq. 1[1,2] provides an excellent correlation, with a standard deviation of ±0.023 and a correlation coefficient of 0.9996 (Fig. 2).[6]

$$\log k/k_0 = -1.56(\sigma^0+0.84\Delta\bar{\sigma}_R^+) - 0.03$$

In this plot, there is no particular deviation. The $\rho(-1.56)$ obtained is identical with the ρ value determined from the 3′-substituents and $+R$(*pi*-acceptor) 4′-substituents ($\rho=-1.57$, $r=0.9987$, $s=\pm0.028$, and $n=5$). The identity indicates that the effects of 3′-substituents (and $+R$ 4′-ones) in the 4-biphenylyl system can be practically treated just as those of the *meta* (and $+R$ *para*) substituents in the phenyl system.

Inukai has reported[7] that the solvolysis data of 1-(4-biphenylyl)-1-methylethyl chlorides also showed downward deviations for $-R$ substituents on the simple σ^+ plot, although the reaction center was the same as that for the reference reaction of σ^+. It was well understood that such deviations resulted from the r^+ (0.67) value, which was smaller than unity (Table 2, Reaction C). Similarly, the recent results of Bolton and Burley for the substituent effects on α-(4-biphenylyl)benzyl chlorides[27] are also best treated with a r^+ value of 0.75 (Table 2, Reaction B). These facts illustrate the assertion that our LArSR Eq. 1 can describe the solvolyses in the 4-biphenylyl system more precisely than does Brown's treatment. The lower r^+ values indicate that the resonance contribution from $-R$ substituents in 4′-position to the stabilization of the transition state is less effective in the biphenylyl system.

The LArSR treatment has been found to be generally applicable to other reactivities in the biphenylyl systems. The results of the correlation analysis are shown in Table 2, in comparison with those in the phenyl systems under the same conditions for the respective reactivities, although the substituent-effect data available are too limited to check the applicability thoroughly. The table includes six typical electrophilic reactions[4a] (solvolyses of secondary and tertiary chlorides, protodesilylation, alkaline hydrolysis of esters, and acid dissociation) and a typical nucleophilic reaction[16] (piperidinodebromination). It is clear at a glance that the correlation for

Table 2. Application of the LArSR Eq. 1 to reactivities for 3′- and 4′-substituted 4-biphenylyl system

Reaction	Solv[a]	Temp (°C)	System	ρ	r^+	R[g]	$\pm s$[h]	n[i]	Ref.
Electrophilic reactions[4a]									
A: Solvolysis	80A	45	Biph	−1.56	0.84	0.999	0.023	9	b)
ArCHMeCl	80A	45	Ph	−4.95	1.15	0.999	0.040	16	2
B: Solvolysis	9: 1EA	25	Biph	−1.30	0.75	0.995	0.057	12	27
ArCH(Ph)Cl	100E	25	Ph	−4.13	1.17	0.998	0.125		28
C: Solvolysis	90A	25	Biph	−1.39	0.67	0.999	0.024	6	7
$ArCMe_2Cl$	90A	25	Ph	−4.54	1.00 (by definition)				8
D: Protodesilylation	AcOH–H^+	50	Biph	−1.31	0.41	0.999	0.013	6	9
$ArSiMe_3+H^+$	AcOH–H^+	50	Ph	−4.99	0.74	0.999	0.068	11	10
E: Alkaline Hydrolysis	88.7E	25	Biph	(0.58)	(0.34)	0.999	0.005	8	11
$ArCOOEt+OH^-$	85E	25	Ph	2.58	0.25	0.997	0.069	16	1c
F: Acid dissociation	50BE	25	Biph	(0.46)	(0.14)	0.978	0.04	8	12
ArCOOH	50BE	20	Biph	(0.49)	(0.36)	0.945	0.06	18	c), 13
	50BE	25	Ph	1.43	0.20	0.991	0.09	6	12
Nucleophilic reactions[4a]									
G: Piperidinodebromination $Ar(NO_2)Br+PiP$	100M	50	Biph[d]	0.95	0.36[f]	0.991	0.038	12	14
H: Ammonium Dissociation	50E	20	Biph	(0.64)	(0.1)	0.988	0.035	10	13
$ArNH_3^+$	50E	25	Ph	(3.11)		0.983	0.120	10	e), 15

a) 80A (80% aq acetone), 9: 1EA (9: 1 EtOH: acetone), 100E (100% EtOH), AcOH–H^+(AcOH-aq H_2SO_4), 50BE (50% 2-butoxyethanol), and 100 M (100% MeOH). b) Present study. c) The points of 3′-CN, 3′-NO_2, 4′-Ph, and 4′-CN were omitted for calculations because of problems with their solubility and purity. d) The reaction of 3′- and 4′-substituted 3-nitro-4-bromobiphenyls with piperidine. e) The point of *p*-F was omitted. Substituents involved are too limited (from *p*-Me to *m*-Br) to get an accurate ρ. f) For the corresponding phenyl system, the r^- of 0.77 was employed (see Text). g) Correlation coefficient. h) Standard deviation. i) Number of substituents involved.

every reaction is excellent ($R>0.99$), except for F reaction, where the biphenylyl system has a very small ρ. Thus, in general, the LArSR treatment is equally applicable to 4-biphenylyl reactivities.

In the comparison between the biphenylyl and phenyl systems, the ratio of ρ values, ρ_{Biph}/ρ_{Ph}, is as a good approximation *ca.* 0.3 in all cases; the ratios of r, r^+_{Biph}/r^+_{Ph}, for A, B, C, and D reaction series (in Table 2) are of the magnitude of 0.5—0.7. For the solvolysis of benzhydryl chlorides, $r^+_{Ph}=1.17$ (in EtOH)[28] was employed for this calculation. The r^+_{Biph} values for E and F series are not quite as reliable as the others, because of the low sensitivities to substituent change ($\rho_{Biph}\simeq 0.5$). In the case of the nucleophilic reaction[4a] of G series, we could not find the substituent-effect data in the phenyl system which corresponded to the same conditions as those in the biphenylyl system. Most recently, we have studied the reactions of 4-substituted 1-chloro-2-nitrobenzenes and 4-substituted 1-fluoro-2-nitrobenzenes with piperidine in MeOH,[17] which could be correlated excellently by means of the LArSR Eq. 1; in the former piperidinodechlorination at 80 °C, $\rho=3.86$, $r^-=0.77$ ($R=0.998$, $s=\pm 0.106$, $n=14$) and in the latter piperidinodefluorination at 25 °C, $\rho=4.02$, $r^-=0.78$ ($R=0.999$, $s=\pm 0.08$, $n=7$). Since the leaving groups of Cl and F gave identical r^- values, it is reasonably estimated that the piperidinodebromination may have a similar amount of nucleophilic resonance exaltation ($r^-=0.77$).[18] Then, the ratio of r^-, r^-_{Biph}/r^-_{Ph}, for G reaction will be of the magnitude of 0.5.

These features of the ratios of r^+ and r^- lead us to the view that there is no simple linear log k-log k relationship between the biphenylyl and phenyl systems for a reaction with $r^\pm_{Ph}>0.5$. However, if a given reaction shows a smaller contribution from the resonance effect ($r^\pm_{Ph}<0.5$), such a linearity may hold practically within experimental uncertainty; in fact both E and F series belong to this case.[11,12]

As far as the comparison of substituent effects between the biphenylyl and phenyl systems are concerned, the relative ρ can be taken as a measure of the transmission of polar effects (more exactly inductive effects) of substituents in biphenylyl relative to the phenyl system. According to a field effect model by Kirkwood-Westheimer,[19] ρ is derived to be proportional to the reciprocal of the square of the distance R,

$$\rho = A\cos\theta/R^2,$$

where A is a constant under given reaction conditions, θ is the angle between a C–X (substituent) dipole and a distance vector to a reaction center, and R is the distance between them. Since $\cos\theta\simeq 1$ (4′- or *para* position of substituents) and $A_{Biph}/A_{Ph}\simeq 1$ can reasonably be expected, the following relation may hold to a first approximation:

$$\rho_{Biph}/\rho_{Ph} = (A_{Biph}/A_{Ph})(R^2_{Ph}/R^2_{Biph}) \simeq R^2_{Ph}/R^2_{Biph}.$$

The relative ρ values are in good agreement with the respective values calculated by using simplified distances (Table 3); this seems to suggest the importance of the transmission mode through the field, as far as the

Table 3. Relative ρ, q_r^+ (q_r^-), and related values

Reaction[a]	ρ_{Biph}/ρ_{Ph}	R^2_{Ph}/R^2_{Biph}	$q^{\pm}_{r,Biph}/q^{\pm}_{r,Ph}$
A: ArCHMeCl	0.32	0.33	0.80
B: ArCHPhCl	0.31	0.33	0.74[b]
C: $ArCMe_2Cl$	0.31	0.33	0.77
D: $ArSiMe_3$	0.26	0.25	0.71
E: ArCOOEt	0.22	0.33	
F: ArCOOH	0.32	0.36	
G: $Ar(NO_2)Br$	(0.2)	0.25	0.73[c]
H: $ArNH_3^+$	(0.2)	0.33	

a) See Table 2. b) $r^+_{Ph}=1.17$ was used (see Text). c) $r^-_{Ph}=0.77$ was used (see Text).

present comparisons are concerned.

Dewar and Grisdale assumed that the factor controlling the inductive effect in ΔpK_a of substituted naphthoic and biphenylcarboxylic acids is solely the electrostatic field effect, the magnitude of which is expressed by a function of the reciprocal of the distance.[20a] As summarized in Tables 2 and 3, the data sets accumulated for biphenylyl reactivities and the results properly analyzed have come to show that the $1/R^2$ approximation is likely to be a more precise description of the ρ (inductive effect) than the Dewar approximation. An alternative mode based on successive polarizations through intervening bonds, however, is not completely ruled out. The transmission factor per one phenyl ring is calculated to be 0.31, as an average of A and C reactions. This figure results in a transmission factor of 0.63[20b] per a sp^2 carbon unit, which is slightly smaller than the values estimated from 1-naphthyl[3] and other side chain reactivities.[4c]

Comparisons of r values in both biphenylyl and phenyl systems also give us interesting facts concerning the loss of resonance in the intervening *pi*-electronic system. Since the apparent substituent constants can be rewritten in terms of σ_i and σ_π,[1] the use of the relative q_r value, instead of the relative r, is reasonable for a net comparison of *pi*-electronic effect.

$$\bar{\sigma} = \sigma^0 + r^+\Delta\bar{\sigma}_R^+ + r^-\Delta\bar{\sigma}_R^- = \sigma_i + q_r^+\sigma_\pi^+ + q_r^-\sigma_\pi^-, \quad (2)$$

where $q_r^+=1+r^+/0.415$ and $q_r^-=1+r^-/0.73$. The relative q_r values, as tabulated in Table 3, reflect the effectiveness of resonance in the biphenylyl relative to the phenyl system and show nearly a constant value of 0.76 ± 0.04. The q_r^+ ratios obtained from the four electrophilic exalted resonance reactions,[4a] A, B, C, and D, agree quite well with the q_r^- ratio of the nucleophilic exalted resonance reaction,[4a] G. It should be noted here that the same type of treatment can be successfully performed with the $+R$ class of substituents in nucleophilic exalted reactions. The resulting relative q_r^- is just equivalent with the well-examined relative q_r^+'s in the electrophilic cases. It is then concluded that the relative effectiveness of *pi*-electronic transmission in the biphenylyl to the phenyl system remains constant in spite of the quite different types of reactions.

In the usual approximation, the reduced effectiveness may be explained in terms of a twisting of two phenyls around the pivot bond in biphenyl.[21] If the total reduced effect is to be caused only by the factor of twisting, the angle can be calculated to be *ca.* 30° from the relation of $\cos^2\theta=0.75$. The angle in a solution has been estimated to be around 35° from some sources.[22] Then the two phenyl rings in biphenyl probably act as if the twisting angle remains nearly the same in all reactions.

The reactivity difference between the present biphenylyl and phenyl derivatives may also be considered as a factor affording lower r^+ values for the biphenylyl system: in the present solvolysis, the former is *ca.* 10 times more reactive than the latter. The increased stabilization of the transition state by the second phenyl ring in biphenylyl should cause a decreased demand for the electron releasing resonance contribution from 4'-substituents. This may predict a lower r^+ value. If this is the case, a much lower r^+ value would be expected in the corresponding fluorenyl system because of the coplanarity of the second phenyl ring. Our experimental results[4c] show clearly that this is not the major factor. A more detailed discussion on the twisting should be done with an alternative comparison between the biphenylyl and fluorenyl systems.

Finally, it is worth particular emphasis that the LArSR relationship, which is based on reactions in the phenyl system, applies equally excellently to reactivities in the other *pi*-system of biphenylyls.

Experimental

Materials. 4-Methyl-, 4-chloro-, 4-bromo-, and 3-chlorobiphenyls were prepared by the Gomberg-Bachmann reaction.[23] 4-Methoxybiphenyl was made by methylation of commercial 4-hydroxybiphenyl in an alkaline solution with slight modifications of the standard Hier's method[24] (87% yield). 3-Bromobiphenyl was prepared as directed by Mowry from 2-aminobiphenyl *via* 2-amino-5-bromobiphenyl.[25]

Almost all 4-acetylbiphenyls were obtained by the usual Friedel-Crafts acetylation of the above monosubstituted biphenyls. 3-Bromo-4'-acetylbiphenyl was prepared by following a slight modification of Berliner's directions.[12] After decomposition of the complex produced, the simple procedure of cooling its solution, instead of successive extraction procedures, gave crude crops (mp 36—37 °C) in 64% yield (recrystd from ligroin; mp 40.5—41 °C). 4-Cyano-4'-acetylbiphenyl was prepared from 4-bromo-4'-acetylbiphenyl by using CuCN in DMF[26] (50% yield, mp 117—120 °C). 4-Nitro-4'-acetylbiphenyl (mp 150—151 °C) was obtained in 27% yield by an acetylation ($AlCl_3$, Ac_2O, nitrobenzene solvent) of 4-nitrobiphenyl. Melting and boiling points of all monosubstituted biphenyls and substituted 4-acetylbiphenyls prepared were equal or very close to the literature values[12,25] and the elemental analysis data agreed with the calculated values.

The acetylbiphenyls were reduced with lithium aluminium hydride or sodium borohydride (especially for the CN and NO_2 derivatives) to the corresponding 1-(4-biphenylyl)ethanol by standard methods. Except for the CN and NO_2 derivatives, every chloride was prepared with dry HCl gas in dry ether as described before.[2] After evaporation of the solvent, crude crops of chlorides were purified by recrystallization from appropriate solvents. 3'-Chloro and 3'-bromo derivatives (liquid) were employed for kinetics without purification; the respective alcohols were purified and, just before kinetics, they were converted into the chlorides for rate measurements. 4'-Cyano and 4'-nitro substituted chlorides were made by the

Table 4. Physical constants of substituted 1-(4-biphenylyl)ethanols and their chlorides

Subst.	Mp or bp of alcohol(°C)	Mp of chloride(°C)
H	95.5—96[a]	52.5—53[b]
4′-MeO	119—119.5	117—118
4′-Me	99—99.5	97—97.5
4′-Cl	107—108	98.5—99.5
4′-Br	148—148.5	118—119
3′-Cl	33.5—34 (160—165/0.75 mmHg)	c)
3′-Br	136—140/0.2 mmHg	c)
4′-CN	135	83.5—84
4′-NO_2	107—108	107—110

a) Lit,[2] mp 97 °C. b) Lit,[2] mp 52.0—52.5 °C.
c) Used without purification.

method of thionyl chloride[2] and purified by recrystallization from hexane-benzene. The physical constants are listed in Table 4.

Solvent and Kinetic Measurements. The 80%(V/V) aqueous acetone was prepared by mixing 4 volumes of purified acetone and 1 volume of distilled water at room temparature (*ca.* 20 °C). Different batches of the solvent in this study were found to give an identical solvolysis rate for the 4′-chloro (or 4′-bromo) derivative within experimental errors; the interpolated rate for the unsubstituted derivative at 45 °C reasonably agreed with the previous rate measured at 45 °C.[2] The determination of the first-order rate constants in 80% aq acetone followed the method described previously;[2] Bromothymol Blue was used as an indicator. Temperatures were controlled within ±0.02 °C.

References

1) a) Y. Yukawa, Y. Tsuno, and M. Sawada, *Bull. Chem. Soc. Jpn.*, **45**, 1198 (1972); b) Y. Tsuno, M. Fujio, Y. Takai, and Y. Yukawa, *ibid.*, **45**, 1519 (1972); c) Y. Tsuno, M. Sawada, M. Fujio, N. Shimizu, T. Uemura, M. Ichihara, T. Nakachi, and Y. Yukawa, *Bull. Chem. Soc. Jpn.*, to be published; d) Private communication by Prof. J. Shorter. Unpublished review with the title "Multiparameter Extensions of the Hammett Equation."

2) Y. Tsuno, Y. Kusuyama, M. Sawada, T. Fujii, and Y. Yukawa, *Bull. Chem. Soc. Jpn.*, **48**, 3337 (1975).

3) Y. Tsuno, M. Sawada, T. Fujii, Y. Tairaka, and Y. Yukawa, *Bull. Chem. Soc. Jpn.*, **48**, 3347, 3356 (1975).

4) a) The term "electrophilic reaction" is used to characterize the reaction in which *pi*-donor($-R$) substituents show an electrophilic exalted resonance effect. On the other hand, the term "nucleophilic reaction" refers to the reaction where *pi*-acceptor($+R$) substituents show a nucleophilic exalted resonance effect. The authors wish to express their thanks to Prof. J. Shorter for his kind comment on these terms.[1d] b) At 45 °C, apparent substituent effects for the present solvolysis can be directly compared with those in the phenyl system under the same conditions. At 25 °C, the effects can be compared with those in the fluorenyl system.[4c] c) Y. Tsuno, Y. Tairaka, M. Sawada, T. Fujii, and Y. Yukawa, *Bull. Chem. Soc. Jpn.*, **51**, 601 (1978).

5) H. C. Brown and Y. Okamoto, *J. Am. Chem. Soc.*, **79**, 1913 (1957); *ibid.*, **80**, 4979 (1958).

6) At 25 °C, $\log k/k_0 = -1.63(\sigma^0 + 0.86\Delta\bar{\sigma}_R^+)$.

7) T. Inukai, *Bull. Chem. Soc. Jpn.*, **35**, 400 (1962).

8) L. M. Stock and H. C. Brown, "Advances in Physical Organic Chemistry," Vol. 1, Academic Press (1963), Chap. 2.

9) R. Baker, R. W. Bott, C. Eaborn, and P. M. Greasley, *J. Chem. Soc.*, **1964**, 627.

10) R. O. C. Norman and R. Taylor, "Electrophilic Substitution in Benzenoid Compounds," Elsevier (1965), Chap. 9; F. B. Deans, C. Eaborn, and D. E. Webster, *J. Chem. Soc.*, **1959**, 3031.

11) E. Berliner and L. H. Liu, *J. Am. Chem. Soc.*, **75**, 2417 (1953).

12) E. Berliner and E. A. Blommers, *J. Am. Chem. Soc.*, **73**, 2479 (1951).

13) D. J. Byron, G. W. Gray, and R. C. Wilson, *J. Chem. Soc., C*, **1966**, 831.

14) C. Dell'Erba, G. Guanti, and G. Garbarino, *Tetrahedron*, **27**, 1807 (1971).

15) G. Baddeley, J. Chadwick, and H. T. Taylor, *J. Chem. Soc.*, **1954**, 2405. See also A. J. Hoefnagel, M. A. Hoefnagel, and B. M. Wepster, *J. Am. Chem. Soc.*, **98**, 6194 (1976); $\rho_m = 3.55$.

16) Another nucleophilic reaction, pK_a of substituted biphenylylammonium ions (reaction H in Table 2) is available, but the data are insufficient for us to calculate the r^- value.[13]

17) Y. Tsuno, N. Goto, *et al.* Unpublished results.

18) The reaction of substituted 2-nitrochlorobenzenes with piperidine in benzene provides r^- of 0.74: W. Greizerstein, R. A. Bonelli, and J. A. Brieux, *J. Am. Chem. Soc.*, **84**, 1026 (1962). Further, the reaction of substituted 2-nitrochlorobenzenes with sodium benzenethiolate in MeOH gives the same r^- value: A. M. Porto, L. Altieri, A. J. Castro, and J. A. Brieux, *J. Chem. Soc., B*, **1966**, 963; M. Fujio, PhD thesis Osaka Univ. (1972).

19) J. G. Kirkwood and F. H. Westheimer, *J. Chem. Phys.*, **6**, 506, 513 (1938); O. Exner, "Advances in Linear Free Energy Relationship," Plenum Press (1972), Chap. 1.

20) a) M. J. S. Dewar and P. J. Grisdale, *J. Am. Chem. Soc.*, **84**, 3548 (1962); b) The value was calculated by $0.31 = 2x^4$: L. M. Stock, *J. Chem. Educ.*, **49**, 400 (1972).

21) For example, P. B. D. dela Mare, E. A. Johnson, and J. S. Lamas, *J. Chem. Soc.*, **1964**, 5317; F. J. Adrian, *J. Chem. Phys.*, **28**, 608 (1958); R. D. Brown, *J. Chem. Soc.*, **1952**, 2229.

22) E. A. Braude and W. F. Forbes, *J. Chem. Soc.*, **1955**, 3776; H. Suzuki, *Bull. Chem. Soc. Jpn.*, **32**, 1340, 1350, 1357 (1959); D. H. Lo and M. A. Whithead, *Can. J. Chem.*, **46**, 2041 (1968).

23) W. E. Bachmann and R. A. Hoffman, *Org. React.*, **2**, 224 (1957).

24) G. S. Hiers and F. D. Hager, *Org. Synth.*, Coll. Vol. I, 58 (1941).

25) D. T. Mowry, M. Renoll, and W. F. Huber, *J. Am. Chem. Soc.*, **68**, 1105 (1946); C. S. Marvel, E. Ginsberg, and M. B. Muller, *ibid.*, **61**, 77 (1939).

26) L. Friedmann and H. Shechter, *J. Org. Chem.*, **26**, 2522 (1961).

27) R. Bolton and R. E. M. Burley, *J. Chem. Soc., Perkin Trans. 2*, **1977**, 426.

28) The correlation parameters are taken from Y. Yukawa, Y. Tsuno, and M. Sawada, *Bull. Chem. Soc. Jpn.*, **39**, 2274 (1966).

The Substituent Effect. XIII. Solvolysis of 1-(7-Substituted 2-Fluorenyl)-ethyl Chlorides and Alkaline Hydrolysis of Ethyl 7-Substituted 2-Fluorenecarboxylates

Yuho Tsuno,* Yoshihiko Tairaka, Masami Sawada, Takahiro Fujii, and Yasuhide Yukawa

The Institute of Scientific and Industrial Research, Osaka University, Suita, Osaka 565
**Department of Chemistry, Faculty of Science, Kyushu University, Hakozaki, Fukuoka 812*

(Received August 13, 1977)

Two sets of rate constants for (i) solvolysis of 1-(7-substituted 2-fluorenyl)ethyl chlorides in both 90 and 80% aqueous acetone and (ii) alkaline hydrolysis of ethyl 7-substituted 2-fluorenecarboxylates in 85% aq EtOH have been determined. Both substituent effects could be correlated excellently with the LArSR relationship; the resulting r^+ values (0.82 and 0.47, respectively) were comparable with the r^+'s in the corresponding biphenylyl system under the same conditions. The comparison of ρ_π^+ values clearly indicates a more efficient transmission of the *pi*-electronic effect in the fluorenyl than in the biphenylyl ststem (1 : 0.75). This can be attributed to a factor of twisting in the latter *pi*-system. The attenuation of the transmission of the *Pi* effect was found to be characteristic of the intervening *pi*-systems independent of reactions: 1.00(4-X-1-phenyl), 0.55(6-X-2-naphthyl), 0.35(7-X-2-fluorenyl), and 0.25(4′-X-4-biphenylyl).

In previous papers of this series, we demonstrated successful applications of the LArSR relationship (Eq. 1), which is based on reactivities in the phenyl system, to reactivities in some extended *pi*-systems, such as 4-biphenylyl[1] and 1-naphthyl systems.[2]

$$\log k/k_0 = \rho(\sigma^0 + r^+\Delta\bar{\sigma}_R^+ + r^-\Delta\bar{\sigma}_R^-) \quad (1)$$

We have been interested further in substituent effects in the fluorenyl system from the viewpoint of the structural similarity in the biphenylyl system,[1] but disregarding the problem of planarity.[3] It can then, be expected that comparisons of substituent effects between fluorenyl and biphenylyl systems under the same conditions can provide important information on the transmission of electronic effects, especially the *pi*-electronic effect, across these *pi*-systems, if Eq. 1 is generally valid.

Although fragmentary data on the pK_a values for some fluorenols and fluorenylamines are available,[4,5] systematic studies of substituent effects in the fluorenyl system have been scarcely reported. Available is only a set of reactivity data for detritiation in CF_3COOH, coupled with biphenylyl data.[6] The reactivity range covered is, however, too limited to estimate and compare the *pi*-electronic effects for our present purposes because of the use of a strongly acidic solvent.[9] Two typical electrophilic reactions in 7-substituted 2-fluorenyl systems with very different amounts of resonance exaltation have been chosen. The one is solvolysis of 1-(2-fluorenyl)ethyl chlorides (Ia), while the other is alkaline hydrolysis of ethyl 2-fluorenecarboxylates. Just before this article was to be submitted, another set of solvolysis data appeared in the literature:[6b] a pair of substituent effects in α-(2-fluorenyl)benzyl chlorides (Ib) and α-(4-biphenylyl)benzyl chlorides (IIb) in 9 : 1 EtOH–acetone. Our systematic substituent-effect data coupled with those in the literature show clearly the characteristics of the intervening fluorenyl and biphenylyl systems.

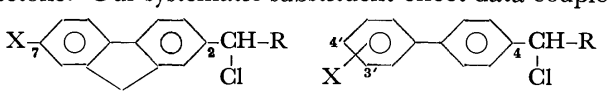

I

a: R=Me
b: R=Ph

II

a: R=Me
b: R=Ph

Results and Discussion

The rates for the solvolysis of seven 1-(7-substituted 2-fluorenyl)ethyl chlorides Ia in 90% (v/v) aqueous acetone were determined at convenient temperatures by means of the usual acid-base titration method. First-order rate constants, $k_1(s^{-1})$, at various temperatures and the relative rates in 2-fluorenyl system with respect to substituents at the 7-position at 25 °C are listed in Table 1, together with some activation parameters; for the MeO, CN, and NO_2 derivatives, the k_1 values at 25 °C were extrapolated from those at other temperatures by means of the Arrhenius equation. Further, the rates for the solvolysis of the same chlorides in 80% (v/v) aq acetone were also determined for the

Table 1. Solvolysis rates of 1-(7-X-2-fluorenyl)-ethyl chlorides in 90%(v/v) aq acetone

X	Temp (°C)	10^5k_1 (s^{-1})	$\log k/k_0$ (at 25°C)	$\Delta H^\ddagger$ (kcal/mol)	$\Delta S^\ddagger$ (e.u.)
MeO	0.0	4.29			
	10.0	15.8			
	20.0	44.4			
	25.0[a]	78.7[a]	1.426[a]	18	−12
C_2H_5	25.0	9.81	0.522		
H	25.0	2.95	0.000		
Cl	25.0	1.14	−0.413		
Br	25.0	0.997	−0.471		
CN	65.0	5.04			
	55.6	2.16			
	45.0	0.731			
	25.0[a]	0.0828[a]	−1.552[a]	20.0	−19.3
NO_2	86.0	20.2			
	75.0	8.34			
	64.2	3.00			
	25.0[a]	0.0495[a]	−1.775[a]	20.4	−19.0

a) Extrapolated from other temperatures.

Table 2. Solvolysis rates of 1-(7-X-2-fluorenyl)-ethyl chlorides in 80% (v/v) aq acetone

X	Temp (°C)	10^5k_1 (s^{-1})	$\log k/k_0$ (at 25 °C)	$\Delta H^{\neq}$ (kcal/mol)	$\Delta S^{\neq}$ (e.u.)
MeO	25.0[a]	1.44×10^3 [a]	1.49[a]		
C_2H_5	0.0	6.48			
	15.0	45.1			
	25.0	147	0.500	19.6	−5.6
H	0.0	1.94			
	15.0	13.2			
	25.0	46.5	0.000	19.9	−6.9
Cl	25.0	16.1	−0.461		
Br	15.0	3.97			
	25.0	13.5	−0.537	20.3	−8.1
CN	25.0	1.04	−1.650		
NO_2	25.0	0.516	−1.955		

a) Extrapolated from a linear free-energy relation between rates in 80 and 90% aq acetone (see Text).

sake of comparison. In the latter solvent, apparent substituent effects in the fluorenyl system can be directly compared with those in biphenylyl and phenyl systems under identical conditions.[1,7] Table 2 contains the kinetic data in 80% aq acetone obtained in the same manner as those in 90% aq acetone.

The k_1 for 7-MeO-2 derivative in 80% aq acetone was extrapolated from the following linear $\log k/k_0$-$\log k/k_0$ correlation between substituent effects in 80 and 90% aq acetone with a high precision (corr coeff, $r=0.9996$, $s=\pm0.031$, $n=6$):

$$(\log k/k_0)_{80\%} = 1.065(\log k/k_0)_{90\%} - 0.029.$$

The minor solvent change from 80 to 90% causes only a small change in the ρ value, but none in the r^+ value of Eq. 1.[8]

On the other hand, the rates for the alkaline hydrolysis of seven ethyl 7-substituted 2-fluorenecarboxylates in 85% (w/w) aq EtOH at 50 °C were measured by means of usual conductivity and/or titration methods. The second-order rate constants, k_2(s^{-1} M^{-1}), and the logarithmic relative rates are listed in Table 3. Unfortunately, we could not get a k_2 for the NO_2 derivative in this ester hydrolysis because the solubility was insufficient to measure it.

Table 3. Rates of alkaline hydrolysis of ethyl 7-X-2-fluorenecarboxylates in 85% (w/w) aq EtOH at 50°C

X[a]	10^3k_2 ($s^{-1}M^{-1}$)	Method[b]	$\log k/k_0$
MeO	2.06	C	−0.259
C_2H_5	2.82	T	−0.123
H	3.74	C,T	0.000
Cl	4.87	C,T	0.115
Br	5.04	C	0.130
COMe	7.46	C	0.300
CN	10.8	C	0.461

a) We could not get a k_2 of the NO_2 deriv. because of the solubility problem. b) T: titration method, C: conductivity method.

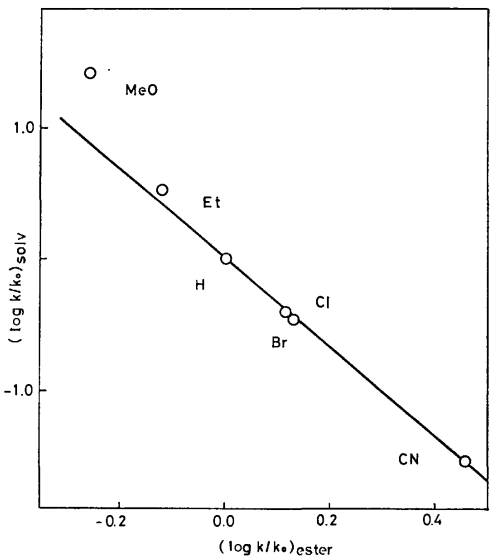

Fig. 1. A plot of $\log k/k_0$ for the solvolysis A (90% acetone, 25 °C) *vs.* the ester hydrolysis D(85% EtOH, 50 °C) in the present 7-X-2-fluorenyl system.

Logarithms of the relative rates for the solvolysis (90% aq acetone) in the fluorenyl system are plotted against those for the ester hydrolysis in Fig. 1. The $-R$(*pi*-donor) substituents deviate upward from the line made with CN and H substituents, for which no exaltation of resonance might be expected. The more electron-releasing the $-R$ substituent at such a conjugative position, the larger the upward deviation. The deviations indicate that the contribution of through-conjugation between substituents and the reaction center for the solvolysis is much more important to the apparent substituent effects than those for the ester hydrolysis, at least at the conjugative (7-)position in the 2-fluorenyl system. Similar upward deviations had also been obtained in the biphenylyl system on the log-log plot of the relative rates between the corresponding solvolysis and ester hydrolysis.[1]

An interesting feature which we found in this study is that there exists an excellent linearity (Fig. 2) of the solvolysis rates (25 °C) between fluorenyl (90%) and biphenylyl (80%) systems, covering a range of substituents from MeO to NO_2 ($r=0.9998$, $s=\pm0.026$, $n=7$):

$$(\log k/k_0)_{\text{Fluo}} = 1.362(\log k/k_0)_{\text{Biph}} - 0.028.$$

The linearity suggests that the blends of the *pi*-electronic (*Pi*) effect and the inductive (*I*) effect are practically equivalent in the two systems for the present solvolysis.

Eaborn *et al.* first observed this kind of behavior in detritiation and pointed out that the effects of 7-substituents in the 2-fluorenyl are similar to those of 4'-substituents in the 4-biphenylyl system;[6] a correlation analysis of their detritiation data in CF_3COOH at 70 °C provides high precision with this relation: $(\log k/k_0)_{\text{Fluo}} = 1.11\ (\log k/k_0)_{\text{Biph}}$ ($r=0.9986$, $s=\pm0.08$, $n=6$). Even though the detritiation has been established as a typical electrophilic exalted resonance reaction, since it inevitably contains serious solvent-substituent interaction, MeO derivatives in both *pi*-systems are less reactive than Me ones; therefore, the reactivity range is limited for only

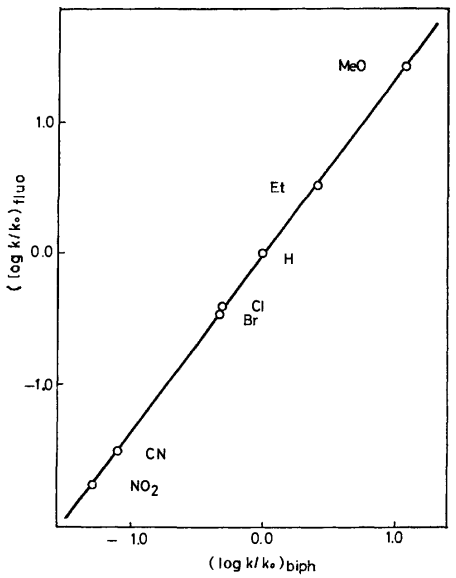

Fig. 2. The linear log k/k_0 —log k/k_0 plot between fluorenyl (90% acetone, 25 °C) and biphenylyl (80% acetone, 25 °C) in the present solvolysis A (Ia *vs.* IIa).

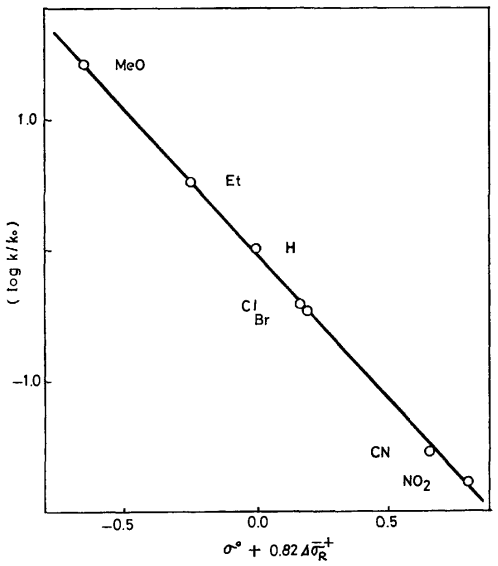

Fig. 3. The LArSR plot for the solvolysis A of 1-(7-X-2-fluorenyl)ethyl chlorides (90%, 25 °C).

weakly conjugating substituents.[9] Bolton and Burley have recently observed a similar linearity between the solvolyses of Ib and IIb (with a slope of 1.45, $r=0.999$), which covers nearly the same range of substituents as ours.

As another example for comparison between the fluorenyl and the biphenylyl systems, the present data of ester hydrolysis are correlated linearly with Berliner's data on the alkaline hydrolysis of ethyl biphenylcarboxylates[10] ($r=0.9935$, $n=5$); since the rates are not very sensitive to substituent changes in either system, it is hard to ascertain whether or not their *Pi* effects relative to *I* effects are different. From the findings in the above reactions, the linear relationships of the substituent effects between the fluorenyl and the biphenylyl systems seem to be quite general.

The present solvolysis of the Ia fluorenyl system

Table 4. Correlation parameters by means of the LArSR Eq. 1

Reaction	Substituted(X) *pi*-system[a]	Solv[b] (%)	Temp (°C)	ρ	r^+	R[f]	$\pm s$[g]	n[h]	Ref.
A: Solvolysis	3,4-X-1-Ph	80A	45	−4.95	1.15	0.999	0.040	16	7
ArCHMeCl		80A	25	−5.15	(1.15)				7
		90A	45	−4.75	1.18	0.999	0.033		12
	7-X-2-Fluo	90A	25	−2.23	0.82	0.999	0.053	7	c)
		80A	25	−2.38	(0.82)			6	c)
	3′,4′-X-4-Biph	80A	45	−1.56	0.84	0.999	0.023	9	1
		80A	25	−1.63	0.86				1
	3,4-X-1-Naph	80A	45	−5.12	1.04	0.999	0.116	10	2
	6-X-2-Naph	80A	45	−3.35	0.84	0.999	0.025	5	13
B: Solvolysis	3,4-X-1-Ph	100E	25	−4.13	1.17	0.998	0.125		36
ArCH(Ph)Cl	7-X-2-Fluo	9: 1EA	25	−1.98	0.73	0.997	0.08	6	6b
	3′,4′-X-4-Biph	9: 1EA	25	−1.30	0.75	0.995	0.06	12	6b
C: Solvolysis	3,4-X-1-Ph	90A	25	−4.54	1.00 (by definition)				d)
$ArCMe_2Cl$	3′,4′-X-4-Biph	90A	25	−1.39	0.67	0.999	0 024	6	d)
	6-X-2-Naph	95A	30	−2.92	0.70	0.999	0.032	5	14
D: Hydrolysis	3,4-X-1-Ph	85E	25	2.58	0.25	0.997	0.069	16	15
ArCOOEt	7-X-2-Fluo	85E	50	0.63	0.47	0.999	0.011	7	c)
	3′,4′-X-4-Biph	90E	25	0.58	0.34	0.999	0.005	8	d)
	3,4-X-1-Naph	85E	50	2.19	0.27	0.999	0 03	10	2
	4-X-1-Naph[e]	85M	30	1.97	0.27	0.989	0.084	6	14
	6-X-2-Naph[e]	70D	25	1.72	0.17	0.995	0.08	7	16
	6-X-2-Naph[e]	85M	30	1.22	0.26	0.996	0.04	9	14

a) Ph(phenyl), Fluo(fluorenyl), Biph(biphenylyl), and Naph(naphthyl) *pi*-systems. b) A (acetone), E (ethanol), EA (EtOH: acetone), M (methanol), and D (dioxane). c) Present study. d) Taken from Table 2 of Ref. 1. e) Methyl esters instead of ethyl esters. f) Correlation coefficient. g) Standard deviation. h) Number of substituents included.

correlates linearly with a single set of neither σ^0 nor σ^+, as has been discussed in the biphenylyl system.[1] The application of the LArSR Eq. 1 to the data Ia in 90% aq acetone (25 °C) gives an excellent correlation (Fig. 3) with the correlation coefficient of 0.9993 and the standard deviation of ± 0.053 ($n=7$), providing nearly the same r^+ value (0.82) as that in the biphenylyl system (0.84):[1]

$$(\log k/k_0)^{\text{Solv}}_{\text{Fluo}} = -2.231(\sigma^0+0.815\Delta\bar{\sigma}_R^+) - 0.050.$$

Further, the substituent effects on the alkaline hydrolysis of ethyl 2-fluorenecarboxylates can be accommodated simply with neither σ^0 nor σ, but can be accommodated successfully with the LArSR Eq. 1:[11]

$$(\log k/k_0)^{\text{Ester}}_{\text{Fluo}} = 0.628(\sigma^0+0.470\Delta\bar{\sigma}_R^+).$$

The results of correlation analysis for the present and the related reactivity data available under closely similar conditions are summarized in Table 4, covering three solvolyses and ester hydrolysis. For comparisons of representative *pi*-systems through which the effects of substituents are effectively transmitted, the table also includes some naphthyl systems as well as the fluorenyl and biphenylyl ones. From nearly perfect fits in every case (Table 4), it may be concluded that substituent effects from conjugative positions in any extended *pi*-systems for any reactions can generally be described by means of the LArSR Eq. 1, at least in electrophilic exalted resonance reactions.

Table 4 shows clearly that substituent effects depend greatly on the structures of the intervening *pi*-systems. The ρ values decrease systematically in the following order: phenyl$\simeq$(1-naphthyl)>2-naphthyl>2-fluorenyl >4-biphenylyl. The ρ values relative to that in the phenyl system (see Table 5) appear to remain constant for the other systems: phenyl (1.00), 2-naphthyl (0.65), 2-fluorenyl (0.46), and 4-biphenylyl (0.32); slight deviations from such a quantitative regularity are found only in the fluorenyl and biphenylyl systems for ester hydrolysis (*ca.* 0.25 and 0.20 respectively). The relative ρ values for 1-naphthyl can not be fairly compared, because their ρ's are usually subject to variation with the steric effects of peri-hydrogen; *e.g.*, on solvation at the reaction center.

On the other hand, each solvolysis gives nearly equal apparent r^+ values for the 2-fluorenyl, 4-biphenylyl, and 2-naphthyl systems in spite of the different ρ values, while the ester hydrolysis offers an apparently larger r^+ in the fluorenyl system. However, it is worth noting that the resonance contribution given by ρr^+ is clearly larger for the 2-fluorenyl than for the 4-biphenylyl system in all the reactions listed (Table 4). As long as the parameters of σ^0 and $\Delta\bar{\sigma}_R^+$ derived from the original phenyl system are utilized for the present LArSR analysis in the fluorenyl and biphenylyl systems, the comparison of ρr^+ is much more reasonable than that of simple r^+ as a measure of the resonance contribution in such extended *pi*-systems.[37] The larger ρr^+ values are exactly in line with the concept of the planar-fluorenyl and nonplanar-biphenylyl systems.

In previous papers,[2] we demonstrated the validity of a more fundamental LSFE Eq. 2 for separating substituent effects into *Pi* and *I* effects in variously substituted 1-naphthyl systems. As the LSFE treatment has been much more useful,[2,18,38] especially in extended *pi*-systems beyond original phenyl systems, it is actually very important to get reliable ρ_i and ρ_π parameters:

$$\log k/k_0 = \rho_i\sigma_i + \rho_\pi^+\sigma_\pi^+ + \rho_\pi^-\sigma_\pi^-. \quad (2)$$

Only when a given set of substituent-effect data covers a sufficient range of reactivity and sufficient numbers of substituents for both $-R$ and $+R$ classes of substituents, we can get reliable ρ_i, ρ_π^+, and ρ_π^- values statistically.[38] In the case of the present data sets, which contain only a few $+R$ substituents, it is, however, perhaps rather dangerous to use statistical ρ_π^- values and then ρ_π^+ values for discussions because of the too limited number of substituents. If it is assumed that ρ_π^- is equal to ρ_i (as in the LArSR treatment), and if σ_i' is provided as $\sigma_i+\sigma_\pi^-$ for $+R$ substituents in electrophilic reactions (and $\sigma_i'=\sigma_i$ for $-R$ substituents), then Eq. 2 should be rewritten as

$$\log k/k_0 = \rho_i\sigma_i' + \rho_\pi^+\sigma_\pi^+,$$

for both $-R$ and $+R$ groups. Consequently, the statistically derived ρ_i and ρ_π^+ values (on the basis of the σ_i' and σ_π^+ correlations) should cover the same range of substituents and should have the same accuracy as in the LArSR treatment. Usually, a data set of an electrophilic reaction involves a few $+R$ substituents such as NO_2 and CN. Therefore, it is recommended in practice that the substituent effects be separated into *Pi* and *I* effects by interconversions of the LArSR parameters to the LSFE parameters, instead of by a direct determination from the LSFE Eq. 2. Based on the definitions of $\sigma^0=\sigma_i+\sigma_\pi^+$ and $\sigma_\pi^+=0.415\ \Delta\bar{\sigma}_R^+$, the LSFE parameters hold the following mathematical relations with the LArSR parameters:[19]

$$\rho_i = \rho, \quad \rho_\pi^+ = \rho(1+r^+/0.415). \quad (3)$$

The ρ_i and ρ_π^+ values can be evaluated by means of Eq. 3 from the ρ and r^+ values in Table 4. Table 5 illustrates the ρ_i, ρ_π^+ values relative to those in the phenyl system; these values show the corresponding

Table 5. Relative ρ_i and ρ_π^+ values in some *pi*-systems

Reaction[a]	*Pi*-system[a]	Relative[b] ρ_i	Relative[b] ρ_π^+
A: Solvolysis	Ph	1.00	1.00
ArCHMeCl	2-Naph	0.68	0.54
	Fluo	0.46	0.36
	Biph	0.32	0.25
	1-Naph	(1.03)	(0.96)
B: Solvolysis	Ph	1.00	1.00
ArCH(Ph)Cl	Fluo	0.48	0.35
	Biph	0.31	0.23
C: Solvolysis	Ph	1.00	1.00
$ArCMe_2Cl$	2-Naph	0.64	0.51
	Biph	0.31	0.23
D: Hydrolysis	Ph	1.00	1.00
$ArCOOEt+OH^-$	2-Naph	0.66	0.58
	Fluo	0.24	0.32
	Biph	0.22	0.25
	1-Naph	(0.85)	(0.87)

a) Taken from Table 4. b) Both relative values are calculated by using ρ and r^+ in Table 4 and Eq. 3.

Table 6. Application of the LArSR Eq. 1 to alkaline hydrolysis in aq EtOH

System[a]	Solv (%)	Temp (°C)	ρ	r^+	R[c]	n[d]	Ref.
ArCOOEt	85E	25	2.58	0.25	0.999	16	15
$ArCH_2COOEt$	85E	25	1.10	0.00[b]	0.996	10	20
$ArCH_2CH_2COOEt$	88E	30	0.64	0.00[b]	0.998	11	20
			0.64	0.00[b]	0.998	6	20
Ar(*c*-C_3H_4)COOEt,*trans*	88E	30	0.88	0.00[b]	0.998	8	20
Ar(*c*-C_3H_4)COOEt, *cis*	88E	30	1.06	0.00[b]	0.995	6	21
ArCH=CHCOOEt, *trans*	85E	25	1.19	0.39	0.999	9	22
	88E	30	1.27	0.31	0.999	6	23
ArCH=CHCOOEt, *cis*	88E	30	1.12	0.26	0.999	4	23

a) Ar(substituted phenyl), *c*-C_3H_4(cyclopropyl). b) σ^0 values were used for correlation. c) Correlation coefficient. d) Number of substituents.

relative effectiveness through which *Pi* and *I* effects are transmitted.

It is worth emphasizing that there exists a remarkable regularity in the attenuation behavior on the transmission of *Pi* effects. That is, a decrement remains constant for any given *pi*-system independent of the reactions or, more exactly, independent of the varied contributions of *Pi* effects in any type of reaction. The effectiveness of transmission is generally 55% for the 2-naphthyl, 35% for the 2-fluorenyl, and 25% for the 4-biphenylyl, as large as that for the phenyl *pi*-system. The variations probably reflect characteristics of the systems.

Because of their geometrical similarity, substituent effects between fluorenyl and biphenylyl systems can be compared most interestingly. The ratio of the *Pi* effects, biphenylyl/fluorenyl, for the present solvolysis is calculated to be 0.72, reflecting the obviously decreased effectiveness of the transmission across the intervening biphenylyl relative to the fluorenyl system. This figure must be well related with the twisting angle of both phenyl rings in biphenyl, because such a twisting is expected to decrease the *Pi* contribution. In the case of ester hydrolysis, the ratio shows a slightly larger value (0.78), probably the result of slight differences in the reaction conditions. Some proper correction will provide a value closer to 0.72. At any rate, the averaged value of 0.75 ± 0.03 is remarkably the same as the previous value obtained on the basis of a different comparison between the biphenylyl and phenyl systems.[1] Table 5 also indicates that the 6-X-2-naphthyl system is 1.6 times more effective than 7-X-2-fluorenyl in transmitting the *Pi* effects, although their r^+ values appear to be equal.

On the other hand, we can not get any regularity in the attenuation of relative *I* effects among the systems studied, though a limited regularity probably holds in three solvolyses, A, B, and C, in Table 4, as has been mentioned above. The results of the A solvolysis (ArCHMeCl) show the ρ_i in the fluorenyl system to be larger than that in the biphenylyl system. Further, for another solvolysis, B (ArCHPhCl), the same thing is true.

These findings are not consistent with the transmission mode of the *I* effect through a field, since the simplified distance between substituents and the reaction center is equivalent for this pair. As a factor controlling the magnitude of the apparent ρ_i, the nature of the intervening bonds, such as the bond-order in the pivot bond in the biphenyl component, may be incorporated with another factor of distance.[1] The excellent linearity between the 2-fluorenyl and the 4-biphenylyl systems may, therefore, imply that the ρ_i is also a function of the interplanar angle. This suggests that the higher the bond-order character of the intervening bond, the larger the ρ_i, even if the simplified distance is equal. This suggestion seems to be consistent with the results shown in Table 6.

The table compares the results of the LArSR treatment for the substituent-effect data available on ester hydrolysis under similar conditions. A major point in which we are interested is the nature of the intervening bond. When the intervening group between a substituted phenyl group and COOEt changes from $-CH_2CH_2-$ to -cyclopropyl- to $-CH=CH-$, the ρ's obviously change from 0.6 to *ca.* 0.9, and *ca.* 1.2 respectively. This suggests some operation of intervening bond-order effects on the transmission of the *I* effect.

In summary, it is particularly important to note that the LArSR relationship can be applied equally well to reactivities in extended *pi*-systems such as 7-X-2-fluorenyl and 6-X-2-naphthyl, other than the phenyl system.

Experimental

Materials. *2-Substituted Fluorenes*: 2-Acetylfluorene (mp 127.5—128 °C),[24] 2-nitrofluorene (mp 160.5 °C), and 2-ethylfluorene (mp 99—100 °C) were prepared by the standard procedures previously reported.[25-27] 2-Chlorofluorene was made as has been described by Sengupta,[28] with slight modifications; chlorine gas was passed through a $CHCl_3$ solution of fluorene under cooling, until the IR absorbance at 764cm^{-1} of the product periodically extracted from the reaction mixture became larger than that at 725 cm^{-1}. Although the product (recrystallized from MeOH) was contaminated with dichloro derivative, it was used without purification in the next acetylation step. 2-Bromofluorene was also prepared by bromination. Bromine (100 g) was rapidly added to a dioxane (600 g) solution of fluorene (70 g) at room temperature. After stirring for 3 h and the subsequent decomposition of the excess Br_2, the solution was poured into water and the precipitate was recrystallized from MeOH–benzene, giving 2-bromofluorene in an 85% yield (mp 109—110 °C, lit,[29] mp 110—111 °C).

7-Substituted 2-Acetylfluorenes: As has been described by Arene

and Taylor in connection with the preparation of 7-methoxy-2-acetylfluorene,[30] 7-ethyl-2-acetylfluorene was obtained by the acetylation of 2-ethylfluorene (with Ac_2O and $AlCl_3$ in nitrobenzene) in an 85% yield; recrystd from EtOH, mp 125.5—126.5 °C. 7-Chloro- or 7-bromo-2-acetylfluorene was synthesized by the addition of Ac_2O(0.6 mol) to a nitrobenzene solution (800 ml) of the respective halofluorene (0.4 mol) and $AlCl_3$ (0.83 mol) under cooling. The mixture was stirred for 3 h and then allowed to stand overnight. After a usual work-up, the product was recrystallized from benzene and then CCl_4; 7-chloro-2-acetylfluorene (83% yield, mp 141—142 °C) and 7-bromo-2-acetylfluorene (75% yield, mp 144—146 °C). 7-Cyano-2-acetylfluorene (recrystd from EtOH–benzene; mp 117—120 °C) was prepared by the use of CuCN from 7-bromo-2-acetylfluorene (60% yield) according to the method described by Fridmann and Shechter.[31]

7-Nitro-2-acetylfluorene was obtained by the literature method[32] in a 72% yield (mp 233—233.5 °C, lit,[32] mp 228 °C); however, because of its low solubility, the purification by recrystallization was difficult. The nitro derivative (50.6 g) was reduced with $SnCl_2 \cdot 2H_2O$(226 g) and concd HCl(280 ml) in AcOH(3500 ml). After treatment with aq KOH, 7-amino-2-acetylfluorene was obtained in a 52% yield; mp 221—221.5 °C. The amine was converted to 7-hydroxy-2-acetylfluorene in a 43% yield *via* diazonium sulfate (recrystd from MeOH–acetone, mp *ca.* 140 °C, dec). The methylation of the hydroxy derivative with Me_2SO_4 afforded 7-methoxy-2-acetylfluorene: mp 137—138 °C, lit,[30] mp 134—135 °C.

All of the above acetylfluorenes except the NO_2 and CN derivatives (low solubilities) were further purified by column chromatography on Al_2O_3 with a benzene eluent[24] and subsequently reduced by appropriate methods to the following alcohols.

1-(7-Substituted 2-Fluorenyl)ethyl Alcohols and Chlorides Ia: The substituted and unsubstituted 2-acetylfluorenes were converted to the corresponding alcohols by a standard reduction with $LiAlH_4$ (for the MeO, Et, H, and Cl derivatives) or $NaBH_4$ (for the Br, CN, and NO_2 derivatives). All the alcohols were recrystallized from benzene–hexane or EtOH–benzene. The physical properties are tabulated in Table 7.

Table 7. Physical constants and analytical data of 1-(7-X-2-fluorenyl)ethyl alcohols

X	Mp(°C)	Calcd(Found) C,%	H,%
MeO	147	79.97(80.08)	6.71(6.62)
C_2H_5	153—154.5	85.67(85.61)	7.61(7.64)
H	131.5—133	85.68(85.66)	6.71(6.51)
Cl	110—111	73.63(73.54)	5.35(5.57)
Br	155—156	62.30(62.57)	4.53(4.50)
CN	151—152	81.68(81.07)	5.57(4.80)
NO_2	178—180,dec	70.58(70.75)	5.13(5.11)

With the exception of the CN and NO_2 derivatives, the 1-(7-substituted 2-fluorenyl)ethyl chlorides were prepared by passing dry HCl gas through an ether (200 ml) solution of the alcohol (*ca.* 5 g); although the solubility of some alcohols was less sufficient, HCl gas was bubbled in and, as the reaction proceeded, the alcohol was dissolved into a solution. After the treatment as has been described before,[7] the chlorides were purified by recrystallization from hexane or ether–petroleum ether and used for kinetics immediately after the evaporation of the solvents *in vacuo*. The CN and NO_2 derivatives were made by the SO_2Cl method[7] and were recrystallized from hexane–benzene.

7-Substituted 2-Fluorenecarboxylic Acids[33] *and Their Ethyl Esters*: The 7-methoxy-, 7-ethyl-, 7-chloro-, 7-bromo-, and unsubstituted 2-acetylfluorenes were moderately oxidized to the respective 7-substituted 2-fluorenecarboxylic acids by the use of iodine in pyridine (20—89% yields) using a method similar to that described by Barnett *et al.*[34] The 7-nitro-2-acetylfluorene was converted to the corresponding acid by following the procedure of Weisburger *et al.*[5] The acid hydrolysis of 7-cyano-2-acetylfluorene gave 7-acetyl-2-fluorenecarboxylic acid (80% yield).

All of the ethyl 7-substituted 2-fluorenecarboxylates were prepared by the esterification of the corresponding acids or acid chlorides with EtOH, except in the case of ethyl 7-cyano-2-fluorenecarboxylate, which was obtained from the bromo derivative (39% yield) in the same manner as was used for 7-cyano-2-acetylfluorene. Every ester was purified by column chromatography on Al_2O_3 with a benzene eluent and by subsequent recrystallization from hexane or hexane–EtOH. The physical properties and analytical data of the esters are given in Table 8.

Table 8. Physical constants and analytical data of ethyl 7-X-2-fluorenecarboxylates

X	Mp(°C)	Calcd(Found) C,%	H,%
MeO	142—143	76.10(76.00)	6.01(6.01)
C_2H_5	109—109.5	81.17(80.95)	6.81(6.89)
H	85—85.5[a]	80.65(80.76)	5.92(5.95)
Cl	131.5—132	70.46(70.61)	4.80(4.59)
Br	137—138	60.59(60.54)	4.13(3.96)
COMe	149—149.5	77.12(76.90)	5.75(5.70)
CN	187—188	77.55(77.53)	4.98(4.90)
NO_2	200.5	67.84(67.62)	4.63(4.46)

a) Lit,[35] mp 81—82 °C.

The protone NMR spectra for the esters, chlorides, and their precursors (the alcohols and ketones) were consistent with the respective assigned structures.

Kinetics and Solvents. *Solvolysis*: The 80%(V/V) and 90%(V/V) aqueous acetones were prepared by mixing nominal volumes of each component at 25 °C. Kinetics were carried out in the concentration of each chloride at *ca.* 0.02 M^{-1}, and the reaction was followed by titration with aq NaOH(*ca.* 0.02 M^{-1}), using Bromothymol Blue or Bromocresol Green as an indicator. All the kinetic runs accurately obeyed the first-order kinetic law, and the determination of $k_1(s^{-1})$ followed the method which we have previously described.[7] The reproducibility of the rate constants from repeated runs was within $\pm 1\%$.

Alkaline Hydrolysis: The 85%(w/w) aqueous EtOH was prepared by mixing 4000 ml of abs EtOH and 545 ml of water at 25 °C;[15] this gave $d_4^{25}=0.826_6$ by means of a pycnometer. A NaOH solution (*ca.* 0.08 M^{-1}) in the solvent was made by dissolving sodium in the solvent and then standardizing it with benzoic acid. The temperature was controlled at 50 ± 0.02 °C.

A polyethylene cell equipped with Pt plates was employed for the conductivity measurements. Bromothymol Blue was used as an indicator for the titration method. The $k_2(s^{-1}M^{-1})$ values from the equimolar reactions of the ester and the OH^- were determined by the method which will be described elsewhere.[15] No initial concentration effects could be detected in the concentration range of 0.012—0.036 M^{-1} of the ester

and the OH^-. Ethyl 7-nitro-2-fluorenecarboxylate showed a low solubility (less than 0.005 M^{-1}), and so the determination of an accurate k_2 value was given up in the present study. The titration and conductivity methods gave the same k_2. The reproducibility of the rate constants from repeated runs was within $\pm 1\%$.

References

1) The Substituent Effect. 12: Y. Tsuno, W.-Y. Chong, Y. Tairaka, M. Sawada, and Y. Yukawa, *Bull. Chem. Soc. Jpn.*, **51**, 596 (1978).

2) Y. Tsuno, M. Sawada, T. Fujii, Y. Tairaka, and Y. Yukawa, *Bull. Chem. Soc. Jpn.*, **48**, 3347, 3356 (1975).

3) For example, B. M. Burns and J. Iball, *Nature*, **173**, 635 (1954); E. A. Braude and W. F. Forbes, *J. Chem. Soc.*, **1955**, 3776; H. Suzuki, *Bull. Chem. Soc. Jpn.*, **27**, 597 (1954), **32**, 1340, 1350, 1357 (1959); J. Dale, *Acta Chem. Scand.*, **11**, 650 (1957); G. Zerbi and S. Sandroni, *Spectrochim. Acta*, **24**, 511 (1968); L. M. Litvinenko and A. P. Grekov, *Chem. Abstr.*, **51**, 12866e (1957).

4) V. P. Kreiter, W. A. Bonner, and R. H. Eastman, *J. Am. Chem. Soc.*, **76**, 5770 (1954).

5) P. H. Grantham, E. K. Weisburger, and J. H. Weisburger, *J. Org. Chem.*, **26**, 1008 (1961).

6) a) R. Baker, R. W. Bott, C. Eaborn, and P. M. Gleasley, *J. Chem. Soc.*, **1964**, 627; b) R. Bolton and R. E. M. Burley, *J. Chem. Soc., Perkin Trans. 2*, **1977**, 426.

7) Y. Tsuno, Y. Kusuyama, M. Sawada, T. Fujii, and Y. Yukawa, *Bull. Chem. Soc. Jpn.*, **48**, 3337 (1975).

8) See Table 4.

9) Usually, such a solvent-modified MeO substituent must be excluded from the line-up of ordinary substituents; then it is hard to get reliable r^+ (and ρ) values from the data of their detritiation in CF_3COOH.

10) E. Berliner and L. H. Liu, *J. Am. Chem. Soc.*, **75**, 2417 (1953).

11) As σ^0 values, 0.72 for CN and 0.47 for COMe were used in this hydrolysis instead of the standard values because of solvent effect (and/or alkaline-condition effects) on such polar substituents.[15])

12) Y. Tsuno, T. Fujii, and M. Mishima, unpublished.

13) Y. Tsuno, M. Sawada, T. Fujii, and Y. Yukawa, unpublished.

14) V. Baliah and P. A. Nadar, *Indian J. Chem.*, **9**, 671, 1241, 1339 (1971).

15) Y. Tsuno, M. Sawada, M. Fujio, N. Shimizu, T. Uemura, M. Ichihara, T. Nakachi, and Y. Yukawa, *Bull. Chem. Soc. Jpn.*, to be published.

16) P. R. Wells and W. Adcock, *Aust. J. Chem.*, **19**, 221 (1966).

17) B. M. Wepster, *J. Am. Chem. Soc.*, **95**, 102 (1973); A. J. Hoefnagel and B. M. Wepster, *ibid.*, **95**, 5357 (1973); A. J. Hoefnagel, J. C. Monshouwery, E. C. G. Snorn, and B. M. Wepster, *ibid.*, **95**, 5350 (1973); H. V. Bekkum, P. E. Verkade, and B. M. Wepster, *Recl. Trav. Chim. Pays-Bas.*, **78**, 815 (1958).

18) Y. Tsuno, M. Fujio, Y. Takai, and Y. Yukawa, *Bull. Chem. Soc. Jpn.*, **45**, 1519 (1972); *ibid.*, **48**, 3324, 3330 (1975).

19) $\rho_{\pi}^{-}=\rho\ (1+r^-/0.73)$ for nucleophilic reactions.

20) Y. Yukawa, Y. Tsuno, and M. Sawada, *Bull. Chem. Soc. Jpn.*, **45**, 1198 (1972).

21) R. Fuchs and J. J. Bloomfield, *J. Org. Chem.*, **28**, 910 (1963).

22) B. Jones and J. G. Watkinson, *J. Chem. Soc.*, **1957**, 4064.

23) J. J. Bloomfield and R. Fuchs, *J. Org. Chem.*, **26**, 2991 (1961).

24) Mp of 2-acetylfluorene was raised to 131—131.5 °C after column chromatography.

25) *Org. Synth.*, Coll. Vol. III, 23 (1955).

26) *Org. Synth.*, Coll. Vol., II, 447 (1943).

27) S. Kajigaeshi, M. Fujimoto, S. Fujisaki, T. Kunishige, and M. Mashihara, *Chem. Abstr.*, **69**, 76991u (1968); E. Sawicki, *J. Am. Chem. Soc.*, **76**, 2269 (1954).

28) S. K. Sengupta, *Indian J. Chem.*, **4**, 235 (1966).

29) F. Dewhurst and P. K. Shah, *J. Chem. Soc., C*, **1970**, 1737; S. D. Ross, M. Finkelstein, and R. C. Peterson, *J. Am. Chem. Soc.*, **80**, 4327 (1958); H. F. Miller and G. B. Bachman, *ibid.*, **57**, 2447 (1935).

30) E. O. Arene and D. A. H. Taylor, *J. Chem. Soc., C*, **1966**, 481.

31) L. Friedmann and H. Shechter, *J. Org. Chem.*, **26**, 2522 (1961).

32) H. F. Oehlschlaeger and I. R. McGregor, *J. Am. Chem. Soc.*, **71**, 3223 (1949).

33) A careful purification of the acids was not performed.

34) M. D. Barnett, G. H. Daub, F. N. Hayes, and D. G. Ott, *J. Am. Chem. Soc.*, **82**, 2282 (1960).

35) D. C. Morrison, *J. Org. Chem.*, **23**, 1772 (1958).

36) See Table 5 in Y. Yukawa, Y. Tsuno, and M. Sawada, *Bull. Chem. Soc. Jpn.*, **39**, 2274 (1966).

37) Wepster mentioned that a through-conjugation interaction in the phenyl system is expressed by:[17])

$$-\Delta\Delta G_p = \rho r^+ \Delta\bar{\sigma}_R^+ 2.3RT = \rho(\sigma-\sigma^0)\,2.3RT.$$

Since the parameters of $(\sigma^0)_{Fluo}$ and $(\Delta\bar{\sigma}_R^+)_{Fluo}$ derived from the fluorenyl system are not utilized for the present analysis, the ρr^+ obtained does not correspond to the through-conjugation in the fluorenyl system.

38) Y. Tsuno, M. Fujio, T. Nakachi, and M. Mishima, *J. Am. Chem. Soc.*, to be published; Y. Tsuno, M. Fujio, T. Nakachi, and Y. Yukawa, unpublished.

Organic Photochemical Reactions. XXVI. Photoaddition of Singlet and Triplet Methyl Pyruvate with 2,3-Dimethyl-2-butene[1]

Kensuke SHIMA, Taisuke SAWADA, and Hiroyuki YOSHINAGA

Department of Industrial Chemistry, Faculty of Engineering, Miyazaki University, Miyazaki 880

(Received September 7, 1977)

UV irradiation of methyl pyruvate in the presence of 2,3-dimethyl-2-butene leads to the formation of four primary photo-products in reasonable quantum yield: two unsaturated ethers (**1** and **2**) and two unsaturated alcohols (**3** and **4**). The effects of olefin concentration on the quantum yield of product formation, as well as quenching studies, suggest that **3** and **4** are formed from the excited singlet state of methyl pyruvate, while **1** and **2** are produced from the triplet state of methyl pyruvate. The role of exciplexes in this reaction is discussed. Quenching data of fluorescence of methyl pyruvate and the kinetic analysis of this reaction support these considerations.

The photocycloaddition of carbonyl compounds with olefins to form oxetanes is a topic of recent preparative and mechanistic interest. An attack of the $^3(n\pi^*)$ carbonyl compound on a ground state olefin is not the only allowed mechanism for photoaddition reaction. Alkanals and alkanones can attack olefins or conjugated dienes by a mechanism involving the singlet excited state of the carbonyl compounds.[2] In some cases, photoaddition may occur by both singlet and triplet mechanisms concurrently, as in the addition of acetone to 1-methoxy-1-butene,[3] or the addition of fluorenone to a ketenimine.[4] Recently, it has been suggested that an exciplex which leads to oxetane formation is formed between excited carbonyl compounds and olefins.[2a,2f,5] Some years ago, we reported that biacetyl and methyl pyruvate add to 2,3-dimethyl-2-butene to afford allylic ethers.[6] In these photoadditions, no detectable amounts of oxetanes were isolated. These results were explained by the reactivity of the 1,4-biradical intermediates. In this paper we wish to report some results concerning the photoaddition of methyl pyruvate to 2,3-dimethyl-2-butene, and our studies concerning the mechanism of this addition.

Results and Discussion

Products Studies. A preparative UV photoreaction of methyl pyruvate in solution in the presence of 2,3-dimethyl-2-butene leads to the formation of four products, which can be detected by VPC analysis. These are separated by preparative VPC and assigned the structures **1**—**4**.

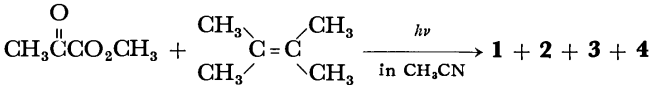

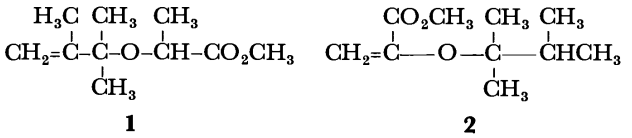

1

2

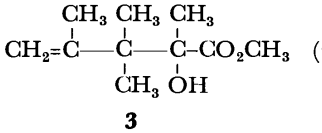

3

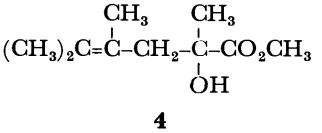

4

Compound **1** was assigned the allylic ether structure on the basis of its IR and NMR spectra (isopropenyl and $-OCH(CH_3)-$ groups). Compound **2** was identified as the isomeric vinyl ether by its IR and NMR spectra (isopropyl and $CH_2=C(CO_2CH_3)-O-$ groups). The compound slowly decomposed on standing and thus the isolation of **2** had to be performed carefully. The structures of the unsaturated alcohols (**3** and **4**) were apparent from an examination and comparison of their IR and NMR spectra. **3** showed terminal methylene absorption in the IR and NMR spectra, and only one $CH_3\dot{C}=$ signal in the NMR spectrum; **4** showed no vinyl proton, but signals for three $CH_3\dot{C}=$ groups and an allylic methylene in the NMR spectrum.

1 and **2** are the products derived from the disproportionation of the 1,4-biradical intermediate (**5**), and **3** and **4** are the products expected from the hydrogen abstraction of excited methyl pyruvate from 2,3-dimethyl-2-butene.

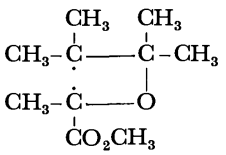

5

Quantum Yields. In order to investigate the quantum yield for product formation as a function of the concentration of reactants, Pyrex tubes containing known concentrations of methyl pyruvate and 2,3-dimethyl-2-butene in acetonitrile were irradiated in a merry-go-round reactor. After irradiation, the photoproduct in each tube was subjected to VPC analysis. The quantum yields for product formation were obtained by tris(oxalato)ferrate(III) actinometry.

Figure 1 shows plots of the reciprocal of quantum yields for the formation of products against the reciprocal of concentration of 2,3-dimethyl-2-butene. This indicates that different precursors exist for the formation of unsaturated alcohols (**3** and **4**) and unsaturated ethers (**1** and **2**). The upward curvature for **1** and **2** seen in Fig. 1 at higher olefin concentration is due to the deactivation of the excited singlet state of methyl pyruvate by interaction with 2,3-dimethyl-2-butene.[7]

Quenching Studies. Quantitative studies were carried out using 2,3-dimethyl-1,3-butadiene as a triplet quencher in acetonitrile in the presence of methyl pyruvate and 2,3-dimethyl-2-butene. Plots of relative

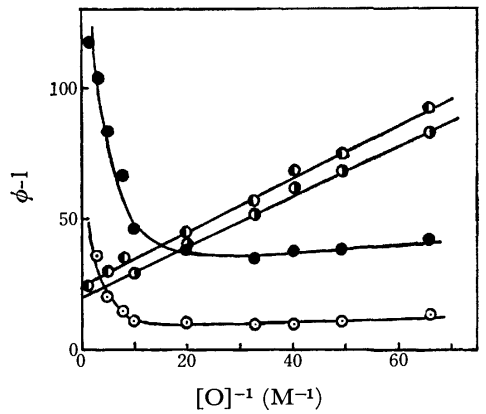

Fig. 1. Dependence of the reciprocal of the quantum yield for products formation on the reciprocal of 2,3-dimethyl-2-butene concentration.
●: Product **1**, ⊙: product **2**, ◐: product **3**, ◑: product **4**. [MP]=0.1 M in acetonitrile.

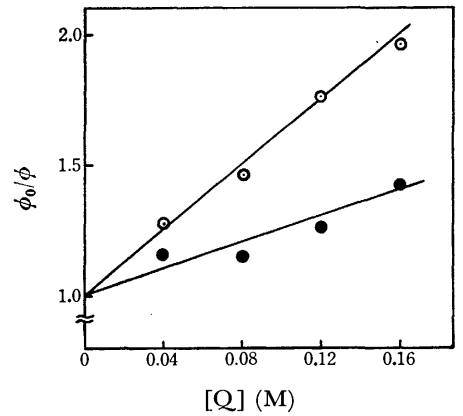

Fig. 2. Stern-Volmer plot of quenching of products **1**+**2** and **3**+**4** against 2,3-dimethyl-1,3-butadiene concentration.
⊙: **1**+**2**, ●: **3**+**4**. [MP]=0.1 M, [O]=0.2 M in acetonitrile.

quantum yields for **1**+**2** and **3**+**4** *vs.* quencher concentration in the presence of 0.2 M olefin concentration in acetonitrile are shown in Fig. 2. Apparently, **1**+**2** are more efficiently quenched than **3**+**4** are. It now seems established that, while conjugated dienes act as efficient quenchers of the triplet state of carbonyl compounds, dienes may also act as quenchers of the carbonyl singlet state.[2a] From the above experiment, we propose that **3**+**4** are formed from the excited singlet state of methyl pyruvate, probably *via* an exciplex, and **1**+**2** are formed from the triplet state of methyl pyruvate. This is confirmed by the kinetic treatment discussed later.

Fluorescence Quenching. 2,3-Dimethyl-2-butene and 2,3-dimethyl-1,3-butadiene quench the fluorescence of methyl pyruvate, as the Stern-Volmer plots in Fig. 3 show. This quenching effect is not due to a ground-state charge-transfer formation between methyl pyruvate and quenchers. Absorption spectra taken of methyl pyruvate with higher concentrations of 2,3-dimethyl-2-butene or 2,3-dimethyl-1,3-butadiene than

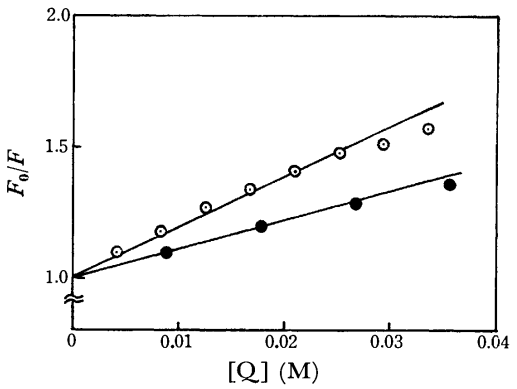

Fig. 3. Stern-Volmer plots for the fluorescence quenching of methyl pyruvate by 2,3-dimethyl-2-butene (⊙) and 2,3-dimethyl-1,3-butadiene (●) in acetonitrile.
[MP]=0.1 M.

those used in the kinetic experiments are identical with the spectra of methyl pyruvate in the absence of quenchers. The fluorescence of methyl pyruvate was also quenched by other dienes and olefins (Table 1). In Fig. 4 the function log k_q is plotted against the ionization potentials of several dienes and olefins. The moderately good linear behavior indicates that a charge

Table 1. Quenching rate constants and ionization potentials of unsaturated compounds

Unsaturated compound	$k_q\tau_s$[a] M^{-1}	$k_q \times 10^{-9}$ $M^{-1}s^{-1}$	IP[b] eV
2,5-Dimethyl-2,4-hexadiene	94.8	11.56	7.84
1,3-Cyclohexadiene	32.1	3.91	8.30
2,3-Dimethyl-2-butene	19.0	2.32	8.42
1,3-Pentadiene	13.4	1.63	8.59, 8.65
2,3-Dimethyl-1,3-butadiene	10.4	1.27	8.72
2-Methyl-1,3-butadiene	10.8	1.32	8.85
2-Methyl-2-butene	11.0	1.34	8.85

a) [MP]=0.1M in CH_3CN, τ_s=8.2 ns. b) Vertical ionization potentials; see Refs. 2a and 8.

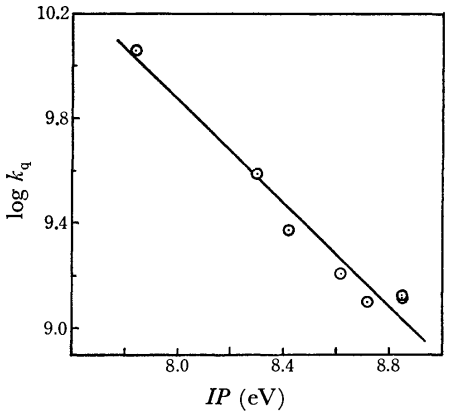

Fig. 4. Dependence of rates of methyl pyruvate fluorescence quenching by unsaturated compounds on their ionization potentials.

transfer interaction contributes to the stabilization of this quenching process. Similar correlations for fluorescence quenching of aromatic hydrocarbons,[8] alkanones,[2a] alkanals,[2e] azoalkanes,[9] and vinylene carbonates[10] by dienes or olefins have been attributed to exciplex formation.

Kinetic Analysis. The following mechanism is consistent with the above experiments:

	Rate Constant
$MP \xrightarrow{h\nu} {}^1MP$	
${}^1MP \longrightarrow MP + \Delta$ or $h\nu$	k_d^1
${}^1MP \longrightarrow {}^3MP$	k_{ST}
${}^1MP + O \longrightarrow {}^1(MP\cdots O)$	k_c^1
${}^1(MP\cdots O) \longrightarrow MP + O$	k_a^1
${}^1(MP\cdots O) \longrightarrow \mathbf{3} + \mathbf{4}$	k_p^1
${}^1MP + Q \longrightarrow MP + Q$	k_q^1
${}^3MP \longrightarrow MP$	k_d^3
${}^3MP + O \longrightarrow {}^3(MP\cdots O)$	k_c^3
${}^3(MP\cdots O) \longrightarrow MP + O$	k_a^3
${}^3(MP\cdots O) \longrightarrow \mathbf{1} + \mathbf{2}$	k_p^3
${}^3MP + Q \longrightarrow MP + {}^3Q$	k_q^3

MP: methyl pyruvate; O: 2,3-dimethyl-2-butene; Q: 2,3-dimethyl-1,3-butadiene; ${}^1(MP\cdots O)$, ${}^3(MP\cdots O)$: singlet and triplet exciplex, respectively.

Steady-state treatment of the species ${}^1MP$, ${}^3MP$, ${}^1(MP\cdots O)$, and ${}^3(MP\cdots O)$ leads to the expressions

$$\phi_{3+4} = \phi_A = \left(\frac{k_p^1}{k_a^1+k_p^1}\right)\left(\frac{k_c^1[O]}{k_d^1+k_{ST}+k_c^1[O]+k_q^1[Q]}\right), \quad (1)$$

$$\phi_{1+2} = \phi_E = \left(\frac{k_{ST}}{k_d^1+k_{ST}+k_c^1[O]+k_q^1[Q]}\right)\left(\frac{k_p^3}{k_a^3+k_p^3}\right) \times\left(\frac{k_c^3[O]}{k_d^3+k_c^3[O]+k_q^3[Q]}\right), \quad (2)$$

where ϕ_E and ϕ_A are the quantum yields for the formation of unsaturated ethers (**1**+**2**) and unsaturated alcohols (**3**+**4**), respectively.

First, consider the formation of **3**+**4**. In the absence of quenching by 2,3-dimethyl-1,3-butadiene, Eq. 1 becomes

$$\phi_A^{-1} = \left(1+\frac{k_a^1}{k_p^1}\right)\left(1+\frac{k_d^1+k_{ST}}{k_c^1[O]}\right). \quad (3)$$

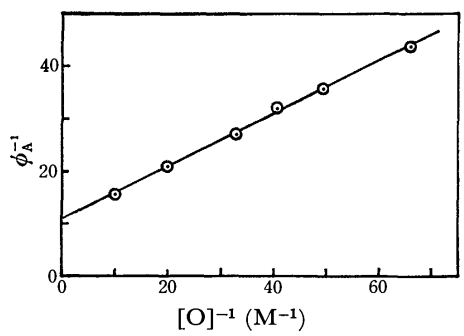

Fig. 5. Dependence of the reciprocal of the quantum yield for the formation of **3**+**4** on the reciprocal of 2,3-dimethyl-2-butene concentration. Slope=0.51 M, Intercept=10.7.

Figure 5 shows plots of the reciprocal of quantum yields for the formation of **3**+**4** against the reciprocal of concentration of 2,3-dimethyl-2-butene. A least-squares analysis of the points gave an intercept of 10.7 and a slope of 0.51 M. The intercept of Fig. 5 is now associated with $1+k_a^1/k_p^1$, and using this value in conjunction with the slope, we obtain the limiting quantum yield, $\phi_A^{lim}=0.0937$, $k_a^1/k_p^1=9.67$, and $k_c^1/(k_d^1+k_{ST})=21.0$.

In the presence of the quencher, Q,

$$\frac{\phi_A^\circ}{\phi_A} = 1 + \frac{k_q^1[Q]}{k_d^1+k_{ST}+k_c^1[O]} = 1 + k_q^1\tau_s[Q], \quad (4)$$

where ϕ_A is the quantum yield for the formation of **3**+**4** in the presence of Q, ϕ_A° is the quantum yield for the formation of **3**+**4** in the absence of Q, and τ_s is the lifetime of the excited singlet state in the absence of Q. 2,3-Dimethyl-1,3-butadiene quenches the formation of **3**+**4** in the presence of 0.2 M 2,3-dimethyl-2-butene in acetonitrile, as the Stern-Volmer plots in Fig. 2 show. From the slope in Fig. 2 we obtain the $k_q^1\tau_s$ value of 2.44; thus, $k_c^1/k_q^1=1.65$. A Stern-Volmer treatment of the fluorescence quenching in Fig. 3 yields a slope of 19.0 M^{-1} for 2,3-dimethyl-2-butene and 10.8 M^{-1} for 2,3-dimethyl-1,3-butadiene; thus, we get $k_c^1/k_q^1=1.82$. This is in good agreement with the value of k_c^1/k_q^1 (=1.65) obtained from the above calculation. These results indicate that the fluorescence quenching and the formation of **3**+**4** proceed *via* the excited singlet state of methyl pyruvate.

Next, consider the formation of **1**+**2**. In the absence of 2,3-dimethyl-1,3-butadiene, Eq. 2 leads to Eq. 5 by taking $k_{ST}\gg k_d^1$, since the triplet quantum yield for carbonyl compound is high:[11]

$$\phi_E^{-1} = \left(\frac{k_{ST}+k_c^1[O]}{k_{ST}}\right)\left(1+\frac{k_a^3}{k_p^3}\right)\left(1+\frac{k_d^3}{k_c^3[O]}\right). \quad (5)$$

Rearranging Eq. 5 gives

$$\left(\frac{k_{ST}}{k_{ST}+k_c^1[O]}\right)\phi_E^{-1} = \left(1+\frac{k_a^3}{k_p^3}\right)\left(1+\frac{k_d^3}{k_c^3[O]}\right). \quad (6)$$

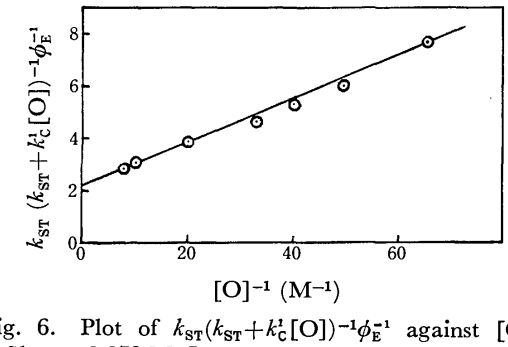

Fig. 6. Plot of $k_{ST}(k_{ST}+k_c^1[O])^{-1}\phi_E^{-1}$ against $[O]^{-1}$. Slope=0.079 M, Intercept=2.22.

Figure 6 shows a plot of $k_{ST}(k_{ST}+k_c^1[O])^{-1}\phi_E^{-1}$ against reciprocal olefin concentration. From the slope (=0.079 M) and intercept (=2.22) in Fig. 6, we obtain $k_a^3/k_p^3=1.22$, and $k_c^3/k_d^3=28.1$.

In the presence of Q,

$$\frac{\phi_E^\circ}{\phi_E} = \left(1+\frac{k_q^1[Q]}{k_d^1+k_{ST}+k_c^1[O]}\right)\left(1+\frac{k_q^3[Q]}{k_d^3+k_c^3[O]}\right). \quad (7)$$

Rearranging Eq. 7 gives

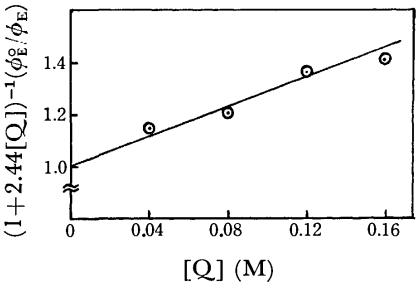

Fig. 7. Plot of $(1+2.44[Q])^{-1}$ (ϕ_E°/ϕ_E) against [Q]. Slope=2.78 M^{-1}.

Table 2. The ratio of rate constants of elementary reactions in acetonitrile and in benzene[a)]

	CH_3CN	C_6H_6
k_c^1/k_{ST}	21.0	22.3
k_c^1/k_q^1	1.65	1.64
k_a^1/k_p^1	9.67	14.5
k_c^3/k_d^3	28.1	37.4
k_c^3/k_q^3	1.53	1.50
k_a^3/k_p^3	1.22	1.05
$k_c^{1b)}$ ($M^{-1}s^{-1}$)	2.5×10^9	2.7×10^9

a) [MP]=0.1 M. b) Fluorescence lifetime of methyl pyruvate: 8.2 ns (in benzene).

$$\left(1+\frac{k_q^1[Q]}{k_d^1+k_{ST}+k_c^1[O]}\right)^{-1}\left(\frac{\phi_E^\circ}{\phi_E}\right)=1+\frac{k_q^3[Q]}{k_d^3+k_c^3[O]}. \quad (8)$$

At 0.2 M olefin concentration, $k_q^1/(k_d^1+k_{ST}+k_c^1[O])=2.44$; the dependence of $(1+2.44[Q])^{-1}(\phi_E^\circ/\phi_E)$ on [Q] are shown in Fig. 7. From the slope (=2.78 M^{-1}) in Fig. 7, we get $k_c^3/k_q^3=1.53$. The results are summarized in Table 2. Table 2 also includes the results in benzene solution. From the above experiments, we could calculate the ratio of the rate constants of elementary reactions; and if we take $\tau_S\simeq k_{ST}^{-1}=8.2$ ns, the rate constant of 2.5×10^9 M^{-1} s^{-1} for the singlet exciplex formation from methyl pyruvate and 2,3-dimethyl-2-butene in acetonitrile can be obtained. In this photoreaction, no predominant solvent effects were observed. In the case of biacetyl and 2,3-dimethyl-2-butene, the unsaturated ether formation and biacetyl phosphorescence quenching by 2,3-dimethyl-2-butene are 3—5 times larger in acetonitrile solution than in benzene solution.[12)]

Experimental

General. NMR spectra were recorded on a JEOL JNM-MH 100 machine, IR spectra on a JASCO IRA-1 spectrometer, mass spectra on a Hitachi Perkin-Elmer RMU-60 spectrometer, and fluorescence spectra on a Hitachi MPF-4 spectrofluorimeter. The fluorescence lifetime was measured using a Hitachi Time Resolved Photometer. VPC were performed on a Shimadzu GC-3BF or GC-6AM apparatus using a column of Carbowax 20M (20% on Celite 545, 3m) at 120 °C.

Methyl pyruvate was prepared by the reaction of pyruvic acid with methanol in the presence of catalytic amounts of *p*-toluenesulfonic acid.[13)] 2,3-Dimethyl-2-butene was prepared by the dehydration of 2,3-dimethyl-2-butanol,[14)] formed from the reaction of isopropylmagnesium bromide with acetone in ether. It was purified by efficient fractional distillation. 2,3-Dimethyl-1,3-butadiene was prepared by dehydration of pinacol with hydrobromic acid, followed by distillation.[15)] 1,3-Cyclohexadiene was prepared as described by Marvel and Hartzell.[16)] 2-Methyl-2-butene was prepared by the method of Whitmore *et al.*[17)] 2,5-Dimethyl-2,4-hexadiene, 1,3-pentadiene, and 2-methyl-1,3-butadiene were obtained commercially, and were purified by distillation before use. Acetonitrile was distilled three times from phosphorus pentaoxide and once from potassium carbonate.

Irradiation of Methyl Pyruvate with 2,3-Dimethyl-2-butene. A solution of methyl pyruvate (10.2 g) and 2,3-dimethyl-2-butene (8.4 g) in acetonitrile was irradiated for 120 h with a 300-W high pressure mercury lamp filtered through a hexane solution of naphthalene. After removal of the unreacted materials under vacuum, the remaining liquid was distilled under reduced pressure to give a liquid (5 g, bp 110—125 °C/30 mmHg) and leave a viscous liquid (1 g). VPC of the distillate showed four products (**1**—**4**) with the area ratios of 22: 15: 26: 37. These products were isolated by preparative VPC on a 3 m 20% Carbowax 20M column at 120 °C.

Methyl 2-(1,1,2-Trimethyl-2-propenyloxy)propionate (**1**): NMR (CCl_4) δ=1.23 (3H, s), 1.25 (3H, d, J=7 Hz), 1.29 (3H, s), 1.73 (3H, s), 3.62 (3H, s), 3.79 (1H, q, J=7 Hz), and 4.86 (2H, s); IR 3100, 2995, 2975, 1740, 1643, and 1120 cm^{-1}.

Methyl 2-(1,1,2-Trimethylpropoxy)acrylate (**2**): NMR (CCl_4) δ=0.97 (6H, d, J=7 Hz), 1.21 (6H, s), 1.92 (1H, sept, J=7 Hz), 3.66 (3H, s), 4.81 (1H, s), and 5.51 (1H, s); IR 2980, 2875, 1740, 1620, and 1140 cm^{-1}.

Methyl 2-Hydroxy-2,3,3,4-tetramethyl-4-pentenoate (**3**): NMR (CCl_4) δ=1.14 (3H, s), 1.16 (3H, s), 1.30 (3H, s), 1.75 (3H, s), 3.37 (1H, s), 3.67 (3H, s), and 4.77 (2H, m); IR 3540, 3085, 2980, 2960, 1720, and 1630 cm^{-1}.

Methyl 2-Hydroxy-2,4,5-trimethyl-4-hexenoate (**4**): NMR (CCl_4) δ=1.33 (3H, s), 1.63 (9H, s), 2.40 (1H, s), 2.45 (1H, s), 3.44 (1H, s), and 3.66 (3H, s); IR 3560, 2960, and 1730 cm^{-1}.

Quantum Yield Studies. Samples (4 ml) containing 0.1 M methyl pyruvate and varying concentrations of 2,3-dimethyl-2-butene in acetonitrile were placed in 10-mm o.d. Pyrex tubes. The samples were degassed using four freeze-pump-thaw cycles at $\approx5\times10^{-4}$ mmHg and sealed. The tubes were photolyzed to $<10\%$ conversion on a merry-go-round apparatus using a HALOS PIH 300 mercury lamp and a potassium chromate filter solution to isolate the 313-nm irradiation. The entire apparatus was immersed in a water bath. After irradiation, an internal standard (naphthalene) was added to each tube, and product yields were measured by VPC analysis on machines with flame ionization detectors. The area ratios of the peak for pure samples of the products (**1**—**4**) and for naphthalene were plotted against the ratios of the amounts actually present. The calibration factors thus obtained were 1.84 for **1**, 4.79 for **2**, 2.74 for **3**, and 2.01 for **4**. Peak areas were measured by a planimeter. Light intensities were measured by tris(oxalato)ferrate(III) actinometry.[18)]

Quenching of Products by 2,3-Dimethyl-1,3-butadiene. Acetonitrile solutions containing 0.1 M methyl pyruvate, 0.2 M 2,3-dimethyl-2-butene, and various concentrations of 2,3-dimethyl-1,3-butadiene (0—0.16 M) were prepared. Four milliliters of each sample were degassed and irradiated at 313 nm. Photolyzed solutions were analyzed for product formation using a VPC column.

Fluorescence Quenching. Solutions of methyl pyruvate (0.1 M) with various concentrations of 2,3-dimethyl-2-butene

or 2,3-dimethyl-1,3-butadiene were made up in acetonitrile. Solutions were placed in a quartz fluorescence cell and the fluorescence spectra were recorded. The excitation wavelength was 360 nm; the intensities of methyl pyruvate fluorescence at the maximum (410 nm) were measured in the absence (F_0) and presence (F) of various concentrations of quenchers. Stern-Volmer quenching plots were drawn of F_0/F against quencher molarity. No shifts in fluorescence maxima were observed upon increase in quencher concentration, and no new fluorescence bands were discernible in any of the measurements.

The authors are grateful to Nissei Sangyo Co. for measuring the fluorescence lifetime of methyl pyruvate. This research was supported by Grants-in-Aid for Scientific Research from the Ministry of Education (No. 747020 and 154163).

References

1) Part XXV: K. Shima, S. Takeo, K. Yokoyama, and H. Yamaguchi, *Bull. Chem. Soc. Jpn.*, **50**, 761 (1977).

2) a) N. C. Yang, M. H. Hui, D. M. Shold, N. J. Turro, R. R. Hautala, K. Dawes, and J. C. Dalton, *J. Am. Chem. Soc.*, **99**, 3023 (1977); b) J. C. Dalton, P. W. Wriede, and N. J. Turro, *ibid.*, **92**, 320 (1970); c) J. A. Barltrop and H. A. J. Carless, *ibid.*, **94**, 1951 (1972); d) J. A. Barltrop and H. A. J. Carless, *ibid.*, **94**, 8761 (1972); e) K. Shima, T. Kubota, and H. Sakurai, *Bull. Chem. Soc. Jpn.*, **49**, 2567 (1976); f) N. J. Turro, J. C. Dalton, K. Dawes, G. Farrington, R. Hautala, D. Morton, M. Niemczyk, and N. Schore, *Acc. Chem. Res.*, **5**, 92 (1972).

3) N. J. Turro and P. A. Wriede, *J. Am. Chem. Soc.*, **90**, 6863 (1968).

4) L. A. Singer, G. A. Davis, and V. P. Muralidharan, *J. Am. Chem. Soc.*, **91**, 897 (1969).

5) a) I. E. Kochevar and P. J. Wagner, *J. Am. Chem. Soc.*, **94**, 3859 (1972); b) R. A. Caldwell, G. W. Sovocool, and R. P. Gajewski, *ibid.*, **95**, 2549 (1973).

6) a) H.-S. Ryang, K. Shima, and H. Sakurai, *J. Org. Chem.*, **38**, 2860 (1973); b) K. Shima, T. Kawamura, and K. Tanabe, *Bull. Chem. Soc. Jpn.*, **47**, 2347 (1974).

7) Similar examples appear in the following papers: Ref. 4 and G. A. Davis, P. A. Carapellucci, K. Szoc, and J. D. Gresser, *J. Am. Chem. Soc.*, **91**, 2264 (1969).

8) D. A. Labianca, G. N. Taylor, and G. S. Hammond, *J. Am. Chem. Soc.*, **94**, 3679 (1972).

9) a) A. C. Day and T. R. Wright, *Tetrahedron Lett.*, **1969**, 1067; b) B. S. Solomon, T. F. Thomas, and C. Steel, *J. Am. Chem. Soc.*, **90**, 2249 (1968).

10) a) F. D. Lewis and R. H. Hirsch, *J. Am. Chem. Soc.*, **98**, 5914 (1976); b) F. D. Lewis, R. H. Hirsh, P. M. Roach, and D. E. Johnson, *ibid.*, **98**, 8438 (1976).

11) A. A. Lamola and G. S. Hammond, *J. Chem. Phys.*, **43**, 2129 (1965).

12) K. Shima, K. Tsukamoto, N. Inoue, and S. Ohta, unpublished results.

13) A. Weissberger and C. J. Kibler, *Org. Synth.*, Coll. Vol. III, 610 (1955).

14) I. Shurman and C. E. Boord, *J. Am. Chem. Soc.*, **55**, 4930 (1933).

15) R. Adams and E. W. Adams, *Org. Synth.*, Coll. Vol. I, 459 (1941); C. F. H. Allen and A. Bell, *ibid.*, Coll. Vol. III, 312 (1955).

16) C. S. Marvel and G. E. Hartzell, *J. Am. Chem. Soc.*, **81**, 448 (1959).

17) F. C. Whitmore, C. S. Rowland, S. N. Wrenn, and G. W. Kilmer, *J. Am. Chem. Soc.*, **64**, 2970 (1942).

18) C. G. Hatchard and C. A. Parker, *Proc. R. Soc. London, Ser. A*, **235**, 518 (1956).

Kinetic Studies on the Lime Sulfurated Solution (Calcium Polysulfide) Process for Removal of Heavy Metals from Wastewater

Kiyochika YAHIKOZAWA, Toshiro ARATANI,* Ryuzo ITO,** Takataro SUDO, and Takeo YANO*

Department of Chemical Engineering, College of Textile Science and Technology, Shinshu University, Tokida, Ueda 386
**Department of Chemical Engineering, College of Engineering, University of Osaka Prefecture, Mozu-Ume, Sakai 591*
***Department of Chemical Engineering, College of Engineering Science, Osaka University, Toneyama, Toyonaka 560*

(Received April 1, 1977)

A new process has been developed for wastewater purification, utilizing "Lime Sulfurated Solution" as a coagulant. Calcium polysulfide, the main component of this solution, decomposes in water on contact with a gas (atmospheric air or CO_2 gas) and reacts with heavy metals. The heavy metals are removed as practically insoluble precipitates. The kinetics of this process were studied in a batch stirred tank vessel to obtain the fundamental data needed for development of a commercial continuous process. The findings are as follows: (1) Processing of bivalent metals Hg^{2+}, Cd^{2+}, Zn^{2+}, Pb^{2+}, and Cu^{2+} are completed in a few minutes to achieve the water quality standards in Japan. (2) Cr^{3+} is flocculated as $Cr(OH)_3$ by the strong alkaline base of CaS_x solution. It takes about 60 minutes for the precipitation with CO_2 blowing, and 30 min with aeration. Cr(VI) is quickly reduced to Cr^{3+} and removed as $Cr(OH)_3$. (3) A simulated wastewater simultaneously contaminated with 6 kinds of heavy metals can be brought well within the standards within 20 min of processing time.

The development of a new process for removal of heavy metals from industrial wastewater is essential for the protection of the environment. A variety of processes have already been proposed and some have been put into practice. For example, ion exchange, reverse osmosis, chemical precipitation, and others have been developed. Among these, the chemical precipitation process is now the most practical and the least expensive.[5] This process can be further divided into the "Hydroxide process" and the "Sulfide process." In the former, heavy metals are precipitated as metal hydroxides. In the ferrite process, which is one kind of hydroxide process, heavy metals are removed by being occluded in the ferrite crystals. Thus, the sludge from this process is less soluble than that from the other hydroxide processes. In the latter process, the heavy metal ions are removed as metal sulfides. A typical example of coagulant is sodium sulfide. The precipitated metal sulfides of a sodium sulfide process, however, are often colloidal and do not grow large enough to allow easy filtration. Consequently, the sodium sulfide process is inevitably followed by the injection of another coagulant (iron(III) chloride or sulfate) for coprecipitation of these colloidal metal sulfides. The sulfide process has the advantage of removing mercury more effectively than the other process, because HgS has the very low solubility products of 10^{-52}.

In the present study, a new sulfide process has been developed, utilizing "Lime Sulfurated Solution" as a single coagulant. The main component of this solution is calcium polysulfide, whose chemical formula is CaS_x, $x=4.7—5.4$.[6] Hereafter, lime sulfurated solution will be briefly written as CaS_x solution. This solution is well known as an insecticide or a disinfectant in agriculture.[1] When used as an insecticide, CaS_x solution decomposes slowly in contact with atmospheric air and produces calcium thiosulfate, hydrogen sulfide, and solid sulfur.[7] For the purification of wastewater contaminated with heavy metals, CaS_x solution decomposes rapidly by blowing a decomposing gas (air or CO_2 gas); heavy metals react with calcium thiosulfate or hydrogen sulfide and are precipitated as metal sulfides or hydroxides. However, the kinetics of these reactions have not been well studied. Thus, some experiments in a batch stirred tank reactor with air or CO_2 blowing were conducted aimed at the removal of heavy metals in order to gain the fundamental kinetic data needed for the design of a commercial continuous process.

Experimental

Apparatus. A batch stirred tank reactor of 2 dm^3 in volume was constructed, as illustrated in Fig. 1, to study the kinetics for the removal of heavy metals from wastewater by CaS_x. The decomposing gas (air or CO_2; flow rate, 500 cm^3/min) is blown in and dispersed into bubbles. The revolution of the impeller was 10 Hz. These revolution and gas flow rates were ascertained to be sufficient for the finest dispersion of the gas bubbles. The excess hydrogen sulfide was caught by the adsorber A, which was packed with appropriate adsorbing pellets. The pH and the temperature in the reactor were measured with a pH meter and a thermometer T.

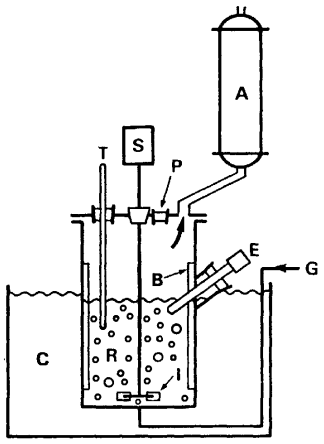

Fig. 1. Experimental apparatus. A: H_2S adsorber, B: baffle plate, C: constant temperature bath, E: glass electrode for pH measurement, G: pipe for gas aspiration, I: turbine impeller, P: plug for CaS_x injection, R: batch reactor, S: stirrer, T: thermometer.

Method. Water contaminated with 6 kinds of heavy metal ions: Hg^{2+}, Cd^{2+}, Pb^{2+}, Cu^{2+}, Zn^{2+}, and Cr^{3+}, was used as simulated wastewater in this experiment. Cr(VI) was also provided for the removal test by dissolving crystals of potassium dichromate. 2 dm^3 of the simulated wastewater was first placed in a constant temperature bath of 25 °C. The brown-colored CaS_x solution was injected into the reactor, and the blowing of the decomposing gas was immediately started. The sample liquors of 20 cm^3 were taken at the predetermined time intervals and filtered through No. 5C filter paper. The concentration of heavy metals in the filtrates was analyzed by an atomic absorption spectrophotometer according to JIS-K0102.[2] Sample liquors were concentrated by extraction with chloroform solution of dithizone, if high sensibilities were required. The initial pH of the simulated wastewater was set at 5.0. The simulated wastewaters were prepared in two ways. One set contained only one chemical species from among 6 heavy metals to investigate the behavior of each metal. The other was simultaneously contaminated with 6 kinds of heavy metals to determine the practical application requirements.

Results

Heavy metal concentrations in the treated water are compared with the water quality standards (criteria) in Japan. The batch processing time to clear the criteria is also checked to obtain the required residence time (or reactor volume) of a continuous process.

Typical examples of the heavy metal concentrations in the filtrate are plotted against the processing time in Figs. 2 to 5. As for the removal of mercury (Fig. 2), the severe criterion (5 ppb) is clearly covered by this CaS_x process; pure H_2S gas blowing and the Na_2S process can not cope with this criterion. The S^{2-} ion which may dissolve HgS can be eliminated by the decomposition of CaS_x with air or CO_2 gas in the case of the CaS_x process. Calcium salts and solid sulfur are also liberated from CaS_x and they work as flocculating aids to precipitate the metal sulfide (HgS). This flocculating ability was ascertained by an auxiliary experiment, in which precipitation of HgS from colloidal HgS solution was observed by adding a solution that had contained only air-decomposed CaS_x. R_m in the figures indicates the mole ratio of sulfur in CaS_x or Na_2S to heavy metal. For quantities of Na_2S injected larger than $R_m=25$, the processing results in a less effective removal of Hg^{2+}. A limited duration (10 s) blowing of H_2S gas does not give any better removal than the $R_m=2$ injection of Na_2S.

For the conditions of $R_m=25$ and the initial metal concentration of 25 ppm, the other metals were tested. For Cd^{2+} and Zn^{2+} (Fig. 3), CO_2 gas blowing can reduce the processing time compared with the aeration.

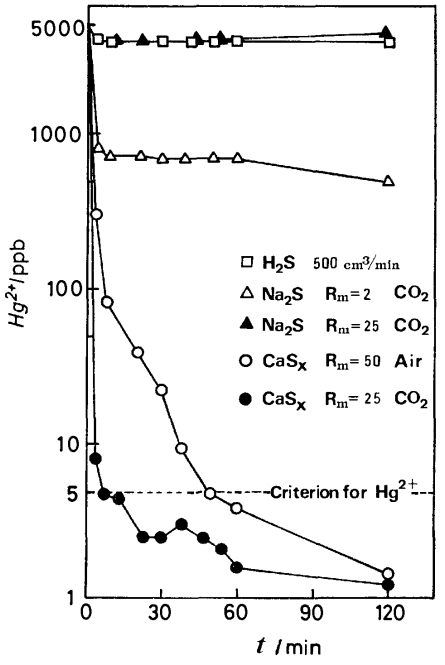

Fig. 2. Removal of Hg^{2+}, initial concentration of Hg^{2+} =5 ppm.

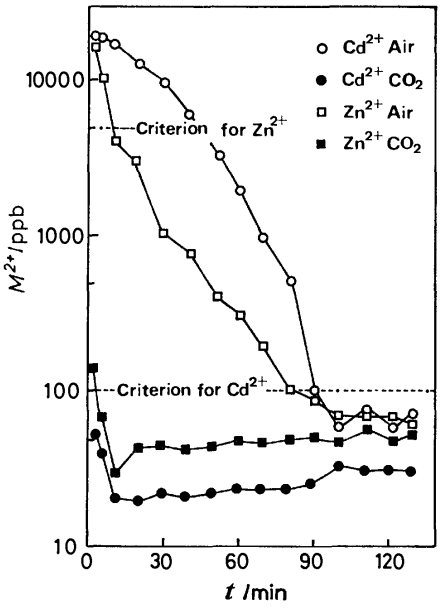

Fig. 3. Removal of Cd^{2+} or Zn^{2+}.

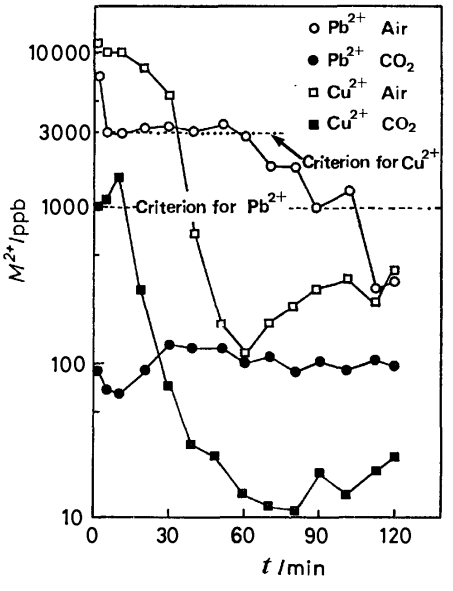

Fig. 4. Removal of Pb^{2+} or Cu^{2+}.

The same tendency is found for Pb^{2+} and Cu^{2+} (Fig. 4). For Cr^{3+} and Cr(VI), the aeration is desirable to shorten the processing time, as illustrated in Fig. 5.

Removal of heavy metals from the simulated wastewater simultaneously contaminated with 6 kinds of heavy metals is shown in Figs. 6 and 7. Long processing time is required for the aeration. CO_2 gas blowing, however, can reduce the processing time to within 30 min.

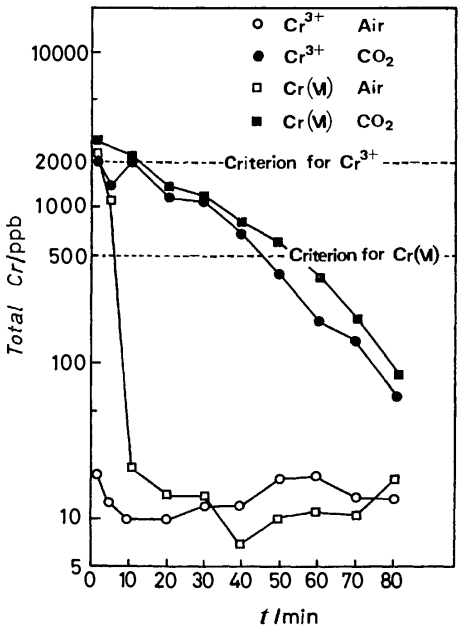

Fig. 5. Removal of Cr^{3+} or Cr(VI).

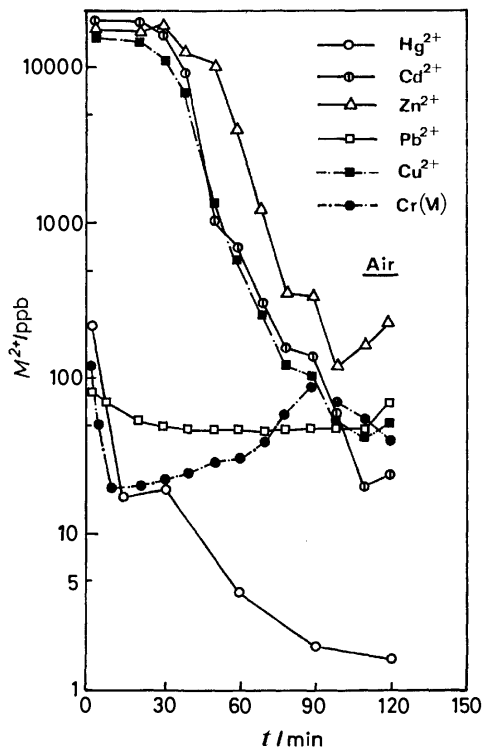

Fig. 6. Simultaneous removal of heavy metals with aeration.

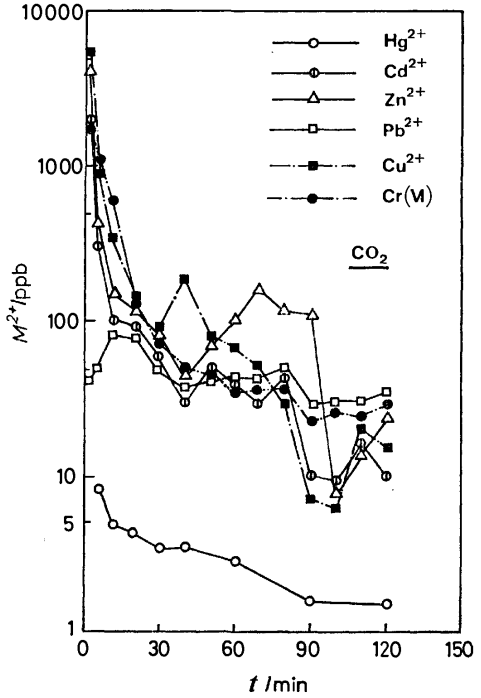

Fig. 7. Simultaneous removal of heavy metals with CO_2 blowing.

Discussion

Apparent kinetic data have been obtained, but it is unsettled question whether the processing time is needed for the decomposition of CaS_x or for the flocculation of the precipitates. The reactions for the decomposition of CaS_x by air or CO_2 and for the precipitation of heavy metals need to be discussed.

The changes in color of the precipitates (or suspended solids) and of the liquid phase were observed while CaS_x was decomposed by air or CO_2, with and without heavy metals. Without any charging of metal ions, the water in the reactor become light brown after the injection of CaS_x, because the CaS_x solution has a reddish brown color.

After the aeration, white particles (solid sulfur) which were liberated from CaS_x could be recognized as a suspension or scum, while the liquid phase was still brown. 60 min after the start of aeration, the brown color had gradually disappeared. When the heavy metal ions were in the water, the color of the suspended particles of metal sulfide was gradually predominating over the color of the sulfur particles. Yellow suspended particles (CdS) could vividly be seen in the water containing Cd^{2+}. Similarly, white (ZnS) for Zn^{2+}, dark gray (PbS) for Pb^{2+}, brown (CuS) for Cu^{2+}, and black particles (HgS) for Hg^{2+} were observed.

Upon blowing CO_2, on the other hand, the brown color of CaS_x solution instantaneously disappeared and white sulfur particles were produced. With the presence of heavy metal ions, the color of the suspended metal sulfide, which was different for each heavy metal, was observed immediately (within 1 s) after the start of CO_2 blowing. Thus the decomposition of CaS_x and the precipitation of bivalent metal ions by aeration was found to be considerably slower than that

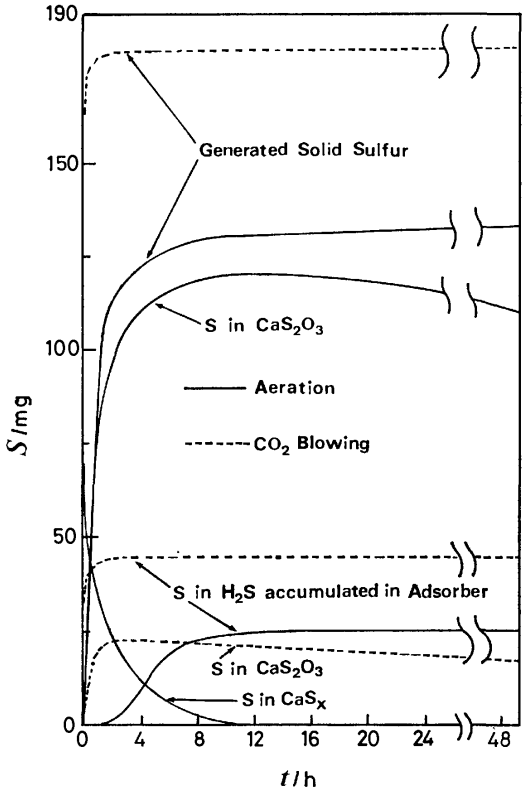

Fig. 8. Decomposition of CaS_x in a flask by aeration or CO_2 blowing; 1 cm^3 of CaS_x solution was added per 1 dm^3 of water.

by CO_2 blowing.

For more detailed research about the reaction kinetics for the decomposition of CaS_x, an auxiliary experiment was undertaken to determine quantitatively how the amounts of generated chemicals vary with time when CaS_x was decomposed in water without heavy metals. The decomposition of CaS_x by air or CO_2 was performed in a flask with a blowing pipe. The substances obtained after the decomposition were chemically analyzed[3,4] as shown in Fig. 8. Hydrogen sulfide, calcium thiosulfate, and solid sulfur (as suspended particles) were clearly recognized. Figure 8 indicates that CO_2 blowing gives rise to a more rapid decomposition of CaS_x than does aeration. This is consistent with the observations of color changes.

From another experiment for the decomposition of CaS_x with pure oxygen gas, it was found that hydrogen sulfide was not evolved by O_2.

The principal reactions of the decomposition of CaS_x by CO_2 and O_2 can be represented as Eqs. 1 and 2, following the above information:

$$CaS_x + \frac{3}{2}O_2 \longrightarrow CaS_2O_3 + (x-2)S, \quad (1)$$

$$CaS_x + CO_2 + H_2O \longrightarrow CaCO_3 + H_2S + (x-1)S. \quad (2)$$

Equations 1 and 2 imply that the decomposition of CaS_x by CO_2 generates a larger quantity of sulfur than that by O_2 or air. This agreed with the result of Fig. 8. Some H_2S, though only a small amount, was detected for the aerated case in Fig. 8. This H_2S was generated due to the decomposition by trace CO_2 in air, according to Eq. 2. For the wastewater containing heavy metal ions, the precipitating reactions can be written as

$$M^{2+} + CaS_2O_3 + H_2O \longrightarrow MS + CaSO_4 + 2H^+, \quad (3)$$

$$M^{2+} + H_2S \longrightarrow MS + 2H^+. \quad (4)$$

The rate of reaction for Eq. 3 was measured experimentally by a batch test. The test showed that formation of CdS precipitate was observed immediately after the injection of Cd^{2+} into the calcium thiosulfate solution. Equation 3 was found to proceed as quickly as the reaction with Eq. 4.

These processes, from Eq. 1 to 4, are known as the heterogeneous gas-liquid reaction with the formation of precipitates. An analytical treatment by a mathematical model is difficult. In the present study, the apparent kinetics are discussed experimentally.

An interesting result was the color change with the processing of Zn^{2+}. As the solid precipitates (ZnS, S, $CaSO_4$, and $CaCO_3$) are all white and CaS_x is brown, the time needed for the decomposition of CaS_x can be observed as the color change in the solution. With aeration, complete decomposition of CaS_x was observed at about 60 minutes of processing. The time when the steep decrease in the concentration of Zn^{2+} ended agreed exactly with the time when the brown color of injected CaS_x had disappeared (see Fig. 3). For removal of heavy metal ions by aeration, Eq. 1 is thought to be rate-controlling step. This slow decomposition was partly supported by pH measurements, for CaS_x which might dissolve heavy metal ions was thought to be stable in the alkaline side until the base of CaS_x solution was neutralized by the trace of CO_2 in air. The initial pH (pH=5) become rapidly alkaline (about pH=11 in this experimental condition with the simulated wastewater contaminated with a heavy metal) on the injection of CaS_x solution, which has a strong alkaline base. After aeration, the pH gradually returned to neutral (pH=7). With CO_2 blowing, the pH returned rapidly to the slightly acidic side (pH=6). These speeds of pH change may have a relation to the neutralizing speeds of alkaline base of CaS_x solution by CO_2 gas (in air or pure CO_2) and, therefore, partly relate to the rate of decomposition of CaS_x. In applying this CaS_x process to wastewater treatment, the treated water has pH values ranging from 6 to 7, and so can pass the water quality criteria for pH range without injecting any other alkaline reagents. Thus, a more economical treatment is expected than the usual chemical precipitation processes.

For the removal of Cr^{3+}, since the sulfide of Cr^{3+} is unstable in water, Cr^{3+} is not precipitated as Cr_2S_3, but easily removed as $Cr(OH)_3$ by the strong alkaline nature of CaS_x solution. The reduction of Cr(VI) (dichromate) to Cr^{3+} ion is easily attained by H_2S or CaS_2O_3 according to either pair of Eqs. 5 and 6 or 5 and 7.

$$Cr_2O_7^{2-} + 2OH^- \longrightarrow 2CrO_4^{2-} + H_2O, \quad (5)$$

$$2CrO_4^{2-} + 3H_2S + 10H^+ \longrightarrow 2Cr^{3+} + 3S + 8H_2O, \quad (6)$$

$$2CrO_4^{2-} + 3S_2O_3^{2-} + 10H^+ \longrightarrow 2Cr^{3+} + 3SO_4^{2-} + 3S + 5H_2O. \quad (7)$$

The reduction sheme from Cr(VI) to Cr^{3+} through CrO_4^{2-} was also confirmed by the observation of the color change in the solution. The color of the solution was initially brown (dichromate), and changed to yellow (chromate) on injection of CaS_x and further to light green ($Cr(OH)_3$). With the aeration, these changes were observed within 10 min. For the CO_2 blowing, however, the changes ended in a few seconds, and a fine floc of $Cr(OH)_3$ which partly passed through the No. 5C filter paper was generated. As shown in Fig. 5, the aeration is more effectively than CO_2 gas blowing, for the faster precipitation of Cr^{3+} and Cr(VI). For the precipitation of Cr^{3+}, the slow change in pH with aeration is thought to be favorable to the flocculation of $Cr(OH)_3$ particles. Rapid decomposition of CaS_x with CO_2 blowing may give to the fast formation of a fine floc of $Cr(OH)_3$ by the alkaline base which has been coordinated to CaS_x and freed by the decomposition. The processing rate of Cr^{3+} may be determined by the step of flocculation of the hydroxide floc. For the aeration, the difference between the curves of Cr^{3+} and Cr(VI) in Fig. 5 shows the time required for the reduction of Cr(VI) to Cr^{3+} according to Eqs. 5, 6, and 7. Figure 7 also indicates that chromium can be precipitated faster in the simultaneous removal than in the removal for the case when the water was contaminated only with chromium. This effect is thought to be due to the coprecipitation of $Cr(OH)_3$ with the other sulfides.

Minimum values are observed in the detected concentrations in Figs. 2 to 7. Thus, in the continuous CaS_x process, the mean residence time of the reactor used for the treatment should be so designed as to be equal to the time when the minimum values in the concentrations are attained in batch tests.

Conclusion

From the preceding experiments and discussion, the kinetics of the CaS_x process can be summarized as follows.

(1) CaS_x is decomposed slowly by aeration and rapidly by CO_2 gas blowing, and produces H_2S, $CaCO_3$, $CaSO_4$, and solid sulfur particles. Bivalent heavy metals are precipitated as metal sulfides. The precipitating rate is determined by the step of CaS_x decomposition. Cr^{3+} can also be precipitated as a metal hydroxide more rapidly with aeration than with CO_2 blowing. The precipitating rate of the hydroxide is determined by the step of the flocculation. Cr(VI) is easily precipitated as $Cr(OH)_3$ after rapid reduction from Cr(VI) to Cr^{3+} by H_2S or CaS_2O_3. The solid sulfur and calcium salts work effectively to coprecipitate the metal sulfides and the hydroxide.

(2) The water treated by a single coagulant, CaS_x, can pass the water quality standards in Japan for 6 kinds of heavy metals, within 60 min of processing time. Based on these batch kinetic data, development of a continuous purification process is thought to be easily possible.

The authors wish to express their thanks to Mr. Shigeki Yasuhara and Mr. Teruyuki Miyazawa for assistance in the experimental work. The present work was partially supported by a Grant-in-Aid for Developmental Scientific Research from the Ministry of Education.

References

1) M. Hori, "Nihon Shin Noyaku Monogatari," Nihon Shokubutsu Boh-eki Kyokai (1973), p. 264.
2) Japanese Industrial Standards, "Testing Methods for Industrial Waste Water," JIS-K0102 (1971).
3) K. H. Mancy and W. L. Weber, Jr., "Analysis of Industrial Wastewater," Wiley Interscience, New York (1973), p. 525.
4) T. Ogami, "Nogyo Bunseki," Asakura Shoten, Tokyo (1942), p. 71.
5) G. A. Sawyer, *Chem. Eng. (N. Y.)*, July 24th, **1972**, 120.
6) G. Shwarzenbach and Adolphe Fisher, *Helv. Chim. Acta*, **43**, 1365 (1960).
7) H. H. Shepard, "The Chemistry and Action of Insecticides," McGraw-Hill, Yew Nork (1951), p. 54.

The Hydrocracking of Polynuclear Aromatic Hydrocarbons over Molten Salt Catalysts[1)]

Yohji NAKATSUJI, Toshio KUBO, Masakatsu NOMURA, and Shōichi KIKKAWA

Department of Applied Chemistry, Faculty of Engineering, Osaka University, Yamadakami, Suita, Osaka 565

(Received May 31, 1977)

The hydrocracking of phenanthrene, anthracene, pyrene, chrysene, and fluoranthene over molten salt catalysts at 400 °C in the batch autoclave systems was examined. The products were mainly identified by means of GC-MS, but the representative products were isolated by preparative GLC and characterized by using NMR, IR, UV, and mass spectrometry. Most of the isolated products are compounds not previously confirmed in detail, although their formation has been expected in the hydrocracking of the corresponding aromatic compounds. Probable reaction routes are offered based on the product distributions. The binary mixture of zinc chloride and copper(I) chloride is considered to act as a molten dual-functional catalyst.

The hydrocracking of the model compounds, which are supposed to be structural units of coal, has frequently been carried out in order to examine the function of catalysts and the reaction process. In the investigation reported by Qader,[2)] the hydrocracking of naphthalene, anthracene, and pyrene was found to proceed through a sequential occurence of hydrogenation, isomerization, and cracking reactions over silica-alumina-based dual-functional catalysts, which are extensively used in the industrial processing of petroleum feedstocks. Zielke *et al.*[3)] had shown molten zinc chloride to be a superior acidic catalyst for the hydrocracking of pyrene and coal extracts when used in high concentrations.

As a part of a study of organic reactions in molten salts,[4)] we examined the catalytic activity of molten salts in the hydrocracking of a heavy anthracene oil.[5)] In this experiment, a binary mixture of CuCl and $ZnCl_2$ was found to be more effective than $ZnCl_2$ alone in obtaining many lower-boiling fractions; both the analysis of the starting oil and the confirmation of the products were also carried out extensively. However, in this hydrocracking of the heavy anthracene oil, the behavior of the representative constituents of the starting oil, that is, anthracene, phenanthrene, chrysene, pyrene, and fluoranthene, could not be clarified in detail. Concerning the hydrocracking of anthracene, the efficient catalytic activity of the binary mixture of $ZnCl_2$ and CuCl was reported in a preliminary paper.[6)] In addition to the above results, this paper will describe the application of this catalyst to the hydrocracking of phenanthrene, chrysene, pyrene, and fluoranthene and their characteristic properties. The effects of two different-batch autoclave systems on their product distributions are also investigated. Moreover, the probable reaction routes for the respective reactions of phenanthrene, chrysene, and fluoranthene will be offered and discussed.

Experimental

Product Analysis. The GLC analyses were performed on a Shimadzu GC-3AH for the gaseous products and on a Shimadzu GC-4BPTF for the liquid and solid products. The GC-MS spectra were taken at 20 eV with a Hitachi RMU-6MG spectrometer connected with a Hitachi M 5201 gas chromatograph by using a 3 m×3 mm column of 5% Silicone OV-1 on Uniport KS. The main products were isolated on a Shimadzu GC-3BT using a 3 m×3 mm column of 10% Pluronic L 84 on Neopack IA (for products from phenanthrene) or a 3 m×3 mm column of 20% Silicone DC 550 on Celite 545 (for products from pyrene, chrysene, and fluoranthene). The NMR spectra were recorded on a Jeol JNM-PS-100 spectrometer, using tetramethylsilane as the internal standard. CCl_4 was used as the solvent for all the compounds. The UV spectra and the IR spectra were taken with a Hitachi 124 spectrometer and a Jasco IR-E spectrometer respectively.

Materials. The chrysene (G.R.), fluoranthene (E.P.), and phenanthrene (E.P.) were obtained from the Tokyo Kasei Kogyo Co., Ltd. The pyrene (G.R.) and anthracene (E.P.) were obtained from Nakarai Chemicals, Ltd., and Wako Pure Chemical Industries, Ltd., respectively. The anthracene and phenanthrene were recrystallized from ethanol. The fluoranthene (98% purity by GLC) contained a small amount of cyclopenta[*j*,*k*]phenanthrene. This impurity was not removed before use. The zinc iodide and the copper(I) bromide were obtained from the Mitsuwa Chemicals Co., Ltd., while the other metal halides used in this investigation were obtained from Nakarai Chemicals, Ltd. These salts were dried before use at 400 °C for 1 h in nitrogen.

General Procedure. All the experiments were carried out in the two different systems (A and B) as follows:

A) A stainless steel vessel containing 8 g of feed and an equimolar amount of the catalyst was placed in a stainless steel (SUS 32) autoclave with a capacity of 200 ml. The system was flashed and filled with hydrogen to 100 kg/cm^2; then the autoclave was heated up to the desired temperature. The time taken to reach the stage was from 60 to 70 min. The reaction system shaken in a horizontal direction (68 strokes/min) was maintained at 400 °C for the desired reaction period. No attempts were made to maintain the hydrogen pressure at a constant level during the reaction.

B) A stainless steel vessel containing 10 g of feed and an equimolar amount of the catalyst was placed in a stainless steel (SUS 32) autoclave with a capacity of 500 ml. Hydrogen was introduced into the autoclave to 100 kg/cm^2. The rate of the temperature rise was controlled to about 3 °C/min up to 400 °C, after which the temperature was held for the desired reaction period. The autoclave was shaken in a horizontal direction (70 strokes/min). No attempts were made to maintain the hydrogen pressure at a constant level during the reaction.

After the system (A or B) had been cooled to room temperature, gases were collected in a gas holder and analyzed by GLC (60—80 mesh Silica gel column). When the products were obtained in a solid state, they were dissolved in a proper solvent and analyzed by GLC (4.5 m×3 mm packed with 20% SE-30 on Uniport B 60—80 mesh, programmed from 30 to 270 °C, 5 °C/min, TCD, H_2 carrier). The products

obtained in a liquid state were also analyzed by GLC in neat. The actual quantitative interpretation of a chromatogram is based on the peak area. The weight correction factors were determined by the measurement of the relative areas of authentic compounds. The values conveniently used in this study were as follows: retention time, 0—11 min, 0.9; 11—32 min, 1.0; 32—37 min, 1.1; 37—42 min, 1.2; 42—50 min, 1.3; 50 min-, 1.4 (Figs. 1—5). The mixture of coke and catalyst obtained after the extraction of the products was washed with hydrochloric acid in order to remove the catalyst. The coke obtained in this manner was dried and weighed.

Classification of Products. In order to characterize the activity of molten salt catalysts, the products were conveniently classified into 27 groups as follows: I, C_1—C_4 gases; II, C_5—C_7 alkanes; III, cycloalkanes; IV, monocyclic aromatics; V, indans and tetralins; VI, bicyclic aromatics; VII, dihydrophenanthrene; VIII, tetrahydrophenanthrene and its isomers; IX, octahydrophenanthrene and its isomers; X, phenanthrene; XI, higher-boiling compounds; XII, coke; XIII, benzindans, tricyclic aromatics, and their hydrogenated compounds; XIV, perhydropyrenes; XV, decahydropyrenes; XVI, tetrahydropyrene; XVII, hexahydropyrenes; XVIII, dihydropyrene; XIX, pyrene; XX, dodecahydrochrysene and its isomers; XXI, octahydrochrysene and its isomers; XXII, dihydrochrysene; XXIII, hexahydrochrysene and its isomers; XXIV, tetrahydrochrysene and its isomers; XXV, chrysene; XXVI, tetrahydrofluoranthene; XXVII, fluoranthene.

Results and Discussion

Identification of Products. The mass spectra of all the products in this study were obtained by means of GC-MS. The molecular weights of the products are given, and the chemical structures can be fairly deduced when specific cleavage patterns are found in the mass spectra. We previously published the results of the identification of the hydrocracked products of anthracene by considering their mass spectra in combination with the eluted order on the gas chromatogram estimated from their boiling points.[7] In that case, the isomerization of the skeleton of anthracene seemed not to occur. However, the isomerization between *sym*-octahydrophenanthrene and *sym*-octahydroanthracene was clearly found in this hydrocracking of anthracene over acidic molten salts,[6,8] so additional analytical methods were considered necessary for more detailed analyses. The main products were isolated by preparative GLC and analyzed by using NMR spectrometry. The NMR spectral data obtained for the isolated products were as follows: 6-butyltetralin, δ=0.92 (3H, t), 1.08—1.68 (4H, m), 1.78 (4H, m), 2.46 (2H, t), 2.66 (4H, m), and 6.6—7.0 (3H, m); 1,2,3,4,4a,9,10,10a-octahydrophenanthrene, 6.90 (4H, s); 1,2,3,4,5,6,7,8-octahydrophenanthrene, 1.75 (8H, m), 2.48 (4H, m), 2.65 (4H, m), and 6.60 (2H, s); 9,10-dihydrophenanthrene, 2.81 (4H, s), 7.02—7.33 (6H, m), and 7.48—7.72 (2H, m); 1,2,3,4-tetrahydrophenanthrene, 1.82 (4H, m), 2.88 (2H,m), 3.07 (2H, m), and 6.96—7.96 (6H, m); 1,2,3,3a,4,5,9,10,10a,10b-decahydropyrene, 6.5—7.0 (3H, m); 1,2,3,3a,4,5,5a,6,7,8-decahydropyrene, 6.64 (2H, s); 4,5,9,10-tetrahydropyrene, 2.84 (8H, s) and 6.92 (6H, s); 1,2,3,3a,4,5-hexahydropyrene, 1.2—2.4 (6H, m), 2.6—3.4 (5H, m), and 6.8—7.7 (5H, m); 1,2,3,6,7,8-hexahydropyrene, 2.01 (4H, m), 3.0 (8H, t), and 6.92 (4H, s); 4,5-dihydropyrene, 3.24 (4H, s) and 7.16—7.68 (8H, m); 5,6,8,9,10,11-hexahydrobenz[*a*]anthracene, 1.80 (4H, m), 2.72 (8H, m) and 6.76—7.80 (6H, m); 1,2,3,4,5,6-hexahydrochrysene, 1.84 (4H, m), 2.73 (8H, m), and 6.8—7.7 (6H, m); 8,9,10,11-tetrahydrobenz[*a*]anthracene, 1.80 (4H, m), 2.92 (4H, m), and 7.3—8.6 (8H, m); 1,2,3,4-tetrahydrochrysene, 1.96 (4H, m), 2.94 (2H, m), 3.16 (2H, m), and 7.2—8.8 (8H, m); 5,6-dihydrochrysene, 2.86 (2H, m), 3.20 (2H, m), and 6.8—8.1 (10H, m); 6-phenyltetralin, 1.82 (4H, m), 2.77 (4H, m), and 6.9—7.6 (8H, m); 5-phenyltetralin, 1.76 (4H, m), 2.56 (2H, m), 2.80 (2H, m), and 6.8—7.5 (8H, m). When the NMR spectrum of an isolated compound is complicated, the information about the molecular weight obtained from the mass-spectral measurements and the ratio of aromatic hydrogen to non-aromatic hydrogen from the NMR method often gave the correct structure (*e.g.*, the distinction between 1,2,3,3a,4,5,9,10,10a,10b-decahydropyrene and 1,2,3,3a,4,5,5a,6,7,8-decahydropyrene). When the amount of a compound isolated was small, UV spectrometry was conventionally used for the structural confirmation. The type of aromatic hydrocarbon (that is, benzene, naphthalene, biphenyl, anthracene, phenanthrene, pyrene, fluoranthene, chrysene, and so on) is clarified based on the characteristic absorption bands. For example, the absorption wave numbers of phenanthrene, 4,5-dihydropyrene, 1,2,3,4-tetrahydrochrysene, and 8,9,10,11-tetrahydrobenz[*a*]-anthracene differed to some degree, but their characteristic absorption bands were similar. This indicates that these compounds all have a phenanthrene skeleton. Of course, IR spectrometry played an important role

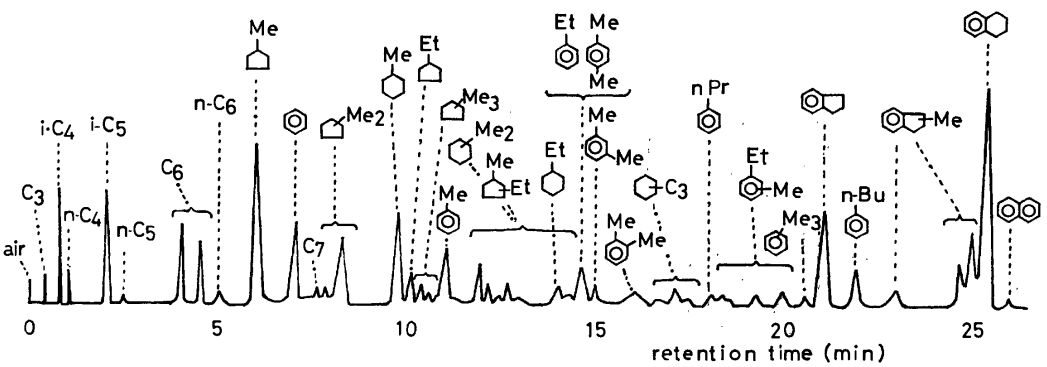

Fig. 1. Gas chromatogram of hydrocracked products of polynuclear aromatic hydrocarbons.

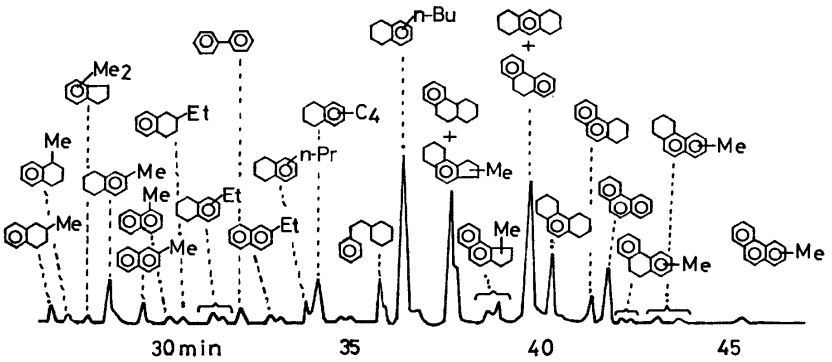

Fig. 2. Gas chromatogram of hydrocracked products of phenanthrene.

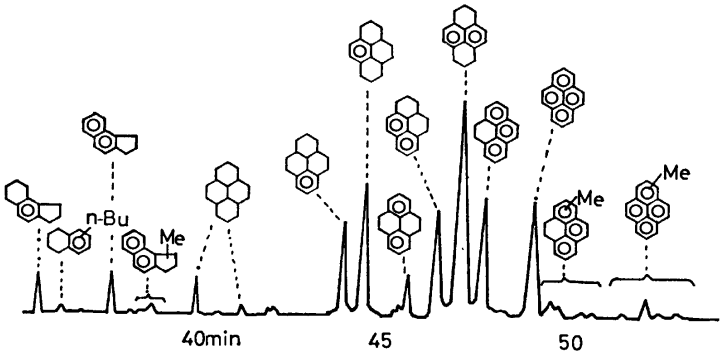

Fig. 3. Gas chromatogram of hydrocracked products of pyrene.

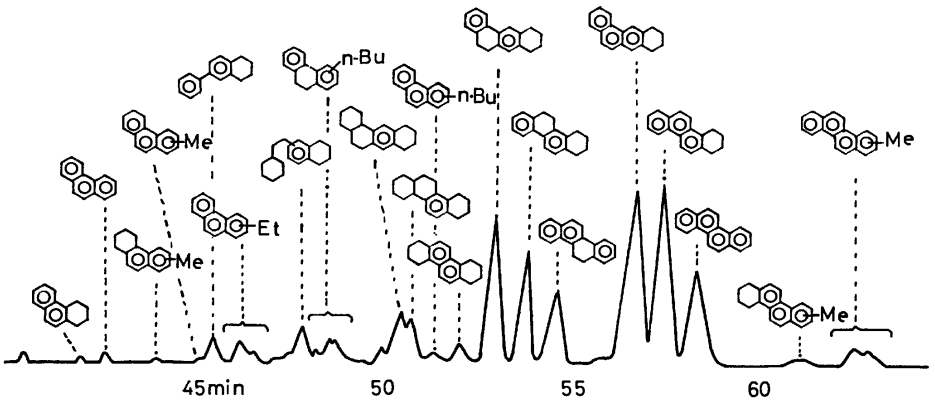

Fig. 4. Gas chromatogram of hydrocracked products of chrysene.

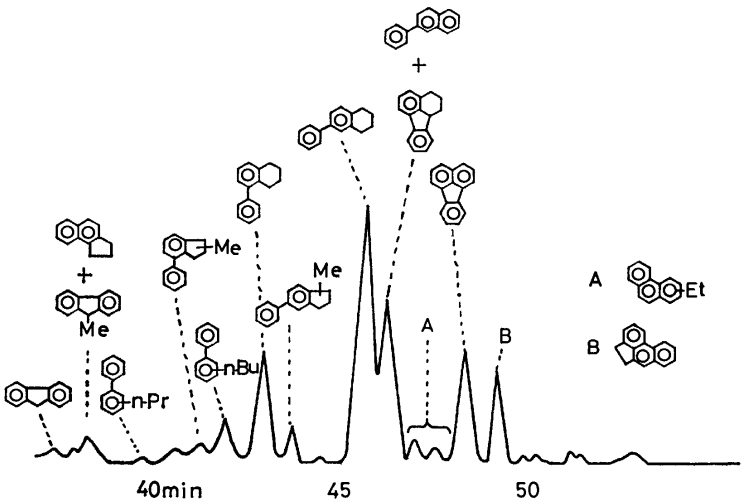

Fig. 5. Gas chromatogram of hydrocracked products of fluoranthene.

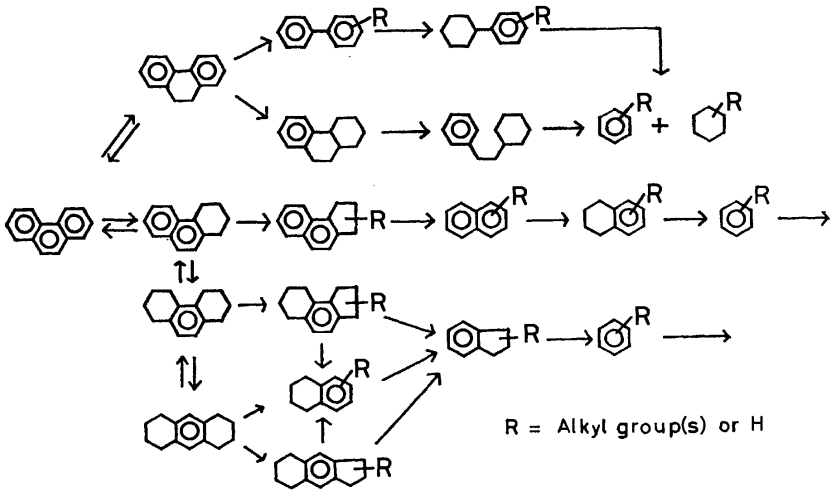

Fig. 6. Probable reaction process of phenanthrene.

in the analysis. The cleavage patterns of the mass spectra of the compounds identified by using these analytical methods could then be applied to other compounds. The GC charts of the hydrocracked products are shown in Figs. 1—5, where the structures characterized or assumed are listed. The structures of benzindan derivatives and their hydrogenated compounds are not certain because the distinction between 2,3-dihydro-1*H*-benz[*e*]indene and 2,3-dihydro-1*H*-benz[*f*]indene is not clear only by considering their mass spectra. Consequently, the structures for these compounds listed in these figures are chosen for convenience. By this exhaustive analysis, the probable reaction process can be estimated and the difference in catalytic activity among the molten salt catalysts can be clarified.

Hydrocracking of Phenanthrene. The most probable reaction process is shown in Fig. 6. The most important characteristic of the hydrocracking of phenanthrene is the isomerization between *sym*-octahydrophenanthrene and *sym*-octahydroanthracene. We also observed the isomerization in the hydrocracking of anthracene in the presence of a Lewis acid.[6,8] A constant ratio of them in equilibrium was observed, so this isomerization is considered to be reversible. This finding is consistent with that observed over aluminum chloride by Schroeter.[9] On the other hand, this isomerization was not observed in their hydrogenation in the presence of alkali metals.[10] These findings suggest that the decomposition process of *sym*-octahydroanthracene must also be considered in the hydrocracking of phenanthrene over acidic catalysts.

The formation of 1-cyclohexyl-2-phenylethane was found in the products[δ=2.56(2H,t,J=8 Hz)]. *unsym*-Octahydrophenanthrene is considered to be cleaved and hydrogenated to that compound, judging from the similarity of the structures of these two compounds. In the presence of aluminum chloride, secondary alkyl-

Table 1. Hydrocracking of phenanthrene

Reaction conditions: initial hydrogen pressure, 100 kg/cm^2; reaction temperature, 400 °C; reaction system A: Catalyst/Feed=1.0 (mol/mol), Hydrogen/Feed=18.8 (mol/mol); B: Catalyst/Feed=1.0, Hydrogen/Feed=26.7.

		Run No.						
		1	2	3	4	5	6	7
Catalyst		$ZnCl_2$	$ZnCl_2$/CuCl	ZnI_2/KI	$ZnCl_2$/$NiCl_2$	—	$ZnCl_2$	$ZnCl_2$/CuCl
(mol: mol)			(60:40)	(80:20)	(90:10)			(60:40)
Reaction system		A	A	A	A	B	B	B
Reaction time (h)		3	3	3	3	1	1	1
Product (wt %)	I	0.4	27.7	0.2	11.2	2.0	1.6	3.2
	II	—	7.2	—	1.4	—	—	0.3
	III	—	7.0	0.1	7.5	—	—	2.2
	IV	0.1	33.2	—	10.5	—	0.3	3.3
	V	0.1	12.4	2.2	11.5	0.1	0.9	10.9
	VI	0.4	2.2	0.1	1.0	0.6	0.4	0.6
	VII	8.0	0.5	14.2	9.8	13.6	21.2	14.8
	VIII	3.5	1.4	13.7	6.9	5.7	9.5	7.5
	IX	—	1.1	5.2	4.8	3.5	7.0	22.6
	X	87.5	1.4	63.4	33.4	74.5	55.5	24.9
	XI	—	1.3	0.9	2.0	—	3.2	5.0
	XII	—	4.6	—	—	—	0.4	4.7

benzene was dealkylated in preference to primary alkylbenzene.[11] If this finding is extended to the case of *unsym*-octahydrophenanthrene, the preferable scisson of its C_{4a}–C_{4b} bond to produce 1-cyclohexyl-2-phenylethane may be reasonable. Although the above decomposition process has never been indicated in this connection, it is one of the most important decomposition routes in the hydrocracking of phenanthrene.

The product distributions are shown in Table 1. From the standpoint of the distribution of the gaseous products, especially the ratio of iso to normal isomers, the catalytic action of molten salts was discussed in a previous paper.[5] The constituents of the gaseous products in Run 2 were as follows: methane, 8.0 wt %; ethane, 7.5%; propane, 33.6%; isobutane, 38.0%; butane, 9.3%; butenes, 3.6%. Since the ratio of isobutane to butane is higher than that in the thermodynamic equilibrium, this hydrocracking is considered to proceed by means of a carbonium-ion mechanism.[12]

The catalytic activity of the binary mixture of zinc iodide and potassium iodide is superior to that of zinc chloride in the hydrogenation of phenanthrene (Runs 1 and 2). In this case, attention must be paid to the fact that the intrinsic cracking activity is lowered by the addition of potassium iodide because of the formation of the complex ions.[5,13] The conversion in the presence of the zinc chloride containing 10 mol % nickel(II) chloride is lower than that in the presence of zinc chloride containing 40 mol % copper(I) chloride, but the product distributions obtained over these two catalysts are similar (Runs 2 and 4). Therefore, the decomposition process of phenanthrene over $NiCl_2/ZnCl_2$ is considered to be intermediate between that over $ZnCl_2$ and that over $ZnCl_2$/CuCl. This finding suggests that zinc chloride has a good intrinsic cracking activity under these reaction conditions, but its hydrogenating activity is not so high. The addition of a good hydrogenating catalyst to zinc chloride will produce an excellent catalyst for the hydrocracking of polynuclear aromatic hydrocarbons. Consequently, these molten salt catalysts act as dual-functional catalysts, and appropriate molten mixtures of metal salts with the hydrogenating activity and metal salts with the cracking activity may be able to become effective catalysts.

A remarkable catalytic action of $ZnCl_2$/CuCl was observed in this investigation (Runs 1 and 2). The hydrogenating activity of zinc chloride is very low in this temperature range (Run 1). The intrinsic cracking activity of zinc chloride may not be able to operate because phenanthrene is little hydrogenated. The addition of copper(I) chloride to zinc chloride must contribute to the improvement of the hydrogenating activity of the catalyst. The difference in the yield of octahydrophenanthrene and its isomers (IX) between Run 6 and Run 7 indicates this improvement in the hydrogenating activity.

By comparing the results of Run 1 and Run 6, phenanthrene was found to be more hydrogenated in Run 6 than in Run 1. From this fact, it can be seen that the ratio of hydrogen to the feed must affect the product distributions. In addition, the material, the capacity, the stirring pattern, and the memory effect of the autoclave are also important factors in dominating these reactions. Therefore, even if the pressure, the temperature, and the ratio of hydrogen to the feed should be maintained at constant levels in the different systems, similar results may not be obtained.

Hydrocracking of Pyrene. Pyrene is liable to accept the hydrogenation (Runs 1 and 9), but is fairly stable to the catalytic cracking (Runs 2 and 10), com-

TABLE 2. HYDROCRACKING OF PYRENE

Reaction conditions: initial hydrogen pressure, 100 kg/cm²; reaction temperature, 400 °C; reaction system A: Catalyst/Feed=1.0 (mol/mol), Hydrogen/Feed=21.3; reaction system B: Catalyst/Feed=1.0, Hydrogen/Feed=30.5.

		Run No.						
		8	9	10	11	12	13	14
Catalyst (mol: mol)		—	$ZnCl_2$	$ZnCl_2$/CuCl (60:40)	ZnI_2/KI (80:20)	$ZnBr_2$/CuBr (60:40)	$ZnCl_2$	$ZnCl_2$/CuCl (60:40)
Reaction system		A	A	A	A	A	B	B
Reaction time (h)		3	3	3	3	3	3	3
Product (wt %)	I	—	0.7	13.7	—	22.8	6.4	11.3
	II	—	—	1.1	—	4.4	0.3	2.5
	III	—	—	1.9	—	9.7	2.9	6.3
	IV	—	—	3.0	—	5.1	2.0	3.8
	V	—	—	3.2	—	4.3	2.1	5.7
	VI	—	—	tr	—	tr	0.2	0.1
	XIII	0.5	0.4	3.6	1.6	5.6	2.1	3.2
	XIV	—	—	1.2	3.5	2.3	4.3	4.8
	XV	—	1.5	7.5	16.7	4.5	20.4	14.4
	XVI	1.0	3.0	2.6	3.5	1.5	4.3	3.5
	XVII	3.6	8.5	21.3	40.4	7.7	31.1	20.9
	XVIII	16.7	23.7	13.5	15.8	4.3	9.6	7.8
	XIX	78.2	62.2	19.7	18.5	4.6	8.5	6.0
	XI	—	—	3.9	—	2.2	4.8	8.2
	XII	—	—	3.8	—	21.0	1.0	1.5

pared with phenanthrene. If the decomposition of dihydropyrene to phenanthrene takes place, the hydrocracking may occur easily. In practice, however, dihydropyrene was converted further to highly hydrogenated pyrenes, and so the probable decomposition routes of pyrene could not be clarified in detail in this investigation. In the hydrocracking of pyrene, a binary mixture of zinc bromide and copper(I) bromide was used for the purpose of examining the effect of the difference of halide (Run 12). A high catalytic activity was found, but a fairly large amount of coke was also formed. This is probably the reason why the reaction conditions are not adequate for this catalyst. There is still much room for an examination of the reaction conditions. No remarkable difference in the product distributions of Runs 13 and 14 was observed because the large amount of hydrogen and the other factors mentioned above might serve to make uniform the characteristics of these two catalysts. This may be considered to be indirect evidence for the improvement of the hydrogenating activity by the addition of copper(I) chloride. The binary mixture of zinc iodide and potassium iodide displayed an excellent hydrogenating activity and a lack of the cracking activity (Run 11).

Hydrocracking of Chrysene. The results of the hydrocracking of chrysene are shown in Table 3. Chrysene is hydrogenated to hydrochrysenes, which then isomerize to hydrobenz[*a*]anthracenes (Fig. 7). For example, 1,2,3,4,5,6-hexahydrochrysene (containing a *sym*-octahydrophenanthrene skeleton) isomerizes to 5,6,8,9,10,11-hexahydrobenz[*a*]anthracene (containing a *sym*-octahydroanthracene skeleton) in the presence of a Lewis acid. The formation of 8,9,10,11-tetrahydrobenz[*a*]anthracene is attributed to either the isomerization of 1,2,3,4-tetrahydrochrysene or the dehydrogenation of 5,6,8,9,10,11-hexahydrobenz[*a*]anthracene; it is not certain which occurred in practice. The main decomposition pathways of hydrochrysenes and their isomers are probably the formations of butylphenanthrene and the hydrogenated compounds. These phenanthrene-type compounds are hydrocracked in a manner similar to that described in the hydrocracking of phenanthrene. The decomposition route from dodecahydrochrysene and benz[*a*]anthracene to 5- and 6-(2-cyclohexylethyl)-tetralin respectively becomes fairly important in the B system (Run 18), because the extent of the hydrogenation is relatively high. Of course, the saturated six-member rings of tetra-, octa-, dodecahydrochrysenes, and hydrobenz[*a*]anthracenes isomerize to five-member rings. The probable reaction process of chrysene is shown in Fig. 7. A high catalytic activity of $ZnCl_2$/CuCl was also observed in the hydrocracking of chrysene. Chrysene accepts hydrogenation relatively easily in comparison with phenanthrene (Runs 1 and 15).

Table 3. Hydrocracking of chrysene

Reaction conditions: initial hydrogen pressure, 100 kg/cm²; reaction temperature, 400 °C; reaction system A: Catalyst/Feed=1.0, Hydrogen/Feed=24.1; reaction system B: Catalyst/Feed=1.0, Hydrogen/Feed=34.4.

		Run No.			
		15	16	17	18
Catalyst		$ZnCl_2$	$ZnCl_2$/CuCl	$ZnCl_2$	$ZnCl_2$/CuCl
(mol: mol)			(60:40)		(60:40)
Reaction system		A	A	B	B
Reaction time (h)		3	3	3	3
Product (wt %)	I	2.3	28.2	6.7	7.0
	II	—	10.7	—	3.7
	III	—	17.6	1.3	19.5
	IV	—	25.2	0.6	8.3
	V	0.4	10.1	4.5	24.1
	VI	—	1.0	0.6	2.2
	XIII	3.6	3.4	12.0	24.3
	XX	—	—	5.1	4.0
	XXI	2.3	0.3	2.9	0.5
	XXII	8.6	—	7.5	0.2
	XXIII	7.3	0.3	14.8	2.2
	XXIV	11.3	0.4	26.0	2.0
	XXV	64.2	0.1	9.2	—
	XI	—	—	7.7	—
	XII	—	2.7	1.1	2.0

Hydrocracking of Fluoranthene. In order to examine the initial decomposition process of fluoranthene, 1 h was used as the reaction time. The results are shown in Table 4. The tetrahydrofluoranthene formed by the hydrogenation of fluoranthene is ruptured to 5-phenyl-

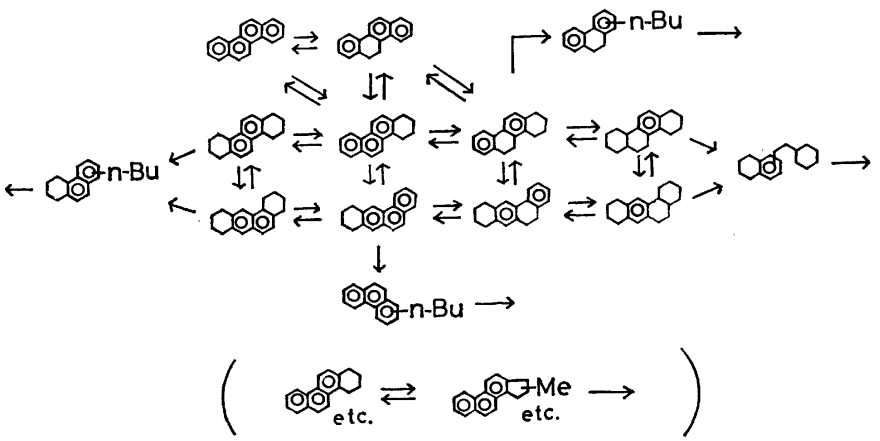

Fig. 7. Probable reaction process of chrysene.

TABLE 4. HYDROCRACKING OF FLUORANTHENE

Reaction conditions: initial hydrogen pressure, 100 kg/cm^2; reaction temperature, 400 °C; reaction system A: Catalyst/Feed=1.0, Hydrogen/Feed=21.3; reaction system B: Catalyst/Feed=1.0, Hydrogen/Feed=30.5.

	Run No.	
	19	20
Catalyst	$ZnCl_2$	$ZnCl_2$/CuCl
(mol: mol)		(60:40)
Reaction system	A	A
Reaction time (h)	1	1
I	—	14.9
II	—	3.3
III	—	5.8
IV	—	10.4
V	—	7.9
VI	—	5.4
XIII	2.4	31.5
XXVI	15.6	4.2
XXVII	80.4	5.2
XI	1.6	6.1
XII	—	5.3

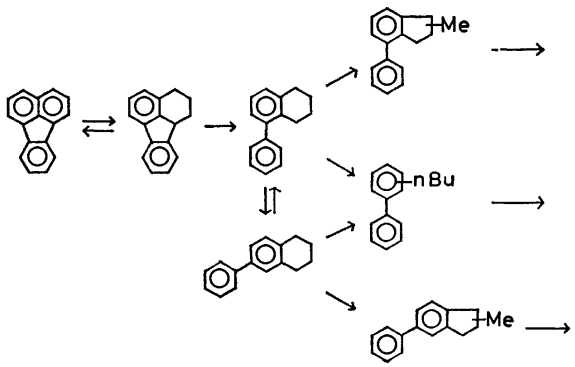

Fig. 8. Probable reaction process of fluoranthene.

tetralin in the presence of hydrogen, followed by isomerization to 6-phenyltetralin. Consequently, the amounts of biphenyl derivatives were fairly large. The great formation of biphenyls in the hydrocracking of a heavy anthracene oil[5] may be attributed to this decomposition pathway. The decomposition process of fluoranthene is shown in Fig. 8.[14]

Hydrocracking of Anthracene. The details of the hydrocracking of anthracene have been reported in a preliminary study.[6] Anthracene is more easily hydrogenated than phenanthrene. The product distribution of anthracene is similar to that of phenanthrene when the hydrocracking proceeds to some degree. This phenomenon is attributable to the fact that the marginal hydrogenated ring is ruptured in preference to the central ring in a dihydro derivative, for the cleavage of a saturated single C–C bond of dihydroanthracene or phenanthrene should result in a different type of compound. In addition, it is necessary to take into account the fact that the isomerization between *sym*-octahydroanthracene and *sym*-octahydrophenanthrene does away with the difference in their product distributions.

Concerning the reaction routes over these molten salt catalysts, the findings in this investigation may be outlined as follows: 1) the isomerization between *sym*-octahydrophenanthrene and *sym*-octahydroanthracene in the hydrocracking of phenanthrene and anthracene, and a similar isomerization in the hydrocracking of chrysene; 2) the decomposition of *unsym*-octahydrophenanthrene to 1-cyclohexyl-2-phenylethane in the hydrocracking of phenanthrene and a similar cleavage in the hydrocracking of chrysene; 3) a decomposition pathway leading to biphenyls in the hydrocracking of fluoranthene. On the other hand, $ZnCl_2$/CuCl salt, which is considered to act as a dual-functional catalyst, displayed a more efficient catalytic activity for *cata*-condensed aromatic hydrocarbons (phenanthrene, anthracene, and chrysene) than for *peri*-condensed aromatic hydrocarbons (pyrene). Moreover, these results (listed in Figs. 1—5) were useful in the identification of the hydrocracked products of Yūbari coal.[16]

References

1) Organic reaction in Fused Salts. Part XIII, Part XII: Y. Nakatsuji, S. Fujioka, M. Nomura, and S. Kikkawa, *Bull. Chem. Soc. Jpn.*, **50**, 3406 (1977); a part of this work was presented at the 36th National Meeting of the Chemical Society of Japan, Osaka, April 1977.

2) S. A. Qader, *J. Inst. Petrol. (London)*, **59**, 178 (1973).

3) C. W. Zielke, R. T. Struck, J. M. Evans, C. P. Costanza, and E. Gorin, *Ind. Eng. Chem., Process Des. Rev.*, **5**, 151, 158 (1966).

4) S. Kikkawa and M. Nomura, *Yuki Gosei Kagaku*, **33**, 593 (1975).

5) Y. Nakatsuji, S. Fujioka, M. Nomura, and S. Kikkawa, *Bull. Chem. Soc. Jpn.*, **50**, 3406 (1977).

6) S. Kikkawa, M. Nomura, T. Kubo, and Y. Nakatsuji, *Chem. Lett.*, **1976**, 1383.

7) S. Kikkawa, M. Nomura, and K. Murase, *Sekiyu Gakkaishi*, **19**, 863 (1976).

8) M. Morita and K. Hirosawa, *Nippon Kagaku Kaishi*, **1976**, 1259.

9) G. Schroeter, *Ber.*, **57**, 1990 (1924).

10) S. Friedman, M. L. Kaufman, and I. Wender, *J. Org. Chem.*, **36**, 694 (1971).

11) K. Itoh, R. Kurashige, S. Hamanaka, and M. Ogawa, *Kogyo Kagaku Zasshi*, **70**, 918 (1967).

12) R. A. Flinn, O. A. Larson, and H. Beuther, *Ind. Eng. Chem.*, **52**, 153 (1960).

13) C. N. Kenney and R. Takahashi, *J. Catal.*, **22**, 16 (1971).

14) Cyclopenta [*j,k*]phenanthrene (M=204; the UV spectrum is coincident with that in the literature[15]) was detected in the feed and the product. The formation of ethylphenanthrenes may be attributed to the cleavage of this compound.

15) W. E. Parham, D. R. Johnson, C. T. Hughes, M. K. Meilahn, and J. K. Rinehart, *J. Org. Chem.*, **35**, 1048 (1970).

16) S. Kikkawa, M. Nomura, and T. Ida, unpublished data.

Reclamation of Vulcanized Rubbers by Chemical Degradation. IX. Oxidative Degradation of *cis*-1,4-Polyisoprene by Phenylhydrazine-Iron(II) Chloride System

Nariyoshi KAWABATA, Shinzo YAMASHITA, and Yoshinori FURUKAWA

Department of Chemistry, Faculty of Polytechnic Science, Kyoto Institute of Technology, Matsugasaki, Sakyo-ku, Kyoto 606

(Received June 29, 1977)

Degradation of *cis*-1,4-polyisoprene by phenylhydrazine–iron(II) chloride system was investigated in benzene solution at 30 °C in the air. Separate use of the two chemicals was much less effective for degradation. The number of chain scission was found to depend upon only the amount of phenylhydrazine, independent of that of iron(II) chloride, indicating that phenylhydrazine plays the leading part of the phenylhydrazine–iron(II) chloride system in the degradation. When iron(III) chloride was used instead of iron(II) chloride, the degradation became slower, but the number of chain scission was not significantly affected.

Reclaiming processes are well established for natural rubber scrap, and the reclaimed matter can be used in the compounding of new rubber products. However, devulcanization and depolymerization is performed by heating at *ca.* 200 °C, which is not desirable from an economical point of view, for several hours under pressure in the presence of cheap oil and organic chemicals. Moreover, the process is limited to natural rubber scrap. The devulcanization and depolymerization stage should be modified for synthetic rubber scrap. Natural rubber vulcanizates behave well under the present reclaiming conditions, since they soften with heat, but it is difficult to reclaim synthetic rubber vulcanizates. As an example, styrene-butadiene rubber (SBR) vulcanizates, after initial softening by heating, quickly harden on further heating.

The phenylhydrazine–iron(II) chloride system is a good reagent for the reclamation of scrap tire[1] and various types of synthetic rubber vulcanizates[2] during several hours at room temperature. Useful elastomers can be obtained by the vulcanization of these reclaimed product. Devulcanization and depolymerization stage of the new reclaiming procedure was shown to be an oxidative degradation of vulcanized rubbers by the atmospheric oxygen.[3] In the presence of iron(II) chloride, phenylhydrazine rapidly absorbs an equimolar amount of oxygen, evolving an equimolar amount of nitrogen.[4] When *cis*-1,4-polyisoprene was added to the reaction mixture, additional oxygen absorption was observed, the molecular weight of polymer decreasing during the course of additional oxygen absorption. The scission efficiency based on the additionally absorbed oxygen was found to be much higher than that for autoxidation of natural rubber. The high scission efficiency seems to be the source of the strong ability of the phenylhydrazine–iron(II) chloride system as a reagent for the reclamation of vulcanized rubbers. In this work, we have investigated the mechanism of the degradation, with attention focussed on the dependence of the number of chain scission upon the composition of the phenylhydrazine–iron(II) chloride system in the degradation.

Experimental

Materials. *cis*-1,4-Polyisoprene (IR-2200, Japan Synthetic Rubber Co., Ltd.) was masticated at room temperature for 20 min, and dissolved in benzene. The gel was removed by filtration, and the soluble polymer recovered by pouring the filtrate into a large excess of methanol was purified by reprecipitation, followed by drying *in vacuo* at room temperature. Benzene was purified by washing with sulfuric acid. After repeated washing with water, it was dried with calcium chloride, then refluxed over calcium hydride and distilled. Commercial phenylhydrazine, iron(II) chloride, anhydrous iron(III) chloride, methanol, and other chemicals were used without further purification. Thermogravimetric analysis of the iron(II) chloride indicated the presence of 40.8 wt% of water.

Procedure. Viscosity measurements of degraded and undegraded *cis*-1,4-polyisoprene solutions were carried out in benzene at 30°C with an Ubbelohde-type dilution viscometer.

The degradation reaction was carried out in a round-bottomed 100 ml flask equipped with a mechanical stirrer in the air. Phenylhydrazine was added *via* a hypodermic syringe to a mixture of 0.5 g of *cis*-1,4-polyisoprene in 48.0 ml of benzene and a prescribed amount of iron(II) chloride or iron(III) chloride in 2.0 ml of methanol at 30 °C under stirring. Part of the reaction mixture was taken out, and the intrinsic viscosity of the solution was immediately determined at 30 °C using Baker's equation[5]

$$[\eta] = a(\eta_r^{1/a} - 1)/c,$$

parameter a for the equation was determined to be 3 prior to experiments on degradation. The dependence of the intrinsic viscosity upon the reaction time was plotted. After the decrease of viscosity became constant, the residue of the reaction mixture was poured into a large excess of methanol, and the polymer was recovered from the solution. The recovered polymer was dried *in vacuo* at room temperature, and the number average molecular weight was determined based on the intrinsic viscosity in benzene solution at 30 °C using the viscosity—molecular weight relationship.[4] The number of chain scission was determined from the decrease in the number average molecular weight during the course of degradation.

Results and Discussion

The relation between the intrinsic viscosity of the reaction mixture determined by use of Baker's equation and the reaction time for the degradation of *cis*-1,4-polyisoprene by the phenylhydrazine–Iron(II) chloride system in benzene at 30 °C, is shown in Fig. 1. In the absence of both chemicals, the intrinsic viscosity did not significantly change at 30 °C within 30 min. Curve 1

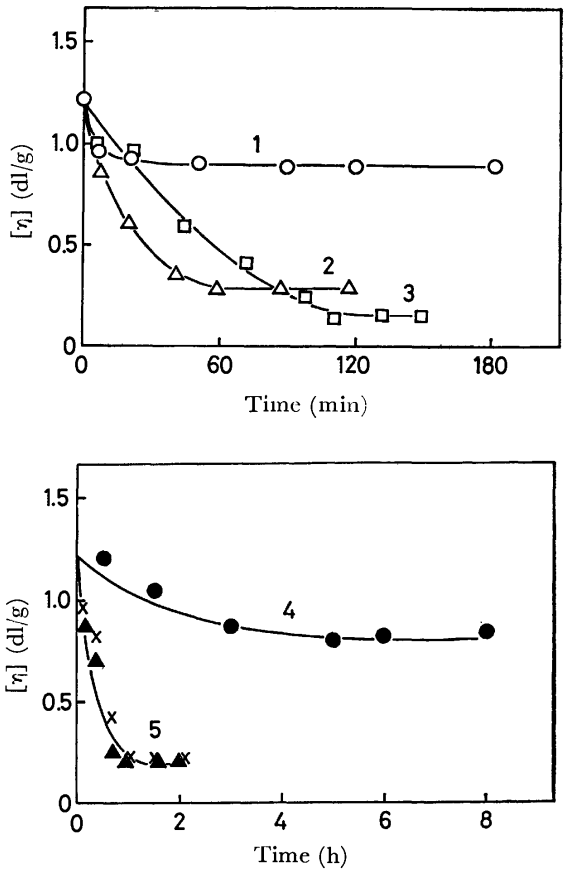

Fig. 1. Time dependence of the intrinsic viscosity of the reaction mixture for the degradation of *cis*-1,4-polyisoprene by the phenylhydrazine–iron(II) chloride system in benzene solution at 30 °C under the atmosphere of air. Conditions: *cis*-1,4-polyisoprene, 0.5 g; benzene, 48.0 ml; methanol, 2.0 ml. (○) iron(II) chloride, 0.10 mmol; phenylhydrazine, 0 mmol. (△) iron(II) chloride, 0.10 mmol; phenylhydrazine, 0.45 mmol. (□) iron(II) chloride, 0.10 mmol; phenylhydrazine, 2.00 mmol. (●) iron(II) chloride 0 mmol; phenylhydrazine, 1.00 mmol. (▲) iron(II) chloride, 0.02 mmol; phenylhydrazine, 1.00 mmol. (×) iron(II) chloride, 0.10 mmol; phenylhydrazine, 1.00 mmol.

was obtained in the presence of iron(II) chloride but in the absence of phenylhydrazine, whereas curves 2 and 3 were obtained in the presence of both compounds. A comparison of the curves indicates that the presence of phenylhydrazine considerably increases the rate of the degradation. Curves 2 and 3 show that degradation was almost complete within 2 h, the number of chain scission increasing with the amount of phenylhydrazine.

Curve 4 was obtained in the presence of phenylhydrazine but in the absence of iron(II) chloride, whereas curve 5 was obtained in the presence of both compounds. We see that separate use of phenylhydrazine and iron(II) chloride is less effective for the degradation of the polymer. This is in line with the fact that separate use of the two compounds is much less effective for the reclamation of scrap tire.

A comparison of curves 4 and 5 indicates that the presence of iron(II) chloride remarkably increases the rate of the degradation. However, curve 5 shows that the number of chain scission is not sensitive to the amount of iron(II) chloride.

After the decrease in the intrinsic viscosity of the reaction mixture (Fig. 1) ceased, the degraded polymer was recovered from the reaction mixture. Based on the number average molecular weight of the degraded and undegraded polymer, the number of chain scission was calculated. The number of chain scission versus the amount of phenylhydrazine is plotted in Fig. 2. Curve A was obtained for the degradation by the phenylhydrazine–iron(II) chloride system. Curve B was obtained for the degradation in the presence of phenylhydrazine but in the absence of iron(II) chloride. Fig. 2 indicates that iron(II) chloride considerably increases not only the rate of the degradation but also the number of chain scission. However, the number of chain scission depends upon only the amount of phenylhydrazine, independent of that of iron(II) chloride. This indicates that phenylhydrazine plays the principal part in the phenylhydrazine–iron(II) chloride system for the degradation of the polymer. Iron(II) chloride seems to be a catalyst in the oxidative degradation of the polymer by phenylhydrazine.

Phenylhydrazine is an accelerator for the mastication of rubber.[6,7] Mastication and our new method of reclamation appear to be closely related to each other. Phenylhydrazine was reported to be oxidized on exposure to free oxygen.[8] Iron(II) chloride seems to accelerate the oxidation.[4] Analysis of the products of the reaction of phenylhydrazine with iron(II) chloride under the atmosphere of oxygen and air showed the formation of benzene, phenol, and biphenyl.[4] Thus it seems that the formation of phenyl radical by the oxidation of phenylhydrazine is accelerated by iron(II)

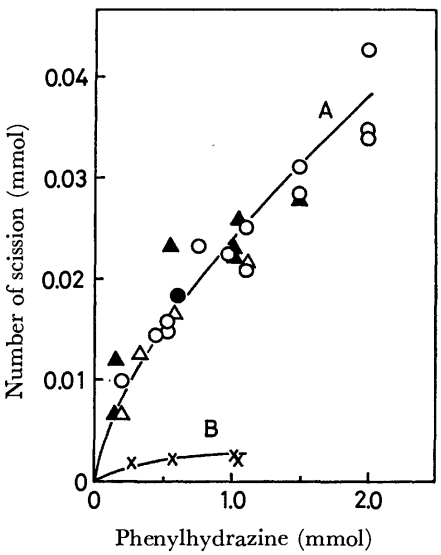

Fig. 2. Plot of the number of chain scission versus the amount of phenylhydrazine for the degradation of *cis*-1,4-polyisoprene by the phenylhydrazine-iron(II) chloride system in benzene solution at 30 °C under the atmosphere of air. Conditions: *cis*-1,4-polyisoprene, 0.5 g; benzene, 48.0 ml; methanol, 2.0 ml; iron(II) chloride, (●) 0.20 mmol, (○) 0.10 mmol, (▲) 0.02 mol, (△) 0.004 mmol, (×) 0 mmol.

chloride. The phenyl radical and related reactive species might attack *cis*-1,4-polyisoprene, causing the degradation of the polymer. Thus the number of the chain scission of the polymer considerably increases with the presence of iron(II) chloride, but not with the amount of iron(II) chloride.

Color change takes place during the course of degradation, showing the change of iron(II) to iron(III). In connection with this the degradation of *cis*-1,4-polyisoprene by the phenylhydrazine–iron(III) chloride system was also studied. The relation between the intrinsic viscosity of the reaction mixture determined by use of Baker's equation and the reaction time for the degradation in benzene at 30 °C, is shown in Fig. 3.

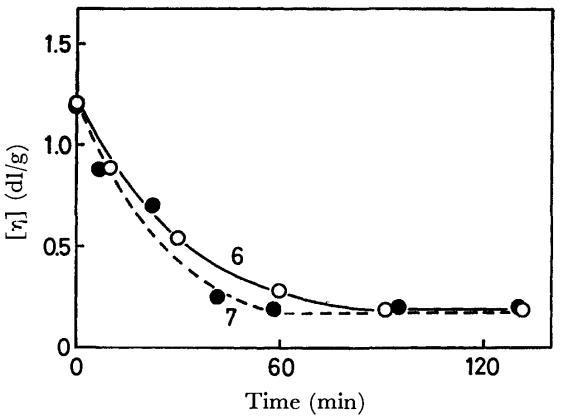

Fig. 3. Time dependence of the intrinsic viscosity of the reaction mixture for the degradation of *cis*-1,4-polyisoprene by the phenylhydrazine–iron(II) chloride system and the phenylhydrazine–iron(III) chloride system in benzene solution at 30 °C under the atmosphere of air. Conditions: *cis*-1,4-polyisoprene, 0.5 g; benzene, 48.0 ml; methanol, 2.0 ml. (●) iron(II) chloride, 0.02 mmol; phenylhydrazine, 1.00 mmol. (○) iron(III) chloride, 0.02 mmol; phenylhydrazine, 1.00 mmol.

Curve 6 was obtained for the degradation by the phenylhydrazine–iron(III) chloride system, and curve 7 for the degradation by the phenylhydrazine–iron(II) chloride system. Iron(III) chloride also considerably increases the rate of degradation of the polymer by phenylhydrazine. However, the degradation becomes slower when iron(III) chloride is used instead of iron(II) chloride, as shown in Fig. 3. This is in line with the fact that phenylhydrazine–iron(III) chloride system is less effective than the phenylhydrazine–iron(II) chloride system in the reclamation of scrap tire.[1] The number of chain scission versus the amount of phenylhydrazine for the degradation of the polymer by the phenylhydrazine–iron(III) chloride system is plotted in Fig. 4. Curve D was obtained in the absence of iron(III) chloride. We see that iron(III) chloride also considerably increases not only the rate of the degradation but also the number of chain scission. However, the number of chain scission depends only upon the amount of phenylhydrazine and not upon the amount of iron(III) chloride. Phenylhydrazine also seems to play the principal role in the phenylhydrazine–iron(III) chloride

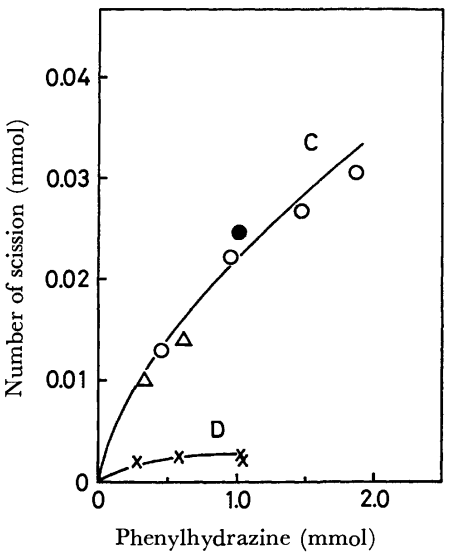

Fig. 4. Plot of the number of chain scission versus the amount of phenylhydrazine for the degradation of *cis*-1,4-polyisoprene by the phenylhydrazine–iron(III) chloride system in benzene solution at 30 °C under the atmosphere of air. Conditions: *cis*-1,4-polyisoprene, 0.5 g; benzene, 48.0 ml; methanol, 2.0 ml; iron(III) chloride, (○) 0.10 mmol, (△) 0.05 mmol, (●) 0.02 mmol, (×) 0 mmol.

system in the degradation of the polymer. A comparison of curve C in Fig. 4 with curve A in Fig. 2 leads us to conclude that the efficiency of the chain scission based on the amount of phenylhydrazine is in the same order of magnitude regardless of whether iron(II) chloride or iron(III) chloride is used. Iron(II) chloride and iron(III) chloride could recycle during the degradation.

The results of the present and previous works suggest a reasonable interpretation of the mechanism of reaction. Experimental evidences are as follows:

1. The infrared spectra of the soluble fractions obtained from various rubber vulcanizates by the treatment with phenlhydrazine–iron(II) chloride system show the presence of carbonyl and hydroxyl groups.[2]

2. The treatment of vulcanized *cis*-1,4-polyisoprene by the phenylhydrazine–iron(II) chloride system in the air reduces the effective network chain density of the vulcanizates, giving a soluble fraction of rubber. Treatment in sealed vessels in the absence of oxygen gives no soluble fraction, not decreasing the effective network chain density.[3]

3. From the decrease of the effective network chain density and the increase of the soluble fraction, it is concluded that the network chain of the vulcanized rubber undergoes a severance reaction by the phenylhydrazine–iron(II) chloride system in the order: polysulfide linkage>monosulfide linkage>carbon-carbon crosslink.[3]

4. Although Chattaway[8] indicated that phenylhydrazine is oxidized on exposure to free oxygen, it has been found that iron(II) chloride considerably accelerates oxidation.[4]

5. In the presence of iron(II) chloride under air or

oxygen atmosphere, phenylhydrazine rapidly absorbs an equimolar amount of oxygen, evolving an equimolar amount of nitrogen.[4] Gas chromatographic analysis of the reaction mixture shows the presence of benzene, phenol, and biphenyl in 37, 35—60, and 4—8% yields, respectively, based on phenylhydrazine.[4] When *cis*-1,4-polyisoprene is added to the reaction mixture, additional absorption of oxygen is observed, the molecular weight of the polymer decreasing during course of additional oxygen absorption.[4]

6. Under nitrogen atmosphere, the reaction of phenylhydrazine with iron(II) chloride in benzene solution rapidly gives a 2: 1 complex, a white solid which is relatively stable under nitrogen but rapidly decomposes in the presence of oxygen; in the air, it is a very effective reagent for the reclamation of vulcanized rubbers.[9]

7. Separate use of phenylhydrazine and iron(II) chloride is much less effective for the degradation of *cis*-1,4-polyisoprene. However, the number of chain scission depends only upon the amount of phenylhydrazine and not upon that of iron(II) chloride.

8. When iron(III) chloride is used instead of iron(II) chloride, the degradation becomes slower, the number of chain scission not being significantly affected.

9. Color change takes place during the course of degradation, showing the change of iron(II) to iron(III).

We postulate the following mechanism for the reclamation of vulcanized rubbers by the phenylhydrazine–iron(II) chloride system. Devulcanization and the depolymerization stage of the new reclaiming procedure is an oxidative degradation of vulcanized rubber by atmospheric oxygen. The function of the phenylhydrazine–iron(II) chloride system is essentially the acceleration of autoxidation of vulcanized rubber.

$$2PhNHNH_2 + FeCl_2 \longrightarrow \underset{\mathbf{1}}{[2PhNHNH_2 \cdot FeCl_2]}, \quad (1)$$

$$\mathbf{1} \xrightarrow{O_2} \underset{\mathbf{2}}{Ph\cdot} + \underset{\mathbf{3}}{PhOOH} + \underset{\mathbf{4}}{HOO\cdot} + N_2, \quad (2)$$

$$\mathbf{2} \xrightarrow{RH} R\cdot + PhH \quad (3)$$

$$\mathbf{2} \xrightarrow{2} PhPh \quad (4)$$

$$\mathbf{2} \xrightarrow{O_2} PhOO\cdot \xrightarrow{RH} R\cdot + \mathbf{3}, \quad (5)$$

$$\mathbf{3} \xrightarrow{Fe^{2+}} \underset{\mathbf{5}}{PhO\cdot} + Fe^{3+} + OH^-, \quad (6)$$

$$\mathbf{4} \xrightarrow{RH} R\cdot + H_2O_2, \quad (7)$$

$$\mathbf{5} \xrightarrow{RH} R\cdot + PhOH \quad (8)$$

$$R\cdot \xrightarrow{O_2} ROO\cdot \xrightarrow{RH} ROOH + R\cdot, \quad (9)[10]$$

$$Fe^{3+} \xrightarrow{ROOH} Fe^{2+} + ROO\cdot + H^+, \quad (10)$$

$$Fe^{3+} \xrightarrow{PhOOH} Fe^{2+} + PhOO\cdot + H^+, \quad (11)$$

$$R\cdot \xrightarrow{O_2} ROO\cdot \longrightarrow R'CHO + HOR'', \quad (12)[10]$$

Where RH represents rubber molecule. In the reclamation of sulfur vulcanizate, the severance of crosslink predominates scission of the main chain.[3] In such a case, we should take into consideration the following mechanism[11] proposed for the severance of monosulfide linkage of the vulcanizate.

$$RSR \xrightarrow{3} RSOR + PhOH, \quad (13)[11]$$

$$RSR \xrightarrow{H_2O_2} RSOR + H_2O, \quad (14)$$

$$RSOR \longrightarrow R'SOH + R''H, \quad (15)[11]$$

where RSR represents the crosslinked part of sulfur vulcanizate. Equations 12 and 15 respectively denote the degradation of main chain and the severance of sulfur crosslink of vulcanized rubber.

This work was supported by a Scientific Research Grant from the Ministry of Education (No. 110311).

References

1) S. Yamashita, N. Kawabata, K. Mori, and T. Fujii, *Nippon Gomu Kyokai Shi*, **49**, 360 (1976).
2) S. Yamashita, N. Kawabata, and K. Hayashi, *Nippon Gomu Kyokai Shi*, **49**, 420 (1976).
3) S. Yamashita, N. Kawabata, S. Sagan, and K. Hayashi, *J. Appl. Polym. Sci.*, **21**, 2201 (1977).
4) S. Yamashita, S. Kato, N. Kawabata, and T. Okamoto, *J. Appl. Polym. Sci.*, in press.
5) W. E. Davis and J. H. Elliott, *J. Colloid Sci.*, **4**, 313 (1949).
6) I. Williams, *Ind. Eng. Chem.*, **26**, 1190 (1934).
7) G. Kraus and K. W. Rollmann, *J. Appl. Polym. Sci.*, **8** 2585 (1964).
8) F. D. Chattaway, *J. Chem. Soc.*, **91**, 1323 (1907).
9) S. Yamashita, K. Kasai, M. Tanaka, and K. Harada, Abstr. No. 3N22, 34th National Meeting of the Chemical Society of Japan, Tokyo, April 1976.
10) S. Yamashita, *Nippon Gomu Kyokai Shi*, **41**, 380 (1968).
11) J. I. Cunneen, *Rubber Chem. Technol.*, **41**, 182 (1968).

NOTES

BULLETIN OF THE CHEMICAL SOCIETY OF JAPAN VOL. 51 (2), 629—630 (1978)

The Extraction of Alkali Metal Picrates into Benzene by Means of 18-Crown-6

Tadashi IWACHIDO, Akira SADAKANE,* and Kyoji TÔEI*

College of Liberal Arts, Okayama University, Tsushima, Okayama 700

**Department of Chemistry, Faculty of Science, Okayama University, Tsushima, Okayama 700*

(Received May 30, 1977)

Synopsis. The distribution of alkali metal picrates between water and benzene was investigated in the presence of 18-crown-6. The overall equilibrium constants, K_{ex}, and some constituent equilibrium constants were determined. The K_{ex} value increases, passes through a maximum (at potassium), and falls off as the size of the alkali metal cation increases.

18-Crown-6 (CR) combines stoichiometrically with alkali metal cations to form complexes, in which the cation is accommodated into the hydrophilic molecular hole of the ligand (diameter: 0.26—0.32 nm).[1-3] The outer surface is then formed by the hydrophobic groups. From the 'metal in the hole' picture, the resulting complexes may be expected to be identical in size and in hydrophobicity. It is well known that there is a striking correlation between the stability of the complex and the size of the cation.[4] Among alkali metal cations, the potassium cation forms the most stable complex with the ligand; cations larger (Rb^+, Cs^+) or smaller (Li^+, Na^+) than the optimum size form destabilized complexes because, in the former, these cations are too large to fit into the ligand hole, while, in the latter, the hydration energy of these cations is predominant.[5]

In this paper, methods for obtaining the overall equilibrium constants will be reported. The extractability of alkali metal cations by CR will be discussed in terms of the stability constant of the complex.

Experimental

Materials. Commercial CR (Nisso Co., Ltd.) was used without further purification. The alkali metal picrates were prepared and purified as has previously been described.[6]

Extraction Procedure. The picrates were each dissolved in water containing lithium hydroxide at a concentration of 5×10^{-5} M (1 M = 1 mol dm^{-3}). The concentrations were 10^{-2} M for sodium picrate, 10^{-3} M for potassium and rubidium picrates, and 5×10^{-3} M for caesium picrate. The CR was made up in benzene solutions, the concentration range being $(0.15-2)\times10^{-3}$ M. Equal volumes (20 cm^3) of the aqueous and benzene solutions were transferred into a 50-cm^3 centrifuge tube equipped with a stopper, shaken in a water bath thermostated at (25±0.01)°C for 20 min, and then allowed to stand for about 20 min. The picrate concentration in the benzene phase was determined spectrophotometrically at 425 nm. The molar absorption coefficients, ε, of the picrates in the benzene phase were determined to be ε=8900, 9400, 9100, and 9000 M^{-1} cm^{-1} at 425 nm for sodium, potassium, rubidium, and caesium picrates respectively. For this purpose, each of the benzene solutions was equilibrated with each of the aqueous picrate solutions as in the above procedure, after which the picrates extracted were completely back-extracted into water. The picrate concentrations were determined spectrophotometrically (ε=14400 M^{-1} cm^{-1} at 354 nm).

The Distribution Coefficient of CR. The CR was made up in benzene solutions ranging in concentration from 0.7×10^{-4} to 3.5×10^{-4} M. Each of the solutions was equilibrated with an aqueous 0.1 M potassium chloride solution containing lithium hydroxide (0.01 M) at 25 °C. The benzene phases separated from the aqueous phase were each shaken with the aqueous potassium chloride solution in the presence of an excess of the potassium salt of 2,2′,4,4′,6,6′-hexanitrodiphenylamine. The concentration of the resulting complex in the benzene phase was determined spectrophotometrically at 425 nm by means of the calibration method. The distribution constants thus obtained were averaged for use in subsequent calculations.

Results and Discussion

The equilibrium between an aqueous solution containing an alkali metal cation, M^+, and a picrate anion, A^-, and a benzene solution containing CR can be written as

$$M^+ + CR_o + A^- \rightleftharpoons MCRA_o,$$

$$K_{ex} = \frac{[MCRA]_o}{[M^+][CR]_o[A^-]}, \quad (1)$$

where MCRA designates ion-pairs between alkali metal complexes, MCR^+, and picrate anions; the subscript o refers to the benzene phase, and the lack of a subscript, to the aqueous phase; the molar concentrations are given in brackets. The constituent equilibria are

$$CR \rightleftharpoons CR_o, \qquad D_c = \frac{[CR]_o}{[CR]}, \quad (2)$$

$$M^+ + CR \rightleftharpoons MCR^+, \qquad K_s = \frac{[MCR^+]}{[M^+][CR]}, \quad (3)$$

$$MCR^+ + A^- \rightleftharpoons MCRA, \qquad K_{ass} = \frac{[MCRA]}{[MCR^+][A^-]}, \quad (4)$$

$$MCRA \rightleftharpoons MCRA_o, \qquad D_{ip} = \frac{[MCRA]_o}{[MCRA]}. \quad (5)$$

The mass balances are

$$T_M = [M^+] + [MCR^+] + [MCRA] + [MCRA]_o, \quad (6)$$

$$T_{CR} = [CR] + [CR]_o + [MCR^+] + [MCRA] + [MCRA]_o, \quad (7)$$

$$T_A = [A^-] + [MCRA] + [MCRA]_o, \quad (8)$$

where T denotes the total concentration.

Table 1. Equilibrium constants for extraction of picrate with 18-crown-6 (CR) and dibenzo-18-crown-6 (DBC)

Ligand	Cation	Ionic diameter (nm)	D_c	log K_{ex}	log K_s	log ($K_{ass}D_{ip}$)	D_{ip}	K_{ass}
CR			0.0572					
	Na^+	0.194		3.31	<0.3[a]	>1.8	>0.4	
	K^+	0.266		6.00	2.06[a]	2.70	3.7	140
	Rb^+	0.294		5.43	1.5	2.7	>1[b]	
	Cs^+	0.334		4.28	0.8[a]	2.2	>1	
DBC			800					
	Na^+			2.21[c]	1.2[d]	3.9		
	K^+			4.65[c]	1.7[d]	5.9		
	Rb^+			3.75[c]	1.1[d]	5.6		
	Cs^+			3.07[c]	0.8[d]	5.2		

a) From Ref. 5. b) Estimated value. c) From Ref. 6. d) From Ref. 7.

Substituting Eqs. 2, 3, and 5 into Eq. 6, we obtain

$$[M^+] = \frac{T_M - [MCRA]_o(1+1/D_{ip})}{1+(K_s/D_c)[CR]_o}. \quad (9)$$

Equations 2, 6, and 7 are combined to give

$$[CR]_o = \frac{[M^+] - T_M + T_{CR}}{1+1/D_c}. \quad (10)$$

From Eq. 8, we obtain

$$[A^-] = T_A - [MCRA]_o(1+1/D_{ip}). \quad (11)$$

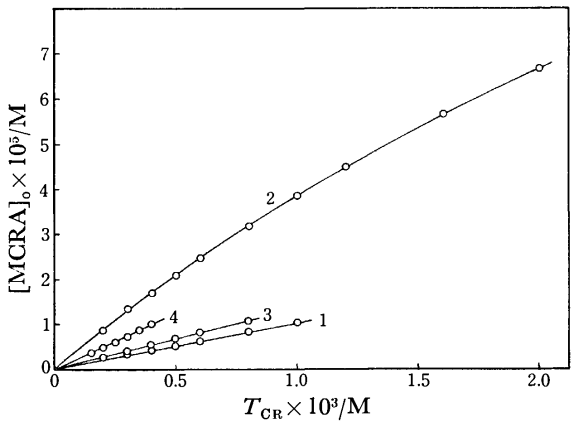

Fig. 1. Extraction of alkali metal picrate into benzene by 18-crwon-6. 1: Na, 2: K, 3: Rb, 4: Cs.

Combining Eqs. 1, 9, 10, and 11, we obtain a single relation with two unknowns, K_{ex} and D_{ip}. These were evaluated by a nonlinear regression fitting of 6—10 points per system, the deviation of the measured variable $[MCRA]_o$ being minimized in the process. In the case of rubidium, the relation thus obtained contains one more unknown, K_s. In view of the structural resemblance between $RbCR^+$ and $CsCR^+$, it is reasonable to estimate that $D_{ip}>1$ for rubidium. Thus, we can likewise estimate K_{ex} and K_s by regression analysis. As can be seen from Fig. 1, the calculated (solid line) and found (open circle) data agree within 2 percent. From Eqs. 9, 10, and 11, on the other hand, it is expected that a much simpler relation will hold between $[MCRA]_o$ and K_{ex} for MCRA of a low extractability:

$$[MCRA]_o = \frac{K_{ex}(T_M)^2}{1+1/D_c} T_{CR}. \quad (12)$$

The K_{ex} values obtained from the slope of each straight line in Fig. 1 ($\log K_{ex}=3.30$ and 4.27 for Na^+ and Cs^+ respectively) are in good agreement with those listed in Table 1. The ion-association constant, K_{ass}, for potassium is calculated from the equation

$$K_{ex} = \frac{1}{D_c}(K_s K_{ass} D_{ip}). \quad (13)$$

The data obtained, together with the values from the literature for dibenzo-18-crown-6 (DBC), are summarized in Table 1.

Table 1 shows that the log ($K_{ass}D_{ip}$) values for CR are almost all equal in magnitude except for sodium. The same is true for its aromatic analogue, DBC. It follows from this finding that the observed sequence of K_{ex} for a given ligand is determined primarily by that of the stability constant, K_s.

Table 1 also shows that the distribution coefficient, D_c, of DBC is more than four decades greater than that of CR; this finding indicates that DBC is much more hydrophobic than CR. The hydrophobicity of the ligand shows virtually no effect on the stability of the complex, but it does have a slight effect on K_{ex}. It follows that the magnitude of K_{ex} for a given alkali metal is chiefly governed by that of $K_{ass}D_{ip}/D_c$ (*cf.* Eq. 13). It is noticeable that the less hydrophobic ligand is preferred as an extracting agent.

References

1) C. J. Pedersen, *J. Am. Chem. Soc.*, **92**, 386 (1970).
2) D. Bright and M. R. Truter, *J. Chem. Soc., B*, **1970**, 1544.
3) M. A. Bush and M. R. Truter, *Chem. Commun.*, **1970**, 1439.
4) J. J. Christensen, J. O. Hill, and R. M. Izatt, *Science*, **174**, 459 (1971).
5) H. K. Frensdorff, *J. Am. Chem. Soc.*, **93**, 600 (1971).
6) A. Sadakane, T. Iwachido, and K. Tôei, *Bull. Chem. Soc. Jpn.*, **45**, 432 (1972).
7) E. Shchori, N. Nae, and J. Jagur-Grodzinski, *J. Chem. Soc., Dalton Trans.*, **1975**, 281.

BULLETIN OF THE CHEMICAL SOCIETY OF JAPAN VOL. 51 (2), 631—632 (1978)

Electronic Spectra and Charge-Transfer Absorption of Solid Anion Radical Salts of 2,3-Dicyano-*p*-benzoquinone and 2,3-Dichloro-5,6-dicyano-*p*-benzoquinone

Yôichi IIDA

Department of Chemistry, Faculty of Science, Hokkaido University, Sapporo 060

(Received August 9, 1977)

Synopsis. The diffuse reflection spectra were measured with solid anion radical salts of 2,3-dicyano-*p*-benzoquinone and 2,3-dichloro-5,6-dicyano-*p*-benzoquinone with rubidium and caesium cations. Strong charge-transfer transition between anion radicals was observed in the low-energy region. The spectroscopic features of the charge-transfer absorption were discussed in terms of one-dimensional Hubbard model.

In most solid ion radical salts, the planar ion radical molecules are known to form, in themselves, a segregated face-to-face stacking into infinite one-dimensional columns so as to make a large overlap between their half-occupied molecular orbitals.[1-3] In this case, since any individual radical molecule interacts through charge-transfer most strongly with two other neighboring radicals, the electronic spectrum of the solid salt differs distinctly from the monomer spectrum of the radical ion in solution but shows a charge-transfer transition between ion radicals in the low-energy region.[1-3]

Several years ago,[1] we examined the solid-state spectra of some stable anion radical salts derived from 2,3-dicyano-*p*-benzoquinone (p-H_2QCy_2) and 2,3-dichloro-5,6-dicyano-*p*-benzoquinone (p-Cl_2QCy_2). We prepared such crystalline salts as Na^+ p-$H_2QCy_2^{\cdot-}$, K^+ p-$H_2QCy_2^{\cdot-}$, Na^+ p-$Cl_2QCy_2^{\cdot-}$, and K^+ p-$Cl_2QCy_2^{\cdot-}$, where we found strong absorptions due to the charge-transfer transition between anion radicals in the low-energy region. In the case of Na^+ p-$Cl_2QCy_2^{\cdot-}$ and K^+ p-$Cl_2QCy_2^{\cdot-}$ salts, the band shape of the charge-transfer absorption was found to be almost symmetrical with respect to the axis of peak energy. However, in the case of Na^+ p-$H_2QCy_2^{\cdot-}$ and K^+ p-$H_2QCy_2^{\cdot-}$ salts, the band shape is no longer symmetrical with respect to the axis of peak energy, but has a distinct shoulder in the higher-energy region. Recently, we could well explain those spectroscopic features of the charge-transfer absorptions in terms of one-dimensional Hubbard model.[2,3] In the present paper, we further examined the solid-state spectra of the anion radical salts of p-H_2QCy_2 and p-Cl_2QCy_2 with rubidium and caesium cations.

p-H_2QCy_2 was synthesized from *p*-benzoquinone according to the method of Thiele *et al.*,[4] while p-Cl_2QCy_2 was commercially available. The anion radical salts of Rb^+ p-$H_2QCy_2^{\cdot-}$, Cs^+ p-$H_2QCy_2^{\cdot-}$, Rb^+ p-$Cl_2QCy_2^{\cdot-}$, and Cs^+ p-$Cl_2QCy_2^{\cdot-}$ were prepared according to the method described in the previous paper.[1] The solid-state spectra of these anion radical salts were measured by diffuse reflection method. The spectra were recorded on a Beckman DK-2A spectroreflectometer in the range from 4000 to 30800 cm^{-1} at room temperature. In order to avoid cation exchange between the salt and the diluent, the samples were ground and diluted with pure naphthalene. The solid-state spectra were obtained by plotting the diffuse reflection spectra using the Kubelka-Munk function, $f(R)=(1-R)^2/2R$, in which R is the reflectance.

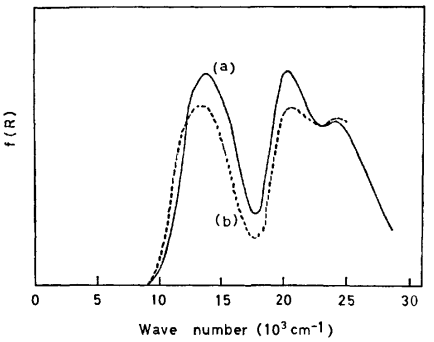

Fig. 1. The solid-state spectra of (a) Rb^+ p-$Cl_2QCy_2^{\cdot-}$ and (b) Cs^+ p-$Cl_2QCy_2^{\cdot-}$.

Figure 1, curve (a), is the observed solid-state spectrum of Rb^+ p-$Cl_2QCy_2^{\cdot-}$ salt, which shows a strong absorption at 13600 cm^{-1} and high-energy bands at 20100 and 24000. These spectroscopic features are found to be very similar to those previously reported on Na^+ p-$Cl_2QCy_2^{\cdot-}$ or K^+ p-$Cl_2QCy_2^{\cdot-}$.[1] The band peaked at 13600 cm^{-1} appears in the low-energy region where the p-Cl_2QCy_2 anion radical monomer does not absorb.[1] This low-energy band seems to be attributable to the charge-transfer transition between the p-Cl_2QCy_2 anion radicals in the segregated stack of the anion radicals, while the bands at 20100 and 24000, cm^{-1} to the shifted bands of the anion radical monomer at 17100 and 21900 cm^{-1}, respectively. Here, we note that the line shape of the charge-transfer absorption at 13600 cm^{-1} is almost symmetrical with respect to the peak-energy axis and that the high-energy bands at 20100 and 24000 cm^{-1} are appreciably blue-shifted, compared to the corresponding absorptions of the monomer spectrum. On the other hand, Fig. 1, curve (b), is the observed solid-state spectrum of Cs^+ p-$Cl_2QCy_2^{\cdot-}$ salt, which also shows a strong charge-transfer band peaked at 13400 cm^{-1} and high-energy bands at 20500 and 24200. In this salt, the line shape of the charge-transfer absorption is again almost symmetrical with respect to the peak-energy axis. As the charge-transfer transition occurs in the segregated stack of the p-Cl_2QCy_2 anion radicals, we can well understand the fact that the energy of the charge-transfer absorption remains nearly constant in going from the rubidium salt to the caesium salt.

On the other hand, Fig. 2, curve (a), is the observed solid-state spectrum of Rb^+ p-$H_2QCy_2^{\cdot-}$. A strong low-

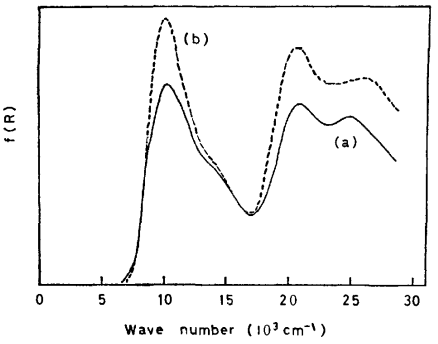

Fig. 2. The solid-state spectra of (a) Rb$^+$ p-$H_2QCy_2^-$ and (b) Cs$^+$ p-$H_2QCy_2^-$.

energy charge-transfer absorption, which arises from the segregated stack of the p-H_2QCy_2 anion radicals, is found at 10300 cm^{-1} with a shoulder around 13500. High-energy bands are located at 20800 and 25000 cm^{-1}, which originate from the monomer absorptions of the p-H_2QCy_2 anion radical at 17100 and 21500 cm^{-1}, respectively.[1] Here, we note that the charge-transfer band is broad and has the shoulder in the higher-energy side and that its line shape is no longer symmetrical with respect to the peak-energy axis. The solid-state spectrum of Cs$^+$ p-$H_2QCy_2^-$ is given in Fig. 2, curve (b). In this case, the charge-transfer band and the high-energy bands are located at 10000 cm^{-1} with a shoulder around 13500 and at 20500 and 25800 cm^{-1}, respectively.

Hereafter, we only discuss the spectroscopic features of the observed charge-transfer absorptions on the basis of our previous theoretical approach.[2] To the segregated stacks of the p-Cl_2QCy_2 or p-H_2QCy_2 anion radicals in their solid salts, we apply non-alternant one-dimensional Hubbard model composed of ion radical molecules with half-occupied orbitals. In the case of paramagnetic state, the intermolecular charge-transfer absorption, $\sigma(\omega)$, is given by

$$\sigma(\omega) \propto \frac{e^2}{4} \frac{I^2}{\omega^2\sqrt{\omega^2-I^2}} \sqrt{4T^2-\omega^2+I^2}. \quad (1)$$

Here, a δ-function was assumed for each elementary transition in which the spin and the wave vector of an electron are conserved; I is the intra-site Coulomb repulsion energy, and T (<0) is the transfer matrix element between nearest neighbor ion radicals in one-dimensional Hubbard model. A schematic representation of the absorption line shape of Eq. 1 has been given in Fig. 1 of Ref. 2. The theoretical charge-transfer absorption has a sharp divergent peak at $\omega=I$. The spectrum has no absorption in the region $\omega<I$, but has a distinct shoulder in the region $I<\omega<\sqrt{I^2+4T^2}$. Actually, however, the elementary absorption is not a δ-function but involves a finite width, and the spectrum will become more smoothed,[2] so that the observed charge-transfer absorption has an intensity even in the energy region lower than the peak position. Therefore, the absorption peak of the observed charge-transfer band corresponds to $\omega=I$, and its band width comes partly from the width due to the elementary absorptions but partly from the width due to non-zero transfer matrix element, $\sqrt{I^2+4T^2}-I$. We divide the two contributions of the widths in a way similar to the previous work.[3] With respect to $\omega=I$, we subtract the lower-energy side from the higher-energy side of the observed charge-transfer absorption. Then, the part symmetrical with respect to $\omega=I$ will correspond to the contribution of the elementary absorptions, while the remaining asymmetric part, to the width due to non-zero transfer matrix element, $\sqrt{I^2+4T^2}-I$, because the absorption in the $\omega<I$ region is solely attributable to the elementary absorptions and the absorption of Eq. 1 appears only in the $\omega>I$ region.

As for the charge-transfer absorptions of Rb$^+$ p-$Cl_2QCy_2^-$ and Cs$^+$ p-$Cl_2QCy_2^-$, the I values for the rubidium and caesium salts are estimated to be 13600 and 13400 cm^{-1}, respectively, from the observed peak energies. In both salts, the band width due to the transfer matrix element, $\sqrt{I^2+4T^2}-I$, is found to be 400 cm^{-1} or less, and the $|T|$ values are estimated to be 1500 cm^{-1} or less by using the observed I values.

On the other hand, from the observed peak energy, the I values for Rb$^+$ p-$H_2QCy_2^-$ and Cs$^+$ p-$H_2QCy_2^-$ are estimated to be 10300 and 10000 cm^{-1}, respectively. In both salts, however, the broad asymmetric charge-transfer absorption with a distinct shoulder in the $\omega>I$ region implies that the band width due to the transfer matrix element is comparable to the width of elementary absorption. By using the above-mentioned method, the asymmetric part in the higher-energy side of the charge-transfer absorption, $\sqrt{I^2+4T^2}-I$, is found to be 2000 cm^{-1} or less for Rb$^+$ p-$H_2QCy_2^-$ and about 2400 cm^{-1} or less for Cs$^+$ p-$H_2QCy_2^-$. Thus, the $|T|$ values for the rubidium and caesium salts are estimated to be $\leq$3400 and $\leq$3700 cm^{-1}, respectively. These values are found to be considerably larger than the corresponding values for the Rb$^+$ p-$Cl_2QCy_2^-$ and Cs$^+$ p-$Cl_2QCy_2^-$ salts.

In conclusion, the solid-state spectra of M$^+$ p-$Cl_2QCy_2^-$ and M$^+$ p-$H_2QCy_2^-$, (M=Na, K, Rb, and Cs), are predominantly governed by the manner of the segregated stacks of the anion radicals, but are hardly influenced by the species of the counter cations. In such stacks of the anion radicals, the p-H_2QCy_2 anion radicals stack more closely than do the p-Cl_2QCy_2 anion radicals. This results in remarkable difference in the charge-transfer absorptions between the p-Cl_2QCy_2 and p-H_2QCy_2 anion radical salts.

References

1) Y. Iida, *Bull. Chem. Soc. Jpn.*, **44**, 1777 (1971), and the references cited therein.

2) Y. Iida, *Bull. Chem. Soc. Jpn.*, **50**, 1445 (1977), and the references cited therein.

3) Y. Iida, *Bull. Chem. Soc. Jpn.*, **50**, 2481 (1977).

4) J. Thiele and J. Meisenheimer, *Ber. Deut. Chem. Gesell.*, **33**, 675 (1900); J. Thiele and F. Günther, *Justus Liebigs Ann. Chem.*, **349**, 59 (1906).

BULLETIN OF THE CHEMICAL SOCIETY OF JAPAN VOL. 51 (2), 633—634 (1978)

Heat of Adsorption of Ammonia on Silica-Alumina at Low Surface Coverage

Tatsuo MASUDA, Hitofumi TANIGUCHI, Kazuo TSUTSUMI, and Hiroshi TAKAHASHI
Institute of Industrial Science, The University of Tokyo, Roppongi, Minato-ku, Tokyo 106

(Received August 23, 1977)

Synopsis. Heats of adsorption of ammonia on silica–alumina at very low surface coverage were measured in details. The effects of ammonia adsorption on the glass wall and on the greese were corrected. The initial heat value agreed fairly well with the heat of neutralization of NH_3(G) and HCl(G). The diffusion of the gas had little effect on the value of heat of adsorption.

The integral heat of adsorption ($\Delta Q/\Delta n_S$) can be obtained by the measurement of heat effect (ΔQ) accompanying adsorption of a small dose (Δn_S) of gas. In order to obtain the differential heat of adsorption ($q=\partial Q/\partial n_S$), a calorimeter is required which is capable of measuring small amount of adsorbed gas and heats evoloved as accurately as possible.

In this study, the heat of adsorption of ammonia on silica–alumina was measured, particularly at very low surface coverage and also the influence of the diffusion of the gas on heat effects was examined.

Experimental

Heats of adsorption were determined in a twin conduction type calorimeter (Tokyo Riko Co., Ltd.) fitted with the apparatus which is schematically drawn in Fig. 1. The heat of adsorption was measured at 25 °C. The amount adsorbed was calculated from pressure change before and after adsorption measured by a MKS capacitance manometer (below≈10 Torr) and a mercury manometer (above≈10 Torr).

Silica–alumina (Al_2O_3, 13 wt%) was supplied by Shokubai Kasei Co., Ltd. and used as granules of 28—60 mesh. The surface area of silica–alumina measured by nitrogen adsorption was 557 m^2/g. About 0.5 g of silica–alumina was placed in a sample cell and pretreated at 400 °C under 10^{-5} Torr for 5 h.

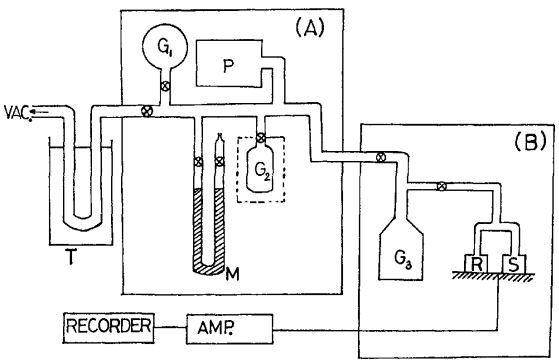

Fig. 1. Schematic diagram of vacuum system [A] and micro calorimeter [B].
T: Liquid nitrogen trap, M: mercury manometer,
P: capacitance manometer, G_1, G_2: gas storage bulb,
G_3: adsorbate reservoir, R: reference cell,
S: sample cell.
Temperatures of [A] and [B] were maintained at 25± 0.1 °C and at 25±0.01 °C, respectively.

The twin conduction type calorimeter contained a reference cell constructed as similarly as the sample cell which eliminates the effects of external thermal disturbance and other effects such as the slight temperature difference between admitted gas and the calorimeter or heat of adiabatic compression. In this apparatus, when herium gas was admitted to the evacuated cell up to 2 Torr, no deflection of base line was detected in 50 μV full scale.

Results and Discussion

The adsorption of ammonia at extremely low coverage must be quite important with regard to the surface acidic nature of silica-alumina. However, detailed studies in this field have been lacking. In Fig. 2, the differential heat curve in the coverage lower than 0.007 is shown. The plots of a—d shown by open circles are the results obtained when about 0.41, 0.81, 2.62, and 4.8 μmol/g of ammonia were admitted several times in each case. In these experiments, no residual gas the pressure of which was higher than 10^{-4} Torr was detected. As can be seen from Fig. 2, discontinuous differential heat curves were obtained along with the difference of the amount of admitted gas. These discontinuity probably resulted from the adsorption of ammonia on the glass wall and on the greese system of gas holder G_3 in Fig. 1, which caused errors of the caluculation of amounts of ammonia adsorbed on the sample. Therefore, the effect of ammonia adsorption on the glass wall and on the greese was corrected by a conventional way.[1] The corrected results of differential heat are shown by closed circles in Fig. 2. The initial heat value was observed to be 41 kcal/mol. This value agrees fairly well to the heat of neutralization of NH_3

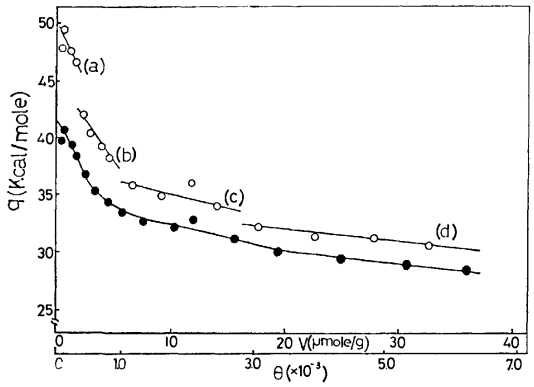

Fig. 2. Heats of adsorption of ammonia on silica–alumina at 25 °C.
○: Observed heat values, ●: corrected values.

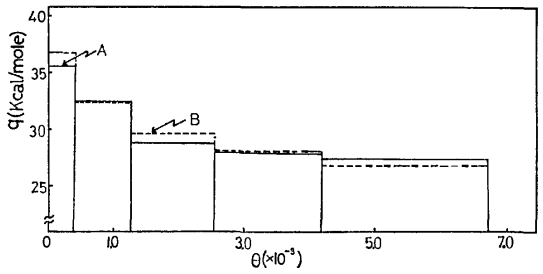

Fig. 3. Heats of adsorption of ammonia on silica–alumina at 25 °C. Stepped curve A, results obtained in case of admission of large doses of ammonia. Stepped curve B, integrated values of differential heats (small doses) in Fig. 2.

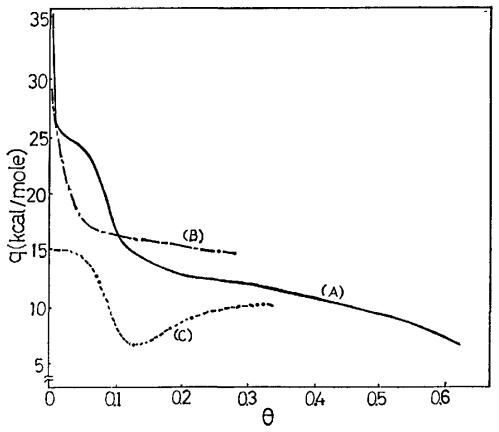

Fig. 4. Heats of adsorption of ammonia on silica–alumina. Curve A, present work (at 25 °C), Curve B, F. S. Stone *et al*, (at 30 °C), Curve C, P. Y. Hsieh (at 0 °C).

(G) and HCl (G). Moreover, differential heat curve decreased progressively and no anomalous behavior was observed.

In Fig. 3, a stepped curve A which shows the heats evolved during adsorptions of larger doses is compared with a stepped curve B which was obtained by integration of the values of differential heats in Fig. 2 (closed circles) in order to examine the influence of diffusion of ammonia in the sample layer. The fact that both curves are well coincident suggests that the diffusion of gas has little effect on the value of heat of adsorption.[2] The use of small dose is, therefore, favorable for adsorption studies on heterogeneous adsorbents and make it possible to measure heats of adsorption approaching true differential ones $(\partial Q/\partial n_S)$.

The differential heat curve up to 0.6 of θ is shown in Fig. 4 together with the results of Hsieh[3] and Stone.[4] Their results, especially that of Hsieh, are very different from ours. The discrepancy may be ascribed to the difference of sensitivity of calorimeters used and also to the fact that they measured the heat by admission of larger dose of ammonia as well as to the difference of sample preparation methods. Our results indicate that there exist very strong chemisorption sites up to 0.02 of θ and almost homogeneous chemisorption sites between 0.02 and 0.06.

Work is in progress to examine the availability of micro calorimetric measurement in the field of acidic character of solid catalysts and will be published.

This work was partly supported by a Grant-in-Aid for Science Research from the Ministry of Education.

References

1) M. Wahba and C. Kemball, *Trans. Faraday Soc.*, **49**, 1351 (1953).
2) P. C. Gravelle, *Adv. Catal.*, **22**, 191 (1972),
3) P. Y. Hsieh, *J. Catal.*, **2**, 211 (1963).
4) F. S. Stone and L. Whalley, *J. Catal.*, **8**, 173 (1967).

BULLETIN OF THE CHEMICAL SOCIETY OF JAPAN VOL. 51 (2), 635—636 (1978)

A Simple Method for the Calculation of the Polycrystalline ESR Lineshape

Kazuo SHIMOKOSHI

Department of Chemistry, Tokyo Institute of Technology, Ohokayama, Meguro-ku, Tokyo 152

(Received September 3, 1977)

Synopsis. A simple interpolation method is developed for calculating the magnetic resonance lineshapes of the polycrystalline samples. The method uses the *spline* function with the optional number of calculated points, at which the spin Hamiltonian is solved most accurately. The calculation procedure and some examples will be given.

The polycrystalline lineshapes of the ESR spectra are generally calculated by integrating the transition fields and probabilities, which are themselves obtained by solving the spin Hamiltonian (1), over the orientational distribution of the spin system:

$$\boldsymbol{H} = \boldsymbol{B}\tilde{\boldsymbol{g}}\boldsymbol{S} + \boldsymbol{S}\tilde{\boldsymbol{D}}\boldsymbol{S} + \sum_i (\boldsymbol{I}_i\tilde{\boldsymbol{A}}_i\boldsymbol{S} + \boldsymbol{I}_i\tilde{\boldsymbol{P}}_i\boldsymbol{I}_i - g_n\beta_n\boldsymbol{B}\boldsymbol{I}_i). \quad (1)$$

Most organic and inorganic free radicals have magnetic nuclei, whose hyperfine tensors do not, in general, have common axes. When these non-coaxial tensors are involved in the Hamiltonian, it takes much time to compute the transition fields accurately, even for a single orientation of the applied field. However, since the resonance field is generally a smoothly varying function of the polar and azimuthal angles (θ, ϕ), the lineshape can be calculated by the use of a suitable interpolation function with a minimum number of data points obtainced by the best solution of the Hamiltonian (1). Herring *et al.*[1] have used Newton's divided-difference polynominal as such an interpolation function. In the present note the application of the *spline* function to the calculation of the polycrystalline ESR lineshapes will be described.

From the transition field $(\boldsymbol{H}_i)$ and the probability $(\boldsymbol{q}_i)$ obtained by the solution of Eq. 1 for a specified transition (i), the monocrystalline component with a given width, λ, can be given as follows:

$$F_i(H, \theta, \phi) = (1/\lambda)(2/\pi)^{1/2} \exp\{-[H-\boldsymbol{H}_i(\theta, \phi)]^2/\lambda^2\}, \quad (2)$$

for the Gaussian, and

$$F_i(H, \theta, \phi) = (2/\lambda)/\{1+(2\pi/\lambda)^2[H-\boldsymbol{H}_i(\theta, \phi)]^2\}, \quad (3)$$

for the Lorentzian. The polycrystalline spectrum is, then, given by

$$S_i(H) = 1/4\pi \int_0^{2\pi} d\phi \int_0^{\pi} d\theta \sin\theta F_i(H, \theta, \phi)\boldsymbol{q}_i(\theta, \phi). \quad (4)$$

This integration 4 is, thereby not generally possible by analytical means. Lefebvre and Maruani[2] have applied the Gaussian quadrature to the numerical integration with an optional number of the data points. However, if one has a sufficient number of functional values in the θ-ϕ space, the integration can be approximated by the corresponding summation (Eq. 5):

$$S_i(H) = \sum_{\theta}\sum_{\phi} F_i(H, \theta, \phi)\boldsymbol{q}_i(\theta, \phi). \quad (5)$$

In order to obtain a sufficient number of F_i and $\boldsymbol{q}_i$ values as functions of θ and ϕ from the least number of calculated grid points, the *spline* function[3] was used as an example of the interpolation function with a better quality.

The *spline* method for the interpolation divides the interval into N consecutive subintervals. In each, the function is approximated by a different polynominal with a certain degree, M. At points between two such intervals, the polynominals of the two sides are connected so as to have the same values and derivatives (up to the M-1th derivative). In the present work, the simplest one with $M=3$ was used. The *spline* function, $f(x)$, with the data points of $x^{(j)}$ and $y^{(j)}$ and with equally spaced variables, $x^{(j)}$ $(j=0,1,2,\ldots,n)$, can be defined as follows:

$$f(x) = \sum_{j=0}^{n} C(j, j'; x)y^{(j)}; \ (x^{(j'-1)} \leq x \leq x^{(j')}), \quad (6)$$

where $y^{(j)}$ is the data value at $x=x^{(j)}$ and where j' specifies the interval at which the variable (x) is found. From the definition of the *spline* function, the coefficient, $C(j,j'; x)$, in Eq. 6 is given as follows:

$$C(j, j'; x) = b_{j'}(x)a_{j'-1,j} + b_{j'-1}(x)a_{j',j} + (x^{(j')}-x)\delta_{j'-1,j}/h + (x-x^{(j'-1)})\delta_{j',j}/h, \quad (7)$$

where $h=x^{(j)}-x^{(j-1)}(=\text{constant})$, $\delta_{j',j}$ is the usual Kronecker delta, and the b's and a's are given by

$$b_{j'}(x) = (x^{(j')}-x)^3/(6h) - (x^{(j')}-x)h/6$$

$$a_{j',j} = h^2[(\boldsymbol{A}^{-1})_{j',j+1} - 2(\boldsymbol{A}^{-1})_{j',j} + (\boldsymbol{A}^{-1})_{j',j+1}]/3.$$

The elements of the inverse matrix $(\boldsymbol{A}^{-1})$ are

$$(\boldsymbol{A}^{-1})_{j',j} = (-1)^{j'+j}D_{j'-1}D_{n-1-j}/(2^{j-j'}D_{n-1}), \quad (1 \leq j' \leq j \leq n)$$

$$(\boldsymbol{A}^{-1})_{j',j} = (-1)^{j'+j}D_{j-1}D_{n-1-j'}/(2^{j'-j}D_{n-1}), \quad (1 \leq j \leq j' \leq n)$$

and

$$(\boldsymbol{A}^{-1})_{j',-1} = (\boldsymbol{A}^{-1})_{j',0} = (\boldsymbol{A}^{-1})_{j',n} = (\boldsymbol{A}^{-1})_{j',n+1} = 0,$$

where D_n is given by $D_n=[(1+\sqrt{3}/2)^{n+1}-(1-\sqrt{3}/2)^{n+1}]\sqrt{3}$. For the present purposes, the interpolation should generally be extended to the case with two variables (θ, ϕ). This can be done by simply multiplying the coefficients for each variable,[3] as is shown in Eq. 8.

$$f(x_1, x_2) = \sum_{i_1}\sum_{i_1} C_1(i_1, i_1'; x_1)C_2(i_2, i_2'; x_2)y^{(i_1, i_2)}, \quad (8)$$

where $x_1^{(i_1'-1)} \leq x_1 \leq x_1^{(i_1')}$ and $x_2^{(i_2'-1)} \leq x_2 \leq x_2^{(i_2')}$. The expanded transition fields and probabilities can be calculated from the original data points $(\boldsymbol{H}_i^0, \boldsymbol{q}_i^0)$ by using the *spline* coefficients as follows:

$$\boldsymbol{H}_i(\theta, \phi) = \sum_{j=0}^{n_\theta}\sum_{k=0}^{n_\phi} C_1(j, j'; \theta)C_2(k, k'; \phi)\boldsymbol{H}_i^0(j, k),$$

$$\boldsymbol{q}_i(\theta, \phi) = \sum_{j=0}^{n_\theta}\sum_{k=0}^{n_\phi} C_1(j, j'; \theta)C_2(k, k'; \phi)\boldsymbol{q}_i^0(j, k), \quad (9)$$

where n_θ and n_ϕ are the number of the original data

points minus one in each direction. By putting Eq. 9 into Eqs. 2 or 3, and using Eq. 5, the lineshape due to the i transition can be obtained. When the system contains many transitions, the total lineshape will be given by the summation of $S_i(H)$ (Eq. 10):

$$S(H) = \sum_i S_i(H). \tag{10}$$

In the calculation of Eq. 9, we need only the tabulated data and the spline coefficients, $C(j,j';x)$. The coefficients can be determined without the values of the variable (x) if the original data are calculated for equally spaced variables. For calculation on a computer, therefore, the *spline* coefficients can be calculated independently and stored for common use in a file specified with the total number of the data points and the desired number of the interpolated points in each interval. Using these tabulated *spline* coefficients and the processes described above, the computation of the polycrystalline spectrum can be much simplified. Thus, we believe the spline interpolation is easier to handle and more convenient than the polynominal interpolation in Ref. 1.

Figure 1 shows the spectrum of the randomly oriented NO_2 radical, where both n_θ and n_ϕ are equal to 5. For the sake of simplicity, the second-order perturbation solution of the spin Hamiltonian[4] was used in the calculation of the original data points. The spectrum is comparable to that of NO_2 observed (Fig. 2).[5]

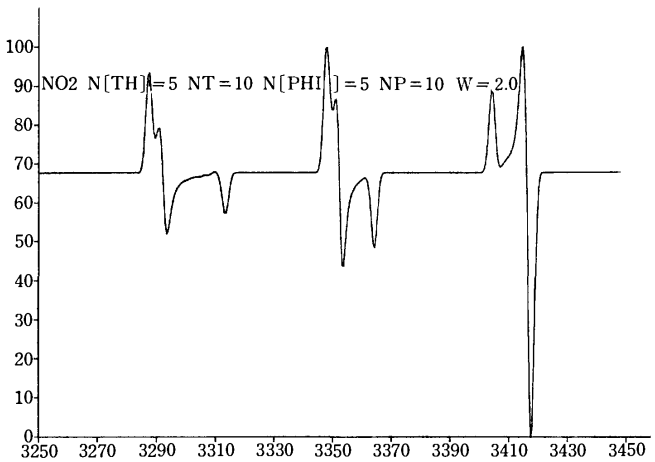

Fig. 1. The X-band spectrum of the randomly oriented NO_2 ($S=1/2$, $I=1$) calculated by the use of the spline function. The number of the data points $n_\theta=n_\phi=5$ ($0\leq\theta$, $\phi\leq\pi/2$) and each interval is further interpolated by 10 points. The magnetic parameters used in the calculation are $g_1=2.0056$, $g_2=1.9956$, $g_3=2.0029$; $A_1=56.0$, $A_2=51.0$, $A_3=65.0$ (G), and component width 2.0 G.

Fig. 2. The X-band spectrum of NO_2 adsorbed on silica gel and measured at 77 K. The resolution of the spectrum is somewhat poor, but the magnetic parameters derived from the spectrum is comparable to those of the spectrum in Fig. 1.

As in the case of the Gaussian integration,[2] the accuracy of of the calculated lineshapes is dependent on the number of the original data points, and also on the smoothness of the angular variation. The smoothness of the variation depends on the anisotropy of the tensors. It is, therefore, necessary to calculate more data points to obtain an accurate lineshape when the anisotropy of the tensors is large. In the case of the spectrum in Fig. 1, the lineshape did not change when the data points were increased from 5 to 10 in each variable if the total interpolated number of the transition field is large enough.

In the above calculations there is no restriction on the source of the transition fields and probabilities. This technique can, therefore, easily be applied to the calculation of the NMR lineshape of the polycrystalline samples by using the nuclear-spin transitions instead of the electron spin's.

References

1) F. G. Herring, C. A. McDowell, and J. C. Tait, *J. Chem. Phys.*, **57**, 4564 (1972).

2) R. Lefebvre and J. Maruani, *J. Chem. Phys.*, **42**, 1480 (1965).

3) J. H. Ahlberg, E. N. Nilson, and J. L. Walsh, "The Theory of Splines and Their Applications," Academic press, New York (1967).

4) M. Iwasaki, *J. Magn. Reson.*, **16**, 417 (1974).

5) T. J. Schaafsma, G. A. V. D. Velde, and J. Kommandeur, *Mol. Phys.*, **14**, 501 (1968).

BULLETIN OF THE CHEMICAL SOCIETY OF JAPAN VOL. 51 (2), 637—638 (1978)

Potassium-Sodium Ion Exchange Isotherm of Crystalline Zirconium Arsenate

Junko SUGISAWA, Takao YONEZAWA, Kazunori TAKAGUCHI, and Isao TOMITA*

Department of Chemistry, Faculty of Science, Tokyo Kyoiku University, Otsuka, Tokyo 112

(Received June 16, 1977)

Synopsis. When the forward and reverse Na^+–K^+ exchange isotherm was investigated for the α-zirconium arsenate ion exchanger, a large hysteresis loop was observed. The interlayer distance of the exchanger decreased with an increase in the ionic fraction of Na^+ in the exchanger. The result may be interpreted in terms of the formation of different types of solid solutions during the processes in both directions.

The ion-exchange behavior of alkali metal ions on zirconium bis(monohydrogen orthoarsenate)monohydrate, $Zr(HAsO_4)_2 \cdot H_2O$ (referred to as α-ZA), has been investigated by several authors.[1-3] A recent study has shown that α-ZA can be converted to a half-exchanged phase, $Zr(HAsO_4)(MAsO_4) \cdot xH_2O$, and a fully exchanged phase, $Zr(MAsO_4)_2 \cdot yH_2O$, for each of the lithium, sodium, and potassium ions as the ion exchange proceeds.[3] With regard to a sodium- or potassium-form exchanger, a half-exchanged form is a monohydrate, while a fully exchanged form is a trihydrate. An attempt has been made to study the forward and reverse exchange isotherm by using both disodium and dipotassium form as the starting exchangers.

Experimental

Preparation of the Materials. The α-ZA was synthesized as has been reported previously.[3] The alkali-metal-form exchanger was prepared by titrating α-ZA with a 0.1 M KOH or NaOH solution by the use of a potentiometric titrimeter. The titration was carried out very slowly (for the period of 60 to 70 h) lest the pH of the solution should exceed 9. The hydrolysis of the exchanger could be avoided in this way as much as possible. At the end point the pH was about 8. The prepared materials were filtered and stored over a saturated LiCl solution (the relative humidity was about 10%).

Ion Exchange. The ion-exchange reaction, $\overline{K}+Na^+ \rightleftharpoons \overline{Na}+K^+$, was studied, here, the superscript bars refer to the exchanger phase. The experiments were carried out by the batch method, the procedure being as follows. Mixed solutions of 0.1 M NaCl and 0.1 M KCl in various mixing ratios were prepared to give various ionic fractions of Na^+ or K^+. Each alkali chloride solution had been adjusted to pH 9 by adding a small amount of the corresponding alkali hydroxide solution. Then, 250 mg of α-ZA in the Na or K form was placed in contact with 25 ml of the above-mentioned mixed solution and the slurry was shaken for 4 days at 25 °C. The reaction vessel had been filled with nitrogen gas to avoid the hydrolytic conversion of the salt form into the hydrogen form. The resulting slurry was centrifuged, and the supernatant was analyzed for K^+ and Na^+ by means of flame photometry. The exchanger phase was subjected to X-ray powder diffractometry and thermal analysis (TG and DSC).

* Present address: Department of Chemistry, The University of Tsukuba, Ibaraki 300-31.

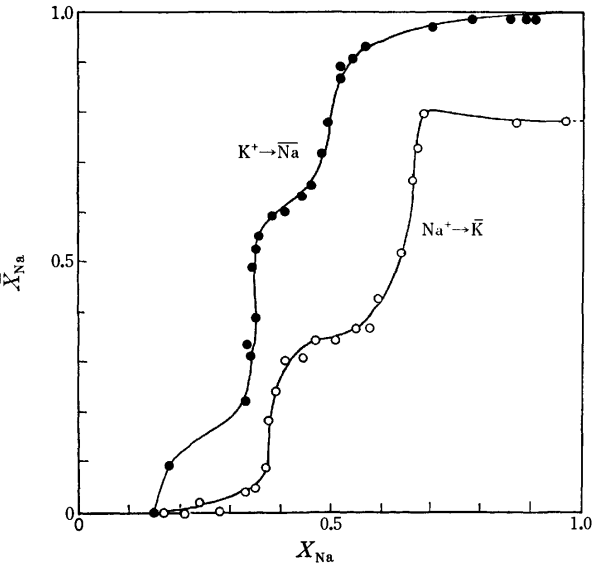

Fig. 1. The forward and reverse Na^+–K^+ exchange isotherm. $Na^+ \rightarrow \overline{K}$ denotes that K^+ ion in the exchanger is replaced with Na^+ ion. $K^+ \rightarrow \overline{Na}$ denotes that Na^+ ion in the exchanger is replaced with K^+ ion.

Results and Discussion

In Fig. 1 the Na^+–K^+ ion-exchange isotherm is shown. It should be noted that about 20% of the total K^+ could not be released from the exchanger, even when the exchanger in the K form was in contact with the solution containing Na^+ ions, *i.e.*, when the ionic fraction of Na^+ in the solution (X_{Na}) was unity. It has previously been found that K^+ could not be released into acidic media with a pH of about 1.5.[3] These facts suggest that the ions with large ionic radii have difficulty in diffusing rapidly inside the exchanger for steric reasons.

In comparison with the Na^+–K^+ exchange isotherm on crystalline zirconium phosphate (α-ZP), quite a large hysteresis loop was observed in α-ZA. Two vertical portions exist on both the forward and reverse exchange isotherm—at the ionic fraction (X_{Na}) of 0.38 and 0.65 for the $Na^+ \rightarrow \overline{K}$ process, while at 0.48 and 0.34 for the $K^+ \rightarrow \overline{Na}$ process. Generally, the presence of vertical portions in the isotherm suggests that two immiscible phases coexist in the exchanger, according to the phase rule.[5] From this point of view, the X-ray powder patterns of the exchanged solid phases were examined carefully. In the $Na^+ \rightarrow \overline{K}$ process, a single (002) reflection peak was observed for each of the samples at various stages of exchange, but the interlayer distance of the exchanger decreased with an increase in $\bar{X}_{Na}$, the ionic fraction of Na^+ in the exchanger: 10.83A

for $\bar{X}_{Na}=0$, 10.55A for $\bar{X}_{Na}=0.30$, 10.34A for $\bar{X}_{Na}=0.43$, and 9.99A for $\bar{X}_{Na}=0.57$—0.80.

In the $K^+\rightarrow\overline{Na}$ process, the interlayer distance again decreased with an increase in $\bar{X}_{Na}$: 10.75A for $\bar{X}_{Na}=0.09$, 10.55A for $\bar{X}_{Na}=0.31$, 10.30A for $\bar{X}_{Na}=0.58$ and 9.35A for $\bar{X}_{Na}=0.89$. However, here the (002) peak width was somewhat broader than those in the $Na\rightarrow\overline{K}$ process, indicating a close overlapping of the two peaks. In fact, at $\bar{X}_{Na}=0.66$ (the corresponding X_{Na} is in the vicinity of 0.48), a splitting into two peaks was clearly observed.

Continuous changes in the interlayer distance can usually be explained by the formation of a solid solution. However, this interpretation can not be accepted in the present case, since the phase rule requires the coexistence of two phases in the $\bar{X}_{Na}$ regions, which give vertical portions in the isotherm. The only possibility is that two kinds of solid solutions with very close interlayer distances are formed. As has been mentioned above, the evidence is found only in the $\bar{X}_{Na}$ regions, 0.7—0.6, in the $K^+\rightarrow\overline{Na}$ process, but the possibility can not be excluded in other regions also if one take the unsatisfactory dissolution of X-ray powder diffractometry into account.

The powder patterns of the solid, in which the exchange reaction proceeded to the same extent, but in the opposite direction, gave somewhat different small peaks. The formation of different solid solutions during the forward and reverse processes should result in a hysteresis loop.

The present work was partially supported by a Grant-in-Aid for Scientific Research from the Ministry of Education.

References

1) E. Torracca, U. Costantino, and M. A. Massucci, *J. Chromatogr.*, **30**, 384 (1967).
2) A. Clearfield, G. D. Smith, and B. Hammond, *J. Inorg. Nucl. Chem.*, **30**, 277 (1968).
3) T. Yonezawa and I. Tomita, *J. Inorg. Nucl. Chem.*, **39**, 1671 (1977).
4) G. Alberti, U. Costantino, S. Allulli, and M. A. Massucci, *J. Inorg. Nucl. Chem.*, **35**, 1339 (1973).
5) For example, A. Clearfield and A. S. Medina, *J. Phys. Chem.*, **75**, 3750 (1971).

BULLETIN OF THE CHEMICAL SOCIETY OF JAPAN VOL. 51 (2), 639—640 (1978)

Polarographic Behavior of Chloramine-T in an Alkaline Solution at a Rotating Platinum Electrode

Toshio MATSUDA

Department of Chemistry, Ritsumeikan University, Kyoto 603

(Received June 22, 1977)

Synopsis. Chloramine-T in alkaline solutions at pH higher than 8 gives a single reduction wave at a rotating platinum electrode. This wave results from the two-electron reduction of the anionic species of *N*-chloro-*p*-toluenesulfonamide. The electrode reaction is polarographically irreversible. Reproducible waves were observed with a freshly reduced electrode. The diffusion current was proportional to the concentration over the range from 0.05 to 0.6 mM chloramine-T.

Chloramine-T (CAT) exhibits a reduction wave in alkaline solutions at a rotating platinum electrode (RPE), as reported previously.[1,2] In this report, the polarographic behavior of CAT at the RPE was further investigated over the pH range from 7 to 13 in order to elucidate the nature of the wave from an analytical viewpoint.

Experimental

The polarograph and synchronous rotator used were the same as those described previously.[1] A vertical platinum-wire microelectrode (5.0 mm, 0.5 mm in diameter) was used at 600 r.p.m. The sensitivity of the electrode was 8.90 μA/mM for hexacyanoferrate(III) in 0.1 M KNO_3 and a Britton-Robinson (B.R.) buffer at pH 10.

Pretreatment of the electrode was performed by means of repetition of electrolytic oxidation and reduction in 0.1 M $HClO_4$.[3] Polarograms were recorded by either forward or backward scans. For forward scans, the electrode potential was shifted from positive to negative potential, and *vice versa*. The scan rate was 200 mV per minute. The cathodic current was taken to be positive.

Preparation of the solutions and other experimental conditions have been reported elsewhere.[1]

Results and Discussion

Polarographic waves of CAT at pH 10 are shown in Fig. 1, and similar waves were obtained over the pH range from 8 to 13. A single reduction wave appeared at a potential near the reduction potential of platinum oxide. Although the slope of the wave was dependent on the direction of scanning, well-developed and reproducible waves were obtained for backward scans with a freshly reduced electrode (curve 1). The values of the half-wave potential of the waves obtained in a manner similar to those shown in curve 1 were reproducible to within ±10 mV. The value of $\Delta E_{1/2}/\Delta$pH was −50 mV per unit pH over the pH range from 8 to 13 (Table 1).

The magnitude of the limiting current was independent of the direction of scanning, provided that a correction for the residual current in each case was applied. This correction remained constant to within ±2% over the above pH range (Table 1), and was

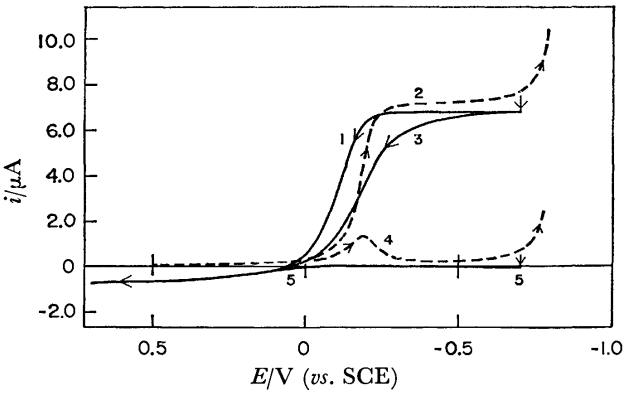

Fig. 1. Polarograms of 0.4 mM CAT in a solution containing 0.1 M KNO_3 and B. R. buffer pH 9.95. Recording procedures: (1) Backward from −0.7 V after preoxidation at +1.3 V for 2 min; (2) forward from +0.5 V after preoxidation at +1.3 V for 2 min; (3) backward from −0.7 V after polarization at −0.5 V for about 5 min; (4) same as in curve 2 (residual current); (5) same as in curve 1 (residual current).

Table 1. Polarographic data for the reduction wave of 0.4 mM CAT[a]

pH	i_d/μA	i_dC^{-1}/μAmM^{-1}	$E_{1/2}$/V (*vs.* SCE)
7.15	6.91	17.3	—[b]
8.20	6.92	17.3	−0.040
9.04	6.95	17.4	−0.080
9.95	6.93	17.3	−0.122
11.05	6.91	17.3	−0.177
11.85	6.93	17.3	−0.220
12.89	6.81	17.0	−0.265

a) These values were obtained in a supporting electrolyte solution containing 0.1 M KNO_3 and a B.R. buffer for various pH values and in the case of backward polarograms. b) No single wave appeared.

proportional to concentrations from 0.05 to 0.6 mM CAT. A plot of log i_d *vs.* log N (N is the number of revolutions per minute, which varied from 600 to 1200 min^{-1}) gave a straight line with a slope of 1/2.7. A similar result was obtained for the diffusion current of the hexacyanoferrate(III) ion. The temperature coefficient of i_d measured in the temperature range from 15 to 40 °C was 1.7% per degree. The limiting current can be concluded to be controlled by diffusion.

The value of i_d/C was found to be (17.3±0.3) μA/mM in the above pH range. This value corresponds to a two-electron reduction, which was calculated from a comparison with the value of i_d/C for the hexacyanoferrate(III) ion. This result suggests that monovalent

positive chlorine is reduced to a chloride ion by the electrode reaction. According to a previous report[4] the *N*-chloro-*p*-toluenesulfonamide anion predominates in alkaline solutions of CAT. It is, therefore, concluded that a single wave results from the reduction of the anion given by the reaction

$$RSO_2NCl^- + 2H_2O + 2e^- \longrightarrow RSO_2NH_2 + Cl^- + 2OH^-,$$

where $R=CH_3C_6H_4$. For the wave obtained in the backward scan with a freshly reduced electrode, a plot of log $[i/(i_d-i)]$ *vs.* E showed a straight line. The values of these slopes were found to be (85 ± 10) mV per log unit over the pH range from 8 to 13. The electrode reduction is considered to be polarographically irreversible.

It has been stated[5] that CAT is hydrolyzed in alkaline solutions and then the hypochlorite produced acts as an active species. In this study, the hypochlorite added to the CAT solution gave a single wave, the half-wave potential of which was more positive than that of the reduction wave of CAT. The value of the half-wave potential for the reduction wave of hypochlorite was the same as that reported previously.[6,7] It is concluded, therefore, that the reduction wave in the CAT solution is free from reduction of the hypochlorite.

The effect of the direction of scanning on the polarogram, as is shown in Fig. 1, can be explained as follows. When the curve was recorded for forward scan with the oxidized electrode, a deformed wave was observed, with the rising portion shifted to more negative potentials (curve 2). This result means that the electrode reduction of CAT is inhibited in the rising portion of the wave by the partially remaining oxide. In fact, the wave obtained for forward scan from 0 V with the reduced electrode was well-defined.

When the curve was recorded in backward scan with the electrode previously polarized at -0.5 V for about 5 min, the wave became markedly ill-defined (curve 3). The half-wave potential tended to shift to more negative potentials with increasing polarization time. The results are considered to be due to the deactivation of the electrode surface that occurred during polarization. This deactivation may be attributed to the adsorption of some constituents on the electrode surface. For example, adsorption of *p*-toluenesulfonamide (TSA), one of the reduction products, could be considered responsible on the basis of the following result. The a.c. polarographic base current used with the RPE with a reduced surface was recorded either in the presence or the absence of TSA. The base current decreased in the presence of 0.2 mM TSA in the potential region over which the platinum electrode had been reduced.

On the other hand, when the curve was recorded in backward scan with a freshly-reduced electrode, after preoxidation, the value of the half-wave potential was more positive than values obtained by other procedures, and the slope was independent of the starting potential (curve 1). This indicates that the electrode surface is free from formation of the oxide and the adsorption of constituents. This result is in line with the fact[3,8] that the electrode reaction tended to be more reversible on the platinum electrode with a fresh layer of finely-divided platinum.

The results described above indicate that the slope of the wave is strongly dependent on the history of the electrode, and that, for amperometric studies, careful attention should be paid to the selection of the potential for which the current is measured.

The author wishes to express his sincere thanks to Professor Taitiro Fujinaga of Kyoto University and to Professor Toyoshi Nagai of Ritsumeikan University.

References

1) T. Matsuda, *Bull. Chem. Soc. Jpn.*, **50**, 1934 (1977).
2) T. Nagai, T. Matsuda, and N. Sugii, *Nippon Kagaku Zasshi*, **90**, 790 (1969).
3) T. Nagai and T. Matsuda, *Rev. Polarogr. (Kyoto)*, **16**, 16 (1969).
4) T. Matsuda, *J. Electroanal. Chem. Interfacial Electrochem.*, **69**, 251 (1976).
5) A. Berka, J. Vulterin, and J. Zýka, "Newer Redox Titrants," Pergamon Press, London (1965), p. 37.
6) O. Schwarzer and R. Landsberg, *J. Electroanal. Chem. Interfacial Electrochem.*, **19**, 391 (1968).
7) J. A. Harrison and Z. A. Khan, *J. Electroanal. Chem. Interfacial Electrochem.*, **30**, 87 (1971).
8) R. N. Adams, "Electrochemistry at Solid Electrodes," Marcel Dekker, New York (1969), p. 187.

BULLETIN OF THE CHEMICAL SOCIETY OF JAPAN VOL. 51 (2), 641—642 (1978)

The Preparation and the Structure of Cobalt(III) Complexes Containing a *cis*-2-Butene-1,4-diamine Chelate Ring

Yoshikuni SOMA* and Fujio MIZUKAMI**

Department of Chemistry, Faculty of Science, Tohoku University, Aoba, Aramaki, Sendai 980

***National Chemical Laboratory for Industry, Honmachi, Shibuya-ku, Tokyo 151*

(Received July 13, 1977)

Synopsis. New cobalt(III) complexes containing a seven-membered chelate ring, $[Co(en)_2(dcb)]^{3+}$, $[Co(acac)_2(dcb)]^+$ and $[Co(dcbta)]^-$, were synthesized and resolved into optical isomers, and their structures were determined; dcb=*cis*-2-butene-1,4-diamine, dcbta=*cis*-2-butene-1,4-diamine-*N,N,N',N'*-tetraacetate ion.

cis-2-Butene-1,4-diamine (dcb) can coordinate to a metal ion as a bidentate or terdentate ligand because dcb has two amino groups and one double bond. However, there have been no reports on the metal complex of dcb. This Note will deal with the preparation and the structure of complexes in which dcb coordinates to a trivalent cobalt ion with two amino groups.

Experimental

cis-*2-Butene-1,4-diamine (dcb).* This was prepared *via* 1,4-diphthalimido-*cis*-2-butene from *cis*-2-butene-1,4-diol according to the usual method;[1,2] yield, 45%. The ^1H NMR spectrum of the diamine gave the following signals: $-NH_2$, δ 1.27 singlet; $-CH_2-$, δ 3.33 doublet; $-CH=$, δ 5.53 double triplets. The diamine was converted to the picrate for analysis. Found: C, 35.35; H, 3.22; N, 20.29%. Calcd for $C_{16}H_{16}N_8O_{14}$: C, 35.30; H, 2.96; N, 20.59%.

Sodium cis-*2-Butene-1,4-diamine*-N,N,N',N'-*tetraacetate (dcbta-Na$_4$).* This was synthesized by a method similar to that used for trimethylenediaminetetraacetate.[3] Chloroacetic acid (10.5 g) in 30 cm^3 of water was neutralized with 4 g of NaOH in 30 cm^3 of water below 20 °C. To the solution we added 2.2 g of dcb, after which the solution was heated at 80 °C for 3 h. During the heating, the pH of the solution was kept at 8 by adding 3 g of NaOH in 30 cm^3 of water in small portions. This solution itself was used for the synthesis of the dcbta complex.

[Co(en)$_2$(dcb)]Br$_3$. This was synthesized by a method similar to that used for $[Co(en)_2(tmd^{***})]Br_3$.[4] To 200 cm^3 of DMSO containing 3 g of *cis*-$[CoCl_2(en)_2]Cl$ we added 0.9 g of dcb in 50 cm^3 of DMSO. The solution was kept at 20—30 °C for two days. The remainder of the procedure used to obtain the complex was identical with the method used for $[Co(en)_2(tmd)]Br_3$. Yield, 0.5 g. Found: C, 19.04; H, 5.32; N, 16.46%. Calcd for $C_8H_{26}N_6CoBr_3$: C, 19.03; H, 5.20; N, 16.65%.

(−)$_{405}$-[Co(en)$_2$(dcb)]Cl$_3$·H$_2$O·HCl. The racemate was resolved according to a method similar to that used for $[Co(amb^{****})(en)_2]^{2+}$.[5] The racemate (0.28 g), adsorbed on an SP-Sephadex column (ϕ4×150 cm), was eluted with a solution of 0.15 M potassium $(+)_{589}$-tartratoantimonate. The eluate containing the $(-)_{405}$-isomer was again passed through an SP-Sephadex column (ϕ1.8×20 cm), and the adsorbed band was eluted with a 0.36 M HCl solution. The eluate was evaporated to dryness in a vacuum desiccator over KOH. Found: C, 22.74; H, 7.00; N, 19.19%. Calcd for $C_8H_{29}N_6Cl_4Co$: C, 22.54; H, 6.87; N, 19.72%.

[Co(acac)$_2$(dcb)]ClO$_4$. The procedure used here is identical with the method used for $[Co(acac)_2(en)]ClO_4$,[6] except for using dcb instead of ethylenediamine. The dcb complex was prepared by mixing $Na[Co(acac)_2(NO_2)_2]\cdot 5H_2O$ and dcb (1:1) in aqueous methanol in the presence of charcol and by then adding $NaClO_4$. Found: C, 38.23; H, 5.41; N, 6.47%. Calcd for $C_{14}H_{26}N_2O_8ClCo$: C, 37.81; H, 5.89; N, 6.30%.

(−)$_{405}$-[Co(acac)$_2$(dcb)]$^+$. The racemate was resolved according to a method similar to that used for $[Co(acac)_2(RS\text{-}2,4\text{-ptn}^{\dagger})]ClO_4$.[7] The racemate and sodium hydrogen dibenzoyltartrate were dissolved in water at 65 °C. A violet powder was precipitated by cooling the solution to 20 °C and then filtered off. The powder was recrystallized from water fractionally until the ratio of the $\Delta\varepsilon$ and ε values of the powder became constant. The pure powder was converted into perchlorate by treating it with aqueous methanol containing $AgClO_4$. The perchlorate of the $(-)_{405}$-isomer was hygroscopic and was obtained in only a slight amount. The quantitative CD curve of this isomer was determined with the aid of the ε values of the racemate.

Na[Co(dcbta)]·2H$_2$O. The procedure used here is almost identical with the method used for $[Co(RR\text{- and }SS\text{-}2,4\text{-ptnta}^{\dagger\dagger})]^-$.[8] To a solution containing 26 mmol of $dcbtaNa_4$ we added 8.1 g of $Na_3[Co(NO_2)_6]$[9], after which the solution was warmed at 55 °C for 40 h. Crystals were obtained by gradually evaporating the solution at 30 °C. Found: C, 33.26; H, 4.07; N, 6.42%. Calcd for $C_{12}H_{18}N_2O_{10}NaCo$: C, 33.35; H, 4.20; N, 6.48%.

K(+)$_{589}$-[Co(dcbta)]·2H$_2$O. The silver salt of the racemate was dissolved in 30 cm^3 of water. To the solution we then added 0.9 g of $(+)_{589}$-$[Co(NO_2)_2(en)_2]Br$[10] in 20 cm^3 of water. The solution was then warmed at 50 °C, and the AgBr was filtered off. The filtrate was evaporated to dryness, and the residue was suspended in a small amount of water. The undissolved powder was filtered off and dissolved in a large amount of hot water. Crystals were obtained fractionally from the solution by evaporation in a vacuum desiccator over P_2O_5. Each fraction was checked by means of its CD, and pure crystals were obtained by repeating such fractional recrystallizations. The pure crystals were suspended in water and converted into potassium salt by stirring with a cation exchanger, Dowex 50W-X8. Found: C, 32.44; H, 3.97; N, 6.44%. Calcd for $C_{12}H_{18}N_2O_{10}KCo$: C, 32.15; H, 4.06; N, 6.25%.

Measurements. The visible and ultraviolet absorption spectra were recorded with a Hitachi 323 spectrophotometer.

* Present address: Research Center, Mitsui Petrochemical Industries Ltd., Wagicho, Kuga-gun, Yamaguchi 740.

*** 1,4-Butanediamine.

**** 4-Aminobutanoate ion.

† (2*R*,4*S*)-2,4-Pentanediamine.

†† 2,4-Pentanediamine-*N,N,N',N'*-tetraacetate ion.

The CD curves were obtained on a JASCO Model ORD/UV-5 spectrophotometer with a CD attachment. The ^1H NMR spectra in D_2O were obtained on Varian T-60 and HA-100 spectrometers, using Na–TMS as the internal standard.

Results and Discussion

The ^1H NMR spectrum of $(-)_{405}$-$[Co(en)_2(dcb)]^{3+}$ (**1**) exhibits only two kinds of broad signals (δ 2.84 and 3.40) and a multiplet signal (δ 5.98). The ^1H NMR spectrum of $(-)_{405}$-$[Co(acac)_2(dcb)]^+$ (**2**) gives only two kinds of singlet signals (δ 1.20 and 1.28) on the methyl groups. These facts suggest that **1** and **2** have a symmetry element other than C_1 and, so the dcb in the

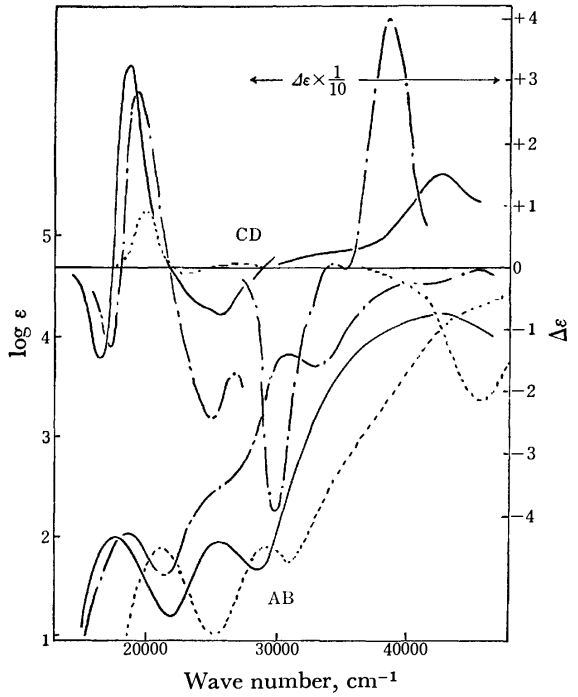

Fig. 1. Absorption (AB) and CD spectra of (----) $(-)_{405}$-$[Co(en)_2(dcb)]^{3+}$, (-·-): $(-)_{405}$-$[Co(acac)_2(dcb)]^+$, (——): $(+)_{589}$-$[Co(dcbta)]^-$ in water.

complexes acts as a bidentate ligand. As Fig. 1 shows, the absorption spectra of **1** and **2** are similar to those of the analogous complexes, $[Co(en)_2(tmd)]^{3+}$,[4] and $[Co(acac)_2(2,4\text{-ptn})]^+$,[7] respectively. The CD curve of **1** is very similar to that of $\Lambda(+)_{589}$-$[Co(en)_3]^{3+}$.[11] In the region from 15000 to 40000 cm^{-1}, the CD curve of **2** is almost enantiomeric with that of $\Lambda(-)_{546}$-$[Co(acac)_2(RR\text{-}2,4\text{-ptn})]^+$.[7] It is thus clear that **1** and **2** have a *cis*-2-butene-1,4-diamine chelate ring (seven-membered ring). In addition, **1** and **2** seem to be assignable to the Λ- and Δ-configurations respectively.

In the region from 15000 to 40000 cm^{-1}, the absorption and CD spectra of $(+)_{589}$-$[Co(dcbta)]^-$ (**3**) are very similar to those of $\Delta(+)_{589}$-$[Co(RR\text{-}2,4\text{-ptnta})]^-$,[8] respectively. This suggests that the dcbta coordinates to the cobalt(III) ion as a sexadentate ligand such as 2,4-ptnta and that **3** has the $\Delta(\lambda)$ structure (C_2 symmetry), as is shown in Fig. 2. This $\Delta(\lambda)$ structure seems also to be supported by the ^1H NMR spectrum of **3**

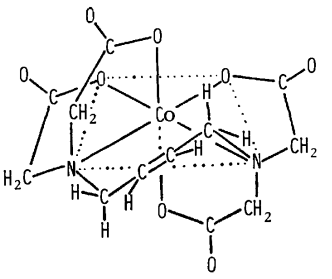

Fig. 2. Schematic structure of $\Delta(\lambda)$-$[Co(dcbta)]^-$.

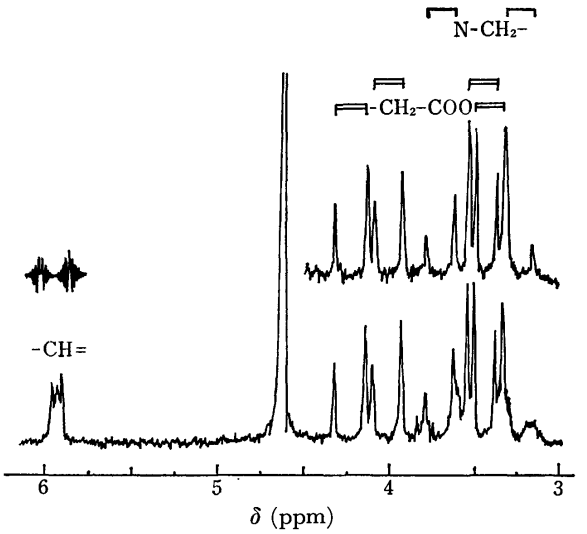

Fig. 3. ^1H NMR spectrum (100 MHz) of $(+)_{589}$-$[Co(dcbta)]^-$ in D_2O.

shown in Fig. 3. The spectrum exhibits a kind of –CH= signal, two kinds of $-CH_2-COO$ signals (two kinds of double doublets), and a kind of $N-CH_2-$ signal. The assignment of the $N-CH_2-$ signal is confirmed by the fact that the complicated signal becomes double doublets (axial H and equatorial H) upon irradiation at δ 5.95.

References

1) L. H. Amundsen, R. H. Mayer, L. S. Pitts, and L. A. Malentacchi, *J. Am. Chem. Soc.*, **73**, 2118 (1951).
2) J. C. Sheehan and W. A. Bolhofer, *J. Am. Chem. Soc.*, **72**, 2786 (1950).
3) J. A. Weyh and R. E. Hamm, *Inorg. Chem.*, **7**, 2431 (1968).
4) H. Ogino and J. Fujita, *Bull. Chem. Soc. Jpn.*, **48**, 1836 (1975).
5) M. Kojima, H. Takayanagi, and J. Fujita, *Bull. Chem. Soc. Jpn.*, **50**, 1891 (1977).
6) L. J. Boucher, *Inorg. Chem.*, **6**, 2162 (1967).
7) F. Mizukami, H. Ito, J. Fujita, and K. Saito, *Bull. Chem. Soc. Jpn.*, **46**, 2410 (1973).
8) F. Mizukami, H. Ito, J. Fujita, and K. Saito, *Bull. Chem. Soc. Jpn.*, **44**, 3051 (1971).
9) E. Billman, *Z. Anal. Chem.*, **39**, 284 (1900).
10) F. P. Dwyer and F. L. Garvan, *Inorg. Synth.*, **6**, 194 (1960).
11) A. J. McCaffery and S. F. Mason, *Mol. Phys.*, **6**, 359 (1963); Y. Saito, K. Nakatsu, M. Shiro, and H. Kuroya, *Bull. Chem. Soc. Jpn.*, **30**, 795 (1957).

BULLETIN OF THE CHEMICAL SOCIETY OF JAPAN VOL. 51 (2), 643—644 (1978)

Nuclear Magnetic Resonance Studies of Cobalt Complexes. Cobalt-59 Nuclear Magnetic Resonance Spectrum of the Hexakis-(trimethyl phosphite)cobalt(III) Complex

Akira YAMASAKI,* Takashi AOYAMA, Shizuo FUJIWARA, and Keikichi NAKAMURA**

Department of Chemistry, Faculty of Science, The University of Tokyo, Hongo, Tokyo 113

(Received July 18, 1977)

Synopsis. The well-resolved septet spectrum was recorded for cobalt-59 NMR of $[Co(P(OCH_3)_3)_6](BF_4)_3$ in an acetonitrile solution. The obtained NMR parameters are: σ(Co-59)=+304 ppm (upfield from $[Co(CN)_6]^{3-}$), ^1J(Co–P)=414 Hz, and ΔH(Co)=340 Hz.

The last member of the symmetric diamagnetic $Co^{III}L_6$-type complexes, the $Co^{III}P_6$-type hexakis(trimethyl phosphite)cobalt(III) complex, was examined by cobalt-59 nuclear magnetic resonance (NMR) spectroscopy. The coordination character of such a $Co^{III}P_6$-type complex seems very interesting because the relatively hard metal ion, Co(III), and the typically soft ligand, $P(OCH_3)_3$, form an octahedral complex which seems to have a very crowded configuration around the small central metal ion.[1] The result of the cobalt-59 NMR study is reported in this paper mainly because of the interest in the metal-ligand coordination bonding.

Experimental

Hexakis(trimethyl phosphite)cobalt(III) tetrafluoroborate was synthesized by a process similar to that of its perchlorate.[1] (Cobalt(II) tetrafluoroborate was used instead of cobalt(II) perchlorate.) The analyses of Co, P, and BF_4 were carried out gravimetrically. (Found: Co, 5.50; P, 17.89; BF_4, 25.03; Calcd for $C_{18}H_{54}O_{18}P_6CoB_3F_{12}$(=$[Co(P(OCH_3)_3)_6](BF_4)_3$): Co, 5.54; P, 17.47; BF_4, 24.48). The ultraviolet spectra and proton NMR spectra (100 MHz) were almost the same as those of the corresponding perchlorate in an acetonitrile solution: ν_{1max}=350 nm, log ε=2.3; $\delta(OCH_3)$=4.00 ppm (symmetric multiplet).

Cobalt-59 NMR spectral measurements were carried out with a Varian VF-16 NMR spectrometer operating at 7.9650 MHz (modulation of about 0.1 gauss). Potassium hexacyanocobaltate(III) was used as an external standard. The complex was dissolved in an acetonitrile, and poured into a 14 mmϕ sample tube for the spectral measurement.

Results and Discussion

The recorded cobalt-59 NMR spectrum is shown in Fig. 1. The well-resolved septet is clearly observed. The origin of this septet can be attributed to the scalar coupling of six equivalent phosphorus-31 nuclei (I=1/2) directly coordinated to the central cobalt-59 nucleus. The chemical shift was +304 ppm from the external standard $[Co(CN)_6]^{3-}$; this is the largest value for high-field resonance among the numerous tervalent cobalt complexes. The discussion of the chemical shifts will be published elsewhere. The line-shape simulation was carried out using the HITAC 8700/8800 computer of the Computer Centre, The University of Tokyo. The best-fitted parameters are: ^1J(Co–P)=414 Hz, and ΔH(Co)=340 Hz (assuming Gaussian curves). Simulation with the Lorentzian curves did not succeed in giving the approximate curves.

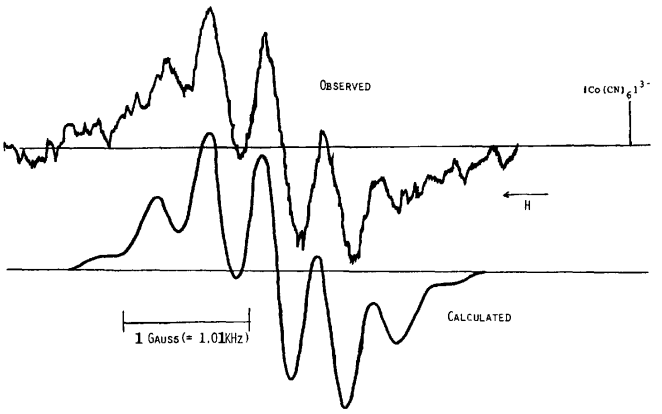

Fig. 1. Cobalt-59 nuclear magnetic resonance spectrum of $[Co(P(OCH_3)_3)_6](BF_4)_3$ in CH_3CN solution (7.9650 MHz), and its simulated spectrum with ^1J(Co–P) of 414 Hz, and ΔH=340 Hz (Gaussian curves).

This multiplet confirms that the quadrupolar relaxation of the central cobalt-59 in this complex is not so effective as those of the other $Co^{III}L_6$-type complexes. The octahedral coordination of the six phosphorus ligands is also confirmed from the septet spectrum.

The magnitude of the spin-spin coupling constant, ^1J(Co–P) is noticeably smaller than that for the $[Co(PF_3)_4]^-$,[2] which was the only previously reported coupling constant between cobalt-59 and phosphorus-31. The coordinating characters of trifluorophosphine and trialkyl phosphite have been assumed to be quite similar, or almost the same.[3,4] Therefore, the difference in the ^1J(Co–P) values between $[Co(PF_3)_4]^-$ and $[Co(P(OCH_3)_3)_6]^{3+}$ can be attributed to the differences in the oxidation state or coordination number of the central cobalt ions. It has been noted that the s-characters of bonding atoms have a large influence on the spin-spin coupling constants.[3,5] For rhodium and platinum complexes, the metal-ligand coupling constants of tetracoordinated complexes (Rh(I), Pt(II)) are about 1.5 times those of the corresponding hexacoordinated complexes (Rh(III), Pt(IV))[3]: tetracoordinated complexes have an s-character of one fourth, while octahedral complexes have one sixth.

Although the contribution of the s-characters of the

* Present address: Laboratory of Applied Chemistry, The University of Electro-Communications, Chofu, Tokyo 182.

** National Research Institute for Metals, Nakameguro, Meguro-ku, Tokyo 153.

coordination bonds to the magnitude of the spin-spin coupling constants is quite attractive as an explanation of the differences among the many complexes, it is not sufficient to describe the quite small coupling constant ^1J(Co–P) in our $[Co(P(OCH_3)_3)_6]^{3+}$ complex. The ^1J(Co–P) in $[Co(PF_3)_4]^-$ is reported to be 1225 Hz,[2] and the corresponding coupling constant in our complex is only 414 Hz, which is much smaller than two thirds of the ^1J(Co–P) in $[Co(PF_3)_4]^-$. Therefore, further contributions should be taken into account.

Another possible factor which would decrease the coupling constants is the bond weakening due to steric or other repulsive interactions, such as so-called trans-effects. The geometric factors should be important in considering the complexes of bulky ligands such as phosphines and phosphites. Tolman[4] studied the steric hindrances by the ligand-cone angles, which is the apex angle of the minimum cones contered several angstroms (metal–phosphorus bond lengths) away from the center of the phosphorus atom along the threefold axis of phosphorus ligands which just touch the outermost extremities of a folded back ligand while maintaining C_3 symmetry. According to his study with CPK models, the cone angle of PF_3 (when coordinated to Ni(0)) is about 104°, and that of $P(OCH_3)_3$ is 107° (uncertainly of ±2°). He used the metal–phosphorus bond length of 2.28 Å, but he suggested that it was too long.

His cone angle estimation cannot be directly applied to our case, because the proton NMR showed that all fifty-four protons in $[Co(P(OCH_3)_3)_6]^{3+}$ are strictly equivalent. The equivalence of the six phosphorus-31 nuclei also confirms that there are no differences in the six phosphite groups. This means that the free rotation of each phosphite group occurs around the threefold axis, namely, the cobalt(III)–phosphorus bond. Therefore, the ligand-cone angles of phosphite esters in the $[Co(P(OCH_3)_3)_6]^{3+}$ should be smaller the 90°, and the bond length between the central cobalt(III) and the ligand phosphorus atom must be elongated to allow the free rotation of phosphite groups. Such bond stretching might cause a smaller spin-spin coupling constant than would occur in the case of no steric hindrances.

One of the authors (A. Y.) wishes to thank Professor Dr. Ekkehard Fluck, Institut für anorganische Chemie, Universität Stuttgart, where a part of this work was carried out. He is also grateful to the Alexander-von-Humboldt Stiftung for the financial support of his stay in the Institute.

References

1) A. Yamasaki, Y. Mihara, and S. Fujiwara, *Inorg. Chim. Acta*, in press.
2) E. A. C. Lucken, K. Noack, and D. F. Williams, *J. Chem. Soc., A*, **1967**, 148.
3) A. Pidcock and J. F. Nixon, *Ann. Rev. NMR Spectrosc.*, **II**, 345 (1969).
4) C. A. Tolman, *J. Am. Chem. Soc.*, **92**, 2956 (1970).
5) J. A. Pople and D. P. Santry, *Mol. Phys.*, **8**, 1 (1964).

BULLETIN OF THE CHEMICAL SOCIETY OF JAPAN VOL. 51 (2), 645—646 (1978)

The Solvent Extraction of Thallium(I) as a Dibenzo-18-crown-6 Complex with the Picrate Ion

Tatsuya SEKINE, Hiroji WAKABAYASHI, and Yuko HASEGAWA

Department of Chemistry, Science University of Tokyo, Kagurazaka, Shinjuku-ku, Tokyo, 162

(Received August 5, 1977)

Synopsis. The solvent extraction of thallium(I) with dibenzo-18-crown-6 (DBC) as the picrate into chloroform and benzene was measured at 25 °C. The extraction was nearly the same as that of potassium(I) and much better than rubidium(I); this tendency was mainly attributed to the difference in the stability of the DBC complexes in the aqueous phase. Thallium(III) was extracted only poorly.

The solvent extraction of alkali metal ions with various macrocyclic polyethers of different ring sizes was employed in the early work on these compounds as a measure of the stability of the complexes of the metal ions with them.[1,2] It was found that, among the alkali metal ions, 18-crown-6 polyethers extracted potassium(I) most effectively; this was explained in terms of the size of K^+ being the most favorable fit for the 18-crown-6 polyether rings. The relationship between the extractability and the stability of the macrocyclic polyether complexes was further considered statistically.[3-5] It was assumed that metal ions trapped in the ring were not hydrated or that they were hydrated similarly.[5]

The extraction of metal ions with macrocyclic polyethers has been further studied by several inorganic chemists with regard to alkali metal ions[4-7] and alkaline earth ions,[4] and the extraction equilibria as well as the nature of the complexes have been discussed in details. Furthermore, extraction with macrocyclic polyethers has been used in the substoichiometric determination of sodium(I)[8] and the separation of strontium(II) from macro amounts of calcium(II).[9]

In the present study, we have measured the solvent extraction of thallium(I) as a dibenzo-18-crown-6 (DBC) complex with the picrate ion into benzene and chloroform. The results were compared with previous data on alkali metal ions obtained under similar conditions.[6]

Experimental

All the procedures were performed at 25±0.3 °C. The DBC was obtained from the Aldrich Co., U.S.A., and was recrystallized several times from chloroform. The other reagents were of an analytical grade. The lithium picrate solution was prepared from lithium hydroxide and picric acid. The standard thallium(I) solution was prepared from thallium(I) nitrate, the concentration being checked by a colorimetric method.[10] A 5-ml portion of an aqueous solution containing lithium picrate and 1×10^{-4} mol dm^{-3} of thallium(I) (pH about 3.3) and the same volume of benzene or chloroform containing a certain amount of DBC were placed in a stoppered glass tube and agitated mechanically until the distribution equilibrium was attained. The two phases were then centrifuged off, and the thallium(I) in the organic phase was back-extracted with 0.1 mol dm^{-3} perchloric acid. The amount of thallium thus back-extracted and that remained in the aqueous phase was measured by an atomic absorption method. The distribution ratio was defined by means of the following equation and was calculated from the experimental data:

$$D = [\mathrm{Tl(I)}]_{\mathrm{org,total}}/[\mathrm{Tl(I)}]_{\mathrm{total}}. \quad (1)$$

Results and Discussion

In the following statistical treatment, a unipositive metal ion, DBC, and a picrate ion are denoted by M^+, E, and A^-, respectively, and the chemical species in the organic and aqueous phases by the subscript "org" and by the lack of any subscript respectively. Then the following equilibrium constants may be defined:

$$\beta_1 = [\mathrm{ME^+}][\mathrm{M^+}]^{-1}[\mathrm{E}]^{-1}, \quad (2)$$

$$K_{\mathrm{ex0}} = [\mathrm{ME^+A^-}]_{\mathrm{org}}[\mathrm{M^+}]^{-1}[\mathrm{E}]_{\mathrm{org}}^{-1}[\mathrm{A^-}]^{-1}, \quad (3)$$

$$K_{\mathrm{ex}} = [\mathrm{ME^+A^-}]_{\mathrm{org}}[\mathrm{ME^+}]^{-1}[\mathrm{A^-}]^{-1}, \quad (4)$$

$$K_{\mathrm{d}} = [\mathrm{E}]_{\mathrm{org}}[\mathrm{E}]^{-1}. \quad (5)$$

Thus,

$$K_{\mathrm{ex}} = K_{\mathrm{ex0}}K_{\mathrm{d}}\beta_1^{-1} \text{ or } K_{\mathrm{ex0}} = K_{\mathrm{ex}}\beta_1 K_{\mathrm{d}}^{-1}. \quad (6)$$

The distribution ratio may generally be written as

$$D = ([\mathrm{ME^+A^-}]_{\mathrm{org}}+[\mathrm{ME^+}]_{\mathrm{org}})([\mathrm{M^+}]+[\mathrm{ME^+}])^{-1}. \quad (7)$$

However, since the dissociation of the ion-pair in the non-polar solvents may be negligible, and since $[ME^+]$ was found to be much smaller than $[M^+]$ under the conditions of the present work, as will be seen, Eq. 7 is written in the present paper as

$$D = K_{\mathrm{ex0}}[\mathrm{E}]_{\mathrm{org}}[\mathrm{A^-}]. \quad (8)$$

The distribution ratio as a function of the DBC concentration showed a straight line with a slope of 1, as is seen from Fig. 1; that as a function of the picrate ion also showed a straight line with a slope of 1 in the picrate concentration range from 10^{-3} to 10^{-2} mol dm^{-3}, although it deviated slightly from the line above this range.

The equilibrium constants obtained from these data are listed in Table 1, together with those from the literature.

It may be seen from these data that the extraction of thallium(I) is much better than that of rubidium(I) and nearly the same as that of potassium(I), which is extracted most effectively with 18-crown-6 polyethers among the alkali metal ions.

By separate experiments, it was found that the extraction of thallium(III) was much poorer than that of thallium(I). For example, the distribution ratio of the former into chloroform, was $10^{-1.14}$ when $[\mathrm{E}]_{\mathrm{org}}$ was 1×10^{-2} mol dm^{-3} and $[A^-]$ was 7.5×10^{-3} mol dm^{-3}, and under identical conditions the distribution ratio

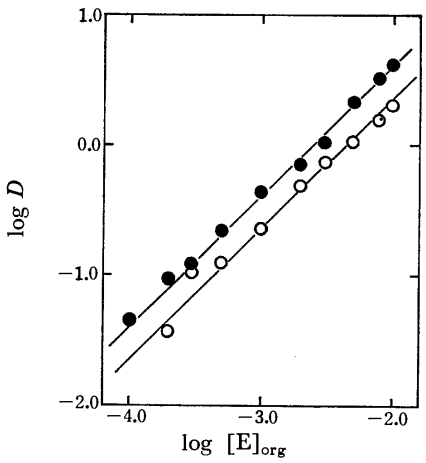

Fig. 1. Extraction curves of thallium(I) complex with DBC as picrate into chloroform (●) and benzene (○). The aqueous phase contained 7.4×10^{-3} mol dm^{-3} of lithium picrate and was at pH about 3.3. The straight lines are calculated by introducing the values of K_{ex0} in Table 1 and the above picrate concentration into Eq. 8.

Table 1. Summary of constants

Metal ion	Na^+	K^+	Rb^+	Cs^+	Tl^+	Remarks
Diameter (nm)	0.19	0.27	0.29	0.33	0.29	Ref. 11
$\log K_{ex0}$ into $CHCl_3$	—	—	—	—	4.74[a]	
$\log K_{ex0}$ into C_6H_6	2.2	4.65	3.75	3.07	4.49[a]	
$\log \beta_1$	1.2	1.7	1.1	0.8	1.5	Ref. 11
$\log K_{ex}$ into C_6H_6[b]	3.9	5.9	5.6	5.2	5.9	

a) Present work, others taken from Ref. 6.
b) $\log K_{ex}=\log K_{ex0}K_d\beta_1^{-1}$ in which $\log K_d=2.9$ (Ref. 6) was employed.

of thallium(I) was $10^{0.62}$.

The apparent tendency of the extraction given by K_{ex0} in Eq. 3 for different metal ions is affected by both the stability and the extractability of the complex in the aqueous phase, as may be seen from Eq. 6. The value of K_{ex}, which represents the latter property of the complex, should be affected by the molar volume of the extracted species and also by the interactions of the complex, probabaly mainly by those of the central metal ion, with water molecules and/or solvent molecules. The molar volumes of the extractable complexes of different metal ions with the same polyether should be rather similar to each other. Thus, when the K_{ex} values of metal ions with the same macrocyclic polyether are different, it is probably due to the difference in the hydration of the complex if no special interactions with the solvent molecules are to be expected.

As may be seen from Table 1, the value of K_{ex} of thallium(I) is similar to that of potassium(I) and not very much different from rubidium(I). Thus, the difference in the extractability of these three ions into benzene may be attributed mainly to the difference in the stability of the complex. The fact that the stability of the thallium(I) complex with 18-crown-6 polyethers is very similar to that of the corresponding potassium(I) complexes has already been pointed out.[11,12]

Since thallium(I) is much more effectively extracted with DBC than thallium(III), the separation of thallium in these oxidation states may be achieved by extraction with this reagent, and, since this tendency is the inverse of that observed in many other extraction systems, it should be useful for such purposes as to separate a small amount of thallium(I) from a large amount of thallium(III).

The authors are very grateful to Dr. Yasuyuki Takeda of the Department of Chemistry, Chiba University, for his valuable discussion and experimental aid in the early stage of this work.

References

1) C. J. Pedersen, *Fed. Proc., Fed. Am. Soc. Exp. Biol.*, **27**, 1305 (1968); *J. Am. Chem. Soc.*, **92**, 391 (1970).
2) G. Eisenman, S. Ciani, and G. Szabo, *Fed. Proc., Fed. Am. Soc. Exp. Biol.*, **27**, 1289 (1968).
3) H. K. Frensdorff, *J. Am. Chem. Soc.*, **93**, 4684 (1971).
4) J. Rais, M. Kyrs, and L. Kadlecova, Proc. Int. Solvent Extraction Conf., 1974, Soc. Chem. Ind., London (1974), p. 1705.
5) P. R. Danesi, H. Meider-Gorican, R. Chiarizia, V. Capuano, and G. Scibona, Proc. Int. Solvent Extraction Conf., **1974**, Soc. Chem. Ind. London (1974), p. 1764; *J. Inorg. Nucl. Chem.*, **37**, 1479 (1975).
6) A. Sadakane, T. Iwachido, and K. Toei, *Bull. Chem. Soc. Jpn.*, **48**, 60 (1975).
7) T. Iwachido, M. Kimura, and K. Toei, *Chem. Lett.*, **1976**, 1101.
8) J. W. Mitchell and D. L. Shanks, *Anal. Chem.*, **47**, 642 (1975).
9) T. Kimura, K. Iwashima, T. Ishimori, and H. Hamaguchi, *Chem. Lett.*, **1977**, 563.
10) H. Goto, Y. Kakita, and N. Ichinose, *Nippon Kagaku Zasshi*, **88**, 640 (1967).
11) E. Shchori, N. Nae, and J. Jagur-Grodzinski, *J. Chem. Soc. Dalton Trans.*, **1975**, 2381.
12) J. J. Christensen, D. J. Eatough, and R. M. Izatt, *Chem. Rev.*, **74**, 351 (1974).

BULLETIN OF THE CHEMICAL SOCIETY OF JAPAN VOL. 51 (2), 647—648 (1978)

Binuclear Metal Complexes. XXI.[1] Copper(I)-Copper(II) Mixed-Valence Complexes with Quadridentate Schiff Bases

Hisashi OKAWA, Visit KASEMPIMOLPORN, and Sigeo KIDA

Department of Chemistry, Faculty of Science, Kyushu University, Hakozaki, Higashi-ku, Fukuoka 812

(Received September 12, 1977)

Synopsis. Copper(I)–copper(II) mixed-valence complexes of the quadridentate Schiff bases were obtained and characterized. ESR and visible spectra showed no evidence for the delocalization of an unpaired electron between copper(I) and copper(II) ions.

It is well known[2] that *N,N'*-di(salicylidene)ethylenediaminatocopper(II) and its homologues react with bivalent metal ions to form binuclear and trinuclear metal complexes. In the previous paper[3] of this series it was shown that vanadium(V)–copper(I) hetero-metal complexes with *N,N'*-di(salicylidene)ethylenediamine and its derivatives are obtained by reacting oxovanadium(IV) complexes with the Schiff bases and copper(II) halides. This fact implies that the "outside" coordination site of these ligands is sterically suitable for a copper(I) ion which prefers tetrahedral or trigonal configuration to square-planar configuration. Thus, it seems possible to synthesize copper(I)–copper(II) mixed-valence complexes using the quadridentate Schiff bases. This report relates to the synthesis and characterization of the mixed-valence complexes, $[Cu_2(R_1,R_2\text{-en})an]ClO_4$, $[Cu_2(H,H\text{-ph})an]ClO_4$, and $[Cu_2(H,H\text{-tn})]ClO_4$ (R_1,R_2=H, CH_3; an=CH_3CN), where $H_2(R_1,R_2\text{-en})$ denotes *N,N'*-di(salicylidene)ethylenediamine with the substituents R_1 and R_2 at the 5- and α-positions respectively, and H_2(H,H-ph) and H_2(H,H-tn) indicate *N,N'*-di(salicylidene)-*o*-phenylenediamine and *N,N'*-di(salicylidene)trimethylenediamine respectively.

Experimental

Syntheses. The synthetic methods of the copper(I)–copper(II) mixed-valence complexes are practically the same. The synthesis of $[Cu_2(H,H\text{-en})an]ClO_4$ is exemplified. Nitrogen was bubbled through a suspension of Cu(H,H-en) (330 mg) in dry methanol (50 ml) for 10 min. Then $[Cu(an)_4]ClO_4$ (326 mg) was added and the mixture was stirred for 3 h under nitrogen atomosphere. Red-purple prisms which separated were collected, washed with dry methanol, and dried over P_2O_5 in vacuum. Elemental analyses are given in Table 1.

The compound used for the ESR study was prepared by a method similar to that described above except for using $Ni(R_1,R_2\text{-en})$ containing a slight amount of copper(II) ion instead of using $Cu(R_1,R_2\text{-en})$. $Cu(R_1,R_2\text{-en})ZnCl_2$ was obtained after the method described by Sinn *et al.*[4]

Measurements. IR spectra were measured with a Hitachi 215 Grating Spectrophotometer on a KBr disk. Reflectance spectra were measured with a Shimadzu Multipurpose Spectrophotometer Model MSP-5000. Magnetic susceptibilities were measured by the Faraday method. Effective magnetic moments were calculated by the expression, $\mu_{eff}=2.828\sqrt{(\chi_M-60\times10^{-6})T}$, where χ_M is molar magnetic susceptibility corrected by the use of Pascal's constants.

Results and Discussion

Selected IR bands, visible spectral bands and effective magnetic moments of the present complexes as well as $Cu(R_1,R_2\text{-en})ZnCl_2$ are given in Table 2. Magnetic moments clearly indicate that the present complexes contain one bivalent and one univalent copper ions in each molecule. One of the skeletal vibrations (near 1550 cm^{-1}) of the mixed-valence complexes is higher in frequency than that of the corresponding mononuclear complex. Furthermore, the frequency of this band is practically the same as that of $Cu(R_1,R_2\text{-en})ZnCl_2$, whose binuclear structure has been demonstrated.[4] These facts imply that the copper atoms in the mixed-valence complexes are bridged by the phenolic oxygens.

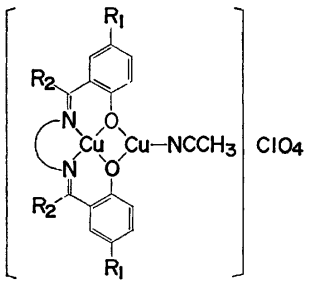

Fig. 1.

Table 1. Elemental analyses of mixed-valence complexes

	Found (%)				Calcd (%)			
	C	H	N	Cu	C	H	N	Cu
$[Cu_2(H,H\text{-en})an]ClO_4$	40.41	3.17	7.86	24.00	40.49	3.21	7.87	23.80
$[Cu_2(H,Me\text{-en})an]ClO_4$	42.54	3.75	7.43	22.60	42.75	3.77	7.48	22.62
$[Cu_2(Me,H\text{-en})an]ClO_4$	43.21	3.88	7.29	22.66	42.75	3.77	7.48	22.62
$[Cu_2(Me,Me\text{-en})an]ClO_4$	44.59	4.23	7.08	20.93	44.79	4.27	7.12	21.54
$[Cu_2(H,H\text{-ph})an]ClO_4$	45.28	2.94	7.29	21.66	45.41	2.94	7.22	21.86
$[Cu_2(H,H\text{-tn})]ClO_4$	40.09	3.47	6.02	25.13	40.36	3.19	5.54	25.12

Table 2. Selected IR bands, visible spectral bands, and effective magnetic moments of complexes

	IR (cm^{-1})			Visible (cm^{-1})		μ_{eff} (B.M.)
	C≡N	skel.	ClO_4^-			
$[Cu_2(H,H\text{-en})an]ClO_4$	2290	1550	1090	17 500	19 500	1.82
$[Cu_2(H,Me\text{-en})an]ClO_4$	2300	1540	1080	18 000	19 600	1.80
$[Cu_2(Me,H\text{-en})an]ClO_4$	2290	1550	1100	17 000	19 600	1.88
$[Cu_2(Me,Me\text{-en})an]ClO_4$	2280	1540	1090	18 500	19 800	1.78
$[Cu_2(H,H\text{-ph})an]ClO_4$	2295	1525	1100	18 000		1.84
$[Cu_2(H,H\text{-tn})]ClO_4$		1550	1100	18 000		1.79
$Cu(H,H\text{-en})ZnCl_2$		1555		17 500	19 600	1.83
$Cu(H,Me\text{-en})ZnCl_2$		1540		18 000	19 800	1.82
$Cu(Me,H\text{-en})ZnCl_2$		1550		17 000	19 700	1.87
$Cu(Me,Me\text{-en})ZnCl_2$		1540		18 500	19 800	1.84

Table 3. Temperature variations of magnetic moment

$[Cu_2(H,H\text{-en})an]ClO_4$											
T(K)	83.5	103.5	125.1	146.3	168.5	190.0	211.3	234.2	256.1	276.1	297.4
μ_{eff}	1.79	1.80	1.81	1.81	1.82	1.81	1.82	1.81	1.82	1.81	1.82
$[Cu_2(H,Me\text{-en})an]ClO_4$											
T(K)	81.7	103.5	124.7	145.5	166.3	186.9	206.1	226.9	249.3	274.3	295.4
μ_{eff}	1.79	1.78	1.78	1.78	1.77	1.78	1.78	1.79	1.79	1.80	1.80
$[Cu_2(H,H\text{-tn})]ClO_4$											
T(K)	81.5	102.0	124.7	145.5	167.4	187.0	207.0	229.0	250.2	274.4	297.4
μ_{eff}	1.54	1.57	1.59	1.60	1.61	1.63	1.67	1.70	1.74	1.77	1.79

The IR spectra of $[Cu_2(R_1,R_2\text{-en})an]ClO_4$ and $Cu(R_1,R_2\text{-en})ZnCl_2$ resemble each other except the bands at 2300—2280 and 1100—1080 cm^{-1} of the former. They are assigned to coordinated acetonitrile and non-coordinated perchlorate ion respectively. Therefore, it is likely that $[Cu_2(R_1,R_2\text{-en})an]ClO_4$ and $[Cu_2(H,H\text{-en})an]ClO_4$ have a structure shown in Fig. 1.

On the other hand, $[Cu_2(H,H\text{-tn})]ClO_4$ differs from the other complexes in lacking acetonitrile in composition. It is likely that the "outside" copper(I) ion is coordinated by a donating atom of another molecule at the third (and forth) coordination position to form a polymeric structure. In fact, the magnetic moment of $[Cu_2(H,H\text{-tn})]ClO_4$ decreases with lowering of temperature, while the moments of $[Cu_2(H,H\text{-en})an]ClO_4$ and $[Cu_2(H,Me\text{-en})an]ClO_4$ are almost constant in the temperature range 78—300 K (Table 3).

The electronic spectra of $[Cu_2(H,H\text{-ph})an]ClO_4$ and $[Cu_2(H,H\text{-tn})]ClO_4$ are practically the same as those of Cu(H,H-ph) and Cu(H,H-tn), respectively. On the other hand, each spectrum of $[Cu_2(R_1,R_2\text{-en})an]ClO_4$ markedly differs from that of $Cu(R_1,R_2\text{-en})$, a new band being found around 19500 cm^{-1}. This band can not be an inter-valence transfer band, but should be one component of the d-d bands of the "inside" copper(II) ion, judging from the fact that the electronic spectra of $[Cu_2(R_1,R_2\text{-en})an]ClO_4$ and $Cu(R_1,R_2\text{-en})ZnCl_2$ resemble each other. It can be concluded that there is no appreciable delocalization of the unpaired electron over the binuclear unit, since the ESR spectra of $Ni(Cu)(R_1,R_2\text{-en})$ and $[Ni(Cu)Cu(R_1,R_2\text{-en})an]ClO_4$ show nearly the same $g_{\parallel}$ and $A_{\parallel}$, respectively.

The authors are grateful to the Ministry of Education for a Scientific Research Grant-in-Aid.

References

1) Part XX: H. Okawa *et al.*, *Mem. Faculty Sci., Kyushu Univ., Ser. C, Chem.*, in press.
2) E. Sinn and C. M. Harris, *Coord. Chem. Rev.*, **4**, 391 (1969).
3) H. Okawa and S. Kida, *Inorg. Chim. Acta*, **23**, 253 (1977).
4) S. J. Gruber, C. M. Harris, and E. Sinn, *J. Inorg. Nucl. Chem.*, **30**, 1805 (1968).

BULLETIN OF THE CHEMICAL SOCIETY OF JAPAN VOL. 51 (2), 649—650 (1978)

Isolation and Photolysis of 2,3-Bis(diphenylmethylene)-5,6-diazaspiro[3.4]octa-5,7-dien-1-ones

Kozaburo UEDA and Fumio TODA

Department of Industrial Chemistry, Faculty of Engineering, Ehime University, Matsuyama 790

(Received June 6, 1977)

Synopsis. Pyrazole given in the title was prepared by the reaction of 2-diazo-3,4-bis(diphenylmethylene)cyclobutanone with acetylenes. Photolysis of the pyrazole afforded 1,2-dihydro-3*H*-benzo[*a*]cyclobuta[*c*]cycloheptan-1-one.

All attempts to isolate 3-acyl-3*H*-pyrazole (**1**) have been unsuccessful because of its easy isomerization to *N*-substituted pyrazole (**2**).[1-3] We report the isolation of the title pyrazole (**4**) and its photochemical conversion into 1,2-dihydro-3*H*-benzo[*a*]cyclobuta[*c*]cycloheptan-1-one (**8**).

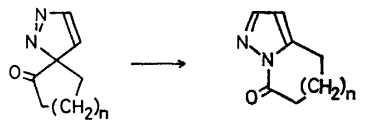

1 2

Treatment of 2-diazo-3,4-bis(diphenylmethylene)-cyclobutanone (**3**) with dimethyl acetylenedicarboxylate, benzoylacetylene, and dibenzoylacetylene afforded 7,8-bis(methoxycarbonyl)- (**4a**, 78%), 7-benzoyl- (**4b**, 82%), and 7,8-dibenzoyl-2,3-bis(diphenylmethylene)-5,6-diazaspiro[3.4]octa-5,7-dien-1-one (**4c**, 80%), respectively. The formation of 3*H*-pyrazole by 1,3-dipolar

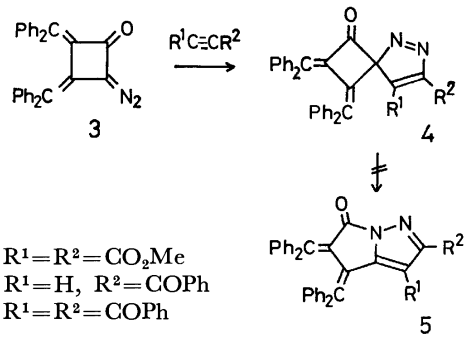

a; $R^1=R^2=CO_2Me$
b; $R^1=H$, $R^2=COPh$
c; $R^1=R^2=COPh$

Scheme 1.

cycloaddition of diazo ketone to acetylene is well established.[1,4,5] The structure of **4b** was characterized by the following experiment. Treatment of **4b** with $ZnCl_2$ in MeOH afforded 3-(1-diphenylmethylene-2-methoxycarbonyl-3,3-diphenyl-2-propenyl)-5-benzoyl pyrazole (**6**, 90%).

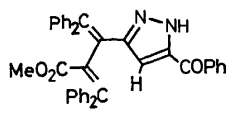

6

Frank-Neumann and Buchecker[2] reported that the easy thermal conversion of **1** into **2** is due to the stability of **2** bearing heteroaromatic pyrazole ring. However, no analogous thermal conversion of **4** into **5** took place even in boiling xylene. The contrast would be due to destabilization of **5** which may not be planar because of ring strain and/or steric repulsion between the two diphenylmethylene groups. This is supported by examination of molecular models.

In contrast to the photochemical conversion of 3*H*-pyrazole into cyclopropane,[6,7] photolysis of **4a—c** afforded 8,9-bis(methoxycarbonyl)- (**8a**), 8-benzoyl- (**8b**), and 8,9-dibenzoyl-3-phenyl-2-diphenylmethylene-1,2-dihydro-3*H*-benzo[*a*]cyclobuta[*c*]cycloheptan-1-one (**8c**), respectively, in quantitative yields. The reaction sequence can be formulated by successive cyclization and hydrogen migration of the initially formed biradical intermediate (**7**),[8,9] as shown in Scheme 2.

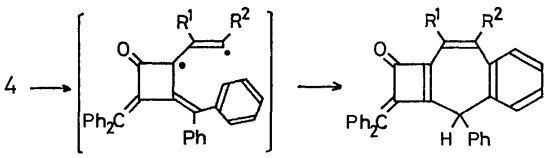

7 8

Scheme 2.

Experimental

All the melting points are uncorrected. Photolysis was carried out at room temperature under N_2, using light from a 100-W high-pressure mercury lamp (Riko Kagaku Sangyo Co.) The IR, UV, and NMR were measured in KBr disk, $CHCl_3$, and $CDCl_3$, respectively. The mass spectra were obtained with an ionization energy of 75 eV.

Cycloaddition of 3 to Acetylenes. A solution of **3**[10] (3 mmol) and an equimolar amount of the acetylenes in benzene (50 ml) was kept at 0 °C for 1 day. Crude crystals remaining after evaporation of the solvent were recrystallized from AcOEt to give cycloadduct as red prisms.

4a: 78%; mp 158—159 °C. IR: 1765, 1740 cm^{-1}; λ_{max}: 335 (22600), 415 nm (ε, 5000); NMR: δ=7.7—6.5 (m, 20H), 3.90 (s, 3H), 3.39 (s, 3H); MS: *m/e* (rel intensity) 566 (M^+, 32), 507 (M^+-CO_2Me, 56), 479 (100). Found: C, 76.15; H, 4.78; N, 4.92%. Calcd for $C_{36}H_{26}O_5N_2$: C, 76.31; H, 4.63; N, 4.94%.

4b: 82%; mp 147—148 °C. IR: 1750, 1640 cm^{-1}; λ_{max}: 325 (25800), 427 nm (ε, 5500); NMR: δ=8.5—8.2 (m, 2H), 7.4—6.5 (m, 23H), 6.06 (s, 1H); MS: *m/e* (rel intensity) 554 (M^+, 25), 449 (M^+-PhCO, 10), 105 ($PhCO^+$, 100). Found: C, 84.30; H, 4.98; N, 5.13%. Calcd for $C_{39}H_{26}O_2N_2$: C, 84.45; H, 4.73; N, 5.05%.

4c: 80%; mp 124—125 °C. IR: 1755, 1660 cm^{-1}; λ_{max}: 320 (26000), 432 nm (ε, 5000); NMR: δ=8.3—6.4 (m); MS:

m/e (rel intensity) 658 (M^+, 22), 553 (M^+-PhCO, 6), 105 ($PhCO^+$, 100). Found: C, 83.64; H, 4.72; N, 4.38%. Calcd for $C_{46}H_{30}O_3N_2$: C, 83.87; H, 4.59; N, 4.25%.

Formation of ***6***. A mixture of **4b** (555 mg, 1 mmol), $ZnCl_2$ (150 mg, 1.1 mmol), and MeOH (20 ml) was stirred at room temperature for 15 min. The reaction mixture was decomposed with dil HCl, and then extracted with benzene. Crude crystals remaining after evaporation of the solvent were recrystallized from MeCN to give **6** as pale yellow needles; 510 mg (90%); mp 176—177 °C. IR: 3350, 1715 cm^{-1}; λ_{max}: 252 (29800), 290 (22300), 335 nm sh (ε, 11000); NMR: δ=9.05 (br s, 1H), 7.9—6.7 (m, 25H), 6.43 (s, 1H),[11] 3.35 (s, 3H). Found: C, 81.62; H, 5.12%. Calcd for $C_{40}H_{30}O_3N_2$: C, 81.88; H, 5.15%.

Photolysis of ***4***. A solution of **4a** (1.13 g, 2 mmol) in MeOH (150 ml) was irradiated for 30 min. Crude crystals remaining after evaporation of the solvent were recrystallized from CH_2Cl_2-MeOH to give **8a** as colorless prisms in a quantitative yield; mp 273—273.5°C. IR: 1785, 1750, 1730 cm^{-1}; λ_{max}: 320 (14500), 343 nm (ε, 16600); NMR: δ= 7.7—6.4 (m, 19H), 5.10 (s, 1H), 3.80 (s, 3H), 3.08 (s, 3H); MS: *m/e* 538 (M^+). Found: C, 80.12; H, 4.86%. Calcd for $C_{36}H_{26}O_5$: C, 80.28; H, 4.87%.

Similar photolysis of **4b** and **4c** afforded **8b** and **8c**, respectively, in quantitative yields.

8b: Colorless prisms: mp 268—270 °C. IR: 1780, 1660 cm^{-1}; λ_{max}: 245 (25200), 329 nm (ε, 17200); NMR: δ=8.3—8.1 (m, 2H), 7.7—6.7 (m, 22H), 6.17 (s, 1H), 5.10 (s, 1H). Found: C, 88.76; H, 4.69%. Calcd for $C_{39}H_{26}O_2$: C, 88.95; H, 4.98%.

8c: Colorless prisms: mp 257—258 °C. IR: 1780, 1660 cm^{-1}; λ_{max}: 258 (30000), 330 nm (ε, 21600); NMR: δ=8.3—6.6 (m, 29H), 5.19 (s, 1H); MS: *m/e* 630 (M^+). Found: C, 87.37; H, 4.76%. Calcd for $C_{46}H_{30}O_3$: C, 87.59; H, 4.79%.

References

1) M. Franck-Neumann and C. Dietrich-Buchecker, *Tetrahedron Lett.*, **1976**, 2069.

2) M. Franck-Neumann and C. Buchecker, *Angew. Chem. Int. Ed. Engl.*, **12**, 240 (1973).

3) M. Franck-Neumann and C. Buchecker, *Tetrahedron Lett.*, **1972**, 937.

4) G. L. Closs and W. A. Boell, *Angew. Chem.*, **75**, 640 (1963).

5) A. C. Day and M. C. Whiting, *J. Chem. Soc., C*, **1966**, 1719.

6) C. Dietrich-Buchecker and M. Franck-Newmann, *Tetrahedron*, **33**, 751 (1977).

7) W. Kirmse, "Carbene Chemistry," Academic Press, New York, N. Y. (1971), p. 23.

8) G. Baum, R. Bernard, and H. Shechter, *J. Am. Chem. Soc.*, **89**, 5307 (1967).

9) G. L. Closs and L. R. Kaplan, *J. Am. Chem. Soc.*, **91**, 2168 (1969).

10) K. Ueda, M. Igaki, and F. Toda, *Bull. Chem. Soc. Jpn.*, **49**, 3173 (1976).

11) The signal can be assigned to the C-4 proton of pyrazole nucleus on the basis of the study by Tensmeyer and Ainsworth: L. G. Tensmeyer and C. Ainsworth, *J. Org. Chem.*, **31**, 1878 (1966).

BULLETIN OF THE CHEMICAL SOCIETY OF JAPAN VOL. 51 (2), 651—652 (1978)

NMR Spectroscopic Studies of the Tautomerism in Tetramic Acid Analogs and Their Anilides. III.[1] Polar Solvent Effects on the Tautomeric Populations*

Kimitoshi SAITO** and Tatsuaki YAMAGUCHI

Laboratory of Organic Chemistry, Chiba Institute of Technology, Tsudanuma, Narashino-shi, Chiba 275

(Received June 10, 1977)

Synopsis. NMR spectroscopic studies of 3-acetyltetramic acid† (3-acetyl-2,4-azolidinedione), 3-acetyltetronic acid† (3-acetyl-2,4-oxolanedione), 3-acetylthiotetronic acid† (3-acetyl-2,4-thiolanedione) and their anilides† (3-(2-phenyliminoethyl) derivatives) showed variations in the tautomeric equilibria with certain polar solvents. For example, the strong solvation effect of DMSO-d_6 causes a predominance of the lactim forms of 3-acetyltetramic acid over the lactam forms and up-field shifts of the enolic protons.

Previously, the tautomeric equilibria of 3-acetyltetramic acid analogs (I—III)† and their anilides (IA—IIIA)† in chloroform-*d* were studied by means of NMR spectroscopy.[1,2] In chloroform-*d*, the spectra of I—III showed the splitting of methylene proton signals by "external" (*cis-trans*) tautomerization (a, b ⇌ c, d), besides the splitting of methyl proton signals by the "internal" prototropy (a⇌b, c⇌d), caused by the different anisotropic effect of the carbonyl group in each tautomer (Chart 1, a—d).[1]

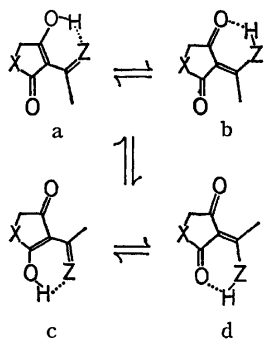

Chart 1.

However, with some exceptions, the splittings in methyl and methylene signals could not be observed in any solvents other than chloroform-*d* (Table 1). For this disappearance of the splittings, two reasons can be considered. The one is the rapid tautomeric interconversion accelerated by the polar solvent over the NMR time-scale. The other is the inclination of the tautomeric equilibria to one side as a result of the solvation effect. When DMSO-d_6 was added to the solution of 3-acetyltetramic acid (I) in chloroform-*d*, the intensity of the methylene signal of the c, d form was successively decreased and extinguished at a DMSO-d_6 content of *ca.* 25%, whereas that of the a, b form was increased. Figure 1a shows the variations in the intensity ratio (c+d)/(a+b) with the DMSO-d_6 content. From this fact, it can be concluded that the acceleration of the prototropy by the polar solvent does not happen in this case.

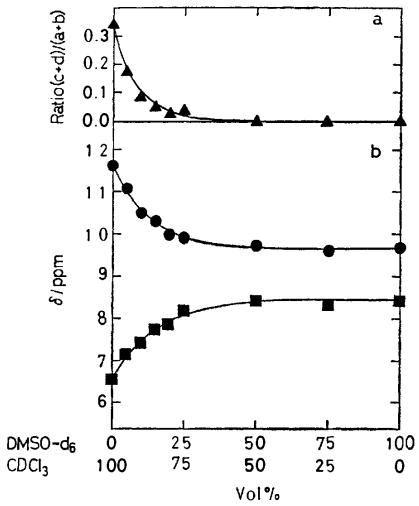

Fig. 1. Variations of the chemical shifts and the tautomeric ratio of 3-acetyltetramic acid (I) in $CDCl_3$-DMSO-d_6 mixed solvent system.
▲: Ratio of c, d form to a, b form, ●: enolic proton, ■: lactam-lactim proton.

Furthermore, along with the addition of DMSO-d_6, the down-field shift of the NH proton signal and the up-field shift of the enolic proton signal were observed throughout this experiment (Fig. 1b). The down-field shift of the NH proton signal suggests the formation of the lactim form, which is then rapidly interconverted with the corresponding lactam form. With the addition of DMSO-d_6, the lactim form should become predominant over the lactam form, since DMSO-d_6 might solvate and stabilize the more polar lactim form.[3]

The up-field shift of the enolic proton is probably caused by the formation of an intermolecular hydrogen

* A preliminary report of this work was presented at the 36th National Meeting of the Chemical Society of Japan, Osaka, April 1977.

** Present address: Department of Applied Chemistry, School of Science and Technology, Waseda University, Nishi-Okubo, Shinjuku-ku, Tokyo 160.

† Common names are consciously introduced for these compounds in order to express the mixed systems of the complicated tautomers. However, the IUPAC names of their keto forms are as follows: 3-acetyl-2,4-azolidinedione (I), 3-acetyl-2,4-oxolanedione (II), 3-acetyl-2,4-thiolandione (III), 3-(2-phenyliminoethyl)-2,4-azolidinedione (IA), 3-(2-phenyliminoethyl)-2,4-oxolanedione (IIA), and 3-(2-phenyliminoethyl)-2,4-thiolanedione (IIIA).

Table 1. NMR chemical shifts and tautomeric populations in various solvents at 34 °C

Compound No.	X	Z	Solvent	Chemical shifts (δ ppm, 100 MHz) CH_3	CH_2	ZH	Tautomeric populations (%) a,b[a]	c,d[a]
I	NH	O	$CDCl_3$	2.49 2.46	3.84 3.97	11.42	77[b]	23
			CD_3CO_2D	2.48	3.75 3.96	c)	24[b]	76
			CF_3CO_2D	2.58	4.18	c)	0	100
			CD_3OD	2.72	4.08	c)	0	100
			DMSO-d_6	2.31	3.70	10.11	100[b]	0
II	O	O	$CDCl_3$	2.55 2.56	4.46 4.68	11.38	36	64
			CD_3CO_2D	2.50	4.60	c)	100	0
			CF_3CO_2D	2.64	4.82	c)	100	0
			CD_3OD	2.80	4.96	c)	100	0
			DMSO-d_6	2.63	4.92	8.20	0	100
			C_5D_5N	2.78	4.53	14.72	0	100
III	S	O	$CDCl_3$	2.54 2.56	3.83 4.04	14.96	24	76
			CCl_4	2.84	3.97 4.20	15.83	17	83
			CD_3CO_2D	2.52	4.05	c)	100	0
			CF_3CO_2D	2.69	4.13	c)	100	0
			CD_3OD	2.80	4.30	c)	100	0
			DMSO-d_6	2.63	4.93	9.62	0	100
IA	NH	NPh	$CDCl_3$	2.53 2.57	3.76 3.82	12.09 12.03	53[b]	47
			CD_3CO_2D	2.52	3.78 3.86	c) c)	32[b]	68
			CF_3CO_2D	2.85	4.18	c) c)	0	100
			CD_3OD	2.78	4.02 4.08	c) c)	64[b]	36
			DMSO-d_6	2.17 2.20	3.56 3.64	12.22 12.31	72[b]	28
IIA	O	NPh	$CDCl_3$	2.54 2.58	4.48 4.53	11.66 12.44	26	74
			CD_3CO_2D	2.50	4.60	c) c)	100	0
			CF_3CO_2D	2.64	4.82	c) c)	100	0
			DMSO-d_6	2.48	4.51	12.01	0	100
IIIA	S	NPh	$CDCl_3$	2.73	4.04 4.13	13.83 14.09	22	78
			CD_3OD	2.78	4.08	c) c)	100	0
			CF_3CO_2D	2.66	4.12	c) c)	100	0
			DMSO-d_6	2.78	4.22	c) c)	0	100

a) For IA-IIIA, the a and c forms were not detected. b) For I and IA, the corresponding lactim forms are included in the populations of the a and b form. c) Extinguished by the rapid H-D exchange reactions with the deuterated solvents.

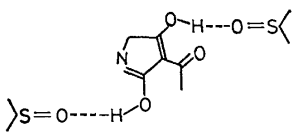

I-b lactim form

Chart 2.

bonding between I and the DMSO-d_6 molecule. Similar shifts could be observed with respect to II and III. However, further investigations might be necessary with regard to this problem.

In a similar way, major tautomers of the other analogs in various solvents were determined by the measurement of the variations in the methylene signal intensities in mixed solvent systems with chloroform-*d*.

Experimental

The compounds (I—IIIA) were prepared by the methods of the literature cited in the preceding papers.[1,2] All the deuterated solvents were obtained from E. Merck, Ltd. Solutions for the measurements were made so as to contain 1.5×10^{-4} mol of the compounds in 0.4 ml of the solvents. The NMR spectra were recorded on a JEOL PS-100 spectrometer at 100 MHz at 34 °C, using TMS as the internal standard.

References

1) Part II: T. Yamaguchi, K. Saito, T. Tsujimoto, and H. Yuki, *J. Heterocycl. Chem.*, **13**, 533 (1976).

2) Part I: T. Yamaguchi, K. Saito, T. Tsujimoto, and H. Yuki, *Bull. Chem. Soc. Jpn.*, **49**, 1161 (1976).

3) A. Page, *J. Am. Chem. Soc.*, **87**, 5333 (1965).

BULLETIN OF THE CHEMICAL SOCIETY OF JAPAN VOL. 51 (2), 653—654 (1978)

The Derivation of a Brominated Algal Component from Myrcene

Kazuo YOSHIHARA and Yoshio HIROSE

The Institute of Food Chemistry, Wakayamadai 1-chome, Shimamotocho, Mishima-gun, Osaka 618

(Received June 24, 1977)

Synopsis. The supposed structure, 5-bromo-4,4-dimethyl-2-vinyl-1-cyclohexene, for a brominated monoterpene from *Desmia (Chondrococuus) hornemanni* was derived from myrcene through a one-step reaction, and the structure was confirmed.

Many halogenated monoterpenes have been isolated from *D. hornemanni* and characterized.[1-4] Most of them are acyclic myrcene derivatives, and one cyclic compound from Japanese *hornemanni* has been supposed to have the structure of 5-bromo-4,4-dimethyl-2-vinyl-1-cyclohexene (I).[2] We presumed that those halogenated monoterpenes were the products of a halogenium-ion attack on the double bond of myrcene, and tried to derive I by the cyclization of myrcene with the bromonium ion.

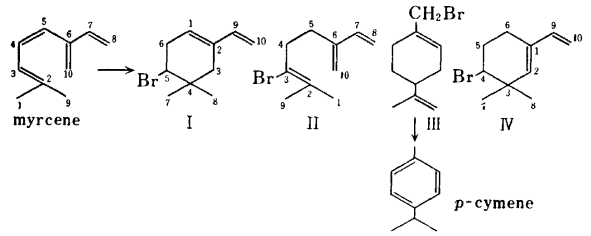

Several cyclizations were carried out. Among the reagents tested, 2,4,4,6-tetrabromo-2,5-cyclohexadien-1-one (TBCO)[5] was the most desirable for our purposes. The reaction of myrcene with TBCO in nitromethane at 0 °C afforded a mixture containing five monobromides and the starting hydrocarbon. The mixture was run out through SiO_2-column and gas chromatography (GC), thus isolating three monobromides. One of them was identified with the natural cyclic monobromide mentioned above in its IR and NMR spectra, except for one singlet signal at δ 1.21. This signal is found in the NMR spectrum of the natural compound, but not in the synthetic one, therefore, we may conclude that this signal is due to contamination. The NMR spectrum (including the irradiation technique), the IR and the mass spectra of the synthetic compound were satisfied with the supposed structure (I). Two other bromides were also isolated, their structures were assigned as 3-bromomyrcene (II) and 7-bromolimonene (III) from a comparison of the NMR spectra with those of 3-bromo-7-chloromyrcene[1] and limonene respectively. The double bond isomer of I, 4-bromo-3,3-dimethyl-1-vinyl-1-cyclohexene (IV), was not separated from I, but from the NMR and GC-mass spectra of the mixture the existence of compound (IV) was sopposed. In our experiment, the isolation using preparative GC was often accompanied with decomposition, and especially, the allyl bromide (III) was coverted to *p*-cymene. I, as well as II, were unstable for long storage, even in an ice stocker. We think that II can be used for the synthesis of 3-bromo-7-chloromyrcene, *etc.* Other attempts at cyclization, such as HOBr attack by NBS–H_2O or NBA–H_2O in acetone and the acid-catalyzed cyclization of myrcene-2,3-epoxide, followed by bromination, could not afford our expected compounds.

Experimental

An analytical GC was performed with a Hitachi 063-type apparatus equipped with a HB-2000 capillary column, and preparative GC with Varian's model 90 fitted OV-17 on Chromosorb-W, operated at 100 °C with a detection filament current of 70 mA. In the operation of the latter apparatus over a filament current of 100 mA, allyl bromide (III) was dehydrobrominated in a detector, as was shown by the unusual base-line dropping. For the measurement of the physical data, Hitachi RM-50GC-type GC-mass (fitted with a OV-17 glass capillary column and operated at an ionization voltage of 70 eV) spectrometer were used.

The Reaction of Myrcene with TBCO. To a solution of CH_3NO_2 (500 ml) containing myrcene (20 g), TBCO (40 g) was added, after which the mixture was stirred for 30 min at 0 °C. The resulting mixture was extracted with pentane. The extract (18.4 g) was chromatographed through a SiO_2 column several times, using pentane as the carrier, the process was monitored by means of analytical GC. First myrcene (10.3 g) was extracted, then a mixture of I, II, and IV (3.3 g), and at last a mixture of I and III (2.8 g). The ratio of the products, I: II: III: IV, was 3: 1: 2: 1.

5-Bromo-4,4-dimethyl-2-vinyl-1-cyclohexene (I). NMR (CCl_4) δ 1.03 and 1.07 (each s, 3H, assigned to C-7 and C-8 dimethyl respectively), 2.02—2.40 (m, 2H, C-3 methylene), 2.69—2.90 (m, centered at 2.75, 2H, C-6 methylene), 4.03 (dd, 1H, J=7.5 and 6.0 Hz, C-5 methylene which changed into a singlet signal upon irradiation with C-6 methylene), 4.88 and 5.00 (each d, 1H, J=11 and 17 Hz, *cis*- and *trans*-olefin protons on C-10, respectively; irradiation with the C-9 olefin proton changed those signals into two broad s, signals), 5.49 (m, 1H, C-1 olefin, which changed into a broad s, upon irradiation with C-6 methylene), and 6.73 (dd, 1H, J=11 and 17 Hz); IR ν 3080, 1660, 1600, 1370, 1350, and 890 cm^{-1}; MS *m/e* 216 and 214 (M^+, $C_{10}H_{16}Br$, 9.7%), 201 and 199 (−Me, $C_9H_{13}Br$, 1%), 135 (−Br, $C_{10}H_{15}$, base peak), 119 (C_9H_{11}, 32%), 107 (30%), 93 (50%), and 79 (36%).

3-Bromomyrcene (II). NMR δ 1.73 and 1.83 (allyl-coupled broad s, each 3H, C-1 and C-9 vinyl methyl), a signal centered at 2.25 (m, 4H, C-4 and C-5 methylenes), 4.98 and 5.20 (each d, 1H, J=12 and 18 Hz, *cis*- and *trans*-olefin protons on C-8), 5.00 (broad s, 2H, C-10 olefin), and 6.22 (dd, 1H, J=12 and 18 Hz, C-7 olefin proton); IR ν 3070, 1640, 1375, 1200, 990, 895, and 660 cm^{-1}; MS *m/e* 216 and 214 (M^+, $C_{10}H_{15}Br$, 3%), 173 and 171 (7%), 135 (−Br, $C_{10}H_{15}$, base peak), 119 (34%), 107 (27%), and 79 (49%).

7-Bromolimonene (III). NMR δ 1.73 (s, 3H, C-9 methyl), 3.83 (s, 2H, C-7 methylene), 4.68 (s, 2H, C-10 olefin protons), and 5.38 (m, 1H, C-2 olefin proton); IR ν 3060,

1640, 1200, 885, 810, and 600 cm^{-1}; MS *m/e* 216 and 214 (M^+, $C_{10}H_{15}Br$, 7%), 171 and 173 ($-C_3H_7$, C_7H_8Br, 15%), 135 ($-Br$, $C_{10}H_{15}$, base peak), 119 (37%), 93 (72%), and 68 (C_6H_6, 67%). The decomposed product in a GC detector with a filament current of 150 mA, *p*-cymene, was identified by a comparison of its IR and mass spectra with those of an authentic sample.

4-Bromo-3,3-dimethyl-1-vinyl-1-cyclohexene (IV). This compound was not purified, but some NMR signals in a mixture with I and the mass spectrum were obtained. NMR 1.15 (s, C-7 and C-8 *gem.* dimethyl), 1.60—2.00 (complex), 5.43 (broad s, C-4 methylene), and 6.25 (dd, $J=12$ and 18 Hz, C-9 vinyl methyl); MS *m/e* 216 and 214 (7%), 201 and 199 (3%), 135 (base peak), 119 (38%), 109 (27%), 93 (52%), and 79 (23%).

We wish to thank Professor Toshio Miwa of Osaka City Univ. for the measurement of 100 MHz NMR, to Mr Hiroshi Nii of the Nagaoka Perfumery Co., Ltd., for providing the myrcene, to Dr. Kiichi Nishimura of the Suntory Co., Ltd., for the measurements using the GC-mass spectrometer, and to Dr. Yoko Naya for providing the spectral data on haloterpenes and useful suggestions.

References

1) N. Ichikawa, Y. Naya, and S. Enomoto, *Chem. Lett.*, **1974**, 1333.

2) N. Ichikawa, Y. Naya, and S. Enomoto, The Abstract of the 18th Symposium of Terpene, Essential Oils, and Aromatic Chemistry, 67 (1974).

3) B. J. Burreson, F. X. Woolard, and R. E. Moore, *Tetrahedron Lett.*, **1975**, 2155.

4) B. J. Burreson, F. X. Woolard, and R. E. Moore, *Chem. Lett.*, **1975**, 1111.

5) T. Kato, I. Ichinose, A. Kamoshita, and Y. Kitahara, *J. Chem. Soc., Chem. Commun.*, **1976**, 516.

BULLETIN OF THE CHEMICAL SOCIETY OF JAPAN VOL. 51 (2), 655—656 (1978)

The Michael Type Alkylation of α,β-Unsaturated Sulfoxide and Reaction of the Resulting α-Sulfinyl Carbanion

Hideki SUGIHARA, Rikuhei TANIKAGA, Kazuhiko TANAKA, and Aritsune KAJI

Department of Chemistry, Faculty of Science, Kyoto University, Kitashirakawa, Sakyo-ku, Kyoto 606

(Received July 4, 1977)

Synopsis. Aryl vinyl sulfoxide was alkylated *via* the Michael-type addition with lithium dialkylcuprates, and the resulting α-sulfinyl carbanions were reacted with various electrophiles (*i.e.* aldehydes, ketones, and alkyl halides) to afford α-substituted alkyl sulfoxides.

α,β-Unsaturated sulfoxides undergo Michael-type addition in the presence of a base.[1] However, no Michael-type alkylation to α,β-unsaturated sulfoxides has been investigated,[2] only a few reactions of secondary α-sulfinyl carbanions being reported.[3]

This paper describes the Michael-type alkylation to aryl vinyl sulfoxides, and the reaction of the initially formed α-sulfinyl carbanions with various electrophiles in one pot.

Results and Discussion

p-Chlorophenyl vinyl sulfoxide (**1**) was polymerised by alkyllithium, and was inert with the Grignard reagents.

On the other hand, vinyl sulfoxide **1** was alkylated by lithium dimethylcuprate, lithium dibutylcuprate and lithium di-*t*-butylcuprate to give *p*-chlorophenyl propyl sulfoxide (**2a**), *p*-chlorophenyl hexyl sulfoxide (**2b**), and *p*-chlorophenyl 3,3-dimethylbutyl sulfoxide (**2c**), respectively.

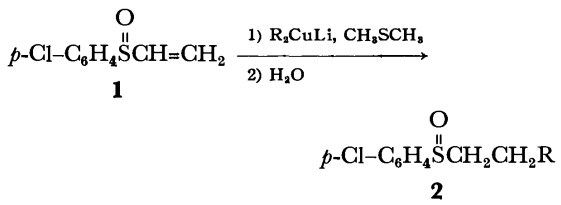

In the above Michael-type reaction, α-sulfinyl carbanion (**3**) was trapped by various electrophiles. β-Hydroxy sulfoxides (**4a**, **b**, **c**) were obtained when benzophenone was added to a solution of **3**. No 1,2-adduct of benzophenone was obtained even when benzophenone and **1** were added to lithium dialkylcuprate at the same time.[4]

Enolizable ketones and aldehydes such as cyclohexanone and propionaldehyde were treated in the same way to give the corresponding condensation products (**4e**, **f**) and **2b**.

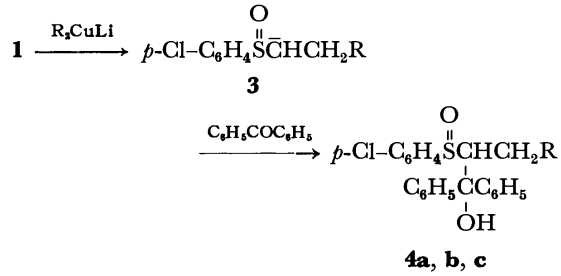

Table 1. Reaction of α-sulfinyl carbanion with electrophiles (yield of **2**, **4**, **5**)

Electrophile	R_2CuLi R= CH_3	n-C_4H_9	t-C_4H_9
H^+	30	75	34
$(C_6H_5)_2CO$	80	73	45
C_6H_5CHO	—	67	—
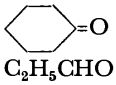	—	26	—
C_2H_5CHO	—	13	—
CH_2=$CHCH_2Br$	—	73	—

Allyl bromide underwent substitution reaction with **3** to afford *p*-chlorophenyl 1-allylhexyl sulfoxide (**5**). The results are given in Table 1.

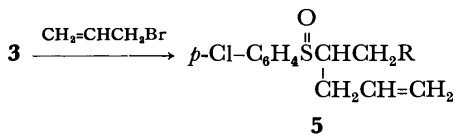

Benzyl *p*-chlorophenyl sulfoxide (**6**), **2b** and 1-phenyl-1-heptene (**7**) were obtained when benzyl bromide was treated in the same way. It is assumed that **3** reacts with benzyl bromide to give alkylated sulfoxide (**8**), and the first formed **8** easily eliminates sulfenate (**9**) under basic conditions to give **7**,[5] the residual benzyl bromide combining with liberated **9** to produce **6**.

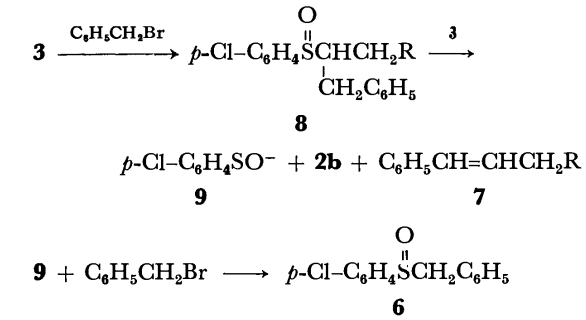

Experimental

Alkylation of p-*Chlorophenyl Vinyl Sulfoxide* ***1***.

p-*Chlorophenyl Propyl Sulfoxide* ***2a***: To an ether–dimethyl sulfide (1: 1, v/v) solution (30 ml) of copper(I) bromide–dimethyl sulfide complex[6] (1.03 g, 5 mmol) was added an ethereal solution of methyllithium (9 mmol) at 0 °C under nitrogen. The solutions was cooled to −60 °C, and **1** (1.31 g, 7 mmol) in ether (10 ml) was added. The temperature of the

mixture was allowed to rise to room temperature. The mixture was then extracted with ether, and dried over magnesium sulfate dehydrate. After removal of the solvent, **2a** was isolated (0.43 g, 30%) by chromatography on silica gel; oil: IR (film) 1030 (S=O) cm^{-1}; NMR (CCl_4) δ=1.02 (3H, t, J=7 Hz), 1.60 (2H, m), 2.64 (2H, t, J=7 Hz), 7.45 (4H, m).

p-*Chlorophenyl Hexyl Sulfoxide* ***2b***: To a solution of the copper(I) bromide complex (5 mmol) was added a hexane solution of butyllithium (9 mmol) at −60 °C under nitrogen. After being left to stand for 30 min, **1** (7 mmol) in ether was added to the mixture. The temperature of the mixture was allowed to rise to room temperature. After the usual work-up **2b** was isolated (1.28 g, 75%) by chromatography on silica gel: oil; IR (film) 1030 (S=O) cm^{-1}; NMR (CCl_4) δ=0.87 (3H, m), 1.30 (8H, m), 2.72 (2H, t, J=7 Hz), 7.48 (4H, m).

p-*Chlorophenyl 3,3-Dimethylbutyl Sulfoxide* ***2c***: To a solution of the copper(I) bromide complex (5 mmol) was added a pentane solution of *t*-butyllithium (9 mmol) at −78 °C under nitrogen. After being left to stand for 30 min, **1** (7 mmol) was added to the mixture. After the usual work-up **2c** (0.57 g, 34%) and *p*-chlorophenyl 1,1-dimethylethyl sulfoxide (0.17 g, 11%) were isolated by chromatography on silica gel. **2c**: mp 65—68 °C; IR (KBr) 1030 (S=O) cm^{-1}; NMR (CCl_4) δ=0.90 (9H, s), 1.50 (2H, m), 2.68 (2H, m), 7.50 (4H, m). *p*-Chlorophenyl 1,1-dimethylethyl sulfoxide: oil; IR (film) 1030 (S=O) cm^{-1}; NMR (CCl_4) δ=1.08 (9H, s), 7.45 (4H, m).

Reaction of α-Sulfinyl Carbanion ***3*** *with Electrophiles.*

p-*Chlorophenyl 1-(Diphenylhydroxymethyl)propyl Sulfoxide* ***4a***: To a solution of lithium dimethylcuprate was added an ethereal solution of **1** (7 mmol) and benzophenone (7 mmol) at −60 °C under nitrogen. The temperature of the mixture was allowed to rise to room temperature. After the usual work-up **4a** (2.16 g, 80%) was obtained: mp 129—131 °C; IR(KBr) 3420 (OH), 1005 (S=O) cm^{-1}; NMR ($CDCl_3$) δ= 0.20 (3H, t, J=7 Hz), 1.80 (2H, m), 3.42 (1H, m), 4.65 (1H, m), 7.42 (14H, m).

p-*Chlorophenyl 1-(Diphenylhydroxymethyl)hexyl Sulfoxide* ***4b***: To a solution of lithium dibutylcuprate was added an ethereal solution of **1** (7 mmol) and benzophenone (7 mmol) at −60 °C. The temperature of the mixture was allowed to rise to room temperature. After the usual work-up **4b** (2.18 g, 73%) was obtained: mp 120—121 °C; IR (KBr) 3420 (OH), 1000 (S=O) cm^{-1}; NMR ($CDCl_3$) δ=0.70 (9H, m), 1.76 (2H, m), 3.43 (1H, m), 7.40 (15H, m).

p-*Chlorophenyl 3,3-Dimethyl-1-(diphenylhydroxymethyl)butyl Sulfoxide* ***4c***: To a solution of lithium di-*t*-butylcuprate was added an ethereal solution of **1** (7 mmol) and benzophenone (7 mmol) at −78 °C. The mixture was treated in a similar way as described in the previous section, and **4c** (1.35 g, 45%) was obtained: mp 119—120 °C; IR (KBr) 3420 (OH), 1005 (S=O) cm^{-1}; NMR ($CDCl_3$) δ=0.12 (7.7 Hz, s), 0.90 (1.3H, s), 1.80 (2H, m), 3.35 (1H, t, J=4 Hz), 4.95 (1H, m), 7.34 (14H, m).

p-*Chlorophenyl 1-(α-Hydroxybenzyl)hexyl Sulfoxide* ***4d***: To a solution of lithium dibutylcuprate was added an ethereal solution of **1** (7 mmol) at −60 °C under nitrogen, an ethereal solution of benzaldehyde (7 mmol) being added after having been left to stand for 30 min. The mixture was then treated in a similar way as described in the section for **4c**, and **4d** (diastereomers) (1.57 g, 67%) were isolated by chromatography on silica gel: mp 80—82 °C; IR (KBr) 3420 (OH), 1000 (S=O) cm^{-1}; NMR ($CDCl_3$) δ=0.80 (11H, m), 1.62 (1H, m), 2.70 (1H, m), 4.80 (1H, d, J=8 Hz), 7.22 (9H, m): mp 103—105 °C; IR (KBr) 3420 (OH), 1000 (S=O) cm^{-1}; NMR ($CDCl_3$) δ=0.80 (11H, m), 1.62 (1H, m), 2.70 (1H, m), 5.22 (1H, d, J=4 Hz), 7.22 (9H, m).

p-*Chlorophenyl 1-(1-Hydroxycyclohexyl)hexyl Sulfoxide* ***4e***: Cyclohexanone (7 mmol) was treated in a similar way as described in the preceding sections **4e** (0.62 g, 26%) and **2b** (0.64 g, 37%) were isolated by chromatography on silica gel. **4e**: mp 130—132 °C; IR (KBr) 3420 (OH), 1005 (S=O) cm^{-1}; NMR ($CDCl_3$) δ=1.20 (21H, m) 2.62 (1H, t, J=4 Hz), 4.23 (1H, s), 7.50 (4H, m).

p-*Chlorophenyl 1-(1-Hydroxypropyl)hexyl Sulfoxide* ***4f***: Propionaldehyde (7 mmol) was treated in a similar way as described in the preceding sections, **4f** (0.26 g, 13%) and **2b** (0.63 g, 37%) were isolated. **4f**: oil; IR (film) 3420 (OH), 1005 (S=O) cm^{-1}; NMR (CCl_4) δ=1.20 (17H, m), 2.42 (1H, m), 3.78 (1H, m), 7.48 (4H, m).

p-*Chlorophenyl 1-Allylhexyl Sulfoxide* ***5***: Allyl bromide (7 mmol) was treated in a similar way as described in the preceding sections, **5** (1.45 g, 73%) was obtained: oil; IR (film) 1030 (S=O) cm^{-1}; NMR (CCl_4) δ=1.40 (14H, m), 5.00 (2H, m), 5.52 (1H, m), 6.45 (4H, m).

Reaction of ***3*** *with Benzyl Bromide*: Benzyl bromide (7 mmol) was treated in a similar way as described in the preceding sections. After the work-up, **2b** (0.40 g, 47%), benzyl *p*-chlorophenyl sulfoxide **6** (0.40 g, 46%) and 1-phenyl-1-hexene **7** (0.25 g, 41%) were isolated by chromatography on silica gel. **6**: mp 133—134 °C; IR (KBr) 1030 (S=O) cm^{-1}; NMR ($CDCl_3$) δ=4.03 (2H, d, J=4 Hz), 7.24 (5H, m). **7**: oil; NMR (CCl_4) δ=0.92 (3H, m), 1.38 (6H, m), 2.20 (2H, m), 6.20 (2H, m), 7.17 (5H, m).

This work was partly supported by a Grant-in-Aid of the Ministry.

References

1) G. Tsuchihashi, S. Mitamura, and K. Ogura, *Tetrahedron Lett.*, **1973**, 2469, and references therin.

2) Only diphenylmethane (pK_a=33—35) undergoes Michael-type alkylation. G. A. Russell and H. D. Beker, *J. Am. Chem. Soc.*, **85**, 3406 (1963).

3) T. Durst, R. Van Den Elzen, and C. H. Nguyen, *Chem. Commun.*, **1971**, 1334.

4) E. J. Corey and I. Kuwajima, *J. Am. Chem. Soc.*, **92**, 395 (1971).

5) T. J. Wallace, J. E. Hofmann, and A. Schriesheim, *J. Am. Chem. Soc.*, **85**, 2739 (1963).

6) H. O. House, Chia-Yeh Chu, J. M. Wilkins, and M. J. Umen, *J. Org. Chem.*, **40**, 1460 (1975).

BULLETIN OF THE CHEMICAL SOCIETY OF JAPAN VOL. 51 (2), 657—658 (1978)

Lactones of Hydrogenated 5,8-Dihydroxy-4-methylnaphthalene-1-carboxylic Acids

Hajime IRIKAWA and Yasuaki OKUMURA

Department of Chemistry, Faculty of Science, Shizuoka University, Oya, Shizuoka 422

(Received July 5, 1977)

Synopsis. The γ- and δ-lactones were derived from the Diels-Alder adduct of *p*-benzoquinone and methyl sorbate.

Generally, whether a γ- or δ-lactone is formed in a reaction depends mainly on the stability of the lactone under the reaction conditions.[1] This paper deals with the lactones of *cis*-octahydro- and *cis*-decahydro-5β,8β-dihydroxy-4β-methylnaphthalene-1β-carboxylic acids.

The Diels-Alder adduct[2] of *p*-benzoquinone and methyl sorbate was reduced with zinc to **1**, which was hydrogenated to **2a** in the presence of palladium-carbon, and to **3a** with platinum oxide. Lactonization of **3a** in methanolic hydrogen chloride afforded the keto δ-lactone (**4**), supporting the cis ring junctions in **1**, **2a**, and **3a**.

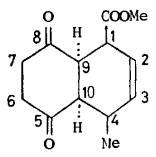

1

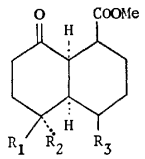

2a R_1,R_2=O R_3=Me
2b R_1,R_2=O R_3=H
3a R_1=OH R_2=H R_3=Me
3b R_1=OH R_2,R_3=H

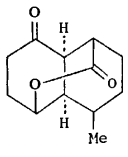

4

Fig. 1.

The reduction of **1** with sodium borohydride followed by treatment with acetic anhydride and pyridine gave the acetoxy δ-lactone (**5**) and the $\Delta^{1,2}$-γ-lactone (**6**), the latter of which afforded the acetate (**7**) by acetylation at elevated temperature. Treatment of **5** with sodium methoxide gave **6**. An attempt to convert **6** into the corresponding saturated γ-lactone (**8a**) by catalytic hydrogenation with platinum oxide failed, but gave the δ-lactone (**9**) and the $\Delta^{1,9}$-γ-lactone (**10**). The δ-lactone **9**, which was stable against treatment with sodium methoxide, was obtained from **2a** or **3a** by sodium borohydride reduction, or from **4** by hydrogenation under the similar conditions to those in the preparation of **3a**. The C-8 carbonyl group of **4** is obviously less hindered than that of **3a**.

On the other hand, Wheeler *et al.* reported the reduction of **2b** under Meerwein-Ponndorf conditions to **8b**, which was also obtained from **8c** by catalytic hydrogenation or sodium borohydride reduction.[3,4]

It is interesting to infer the conformations of **2a** and **3a**. The signal for the equatorial proton on C-5 (CH–O–) in the ^{1}H NMR spectrum of **4** appears at 4.95 ppm as a broad singlet (W_H=7 Hz), while a multiplet signal at 4.40 ppm (W_H=17 Hz) in the spectrum of **3a** must be attributed to the axial proton on C-5 (CH–OH). The

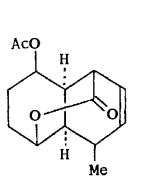

5

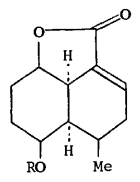

6 R=H
7 R=Ac

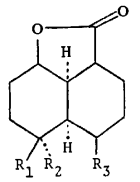

8a R_1=OH R_2=H R_3=Me
8b R_1=OH R_2,R_3=H
8c R_1,R_2=O R_3=H

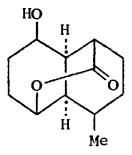

9

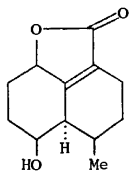

10

Fig. 2.

signals for C-1 in the ^{13}C NMR spectra of **3a** and **3b** appear at nearly the same fields. The signals for C-2 and -9 in **3a** are observed at fields higher than those of the corresponding carbons in **3b** as a consequence of the γ gauche effect of the methyl group. The similar shielding trends are also found for C-1, -2, and -9 in the spectra of **2a** and **2b**. These data indicate that **2a** and **3a** exist predominantly in the conformations similar to those of **2b** and **3b** which bear the equatorial methoxycarbonyl groups. Details will be published elsewhere.

Therefore, the conformations of the intermediate diol esters from **2a** and **2b** might affect the way of lactonization. The formation of **8b** seems to proceed through the preferred conformer **A** (R=H) similar to those of **2b** and **3b**. In the case of R=Me, **9** might be formed *via* the stable conformer **B**, since **A** is unstable on account of the steric effect of the methyl group.

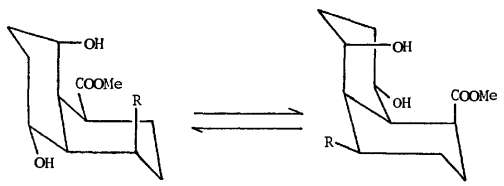

A B

Fig. 3.

Experimental

Melting points are uncorrected. The IR spectra were recorded on a Hitachi Infrared Spectrometer EPI-G_3 in

nujol, unless otherwise noted. The UV spectra were recorded on a Shimadzu MPS-50L in EtOH. The ^1H and ^{13}C NMR spectra were obtained on a JNM-PS-100 or JNM-PFT-60 in $CDCl_3$. Chemical shifts are given in δ-values with respect to TMS as an internal standard. Assignment of chemical shifts for close-lying peaks marked with asterisk may be reversed. Compounds **2b** and **3b** were prepared according to literature procedures.[5]

Preparation of ***1***. A solution of 18.0 g of *p*-benzoquinone and 17.6 g of methyl sorbate in 150 ml of benzene was refluxed for 19 h, and concentrated *in vacuo*. The residue was treated with 50 g of zinc in 150 ml of AcOH at room temperature for 2 h to give 2.30 g of the unreduced adduct[2] and 6.95 g of **1**: mp 136—137 °C (from EtOH); IR 1735 and 1702 cm^{-1}; ^1H NMR 0.88 (3H, d, J=7 Hz, CMe), 2.4—3.4 (7H), 3.71 (3H, s, OMe), *ca.* 3.8 (1H, m), 5.65 (1H, m, -CH=), and 6.04 ppm (1H, br d, J=11 Hz, -CH=); ^{13}C NMR 17.04 (CMe), 30.55 (C-4), 34.73 (C-6), 37.61 (C-7), 39.44 (C-1), 46.05 (C-9), 48.33 (C-10), 52.10 (OMe), 121.37 (C-2), 131.27 (C-3), 172.06 (COO), 207.85 (C-5*), and 210.29 ppm (C-8*). Found: C, 66.19; H, 6.86%. Calcd for $C_{13}H_{16}O_4$: C, 66.08; H, 6.83%.

Preparation of ***2a***. Hydrogenation of 2.84 g of **1** with 266 mg of 5% Pd-C in 120 ml of MeOH gave 2.51 g of **2a**: mp 110—111 °C (from EtOH); IR 1721 and 1706 cm^{-1}; ^1H NMR 0.84 (3H, d, J=7 Hz, CMe), 1.4—3.1 (11H), *ca.* 3.5 (1H, m), and 3.69 ppm (3H, s, OMe); ^{13}C NMR 15.82 (CMe), 20.08 (C-2), 30.47 (C-3), 31.45 (C-4), 35.10 (C-6), 37.41 (C-7), 41.35 (C-1), 47.68 (C-9), 51.13 (C-10), 51.78 (OMe), 173.52 (COO), 208.91 (C-5*), and 209.80 ppm (C-8*). Found: C, 65.32; H, 7.68%. Calcd for $C_{13}H_{18}O_4$: C, 65.53; H, 7.61%.

^{13}C NMR of ***2b***. 23.49 (C-3*), 23.98 (C-2*), 26.62 (C-4), 35.83 (C-6), 36.56 (C-7), 41.23 (C-1), 48.41 (C-10), 49.22 (C-9), 51.82 (OMe), 173.60 (COO), 207.85 (C-8*), and 209.56 ppm (C-5*).

Preparation of ***3a***. Hydrogenation of 2.92 g of **1** with 95 mg of PtO_2 in 120 ml of MeOH gave 2.33 g of **3a**: mp 124—125 °C (from benzene); IR 3370, 1744, and 1693 cm^{-1}; ^1H NMR 0.97 (3H, d, J=7 Hz, CMe), 1.3—2.8 (12H), 3.18 (1H, br t, J=5 Hz), 3.65 (3H, s, OMe), and 4.40 ppm (1H, m, W_H=17 Hz, C<u>H</u>-OH); ^{13}C NMR 17.12 (CMe), 19.55 (C-2), 27.67 (C-4), 31.61 (C-6), 34.04 (C-3), 37.90 (C-7), 42.69 (C-1), 47.27 (C-9*), 47.56 (C-10*), 51.61 (OMe), 70.20 (C-5), 174.57 (COO), and 210.94 ppm (C-8). Found: C, 64.97; H, 8.65%. Calcd for $C_{13}H_{20}O_4$: C, 64.98; H, 8.39%.

^{13}C NMR of ***3b***. 21.18 (C-4), 23.98 (C-2*), 24.83 (C-3*), 29.21 (C-6), 38.51 (C-7), 42.56 (C-1), 45.69 (C-10), 49.75 (C-9), 51.70 (OMe), 70.45 (C-5), 174.57 (COO), and 209.48 ppm (C-8).

Lactonization of ***3a*** *to* ***4***. Treatment of 160 mg of **3a** with 5 ml of 6% methanolic hydrogen chloride at 20 °C overnight gave 101 mg of **4**: mp 100—101 °C (from benzene–hexane); IR 1733 and 1712 cm^{-1}; ^1H NMR 1.14 (3H, d, J=6 Hz, CMe), 1.3—2.9 (12H), and 4.95 ppm (1H, br s W_H=7 Hz, CH-O-). Found: C, 69.18; H, 7.91%. Calcd for $C_{12}H_{16}O_3$: C, 69.21; H, 7.74%.

$NaBH_4$ Reduction of ***1*** *and Subsequent Acetylation.* Reduction of 1.69 g of **1** with 0.8 g of $NaBH_4$ in 80 ml of MeOH at 0 °C for 1.5 h gave an oily product, which was treated with 7 ml of Ac_2O and 10 ml of pyridine at room temperature overnight to afforded 527 mg of **5** and 356 mg of **6**. **5**: mp 114—116 °C (from benzene–hexane); IR 1733 and 1252 cm^{-1}; ^1H NMR 1.21 (3H, d, J=7 Hz, CMe), 1.5—2.9 (7H), 2.08 (3H, s, OAc), 3.25 (1H, m, W_H=10 Hz, CH-COO), 4.76 (1H, br s, W_H=8 Hz, CH-O-), 4.98 (1H, m, W_H=18 Hz, C<u>H</u>-OAc), 5.70 (1H, dd, J=10 and 3 Hz, -CH=), and 5.93 ppm (1H, m, -CH=). Found: C, 67.26; H, 7.35%. Calcd for $C_{14}H_{18}O_4$: C, 67.18; H, 7.25%. **6**: mp 155—157 °C (from EtOH); IR ($CHCl_3$) 3600, 3480, 1754, and 1691 cm^{-1}; UV max 225 nm (ε 8500); ^1H NMR 1.23 (3H, d, J=6 Hz, CMe), 1.3—2.6 (9H), 3.05 (1H, m), 4.23 (1H, br s, W_H= 13 Hz, C<u>H</u>-OH), 4.70 (1H, m, W_H=14 Hz, CH-O-), and 6.85 ppm (1H, q, J=6 and 3 Hz, -CH=). Found: C, 69.37; H, 7.84%. Calcd for $C_{12}H_{16}O_3$: C, 69.21; H, 7.74%.

The Acetate ***7***. Treatment of 257 mg of **6** with 5 ml of Ac_2O and 7 ml of pyridine at 100—105 °C for 6 h gave 177 mg of **7**: mp 138—139 °C (from benzene–hexane); IR 1760, 1733, 1689, and 1250 cm^{-1}; UV max 222 nm (ε 9700); ^1H NMR 1.09 (3H, d, J=6 Hz, CMe), 1.2—2.7 (8H), 1.97 (3H, s, OAc), 3.15 (1H, m), 4.77 (1H, m, W_H=14 Hz, CH-O-), 5.25 (1H, br s, W_H=8 Hz, CH-OAc), and 6.90 ppm (1H, br d, J=3 Hz, -CH=). Found: C, 67.01; H, 7.25%. Calcd for $C_{14}H_{18}O_4$: C, 67.18; H, 7.25%.

Conversion of ***5*** *into* ***6***. Treatment of 99 mg of **5** with 3 ml of 1 M NaOMe at room temperature overnight gave 41 mg of **6**.

Catalytic Hydrogenation of ***6***. Hydrogenation of 343 mg of **6** with 36 mg of PtO_2 in 50 ml of AcOEt gave 125 mg of **9** and 142 mg of **10**. **9**: mp 105—106 °C (from benzene–hexane); IR ($CHCl_3$) 3600, 3430, and 1725 cm^{-1}; ^1H NMR 1.08 (3H, d, J=6 Hz, CMe), 1.3—2.4 (11H), 2.95 (2H, br s, W_H=9 Hz, O<u>H</u> and C<u>H</u>-COO), 3.80 (1H, m, W_H=17 Hz, C<u>H</u>-OH), and 4.70 ppm (1H, br s, W_H=8 Hz, CH-O-). Found: C, 68.42; H, 8.82%. Calcd for $C_{12}H_{18}O_3$: C, 68.54; H, 8.63%. **9** was stable against teratment with 1 M NaOMe at room temperature overnight. **10**: mp 181—182 °C (from benzene); IR ($CHCl_3$) 3600, 3470, 1750, and 1696 cm^{-1}; UV max 223 nm (ε 12500); ^1H NMR 1.21 (3H, d, J=6 Hz, CMe), 1.3—2.6 (11H), 4.30 (1H, m, W_H=12 Hz, C<u>H</u>-OH), and 4.70 ppm (1H, m, W_H=15 Hz, CH-O-). Found: C, 69.34; H, 7.71%. Calcd for $C_{12}H_{16}O_3$: C, 69.21; H, 7.74%.

$NaBH_4$ Reduction of ***2a***. Reduction of 1.56 g of **2a** with 0.7 g of $NaBH_4$ in 50 ml of MeOH at 0 °C for 2 h gave 1.07 g of **9**. In a similar way, **9** was obtained from **3a** (204 mg from 323 mg of **3a**).

Catalytic Hydrogenation of ***4***. Hydrogenation of 81 mg of **4** with 2 mg of PtO_2 in 20 ml of MeOH gave 75 mg of **9**.

References

1) M. F. Ansell and M. H. Palmer, *Quart. Rev.*, **18**, 211 (1964).

2) J. Weichet, B. Kakac, and L. Blaha, *Collect. Czech. Chem. Commun.*, **27**, 843 (1962).

3) A. C. Ghosh, K. Mori, A. C. Rieke, S. K. Roy, and D. M. S. Wheeler, *J. Org. Chem.*, **32**, 722 (1967).

4) S. K. Roy and D. M. S. Wheeler, *J. Chem. Soc.*, **1963**, 2155.

5) R. B. Woodward, F. E. Bader, H. Bickel, A. J. Frey, and R. W. Kierstead, *Tetrahedron*, **2**, 1 (1958).

BULLETIN OF THE CHEMICAL SOCIETY OF JAPAN VOL. 51 (2), 659—660 (1978)

The Reaction of Cyclohexyl Isocyanide with Aromatic Diacyl Disulfides

Sakuya TANAKA, Kenji MASUE, and Masaya OKANO*
Institute for Chemical Research, Kyoto University, Uji, Kyoto 611

(Received July 30, 1977)

Synopsis. The reaction of cyclohexyl isocyanide with dibenzoyl disulfide in toluene at a reflux temperature gives cyclohexyl isothiocyanate, together with some unidentified compounds. Based on the substituent effects on the rate, a probable reaction path is proposed. The distinction between two reactions conducted in the absence and in the presence of soft metal salts is also described.

It has been reported previously that diacyl disulfides reacted smoothly with isocyanides in boiling chloroform (61 °C) to give only isothiocyanates in the presence of the salts of such soft metal ions as Tl^{I} and Pb^{II}, while without added metal salts there was only a low yield of the product.[1] It seemed that it would be of interest to investigate what kind of reaction occurs between isocyanide and dibenzoyl disulfide (DBDS) in the absence of metal salts, but at a higher temperature where a radical fission of the disulfide is still unexpected.[2] In relation to this, Shono *et al.* have reported that cyclohexyl isocyanide reacted with dibenzoyl peroxide at 80—90 °C to afford products derived from benzoyloxyl radical ($PhCO_2\cdot$).[3]

Results and Discussion

When cyclohexyl isocyanide (**1**) was heated with an equimolar amount of DBDS in toluene at a reflux temperature (111 °C) for 24 h, cyclohexyl isothiocyanate (**2**) was formed in a 49% yield; **1** was completely consumed, while 24% of DBDS was recovered (Scheme 1). At the same time we observed the formation of considerable amounts of brown solids which seemed to be a mixture of the reaction products between **1** and the initially formed dibenzoyl sulfide (DBS) (as determined by a study of the NMR, IR, and mass spectra) (Scheme 2); this was confirmed by a separate experiment (See Experimental). Several attempts to separate the solids into pure components have failed, and so each of them remains unidentified. It should be noted that the reaction (2) was accompanied by the formation of only a very low yield (3%) of **2**. The fact that the yield of **2** from DBDS does not exceed 50% in this

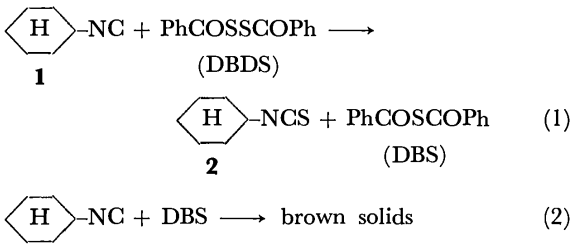

case may suggest that the latter reaction is faster than the former one. In fact, when two equivalents of **1** were treated with DBDS, the yield of **2** increased to 94% (based on DBDS). Some typical results are shown in Table 1, together with those obtained by the use of *p,p'*-disubstituted DBDS. The addition of several radical scavengers, such as *p*-benzoquinone and *p-t*-butylcatechol, had no effect on the yield of the product, suggesting an ionic nature of the reaction. In accordance with this, the reaction rate increased with an increase in the solvent polarity; the treatment of DBDS with two equivalents of **1** in refluxing acetonitrile (bp 82 °C, $\varepsilon=37.5$) and in refluxing cyclohexane (bp 81 °C, $\varepsilon=2.02$) for 10 h gave **2** in 68% and 4% yields respectively.

Table 1. The reaction of **1** with aromatic diacyl disulfides[a]

R'SSR' (1 mmol)	**1** (mmol)	Time[b] (h)	**2** (%)[c]
R'=*p*-$NO_2C_6H_4CO$	1	10	47
p-$NO_2C_6H_4CO$	2	10	85
R'=C_6H_5CO	1	24	49
C_6H_5CO	2	24	94
C_6H_5CO[d]	2	24	92
C_6H_5CO[e]	2	24	84
R'=*p*-$MeOC_6H_4CO$	1	32	67
p-$MeOC_6H_4CO$	2	32	93

a) Toluene (10 ml) was used as the solvent; at reflux. b) **1** was completely consumed during this reaction time. c) By GLC (based on disulfide). d) *p*-Benzoquinone (0.5 mmol) was added. e) *p-t*-Butylcatechol (0.5 mmol) was added.

Table 2. The effect of *p*- and *p'*-substituents in DBDS on the rate of formation of **2** from **1**[a,b]

R'SSR' (1 mmol)	Time (h)	**2** (%)[c]	Consumed **1** (%)[c]
R'=*p*-$NO_2C_6H_4CO$	1	15	56
	3	25	88
	5	38	91
R'=C_6H_5CO	1	6	22
	5	12	39
	10	16	50
R'=*p*-$MeOC_6H_4CO$	5	9	9
	10	11	16

a) **1** (1 mmol). b) Toluene (10 ml) was used as the solvent; at reflux. c) By GLC (based on disulfide).

In order to ascertain some characteristics of the reaction, the following experiments were also carried out. First, the rates of the formation of **2** from **1** and aromatic diacyl disulfides were roughly examined in refluxing toluene. The results in Table 2 show that rates decrease in the following order; *p*-NO_2>H>*p*-

* To whom correspondence should be addressed.

MeO. Second, the competitive reaction between **1** and phenyl isocyanide with DBDS (1 mmol of each reactant) in refluxing toluene (10 ml) for 6 h afforded **2** (20%) and phenyl isothiocyanate (14%), in addition to unreacted **1** (33%) and phenyl isocyanide (84%), showing that the more nucleophilic **1** reacted faster.

Based on all our results, we propose Scheme 3 for this reaction. It involves the initial nucleophilic attack of isocyanide on the sulfur atom of DBDS. The subsequent removal of benzoyl cation from the transient imidoyl cation affords isothiocyanate. The combination of the benzoyl cation with thiobenzoate anion gives DBS, which then reacts with **1** to give brown solids.

$$\mathrm{RNC + ArCOSSCOAr} \xrightarrow{(A)} \mathrm{R{-}N{=}\overset{+}{C}{-}SCOAr + ArCOS^-}$$

$$\mathrm{R{-}N{=}\overset{+}{C}{-}SCOAr} \longrightarrow \mathrm{R{-}NCS + ArCO^+} \qquad (3)$$

$$\mathrm{ArCO^+ + ArCOS^-} \longrightarrow \mathrm{ArCOSCOAr} \xrightarrow[(B)]{\mathrm{RNC}} \text{brown solids}$$

Now we can compare the reactions with or without added soft metal salts. In the absence of metal salts, the rates of (A) and (B) are comparable, or Step (B) may be faster than (A). On the other hand, the presence of soft metal salts considerably accelerates Step (A) by coordination with the sulfur atom, as was clarified in the previous report,[1] and therefore Step (B) becomes comparatively very slow if such acceleration is not significant in it. In fact, when **1** was treated with DBS in the presence of TlSCOPh in chloroform at reflux for 3 h (1 mmol of each reactant), the consumption of **1** was only 25%, much lower than that in the case of DBDS (79%).

Experimental

The IR and NMR spectra analyses and GLC analyses were carried out as has been described in a previous paper.[1] The mass spectra were recorded on a JEOL-01SG spectrometer.

Materials. The isocyanides (RNC: R=*c*-C_6H_{11}, Ph) and disulfides (R'SSR': R'=PhCO, *p*-$MeOC_6H_4CO$, *p*-$NO_2C_6H_4CO$) were prepared by a method reported previously.[1] Dibenzoyl sulfide was prepared by a modification of the method of Kodomari *et al.*[4] Cyclohexyl isothiocyanate (**2**) prepared previously in our laboratory and commercial phenyl isothiocyanate were used as authentic samples for the GLC analyses. TlSCOPh was prepared by the reported method.[5]

*Reaction of **1** with DBDS.* A mixture of **1** (0.545 g, 5 mmol) and DBDS (1.37 g, 5 mmol) in toluene (10 ml) was stirred at reflux for 24 h. After it had been cooled, the GLC analysis of toluene solution revealed the presence of 2.45 mmol of **2** (49% yield: based on DBDS). The evaporation of the solvent, followed by the addition of ether to the residue, gave 0.33 g (24%) of DBDS as an insoluble precipitate. By removing the ether from the above ether washing and by adding hexane to the residue, brown solids (1.12 g, mp 186—192 °C) were separated out as precipitates. The hexane washing contained **2**. The NMR spectrum of this solid revealed the presence of cyclohexyl and phenyl groups, and the IR spectrum had strong absorptions at 1660 and 1630 cm^{-1}, these spectra being the same as those of the solids obtained from **1** and DBS (in toluene, 111 °C, 14 h). The mass spectrum showed peaks at *m/e* 351, 460, and 569 which may correspond to the three adducts of DBS-**1**, 1:1, 1:2, and 1:3 respectively. None of the compounds could be separated by column chromatography or preparative TLC on activated alumina.

The helpful comments of Dr. Sakae Uemura are gratefully acknowledged.

References

1) S. Tanaka, S. Uemura, and M. Okano, *Bull. Chem. Soc. Jpn.*, **50**, 2785 (1977).

2) a) K. Tsuda and T. Otsu, *Bull. Chem. Soc. Jpn.*, **39**, 2206 (1966); b) S. Kondo and K. Tsuda, *Makromol. Chem.*, **175**, 2111 (1974).

3) T. Shono, M. Kimura, Y. Ito, K. Nishida, and R. Oda, *Bull. Chem. Soc. Jpn.*, **37**, 635 (1964).

4) M. Kodomari, T. Sodeyama, K. Itabashi, *Yuki Gosei Kagaku Kyokai Shi*, **31**, 416 (1973).

5) S. Uemura, S. Tanaka, and M. Okano, *Bull. Chem. Soc. Jpn.*, **50**, 220 (1977).

BULLETIN OF THE CHEMICAL SOCIETY OF JAPAN VOL. 51 (2), 661—662 (1978)

Absolute Stereochemistry of Cacalol

Mahito TERABE, Masahiro TADA, and Takeyoshi TAKAHASHI

Department of Chemistry, Faculty of Science, The University of Tokyo, Bunkyo-ku, Tokyo 113

(Received August 11, 1977)

Synopsis. Descriptions on the absolute configuration at C-5 of cacalol have been confused. Ozonolysis of cacalol afforded (*S*)-(+)-2-methylhexanedioic acid. The asymmetric center at C-5 of cacalol, cacalone, and of sesquiterpenes related to these compounds was therefore established to be (*S*)-configuration.

Since cacalol and cacalone were isolated from *Cacalia decomposita* A. Gray,[1] a number of sesquiterpenes related to these compounds have been isolated from plants of the genus *Cacalia*.[2–7] Among these sesquiterpenes, cacalone,[1] maturinone,[2–8] and decompostin[3,9,10] have been chemically correlated with cacalol. Through a series of revisions (**1a**,[1] **1b**,[8] and **1c**), the structure of cacalol was established to be 5,6,7,8-tetrahydro-3,4,5-trimethylnaphtho[2,3-*b*]furan-9-ol (**1c**)[9,11–15] by unambiguous syntheses of maturinone (**2**)[9,11–13] and (±)-cacalol (**1c**).[12,14,15] Based on conversion of cacalol into cacalone,[16,17] a *p*-quinol structure (**3**)[16–18] was recently shown for cacalone, and previously presented formulas (**4a**,[1] **4b**,[8] and **4c**[9,11,13]) were excluded.

Descriptions on the absolute configuration at C-5 hitherto reported for cacalol have been confused. In the present paper, we wish to report evidence leading to a (5*S*)-configuration for cacalol (**1c-B**).

In early studies on cacalol and cacalone, a stereostructure (**1b-A**) with 8β-methyl group was proposed for cacalol because of the formation of (*R*)-(+)-β-methyladipic acid [**5**; (*R*)-(+)-3-methylhexanedioic acid] on ozonolysis of cacalol.[8] However, the formation of **5** from cacalol can not be explained by the present structure (**1c**) for cacalol. The stereostructures (**1c-A**, **4c-A**, and **6A**) with (5*R*)-configuration were then suggested[19] for cacalol, cacalone, and for a nor-*p*-quinone,[1,7,20] respectively, based on an interpretation of their anomalous ORD curves by means of the presence of inherently dissymmetric chromophores.[19] This result[19] seems to be inconvincing, as the reference compounds cited therein[19] are inadequate for the arguments, and the structure of cacalone was later revised from **4c** to **3**.[16,17]

Decompostin is a natural eremophilane derivertive coexisting with cacalol, cacalone, and maturinone in *C. decomposita*.[3] Biogenetic considerations that cacalol and its related compounds are derived from sesquiterpenes of eremophilane type such as decompostin have been proposed.[13,21] As an absolute configuration of decompostin was determined to be **7a**,[3,22] the biogenetic pathway is shown as in Scheme 1, suggesting a (5*S*)-configuration for cacalol (**1c**) and for its related sesquiterpenes (**3**, **6**, *etc.*).[20] It was reported that deacetyl-6-epidecompostin (**7b**)[9] [or its mesylate[10]] was converted chemically into naphthofuran derivertive (**8b**)[9,10] which was derived from cacalol.[1] However, no information on the stereochemistry at C-5 of cacalol can be

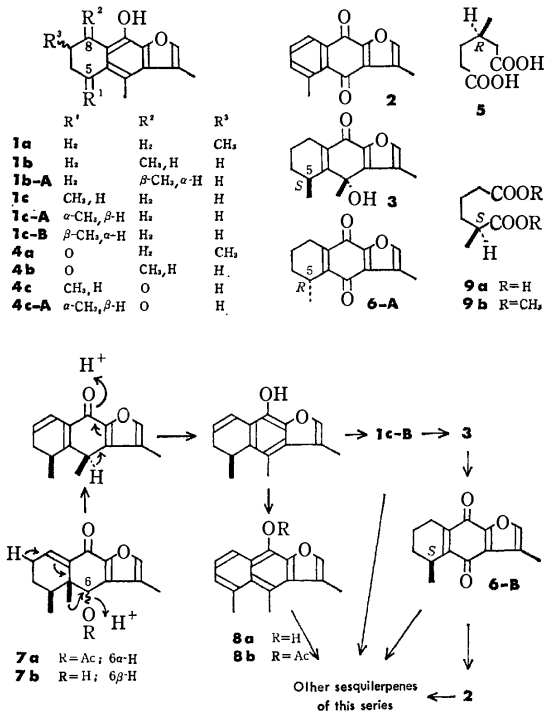

Scheme 1.

drawn from the above result, as **8b** bears no asymmetric center. Therefore, the ozonolysis of cacalol (**1c**) was reexamined.

Cacalol was ozonized in acetic acid and treated successively with hydrogen peroxide and with palladium on charcoal. The major component of acidic products was shown to be 2-methylhexanedioic acid by PMR examination. Purification of the acid fraction using an ion-exchange resin column and then by recrystallization gave (*S*)-(+)-2-methylhexanedioic acid (**9a**),[23,24] mp 76.5—77.5 °C, $[\alpha]_D$ +12° (EtOH), whose IR ($CHCl_3$) and PMR ($CDCl_3$) spectra were found to be identical with those of authentic (±)-**9a** prepared from 2-methyl-1-cyclohexanone. This led to a (5*S*)-configuration for cacalol and for its related sesquiterpenes in accordance with the biogenetic considerations (Scheme 1).

Experimental

Melting points were determined on a Mel-temp capillary melting point apparatus (Laboratory Devices) and are uncorrected. IR and UV spectra were measured on a Hitachi EPI-G2 spectrometer and a Hitachi EPS-3 spectrometer, respectively. Optical rotations were measured on a JASCO DIP-SL polarimeter. Mass spectra were taken on a Hitachi RMU-6-Tokugata mass spectrometer operating at 70 eV. PMR spectra were taken on a Hitachi R-20 spectrometer using TMS as internal standard. For column chromatography

Wakogel C-200 (Wako Pure Chem. Ind.) was used.

*Isolation of Cacalol (**1c-B**).* Cacalol was isolated from *Cacalia delphiniifolia* Sieb. et Zucc. according to the descriptions reported by Naya *et al.*[7] Crystallization from ether–hexane gave pure cacalol (**1c-B**), mp 92—93 °C (lit,[1] 92—94 °C), $[\alpha]_D^{24}$ +6° (*c* 1.0, $CHCl_3$) [lit,[1] +10° ($CHCl_3$)]. For an identification purpose, this natural product was acetylated (acetic anhydride, pyridine, at room temperature) to give cacalol acetate, mp 104—105 °C (lit,[1] 103—104 °C; lit,[7] 103.5—104.5 °C), $[\alpha]_D^{20}$ −10° (*c* 1.0, $CHCl_3$) [lit,[1] −9° ($CHCl_3$); lit,[7] −96.5° ($CHCl_3$)[25]]. Spectral data (IR, UV, and PMR) of cacalol and of its acetate were identical with the reported values.[1]

*Ozonolysis of Cacalol (**1c-B**).* Oxygen containing ozone (*ca.* 3%) was passed through the solution of cacalol (500 mg) in acetic acid (20 ml) at room temperature for 12 h. To this solution was added 30% hydrogen peroxide (2.5 ml), and the mixture was stirred at room temperature for 2 h and then at 60 °C for 2.5 h. After addition of water (10 ml) and 10% palladium–charcoal (100 mg), the reaction mixture was stirred at room temperature for 17 h to complete decomposition of the peracid. The catalyst was filtered off and the solution was evaporated to give an oil, which was dissolved in ether, washed with saturated aqueous sodium chloride solution, and extracted with 5% sodium hydrogencarbonate. The aqueous layer was acidified (pH 1) with concentrated hydrochloric acid and extracted with ether. The ethereal solution was dried over anhydrous sodium sulfate and evaporated to give an oil (174 mg). This oil was shown to consist mainly of 2-methylhexanedioic acid by PMR ($CDCl_3$) examination [δ 1.21 (3H, d, J=7 Hz), 1.70 (4H, m), 2.42 (3H, m), and 9.41 (2H, br s)]. The oil was dissolved in water (2 ml), neutralized with 1 M sodium hydroxide, and chromatographed on an Amberlite IR-120 cation exchange resin column (50 g; elution with water). Several fractions gave crystals [$[\alpha]_D^{20}$ +18° (*c* 0.5, EtOH)] on removal of water. These were combined and recrystallized from ether–hexane to afford (*S*)-(+)-2-methylhexanedioic acid (**9a**), mp 76.5—77.5 °C (lit,[23] 81—83 °C; lit,[24] 81—82 °C), $[\alpha]_D^{25}$ +12° (*c* 0.2, EtOH) [lit,[23] +13.8° (*c* 1.91, EtOH); lit,[24] −13.4° (*c* 2.15, EtOH)]; IR ($CHCl_3$) 3100, 2940, 2890, and 1700 cm^{-1}; PMR ($CDCl_3$) δ 1.20 (3H, d, J=7 Hz), 1.68 (4H, m), 2.36 (3H, m), and 8.9 (2H, br s) [lit,[24] PMR ($CDCl_3$) δ 1.22 (3H, d, J=7 Hz), 1.67 (4H, m), 2.38 (3H, m), and 11.6 (2H, s)]. The IR and PMR spectra were identical with those [IR ($CHCl_3$) and PMR ($CDCl_3$)] of authentic (±)-2-methylhexanedioic acid, respectively.

The acid (**9a**) was treated with diazomethane in ether to give a dimethyl ester (**9b**), an oil, IR (neat) 2960, 1735, 1435, and 1165 cm^{-1}; PMR (CCl_4) δ 1.15 (3H, d, J=7 Hz), *ca.* 1.5 (4H, m), 2.23 (3H, m), and 3.62 (6H, s) [lit,[26] PMR (CCl_4) δ 1.13 (3H, d, J=7 Hz), 1.57 (4H, m), *ca.* 2.30 (1H, m), 2.25 (2H, m), and 3.62 (6H, s)]; mass spectrum *m/e* 157 [$(M-OCH_3)^+$], *m/e* 129 [$(M-CO_2CH_3)^+$], *m/e* 128, *m/e* 88, and *m/e* 74. The IR, PMR, and mass spectra were found to be identical with those [IR (neat), PMR (CCl_4), and mass spectra)] of authentic dimethyl (±)-2-methylhexanedioate, respectively.

(±)-2-Methylhexanedioic Acid from 2-Methyl-1-cyclohexanone. 2-Formyl-6-methyl-1-cyclohexanone was prepared from 2-methyl-1-cyclohexanone according to the procedures described by Dallacker *et al.*[27] The formylated ketone in acetone was oxidized with potassium permanganate in a usual manner to give (±)-2-methylhexanedioic acid [(±)-**9a**].[28] This acid was esterified with diazomethane in ether to afford dimethyl (±)-2-methylhexanedioate [(±)-**9b**].[26]

The authors wish to thank Mr. Masaya Sakata and Mr. Noboru Saito, University Forest at Chichibu, the University of Tokyo, for collecting *Cacalia delphiniifolia* Sieb. et Zucc.

References

1) J. Romo and P. Joseph-Nathan, *Tetrahedron*, **20**, 2331 (1964).
2) J. Correa and J. Romo, *Tetrahedron*, **22**, 685 (1966).
3) L. Rodríguez-Hahn, A. Guzmán, and J. Romo, *Tetrahedron*, **24**, 477 (1968).
4) P. Joseph-Nathan, Ma. C. Negrete, and Ma. P. González, *Phytochemistry*, **9**, 1623 (1970).
5) K. Hayashi, H. Nakamura, and H. Mitsuhashi, *Phytochemistry*, **12**, 2931 (1973).
6) T. Takemoto, G. Kusano, K. Aota, M. Kaneshima, and N. A. El. Emary, *Yakugaku Zasshi*, **94**, 1593 (1974).
7) K. Naya, Y. Miyoshi, H. Mōri, K. Takai, and M. Nakanishi, *Chem. Lett.*, **1976**, 73.
8) P. Joseph-Nathan, J. J. Morales, and J. Romo, *Tetrahedron*, **22**, 301 (1966).
9) H. Kakisawa, Y. Inouye, and J. Romo, *Tetrahedron Lett.*, **1969**, 1929.
10) J. Romo, *Bol. Inst. Quim. Univ. Nac. Auton. Mex.*, **21**, 92 (1969); *Chem. Abstr.*, **73**, 15021P (1970).
11) P. M. Brown and R. H. Thomson, *J. Chem. Soc., C*, **1969**, 1184.
12) Y. Inouye, Y. Uchida, and H. Kakisawa, *Bull. Chem. Soc. Jpn.*, **50**, 961 (1977).
13) R. M. Ruiz, J. Correa, and L. A. Maldonado, *Bull. Soc. Chim. Fr.*, **1969**, 3612.
14) Y. Inouye, Y. Uchida, and H. Kakisawa, *Chem. Lett.*, **1975**, 1317.
15) F. Yuste and F. Walls, *Aust. J. Chem.*, **29**, 2333 (1976).
16) A. Casares and L. A. Maldonado, *Tetrahedron Lett.*, **1976**, 2485.
17) F. Yuste, E. Díaz, F. Walls, and K. Jankowski, *J. Org. Chem.*, **41**, 4103 (1976).
18) A *cis* relationship of the two methyl groups (at C-4 and C-5) was demonstrated (Refs. 16 and 17). A 5β-methyl configuration was derived (Ref. 17) from the evidence (formation of **5** from cacalol, related to cacalone) reported in Ref. 8; however, this is not a convincing fact leading to 5β-methyl stereochemistry for **3** as described in the text (*cf.* also Ref. 20).
19) P. Joseph-Nathan and Ma. P. González, *Can. J. Chem.*, **47**, 2465 (1969).
20) Indeed, a number of natural sesquiterpenes related to cacalol were formulated with (5*S*)-configuration (*e.g.* Refs. 7, 16; *cf.* Ref. 17).
21) *Cf.* also Refs. 5, 7, 9, 10, 11, and 16.
22) Z. Samek, J. Harmatha, L. Novotný, and F. Šorm, *Collect. Czech. Chem. Commun.*, **34**, 2792 (1969).
23) I. Kawasaki and T. Kaneko, *Bull. Chem. Soc. Jpn.*, **41**, 1482 (1968).
24) C. F. Wong, E. Auer, and R. T. LaLonde, *J. Org. Chem.*, **35**, 517 (1970). (*R*)-(−)-2-Methylhexanedioic acid was described.
25) This value might be erroneous.
26) "The Sadtler Standard Spectra," Sadtler Research Laboratories, Philadelphia (1967), No. 3893 M; the PMR spectrum of dimethyl (±)-2-methylhexanedioate [(±)-**9b**] was registered.
27) F. Dallacker, I. Alroggen, H. Krings, B. Laurs, and M. Lipp, *Justus Liebigs Ann. Chem.*, **647**, 23 (1961).
28) Infrared Data Committee of Japan, Ed., "IRDC Cards," Nankodo, Tokyo (1962), No. 2687.

BULLETIN OF THE CHEMICAL SOCIETY OF JAPAN VOL. 51 (2), 663—664 (1978)

The Reaction of *ortho*-Palladated Ferrocene Complexes with Olefins

Taeko IZUMI, Kazuyoshi ENDO, Osamu SAITO, Iwao SHIMIZU,
Mitsugi MAEMURA, and Akira KASAHARA
Department of Applied Chemistry, Faculty of Engineering, Yamagata University, Yonezawa 992

(Received August 22, 1977)

Synopsis. *ortho*-Palladation products of (dimethylaminomethyl)ferrocene and 2-pyridylferrocene were treated with various olefins under mild conditions. A variety of unusual 1,2-disubstituted ferrocene derivatives were obtained from these reactions.

Following the first report that a palladium-carbon bond is formed directly upon the reaction of palladium(II) salt with azobenzene,[1] considerable interest developed in this area.[2] The *ortho*-palladation reaction is ideally suited for use in the synthesis of *ortho*-disubstituted compounds, since the metalated complexes can be made directly from monosubstituted aromatics. Previously, for example, the reactions of *ortho*-palladation products from numerous α-aryl nitrogen derivatives with carbon monoxide,[3,4] halogen,[5] alkyllithium or a Grignard reagent,[6] and olefins[7-9] have been reported. Furthermore, we ourselves have reported the reactions of an *ortho*-palladated complex of 2-pyridylferrocene with carbon monoxide, alkyllithium, and bromine.[10] In this report, we wish to report on the reactions of various olefins with *ortho*-palladated ferrocenyl derivatives: di-μ-chloro-bis[2-(dimethylaminomethyl)ferrocenyl]dipalladium(II) (**1**) and di-μ-chloro-bis[2-(2-pyridyl)ferrocenyl]dipalladium(II) (**2**).

Tsuji[7] has previously reported that the reaction of the *ortho*-palladated *N,N*-dimethylbenzylamine complex with styrene in acetic acid led to the formation of the arylated styrene derivative. Holton[9] has also reported the reaction of *ortho*-palladated benzylamine-type complexes with enones in the presence of triethylamine. The attempted reaction of olefin with **1** in acetic acid was unsuccessful even at 100 °C. On the other hand, in the presence of triethylamine, the **1** complex reacted with simple olefins, such as styrene, ethyl acrylate, methyl methacrylate, acrylonitrile, methyl vinyl ketone, and phenyl vinyl ketone, in toluene at 100 °C, leading to the formation of 1-dimethylaminomethyl-2-alkenyl ferrocene (**3**—**8**) in moderate yields. Compounds **3**—**8** exhibited absorptions near 1100, 1000, and 910 cm^{-1} characteristic of homoannularly 1,2-disubstituted ferrocene derivatives.[11] Moreover, the NMR and mass spectra of Compounds **3**—**8** were all consistent with the proposed structures. Complex **2**, similarly, reacted with olefins, such as methyl vinyl ketone and phenyl vinyl ketone, to afford the substitution products (**9** and **10**). The order of the reactivity of the complexes with olefin is **1**>**2**. The reactions carried out are summarized in Table 1, while the properties of the products are given in Table 2.

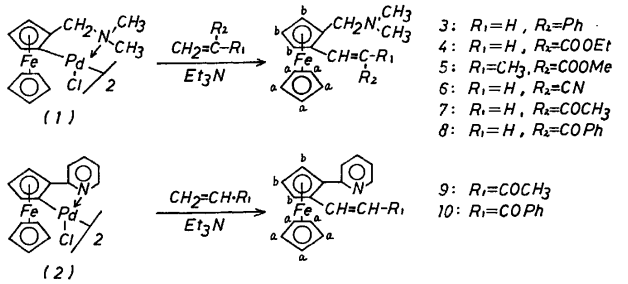

Fig. 1.

Experimental

Materials. The following compounds were synthesized by the methods described in the literature: di-μ-chloro-bis-[2-(dimethylaminomethyl)ferrocenyl]dipalladium(II) (**1**)[12] and di-μ-chloro-bis[2-(2-pyridyl)ferrocenyl]dipalladium(II) (**2**).[10]

General Procedure for the Reaction of a Complex with Olefins. A mixture of 2 mmol of a complex (**1** or **2**), 5 mmol of olefin, and 0.29 g (5 mmol) of triethylamine in toluene (40 ml) was heated at 100 °C under a nitrogen atmosphere. The reaction mixture was then cooled and filtered to remove the precipitated palladium, 100 ml of toluene was added, and the mixture was washed with water, dried over anhydrous magnesium sulfate, filtered, and concentrated under reduced pressure. The residue was then purified by column chromatography (Al_2O_3–benzene or chloroform). The structure of the products

TABLE 1. REACTIONS OF *ortho*-PALLADATED FERROCENYL COMPLEXES WITH OLEFINS

Complex	olefin	Reaction time (h)	Product	Yield[a]
1	Styrene	5	1-Dimethylaminomethyl-2-styrylferrocene (**3**)	33
1	Ethyl acrylate	5	1-Dimethylaminomethyl-2-(2-ethoxycarbonylvinyl)ferrocene (**4**)	55
1	Methyl methacrylate	5	1-Dimethylaminomethyl-2-(2-methoxycarbonyl-2-methylvinyl)-ferrocene (**5**)	28
1	Acrylonitrile	5	1-(2-Cyanovinyl)-2-(dimethylaminomethyl)ferrocene (**6**)	30
1	Methyl vinyl ketone	5	1-(2-Acetylvinyl)-2-(dimethylaminomethyl)ferrocene (**7**)	27
1	Phenyl vinyl ketone	5	1-(2-Benzoylvinyl)-2-(dimethylaminomethyl)ferrocene (**8**)	59
2	Methyl vinyl ketone	19	1-(2-Acetylvinyl)-2-(2-pyridyl)ferrocene (**9**)	8
2	Phenyl vinyl ketone	12	1-(2-Benzoylvinyl)-2-(2-pyridyl)ferrocene (**10**)	20

a) The yields are based upon Complex **1** or **2**.

Table 2. Properties and analyses of reaction products[a)]

Compound	
3	Heavy, reddish-brown oil. Found: C, 72.87; H, 6.56; N, 3.91%; M^+, 345. Calcd for $C_{21}H_{23}FeN$; C, 73.05; H, 6.71; N, 4.05%; mol wt, 345. IR: 1100, 1000, 915 (1,2-disubstituted ferrocene); 1630, 960 (*trans* -CH=CH-); 1600, 1500, 745, 690 cm^{-1} (phenyl). NMR: δ 2.25 (s, 6H, $-N(CH_3)_2$), 3.34 (d-d, 2H, $-CH_2N-$:), 4.10 (s, 5H, H_a), 4.40 (m, 3H, H_b), 6.72 (d, J=12 Hz, 1H, -C=CH-Ph), 7.11—7.28 ppm (m, 6H,-CH=C-Ph+phenyl protons).
4	Heavy, reddish-brown oil. Found: C, 63.51; H, 6.88; N, 4.25% M^+, 341. Calcd for $C_{18}H_{23}FeNO_2$:C, 63.38; H, 6.75; N, 4.18%; mol wt, 341. IR: 1710 (ester); 1100, 1000, 910 (1,2-disubstituted ferrocene); 1625, 960 cm^{-1} (*trans* -CH=CH-). NMR: δ 1.23 (t, 3H, $-COOCH_2CH_3$), 2.09 (s, 6H, $-N(CH_3)_2$), 3.29 (d-d, 2H, $-CH_2N-$), 3.99 (s, 5H, H_a), 4.11 (q, 2H, $-COOCH_2CH_3$), 4.33 (m, 3H, H_b), 5.95 (d, J=14 Hz, 1H, -C=CH-COOEt), 7.53 ppm (d, J=14 Hz, 1H, Fc-CH=C-).
5	Heavy, reddish brown oil. Found: C, 63.44; H, 6.85; N, 4.20%; M^+, 341. Calcd for $C_{18}H_{23}FeNO_2$: C, 63.38; H, 6.75; N, 4.18%; mol wt, 341. IR: 1710 (ester); 1100, 1000, 915 (1,2-disubstituted ferrocene); 1620, 810 cm^{-1} (-C=CH-). NMR: δ 1.93 (d, 3H, $-CH=C(CH_3)-$), 2.04 (s, 6H, $-N(CH_3)_2$), 3.24 (d-d, 2H, $-CH_2N-$), 3.69 (s, 3H, $-COOCH_3$), 3.98 (s, 5H, H_a), 4.30 (m, 3H, H_b), 7.44 ppm (q, 1H, Fc-CH=C-).
6	Heavy, reddish oil. Found: C, 65.27; H, 6.03; N, 9.43%; M^+, 294. Calcd for $C_{16}H_{18}FeN_2$: C, 65.35; H, 6.12; N, 9.52%; mol wt, 294. IR: 2200 (-CN); 1610, 955 (*trans* -CH=CH-), 1100, 1000, 910 (1,2-disubstituted ferrocene). NMR: δ 2.13 (s, 6H, $-N(CH_3)_2$), 3.33 (d-d, 2H, $-CH_2N-$), 4.08 (s, 5H, H_a), 442 (m, 3H, H_b), 5.13 (d, J=12 Hz, 1H, -C=CH-CN), 7.07 ppm (d, J=12 Hz, 1H, Fc-CH=C-).
7	Heavy, reddish-brown oil. Found: C, 65.58; H, 6.69; N, 4.41%; M^+, 311. Calcd for $C_{17}H_{21}FeNO$: C, 65.63; H, 6.75; N, 4.50%; mol wt, 311. IR: 1660 (C=O); 1610, 960 (*trans* -CH=CH-); 1100, 1000, 910 cm^{-1} (1,2-disubstituted ferrocene). NMR: δ 2.07 (s, 6H, $-N(CH_3)_2$), 2.19 (s, 3H, $-COCH_3$), 3.33 (d-d, 2H, $-CH_2N-$), 4.00 (s, 5H, H_a), 4.40 (m, 3H, H_b), 6.27 (d, J=12 Hz, 1H, -C=CH-CO-), 7.40 ppm (d, J=12 Hz, 1H, Fc-CH=C-).
8	Heavy, reddish-brown oil. Found: C, 70.68; H, 6.08; N, 3.70%; M^+, 373. Calcd for $C_{22}H_{23}FeNO$: C, 70.81; H, 6.16; N, 3.75%; mol wt, 373. IR: 1660 (C=O); 1610, 965 (*trans* -CH=CH-); 1100, 1010, 910 (1,2-disubstituted ferrocene); 1600, 1500, 745, 690 cm^{-1} (phenyl). NMR: δ 2.15 (s, 6H, $-N(CH_3)_2$), 3.43 (d-d, 2H, $-CH_2N-$), 4.08 (s, 5H, H_a), 4.56 (m, 3H, H_b), 7.08 (d, J=12 Hz, -C=CH-CO-), 7.28 (broad s, 5H, phenyl protons), 7.82 ppm (d, J=12 Hz, 1H, -CH=C-CO-).
9	Heavy, reddish brown oil. Found: C, 68.81; H, 5.06; N, 4.21%; M^+, 331. Calcd for $C_{19}H_{17}FeNO$: C, 68.92; H, 5.13; N, 4.23%; mol wt, 331. IR: 1660 (C=O); 1610, 960 (*trans* -CH=CH-); 1100, 1005, 915 cm^{-1} (1,2-disubstituted ferrocene). NMR: δ 2.31 (s, 3H, $-CO-CH_3$), 4.00 (s, 5H, H_a), 4.56 (m, 3H, H_b), 6.27 (d, J=12 Hz, 1H, -C=CH-CO-), 7.19 (d, J=12 Hz, 1H, Fc-CH=C-), 7.31—8.39 ppm (m, 4H, pyridyl protons).
10	Reddish crystals, mp 149—150°C. Found: C, 73.39; H, 4.88; N, 3.53%; M^+, 393. Calcd for $C_{24}H_{19}FeNO$: C, 73.31; H, 4.83; N, 3.56%; mol wt, 393. IR: 1655 (C=O); 1630, 960 (*trans* -CH=CH-); 1100, 1000, 910 (1,2-disubstituted ferrocene); 1600, 1500, 745, 690 cm^{-1} (phenyl). NMR: δ 4.02 (s, 5H, H_a), 4.68 (m, 3H, H_b), 6.98 (d, J=12 Hz, 1H, -C=CH-CO-), 7.18—8.13 ppm (m, 10H, Fc-CH=C-+phenyl and pyridyl protons).

a) The IR and mass spectra were measured using a Hitachi 215 spectrophotometer and a Model RMU-6M mass spectrometer at 70 eV. The NMR spectra were observed in $CDCl_3$ on a Hitachi Model R-22 (90 MHz), using TMS as the internal standard (δ, ppm). The chemical shifts were followed by means of the splitting pattern (s, singlet; d, doublet; d-d, double doublet; t, triplet; q, quartet; m, multiplet) and the relative strengths.

was confirmed by an elemental analysis and by the observation of the IR, NMR, and mass spectra. The results are summarized in Tables 1 and 2.

References

1) A. C. Cope and R. W. Siekman, *J. Am. Chem. Soc.*, **87**, 3272 (1965).

2) a) P. M. Maitlis, "The Organic Chemistry of Palladium," Academic Press, Vol. 1, New York (1971), p. 82; b) J. Tsuji, *Yuki Gosei Kagaku Kyokai Shi*, **35**, 10 (1977).

3) H. Takahashi and J. Tsuji, *J. Organomet. Chem.*, **10**, 511 (1967).

4) J. M. Thompson and R. F. Heck, *J. Org. Chem.*, **40**, 2667 (1975).

5) a) D. R. Fahey, *Chem. Commun.*, **1970**, 417; b) D. R. Fahey, *J. Organomet. Chem.*, **27**, 283 (1971).

6) a) S.-I. Murahashi, Y. Tanba, M. Yamamura, and I. Moritani, *Tetrahedron Lett.*, **1974**, 3749; b) M. Yamamura, I. Moritani, and S.-I. Murahashi, *Chem. Lett.*, **1974**, 1423.

7) J. Tsuji, *Acc. Chem. Res.*, **2**, 144 (1969).

8) M. Julia, M. Duteil, and J. Y. Lallemand, *J. Organomet. Chem.*, **102**, 239 (1975).

9) R. A. Holton, *Tetrahedron Lett.*, **1977**, 355.

10) A. Kasahara, T. Izumi, and M. Maemura, *Bull. Chem. Soc. Jpn.*, **50**, 1878 (1977).

11) a) M. Rosenblum, *J. Am. Chem. Soc.*, **81**, 4530 (1959); b) M. Rosenblum and W. G. Howells, *ibid.*, **84**, 1167 (1962).

12) J. C. Gaunt and B. L. Shaw, *J. Organomet. Chem.*, **102**, 511 (1975).

BULLETIN OF THE CHEMICAL SOCIETY OF JAPAN VOL. 51 (2), 665—666 (1978)

A Convenient Method for the Introduction of 1,3-Dithiolan-2-yl Group into Active Methylene Compounds

Shigeo TANIMOTO, Yasuo MATSUMURA, Toyonari SUGIMOTO, and Masaya OKANO
Institute for Chemical Research, Kyoto University, Uji, Kyoto 611

(Received August 22, 1977)

Synopsis. The reaction of 2-ethoxy-1,3-dithiolane with a variety of active methylene compounds in the presence of a zinc chloride catalyst was investigated. By this reaction the introduction of a 1,3-dithiolan-2-yl group into the active methylene compounds was achieved. Some behavior of the 1,3-dithiolan-2-yl derivative of ethyl acetoacetate, which is one of the newly obtained compounds, was also briefly examined.

Recently, 2-alkoxy-1,3-benzodithioles (**1**) have become readily available by means of the action of benzyne on carbon disulfide in the presence of alcohols,[1] and their behavior toward carbon nucleophiles has been studied.[2,3]

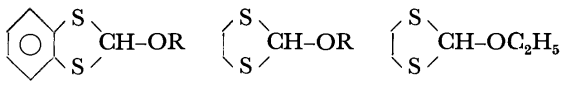

1 **2** **3**

In contrast, no description of the chemistry of 2-alkoxy-1,3-dithiolanes (**2**), the corresponding saturated system of **1**, is to be found in the literature, except for our own earlier report,[4] which involves the synthesis of 2-ethoxy-1,3-dithiolane (**3**) and its reaction with *n*-BuLi.

We wish now to report the reaction of **3** with a variety of active methylene compounds (**4**), by which the introduction of a 1,3-dithiolan-2-yl group into **4** was conveniently achieved.

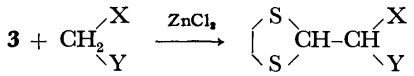

4 **5**

a: X=$COCH_3$, Y=$CO_2C_2H_5$
b: X=$COCH_3$, Y=CO_2CH_3
c: X=Y=$CO_2C_2H_5$
d: X=Y=CO_2CH_3
e: X=Y=$COCH_3$
f: X=CN, Y=$CO_2C_2H_5$
g: X=COC_6H_5, Y=$CO_2C_2H_5$

The reaction of **4** with **3** proceeded smoothly without a solvent under the catalytic action of a metal halide such as zinc chloride or iron(III) chloride, and 1,3-dithiolan-2-yl derivatives of **4** (**5**) could be isolated in quite good yields (Table 1).

The reaction may involve the initial loss of the exocyclic ethoxyl group of **3** to give the 1,3-dithiolan-2-ium ion and its subsequent attack on the active methylene compound.

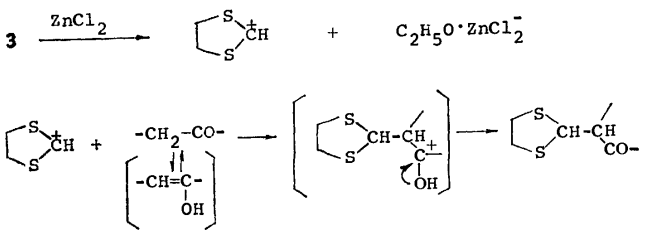

In order to investigate the possibility of the synthesis of a novel class of compound (**9**) with three different carbonyl groups at the same carbon atom, we examined the reaction of **5a** with mercury(II) acetate[6] under conditions similar to those employed for the cleavage of cyclic ethylene thioacetals.[7] However, the product thus obtained was ethyl acetoacetate, and no trace of **9** was isolated. This means that the reaction proceeded only with an exclusive bond fission between 2-C and 6-C.

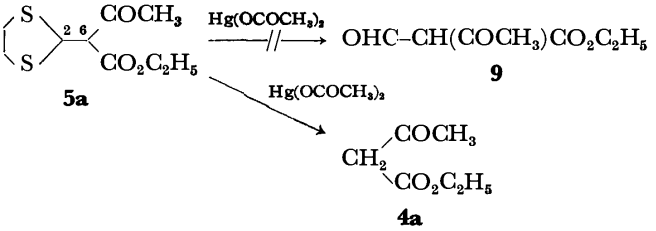

5a **9** **4a**

On the other hand, the hydrolysis of **5a** with a large excess of boiling conc. HCl for 5—6 h gave a bis(1,3-dithiolan-2-yl) derivative, acetoacetaldehyde bis(ethylene thioacetal) (**10**), in a 48% yield[mp 31—33 °C (hexane) (lit,[8] 30—32 °C)], but formylacetone or its derivative, which seems to be simultaneously obtainable, could not be detected.

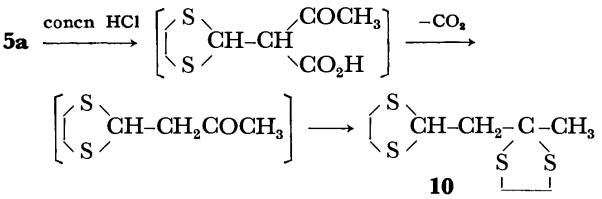

10

Experimental

Reaction of 2-Ethoxy-1,3-dithiolane (3) with Active Methylene Compounds (4). General Procedure: A mixture of 33 mmol of **3**, 39—40 mmol of an active methylene compound, and *ca.* 15 mmol of a catalyst was stirred at room temperature for 24 h, with the exclusion of any moisture, and then poured into a large quantity of an aqueous sodium carbonate solution. The organic layer was separated, combined with an ethereal extract of the aqueous phase, and dried ($MgSO_4$), and the ether was removed. The oily residue was distilled *in vacuo* to afford the desired product. The product can be purified further by column chromatography if necessary. Only in the case of the reaction with ethyl benzoylacetate, the removal of ether and the excess ethyl benzoylacetate leave a solid residue, which was purified by recrystallization from ethanol.

Reaction of 1,3-Dithiolan-2-yl Derivative of Ethyl Acetoacetate (5a) with Mercury(II) Acetate. To a solution of 5 g (21 mmol) of **5a** in 200 ml of acetone, we added 50 ml of water,

Table 1. Reactions of 2-ethoxy-1,3-dithiolane (**3**) with various active methylene compounds (**4**)

Run	Active methylene compound	Catalyst	Products[a] and yields[b] (%)
1	**4a**	$ZnCl_2$	**5a**[c] (70), $(CH_3)CH_2CO_2C_2H_5$[d] (trace) **6**
2	**4a**	$ZnBr_2$	**5a**[c] (72), **6**[d] (trace)
3	**4a**	$AlCl_3$	**5a**[c] (14), **6**[d] (39)
4	**4a**	$FeCl_3$	**5a**[c] (65), **6**[d] (26)
5	**4b**	$ZnCl_2$	**5b**[e] (68), $(CH_3)CH_2CO_2CH_3$[f] (trace) **7**
6	**4c**	$ZnCl_2$	**5c**[g] (49)
7	**4d**	$ZnCl_2$	**5d**[h] (53)
8	**4e**	$ZnCl_2$	**5e**[i] (39), $(CH_3)CH_2COCH_3$[j] (trace) **8**
9[k]	**4f**	$ZnCl_2$	**5f**[l] (24)
10	**4g**	$ZnCl_2$	**5g**[m] (60)

a) Satisfactory elemental analyses were obtained for all new compounds. b) Yields were based upon **3**, and referred to isolated ones. c) Bp 137.5—139.5 °C/2 mmHg. NMR ($CDCl_3$): δ 1.30 (t, 3H), 2.30 (s, 3H), 3.23 (s, 4H), 3.87 (d, 1H), 4.22 (q, 2H), 5.04 (d, 1H). d) The structure proposed for **6** is in agreement with the results of elemental analysis, the mass spectra, and the NMR spectroscopic data. Bp 99—103 °C/1.5 mmHg (lit,[5] 86 °C/0.1 mmHg. NMR ($CDCl_3$): δ 1.28 (t, 3H), 1.93 (s, 3H), 3.04 (s, 2H), 3.36 (s, 4H), 4.18 (q, 2H). e) Bp 136.5—139.5 °C/2 mmHg. NMR ($CDCl_3$): δ 2.30 (s, 3H), 3.24 (s, 4H), 3.78 (s, 3H), 3.91 (d, 1H), 5.06 (d, 1H). f) The structure proposed for **7** is in agreement with the results of elemental analysis, the mass spectra, and the NMR spectroscopic data. Bp 94—97 °C/2 mmHg. NMR ($CDCl_3$): δ 1.90 (s, 3H), 3.03 (s, 2H), 3.35 (s, 4H), 3.69 (s, 3H). g) Bp 138—139 °C/1.5 mmHg. NMR ($CDCl_3$): δ 1.24 (t, 3H), 3.23 (s, 4H), 3.62 (d, 1H), 4.23 (q, 2H), 5.03 (d, 1H). h) Bp 137—138 °C/2 mmHg. NMR ($CDCl_3$): δ 3.26 (s, 4H), 3.67 (d, 1H), 3.79 (s, 3H), 5.03 (d, 1H). i) Purified by column chromatography on silica gel (eluent 50% ether–50% hexane). Mp 50—52.5 °C (ethanol). NMR ($CDCl_3$): δ 2.26 (s, 3H), 3.28 (s, 4H), 4.06 (d, 1H), 5.16 (d, 1H). j) The structure proposed for **8** is in agreement with the results of elemental analysis, the mass spectra, and the NMR spectroscopic data. Bp 142—145 °C/18 mmHg. NMR ($CDCl_3$): δ 1.86 (s, 3H), 2.17 (s, 3H), 3.20 (s, 2H), 3.32 (s, 4H). k) The reaction was performed at 90—100 °C for 8 h. l) Bp 140—142 °C/2 mmHg. NMR ($CDCl_3$): δ 1.30 (t, 3H), 3.38 (broad s, 4H), 4.07 (d, 1H), 4.32 (q, 2H), 5.07 (d, 1H). m) Mp 46—49 °C (ethanol). NMR ($CDCl_3$): δ 1.16 (t, 3H), 3.21 (s, 4H), 4.19 (q, 2H), 4.74 (d, 1H), 5.41 (d, 1H), 7.40—8.33 (m, aromatic 5H).

15 g (47 mmol) of mercury(II) acetate, and 15 g (87 mmol) of cadmium carbonate.[9] This mixture was stirred for 72 h at an ambient temperature, and then the mixture was filtered. After the removal of acetone from the filtrate, the residue was taken up in ether. The evaporation of the solvent under reduced pressure afforded 0.96 g (35%) of ethyl acetoacetate.

References

1) J. Nakayama, *Synthesis*, **1975**, 38.
2) J. Nakayama, *J. Chem. Soc., Perkin Trans. 1*, **1976**, 540.
3) S. Ncube, A. Pelter, and K. Smith, *Tetrahedron Lett.*, **1977**, 255.
4) S. Tanimoto, T. Miyake, and M. Okano, *Bull. Inst. Chem. Res. Kyoto Univ.*, in press.
5) J. F. Harris, Jr., U. S. Patent 2839445; *Chem. Abstr.*, **52**, 17289 (1958).
6) By the employment of mercury(II) chloride an unidentified white solid was isolated.
7) G. P. Pollini, A. Barco, M. Anastasia, and G. Traverso, *Chem. Abstr.*, **69**, 58862y (1968).
8) R. H. Shapiro, T. E. McEntee Jr., and D. L. Coffen, *Tetrahedron*, **24**, 2809 (1968).
9) Under similar conditions, but with cadmium carbonate omitted, almost the same yield of ethyl acetoacetate was obtained; *i.e.*, the cadmium carbonate is not essential to the reaction.

BULLETIN OF THE CHEMICAL SOCIETY OF JAPAN VOL. 51 (2), 667—668 (1978)

Studies on Heterocyclic Analogs of Azulenes. III.[1] The Reactions of 2-Chloro-3-ethoxycarbonylcyclohepta[*b*]pyrrole with the Carbanions Derived from Active Methylene Compounds

Noritaka ABE and Tarozaemon NISHIWAKI*

Department of Chemistry, Yamaguchi University, Yamaguchi 753

(Received September 1, 1977)

Synopsis. 2-Chloro-3-ethoxycarbonylcyclohepta[*b*]-pyrrole reacts with the carbanions derived from active methylene compounds to give substitution products and/or addition products depending on the reaction conditions.

2-Chloro-3-ethoxycarbonylcyclohepta[*b*]pyrrole (**1**) was reported by Matsumura to be substituted at C-2 with malononitrile in hot dioxane.[2] As our findings that **1** affords an addition product at C-8 when treated with Grignard reagents[3] led us to suspect the claim of Matsumura, we repeated his reaction. In our hands the reaction was more complicated than reported,[2] giving a number of products depending on the reaction conditions.

Treatment of **1** with malononitrile in boiling dioxane in the presence of sodium hydride produced two compounds in the ratio of 19: 1. The major one was the Matsumura's compound (**3a**), which is present as the methide form as confirmed by spectral methods, and the minor one was 1,6-dihydro-2-chloro-6-(dicyanomethylene)-3-(ethoxycarbonyl)cyclohepta[*b*]pyrrole(**6a**), a product formed by addition at C-6 of **1** followed by dehydrogenation. Reaction of **1** with ethyl cyanoacetate under the similar conditions afforded the corresponding **3b** and **6b** is the ratio of 4: 1. Although the reaction of **1** with phenylacetonitrile proceeded to give a substitution product and the compound (**6c**) in the ratio of 35: 1, the former takes the structure of 3-ethoxycarbonyl-2-(α-cyanobenzyl)cyclohepta[*b*]pyrrole (**2c**) in solid and in solution as shown by IR and NMR spectra. Predominant shift of the tautomeric equilibrium in favor of the 2-methylene forms (**3a**) and (**3b**), though unusual,[4] must be due to the high stability of the formal negative charge in **4**.

However, the product ratio changed dramatically when the reaction of **1** with ethyl cyanoacetate or phenylacetonitrile was undertaken at room temperature. For instance, the reaction with phenylacetonitrile yielded 1,6-dihydro-2-chloro-3-ethoxycarbonyl-6-(α-cyanobenzyl)cyclohepta[*b*]pyrrole (**5c**) (65%) and **6c** (2%) without giving a trace of **2c**. The structure of **5c** was proved by the presence of a 1H quartet at δ 2.63 and a 1H doublet at δ 4.05 in its NMR spectrum. **5** was unstable, changing into **6** on storage in air.

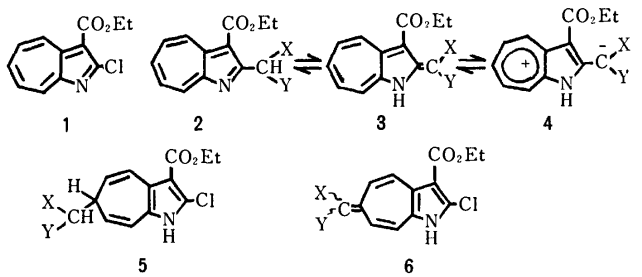

a: X=Y=CN; b: X=CN, Y=CO_2Et; c: X=CN, Y=Ph

Formation of the addition product **5** or its dehydrogenation product **6** was also observed when the reaction was carried out in ethanol in the presence of sodium ethoxide at room temperature or under reflux. These results are collected in Table 1. Dependence of the formations of the substitution product and the addition product[5] (or its dehydrogenation product) of **1** upon the solvent polarity and the reaction temperature is interesting, but we were unable to advance a rationale for these observations.

Table 1. Ratio of the substitution and addition products of **1**

Reagent	Conditions		Ratio (%)	
	Solvent	Temperature (°C)	Substitution (**2** or **3**)	Addition (**5**+**6**)
$CH_2(CN)_2$	Dioxane	25	70	30
$CH_2(CN)_2$	Dioxane	101	95	5
$CH_2(CN)_2$	EtOH	78	11	89
$CNCH_2CO_2Et$	Dioxane	25	21	79
$CNCH_2CO_2Et$	Dioxane	101	82	18
$CNCH_2CO_2Et$	EtOH	25	24	76
$PhCH_2CN$	Dioxane	25	0	100
$PhCH_2CN$	Dioxane	101	97	3
$PhCH_2CN$	EtOH	78	1	99

Experimental

Melting points were uncorrected. NMR spectra were recorded in $CDCl_3$ unless otherwise stated with a Varian HA-100 spectrometer at 100 MHz and the assignments were confirmed by decoupling techniques where necessary. IR spectra were obtained as Nujol mulls, and UV spectra were measured for chloroform solutions unless otherwise stated. Chromatography was performed on Kiesel gel 60 with chloroform. Yields are based on unrecovered starting materials.

*Reaction of **1** with Malononitrile.* (a) Malononitrile (2.00 g) was added into dry dioxane (100 ml) in which sodium hydride (66% in mineral oil) (0.70 g) was suspended. A solution of **1** (1.00 g) in dry dioxane (50 ml) was added into this mixture, stirred at room temperature for 2 days, acidified with acetic acid, and extracted with chloroform. The dried (Na_2SO_4) extracts were evaporated and the residue was chromatographed to give the starting material (0.771 g), **3a** (0.083 g, 30%), and **6a** (0.036 g, 17%), successively. **3a**: Red prisms

* The author to whom correspondence should be addressed.

(from chloroform), mp >300 °C (lit,[2] mp >260 °C), NMR (DMSO-d_6) δ=1.38 (3H, t, J=7 Hz), 4.38 (2H, q, J=7 Hz), 7.7—8.3 (4H, m), 8.67 (1H, bd, J=10 Hz);[6] UV_{max} (MeOH) 257 nm (log ε 4.26), 290 (4.32), 336 (3.78), 438 (4.29); IR 3140 (NH), 2200 (C≡N), 2150 (C≡N), 1680 cm^{-1} (C=O). Found: C, 67.75; H, 4.03; N, 15.69%. **6a**: Yellow needles (from chloroform), mp >300 °C, NMR (DMSO-d_6) δ=1.38 (3H, t, J=7 Hz), 4.33 (2H, q, J=7 Hz), 7.12 (1H, dd, J=12 and 2 Hz), 7.16 (1H, dd, J=12 and 2 Hz), 7.44 (1H, d, J=12 Hz), 8.22 (1H, d, J=12 Hz);[6] UV_{max} 260 nm (log ε 4.29), 282 (4.02), 290^{sh} (4.02), 433 (4.51), 448^{sh} (4.48), 472^{sh} (4.17); IR 3100 (NH), 2200 (C≡N), 1695 cm^{-1} (C=O). Found: C, 59.95; H, 3.18; Cl, 12.01; N, 14.03%. Calcd for $C_{15}H_{10}ClN_3O_2$: C, 60.13; H, 3.36; Cl, 11.84; N, 14.02%. (b) When the above reaction (**1** (2.00 g), dioxane (50 ml), NaH (1.40 g) in dioxane (100 ml), and the nitrile (4.00 g)) was repeated under reflux for 2 h, **3a** (2.074 g, 92%) and **6a** (0.106 g, 4%) were obtained. (c) The nitrile (2.00 g) was added into a solution of sodium ethoxide (Na (0.40 g) and abs ethanol (80 ml)). A solution of **1** (1.00 g) in abs ethanol (40 ml) was added into this mixture, heated under reflux for 1 h, and worked up as above to give **5a** (0.037 g, 4%), the starting material (0.306 g), **3a** (0.060 g, 7%), and **6a** (0.461 g, 52%), successively. **5a**: Needles (from cyclohexane), mp 118—120 °C, NMR δ=1.40 (3H, t, J=7 Hz), 2.46 (1H, q, J=7 Hz), 4.30 (1H, d, J=7 Hz), 4.35 (2H, q, J=7 Hz), 5.2—5.6 (2H, m), 6.40 (1H, d, J=9.5 Hz), 7.01 (1H, d, J=9.5 Hz), 8.92 (1H, bs); IR 3200 (NH), 2200 (C≡N), 1670 cm^{-1} (C=O). **5a** was unstable, changing into **6a** in 27% yield on storage for 5 days.

Reaction of 1 with Ethyl Cyanoacetate. (a) A solution of **1** (1.00 g) in dry dioxane (40 ml) was added into a mixture of ethyl cyanoacetate (1.00 g), sodium hydride (0.70 g), and dry dioxane (40 ml), stirred at room temperature for 1 day, and worked up as above to give **5b** (0.210 g, 16%), the starting material (0.133 g), **3b** (0.206 g, 18%), and **6b** (0.576 g, 52%), successively. **5b**: Needles (from cyclohexane), mp 130—132 °C, NMR δ=1.37 (3H, t, J=7 Hz), 1.39 (3H, t, J=7 Hz), 2.39 (1H, t, J=6.5 Hz), 3.05 (1H, d, J=6.5 Hz), 4.32 (2H, q, J=7 Hz), 4.34 (2H, q, J=7 Hz), 5.4—5.6 (2H, m), 6.39 (1H, d, J=10 Hz), 7.00 (1H, d, J=10 Hz), 8.85 (1H, bs); IR 3200 (NH), 2200 (C≡N), 1675 (C=O), 1663 cm^{-1} (C=O). **3b**: Red needles (from benzene), mp 163—165 °C (lit,[2] mp 163—165 °C), NMR δ=1.37 (3H, t, J=7 Hz), 1.46 (3H, t, J=7 Hz), 4.31 (2H, q, J=7 Hz), 4.51 (2H, q, J=7 Hz), 7.3—7.7 (4H, m), 8.53 (1H, bd, J=10.5 Hz); UV_{max} 259 nm (log ε 4.39), 292 (4.42), 341 (3.98), 500 (4.18). **6b**: Orange plates (from benzene), mp 255—256 °C (dec), NMR (DMSO-d_6) δ=1.27 (6H, t, J=7 Hz), 1.35 (6H, t, J=7 Hz), 4.15 (4H, q, J=7 Hz), 4.27 (4H, q, J=7 Hz), 7.14 (1H, dd, J=12 and 2 Hz), 7.21 (2H, d, J=12.5 Hz), 7.36 (1H, d, J=12 Hz), 7.94 (1H, d, J=12.5 Hz), 8.04 (1H, d, J=12.5 Hz), 8.48 (1H, dd, J=12.5 and 1.5 Hz), 8.56 (1H, d, J=12.5 and 2 Hz);[6,7] UV_{max} 258 nm (log ε 4.42), 281 (4.17), 444 (4.56); IR 3150 (NH), 2200 (C≡N), 1695 (C=O), 1650 cm^{-1} (C=O). Found: C, 58.69; H, 4.29; Cl, 10.38; N, 7.96%. Calcd for $C_{17}H_{15}ClN_2O_4$: C, 58.85; H, 4.32; Cl, 10.23; N, 8.07%. **5b** changed into **6b** in 45% yield on storage for 4 days. (b) The above reaction was carried out under reflux for 1 h to give the starting material (0.028 g), **3b** (1.005 g, 78%), and **6b** (0.228 g, 16%). (c) A solution of 1 (1.00 g) in abs ethanol (40 ml) was added into a mixture of the ester (1.00 g), sodium (0.40 g), and abs ethanol (60 ml) and stirred at room temperature for 1 days. Works-up gave **5b** (0.096 g, 11%), the starting material (0.347 g), **3b** (0.198 g, 24%), and **6b** (0.516 g, 56%).

Reaction of 1 with Phenylacetonitrile. (a) A solution of **1** (2.00 g) in dry dioxane (80 ml) was added into a mixture of phenylacetonitrile (2.00 g), sodium hydride (1.40 g), and dry dioxane (120 ml), stirred at room temperature for 1 day, and worked up as above to give **5c** (1.950 g, 65%) and **6c** (0.054 g, 2%), successively. **5c**: Needles (from methanol), mp 184—185 °C, NMR δ=1.40 (3H, t, J=7 Hz), 2.63 (1H, bq, J=9 Hz), 4.05 (1H, d, J=9 Hz), 4.35 (2H, q, J=7 Hz), 5.1—5.6 (2H, m), 6.42 (1H, d, J=9.5 Hz), 7.19 (1H, d, J=9.5 Hz), 7.32 (5H, s), 8.68 (1H, bs); UV_{max} 280 nm (log ε 3.89); IR: 3200 (NH), 2240 (C≡N), 1657 cm^{-1} (C=O). Found: C, 68.24; H, 4.92; Cl, 10.31; N, 7.79%. Calcd for $C_{20}H_{17}ClN_2O_2$: C, 68.07; H, 4.85; Cl, 10.05; N, 7.94%. **6c**: Yellow prisms (from benzene), mp 249.5—250 °C, NMR δ=1.50 (3H, t, J=7 Hz), 4.50 (2H, q, J=7 Hz), 7.4—7.9 (5H, m), 8.22 (2H, d, J=11 Hz), 8.73 (1H, d, J=11 Hz), 9.60 (1H, d, J=11 Hz);[6] UV_{max} 257 nm (log ε 4.46), 290 (4.25), 400 (4.45); IR 3190 (NH), 2200 (C≡N), 1707 cm^{-1} (C=O). Found: C, 68.14; H, 4.52; Cl, 10.21; N, 7.68%. Calcd for $C_{20}H_{15}ClN_2O_2$: C, 68.45; H, 4.31; Cl, 10.10; N, 7.98%. When a solution of **5c** in benzene was set aside for 4 days, **6c** was obtained in 24% yield. (b) The above reaction (**1** (1.00 g), dioxane (50 ml), the nitrile (0.50 g), and NaH (0.154 g) in dioxane (50 ml)) was carried out under reflux for 1 h to give the starting material (0.240 g), **2c** (0.882 g, 87%), and **6c** (0.025 g, 3%). **2c**: Yellow prisms (from benzene), mp 165—166 °C, NMR δ=1.43 (3H, t, J=7 Hz), 4.43 (2H, q, J=7 Hz), 6.57 (1H, s), 7.2—7.7 (5H, m), 7.8—8.2 (3H, m), 8.87 (1H, bd, J=9 Hz), 9.95 (1H, bd, J=9 Hz); UV_{max} 287 nm (log ε 4.59), 324 (3.90), 345 (3.58), 462 (2.97); IR 2250 (C≡N), 1675 cm^{-1} (C=O). Found: C, 75.63; H, 5.22; N, 8.58%. Calcd for $C_{20}H_{16}N_2O_2$: C, 75.93; H, 5.10; N, 8.86%. (c) A solution of **1** (1.00 g) in abs ethanol (30 ml) was added into a mixture of the nitrile (1.00 g), sodium (0.20 g), and abs ethanol (70 ml), heated under reflux for 1 h, and worked up to give **2c** (0.008 g, 1%), **5c** (1.05 g, 70%), and **6c** (0.025 g, 2%), successively.

We thank Dr. T. Morita, Tohoku University, for NMR spectral determinations.

References

1) Part II, N. Abe, Y. Tanaka, and T. Nishiwaki, *J. Chem. Soc., Perkin Trans. 1*, in press.
2) S. Matsumura, *Bull. Chem. Soc. Jpn.*, **34**, 1361 (1961).
3) N. Abe, *Heterocycles*, **4**, 221 (1976).
4) Swee-Ong Chua, M. J. Cook, and A. R. Katritzky, *J. Chem. Soc., Perkin Trans. 2*, **1973**, 2111.
5) The reaction of 2-chloroazulene with fluorenide anion takes place at C-6: T. Nozoe, "The Chemistry of Nonbenzenoid Aromatic Compounds," ed by M. Oki, Butterworth, London (1970), p. 267.
6) The NH proton was not observed.
7) The NMR spectrum indicates that this compound is a mixture of geometrical isomers.

BULLETIN OF THE CHEMICAL SOCIETY OF JAPAN VOL. 51 (2), 669—670 (1978)

Oxyhydrative Scission of *trans*-2-Butene in the Liquid Phase under Pressure

Yusaku TAKITA, Takashi MAEHARA, Noboru YAMAZOE, and Tetsuro SEIYAMA

Department of Materials Science and Technology, Faculty of Engineering, Kyushu University 36, Hakozaki, Higashi-ku, Fukuoka 812

(Received June 25, 1977)

Synopsis. The liquid phase oxidation of *trans*-2-butene under pressure using a V_2O_5–MoO_3 catalyst suspended in water has been proved to yield acetic acid and aldehyde selectively at 170 °C. Taking into account the results of the oxidation of intermediate compounds, it is suggested that the reaction follows the same oxyhydrative scission mechanism as has been proposed for the gas phase oxidation.

The authors have reported the partial oxidation of lower olefins over V_2O_5–MoO_3 catalyst in the presence of water vapor at 160—290 °C.[1,2] The reaction is unique in that the carbon skeletons are oxidatively cleaved into smaller aldehydes and/or carboxylic acids. The following "Oxyhydrative Scission" mechanism has been proposed.[3]

$$\mathrm{R\text{-}CH{=}CH\text{-}R' \xrightarrow{H^+} R\text{-}\overset{+}{C}H_2\text{-}CH\text{-}R' \xrightarrow[\text{or } OH^-]{H_2O}}$$

$$\mathrm{R\text{-}CH_2\text{-}\underset{\displaystyle OH}{\underset{|}{CH}}\text{-}R' \xrightarrow{[O]} R\text{-}CH_2\text{-}\underset{\displaystyle O}{\overset{\|}{C}}\text{-}R' \xrightarrow{[O]}}$$

$$\mathrm{RCHO + R'COOH} \qquad (1)$$

In the oxidation of higher olefins, however, desorption of acidic products from the catalyst surface requires higher reaction temperatures, which are less favorable for the hydration process involved in Eq. 1. Too great a rise in temperature is also undesirable for the selectivity of the reaction. This dilemma may be solved if the same reaction can be carried out effectively in the liquid phase. Therefore, oxidation of *trans*-2-butene and the proposed intermediate products has been examined in various solvents by using a V_2O_5–MoO_3 catalyst suspension.

Experimental

The V_2O_5–MoO_3 (V/Mo=9/1) catalyst was prepared from aqueous solutions of ammonium methavanadate and ammonium paramolybdate. The powder obtained was calcined at 550 °C for 5 h in air, and sieved to 30—40 mesh.

The liquid phase oxidation under atmospheric pressure was examined in a closed gas-liquid reactor equipped with a gas burette. The catalyst (2 g) was suspended in water or other solvents (30 cm^3) in the reactor. After degassing the reactor briefly, a gaseous reactant (*trans*-2-butene) was introduced as a mixture with oxygen, while the liquid reactants (10—50 mmol) were injected into the reactor through a sampling port. Oxidation under pressure was carried out in a SUS autoclave with an internal volume of 300 cm^3. After introduction of 3 g of catalyst and 60 g of water, *trans*-2-butene (38.57 mmol) and oxygen were introduced to a total pressure of 20 kg/cm^2 at 0 °C. After the reaction, the liquid and gas phases were separately subjected to gas chromatographic analyses.

Results and Discussion

In the gas phase oxidation, butenes are oxidized to acetic acid and acetaldehyde *via* *s*-butyl alcohol (*s*-BuOH) and ethyl methyl ketone (EMK).

1) Liquid Phase Oxidation under Ordinary Pressure. Gaseous mixtures of *trans*-2-butene and oxygen with the butene/O_2 ratios of 1/9 and 9/1 were brought into contact with the V_2O_5–MoO_3 catalyst suspended in water at 50, 70, and 90 °C, but no oxidation products could be detected. This appears to be due to insufficient reaction conditions. For the oxidation of *trans*-2-butene, solvents other than water were not examined, because the first step of the reaction (Eq. 1) necessitates the presence of water.

The liquid phase oxidation of *s*-BuOH was examined in various solvents. As a result, while no reaction occurred in water, benzene, or chlorobenzene, EMK was selectively obtained in dimethyl sulfoxide (DMSO). For example, the oxidation in DMSO at 125 °C for 13 h converted 10.8% of *s*-BuOH and the selectivity to EMK was 89%. No reaction of *s*-BuOH took place in DMSO without catalyst. In contrast to the gas phase oxidation of *s*-BuOH over the same catalyst, where considerable amounts of butenes are co-produced, no butenes were detected. The role of DMSO is not clear.

Liquid EMK could be oxidized at a considerable

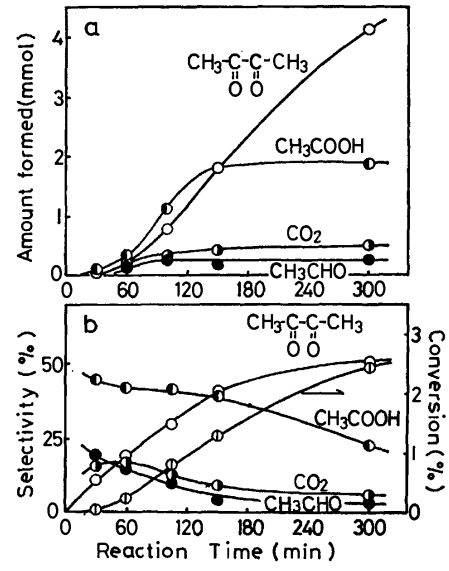

Fig. 1. Liquid phase oxidation of ethyl methyl ketone (EMK). Catalyst: V_2O_5–MoO_3 (V/Mo=9/1) 2 g, EMK: 335.4 mmol, 55 °C, 1 atm.

rate even at 55 °C without the addition of any other solvents (Fig. 1). Acetic acid, acetaldehyde, and CO_2 were formed only in the earlier periods up to 150 min, while the formation of biacetyl continued over the whole reaction period. It is known that the autoxidation of ketone in a homogeneous liquid phase proceeds *via* a hydroperoxide intermediate which is formed by the abstraction of a hydrogen atom at the α-position, followed by the addition of an oxygen molecule there.[4-6] The hydroperoxide intermediate then decomposes in the following two ways.[7]

$$\mathrm{R\text{-}CH(OOH)\text{-}C(=O)\text{-}R'} \longrightarrow \mathrm{R\text{-}C(=O)\text{-}C(=O)\text{-}R' + H_2O} \quad (2)$$

$$\mathrm{R\text{-}CH(OOH)\text{-}C(=O)\text{-}R'} \longrightarrow \mathrm{RCHO + R'COOH} \quad (3)$$

This mechanism can account for the main products in the present reaction. However, the time course of the reaction does not seem to be fully consistent with this mechanism. It is known that the latter reaction (Eq. 3) is accelerated in the presence of carboxylic acids owing to the intervention of a carbonium ion mechanism, and the formation of acetic acid should then increase with time in an autocatalytic manner, provided that a hydroperoxide is a substantial intermediate. This is not the case in the present reaction, suggesting an intermediate other than a hydroperoxide. A surface complex between molecular oxygen adsorbed on the catalyst and EMK might be suggested as the intermediate by analogy with the gas phase oxidation.

2) Liquid Phase Oxidation of trans-*2-Butene under Pressure.* As described above, neither the hydration of *trans*-2-butene nor the oxidative dehydrogenation of *s*-BuOH could be attained in the liquid phase under atmospheric pressure below 90 °C. Accordingly, the liquid phase oxidation of *trans*-2-butene was examined at temperatures above 100 °C under pressure.

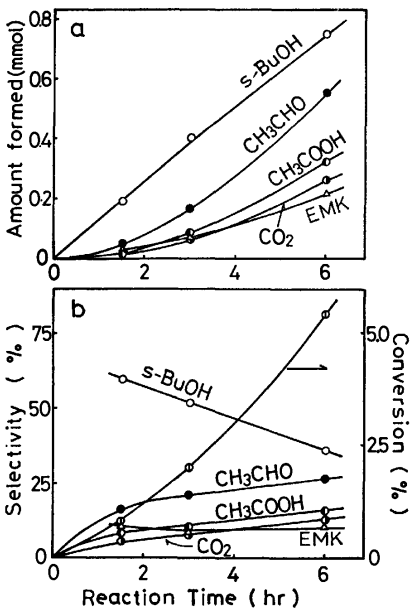

Fig. 2. Oxidation of *trans*-2-butene.
Catalyst; V_2O_5–MoO_3 (V/Mo=9/1) 3.0 g *trans*-2-butene 38.57 mmol, H_2O 60 cm³, O_2 20 kg/cm², 170 °C, total pressure 36 kg/cm².

Figure 2 shows the results of the oxidation at 170 °C under pressure of 36 kg/cm². *s*-BuOH, EMK, acetaldehyde, acetic acid, and CO_2 were obtained, together with small amounts of propionic and butyric acids.

In the homogeneous oxidation of paraffins in nonaqueous solvents in the presence of soluble metal naphthenate catalysts, it has been reported that the formation of hydroperoxides (HPO) and their decomposition to alcohols, ketones, and acids proceed *via* the Haber-Weiss mechanism.[8] In the autoxidation of lower olefins, however, it is known that the product distributions are different. Imamura *et al.*[9] have investigated the oxidation of butenes in benzene at 145 and 175 °C under a pressure of 45 atm with a homogeneous catalyst of manganese naphthenate, and obtained butene oxides (19—26% selectivity), butanediol esters (≈15.8%), and a residue with higher boiling points (41—48%), together with small amounts of aldehydes, ketones, and carboxylic acids.

In the present heterogeneous reaction, the product distribution was similar to that in the catalytic oxidation of butenes in the gas phase, and did not include products characteristic of autoxidation, such as epoxides and glycol esters. While the yields of all the products increased with time, the selectivity to *s*-BuOH was relatively high in the initial stage. This fact suggests that *s*-BuOH is a primary product from the starting olefin, as in the gas phase catalytic oxidation. The *s*-BuOH formed is likely to be oxidized to EMK and then to acetaldehyde and acetic acid, as in the gas phase oxidation. It seems reasonable to assume that these oxidation processes also take place on the catalyst surface, though further experiments are needed to verify this assumption. We consider that the mechanism of the liquid phase oxidation of *trans*-2-butene over the suspended V_2O_5–MoO_3 catalyst would be similar to that of the gas phase oxidation over the same catalyst.

References

1) T. Seiyama, K. Nita, T. Maehara, N. Yamazoe, and Y. Takita, *J. Catal.*, **49**, 164 (1977).
2) Y. Takita, K. Nita, T. Maehara, N. Yamazoe, and T. Seiyama, *J. Catal.*, **50**, 364 (1977).
3) Y. Takita, T. Maehara, N. Yamazoe, and T. Seiyama, *J. Catal.*, to be submitted.
4) D. B. Sharp, L. W. Patton, and S. E. Whitecomb, *J. Am. Chem. Soc.*, **73**, 5600 (1951).
5) A. G. Pinkus, W. C. Serross, and K. K. Lum, *J. Org. Chem.*, **32**, 2649 (1967).
6) W. H. Richardson and R. F. Steed, *J. Org. Chem.*, **32**, 771 (1967).
7) W. Pritzkow, *Ber. B*, **88**, 572 (1955).
8) N. M. Emanuel, E. T. Denisov, and Z. K. Maizus, "Liquid Phase Oxidation of Hydrocarbons," Plenum Press, (1967).
9) J. Imamura, T. Saito, and N. Ohta, *Kogyo Kagaku Zasshi*, **71**, 1642 (1968).

BULLETIN OF THE CHEMICAL SOCIETY OF JAPAN, VOL. 51 (2), 671—672 (1978)

A Study of Ion-Solvent Interaction of Tetraalkylammonium and Common Alkali Metal Ions in Ethylene Carbonate from Electrolytic Conductance Data

Ram GOPAL and Sudha SINGH

Chemistry Department, Lucknow University, Lucknow, U. P., India

(Received May 6, 1977)

Synopsis. Ion-solvent interaction in solutions of some tetraalkylammonium and common alkali metal iodides in ethylene carbonate, from the point of view, of electrical conductance and the derived Walden product, has been examined in this communication. The Debye-Hückel-Onsager equation appears to hold good for all the salts in the temperature and concentration range studied here. Dependence of the Walden product on temperature and radius of cation reveals that the R_4N^+ ions do not interact appreciably with the solvent but Li^+, Na^+, K^+, and Rb^+ ions appear to be solvated.

Ion-solvent interaction studies in some highly polar and non-hydrogen bonded solvents, having medium dielectric constant, namely, dimethylsulfoxide (DMSO)[1,2] and propylene carbonate (PC),[3,4] have been reported in earlier communications from this laboratory. It appears interesting to study the behavior of these salts in an aprotic, dipolar solvent of high dielectric constant like ethylene carbonate (EC) in order to have a wider picture of solute-solvent interaction. This solvent is, like DMSO and PC, highly polar and non-hydrogen bonded; its dielectric constant[5] is 85.81 at 40 °C. A few studies on conductance of electrolytes have been reported in this solvent,[6] but these are confined to 40 °C only and hence of little use in studying ion-solvent interaction. This situation and the interesting solvent properties of ethylene carbonate prompted the investigation reported in this communication.

Experimental

Ethylene carbonate (Fluka, purum) was fractionally crystallized three times. The sample thus obtained was distilled under reduced pressure. The middle fraction of the distillate was collected in a dark colored bottle and kept in a dry box. The sample was found to melt sharply at 36.5 °C and its electrical conductance was of the order of 10^{-6} Ω^{-1} cm^{-1}.

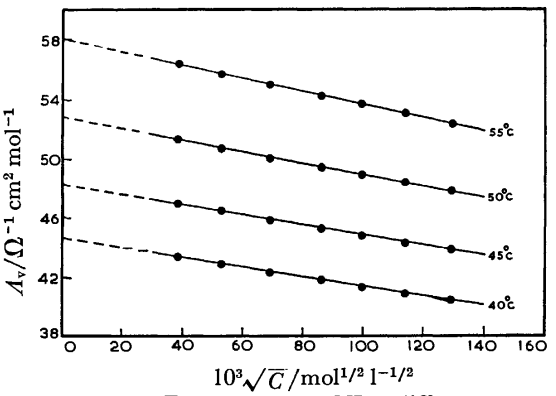

Fig. 1. Λ_v *vs.* $\sqrt{C}$ curves for Me_4NI at different temperatures in ethylene carbonate.

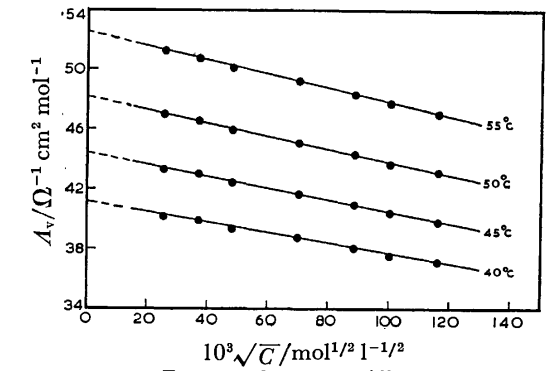

Fig. 2. Λ_v *vs.* $\sqrt{C}$ curves for KI at different temperatures in ethylene carbonate.

Tetraalkylammonium iodides (DPI, USA) and the common salts (BDH, AR) were purified in the usual manner.[7] The experimental procedure for measuring the electrical conductance was the same as described earlier. The precision of measurement was about ±0.03%.

Table 1. Limiting equivalent conductivities Λ_0/Ω^{-1} cm^2 mol^{-1} of some salts in EC

Salt	Limiting equivalent conductivity at			
	40 °C	45 °C	50 °C	55 °C
LiI	32.18	34.76	38.06	42.15
NaI	37.89	40.94	44.53	48.85
KI	41.20	44.42	48.10	52.50
RbI	42.35	45.52	49.20	53.80
Me_4NI	44.75 (44.81)	48.19	52.88	58.20
Et_4NI	42.70 (42.83)	45.87	49.49	53.84
Pr_4NI	39.75	42.60	46.16	50.30
Bu_4NI	37.45 (37.40)	40.70	44.08	47.86
Pen_4NI	35.68	38.25	41.50	45.52
Hex_4NI	33.40	35.70	38.94	47.81
Hep_4NI	31.96	34.25	37.05	40.50

Values in parenthesis are from Ref. 6.

Table 2. Slopes S_T and S_E in ethylene carbonate at 40 °C

Salt	S_T/Ω^{-1} cm^2 $mol^{-3/2}$ $l^{3/1}$ (Theoretical slope)	S_E/Ω^{-1} cm^2 $mol^{-3/2}$ $l^{1/2}$ (Experimental slope)	Deviation $\frac{(S_T-S_E)}{S_E}\times 100$
LiI	32.15	30.58	−4.6
NaI	33.30	31.45	−5.8
KI	33.72	33.50	+0.65
RbI	33.92	34.65	+1.8
Me_4NI	34.34	33.60	−2.2
Et_4NI	33.98	34.58	+1.7
Pr_4NI	33.47	35.40	+5.4
Bu_4NI	33.07	36.50	+9.5
Pen_4NI	32.76	40.45	+19.2
Hex_4NI	32.37	38.45	+15.8
Hep_4NI	32.11	34.34	+6.5

Table 3. Walden product of some salts in ethylene carbonate

Salt	Walden product ($\Lambda_0\eta_0/\Omega^{-1}$ g cm^{-1} mol^{-1}) at			
	40 °C	45 °C	50 °C	55 °C
LiI	0.555	0.599	0.606	0.615
NaI	0.702	0.705	0.709	0.713
KI	0.762	0.765	0.766	0.766
RbI	0.783	0.784	0.784	0.785
Me_4NI	0.828	0.836	0.832	0.835
Et_4NI	0.789	0.790	0.788	0.785
Pr_4NI	0.735	0.734	0.738	0.734
Bu_4NI	0.693	0.701	0.702	0.698
Pen_4NI	0.660	0.658	0.662	0.664
Hex_4NI	0.618	0.615	0.620	0.610
Hep_4NI	0.590	0.591	0.590	0.592

Results and Discussion

From the electrolytic conductance data thus obtained, Λ_v *vs.* $\sqrt{C}$ curves were drawn for different salts at various temperatures. The plots for Me_4NI and KI are given in Figs. 1 and 2, as typicals of tetraalkylammonium and common salts respectively. It may be noted that the plots are almost straight lines suggesting that the simple Debye-Hückel-Onsager theory of electrolytic conductance is applicable to these solutions and the salts are completely ionized in ethylene carbonate. The limiting equivalent conductivities of different salts at various temperatures, obtained from the usual extrapolation procedure, are given in Table 1.

The theoretical slope S_T of the Λ_v *vs.* $\sqrt{C}$ curves, according to Debye-Hückel theory is given by

$$S_T = A + B\Lambda_0,$$

where $A = \frac{82.42}{\eta_0(\varepsilon T)^{1/2}}$ and $B = \frac{8.203\times 10^5}{(\varepsilon T)^{3/2}}$.

From the Λ_0 values given in Table 1, S_T values for different cases at 40 °C have been calculated and compared with the corresponding experimental slopes S_E in Table 2. The value of the dielectric constant used for calculating the experimental slope is $\varepsilon_{40\,°C}=85.81$ and viscosity η/g m^{-1} s^{-1}=1.850, as determined experimentally in this laboratory. Table 2 clearly shows that there is a good agreement between the experimental and theoretical slopes indicating that the simple Debye-Hückel-Onsager theory of strong electrolytic conductivity is applicable to these solutions.

The nature of ion-solvent interaction in EC may be examined from the temperature and ionic radius dependence of the Walden product. Unfortunately, due to lack of the ionic conductance data, at different temperature, only the electrolytic Walden product can be used for the present study. It is assumed that the variations in the Walden product are mainly due to cations since large anions do not interact appreciably in aprotic solvents. Viscosities of the solvent at different temperatures, required to calculate the Walden product, were obtained experimentally and are η/g m^{-1} s^{-1}= 1.850 (40 °C), 1.722 (45 °C), 1.590 (50 °C) and 1.459 (55 °C). The values of the Walden product, $\Lambda_0\eta_0$, for different salts at various temperatures, are given in Table 3.

Although the temperature dependence of the Walden product, can be examined from the data given in Table 3, the plots of $\Lambda_0\eta_0$ against temperature, given in Fig. 3, make it more explicit. It may be noted that $\Lambda_0\eta_0$ for the smaller alkali metal iodides appears to increase slightly with the rise in temperature, indicating a net structure promoting effect of these salts in EC. As pointed out in the earlier paragraph, anions, more particularly the larger ones, are not expected to interact strongly with the aprotic solvents, it is reasonable to presume that the structure enhancement is due to the cation-solvent interaction. Besides, since the Walden product of the larger alkali metal and R_4N-iodides in which the cation may be expected to interact very weakly, if at all, with the solvent, is almost independent of temperature, I^- ion would also be more or less unsolvated. Thus increase in the Walden product with the rise of temperature for smaller alkali metal iodides must be ascribed to the cations which interact appreciably with the solvent molecules and are solvated. The large R_4N^+ ions do not appear to interact significantly, with EC.

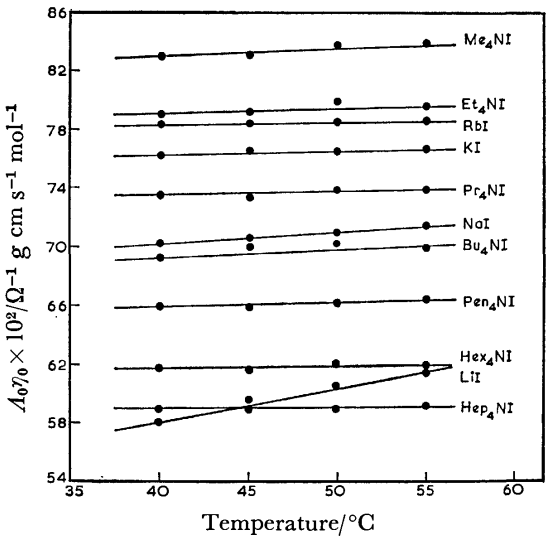

Fig. 3. Walden product $\Lambda_0\eta_0$ *vs.* temperature plots in ethylene carbonate for some electrolytes.

The same conclusions can be arrived at if the variation of the Walden product with the radius of the cation is examined. Since iodide ion is common to all the salts studied here, it may be assumed, as before, that the variation in the Walden product is due to cation only. It may be noted that for the alkali metal salts, the Walden product varies directly with the radius of the cation; this indicates that the size of the cation in solution is larger, the smaller its radius or in other words, the smaller the cation, the more highly solvated it is. Opposite appears to be the case with the R_4N^+ ions. for which the Walden product varies inversely as the radius showing that these ions are not solvated to any appreciable extent. Their size remains almost unchanged in solution and there is no appreciable electrostatic ion-solvent interaction with EC.

Authors are grateful to the Society of the Sigma Xi of USA for financial assistance and to the Head, Chemistry Department, Lucknow University, for research facilities for undertaking this investigation.

References

1) J. S. Jha, S. Singh, and R. Gopal, *Bull. Chem. Soc. Jpn.*, **48**, 2782 (1975).
2) R. Gopal and P. Singh, *Indian J. Chem.*, **14A**, 388 (1976).
3) S. Singh, J. S. Jha, and R. Gopal, *Indian J. Chem.*, **14A**, 127 (1976).
4) R. Gopal and S. Singh, *Indian J. Chem.*, **14A**, 2782 (1976).
5) R. Payne and I. E. Theodrou, *J. Phys. Chem.*, **76**, 28921 (1972).
6) R. F. Kempa and W. H. Lee, *J. Chem. Soc.*, **1961**, 100.
7) R. D. Singh, P. P. Rastogi, and R. Gopal, *Can. J. Chem.*, **46**, 3525 (1968).

The Microenvironmental Effect of Cyclodextrin on the Acid Dissociation of Some Azo Dyes in Aqueous Solutions

Yoshihisa MATSUI and Kazuo MOCHIDA

Department of Agricultural Chemistry, Shimane University, Nishikawazu, Matsue 690

(Received May 14, 1977)

The effects of α- and β-cyclodextrins (CD) on the acid dissociations and tautomeric equilibria of sodium 4-(4′-hydroxy-1′-naphthylazo)-1-naphthalenesulfonate (**1**) and of the conjugate acid (**2**) of Methyl Orange were spectrophotometrically examined and were compared with the effect of a nonpolar solvent (THF). The apparent pK_a values for the dyes decreased with increasing CD concentration. The effect of CD is mainly explained in terms of the hydrophobic interactions between the azo dyes and CD, resulting in a shift in the tautomeric equilibria from less acidic azonium or hydrazone forms to more acidic azo forms of **1** and **2** in an aqueous solution.

The acid dissociation of an indicator dye is generally facilitated by the formation of an inclusion complex between the dye and cyclodextrin (CD) in an aqueous solution.[1-6] This phenomenon is interesting in connection with the microenvironmental effect of an enzyme on the acid dissociation of ionizing groups at the bonding or catalytic site.[7,8] The decrease in pK_a of a dye upon formation of a CD complex has been tentatively attributed to the space alkalinity of CD[1,2] which involves a number of electronegative oxygen atoms in a molecule. On the other hand, Broser *et al.*[4-6] have explained the change in pK_a in terms of a dipole-ion interaction between CD and a dye as follows. A dissociated dye may be more polarizable than the corresponding undissociated dye, so that a dipolar CD molecule associates more tightly to the former than the latter, resulting in enhancement of the acid dissociation of the dye. These arguments, however, completely neglect the hydrophobic property of the cavity of a CD molecule, a property later recognized to play an important role in the binding and catalytic processes of CD.[3,9] In a protein-[7,8] or micellar-[10] dye system, it has frequently been shown that the hydrophobic microenvironment of a binding site significantly affects the pK_a value of a dye. Recently, Connors and Lipari[11] and Miyaji *et al.*[12] reported that the dissociation of carboxylic and barbituric acids in aqueous solutions is retarded by the addition of CD. These observations cannot be explained in terms of the idea of Broser *et al.*, but are well explained in terms of the hydrophobic microenvironment of the CD cavity.

The present study was undertaken to elucidate the contribution of the hydrophobicity of the CD cavity to the acid dissociation of indicator dyes. For this purpose, the behavior of sodium 4-(4′-hydroxy-1′-naphthylazo)-1-naphthalenesulfonate (**1**) and of the conjugate acid (**2**) of Methyl Orange was examined in detail. Both dyes ate known to be good hydrophobic probes, which exhibit absorption spectra that are very sensitive to the microscopic environment around the dye molecules.[13-16] The association of CD with **2** has been examined in some detail by Broser *et al.*[4-6] and Yamada *et al.*[17]

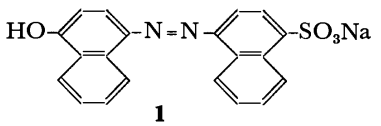

1

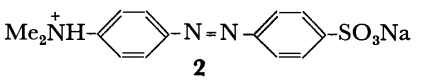

2

Experimental

Materials. α-CD and β-CD were prepared by the method of Lane and Pirt.[18] These substances were separated and purified according to the directions given by Cramer and Henglein.[19] Methyl α-D-glucopyranoside and Methyl Orange of reagent grade were used without further purification. Dye **1** was prepared by coupling 4-diazonio-1-naphthalenesulfonate to 1-naphthol. The crude product was purified by repeated salting-out from an aqueous solution with sodium acetate, followed by recrystallization from water and then washing with hot ethanol. Tetrahydrofuran (THF) of reagent grade was used after distillation, bp 66—67 °C. The aqueous buffer solutions used in the present study were H_2SO_4–Na_2SO_4 (pH 1—2), sodium citrate–HCl (pH 2—4), citric acid–Na_2HPO_4 (pH 3—7), citric acid–NaOH (pH 4—6), Na_2HPO_4–KH_2PO_4 (pH 6—7), KH_2PO_4–$Na_2B_4O_7$ (pH 6—9), and $Na_2B_4O_7$–NaOH (pH 9—12). The ionic strengths (I_c) of buffer solutions were adjusted using Na_2SO_4 to 0.05 M for CD–**1** systems and 0.50 M for CD–**2** systems unless otherwise noted.

Apparatus. Absorption spectra were recorded using a Hitachi Model 124 spectrophotometer. The cells (1.0 cm) were maintained at 25±0.1 °C by means of a jacket through which water was circulated from a constant-temperature bath. The pH of each aqueous solution was measured by means of an Orion Model 801 A digital pH/mV meter.

Spectrophotometric Determination of an Apparent Dissociation Constant for a CD-Dye Inclusion Complex. The absorption spectra of dyes **1** and **2**, at a given concentration (*ca.* 0.03 mM for **1** and *ca.* 0.02 mM for **2**) and at a given pH, were recorded for various CD concentrations (0.0—2.0 mM). Each CD–dye system gave an isosbestic point, indicating the formation of a 1 : 1 complex of CD and the dye. The changes in absorbance with CD concentration were measured at 482 and 528 nm for β-CD–**1** systems in acidic and basic solutions, respectively, and at 507 and 530 nm for CD–**2** systems in strongly and weakly acidic solutions, respectively. According to Hildebrand and Benesi,[20] the change in absorbance (ΔA) is related to the total concentration (c_0) of CD by the following equation:

$$\frac{c_0 s_0}{\Delta A} = \frac{K_d}{\Delta\varepsilon} + \frac{c_0}{\Delta\varepsilon}, \quad (1)$$

where s_0 is the total dye concentration, and K_d and $\Delta\varepsilon$, the apparent dissociation constant of a CD–dye inclusion complex and the difference in the molar absorption coefficient between the free and complexed dyes, respectively. The plot of $c_0 s_0/\Delta A$ *vs.* c_0 gave a straight line for each CD–dye system, and the values of K_d and $\Delta\varepsilon$ were determined from the slope and intercept of the line.

Spectrophotometric Determination of the Apparent Acid Dissocia-

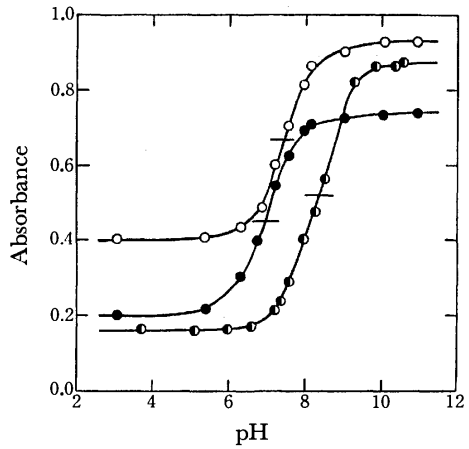

Fig. 1. Plots of absorbances of **1** (3×10^{-5} M) *vs.* pH's at 25 °C.
○: No additive and $\lambda=528$ nm, ●: [β-CD] = 2.02 mM and $\lambda=528$ nm, ◐: [THF] = 3.72 M and $\lambda=535$ nm.

tion Constant ($K_{a,app}$) for an Indicator Dye. Seven to ten buffer solutions were prepared with given concentrations of a dye and an additive, such as CD or THF, and with different pH values. The absorbance at an appropriate wavelength for each solution was plotted against the pH of the solution. Figure 1 illustrates examples of such plots for **1**. The $pK_{a,app}$ values were determined by graphical evaluations of the pH at which $A=(A_a+A_b)/2$, where A_a and A_b are the absorbances under sufficiently acidic and basic conditions, respectively.

Results and Discussion

Change in Absorption Spectrum of a Dye upon the Addition of CD. The absorption spectra of dyes **1** and **2** in a sufficiently acidic solution were markedly changed by the addition of CD, except for the case of the α-CD–**1** system for which the addition of α-CD gave only a slight change in the spectrum of **1**. The molecular cavity of α-CD may be too small to include the naphthyl groups of **1**. Methyl α-D-glucopyranoside had virtually no effect on the spectra of **1** and **2**. The spectral change in the β-CD–**1** system is illustrated in Fig. 2.

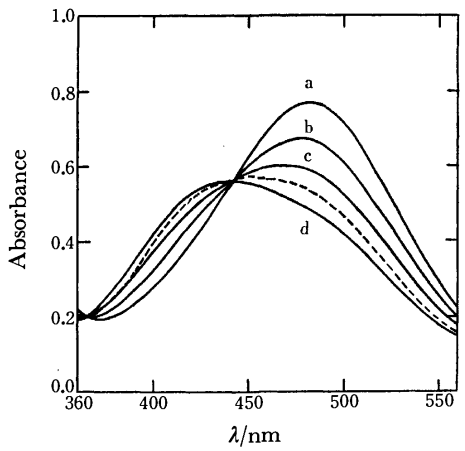

Fig. 2. Absorption spectra of **1** (3.97×10^{-5} M) at pH 4.19 and 25 °C.
Solid line: [β-CD] = (a) 0.00 mM, (b) 0.20 mM, (c) 0.51 mM, (d) 2.03 mM.
Dashed line: [THF] = 3.77 M.

The absorbance around 480 nm markedly decreased and that around 420 nm increased with increasing β-CD concentrations. Isosbestic points were observed at 365 and 441 nm, indicating that β-CD forms a 1 : 1 complex with **1**. The spectral change in **2** upon the addition of α- or β-CD was also very large as reported by Broser,[5] who also showed that both α- and β-CD form 1 : 1 complexes with **2** at low CD concentrations.

When a nonpolar solvent, THF, was added to a sufficiently acidic solution of **1** or **2**, a significant spectral change was observed, which was quite similar to that caused by the addition of CD. An absorption spectrum of **1** in the presence of THF is shown by the dashed line in Fig. 2. It is known that 4-(arylazo)-1-naphthols[14,16,21] and the conjugate acids of 4-aminoazobenzene derivatives[5,13,21] are in tautomeric equilibria.

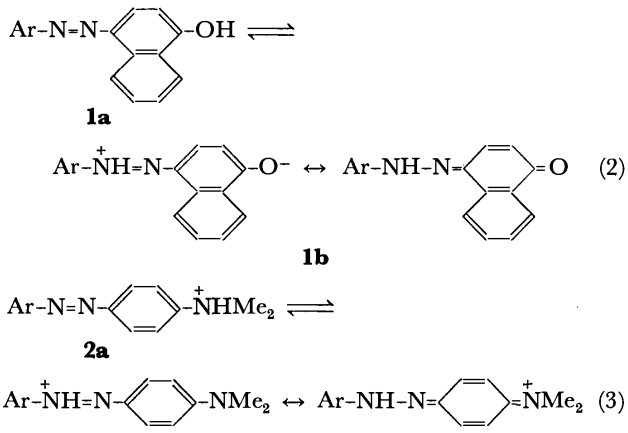

The azonium or hydrazone forms (**1b** and **2b**) are predominant species in aqueous solutions, whereas the azo forms (**1a** and **2a**) are predominant in apolar solutions or microenvironments. Thus, the above spectral changes indicate that both **1** and **2** are bound to the hydrophobic regions of CD molecules to give mainly **1a**– and **2a**–CD complexes, respectively.

Effect of Ionic Strength on the K_d Values for CD–Dye Complexes. In order to determine which dipole-ion interactions and hydrophobic interactions contribute

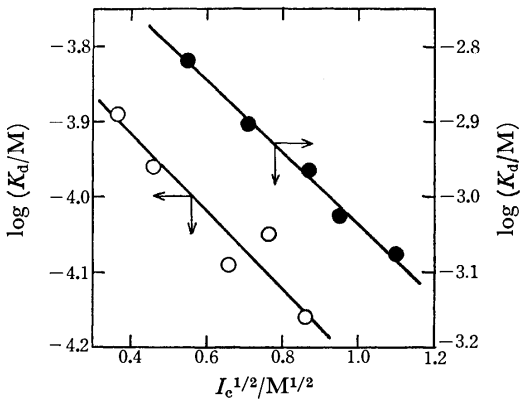

Fig. 3. Plots of log K_d *vs.* $I_c^{1/2}$ for α-CD–**2** systems at 25 °C. The I_c's were adjusted by the addition of Na_2SO_4.
○: pH = 6.7±0.1 (phosphate buffer),
●: 0.10 M H_2SO_4.

mainly to the association of the CD with the dyes, the effect of ionic strength (I_c) on the K_d values were examined for the CD–dye complexes. Electrostatic interactions, in general, weaken with increasing I_c.[7] If the dipole-ion interactions are dominant, as has been suggested by Broser,[5] the K_d value should increase with increasing I_c. On the other hand, hydrophobic interactions are generally enhanced by an increase in I_c (salting-out effect).[22] Figure 3 shows the plot of $\log K_d$ *vs.* $I_c^{1/2}$ for complexes of α-CD with **2** and its conjugate base. All $\log K_d$ values decrease with increasing I_c.

Dye **1** is too insoluble in an aqueous solution for I_c above 0.05 M to permit a precise examination of the effect of I_c on the K_d value for a β-CD–**1** system. However, Mochida *et al.* previously showed[23] that the K_d value for the complex of β-CD with Orange I (**3**), an analog of **1**, decreases with increasing I_c.

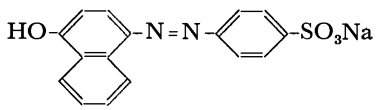

3

These observations strongly suggest that hydrophobic, rather than electrostatic, interactions play a dominant role in the associations of CD with dyes.

Effect of CD on the $pK_{a,app}$ *Values of Azo Dyes.* Table 1 gives the $pK_{a,app}$ values for dyes **1**—**3** in the absence and in the presence of α-CD, β-CD, and/or THF. The observed $pK_{a,app}$ values decrease with increasing CD concentration for all CD–dye systems. The addition of methyl α-D-glucopyranoside up to 100 mM had virtually no effect on the $pK_{a,app}$ values of the azo dyes.

In order to explain the dependence of the $pK_{a,app}$ values on the CD concentrations, a reaction system is postulated which involves inclusion, acid-dissociation, and tautomeric equilibrium processes, thus

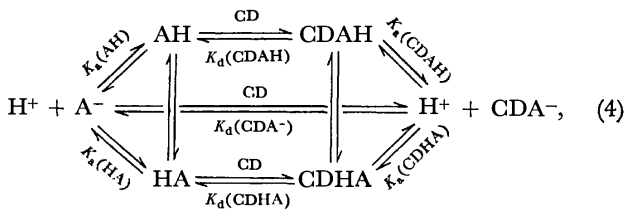

where AH and HA represent the azo form and the azonium or hydrazone form of the azo dye, respectively, K_d and K_a, the dissociation constant of the inclusion complex and the acid-dissociation constant, respectively, for each species given in parenthesis. From reaction

Table 1. Observed and calculated values of $pK_{a,app}$ for CD-azo dye systems at 25 °C

Dye	Additive	Concentration / mM	$pK_{a,app}$ (obsd)	$pK_{a,app}$ (calcd)
1[a]	none	0.000	7.43	(7.43)
	α-CD	10.4	7.50	—
	β-CD	0.591	7.10	7.10
		2.02	7.02	7.01
	THF	3720	8.44	—
2[b]	none	0.000	3.37	(3.37)
	α-CD	0.104	3.07	3.07
		0.520	2.72	2.68
		1.00	2.58	2.53
	β-CD	0.402	3.16	3.12
		1.00	2.96	2.95
	THF	3720	2.88	—
3[c]	none	0.000	8.20	(8.20)
	β-CD	0.500	8.00	8.01
		1.00	7.89	7.89
		2.50	7.72	7.74
		5.00	7.62	7.65
		10.0	7.60	7.59

a) $I_c=0.050$ M; b) $I_c=0.50$ M; c) $I_c=0.025$ M.

4, we can easily derive the following relations from the law of mass action:

$$pK_{a,app}(c_0=0) = \log\{K_a(AH)^{-1}+K_a(HA)^{-1}\}, \quad (5)$$

$$pK_{a,app} = pK_{a,app}(c_0=0) - \log\frac{1+c_0K_d(CDA^-)^{-1}}{1+c_0\{K_d(CDAH)+K_d(CDHA)\}^{-1}}, \quad (6)$$

and

$$pK_{a,app}(c_0=\infty) = pK_{a,app}(c_0=0) - \log\frac{K_d(CDAH)+K_d(CDHA)}{K_d(CDA^-)}, \quad (7)$$

where $pK_{a,app}$ $(c_0=0)$ and $pK_{a,app}$ $(c_0=\infty)$ are the $pK_{a,app}$ values at null and infinite CD concentrations, respectively. Equations similar to Eq. 6 have been derived[11,12] for reaction systems which involve inclusion and acid-dissociation processes, but which did not involve tautomeric equilibrium processes. The values of $\{K_d(CDAH)+K_d(CDHA)\}$ and $K_d(CDA^-)$ in Eqs. 6 and 7 are equal to the K_d in Eq. 1 for each CD–dye system in sufficiently acidic and basic solutions, respectively, and can be experimentally determined (Table 2). The $pK_{a,app}$ values in the presence of CD were calculated on the basis of Eq. 6 using the data in Table 2 and the $pK_{a,app}$ $(c_0=0)$ values determined experimentally, and are compared with the observed values (Table 1). They are in good agreement with

Table 2. The values of $\{K_d(CDAH)+K_d(CDHA)\}$, $K_d(CDA^-)$ and $\{pK_{a,app}(c_0=0)-pK_{a,app}(c_0=\infty)\}$ for CD-azo dye systems at 25 °C

System	$K_d(CDAH)+K_d(CDHA)$ / mM	$K_d(CDA^-)$ / mM	$pK_{a,app}(c_0=0)-pK_{a,app}(c_0=\infty)$
β-CD-**1**	0.390	0.134	0.46
α-CD-**2**	1.25	0.0882	1.15
β-CD-**2**	2.70	0.380	0.85
β-CD-**3**	3.00	0.588	0.71

each other to within the experimental error. This fact indicates that the chemical equilibria of Reaction 4 are valid.

The azonium and hydrazone forms (HA in Eq. 4) are the dominant species in aqueous solutions. This fact means that they are of weaker acidity than the corresponding azo form (AH).[21] However, the latter becomes dominant in the CD complexes. This shift in tautomeric equilibrium may contribute significantly to the decrease in the $pK_{a,app}$ of the dye. The change in microscopic dielectric constant around the dissociative groups of the dyes upon inclusion in the hydrophobic CD cavity may also affect the $pK_{a,app}$ values.[11,12] As the effect of THF on the $pK_{a,app}$ values shows (Table 1), the decrease in dielectric constant causes an increase in the $pK_{a,app}$ of **1**, but a decrease in that of **2**. Thus, the decrease in $pK_{a,app}$ with the formation of the inclusion complexes should be larger for the CD–**2** system than for the CD–**1** system. Indeed, this is the case, as the differences between the $pK_{a,app}(c_0=0)$ and $pK_{a,app}(c_0=\infty)$, calculated on the basis of Eq. 7, show (Table 2).

The authors are indebted to Mr. Etsuji Abe for his help in making some of the measurements.

References

1) F. Cramer, *Chem. Ber.*, **84**, 851 (1951).
2) F. Cramer, *Angew. Chem.*, **64**, 136 (1952); *ibid.*, **64**, 437 (1952).
3) F. Cramer, W. Saenger, and H.-Ch. Spatz, *J. Am. Chem. Soc.*, **89**, 14 (1967).
4) W. Broser and W. Lautsch, *Z. Naturforsch., Teil B*, **8**, 711 (1953).
5) W. Broser, *Z. Naturforsch., Teil B*, **8**, 722 (1953).
6) W. Lautsch, W. Broser, W. Biedermann, and H. Gnichtel, *Angew. Chem.*, **66**, 123 (1954).
7) H. Gutfreund, "Enzymes: Physical Principles," Wiley-Interscience, New York, N. Y. (1972), p. 32.
8) K. J. Laidler and P. S. Bunting, "The Chemical Kinetics of Enzyme Action," 2nd ed, Clarendon Press, Oxford (1973), p. 142.
9) D. W. Griffiths and M. L. Bender, *Adv. Catal.*, **23**, 209 (1973).
10) J. H. Fendler and E. J. Fendler, "Catalysis in Micellar and Macromolecular Systems," Academic Press, New York, N. Y. (1975), p. 194.
11) K. A. Connors and J. M. Lipari, *J. Pharm. Sci.*, **65**, 379 (1976).
12) T. Miyaji, Y. Kurono, K. Uekama, and K. Ikeda, *Chem. Pharm. Bull.*, **24**, 1155 (1976).
13) R. L. Reeves, *J. Am. Chem. Soc.*, **88**, 2240 (1966).
14) R. L. Reeves and R. S. Kaiser, *J. Org. Chem.*, **35**, 3670 (1970).
15) R. L. Reeves, R. S. Kaiser, M. S. Maggio, E. A. Sylvestre, and W. H. Lawton, *Can. J. Chem.*, **51**, 628 (1973).
16) R. L. Reeves, M. S. Maggio, and L. F. Costa, *J. Am. Chem. Soc.*, **96**, 5917 (1974).
17) K. Yamada, J. Morimoto, and H. Iida, *J. Fac. Eng. Chiba Univ.*, **24**, 71 (1973).
18) A. G. Lane and S. J. Pirt, *J. Appl. Chem. Biotechnol.*, **21**, 330 (1971).
19) F. Cramer and F. M. Henglein, *Chem. Ber.*, **91**, 308 (1958).
20) J. H. Hildebrand and H. A. Benesi, *J. Am. Chem. Soc.*, **71**, 2703 (1949).
21) H. Zollinger, "Azo and Diazo Chemistry. Aliphatic and Aromatic Compounds," Interscience Publishers, New York, N. Y. (1961), p. 322.
22) H. von Hippel and T. Schleich, "Biological Macromolecules," ed by S. N. Timasheff and G. D. Fasman, Vol. 2, Marcel Dekker, New York, N. Y. (1969), p. 417.
23) K. Mochida, A. Kagita, Y. Matsui, and Y. Date, *Bull. Chem. Soc. Jpn.*, **46**, 3703 (1973).

A Carbon-13 Spin-Lattice Relaxation Study of Side Chains of Poly(alkyl methacrylate)

Yoshiyuki HIRAI, Taizo ITO, and Yoshio IMAMURA

Department of Chemistry, Faculty of Science, Science University of Tokyo, Kagurazaka, Shinjuku-ku, Tokyo 162

(Received May 26, 1977)

The carbon-13 spin-lattice relaxation times (T_1) of the carbons in the alkyl side chains of poly(alkyl methacrylate) (butyl, octyl, dodecyl, and octadecyl), including poly(butyl methacrylate) of low molecular weights, were determined from partially-relaxed Fourier transform spectra. The T_1 for polymers of high molecular weights were found to be determined by the internal motion of the side chains, and not by the overall motion of the polymer molecules. The relaxation data indicate that the internal motion of the short side chains (butyl and octyl) is restricted by interactions between the side chains, although this effect was ineffective near the free ends of long chains (dodecyl and octadecyl). These observations are interpreted in terms of the local environment around the side chains.

The measurements of carbon-13 spin-lattice relaxation times (^{13}C-T_1) have been applied to investigations of the molecular dynamics of polymers in solutions.[1] Many of those investigations were concerned with the segmental mobility of backbone chains. On the other hand, a few papers have been published on localized motion, such as the internal motion of side groups, the internal motion of methyl groups of polypropyrene[2] and the ring motion of pyrrolidine residues of polypeptides.[3]

In a previous study, Hirai *et al.* evaluated the internal motion of the side groups of polyacrylamides having various molecular weights using ^{1}H-NMR spectroscopy and discussed the change in the local environment around the side groups arising from increase in molecular weight.[4] In the present investigation, samples of poly(normal alkyl methacrylate), including poly(butyl methacrylate) of low molecular weights, were studied. In these polymers, one end of the alkyl side chains is attached to the polymer backbone; such alkyl chains are termed anchored chains. In such cases, a marked gradation of the ^{13}C-T_1 along the alkyl chains was observed.[5] The gradation of T_1 reflects a change in internal motion along the side chains. Therefore, poly(alkyl methacrylate) is an ideal sample for discussing the internal motion of side groups.

The ^{13}C-T_1 for the side chains of poly(alkyl methacrylate) (butyl, octyl, dodecyl, and octadecyl) were determined from partially-relaxed Fourier transform spectra, and the correlation times were estimated. The internal motion of the side chains and the local environment around these chains is discussed on the basis of the relaxation data.

Experimental

Samples of poly(butyl methacrylate), poly(octyl methacrylate), poly(dodecyl methacrylate), and poly(octadecyl methacrylate) were prepared by polymerization of 10 g of the respective monomers in 20 ml of carbon tetrachloride for 5 h at 70 °C, using about 0.1 g of α,α'-azobisisobutyronitrile as an initiator. Samples of poly(butyl methacrylate) of various molecular weights were also prepared by changing the amount of the initiator (over the range from 0.3 to 3 g). The polymers were precipitated in a large amount of methanol in order to free them from any residual monomer, and were dried *in vacuo*. The number-average molecular weights of these polymers were determined using a Kunauar membrane osmometer and a vapor-pressure osmometer in chloroform solutions at 37 °C. The average molecular weights of the polymer samples were as follows: poly(butyl methacrylate) 1.36×10^3—7.95×10^4, poly(octyl methacrylate) 13.4×10^4, poly(dodecyl methacrylate) 8.26×10^4, and poly(octadecyl methacrylate) 11.3×10^4.

Polymer solutions for ^{13}C-NMR spectral measurements were prepared by dissolving of 0.3 g of the polymers in 0.7 ml of chloroform-*d*; the concentration of the polymers was 30% (wt/vol). The solutions were transferred to 8 mm o.d. NMR tubes, which were sealed after the air had been replaced with nitrogen gas. The sample volume was confined to a volume which was designed to be about 15% less than that of the rf sample coil, since it has been pointed out by Farrar and Becker[6] that, in order to avoid systematic errors introduced in T_1, the sample volume should not extend above or below the rf sample coil.

The carbon-13 NMR spectra were measured using a JEOL JNM PS-100 spectrometer equipped with a PFT-100 Fourier transform system operating at 25.03 MHz, and a EC-100 computer with a memory capacity of 16 kirowords. The 90° pulse width was about 23 μs. The apparatus was equipped with an internal ^{2}D field-frequency lock and a noise-modulated proton decoupler. The time-domain signal was digitized in 8192 channels, to provide 4096 data points after Fourier transformation. The recycle times of the 90° pulse were chosen to be at least four times the longest spin-lattice relaxation time. The experiments on spin-lattice relaxation were restricted to a spectral width of 2000 Hz. Over this widths, the ^{13}C rf field is sufficiently effective. All spectra were observed at 27 °C.

The T_1 were calculated, for six significant time intervals in the range from 30 ms to 6.0 s, using the least-squares method. The error in T_1 was estimated from the values of $\lim_{t\to0} \ln\{A_0-A(t)\}/A_0$; the maximum error was within ±10%.

Results and Discussion

^{13}C-NMR Spectra of Poly(alkyl methacrylate). Figure 1 shows the proton-decoupled ^{13}C-NMR spectra of poly(alkyl methacrylate) (butyl, octyl, dodecyl, and octadecyl). In examining these spectra, attention is called to the peaks of the side chain carbons.

The chemical shifts of the carbons of alkyl chains can be estimated from the empirical equation of Grant and Paul[7] or that of Lindeman and Adams;[8] these equations are often used for spectral assignments. The chemical shifts of the carbons of the alkyl side chains were estimated using the equation of Lindeman and Adams.[8] In the calculations, the effect of substitution

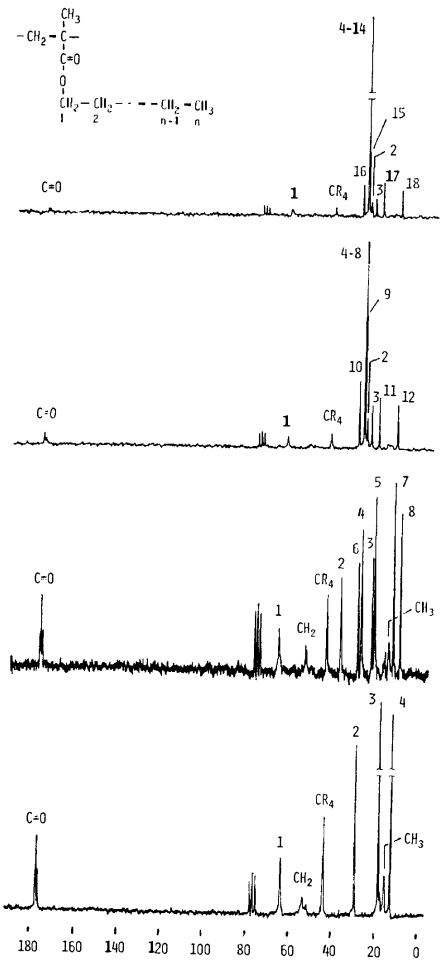

Fig. 1. Proton-decoupled natural-abundance ^{13}C Fourier transform NMR spectra of poly(alkyl methacrylate) in chloroform-*d* (30% (w/v)), at 25.03 MHz and 27 °C. From the top, poly(octadecyl methacrylate), poly(dodecyl methacrylate), poly(octyl methacrylate), and poly(butyl methacrylate). Assignments are indicated near the top of each peak. The numbering system for the alkyl chain starts at the $O-CH_2$ carbon. The horizontal scale is ^{13}C chemical shifts (ppm) relative to tetramethylsilane.

by –OCOR groups[9] was also taken into account. The calculated values are listed in the column marked "Calcd" in Table 1.

The values of the observed chemical shifts are given in the column marked "Obsd". For carbons near the anchored end, the chemical shifts of the peaks yielding short spin-lattice relaxation times are given (the ^{13}C-T_1 values are given in the following section). The basis for this arrangement of the observed chemical shifts is as follows. The ^{13}C-T_1 values for various anchored chains (one end of alkyl chains is anchored to massive materials or to some solvent matrix) have been measured by various investigators.[5,10–14] The ^{13}C-T_1 for all anchored chains increases along the chain from the carbon at the anchored end toward the terminal methyl carbon; there are no exceptions to this rule. One end of each of the alkyl side chains of poly(alkyl methacrylate) is anchored to the polymer backbone; the T_1 for the side chains should be similar to those for the anchored chains already examined.[5,10–14]

For poly(butyl methacrylate), poly(dodecyl methacrylate), and poly(octadecyl methacrylate), the calculated values are in fair agreement with the observed values. Only for poly(octyl methacrylate), is the agreement poor. The origin of this disagreement is obscure; in the assignment of the octyl chain the rule of chemical shifts for linear alkanes was also taken into account. However, it is evident that the assignments for carbons 7 and 8, which have long relaxation times, can be made without error. This means that the disagreement for the octyl chain does not affect the main discussion of the present study given in the following section.

Internal Motion of Alkyl Side Chains. The spin-lattice relaxation times of ^{13}C nuclei in polymers are determined predominantly by ^{13}C–H dipolar interactions.[15] Other possible relaxation mechanisms can be ignored.[1,15] Therefore, only the intramolecular dipolar interactions between a carbon and nearby completely saturated spin-spin decoupled protons are assumed here. If the "extreme narrowing condition" is satisfied, the relaxation time T_1 is given as follows (this condition is valid for side-chain carbons having moderately long spin-lattice relaxation times):

TABLE 1. OBSERVED AND CALCULATED CHEMICAL SHIFTS[a] FOR SIDE CHAINS OF POLY(ALKYL METHACRYLATE)

	Butyl			Octyl			Dodecyl			Octadecyl	
n[b]	Obsd	Calcd	n	Obsd	Calcd	n	Obsd	Calcd	n	Obsd	Calcd
1	64.8	65.4	1	67.1	65.7	1	65.0	65.7	1	65.3	65.7
2	30.3	32.8	2	38.4	30.4	2	28.2	30.4	2	28.3	30.4
3	19.4	21.4	3	23.8	28.7	3	26.1	28.7	3	26.2	28.7
4	13.8	13.9	4	28.8	30.0	4—8	29.7	30.0	4—14	29.9	30.0
			5	22.8	29.7	9	29.4	29.7	15	29.5	29.7
			6	30.3	32.4	10	32.0	32.4	16	32.0	32.4
			7	13.9	22.7	11	22.7	22.7	17	23.0	22.7
			8	10.8	13.9	12	14.2	13.9	18	14.2	13.9

a) ppm relative to tetramethylsilane. b) $-(-CH_2-\underset{\displaystyle C-O-CH_2-CH_2\cdots\cdots CH_2-CH_3}{\overset{\displaystyle CH_3}{\overset{|}{C}}}-)-$ (1 2 $n-1$ n; O)

$$1/T_1 = \hbar^2\gamma_C^2\gamma_H^2\tau \sum_N r_N^{-6}, \quad (1)$$

where $\hbar$ is Planck's constant divided by 2π, γ_C and γ_H are the carbon and proton gyromagnetic ratios, respectively, τ is the correlation time (τ is often expressed as τ_{eff}, the "effective correlation time"), and r_N is the internuclear C–H distance for the N-th proton. In the calculation of $\sum_N r_N^{-6}$, account is taken of the directly bonded protons only.

T_1 of Butyl Chains and Molecular Weights: Table 2 shows the T_1 values for the side chains of poly(butyl methacrylate) of various molecular weights. The effective correlation times (τ_{eff}) were calculated from Eq. 1 using these T_1 values and are listed in Table 3.

Tables 2 and 3 indicate the typical behavior of T_1 and τ_{eff} for anchored chains: the values of T_1 increase steeply from the 1-CH_2 carbon to the terminal carbon (of course, τ_{eff} decreases steeply). These findings are similar to the observations of Levy.[5] The gradation of T_1 and τ_{eff} reflects increasing internal motion toward the terminal methyl groups. Tables 2 and 3 also indicate that the values of T_1 and τ_{eff} for each carbon depend on the molecular weight in the region of low molecular weights. The values of T_1 for each carbon decrease with increasing molecular weight, while τ_{eff} increases with increasing molecular weight. For polymers of high molecular weight, T_1 and τ_{eff} are independent of the molecular weight. Similar results have also been reported for the ^{13}C-T_1 of polystyrene[16] and polyisobutylene[17] in solutions. These findings indicate that T_1 and τ_{eff} for polymers of high molecular weight (in the present experiment, $\overline{M}_n \geq 24900$) are determined by the internal motion of the side chains and not by the overall motion of the polymer molecules. The reciprocal of the correlation time $(\tau_{eff})^{-1}$ can be taken as the sum of the rates for internal and overall motion, *i.e.*, $(\tau_{eff})^{-1}=(\tau_o)^{-1}+(\tau_1)^{-1}$. For polymers having $\overline{M}_n \geq 24900$, the condition $(\tau_o)^{-1} \ll (\tau_1)^{-1}$ is valid, and $(\tau_{eff})^{-1}$ is approximately equal to $(\tau_1)^{-1}$.

T_1 of Alkyl Side Chains: Table 4 shows the values of T_1 for the side chains of poly(butyl methacrylate), poly(octyl methacrylate), poly(dodecyl methacrylate), and poly(octadecyl methacrylate). From these values of T_1, the effective correlation times ($^j\tau_{eff}$, where j is the j-carbon) for each carbon of the side chains can be calculated. Table 5 shows the reciprocals of the correlation times, $^j\tau_{eff}^{-1}$. $^j\tau_{eff}^{-1}$ reflects only the rate of internal motion of the j-carbon in the chain, because, as described in the preceding section, the condition $(\tau_o)^{-1} \ll (\tau_1)^{-1}$ is valid for these polymer samples. Figure 2 shows a plot of $^j\tau_{eff}^{-1}$-j for the side-chain carbons of poly(alkyl methacrylate).

The values of $^j\tau_{eff}^{-1}$ for the butyl and octyl chains increase progressively toward the free end. The $^j\tau_{eff}^{-1}$ curves for the dodecyl and octadecyl chains have flat regions (dotted lines in Fig. 2), which contain carbons 4 to 8 and carbons 4 to 14. The $^j\tau_{eff}^{-1}$ values for the last four carbons (the four carbons near the free end) of these chains increase sharply. Figure 2 also indicates that the $^j\tau_{eff}^{-1}$ for the last four carbons depends on the chain length of these side chains. The $^j\tau_{eff}^{-1}$ values for the butyl chain are small, and those for the octyl chain are comparably small. The $^j\tau_{eff}^{-1}$ values for the last four carbons of the dodecyl and octadecyl chains are rather large. This $^j\tau_{eff}^{-1}$ behavior resembles that of the anchored chains discussed below.

Figure 3 shows the $^j\tau_{eff}^{-1}$ curves for various anchored

Table 2. Carbon-13 spin-lattice relaxation times for side chains of poly(butyl methacrylate)

$\overline{DP}$[b]	T_1[a]			
	1-CH_2	2-CH_2	3-CH_2	4-CH_3
10	0.083	0.36	0.84	1.54
38	0.080	0.29	0.85	1.55
175	0.081	0.26	0.68	1.29
560	0.071	0.25	0.73	1.30

a) In seconds, error ±10%.
b) Average degrees of polymerization.

Table 3. Effective correlation times for side chains of poly(butyl methacrylate)

$\overline{DP}$[b]	τ_{eff}[a]			
	1-CH_2	2-CH_2	3-CH_2	4-CH_3
10	2.8	0.66	0.28	0.10
38	2.9	0.83	0.28	0.10
175	2.9	0.91	0.34	0.12
560	3.3	0.95	0.32	0.12

a) In 10^{-10} s. b) Average degrees of polymerization.

Table 4. Carbon-13 spin-lattice relaxation times[a] for side chains of poly(alkyl methacrylate)

Butyl		Octyl		Dodecyl		Octadecyl	
n[b]	T_1	n	T_1	n	T_1	n	T_1
1	0.071	1		1		1	
2	0.25	2	0.14	2	0.087	2	0.071
3	0.73	3	0.14	3	0.22	3	0.32
4	1.30	4	0.26	4—8	0.56	4—14	0.64
		5	0.48	9	0.58	15	0.64
		6	0.32	10	1.21	16	1.91
		7	1.24	11	2.34	17	2.78
		8	1.55	12	3.32	18	3.98

a) In seconds, error ±10%.
b) See footnote b) of Table 1.

Table 5. $^j\tau_{eff}^{-1}$:[a] the rates of rotational reorientation of the j-carbon in side chains of poly(alkyl methacrylate)

Butyl		Octyl		Dodecyl		Octadecyl	
n[b]	$(^j\tau_{eff})^{-1}$	n	$(^j\tau_{eff})^{-1}$	n	$(^j\tau_{eff})^{-1}$	n	$(^j\tau_{eff})^{-1}$
1	0.3	1		1		1	
2	1.1	2	0.6	2	0.4	2	0.3
3	3.1	3	0.6	3	0.9	3	1.3
4	8.3	4	1.1	4—8	2.4	4—14	2.7
		5	2.0	9	2.5	15	2.7
		6	1.4	10	5.1	16	8.1
		7	5.3	11	9.9	17	11.8
		8	9.9	12	21.2	18	25.4

a) In 10^{10} s^{-1}. b) See footnote b) of Table 1.

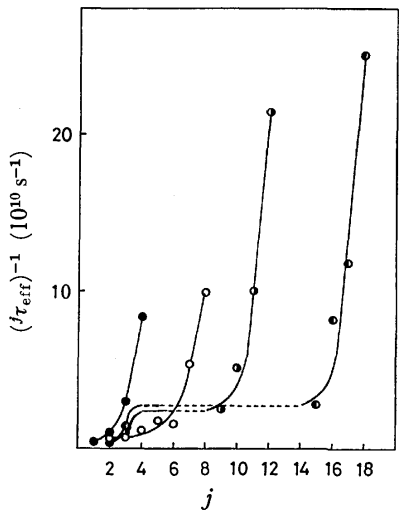

Fig. 2. The plots of $(^jT_{eff})^{-1}$-j for the carbons of the side chains of poly(alkyl methacrylate). ●: Butyl chain, ○: octyl chain, ◑: dodecyl chain, ◐: octadecyl chain.

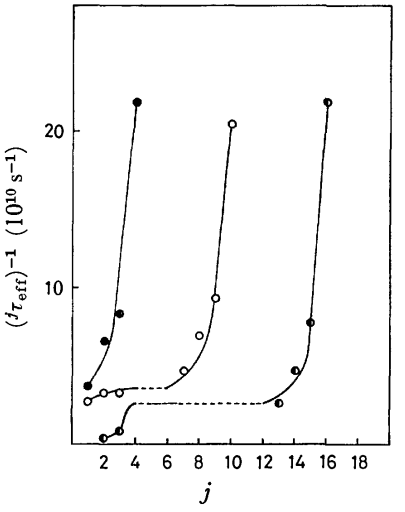

Fig. 3. The plots of $(^jT_{eff})^{-1}$-j for various anchored alkyl chains. ●: Butylammonium ion, ○: 1-decanol, ◐: dipalmitoyllecithin.

chains (the alkyl chains of the butylammonium ion, 1-decanol, and dipalmitoyllecithin). These curves were prepared from ^{13}C-T_1 data for these chains.[10,13,14] The $^jT_{eff}^{-1}$ behavior of the last four carbons of these alkyl chains is different from that of the side chains of poly(alkyl methacrylate). In the case of these anchored chains, the $^jT_{eff}^{-1}$ values for the four carbons is large and give quite similar curves, in spite of the very different properties of these alkyl chains (the curves for *N*,*N*-di-*n*-butyl formamide[12] and lecithin derivatives[11] are also similar to these curves). This constancy of $^jT_{eff}^{-1}$ for the last carbons is called the "limiting microviscosity effect."[18,19] The $^jT_{eff}^{-1}$ values for the last four carbons of these chains do not depend on the chain length or on the type of molecular anchor.

However, the change of $^jT_{eff}^{-1}$ for anchored chains shown in Fig. 3 results only from the restriction of the motion of the anchored end (the anchoring effect). For the side chains of poly(alkyl methacrylate), in addition to this "anchoring effect", the effect of intramolecular packing of the side chains[4] should also be considered. The local environment of the alkyl side chains of poly(alkyl methacrylate) differs from that of the anchored chains in Fig. 3 only in the existence of this intramolecular packing of chains. Therefore, the difference in the $^jT_{eff}^{-1}$ behavior for the last carbons of the side chains of poly(alkyl methacrylate) from those for the various anchored chains, namely the dependence of the $^jT_{eff}^{-1}$ curves on the chain length, can be attributed to this intramolecular packing effect.

The relaxation data presented above indicate that the intramolecular packing effect is ineffective for the last four carbons of the dodecyl and octadecyl chains, although it is effective for the butyl and octyl chains.

The effect of intramolecular packing on internal motion should become measurable when the side chains are unable to escape each other due to the increase in the backbone-chain length[4,20] (this requires that side groups be bulky and rigid). Such examples, in fact, have been observed for the internal rotation of amide groups of polyacrylamide[4] or the tumbling motion of phenyl groups of polystyrene.[21]

The side chains of poly(alkyl methacrylate) differ considerably from the side groups of polyacrylamide and polystyrene in the degree of freedom for interanl motion. Evidently, the degree of freedom for internal motion of alkyl side chains is larger than that of the side groups of polyacrylamide and polystyrene. The degree of freedom of the alkyl side chains is very large at carbons remote from the anchored end. In such cases, the carbons of the side chains can easily exchange equilibrium positions, even if intramolecular packing of the side chains occurs for the polymer chains. As a result, the packing effect is ineffective for restricting internal motion; the side chains behave similarly to the anchored chains, for which the intramolecular packing effect is absent.

From these considerations, the $^jT_{eff}^{-1}$ behavior for the alkyl side chains of poly(alkyl methacrylate) can be interpreted as follows. The internal motion of the last four carbons of the dodecyl and octadecyl chains is not affected by the intramolecular packing of the side chains, because these chains can easily exchange positions with each other. On the other hand, the degrees of freedom of the internal motion for the butyl and octyl chains are less than those for the carbons near the free ends of the dodecyl and octadecyl chains. The butyl and octyl chains are not long enough to permit relaxation of the packing effects, and reduced $^jT_{eff}^{-1}$ values, which arise from the intramolecular packing of the side chains, can be observed. The observations for the side chains of poly(alkyl methacrylate) are interpreted well using the above considerations.

It is concluded that the internal motion of the short side chains (butyl and octyl) is restricted by the intramolecular packing of the side groups, but that this effect is ineffective near the free ends of long chains (dodecyl and octadecyl).

References

1) For example, see J. Schaefer, "Topics in Carbon-13 NMR Spectroscopy," ed by G. C. Levy, John Wiley and

Sons, Vol. 1, New York (1974), Chap. 4.
2) Y. Inoue, A. Nishioka, and R. Chujo, *Makromol. Chem.*, **168**, 163 (1973).
3) D. A. Torchia and J. R. Lyerla, Jr., *Biopolymers*, **13**, 97 (1974).
4) Y. Hirai, M. Yukawa, and Y. Imamura, *Bull. Chem. Soc. Jpn.*, **50**, 1028 (1977).
5) G. C. Levy, *J. Am. Chem. Soc.*, **95**, 6117 (1973).
6) T. C. Farrar and E. D. Becker, "Pulse and Fourier Transform NMR," Academic Press, New York (1971), p. 43.
7) D. M. Grant and E. G. Paul, *J. Am. Chem. Soc.*, **86**, 2984 (1964).
8) L. P. Lindeman and J. Q. Adams, *Anal. Chem.*, **43**, 1245 (1971).
9) G. C. Levy and G. L. Nelson, "Carbon-13 Nuclear Magnetic Resonance for Organic Chemists," Wiley-Interscience, New York (1972), p. 47.
10) J. C. Metcalfe, N. J. M. Birdsall, J. Feeny, A. G. Lee, Y. K. Levine, and P. Partington, *Nature*, **233**, 199 (1971).
11) Y. K. Levine, N. J. M. Birdsall, A. G. Lee, and J. C. Metcalfe, *Biochemistry*, **11**, 1416 (1972).
12) G. C. Levy and G. L. Nelson, *J. Am. Chem. Soc.*, **94**, 4897 (1972).
13) D. Doddrell and A. Allerhand, *J. Am. Chem. Soc.*, **93**, 1558 (1971).
14) G. C. Levy, *J. Chem. Soc., Chem. Commun.*, **1972**, 768.
15) J. Schaefer and D. F. S. Natusch, *Macromolecules*, **5**, 416 (1972).
16) A. Allerhand and R. K. Hailstone, *J. Chem. Phys.*, **56**, 3718 (1972).
17) Y. Inoue, A. Nishioka, and R. Chujo, *J. Poly. Sci., Poly. Phys. Ed.*, **11**, 2237 (1973).
18) J. R. Lyerla, Jr., and G. C. Levy, Ref. 1, p. 118.
19) G. C. Levy, *Acc. Chem. Res.*, **6**, 161 (1973).
20) Y. Hirai, Y. Nunomura, and Y. Imamura, *Bull. Chem. Soc. Jpn.*, **49**, 2200 (1976).
21) H. Nomura and Y. Miyahara, *Polym. J.*, **8**, 30 (1976).

A Molecular-orbital Calculation of Chemically-interacting Systems. Interaction between Two Radicals. Self-reaction of Peroxyl Radicals

Tsutomu MINATO, Shinichi YAMABE,* Hiroshi FUJIMOTO, and Kenichi FUKUI

Faculty of Engineering, Kyoto University, Sakyo-ku, Kyoto 606

** Department of Chemistry, Nara University of Education, Takabatake-cho, Nara 630*

(Received May 31, 1977)

The path of the termination reaction of peroxyl radicals (self-reaction) was studied by means of a perturbational method and its reaction mechanism was elucidated theoretically. It was ascertained from this calculation that the self-reaction of tertiary alkylperoxyl radicals yielding a tetroxide does not have a four-centered transition state with four oxygen atoms of the two peroxyl radicals participating, but has a two-centered transition state with only the terminal oxygen atoms. The self-reaction of primary or secondary alkylperoxyl radicals is found to have a six-centered transition state. The self-reaction of acylperoxyl radicals is also shown to have a six-centered transition state. The mechanism of these self-reactions is clarified in terms of the mode of the particular orbital interaction.

One of the termination reactions of autoxidation is the reaction wherein two peroxyl radicals are converted into non-radical products (self-reaction). Such self-reactions of peroxyl radicals have been studied and various kinds of products have been reported.[1] When a peroxyl radical is represented by ROO·, the products of the self-reaction can be shown to be a function of R. This is displayed in Table 1. When R is a *t*-alkyl group (T) or an acyl group (A), the products of the self-reaction are a peroxide and an oxygen molecule (self-reaction T or A). When R is a *p*-alkyl group (P) or an *s*-alkyl group (S), the products are a carbonyl, an alcohol, and an oxygen molecule (self-reaction SP).

The mechanism involved in these self-reactions has received considerable attention in the last few years because of the fundamental importance of these reactions to a complete understanding of autoxidation. For self-reaction T, the overall process can be represented as follows:[1]

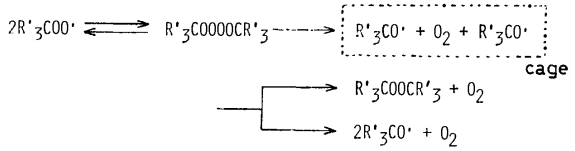

Scheme 1. (for self-reaction T).

This scheme is generally accepted and Bartlett and Guaraldi[2] have provided convincing evidence for the existence of the tetroxide by direct monitoring, using ESR, the concentration of the *t*-butylperoxyl radical, which is present in equilibrium with the tetroxide at very low temperature. Regarding self-reaction SP, its exact mechanism is not yet clear. In this reaction, the carbonyl compounds and alcohol are obtained in high yields, whereas no peroxide, which is present for self-reaction T, was detected.[3] In addtion, when the α-hydrogens of the *s*-, or *p*-alkylperoxyl radicals are replaced by deuterium, an isotopic effect on the rate constant of the overall termination process (*i.e.*, $k_t^H/k_t^D = 1.4$) is observed.[4] k_t is the rate constant of the overall termination process. To explain these experimental results, Russell[5] has proposed a unique mechanism for self-reaction SP which involves the intermediacy of a "cyclic" transition state, as is shown in the following figure:

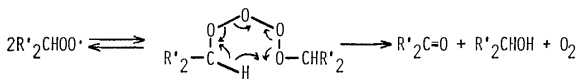

Scheme 2. (for self-reaction SP).

While a mechanism analogous to Scheme 1 with the intermediacy of alkoxyl radicals can be discounted on the basis of experimental results,[3,5] the mechanism of Scheme 2 is supported by most data. However, it has been pointed out that some doubt still remains as to the validity of Russell's mechanism of Scheme 2.[6] Bowman and co-workers[6a] have concluded from thermochemical calculations that, if Scheme 2 is the only viable mechanism for self-reaction SP, the overall activation energy (E_t) should be negative. This is contrary to experimental observations. For example, Howard and Bennett[6b] have found a value of +3 kcal/mol for the E_t of the self-reaction of cyclopentylperoxyl radicals. This discrepancy led Benson propose the following mechanism for self-reaction SP.[6a]

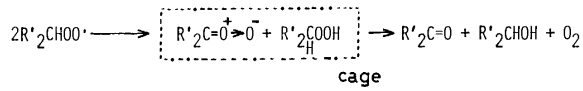

Scheme 3. (for self-reaction SP).

However, there is no experimental evidence for the production of a zwitterion and a hydroperoxide from self-reaction SP[1a] and, consequently, this mechanism is not taken into account in this work. Next, for self-reaction A, the mechanism is also controversial. McDowell and Sifniades have suggested a four-centered transition state as shown by the following scheme:[7]

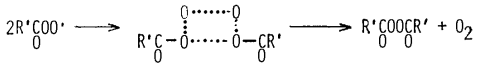

Scheme 4. (for self-reaction A).

However, this scheme appears rather unlikely. While *t*-alkylperoxyl radicals are expected to interact in a manner similar to Scheme 4, the overall rate constant of self-reaction T is much lower than that of self-reaction A, as is shown later in Table 3. Ingold has proposed a six-centered transition state for self-reaction A analogous to Scheme 2,[1b] thus we can write as

Table 1. The products of self-reactions of peroxyl radicals with various substituent groups

R	Reaction	Product	Self-reaction
t-Alkyl group (R'_3C-)	$R'_3COO\cdot + R'_3COO\cdot$	$R'_3COOCR'_3 + O_2$	Self-reaction T
s-Alkyl group (R'_2CH-)	$R'_2CHOO\cdot + R'_2CHOO\cdot$	$R'_2CHOH + R'_2C{=}O + O_2$	Self-reaction SP
p-Alkyl group ($R'CH_2$-)	$R'CH_2OO\cdot + R'CH_2OO\cdot$	$R'CH_2OH + R'CH{=}O + O_2$	Self-reaction SP
Acyl group ($R'CO$-)	$R'C(=O)OO\cdot + R'C(=O)OO\cdot$	$R'C(=O)OOC(=O)R' + O_2$	Self-reaction A

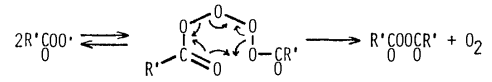

Scheme 5. (for self-reaction A).

Thus, the mechanisms of self-reactions SP and A are still in doubt, although it is accepted that the mechanism of self-reaction T is expressed by Scheme I. Under such circumstances, it is interesting to theoretically study the destruction process of peroxyl radicals. Recently, the ΔW method, which deals with a radical-radical reacting system in terms of the molecular interaction, was developed by the present authors.[8] Some calculations of the ΔW method presented in a previous paper[9] elucidated the difference between recombination and disproportionation mechanisms. In the present work, first, the self-reaction mechanisms will be examined theoretically using the ΔW method. Second, the general aspect of the self-reaction of peroxyl radicals will be explained schematically using the mode of interaction between particular molecular orbitals (MO) of several isolated peroxyl radicals. The reactivity of these radicals can be simply discussed by analyzing the extent of such MO interactions.[10]

Calculation for Assumed Reaction Models

Method of Calculation. In the ΔW method, the wavefunction (Ψ) of a chemically-interacting system consisting of two peroxyl radicals is represented by the sum of various electronic configurations according to the configuration interaction (CI) procedure. Our attention is focused on the reaction system involving singlet spin states because, for triplet spin states, a radical-radical reaction is far from occurring. In this calculation, no electronic configurations for intramolecular excitations are taken into account, as in a previous paper.[9] When the CI secular equation is expanded perturbationally, the total stabilization energy (ΔW) due to the CI mentioned above can be partitioned into the following three terms, Coulomb (E_Q), exchange (E_K) and delocalization (D) terms:

$$\Delta W = E_Q + E_K - D, \quad (1)$$

where E_Q is the classical electrostatic interaction energy between two peroxyl radicals. The exchange energy, E_K, is caused by the overlap between both occupied MO, which are doubly-occupied (DO) or singly-occupied (SO) MO. For the singlet spin state, as well as for the triplet spin state, E_K is found to be repulsive (>0) for systems composed of radicals of usual organic-chemical size.[8] E_K can be further partitioned into four terms, thus

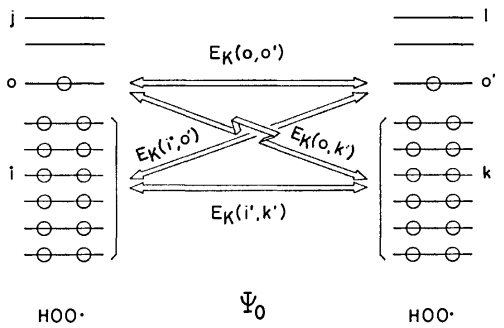

Fig. 1. The adiabatically-interacting configuration (Ψ_0) and the schematic representation of four types of exchange interaction between two hydroperoxyl radical. The lowest and second lowest DOMO's of each HOO·, *i.e.*, the 1s-type ones, are omitted in this figure.

$$E_K = E_K(i', k') + E_K(i', o') + E_K(o, k') + E_K(o, o'). \quad (2)$$

In Fig. 1, the four components of E_K are shown schematically. D is the stabilization energy due to the mixing-in of the charge-transfer configurations with the adiabatically-interacting configuration (Ψ_0). D can be represented by the sum of eight components, thus

$$D = D(i\rightarrow l) + D(k\rightarrow j) + D(i\rightarrow o') + D(k\rightarrow o) + D(o\rightarrow l) + D(o'\rightarrow j) + D(o\rightarrow o') + D(o'\rightarrow o). \quad (3)$$

A system composed of two hydroperoxyl radicals (2HOO·) is selected as the reaction model for the calculation using the ΔW method. The MO of the hydroperoxyl radical, which are needed to evaluate the CI matrix elements are obtained using the semi-empirical all-valence-electron SCF-UHF method, including overlap integrals.[11] The way of estimating the semi-empirical parameters for evaluating the MO integrals is the same as that used in a previous paper.[12] Since the hydroperoxyl radical has 17 electrons, it has six DOMO, excluding the two lowest ls-like MO.

The geometry of the assumed reaction models is illustrated in Fig. 2. The geometry of the isolated hydroperoxyl radical comes from the CNDO calculation of Pople and Beveridge[13] and is frozen in the present calculation. In Fig. 2, Model I is a reaction model representing a four-centered reaction path. This model corresponds to Scheme 4. Model II is a two-centered reaction path in which two terminal oxygen atoms (O_1 and $O_{1'}$) are close to each other. Two radical species form the trans conformation. In

TABLE 2. THE CALCULATED INTERACTION ENERGIES FOR THE REACTION OF TWO HYDROPEROXYL RADICALS
The geometrical parameters, R and θ, are those shown in Fig. 2. The smaller value of ΔW indicates higher reactivity. Due to the symmetrical arrangement of the two radicals, $E_K(i', o') = E_K(o, k')$, $D(i \rightarrow l) = D(k \rightarrow j)$, $D(i \rightarrow o') = D(k \rightarrow o)$, $D(o \rightarrow l) = D(o' \rightarrow j)$ and $D(o \rightarrow o') = D(o' \rightarrow o)$.

	Model I					Model II	
	Ia $\theta=0°$		Ib $\theta=+5°$		Ic $\theta=-5°$		
R [Å]	2.4	2.0	2.4	2.0	2.4	2.4	2.0
E_Q [eV]	0.061	0.101	0.088	0.144	0.033	−0.014	0.033
$E_K(i', k')$	0.313	2.239	0.325	2.166	0.444	0.127	0.952
$E_K(i', o')$, $E_K(o, k')$	0.011	0.102	0.023	0.168	0.016	0.020	0.156
$E_K(o, o')$	−0.025	−0.222	−0.034	−0.264	−0.025	−0.003	−0.037
E_K [eV]	0.310	2.221	0.337	2.238	0.451	0.164	1.227
$D(i \rightarrow l)$, $D(k \rightarrow j)$	0.002	0.005	0.002	0.006	0.003	0.002	0.012
$D(i \rightarrow o')$, $D(k \rightarrow o)$	0.008	0.069	0.016	0.120	0.013	0.019	0.155
$D(o \rightarrow l)$, $D(o' \rightarrow j)$	0.000	0.002	0.000	0.001	0.000	0.000	0.001
$D(o \rightarrow o')$, $D(o' \rightarrow o)$	0.034	0.275	0.042	0.324	0.031	0.005	0.050
D [eV]	0.088	0.702	0.120	0.902	0.094	0.052	0.436
ΔW [eV]	0.283	1.620	0.305	1.480	0.390	0.098	0.824

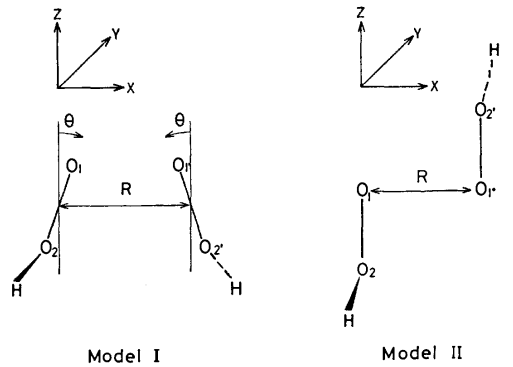

Fig. 2. Two assumed reaction models employed for the calculation of the interaction energy.

Model I, parameter R is the intermolecular distance between the center of the O_1–O_2 group and that of the O_1'–O_2' group, and θ is defined as the angle between the O_1–O_2 group and the Z-axis. In Model II, R is the distance between the two terminal oxygen atoms (O_1 and O_1'). In both models, the four oxygen atoms (O_1, O_2, O_1', and O_2') are always in the X-Z plane. In Model I, the reacting system belongs to the C_2 point group, whereas, in Model II, to the C_i point group.

Results. The interaction energies (ΔW) for Models I and II are given in Table 2. The ΔW of Model Ia (R=2.4 Å, θ=0°) is compared with that of Model II (R=2.4 Å). This comparison shows that Model II is more favorable than Model Ia for the self-reaction. At R=2.0 Å, the same result is obtained from Table 2. This preference of the self-reaction is thoroughly attributable to the exchange energy term, $E_K(i', k')$ (see Fig. 1). Here, let us examine in more detail the possibility of the four-centered reaction path. In Model I, a variation in θ may bring about a change in ΔW.[14] To see the effect of this angle variation for each energy, two other geometries of Model I are employed. In Model Ib, θ is 5° and, in Model Ic, θ is −5°. Model Ib is a closer approach of two terminal oxygen atoms than Model Ia, whereas Model Ic is a closer approach of the two inner oxygen atoms (O_2 and O_2'). At R=2.4 Å, the approach of the inner oxygen atoms is found to bring about a larger ΔW value (0.390 eV), *i.e.*, destabilization of the system. An analysis of the components of ΔW shows that this destabilization comes primarily from an increase in the exchange energy, E_K. In the three models (Ia, Ib, and Ic), the order of the numerical values of ΔW and its three components are as follows:

for E_Q, Ib>Ia>Ic
for E_K, Ic>Ib>Ia
for D, Ib>Ic>Ia
and for ΔW, Ic>Ib>Ia. } R=2.4 Å

Thus, the superiority of Model Ia is ascribed to the small repulsive terms (E_Q and E_K), in spite of the even smaller attractive term (D). The change in E_Q is very smooth as the intermolecular distance is shortened,[8] whereas E_K and D which are of second order in the MO overlap are shown to increase sharply. Since the rate of growth of D is greater than that of E_K, the approach of two radical species may render Model Ib more favorable than Model Ia. Comparing the ΔW of Model Ia (1.620 eV) with that of Model Ib (1.480 eV) at R=2.0 Å, one really finds this trend. At any rate, Model II is the more favorable pathway of the four assumed reaction models.

The difference in the interaction energies, ΔW, of the models adopted here can be interpreted qualitatively in terms of the shape of the particular MO of the hydroperoxyl radical as follows.[10] The SOMO of the hydroperoxyl radical, which is the seventh MO from the bottom shown in Fig. 1, is a π-type one along the X-axis. It has larger lobes at the terminal oxygen atom than those at the inner atom, as is depicted on the left-hand side of the figure.

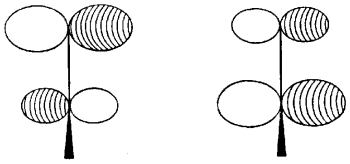

The hydroperoxyl radical also has a π-type DOMO (the fifth MO from the bottom in Fig. 1), as is shown on the right-hand side of the figure, which has larger lobes at the inner oxygen atom. In Model Ic ($\theta=-5°$), the approach of the two inner oxygen atoms enlarges the overlapping between these two equivalent DOMO and, at the same time, reduces the overlap between the two SOMO. The increase of the former overlapping makes E_K(i′, k′) grow large and the reduction of the latter overlapping makes the stabilization terms, E_K(o, o′), D(o→o′) and D(o′→o), become small. The combination of such an increase and reduction results in an unfavorably large ΔW in Model Ic. Since, in Model Ib, the trend of the MO overlapping is opposite (*i.e.*, the SOMO-SOMO overlapping is larger and the DOMO-DOMO overlapping is smaller) to that in Model Ic, the ΔW of the former model becomes favorably small. The even smaller value of ΔW in Model II can be explained in the same way. The favorable results for Model II are attributed to the avoidance of the large overlap between the two DOMO (as shown above) which gives the dominant component of the repulsive term, E_K(i′, k′). Thus, the loss of the SOMO-SOMO overlapping, which produces three attractive terms, E_K(o, o′), D(o→o′), and D(o′→o), has a negligible influence on the superiority of Model II.

In order to seek the charge-transfer configuration that contributes most to the stabilization of the reaction system, the CI coefficients of Ψ were obtained with respect to Models Ib and II (R=2.0 Å), thus

$$\Psi_{\text{Model Ib}} = 0.951\Psi_0 - 0.115\Psi_{o\to o'} - 0.115\Psi_{o'\to o} + 0.052\Psi_{i_2\to o'} + 0.052\Psi_{k_2\to o} + 0.046\Psi_{i_5\to o'} + 0.046\Psi_{k_5\to o} + \cdots, \quad (4)$$

and

$$\Psi_{\text{Model II}} = 0.969\Psi_0 + 0.107\Psi_{i_5\to o'} + 0.107\Psi_{k_5\to o} - 0.049\Psi_{o\to o'} - 0.049\Psi_{o\to o'} + \cdots. \quad (5)$$

In Eqs. 4 and 5, the CI coefficients larger than 0.040 (absolute value) are shown. i_2, i_5, k_2, and k_5 denote the DOMO and the subscripts of i and k are the orbital numbers counted from the lowest DOMO (see Fig. 1). i_5 and k_5 are the π-type MO mentioned above. Equation 4 shows that, except for Ψ_0, the SOMO-SOMO interaction ($\Psi_{o\to o}$ and $\Psi_{o'\to o}$) is the most important in Model Ib, whereas Eq. 5 indicates that the charge transfer (CT) interaction from the π-type MO (i_5 and k_5) to the SOMO (o and o′) is more important than the SOMO-SOMO interaction in Model II.

In the course of the reaction, some bonds to be broken are weakened and new bonds begin to form. To see this effect of bond interchange, the atomic bond population[15] of the chemically-interacting system was calculated using wavefunction Ψ. Models Ia, Ib, and II (R=2.0 Å) were adopted for the calculation and the results are shown in Fig. 3. Judging from the energy results in Table 2, Model Ic is definitely an unfavorable pathway and will not be considered hereinafter. This figure shows that for Models Ia and Ib, a positive intermolecular bond population between the two terminal oxygen atoms (O_1 and $O_{1'}$) appears (0.0058 and 0.0061, respectively). For these two models, however, the intermolecular bond populations between the two inner oxygen atoms (O_2 and $O_{2'}$) are negative (−0.0073 in Model Ia and −0.0036 in Model Ib), which shows that the formation of the new $O_2\cdots O_{2'}$ bond cannot be expressed by them. The O_1–O_2 (or $O_{1'}$–$O_{2'}$) bond population of these two models is larger than that of the isolated HOO·. This can be explained in the following manner. The SOMO of the hydroperoxyl radical is an antibonding π-type orbital, as is sketched above, and therefore the SOMO-SOMO interaction decreases the electron occupancy of the SOMO.[16] If the reaction proceeds *via* Scheme 4, the O_1–O_2 bond should break in the course of the reaction. However, the present calculated results for the O_1–O_2 bond population together with the negative $O_2\cdots O_{2'}$ population indicate that Scheme 4 is an unfavorable pathway from the standpoint of bond interchange. This is an alternative expression of the improbability of the four-centered pathway. In Model II, a small positive population between the two terminal oxygen atoms appears (0.0005) and that of the O_1–O_2 bond increases only slightly (0.1224→0.1234). The smaller accumulation of the $O_1\cdots O_{1'}$ bond population for Model II than for Model Ib is due to the smaller SOMO-SOMO overlap which is the origin of the intermolecular bonding component.[8,9] Aside from this comparison of the $O_1\cdots O_{1'}$ bond population, the present results for the atomic bond population show that, in the self-reaction, the two terminal oxygen atoms forms a new $O_1\cdots O_{1'}$ bond, the O_1–O_2 (or $O_{1'}$–$O_{2'}$) bond of the peroxyl radical remaining un-

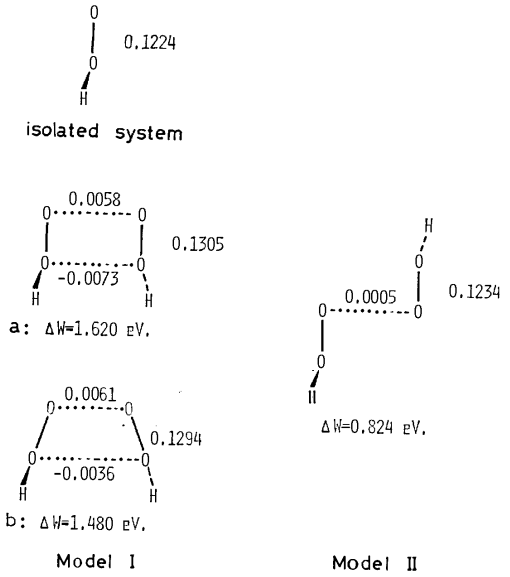

Fig. 3. The change of the atomic bond population by the exchange and CT interactions at R=2.0 Å.

cleaved. Also, the self-reaction is found to produce a tetroxide. However, we have here two incompatible results with respect to the superiority of the assumed reaction models. The value of ΔW in Table 2 shows that Model II is the most favorable reaction pathway for the self-reaction, whereas the atomic bond population in Fig. 3 shows that Model Ib is more favorable for the formation of a new $O_1 \cdots O_{1'}$ bond.

Whichever of the pathways corresponding to Model Ib and II the self-reaction takes, the present calculation demonstrates that the reaction path is that for which the two terminal oxygen atoms approach each other and the two inner oxygen atoms do not approach each other as much as the terminal atoms, with the production of a tetroxide resulting. Consequently, the self-reaction process is not that described by Scheme 4. In the present calculation, the system composed of two hydroperoxyl radicals was selected as the reaction model. It is reasonable to consider that a peroxyl radical has an SOMO which is localized mainly over the two oxygen atoms even if the H atom of the hydroperoxyl radical is replaced by any substituent group. Consequently, the results obtained from the present calculation for such a simple system do not appear to be changed markedly upon the replacement of the H atom by a substituent group.

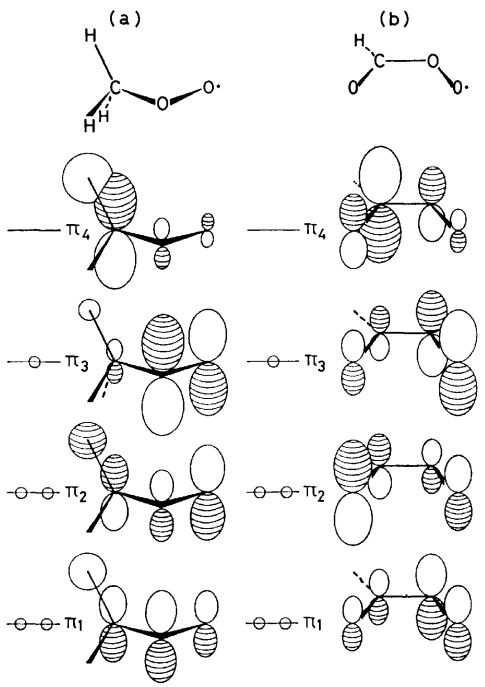

Fig. 4. (a); The schematic representation of the π-type MO's of the methylperoxyl radical. (b); The schematic representation of the π-type MO's of the formylperoxyl radical.
These MO's are obtained by the EH MO method. The geometry of these radicals is obtained from the Pople's standard bond length and bond angle (see Ref. 13).

Discussion

In the previous section, the pathways and mechanisms for the self-reactions of peroxyl radicals were investigated using the ΔW method and the self-reaction was shown to give a tetroxide if the terminal oxygen atoms are initially in contact with each other. However, the overall rate constant ($2k_t$) of self-reaction T is quite different from those of self-reactions SP and A, as is shown in Table 3.[1b] The slowness of self-reaction T is primarily due to the fact that the decomposition of the tetroxide intermediate into two alkoxyl radicals and an oxygen molecule requires significant activation energy.[17] Generally, the difference in the rate constants for the three types of self-reactions is ascribed mainly to the differences in the activation energy for tetroxide decomposition.[17b] However, since the difference in the rate constants between self-reaction T and self-reaction SP (or self-reaction A) is much more significant than that expected from the tetroxide decomposition, these may have quite different mechanisms.

The interaction energy, ΔW, is entirely dependent upon the extent of MO overlapping obtained independently for two peroxyl radicals and, therefore, its value can be estimated roughly by analyzing the shape of these MO.[10] Then, even without actually calculating the ΔW, the self-reaction mechanism can be conveniently discussed in terms of the shape of some particular (*frontier*) MO. On this basis, the mechanism of self-reaction SP and self-reaction A will be discussed.

Self-reaction of p- *and* s-*Alkylperoxyl Radicals.* First, the shapes of the MO of a methylperoxyl radical are obtained conveniently by the extended Hückel (EH) MO method[18] and are sketched in Fig. 4(a). In this figure, only the π-type MO are illustrated, because none of the residual MO are as active in causing the important orbital interaction. It was found that the π_3 orbital is the SOMO of the methylperoxyl radical localized over two oxygen atoms. In self-reaction SP, one peroxyl radical abstracts the methyl hydrogen atom of the other and an alcohol is produced. For the geometrical position of two methylperoxyl radicals such that the SOMO-SOMO interaction becomes large, the tetroxide may be produced as was discussed in the previous section. However, for this geometry, the process of hydrogen abstraction cannot be explained. In consideration of this, the CT interaction between the MO of one radical species localized at the C–H bond of a methyl group and the SOMO (π_3) of the other appears to be important in causing reactions other than that producing the tetroxide. In Fig. 4(a), the π_2 orbital is the highest occupied (HO) MO spreading over the C–H bond. When the reacting system has the geometry shown in Fig. 5, the CT interaction from the HOMO (π_2) to the SOMO (π_3) shown in Fig. 5(a and b) is found to contribute to the stabilization of the system. This stabilization corresponds to the higher reactivity of each radical species. This is because, in the reacting regions ($H_4 \cdots O_{2'}$ and $O_1 \cdots O_{1'}$), the lobes of two MO's (π_2 and π_3) overlap in phase. On the other hand, for this geometry, the SOMO-SOMO interaction does not contribute as much because of its nodal properties. Especially, the (HOMO→SOMO) CT interaction shown in Fig. 5(b) is more important than that shown in Fig. 5(a), for these MO have large lobes at the reacting regions ($H_4 \cdots O_{2'}$ and $O_1 \cdots O_{1'}$). The roles of the CT interactions other

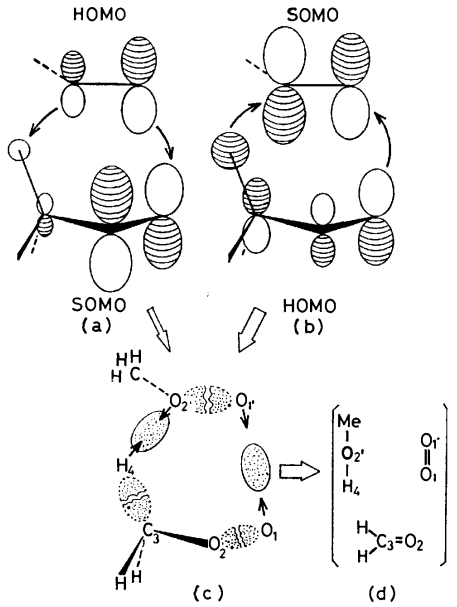

Fig. 5. The CT interaction between the HOMO and SOMO in the self-reaction of the methylperoxyl radicals.

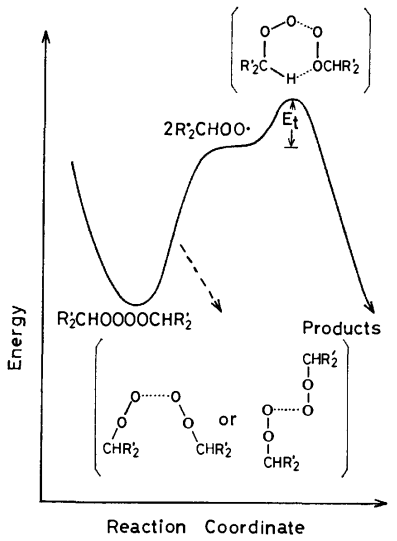

Fig. 6. The potential energy-reaction coordinate curve of the self-reaction SP taken from Ref. 6(b). The six-centered transition state obtained in the present work is additionally depicted and the two-centered path producing a tetroxide is also pictured.

than those depicted in Fig. 5 are minor due to the small value of the corresponding MO overlapping. The CT interaction depicted in Fig. 5(b) will be examined in more detail. This CT interaction contributes to the formation of the new $O_1 \cdots O_{1'}$ and $H_4 \cdots O_{2'}$ bonds and the disappearance of the C_3–H_4 and O_1–O_2 bonds through the loss of bonding electrons. Furthermore, the formation of the C_3=O_2 double bond and the disappearance of the $O_{1'}$–$O_{2'}$ bond can also be explained in terms of this CT interaction. Thus, self-reaction SP gives an alcohol, a carbonyl and an oxygen molecule *via* the *six-centered configuration.*

From the above discussion, self-reaction SP can be described as follows. In the initial stage of the reaction, two terminal oxygen atoms (O_1 and $O_{1'}$ in Fig. 5) approach each other. In this step, if the tetroxide intermediate is not produced, then the reaction system has the six-centered configuration shown in Fig. 5. In this case, the CT interaction between the HOMO spreading over the C_3–H_4 bond and the SOMO is of importance in causing the above-mentioned bond interchange. At this point, the self-reaction produces non-radical products without forming a tetroxide intermediate, as proposed by Russell (see Scheme 2). This picture of the reaction mechanism corresponds to a single-step concerted reaction. However, the bond formation is considered to be concerted, but non-synchronous, as is proposed in many cases of concerted cycloaddition.[14,19] While for cycloaddition (*e.g.*, 1,3-dipolar cycloaddition) two bonds are formed, the bond formation of one of these is, however, advanced with respect to that of the other in the transition state. When self-reaction SP does not have the six-centered configuration, it may readily produce a tetroxide. There is ESR evidence for the formation of a diamagnetic dimer (probably a tetroxide) from two cyclopentylperoxyl radicals.[6b] In short, there are probably two paths for self-reaction SP. One is the path in which a tetroxide is produced, and the other gives an alcohol, a carbonyl and an oxygen molecule. This reaction picture is in agreement with that suggested by Howard and Bennett.[6b] Although these authors gave no detailed discussion of the structure of the transition state in their mechanism, they suggested that in self-reaction SP one pathway giving non-radical products is different from the other which produces a tetroxide. Furthermore, they represented this suggestion schematically using the potential energy-reaction coordinate curve drawn in Fig. 6. When we examine the six-centered configuration of the transition state introduced in this work, it is seen that the present picture of self-reaction SP is in line with their suggestion. According to this picture and the experimental evidence mentioned above, the products and, furthermore, the isotopic effect are easily interpreted. If two peroxyl radicals react in the singlet spin state, the spin-conservation rule requires either that the oxygen molecule evolved in the self-reaction should be formed in an excited singlet spin state or that it should be in a ground triplet state and the carbonyl in an excited triplet state.[1b] Many experiments show that the oxygen molecule is formed in an excited singlet state.[20] Such data is in line with the present picture of the single-step concerted reaction. Thus, it is probable that self-reaction SP has a six-centered transition state as proposed by Russell, although the Russell scheme (Scheme 2) should be somewhat modified to the present picture mentioned above.

Self-reaction of Acylperoxyl Radicals. The overall rate constant for self-reaction A is much larger than that of self-reaction T, as is shown in Table 3. The acylperoxyl radical has a C=O bond at the α-carbon atom which corresponds to the C–H bond of the *p*- and *s*-alkylperoxyl radicals. For self-reaction A, the possibility of a six-centered transition state of the self-reaction

TABLE 3. THE OVERALL RATE CONSTANTS ($2k_t$) FOR THE SELF-REACTIONS[1b)]

Radical	$2k_t$, $M^{-1}s^{-1}$	Self-reaction[a)]
t-Alkylperoxyl	$0.1—60\times10^4$	T
s-Alkylperoxyl	$1—40\times10^6$	SP
p-Alkylperoxyl	$2—8\times10^8$	SP
Acylperoxyl	$10^6—10^{11}$	A

a) The classification of the self-reactions is given in Table 1.

will be examined. To determine the shape of the MO of the acylperoxyl radical, those of a formylperoxyl radical were obtained simply using the EH MO method. In Fig. 4(b), only the π-type MO are depicted according to the same criterion as that for the methylperoxyl radical. From Fig. 4(b), it is found that the π_3 orbital is an SOMO localized appreciably about two oxygen atoms (O–O bond) and that the π_2 orbital is the HOMO spread over the C=O double bond. In Fig. 7 is shown the mode of the mutual CT interaction between the HOMO of one radical species and the SOMO of the other. The CT interactions other than those are not as important for the same reason as the case of the methylperoxyl radical. The (HOMO→SOMO) CT interaction in Fig. 7(a) is more important than that in Fig. 7(b) in the sense that the former interaction is caused by the larger overlap in the reacting regions ($O_2\cdots O_4'$ and $O_1\cdots O_1'$). Looking at the mode of the (HOMO→SOMO) CT interaction of Fig. 7(a and b), one can reasonably understand the process of bond interchange which is similar to the case of the methylperoxyl radical. The intermolecular $O_1\cdots O_1'$ and $O_2\cdots O_4'$ bonds are formed and the O_2'–C_3' single bond is converted to the O_2'=C_3' double bond. Furthermore, the O_1–O_2 and O_1'–O_2' bonds disappear and the C_3'=O_4' double bond is converted to the C_3'–O_4' single bond. Thus, it is anticipated that, in order to

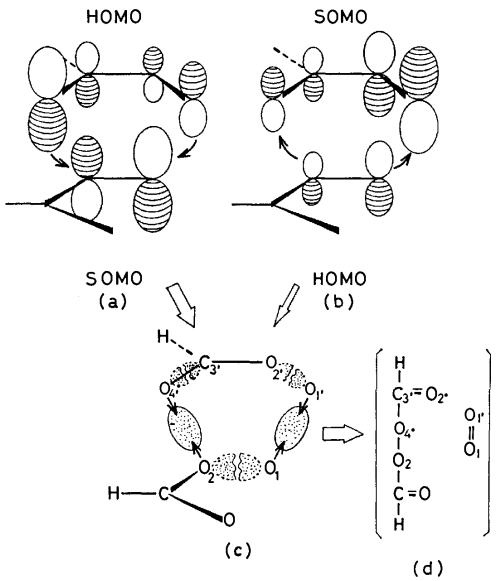

Fig. 7. The CT interaction between the HOMO and SOMO in the self-reaction of the formylperoxyl radicals.

bring about effective (HOMO→SOMO) CT interactions, self-reaction A has the six-centered configuration giving no tetroxide, but non-radical products (the peroxide and oxygen molecules). This picture of the reaction mechanism also corresponds to a single-step concerted reaction. If self-reaction A proceeds along this reaction path, it leads again to the prediction that self-reaction A gives an oxygen molecule in the excited singlet state. Unfortunately, since the data for the spin state of the oxygen molecule produced in self-reaction A do not yet appear to be available, further experimental verification is desirable. It should be noted that in the approach of the two terminal oxygen atoms, self-reaction A may also give a tetroxide as in the case of self-reaction SP.

Conclusion

From this work, a discussion based on the ΔW method was made with respect to the self-reaction of peroxyl radicals. First, the interaction energy, ΔW, was calculated using the simplest peroxyl radical (HOO·). One implication derived from this calculation is that, aside from the superiority of either the trapezoid or trans configurations, the two-centered transition state is more probable than the four-centered one. Second, when three types of substituents (*t*-alkyl, *s*- and *p*-alkyl, and acyl) are taken into account, other reaction mechanisms involving them are introduced. In the case of the self-reaction of both *s*- and *p*-alkylperoxyl and acylperoxyl radicals, the termination is a single-step concerted reaction with a six-centered geometrical configuration. In the former self-reaction, a C_α–H bond is ruptured whereas, in the latter self-reaction, a C_α=O double bond is converted into a single C_α–O bond. There, the CT interaction between the HOMO spread over the C–H or the C=O bond of one peroxyl radical and the SOMO of the other is of importance in triggering the bond interchange. However, in the self-reaction, *t*-alkylperoxyl radicals which do not have a C_α–H bond cannot undergo this termination reaction, but produce solely a tetroxide.

The authors would like to express their graditude to the Data Processing Center of Kyoto University for its generous permission to use the FACOM 230-75 computer. The MO calculations were carried out under financial support from the Ministry of Education of Japan (Grant-in-Aid No. 139012).

References

1) (a) J. A. Howard, "Free Radicals," ed by J. K. Kochi, John Wiley & Sons, Vol. 2, New York, N. Y. (1973); (b) K. U. Ingold, *Acc. Chem. Res.*, **2**, 1 (1969).
2) P. D. Bartlett and G. Guaraldi, *J. Am. Chem. Soc.*, **89**, 4799 (1967).
3) R. Hiatt and L. Zigmund, *Can. J. Chem.*, **48**, 3967 (1970).
4) J. A. Howard, *Adv. Free Radical Chem.*, **4**, 49 (1972).
5) G. A. Russell, *J. Am. Chem. Soc.*, **79**, 3871 (1957).
6) (a) D. F. Bowman, T. Gillan, and K. U. Ingold, *J. Am. Chem. Soc.*, **93**, 6555 (1971); (b) J. A. Howard and J. E. Bennett, *Can. J. Chem.*, **50**, 2374 (1972).

7) C. A. McDowell and S. Sifniades, *Can. J. Chem.*, **41**, 300 (1963).
8) S. Yamabe, T. Minato, H. Fujimoto, and K. Fukui, unpublished results (1977).
9) T. Minato, S. Yamabe, H. Fujimoto, and K. Fukui, *Bull. Chem. Soc. Jpn.*, **51**, 1 (1978).
10) K. Fukui, "Theory of Orientation and Stereoselection," Springer Verlag, Berlin (1970).
11) T. Yonezawa, K. Yamaguchi, and H. Kato, *Bull. Chem. Soc. Jpn.*, **40**, 536 (1967).
12) K. Fukui, H. Fujimoto, and S. Yamabe, *J. Phys. Chem.*, **76**, 232 (1972).
13) J. A. Pople and D. L. Beveridge, "Approximate Molecular Orbital Theory," McGraw-Hill, New York, N. Y. (1970).
14) T. Minato, S. Yamabe, S. Inagaki, H. Fujimoto, and K. Fukui, *Bull. Chem. Soc. Jpn.*, **47**, 1619 (1974).
15) R. S. Mulliken, *J. Chem. Phys.*, **23**, 1833, 1841, 2338, 2343 (1955).
16) H. Fujimoto and T. Sugiyama, *J. Am. Chem. Soc.*, **99**, 15 (1977).
17) (a) J. R. Thomas, *J. Am. Chem. Soc.*, **87**, 3935 (1965); (b) J. R. Thomas and K. U. Ingold, Advances in Chemistry Series, No.75, American Chemical Society, Washington, D. C., 1968.
18) R. Hoffmann, *J. Chem. Phys.*, **39**, 1397 (1963).
19) K. N. Houk, J. Sims, C. R. Watts, and L. J. Luskus, *J. Am. Chem. Soc.*, **95**, 7301 (1973).
20) (a) J. A. Howard and K. U. Ingold, *J. Am. Chem. Soc.*, **90**, 1056 (1968); (b) M. Nakano, K. Takayama, Y. Shimizu, Y. Tsuji, H. Inaba, and T. Migita, *ibid.*, **98**, 1974 (1976).

Mixed Monolayers of Long Normal Chain Fatty Acids with Long Normal Chain Fatty Alcohols

Hirosi MATUO, Kimio HIROMOTO, Kinsi MOTOMURA, and Ryohei MATUURA

Department of Chemistry, Faculty of Science, Kyushu University, Fukuoka 812

(Received June 23, 1977)

The mixed monolayers of long normal chain fatty acids with long normal chain fatty alcohols were studied at various compositions and temperatures. The π-A curves of these systems were measured and the two-dimensional phase diagrams were obtained. The partial molar enthalpy change from the expanded to the condensed state was calculated. It was observed that the phase diagram and enthalpy change of these systems are similar to those previously obtained from the mixed monolayers of long normal chain fatty acids. The miscibility of these systems changes with the increase in the difference of the chain length, as in the systems of fatty acids. It was concluded that the monolayer behavior of the mixed system of an acid and an alcohol is analogous to that of the mixed system of the acid and an acid which contains one more carbon atom in a molecule than the corresponding alcohol.

Many workers have extensively studied the monolayers of long normal chain fatty acids.[1-3] Previously we reported some mixed monolayers of these acids and analyzed the phase behavior of the mixed films.[4,5] The thermodynamic treatment of multicomponent surface films was employed.[6,7] It was found that the miscibility of these films varies with the difference of the chain length. But investigations of mixed films of acids with alcohols have been reported much less frequently. The aim of this paper is to clarify the thermodynamic behavior of the mixed film of a fatty acid and an alcohol by taking advantage of the results for mixed films of fatty acids.

Experimental

Tetradecanoic (C_{14}), pentadecanoic (C_{15}), and octadecanoic (C_{18}) acids were employed in this experiment. 1-Tetradecanol ($C_{14}OH$) and 1-hexadecanol ($C_{16}OH$) were used as the long normal chain fatty alcohols. They were purified by fractional distillation and recrystallizations. Benzene, a spreading solvent, was purified carefully by the usual method. The substrate, 0.001 M HCl, was prepared by using twice distilled water and hydrochloric acid (Wako super special grade).

The surface pressure of the monolayers was measured by a Wilhelmy-type surface balance. The temperature was kept constant within $\pm$0.2 °C during the experiment.

Results and Discussion

Typical surface pressure-area curves obtained for the C_{14}–$C_{14}OH$ and C_{14}–$C_{16}OH$ systems at 25 °C are shown in Figs. 1 and 2, respectively. These isotherms are similar to those previously reported for the C_{14}–C_{15} and C_{14}–C_{17} (acid–acid) systems.[4,7] The characteristics of each system may be expressed briefly as follows:

C_{14}–$C_{14}OH$ system (Fig. 1) : the π-A curves of pure tetradecanoic acid and 1-tetradecanol are of the expanded type at 25 °C. When they are mixed, the transition pressure decreases from the value of C_{14} to that of $C_{14}OH$ with increase in the content of the latter. Recently, Roberts, Österlund, and Axberg[8] have claimed that a mixture of 6.12×10^{15} molecules tetradecanoic acid and 1.53×10^{15} molecules 1-hexadecanol spread from petroleum ether together has no transition from the liquid expanded state to the liquid condensed state at 20 °C and pH 2. But in our experimental data at 20 °C and pH 3, the mixed monolayer of the system in which the mole fraction of C_{14} is 0.8 clearly shows a transition at the surface pressure 2.9 dyne/cm.

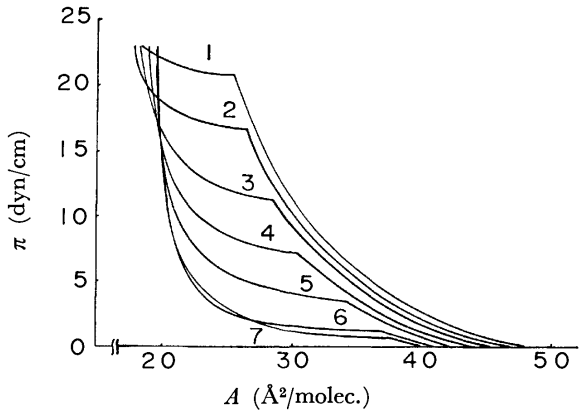

Fig. 1. Surface pressure *vs.* mean area curves of the tetradecanoic acid–1-tetradecanol monolayers at 25 °C: 1, $X_2^\sigma=1$(tetradecanoic acid); 2, 0.9; 3, 0.7; 4, 0.5; 5, 0.3; 6, 0.1; 7, 0(1-tetradecanol).

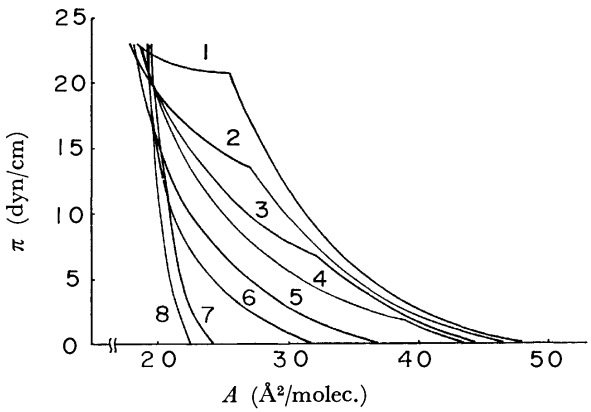

Fig. 2. Surface pressure *vs.* mean area curves of the tetradecanoic acid–1-hexadecanol mixed monolayers at 25 °C: 1, $X_2^\sigma=1$(tetradecanoic acid); 2, 0.9; 3, 0.8; 4, 0.7; 5, 0.6, 6, 0.5; 7, 0.3; 8, 0(1-hexadecanol).

C_{14}–$C_{16}OH$ system (Fig. 2) : the pure $C_{16}OH$ forms a stable condensed film. The mixtures of the acid and alcohol with molar ratios from 9:1 to 7:3 give expanded monolayers which have transition pressures. On the other hand, in mixtures less than 3 : 2 in the

molar ratio, the monolayers are considerably condensed and the transition pressure disappears.

When a binary condensed monolayer is in equilibrium with a binary expanded monolayer, the variation of the equilibrium surface pressure π^{eq} with mole fraction of component 2 in the expanded monolayer $X_2^{\pi,e}$ is related to thermodynamic quantities of the monolayers.[6] According to Eq. 38 in the preceding paper,[6]

$$X_2^{\pi,c} = X_2^{\pi,e} + [(A^c - A^e)X_1^{\pi,e}X_2^{\pi,e}/kT] \times (\partial\pi^{eq}/X_2^{\pi,e})_{T,p}, \quad (1)$$

where the mean area per molecule A has been used with superscripts c and e indicating condensed and expanded films, respectively. We can calculate the numerical values of $X_2^{\pi,c}$, the mole fraction of component 2 in the condensed film, from the dependence of π^{eq} on $X_2^{\pi,e}$. The results evaluated for the C_{14}–$C_{14}OH$ and C_{14}–$C_{16}OH$ systems at 25 °C are shown in Figs. 3 and 4.

The C_{14}–$C_{14}OH$ system (Fig. 3) gives a typical pattern of a simple mixed system in which the two components are miscible in all compositions. This behavior is identical with that of the C_{14}–C_{15} system previously obtained at 20 °C.[7] In the C_{14}–$C_{16}OH$ system, as shown in Fig. 4, the situation of miscibility is somewhat different from the C_{14}–$C_{14}OH$ system. The expanded phase disappeared in the monolayers in which the mole fractions of tetradecanoic acid are below 0.65. A similar phase diagram has been observed for the C_{14}–C_{17}[7] and C_{14}–$C_{14}OH$ systems at 20 °C. We consider that, in this region, the mixed film changes from the expanded to the condensed state in the process of compression at low surface pressures. This shows that the miscibility of the two components at the same temperature gradually decreases with increase in the difference of carbon number between the two film components. When the surface pressure reaches 20.8 dyne/cm, the transition pressure of the pure tetradecanoic acid monolayer at 25 °C, the mixed film perfectly changes into the condensed film.

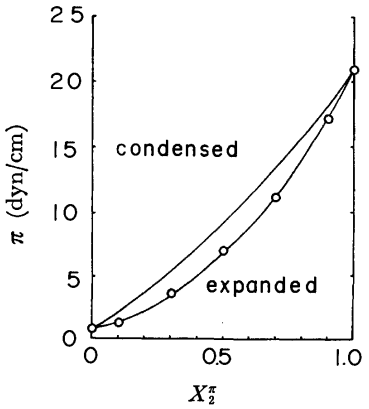

Fig. 3. Phase diagram of the tetradecanoic acid-1-tetradecanol mixed monolayer at 25 °C.

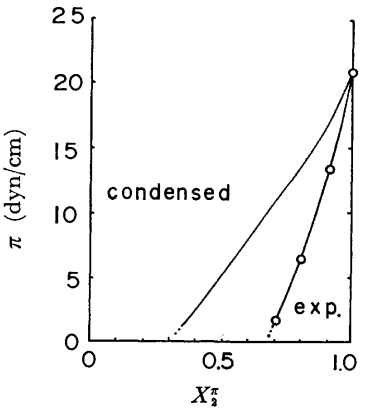

Fig. 4. Phase diagram of the tetradecanoic acid-1-hexadecanol mixed monolayer at 25 °C.

Phase diagrams of the C_{15}–$C_{14}OH$ and C_{15}–$C_{16}OH$ systems are also shown in Figs. 5 and 6. The appearance of these phase diagrams corresponds to that of the C_{14}–$C_{14}OH$ and C_{14}–$C_{16}OH$ systems, respectively. In the C_{15}–$C_{14}OH$ system, as shown in Fig. 5, the transition range is somewhat smaller in composition than that in the C_{14}–$C_{14}OH$ system. This indicates that the miscibility of the C_{15}–$C_{14}OH$ system is likely to be more ideal than that of the latter.[7] This is also applicable to the C_{15}–$C_{16}OH$ system (Fig. 6) as compared with the C_{14}–$C_{16}OH$ system. According to these results, we would conclude that the monolayer of a long normal chain fatty alcohol is analogous to that of a fatty acid which has one more carbon atom than the corresponding alcohol molecule.

The π^{eq}-$X_2^{\pi,e}$ curves obtained for the $C_{14}OH$–$C_{16}OH$ and C_{18}–$C_{14}OH$ systems at 30 °C are shown in Figs. 7 and 8. The two-dimensional phase diagram for the $C_{14}OH$–$C_{16}OH$ system (Fig. 7) seems to be the same type as that of the C_{14}–$C_{16}OH$ and C_{15}–$C_{16}OH$ systems.

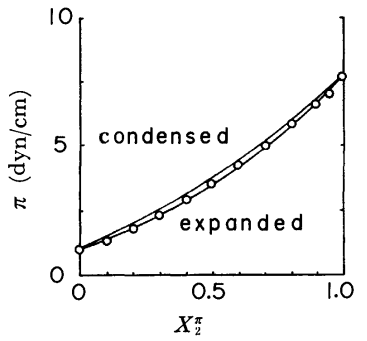

Fig. 5. Phase diagram of the pentadecanoic acid-1-tetradecanol mixed monolayer at 25 °C.

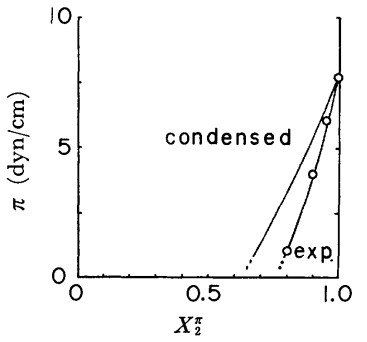

Fig. 6. Phase diagram of the pentadecanoic acid-1-hexadecanol mixed monolayer at 25 °C.

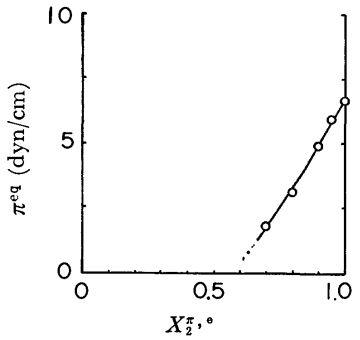

Fig. 7. π^{eq}-$X_2^{\pi,e}$ curve of the 1-tetradecanol-1-hexadecanol mixed monolayer at 30 °C.

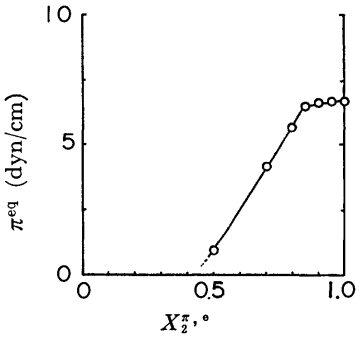

Fig. 8. π^{eq}-$X_2^{\pi,e}$ curve of the octadecanoic acid–1-tetradecanol mixed monolayer at 30 °C.

In the C_{18}–$C_{14}OH$ system (Fig. 8), the π^{eq}-$X_2^{\pi,e}$ curve is complicated because of the presence of the break point. However, by the analysis of the fatty acid's phase diagram,[7] it was found that this system is similar to the C_{14}–C_{19} system.

From the variation of the transition pressure with temperature, we can calculate the thermodynamic quantities such as the partial molar entropy and enthalpy of the transfer from expanded to condensed phase. We have reported the following expression (Eq. 42 in Ref. 6):

$$\bar{s}_i^c - \bar{s}_i^e = (\bar{s}_i^{\pi,c} - \bar{s}_i^{\pi,e}) + (a^e - \bar{a}_i^e)(\partial\pi^e/\partial T)_{p,x_w^e,x_2^{\pi,e}} - (\bar{a}_i^c - \bar{a}_i^e)(\partial\gamma^0/\partial T)_p, \quad i = 1, 2 \qquad (2)$$

where $\bar{a}_i$ is the partial molar area of component i in the monolayer $\partial\pi^e/\partial T$ is the variation of surface pressure with respect to temperature at a given state of the expanded monolayer, γ^0 is the surface tension of water, and the subscript w represents water. In the above equation, $\bar{s}_i^\pi$ is the partial molar entropy of component i in the equilibrium monolayer, and $\bar{s}_i^c - \bar{s}_i^e$ is the thermodynamically well-defined partial molar change in entropy at the phase transition from the expanded to the condensed state.[5,6] The corresponding enthalpy change can be evaluated by the following expression, which has been obtained as Eq. 43 in Ref. 6:

$$\bar{h}_i^c - \bar{h}_i^e = T(\bar{s}_i^c - \bar{s}_i^e). \qquad (3)$$

We have assumed that $\bar{A}_1^e = \bar{A}_2^e = 20$ Å^2/molec. and $\bar{A}_1^c = \bar{A}_2^c = 18$ Å^2/molec.; then we can calculate the values of $\bar{s}_i^c - \bar{s}_i^e$ from Eq. 2. $\bar{h}_i^c - \bar{h}_i^e$ can also be evaluated from Eq. 3.

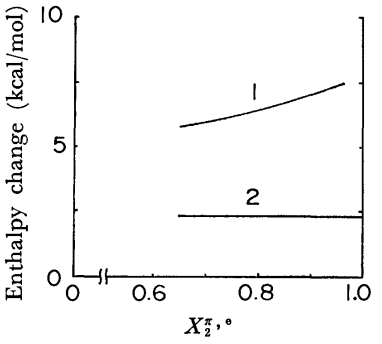

Fig. 9. Partial molar enthalpy change of the phase transition, $-(\bar{h}_i^c - \bar{h}_i^e)$ *vs.* mole fraction in the expanded monolayer, $X_2^{\pi,e}$, curves of the tetradecanoic acid–1-tetradecanol at 20 °C: 1, 1-tetradecanol; 2, tetradecanoic acid.

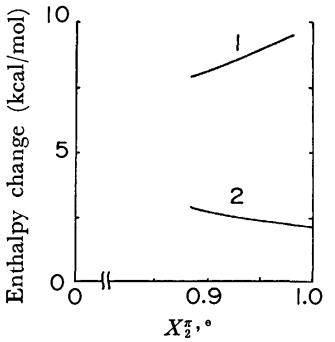

Fig. 10. Partial molar enthalpy change of the phase transition, $-(\bar{h}_i^c - \bar{h}_i^e)$ *vs.* mole fraction in the expanded monolayer, $X_2^{\pi,e}$, curves of the tetradecanoic acid–1-hexadecanol at 20 °C: 1, 1-hexadecanol; 2, tetradecanoic acid.

The calculated values for the C_{14}–$C_{14}OH$ and C_{14}–$C_{16}OH$ systems at 20 °C are shown in Figs. 9 and 10. In the former system (Fig. 9), the enthalpy change of the tetradecanoic acid has a nearly constant value independent of $X_2^{\pi,e}$ in the range of the composition shown. The partial molar enthalpy change of the tetradecanoic acid, 2.2 kcal/mol, is fully acceptable in comparison with that of a mixed film of long normal chain fatty acids.[7] On the other hand, the partial molar enthalpy change of the 1-tetradecanol decreases slightly with decreasing $X_2^{\pi,e}$. The enthalpy change of 1-tetradecanol is larger than that of tetradecanoic acid at the same composition. This indicates that this alcohol is less stable in the expanded state and needs much more heat for the transition from the liquid condensed to the expanded state. This agrees with the experimental result that the transition pressure is elevated by the addition of tetradecanoic acid. In the case of the C_{14}–$C_{16}OH$ system (Fig. 10), the change of partial molar enthalpy of the tetradecanoic acid decreases, while that of the 1-hexadecanol increases, with increasing $X_2^{\pi,e}$, in the range of the composition shown in the figure. The pattern of these two curves is identical with that of the C_{14}–C_{17} system,[7] but the slope of these curves is smaller than that of the latter. This is related to

the miscibility of the two components. Taking advantage of the results for C_{14}–C_{15}, C_{14}–C_{17}, and C_{14}–C_{19} systems,[7] it seems that the more ideal the miscibility, the smaller the inclination is.

In conclusion, mixed monolayers of long normal chain fatty acids with long normal chain fatty alcohols have the same behavior as that of mixed monolayers of fatty acids. That is to say, the acids and alcohols are miscible with each other in the expanded as well as in the condensed state. And the miscibility of two components gradually decreases with an increase in the difference of carbon number between the two components. Finally, we conclude that the monolayer of the alcohol is analogous to that of a fatty acid which contains one more carbon atom in the molecule than the corresponding alcohol.

References

1) G. L. Gaines, "Insoluble Monolayers at Liquid-Gas Interfaces," Interscience Publishers, New York, (1966), Chap. 5.
2) G. E. Boyd and F. Vaslow, *J. Colloid Sci.*, **13**, 275 (1958).
3) H. E. Ries, Jr., and H. D. Cook, *J. Colloid Sci.*, **9**, 535 (1954).
4) N. Kuramoto, K. Sekita, K. Motomura, and R. Matuura, *Mem. Fac. Sci. Kyushu Univ.*, **C8**, 67 (1972).
5) K. Motomura, *J. Colloid Interface Sci.*, **48**, 307 (1974).
6) K. Motomura, K. Sekita, and R. Matuura, *J. Colloid Interface Sci.*, **48**, 319 (1974).
7) K. Sekita, M. Nakamura, K. Motomura, and R. Matuura, *Mem. Fac. Sci. Kyushu Univ.*, **C10**, 51 (1976).
8) K. Roberts, R. Österlund, and C. Axberg, *J. Colloid Interface Sci.*, **55**, 563 (1976).

The application of an Improved d.c. Polarization Technique to the Electronic Conductivity Measurements of α-AgI and AgBr

Junichiro MIZUSAKI, Kazuo FUEKI, and Takashi MUKAIBO

Department of Industrial Chemistry, Faculty of Engineering, The University of Tokyo, Hongo, Bunkyo-ku, Tokyo 113

(Received June 27, 1977)

An improvement was made in the d.c. polarization technique which is used for the measurement of the electronic conductivity of solid electrolytes. In the electrochemical cell, Ag/AgX (X=Br or I)/carbon, the carbon electrode was sealed with AgX in the bottom of a Pyrex tube so that the electrode reaction at the AgX/carbon interface could be suppressed in the steady state. Using the improved d.c. polarization cell, measurement was made of the electronic conductivity of AgI in the temperature range from 330 to 500 °C, and that of AgBr, at temperatures from 375 to 400 °C, as a function of the halogen partial pressure, P_{X_2}. It was found that the electronic conduction of α-AgI is *p*-type and that the electronic conductivity is proportional to $P_{I_2}^{1/2}$. The electronic conductivity of AgBr was found to be proportional to $P_{Br_2}^{-1/2}$ in a low-pressure range of bromine, and proportional to $P_{Br_2}^{1/2}$ in a high-pressure range.

Hebb-Wagner's d.c. polarization technique[1,2] is generally used for the determination of the electronic conductivity of solid electrolytes. For the determination of electronic conductivity by this technique, a complete blocking of the ionic current is necessary. Thus far, the following two types of cell arrangement have been employed for the measurement of AgI and AgBr:

(I) ⊖ Ag/AgX/carbon, inert atmospere ⊕

(II) ⊖ carbon, inert atmospere/AgX/carbon, halogen gas atmospere ⊕

where AgX denotes AgI or AgBr. However, in these cells the ionic current can not be blocked completely, because one of the carbon electrodes is open to the inert atmospere, and the chemical equilibrium can not be established at the electrode/AgX interface.

Using a cell of Type (I), Ilschner[3] measured the electronic conductivity of AgI and AgBr and found that AgI shows the *p*-type electronic conduction in the temperature range from 267 to 332 °C, but the slope of the logarithmic plots of the current against the applied potential difference was 1.2 times larger than that expected by Wagner's theory.[2] Above 332 °C, the electronic conductivity could not be determined because of the increased decomposition current. In the case of AgBr, the *n*-type conduction was observed under the small applied potential difference in the temperature range from 333 to 372 °C, but the decomposition current increased with the increase in the applied potential difference.

Raleigh investigated the electronic conduction of AgBr at temperatures between 250 and 400 °C using a cell of Type (II); he observed both *n*- and *p*-type conductions, in accordance with the applied potential difference, but the decomposition current became large with a decrease in the applied potential difference.[4]

As has been mentioned above, as to α-AgI (stable above 146 °C) and AgBr, no work[3-6] has succeeded in showing whether or not the relation between the current and the applied potential difference coincides with the prediction by Wagner's theory.

The purpose of the present study is to devise a d.c. polarization cell in which the decomposition current is completely blocked and to determine the electronic conductivity of α-AgI and AgBr as a function of the halogen partial pressure.

Improved d.c. Polarization Cell

A conventional d.c. polarization cell of Type (I) is shown in Fig. 1. In the cell, inert gas flows over the electrodes and carries halogen gas from the AgX/carbon interface. Therefore, a polarization cell of this type can not block the decomposition current completely.

In order to obtain a complete ion-blocking condition, the authors devised the d.c. polarization cell shown in Fig. 2. In this cell, AgX seals the carbon electrode completely in a small space at the bottom of a Pyrex tube. When an electrical potential difference is applied between the carbon (positive) and the silver (negative) electrodes, the partial pressure of halogen gas, P_{X_2}*, in the space changes as a result of charging and discharging, finally reaching the value

$$P_{X_2}^* = P_{X_2}^\circ \exp\left(\frac{2FE}{RT}\right), \quad (1)$$

where $P_{X_2}^\circ$ denotes the halogen partial pressure in equilibrium with the AgX co-existing with metallic silver and where E denotes the applied potential difference. Under this condition, the ionic current ceases to flow and Hebb-Wagner's d.c. polarization technique can be applied. We call a cell of this type an improved

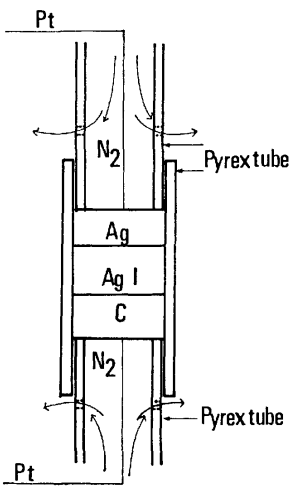

Fig. 1. Conventional type cell.

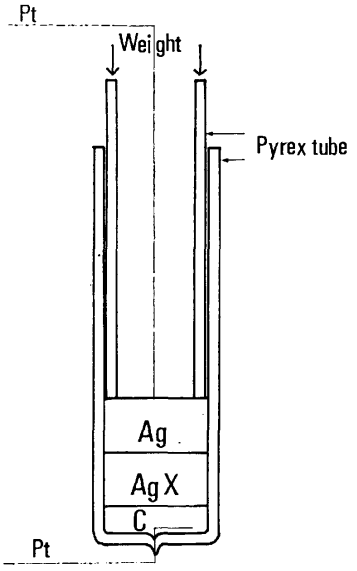

Fig. 2. Improved cell.

d.c. polarization cell.

Equation 1 can be rewritten as follows by using the silver chemical potential, μ_{Ag}:

$$EF = \mu_{Ag}^{\circ} - \mu_{Ag}^{*}, \quad (2)$$

where μ_{Ag}° denotes μ_{Ag} in AgX in equilibrium with metallic silver and where μ_{Ag}^{*} is that of AgX at the AgX/carbon interface. Using the silver activity, a_{Ag}, we obtain

$$EF = -RT \ln a_{Ag}^{*}, \quad (3)$$

where a_{Ag}^{*} denotes the a_{Ag} in AgX at the AgX/carbon interface and where the a_{Ag} in AgX co-existing with metallic silver is taken as unity.

Experimental

Cells and Samples. In order to compare the improved cell with the conventional-type cell, measurements were carried out using both types of cells (Figs. 1 and 2). The cells were constructed in a Pyrex tube, 10 mm in inner diameter. The silver electrode, carbon electrode, and AgX pellet used were the same as those used in a previous work.[7] The AgX pellet was sandwiched by the silver and carbon electrodes and pressed by means of a spring to ensure contact. In a conventional-type cell, purified nitrogen gas was let flow over the surface of the electrodes. In an improved cell, a Pt lead wire was sealed at the lower end of the Pyrex tube. Then the cell was heated at about 400 °C so that the AgX pellet could deform plastically by a slight pressure and come in close contact with the wall of the Pyrex tube. Thus, the carbon electrode was completely sealed in a small space.

Coulometric Study. Prior to the construction of the cells, the weights of the silver electrode and the AgI pellet were measured. After the cell construction, a constant potential difference of 400 or 450 mV was applied at 500 °C for several days. The current decay was recorded by means of an electric recorder. The electricity passed through the cell was calculated by integrating the current-time curve. Then, the cell was disassembled and the weights of the silver electrode and AgI pellet were measured again.

Measurement of the Current and Potential in the Steady State. Measurements were performed at temperatures from 330 to 500 °C for AgI, and at 375 and 400 °C for AgBr, by the use of the improved cell. For comparison, a conventional-type cell was also used for AgI at 500 °C. When the steady state current exceeds about 5 μA, the measurement could be carried out by applying a constant potential difference between the electrodes by means of a d.c. voltage regulator. However, current fluctuation was caused even in the steady state by the unavoidable slight fluctuations in the temperature or the applied potential difference. This current fluctuation became a serious obstacle to the measurement when the steady-state current was lower than about 5 μA. The use of the circuit shown in Fig. 3 was found to be very effective in avoiding such difficulty, and so it was mainly employed in the present work. In this circuit, the standard resistance, R, was connected in series with the cell, and a constant potential difference was applied between the two ends of the series. The resistance showed a kind of buffer action on the fluctuation. When E deviated positively from the relation in Eq. 1, the drop in the current or the ohmic value due to the resistance increased. Consequently, the potential difference loaded to the cell E decreased. Thus, the fluctuation was dampened. When the value of R was chosen so that the ohmic drop at this resistance was 1 to 10% of the applied potential difference in the steady state, the fluctuation of the current and E was effectively suppressed.

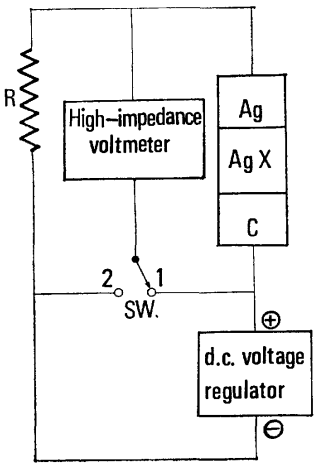

Fig. 3. Circuit diagram for the measurement.
$R = 100\ \Omega - 10\ k\Omega$

The current passed through the cell was determined from the ohmic drop at the resistance measured by means of a high-impedance voltmeter, which was also used for the measurement of the applied potential difference between the electrodes. The steady state was confirmed from the current and potential difference, which had been kept constant for at least 2 or 3 h.

The electric furnace and the temperature-controlling system were already described in a previous paper.[7]

Results and Discussion

Comparison of the Improved Cell with the Conventional-type One. The results of coulometry using both types of cells are shown in Table 1. When AgI is electrolysed, silver deposits on the silver electrode and iodine gas is released in the nitrogen atmosphere or diffuses into the carbon electrode. Therefore, the change in the sum of the weights of the silver electrode and the AgI pellet is equal to the quantity of iodine gas released by the electrolysis. The difference between the quantity

Table 1. Estimation of the ratio of the decomposition current to the electronic current

	Conventional-type cell		Improved cell	
	Run 1	Run 2	Run 11	Run 12
E/mV	450	400	450	400
Quantity of electricity passed through the cell; $[A]$/Faraday	1.90×10^{-3}	1.20×10^{-3}	11×10^{-4}	55×10^{-5}
Initial weight/g of sample				
Ag	2.41	2.65	2.72	7.37
AgI	1.51	1.43	1.37	1.66
Ag+AgI	3.93	4.08	4.09	9.02
Final weight/g of sample				
Ag+AgI	3.74	3.94	4.07	9.01
Weight loss/g	0.19	0.14	0.02	0.01
Released iodine; $[B]$/eqv.	1.5×10^{-3}	1.1×10^{-3}	2×10^{-4}	8×10^{-5}
The ratio; $[B]/([A]-[B])$	3.8	1.1×10	0.2	0.2

of the electricity passed through the cell in Faraday, $[A]$, and the quantity of released iodine in the equvalent, $[B]$, is equal to the quantity of electricity carried by the electrons. Thus, $[B]/([A]-[B])$ gives the ratio of the decomposition current to the electronic current. As is clearly shown in Table 1, the decomposition current is predominant in the conventional-type cell, while the electronic current is predominant in the improved cell.

It should be noted that even when an improved cell is used, the electrolysis of AgI occurs until the carbon electrode is saturated with iodine gas with a partial pressure of P_{I_2}*. The weight loss and the quantity of electricity, due to the electrolysis, are included in the values in Table 1. In the steady state, ion blocking would be effected more completely than that indicated in Table 1.

According to Wagner,[2] when AgX shows a p-type electronic conduction and when the electronic conductivity due to electron holes is expressed by Eq. 4, the relation between the current density, I and E under the complete ion-blocking condition can be represented by Eq. 5:

$$\sigma_h = \sigma_h^\circ \exp\left(\frac{\mu_{Ag}^\circ - \mu_{Ag}}{RT}\right), \quad (4)$$

$$\frac{IFL}{RT} = \sigma_h^\circ \left\{\exp\left(\frac{EF}{RT}\right) - 1\right\}, \quad (5)$$

where σ_h denotes the electronic conductivity in AgX, the silver chemical potential of which is kept at μ_{Ag}, where σ_h° denotes the σ_h of AgX in equilibrium with the metallic silver, and where L denotes the thickness of the AgX pellet. In the previous paper,[7] the authors showed, by the measurement of the chemical potential profile, that Eq. 5 holds for AgI at 500 °C.

When $EF \gg RT$, Eq. 5 can be rewritten as

$$\frac{IFL}{RT} = \sigma_h^\circ \exp\left(\frac{EF}{RT}\right), \quad (6)$$

that is

$$\log\frac{IFL}{RT} = \log\sigma_h^\circ + \frac{EF}{2.303RT}. \quad (7)$$

Therefore, if the decomposition current is completely blocked, the slope of the $\log I$-E plot should be $F(2.303RT)^{-1}$ and I should depend on L. However, if the decomposition current is predominant, I should be independent of L.

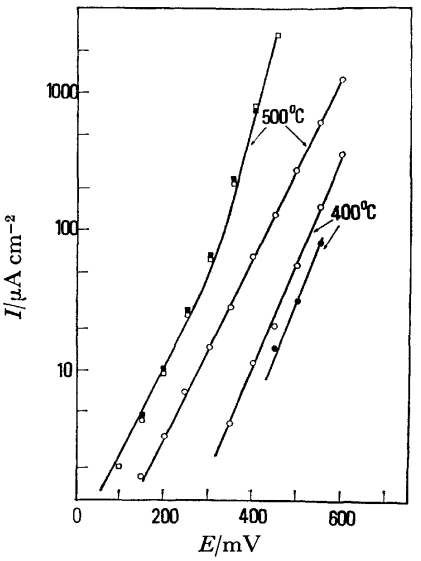

Fig. 4. Plots of I *vs.* E for AgI.
□: Conventional type cell, L=2.7 mm, ■: conventional type cell, L=6.0 mm, ○; improved cell, L=3.3 mm, ●: improved cell, L=6.5 mm.

The plots of the logarithm of I against E in the steady state, obtained by the use of both types of cells, are shown in Fig. 4. When the conventional-type cell is used, the slope of the plots is equal to $F(2.303RT)^{-1}$ in the $E<300$ mV region, while in the $E>300$ mV region the slope is $2F(2.303RT)^{-1}$. The current density is independent of L. When the improved cell is used, the slope of the plots is $F(2.303RT)^{-1}$ and is independent of E. The current density depends on L.

Those results indicate that the improved cell blocks the ionic current completely in the steady state and that the improved cell makes it possible to apply the d.c. polarization technique even when the conventional-type cell can not be used because of the predominant decomposition current.

The results obtained by means of the improved cell will be given below.

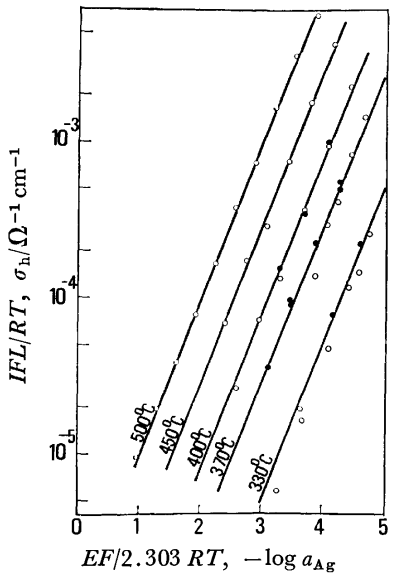

Fig. 5. Plots of σ_h *vs.* $\log a_{Ag}$ for AgI.
○: L=3.8 mm, ●: L=6.5 mm.

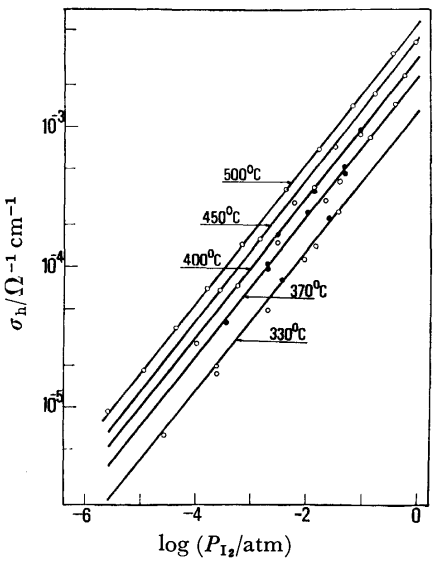

Fig. 6. Plots of σ_h *vs.* $\log P_{I_2}$ for AgI.
○: L=3.8 mm, ●: L=6.5 mm.

Electronic Conductivity of α-AgI. The results for AgI are given in Fig. 5 as a semi-logarithmic plot of $IFL(RT)^{-1}$ against $EF(2.303RT)^{-1}$. Using Eqs. 2, 4, and 6, we obtain

$$\sigma_h^* = \frac{IFL}{RT}, \tag{8}$$

where σ_h^* is the electronic conductivity of AgI at the AgI/carbon interface. By the help of Eq. 3. $EF(2.303RT)^{-1}$ can be substitued for $\log a_{Ag}^*$. Therefore, Fig. 5 also indicates the plots of σ_h against the a_{Ag} of AgI. The combination of Eqs. 1 and 3 yields

$$\log a_{Ag}^* = -\frac{1}{2}\log\frac{P_{I_2}^*}{P_{I_2}^\circ}. \tag{9}$$

Thus, $\log a_{Ag}^*$ can be expressed in terms of $P_{I_2}^*$. The plots of σ_h against P_{I_2} are shown in Fig. 6. The thermodynamic data summarized by Worrell and Hladik[8] are used for the calculation of $P_{I_2}^\circ$ in Eq. 9. We can see from Fig. 6 that the σ_h of AgI is proportional to $P_{I_2}^{1/2}$.

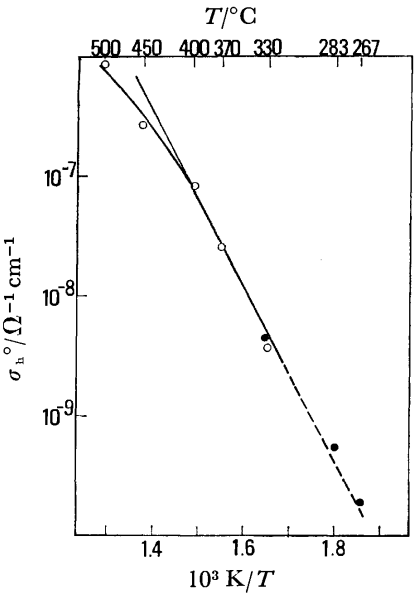

Fig. 7. Arrhenius plots of σ_h° for AgI.
○: This work, ●: by Ilschner.

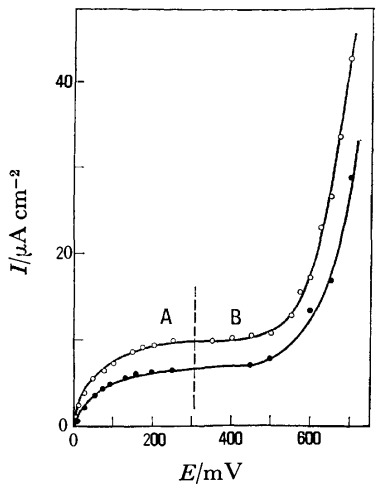

Fig. 8. Plots of I *vs.* E for AgBr at 400 °C.
○: L=2.2 mm, ●: L=3.3 mm.

The plots of σ_h° against T^{-1} are shown in Fig. 7. In the figure, the σ_h° values obtained by Ilschner[3] by the use of the conventional-type cell in a lower temperature range are also shown for the sake of comparison. The two sets of data agree well with each other. The data for the σ_h° of AgI in the temperature range from 267 to 400 °C are expressed as

$$\sigma_h^\circ = 2.76\times10^3 \exp(-1.64\times10^4\,T^{-1})\ (ohm^{-1}\,cm^{-1}). \tag{10}$$

Above 400 °C, the Arrhenius plot for σ_h° is curved. The reason for this is not clear, since the drift mobility or the concentration of electron holes have not been measured in this temperature range.

Electronic Conductivity of AgBr. The plots of I against E at 400 °C are shown in Fig. 8. In the present results, I is proportional to L^{-1}, so a complete ion

blocking is indicated. The curve can be divided into two parts, A and B. In Part A ($E<300$ mV) I asymptotically reaches a plateau, I_{pl}, while in Part B ($E>300$ mV) I increases exponentially from the plateau. It is known that AgBr shows an n-type electronic conduction when $E<300$ mV[7] and shows a p-type electronic conduction when the equilibrium bromine partial pressure is high. Therefore, Part A may correspond to the n-type region, and Part B to the region in which the p-type electronic conduction is predominant.

According to Wagner,[2] when the electronic conductivity of AgBr due to the conduction electrons is expressed by Eq. 11, the I-E relation under the complete ion-blocking condition can be represented by Eq. 12;

$$\sigma_e = \sigma_e^\circ \exp\left(\frac{\mu_{Ag}-\mu_{Ag}^\circ}{RT}\right), \tag{11}$$

$$\frac{IFL}{RT} = \sigma_e^\circ \left\{1-\exp\left(-\frac{EF}{RT}\right)\right\}. \tag{12}$$

Here, σ_e denotes the electronic conductivity at μ_{Ag}, while σ_e° denotes the σ_e of AgBr in equilibrium with metallic silver. The authors showed in the previous paper[7] that Eq. 12 holds for AgBr in the temperature range from 350 to 400 °C when $E<300$ mV.

Equation 12 indicates that, when $EF \gg RT$, I is equal to a constant value, I_{pl}, that is,

$$\frac{I_{pl}FL}{RT} = \sigma_e^\circ. \tag{13}$$

Using Eqs. 12 and 13, we obtain

$$\frac{(I_{pl}-I)}{RT} = \sigma_e^\circ \exp\left(-\frac{EF}{RT}\right), \tag{14}$$

or

$$\log \frac{(I_{pl}-I)FL}{RT} = \log \sigma_e^\circ - \frac{EF}{2.303RT}. \tag{15}$$

The semi-logarithmic plots of $(I_{pl}-I)FL(RT)^{-1}$ against $EF(2.303RT)^{-1}$ for Part A are shown in Fig. 9. The data fall on a straight line with a slope of -1. Clearly, the present results obey Eq. 15. This confirms that Eq. 11 holds for AgBr when $E<300$ mV.

On the assumption that Eq. 4 holds for AgBr under the conditions of complete ion blocking and when $E>300$ mV, we obtain[2]

$$\frac{IFL}{RT} = \sigma_e^\circ + \sigma_h^\circ \exp\left(\frac{EF}{RT}\right). \tag{16}$$

Using Eq. 13, we obtain

$$\frac{(I-I_{pl})FL}{RT} = \sigma_h^\circ \exp\left(\frac{EF}{RT}\right), \tag{17}$$

or

$$\log \frac{(I-I_{pl})FL}{RT} = \log \sigma_h^\circ + \frac{EF}{2.303RT}. \tag{18}$$

The semi-logarithmic plots of $(I-I_{pl})FL(RT)^{-1}$ against $EF(2.303RT)^{-1}$ for Part B are also shown in Fig. 9. The solpe of the plots is unity. Therefore, Eq. 18 holds when $E>300$ mV. This result indicates that the electronic conduction in AgBr under a high bromine partial pressure can be well interpreted as the predominant electron-hole conduction expressed by Eq. 4.

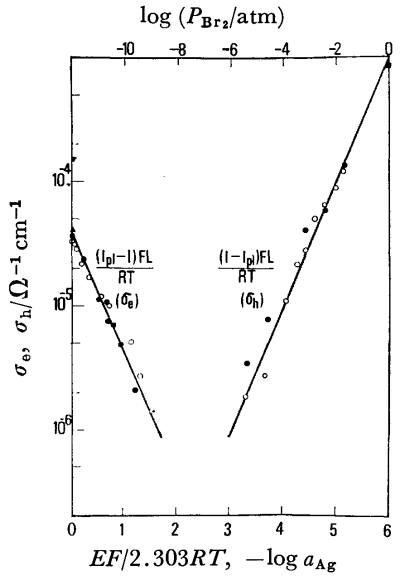

Fig. 9. Plots of σ_e and σ_h *vs.* $\log a_{Ag}$ and $\log P_{Br_2}$ at 400 °C for AgBr.
○: $L=2.2$ mm, ●: $L=3.3$ mm, ▼: by Weiss, ▲; by Ilschner, ■: by Raleigh.

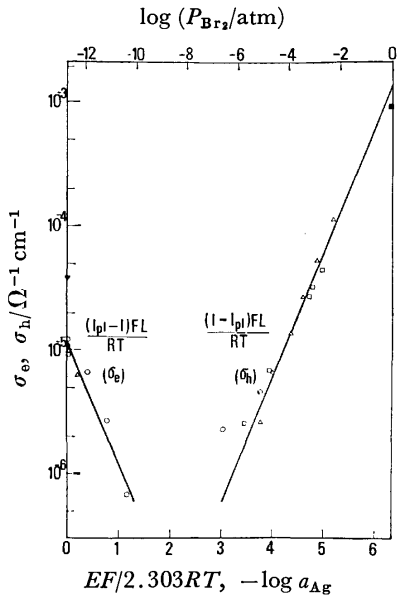

Fig. 10. Plots of σ_e and σ_h *vs.* $\log a_{Ag}$ and $\log P_{Br_2}$ at 375 °C for AgBr.
△: $L=2.5$ mm, □: $L=1.3$ mm, ○: $L=2.2$ mm, ▼: by Weiss, ▲: by Ilschner, ■: by Raleigh.

By inserting Eq. 2 into Eqs. 14 and 17 respectively, we obtain

$$\frac{(I_{pl}-I)FL}{RT} = \sigma_e^* \tag{19}$$

and

$$\frac{(I-I_{pl})FL}{RT} = \sigma_h^*, \tag{20}$$

where σ_e^* and σ_h^* denote the σ_e and σ_h of AgBr at the AgBr/carbon interface respectively. Using Eqs. 1 and 3, $EF(2.303RT)^{-1}$ is rewritten in terms of $\log a_{Ag}^*$ and $\log P_{Br_2}^*$. Figure 9 shows the plots of σ_e and σ_h against $\log a_{Ag}$ and $\log P_{Br_2}$. The corresponding values

of log a_{Ag} and log P_{Br_2} are also shown in Fig. 9. For the calculation of P_{Br_2}, the data in the literature were employed.[8]

The results at 375 °C are shown in Fig. 10. Also, Figs. 9 and 10 show the σ_e° values obtained by Ilschner[3] and Weiss[5] and the σ_h ($P_{Br_2}=1$ atm) obtained by Raleigh[4] by the use of conventional-type cells. The data by Ilschner and by Raleigh are in good agreement with the present results.

From the results presented above, it may be concluded that the improved cell can achieve complete ion blocking and that the electronic conductivity of silver halides can be determined strictly even under when the conventional-type cell can not be used.

Summary

(1) In order to block the ionic current completely in the Hebb-Wagner d.c. polarization cell, an improved cell assembly was devised and used for the accurate determination of the electronic conductivity of α-AgI and AgBr.

(2) The electronic conductivity of α-AgI (330 to 500 °C) was found to be proportional to $P_{I_2}^{1/2}$, and σ_h° (267 to 400 °C) is expressed as:

$$\sigma_h^\circ = 2.76\times10^3 \exp(-1.64\times10^4\, T^{-1}) \quad (\text{ohm}^{-1}\,\text{cm}^{-1})$$

The electronic conductivity of AgBr at 375 and 400 °C was found to be proportional to $P_{Br_2}^{-1/2}$ in the low-pressure range of bromine, and proportional to $P_{Br_2}^{1/2}$ in the high-pressure range.

References

1) M. Hebb, *J. Chem. Phys.*, **20**, 185 (1952).
2) C. Wagner, *Proc. C. I. T. C. E.*, **7**, 361 (1955).
3) B. Ilschner, *J. Chem. Phys.*, **28**, 1109 (1958).
4) D. O. Raleigh, *J. Phys. Chem. Solids*, **26**, 329 (1965).
5) K. Weiss, *Z. Phys. Chem.*, **NF59**, 242 (1968).
6) K. Weiss, *Electrochim. Acta*, **16**, 201 (1971).
7) J. Mizusaki, K. Fueki, and T. Mukaibo, *Bull. Chem. Soc. Jpn.*, **48**, 428 (1975).
8) W. L. Worrell and J. Hladik, "Physics of Electrolyte," ed by J. Hladik, Academic Press, London-New York (1972), p. 747.

Photo-effects of Metal Oxide Electrode. I. Photoelectrochemical Processes on a Silver–Silver Oxide Electrode and the Influence of Ethylene Glycol

Akira KUNUGI, Shuji MIYOSHI, and Shigeo NAGAURA
Department of Applied Chemistry, Faculty of Engineering, Osaka City University, Sugimoto-cho, Sumiyoshi-ku, Osaka 558

(Received July 7, 1977)

The influence of light excitation on the anodic oxidation of a silver electrode in alkaline solutions has been studied. The experimental results have shown that, in addition to the formation of Ag(II) species by a reaction of Ag(I) species with photo-generated holes, illumination in the Ag_2O formation region causes the photogeneration of Ag(I) species at the metal/oxide interface. In the presence of ethylene glycol, the so-called current doubling phenomenon was found. This phenomenon has been interpreted in terms of a mechanism involving a catalytic reaction of the glycol with the photogenerated Ag(II) species, and not by a mechanism involving the oxidation of glycol by the photo-generated holes.

A silver–silver oxide electrode is very useful as a cathode in batteries with a high energy-to-mass ratio; hence, to date, the anodic behavior of silver in alkaline solutions has been extensively studied.[1] Also, the use of silver–silver oxide electrode in organic synthesis has received considerable attention[2] because silver oxides are known to react selectively with certain organic groups.[3]

In recent years, some work has been done on the photoeffects of silver–silver oxide electrodes.[4–7] Illumination definitely increases an anodic current in the Ag_2O formation region; the increment is generally accepted to be a photocurrent due to light absorption by an Ag_2O layer. There is, however, some disagreement concerning what kind of product is formed by light excitation. For example, Göhr and Breitenstein[4] explained the production of the photocurrent by assuming a photo-decomposition of Ag_2O into oxygen and silver, which is reoxidized either to Ag_2O or directly to AgO, depending on the electrode potential adjusted, whereas Memming *et al.*[5] suggested that light absorption by an Ag_2O layer leads to an anodic oxidation to AgO by the interaction of the photo-generated holes in the Ag_2O with Ag_2O. Perkins *et al.*[6] proposed that, in addition to the oxidation of interstitial Ag^+ to Ag^{2+}, which acts as a catalytic center for AgO formation, illumination enhances the rate of the primary Ag^+-formation process at the metal/oxide interface, resulting in a substantial increase in the Ag_2O formation.

In order to obtain more information about the photoelectrochemical process in the anodic oxidation of silver in alkaline solutions, the present work was performed. Furthermore, the influence of ethylene glycol on the electrode process was examined. Ethylene glycol was selected because it has a relatively high reactivity for a reaction with AgO and is virtually inactive for Ag_2O.[8]

Experimental

The working electrode was made from a wire of silver (purity > 99.99%) in the form of a disk (5 mm dia.) surrounded by a Teflon sheath. The reference electrode, against which all the potentials in the present paper are quoted, was Hg/HgO in 1 M KOH, and it was separated from the working electrode by a Luggin capillary. The electrolyte solutions were prepared from extra-pure-grade potassium hydroxide and water, twice distilled from deionized stock. Extra-pure-grade ethylene glycol was used without further purification.

The silver electrode was polished by means of a fine emery paper (number 0/8), cleaned in acetone and distilled water, and washed with a 1 M KOH solution. In addition, the electrode was subjected to the repeating of the potential cycle over the potential of from 0.0 to 0.8 V, with a sweep rate of 2.9 mV/s, in a 1 M KOH solution in the dark, using a potentiostat in conjunction with a linear sweep generator. After several cycles (in most cases, 6 times) the electrode was introduced into another cell filled with the solution to be studied, and then cyclic voltammograms were recorded on a x-y recorder. Simple H-shaped cells with a quartz window, which allowed the illumination of the working electrode, were used.

Coulomb-potential curves, which were measured simultaneously with the cyclic voltammograms, were displayed on a x-y recorder by means of a device constructed in our laboratory. From these curves, the amounts of charge for each peak were obtained.

In the experiments on the photo-effects, a 500 W Xenon arc lamp UXL-500D (Ushio Electric Inc.), which was enclosed in a lamp housing and powered by a dc power supply, was used as the light source. A fairly homogeneous and

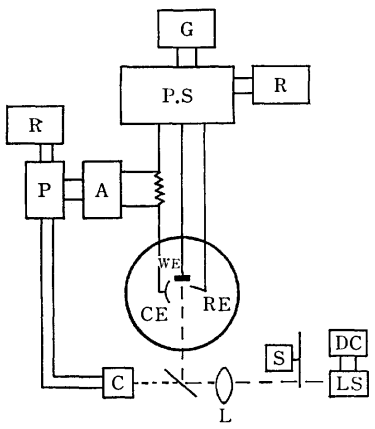

Fig. 1. Block diagram of experimental setup.
G: Function generator, PS: potentiostat, R: x-y recorder, P: prebox for a.c. Voltage measurement, A: differential amplifier, C: photo-cell, S: rotated sector, LS: Xenon lamp house, DC: d.c. power supply, L: lens, WE: working electrode, CE: counter electrode, RE: reference electrode.

horizontal beam was focussed on the working electrode by means of appropriate quartz lenses. For measuring photocurrents, as is shown in Fig. 1, the light was chopped with a rotated sector (35 Hz), and the resulting photocurrent was amplified and displayed on a x-y recorder, in which the dark current is eliminated. The procedure for the determination of the relative intensity of the light was described previously.[9]

The additional amount of silver oxides produced by illumination was determined as follows. Silver oxides formed under illumination in the Ag_2O formation region were dissolved into a 1 M ammonium acetate solution, and then the amount of silver ion in the solution was determined by means of atomic absorption spectrometry. The same measurements were carried out in the dark. The difference in the amount of silver ions between under illumination and in the dark was taken as equivalent to the amount of oxides produced by light excitation. The charges consumed during the formation of the silver oxides were measured by means of a Coulomb meter CLM-2A (Hokuto Denko Corp.). The composition of the oxides produced by light excitation was estimated on the basis of the data obtained above.

All measurements were carried out at ambient temperatures (25±2 °C). Oxygen was removed from solution by bubbling with nitrogen before every measurement.

Results and Discussion

Photo-effects on Oxidation to Silver Oxides in 1 M KOH. A potentiodynamic voltammogram for a silver electrode in an alkaline solution exhibits two major anodic and two major cathodic peaks corresponding to the formation and reduction of Ag_2O and AgO. A typical voltammogram run in 1 M KOH with the sweep rate of 2.9 mV/s is shown in Fig. 2, which also illustrates the effect of light during one cyclic sweep. Figure 2 definitely shows that, in addition to the increase in the magnitude of all the peaks, illumination causes the threshold potential for the commencement of AgO formation to shift to a more negative potential. This potential shift may be interpreted in terms of an overvoltage effect in the formation of AgO as well as in terms of the explanation by Parkins *et al.*;[6] *i. e.*, the overvoltage for the AgO formation is reduced by the Ag(II) species generated photoelectrochemically in the Ag_2O formation region, so that the cathodic shift occurs. The existence of such photo-generated Ag(II) species may be easily proved, as will be shown later.

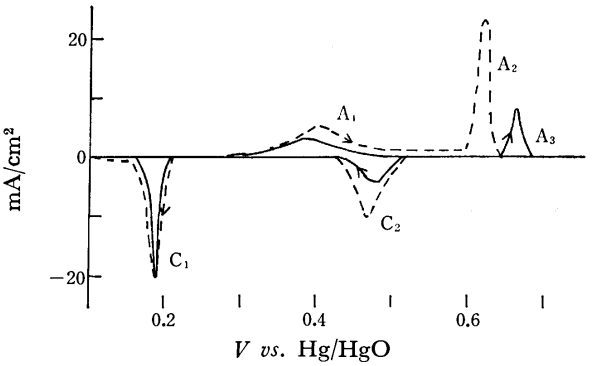

Fig. 2. Potentiodynamic current/potential profile for formation and reduction of oxides at a silver electrode in 1 M KOH. Sweep rate: 2.9 mV/s, ——: in the dark, ----: under illumination.

The potential dependence of a photocurrent was examined by using the chopped light described in a previous section. The general shape of the photocurrent-potential curve for 1 M KOH was the same as that reported by Memming *et al.*[5] The influence of the light intensity on the photocurrent is demonstrated in Fig. 3-a. Figure 3-b presents the ordinary current-potential curve measured simultaneously with Curve A in Fig. 3-a. In spite of the fact that both Ag_2O and AgO films exhibit *n*-type semiconducting behavior,[10] the anodic photocurrent arose only over the range of potentials at which the Ag_2O film exists, but did not appear at more positive potentials than the end of the AgO formation region. The maximum anodic photocurrent increased linearly with the light intensity of the illumination. In the cathodic direction of the potential sweep, photocurrents of different signs were observed in the region between the reduction peaks of AgO and Ag_2O. Such cathodic photocurrents have been examined in detail by Perkins *et al.*[6]

The charges consumed for each peak in Fig. 2 are presented in Table 1. It was found that the ratio of the total cathodic charge to the total anodic one was substantially unity, even under the illumination, indicating that the dissolution of reaction products into the alkaline solution may be neglected during one cycle of the potential. Furthermore, as can be seen from Table 1, the charge for the A_1 peak was increased by

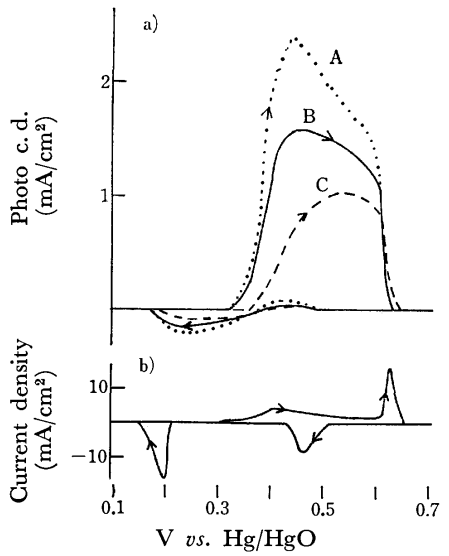

Fig. 3. (a) Photocurrent *vs.* electrode potential for a silver electrode in 1 M KOH (Dark current is eliminated). (b) Current *vs.* electrode potential measured simultaniously with the curve A in (a). Sweep rate: 2.9 mV/s, A, B, and C: light intensity of 110, 64.7, and 32.8 (a.u.), respectively.

Table 1. The amount of charge for each peak in Fig. 1 (mC/cm²)

	A_1	A_2	A_3	C_2	C_1	Total anodic charge	Total cathodic charge
Dark	103	67	0	47	125	170	168
Light	178	128	6	123	186	312	309

about 70% by the illumination, and the charge for A_2 peak under the illumination was larger by about 20% than the charge for the A_1 peak in the dark. From these facts it is clear that, in addition to the formation of Ag(II) species, illumination in the Ag_2O formation region causes a substantial increase in the formation of Ag(I) species at the metal/oxide interface. Therefore, the anodic photocurrent must be due to the photo-generation of both Ag(I) and Ag(II) species.

Composition of Photo-generated Products. In order to determine whether the photo-generated species in the Ag_2O formation region is mainly the Ag(I) or the Ag(II) species, the increment in silver species upon illumination and the corresponding charge were determined as follows. The pretreated electrode was subjected to the potential sweep from 0.0 to 0.575 V at the sweep rate of 2.9 mV/s under illumination. Immediately after the circuit had been opened, the electrode was taken out from the cell and then dipped in a 1 M ammonium acetate solution to remove from the silver substrate the silver oxides which were produced during the potential sweep. The analysis of the silver species in the acetate solution was made by atomic absorption spectrometry. The potential of 0.575 V corresponds to a less positive potential than that at which the electrochemical formation of AgO begins to appear. The anodic charge consumed during this potential sweep was simultaneously determined by means of a Coulomb meter. Blank runs in the dark were carried out as well. The results thus obtained are presented in Table 2. It was found that the illumination during the anodic sweep (0.0—0.575 V) causes the amount of silver ions to increase considerably, as well as the anodic charge. The current efficiency[11] for the additional amount of silver oxides formed by the illumination was 61%. If the photo-associated reaction were only the formation of Ag(II) species from Ag(I) species, the current efficiency for the additional amount of silver oxides would be zero. On the other hand, if only the formation of Ag(I) species from the silver substrate had arisen, the current efficiency of 100% would be obtained. No such results were obtained in this experiment. Accordingly, these experimental results also indicate that the photo-generated species are both Ag(I) and Ag(II) species.

The Ag(II)/Ag(I) ratio on the silver oxides produced only by the light excitation was estimated to be 1.8. This value was calculated on the basis of the current efficiency of 61% and by assuming that the anodic photocurrent arises according the following scheme:

$$Ag/Ag_2O \xrightarrow{h\nu} Ag(I)/Ag_2O + e, \quad (1)$$

$$Ag(I) \text{ and } Ag_2O \xrightarrow{h\nu} Ag(II) \text{ species} + e. \quad (2)$$

That is,

$$E_{eff} = \frac{q_1}{q_1+q_2} \cdot 100. \quad (3)$$

In the case of $E_{eff} > 50\%$

$$\frac{Ag(II)}{Ag(I)} = \frac{q_2}{q_1-q_2}. \quad (4)$$

From Eqs. 3 and 4, we obtain

$$\frac{Ag(II)}{Ag(I)} = \frac{100-E_{eff}}{2E_{eff}-100} = 1.8,$$

where q_1 and q_2 are the charges consumed in Eqs. 1 and 2 respectively.

From Table 1 and 2, it is clear that illumination causes the efficiency for the conversion of Ag_2O and AgO to increase. That is, the conversion was about 65% in the dark, whereas under illumination it was estimated to be almost 100%.[12] One may easily understand such a photo-effect by assuming that the photo-generated Ag(II) species, which act as nuclei for the AgO formation, exist widely within the Ag_2O film.

In further experiments, the effect of the time interval of illumination on the composition of the silver oxides was examined by the above method except for the procedures of illumination and polarization. An Ag_2O film was produced by the anodic potential sweep from 0.0 to 0.5 V (sweep rate, 2.9 mV/s), and then the electrode potential was stepped up to 0.45 V, at which no AgO is electrochemically formed. After the current had decreased to a very low value, the electrode was illuminated for a given period. Immediately afterward, the electrode was taken out from the cell and was worked up according to the above procedure. The charges consumed before and during illumination were measured by means of a Coulomb meter at the same time. In addition, the charges necessary for the reduction of the silver oxides formed under the above conditions were separately determined by sweeping back

Table 2. The composition of silver oxides produced by light excitation during the anodic potential sweep from 0.0 to 0.575 V

	Q_a[a] (mC/cm²)	M_{Ag}[b] (10^{-3}mmol/cm²)	Current efficiency (%)	Ag(II)/Ag(I) ratio
Dark	103	1.06	99	
Light	176	1.52	83	
Difference between light and dark	73	0.46	61[c]	1.8

a) Q_a: the charge consumed during the anodic sweep. b) M_{Ag}: the amount of silver ion, determined by means of atomic absorption spectrometry. c) See Ref. 11.

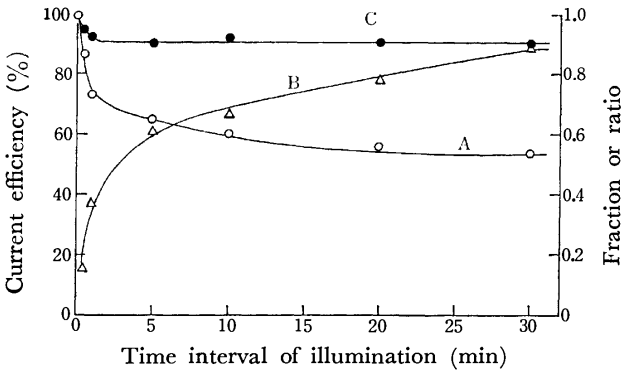

Fig. 4. Effect of illumination time on the current efficiency (curve A), the fraction of Ag(II) in the oxides (curve B), and the ratio of cathodic charge to anodic charge (curve C) about the silver oxides produced by illumination.

from 0.45 to −0.1 V as soon as the light was extinguished. Figure 4 illustrates the effect of the illumination time on the current efficiency for the photo-generated oxides (Curve A), on the fraction[13] of Ag(II) in the oxides (Curve B), and the ratio of the anodic charge consumed only during the illumination and the cathodic charge necessary for the reduction of the photo-generated oxides (Curve C). The current efficiency and the fraction of Ag(II) species varied, as is shown in Fig. 4, as the time interval of illumination increased. That is, the ratio of Ag(II)/Ag(I) increased with an increase in the time interval of illumination. On the other hand, the anodic charges, increased by the light excitation, were always somewhat larger than the corresponding cathodic charges. This fact indicates that only a small part of the anodic photocurrent was used for the photo-decomposition of Ag_2O into silver and oxygen. Therefore, the photo-decomposition of Ag_2O postulated by Göhr *et al.*[4] is not considered to be the main origin of the photocurrent.

If the photo-generation of Ag(II) species is due only to the photoelectrochemical oxidation of interstitial Ag^+, as was proposed by Perkins *et al.*,[6] or if the anodic photocurrent is due only to the formation of AgO, as was reported by Memming *et al.*,[5] the results obtained in the present experiments can not be interpreted. Our conclusion is that the anodic photocurrents are due to the formation of both Ag(I) and Ag(II) species according to Eqs. 1 and 2. In addition, it must be noted that a small part of the anodic photocurrent is used for the evolution of oxygen.

Influence of Ethylene Glycol on the Photo-effects. Figure 5 shows the influence of ethylene glycol on the photocurrent during a cyclic potential sweep of silver in 1 M KOH. The addition of the glycol to the base electrolyte caused the anodic photocurrent to increase considerably. The relation between the photocurrent and the glycol concentration is presented in Fig. 6 as plots of i_p/i_a *vs.* log C, where i_p and i_a imply the maximum photocurrent (peak value) in the presence and absence of the glycol respectively, and C, the bulk concentration of the glycol. The value of i_p/i_a increased with an increase in the glycol concentration and reached a factor of two. Such a current doubling phenomenon had previously been found at a zinc oxide single-crystal electrode by Morrison and Freund.[14] They interpreted it by means of the following two-step mechanism:

$$R + h^+ \longrightarrow R^+, \quad (5)$$

$$R^+ \longrightarrow R^{2+} + e, \quad (6)$$

where h^+ is a photo-generated hole in the crystal; R, a current-doubling agent; R^+, a radical-type species, and e, an electron. However, it seems that current-doubling phenomenon in the silver oxide electrode system can not be interpreted by the mechanism indicated above, but rather by a alternative mechanism, as will be shown below.

Figure 7 shows typical voltammograms for the silver electrode in a 1 M KOH solution containing 0.2 M ethylene glycol in the dark and under illumination. In the presence of glycol, a specific anodic peak (Peak A_4) was observed between the AgO formation and its

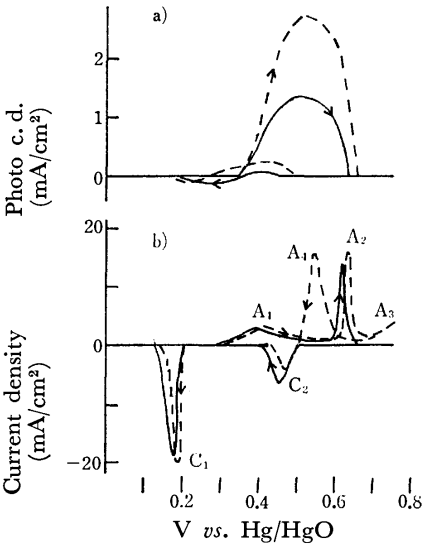

Fig. 5. (a) Influence of ethylene glycol on the photocurrent. (b) Current *vs.* electrode potential measured simultanously with the curve in (a). Sweep rate: 2.9 mV/s, ——: 1 M KOH, ----: 1 M KOH +0.2 M ethylene glycol.

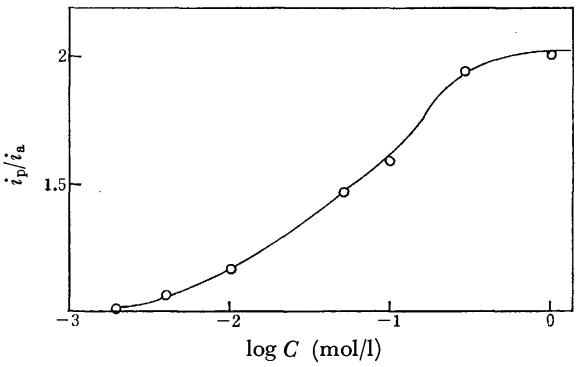

Fig. 6. Maxmum photocurrent *vs.* concentration of ethylene glycol. i_a and i_p: the maxmum photocurrent in the absence and presence of the glycol, respectively, C: the bulk concentration of the glycol.

reduction peaks under a cathodic sweep. The values in both cases, light and dark, increased linearly with an increase in the glycol concentration. The illumination increased the peak value. The appearance of such a peak can be explained by the catalytic mechanism proposed by Sasaki and Toshima,[15] in which a reaction of alcohols with AgO leads to the formation of Ag_2O (or Ag), which is then electrochemically oxidized to AgO. The question arises, however, of why such a catalytic reaction does not easily occur in the AgO formation region under an anodic sweep. This question might be answered by assuming the competitive adsorption of glycol and OH^-; *i.e.*, with an increase in the anode potential, the surface concentration of glycol decreases, whereas that of OH increases.

As can be seen from a comparison of Figs. 2 and 7, the anodic current in the region (A_3) between the AgO formation peak and the oxygen evolution was increased by the addition of glycol, and it was further increased by the illumination. We have no idea, however, how to explain such an increase at the A_3 peak.

The amounts of charge for each peak in Fig. 7 are

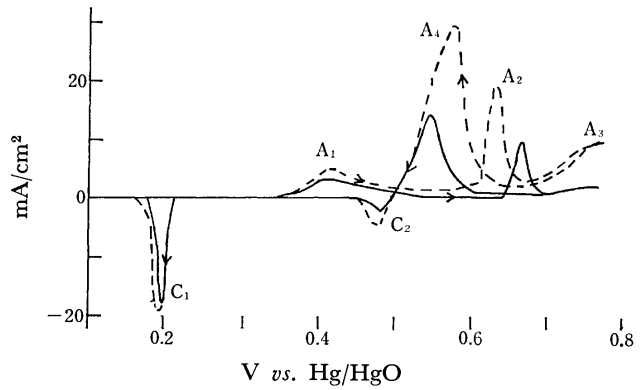

Fig. 7. Potentiodynamic voltammograms for a silver electrode in 1 M KOH +0.2 M ethylene glycol. ——: in the dark, ----: under illumination, sweep rate: 2.9 mV/s.

listed in Table 3. The illumination considerably increased the charges for all peaks. It should be noted that, in spite of the fact that the photocurrent does not arise in the region of either A_3 or A_4 as is shown in Fig. 5, the amounts of charge for these peaks (A_3 and A_4) increased remarkably under the illumination. The remarkable increase in the specific anodic current (A_4) by the illumination is considered to be due to an increase in the surface roughness of the electrode, although the variation in the roughness was not directly examined by means of a microscope. The increase in the surface roughness mainly occurs in the Ag_2O formation region. This idea came from such observations as: (i) When an upper limit of a potential cycle was set at the end of the A_2 peak, when the illumination was limited to the Ag_2O formation region, or when one cyclic voltammogram was run in the solution containing the glycol under illumination, and the next cyclic one was recorded in the dark, little change in the amount of charge for the A_4 peak was observed. (ii) In the presence of glycol, illumination rather decreased both the amount of silver oxides, which formed during the anodic sweep from 0.0 to 0.575 V, and the corresponding cathodic charge, although the anodic charge for the Ag_2O formation region was considerably increased by illumination.

If the anodic photocurrent observed in the present study had arisen according to a mechanism similar to that proposed by Morrison and Freund,[14] the increase in the surface roughness by the light excitation would not occur. Therefore, an alternative mechanism for the current-doubling phenomenon should be proposed in the case of the present electrode system. For example, the following catalytic mechanism are considered: (i) Ethylene glycol reacts with the photo-generated AgO to give a radical intermediate to inject an electron into the electrode. In this case, the AgO is reduced to Ag_2O, which is also oxidized to AgO according to Eq. 7; *i. e.*,

$$Ag_2O + h^+ \longrightarrow AgO, \quad (7)$$
$$AgO + Glycol \longrightarrow Ag_2O + Intermediate, \quad (8)$$
$$Intermediate \longrightarrow Aldehyde + e, \quad (9)$$

or (ii) similarly, the reaction of glycol with the AgO results in the formation of aldehyde and Ag, followed by the electrochemical reoxidation of the latter to Ag_2O, which is then oxidized by the photo-generated hole; *i. e.*,

$$Ag_2O + h^+ \longrightarrow AgO, \quad (7)$$
$$AgO + Glycol \longrightarrow Ag + Aldehyde, \quad (10)$$
$$Ag \longrightarrow Ag_2O + e. \quad (11)$$

Such chemical decomposition and photochemical reformation of AgO is repeated on the electrode surface, and this causes the surface roughness of the electrode to increase.

Consequently, the current-doubling phenomenon at the silver oxide electrode may be interpreted by either mechanism indicated above, and not by a mechanism involving a reaction of glycol with the photo-generated hole.

TABLE 3. THE AMOUNT OF CHARGE FOR EACH PEAK IN Fig. 7 (mC/cm²)

	A_1	A_2	A_3	A_4	C_2	C_1	Total anodic charge	Total cathodic charge
Dark	108	79	75	246	23	119	508	142
Light	223	175	451	619	35	129	1468	168

References

1) B. V. Tilak, R. S. Perkins, H. A. Kozlowska, and B. E. Conway, *Electrochim. Acta*, **17**, 1447 (1972), and references therein.
2) N. A. Hampson, J. B. Lee, and K. I. MacDonald, *Electrochim. Acta*, **17**, 921 (1972).
3) J. A. McMillan, *Chem. Rev.*, **62**, 65 (1962).
4) H. Göhr and A. Breitenstein, *Electrochim. Acta*, **13**, 1377 (1968).
5) R. Memming, F. Mollers, and G. Neumann, *J. Electrochem. Soc.*, **117**, 451 (1970).
6) R. S. Perkins, B. V. Tilak, B. E. Conway, and H. A. Kozlowska, *Electrochim. Acta*, **17**, 1471 (1972).
7) V. I. Veselovsky, T. I. Borisova, A. A. Jakovleva, and S. O. Izidinov, *Electrochim. Acta*, **10**, 325 (1965).
8) S. Toshima, H. Sasaki, and K. Itaya, *Denki Kagaku*, **40**, 234 (1972).
9) T. Shimizu, A. Kunugi, and S. Nagaura, *Denki Kagaku*, **44**, 187 (1976).
10) M. J. Dignam, H. M. Barret, and G. D. Nagy, *Can. J. Chem.*, **47**, 4253 (1969).
11) The current efficiency, E_{eff} was defined by: $E_{eff}=(M_1-M_D)F/(Q_L-Q_D)$. 100(%), where M and Q are the amount (mol) of silver ion formed and the charge (coulomb) consumed during the anodic sweep (0.0—0.575 V) respectively; the subscripts L and D indicate under illumination and in the dark respectively, and F is Faraday's constant.
12) The additional charge for the A_1 peak by the illumination $=(Q_{A_1})_L-(Q_{A_1})_D=178-103=75$ mC/cm², and the fraction of Ag(I) in the oxide produced by the illumination $=1-[Ag(II)/Ag(I)]/[Ag(II)/Ag(I)+1]=1-1.8/(1.8+1)=0.36$. Therefore, the charge corresponding to the amount of Ag(I) species produced by illumination $=75\times0.36=27$ mC/cm². Thus, the charge corresponding to the total amounts of Ag(I) species produced in the A_1 region $=103+27=130$ mC/cm². Consequently, the electrochemical conversion of Ag(I) to Ag(II) $=(128/130)\times100=98\%$.
13) The fraction of Ag(II) in the oxides $=[Ag(II)/Ag(I)]/[Ag(II)/Ag(I)+1]$.
14) S. R. Morrison and T. Freund, *Electrochim. Acta*, **13**, 1343 (1968).
15) H. Sasaki and S. Toshima, *Electrochim. Acta*, **20**, 201 (1975).

Solvent Extraction Equilibria of Acids. VI. The Extraction of Several Mono- and Dicarboxylic Acids with Trioctylphosphine Oxide in Hexane

Masaru NIITSU and Tatsuya SEKINE*

Faculty of Pharmaceutical Sciences, Josai University, Sakado, Saitama 350-02

**Department of Chemistry, Science University of Tokyo, Kagurazaka, Shinjuku-ku, Tokyo 162*

(Received August 11, 1977)

The solvent extraction equilibria of acetic, propionic, and butyric acid and mono-, di-, and trichloroacetic acid (HA), as well as those of oxalic, malonic, succinic, glutaric, and adipic acid (H_2A), have been determined in liquid-liquid systems of hexane containing none or a certain amount of trioctylphosphine oxide (E) and an aqueous 1 mol dm^{-3} chloride solution at 25 °C. The constants, $K_d=[HA]_{org}/[HA]$, $K_{dim}=[(HA)_2]_{org}/[HA]_{org}^2$, $K_{ex1}'=[HAE]_{org}/[HA][E]_{org}$, $K_{ex2}'=[H_2AE_2]_{org}/[H_2A][E]_{org}^2$, and $\beta_{1(org)}=[HAE]_{org}/[HA]_{org}[E]_{org}$, have then been determined from the data. It was found that, among the three fatty acids, the value of K_{ex1}' was higher as the chain length increased, but the values of $\beta_{1(org)}$ were nearly all the same, while among the chloroacetic acids they were higher as the number of chloride atom increased. The extraction of the dicarboxylic acids with E was not very different, although the number of the $-CH_2-$ between the two carboxyl groups changed from zero to four.

In this series of reports, we have reported on the solvent extraction behavior of various inorganic acids with trioctylphosphine oxide (TOPO) in organic solvents.[1-5] In the present paper, we will study the extraction equilibria of acetic, propionic, and butyric acid, mono-, di-, and trichloroacetic acid, and oxalic, malonic, succinic, glutaric, and adipic acid, in 1 mol·dm^{-3} chloride solutions with TOPO in hexane at 25 °C.

Experimental

The experiments were performed much as has previously been described.[1-5] All the reagents were of an analytical grade. The acid was dissolved in 1 mol dm^{-3} hydrochloric acid or 1 mol dm^{-3} (H, Na)Cl ionic media, placed in contact with the same volume of hexane containing none or a certain amount of TOPO in a stoppered glass tube by means of a mechanical shaker, and centrifuged. A certain amount of the organic phase was then pipetted off and titrated with a standard barium hydroxide solution, using phenolphthalein as the indicator.

Statistical

Here the subscript "org" and the lack of subscript denote the species in the organic and aqueous phases respectively. The mono- and dicarboxylic acids are represented by HA and H_2A respectively, while TOPO is represented by E. Since the extraction of dicarboxylic acid species containing no E was negligible, and that of the HAE_2 and H_2AE species was also found to be negligible, the following equilibrium constants were employed for the data analysis:

$$K_d = [HA]_{org}[HA]^{-1}, \quad (1)$$

$$K_{dim} = [(HA)_2]_{org}[HA]_{org}^{-2}, \quad (2)$$

$$K_{ex1}' = [HAE]_{org}[HA]^{-1}[E]_{org}^{-1}, \quad (3)$$

$$K_{ex2}' = [H_2AE_2]_{org}[H_2A]^{-1}[E]_{org}^{-2}. \quad (4)$$

The distribution ratio, D, was defined by the ratio of total acid concentrations in the organic and aqueous phases. The latter was calculated from the initial acid concentration in the aqueous phase and the equilibrium acid concentration in the organic phase. The dissociation in 1 mol dm^{-3} hydrochloric acid was negligible except for trichloroacetic acid, and the observed distribution ratio of the dicarboxylic acids was found to be

$$D = [H_2AE_2]_{org}[H_2A]^{-1} = K_{ex2}'[E]_{org}^2. \quad (5)$$

The distribution ratio for the monocarboxylic acids should generally be written as

$$D = ([HA]_{org}+2[(HA)_2]_{org}+[HAE]_{org})([HA]+[A^-])^{-1} = (K_d+2K_d^2K_{dim}[HA]+K_{ex1}'[E]_{org})(1+K_a[H^+]^{-1})^{-1}. \quad (6)$$

The $[A^-]$ or $K_a[H^+]^{-1}$ term was found to be negligible except for trichloroacetic acid; furthermore, the $[HA]_{org}$ and $[(HA)_2]_{org}$ terms or the K_d and $2K_d^2K_{dim}$ [HA] terms were found to be negligible in the presence of TOPO except for the case of butyric acid.

The free TOPO concentration at equilibrium was calculated by subtracting the fraction combined with acid, which could be written as $[HAE]_{org}$ or $2[H_2AE_2]_{org}$. In the case of butyric acid, however, the extraction of the HA and $(HA)_2$ species was corrected by using the data obtained in the absence of TOPO.

The distribution ratio of the fatty acids in the absence of TOPO was plotted as a function of [HA]:

$$\log D = \log (K_d+2K_d^2K_{dim}[HA]), \quad (7)$$

and the constants were obtained by a curve-fitting method.[6]

The other equilibrium constants were obtained by introducing the experimental data into Eq. 5 or 6. Since the acid dissociation was not negligible for trichloroacetic acid, the distribution ratio was obtained at a certain $[E]_{org,initial}$ value as a function of $[H^+]$ in 1 mol dm^{-3} (H, Na)Cl solutions. Then, from these experimental data and a certain assumed value of K_a, the values of K_{ex1}' in Eq. 6 were calculated. Trials were repeated by introducing other assumed values of K_a and the standard deviation of the K_{ex1}' was calculated from each set of values of K_{ex1}'. Then, the values of the standard deviation were plotted against the K_a value. The K_a value which gave the minimum standard deviation was estimated from the plot and was subsequently employed for the data analysis of trichloroacetic acid.

Results

In the present work, a 1 mol dm^{-3} chloride solution was always employed as the aqueous phase. How-

Table 1. Distribution data of mono-, di-, and trichloroacetic acid between hexane containing no TOPO and 1 mol dm^{-3} HCl
The concentrations are in the mol dm^{-3} units.

(a) Monochloroacetic acid					
$[HA]_{org,total}\times10^{4}$ a)	$[HA]_{total}\times10$	$[HA]\times10$	$[A^-]$ b)	$[HA]_{org}\times10^{4}$	$[(HA)_2]_{org}\times10^{5}$
7.99	8.01	8.01	—	5.80	21.8
4.97	5.34	5.34	—	3.87	9.69
3.89	4.45	4.45	—	3.22	6.73
3.02	3.56	3.56	—	2.58	4.30
(b) Dichloroacetic acid					
$[HA]_{org,total}\times10^{4}$ a)	$[HA]_{total}\times10$	$[HA]\times10$	$[A^-]$ b)	$[HA]_{org}\times10^{4}$	$[(HA)_2]_{org}\times10^{4}$
21.2	7.45	7.45	—	14.2	5.87
12.1	4.97	4.97	—	9.49	2.61
9.50	4.14	4.14	—	7.91	1.81
7.34	3.31	3.31	—	6.32	1.16
5.40	2.48	2.48	—	4.74	0.651
(c) Trichloroacetic acid					
$[HA]_{org,total}\times10^{3}$ a)	$[HA]_{total}\times10$	$[HA]\times10$	$[A^-]\times10^{2}$	$[HA]_{org}\times10^{4}$	$[(HA)_2]_{org}\times10^{3}$
5.01	7.86	6.49	13.7	15.2	3.58
2.59	5.24	4.30	9.4	10.1	1.57
1.94	4.37	3.58	7.9	8.38	1.09
1.38	3.50	2.86	6.4	6.69	0.695
0.886	2.63	2.14	4.9	5.01	0.389

a) Experimentally observed values; the other values were calculated from these as in the text. b) The dissociation of mono- and dichloroacetic acid in 1 mol dm^{-3} HCl was negligible.

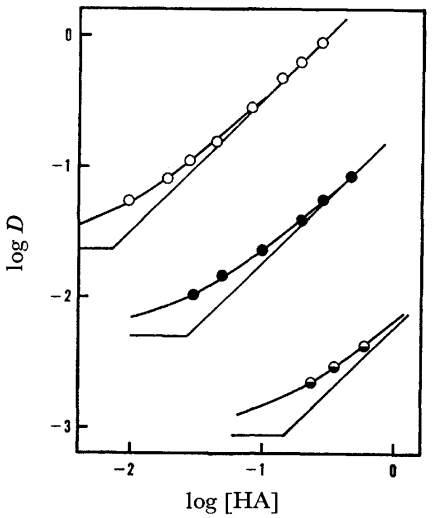

Fig. 1. Distribution ratio of acetic (◒), propionic (●), and butyric (○) acid between hexane and 1 mol dm^{-3} HCl as a function of the acid concentration in the aqueous phase at equilibrium. The solid curves were obtained by introducing the constants K_d and K_{dim} into Eq. 7.

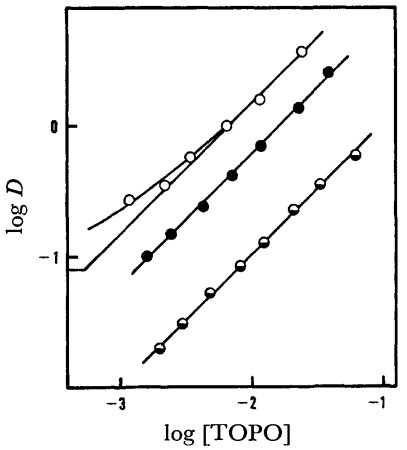

Fig. 2. Distribution ratio of acetic (◒), propionic (●), and butyric (○) acid between hexane containing various amounts of TOPO and 1 mol dm^{-3} HCl initially containing 1×10^{-1}, 3×10^{-2} and 2×10^{-2} mol dm^{-3} of acetic, propionic, and butyric acid, respectively, as a function of the free TOPO concentration. The solid curves were obtained by introducing the extraction constants K_d, K_{dim}, and K_{ex1}' into Eq. 6.

ever, no chloride was ever detected in the organic phase by means of a silver-nitrate-solution test. Thus, the extraction or co-extraction of chloride was concluded to be negligible. This is quite acceptable in view of previous results of this series of reports.[2)]

Figure 1 gives the extraction curves of the three fatty acids in the absence of TOPO as a function of the acid concentration in the aqueous phase, and Fig. 2 shows them as a function of the TOPO concentration. Table 1 lists the distribution data of mono-, di-, and trichloroacetic acid between 1 mol dm^{-3} hydrochloric acid and hexane containing no TOPO, and Fig. 3 shows the extraction curves of mono- and dichloroacetic acid with TOPO, while Table 2 lists the results of the extraction of trichloroacetic acid in 1 mol dm^{-3} (H, Na)Cl solutions with TOPO in hexane. The equilibrium constants obtained from these data by the method described are listed in Table 3. Figure 3 also shows the data of acetic acid in Fig. 2 and the curve for trichloroacetic acid calculated by means of the K_{ex1}' value in Table 3.

Table 2. Extraction data of trichloroacetic acid
Aq. phase: 1 mol dm^{-3} (H, Na)Cl initially containing 2×10^{-2} mol dm^{-3} of the acid. Org. phase: hexane containing 2×10^{-2} mol dm^{-3} of TOPO. All the concentrations are in mol dm^{-3} units.

$[H^+]\times10^2$	$[HA]_{org}\times10^2$	$[HA]\times10^3$	$[E]_{org}\times10^3$	$\log K_{ex1}'$
100	1.82	1.6	1.78	3.90
60.0	1.79	1.9	2.08	3.80
40.0	1.76	2.2	2.38	3.72
24.0	1.73	2.5	2.68	3.71
16.0	1.70	2.8	2.98	3.71
9.55	1.66	3.2	3.38	3.73
5.75	1.61	3.7	3.88	3.76
3.98	1.55	4.3	4.48	3.77
2.63	1.47	5.1	5.28	3.75
1.95	1.43	5.5	5.68	3.78
1.45	1.35	6.3	6.48	3.76
1.17	1.32	6.6	6.78	3.83
1.00	1.30	6.8	6.98	3.83
0.708	1.19	7.9	8.08	3.81
				(Av. 3.78)

$\log K_{ex1}'$ was calculated by using the value, $K_a=0.24$, which gave the mininum standard deviation of the K_{ex1}'.

Discussion

The extraction and dimerization of fatty acids in liquid–liquid systems have been studied for a long time.[7] Most of the previous data have been obtained by employing an aqueous fatty acid solution containing no or only a small amount of an electrolyte as the aqueous phase. In the present study, however, 1 mol dm^{-3} of chloride was always in the aqueous phase; this could cause a salting-out effect, as was found previously.[8] However, the K_d values of the fatty acids from the present ionic medium into hexane were still lower than those in the previous study[8] from an aqueous solution containing no other salts into carbon tetrachloride (the K_d values were 3.20×10^{-3}, 1.51×10^{-2}, and 3.83×10^{-2} respectively for acetic, propionic, and butyric acid).

There has been a report on the dimerization constant of acetic acid in hexane[9] and also one on the distribution and dimerization constants of propionic acid in the hexane–aqueous 0.1 mol dm^{-3} (H, Na)ClO_4 system.[10] The present dimerization constants of these fatty acids in hexane are very similar to each other. The same tendency, a constancy of the dimerization constants among fatty acids of different chain lengths, was also found in several other organic solvents.[10] At the same time, it was also reported that the values increased upon an increase in the chain length of these fatty acids in carbon tetrachloride.[8]

In Fig. 2, the extracted acid species in the organic phase in the presence of TOPO was, for all practical purposes, monomeric except the butyric acid in the lower TOPO concentration region.

From Eqs. 1 and 3, the following equation is obtained:

$$K_{ex1}' = K_d\beta_{1(org)}, \quad (8)$$

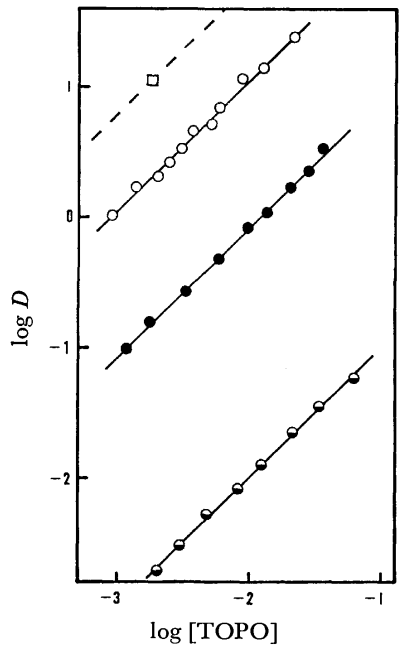

Fig. 3. Distribution ratio of mono- (●), di- (○), and trichloroacetic acid (□), and acetic acid (◒) between hexane containing various amounts of TOPO and 1 mol dm^{-3} HCl initially containing 3.2×10^{-2} and 3.0×10^{-2} mol dm^{-3} of mono- and dichloroacetic acid, respectively as a function of the free TOPO concentration. The curve for trichloroacetic acid was calculated from K_{ex1}' in Table 3 and for acetic acid was taken from Fig. 2.

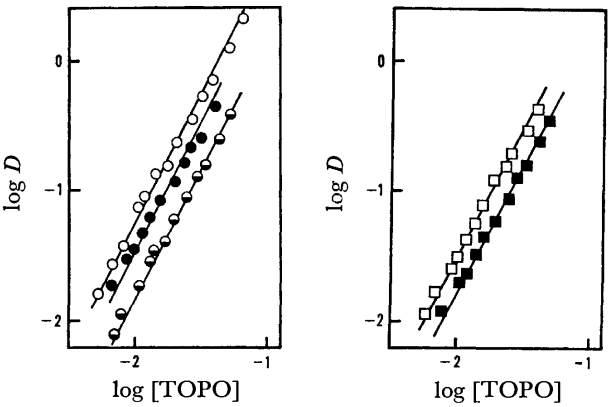

Figs. 4 and 5. Distribution ratio of five dicarboxylic acids between hexane containing various amounts of TOPO and 1 mol dm^{-3} HCl initially containing 2.6×10^{-2}, 9.6×10^{-2}, 9.9×10^{-2}, 1.0×10^{-1}, and 1.0×10^{-1} mol dm^{-3} of adipic (○), glutaric (●), succinic (◒), malonic (■), and oxalic (□) acid, respectively, as a function of the free TOPO concentration.

where $\beta_{1(org)}$ is the association constant of TOPO with monomeric acid in the organic phase. This is written for a monocarboxylic acid as

$$\beta_{1(org)} = [HAE]_{org}[HA]_{org}^{-1}[E]_{org}^{-1}. \quad (9)$$

As may be seen from Table 3, the values of $\beta_{1(org)}$ were nearly the same among all these fatty acids. Furthermore, the association constants of these acids with TOPO

Table 3. Summary of equilibrium constants

(a) Fatty acids					
Acid	pK_a	$\log K_d$	$\log K_{dim}$	$\log K_{ex1}'$	$\log \beta_{1(org)}$
CH_3COOH	4.30	−3.06	3.59	1.01	4.07
C_2H_5COOH	4.66***	−2.30	3.56	1.77	4.07
C_3H_7COOH	4.74**	−1.64	3.48	2.17	3.81
(b) Chloroacetic acids					
Acid	pK_a	$\log K_d$	$\log K_{dim}$	$\log K_{ex1}'$	$\log \beta_{1(org)}$
$CH_2ClCOOH$	2.66	−3.14	2.51	1.93	5.07
$CHCl_2COOH$	1.30†	−2.72	2.16	3.06	5.78
CCl_3COOH	0.62††	−2.63	2.89	3.78	6.41
(c) Dicarboxylic acids					
Acid	pK_{a1}	pK_{a2}	$\log K_{ex2}'$		
$(COOH)_2$	1.07	3.57	2.49		
$CH_2(COOH)_2$	2.74	5.11	2.22		
$C_2H_4(COOH)_2$	3.98	5.50	2.18		
$C_3H_6(COOH)_2$	4.09*	4.84*	2.52		
$C_4H_8(COOH)_2$	4.28***	5.00***	2.74		

The pK_a values were taken from Ref. 11. The ionic concentration and temperature were: (no mark) 1 mol dm^{-3} and at 30 °C for acetic acid, 20 °C for monochloroacetic acid and 25 °C for the others; (*) 0.5 mol dm^{-3} and at 25 °C; (**) 0.2 mol dm^{-3} and at 25 °C; (***) 0.1 mol dm^{-3} and at 20 °C for propionic acid and 25 °C for adipic acid; (†) no specification on the ionic medium and at 25 °C; (††) 1 mol dm^{-3} and at 25 °C obtained in the present work.

were larger than the values of K_{dim}. This seems to be reasonable because the phosphoryl-oxygen in TOPO should be a stronger accepter of hydroxyl-hydrogen in the carboxyl group than the carbonyl-oxygen in the carboxyl group; thus, the former can combine with the hydroxyl group more strongly than the latter.

The dissociation of mono- and dichloroacetic acid is negligible in 1 mol dm^{-3} hydrochloric acid. However, that of trichloroacetic acid should be taken into account. A pK_a value of 0.62 was finally obtained from the data analysis in 1 mol dm^{-3} (H, Na)Cl. The above present value agrees with an estimated value, 0.7, in the literature.[11]

The distribution constant of the monomer, K_d, of monochloroacetic acid was nearly the same as that of acetic acid. However, it was higher as the number of the chlorine atom increased. The replacement of a hydrogen atom with a chlorine atom should change the charge distribution in the molecule, and it could cause an decrease in the K_d by increasing the aquophilic character. However, at the same time, it should cause an increase in the molar volume, which should in turn increase the K_d value by increasing the aquofobic character. The observed value of K_d should be caused by the over-all effect of these two factors.

The extraction of three chloroacetic acids with TOPO was much better than acetic acid, and, among them, the extraction was better when the acid was stronger. The distribution ratio of trichloroacetic acid was too high to measure accurately under the conditions employed for the other two acids; only a calculated extraction curve could be obtained from the data in Table 2, as is given in Fig. 3. The extraction of these chloroacetic acids into hexane containing no TOPO was found to be very poor, as may be seen from Tables 1 and 3. Thus, the good extraction of these acids with TOPO should be attributed to their great tendency to associate with it in the organic phase.

The $\log \beta_{1(org)}$ value between dibutylphosphoric acid and TOPO in hexane was reported to be 4.88;[12] this is lower than chloroacetic acids, but higher than the fatty acids.

It was found that the distribution ratio of all the five dicarboxylic acids studied in the present work was very low in the absence of TOPO; the values of D were estimated to be always lower than 10^{-3}.

These low D values in the absence of TOPO are probably due to a strong hydration of these acids. However, these hydrating water molecules could be replaced by TOPO. Since two TOPO molecules solvated one acid molecule in the organic phase, each carboxyl group should combine with one TOPO by means of a hydrogen-bond; thus, the aquophilic character diminished. It is noticeable that the extraction constants of these dicarboxylic acids are rather similar to each other; this was not observed among the fatty acids which were extracted better when the chain was longer. Among the fatty acids, the values of pK_a are rather similar to each other; consequently, the abilities to associate with TOPO are probably also similar to each other, as is indicated by the values of $\log \beta_{1(org)}$. Thus, the chain length, in other words, the difference in the molar volume, was the main factor affecting the extraction behavior of the fatty acids. On the other hand, two inverse effects probably determine the degree of extraction of the dicarboxylic acids. The strength of the acid, especially that which dissociates first proton, is greater when the chain is shorter, and, although the values of $\beta_{1(org)}$ could not be determined for these acids, it seems a reasonable guess that the stronger the acids, the stronger the interaction with TOPO. Thus, acids of shorter chains are favorable for the extraction. An increase in the chain length, however, probably increases the aquofobic

character of the molecule, and, from this standpoint, longer chains are more favorable for the extraction. The fact that the extraction constants of these dicarboxylic acids are rather similar to each other seems to indicate that two inverse effects are cancelling each other out. We can not yet make a comment on the steric effect of the two TOPO molecules combined with one dicarboxylic acid molecule.

References

1) M. Niitsu and T. Sekine, *J. Inorg. Nucl. Chem.*, **37**, 1054 (1975).
2) M. Niitsu and T. Sekine, *J. Inorg. Nucl. Chem.*, **38**, 1053 (1976).
3) M. Niitsu and T. Sekine, *J. Inorg. Nucl. Chem.*, **38**, 1057 (1976).
4) T. Sekine, Y. Zeniya, and M. Niitsu, *Bull. Chem. Soc. Jpn.*, **49**, 2629 (1976).
5) M. Niitsu and T. Sekine, *Bull. Chem. Soc. Jpn.*, **50**, 1015 (1977).
6) T. Sekine and Y. Hasegawa, "Solvent Extraction Chemistry," Marcel Dekker, New York (1977), p. 71.
7) G. C. Pimentel and A. L. McClellan, "The Hydrogen Bond," W. H. Freeman, San Francisco (1960).
8) T. Sekine, M. Isayama, S. Yamaguchi, and H. Moriya, *Bull. Chem. Soc. Jpn.*, **40**, 27 (1967).
9) M. Davies, P. Jones, D. Patnik, and E. A. Moelwyn-Hughes, *J. Chem. Soc.*, **1951**, 1249.
10) I. Kojima, M. Yoshida, and M. Tanaka, *J. Inorg. Nucl. Chem.*, **32**, 987 (1970).
11) A. E. Martell and L. G. Sillen, "Stability Constants," Spec. Pub. 17, The Chemical Society (1964); Supplement No. 1, Spec. Pub. 25, The Chemical Society (1971).
12) D. H. Liem, *Acta Chem. Scand.*, **22**, 753 (1968).

Nuclear Quadrupole Resonances of Phosphorus Iodides and Some Phosphorus Trihalide–Boron Trihalide Complexes

Hiromitsu TERAO,* Tsutomu OKUDA, and Hisao NEGITA

*Department of Chemistry, Faculty of Education, Tokushima University, Tokushima 770
Department of Chemistry, Faculty of Science, Hiroshima University, Hiroshima 730

(Received August 12, 1977)

Nuclear quadrupole resonance (NQR) frequencies due to ^{79}Br and ^{127}I are examined in phosphorus iodides, PI_3 and P_2I_4, and the complexes $PBr_3 \cdot BBr_3$, $PBr_3 \cdot BI_3$, and $PI_3 \cdot BBr_3$. The quadrupole coupling constants and asymmetry parameters are also derived for ^{127}I in PI_3, P_2I_4, and $PBr_3 \cdot BI_3$. The resonance lines of PI_3 fade out above 257 K, at which temperature a structural phase transition is suggested. The number of resonance lines in P_2I_4 shows that the molecular symmetry of P_2I_4 is $\bar{1}$ instead of 2/m in its crystal. The similarity of the resonance patterns of the three complexes indicates that they are isomorphous with one another. The electronic structures of the halogens in the compounds mentioned above have been discussed by using the Townes-Dailey theory. On complexing, the electric charge of the halogen atoms in the donor PX_3 decreases due to the polarization of $p\sigma$ bonds, whereas that of the halogen atoms in the acceptor BY_3 increases owing to the backdonation through $p\pi$ bonds.

Two kinds of phosphorus iodides, PI_3 and P_2I_4, are known,[1] but no NQR investigation of these compounds has yet been reported. Phosphorus halides can form complexes with boron halides, in which the former act as electron donors and the latter as acceptors.[2] Only the complexes involving the heavier halogen atoms are stable at room temperature. In the case of these complexes, somewhat large shifts of the quadrupole coupling constants are expected on complexing. We have therefore observed NQR spectra due to ^{79}Br and ^{127}I in two kinds of phosphorus iodides and three complexes: $PBr_3 \cdot BBr_3$, $PBr_3 \cdot BI_3$, and $PI_3 \cdot BBr_3$, and have examined the bond character of these compounds. In the related complexes, $PI_3 \cdot BI_3$ and $P_2I_4 \cdot 2BBr_3$, NQR could not be observed. This failure may be caused by the imperfection of the samples.

Experimental

PI_3 and P_2I_4 were obtained by the reaction of the relevant elements in carbon disulfide, followed by recrystallization.[3] PBr_3 and BBr_3 were obtained from commercial sources. BI_3 was synthesized by the method of Renner[4] and was purified by sublimation. The complexes were prepared according to the methods in the literature.[2] All the procedures were performed under a nitrogen or helium atmosphere.

The NQR spectra were obtained with an externally quenched super-regenerative Lecher-line oscillator; the absorption lines were observed on an oscilloscope. The resonance frequencies were measured by the use of a signal generator and a frequency counter with an estimated accuracy of ± 0.01 MHz.

Results and Discussions

Phosphorus Iodides, PI_3 and P_2I_4. In Table 1 are listed the observed frequencies for ^{127}I at liquid nitrogen temperature with the approximate signal to noise ratios observed on an oscilloscope. These frequencies were assigned to the pairs of ν_1 and ν_2, which correspond to the transitions $m=\pm 1/2 \leftrightarrow \pm 3/2$ and $\pm 3/2 \leftrightarrow \pm 5/2$, respectively. However, there is an ambiguity in pairing the resonance frequencies of PI_3, so that the pairing was done in the order of frequency. This pairing is very likely, because the middle line of each group is slightly weaker than those of both sides. Using ν_1 and ν_2, the quadrupole coupling constants e^2Qq/h and the asymmetry parameters η were derived from the table of eigenvalues for the spin 5/2,[5] and are listed also in Table 1.

The crystal structure of PI_3 was reinvestigated recently by Lance *et al.*[6] at room temperature. The structure is hexagonal, and belongs to the space group $P6_3$ with $Z=2$. A pyramidal molecular geometry is maintained in solid PI_3. In this symmetry all the iodine atoms are equivalent and only one NQR line is expected. However, three lines of almost the same intensity were observed on each transition at low temperatures, showing the existence of three crystallographically non-equivalent iodine atoms, and no resonance was observed at room temperature. The temperature dependence of each ν_1 line of PI_3 was investigated. As the temperature rose from 77 K, the resonance frequencies decreased monotonously with the average temperature coefficients $\langle\alpha\rangle=2(\nu_{77}-\nu_{202})/(77-202)(\nu_{77}+\nu_{202})=-3.7 \times 10^{-5}$, -3.1×10^{-5}, and -2.8×10^{-5} deg^{-1} for the lowest, the middle, and the highest lines respectively. All the resonance lines faded out abruptly at about 257 K, which is far below the melting point of 334 K. This indicates that a structural phase transition may occur at about 257 K, because the existence of the three non-equivalent iodine atoms at the lower temperature is inconsistent with the crystal structure analysed at room temperature.

The X-ray analysis by Leung and Waser shows that P_2I_4 is triclinic, space group $P\bar{1}$, and $Z=1$.[7] The two P atoms are linked together, and each P atom is linked to two I atoms at the same distance within the experimental accuracy. The molecular symmetry is 2/m within the experimental accuracy, while only the inversion center is required crystallographically. However, two pairs of NQR lines corresponding to the two non-equivalent iodine atoms are observed instead of the single pair of NQR lines which is expected for the symmetry 2/m. In view of this fact the molecular symmetry should be reduced from 2/m to $\bar{1}$ in the crystalline state.

The temperature dependencies of the ν_1 lines of P_2I_4 were also investigated from 77 K to room temperature. When the temperature is above room temperature, P_2I_4(mp, 397 K) decomposes gradually and the signals

Table 1. Nuclear quadrupole resonance frequencies, quadrupole coupling constants, and asymmetry parameters in phosphorus iodides at 77 K

Compound	ν_1/MHz	S/N	ν_2/MHz	S/N	e^2Qqh^{-1}/MHz	η
PI_3	230.46	(7)	457.90	(2.5)	1527.9	0.071
	231.63	(5)	460.00	(2)	1535.1	0.074
	233.80	(7)	463.87	(2.5)	1548.2	0.079
P_2I_4	239.14	(4)	478.20	(2)	1594.1	0.011
	243.09	(4.5)	486.07	(2)	1620.3	0.013

are rapidly broadened and weakened. Within the observed temperature range the temperature dependencies of the resonance lines are normal, with the average temperature coefficients $\langle\alpha\rangle = -5.4\times10^{-5}$ and -6.3×10^{-5} deg^{-1} for the lower and the upper lines, respectively. These coefficients are larger than those of PI_3.

The observed quadrupole coupling constants of the halogen atoms were qualitatively estimated by the following equations:[8]

$$e^2Qq/h = |e^2Qq/h|_{\text{atom}}\left\{(1-s)(1-i)-\frac{f}{2}\right\}, \quad (1)$$

and

$$f = \frac{2}{3}\eta\frac{e^2Qq/h}{|e^2Qq/h|_{\text{atom}}}. \quad (2)$$

Here $|e^2Qq/h|_{\text{atom}}$ is the atomic quadrupole coupling constant, which is 2292.71 MHz for ^{127}I,[9] s is the degree of the s-hybridization, and f is the degree of the decrease of pπ electrons. s is assumed to be equal to 0.15 in accordance with Townes and Dailey.[10] Then, using the average values of e^2Qq/h and η at 77 K, i and f are calculated to be 0.19 and 0.03 for PI_3 and 0.17 and 0.01 for P_2I_4, respectively. If the π-bonding of the P–I bonds is not different in both iodides, the slightly larger value of f (or η) of PI_3 than that of P_2I_4 may be ascribed to the intermolecular bonding involving I atoms. According to the crystal structure of PI_3,[6] the shortest P···I intermolecular distance (3.670 Å) is smaller than the sum of the relevant van der Waals radii (4.0 Å). Possibly such P···I intermolecular interactions may exist in the low temperature phase as well, where NQR spectra were observed. On the other hand the shortest intermolecular P···I distance is 3.9 Å in P_2I_4.[7] The ionic character of the P–I bonds in PI_3 is somewhat larger than in P_2I_4. This may be attributed to the larger electron withdrawing ability of PI_2 groups than that of I atoms.

Complexes: $PBr_3 \cdot BBr_3$, $PBr_3 \cdot BI_3$, and $PI_3 \cdot BBr_3$. Table 2 shows the observed frequencies of ^{79}Br and ^{127}I of the complexes at liquid nitrogen temperature with the approximate signal to noise ratios. For bromine the resonances of ^{81}Br were also detected; these satisfy the quadrupole moment ratio $Q(^{79}Br)/Q(^{81}Br) = 1.1974$ within the experimental accuracy. The ν_2 lines of the I atoms of the $PI_3 \cdot BBr_3$ may probably exist in the region of about 570 MHz, at which our spectrometer did not operate.

The resonance lines of each complex are divided into two or three groups, in which two closely spaced lines exist with the intensity ratio of about 1 : 2. Referring to the fact that the resonance lines of a component in the complex are shifted to a small extent, the bromine and iodine lines can be identified easily, as shown in Table 2. This identification can be confirmed by the doublet structure,[11,12] which arises from the isotope effect of ^{10}B and ^{11}B.[12] The frequency measurements of the doublet were done at the maximum intensity position of the signals.

Table 2. Nuclear quadrupole resonance frequencies of ^{79}Br and ^{127}I in the complexes $PBr_3 \cdot BBr_3$, $PBr_3 \cdot BI_3$, and $PI_3 \cdot BBr_3$ at 77 K

Compound	Species		ν/MHz	S/N
$PBr_3 \cdot BBr_3$	PBr_3		258.93	(8)
			259.40	(4)
	BBr_3		181.89	(6)
			184.30	(12)
$PBr_3 \cdot BI_3$	PBr_3		258.78	(3)
			259.60	(1.5)
	BI_3	ν_1	203.41	(3)
			207.58	(1.5)
		ν_2	399.80	(7)
			401.22	(15)
$PI_3 \cdot BBr_3$	PI_3	ν_1	289.61	(12)
			289.91	(7)
	BBr_3		176.39	(1.5)
			180.32	(3)

The similarity of the resonance patterns of the complexes shows that these complexes are presumably isomorphous with one another, though the crystal structures of the complexes have not yet been clarified. Possibly one halogen atom is non-equivalent to the remaining two halogen atoms in each species of the complexes.

In the case of $PBr_3 \cdot BI_3$, both ν_1 and ν_2 due to ^{127}I were measured. Where the pairings were done easily due to the intensity difference of the two resonances, and the e^2Qq/h and η were obtained as 1340.3 MHz and 0.104 for the stronger line and 1340.7 MHz and 0.173 for the weaker line. The values of η are greatly decreased compared to the parent BI_3, in which η is 0.455.[12]

In Table 3 the mean values of the coupling constants $\langle e^2Qq/h\rangle_{\text{AV}}$ and asymmetry parameters $\langle\eta\rangle_{\text{AV}}$ at 77 K are listed for the complexes and the parent molecules;[11-13] here $\langle e^2Qq/h\rangle_{\text{AV}}$ were calculated by neglecting the assumed small $\langle\eta\rangle_{\text{AV}}$ for the atoms in which the asymmetry parameters could not be obtained. In the last two columns of Table 3, i and f are listed; these are calculated from Eqs. 1 and 2 with $|e^2Qq/h|_{\text{atom}}$

Table 3. Mean coupling constants, mean asymmetry parameters, ionic characters, and the degree of the decrease of pπ electrons in the complexes and the parent molecules at 77 K

Compound	Species	$\langle e^2Qq/h\rangle_{AV}$/MHz	$\langle\eta\rangle_{AV}$	i	f
$PBr_3 \cdot BBr_3$	PBr_3	518	assumed to be 0	0.21	—
$PBr_3 \cdot BI_3$	PBr_3	518	assumed to be 0	0.21	—
PBr_3[a]	—	439	assumed to be 0	0.33	—
$PI_3 \cdot BBr_3$	PI_3	1931	assumed to be 0	0.01	—
PI_3	—	1537	0.075	0.19	0.03
$PBr_3 \cdot BBr_3$	BBr_3	367	assumed to be 0	0.44	—
$PI_3 \cdot BBr_3$	BBr_3	358	assumed to be 0	0.45	—
BBr_3[b]	—	340	0.45	0.41	0.12
$PBr_3 \cdot BI_3$	BI_3	1340	0.127	0.29	0.05
BI_3[c]	—	1185	0.455	0.30	0.16

a) Calculated from Ref. 13 (at 83 K). b) Ref. 11. c) Ref. 12 (at 78 K).

$=769.756$ MHz for ^{79}Br.[14]

On complexing, the phosphorus halide molecule will transfer a charge to the boron halide without a significant change in its pyramidal form. This charge transfer will decrease the ionicity of the P–X bonds, and therefore the coupling constants of phosphorus halide in the complex will increase compared to the parent phosphorus halide, as seen in Eq.1. It is apparent from Table 3 that the $\langle e^2Qq/h\rangle_{AV}$ values increased significantly, that is, the i values decreased, in the complex as compared to the parent molecule.

On the other hand, in going from the parent molecule to the complex, the boron halide changes its structure from planar triangle to pyramid, so that the forming of a π bond between boron and halogen atoms becomes difficult. The two asymmetry parameters in $PBr_3 \cdot BI_3$ are somewhat different, as stated above. This may be attributed to the intermolecular bonding containing I atoms and/or the crystal field effects. However, since these effects can not be estimated due to the lack of information about the crystal structure, average values of η were used tentatively in order to see the extent of π bondings. From Table 3, the π bond character obviously decreases on complexing, whereas the ionic character remains almost the same. Therefore, the π electrons which participated in the π bond between I and B atoms are mostly given back to the I atom. The same situation may also be expected for BBr_3 of the complexes in which η have not been obtained. The decrease of f is accompanied by the increase in the coupling constants, as is seen from Eq. 1. This is the case for the boron halides of the complexes.

On forming the complexes of $PBr_3 \cdot BBr_3$ and $PI_3 \cdot BBr_3$, the ionic character of the P–X bond, i, decreases in PI_3 much more than in PBr_3, and i of the B–Br bond increases in the latter a little more than in the former complex. Accordingly, it is evident that electrons are transferred from PI_3 to BBr_3 much more than from PBr_3 to BBr_3. This is consistent with the order of the Lewis base strengths, $PI_3 > PBr_3$, which was determined by other methods.[15]

One of the authours (H.T.) wishes to thank Professor Takeshi Waki in Tokushima University for his encouragement throughout this research.

References

1) "Mellor's Comprehensive Treatise on Inorganic and Theoretical Chemistry," Vol. VIII, Supplement III, Longman, London (1971), pp. 528—532.
2) A. F. Armington, J. R. Weiner, and G. H. Moates, *Inorg. Chem.*, **5**, 483 (1966), and the references therein.
3) F. E. E. Germann and R. N. Traxler, *J. Am. Chem. Soc.*, **49**, 307 (1927).
4) Th. Renner, *Angew. Chem.*, **69**, 478 (1957).
5) R. Livingston and H. Zeldes, "Table of Eigenvalues for Pure Quadrupole Spectra, Spin 5/2," ONRL Report 1913, Oak Ridge National Laboratory, Oak Ridge, Tenn. (1955).
6) E. T. Lance, J. M. Haschke, and D. R. Peacor, *Inorg. Chem.*, **15**, 780 (1976).
7) Y. C. Leung and J. Waser, *J. Phys. Chem.*, **60**, 539 (1956).
8) E. A. C. Lucken, "Nuclear Quadrupole Coupling Constants," Academic Press, New York (1969).
9) V. Jaccarino, J. G. King, R. H. Satten, and H. H. Stroke, *Phys. Rev.*, **94**, 1798 (1954).
10) B. P. Dailey and C. H. Townes, *J. Chem. Phys.*, **23**, 118 (1955).
11) T. Chiba, *J. Phys. Soc. Jpn.*, **13**, 860 (1958).
12) W. G. Laurita and W. S. Koski, *J. Am. Chem. Soc.*, **81**, 3179 (1959); The value at 78 K was extracted from I. P. Biryukov, M. G. Voronkov, and I. A. Safin, "Tables of Nuclear Quadrupole Resonance Frequencies," Israel, IPST Press (1969).
13) a) H. Robinson, H. G. Dehmelt, and W. Gordy, *J. Chem. Phys.*, **22**, 511 (1954); b) S. Kojima, K. Tsukada, S. Ogawa, and A. Shimauchi, *J. Chem. Phys.*, **21**, 1415 (1953).
14) J. G. King and V. Jaccarino, *Phys. Rev.*, **94**, 1610 (1954).
15) See *e.g.* A. Finch, P. J. Gardner, and K. K. Sen Gupta, *Inorg. Chem.*, **6**, 386 (1966).

On the Diffusivity of Nonelectrolytes in Infinitely Dilute Solution

Koichiro NAKANISHI

Department of Industrial Chemistry, Faculty of Engineering, Kyoto University, Kyoto 606

(Received August 24, 1977)

The validity of the plot, isoviscous diffusion coefficient $D_1\eta_2$ *vs.* molar volume V_2, where D_1 is the diffusion coefficient of solute at infinite dilution, η_2 the viscosity coefficient of solvent, and V_2 the molar volume of solvent, proposed by Hammond and Stokes for carbon tetrachloride, was examined and confirmed with several solutes. General features of the behavior of diffusivity in dilute solution are discussed in terms of solvent association, complex formation and other factors. The experimental results for iodine are given.

The diffusivity of solute in dilute solution has been the subject of many studies primarily because of its practical importance. From a theoretical point of view, this quantity is of fundamental importance in describing transport properties of fluid systems. If the interdiffusion coefficients measured as a function of concentration in dilute solution are extrapolated to infinite dilution, the limiting value, D_1, represents the motion of a single particle in a medium having uniform but different intermolecular force field from that exerted by itself. Thus, the physical meaning of this quantity can be regarded to be almost the same as that of self-diffusion coefficient.

Stokes and co-workers[1,2] carried out extensive studies on the diffusion of carbon tetrachloride and iodine diluted with various organic solvents. An interesting result is a plot of the viscosity-reduced diffusion coefficient $D_1\eta_2$ (η_2; viscosity coefficient of solvent) of carbon tetrachloride against the molar volume, V_2, of the solvent. For the sake of convenience, the plot will be referred to hereafter as the HS (Hammond-Stokes) plot.[2] There are three linear relationships, each corresponding to a group of solvents, namely, spherical molecules, alcohols and the homolog of normal paraffins. All these plots have a positive slope and converge to a common point when extrapolated to $V_2=0$. This is the Stokes-Einstein limit where large particles diffuse in an essentially continuous medium.

The purpose of this paper is to examine the HS plot for other diffusates which sometimes show more complex interactions with solvents. New data are presented for iodine in six organic solvents.

Experimental

Apparatus and Procedure. The diffusion coefficient of iodine in six organic solvents was determined by the capillary cell method. The procedure was reported previously.[3] The diaphragm cell method was also used in part of the measurements. The apparatus and procedure were similar to those given by Hammond and Stokes[2] and Mills and Woolf.[4] The solution-filled procedure was adopted throughout the measurement. The diaphragm used was a micropore glass filter, No. 4. In order to determine the cell constant of the diaphragm, several runs were performed with aqueous KCl solutions. The cell constant was found to be 0.315 cm^2. The concentration changes in two compartments of the cell were determined by measuring the density of solution. A precision vibration-type densimeter(Shibayama Sci. Instr. Co., Model SS·D 200) was used. The concentration change of iodine in the diaphragm cell experiment was determined by titration using sodium thiosulfate solution. The methods of calculation of diffusion coefficient from these two types of measurement have been described.[3,4]

TABLE 1. DIFFUSION COEFFICIENTS OF IODINE DILUTE IN SIX ORGANIC SOLVENTS AT 298.15 K

Solvent	D_1 10^5 cm^2 s^{-1}	η_2 cP[a]	$D_1\eta_2$ 10^{10} dyn[b]
Heptane	3.40±0.10	0.395	1.34
2,2,4-Trimethylpentane	2.93±0.04	0.484	1.38
1,4-Dioxane	0.96±0.03	1.190	1.14
Tetrahydrofuran	2.35±0.08	0.480	1.09
1-Propanol	1.07 1.00[c]	1.95	2.03
2-Propanol	0.89 0.84[c]	2.10	1.83

a) cP=centipoise=0.01 P. 1P=0.1 Pa s throughout this paper. b) 1 dyn=10^{-5} N throughout this paper. c) Data obtained by the diaphragm cell method.

Results. In connection with the study of diffusion in mixed solvents, the values for the diffusion coefficients of iodine diluted in nine pure solvents have been reported.[3,5,6] The six new data obtained with capillary and diaphragm cell methods are summarized in Table 1. Whenever measurements are duplicated by the two methods, both results agree fairly well with each other. The datum for iodine in heptane agrees with the literature value,[1] while there is a small discrepancy between the two data for iodine in 1,4-dioxane.[1]

Hammond-Stokes Plot for a Solute in Different Solvents

Our literature survey indicates that the diffusion coefficients of a solute in a variety of solvents are available only for limited solutes at 298.15 K. We have tested the validity of the HS plot for these solutes. In the case of CCl_4 and I_2, additional data have been reported since the original works by Stokes *et al.* The HS plots for these two solutes are shown in Figs. 1a and 1b. Other typical examples are also given in Figs. 2a—2f.

We see that the product $D_1\eta_2$ increases when V_2 becomes large. In a limited range where V_2 is between 50 and 200 cm^3 mol^{-1}, $D_1\eta_2$ *vs.* V_2 relation may be approximated by three straight lines. The line with the largest slope is associated with alcohols, aniline, and other associated solvents. Sometimes water can be included in this category. The other two lines are respectively for spherical molecules and for normal paraffins and related chain-like molecules. Extrapolation of these three straight lines may converge to a

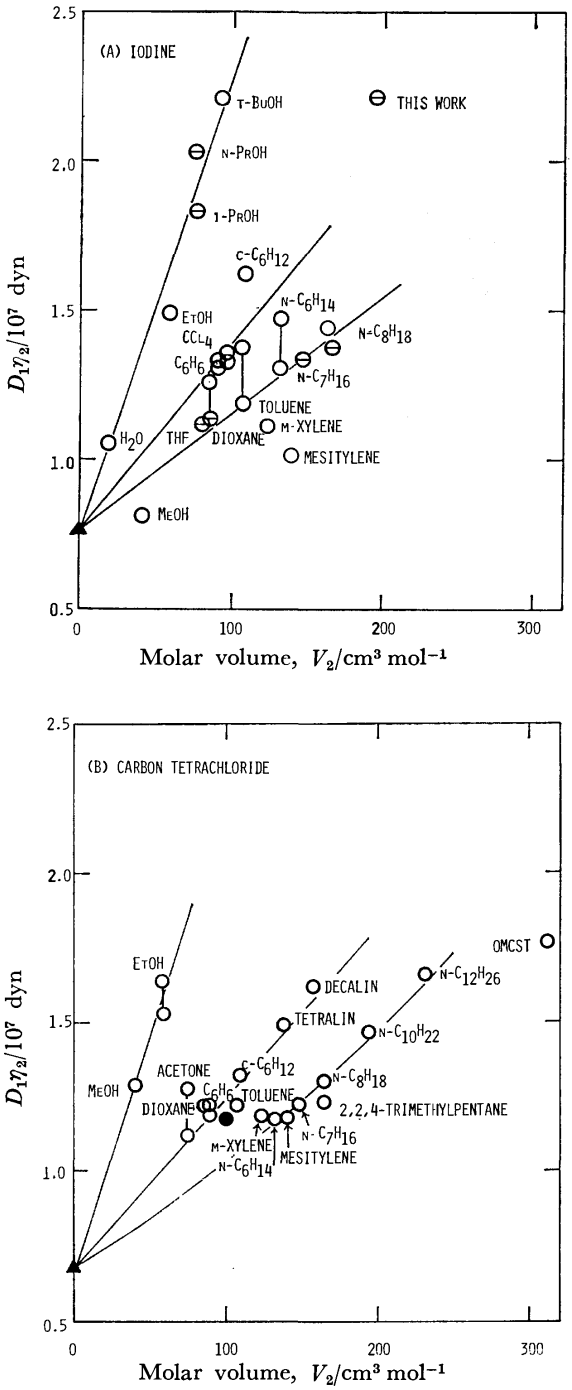

Fig. 1. Hammond-Stokes plot for the diffusion of iodine and carbon tetrachloride in various solvents at 298.15 K. (A) Iodine, (B) carbon tetrachloride. ○, ⊖: $D_1\eta_2$, ●: $(D_1)_{self}\eta_2$, ▲: $D_1\eta_2$ at the Stokes-Einstein limit. Perpendicular lines connect two or more data for the same solvent from different sources.

common point at $V_2=0$. The point given as a triangle represents the D_1 value at the Stokes-Einstein limit and its $D_1\eta_2$ value can be calculated from the Stokes-Einstein equation,

$$D_1\eta_2 = kT/6\pi r_1,$$

where the radius of solute, r_1, is given by

$$r_1 = (3V_1/4\pi N_{av})^{1/3}.$$

Here V_1 is the molar volume of solute at 298.15 K and N_{av} is the Avogadro number.

Although generalization of the original treatment by Hammond and Stokes[2] can be fully verified as above, we have made several interesting observations. In the following discussion, the self-diffusion coefficient, $(D_1)_{self}$, can be included in the correlation. The literature values of $(D_1)_{self}\eta_2$ are taken mainly from the compilations of Dullien[7] and Tyn and Calus.[8]

(1) Whenever a constant slope of $D_1\eta_2$ *vs.* V_2 relation for the same group of solvents can be established, it is almost independent of the solute used. Estimated values for the group of nearly spherical molecules are between 0.95 and 0.55×10^{-9} dyn·mol·cm³, with the exception of carbon dioxide and other smaller solutes which have a larger slope. This is to be compared with 0.60×10^{-9} for CCl_4 reported by Hammond and Stokes.[2]

(2) It should be noted that the $D_1\eta_2$ *vs.* V_2 plot for nonpolar liquids deviates upward from linearity as V_2 increases beyond 200 cm³ mol⁻¹ or so. This tendency seems to be evident for smaller solutes such as ethane (Fig. 2a) and carbon dioxide (Fig. 2b). Perhaps the larger difference in molar volume between solute and solvent may be responsible for this deviation.

(3) Benzene, cyclohexane and CCl_4 form a triplet of simple organic liquid. They are all spherical or disk-like molecules and their molar volume is as large as 100 cm³ mol⁻¹. However, when examined in detail, the molar volume is in the order, c-C_6H_{12}>CCl_4>C_6H_6, while their diffusion coefficient in the same solvent always increases in the order, C_6H_6>c-C_6H_{12}>CCl_4. This indicates that, in spite of larger molar volume, the diffusivity of cyclohexane is somewhat higher than that of CCl_4.

(4) If the diffusing solute has a strong interaction with solvent, that is, there is a solvation between unlike molecules, the product $D_1\eta_2$ takes somewhat lower values.[8,9] A typical example is the case of acetone in chloroform (Fig. 2e), a classical example of binary solution in which the hydrogen bonding between unlike molecules is a source of negative deviation from the ideal solution law. A similar decrease in $D_1\eta_2$ values is also observed for chloroform in ethers, and esters, and in the present data, I_2 in 1,4-dioxane and THF.

(5) The $D_1\eta_2$ *vs.* V_2 plot for various solutes in aliphatic alcohols has a larger slope.[2] A similar tendency is observed for the cases of ethylene glycol (Fig. 2b) and aniline (Fig. 2d) as solvents.

(6) The behavior of water as a solute in various kinds of solvents is puzzling. According to Fig. 2f, the $D_1\eta_2$ values for water in hydrophilic solvents such as alcohols, ketones, esters and carboxylic acids are generally small and close to the value at the Stokes-Einstein limit. However, they are higher in nonpolar solvents. No consistent interpretation can be given at the present stage.

Diffusivity of Different Solutes in the Same Solvent

Let us examine a variation of the diffusion coefficient of different solutes in the same solvent with the molar

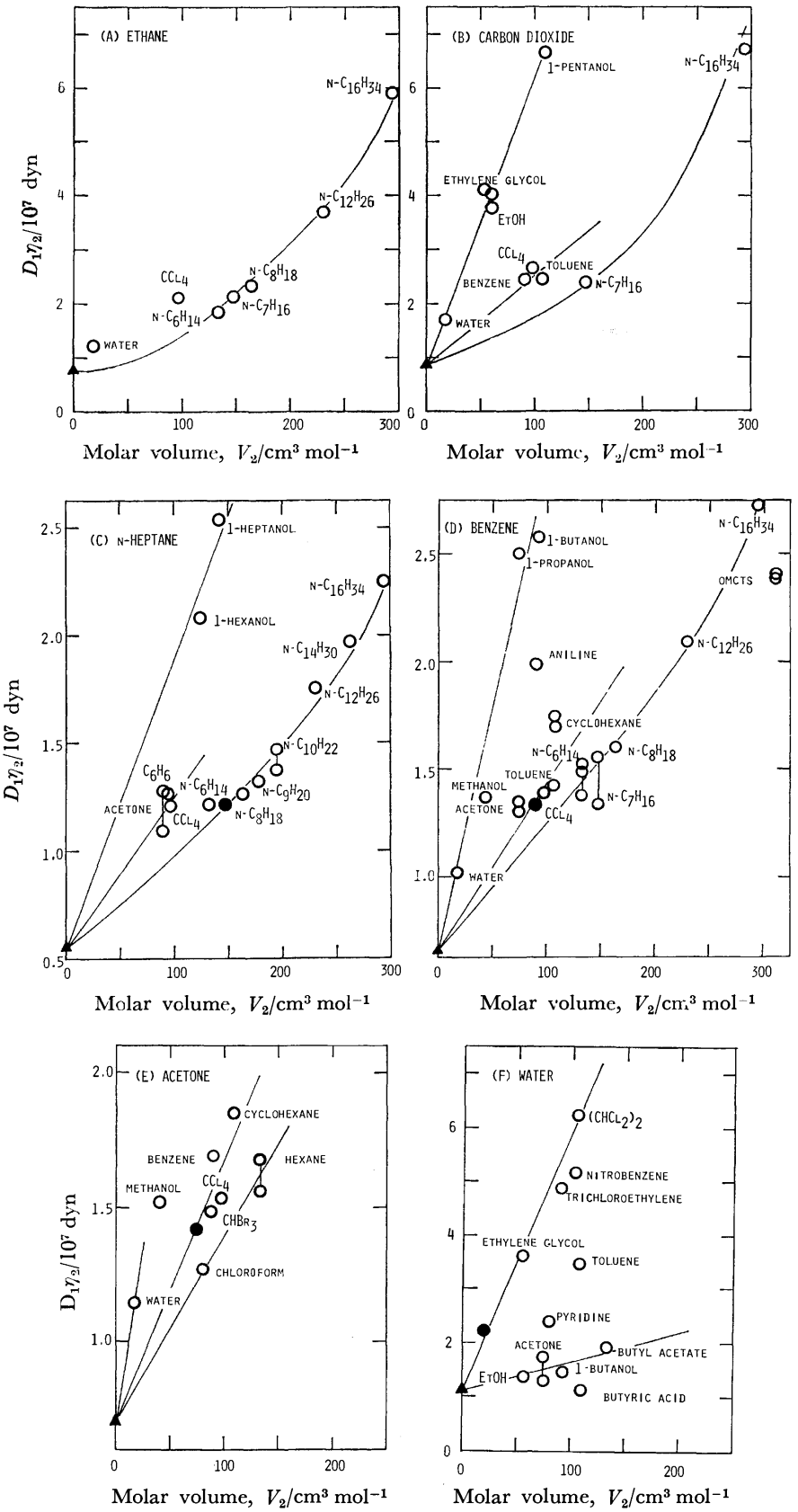

Fig. 2. Hammond-Stokes plot for six solutes at 298.15 K. (A) Ethane, (B) carbon dioxide, (C) heptane, (D) benzene, (E) acetone, (F) water. The notations are the same as those in Fig. 1.

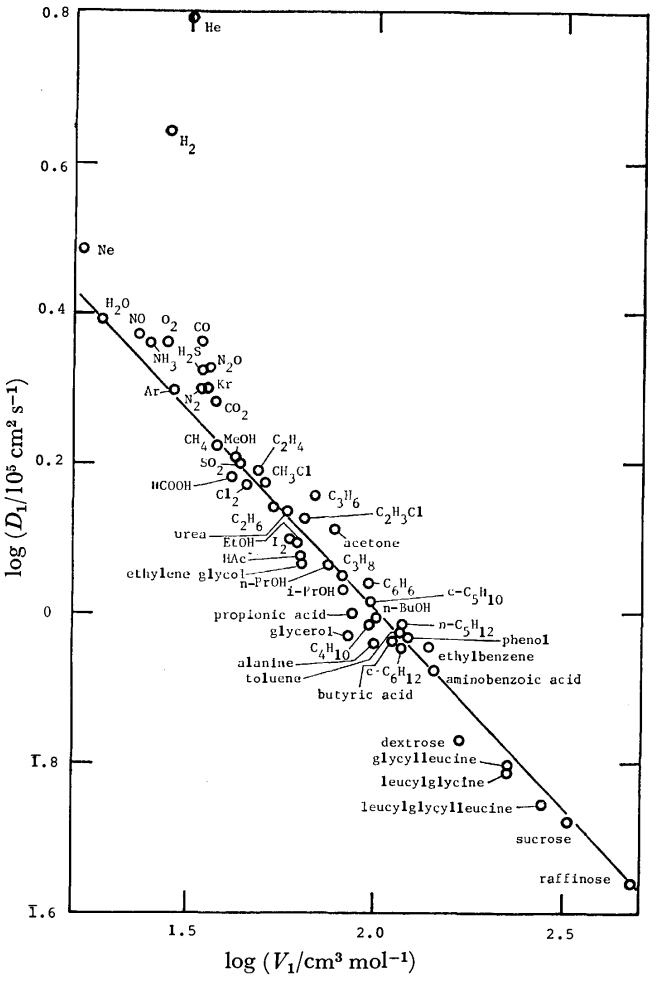

Fig. 3. Log D_1 *vs.* log V_1 plot for various solutes in water at 298.15 K.

volume of solute. Abundant data are available for only limited solvents at 298.15 K. Since no successful procedure has been given for this kind of analysis on diffusivity, we will follow a simple empirical rule proposed by Hildebrand *et al.*[10]

They claimed that the product $D_1\sigma_1^2$ or $D_1(V_c)_1^{2/3}$ where σ_1 is the diameter of molecule and V_c is the critical volume, is found to be constant for non-quantum gases diffusing in CCl_4 and $(n\text{-}C_4F_9)_3N$. We will therefore examine the log D_1 *vs.* log V_1 plot in some selected solvents at 298.15 K. The results are shown in Figs. 3 and 4.

In the case of water as solvent, we see that a good correlation can be established in a V_1 range between 16.8 (neon) and 480 (raffinose) (Fig. 3). All the points scatter properly around a straight line; and large deviations, both positive and negative, can be seen. Helium, hydrogen, and deuterium show a large positive deviation which can be ascribed to a mass effect.[10b] On the other hand, hydrophilic solutes seem to show small negative deviations. We may cite the following solutes: glycerol, ethylene glycol, carboxylic acids, and to a lesser extent, ethanol and 2-propanol The slope of the straight line in log D_1 *vs.* log V_1 plot obtained for water is very close to 2/3, which is equivalent to the rule of the constancy of $D_1\sigma_1^2$ proposed by Hildebrand.[10]

Water(0.89)–cyclohexane(0.89)–carbon tetrachloride (0.90) forms a triplet of isoviscous solvents (Values in parentheses indicate the viscosity coefficient in centipoise for each solvent). The log D_1 *vs.* log V_1 plot for solutes in the latter two solvents is illustrated in Fig. 4. The points for each solute can be classified into three groups; (i) nearly spherical molecules, (ii) normal paraffins, and (iii) other solutes. The slope of linear relation representing group (i) is slightly larger than that for group (ii). Such a difference in slope is ambiguous in the case of water, and the slope for water as solvent

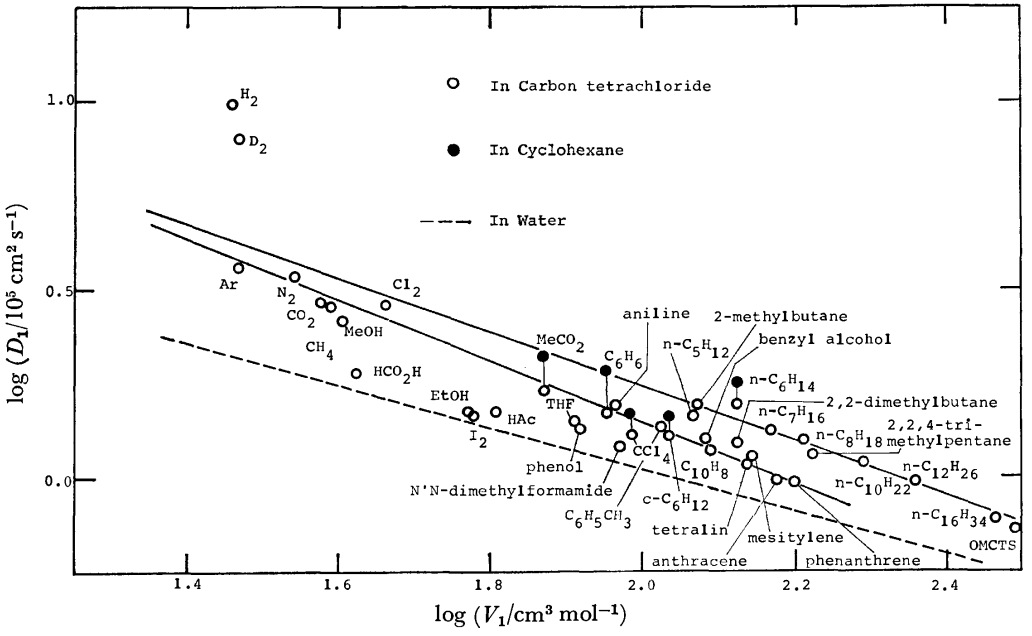

Fig. 4. Log D_1 *vs.* log V_1 plots for various solutes in carbon tetrachloride and cyclohexane at 298.15 K.

being in an intermediate between those for two groups in CCl_4 (dashed line in Fig. 4). The values of diffusion coefficient in water are generally smaller than those in CCl_4 and cyclohexane, indicating that the decrease in diffusivity due to the hydration of each solute cannot be negligible.[11]

The effect of attractive interaction on diffusivity seems to be evident as in the case of the HS plot (Figs. 3 and 4). These observations are supported by recent molecular dynamics calculations on Lennard-Jones liquid mixtures.[12]

In conclusion, the present analysis of the data for the diffusion coefficient in dilute solution reveals general validity of the Hammond-Stokes plot and the presence of the effect of strong specific interaction which causes a decrease in the diffusivity of polar and associated solutes. The analysis will be useful as the basis for empirical methods for predicting the diffusion coefficient in dilute solutions.

The author thanks Messrs. Y. Furusawa and Y. Nishimoto for carrying out the measurements with iodine solutions.

References

1) R. H. Stokes, P. J. Dunlop, and J. R. Hall, *Trans. Faraday Soc.*, **49**, 886 (1953).
2) B. R. Hammond and R. H. Stokes, *Trans. Faraday Soc.*, **51**, 1641 (1955).
3) K. Nakanishi and T. Ozasa, *J. Phys. Chem.*, **74**, 2956 (1970).
4) R. Mills and L. A. Woolf, "Diaphragm Cell," Australian National University Press, Canberra (1968).
5) K. Nakanishi, T. Ozasa, and K. Ashitani, *J. Phys. Chem.*, **75**, 963 (1971).
6) K. Nakanishi and S. Kitajima, *J. Phys. Chem.*, **76**, 2470 (1972).
7) F. A. L. Dullien, *AIChE J.*, **18**, 62 (1972).
8) M. T. Tyn and W. F. Calus, *J. Chem. Eng. Data*, **20**, 106 (1975).
9) G. A. Ratcliff and M.A. Lusis, *Ind. Eng. Chem., Fundam.*, **10**, 474 (1971).
10) (a) M. Ross and J. H. Hildebrand, *J. Chem. Phys.*, **40**, 2397 (1964); (b) K. Nakanishi, E. M. Voigt, and J. H. Hildebrand, *ibid.*, **42**, 1960 (1965); (c) R. J. Powell and J. H. Hildebrand, *ibid.*, **55**, 4715 (1971).
11) J. H. Hildebrand, *Proc. Natl. Acad. Sci. U.S.A.*, **64**, 1329 (1969).
12) K. Toukubo and K. Nakanishi, *J. Chem. Phys.*, **65**, 1937 (1976).

Photochemical Oxidation of Benzene, Toluene, and Ethylbenzene Initiated by OH Radicals in the Gas Phase

Mikio Hoshino, Hajime Akimoto, and Michio Okuda
The National Institute for Environmental Studies, Yatabe, Ibaraki 300-21

(Received September 2, 1977)

Photochemical oxidation of benzene, toluene, and ethylbenzene initiated by OH radicals in the presence of NO and NO_2 was studied in the air by using a 67 dm^3 reaction chamber made of Pyrex glass. OH radicals were produced by photochemical decomposition of nitrous acid, the products being phenol and nitrobenzene for benzene; cresols, benzaldehyde, *m*- and *p*-nitrotoluenes, and benzyl nitrate for toluene; ethylphenols, benzaldehyde, acetophenone, and *m*- and *p*-nitroethylbenzene for ethylbenzene. The reaction mechanisms are proposed based on the addition of OH radicals to aromatic rings and the hydrogen abstraction of OH radicals from alkyl groups.

Photochemical oxidation of hydrocarbons related to air pollution has been discussed since Haagen-Smit proposed[1] a mechanism for photochemical smog formation in Los Angeles whereby harmful oxidants were produced by nitrogen oxides and hydrocarbons under sunlight. Recent studies[2–5] have shown that OH radicals play the most important role in the photo-oxidation of hydrocarbons.

From the standpoint of air pollution, the major concerns are information on the rate constants and that on the final products of the reactions of OH radicals with hydrocarbons. The former is useful for modeling the urban atmosphere, and the latter for taking precaution against injury to both plants and humans. As far as aromatic hydrocarbons are concerned the rate constants and their Arrehenius parameters of the reactions of OH radicals have been thoroughly studied by flash-resonance fluorescence[6,7] and smog chamber experimental techniques,[8,9] but no report was given on the final products.

The present work deals with the photo-oxidation products of aromatic molecules initiated by OH radicals produced by the photolysis of nitrous acid (HNO_2). The final products observed for benzene, toluene, and ethylbenzene in the presence of NO and NO_2 are reported and the reaction mechanisms are discussed.

Experimental

The reaction cell used was a 67 dm^3 Pyrex glass chamber (diam. 22.5 cm, length 170 cm) which can be evacuated to 10^{-7} Torr by a rotary, sorption, and titanium getter and spatter ion pumps. Aromatic hydrocarbons in a 105 cm^3 glass bulb at a known pressure were first introduced into the reaction chamber. Nitrous acid was produced from sodium nitrite and sulfuric acid according to the method of Cox.[10] A round-bottomed flask (500 cm^3) containing 5% sulfuric acid was filled with pure air after evacuation. Aqueous sodium nitrite (5×10^{-2} mol/dm^3 or 5×10^{-3} mol/dm^3) was added drop by drop under a stream of pure air carrying the gaseous nitrous acid produced into the reaction chamber. To avoid excess moisture, pure air was introduced into the reaction chamber, by-passing the flask after the sodium nitrite solution had been consumed. Two Capsulon pressure gauges (Edward High Vacuum Co.) calibrated by means of a mercury manometer were used for measuring pressures.

The light source was a 500W xenon lamp. A parallel light beam of *ca.* 200 mmϕ was obtained by using an elliptic mirror, a lens, and an off-axis parabolic mirror. The reaction mixtures were irradiated through a Pyrex window. The wavelengths of the irradiated light were longer than 320 nm.

Product identification and quantitative analysis were performed using a gas chromatograph (Shimadzu 6A) and G. C. mass spectrometer (JOEL, JMS-D100). Glass columns (3 m) with 5% SE-30 on Shimalite W were used. The oven temperature was elevated from 80 to 200 °C at a programmed rate of 4 °C/min.

It should be noted that the conversion of aromatic molecules was limited to below 1% in order to avoid reactions of primary products. Dark reactions were found to be negligible. Because of the low conversion of reactants, the sampled gas had to be concentrated before introduction into the gas chromatograph or G. C. mass spectrometer. The reaction mixtures were first sampled from the reaction chamber into a 700 cm^3 glass bulb which had been evacuated before use. The sampled gas in the bulb was exhausted out slowly through a cooled spiral glass tube in order to collect products. The temperature of the spiral tube had to be kept between −80 and −60 °C, since the relatively volatile products escape above −60 °C. Nitrogen dioxide which causes thermal reaction with the reactants and products in the tube was captured below −80 °C. After the concentration the tube was warmed with hot water, and the products trapped in the tube were introduced directly into the gas chromatograph.

The concentrations of nitrogen oxides were measured with a commerical chemiluminescence NO_x analyzer (Monitor Labs, Model 8440). The analyzer is capable of measuring simultaneously the concentrations of NO and NO_x, where NO_x here is the sum of HNO_2, NO and NO_2.

$$[NO_x] = [HNO_2] + [NO] + [NO_2] \quad \text{(i)}$$

The concentrations of HNO_2, NO, and NO_2 were determined by the method of Cox[10] as follows. When the mixture of HNO_2, NO_2, and NO is bubbled through an aqueous alkaline solution (0.1 M NaOH), HNO_2 and a certain amount of NO_2 and NO are removed. Thus the concentrations of HNO_2, NO, and NO_2 are determined, from Eq. i and the following relation.

$$[NO_x]_{alkaline} = (1-a)[NO] + (1-b)[NO_2] \quad \text{(ii)}$$

Factors a and b were obtained by independent measurement of the loss of NO and NO_2 after bubbling through alkaline solution. The values of a and b were determined to be 0.1 and 0.2, respectively.

Benzene, toluene and ethylbenzene were supplied by Wako Pure Chem. Ind. Co. Pure air and nitrogen gases (Takachiho Chem. Ind. Co.) were used without purification. As an authentic sample, benzyl nitrate was prepared by fractional distillation of the reaction mixture of benzyl chloride and silver nitrate in a dried acetonitrile solution.

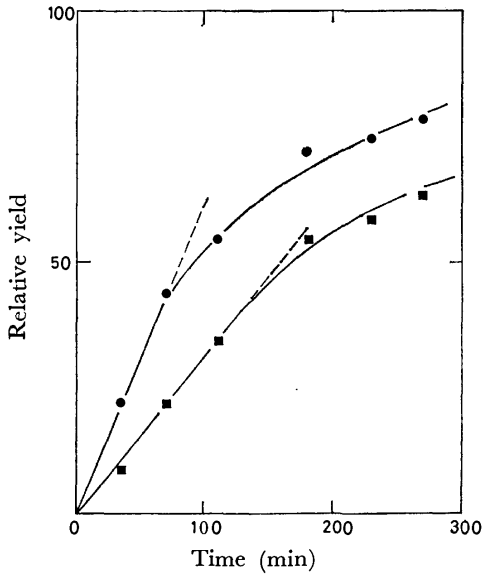

Fig. 1. Relative yields of phenol (●) and nitrobenzene (■) *vs.* irradiation time in the photo-oxidation of benzene-HNO_2-air system.

Results

Phenol and nitrobenzene were the major products when the mixture of benzene and HNO_2 in the air was irradiated. A small amount of nitrophenols was detected as well.

Figure 1 shows typical formation curves of the products as a function of irradiation time when the initial concentrations of benzene and HNO_2 were 31 and 3.2 ppm, respectively. NO_2 at 1.4 ppm and NO at 1.2 ppm were present in the initial reaction mixture, since HNO_2 partially decomposes into NO and NO_2.

As shown in Fig. 1, the amounts of phenol and nitrobenzene first increase linearly with time, then show convex curvatures, which would be due to the decrease of the concentration of HNO_2 by photochemical decomposition. The ratio of nitrobenzene to phenol was found to increase as the reaction proceeds, the increase of NO_2 concentration during irradiation being responsible for this. The ratios of nitrobenzene to phenol determined from the initial inclinations of their formation curves are shown in Table 1. The ratio changes with the initial concentration of NO_2. Nitophenols were minor products and a relative yield less than 1% of phenol was dependent on the temperature of the spiral trap. They might be produced by a thermal reaction of phenol and NO_2 in the spiral trap, although photochemical formation is not excluded.

The major products in the toluene–HNO_2–air system were cresols, benzaldehyde, and *m*-nitrotoluene. Small amounts of *p*-nitrotoluene, benzyl nitrate, and nitrocresols were observed. A trace amount of an unidentified substance giving mass peaks at *m/e*: 124(39), 123(18), 122(100), 94(93), 82(54), 66(48), and 54(69) was also observed. The relative yield of *o*-cresol was found to be *ca.* 80% of the total amount of cresols and that of *m*- and *p*-cresol *ca.* 20%. *m*- and *p*-cresols could not be separated by gas chromatograph column. The yield of nitrocresols was less than 5% that of cresols. Since most nitrocresols are considered to be produced thermally from cresol and NO_2 in the trap as in the case of nitrophenol, the yield of nitrocresols was added to that of cresols (Table 2 and Figs. 2 and 3).

Table 1. Relative product yields in the photo-oxidation of the benzene-HNO_2-NO_x-air system

Initial concentration			Relative yield	
HNO_2 ppm	NO_2 ppm	NO ppm	Phenol	Nitro-Benzene
0.52	0.02	0.06	1.0	0.08
3.2	1.4	1.2	1.0	0.50

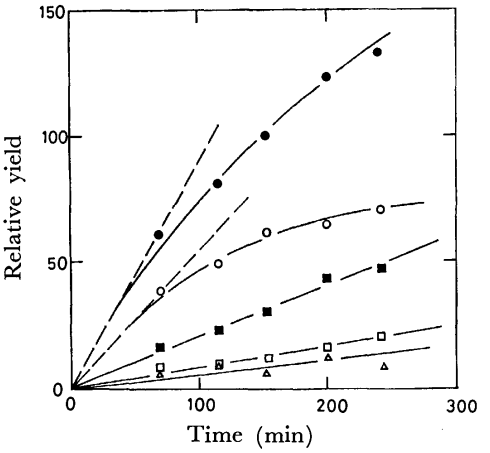

Fig. 2. Relative yields of cresols (●), benzaldehyde (○), *m*-nitrotoluene (■), *p*-nitrotoluene (□), and benzyl nitrate (△) *vs.* irradiation time in the photo-oxidation of toluene-HNO_2-air system.

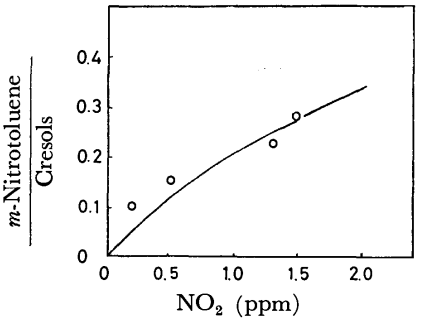

Fig. 3. Yields of *m*-nitrotoluene relative to cresols as a function of initial concentration of NO_2 in the photo-oxidation of toluene-HNO_2-air system.

The plots of [cresol+nitrocresol] and benzaldehyde *vs.* irradiation time are convex upwards. This would be due to the consumption of HNO_2 (Fig. 2). 6 ppm of HNO_2 were reduced to 2.3 ppm after 4 h irradiation. On the other hand, *m*-nitrotoluene seems to increase linearly with time. Both HNO_2 and NO_2 contribute to the formation of *m*-nitrotoluene. Thus an increase of NO_2 during the course of irradiation would compensate a decrease of HNO_2, resulting in an apparent linear increase of *m*-nitrotoluene. 1.3 ppm of NO_2 observed before irradiation was increased to 2.1 ppm after 4 h irradiation.

Table 2. Relative product yields (cresol = 1.0) in the photo-oxidation of the toluene-HNO_2-O_2/N_2 system

Initial concentration				Relative yield			
HNO_2 ppm	NO_2 ppm	NO ppm	Atmosphere	Benzaldehyde	Benzyl-nitrate	*m*-Nitro-toluene	*p*-Nitro-toluene
4	0.2	0.4	air	0.45	0.06	0.10	0.10
7	0.5	1.0	air	0.42	0.06	0.15	0.10
6	1.3	2.1	air	0.61	0.06	0.23	0.09
12	1.5	1.5	air	0.48	0.05	0.28	0.11
3	0.3	0.4	N_2	—	—	0.43	0.17
12	2.0	3.6	N_2	—	—	0.97	0.14

Table 3. Relative product yields (ethylphenol = 1.0) in the photo-oxidation of the ethylbenzene(EB)-HNO_2-NO_x-air system

Initial concentration			Relative yield			
HNO_2 ppm	NO_2 ppm	NO ppm	Benzaldehyde	Acetophenone	*m*-Nitro-EB	*p*-Nitro-EB
1.7	0.5	0.2	0.60	1.73	0.11	0.08
7.9	1.2	3.0	0.65	2.02	0.37	0.16

The ratios of products determined from the initial slopes on the formation curves of the products are shown in Table 2. It is evident that the ratio of benzaldehyde to cresols is constant irrespective of the concentration of NO_2. On the other hand, the ratio of *m*-nitrotoluene to cresols increases with increasing initial concentration of NO_2 as shown in Fig. 3.

When the reaction was carried out in a nitrogen atmosphere, the products obtained were cresols and *m*- and *p*-nitrotoluene. It should be noted that the ratio of *m*-nitrotoluene to cresols is four times greater than that observed in the air with the same concentration of NO_2. The ratio of *o*-cresol to *m*- and/or *p*-cresol was the same as that for the air system.

In the photochemical oxidation of ethylbenzene, the products identified were ethylphenols, acetophenone, benzaldehyde, *m*-nitroethylbenzene, and *p*-nitroethylbenzene. Nitroethylphenols were also observed as minor products. Phenyl acetaldehyde was not obtained. The formation curves of the products were essentially the same as in the cases of benzene and toluene.

The ratios of the products to ethylphenols are shown in Table 3. With increase in the initial concentration of NO_2 the yield of *m*-nitroethylbenzene increases markedly. The ratios of acetophenone and benzaldehyde to ethylphenols are independent of the concentrations of NO_2. The main product was acetophenone, the yield of which was approximately twice that of ethylphenols.

Discussion

In an aromatic hydrocarbon–HNO_2–air system, photochemical oxidation is initiated by OH radicals formed in the photolysis of HNO_2.[10,11]

$$HNO_2 + h\nu(330\text{—}390\ \text{nm}) \longrightarrow OH + NO. \quad (1)$$

The reaction of the OH radicals with aromatic hydrocarbons competes with the reactions,

$$OH + NO \xrightarrow{M} HNO_2, \quad (2)$$

$$OH + NO_2 \xrightarrow{M} HNO_3, \quad (3)$$

$$OH + HNO_2 \xrightarrow{M} H_2O + NO_2, \quad (4)$$

where NO and NO_2 are unavoidably present in the initial reaction mixture and also formed in the photolysis of HNO_2. In such a reaction system, a part of the OH radicals would be reproduced by the reaction

$$HO_2 + NO \longrightarrow OH + NO_2, \quad (5)$$

since HO_2 radicals are expected to be produced in the reaction of OH radicals with aromatic hydrocarbons. Thus, the photochemical oxidation in the present system is a chain process in which an OH radical acts as a chain carrier.

Benzene–HNO_2 System. In the photochemical reaction of the benzene–HNO_2–air system, the initial step should be the OH radical addition to the benzene ring followed by the reactions with O_2 and NO_2 (Scheme 1).

Addition of OH radicals to benzene has been shown to occur in the radiolysis[12,13] and photolysis[14] studies of aqueous solutions of benzene. In pulse radiolysis[12] of the aqueous solution of benzene, a transient absorption spectrum assigned to hydroxycyclohexadienyl radical has been detected. The final products in the aerated solution were phenol, peroxide, and hydroperoxide, whose yields were dependent on the pulse intensity. At low pulse intensities where the formation of peroxide and hydroperoxide due to radical-radical reactions was unfavorable, phenol was the main product and could account for 80% of the yield of OH radicals. On the other hand, photolysis[14] of benzene–H_2O_2 and γ-radiolysis[13] of benzene, both in aqueous solutions in the presence of oxygen, are known to give phenol and hydroxy-2,4-hexadienedial (CHO–C(OH)=CH–CH=CH–CHO and CHO–CH=C(OH)–CH=CH–CHO) as final products.

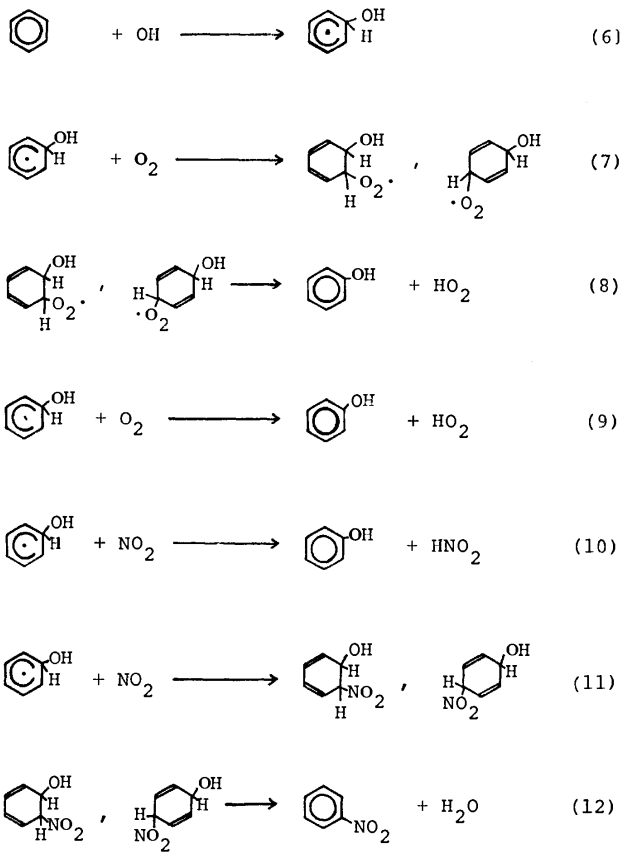

Scheme 1.

In the present reaction system, the final products were phenol and nitrobenzene and the formation mechanism can be visualized as in Scheme 1. The reaction sequence (7)—(8) is the same as the one suggested[12–14] for the formation of phenol in aqueous solutions. In the gas phase, however, Reactions 9 and 10, direct abstraction of the hydrogen atom by O_2 and NO_2, might also occur.

No formation of hydroxy-2,4-hexadienedial was observed. The compound is thought[13,14] to be formed *via* bimolecular reaction of 4-hydroxy-2,5-cyclohexadienylperoxyl radicals in aqueous systems. Since the concentration of benzene is two orders of magnitude lower than that in the aqueous studies, absence of the product due to the bimolecular radical-radical reaction is reasonable.

When NO_2 is present, it will add to the 4-hydroxy-2,5-cyclohexadienyl radicals to give nitrocyclohexadienols as a reaction intermediate and the elimination of H_2O from the intermediate will give nitrobenzene as a final product. Formation of nitrobenzene has been reported[15] in the radiolysis of aqueous $NaNO_3$ solution containing benzene, and the reaction mechanism based on the addition of NO_2 to the 4-hydroxy-2,5-cyclohexadienyl radicals followed by the elimination of H_2O has been postulated. The fact that the relative yield of nitrobenzene to phenol increases with increase in the initial concentrations of NO_2 can be explained by the mechanism shown in Scheme 1.

Nitrophenol was obtained as a very minor product. This is in line with the study of the radiolysis of aqueous $NaNO_3$–benzene system,[15] but differs from the one in the gas phase photo-oxidation systems[16,17] containing much higher concentrations ($\approx$1000 ppm of each reactant) of benzene and NO or NO_2 in the air. Formation of nitrophenol instead of phenol was probably due to the secondary nitration of phenol either in the gas phase or during the analytical procedure.

Toluene–HNO_2 System. In the reaction of the toluene–HNO_2–air system, cresols and *m*-nitrotoluene seem to be produced by the same reaction sequences as those for benzene. Approximately 80% of the total cresol formed was *o*-cresol. Predominant formation of *o*-cresol has recently been reported[18] in the reaction of toluene with oxygen atoms produced in the mercury photosensitization of N_2O. On the other hand, the formation ratio of *m*- and *p*-cresol to *o*-cresol is much higher in the radiation-induced hydroxylation[19] of toluene in aqueous solutions both in the presence and absence of metal salts. Hence it is concluded that the ortho position of toluene is regarded as the predominant reactive site both for OH radicals and oxygen atoms in the gas phase and that OH radicals discriminate the attacking site of substituted benzene more specifically in the gas phase than in aqueous solutions. The formation mechanism of cresols and *m*-nitrotoluene is proposed to be as follows.

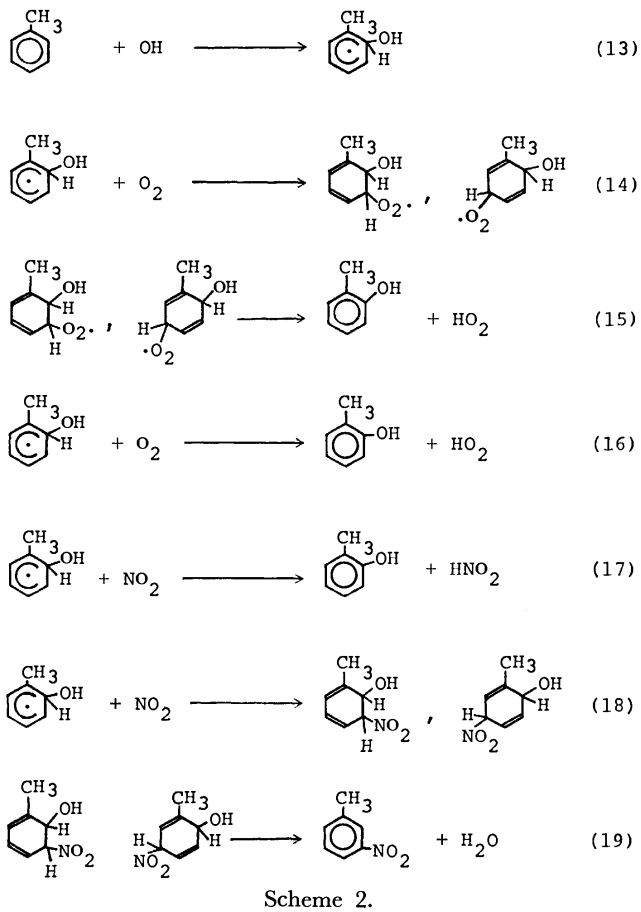

Scheme 2.

A marked increase in the yield of *m*-nitrotoluene relative to cresols with an increase of initial concentration of NO_2 (Table 2 and Fig. 3) is in line with the proposed mechanism. It should be noted that the addition

of OH radicals to the para position (not shown in Scheme 2) also leads to *m*-nitrotoluene when NO_2 adds to the methyl-substituted hydroxycyclohexadienyl radicals followed by elimination of H_2O. A minor product, *p*-nitrotoluene, might be produced *via* an intermediate radical of an OH adduct at the meta position followed by elimination of H_2O. However, the increase of *p*-nitrotoluene with an increase of the initial concentration of NO_2 is much less marked (Table 2), no *o*-nitrotoluene, which is also expected from the OH adduct at the meta position, being obtained. This suggests a different reaction path for *p*-nitrotoluene although an alternate mechanism can not be specified.

Benzaldehyde and benzyl nitrate are reasonably assumed to be formed from benzyl radicals as intermediates. Hydrogen atom abstraction by OH radicals from the methyl group of toluene occurs at slightly elevated temperatures in gas phase reactions.[20] Since the C–H bond-dissociation energy[21] in the methyl group of toluene is only 83 kcal/mol as compared to 91 kcal/mol for the tertiary C–H bond of isobutane, it is reasonable to assume that the hydrogen abstraction competes with the addition to the aromatic ring even at room temperature. Kinetic studies[6,7] on the determination of rate constants for the reaction of OH radicals with toluene also suggest the competitive abstraction of hydrogen atom from the methyl group. The formation mechanism of benzaldehyde and benzyl nitrate is thus proposed as follows, in analogy with the reaction sequence postulated[2] for alkyl radicals in the presence of O_2, NO, and NO_2.

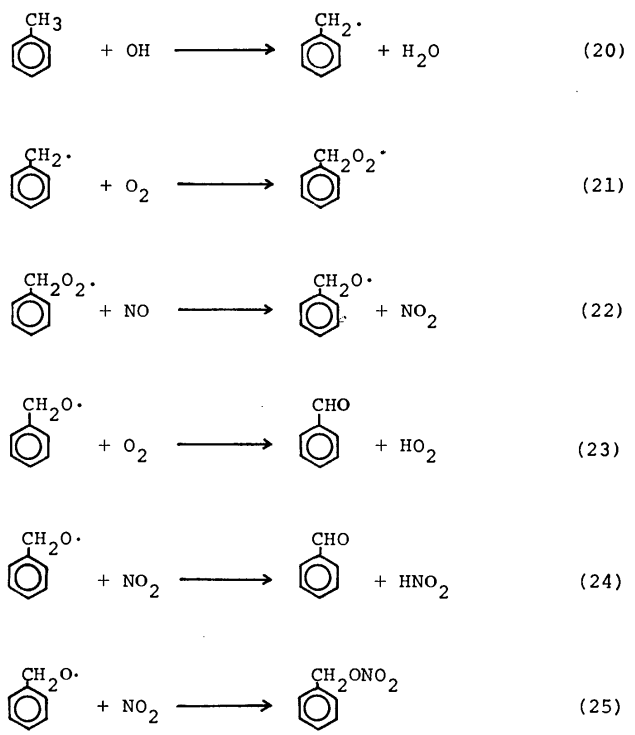

Scheme 3.

Reactions 22—25 to produce benzaldehyde and benzyl nitrate are assumed to be analogous to the reactions of methylperoxyl and methoxyl radicals to give formaldehyde and methyl nitrate.[2] If we assume the distribution of the final products given in Table 2 represents the initial step ratio of the OH addition to hydrogen atom abstraction, the percentage of the abstraction is estimated to be 25—35%. The value is in line with the suggestion by Davis *et al.*[6] that over half of the time, the reaction at room temperature proceeds *via* addition based on the pressure dependence of the rate constants. However, since no material balance has been studied, the above value should be taken as a first approximation. Formation of benzyl nitrate apparently did not increase with the increase of the initial concentration of NO_2, and an alternative path

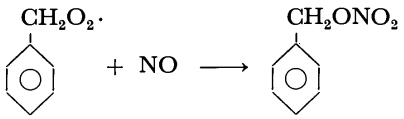

might take place as proposed by Darnall *et al.*[22] in the case of alkylperoxyl radicals containing more than four carbon atoms.

The unidentified minor product in the photo-oxidation of toluene, giving mass peaks at *m/e*, 124, 123, 122, 94, 82, 66, and 54, might be 2-methyl-2,4-hexadienedial. A possible reaction mechanism to give the product is as follows.

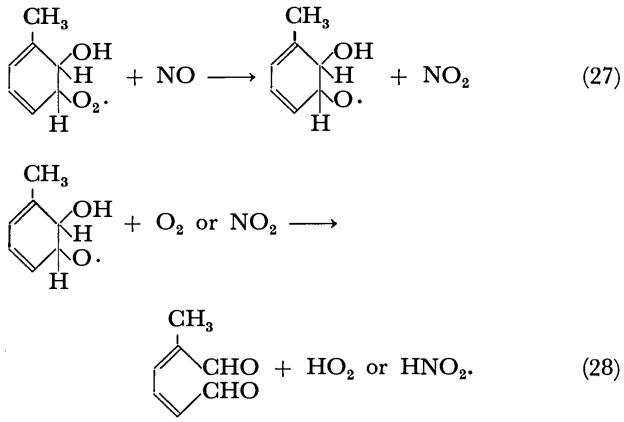

Although the mass pattern observed is what is expected for the compound, the identification is tentative since no authentic sample was available.

In an atmosphere of N_2 instead of air, the products obtained are cresols and *m*- and *p*-nitrotoluene. Benzaldehyde and benzyl nitrate, thought to be produced *via* benzylperoxyl radicals, were not observed. The results are in line with the proposed schemes 2 and 3. On the other hand, in the absence of O_2 bibenzyl and/or α-nitrotoluene derived from benzyl radicals can be expected as final products. Neither of them, however, was detected. Presumably, the poor yields of these products may be due to the low concentration of the radicals and NO_2. The ratio of *m*-nitrobenzene to phenol in the N_2 atmosphere was four times greater than that in the air. This observation is qualitatively explained by the fact that the hydrogen atom abstraction by O_2, Reactions 14, 15, and/or 16, does not contribute to the formation of cresols in the absence of O_2, resulting in a greater ratio of *m*-nitrotoluene to cresols as compared with that obtained in the air.

Ethylbenzene–HNO_2 System. Of the products obtained in the ethylbenzene–HNO_2–air system, ethyl

phenol and *m*- and *p*-nitroethylbenzene will be derived from the addition of OH radicals to an aromatic ring as in the case of toluene. The reaction mechanism is analogous to Scheme 2 for toluene. Acetophenone is considered to be produced *via* 1-phenylethyl radicals formed by the abstraction of an α-hydrogen atom by OH radicals. The proposed mechanism is as follows.

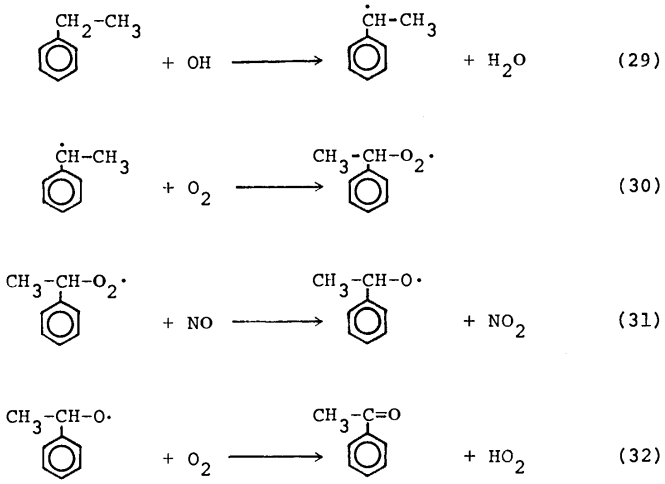

Scheme 4.

Another major product, benzaldehyde, is thought to be produced by the decomposition of 1-phenylethoxyl radicals as follows.

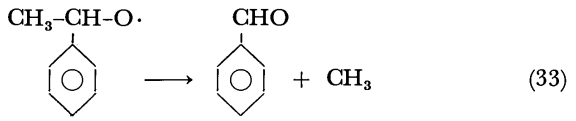

Bond cleavage in alkoxyl radicals to give a carbonyl compound and methyl radical has been assumed[23] in the photochemical oxidation of isobutane in the presence of NO and NO_2. Another possibility for the formation of benzaldehyde is the one initiated by the abstraction of a β-hydrogen atom in ethyl group of ethylbenzene. The reaction scheme is shown as Scheme 5.

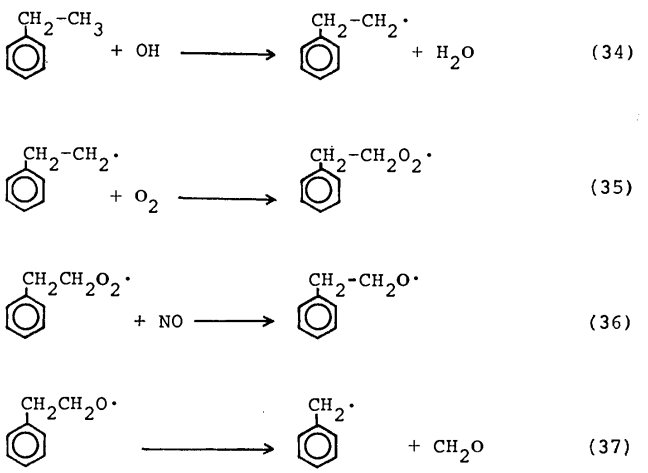

Scheme 5.

According to Eqs. 21 and 22, benzyl radicals produced may be oxidized to give benzaldehyde. However, if this reaction mechanism holds, phenylacetaldehyde should also be expected as

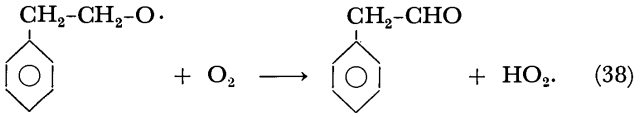

Benzyl nitrate is also expected as in the case for toluene. Since neither of these products was obtained, we conclude that the β-hydrogen abstraction does not occur in the reaction of OH radicals with ethylbenzene, and Scheme 4 should be adopted to interpret the formation of benzaldehyde.

The ratio of yield of products formed *via* hydrogen atom abstraction to those *via* OH radical addition increases markedly for ethylbenzene as compared with the case of toluene. Thus, from the product distribution (Table 3) the percentage of the hydrogen abstraction may be deduced to be 60—70%. The apparent increase in percentage of the hydrogen abstraction reaction would be due to the weaker bond energy of α-hydrogen-carbon bond in the ethyl group of ethylbenzene than that in the methyl group of toluene.

Atmospheric Importance. It is well-known that aromatic hydrocarbons (alkylbenzenes) constitute a substantial fraction of hydrocarbons in the polluted urban atmosphere. For example, the average percentage of aromatic hydrocarbons in the Los Angeles Basin was reported[24] to be roughly 20%. In Japan, the presence of a higher percentage of aromatic hydrocarbons has been noted,[25,26] amounting to 30—35% in average. Thus it is expected that the reaction products observed in the present study should also be formed in such an ambient air. Phenols, aromatic carbonyl compounds and nitrobenzenes, and nitrates should be of concern since they are found to be formed even at atmospheric concentrations of NO and NO_2. Recently, nitrocresols were observed[16] in rain drops collected in Yokohama. This suggests that the nitration of phenols occurs easily in both gas phase secondary reactions and in aerosol droplets, since the nitrocresols are only a minor products in the primary reaction of OH radicals in the presence of atmospheric concentration of NO and NO_2.

We thank Drs. N. Washida and G. Inoue for many helpful discussions on the reaction mechanism. The assistance of Mr. K. Nagasawa throughout this study is gratefully acknowledged.

References

1) A. J. Haagen-Smit, *Ind. Eng. Chem.*, **44**, 1342 (1952).
2) J. Heicklen, K. Westberg, and N. Cohen, in "Chemical Reactions in Urban Atmosphere," ed by C. Tuesday, Elsevier, New York, N. Y. (1971), p. 55.
3) J. G. Calvert and R. D. McQuigg, *Int. J. Chem. Kinet., Symp.*, **1**, 113 (1975).
4) C. C. Wang, L. I. Davis, Jr., C. H. Wu, S. M. Jasper, H. Niki, and W. Weinstock, *Science*, **189**, 797 (1975).
5) C. H. Wu, C. C. Wang, S. M. Jasper, L. I. Davis, Jr., M. Hanabusa, D. Killinger, H. Niki, and B. Weinstock, *Int. J. Chem. Kinet.*, **8**, 765 (1976)

6) D. D. Davis, W. Bollinger, and S. Fischer, *J. Phys. Chem.*, **79** 293 (1975).
7) R. A. Perry, R. Atkinson, and J. N. Pitts, Jr., *J. Phys. Chem.*, **81**, 296 (1977).
8) A. C. Lloyd, K. R. Darnall, A. M. Winer, and J. N. Pitts, Jr., *J. Phys. Chem.*, **80**, 789 (1976).
9) G. J. Doyle, A. C. Lloyd, K. R. Darnall, A. M. Winer, and J. N. Pitts, Jr., *Environ. Sci. Technol.*, **9**, 237 (1975).
10) R. A. Cox, *J. Photochem.*, **3**, 175 (1974).
11) R. A. Cox and R. G. Derwent, *J. Photochem.*, **6**, 23 (1976/1977).
12) L. M. Dorfman, I. A. Taub, and R. E. Bühler, *J. Chem. Phys.*, **36**, 3051 (1962).
13) (a) T. K. K. Srinivasan, I. Balakrishnan, and M. P. Reddy, *J. Phys. Chem.*, **73**, 2071 (1969); (b) I. Balakrishnan and M. P. Reddy, *ibid.*, **76**, 1273 (1972).
14) N. Jacob, I. Balakrishnan, and M. P. Reddy, *J. Phys. Chem.*, **81**, 17 (1977).
15) M. K. Eberhardt, *J. Phys. Chem.*, **79**, 1067 (1975).
16) K. Nojima, K. Fukaya, S. Fukui, and S. Kanno, *Chemosphere*, **2**, 77 (1975).
17) W. Ando, private communication.
18) J. S. Gaffney, R. Atkinson, and J. N. Pitts, Jr., *J. Am. Chem. Soc.*, **98**, 1828 (1976).
19) M. K. Eberhart and M. I. Martinez, *J. Phys. Chem.*, **79**, 1917 (1975).
20) A. F. Trotman-Dickenson and E. W. R. Steacie, *J. Chem. Phys.*, **19**, 329 (1951).
21) J. G. Calvert and J. N. Pitts, Jr., "Photochemistry," John Wiley, New York, N. Y. (1966), p. 824.
22) K. R. Darnall, W. P. L. Carter, A. M. Winer, A. C. Lloyd, and J. N. Pitts, Jr., *J. Phys. Chem.*, **80**, 1948 (1976).
23) J. Heicklen, "Atmospheric Chemistry," Academic Press, New York, N. Y. (1976), p. 389.
24) A. P. Altshuller, W. A. Lonneman, F. D. Sutterfield, and S. L. Kopczynski, *Environ. Sci. Technol.*, **5**, 1009 (1971).
25) J. Kondo and H. Akimoto, *Adv. Environ. Sci. Technol.*, **5**, 1 (1975).
26) T. Katou, Y. Hanai, Y. Horimoto, and H. Kachi, *Bull. Inst. Sci. Tech., Yokohama Natl. Univ.*, **1**, 37 (1974).

The Formation of Nitrogeneous Compounds in the γ-Radiolyses of Liquid Nitrogen Solutions of Hydrogen, Methane, and Ethane

Keiichi HORIGOME, Shun-ichi HIROKAMI,* and Shin SATO

Department of Applied Physics, Tokyo Institute of Technology, Ookayama, Meguro-ku, Tokyo 152

(Received September 9, 1977)

The γ-radiolyses of liquid nitrogen solutions of hydrogen, methane, and ethane have been reinvestigated. A complete survey of nitrogen-containing products has been attempted. The nitrogeneous compounds observed were ammonia (0.7) and hydrogen azide (0.02) in the case of hydrogen, ammonia (0.3), hydrogen cyanide (0.1), methyl azide (0.01), and a polymer in the case of methane, and ammonia (0.3), hydrogen cyanide (0.05), acetonitrile (0.04), ethyl azide (0.01), and a polymer in the case of ethane. The values in parentheses are the *G*-values obtained at optimum conditions. The hydrolysis of the polymer obtained with methane gave formaldehyde in amounts which correspond to the fact that the *G*-value of the nitrogen atoms which were converted into the polymer is about 1.0. In order to explain these results, possible reaction mechanisms are discussed.

The reactions of nitrogen atoms with hydrocarbons have been investigated in the gas phase, using active nitrogen produced in a discharge;[1] however, probably because of the low pressure and of the high temperature, more than 90% of the nitrogeneous compounds observed were hydrogen cyanide, irrespective of the hydrocarbon used. Consequently, it was almost impossible to elucidate any details of the reaction mechanism.

A few years ago, our laboratory started to use the γ-radiolysis of liquid nitrogen as the source of nitrogen atoms and studied the reactions with several olefins which are soluble in liquid nitrogen with the hope that the addition products might not decompose into hydrogen cyanide.[2] In fact, we observed the formations of acetonitrile, propionitrile, and acrylonitrile, respectively, in the reactions with propylene, 1-butene, and allene, and we could propose a generalized reaction mechanism:[3]

$$RCH{=}CH_2 + N \rightarrow R\text{-}\underset{\displaystyle N}{\overset{\displaystyle H}{C}}\text{-}CH_2 \rightarrow RCN + CH_3.$$

However, the *G*-values of these nitrile compounds, including hydrogen cyanide obtained in the reaction with ethylene were very small—less than 0.2. During these measurements, we recognized the formation of a polymer and measured the *G*-value of the nitrogen atoms which were converted into the polymer by using Conway's method. This method is one of the techniques frequently used in biochemistry. A sample containing amine and/or imine is hydrolyzed in an alkaline solution and the ammonia evolved is absorbed in dilute sulfuric acid in a specially designed vessel, and then the amount of ammonia is measured photometrically. The *G*-value of nitrogen atoms thus estimated was strongly dependent upon the hydrocarbons used and ranged from 0.1 to 0.7.[4] We tentatively explained this dependency to be due to the solubilities of hydrocarbons into liquid nitrogen.

In a short note, Siderer and Sato reported the results obtained in the γ-radiolysis of the liquid nitrogen solution of methane. The *G*-value of hydrogen cyanide was 0.08 at the optimum condition, while that of ammonia obtained by using Conway's method was 0.6.[5] On the basis of these results, they suggested that the nitrogen atoms which give nitrile compounds are not in the ground state, ^4S, but in the excited state, ^2D and/or ^2P, while the nitrogen atoms in the ground state lead to the formation of a basic polymer.

Experimental

The dried high-purity nitrogen was purchased from the Takachiho Shoji Co., and was used after having been passed through sulfuric acid (Yotsuhata Chemical Co.). The hydrogen, methane, ethane, ammonia, and various hydrocarbons used for identification were also purchased from the Takachiho Shoji Co. The hydrogen cyanide was synthesized from sodium cyanide and sulfuric acid. The nitrile compounds were supplied by the Tokyo Kasei Co. The sodium 4,5-dihydroxy-2,7-naphthalenedisulfonate used for the quantitative estimation of formaldehyde was purchased from the Wako Chemical Co.

The samples for γ-irradiation were prepared in the same manner as has been described before;[5] *i.e.*, a known amount of hydrogen, methane, or ethane was first introduced into a sampling tube 20 cm long and 3 cm in diameter. The pressure was measured by means of an oil manometer. Then pure nitrogen was introduced into the tube at 77 K under the pressure a little higher than the atmosphere. The nitrogen was then easily liquefied. The amount of the liquid was measured by the scale on the sampling tube. Since the amounts of substrates, hydrogen, methane, and ethane introduced were small, all of the gases were assumed to be dissolved into the liquid nitrogen.[6]

The samples thus prepared were irradiated by ^{60}Co γ-rays in a liquid nitrogen-Dewar flask at a dose rate of about 1.2×10^6 R h^{-1}, usually for 1 h. After irradiation, the sampling tube was connected to a vacuum system and the inside was slowly pumped out at 77 K. Usually two hours were taken for complete evacuation. The products thus obtained were subjected to analysis.

In order to identify the volatile products, use was made of a quadrupole mass-spectrometer (Nichiden-Varian TE-600) after separating the products with a gas chromatograph, the column of which was made of 6 m Silicone SE-52 supported by Uniport KS 60—80 mesh 80% w/w. Helium was used for the carrier gas.

Several analytical methods were applied to the identification of the polymer obtained in the reaction with methane: mass-spectrometry for the solid state, NMR spectroscopy, and thin layer chromatography. However, no conclusive results could be obtained except that the polymer contains N–H bonds, which was shown by the NMR spectroscopy.

* Present address: Faculty of Pharmaceutical Sciences, Toyama Medical and Pharmaceutical University, Sugitani, Toyama 930-01.

Since the polymer was easily hydrolyzed with a dilute aqueous solution of hydrochloric acid to produce formaldehyde, we measured the amount of the aldehyde photometrically using sodium 4,5-dihydroxy-2,7-naphthalenedisulfonate as a chromophoric reagent.[7]

Results

Hydrogen. As the reaction products, we observed two compounds: ammonia and hydrogen azide. Both compounds were identified by the mass-spectra. Figure 1 shows the G-values of the two products as functions of the concentration of hydrogen introduced into the sampling tube. The extrapolation of the plots between $1/G(NH_3)$ and $1/[H_2]$ gave $G(NH_3) = 0.7$ at the infinite concentration of hydrogen. We looked for hydrazine as a product, since it is another simple compound composed of nitrogen and hydrogen atoms; however, we could not observe the formation of this compound.

Methane. Ammonia, ethane, hydrogen cyanide, methyl azide, and small amounts of acetonitrile and propane were observed as volatile products. As is shown in Fig. 2, the G-values of ammonia and ethane showed a small dependence on the total dose. Figure 3 shows the G-values of the four main products at the dose of 5×10^{20} eV cm^{-3} as functions of the concentration of methane. It is noticeable that the three nitrogeneous compounds, ammonia, hydrogen cyanide, and methyl azide, showed different dependences on the concentration of methane.

Table 1 shows the G-values of formaldehyde produced by the hydrolysis of the polymer. The G-values were about 1.0 in the concentration range from 0.02 to 0.5 mol l^{-1} of methane.

Ethane. Only volatile products were analyzed. The G-values of the main products at the dose of 5×10^{20} eV cm^{-3} are shown in Fig. 4 as functions of the concentration of ethane. The nitrogeneous compounds ob-

Table 1. The yield of formaldehyde produced by the hydrolysis of the polymer obtained in the γ-radiolysis of the liquid nitrogen solution of methane

Methane mol l^{-1}	Formaldehyde G
0.024	1.00
0.042	1.07
0.071	0.85
0.11	0.93
0.37	1.00
0.54	0.91

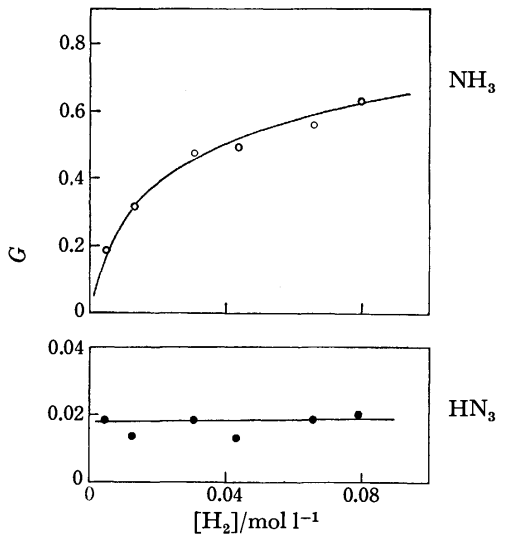

Fig. 1. G-Values of ammonia (○) and hydrogen azide (●) as functions of the concentration of hydrogen from the liquid nitrogen solution.

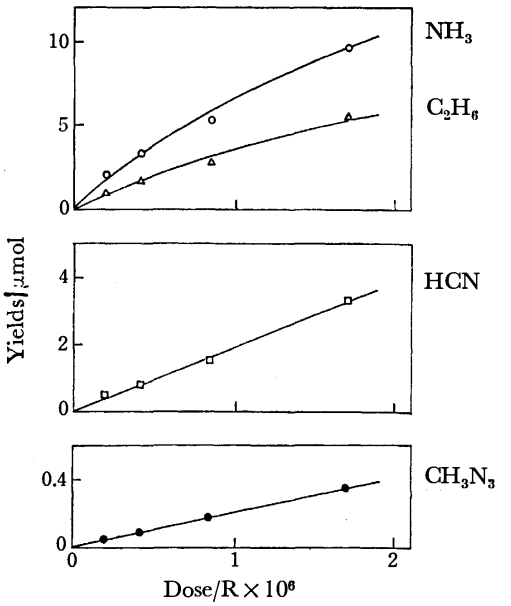

Fig. 2. The dose dependence of the yields of ammonia (○), ethane (△), hydrogen cyanide (□), and methyl azide (●) from the γ-radiolysis of a liquid nitrogen solution of 0.03 mol l^{-1} methane.

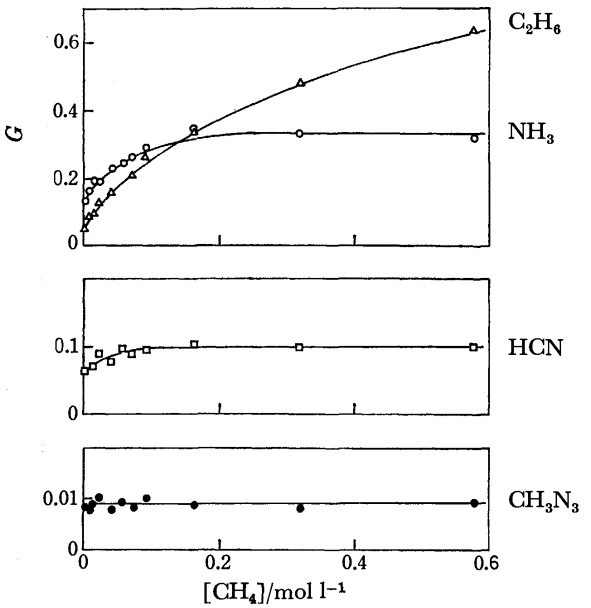

Fig. 3. G-Values of ammonia (○), ethane (△), hydrogen cyanide (□), and methyl azide (●) as functions of the concentration of methane from the liquid nitrogen solution.

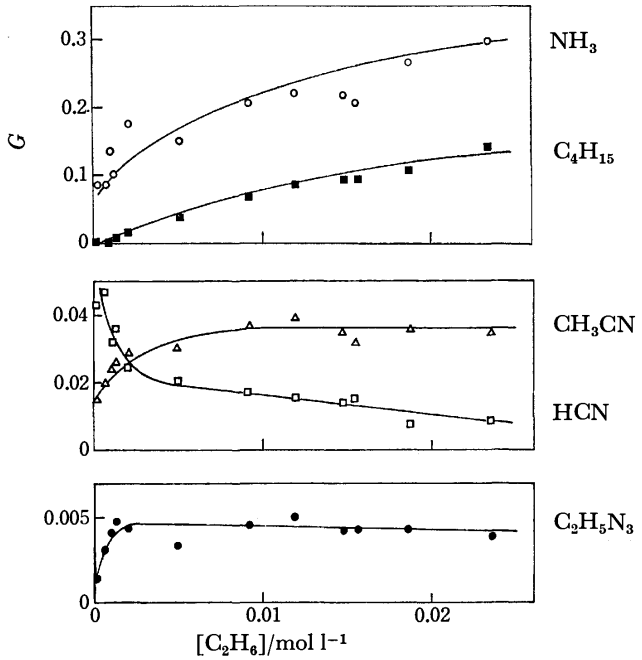

Fig. 4. *G*-Values of ammonia (○), butane (■), acetonitrile (△), hydrogen cyanide (□), and ethyl azide (●) as functions of the concentration of ethane from the liquid nitrogen solution.

served were ammonia, acetonitrile, hydrogen cyanide, and ethyl azide. The ethane concentration-dependence of the *G*-value of hydrogen cyanide was different from those of other products: *i.e.*, the *G*(HCN) decreased with increasing concentration of ethane. Repeated measurements showed the same dependence.

In the gas chromatographic analysis, the peaks of hydrogen azide and methyl azide overlapped with those of ethane and butane, respectively; therefore, the *G*-value of these two azides could not be measured.

Discussion

Formation of Ammonia. When ethylene was used as a solute, the formation of ammonia could not be observed in the gas chromatographic analysis.[8] As are shown in Figs. 1, 3, and 4, ammonia is one of the main products when hydrogen, methane, and ethane are used as solutes. This observation suggests that the presence of hydrogen atoms in the reacting system is indispensable for the formation of ammonia. Even at the temperature of liquid nitrogen, the addition reaction of hydrogen atoms to the double bond of olefins is a fast process.[9]

On the way to the formation of ammonia, the NH_2 radicals must be produced. If so, the formation of hydrazine, N_2H_4, can be expected; however, no hydrazine could be found even in the radiolysis of the liquid nitrogen–hydrogen system. Similarly, when methane or ethane is used as a solute, the formation of alkyl amines such as CH_3NH_2 and $C_2H_5NH_2$ can be expected; however, as stated in the Results section, no amines could be observed.

In order to explain these results, we tentatively considered the following reactions:

$$NH_2 + NH_2 \rightarrow NH_3 + NH,$$
$$CH_3 + NH_2 \rightarrow CH_4 + NH,$$
$$C_2H_5 + NH_2 \rightarrow C_2H_6 + NH,$$
$$NH + NH \rightarrow N_2 + H_2.$$

All of these reactions are exothermic by more than 10 kcal mol^{-1}. According to the measurement of Gillis,[10] the ratio of rate constants for disproportionation to combination of ethyl radicals at −181 °C is larger than four and the activation energy for combination exceeds that for disproportionation by about 300 cal mol^{-1}. Similar relations might also applicable to the reactions of NH_2 radicals and to the reactions between CH_3 and NH_2, and C_2H_5 and NH_2 radicals.

Formation of Nitrile Compounds. It is now well known that nitrogen atoms in the ground state, ^4S, are inactive to alkane molecules.[11] The formation of nitrogeneous compounds in the presence of alkane molecules, therefore, is due to the reactions of nitrogen atoms with alkyl radicals eventually formed in the system. However, the *G*-value of hydrogen cyanide obtained in the γ-radiolysis of the liquid nitrogen–methane system is only 0.1, as is shown in Fig. 3, a value which suggests that less than 10% of the nitrogen atoms are converted into nitrogeneous compounds. Consequently, as has been discussed in a previous paper,[5] we propose that the nitrile compounds observed in the gas chromatographic analysis are not the products of the reactions of nitrogen atoms in the ground state, ^4S, but those of nitrogen atoms in the excited state, ^2D.

$$CH_3 + N(^2D) \rightarrow HCN + H_2$$
$$C_2H_5 + N(^2D) \rightarrow CH_3CN + H_2$$

The presence of the excited state, ^2D, in the active nitrogen has been confirmed[12] and is known to have a long life. Moreover, if the nitrogen atoms are in the state of ^4S, the above reactions are not spin-allowed ones.

When ethane was used as a solute, the *G*-value of hydrogen cyanide decreased with increasing concentration of ethane. This decrease may be explained by the competition of nitrogen atoms (^2D) and ethylene, which is produced in the system, for methyl radicals. The formation of alkyl radicals and olefins may be described as follows:[3]

$$N_2(^3\Sigma_u^+) + CH_4 \rightarrow N_2 + CH_3 + H,$$
$$N_2(^3\Sigma_u^+) + C_2H_6 \rightarrow N_2 + 2CH_3,$$
$$\rightarrow N_2 + C_2H_5 + H,$$
$$C_2H_5 + H \rightarrow C_2H_4 + H_2,$$
$$\rightarrow C_2H_6.$$

Formation of Polymer. As has been stated in the Results section, most of nitrogen atoms produced in the methane solution contribute to the formation of a polymer. The initiating reaction must be as follows:

$$CH_3 + N(^4S) \rightarrow CH_3N \rightarrow CH_2{=}NH.$$

This type of imine is not stable at room temperature and easily polymerizes into a complex polymer.

According to the infrared spectroscopic study of the photolysis of methyl azide in a rigid matrix by Milligan,[13] methylimino radicals (CH_3N) produced in the

photolysis of methyl azide isomerize to methylene imine in the matrix, and when the product is warmed up to temperatures where the matrix material is lost, a white solid is observed to remain on the wall. He measured the infrared spectrum of this solid and suggested that a part of it is hexamethylenetetramine.

We therefore looked for hexamethylenetetramine in our polymer by using gas chromatography, but we could not find it. Probably the main polymerization process is not the formation of this compound.

Formation of Azide. Because of the characteristic mass-spectra, the formation of azides was confirmed in the present experiment. As are shown in Figs. 1, 3, and 4, the *G*-values of all azides are not affected by concentrations of solutes in excess of 2×10^{-3} mol l^{-1}. If nitrogen atoms are the precursors of these azides, the yields should change with the concentration of solutes as do those of the ammonia and nitrile compounds. The N_3 radicals, therefore, may be produced by a process which is independent of the main process of the formation of nitrogen atoms—probably ion-molecule reactions, although we cannot specify them.

The authors wish to express their thanks to Dr. Masuo Funabashi of this Institute for the measurements of NMR spectroscopy and thin layer chromatography.

References

1) H. G. Evans, G. R. Freeman, and C. A. Winkler, *Can. J. Chem.*, **34**, 1271 (1956).
2) T. Oka and S. Sato, *Bull. Chem. Soc. Jpn.*, **42**, 582 (1969).
3) T. Oka, Y. Suda, and S. Sato, *Bull. Chem. Soc. Jpn.*, **42**, 3083 (1969).
4) K. Ishizaki and S. Sato, *Bull. Chem. Soc. Jpn.*, **47**, 2597 (1974).
5) Y. Siderer and S. Sato, *Bull. Chem. Soc. Jpn.*, **48**, 2383 (1975).
6) S. Hirokami and R. J. Cvetanović, *J. Am. Chem. Soc.*, **96**, 3738 (1974).
7) F. Feigl and V. Anger, "Spot Tests in Organic Analysis," translated by R. E. Oesper, Elsevier Publishing Co. (1966), p. 434.
8) T. Oka and S. Sato, *Bull. Chem. Soc. Jpn.*, **43**, 3711 (1970).
9) S. Hirokami and R. J. Cvetanović, *J. Plys. Chem.*, **78**, 1254 (1974).
10) H. A. Gillis, *Can. J. Chem.*, **49**, 2861 (1971).
11) D. R. Safrany, "Progress in Reaction Kinetics," ed by K. R. Jennings and R. B. Cundall, Pergamon Press, Vol. 6, Oxford (1972), p. 1.
12) B. Brocklehurst and K. R. Jennings, "Progress in Reaction Kinetics," ed by G. Porter, Pergamon Press, Vol. 4, Oxford (1967), p. 1.
13) D. E. Milligan, *J. Chem. Phys.*, **35**, 1491 (1961).

Fluorescence and Dual Phosphorescence Spectra of Quinoxaline in Fluid Solution

Kohzaburo YAMAMOTO, Takeshi TAKEMURA, and Hiroaki BABA

Division of Chemistry, Research Institute of Applied Electricity, Hokkaido University, Sapporo 060

(Received September 21, 1977)

Fluorescence and phosphorescence spectra of quinoxaline in isooctane (2,2,4-trimethylpentane) have been measured under fluid conditions. The fluorescent emission with a spectral maximum at 410 nm is assigned to the $^1(n,\pi^*)\rightarrow S_0$ fluorescence of quinoxaline. A new phosphorescence spectrum appears in a wavelength region longer than 520 nm as the concentration of quinoxaline increases, in addition to the phosphorescence spectrum of the monomer. From the results of photostationary and transient experiments on the concentration and/or temperature dependence of phosphorescence, it has been confirmed that the phosphorescence consists of two components attributable to the monomer and the excimer.

Triplet excimers have been a subject of considerable interest.[1-8] Recently, we have confirmed the existence of the triplet excimer for naphthalene and its derivatives and phenanthrene in fluid solution by means of photostationary and transient phosphorescence measurements.[1-4] On the other hand, Chandross and Dempster showed that practically no triplet excimer is formed even with a sandwich-pair conformation of the two naphthalene rings in 1,3-di(1-naphthyl)propane in a rigid glass. Such a sandwich-pair is favorable for the formation of singlet excimer.[5]

More recently, Subudhi and Lim observed intramolecular excimer phosphorescence spectra of 1,3-di(1-naphthyl)propane[6] and 1,2-di(1-naphthyl)ethane[7] in a fluid solution. The spectra of these compounds are very similar to those of naphthalene and its derivatives reported by us.[1,2]

The experimental results described above seem to be reasonably explained in terms of the idea that there is a conformational difference between singlet and triplet excimers.[2,7] However, there still remain unsolved problems concerning the stability and geometrical structure of triplet excimers. In order to settle the problems, it is desirable to examine whether or not the triplet excimer is formed in fluid solution in compounds other than aromatic hydrocarbons.

Quinoxaline is similar to naphthalene in electronic structure except that the former has lower-lying (n,π^*) states. The presence of the (n,π^*) states will make it relatively easy to detect the phosphorescence of quinoxaline in fluid solution.

This paper reports the phosphorescence spectrum of quinoxaline in fluid solution, together with its fluorescence spectrum which has not been observed so far. The phosphorescence of quinoxaline is shown to be due to both the monomer and the excimer as in the case of aromatic hydrocarbons.

Experimental

Quinoxaline (Nakarai Chemical Co.) was purified by vacuum sublimation. Isooctane (2,2,4-trimethylpentane, Wako Pure Chemical Co.) was passed through a silica-gel column. The solution of quinoxaline in isooctane was fully degassed by repeated freeze-thaw cycles (7 or 8 times). Emission spectra were measured with a high-resolution, high-sensitivity emission spectrophotometer[1,2] equipped with a photon-counting detector. A specially designed spectrophosphorimeter was used for measuring the phosphorescence or delayed emission spectra as well as the time-resolved emission spectra with the lifetimes ranging from 10^2 to 10^{-5} s by means of the photon-counting method combined with a multichannel digital boxcar technique.[1,2] Representative emission and excitation spectra were corrected for the spectral sensitivity of the monochromator-photomultiplier system and for the spectral intensity of exciting light, respectively. The fluorescence quantum yield of quinoxaline was determined by comparing the corrected fluorescence spectrum with that of quinine sulfate in 1/2 M sulfuric acid used as a reference.

Results and Discussion

Uncorrected emission spectra are shown in Fig. 1, which were measured for both the aerated and the degassed isooctane solutions of 1.1×10^{-4} M quinoxaline at 25 °C. The emission spectrum of the aerated sample (A in Fig. 1) may be assigned to $^1(n,\pi^*)\rightarrow S_0$ fluorescence of quinoxaline on the basis of the following facts: (1) There is a mirror image relation between the emission spectrum and the lowest $^1(n,\pi^*)\leftarrow S_0$ absorption spectrum of quinoxaline; (2) the emission spectrum is very similar to the fluorescence spectrum of gaseous quinoxaline reported by McDonald and Brus,[9,10] and Soep and Tramer,[11] although it differs from the spectrum obtained by Dewey and Hadley;[12] (3) the exci-

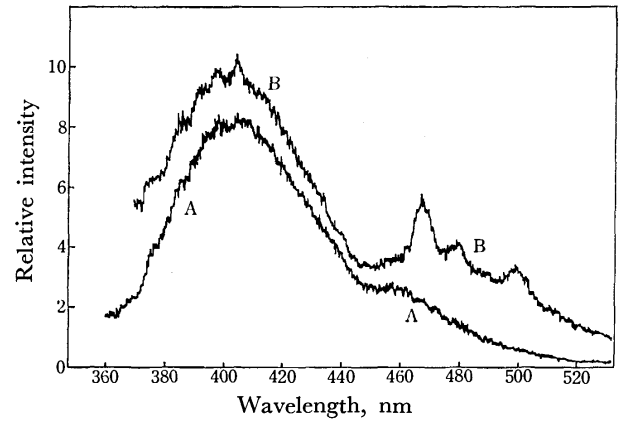

Fig. 1. Emission spectra (uncorrected) of quinoxaline in isooctane at 25 °C: A, aerated sample; B, degassed sample. The exciting wavelength is 315 nm with a band width of 10 nm; the band width for the emission is 3 nm. The concentration of quinoxaline is 1.1×10^{-4} M.

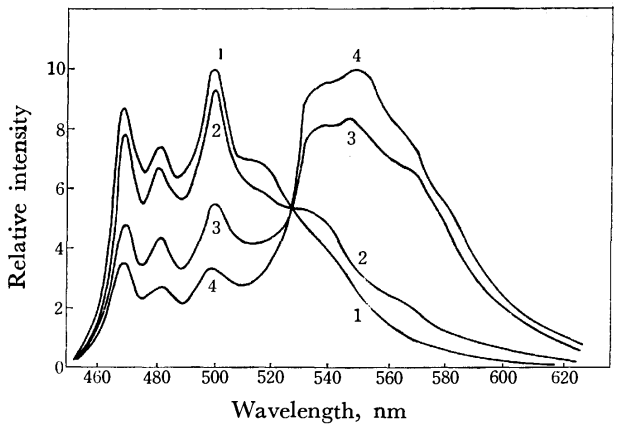

Fig. 2. Changes in the delayed emission spectrum (uncorrected) of quinoxaline in isooctane at 25 °C caused by the increase of the concentration. The concentrations of quinoxaline: (1) 1.1×10^{-4}; (2) 1.1×10^{-3}; (3) 1.1×10^{-2}; (4) 1.1×10^{-1} M. The spectral intensities are normalized at 528 nm.

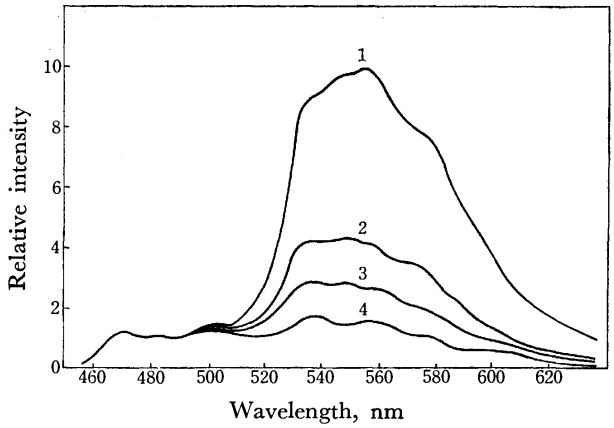

Fig. 3. Changes in the delayed emission spectrum (uncorrected) of quinoxaline in isooctane with temperature. The temperatures of the solution: (1) 0; (2) 25; (3) 43; (4) 60 °C. The concentration of quinoxaline is 6.0×10^{-2} M. The spectral intensities are normalized at 470 nm.

tation spectrum monitored at any emission wavelength between 370 and 520 nm is in fair agreement with the absorption spectrum in the range of the $^1(n,\pi^*)\leftarrow S_0$ transition of quinoxaline; (4) the emission concerned has a quantum yield of 7.5×10^{-5} and a lifetime shorter than 2 ns in isooctane at 25 °C; and (5) the quantum yield is independent of concentration and is not changed by degassing the sample solution. It should be noted here that the appearance of a shoulder at about 460 nm is due to the fact that the spectrum is not corrected for the sensitivity of the spectrophotometer used.

On the other hand, the degassed sample (B in Fig. 1) exhibits, in addition to the fluorescence spectrum described above, a structured emission spectrum in a wavelength region longer than 465 nm. This emission has an apparent lifetime of the order of 10^{-3} s. The excitation spectrum with respect to the structured emission spectrum agrees with the absorption spectrum of quinoxaline.

Figure 2 shows the delayed emission spectra (uncorrected) of quinoxaline in isooctane at 25 °C, which were measured with the spectrophosphorimeter. The emission spectrum of quinoxaline for a relatively low concentration (1.1×10^{-4} M) is in good agreement with the phosphorescence spectrum in EPA at 77 K, but the former spectrum is red-shifted by about 300 cm^{-1} compared with the latter.

The experimental results described above indicate that the structured spectrum extending from 465 nm towards longer wavelengths at a relatively low concentration is attributable to the phosphorescence from the monomer of quinoxaline.

The delayed emission spectrum, however, exhibits strong concentration dependence as shown in Fig. 2, where the spectral intensities are normalized at 528 nm. A new emission spectrum grows in a wavelength region from 520 to 620 nm with the increase of concentration; hereafter, it will be called emission spectrum E. Although the excitation spectrum cannot be obtained accuratcly by monitoring the emission spectrum E because of the high solute concentration, the onset at the longest wavelength of the excitation spectrum coincides with that of the absorption spectrum of quinoxaline. It is seen in Fig. 2 that the intensity ratio of the emission E to the monomer phosphorescence increases as the concentration increases. It should be noted that the emission E is not due to a photochemical product, because practically no change was produced in the intensity of the emission E by exposing the sample solution to UV light. It is also noted that the solvent used showed no delayed emission under the present experimental conditions.

By reference to the excimer phosphorescence of naphthalene and phenanthrene,[1-4] the experimental results regarding the concentration dependence of the delayed emission are found to suggest that the emission E is due to the excimer phosphorescence of quinoxaline. However, there still remains the possibility that the emission E is an impurity phosphorescence resulting from T-T energy transfer from quinoxaline to an impurity involved originally in the solute.

In order to decide whether the emission E is due to the triplet excimer of quinoxaline or not, temperature dependence of the phosphorescence spectrum must be examined. The temperature dependence of the delayed emission spectrum for 6.0×10^{-2} M quinoxaline in isooctane is shown in Fig. 3, where the intensities of emission spectra are normalized at 470 nm. It is clearly seen in Fig. 3 that the intensity ratio of the emission E to the monomer phosphorescence markedly decreases as the temperature rises. This means that the emission E is not due to an impurity triplet resulting from the T-T energy transfer, since in the case of T-T energy transfer in fluid solution the intensity ratio of phosphorescence of the energy donor to that of the acceptor must be independent of temperature.[13] When the sample solution is frozen, the emission E vanishes, while the monomer phosphorescence intensifies remarkably. Thus, all the experimental results obtained indicate that the emission E is the excimer phosphorescence of quinoxaline itself.

Figure 4 shows collectively the absorption spectrum

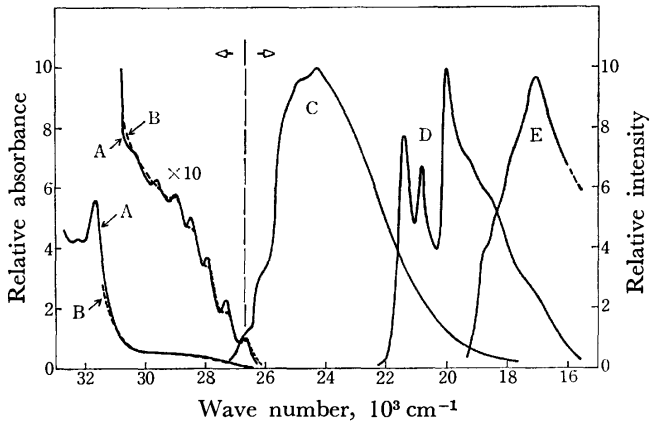

Fig. 4. Absorption, excitation (corrected), and emission (corrected) spectra of quinoxaline in isooctane at 20 °C: A, absorption; B, excitation spectra of the fluorescence and the monomer phosphorescence; C, fluorescence; D, monomer phosphorescence; and E, excimer phosphorescence.

and corrected emission and excitation spectra of quinoxaline in isooctane at 20 °C.

By solving the rate equations with regard to the kinetic scheme 1 appropriate for the deactivation of the triplet state involving excimer formation,[2] one can easily obtain Eqs. 2 and 3 for the time dependence of the intensities, I, of the monomer (m) and excimer (d) phosphorescence:

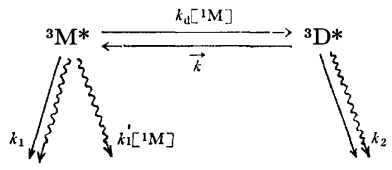

(1)

$$I_m(t) = \frac{C_1(\theta_2 - X)}{\theta_2 - \theta_1}\{e^{-\theta_1 t} + Ae^{-\theta_2 t}\}, \quad (2)$$

$$I_d(t) = \frac{C_2[^1M]}{\theta_2 - \theta_1}\{e^{-\theta_1 t} - e^{-\theta_2 t}\}, \quad (3)$$

with

$$\left.\begin{matrix}\theta_1 \\ \theta_2\end{matrix}\right\} = \frac{1}{2}[X + Y \mp \{(Y-X)^2 + 4k_d\overleftarrow{k}[^1M]\}^{1/2}], \quad (4)$$

$$X = k_1 + (k_1' + k_d)[^1M], \qquad Y = k_2 + \overleftarrow{k}, \quad (5)$$

$$A = (X - \theta_1)/(\theta_2 - X), \quad (6)$$

and C_1 and C_2 are constants with positive values. Here, ^{1}M, ^{3}M*, and ^{3}D* stand for the ground singlet monomer, excited triplet monomer, and excited triplet dimer (triplet excimer), respectively; k_1 and k_2 are the sums of the radiative and nonradiative decay constants for the triplet monomer and excimer, respectively; k_d and $\overleftarrow{k}$ are the rate constants for the formation and dissociation of the triplet excimer, respectively; and k_1' is the rate constant for quenching by the ground state molecule.

Figure 5 shows representative decay curves of the phosphorescence monitored at 480 nm (M) and at 540 nm (D) for 1.1×10^{-2} M and 1.1×10^{-1} M quinoxaline in isooctane at 20 °C. According to Eqs. 2 and 3, it is expected that $I_m(t)$ should yield a curve consisting of two exponential decays, while $I_d(t)$ a rise-and-decay curve. It is clearly seen in Fig. 5 that the decay curves for the monomer phosphorescence at 480 nm correspond well to $I_m(t)$ predicted by Eq. 2 with $\theta_1 = 5.4\times10^2$ s^{-1} and $\theta_2 = 1.9\times10^4$ s^{-1} for a solute concentration of 1.1×10^{-2} M and with $\theta_1 = 1.2\times10^3$ s^{-1} and $\theta_2 = 2.7\times10^4$ s^{-1} for 1.1×10^{-1} M. The $I(t)$ curve monitored at 540 nm for 1.1×10^{-1} M shows clearly a rise-and-decay curve corresponding to $I_d(t)$ in Eq. 2, with a decaying rate constant very close to the value of θ_1 in $I_m(t)$. On the other hand, the $I(t)$ curve at 540 nm for 1.1×10^{-2} M shows almost a single exponential decay. This fact may be attributed to the coexistence of the monomer and the excimer phosphorescence emissions at 540 nm.

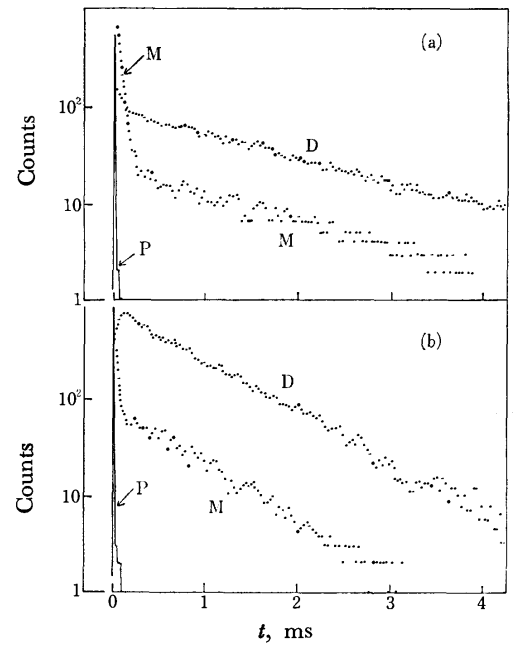

Fig. 5. Representative $I(t)$ curves for the phosphorescence of quinoxaline in isooctane at 20 °C. The concentrations of quinoxaline: (a) 1.1×10^{-2} M; and (b) 1.1×10^{-1} M. Monitoring wavelengths: M, 480 nm (monomer region); D, 540 nm (monomer+excimer region). P represents the exciting light pulse.

Here again, we shall examine the possibility that the emission E is due to an impurity. In this case, ^{1}M and ^{3}D* in the kinetic scheme (1) must be replaced by ^{1}A and ^{3}A*, respectively, where ^{1}A and ^{3}A* are the ground state and the excited triplet state of the impurity molecule. Since the energy separation between the structured phosphorescence spectrum of the quinoxaline monomer and the broad emission spectrum E is about 3000 cm^{-1}, the reverse T-T energy transfer from the triplet state of the impurity to that of quinoxaline can be completely neglected; that is, $\overleftarrow{k}=0$.

In such a case, the $I(t)$ curve of the phosphorescence observed at 480 nm should give a single exponential decay, since the phosphorescence emission at 480 nm is due to the quinoxaline monomer which is regarded as the energy donor. This contradicts the observation that the $I(t)$ curves M in Fig. 5 consist of two exponential decays. In other words, the results of dynamic measurement of the phosphorescence also indicate that the

broad emission cannot be due to an impurity.

It is thus concluded that the broad emission spectrum, which appears in the range of 520—620 nm upon increasing the concentration of quinoxaline, is ascribable to the triplet excimer of quinoxaline.

References

1) T. Takemura, H. Baba, and Y. Shindo, *Chem. Lett.*, **1974**, 1091.
2) T. Takemura, M. Aikawa, H. Baba, and Y. Shindo, *J. Am. Chem. Soc.*, **98**, 2205 (1976).
3) T. Takemura, M. Aikawa, and H. Baba, *J. Luminescence*, **12/13**, 819 (1976).
4) M. Aikawa, T. Takemura, and H. Baba, *Bull. Chem. Soc. Jpn.*, **49**, 473 (1976).
5) E. A. Chandross and C. J. Dempster, *J. Am. Chem. Soc.*, **92**, 704 (1970).
6) P. C. Subudhi and E. C. Lim, *J. Chem. Phys.*, **63**, 5491 (1975).
7) P. C. Subudhi and E. C. Lim, *Chem. Phys. Lett.*, **44**, 479 (1976).
8) W. Klöpffer, "Organic Molecular Photophysics," Vol. 1, ed by J. B. Birks, Wiley-Interscience, London (1973), p. 396.
9) J. R. McDonald and L. E. Brus, *Chem. Phys. Lett.*, **23**, 87 (1973).
10) J. R. McDonald and L. E. Brus, *J. Chem. Phys.*, **61**, 3895 (1974).
11) B. Soep and A. Tramer, *Chem. Phys.*, **7**, 52 (1975).
12) H. J. Dewey and S. G. Hadley, *Chem. Phys. Lett.*, **17**, 574 (1972).
13) T. Takemura, M. Aikawa, and H. Baba, *Bull. Chem. Soc. Jpn.*, **47**, 2476 (1974).

The Crystal and Molecular Structures of *trans*-Dichlorobis(dimethylneomenthylphosphine)palladium(II)* and *trans*-Dichlorobis(dimethylmenthylphosphine)palladium(II), Asymmetric Hydrosilylation Catalysts of Olefin

Kojiro KAN, Kunio MIKI, Yasushi KAI, Noritake YASUOKA, and Nobutami KASAI**

Department of Applied Chemistry, Faculty of Engineering, Osaka University, Yamadakami, Suita, Osaka 565

(Received September 24, 1977)

The molecular structures of $[PdCl_2\{(Me_2neoMen)P\}_2]$ and $[PdCl_2\{(Me_2Men)P\}_2]$, asymmetric hydrosilylation catalysts of olefin, were determined by means of X-ray diffraction. Both complexes form yellow prismatic crystals. The former belongs to the monoclinic system: $a=13.512(5)$, $b=13.082(1)$, $c=8.472(1)$ Å, and $\beta=97.00(2)°$, space group $P2_1$ with $Z=2$; the latter belongs to the tetragonal system: $a=9.662(1)$ and $c=32.459(2)$ Å, space group $P4_32_12$ with $Z=4$. Both structures were determined by the heavy atom method and have been refined anisotropically by a least-squares procedure ($R=0.0697$ for 2606 non-zero reflections for the former and $R=0.0713$ for 1388 non-zero reflections for the latter). The former molecules is not iso-structural with its nickel analog. The central palladium atom has *trans*-square planar geometry [Pd-Cl 2.304(5) and 2.297(5), Pd-P 2.344(4) and 2.361(5) Å]. The molecule has an approximate two-fold symmetry around the normal to the co-ordination plane. The neomenthyl groups are on the same side of the co-ordination plane. The latter molecule has exact C_2 symmetry: the two-fold axis passes through the Cl(1), Pd, and Cl(2) atoms which lie on the co-ordination plane. The geometry around the palladium slightly deviates from the *trans*-square planar [Pd–Cl 2.296(9) and 2.267(9) Å and Pd–P 2.310(6) Å]. The menthyl groups are located on either side of the co-ordination plane.

In a series of structural studies of catalytically active organometallic complexes, the molecular structures of some organoaluminium complexes have been determined;[1-4] their roles in the stereospecific polymerization of acetaldehyde have also been discussed.[4,5] The X-ray molecular structure of $[Zn(OMe)_2(EtZnOMe)_6]$,*** which is considered as the key substance for the polymerization of methyloxirane, has recently been reported.[6]

A variety of dihalophosphine-transition metal(II) complexes have been found to be effective catalysts for the hydrosilylation of olefins and acetylenes by M. Kumada and co-workers.[7-9] *trans*-Dichlorobis(dimethylneomenthylphosphine)nickel(II) $[NiCl_2\{(Me_2neoMen)P\}_2]$† and -palladium(II) $[PdCl_2\{(Me_2neoMen)P\}_2]$ and *trans*-dichlorobis(dimethylmenthylphosphine)palladium(II) $[PdCl_2\{(Me_2Men)P\}_2]$† are complexes in which each phosphine has a chiral substituent; they are catalysts for the asymmetric hydrosilylation of olefin.[10]

The X-ray molecular structure of the nickel complex $[NiCl_2\{(Me_2neoMen)P\}_2]$ has been reported very recently.[11] In this paper the molecular structures of the palladium analogs $[PdCl_2\{(Me_2neoMen)P\}_2]$ and $[PdCl_2\{(Me_2Men)P\}_2]$ are described.

Experimental

Crystals of $[PdCl_2\{(Me_2neoMen)P\}_2]$ and $[PdCl_2\{(Me_2Men)P\}_2]$ were provided by Professor M. Kumada and co-workers of Kyoto University. They are both yellow and prismatic. Preliminary photographic data showed that crystals of $[PdCl_2\{(Me_2neoMen)P\}_2]$ and $[PdCl_2\{(Me_2Men)P\}_2]$ belong to monoclinic and tetragonal system, respectively. Since these complexes are both optically active, the corresponding space groups should be non-centrosymmetric. The systematic absence of reflections of the former ($0k0$, $k=2n+1$) indicated that its space group was $P2_1$; in the latter the absences ($h00$, $h=2n+1$ and $00l$, $l=2n+1$) suggested the space group $P4_12_12$ or $P4_32_12$.

The unit-cell dimensions of the two crystals were determined by the least-squares fit from 2θ values of 16 and 11 high-angle reflections measured on a G.E. single crystal orienter mounted on a Rigaku SG-2 goniometer. The crystal densities were measured by flotation in aqueous solutions of potassium tartarate. Crystal data of the two complexes are given in Table 1.

A crystal of $[PdCl_2\{(Me_2neoMen)P\}_2]$ with dimensions of $0.23\times0.20\times0.18$ mm was chosen for the intensity measurement. A Rigaku automated four-circle diffractometer was used, with Zr-filtered Mo $K\alpha$ radiation. The θ-2θ scan technique was employed. The integrated intensities of each reflection were determined by scanning over a peak at a rate of 4 °min^{-1}, and subtracting the background obtained by averaging the two values measured for 5 s at both ends of a scan. The 2θ scan width was from $-1.0°$ for the $K\alpha_1$ peak to 1.0° for the $K\alpha_2$ peak. For the intensity data collection of $[PdCl_2\{(Me_2Men)P\}_2]$ the crystal used had dimensions of

Table 1. Crystal data

	$[PdCl_2\{(Me_2neoMen)P\}_2]$ $C_{24}H_{50}Cl_2P_2Pd$	$[PdCl_2\{(Me_2Men)P\}_2]$ $C_{24}H_{50}Cl_2P_2Pd$
F. W.	577.9	577.9
Crystal system	Monoclinic	Tetragonal
Space group	$P2_1$	$P4_32_12$
a [Å]	13.512(5)	9.662(1)
b [Å]	13.082(1)	
c [Å]	8.472(1)	32.459(2)
β [°]	97.00(2)	
U [Å^3]	1486.4(6)	3030.2(4)
Z	2	4
D_m [g cm^{-3}]	1.29	1.27
D_c [g cm^{-3}]	1.29	1.27
μ [cm^{-1}]	9.1 (for Mo $K\alpha$)	77.6 (for Cu $K\alpha$)

* Read at the 21st symposium on Organometallic Chemistry Japan, Sendai, Oct. 4 (1973).

** To whom correspondence should be addressed.

*** Me: methyl group, Et: ethyl group.

† *neo*Men: neomenthyl group, Men: menthyl group.

$0.20\times0.17\times0.15$ mm. This crystal was rather small to give sufficient intensity using Mo $K\alpha$ radiation, but no other good, larger crystal could be selected. It was therefore necessary to use Cu $K\alpha$ radiation in order to obtain strong reflection intensities. Intensity measurements were carried out in a way similar to those for $[PdCl_2\{(Me_2neoMen)P\}_2]$. Totals of 2814 independent reflections for $[PdCl_2\{(Me_2neoMen)P\}_2]$ and 1440 for $[PdCl_2\{(Me_2Men)P\}_2]$ were collected at room temperature. In each case three standard reflections were measured after every 50 reflections. The intensities were corrected for the usual Lorentz and polarization effects. The absorption correction was ignored. This might limit the accuracy of the structures obtained, especially that of $[PdCl_2\{(Me_2Men)P\}_2]$ (μ(Cu $K\alpha$)$=77.6$ cm^{-1}).

TABLE 2. POSITIONAL AND THERMAL PARAMETERS OF ATOMS FOR $[PdCl_2\{(Me_2neoMen)P\}_2]$ (e.s.d.'s in parentheses)

(a) Fractional co-ordinates ($\times10^4$).

Atom	x	y	z	Atom	x	y	z
Pd	−2711.6(6)	−2500	− 191.5(10)	C(19)	758(18)	−2754(14)	3098(22)
Cl(1)	−1556(3)	−3779(3)	− 355(5)	C(20)	1363(12)	−1741(16)	849(28)
Cl(2)	−3884(3)	−1229(3)	− 184(6)	C(3)	−5145(11)	−3382(16)	− 741(20)
P(1)	−1563(3)	−1300(3)	− 926(4)	C(4)	−3723(12)	−4921(12)	− 862(21)
P(2)	−3934(3)	−3727(3)	230(5)	C(31)	−2398(13)	−4688(18)	3331(20)
C(1)	− 740(12)	−1835(13)	−2294(17)	C(32)	−3425(16)	−5039(15)	2868(22)
C(2)	−2210(14)	− 321(13)	−2177(18)	C(33)	−4186(11)	−4161(13)	2219(19)
C(11)	−1907(11)	3085(15)	2205(18)	C(34)	−4194(13)	−3361(15)	3543(21)
C(12)	−1129(10)	4529(12)	1032(16)	C(35)	−3116(14)	−2975(15)	4041(19)
C(13)	− 698(9)	− 540(10)	504(14)	C(36)	−2432(16)	−3828(20)	4577(22)
C(14)	− 195(10)	−1153(12)	1983(17)	C(37)	−1783(21)	−5577(25)	4018(30)
C(15)	− 985(13)	−1368(15)	3085(18)	C(38)	−4943(14)	−2538(25)	3187(20)
C(16)	−1451(12)	− 389(19)	3582(19)	C(39)	−4819(25)	−1661(23)	4458(29)
C(17)	−2278(16)	1350(19)	2752(26)	C(40)	−6026(16)	−2899(32)	3040(33)
C(18)	464(13)	−2073(11)	1613(19)				

(b) Anisotropic temperature factors ($\times10^4$) expressed in the form $\exp\{-(\beta_{11}h^2+\beta_{22}k^2+\beta_{33}l^2+\beta_{12}hk+\beta_{13}hl+\beta_{23}kl)\}$.

Atom	β_{11}	β_{22}	β_{33}	β_{12}	β_{13}	β_{23}
Pd	63.1(5)	60.2(5)	165.0(12)	−13.0(14)	13.0(11)	1.5(20)
Cl(1)	80.1(25)	65.4(25)	344.0(89)	4.9(40)	62.4(75)	− 2.8(77)
Cl(2)	73.5(25)	82.5(29)	384.5(99)	20.8(44)	45.7(78)	13.0(91)
P(1)	81.0(24)	66.4(23)	145.4(47)	−12.5(39)	29.4(52)	5.2(57)
P(2)	75.0(24)	75.5(28)	232.8(68)	−29.6(43)	22.7(65)	− 4.8(73)
C(1)	125(13)	113(14)	175(23)	−28(22)	134(29)	−55(30)
C(2)	158(16)	87(12)	174(24)	−18(23)	−44(31)	106(29)
C(11)	87(11)	139(17)	231(28)	−13(23)	17(28)	−118(37)
C(12)	80(9)	79(10)	213(24)	− 8(16)	28(24)	−57(26)
C(13)	65(8)	66(9)	176(21)	−20(14)	55(20)	−37(22)
C(14)	80(10)	98(12)	219(25)	−49(18)	−16(24)	61(29)
C(15)	139(15)	122(16)	202(26)	−94(27)	−70(32)	31(35)
C(16)	99(13)	204(24)	195(27)	2(30)	22(30)	−49(43)
C(17)	146(19)	165(23)	429(51)	41(33)	60(50)	−314(60)
C(18)	137(14)	62(9)	302(33)	22(19)	−140(35)	−56(29)
C(19)	233(24)	89(18)	317(38)	66(31)	−179(49)	−9(37)
C(20)	79(12)	110(16)	607(62)	−61(23)	130(43)	−97(53)
C(3)	63(9)	160(18)	300(34)	−68(22)	−92(28)	70(42)
C(4)	96(12)	72(11)	354(37)	−66(19)	77(33)	−99(33)
C(31)	111(14)	181(23)	236(31)	−1(30)	−29(33)	89(45)
C(32)	180(20)	104(15)	288(36)	34(29)	116(44)	122(39)
C(33)	90(11)	91(12)	287(32)	−56(19)	116(30)	−0(32)
C(34)	114(14)	110(15)	297(34)	7(24)	126(36)	− 8(37)
C(35)	137(15)	147(19)	216(28)	−76(27)	50(34)	−34(36)
C(36)	138(17)	213(28)	259(35)	−30(36)	7(39)	163(54)
C(37)	245(30)	264(37)	424(60)	331(58)	107(69)	237(79)
C(38)	163(16)	138(17)	333(35)	80(50)	169(39)	22(68)
C(39)	346(41)	188(29)	394(59)	218(60)	223(79)	−124(68)
C(40)	115(17)	408(73)	656(77)	154(57)	304(60)	281(119)

TABLE 2. (CONTINUED)

(c) Calculated co-ordinates ($\times 10^3$) and assigned isotropic temperature factors for hydrogen atoms (except methyl hydrogen atoms).

Atom	x	y	z	B	Atom	z	y	z	B
H(11)	−256	− 13	166	5.0	H(31)	−211	−434	230	5.0
H(12A)	−149	85	− 1	5.0	H(32A)	−343	−563	193	5.0
H(12B)	− 53	93	159	5.0	H(32B)	−371	−541	387	5.0
H(13)	−101	− 36	−21	5.0	H(33)	−496	−441	196	5.0
H(14)	38	− 68	262	5.0	H(34)	−439	−376	460	5.0
H(15A)	−158	−185	248	5.0	H(35A)	−284	−256	307	5.0
H(15B)	− 66	−178	414	5.0	H(35B)	−312	−243	504	5.0
H(16A)	− 88	3	433	5.0	H(36A)	−264	−419	563	5.0
H(16B)	−203	− 59	434	5.0	H(36B)	−166	−356	484	5.0
H(18)	− 5	−255	76	5.0	H(38)	−482	−236	194	5.0

TABLE 3. POSITIONAL AND THERMAL PARAMETERS OF ATOMS FOR $[PdCl_2\{(Me_2Men)P\}_2]$ (e.s.d.'s in parentheses)

(a) Fractional co-ordinates ($\times 10^4$).

Atom	x	y	z	Atom	x	y	z
Pd	−1962.3(22)	−1962.3(22)	0	C(13)	955(14)	−3176(15)	− 529(4)
Cl(1)	− 282(9)	− 282(9)	0	C(14)	1241(15)	−4623(16)	− 356(4)
Cl(2)	−3621(9)	−3621(9)	0	C(15)	2831(19)	−4799(21)	− 311(5)
P	− 937(4)	−2855(5)	− 585(1)	C(16)	3563(16)	−4660(18)	− 731(5)
C(1)	−1676(19)	−4435(20)	− 812(5)	C(17)	3979(20)	−3052(27)	−1333(6)
C(2)	−1171(19)	−1594(21)	−1006(5)	C(18)	488(18)	−4829(19)	82(6)
C(11)	3258(17)	−3259(20)	− 912(5)	C(19)	1103(24)	−3989(26)	436(5)
C(12)	1667(16)	−3026(20)	− 963(5)	C(20)	557(28)	−6399(26)	209(8)

(b) Anisotropic temperature factors ($\times 10^4$) expressed in the form $\exp\{-(\beta_{11}h^2+\beta_{22}k^2+\beta_{33}l^2+\beta_{12}hk+\beta_{13}hl+\beta_{23}kl)\}$.

Atom	β_{11}	β_{22}	β_{33}	β_{12}	β_{13}	β_{23}
Pd	99.6(18)	99.6(18)	11.3(1)	15.1(30)	− 2.4(13)	2.4(13)
Cl(1)	151.4(108)	151.4(108)	34.8(13)	−66.6(139)	48.8(97)	−48.8(97)
Cl(2)	190.4(122)	190.4(122)	21.9(9)	−142.6(153)	24.1(88)	−24.1(88)
P	112.6(47)	152.3(58)	11.4(4)	53.2(89)	− 3.6(24)	5.6(28)
C(1)	174(28)	250(33)	15(2)	−44(47)	− 5(13)	−66(14)
C(2)	200(28)	253(34)	14(2)	205(51)	9(12)	55(13)
C(11)	103(21)	201(29)	23(2)	52(37)	21(13)	10(15)
C(12)	139(22)	209(27)	16(2)	94(45)	34(11)	34(14)
C(13)	104(17)	118(19)	14(2)	68(31)	− 6(9)	17(10)
C(14)	129(21)	162(23)	11(1)	77(35)	13(9)	7(10)
C(15)	166(27)	269(35)	15(2)	192(51)	8(13)	31(15)
C(16)	115(20)	180(26)	17(2)	70(37)	−2(11)	−4(13)
C(17)	189(30)	344(45)	27(3)	150(69)	87(17)	75(22)
C(18)	208(30)	186(27)	20(3)	159(46)	33(15)	58(14)
C(19)	288(41)	383(50)	12(2)	110(77)	−14(15)	−33(17)
C(20)	349(52)	272(45)	37(4)	118(76)	52(26)	118(24)

(c) Calculated co-ordinates ($\times 10^3$) and assigned isotropic temperature factors for hydrogen atoms (except methyl hydrogen atoms).

Atom	x	y	z	B	Atom	x	y	z	B
H(11)	366	−251	− 70	5.0	H(15A)	305	−581	− 18	5.0
H(12A)	125	−379	−117	5.0	H(15B)	322	−402	− 10	5.0
H(12B)	148	−200	−109	5.0	H(16A)	467	−478	− 69	5.0
H(13)	137	−243	− 32	5.0	H(16B)	320	−546	− 94	5.0
H(14)	83	−540	− 56	5.0	H(18)	− 56	−446	4	5.0

Solution and Refinement of the Structure

Both structures were solved by the heavy-atom method, and refined anisotropically by the block-diagonal least-squares procedure using the HBLS V program.[12] The function minimized was $\Sigma(|F_o|-k\cdot|F_c|)^2$, where k is a scale factor. The atomic scattering factors used were those of Hanson, Herman, Lea, and Skillman.[13]

[PdCl$_2${(Me$_2$neoMen)P}$_2$]. From a three-dimensional Patterson function, the approximate co-ordinates of the palladium, two chlorine, and two phosphorus atoms were easily determined. All the non-hydrogen atoms were located in the subsequent Fourier synthesis. In the least-squares refinement, the y parameter of the palladium atom was fixed at 0.25 in order to define the origin of the unit-cell. When the R value fell down to 0.075, a difference synthesis revealed some but not all positions of the hydrogen atoms. All the hydrogen atoms except methyl hydrogen were then located assuming the C–H bond length of 1.08 Å and a tetrahedral angle for each carbon atom. In the subsequent refinement their contributions were included in the structure factor calculations, under the condition of fixed parameters. The effect of anomalous dispersion[14] for palladium, chlorine, and phosphorus atoms was then corrected for. The final R values for the structure obtained and its enantiomorph were 0.0702 (R_w=0.067) and 0.0697 (R_w=0.066) for 2606 non-zero reflections. The final positional and thermal parameters of the latter, which confirmed the absolute configuration of the neomenthyl group, are given in Table 2.††

[PdCl$_2${(Me$_2$Men)P}$_2$]. Since four molecules are contained in a unit-cell with the space group $P4_12_12$ or $P4_32_12$, the molecules must have special positions. The following two cases can satisfy the requirements: (1) only the palladium atom lies on the two-fold axis normal to the co-ordination plane, or (2) the palladium and the two chlorine atoms lie on the two-fold axis on the co-ordination plane.

A three-dimensional Patterson function could be interpreted for the latter case for the space group of either $P4_12_12$ or its enantiomorph $P4_32_12$; after assuming the $P4_32_12$ group, the subsequent Fourier synthesis revealed all the non-hydrogen atoms. At the final stage of the refinement, the effect of the anomalous dispersion for heavy atoms[14] was considered, and the contributions of all the hydrogen atoms except the methyl hydrogens were included in the structure factor calculations in the same manner as in [PdCl$_2${(Me$_2$*neo*Men)P}$_2$]. The final R value for the structure obtained and its enantiomorph was 0.0713 (R_w=0.0778) and 0.0803 (R_w=0.0899) for 1388 non-zero reflections. The former structure confirmed the absolute configuration of the menthyl group and determined the space group to be $P4_32_12$. The positional and thermal parameters are also given in Table 3.†††

Results and Discussion

The molecular structures of [PdCl$_2${(Me$_2$*neo*Men)P}$_2$] and [PdCl$_2${(Me$_2$Men)P}$_2$] are shown in Figs. 1 and 2 respectively, along with the numbering scheme of the atoms. The stereoscopic drawings of the molecules are given in Figs. 3 and 4. Bond lengths and bond angles are listed in Tables 4 and 5.

[PdCl$_2${(Me$_2$neoMen)P}$_2$]. The molecule has an approximate two-fold symmetry around the normal to the co-ordination plane, which passes through the palladium atom. The present complex is not iso-struc-

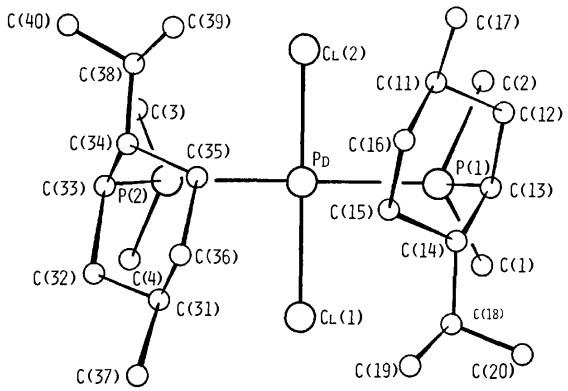

Fig. 1. Molecular structure of [PdCl$_2${(Me$_2$*neo*Men)P}$_2$] with the numbering scheme of atoms.

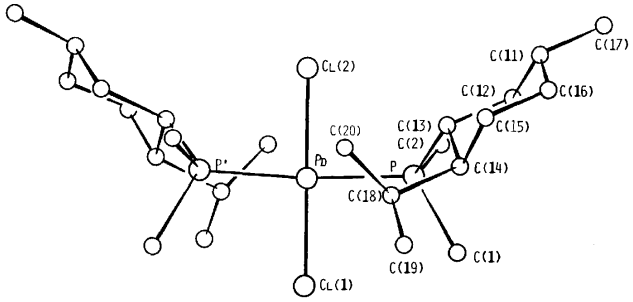

Fig. 2. Molecular structure of [PdCl$_2${(Me$_2$Men)P}$_2$] with the numbering scheme of atoms.

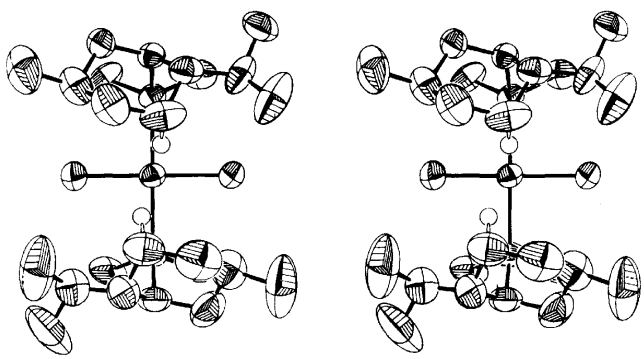

Fig. 3. A stereoscopic drawing of the [PdCl$_2${Me$_2$*neo*-Men)P}$_2$] molecule. Non-hydrogen atoms are represented by thermal ellipsoids at 50% probability levels.

†† This table of observed and calculated structure factors is kept as Document No. 7806a at the Chemical Society of Japan.

††† This table of observed and calculated structure factors is kept as Document No. 7806b at the Chemical Society of Japan.

TABLE 4. BOND LENGTHS AND BOND ANGLES IN $[PdCl_2\{(Me_2neoMen)P\}_2]$
(e.s.d.'s in parentheses)

Bond lengths [l/Å]			
Pd-Cl(1)	2.304(5)	Pd-Cl(2)	2.297(5)
Pd-P(1)	2.344(4)	Pd-P(2)	2.361(5)
P(1)-C(1)	1.839(18)	P(1)-C(2)	1.817(19)
P(1)-C(13)	1.865(14)	P(2)-C(3)	1.796(21)
P(2)-C(4)	1.856(18)	P(2)-C(33)	1.849(17)
C(11)-C(12)	1.544(25)	C(11)-C(16)	1.548(31)
C(11)-C(17)	1.542(31)	C(12)-C(13)	1.513(20)
C(13)-C(14)	1.570(21)	C(14)-C(15)	1.527(25)
C(14)-C(18)	1.551(24)	C(15)-C(16)	1.509(31)
C(18)-C(19)	1.553(30)	C(18)-C(20)	1.508(29)
C(31)-C(32)	1.468(32)	C(31)-C(36)	1.548(36)
C(31)-C(37)	1.504(41)	C(32)-C(33)	1.594(27)
C(33)-C(34)	1.535(25)	C(34)-C(35)	1.551(28)
C(34)-C(38)	1.483(38)	C(35)-C(36)	1.485(33)
C(38)-C(39)	1.569(47)	C(38)-C(40)	1.529(53)
Bond angles [ϕ/°]			
C(1)-Pd-Cl(2)	176.7(2)	Cl(1)-Pd-P(1)	89.7(2)
Cl(1)-Pd-P(2)	90.4(2)	Cl(2)-Pd-P(1)	89.7(2)
Cl(2)-Pd-P(2)	89.8(2)	P(1)-Pd-P(2)	173.3(2)
Pd-P(1)-C(1)	112.5(6)	Pd-P(1)-C(2)	109.8(6)
Pd-P(1)-C(13)	124.6(5)	Pd-P(2)-C(3)	112.0(7)
Pd-P(2)-C(4)	110.1(6)	Pd-P(2)-C(33)	123.8(6)
C(13)-P(1)-C(1)	103.5(7)	C(13)-P(1)-C(2)	102.8(7)
C(1)-P(1)-C(2)	100.7(8)	C(3)-P(2)-C(4)	99.8(9)
C(33)-P(2)-C(3)	103.7(9)	C(33)-P(2)-C(4)	104.6(8)
C(12)-C(11)-C(16)	108.5(16)	C(12)-C(11)-C(17)	110.9(16)
C(16)-C(11)-C(17)	114.1(18)	C(11)-C(12)-C(13)	113.7(13)
C(12)-C(13)-P(1)	114.6(10)	C(12)-C(13)-C(14)	110.3(12)
C(14)-C(13)-P(1)	115.0(10)	C(13)-C(14)-C(15)	108.4(13)
C(13)-C(14)-C(18)	116.0(13)	C(15)-C(14)-C(18)	116.2(14)
C(14)-C(15)-C(16)	111.1(16)	C(15)-C(16)-C(11)	115.5(19)
C(14)-C(13)-C(19)	112.2(15)	C(14)-C(16)-C(20)	112.1(15)
C(19)-C(18)-C(20)	111.9(17)	C(32)-C(31)-C(36)	107.7(20)
C(32)-C(31)-C(37)	108.8(21)	C(36)-C(31)-C(37)	111.0(22)
C(31)-C(32)-C(33)	114.6(18)	C(32)-C(33)-P(2)	110.7(12)
C(32)-C(33)-C(14)	107.5(14)	C(34)-C(33)-P(2)	118.4(12)
C(33)-C(34)-C(35)	109.3(15)	C(33)-C(34)-C(38)	114.3(19)
C(35)-C(34)-C(38)	114.4(19)	C(34)-C(35)-C(36)	111.6(18)
C(35)-C(36)-C(31)	114.0(20)	C(34)-C(38)-C(39)	112.2(25)
C(34)-C(38)-C(40)	114.5(27)	C(39)-C(38)-C(40)	107.6(28)
Short atomic contact [l/Å] and angles [ϕ/°]			
Pd···H(15A)	2.71	P(1)···Pd···H(15A)	71.8
H(15A)···H(35A)	2.06	P(2)···Pd···H(35A)	72.6

tural with its Ni-analog, $[NiCl_2\{Me_2neoMen)P\}_2]$. A remarkable difference between these two complexes is the arrangement of the two neomenthyl groups about the co-ordination plane. The neomenthyl groups are located on the same side of the co-ordination plane in the present complex, whereas they are on opposite sides of the plane in the Ni-analog. This structural difference may affect the different catalytic activities of these two complexes in the hydrosilylation of olefins.

The co-ordination around the palladium atom is rather square-pyramidal, and deviates from the *trans*-square planar geometry; the deviations of the Pd, Cl(1), Cl(2), P(1), and P(2) atoms from the co-ordination plane are relatively large: 0.08, 0.02, 0.02, −0.04, and −0.06 Å, respectively. The Pd–Cl bond lengths are nearly equal, 2.304(5) and 2.297(5) Å (av 2.301 Å); these are the ordinary values found in *trans* Pd–Cl bonds.[15-20] The Cl(1)–Pd–Cl(2) is not linear, [176.7 (2)°]. The Pd–P bond lengths are unequal, 2.344(4) and 2.361(5) Å (av 2.353 Å). These are the longest values so far reported for complexes which have the *trans* Pd–P bonds.[22-28] The P(1)–Pd–P(2) angle of 173.3(2)° significantly deviates from 180° (Fig. 5), in

TABLE 5. BOND LENGTHS AND BOND ANGLES IN $[PdCl_2\{Me_2Men)P\}_2]$
(e.s.d.'s in parentheses)

Bond lengths [l/Å]			
Pd-Cl(1)	2.296(9)	Pd-Cl(2)	2.267(9)
Pd-P	2.310(5)	P-C(1)	1.839(20)
P-C(2)	1.843(20)	P-C(13)	1.863(16)
C(11)-C(12)	1.563(27)	C(12)-C(13)	1.575(24)
C(13)-C(14)	1.532(22)	C(14)-C(15)	1.552(26)
C(15)-C(16)	1.541(27)	C(16)-C(11)	1.504(26)
C(11)-C(17)	1.548(33)	C(14)-C(18)	1.610(25)
C(18)-C(19)	1.525(32)	C(18)-C(20)	1.573(33)
Bond angles [ϕ/°]			
Cl(1)-Pd-Cl(2)	180	P-Pd-P′	175.5(5)
Cl(1)-Pd-P	87.8(3)	Cl(2)-Pd-P	92.3(3)
Pd-P-C(1)	118.2(7)	Pd-P-C(2)	108.0(7)
Pd-P-C(13)	113.7(5)	C(1)-P-C(2)	101.8(9)
C(1)-P-C(13)	106.4(8)	C(2)-P-C(13)	107.6(8)
C(12)-C(11)-C(16)	111.3(15)	C(12)-C(11)-C(17)	109.2(17)
C(16)-C(11)-C(17)	111.9(17)	C(11)-C(12)-C(13)	108.7(15)
C(12)-C(13)-C(14)	109.5(13)	C(12)-C(13)-P	109.0(11)
C(14)-C(13)-P	111.4(10)	C(13)-C(14)-C(15)	108.2(14)
C(13)-C(14)-C(18)	110.9(13)	C(15)-C(14)-C(18)	110.6(14)
C(14)-C(15)-C(16)	111.2(16)	C(15)-C(16)-C(11)	109.5(15)
C(14)-C(18)-C(19)	115.0(16)	C(14)-C(18)-C(20)	109.3(16)
C(19)-C(18)-C(20)	107.5(18)		
Short atomic contact [l/Å]			
Pd···H(18) 2.78			

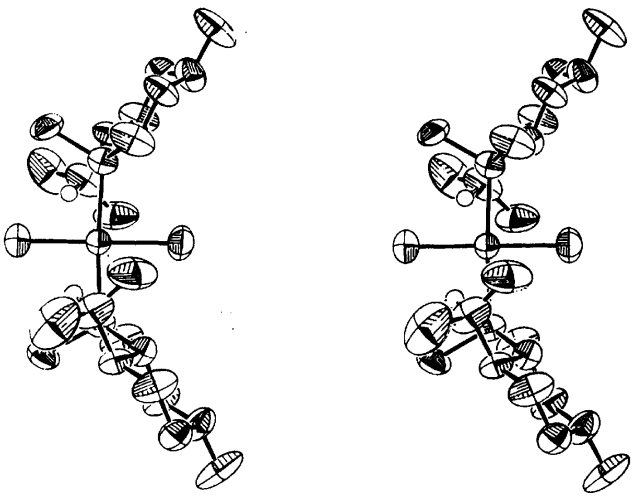

Fig. 4. A stereoscopic drawing of the $[PdCl_2\{(Me_2$-Men)$P\}_2]$ molecule.

order to decrease the steric repulsion between two neomenthyl groups in the molecule.

The conformation about the P(1)–Pd–P(2) is approximately eclipsed (Fig. 6) in a way different from the Nickel analog. The P(1) and P(2) atoms deviates slightly away from the approximate co-ordination plane. There is no significant difference between the conformations about the P(1)–C(13) (Fig. 7) and P(2)–C(33) bonds, which are intermediates between the staggered and eclipsed conformations.

The P–C bond lengths, ranging from 1.796(21) to 1.865(14) Å, are equal within the limits of error. However, the geometries around the phosphorus atoms show distortions. The Pd–P(1)–C(13) and Pd–P(2)–C(33) angles, 124.6(5) and 123.8(6)°, deviate greatly from the tetrahedral angle, whereas the C–P–C angles are rather small [99.8(9)—104.6(8)°]. The large Pd–P(1)–C(13) and Pd–P(2)–C(33) angles are also due to the steric repulsion between the neomenthyl groups in the molecule.

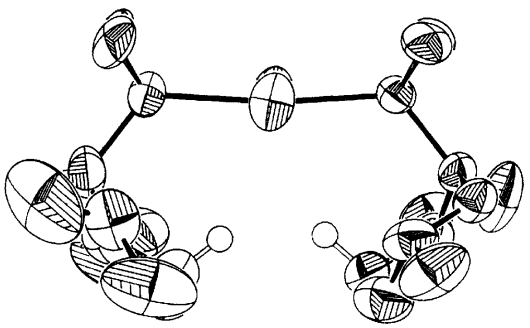

Fig. 5. $[PdCl_2\{(Me_2neoMen)P\}_2]$ molecule projected along the Cl(1)-Pd bond.

The P(1)–C(13)–C(12), P(1)–C(13)–C(14), and P(2)–C(33)–C(34) angles 114.6(10), 115.0(10), and 118.4(12)°, are larger than the normal value of 109.5°. Similar distortions of the P–C–C angles, which are considered to be due to the steric hindrance between the neomenthyl and methyl groups, were observed in the Ni-analog.[11]

$[PdCl_2\{(Me_2Men)P\}_2]$. The molecule has C_2 symmetry; the two fold axis passes through the Cl(1),

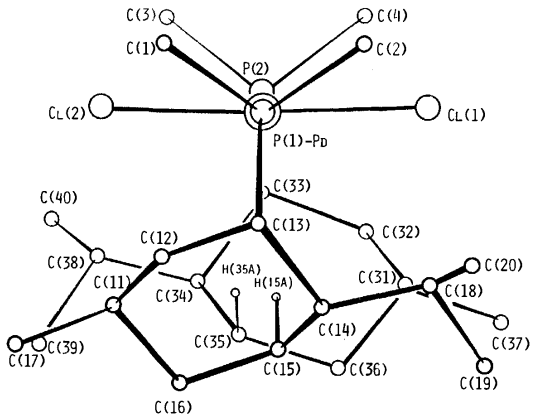

Fig. 6. The conformation about the P(1)-Pd bond in $[PdCl_2\{(Me_2neoMen)P\}_2]$.

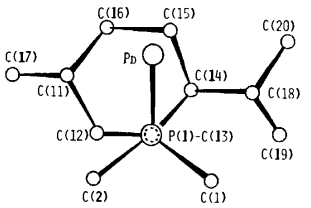

Fig. 7. The conformation about the P(1)-C(13) bond in $[PdCl_2\{(Me_2neoMen)P\}_2]$. The conformation about the P(2)-C(33) bond is similar to this.

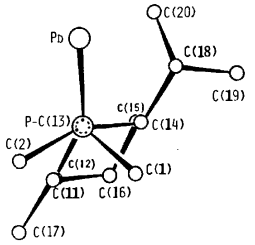

Fig. 8. The conformation about the P-C(13) bond in $[PdCl_2\{(Me_2Men)P\}_2]$.

Pd, and Cl(2) atoms which are on the co-ordination plane (Figs. 2 and 4). The geometry around the palladium atom is *trans*-square planar. The two menthyl groups are located on either side of the co-ordination plane.

The Pd–Cl bond lengths 2.296(9) and 2.267(9) Å (av 2.282 Å) are equal to those in $[PdCl_2\{(Me_2neo-Men)P\}_2]$. The Pd–P bond length 2.310(5) Å is significantly shorter than those in $[PdCl_2\{(Me_2neoMen)-P\}_2]$. The longer Pd–P lenghts in the latter are considered to result from the steric hindrance between the two neomenthyl groups. The P–Pd–P′ angle (175.5 (5)°) is not linear.

The conformation about the P–C(13) bond (Fig. 8) is an intermediate between the staggered and eclipsed conformations, which is rather similar to the one in $[NiCl_2\{Me_2neoMen)P\}_2]$.

The conformation about the C(14)–C(18) bond of the menthyl group is different from those of the neomenthyl groups in $[NiCl_2\{(Me_2neoMen)P\}_2]$ and $[PdCl_2-\{(Me_2neoMen)P\}_2]$, since the isopropyl group is rotated about 120° around the C(14)–C(18) bond. This is

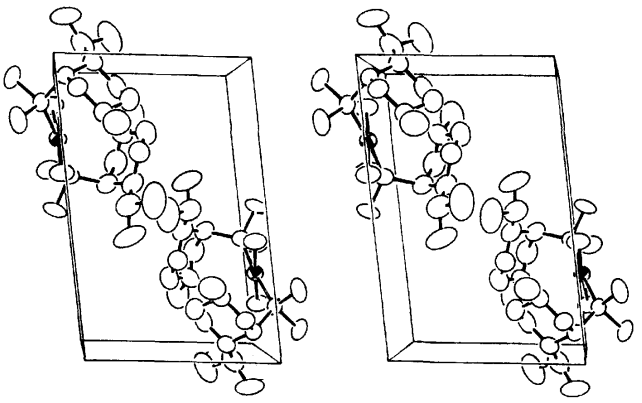

Fig. 9. A stereoscopic view of the crystal structure, $[PdCl_2\{(Me_2neoMen)P\}_2]$.

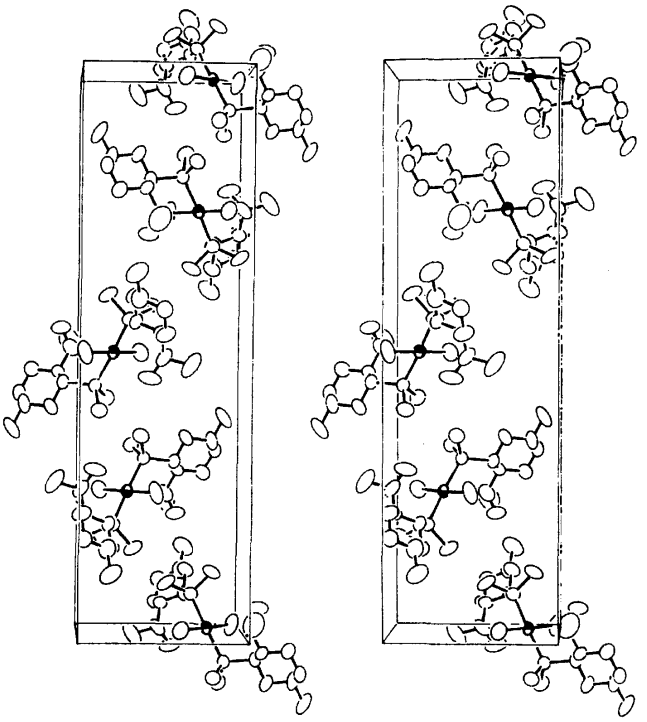

Fig. 10. A stereoscopic view of the crystal structure, $[PdCl_2\{(Me_2Men)P\}_2]$.

due to the steric interaction between the palladium atom and the isopropyl group of the menthyl group. Two hydrogen atoms, H(18) and H(18′), of the menthyl group occupy the vacant sites of the octahedron centered by the palladium and make short contacts (2.78 Å) with the palladium atom.

Crystal Structure. The Crystal structure of $[PdCl_2-\{(Me_2neoMen)P\}_2]$ is given in Fig. 9. The packing of $[PdCl_2\{(Me_2Men)P\}_2]$ molecules in a unit-cell is shown in Fig. 10. There is no short intermolecular atomic contact less than 3.8 Å between non-hydrogen atoms in either crystal.

The calculations were carried out on the NEAC 2200-700 computer at Osaka University and the FACOM 230-60 at Kyoto University. Figures 3, 4, 5, 9, and 10 were drawn on a NUMERICON 7000 system at Osaka University with a local version of ORTEP.[28]

This work was supported in part by a Grant-in-aid for Scientific Research from the Ministry of Education (No. 84305), for which the authors express their gratitude. The authors express their deep thanks to Professor Makoto Kumada and his co-workers of Kyoto University for kindly providing the crystals and for many helpful discussions.

References

1) Y. Kai, N. Yasuoka, N. Kasai, and M. Kakudo, *J. Organomet. Chem.*, **32**, 165 (1971).
2) Y. Kai, N. Yasuoka, N. Kasai, and M. Kakudo, *Bull. Chem. Soc. Jpn.*, **45**, 3388 (1972).
3) Y. Kai, N. Yasuoka, N. Kasai, and M. Kakudo, *Bull. Chem. Soc. Jpn.*, **45**, 3397 (1972).
4) Y. Kai, N. Yasuoka, N. Kasai, and M. Kakudo, *Bull. Chem. Soc. Jpn.*, **45**, 3408 (1972).
5) H. Yasuda and H. Tani, *Macromolecules*, **6**, 17 (1973).
6) M. Ishimori, T. Hagihara, T. Tsuruta, Y. Kai, N. Yasuoka, and N. Kasai, *Bull. Chem. Soc. Jpn.*, **49**, 1165 (1976).
7) Y. Kiso, M. Kumada, K. Tamao, and M. Umeno, *J. Organomet. Chem.*, **50**, 297 (1973).
8) Y. Kiso, M. Kumada, K. Maeda, K. Sumitani, and K. Tamao, *J. Organomet. Chem.*, **50**, 311 (1973).
9) M. Kumada, K. Sumitani, Y. Kiso, and K. Tamao, *J. Organomet. Chem.*, **50**, 319 (1973).
10) Y. Kiso, K. Tamao, and M. Kumada, private communication.
11) K. Kan, Y. Kai, N. Yasuoka, and N. Kasai, *Bull. Chem. Soc. Jpn.*, **50**, 1051 (1977).
12) T. Ashida, The Universal Crystallographic Computing System-Osaka, The Computation Center, Osaka University (1973), p. 55.
13) H. P. Hanson, P. Herman, J. D. Lea, and S. S. Skillman, *Acta Crystallogr.*, **18**, 511 (1965).
14) "International Tables for X-Ray Crystallography," The Kynoch Press, Vol. IV, Birmingham (1974), p.149.
15) R. G. Little and R. J. Doedens, *Inorg. Chem.*, **12**, 537 (1973).
16) G. P. Khare, R. G. Little, J. T. Veal, and R. J. Doedens, *Inorg. Chem.*, **14**, 2475 (1975).
17) R. J. Williams, W. H. Watson, M. J. Bennett, F. A. Cotton, and D. L. Weaver, *Acta Crystallogr.*, **23**, 788 (1967).
18) L. C. Satek, H. L. Ammon, and J. M. Stewart, *Acta Crystallogr., Sect. B*, **31**, 2691 (1975).
19) P. E. Skakke and S. E. Rasmussen, *Acta Chem. Scand.*, **24**, 2634 (1970).
20) T. Debaerdemaeker, A. Kutoglu, G. Schmid, and L. Weber, *Acta Crystallogr., Sect. B*, **29**, 1283 (1973).
21) N. A. Bailey and R. Mason, *J. Chem. Soc., A*, **1968**, 2594.
22) G. Beran, A. J. Carty, P. C. Chieh, and H. A. Patel, *J. Chem. Soc., Dalton Trans.*, **1973**, 488.
23) S. Jacobson, Y. S. Wong, P. C. Chieh, and A. J. Carty, *J. Chem. Soc., Chem. Commun.*, **1974**, 520.
24) M. L. Schneider and H. M. M. Shearer, *J. Chem. Soc., Dalton Trans.*, **1973**, 354.
25) J. Fayos, E. Dobrzynski, R. J. Angelici, and J. Clardy, *J. Organomet. Chem.*, **59**, C33 (1973).
26) D. L. Weaver, *Inorg. Chem.*, **9**, 2250 (1970).
27) G. Bonbieri, A. Immirzi, and L. Toniolo, *Acta Crystallogr., Sect. A*, **31**, S141 (1975).
28) C. K. Johnson, *ORTEP-II*, Report ORNL-5138, Oak Ridge National Laboratory Tennessee, 1976.

The Spatial Distribution of Secondary Electrons Produced in the γ-Radiolysis of Water

Ken-ichi KOWARI and Shin SATO

Department of Applied Physics, Tokyo Institute of Technology, Ookayama, Meguro-ku, Tokyo 152

(Received October 19, 1977)

The spatial distribution of secondary electrons produced in the γ-radiolysis of water in the liquid phase has been theoretically calculated. The method consists of the combination of the procedure previously developed for the calculation of the G-value of electrons with the theory proposed by Fröhlich and Platzman for the slowing down of electrons in polar liquids. The G-value of the ion-pairs initially produced was calculated to be 6.8 on the assumption that the binding energies of electrons in water are equal to those in solid water at 77K. 27% of the ion-pairs were generated in isolated spurs. Another 27% of the ion-pairs were generated in condensed spurs, each of which contains more than one hundred ion-pairs. The other ion-pairs formed less condensed spurs, each of which contains from 2 to 100 ion-pairs. A new definition was given for the classification of spurs: isolated spurs, blobs, and short tracks; the original proposal was by Mozumder and Magee. The diameter of the isolated spur was estimated to be about 100 Å. The distribution of the distance between the parent positive ion and the thermalized electron in the isolated spur was well expressed by the function proposed by Abell and Funabashi, except at very short distances.

When ionizing radiation interacts with a material in the condensed phase, the energy transfer from the radiation to the material occurs through the kinetic energy of the secondary electrons produced, and the energy deposits are heterogeneously distributed in the system. In radiation chemistry, the region in which active species are produced by radiation is called a spur. Mozumder and Magee classified these spurs into three types, on the basis of the amount of energy deposited in the region: isolated spurs, blobs, and short tracks.[1] Experimentally the distribution of such spurs can be estimated from the number of clusters produced in a cloud chamber. According to the measurement of Wilson, who used 25 keV electrons as the radiation source, 42.6% of the observed clusters contained one ion-pair, 22.5% two pairs, 12.4% three pairs, 10.1% four pairs, and 12.4% more than five pairs.[2] From the point of view of radiation chemistry, the number of ion-pairs involved in a spur is important, because the reactions occurring in a spur may be dependent upon the number of ion-pairs involved in the spur; for example, the neutralization reaction between positive ions and ejected electrons in a condensed spur may be faster than that in an isolated spur.

We have previously developed a calculation method for the G-values of ionization and excitation.[3] Using this method, we can calculate the initial energy distribution of subexcitation electrons. Therefore, if we can estimate the slowing down process of electrons in the condensed phase, we can construct the spatial distribution of secondary electrons produced in the radiolysis. As for the slowing down process of electrons in the condensed phase, Fröhlich and Platzman proposed a theory with which they estimated the rate of slowing down of electrons in water.[4] Recently Magee and Helman examined this theory numerically and estimated the rates of energy loss of electrons in a few hydrocarbons as well as in water.[5] As has been stated in their paper, the absolute value of the rate of energy loss is somewhat obscure, because the theory proposed by Fröhlich and Platzman treated only the "indirect" interaction between electrons and surrounding molecules. The treatment of the "direct" interactions, such as the formation of short-lived negative ions, has not been formulated yet. Consequently, we cannot avoid the appearance of a somewhat arbitrary factor in the estimation of the rate of slowing down of subexcitation electrons.

So far the spatial distribution of secondary electrons has been discussed in connection with the electron scavenging in the γ-irradiated hydrocarbons and with the electric conductivity of the irradiated hydrocarbons. The simplest assumed function was a Gaussian; however, it is now well known that the spatial distribution has a long tail compared with a Gaussian. Freeman and his group used a function which is composed of a Gaussian and a power function.[6] One of the present authors also discussed the spatial distribution of secondary electrons in the γ-irradiated hydrocarbons and derived a function from the experimental data of the electron scavenging by assuming a diffusion model.[7] Similar attempts have been made by several investigators.[8] Among them, Abell and Funabashi proposed a simple exponential function to express the spatial distribution and showed that this function is suitable to explain the experimental data both for the electron scavenging and for the voltage dependence of the electric conductivity of the irradiated hydrocarbons.[9] However, all of these attempts are empirical and have no rigid theoretical backgrounds. We, therefore, thought that the theoretical derivation of the function expressing the spatial distribution of secondary electrons would be worthwhile carrying out even if several assumptions are involved.

G-Value of Ionization

Procedure of Calculation. When water is exposed to the γ-rays from ^{60}Co, the energy transfer mainly occurs through the Compton effect. The energy distribution of the Compton electrons can be calculated by using the equation

$$\frac{d\sigma(T)}{dT} = \frac{\pi r_0^2}{\alpha h\nu}\left[1+\frac{T^2}{(h\nu-T)h\nu}+\left\{1-\frac{T}{\alpha(h\nu-T)}\right\}^2\right], \quad (1)$$

which was derived by Davison and Evans[10] from the

famous Klein-Nishina formula. Here, $\sigma(T)$ is the cross section for the formation of Compton electrons with the energy T, $h\nu$ is the energy of the incident γ-rays, $\alpha = h\nu/mc^2$, and $r_0 = e^2/mc^2$. m is the mass of electron, e is the charge, and c is the velocity of light.

Previously we have calculated the energy distribution of Compton electrons from helium gas irradiated by ^{60}Co γ-rays.[11] The fraction of the Compton electrons with energy of T was expressed by $f(T)$. This function is common to any material, because Eq. 1 does not discriminate target electrons. The total energy absorbed by the material, T_0, therefore, is expressed as follows:

$$T_0 = \int_0^{T_{max}} T\, f(T)\, dT. \tag{2}$$

Here, $T_{max} = 2\alpha h\nu/(1+2\alpha)$.

Using the function $f(T)$, we can calculate the degradation spectrum of the Compton electrons:

$$y_1(T) = \int_T^{T_{max}} f(T)\, dT/S(T). \tag{3}$$

$S(T)$ is the stopping power of water and may be expressed as follows:

$$S(T) = N\sum_i n_i \left\{ \int_{E_{si}}^{(T+I_i)/2} E(\sigma_{E,dir} + \sigma_{E,exc})dE + \frac{1}{2}\int_{E_{ti}}^{E_{si}} E\sigma_{E,exc}dE \right\}. \tag{4}$$

N is the number of molecules in a unit volume, n_i the number of electrons in the i-th shell of water, I_i the binding energy of the electron in the i-th shell, and E_{si} and E_{ti} the energies of the singlet and triplet excitations for the electrons in the i-th shell. $\sigma_{E,dir}$ and $\sigma_{E,exc}$ are the differential cross sections of the energy loss E due to the direct excitation and due to the excitation accompanied with the exchange of electrons, respectively.

In the procedure we developed for the calculation of G-values, the cross sections of the energy loss are estimated by using the classical binary-encounter-collision theory. For the direct excitation,

$$\sigma_{E,dir} = \frac{\pi e^4}{T+I_i+E_i}\left(\frac{1}{E^2} + \frac{4E_i}{3E^3}\right), \tag{5}$$

where E_i is the average kinetic energy of the target electron. For the excitation accompanied with the exchange of electrons, E in Eq. 5 is replaced by $T+I_i-E$.

Once the degradation spectrum of Compton electrons is obtained, we can calculate the degradation spectra of electrons ejected in the later steps of ionization due to the impact of electrons.

$$y_2(T) = \frac{N}{S(T)}\sum_i n_i \int_T^{(T_{max}-I_i)/2} \times \int_{2T_2+I_i}^{T_{max}} y_1(T_1)\sigma(T_1T_2)dT_1dT_2, \tag{6}$$

$$y_3(T) = \frac{N}{S(T)}\sum_i n_i \int_T^{(T_{max}-3I_i)/4} \times \int_{2T_2+I_i}^{(T_{max}-I_i)/2} y_2(T_1)\sigma(T_1T_2)dT_1dT_2. \tag{7}$$

Here, $\sigma(T_1T_2)$ is the differential cross section for the production of a secondary electron with energy of T_2 in the collision between the incident electron with energy of T_1 and the target electron in the i-th shell and is expressed as follows, by using Eq. 5:

$$\sigma(T_1T_2) = \frac{\pi e^4}{T+I_i+E_i}\left[\frac{1}{(T_2+I_i)^2} + \frac{4E_i}{3(T_2+I_i)^3} + \frac{1}{(T_1-T_2)^2} + \frac{4E_i}{3(T_1-T_2)^3}\right]. \tag{8}$$

Equations similar to $y_2(T)$ and $y_3(T)$ may be constructed for the later steps. The total degradation spectrum is obviously the sum of the degradation spectra of the electrons ejected in all steps:

$$y(T) = \sum_m y_m(T). \tag{9}$$

The degradation spectrum of electrons is one of the most important values for the irradiated system; from it we can deduce many interesting values concerning the reactions occurring in the system. The G-value of ionization is one of them.

In order to calculate the G-value of ionization, we need the total cross section of ionization due to the impact of an electron with the energy T, which is expressed per target electron as follows:

$$Q_{ion} = \int_{I_i}^{(T+I_i)/2} (\sigma_{E,dir} + \sigma_{E,exc})dE = \frac{\pi e^4}{T+I_i+E_i}\left[\left(\frac{1}{I_i} - \frac{1}{T}\right) + \frac{2E_i}{3}\left(\frac{1}{I_i^2} - \frac{1}{T^2}\right)\right]. \tag{10}$$

Then, the number of ions produced by the ejection of the electron in the i-th shell can be calculated by the equation

$$N_{ion} = Nn_i \int_{I_i}^{T_{max}} Ty(T)Q_{ion}(T)\, d\ln T. \tag{11}$$

The G-value of ionization through this process is obviously

$$G_{ion} = 100N_{ion}/T_0. \tag{12}$$

Similar formulations can be made for other processes, including singlet and triplet excitations.

Calculated Results. The constants used for the calculation are summarized in Table 1. Since no experimental values were available, we had to estimate them somewhat arbitrarily. For the binding energies of electrons in water in the liquid phase, we estimated the values from the spectrum of X-ray induced photoelectron spectroscopy obtained with solid state water at 77 K.[12] The E_s and E_t values for the $1b_1$ orbital are those reported for the gas phase. For other orbitals, the equations shown in the note of Table 1 were used.

TABLE 1. CONSTANTS USED FOR CALCULATION

Orbital	I_i	E_i	E_s	E_t
$1b_1$	7.6	45.0	7.42	5.0
$3a_1$	9.8	54.9	9.6[a]	7[b]
$1b_2$	14.5	74.7	14[a]	12[b]
$2a_1$	26.3	119	26[a]	24[b]
$1a_1$	533	1265	533[a]	531[b]

a) $E_s = I_i - (I_i - E_s)_{1b_1} = I_i - 0.2$.
b) $E_t = I_i - (I_i - E_t)_{1b_1} = I_i - 2.6$.

Table 2. The G-values of ionization and singlet and triplet excitations from each orbital
The values in parentheses are the G-values of superexcited states.

Orbital	G_e	G_s	G_t
$1b_1$	3.13	0.23	1.18
$3a_1$	1.87	(0.096)	0.15 (0.12)
$1b_2$	0.96	(0.075)	(0.018)
$2a_1$	0.39	(0.009)	(0.002)
$1a_1$	0.008	(5×10^{-6})	(4×10^{-7})

Table 3. The G-values of ionization, including the ionization from the superexcited state (G_{ion}) and of singlet and triplet excitations ($G_{singlet}$ and $G_{triplet}$)

G_{ion}	6.76
$G_{singlet}$	0.23
$G_{triplet}$	1.21

In order to estimate the average kinetic energies, E_i, we deduced an equation:

$$E_i = 9.15I_i^{0.785}, \quad (13)$$

by plotting the reported values of E_i and I_i for five noble gases.[13]

The G-values calculated are summarized in Table 2. In this Table, the G-values of the superexcited states which are in the parentheses are involved in those of singlet and triplet excitations. If all of the superexcited states are assumed to be ionized, then the G-value of ionization should be increased by 0.32. In Table 3 are listed the corrected G-values.

Since the G-value of ionization is sensitive to the ionization potential assumed, *i.e.*, the I_i value for the $1b_1$ orbital, we calculated the G-values by assuming several I_i values. The results are shown in Fig. 1. The value obtained with I_i=12.6 eV is that for the gas phase.

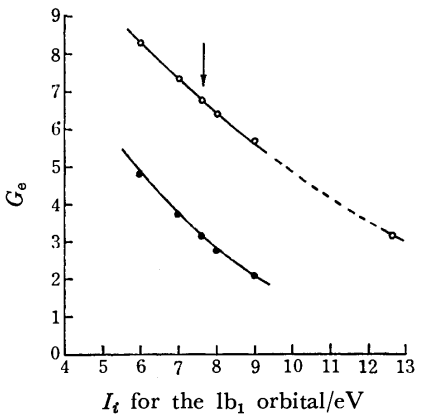

Fig. 1. The calculated G-value of electrons as a function of the energy assumed for the electron in the $1b_1$ orbital. ○, for the total; ●, for the G-value from the $1b_1$ orbital only. The arrow shows the value used in the following calculation.

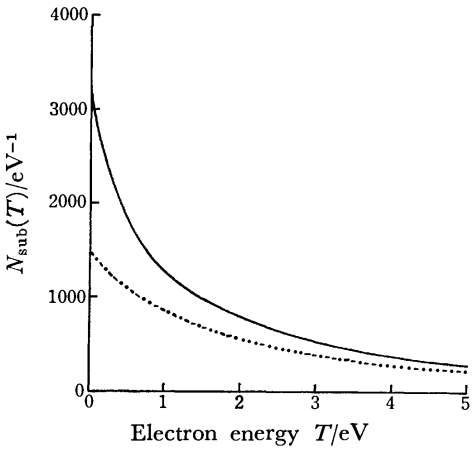

Fig. 2. The initial energy distribution of subexcitation electrons. Solid line is for the total and dotted line for the "child" electrons.

Subexcitation Electrons

Initial Energy Distribution. Since the degradation spectrum of electrons in γ-irradiated water has been obtained, the initial energy distribution of subexcitation electrons can be calculated by using the following equations:[14]

$$N_{sub}(T) = f(T) + N_p(T) + N_c(T);\ T<E_t, \quad (14)$$

$$N_p(T) = N\sum_i n_i \int_{E_t}^{T+I_i} y(T+E)\sigma(T+E,E)\mathrm{d}E,$$

$$N_c(T) = N\sum_i n_i \int_{2T+I_i}^{T_{max}} y(T')\sigma(T',T+I_i)\mathrm{d}T'.$$

The first term, $f(T)_{T<E_t}$, represents the contribution of Compton electrons and is negligibly small compared with the second and third terms when the energy of the incident γ-rays is higher than the binding energy of the electron in the innermost shell. The second term corresponds to the electrons which had the energy higher than the threshold, $E_t(1b_1)$ in the present case, before the last collision. We may call them "parent" electrons. The third term represents the electrons generated in the last collision with the energy lower than $E_t(1b_1)$, which we may call "child" electrons.

Figure 2 shows the calculated result for the initial energy distribution of subexcitation electrons produced in water. The dotted curve corresponds to the "child" electrons. The number of "child" electrons is about twice that of "parent" electrons. Douthat calculated the energy distribution of subexcitation electrons in helium gas irradiated by 1.99 keV electrons.[14] The curve reported is similar to that shown in Fig. 2.

If the irradiated material is in the gas phase at a low pressure, these subexcitation electrons are homogeneously distributed in the material and collide with the surrounding molecules to excite their vibrations and rotations. The rate of the energy loss, however, is much slower than that due to electronic excitations when the electron energy is higher than the threshold.[15]

Thermalization Distance. According to the theory proposed by Fröhlich and Platzman, the rate of the energy loss of an electron in the 1—10 eV energy region due to dielectric relaxation is expressed by this equation:

$$-\frac{dT}{dt}=\frac{2e^2}{\pi v}\int_0^\infty \frac{\omega\varepsilon^2(\omega)}{\varepsilon_1^2(\omega)+\varepsilon_2^2(\omega)}xK_0(x)K_1(x)dx. \quad (15)$$

Here v is the velocity of the moving electron, x is defined by $x=\omega b_{min}/v$, $\omega/2\pi$ is the frequency, b_{min} is the minimum value of the collision parameter, ε_1 and ε_2 are the real and imaginary part of the complex dielectric constant of the solvent, and K_0 and K_1 are the modified Bessel functions of the second kind, of order 0 and 1. In the case of polar solvents such as water, the dipolar relaxation is the main process for the energy loss and the rate of energy loss can be approximated as follows:

$$-\frac{dT}{dt}\simeq\frac{\pi e^2}{4d}\frac{\varepsilon_s-\varepsilon_{1r}}{\tau n^4}. \quad (16)$$

Here d is the intermolecular distance, τ the relaxation time, n the refractive index, ε_s the static dielectric constant, and ε_{1r} the dielectric constant at frequencies lower than the lowest main infrared absorption frequency.

Fröhlich and Platzman substituted the experimental values of water at 20 °C into Eq. 16 and obtained 10^{13} eV s^{-1} for $-dT/dt$.

Magee and Helman recently discussed Eq. 15 and calculated the rate of energy loss of subexcitation electrons in benzene and polyethylene, which have no dipole moments, as well as in water. The rates of the energy loss calculated in benzene and polyethylene were a little smaller than that in water.

As stated in the Introduction, the theory of Fröhlich and Platzman treats only the "indirect" interaction of moving electrons with surrounding molecules. Magee and Helman estimated the rate of the energy loss due to the "direct" interaction in water and suggested that $-dT/dt\simeq10^{14}$ eV s^{-1}. In the present calculation, therefore, we used two values, 10^{13} and 10^{14} eV s^{-1} for $-dT/dt$.

If the rate of energy loss is independent of the electron energy, the path length over which an electron with the energy T loses energy down to T_{min} may be calculated by the equation

$$R=\frac{2}{3}\left(\frac{2}{m}\right)^{1/2}\frac{1}{k}[T^{3/2}-T_{min}^{3/2}], \quad (17)$$

where m is the electron mass and k is the rate of energy loss.

The relation between the crooked path, R, and the straight distance, r, between the starting point and the point where the electron energy is degraded to T_{min} can be given by the theory of random walks.[16] With given R, the distribution in r, *i.e.*, the probability of arriving at a point r, $P(r)$, is given by

$$P(r)=4\pi r^2W(r) \quad (18)$$

and

$$W(r)=(2\pi RL/3)^{-3/2}\exp(-3r^2/2RL). \quad (19)$$

Here L is the mean free path of an electron in the solvent.

As will be discussed later, about 30% of the ion-pairs produced in the γ-irradiated water are generated in isolated spurs. The electrons in these do not interact with active species in other spurs before they are thermalized, and the initial energy distribution of electrons in the isolated spurs are similar to that of the "child" electrons discussed above. Consequently, the spatial

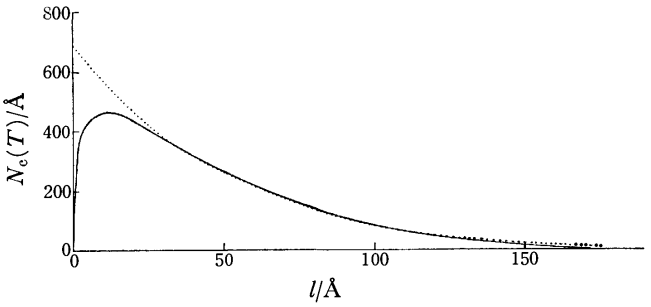

Fig. 3. The spatial distribution of thermalized electrons in the isolated spurs. $-dT/dt=10^{13}$ eV s^{-1}. For the dotted line, see the Text.

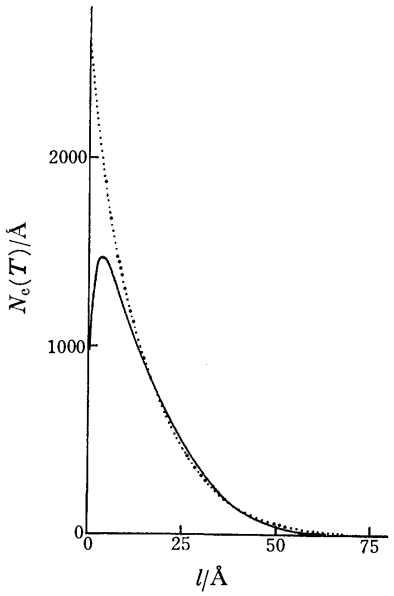

Fig. 4. The spatial distribution of thermalized electrons in the isolated spurs. $-dT/dt=10^{14}$ eV s^{-1} For the dotted line, see the Text.

distribution of electrons when they are thermalized in the isolated spurs can be expressed by

$$F(r)=\int_0^{E_t}W(r)N_e(T)dT. \quad (20)$$

Here, T_{min} should be taken as thermal energy.

For the actual calculation, we took, $L=3$ Å and $T_{min}=0$. The calculated results are shown in Figs. 3 and 4, where the rate of energy loss k is assumed to be 10^{13} and 10^{14} eV s^{-1}, respectively. The dotted lines shown in both figures are drawn by using the function $4\pi r^2F(r)=A\exp(-r/b)$; $A=690$ and $b=48$ Å for Fig. 3 and $A=3000$ and $b=14$ Å for Fig. 4. Except for the very small value of r, both curves coincide with those theoretically estimated.

The Number of Ion-pairs in a Spur

The energy of the secondary electrons ejected from the parent molecules into the solvent ranges from zero to the maximum value, T_{max}. If the initial energy is low, the electron will be thermalized close by the parent molecule ion and will make an ion-pair.

The initial energy distribution of secondary electrons

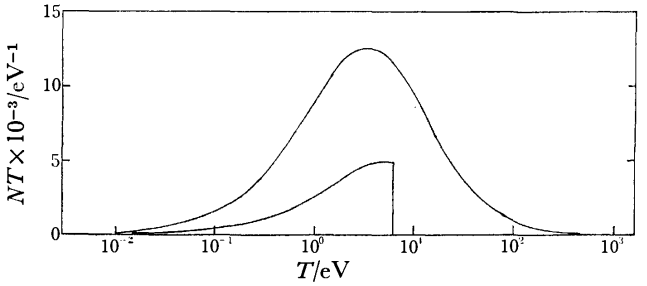

Fig. 5. The initial energy distribution of secondary electrons. The lower curve is for the subexcitation electrons in the isolated spurs.

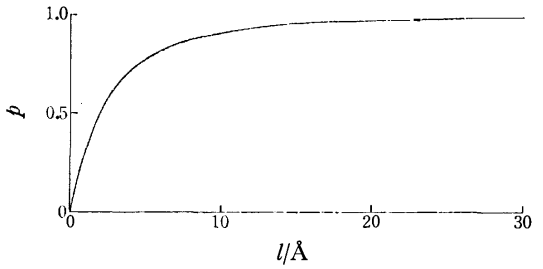

Fig. 6. The distance between two successive ionizations occurring in the γ-irradiated water.

can be calculated also from the degradation spectrum obtained above:

$$N(T) = f(T) + N\sum_i n_i \int_{2T+I_i}^{T_{max}} y(T')\sigma(T',T)\mathrm{d}T', \qquad (21)$$

where $f(T)$ is the contribution of Compton electrons. $\sigma(T',T)$ is the differential cross section which appears in Eq. 8. The calculated result for the secondary electrons in the γ-irradiated water is shown in Fig. 5. Here the relation $TN(T)$ *vs.* ln T is plotted, so that the area under the curve is proportional to the number of secondary electrons. The electrons whose energy is higher than the threshold, E_t, correspond to the "parent" electrons discussed in the previous section and the electrons whose energy is lower than E_t are the "child" electrons.

If a "parent" electron has a higher energy than the ionization potential of water, it will give rise to another ionization. The number of the "child" electrons produced in this second ionization has already been counted in Fig. 5. The average probability with which "parent" electrons give rise to such ionizations within the distance, l, from the last ionization is expressed by the following equation:

$$p = \int_I^{T_{max}} [1-\exp(-N\sum_i n_i Q_i(T)l]N(T)\mathrm{d}T/ \int_I^{T_{max}} N(T)\mathrm{d}T. \qquad (22)$$

Here $Q_i(T)$ is the total ionization cross section due to a "parent" electron with the energy T. The values of p are plotted in Fig. 6 as a function of the distance l. Obviously, most of "parent" electrons in the γ-irradiated water give rise to their second ionizations very close to the first ionizations.

As has been shown in the previous section, if two successive ionizations occur within a short distance——let us take 150 Å as the upper limit——the two ion-pairs produced may interact with each other during their thermalization; *i.e.*, these two ion-pairs may be regarded to be in the same spur.

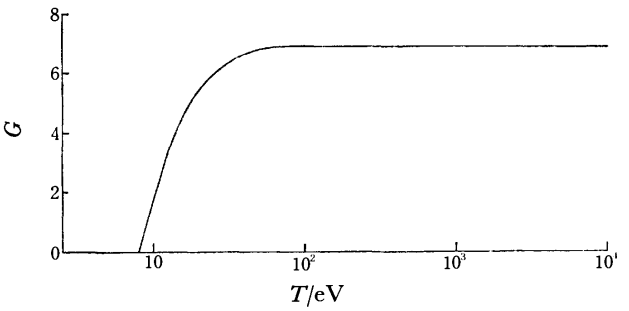

Fig. 7. The G-value of electrons as a function of the energy of the incident electron.

The energy of a "parent" electron which induces two successive ionizations within the interval of 150 Å on the average corresponds to 10 keV. Consequently, if a "parent" electron has the energy higher than 10 keV, "child" electrons produced by this "parent" electron will be isolated from other ionizations. In Fig. 5, the initial energy distribution of "child" electrons in isolated spurs is also plotted. If we plot these values in Fig. 2, the curve obtained is similar to that for N_e. The percentage of the "child" electrons in isolated spurs against the total electrons has been calculated to be 27%.

If the energy of "parent" electrons is lower than 10 keV and sufficiently higher than the ionization potential of water, these electrons will produce condensed spurs, and if the energy of "parent" electrons is a little higher than the ionization potential of water, the spurs generated will contain a few ion-pairs.

In order to calculate the number of ion-pairs in spurs, we need the relationship between the G-value of electrons and the energy of the incident electron. This type of calculation has already been made for helium gas.[11] Figure 7 is the result for water in the liquid phase. By combining this result with the number of "parent" electrons, we can calculate the number of ion-pairs produced in each spur. The calculated numbers, however, are not always integers. Therefore, we tentatively allotted the numbers proportionally to the adjacent integral numbers; for example, when the number was 2.6, we read it as 40% for two ion-pairs and 60% for three ion-pairs. The results thus calculated are summarized in Tables 4 and 5.

Table 4 shows the percentage of the number of spurs which contain different numbers of ion-pairs against the total number of spurs. This result may be compared with the observation of Wilson discussed in the Introduction. Similar observations have been made by Beekman with electrons at higher energies.[17] Both observations are included in Table 4.

On the other hand, Table 5 shows the distribution of ion-pairs in the spurs of different types. It is noticeable that 27% of the ion-pairs are generated in isolated spurs and another 27% of the ion-pairs are generated in very condensed spurs which consist of more than one

TABLE 4. CALCULATED RELATIVE FREQUENCIES OF SPURS IN WATER AND RELATIVE FREQUENCIES OF CLUSTERS OBSERVED IN A CLOUD CHAMBER

Ion-pairs per spur	1	2	3	4	>4
Relative frequency %	73.6	11.7	5.0	3.1	6.6
Ion-pairs per cluster	1	2	3	4	>4
Relative frequency %					
Source: 25 keV[2]	42.6	22.5	12.4	10.1	12.4
150 keV[17]	60	23	8	4	5
320 keV[17]	62	20	9	4	5

TABLE 5. RELATIVE NUMBERS OF ION-PAIRS IN DIFFERENT SPURS

Ion-pairs per spur	Relative number %	
1	26.8	Isolated spurs
2	8.5	Blobs
3	5.4	
4	4.5	
5—10	10.9	
11—100	16.5	Short tracks
101—	27.4	

hundred ion-pairs.

Mozumder and Magee classified spurs into three types: isolated spurs, blobs, and short tracks, on the basis of the energy deposited in them. A similar classification may be applied to the result shown in Table 5: *i.e.*, isolated spurs for the spurs containing only one ion-pair, blobs for the spurs containing two to ten ion-pairs, and short tracks for the spurs containing more than ten ion-pairs.

Discussion

G-Value of Electrons. Figure 8 shows the contribution of different portions of the electron degradation spectrum to the ionization and excitations, singlet and triplet, induced by one keV electrons in water. This type of figure has already been discussed in previous papers.[3,11] From this figure, we can estimate the number of ionizations and excitations during the slowing down of the incident electron.

Let us consider the track of ionizations in water induced by a 1keV electron. Since the ionization probability along the path of a high energy electron is roughly proportional to the reciprocal of the electron energy, the average distance between two successive ionizations near the starting point is about 15 Å. The direction of the path will not be changed so often, because the cross section for small energy loss, around 10 eV, is much larger than that for the larger energy loss. After having induced about 20 ionizations and a few electronic excitations, the energy of the "parent" electron is degraded to 500 eV, a value which is comparable to the binding energy of the electrons in the inner-most shell. After the electron energy reached 500 eV, the path of the "parent" electron may change direction often. The average interval of two successive ionizations is now 9 Å, a distance which corresponds to three times the diameter of a water molecule. Consequently, about 50 ion-pairs may be produced in a very small space at the end of the track of ionizations. Since the diameter of the isolated spur is about 100 Å, as shown in Fig. 3, the density of charged species at the end of the track must be very high. A schematic picture of a short track is shown in Fig. 9.

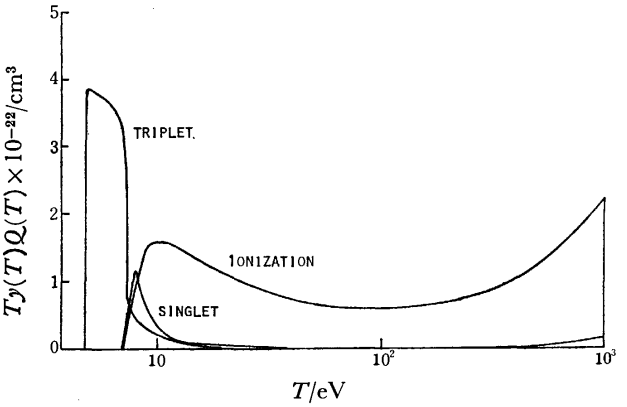

Fig. 8. The contribution of the different portions of the electron degradation spectrum to ionization and singlet and triplet excitations.

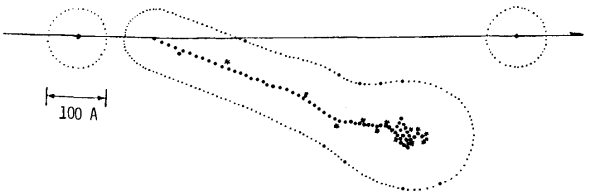

Fig. 9. A schematic picture of an example of short tracks produced by a 1 keV electron. A dot corresponds to an ionization and an asterisk to an excitation.

According to the measurement of Hunt *et al.*, the initial G-value of dry electrons in water is 4.8.[18] They used one mol l^{-1} cadmium ions as the scavenger for electrons. This concentration corresponds to one scavenger ion per 55 water molecules. At the end of the track of a high energy electron, the density of ion-pairs must be comparable to or higher than that of scavenger ions. A large part of the electrons, a percentage which we cannot calculate at present, may escape from the scavenging and be neutralized with their counter ions. Consequently, we do not think that the value $G_e=6.8$ obtained in the present calculation is absurdly large.

The Rate of Slowing Down of Subexcitation Electrons. For the rate of slowing down of subexcitation electrons, we took two values, 10^{13} and 10^{14} eV s^{-1}. These values are somewhat arbitrary, as was stated when we introduced them. If more reliable values become available, these values should be replaced by them. Another point important for the present calculation is the assumption that the rate of energy loss is independent of the electron energy. This assumption might be acceptable for the energy loss due to the "indirect" interaction, but since the "direct" interaction is a kind of resonance effect, the rate of the energy loss must be strongly dependent on the electron energy. Although this process has not been formulated yet, it may be better for the calculation to treat the "direct" interaction as if it were a kind of

electronic excitation.

In the present calculation, only one value of the rate of energy loss has been assumed for all subexcitation electrons ranging from thermal energy to the maximum, E_t. However, when the electron energy is degraded to subvibrational energy ($\approx$0.4 eV), no process of the energy loss but that due to the intermolecular vibrations remains. In a polar solvent, such a slow electron may be solvated by surrounding molecules. In non-polar solvents, however, these electrons may migrate further into the solvent, as suggested by Hummel *et al.*[19] and estimated by Mozumber and Magee.[20]

According to the estimate of Mozumder and Magee, the themalization distance of the subvibrational electrons in hexane is in the order of 50 Å, a distance which is of the same order as that estimated here to be the thermalization distance of the subexcitation electrons.

Spatial Distribution of Ion-pairs in Spurs. Most of electrons and positive ions generated in blobs and short tracks may be neutralized pairwise before they are thermalized. If the concentration is low, electron scavengers can capture only electrons which have escaped the neutralization. The spatial distribution function of ion-pairs derived for the interpretation of the experimental results of electron scavenging and of electric conductivity is, therefore, composed of the sum of two parts: one is the distribution of ion-pairs in isolated spurs and the other is the distribution of ion-pairs which have escaped the neutralization in blobs and short tracks.

As has been shown in the Results section, the spatial distribution of ion-pairs in isolated spurs was well expressed by the function proposed by Abell and Funabashi. However, we think that this agreement resulted from a somewhat fortuitous cancellation.

Let us assume that only one ion-pair is left after the neutralization in each blob and short track. Then, all spurs now contain only one ion-pair, the G-value of which is 2.5 ($\simeq 6.8 \times 26.8/73.6$). As Table 4 shows, 74% of them come from the original isolated spurs and the rest, 26%, from blobs and short tracks. Although we cannot calculate it numerically, the spatial distribution of ion-pairs which have escaped the neutralization in blobs and short tracks may be much broader than that in the original isolated spurs. If we take this contribution into account, the spatial distribution should have a long tail.

On the other hand, the function of Abell and Funabashi has been proposed to explain the experiments carried out with hydrocarbons, in which the thermalization of subvibration electrons has to be considered. As Mozumder suggested,[21] the spatial distribution of electrons during the degradation of subvibrational energies is getting close to a Gaussian, which is sharper than the function of Abell and Funabashi. This effect might cacel the broader distribution of ion-pairs which escaped the neutralization in blobs and short tracks.

References

1) A. Mozumder and J. L. Magee, *Radiat. Res.*, **28**, 203 (1966).
2) C. T. R. Wilson, *Proc. R. Soc. London, Ser. A*, **104**, 1, 192 (1923).
3) S. Sato, K. Okazaki, and S. Ohno, *Bull. Chem. Soc. Jpn.*, **47**, 2174 (1974).
4) H. Fröhlich and R. L. Platzman, *Phys. Rev.*, **92**, 1152 (1953).
5) J. L. Magee and W. P. Helman, *J. Chem. Phys.*, **66**, 310 (1977).
6) J.-P. Dodelet, K. Shinsaka, U. Kortsch, and G. R. Freeman, *J. Chem. Phys.*, **59**, 2376 (1973).
7) S. Sato and T. Oka, *Bull. Chem. Soc. Jpn.*, **44**, 856 (1971).
8) M. Tachiya, *J. Chem. Phys.*, **56**, 4377 (1972); M. Baba and K. Fueki, *Bull. Chem. Soc. Jpn.*, **48**, 2240 (1975).
9) G. C. Abell and K. Funabashi, *J. Chem. Phys.*, **58**, 1079 (1973).
10) C. M. Davison and R. D. Evans, *Rev. Mod. Phys.*, **24**, 79 (1952).
11) S. Sato, K. Kowari, and K. Okazaki, *Bull. Chem. Soc. Jpn.*, **49**, 933 (1976).
12) K. Siegbahn *et al.*, "ESCA Applied to Free Molecules," North-Holland, Amsterdam (1971).
13) Y.-K. Kim, *Radiat. Res.*, **61**, 21 (1975); private communication.
14) D. A. Douthat, *Radiat. Res.*, **61**, 1 (1975).
15) M. Inokuti, *Rev. Mod. Phys.*, **43**, 297 (1971).
16) S. Chandrasekhar, *Rev. Mod. Phys.*, **15**, 1 (1943).
17) W. J. Beekman, *Physica*, **15**, 327 (1949); A. Orc and A. Larsen, *Radiat. Res.*, **21**, 331 (1964).
18) J. W. Hunt, "Advances in Radiation Chemistry," ed by M. Burton and J. L. Magee, John Wiley & Sons, Vol. 5, New York (1976), p. 185.
19) A. Hummel, A. O. Allen, and F. H. Watson, Jr., *J. Chem. Phys.*, **44**, 3431 (1966).
20) A. Mozumder and J. L. Magee, *J. Chem. Phys.*, **47**, 939 (1967).
21) A. Mozumder, "Advances in Radiation Chemistry," ed by M. Burton and J. L. Magee, John Wiley & Sons, Vol. 1, New York (1969), p. 1.

Vibration Spectra and Rotational Isomerism of Chain Molecules. VII.[1] 1-Chloro-, 1-Bromo-, and 1-Iodopropanes, and 1-Chloro-, 1-Bromo-, and 1-Iodobutanes

Yoshiki OGAWA, Shuji IMAZEKI, Hiroko YAMAGUCHI, Hiroatsu MATSUURA,*
Issei HARADA, and Takehiko SHIMANOUCHI**
Department of Chemistry, Faculty of Science, University of Tokyo, Hongo, Bunkyo-ku, Tokyo 113
(Received November 8, 1977)

The Raman and infrared spectra of 1-chloro-, 1-bromo-, and 1-iodopropanes, $CH_3CH_2CH_2X$ (X=Cl, Br, and I), and 1-chloro-, 1-bromo-, and 1-iodobutanes, $CH_3CH_2CH_2CH_2X$ (X=Cl, Br, and I), were measured for the gaseous, liquid, glassy, and crystalline states. The normal vibration frequencies were calculated, a consistent set of force constants explaining the frequencies of basic halogenoalkanes being assumed. The rotational isomerism was studied on the basis of the spectral observations and the normal coordinate calculations. The enthalpy differences among the rotational isomers were examined.

The study of the vibration spectra and rotational isomerism of 1-halogenopropanes was started by Mizushima and coworkers[2] and Radinger and Wittek[3] about thirty years ago. Many studies have been made by means of Raman and infrared,[4-17] microwave,[18,19] and electron-diffraction[20] measurements. As a result, it has been established that the *trans* (T) form exists in the crystalline state except 1-fluoropropane for which the *gauche* (G) form exists[7a,b] and both the T and G forms exist in the liquid and gaseous states. The enthalpy difference between the T and G forms has also been determined by many investigators.[4-6,10,11,17-20] However, as has been indicated previously,[17] the reported values of the enthalpy difference are quite different from one another and there are some disagreements in the vibrational assignments among different authors. These problems remain to be settled.

The rotational isomerism of 1-halogenobutanes has been studied also by means of Raman and infrared,[4-9,14,16,21-25] and electron-diffraction[26] measurements. Ukaji and Bonham[26a] concluded that 1-chlorobutane had an isomer distribution of 37% TG, 24% GG', 17% GG, 11% TT, and 11% GT in the gaseous state at room temperature. Snyder and Schachtschneider[14] observed the infrared spectra of $CH_3(CH_2)_n$-Cl (n=1—5) in the crystalline (annealed solid) and glassy (unannealed solid) states and obtained the refined valence force field through the normal coordinate analysis. They indicated that the vibrational spectra of 1-chlorobutane in the crystalline state are explained by the existence of the TT form and those in the glassy state by the coexistence of the TT form and the TG form with the *gauche* CC–CCl axis. More recently, Crowder and coworkers[7,8] interpreted the vibrational spectra of 1-fluoro- and 1-iodoalkanes, taking into account only two among various isomers, the all-*trans* form and the form which has a *gauche* conformation about the CC–CX axis and a *trans* conformation about the remaining axes. Thus, the whole aspect of the rotational isomers existing in the various states of 1-halogenobutanes is still unknown and the enthalpy differences among the isomers have not yet been determined.

In the previous papers,[27-31] we compared the Raman and infrared spectra of unbranched ethers, paraffins, and sulfides in the crystalline, glassy, liquid, and gaseous states with the results of normal vibration calculations and determined the rotational isomers existing in each state. As a continuation of such studies, the same method has been applied to 1-halogenopropane and 1-halogenobutane molecules. The results show that the method is useful in the study of rotational isomerism. In the course of the research, several new findings including the identification of less stable rotational isomers and the enthalpy differences among the isomers in the liquid state have been obtained. The present paper describes the rotational isomerism and vibrational assignments of 1-halogenopropanes, $CH_3CH_2CH_2X$, and 1-halogenobutanes, $CH_3CH_2CH_2CH_2X$ (X=Cl, Br, and I).

Experimental

Samples used in the present study were purchased from Tokyo Kasei Kogyo Co., Ltd. and were distilled prior to the measurements. The Raman and infrared spectra were measured for the gaseous, liquid, glassy, and crystalline states by the method reported previously.[27,28,30]

The glassy state for the Raman measurements was obtained by immersing the sample enclosed in an ampoule in liquid nitrogen for rapid cooling, and that for the infrared measurements by depositing the sample onto a cooled window of KBr or KRS-5.

For the determination of the enthalpy difference, the Raman spectra in the liquid state were recorded twice at each of nine different temperatures between −105 and 15 °C for 1-chloropropane, nine different temperatures between −100 and 15 °C for 1-bromopropane, eight different temperatures between −85 and 15 °C for 1-iodopropane, and eight different temperatures between −90 and 15 °C for 1-chloro-, 1-bromo-, and 1-iodobutanes. The Raman spectra in the gaseous state were also measured three times at each of four different temperatures between 23 and 80 °C for 1-chloropropane.

Normal Coordinate Treatment

The normal coordinate treatment of the unbranched halogenoalkanes (see Table 1) was carried out with a computer program NCTB2[32] and a HITAC 8700/8800

* Present address: Department of Chemistry, Faculty of Science, Hiroshima University, Higashisenda-machi, Hiroshima 730.

** Present address: College of Information Sciences, University of Tsukuba, Sakura-mura, Niihari-gun, Ibaraki 300-31.

Table 1. Procedure of the least-squares calculation

(i) Chloroalkanes

Step	C_3H_7Cl[a]	C_4H_9Cl[b]	$C_5H_{11}Cl$[c]	ClC_3H_6Cl[d]	ClC_4H_8Cl[c]
1	T (19)	TT (26)			
2	G (17)	TG (13)			
3			TTT (29)		
4			TTG (18)	GG (19)	GTG′ (24)
				TG (12)	
				TT (13)	
5		GT (5)	TGT (14)		TTT (17)
		GG (11)	TGG (11)		TTG (20)
			GTG (9)		TGG (18)
			GTG′ (8)		GTG (16)
					GGG (17)

(ii) Bromoalkanes

Step	C_3H_7Br[a]	C_4H_9Br[b]	$C_5H_{11}Br$[c]	BrC_3H_6Br[d]	BrC_4H_8Br[c]
1	T (19)	TT (24)			
2	G (16)	TG (14)			
3			TTT (31)		
4			TTG (29)	GG (19)	GTG′ (24)
				TG (10)	
				TT (7)	
5		GT (4)	TGT (10)		TTT (19)
		GG (8)	GTT (7)		TTG (20)
			TGG (10)		TGT (17)
			GTG (10)		TGG (20)
			GTG′ (7)		GTG (16)
					GGG (19)
6	CH_3CHDCH_2Br[e]	T (17) G (6)	G′ (6)		
	CH_3CH_2CHDBr[e]	T (16) G (5)	G′ (9)		

(iii) Iodoalkanes

Step	C_3H_7I[a]	C_4H_9I[b]	$C_5H_{11}I$[c]	IC_3H_6I[d]
1	T (19)	TT (24)		
2	G (13)	TG (15)		
3			TTT (28)	
4			TTG (16)	GG (19)
				TG (13)
				TT (19)
5		GT (7)	TGT (12)	
		GG (13)	GTT (9)	
			TGG (14)	
			GTG (10)	
			GTG′ (11)	

(iv) Fluoroalkanes

Step	C_3H_7F[f]	C_4H_9F[f]	$C_5H_{11}F$[f]
1	G (17)	TG (24)	
2			TTG (27)
3	T (9)	TT (7)	
4			TTT (6)
5		GT (3)	TGT (3)
		GG (1)	GTT (3)

Table 1. Continued

The least-squares calculation begins with the simplest halogenoalkanes given in the first step and the first set of force constants is determined so as to give the best fit between the observed and calculated frequencies. This set of force constants gives the definite vibrational assignments of the halogenoalkanes given in the second step and the second set of force constants is subsequently determined from the observed frequencies in this step in addition to those in the first step. By repeating this procedure, the final set of force constants is obtained. The figures in parentheses give the numbers of observed frequencies used for the least-squares calculation. The observed frequencies of the CH and CD stretching vibrations are not included in the calculation and accordingly the force constants associated with these vibrations are not refined. The results of the following references are utilized in the least-squares calculation. a) This study and Ref. 13. b) This study. c) Ref. 34. d) Ref. 35. e) Ref. 15. f) Ref. 7.

computer system at the Computer Center of the University of Tokyo. The calculation made it possible to assign the observed Raman and infrared bands to individual rotational isomers and to determine a consistent set of force constants of halogenoalkanes. Structural parameters and symmetry coordinates used in the calculation and a final set of the force constants will be reported in a separate paper.[33]

The force constants of halogenoalkanes were determined in the following way. The force constants associated with a methyl or methylene group which is not bound directly to a halogen atom were assumed to be the same as those for the paraffin molecules.[32] The force constants associated with the halogen atom, including those of the methyl or methylene group adjacent to the halogen atom, were refined in the least-squares adjustment. The initial values for the chlorine part were transferred from the result by Snyder and Schachtschneider.[14] The initial values for the bromine and iodine parts were estimated from the corresponding values of the chlorine part. Some of the halogenoalkane force constants including those which were unestimable from the observed frequencies were assumed to be the same values as those for the corresponding paraffin force constants.

Table 1 shows the procedure of the least-squares calculation. The calculation began with the simplest halogenoalkanes in the extended form, and then the molecules to be treated were extended to the longer halogenoalkanes and the non-extended forms. In the force constant refinement, we also used the observed frequencies of the deuterated derivatives of 1-bromopropane,[15] 1-halogenopentanes,[34] 1,3-dihalogenopropanes,[35] and 1,4-dihalogenobutanes.[34] A total of 23 force constants associated with the chlorine part were determined from 336 Raman and infrared frequencies of 21 forms of 5 molecular species, 21 force constants associated with the bromine part from 419 frequencies of 29 forms of 7 molecular species, and 23 force constants associated with the iodine part from 242 frequencies of 16 forms of 4 molecular species.

The normal vibration calculation of fluoroalkanes was also carried out in the same way as the other halogenoalkanes on the basis of the experimental data by Crowder and Mao.[7] The procedure of the least-squares calculation of fluoroalkanes is also included in Table 1. A total of 22 force constants associated with the fluorine part were determined from 100 Raman and infrared frequencies of 10 forms of 3 molecular species.

Results

Figures 1—16 show the Raman and infrared spectra in the gaseous, liquid, glassy, and crystalline states. The observed frequencies and the vibrational assignments based on the calculated potential-energy distributions are listed in Tables 2—7. The observed spectra were analyzed with reference to the results of the normal coordinate treatment. The values of enthalpy differences obtained from the intensity variation of the Raman bands with temperature are given in Figs. 17 and 18.

In the following subsections, the rotational isomerism of the individual halogenopropane and halogenobutane molecules is described.

1-Halogenopropanes. These molecules have two possible rotational isomers, T and G, as given in Table 1 of Part I of this series.[27] The observed Raman and infrared spectra and the calculated frequencies are compared in Figs. 7 and 8. These figures show that the T form exists in the crystalline state of 1-chloro-, 1-bromo-, and 1-iodopropanes and the T and G forms coexist in the glassy, liquid, and gaseous states.

The individual rotational isomers of each molecule are discriminated from each other by the Raman key bands of the liquid state, their frequencies being given in parentheses: T form (364 and 723 cm^{-1}) and G form (292, 424, 648, and 787 cm^{-1}) of 1-chloropropane, T form (311 and 648 cm^{-1}) and G form (274, 402, 563, and 777 cm^{-1}) of 1-bromopropane, and T form (288 and 593 cm^{-1}) and G form (390, 503, and 763 cm^{-1}) of 1-iodopropane. These Raman bands were used for the determination of the enthalpy difference between the T and G forms of each molecule. Figure 17 shows the obtained results of the enthalpy differences in the liquid state. As is evidently seen in Fig. 17, the G form is slightly more stable than the T form for any of 1-chloro-, 1-bromo-, and 1-iodopropanes in the liquid state.

The enthalpy difference in the gaseous state of 1-chloropropane was also determined. The ΔH_{G-T} value of 15 ± 30 cal/mol and -210 ± 100 cal/mol were obtained from the pairs of the Raman bands at 663 and 745 cm^{-1} and at 793 and 745 cm^{-1}, respectively. Thus, the G form is as stable as or slightly more stable than the T form in gaseous 1-chloropropane.

1-Halogenobutanes. These molecules have five possible isomers, TT, TG, GT, GG, and GG′,[27] where the first and second conformation symbols in each isomer designation are those for the CC–CC and CC–CX axes,

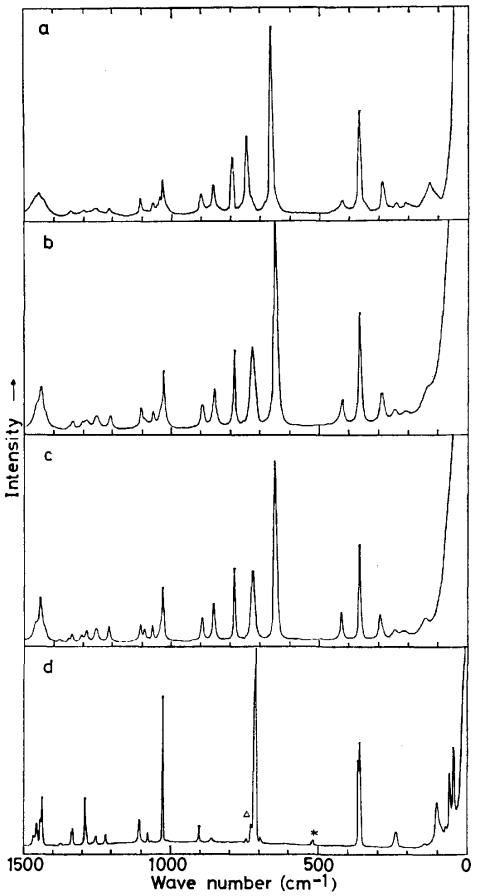

Fig. 1. Raman spectra of 1-chloropropane.
a: Gas (23 °C), b: liquid (23 °C), c: liquid (−100 °C), d: crystal (liquid nitrogen temperature). Following symbols are used in Figs. 1—16. *: Emission line of Ar^+, △: origin unknown, ×: impurity.

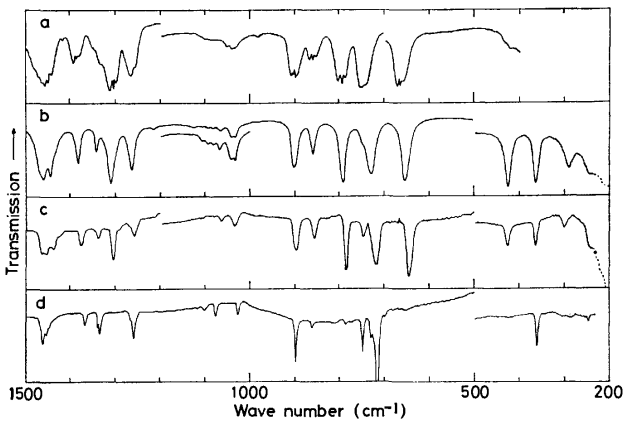

Fig. 2. Infrared spectra of 1-chloropropane.
a: Gas (room temperature), b: liquid (room temperature), c: glass, d: crystal.

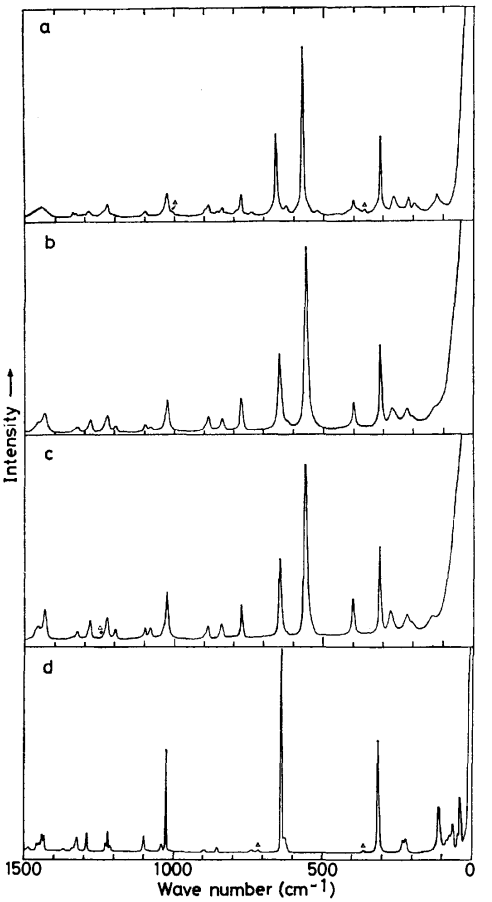

Fig. 3. Raman spectra of 1-bromopropane.
a: Gas (23 °C), b: liquid (23 °C), c: liquid (−90 °C), d: crystal (liquid nitrogen temperature).
The symbol is explained in the caption of Fig. 1.

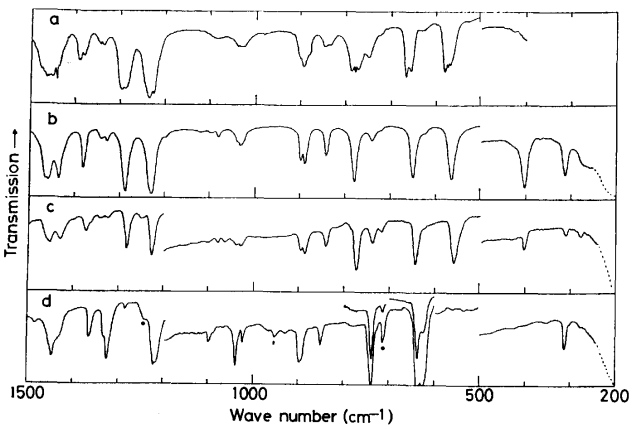

Fig. 4. Infrared spectra of 1-bromopropane.
a: Gas (room temperature), b: liquid (room temperature), c: glass, d: crystal.
The symbol is explained in the caption of Fig. 1.

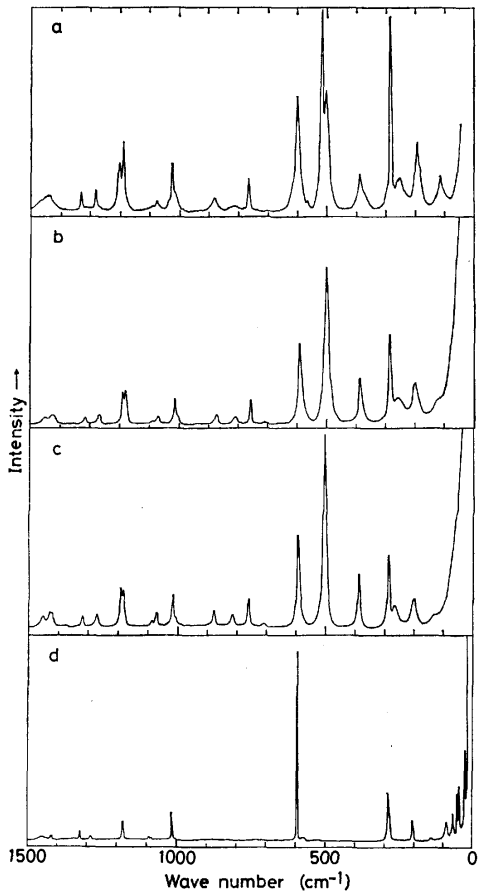

Fig. 5. Raman spectra of 1-iodopropane.
a: Gas (23 °C), b: liquid (23 °C), c: liquid (−80 °C), d: crystal (liquid nitrogen temperature).

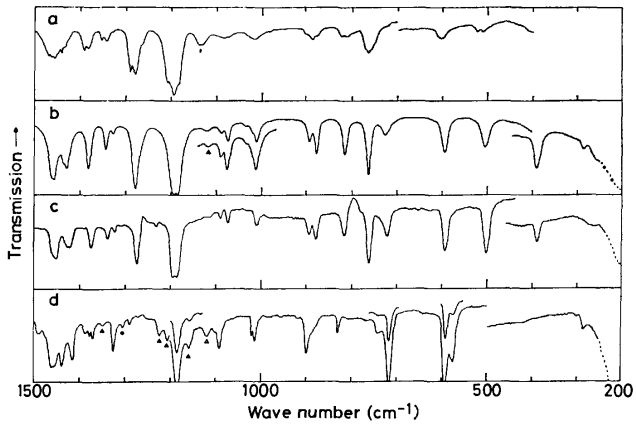

Fig. 6. Infrared spectra of 1-iodopropane.
a: Gas (room temperature), b: liquid (room temperature), c: glass, d: crystal.
The symbol is explained in the caption of Fig. 1.

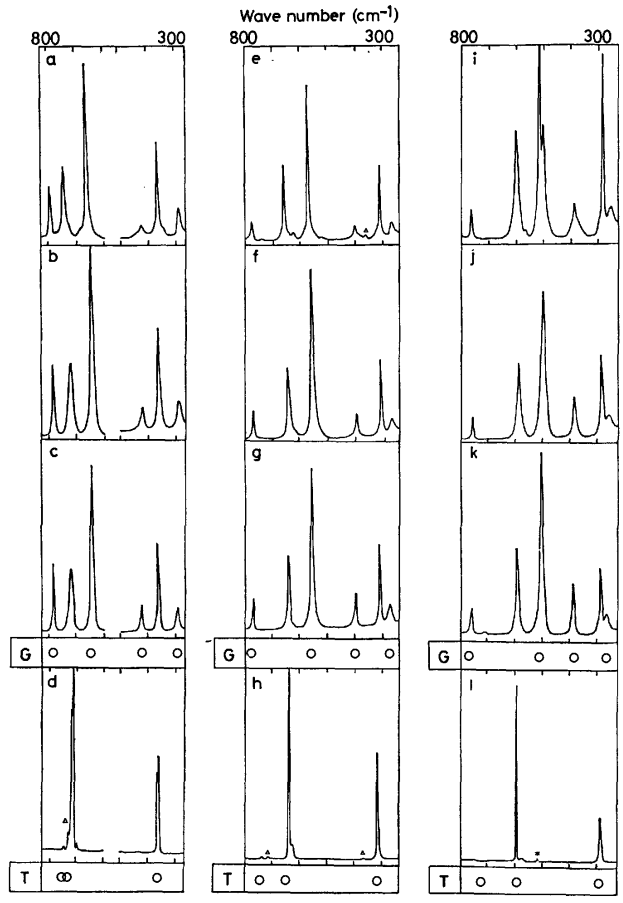

Fig. 7. Comparison between the Raman spectra and the calculated frequencies of 1-halogenopropanes.
1-Chloropropane,
a: gas (23 °C), b: liquid (23 °C), c: liquid (−100 °C), d: crystal (liquid nitrogen temperature).
1-Bromopropane,
e: gas (23 °C), f: liquid (23 °C), g: liquid (−90 °C), h: crystal (liquid nitrogen temperature).
1-Iodopropane,
i: gas (23 °C), j: liquid (23 °C), k: liquid (−80 °C), l: crystal (liquid nitrogen temperature).
The symbols are explained in the caption of Fig. 1.

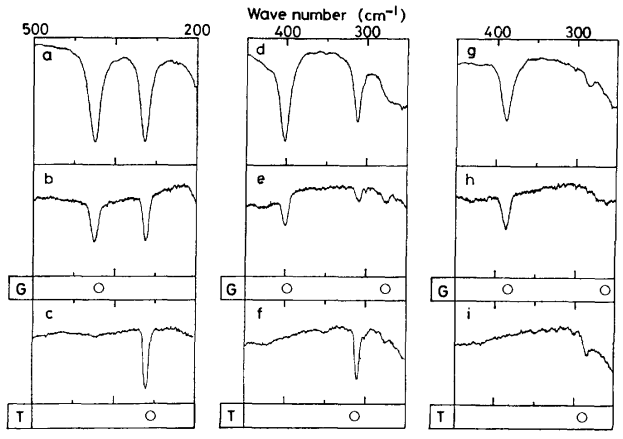

Fig. 8. Comparison between the infrared spectra and the calculated frequencies of 1-halogenopropanes.
1-Chloropropane,
a: liquid (room temperature), b: glass, c: crystal.
1-Bromopropane,
d: liquid (room temperature), e: glass, f: crystal.
1-Iodopropane,
g: liquid (room temperature), h: glass, i: crystal.

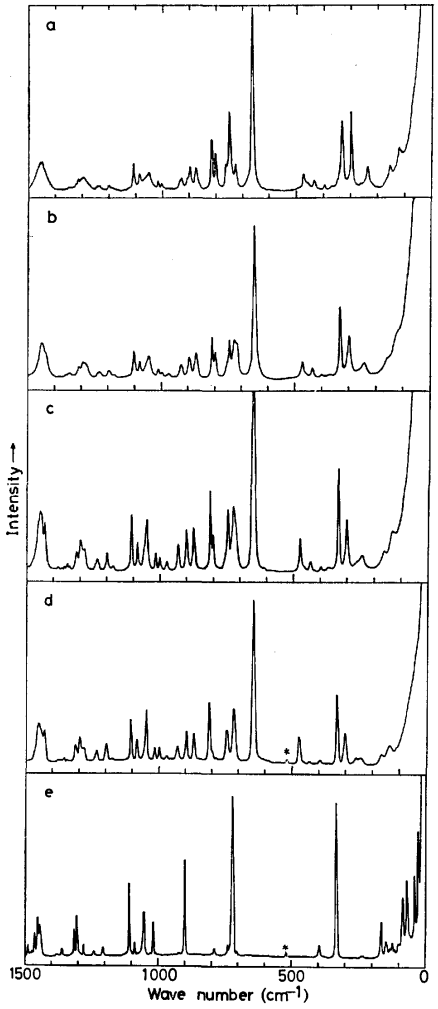

Fig. 9. Raman spectra of 1-chlorobutane.
a: Gas (23 °C), b: liquid (23 °C), c: liquid (−90 °C), d: glass (liquid nitrogen temperature), e: crystal (liquid nitrogen temperature).
The symbol is explained in the caption of Fig. 1.

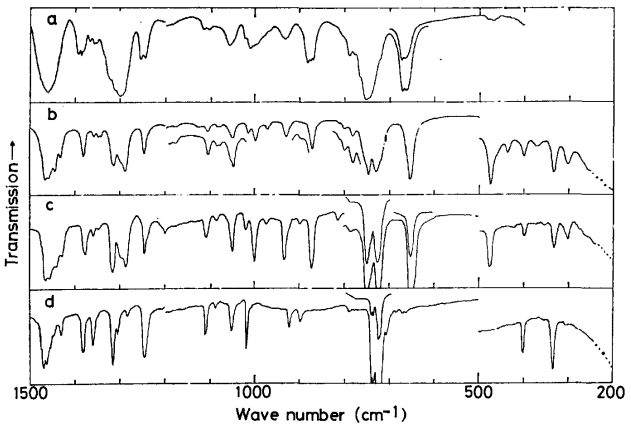

Fig. 10. Infrared spectra of 1-chlorobutane.
a: Gas (room temperature), b: liquid (room temperature), c: glass, d: crystal.

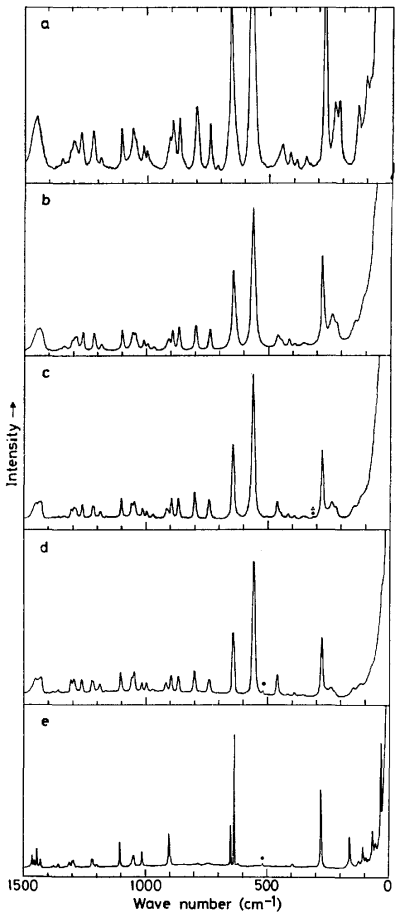

Fig. 11. Raman spectra of 1-bromobutane.
a: Gas (23 °C), b: liquid (23 °C), c: liquid (−90 °C), d: glass (liquid nitrogen temperature), e: crystal (liquid nitrogen temperature).
The symbols are explained in the caption of Fig. 1.

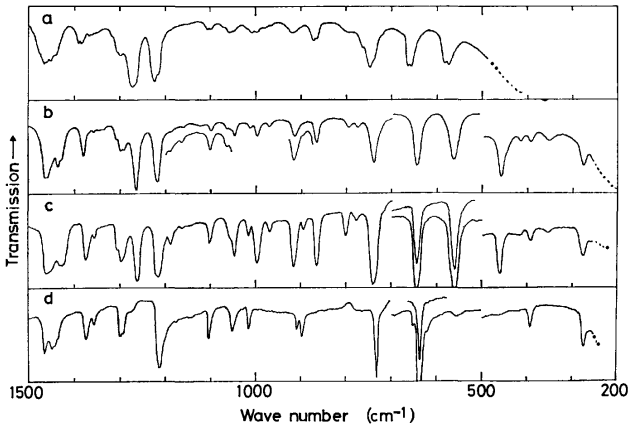

Fig. 12. Infrared spectra of 1-bromobutane.
a: Gas (room temperature), b: liquid (room temperature), c: glass, d: crystal.

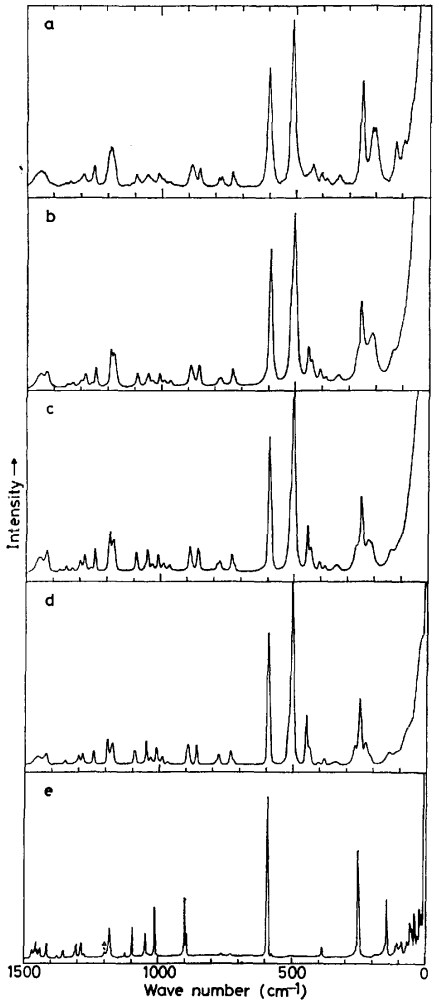

Fig. 13. Raman spectra of 1-iodobutane.
a: Gas (42 °C), b: liquid (23 °C), c: liquid (−95 °C), d: glass (liquid nitrogen temperature), e: crystal (liquid nitrogen temperature).
The symbol is explained in the caption of Fig. 1.

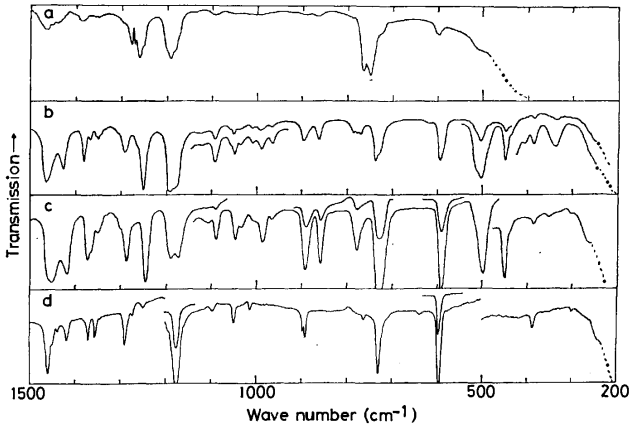

Fig. 14. Infrared spectra of 1-iodobutane.
a: Gas (room temperature), b: liquid (room temperature), c: glass, d: crystal.

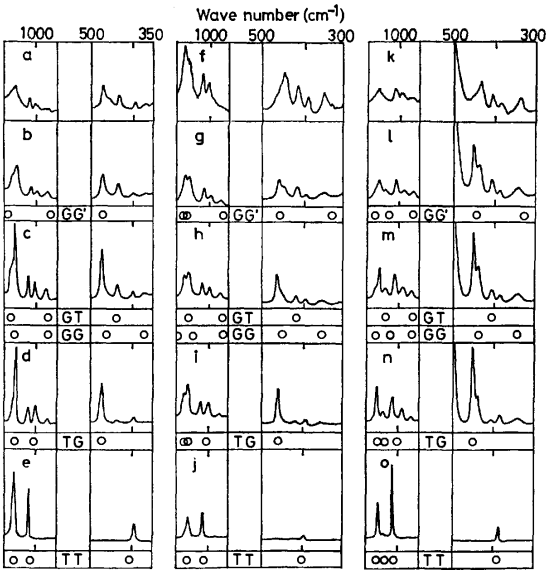

Fig. 15. Comparison between the Raman spectra and the calculated frequencies of 1-halogenobutanes.
1-Chlorobutane,
a: gas (23 °C), b: liquid (23 °C), c: liquid (−90 °C), d, glass (liquid nitrogen temperature), e: crystal (liquid nitrogen temperature).
1-Bromobutane,
f: gas (23 °C), g: liquid (23 °C), h: liquid (−90 °C), i: glass (liquid nitrogen temperature), j: crystal (liquid nitrogen temperature).
1-Iodobutane,
k: gas (42 °C), l: liquid (23 °C), m: liquid (−95 °C), n: glass (liquid nitrogen temperature), o: crystal (liquid nitrogen temperature).

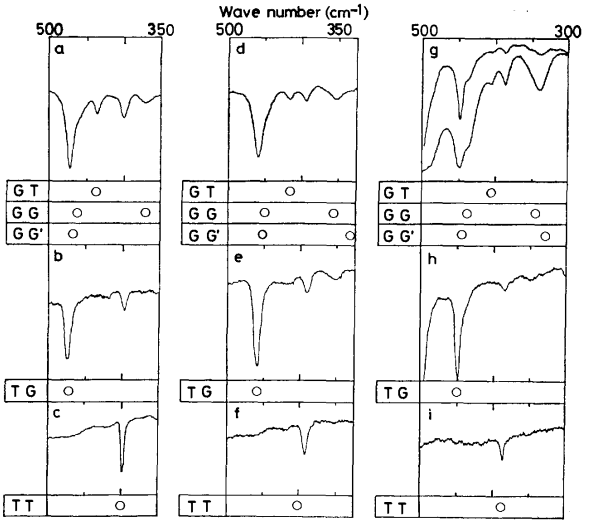

Fig. 16. Comparison between the infrared spectra and the calculated frequencies of 1-halogenobutanes.
1-Chlorobutane,
a: liquid (room temperature), b: glass, c: crystal.
1-Bromobutane,
d: liquid (room temperature), e: glass, f: crystal.
1-Iodobutane,
g: liquid (room temperature), h: glass, i: crystal.

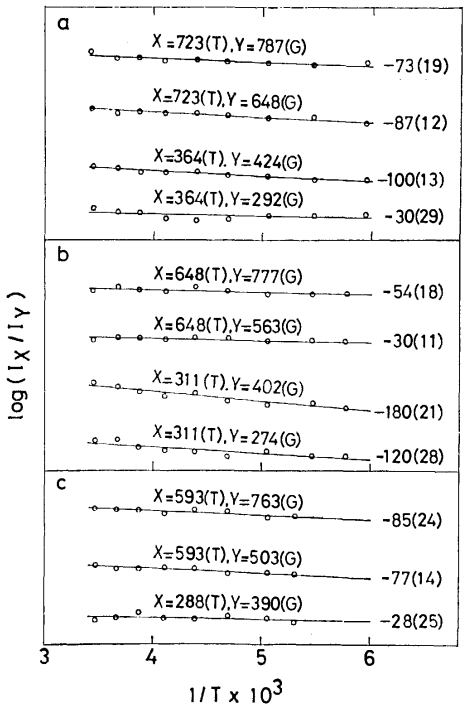

Fig. 17. Enthalpy differences between the T and G forms of 1-halogenopropanes.
a: 1-Chloropropane, b: 1-bromopropane, c: 1-iodopropane.
X and Y denote the band pairs (cm^{-1}). The values of ΔH_{G-T} (cal/mol) are given on the right side of the straight lines. The standard deviations obtained by the method of least-squares are also given in parentheses.

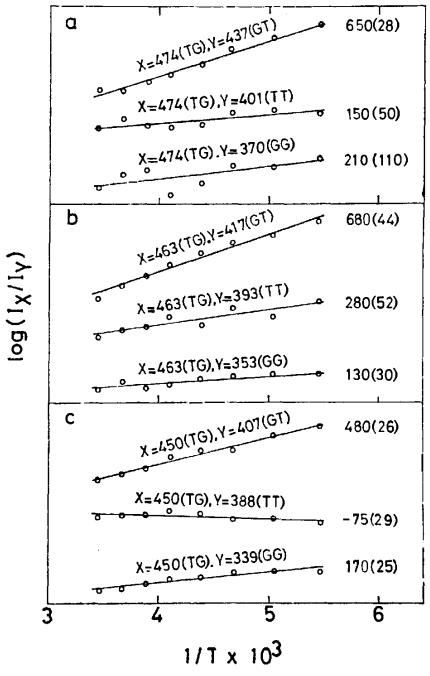

Fig. 18. Enthalpy differences among the TT, TG, GT, and GG forms of 1-halogenobutanes.
a: 1-Chlorobutane, b: 1-bromobutane, c: 1-iodobutane.
X and Y denote the band pairs (cm^{-1}). The values of ΔH_{Y-X} (cal/mol) are given on the right side of the straight lines. The standard deviations obtained by the method of least-squares are also given in parentheses.

respectively. The observed Raman and infrared spectra and the calculated frequencies are compared in Figs. 15 and 16.

For 1-chlorobutane (see Figs. 15a—e and 16a—c), the spectra in the crystalline state show that only the TT form exists. The Raman band at 397 cm^{-1} and the infrared band at 400 cm^{-1} persisting in the crystalline state can be explained only by the existence of the TT form. In the glassy, liquid, and gaseous states, the observed spectra are explained by the coexistence of the TT, TG, GT, and GG forms. The Raman band at 476 cm^{-1} and the infrared band at 474 cm^{-1} in the glassy state, whose intensities relative to those of other bands increase in going from the liquid state to the glassy state, can be explained only by the existence of the TG form. The Raman band at 437 cm^{-1} and the infrared band at 436 cm^{-1} observed in the liquid state are assigned to the GT form, while the Raman bands at 458 (a shoulder of the 474 cm^{-1} band) and 370 cm^{-1} and the infrared bands at 458 (a shoulder of the 473 cm^{-1} band) and 370 cm^{-1} in the liquid state are assigned to the GG form.

For 1-bromobutane (see Figs. 15f—j and 16d—f), the comparison between the observed spectra and the calculated frequencies indicates that the TT form exist in the crystalline state. The Raman band at 397 cm^{-1} and the infrared band at 394 cm^{-1} are assigned only to the TT form. The glassy-, liquid-, and gaseous-state spectra show the coexistence of the TT, TG, GT, and GG forms in these states. The Raman band at 462 cm^{-1} and the infrared band at 459 cm^{-1} in the glassy state, whose intensities are enhanced as compared with those of the liquid state at room temperature, are assigned only to the TG form. The existence of the GT form is confirmed by the Raman and infrared bands at 417 cm^{-1} in the liquid state, and the existence of the GG form is also clear from the observation of the Raman bands at 448 (a shoulder of the 463 cm^{-1} band) and 353 cm^{-1} and the infrared bands at 445 (a shoulder of the 459 cm^{-1} band) and 352 cm^{-1} in the liquid state. In the gaseous state, the Raman spectral pattern around 450 cm^{-1} is different from that in the liquid state. The existence of the TG and GG forms is, however, confirmed definitely by the observation of the Raman bands at 1000 and 350 cm^{-1}, respectively.

For 1-iodobutane (see Figs. 15k—o and 16g—i), the spectra of the crystalline state are explained by the existence of the TT form and those of the glassy, liquid, and gaseous states by the coexistence of the TT, TG, GT, and GG forms similarly to the cases of 1-chloro- and 1-bromobutanes. The Raman band at 389 cm^{-1} and the infrared band at 387 cm^{-1} in the crystalline state are assigned only to the TT form and the Raman band at 452 cm^{-1} and the infrared band at 449 cm^{-1} in the glassy state only to the TG form. The Raman band at 407 cm^{-1} and the infrared band at 406 cm^{-1} in the liquid state indicate the existence of the GT form and the Raman bands at 438 (a shoulder of the 450

TABLE 2. OBSERVED FREQUENCIES AND VIBRATIONAL ASSIGNMENTS OF 1-CHLOROPROPANE

Observed frequency (cm^{-1})[a]							Assignment[b]
Gas		Liquid		Glass	Crystal		
R	IR	R	IR	IR	R	IR	
	1464 S, sh		1464 S, sh	1463 M	1465 VW	1463 M	CH_2 scis
1452 W, b	1457 S 1450 S, sh	1458 W, sh	1457 S	1453 M	1453 W	1455 M 1448 W, sh	CH_3 op-d-deform CH_3 ip-d-deform
	1441 M, sh	1443 M	1442 S	1438 M	1441 W, sh 1434 M	1443 W, sh	CH_2 scis (T)
		1431 VW,sh*	1436 M, sh	1425 VW, sh			CH_2 scis (G)
	1395 M 1388 M 1383 M, sh	1382 VW	1381 M	1378 M	1372 VW	1375 W, sh 1372 W	CH_3 s-deform
	1352 W, sh	1347 VW, sh	1352 VW, sh				CH_2 wag (G)
1343 VW	1335 M, sh	1337 W	1339 M	1339 M	1336 VW 1332 VW	1343 W 1338 M	CH_2 wag (T)
1304 VW	1315 S 1307 S 1300 S	1305 VW, sh	1306 S	1307 M			CH_2 wag (G)
		1288 VW	1300 M, sh	1295 VW, sh	1288 M 1284 VW, sh		CH_2 twist (T)
1259 VW	1266 S 1258 M, sh	1256 W	1266 M, sh 1260 S	1266 W, sh 1261 M	1262 VW, sh 1254 VW	1268 VW, sh 1262 M	CH_2 wag (T) CH_2 twist (G)
1212 VW		1217 VW, sh 1209 W	1211 VW	1215 VW	1220 VW		CH_2 twist (T) CH_2 twist (G)
1108 W	1098 VW, b	1104 W 1090 VW, sh	1103 VW 1090 VW	1105 VW	1104 W	1104 VW	CC stretch (T) CC stretch (G)
1079 VW	1068 VW, sh		1078 VW	1080 VW	1078 VW	1079 W	CH_3 op-rook (T)
1067 W		1063 W	1063 W	1065 W			CC stretch (G)
1042 W, sh	1051 W						
1032 M	1038 W	1038 W, sh 1027 M	1038 W 1030 W	1035 M	1028 VS	1029 W	CH_3 op-rock (G) CC stretch (T)
899 W	908 S 903 S, sh	899 W, sh*	899 S	897 S	904 W	898 S	CH_3 ip-rock (T)
	898 S	895 W	895 S, sh				CH_3 ip-rock (G)
					861 VW	863 VW	CH_2 rock (T)
857 M	866 M 859 M 852 M, sh	856 W	856 M	857 M			CH_2 rock (G)
793 S	802 S 793 S 787 S	787 S	789 VS	786 VS			CH_2 rock (G)
			746 W, sh	748 M	745 VW	748 S	CH_2 rock (T)
					728 VW	730 VW, sh	Origin unknown
745 S	748 S, b	723 S	727 S	720 S	717 S, sh 712 VS	715 VS	CCl stretch (T)
					698 VW		^{13}CCl stretch (T)?
663 VS	671 S 665 S 658 S	648 VS	651 VS	645 VS			CCl stretch (G)
422 VW		424 W	425 VW	425 VW			CCC deform (G)
364 S		364 S	365 VW	362 VW	367 S, sh 361 S	361 VW	CCC deform (T)
288 M		292 M	291 VW	296 VW			CCCl deform (G)
242 VW		248 W	246 VW	245 VW	241 W	245 VW	CCCl deform (T)
207 VW		214 VW					CH_3 torsion (G)
130 W		140 VW			145 W		CC torsion (T, G)

Table 2. Continued

Observed frequency (cm^{-1})[a]							Assignment[b]
Gas		Liquid		Glass	Crystal		
R	IR	R	IR	IR	R	IR	
					103 S 88 W, sh 74 W 59 S 47 S		Lattice vibrations

a) VS: Very strong, S: strong, M: medium, W: weak, VW: very weak, b: broad, sh: shoulder. The broadness of the band shapes in the gaseous state does not always allow us to correlate the individual bands in the liquid state to those in the gaseous state. Only approximate correlations are made in such cases and in other cases of similar situations. The bands denoted with * were observed in the liquid-state Raman spectra at lower temperature. b) For the notation and definition of the local symmetry coordinates, see Ref. 36. According to the results of the normal coordinate treatment,[33] the CH_3 rocking, CH_2 rocking, CH_2 twisting, and CC stretching coordinates are highly coupled to yield complicated vibrational modes. The listed assignments are thus only approximate ones.

Table 3. Observed frequencies and vibrational assignments of 1-bromopropane

Observed frequency (cm^{-1})[a]							Assignment[b]
Gas		Liquid		Glass	Crystal		
R	IR	R	IR	IR	R	IR	
					1485 VW	1484 VW	Overtone or combination?
	1464 S		1464 S			1463 W, sh	CH_2 scis
1452 VW, sh	1451 S	1458 VW, sh	1458 S	1453 M	1457 VW 1450 VW	1458 M, sh 1446 S	CH_3 op-d-deform CH_3 ip-d-deform
1443 W	1443 M, sh	1436 W	1435 S	1428 M	1438 W 1432 W	1440 M, sh 1433 W, sh	CH_2 scis
1387 VW	1393 M 1383 M	1381 VW*	1382 S	1375 M 1363 W, sh	1365 VW	1368 M	CH_3 s-deform (G) CH_3 s-deform (T)
1338 VW	1348 VW	1336 VW, sh	1343 VW	1342 VW			CH_2 wag (G)
1331 VW	1340 VW	1326 VW	1330 W	1327 VW	1335 VW, sh 1321 W	1336 M, sh 1327 S	CH_2 wag (T)
1288 VW	1296 S 1288 S	1290 VW, sh 1283 VW	1287 VS	1283 S	1289 W	1291 VW	CH_2 twist (T) CH_2 twist (G)
				1253 VW		1245 VW, sh	Origin unknown
1233 VW, sh	1235 VS	1233 VW, sh	1233 VS, sh	1226 VS			CH_2 wag (G)
1226 W	1227 VS	1226 W	1228 VS		1226 VW 1219 W	1222 S 1218 S	CH_2 wag (T)
		1213 VW*			1211 VW		CH_2 twist (T)
1200 VW		1198 VW	1200 W				CH_2 twist (G)
1099 VW	1085 W, b	1100 VW	1099 VW	1102 VW	1099 W	1099 W	CC stretch (T)
		1081 VW	1082 VW	1080 VW			CC stretch (G)
				1065 W			CH_3 ip-rock (G)
		1041 VW,sh*	1042 W, sh	1040 W	1039 W	1039 M	CH_3 op-rock (T)
1027 W	1033 W, b	1031 W, sh	1032 M	1029 W			CH_3 op-rock (G)
		1025 M	1025 W, sh		1025 S	1025 W	CC stretch (T)
1008 VW, sh							Origin unknown
						953 VW	Origin unknown
896 VW, sh	903 W, sh 895 M	896 VW, sh	897 M	896 M	895 VW	898 M 894 M, sh	CH_3 ip-rock (T)
887 VW	883 W, sh	886 W	888 M	888 M			CC stretch (G)
856 VW	848 W	850 VW, sh	841 M	842 M	852 VW	851 W	CH_2 rock (T)
840 VW	836 W	840 W					CH_2 rock (G)

Table 3. Continued

Observed frequency (cm^{-1})[a]							
Gas		Liquid		Glass	Crystal		Assignment[b]
R	IR	R	IR	IR	R	IR	
792 VW, sh 778 W	788 M 780 M 773 M	777 M	778 S	774 VS			CH_2 rock (G)
742 VW	752 W		740 W	738 M	736 VW	738 VS	CH_2 rock (T)
				720 VW	714 VW	714 W	Origin unknown
660 S	666 S 657 S	648 S	648 S	644 VS	638 VS	637 VS	CBr stretch (T)
627 W	630 W, b	620 VW, sh	620 VW, sh		625 VW, sh	623 VW, sh	2×313 cm^{-1} or ^{13}CBr stretch (T)?
572 VS	580 S 573 S 567 S	563 VS	563 VS	559 VS			CBr stretch (G)
523 VW							Origin unknown
401 W		402 M	401 VW	402 VW			CCC deform (G)
363 VW					363 VW		Origin unknown
311 S		311 S	312 VW	311 VW	313 S	311 VW	CCC deform (T)
268 W		274 W	273 VW	277 VW			CCBr deform (G)
					232 W		CH_3 torsion (T)
217 W		224 W			222 W		CCBr deform (T)
198 VW		205 VW, sh					CH_3 torsion (G)
122 W		133 W					CC torsion (T)
					115 W, sh 111 M 86 W, sh 77 W, sh 65 M 48 W, sh 39 M		Lattice vibrations

a), b) See a) and b), respectively, of Table 2.

Table 4. Observed frequencies and vibrational assignments of 1-iodopropane

Observed frequency (cm^{-1})[a]							
Gas		Liquid		Glass	Crystal		Assignment[b]
R	IR	R	IR	IR	R	IR	
						1488 W	$591+898$ cm^{-1}?
		1469 VW, sh*	1460 S			1473 W, sh	CH_2 scis
	1458 M 1443 W, sh	1455 W	1456 S	1452 M	1460 VW 1454 VW 1448 VW 1443 VW	1460 S 1451 S 1438 S	CH_3 op-d-deform CH_3 ip-d-deform
1435 W, b		1433 W	1435 M, sh	1423 M			CH_2 scis (G)
		1427 W	1428 S		1418 VW	1415 S	CH_2 scis (T)
1383 VW	1392 M 1383 M	1378 VW	1380 S	1376 M	1375 VW 1367 VW	1386 W 1376 W 1370 W	CH_3 s-deform
						1349 VW	Origin unknown
	1354 W 1343 W	1338 VW, sh*	1344 M	1340 W			CH_2 wag (G)
1332 W		1323 W	1328 W	1325 VW	1324 W	1325 M	CH_2 wag (T)
						1304 VW	Origin unknown
1282 W	1291 S 1279 S	1285 VW, sh* 1273 W	1279 S	1275 S	1286 VW	1289 VW	CH_2 twist (T) CH_2 twist (G)
						1212 VW	Origin unknown
						1206 VW	Origin unknown

TABLE 4. CONTINUED

Observed frequency (cm^{-1})[a]							Assignment[b]
Gas		Liquid		Glass	Crystal		
R	IR	R	IR	IR	R	IR	
1202 M	1208 S 1195 VS	1194 M	1195 VS	1194 VS			CH_2 wag (G)
1189 M	1185 VS, sh	1184 M	1185 VS	1186 VS	1182 W	1185 VS	CH_2 wag (T), CH_2 twist (T)
						1158 W, sh	Origin unknown
	1133 W		1121 VW			1117 W	Origin unknown
1089 VW 1076 W	1083 W, b	1088 VW 1073 W	1089 VW 1075 W	1090 VW 1075 W	1092 VW 1087 VW	1090 M	CC stretch (T) CC stretch (G)
1035 VW, sh		1032 VW, sh	1036 VW, sh				CH_3 op-rock (G)
1024 M 1013 W, sh	1016 W, b	1019 M 1011 W, sh	1020 W, sh 1012 M	1010 W	1016 W 1011 VW	1020 W 1013 W	CC strech (T) CH_3 op-rock (T), CC stretch (G)
895 VW, sh 880 W	888 M	894 VW, sh 879 W	895 M 880 M	895 M 880 M	898 VW	898 M 880 W, sh	CH_3 ip-rock (T) CH_3 ip-rock (G)
	823 W, sh	828 VW, sh			828 VW	829 W	CH_2 rock (T)
817 VW	812 W	816 VW	816 M	817 M			CH_2 rock (G)
765 W	765 M	763 M	764 S	762 S			CH_2 rock (G)
		711 VW	726 W	722 M	724 VW	716 VS	CH_2 rock (T)
602 S	603 W	593 S	594 M	593 S	594 VS	591 VS	CI stretch (T)
					578 VW	575 W	^{13}CI stretch (T)
518 VS 503 S	523 W 512 W	503 VS	503 M	500 S			CI stretch (G)
388 W		390 M	388 VW	388 VW			CCC deform (G)
285 VS		288 S	285 VW	270 VW	286 S	285 VW	CCC deform (T)
256 W		263 W	263 VW				CCI deform (G)
					240 VW		CH_3 torsion (T)
197 M		203 M			206 M		CCI deform (T)
189 W, sh							CH_3 torsion (G)
116 W		130 VW			144 VW		CC torsion (T)
					116 VW 91 M 69 M 53 S 46 S 28 S		Lattice vibrations

a), b) See a) and b), respectively, of Table 2.

cm^{-1} band) and 339 cm^{-1} and the infrared bands at 438 (a shoulder of the 449 cm^{-1} band) and 339 cm^{-1} indicate the existence of the GG form. In the gaseous state, a trend similar to the case of 1-bromobutane is observed in the Raman spectral pattern around 440 cm^{-1}. The existence of the TG and GG forms is confirmed by the observation of the Raman bands at 995 and 337 cm^{-1}, respectively.

It is not probable that the GG′ form of 1-bromobutane exists, since no bands are observed in the gaseous, liquid, or glassy state around its characteristic frequency of 331 cm^{-1}. The distance between the terminal methyl group and the bromine atom seems to be too short for the GG′ form to be stable. Thus, it is also improbable that the GG′ form of 1-chloro- or 1-iodobutane exists, although its existence is uncertain from the normal coordinate analysis because of the coincidence of the frequencies of the GG′ and other forms.

As has been described above, the key bands for the individual isomers of each molecule in the skeletal deformation region have become clear. These key bands were used for the determination of the enthalpy differences among the isomers in the liquid state. Figure 18 shows the obtained results of the enthalpy differences.

For 1-chlorobutane, the intensity ratios of the Raman bands at 370 (GG form) and 474 cm^{-1} (TG form), those at 401 (TT form) and 474 cm^{-1}, and those at 437 (GT form) and 474 cm^{-1} gave the enthalpy differences, $\Delta H_{GG-TG}=210\pm110$ cal/mol, $\Delta H_{TT-TG}=150\pm50$ cal/

Table 5. Observed frequencies and vibrational assignments of 1-chlorobutane

Observed frequency (cm^{-1})[a]								Assignment[b]
Gas		Liquid		Glass		Crystal		
R	IR	R	IR	R	IR	R	IR	
		1480 VW, sh	1476 M, sh	1483 VW, sh	1474 M, sh	1488 W	1486 VW	CH_2 scis
		1468 M, sh*	1467 VS	1468 W, sh	1465 S	1477 VW 1471 VW	1475 M, sh 1469 S	CH_3 op-d-deform, CH_2 scis
1454 M, b	1460 VS, b	1458 M*	1460 VS	1454 M	1456 S	1462 W 1451 M	1462 S 1454 M, sh	CH_2 scis, CH_3 op-d-deform
		1447 M	1446 S	1443 M	1442 M, sh	1444 M	1447 W, sh	CH_3 ip-d-deform
		1434 W, sh	1433 M	1432 M	1428 M, sh	1438 W, sh	1432 W	CH_2 scis
	1393 M 1387 M	1383 VW	1383 M	1380 VW	1377 M	1378 VW	1383 M	CH_3 s-deform
	1368 W	1369 VW		1370 VW				CH_2 wag (TG)
	1359 W	1358 VW	1360 VW	1360 VW	1359 W	1360 VW	1362 M	CH_2 wag (TT, GG)
1348 VW	1352 W 1340 W, sh	1346 VW	1349 VW 1344 W	1346 VW	1348 VW			CH_2 wag (GT) CH_2 wag (GG, GT)
	1322 M, sh		1319 M, sh					CH_2 wag (TG)
1313 W, sh	1312 S, sh	1311 W	1316 M	1315 W	1315 S	1324 VW 1314 W	1316 S 1307 W	CH_2 wag (TT, GG)
1297 W	1300 VS	1300 W	1302 M, sh	1299 W	1298 M, sh	1303 M		CH_2 twist (TT, TG)
		1285 W, sh	1291 S	1284 VW	1285 S			CH_2 wag (TG), CH_2 twist (GT)
						1280 VW	1284 VW	CH_2 twist (TT)
1250 VW	1253 M 1244 M	1242 VW, sh	1248 M	1242 VW, sh	1245 M	1240 VW	1246 S	CH_2 wag (TT), CH_2 twist (GT)
1238 VW		1234 VW	1234 VW, sh	1236 W	1237 W, sh			CH_2 twist (TG)
1228 VW		1230 VW, sh						CH_2 twist (GG)
						1205 W	1208 VW	CH_2 twist (TT)
1198 W	1195 VW	1198 VW	1200 VW	1199 W	1200 W			CH_2 twist (TG)
			1190 VW					CH_2 twist (GT)
		1178 VW, sh	1178 VW	1178 VW				CH_2 twist (GG)
1107 W	1113 W 1102 W	1107 W	1106 W	1108 M	1106 W	1109 S 1100 VW	1109 M	CC stretch (TT, TG, GT)
1085 W		1084 W	1085 VW	1086 W	1083 VW	1087 W	1088 VW	CH_2 rock (TT), CH_3 ip-rock (TG), CC stretch (GT)
			1080 VW					CH_3 op-rock (GG)
1064 W, sh	1057 W	1058 W, sh	1058 VW, sh					CC stretch (GG, GT)
1050 W	1050 W, sh	1050 W	1051 W	1049 M	1048 M	1052 M	1052 M	CC stretch (TT, TG)
1017 VW	1023 W, sh	1015 VW	1017 W	1018 W	1017 W	1017 M	1018 M	CC stretch (TT)
1000 VW	1010 W	998 VW	1000 W	1000 W	999 M			CC stretch (TG)
976 VW	972 W, sh	972 VW	973 VW	973 VW	972 VW			CH_3 ip-rock (GG), CH_3 op-rock (GT)
929 VW	934 W	932 VW, sh	932 W	932 W	931 M			CH_2 rock (TG)
		927 W			922 VW, sh	920 VW	924 W	CH_3 op-rock (TT), CH_2 rock (GG, GT)
897 W		896 W	898 VW	899 W	897 VW	900 S	898 W	CH_3 ip-rock (TT, GT)
876 W	882 M 877 M 872 M	872 W	875 M	872 W	870 S			CH_3 op-rock (TG), CH_2 rock (GG)
813 M		811 M	812 VW	813 M	812 VW			CH_2 rock (TG)
800 M		800 W	801 VW	803 VW, sh	804 VW, sh			CC stretch (GG), CH_2 rock (GT)
	790 M		783 W	786 VW	783 VW	788 VW	787 VW	CH_2 rock (TT)
761 W	767 M, sh	755 VW, sh	757 M, sh					CH_2 rock (GG, TT)
	753 VS	746 M	747 S	746 W	747 VS			CH_2 rock (TG)
					738 M, sh	743 VW 738 VW	740 S 736 S	CH_2 rock (TT)

Table 5. Continued

Observed frequency (cm^{-1})[a]								
Gas		Liquid		Glass		Crystal		Assignment[b]
R	IR	R	IR	R	IR	R	IR	
748 S	743 VS	727 M	730 S	721 M	723 VS	725 S 718 VS	722 VS	CCl stretch (TT)
726 W	722 M, sh	718 M, sh	718 M, sh					CCl stretch (GT)
665 VS	671 S 663 S	653 VS	653 VS	647 VS	650 VS			CCl stretch (TG, GG)
473 W		474 W	473 VW	476 W	474 VW			CCC deform (TG)
459 VW, sh		458 VW, sh	458 VW, sh					CCC deform (GG)
434 VW		437 VW	436 VW	438 VW				CCC deform (GT)
397 VW		401 VW	399 VW	398 VW	398 VW	397 W	400 VW	CCC deform (TT)
370 VW		370 VW	370 VW	370 VW				CCC deform (GG)
332 S		334 S	333 VW	334 S	332 VW	333 VS	334 VW	CCC deform (TT)
298 S		302 M	300 VW	305 W	302 VW			CCCl deform (TG), CCC deform (GT)
262 VW		265 VW, sh		266 VW				CCC deform (TG), CCCl deform (GT)
238 VW		243 VW		247 VW				CCCl deform (GG)
						237 VW		CH_3 torsion (TT)
154 VW		161 VW		170 VW		166 M		CCCl deform (TT)
						148 W		
120 VW		125 VW		139 W		133 VW		
						124 W		
						100 VW		Torsions (TT) and
						85 M		lattice vibrations
						69 S		
						41 S		
						28 S		

a), b) See a) and b), respectively, of Table 2.

Table 6. Observed frequencies and vibrational assignments of 1-bromobutane

Observed frequency (cm^{-1})[a]								
Gas		Liquid		Glass		Crystal		Assignment[b]
R	IR	R	IR	R	IR	R	IR	
		1488 VW*	1473 W, sh	1488 VW, sh		1478 VW		CH_2 scis
	1465 M	1465 W, sh*	1466 S	1468 W, sh	1462 S	1462 W	1466 M	CH_3 op-d-deform, CH_2 scis
1453 M, sh		1456 W, sh*	1458 S, sh			1454 VW	1448 M	CH_2 scis
	1452 M, sh							
1448 M		1448 M	1452 M, sh	1448 M		1443 W	1442 M	CH_3 ip-d-deform
	1442 M, sh	1438 M	1437 S					CH_2 scis
		1429 W, sh	1430 M, sh	1427 M	1430 S	1433 VW 1428 W	1435 W, sh	CH_2 scis
	1390 W 1386 W	1381 VW	1382 M	1378 VW	1378 M	1376 VW	1375 M	CH_3 s-deform
	1368 VW		1370 VW, sh		1368 M, sh			CH_2 wag (TG)
1363 VW		1357 VW	1360 VW	1356 VW	1358 W	1356 VW	1358 W	CH_2 wag (TT)
			1355 VW					CH_2 wag (GG)
			1347 VW					CH_2 wag (GT)
1343 VW		1337 VW	1340 VW					CH_2 wag (GG, GT)
1308 W, sh	1307 M, sh	1305 W	1308 W, sh	1305 W	1308 M, sh	1312 W		CH_2 twist (TT,TG)
1295 W	1300 M	1295 W	1299 M	1294 W	1298 M	1300 W 1296 W	1299 M 1293 M	CH_2 wag (TT, TG)
	1297 M	1288 W	1293 M		1292 M, sh			CH_2 twist (GG, GT)
				1273 VW		1275 VW 1270 VW	1277 VW	CH_2 twist (TT)
1267 M	1272 VS	1262 M	1267 VS	1261 W	1263 VS			CH_2 twist (TG, GG, GT)

Table 6. Continued

Observed frequency (cm^{-1})[a]								Assignment[b]
Gas		Liquid		Glass		Crystal		
R	IR	R	IR	R	IR	R	IR	
1217 M	1224 VS 1217 S, sh	1220 W, sh* 1215 M	1219 VS	1218 W	1222 VS 1217 VS	1217 W 1209 VW, sh	1213 S	CH_2 wag (TG, GG, GT) CH_2 wag (TT)
				1198 VW	1203 W, sh	1199 VW		CH_2 rock (TT)
1189 VW		1186 VW	1189 VW	1187 W	1189 W			CH_2 twist (TG, GT)
1155 VW		1160 VW	1164 VW	1162 VW	1164 VW			CH_2 twist (GG)
1103 M	1107 W 1100 W	1100 M	1100 W	1101 M	1103 W	1104 M	1104 M	CC stretch (TT, GT)
					1100 W, sh			CC stretch (TG)
	1074 VW, sh			1080 VW				CC stretch (GT)
			1064 VW					CH_3 op-rock (GG)
1060 M	1057 W	1057 M	1053 VW, sh	1056 W, sh	1056 W, sh	1056 W, sh	1051 M	CC stretch (TT), CH_3 ip-rock (TG)
1048 W, sh	1048 W, sh	1048 M	1048 W	1046 M	1047 M	1047 W		CH_2 twist (TT), CC stretch (TG, GT)
1013 W	1022 VW, sh 1008 W	1013 W	1014 VW	1014 W	1016 W	1013 W	1016 W	CC stretch (TT)
1000 VW	997 W	997 VW	996 W	996 W	997 S			CC stretch (TG)
973 VW, sh		972 VW	970 VW	969 VW	970 W			CH_3 ip-rock (GG), CH_3 op-rock (GT)
915 VW, sh	918 W	915 VW, sh	915 W	913 W	916 S			CH_2 rock (TG, GG)
907 W, sh		907 W					908 W	CH_3 op-rock (TT), CH_2 rock (GT)
896 M		893 M	895 VW	893 W	895 W	902 M 897 W, sh	898 W	CH_3 ip-rock (TT)
869 M	873 W 868 W	868 M	867 M	864 W	865 S			CH_3 op-rock (TG), CH_2 rock (GG), CH_3 ip-rock (GT)
800 S	800 W	799 M	797 W	801 M	801 W			CH_2 rock (TG), CC stretch (GG)
	783 W	777 VW*	777 W	775 VW	778 W	776 VW		CH_2 rock (TT, GT)
743 M	764 W, sh 748 S	740 M	742 S	740 W	740 VS			CH_2 rock (TG, GG, GT)
	738 M, sh		732 M, sh		733 VS	741 VW	733 VS	CH_2 rock (TT)
658 VS	664 M 657 M	643 S	646 S	640 S	642 VS	649 M 636 VS	650 VW, sh 637 VS	CBr stretch (TT, GT)
					621 VW	620 VW	620 W, sh	^{13}CBr stretch (TT)?
576 VS	582 M 574 M	562 VS	564 S	558 VS	558 VS			CBr stretch (TG, GG)
456 VW, sh		463 W	459 VW	462 M	459 VW			CCC deform (TG)
448 W		448 VW, sh	445 VW, sh	448 VW, sh	444 VW, sh			CCC deform (GG)
415 VW		417 VW	417 VW	419 VW	417 VW			CCC deform (GT)
390 VW		393 VW	393 VW	392 VW	392 VW	397 VW	394 VW	CCC deform (TT)
350 VW		353 VW	352 VW	355 VW	352 VW			CCC deform (GG)
276 VS		279 S	277 VW	278 S	275 VW	280 S	274 VW	CCC deform (TT, GT), CCBr deform (TG)
				267 W, sh				CCC deform (TG)
232 S		238 M		242 W				CCBr deform (GT)
215 S		224 M, sh		227 VW, sh				CH_3 torsion
138 M		143 W		153 VW		162 M		CCBr deform (TT)
105 W		115 VW		122 VW		125 VW		CC torsion
						108 W 93 VW 84 VW 67 M 57 W 42 VW, sh 36 S		Torsion (TT) and lattice vibrations

a), b) See a) and b), respectively, of Table 2.

TABLE 7. OBSERVED FREQUENCIES AND VIBRATIONAL ASSIGNMENTS OF 1-IODOBUTANE

Observed frequency (cm^{-1})[a]								Assignment[b]
Gas		Liquid		Glass		Crystal		
R	IR	R	IR	R	IR	R	IR	
			1474 W, sh	1481 VW		1470 VW		CH_2 scis
	1465 VW, sh	1466 VW*	1463 S	1465 VW, sh	1458 VS, sh	1457 W	1459 S	CH_3 op-d-deform, CH_2 scis
	1460 W	1453 W, sh*	1457 S, sh	1452 W	1451 VS	1452 VW	1450 M, sh	CH_2 scis
1448 W, b	1452 W, sh	1446 W	1445 M, sh			1441 VW	1438 VW	CH_3 ip-d-deform
	1437 W, sh	1429 W	1431 M, sh	1430 W, sh				CH_2 scis
		1423 W, sh*	1425 M, sh	1424 W				CH_2 scis
			1419 M		1419 S	1417 W	1419 W	CH_2 scis
	1384 W	1379 VW	1380 M	1377 VW	1373 S	1377 VW 1372 VW	1371 W	CH_3 s-deform
		1368 VW	1367 W	1366 VW	1365 M, sh			CH_2 wag (TG)
1355 VW	1352 VW	1353 VW	1354 W, sh	1353 VW	1353 W	1354 VW	1356 W	CH_2 wag (TT, GG)
			1350 W					CH_2 wag (GT)
1339 VW		1343 VW 1333 VW	1343 W, sh 1336 VW, sh	1343 VW 1332 VW	1333 VW, sh			CH_2 wag (GG) CH_2 wag (GT)
		1303 VW	1306 VW, sh	1302 W	1304 W, sh	1308 W		CH_2 twist (TT, TG)
	1298 VW, sh		1295 W, sh					CH_2 wag (TG)
1289 VW		1288 W	1290 W	1287 W	1288 S	1290 W 1276 VW	1289 M 1274 VW	CH_2 wag (TT)
	1278 M 1271 M, sh			1272 VW	1272 W, sh			CH_2 twist (GG)
	1261 M	1263 VW	1264 W, sh	1263 VW				CH_2 twist (GT)
1250 W	1252 M, sh	1248 W	1250 VS	1247 W	1246 VS		1250 VW	CH_2 twist (TT, TG, GG, GT)
						1201 VW		Origin unknwn
1193 M, sh	1203 M, sh 1193 M	1191 M	1192 VS	1192 W	1190 M			CH_2 wag (TG, GG)
1185 M	1183 M, sh	1183 M	1183 VS, sh	1182 W, sh		1187 W, sh 1183 W		CH_2 wag (TT, GT)
		1175 M, sh	1175 VS, sh	1176 W	1173 M	1178 VW	1175 VS	CH_2 rock (TT), CH_2 twist (GT)
		1153 VW, sh*		1157 VW	1153 W, sh			CH_3 ip-rock (TG)
			1122 VW					CC stretch (GG)
1095 W	1094 VW	1093 W	1093 W	1093 W	1089 VW	1098 W	1095 VW	CC stretch(TT,TG)
		1089 VW, sh		1091 W, sh				CC stretch (GT)
		1059 VW, sh	1058 VW, sh					CH_3 op-rock (GG)
1050 W		1049 W	1050 VW	1050 W	1047 VW	1050 W	1049 W	CC stretch (TT, TG)
		1037 VW	1039 VW, sh					CH_3 ip-rock (GT)
		1032 VW, sh	1032 VW, sh	1036 VW	1035 VW, sh	1034 VW 1024 VW	1029 VW	CH_2 twist (TT, TG)
1010 W		1008 W	1011 VW	1013 W	1008 VW, sh	1014 M 1006 VW	1013 VW	CC stretch (TT)
995 VW		990 VW	991 VW	990 VW	987 W			CC stretch (TG)
970 VW		968 VW	968 VW	970 VW	966 VW, sh			CH_3 ip-rock (GG), CH_3 op-rock (GT)
	898 VW	896 W, sh	896 W	895 W, sh				CH_2 rock (TG, GT)
889 W		889 W	891 VW, sh	892 W	893 W	901 M 895 W	898 W 892 M	CH_3 ip-rock (TT), CH_3 op-rock (TT)
		886 W, sh						CH_2 rock (GG)
860 W	870 VW 863 VW	861 W	863 W	861 W	859 W			CH_3 op-rock (TG), CH_2 rock (GG)
786 W	790 VW, sh	786 VW	787 W	792 VW, sh	788 VW, sh			CC stretch (GG)
778 W		779 VW	779 W	781 VW	778 W			CH_2 rock (TG, GT)
	765 VS 759 VS, sh 750 VS		772 W	763 VW	765 VW, sh	764 VW	762 VW	CH_2 rock (TT)

Table 7. Continued

Observed frequency (cm^{-1})[a]								Assignment[b]
Gas		Liquid		Glass		Crystal		
R	IR	R	IR	R	IR	R	IR	
736 W		736 W	735 M	735 W	728 M			CH_2 rock (TG, GG)
728 VW, sh	724 W, sh	728 W, sh	726 M, sh	723 VW, sh		731 VW	730 S	CH_2 rock (TT, GT)
601 S	600 W	593 S	592 M	593 S	590 M	595 S 592 VS 589 S	596 VS	CI stretch(TT, GT)
						577 VW		^{13}CI stretch (TT)?
		515 S, sh	518 VW, sh	517 M, sh	520 VW, sh			CI stretch (GG)
511 VS		506 VS	504 W	503 VS	500 W			CI stretch (TG)
453 VW, sh		450 M	449 VW	452 M	449 VW			CCC deform (TG)
436 VW		438 W, sh	438 VW, sh	442 W, sh	435 VW			CCC deform (GG)
408 VW		407 W	406 VW	407 VW				CCC deform (GT)
385 VW		388 VW	387 VW	386 VW	384 VW	389 VW	387 VW	CCC deform (TT)
337 W		339 VW	339 VW	341 VW	348 VW			CCC deform (GG)
		267 M, sh	268 VW	270 W	267 VW			CCC deform (TG, GT)
251 S		251 S	247 VW	250 M		256 S	245 VW	CCC deform (TT), CH_3 torsion (TG)
		231 M, sh		230 W				CH_3 torsion (TT)
		223 M, sh*						CH_3 torsion (GG)
213 M		212 M		213 VW, sh				CCI deform (TG, GT)
203 M								CCI deform (GG)
		190 W, sh*		188 VW				CH_3 torsion (GT)
127 M		132 W		141 W		149 M		CCI deform (TT), CC torsion (TT)
96 W		110 VW		114 VW		112 W		Torsions and lattice vibrations
						95 W		
70 VW				75 VW		74 W		
						60 W		
						55 W		
						45 M		
						34 VW		
						25 M		
						20 W		

a), b) See a) and b), respectively, of Table 2.

Table 8. Rotational isomers of 1-halogenopropanes and 1-halogenobutanes

	Gas				Liquid				Glass				Crystal
$CH_3CH_2CH_2F$[a]		T	G			——				T	G		G
$CH_3CH_2CH_2Cl$		T	G			T	G			T	G		T
$CH_3CH_2CH_2Br$		T	G			T	G			T	G		T
$CH_3CH_2CH_2I$		T	G			T	G			T	G		T
$CH_3CH_2CH_2CH_2F$[b]		——			TT	TG	GT	GG		——			TG
$CH_3CH_2CH_2CH_2Cl$	TT	TG	GT	GG	TT	TG	GT	GG	TT	TG	GT	TT	TT
$CH_3CH_2CH_2CH_2Br$	TT	TG	GT	GG	TT	TG	GT	GG	TT	TG	GT	GG	TT
$CH_3CH_2CH_2CH_2I$	TT	TG	GT	GG	TT	TG	GT	GG	TT	TG	GT	GG	TT

a) Refs. 7 and 19. b) Ref. 7.

mol, and $\Delta H_{GT-TG}=650\pm28$ cal/mol, respectively. The relatively large error is estimated for the ΔH_{GG-TG} value because of the very weak intensity of the band at 370 cm^{-1}. Thus, the stability of the rotational isomers in the liquid state is in the order of TG, TT, GG, and GT, with the TG form being the most stable.

For 1-bromobutane, the intensity ratios of the Raman bands at 353 (GG form) and 463 cm^{-1} (TG form), those at 393 (TT form) and 463 cm^{-1}, and those at 417 (GT form) and 463 cm^{-1} gave the enthalpy differences, $\Delta H_{GG-TG}=130\pm30$ cal/mol, $\Delta H_{TT-TG}=280\pm52$ cal/mol, and $\Delta H_{GT-TG}=680\pm44$ cal/mol, respective-

ly. In the liquid state, the stability of the rotational isomers is in the order of TG, GG, TT, and GT.

For 1-iodobutane, the enthalpy differences, $\Delta H_{GG-TG}=170\pm25$ cal/mol, $\Delta H_{TT-TG}=-75\pm29$ cal/mol, and $\Delta H_{GT-TG}=480\pm26$ cal/mol were obtained from the pairs of the Raman bands at 339 (GG form) and 450 cm^{-1} (TG form), those at 388 (TT form) and 450 cm^{-1}, and those at 407 (GT form) and 450 cm^{-1}, respectively. Thus, the stability of the rotational isomers in the liquid state is in the order of TT, TG, GG, and GT.

Comparison with Previous Results. Table 8 shows the rotational isomers of 1-halogenopropanes and 1-halogenobutanes existing in the various states, including those of 1-fluoropropane and 1-fluorobutane reported by Crowder and Mao.[7] In the crystalline state, 1-fluoropropane takes the G form and 1-fluorobutane takes the TG form, in contrast with other 1-halogenopropanes and 1-halogenobutanes.

Many investigations[2-6,8-18,20] indicated for 1-chloro-, 1-bromo-, and 1-iodopropanes that the T form exists in the crystalline state and the T and G forms coexist in the glassy, liquid, and gaseous states. These conclusions have been further confirmed by the present normal vibration calculation of these compounds in conjunction with longer halogenoalkanes.

The quite different values of the enthalpy differences were reported by many authors[4-6,10,11,18-20] for 1-halogenopropanes. Tanabe and Saëki[17] discussed this problem and obtained their values of the enthalpy differences by the absolute-intensity method and the temperature-variation method applied to the infrared spectra of the liquid state. The values by the latter method were $\Delta H_{G-T}=-140$ cal/mol for 1-chloropropane, $\Delta H_{G-T}=220$ cal/mol for 1-bromopropane, and $\Delta H_{G-T}=580$ cal/mol for 1-iodopropane. However, the present results show that the G form is more stable than the T form by about 100 cal/mol for these three compounds in common in the liquid state. Tanabe and Saëki mentioned that the good air-tightness of the high temperature cell allowed the experiment at temperatures higher than the boiling point of 1-chloro- or 1-bromopropane. This implies that the enthalpy differences obtained are those at pressures higher than 1 atm. The disagreement between their and our values is ascribed, at least in part, to the above fact. As for gaseous 1-fluoropropane, the ΔH_{G-T} value of -50 ± 30 cal/mol was obtained by the microwave measurement.[19]

There has been disagreement concerning the assignment of the CH_2 twisting bands of 1-halogenopropanes. Snyder and Schachtschneider[14] assigned the 1292 cm^{-1} band of 1-chloropropane to the *trans* CH_2 twisting mode on the basis of the normal vibration calculation of many kinds of chloroalkanes and Hayashi *et al.*[15] assigned the 1288 cm^{-1} band of 1-bromopropane to the *trans* CH_2 twisting mode. These assignments agree with those by Brown and Sheppard[9] and Komaki *et al.*[11] On the other hand, Tanabe and Saëki[17] had doubts of these assignments from the viewpoint that the twisting frequencies of the CH_2 group (adjacent to CH_3) in 1-halogenopropanes should be lower than that of propane, 1278 cm^{-1}, and that the twisting frequency of the CH_2 group (adjacent to CH_3) should be lower than the wagging frequency of the CH_2 group (adjacent to halogen) in the *trans* form. Thus, they assigned the 1256, 1200, and 1180 cm^{-1} bands of 1-chloro, 1-bromo-, and 1-iodopropanes, respectively, to the *trans* CH_2 twisting mode. In the present study, however, the Raman band of 1-chloropropane at 1288 cm^{-1}, the Raman and infrared bands of 1-bromopropane at 1289 and 1291 cm^{-1}, respectively, and the Raman and infrared bands of 1-iodopropane at 1286 and 1289 cm^{-1}, respectively, all of which are definitely observed in the crystalline state (see Figs. 1—6), are assigned consistently to the *trans* CH_2 twisting mode on the basis of our normal vibration calculation including the data of longer halogenoalkanes. Tanabe and Saëki did not assign these bands to any vibration of the T form of 1-halogenopropanes. Also, their grounds for interpreting the spectra are not appropriate, since it is generally acceptable that the twisting frequency of the CH_2 group (adjacent to CH_3) can be higher than the twisting frequency of a single isolated CH_2 group in propane owing to the vibrational coupling between the two CH_2 twisting modes in 1-halogenopropanes, and that it can be higher than the wagging frequency of the CH_2 group (adjacent to halogen) owing to the mass effect by the halogen atom. The situation is almost the same for the *gauche* twisting frequencies.

Many studies[4-9,14,16,21-26] have been made on the rotational isomerism of 1-halogenobutanes. Ukaji and Bonham[26a] proposed for 1-chlorobutane an isomer distribution of 37% TG, 24% GG′, 17% GG, 11% TT, and 11% GT in the gaseous state and Momany *et al.*[26b] proposed for 1-bromobutane 36% TT, 24% TG, 24% GT, and 16% GG in the gaseous state by the electron-diffraction method. Snyder and Schachtschneider[14] concluded for 1-chlorobutane that the TT form exists in the crystalline state and the TT and TG forms coexist in the glassy state on the basis of the comparison of the crystalline- and glassy-state spectra and of the normal coordinate analysis. Crowder and Ali[8a] interpreted the spectra of 1-iodobutane, taking into account only two among various isomers, the TT and TG forms. In the present study, it has been also found that the GT and GG forms of each of 1-halogenobutanes exist in the gaseous, liquid, and glassy states in addition to the TT and TG forms. However, the existence of the GG′ form was not identified in any state of these compounds. The skeletal deformation vibrations of 1-chlorobutane[22] and 1-bromobutane[22,23] were discussed in relation to the identification of existing rotational isomers. The results of these studies, however, do not agree with ours.

Studies concerning the relative stability of the isomers of 1-halogenobutanes have not yet been fully made. So far, only the apparent enthalpy difference between the mixture of the TT and GT forms and that of the TG and GG forms has been determined from the C–Br stretching bands of 1-bromobutane by the infrared and Raman methods,[5,6] and the relative stabilities of the *trans* and *gauche* conformations about the CC–CX and CC–CCX axes have been estimated by the electron-diffraction method.[26] In the present study, it has been possible to determine the enthalpy differences among the

individual isomers of 1-chloro-, 1-bromo-, and 1-iodobutanes, as the key bands in the skeletal deformation region have been clarified.

Discussion

Several consistent trends have been observed for 1-halogenopropanes and 1-halogenobutanes. (1) The forms existing in the various states are same for all the compounds except 1-fluoroalkanes (Table 8). (2) The enthalpy difference ΔH_{G-T} in the liquid state is about -100 cal/mol for 1-halogenopropanes studied in this work in common. For 1-halogenobutanes in the liquid state, the GT form is the least stable and the TG form is the most stable with an exception that the TT form of 1-iodobutane is slightly more stable than the TG form (Figs. 17 and 18). (3) The force constants of the halogen part[33] show a systematic trend in their values.

The diagonal force constants of the CCX skeletal deformation for different halogen atoms are about the same and the frequency shifts are mainly due to the difference in the masses of halogen atoms. Together with the similarity of the relative stabilities of the rotational isomers, this is one of the principal reasons for the similarity of the spectral patterns. Thus, the skeletal deformation region of 1-halogenobutanes has good key bands for discriminating the individual isomers. In particular, the bands in the 300—500 cm^{-1} region of 1-halogenobutanes are explicit examples, since these bands are associated predominantly with the CCC skeletal deformation (see Tables 5—7) and the frequency shift due to the mass difference is smaller than that for 1-halogenopropanes. In the study of the longer halogenoalkanes,[34] the key bands in the skeletal deformation region are efficiently used together with those in the skeletal stretching and CH_2 rocking regions.

It is noticed for the halogenoalkane molecules studied in this work except 1-iodobutane that the most stable isomer in the liquid or glassy state does not exist in the crystalline state. This is reasonably understood by considering that the T or TT form is less stable than the G or TG form by only 100—300 cal/mol in the liquid state and the intermolecular forces favoring the T or TT form in crystal may well overwhelm the intramolecular forces favoring the G or TG form.

Care must be taken in the interpretation of the Raman spectra in the gaseous state on the analogy of that in the liquid state. An apparent band or shoulder observed only in the gaseous-state Raman spectra can be that due to some rotational isomer which is not identified in the liquid-state spectra, part of the rotational contour of the vibrational band, or a hot band. The relative peak intensities of the bands belonging to the same isomer can also be different from those in the liquid state. Such examples are found in the Raman spectra of 1-iodopropane. The C–I stretching band of the G form is observed as doublet at 518 and 503 cm^{-1}. This doublet may be the contour of the B-type vibration since the corresponding infrared band is also observed as the B-type doublet. The relative peak intensities of the 602 and 285 cm^{-1} bands, both assigned to the T form, in the gaseous-state spectrum are significantly different from those in the liquid-state spectrum. In the cases of 1-bromo- and 1-iodobutanes, the relative intensities of the Raman bands in the gaseous state at 448 and 456 cm^{-1} and at 436 and 453 cm^{-1}, respectively, are different from those in the liquid state.

As has been shown in the present work, the skeletal deformation vibrations are useful for the determination of the enthalpy differences because of the relatively few overlapping bands due to different isomers. The measurement of the Raman spectra in this region is more effective for this purpose than that of the infrared spectra. Experiments of the temperature dependence of Raman intensities, especially at lower temperatures, can be performed without much difficulty, but the measurement of infrared intensities is difficult because of the interference by infrared emissions from the sample and the reference experimental apparatus.

References

1) Part VI: H. Matsuura, M. Kono, H. Iizuka, Y. Ogawa, I. Harada, and T. Shimanouchi, *Bull. Chem. Soc. Jpn.*, **50**, 2272 (1977).
2) S. Mizushima, Y. Morino, and S. Nakamura, *Sci. Pap. Inst. Phys. Chem. Res. Tokyo*, **37**, 205 (1940).
3) G. Radinger and H. Wittek, *Z. Phys. Chem.*, **B45**, 329 (1940).
4) J. Goubeau and H. Pajenkamp, *Acta Phys. Austriaca*, **3**, 283 (1949).
5) T. Yoshino and H. J. Bernstein, *Can. J. Chem.*, **35**, 339 (1957).
6) M. W. Anderson, J. A. Taylor, and C. T. Walker, *J. Chem. Phys.*, **64**, 2695 (1976).
7) a) G. A. Crowder and H.-K. Mao, *J. Mol. Structure*, **16**, 165 (1973); b) G. A. Crowder and H.-K. Mao, *ibid.*, **18**, 33 (1973); c) G. A. Crowder and H.-K. Mao, *ibid.*, **23**, 161 (1974).
8) a) G. A. Crowder and S. Ali, *J. Mol. Structure*, **25**, 377 (1975); b) G. A. Crowder and S. Ali, *ibid.*, **30**, 181 (1976).
9) a) J. K. Brown and N. Sheppard, *Discuss. Faraday Soc.*, **9**, 144 (1950); b) J. K. Brown and N. Sheppard, *Trans. Faraday Soc.*, **50**, 535 (1954); c) J. K. Brown and N. Sheppard, *ibid.*, **50**, 1164 (1954).
10) Y. A. Pentin and V. M. Tatevskii, *Dokl. Akad. Nauk. SSSR*, **108**, 290 (1956); Y. A. Pentin, V. M. Tatevskii, and V. A. Pozdyshev, *Fiz. Sbornik L'vov. Univ.*, **1957**, 300; *Chem. Abstr.*, **55**, 21797c (1961).
11) C. Komaki, I. Ichishima, K. Kuratani, T. Miyazawa, T. Shimanouchi, and S. Mizushima, *Bull. Chem. Soc. Jpn.*, **28**, 330 (1955).
12) N. T. McDevitt, A. L. Rozek, F. F. Bentley, and A. D. Davidson, *J. Chem. Phys.*, **42**, 1173 (1965).
13) K. Radcliffe and J. L. Wood, *Trans. Faraday Soc.*, **62**, 1678 (1966).
14) R. G. Snyder and J. H. Schachtschneider, *J. Mol. Spectrosc.*, **30**, 290 (1969).
15) M. Hayashi, K. Ohno, and H. Murata, *Bull. Chem. Soc. Jpn.*, **46**, 2332 (1973).
16) A. J. Barnes, H. E. Hallam, J. D. R. Howells, and G. F. Scrimshaw, *J. Chem. Soc., Faraday Trans. 2*, **69**, 738 (1973).
17) K. Tanabe and S. Saëki, *J. Mol. Structure*, **27**, 79 (1975).
18) T. N. Sarachman, *J. Chem. Phys.*, **39**, 469 (1963).
19) E. Hirota, *J. Chem. Phys.*, **37**, 283 (1962).
20) Y. Morino and K. Kuchitsu, *J. Chem. Phys.*, **28**, 175 (1958).

21) L. Kohovec and K. W. F. Kohlrausch, *Z. Phys. Chem.*, **B48**, 7 (1940/41).
22) T. Fujiyama, *Bull. Chem. Soc. Jpn.*, **44**, 1194 (1971); T. Fujiyama, *ibid.*, **45**, 3016 (1972).
23) R. Schröder, H. Böhlig, J. Fruwert, and G. Geiseler, *J. Mol. Structure*, **41**, 37 (1977).
24) F. F. Bentley, N. T. McDevitt, and A. L. Rozek, *Spectrochim. Acta*, **20**, 105 (1964).
25) H. Goetz and S. Domin, *Z. Anal. Chem.*, **246**, 302 (1969).
26) a) T. Ukaji and R. A. Bonham, *J. Am. Chem. Soc.*, **84**, 3631 (1962); b) F. A. Momany, R. A. Bonham, and W. H. McCoy, *ibid.*, **85**, 3077 (1963).
27) Part I: T. Shimanouchi, Y. Ogawa, M. Ohta, H. Matsuura, and I. Harada, *Bull. Chem. Soc. Jpn.*, **49**, 2999 (1976).
28) Part II: I. Harada, H. Takeuchi, M. Sakakibara, H. Matsuura, and T. Shimanouchi, *Bull. Chem. Soc. Jpn.*, **50**, 102 (1977).
29) Part III: M. Sakakibara, H. Matsuura, I. Harada, and T. Shimanouchi, *Bull. Chem. Soc. Jpn.*, **50**, 111 (1977).
30) Part IV: M. Ohta, Y. Ogawa, H. Matsuura, I. Harada, and T. Shimanouchi, *Bull. Chem. Soc. Jpn.*, **50**, 380 (1977).
31) Part V: Y. Ogawa, M. Ohta, M. Sakakibara, H. Matsuura, I. Harada, and T. Shimanouchi, *Bull. Chem. Soc. Jpn.*, **50**, 650 (1977).
32) T. Shimanouchi, H. Matsuura, Y. Ogawa, and I. Harada, *J. Phys. Chem. Ref. Data*, to be published.
33) T. Shimanouchi, H. Matsuura, Y. Ogawa, and I. Harada, to be published.
34) Part VIII: S. Imazeki, Y. Ogawa, M. Sakakibara, H. Matsuura, I. Harada, M. Tasumi, and T. Shimanouchi, to be published.
35) J. Thorbjørnsrud, O. H. Ellestad, P. Klaboe, and T. Torgrimsen, *J. Mol. Structure*, **15**, 61 (1973).
36) T. Shimanouchi, "Tables of Molecular Vibrational Frequencies," Consolidated Vol. I, U. S. Govt. Printing Office, No. C13.48 : 39 (1972).

The Electronic Structure of Ru(III)–Ammine Complexes and the Product Distribution from Solid-state Thermal Reaction

Susumu KOHATA, Shigeyoshi SAKAKI,* and Akira OHYOSHI*

Yatsushiro College of Technology, Hirayama-shinmachi, Yatsushiro 866

** Department of Industrial Chemistry, Faculty of Engineering, Kumamoto University, Kurokami, Kumamoto 860*

(Received April 2, 1977)

INDO-type UHF-MO calculations were carried out for Ru(III)-ammine complexes in order to investigate their electronic structures and bonding nature. It was revealed that the ground state of $RuX(NH_3)_5^{2+}$(X=F, Cl, Br, or I) is the ^2E state and that that of *cis*-$RuX_2(NH_3)_4^+$ is the $^2A_1$ state; in $RuX(NH_3)_5^{2+}$, the odd electron exists not on the d_{xy} orbital but on the d_{xz} or d_{yz} orbital which interacts with the p_π orbital of the halide ligand, and in *cis*-$RuX_2(NH_3)_4^+$, this electron exists not on the d_{xz} or d_{xy} orbital but on the d_{yz} orbital which interacts with the p_π orbitals of the two halide ligands. Concenring the bonding nature, the following results were obtained: (1) the strength of the Ru–NH_3 bond in these complexes increases in the order, *cis*-$RuX_2(NH_3)_4^+$<$RuX(NH_3)_5^{2+}$ <$Ru(OH_2)(NH_3)_5^{3+}$<$Ru(NH_3)_6^{3+}$; (2) in the aqua-ammine complex, the Ru–OH_2 bond is weaker than the Ru–NH_3 bond; and (3) in the halogeno-ammine complexes, the *trans*-Ru–NH_3 bond is weaker than the *cis*-Ru–NH_3 bond. MO calculations were also carried out for some distorted states of $RuCl(NH_3)_5^{2+}$. From these results, a discussion is presented on the relation between the thermal reaction product and the reaction mechanism; *cis*-$RuCl_2(NH_3)_4^+$ is expected to be produced *via* an associative reaction mechanism, while the *trans*-form product is expected to result from a dissociative mechanism.

It is known that the ammine or aqua ligand of Ru(III)–ammine complexes can be substituted for the outer-sphere halide ion *via* a solid-state thermal (30—210 °C) reaction.[1–3] This reaction is interesting from the viewpoint of the synthesis of certain Ru(III)–ammine complexes, because the halide ligand is substituted for the water molecule in the aqueous solution, while the ammine or aqua ligand is substituted for the halide ion. It has been suggested that the main product of this monohalogenopentaammine complex reaction is the *cis*-dihalogenotetraammine complex,[4] although the *trans*-form is expected as the main product due to the fact that the *trans*-effect of the halide ligand is greater than that of the ammine ligand. In order to clarify the reason why this reaction gives a *cis*-form product, not only experimental results, but also theoretical work are necessary, since calculations can give meaningful information about the electronic structure and the bonding nature of these complexes. Although some experimental work, such as UV-VS spectroscopic and ESR studies have been reported, only a few studies of MO calculations have been published on these complexes.[5,6]

In this work, a semi-empirical UHF-MO study was carried out for the hexaammine-, aquapentaammine-, monohalogenopentaammine-, and *cis*-dihalogenotetraammine–ruthenium(III) complexes. A discussion is presented on thier electronic structures, including electron configuration, the bond strength between metal and ligand, and the *trans*-effect of the ligand. From the results of MO calculations on the distorted state, which is considered to be a thermally-excited state, a discussion is presented on the reaction products and the mechanism of the solid-state thermal-substitution reaction.

Calculations and Geometries

Calculations. The method used here is the INDO-type UHF-MO method, which has been presented in detail elsewhere.[7] The resonance integrals were evaluated by means of the Wolfsberg-Helmholz approximation.[8] For the Ru and Rh atoms, the valence-state ionization potentials, I_μ, were evaluated from atomic spectra.[9] One-center Coulomb-repulsion integrals, $\gamma_{\mu\mu}$, were taken from the work of Di Sipio *et al.*[10] Two-center Coulomb-repulsion integrals were approximated using a modification of the Ohno equation.[11,12] For the atoms of the ligand, the values of I_μ were taken from the Hinze and Jaffé work,[13] and those of $\gamma_{\mu\mu}$ were estimated from the same work using the Pariser-Parr approximation.[14] A double-ζ type d-orbital was used for the 4d orbitals of the Ru and Rh atoms,[15] while single Slater-type orbitals[16,17] were used for all s and p orbitals. The quantity, E_{AB}, is used as the bond index, which gives the energy contribution of the AB bond to the total energy. Thus, a large absolute value of E_{AB} indicates a strong interaction between atoms A and B.[18,19]

Geometries. The Rh–Cl bond length is taken to be 2.50 Å from that corresponding to $RhCl_6^{3-}$,[20] and that of Rh–Br is estimated to be 2.6475 Å. The geometries of (a) $RuX(NH_3)_5^{2+}$, (b) $Ru(OH_2)(NH_3)_5^{3+}$, and (c) *cis*-$RuX_2(NH_3)_4^+$(X=F, Cl, Br, and I) are shown in Fig. 1. The Ru–N and Ru–O interatomic distances are taken to be 2.23 and 2.50 Å from the corresponding values for $[Ru(OH)(NO)(NH_3)_4]Cl_2$,[21] respectively. The Ru–Cl bond length is taken to be 2.40 Å from the corresponding value of the similar $[RhCl(NH_3)_5]Cl_2$.[22] The Ru–F, Ru–Br, and Ru–I bond lengths are estimated to be 2.115, 2.5475, and 2.7191 Å, respectively. For all the complexes, the geometries of the ammine and aqua ligands are taken to be those of free molecules.[23]

Results and Discussion

Parametrization. In order to determine the values of the Wolfsberg-Helmholz parameter, K, MO calculations were carried out for $RhCl_6^{4-}$ and $RhBr_6^{4-}$, since the electronic structures of these complexes have been investigated in detail. The calculated spin densities on the ligand are given in Table 1, together with experimental values.[24] All the calculations give rather rea-

Table 1. Effects of K values in INDO-type UHF-MO calculations of RhX_6^{4-}

Compound	$RhCl_6^{4-}$						$RhBr_6^{4-}$			
Calculation	I[a]	II[a]	III[a]	IV[b]	V[b]	Obsd[c]	I[a]	II[a]	III[b]	Obsd[c]
K	0.50	0.60	0.70	0.50	0.70		0.50	0.70	0.70	
Spin fraction										
f_s (%)	0.71	0.94	1.18	0.73	1.21	1.1	0.54	0.91	0.96	1.2
$f_{p\sigma}$ (%)	2.88	3.52	4.11	3.13	4.54	8.6	2.85	4.12	4.64	9.5

a) The AO exponents of Richardson *et al.* were used. b) The AO exponts of Basch and Gray were used. c) Ref. 24.

Table 2. Comparison between the total energies, electron densities, and the d_π-p_π bonding interaction of configurations I and II

Compound	$RuCl(NH_3)_5^{2+}$		*cis*-$RuCl_2(NH_3)_4^+$	
Configuration[a]	I	II	I	II
Total energy (eV)	−2148.06	−2147.83	−2202.97	−2201.38
Electron density (e)				
Ru { d	6.234	6.201	6.252	6.246
Ru { s, p	1.098	1.112	1.135	1.132
Cl	7.368	7.434	7.432	7.447
cis-NH_3	7.656	7.639	7.667	7.667
trans-NH_3	7.675	7.698	7.703	7.678
E_{Ru-Cl} (eV)	−15.08	−14.31	−14.75	−14.37
$E_{d_\pi-p_\pi}^{(1)+(2)}$ (eV)	−1.21	0.0	− 0.99	− 0.55

a) See Fig. 2.

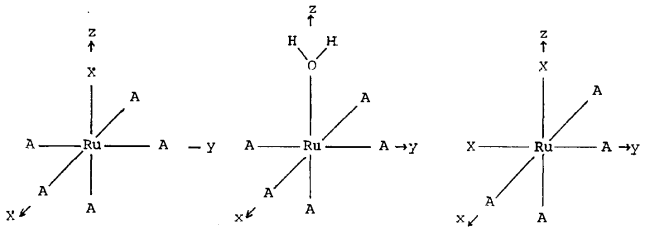

(a) $RuX(NH_3)_5^{2+}$ (b) $Ru(OH_2)(NH_3)_5^{3+}$ (c) *cis*-$RuX_2(NH_3)_4^+$

Fig. 1. Coordinate systems of Ru(III)-ammine complexes (A=NH_3 and X=F, Cl, Br, or I).

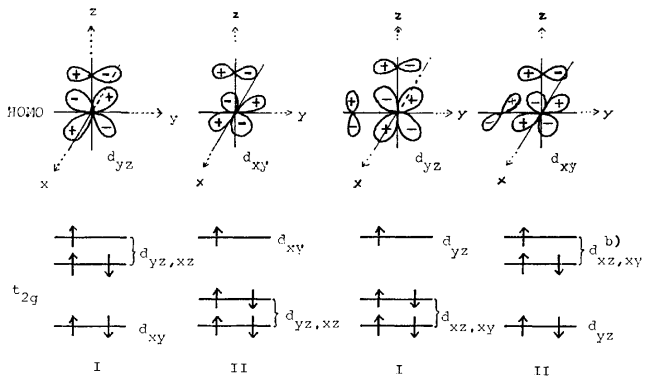

$RuX(NH_3)_5^{2+}$ *cis*-$RuX_2(NH_3)_4^+$

Fig. 2. Two types of electron configuration and the orbital interaction schemes[a] of $RuX(NH_3)_5^{2+}$ and *cis*-$RuX_2(NH_3)_4^+$. a) The d_π-p_π anti-bonding orbitals are shown here. The bonding orbitals are omitted, since the electron occupancy of these MO's are not different between the two types of electron configuration. b) The d_{xy}-p_{2x} interaction is given here. The d_{xz}-p_{1x} one is similar to this interaction.

sonable spin fractions, f_s, for both the Cl 3s-orbital and the Br 4s-orbital, while they give values that are too small for the spin fractions, $f_{p\sigma}$, of both the Cl $3p_\sigma$-orbital and the Br $4p_\sigma$-orbital. Calculation III (K= 0.70) appears to be the most reasonable, although the value of $f_{p\sigma}$ is also too small. When orbital exponents of Basch and Gray[16] are used instead of those of Richardson *et al.*,[15] the results for f_s and $f_{p\sigma}$ improve slightly. These results do not appear to be unreasonable, since a large uncertainty may be included in experimental spin fraction. From these calculations, the empirical parameter K was taken to be 0.70 and Basch and Richardson orbital exponents were used in the UHF-MO calculation.

Electron Configuration. Ru(III) complexes have a low-spin d^5 electron configuration. As is shown in Fig. 2, there are two possibilities: the complexes may be of configuration I or II. For $RuX(NH_3)_5^{2+}$(X=Cl and Br), Verdonck and Vanqickenborne[5] have suggested that configuration I is reasonable. Kaplan and Navon[6] have also reported from their ESR study of RuX $(NH_3)_5^{2+}$ (X=Cl and Br) that the d_{xz} and d_{yz} orbitals are unstable relative to the d_{xy} orbital. Unfortunately no theoretical interpretation has been reported on this issue. Thus, it is necessary to theoretically ascertain the orbital order.

In the present work, an investigation was made to determine which configuration, I or II, are the ground states of $RuCl(NH_3)_5^{2+}$ and *cis*-$RuCl_2(NH_3)_4^+$. As is shown in Table 2, configuration I has a lower total energy than configuration II by *ca.* 0.23 eV for the former complex and by *ca.* 1.6 eV for the latter.

TABLE 3. ELECTRON DISTRIBUTION AND BOND STRENGTH OF Ru(III)-AMMINE COMPLEXES

Compound	$RuX(NH_3)_5^{2+}$				*cis*-$RuX_2(NH_3)_4^+$				$RuX(NH_3)_5^{3+}$	
	F	Cl	Br	I	F	Cl	Br	I	NH_3	H_2O
Electron density (e)										
Ru { d	6.137	6.234	6.261	6.278	6.085	6.252	6.287	6.318	6.226	6.146
Ru { s, p	0.971	1.098	1.119	1.148	0.888	1.135	1.175	1.219	1.148	0.948
X	7.607	7.368	7.316	7.262	7.632	7.432	7.389	7.349	—	7.822
cis-NH_3	7.653	7.656	7.657	7.659	7.684	7.667	7.684	7.686	7.604	7.622
trans-NH_3	7.675	7.675	7.674	7.670	7.698	7.703	7.695	7.696	7.604	7.596
Net charge										
Ru	0.892	0.668	0.620	0.574	1.027	0.613	0.538	0.643	0.626	0.906
E_{AB} (eV)										
cis-Ru-NH_3	−10.43	−10.64	−10.69	−10.68	− 9.90	−10.34	−10.63	−10.56	−13.33	−10.61
trans-Ru-NH_3	−10.40	−10.47	−10.47	−10.33	−10.16	−10.33	−10.40	−10.41	−13.33	−11.02
Ru-X	−15.49	−15.26	−13.60	−12.78	−15.89	−14.75	−13.03	−12.35	—	− 5.75

To investigate the reason why configuration I is the ground state, the E_{Ru-Cl} value of that configuration are compared with that of configuration II for $RuCl(NH_3)_5^{2+}$ in Table 2. The absolute value of E_{Ru-Cl} is greater for configuration I (−15.08 eV) than for II (−14.31 eV), which suggests that the stability of these two electron configuration depends largely on the Ru–Cl bond strength.[25] In more detail, a large difference is found not between $E_{d\pi-sp\sigma}$ and $E_{p\pi-p\pi}$ but for $E_{d\pi-p\pi}$ of E_{Ru-Cl}; in configuration I ($E_{d\pi-p\pi}=-1.21$ eV), the halogen donates a p_π-electron to the d_π-orbital of the metal ion, since the d_π-orbital of the Ru atom has only one electron and is able to accept electrons from the ligand. On the other hand, the halogen cannot donate an electron in configuration II ($E_{d\pi-p\pi}=0.0$ eV), since the d_π-orbital interacting with the halogen-atom p_π-orbital is filled. The difference between the $E_{d\pi-p\pi}$ values for configurations I and II is almost the same as the difference of between their total E_{Ru-Cl} values. Thus, the d_π-p_π bonding interaction between the Ru and Cl atoms stabilizes configuration I. For *cis*-$RuCl_2(NH_3)_4^+$, the same results were obtained, as is shown in Table 2; configuration I has two d_π-p_π interactions, while configuration II has only one, which makes configuration I more stable than II.

Therefore, the π-electrons of the halide ligand delocalize onto the d_π-orbital of the Ru atom in configuration I, while they cannot do so in configuration II. These results are reflected in the electron distributions of these complexes; the electron density of the p_π-orbital of the Cl atom is smaller in configuration I than in II. The d_π-orbital of the Ru atom, on the other hand, has more electrons in configuration I than does configuration II. It should be noted that the difference in electron density of the p_π-orbitals of the Cl atoms is almost the same as that of the electron density of the d_π-orbital of the Ru atom. In conclusion, the electron configuration in the ground state is I, which results from the interaction of the Cl-atom p_π-orbital with the half-occupied d_π-orbital of the Ru atom.

Electron Density and Bond Strength. The result for Ru(III)–ammine complexes are shown in Table 3. The electron densities of the Ru atom for these complexes increase in the order: $Ru(OH_2)(NH_3)_5^{3+}$<$Ru(NH_3)_6^{3+}$ < $RuX(NH_3)_5^{2+}$ < *cis*-$RuX_2(NH_3)_4^+$. The electron numbers of the ammine ligand for these complexes decrease in the order *cis*-$RuX_2(NH_3)_4^+$ > $RuX(NH_3)_5^{2+}$ > $Ru(OH_2)(NH_3)_5^{3+}$ > $Ru(NH_3)_6^{3+}$; *i.e.*, the numbers of electrons transfered from the ammine ligand to the metal decrease in reverse order. The net charges of the Ru(III) ion decrease in the order: $Ru(OH_2)(NH_3)_5^{3+}$ > $Ru(NH_3)_6^{3+}$ > $RuX(NH_3)_5^{2+}$(X= Br,I) > *cis*-$RuX_2(NH_3)_4^+$(X=Cl,Br,I). For both halogeno ammine complexes, the electron densities of the 4d-orbital of the Ru atom increase in the order; fluoro < chloro < bromo < iodo, and the electron densities of the p_π-orbital of the halide ligand decrease in reverse order, which suggests that the d_π-p_π interactions increase in the forward order.

For both $RuX(NH_3)_5^{2+}$ and *cis*-$RuX_2(NH_3)_4^+$, the electron densities of the ammine, which is in the *cis*-position with respect to the halide ligand are smaller than those in the *trans*-position. Since the ammine ligand coordinates with the metal ion by donating its lone-pair electrons, it is expected that the *cis*-ammine coordinates more strongly with the Ru atom than the *trans*-ammine, which will be revealed in the following section on the basis of the E_{Ru-NH_3} value. In the aqua-complex, on the other hand, the electron density decreases for the ammine in *trans*-position more than for that in *cis*-position. From these results, it is conceivable that the *trans*-ammine coordination bond is stronger than that of the *cis*-ammine, which suggests that the aqua ligand has a weaker *trans*-effect than does the ammine ligand.

With the value of E_{AB} and electron-density contour maps, the bond strength of the Ru(III)–ligand can be investigated in more detail. The absolute values of E_{Ru-NH_3} for the complexes decrease in the order: $Ru(NH_3)_6^{3+}$ > $Ru(OH_2)(NH_3)_5^{3+}$ > $RuX(NH_3)_5^{2+}$ > *cis*-$RuX_2(NH_3)_4^+$ (see Table 3). It is of note that the Ru–NH_3 bond strength of $Ru(NH_3)_6^{3+}$ is the strongest of all these Ru(III)–ammine complexes. This result is in accord with the fact that the Ru–N stretching force constant of $Ru(NH_3)_6^{3+}$(2.01 mdyn/Å)[26] is the

Table 4. Electronic structure of the distorted state of $RuCl(NH_3)_5^{2+}$

Structure[a]	(1)	(2)	(3)	(4)[b]
Electron density (e)				
Ru { d	6.228	6.220	6.216	6.234
Ru { s, p	1.096	1.096	1.092	1.098
cis-NH_3(1)	7.656	7.645	7.667	7.666
trans-NH_3	7.685	7.667	7.704	7.675
Cl	7.365	7.390	7.342	7.368
E_{AB} (eV)				
cis-Ru-NH_3(1)	−10.58	−10.93	−10.72	−10.41
trans-Ru-NH_3	−10.35	− 9.15	−10.17	−10.47
Ru-Cl	−15.07	−14.64	−15.27	−15.26
Total energy (eV)	−2148.12	−2148.13	−2151.59	−2148.06

a) Corresponing to Fig. 4. b) Ground-state structure.

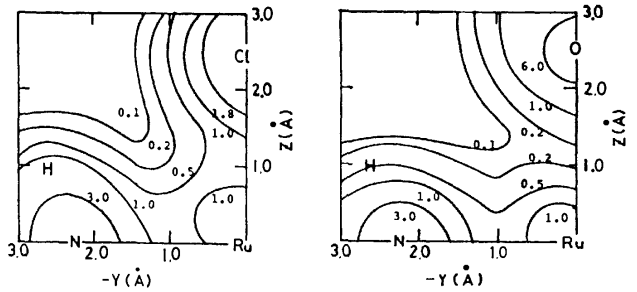

(3-a) $RuCl(NH_3)_5^{2+}$ (3-b) $Ru(OH_2)(NH_3)_5^{3+}$

Fig. 3. Electron density contour maps.

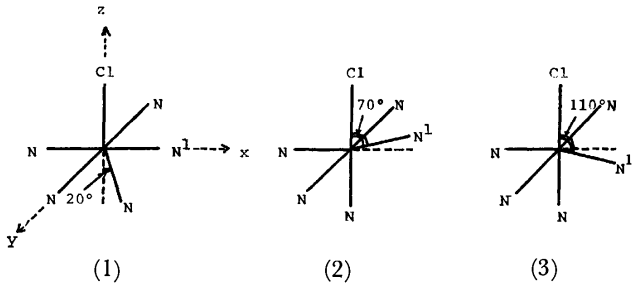

Fig. 4. Examined distorted states of $RuCl(NH_3)_5^{2+}$.

largest of all these complexes (*ca.* 1.6—1.9 mdyn/Å for $RuX(NH_3)_5^{2+}$).[27] The Ru–NH_3 bond strength in $Ru(OH_2)(NH_3)_5^{3+}$ is almost the same as those in halogeno ammine complexes, while the Ru–OH_2 bond strength is rather weak (see the value of E_{Ru-OH_2}). A weak coordination bond of the aqua ligand is also expected from the small electron distribution between the Ru atom and the aqua ligand (see the density contour map of 0.2 e in Figs. 3a and b). For both monohalogeno and *cis*-dihalogeno ammine complexes, the Ru–NH_3 bond strength in the position *trans* to the halide ligand is weaker than in the position *cis* for all complexes by *ca.* 0.1—0.3 eV (see Table 3). These results suggest that the *trans*-effect of halide ligand is stronger than that of the ammine ligand.

Electronic Structures of Some Distorted State. As described above, the *cis*-ammine ligand coordinates with the Ru atom more strongly than does the *trans*-ammine ligand. It is unexpected that the *cis*-ammine ligand is mainly substituted for the outer-sphere halide ion in the solid-state thermal reaction in spite of the strong *cis*-Ru–NH_3 bond.[3,4] In order to clarify this problem, an MO study was carried out on the distorted state of $RuCl(NH_3)_5^{2+}$, because the distortion is expected to occur in the thermally-activated state.

UHF-MO calculations were carried out on the following distorted states of $RuCl(NH_3)_5^{2+}$: those for which (1) the angle between the z-axis and the *trans*-Ru–NH_3 bond is 20°, (2) the angle between the z-axis and the *cis*-Ru–NH_3 bond is 70° and (3) 110°. All of these distortions were examined in the plane including mainly the unpaired electron (see Fig. 4). These results are given in Table 4, accompanied by the ground state

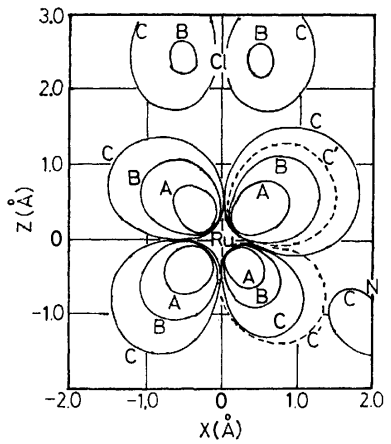

Fig. 5. LUMO contour map of $RuCl(NH_3)_5^{2+}$ ($\angle$X-Ru-NH_3=110°, A=0.25 e, B=0.05 e, C=0.005 e in distorted state and C′=0.005 e in ground state).

result. In terms of the total energy, distorted state (3) is the most stable.[28]

Thus, it is reasonable to conclude that the reaction mainly occurs from state (3). In the case of (3), the bent *cis*-Ru–NH_3 bond becomes stronger, while the *trans*-Ru–NH_3 bond becomes weaker. If the solid-state thermal-substitution reaction proceeds *via* a dissociative mechanism, the weak *trans*-Ru–NH_3 bond should dissociate to produce a complex with a *trans*-substituted structure.

The LUMO, which plays an important role in the nucleophilic attack, extends to the area between the bent Ru–NH_3 bond and the Ru–Cl bond more greatly than does that of non-distorted state, as is shown in Fig. 5. Thus, the nucleophilic attack of the outer-

sphere anion is accelerated by the distortion, and the attack occurs in the direction is shown in Fig. 5. If the reaction proceeds *via* an associative mechanism, the entering group attacks the Ru atom in the direction in which the LUMO largely extends, followed by bond dissociation of the *trans*-Ru–NH_3 bond. Then, as the *cis*-ammine ligand transfers to the vacant position, the entering group transfers to the initial position of the *cis*-ammine ligand. Since the *cis*-substituted tetraammine complex is obtained as a main product,[4] the associative mechanism is expected to be the main reaction path in the thermal-substitution reaction of halogenopentaammine complexes in the solid state, which agrees with the negative values of the activated entropy for these reactions.

In conclusion, the present INDO-type UHF-MO study of Ru(III)–ammine complexes provides useful information about their electron configurations in the ground state and the bonding nature between the metal and ligand. Some other useful information has also been obtained with this method, which successfully suggests the relation between the distribution of the reaction products and the reaction mechanism. These results agree with experimental results.

References

1) A. Ohyoshi, S. Hiraki, T. Odate, S. Kohata, and J. Oda, *Bull. Chem. Soc. Jpn.*, **48**, 230 (1975).
2) A. Ohyoshi, S. Hiraki, T. Odate, S. Kohata, and J. Oda, *Bull. Chem. Soc. Jpn.*, **48**, 262 (1975).
3) A. Ohyoshi, S. Kohata, M. Nishimori, Y. Shimura, and N. Iwasaki, *Bull. Chem. Soc. Jpn.*, **49**, 1284 (1976).
4) For example, $[RuCl(NH_3)_5]Cl_2$ gives $[RuCl_2(NH_3)_4]Cl$ in the solid-state thermal reaction. This reaction product has three Ru-N stretching bands at 483, 460, and 449 cm^{-1}. *cis*-$[RuCl_2(NH_3)_4]Cl$ has three Ru-N stretching bands at 480, 464, and 452 cm^{-1}, while *trans*-form one has only one band at 454 cm^{-1}. Thus, the reaction product appears to have a *cis*-form. (N. Iwasaki, S. Kohata, *et al.*, to be published.)
5) E. Verdonck and L.G. Vanquickenborne, *Inorg. Chem.*, **13**, 764 (1974).
6) D. Kaplan and G. Navon, *J. Phys. Chem.*, **78**, 700 (1974).
7) S. Sakaki, H. Kikkawa, H. Kato, and S. Yoshida, *Bull. Chem. Soc. Jpn.*, **49**, 76 (1976).
8) M. Wolfsberg and L. Helmholz, *J. Chem. Phys.*, **20**, 837 (1952).
9) C. E. Moore, "Atomic Energy Levels," U. S. Natl. Bur. Std. Circ., No. 467 (1958).
10) L. Di Sipio, E. Tondello, G. De Michelis, and L. Oleari, *Chem. Phys. Lett.*, **11**, 287 (1971).
11) K. Ohno, *Theor. Chim. Acta*, **2**, 219 (1964).
12) S. Sakaki, H. Kato, and T. Kawamura, *Bull. Chem. Soc. Jpn.*, **48**, 195 (1975). The values of a_{5s} and a_{5p} were taken to be 1.41 and 2.18 eV, and 1.31 and 2.02 eV for the Rh and Ru atoms, respectively.
13) J. Hinze and H. H. Jaffé, *J. Am. Chem. Soc.*, **84**, 540 (1962).
14) T. Pariser and R. G. Parr, *J. Chem. Phys.*, **21**, 767 (1953).
15) J. W. Richardson, M. J. Blackman, and J. E. Ranochak, *J. Chem. Phys.*, **58**, 3010 (1973).
16) H. Basch and H. B. Gray, *Theor. Chim. Acta*, **4**, 367 (1966).
17) E. Clementi, D. L. Raimond, and W. P. Reinhart, *J. Chem. Phys.*, **47**, 1330 (1967).
18) M. S. Gordon, *J. Am. Chem. Soc.*, **91**, 3122 (1969).
19) S. E. Ehrenson and S. Seltzer, *Theor. Chim. Acta*, **20**, 17 (1971).
20) L. E. Sutton, "Table of Interatomic Distances and Configurations in Molecules and Ions," The Chem. Soc., Buolington House, Vol. 1 (1958).
21) G. B. Bokii and N. A. Parpiyev, *Krystallografiya*, **2**, 691 (1957).
22) R. S. Evans, E. A. Hopcus, J. B, and A. F. Schreiner, *J. Cryst. Mol. Struct.*, **3**, 235 (1973).
23) W. S. Benedict and E. K. Plylor, *Can. J. Phys.*, **35**, 1235 (1957).
24) J. R. Shock and M. T. Rogers, *J. Chem. Phys.*, **62**, 2640 (1975).
25) It should be noted that there exist the π interactions between the π-orbital of the ammine and the d_π-orbital of the metal ion. However, such an interaction is minor relative to the d_π-p_π interaction of Ru-Cl.
26) K. H. Schmidt and A. Müller, *Inorg. Chem.*, **14**, 2183 (1975).
27) Unpublished work.
28) This stabilization should be due to the Jahn-Teller effect, since the ground state is the ^2E state. Therefore, distortion is brought about not only by the thermal excitation, but also by the Jahn-Teller effect.

Spectrophotometric Determination of Iron(III) and Aluminium with Semimethylxylenol Blue

Joichi UEDA

Department of Chemistry, Faculty of Education, Kanazawa University, Marunouchi, Kanazawa-shi 920

(Received June 6, 1977)

Semimethylxylenol Blue (SMXB) reacts with iron(III) and aluminium to form water-soluble colored complexes. The colored solution of the iron(III) complex shows a maximum absorption at 580—581 nm, while that of the aluminium complex shows it at 554—555 nm. The absorbances of the solutions are constant over the pH range from 1.2 to 1.5 and from 2.5 to 2.9, respectively. Beer's law is obeyed up to 1.4 μg cm^{-3} of iron(III) and 1.0 μg cm^{-3} of aluminium. Their molar extinction coefficients are 3.38×10^4 and 2.91×10^4, respectively. As a result of the investigation of the composition of the iron(III) or aluminium complex, the mole ratio of metal and SMXB was estimated to be 1 : 1. Among the 45 diverse ions examined, gallium, tin(IV), bismuth(III), zirconium, and vanadium(V) interfered with iron(III) determination, and gallium, indium, bismuth(III), scandium, titanium(IV), zirconium, vanadium(V), iron(III), fluoride, and oxalate interfered with aluminium determination. Consecutive determination of iron(III) and aluminium was also studied.

Semimethylxylenol Blue (SMXB) is obtained as one of the products in the synthesis of Methylxylenol Blue by the Mannich condensation of Paraxylenol Blue, formaldehyde, and iminodiacetic acid. It is a monosubstituted derivative of Paraxylenol Blue, while Methylxylenol Blue is a disubstituted derivative.[1] In the preceding paper,[2] the author proposed a method for the determination of thorium, based on the sensitive color reaction of SMXB with thorium. This reagent also reacts with iron(III) and aluminium to form water-soluble colored complexes. So the possibility of using this reagent for the spectrophotometric determinations of these elements was examined, and it was found that SMXB was a suitable reagent for these elements, especially for iron(III), as regards both sensitivity and selectivity, and could be applied to the determinations of up to 1.4 μg cm^{-3} of iron(III) and up to 1.0 μg cm^{-3} of aluminium. In the present methods, iron(III) interferes with the determination of aluminium, giving a positive error, but it can be determined without interference from aluminium. Utilizing these facts, the consecutive determination of iron(III) and aluminium was also studied, and satisfactory results were obtained with the solutions containing 0.16—2.0 μg cm^{-3} of iron(III) and 0.16—1.2 μg cm^{-3} of aluminium.

The present methods for both iron(III) and aluminium are nearly as specific as the methods using such reagents with similar structures to SMXB as Xylenol Orange,[3,4] Methylthymol Blue,[5,6] and Methylxylenol Blue,[7,8] and have higher sensitivities than these methods. Further, this reagent is more sensitive than the most common reagents for iron, such as 1,10-phenanthroline,[9] 4,7-dihydroxy-1,10-phenanthroline,[10] 2,2'-bipyridine,[9] and 2,4,6-tri-2-pyridyl-1,3,5-triazine,[11] and more sensitive than those for aluminium such as Aluminon,[12] Alizarin S,[12] Eriochrome Cyanine R,[13] Stilbazo,[14] and Chromazurol S.[15]

Experimental

Reagents. *Standard Iron(III) Solution*: A solution containing about 1 mg cm^{-3} of iron(III) was prepared by dissolving guaranteed reagent grade iron(III) nitrate in a small amount of nitric acid and diluting with distilled water. The solution was standardized by the complexometric back-titration with a standard solution of thorium using Xylenol Orange as an indicator. This solution was diluted as required.

Standard Aluminium Solution: A solution containing about 1 mg cm^{-3} of aluminium was prepared by dissolving guaranteed reagent grade aluminium nitrate in a small amount of hydrochloric acid and diluting with distilled water. The solution was standardized by the complexometric back-titration with a standard solution of zinc using Xylenol Orange as an indicator. This solution was diluted as required.

SMXB Solution: A 0.05% SMXB solution was prepared by dissolving a weighed amount of the reagent in distilled water. The SMXB was prepared by the method described in the preceding paper[2] : it was synthesized from Paraxylenol Blue, iminodiacetic acid, and formaldehyde by the Mannich condensation, separated from the reaction mixture on a cellulose column by 1-butanol saturated with 0.1% acetic acid, and then obtained in the free acid form by passing the fraction of SMXB through a column of cation-exchange resins.

Buffer Solutions: The pH was adjusted with 1 mol dm^{-3} sodium acetate-1 mol dm^{-3} hydrochloric acid for the determination of iron(III) and 0.1 mol dm^{-3} glycine-0.1 mol dm^{-3} sodium chloride-0.1 mol dm^{-3} hydrochloric acid for that of aluminium.

All the other reagents used were of guaranteed reagent grade.

Apparatus. A Hitachi-Perkin-Elmer model 139 spectrophotometer with 1 cm glass cells was used for the absorbance measurements, and a Hitachi-Horiba model M-5 glass electrode pH meter for the pH measurements.

Recommended Procedures. *Determination of Iron(III)*: A sample solution containing up to 35 μg of iron(III) is transferred to a 25 cm^3 volumetric flask. Then 10 cm^3 of the buffer solution of sodium acetate-hydrochloric acid and 3 cm^3 of 0.05% SMXB solution are added. After making up the volume to 25 cm^3 (the final pH: 1.3) and allowing it to stand for 20 min, the absorbance is measured at 580 nm against the reagent blank.

Determination of Aluminium: A sample solution containing up to 25 μg of aluminium is taken into a 50 cm^3 Erlenmeyer's flask. Then, 5 cm^3 of the buffer solution of glycine-sodium chloride-hydrochloric acid, 2 cm^3 of 0.05% SMXB, and 10 cm^3 of dioxane are added. After being kept for a few minutes in a boiling water bath, the solution is cooled with running water, transferred to a 25 cm^3 volumetric flask, and diluted to the mark with water (the final pH : 2.6). The absorbance is measured at 555 nm within 1 h against the reagent blank.

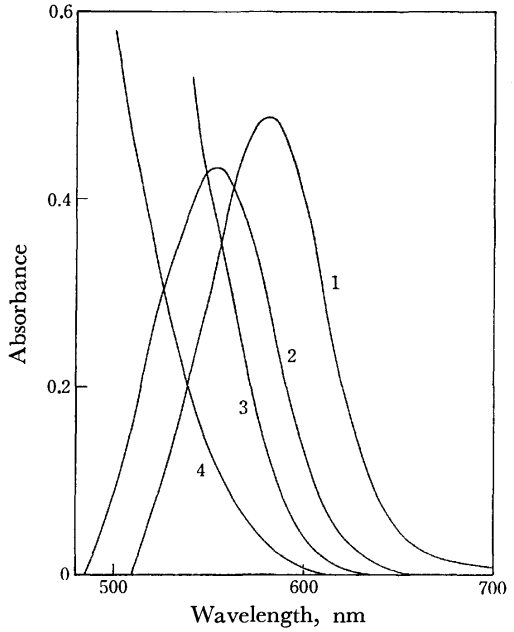

Fig. 1. Absorption curves of iron(III) and aluminium complexes.
1: Fe(III) 20 μg/25 cm³, 0.05% SMXB 3 cm³, pH 1.3, reference: reagent blank.
2: Al 10 μg/25 cm³, 0.05% SMXB 2 cm³, dioxane 10 cm³, pH 2.6, reference: reagent blank.
3, 4: Reagent blanks of 1 and 2 respectively, reference: water.

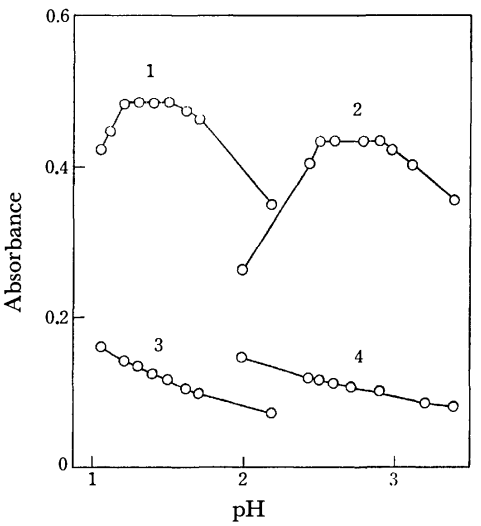

Fig. 2. Effect of pH.
1: Fe(III) 20 μg/25 cm², 0.05% SMXB 3 cm³, wavelength 580 nm, reference: reagent blank.
2: Al 10 μg/25 cm³, 0.05% SMXB 2 cm³, dioxane 10 cm³, wavelength 555 nm, reference: reagent blank.
3, 4: Reagent blanks of 1 and 2 respectively, reference: water.

Results and Discussion

Absorption Curves. The absorption curves of iron(III) and aluminium complexes obtained by the recommended procedures are shown in Fig. 1.

The colored solution of the iron(III) complex had an absorption maximum at 580—581 nm, while that of the aluminium complex had it at 554—555 nm.

The Effect of pH. As shown in Fig. 2, the ranges in which the maximum and nearly constant absorbance was obtained were found to be pH 1.2—1.5 for iron(III) and pH 2.5—2.9 for aluminium.

The Stability of the Color. Iron(III) Complex: The full color development was obtained about 10 min after the reagent was added. The color, once developed, was very stable, and the absorbance remained constant for at least several hours.

Aluminium Complex: The color reaction of SMXB with aluminium was very slow at a room temperature. But the reaction time could be considerably shortened by heating the solution in a boiling water bath, and the maximum color development was obtained within only a few minutes. So heating for 3 min in a hot water bath was adopted in further experiments. On the other hand, the absorbance of the resultant colored solution decreased gradually with the time of standing. However, it was found that by adding 7 to 13 cm³ of dioxane the absorbance remained almost constant for at least 1 h after the color development and was higher by about 14% than the absorbance of the colored solution in the absence of dioxane. Accordingly, 10 cm³ of dioxane was always used in these experiments.

The Effect of the Amount of SMXB. The maximum and almost constant absorpances were obtained by adding from 2.7 to 6 cm³ of 0.05% SMXB solution for 20 μg of iron(III) and from 1.5 to 6 cm³ for 10 μg of aluminium.

The Effect of the Amount of the Buffer Solution. The addition of from 3 to 15 cm³ of 1 mol dm^{-3} sodium acetate–1 mol dm^{-3} hydrochloric acid buffer solution had no effect on the color intensity of the iron(III) complex. In the case of aluminium, there was no change in the absorbance when 3 to 10 cm³ of 0.1 mol dm^{-3} glycine–0.1 mol dm^{-3} sodium chloride–0.1 mol dm^{-3} hydrochloric acid buffer solution was used. In this case, the use of the acetate buffer instead of the glycine–sodium chloride–hydrochloric acid buffer was unsatisfactory, because the decrease of the absorbance was induced immediately after the color development, even if dioxane was present.

Calibration Curves. Under the conditions described in the recommended procedures, Beer's law was obeyed up to 1.4 μg cm^{-3} of iron(III) and up to 1.0 μg cm^{-3} of aluminium. The molar absorptivities calculated from the curves were found to be 3.38×10^4 for iron(III) and 2.91×10^4 for aluminium, while the sensitivities for $\log I_0/I = 0.001$ were 0.0016 μg Fe(III)/cm² and 0.0009 μg Al/cm². The reproducibilities of the methods, expressed by the relative standard deviations of the absorbances which were obtained from five repeat determinations, were 0.47% for iron(III) and 0.87% for aluminium.

The Effect of Diverse Ions. The effect of 45 diverse ions on the determination of 20 μg of iron(III) or 10 μg of aluminium was examined. The results obtained are summarized in Table 1.

For the iron(III) determination, 24 cations such as alkali metals, alkaline earth metals, lead, copper, zinc,

Table 1. Effects of diverse ions

Ion	A		B		Ion	A		B	
	Amount added (mg)	Fe(III) found (μg)	Amount added (μg)	Al found (μg)		Amount added (mg)	Fe(III) found (μg)	Amount added (μg)	Al found (μg)
Li^{+}	1	20.0	500	9.9	Ce^{3+}	1	19.9	500	10.5
K^{+}	1	20.3	500	9.9	Ti^{4+}	0.1	20.2	10	12.4
Be^{2+}	1	20.3	500	10.4	Zr^{4+}	0.02	54.3	10	22.1
Mg^{2+}	1	20.0	500	9.9	Th^{4+}	0.02	20.1	10	12.1
Ca^{2+}	1	19.9	500	9.9	Th^{4+}	—	—	10[a]	10.0
Sr^{2+}	1	19.9	500	10.0	V(V)	0.02	22.5	10	12.5
Ba^{2+}	1	20.3	500	10.0	Cr^{3+}	1	20.7	50	10.3
Al^{3+}	0.2	20.1	—	—	Mo(VI)	0.04	20.0	20	9.9
Ga^{3+}	0.02	25.2	10	13.5	W(VI)	0.5	19.5	100	9.7
In^{3+}	0.5	20.6	10	11.4	UO_2^{2+}	1	20.0	500	10.5
Sn^{4+}	0.02	24.2	10	10.3	Mn^{2+}	1	19.7	500	9.9
Pb^{2+}	1	20.1	100	10.2	Fe^{3+}	—	—	10	13.5
As(V)	1	19.5	100	10.0	Co^{2+}	1	19.9	50	10.3
Sb^{3+}	0.1	20.8	100	9.8	Ni^{2+}	1	19.7	10	10.5
Bi^{3+}	0.02	23.7	10	11.9	Rh^{3+}	1	20.2	100	9.9
Cu^{2+}	1	20.0	10	12.1	Pd^{2+}	0.5	20.7	20	10.4
Cu^{2+}	—	—	20[a]	9.9	Ir^{4+}	1	19.0	250	9.8
Au^{3+}	1	20.4	500	9.9	Pt(IV)	1	20.3	500	10.0
Zn^{2+}	1	20.0	250	10.5	F^{-}	0.1	19.5	10	6.6
Cd^{2+}	1	19.8	500	10.0	PO_4^{3-}	10	19.1	1000	9.8
Hg^{2+}	0.5	20.6	500	10.2	SO_4^{2-}	10	20.0	1000	9.6
Sc^{3+}	0.1	20.1	10	17.2	Oxalate	0.02	19.4	10	9.0
Y^{3+}	1	20.0	10	10.3	Tartrate	10	19.9	1000	10.2
La^{3+}	1	19.9	500	10.3	Citrate	10	19.8	1000	10.0

A: Effect on iron(III) determination (20 μg of iron(III) was taken). *B*: Effect on aluminium determination (10 μg of aluminium was taken). a) 2 cm^3 of 1 mmol dm^{-3} EDTA solution was added after color development.

lanthanoids, manganese(II), cobalt, and nickel did not interfere, even if they were present at a concentration of 50 times that of iron(III). With regard to the anions, 500 fold amounts of tartrate, citrate, phosphate, or sulfate did inotnterfere. Gallium, tin(IV), bismuth(III), zirconium, and vanadium(V), however, interfered seriously. For the aluminium determination, gallium, indium, bismuth(III), copper, scandium, titanium(IV), zirconium, thorium, vanadium(V), iron(III), fluoride, and oxalate interfered seriously, but copper and thorium could be masked partly by the addition of 2 cm^3 of 1 mmol dm^{-3} EDTA solution at room temperature after color development.

Consecutive Determination of Iron(III) and Aluminium. Iron(III) interferes with the aluminium determination at pH 2.6 by the formation of iron(III)–SMXB complex, giving a positive error, but it can be determined at pH 1.3 without interference from aluminium. Utilizing these facts, the consecutive determination of iron(III) and aluminium has also been studied. The procedure for the determination is as follows.

The sample solution containing iron(III) and aluminium is divided equally. In one solution, the absorbance of the iron(III) complex alone is measured at 580 nm by using a recommended procedure for iron(III). In the other, the sum of the absorbances of the iron(III) and aluminium complexes is measured at 555 nm by using a recommended procedure for aluminium, by adding 5 cm^3 of reagent solution. From these data, the contents of both iron(III) and aluminium in the original samplesolution can be determined by using the following equations:

$$C_{Fe} = 2 \times \frac{A_{580}}{a_{580}^{Fe}}, \qquad C_{Al} = 2 \times \frac{A_{555} - (a_{555}^{Fe}/a_{580}^{Fe})A_{580}}{a_{555}^{Al}},$$

where C_{Fe} and C_{Al} are the contents of iron(III) and aluminium, and A_{580} and A_{555} are the absorbances at 580 and 555 nm, respectively. Further, a_{580}^{Fe} and a_{555}^{Fe} are the absorbances per 1 microgram of iron(III) at 580 and 555 nm respectively, and a_{555}^{Al} is that of aluminium at 555 nm. As shown in Table 2, satisfactory results were obtained with the solutions contain-

Table 2. Consecutive determination of iron(III) and aluminium

Taken (μg)		Found (μg)	
Fe(III)	Al	Fe(III)	Al
4	4	4.0	3.9
4	20	4.0	20.0
4	30	4.0	31.0
20	20	20.6	20.4
20	30	20.0	30.0
50	4	49.8	4.0
50	30	50.6	31.0

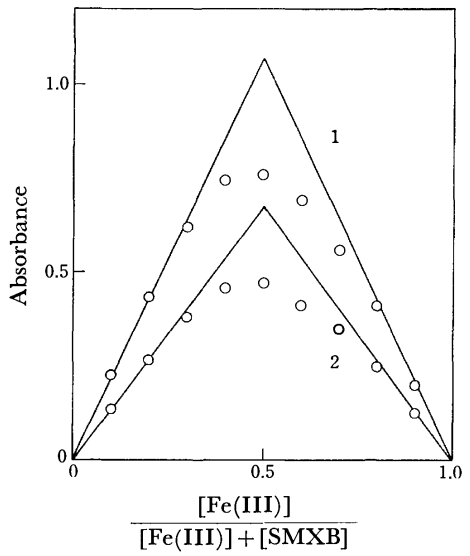

Fig. 3. Mole ratio of iron(III) complex determined by continuous variation method.
$[Fe(III)]+[SMXB]=7.16\times10^{-5}$ mol dm^{-3}, pH: 1.3, wavelength(nm)—1: 580, 2: 610.

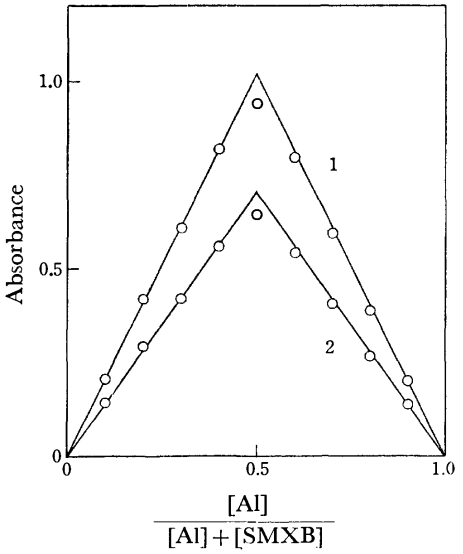

Fig. 4. Mole ratio of aluminium complex determined by continuous variation method.
$[Al]+[SMXB]=7.41\times10^{-5}$ mol dm^{-3}, dioxane: 10 cm^3, pH: 2.6, wavelength(nm)—1: 555, 2: 525.

ing 0.16—2.0 μg cm^{-3} of iron(III) and 0.16—1.2 μg·cm^{-3} of aluminium.

The Composition of the Complexes. The results obtained by the continuous variation method are shown in Figs. 3 and 4, from which it can be assumed that both iron(III) and aluminium formed the 1:1 complex with SMXB, though other iron(III) complexes may be formed at higher concentrations of iron(III). The same results were also obtained by the mole ratio method.

References

1) M. Otomo, *Bunseki Kagaku*, **21**, 442 (1972).
2) J. Ueda, *Nippon Kagaku Kaishi*, **1977**, 350.
3) M. Otomo, *Bunseki Kagaku*, **14**, 677 (1965).
4) M. Otomo, *Bull. Chem. Soc. Jpn.*, **36**, 809 (1963).
5) K. Tonosaki, *Bull. Chem. Soc. Jpn.*, **39**, 425 (1966).
6) V. N. Tikhonov, *Zh. Anal. Khim.*, **21**, 275 (1966); *Anal. Abstr.*, **14**, 6707 (1967).
7) M. Deguchi, S. Yamabuki, and M. Yashiki, *Bunseki Kagaku*, **20**, 891 (1971).
8) J. Ueda, *Nippon Kagaku Kaishi*, **1974**, 273.
9) E. B. Sandell, "Colorimetric Determination of Traces of Metals," Interscience Pub. Inc., New York (1959), p. 537.
10) A. A. Schilt, G. F. Smith, and A. Heimbuch, *Anal. Chem.*, **28**, 809 (1956).
11) F. Nakashima and K. Sakai, *Bunseki Kagaku*, **11**, 73 (1962).
12) E. B. Sandell, "Colorimetric Determination of Traces of Metals," Interscience Pub. Inc., New York (1959), pp. 228, 240.
13) U. T. Hill, *Anal. Chem.*, **28**, 1419 (1956).
14) M. Jean, *Anal. Chim. Acta*, **10**, 526 (1954).
15) P. Pakalns, *Anal. Chim. Acta*, **32**, 57 (1965).

X-Ray Fluorescence Spectroscopy of Metal Sulfides

Takashi MAEKAWA, Niro KIKUCHI, Noriyuki FUKUDA, and Toshio YOKOKAWA

Department of Chemistry, Faculty of Science, Hokkaido University, Sapporo 060

(Received June 8, 1977)

The S K_α spectra of the sulfur compounds were measured. The S K_α energies of metal sulfides were less than that of the pure sulfur in accordance with the theoretical prediction. The S K_α shift for CaS (−0.239 eV) is the largest among those of metal sulfides examined in this study. In the sulfur+selenium binary mixtures, the S K_α energy goes more negative than that of sulfur with increasing the selenium content. These results can be interpreted in terms of the electronegativity of the counter atoms.

The study of physico-chemical properties of non-crystalline solids has grown into one of the important fields of solid state chemistry. Various materials of this class have been studied extensively as to their thermodynamic, structural, and electrical properties.[1] In these materials all long-range order is destroyed and many of the experimental techniques for investigating structural details of crystals become of no use. However, optical spectra often remain similar if the short-range order does not change much. X-Ray emission spectroscopy might be one of the powerful means as well for exploring the short range and electronic structure.[2,3] For example, the energy of inner levels, though not participating in the chemical bonds, slightly changes depending on the valence electron configuration. Thus, the wavelengths of the X-rays due to the transitions of electrons between inner levels of an atom change from compound to compound. This is called the chemical shift of the X-ray energy. X-Ray emission studies for sulfur compounds have been examined extensively by many authors.[4–8] In the present study, a two-crystal spectrometer was applied for the close examination of the chemical shifts of metal sulfides, since they have not been surveyed as extensively as the other sulfur compounds. The sulfur + selenium amorphous mixtures were also examined. The way of analysis proposed in this paper will easily be applicable to other elements like Al, Si, and P, which are the main constituents of the inorganic amorphous materials like silicate glasses.

Experimental

The sulfur K_α emission spectra were obtained by the X-ray excitation method. The spectrometer used in this experiment is of the two crystal type (Toshiba Elec. Co. AFV-701).[9] The conditions for the measurements are listed in Table 1. The angle 2θ was scanned repeatedly to gain the spectra of an appropriate intensity. Pulses from the gas flow-proportional counter were stored in a multichannel analyzer and recorded on a paper tape. In order to minimize an error due to the thermal expansion of the analyzing crystals the measurement was performed in an air controlled room. For the sake of calibration, the same procedure as on the samples was performed on the reference material (orthorhombic sulfur) both before and after every measurement.

In Fig. 1 the upper parts of the sulfur K_α spectra of pure sulfur and CaS are shown as an example. The interval between neighboring points was 0.01 eV in this case. It is seen that K_{α_1} and K_{α_2} peaks overlap; the latter appears on a shoulder of the former one. However one easily sees a considerable shift between the maximum points of the two spectra.

In order to seek the maximum point of the spectrum, we postulated that the least square curve fit by a fourth order equation of energy can be applied to 120 intensity values (points) in the uppermost part of the spectrum, as shown in Fig. 1. The root mean square per cent deviation, σ_p, of the curve fit for the above S and CaS were 0.66 and 0.85% respectively.† The chemical shift was evaluated from the energy of the maximum referred to that of the orthorhombic sulfur.

Table 1. Conditions for the measurement of S K_α spectra

X-Ray tube	Cr
voltage	50 kV
current	30 mA
Analyzing crystal	Ge(111) ($2d$=6.533 Å)
Detector	PR Gas, Proportional counter
PHA	differential
Scan range (2θ)	110.66—110.80°
Scan speed (2θ)	0.02°/min
Storing time interval	2 s/channel, scan
Number of repeated scans	4—5

The alkaline earth sulfides were prepared by heating the corresponding carbonates in a dry H_2S stream at about 1000 °C. The sulfur+selenium mixtures were prepared by melting the desired quantities of sulfur and selenium in an evacuated glass ampoule and quenching it to the room temperature. The other compounds of commercial source were of reagent grade. These were ground and pressed into pellets of 34 mm diameter inside a poly-vinyl chloride ring.

Results and Discussion

In Table 2 are given the energy differences of sulfur K_α of several sulfides, sulfur + selenium mixtures, and sulfate referred to that of pure sulfur. The error limits were estimated by a t-distribution method which was applied to several measurements, shown in parentheses. The literature values are also included in the table. Contamination with sulfate was detected in SrS and BaS.†† In sulfur + selenium the absolute values

† $\sigma_p = 100 \times [\sum(y_i/y_i(\text{calcd}) - 1)^2/(n-1)]^{1/2}$

†† The contamination of sulfates causes large errors in the K_α shifts of sulfur in metal sulfides, because the K_α shifts of sulfates are large and opposite in direction. This contamination can be checked spectroscopically by examining the K_β spectra of sulfur. In the sulfate the so-called K_β' satellite peak appears at the lower energy side of the main peak. The intensity of the S K_β' peak of sulfates is about 20—30% of that of the main K_β peak. The detection of the sulfate by this satellite spectrum is useful, because it does not appear in the metal sulfides. Quantitative analysis, however, cannot be accomplished by this method.

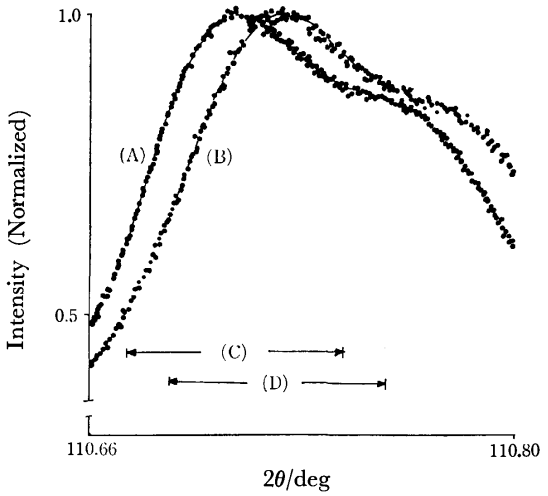

Fig. 1. Sulfur K_α spectra of pure sulfur and CaS (upper part only). The solid line is obtained by a least square fit of a fourth order equation of energy. (A), sulfur; (B), CaS; (C) and (D), ranges used in the least square. Maximum intensity; 28000 and 14000 counts for S and CaS respectively.

of the shifts are very small compared with those of the metal sulfides. It is seen, however, that the shift of S K_α became more negative with increase of the selenium content.

Data Treatment. Before considering the results, some discussion will be necessary about the data treatment employed in this work. The determination of the peak position is very difficult. However, the use of computer calculations on repeatedly stored data can avoid the complexity inherent to the graphical method. Among many proposed ways, the method in which the peak position is decided by the middle point of the half maximum is simple, but it requires the full spectrum and causes some uncertainties when the intensity is small. The most severe difficulty arises when the spectrum is not symmetric, as is observed in the present S K_α spectrum, where K_{α_1} and K_{α_2} overlap. Thus in order to seek the peak position of each component strictly, it is necessary to separate the curve into two by assuming appropriate functions, say Gaussian or Lorentzian. This procedure, however, has some mathematical complexity and gives rise to an additional uncertainty in the possible analysis. Now in the case where only the energy differences rather than the absolute values are required, almost identical results are expected to be obtained independent of the different mathematical procedures, provided the shapes of the spectra do not change as in the present case. Thus the curve fit by a polynomial equation without a process of the peak separation can also be used for the determination of the energy differences among the spectra. The parabolic fit was employed in some references.[10] However, in the spectrum obtained in this work, it is questionable whether the data can be fit by a parabola even in the top region. Actually, the range which can be approximated by a parabolic equation is restricted to the uppermost part of the spectrum and the number of points used is too small to produce a better fit. The present curve which is fit by a fourth order equation

Table 2. Sulfur K_α shifts for several compounds and sulfur + selenium mixtures

$\Delta E = E(\text{specimen}) - E(\text{S})$

Specimen	ΔE/eV This work		[1][a]	[2][b]
ZnS	−0.208±0.005[e]	(10)[d]	−0.1	—
CdS	−0.171±0.010	(11)	−0.3	−0.12
PbS	−0.161±0.006	(10)	—	—
Sb_2S_3	−0.160±0.003	(10)	−0.2	−0.16
Ag_2S	−0.117±0.006	(10)	—	−0.12
FeS	−0.160±0.005	(10)	−0.2	−0.14
BaS[e]	−0.201±0.005	(3)	—	−0.14
SrS[e]	−0.216±0.005	(3)	—	—
CaS	−0.239±0.005	(8)	−0.2	−0.22
$FeSO_4$	+1.18	(2)		
Sulfate (av)	—		+1.0	+1.18
S(5)-Se(95)[f]	−0.033±0.005	(3)		
S(10)-Se(90)	−0.027±0.005	(3)		
S(25)-Se(75)	−0.024±0.012	(3)		

a) Sato *et al.*, Ref. 4. b) Nefedow, Ref. 5. c) Error limit: t-distribution, 95% certainty. d) Number of measurements. e) Small contaminations of sulfate were detected in the present samples. f) Mol per cent of selenium.

seems to be acceptable judging from the per cent deviation of the curve fit.

Metal Sulfides. As stated previously, metal sulfides have not been thoroughly studied as to the S K_α line, because the chemical shift is not so distinct from one sulfide to the other, compared with the sulfide-sulfur-sulfite-sulfate series. The data of Sato *et al.* and of Nefedow are to be compared with the present results. The general agreement is satisfactory, although the precision was greatly improved in the present study. It is to be noted that any contamination of sulfate makes the negative shift less; some literature values of smaller shift might be explained by this reason. The same reasoning may be applicable to the values of SrS and BaS (in comparison with that of CaS).

Coulson and Zauli proposed an equation combining the chemical shifts and the partial charges on the sulfur atoms.[7] The energy shifts were expressed by a parabolic equation

$$\Delta E\, K_\alpha/\text{eV} = q(q+3)/8,$$

where q is the partial charge on the sulfur. Thus the K_α lines of sulfur shift to the lower energy side with an accumulation of electrons on the sulfur atoms, while in sulfates and sulfites the positive shifts were predicted. As is easily seen from the above equation, the magnitudes of the negative shifts, which were expected for the metal sulfides, are very small. Thus the previous authors mainly discussed the shifts for sulfates or sulfites, in which the shifts are large and can be detected comparatively easily.

In Fig. 2 the relation between the K_α energy shifts from this work and Pauling's electronegativity of the counter atoms are plotted.[11] It is seen that the negative shifts increase with decrease in the electronegativity of the metals. Since the electronegativity difference

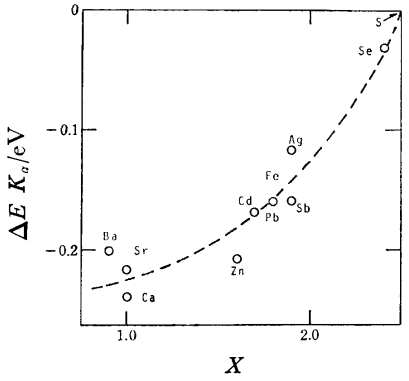

Fig. 2. Relation between S K_α energy shifts of metal sulfides ($\Delta E\ K_\alpha$) and Pauling's electronegativities of the counter metals (X). The shift at the lowest sulfur content of S+Se mixture is also included.

gives the ionicity of a bond as a first approximation, the shifts are more negative with increasing negative partial charges on the sulfur atoms. Thus it is concluded that the above theoretical equation can also be applicable to the metal sulfides. For an estimation of absolute values, however, there are some difficulties. In the condensed state the partial charges are not determined by the electronegativity difference alone. Further, since the above theoretical equation was based on the free ion model, it is not plausible to apply it straightforwardly to the estimation of the absolute charges in real crystals.

Sulfur + Selenium. Sulfur and selenium are quite similar elements. The Pauling's electronegativity of sulfur (2.5) is somewhat larger than that of selenium (2.4), while selenium is more electronegative by the Sanderson's scale.[12] Our previous enthalpy measurement of the liquid binary S + Se solution shows that the enthalpy is positive at all compositions and is symmetric.[13] The positive values of the enthalpy imply that the electrochemical effect is small, if present.[14] The present results show that if the chemical shifts are caused mainly by the partial charges on the sulfur atoms, sulfur bears some negative charges in the binary mixture. Further, if it is accepted that the direction of the charge transfer can be determined mainly by the electronegativity difference, the electronegativity of sulfur is larger than that of selenium, in accordance with Pauling. In the present samples quenched from the liquid state, sulfur and selenium are expected to mix randomly to form various co-rings and co-chains, as in the liquid mixture. In the dilute solution of sulfur, each sulfur atom is coordinated mainly by selenium atoms. Accordingly the electron transfer to sulfur from selenium is relatively large and the shifts are bigger at lower sulfur content, as is found (see Table 2). The shift at the lowest sulfur content was plotted in Fig. 2. As judged from the present results, the Pauling's scale is superior to the Sanderson's scale of electronegativity, although the latter is concerned with a condensed state and should be better applicable to the present system, compared with the former which is strictly applicable only to diatomic gas molecules.

This work was supported by a Grant-in-Aid (No. 943001) for Scientific Research from the Ministry of Education.

References

1) J. Tauc, Ed., "Amorphous and Liquid Semiconductors," Plenum Press, London (1974).
2) L. V. Azaroff, Ed., "X-Ray Spectroscopy," McGraw-Hill, New York (1974).
3) D. J. Fabian, Ed., "Soft X-Ray Band Spectra," Academic Press, London (1968).
4) T. Sato, Y. Takahashi, and K. Yabe, *Bull. Chem. Soc. Jpn.*, **40**, 298 (1967).
5) W. Nefedow, *Phys. Status Solidi*, **2**, 904 (1962).
6) R. Manne, *J. Chem. Phys.*, **46**, 4645 (1967).
7) C. A. Coulson and C. Zauli, *Mol. Phys.*, **6**, 525 (1963).
8) C. Sugiura, Y. Gohshi, and I. Suzuki, *Phys. Rev. B*, **10**, 338 (1974).
9) Y. Gohshi, Y. Hukao, and K. Hori, *Spectrochim. Acta, part B*, **27**, 135 (1972).
10) A. S. Koster and G. D. Rieck, *J. Phys. Chem. Solids*, **31**, 2505 (1970).
11) L. Pauling, "The Nature of the Chemical Bond," Cornell Univ. Press, Ithaca (1960).
12) R. T. Sanderson, "Chemical Bonds and Bond Energy," Academic Press, London (1971).
13) T. Maekawa, T. Yokokawa, and K. Niwa, *Bull. Chem. Soc. Jpn.*, **46**, 761 (1973).
14) B. W. Mott, *Phil. Mag.*, **2**, 259 (1957).

X-Ray Fluorescence Spectroscopy of Binary Silicate Glasses

Takashi MAEKAWA, Niro KIKUCHI, Shigekazu SUMITA, and Toshio YOKOKAWA
Department of Chemistry, Faculty of Science, Hokkaido University, Sapporo 060

(Received June 8, 1977)

The Si K_α emission lines of the several silicon compounds and binary silicate (Na, K, Rb, and B-silicates) glasses were measured. In the binary silicates, negative energy shifts from that of SiO_2 were observed. They were interpreted as indicating a relative decrease of the quantity of charge transfer from silicon to oxygen, when more electropositive elements like alkali metals are located on the next nearest neighbor positions of the silicon atoms. The Si K_α shifts of silicate glasses have a good correlation with the basicity of their melts.

As shown in the previous paper, the X-ray emission spectra provide important information about the chemical bonds in the compounds.[1] It is particularly useful to apply this technique to the study of non-crystalline materials, since the long range order disappears and the data on the bond character are quite limited. Among the many inorganic materials, the silicate glasses have drawn special attention in many fields. The network structure of these glasses has been confirmed from their thermodynamic as well as structural properties. However, the details of the Si–O bond, especially its relation to the chain or ring structures and their composition dependences are not satisfactorily understood. Recently, Sakka and Matusita reported Si K_α and K_β spectra of simple binary silicates.[2] Although they found some changes of the peaks of K_β spectra and their widths, no chemical shift of Si K_α was observed. On the other hand, Zopf *et al.* reported the chemical shifts of Si K_α for several silicates.[3] It has been implicitly assumed that Si–O–Si and Si–O^- bonds in silicates stay in the same energy values irrespective of the counter basic oxides. In the present work we applied an improved spectrometer to measure the chemical shifts of Si K_α, if any, and to look for a possible relation between the shifts and the basicity of the glasses.

Experimental

The apparatus used in this experiment is the same as that described in the previous paper.[1] The conditions of the measurement for the Si K_α are shown in Table 1. The features and the scanned ranges for the K_α spectra of silicon metal and SiO_2 are shown in Fig. 1. Because of the low reflecting power of the analyzing crystal (ADP) and the low concentration of silicon in the sample, the intensity of Si K_α was very weak compared with those of S K_α. The curve fit using a fourth order equation was applied to look for the maximum point of the spectrum. The chemical shifts were also obtained by the same procedure as noted in the previous paper.

Melts of M_2O+SiO_2 (M=Na, K, and Rb) were prepared by melting SiO_2 and M_2CO_3 in a platinum crucible. $PbO+SiO_2$ melts were prepared by heating the desired quantities of the two oxides in an alumina crucible. These melts were poured onto a stainless steel plate and quenched into flat glass samples. On the other hand, $B_2O_3+SiO_2$ has high viscosity and it is difficult to prepare flat glasses by such a procedure. In this case the melts were prepared and quenched in a platinum dish, which could be inserted directly into a sample holder of the spectrometer. The effects due to the surface roughness can be avoided by rotating the samples while the fluorescence spectrum was measured. SiC, Na_2SiF_6, and

Table 1. Conditions for the measurement of Si K_α spectra[a)]

X-Ray tube	Cr or Rh
voltage	50 kV (Cr) or 40 kV (Rh)
current	30 mA
Analyzing crystal	ADP ($2d=10.648$ Å)
Detector	PR Gas, proportional counter
PHA	differential
Scan speed (2θ)	0.02°/min
Storing time interval	2 s/channel, scan
Number of repeating scans	5—30
Energy interval	0.011 eV
Number of points used in the least square (fourth order)	70
σ_p (Si)[b)]	1.5%
σ_p (SiO_2)	1.7%

a) See Fig. 1 and Ref. 1. b) $\sigma_p=100\times[\Sigma(y_i/y_i(\text{calcd})-1)^2/(n-1)]^{1/2}$

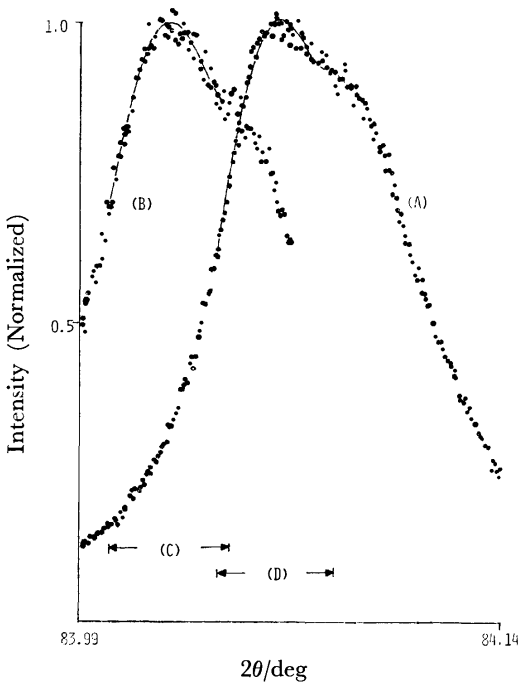

Fig. 1. Silicon K_α spectra of pure silicon and SiO_2 (upper part only). The solid line is obtained by a least square fit by a fourth order equation. (A): Si, (B): SiO_2, (C) and (D): ranges used in the least square. Maximum intensity; 5000 and 2800 counts for Si and SiO_2 respectively.

TABLE 2. SILICON K_α ENERGY SHIFTS FOR SOME SILICON COMPOUNDS

$\Delta E = E(\text{specimen}) - E(\text{Si})$

Compound	ΔE/eV		
	This work		Literature[a]
SiC	0.228±0.005[b]	(3)[c]	0.25
Si_3N_4	0.446±0.001	(5)	0.49
SiO_2 (α-quartz)	0.606±0.007	(6)	0.60
Na_2SiF_6	0.971±0.017	(3)	0.90

a) W. Nefedow, Ref. 4. b) Error limit: t-distribution, 95% certainty. c) Number of measurements.

TABLE 3. CHEMICAL SHIFTS OF Si K_α FOR BINARY SILICATE GLASSES

$\Delta E = E(\text{specimen}) - E(SiO_2)$

Specimen		ΔE/eV	
Na_2O	(33.3)[a] $-SiO_2$	−0.058±0.019[b]	(4)[c]
	(50.0) $-SiO_2$	−0.094±0.013	(5)
K_2O	(20.0) $-SiO_2$	−0.041±0.009	(7)
	(33.3) $-SiO_2$	−0.072±0.019	(5)
	(50.0) $-SiO_2$	−0.095±0.016	(6)
	(66.7) $-SiO_2$	−0.117±0.022	(6)
Rb_2O	(20.0) $-SiO_2$	−0.049±0.016	(6)
	(50.0) $-SiO_2$	−0.085±0.021	(5)
PbO	(33.3) $-SiO_2$	−0.064±0.022	(4)
	(50.0) $-SiO_2$	−0.067±0.014	(6)
	(60.0) $-SiO_2$	−0.072±0.039	(4)
	(66.7) $-SiO_2$	−0.093±0.012	(5)
	(80.0) $-SiO_2$	−0.081±0.026	(5)
B_2O_3	(50.0) $-SiO_2$	−0.002±0.010	(5)
	(66.7) $-SiO_2$	−0.006±0.021	(6)

a) Mole per cent for binary silicates. b) Error limit: t-distribution, 95% certainty. c) Number of measurements.

other crystalline samples were prepared in pellet forms of 34 mm diameter.

Results and Discussion

In Table 2 the results of the Si K_α energy shifts of some silicon compounds referred to the energy of metallic silicon are listed. The positive shift of Si K_α in Na_2SiF_6 is the largest among them. This result agrees well with that by a previous author.[4] The silicon K_α shifts of binary silicates from that of SiO_2 are shown in Table 3 and are plotted in Fig. 2. The chemical shifts are all negative, but depend on the composition and the kind of the counter oxides. The following points may be noted from the results.

i) In M_2O+SiO_2 (M=Na, K, and Rb) systems, the Si K_α energy goes more negative with increase of M_2O concentration. No differences among the three alkali oxides can be detected.

ii) In $PbO+SiO_2$, the shifts are similar to those of the above systems. But the absolute value is somewhat smaller than that of the former systems.

iii) In $B_2O_3+SiO_2$, the shifts are too small to give any composition dependence.

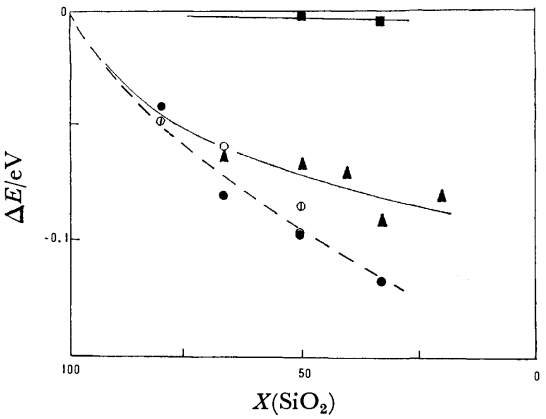

Fig. 2. Chemical shifts of Si K_α for binary silicates. $X(SiO_2)$ is the mole percent of SiO_2 in binary silicates.
○: Na_2O-SiO_2, ●: K_2O-SiO_2, ◑: Rb_2O-SiO_2, ▲: PbO-SiO_2, ■: B_2O_3-SiO_2.
Error limits are shown in Table 3.

K_α Shifts and the Effective Charges. It is known that the energy of X-ray emission spectrum from an atom in its compounds depends upon the chemical environment of the atom, *i.e.* partial charges, bond lengths, and coordination numbers.[5-8] Generally the positive shifts of X-ray energy in the third period elements in the periodic table correspond chiefly to cationic charges on the atom.[6] In the previous paper we observed the relation between S K_α energy shifts of sulfides and the electronegativity of the counter atoms. The present experimental results (Table 2) coincide with the general trend that the shifts go more positive with an increase of the electronegativity differences between silicon and the combined atoms. The silicon atom in Na_2SiF_6 coordinates six fluorine atoms and cannot be compared in a straightforward way with the others.

In the homogeneous mixtures of SiO_2 with other metal oxides, the three dimensional network structure of SiO_2 is modified by the following reaction.

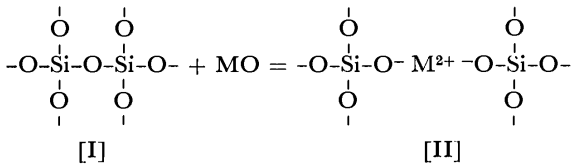

The size and number of the resulting descrete anions depend on the composition as well as the kind of the metal oxides.[9] Although SiO_4 tetrahedra remains as a structural unit through the above reaction, the electronic density of an Si–O bond should change from [I] to [II]. The ionic structure of an O–M bond should cause some effects on the neighboring Si–O bond character. Thus we must compare the electronic structure between Si–O–Si and $Si-O^-$–M^{2+} instead of considering the Si–O bond only. The source of the charge transferred to oxygen is restricted to silicon atoms in SiO_2, while the main source of the electron is the electropositive element (M in the above equation) in silicates. Mixing SiO_2 with a M_2O results in a relative decrease of the positive charge on the silicon

atom compared with that of SiO_2. This idea coincides with the principle of the electronegativity equalization proposed by Sanderson.[10] The positive charge on silicon atoms will decrease with the increase of the concentration of the metal oxides. This is again in accord with the experimental findings.

K_α Shifts and the Basicity. The thermodynamic studies of these liquid silicates show that the activity of SiO_2 drastically decreases from that of pure SiO_2.[11] In these mixed oxide melts, an useful idea called the basicity of the melt is often employed. Basicity is defined by the oxygen ion activity in the melts.[12] It depends on the metal oxide solute and its concentration. Thus the basicity of the lead silicates is smaller than that of alkali silicates at the same SiO_2 content. Both components of $B_2O_3+SiO_2$, on the other hand, are considered to be acidic in nature. Addition of B_2O_3 to SiO_2 gives a negligible shift of Si K_α energy. Therefore, the basicity reflects the degree of the positive charges on the silicon atoms, although the former is directly determined by the activity of the metal oxide and the latter is primarily determined by the ionic potential (Coulombic force) of a metal ion. There will even be a possibility of finding the basicity scale of the silicate melts by measuring the Si K_α energy of their glassy samples. The significance of the X-ray energy shifts will be similar to the ultraviolet spectra of a probe ion (for example, $^3P_1 \leftarrow {}^1S_0$ of Pb^{2+} ion) under the presence of polarizing elements like Si, P, and others.[13]

This work was supported by a Grant-in-Aid (No. 943001) for Scientific Research from the Ministry of Education.

References

1) T. Maekawa, N. Kikuchi, N. Fukuda, and T. Yokokawa, *Bull. Chem. Soc. Jpn.*, **51**, 777 (1978).
2) S. Sakka and K. Matusita, *J. Non-Cryst. Solids*, **22**, 57 (1976).
3) G. W. E. Zopf, H.-U. Chun, and R. Bruckner, *J. Non-Cryst. Solids*, **21**, 251 (1976).
4) W. Nefedow, *Phys. Status Solidi*, **2**, 904 (1962).
5) L. V. Azaroff, Ed., "X-Ray Spectroscopy," McGraw-Hill, New York (1974).
6) G. Leonhardt and A. Meisel, *J. Chem. Phys.*, **52**, 6189 (1970).
7) K. Lauger, *J. Phys. Chem. Solids*, **32**, 609 (1971).
8) F. A. Gianturco and C. A. Coulson, *Mol. Phys.*, **14**, 223 (1968).
9) F. D. Richardson, "Physical Chemistry of Melts in Metallurgy," Academic Press, Vol. 1, London (1974).
10) R. T. Sanderson, "Chemical Bonds and Bond Energy," Academic Press, London (1971).
11) M. G. Frohberg, E. Caune, and M. L. Kapoor, *Arch. Eisenhuttenwes.*, **44**, 585 (1973).
12) H. Flood and T. Forland, *Acta Chem. Scand.*, **1**, 592 (1947).
13) J. A. Duffy and M. D. Ingram, *J. Non-Cryst. Solids*, **21**, 373 (1976).

Experimental Studies of the Liquid Junction Potential between Electrolyte Solutions in Different Solvents. I. Water–Organic Solvent Junctions

Kosuke IZUTSU, Toshio NAKAMURA, Toshihiko KITANO, and Chieko HIRASAWA

Department of Chemistry, Faculty of Science, Shinshu University, Asahi, Matsumoto 390

(Received June 6, 1977)

The liquid junction potential (ljp) between water and organic solvents was investigated by measuring the emfs of cells with free-diffusion junctions of various electrolyte solutions. In most experiments, the concentration of the electrolyte on one side of a junction was kept much larger than that on the other side (c MX in S//c' M'X' in S'; S or S' is H_2O and $c \gg c'$); thus the ljp was mainly determined by MX. The ljp may practically be expressed by the sum of $E_{j,ion}$ (concn) (I), $E_{j,ion}$ (ion-solv.) (II), and $E_{j,solv.}$ (III). I and II are contributions from ionic species: I is the concentration term, which can be estimated approximately from the Henderson equation, and II is the term due to the difference in ionic solvations in S and S'. III is the contribution from the transfer of solvent molecules. The sum of II and III for the case in which S=H_2O is approximately equal in absolute value but opposite in sign to that for the case in which S'=H_2O. The change of II with the anion X^- is in linear relation with free energy of transfer of the anion from S to S'. The change of III with the bridge solvent is also a linear function of the heat (or free energy) of solution of S into S'. The rate of the change with the heat of solution can be divided in two classes by the species of the cation M^+: the rate for R_4N^+ ions is just a half of that for such ions as Li^+, Na^+, Mg^{2+}, and Ba^{2+}. The effect of the mixed bridge electrolytes and the mixed bridge solvents was also examined.

Because the problem of the liquid junction potential (abbreviated 'ljp') between electrolyte solutions in different solvents is of considerable importance in the electrochemistry of non-aqueous solvents, many reports have recently appeared concerning this problem.[1–10] According to Alfenaar, DeLigny, and Remijnse,[3] the value of the ljp, E_j, at such a junction as (A) can, in principle, be estimated by carrying out the integration of Eq. 1

$$c\,\mathrm{MX}\ \text{in solvent S} \underset{\mathrm{J}}{//} c'\,\mathrm{M'X'}\ \text{in solvent S'} \qquad \text{(A)}$$

$$E_j = -\frac{1}{F}\int_S^{S'} \sum_i t_i^r \mathrm{d}\mu(i), \qquad (1)$$

where t_i^r and $\mu(i)$ are the reduced transport number[11] and the chemical potential, respectively, of chemical species i, and the sum extends over all species, charged and uncharged, present at the junction. The reduced transport number t_i^r is equal to t_i/z_i for an ion with charge z_i and transport number t_i, while t_i^r for an uncharged species can be defined by nF/Q, where n is the amount of substance of the uncharged species transported across the junction when a quantity of charge Q flows through the cell. Alfenaar *et al.*[3] considered that E_j can be expressed by the sum of two terms, *i.e.*, $E_{j,ion}$, which is the contribution from ionic species, and $E_{j,solv.}$, which is the contribution from solvent molecules:

$$E_j = E_{j,ion} + E_{j,solv.}, \qquad (2)$$

$$E_{j,ion} = -\frac{1}{F}\int_S^{S'} \sum_{ions} \frac{t_i}{z_i}\mathrm{d}\mu(i), \qquad (3)$$

$$E_{j,solv.} = -\frac{1}{F}\int_S^{S'} \sum_{\substack{solvent\\ molecules}} t_i^r \mathrm{d}\mu(i). \qquad (4)$$

To carry out the above integrations, however, is difficult because of the difficulties in getting enough knowledge concerning t_i^r and $\mathrm{d}\mu(i)$, which actually determine the ljp between different solvents. Therefore, at the present stage, it seems important to get detailed experimental information about the factors influencing the ljp. An interesting approach from this standpoint has been reported by Cox *et al.*[5] But experimental results are still too scarce to elucidate this problem completely.

In the present study, we have measured emfs of many cells with liquid junction(s) between different solvents, in order to learn how the ljp is influenced by the solvents and electrolytes present at the junction(s). A simple cell, which was constructed by using a dual four-way stopcock, gave free-diffusion junctions and was convenient for rapid, repeated measurements of the emf. We also tried to correlate the results of these emf measurements with the literature data of ion-solvent and solvent-solvent interactions. For such data, we mainly referred to the report of Parker and his coworkers.[5,12]

If we carry out the integrations in Eqs. 3 and 4 under the following simplifying assumptions

(i) c' is negligibly small compared to c,

(ii) the molar conductivity for each ion and t_i^r for each molecule do not vary throughout the boundary, and

(iii) the concentration of each ion changes linearly at the boundary, then we can get Eqs. 5—8 from Eqs. 2—4

$$E_j = E_{j,ion}(\text{concn}) + E_{j,ion}(\text{ion-solv.}) + E_{j,solv.}, \qquad (5)$$

$$E_{j,ion}(\text{concn}) = \frac{RT}{F}(t_{M^+} - t_{X^-})\ln\frac{c\Lambda(\mathrm{MX})}{c'\Lambda(\mathrm{M'X'})}, \qquad (6)$$

$$E_{j,ion}(\text{ion-solv.}) = -\frac{1}{F}[t_{M^+}{}^S\Delta\mu^{S'}(M^+) - t_{X^-}{}^S\Delta\mu^{S'}(X^-)], \qquad (7)$$

$$E_{j,solv.} = -\frac{1}{F}t_S^r{}^S\Delta\mu^{S'}(S), \qquad (8)$$

where ${}^S\Delta\mu^{S'}(M^+)$, ${}^S\Delta\mu^{S'}(X^-)$, and ${}^S\Delta\mu^{S'}(S)$ represent changes in standard chemical potentials of M^+, X^-, and S, respectively, on crossing the boundary from S to S' in the process which actually determines the ljp. Equations 6 and 7 are similar to those recently reported by Gaboriaud.[8] In obtaining Eq. 8, we consider that $E_{j,solv.}$ receives its chief contribution from the solvent

molecule S which is transported from S to S′ with the transfer of electrolyte MX. As is apparent from Eqs. 5 to 8, when condition (i) is satisfied, the effect of M′X′ appears only in the term $E_{j,ion}$(concn) and the ljp should be almost independent of the species of M′X′, provided that c' and Λ(M′X′) are kept constant. In the present study, we carried out most experiments in cells in which condition (i) is satisfied, after confirming experimentally that the above prediction actually holds.*

By the help of the above simplified equations, we could find some correlations between the ljp and the literature data of ion-solvent and solvent-solvent interactions. In this report, we present the results obtained concerning the water-organic solvent junctions. Detailed results concerning the ljp between different organic solvents will be reported elsewhere.

Experimental

Reagents. The preparation and purification of all tetraethylammonium and tetrabutylammonium salts used in this study were carried out by the conventional procedures. Tetramethylammonium perchlorate was obtained from the Nakarai Chemicals Co., Ltd., and was a product for polarographic use. Anhydrous silver perchlorate and lithium perchlorate, both obtained commercially, were used after drying at 70 and 200 °C, respectively, under a vacuum. Anhydrous sodium perchlorate was prepared by recrystallizing from a hot aqueous solution and was dried at 200 °C under a vacuum. All the other reagents were of analytical reagent grade.

Dimethyl sulfoxide (DMSO), *N,N*-dimethylformamide (DMF), propylene carbonate (PC), and acetonitrile (AN) were purified following the methods described in Ref. 13. Nitromethane (NM), acetone (Ac), and methanol (MeOH) were of analytical reagent grade and were purified by distillation.

Apparatus. For emf measurements, the cell shown schematically in Fig. 1 was constructed by using a dual four-way stopcock obtained from the Kyowa Seimitsu Co., Ltd. This stopcock is the one used for high speed liquid chromatography; its liquid path is made of Teflon and has a bore of 1 mm. By turning the stopcock to the position of Fig. 1(A), each of the three compartments of the cell is filled with an appropriate solution. The stopcock is then turned to the position of Fig. 1(B), which results in the formation of sharp liquid boundaries (free-diffusion junctions) at J_1 and J_2. The emf of the cell is established soon after turning the stopcock and remains constant within ±1 mV for a few minutes. After the measurement of the emf, the stopcock is turned back to the position of Fig. 1(A) and the solution in each compartment is renewed. Then, by turning the stopcock to the position of Fig. 1(B), the emf can be measured repeatedly. The ljps obtained with this cell were reproducible within ±1 mV. The emf was measured with a voltmeter with an input impedance of 10^{11} ohms. All measurements were carried out in a room thermostated at about 25 °C.

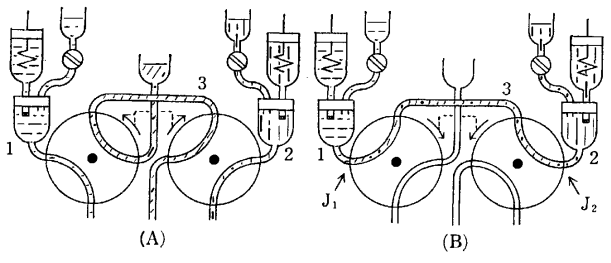

Fig. 1. Cell for emf measurements.

* An example of such an experiment was that the emf of the cell, Ag/0.01 M $AgClO_4$, 0.1 M Et_4NClO_4(AN)//0.1 M Et_4NClO_4(AN)$//_{j1}$$10^{-3}$ M Et_4NX(AN)$//_{j3}$0.1 M Et_4NClO_4(H_2O)//0.01 M $AgClO_4$, 0.1 M Et_4NClO_4(H_2O)/Ag, was constant within several millivolts even when the anion X^- was changed from Pic^- to Cl^-. When compared with the large emf changes of cell III with the anion X^- (Fig. 4(C)), this result may be regarded as a confirmation of the above prediction.

Results and Discussion

Emf Measurements of Cells I and II. Emfs of cells I and II were measured by changing solvents S_1 and S_2 and electrolyte MX:

Ag/10^{-3} M $AgClO_4$, 1M $NaClO_4(S_1)//_{j1}$1M $NaClO_4(S_1)//_{j1}$ 0.1 M $MX(S_1)//_{j2}$$10^{-3}$ M $Et_4NClO_4(S_2=S_1$ or $H_2O)//_{j2}$5×10^{-3} M $AgClO_4$, 5×10^{-3} M $Et_4NClO_4(S_2=S_1$ or $H_2O)$/Ag Cell I**

aq SCE$//_{j1}$3M $NaCl(S_1=H_2O)//_{j1}$0.1 M $MX(S_1=H_2O)//_{j2}$ 10^{-3} M $Et_4NClO_4(S_2)//_{j2}$5×10^{-3} M $AgClO_4$, 5×10^{-3} M $Et_4NClO_4(S_2)$/Ag Cell II

where S_1 in cell I was MeOH, AN, PC, DMSO, or DMF, S_2 in cell II was H_2O, MeOH, AN, PC, DMSO, or DMF, and MX was Me_4NClO_4, Et_4NClO_4, Pr_4NClO_4, Bu_4NClO_4, $LiClO_4$, $NaClO_4$, $Mg(ClO_4)_2$, $Ba(ClO_4)_2$, Et$_4$NPic, Et_4NI, Et_4NBr, Et_4NCl, or Et_4NNO_3. The measured emf values were corrected for the ljps at j_1, j_2, and J_1, which were calculated by using the Henderson equation (Eq. 23 in Ref. 14) and the conductivity data.[15] The corrected emf values are shown in Tables 1 and 2. The change in corrected emf values with the change of MX corresponds to the change in the ljp at J_2. In Table 3, the values of ΔE(I)=[corrected emf($S_2=H_2O$)−corrected emf($S_2=S_1$)] for cell I and ΔE(II)=[corrected emf($S_2\neq H_2O$)−corrected emf($S_2=H_2O$)] for cell II are tabulated. If we consider that $E_{j,ion}$(concn) for the case in which $S_2\neq S_1$ is nearly equal to that for the case in which $S_2=S_1$ (see Eq. 6), then we can think that ΔE(I) and ΔE(II) are nearly equal to $[E_{Ag/Ag^+}(S_2=H_2O)-E_{Ag/Ag^+}(S_2=S_1)+E_{j,ion}$(ion-solv.)$+E_{j,solv.}]$ for cell I and $[E_{Ag/Ag^+}(S_2\neq H_2O)-E_{Ag/Ag^+}(S_2=H_2O)+E_{j,ion}$(ion-solv.)$+E_{j,solv.}]$ for cell II, respectively. Though both ΔE(I) and ΔE(II) changed considerably (sometimes by more than 200 mV) with the change of MX, it is interesting to note that, for most kinds of MX used, the absolute values of ΔE(I) and ΔE(II) for the case in which S_1 for cell I and S_2 for cell II were the same organic solvent agreed with each other within several millivolts. Because, in this case, $E_{Ag/Ag^+}(S_2=H_2O)$ and $E_{Ag/Ag^+}(S_2=S_1)$ for cell I should be equal to $E_{Ag/Ag^+}(S_2=H_2O)$ and $E_{Ag/Ag^+}(S_2\neq H_2O)$ for cell II, the

** M=mol dm^{-3}.

Table 1. Corrected emfs of cell I (in mV)

MX	S_1					S_1				
	MeOH	AN	PC	DMSO	DMF	MeOH	AN	PC	DMSO	DMF
			$S_2=S_1$					$S_2=H_2O$		
Me_4NClO_4	(−39)	−18	−48	−77	−71	(−131)	173	−246	184	0
Et_4NClO_4	(−38)	−22	−51	−83	−77	(−157)	140	−273	172	−17
Pr_4NClO_4	−47	−31	−63	−95	−85	−191	110	−303	148	−47
Bu_4NClO_4	−54	−37	−70	−103	−91	−213	91	−321	134	−66
$LiClO_4$	−52	−31	−70	−100	−92	−164	179	−227	141	−38
$NaClO_4$	−46	−26	−65	−97	−84	−130	200	−204	155	−16
$Mg(ClO_4)_2$*	−68	−45	−77	−112	100	−176	172	−234	128	−50
$Ba(ClO_4)_2$*	−66	−45	−81	−113	102	−158	181	−234	135	−48
Et_4NCl	−26	−21	−45	−87	−77	−203	17	−427	38	−162
Et_4NBr	−29	−21	−44	−87	−75	−193	46	−397	73	−127
Et_4NI	−33	−22	−50	−88	−76	−173	87	−344	122	−77
Et_4NNO_3	−32	−23	−54	−90	−78	−181	64	−374	97	−103
Et_4NPic	(−23)	−10	−34	−73	−63	(−94)	185	−222	218	32

* The correction was made by assuming that the ljp at J_1 is equal to that for $MX=LiClO_4$. Values in parentheses show that the solubility of MX was less than 0.1 M.

Table 2. Corrected emfs of cell II (in mV)

MX	S_2					
	H_2O	MeOH	AN	PC	DMSO	DMF
Me_4NClO_4	378	471	186	572	117	307
Et_4NClO_4	361	480	196	585	104	298
$LiClO_4$	372	477	158	526	127	316
$NaClO_4$	386	467	154	530	138	320
$Mg(ClO_4)_2$*	359	462	138	524	117	305
$Ba(ClO_4)_2$*	363	455	136	520	119	308
Et_4NCl	355	525	323	734	226	434
Et_4NBr	353	512	288	704	189	398
Et_4NI	354	488	248	653	142	348
Et_4NNO_3	359	506	272	682	167	376

* The correction was made by assuming that the ljp at J_1 is equal to that for $MX=LiClO_4$.

Table 3. ΔE(I) and ΔE(II) (in mV)*

MX	Organic solvent									
	MeOH		AN		PC		DMSO		DMF	
	ΔE(I)	ΔE(II)	ΔE(I)	ΔE(II)	ΔE(I)	ΔE(II)	ΔE(I)	ΔE(II)	ΔE(I)	ΔE(II)
Me_4NClO_4	(−92)	+93	+191	−192	−198	+194	+261	−261	+71	−71
Et_4NClO_4	(−119)	+119	+162	−165	−222	+224	+255	−257	+60	−63
Pr_4NClO_4	−144	—	+141	—	−240	—	+243	—	+38	—
Bu_4NClO_4	−159	—	+128	—	−251	—	+237	—	+25	—
$LiClO_4$	−112	+105	+210	−214	−157	+154	+241	−245	+54	−56
$NaClO_4$	−84	+81	+226	−232	−139	+144	+252	−248	+68	−66
$Mg(ClO_4)_2$	−108	+103	+217	−221	−157	+165	+240	−242	+50	−54
$Ba(ClO_4)_2$	−92	+92	+226	−227	−153	+157	+248	−244	+54	−55
Et_4NCl	−177	+170	+38	−32	−382	+379	+125	−129	−85	+79
Et_4NBr	−164	+159	+67	−65	−353	+351	+160	−164	−52	+45
Et_4NI	−140	+134	+109	−106	−294	+299	+210	−212	−1	∸6
Et_4NNO_3	−149	+147	+87	−87	−320	+323	+187	−192	−25	+17
Et_4NPic	(−71)	—	+195	—	−188	—	+291	—	+95	—

* ΔE(I) = [corrected emf($S_2=H_2O$) − corrected emf($S_2=S_1$)] for cell I and ΔE(II) = [corrected emf($S_2 \neq H_2O$) − corrected emf($S_2=H_2O$)] for cell II.

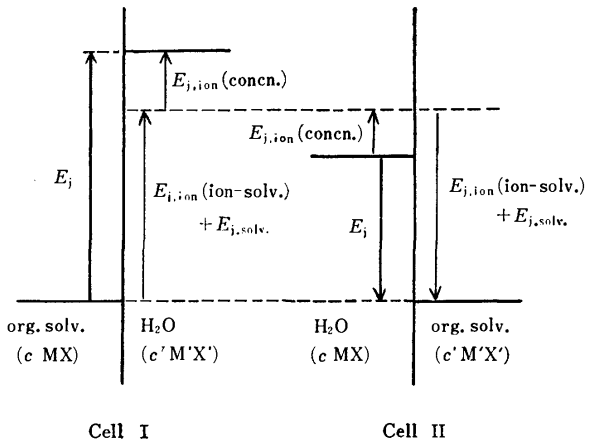

Fig. 2. Schematic representation of the ljp at J_2 in cells I and II ($c \gg c'$).

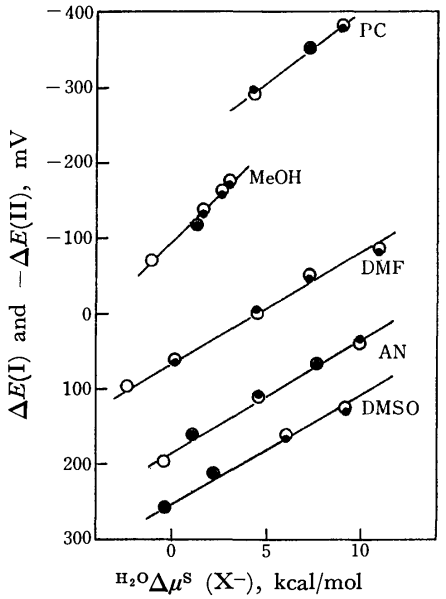

Fig. 3. ΔE(I) (○) and $-\Delta E$(II) (●) as the function of $^{H_2O}\Delta\mu^S(X^-)$. Organic solvent is given along each line. X^- on each line are, from right to left, Cl^-, Br^-, I^-, ClO_4^-, and Pic^-. (Plots for ClO_4^- and Pic^- are not given when the values of $^{H_2O}\Delta\mu^S(X^-)$ are not available.)

above results seem to show that the absolute values of $E_{j,ion}$(ion-solv.)$+E_{j,solv.}$ for cells I and II agree with each other within several millivolts. (We found that similar relations can be obtained at any junctions possible between such organic solvents as MeOH, AN, DMSO, and DMF.[16]) This situation is illustrated schematically in Fig. 2. Probably it would be reasonable to consider that the above statement holds for each $E_{j,ion}$(ion-solv.) and $E_{j,solv.}$.

In Fig. 3, the values of ΔE(I) and ΔE(II) at various water-organic solvent junctions with Et_4NX as MX are plotted as functions of the free energies of transfer of X^- from H_2O to organic solvent S, $^{H_2O}\Delta\mu^S(X^-)$. For $^{H_2O}\Delta\mu^S(X^-)$, we referred to the values of Ref. 12 which were obtained under the extrathermodynamic assumption of $^{H_2O}\Delta\mu^S(Ph_4As^+)=^{H_2O}\Delta\mu^S(Ph_4B^-)$. Excellent linear correlations are always obtained between ΔE and $^{H_2O}\Delta\mu^S(X^-)$, as can be expected from Eq. 7. (If $E_{j,solv.}$ is independent of X^-, the change in ΔE can be considered to correspond to that in $E_{j,ion}$(ion-solv.). Because the molar ion conductivities of the anions other than picrate are nearly equal to each other,[15] t_{M^+} and t_{X^-} in the present case may be considered to remain approximately constant, irrespective of the species of X^-.) The slopes, however, change with the organic solvents: the slopes are between 14 and 15 mV/(kcal/mol) for AN, DMSO, and DMF, but *ca.* 17 mV/(kcal/mol) for PC and *ca.* 25 mV/(kcal/mol) for MeOH. According to Eq. 7, the slopes in Fig. 3 for such organic solvents as AN, DMSO, and DMF correspond to t_{X^-} of about 0.3_5, which seems to be smaller than that expected from the conductivity data ($t_{X^-}>0.6$).[15] Therefore, the linear correlation in Fig. 3 cannot be regarded as in quantitative agreement with Eq. 7. The larger slopes for PC and MeOH cannot be explained from the conductivity data. Though the mechanism determining these slopes cannot be elucidated from the present study, it may be that $\Delta\mu(X^-)$ and/or t_{X^-} expected from the literature data are effective only partially in the processes which determine the ljp.

The change in E_j with the cations of MX is somewhat more complicated and will be discussed in the next section.

Emf Measurements of Cell III. The emf of cell III was measured by changing the bridge electrolytes and solvents:

$$\mathrm{Ag/5\times10^{-3}\,M\ AgClO_4,\ 5\times10^{-3}\,M\ Et_4NClO_4(S_1{=}AN)}\underset{j1}{//}$$

$$\mathrm{10^{-3}\,M\ Et_4NClO_4(S_1{=}AN)}\underset{j1}{//}\mathrm{0.1\,M\ MX(S_3)}\underset{j2}{//}\mathrm{10^{-3}\,M}$$

$$\mathrm{Et_4NClO_4(S_2{=}H_2O)}\underset{j2}{//}\mathrm{5\times10^{-3}\,M\ AgClO_4,\ 5\times10^{-3}\,M}$$

$$\mathrm{Et_4NClO_4(S_2{=}H_2O)/Ag} \qquad \text{Cell III}$$

where S_3 was AN, PC, NM, Ac, DMSO, or DMF, and MX was Et_4NClO_4, Me_4NClO_4, Pr_4NClO_4, Bu_4NClO_4, $LiClO_4$, $NaClO_4$, $Mg(ClO_4)_2$, $Ba(ClO_4)_2$, Et_4NPic, Et_4NBF_4, Et_4NI, Et_4NBr, Et_4NCl, or Et_4NNO_3. The results are summarized in Fig. 4. Solvents S_3 are designated on the abscissa at the corresponding emfs of cell III, in which the bridge electrolyte is 0.1 M Et_4NClO_4.

Figures 4(A) and 4(B) show that the emf for each bridge electrolyte changes approximately linearly against the abscissa, and that the slopes of these straight lines can be classified according to the bridge cations in two groups, *i.e.*, one for tetraalkylammonium ions and the other for such cations as Li^+, Na^+, Mg^{2+}, and Ba^{2+}. The slope of the second group is just twice that of the first group.*** In Fig. 4(A) the values of $\Delta\Delta H_s=^{S3}\Delta H^{S1}(S_3)-^{S3}\Delta H^{S2}(S_3)$ obtained from Table I in Ref. 5 are also plotted against a similar abscissa (here, $^{S3}\Delta H^{S1}(S_3)$ represents the heat per mole of transfer of S_3 from S_3 to S_1). A good linear relation is observed for all aprotic solvents used as S_3 (*cf.* Ref. 5).

When the bridge solvent S_3 in cell III changes, the ljps at both J_1 and J_2 may change. From Eqs. 6 to 8,

*** A similar phenomenon was also observed when picrates, instead of perchlorates, were used as MX.

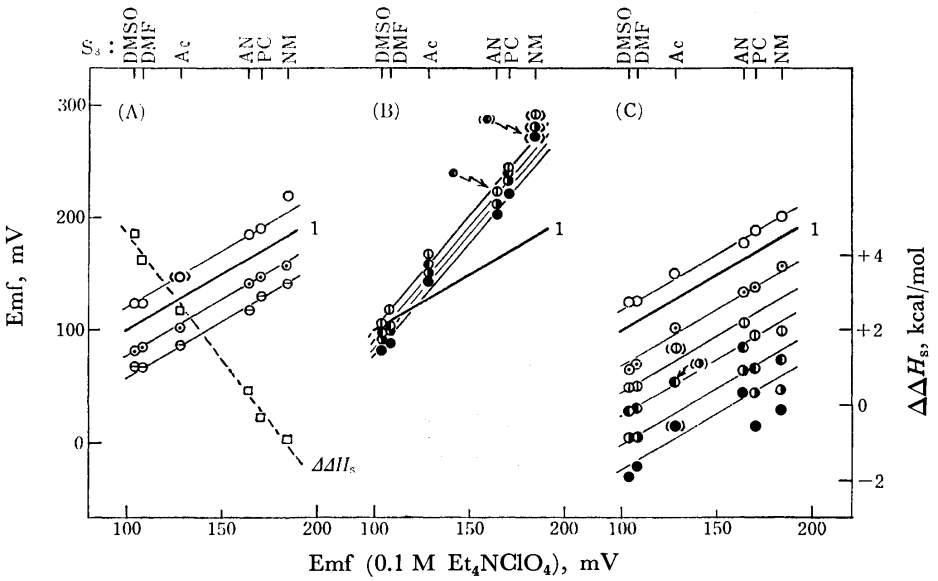

Fig. 4. Emf of cell III and $\Delta\Delta H_s$ (see text).
(A) and (B) for $MX=MClO_4$. M^+: 1 Et_4N^+; ○ Me_4N^+; ⊙ Pr_4N^+; ⊖ Bu_4N^+; ⓘ Na^+; ◑ Li^+; ◐ Ba^{2+}; and ● Mg^{2+}. (C) for $MX=Et_4NX$. X^-: 1 ClO_4^-; ○ Pic^-; ⊙ BF_4^-; ⓘ I^-; ◐ NO_3^-; ◑ Br^-; and ● Cl^-.

the sum of the ljps at J_1 and J_2 can be expressed by the sum of the following three terms:

$$E_{j,ion}(\text{concn})_{(J1+J2)} \approx 0, \quad (9)$$

$$E_{j,ion}(\text{ion-solv.})_{(J1+J2)} = -\frac{1}{F}[t_{M^+}{}^{S1}\Delta\mu^{S2}(M^+) - t_{X^-}{}^{S1}\Delta\mu^{S2}(X^-)], \quad (10)$$

$$E_{j,solv.(J1+J2)} = \frac{1}{F}t^r_{S3}[{}^{S3}\Delta\mu^{S1}(S_3) - {}^{S3}\Delta\mu^{S2}(S_3)] = \frac{1}{F}t^r_{S3}\Delta\Delta\mu_s. \quad (11)$$

If these simplified equations may be assumed to hold in cell III, the change of the bridge solvent (S_3) affects only the term of $E_{j,solv.(J1+J2)}$, and the emf of cell III is expected to change linearly with the change of $\Delta\Delta\mu_s = [{}^{S3}\Delta\mu^{S1}(S_3) - {}^{S3}\Delta\mu^{S2}(S_3)]$. Here, the following relations have been found by Cox *et al.*:[5] ${}^{S}\Delta\mu^{H_2O}(S) \approx ({}^{S}\Delta H^{H_2O}(S) + 3 \text{ kcal mol}^{-1})/2$ and ${}^{S}\Delta\mu^{AN}(S) \approx {}^{S}\Delta H^{AN}(S)/2$, where S denotes an organic solvent. Therefore, the good linear correlations in Figs. 4(A) and 4(B) between $\Delta\Delta H_s$ and the change in emf indicate that Eq. 11 is, at least qualitatively, a reasonable representation.† Here we must point out that, as was found by Cox *et al.*,[5] the change in ${}^{S}\Delta\mu^{H_2O}(S)$ is generally much larger than the change in ${}^{S}\Delta\mu^{AN}(S)$. Thus, most of the change in emf of cell III with the bridge solvent should be attributed to the change in $E_{j,solv.}$ at J_2 (water–organic solvent junction). This has been confirmed experimentally from the investigation of the ljp between different aprotic solvents.[16]

In deriving Eq. 8, we assumed that solvent molecules which are transferred across the boundary with the bridge electrolyte determine $E_{j,solv.}$. The fact that two classes of straight lines with a simple slope ratio (1 : 2) are obtained might be an indication that solvent molecules are really carried across the junction with the bridge electrolyte and that the number of the solvent molecules determines the ljp. It is difficult, however, to understand why the slopes are the same for all tetraalkylammonium perchlorates, on one hand, and for the perchlorates of Li^+, Na^+, Mg^{2+}, and Ba^{2+}, on the other hand, even though there exist considerable differences in ionic mobilities and solvations among the cations in each group.

We showed in Table 3 that the difference of ΔE between such bridge cations as Li^+, Na^+, Mg^{2+}, and Ba^{2+} is relatively small. The results in Fig. 4(B) also show that these cations behave in approximately the same way. Similar phenomena have also been observed at junctions between different organic solvents.[16] Cox *et al.*[5] tried to attribute this small difference in ljp among these cations to the compensating effect of two factors, the free energies of transfer of cations and their mobilities. We would rather consider, however, that it is because the contribution from these cations to $E_{j,ion}$(ion-solv.) is actually relatively small. This can be supported by the following reasoning: Parker and his coworkers[4,5] considered that, when the bridge electrolyte is 0.1 M Et_4NPic, the value of $E_{j,ion}$(ion-solv.) is generally small. If this is correct, the ljp of cell III with 0.1 M Et_4NPic as the bridge electrolyte may be considered to be small when $\Delta\Delta H_s$ becomes +3 kcal/mol, because $\Delta\Delta\mu_s$ is then approximately zero and $E_{j,solv.}$ may also be expected to be small. From Fig. 4(C), the emf of cell III with 0.1 M Et_4NPic bridge electrolyte is *ca.* 140 mV at 123 mV of the abscissa at which $\Delta\Delta H_s = +3$ kcal/mol. We find from Fig. 4(B) that the emfs of cell III with such bridge cations as Li^+, Na^+, Mg^{2+}, and Ba^{2+} are also near 140 (±15) mV at $\Delta\Delta H_s = +3$ kcal/mol, a good coincidence with the above emf value (here the contribution from the perchlorate ion may be considered to be relatively

† The results in Fig 4 show that t^r_{S3} in Eq. 11 has negative values.

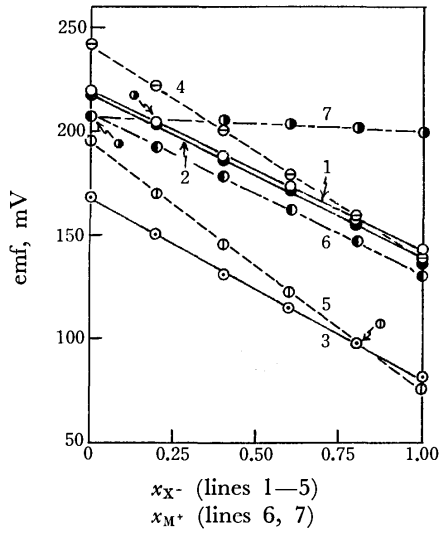

Fig. 5. Changes of emfs of cells IV and IV′ with the molar ratios of the mixed bridge electrolytes.
Lines 1—5 are for cell IV and lines 6 and 7 for cell IV′. $X^-=Br^-$ and $Y^-=ClO_4^-$ for lines 1(○), 2(●), and 3(⊙), $X^-=Br^-$ and $Y^-=Pic^-$ for lines 4(⊖) and 5(◫), $M^+=Bu_4N^+$ and $N^+=Na^+$ for line 6(◐), and $M^+=Li^+$ and $N^+=Na^+$ for line 7(◑). Solvent S_3 is AN for lines 2, 4, 6, and 7, H_2O for line 1, and DMF for lines 3 and 5.

small). A similar coincidence between the emf of the cell with 0.1 M Et_4NPic bridge electrolyte and those with 0.1 M bridge electrolytes of the perchlorates of these cations was observed at $\Delta\Delta\mu_s\approx 0$ also in the case in which MeOH, instead of H_2O, was used as S_2 in cell III.[16]

The effect of tetraalkylammonium ions on the ljp at water–organic solvent junctions was considerable, as is shown in Table 3. When these ions were used as the bridge cations in cell III, the emf decreased with the increase of the cationic size, as can be expected from Eq. 10 (Fig. 4(A)). But quantitative study is difficult because the available data concerning the free energy of transfer of these ions is insufficient.

Figure 4(C) shows that the effect of bridge anions on the emf of cell III is quite large. If we consider the emfs of the cell in which the bridge solvents are AN, DMSO, and DMF, we find that the emf changes linearly with the bridge solvents, with slopes approximately equal for all bridge anions, and the lines shift to smaller emf values from picrate to chloride ions. Because ${}^{S}\Delta\mu^{AN}(X^-)$ is smaller than ${}^{S}\Delta\mu^{H_2O}(X^-)$, most of the change in the emf with the bridge anions corresponds to the change in ljp at J_2 (see Fig. 3). When the bridge solvent was PC or NM, however, deviations from linearity occurred, especially with halogenide and nitrate ions, as can also be expected from the results in Fig. 3.

Use of a Salt Bridge Consisting of Mixed Electrolytes or Mixed Solvents. Salt Bridge Consisting of Mixed Electrolytes: The emfs of cells IV and IV′ were measured by changing the ratio of the mixed electrolytes in the salt bridge. The results are represented in Fig. 5.

$$Ag/5\times10^{-3}\,M\ AgClO_4,\ 10^{-2}\,M\ Et_4NClO_4(AN)\underset{j1}{//}10^{-2}\,M\ Et_4NClO_4(AN)\underset{J1}{//}0.1\,xM\ Et_4NX\text{-}0.1(1-x)M\ Et_4NY(S_3)\underset{J2}{//}$$
$$10^{-2}\,M\ Et_4NClO_4(H_2O)\underset{j2}{//}5\times10^{-3}\,M\ AgClO_4,\ 10^{-2}\,M\ Et_4NClO_4(H_2O)/Ag \qquad \text{Cell IV}$$

$$Ag/10^{-2}\,M\ AgClO_4(AN)\underset{J1}{//}0.1x\,M\ MClO_4\text{=}0.1(1-x)M\ NClO_4(S_3)\underset{J2}{//}10^{-2}\,M\ AgClO_4(H_2O)/Ag \qquad \text{Cell IV′}$$

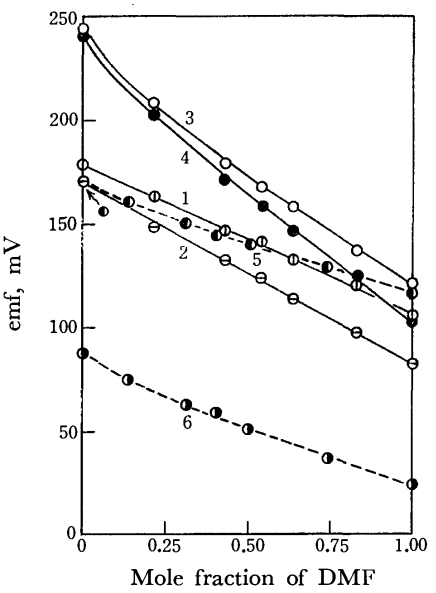

Fig. 6. Changes of emfs of cells V and V′ with the mole fractions of mixed bridge solvents.
Lines 1—4 for cell V′. M^+: 1(◫) Et_4N^+; 2(⊖) Bu_4N^+; 3(○) Na^+; and 4(●) Li^+. Lines 5 and 6 for cell V. X^-: 5(◐) ClO_4^-; and 6(◑) Br^-.

Lines 1—3 were obtained for cell IV in which $X^-=Br^-$, $Y^-=ClO_4^-$, and solvent S_3 was AN, H_2O, and DMF, respectively. All these lines were straight. Because the molar conductivities of Br^- and ClO_4^- are approximately equal in all the solvents concerned, this linear relation is what can be expected. If $X^-=Br^-$ and $Y^-=Pic^-$ in cell IV or $M^+=Bu_4N^+$ or Li^+ and $N^+=Na^+$ in cell IV′, there exist some differences between the molar conductivities of X^- and Y^- or M^+ and N^+.[15] But the changes of emfs with the molar ratio of the mixed electrolyte were also almost linear, as shown by lines 4 to 7. This can be understood if we consider that the relations $x\Lambda_{Et_4NX}/[x\Lambda_{Et_4NX}+(1-x)\Lambda_{Et_4NY}]$ *vs.* x and $x\Lambda_{MClO_4}/[x\Lambda_{MClO_4}+(1-x)\Lambda_{NClO_4}]$ *vs.* x are almost linear even when there exist some differences in molar conductivities.

Salt Bridge Consisting of Mixed Solvents: The results in Fig. 6 were obtained by measuring emfs of cells V and V′ for various ratios of the mixed bridge solvents.

$$Ag/5\times10^{-3}\,M\ AgClO_4,\ 10^{-2}\,M\ Et_4NClO_4(AN)\underset{j1}{//}10^{-2}\,M\ Et_4NClO_4(AN)\underset{J1}{//}0.1\ M\ Et_4NX(AN+DMF)\underset{J2}{//}10^{-2}\,M$$
$$Et_4NClO_4(H_2O)\underset{j2}{//}5\times10^{-3}\,M\ AgClO_4,\ 10^{-2}\,M\ Et_4NClO_4(H_2O)/Ag \qquad \text{Cell V}$$

$$Ag/10^{-2}\,M\ AgClO_4(AN)\underset{J1}{//}0.1\ M\ MClO_4(PC+DMF)\underset{J2}{//}10^{-2}\,M\ AgClO_4(H_2O)/Ag \qquad \text{Cell V′}$$

When M^+ in cell V′ was Et_4N^+ or Bu_4N^+, the emfs changed almost linearly with the mole fraction of the solvents. But deviations from linearity occurred when M^+ in cell V′ was Na^+ or Li^+, and X^- in cell V was Br^- or ClO_4^-. To predict the effect of the mixed solvents is rather difficult. Besides the effect to the solvent component of the ljp, $E_{j,solv.}$, the effect of the preferential ionic solvation by one of the mixed solvents must be taken into account. In the cases of Fig. 6, lines 3 and 4, the deviation from linearity seems to be due to the preferential solvation of DMF to the bridge cations (Na^+ and Li^+).

In the present report, we have examined in detail how the ljps between water and organic solvents are influenced by the solvents and electrolytes present at the junctions and found that some of the influence can be correlated, at least qualitatively, with the literature data concerning ion-solvent and solvent-solvent interactions. The influence at the junctions between water and organic solvents is much larger than that at any junctions possible between such organic solvents as MeOH, AN, PC, DMF, and DMSO.[16] Therefore, we must take this influence carefully into account when we measure emfs of cells involving water-organic solvent junctions. The results in the present report will be of use in such cases.

References

1) I. M. Kolthoff, *J. Polarogr. Soc.*, **10**, 22 (1964).

2) J. F. Coetzee and J. J. Campion, *J. Am. Chem. Soc.*, **89**, 2513, 2517 (1967).

3) M. Alfenaar, C. L. DeLigny, and A. G. Remijnse, *Recl. Trav. Chim. Pays-Bas*, **86**, 986 (1967).

4) R. Alexander, A. J. Parker, J. H. Sharp, and W. E. Waghorne, *J. Am. Chim. Soc.*, **94**, 1148 (1972).

5) B. G. Cox, A. J. Parker, and W. E. Waghorne, *J. Am. Chem. Soc.*, **95**, 1010 (1973).

6) N. Matsuura and K. Umemoto, *Bull. Chem. Soc. Jpn.*, **47**, 806, 813, 1334 (1974).

7) J. W. Diggle and A. J. Parker, *Aust. J. Chem.*, **27**, 1617 (1974).

8) R. Gaboriaud, *J. Chim Phys.*, **72**, 347 (1975).

9) R. C. Murray, Jr., and D. A. Aikens, *Electrochim. Acta*, **21**, 1045 (1976).

10) M. Cappelletti, P. Longhi, and T. Mussini, *Gazz. Chem. Ital.*, **106**, 241 (1976).

11) A. J. Staverman, *Trans. Faraday Soc.*, **48**, 176 (1952).

12) B. G. Cox, G. R. Hedwig, A. J. Parker, and D. W. Watts, *Aust. J. Chem.*, **27**, 477 (1974).

13) K. Izutsu, "Denkyoku-hanno no Kiso," ed by T. Osa, Kyoritsu Shuppan, Tokyo (1973), Chap. 2.

14) D. A. MacInnes, "The Principles of Electrochemistry," Dover Publications, New York (1961), p. 232.

15) M. Spiro, "Physical Chemistry of Organic Solvent Systems," ed by A. K. Covington and T. Dickinson, Plenum Press, New York (1973), pp. 673—680; M. L. Jansen and H. L. Yeager, *J. Phys. Chem.*, **77**, 3089 (1973).

16) K. Izutsu, unpublished results.

The Crystal Structure of the Ammonium Bromide Complex of 1,4,7,10,13,16-Hexaoxacyclooctadecane (18-Crown-6), $C_{12}H_{24}O_6 \cdot NH_4Br \cdot 2H_2O$

Osamu NAGANO, Akiko KOBAYASHI, and Yukiyoshi SASAKI

Department of Chemistry, Faculty of Science, The University of Tokyo, Hongo, Tokyo 113

(Received July 1, 1977)

Ammonium bromide forms a 1 : 1 complex with cyclic polyether "18-crown-6." The crystals of $C_{12}H_{24}O_6 \cdot NH_4Br \cdot 2H_2O$ are orthorhombic, with the space group of Pnam and with cell constants of $a=10.002(3)$, $b=12.716(4)$, $c=15.073(4)$ Å, and $Z=4$. The structure was solved by the conventional heavy-atom technique and refined by the full matrix least-squares method to $R=0.099$ for 1033 independent reflections. The 18-crown-6 has a conformation with a pseudo D_{3d} symmetry. The ammonium cation is displaced by 1.00 Å from the mean oxygen plane of the 18-crown-6 and interacts with the nearest bromide anion. The relationship between the cation and the 18-crown-6 resembles those of the $C_{12}H_{24}O_6 \cdot RbNCS$ and $C_{12}H_{24}O_6 \cdot CsNCS$ complexes. On the difference Fourier maps, four electron-density peaks were detected at reasonable positions for the hydrogen atoms of the amonium cation.

Macrocyclic polyethers, often called "crown" compounds, form complexes with many different inorganic cations, such as alkaline metal, alkaline-earth metal, and ammonium cations.[1] They have the possibility to increase the salt solubility and the anion reactivity in organic solvents.

In the last decade, therefore, many macrocyclic polyethers have been studied as catalysts for organic syntheses,[2,3] reagents for solvent extraction in analytical chemistry,[4,5] and packing material for the separation of *d,l*-amino acids by column chromatography.[7-9] Our main interest in the present structure study of $C_{12}H_{24}O_6 \cdot NH_4Br \cdot 2H_2O$ lies in the difference between the interaction of an alkaline or alkaline-earth metal cation-crown compound[10-16] and that of an ammonium cation-crown compound.

Experimental

18-Crown-6 was synthesized from bis(2-chloroethyl) ether and tetraethylene glycol according to the following scheme:[17,18]

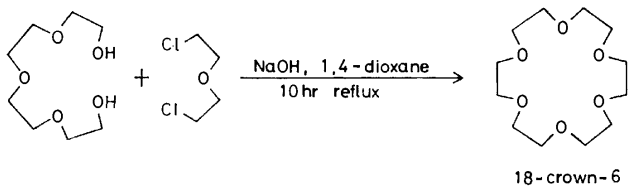

18-crown-6

The crystal of $C_{12}H_{24}O_6 \cdot NH_4Br \cdot 2H_2O$ was obtained from an aqueous solution of the 18-crown-6 and ammonium bromide (18-crown-6 : NH_4Br = 1 : 1). The crystal used was made nearly spherical, and its radius was 0.18 mm.

The intensities of the reflections were measured with a Rigaku automatic four-circle diffractometer (graphite monochrometer, Mo $K\alpha$ radiation, ω-2θ scan method). The scanning range was determined according to the formula of $1.2° + 0.6° \tan\theta$, and the scanning rate was 0.5° per min in ω when $2\theta < 60°$. Background counts of 10 s were taken at both limits of the scanning range. Three reference reflections were measured after every 50 reflections; no significant changes were observed over the period of data collection. The intensities of 1033 reflections ($\sigma(F) > 3.0$) were adopted for the structure determination.

The crystal data are: $C_{12}H_{24}O_6 \cdot NH_4Br \cdot 2H_2O$, orthorhombic, space group Pnam, $a=10.002(3)$, $b=12.716(4)$ $c=15.073(4)$ Å, $U=1917.1(9)$ Å^3 at 23 °C, $Z=4$, $D_m=1.35$, $D_x=1.380$ g cm^{-3}, $F.W.=398.29$ and μ(Mo $K\alpha$)$=23.07$ cm^{-1}.

Structure Determination

The structure was solved by the heavy-atom technique and refined by the full matrix least-squares program LINUS.[19] The function minimized was $\Sigma w(|F_o|-|F_c|)^2$, where $w=1/\sigma^2(F)$. The atomic scattering factors used were taken from the International Tables for X-Ray Crystallography, Vol. IV.[20] Corrections for anomalous dispersion and absorption were included in the refinement. An extinction correction was applied at the final stage of the refinement, but the R value, 0.099 ($R=\Sigma w||F_o|-|F_c||/\Sigma w|F_o|$), did not change. The R value was relatively large, possibly because of the sensitivity of the crystal to X-ray, but possibly also because of the release of water molecules from the crystal during the measurement. In a test of the R-factor ratio based on the hypothesis that $Pna2_1$ was the correct space group, the R-factor ratio, $R(\text{Pnam})/R(Pna2_1)$, was found to be 1.016. We could not reject, at the 50% significance level, the hypothesis that Pnam was the correct space group. However, the result for $Pna2_1$ indicated unreasonable values in the bond distances and bond angles. Hence, we selected centro-symmetric Pnam as the space group of the crystal.[21] The atomic coordinates and temperature factors are listed in Tables 1—3. The F_o-F_c table is kept at the office of this Bulletin as Document No. 7807.

Results and Discussion

Crystal Structure. The two oxygen atoms of the 18-crown-6, O(1) and O(4), the nitrogen atom and two hydrogen atoms, H_{Br} and $H_{O(4)}$, of the ammonium cation and the bromide anion lie on the mirror plane at $z=1/4$ and 3/4. The cation interacts with the 18-crown-6 and the nearest bromide anion, which is weakly bound to four water molecules. The NH_4^+–Br^- distance (3.438 Å) is slightly longer than the sum of the two corresponding ionic radii (3.39 Å = 1.43 + 1.96 Å). The Br^-–OH_2 distances (average, 3.365 Å) are in fair agreement with the sum of corresponding ionic and van der Waals radii (3.36 Å = 1.96 + 1.40 Å). There is

Table 1. Fractional coordinates (and estimated standard deviations) of the non-hydrogen atoms (Values are $\times 10^4$)

	x	y	z
Br	1456(2)	1412(2)	2500
O(1)	−338(13)	2169(11)	7500
O(2)	562(9)	1250(8)	9120(5)
O(3)	3138(9)	356(8)	9177(6)
O(4)	4072(14)	−370(12)	7500
O(H_2O)	3716(14)	2850(12)	3629(10)
N	1308(16)	196(11)	7500
C(1)	−1120(16)	2128(16)	8280(11)
C(2)	−224(19)	2178(14)	9073(11)
C(3)	1329(16)	1204(15)	9910(10)
C(4)	2196(17)	268(17)	9862(10)
C(5)	3959(20)	−546(16)	9047(13)
C(6)	4875(17)	−347(15)	8273(13)

Table 2. Fractional coordinates (and estimated standard deviations) of the hydrogen atoms (Values are $\times 10^3$)

	x	y	z
H(1)	−164(11)	147(8)	829(7)
H(1)*	−174(11)	247(8)	828(7)
H(2)	−78(11)	226(9)	963(7)
H(2)	35(10)	282(8)	902(7)
H(3)	74(11)	116(8)	1044(7)
H(3)*	190(10)	184(8)	995(7)
H(4)	165(11)	−36(8)	976(7)
H(4)	265(11)	17(9)	1044(7)
H(5)	341(11)	−118(8)	892(7)
H(5)*	448(11)	−69(8)	959(7)
H(6)	553(11)	−92(8)	824(7)
H(6)*	530(11)	39(9)	834(7)
H_{Br}	69(16)	−51(13)	750
$H_{O(2)}$	108(10)	56(8)	803(6)
$H_{O(4)}$	220(18)	0(14)	750

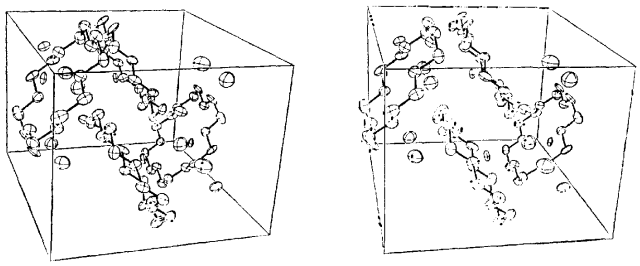

Fig. 1. Stereoscopic view of the crystal structure looking along the c axis. The c axis vertical, the a axis horizontal.

no direct interaction between the cation and the water molecules. The TG measurement of $C_{12}H_{24}O_6·NH_4Br·2H_2O$ showed that the water molecules of crystallization were released from the crystal lattice at *ca.* 55 °C. They are distributed in the holes of the crystal lattice as is shown in Fig. 1.

The Structure of the NH_4^+·18-Crown-6 Complex Cation. The pseudo D_{3d} symmetrical conformation of the 18-crown-6 is the same as those found in the KNCS, RbNCS, and CsNCS complexes.[22] Table 4 shows the bond distances, the bond angles, and the torsion angles in the 18-membered ring. The six oxygen atoms of the 18-crown-6 are alternately 0.25 Å above and below their mean plane and form a nearly planar hexagon of approximately 2.84 Å (2.819—2.853 Å; average, 2.840 Å). The C–C distances (1.474—1.506 Å; average, 1.492 Å) and the C–O distances (1.403—1.424 Å; average, 1.416 Å) appear to be somewhat shorter than those in the $C_{12}H_{24}O_6$·KNCS complex, possibly because of the internal motion in the ring, as is observed in other complexes.[16-20,22] The temperature factors of the oxygen and carbon atoms are remarkably anisotropic (Table 3). The C–O–C bond angles (110.8—115.1°; average, 113.0°) are larger than the C–C–O bond angles (106.8—111.5°; average, 109.0°). The average of the torsion angles about C–C bonds is 67.9°, while that about C–O bonds is 4.3°. All the C–H distances are between 0.96 and 1.05 Å.

The nitrogen atom of the ammonium cation has the smallest thermal ellipsoid of all the non-hydrogen atoms,

Table 3. Anisotropic vibration parameters (Å²) of the $\exp[-2\pi^2(U_{11}h^2a^{*2}+U_{22}k^2b^{*2}+U_{33}l^2c^{*2}+2U_{12}hka^*b^*+2U_{13}hla^*c^*+2U_{23}klb^*c^*)]$ form (Values are $\times 10^4$)

	U_{11}	U_{22}	U_{33}	U_{12}	U_{13}	U_{23}
Br	58(1)	105(2)	76(2)	−21(2)	0	0
O(1)	58(9)	87(12)	59(8)	15(8)	0	0
O(2)	68(6)	74(8)	45(5)	4(5)	−5(5)	−9(5)
O(3)	61(6)	73(7)	65(6)	−5(5)	1(5)	13(6)
O(4)	53(8)	88(12)	72(10)	10(8)	0	0
O(H_2O)	120(11)	155(14)	153(12)	0(10)	1(11)	−39(11)
N	73(10)	20(7)	33(7)	−11(8)	0	0
C(1)	68(11)	80(14)	73(11)	13(10)	8(9)	1(10)
C(2)	94(13)	59(12)	59(9)	6(10)	9(10)	−11(8)
C(3)	55(9)	100(14)	49(8)	−16(10)	11(8)	−7(9)
C(4)	74(11)	110(16)	42(9)	−34(12)	6(8)	32(10)
C(5)	99(14)	74(13)	80(13)	22(11)	−28(12)	4(11)
C(6)	69(10)	81(13)	102(14)	55(11)	−5(10)	−11(12)

TABLE 4. BOND DISTANCES (Å), BOND ANGLES (°), AND TORSION ANGLES (°) IN THE 18-REFER MEMBERED RING

Prime marks as superscripts refer to the following equivalent position: $x, y, 3/2-z$.

Atoms				Distance	Angle	Torsion angle
1	2	3	4	2-3	1-2-3	1-2-3-4
C (1')	-O (1)	-C (1)	-C (2)	1.414	112.6	0.18
O (1)	-C (1)	-C (2)	-O (2)	1.496	109.4	67.10
C (1)	-C (2)	-O (2)	-C (3)	1.420	109.6	6.20
C (2)	-O (2)	-C (3)	-C (4)	1.418	112.1	4.97
O (2)	-C (3)	-C (4)	-O (3)	1.474	108.1	65.20
C (3)	-C (4)	-O (3)	-C (5)	1.403	111.5	3.96
C (4)	-O (3)	-C (5)	-C (6)	1.424	115.1	2.12
O (3)	-C (5)	-C (6)	-O (4)	1.506	108.8	71.36
C (5)	-C (6)	-O (4)	-C (6')	1.415	106.8	8.79
C (6)	-O (4)	-C (6')	-C (5')	1.415	110.8	8.79

TABLE 5. DISTANCES (Å) INVOLVING THE AMMONIUM AND BROMIDE IONS

Roman numerals refer to the following equivalent positions:

I; $-1/2+x, 1/2-y, 1/2-z$

II; $x, y, 1/2-z$

III; $-1/2+x, 1/2-y, z$.

N-O(1)	3.000	Br-N	3.438
N-O(2)	2.884	Br-H_{Br}	2.43
N-O(3)	3.128	Br-O(H_2O)	3.369
N-O(4)	2.857	Br-O(H_2O) I	3.360
N-H_{Br}	1.09	Br-O(H_2O) II	3.369
N-$H_{O(2)}$	0.95	Br-O(H_2O) III	3.360
N-$H_{O(4)}$	0.93		

suggesting that the cation strongly interacts with the 18-crown-6 as is shown in Figs. 2 and 3. This nitrogen atom is displaced by 1.00 Å from the mean oxygen plane of the 18-crown-6. The ammonium cation is too large to fit in the cavity of the 18-crown-6. Dunitz *et al.*[22] reported that, in the RbNCS and CsNCS complexes of the 18-crown-6, the cations were displaced from the mean oxygen plane by 1.19 Å (Rb^+) and 1.44 Å (Cs^+). The distance, 1.00 Å for NH_4^+, is a suitable length considering the size of the cations and that of the cavity of the 18-crown-6 (cavity < NH_4^+ < Rb^+ < Cs^+). The straight line passing through the bromine and nitrogen atoms intersects the mean oxygen plane at an angle of 68.8° (Fig. 3). The N–O distances are divided into two groups (3.000—3.128 Å; average, 3.064 Å for N–O(1), N–O(3) and N–O(3'); 2.857—2.844 Å; average, 2.871 Å for N–O(2), N–O(2') and N–O(4)). On the difference Fourier maps, four electron-density peaks (0.6—0.8 e/Å^3) were detected at reasonable positions for the hydrogen atoms of the ammonium caion. The electron-densities of the ghost peaks around the nitrogen atom were lower than 0.55 e/Å^3. Three peaks are between N and O(2), N and O(2'), and N and O(4), suggesting the existence of three hydrogen bonds (Fig. 2). The last peak is between N and Br^- (Fig. 3). The N–H distances are between 0.9 and 1.1 Å. Table 5 shows the distances in-

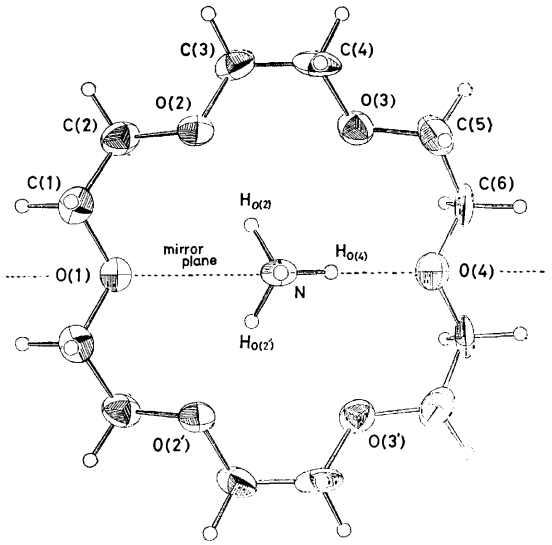

Fig. 2. $NH_4^+ \cdot C_{12}H_{24}O_6$ complex cation viewed in direction normal to the mean plane. The vibration ellipsoids are drawn at the 30% probability level.[23]

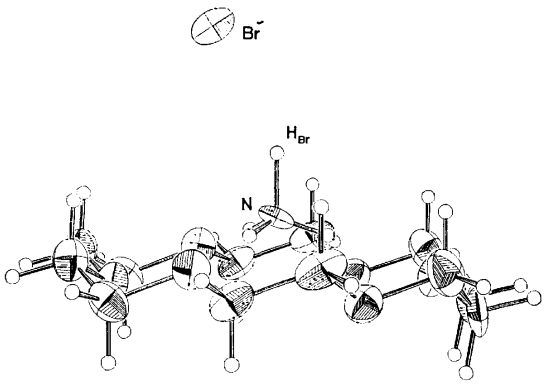

Fig. 3. $NH_4^+ \cdot C_{12}H_{24}O_6$ complex cation viewed along a direction in the mean plane. The vibration ellipsoids are drawn at the 30% probability level.[23]

volving the ammonium and bromide ions. The structure of $NH_4^+ \cdot$18-crown-6 closely resembles those of $Rb^+ \cdot$ 18-crown-6 and $Cs^+ \cdot$18-crown-6, but the distortion from the D_{3d} symmetry in $NH_4^+ \cdot$18-crown-6 is slightly larger than those in $Rb^+ \cdot$18-crown-6 and $Cs^+ \cdot$18-crown-6 because of the hydrogen bonds. In brief, the present complex differs from alkaline or alkaline-earth metal salts-"crown" complexes in the presence of the hydrogen bonds.

References

1) C. J. Pedersen, *J. Am. Chem. Soc.*, **89**, 7017 (1967).
2) R. A. Bartsch and R. H. Kayser, *J. Am. Chem. Soc.*, **96**, 4346 (1974).
3) D. J. Sum and H. F. Simmons, *J. Am. Chem. Soc.*, **94**, 4024 (1972).
4) J. W. Mitchell and D. L. Shanks, *Anal. Chem.*, **47**, 642 (1975).
5) A. Sadakane, T. Iwachido, and K. Toei, *Bull. Chem. Soc. Jpn.*, **48**, 60 (1975).
6) Yu. A. Ovchinnikov, V. T. Ivanov, and A. M. Shkrob, "Membrane-active Complexones," B. B. A. Library, Vol. 12.

7) J. P. Behr, J. M. Lehn, and P. Vierling, *J. Chem. Soc., Chem. Commun.*, **1976**, 621.
8) D. A. Laidler and J. F. Stoddart, *J. Chem. Soc., Chem. Commun.*, **1976**, 979.
9) G. Dotsivi, Y. Sogah, and D. J. Cram, *J. Am. Chem. Soc.*, **98**, 3038 (1976).
10) P. R. Mallinson and M. R. Truter, *J. Chem. Soc., Perkin Trans. 2*, **1973**, 1818.
11) D. E. Fenton, M. Mercer, N. S. Poonia, and M. R. Truter, *J. Chem. Soc., Chem. Commun.*, **1972**, 66.
12) P. P. North, E. C. Steiner, F. P. van Remoortere, and F. P. Boer, *Acta Crystallogr., Sect. B*, **32**, 370 (1976).
13) M. A. Bush and M. R. Truter, *J. Chem. Soc., Perkin Trans. 2*, **1972**, 341.
14) N. K. Dalley, D. E. Smith, R. N. Izatt, and J. J. Christensen, *J. Chem. Soc., Chem. Commun.*, **1972**, 90.
15) J. D. Owen and J. N. Wingfield, *J. Chem. Soc., Chem. Commun.*, **1976**, 318.
16) M. A. Bush and M. R. Truter, *J. Chem. Soc., Sect. B*, **1971**, 1440.
17) G. W. Gokel and D. J. Cram, *J. Org. Chem.*, **39**, 2445 (1974).
18) F. L. Cook, T. C. Caruso, M. P. Byrne, C. W. Bowers, D. H. Speck, and C. L. Liotta, *Tetrahedron Lett.*, **1974**, 4029.
19) P. Coppens and W. C. Hamilton *Acta Crystallogr., Sect. A*, **26**, 71 (1970).
20) "International Tables for X-Ray Crystallography," Kynoch Press, Vol. IV. Birmingham (1974),
21) W. C. Hamilton, *Acta Crystallogr.*, **18**, 502 (1965).
22) J. D. Dunitz, M. Dobler, P. Seiler, and R. P. Phizackerley, *Acta Crystallogr., Sect. B*, **30**, 2733 (1974).
23) C. K. Johnson. ORTEP. Report ORNL-3794, Oak Ridge National Laboratory, Oak Ridge, Tennessee.

Studies of the Hydrous Titanium Oxide Ion Exchanger. IV. The Effect of Radiation and Heat Treatment*

Yasushi INOUE and Masamichi TSUJI**

Department of Nuclear Engineering, Faculty of Engineering, Tohoku University, Aramaki, Sendai 980

(Received July 20, 1977)

The effects of ^{60}Co γ-ray irradiation and of heat treatment in air have been studied on the properties of the hydrous titanium oxide ion exchanger. The ion-exchange capacity of the sodium form did not change at all, while that of the hydrogen form decreased a little, by the exposure of 5.2×10^8 R. The color of the exchanger, initially white, turned yellow upon irradiation. This exchanger was stable against heat treatment up to around 80 °C; thereafter the exchange capacity gradually decreased with the temperature until 324 °C, where it was abruptly reduced to about a quarter of the initial value. The examination of the titration curves showed that the most acidic exchange site was weaker than less acidic sites against heat treatment. The structural formula of this hydrous titanium oxide ion exchanger has been suggested on the basis of the ion-exchange capacity, the thermal decomposition curves, and such auxiliary data as the X-ray diffraction and the infrared spectra.

In the field of nuclear chemical engineering, an ion exchanger is often exposed to an intense radiation and to a high temperature. Since most inorganic ion exchangers are expected to be superior to ion-exchange resins in these respects,[1] it is very important to study their radiation- and thermal stabilities. Moreover, these studies may be helpful in considering the structure of the exchanger. However, the radiation- and thermal stabilities of the hydrous titanium oxide ion exchanger have not yet been studied in detail. On the other hand, many propositions have been made concerning the structure of hydrous titanium oxide based on various circumstantial evidence.[4-11] However, neither the composition nor the ion-exchange properties, such as the ion-exchange capacity and the acid-base property, deduced from these structural formulas are compatible with those actually observed in the hydrous titanium ion exchanger prepared by the method previously proposed by the present authors.[2,3]

The present paper will describe the effect of ^{60}Co γ-ray irradiation and of heat treatment in air on the ion-exchange properties of the hydrous titanium oxide. Furthermore, the structural formula of the exchanger have been inferred from those results and from the data obtained by the previous studies.[2,3]

Experimental

Reagents and Apparatus. The hydrous titanium oxide ion exchanger was prepared by the method described previously[2] and then converted into H^+ or Na^+ forms. The other chemicals were of the highest purity grade and were obtained from Wako Pure Chemical Industries, Ltd.

γ-Ray irradiation was carried out using the ^{60}Co γ-ray irradiation facility of Tôhoku University. About 6 g of the exchanger in a desired ionic form was placed in a stoppered test tube with either 10 cm^3 of water or a 0.1 M NaOH (1 M= mol/dm^3) solution, or without them, and irradiated intermittently at an average exposure rate of 3.2×10^5 or 2.5×10^5 R/h (1 R=258 μC/kg).

The thermal analysis was undertaken with a Shimadzu micro thermal analyzer, Model DT-20B, connected to a thermal balance, Model TGC-20H, for thermogravimetric analysis (TGA), and a high-temperature-sample holder, Model MDH-20, for differential thermal analysis (DTA). The reference material for DTA was α-alumina. The measurement was performed in air at a heating rate of 10 °C/min.

The infrared (IR) absorption spectra were measured with a Nihon Bunko infrared spectrometer, Model IRA-I, using the KBr disk method. The wave number was calibrated with polystyrene.

Heat Treatment. The exchanger in a desired ionic form was heated in air to a constant weight at a constant temperature. After cooling, the sample in the Na^+-form was converted into the H^+ form by immersing it in a 0.1 M HCl solution, while that in the H^+-form was immersed in water. Thereafter, they were both subjected to the humidifying operation described previously.[3]

The other experimental procedures were the same as those previously been described.[2,3]

Results and Discussion

Radiation Stability. Table 1 represents the effect of γ-irradiation on the properties of the exchanger, together with that of the ion-exchange resin, Dowex-50, for comparison. It took 1.5 y to reach a total exposure of 5.2×10^8 R. Even if the exchanger was not irradiated, the ion-exchange capacity decreased to about a half of the initial value when the exchanger in the hydrogen from was allowed to stand for 1.5 y. The decrease in the ion-exchange capacity is, thus, largely due to aging of the exchanger, and only slightly to the effect of the γ-rays. The ion-exchange capacity of the sodium form, however, did not change at all upon a γ-ray irradiation of up to 5.2×10^8 R. The amount of titanium dissolved in the supernatant solution during irradiation was 7.2×10^{-5} g. Since this value is compatible with the data concerning chemical stability described previously,[2] it can be said that γ-ray irradiation does not influence the solubility of the material. After irradiation, all the samples turned yellow except for the sample in the hydrogen form exposed up to 2.2×10^8 R. The yellow color of the exchanger in the hydrogen form disappeared when it was immersed in a 1.0 M sodium hydroxide solution, but appeared again by reconversion to the hydrogen form. In contrast, the yellow color

* Thesis submitted by one of the authors (M. T.) to Tôhoku University in partial fulfillment of the requirements for the degree of Kogaku-Hakushi (Ph. D).

** Present address: Department of Chemistry, Tokyo Institute of Technology, Ookayama, Meguro-ku, Tokyo 152.

Table 1. Effect of γ-irradiation on the properties of the exchanger[a)]

Sample No.	Exchanger (ionic form)	Environment	Exchange capacity[c)] meq. Na^+/g		Color of the exchanger after irradiation
			Irradiated	Unirradiated	
1	HTO(H^+)[b)]	Water	2.27±0.10	2.72±0.05	Yellow
2	HTO(H^+)	Air	2.64±0.07	2.85±0.08	Light creamy
3	HTO(Na^+)	0.1 M NaOH	4.31±0.00	4.30±0·10	Yellow
4	HTO(Na^+)	Air	4.68±0.07	4.61±0.05	Yellow
5	Dowex 50×8(H^+)	Water	4.37±0.05	4.71±0.13	Brown
6	Dowex 50×8(Na^+)	0.1 M NaOH	4.74±0.21	4.72±0.10	Brown
7	HTO(H^+)	Air	2.97	2.98	White
8	HTO(H^+)	Water	2.90	—	Yellow

a) Average exposure rate (R/h): No. 1—6; 2.5×10^5, No. 7—8; 3.2×10^5. Time of irradiation (h): No. 1—6; 2141, No. 7—8; 680. Time of standing: No. 16; 1.5 y, No. 78; 36 d. Exposure (R): No. 1—6; 5.2×10^8, No. 78; 2.2×10^8. b) Hydrous titanium oxide, c) No. 16: 1.0 M NaOH batch exchange capacity[3)], No. 7—8: 0.10 M NaOH column exchange capacity.[2)]

Table 2. Effect of the heat treatment of the H^+-form exchanger on the composition and the ion-exchange capacity

Sample No.	Temperature (°C)	Weight loss (wt%)	Composition, molar ratio of H_2O/Ti after		Exchange capacity[a)]		
			Heated	Humidified	meq. Na^+/g	eq. Na^+/mol Ti	mol H_2O/mol Ti
1	R.T.	—	1.892	1.892	4.54±0.22	0.517±0.025	0.258±0.012
2	80±0.5	23.50	0.303	1.536	4.78±0.27	0.514±0.029	0.257±0.014
3	122±1	24.74	0.241	1.426	4.42±0.25	0.466±0.026	0.233±0.013
4	159±1	26.32	0.165	1.269	3.92±0.27	0.402±0.027	0.201±0.013
5	324±2	29.06	0.038	0.996	1.33±0.24	0.130±0.023	0.065±0.011
6	623±7	29.39	0.023	0.111	0.54±0.21	0.044±0.017	0.022±0.008
7	830±10	29.91	0	—	—	—	—

a) 1.0 M NaOH batch exchange capacity.

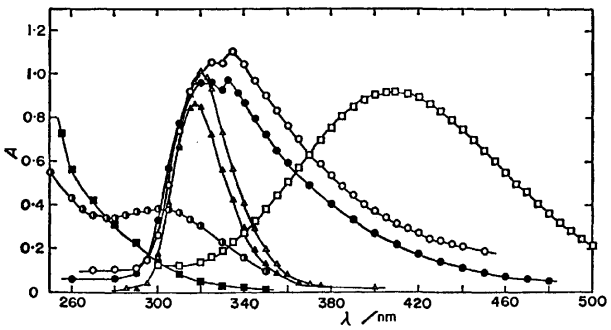

Fig. 1. Absorption spectra of the exchanger and the supernatant solution after irradiation.
●: Supernatant solution diluted by H_2O(Ti: 1.2×10^{-5} M), ○: Supernatant solution diluted by 1 M H_2SO_4 (Ti: 1.2×10^{-5} M), ▲: Exchanger, 5.9×10^{-2} M Ti/1 M H_2SO_4, △: Exchanger, $<5.9\times10^{-2}$ M Ti/1 M $HClO_4$, □: 1.25×10^{-3} M Ti(IV), 3.75×10^{-2} M H_2O_2 in 1 M H_2SO_4, ■: 200 ppm Ti(IV) in 1.8 M H_2SO_4 (Ref. 13), ◑: 10 ppm Fe(III) in 1.8 M H_2SO_4 (Ref. 13).

in the sodium form did not disappear when the sample was converted to the hydrogen form, but it almost disappeared when it was converted back to the sodium form again. Moreover, a sodium hydroxide solution wherein the sodium-form exchanger was immersed turned brownish yellow.

The change in color might be caused by the reaction of titanium with the radiolytic products of water. The absorption spectra were measured in order to identify the species responsible for yellow coloration (*cf.* Fig. 1). Sample No. 3 in Table 1 was dissolved with heating it in concentrated sulfuric or perchloric acid, followed by dilution to an acidity of 1 M. The absorption spectra of these solutions showed a single peak. Its position agreed approximately with one of the two peaks which appeared in the spectra of the solutions prepared by diluting the supernatant solution of the same sample with the respective acids. This observation leads to the conclusion that, besides the species formed in the exchanger, some other species are present in the supernatant solution. These absorption spectra differ from those of sulfuric acid—hydrogen peroxide and sulfuric acid solutions of titanium(IV) and of a sulfuric acid solution of iron(III)[13)], which may be present as an impurity. The peroxoc-omplex of titanium contained in solid titanium dioxide is reported to show the absorption band in the same position as in the sulfuric acid solution.[14)] Therefore, the species giving rise to the yellow color appearing in the irradiated hydrous titanium oxide and in the supernatant solution cannot be ascribed to the peroxo-complex. From these observations we can conclude that the sodium form is suitable for the preservation of the hydrous titanium oxide ion exchanger. Compared with Dowex-50, this ex-

Table 3. Effect of the heat treatment of the Na^+-form exchanger on the composition and the ion-exchange capacity[a]

Sample No.	Temperature (°C)	Weight loss (wt%)	Composition[b] mole ratio			Exchange capacity[c] meq. Na^+/g
			H_2O/Ti	Na/Ti	H_2O/Na	
1	R.T.	—	1.634	0.517	3.16	4.54±0.22
2	80±0.5	14.53	0.622	0.517	1.20	4.73±0.22
3	122±1	18.12	0.372	0.517	0.719	4.59±0.32
4	159±1	19.19	0.297	0.517	0.574	3.04±0.20
5	324±2	23.95	≈0	0.517	≈0	0.93±0.27
6	623±7	24.80	≈0	0.517	≈0	0.26±0.25

a) The exchangers were subjected to conditioning and humidifying operation and converted to H^+-form. b) Immediately after heat treatment. c) 1.0 M NaOH batch exchange capacity.

changer is stable against radiation, at least to the same extent as the ion-exchange resin. Further studies are, however, required to reach a definite conclusion on the radiation stability; irradiation by γ-rays in much higher doses and by α- or β-rays emitted from isotopes adsorbed on the exchanger, and the identification of the yellow species.

Thermal Stability. The results for the hydrogen-form exchanger are shown in Table 2. It should be noted that the left of the three columns showing the exchange capacity represents the exchange capacity per 1 g of a humidified sample. The middle column shows the normalized exchange capacity per 1 mol of titanium. The right shows the amount of water per 1 mol of titanium that should be liberated by the condensation of the hydroxyl group which may act as an exchange site (bound water).

The exchange capacity did not change up to 80 °C; then it gradually decreased with the temperature, while at 324 °C it was suddenly reduced to a quarter of the original value. At 623 °C more than 90% of the exchange site was destroyed.

The amount of water contained in the exchanger immediately after the heat treatment (the fourth column in Table 2) at temperatures below 122 °C was more than that of the bound water, but the relation was reversed at a higher temperature. The latter relation indicates that the exchanger recovers bound water to a certain degree during the humidifying operation. However, no bound water was recovered for the sample heated at 623 °C.

Next, let us consider the relation between the water content after heat treatment and the water content of the exchanger subjected to the humidifying operation (the fifth column in Table 2). In the case of heat treatment in the range of 80—159 °C, the difference between these water contents, that is, the amount of water recovered by humidifying, is almost constant, 1.1—1.2 mol per mol of titanium. The exchanger heated at 623 °C recovered water only slightly.

The sudden decrease in both the exchange capacity and the degree of recovery of water at a heating temperature of 324 °C might be associated with the crystallization of the exchanger, because no X-ray diffraction pattern appeared until 324 °C, where two weak and broad peaks (d=3.52, 3.42 Å) appeared. (1 Å=0.1nm)

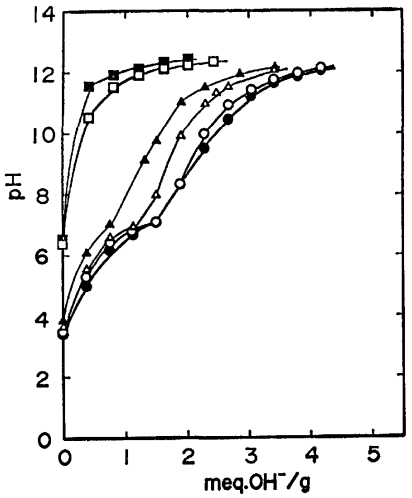

Fig. 2. Titration curves of the exchanger subjected to heat treatment in H^+-form.
I (Ionic strength); 0.10 M, ●: R.T. ○: 80 °C, △: 122 °C, ▲: 159 °C, □: 324 °C, ■: 623 °C.

When the heating temperature was raised to 623 °C, the diffraction line, d=3.52 Å, became sharper and many other lines appeared. This pattern is attributable to the mixture of anatase and brookite.

In order to examine the effect of heat treatment on the acid-base property of the exchanger, the titration curves were measured and found to be as shown in Fig. 2. For samples heated at a temperature not higher than 159 °C, the pH of the breaking point in the titration curves was independent of the temperature and the curves in the pH range higher than that point were parallel with each other. On the other hand, when the exchangers were heat-treated at 324 °C or higher, the curves started at pH 6.5, the point of breaking mentioned above. This means that the exchange site with the smallest pK_a value is responsible for the decrease in the capacity of the exchanger with heating at a temperature lower than 159 °C. The most acidic sites were completely destroyed at 324 °C, and the loss of less acidic sites began to occur at the same temperature. At 623 °C, almost all of the exchange sites were destroyed.

The effect of heat treatment on the sodium form is shown in Table 3 and Fig. 3. Obviously, the change

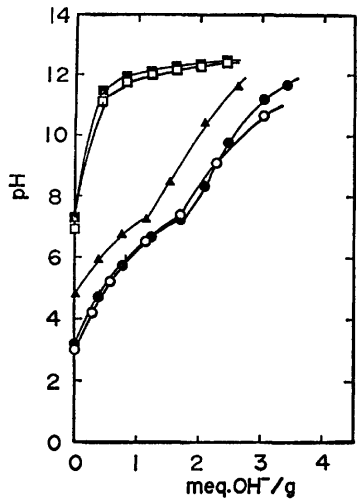

Fig. 3. Titration curves of the exchanger subjected to heat treatment in Na^+-form, followed by conditioning.
I; 0.10 M, ●: 80 °C, ○: 122 °C, ▲: 159 °C, □: 324 °C, ■: 623 °C.

in both the exchange capacity and the acid-base property with a rise in the temperature followed a tendency similar to that of the exchanger heat-treated in hydrogen form. On the other hand, a considerable difference in the release of water by heat treatment between the sodium and the hydrogen forms was observed; that is, at 80 °C the former left twice as much water behind as the latter, in which major part of the residual water was bound water. This cannot be understood by simply considering the hydrating power of the cations, because that of the sodium ion is weaker than that of the hydrogen ion; instead, it must be considered that the sodium ion hinders the release of water by exerting some special effect on the structure. X-Ray analysis exhibited no sign of crystallization until 850 °C, where the diffraction pattern attributable to rutile began to appear. These observations suggest a difference between the two ionic forms in the mechanism for the decrease in the exchange capacity with heat treatment. In the hydrogen form, the dehydrating condensation of hydroxyl groups plays an important role in both the loss in exchange capacity and the crystallization of the material, while, in the sodium form, the sodium ion forms a stable chemical bond with titanium dioxide and the exchange site loses its function as a result.

Structure. The structural formula of the hydrous titanium oxide ion exchanger can be deduced from the various properties described previously as well as by such supplementary data as DTA, TGA, the IR spectra, and X-ray diffraction.

The titration curves and the effect of heat treatment on them strongly suggest that the most acidic exchange site differs intrinsically from the others and accounts for a half of the total exchange capacity. The other, less acidic sites might be distinguished from each other by the change in the electronic structure caused by the adsorption of the sodium ion. When the exchange capacities corresponding to the first-, second-, and third plus fourth dissociable exchange sites are converted to the simplest integral ratio, it is 2 : 1 : 1. Considering this fact and the total exchange capacity of 0.5 eq./mol of titanium, the unit structure must contain 4 hydroxyl groups per 8 atoms of titanium.

Figure 4 shows the TGA and DTA curves of the exchanger in hydrogen form. The TGA curves indicate that the samples heat-treated at 159 °C and lower lost weight suddenly up to about 150 °C, and then gradually up to about 500 °C, where the weight became constant. In contrast, most of the water in the sample heat-treated at 324 °C was released below 80 °C. In the DTA curves, large endothermic peaks appearing in the temperature range lower than 150 °C sharpened as the temperature for heat treatment became higher. The position of the peak, initially at 100 °C, shifted to 75 °C when the exchanger was heat-treated at 80 °C. The shoulder observed in the peak became less pronounced with the rise in the temperature for heat treatment. When the sample was heated at 324 °C, it showed a sharp peak with a very small shoulder.

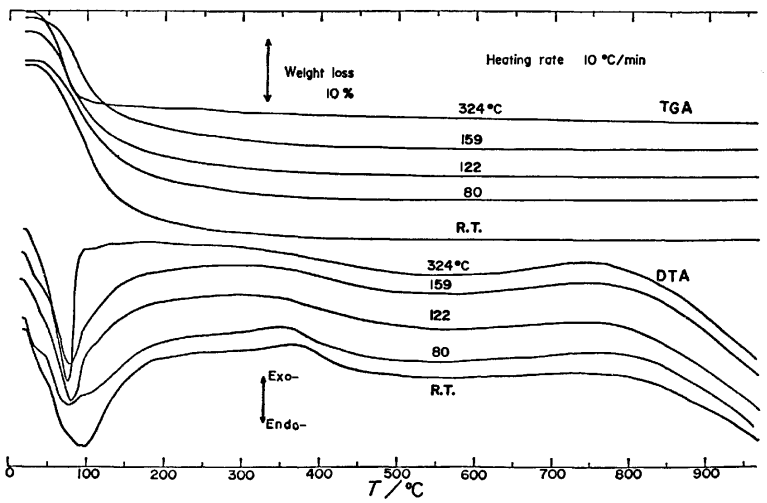

Fig. 4. TGA and DTA curves of the exchanger subjected to heat treatment in H^+-form.

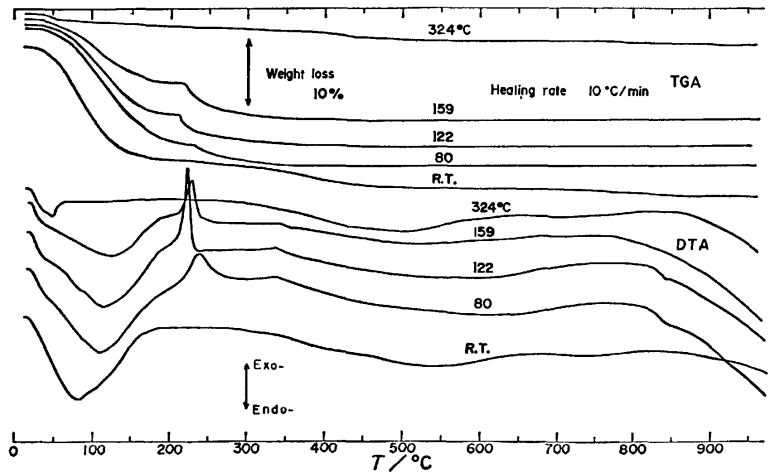

Fig. 5. TGA and DTA curves of the exchanger subjected to heat treatment in Na^+-form, followed by conditioning.

Apparently, the observation just described is compatible with the change in the exchange capacity and in the degree of the recovery of water with temperatures for heat treatment, if the peak near 75 °C is considered to correspond to the water recoverable by humidifying, and the shoulder, to the bound water.

The observations described above can be summarized as follows. When the exchanger in the hydrogen form is heated at 80 °C, the release of water is accompanied by the stabilization of the network structure. By the heat treatment at 122—159 °C the network structure remains essentially unchanged except for a slight modification. This stabilized network can accommodate an approximately constant amount of water. The release of the bound water becomes pronounced at temperatures higher than 324 °C and a partial crystallization occurs. Therby the exchange capacity decreases suddenly. At 623 °C the crystallization proceeds to an extreme end and the structure changes completely. Therefore, almost all the water, including the bound water lost by heat-treatment at 623 °C, is not recovered by the humidifying operation.

Figure 5 shows the DTA and TGA curves of the exchanger heat-treated as the sodium form. The TGA curve of the sodium form dried at room temperature consists of three steps: R.T.—170 °C, 350—450 °C, and 730—900 °C. The samples heat-treated at 80, 122, and 159 °C lost weight in two steps. The TGA curve observed for the sample subjected to heat treatment at 324 °C corresponds to the poor recovery of water. The slight weight loss above 730 °C, which is also observed for the exchanger dried at room temperature, is probably due to the decomposition of the sodium carbonate accidentally remaining in the exchanger after treatment with a 0.1 M hydrochloric acid solution. In the DTA curves, the endothermic peak corresponding to dehydration was displaced toward a temperature higher by about 30 °C by heat treatment at a temperature lower than 324 °C. After this shift, the position of the peak approximately agrees with that of the hydrogen form dried at room temperature. These samples also showed the exothermic peak in the range of 210—230 °C, where some weight loss was observed on the

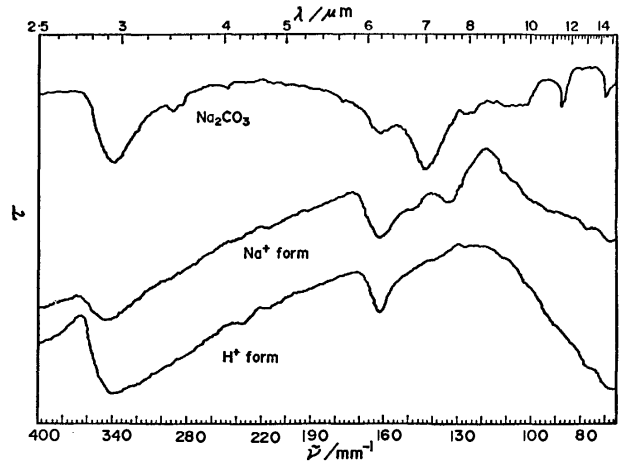

Fig. 6. IR spectra of the exchanger.

corresponding TGA curves. Because dehydration is an endothermic reaction, this peak cannot be accounted for by dehydration. This kind of exothermic peak has also been reported to be observed for the hydrous titanium oxide synthesized by the addition of ammonia water to a titanium tetrachloride solution.[10,12] Imoto *et al.*[10] ascribed the peak to the release of ammonia, while Vivien *et al.*[12] attributed it to crystallization. Since the present hydrous titanium oxide ion exchanger contains no ammonia, this exothermic peak cannot be attributed to the release of ammonia, but to the reaction which is responsible for the sudden decrease in the exchange capacity mentioned above.

Figure 6 shows the IR spectra of the exchanger in the hydrogen and the sodium forms dried at room temperature. The asymmetric absorption band observed near 3400 cm^{-1} is attributable to the sum of the contributions from water and hydroxyl-group bonding to titanium, the former at the lower, and the latter at the higher, wave number sides respectively.[12] The absorption band near 1625 cm^{-1} is due to the bending mode of water, and the absorption in the <1000 cm^{-1} range, the titanium–oxygen bond. The IR spectrum of the exchanger in the sodium form is similar to that of the exchanger in the hydrogen form except for the appear-

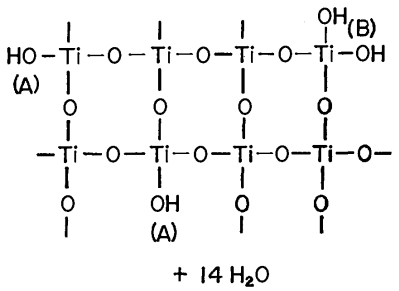

Fig. 7. Structural formula of the exchanger.

ance of the absorption band in 1380—1300 cm^{-1}. This absorption band disappeared when the samples was subjected to heat treatment at 825 °C. Further study is needed before this absorption band can be identified.

On the basis of the results concerning the properties of the exchanger presented above, the structural formula represented in Fig. 7 is inferred for the exchanger in the hydrogen form, though the arrangement of such a unit structure is not very regular because the X-ray diffraction pattern displays a nearly amorphous structure. Of the exchange sites in this model, (A) is the most acidic, and (B), the least acidic, ion-exchange group. The exchange site (A) is easily destroyed by condensation with the neighboring exchange site of the same kind. The appearance of anatase and brookite in the first crystallization step can also be understood by assuming this structure.

The authors wish to express their thanks to Professor Wataru Suëtaka, Department of Metal Processing and Mechanical Metallurgy, Faculty of Engineering, Tohoku University, for his valuable suggestions on the measurement of IR spectra. They also would like to thank Mr. Shigenori Sakagami for obtaining some of the data.

References

1) E. V. Egorov and P. D. Novikov, "Action of Ionizing Radiation on Ion-Exchange Materials," Israel Program for Scientific Translations, Jerusalem (1967), Chap. V.
2) Y. Inoue and M. Tsuji, *J. Nucl. Sci. Technol.*, **13**, 85 (1976).
3) Y. Inoue and M. Tsuji, *Bull. Chem. Soc. Jpn.*, **49**, 111 (1976).
4) C. B. Amphlett, "Inorganic Ion Exchanger," Elsevier, Amsterdam (1964), p. 97.
5) C. Heitner-Wirguin and A. Albu-Yaron, *J. Appl. Chem.*, **15**, 445 (1965).
6) M. Herrmann and H. P. Boehm, *Z. Anorg. Allg. Chem.*, **368**, 73 (1969).
7) Yu. D. Dolmatov, Z. N. Bulavina, and M. Yu. Dolmatova, *Radiokhimiya*, **16**, 116 (1974).
8) N. Ogata and N. Inoue, *Nippon Kaisui Gakkai Shi*, **24**, 149 (1971).
9) N. Sakai, K. Yoshikawa, M. Suzuki, and S. Kobayashi, *Kogyo Kagaku Zasshi*, **64**, 613 (1961).
10) H. Imoto and M. Kaneko, *Kogyo Kagaku Zasshi*, **74**, 591 (1971).
11) A. Clearfield, *Rev. Pure Appl. Chem.*, **14**, 91 (1964).
12) D. Vivien, J. Livage, and C. Mazieres, *J. Chim. Phys. Phys.-Chim. Biol.*, **67**, 199 (1970).
13) M. Ishibashi, T. Shigematsu, Y. Yamamoto, M. Tabushi, and T. Kitagawa, *Nippon Kagaku Zasshi*, **76**, 758 (1955).
14) A. H. Boonstra and C. A. H. A. Mutsaers, *J. Phys. Chem.*, **79**, 1940 (1975).

Polarographic Behavior of Tris(acetylactonato)ruthenium(III) in Aqueous and Acetonitrile Solutions

Akira ENDO, Masayuki WATANABE,* Sadayuki HAYASHI,**
Kunio SHIMIZU, and Gen P. SATÔ

Department of Chemistry, Faculty of Science and Technology, Sophia University, Kioicho, Chiyoda-ku, Tokyo 102

(Received September 12, 1977)

In tetraethylammonium perchlorate–acetonitrile solution, $[Ru(acac)_3]$ was reversibly reduced at the dropping mercury electrode to $[Ru(acac)_3]^-$ with a conditional electrode reaction rate-contsant estimated to be *ca.* 0.2 cm s^{-1} or larger. The reduced form was stable in the solution under an inert gas atmosphere. In aqueous solutions, $[Ru(acac)_3]$ was reduced reversibly when the depolarizer concentration was less than 0.07 mol m^{-3} at 25 °C. At higher depolarizer concentrations, $[Ru(acac)_3]$ molecules were adsorbed onto the mercury surface, and the free molecules in solution were reduced through the adsorbed layer at a smaller rate; the adsorbed layer was removed at a certain negative potential, and the reversible reduction took place normally at the bare surface. The difference between reversible half-wave potentials observed in acetonitrile and aqueous solutions was discussed in terms of solvation energies of the oxidized and reduced forms.

Many electrochemical investigations have been carried out on various metal acetylacetonato-complexes.[1–5] In the course of studying some ruthenium complexes, tris(acetylacetonato)ruthenium(III), $[Ru(acac)_3]$, attracted our attention. It is known to act as a catalyst in organic reactions, for instance, hydrogenation of nitroarenes to amines.[6] Since tris(acetylacetonato)-metal complexes are usually poorly soluble in water, they have been studied in non-aqueous solvents such as acetonitrile and *N*,*N*-dimethylformamide. However, $[Ru(acac)_3]$ is exceptionally soluble in aqueous solution to as much as about 0.5 mmol dm^{-3} at 25 °C. In the present work its electrochemical behavior was examined in acetonitrile and aqueous solutions.

Experimental

Materials. The complex was prepared by the following procedure.[7] Ruthenium(III) chloride (1.9 g as Ru, dissolved in 150 cm^3 of 1 mol dm^{-3} HCl) was reduced with ethanol, and the mixture was evaporated nearly to dryness on a water bath. The blue residue was dissolved in 50 cm^3 of water, and the pH of the solution was adjusted to about 6 with 1 mol dm^{-3} KOH solution. The solution was refluxed with 15 cm^3 of acetylacetone and 50 cm^3 of ethanol for about 4 h. Then the solution was concentrated to about one-fifth the initial volume. Crystals of crude $[Ru(acac)_3]$ precipitated on cooling. The product, after being thoroughly washed with ethyl ether, was recrystallized from methanol and dried under vacuum at room temperature. The recrystallized, dark red crystals were readily soluble in acetonitrile, methanol, ethanol, and to a lesser extent in water. Found: C, 45.2; H, 5.2%. Calcd for $RuC_{15}H_{21}O_6$: C, 45.2; H, 5.3%. Further purification, when required, was carried out by sublimatography;[8] the crystals which condensed at 120 °C under a vacuum were collected.

Tetraethylammonium perchlorate (TEAP) was prepared from perchloric acid and tetraethylammonium iodide according to Given *et al.*[9] Acetonitrile was purified according to the procedure described by Forcier and Olver[10] and used within 10 days at the most. The water content of the solvent as determined by the Karl Fischer titration was less than 1 mmol dm^{-3}.

Other chemicals were of guaranteed reagent grade and used as received except for aluminium perchlorate, which was prepared by dissolving aluminium hydroxide in perchloric acid. Water was obtained by distilling deionized water in an all-glass apparatus and used throughout the experiments except for syntheses, in which deionized water was used.

Measurements. All the potentials were measured against an aqueous saturated calomel electrode (SCE), and all the measurements were carried out at (25.0±0.1) °C unless otherwise stated. For aqueous systems, an H-type salt bridge (saturated KCl solution) with filter-paper plugs was used for connecting the test solution with the SCE; for acetonitrile systems, the connection was made through an aqueous agar-plugged KCl bridge. As counter electrode, a spiral of platinum wire was used.

Deoxygenation of aqueous solutions was carried out with nitrogen which had been passed through an acidic vanadium(II) sulfate solution and water, successively; for acetonitrile systems, the purified nitrogen was passed through a calcium chloride column and then a wash bottle containing the solvent kept at 25 °C.

For acetonitrile systems, 0.05 mol dm^{-3} TEAP and 0.05 mol dm^{-3} $NaClO_4$ base solutions were used. Seven base solutions were used for aqueous systems: 0.2 mol dm^{-3} KCl, 0.033 mol dm^{-3} $Al(ClO_4)_3$, 0.066 mol dm^{-3} Na_2SO_4, 0.2 mol dm^{-3} $NaNO_3$, 0.2 mol dm^{-3} sodium *p*-toluenesulfonate, Sørensen buffer ($4.49 \leqq pH \leqq 6.81$), and Kolthoff buffer (pH = 7.0).

Dc and conventional ac polarograms were recorded with a potentiostat-type polarograph constructed in this laboratory. The instrument for phase selective ac (PSAC) polarography has been described elsewhere.[11] The root-mean-square amplitude of the superimposed ac signal was 3 mV for PSAC and 5 mV for conventional ac polarography. Two dropping mercury electrodes (DME) were used; their *m* values were as follows at 25 °C under a mercury head of 50 cm: No. 1, 1.78 mg s^{-1}; No. 2, 1.36 mg s^{-1}. Instantaneous currents at 3.50 s after beginning of drop growth were sampled by means of a dislodger-cutoff device previously described,[12,13] unless otherwise stated.

In PSAC measurements, correction was made for the uncompensated resistance, which was calculated from the PSAC polarograms of the base solution by assuming that the admittance was purely capacitive. The faradaic conductance (G_f) and susceptance (B_f) were obtained by subtracting the corresponding values for the base solution from the electrode conductance and susceptance in the presence of the depolar-

* Present Address: Senzoku Gakuen College First High School, Senzoku 1, Meguro-ku, Tokyo 152.

** Present Address: Meiji Senior High School, Shiroganedai 1, Minato-ku, Tokyo 108.

izer.[11]

Controlled potential coulometry was carried out as described earlier[14] except that integration of the electrolytic current was carried out on a digital counter (Takedariken, Universal Counter TR-5104) by converting the current signal into pulses with a voltage-frequency converter (Aiko, VF500).[15] The electrolytic cell with a mercury pool working elecrode (surface area, about 7.1 cm^2) previously described[14] was used for both systems. When an acetonitrile test solution was placed in the working electrode compartment, the counter and reference electrode compartments were filled with aqueous potassium chloride solution. Contamination by a small amount of water leaking from the bridges was inevitable when electrolysis was prolonged, but no appreciable effect was noticed.

Cyclic voltammetry was carried out by means of the dc polarograph to which a programmable triangular signal generator[16] was connected. Voltammograms were displayed on an X-Y recorder (Riken Denshi, Model F-3D) for lower scan rates or on a cathode ray oscilloscope screen (National, Model VP-526) for higher scan rates. A Princeton Applied Research hanging mercury electrode assembly (Model 9323) was used, the radius of the mercury drops being about 0.44 mm.

A Hitachi 624 digital spectrophotometer was used for recording absorption spectra. Quartz cells of 1 cm and 0.5 cm were used for lower concentrations and a spacer cell of 1 mm, for higher concentrations.

Results and Discussion

Acetonitrile Systems. In 0.05 mol dm^{-3} TEAP solutions, a reduction step with half-wave potential ($E_{1/2}$) of -0.72_5 V was observed on the dc polarogram. The limiting current of the step was directly proportional to the depolarizer concentration and inversely proportional to the square root of the drop time of a mercury electrode dropping freely. As described below the step corresponds to the one-electron reduction to [Ru(acac)$_3$]$^-$. The log-plot resulted in a straight line with a reciprocal slope of -61 mV.

When the complex was partially reduced at the mercury pool electrode kept at a potential of the diffusion current plateau (-1.0 V), a single redox step appeared at the same half-wave potential. When the cathodic and anodic diffusion currents recorded intermittently in the course of the electrolytic reduction were plotted against the quantity of electricity, the magnitude of the former decreased and the latter increased linearly, and the plots indicated that the process was a one-electron reduction to [Ru^{II}(acac)$_3$]$^-$.

The reduced form was quantitatively reoxidized when it was electrolyzed at a potential of the anodic diffusion current plateau. It was readily oxidized also by atmospheric oxygen, but was not oxidized by perchlorate ions in the solution.

The polarographically reversible nature of the reduction is more clearly shown by the results of PSAC polarography (Table 1 and Fig. 1). Both the conductance and susceptance peak potentials coincided with $E_{1/2}$. The peak conductance and susceptance measured in the frequency range of 35—90 Hz agreed reasonably well with the theoretical value for a reversible or nernstian one-electron transfer. At higher frequencies

Table 1. cot ϕ of 0.50 mmol dm^{-3} [Ru(acac)$_3$] in acetonitrile 0.05 mol dm^{-3} TEAP solution, 25 °C

f/Hz	35	70	90	190	270
cot ϕ	1.0_3	0.9_2	0.9_3	1.4_4	1.5_7

f, frequency; ϕ, phase angle of faradaic admittance; estimated error in cot ϕ is about 10%.

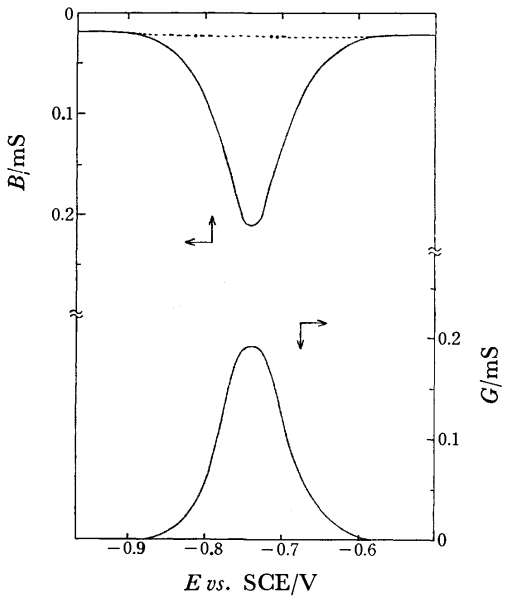

Fig. 1. PSAC polarograms of 0.50 mmol dm^{-3} [Ru(acac)$_3$] in acetonitrile 0.05 mol dm^{-3} TEAP solution. 35 Hz, 3 mV (r.m.s.); DME, No. 1; 25 °C; dashed line, base solution.

cot ϕ, where ϕ is the phase angle of the faradaic admittance, tended to increase. The limited accuracy of the instrument, however, allowed us only to estimate that the lower limit of the conditional electrode reaction rate constant (at $E_{1/2}$) was about 0.2 cm s^{-1}.

Aqueous Systems. Typical dc and ac polarograms are shown in Fig. 2. When the depolarizer concentration was less than 0.07 mmol dm^{-3}, a one-electron reduction dc step with $E_{1/2}=-0.51_6$ (curve A) and the corresponding ac wave, similar to those observed in acetonitrile solution, were observed. This step was reversible, as demonstrated by the PSAC polarographic data (Table 2).

At higher depolarizer concentrations, however, peculiar dc and ac polarograms were observed. The dc polarogram showed a small step prior to the main reduction step and a kink or a sudden increase in current magnitude at a potential of the shoulder of the main step. The ac polarogram was characterized by a marked depression of admittance starting from the potential of the small dc step and continuing to a round wave corresponding to the main dc step followed by a sharp peak at the potential where the sudden increase in dc current took place. When the temperature of the solution was varied (15—40 °C), the effect of its increase on the shape of the polarograms was similar to that of the decrease in the concentration: the potential of the small dc step shifted to negative, while that of the kink on the shoulder remained almost the same, and the ac polarogram changed correspondingly.

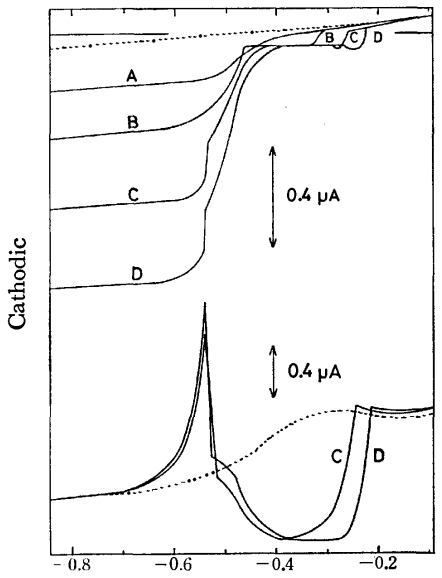

Fig. 2. Dc (upper) and conventional ac (lower) polarograms of $[Ru(acac)_3]$ in aqueous 0.2 mol dm^{-3} KCl solution.
Depolarizer concentration/mmol dm^{-3} = 0.05 (A), 0.1 (B), 0.2 (C), 0.3 (D). 35 Hz, 5 mV (r.m.s.); DME, no. 1; 25 °C; dashed lines, base solution. Ac polarograms for A and B are not shown for the sake of simplicity.

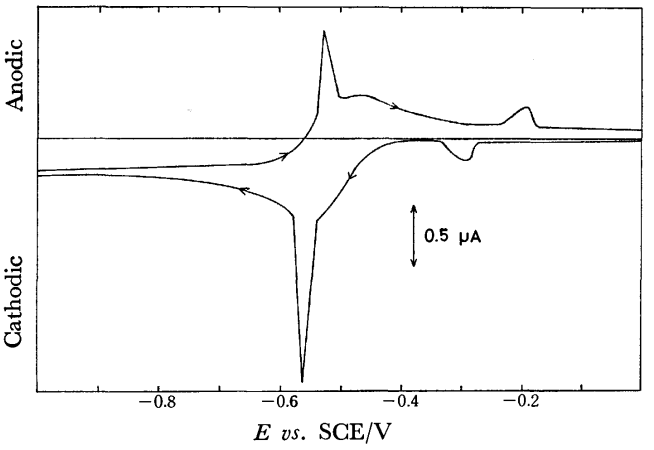

Fig. 3. Typical cyclic voltammogram of 0.20 mmol dm^{-3} $[Ru(acac)_3]$ in aqueous 0.2 mol dm^{-3} $NaNO_3$ solution.
Scan rate, 168 mV s^{-1}; 25 °C.

Table 2. Faradaic peak conductance of 0.05 mmol dm^{-3} $[Ru(acac)_3]$ in aqueous 0.2 mol dm^{-3} $NaNO_3$ solution, 25 °C

f/Hz	$G_{p,N}$/μS	$G_{p,obs}$/μS
23	24.15	24.7_2
58	38.36	39.5_9
90	47.78	50.3_7

f, frequency; $G_{p,N}$, peak conductance calculated for nernstian one-electron transfer; $G_{p,obsd}$, observed peak conductance.

The controlled potential coulometry of $[Ru(acac)_3]$ at −0.7 V showed that the reduction was one-electron process and the reduced form was stable in the absence of oxygen. A partially reduced solution showed a single redox dc step at the same half-wave potential; the anodic step was accompanied by a small kink at the potential where the small step had appeared on the polarogram before the electrolysis. The reduced form was not oxidized by perchlorate ions, in contradistinction to the case of $[Ru^{II}(Hedta)(H_2O)]^-$, which was reoxidized in aqueous perchlorate solutions.[14] The reduced form reacted with formate ions to produce electro-inactive entities, most probably some carbonyl species. The details of the reaction are under investigation; but the rate was much less than that of $[Ru^{II}(Hedta)(H_2O)]^-$–formate reaction.[17] That $[Ru^{II}(acac)_3]^-$ is less reactive than $[Ru(Hedta)(H_2O)]^-$ seems to be attributable to its symmetrical shape.

The dc and ac polarograms at higher depolarizer concentrations indicate the presence of adsorption; it was more clearly shown by the electrocapillary curves, in which a decrease in the interfacial tension was observed at the potentials between the small dc step and the kink. The possibility that the adsorption might be due to some impurities contained in the sample was excluded by the fact that the dc and ac polarograms of a purer sample obtained by sublimatography were identical with those of the simply recrystallized sample.

The concentration dependence of the dc polarogram clearly suggests that the adsorbed species is the oxidized form, not the reduced form (Fig. 2). This view is supported by the shape of the electrocapillary curve showing the adsorption of a neutral species and by the fact that the polarograms remained practically unchanged irrespective of the supporting electrolytes: KCl, $NaNO_3$, Na_2SO_4, $Al(ClO_4)_3$, and Sørensen and Kolthoff buffers of various pH (with the exception of sodium *p*-toluenesulfonate; see below).

Bis(acetylacetonato)cobalt(II)[18] and bis(acetylacetonato)nickel(II)[19] are known to dimerize in some non-aqueous solutions at higher concentrations. In the case of aqueous solutions of $[Ru(acac)_3]$, however, no indication of such association was detected by the visible and ultraviolet spectra in the range of 190—650 nm even at 0.4 mmol dm^{-3} (about 80% of saturation), and the spectra agreed with those in acetonitrile solution.

These observations lead us to conclude that $[Ru(acac)_3]$ is adsorbed onto the mercury surface in the potential region between the small step and the kink.

A typical cyclic voltammogram shown in Fig. 3 reflects the same situation: on each of the cathodic and anodic branches, two sharp adsorption-desorption peaks appeared, between which a round peak corresponding to the main dc step was seen. At higher scan rates the relative heights of the adsorption-desorption peaks to the round peak increased; at the same time, the potential separations between the anodic and cathodic peaks for each of the two pairs of the sharp peaks increased, suggesting that the adsorption-desorption process involved some kinetic character.

In the PSAC polarograms of 0.05 mmol dm^{-3} [Ru-

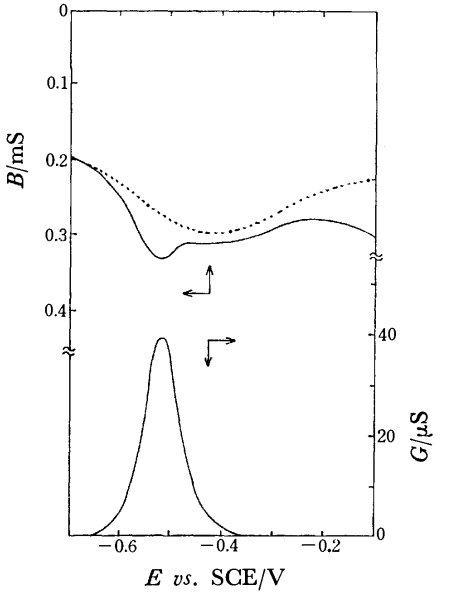

Fig. 4. PSAC polarograms of 0.05 mmol dm^{-3} [Ru(acac)$_3$] in aqueous 0.2 mol dm^{-3} $NaNO_3$ solution. 58 Hz, 3 mV (r.m.s.); DME, No. 2; 25 °C; dashed line, base solution.

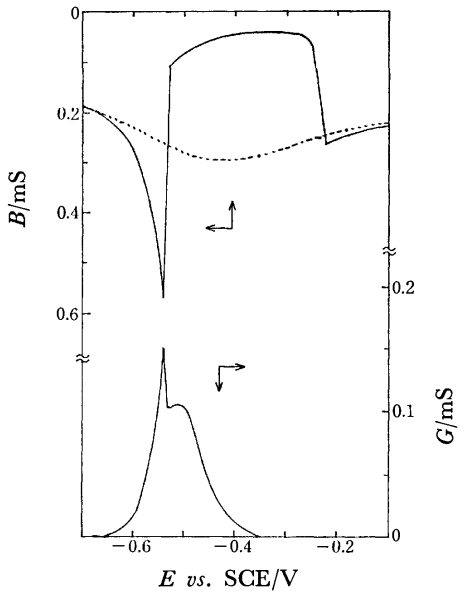

Fig. 5. PSAC polarograms of 0.3 mmol dm^{-3} [Ru(acac)$_3$] in aqueous 0.2 mol dm^{-3} KNO_3 solution. Conditions are the same as in Fig. 4.

(acac)$_3$] (Fig. 4) a shoulder at the positive side of the susceptance polarogram indicates that even at this concentration there was still some adsorption. However, the conductance component corresponded to a nernstian one-electron transfer as indicated by the value of the peak conductance (Table 2; the excessive values of the experimental peak conductance at higher frequencies may be due to the contribution of adsorption and/or instrumental errors).

The adsorption seems to affect the electron transfer. When the concentration was 0.30 mmol dm^{-3}, the susceptance polarogram showed a well-like depression corresponding to the adsorption, and the conductance polarogram showed a round peak followed by a sharp rise at its negative shoulder (Fig. 5). The potential of the latter coincided with the potential at which the sudden increase in current was observed on the dc polarogram. The height of the round peak was much less than the theoretical value for a nerstian one-electron transfer, but the values of the conductance at the potentials more negative than the sharp rise were roughly equal to those expected for a hypothetical nernstian wave with a peak potential of −0.52 V.

The susceptance polarogram showed a small peak at the positive edge of the depression (−0.23 V) when the frequency was 23 Hz, but no appreciable peak was observed at this potential on the conductance polarogram, so that the process was essentially capacitive. The susceptance peak became less clear with increasing frequency, probably owing to the kinetic character of the adsorption-desorption process as observed in the cyclic voltammetry.

The electrochemical behavior of [Ru(acac)$_3$] in the aqueous solutions is interpreted as follows. The complex is reduced at the mercury electrode to the corresponding Ru(II) species. This process is essentially reversible or nerstian as indicated by the results obtained at the lower concentrations. However, the Ru(III) complex molecules are adsorbed onto the electrode when the concentration is higher. The adsorbed molecules are stabilized and its reduction potential becomes more negative than that of the free molecules. The free molecules undergo reduction through the layer of adsorbed [Ru(acac)$_3$] at a lower rate. Beyond a certain potential (−0.54 V) the adsorbed layer of [Ru(acac)$_3$] no longer exists, and the reversible reduction takes place normally at the bare surface of the electrode. In view of the fact that this potential was practically independent of the depolarizer concentration and temperature, the adsorbed [Ru(acac)$_3$] molecules seem to be reduced at this potential to [Ru(acac)$_3$]$^-$, which is not adsorbable.

Interestingly, in 0.2 mol dm^{-3} aqueous sodium *p*-toluenesulfonate solution, a reversible one-electron dc step was observed even at higher depolarizer concentrations. The half-wave potential was the same as that of the reversible step observed at lower concentrations in the other aqueous base solutions. The positive branch of the electrocapillary curve of [Ru(acac)$_3$] in this solution lied below those obtained in the other supporting electrolyte solutions, whereas the negative branch was essentially the same. Probably, *p*-toluenesulfonate ions replaced the adsorbed [Ru(acac)$_3$] at least partially, and the adsorbed layer of the anions did not retard the electron transfer to any appreciable extent.

Half-wave Potentials. The observed reversible half-wave potentials of [Ru(acac)$_3$] in acetonitrile–TEAP system and in aqueous potassium chloride and other systems were -0.72_5 V and -0.51_6 V, respectively, both being measured against the aqueous SCE as described. The liquid-junction potential between the acetonitrile and the aqueous phases is unknown, but Coetzee and Campion[20] have given a semiempirical value of 0.034 V (aqueous side positive) for the junc-

tion Et_4NClO_4 (0.1 mol dm^{-3} in acetonitrile)|KCl (saturated in water). Correcting the half-wave potential in acetonitrile for this value, we have a net difference of $E_{1/2}$(acetonitrile)$-E_{1/2}$(water)$=-0.17_5$ V, which may be related to the activities of $[Ru(acac)_3]$ and $[Ru(acac)_3]^-$ in both systems by the following equation:

$$\Delta E_{1/2} = -\frac{1}{nF}(\Delta\mu_{II}^{\ominus} - \Delta\mu_{III}^{\ominus}), \quad (1)$$

where $\Delta\mu_{III}^{\ominus}$ and $\Delta\mu_{III}^{\ominus}$ are the differences of the standard chemical potentials of $[Ru^{II}(acac)_3]^-$ and $[Ru^{III}(acac)_3]$, respectively, when each species is transferred from water to acetonitrile. The diffusion coefficients of the two species are assumed to be equal for each solvent, and the contribution of the activity coefficients are ignored.

We assume that $\Delta\mu_{II}^{\ominus}$ is approximated by the Born equation[21]

$$\Delta\mu_{II}^{\ominus} = -\frac{z^2 e^2 N}{8\pi \varepsilon_0 a}\left\{\frac{1}{\varepsilon_W} - \frac{1}{\varepsilon_{AN}}\right\}, \quad (2)$$

and $\Delta\mu_{III}^{\ominus}$ by

$$\Delta\mu_{III}^{\ominus} = -RT\ln(c_{AN}^s/c_W^s), \quad (3)$$

where e is the elementary charge; N, Avogadro constant; z, the charge number of the ion ($=-1$); ε_0, the permittivity of vacuum; ε_W and ε_{AN}, the relative permittivities of water and acetonitrile, respectively; c_W^s and c_{AN}^s, the concentrations of the saturated solutions of $[Ru^{III}(acac)_3]$ in the respective solvent. Estimating the ionic radius a to be 0.5 nm, a not unreasonable value, we obtain $\Delta\mu_{II}^{\ominus} \approx 1.9$ kJ mol^{-1} from Eq. 1. The solubility of $[Ru^{III}(acac)_3]$ in water was about 0.5 mmol dm^{-3}; no reliable estimate of its solubility in acetonitrile was made, but it seemed to be soluble up to about 0.2 mol dm^{-3}. These values lead to $\Delta\mu_{III}^{\ominus} \approx -14.8$ kJ mol^{-1}. The value of $\Delta E_{1/2}$ thus estimated is about -0.17 V. This unexpectedly good agreement should not be given much confidence in view of the oversimplified model and very rough estimation involved. However, it does suggest that the half-wave potential observed in the acetonitrile–TEAP system represents the reversible half-wave potential of the $[Ru^{III}(acac)_3]/[Ru^{II}(acac)_3]^-$ couple in this solvent.

The reduction step in acetonitrile was shifted to positive potential when TEAP was replaced by sodium perchlorate. But the half-wave potential was independent of the depolarizer concentration at a given concentration of sodium ions. If the half-wave potential in the absence of sodium ions corresponds to the simple reduction as discussed above, this shift must be attributed to sodium ions. Such a shift of half-wave potential caused by alkali metal ions in solvents of lower dielectric constants have been explained by ion-pairing interaction or coordinative relaxation between the reduced form and the cation.[22,23] In the former case the half-wave potential is independent of the depolarizer concentration. Thus, the observed half-wave potential shifts were accounted for by ion-pair formation between $[Ru(acac)_3]^-$ and sodium ions. The details will be reported separately.

Authors' thanks are due to Assistant Professor Shinichi Saito of Sophia University for his halp in sublimatographic purification of the complex. They also thank Sr. Jean Michalec for correcting the manuscript. The present work was partly supported by a Grant-in-Aid for Scientific Research from the Ministry of Education.

References

1) G. S. Patterson and R. H. Holm, *Inorg. Chem.*, **11**, 2285 (1972).
2) K. Shimizu, K. Morinaga, and K. Nakano, *Nippon Kagaku Zasshi*, **90**, 564 (1969).
3) J. N. Burnett, L. K. Hiller, Jr., and R. W. Murray, *J. Electrochem. Soc.*, **117**, 1028 (1970).
4) B. Ćosović and M. Branica, *J. Electroanal. Chem.*, **20**, 269 (1969).
5) B. Ćosović, M. Verži, and M. Branica, *J. Electroanal. Chem.*, **22**, 325 (1969).
6) J. F. Knifton, *J. Org. Chem.*, **41**, 1200 (1976).
7) M. Mukaida, private communication.
8) E. Shibata and S. Saito, *Nippon Kagaku Zasshi*, **80**, 604 (1959).
9) P. H. Given, M. E. Peover, and J. Schoen, *J. Chem. Soc.*, **1958**, 2674.
10) G. A. Forcier and J. W. Olver, *Anal. Chem.*, **37**, 1447 (1965).
11) G. P. Satô and M. Kobayashi, *Rev. Polarogr. (Kyoto)*, **20**, 27 (1974).
12) K. Shimizu, M. Kobayashi, and G. P. Satô, *Bunseki Kagaku*, **23**, 1537 (1974).
13) K. Shimizu and M. Kobayashi, *Bunseki Kiki*, **12**, 687 (1974).
14) K. Shimizu, T. Matsubara, and G. P. Satô, *Bull. Chem. Soc. Jpn.*, **47**, 1651 (1974).
15) S. Hayashi, K. Shimizu, and G. P. Satô, *Rev. Polarogr. (Kyoto)*, **21**, 13 (1975).
16) K. Tsuji and K. Takahashi, *Anal. Chim. Acta*, **57**, 473 (1971).
17) K. Shimizu, *Bull. Chem. Soc. Jpn.*, 50, 2921 (1977).
18) F. A. Cotton and R. H. Sodergerg, *Inorg. Chem.*, **3**, 1 (1964).
19) F. A. Cotton and J. P. Fackler, Jr., *J. Am. Chem. Soc.*, **83**, 2818 (1961).
20) J. F. Coetzee and J. J. Campion, *J. Am. Chem. Soc.*, **89**, 2517 (1967).
21) J. F. Coetzee and J. J. Campion, *J. Am. Chem. Soc.*, **89**, 2513 (1967).
22) R. W. Murray and L. K. Hiller, Jr., *J. Am. Chem. Soc.*, **39**, 1221 (1967).
23) S. Misumi, M. Aihara, and Y. Nonaka, *Bull. Chem. Soc. Jpn.*, **43**, 774 (1970).

Thermodynamic Study on Adduct Formation of Copper(II) β-Diketonates with Heterocyclic Bases

Kazumasa UEDA

Department of Industrial Chemistry, Faculty of Technology, Kanazawa University, Kodatsuno, Kanazawa 920

(Received September 14, 1977)

The stability constants and thermodynamic functions for 1:1 adduct formation of unidentate heterocyclic bases with copper(II) β-diketonates were determined in non-aqueous solvents by the spectrophotometric method. The main factors controlling the stability of the adducts were investigated and the bases were classified into two groups in adduct formation from the plots of the stability constants against pK_H values of the bases: steric hindered and unhindered bases. Large negative entropy changes were observed for pyridine, β-picoline, and γ-picoline; these were ascribed to the π-bond character of the adduct bonds. A solvent effect was observed; the order of increasing adduct stability was as follows: acetone < butyl acetate < 4-methyl-2-pentanone < chloroform < nitrobenzene < toluene ≃ benzene < chlorobenzene. This order agreed with the decreasing order of the solvent-chelate interaction and of the solvent-base interaction. In all cases, the adducts were stabilized by large exothermic enthalpy changes. Moreover, the introduction of a CF_3 group into β-diketones also brought about a considerable entropy change which promoted the stabilization of the chelate. The effect of the other terminal groups was not clearly observed.

It is well known that copper(II) β-diketonates behave as Lewis acids and react with nitrogen bases to form addition compounds.[1] The formation equilibria of such synergistic adducts have been widely investigated for many metals under a variety of conditions.[2,3]

Most investigations of the adduct formation have been carried out by means of solvent extraction. Therefore, complications inherent to the heterogeneous equilibrium, *e.g.*, the displacement reaction of a Lewis base for water molecules in metal chelates, would be involved.

Since the direct observation of the equilibria in non-aqueous solvents is free from these complications, some detailed studies have been undertaken by using spectrophotometric,[4-6] titrimetric,[7,8] ESR, and NMR[9,10] techniques. Planar, four-coordinate copper(II) complexes of β-diketones react with Lewis bases to form five-coordinate 1:1 adducts and six-coordinate 1:2 adducts, and the formation constants for 1:1 adducts with various bases have been determined. Nevertheless, comparatively little information is available about the thermodynamics of these equilibria.

In the present investigation, the author has undertaken to obtain the thermodynamic data for the adduct formation of several different β-diketonato complexes of copper with a variety of bases, and quantitative information on factors affecting the stability of the adducts formed in non-aqueous solvents.

Experimental

Apparatus and Materials. The absorption measurements were carried out with a Hitachi 124 spectrophotometer equipped with a thermostated cell holder, which was held at the required temperature by water from a HAAKE FJ thermoelectric circulating bath. β-Diketones with a CF_3 terminal group such as benzoyltrifluoroacetone(Hbfa), 2-thenoyltrifluoroacetone(Htta), 2-furoyltrifluoroacetone(Hfta), pivaloyltrifluoroacetone(Hpta), trifluoroacetylacetone(Htaa), and the nonfluorinated β-diketones such as acetylacetone(Haa), benzoylacetone(Hba), and dipivaloylmethane(Hdpm) were commercially available and used without further purification. All the nitrogen bases were of guaranteed grade and usually dried over potassium hydroxide; a constant boiling fraction was collected under a reduced pressure. Solvents were of guaranteed grade and freshly distilled before use.

Preparation of Copper Chelates. The copper chelates were prepared by mixing equivalent quantities of copper(II) chloride solution and β-diketone methanol solution and adding 2M sodium acetate solution under continuous stirring. The mixture was allowed to stand in a refrigerator for several hours, after heated for a short while on a hot plate. The filtered complex was washed with water and dried in a desiccator. After being recrystallized from benzene, the crystalline chelate was dried by standing over diphosphorus pentaoxide *in vacuo*. The results of elementary analysis are shown in Table 1.

Calculation of Stability Constants and Thermodynamic Functions. The stability constants of the 1:1 adduct in non-aqueous solvent were obtained by the following equation:

$$K = \frac{[\text{Adduct}]}{[\text{Diketonate}][\text{Base}]} = \frac{1-\alpha}{\alpha[\text{Base}]}. \quad (1)$$

The concentration of the free base is

$$[\text{Base}] = B_0 - C_0(1-\alpha), \quad (2)$$

where α is the fraction of the free diketonate and B_0 and C_0 are the total concentrations of the base and the copper chelate. Since the bases do not absorb at the wavelength concerned,

$$A = A_0\alpha + A_\infty(1-\alpha), \quad (3)$$

where A and A_0 are the absorbances of the system and the diketonate only. A_∞ is the absorbance found, by trial and error, to give the most reproducible value of K.[4,11] The stability constant can be expressed in terms of the absorbance

Table 1. Analysis of copper(II) chelates

Chelate	Found (Calcd) %		
	C	H	Cu
$Cu(bfa)_2$	48.55 (48.64)	2.48 (2.44)	12.84 (12.86)
$Cu(tta)_2$	38.00 (37.99)	1.60 (1.59)	12.54 (12.56)
$Cu(fta)_2$	40.53 (40.56)	1.71 (1.70)	13.45 (13.41)
$Cu(pta)_2$	41.84 (42.34)	4.37 (4.44)	14.08 (14.00)
$Cu(taa)_2$	32.38 (32.48)	2.11 (2.18)	17.17 (17.18)
$Cu(ba)_2$	62.14 (62.24)	4.62 (4.70)	16.38 (16.38)
$Cu(aa)_2$	45.65 (45.88)	5.35 (5.39)	24.10 (24.09)
$Cu(dpm)_2$	61.51 (61.43)	8.86 (8.90)	14.73 (14.71)

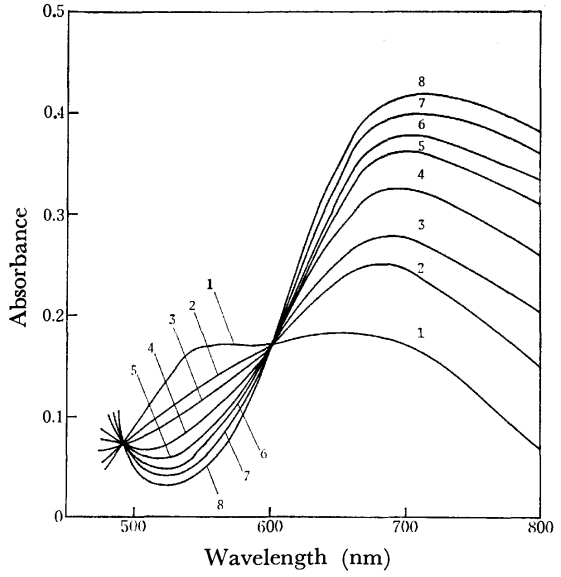

Fig. 1. Absorption spectra of $Cu(bfa)_2$-pyridine system in benzene at 298 K. $[Cu(bfa)_2]=0.005$ M, [pyridine]; 1: 0, 2: 0.002 M, 3: 0.003 M, 4: 0.005 M, 5: 0.007 M, 6: 0.01 M, 7: 0.015 M, 8: 0.04 M.

from Eqs. 1, 2, and 3:

$$K=\frac{[A-A_0]}{[A_\infty-A]B_0-C_0[A-A_0]/[A_\infty-A_0]}. \quad (4)$$

At least ten experimental points were used in each system and each measured absorbance was the average of three independent determinations. The standard molar thermodynamic functions were calculated by the usual methods: $-RT\ln K=\Delta G^\circ=\Delta H^\circ-T\Delta S^\circ$ and $\Delta H^\circ/RT^\circ=d\ln K/dT$. ΔH° was constant within the experimental error over the range of temperature, as shown in Fig. 3. Under the present experimental conditions, the values of $\log K$ were reproducible within ±0.05, values of ΔG within ±0.9 kJ mol^{-1}, and the values of ΔS within ±0.2 J K^{-1} mol^{-1}.

Results and Discussion

It has already been recognized that copper(II) β-diketonates react with nitrogen bases to form several adducts and that the 1:1 adduct is preferentially formed in non-polar organic solvents.[2,12] The absorption spectra of $Cu(bfa)_2$–pyridine system are shown in Fig. 1, as a typical example. These spectra form a family with isobestic points at these intersections, indicating the formation of a mono-adduct. Similar spectra with sharp isobestic points are obtained for all the bases employed. The analytical results by the molar ratio method also show that the present chelates form only 1:1 type adducts and 1:2 type equilibria do not take place, as shown in Fig. 2. Therefore, the author investigated only 1:1 type adduct formation equilibria with unidentate nitrogen bases, though several types of adducts with unidentate nitrogen bases have been identified, especially when the neutral ligand is a strong base and the chelate ligand contains an electron withdrawing nitro- or cyano-group.[13,14]

Stability Constants of Base Adducts. Figure 3 shows the changes in the stability constants of $Cu(bfa)_2$ adduct as a function of temperature. The stabilities decrease

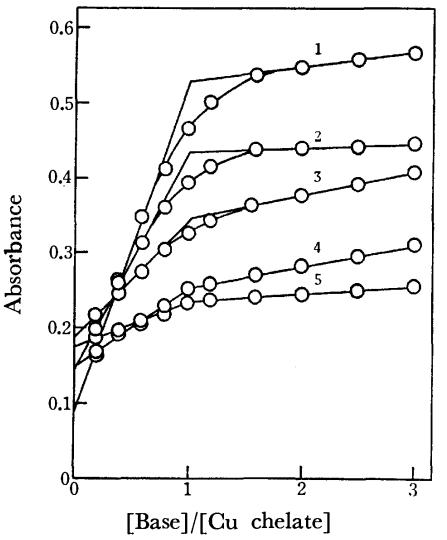

Fig. 2. Determination of the adduct composition by mole ratio method in benzene at 298 K. [Cu chelate] $=0.005$ M. 1: $Cu(bfa)_2$-2-methylpiperidine (850 nm), 2: $Cu(tta)_2$-γ-picoline (740 nm), 3: $Cu(fta)_2$-2,4-lutidine(700 nm), 4: $Cu(taa)_2$-α-picoline (690 nm), 5: $Cu(pta)_2$-pyridine (620 nm).

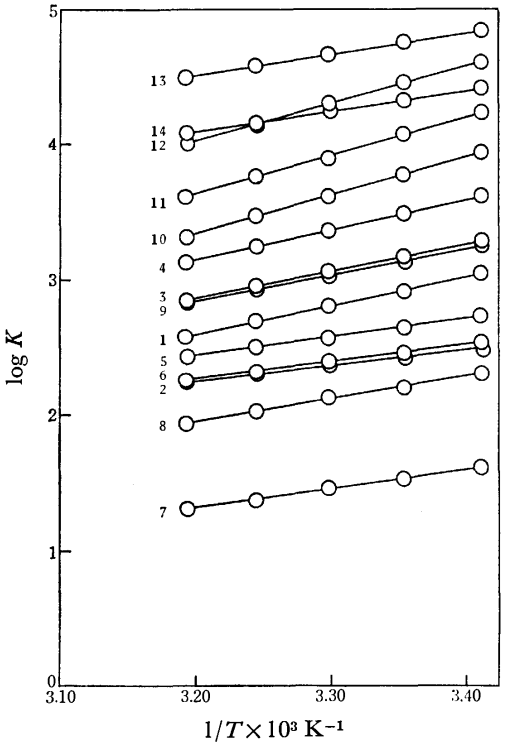

Fig. 3. Temperature dependence of stability constants for $Cu(bfa)_2$ adduct. For numerals, see Table 2.

linearly on every base as temperature rises. The adduct chelate dissociation must be much enhanced with the increase of thermal energy. From the slope of these linear plots, the standard enthalpy change of adduct formation was obtained. It seems remarkable that the enthalpies for pyrrolidine and piperidine show smaller changes in spite of their high stabilities. The stability constants increase in the following order: 2,6-lutidine $\ll$ quinoline $<$ α-picoline $\leq$ 2,5-lutidine $<$ 2,4-lutidine $<$ pyridine $<$ isoquinoline $<$ β-picoline $<$

Table 2. The effect of nitrogen bases on adduct formation

No.	Base	log K_{298}	$-\Delta G_{298}$ (kJ mol^{-1})	$-\Delta H$ (kJ mol^{-1})	$-\Delta S_{298}$ (J K^{-1} mol^{-1})
1	Pyridine	2.91	16.61	44.31	92.89
2	α-Picoline	2.43	13.85	22.80	30.03
3	β-Picoline	3.17	18.07	38.70	69.18
4	γ-Picoline	3.48	19.87	41.63	72.97
5	2,4-Lutidine	2.64	15.06	26.40	38.03
6	2,5-Lutidine	2.46	14.01	23.01	30.17
7	2,6-Lutidine	1.53	8.70	25.44	56.13
8	Quinoline	2.20	12.55	31.96	65.11
9	Isoquinoline	3.13	17.91	35.69	59.64
10	2-Methylpiperidine	3.77	21.55	54.73	111.28
11	3-Methylpiperidine	4.08	23.26	55.18	107.06
12	4-Methylpiperidine	4.45	25.39	53.22	93.32
13	Pyrrolidine	4.76	27.19	30.37	10.66
14	Piperidine	4.32	24.64	29.87	17.54

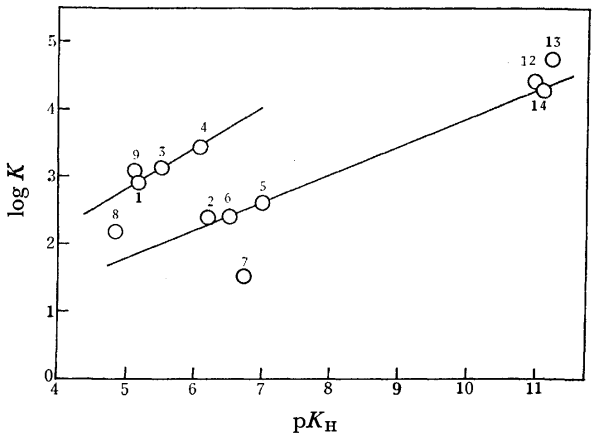

Fig. 4. Plots of log K *vs.* pK_H in benzene at 298 K. For numerals, see Table 2.

γ-picoline < 2-methylpiperidine < 3-methylpiperidine < piperidine < 4-methylpiperidine < pyrrolidine. The order is related not only to the basicity of the bases, but also to the steric effect due to substitution. The high stabilities in the secondary cyclic amines correspond to their large donor properties. The higher stability of γ-picoline as compared with that of pyridine also reflects the increased donor power of the nitrogen atom due to the introduction of a methyl group. A similar effect would be expected for α-picoline and lutidines from these pK_H values, but much lower stabilities were observed. This fact may be caused by the steric interference of the α-methyl group. In order to make the point clearer, the stability constants of these mono-adducts are plotted against the pK_H values of the bases, as shown in Fig. 4. The values of the stability constants are classified roughly into two types, the higher and lower stability groups. The values of 2,6-lutidine and quinoline lie apart from these two groups. The lower stabilities of the second group compared to those of the first may be attributed to the steric hindrance of the methyl group in the α-position. This interference is significant in 2,6-lutidine. Owing to the steric hindrance from the hydrogen atom attached to the nitrogen atom of pyrrolidine and piperidine, the adduct stabilities of those bases are reduced to the second group. The lower stability of quinoline may be caused by the steric effect of the adjacent benzene ring. Thus, both the pK_H and the steric hindrance of the bases have an effect on the stability of the base adduct.

Thermodynamics of Adduct Formation. The stability constants of Cu(bfa)$_2$ adduct in benzene at 298 K and some related thermodynamic functions are summarized in Table 2. The values of ΔG for all the donor systems are negative, so it is obvious that the acceptor mother chelate is stabilized by the adduct chelate formation. Both the enthalpy and the entropy terms contribute to the negative values of the free energy. The introduction of a fluorine atom into β-diketone greatly increases the stability of its base adduct.[6,15] This is supported by the highly negative values of ΔH.

In the present system, the energy contribution from the structural rearrangement is significant. The enthalpy values for α-substituted pyridines are less negative and the entropy more positive than those for the other substituted pyridines. These differences may confirm the presence of some motional freedoms of α-substituted pyridines. In the α-substituted pyridines, the free rotation of the α-methyl group prevents any base with an α-methyl group from penetrating easily the chelate plane. Consequently, the approach of the base to the central copper atom will be hindered, and the chelate rings are distorted. Quinoline shows a structural difference from the α-substituted pyridines. The planar aromatic molecules will tend to arrange themselves in one of the two planes perpendicular to the coordination plane of the copper atom. Thus, the hydrogen atom of the ortho C–H group can easily penetrate the chelate plane; the rotational freedom of isoquinoline is more effective than quinoline.

In the case of pyrrolidine and piperidine, ΔG is exceedingly negative, while ΔH is not so much; as for ΔS, it is even close to zero. On the other hand, pyridine gives appreciably negative values of ΔH and ΔS, but not so great a negative value of ΔG. The difference between these two sets of data is probably owing, at least in part, to the smaller size of pyridine molecules. However, there is evidence that a π-bond is formed

Table 3. The effect of organic solvents on adduct formation

Solvent	log K_{298}	$-\Delta G_{298}$ (kJ mol^{-1})	$-\Delta H$ (kJ mol^{-1})	$-\Delta S_{298}$ (J K^{-1} mol^{-1})
Chlorobenzene	3.07	17.53	44.26	89.67
Benzene	2.91	16.61	44.31	92.89
Toluene	2.87	16.40	28.99	42.24
Nitrobenzene	2.62	14.98	25.60	35.64
Chloroform	2.57	14.68	28.16	45.19
4-Methyl-2-pentanone	2.10	11.96	14.64	8.98
Butyl acetate	2.07	11.84	15.27	11.51
Acetone	1.91	10.92	14.22	11.08

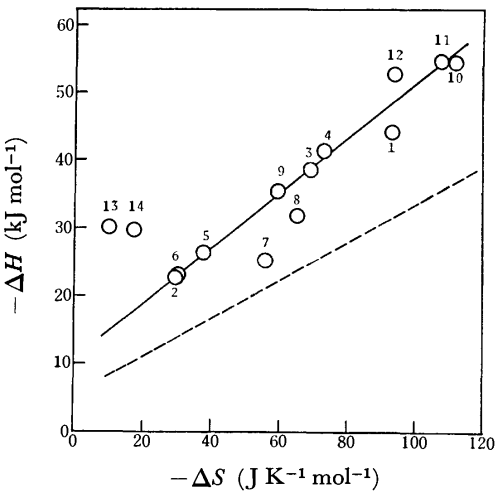

Fig. 5. Plots of $-\Delta H$ *vs.* $-\Delta S$ for $Cu(bfa)_2$ adducts (——) and non-fluorinated copper adducts (----). For numerals, see Table 2.

between the silver and the heterocyclic bases.[16] Though the systems are different, a π-bond is operative also in the case of the non-ortho-substituted pyridines. Thus, these pyridines make strong adduct bonds through their large π-bonding character, and the systems are generally rigid, owing to the restriction of rotational freedom. On the other hand, in pyrrolidine and piperidine there would be free rotation of the base molecule in the adduct bond with σ-bond character. The disorder of those systems will be attributed mostly to the rotational freedom of the bases. The smaller pyrrolidine has more kinetic freedom. It is surprising that the adduct bond in pipecolines is most rigid and is little influenced by the position of the substituent group. This will depend upon the larger size of the base molecules and their high basicity, even though the π-bond character is low.

Effect of Organic Solvents. The effect of solvents on the $Cu(bfa)_2$–pyridine system is shown in Table 3. The chelate is generally soluble in polar solvents but sparingly soluble in non-polar solvents, *e.g.*, hexane, cyclohexane, cyclohexanon, and carbon tetrachloride, though the latter solvents show a remarkable synergistic enhancement in the solvent extraction of metal chelates.[2,17] Among the non-polar solvents, benzene dissolves the chelate easily. The general order of increasing adduct stability is: acetone<butyl acetate <4-methyl-2-pentanone <chloroform <nitrobenzene < toluene≃benzene <chlorobenzene.

This order does not agree with that of the dipole moments, the dielectric constants, nor the transition energy of ligand field of the solvents, but it agrees with the decreasing order of the interaction between the solvent and the copper chelate or of the solvation energy of pyridine with various solvents. Libutti[18] measured the solvation energy of pyridine in benzene(—0.01 kcal/mol) and chloroform(—1.82 kcal/mol) and suggested that chloroform interacts very strongly with pyridine through hydrogen bonding. Data from NMR[19] and calorimetry[20] convince us of a weak interaction of pyridine with benzene. The existence of a large solvation energy will lower the activity and base strength of pyridine. This leads to the decrease of adduct stability and would account for the less exothermic nature observed in nitrobenzene and chloroform. On the contrary, chlorobenzene and benzene form weak solvates, which serve to reduce the endothermic effect of deaggregating pyridine molecules in these solvents. In 4-methyl-2-pentanone, butyl acetate, and acetone, the adduct stabilities are very low, and the reactions are least exothermic. This phenomena may be explained by the solvation of the copper chelate. The electron-withdrawing CF_3 group of the chelate ligand decreases the electron density around the central copper atom and, at the same time, it enhances the ability to solvate with such polar oxygen-containing solvents as 4-methyl-2-pentanone, butyl acetate, and acetone, although even weak solvates are not produced in non-fluorinated β-diketonate chelates.[21] It will require much energy to substitute a solvent molecule in addition to removing the dipole interaction of the pyridine with the solvent, and this fact promotes the irregular nature of the systems.

Effect of Chelate Ligands. Adduct stability will be much influenced by the Lewis acidity of the chelate, which is affected by the terminal group of the chelate ligand. The effect of chelate ligands involving non-fluorinated β-diketones in the pyridine system is shown in Table 4. The adduct stabilities in the fluorinated ligands differ little from those expected from the pK_H values. The constants increase in the following order: Hdpm < Haa < Hba ≪ Htaa < Hpta ≤ Hbfa < Hfta< Htta. For the fluorinated ligands, the electron-withdrawing effect of the CF_3 group is quite large, and the effect of the other terminal substituent is not so obviously recognized. But the order seems to correlate with the pK_H values, except Hpta, and to be just the reverse of the trend that the weaker the acidity of

Table 4. The effect of chelate ligands on adduct formation

Ligand	Base	$\log K_{298}$	$-\Delta G_{298}$ (kJ mol^{-1})	$-\Delta H$ (kJ mol^{-1})	$-\Delta S_{298}$ (J K^{-1} mol^{-1})
Htta	Pyridine	3.27	18.66	42.76	80.83
(6.28) [a]	α-Picoline	2.55	14.56	22.17	25.54
	γ-Picoline	3.62	20.67	38.95	61.32
	2,4-Lutidine	2.82	16.11	24.02	26.52
	2,6-Lutidine	1.74	9.91	26.61	55.99
Hfta	Pyridine	3.18	18.11	42.05	80.27
(6.18)	α-Picoline	2.46	14.06	28.24	47.57
	γ-Picoline	3.57	20.37	36.44	53.88
	2,4-Lutidine	2.79	15.94	24.27	27.92
	2,6-Lutidine	1.69	9.62	28.45	63.15
Hbfa	Pyridine	2.91	16.61	44.31	92.89
(6.01)	γ-Picoline	3.48	19.87	41.63	72.97
Hpta	Pyridine	3.02	17.24	44.60	91.77
(6.90)	α-Picoline	2.38	13.60	33.01	65.11
	γ-Picoline	3.43	19.58	37.07	58.65
	2,4-Lutidine	2.58	14.68	24.64	33.40
	2,6-Lutidine	1.61	9.16	23.76	48.98
Htaa	Pyridine	2.99	17.03	35.27	61.18
(6.09)	α-Picoline	2.25	12.84	22.01	30.73
	γ-Picoline	3.33	18.99	33.60	48.97
	2,4-Lutidine	2.48	14.14	20.58	21.61
	2,6-Lutidine	1.60	9.12	20.29	37.46
Hba	Pyridine	1.25	7.15	18.49	38.03
(8.55)					
Haa	Pyridine	1.07	6.11	14.43	27.92
(8.99)					
Hdpm	Pyridine	0.81	4.64	19.50	49.81

a) The pK_H values in parentheses are taken from T. Sekine, R. Murai, M. Niitsu, and N. Ihara, *J. Inorg. Nucl. Chem.*, **36**, 2569 (1974).

the ligand is, the weaker is the adduct stability.[17] To a certain extent, thenoyl, furoyl, and phenyl groups contribute to the resonance stabilization of those adducts, and the pivaloyl group shows some steric interference. However, we have no independent data available on the dissociation constants of the β-diketones in benzene solution; hence, further investigation will be required before a detailed discussion can be done. Nevertheless, the effect of bases definitely appears in the present experiment.

In the reaction of non-fluorinated copper chelates with nitrogen bases, Graddon pointed out a linear relationship between ΔH and ΔS, which was interpreted as indicating a common interaction mechanism.[22] The isoequilibrium temperature of the system containing 2-substituted 1,3-diketones was 310 K in benzene solution. A similar relationship was observed in the present fluorinated ligands, though a few points did not fit well in the case of Hbfa, as shown in Fig. 5. The line itself is situated considerably above that for the non-fluorinated ligands, and possesses a large slope. The isoequilibrium temperature is 413 K. These facts indicate rather clearly that fluorinated adducts are entropy-stabilized, while the non-fluorinated adducts show higher entropy-resistance. Thus, the extra stability of fluorinated adducts can mainly be ascribed to the entropy factor.

The author wishes to express his deep gratitude to Professor Shunzo Ueda, of Kanazawa University, for his continual encouragement and advice throughout this work. The author also wishes to express his thanks to Professor Tsunenobu Shigematsu and Assistant Professor Masakazu Matsui, of Kyoto University, for their valuable guidance and discussion.

References

1) D. P. Graddon, *Coord. Chem. Rev.*, **4**, 1 (1969).
2) Y. Marcus and A. S. Kertes, "Ion Exchange and Solvent Extraction of Metal Complexes," Wiley-Interscience, London (1969), p. 815.
3) T. Sekine, *Nippon Kagaku Zasshi*, **90**, 951 (1969).
4) D. P. Graddon and E. C. Watton, *J. Inorg. Nucl. Chem.*, **21**, 49 (1961).
5) T. Shigematsu, M. Tabushi, M. Matsui, and M. Munakata, *Bull. Chem. Soc. Jpn.*, **41**, 2656 (1968).
6) W. Partenheimer and R. S. Drago, *Inorg. Chem.*, **9**, 47 (1970).
7) E. F. Kassierer and A. S. Kertes, *J. Inorg. Nucl. Chem.*, **34**, 3209 (1972).
8) D. P. Graddon and W. K. Ong, *J. Inorg. Nucl. Chem.*, **37**, 469 (1975).
9) A. F. Garito and B. B. Wayland, *J. Am. Chem. Soc.*, **91**, 866 (1969).
10) T. Kogane, H. Yukawa, and R. Hirota, *Chem. Lett.*,

1974, 477.
11) P. Gans and H. M. N. H. Irving, *J. Inorg. Nucl. Chem.*, **34**, 1885 (1972).
12) W. R. Walker and N. C. Li, *J. Inorg. Nucl. Chem.*, **27**, 2255 (1965).
13) L. L. Funch and T. R. Ortolano, *Inorg. Chem.*, **7**, 567 (1968).
14) T. M. Shepherd, *J. Chem. Soc., Dalton Trans.*, **1972**, 813.
15) D. P. Graddon and W. K. Ong, *Aust. J. Chem.*, **27**, 741 (1974).
16) R. K. Murman and F. Basolo, *J. Am. Chem. Soc.*, **77**, 3484 (1955).
17) T. Honjyo and T. Shigematsu, *Kagaku*, **23**, 708 (1968).
18) B. L. Libutti, B. B. Wayland, and A. F. Garito, *Inorg. Chem.*, **8**, 1510 (1969).
19) J. N. Murrell and V. M. S. Gill, *Trans. Faraday Soc.*, **60**, 248 (1965).
20) P. R. Garrett, J. M. Pollock, and K. W. Morrow, *J. Chem. Thermodyn.*, **3**, 135 (1971).
21) F. R. Clarke, J. F. Steinbach, and W. F. Wagner, *J. Inorg. Nucl. Chem.*, **26**, 1311 (1964).
22) D. P. Graddon and K. B. Heng, *Aust. J. Chem.*, **24**, 1781 (1971).

A Molecular Orbital Study of Silylated Carbenes

Ryoji NOYORI, Masashi YAMAKAWA, and Wataru ANDO*

Department of Chemistry, Nagoya University, Chikusa, Nagoya 464

** Department of Chemistry, The University of Tsukuba, Niihari-gun, Ibaraki, 300-31*

(Received May 11, 1977)

The geometry and electronic properties of methylene, methylcarbene, carboxycarbene, phenylcarbene, trimethylsilylcarbene, silylcarbene, carboxysilylcarbene, and phenylsilylcarbene have been determined by MINDO/3 calculation. Introduction of a silyl group results in considerable decrease in ionization potential of carbenes. The electron affinity is increased to some extent by such substitution. The computation suggests a bent geometry for optimized triplet trimethylsilylcarbene structure, in conflict with a recent postulate that the ground-state molecule has an essentially linear structure.

Silylcarbenes generated by photolysis of the corresponding diazo compounds display intriguing behavior.[1-9] One is the relative reactivity of alkenes in the cyclopropanation of these carbenes. Ordinary carbenes are electrophilic and in most cases undergo cycloaddition preferentially to the more alkylated alkenes,[10] whereas the reactivity of ethoxycarbonyltrimethylsilylcarbene toward alkenes decreases with increasing methyl substitution on the double bond.[3] Another is the mode of reaction with dialkyl sulfides. Most carbenes react with sulfides in an electrophilic manner to produce sulfur ylides;[10] in contrast, reaction of silylcarbenes results in the formation of formal sulfur–carbon bond

$$RC(N_2)COOC_2H_5 \xrightarrow{h\nu} RCCOOC_2H_5 + N_2$$

R=H or $Si(CH_3)_3$

$$RCCOOC_2H_5 + \text{Olefin} \longrightarrow \text{cyclopropane-}COOC_2H_5$$

$$HCCOOC_2H_5 + R'_2S \longrightarrow R'_2\overset{+}{S}-\overset{-}{C}HCOOC_2H_5$$

$$(CH_3)_3SiCCOOC_2H_5 + R'_2S \longrightarrow R'S-\underset{\displaystyle COOC_2H_5}{\overset{\displaystyle Si(CH_3)_3}{\overset{|}{\underset{|}{C}}}}-R'$$

insertion products.[11] In addition, trimethylsilylcarbene has received attention as a precursor of a silaethylene.[6-9] These interesting features have prompted us

$$(CH_3)_3SiCHN_2 \xrightarrow{h\nu} (CH_3)_3SiCH + N_2$$

$$(CH_3)_3SiCH \longrightarrow (CH_3)_2Si{=}CHCH_3$$

to examine the electronic structures of the carbenes by semi-empirical SCF MO calculations.

Results and Discussion

A linear carbene has two perpendicular 2p orbitals into which two valence electrons are to be placed. Degeneracy is removed on bending, giving a σ orbital (in the plane in which bending takes place) and leaving p orbital (perpendicular to the plane).[12] When a conjugative group is attached to the divalent carbon, bending can occur in either in-plane or out-of-plane manner. The levels of these orbitals are affected in various ways by interaction with the adjacent carbene substituents. Thus total molecular energies vary as a function of bond angle, θ. We calculated the structures of four silylcarbenes and some related species according to the MINDO/3 method.[13] Contribution of silicon d orbitals was not explicitly considered. In order to perform the calculation, the program supplied by the Quantum Chemistry Program Exchange (QCPE) was modified for use with the FACOM 230-60 computer at Nagoya University. For carbenes **1**—**7**, the bond lengths, bond angles, and torsional angle were optimized. For large substituents such as phenyl or carboxyl, some fixed parameters were used. The molecular structures thus obtained are given in the molecular formulas; the details are summarized in Table 1. Geometries of the triplet states were determined by this method and the electronic structures by unrestricted Hartree-Fock type SCF calculations, not by the conventional *half-electron method*.[13] Electronic properties of the carbenes are given in Table 2. The ionization potential (IP) of the carbenes and the electron affinity (EA),

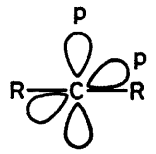

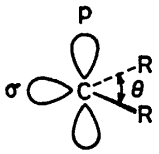

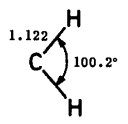

1S

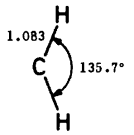

1T

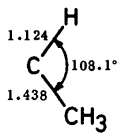

2S

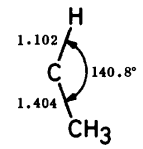

2T

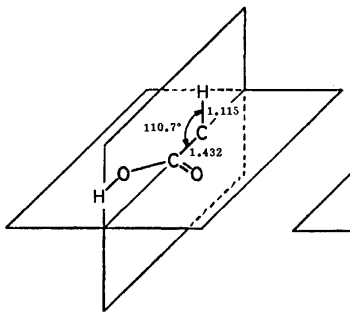

3S

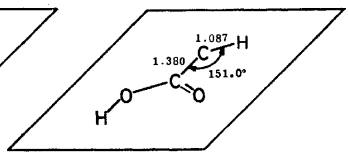

3T

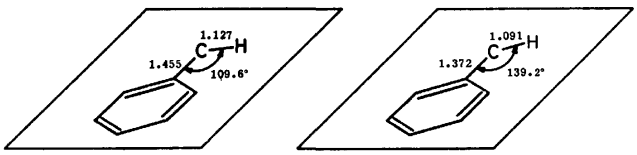

4S

4T

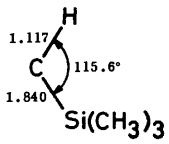

5S

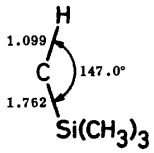

5T

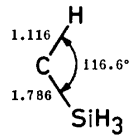

6S

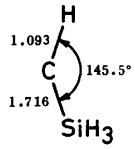

6T

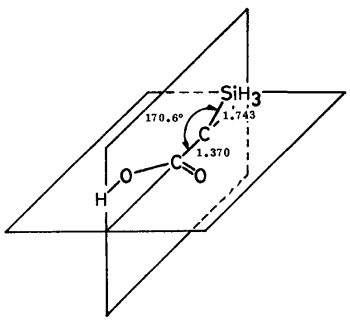

7S

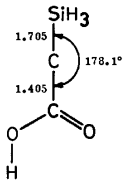

7T

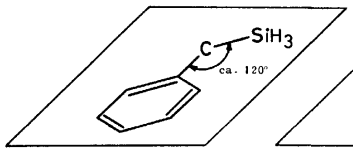

8S

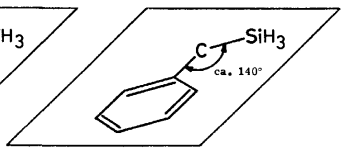

8T

as estimated as IP of the corresponding radical anions, provide the indication of nucleophilicity and electrophilicity, respectively. Electron density of the formally vacant p orbital ($d_{p\pi}$) and net atomic charge of the carbenic center might be related to the reactivity of these carbenes as well.[17]

Methylene (1). Calculations indicate that the triplet state (**1T**) is the ground state with minimum energy at an HCH bond angle of 135.7°, lying 11.8 kcal/mol below the lowest singlet state (**1S**) with bond angle of 100.2°. Calculated IP of **1S** is 9.94 eV. The result for this parent carbene species is in good agreement with experimental results.[18,19] The calculated EA value, 0.09 eV, is somewhat lower than the observed value, 0.21 eV.[18] The MINDO/3 calculation for **1** has been carried out,[13] but the IP of **1T** has not been reported.[20]

Methylcarbene (2). The 140.8° triplet (**2T**) was found to be the ground state. The 108.1° singlet (**2S**) lies 16.9 kcal/mol above **2T** and has IP of 8.86 eV. This value is 1.08 eV lower than that of **1S**. The EA value, 0.83 eV, is larger than that of simple methylene. Introduction of methyl group increases $d_{p\pi}$ by 0.12.[21]

Carboxycarbene (3). The carboxyl group was used as a model of the alkoxycarbonyl group. Both singlets and triplets with minimum energies have bent structures. The in-plane triplet is more stable than the singlet of out-of-plane bent structure. This is to be noted because alkoxycarbonylcarbenes formed from diazoacetates are known to behave usually as a singlet species.[22,23] The orbital stabilization of **3S** is attained as a result of both bending to acquire s character and π conjugation between the occupied σ orbital and carboxyl group. IP of **3S** is nearly identical with that of **1S**. As expected, this electron-withdrawing group increases the EA value, predicting the eminent electrophilic nature of carbene.

Phenylcarbene (4). In both **4S** and **4T**, all the atoms lie nearly on the same plane. In accord with experimental findings,[24] the ground state is a bent triplet (**4T**). The low IP (8.22 eV) and high EA (1.55 eV) for the singlet species (**4S**) characterize the electronic property. Its $d_{p\pi}$, 0.20 is rather high.[25]

Trimethylsilylcarbene (5). The ground state was indicated to be triplet, as has recently been demonstrated by experiments.[9] According to the present calculation, however, the ground state has a 147° bent structure (**5T**), which lies in marked contrast with the recent postulate that **5T** has a linear structure.[9] The lowest singlet state (**5S**) with bond angle of 115.6°, lying 32.9 kcal/mol above **5T**, has an IP of 8.25 eV. The IP is much lower than that of **1S** (9.94 eV) or **2S** (8.86 eV) but comparable with the one of the phenylated carbene **4S**. Electron density of the carbenic carbon, $d_{p\pi}$, is smaller than that in the case of **2S**. Thus the trimethylsilyl group, as compared with the methyl group, has been shown to decrease IP greatly but not to increase electron density of the divalent carbon. Lack of hyperconjugative stabilization of the vacant orbital may be the cause. On going from **2S** to **5S**, EA value increases by 0.93 eV.

Silylcarbene (6). The optimized geometry and electronic properties are quite similar to those of the trimethyl derivative **5**.

Carboxysilylcarbene (7). For the sake of economy of calculation, silyl group was used as a model of the trimethylsilyl group. The carbene has also triplet ground state (**7T**). Unlike carboxy- or silylcarbene, the triplet state with minimum energy is of linear structure. The lowest singlet state (**7S**) of 170.6° bent structure, lying 23.5 kcal/mol above the ground state **7T**, is stabilized to a considerable extent through conjugation of the σ orbital (99.9% p-character) containing paired electrons with the adjacent carboxyl group. Notably, silyl group introduced into the carbene **3S** decreases the IP value by 1.11 eV, suggesting endowment of nucleophilicity. On the other hand, no change in electrophilicity can be expected, as seen from the comparable EA value. The $d_{p\pi}$ and net atomic charge of the carbene center were found to increase to some extent.

Phenylsilylcarbene (8). The structure could not be optimized because of the large framework. The ground

Table 1. Calculated molecular geometries of carbenes **2**—**7**

Carbene	Calcd bond length (Å), bond angles, and torsional angles
$CHCH_3$, **2S**	C-C; 1.438, CH_2-H; 1.112—1.113, C(carbene)-H; 1.124, ∠H-C-CH_3; 108.1°, ∠CH-CH_2-H; 112.5—114.0°, τ(H-C-CH_2-H); 60°[a]
2T	C-C; 1.404, CH_2-H; 1.106—1.123, C(carbene)-H; 1.102, ∠H-C-CH_3; 140.8°, ∠CH-CH_2-H; 112.1—113.4°, τ(H-C-CH_2-H); 60°[a]
CHCOOH, **3S**	C-C; 1.432, C=O; 1.230, C-O; 1.350, O-H; 0.955,[b] C-H; 1.115, ∠H-C-C; 110.7°, τ(H-C-C=O); 90.2°
3T	C-C; 1.380, C=O; 1.236, C-O; 1.355, O-H; 0.955,[b] C-H; 1.087, ∠H-C-C; 151.0°, τ(H-C-C=O); 0.0°
CHC_6H_5, **4S**	C(carbene)-C; 1.455, C(carbene)-H; 1.127, ∠H-C(carbene)-C; 109.6°, τ(H-C(carbene)-C=C); 5.8°[c]
4T	C(carbene)-C; 1.372, C(carbene)-H; 1.091, ∠H-C(carbene)-C; 139.2°, τ(H-C(carbene)-C=O); 5.8°[c]
$CHSi(CH_3)_3$, **5S**	C(carbene)-Si; 1.840, Si-CH_3; 1.885—1.888, CH_2-H; 1.114—1.115, ∠C(carbene)-Si-CH_3; 108.9—110.5°; ∠Si-CH_2-H; 115.0—115.5°,[a,d] C(carbene)-H; 1.117, ∠H-C(carbene)-Si; 115.6°, τ(H-C(carbene)-Si-CH_3); 60.1°
5T	C(carbene)-Si; 1.762, Si-CH_3; 1.889—1.895, CH_2-H; 1.116—1.117, ∠C(carbene)-Si-CH_3; 108.9—110.5°; ∠Si-CH_2-H; 115.0—115.6°,[a,d] C(carbene)-H; 1.099, ∠H-C(carbene)-Si; 147.0°, τ(∠H-C(carbene)-Si-CH_3); 60.1°
$CHSiH_3$, **6S**	C-Si; 1.786, Si-H; 1.480—1.481, ∠C-Si-H; 111.7—113.5°,[a] C-H; 1.116, ∠H-C-Si; 116.6°, τ(H-C-Si-H); 60.2°
6T	C-Si; 1.716, Si-H; 1.481—1.483, ∠C-Si-H; 110.1—110.5°,[a] C-H; 1.093, ∠H-C-Si; 145.5°, τ(H-C-Si-H); 60.0°
$C(SiH_3)COOH$, **7S**	C-C; 1.370, C=O; 1.245, C-O; 1.354, O-H; 0.954,[b] C-Si; 1.743, Si-H; 1.472—1.479, ∠C-Si-H; 108.3—112.8°,[a] ∠C-C-Si; 170.6°, τ(Si-C-C=O); 90.0°, τ(C-C-Si-H); 30.0°
7T	C-C; 1.405, C=O; 1.239, C-O; 1.342, O-H; 0.957,[b] C-Si; 1.705, Si-H; 1.487, ∠C-Si-H; 112.0—112.7°,[a] ∠C-C-Si; 178.1°, τ(Si-C-C=O); 0.0°, τ(C-C-Si-H); 60.0°

a) CH_3, $Si(CH_3)_3$, and SiH_3 groups are assumed to have approximately C_{3v} symmetry. b) Planar structure for COOH group was assumed; ∠C-C=O; 120°, ∠C-C-O; 120°, ∠C-O-H; 110°. c) Phenyl ring was treated as regular hexagon; C-C; 1.397 A, C-H; 1.084 A, bond angle; 120°. d) Angles of 60, 180, 300° are used for the torsional angle, τ(C(carbene)-Si-CH_2-H).

Table 2. Electronic properties of certain carbenes obtained by MINDO/3 method

Carbene	Occupation	θ, deg	IP, eV[a]	EA, eV[b]	$d_{p\pi}$[c,d]	Net atomic charge[d]	ΔH_f,[e] kcal/mol
CH_2, **1S**	σ^2	100.2	9.94	0.09	0.0	+0.19	100.2
1T	σp	135.7	9.92	−1.18[f]	1.0	−0.14	88.4
$CHCH_3$, **2S**	σ^2	108.1	8.86	0.83	0.12	+0.06	75.6
2T	σp	140.8	9.09	−0.39[f]	—	−0.15	58.7
CHCOOH, **3S**	σ^2	110.7	9.89	2.20	0.11	+0.04	−8.5
3T	σp	151.0	10.77	1.17	—	−0.13	−24.8
CHC_6H_5, **4S**	σ^2	109.6	8.22	1.55	0.20	0.0	118.9
4T	σp	139.2	8.08	0.69	—	−0.14	98.5
$CHSi(CH_3)_3$, **5S**	σ^2	115.6	8.25	1.76	0.05	−0.04	30.6
5T	σp	147.0	9.26	0.41	—	−0.21	−2.3
$CHSiH_3$, **6S**	σ^2	116.6	8.28	1.29	0.06	0.0	83.2
6T	σp	145.5	9.26	−0.09[f]	—	−0.15	50.8
$C(SiH_3)COOH$, **7S**	σ^2	170.6	8.78	2.58	0.21	−0.12	−38.2
7T	pp′	178.1	9.72	1.87	—	−0.18	−61.7

a) Ionization potential. b) Electron affinity. c) Electron density of carbene p orbital. d) In units of electron charge. e) Heat of formation. f) The negative value may be due to the underestimation of the core resonance integrals in this method.

state was estimated to be *ca.* 140° bent triplet (**8T**), the lowest singlet (**8S**) prefering an in-plane bent (*ca.* 120°) geometry.

Thus MINDO/3 method shows that introduction of silyl groups into the carbene center results in considerable decrease in IP's, thereby increasing nucleophilic character. The same perturbation, however, is observed with other substituents, particularly phenyl and methyl groups. Electrophilicity, as judged from the EA's, is affected by silyl substitution, the effect being highly dependent on the nature of other substituents on divalent carbon. Silyl moieties increase

electron density, $d_{p\pi}$, of the carbenic carbon, but the degree of the effect is less than methyl or phenyl substituent. Thus when the electronic properties of the silylcarbenes are compared with those of the related nonsilylated carbenes of the same singlet electronic configuration, we cannot anticipate any peculiar behavior of the former species. In order to interpret the unique reactivity of silylcarbenes, the bulkiness of silyl group[3] and efficiency of the S-T intersystem crossing should be taken into account. The silyl groups may exert strong influence on the nature of the transition state or intermediate of carbene *reactions* rather than the properties of the divalent species itself.

The MINDO/3 procedure is the most sophisticated semi-empirical SCF MO method at present and the accuracy of the calculations has been demonstrated by excellent agreement with experimental observations for a large number of ground state molecules. This is also the case for organosilicon compounds.[16] Nevertheless, the calculated bent geometry of **5** is inconsistent with the recent postulate that ground-state trimethylsilylcarbene has a linear geometry.[9] If the conclusion based on ESR study is correct,[26] one of the major causes of this controversy might be the influence of possible $d\pi$-$p\pi$ interaction, although such orbital effect is usually considered to be negligible.[27-29] If this were the case, it might present a rare example of d-orbital participation.

References

1) U. Schöllkopf and N. Rieber, *Angew. Chem.*, **79**, 906 (1967).
2) D. Seyferth, A. W. Dow, H. Menzel, and T. C. Flood, *J. Am. Chem. Soc.*, **90**, 1080 (1968).
3) U. Schöllkopf, D. Hoppe, N. Rieber, and V. Jacobi, *Justus Liebigs Ann. Chem.*, **730**, 1 (1969).
4) A. G. Brook and P. F. Jones, *Can. J. Chem.*, **49**, 1841 (1971).
5) R. N. Hazeldine, D. L. Scott, and A. E. Tipping, *J. Chem. Soc., Perkin Trans. 1*, **1974**, 1440.
6) R. L. Kreeger and H. Shechter, *Tetrahedron Lett.*, **1975**, 2061.
7) W. Ando, A Sekiguchi, and T. Migita, *Chem. Lett.*, **1976**, 779.
8) O. L. Chapman, C.-C. Chang, J. Kolc, M. E. Jung, J. A. Lowe, T. J. Barton, and M. L. Tumey, *J. Am. Chem. Soc.*, **98**, 7844 (1976).
9) M. R. Chedekel, M. Skoglund, R. L. Kreeger, and H. Shechter, *J. Am. Chem. Soc.*, **98**, 7846 (1976).
10) W. Kirmse, "Carbene Chemistry," 2nd ed, Academic Press, New York, N. Y. (1971); M. Jones, Jr., and R. A. Moss, "Carbenes," Vol. 1, John Wiley, New York, N. Y. (1973).
11) W. Ando, *Acc. Chem. Res.*, **10**, 179 (1977).
12) R. Hoffmann, G. D. Zeiss, and G. W. Van Dine, *J. Am. Chem. Soc.*, **90**, 1485 (1968).
13) M. J. S. Dewar, R. C. Haddon, and P. K. Weiner, *J. Am. Chem. Soc.*, **96**, 253 (1974); R. C. Bingham, M. J. S. Dewar, and D. H. Lo, *ibid.*, **97**, 1285, 1294 (1975).
14) N. C. Baird and M. J. S. Dewar, *J. Chem. Phys.*, **50**, 1262 (1969).
15) N. C. Baird, M. J. S. Dewar, and R. Sustman, *J. Chem. Phys.*, **50**, 1275 (1969).
16) M. J. S. Dewar, D. H. Lo, and C. A. Ramsden, *J. Am. Chem. Soc.*, **97**, 1311 (1975), and references cited therein.
17) R. Hoffmann, R. Gleiter, and F. B. Mallory, *J. Am. Chem. Soc.*, **92**, 1460 (1970); J. F. Harrison, *ibid.*, **93**, 4113 (1971).
18) P. F. Zittel, G. B. Ellison, S. V. ONeil, E. Herbst, W. C. Lineberger, and W. P. Reinhardt, *J. Am. Chem. Soc.*, **98**, 3731 (1976), and references cited therein.
19) E. Wasserman, V. J. Kuck, R. S. Hutton, E. D. Anderson, and W. A. Yager, *J. Chem. Phys.*, **54**, 4120 (1971); R. A. Bernheim, H. W. Bernard, P. S. Wang, L. S. Wood, and P. S. Skell, *J. Chem. Phys.*, **54**, 3223 (1971).
20) *Ab initio* calculation for CH_2: see J. F. Harrison, *J. Chem. Phys.*, **54**, 5413 (1971).
21) *Ab initio* calculation for $CHCH_3$: J. A. Altmann, I. G. Csizmadia, and K. Yates, *J. Am. Chem. Soc.*, **96**, 4196 (1974).
22) V. Dane and E. W. Warnhoff, *Org. React.*, **18**, 217 (1970); A. P. Marchand and N. M. Brockway, *Chem. Rev.*, **74**, 431 (1974).
23) Sensitized photolysis of methyl diazoacetate produces triplet carbomethoxycarbene: M. Jones, Jr., W. Ando, M. E. Hendrick, A. Kulczycki, Jr., P. M. Howley, K. F. Hummel, and D. S. Malament, *J. Am. Chem. Soc.*, **94**, 7469 (1972).
24) J. Higuchi, *J. Chem. Phys.*, **39**, 1339 (1963).
25) MINDO/3 calculation of singlet para-substituted phenylcarbenes was recently reported. See R. J. Miller, L. S. Yang, and H. Shechter, *J. Am. Chem. Soc.*, **99**, 938 (1977).
26) The estimate[9] may not be very reliable, since the bond angle was derived by comparison of the proton hyperfine splitting constant with the value of *methylene*.
27) For example, J. I. Musher, *J. Am. Chem. Soc.*, **94**, 1370 (1972); J.-M. Lehn and G. Wipff, *ibid.*, **98**, 7498 (1976); F. Bernardi, I. G. Csizmadia, A. Mangini, H. B. Schlegel, M.-H. Whangbo, and S. Wolfe, *ibid.*, **97**, 2209 (1975).
28) In special cases, however, such interaction is significant. See L. M. Loew and W. R. MacArthur, *J. Am. Chem. Soc.*, **99**, 1019 (1977).
29) In order to estimate the effect of d functions of silicon atom, CNDO/2 calculation[30] was carried out for singlet silylcarbene (6S). When only s and p atomic orbitals were considered, a 123° bent geometry was obtained as the optimal structure. The computation using an spd basis set[31] afforded nearly the same optimized geometry, $\theta=125°$. As usual, the addition of d orbital lowered the total energy of the carbene because of the polarization effect, but did not alter the shape of potential surface curve. This result implies relative unimportance of the d-orbital participation.
30) J. A. Pople and D. L. Beveride, "Approximate Molecular Orbital Theory," McGraw-Hill, New York, N. Y. (1970). In the original CNDO/2 program, same values have been used for 3s-, 3p-, and 3d-orbital exponents. However, the 3d-orbital exponent value 0.30 was used in this calculation.[31]
31) B. Roos and P. Siegbahn, *Theor. Chim. Acta*, **17**, 199 (1970).

Reaction of Organic Tin(II) Compounds with Ethyl Isocyanate

Ikuko WAKESHIMA and Ichiro KIJIMA

Department of Industrial Chemistry, Faculty of Engineering, Science University of Tokyo, Kagurazaka, Shinjuku-ku, Tokyo 162

(Received June 3, 1977)

The reaction of Sn–OC bond-containing tin(II) compounds with ethyl isocyanate was investigated. From the ν_{NCO} absorption bands, it is recognized that the reactivity, in terms of tin(II) compounds, decreases in the order: bis[2-(dimethylamino)ethoxo]tin(II) > bis[*o*-(ethoxycarbonyl)phenolato]tin(II) > di(phenolato)tin(II)> bis(ethoxycarbonylacetonato)tin(II) > bis(3-ethoxycarbonyl-2-pentanoato)tin(II) > bis(1-phenylbutane-1,3-dionato)tin(II) > bis(dibenzoylmethanato)tin(II). Bis[2-(dimethylamino)ethoxo]tin(II), bis[*o*-(ethoxycarbonyl)-phenolato]tin(II), and di(phenolato)tin(II) yielded triethyl isocyanurate as a main product from reactions with ethyl isocyanate, while bis(ethoxycarbonylacetonato)tin(II), bis(3-ethoxycarbonyl-2-pentanoato)tin(II), bis(1-phenylbutane-1,3-dionato)tin(II), and bis(dibenzoylmethanato)tin(II) gave mixtures of the isocyanurate and 6-ethylimino-1,3,5-triethylhexahydro-1,3,5-triazine-2,4-dione. The mechanism for the formation of these products is discussed.

Certain kinds of organic tin(II) compounds are widely used as catalysts for the synthesis of polyurethanes and as curing agents for silicones. Recently, many kinds of organic tin(II) compounds[1–10] have been prepared, and the reactivities of some have been investigated. Previously, the present authors reported that the reaction of bis(acetylacetonato)tin(II) with ethyl isocyanate resulted in 6-ethylimino-1,3,5-triethylhexahydro-1,3,5-triazine-2,4-dione in an excellent yield.[11] In the present paper, the reaction of several organic tin(II) compounds with ethy isocyanate will be described.

Results and Discussion

Reaction of Tin(II) Dialkoxide with Ethyl Isocyanate. Ethyl isocyanate was added to a solution of bis[2-(dimethylamino)ethoxo]tin(II) (**1**), bis[*o*-(ethoxycarbonyl)phenolato]tin(II) (**2**), and di(phenolato)tin(II) (**3**) in benzene at room temperature and then heated for several hours (as indicated in Table 1). The reaction mixtures were hydrolyzed to isolate the products. There results are shown in Table 1.

In the reaction of tin(II) compound **1** with ethyl isocyanate at 20—24 °C, IR spectroscopy demonstrated the absence of the characteristic absorption band of the ν_{NCO} group within 1 h. When the reaction mixture was further refluxed for 3 h, the yield of triethyl isocyanurate was much higher compared with that of the reaction without heating (runs 1 and 2). This indicates that the reaction proceeds through the intermolecular reaction of the intermediate, as described in a previous paper.[13] Judging from the time required for the disappearance of the ν_{NCO} absorption band observed in ethyl isocyanate, it was found that tin(II) compounds **2** and **3** were less reactive than tin(II) compound **1**, and that the reactivity of tin(II) compound **3** was inferior to that of tin(II) compound **2**. These facts indicate that the reduction in the electron density on the oxygen atom of the Sn–OC bond due to the M-effect of the R group results in a decrease in the nucleophilicity of the oxygen atom toward ethyl isocyanate and that the low solubility[6] of tin(II) compound **3** reduced the reaction of that compound **3** toward ethyl isocyanate. In the reaction of tin(II) compound **2**, triethyl isocyanurate was obtained as the main product accompanied by a small amount of the carbamate derivative and tin(II) compound **3** gave triethyl isocyanurate as the only product. This suggests that the Sn–N bond formed by the insertion of ethyl isocyanate into the Sn–OC bond is considerably more active.

Table 1. Reaction of $Sn(OR)_2$ with ethyl isocyanate in benzene[a]

Run	$Sn(OR)_2$	Reaction time (h)	Yield (%) of products[b]	
			$C_2H_5NHCO_2R$	$(C_2H_5NCO)_3$
1	**1**	3[c]	45.4[e]	38.6[g]
2	**1**	3[d]	25.9	56.1
3	**2**	3	4.9[f]	90.2
4	**2**	8		86.3
5	**3**	8		86.9

a) $[Sn(OR)_2] : [C_2H_5NCO] = 1 : 2$ b) Satisfactory analytical and IR or NMR spectroscopic data were obtained for all compounds prepared. c) Reaction temperature 20—24 °C. d) After the disappearance of the ν_{NCO} band, the reaction mixture was heated for 3 h. e) Bp 70—71 °C at 0.3 mmHg. f) Bp 98—100 °C at 0.3 mmHg. g) Mp 94—95 °C (Lit, 95 °C[12]).

Reactions of the β-Keto Ester and the β-Diketone Tin(II) Derivative with Ethyl Isocyanate. These reactions were carried out using a similiar procedure. The results are summarized in Table 2.

The reaction between the bis(β-keto ester)tin(II) derivative and ethyl isocyanate: bis(ethoxycarbonylacetonato)tin(II) (**4**) reacted with ethyl isocyanate in various molar ratios to give mixtures of ethyl α-(ethylcarbamoyl)acetoacetate (**9**), triethyl isocyanurate (**10**), and 6-ethylimino-1,3,5-triethylhexahydro-1,3,5-triazine-2,4-dione (**11**), as shown in Reaction 1.

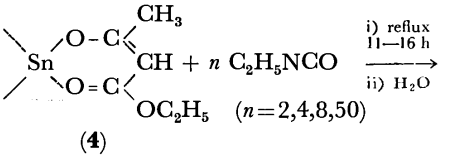

(**4**)

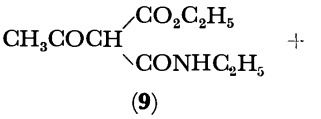

(**9**)

TABLE 2. REACTION OF $Sn(OR)_2$ WITH ETHYL ISOCYANATE IN BENZENE

Run	$Sn(OR)_2$	Molar ratio $RNCO/Sn(OR)_2$	Reaction time (h)	Yield (%) of products		
				9[a]	**10**	**11**[b]
6	**4**	2	11	79.7		
7	**4**	4	11	60.0	13.9	
8	**4**	8	11	43.0	22.1	9.6
9	**4**	50	16		40.0	27.7
10	**5**	4	15		75.0	trace
11	**5**	50	38		47.7	34.4
12	**6**	4	9		16.1	62.0
13	**6**	50	26		24.5	60.4
14	**7**	2	40		16.7	37.7

a) Bp 80 °C at 0.05 mmHg. b) Bp 84—87 °C at 0.05 mmHg (84—87 °C at 0.05 mmHg[11]).

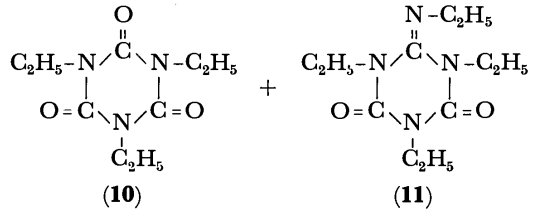

(**10**) (**11**) (1)

Judging from the reaction time required for the completion of the reaction, β-keto ester tin(II) compounds have been found to be less reactive toward ethyl isocyanate than tin(II) alkoxides. Although all of the reactions between bis(acetylacetonato)tin(II) (**8**) and ethyl isocyanate in various molar ratios gave only compound **11**, the reaction of tin(II) compound **4** with ethyl isocyanate of a molar ratio of 1 : 2 (run 6) yielded compound **9** in a yield of 79.6%. This difference may be related to the lesser nucleophilicity of the oxygen atom of the Sn–OC bond and the preferential reactivity of the methine proton in the chelate ring due to the greater electron-withdrawing force of the ethoxyl group. The reaction of a molar ratio of 1 : 4 (run 7) yielded compound **10** (13.9%) besides the formation of compound **9** (60.0%). In the cases of $n=8$ (run 8) and 50 (run 9), compound **11** was obtained in yields of 9.6 and 27.7%, respectively, together with the formation of compound **10** in 22.1 and 40 % yields, respectively. From these results, it is clear that the yield of compound **11** increases with increasing molar ratio of ethyl isocyanate to tin(II) compound **4**. The reaction of bis(3-ethoxycarbamoyl-2-pentanoato)tin(II) (**5**) with ethyl isocyanate in a molar ratio of 1 : 4 (run 10) gave compound **10** as a main product accompanied by a small amount of compound **11**. When a large amount of ethyl isocyanate ($n=50$, run 11) was treated with tin(II) compound **5**, compounds **10** and **11** were obtained in yields of 47.7 and 34.4 %, respectively. It is worth noting that compound **11** is produced by a reaction with the β-keto ester tin(II) compound, in which the methin proton of the chelate ring is substituted by an ethyl or ethylcarbamoyl group. From these results, the following scheme is given as a plausible reaction path:

TABLE 3. YIELD AND PROPORTION OF PRODUCTS FROM IN THE REACTION OF VARIOUS TIN(II) COMPOUNDS WITH ETHYL ISOCYANATE

$Sn(OC(R)=CHCOR')_2$			Total yield of product (%)	Proportion of products	
	R	R′		**10**	**11**
8	CH_3	CH_3	89		100
6	C_6H_5	CH_3	85	29	71
7	C_6H_5	C_6H_5	54	31	69
4	CH_3	OC_2H_5	68	59	41

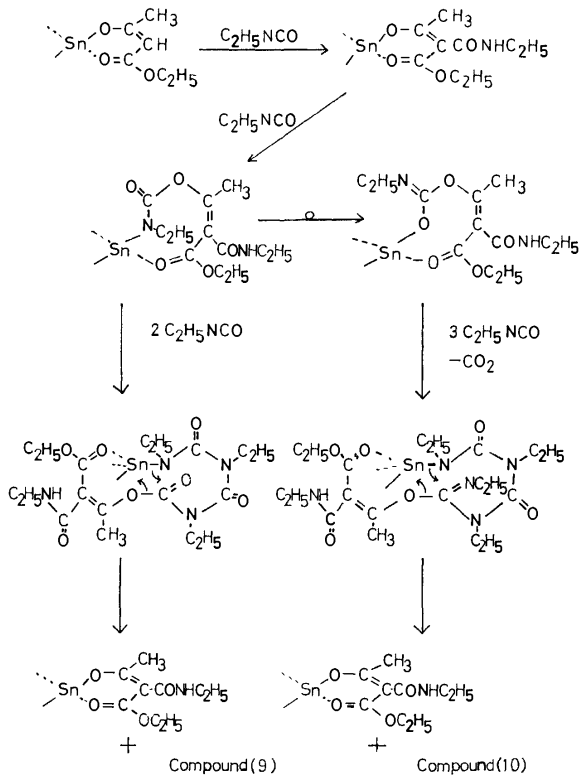

Scheme.

The extent to which N→O migration of the tin atom correlates with the formation of compounds **10** and **11** is considerable.

The Reaction of Bis(β-diketonato)tin(II) Derivatives with Ethyl Isocyanate: When bis(1-phenylbutane-1,3-dionato)tin(II) (**6**) was allowed to react with ethyl isocyanate, compounds **10** and **11** were obtained without the forma-

tion of 2-ethylcarbamoyl-1-phenyl-1,3-butanedione. The reaction in a 1:4 molar ratio required 4 h for the disappearance of the ν_{NCO} absorption band at about 2270 cm^{-1} and 26 h in a 1:50 molar ratio. On the other hand, it was found that the reaction of bis(dibenzoylmethanato)tin(II) (**7**) with ethyl isocyanate was very slow; after heating for 40 h, 96 % of tin(II) compound **7** and 45.6% of ethyl isocyanate were recovered and compounds **10** and **11** were obtained in low yields. Tin(II) compound **8** gave only compound **11** and the other bis(β-diketonato)tin(II) derivatives afforded a mixture of compounds **10** and **11** as reaction products. The bis(β-diketonato)tin(II) derivatives provided compound **11** in higher yields in comparison with the bis(β-keto ester)tin(II) derivatives as described above. It may be assumed that N→O migration of the tin atom occurs more easily in tin(II) compounds **6** and **7** than in tin(II) compounds **4** and **5**.

As can be seen from Table 3, the proportion of products is influenced by the substituent, R′, bonded to the chelate ring; the production of compound **11** increases in the order: $CH_3 > C_6H_5 > OC_2H_5$. Taking account of the $\nu_{C=O}$ absorption band of tin(II) compound **4** ($\nu_{C=O}$ 1600 cm^{-1}),[1] tin(II) compound **6** ($\nu_{C=O}$ 1565 cm^{-1}),[4] tin(II) compound **7** ($\nu_{C=O}$ 1548 cm^{-1}),[4] and tin(II) compound **8** ($\nu_{C=O}$ 1567 cm^{-1}),[1] the strength of co-ordination of the oxygen atom on the R′CO group toward the tin atom appears to play an important role in the formation of compounds **10** and **11**.

Experimental

Experiments were carried out in a nitrogen atmosphere dried using liquid nitrogen. The measured melting and boiling points are uncorrected. The IR spectra were recorded with a Hitachi EPI-2S spectrometer and the ^{1}H-NMR spectra on a Hitachi R-24 (60 MHz) using TMS as an internal standard. The abbreviations s, t, q, br, and m in the NMR spectra denote singlet, triplet, quartet, broad, and multiplet, respectively. Elemental analysis were carried out using a Yanagimoto M-2 CHN corder.

Reagents. Hexane, benzene, and ethanol were dried using the methods given a previous paper.[6] Ethyl acetoacetate, ethyl salicylate, benzoylacetone, phenol, and 2-(dimethylamino)ethanol were dried using an azeotropic distillation method using benzene. Ethyl 3-ethylacetoacetate was prepared by a method given in the litrature.[11] Ethyl isocyanate was obtained commercially and purified by distillation just prior to use. Tin(II) derivatives were prepared by reactions of tin(II) diethoxide with the corresponding alcohol, phenol, ester, or ketone.

General Procedure. Ethyl isocyanate was added dropwise to a benzene (1.4—1.5 ml/$Sn(OR)_2$ mmol) solution of $Sn(OR)_2$ (100 mmol) at 25—30 °C with stirring. After standing at room temperature for 1 h, the solution was heated to 79—81 °C for fixed time intervals and the disappearance of the ν_{NCO} absorption band was observed. After the solution distilled off, the oily residue was hydrolyzed with a water (5—6 ml) and acetone (100 ml) or benzene mixed solution. Removal of the inorganic tin with a centrifugal separator gave a pale yellow solution, which was then concentrated and distilled *in vacuo*. Products **9** and **11** were fractionally distilled under reduced pressure through a 20-cm Widmer fractionating column. The residue (compound **10**) was recrystallized from hexane. In the case of the reaction with tin(II) compound **3**, the unreacted tin(II) compound was filtered off before hydrolysis. The products obtained were identified on the basis of IR, NMR, and mass spectra and elemental analysis. Proof of the structure of compound **11** was also provided by its conversion to triethyl isocyanurate a 2M-HCl alcoholic solution.[11]

$CH_3COCH(CONHC_2H_5)CO_2C_2H_5$ bp 80 °C at 0.05 mmHg, M^+ 201, IR(cm^{-1}); ν_{N-H} 3340, $\nu_{C=O}$ 1730, $\nu_{C=O}$ and $\delta_{O-H\,enol}$ 1650, δ_{N-H} 1550, $\nu_{C=N}$ 1400, $\nu_{C=C}$ 955, 790, NMR (δ); CH_3CH_2N and CH_3CH_2O 1.3 district (m), $CH_3C{=}O$ 2.39(s), CH_3CH_2N 3.38, CH_3CH_2O 4.24(q), N**H** 9.23(t), OH 18.69(s). Found: C, 53.61; H, 7.71; N, 7.16%. Calcd for $C_9H_{15}O_4N$: C, 53.72; H, 7.51; N, 6.96%.

$C_2H_5NHCO_2CH_2CH_2N(CH_3)_2$ bp 70—71 °C at 0.3 mmHg, IR(cm^{-1}); ν_{N-H} 3350, $\nu_{C=O}$ 1680, NMR(δ); CH_3CH_2N 1.11(t), CH_3N 2.19(s), CH_2N 2.43(t), CH_3CH_2 3.12(m), CH_2O 4.02(t), N–H 5.5(br). Found: 52.46; H, 9.88; N, 17.14%. Calcd for $C_7H_{16}N_2O_2$: C, 52.47; H, 10.07; N, 17.49%.

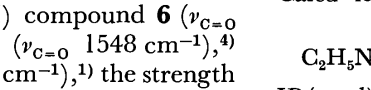

bp 98—100 °C at 0.3 mmHg, IR(cm^{-1}); ν_{N-H} 3340, $\nu_{C=O}$ 1710, NMR(δ); CH_3CH_2 1.11(t), CH_3CH_2O 1.30(t), CH_3CH_2N 3.23(m), CH_3CH_2O 4.20(q), N-**H** 5.35(s), phenyl proton 7.20—7.80(m). Found: C, 61.07; H, 6.40; N, 5.80%. Calcd for $C_{12}H_{15}NO_4$: C, 60.75; H, 6.37; N, 5.90%.

References

1) I. Wakeshima and I. Kijima, *Chem. Lett.*, **1972**, 325.
2) K. D. Bos, H. A. Budding, E. J. Bulten, and J. N. Noltes, *Inorg. Nucl. Chem. Lett.*, **9**, 961 (1973).
3) S. Gopinathan, C. Gopinathan, and J. Gupta, *Indian J. Chem.*, **11**, 1067 (1973).
4) P. F. R. Ewings, D. E. Fenton, and P. G. Harrison, *Inorg. Nucl. Chem. Lett.*, **10**, 43 (1974).
5) P. F. R. Ewings, P. G. Harrison, and D. E. Fenton, *J. Chem. Soc., Dalton Trans.*, **1975**, 821.
6) I. Wakeshima and I. Kijima, *Nippon Kagaku Kaishi*, **1974**, 536.
7) C. D. Schaeffer and J. J. Zuckerman, *J. Am. Chem. Soc.*, **96**, 7160 (1974).
8) D. H. Harrison and M. F. Lappert, *J. Chem. Soc., Chem. Commun.*, **1974**, 895.
9) M. Veith, *Angew. Chem.*, **87**, 287 (1975).
10) P. Foley and M. Zeldin, *Inorg. Chem.*, **14**, 2264 (1975).
11) I. Wakeshima and I. Kijima, *Bull. Chem. Soc. Jpn.*, **48**, 953 (1975).
12) *Beilstein*, **26**, 250.
13) I. Wakesima, H. Suzuki, and I. Kijima, *Bull. Chem. Soc. Jpn.*, **48**, 1069 (1975).
14) I. Wakeshima, Y. Hara, and I. Kijima, 24th National Meeting of the Chemical Society Japan, Osaka, April 1971: **3**, 1205.

Syntheses of Unsymmetrical Sulfides and Bis(alkylthio)methanes from Diphenylphosphinodithioate Esters

Koshiro GODA, Fumito HANAFUSA, and Naoki INAMOTO

Department of Chemistry, Faculty of Science, The University of Tokyo, Hongo, Tokyo 113

(Received June 7, 1977)

Unsymmetrical sulfides were prepared by the reactions of diphenylphosphinodithioate esters with organolithiums in tetrahydrofuran (THF) at −78 °C or at room temperature in fairly good or excellent yields. Similarly, methylene bis(diphenylphosphinodithioate) gave bis(alkylthio)methanes by reactions with organolithiums in good yields. The use of bad-smelling thiols is avoided and the phosphorus part can be recycled after sulfurization and esterification. Allyl diphenylphosphinodithioate gave allylbenzene *via* $S_N2(C)$ reaction upon treatment with phenylmagnesium bromide in refluxing THF.

The reaction of alkyl diphenylphosphinodithioates (**1**) with butyllithium affords [Ph_2PS]Li and butyl sulfides by $S_N2(S)$ mechanism.[1]

$$Ph_2P(S)SR + R'Li \longrightarrow [Ph_2PS]Li + R\text{-}S\text{-}R' \quad (1)$$
1 **2**

This is utilized for the preparation of unsymmetrical sulfides (**2**).[2] This paper describes in detail the syntheses of unsymmetrical sulfides and bis(alkylthio)-methanes from diphenylphosphinodithioate esters.

Preparation of Unsymmetrical Sulfides. The esters (**1**) were allowed to react with organolithiums in tetrahydrofuran (THF) at −78 °C or at room temperature for 0.5 h. After the reaction mixture had been quenched with water, the yields of sulfides (**2**) obtained were determined by gas chromatography (GLC) or by isolation with dry column chromatography (DCC). The results are summarized in Table 1.

In the case of the allyl ester, the yield of the corresponding sulfide is comparatively low, probably because of competitive Wittig type rearrangement.[1]

The reactions with Grignard reagents in refluxing THF, except for phenylmagnesium bromide, gave the corresponding sulfides (**2**) only in low yields accompanied by recovery of the starting esters (**1**).[1] The reaction of the allyl ester with phenylmagnesium bromide in THF at room temperature afforded allyldiphenylphosphine sulfide (**3**) (7%) and diphenylphosphinodithioic acid (19%) accompanied by 41% of unchanged ester and a small amount of allylbenzene. In refluxing THF, the reaction gave allylbenzene (70%) and diphenylphosphinodithioic acid (89%) together with a trace amount of triphenylphosphine sulfide ($S_N2(P)$ reaction).

TABLE 1. REACTIONS OF **1** WITH ORGANOLITHIUMS IN THF

R	R′	Reaction temp (°C)	**2** (%)[a]
Me	Bu	−78	98
	Ph	r. t.	95
Et	Bu	−78	88
	Ph	r. t.	89
Ph	Bu	−78	95[b]
	Ph	r. t.	90
$PhCH_2$	Bu	−78	86
	Ph	−78	79[b]
	Ph	r. t.	60[b]
CH_2=$CHCH_2$	Bu	−78	63
	Ph	r. t.	72[b]

a) Determined by GLC unless noted otherwise. b) Isolated by DCC.

The formation of allylbenzene and **3** is illustrated as follows:

$$Ph_2P(S)SCH_2CH{=}CH_2 + PhMgBr \xrightarrow{S_N2(C)} Ph_2P(S)SMgBr + PhCH_2CH{=}CH_2$$

$$Ph_2P(S)\bar{S}CHCH{=}CH_2 \xrightarrow[\text{rearr.}]{\text{Wittig}} Ph_2P(S)CH(S^-)CH{=}CH_2 \xrightarrow{-S} \xrightarrow{H^+} Ph_2P(S)CH_2CH{=}CH_2$$
3

Namely, phenylmagnesium bromide attacks the α-carbon atom of the ester in $S_N2(C)$ manner at higher temperature to afford allylbenzene, while it abstracts the α-hydrogen atom in the ester at room temperature to form **3** through Wittig type rearrangement followed by desulfurization by a small amount of [Ph_2PS]MgBr produced according to Eq. 1.

A possibility of $S_N2'(C)$ mechanism for the formation of allylbenzene can be excluded based on the results of the reactions of phenylmagnesium bromide with the 2-butenyl and 1-methylallyl esters, as shown below.

$$Ph_2P(S)SCH_2CH{=}CHCH_3 + PhMgBr \longrightarrow PhCH_2CH{=}CHCH_3 + PhCH(CH_3)CH{=}CH_2 \quad (94 : 6)$$
$$+ Ph_2P(S)SH$$

$$Ph_2P(S)SCH(CH_3)CH{=}CH_2 + Ph_2P(S)SCH_2CH{=}CHCH_3 \quad (54 : 46)$$
$$\xrightarrow{PhMgBr} PhCH(CH_3)CH{=}CH_2 + PhCH_2CH{=}CHCH_3 \quad (44 : 56)$$
$$+ Ph_2P(S)SH$$

However, the $S_N2'(C)$ mechanism is not completely ruled out.

Thus, the Grignard reagents can not be used for the preparation of **2**, because of the low thiophilicity.[1]

Unsymmetrical sulfides are usually prepared by the reactions of alkali thiolates with alkyl halides,[3] alkyl phosphinates,[4] or dialkyl carbonates,[5] and by the reaction of 1-methyl-2-fluoropyridinium salt with alcohols and then thiols.[6] On the other hand, the present method can be carried out without the use of bad-smelling thiol, and [Ph_2PS]Li produced in the reaction can be reconverted into diphenylphosphinodi-

Table 2. Reactions of **4** with RLi (at −78 °C in THF)

R	**5** (%)
Me	89[a]
Et	61[a]
Bu	99[b]
Ph	61[b]

a) By GLC. b) By isolation.

thioic acid, which is converted easily into the ester, by treatment with sulfur, indicating that the phosphorus part can be recycled.

Organosodiums can be used. For example, phenylsodium reacted with methyl and phenyl esters at room temperature to afford methyl phenyl sulfide and diphenyl sulfide in 67 and 82% yields, respectively.

Preparation of Bis(alkylthio)methanes. If methylene bis(diphenylphosphinodithioate) (**4**) is prepared from diphenylphosphinodithioic acid and dihalomethane, the preparation of bis(alkylthio)methanes (**5**) would be possible as follows.

$$2Ph_2P(S)SH + CH_2X_2 \longrightarrow (Ph_2P(S)S)_2CH_2 \xrightarrow{2RLi} (RS)_2CH_2$$

4 **5**

Compound **4** was prepared from dibromo- and diiodomethanes in 14 and 67% yields, respectively, but not from dichloromethane.

The reactions of **4** with organolithiums are summarized in Table 2. The yields of **5** are good or excellent.

When **4** is allowed to react with more than three moles of organolithium and the reaction mixture is treated with alkyl halides, 1,1-bis(alkylthio)alkanes can be prepared by one-pot reaction (see Experimental), which can be easily converted into the corresponding aldehydes.

It is interesting that the diphenylphosphinodithioates act as alkylthio-transfer reagent.

Experimental

Materials. Methyl-, ethyl-, and phenyllithiums were prepared by the method of Gilman *et al.*[7] Alkyl diphenylphosphinodithioates (**1**) were prepared by the methods described in the preceding paper.[1] 1-Phenyl-2-butene and 3-phenyl-1-butene were prepared by the reported method[8] and purified by fractional distillation.

The reactions were carried out under nitrogen or argon.

Preparation of Unsymmetrical Sulfides. General Procedure. Organolithium (*ca.* 3 mmol) was added to a solution of **1** (*ca.* 1.5 mmol) in THF (20 ml) cooled at −78 °C and the mixture was stirred for 0.5 h. After addition of water (0.5 ml) to a small amount of the reaction mixture was added an internal reference such as mesitylene, naphthalene, butyl ethyl sulfide, or phenanthrene. The yield of sulfide (**2**) was determined by GLC (H 523 on Diasolid at 100—150 °C). The sulfide was isolated from the residual part of the reaction mixture by DCC (SiO_2, CCl_4).

Reaction of [Ph_2PS]Li with Sulfur. To the reaction mixture from phenyl diphenylphosphinodithioate (0.99 g, 3.0 mmol) and butyllithium (3.0 mmol) in THF (100 ml) was added an excess amount of sulfur, and the mixture was allowed to stand overnight. After addition of 10% aq sodium hydroxide, the reaction mixture was washed with benzene in order to extract sulfide, and filtered for removal of excess sulfur. The filtrate was acidified with hydrochloric acid and extracted with benzene to give diphenylphosphinodithioic acid (0.635 g, 84%).

Reaction of Allyl Diphenylphosphinodithioate with Phenylmagnesium Bromide. 1) A mixture of the ester (1.12 g, 3.8 mmol) in THF (10 ml) and phenylmagnesium bromide (10.6 mmol) in THF (15 ml) was heated for several minutes and then stirred for 4 h at room temperature. The reaction mixture was acidified with dilute hydrochloric acid and extracted with benzene. The benzene extract was washed with aq sodium hydroxide. The aq alkaline extract gave diphenylphosphinodithioic acid (0.19 g, 19%) after acidification. The benzene solution was treated with DCC (SiO_2, AcOEt). The unchanged ester (0.45 g, 41%) was recovered and allyldiphenylphosphine sulfide (69 mg, 7%) was obtained as an oily substance. IR (neat): 1590 (C=C), 1430, 1110 (P–Ph), and 640 cm^{-1} (P=S); NMR (CCl_4): δ 3.30 (dd, J_{PCH}=16 Hz, J_{HH}=6 Hz, 2H, PCH_2), 4.85—5.15 (m, 1H, CH=C), 5.25 (d, J_{HH}=5 Hz, 1H, CH), 5.55—6.10 (m, 1H, –CH=), and 7.25—8.10 (m, 10H, 2P–Ph); MS: *m/e* 258 (M^+, 23%) and 217 (Ph_2PS^+, 100).

Found: C, 70.00; H, 6.12%. Calcd for $C_{15}H_{15}PS$: C, 69.74; H, 5.85%.

2) A mixture of the ester (0.345 g, 1.2 mmol) and phenylmagnesium bromide (2 mmol) in THF (12 ml) was refluxed for 2 h. The yield of allylbenzene was determined to be 70% by GLC using dibutyl ether as an internal reference. Ethyl acetate was added to the reaction mixture, and the mixture was washed with aq sodium hydroxide. The aq layer was acidified with hydrochloric acid and extracted with ethyl acetate to give diphenylphosphinodithioic acid (0.264 g, 89%). A trace amount of triphenylphosphine sulfide was isolated by DCC of the first ethyl acetate solution.

Preparation of 2-Butenyl Diphenylphosphinodithioate. A mixture of diphenylphosphinodithioic acid (25 g, 0.10 mol) and sodium hydroxide (4 g, 0.10 mol) in THF (50 ml) was stirred at room temperature for 1.5 h. 2-Butenyl chloride (9.3 g, 0.10 mol) was then added, and the mixture was refluxed for 2 h. After removal of THF, the residue was extracted with benzene to give crude ester (30.0 g, 98%) as oil, which was purified by means of DCC, because of the decomposition on vacuum distillation. IR (neat): 1420, 1100 (P–Ph), and 650 cm^{-1} (P=S); NMR ($CDCl_3$): δ 1.52 (d, J=6 Hz, 3H), 3.55 (dd, J_{PSCH}=14 Hz, J=6 Hz, 2H), 5.50 (m, 2H), and 7.3—8.3 (m, 10H).

Reaction of 2-Butenyl Diphenylphosphinodithioate with Phenylmagnesium Bromide. A mixture of the ester (1.16 g, 3.60 mmol) and phenylmagnesium bromide (5 mmol) in THF (30 ml) was refluxed for 4.5 h. After treatment with 0.2 M hydrochloric acid, the reaction mixture was extracted with carbon tetrachloride. The carbon tetrachloride extract was further extracted with aq sodium hydroxide. The aqueous layer afforded diphenylphosphinodithioic acid (0.21 g, 22%) after acidification and extraction with benzene. A mixture of 1-phenyl-2-butene and 3-phenyl-1-butene (94 : 6) was obtained from the carbon tetrachloride layer in 71% yield (by GLC).

Reaction of Sodium Diphenylphosphinodithioate with 1-Methylallyl Chloride Followed by Reaction with Phenylmagnesium Bromide. A mixture of diphenylphosphinodithioic acid (17.1 g, 68 mmol) and sodium hydroxide (3 g, 75 mmol) in THF (50 ml) was stirred at room temperature for 1.5 h. After addition of 1-methylallyl chloride (6.5 g, 72 mmol) the mixture was refluxed for 3 h. After removal of THF the residue was

extracted with benzene and the dried benzene extract was evaporated to afford a mixture of 1-methylallyl and 2-butenyl diphenylphosphinodithioates (54 : 46 by NMR), yield 4.2 g (20%). NMR ($CDCl_3$; due to 1-methylallyl ester): δ 1.38 (d, J=6 Hz), 3.9—4.4 (m), 4.9—5.2 (m), 5.4—6.0 (m), and 7.3—8.3 (m). The ratio of both esters was determined on the basis of the peak areas at δ 3.55 (due to 2-butenyl ester, NMR data of which have been described already) and 3.9—4.4 (due to 1-methylallyl ester). Since separation of the two esters was unsuccessful, the mixture was used for the following reaction.

A solution of the ester mixture (0.72 g, 2.40 mmol) and phenylmagnesium bromide (3.5 mmol) in THF (30 ml) was refluxed for 4 h and the reaction mixture was subjected to the treatment similar to that in the reaction of 2-butenyl ester. Diphenylphosphinodithioic acid and a mixture of 1-phenyl-2-butene and 3-phenyl-1-butene (56 : 44 by GLC) were obtained in 57 and 51% yields, respectively.

Preparation of **4**. *1) From Dibromomethane*: Dibromomethane (25 g, 0.14 mol) was added to a mixture of diphenylphosphinodithioic acid (30 g, 0.12 mol) and sodium hydroxide (5 g, 0.13 mol) in ethanol (200 ml), and the mixture was refluxed for 3 h. The reaction mixture was washed with water and extracted with benzene. After evaporation of benzene from the benzene extract, a small amount of ethanol was added to the residual oil and the mixture was allowed to stand at 0 °C. The resulting crystals were collected and recrystallized from acetonitrile, mp 90—91 °C, yield 4.4 g (14%). IR (KBr): 1425, 1095 (P–Ph), 650 (P=S), and 520 cm^{-1} (P–S); ^{1}H-NMR ($CDCl_3$): δ 4.56 (t, J_{PSCH}=16 Hz, 2H, CH_2) and 7.10—8.10 (m, 20H, 4Ph); ^{31}P-NMR (THF): δ_P −63.8 ppm.

Found: C, 58,32; H. 4.33; S, 24.86%. Calcd for $C_{25}H_{22}P_2S_4$: C, 58.57; H, 4.33; S, 25.02%.

2) From Diiodomethane: Diiodomethane (25 g, 0.09 mmol) was added to a mixture of diphenylphosphinodithioic acid (45 g, 0.18 mol) and sodium hydroxide (7.4 g, 0.19 mol) in THF (200 ml), and the mixture was refluxed for 16 h under stirring. A similar treatment of the reaction mixture gave 32 g (67%) of **4**, mp 90—91 °C.

Reaction of **4** *with Butyllithium*. A typical procedure is as follows.

Butyllithium (3.0 mmol) in hexane (2 ml) was added to a solution of **4** (0.425 g, 0.83 mmol) in THF (15 ml) at —78 °C, and the mixture was stirred for 15 min. After addition of methyl iodide (1 ml), the reaction mixture was subjected to DCC (SiO_2, CCl_4) to give methyl diphenylphosphinodithioate (0.36 g, 85%) and bis(butylthio)methane (0.16 g, 99%); NMR (CCl_4): δ 0.91 (t, J_{HH}=6 Hz, 6H, 2Me), 1.53 (m, 8H, $4CH_2$), 2.63 (t, J_{HH}=7 Hz, 4H, $2SCH_2$), and 3.68 (s, 2H, S–CH_2–S).

One-Pot Synthesis of 1,1-Bis(phenylthio)ethane from **4**. To a solution of **4** (1.14 g, 2.2 mmol) in THF (20 ml) was added phenyllithium (10 mmol) in ether (10 ml) at −78 °C and the mixture was stirred at this temperature for 30 min. After addition of methyl iodide (0.7 ml, 10 mmol) at 0 °C, the mixture was stirred for 20 min and subjected to DCC (SiO_2, CCl_4) to give 1,1-bis(phenylthio)ethane (0.21 g, 41%); NMR (CCl_4): δ 1.68 (d, J=7 Hz, 3H, $CHC\underline{H}_3$), 4.62 (q, J=7 Hz, 1H, C$\underline{H}$Me), and 7.20—7.60 (m, 10H, 2Ph), and methyl phenyl sulfide (50 mg).

Reactions of Phenylsodium. *1) With Methyl Diphenylphosphinoditioate*: Phenylsodium (8 mmol) in THF (3 ml) was added to a solution of the ester (0.54 g, 2.0 mmol) in THF (15 ml) and the mixture was stirred at room temperature for 1 h. After addition of methanol, the reaction mixture was evaporated and analyzed by GLC. The yield of methyl phenyl sulfide was 67%.

2) With Phenyl Diphenylphosphinoditioate: Phenylsodium (8 mmol) in THF (3 ml) was added to a solution of the ester (0.49 g, 1.5 mmol) in THF (15 ml) and the mixture was stirred at room temperature for 1 h. After addition of methanol, diphenyl sulfide (0.23 g, 82%) was isolated from the reaction mixture by DCC (SiO_2, $CHCl_3$, and then SiO_2, CCl_4).

References

1) K. Goda, R. Okazaki, K. Akiba, and N. Inamoto, *Tetrahedron Lett.*, **1976**, 181; *Bull. Chem. Soc. Jpn.*, **51**, 260 (1978).

2) For preliminary report see: K. Goda and N. Inamoto, *Chem. Lett.*, **1975**, 1009.

3) a) S. R. Sandler and W. Karo, "Organic Functional Group Preparation," Academic Press, New York (1968), p. 486; b) For use of phase-transfer catalysis see: A. W. Herriott and D. Picker, *Synthesis*, **1975**, 447.

4) S. Savignac and P. Coutrot, *Synthesis*, **1974**, 818.

5) Y. Tamura, T. Saito, H. Ishibashi, and M. Ikeda, *Synthesis*, **1975**, 641.

6) T. Mukaiyama, S. Ikeda, and S. Kobayashi, *Chem. Lett.*, **1975**, 1159.

7) H. Gilman, E. A. Zoellner, and W. M. Selby, *J. Am. Chem. Soc.*, **55**, 1252 (1933).

8) K. W. Wilson, J. D. Roberts, and W. G. Young, *J. Am. Chem. Soc.*, **71**, 2019 (1949).

The Template-directed Synthesis of Oligonucleotide. II.[1] The Interactive Properties of Nucleic Acid Base-binding Poly(4-vinylpyridine) and Its Related Compound with Nucleotides

Takeo SHIMIDZU,* Akira MURAKAMI, Yoshiyuki KONISHI, and Manabu MINAMI

Department of Hydrocarbon Chemistry, Faculty of Engineering, Kyoto University, Yoshida, Sakyo-ku, Kyoto 606

(Received June 11, 1977)

The interactive properties of positively charged polynucleotide analogs, such as nucleic acid base-binding poly(4-vinylpyridine)s and their derivatives, with nucleotides have been investigated. The interactions of the positively charged polynucleotide analogs such as *N*-alkylated poly(4-vinylpyridine)s with 9-(ω-chloroalkyl)adenine and of *N*-alkylated poly(4-vinylpyridine) with 1-(2-bromoethyl)thymine with nucleotides were attributed predominantly to a base-base stacking under reinforcement by the coulombic attractive force. The purine-purine base interaction was found to be stronger than the purine-pyrimidine and the pyrimidine-pyrimidine interactions. The interaction was reduced by an increase in the ionic strength. The higher the charge density of the nucleotide was, the stronger was the interaction observed. On the other hand, a cross-linked positively charged polynucleotide analog such as *N*-alkylated cross-linked poly(4-vinylpyridine) with 9-(2-chloroethyl)adenine showed considerable selective interaction with the complementary nucleotide, uridine-5′-phosphate (pU), in both aqueous and pyridine solutions.

Various kinds of polynucleotide analogs have been prepared by the literature procedures.[2–12] Template-directed syntheses of oligonucleotide have also been attempted using neutral polynucleotide analogs such as poly(1-vinyluracil)[13] and oligonucleotide whose phosphoric acid moiety was blocked.[1] In general, interactions between the condensing nucleotide and the polynucleotide analogs are not very strong except for the interaction between the nucleotide and the polynucleotide analog with a positive charge. The polynucleotide analog with a positive charge is noteworthy for its coulombic interactive force with the condensing nucleotide. One of the polynucleotide analogs with a positive charge has been materialized by Okubo and Ise with poly(4-vinylpyridine) *N*-alkylated with a halogenoalkylated nucleic acid base;[14,15] they have also reported a noteworthy study of the interactions with polynucleotide and a nucleic acid base. The contribution of the coulombic force to the interaction is remarkable. However, the base-base stacking takes place predominantly in the interaction.

On the template-directed condensation of nucleotide, the most essential requirement for the template is a selective interaction between the template molecule and the condensing nucleotide. In this paper, we will describe our studies of the interactive properties of nucleotides with nucleic acid base binding poly(4-vinylpyridine)s and their derivatives.

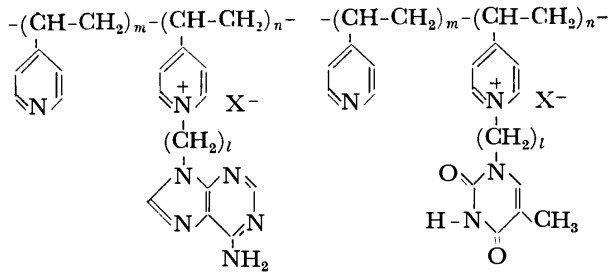

$l=2,3,4,6$
(PVP)-C$_l'$-Ade$_n$

$l=2$
(PVP)-C$_l'$-Thy$_n$

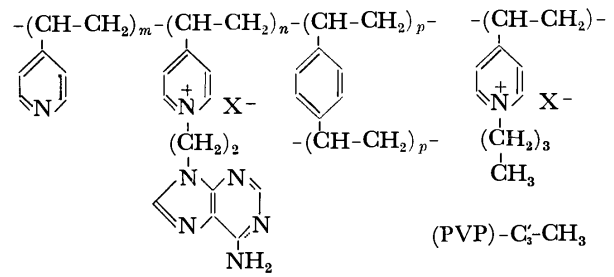

$p=2$
$n=61$
[PVP]$_p$-C$_2'$-Ade$_n$

(PVP)-C$_3'$-CH$_3$

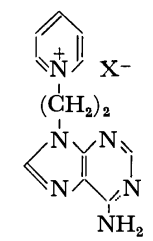

Py-C$_2'$-Ade

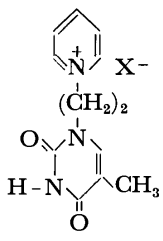

Py-C$_2'$-Thy

Results and Discussion

Nucleic acid base-binding poly(4-vinylpyridine)s were synthesized by the alkylation of poly(4-vinylpyridine) with the halogenoalkyl derivatives of nucleic acid bases. The nucleic acid base-binding poly(4-vinylpyridine)s and their related compounds adopted in the present paper are shown on the right.

The polymers, nucleic acid base-binding poly(4-vinylpyridine)s (PVP)–C$_l'$–Ade$_n$ and (PVP)–C$_l'$–Thy$_n$ and their related compounds, were soluble in water and interacted with nucleotides. The solution of the nucleic acid base-binding poly(4-vinylpyridine) followed Beer's law in the range from 10^{-5} mol/dm^3 to 8×10^{-4} mol/dm^3. No conformational change which affects an intramolecular base-base interaction occurred in the present concentration range.

For example, the mixing curve of (PVP)–C$_2'$–Ade$_{48}$ and adenosine-5′-phosphate, pA, is shown in Fig. 1. The hypochromicity was calculated at the wavelength where the differences in the UV absorbances of the solu-

Table 1. Maximum hypochromicities in the mixing curves of (PVP)-C_l'-Ade_n, (PVP)-C_l'-Thy_n and nucleoside

Analog	Nucleoside	Hypochromicity %	Ratio[a]	Wavelength[b] nm	Concentration[c] mol/dm³
(PVP)-C_2'-Ade_{48}	Ado	1.7±0.2	1 : 2.1	260	4.8×10^{-4}
	Guo	1.0±0.1	1 : 5.5	255	4.8×10^{-4}
	Urd	1.8±0.2	1 : 0.5	261	4.8×10^{-4}
(PVP)-C_2'-Ade_{52}	Ado	1.6±0.2	1 : 2.0	260	5.0×10^{-4}
	Guo	1.0±0.2	1 : 3.0	255	5.0×10^{-4}
	Thy	2.2±0.3	1 : 0.7	263	5.0×10^{-4}
(PVP)-C_2'-Thy_{100}	Ado	5.7±0.3	1 : 0.7	260	6.7×10^{-4}
	Guo	6.2±0.3	1 : 0.4	258	6.7×10^{-4}
	Cyd	1.9±0.2	1 : 2.9	268	6.7×10^{-4}
	Urd	2.1±0.2	1 : 0.7	263	6.7×10^{-4}

a) The ratio of the polynucleotide analog and nucleoside where the maximum hypochromicity was given. b) The wavelength where the hypochromicity was calculated. c) Concentration shows the total concentration of nucleic acid bases in the mixture.

Table 2. Maximum hypochromicities in the mixing curves of (PVP)-C_l'-Ade_n, (PVP)-C_l'-Thy_n and nucleotide[a]

Analog	Nucleotide	Hypochromicity %	Ratio[b]	Wavelength[c] nm	Concentration[d] mol/dm³
(PVP)-C_2'-Ade_{48}	pA	11.8±0.2	1 : 0.6	260	4.8×10^{-4}
	pG	7.5±0.2	1 : 0.5	255	4.8 ± 10^{-4}
	pC	6.7±0.2	1 : 2.2	265	4.8 ± 10^{-4}
	pU	5.4±0.2	1 : 2.5	260	4.8 ± 10^{-4}
	ATP	ppt.	—	—	4.8 ± 10^{-4}
(PVP)-C_2'-Ade_{52}	pA	10.9±0.3	1 : 0.8	260	5.7×10^{-4}
	pG	7.2±0.3	1 : 1.5	255	5.7×10^{-4}
	pC	7.0±0.3	1 : 0.9	265	5.7×10^{-4}
	pU	5.2±0.3	1 : 0.5	260	5.7×10^{-4}
(PVP)-C_3'-Ade_{56}	pA	9.8±0.3	1 : 1.1	260	5.7×10^{-4}
	pC	6.9±0.3	1 : 0.8	265	5.7×10^{-4}
	pU	6.0±0.3	1 : 0.6	260	5.7×10^{-4}
(PVP)-C_4'-Ade_{39}	pA	9.7±0.3	1 : 1.3	260	5.7×10^{-4}
	pC	7.0±0.3	1 : 0.6	265	5.7×10^{-4}
	pU	6.1±0.3	1 : 0.4	260	5.7×10^{-4}
(PVP)-C_6'-Ade_{47}	pA	10.0±0.3	1 : 1.1	260	5.7×10^{-4}
	pC	7.0±0.3	1 : 0.8	265	5.7×10^{-4}
	pU	5.9±0.3	1 : 0.4	260	5.7×10^{-4}
(PVP)-C_2'-Thy_{100}	pA	10.9±0.4	1 : 0.8	263	6.7×10^{-5}
	pG	9.0±0.4	1 : 4.0	259	6.7×10^{-5}
	pC	4.3±0.4	1 : 1.0	269	6.7×10^{-5}
	pU	5.3±0.4	1 : 0.4	264	6.7×10^{-5}
	ATP	ppt.	—	—	6.7×10^{-5}

a) Disodium salts of nucleotides were used. b) This shows the ratio of the polynucleotide analog and nucleotide where the maximum hypochromicity was given. c) This shows the wavelength where the hypochromicity was calculated. d) Concentration shows the total concentration of nucleic acid bases in the mixture.

tion mixtures were most extended. However, the magnitude of the hypochromicity was effectively the same as that observed at 260 nm. The hypochromicity is seen as resulting from interaction between the nucleic acid bases of two molecules. In the present paper, the maximum hypochromicities are listed in the Tables. The maximum hypochromicities were not given at a 1 : 1 molar ratio of those two molecules.

Tables 1 and 2 show the maximum hypochromicities in the mixing curves of (PVP)–C_l'–Ade_n and nucleoside, (PVP)–C_l'–Thy_n and nucleoside, (PVP)–C_l'–Ade_n and nucleotide, and (PVP)–C_l'–Thy_n and nucleotide. Polynucleotide analogs, such as (PVP)–C_l'–Ade_n (l=2, 3, 4, 6) and (PVP)–C_l'–Thy_n (l=2), had a stronger interaction with a purine base than with a pyrimidine base. This tendency is similar to the result which was obtained by Okubo *et al.*[15] in the cases of the interactions of the nucleic acid base-binding poly(4-vinylpyridine) both with polynucleotide and with a nucleic acid base. It was also observed that the interaction of the poly-

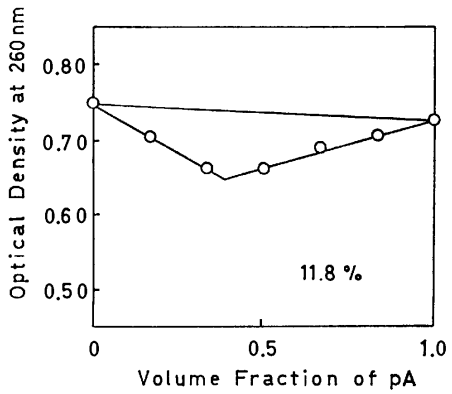

Fig. 1. Apparent hypochromicity in the mixing curve of (PVP)-C_2'-Ade_{48}-pA mixture.
Concentration, 4.8×10^{-4} mol/dm^3; temp, 15 °C.

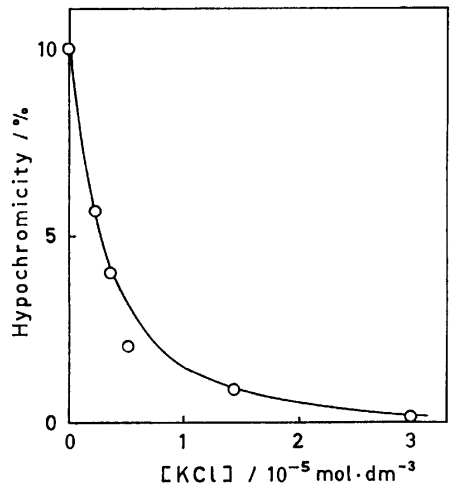

Fig. 2. Influence of salt on the apparent hypochromicity of (PVP)-C_2'-Thy_{100}-pA mixture.
Concentration, 6.7×10^{-5} mol/dm^3; temp, 15 °C; (PVP)-C_2'-Thy_{100}: pA=1 : 1.

nucleotide analog with nucleotide was stronger than that with nucleoside. On the interaction of the polynucleotide analog with adenosine triphosphate, ATP, a precipitation took place. Generally, a UV hypochromicity is not observed in mixtures of polynucleotide and nucleotide in the present concentration range. Such a stronger interaction suggests a dominant contribution of a coulombic force in the interaction between a polynucleotide analog with a positive charge and a nucleotide with a negative charge. Even in the case of the interaction of the polynucleotide analog with nucleoside, no repulsive coulombic force takes place. In neither cases was the quantitative ratio of the bases in the interaction, which was shown as the ratio at the maximum hypochromicity being given, always unity. This fact shows that the hydrogen-bond formation between complementary bases is not main force participating in the intermolecular interactions of the bases; rather, it suggests that a hydrophobic interaction is overwhelming. The influence of the side-chain length of the polynucleotide analog, (PVP)-C_l'-Ade_n, in the interaction between (PVP)-C_l'-Ade_n and nucleotide was not obvious where the length, l was below 6.

Table 3. pH dependence of apparent hypochromicities in the mixing curve of (PVP)-C_2'-Ade_{48} and pA[a)]

pH	4.0	5.0	5.5
Hypochromicity/%	1.8	2.4	11.8

(PVP)-C_2'-Ade_{48}: pA=1 : 0.6; Wavelength, 260 nm; concn, 4.8×10^{-4} mol/dm^3.
a) Disodium salt of pA was used.

Table 4. Apparent hypochromicities in the mixing curves of (PVP)-C_3'-CH_3 and nucleotide[a)]

Analog	pA	pU	ATP
(PVP)-C_3'-CH_3	1.5	0.6	15.8

Concn, 6.7×10^{-4} mol/dm^3.
a) Disodium salts of nucleotides were used.

Table 3 shows the pH dependence of the interaction of (PVP)-C_2'-Ade_{48} with adenosine-5'-phosphate, pA. A decrease of the pH of the solution made the maximum hypochromicity decrease. This result can be explained as follows; the lower pH makes the dissociation of the phosphate group in the nucleotide, pA, decrease and the amino group in the adenine moiety protonate, followed by a repulsion between the positively charged amino group and the positively charged (PVP)-C_2'-Ade_{48} upon the interaction.

In general, the addition of salt to the solution reduces the coulombic interaction of charged molecules. Figure 2 shows the influence of KCl added to the solution of the maximum hypochromicity of the (PVP)-C_2'-Thy_{100}-pA mixture. An increase in the ionic strength made the hypochromicity decrease. This shows that the interaction between the polynucleotide analog and nucleotide is governed by the coulombic attractive force.

Table 4 shows the maximum hypochromicity in the mixing curve of (PVP)-C_3'-CH_3 and nucleotide. In the case of (PVP)-C_3'-CH_3-monoculeotide, the magnitude of the hypochromicity was low. This result indicates that the interaction among the nucleotides which are concentrated in the vicinity of the positively charged polynucleotide analog can scarecely be evaluated. The result also shows that it is not necessary to take the interaction between the pyridinium moiety and the nucleotide into account in considering the hypochromicity. On the other hand, the certain magnitude of the hypochromicity for (PVP)-C_3'-CH_3 and ATP suggests that there exists a stacking among the ATPs concentrated at the cationic (PVP)-C_3'-CH_3. The distinction between the nucleotides and the ATP may be due to the charge density following its concentration.

The monomeric analogs of such polynucleotide analogs as Py-C_2'-Ade and Py-C_2'-Thy all have a single cationic charge. Table 5 shows the muximum hypochromicity in the mixing curve of the monomeric analogs and the nucleotides. The hypochromicity was not observed in the single-single charge system, although the two species were oppositely charged. On the other hand, a definite interaction between the monomeric

Table 5. Apparent hypochromicities in the mixing curves of Py-C_2'-Ade, Py-C_2'-Thy and nucleotide[a)]

Mono. analog	pA	pU	ATP
Py-C_2'-Ade	0	0	1.0[b)]
Py-C_2'-Thy	0	0	1.0[b)]

Concn, 6.7×10^{-4} mol/dm^3.
a) Disodium salts of nucleotides were used. b) [Py-C_2'-Ade]/[ATP] and [Py-C_2'-Thy]/[ATP] were 4.2 and 5.2, respectively.

Table 6. Selective adsorption of nucleotide on [PVP]$_2$-C_2'-Ade$_{61}$ in aqueous solution

Nucleotide mmol	H_2O cm^3	Adsorbed nucleotide mmol
pA (0.50)	1.0	pA (0.19)
pU (0.50)	1.0	pU (0.17)
pA (0.50), pU (0.50)	1.0	pA (0.07), pU (0.12)
pA (0.50), pU (0.50), pC (0.50)	2.0	pA (0.03), pU (0.12), pC (0.05)

[PVP]$_2$-C_2'-Ade$_{61}$, 2.5×10^{-4} mol equiv; Column, 2 mm id; Eluent (H_2O), 20 cm^3.

Table 7. Selective adsorption of nucleotide on [PVP]$_2$-C_2'-Ade$_{61}$ in pyridine

Nucleotide mmol	Pyridine cm^3	Adsorbed nucleotide mmol
pA (0.50)	1.0	pA (0.20)
pU (0.50)	1.0	pU (0.20)
pA (0.50), pU (0.50)	1.0	pA (0.08), pU (0.16)
pA (0.50), pU (0.50), pC (0.50)	1.0	pA (0.04), pU (0.15), pC (0.05)

Eluent (pyridine), 20 cm^3: The other conditions are the same as Table 6.

analogs and ATP, which has a multi-charge, was observed. This result suggests that an effective interaction requires the charge of one interactive species to be more than unity, at least.

The nucleic acid base-binding cross-linked poly(4-vinylpyridine) such as [PVP]$_2$–C_2′–Ade$_{61}$ was synthesized by the reaction of 9-(2-chloroethyl)adenine and poly(4-vinylpyridine), which had been cross-linked by divinylbenzene. Tables 6 and 7 show the adsorptions of nucleotides on [PVP]$_2$–C_2′–Ade$_{61}$ in water and in pyridine, respectively. Compared with the above-described water-soluble polynucleotide analogs such as (PVP)–C_l'–Ade$_n$ and (PVP)–C_l'–Thy$_n$, the [PVP]$_2$–C_2′–Ade$_{61}$ had a considerable tendency to interact with the complementary nucleotide. In both solvent systems, the total amount of the adsorbed nucleotides on the [PVP]$_2$–C_l'–Ade$_{61}$ was constant, independent of the kind of nucleotide. That is, the total amount of the nucleotide adsorbed depended on the total number of charges in the [PVP]$_2$–C_2′–Ade$_{61}$. The selectivity in the adsorption as the complementary interaction rose and appeared to be marginal when more than one nucleotides were used. The order of the addition of the nucleotide did not affect the selectivity in the adsorption. This means that the adsorption is reversible. The occurrence of the considerable complementary base-base interaction in this case is important in connection with the template molecule in the template-directed synthesis of oligonucleotide. The formation of the cross-linked structure is preferable to the complementary base-base interaction, though it gives a heterogeneous reaction system. It is though that a matrix which is formed by the cross-linked structure is advantageous for the stability of the hydrogen-bond formation. The adsorbed nucleotide can be eluted with a concentrated salt solution. These properties suggest that the nucleic acid base-binding cross-linked poly(4-vinylpyridine) is useful for the template-directed synthesis of oligonucleotide and for affinity chromatography.

Experimental

UV Measurements. Standardized solutions of the polynucleotide analogs, nucleotides, their analogs, and nucleosides were mixed in varying proportions. The solutions were not buffered. The mixtures were stored for periods of up to 6 h at 5 °C, until no further optical density change occurred. UV measurements were then carried out on Hitachi EPS-3T spectrophotometer at 15 °C. The hypochromicity was calculated according to the following equation:[18)]

$$\text{Hypochromicity } (\%) = \left(1-\frac{I_{a+b}}{mI_a+nI_b}\right)\times 100,$$

where m and n are the volume fractions of the a and b solutions and where I_a, I_b, and I_{a+b} are the absorbances of solutions of the a, the b, and the mixture solution, respectively.

Alkylating Reagents. 9-(2-Chloroethyl)adenine was synthesized by a literature procedure.[16)]

All the 9-(ω-chloroalkyl)adenines except 9-(2-chloroethyl)-adenine were synthesized by a literature procedure.[17)]

1-(2-Bromoethyl)thymine was synthesized by a modification of the procedure of Ueda *et al.*[16)] A mixture of 31.6 g (0.19 mol) of 1-(2-hydroxyethyl)thymine and 126 g (0.61 mol) of thionyl bromide, plus a few drops of pyridine, was heated under reflux for 45 min. Then the excess thionyl bromide was removed under reduced pressure, and the remainder was washed with water. The residual solid was extracted with chloroform in a Soxleht extractor. A white, powdery 1-(2-bromoethyl)thymine was obtained from the chloroform solution (18.1 g, 41 %); IR(KBr): 3000, 2330, 1710, 1663, 1360, 1280, 900, 515 cm^{-1}; R_f (2-propanol : concn NH_4OH : H_2O = 7 : 1 : 2, Whatman 3MM) : 0.72; Found: C, 35.57; H, 3.79; N, 11.94; Br, 32.13%. Calcd for $C_7H_9N_2O_2Br$: C, 36.07; H, 3.89; N, 12.02; Br, 34.29%.

Polynucleotide Analogs, (PVP)–C_l'–Ade$_n$ and (PVP)–C_l'–Thy$_n$. The alkylations of poly(4-vinylpyridine) were carried out using the corresponding ω-halogenoalkylated nucleic acid bases mentioned above, according to a literature procedure.[14)] The degree of alkylation was estimated by means of elementary analysis. The results are tabulated in Table 8.

Cross-linked Polynucleotide Analog, [PVP]$_2$–C_2'–Ade$_{61}$. Freshly distilled 4-vinylpyridine and 1.5 mol% of divinylbenzene (55% solution of ethylbenzene) were placed in a flask with a few seeds of cross-linked polystyrene. After the reaction mixture has then been kept at 60 °C for 1 day, a faint coral-reddish, porous popcorn polymer was obtained. The polymer was ground and thoroughly washed with ethanol. The degree of the cross-linkage was calculated to be 2 % by means of the C/N ratio in the elementary analysis (Found: C, 79.81; H, 7.27; N, 12.92%).

Two grams of the resulting polymer, 4.0 g of 9-(2-chloro-

Table 8. Results of the alkylation of poly(4-vinylpyridine) with halogenoalkylated nucleic acid bases

Alkylating reagent g		DMF cm³	Time h	Degree of alkylation %	λ_{max} nm
9-(2-Chloroethyl)adenine	1.0	1.5	73	48	261
9-(2-Chloroethyl)adenine	1.5	2.0	72	52	261
1-(2-Bromoethyl)thymine	11.8	10.8	72	100	267
9-(3-Chloropropyl)adenine	1.7	2.0	72	56	261
9-(4-Chlorobutyl)adenine	2.0	2.5	70	39	261
9-(6-Chlorohexyl)adenine	2.0	2.5	85	47	261

Poly(4-vinylpyridine) 0.5 g was used. React. temp, 95—100 °C. Products were washed with alcohol and ether, until no ultraviolet absorption was observed in the washings.

ethyl)adenine, and 7 cm³ of DMF were placed in a sealed bottle, and the mixture was heated at 80 °C with stirring for a week. The resulting material was thoroughly washed with hot ethanol and water. The degree of alkylation was calculated to be 63 % (*cf.* the pyridine moiety in the polymer) by the change in the C/N ratio in the elementary analysis from that of the starting polymer (Found: C, 60.50; H, 5.62; N, 24.59, Cl, 9.29%).

Poly(1-butyl-4-vinylpyridinium bromide), (PVP)–C_3'–CH_3.

Twenty-six cm³ of 4-vinylpyridine and 32 cm³ of butyl bromide were dissolved in 100 cm³ of benzene, and the mixture was heated at 50 °C with stirring for 115 h. A reddish violet solution resulted. The benzene was then removed, and the residue was dissolved in water, followed by dialysis. The resulting solution was lyophilized. A hygroscopic, faint yellow, powdery product was thus obtained (11.2 g).

1-[2-(Adenin-9-yl)ethyl]pyridinium Chloride, Py–C_2'–Ade.

In 2 cm³ of a freshly distilled pyridine, 0.11 g of 9-(2-chloroethyl)adenine was dissolved. The mixture was sealed under nitrogen and then heated in boiling water for 68 h. A white precipitate was filtered, washed with ethyl acetate, and then dried (46 mg); mp 290—291 °C, $\lambda_{max}^{H_2O}$, 260 nm; $\varepsilon_{max}^{H_2O}$, 1.63×10^4; Found: C, 52.16; H, 4.90; N, 30.30; Cl, 12.69%. Calcd for $C_{12}H_{13}N_6Cl$: C,52.08; H,4.74; N,30.37; Cl,12.81%.

1-[2-(Thymin-1-yl)ethyl]pyridinium Chloride, Py–C_2'–Thy.

In 5 cm³ of freshly distilled pyridine, 1.0 g of 1-(2-chloroethyl)thymine was dissolved. The mixture was then refluxed on a steam bath for 5 h. A white needle crystal was obtained after cooling. It was washed with ethanol and then dried (230 mg): $\lambda_{max}^{H_2O}$, 266 nm; $\varepsilon_{max}^{H_2O}$, 1.3×10^4; Found: C, 52.33; H, 5.34; N, 15.14; Cl, 13.15%. Calcd for $C_{12}H_{14}N_3O_2Cl$: C, 53.84; H, 5.27; N, 15.70; Cl, 13.24%.

Adosorption. One half mmol of nucleotide was dissolved in a certain amount of water and then placed on 100 mg (2.5×10^{-4} mol equiv) of the [PVP]$_2$–C_2'–Ade$_{61}$. The adsorption of the nucleotide on the [PVP]$_2$–C_2'–Ade$_{61}$ was completed within 1 h, with stirring. The whole mixture was then placed in a column whose inner diameter was 2 mm. Then the column was washed by the addition, drop by drop, of 20 cm³ of water for a 10 min period. The content of the nucleotide in the effluent was analyzed by paper chromatography and by liquid chromatography (Shimadzu-Dupont 830, Permaphase AAX). From the composition of the nucleotides in the effluents, the amounts of nucleotides adsorbed on the [PVP]$_2$–C_2'–Ade$_{61}$ were calculated. For the experiment in the pyridine-solution system, the pyridinium form of the nucleotides was used, and pyridine was used as the effluent in lieu of water. Before analysis, the pyridine was evaporated; the residue was dissolved in water and then analyzed.

The authors are indebted to Professor K. Fukui for his encouragement and to Mr. H. Azuma and Mr. Y. Yonehara for their technical assistances. The present work was supported by a Grant-in-Aid from the Ministry of Education.

References

1) Part I. T. Shimidzu and A. Imai, *Bull. Chem. Soc. Jpn.*, **49**, 349 (1976).
2) A. S. Jones and D. G. Pearson, *Proc. Chem. Soc.*, **1961**, 78.
3) M. G. Boulton, A. S. Jones, and R. T. Walker, *J. Chem. Soc., C*, **1968**, 1216.
4) A. S. Jones, M. K. Khan, and R. T. Walker, *J. Chem. Soc., C*, **1968**, 1454.
5) F. Cassidy and A. S. Jones, *Eur. Polym. J.*, **2**, 319 (1966).
6) K. Kondo, H. Iwasaki, K. Nakatani, N. Ueda, K. Takemoto, and M. Imoto, *Makromol. Chem.*, **125**, 42 (1969).
7) K. Kondo, H. Iwasaki, N. Ueda, K. Takemoto, and M. Imoto, *Makromol. Chem.*, **125**, 298 (1969).
8) K. Takemoto, *J. Macromol. Sci., Part C*, **5**, 29 (1970).
9) T. Seita, K. Yamaguchi, M. Kinoshita, and M. Imoto, *Makromol. Chem.*, **154**, 255, 263 (1972).
10) H. Schott and G. Greber, *Makromol. Chem.*, **136**, 303, 307 (1970).
11) J. Pitha and P. O. P. Ts'o, *J. Org. Chem.*, **33**, 1341 (1968).
12) P. M. Pitha and J. Pitha, *Biopolymers*, **9**, 965 (1970).
13) P. M. Pitha and J. Pitha, *Nature New Biology*, **240**, 78 (1972).
14) T. Okubo and N. Ise, *Polym. J.*, **4**, 675 (1973).
15) T. Okubo, K. Ban, and N. Ise, *Makromol. Chem.*, **175**, 49 (1974).
16) N. Ueda, K. Kondo, M. Kono, K. Takemoto, and M. Imoto, *Makromol. Chem.*, **120**, 13 (1968).
17) D. T. Browne, J. Eisinger, and N. J. Leonard, *J. Am. Chem. Soc.*, **90**, 7302 (1968).
18) M. N. Lipsett, L. A. Happel, and D. F. Bradley, *J. Biol. Chem.*, **236**, 857 (1961).

Regioselective, Abnormal Ring Opening of the Epoxide of Quinone Epoxide-Cyclopentadiene Adducts

Akitami ICHIHARA, Makio KOBAYASHI, Kengo ODA, and Sadao SAKAMURA

Department of Agricultural Chemistry, Faculty of Agriculture, Hokkaido University, Sapporo 060

(Received June 28, 1977)

Treatment of quinone epoxide-cyclopentadiene adducts with sulfuric acid gave abnormal ring opening products, whose structures were determined by the spectral data and identification of the degradation product. Regioselectivity of the reaction was confirmed. The mechanism of the reaction is discussed.

In the course of the synthetic studies of highly oxygenated cyclohexane derivatives,[1] it was needed to prepare compound **5** which would be served as a pertinent intermediate for the synthesis of crotepoxide[2] and senepoxide.[3] For this purpose, a derivative **3a** which was obtained by epoxidation of the benzoate **2d** of Diels-Alder adduct **2a** from cyclopentadiene and 2-(hydroxymethyl)-1,4-benzoquinone **1a** was prepared. The stereochemistry of **3a** was deduced from analogy and the spectral similarity with those of **3b** and **3c**, whose stereo-

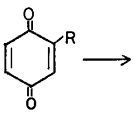

1a R=CH_2OH
1b R=CH_3
1c R=H
1d R=CH_2OCOCH_3

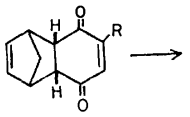

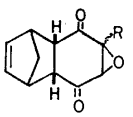

2a R=CH_2OH
2b R=CH_3
2c R=H
2d R=$CH_2OCOC_6H_5$
2e R=CH_2OCOCH_3

3a R=$CH_2OCOC_6H_5$
3b R=CH_3
3c R=H
3d R=CH_2OCOCH_3

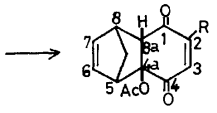

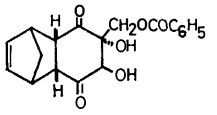

4a R=$CH_2OCOC_6H_5$
4b R=CH_3
4c R=H
4d R=CH_2OCOCH_3

5

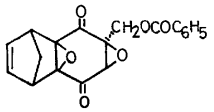

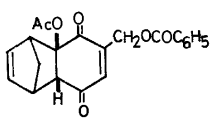

6 **7**

structure has been unequivocally established.[4] Treatment of the epoxide **3a** with various acids yielded only complex mixtures resulting from polymerization and decomposition. However, when the epoxide **3a** was treated with acetic acid–sulfuric acid (10:1 v/v) at 25 °C for 3 days, an unknown product, $C_{21}H_{18}O_6$, was obtained. The infrared spectrum showed absorption bands at 1728 cm^{-1} due to acetoxy carbonyl group and at 1673 cm^{-1} attributed to enedione carbonyl and benzoyl carbonyl groups. In the PMR spectrum (Table 1), a signal at δ 6.65 (1H, t) due to a β-olefinic proton of enedione moiety and a signal at δ 2.04 (3H, s) due to an acetate methyl group were observed. Epoxidation of **4a** with hydrogen peroxide in alkaline solution gave, with loss of acetic acid, a diepoxide **6**, whose structure was supported by elemental analysis, $C_{19}H_{14}O_6$, and the spectral data. From these observations **4a** or **7** was deduced for the product as possible structures. At this stage, however, it was difficult to decide the correct structure on the basis of spectral data. In order to confirm the structure, further investigation was carried out on the adduct **3b** of toluquinone epoxide, since the quinone **1b** is easily available and retro Diels-Alder reaction of the product **4b** would yield known compound, 5-acetoxytoluquinone. Thus, the epoxide **3b** was prepared and treated with sulfuric acid in acetic acid at 25 °C for 3 days in the same manner. The resultant product, $C_{14}H_{12}O_4$, exhibited absorption bands at 1733 cm^{-1} ascribable to acetate carbonyl group and at 1688 cm^{-1} due to enedione system in the IR spectrum. In the PMR spectrum (Table 1), signals at δ 2.02 due to acetoxy methyl group and at δ 6.52 due to a vinylic proton in enedione moiety were observed. These data are certainly in accord with the structure of the abnormal ring opening product. In order to confirm the correct structure, retro Diels-Alder reaction was carried out by heating the compound **4b** at 350 °C under an atmosphere of nitrogen to give a product, mp 72—73 °C, whose structure is compatible to an acetoxyquinone. Since the location of the acetoxyl group was still not obvious, the acetoxyquinone was reduced with lithium aluminum hydride to yield a 1,2,4-benzenetriol. The PMR spectrum exhibited two signals at δ 6.38 and 6.56 as singlets, which indicate that these protons are located in a *para* position and the structure was deduced to be 5-methyl-1,2,4-benzenetriol. This means that the abnormal reaction product must be **4b**. Conclusive result was obtained by the direct comparison of the acetoxyquinone with an authentic sample, 2-acetoxy-1,4-benzoquinone, which was prepared according to the known procedure.[5] The sample thus prepared was identical with thermally decomposed product of **4b** in all respects. Accordingly, the structure of the abnormal reaction product was unambiguously identified as **4b**. The stereochemistry of **4b** was assigned to have the *endo*-configuration on the basis of following facts. Since in those compounds having *endo*-structure with 4a-substituent, the H-8a appears as a doublet with a coupling constant of 3 to 4Hz,[4] the signal at δ 2.95 with a coupling constant,

Table 1. PMR Spectra of abnormal ring cleavage products

PMR (δ) in $CDCl_3$

4 R	H-9	$OCCH_3$ (O)	H-8a	H-8	H-5	H-6,7	H-3	R
CH_2OCOPh (**4a**)	1.70 1.90 ABq J=9 Hz	2.04 s	2.98 d J=4 Hz	3.28 br s	3.41 br s	5.94, d d J=3 and 6 Hz 6.20, d d J=3 and 6 Hz	6.65 t J=2 Hz	5.07 d, J=2 Hz 8.03 7.42, J=5 Hz
CH_3(**4b**)	1.66 1.87 ABq J= 9Hz	2.02 s	2.95 d J=4 Hz	3.26 br s	3.46 br s	5.93, d d J=3 and 6 Hz 6.14, d d	6.52 q J=1.5 Hz	1.88 d J=1.5 Hz
H(**4c**)	1.68 1.90 ABq J=9 Hz	2.64 s	2·84 d J=4 Hz	3.28 br s	3.38 br s	5.93, d d J=3 and 6 Hz 6.19, d d J=3 and 6 Hz	6.61 d J=2 Hz	6.61 d J=2 Hz
CH_2OAc(**4d**)	1.64 1.86 ABq J=9 Hz	2.00 s	2.91 d J=4 Hz	3.22 br s	3.35 br s	5.93, d d J=3 and 6 Hz 6.19, d d J=3 and 6 Hz	6.46 t J=2 Hz	2.00 s 4.76 d, J=2 Hz

J=4Hz, in **4b** is also consistent with the *endo*-assignment. The structure of **4a** (**4c** and **4d**) was deduced from the PMR spectrum which shows similar spectral pattern with that of **4b** (Table 1).

For the purpose to investigate generality of this reaction, two more compounds, **3c** and **3d**, were prepared from **1c** and **1d** respectively and treated with sulfuric acid under the same conditions to yield analogous compounds, **4c** and **4d**. The PMR spectral data of the abnormal ring opening products are summarized in Table 1.

The results mentioned above are of quite interest since in the case of substituted quinone epoxide adducts (**3a**, **3b**, and **3d**), all of the reactions proceeded regioselectively to give **4a**, **4b**, and **4d**.

Finally, the mechanism of the abnormal reaction was presumed as follow. Ring contraction of piperitone epoxide, an α-epoxy ketone, under basic conditions was reported, for which Favorskii type mechanism was postulated.[6] On the other hand, in the reaction of a steroid α-epoxy ketone with acids, another plausible mechanism which involves an enol intermediate was suggested.[7] Since extremely strained structure resulted from Favorskii type reaction (path B in Scheme 1) excludes the possibility involving cyclopropanone intermediate and in fact, none of the compounds as **i** derived *via* the intermediate was obtained, enol intermediate (path A) might be involved in the present reaction as shown in Scheme 1. From the mechanistic point of view, it is interesting to note that another possible product **7** had not been recognized in the reaction.

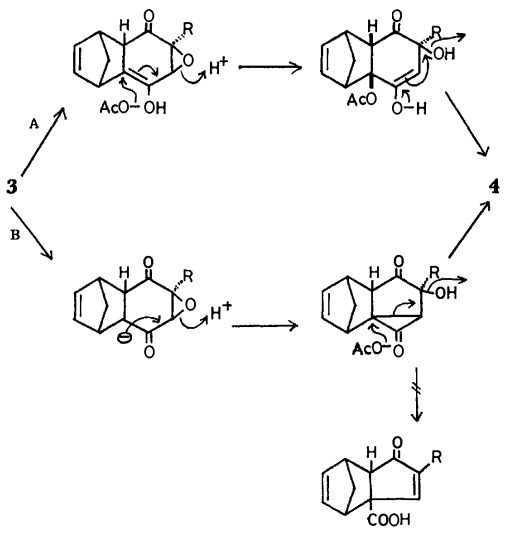

i

Scheme 1.

The abnormal ring opening reaction would be useful for the synthesis of some 2-acetoxy-1,4-benzoquinones *via* retro Diels-Alder reaction.

Experimental

All melting points were uncorrected. The IR spectra were taken on a Hitachi EPI-S2 Spectrophotometer and the PMR spectra were measured with a Hitachi R-22 Spectrometer (90MHz), using tetramethylsilane as an internal standard.

*2-(Hydroxymethyl)-1,4-benzoquinone (**1a**).* This compound was prepared according to the known procedure involving oxidation of 2,5-dihydroxybenzyl alcohol with lead tertaacetate.[8]

endo-*2-Hydroxymethyl-5,8-methano-4a,5,8,8a-tetrahydro-1,4-naphthoquinone (**2a**).* A solution of 1.5 g of the benzoquinone **1a** and 2 ml of cyclopentadiene in 6 ml of methanol was allowed to stand until the spot of the starting material disappeared on TLC. The reaction mixture was concentrated *in vacuo* to give a residue, which was recrystallized from benzene to yield pure **2a**, mp 65—66 °C; IR ν_{max}^{KBr} 1653, 3530 cm^{-1}; PMR ($CDCl_3$) δ 1.42 (2H, m, CH_2), 3.10 (2H, br s, $=CH$), 6.52 (1H, t, J=3Hz, $=CH$). Found: C, 70.72; H, 5.95%. Calcd for $C_{12}H_{12}O_3$: C, 70.57; 5.92%.

endo-*2-(Benzoyloxymethyl)-5,8-methano-4a,5,8,8a-tetrahydro-1,4-naphthoquinone (**2d**).* A solution of 2.1 g of the adduct and 1.6 ml of benzoyl chloride in 10 ml of pyridine was allowed to stand at room temperature. The reaction mixture was washed with water and organic layer was separated. The water layer was extracted twice with benzene and the combined extracts were dried over anhydrous sodium sulfate and concentrated. The resultant crystals were recrystallized from

benzene to give 2.86 g of the benzoate, mp 147—148 °C; IR ν_{max}^{KBr} 1723, 1664, 1636, 1600 cm^{-1}; PMR ($CDCl_3$) δ 1.34—1.58 (2H, m, CH_2), 3.22 (2H, m, CH), 3.52 (2H, br s, -CH), 5.08 (2H, d, J=2Hz, CH_2), 6.06 (2H, t, J=2Hz, =CH), 6.60 (1H, t, J=2Hz, =CH), 7.33—7.59 (3H, m, ArH), 8.03 (2H, dd, J=2Hz, J=8Hz, ArH). Found: C, 73.79; H, 5.17%. Calcd for $C_{19}H_{16}O_4$: C, 74.01; H, 5.23%.

*r-2-(Benzoyloxymethyl)-2,3-epoxy-t-5,8-methano-2,c-3,t-4a,5,8,t-8a-hexahydro-1,4-naphthoquinone (**3a**).* A mixture of 100 mg of the benzoate **2d** and 2 ml of solution made from 25 ml of hydrogen peroxide (30%) and 5 g of sodium carbonate in 125 ml of water was allowed to stand for *ca.* 40 min. The reaction mixture was extracted with benzene and the combined extracts were dried on anhydrous sodium sulfate. Removal of the solvent gave 66 mg of crystals which were recrystallized from benzene to yield the pure epoxide **3a**, mp 139—140 °C; IR ν_{max}^{KBr} 1715, 1600 cm^{-1}; PMR ($CDCl_3$) δ 1.22, 1.44 (2H, ABq, J=8Hz, CH_2), 3.25 (2H, br s, CH), 3.38 (2H, br s, CH), 3.52 (1H, s, COCH), 4.82, 4.54 (2H, ABq, J=13Hz, CH_2), 6.00 (2H, t, J=2Hz, =CH), 7.20—7.49 (3H, m, ArH), 7.90 (2H, dd, J=8Hz, J=2Hz, ArH); MS *m/e* 324 (M^+). Found: C, 70.21; H, 4.97%. Calcd for $C_{19}H_{16}O_5$: C, 70.36; H, 4.98%.

*endo-4a-Acetoxy-2-(benzoyloxymenthyl)-5,8-methano-4a,5,8,8a-tetrahydro-1,4-naphthoquinone (**4a**).* To a solution of 139.7 mg of the epoxide **3a** in 2 ml of acetic acid was added a mixture of 2.2 ml of sulfuric acid-acetic acid (1 : 10 v/v), and the mixture was stand for 3 days at 25 °C and the completion of the reaction was checked by TLC. The reaction mixture was extracted with chloroform and washed with water. The combined extracts were dried on anhydrous sodium sulfate and concentrated *in vacuo*. The residue was chromatographed on silicic acid and eluted with benzene-ethyl acetate (95 : 5 v/v) to give 34.5 mg of a crystalline material. The crude crystals were recrystallized from benzene to give a pure compound, **4a**, mp 166—167 °C. IR ν_{max}^{KBr} 1728, 1673, 1640 cm^{-1}; PMR spectra are cited on Table 1. MS *m/e* 367 (M^+ + 1). Found: C, 67.89; H, 4.75%. Calcd for $C_{21}H_{18}O_6$: C, 68.84; H, 4.95%.

*Epoxidation of **4a**.* To a solution of 546 mg of **4a** in 6 ml of tetrahydrofuran was added a mixture of 0.2 g of potassium carbonate and 1 ml of hydrogen peroxide (30%) in 5 ml of water. After 10 min, the reaction mixture was extracted with chloroform and the extracts were dried on anhydrous sodium sulfate and concentrated. The residue was chromatographed on 20 g of silicic acid using benzene-ethyl acetate (95 : 5 v/v) as eluent to give 82 mg **6** as crystals, mp 132—133 °C; IR ν_{max}^{KBr} 1732, 1704, 1604 cm^{-1}; PMR ($CDCl_3$) δ 1.47 (2H, m, CH_2), 3.23 (2H, m, CH), 3.65 (1H, s, COCH), 4.53, 4.76 (2H, ABq, J=13Hz, $-CH_2O$), 6.42 (2H, t, J=2Hz, =CH), 7.32—7.57 (3H, m, ArH), 7.92 (2H, dd, J=8Hz, 2Hz, ArH); MS *m/e* 338 (M^+). Found C, 67.53; H, 4.16%. Calcd for $C_{19}H_{14}O_6$: C, 67.45; H, 4.17%.

*2-Methyl-5,8-methano-4a,5,8,8a-tetrahydro-1,4-naphthoquinone (**2b**).* This compound was prepared from toluquinone **1b** and cyclopentadiene in methanol heating at 50 °C for 4 h.[4] Mp 61—62.4 °C.

*r-2,3-Epoxy-2-methyl-c-5,8-methano-2,3,c-4a,5,8,c-8a-hexahydro-1,4-naphthoquinone (**3b**).* This compound was prepared in the same way used for the synthesis of **3a** starting from toluquinone.[4]

*endo-4a-Acetoxy-2-methyl-5,8-methano-4a,5,8,8a-tetrahydro-1,4-naphthoquinone (**4b**).* To a solution of 8 g of the epoxide **3b** in 40 ml of acetic acid was added a mixture of 70 ml of acetic acid and 7 ml of sulfuric acid. After allowing to stand for two days at room temperature, the reaction mixture was extracted with chloroform and the extracts were concentrated *in vacuo* to give a residue which was chromatographed on silicic acid to yield 10 g of the product. Pure **4b** was obtained by recrystallization from benzene, mp 61—62 °C, IR ν_{max}^{KBr} 1733, 1668 cm^{-1}; PMR data, see Table 1. MS *m/e* 246 (M^+); Found: C 68.50; H, 6.00%, Calcd for $C_{14}H_{12}O_4$: C, 68.28; H, 5.73%.

5-Acetoxy-2-methyl-1,4-benzoquinone. A column packed with glass beads was evacuated from lower end of the column with an aspirator at 0.4 mmHg and heated at 350 °C. From the bottle equipped on the column, 100 mg of **4a** was dropped five times into the column, and after cooling, the reaction vessel was washed with chloroform to give a crude product, which was chromatographed on silicic acid using benzene-ethyl acetate (95 : 5 v/v) to yield 53 mg of 5-acetoxytoluquinone, mp 72—73.5 °C (lit,[5] 74.5—76 °C).

Reduction of 5-Acetoxy-2-methyl-1,4-benzoquinone. A mixture of 20 mg of the quinone in 7 ml of anhydrous ether and 17 mg of $LiAlH_4$ was refluxed for 2 h. To the reaction mixture was added ethyl acetate to decompose excess $LiAlH_4$, and then 10%-sulfuric acid to acidify. The mixture was extracted with ethyl acetate and the extracts were dried over anhydrous sodium sulfate, and evaporated *in vacuo* to give a residue. PMR ($CDCl_3$) δ 6.38 (1H, s, ArH), 6.55 (1H, s, ArH), 7.90—6.78 (3H, br, ArOH).

*endo-4a-Acetoxy-5,8-methano-4a,5,8,8a-tetrahydro-1,4-naphthoquinone (**4c**).* The epoxide **3c** prepared from 1 g of *p*-benzoquinone (**1c**) according to the known procedure[5] was dissolved into 10 ml of acetic acid. To the solution was added a mixture of 3 ml of concd sulfuric acid and 30 ml of acetic acid. After allowing to stand for 3 days at room temperature, the reaction mixture was extracted with chloroform and the extracts were washed with brine and dried over anhydrous sodium sulfate, evaporated *in vacuo* to give a crude residue. The residue was chromatographed on silicic acid to give 600 mg of **4c**, mp 102—103 °C, IR ν_{max}^{KBr} 1736, 1683, 1671 cm^{-1}; PMR data (Table 1); MS *m/e* 232 (M^+). Found: C, 67.31; H, 5.34%. Calcd for $C_{13}H_{12}O_4$: C, 67.23; H, 5.21%.

*r-2-(Acetoxymethyl)-2,3-epoxy-t-5,8-methano-2,c-3,t-4a,5,8,t-8a-hexahydro-1,4-naphthoquinone (**3d**).* A solution of 13 g of 3-(acetoxymethyl)-1,4-benzoquinone (**1d**) and 8 ml of cyclopentadiene was allowed to stand for 1 h at room temperature. The reaction mixture was concentrated *in vacuo*. To the residue dissolved into tetrahydrofuran was added 100 ml of hydrogen peroxide (30%) under ice-cooling. The mixture was heated at 55—60 °C for 1 h and then cooled at room temperature. After excess hydrogen peroxide had been decomposed with sodium bisulfite, the reaction mixture was extracted twice with benzene and the extracts were dried on anhydrous sodium sulfate and concentrated *in vacuo* to yield a product, which was recrystallized from benzene to give 3.07 g of the epoxide **3d**, mp 125—126 °C, IR ν_{max}^{KBr} 1725, 1260 cm^{-1}; PMR ($CDCl_3$) δ 1.27, 1.47 (2H, ABq, J=9Hz, CH_2), 2.02 (3H, s, $COCH_3$), 3.32 (2H, br s, CH), 3.49 (2H, br. s, CH), 3.54 (1H, s, COCH), 4.69, 4.31 (2H, ABq, J=13Hz, CH_2OAc), 6.09 (2H, t, J=2Hz, =CH); MS *m/e* 262 (M^+): Found C, 64.22; H, 5.39%. Calcd for $C_{14}H_{14}O_5$: C, 64.11; H, 5.38%.

*endo-4a-Acetoxy-2-(acetoxymethyl)-5,8-methano-4a,5,8,8a-tetrahydro-1,4-naphthoquinone (**4d**).* To a solution of 3.07 g of the epoxide **3d** in 10 ml of acetic acid was added a mixture of 6 ml of concd sulfuric acid and 60 ml of acetic acid, and the reaction mixture was allowed to stand for 3 days at room temperature and extracted with chloroform. The extracts

were washed with brine and dried on anhydrous sodium sulfate and concentrated *in vacuo*. The residue was chromatographed on silicic acid eluting with benzene-ethyl acetate (95 : 5 v/v) to yield 1 g of the product, **4d**, mp 102—103 °C. IR ν_{max}^{KBr} 1752, 1732, 1682 cm^{-1}; PMR data, see Table 1. MS *m/e* 304 (M^+). Found: C, 67.31; H, 5.34%. Calcd for $C_{16}H_{16}O_6$: C, 67.23; H, 5.21%.

References

1) This paper constitutes part X of "Synthetic Studies of Highly Oxygenated Cyclohexane Derivatives." For part IX, A. Ichihara, M. Ubukata, and S. Sakamura; *Tetrahedron Lett.*, **1977**, 3473.

2) An antitumor compound isolated from *Croton macrostachys*, S. M. Kupchan, R. J. Hemingway, and R. M. Smith, *J. Org. Chem.*, **34**, 3898 (1969). (Synthesis) K. Oda, A. Ichihara, and S. Sakamura, *Tetrahedron Lett.*, **1975**, 3187; M. R. Demuth, P. E. Garrett, and J. D. White. *J. Am. Chem. Soc.*, **98**, 634 (1976)

3) F. Hollands, D. Becher, J. Gaudemer, and J. Polonsky, *Tetrahedron*, **24**, 1633 (1968). (Synthesis) A. Ichihara, K. Oda, M. Kobayashi, and S. Sakamura, *Tetrahedron Lett.*, **1974**, 4235

4) D. F. O'Brien and J. W. Gates, Jr., *J. Org. Chem.*, **30**, 2593 (1965)

5) H. S. Wilgus and J. W. Gates, Jr., *Can. J. Chem.*, **45**, 1975 (1967). J. Posvisil and V. Ettel, *Collect. Czech. Chem. Commun.*, **24**, 729 (1959)

6) H. O. House and W. F. Gilmore, *J. Am. Chem. Soc.*, **83**, 3972, 3980 (1961)

7) M. Tomoeda, M. Ishizaki, H. Kobayashi, S. Kanatomo, T. Koga, M. Inuzuka, and T. Furuta, *Tetrahedron*, **21**, 733 (1965)

8) A. Black, *Helv. Chim. Acta*, **30**, 1 (1974)

Ligand Effects of 2,2′-Bipyridine in the Decomposition of 1,2,3,4-Tetrahydro-1-naphthyl Hydroperoxide Catalyzed by Cobalt(II) Salt

Teruaki YAMADA and Yoshio KAMIYA

Department of Reaction Chemistry, Faculty of Engineering, The University of Tokyo, Bunkyo-ku, Tokyo 113

(Received June 28, 1977)

The ligand effect of 2,2′-bipyridine on the rate of the decomposition of 1,2,3,4-tetrahydro-1-naphthyl hydroperoxide catalyzed by cobalt(II) decanoate in chlorobenzene was kinetically studied and compared with the redox potentials and the spectral data of cobalt(II) complexes. The activity of the anhydrous cobalt(II) decanoate increased by a factor of from three to seven by the addition of 2,2′-bipyridine when the molar ratio of 2,2′-bipyridine to cobalt was 0.25 to 2. It was found that the catalytic activity of the anhydrous cobalt(II) decanoate–2,2′-bipyridine complex shows a remarkable maximum value at the molar ratio of 2,2′-bipyridine to cobalt of 0.5. This novel finding can be explained on the basis of the redox potential measured by cyclic voltammetry in dichloromethane, the IR data, and the structure of the catalyst. The coordination of 2,2′-bipyridine causes the redox potential to change from 0.80—0.84 V to 0.60—0.64 V (*vs.* SCE) and also weakens the Co–O(decanoate) bond strength, resulting in a facile coordination of hydroperoxide to the cobalt ion as well as the acceleration of cleavage of hydroperoxide. The maximum activity was explained by the proposed structure of the cobalt(II) decanoate–2,2′-bipyridine (1 : 1/2) complex with a fairly low redox potential and a vacant coordination site.

The metal-catalyzed decomposition of alkyl hydroperoxide is the most common pathway of catalysis by transition-metal complexes in the autoxidation reaction. A catalytic cycle is possible *via* the following reduction oxidation reaction by two valency-state metal ions:

$$ROOH + M^{(n-1)+} \longrightarrow RO\cdot + M^{n+} + OH^-$$

$$ROOH + M^{n+} \longrightarrow RO_2\cdot + M^{(n-1)+} + H^+$$

Many kinetic investigations[1] of metal-catalyzed decomposition have been undertaken, but many points about the role of the metal are still obscure. A "ligand-effect" investigation must be one of the most valid probes to elucidate the role of the metal and also to serve as a gateway to many applications. Although, in some works[2] dealing with the kinetics of autoxidation, the fact of the activation or deactivation of a metal catalyst by a chelating agent has been mentioned, no systematic study has yet been presented.

The ligand effect in autoxidation seems to depend on the kind of metal, ligand and solvent, but it is hard to explain it because of its complexity. The difficulties derived from its complexity will be clarified only by the quantitative investigation of each factor affecting the catalytic activity. Not only a kinetic but also a structural study is needed to clarify the reaction mechanism. In this paper, we will report the interesting ligand effect of 2,2′-bipyridine in the cobalt salt-catalyzed decomposition of hydroperoxide.

Experimental

Materials. Cobalt(II) decanoate ($CoDe_2$) was prepared according to the method of Heaton and Uri.[3] An aqueous solution of cobalt(II) sulfate was added to an aqueous solution of sodium decanoate. The resulting precipitate was washed with hot water and dried in two ways. The pink-colored catalyst, defined as the cobalt(II) decanoate (A) ($CoDe_2$(A)), was air-dried at room temperature. The other, blue-colored catalyst, defined as the cobalt(II) decanoate (B) ($CoDe_2$(B)), was obtained by drying under a vacuum at 70 °C for 5 h. Elemental analyses were carried out on both $CoDe_2$(A) and $CoDe_2$(B). Found: C, 54.6; H, 10.4%. Calcd for $CoDe_2$(A) [$Co(C_{10}H_{19}O_2)_2\cdot 2H_2O$]: C, 54.9; H, 10.0%. Found: C, 58.2; H, 10.0%. Calcd for $CoDe_2$(B) [$Co(C_{10}H_{19}O_2)_2$]: C, 59.8; H, 9.0%. 2,2′-Bipyridine (bpy) was further purified by recrystallization from heptane and dried under a vacuum at room temperature. Mixed solutions of cobalt(II) decanoate and 2,2′-bipyridine, a very strong chelating agents with a high stability constant,[4] were allowed to stand at room temperature for 15 h to equilibrate and then submitted to the reaction and other measurements. 1,2,3,4-Tetrahydro-1-naphthyl hydrperoxide (THP) was prepared by a modification of the conventional method.[5] After the autoxidation of 1,2,3,4-tetrahydronaphthalene (tetralin) initiated by azobisisobutyronitrile at 50 °C for 60 h, the oxidation products were concentrated by distillation under reduced pressure and then crystallized from a solution upon cooling to 0 °C. This crystal was recrystallized from heptane and then dried under a vacuum at room temperature. The purified hydroperoxide was confirmed to be 99.0% pure by iodometric titration. Dichloromethane was dried by calcium chloride and purified by repeated distillations. All the other chemicals were of a reagent grade.

Decomposition of THP. A 50-ml three-necked round-bottomed flask was filled with a solution (40 ml) containing a catalyst and maintained at the reaction temperature. Argon gas was introduced into the system to remove any dissolved oxygen. A solution of THP (10 ml) was prepared separately and heated to the reaction temperature. The reaction was started by the addition of all the THP solution. A certain portion of the solution (2 ml) was withdrawn from the reaction mixture at regular intervals and subjected to iodometric titration to determine the concentration of hydroperoxide. The decomposition products were analyzed by gas chromatography on a 3-m column packed with PEG-20M. The carrier gas was helium, and the column temperature was 200 °C.

Electrochemical and Spectral Measurements. Cyclic voltammetry was done using a potentiostat, a function generator, and a X-Y recorder. The electrode system consisted of a saturated calomel reference electrode (SCE), a platinum plate used as working electrode, and a platinum wire used as a counter electrode. Measurements were made at room temperature in a glass cell to which the reference electrode was connected with a double salt bridge. A solution of the complex (1—10 mM) was prepared by dissolving a weighed quantity in a measured volume of dichloromethane. As the supporting electrolyte tetrabutylammonium perchlorate was added to this solution, which was flushed with nitrogen for ten minutes prior to measurement. The visible and ultra-

violet spectra were obtained in chlorobenzene using a Hitachi-124 spectrophotometer. The infrared spectra were obtained by the Nujol method using a JASCO-IRA 2 spectrophotometer.

Results

Effects of 2,2'-Bipyridine in Chlorobenzene. The effect of 2,2'-bipyridine on the rate of the $CoDe_2$-catalyzed decomposition of THP in chlorobenzene is shown in Fig. 1. The rate of decomposition was increased by the addition of 2,2'-bipyridine. The $CoDe_2$(A)–bpy complexes showed a monotonous increase in their activity, but surprisingly, the $CoDe_2$(B)–bpy complexes showed a maximum activity at the molar ratio of [bpy]/[$CoDe_2$]=1/2. Both $CoDe_2$(A)–bpy and $CoDe_2$(B)–bpy complexes showed almost the same activity at ratios of [bpy]/[$CoDe_2$] higher than 1. Incidentally, the rate of the autoxidation of tetralin was increased by the addition of 2,2'-bipyridine and did not exceed

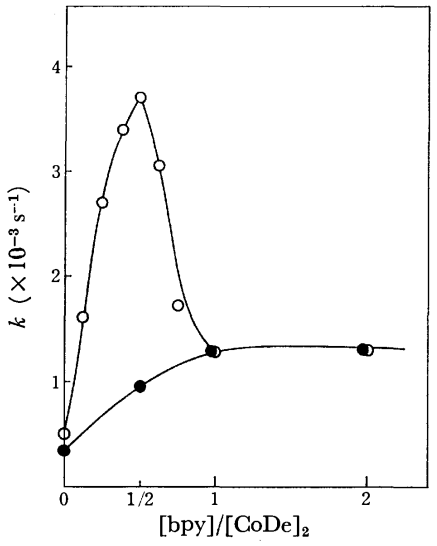

Fig. 1. Effect of 2,2'-biyridine on the rate of decomposition of THP catalyzed by $CoDe_2$ in chlorobenzene at 45 °C.
(-●-) $CoDe_2$(A), (-○-) $CoDe_2$(B), [$CoDe_2$]=2×10⁻⁴ M, [THP]=5×10⁻² M.

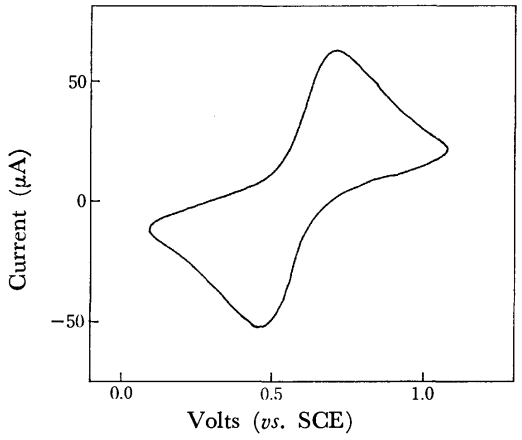

Fig. 2. Cyclic voltammogram of $CoDe_2$(B)-bpy(1:1) in dichloromethane.
Scan rate was 0.05 V/s.

Table 1. Comparison of the voltammetric data with the decomposition rates of THP for $CoDe_2$-bpy complexes

Complex	Electrode reaction	$E_{1/2}$, V	k, 10^{-3} s^{-1}
$CoDe_2$(B)	Co(II) − e → Co(III)	0.80	0.5
	Co(III) + e → Co(II)	0.84	
$CoDe_2$(B)-bpy(1 : 1/2)	Co(II) − e → Co(III)	0.67	3.7
	Co(III) + e → Co(II)	0.70	
$CoDe_2$(B)-bpy(1 : 1)	Co(II) − e → Co(III)	0.60	1.3
	Co(III) + e → Co(II)	0.63	
$CoDe_2$(B)-bpy(1 : 2)	Co(II) − e → Co(III)	0.59	1.3
	Co(III) + e → Co(II)	0.59	

Table 2. Infrared absorption bands and decomposition rates of THP for $CoDe_2$-bpy complexes

Complex	C–O st., cm^{-1}	k, ×10^{-3} s^{-1}
$CoDe_2$(B)	1550	0.5
$CoDe_2$(B)-bpy(1 : 1/2)	1570	3.7
$CoDe_2$(B)-bpy(1 : 1)	1590	1.3
$CoDe_2$(B)-bpy(1 : 2)	1595	1.3

the limiting rate. A large excess of 2,2'-bipyridine, one hundred times the quantity of $CoDe_2$(B), decreased the decomposition rate to half the value of $CoDe_2$(B) alone.

The redox potentials of the $CoDe_2$(B)–bpy complexes, the determining factor for the activity of a catalyst in the redox reaction, were measured by cyclic voltammetry in dichloromethane. Table 1 shows the values of the redox potential and the decomposition rates for $CoDe_2$(B)–bpy complexes. The redox potential was shifted in the negative direction by the coordination of 2,2'-bipyridine. This shows that the reductive force of a cobalt(II) ion or the electron density on a cobalt(II) ion is increased by the coordination of 2,2'-bipyridine. Figure 2 shows the reversible change in the potential for anodic and cathodic sweeps of the Co(II)-Co(III) couple as established by cyclic voltammetry.

Table 2 shows the C–O stretching absorptions of the decanoate ligands of $CoDe_2$(B)–bpy complexes. The absorption peak shifts to a higher wave number with an increase in the amount of 2,2'-bipyridine added. This shows the increase in the double-bond character in the C–O bond. The C-T bands and d-d bands measured on $CoDe_2$(A)–bpy, and $CoDe_2$(B)–bpy complexes are shown in Table 3. The C-T band shifted to a longer wavelength, and the d-d band, to a shorter are, upon the addition of 2,2'-bipyridine. Both $CoDe_2$(A)–bpy and $CoDe_2$(B)–bpy complexes have shown the same absorption band at the [bpy]/[$CoDe_2$] ratios of both 1 and 2.

As is shown in Fig. 3, product analysis[6] showed that the ratio of [C]/([C]+[D]) was about 0.29 for the $CoDe_2$(B) complex and about 0.39—0.45 for the $CoDe_2$(B)–bpy complexes; C and D are 1,2,3,4-tetrahydro-1-naphthol (α-tetralol) and 1,2,3,4-tetrahydro-1-naphthalenone (α-tetralone) respectively. The ratio of α-tetralol to α-tetralone was independent of the metal or hydroperoxide concentration.

TABLE 3. ULTRAVIOLET AND VISIBLE ABSORPTION BANDS OF $CoDe_2$-bpy COMPLEXES

Complex	d-d band, nm (ε, $1\,mol^{-1}\,cm^{-1}$)		C-T band, nm (ε, $1\,mol^{-1}\,cm^{-1}$)	
$CoDe_2$(A)	526	(22.7)		
$CoDe_2$(A)-bpy(1 : 1/2)	522	(46.5)	361	(322)
$CoDe_2$(A)-bpy(1 : 1)	522	(41.8)	363	(569)
$CoDe_2$(A)-bpy(1 : 2)	520	(38.1)	365	(608)
$CoDe_2$(B)	526	(21.0)		
$CoDe_2$(B)-bpy(1 : 1/2)	522	(57.1)	355	(384)
$CoDe_2$(B)-bpy(1 : 1)	522	(50.7)	365	(560)
$CoDe_2$(B)-bpy(1 : 2)	520	(40.2)	365	(585)

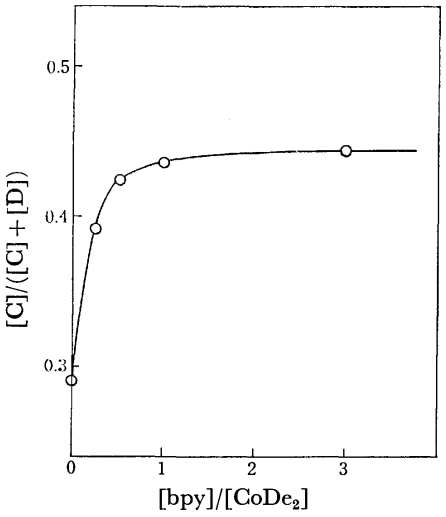

Fig. 3. Variation of [C]/([C]+[D]) in the decomposition of THP in chlorobenzene at 45 °C.
C: α-Tetralol, D: α-tetralone, $[CoDe_2(B)]=2\times10^{-4}$ M, $[THP]=5\times10^{-2}$ M.

TABLE 4. DECOMPOSITION RATES OF THP FOR $CoDe_2$-(bipyridine derivative) COMPLEXES IN CHLOROBENZENE AT 40 °C

Complex	k, $\times10^{-4}\,s^{-1}$
$CoDe_2$(B)-(2,2′-biquinoline)	3.5
$CoDe_2$(B)-(2,2′-bipyridine)	4.8
$CoDe_2$(B)-(6,6′-dimethyl-2,2′-bipyridine)	5.9
$CoDe_2$(B)-(4,4′-dimethyl-2,2′-bipuinoline)	6.5

[bipyridine derivative]/$[CoDe_2]=2$,
$[CoDe_2]=2\times10^{-4}$ M, $[THP]=5\times10^{-2}$ M.

Table 4 shows the catalytic activities of the $CoDe_2$(B)–bipyridine derivative complexes. These results show that the activity of a catalyst increases with an increase in the electron-donating property of the ligand; this supports the proposition that the increase in the electron density of the cobalt(II) ion causes an increase in the catalytic activity. The deviation of 6,6′-dimethyl-2,2′-bipyridine can be ascribed to the steric hindrance to the coordination to the cobalt(II) ion.

Effects of 2,2′-Bipyridine in Acids. Figure 4 shows the effect of 2,2′-bipyridine on the rate of the cobalt(II) acetate ($Co(OAc)_2$)-catalyzed decomposition of THP in acetic acid. Unlike the case of the decomposition in chlorobenzene, the decomposition rate in acetic acid decreased with an increase in the amount of 2,2′-bipyridine added. Similar reactions were carried out in various acid solvents as is shown in Table 5. The decomposition rate was decreased by the addition of 2,2′-bipyridine to all the solvents, suggesting that the inhibitive effect of 2,2′-bipyridine is independent of the strength of acids.

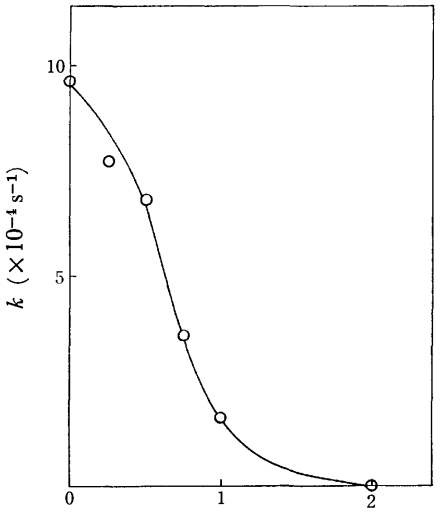

Fig. 4. Effect of 2,2′-bipyridine on the rate of decomposition of THP catalyzed by $Co(OAc)_2$ in acetic acid at 50 °C.
$[Co(OAc)_2]=10^{-3}$ M, $[THP]=5\times10^{-2}$ M.

TABLE 5. DECOMPOSITION RATE OF THP IN FATTY ACIDS[a]

	k, $\times10^{-4}\,s^{-1}$	k_2, $\times10^{-4}\,s^{-1}$	k_2/k
Acetic acid(C_2)	0.89	0.18	0.20
Propionic acid(C_3)	1.35	0.35	0.26
Butyric acid(C_4)	2.00	0.68	0.34
Valeric acid(C_5)	3.08	1.08	0.35
Heptanoic acid(C_7)	5.83	1.94	0.33
Nonanoic acid(C_9)	7.61	2.21	0.29

a) k and k_2 are pseudo-first-order rate constants of the THP decomposition reactions by 10^{-3} M $Co(OAc)_2$ and 10^{-3} M $Co(OAc)_2$-bpy(1 : 1) respectively. $[THP]=5\times10^{-2}$ M, temperature = 50 °C.

Discussion

Increase in Activity. It can be presumed that the redox potential of a catalyst is the most influential factor in hydroperoxide decomposition. The redox potentials of

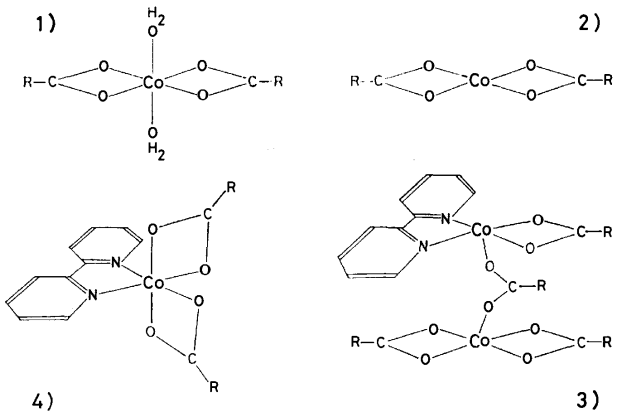

Fig. 5. Proposed structure of $CoDe_2$-bpy complexes. 1) $CoDe_2$(A), 2) $CoDe_2$(B), 3) $CoDe_2$(B)-bpy(1 : 1/2), 4) $CoDe_2$(B)-bpy(1 : 1).

metal ions were compared with the catalytic activity in oxidation reactions by Chalk and Smith,[7] who reported that the redox potentials of metal ions in aqueous solution could not be correlated with the catlytic activity in non-polar media, though the values in absolute alcohol could be correlated fairly well.

As redox potentials are very sensitive to the ligand and the solvent, it is necessary to measure them in a similar non-polar solvent in order to make a comparison with the catalytic activities of the hydroperoxide decomposition in chlorobenzene. Recent progress in the field of electrochemistry in non-aqueous media[8] enable us to measure the redox potentials of many complexes in various non-aqueous solvents. We measured the redox potentials of the $CoDe_2$(B)–bpy complexes in dichloromethane and compared them to their catalytic activities (Table 1). The catalytic activities seem to be correlated to their redox potentials except in the case of $CoDe_2$(B)–bpy(1:1/2). The increase in the activity upon the addition of 2,2′-bipyridine can be attributed to the change in the redox potential of the catalyst. Such a change in the redox potential of the cobalt ion by 2,2′-bipyridine will bring about two effects; one is the increase in the reductive force of the cobalt(II) ion, which accelerates the cleavage of the hydroperoxide molecule, while the other is the increase in the electron density on the cobalt(II) ion, which will stabilize the $CoDe_2$–hydroperoxide complex.

From the IR data (Table 2), another change was found in the first ligand decanoate, an increase in the double-bond character of the C–O bond. This suggests a weakening in the Co–O bond strength, which must bring about the facile coordination of the hydroperoxide molecule to the central cobalt(II) ion. The decomposition of hydroperoxide by the metal ion must take the pathway in which the coordination of hydroperoxide to the metal ion occurs. Then the facile coordination of hydroperoxide to the metal ion must lead to a higher decomposition rate.

Therefore, the increase in the rate of decomposition of hydroperoxide due to 2,2′-bipyridine can be ascribed to the change in the redox potential of the cobalt(II) ion and the weakening of the Co–O bond strength. The results of product analysis seem to indicate that there is a non-radical decomposition in the $CoDe_2$(B)–THP system and that the portion of radical decomposition increases upon the addition of 2,2′-bipyridine.

In acetic or other fatty acids, the effect of 2,2′-bipyridine was quite the reverse of that in chlorobenzene. The acid solvent may suppress the positive ligand effect; that is, there may be no weakening of the Co–O(acetate) bond strength in an acetic acid solvent. The 2,2′-bipyridine will just retard the decomposition of hydroperoxide by occupying the coordination site of the cobalt(II) ion.

Maximum Activity. The electrochemical and spectral data can not fully explain the maximum activity of the $CoDe_2$(B)–bpy(1:1/2). It can, however, be explained on the basis of the structural variation in the complexes. Figure 5 shows the proposed structure of these complexes. $CoDe_2$(A) (Structure 1) was pink and a six-coordination complex.[9] The disappearance of the OH absorption at 3420 cm^{-1} and the weight decrease correspond to the loss of two coordinated H_2O molecules by drying Complex 1 under a vacuum at 70 °C for 5 h, leading inevitably to Structure 2. This is a four-coordination complex. The color change from pink to blue[10] is consistent with the above structural change. From the spectral and electrochemical data and from the steric difficulties of 2,2′-bipyridine, it seems that $CoDe_2$–bpy(1:1) and $CoDe_2$–bpy(1:2) will take Structure 4. We propose Structure 3 for $CoDe_2$(B)–bpy(1:1/2), though a five-coordination complex with one vacant coordination site can not be excluded.

These catalytic activities can be explained according to these structures. The fact that the activities of $CoDe_2$(A) and $CoDe_2$(B) are lower than the others can be attributed to their weak reductive force because of no coordination of 2,2′-bipyridine. The slight difference in activity between $CoDe_2$(A) and $CoDe_2$(B) might be brought about by the two vacant coordination sites of $CoDe_2$(B). $CoDe_2$(B)–bpy(1:1/2) shows the highest activity of all the catalysts. This is explained by Structure 3 having a vacant coordination site and an adequate reductive force to cleave the hydroperoxide molecule. $CoDe_2$(A)–bpy (1:1/2) may not have the highest activity because of the coordinated H_2O molecule, which probably interferes with the coordination of the hydroperoxide molecule. The activity of $CoDe_2$(B)–bpy(1:1), which is between those of $CoDe_2$(B) and $CoDe_2$(B)–bpy(1:1/2), can be attributed to Structure 4, which may have a strong reductive force but no vacant coordination site. The fact that the activity is higher than that of $CoDe_2$(B) may be attributed to the strong reductive force, while the lower activity than $CoDe_2$(B)–bpy(1:1/2) may be attributable to the lack of any vacant coordination site. Judging from their spectral data, $CoDe_2$(A)–bpy(1:1) and $CoDe_2$(B)–bpy(1:1) must take the same structure; the data show a complete agreement with the results of catalytic activity.

We would like to thank Professor Testuo Osa (Tohoku University) for his assistance with the cyclic voltammetry.

References

1) R. Hiatt, K. C. Irwin, and C. W. Gould, *J. Org. Chem.*, **33**, 1430 (1968); N. M. Emanuel, Z. K. Maizus, and I. P. Skibida, *Angew. Chem. Int. Ed. Engl.*, **8**, 97 (1969); R. A. Sheldon and J. K. Kochi, "Advances in Catalysis," ed by D. D. Eley, Academic Press, Vol. 25, New York (1976), p. 272.
2) A. J. Chalk and J. F. Smith, *Trans. Faraday Soc.*, **53**, 1235 (1957); G. M. Bulgakova, I. P. Skibida, E. G. Rukhadaze, and G. P. Talyzenkova, *Kinet. Katal.*, **12**, 359 (1971).
3) F. W. Heaton and N.Uri, *J. Lipid Res.*, **2**, 152 (1961).
4) R. Griesser and H. Sigel, *Inorg. Chem.*, **10**, 2229 (1971).
5) N. Rabjohn, *Org. Synth.*, Coll. Vol. IV, 895 (1963).
6) K. Ishida, Master's Thesis, Univ. of Tokyo (1973).
7) A. J. Chalk and J. F. Smith, *Trans. Faraday Soc.*, **53**, 1214 (1957).
8) T. Inoue, *Rev. Polarog. (Kyoto)*, **17**, 29 (1971); C. K. Mann and K. K. Barnes, "Electrochemical Reactions in Nonaqueous Systems," Marcel Dekker, New York (1970).
9) C.Oldam, "Progress in Inorganic Chemistry," ed by F. A. Cotton, Interscience, Vol. 10, New York (1966), p. 243.
10) L. E. Orgel, "An Introduction to Transition-Metal Chemistry," 2nd ed, Methuen, London (1966).

The Reductive Deacylation of the Knoevenagel Condensates by the Use of the Tetracarbonylhydridoferrate(0) Anion. A New Synthetic Route of Ketones from Aldehydes

Masakazu YAMASHITA,* Yoshihisa WATANABE,** Take-aki MITSUDO,** and Yoshinobu TAKEGAMI**

Department of Applied Chemistry, Faculty of Engineering, Doshisha University, Kamigyo-ku, Kyoto 602

*** Department of Hydrocarbon Chemistry, Faculty of Engineering, Kyoto University, Sakyo-ku, Kyoto 606*

(Received July 18, 1977)

The Knoevenagel condensates prepared from 2,4-pentanedione with aldehydes were allowed to react with the tetracarbonylhydridoferrate(0) anion in ethanol to give reductively deacylated monoketones in high yields. However, the exclusive reduction of the α,β-unsaturated double bond of the same condensates was encountered when the reaction was carried out in such a solvent as tetrahydrofuran and acetone. The Knoevenagel condensates, derived from the reaction of ethyl acetoacetate and/or ethyl benzoylacetate with aldehydes, were simply reduced even in ethanol. The reaction mechanism is briefly discussed.

The tetracarbonylhydridoferrate anion $[FeH(CO)_4]^-$ (**1**) is a useful reagent for the dehalogenation of organic halides,[1,2] the reductive alkylation[3,4] and amination[5,6] of carbonyl compounds, the desulfurization of thioketones,[7] and so on. The **1** ferrate is also an effective hydrogenating reagent for α,β-unsaturated carbonyl compounds, giving saturated ones.[8] Conjugated dienes can be converted into monoenes,[9] and the C=N double bond of *N*-benzylideneaniline can also be hydrogenated to give *N*-benzylaniline.[5]

Previously, we briefly reported the reaction of **1** with 3-alkylidene-2,4-pentanedione, **2**, a Knoevenagel condensate.[10] In this reaction, reductively deacetylated products, alkyl methyl ketones, **3**, were obtained in high yields.

This study will deal with the unusual reaction of **1** with 3-alkylidene-2,4-pentanediones, along with several other types of Knoevenagel condensates, **5**, **6**, **7**, and **8**.

Results and Discussion

3-Alkylidene-2,4-pentanediones, prepared from aldehydes and 2,4-pentanedione, such as 3-butylidene-2,4-pentanedione and 3-benzylidene-2,4-pentanedione, were allowed to react with an equimolar amount of **1** for 1 h at room temperature under an argon atmosphere in ethanol. The reaction proceeded rapidly, with a color change from pale yellow to red-brown, giving only the corresponding alkyl methyl ketones, **3**, in high yields (Table 1).

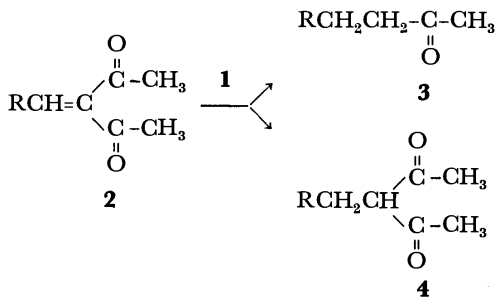

Table 1 shows that this reaction is dramatically affected by the solvent employed. In ethanol, the methyl ketones, **3**, were unexpectedly obtained as products, whereas in tetrahydrofuran or acetone, only the expected reduced products, **4**, were isolated.

The crude condensates, **2**, prepared from 2,4-pentanedione and aldehydes after the removal of the unreacted substrates by distillation, could be converted into **3** smoothly. The results are shown in Table 2.

In the reduction of enamines,[11] Schiff's bases,[12] or α,β-unsaturated carbonyl compounds[12] with **1**, the yields of the products, amines or saturated carbonyl compounds, do not exceed 1.0 mol*** under an argon or nitrogen atmosphere. However, under a carbon monoxide atmosphere, the reaction proceeds with the absorption of carbon monoxide, yielding the products in amounts of about 2—3 mol without forming carbonylated products. In these reactions, it is considered that a major portion of the carbon monoxide absorbed is used to generate the pentacarbonyliron, which is then converted by the base into the ferrate, **1**.

The reaction of **2** (R=Ph) with **1** gave 1.6 mol of 4-phenyl-2-butanone, **3** (R=Ph), even under an argon atmosphere, showing that an active species was reproduced in the course of this reaction. In the reaction in tetrahydrofuran, the yield of 3-benzyl-2,4-pentanedione (**4**, R=Ph) did not exceed 1.0 mol under argon. Now we assume that the carbon monoxide used for the reproduction of pentacarbonyliron might be provided by the eliminated acetyl group.

In further KOH is added to the reaction solution, **1** may be generated according to Eq. 1.[13] Therefore, we examined the effect of the addition of KOH. The results are shown in Table 3.

$$Fe(CO)_5 + 3KOH \longrightarrow KHFe(CO)_4 + K_2CO_3 + H_2O. \quad (1)$$

The yield of **3** (R=Ph) increased to about 4 mol at a maximum (Run 15), supporting the above assumption. However, the addition of a large excess of KOH disturbed the reaction (Run 16). In this case, the concentration of the active hydride, **1**, decreases according to

$$KHFe(CO)_4 + KOH \rightleftarrows K_2Fe(CO)_4 + H_2O. \quad (2)$$

In order to investigate the scope and limitation of this reductive deacylation reaction with **1**, the re-

* To whom correspondence should be addressed.

*** 'mol' means mol/mol-ferrate hereafter.

TABLE 1. THE REACTION OF $[FeH(CO)_4]^-$ WITH 3-ALKYLIDENE-2,4-PENTANEDIONE[a)]

Run	$RCH{=}C(COCH_3)_2$ R	Solvent	Product	Yield (%)[b)]
1	$CH_3CH_2CH_2-$	EtOH	$CH_3CH_2CH_2CH_2CH_2-C(=O)-CH_3$	69 (89)
2	$(CH_3)_2CH-$	EtOH	$(CH_3)_2CHCH_2CH_2C(=O)CH_3$	60
3	CH_3CH_2-	EtOH	$CH_3CH_2CH_2CH_2C(=O)CH_3$	71 (92)
4		EtOH	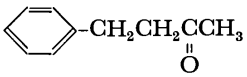	76 (90)
5		THF	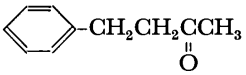 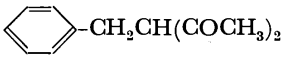	— 75
6		Acetone	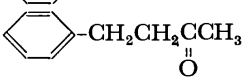 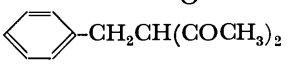	trace 65
7		EtOH	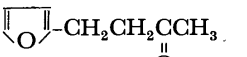	82

a) At room temperature for 1 h under an argon atmosphere. b) Isolated yield based on the amount of the condensate. Yields in parentheses were determined by GLPC using internal standards.

TABLE 2. THE SUCCESSIVE REACTION OF A MIXTURE OF ALDEHYDES AND 2,4-PENTANEDIONE WITH $[FeH(CO)_4]^-$ IN ETHANOL[a)]

Run	Aldehyde	Product	Yield (%)[b)]
8	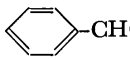	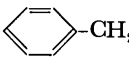	56
9	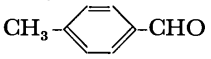	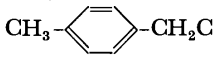	54
10	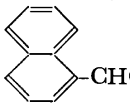	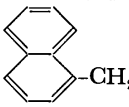	63
11	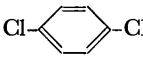	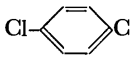	58
12	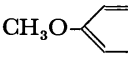	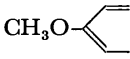	47
13	$CH_3CH_2CH_2CHO$	$CH_3CH_2CH_2CH_2CH_2COCH_3$	57

a) At room temperature under an argon atmosphere. b) Isolated yield based on the amount of aldehydes.

TABLE 3. EFFECT OF ADDED KOH IN THE REACTION OF 3-BENZYLIDENE-2,4-PENTANEDIONE WITH $[FeH(CO)_4]^-$ IN ETHANOL[a)]

Run	3-Benzylidene-2,4-pentanedione (mmol)	**1** (mmol)	Added KOH (mol/mol-ferrate)	Yield of 4-phenyl-2-butanone (mmol)
14	22	5.5	0	8.0
15	22	5.5	5.5	21.0
16	20	1.0	100	0.7

a) At room temperature for 1 h under an argon atmosphenere.

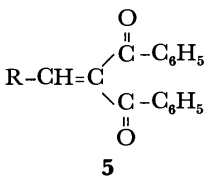

5

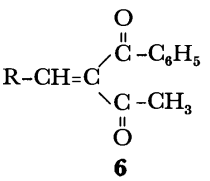

6

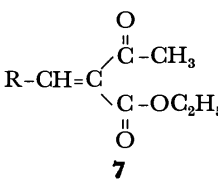

7

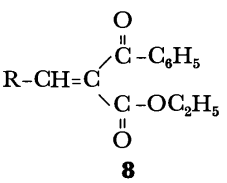

8

action of the other Knoevenagel condensates, **5**, **6**, **7**, and **8**, with **1** was attempted. The results are shown in Table 4.

2-Benzylidene-1,3-diphenyl-1,3-propanedione, **5**, gave 1,3-diphenyl-1-propanone exclusively. The reaction of **6** with **1** afforded 4-phenyl-2-butanone (17%) and 1,3-diphenyl-1-propanone (69%) respectively. This shows that the acetyl group is more releasable than the

Table 4. The reaction of several Knoevenagel condensates with $[FeH(CO)_4]^-$ in ethanol

Run	Knoevenagel condensate	Reaction conditions		Product	Yield (%)
		Temp (°C)	Time (h)		
17	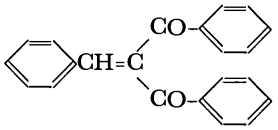	r. t.	2	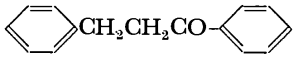	80
18	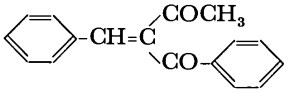	r. t.	2	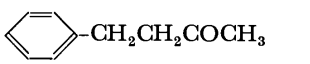	17
				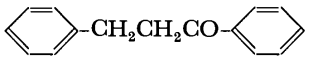	69
19	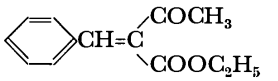	r. t.	17	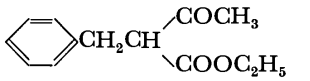	90
				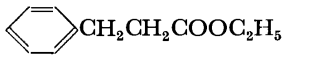	< 1
20	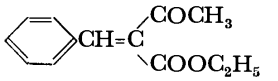	80	5	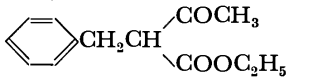	40
				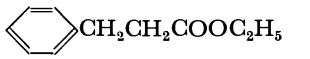	< 1
				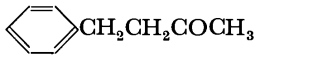	39
21	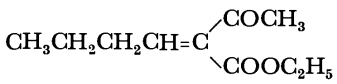	r. t.	24	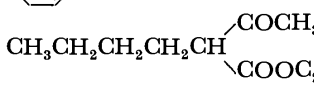	70
					6
				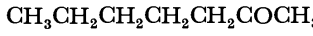	< 1
22	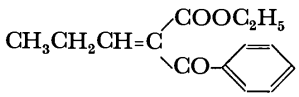	r. t.	18	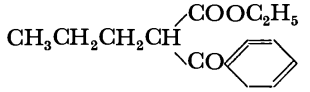	70

benzoyl group under these reaction conditions. However, the reaction of the **7** condensates with **1** in ethanol gave simply reduced compounds, along with a trace of deacetylated compounds, at room temperature. However, at higher temperatures, 4-phenyl-2-butanone was obtained in a 39% yield. The condensate of ethyl benzoylacetate and propionaldehyde (**8**, R=Et) gave similar results.

A tentative mechanism of the reductive deacylation reactions of 3-benzylidene-2,4-pentanedione with **1** is illustrated in Scheme 1. First, **1** attacks an olefinic

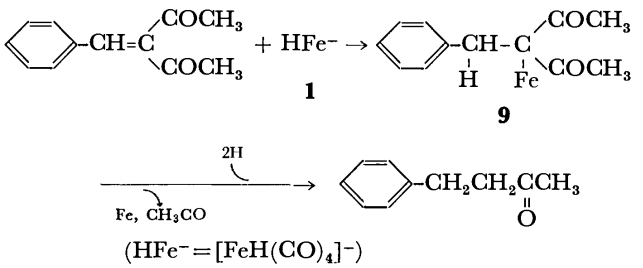

Scheme 1.

double bond of **2** to give a complex, **9**. It has been reported that the iron atom is attached to the α-carbon of the olefinic bond in the reduction of α,β-unsaturated carbonyl compounds[8] and the hydroacylation of α,β-unsaturated carboxylic esters.[14] The elimination of carbonyliron and acetyl groups, followed with the abstraction of the proton from the solvent, would then give **3**. Some of the products obtained by the elimination of acyl and carbonyliron groups are assumed to be exist as acylcarbonylferrates ($[RCOFe(CO)_4]^-$), which are then protonated to give aldehydes.[15,16] In the reaction of **1** with 2-benzylidenebenzoylacetone, about 10% of the benzaldehyde was detected in the reaction mixture by GLPC, a finding which would support the formation of acylcarbonylferrate.

Experimental

All the melting points and boiling points are uncorrected. The acetylacetone, dibenzoylmethane, benzoylacetone, ethyl acetoacetate, ethyl benzoylacetate, and aldehydes were all commercial products. The benzene, tetrahydrofuran, and piperidine were obtained from commercial sources and were dehydrated and distilled before use. The pentacarbonyliron was also a commercial product and was used without purification.

3-Alkylidene-2,4-pentanedione. General procedure was as follows. After an equimolar mixture of 2,4-pentanedione and an aldehyde had been cooled in an ice-bath, 0.4—0.5 mol% of piperidine was added, drop by drop; thereafter the mixture was stirred for 5 h at 0 °C and then at room temperature for 5 h. The reaction mixture was then subjected to fractional distillation. The yields were 60—75% in all cases. The analytical data were as follows. 3-Propylidene-2,4-pentanedione; bp 81—89 °C/14.5 mmHg. Found: C, 68.64; H, 8.80%. Calcd for $C_8H_{12}O_2$: C, 68.54; H, 8.90%. 3-Butylidene-2,4-pentanedione; bp 104—109 °C/13 mmHg. 3-Benzylidene-2,4-pentanedione; bp 108 °C/0.09 mmHg.

Found: C, 76.30; H, 6.61%. Calcd for $C_{12}H_{12}O_2$: C, 76.57; H, 6.43%. 3-Furfurylidene-2,4-pentanedione; bp 116 °C/0.8 mmHg (lit,[17] bp 128—129 °C/4 mmHg). 3-Isobutylidene-2,4-pentanedione; bp 89—93 °C/14 mmHg. These compounds gave satisfactory IR and NMR spectroscopic data.

Other Knoevenagel Condensates. The condensates of aldehydes with ethyl acetoacetate or ethyl benzoylacetate were prepared according to a method similar to that used for 3-alkylidene-2,4-pentanediones. Ethyl 2-acetyl-2-hexenoate; bp 100—109 °C/15 mmHg. Found: C, 65.17; H, 8.67%. Calcd for $C_{10}H_{16}O_3$: C, 65.19; H, 8.76%. Ethyl 2-acetyl-3-phenyl-2-propenoate; bp 110—114 °C/0.2 mmHg. Found: C, 71.58; H, 6.51%. Calcd for $C_{13}H_{14}O_3$: C, 71.54; H, 6.47%. Ethyl 2-benzoyl-2-pentenoate; bp 108—109 °C/0.38 mmHg. Found: C, 72.35; H, 6.69%. Calcd for $C_{14}H_{16}O_3$: C, 72.39; H, 6.94%. Satisfactory IR and NMR data were obtained for these compounds. The 2-benzylidenedibenzoylmethane and 2-benzylidenebenzoylacetone were prepared according to the methods described in the literature.[18]

*Preparation of Tetracarbonylhydridoferrate (**1**).* All the reactions were carried out in a 200-ml, three-necked flask equipped with a buret and a magnetic stirrer under an argon atmosphere. **1** in ethanol was prepared according to the method described in a previous paper.[19] **1** in tetrahydrofuran was prepared as follows. To a stirred suspension of the sodium amalgam in dry tetrahydrofuran (50 ml) prepared from mercury (100 g) and sodium (0.70 g), pentacarbonyliron (1.5 ml, 11 mmol) was added, drop by drop, under argon. The mixture was then stirred for 2 h at room temperature, and the excess of the amalgam was removed through a side arm. The suspension containing the dianion, disodium tetracarbonylferrate(−II) ($Na_2Fe(CO)_4$), was treated with acetic acid (11 mmol).[20] **1** in acetone was prepared by adding 1.5 ml (11 mmol) of $Fe(CO)_5$ to a mixture of acetone (30 ml) and a 10-M KOH aqueous solution (3 ml).

*Reaction of the Knoevenagel Condensates with **1**.* The reaction of 3-benzylidene-2,4-pentanedione with **1** illustrates a typical procedure. To an ethanol solution (33 ml) of **1** (11 mmol), an ethanol solution of 3-benzylidene-2,4-pentanedione (11 mmol) was added, after which the reaction mixture was stirred for 1 h at room temperature under argon. After the solvent had then been evaporated, the residue was extracted with diethyl ether and the ether layer was washed twice with water and dried over sodium sulfate. The solvent was removed *in vacuo*, and the liquid remaining was then subjected to fractional distillation. The product was identified as 4-phenyl-2-butanone by IR, NMR, and GLPC using an authentic sample; bp 106 °C/12.5 mmHg. Yield, 76% (GLPC yield, 90%). The analytical data of some of the other results were as follows. 4-(2-Furyl)-2-butanone; bp 76—77 °C/13 mmHg. Found: C, 69.29; H, 7.23%. Calcd for $C_8H_{10}O_2$: C, 69.54; H, 7.30%. 3-Benzyl-2,4-pentanedione; bp 95—97 °C/0.25 mmHg (lit,[21] bp 115—118 °C/4 mmHg). Found: C, 75.87; H, 7.46%. Calcd for $C_{12}H_{14}O_2$: C, 75.76; H, 7.42%. Ethyl 2-acetyl-3-phenylpropionate; bp 85 °C/0.06 mmHg. Found: C, 71.51; H, 7.53%. Calcd for $C_{13}H_{16}O_3$: C, 70.88; H, 7.32%.

*The Successive Reaction of the Mixtures of Aldehydes and 2,4-Pentanedione with **1**.* The synthesis of 4-(*p*-tolyl)-2-butanone from *p*-tolualdehyde illustrates a typical procedure. After a mixture of *p*-tolualdehyde (11 mmol) and 2,4-pentanedione had been cooled in an ice-bath, 0.05 mmol of piperidine was added, drop by drop, by the use of a micro syringe, after which the mixture was stirred for 5 h at 0 °C and then at room temperature for 5 h. The reaction mixture was then evaporated, and the residual liquid was added to the ethanol solution of **1** (11 mmol). The mixture was stirred for 1 h at room temperature under argon. After the solvent had been evaporated, the residue was extracted with diethyl ether, and the ether layer was washed twice with water and dried over sodium sulfate. The solvent was evaporated, and the liquid remaining was subjected to fractional distillation. The product was identified as 4-(*p*-tolyl)-2-butanone by IR, NMR, and elemental analysis; bp 69 °C/0.6 mmHg; yield, 54%. Found: C, 81.36; H, 8.84%. Calcd for $C_{11}H_{14}O$: C, 81.44; H, 8.70%. The analytical data of the other results were as follows. 4-(α-Naphthyl)-2-butanone; bp 100—102 °C/0.15 mmHg. Found: C, 84.83; H, 7.10%. Calcd for $C_{14}H_{14}O$: C, 84.81; H, 7.12%. 4-(*p*-Methoxyphenyl)-2-butanone; bp 100—103 °C/0.23 mmHg. 4-(*p*-Chlorophenyl)-2-butanone; bp 89—90 °C/0.26 mmHg. Found: C, 65.55; H, 6.25%. Calcd for $C_{10}H_{11}ClO$: C, 65.76; H, 6.07%. Satisfactory IR and NMR data were obtained for these compounds.

References

1) Y. Takegami, Y. Watanabe, T. Mitsudo, and T. Okajima, *Bull. Chem. Soc. Jpn.*, **42**, 1992 (1969).
2) H. Alper, *Tetrahedron Lett.*, **1975**, 2257.
3) G. F. Cainelli, M. Panunzio, and A. Umani-Ronch, *Tetrahedron Lett.*, **1973**, 2491.
4) G. F. Cainelli, M. Panunzio, and A. Umani-Ronch, *J. Chem. Soc., Perkin Trans. 1*, **1975**, 1273.
5) Y. Watanabe, S. C. Shim, T. Mitsudo, M. Yamashita, and Y. Takegami, *Bull. Chem. Soc. Jpn.*, **49**, 2302 (1976), and the references cited therein.
6) G. P. Boldrini, M. Panunzio, and A. Umani-Ronch, *Synthesis*, **1974**, 733.
7) H. Alper, *J. Org. Chem.*, **40**, 2694 (1975).
8) R. Noyori, I. Umeda, and T. Ishigami, *J. Org. Chem.*, **37**, 1542 (1972).
9) Y. Takegami, Y. Watanabe, I. Kanaya, T. Mitsudo, T. Okajima, Y. Morishita, and H. Masada, *Bull. Chem. Soc. Jpn.*, **41**, 2990 (1968).
10) M. Yamashita, Y. Watanabe, T. Mitsudo, and Y. Takegami, *Tetrahedron Lett.*, **1975**, 1867.
11) T. Mitsudo, Y. Watanabe, M. Tanaka, S. Atsuta, K. Yamamoto, and Y. Takegami, *Bull. Chem. Soc. Jpn.*, **48**, 1506 (1975).
12) M. Yamashita, unpublished results.
13) P. Krumholz and H. M. A. Stettiner, *J. Am. Chem. Soc.*, **71**, 3035 (1949).
14) T. Mitsudo, Y. Watanabe, M. Yamashita, and Y. Takegami, *Chem. Lett.*, **1974**, 1385.
15) M. P. Cooke, Jr., *J. Am. Chem. Soc.*, **92**, 6080 (1970).
16) Y. Watanabe, M. Yamashita, T. Mitsudo, M. Igami, and Y. Takegami, *Bull. Chem. Soc. Jpn.*, **48**, 2490 (1975), and the references cited therein.
17) H. Midorikawa, *Bull. Chem. Soc. Jpn.*, **27**, 213 (1954).
18) M. Sekiya and K. Suzuki, *Chem. Pharm. Bull.*, **18**, 153 (1970).
19) Y. Takegami, Y. Watanabe, H. Masada, and I. Kanaya, *Bull. Chem. Soc. Jpn.*, **40**, 1456 (1967).
20) $[FeH(CO)_4]^-$ was quantitatively isolated as a bis(triphenylphosphine)iminium salt; see Ref. 14.
21) Y. Murakami and K. Nakamura, *Bull. Chem. Soc. Jpn.*, **39**, 901 (1966).

The Photo-cycloaddition of 3-Cyano-2,4-pentanedione with Cyclohexene and Its Quenching by Enol Ether

Masaru TADA, Hidetoshi HARADA, and Kyo MIURA

Department of Chemistry, School of Science and Engineering, Waseda University, Shinjuku, Tokyo 160

(Received July 28, 1977)

The 1,3-dicarbonyl compound, with an electro-negative substituent, 3-cyano-2,4-pentanedione, gives the photo-addition product with cyclohexane. The adduct must be formed by the retro-aldol reaction of the "2+2" cyclo-addition product and the hemiacetalization of the resulting 1,5-dicarbonyl compound. Enol ether, with a lower ionization potential, does not photoadd to 3-cyano-2,4-pentanedione but quenches the photoaddition between 3-cyano-2,4-pentanedione and cyclohexene. The solvent effect, the ionization potential, and quenching experiments show that the photoaddition follows a process involving a singlet excited complex.

It is well known that 2,4-pentanedione (**1**), a non-cyclic 1,3-dicarbonyl compound, gives a photoaddition product with olefin through its enol form. The classical work by de Mayo *et al.*,[1] however, was not followed by frequent application, even though this type of reaction seems to be a useful method for the preparation of 1,5-diketone and cyclohexenone derivative by the base-catalyzed condensation of the diketone (Eq. 1). To determine the scope and limitation of this type of reaction, we attempted the photocycloaddition of Compounds **2**—**6** with cyclohexene. None of these compounds, however, showed any photo-reactivity. Several factors may influence the reactivity of these compounds such as; a) the electronic configuration of the lowest excited state, $n\pi^*$ or $\pi\pi^*$; b) the importance of the enol form in keto-enol equilibrium; c) the fixation of the cyclic *s-cis* conformation by intramolecular hydrogen bonding, and d) the effect of excitation on the intramolecular hydrogen bonding. Non-cyclic 1,3-dicarbonyl compounds with an additional electronegative group, such as methyl 2,4-dioxopentanoate (**7**) or 2-(methoxycarbonyl)-1,3-propanedial (**8**), have been reported to give photo-adducts with olefins.[2,3] This fact strongly suggests the importance of charge transfer interaction between these electronegative dicarbonyl compounds and olefin for the photo-cycloaddition. We selected 3-cyano-2,4-pentanedione (**9**) as a dicarbonyl compound and wish to report on the nature of the photo-cycloaddition of **9** with olefin.

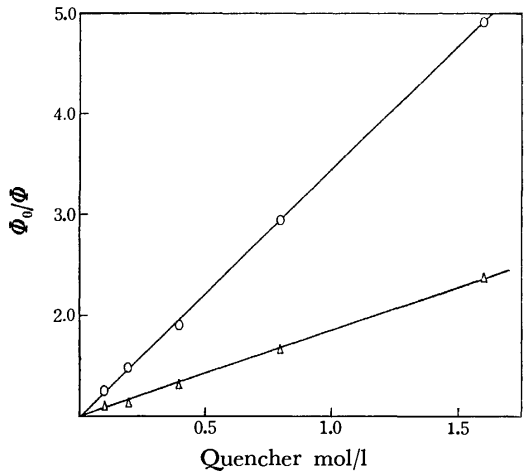

Fig. 1. Quenching of photo-cycloaddition of **9** to cyclohexene by enol ethers.

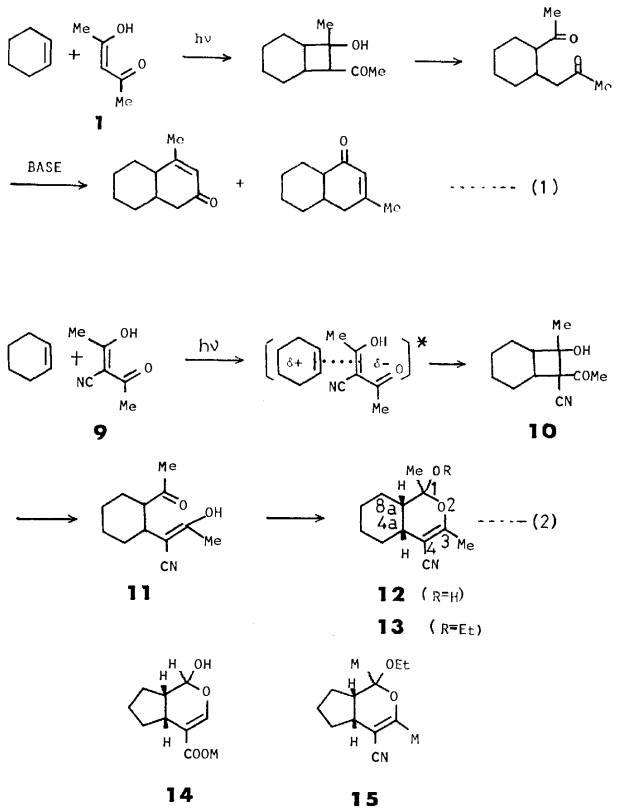

The irradiation of 3-cyano-2,4-pentanedione (**9**) in the presence of excess cyclohexene in variety of solvents gave the photoadduct **12** in variable yields; a cyclic ethyl acetal, **13**, was obtained when absolute ethanol was used as the solvent. The structure of **12** was deduced from the spectral data and by analogy with the structure of the adduct between 2-(methoxycarbonyl)-1,3-propanedial (**8**).[3]

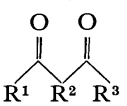

	R_1	R_2	R_3
1	Me	H	Me
2	Me	Me	Me
3	Me	Ph	Me
4	Me	H	Ph
5	Me	H	OMe
6	Ph	H	OEt
7	Me	H	COOMe
8	H	COOMe	H
9	Me	CN	Me

As a precedent, the photoadduct **12** must be derived from the 2+2 adduct, **10**, of 3-cyano-2,4-pentanedione and cyclohexene, which opens the cyclobutane ring by means of retro-aldol-type cleavage, giving the 1,5-dicarbonyl compound, **11**, followed by the hemiacetalization (Eq. 2). The sharp IR absorptions at 3420, 2210, and 1617 cm^{-1} show the presence of hydroxyl, conjugate cyano, and conjugate enol ether groups respectively. The NMR signals at $\delta=1.53$ (singlet) and 2.10 ppm (doublet, $J=2$ Hz) are due to the methyls at the hemiacetal carbon (C_1) and enol ether moieties. The long-range coupling of the latter signal with the hydrogen at C_{4a} (2.96 ppm) has been evidenced by a decoupling experiment.[4] The NMR signal at $\delta=2.96$ due to the hydrogen at C_{4a} is a multiplet with the half-band width of 10 Hz, which shows the lack of vicinal diaxial coupling and the equatorial nature of the H_{4a} on the cyclohexane ring. The observation of Dreiding molecular models indicates that H_{4a} bisects the methylene at C_5 and that the dihedral angle between H_{4a} and H_{8a} is *ca.* 50°. The vicinal couplings between these hydrogens, in addition to the long-range coupling between H_{4a} and C_3-methyl, meet the requirements for H_{4a} being equatorial. These aspects of the NMR spectrum lead us to deduce that the stereochemistry of the ring junction of the adduct is *cis*.

The photoreaction between 3-cyano-2,4-pentanedione (**9**) and cyclopentene in absolute ethanol gave a similar product, **15**, with *cis*-ring fusion, this is completely parallel to the photoreaction of 2-(methoxycarbonyl)-1,3-propanedial to cyclopentene to give the adduct **14**. The photoreaction of **9** was carried out in a variety of solvents, such as hexane, benzene, ether, THF, ethanol, methanol, and methanol–acetonitrile (1 : 1); the yield of the adduct **12** is generally better in alcoholic solvents than in non-polar solvents or in acetonitrile. Casal *et al.*[5] reported that an aromatic 1,3-dicarbonyl compound, **4**, adds photochemically to styrenes or stilbens, though in our trial **4** failed to enter the photo-addition to cyclohexene. From the discussion above, the 1,3-dicarbonyl system with an electronegative group or the conjugated olefin with an aromatic system seems to be required for the photo-addition. The UV spectrum of mixture of **9** and cyclohexene does not show any evidence for the formation of a CT complex, at least in dilute concentrations, in the ground state. These results, in conjunction with the solvent effect, suggest that the photo-addition takes an excited complex process of charge transfer. The attempted photoreaction of **9** with an olefin having a lower ionization potential, such as ethyl vinyl ether (I_p: 8.6 eV),[6] 2,3-dihydro-1,4-dioxin (I_p: *ca.* 7.6 eV),[7] or *cis*-1,2-dimethoxyethylene (I_p: 8.0 eV)[6] in ether, does not give any photoadduct, but the starting material is recovered. On the other hand, cyclohexene (I_p: 8.9 eV), with higher ionization potential, shows photoreactivity in the same solvent; hence, the excited complexes with olefins having lower ionization potentials are considered to be dissociated into radical-ion pairs by electron transfer in ether. Since the excited complex formation is favored with such olefins, enol ethers are expected to quench the photo-addition between **9** and cyclohexene. Such was found to be true in the photo-addition of 2-buten-4-olide with olefins and its quenching by 1,1-dimethoxyethylene.[9] Stern-Volmer plots of the quenching experiments on the photoaddition of **9** indeed show a straight line with the slopes of 2.46 and 0.85 M^{-1} for 2,3-dihydro-1,4-dioxin and ethyl vinyl ether respectively (Fig. 1). The importance of charge transfer and electron transfer for this quenching is evident from the quenching-rate constants being dependent upon the ionization potential of the quencher. 1,3-Pentadiene (I_p: 8.7 eV)[8] and oxygen do not quench the photo-addition of **9** in a normal manner for a triplet quenching, but a higher concentration of 1,3-pentadiene quenches the reaction and gives the 1 : 1 adduct, in a poor yield, from the excited complex between **9** and 1,3-pentadiene.

In conclusion, the photo-cycloaddition of 3-cyano-2,4-pentenedione (**9**) to olefin takes a singlet excited complex process, and the cyclization competes with the electron-transfer process, employing **9** as an electron accepter (A) and olefin as a donor (D).

$$\text{"A"} \xrightarrow{h\nu} [\text{A}]^{*1} \xrightarrow{\text{"D"}} [\text{A}\cdots\cdots\text{D}]^{*} \longrightarrow \text{Adduct}$$

$$\downarrow \text{solvent}$$

$$[\text{A(solvent)}]^{-} + [\text{D(solvent)}]^{+}$$

Experimental

Preparation of Materials. The 3-cyano-2,4-pentanedione (**9**) (mp 51 °C, UV: λ_{max}^{EtOH} 276 nm (10300)), was synthesized by the method of Traub[10] from 2,4-pentanedione and cyanogen generated by the addition of a sodium cyanide solution to a solution of copper(II) sulfate.[11] The cyclohexene was prepared by the acid-catalyzed dehydration of cyclohexanol and was distilled before use. Commercially available ethyl vinyl ether was distilled (bp 36—37 °C) immediately before use to remove the stabilizer. The 2,3-dihydro-1,4-dioxin (bp 94—95 °C) was prepared by the method of Sammerbell *et al.*[12,13] by the dechlorination of *trans*-2,3-dichloro-1,4-dioxane. The *cis*-1,2-dimethoxyethylene (bp 97 °C) was prepared by the method of Shostakoviskii *et al.*[14] by the gas-phase elimination of methanol from 1,1,2-trimethoxyethane[15] catalyzed by silica gel–BaO at 350—370 °C. The collection of the fraction boiling at 97 °C by repeated distillations gave *cis*-1,2-dimethoxyethylene.

Photo-cycloaddition of 3-Cyano-2,4-pentanedione(9) with Cyclohexene. To **9** (125 mg, 1 mmol) and cyclohexene (5 g, 60 mmol) we added one of the solvents, and the total volume was adjusted to 10 ml. The solution, placed in a Pyrex tube was sealed by means of a rubber septum and the solution was bubbled by argon for several minutes through a syringe needle. Irradiation was carried out externally with a 450-W high-pressure mercury lamp mounted in the center of a rotary irradiation apparatus (Rikosha Merry-go-round type; the distance between the lamp and the tube is *ca.* 5 cm) for 50—60 h, the reaction being monitored by TLC analyses. In the case of the methanol solution, the starting **9** disappeared after 55 hs' irradiation, at this time the solution was condensed *in vacuo*. The chromatography of the residue on alumina (Merck act. II-III) eluted with 1) benzene, 2) benzene–ether (1:1), and 3) ether gave a crystal of the adduct **12** from the benzene-ether eluate (125 mg, 60%). **12**, mp 113.8—114.3

°C(recrystalyzed from ether). Found: C, 70.01; H, 8.37; N, 6.98%. Calcd for $C_{12}H_{17}NO_2$: C, 69.54; H, 8.27; N, 6.76%. MS (80 eV): *m/e*(%) 207(M^+, 10), 189(7), 165(50), 164(39), 149(19), 136(53), 125(100), 122(75), 81(72), 71(66), and 43(92). UV: λ_{max}^{EtOH} 236 nm (16900). IR(Nujol): 3420, 2210, 1617, 1275, 1155, and 1065 cm^{-1}. NMR($CDCl_3$): (δ) 4.00(3H, s), 2.96(1H, diff. s $W_{1/2}$: 10 Hz), 2.10(3H, d, J=2 Hz), 1.53(3H, s), and 2.1—0.8 ppm(10H). The yield of the adduct **12** was best in methanol or ethanol (60—70%), and worse in a non-polar solvent or in acetonitrile. Ethyl acetal was obtained when absolute ethanol was used as a solvent. The refluxing of the methanol solution of **9** without irradiation as a dark reference gave no adduct at all.

Quenching Experiments. *a) Quenching by Enol Ether or 1,3-Pentadiene*: A solution of 3-cyano-2,4-pentenedione (**9**) (0.05 mol/l), cyclohexene (1.5 mol/l), and 0—0.6 mol/l of a quencher (2,3-dihydro-1,4-dioxin, ethyl vinyl ether, or 1,3-pentadiene) in ether was placed in Pyrex tubes and irradiated by using a rotary irradiation apparatus after the deoxygenation of the system. After irradiation for 17 h, GLC analyses showed that the starting material was still a major component in the reaction mixture; to each reaction mixture we added the same amount of 1,2-di-*m*-tolylethane as an internal reference. Stern-Volmer plots obtained by GLC analyses of the adduct in each reaction mixture gave the straight lines with the slopes of 2.46 and 0.85 M^{-1} for 2,3-dihydro-1,4-dioxin and ethyl vinyl ether respectively.

b) Quenching by Oxygen: The mixture of **9** (0.05 mol/l) and cyclohexene (1.5 mol/l) in ether was placed in two Pyrex tubes; one of the solutions was bubbled by oxygen under cooling in an ice-salt bath, while the other was purged with argon. Irradiation of both solutions for 15 h and GLC analyses did not show any distinct difference in the photoreactivity.

References

1) P. de Mayo, H. Takeshita, and A. B. M. A. Sattar, *Proc. Chem. Soc.*, **1962**, 119; *Can. J. Chem.*, **41**, 440 (1963).
2) H. Takeshita and S. Tanno, *Bull. Chem. Soc. Jpn.*, **46**, 880 (1973).
3) (a) J. J. Partridge, N. K. Chadha, and M. R. Uskovic, *J. Am. Chem. Soc.*, **95**, 532 (1973); (b) G. Büchi, J. A. Carlson, J. E. Powel, Jr., and L. F. Tietze, *ibid.*, **95**, 540 (1973).
4) D. Gagnaire and E. Payo-Subiza, *Bull. Soc. Chim. Fr.*, **1963**, 2633.
5) P-F. Casals, J. Ferard, and R. Ropert, *Tetrahedron Lett.*, **1976**, 3077.
6) D. Brith-Smith, A, Gilbert, B, Orger, and H, Tyrrel, *J. Chem. Soc., Chem. Commun.*, **1974**, 334.
7) Calculated from the absorption maximum of the CT-complex between 2,3-dihydro-1,4-dioxin and TCNE in cyclohexane. See M. P. Niemayk, N. E. Shore, and N. J. Turro, *Mol. Photochem.*, **5**, 69 (1973).
8) S. L. Murov, "Handbook of Photochemistry," Marcel Decker, New York (1973), p. 198.
9) M. Tada, T. Kokubo, and T. Sato, *Tetrahedron*, **28**, 2121 (1972).
10) W. Traub, *Chem. Ber.*, **31**, 2944 (1898).
11) G. J. Jang, *Inorg. Synth.*, **5**, 43 (1957).
12) R. K. Summerbell and R. R. Umhoefer, *J. Am. Chem. Soc.*, **61**, 3016 (1939).
13) R. K. Summerbell and L. N. Bauer, *J. Am. Chem. Soc.*, **57**, 2364 (1935).
14) M. F. Schostakovskii, N. V. Kuznetsov, and C-M. Yang, *Izv. Akad. Nauk. USSR, Otd. Khim. Nauk.*, **1962**, 710; *Chem. Abstr.*, **57**, 16389a (1962).
15) S. M. McElvin and C. H. Stammer, *J. Am. Chem. Soc.*, **73**, 915 (1951).

Structure of Aloenin, a New Biologically-active Bitter Glucoside from *Aloe arborescens* var. *natalensis*

Toshifumi HIRATA and Takayuki SUGA*

Department of Chemistry, Faculty of Science, Hiroshima University, Higashisenda-machi, Hiroshima 730

(Received August 5, 1977)

Aloenin, a new bitter glucoside with an inhibitory activity for the gastric juice secretion of rats, was isolated from the leaves of *Aloe arborescens* Mill. var. *natalensis* Berger, and the structure was confirmed to be 4-methoxy-6-(2-β-D-glucopyranosyloxy-4-hydroxy-6-methylphenyl)-2-pyrone by means of chemical, spectroscopic, and X-ray crystallographic methods. Ambiguity in the assignment of 2-pyrone-ring carbon signals was clarified by examination of the ^{13}C-NMR spectra of aloenin and the related compounds.

The plants of Aloe species have been widely used for folk remedies, and their chemical constituents have been studied by several workers.[1-11] Recently, Soeda[12] and Yamamoto[13] have tested the effectiveness of "Cape Aloe" as material for medical treatment. In Japan, *Aloe arborescens* Mill. var. *natalensis* Berger (Kidachirokai or Kidachiaroe in Japanese) has been traditionally used as material for folk remedies for gastro-intestinal disturbances, burns, insect bites, athlete's foot, *etc.* In the course of chemical and biochemical examinations of this plant, a new bitter glucoside, named aloenin, was isolated, its structure being postulated to be a chromene derivative (**1**).[8] Aloenin was identified with aloearbonaside which was independently isolated and named by Makino *et al.*[9] They also assigned the same structure **1** to this compound. It was decided upon mutual agreement to use thereafter the name "aloenin".[8] However, doubts concerning the proposed structure were aroused by anomalous intensity enhancement found in intramolecular nuclear Overhauser effect (NOE)[14] of some derivatives of aloenin, as well as ambiguity in assignments of the ^{13}C-NMR spectrum. The structure of aloenin was reexamined by means of chemical, spectroscopic, and X-ray crystallographic methods, and a report given on a revised structure of aloenin.[15-17] We wish to describe *en bloc* the results of studies on the revised structure **2** for aloenin, the assignment of 2-pyrone-ring carbon signals in the ^{13}C-NMR spectra of aloenin and its derivatives, and tests of the inhibitory activity to the gastric juice secretion of rats.

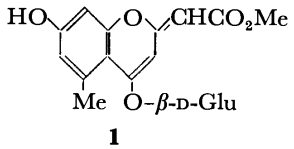

1

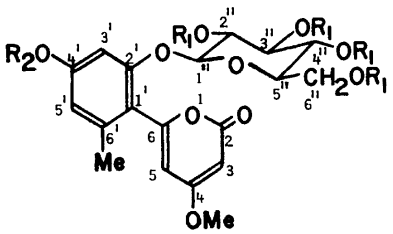

2: $R_1=R_2=H$
5: $R_1=R_2=Me$
10: $R_1=H$, $R_2=Me$
18: $R_1=R_2=Ac$
19: $R_1=Ac$, $R_2=Me$

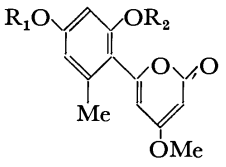

3: $R_1=R_2=H$
4: $R_1=R_2=Me$
6: $R_1=Me$, $R_2=H$
20: $R_1=Me$, $R_2=Ac$
21: $R_1=R_2=Ac$

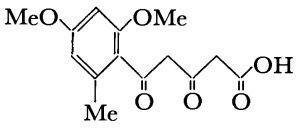

7

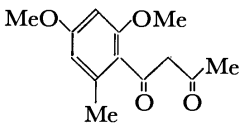

8

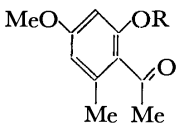

9: R=Me
11: R=β-D-glucosyl
12: R=H
16: R=Ac
17: R=tetra-*O*-acetyl-β-D-glucosyl

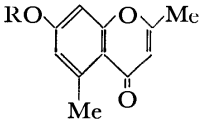

13: R=H
14: R=Me

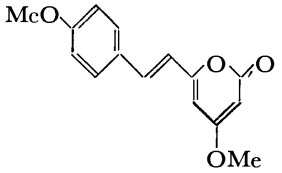

15

* To whom all inquiries should be addressed.

Results and Discussion

Structure Elucidation. Aloenin (**2**)** was isolated as a major component by chromatography on silica gel from the leaf juice of the Aloe plants cultivated in pots. The IR spectrum of aloenin exhibited bands (1714 and 1642 cm^{-1}) due to a conjugated ester or a lactone group. The UV spectrum in an alkaline solution showed a bathochromic shift by 46 nm. The IR and UV spectra closely resemble those of 2-pyrone derivatives.[18] The PMR spectrum in acetone-d_6 showed the presence of an aromatic methyl, a methoxyl, and four olefinic or aromatic protons.

Hydrolysis of aloenin with 3% methanolic hydrochloric acid afforded an aglycone **3** and D-glucose. Methylation of **3** with diazomethane gave a trimethyl ether **4**, whose PMR spectrum in $CDCl_3$ showed signals due to an aromatic methyl, three methoxyl, and four olefinic or aromatic protons. Exhaustive methylation of aloenin by Hakomori's method[19] yielded a hexamethyl ether **5**, which could be hydrolyzed with 3% methanolic hydrochloric acid to a dimethyl ether **6** and 2,3,4,6-tetra-*O*-methyl-D-glucose. This suggests that the sugar moiety is linked with the aglycone through the C-1 hydroxyl group of D-glucose. Methylation of **6** with diazomethane afforded **4**. Treatment of **4** with 5% methanolic potassium hydroxide at room temperature yielded potassium salt of the corresponding β-diketo acid, which on acidification with dilute hydrochloric acid gave an unstable β-diketo acid **7**. The structure of **7** was assigned by the fact that it

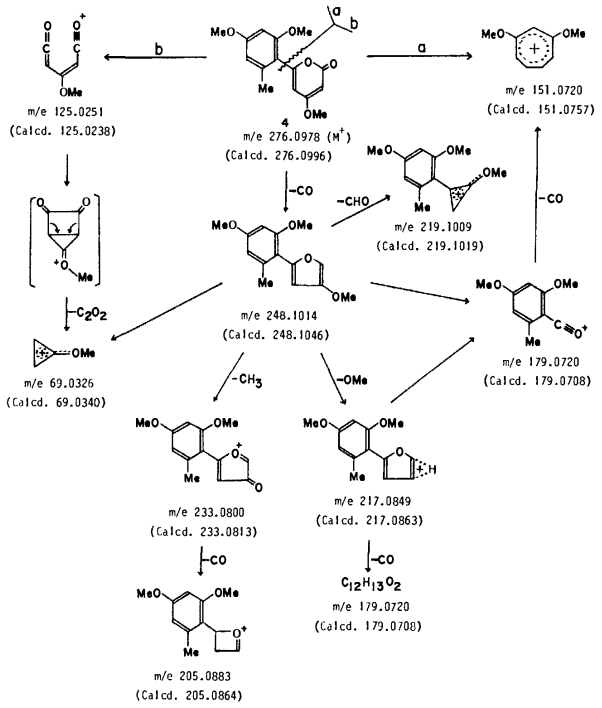

Scheme 1. Fragmentation patterns in the mass spectrum of **4**.

** In this paper, for convenience, the carbon atoms of aloenin (**2**) and its derivatives are numbered as shown in the structural formulae.

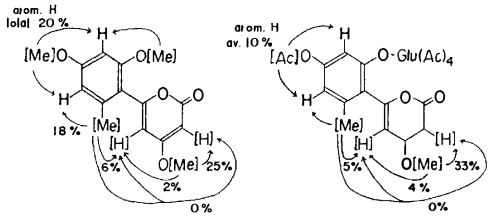

4 **20**

Fig. 1. NOE values of **4** and **20** in $CDCl_3$.

underwent facile decarboxylation on heating to yield 1-(2,4-dimethoxy-6-methylphenyl)butane-1,3-dione (**8**), which was identified by comparison with an authentic sample synthesized from 3,5-dihydroxytoluene by acetoacetic ester condensation. The results demonstrate the presence of a C-4 hydroxylated 2-pyrone skeleton.[20] The product **8** possesses a new acetyl group which is not present in the parent compound **4**. The absence of the acetyl group in **4** warrants a carboxyl group in **7** to be attached to the end of the side chain of **8**. This indicates that the structure of **4** should be represented as 4-methoxy-6-(2,4-dimethoxy-6-methylphenyl)-2-pyrone. A typical mass-spectral fragmentation pattern of C-6 substituted 4-methoxy-2-pyrone derivatives[21] was observed for **4**. The fragments were completely characterized by high-resolution mass-spectral measurements as shown in Scheme 1. The results of the NOE experiments are in line with structure **4** for the dimethyl ether of aglycone **3** as shown in Fig. 1.

Structure **4** was further confirmed by synthesis according to the following procedure. β-Diketone (**8**) prepared from 2,4-dimethoxy-6-methylacetophenone (**9**)[22] was first converted into **7** by treatment with sodium amide in liquid ammonia followed by carbon dioxide.[23] Cyclization of **7** in the presence of acetic anhydride gave 2-pyrone derivative,[23] which was then converted into trimethyl ether **4** with diazomethane. Trimethyl ether **4** derived from aloenin was found to be identical with the synthesized trimethyl ether (**4**). In the course of synthetic studies of **4**, we found that some 2,4,6-trisubstituted acetophenones had been erroneously correlated[24] with their PMR and IR spectra, *i.e.*, the 2,4,6-trisubstituted acetophenones prepared from 3,5-dihydroxytoluene and acetyl chloride by the Friedel-Crafts reaction were identified as 2,6-dimethoxy-4-methyl-, 2,4-dimethoxy-6-methyl-, 2-hydroxy-6-methoxy-4-methyl-, and 2-hydroxy-4-methoxy-6-methyl-acetophenones. However, the acetophenone derivatives were established to be 2,4-dimethoxy-6-methyl-, 2,6-dimethoxy-4-methyl-, 2-hydroxy-4-methoxy-6-methyl-, and 2-hydroxy-6-methoxy-4-methyl-acetophenones, respectively, by reexamination of the signal assignments in the PMR spectra and the conversion of the acetophenone derivatives into known *o*- or *p*-orsellinates.[22]

The alkaline degradation of a monomethylated product **10** of aloenin by refluxing with 5% methanolic potassium hydroxide yielded a glucoside **11**, which could be hydrolyzed to 2-hydroxy-4-methoxy-6-methylacetophenone (**12**)[22] and D-glucose. This shows that the glucose moiety in aloenin is located on the C-2' hydroxyl group of the aglycone **3**. The aglycone (**3**) was converted into 2,5-dimethyl-7-hydroxychromone

TABLE 1. ATOMIC PARAMETERS[a)]

Atoms	x/a	y/b	z/c
C (1)	0.6099 (5)	0.1251 (3)	0.1062 (2)
C (2)	0.5120 (5)	0.0190 (3)	0.1261 (2)
C (3)	0.3271 (5)	0.0134 (3)	0.0950 (2)
C (4)	0.2339 (5)	0.1148 (4)	0.0436 (3)
C (5)	0.3301 (4)	0.2153 (3)	0.0252 (2)
C (6)	0.2608 (4)	0.3284 (3)	−0.0262 (2)
C (7)	0.1785 (4)	0.3207 (3)	−0.1214 (2)
C (8)	0.1097 (4)	0.4264 (3)	−0.1718 (2)
C (9)	0.1237 (4)	0.5396 (3)	−0.1250 (2)
C (10)	0.2029 (4)	0.5496 (3)	−0.0306 (2)
C (11)	0.2727 (4)	0.4448 (3)	0.0194 (2)
C (12)	0.3541 (5)	0.4571 (4)	0.1216 (2)
C (13)	0.3049 (6)	−0.1883 (4)	0.1592 (3)
O (1)	0.5157 (3)	0.2206 (2)	0.0555 (2)
O (2)	0.7755 (3)	0.1420 (3)	0.1296 (2)
O (3)	0.2201 (4)	−0.0833 (3)	0.1084 (2)
O (4)	0.1782 (4)	0.2059 (3)	−0.1626 (2)
O (5)	0.0559 (5)	0.6423 (3)	−0.1743 (2)

a) E.s.d. in parentheses ($\times 10^4$).

TABLE 2. ANISOTROPIC THERMAL PARAMETERS[a)]

Atoms	B_{11}	B_{22}	B_{33}	B_{12}	B_{23}	B_{31}
C-1	2.36	2.20	2.81	0.03	−0.53	0.15
C-2	2.71	2.38	2.58	−0.12	−0.15	0.25
C-3	2.62	2.16	2.84	−0.40	0.31	0.12
C-4	2.46	2.69	3.20	−0.34	−0.38	0.43
C-5	2.05	2.53	2.42	0.14	−0.43	0.04
C-6	2.09	2.53	2.29	0.20	−0.37	0.17
C-7	2.23	2.58	2.74	0.07	−0.37	−0.13
C-8	2.48	2.96	2.28	0.04	−0.48	0.19
C-9	1.81	2.57	2.58	−0.12	−0.31	0.50
C-10	2.34	2.48	2.27	−0.04	−0.06	0.19
C-11	1.88	2.57	2.02	−0.18	−0.03	0.20
C-12	3.13	3.50	1.98	0.26	−0.37	0.12
C-13	4.17	2.51	3.82	−0.08	0.64	0.75
O-1	2.00	2.17	3.14	0.09	−0.51	0.49
O-2	2.29	2.70	5.49	0.00	−1.16	0.67
O-3	2.92	2.69	4.63	−0.70	0.10	0.98
O-4	4.44	2.84	3.42	0.77	−1.68	−1.05
O-5	3.67	2.30	3.42	−0.34	−1.12	0.95

a) In the expression $F_o \cdot \exp[-1/4(B_{11}h^2a^{*2} + \cdots\cdots + B_{13}2hla^*c^*)]$.

(**13**)[25] by treatment with 5% hydrochloric acid. On the other hand, a similar treatment of **6** gave 2,5-dimethyl-7-methoxychromone (**14**). This suggests the presence of a hydroxyl group attached to the C-4′ position of the aromatic ring in aloenin. The authentic chromones, **13** and **14**, were obtained by the Pechman condensation, followed by decarboxylation, of *p*-orsellinic acid with ethyl acetoacetate.[25] Sethna and Shah[26] reported that such reactions as above yield 4,5-dimethyl-7-hydroxycoumarin. We reexamined the reported structure by spectroscopic and chemical methods in connection with the syntheses of the chromones, **13** and **14**, and found that the product is 2,5-dimethyl-7-hydroxychromone, not coumarin.

TABLE 3. BOND DISTANCES[a)]

Bonds	Distances	Bonds	Distances
C (1)-C (2)	1.404 (5)	C (6)-C (11)	1.407 (4)
C (1)-O (1)	1.378 (4)	C (7)-C (8)	1.395 (5)
C (1)-O (2)	1.233 (4)	C (7)-O (4)	1.366 (5)
C (2)-C (3)	1.372 (5)	C (8)-C (9)	1.384 (5)
C (3)-C (4)	1.427 (5)	C (9)-C (10)	1.392 (5)
C (3)-O (3)	1.340 (4)	C (9)-O (5)	1.360 (5)
C (4)-C (5)	1.343 (5)	C (10)-C (11)	1.388 (4)
C (5)-C (6)	1.468 (5)	C (11)-C (12)	1.501 (5)
C (5)-O (1)	1.376 (4)	C (13)-O (3)	1.430 (5)
C (6)-C (7)	1.407 (5)		

a) E.s.d. in parentheses ($\times 10^3$).

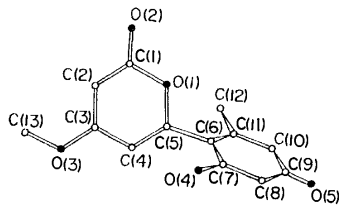

Fig. 2. Atomic numbering in aglycone **3** for X-ray analysis. The atoms indicated with ○ and ● denote carbon and oxygen atoms, respectively.

In order to establish the complete structure of aloenin, we examined the structure by X-ray crystallographic analysis. However, due to the lack of a good single crystal of aloenin, the analysis was carried out with aglycone **3**. Cell dimentions were obtained by least-squares calculations from 2θ values of 13 well-centered, resolved Cu $K\alpha$ diffraction peaks. Crystal data: monoclinic (space group $P2_1/c$), four molecules per unit cell with dimensions $a=7.422(2)$, $b=10.719(4)$, $c=14.393(4)$ Å, $\beta=99.54(2)°$; $U=1129.1$ Å^3; $D_c=1.46$ g cm^{-3}. A total of 2292 reflections were collected on a four circle automatic diffractometer; 198 reflections were smaller than 1.96 times of the standard deviations in intensity and were recorded as "unobserved." The phases of 153 strong reflections with $|E| > 1.85$ were determined by direct methods using the program MULTAN.[27] The E map for the best solution showed the 18 non-hydrogen atoms as the largest peaks. The structure was refined by full-matrix least-squares method. Four cycles of anisotropic refinement for carbon and oxygen atoms and of isotropic refinement for hydrogen atoms reduced the R index to 0.073. The final atomic coordinates and anisotropic thermal parameters of the non-hydrogen atoms are given in Tables 1 and 2, and bond distances and angles in Tables 3 and 4, with atoms designated as shown in Fig. 2. The results indicate that the structure of the aglycone is of structural formula **3**.

The crystal structure consists of two stackings of the planes of phenyl and pyrone groups of the aglycone molecules, which are packed along the a-axis and the c-axis, respectively (Fig. 3), the dihedral angle between the planes being 117°. One carbonyl and two hydroxyl groups participate in the formation of the

Table 4. Bond angles[a]

Angles	θ	Angles	θ
C (2) - C (1) - O (1)	118.4 (3)	C (6) - C (7) - C (8)	121.4 (3)
C (2) - C (1) - O (2)	126.1 (3)	C (6) - C (7) - O (4)	116.4 (3)
O (1) - C (1) - O (2)	115.5 (3)	C (8) - C (7) - O (4)	122.1 (3)
C (1) - C (2) - C (3)	119.5 (3)	C (7) - C (8) - C (9)	117.9 (3)
C (2) - C (3) - C (4)	120.6 (3)	C (8) - C (9) - C (10)	121.9 (3)
C (2) - C (3) - O (3)	124.9 (3)	C (8) - C (9) - C (5)	117.6 (3)
C (4) - C (3) - O (3)	114.5 (3)	C (10) - C (9) - O (5)	120.5 (3)
C (3) - C (4) - C (5)	119.0 (3)	C (9) - C (10) - C (11)	120.3 (3)
C (4) - C (5) - C (6)	127.5 (3)	C (6) - C (11) - C (10)	119.2 (3)
C (4) - C (5) - O (1)	120.5 (3)	C (6) - C (11) - C (12)	121.3 (3)
C (6) - C (5) - O (1)	112.0 (3)	C (10) - C (11) - C (12)	119.5 (3)
C (5) - C (6) - C (7)	120.1 (3)	C (1) - O (1) - C (5)	122.1 (3)
C (5) - C (6) - C (11)	120.5 (3)	C (3) - O (3) - C (13)	117.5 (3)
C (7) - C (6) - C (11)	119.3 (3)		

a) E.s.d. in parentheses ($\times 10$).

Table 5. ^{13}C-Chemical shifts of aloenin (**2**) and its derivatives, **4**, **6**, **18**, **19**, **20**, and **21**

Carbon No.	**2**[a]	**4**[b,e]	**6**[c]	**18**[c,d,e]	**19**[c,e]	**20**[c]	**21**[c]
2	165.5	165.2 (+2.6)	166.2	164.3 (+2.0)	164.7 (+2.0)	164.5	164.2
3	88.4	88.2 (+0.4)	88.2	88.5 (+0.4)	88.2 (+0.3)	88.6	88.9
4	171.7	171.2 (+2.0)	171.7	170.7 (+1.3)	171.1 (+0.9)	170.7	170.5
5	105.0	104.6 (+1.4)	104.8	105.0 (+1.0)	105.0 (+0.8)	104.1	104.4
6	159.3	158.9 (+1.2)	156.4	156.4[f] (+0.8)	157.4 (+0.7)	157.7	156.8
1′	114.7	114.8 (+0.5)	113.0	120.3 (+0.3)	115.6 (0.0)	118.4	123.3
2′	157.8	158.9 (+1.3)	159.2	155.1[f] (+0.7)	155.5 (+0.6)	150.0	149.4
3′	102.0	96.1 (+0.8)	99.5	106.2 (+0.8)	99.7 (+0.4)	106.1	114.2
4′	161.0	161.8 (+1.4)	161.6	152.1 (+0.8)	161.5 (+0.6)	161.2	151.8
5′	112.4	107.0 (+1.1)	108.1	117.7 (+0.7)	108.9 (+0.6)	114.0	121.1
6′	140.0	139.9 (+0.8)	139.8	140.2 (+0.6)	140.2 (+0.3)	140.0	140.1
1″	102.7	—	—	98.7 (+0.1)	98.8 (+0.1)	—	—
2″	74.5	—	—	70.5 (+0.8)	70.6 (+0.7)	—	—
3″	78.1	—	—	72.5 (+0.6)	72.6 (+0.4)	—	—
4″	71.0	—	—	68.2 (+0.7)	68.3 (+0.6)	—	—
5″	78.1	—	—	72.0 (+0.4)	72.0 (+0.3)	—	—
6″	62.3	—	—	62.0 (+0.6)	62.0 (+0.5)	—	—
4-OMe	56.0	55.8 (+1.0)	56.0	55.9 (+0.7)	55.9 (+0.5)	55.9	56.0
4′-OMe	—	55.3 (+0.4)	55.2	—	55.3 (+0.3)	55.5	—
6′-Me	20.2	20.2 (0.0)	20.4	19.7[g] (0.0)	20.3 (0.0)	20.3	20.1[h]
2′-OMe	—	58.8 (+0.4)	—	—	—	—	—
4′-OCOMe	—	—	—	21.2[g]	—	20.8	20.7[h] / 21.1[h]
4′-OCOMe	—	—	—	168.5	—	169.2	168.7×2

a) Determined in C_5D_5N at 60°. b) Determined in $CDCl_3$-CD_3OD (9 : 1). c) Determined in $CDCl_3$ (TMS = 0). d) The δ_c values for the tetraacetyl groups at glucose moiety are 20.5×4, 170.1, 169.7, 169.1, and 168.8 ppm. e) Figures in parentheses are shift values observed in $CDCl_3$: CD_3OH(1 : 1) in ppm. f), g), and h) Assignments are interchangeable.

intermolecular hydrogen bond. One chain is formed through O(2)-carbonyl and O(5)-hydroxyl groups. The other chains O(4)- and O(5)-hydroxyl groups belonging to the neighboring molecules are correlated by a 2_1 screw axis. The crystal structure is stabilized by the networks of these hydrogen bonds.

The β-glucopyranosyloxyl structure was established by the enzymic hydrolysis of **2** with β-glucosidase (emulsin) and the J-value of 5.5 Hz obtained from the anomeric proton signal at δ 4.78 in the PMR spectrum of **5**. The structure of aloenin has now been established as 4-methoxy-6-(2-β-D-glucopyranosyloxy-4-hydroxy-6-methylphenyl)-2-pyrone (**2**).

^{13}C-NMR Study. In the ^{13}C-NMR spectroscopic study of aloenin (**2**) and its derivatives during the course of structure confirmation, it was found that preliminary assignments[15] in accord with reported results[30] differ from those for yangonin (**15**).[28] In order to clarify the ambiguity and disagreement[28–31] in the signal assignment of C-2, C-4, and C-6 in 6-

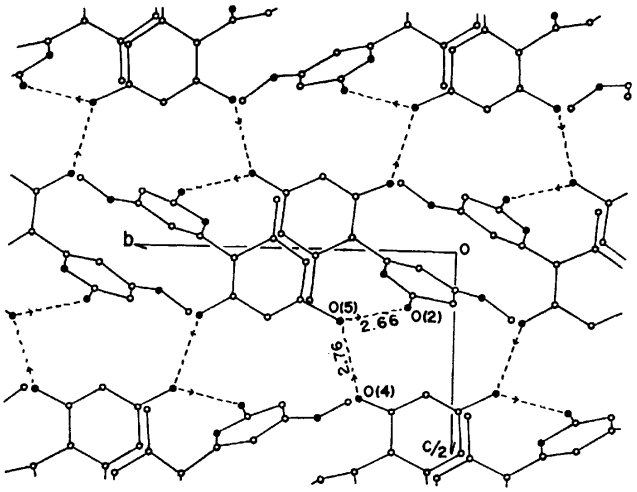

Fig. 3. The projection of aglycone **3** viewed along the a-axis. Hydrogen bonds are shown by a broken line. The atoms indicated with ○ and ● denote carbon and oxygen atoms, respectively.

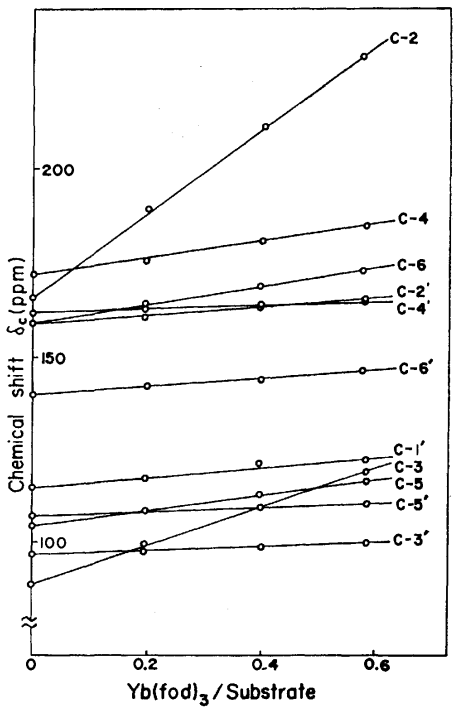

Fig. 4. Variations in the ^{13}C chemical shift of **4** in $CDCl_3$ with increasing concentration of $Yb(fod)_3$.

substituted 4-methoxy-2-pyrone rings, we investigated natural-abundance ^1H noise-decoupled ^{13}C FT NMR spectra of aloenin (**2**) and its derivatives (Tables 5 and 6).

Signals due to C-2, C-4, and C-6 in the 2-pyrone ring were distinguished as follows. Selective ^1H decoupling irradiated at H-3, H-5, and 4-OCH_3 frequencies revealed the C-2, C-4, and C-6 signal assignments, since $^2J_{C(2)-C(3)-H(3)} < ^2J_{C(6)-C(5)-H(5)}$ is known for 2-pyrone.[32] Hydrogen-bonding shifts[33] of the C-2 carbonyl peaks were distinguished when a $CDCl_3$–CD_3OH (1 : 1) mixed solvent was used for **4**, **18**, and **19**

Table 6. ^{13}C-Chemical shifts[a] of acetophenone derivatives, **9**, **12**, **16**, and **17**

Carbon No.	**9**	**12**	**16**	**17**
1	124.1	115.2	127.2	125.8
2	158.5	167.2	148.7	154.9
3	96.1	99.1	105.8	100.6
4	161.2	164.4	160.5	160.8
5	107.4	111.8	114.2	109.8
6	137.9	141.9	137.8	137.5
COMe	204.4	203.9	202.1	204.1
COMe	32.4	33.0	31.9	32.4
4-OMe	55.3	55.3	55.4	55.4
6-Me	20.0	25.1	20.1	19.6

a) Determined in $CDCl_3$ (TMS=0).

Table 7. Inhibition of gastric juice secretion of rats by aloenin (**2**)

Compound	Dose (mg/kg)	pH	Secretion (ml/100 g body weight)	Inhibition (%)
Control	—	1.8	4.7	0
Aloenin (**2**)	100	1.8	3.6	23

(Table 5). The lanthanide-induced shift (LIS) method[34,35] was applied to **4** employing $Yb(fod)_3$ in $CDCl_3$. The largest lanthanide-induced shift value was obtained for the C-2 peak as indicated in Fig. 4.

For assignments of the benzene ring carbons, we examined the substituent effects[36] of some acetophenone derivatives, **9**, **12**, **16**, and **17** (Table 6). The methylation and acetylation shifts in *o*-hydroxyacetophenone[37,38] were utilized for assigning the benzene ring carbons of all the compounds examined. The deuteration effect[39] (−0.6 ppm) was detected for C-2 of **12**, which has an abnormal chemical shift due to an intramolecular hydrogen-bond. The substituent effects were useful for assigning the benzene-ring carbons of aloenin derivatives (Table 5).

The signals due to the sugar moiety of **2** appear at almost the same positions as those of methyl β-D-glucopyranoside[32] in pyridine-d_5 except for the anomeric C-1 signal which was shifted upfield by about −3 ppm from the position of the C-1 signal of methyl glucoside. A similar behavior was observed for the sugar moieties of **17**, **18**, and **19** and methyl tetra-*O*-acetyl-β-D-glucopyranoside in $CDCl_3$. On the other hand, anomeric carbon signals in sugar moieties of some steroid and triterpenoid glycosides were found to resonate at almost the same position as that in the corresponding methyl glycosides.[40] Chemical shift changes in aromatic aglycone carbons due to glycosidation (**6**→**19** as shown in Table 5) will also be useful for structure determination of natural glycosides having aromatic aglycones.

Thus, the assignments for all carbon atoms of aloenin (**2**) and its derivatives were established as shown in Tables 5 and 6; the present ^{13}C-NMR data on derivatives, **4**, **6**, **9**, **12**, and **16**—**21**, are in line with the structure of aloenin (**2**).

Test of Inhibitory Action on Gastric Juice Secretion. Since Aloe juice is widely used as domestic medicine for gastro-intestinal disturbance, the action of aloenin (**2**) on the gastric juice secretion of rats was tested by the method of Shay *et al.*[41] (Table 7). Aloenin (**2**) was found to exhibit an inhibitory action on gastric juice secretion.

Experimental

MS analyses were performed on Hitachi mass spectrometers, Model RMU-7L (for the high-resolution mass spectrum measurements) and Model RMS-4 (for the usual measurements), ionizing at the order of 70 eV. The 100 MHz and 60 MHz PMR spectra were recorded on Varian HA-100 and Hitachi Perkin-Elmer R-20 spectrometers, respectively, using TMS as an internal standard. The natural-abundance ^{13}C FT NMR spectra were taken on a Varian NV-14 FT NMR spectrometer operating at 15.087 MHz at 30 °C, using TMS as an internal reference ($\delta_c=0$) in a 8-mm spining tube, precision of δ_c being *ca.* ±0.1. The ^{13}C signals were assigned using known chemical shift rules,[33] ^1H single-frequency off-resonance (SFORD) and/or selective decoupling techniques[33] in combination with C_6D_6-induced ^1H shifts.[42] The NOE experiments were carried out on a Varian HA-100 spectrometer operating at 100 MHz in the frequency-swept and internal-TMS-locked mode. Samples were prepared in concentration of 5% (w/v) in $CDCl_3$ and carefully degassed just prior to measurements. The NOE values are represented by an increase in integrated intensities, precision of the values being *ca.* $\pm2\%$. Crystallographic analysis was performed on a Syntex $P2_1$ diffractometer using ω-scan technique with Cu $K\alpha$ radiation and a Ni-filter. The differential thermal and thermal gravimetric analyses were carried out on a Rigakudenki 8002 DTA-TGA analyzer. Melting points determined with a micro hot stage apparatus are uncorrected.

Extraction and Isolation. The leaves (3.7 kg) of *Aloe arborescens* Mill. var. *natalensis* Berger, which had been cultivated in pots for 3—4 years after planting the cuttings of lateral buds *ca.* 5 cm long, were collected in late April, minced mechanically, and squeezed on a three fold gauze to give a green leaf juice. The leaf juice on evaporation of water on a steam bath afforded a brown viscous mass, which was subjected to column chromatography on silica gel with a $CHCl_3$–MeOH mixture with MeOH increasing from 0 to 100% and then preparative TLC on silica gel with a $CHCl_3$–MeOH (3:1) mixture to give aloenin (**2**) (1.78 g).

*Aloenin (**2**).* Mp 145—147 °C (monohydrate) and 204—205 °C (anhydrous): the melting points and water of crystallization were determined by differential thermal and thermal gravimetric analyses; $[\alpha]_D^{25}$ −26.79° (*c* 2.2, MeOH); IR (dioxane) 3300, 1714, 1642, 1608, 1560 cm^{-1}; UV (EtOH) λ_{max} 307 nm (log ε 3.91), 245 (3.81), 232 (3.87), (0.05 M KOH-EtOH) 353 nm (log ε 4.16), 253 (4.14), 225 (3.98); PMR (Acetone-d_6) δ 2.19 (s, 3H, C(6′)-Me), 3.86 (s, 3H, C(4)-Me), 5.47 (d, J=2.5 Hz, 1H, C(3)-H), 6.15 (d, J=2.5 Hz, 1H, C(5)-H), 6.45 (d, J=2.2 Hz, 1H, arom. H), 6.62 (d, J=2.2 Hz, 1H, arom. H); ^{13}C-NMR (C_5D_5N) (Table 5). Found: C, 53.02; H, 5.76%. Calcd for $C_{19}H_{22}O_{10}\cdot H_2O$: C, 53.27; H, 5.65%.

*Dimethyl Ether **10**.* Methylation of **2** (100 mg) with diazomethane gave dimethyl ether **10** (102 mg): Mp 117—118 °C; IR (KBr) 3400, 1680, 1635, 1610, 1561 cm^{-1}; PMR (C_5D_5N) δ 2.29 (s, 3H, C(6′)-Me), 3.54 (s, 3H, C(4′)-OMe), 3.71 (s, 3H, C(4)-OMe), 5.60 (d, J=2.5 Hz, 1H, C(3)-H), 6.05 (d, J=2.5 Hz, 1H, C(5)-H). Found: C, 56.35; H, 5.65%. Calcd for $C_{20}H_{24}O_{10}$: C, 56.60; H, 5.70%.

*Pentaacetate **18**.* A pentaacetate derivative (**18**) of **2** was prepared by treatment with acetic anhydride in pyridine for 1 day at room temp: Mp 192—193 °C; IR ($CHCl_3$) 1758, 1714, 1698, 1645, 1608, 1567 cm^{-1}; PMR ($CDCl_3$) δ 1.98 (s, 6H, 2×OAc), 2.02 (s, 3H, OAc), 2.08 (s, 3H, OAc), 2.27 (s, 3H, C(6′)-Me), 2.29 (s, 3H, C(4′)-OAc), 3.86 (s, 3H, C(4)-OMe), 5.52 (d, J=2.5 Hz, 1H, C(3)-H), 5.99 (d, J=2.5 Hz, 1H, C(5)-H), 6.72 (bs, 2H, arom. 2H), 3.5—5.3 (7H); NOE (Fig. 1); ^{13}C-NMR ($CDCl_3$) (Table 5). Found: C, 49.60; H, 4.52%. Calcd for $C_{29}H_{32}O_{20}$: C, 49.72; H, 4.60%.

*Exhaustive Methylation of Aloenin (**2**).* Aloenin (**2**) (120 mg) was treated according to Hakomori's method[19] with sodium hydride and methyl iodide in dimethyl sulfoxide to give hexamethyl ether **5** (67 mg): Mp 143—143.5 °C; IR (KBr) 3050, 1720, 1648, 1615, 1572 cm^{-1}; PMR ($CDCl_3$) δ 2.22 (s, 3H, C(6′)-Me), 3.35 (s, 3H, OMe), 3.38 (s, 3H, OMe), 3.49 (s, 3H, OMe), 3.58 (s, 3H, OMe), 3.76 (s, 3H, OMe), 3.78 (s, 3H, OMe), 4.78 (d, J=5.5 Hz, 1H, C(1″)-H), 5.46 (d, J=2.0 Hz, 1H, C(3)-H), 6.08 (d, J=2.0 Hz, 1H, C(5)-H), 6.46 (d, J=2.0 Hz, 1H, arom. H), 6.59 (d, J=2.0 Hz, 1H, arom. H). Found: C, 59.71; H, 6.75%. Calcd for $C_{24}H_{32}O_{10}$: C, 59.99; H, 6.71%.

*Acid Hydrolysis of Aloenin (**2**).* After aloenin (**2**) (100 mg) dissolved in 3% methanolic hydrochloric acid (5 ml) had been heated under reflux for 2 h, the mixture was diluted with water and extracted with ether. The ether extract gave the aglycone (**3**) (41 mg): Mp 213—214 °C; IR (KBr) 3350, 1670, 1628, 1600, 1562 cm^{-1}; PMR (C_5D_5N) δ 2.33 (s, 3H, C(6′)-Me), 3.61 (s, 3H, C(4)-OMe), 5.67 (d, J=2.5 Hz, 1H, C(3)-H), 6.38 (d, J=2.5 Hz, 1H, C(5)-H). Found: C, 62.75; H, 4.81%. Calcd for $C_{13}H_{12}O_5$: C, 62.90; H, 4.87%. The aqueous layer was passed through an Amberlite resin IR-45 (OH) column until all chloride ions had been removed. The neutral solution on concentration under reduced pressure gave D-glucose (30 mg): mp 144—145 °C, $[\alpha]_D^{25}$ +109°→+49° (*c* 0.2, H_2O).

*Enzymic Hydrolysis of Aloenin (**2**).* A suspension of aloenin (**2**) (20 mg) and emulsin (50 mg) in a phosphate buffer solution (pH 6.5) (5 ml) was stirred at 35 °C for 2 days. Formation of the aglycone (**3**) and glucose was confirmed by TLC and PPC analyses.

*Trimethyl Ether **4**.* Methylation of aglycone (**3**) (20 mg) with diazomethane gave the trimethyl ether **4** (20 mg): Mp 133—134 °C; IR (Nujol) 1725, 1641, 1613 cm^{-1}; PMR ($CDCl_3$) δ 2.26 (s, 3H, C(6′)-Me), 3.74 (s, 3H, C(2′)-OMe), 3.81 (s, 3H, C(4′)-OMe), 3.83 (s, 3H, C(4)-OMe), 5.50 (d, J=2.5 Hz, 1H, C(3)-H), 5.99 (d, J=2.5 Hz, 1H, C(5)-H), 6.34 (s, 2H, C(3′)- and C(5′)-H); NOE (Fig. 1); MS *m/e* (rel intensity) 276 (M^+, 100), 261 (5), 248 (52), 233 (33), 217 (12), 205 (44), 191 (13), 189 (17), 179 (29), 178 (30); High-resolution MS (Scheme 1); ^{13}C-NMR ($CDCl_3$) (Table 5). Found: C, 65.00; H, 5.72%. Calcd for $C_{15}H_{16}O_5$: C, 65.21; H, 5.84%.

*Acid Hydrolysis of the Hexamethyl Ether (**5**).* The hexamethyl ether (**5**) (100 mg) was refluxed with 5 ml of 3% methanolic hydrochloric acid for 2 h and then the mixture, after being diluted with water, was extracted with chloroform. The chloroform extract gave a product **6** (35 mg) [mp 194—195 °C; IR (KBr) 1665, 1605, 1546, 1504, 844, 810, 750 cm^{-1}; PMR ($CDCl_3$) δ 2.32 (s, 3H, C(6′)-Me), 3.78 (s, 3H, C(4′)-OMe), 3.85 (s, 3H, C(4)-OMe); ^{13}C-NMR ($CDCl_3$) (Table 5)] and 2,3,4,6-tetra-*O*-methyl-D-glucose (mp 90—94 °C). Methylation of the product (**6**) (10 mg) with diazomethane gave trimethyl ether (**4**) (10 mg). The tetra-*O*-methyl-D-glucose was identified by comparing the mp and IR spectrum

with those of a synthetic sample.

*Acid Hydrolysis of the Dimethyl Ether (**10**).* The dimethyl ether (**10**) (50 mg) was refluxed with 3 ml of 3% methanolic hydrochloric acid for 2 h. The same treatment as in the case of **5** gave the compound **6** (17 mg) [mp 194—195 °C; IR (KBr) 1665, 1605, 1546, 1504 cm^{-1}] and glucose.

*Conversion of **3** and **6** into Chromone Derivatives.* The aglycone (**3**) (50 mg) was heated with 5% hydrochloric acid (5 ml) under reflux for 1 h, giving 2,5-dimethyl-7-hydroxychromone (**13**) (30 mg; mp 244—245 °C).[25] The same treatment of **6** as above gave 2,5-dimethyl-7-methoxychromone (**14**) (32 mg; mp 116—117 °C).

*Alkaline Cleavage of the Trimethyl Ether (**4**).* A solution of trimethyl ether (**4**) (200 mg) in 5% methanolic potassium hydroxide (20 ml) was stirred at room temp in an atmosphere of nitrogen. Crystals which started to appear after 12 h were filtered after 2 days and washed with absolute ethanol and then chloroform. They showed red coloration with ethanolic ferric chloride. A solution of the crystals (132 mg) in water (10 ml) was acidified carefully with a few drops of dilute hydrochloric acid and then immediately extracted with ether to give β-keto acid **7** (110 mg): IR (liquid) 3500—2500, 1725, 1600 cm^{-1}; PMR ($CDCl_3$) δ 2.33 (s, 3H, arom. Me), 3.73 (s, 6H, 2×OMe), 6.62 (s, 2H, arom. 2H); the reddish violet coloration is characteristic of β-keto acids with ethanolic ferric chloride. The keto acid (**7**) underwent facile decarboxylation during the course of purification by recrystallization. Without any purification, **7** (80 mg) dissolved in $CHCl_3$ (10 ml) was heated under reflux for 5 h in a stream of nitrogen to undergo decarboxylation. This was confirmed by the formation of barium carbonate in a barium hydroxide trap attached to the reflux apparatus. Removal of the solvent from the chloroform solution gave 1-(2,4-dimethoxy-6-methylphenyl)butane-1,3-dione (**8**) (61 mg; mp 72—73 °C, M^+ 236), which was identified by direct comparison with a synthetic specimen described below.

*Alkaline Cleavage of the Dimethyl Ether (**10**).* A solution of the dimethyl ether (**10**) (100 mg) in 5% methanolic potassium hydroxide (10 ml) was refluxed for 12 h. The mixture, after neutralization with hydrochloric acid and subsequent removal of the solvent, was subjected to preparative TLC on silica gel to give an oily product **11** (32 mg): IR (Nujol) 3450, 1600, 1180 cm^{-1}, which was treated with acetic anhydride in pyridine at room temp to afford tetraacetate **17**: mp 144—146 °C; IR (KBr) 1753, 1690, 1610, 1382, 1320, 1239 cm^{-1}; PMR ($CDCl_3$) δ 2.00 (s, 3H, OAc), 2.05 (s, 6H, 2×OAc), 2.10 (s, 3H, OAc), 2.22 (s, 3H, Me), 2.40 (s, 3H, COMe), 3.78 (s, 3H, OMe), 6.52 (s, 2H, arom. 2H); ^{13}C-NMR (Table 6). Found: C, 64.37; H, 6.70%. Calcd for $C_{24}H_{30}O_8$: C, 64.56; H, 6.77%. Hydrolysis of **11** (20 mg) with 3% methanolic hydrochloric acid (5 ml) gave 11 mg of 2-hydroxy-4-methoxy-6-methylacetophenone (**12**) (mp 78.0—78.5 °C; *m/e* 180 (M^+)), a trace of 2,5-dimethyl-7-methoxychromone (**14**), and glucose. The products, **12** and **14**, were identified by comparison with an authentic specimen,[22,25] glucose being detected by TLC and PPC analyses.

*2-Acetoxy-4-methoxy-6-methylacetophenone (**16**).* Acetylation of **12** (66 mg) with acetic anhydride in pyridine at room temp gave a methylacetophenone derivative (**17**) (80 mg): IR (liquid) 1760, 1680, 1605 cm^{-1}; PMR ($CDCl_3$) δ 2.28 (s, 3H, OAc), 2.33 (s, 3H, Me), 2.44 (s, 3H, COAc), 3.78 (s, 3H, OMe), 6.52 (d, J=2.0 Hz, 1H, arom. H), 6.65 (d, J=2.0 Hz, 1H, arom. H); ^{13}C-NMR (Table 6).

*Tetraacetate **19**.* Acetylation of the dimethyl ether (**10**) (50 mg) with acetic anhydride in pyridine at room temp gave tetraacetate **19** (53 mg): Mp 182—183 °C; IR (KBr) 1755, 1720, 1650, 1615, 1574 cm^{-1}; PMR ($CDCl_3$): δ 1.98 (s, 6H, 2×OAc), 2.03 (s, 3H, OAc), 2.10 (s, 3H, OAc), 2.30 (s, 3H, arom. Me), 3.82 (s, 3H, OMe), 3.87 (s, 3H, OMe), 5.50 (d, J=2.5 Hz, 1H, C(3)–H), 5.98 (d, J=2 Hz, 1H, C(5)–H), 6.50 (s, 2H, C(3′)- and C(5)–H); ^{13}C-NMR (Table 5).

*Methoxyacetate **20**.* Acetylation of the compound **6** (61 mg) with acetic anhydride in pyridine at room temp gave methoxyacetate **20** (58 mg): Mp 159—160 °C; IR (KBr) 1765, 1735, 1635, 1620, 1560 cm^{-1}; PMR ($CDCl_3$) δ 2.20 (s, OAc) 2.32 (s, Me), 3.83 (s, C(4′)–OMe), 3.86 (s, C(4)–OMe), 5.52 (d, J=2.0 Hz, C(3)–H), 5.95 (d, J=2.0 Hz, C(5)–H), 6.53 (d, J=2.0 Hz, arom. H), 6.72 (d, J=2.0 Hz, arom. H); ^{13}C-NMR (Table 5).

*Diacetate **21**.* Acetylation of the aglycone (**3**) (100 mg) with acetic anhydride in pyridine at room temp gave diacetate **21** (32 mg): Mp 151—152.5 °C; IR (KBr) 1764, 1725, 1640, 1614, 1565 cm^{-1}; PMR ($CDCl_3$) δ 2.20 (s, 3H, OAc), 2.30 (s, 3H, OAc), 2.33 (s, 3H, Me), 3.87 (s, 3H, OMe), 5.52 (d, J=2.0 Hz, 1H, C(3)–H), 5.98 (d, J=2.0 Hz, 1H, C(5)–H), 6.87 (m, 2H, arom. 2H); ^{13}C-NMR (Table 5).

*Synthesis of 1-(2,4-Dimethoxy-6-methylphenyl)butane-1,3-dione (**8**).* Sliced metallic sodium (25 mg) was added under ice-cooling to a mixture of ethyl acetate (0.5 ml) and 2,4-dimethoxy-6-methylacetophenone (**9**) (100 mg), which was prepared from 3,5-dihydroxytoluene by acetoacetic ester condensation.[22] The reaction mixture was left to stand at room temp for 5 min and then heated at 110 °C for 2 h. The mixture, after cooling and addition of water (5 ml), was extracted with ether to remove the unchanged substance. The separated alkaline solution was acidified with dilute acetic acid and extracted with ether to yield dione **8** (55 mg): Mp 72—73 °C; IR (KBr) 3500—2500, 1600 cm^{-1} (enol form of β-diketone); UV (EtOH) λ_{max} 282 nm (log ε 4.04), 222 (3.92); PMR ($CDCl_3$) δ 2.15 (s, 3H, COMe), 2.34 (s, 3H, arom. Me), 3.78 (s, 6H, 2×OMe), 5.69 (s, 1H, C(2)–H (enol form)), 6.32 (bs, 2H, arom. 2H); MS *m/e* (rel intensity) 236 (M^+, 31), 219 (30), 205 (20), 179 (100), 152 (36). Found: C, 66.02; H, 6.57%. Calcd for $C_{13}H_{16}O_4$: C, 66.08; H, 6.83%. The product (**8**) gave a reddish violet coloration characteristic of a β-diketone structure by the ferric chloride test.

*Test of Inhibitory Action of Aloenin (**2**) on Gastric Juice Secretion.* Inhibitory activity to gastric juice secretion was tested by the method of Shay *et al.*[41] Male rats of Donryu strain, 130—170 g in weight, were used for the tests. Table 7 gives the amount and pH of the gastric juice secreted during a period of 4 h after oral administration of the sample through a gastro-tube, together with the results of the control experiment.

We are grateful to Dr. Kazuo Tori, Shionogi Research Laboratory, Shionogi & Co., Ltd. and Mr. Osamu Koshitani, Hiroshima University, for their help in the ^{13}C-NMR study, and to Dr. Yoshihiko Kushi, Hiroshima University, and Dr. Arild Christensen, Syntex Analytical Instruments, Inc., for their assistance in the X-ray study. The investigation was partially supported by a Grant-in-Aid (074176, 047089, and 034058) for Scientific Research in 1975 from the Ministry of Education.

References

1) J. E. Hay and L. J. Haynes, *J. Chem. Soc.*, **1956**, 3141.
2) L. J. Haynes, J. I. Henderson, and J. M. Tyler, *J. Chem. Soc.*, **1960**, 4879.
3) L. Horhammer, H. Wagner, and G. Bittner, *Z. Natur-*

forsh., **19b**, 222 (1964).
4) T. J. McCarthy, *Planta Med.*, **17**, 1 (1969).
5) E. Constantinescu, M. Palade, A. Grasu, and E. Rotaru, *Farmacia*, **17**, 591 (1969).
6) L. J. Haynes, D. K. Holdsworth, and R. Russell, *J. Chem. Soc., C*, **1970**, 2581.
7) D. K. Holdwsorth, *Planta Med.*, **19**, 322 (1971).
8) T. Suga, T. Hirata, and M. Odan, *Chem. Lett.*, **1972**, 547.
9) K. Makino, A. Yagi, and I. Nishioka, *Chem. Pharm. Bull.*, **21**, 149 (1973).
10) A. Yagi, K. Makino, and I. Nishioka, *Chem. Pharm. Bull.*, **22**, 1159 (1974).
11) K. Makino, A. Yagi, and I. Nishioka, *Chem. Pharm. Bull.*, **22**, 1565 (1974).
12) M. Soeda, *J. Med. Soc. Toho, Jpn.*, **16**, 365 (1969), and references cited therein.
13) I. Yamamoto, *J. Med. Soc. Toho, Jpn.*, **17**, 361 (1970).
14) J. H. Noggle and R. E. Schirmer, "The Nuclear Overhauser Effect. Chemical Application," Academic Press Inc., New York (1971).
15) T. Suga, T. Hirata, and K. Tori, *Chem. Lett.*, **1974**, 715.
16) T. Hirata, Y. Kushi, T. Suga, and A. Christensen, *Chem. Lett.*, **1976**, 393.
17) K. Tori, T. Hirata, O. Koshitani, and T. Suga, *Tetrahedron Lett.*, **1976**, 1311.
18) A. K. Ganguly, T. R. Govindachari, and P. A. Mohamed, *Tetrahedron*, **21**, 93 (1965).
19) S. Hakomori, *J. Biochem.*, **55**, 205 (1964).
20) W. B. Mors, O. R. Gottlieb, and C. Djerassi, *J. Am. Chem. Soc.*, **79**, 4507 (1957).
21) Q. N. Porter and J. Baldas, "Mass Spectrometry of Heterocyclic Compounds," Wiley-Interscience Inc., New York (1971).
22) T. Suga, T. Hirata, and F. Walls, *J. Sci. Hiroshima Univ., Ser. A*, **38**, 327 (1974).
23) T. M. Harris and C. S. Combs, *J. Org. Chem.*, **33**, 2399 (1968).
24) E. Guzman-Lopez, N. Rosas, and F. Walls, *Bol. Inst. Quim. Univ. Nacl. Auton. Mex.*, **22**, 125 (1970).
25) T. Hirata and T. Suga, *Bull. Chem. Soc. Jpn.*, **47**, 244 (1974).
26) S. M. Sethna and R. C. Shah, *J. Indian Chem. Soc.*, **17**, 211 (1940).
27) G. Germain, P. Main, and M. M. Woolfson, *Acta Crystallogr., Sect. A*, **27**, 368 (1971).
28) M. Tanabe, H. Seto, and L. Johnson, *J. Am. Chem. Soc.*, **92**, 2157 (1970).
29) W. V. Turner and W. H. Pirkle, *J. Org. Chem.*, **39**, 1935 (1974).
30) L. J. Mulheirn, R. B. Beechey, D. P. Leworthy, and M. D. Osselton, *J. Chem. Soc., Chem. Commun.*, **1974**, 874.
31) M. S. R. Nair and S. T. Carey, *Tetrahedron Lett.*, **1975**, 1655.
32) A. A. Chalmers and K. G. R. Pachler, *Can. J. Chem.*, **53**, 1980 (1975).
33) J. B. Stothers, "Carbon-13 NMR Spectroscopy," Academic Press, New York (1972).
34) B. C. Mayo, *Chem. Soc. Rev.*, **2**, 49 (1973).
35) N. J. Cussans and T. N. Huckerby, *Tetrahedron*, **31**, 2719 (1975).
36) G. C. Levy and G. L. Nelson, "Carbon-13 Nuclear Magnetic Resonance for Organic Chemists," Wiley-Interscience Inc., New York (1972).
37) M. Kobayashi, Y. Terui, K. Tori, and N. Tsuji, *Tetrahedron Lett.*, **1976**, 619.
38) Y. Terui, K. Tori, and N. Tsuji, *Tetrahedron Lett.*, **1976**, 621.
39) F. W. Wehrli, *J. Chem. Soc., Chem. Commun.*, **1975**, 663.
40) L. Radics, M. Katar-Peredy, S. Corsano, and L. Standoli, *Tetrahedron Lett.*, **1975**, 4287.
41) H. Shay, S. A. Komarov, S. S. Fels, D. Meranze, M. Gruentein, and M. Siplet, *Gastroenterology*, **5**, 43 (1945).
42) K. Nikki, N. Nakagawa, and Y. Takeuchi, *Bull. Chem. Soc. Jpn.*, **48**, 2902 (1975).

Chemical Studies on Tuberactinomycin. XIV.[1] Novel Synthesis of DL-Capreomycidine[2]

Tateaki WAKAMIYA, Katsutoshi MIZUNO, Tatsuzo UKITA, Tadashi TESHIMA, and Tetsuo SHIBA

Department of Chemistry, Faculty of Science, Osaka University, Toyonaka, Osaka 560

(Received August 8, 1977)

Cyclic guanidino amino acid, capreomycidine, is a component of antituberculous peptides, capreomycin and tuberactinomycin N and O. Its epimer was also found in protease inhibitors, chymostatin and elastatinal. A new synthetic approach to DL-capreomycidine *via* β-hydroxyornithine was studied for the purpose of total synthesis of capreomycidine and epicapreomycidine of natural forms or its hydroxy derivative, tuberactidine.

Antituberculous peptide, capreomycin, contains a unique cyclic guanidino amino acid capreomycidine (**1**) as a component.[3] A second case of its natural occurrence was revealed in the recent studies on similar antibiotics, tuberactinomycins, also as a constituent amino acid of two congeners N and O.[4] After the chemical structure of capreomycidine had been determined by Herr,[3] its stereochemistry was assumed by Bycroft *et al.*[5,6] to be (*S*)-α-[(4*R*)-2-iminohexahydro-4-pyrimidyl]glycine (L-capreomycidine) (**1**) and confirmed by X-ray analysis of tuberactinomycin O.[4a] A diastereoisomer of L-capreomycidine, (*S*)-α-[(4*S*)-2-iminohexahydro-4-pyrimidyl]glycine (L-epicapreomycidine) (**2**) was recently found as a component amino acid in protease inhibitors such as chymostatin[7] and elastatinal.[8] Occurrence of two diastereoisomers of one amino acid in nature is not so rare, particularly in the field of peptide antibiotics, but capreomycidine can be regarded as an example for consideration of amino acid biosynthesis from the view point of stereochemistry.

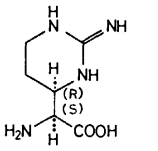

1

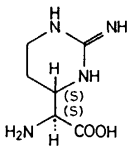

2

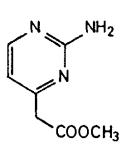

3

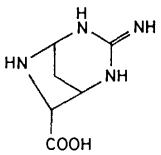

4

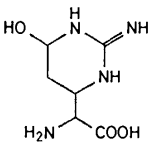

5

Concerning the synthesis of capreomycidine, Bycroft *et al.* presented a synthetic approach to DL-compound in 1971.[9] Their method is based on oximation of methyl (2-amino-4-pyrimidyl)acetate (**3**) followed by hydrogenation. However, according to their scheme, synthesis of an optically active form of this amino acid would require much effort particularly in the procedure of optical resolution. In fact they have not yet succeeded in preparing L-capreomycidine. As regards their failure in the synthesis of viomycidine (**4**) from 6-hydroxy analog of **3**, the approach seems unpromising for the synthesis of tuberactidine (**5**) which is another cyclic guanidino amino acid in tuberactinomycin group. The situation prompted us to search for a more favorable synthetic route to secure a common intermediate from which both optically active capreomycidine and tuberactidine could be obtained. This may offer a requisite tool for the synthesis of biologically important peptides containing cyclic guanidino amino acid.

In this connection, we describe a new synthetic method of DL-capreomycidine through β-hydroxyornithine for the preparation of optically active isomer. β-Hydroxyornithine was prepared in a previous synthesis of γ-hydroxy-β-lysine through rather tedious steps *via* 5-phthalimino-2-pentenoic acid.[10] We have improved the approach by a completely different method based on aldol condensation of 3-phthalimidopropionaldehyde (**6**)[11] with [*N*-(1-carboxylatoethylidene)glycinato]aquacopper(II) (**7**)[12] introduced by Ichikawa *et al.*[13] (Scheme 1).

After removal of copper(II) ion from the condensate, N^{δ}-phthaloyl-β-hydroxyornithine (**8**) was obtained as a mixture of *threo* (**8a**) and *erythro* (**8b**) forms in the ratio 89 : 11.[14] Each isomer was separated by fractional crystallization from water. Such a remarkable stereoselectivity was favorable for our purpose of preparing

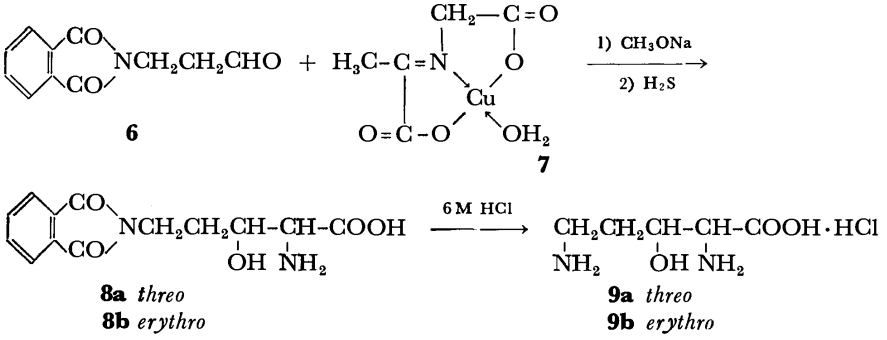

6 **7**

8a *threo*
8b *erythro*

9a *threo*
9b *erythro*

Scheme 1.

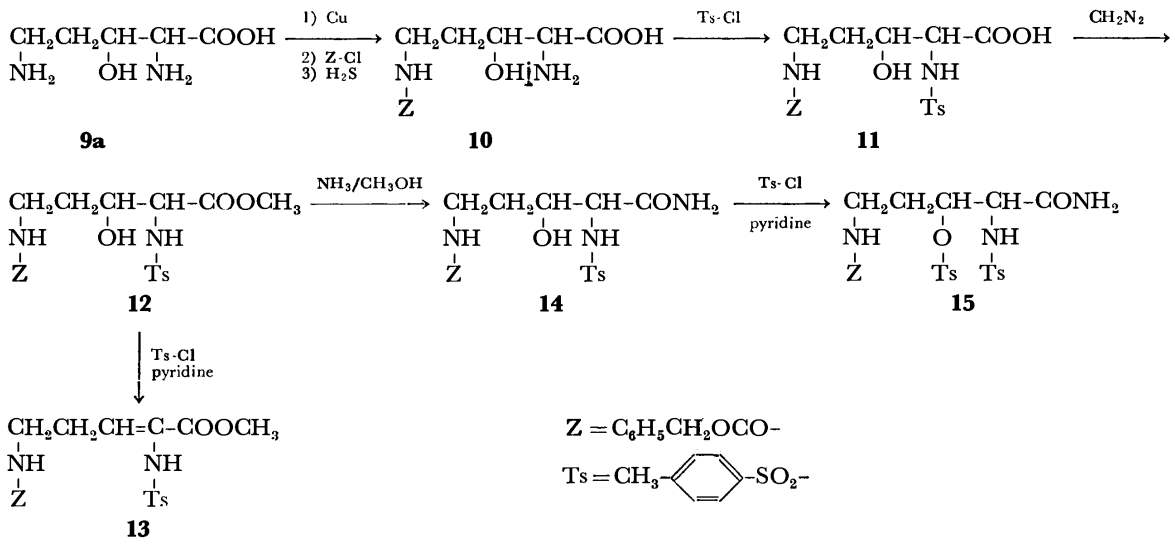

9a 10 11 12 13 14 15

Scheme 2.

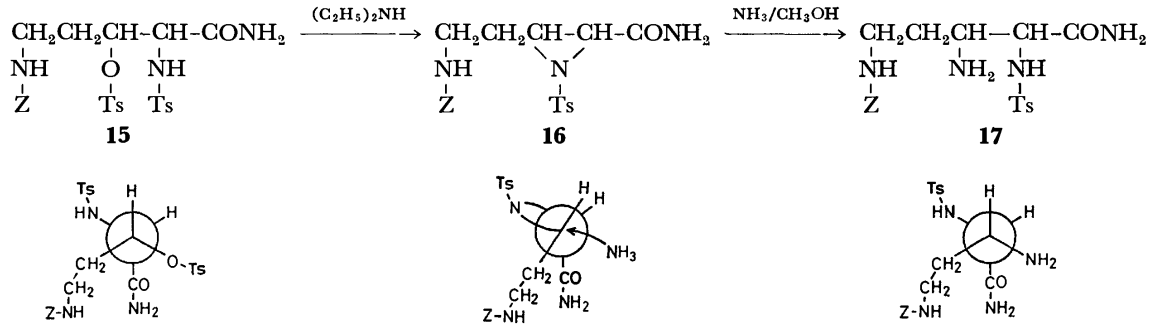

15 16 17

Scheme 3.

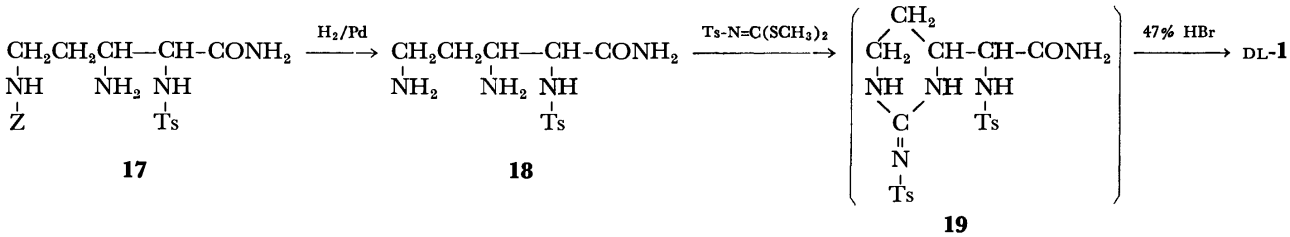

17 18 19

Scheme 4.

capreomycidine of natural *threo* form, if the β-hydroxyl group could be converted into amino group without inversion of its configuration.

Removal of phthaloyl group from **8a** gave *threo*-β-hydroxyornithine (**9a**) which was anew benzyloxycarbonylated selectively at δ-amino group *via* copper(II) complex. Such an exchange of the protecting group was required for smooth deprotection in later synthetic step. N^{δ}-Benzyloxycarbonyl derivative **10** thus obtained was then tosylated at α-amino group to afford N^{δ}-benzyloxycarbonyl-N^{α}-tosyl-β-hydroxyornithine (**11**). (Scheme 2).

For conversion of β-hydroxyl into β-amino group, *O*-tosylation had been first carried out. However, *O*-tosylate of β-hydroxy acid is liable to turn to α,β-unsaturated compound by treatment with base when carboxyl group is free or esterified, whereas its acid amide often gives the desired *O*-tosylate.[15] In fact, methyl ester **12** readily gave α,β-unsaturated compound **13** even during the course of *O*-tosylation of **12** in pyridine. Thus, we converted methyl ester **12** into amide **14** with ammonia in methanol prior to *O*-tosylation. Amide **14** thus obtained afforded the desired *O*-tosyl derivative **15** in a satisfactory yield. *O*-Tosylate **15** was treated with diethylamine in tetrahydrofuran to yield aziridine compound **16**,[15] which was then converted into β-aminoornithine derivative **17** with ammonia in methanol (Scheme 3). In order to confirm the position and configuration of the newly introduced amino group, **17** was reversely deaminated with sodium nitrite to give hydroxy compound identified with the starting material **14** on thin-layer chromatography, affording *threo*-β-hydroxyornithine (**9a**) on hydrolysis. The fact that *threo* configuration was maintained in **17** was elucidated by the double inversion throughout the course of reaction (Scheme 3). Triamino deriva-

tive **17** thus established was debenzyloxycarbonylated by catalytic hydrogenation and then guanidinated with *N*-(*p*-tolylsulfonyl)bis(methylthio)methanimine[16] to afford a cyclic guanidino compound **19**, which, without isolation, was hydrolyzed with hydrobromic acid to give the final product (**1**). (Scheme 4). It was identical with that of natural L-capreomycidine on thin-layer chromatogram and amino acid analysis. IR and NMR spectra of the synthetic flavianate were also superposable with those of a natural specimen.

The novel synthesis of DL-capreomycidine, being entirely different from the former method,[9] is promising in view of preparation of an optically active guanidino amino acid particularly L-capreomycidine, L-epicapreomycidine or L-tuberactidine.[17]

Experimental

N$^{\delta}$-*Phthaloyl-β-hydroxyornithine (**8**).* Phthalimide (147 g, 1.00 mol) was suspended in 300 ml of absolute ethanol in which sodium metal (0.45 g) had been dissolved. Acrylaldehyde (56.1 g, 1.00 mol) in 50 ml of absolute ethanol was added dropwise to the suspension at room temperature for 50 min with stirring under nitrogen atmosphere. [*N*-(1-carboxylatoethylidene)glycinato]aquacopper(II) dihydrate (**7**)[13] (162 g, 0.621 mol) and 350 ml of absolute methanol were immediately added to the viscous pale yellow solution obtained. To the suspension was added sodium methoxide (54.0 g, 1.00 mol) in 150 ml of absolute methanol for 50 min. After being stirred at 30 °C overnight under nitrogen atmosphere, the reaction mixture was neutralized with 9 ml of acetic acid, and diluted with 1 litre of water. Greenish viscous precipitate was filtered off, and the filtrate was kept for further treatment (filtrate A).

The precipitate was dissolved in 1 M hydrochloric acid and the insoluble material was filtered off. Hydrogen sulfide was bubbled through the filtrate for 1 h. Cupric sulfide was filtered off and washed with 1 M hydrochloric acid. Filtrate and washings were combined, aerated, concentrated *in vacuo*, and neutralized with pyridine. Addition of ethanol gave precipitate of crude *threo* *N*$^{\delta}$-phthaloyl compound **8a** (77.6 g). This was recrystallized from water to give pure **8a**: yield 48.2 g (28%), mp 214.5 °C (dec).

Found: C, 52.65; H, 5.59; N, 9.46%. Calcd for $C_{13}H_{14}N_2O_5 \cdot H_2O$: C, 52.70; H, 5.44; N, 9.46%.

Filtrate A was treated as above to recover **8a** (2.28 g, 1.3%). Pure *erythro* compound (**8b**) was obtained from the mother liquor: yield 0.71 g (0.4%), mp 245 °C (dec).

Found: C, 55.49; H, 5.12; N, 10.03%. Calcd for $C_{13}H_{14}N_2O_5$: C, 56.11; H, 5.07; N, 10.07%.

threo-*β-Hydroxyornithine Hydrochloride (**9a**).* *N*$^{\delta}$-Phthaloyl-*threo*-*β*-hydroxyornithine (**8a**) (5.40 g, 18.2 mmol) was dissolved in 130 ml of 6 M hydrochloric acid and heated under reflux for 12 h. Phthalic acid was filtered off and the filtrate was extracted with ethyl acetate. Aqueous layer was concentrated *in vacuo*. Concentration after addition of a small amount of water was repeated several times to remove excess hydrochloric acid. Oily product was dissolved in a small amount of water, neutralized with pyridine, and then precipitated by addition of ethanol. Crystallization from water and ethanol gave **9a**: yield 3.20 g (87%), mp 189—190 °C (dec).

Found: C, 29.54; H, 7.56; N, 13.97; Cl, 17.47%. Calcd for $C_5H_{13}N_2O_3Cl \cdot H_2O$: C, 29.63; H, 7.46; N, 13.83; Cl, 17.50%.

erythro-*β-Hydroxyornithine Hydrochloride (**9b**).* *N*$^{\delta}$-Phthaloyl-*erythro*-*β*-hydroxyornithine (**8b**) (1.00 g, 3.60 mmol) was hydrolyzed with 60 ml of 6 M hydrochloric acid and treated as above: yield 580 mg (87%), mp 225 °C (dec).

Found: C, 32.26; H, 7.18; N, 15.30; Cl, 19.29%. Calcd for $C_5H_{13}N_2O_3Cl$: C, 32.53; H, 7.10; N, 15.17; Cl, 19.20%.

N$^{\delta}$-*Benzyloxycarbonyl*-threo-*β-hydroxyornithine (**10**).* Basic copper carbonate (23.9 g, 100 mmol) was added portionwise under boiling to a solution of *threo*-*β*-hydroxyornithine hydrochloride (**9a**) (10.1 g, 50.0 mmol) in 250 ml water. After additional 15 min boiling, excess copper carbonate was filtered off and washed with hot water. The combined filtrate and washings were subjected to acylation with benzyloxycarbonyl chloride (14.5 g, 85.0 mmol) and sodium hydrogencarbonate in the usual way. The reaction product precipitated was filtered, suspended in 200 ml of water, and 6 M hydrochloric acid was added to the suspension until precipitate dissolved. Hydrogen sulfide was passed through the solution, and the resulting cupric sulfide was filtered off. Neutralization of the solution with sodium hydrogencarbonate gave crystals (12.4 g) which were recrystallized from water: yield 10.3 g (71%), mp 212—213 °C (dec).

Found: C, 53.55; H, 6.58; N, 9.61%. Calcd for $C_{13}H_{18}N_2O_5 \cdot 1/2H_2O$: C, 53.60; H, 6.57; N, 9.62%.

N$^{\alpha}$-*Benzyloxycarbonyl*-N$^{\alpha}$-p-*tolylsulfonyl*-threo-*β-hydroxyornithine (**11**).* Triethylamine (3.00 g, 29.7 mmol) and *p*-toluenesulfonyl chloride (2.80 g, 14.7 mmol) were added portionwise during a period of 30 min to a suspension of *N*$^{\delta}$-benzyloxycarbonyl-*threo*-*β*-hydroxyornithine (**10**) (2.77 g, 9.52 mmol) in 24 ml of aqueous tetrahydrofuran (H_2O–THF = 2 : 1). The reaction mixture was stirred at room temperature for 1.5 h, concentrated to approximately 8 ml *in vacuo*, and extracted several times with ether. The aqueous layer was acidified with 2 M hydrochloric acid to produce an oily material which was extracted with ethyl acetate. The extract was washed with water, dried over anhydrous sodium sulfate, and concentrated *in vacuo*. The oily residue was triturated with ether to crystallize. It was recrystallized from ethanol, ether, and hexane: yield 3.75 g (90%), mp 169.5—170 °C.

Found: C, 54.69; H, 5.59; N, 6.41; S, 7.20%. Calcd for $C_{20}H_{24}N_2O_7S$: C, 55.03; H, 5.54; N, 6.42; S, 7.32%.

N$^{\delta}$-*Benzyloxycarbonyl*-N$^{\delta}$-p-*tolylsulfonyl*-threo-*β-hydroxyornithine Methyl Ester (**12**).* Compound **11** (5.62 g, 12.9 mmol) was dissolved in a mixture of 15 ml each of anhydrous dioxane and anhydrous tetrahydrofuran. Diazomethane in ether was added to the solution under ice cooling until its yellow color remained. Excess diazomethane was decomposed with acetic acid with stirring for 30 min. The reaction mixture was concentrated *in vacuo* to give an oily residue, which was crystallized by addition of a small amount of ether.

It was recrystallized from ethyl acetate and hexane: yield 5.37 g (93%), mp 127—128 °C.

Found: C, 55.81; H, 5.83; N, 6.20; S, 7.19%. Calcd for $C_{21}H_{26}N_2O_7S$: C, 55.99; H, 5.82; N, 6.22; S, 7.12%.

N$^{\delta}$-*Benzyloxycarbonyl*-N$^{\delta}$-p-*tolylsulfonyl*-*α,β-dehydroornithine Methyl Ester (**13**).* To a solution of methyl ester **12** (1.02 g, 2.27 mmol) in 3 ml of anhydrous pyridine was added dropwise a solution of *p*-toluenesulfonyl chloride (864 mg, 4.53 mmol) in anhydrous pyridine with stirring under ice cooling. Stirring was continued under cooling for 30 min and then at room temperature overnight. The reaction mixture was concentrated *in vacuo*, dissolved in 20 ml of water, and extracted three times with 10 ml of ethyl acetate. The extract was washed with water, 1 M hydrochloric acid, saturated sodium chloride solution and dried over anhydrous sodium sulfate. The oily residue obtained after vacuum concentration was purified on silica gel column using benzene–ethyl acetate (3 : 1) as a solvent. Pure unsaturated compound

was obtained from the eluate: yield 0.70 g (71%), mp 85—86 °C, after recrystallization from ethyl acetate and hexane.

Found: C, 58.33; H, 5.60; N, 6.58; S, 7.36%. Calcd for $C_{21}H_{24}N_2O_6S$: C, 58.32; H, 5.59; N, 6.48; S, 7.41%.

*N$^{\delta}$-Benzyloxycarbonyl-N$^{\delta}$-p-tolylsulfonyl-threo-β-hydroxyornithine Amide (**14**).* Methyl ester **12** (4.50 g, 10.0 mmol) was dissolved in 80 ml of methanol. The solution was saturated with ammonia in a pressure bottle and kept at room temperature for 2 days. Concentration *in vacuo* gave an oily residue, which was crystallized by trituration with hexane. It was recrystallized from ethyl acetate and hexane: yield 4.17 g (96%), mp 134.5 °C.

Found: C, 54.94; H, 5.83; N, 9.48; S, 7.44%. Calcd for $C_{20}H_{25}N_3O_6S$: C, 55.16; H, 5.79; N, 9.65; S, 7.36%.

*N$^{\delta}$-Benzyloxycarbonyl-N$^{\alpha}$,O-bis(p-tolylsulfonyl)-threo-β-hydroxyornithine Amide (**15**).* *p*-Toluenesulfonyl chloride (9.33 g, 48.9 mmol) in 20 ml of pyridine was added dropwise to a solution of amide **14** (3.55 g, 8.15 mmol) in 15 ml of pyridine for 4 h under stirring and cooling in ice–salt bath. After additional 4 h stirring in a chilled bath, the reaction mixture was poured on crushed ice in 35 ml of concentrated hydrochloric acid. Aqueous solution was extracted with ethyl acetate. The extract was washed with water, dried over sodium sulfate, and concentrated *in vacuo*. The oily residue obtained was purified by silica gel column chromatography: Silica gel 50 g; column 2.3 × 30 cm; each 10 g fraction. The following solvents were used successively, benzene (100 ml), benzene–ethyl acetate (4 : 1 = 250 ml, 3 : 1 = 400 ml, 2 : 1 = 350 ml), ethyl acetate (850 ml). Fractions 16 to 35 gave α,β-unsaturated amide as an oily substance (340 mg, 10%). Desired *O*-tosylate was obtained as crystals from fractions 36—84 (2.35 g, 49%), the starting material **14** being recovered from fractions 101—145 (1.15 g, 32%). *O*-Tosylate was recrystallized from chloroform and ether for elemental analysis, mp 146—147 °C.

Found: C, 55.03; H, 5.32; N, 7.10; S, 10.82%. Calcd for $C_{27}H_{31}N_3O_8S_2$: C, 54.99; H, 5.30; N, 7.13; S, 10.88%.

*5-Benzyloxycarbonylamino-cis-2,3-(p-tolylsulfonylepimino)pentanamide (**16**).* Diethylamine (114 mg, 1.55 mmol) was added at 35—37 °C to a solution of ditosyl amide **15** (457 mg, 0.774 mmol) in 5 ml of anhydrous tetrahydrofuran. The reaction mixture was stirred for 3 h at the temperature and concentrated *in vacuo*. The residue was dissolved in ethyl acetate and washed with water, 1 M hydrochloric acid, and again water to neutral. Organic layer was dried over anhydrous sodium sulfate and concentrated *in vacuo*. The crystalline residue was recrystallized from chloroform and ether: yield 289 mg (89%), mp 136—137 °C.

Found: C, 57.16; H, 5.62; N, 10.08; S, 7.71%. Calcd for $C_{20}H_{23}N_3O_5S$: C, 57.54; H, 5.55; N, 10.07; S, 7.68%.

*threo-3-Amino-5-benzyloxycarbonylamino-2-(p-tolylsulfonylamino)-pentanamide (**17**).* Gaseous ammonia was bubbled into a solution of aziridine compound **16** (1.02 g, 2.44 mmol) in 200 ml of methanol until saturation. It was kept in a pressure bottle at room temperature for 4 days, and concentrated *in vacuo*. Evaporation was repeated twice after dissolution of the residue in methanol. Finally, residual oil was dissolved in 15 ml of 0.2 M hydrochloric acid and extracted with ethyl acetate. The aqueous layer was concentrated *in vacuo* and the oily residue was crystallized by trituration with ether: yield 1.01 g (87%). It was recrystallized from methanol and ether, mp 115—117 °C.

Found: C, 49.26; H, 5.86; N, 11.58; S, 6.52; Cl, 7.25%. Calcd for $C_{20}H_{26}N_4O_5S \cdot HCl \cdot H_2O$: C, 49.12; H, 5.98; N, 11.46; S, 6.56; Cl, 7.25%.

*threo-3,5-Diamino-2-(p-tolylsulfonylamino)pentanamide (**18**).* 3-Amino compound **17** (1.01 g, 2.14 mmol) obtained above was dissolved in 20 ml of methanol containing 0.18 ml (2.16 mmol) of concentrated hydrochloric acid and hydrogenated in the presence of palladium black. After the completion of reduction had been checked on TLC, the catalyst was filtered off and the filtrate was concentrated *in vacuo*. The crystalline residue was recrystallized from methanol and ether: yield 0.73 g (91%), mp 189—191 °C.

Found: C, 37.00; H, 5.93; N, 14.62; S, 8.31; Cl, 18.11%. Calcd for $C_{12}H_{20}N_4O_3S \cdot 2HCl \cdot H_2O$: C, 36.83; H, 6.18; N, 14.32; S, 8.19; Cl, 18.12%.

*DL-Capreomycidine (**1**) Diflavianate.* 3,5-Diamino compound **18** (200 mg, 0.511 mmol), *N-(p*-tolylsulfonyl)bis(methylthio)methanimine[16] (141 mg, 0.511 mmol) and 0.51 ml of 1 M sodium hydroxide were dissolved in 95% ethanol. The solution was heated under reflux for 3 h. After addition of 0.51 ml of 1 M sodium hydroxide, heating was continued for 6 h. The reaction mixture was concentrated *in vacuo* to yield a residue which was extracted with ethyl acetate. The extract was washed with saturated sodium chloride solution, dried over anhydrous sodium sulfate, and concentrated *in vacuo*. The oily residue was immediately hydrolyzed with 47% hydrobromic acid in the presence of 2 ml of anisole under reflux for 24 h. The hydrolyzate was extracted with benzene several times, diluted with water, and extracted with ethyl acetate. The aqueous layer was concentrated *in vacuo* and ethanol was added to the residue. After removal of insoluble material by filtration, the filtrate was concentrated again. The residue was dissolved in 2 ml of water containing excess flavianic acid, 2 ml of ethanol being added. It was allowed to stand to yield yellow needles: Yield 90 mg (21%). For elemental analysis, it was recrystallized from water, mp 217—219 °C (dec).

Found: C, 36.42; H, 3.55; N, 13.34; S, 7.49%. Calcd for $C_{26}H_{24}N_8O_{18}S_2 \cdot 3H_2O$: C, 36.54; H, 3.54; N, 13.11; S, 7.50%.

References

1) Part XIII. S. Nomoto and T. Shiba, *J. Antibiot.*, **30**, 1008 (1977).

2) Presented at the 34th National Meeting of the Chemical Society of Japan, Kanagawa, April 1976, II, p. 698.

3) a) E. B. Herr, Jr., *Antimicrob. Agents Chemother.*, **1963**, 201; b) E. B. Herr, Jr., and M. O. Redstone, *Ann. N. Y. Acad. Sci.*, **135**, 940 (1966).

4) a) H. Yoshioka, T. Aoki, H. Goko, K. Nakatsu, T. Noda, H. Sakakibara, T. Take, A. Nagata, J. Abe, T. Wakamiya, T. Shiba, and T. Kaneko, *Tetrahedron Lett.*, **1971**, 2043; b) T. Ando, K. Matsuura, R. Izumi, T. Noda, T. Take, A. Nagata, and J. Abe, *J. Antibiot.*, **24**, 680 (1971); c) T. Wakamiya, T. Shiba, T. Kaneko, H. Sakakibara, T. Noda, and T. Take, *Bull. Chem. Soc. Jpn.*, **46**, 949 (1973).

5) B. W. Bycroft, D. Cameron, L. R. Croft, and A. W. Johnson, *J. Chem. Soc., Chem. Commun.*, **1968**, 1301.

6) B. W. Bycroft, L. R. Croft, A. W. Johnson, and T. Webb, *J. Antibiot.*, **22**, 133 (1969).

7) K. Tatsuta, N. Mikami, K. Fujimoto, S. Umezawa, H. Umezawa, and T. Aoyagi, *J. Antibiot.*, **26**, 625 (1973).

8) a) H. Umezawa, T. Aoyagi, A. Okura, H. Morishima, T. Takeuchi, and Y. Okami, *J. Antibiot.*, **26**, 787 (1973); b) A. Okura, H. Morishima, T. Takita, T. Aoyagi, T. Takeuchi, and H. Umezawa, *ibid.*, **28**, 337 (1975).

9) B. W. Bycroft, D. Cameron, and A. W. Johnson, *J. Chem. Soc., C*, **1971**, 3040.

10) T. Wakamiya, T. Teshima, I. Kubota, T. Shiba, and T. Kaneko, *Bull. Chem. Soc. Jpn.*, **47**, 2292 (1974).

11) O. A. Moe and D. T. Werner, *J. Am. Chem. Soc.*, **71**,

1251 (1949).
12) A. Nakahara, H. Yamamoto, and H. Matsumoto, *Bull. Chem. Soc. Jpn.*, **37**, 1137 (1964).
13) a) T. Ichikawa, S. Maeda, Y. Araki, and Y. Ishido, *J. Am. Chem. Soc.*, **92**, 5514 (1970); b) T. Ichikawa, S. Maeda, T. Okamoto, Y. Araki, and Y. Ishido, *Bull. Chem. Soc. Jpn.*, **44**, 2779 (1971); c) S. Ohdan, T. Okamoto, S. Maeda, T. Ichikawa, Y. Araki, and Y. Ishido, *ibid.*, **46**, 981 (1973).
14) The observed ratio was obtained from amino acid analysis (55 cm column, pH 5.28, 0.35 M sodium citrate buffer).
15) a) K. Okawa, T. Kinutani, and K. Sakaki, *Bull. Chem. Soc. Jpn.*, **41**, 1353 (1968); b) Y. Nakagawa, T. Tsuno, K. Nakajima, M. Iwai, H. Kawai, and K. Okawa, *Bull. Chem. Soc. Jpn.*, **45**, 1162 (1972).
16) J. V. Rodricks and H. Rapoport, *J. Org. Chem.*, **36**, 46 (1971).
17) Recently, we have succeeded to synthesize L-capreomycidine according to this synthetic principle. T. Shiba, T. Ukita, K. Mizuno, T. Teshima, and T. Wakamiya, *Tetrahedron Lett.*, **1977**, 2681.

Nucleoside Analogs. 6. A Synthesis of Carbocyclic Puromycin Analogs[1)]

Tetsuo SUAMI,* Kin-ichi TADANO, Mitsukuni AYABE, and the late Yasufumi EMORI
Department of Applied Chemistry, Faculty of Engineering, Keio University, Hiyoshi, Yokohama 223
(Received August 9, 1977)

Eight carbocyclic puromycin analogs, in which the furanosyl ring of puromycin is replaced with a cyclopentyl system, were synthesized. Their minimum degeneration concentration (MDC) was determined against *HeLa* cells in a tissue culture. The two analogs were found to be remarkably active.

A nucleoside antibiotic puromycin (**1**) was isolated from a culture broth of *Streptomyces alboniger* by Porter *et al.*,[2)] its synthesis being accomplished by Baker *et al.*[3)] Various analogs have been prepared for clarification of the relationship between structure and biological activity.[4-7)]

In particular, Daluge and Vince[7)] demonstrated the essential structural requirement for biological activity in puromycin analogs by the synthesis of a carbocyclic analog: 6-dimethylamino-9-[(1*R*,2*R*,3*R*)-2-hydroxy-3-(*p*-methoxyphenyl-L-alanylamino)cyclopentyl]purine. They showed that the removal of the hydroxymethyl moiety from the puromycin molecule is not detrimental to activity and the furanosyl ring can be replaced with a cyclopentane ring with no loss in activity. Their assessment of the structural requirement in the puromycin molecule stimulated us to prepare a carbocyclic puromycin analog in which the 3-amino-3-deoxy-β-D-ribofuranosyl moiety of puromycin is replaced by 3-amino-2,4,5-trihydroxycyclopentyl group.

The structure of puromycin resembles that of the aminoacyl–adenyl terminus of aminoacyl-tRNA, this being strongly connected with its biological activity. Since a cyclopentane ring is conformationally similar to a furanosyl ring, 3-amino-2,4,5-trihydroxycyclopentyl group might replace the furanosyl moiety of puromycin, favorably resulting in biological activity.

Carbocyclic analogs of adenosine and pyrimidine nucleosides, in which the ribofuranosyl moiety was replaced by the polyhydroxycyclopentyl or polyhydroxycyclohexyl group, have been prepared.[8-12)] In connection with the preceding studies and to extend the Daluge and Vince evaluation of the structural requirement of the puromycin molecule, we have synthesized eight diastereoisomeric 6-dimethylamino-9-[2,4,5-trihydroxy-3-(*p*-methoxyphenyl-L-alanylamino)cyclopentyl]purines (**8a,b, 15a,b, 22a,b,** and **30a,b**), and their biological activities were dtermined against *HeLa* cells.

Results and Discussion

The carbocyclic puromycin analogs were prepared by the reaction processes shown in Schemes 2 and

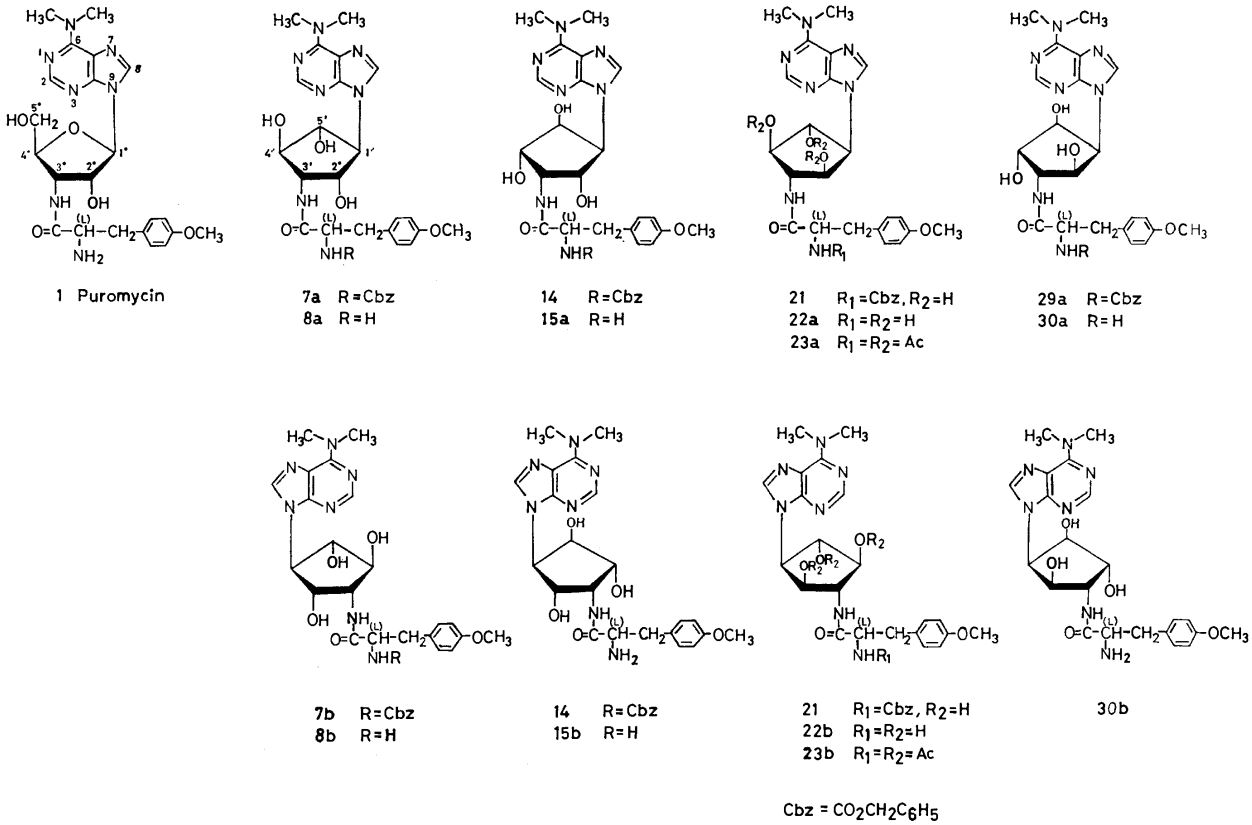

Scheme 1.

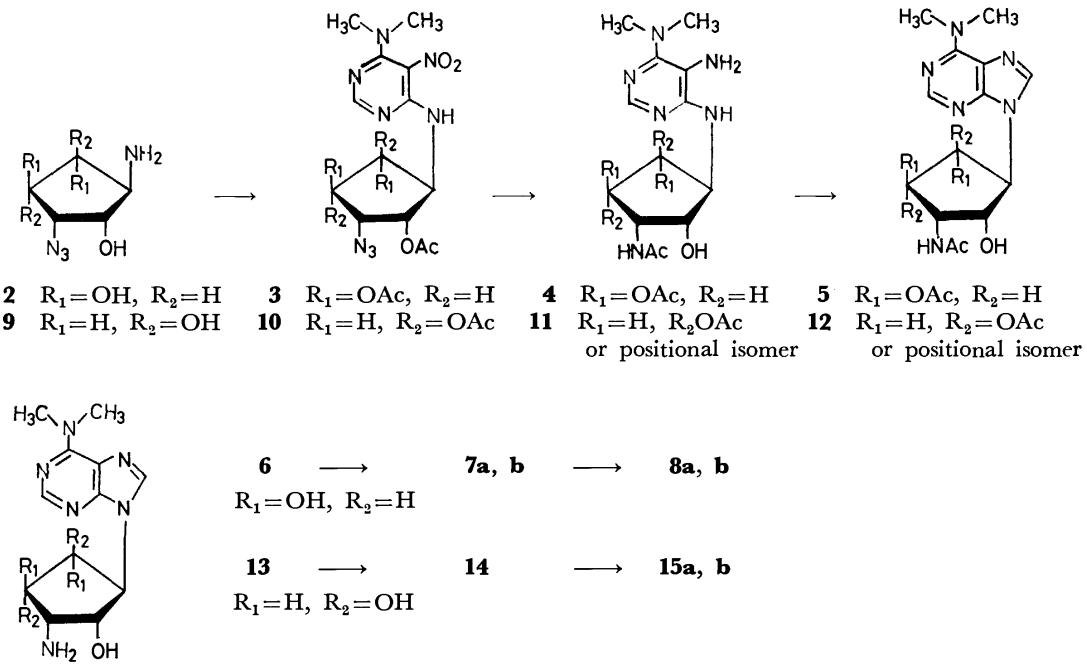

Scheme 2.[19]

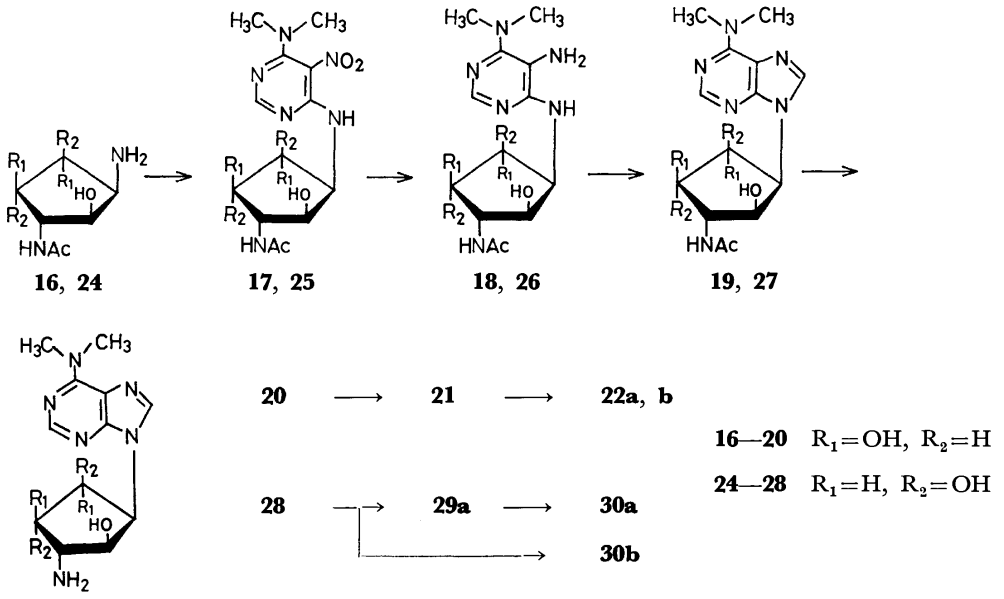

Scheme 3.[19]

3. The processes are divided into two categories, 1-amino-3-azido-2,4,5-cyclopentanetriols (**2** and **9**) being used as the starting material in the former two (Scheme 2) and 3-acetamino-1-amino-2,4,5-cyclopentanetriols (**16** and **24**) in the latter two.

When 1-amino-3-azido-2,4,5-cyclopentanetriol[11] (**2**) was heated with 6-chloro-4-dimethylamino-5-nitropyrimidine[13] in 2-methoxyethanol in the presence of triethylamine, 6-[(3-azido-2,4,5-triacetoxycyclopentyl)-amino]-4-dimethylamino-5-nitropyrimidine (**3**) was obtained, after acetylation. The structure of **3** was confirmed by the ^{1}H NMR spectrum in which NH revealed a doublet at δ 8.38 (J=7 Hz).

Catalytic hydrogenation of **3** with Raney nickel afforded 6-[(3-acetamido-4,5-diacetoxy-2-hydroxycyclopentyl)amino]-5-amino-4-dimethylaminopyrimidine (**4**). During the course of the reaction, acetyl group migration took place from O to N in the *cis*-arrangement.

Ring closure of **4** was performed with triethyl orthoformate in the presence of *p*-toluenesulfonic acid to give the purine derivative (**5**) in 87% yield. Hydrolysis of **5** in aqueous barium hydroxide, followed by purification on a column of Amberlite CG-120(H$^+$) resin gave 9-(3-amino-2,4,5-trihydroxycyclopentyl)-6-dimethylaminopurine (**6**). Compound **6** was converted into the crystalline hydrochloride which was proved to be the 9-substituted adenine derivative by a characteristic UV absorption.[16]

Table 1. Minimum degeneration concentration (MDC) with *HeLa S3* cells in a tissue culture by the two-fold serial liquid medium dilution method[18]

Compound	MDC (μg/ml)
8a	15.6
8b	250
15a	31.2
15b	125
22a	1000
22b	1000
30a	250
30b	500

When **6** was treated with *N*-benzyloxycarbonyl-*p*-methoxyphenyl-L-alanine[14] and *N*-hydroxysuccinimide in the presence of dicyclohexylcarbodiimide, a mixture of two diastereoisomers (**7a** and **7b**) was obtained, since **6** is of DL form. Compounds **7a** and **7b** were successfully separated by fractional recrystallization. Hydrogenolysis of **7a** and **7b** in glacial acetic acid with palladium black gave **8a** and **8b**, respectively. The overall yields of **8a** and **8b** were 11 and 19%, respectively.

Compounds **15a** and **15b** were obtained by analogous reactions (Scheme 2) in 7 and 8% overall yields, respectively.

On the other hand, when 3-acetamido-1-amino-2,4,5-cyclopentanetriol (**16**) was subjected to react with 6-chloro-4-dimethylamino-5-nitropyrimidine,[13] 6-[(3-acetamido-2,4,5-trihydroxycyclopentyl)amino]-4-dimethylamino-5-nitropyrimidine (**17**) was obtained in 77% yield. The successive reactions leading to **22a** and **22b** were carried out by following the reactions used in the preparation of **8a** and **8b** (Scheme 3). The overall yields of **22a** and **22b** were 8 and 14%, respectively.

By an analogous reaction (Scheme 3), **30a** and **30b** were obtained each in 8% overall yield.

A biological activity of the carbocyclic puromycin analogs thus obtained was determined by the usual two-fold serial liquid medium dilution method with *HeLa S3* cells in a tissue culture. The minimum degeneration concentration (MDC) was appraised, the result being given in Table 1. We see that **8a** and **15a** are remarkably active, in contrast with other diastereoisomers.

The stereochemistry of **8a** and **15a** is tentatively assigned as that depicted in Scheme 1, on the basis of their biological activity and the absolute configuration of puromycin with respect to that on C-1′, 2′, and 3′.

The stereochemistry of **22a** and **30a** is assigned tentatively on the observation that, in the cases of **8a** and **15a**, their specific rotations are more levorotatory than those of the respective diastereoisomers: **8b** and **15b**. Therefore, the absolute configurations of **22a** and **30a** depicted in Scheme 1 are assigned to the strongly levorotatory diastereoisomers.

Experimental

Melting points were determined in capillary tubes in a liquid bath and are uncorrected. Solutions were evaporated under reduced pressure. Optical rotations were measured with a Japan Spectroscopic DIL-SL polarimeter. ^{1}H NMR spectra were recorded at 60 MHz with a Varian A-60D spectrometer for solutions in chloroform-*d*, unless otherwise stated, with tetramethylsilane as an internal standard, the peak positions being given in δ values.[17] IR spectra were recorded on potassium bromide disks with a Hitachi Perkin-Elmer 225 spectrometer. UV spectra were determined with a Hitachi Perkin-Elmer UV-VIS 139 spectrometer. Acetylation was performed with acetic anhydride and pyridine. Catalytic hydrogenation of a nitro group to an amino group was carried out in the presence of Raney nickel in a hydrogen atmosphere (3.4 kg/cm^2) with a Parr apparatus. TLC was performed on Wakogel B-10 Wako Pure Chemical Co. Ltd.) plates. Silica gel (Wakogel C-300) was used for column chromatography.

DL-(1,4/2,3,5)-1-Amino-3-azido-2,4,5-cyclopentanetriol (2). The compound was prepared by the method of Tadano *et al.*[11]

6-[(DL-(1,4/2,3,5)-3-Azido-2,4,5-triacetoxycyclopentyl)amino]-4-dimethylamino-5-nitropyrimidine (3). A mixture of **2** (1.0 g) and 6-chloro-4-dimethylamino-5-nitropyrimidine[13] (2.33 g) in 2-methoxyethanol (50 ml) containing triethylamine (1 ml) was heated at 100 °C for 5 h with mechanical agitation. The mixture was evaporated and the residue was dissolved in warm water (50 ml). The aqueous solution was washed with benzene repeatedly and the aqueous layer was evaporated. The residue was acetylated and the resulting solution was poured into ice cold water. The solution was extracted with chloroform and the chloroform solution was evaporated to give a pale yellow crystalline residue. The residue was washed with warm ethyl acetate to give 1.92 g (72%) of **3**, mp 190—191 °C. ^{1}H NMR: δ 2.06 (s, 3, OAc), 2.14 (s, 3, OAc), 2.15 (s, 3, OAc), 3.08 (s, 6, 2×NCH$_3$), 8.04 (s, 1, pyrimidine H-2), 8.38 (d, 1, J=7 Hz, NH).

Found: C, 43.98; H, 4.79; N, 24.26%. Calcd for $C_{17}H_{22}N_8O_8$: C, 43.78; H, 4.76; N, 24.03%.

6-[(DL-(1,4/2,3,5)-3-Acetamido-4,5-diacetoxy-2-hydroxycyclopentyl)amino]-5-amino-4-dimethylaminopyrimidine (4). Compound **3** (300 mg) was catalytically hydrogenated in ethyl acetate (50 ml) for 3 h. The catalyst was filtered off and the filtrate was evaporated to give 253 mg (96%) of **4** as crystals, mp 206—207 °C (dec). ^{1}H NMR (DMSO-d_6): δ 1.94 (s, 3, NAc), 2.05 (s, 3, OAc), 2.06 (s, 3, OAc), 2.81 (s, 6, 2×NCH$_3$), 5.73 (d, 1, J=4 Hz, OH), 6.75 (d, 1, J=7 Hz, pyrimidine H-6), 8.08 (s, 1, pyrimidine H-2), 8.13 (d, 1, J=8 Hz, NH).

Found: C, 50.05; H, 6.50; N, 20.20%. Calcd for $C_{17}H_{26}N_6O_6$: C, 49.75; H, 6.39; N, 20.48%.

9-[DL-(1,4/2,3,5)-3-Acetamido-4,5-diacetoxy-2-hydroxycyclopentyl]-6-dimethylaminopurine (5). A mixture of **4** (204 mg) and triethyl orthoformate (0.11 ml) in *N*,*N*-dimethylformamide (10 ml) was stirred for 6 h in the presence of *p*-toluenesulfonic acid (9 mg). After being neutralized with Amberlite IRA-400 (OH$^-$) resin, the solution was evaporated. The residue was recrystallized from ethyl acetate to give 182 mg (87%) of **5**, mp 200—201 °C. ^{1}H NMR (DMSO-d_6): δ 1.95 (s, 3, NAc), 1.97 (s, 3, OAc), 2.12 (s, 3, OAc), 3.59 (s, 6, 2×NCH$_3$), 5.95 (d, 1, J=5 Hz, OH), 8.31 (d, 1, J=8 Hz, NH), 8.56 (s, 1, purine H-2 or 8), 8.60 (s, 1, purine H-8 or 2).

Found: C, 51.64; H, 5.75; N, 19.74%. Calcd for $C_{18}H_{24}N_6O_6$: C, 51.42; H, 5.75; N, 19.99%.

*9-[DL-(1,4/2,3,5)-3-Amino-2,4,5-trihydroxycyclopentyl]-6-dimethylaminopurine (**6**).* A mixture of **5** (1.65 g) and barium hydroxide octahydrate (8.0 g) in water (96 ml) was heated at 100 °C for 3 h with mechanical agitation. Carbon dioxide was bubbled into the solution and barium carbonate was filtered off. The filtrate was concentrated and the residue was purified on a column of Amberlite CG-120(H^+) resin. After being washed with water, the column was eluted with dil NH_4OH and the effluent was concentrated to give 1.14 g of **6** as a crude product. A part of the product was converted into crystalline hydrochloride, mp 250 °C (dec). UV: $\lambda_{max}^{0.1M\ HCl}$ 269 nm ($\varepsilon=1.7\times10^4$), $\lambda_{max}^{H_2O}$ 277 nm ($\varepsilon=1.7\times10^4$), $\lambda_{max}^{0.1M\ NaOH}$ 277 nm ($\varepsilon=1.7\times10^4$).

Found: C, 43.35; H, 5.74; N, 25.19; Cl, 10.88%. Calcd for $C_{12}H_{19}N_6O_3Cl$: C, 43.57; H, 5.79; N, 25.41; Cl, 10.72%.

*6-Dimethylamino-9-[(1S,2R,4R,5R)-2,4,5-trihydroxy-3-(N-benzyloxycarbonyl-p-methoxyphenyl-L-alanylamino)cyclopentyl]purine (**7a**)* and *6-Dimethylamino-9-[(1R,2S,4S,5S)-2,4,5-trihydroxy-3-(N-benzyloxycarbonyl-p-methoxyphenyl-L-alanylamino)cyclopentyl]-purine (**7b**).* Dicyclohexylcarbodiimide (DCC, 838 mg) was added under ice-cooling with agitation to a solution of **6** (1.14 g) and *N*-benzyloxycarbonyl-*p*-methoxyphenyl-L-alanine[14] (1.34 g) in *N,N*-dimethylformamide (DMF, 57 ml) containing *N*-hydroxysuccinimide (468 mg). After 30 min, the solution was left to settle at ambient temperature for 18 h. The mixture was filtered in order to remove *N,N'*-dicyclohexylurea and the filtrate was concentrated. The residue was recrystallized from ethanol to give 670 mg (29%) of **7a** as needles, mp 179—180 °C, $[\alpha]_D^{20}$ −24.4° (*c* 1.07, DMF). ^{1}H NMR (DMSO-d_6): 3.62 (s, 6, 2×NCH_3), 3.90 (s, 3, OCH_3), 5.18 (s, 2, benzyl CH_2), 7.34 (q, 4, C_6H_4), 7.58 (s, 5, C_6H_5), 8.28 (d, 1, J=8 Hz, NH on C-3'), 8.54 (s, 1, purine H-2 or 8), 8.57 (s, 1, purine H-8 or 2).

Found: C, 59.62; H, 5.86; N, 16.20%. Calcd for $C_{30}H_{35}N_7O_7$: C, 59.49; H, 5.83; N, 16.19%.

The ethanolic mother liquor of **7a** was stored in a refrigerator to give 1.12 g of a product. Recrystallization from methanol gave 931 mg (40%) of **7b** as needles, mp 210—211 °C, $[\alpha]_D^{20}$ +17.5° (*c* 1.03, DMF). ^{1}H NMR (DMSO-d_6): 3.64 (s, 6, 2×NCH_3), 3.90 (s, 3, OCH_3), 5.21 (s, 2, benzyl CH_2), 7.36 (q, 4, C_6H_4), 7.62 (s, 5, C_6H_5), 8.27 (d, 1, J=6 Hz, NH on C-3'), 8.57 (s, 1, purine H-2 or 8), 8.61 (s, 1, purine H-8 or 2).

Found: C, 59.23; H, 5.83; N, 16.33%. Calcd for $C_{30}H_{35}N_7O_7$: C, 59.49; H, 5.83; N, 16.19%.

*6-Dimethylamino-9-[(1S,2R,4R,5R)-2,4,5-trihydroxy-3-(p-methoxyphenyl-L-alanylamino)cyclopentyl]purine (**8a**).* A solution of **7a** (300 mg) in glacial acetic acid (20 ml) was hydrogenated in the presence of palladium black (200 mg) in a hydrogen atmosphere (1.4 kg/cm^2) for 3 h. The catalyst was filtered off, and the filtrate was concentrated. A methanolic solution of the residue was passed through a column of Amberlite IRA-400(OH^-) resin and the effluent was concentrated. The residue was recrystallized from methanol to give 146 mg (63%) of **8a**, mp 190—191 °C (dec), $[\alpha]_D^{19}$ −55.0° (*c* 0.98, DMF). UV: $\lambda_{max}^{0.1M\ HCl}$ 268 nm ($\varepsilon=2.7\times10^4$), $\lambda_{max}^{H_2O}$ 276 nm ($\varepsilon=1.9\times10^4$), $\lambda_{max}^{0.1M\ NaOH}$ 275 nm ($\varepsilon=2.1\times10^4$). ^{1}H NMR (DMSO-$d_6$): 3.62 (s, 6, 2×$NCH_3$), 3.89 (s, 3, OCH_3), 7.31 (q, 4, C_6H_4), 8.54 (s, 1, purine H-2 or 8), 8.57 (s, 1, purine H-8 or 2).

Found: C, 55.92; H, 6.28; N, 20.54%. Calcd for $C_{22}H_{29}N_7O_5$: C, 56.04; H, 6.20; N, 20.79%.

*6-Dimethylamino-9-[(1R,2S,4S,5S)-2,4,5-trihydroxy-3-(p-methoxyphenyl-L-alanylamino)cyclopentyl]purine (**8b**).* Catalytic hydrogenation of **7b** (300 mg) was carried out as in the preparation of **8a**. The product was recrystallized from methanol to give 182 mg (78%) of **8b**, mp 196—197 °C, $[\alpha]_D^{19}$ +0.39° (*c* 0.98, DMF). UV: $\lambda_{max}^{0.1M\ HCl}$ 269 nm ($\varepsilon=1.8\times10^4$), $\lambda_{max}^{H_2O}$ 276 nm ($\varepsilon=2.0\times10^4$), $\lambda_{max}^{0.1M\ NaOH}$ 276 nm ($\varepsilon=2.3\times10^4$). ^{1}H NMR (DMSO-$d_6$): 3.61 (s, 6, 2×$NCH_3$), 3.89 (s, 3, OCH_3), 7.35 (q, 4, C_6H_4), 8.56 (s, 1, purine H-2 or 8), 8.58 (s, 1, purine H-8 or 2).

Found: C, 55.95; H, 6.18; N, 20.52%. Calcd for $C_{22}H_{29}N_7O_5$: C, 56.04; H, 6.20; N, 20.79%.

*DL-(1,5/2,3,4)-1-Amino-3-azido-2,4,5-cyclopentanetriol (**9**).* Hydrolysis of DL-(1,5/2,3,4)-1-acetamido-3-azido-2,4,5-triacetoxycyclopentane[15] (1.68 g) in 3 M HCl, followed by deionization with Amberlite IRA-400 (OH^-) resin gave 837 mg (98%) of **9** as a crude syrup. The product was used for successive reaction without purification.

*6-[(DL-(1,5/2,3,4)-3-Azido-2,4,5-triacetoxycyclopentyl)amino]-4-dimethylamino-5-nitropyrimidine (**10**).* A mixture of **9** (837 mg) and 6-chloro-4-dimethylamino-5-nitropyrimidine[13] (1.46 g) in 2-methoxyethanol (42 ml) containing triethylamine (1 ml) was heated at 90 °C for 3.5 h. The mixture was treated as in the preparation of **3**. The product was recrystallized from ethanol to give 1.15 g (51%) of **10**, mp 146—147 °C. ^{1}H NMR: 2.03 (s, 3, OAc), 2.11 (s, 3, OAc), 2.15 (s, 3, OAc), 3.05 (s, 6, 2×NCH_3), 7.97 (s, 1, pyrimidine H-2), 8.22 (d, 1, J=6 Hz, NH).

Found: C, 44.00; H, 4.87; N, 23.70%. Calcd for $C_{17}H_{22}N_8O_8$: C, 43.78; H, 4.76; N, 24.03%.

*6-[(DL-(1,5/2,3,4)-3-Acetamido-2,5-(or 4,5)-diacetoxy-4(or 2)-hydroxycyclopentyl)amino]-5-amino-4-dimethylaminopyrimidine (**11**).* Compound **10** (1.42 g) was catalytically hydrogenated in ethyl acetate (60 ml). The product was recrystallized from ethanol to give 1.08 g (86%) of **11**, mp 155—156 °C (dec).

Found: C, 49.73; H, 6.53; N, 20.14%. Calcd for $C_{17}H_{26}N_6O_6$: C, 49.75; H, 6.39; N, 20.48%.

*9-[DL-(1,5/2,3,4)-3-Acetamido-2,5-(or 4,5)-diacetoxy-4(or 2)-hydroxycyclopentyl]-6-dimethylaminopurine (**12**).* A mixture of **11** (902 mg) and triethyl orthoformate (8.6 ml) in DMF (28 ml) containing *p*-toluenesulfonic acid (30 mg) was stirred for 4 h. The reaction mixture was worked up as in the preparation of **5**. The product was washed with warm ethyl acetate to give 770 mg (83%) of **12** as amorphous powder, mp 218—219 °C (dec). ^{1}H NMR (DMSO-d_6): 1.89 (s, 3, NAc), 2.03 (s, 6, 2×OAc), 3.50 (s, 6, 2×NCH_3), 6.14 (d, 1, J=9 Hz, NH), 8.50 (s, 1, purine H-2 or 8), 8.62 (s, 1, purine H-8 or 2).

Found: C, 51.26; H, 5.80; N, 20.06%. Calcd for $C_{18}H_{24}N_6O_6$: C, 51.42; H, 5.75; N, 19.99%.

*9-[DL-(1,5/2,3,4)-3-Amino-2,4,5-trihydroxycyclopentyl]-6-dimethylaminopurine (**13**).* A mixture of **12** (769 mg) and barium hydroxide octahydrate (4.0 g) in water (51 ml) was heated at 100 °C for 3.5 h. The mixture was worked up as in the preparation of **6** to give 502 mg (93%) of **13** as a crude product. The product was converted into the crystalline hydrochloride in 76% yield, mp 259—260 °C (dec). UV: $\lambda_{max}^{0.1M\ HCl}$ 268 nm ($\varepsilon=2.11\times10^4$), $\lambda_{max}^{H_2O}$ 276 nm ($\varepsilon=2.12\times10^4$), $\lambda_{max}^{0.1M\ NaOH}$ 276 nm ($\varepsilon=2.10\times10^4$).

Found: C, 39.30; H, 5.43; N, 22.61; Cl, 18.99%. Calcd for $C_{12}H_{20}N_6O_3Cl_2$: C, 39.25; H, 5.49; N, 22.88; Cl, 19.31%.

*A Mixture of 6-Dimethylamino-9-[(1S,2R,4S,5S)-2,4,5-trihydroxy-3-(N-benzyloxycarbonyl-p-methoxyphenyl-L-alanylamino)cyclopentyl]purine and 6-Dimethylamino-9-[(1R,2S,4R,5R)-2,4,5-trihydroxy-3-(N-benzyloxycarbonyl-p-methoxyphenyl-L-alanylamino)cyclopentyl]purine (**14**).* DCC (184 mg) was added under ice-cooling to a solution of **13** (249 mg) and *N*-benzyloxycarbonyl-*p*-methoxyphenyl-L-alanine[14] (293 mg) in DMF (9 ml) containing *N*-hydroxysuccinimide (103 mg). The mixture was worked up as in the preparation of **7a** and **7b** to give 362 mg (71%) of **14**, mp 125—132 °C. ^{1}H NMR (DMSO-

d_6): δ 3.63 (s, 6, $2\times NCH_3$), 3.90 (s, 3, OCH_3), 5.21 (s, 2, benzyl CH_2), 8.59 (s, 2, purine H-2 and 8).

Found: C, 59.25; H, 5.81; N, 16.10%. Calcd for $C_{30}H_{35}N_7O_7$: C, 59.49; H, 5.83; N, 16.19%.

*6-Dimethylamino-9-[(1*S,*2*R,*4*S,*5*S*)-2,4,5-trihydroxy-3-(*p*-methoxyphenyl-L-alanylamino)cyclopentyl]purine (**15a**) and 6-Dimethylamino-9-[(1*R,*2*S,*4*R,*5*R*)-2,4,5-trihydroxy-3-(*p*-methoxyphenyl-L-alanylamino)cyclopentyl]purine (**15b**).* A solution of **14** (543 mg) in glacial acetic acid (40 ml) was hydrogenated in the presence of palladium black in a hydrogen atmosphere (3.0 kg/cm^2) for 3 h. The catalyst was filtered off and the filtrate was evaporated. The methanolic solution of the residue was passed through a column of Amberlite IRA-400(OH^-) resin. The effluent was evaporated and the residue was purified by column chromatography using 6:1 (v/v) chloroform–methanol. Fractions showing a single spot at R_f 0.25 on TLC in the same solvent system were combined and evaporated to give 137 mg (32%) of **15a**, mp 190—191 °C, $[\alpha]_D^{21}$ −96.4° (*c* 1.00, DMF). UV: $\lambda_{max}^{0.1M\ HCl}$ 269 nm ($\varepsilon=2.39\times10^4$), $\lambda_{max}^{H_2O}$ 275 nm ($\varepsilon=2.51\times10^4$), $\lambda_{max}^{0.1M\ NaOH}$ 276 nm ($\varepsilon=2.53\times10^4$). ^{1}H NMR (DMSO-$d_6$): δ 3.64 (s, 6, $2\times NCH_3$), 3.91 (s, 3, OCH_3), 8.59 (s, 2, purine H-2 and 8).

Found: C, 55.84; H, 6.09; N, 20.58%. Calcd for $C_{22}H_{29}N_7O_5$: C, 56.04; H, 6.20; N, 20.79%.

Fractions showing a single spot at R_f 0.20 on TLC in the same solvent were combined and evaporated to give 145 mg (34%) of **15b**, mp 121—122 °C, $[\alpha]_D^{21}$ +9.0° (*c* 1.00, DMF). UV: $\lambda_{max}^{0.1M\ HCl}$ 269 nm ($\varepsilon=2.11\times10^4$), $\lambda_{max}^{H_2O}$ 276 nm ($\varepsilon=2.17\times10^4$), $\lambda_{max}^{0.1M\ NaOH}$ 276 nm ($\varepsilon=2.18\times10^4$). ^{1}H NMR (DMSO-$d_6$): δ 3.63 (s, 6, $2\times NCH_3$), 3.91 (s, 3, OCH_3), 8.59 (s, 2, purine H-2 and 8).

Found: C, 55.82; H, 6.31; N, 20.95%. Calcd for $C_{22}H_{29}N_7O_5$: C, 56.04; H, 6.20; N, 20.79%.

*DL-(1,2,4/3,5)-3-Acetamido-1-amino-2,4,5-cyclopentanetriol (**16**).* The compound was prepared by the method of Tadano *et al.*[11]

*6-[DL-(1,2,4/3,5)-3-Acetamido-2,4,5-trihydroxycyclopentyl]amino-4-dimethylamino-5-nitropyrimidine (**17**).* A mixture of **16** (990 mg) and 6-chloro-4-dimethylamino-5-nitropyrimidine[13] (1.27 g) in 2-methoxyethanol (51 ml) containing triethylamine (2 ml) was heated at 98 °C for 2 h with mechanical agitation. The solution was evaporated and the residue was recrystallized from ethanol to give 1.43 g (77%) of **17**, mp 216—218 °C (dec).

Found: C, 43.61; H, 5.60; N, 23.42%. Calcd for $C_{13}H_{20}N_6O_6$: C, 43.82; H, 5.66; N, 23.58%.

*6-[(DL-(1,2,4/3,5)-3-Acetamido-2,4,5-trihydroxycyclopentyl)-amino]-5-amino-4-dimethylaminopyrimidine (**18**).* Compound **17** (1.43 g) was catalytically hydrogenated in 50% aqueous ethanol (25 ml) for 15 h. The product was recrystallized from ethanol to give 1.19 g (91%) of **18**, mp 187—189 °C (dec).

Found: C, 47.52; H, 7.00; N, 25.31%. Calcd for $C_{13}H_{22}N_6O_4$: C, 47.84; H, 6.80; N, 25.75%.

*9-[DL-(1,2,4/3,5)-3-Acetamido-2,4,5-trihydroxycyclopentyl]-6-dimethylaminopurine (**19**).* A mixture of **18** (552 mg) and formamide (16 ml) was heated at 180 °C for 1.5 h. The solution was evaporated and the residue was dissolved in boiling water. After being decolorized with active charcoal, the solution was settled in a refrigerator to give 427 mg (75%) of **19** as needles, mp 295—297 °C (dec). UV: $\lambda_{max}^{0.1M\ HCl}$ 269 nm ($\varepsilon=2.04\times10^4$), $\lambda_{max}^{H_2O}$ 277 nm ($\varepsilon=2.04\times10^4$), $\lambda_{max}^{0.1M\ NaOH}$ 276 nm ($\varepsilon=2.33\times10^4$).

Found: C, 50.24; H, 6.00; N, 25.24%. Calcd for $C_{14}H_{20}N_6O_4$: C, 49.99; H, 5.99; N, 24.99%.

*9-[DL-(1,2,4/3,5)-3-Amino-2,4,5-trihydroxycyclopentyl]-6-dimethylaminopurine (**20**).* A mixture of **19** (1.48 g) and barium hydroxide octahydrate (19 g) in water (300 ml) was heated under reflux for 4 h. The mixture was worked up as in the preparation of **6** to give 1.16 g (90%) of **20**, mp 204—205 °C (dec). An analytically pure sample was obtained by recrystallization from aqueous ethanol.

Found: C, 48.72; H, 6.20; N, 28.71%. Calcd for $C_{12}H_{18}N_6O_3$: C, 48.97; H, 6.16; N, 28.55%.

*A Mixture of 6-Dimethylamino-9-[(1*S,*2*S,*4*R,*5*R*)-2,4,5-trihydroxy-3-(N-benzyloxycarbonyl-p-methoxyphenyl-L-alanylamino)cyclopentyl]purine and 6-Dimethylamino-9-[(1*R,*2*R,*4*S,*5*S*)-2,4,5-trihydroxy-3-(N-benzyloxycarbonyl-p-methoxyphenyl-L-alanylamino)-cyclopentyl]purine (**21**).* To a solution of **20** (218 mg) and *N*-benzyloxycarbonyl-*p*-methoxyphenyl-L-alanine[14] (256 mg) in DMF (10 ml) containing *N*-hydroxysuccinimide (90 mg), DCC (161 mg) was added under ice-cooling. The mixture was worked up as in the preparation of **7a** and **7b** to give 334 mg (74%) of **21**, mp 214—216 °C.

Found: C, 59.52; H, 5.84: N, 16.37%. Calcd for $C_{30}H_{35}N_7O_7$: C, 59.49; H, 5.83; N, 16.19%.

*6-Dimethylamino-9-[(1*S,*2*S,*4*R,*5*R*)-2,4,5-trihydroxy-3-(p-methoxyphenyl-L-alanylamino)cyclopentyl]purine (**22a**)* and *6-Dimethylamino-9-[(1*R,*2*R,*4*S,*5*S*)-2,4,5-trihydroxy-3-(p-methoxyphenyl-L-alanylamino)cyclopentyl]purine (**22b**).* A solution of **21** (500 mg) in glacial acetic acid (15 ml) was hydrogenated in the presence of 10% palladium on charcoal in a hydrogen atmosphere (3.0 kg/cm^2) for 2 h. The solution was worked up as in the preparation of **8a**, and the product was purified by column chromatography using 3 : 1 (v/v) chloroform–methanol. Fractions showing a single spot at R_f 0.45 on TLC in the same solvent system were combined and concentrated to give 90 mg (23%) of **22a**, mp 259—261 °C (dec), $[\alpha]_D^{20}$ −31.9° (*c*, 0.99, DMF).

Found: C, 55.85; H, 6.24; N, 20.47%. Calcd for $C_{22}H_{29}N_7O_5$: C, 56.04, H, 6.20; N, 20.79%.

Fractions showing a single spot at R_f 0.31 on TLC in the same solvent were combined and concentrated to give 104 mg (27%) of **22b**, mp 258—260 °C (dec), $[\alpha]_D^{20}$ −3.6° (*c* 1.01, DMF).

Found: C, 56.04; H, 6.19; N, 20.60%. Calcd for $C_{22}H_{29}N_7O_5$: C, 56.04; H, 6.20; N, 20.79%.

N,O-*Tetraacetyl Derivative of **22a** (**23a**).* Compound **22a** (30 mg) was acetylated and the product was purified by a column chromatography using 5 : 1 (v/v) benzene–ethanol. The product was washed with ether to give 37 mg (91%) of **23a**, mp 188—189 °C. ^{1}H NMR: δ 1.80 (s, 3, NAc), 1.91 (s, 3, OAc), 1.97 (s, 3, OAc), 2.06 (s, 3, OAc), 3.01 (d, 2, J= 7 Hz, $C\underline{H}_2C_6H_4$), 3.46 (s, 6, $2\times NCH_3$), 3.69 (s, 3, OCH_3), 6.58 (d, 1, J=8 Hz, NH), 6.89 (q, 4, C_6H_4), 7.67 (d, 1, J= 6 Hz, NH), 7.72 (s, 1, purine H-2 or 8), 8.18 (s, 1, purine H-8 or 2).

Found: C, 56.28; H, 5.90; N, 15.04%. Calcd for $C_{30}H_{37}N_7O_9$: C, 56.33; H, 5.83; N, 15.33%.

N,O-*Tetraacetyl Derivative of **22b** (**23b**).* Compound **22b** (30 mg) was acetylated and the product was purified as in the preparation of **23a** to give 28 mg (69%) of **23b** as a glass. ^{1}H NMR: δ 1.83 (s, 3, NAc), 1.90 (s, 3, OAc), 1.98 (s, 3, OAc), 2.05 (s, 3, OAc), 3.00 (d, 2, J=6 Hz, $C\underline{H}_2C_6H_4$), 3.47 (s, 6, $2\times NCH_3$), 3.69 (s, OCH_3), 6.45 (d, 1, J=8 Hz, NH), 6.87 (q, 4, $CH_2C_6\underline{H}_4$), 7.56 (d, 1, J=7 Hz, NH), 7.72 (s, 1, purine H-2 or 8), 8.18 (s, 1, purine H-8 or 2).

Found: C, 56.29; H, 6.09; N, 14.95%. Calcd for $C_{30}H_{37}N_7O_9$: C, 56.33; H, 5.83; N, 15.33%.

*DL-(1,2,5/3,4)-3-Acetamido-1-amino-2,4,5-cyclopentanetriol (**24**)* The compound was prepared by the method of Tadano *et al.*[11]

*6-[(DL-(1,2,5/3,4)-3-Acetamido-2,4,5-trihydroxycyclopentyl)-amino]-4-dimethylamino-5-nitropyrimidine (**25**).* A mixture of **24** (402 mg) and 6-chloro-4-dimethylamino-5-nitropyrim-

idine[13] (514 mg) in 2-methoxyethanol (21 ml) containing triethylamine (1 ml) was heated at 80 °C for 2.5 h. The solution was evaporated and the residue was washed with warm ethanol to give 564 mg (75%) of **25**, mp 215—216 °C (dec).

Found: C, 43.96; H, 5.64; N, 23.72%. Calcd for $C_{13}H_{20}N_6O_6$: C, 43.82; H, 5.66; N, 23.58%.

*6-[(DL-(1,2,5/3,4)-3-Acetamido-2,4,5-trihydroxycyclopentyl)-amino]-5-amino-4-dimethylaminopyrimidine (**26**).* Compound **25** (796 mg) was catalytically hydrogenated in water (50 ml) for 5.5 h. The catalyst was filtered off and the filtrate was evaporated to give 635 mg (87%) of **26**, mp 229—230 °C (dec).

Found: C, 48.13; H, 6.75; N, 26.10%. Calcd for $C_{13}H_{22}N_6O_4$: C, 47.84; H, 6.80; N, 25.75%.

*9-[DL-(1,2,5/3,4)-3-Acetamido-2,4,5-trihydroxycyclopentyl]-6-dimethylaminopurine (**27**).* A mixture of **26** (319 mg) and triethyl orthoformate (1.6 ml) in DMF (53 ml) was heated at 67 °C for 4 h in the presence of *p*-toluenesulfonic acid (10 mg). After being neutralized with Amberlite IRA-400 (OH^-) resin, the solution was evaporated. The residue was dissolved in 0.1 M HCl (33 ml). After 2 h, the solution was evaporated. The residue was dissolved in water and neutralized with 0.1 M NaOH. The solution was allowed to settle in a refrigerator to give 291 mg (89%) of **27** as crystals, mp 233—234 °C (dec).

Found: C, 49.71; H, 5.95; N, 24.65%. Calcd for $C_{14}H_{20}N_6O_4$: C, 49.99; H, 5.99; N, 24.99%.

*9-[DL-(1,2,5/3,4)-3-Amino-2,4,5-trihydroxycyclopentyl]-6-dimethylaminopurine (**28**).* A mixture of **27** (340 mg) and barium hydroxide octahydrate (2.7 g) in water (34 ml) was heated at 100 °C for 4 h. The solution was worked up as in the preparation of **6** to give 278 mg (93%) of **28**. UV: $\lambda_{max}^{0.1M\ HCl}$ 268 nm ($\varepsilon=1.48\times10^4$), $\lambda_{max}^{H_2O}$ 275 nm ($\varepsilon=1.64\times10^4$), $\lambda_{max}^{0.1M\ NaOH}$ 275 nm ($\varepsilon=1.64\times10^4$). ^1H NMR (DMSO-d_6): δ 3.63 (s, 6, $2\times NCH_3$), 8.47 s, (1, purine H-2 or 8), 8.58 (s, 1, purine H-8 or 2).

Hydrochloride of **28** was obtained as crystals in 46% yield by recrystallization from methanol, mp 163—164 °C.

Found: C, 41.67; H, 5.97; N, 23.86; Cl, 10.01%. Calcd for $C_{12}H_{19}N_6O_3Cl\cdot H_2O$: C, 41.32; H, 6.06; N, 24.09; Cl, 10.16%.

*6-Dimethylamino-9-[(1S,2S,4S,5S,)-2,4,5-trihydroxy-3-(N-benzyloxycarbonyl-p-methoxyphenyl-L-alanylamino)cyclopentyl] Purine (**29a**).* DCC (202 mg) was added under ice-cooling with agitation to a solution of **28** (274 mg) and *N*-benzyloxycarbonyl-*p*-methoxyphenyl-L-alanine[14] (323 mg) in DMF (11 ml) containing *N*-hydroxysuccinimide (113 mg). The mixture was worked up as in the preparation of **7a** to give 165 mg (29%) of **29a**, mp 222—223 °C (dec) (from methanol).

Found: C, 58.52; H, 5.80; N, 15.58%. Calcd for $C_{30}H_{35}N_7O_7$–CH_3OH: C, 58.39; H, 6.16; N, 15.38%.

The product was acetylated to give tri-*O*-acetyl derivative of **29a** in a quantitative yield as a syrup. ^1H NMR (DMSO-d_6): δ 1.85 (s, 3, OAc), 1.97 (s, 3, OAc), 2.00 (s, 3, OAc), 2.98 (d, 2, $J=7$ Hz, $CH_2C_6H_4$), 3.46 (s, 6, $2\times NCH_3$), 3.70 (s, 3, OCH_3), 5.02 (s, 2, benzyl CH_2), 7.79 (s, 1, purine H-2 or 8), 8.23 (s, 1, purine H-8 or 2).

Found: C, 59.06; H, 5.76; N, 13.14%. Calcd for $C_{36}H_{41}N_7O_{10}$: C, 59.09; H, 5.65; N, 13.40%.

*6-Dimethylamino-6-[(1S,2S,4S,5S)-2,4,5-trihydroxy-3-(p-methoxyphenyl-L-alanylamino)cyclopentyl]purine (**30a**).* A solution of **29a** (32 mg) in glacial acetic acid (8 ml) was hydrogenated in the presence of palladium black in a hydrogen atmosphere (3.0 kg/cm²) for 4 h. The solution was worked up as in the preparation of **8a** to give 12 mg (48%) of **30a**, mp 139—140 °C (from methanol), $[\alpha]^{19}$ −49.4° (*c* 1.13, methanol). UV: $\lambda_{max}^{0.1M\ HCl}$ 269 nm ($\varepsilon=2.11\times10^4$), $\lambda_{max}^{H_2O}$ 275 nm ($\varepsilon=2.15\times10^4$), $\lambda_{max}^{0.1M\ NaOH}$ 275 nm ($\varepsilon=2.00\times10^4$). ^1H NMR (DMSO-d_6): δ 3.64 (s, 6, $2\times NCH_3$), 3.90 (s, 3, OCH_3), 8.55 (s, 1, purine H-2 or 8), 8.61 (s, 1, purine H-8 or 2).

Found: C, 55.78; H, 6.35; N, 20.41%. Calcd for $C_{22}H_{29}N_7O_5$: C, 56.04; H, 6.20; N, 20.79%.

*6-Dimethylamino-9-[(1R,2R,4R,5R)-2,4,5-trihydroxy-3-(p-methoxyphenyl-L-alanylamino)cyclopentyl]purine (**30b**).* The methanolic mother liquor of **29a** was concentrated to give 741 mg of a residual syrup. A solution of the residue in glacial acetic acid (14 ml) was hydrogenated in the presence of palladium black in a hydrogen atmosphere (3.0 kg/cm²) for 3 h. The solution was worked up as in the preparation of **8a**. The product was purified by column chromatography using 5 : 1 (v/v) chloroform–methanol. Fractions showing a single spot at R_f 0.27 on TLC in the same solvent were combined and evaporated to give 51 mg of **30a**. Fractions showing a single spot at R_f 0.21 on TLC in the same solvent were combined and evaporated to give 113 mg (26% from **28**) of **30b**, mp 201—202 °C (dec), $[\alpha]_D^{19}$ +42.0° (*c* 1.13, methanol). UV: $\lambda_{max}^{0.1M\ HCl}$ 269 nm ($\varepsilon=1.96\times10^4$), $\lambda_{max}^{H_2O}$ 275 nm ($\varepsilon=2.05\times10^4$), $\lambda_{max}^{0.1M\ NaOH}$ 276 nm ($\varepsilon=2.19\times10^4$). ^1H NMR (DMSO-d_6): δ 3.63 (s, 6, $2\times NCH_3$), 3.89 (s, 3, OCH_3), 8.53 (s, 1, purine H-2 or 8), 8.59 (s, 1, purine H-8 or 2).

Found: C, 55.78; H, 6.29; N, 20.64%. Calcd for $C_{22}H_{29}N_7O_5$: C, 56.04; H, 6.20; N, 20.79%.

The authors are indebted to Mr. Saburo Nakada for Carrying out elemental analyses.

References

1) This article is dedicated to the memory of Yasufumi Emori, an exceptionally able coworker who died tragically in a mountain climbing accident in 1976. The numbering of aminocyclitols in this article does not follow the IUPAC and IUB tentative rules for cyclitol nomenclature [*J. Biol. Chem.*, **243**, 5809 (1968)]. Aminocyclitols are numbered in accordance with the numbering of 3-amino-3-deoxy-D-ribofuranose, since it will avoid change in the numbering before and after the condensation of the aminocyclitols with pyrimidine and purine derivatives.

2) J. N. Porter, R. I. Hewitt, G. W. Hesseltine, G. Krupka, J. A. Lowery, W. S. Wallace, N. Bohonos, and J. H. Williams, *Antibiot. Chemotherapy*, **2**, 409 (1952).

3) B. R. Baker, J. P. Joseph, and J. H. Williams, *J. Am. Chem. Soc.*, **77**, 1 (1955).

4) J. A. Montgomery and H. J. Thomas, *Adv. Carbohydr. Chem.*, **17**, 301 (1962).

5) R. H. Symons, R. J. Harris, L. P. Clarke, J. F. Wheldrake, and W. H. Elliott, *Biochem. Biophys. Acta*, **179**, 248 (1969).

6) L. V. Fisher, W. W. Lee, and L. Goodman, *J. Med. Chem.*, **13**, 775 (1970).

7) S. Daluge and R. Vince, *J. Med. Chem.*, **15**, 171 (1972).

8) T. Suami, Y. Sato, Y. Fukai, and Y. Sakota, *J. Hetercycl. Chem.*, **6**, 663 (1969).

9) T. Suami, Y. Fukai, Y. Sakota, M. Karimoto, N. Takoi, and Y. Tsukamoto, *Bull. Chem. Soc. Jpn.*, **44**, 1695 (1971).

10) T. Suami, S. Nishiyama, K. Tadano, and F. W. Lichtenthaler, *Bull. Chem. Soc. Jpn.*, **46**, 2562 (1973).

11) K. Tadano, Y. Emori, M. Ayabe, and T. Suami, *Bull. Chem. Soc. Jpn.*, **50**, 1572 (1977).

12) K. Tadano, S. Horiuchi, and T. Suami, *Bull. Chem. Soc. Jpn.*, submitted.
13) F. L. Rose, *J. Chem. Soc.*, **1954**, 4116.
14) H. E. Carter and J. W. Hinman, *J. Biol. Chem.*, **178**, 403 (1949).
15) K. Tadano, Y. Emori, M. Ayabe, and T. Suami, *Bull. Chem. Soc. Jpn.*, **49**, 1108 (1976).
16) R. K. Robins, K. J. Dille, C. H. Willitis, and B. E. Christensen, *J. Am. Chem. Soc.*, **75**, 263 (1953).
17) In NMR descriptions s=singlet, d=doublet, t=triplet, q=quartet, and m=multiplet.
18) The end point dilution in μg/ml represents the lowest dilution at which degeneration of cells was observed by microscopic observation after incubation at 37 °C for 48 h.
19) In Schemes 2 and 3, the structures depict only one enantiomer of the racemic form actually obtained.

Evidence of Existence of Two Stereospecific Control Mechanisms in Asymmetric Transformation of 2-Phenylpropanal *via* Enamines

Hajime MATSUSHITA, Yasuko TSUJINO, Masao NOGUCHI, Masahiko SABURI,* and Sadao YOSHIKAWA*

Central Research Institute, The Japan Tobacco and Salt Public Corporation, Umegaoka, Midori-ku, Yokohama, Kanagawa 227

** Department of Synthetic Chemistry, Faculty of Engineering, The University of Tokyo, Bunkyo-ku, Tokyo 113*

(Received August 16, 1977)

The temperature dependence of asymmetric transformation of 2-phenylpropanal *via* achiral enamine salt of *d*-10-camphorsulfonic acid was examined. The relation between the rotation of 2-phenylpropanal obtained and reaction temperature showed a notable change in specific rotation of the aldehyde obtained. Two courses are postulated for the optical activation.

Asymmetric transformation of racemic α-substituted carbonyl compounds was achieved by treatment of the enamines with chiral acids.[1] This is attributed to the difference in free energy between mutually interconvertible diastereoisomeric iminium salt (thermodynamical control).[2-4] However, Duhamel and Plaquevent recently reported some experimental facts explicable in terms of kinetic control, though the mechanism was not described in detail.[5]

The rotation of the α-substituted carbonyl compounds obtained depends remarkably on the reaction temperature as well as the solvent used.[1] Accordingly, the temperature effect on the asymmetric transformation was examined in detail using 2-phenylpropanal (hereafter called PPA) as a model α-substituted carbonyl compound. From the relation between reaction temperature and specific rotations of PPA, it was found that thermodynamical control or kinetic control alone is not sufficient to account for the results.

Achiral enamines **1**, **2**, **3**, and **4** are morphorine, piperidine, pyrrolidine, and *N*-methylpiperazine enamines, respectively, of racemic PPA.

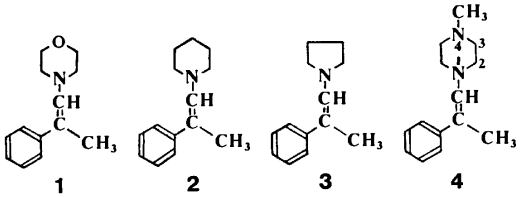

1 **2** **3** **4**

Experimental

Optical rotations were determined with a JASCO Digital Automatic Polarimeter Model DIP 181. Gas chromatographic analyses were carried out using a 2 m column of 20% SE-30 on Chromosorb W with a Hitachi Gas Chromatograph Model K53. Nuclear magnetic resonance spectra were measured with a JNM-PS-100 Spectrometer using tetramethylsilane as an internal standard. Chemical shifts are given in δ values. Infrared spectra were obtained with a JASCO Model IR-G and mass spectra with a Hitachi GC-MS RM-50 (column: 10% SE-30 on Chromosorb W, 3 mm × 1 m).

Reagents and Solvent. *d*-10-Camphorsulfonic acid was prepared according to the directions of Reychler.[6] $[\alpha]_D^{23}$ +21.8° (*c* 8.81 H_2O), lit, $[\alpha]_D^{20}$ +22.6° (*c* 8.3, H_2O). Chloroform was purified by being shaken 7 times with water, dried over calcium chloride, and distilled.

Preparation of Enamines. Enamines were prepared by the usual azeotropic procedure using benzene as a solvent.

*1-(β-Methylstyryl)morphorine (**1**)*: Bp 108—111 °C (0.5 mmHg). Yield 90.8%. Mp 59.5—62 °C. MS *m/e* 203 (M^+), 144 (base), 130, 91. IR (film) 1685, 1640, 1600, 1499, 1450, 1378, 1298, 1260, 1120, 865, 760, 705, 650, 605, 545 cm^{-1}. NMR ($CDCl_3$) mixture of two geometrical isomers in the ratio 77 : 23 at room temperature. Major isomer 1.08 (d, J=1.1 Hz, CH=C-CH_3), 2.78 (m), 3.7 (m), 6.02 (q, J=1.1 Hz, CH=C-CH_3), 7.3 (m, phenyl). Minor isomer 1.96 (d, J=1.3 Hz, CH=C-CH_3), 2.64 (m), 3.55 (m), 5.76 (q, J=1.3 Hz, CH-C-CH_3), 7.3 (m, phenyl). Found: C, 76.53; H, 8.50; N, 6.88%. Calcd for $C_{13}H_{17}ON$: C, 76.81; H, 8.48; N, 6.89%.

*1-(β-Methylstyryl)piperidine (**2**)*: Reported previously.[1] Found: C, 83.46; H, 9.91; N, 6.83%. Calcd for $C_{14}H_{19}N$: C, 83.53; H, 9.51; N, 6.96%.

*1-(β-Methylstyryl)pyrrolidine (**3**)*: Also reported.[1] Found: C, 83.11; H, 9.26; N, 7.37%. Calcd for $C_{13}H_{17}N$: C, 83.37; H, 9.15; N, 7.48%.

*1-(β-Methylstyryl)-4-methylpiperazine (**4**)*: Bp 111—114 °C (2.5 mmHg). Yield 97.7%. MS *m/e* 216 (M^+, base), 144, 131, 115, 91. IR (film) 2950, 2800, 1640, ($\nu_{C=C}$), 1600, 1495, 1455, 1375, 1290, 1118, 1148, 1015, 760, 700 cm^{-1}. NMR ($CDCl_3$) mixture of two geometrical isomers in the ratio 7 : 4 at room temperature. Major isomer 2.09 (d, J=1.0 Hz, CH=C-CH_3), 2.30 (s, N-CH_3), 2.5 (m), 6.12 (q, J=1.0 Hz, N-CH=C), 7.3 (m, phenyl). Minor isomer 1.97 (d, J=1.2 Hz, CH=C-CH_3), 2.22 (s, N-CH_3), 2.3 (m), 2.7 (m), 5.89 (q, J=1.2 Hz, N-CH=C), 7.5 (m, phenyl). Found: C, 77.68; H, 9.42; N, 12. 84%. Calcd for $C_{14}H_{20}N_2$: C, 77.73; H, 9.32; N, 12.95%.

Asymmetric Transformation of Enamine. Under vigorous stirring with a homogenizer, enamine **1**, **2**, or **3** (0.01 mol) and *d*-10-camphorsulfonic acid monohydrate (0.01 mol) were added to 50 ml of chloroform. In order to control the temperature in the reaction flask, the temperature of the bath in which the flask was immersed was regulated with Dry Ice–ethanol or ice–water. Temperature in the flask was measured with a thermocouple. The reaction was continued for 30 min. The reaction mixture was washed with three 20 ml portions of water in order to remove *d*-10-camphorsulfonic acid completely. After the chloroform layer had been dried, the optical rotation was measured. The concentration of PPA in the chloroform solution was measured gas chromatographically. The yield of PPA was 90—100% in every case. Use of double the molar quantity of the acid to be hydrolyzed is necessary for enamine **4**. Two cases were examined: (a) 0.01 mol of **4** was treated with 0.02 mol of *d*-10-camphorsulfonic acid monohydrate, and (b) 0.01 mol of **4** was treated with a mixture of 0.01 mol of *d*-10-camphorsulfonic acid

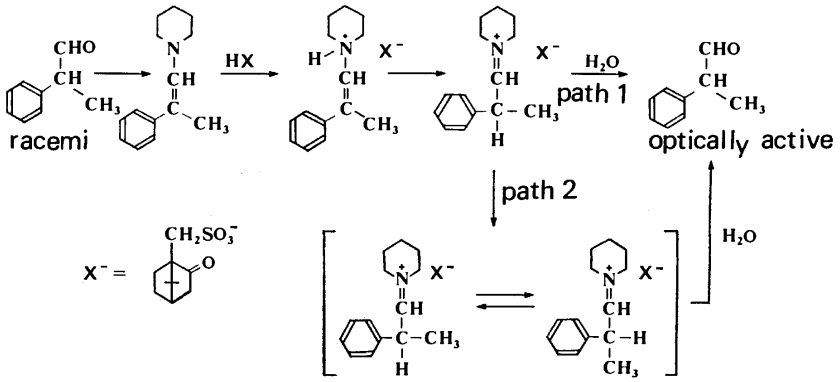

Scheme 1.

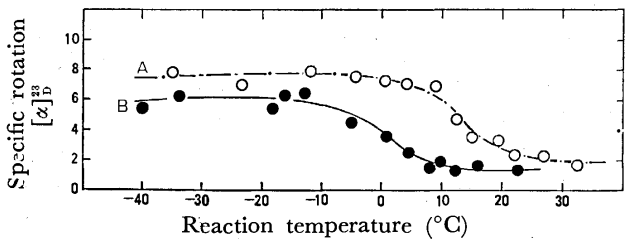

Fig. 1. Relationship between reaction temperature and rotation of 2-phenylpropanal.
Curve A; 1-(β-Methylstyryl)piperidine (**2**).
Curve B; 1-(β-Methylstyryl)pyrrolidine (**3**).

monohydrate and 0.01 mol of *p*-toluenesulfonic acid monohydrate. The subsequent procedure is identical with that described in the hydrolyses of **1**, **2**, and **3**.

Results and Discussion

1-(β-methylstyryl)piperidine and 1-(β-methylstyryl)-pyrrolidine salts of *d*-10-camphorsulfonic acid were hydrolyzed at various temperatures. The relation between the rotation of PPA obtained from the hydrolyzates and the hydrolysis temperature is shown in Fig. 1.

Two flat levels and a transient stage between them are seen in each case, suggesting that optical activation is induced by two courses. In the transient stage, the two reaction courses would participate in the induction of optical activity. There are two types of enamine salt, enaminium and iminium.[7,8] Protonation to an enamine first occurs rapidly on a nitrogen atom, transfer of the proton to the β-carbon atom taking place. The following two reaction courses are presumed: a) asymmetric rearrangement of the proton from the nitrogen atom in the enaminium salt to the β-carbon atom in the iminium salt under the asymmetric circumstance caused by chiral acid anion, and b) a thermodynamic equilibrium between the resulting two enantiomeric iminium salts since the proton attached to the β-carbon atom is fairly labile.[9] On account of the instability of enaminium structure, the optical activity induced by the former course might be retained at a low temperature. At a high temperature, the asymmetrically attached proton to the β-carbon atom in the iminium salt becomes easily exchangeable, and a thermodynamic equilibrium would be attained between the two diastereomeric iminium salts. The optical activities of the

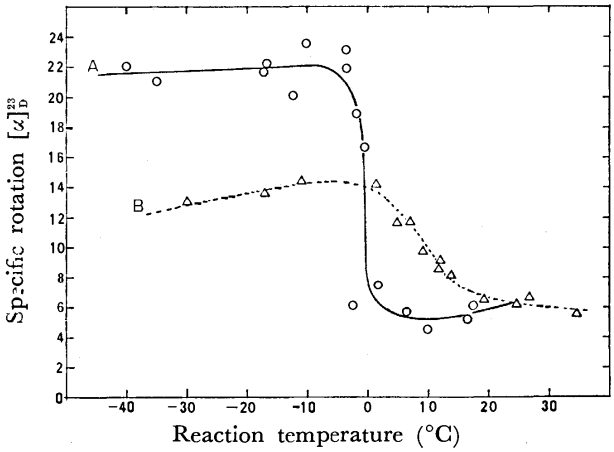

Fig. 2. Relationship between reaction temperature and rotation of 2-phenylpropanal obtained from the hydrolyzate of 1-(β-methylstyryl)morphorine salt of *d*-10-camphorsulfonic acid.
Curve A; Solvent $CHCl_3$.
Curve B; Solvent $CHCl_3$: CH_3OH(9 : 1).

PPA obtained would reflect the equilibrium. Path 1 (Scheme 1) represents the former mechanism controlled kinetically and path 2 the latter mechanism controlled thermodynamically. The higher flat level (Fig. 1) corresponds to the former, and the lower flat level corresponds to the latter.

In the case of asymmetric transformation of racemic PPA *via* chiral enamines using *S*(−)-prolinamide or *N*-(L-prolyl)piperidine as an amine component, hydrolysis at low temperature gave *R*(−)-PPA and that at a high temperature *S*(+)-PPA. This phenomenon was also interpreted in the same way discussed above.[10]

Figure 2 shows the correlation between reaction temperature and the optical rotation of PPA obtained from 1-(β-methylstyryl)morphorine enamine salt of *d*-10-camphorsulfonic acid. A sharp decrease in specific rotation in the temperature range −5—0 °C (Fig. 2-A) is noted, the transient stage (Fig. 1) being almost absent. This phenomenon may be due to the fact that the existence of oxygen atom in morphorine moiety stabilizes the enaminium structure by intramolecular hydrogen bonding with the hydrogen atom attached to the nitrogen atom. It is known that severance of the hydrogen bond takes place in narrow temperature range.

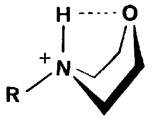

Fig. 3.

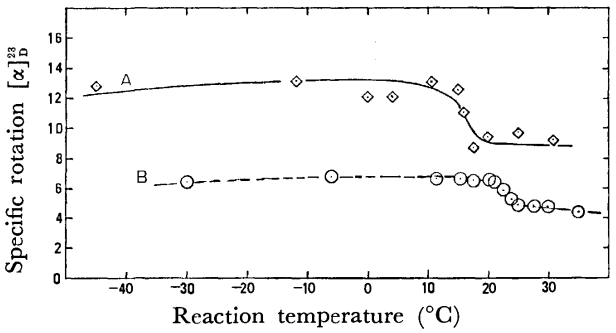

Fig. 4. Relationship between reaction temperature and rotation of 2-phenylpropanal obtained from the hydrolyzate of 1-(β-methylstyryl)-4-methylpiperazine salt.
Curve A; *d*-10-Camphorsulfonic acid : enamine (2 : 1).
Curve B; *d*-10-Camphorsulfonic acid : *p*-toluensulfonic acid : enamine (1 : 1 : 1).

Marman and Doty[11] examined the thermal transition profiles of the double helical complex of deoxyribonucleic acids into random coiles in neutral solutions and showed that the cleavage occurs in a narrow temperature range. Similar phenomena were reported by other workers.[12-15] Thus, the kinetical control disappears rapidly with severance of the hydrogen bond.

The ratio of the geometrical isomers at room temperature and the optical yield are given in Table 1. Low optical yields in the range of kinetical control (lower temperature range) are attributable to the mixture of two geometrical isomers. If the two isomers are separated from each other, higher optical yields are expected as shown by Duhamel and Plaquevent.[5] The stability of the enaminium salt of **1** at lower temperature may be responsible for the high optical yield. The stable enaminium structure controls the course of the transfer of the hydrogen atom from the nitrogen atom to the β-carbon atom.

When methanol (5 ml) was added to the solvent ($CHCl_3$, 45 ml) before hydrolysis to weaken hydrogen bonding, the curve became similar to that in the case of **2** and **3** as shown by curve B in Fig. 2. The addition gave rise to the lowering of optical yield especially in the lower temperature range. This confirms the stabilization of the enaminium structure by hydrogen bond in the case of **1**.

The relation between the rotation of PPA obtained with 1-(β-methylstyryl)-4-methylpiperazine and reaction temperature is shown in Fig. 4. The enamine could not be hydrolyzed easily by equimolar addition of acid such as *d*-10-camphorsulfonic acid monohydrate of *p*-toluenesulfonic acid monohydrate. The acid is apparently first consumed for protonation to the nitrogen atom at the 4-position, and use of double the molar quantity of acid is necessary.

Table 1. The ratio of the geometrical isomers and the optical yield

Enamine	Ratio of geometrical isomers	Optical yield (ee)[a] %	
		Lower temp range[b]	Higher temp range[c]
1	77 : 23	9.2	2.5
2	87 : 13	3.4	0.8
3	84 : 16	2.5	0.8

a) Optical yields are calculated based on $[\alpha]_D^{25}$ +238°.[5] b) The temperature range in which the asymmetric transformation is controlled kinetically. c) The temperature range in which the asymmetric transformation is controlled thermodynamically.

Curve A in Fig. 4 shows a case of the hydrolysis of enamine salt of *d*-10-camphorsulfonic acid monohydrate (molar ratio of the enamine and the acid; 1 : 2). It has two flat levels with a transient stage between them, as in the case of the curves in Figs. 1 and 2. The temperature range corresponding to the transient stage is 10—20 °C, narrower as compared to that of **2** and **3**. This tendency is similar to that of **1**, suggesting that the nitrogen atom at 4-position and hydrogen atom attached to the nitrogen atom at 1-position have a mutual interaction similar to the hydrogen bonding observed in the morphorine enamine salt, although the nitrogen atom at 4-position cannot operate as effectively as the oxygen atom in the morphorine enamine salt because of quaternarization.

Curve B shows a case of hydrolysis of the enamine salt of *d*-10-camphorsulfonic acid monohydrate and *p*-toluenesulfonic acid monohydrate (molar ratio of the enamine, *d*-10-camphorsulfonic acid monohydrate, and *p*-toluenesulfonic acid monohydrate; 1:1:1). The optical yield is reduced to one half its former results (Curve A, Fig. 4). An explanation of this result would be as follows: *d*-10-camphorsulfonate anion and *p*-toluenesulfonate anion form ion pairs with the two protonated nitrogen atoms in **4**, and only one acid anion of the two, probably the one that associated with the nitrogen atom at 1-position, can participate in the asymmetric transformation of PPA.

In order to get evidence for the two courses, isotopic labeling studies were carried out. As soon as dry DCl gas was added to enamine **2** in $CDCl_3$, the salt was hydrolyzed with H_2O (Scheme 2). Hydrolysis at 0 and 35 °C gave non-deuterated PPA (yield 100 %). This shows that the deuterium atom attached to the nitrogen atom exchange undergoes easily with hydrogen atoms in excess H_2O, the proton rearrangement from nitrogen atom to the β-carbon atom then occurring. Ease of this deuterium-proton exchange was already reported.[16] The above enaminium salt was completely rearranged to the corresponding iminium salt[16] and the resulting iminium salt was hydrolyzed with H_2O at 0 and 35 °C.

Hydrolysis at 0 °C gave Cα-deuterated PPA, indicating that the proton at β-carbon atom in the iminium salt is not exchangeable with hydrogen atom or deuterium atom at low temperature. In other words, optical yield is determined in the course of the rearrange-

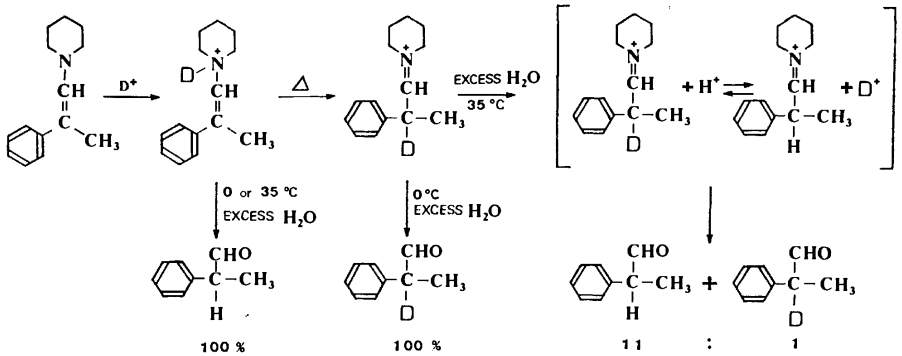

Scheme 2.

ment from enaminium salt to iminium salt.

On the other hand, hydrolysis at 35 °C gave a mixture of the deuterated and non-deuterated PPA (1:11), indicating that the asymmetrically attached deuterium atom to the β-carbon atom in the iminium salt becomes easily exchangeable at 35 °C and the optical activation is controlled thermodynamically at the step of the iminium salt. The results of isotopic labeling studies also strongly support the existence of the two asymmetric transformation courses.

References

1) H. Matsushita, M. Noguchi, M. Saburi, and S. Yoshikawa, *Bull. Chem. Soc. Jpn.*, **48**, 3715 (1975).
2) J. Read and A. M. McMath, *J. Chem. Soc.*, **1925**, 1572.
3) M. M. Jamison and E. E. Turner, *J. Chem. Soc.*, **1942**, 437.
4) H. Leuchs, *Chem. Ber.*, **54**, 830 (1921).
5) L. Duhamel and J. Plaquevent, *Tetrahedron Lett.*, **1977**, 2285.
6) A. Reychler, *Bull. Soc. Chim. Fr.*, **19**, 120 (1898).
7) G. Opitz and A. Griesinger, *Ann.*, **665**, 101 (1963).
8) E. J. Stamhuis and W. Maas, *J. Org. Chem.*, **30**, 2156 (1965).
9) H. Matsushita, Y. Tsujino, M. Noguchi, and S. Yoshikawa, *Bull. Chem. Soc. Jpn.*, **49**, 3629 (1976).
10) H. Matsushita, Y. Tsujino, M. Noguchi, M. Saburi, and S. Yoshikawa, *Bull. Chem. Soc. Jpn.*, **51**, 201 (1978).
11) J. Marmur and P. Doty, *Nature*, **183**, 1427 (1959).
12) K. Matsuo and M. Tsuboi, *Bull. Chem. Soc. Jpn.*, **39**, 347 (1966).
13) H. R. Mahler, B. D. Mehrotra, and C. W. Sharp, *Biochem. Biophys. Res. Commun.*, **4**, 79 (1961).
14) M. Mandel, *J. Mol. Biol.*, **5**, 435 (1962).
15) H. Tabor, *Biochemistry*, **1**, 496 (1962).
16) H. Matsushita, Y. Tsujino, M. Noguchi, and S. Yoshikawa, *Bull. Chem. Soc. Jpn.*, **50**, 1513 (1977).

Synthesis of Hindered *t*-Alkyl Ethers

Hiromitsu MASADA* and Tadahide SAKAJIRI

Department of Industrial Chemistry, Faculty of Engineering, Kanazawa University, Kodatsuno, Kanazawa 920

(Received August 26, 1977)

Di-*t*-butyl ether was prepared in 6—73% yields by the reactions of *t*-butyl halide with Ag_2CO_3, Ag_2O, HgO, ZnO, $ZnCO_3$, PbO_2, $Cu_2(CO_3)(OH)_2$, and Tl_2O_3 at 20—65 °C in hydrocarbons under nitrogen. Similar reactions gave seven new hindered di-*t*-alkyl ethers: di-*t*-pentyl ether, bis(1,1-dimethylbutyl) ether, bis(1-ethyl-1-methylpropyl) ether, bis(1,1-dimethylpentyl) ether, bis(1-ethyl-1-methylbutyl) ether, bis(1,1-diethylpropyl) ether, and bis(1,1-dimethylhexyl) ether. The yield of di-*t*-alkyl ether decreased as the *t*-alkyl group became bulky. A slight difference in the skeletal structure of the *t*-alkyl halide markedly influences the substitution. The reaction pathways are elucidated on the basis of the experimental results.

Sterically hindered di-*t*-alkyl ethers have never been prepared by any usual procedure, such as dehydration of alcohols or the Williamson synthesis. Only di-*t*-butyl ether has been obtained by some specific procedures.[1-3]

This work deals with the syntheses of unknown di-*t*-alkyl ethers by the reactions of *t*-alkyl halides with various metal compounds. Furthermore the reaction pathways and the steric effects of *t*-alkyl groups on their reactivity were investigated in detail.

Results and Discussion

A series of *t*-alkyl halides was allowed to react with various metal compounds in pentane and hexane under optimum conditions. The products were di-*t*-alkyl ether, *t*-alkyl alcohol, and olefins, as illustrated in Scheme 1.

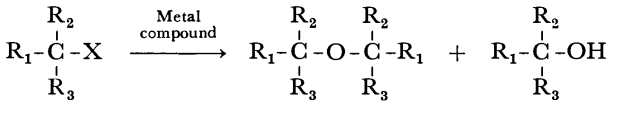

1—**8** + Olefins

1: $R_1=R_2=R_3=$Me **5**: $R_1=R_2=$Me, $R_3=n$-Bu
2: $R_1=R_2=$Me, $R_3=$Et **6**: $R_1=$Me, $R_2=$Et, $R_3=n$-Pr
3: $R_1=R_2=$Me, $R_3=n$-Pr **7**: $R_1=R_2=R_3=$Et
4: $R_1=$Me, $R_2=R_3=$Et **8**: $R_1=R_2=$Me, $R_3=n$-C_5H_{11}

Scheme 1.

Table 1 shows the results in detail. The reaction of *t*-butyl chloride with silver carbonate at 20 °C for 20 h gave **1** in 73% yield (Run 1). A similar reaction of silver(I) oxide at 35 °C also gave **1** in 63% yield (Run 2). Mercury(II) oxide reacted more slowly with *t*-butyl and *t*-pentyl chlorides, and 2-chloro-2-methylpentane to give **1**, **2**, and **3** respectively in reasonable yields (Runs 3, 14, and 19). In the case of zinc compounds, **1** and **2** were afforded only on addition of *t*-alkyl alcohol to the system (Runs 4, 5, and 15). This result suggests the participation of the alcohol in the formation of **1** and **2**. Lead(IV) oxide and copper(II) carbonate hydroxide failed to complete the reaction even under certain strict conditions (Runs 6 and 7). Thallium(III) oxide readily reacted with *t*-butyl chloride to give **1**, but in only 6% yield (Run 8). Consequently, silver(I) oxide and carbonate gave better results than the other metal compounds. *t*-Butyl and *t*-pentyl bromides also reacted with two equivalents of silver compound at much lower temperatures than the corresponding chlorides (Runs 9, 10, and 16). Calcium hydride retarded the reaction and decreased markedly the distributions of both *t*-pentyl alcohol and **2** (Run 13).

On the whole, the yield of the ether decreased as the *t*-alkyl group became bulky (Runs 11—27). When one of the methyl groups of *t*-butyl chloride was substituted for ethyl, propyl butyl, and pentyl groups, the yields of **2**, **3**, **5**, and **8** were 47, 37, 29, and 11% respectively. The substitution of methyl groups of the chloride for two or three ethyl groups resulted in a more remarkable decrease: the yields of **4** and **7** were 21 and 2%, respectively. Scheme 2 illustrates the relationship between the structure of the *t*-alkyl group and the yield of di-*t*-alkyl ether.

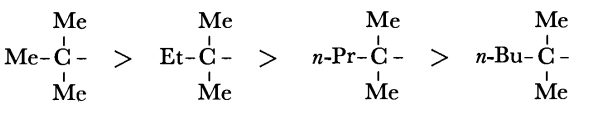

1: 73% **2**: 47% **3**: 37% **5**: 29%

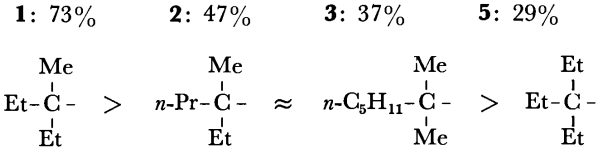

4: 21% **6**: 11% **8**: 11% **7**: 2%

Scheme 2.

It is interesting from a structural point of view that the yields of isomeric **3** and **4** are quite different (Runs 17 and 20). An analogous tendency is observed in isomeric **5**, **6**, and **7** (Runs 22, 24, and 26). To sum up, the yield is greatly influenced by the degree of bulkiness and the structure of the *t*-alkyl group.

Table 2 shows the time-course of the reaction of *t*-pentyl chloride with a small excess of silver carbonate at 20 °C (*cf.* Run 11). The proportions of the chloride and the products were followed by GLPC at regular time intervals. The initial step of this reaction was so fast that half of the chloride was consumed in a few hours. The proportions of **2** and of the olefins (2-methyl-1-butene and 2-methyl-2-butene) increase with an increase in reaction time, while that of *t*-pentyl alcohol remains almost constant over several hours.

*To whom correspondence should be addressed.

Table 1. Reactions of *t*-alkyl halides with metal compounds

Run	Substrates[a]		Conditions			Yield (%) of products[c]		
	t-Alkyl halide	Metal compound (mmol)	Solvent[b]	Temp °C	Time h	Ether	Alcohol	Olefin
1	*t*-BuCl	Ag_2CO_3	P	20	20	**1**, 73	7	16
2	*t*-BuCl	Ag_2O	P	35	20	**1**, 63	12	21
3	*t*-BuCl	HgO	P	35	20	**1**, 59	24	13
4	*t*-BuCl[d]	ZnO (26)	H	55	20	**1**, 37	—	42
5	*t*-BuCl[d]	$ZnCO_3$	P	35	20	**1**, 10	—	11
6	*t*-BuCl	PbO_2	H	65	50	**1**, 15	15	48
7	*t*-BuCl	$Cu_2(CO_3)(OH)_2$	P	35	200	**1**, 12	18	28
8	*t*-BuCl	Tl_2O_3	P	20	6	**1**, 6	49	41
9	*t*-BuBr	Ag_2CO_3 (40)	P	−20	5	**1**, 56	16	24
10	*t*-BuBr	Ag_2O (40)	P	0	5	**1**, 55	34	7
11	$Et(Me)_2CCl$	Ag_2CO_3	H	20	20	**2**, 47	21	32
12	$Et(Me)_2CCl$	Ag_2O	H	35	20	**2**, 34	27	39
13	$Et(Me)_2CCl$[e]	Ag_2O	H	35	40	**2**, 16	1	83
14	$Et(Me)_2CCl$	HgO	H	40	40	**2**, 16	30	54
15	$Et(Me)_2CCl$[f]	ZnO (26)	H	55	13	**2**, 10	—	45
16	$Et(Me)_2CBr$	Ag_2CO_3 (40)	H	−20	5	**2**, 35	15	50
17	*n*-$Pr(Me)_2CCl$	Ag_2CO_3	P	20	20	**3**, 37	26	37
18	*n*-$Pr(Me)_2CCl$	Ag_2O	P	35	20	**3**, 36	24	35
19	*n*-$Pr(Me)_2CCl$	HgO	P	35	100	**3**, 13	40	45
20	$Me(Et)_2CCl$	Ag_2CO_3	P	20	20	**4**, 21	37	42
21	$Me(Et)_2CCl$	Ag_2O	P	35	20	**4**, 10	40	49
22	*n*-$Bu(Me)_2CCl$	Ag_2CO_3	P	20	20	**5**, 29	30	40
23	*n*-$Bu(Me)_2CCl$	Ag_2O	P	35	20	**5**, 31	25	40
24	*n*-Pr(Et)(Me)CCl	Ag_2CO_3	P	20	20	**6**, 11	35	54
25	*n*-Pr(Et)(Me)CCl	Ag_2O	P	35	20	**6**, 9	18	66
26	Et_3CCl	Ag_2CO_3	P	20	20	**7**, 2	40	50
27	*n*-$C_5H_{11}(Me)_2CCl$	Ag_2CO_3	P	20	20	**8**, 11	38	51

a) *t*-Alkyl halide 40 mmol and metal compound 22 mmol used unless otherwise stated. b) Pentane (P) or hexane (H) 20 cm^3 used. c) GLPC yields based on *t*-alkyl halide. d) *t*-Butyl alcohol 40 mmol added. e) Calcium hydride 20 mmol added. f) *t*-Pentyl alcohol 40 mmol added.

This observation suggests that the alcohol is consumed during the reaction. The other *t*-alkyl chloride also gave similar results.

The following pathways therefore are proposed for the reaction of *t*-alkyl halide with silver carbonate:

$$R\text{-}X + Ag_2CO_3 \xrightarrow{E} R'\text{-}C{=}C + AgX + AgOH + CO_2 \quad (1)$$

$$R\text{-}X + AgOH \longrightarrow R\text{-}OH + AgX \quad (2)$$

$$R\text{-}X + R\text{-}OH + Ag_2CO_3 \xrightarrow{S} R\text{-}O\text{-}R + AgX + AgOH + CO_2 \quad (3)$$

The elimination of *t*-alkyl halide with silver carbonate gives olefins, silver halide, and silver hydroxide (Eq. 1). Silver hydroxide reacts with *t*-alkyl halide to give *t*-alkyl alcohol (Eq. 2). A desiccant such as calcium hydride would partly react with silver hydroxide and suppress the conversion into the alcohol.[4] The desired ether is formed from the halide and the alcohol in the presence of silver carbonate (Eq. 3). As the reaction is carried out in nonpolar solvents, the ether is given by bimolecular nucleophilic substitution. Such pathways can also be estimated for the reactions of the other metal compounds. These equations explain successfully the distribution of the products, the steric hindrance of the *t*-alkyl group, and the additive effect of the alcohol or calcium hydride.

Table 2. Proportions of *t*-pentyl chloride and its products during the reaction

Time h	Proportions[a] (%)			
	t-$C_5H_{11}Cl$	**2**	*t*-$C_5H_{11}OH$	Olefins[b]
0	100	0	0	0
0.5	76	7	7	10
1	68	10	10	12
2	53	18	12	17
3	41	24	14	21
5	27	32	18	23
7	16	37	21	26
10	11	40	21	28
15	5	44	21	30
20	0	47	21	32

a) The proportions were available from the more detailed results on Run 11 in Table 1. b) 2-Methyl-1-butene and 2-methyl-2-butene.

Experimental

Materials. All inorganic chemicals were commercial extra pure or GR grade reagents, dried over silica gel, and used without further purification. 2-Chloro-2-methylpentane, 3-chloro-3-methylpentane, 2-chloro-2-methylhexane, 3-chloro-3-methylhexane, 3-chloro-3-ethylpentane, and 2-chloro-2-methylheptane were derived from the corresponding alcohols.[5-8] Organic chemicals were distilled from calcium hydride before use and their purities were checked by GLPC.

Procedure and Analysis. In a three-necked flask, fitted with a reflux condenser, a dropping funnel, and a magnetic stirrer, 40 mmol of *t*-alkyl halide was added to 22 mmol of metal compound in 20 cm^3 of pentane or hexane medium. The mixture was stirred at a given temperature under nitrogen. The products in the solution were determined by GLPC comparison with authentic samples using toluene, *o*-xylene, and mesitylene as internal standards (Table 1). GLPC analyses were performed on a Shimadzu GC-3AH chromatograph using 3 m × 3 mm columns packed with 5% DNDP and 5% Silicone DC 550 on 80—100 mesh Celite support. NMR spectra were determined with a JEOL-PS-100 high resolution spectrometer operating at 100 MHz. Chemical shifts are reported in δ units from internal TMS. IR spectra were recorded on a JASCO DS-301 spectrometer. Mass spectra were recorded on a JEOL JMS-01SG spectrometer with ionization current 75 eV. The molecular weights of some ethers were measured by cryoscopy in benzene.

Characterization of Di-t-alkyl Ethers. The preparative scale reaction of *t*-alkyl chloride (0.2 mol) with silver carbonate (30.33 g, 0.11 mol) in pentane (100 cm^3) was carried out at 20 °C for 20 h in a manner similar to that above. The reaction mixture was filtered. The filtrate was concentrated and rectified over potassium carbonate, giving di-*t*-alkyl ether (purity > 99.5%), which was identified by its physical constants, NMR, IR, and mass spectra.

*Di-t-butyl Ether (**1**)*: Yield, 5.60 g (43%); bp 106 °C; IR (neat) 1384, 1363 (*t*-Bu), and 1173 cm^{-1} (C-O-C); NMR ($CDCl_3$) δ=1.26 (18H, s, *t*-Bu).

*Di-t-pentyl Ether (**2**)*: Yield, 5.56 g (35%); bp 151.5—152 °C; IR (neat) 1380, 1365 (*gem*-CH_3), and 1162 cm^{-1} (C-O-C); NMR ($CDCl_3$) δ=0.89 (6H, t, J=7.2 Hz, CH_2CH_3), 1.21 (12H, s, O-C-CH_3), and 1.47 (4H, q, J=7.4 Hz, CH_2).

*Bis(1,1-dimethylbutyl) Ether (**3**)*: Yield, 5.60 g (30%); bp 79.5—80 °C/17 Torr; mol wt, found, 187.9, calcd for $C_{12}H_{26}O$, 186.3; IR (neat) 1380, 1365 (*gem*-CH_3), and 1164 cm^{-1} (C-O-C); MS *m/e* (rel intensity), 143 (M^+—Pr, 50), 99 (79), 85 (PrC^+Me_2, 100), 59 (HOC^+Me_2, 83), and 43 (50).

*Bis(1-ethyl-1-methylpropyl) Ether (**4**)*: Yield, 2.40 g (13%); bp 78—79 °C/15 Torr; IR (neat) 1456, 1375, and 1142 cm^{-1} (C-O-C); NMR ($CDCl_3$) δ=0.85 (12H, t, J=7.2 Hz, CH_2CH_3), 1.20 (6H, s, O-C-CH_3), and 1.50 (8H, q, J=7.4 Hz, CH_2).

*Bis(1,1-dimethylpentyl) Ether (**5**)*: Yield, 6.00 g (28%); bp 109—110 °C/20 Torr; mol wt, found, 215.8, calcd for $C_{14}H_{30}O$, 214.4; IR (neat) 1380, 1364 (*gem*-CH_3), and 1161 cm^{-1} (C-O-C); MS *m/e* (rel intensity), 157 (M^+—Bu, 30), 101 (26), 99 (BuC^+Me_2, 100), 59 (HOC^+Me_2, 39), 57 (78), and 43 (16).

*Bis(1-ethyl-1-methylbutyl) Ether (**6**)*: Yield, 2.36 g (11%); bp 111—112 °C/20 Torr; mol wt, found, 214.6, calcd for $C_{14}H_{30}O$, 214.4; IR (neat) 1463, 1380, and 1145 cm^{-1} (C-O-C); MS *m/e* (rel intensity), 185 (M^+—Et, 8), 171 (M^+—Pr, 13), 101 (10), 99 (71), 87 (HOC^+PrMe, 58), 73 (45), 57 (100), and 43 (19).

*Bis(1,1-diethylpropyl) Ether (**7**)*: Yield, 0.20 g (1%); IR (neat) 1455, 1380, and 1131 cm^{-1} (C-O-C); MS *m/e* (rel intensity), 185 (M^+—Et, 31), 99 (C^+Et_3, 88), 87 (HOC^+Et_2, 100), 57 (98), 45 (29), and 29 (19).

*Bis(1,1-dimethylhexyl) Ether (**8**)*: Yield, 2.66 g (11%); bp 131—131.5 °C/16 Torr; IR (neat) 1382, 1367 (*gem*-CH_3), and 1152 cm^{-1} (C-O-C); MS *m/e* (rel intensity), 242 (M^+, 5), 171 ($M^+-C_5H_{11}$, 62), 115 (13), 113 ($C_5H_{11}C^+Me_2$, 80), 71 (66), 59 (HOC^+Me_2, 100), 57 (68), and 43 (79).

References

1) J. L. E. Erickson and W. H. Ashton, *J. Am. Chem. Soc.*, **63**, 1769 (1941); A. G. Anderson, Jr., and F. J. Freenor, *J. Org. Chem.*, **37**, 628 (1972).

2) S. O. Lawesson and N. C. Yang, *J. Am. Chem. Soc.*, **81**, 4232 (1959).

3) G. A. Olah, Y. Halpern, and H. C. Lin, *Synthesis*, **1975**, 315.

4) G. Wulff and G. Röhle, *Angew. Chem. Int. Ed. Engl.*, **13**, 161 (1974).

5) A. Deschamps, *J. Am. Chem. Soc.*, **42**, 2671 (1920).

6) G. Edgar, G. Calingaert, and R. E. Marker, *J. Am. Chem. Soc.*, **51**, 1485 (1929).

7) W. W. Moyer and C. S. Marvel, *Org. Synth.*, Coll. Vol. II, 602 (1950).

8) F. C. Whitmore and D. E. Badertscher, *J. Am. Chem. Soc.*, **55**, 1559 (1933).

Synthetic Studies of Pyridomycin. II.[1] Synthesis of a Model Twelve-membered Ring Compound Related to Pyridomycin

Mitsuhiro KINOSHITA and Masaki AWAMURA

Department of Applied Chemistry, Faculty of Engineering, Keio University, Hiyoshi, Kohoku-ku, Yokohama 223

(Received August 31, 1977)

A prototypic compound of pyridomycin, 6-(3-hydroxypicolinoylamino)-5-methyl-8-aza-1,4-dioxacyclododecane-3,7,12-trione (**11**), was synthesized. 4-(Benzyloxycarbonylamino)butyric acid was coupled with *t*-butyl glycolate in the presence of DCCI and pyridine to afford *t*-butyl [4-(benzyloxycarbonylamino)butyryloxy] acetate (**4**). De-*t*-butylation of **4** followed by condensation with *N*-*t*-butoxycarbonyl-L-threonine benzyl ester by the DCCI method gave *O*-[{4-(benzyloxycarbonylamino)butyryloxy}acetyl]-*N*-*t*-butoxy-carbonyl-L-threonine benzyl ester (**6**). Deprotection of **6** followed by cyclization with Woodward's reagent K afforded 6-(*t*-butoxy-carbonylamino)-5-methyl-8-aza-1,4-dioxacyclododecane-3,7,12-trione (21% yield), which was transformed into the title compound **11**.

Pyridomycin is an antimycobacterial antibiotic[2] produced by *Streptomyces pyridomyceticus*.[3] The structure of pyridomycin (**1**) was determined by means of X-ray analysis[4] and chemical degradation.[5] The most striking characteristic of the structure is its novel heterocyclododecane system containing unique exocyclic *s*-butylidene and 3-pyridylmethyl side chains.

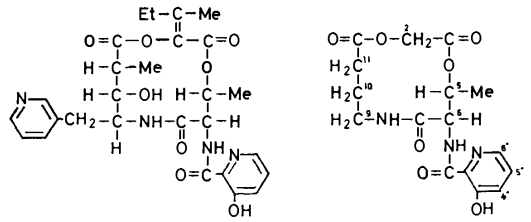

1 **11**

Chart 1.

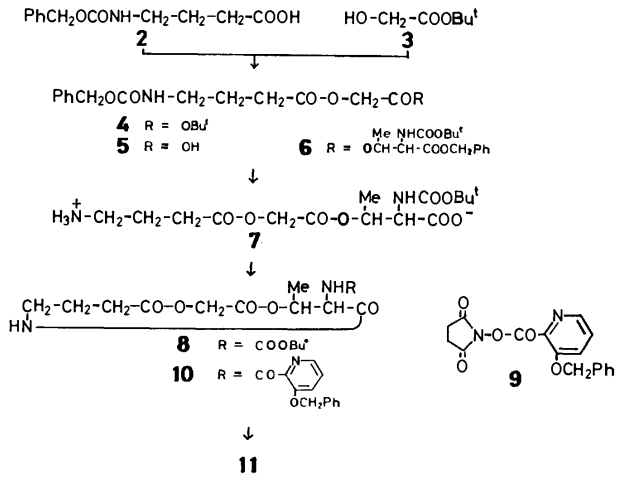

Chart 2.

During the course of studies on the total synthesis of pyridomycin, the natural (−)-4-amino-3-hydroxy-2-methyl-5-(3-pyridyl)pentanoic acid, which is a building block containing the 3-pyridylmethyl side chain of the pyridomycin ring system, was synthesized.[1] So far no attempt seems to have been made for the preparation of this new type of medium ring system present in pyridomycin. We therefore tried to synthesize a prototype in which, except for the moiety of L-threonine, the structure was made simpler than that of the natural antibiotic. This paper deals with the synthesis of 6-(3-hydroxypicolinoylamino)-5-methyl-8-aza-1,4-dioxacyclododecane-3,7,12-trione (**11**) whose cyclic structure is composed of *N*-(3-hydroxypicolinoyl)-L-threonine, 4-aminobutyric acid, and glycolic acid (Chart 1). In the synthesis of **11**, we adopted the method of cyclization by amide bond formation. The pathway is most commonly used for the synthesis of peptolides and peptide lactones. The synthetic scheme is shown in Chart 2.

4-(Benzyloxycarbonylamino)butyric acid (**2**) was prepared by the Schotten-Baumann reaction of 4-aminobutyric acid with benzyl chloroformate. *t*-Butyl glycolate (**3**)[6] was prepared by selective saponification of *t*-butyl acetoxyacetate[6] obtained by *t*-butylation of acetoxyacetic acid[7] with 2-methylpropene in the usual way. Condensation of **2** with **3** was carried out in the presence of dicyclohexylcarbodiimide (DCCI) and pyridine in THF to afford *t*-butyl [4-(benzyloxycarbonylamino)butyryloxy]acetate (**4**) in 64.5% yield after being subjected to silica gel chromatography. Treatment of **4** with trifluoroacetic acid gave [4-(benzyloxycarbonylamino)butyryloxy]acetic acid (**5**) in 96.7% yield. *N*-*t*-Butoxycarbonyl-L-threonine benzyl ester[8] was acylated with **5** in THF using DCCI and pyridine to afford the protected open-chain intermediate (**6**) in 90.4% yield after silica gel chromatography. Deprotection of **6** by hydrogenolysis over palladium black gave the linear system **7** with terminal amino and carboxy group in 99.5% yield. Cyclization of **7** was performed with *N*-ethyl-5-phenylisoxazolium-3'-sulfonate (Woodward's reagent K)[9] according to the procedure of Bláha and Rudinger,[10] and of Gisin and Merrifield[11] to afford the intramolecular cyclization product, 6-(*t*-butoxycarbonylamino)-5-methyl-8-aza-1,4-dioxacyclodecane-3,7-12-trione (**8**) as colorless needles in 21.1% yield. The structure of **8** was confirmed by PMR analysis and molecular weight determination by mass spectrum. The cyclization of **7** which was carried out with large excess of DCCI by the method of Vogler *et al.*,[12] or with 1-ethyl-3-(3-dimethylaminopropyl)carbodiimide hydrochloride in dichloromethane at 10^{-2}—10^{-3} M concentration of **7** by the method of Sheehan and Ledis,[13] yielding the cyclized product **8** in lower yields (4—8.3%). In all the cyclization reactions abovementioned, no appreciable amount of intermolecular

cyclization products could be isolated.

De-*t*-butoxycarbonylation of **8** followed by *N*-acylation with *N*-(3-benzyloxypicolinoyloxy)succinimide (**9**) gave the 3-benzyloxypicolinamide derivative **10** in 85.2% yield. Removal of the benzyl group of **10** by hydrogenolysis over palladium black afforded the pyridomycin analog **11** as colorless plates in 80.7% yield. The structure was confirmed by elemental and PMR analyses.

Experimental

Melting points were determined on a micro hot-stage and are uncorrected. IR spectra were taken on a Hitachi 225 spectrophotometer and PMR spectra on a Varian A-60D spectrometer using TMS as an internal standard. Specific rotations were determined with a Zeiss Photoelectric Polarimeter. TLC and column chromatography were performed on Wakogel B-5 and C-200, respectively. Concentration was carried out below 40 °C under reduced pressure.

4-(Benzyloxycarbonylamino)butyric Acid (2). *N*-Benzyloxycarbonylation of 4-aminobutyric acid was carried out with benzyl chloroformate and 2M NaOH solution under the Schotten-Baumann conditions to afford **2** as colorless needles in 64.9% yield: Mp 63—64 °C (ether-petroleum ether).

Found: C, 60.46; H, 6.25; N, 5.89%. Calcd for $C_{12}H_{15}NO_4$: C, 60.75%; H, 6.37; N, 5.90%.

t-*Butyl Glycolate (3).*[6] Liquid 2-methylpropene (86 ml) was added to a solution of acetoxyacetic acid[7] (16.7 g) in dichloromethane (141 ml) containing concd H_2SO_4 (1.41 ml) at −30 °C under cooling. The stoppered flask was allowed to stand at room temperature for 3 days. The usual work-up followed by distillation afforded a fraction of *t*-butyl acetoxyacetate boiling at 59—62 °C/5 Torr; yield 19.0 g (77.2%), n_D^{19} 1.4131 (lit,[6] bp 79—81 °C/12 Torr n_D^{20} 1.4142); TLC [silica gel, petroleum ether-diisopropyl ether (3 : 1)] of the sample showed a single spot detected by H_2SO_4. A solution of the ester (12.106 g, 69.52 mmol) in acetone (35 ml) was cooled to 0 °C and 2M NaOH solution (38.2 ml) was added slowly under stirring. After the addition of NaOH, stirring was continued at 0 °C for 1 h until the reaction mixture showed a constant pH value (*ca.* 9). The mixture was then neutralized with 5% citric acid and concentrated in order to remove acetone. The residue was extracted four times with ether, the combined ethereal extracts were washed with saturated $NaHCO_3$ and saturated NaCl solutions, dried, and immediately evaporated to give a colorless syrup of **3** (3.908 g, 42.6%). The fresh sample of **3** was homogeneous on TLC with petroleum ether-diisopropyl ether (3 : 1). However, when a fresh sample was stored in a desiccator overnight, it showed on TLC a new spot with lower R_f-value in addition to the original spot of the fresh sample. Although the sample of **3** could be distilled at 40—57 °C/7—14 Torr [lit,[6] bp 56 °C/12 Torr], all of the distillates were not homogeneous on TLC.

t-*Butyl [4-(Benzyloxycarbonylamino)butyryloxy]acetate (4).* A solution of **2** (7.017 g, 29.6 mmol) in dry THF (15.5 ml) was added slowly dropwise to a stirred solution of the freshly prepared sample of **3** (3.908 g, 29.6 mmol), DCCI (6.782 g, 32.9 mmol) and pyridine(2.45 ml, 31.2 mmol) in dry THF (11.6 ml), cooled at 0 °C. Stirring was continued at 0 °C for 1 h and then at room temperature for 3 days. The precipitate of *N,N'*-dicyclohexylurea (DCU) was filtered off and the filtrate was treated with acetic acid (*ca.* 0.25 ml) for 1 h. The resulting DCU was removed and the filtrate was diluted with ethyl acetate and washed with saturated $NaHCO_3$ and saturated NaCl solutions. The dried solution was evaporated to afford yellow syrup (8.533 g), which was chromatographed on silica gel (341 g) with benzene–ethyl acetate (2 : 1) to give **4** (6.701 g, 64.5%) as colorless crystals: Mp 63.5—64.5 °C from ethyl acetate); $\delta(CDCl_3)$ 1.48(s, 9H, OBu^t), *ca.* 1.9 (m, 2H, H-10*), *ca.* 2.5(m, 2H, H-11), 3.34(dd, 2H, H-9, $J_{9,10}=J_{9,NH}=6.8$ Hz), 4.57(s, 2H, H-2), 5.20(s, 2H, OCH_2-Ph), *ca.* 5.1 (br, 1H, NH), and 7.35(s, 5H, Ph).

Found: C, 61.63; H, 7.20; N, 3.79%. Calcd for $C_{18}H_{25}NO_6$: C, 61.52; H, 7.17; N, 3.99%.

[4-(Benzyloxycarbonylamino)butyryloxy]acetic Acid (5). A mixture of **4** (5.200 g, 14.8 mmol) and trifluoroacetic acid (15.9 ml) was kept at room temperature for 40 min and then evaporated. The residual syrup was coevaporated with ether repeatedly and dried over NaOH pellets in a desiccator to afford a crystalline solid, which was recrystallized from ethyl acetate to yield the first crop of **5** (3.418 g, 78.2%), mp 78—79.5 °C. From the mother liquor the second and third crops were obtained, the total yield amounting to 96.7%: $\delta(CDCl_3)$ 1.92(m, 2H, H-10), 2.53(t, 2H, H-11, $J=7$ Hz), 3.38(m, 2H, H-9), 4.72(s, 2H, H-2), 5.21(s, 2H, OCH_2Ph), 5.36(br, 1H, NH), 7.48(s, 5H, Ph), and 8.0(br, 1H, COOH).

O-[{*4-(Benzyloxycarbonylamino)butyryloxy}acetyl*]-N-t-*butoxycarbonyl*-L-*threonine Benzyl Ester (6).* A solution of **5** (1.405 g, 4.78 mmol) in THF (3.0 ml) was added slowly to a stirred solution of *N*-*t*-butoxycarbonyl-L-threonine benzyl ester[8] (1.486 g, 4.78 mmol), DCCI (1.183 g, 5.735 mmol), and pyridine (0.387 ml, 4.78 mmol) in THF (7.8 ml) at 0 °C. Stirring was continued at 0 °C for 10 min and then at room temperature for 3 days. Work-up of the reaction mixture in the same way as in the preparation of **4** afforded a yellow syrup of crude product. The product (3.103 g) was chromatographed on silica gel (175 g) with hexane–ethyl acetate(2 : 1) to give **6** (2.532 g, 90.4%). A sample of this syrup (107 mg) was chromatographed again on silica gel (5 g) with the solvent system to afford the analytical sample (84 mg) as a colorless syrup: $[\alpha]_D^{15}$ +17°(*c*, 1.0, $CHCl_3$); $\delta(CDCl_3)$ 1.38(d, 3H, 5-Me, $J=6.5$ Hz), 1.47(s, 9H, *t*-Bu), 1.90(m, 2H, H-10), 2.50 (m, 2H, H-11), 3.30(m, 2H, H-9, $J_{9,10}=J_{9,NH}=6$ Hz), 4.35 and 4.53 (each d, H-2, $J_{gem}=16$ Hz), 4.4—4.67(m, 1H, H-6), 5.15 and 5.20(each s, 4H, OCH_2Ph), 5.1—5.3(m, 2H, NH), 5.53 (dq, 1H, H-5, $J_{5,6}=3$ Hz), and 7.40(s, 10H, Ph).

Found: C, 61.51; H, 6.57; N, 4.62%. Calcd for $C_{30}H_{38}N_2O_{10}$: C, 61.42; H, 6.53; N, 4.78%.

O-[*(4-Aminobutyryloxy)acetyl*]-N-t-*butoxycarbonyl*-L-*threonine (7).* A solution of **6** (150 mg) in methanol (5.3 ml) was stirred with palladium black under bubbling with hydrogen gas for 30 min. The filtered solution was evaporated and then coevaporated with hexane to afford **7** as a colorless glassy solid showing a single spot (ninhydrin and H_2SO_4 reagents) on TLC (silica gel) with 1-butanol-acetic acid–water (4 : 1 : 1): Yield, 92.1 mg (99.5%); $\nu_{max}^{CHCl_3}$ 3430 (NH), 2800—2500(NH_3^+), 1735 (ester), 1700(amide I), 1610(COO^-), and 1490 cm^{-1}(amide II); $\delta(CDCl_3)$ 1.35(d, 3H, 5-Me, $J=6.5$ Hz), 1.46(s, 9H, *t*-Bu), 2.10(m, 2H, H-10), 2.67(m, 2H, H-11), 3.17(m, 2H, H-9), 4.30(m, 1H, H-6), 4.68(s, 2H, H-2), and 5.46—5.80(m, 2H, H-5 and NH).

6-(t-Butoxycarbonylamino)-5-methyl-8-aza-1,4-dioxacyclododecane-3,7,12-trione (8). Compound **7** (368 mg, 1.02 mmol) was activated in DMF (35 ml) with Woodward's reagent K[9] (273 mg (purity 95%), 1.02 mmol) at 0—10 °C for 3.5 h, according to the procedure of Bláha and Rudinger[10] and Gisin and Merrifield.[11] The resulting turbid solution

* Numbering of the protons corresponds to that of compound **11** in Chart 1.

was diluted with DMF (25 ml) and dichloromethane (1.02 l). Triethylamino (0.143 ml, 1.02 mmol) was added to the solution, and the mixture was stirred at room temperature for 60 h. The clear solution was evaporated and the residue was extracted with ethyl acetate. The extract was washed twice with water and the aqueous layers were extracted with ethyl acetate. The combined organic layers were washed with saturated NaCl solution, dried, and evaporated to afford a yellow syrup (356 mg). The syrup was chromatographed on silica gel (36 g) with hexane-acetone (2 : 1) to give **8** (74.2 mg, 21.1%) as colorless needles. Recrystallization from ethyl acetate afforded the analytical sample: Mp 216—217 °C(sub.); $[\alpha]_D^{14}$ −5° (*c* 1.0, $CHCl_3$); ν_{max}^{KBr} 1757, 1737 (lactone), 1715(urethane), 1654(amide I), and 1515 cm^{-1} (amide II); $\delta(CDCl_3)$, 1.26(d, 3H, 5-Me, J=6.5 Hz), 1.42 (s, 9H, *t*-Bu), *ca.* 2.0(m, 2H, H-10), *ca.* 2.5(m, 2H, H-9), 2.8—4.0(m, 2H, H-11), 4.20(dd, 1H, H-6, $J_{5,6}$=5 Hz, $J_{6,NH}$ =8 Hz), 4.50 and 4.80(each d, 2H, H-2, J_{gem}=15 Hz), 5.27 (m, 1H, H-5) and *ca.* 6.1(br, NH); molecular ion at *m/e* 344.162(calcd, 344.1583).

Found: C, 52.14; H, 6.98; N, 8.09%. Calcd for $C_{15}H_{24}N_2O_7$: C, 52.32; H, 7.03; N, 8.14%.

*N-(3-Benzyloxypicolinoyloxy)succinimide (**9**).* 3-Benzyloxypicolinic acid hydrochloride sesquihydrate[14] (500 mg, 1.71 mmol) was suspended in a mixture of ethyl acetate (7.3 ml) and triethylamine (0.25 ml) and stirred at room temperature for 1 h. The crystals of triethylamine hydrochloride were filtered off and washed with ethyl acetate. *N*-Hydroxysuccinimide (210 mg, 1.82 mmol) and DCCI (370 mg, 1.82 mmol) were added to the combined filtrates. The mixture was stirred at room temperature for 2 h, and then kept at 0 °C for 0.5 h. The resulting crystalline product (a mixture of **9** and DCU) was collected by filtration and extracted with DMF (10 ml) under stirring at room temperature for 1 h. After removal of undissolved DCU, the DMF solution was evaporated to give a crystalline solid (528 mg). The solid was again dissolved in DMF (6.9 ml) at 50 °C in order to remove DCU and the filtered solution was evaporated. The residual crude crystals of **9** (443 mg, 79.6%) were recrystallized from a mixture of DMF (3.2 ml) and ethyl acetate (68 ml) to afford a practically pure sample of **9** (348 mg, 62.3%), mp 179—183 °C. The sample was again recrystallized from the same solvent system to give an analytical sample, mp 181—183 °C.

Found: C, 62.35; H, 4.51; N, 8.49%. Calcd for $C_{17}H_{14}N_2O_5$: C, 62.57; H, 4.32; N, 8.59%.

*6-(3-Benzyloxypicolinoylamino)-5-methyl-8-aza-1,4-dioxacyclododecane-3,7,12-trione (**10**).* A sample of **9** (20.0 mg, 0.0581 mmol) was dissolved in trifluoroacetic acid (0.1 ml). The solution was kept at room temperature for 5 min and then evaporated to afford a colorless glassy solid (20.8 mg) of the trifluoroacetate of the amino peptide dilactone. 3-Benzyloxypicolinic acid active ester **9** (19.0 mg, 0.0581 mmol) was added to a solution of the trifluoroacetate(20.8 mg) in DMF (0.25 ml). Triethylamine was then added until the solution became neutral (pH 7), and the mixture was allowed to stand at 37 °C for 4 days. The reaction mixture was evaporated and dissolved in ethyl acetate. The solution was washed with water and saturated NaCl solution, dried and evaporated. The residual pale-yellow syrup (40 mg) was chromatographed on silica gel (3 g) with benzene-acetone (1 : 1) to afford a colorless syrup of **10** (22.5 mg, 85.2%); $\delta(CDCl_3)$, 1.28(d, 3H, 5-Me, J=6.8 Hz), *ca.* 2.1(m, 2H, H-10), *ca.* 2.5(m, 2H, H-9), 3.0—4.0 (m, 2H, H-11), 4.56 and 4.82(each d, 2H, H-2, J_{gem}=15 Hz), 4.77(dd, 1H, H-6, $J_{6,NH}$=8 Hz, $J_{5,6}$=5 Hz), 5.27(s, 2H, OCH_2Ph), 5.42(m, 1H, H-5), *ca.* 6.2(m, 1H, NH), 7.39 (s, 5H, Ph), *ca.* 7.5(m, 2H, picolinyl H-4′, 5′), 8.3(m, 1H, picolinyl H-6′), and 8.45(m, 1H, NH).

*6-(3-Hydroxypicolinoylamino)-5-methyl-8-aza-1,4-dioxacyclododecane-3,7,12-trione (**11**).* A solution of **10** (22.4 mg) in methanol(3 ml) was stirred with palladium black for 10 min under bubbling with hydrogen gas. Acetone was added to the reaction mixture, the catalysts were filtered off, and the filtrate was evaporated to give **11** (14.3 mg, 80.7%). TLC (silica gel, benzene-acetone(1 : 1)) of the sample showed a single spot (R_f 0.68) detected by means of $FeCl_3$ and H_2SO_4. The sample was recrystallized from acetone to afford the pure sample: Mp 253—255 °C; $[\alpha]_D^{26}$ +9° (*c* 0.45, $CHCl_3$); δ ($CDCl_3$), 1.36(d, 3H, 5-Me, J=6.8 Hz), *ca.* 2.0(m, 2H, H-10), *ca.* 2.5(m, 2H, H-9), *ca.* 3.8(m, 2H, H-11), 4.57 and 4.96(each d, 2H, J_{gem}=15 Hz), 4.60(dd, 1H, H-6, $J_{5,6}$=5 Hz, $J_{6,NH}$ =8 Hz), 5.42(m, 1H, H-5), *ca.* 6.0(br, 1H, NH), *ca.* 7.4(m, picolinyl H-4′,5′), 8.2(m, 1H, H-6′), and 8.7(m, 1H, NH).

Found: C, 52.82; H, 5.31; N, 11.61%. Calcd for $C_{16}H_{19}N_3O_7$: C, 52.60, H, 5.24; N, 11.50%.

The authors wish to thank Mr. Saburo Nakada for carrying out the microanalyses, and Mrs. Shinoka Fujita(née Yamamoto) and Mr. Haruyoshi Kawazoe for their assistance.

References

1) Part I: M. Kinoshita and S. Mariyama, *Bull. Chem. Soc. Jpn.*, **48**, 208(1975).
2) K. Maeda, H. Kosaka, Y. Okami, and H. Umezawa, *J. Antibiot.*, **6A**, 140 (1953).
3) Y. Okami, K. Maeda, and H. Umezawa, *J. Antibiot.*, **7A**, 55 (1954).
4) G. Koyama, Y. Iitaka, K. Maeda, and H. Umezawa, *Tetrahedron Lett.*, **1967**, 3587.
5) H. Ogawara, K. Maeda, G. Koyama, H. Naganawa, and H. Umezawa, *Chem. Pharm. Bull.*, **16**, 679 (1968).
6) E. Müller and H. Huber-Emden, *Liebigs Ann. Chem.*, **660**, 54 (1962); L. A. Carpino, *J. Org. Chem.*, **29**, 2820 (1964).
7) R. Anschütz and W. Bertram, *Ber.*, **36**, 467 (1904).
8) E. Wünsch and J. Tentsch, *Chem. Ber.*, **97**, 2490 (1964).
9) R. B. Woodward, R. A. Olofson, and H. Mayer, *Tetrahedron, Suppl.*, **8**, 321 (1966); Aldrich Chemical Co., Inc.
10) K. Bláha and J. Rudinger, *Collect. Czech. Chem. Commun.*, **30**, 3325 (1965).
11) B. F. Gisin and R. B. Merrifield, *J. Am. Chem. Soc.*, **94**, 6165 (1972).
12) K. Vogler, R. O. Studer, P. Lanz, W. Lergier, and E. Böhni, *Helv. Chim. Acta*, **48**, 1161 (1965).
13) J. C. Sheehan, S. L. Ledis, *J. Am. Chem. Soc.*, **95**, 875 (1973).
14) J. T. Sheehan, *J. Org. Chem.*, **31**, 636 (1966).

Biosynthesis of Aloenin in *Aloe arborescens* var. *natalensis**

Takayuki SUGA and Toshifumi HIRATA

Department of Chemistry, Faculty of Science, Hiroshima University, Higashisenda-machi, Hiroshima 730

(Received September 12, 1977)

The ^{14}C- and ^{3}H-labeling patterns in aloenin biosynthesized by uptake of acetate-1-^{14}C, malonate-2-^{14}C, phenylalanine-1-^{14}C and -3-^{14}C, methionine-*methyl*-^{14}C, and glucose-3-^{3}H to *Aloe arborescens* var. *natalensis* demonstrated that the carbon skeleton of aloenin is arisen *via* a biological polyketide by the acetate-malonate pathway and the *O*-methyl group originates from methionine. Further, feeding experiments of $^{3}H/^{14}C$-doubly labeled 4-methoxy-6-(2,4-dihydroxy-6-methylphenyl)-2-pyrone and 5-(2-β-D-glucopyranosyloxy-4-hydroxy-6-methylphenyl)-3,5-dioxopentanoic acid in the Aloe plant revealed that an immediate intermediate is the pyrone derivative and not the dioxopentanoic acid derivative. Aloenin was demonstrated to be biosynthesized in such a way that the first formation of the pyrone by cyclization of the biological polyketide and then *O*-methylation of the cyclized intermediate is followed by introduction of a glucose molecule into the pyrone derivative.

Aloe arborescens Mill. var. *natalensis* Berger has been widely used for folk remedies.[3–5] A new bitter glucoside, named aloenin, with an inhibitory activity for the gastric juice secretion of rats was isolated from the plant, and its structure was reported to be a chromene derivative (**1**).[6–7] However, reexaminations of the structure by means of spectroscopic and chemical methods had proposed revised structure **2**,[8] which was recently confirmed by X-ray crystallographic and ^{13}C NMR spectroscopic studies.[9–11] We also examined other bioactive components and chemical constituents of the plant.[12]

The biosynthetic pathway of aloenin (**2**) is of considerable interest because of "the masked polyketide structure".[13–15] In parallel with the structural studies of aloenin, we carried out feeding experiments of the tracer compounds, such as ^{14}C-labeled acetate, malonate, phenylalanine, and methionine, ^{3}H-labeled glucose, and $^{3}H/^{14}C$-doubly labeled 4-methoxy-6-(2,4-dihydroxy-6-methylphenyl)2-pyrone (**3**) and 5-(2-β-D-glucopyranosyloxy-4-hydroxy-6-methylphenyl)-3,5-dioxopentanoic acid (**4**), in the Aloe plants to elucidate the biosynthetic pathway for generating the carbon skeleton of aloenin, the immediate intermediate for the biosynthesis of aloenin, and the biosynthetic sequence in the stage leading to aloenin from the biological polyketide. The results have been partly outlined in the preliminary communications,[1,2] but we wish to describe *en bloc* details of the results.

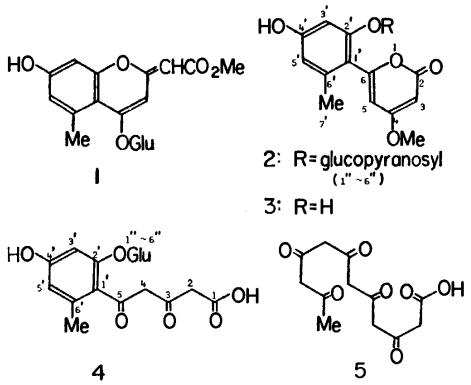

Results and Discussion

Feeding experiments of the ^{14}C- and ^{3}H-labeled tracer compounds, such as sodium acetate-1-^{14}C, sodium malonate-2-^{14}C, DL-phenylalanine-1-^{14}C, DL-phenylalanine-3-^{14}C, L-methionine-*methyl*-^{14}C, and D-glucose-3-^{3}H, were carried out in the potted plants by the cotton thread method.[16] Sodium acetate-1-^{14}C and sodium malonate-2-^{14}C were incorporated to a considerable extent in contrast to the other ^{14}C- and ^{3}H-labeled tracers, as shown in Table 1. This suggests that aloenin (**2**) may be biosynthesized by the acetate-malonate pathway, which probably involves a biological polyketide intermediate **5**. Further, the seasonal changes in the incorporations of ^{14}C-labeled acetate and malonate into aloenin indicated that the biosynthesis of aloenin (**2**) was favored in April rather than in July or October.

In order to establish the biosynthetic pathway suggested by the foregoing feeding experiments, aloenin biosynthesized by incorporation of the above-described ^{14}C- and ^{3}H-labeled precursors, respectively, was subjected to the degradation to determine the labeling pattern. Aloenin was first degraded using 5% hydrochloric acid to 2,5-dimethyl-7-hydroxychromone (**6**), glucose, and carbon dioxide,[8,11] which, in turn, originate from the C-3—C-6 and C-1′—C-7′, the C-1″—C-6″, and the C-2 moieties of **2**,** respectively. The alkaline degradation of the methylated compound (**7**) derived from **6** gave 2-hydroxy-4-methoxy-6-methylacetophenone (**8**)[17] corresponding to the C-5—C-6 and C-1′—C-7′ moiety. Methylation of **8** by Hakomori's method gave 2,4-dimethoxy-6-methylacetophenone (**9**), which was then transformed to 3,5-dimethoxytoluene (**10**) on treatment with 10% hydrochloric acid. Nitra-

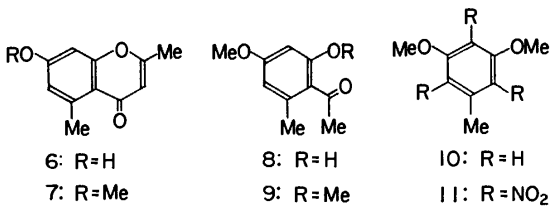

* Preliminary accounts of this work have been communicated in references 1 and 2.

** In this paper, for convenience, the carbon atoms of aloenin (**2**), the aglycone (**3**), and the diketo acid (**4**) are numbered as shown in the formulae.

Table 1. Incorporation of the radioactive tracers into aloenin (**2**) by the aloe plants

Exp. No.	Precursor[a] (μCi)	Feeding time (day)	Season	Sp. act. of **2** (dpm/mmol)	Incorporation (%)
1	AcNa-1-^{14}C (1.00×10^{2})	7	April	1.87×10^{5}	0.062
2	AcNa-1-^{14}C (1.00×10^{3})	7	April	2.76×10^{6}	0.030
3	AcNa-1-^{14}C (1.00×10^{2})	7	October	1.85×10^{4}	0.008
4	MaNa-2-^{14}C (5.00)	3	April	2.17×10^{4}	0.020
5	MaNa-2-^{14}C (5.00)	7	April	1.21×10^{5}	0.180
6	MaNa-2-^{14}C (1.00×10^{2})	7	July	2.73×10^{4}	0.049
7	MaNa-2-^{14}C (1.00×10^{2})	7	October	3.79×10^{3}	0.004
8	Phe-1-^{14}C (5.00×10)	7	October	5.03×10^{2}	0.001
9	Phe-3-^{14}C (5.00)	3	April	2.28×10^{3}	0.007
10	Phe-3-^{14}C (5.00)	7	April	4.00×10^{3}	0.004
11	Phe-3-^{14}C (2.00×10)	7	July	1.18×10^{3}	0.002
12	Phe-3-^{14}C (5.00×10)	7	July	4.44×10^{3}	0.004
13	Met-*m*-^{14}C (3.00×10)	7	July	4.36×10^{3}	0.012
14	Met-*m*-^{3}H (2.50×10^{3})	7	June	5.07×10^{6}	0.036
15	Glc-3-^{3}H (2.50×10^{3})	7	June	1.12×10^{6}	0.003

a) AcNa-1-^{14}C, MaNa-2-^{14}C, Phe-1-^{14}C, Phe-3-^{14}C, Met-*m*-^{14}C, Met-*m*-^{3}H, and Glc-3-^{3}H denote sodium acetate-1-^{14}C, sodium malonate-2-^{14}C, D,L-phenylalanine-1-^{14}C, DL-phenylalanine-3-^{14}C, L-methionine-*methoxyl*-^{14}C, L-methionine-*methoxyl*-^{3}H, and D-glucose-3-^{3}H, respectively.

Table 2. Distribution of radioactivity in aloenin (**2**) after uptake of sodium acetate-1-^{14}C

Compound	Carbons originated from **2**	Sp. act. (dpm/mmol)	Distribution (%)	
			Found	Expected[a]
2	C-2—C-6, C-1′—C-7′, MeO, and C-1″—C-6″	2.27×10^{4}	100	100
Glucose	C-1″—C-6″	8.30×10^{3}	36.6	—
7	C-3—C-6 and C-1′—C-7′	1.29×10^{4}	56.8	52.8
8	C-5, C-6 and C-1′—C-7′	1.05×10^{4}	46.3	42.2
10	C-1′—C-7′	7.56×10^{3}	33.3	31.7
Bromopicrin	C-1′, C-3′, and C-5′	0	0	0

a) Theoretical values calculated on the basis of the acetate-malonate pathway, after subtracting the radioactivity of glucose moiety from that of **2**.

Table 3. Distribution of radioactivity in aloenin (**2**) after uptake of sodium malonate-2-^{14}C

Compound	Carbons originated from **2**	Sp. act. (dpm/mmol)	Distribution (%)	
			Found	Expected[a]
2	C-2—C-6, C-1′—C-7′, MeO, and C-1″—C-6″	3.82×10^{4}	100	100
Glucose	C-1″—C-6″	1.20×10^{4}	31.4	—
7	C-3—C-6 and C-1′—C-7′	2.60×10^{4}	68.1	68.6
8	C-5, C-6 and C-1′—C-7′	2.25×10^{4}	58.9	57.2
10	C-1′—C-7′	1.76×10^{4}	46.1	45.8
Bromopicrin	C-1′, C-3′, and C-5′	1.14×10^{4}	29.8	34.2

a) Refer a) in Table 2.

Table 4. Distribution of radioactivity in aloenin (**2**) after uptake of DL-phenylalanine-1-^{14}C

Compound	Carbons originated from **2**	Sp. act. (dpm/mmol)	Distribution (%)	
			Found	Expected[a]
2	C-2—C-6, C-1′—C-7′, MeO, and C-1″—C-6″	5.03×10^{2}	100	100
Glucose	C-1″—C-6″	8.30×10	16.5	—
7	C-3—C-6 and C-1′—C-7′	2.92×10^{2}	58.1	83.5
8	C-5, C-6, and C-1′—C-7′	2.26×10^{2}	44.9	0

a) Theoretical values calculated on the basis of the shikimate pathway, after subtracting the radioactivity of glucose moiety from that of **2**.

TABLE 5. DISTRIBUTION OF RADIOACTIVITY IN ALOENIN (**2**) AFTER UPTAKE OF DL-PHENYLALANINE-3-^{14}C

Compound	Carbons originated from **2**	Sp. act. (dpm/mmol)	Distribution (%)	
			Found	Expected[a]
2	C-2—C-6, C-1′—C-7′, MeO, and C-1″—C-6″	4.44×10^3	100	100
Glucose	C-1″—C-6″	7.50×10^2	16.9	—
7	C-3—C-6 and C-1′—C-7′	3.20×10^3	72.0	83.1
8	C-5, C-6, and C-1′—C-7′	2.85×10^3	64.1	83.1
10	C-1′—C-7′	2.38×10^3	53.5	0

a) Refer a) in Table 4.

TABLE 6. DISTRIBUTION OF RADIOACTIVITY IN ALOENIN (**2**) AFTER UPTAKE OF L-METHIONINE-*methyl*-^{14}C

Compound	Carbons originated from **2**	Sp. act. (dpm/mmol)	Distribution (%)	
			Found	Expected[b]
2	C-2—C-6, C-1′—C-7′, MeO, and C-1″—C-6″	4.36×10^3	100	100
7	C-3—C-6 and C-1′—C-7′	9.79×10	2.3	0
Glucose	C-1″—C-6″	0	0	0
CO_2	C-2	5.50×10	1.3	0
—	MeO	—	(96.4)[a]	100

a) Balance amount. b) Theoretical values calculated on the basis that the methyl of the methoxyl group at C-4 is originated from L-methionine.

TABLE 7. DISTRIBUTION OF RADIOACTIVITY IN ALOENIN (**2**) AFTER UPTAKE OF D-GLUCOSE-3-^3H

Compound	Carbons originated from **2**	Sp. act. (dpm/mmol)	Distribution (%)	
			Found	Expected[a]
2	C-2—C-6, C-1′—C-7′, MeO, and C-1″—C-6″	4.80×10^3	100	100
Glucose	C-1″—C-6″	4.52×10^3	94.2	100
7	C-3—C-6 and C-1′—C-7′	2.00×10^2	4.1	0

a) Theoretical values calculated on the basis that the glucose moiety of **2** is originated from D-glucose.

tion of **10** afforded the trinitro derivative (**11**), which on bromopicrin cleavage[18,19] afforded bromopicrin originated, respectively, from C-1′, C-3′, and C-5′ of **2**. The radioactivities of these compounds are listed in Tables 2—7. It was observed that the ^{14}C-labeling patterns of **2** biosynthesized from acetate-1-^{14}C and malonate-2-^{14}C, respectively, were in complete agreement with the pattern anticipated from the acetate-malonate pathway (Tables 2 and 3). In feeding experiments of phenylalanine-1-^{14}C and -3-^{14}C (Tables 1, 4, and 5), the low incorporation of the tracers and the random distribution of radioactivities were observed in contrast with the incorporations of the acetate and the malonate. These facts unambiguously establish that the carbon skeleton of aloenin is generated by the acetate-malonate pathway and not by the shikimate pathway. The above results obtained in the incorporations of phenylalanine may be explained by participation of these precursors in the formation of polyketide **5** *via* acetoacetyl-CoA which is probably produced from phenylalanine through such an intricate metabolic pathway[20] as involving the cleavage of even the aromatic ring.

After uptake of L-methionine-*methyl*-^{14}C, almost all the amount of the total radioactivities were located on the *O*-methyl group of aloenin, as shown in Table 6. The distribution of radioactivity on the C-2—C-6, C-1′—C-7′, and C-1″—C-6″ carbon atoms was negligibly small and was within the experimental error. This demonstrates that the *O*-methyl group at C-4 of aloenin (**2**) originates from the *S*-methyl group of L-methionine. On the other hand, the ^3H-labeling pattern in aloenin biosynthesized by incorporation of D-glucose-3-^3H are shown in Table 7. The pattern indicates that the glucose moiety (C-1″—C-6″) is produced by introduction of a molecule of glucose. In the stage leading to aloenin from the biological polyketide (**5**), the introduction of the glucose molecule and the creation of the methoxyl group may occur through pathway (a) or (b) involving a different compound, 4-methoxy-6-(2,4-dihydroxy-6-methylphenyl)-2-pyrone (**3**) or 5-(2-*β*-D-glucopyranosyloxy-4-hydroxy-6-methylphenyl)-3,5-dioxopentanoic acid (**4**), which are possible as an immediate intermediate for the biosynthesis of aloenin, as shown in Scheme 1. In order to prove the immediate intermediate and the biosynthetic sequence in the stage, the $^3H/^{14}C$-doubly labeled compounds, (**3**) and (**4**), were prepared from the labeled aloenin and subjected to feeding experiments as follows. The ^{14}C- and ^3H-labeled specimens of aloenin were synthesized biologically by feeding acetate-1-^{14}C, L-methionine-*methyl*-^3H, and D-glucose-3-^3H to the Aloe plant (Table 1). The incorporation of these labeled compounds into aloenin should yield 2, 4, 6, 2′, 4′, 6′-^{14}C-, *methoxyl*-^3H-, and

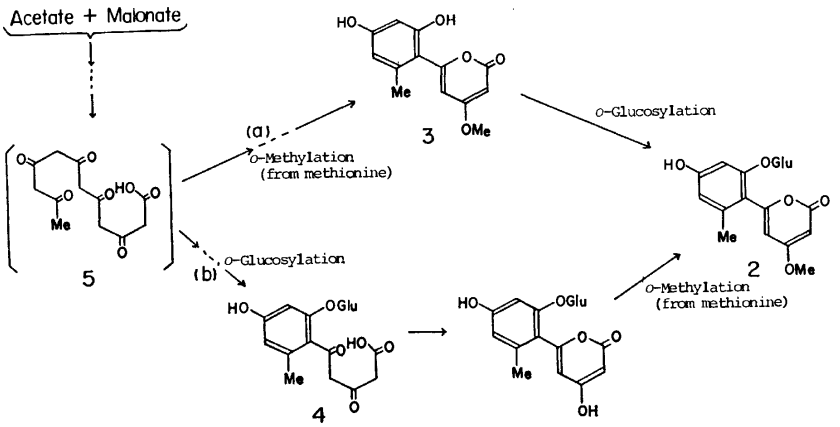

Scheme 1. Possible biosynthetic pathways of aloenin (**2**) in aloe plants.

TABLE 8. INCORPORATION OF THE DOUBLY LABELED TRACERS, **3** AND **4**, INTO ALOENIN (**2**) BY THE ALOE PLANTS

Exp. No.	Precursor[a,b] (μCi)	Feeding time (day)	Season	Sp. act. of **2** (dpm/mmol)[b]	Incorporation (%)[c]
16	Pyrone-^3H; ^{14}C (1.22×10^{-3})	5	July	8.44×10^2	8.1
17	Pyrone-^3H; ^{14}C (1.31×10^{-3})	5	July	6.52×10^2	5.5
18	Pyrone-^3H; ^{14}C (4.06×10^{-3})	3	August	8.48×10^2	13.4
19	Acid-^3H; ^{14}C (5.00×10^{-2})	5	July	0	0
20	Acid-^3H; ^{14}C (2.55×10^{-2})	3	August	0	0
21	Acid-^3H; ^{14}C (2.80×10^{-2})	3	August	0	0

a) Pyrone-^3H; ^{14}C and acid-^3H; ^{14}C denote 4-methoxy-6-(2,4-dihydroxy-6-methylphenyl)-2-pyrone-*methoxyl*-^3H; 2,4,6,2′,4′,6′-^{14}C (**3**) and potassium salt of 5-(2-β-D-glucopyranosyloxy-4-hydroxy-6-methylphenyl)-3,5-dioxopentanoic acid-3″-^3H; 1,3,5,2′,4′,6′-^{14}C (**4**), respectively. b) Radioactivities of the doubly labeled compounds refer to only ^{14}C. c) The incorporations were calculated with respect to only ^{14}C.

TABLE 9. THE $^3H/^{14}C$ LABELING RATIOS IN ALOENIN (**2**) AFTER UPTAKE OF DOUBLY LABELED PYRONE **3**

Exp. No.[a]	Pyrone **3** Sp. act. (dpm/mmol) ^3H	Pyrone **3** Sp. act. (dpm/mmol) ^{14}C	Pyrone **3** $^3H/^{14}C$ Ratio	Aloenin (**2**) Sp. act. (dpm/mmol) ^3H	Aloenin (**2**) Sp. act. (dpm/mmol) ^{14}C	Aloenin (**2**) $^3H/^{14}C$
16	3.30×10^5	5.01×10^1	6.59	5.34×10^3	8.44×10^2	6.33
17	3.30×10^5	5.01×10^1	6.59	4.07×10^3	6.52×10^2	6.24
18	2.80×10^5	2.46×10^1	11.4	8.74×10^3	8.48×10^2	10.3

a) "Exp. No." corresponds to the number in Table 8.

3″-^3H-labeled aloenin, respectively, since the carbon skeleton, the methoxyl group, and the glucose moiety have been established to be arisen from acetate, methionine, and glucose as described above. Aloenin-2,4,6,2′,4′,6′-^{14}C was mixed with aloenin-*methoxyl*-^3H and then the combined material was hydrolyzed[8,11] with 3% HCl–MeOH to yield 4-methoxy-6-(2,4-dihydroxy-6-methylphenyl)-2-pyrone-*methoxyl*-^3H; 2,4,6,2′,4′,6′-^{14}C (**3**). On the other hand, following the method established for the synthesis of the corresponding diketo acid by alkaline degradation of the 6-substituted 4-methoxy-2-pyrone derivatives,[8,11] a combined sample of aloenin-3″-^3H and aloenin-2,4,6,2′,4′,6′-^{14}C was treated with 5% KOH–MeOH to yield potassium salt of 5-(2-β-D-glucopyranosyloxy-4-hydroxy-6-methylphenyl)-3,5-dioxopentanoic acid-3″-^3H; 1,3,5,2′,4′,6′-^{14}C (**4**).

Feeding experiments of the doubly labeled pyrone (**3**) and the potassium salt of diketo acid **4** to the Aloe plant were carried out in the same manner as above. The labeled pyrone **3** was incorporated into aloenin to an extremely large extent (Exp. 16—18) in comparison with the incorporation of such labeled compounds as acetate-1-^{14}C, malonate-2-^{14}C, glucose-3-^3H, and methionine-*methyl*-^3H, as shown in Tables 1, 8, and 9. In contrast to this, no incorporation of the diketo acid (**4**) into aloenin occurred in all of the three trials (Exp. 19—21). These results demonstrate that the pyrone **3**, but not the diketo acid **4**, is an immediate intermediate for the biosynthesis of aloenin. Further, the $^3H/^{14}C$ ratio of the doubly labeled pyrone (**3**) was retained in aloenin biosynthesized by uptake of the labeled pyrone, as shown in Table 9. This indicates the occurrence of *O*-glucosylation at the C-2′ hydroxyl group of the pyrone **3**. Thus, the biosynthesis of aloenin (**2**) was demonstrated to proceed in pathway (a) as shown in Scheme 1, that is, the first formation of aglycone **3** by cyclization of biological polyketide 5

produced by the acetate-malonate pathway and then by creation of the C-4 methoxyl group by *O*-methylation with methionine is followed by introduction of a glucose molecule into the C-2′ hydroxyl group of the aglycone (**3**).

Experimental

The radioactive products were purified to constant specific radioactivity by a combination of preparative TLC (silica gel; 0.75 mm in thickness) and repeated recrystallization. All the products had PMR, IR, and MS spectra consistent with the structure, and the melting points and spectral data agreed with the corresponding authentic samples.[8,11] Radioactivities were measured on a liquid scintillation spectrometer using Bray's scintillation solvent.[21] The counting error was within ±2%.

Incorporation of the Labeled Compounds into Aloenin by the Aloe Plants. A phosphate buffered solution (pH 7.38) of each of the ^{14}C- and ^{3}H-labeled compounds was fed to the potted whole plants (*ca.* 30 cm in length) through the stem perforated with a cotton thread for sucking up the solution.[16] After 3—7 days, the leaves (*ca.* 200 g) were minced mechanically and extracted with MeOH by means of a Soxhlet apparatus. Removal of the solvent gave a brown viscous mass, which was chromatographed on a silica gel column with $CHCl_3$-MeOH (3:1) to give aloenin (**2**) (*ca.* 220 mg): Mp 145—147 °C (lit,[8,11] mp 145—147 °C); IR (Nujol) 3350 (OH), 1710 (C=O), and 1640 cm^{-1} (C=C); PMR (acetone-d_6) δ 2.19 (s, 3H, Ar-Me) and 3.86 (s, 3H, OMe). The radioactivities are shown in Table 1.

*Degradation of **2** with Hydrochloric Acid.* Aloenin (**2**) (100 mg), obtained by incorporating the tracer compounds, was refluxed[8,11] with 5% HCl (10 ml) for 2 h using the $Ba(OH)_2$ trap attached to the reflux apparatus. Carbon dioxide liberated was converted to $BaCO_3$ by absorbing it in the $Ba(OH)_2$ solution. The reaction mixture was then extracted with ether to give 2,5-dimethyl-7-hydroxychromone (**6**) (45 mg): Mp 245 °C (dec) (lit,[17] mp 245 °C (dec)); IR (Nujol) 1665 (C=O) and 1618 cm^{-1} (C=C). The aqueous layer was passed through an Amberlite resin IR-45 (OH) column until all chloride ions had been removed to give D-glucose (18 mg): Mp 144—145 °C. Methylation of **6** (30 mg) with CH_2N_2 gave 2,5-dimethyl-7-methoxychromone (**7**) (29 mg): Mp 116—117 °C (lit,[17] mp 116—117 °C); IR (Nujol) 3050, 1650, 1630, and 1570 cm^{-1}; PMR ($CDCl_3$) δ 2.25 (s, 3H, C(2)-Me), 2.77 (s, 3H, Ar-Me), and 3.81 (s, 3H, OMe).

*Degradation of **7** with Sodium Hydroxide.* To a solution of **7** (45 mg) in MeOH (4 ml), 30% KOH solution (10 ml) was added, and the mixture was refluxed under an atmosphere of N_2.[17] The reaction mixture, after acidification, was extracted with ether to give 2-hydroxy-4-methoxy-6-methylacetophenone (**8**) (15 mg): Mp 78.0—78.5 °C (lit,[17,22] mp 78.0—78.5 °C); IR (KBr) 1612, 1590, 1500, 859, and 821 cm^{-1}; PMR ($CDCl_3$) δ 2.53 (s, 3H, Ar-Me), 2.58 (s, 3H, COMe), 3.77 (s, 3H, OMe), 6.25 (s, 2H, arom. H), and 13.48 (s, 1H, OH). Methylation of **8** (10 mg) by Hakomori's method[23] gave 2,4-dimethoxy-6-methylacetophenone (**9**) (7 mg): Mp 41—42 °C (lit,[22] mp 41—42 °C); IR ($CDCl_3$) 1682 and 1600 cm^{-1}; PMR ($CDCl_3$) δ 2.23 (s, 3H, Ar-Me), 2.44 (s, 3H, COMe), 3.76 (s, 6H, 2×OMe), and 6.28 (s, 2H, arom. H).

*Degradation of **9** with Hydrochloric Acid.* A solution of **9** (140 mg) in 5% HCl (25 ml) was refluxed for 10 h, and the reaction mixture was extracted with ether to give an oily product (103 mg), which was separated on preparative TLC with hexane-EtOAc (3:1) to afford 3,5-dimethoxytoluene (**10**) (95 mg): Bp 130—132 °C (7.0 mmHg); n_D^{25} 1.5239; IR (liq.) 1600, 1298, and 1207 cm^{-1}; PMR ($CDCl_3$) δ 2.32 (s, 3H, Ar-Me), 3.73 (s, 6H, 2×OMe), and 6.30 (s, 3H, arom. H).

*Nitration of **10**.* To a solution of **10** (250 mg) in concd H_2SO_4 (3 ml), a mixture of concd HNO_3 (3 ml) and concd H_2SO_4 (3 ml) was added under ice-cooling. After heating for 3 min at 60 °C, the reaction mixture was poured into H_2O (60 ml) and then allowed to stand overnight to give yellow powders (119 mg). Recrystallization of the powders afforded pale yellow crystals of the trinitro derivative (**11**): Mp 70—71 °C; *m/e* 287 (M^+); IR (KBr) 1625, 1570, 1500, 1380, and 882 cm^{-1}; PMR ($CDCl_3$) δ 2.38 (s, 3H, Ar-Me) and 4.12 (s, 6H, 2×OMe).

*Bromopicrin Cleavage of **11**.* According to the procedure of bromopicrin cleavage,[18,19] a paste of $Ca(OH)_2$ (7.0 g in 30 ml of H_2O) was added at 0 °C to a solution of **11** (20 mg) in a saturated solution of $Ca(OH)_2$ (1.0 ml), and Br_2 (2.5 ml) was then dropped into the mixture under stirring. After the mixture had been kept at 10 °C for 2 h until disappearance of the yellow color, it was steam-distilled to give bromopicrin (6 mg): IR (liq.) 1560 and 1351 cm^{-1} (NO_2).

Preparation of 4-Methoxy-6-(2,4-dihydroxy-6-methylphenyl)-2-pyrone-methoxy-^{3}H;*2,4,6,2′,4′,6′*-^{14}C (***3***). The singly labeled tracers, aloenin-2,4,6,2′,4′,6′-^{14}C and *-methoxyl-*^{3}H, were synthesized biologically by administration of acetate-1-^{14}C and L-methionine-*methyl*-^{3}H, respectively, into the Aloe plant in the same manner as described above (Table 1). A mixture of the ^{14}C-labeled aloenin (40 mg) and the ^{3}H-labeled aloenin (40 mg) was refluxed[8,11] with 3% HCl-MeOH (10 ml) for 2 h. The reaction mixture was diluted with H_2O (30 ml) and extracted with ether using a continuous extractor to give a crude product (32 mg), which was purified to constant specific radioactivity by preparative TLC with MeOH-$CHCl_3$ (1:4) followed by recrystallization to afford pure doubly-labeled pyrone **3**: Mp 213—214 °C; IR (KBr) 3350, 1670, 1628, and 1600 cm^{-1}; PMR (acetone-d_6) δ 2.19 (s, 3H, Ar-Me), 3.92 (s, 3H, OMe), 5.94 (d, J=2.2 Hz, 1H), 6.07 (d, J=2.2 Hz, 1H), and 6.33 (s, 2H, arom. 2H). The radioactivities are shown in Table 8.

Preparation of Potassium Salt of 5-(2-β-D-Glucopyranosyloxy-4-hydroxy-6-methylphenyl)-3,5-dioxopentanoic acid-3″-^{3}H;*1,3,5,2′,4′,6′*-C^{14} (***4***). The singly labeled tracers, aloenin-2,4,6,2′,4′,6′-^{14}C and -3″-^{3}H, were prepared biologically from acetate-1-^{14}C and D-glucose-3-^{3}H, respectively (Table 1). According to the reported procedure,[8,11] a mixture of the ^{14}C-labeled aloenin (36 mg) and the ^{3}H-labeled aloenin (70 mg) dissolved in 5% KOH-MeOH (10 ml) was stirred at room temperature under an atmosphere of N_2. After 3 days, the reaction mixture was subjected to preparative TLC with 1-BuOH-MeOH-H_2O (7:3:3) to give potassium salt (37 mg) of doubly labeled **4**: IR (Nujol) 3400 (OH) and 1610 cm^{-1} (COO^-); PMR (D_2O) δ 2.30 (s, 3H, Ar-Me) and 6.63 (s, 2H, arom. 2H). The radioactivities are shown in Table 8.

This investigation was partially supported by a Grant-in-Aid (074176 and 047089) for Scientific Research in 1975 from the Ministry of Education.

References

1) T. Suga, T. Hirata, F. Koyama, and E. Murakami, *Chem. Lett.*, **1974**, 873.

2) T. Hirata, O. Koshitani, and T. Suga, *Chem. Lett.*, **1977**, 479.

3) T. J. McCarthy, *Planta Med.*, **16**, 348 (1968).
4) M. Soeda, *J. Med. Soc. Toho, Jpn.*, **16**, 365 (1969) and references cited therein.
5) I. Yamamoto, *J. Med. Soc. Toho, Jpn.*, **17**, 361 (1970).
6) T. Suga, T. Hirata, and M. Odan, *Chem. Lett.*, **1972**, 547.
7) K. Makino, A. Yagi, and I. Nishioka, *Chem. Pharm. Bull.*, **21**, 149 (1973).
8) T. Suga, T. Hirata, and K. Tori, *Chem. Lett.*, **1974**, 715.
9) T. Hirata, Y. Kushi, T. Suga, and A. Christensen, *Chem. Lett.*, **1976**, 393.
10) K. Tori, T. Hirata, O. Koshitani, and T. Suga, *Tetrahedron Lett.*, **1976**, 1311.
11) T. Hirata and T. Suga, *Bull. Chem. Soc. Jpn.*, **51**, 842 (1978).
12) T. Hirata and T. Suga, *Z. Naturforsch.*, **32C**, 731 (1977).
13) A. J. Birch and F. W. Donovan, *Aust. J. Chem.*, **6**, 360 (1953).
14) A. J. Birch, *Proc. Chem. Soc.*, **1962**, 3.
15) A. J. Birch, *Science*, **156**, 202 (1967).
16) D. J. Austin and H. B. Meyers, *Phytochemistry*, **4**, 245 (1965).
17) T. Hirata and T. Suga, *Bull. Chem. Soc. Jpn.*, **47**, 244 (1974).
18) J. M. Essery, P. F. Juby, L. Marion, and E. Trumbull, *Can. J. Chem.*, **41**, 1142 (1963).
19) M. Yamasaki, T. Usui, and S. Shibata, *Chem. Pharm. Bull.*, **11**, 363 (1963).
20) P. Karlson, "Introduction to Modern Biochemistry," 2nd ed, Academic Press, New York (1965), p. 159.
21) G. A. Bray, *Analyt. Biochem.*, **1**, 279 (1960).
22) T. Suga, T. Hirata, and F. Walls, *J. Sci. Hiroshima Univ., Ser. A.*, **38**, 327 (1974).
23) S. Hakomori, *J. Biochem.*, **55**, 205 (1964).

Studies of Unusual Amino Acids and Their Peptides. IX. The Synthetic Study of Bottromycins B_1 and B_2[1)]

Takashi YAMADA, Katsumi TAKASHIMA, Toshifumi MIYAZAWA, Shigeru KUWATA, and Hiroshi WATANABE

Laboratory of Chemistry, Faculty of Science, Kōnan University, Okamoto, Higashinada-ku, Kobe 658

(Received September 16, 1977)

Bottromycins B_1 and B_2, peptide antibiotics, were synthesized according to the structures proposed by Nakamura *et al.* B_1 was obtained by the condensation of the imidate, Piv–Tle–Val–ImPro–OEt·HCl with the ester, H–Gly–Phe(βMe)–β-Tha–OH in the presence of Et_3N, and B_2 by the replacement of the Z group of Z–Tle–Val–ImPro–Gly–Phe(βMe)–β-Tha–OMe by the *trans*-4-methyl-2-pentenoyl group. The structures of the synthetic B_1 and B_2 were confirmed by elemental analyses, amino acid analyses, and CI-mass spectra. However, the synthetic bottromycins differed from the natural ones in many respects, *e.g.*, IR spectra, behavior in TLC, and pK_a values. Most significantly, no antimicrobial activities were detected in the synthetic B_1. On the basis of these results, it is concluded that the structures proposed by Nakamura *et al.* for bottromycins are erroneous and should be revised.

Bottromycin is a peptide antibiotic which was first isolated from the culture broth of *Streptomyces bottropensis* by Waisvisz *et al.*[2)] They determined the *C*-terminal dipeptide to be β-methylphenylalanyl-β-(2-thiazolyl)-β-alanine methyl ester, though they gave no information about the configurations of the two amino acids. Later, Nakamura *et al.*,[3)] who studied this antibiotic in detail, were able to separate it into 5 species and gave these components the structures shown in Fig. 1. Wolf and his co-workers[4)] also isolated bottromycin and separated it into 5 species, 3 species of which, however, could not be identified. The configurations of the two unusual amino acids, β-methylphenylalanine and β-(2-thiazolyl)-β-alanine, were determined to be *erythro*-L by Arold *et al.*[5)] and L by our group,[6)] respectively.

Compared with other peptide antibiotics, the structure proposed for bottromycin is very unique, because it consists of a linear acyl peptide ester containing an iminopeptide bond[7a)] in the middle of the molecule, and contains many unusual amino acids, but no D-amino acid. These structural features had strongly aroused our interest in the relationship between the structures and the biological activities, and prompted us to synthesize bottromycin.

A preliminary trial[8)] to build up bottromycin by coupling the three known dipeptide fragments, *i.e.*, pivaloyl-*t*-leucylvaline,[9)] (iminoproly)glycine,[8)] and β-methylphenylalanyl-β-(2-thiazolyl)-β-alanine methyl ester,[10)] failed due to the easy cyclization of the (iminoprolyl)glycine fragment into an imidazolone when the carboxyl group was activated. The imidazolone formation could successfully be avoided by locating a carboxyl (or alkoxycarbonyl) group sufficiently apart from the imino group in the molecule, as seen in the syntheses of model iminopeptides.[11)] On the basis of these previous results, we adopted the synthetic routes through the condensation of the tripeptide imidate with the tripeptide ester to form an iminopeptide bond, as is shown in Schemes 1 and 2.

For the preparation of the *N*-terminal fragment of B_1, Z–Tle–OH[7b)] (**1**) was coupled with H–Val–Pro–NH_2

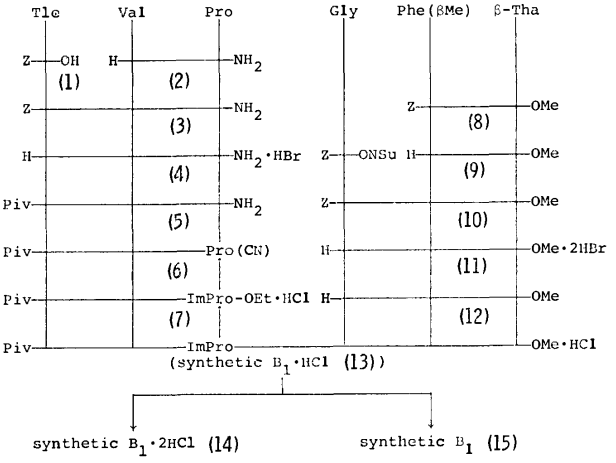

Scheme 1. Synthesis of bottromycin B_1.

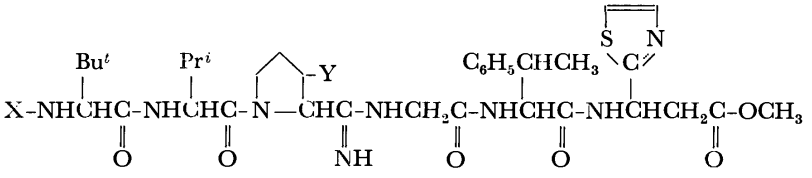

	Bottromycins				
	A_1	A_2	B_1	B_2	C_2
X	Piv	MPE	Piv	MPE	MPE
Y	CH_3	CH_3	H	H	a)

a) Dimethyl- or ethyl-proline in the proline moiety.

Fig. 1. The structure of bottromycin group proposed by Nakamura *et al.*[3)]

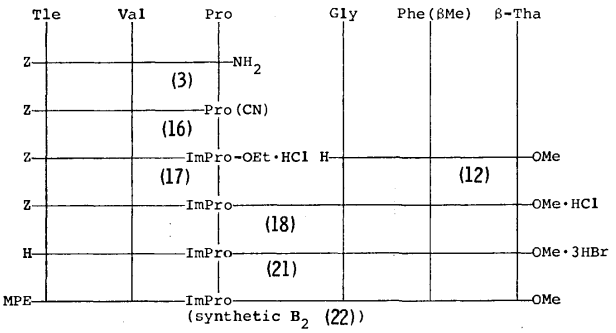

Scheme 2. Synthesis of bottromycin B_2.

(**2**) by the mixed anhydride method, and the protected tripeptide amide (**3**) was obtained in 88% yield. The Z group of the amide (**3**) was replaced by the pivaloyl group through the debenzyloxycarbonylation of **3** with hydrogen bromide in acetic acid and the successive acylation with pivaloyl chloride in the presence of *N*,*N*-diisopropylethylamine, to give *N*-pivaloyl tripeptide amide (**5**). The amide (**5**) was dehydrated to the nitrile (**6**) with phosphoryl chloride in pyridine in 87% yield, and then converted into the imidate hydrochloride (**7**) by the method of Pinner[8,11,12] in 98% yield.

The *C*-terminal fragment was prepared by the coupling of Z–Gly–ONSu with H–Phe(*β*Me)–*β*-Tha–OMe (**9**), followed by the debenzyloxycarbonylation of the resulting protected tripeptide (**10**) with hydrogen bromide in acetic acid. The tripeptide ester (**11**) was obtained as the dihydrobromide in 79% yield, based on the protected dipeptide ester[10] (**8**).

The tripeptide imidate hydrochloride (**7**) was condensed with the tripeptide ester (**12**) derived from the dihydrobromide (**11**) in methanol in the presence of triethylamine and afforded bottromycin B_1 as the monohydrochloride (**13**) in 50% yield. The free B_1 (**15**) was obtained by the treatment of the hydrochloride (**13**) with an ion exchange resin, while the treatment of the compound (**13**) with 4.7% hydrogen chloride in methanol gave the B_1 dihydrochloride (**14**).

Bottromycin B_2 was synthesized as follows: The protected tripeptide amide (**3**) was dehydrated with phosphoryl chloride in pyridine in 97% yield, and the resulting nitrile (**16**) was converted into the tripeptide imidate hydrochloride (**17**) by the method of Pinner. From the hydrochloride (**17**) and the tripeptide ester (**12**), the *N*-Z-iminohexapeptide ester (**18**) was obtained in 37% yield in the same manner as was used for the preparation of the B_1 hydrochloride (**13**). The compound (**18**) was debenzyloxycarbonylated with hydrogen bromide in acetic acid, acylated with *trans*-4-methyl-2-pentenoyl chloride (MPE-Cl) in pyridine, and treated with Amberlyst A-29; thus the desired bottromycin B_2 was obtained in 43% yield. Although no information about the geometry of the MPE group in bottromycins A_2 and B_2 had been given, we used the *trans*-MPE-Cl for the preparation of B_2 after assuming that the MPE group of the natural compounds would be in the more stable *trans* form.

Near the end of this synthetic work, we received some information[1b] about a revised study of bottromycin A_2, which was published later.[1c] The revised structure was quite different from the old one.[3] Though nothing was mentioned about bottromycins A_1 and B_1, these structures also became doubtful. Therefore, we carefully investigated the properties of the compounds synthesized here according to the structures proposed by Nakamura *et al.*, by comparing with the structure of the natural A_2.[13]

The coincidence of the structures of the synthetic bottromycins B_1 and B_2 with the proposed structures was confirmed by elemental analyses, amino acid analyses (Table 1), and the chemical ionization (CI) mass spectra (Fig. 2).

However, these synthetic bottromycins differed from the natural ones[13] in many respects: the IR spectra of the natural B_1 and the synthetic B_1 did not coincide with each other, though those of the synthetic B_1 and B_2 very much resemble each other and those of the natural B_1 and A_2 also resemble each other. It should be pointed out that the synthetic B_2 had an absorption band assigned to C–H bending deformation of *trans* disubstituted C=C at 980 cm^{-1}, while the natural A_2 had not absorption band in the same region. (Fig. 3) The R_f values (TLC, MeOH:AcOEt = 1:3) of the synthetic B_1 and B_2 were 0.37 and 0.33, respectively, while that of the natural A_2 containing some B_2[13] was

Table 1. Analytical data of synthetic bottromycins

Bottromycin	$[\alpha]_D$ (MeOH)	Molecular formula	Found (Calcd) (%) C	H	N
Synthetic B_1 (**15**)	−54.1°[a]	$C_{40}H_{60}N_8O_7S \cdot H_2O$	58.80 (58.95)	7.61 (7.67)	12.87 (13.75)
Synthetic $B_1 \cdot HCl$ (**13**)	−34.6°[b]	$C_{40}H_{60}N_8O_7S \cdot HCl \cdot 2H_2O$	55.41 (55.25)	7.41 (7.53)	12.18 (12.89)
Synthetic $B_1 \cdot 2HCl$ (**14**)	−34.2°[c]	$C_{40}H_{60}N_8O_7S \cdot 2HCl \cdot H_2O$	54.32 (54.11)	7.34 (7.26)	11.96 (12.62)
Synthetic B_2 (**22**)	−55.5°[d]	$C_{41}H_{60}N_8O_7S \cdot 2H_2O$	58.68 (58.27)	7.45 (7.63)	12.38 (13.25)

Amino acid analyses: *6 M HCl, 110 °C, 5 days in sealed tube.*
Synthetic B_1 (**15**): Tle 1.06, Val 1.09, Pro 0.98, Gly 1, Phe(*β*Me) 1.04, *β*-Tha 0.77[e]
Synthetic B_2 (**22**): Tle 1.01, Val 1.11, Pro 1.06, Gly 1, Phe(*β*Me) 1.02, *β*-Tha 0.74[e]

a) *c* 1 at 25 °C. b) *c* 1 at 20 °C. c) *c* 0.5 at 20 °C. d) *c* 0.988 at 25 °C. e) Amino acid produced from *β*-Tha in hydrolysis: Asp 0.05 (for B_1), 0.06 (for B_2).

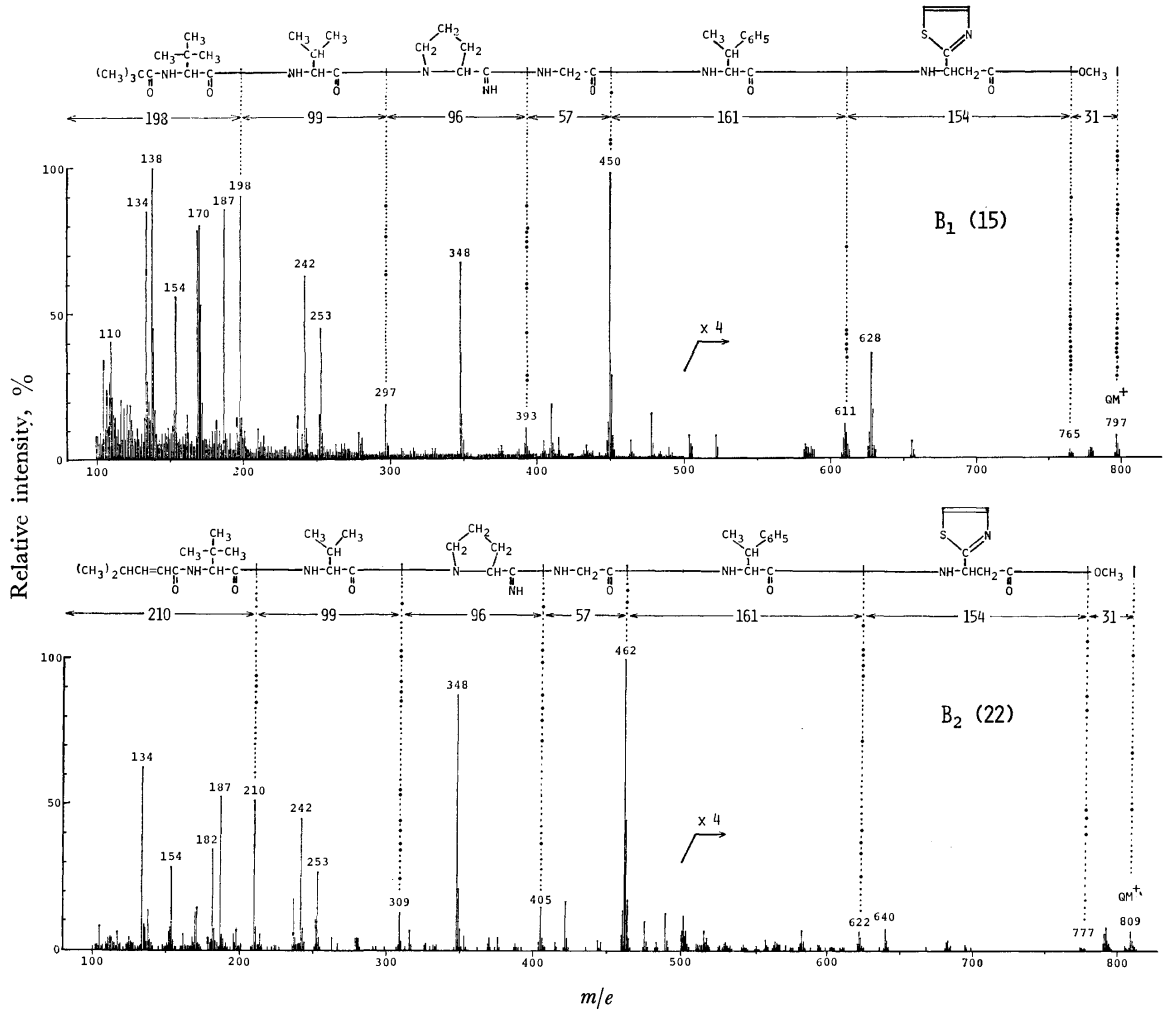

Fig. 2. CI(CH_4)-mass spectra of synthetic bottromycins B_1 (**15**) and B_2 (**22**).

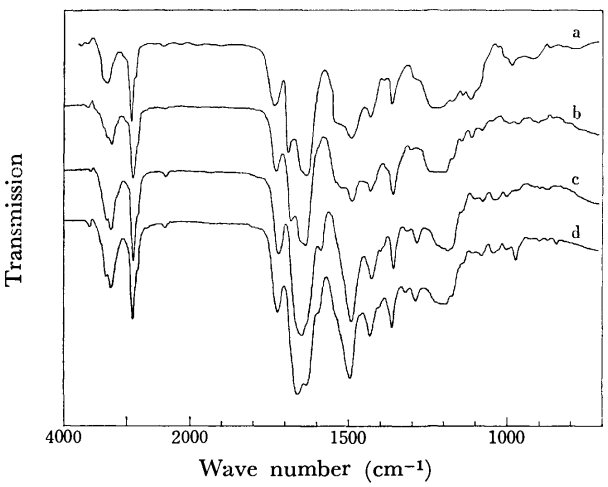

Fig. 3. IR spectra of natural and synthetic bottromycins in $CHCl_3$. a: Natural B_1 (This spectrum is reproduced from Fig. 3 in Ref. 19), b: natural A_2,[13] c: synthetic B_1 (**15**), d: synthetic B_2 (**22**).

0.78,[14] a quite different value. Further, the behavior of the synthetic B_2 and the natural A_2 against $KMnO_4$ solution was striking: when a dilute $KMnO_4$ solution was sprayed on the thin-layer chromatogram, the synthetic B_2 immediately decolorized $KMnO_4$, but, unexpectedly, the natural A_2 remained unchanged, though it has been proposed that it contains an ethylene linkage. Furthermore, the pK_a values were also different: the pK_a value (in MeOH:H_2O = 3:2) of the synthetic B_1 was 9.1, similar to those of its related iminopeptides,[11] while that of the natural A_2 was 8.3 (lit,[3c] 8.1—8.3). The most conclusive results were obtained from the comparison of the antimicrobial activities: no activities were detected in the synthetic B_1 so far examined; this can be seen in Table 2.

From all of the above results, we conclude that the structures of bottromycins proposed by Nakamura *et al.*, not only for A_2 and B_2, but also for B_1 and probably A_1, are erroneous and should be revised.

Experimental

All the melting points are uncorrected. The optical rotations were measured by means of a Yanagimoto polarimeter, OR-10, or a Perkin-Elmer 141 polarimeter. The NMR spectra were recorded on a JEOL PS-100 spectrometer or a Hitachi R-24A spectrometer. The IR spectra were recorded on a Hitachi EPI-S2 spectrophotometer. The pK_a values were measured by means of a Hitachi-Horiba pH meter, F-7. GLC analyses were carried out on a Hitachi 063 Gas

Table 2. Antimicrobial activities of synthetic bottromycin B_1 and natural A_2

Microorganism	MIC (μg/ml) Synthetic B_1	Natural A_2
Staphylococcus aureus 209-p	>50	0.1
Terashima	>50	0.19
Smith	>50	0.19
252 R	>50	0.19
199 R	>50	0.19
664 R	>50	0.19
Staphylococcus epidermidis 10131 R	>50	≦0.005
Kawamura	>50	0.1
Streptococcus faecalis	>50	0.19
Urayama R	>50	0.19
Sarcina lutea PCI-1001	>50	0.1
Bacillus subtilis PCI-219	>50	≦0.05
Escherichia coli NIHJ	>50	50
K-12	>50	12.5
6065 R	>100	25
Salmonella typhi T-58	>100	>100
Salmonella enteritidis	>100	25
Shigella flexneri 2a	>100	25
Shigella sonnei	>100	25
Citrobacter freundii TU-786	>100	50
Enterobacter cloacae TL-14	>100	>100
Serratia marcescens OU-29	>100	>100
Klebsiella pneumoniae PCL-602	> 50	50
Proteus mirabilis 1698	> 50	>50
Proteus vulgaris IID-874	>100	>100
Pseudomonas aeruginosa PI-67	> 50	>50
No. 12	>100	50
No. 45	>100	>100
150	>100	50

Agar dilution method: Inoculumn size: 10^6 cells/ml. Medium: Heat infusion agar (pH 7.2). Cultivation: 18 h, 37 °C.

Chromatograph. TLC was done on Merck's Kieselgel GF_{254} (Type 60) or precoated Kieselgel 60 F_{254}. For column chromatography, Merck's Kieselgel 60 (0.063—0.200 mm) was employed.

L-t-*Leucine (Tle)*.[20] This compound was prepared from DL-*t*-leucine according to the method of Weygand,[9] and was proved to be optically pure by GLC of Piv-Tle-Val-OMe[15] derived from it without any purification; mp 250.5—251 °C (sublim.), $[\alpha]_D^{21}$ −10.8° (*c* 1, H_2O). Lit, $[\alpha]_D^{21}$ −9.4° (*c* 1, H_2O);[16] $[\alpha]_{546}^{20}$ −10.9° (*c* 2, H_2O);[9] $[\alpha]_D$ −8.3° (*c* 0.53, H_2O).[17]

Z-Tle-OH (1). Into a cold solution of *t*-leucine (2.5 g, 19.1 mmol) in 1M NaOH (19.1 ml), Z-Cl (3.9 g, 22.9 mmol) and 1M NaOH (22.9 ml) were simultaneously added with vigorous stirring at 0—2 °C, and the mixture was stirred at about 0 °C for 1 h and then at room temperature for 1 h. After the usual treatment,[9] the desired compound was obtained as an oil: Yield, 4.9 g (97%); $[\alpha]_D^{20}$ −5.9° (*c* 1, MeOH); $[\alpha]_D^{20}$ +4.0° (*c* 1, DMF). Lit,[17] $[\alpha]_D$ +3.8° (*c* 0.39, DMF) *Dicyclohexylammonium Salt*: Mp 165.5—166.5 °C, $[\alpha]_D^{20}$ −8.3° (*c* 1, MeOH). Lit,[17] mp 165—168 °C, $[\alpha]_D$ −8.4° (*c* 0.59, MeOH).

Z-Tle-Val-Pro-NH_2 (3). Into a cold solution of Z-Tle-OH (**1**) (1.857 g, 7 mmol) and *N*-methylmorpholine (708 mg, 7 mmol) in THF (15 ml), isobutyl chloroformate (956 mg, 7 mmol) was added, drop by drop, with vigorous stirring below −10 °C, and the mixture was stirred at the same temperature for 15 min. To the mixture was added H-Val-Pro-NH_2·HBr[9] (**2**·HBr) (2.059 g, 7 mmol) and *N*-methylmorpholine (708 mg, 7 mmol) in DMF (15 ml) at about −10 °C. The mixture was stirred at about −10 °C for 20 min, at −5 °C for 1 h, at 0 °C for 1 h, and at room temperature overnight. After the removal of the precipitate, the yellow filtrate was evaporated under reduced pressure and the residual DMF solution was diluted with water (200 ml), extracted with AcOEt, washed with water, 1M $NaHCO_3$, and water again, and dried over $MgSO_4$. The solution was concentrated to give a colorless foamy solid: Yield, 2.845 g (88.2%). This product was used for the next reaction without further purification. The analytical sample was obtained by chromatography on a silica gel column with AcOEt–MeOH (15 : 1); $[\alpha]_D^{20}$ −88.7° (*c* 1, MeOH). Found: C, 61.97; H, 8.07; N, 12.18%. Calcd for $C_{24}H_{36}N_4O_5$: C, 62.59; H, 7.88; N, 12.16%.

H-Tle-Val-Pro-NH_2·HBr (4). This compound was prepared by the removal of the Z group from **3** (2.073 g, 4.5 mmol) with 25% HBr in AcOH (4.5 g) as usual. The crude product was recrystallized from MeOH–ether to colorless crystals: Yield, 1.570 g (85.6%); mp 193—196 °C. Found: C, 45.22; H, 8.19; N, 13.19%. Calcd for $C_{16}H_{30}N_4O_3$·HBr·H_2O: C, 45.18; H, 7.82; N, 13.17%.

Piv-Tle-Val-Pro-NH_2 (5). Into a cold solution of **4** (522 mg, 1.28 mmol) and *N,N*-diisopropylethylamine (381 mg, 2.95 mmol) in CH_2Cl_2 (4 ml), pivaloyl chloride (201 mg, 1.67 mmol) in CH_2Cl_2 (2 ml) was stirred, drop by drop, at 2—3 °C, and stirring was continued at room temperature for 1 h. To the resulting clear solution, 1-(2-aminoethyl)piperazine (99 mg, 0.77 mmol) in CH_2Cl_2 (1 ml) was added. After the mixture was stirred at room temperature for 10 min, the precipitate was filtered off. The filtrate was evaporated under reduced pressure and the residue was treated with AcOEt to remove any insoluble materials. The AcOEt solution was washed with water, 0.5 M citric acid, 1M $NaHCO_3$, and water again, and dried over $MgSO_4$. After the removal of the solvent, a foamy solid was obtained: Yield, 368 mg (69.9%). The analytical sample was obtained by chromatography on a silica gel column with AcOEt–MeOH (1 : 9); $[\alpha]_D^{20}$ −109.8° (*c* 1, MeOH). Found: C, 61.15; H, 9.45; N, 13.02%. Calcd for $C_{21}H_{38}N_4O_4$: C, 61.43; H, 9.33; N, 13.65%.

N-*(Piv-Tle-Val)-2-cyanopyrrolidine (6)*. To a stirred solution of **5** (493 mg, 1.2 mmol) in dry pyridine (2.5 ml), $POCl_3$ (0.14 ml, 1.44 mmol) in CH_2Cl_2 (0.4 ml) was added, drop by drop, below −10 °C. The solution was stirred at the same temperature for 1 h, treated with ice (10 g), and then extracted with AcOEt. The organic layer was washed with 1M HCl, 1M $NaHCO_3$, and water, and dried over $MgSO_4$: Yield, 408 mg (86.6%); a foamy solid, $[\alpha]_D^{20}$ −118.2° (*c* 1, MeOH). Found: C, 63.80; H, 9.29; N, 13.94%. Calcd for $C_{21}H_{36}N_4O_3$: C, 64.25; H, 9.24; N, 14.27%.

Piv-Tle-Val-ImPro-OEt·HCl (7). To a cold solution of **6** (385 mg, 0.98 mmol) and absolute EtOH (60 mg, 1.3 mmol) in dry ether (10 ml), dry HCl was passed with stirring at about −15 °C until saturation, and then at 0 °C for 30 min and at room temperature for 30 min. The reaction mixture was evaporated under reduced pressure to afford a colorless foamy solid: Yield, 457 mg (98.2%). This imidate hydrochloride was immediately used for the next reaction without any purification.

Z-Gly-Phe(βMe)-β-Tha-OMe (10). Into a solution

of the crude product of H–Phe(βMe)–β-Tha–OMe·2HBr (**9**·2HBr) (prepared by the removal of the Z group from Z–Phe(βMe)–β-Tha–OMe[10] (**8**) (960 mg, 1.99 mmol) with 25% HBr in AcOH as usual) and Et_3N (450 mg, 4.46 mmol) in CH_2Cl_2 (40 ml), Z-Gly-ONSu (660 mg, 2.15 mmol) was added with stirring and the mixture was allowed to stand at room temperature overnight. After the removal of the solvent, the residue was dissolved in AcOEt, washed with water, 1M HCl, water, 1M $NaHCO_3$, and water again, and dried over Na_2SO_4. The solution was evaporated under reduced pressure to leave a solid, which was recrystallized from MeOH: Yield, 852 mg (79.3%); mp 159.5—160 °C, $[\alpha]_D^{20}$ +18.4° (*c* 1, MeOH). Found: C, 60.32; H, 5.59; N, 10.25%. Calcd for $C_{27}H_{30}N_4O_6S$: C, 60.21; H, 5.61; N, 10.40%.

*H–Gly–Phe(βMe)–β-Tha–OMe·2HBr (**11**).* This compound was prepared by the treatment of **10** (539 mg, 1 mmol) with 25% HBr in AcOH (1.5 g) as usual. The crude product was purified by the reprecipitation from MeOH–ether: Yield, 581 mg (99.5%); mp 149—152 °C. Found: C, 38.96; H, 4.86; N, 9.42%. Calcd for $C_{19}H_{24}N_4O_4S\cdot 2HBr\cdot H_2O$: C, 39.06; H, 4.83; N, 9.59%.

The free ester, H–Gly–Phe(βMe)–β-Tha–OMe (**12**), was prepared by the treatment of **11** with Et_3N (in double the mole concentration of **11**) in THF, followed by the filtration of a precipitate and the removal of the solvent. The residual oil, the tripeptide ester (**12**), was used for the next reaction without any purification.

Piv–Tle–Val–ImPro–Gly–Phe(βMe)–β-Tha–OMe (Synthetic Bottromycin B_1). *a) HCl Salt (**13**):* A solution of the imidate hydrochloride (**7**) (457 mg, 0.96 mmol), the tripeptide ester (**12**) prepared from **11** (453 mg, 0.8 mmol), and Et_3N (97 mg, 0.96 mmol) in dry MeOH (5 ml) was stirred at room temperature for 3 days. The solution was then evaporated under reduced pressure, leaving a foamy solid. The solid was taken up in AcOEt and freed from any insoluble materials by filtration. The filtrate was evaporated under reduced pressure, and the residue was chromatographed on preparative layers of silica gel with $CHCl_3$–MeOH–AcOH (95 : 15 : 3) to give a foamy solid: Yield, 344 mg (49.5%).

*b) 2HCl Salt (**14**).* The hydrochloride (**13**) (100 mg) was treated with 4.7% HCl in MeOH (10 ml), and evaporated under reduced pressure, leaving a colorless solid: Yield, 98 mg; mp 156—160 °C (dec). pK_a (amidine group): 9.1 (MeOH–H_2O (3 : 2), 20 °C).

*c) Free Compound (**15**):* This compound was obtained by passing the HCl salt (**13**) (120 mg) through a Dowex 1×8 column (25% MeOH) or an Amberlyst A-29 column (90% MeOH): Yield, 112 mg, a foamy solid.

Analytical results of the compounds (**13**, **14**, and **15**) are summarized in Table 1.

*N-(Z–Tle–Val)-2-cyanopyrrolidine (**16**).* This compound was prepared by the dehydration of the tripeptide amide (**3**) (553 mg, 1.2 mmol) with $POCl_3$ (0.14 ml, 1.44 mmol) in a mixture of dry pyridine (2.5 ml) and CH_2Cl_2 (0.4 ml) at about −10 °C, as has been described above for the preparation of **6**: Yield, 455 mg (85.7%); a foamy solid, $[\alpha]_D^{20}$ −98.3° (*c* 1, MeOH). Found: C, 64.78; H, 7.97; N, 12.73%. Calcd for $C_{24}H_{34}N_4O_4$: C, 65.14; H, 7.74; N, 12.66%.

*Z–Tle–Val–ImPro–OEt·HCl (**17**).* This compound was prepared by passing dry HCl into a mixture of **16** (398 mg, 0.9 mmol) and absolute EtOH (55 mg, 1.2 mmol) in dry ether, as has been described above for the preparation of **7**: Yield, 457 mg (96.7%); a foamy solid. This product was immediately used for the next reaction.

*Z–Tle–Val–ImPro–Gly–Phe(βMe)–β-Tha–OMe·HCl (**18**).* A solution of the imidate hydrochloride (**17**) (457 mg, 0.87 mmol), the tripeptide ester (**12**) prepared from **11** (396 mg, 0.7 mmol), and Et_3N (88 mg, 0.87 mmol) in dry MeOH (5 ml) was stirred at room temperature for 3 days. After being treated as described above for **13**, the resulting foamy solid was chromatographed on preparative layers of silica gel with $CHCl_3$–MeOH–AcOH (95 : 15 : 3) to give a foamy solid: Yield, 229 mg (36.7%); $[\alpha]_D^{20}$ −21.2° (*c* 0.5, MeOH). Found: C, 58.10; H, 6.85; N, 12.19%. Calcd for $C_{43}H_{58}N_8O_8S\cdot HCl\cdot 1/2H_2O$: C, 57.87; H, 6.78; N, 12.55%.

trans-*4-Methyl-2-pentenoic Acid (**19**).* This compound was prepared from malonic acid and isobutyraldehyde in pyridine containing a small amount of piperidine.[18] This acid obtained here was proved to be the *trans* isomer by the NMR and IR spectra, as shown below: Yield, 65.1%; bp 107—109 °C/14 Torr, n_D^{19} 1.4469 (lit,[18] bp 115—116 °C/20 Torr, $n_D^{20.6}$ 1.4489); IR(neat): 985 cm^{-1} (σ C–H of *trans*-disubstituted olefin); NMR($CDCl_3$): δ=1.09 (6H, d, *J*=7 Hz, $(C\underline{H}_3)_2CH$–), 2.52 (1H, o, *J*=7 Hz, $(CH_3)_2C\underline{H}CH$=), 5.82 (1H, dd, *J*=16 and *ca.* 1 Hz, –CH=C<u>H</u>–COOH), 7.11 (1H, dd, *J*=16 and 6.5 Hz, >CH–C<u>H</u>=CH–), 12.26 (1H, s, –COO<u>H</u>).

trans-*4-Methyl-2-pentenoyl Chloride (**20**).* This compound was prepared from **19** and $SOCl_2$ as usual:[18] Yield, 73%; bp 65—66 °C/25 Torr (lit,[18] bp 58—59 °C/18 Torr); NMR($CDCl_3$): δ=1.12 (6H, d, *J*=7 Hz, $(C\underline{H}_3)_2CH$–), 2.58 (1H, o, *J*=7 Hz, $(CH_3)_2C\underline{H}CH$=), 6.04 (1H, dd, *J*=16 and *ca.* 1 Hz, –CH=C<u>H</u>–COCl), 7.19 (1H, dd, *J*=16 and 6.5 Hz, >CH–C<u>H</u>=CH–).

*MPE–Tle–Val–ImPro–Gly–Phe(βMe)–β-Tha–OMe (Synthetic Bottromycin B_2) (**22**).* The compound (**18**) (121 mg, 0.136 mmol) was treated with 25% HBr in AcOH (2 g) at room temperature. The reaction mixture was diluted with dry ether, and the separated gummy material was trituated and throughly washed with dry ether. It afforded the iminohexapeptide methyl ester trihydrobromide(**21**) as a brownish amorphous powder (133 mg). Into a solution of the crude trihydrobromide (131 mg) in pyridine (2.5 ml), was stirred *trans*-MPE-Cl (**20**) (55 mg, 0.415 mmol) in benzene (1.5 ml) under ice-cooling, and the mixture was stirred at room temperature overnight. The solvent was throughly removed by repeated concentrations under reduced pressure after each addition of benzene. The residual syrup was chromatographed on preparative layers of silica gel with $CHCl_3$–MeOH–AcOH (96 : 15 : 3) to give a foamy solid, which was then passed through an Amberlyst A-29 column with 90% MeOH as a solvent. The eluent was evaporated under reduced pressure to afford a foamy solid: yield, 52 mg (43.3% based on **18**). Analytical results are summarized in Table 1.

This work was supported by a Grant-in-Aid for Scientific Research from the Ministry of Education (14703, 1976). We thank Drs. Hamao Umezawa, Tomohisa Takita, and Hiroshi Naganawa of the Institute of Microbial Chemistry, for measuring the mass spectra and for supplying bottromycin A_2, and Dr. Ichiro Chibata and his co-workers at Tanabe Seiyaku Co., Ltd., for the amino acid analyses and the microbiological assays.

References

1) a) This work was presented at the 14th Symposium on Peptide Chemistry (Japan), Hiroshima, November, 1976; T. Yamada, T. Miyazawa, S. Kuwata, and H. Watanabe, Proceedings of the 14th Symposium on Petide Chemistry, Japan (1976), p. 113; b) T. Takita, private communication

(August, 1976); c) Y. Takahashi, H. Naganawa, T. Takita, H. Umezawa, and S. Nakamura, *J. Antibiot.*, **29**, 1120 (1976); this was also presented at the 14th Symposium on Peptide Chemistry (Japan), Hiroshima, November, 1976 (Y. Takahashi, H. Naganawa, T. Takita, H. Umezawa, and S. Nakamura, Proceedings of the 14th Symposium on Peptide Chemistry, Japan (1976), p. 117), at the same time as our study.

2) J. M. Waisvisz, M. G. van der Hoeven, J. van Peppen, and W. C. M. Zwennis, *J. Am. Chem. Soc.*, **79**, 4520 (1975); J. M. Waisvisz, M. G. van der Hoeven, J. F. Hölscher, and B. te Nijenhuis, *ibid.*, **79**, 4522 (1957); J. M. Waisvisz, M. G. van der Hoeven, and B. te Nijenhuis, *ibid.*, **79**, 4524 (1957); J. M. Waisvisz and M. G. van der Hoeven, *ibid.*, **80**, 383 (1958).

3) a) S. Nakamura, T. Chikaike, K. Karasawa, N. Tanaka, H. Yonehara, and H. Umezawa, *J. Antibiot.*, **18A**, 47 (1965); b) S. Nakamura, T. Chikaike, H. Yonehara, and H. Umezawa, *ibid.*, **18A**, 60 (1965); S. Nakamura, T. Chikaike, H. Yonehara, and H. Umezawa, *Chem. Pharm. Bull.*, **13**, 599 (1965); c) S. Nakamura, N. Tanaka, and H. Umezawa, *J. Antibiot.*, **19A**, 10 (1966); S. Nakamura and H. Umezawa, *Chem. Pharm. Bull.*, **14**, 981 (1966); d) S. Nakamura, T. Yajima, Y. C. Lin, and H. Umezawa, *J. Antibiot.*, **20A**, 1 (1967).

4) W. J. Miller, L. Chaiet, G. Rasmussen, B. Christensen, J. Hannah, A. K. Miller, and F. J. Wolf, *J. Med. Chem.*, **11**, 746 (1968).

5) H. Arold, M. Eule, and S. Reissmann, *Z. Chem.*, **9**, 447 (1969).

6) Y. Seto, K. Torii, K. Bori, K. Inabata, S. Kuwata, and H. Watanabe, *Bull. Chem. Soc. Jpn.*, **47**, 151 (1974).

7) a) An iminopeptide bond means a -C(=NH)-NH- group situated between amino acid residues. The nomenclatures and abbreviations for iminopeptides and their derivatives were described previously.[8,11] b) Abbreviations according to the IUPAC-IUB Commission (*J. Biol. Chem.*, **247**, 977 (1972)) are used throughout. Additional abbreviations: Tle, *t*-leucine; Phe(βMe), *erythro*-β-methylphenylalanine; β-Tha, β-(2-thiazolyl)-β-alanine; Pro(CN), 2-cyanopyrrolidine; ImPro, iminoproline;[7a] Bu^t, *t*-butyl; Pr^i, isopropyl; Z, benzyloxycarbonyl; Piv, pivaloyl; MPE, 4-methyl-2-pentenoyl; ONSu, succinimidooxy; DCC, dicyclohexylcarbodiimide; THF, tetrahydrofuran; DMF, *N*,*N*-dimethylformamide; BuOH, 1-butanol. The amino acids and their derivatives used here are all of the L-configuration.

8) T. Yamada, K. Suegane, S. Kuwata, and H. Watanabe, *Bull. Chem. Soc. Jpn.*, **50**, 1088 (1977).

9) W. Steglich, E. Frauendorfer, and F. Weygand, *Chem. Ber.*, **104**, 687 (1971).

10) Y. Kataoka, Y. Seto, M. Yamamoto, T. Yamada, S. Kuwata, and H. Watanabe, *Bull. Chem. Soc. Jpn.*, **49**, 1081 (1976).

11) T. Yamada, T. Miyazawa, S. Kuwata, and H. Watanabe, *Bull. Chem. Soc. Jpn.*, **50**, 1827 (1977).

12) R. Roger and D. G. Neilson, *Chem. Rev.*, **61**, 193 (1961); S. Patai, Ed., "The Chemistry of Amidines and Imidates," John Wiley & Sons, London (1975), p. 389.

13) Throughout this investigation, we were forced to use only bottromycin A_2 containing 5% of B_2 provided by Dr. T. Takita, as a natural standard sample, because neither Umezawa's group nor Wolf's group has any A_1 and B_1 (private communications from Dr. T. Takita (September, 1976) and from Dr. F. J. Wolf (September, 1976)), and they are the only two groups who have reported that they could isolate bottromycins.

14) Although this sample of the natural A_2 contained some B_2,[13] TLC showed only one spot. This is understandable because bottromycin B_2 has been reported to behave like A_2 in TLC: *e.g.*, R_f values of A_2 and B_2 were 0.81 and 0.80 (BuOH : AcOH : H_2O = 100 : 12 : 100), respectively.[3d]

15) E. Frauendorfer, W. Steglich, and F. Weygand, *Chem. Ber.*, **106**, 1019 (1973).

16) H. Pracejus and S. Winter, *Chem. Ber.*, **97**, 3173 (1964).

17) J. Pospíšec and K. Bláha, *Collect. Czech. Chem. Commun.*, **42**, 1069 (1977).

18) R. P. Linstead, *J. Chem. Soc.*, **1929**, 2498.

19) Y. Sumiki, "Koseibusshitsu," Supplement I, Tokyo Daigaku Shuppankai, Tokyo (1970), p. 325. See also Ref. 3c.

20) The configuration of *t*-leucine isolated from bottromycin has been assigned to the L-series by Nakamura *et al.*,[3b] although the compound showed the positive specific rotation, $[\alpha]_D^{22}$ +4° (*c* 1, H_2O), contrary to L-*t*-leucine prepared by us or all others.

13αH-Olean-18-ene Derivatives. Forced Wolff-Kishner Reduction Products of 19-Oxoolean-12-ene Derivatives[1]

Tadashi HONDA, Tatsushi MURAE, Takahiko TSUYUKI, and Takeyoshi TAKAHASHI
Department of Chemistry, Faculty of Science, The University of Tokyo, Hongo, Bunkyo-ku, Tokyo 113
(Received October 13, 1977)

Methyl 2α,3β,23-triacetoxy-13αH-olean-18-en-28-oate (**4**) and methyl 2α,3β-diacetoxy-13αH-olean-18-en-28-oate (**7**) were obtained from methyl 2α,3β,23-triacetoxy-19-oxoolean-12-en-28-oate (**2**) and from methyl 2α,3β-diacetoxy-19-oxoolean-12-en-28-oate (**5**), respectively, by the forced Wolff-Kishner reduction and subsequent acetylation and methylation. Methyl 2α,3β-diacetoxy-13βH-olean-18-en-28-oate (**10**), prepared from methyl 2,3-di-*O*-acetylarjunate (**13**) *via* methyl 2α,3β-diacetoxy-19α-hydroxy-12-oxooleanan-28-oate (**18**) and methyl 2α,3β-diacetoxy-19α-hydroxyoleanan-28-oate (**19**), was shown to be not identical with **7**. This led to a 13αH-olean-18-ene structure for **7**.

It is well known that the reduction of sterically hindered ketones, such as 11-oxosteroids, is not easily effected using the usual Wolff-Kishner procedure, while modified procedures under forced reaction conditions developed by Barton[2] or Nagata[3] are successfully applied to the reduction of hindered or masked carbonyl groups.

In connection with the structure determination of arjungenin (**1**),[4] a new constituent of *Terminalia arjuna*, a forced Wolff-Kishner reduction of methyl 2α,3β,23-triacetoxy-19-oxoolean-12-en-28-oate (**2**)[4] derived from **1**, was attempted aiming at the conversion into the known compound, methyl 2,3,23-tri-*O*-acetylarjunolate (**3**).[5] The 19-oxoolean-12-ene derivative (**2**) was subjected to a forced Wolff-Kishner reduction modified by Nagata under conditions described as procedures "A" and "B",[3] followed by acetylation and methylation. However, the resulting products were so complex that no definite product could be separated. The reduction of **2** using Barton's procedure[2] and subsequent methylation and acetylation gave a trisubstituted olefin (**4**; yield 32 %) as a sole reaction product, which was found to be not identical with methyl 2,3,23-tri-*O*-acetylarjunolate (**3**).

In order to obtain information on the structure of the reduction product (**4**), a simpler model compound of **2**, methyl 2α,3β-diacetoxy-19-oxoolean-12-en-28-oate (**5**)[6] derived from arjunic acid (**6**),[6] was subjected to the Wolff-Kishner reduction by Barton's procedure.[2] The reduction product, after acetylation and methylation, was separated by column chromatography into an olefin (**7**; yield 46 %) and an α,β-unsaturated ketone (**8**; yield 20 %). This olefin (**7**), mp 224—225 °C, $[\alpha]_D$ +71°, was indicated to be a pentacyclic trisubstituted monoolefin having a methoxycarbonyl and two acetoxyl groups by IR (1740 and 1630 cm^{-1}), PMR [δ 1.98, 2.05 (each 3H, s; 2×CH_3COO–), 3.64 (3H, s; –$COOCH_3$), and 5.30 (1H, sharp singlet)], and mass spectrum ($C_{35}H_{54}O_6$), but was shown not to be an expected deoxygenated product, methyl 2,3-di-*O*-acetylmasulinate (**9**; =methyl 2α,3β-diacetoxyolean-12-en-28-oate, mp 184—186 °C, $[\alpha]_D$ +33.5°, IR 1730, 1720, 1659, and 819 cm^{-1})[7] by comparison with their melting points and spectral data. Although the mass spectrum of **7** showed peaks at *m/e* 249, 248, and 189, characteristic for Δ^{18}-oleanene derivatives,[8] this olefin (**7**) was found to be not identical with methyl 2α,3β-diacetoxyolean-18-en-28-oate (**10**) as described below. The olefin (**7**), therefore, was inferred to be methyl 2α,3β-diacetoxy-13αH-olean-18-en-28-oate, and the proposed structure was supported by the following transformation and evidence.

On oxidation with selenium dioxide in acetic acid, the olefin (**7**) gave a known diene, methyl 2α,3β-diacetoxyoleana-12,18-dien-28-oate (**11**),[6] which was further converted into methyl 2α,3β-diacetoxyoleana-11,13(18)-dien-28-oate (**12**) by treatment with hydrochloric acid in chloroform. This diene (**12**) proved to be identical with the diene (**12**)[6] prepared by dehydration of methyl 2,3-di-*O*-acetylarjunate (**13**)[6] followed by isomerization according to the known procedures.[6]

Methyl *O*-acetylmorolate (**14**; =methyl 3β-acetoxyolean-18-en-28-oate) has been prepared from methyl 3-*O*-acetylsiaresinolate (**15**; =methyl 3β-acetoxy-19α-hydroxyolean-12-en-28-oate) *via* a 12-keto 19α-ol (**16**) and a 19α-ol (**17**) by Barton *et al.*[9] By the same procedures, methyl 2,3-di-*O*-acetylarjunate (**13**; =methyl 2α,3β-diacetoxy-19α-hydroxyolean-12-en-28-oate)[4,6] was converted into methyl 2α,3β-diacetoxyolean-18-en-28-oate (**10**). Arjunic acid (**6**), isolated from *Terminalia arjuna*,[4,6] was converted into methyl 2,3-di-*O*-acetylarjunate (**13**), which was treated with hydrogen peroxide in acetic acid to yield a 12-keto alcohol (**18**). The keto alcohol (**18**) showed IR absorption bands at 3500, 1750, 1730, 1720, and 1690 cm^{-1}. In the PMR spectrum of **18**, a signal due to $C_{(19\beta)}$–H appears at δ 4.55 as a triplet-like, which, on addition of D_2O, changes into a doublet (J=3.5 Hz). A doublet (J=7 Hz) due to $C_{(13\beta)}$–H was also observed at δ 3.10 and a double doublet (J=7 and J=3.5 Hz) due to $C_{(18\beta)}$–H at δ 2.90. The 13βH-configuration of **18** was suggested by the following attempted isomerization reaction. The ketone (**18**) was treated with potassium hydroxide in boiling ethanol and the reaction product was then acetylated to give the starting material in 50 % yield.

The ketone (**18**) was subjected to the Wolff-Kishner reduction and the product was then methylated and acetylated to give a mixture of deoxygenated alcohols (**19** and **20**), which was separated by silica gel column chromatography. An alcohol (**19**) showed a doublet (J=2 Hz) due to $C_{(19\beta)}$–H at δ 3.37, while a diastereomeric alcohol (**20**) at δ 3.40 as a doublet (J=5 Hz). The alcohols (**19** and **20**) were then oxidized with the Jones reagent to yield the corresponding ketones (**21** and **22**), respectively. In the PMR spectrum of **21**, a signal due to $C_{(18\beta)}$–H appeared at δ 3.15 as a doublet

($J_{13\beta,18\beta}$=4 Hz), while in **22** $C_{(18\beta)}$–H resonated at δ 3.28 as a doublet ($J_{13\alpha,18\beta}$=12 Hz). The CD values were $\Delta\varepsilon_{302}$=+1.60 and $\Delta\varepsilon_{302}$=−0.11 for **21** and **22**, respectively. The coupling constant, $J_{13,18}$ and CD values led to a 13β*H*- and a 13α*H*-configuration for **21** and **22**, respectively. Therefore a configuration at C-13 of the alcohol (**19**) was inferred to be 13β*H* (with an axial 19α-OH), and that of **20** 13α*H* (with an equatorial 19α-OH).

The alcohol (**19**) was treated with phosphoryl chloride in pyridine to afford an 18-ene (**10**), whose configuration at C-13 must be β*H*. The PMR spectrum of **10** showed a signal due to $C_{(19)}$–H at δ 5.10 as a singlet, and the mass spectrum gave fragment peaks characteristic for Δ^{18}-oleanene derivatives[8] at *m/e* 249 and 189, together with a molecular ion peak at *m/e* 570.3912 (M^+; *m/e* 570.3917 calcd for $C_{35}H_{54}O_6$). The isomeric alcohol (**20**), on dehydration under the same conditions, gave a 13(18)-ene (**23**), whose PMR spectrum showed no signal due to olefin proton. This olefin (**23**) was also obtainable by catalytic hydrogenation of the known methyl 2α,3β-diacetoxyoleana-11,13(18)-dien-28-oate (**12**).[6]

The 13β*H*-18-ene (**10**) thus prepared was found to be not identical with the olefin (**7**), obtained by the forced Wolff-Kishner reduction of methyl 2α,3β-diacetoxy-19-oxoolean-12-en-28-oate (**5**). The structure of the olefin (**7**) should therefore be formulated as methyl 2α,3β-diacetoxy-13α*H*-olean-18-en-28-oate.

From this observation, the structure of the trisubstituted olefin (**4**), formed by the forced Wolff-Kishner reduction of methyl 2α,3β,23-triacetoxy-19-oxoolean-12-en-28-oate (**2**)[4,10] and by successive methylation and acetylation, was suggested to be methyl 2α,3β,23-triacetoxy-13α*H*-olean-18-en-28-oate. The spectral data are compatible with the proposed structure (**4**). The mass spectrum of **4** showed peaks characteristic for Δ^{18}-oleanene derivatives[8] at *m/e* 249, 248, and 189. In the PMR spectrum, a sharp singlet due to an olefinic proton at C-19 appeared at δ 5.30. This δ-value was identical with that for $C_{(19)}$–H of methyl 2α,3β-diacetoxyolean-18-en-28-oate (**7**) with a 13α*H*-configuration, while differed from those for $C_{(19)}$–H of the 13β*H*-18-ene (**10**; δ 5.10) and of methyl *O*-acetylmorolate (**14**; δ 5.07)[11] with a 13β*H*-configuration.

Triterpenes with an olean-18-ene framework hitherto reported, germanicol (**24**),[12] miliacin (**25**),[13] morolic acid (**26**),[9,14] germanidiol (**27**; =2β-hydroxygermanicol),[15] and epigermanidiol (**28**; =2α-hydroxygermanicol)[16], are all in $C_{(13)}$-β*H* configuration, and neither isolation nor preparation of olean-18-ene derivative with a 13α*H*-configuration has yet been described. Methyl 2α,3β,23-triacetoxy-13α*H*-olean-18-en-28-oate (**4**) and methyl 2α,3β-diacetoxy-13α*H*-olean-18-en-28-oate (**7**) are the first examples of 13α*H*-olean-18-ene derivatives.

The structure of the α,β-unsaturated ketone (**8**), obtained by the forced Wolff-Kishner reduction of **5**, was inferred to be **8** from the IR (1730 and 1680 cm^{-1}), UV λ_{max} 253 nm (log ε 3.81), PMR (absence of olefinic proton), and mass spectral data *m/e* 584.3682 (M^+; *m/e* 584.3709 calcd for $C_{35}H_{52}O_7$) and *m/e* 188.

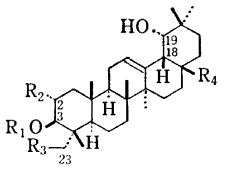

	R_1	R_2	R_3	R_4
1	H	OH	OH	COOH
6	H	OH	H	COOH
13	Ac	OAc	H	$COOCH_3$
15	Ac	H	H	$COOCH_3$

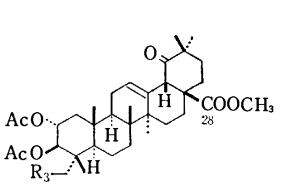

	R_3
2	OAc
5	H

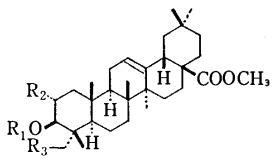

	R_1	R_2	R_3
3	Ac	OAc	OAc
9	Ac	OAc	H
29	H	OH	OH

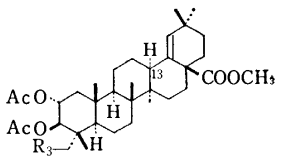

	R_3
4	OAc
7	H

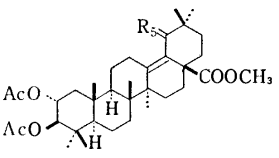

	R_5
8	O
23	H_2

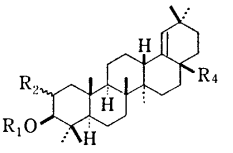

	R_1	R_2	R_4
10	Ac	α-OAc	$COOCH_3$
14	Ac	H	$COOCH_3$
24	H	H	CH_3
25	CH_3	H	CH_3
26	H	H	COOH
27	H	β-OH	$COOCH_3$
28	H	α-OH	$COOCH_3$

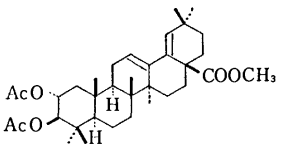

11

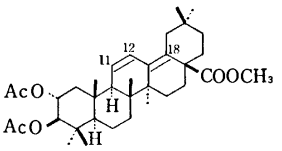

12

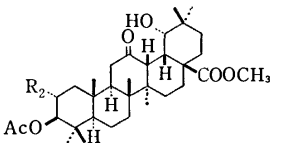

	R_2
16	H
18	OAc

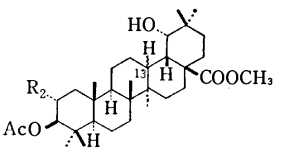

	R_2	13H
17	H	β
19	OAc	β
20	OAc	α

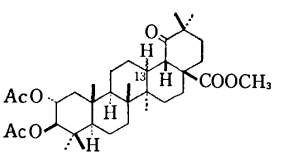

21	13β-H
22	13α-H

Although the formation mechanism of 13α*H*-olean-18-ene derivatives from 19-oxoolean-12-enes is not clearly elucidated, a mechanism *via* 19-oxoolean-13(18)-ene seems to be likely. It has been reported that olean-12-en-19-one derivatives undergo isomerization in the presence of alkali to give the corresponding olean-13(18)-en-19-one derivatives.[6,10,17] And α,β-unsaturated carbonyl compounds, on Wolff-Kishner reduction, often afford abnormal deoxygenated products in which a migration of the double bond has occurred, together with the normal products.[18] Under the forced Wolff-Kishner reduction conditions, a 19-oxoolean-12-ene derivative (**5**) must have isomerized into the corresponding α,β-unsaturated ketone (**8**). This compound (**8**) was subjected to the forced Wolff-Kishner reduction to give 13α*H*-olean-18-ene (**7**) in 19 % yield, after acetylation and methylation of the product, while the corresponding normal deoxygenated product, olean-13(18)-ene derivative (**23**) was not obtained.

The formation reaction of 13α*H*-olean-18-ene derivatives (**4** and **7**) was stereospecific and no 13β*H*-diastereomer was detected. The stereospecificity may be due to a structure feature around the C/D/E rings of olean-13(18)-en-19-one derivatives and/or of their nitrogen-containing intermediates.

Experimental

General indications in Experimental were the same as described in a previous paper.[4] Anhydrous hydrazine was prepared by Kusama's procedure.[19] Diethylene glycol was distilled and dried over Molecular Sieves. The forced Wolff-Kishner reduction was carried out in an argon atmosphere.

Forced Wolff-Kishner Reduction of Methyl 2α,3β,23-Triacetoxy-19-oxoolean-12-en-28-oate (2) Followed by Methylation and Acetylation. Methyl 2α,3β,23-triacetoxy-19-oxoolean-12-en-28-oate (**2**; 66 mg)[4] was treated with diethylene glycol (3 ml), sodium (68 mg), and anhydrous hydrazine (1 ml) according to the Barton procedure.[2] The reaction product, without purification, was subjected to methylation with diazomethane in ether and then to acetylation with acetic anhydride in pyridine to give a crude product (*ca.* 47 mg). The product in benzene was passed through a column of silica gel (10 g) and the following solvents were used as eluent (each 40 ml): fr. 1, benzene; fr. 2, benzene-acetone (200:3); frs. 3—8, benzene-acetone (100:3). Fractions 5 and 6 were combined (*ca.* 17 mg) and purified by preparative TLC, developed with benzene-acetone (16:1) to give methyl 2α,3β,23-triacetoxy-13α*H*-olean-18-en-28-oate (**4**; 13 mg), as amorphous solid, $[\alpha]_D$ +70° (*c* 0.16, EtOH), IR (Nujol) 1740 (br), 1730, 1715 (sh), 1240, 1225, 1045, and 1030 cm^{-1}; PMR* ($CDCl_3$) δ 0.83, 0.90, 1.12 (each 3H, s; *t*-Me), 0.98 (9H, s; 3×*t*-Me), 1.99, 2.01, 2.08 (each 3H, s; -OAc), 3.65 (3H, s; $-CO_2Me$), 3.58, 3.82 (2H, ABq, *J*=12 Hz; $C_{(23)}H_2$-OAc), 5.10 (2H, m; $C_{(2\beta)}$-H and $C_{(3\alpha)}$-H), 5.30 (1H, s; $C_{(19)}$-H); MS *m/e* 628 (M^+), 626, 569, 568, 466, 449, 448, 435, 433, 392, 262, 249, 248, 245, 203, 189 (base peak), 185, and 175.

Forced Wolff-Kishner Reduction of Methyl 2α,3β-Diacetoxy-18-oxoolean-12-en-28-oate (5) Followed by Acetylation and Methylation. Methyl 2α,3β-diacetoxy-19-oxoolean-12-en-28-oate (**5**; 120 mg) was subjected to the forced Wolff-Kishner reduction by the same procedure [diethylene glycol (*ca.* 6 ml), sodium (136 mg), and anhydrous hydrazine (1.5 ml)] as above, and the reaction product (*ca.* 84 mg) was acetylated with acetic anhydride in pyridine to give an acetylated product. This was purified by column chromatography on silica gel (15 g) eluting with the following solvents; fr. 1, benzene-acetone (100:1, 30 ml); fr. 2, benzene-acetone (50:1, 30 ml); frs. 3 and 4, benzene-acetone (100:3, each 30 ml); frs. 5—10, benzene-acetone (25:1, each 15 ml), and frs. 11—21, benzene-acetone (20:1, each 30 ml). From the fractions 6—8, a diacetate (*ca.* 52 mg) was obtained as amorphous solid, IR (KBr) 1738, 1700, 1630, 1250, 1230, 1045, and 1035 cm^{-1}; PMR ($CDCl_3$) δ 0.92, 0.98 (each 9H, s; 3×*t*-Me), 1.09 (3H, s; *t*-Me), 1.98, 2.05 (each 3H, s; -OAc), 4.75 (1H, d, *J*=11 Hz; $C_{(2\alpha)}$-H), 5.15 (1H, ddd, *J*=11, *J*=11, and *J*=4 Hz; $C_{(2\beta)}$-H), and 5.34 (1H, s; $C_{(19)}$-H); MS *m/e* 512 (M^+-CO_2), 510, 497, 452, 437, 409, 392, 349, 334, 247, 233, 215, 203, and 190 (base peak). Fractions 14—19 gave an α,β-unsaturated keto acid (23 mg).

The diacetate, above obtained, was treated with diazomethane in ether to give methyl 2α,3β-diacetoxy-13α*H*-olean-18-en-23-oate (**7**), which was crystallized from ethanol to afford white needles (38 mg), mp 224—225 °C, $[\alpha]_D$ +71° (*c* 1.38, EtOH); IR (KBr) 1740, 1725 (sh), 1630, 1250, and 1230 cm^{-1}; PMR ($CDCl_3$) δ 0.83, 1.10 (each 3H, s; *t*-Me), 0.91 (9H, s; 3×*t*-Me), 0.98 (6H, s; 2×*t*-Me), 1.98, 2.05 (each 3H, s; -OAc), 3.64 (3H, s; $-CO_2Me$), 4.75 (1H, d, *J*=11 Hz; $C_{(2\alpha)}$-H), 5.15 (1H, ddd, *J*=11, *J*=11, and *J*=4 Hz; $C_{(2\beta)}$-H), and 5.30 (1H, s; $C_{(19)}$-H); mol wt *m/e* 570.3830. Calcd for $C_{35}H_{54}O_6$: *m/e* 570.3917. MS *m/e* 570 (M^+), 568, 511, 510, 495, 450, 435, 409, 407, 334, 259, 249, 248, 247, 235, 234, 233, 215, 203, 189 (base peak), 187, and 175.

The α,β-unsaturated keto acid, on treatment with diazomethane, was converted into methyl 2α,3β-diacetoxy-19-oxo-olean-13(18)-en-28-oate (**8**), mp 223—224°C (crystallized from ether); $[\alpha]_D$ −154° (*c* 0.94, $CHCl_3$); IR (KBr) 1730, 1680, 1240, 1230, and 1040 cm^{-1}; UV (EtOH) λ_{max} 253 nm (log ε 3.81); PMR ($CDCl_3$) δ 0.85, 1.12, 1.23 (each 3H, s; *t*-Me), 0.90, 1.06 (each 6H, s; 2×*t*-Me), 1.99, 2.06 (each 3H, s; -OAc), 3.64 (3H, s; $-CO_2Me$), 4.76 (1H, d, *J*=11 Hz; $C_{(3\alpha)}$-H), 5.18 (1H, ddd, *J*=11, *J*=11 and *J*=4 Hz; $C_{(2\beta)}$-H), and the absence of olefinic proton; mol wt *m/e* 584.3682. Calcd for $C_{35}H_{52}O_7$: *m/e* 584.3709. MS *m/e* 584 (M^+), 524, 482, 464, 405, and 188 (base peak).

*Oxidation of Methyl 2α,3β-Diacetoxy-13α*H*-olean-18-en-28-oate (7) with Selenium Dioxide.* A mixture of **7** (32.5 mg) and selenium dioxide (15.2 mg) in acetic acid (3 ml) was heated under reflux for 6 h. Usual work-up gave a residue (33 mg), which was subjected to purification by preparative TLC, developed with benzene-acetone (50:3), to give methyl 2α,3β-diacetoxyoleana-12,18-dien-28-oate (**11**; 21 mg), mp 245—247 °C (crystallized from ethanol); $[\alpha]_D$ +64° (*c* 1.0, EtOH); IR (KBr) 1733, 1720 (sh), 1630, 1250, 1225, and 1040 cm^{-1}; UV (EtOH) λ_{max} 235 nm (log ε 3.9); PMR ($CDCl_3$) δ 0.90, 1.11 (each 3H, s; *t*-Me), 0.91 (6H, s; 2×*t*-Me), 1.00 (9H, s; 3×*t*-Me), 1.99, 2.05 (each 3H, s; -OAc), 3.61 (3H, s; $-CO_2Me$), 4.76 (1H, d, *J*=11 Hz; $C_{(2\alpha)}$-H), 5.16 (1H, ddd, *J*=11, *J*=11, and *J*=4 Hz; $C_{(2\beta)}$-H), 5.47 (1H, s; $C_{(19)}$-H), and 5.57 (1H, t-like; $C_{(12)}$-H); mol wt *m/e* 568.3708. Calcd for $C_{35}H_{52}O_6$: *m/e* 568.3760; MS *m/e* 568 (M^+), 509, 448, 433, 389, 367, 260, 247, and 201 (base peak).

Isomerization of Methyl 2α,3β-Diacetoxyoleana-12,18-dien-28-oate (11) into Methyl 2α,3β-Diacetoxyoleana-11,13-dien-28-oate (12). The diene (**11**; 21 mg) was dissolved in chloroform (3 ml) and dry hydrogen chloride was passed through the solution for 1.5 h. Usual treatment gave a residue (16 mg), which

* PMR spectra were measured using a Hitachi R-20 (60 MHz) spectrometer unless otherwise stated.

was shown to be completely isomerized into methyl 2α,3β-diacetoxyoleana-11,13-dien-28-oate (**12**) by PMR examination. The diene (**12**): mp 186.5—188.5 °C (crystallized from ethanol); $[\alpha]_D$ −128° (*c* 0.125, EtOH); IR (KBr) 1730, 1725 (sh), 1700 (sh), 1630, 1245, 1230 (sh), 1042, and 1030 cm^{-1}; UV (EtOH) λ_{max} 243.5 (log ε 4.31), 251.5 (4.36), and 260.5 nm (4.16); PMR ($CDCl_3$) δ 0.80 (6H, s; 2×*t*-Me), 0.91 (12H, s; 4×*t*-Me), 1.08 (3H, s; *t*-Me), 2.00, 2.06 (each 3H, s; -OAc), 3.66 (3H, s; $-CO_2Me$), 4.76 (1H, d, *J*=11 Hz; $C_{(3\alpha)}$-H), 5.15 (1H, ddd, *J*=11, *J*=11, and *J*=4 Hz; $C_{(2\beta)}$-H), 5.58 (1H, d, *J*=11 Hz; $C_{(12)}$-H), and 6.48 (1H, dd, *J*=11 and *J*=2 Hz; $C_{(11)}$-H); mol wt *m/e* 568.3698. Calcd for $C_{35}H_{52}O_6$: *m/e* 568.3760; MS *m/e* 568 (M^+), 509, 448, 433, 389, 367, and 187 (base peak). This diene was found to be identical with the diene (**12**)[6] prepared from methyl 2,3-di-*O*-acetylarjunate (**13**)[4,6] according to the known procedures.[6]

*Oxidation of Methyl 2,3-Di-O-acetylarjunate (**13**) with Hydrogen Peroxide.* A solution of methyl 2,3-di-*O*-acetylarjunate (**13**; 102 mg)[4,6] in acetic acid (8 ml) was treated dropwise at 70—75 °C with a mixture of acetic acid (1 ml) and hydrogen peroxide (35 %, 1 ml) according to the Barton procedure.[9] Usual treatment gave a residue (*ca.* 100 mg), which was purified by column chromatography on silica gel (15 g). Elution was carried out with the following solvents: fr. 1, benzene-acetone (50:1, 30 ml); fr. 2, benzene-acetone (100:3, 30 ml); frs. 3 and 4, benzene-acetone (25:1, each 15 ml), frs. 5—10 (each 10 ml), frs. 11 and 12 (each 15 ml). Fractions 6—8, on evaporation of the solvents, gave a residue (*ca.* 70 mg), which was crystallized from ether to give methyl 2α,3β-diacetoxy-19α-hydroxy-12-oxooleanan-28-oate (**18**; 32 mg) as white needles, mp 272—273 °C; $[\alpha]_D$ −25° (*c* 1.11, $CHCl_3$); IR (Nujol) 3500, 1750, 1730, 1720, 1690, 1260, 1230, and 1045 cm^{-1}; PMR ($CDCl_3$) δ 0.91, 0.98, 1.01 (each 6H, s; 2×*t*-Me), 1.15 (3H, s; *t*-Me), 1.99, 2.05 (each 3H, s; -OAc), 2.90 (1H, dd, *J*=7 and *J*=3.5 Hz; $C_{(18\alpha)}$-H), 3.10 (1H, d, *J*=7 Hz; $C_{(13\alpha)}$-H), 3.70 (3H, s; $-CO_2Me$), 4.55 [1H, t-like; $C_{(19\beta)}$-H; on addition of D_2O. this signal changes into a doublet (*J*=3.5 Hz)], 4.75 (1H, d, *J*=11 Hz; $C_{(3\alpha)}$-H), and 5.10 (1H, ddd, *J*=11, *J*=11, and *J*=4 Hz; $C_{(2\alpha)}$-H); MS *m/e* 602 (M^+), 584, 569, 543, 525, 524, 482, 465, 464, and 276 (base peak); Found: C, 68.59; H, 9.09%. Calcd for $C_{35}H_{54}O_9 \cdot 1/2\ H_2O$: C, 68.71; H, 9.06%.

*Treatment of Methyl 2α,3β-Diacetoxy-19α-hydroxy-12-oxooleanan-28-oate (**18**) with Alkali.* A mixture of **18** (28 mg) in methanol (5 ml) containing potassium hydroxide (400 mg) was heated under reflux for 2 h. After usual work-up, a residue was acetylated with acetic anhydride in pyridine and crystallized from ether to afford white needles, which were chromatographed on silica gel (5 g), eluting with the following solvents: fr. 1, benzene-acetone (50:1, 10 ml); fr. 2, benzene-acetone (100:3, 10 ml); and frs. 3—11, benzene-acetone (25:1, each 5 ml). Fractions 6—8, on evaporation of the solvents, afforded crystals, which were identical with the starting material in respect to IR, PMR, and TLC.

*Wolff-Kishner Reduction of Methyl 2α,3β-Diacetoxy-19α-hydroxy-12-oxooleanan-28-oate (**18**) Followed by Methylation and Acetylation. i) By the Barton Procedure.* To a boiling mixture of sodium (106 mg) in diethylene glycol (5 ml) and anhydrous hydrazine (1 ml), methyl 2α,3β-diacetoxy-19α-hydroxy-12-oxo-oleanan-28-oate (**18**; 100 mg) was added. The reaction mixture was treated according to the Barton procedure[2] to afford a residue, which was methylated with diazomethane and then acetylated with acetic anhydride in pyridine. The product, dissolved in benzene, was passed through a column of silica gel (15 g) and eluted with the following solvents: fr. 1, benzene-acetone (100:1, 30 ml); frs. 2 and 3, benzene-acetone (50:1, each 15 ml); frs. 4—15, benzene-acetone (100:3, each 10 ml). A 13β*H*-alcohol (**19**; 33 mg) was obtained from fractions 7 and 8, as amorphous solid, IR (Nujol) 3500, 1740, 1240, and 1230 cm^{-1}; PMR ($CDCl_3$) δ 0.88 (12H, s; 4×*t*-Me), 0.96 (6H, s; 2×*t*-Me), 1.17 (3H, s; *t*-Me), 1.97, 2.03 (each 3H, s; -OAc), 3.37 (1H, d, *J*=2 Hz; $C_{(19\beta)}$-H), 3.70 (3H, s; $-CO_2Me$), 4.75 (1H, d, *J*=11 Hz; $C_{(3\alpha)}$-H), and 5.13 (1H, ddd, *J*=11, *J*=11, *J*=4 Hz; $C_{(2\beta)}$-H); MS *m/e* 570 (M^+-H_2O), 528, 510, 495, 486, 468, 450, 435, and 189 (base peak). Fractions 9—12 gave a 13α*H*-alcohol (**20**; 26 mg) as amorphous solid, IR (Nujol) 3500, 1740, 1725 (sh), 1245, and 1225 cm^{-1}; PMR ($CDCl_3$) δ 0.90 (9H, s; 3×*t*-Me), 0.97, 1.03, 1.09, 1.25 (each 3H, s; *t*-Me), 1.98, 2.04 (each 3H, s; -OAc), 3.40 (1H, d, *J*=5 Hz; $C_{(19\beta)}$-H), 3.69 (3H, s; $-CO_2Me$), 4.75 (1H, d, *J*=11 Hz; $C_{(3\alpha)}$-H), and 5.15 (1H, ddd, *J*=11, *J*=11, and *J*=4 Hz; $C_{(2\beta)}$-H); MS *m/e* 570 (M^+-H_2O), 528, 510, 495, 486, 468, 450, 435, and 189 (base peak). *ii) By the Huang-Minlon Procedure.* A mixture of **18** (47 mg), potassium hydroxide (500 mg), anhydrous hydrazine (0.6 ml), and diethylene glycol (4.7 ml) was heated under reflux for 1.5 h and excess hydrazine and water were distilled off. Then reflux was continued at 220 °C for 7 h. After usual work-up, acetylation and methylation were followed. The reaction mixture was subjected to column chromatographic separation on silica gel (5 g), eluting with benzene-acetone (100:1, 10 ml; fr. 1); benzene-acetone (50:1, 10 ml; fr. 2), and then benzene-acetone (100:3, each 5 ml; frs. 3—12). Fractions 5 and 6 gave the 13β*H*-alcohol (**19**; 21.4 mg) and fractions 7—9 the 13α*H*-alcohol (**20**; 14.5 mg).

*Oxidation of Methyl 2α,3β-Diacetoxy-19α-hydroxyoleanan-28-oate (**19**) with Jones Reagent.* A solution of **19** (19 mg) in acetone (1.5 ml) was cooled at 0 °C and Jones reagent (0.2 ml) was added with stirring. After usual work-up, the reaction product was dissolved in benzene and passed through a column of silica gel (5 g) and eluted with the following solvents: fr. 1, benzene-acetone (200 : 1, 20 ml); frs. 2—17, benzene-acetone (50 : 1, each 2.5 ml). Fractions 10 and 11, on evaporation of the solvents, gave methyl 2α,3β-diacetoxy-19-oxooleanan-28-oate (**21**; 9.6 mg) as amorphous solid, IR (KBr) 1730, 1720 (sh), 1695 (sh), 1245, and 1230 cm^{-1}; CD (*c* 0.0024, EtOH) $\Delta\varepsilon_{302}$ +1.60; PMR (100 MHz**, $CDCl_3$) δ 0.84, 0.94, 0.98, 1.01, 1.12 (each 3H, s; *t*-Me), 0.86 (6H, s; 2×*t*-Me), 1.94, 2.01 (each 3H, s; -OAc), 3.15 (1H, d, $J_{13\beta,18\beta}$=4 Hz; $C_{(18\beta)}$-H), 3.70 (3H, s; $-CO_2Me$), 4.70 (1H, d, *J*=11 Hz; $C_{(3\alpha)}$-H), and 5.06 (1H, ddd, *J*=11, *J*=11, and *J*=4 Hz; $C_{(2\beta)}$-H); mol wt *m/e* 586.3899. Calcd for $C_{35}H_{54}O_7$: *m/e* 586.3867; MS *m/e* 586 (M^+), 527, 526, 484, 467, 466, 451, 425, 407, and 205 (base peak).

*Oxidation of Methyl 2α,3β-Diacetoxy-19α-hydroxy-13α*H*-oleanan-28-oate (**20**) with Jones Reagent.* A solution of **20** (14 mg) in acetone (1.5 ml) was oxidized with Jones reagent (0.2 ml) as the same as above. Usual treatment and purification gave methyl 2α,3β-diacetoxy-19-oxo-13α*H*-oleanan-28-oate (**22**), mp 204—209 °C; IR (KBr) 1730, 1710 (sh), 1690, 1240, and 1225 cm^{-1}; CD (*c* 0.0025, EtOH) $\Delta\varepsilon_{302}$ −0.11; PMR (100 MHz, $CDCl_3$) δ 0.86, 0.88, 1.08, 1.14 (each 3H, s; *t*-Me), 1.02 (9H, s; 3×*t*-Me), 1.95, 2.00 (each 3H, s; -OAc), 3.28 (1H, d, $J_{13\alpha,18\beta}$=12 Hz, $C_{(18\beta)}$-H), 3.64 (3H, s; $-CO_2Me$), 4.69 (1H, d, *J*=11 Hz; $C_{(3\alpha)}$-H), and 5.10 (1H, ddd, *J*=11, *J*=11, and *J*=4 Hz; $C_{(2\beta)}$-H); MW *m/e* 586.3879. Calcd for $C_{35}H_{54}O_7$: *m/e* 586.3867; MS *m/e* 586 (M^+), 527, 526, 484, 467, 466, 451, 425, 407, and 205 (base peak).

** PMR (100 MHz) spectra were measured with a JEOL 4H-100 spectrometer.

*Dehydration of Methyl 2α,3β-Diacetoxy-19α-hydroxyoleanan-28-oate (**19**).* A solution of **19** (21 mg) in pyridine (0.7 ml) and phosphoryl chloride (0.1 ml) was heated under reflux for 4 h and then treated as usual to afford a residue (19 mg). The residue was dissolved in benzene and passed through a column of silica gel (3 g) and eluted with benzene (6 ml; fr. 1), benzene-acetone (100 : 1, 6 ml; fr. 2), and with benzene–acetone (50 : 1, each 6 ml; frs. 3—9) successively. The fractions 5 and 6 were combined and further subjected to purification by preparative TLC on Kieselgel PF_{254} developed with benzene–acetone (20 : 1) to give methyl 2α,3β-diacetoxy-olean-18-en-28-oate (**10**; 6 mg), mp 232—233 °C (crystallized from ethanol), $[\alpha]_{450}$ −38° (*c* 0.13, EtOH); IR (KBr) 1740 (br), 1630, 1245, and 1230 cm^{-1}; PMR ($CDCl_3$) δ 0.78, 1.02 (each 3H, s; *t*-Me), 0.90 (6H, s; 2×*t*-Me), 0.98 (9H, s; 3×*t*-Me), 1.98, 2.04 (each 3H, s; -OAc), 3.66 (3H, s; $-CO_2Me$), 4.75 (1H, d, J=11 Hz; $C_{(3\alpha)}$-H), 5.10 (1H, s; $C_{(19)}$-H), and 5.15 (1H, ddd, J=11, J=11, and J=4 Hz; $C_{(2\beta)}$-H); mol wt *m/e* 570.3912. Calcd for $C_{35}H_{54}O_6$: *m/e* 570.3917; MS *m/e* 570 (M^+), 555, 538, 511, 510, 495, 468, 451, 450, 436, 435, 409, 407, 391, 249, 203, and 189 (base peak). This ester (**10**) gave the same R_f value on TLC as that of **7**, but the IR and PMR spectra were distinctly different to each other.

*Dehydration of Methyl 2α,3β-Diacetoxy-19α-hydroxy-13αH-oleanan-28-oate (**20**).* A solution of **20** (12 mg) in pyridine (0.7 ml) and phosphoryl chloride (0.1 ml) was refluxed for 1 h. After usual treatment, purification by preparative TLC was carried out as before. Methyl 2α,3β-diacetoxyolean-13(18)-en-28-oate (**23**) was obtained, mp 202—203 °C (crystallized from ether); IR (KBr) 1720, 1700 (sh), 1620, 1240, 1230, and 1030 cm^{-1}; PMR ($CDCl_3$) δ 0.74, 1.02, 1.15 (each 3H, s; *t*-Me), 0.90 (12H, s; 4×*t*-Me), 1.98, 2.04 (each 3H, s; -OAc), 3.65 (3H, s; $-CO_2Me$), 4.75 (1H, d, J=11 Hz; $C_{(3\alpha)}$-H), 5.15 (1H, ddd, J=11, J=11, and J=4 Hz; $C_{(2\beta)}$-H), and the absence of olefinic proton; mol wt *m/e* 570.3916. Calcd for $C_{35}H_{54}O_6$: *m/e* 570.3917; MS *m/e* 570 (M^+), 555, 538, 511, 510, 495, 468, 451, 450, 436, 435, 407, 391, 249, 203, and 189 (base peak).

*Catalytic Hydrogenation of Methyl 2α,3β-Diacetoxyoleana-11,13-dien-28-oate (**12**).* The 11,13-diene (**12**; 23 mg) in acetic acid was hydrogenated under an atmospheric pressure in the presence of platinum oxide (5 mg) for 20 h and worked up as usual to give a residue. The residue was subjected to preparative TLC on Kieselgel PF_{254} developed with benzene–acetone (50 : 3). The crude product (11 mg) was crystallized from ether to afford methyl 2α,3β-diacetoxyolean-13(18)-en-28-oate (**23**), mp 205.5—206.5 °C; $[\alpha]_{450}$ −66° (*c* 0.076, EtOH); mol wt *m/e* 570.3827. Calcd for $C_{35}H_{54}O_6$: *m/e* 570.3917. The IR, PMR, and MS spectra and TLC were completely identical with those of the specimen obtained by the dehydration of **20**.

*Forced Wolff-Kishner Reduction of Methyl 2α,3β-Diacetoxy-19-oxoolean-13(18)-en-28-oate (**8**) Followed by Acetylation and Methylation.* The α,β-unsaturated keto ester (**8**; 38 mg) was subjected to the forced Wolff-Kishner reduction (sodium 38 mg, diethylene glycol 1.5 ml, and anhydrous hydrazine 0.4 ml) under the same conditions as before. After usual work-up, a residue was acetylated with acetic anhydride in pyridine. The crude acetate was purified by column chromatography on silica gel (5 g), using the following solvents as eluent (each 10 ml): fr. 1, benzene–acetone (100 : 1); fr. 2, benzene–acetone (50 : 1); frs. 3 and 4, benzene–acetone (100 : 3); frs. 5—8, benzene-acetone (25 : 1); fr. 9, benzene–acetone (20 : 1). Fractions 5 and 6 were combined and methylated with diazomethane in ether. The reaction product was purified by preparative TLC on Kieselgel PF_{254} developed with benzene–acetone (20 : 1) to afford methyl 2α,3β-diacetoxy-13α*H*-olean-18-en-28-oate (**7**), which was shown to be identical (IR, PMR, MS, and TLC) with a specimen obtained by the forced Wolff-Kishner reduction of **5**.

References

1) This work was reported in a preliminary form: T. Honda, T. Murae, T. Tsuyuki, and T. Takahashi, *Chem. Lett.*, **1977**, 271,

2) D. H. R. Barton, D. A. J. Ives, and B. R. Thomas, *J. Chem. Soc.*, **1955**, 2056.

3) W. Nagata and H. Itazaki, *Chem. & Ind.*, **1964**, 1194.

4) T. Honda, T. Murae, T. Tsuyuki, and T. Takahashi, *Chem. Pharm. Bull.*, **24**, 178 (1976); T. Honda, T. Murae, T. Tsuyuki, T. Takahashi, and M. Sawai, *Bull. Chem. Soc. Jpn.*, **49**, 3213 (1976).

5) F. E. King, T. J. King, and J. D. White, *J. Chem. Soc.*, **1958**, 2830.

6) L. R. Row, P. S. Murty, G. S. R. S. Rao, C. S. P. Sastry, and K. V. J. Rao, *Indian J. Chem.*, **8**, 716 (1970).

7) L. Caglioti, G. Cainelli, and F. Minutilli, *Gazz. Chim. Ital.*, **91**, 1387 (1961); L. Caglioti and G. Cainelli, *Tetrahedron*, **18**, 1061 (1962).

8) Cf. H. Budzikiewicz, J. M. Wilson, and C. Djerassi, *J. Am. Chem. Soc.*, **85**, 3688 (1963).

9) D. H. R. Barton, C. J. W. Brooks, and N. J. Holness, *J. Chem. Soc.*, **1951**, 278.

10) L. R. Row and G. S. R. S. Rao, *Tetrahedron*, **18**, 827 (1962). They described a formation of methyl arjunolate (**29**) on a forced Wolff-Kishner reduction of **2**. However, no such deoxygenated product (**3**) was obtained in the present work.

11) M. Shamma, R. E. Glick, and R. O. Mumma, *J. Org. Chem.*, **27**, 4514 (1962).

12) a) J. M. Beaton, J. D. Johnston, L. C. McKean, and F. S. Spring, *J. Chem. Soc.*, **1953**, 3660; b) R. E. Ireland, S. W. Baldwin, D. J. Dawson, M. I. Dawson, J. E. Dolfini, J. Newbould, W. S. Johnson, M. Brown, R. J. Crawford, P. F. Hudrilik, G. H. Rasmussen, and K. K. Schmiegel, *J. Am. Chem. Soc.*, **92**, 5743 (1970); c) M. Tori, T. Tsuyuki, and T. Takahashi, *Chem. Lett.*, **1977**, 699.

13) S. Abe, *Bull. Chem. Soc. Jpn.*, **33**, 271 (1960).

14) D. H. R. Barton and C. J. W. Brooks, *J. Chem. Soc.*, **1951**, 257; D. H. R. Barton and N. J. Holness, *ibid.*, **1952**, 78.

15) S. Nakamura, T. Yamada, H. Wada, Y. Inoue, T. Goto, and Y. Hirata, *Tetrahedron Lett.*, **1965**, 2017.

16) H. Wada, G. Goto, T. Goto, and Y. Hirata, *Tetrahedron Lett.*, **1966**, 3461.

17) P. Bilham, G. A. R. Kon, and W. C. J. Ross, *J. Chem. Soc.*, **1942**, 540; L. Ruzicka, R. Grob, R. Egli, and O. Jeger, *Helv. Chim. Acta*, **26**, 1218 (1943).

18) R. A. Sneen and N. P. Matheny, *J. Am. Chem. Soc.*, **86**, 5503 (1964).

19) K. Kusama, *J. Biochem.*, **44**, 375 (1957).

Formation of Bis(methylthio)(methylsulfinyl)methane in the Reaction of Methyl (Methylthio)methyl Sulfoxide with Sodium Hydride

Katsuyuki OGURA, Nobuko KATOH, and Gen-ichi TSUCHIHASHI

Sagami Chemical Research Center, Nishi-Ohnuma Sagamihara, Kanagawa 229

(Received October 19, 1977)

Treatment of methyl (methylthio)methyl sulfoxide (**1**) with sodium hydride gave bis(methylthio)(methylsulfinyl)methane (**3**) which might be formed by abnormal attack of the carbanion (**2**) of **1** on the sulfide linkage of **1**. The additon of butyl iodide to this system completely suppressed the formation of **3**, showing that **2** reacts faster with butyl iodide than with **1**. The mechanism to account for these phenomena is discussed.

Recently, new synthetic methods using methyl (methylthio)methyl sulfoxide (**1**) have been developed.[1-7] This compound can be converted into the carbanion (**2**) by the action of sodium hydride, potassium hydride, or butyllithium. In tetrahydrofuran (THF), treatment of **1** with either potassium hydride[6,9] or butyllithium[6,7,9] generates **2** instantaneously at from −70 °C to an ambient temperature. On the other hand, when sodium hydride is employed as a base, warming is necessary to form **2**.[2,3,8,10] Thus, alkylation of **1** with an alkyl halide and sodium hydride can be achieved by agitation of these compounds together in THF at an elevated temperature.[2,3,8] During the course of our investigation on the solvent-effect for the formation of **2** using sodium hydride, we have found the following interesting reaction of **1** with **2** to form bis(methylthio)-(methylsulfinyl)methane (**3**) and dimethyl sulfoxide.

A solution containing **1** (34.6 mmol) and sodium hydride (22.5 mmol) in hexamethylphosphoric triamide (HMPT; 10 ml) was stirred under cooling with ice-water for 2 h and at room temperature for 36.5 h. A usual work-up gave **3** as colorless crystals, mp 69—70 °C, in 45% yield. The structure of this product was confirmed by its IR and NMR spectra, the elemental analysis, and the independent synthesis achieved by the oxidation of tris(methylthio)methane with hydrogen peroxide and a catalytic amount of sodium tungstate. Even when one equivalent of sodium hydride was employed, the similar result was obtained. The formation of **3** was also observed in THF although the reaction went more slowly than in HMPT. Furthermore, it should be noted that the addition of butyl iodide to the solution containing **1** and sodium hydride in HMPT completely suppressed the formation of **3** and a butylated product, 1-(methylsulfinyl)-1-(methylthio)pentane (**4**) was produced instead.

These facts may be reasonably explained by the mechanism depicted in Scheme 1. During the reaction of **1** with sodium hydride, the carbanion (**2**) coexists with the unreacted **1** because of the slow reaction of **1** with sodium hydride. Then, **2** attacks on the sulfide linkage of **1** as shown in Scheme 1, forming the carbanion of dimethyl sulfoxide (**5**) and **3** which are further converted into **5**[11] and the carbanion (**6**) of **3**, respectively, by a proton transfer. When butyl iodide is added to this system, the formed carbanion (**2**) reacts with the iodide faster than with **1** to afford the butylated product (**4**).

Existence of **6** at the final stage of the reaction might be supported by the fact that the addition of benzyl chloride, followed by stirring of the solution at from room temperature to 40 °C gave *β,β*-bis(methylthio)styrene (**8**) which was very likely formed by dehydrosulfenylation of the benzylated product (**7**) of the carbanion (**6**).

Since the alkylation of **1**, followed by the hydrolysis of the thioacetal *S*-oxide group provides a convenient synthetic route to aldehydes, we would like to emphasize that the necessary conditions for the alkylation of **1** by an alkyl halide–sodium hydride system is to stir a solution containing these reagents together at a temperature of *ca.* 50 °C.

Experimental

Formation of Bis(methylthio)(methylsulfinyl)methane (3) from Methyl (Methylthio)methyl Sulfoxide (1). To a solution

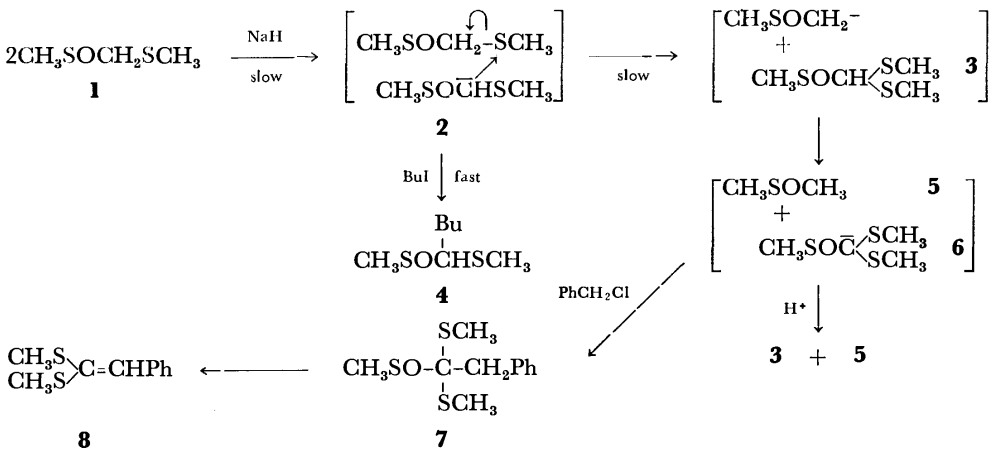

Scheme 1.

containing **1** (4.290 g, 34.6 mmol) in HMPT (10 ml), was added sodium hydride (65% oil-dispersion; 830 mg, 22.5 mmol), and the mixture was stirred under cooling with ice-water for 2 h and at room temperature for 36.5 h. After the addition of dichloromethane (150 ml) and washing with water (100 ml), the organic layer was dried over anhydrous sodium sulfate and evaporated *in vacuo*. The residue was separated by twofold column-chromatography on silica gel (eluted with dichloromethane) to afford **3** (1.337 g, 7.86 mmol; 45%) as colorless crystals. An analytical sample was obtained by recrystallization from diethyl ether–hexane: Mp 69—70 °C; IR (KBr) 1032 cm^{-1}; NMR ($CDCl_3$): δ=2.36 (6H, s), 2.72 (3H, s), and 4.53 (1H, s). Found: C, 28.11: H, 5.90%. Calcd for $C_4H_{10}OS_3$: C, 28.21; H, 5.91%.

This compound is thermally unstable even at room temperature and decomposes completely within 1 h at 50 °C.

Oxidation of Tris(methylthio)methane into ***3***. To a solution of tris(methylthio)methane(1.505 g, 9.77 mmol) in methanol (10 ml), were added sodium tungstate dihydrate (10 mg) and 30% aqueous solution (1.1 ml, 9.7 mmol) of hydrogen peroxide under cooling with ice-water. Then, the mixture was stirred under cooling with ice-water for 1 h, and water (25 ml) was added. After the extraction with four 30 ml-portions of dichloromethane, the organic layer was dried over anhydrous sodium sulfate and evaporated *in vacuo*. The residue was column-chromatographed on silica gel (eluted with dichloromethane–ethyl acetate) to yield 927 mg (56%) of colorless crystals which were identified with **3** by the comparison of their IR and NMR spectra with those of the product obtained by the reaction of **1** with sodium hydride.

Reaction of ***1*** *with Sodium Hydride in the Presence of Butyl Iodide*. To a solution of **1** (1.385 g, 11.69 mmol) in HMPT (2 ml) were added sodium hydride (65% oil-dispersion; 538 mg, 14.6 mmol) and butyl iodide (2.888 g, 15.70 mmol). The mixture was stirred under cooling with ice-water for 2 h, at room temperature for 25 h, and at 45 °C for 24 h. After the addition of dichloromethane (30 ml), the deposited solid was filtered off and the filtrate was evaporated *in vacuo*. The residue was separated by column-chromatography on silica gel (eluted with dichloromethane and ethyl acetate) to afford 1.327 g (7.37 mmol: 66%) of **4** which was identified with the product previously reported[8] by the comparison of their NMR spectra.

*Detection of DMSO (****5****) in the Reaction of* ***2*** *with* ***1***. To a suspension of potassium hydride (24% oil-dispersion; 2.166 g, 13.0 mmol) in THF (10 ml) was added **1** (3.026 g, 24.44 mmol) under cooling with ice-water for 30 min, at room temperature for 16.5 h, and at 40 °C for 9 h. After the addition of dichloromethane (100 ml) and water (1 ml), stirring at room temperature for 5 min, and the addition of anhydrous sodium sulfate, the insoluble matter was filtered off and the filtrate was evaporated *in vacuo*. The residue was separated by column-chromatography on Florisil (eluted with dichloromethane, ethyl acetate, and methanol) to give 203 mg (10%) of **3** and 1.275 g of a colorless oil which was shown by an NMR analysis to consist of **1** (959 mg) and **5** (316 mg; 33%).

Reaction of ***6*** *with Benzyl Chloride*. A mixture containing **1** (5.159 g, 41.60 mmol) and sodium hydride (65% oil-dispersion; 860 mg, 23.3 mmol) in HMPT (15 ml) was stirred under cooling with ice-water and at room temperature for 49.5 h. After the addition of benzyl chloride (2.818 g, 22.28 mmol), the mixture was further stirred at room temperature for 1 week and at 40 °C for 4 h. Then, water (50 ml) and dichloromethane (100 ml) were added and the solution was shaken. After the organic layer was separated, the aqueous layer was extracted with two 30 ml-portions of dichloromethane. The organic layers were combined, dried over anhydrous sodium sulfate, and evaporated *in vacuo*. The residue was column-chromatographed on silica gel (eluted with hexane–benzene) to give a pale yellow oil which was shown by an NMR analysis(using piperonal as an internal standard) to contain 1.149 g (28%) of β,β-bis(methylthio) styrene (**8**). A pure sample of **8** could be obtained by distillation under reduced pressure and it was identified by comparison of its IR and NMR spectra with those of an authentic sample which was given by reduction of β-(methylsulfinyl)-β-(methylthio)styrene[12] as described in the following.

Reduction of β-(Methylsulfinyl)-β-(methylthio)styrene with Titanium Trichloride. To a solution containing β-(methylsulfinyl)-β-(methylthio)styrene[12] (7.106 g) in 30 ml of dichloromethane and 60 ml of hexane, was added 20% aqueous solution (30 ml) of titanium trichloride and the resulting mixture was stirred at room temperature for 1 h. After the addition of benzene (100 ml), the organic layer was separated, washed with water, dried over anhydrous potassium carbonate, and evaporated *in vacuo*. The residue was column-chromatographed on Florisil to give 1.595 g of a pale yellow oil, whose structure was assigned as **8** by its physical data and an elemental analysis: Bp 104—105 °C/0.3 Torr (lit,[13] bp 94—95 °C/0.25 Torr); NMR ($CDCl_3$): δ=2.27 (3H, s), 2.32 (3H, s), 6.71 (1H, s), and 7.10—7.60 (5H, m); MS(70 eV): *m/e* (rel. intensity) 196 (66), 149 (31), and 134 (100). Found: C, 61.02; H, 6.10; S, 32.56%. Calcd for $C_{10}H_{12}S_2$: C, 61.17; H, 6.16; S, 32.66%.

References

1) K. Ogura, S. Furukawa, and G. Tsuchihashi, *Bull. Chem. Soc. Jpn.*, **48**, 2219 (1975) and the references cited therein.

2) G. Schill and P. R. Jones, *Synthesis*, **1974**, 117.

3) G. R. Newkome, J. M. Robinson, and J. D. Sauer, *J. Chem. Soc. Chem. Commun.*, **1974**, 410.

4) K. Ogura, M. Yamashita, and G. Tsuchihashi, *Synthesis*, **1975**, 385.

5) K. Ogura, I. Yoshimura, N. Katoh, and G. Tsuchihashi, *Chem. Lett.*, **1975**, 803.

6) K. Ogura, M. Yamashita, S. Furukawa, M. Suzuki and G. Tsuchihashi, *Tetrahedron Lett.*, **1975**, 2767.

7) K. Ogura, M. Yamashita, and G. Tsuchihashi, *Tetrahedron Lett.*, **1976**, 759.

8) K. Ogura and G. Tsuchihashi, *Tetrahedron Lett.*, **1971**, 3151.

9) K. Ogura and G. Tsuchihashi, *Tetrahedron Lett.*, **1972**, 2681.

10) K. Ogura and G. Tsuchihashi, *J. Am. Chem. Soc.*, **96**, 1960 (1974).

11) Formation of **5** was confirmed by the experiment using **1** and potassium hydride (0.5 equivalent to **1**) in THF (see Experimental section).

12) K. Ogura and G. Tsuchihashi, *Tetrahedron Lett.*, **1972**, 1383.

13) G. A. Russell and L. A. Ochrymowycz, *J. Org. Chem.*, **35**, 764 (1970).

Substrate-Nucleophile Association in the Finkelstein Reaction System in Dipolar Aprotic Solvent. Formation of Complex between Substituted Chloromethanes and Halide Ion in Acetonitrile*

Jun-ichi HAYAMI, Tohru KOYANAGI, Nobuhisa HIHARA, and Aritsune KAJI

Department of Chemistry, Faculty of Science, Kyoto University, Kyoto 606

(Received January 14, 1977)

Substrate-nucleophile association was found between substituted chloromethanes ($ArXCH_2Cl$: X=NONE, S, SO, SO_2, and CO) and halide ion (Cl^-, Br^-, and I^-) in dipolar aprotic solvent. The equilibrium constant (K), limiting shift (Δ_c), the enthalpy of formation ($\Delta H°$), and the entropy of formation ($\Delta S°$), for complexing were determined by NMR measurement. The measurement of spin-lattice relaxation time (T_1) gave an information on the conformation of this complex. Halide ion seems to locate closest to α-methylene protons at the site of potential S_N2 reaction.

In the course of studies on the symmetrical Finkelstein reaction in a dipolar aprotic solvent,[1,2] the present authors found the specific interaction between a strong nucleophile and a substrate (substituted chloromethanes).

$$ArXCH_2Cl + Y^- \overset{K}{\rightleftharpoons} ArXCH_2Cl \cdot Y^- \quad (1)$$

Ar = Phenyl and substituted phenyl

X = NONE, S, SO, SO_2, and CO

Y = Cl, Br, and I

Y^- was used in the form of tetraalkylammonium salt (R_4NY; R=ethyl or butyl).

The interaction was observed as a low field shift of the absorption in a PMR spectrum of substrate, on the addition of nucleophilic anion to the solution of the substrate in dipolar aprotic solvent. Martin, Hayami and Lemieux reported the formation of an anion-substrate complex for β-glycopyranosyl derivatives.[3] Green and Martin extended the study to trihalomethanes and other substrates.[4] They attributed such an interaction mainly to hydrogen bonding. Since then, such hydrogen bonding equilibria have been studied extensively between various nucleophilic anions and hydrogen donors. Typical examples were found in the interaction of carboxylic acids[5] or phenols[6] with various anions.

The most important feature of the present study lies in the fact that the complex formation is operative under the same conditions where the symmetrical Finkelstein reaction with radioactive chloride ion actually proceeds.

$$ArXCH_2Cl + *Cl \overset{k}{\longrightarrow} ArXCH_2{*}Cl + Cl^- \quad (2)$$

In the present study, thermodynamic aspects of the complex formation are described. Measurements of the proton spin-lattice relaxation time were made to indicate the partial freezing of the intramolecular rotation about the potential S_N2 reaction center.

Experimental

Materials. Acetonitrile was distilled five times from P_2O_5 and once from K_2CO_3 initially, and finally distilled with no reagent added. The dry solvent was stored in a dry box.

Substituted chloromethanes[7] were synthesized according to the standard procedure.

Tetraalkylammonium Salts: Tetraalkylammonium halides were prepared by the reaction of the corresponding alkyl halides and trialkyl amines in acetonitrile.[3] Tetraethylammonium perchlorate was prepared by the reaction of tetraethylammonium bromide and perchloric acid. Immediately before each measurement, all the salts were dried under reduced pressure over P_2O_5 at the refluxing temperature of toluene (or benzene for perchlorate) for 2 h.

Proton Magnetic Shift Measurement. An aliquot of the stock solution of substituted chloromethane (0.1 mmol) and TMS in acetonitrile was placed in volumetric tubes (1 ml) containing ammonium salts (0.2—1.2 mmol). The solutions were made up to the mark, and then were transferred to the NMR sample tubes. All the samples were prepared inside a dry box. The PMR spectra were measured in an internal lock mode for the solvent acetonitrile, with a JEOL PS-100 spectrometer operating at 100 MHz. The line positions were measured to 0.1 Hz by reading the frequencies at each resonance of substrate and the internal standard, TMS, with a built-in frequency counter at least four times and averaging the results.

Analysis of PMR Shift vs. Concentration. Equilibrium constant, K, and limiting shift of the complex, Δ_c, were determined by means of Scott's modification of the Benesi-Hildebrand equation,[8,9] assuming only 1 : 1 complex of substrate and halide ion. In this treatment the degree of dissociation of ammonium salt was assumed to be constant in the concentration range of measurements.[10,11] Analysis was repeated until a self-consistent set of values was obtained. It was carried out automatically on the programmable calculator, Canon SX-110. The use of PMR measurement is an authorized method for the study of hydrogen bonding interaction, being essentially similar to that given by Martin and coworkers.[3]

Measurements of Spin-lattice Relaxation Time (T_1). Spin-lattice relaxation curves of protons were obtained on a JEOL PS-100 NMR spectrometer equipped with a pulse Fourier-transform unit (PFT-100) and a spectrum computer (EC-100), by application of 180°-t-90° pulse sequences at 100 MHz. The spin-lattice relaxation time (T_1) was deduced by the least-squares approximation of the observed value of $I_{(t)}$ to $I_0[1-2\exp(-t/T_1)]$, where $I_{(t)}$ is longitudinal magnetization at time t, and I_0 is the equilibrium magnetization.[12] Measurements were carried out with two samples for each series of substituted chloromethanes, the standard acetonitrile solution of the substrate (0.1 M), and a solution in which the appropriate amount of tetraethylammonium chloride

* S_N2 Reactions in Dipolar Aprotic Solvents. VI. Part of this work was presented before the 2nd IUPAC Conference on Physical Organic Chemistry (Nordwijkerhout, 1974), and was published in *Tetrahedron Lett.*, **1973**, 385.

was added to the standard solution.

Since the equilibration is very fast as compared with the $1/T_1$ of the protons in both the free and the complexed substrate, the observed $T_1(T_1^{obsd})$ in the present case can be expressed as the weighted means.[13]

$$1/T_1^{obsd} = f^c/T_1^c + f^\circ/T_1^\circ = f^c R_1^c + f^\circ R_1^\circ, \quad (3)$$

where f^c and f° denote the fractions, T_1^c and T_1°, the relaxation time, and R_1^c and R_1°, the rate of relaxation of complexed and uncomplexed species, respectively. Since f^c and f° can be calculated from the equilibrium constant (K), the values of R_1^c are easily deduced. The rotational correlation time (τ_c) can be calculated from R_1 by means of

$$R_1 = (3/2)\hbar^2\gamma_H^4\tau_c/r_{HH}^6, \quad (4)$$

where $\hbar$ is the Planck constant divided by 2π, γ_H is the gyromagnetic ratio of proton, and r_{HH} is the distance between neighboring protons.[14] The effect of complexing on the intramolecular rotation is sharply reflected on τ_c. τ_c^c and τ_c° denote the rotational correlation time of the complexed and the uncomplexed species, respectively.

Results and Discussion

On addition of tetraalkylammonium halide to the acetonitrile solution of substituted chloromethanes, the PMR absorption showed low field shift. The amount of shift of each proton was analyzed by the Scott modification of the Benesi-Hildebrand equation,[3] which gave a good linear relationship in each case. α-Methylene protons of (arylsulfinyl)chloromethanes, which appear as AB quartet in acetonitrile solution, exhibit a different response on complexing; the proton in a higher field showing apparently a larger shift (Fig. 1). The difference in the response was also substantiated in the measurement of spin-lattice relaxation time (T_1). On addition of chloride ion, the rate of relaxation became higher at the proton lying in the higher field.

Effect of the Ammonium Salts. The effect of tetraalkylammonium salts on the formation of the complex was investigated by using (*p*-chlorophenylsulfonyl)chloromethane as substrate, which showed a low reactivity

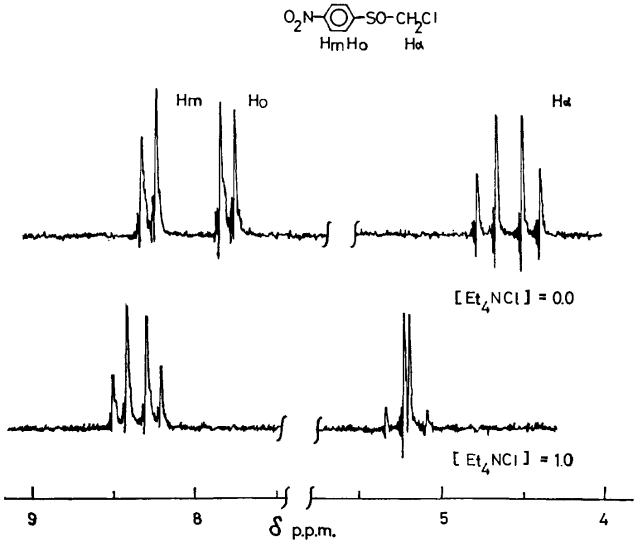

Fig. 1. Change of pmr spectra of (*p*-nitrophenylsulfinyl)chloromethane in acetonitrile after addition of TEACl.

in S_N2 reactions and gave no detectable amount of the substitution product with various halide ions under the conditions of the PMR measurement. The results are given in Table 1.

Since tetraethylammonium perchlorate showed essentially no ability in the formation of complex, and the other salts studied gave rise to significant changes in the chemical shift of the substrate, it is understood that the cation portion of the ammonium salts plays no essential role in the change of PMR shift, and that the anion portion eventually controls these equilibria.

The most electronegative chloride ion forms a more stable complex than other halide ions (Br^- or I^-) do. The results suggest that the interaction is similar to that studied by Martin and coworkers,[3,4] and that it might be of hydrogen bonding. The present results also suggest that such a phenomenon is general for substances with "acidic" proton(s) as were the cases with certain β-glycopyranosyl derivatives and with trihalomethanes.

Tetraethylammonium bromide and tetrabutylammonium bromide differ in the formation constant of the complex (K), although these salts have bromide ion in common. The difference can be ascribed to the difference in the ion pair dissociation of the salt in the organic solution.[15] Tetrabutylammonium iodide is apparently a more effective hydrogen bond acceptor than expected from the basicity of iodide ion. This might also be ascribed to the ion pairing phenomena of the ammonium iodide.[15] However, lack of information on the behavior of the ammonium salts in high concentrations allows no further discussion.

Effect of the Solvent. The substituted chloromethanes form a complex with the halide ion, not only in acetonitrile but also in other dipolar aprotic solvents (DMSO or DMF). However, addition of a protic solvent (methanol) to the solution in acetonitrile retards the substrate-anion complex formation (Table 2). This can be explained in terms of the competitive hydrogen bonding between a protic solvent and the halide ion.[16] Methanol exhibits a strong tendency to undergo hydrogen bonding association with chloride ion.[17]

PMR Shift. Equilibrium constant (K) and the limiting shift of the complex (Δ_c) for *p*-nitrophenyl derivatives of substituted chloromethanes, with tetraethylammonium chloride as hydrogen bond acceptor,[18]

Table 1. Effect of tetraalkylammonium salts on the formation of complex [*p*-Cl-Ph-SO_2-CH_2Cl + R_4NX][a]

R_4NX R	R_4NX X	K (M^{-1})[b]
C_2H_5	Cl	0.820
C_2H_5	Br	0.358
n-C_4H_9	Br	0.555
n-C_4H_9	I	0.711
C_2H_5	ClO_4	0

Throughout this paper 1 M = 1 mol dm^{-3}, 1 cal_{th} = 4.184 J, 1 Å = 0.1 nm.

a) In acetonitrile, at 25 °C. b) Errors estimated to be within 0.005.

Table 2. Effect of the protic solvent (MeOH) on the formation of complex [p-NO_2-Ph-CH_2Cl + TEACl][a]

MeOH	K (M^{-1})[b]
0	0.258
0.061	0.232
0.123	0.188
0.245	0.141
0.491	0.084

a) In acetonitrile, at 32 °C. b) Errors estimated to be within 0.005.

Table 3. Summary of the formation of complex between substituted chloromethanes and TEACl in acetonitrile [p-NO_2-Ph-X-CH_2Cl + Cl^-][a]

Substrate (-X-)	Δ_c(*meta*)	Δ_c(*ortho*) (ppm)[b]	Δ_c(α-CH_2)	K[c] (M^{-1})	$\rho(K)$
NONE	−0.220	−0.681	−0.943	0.258	0.63
S	−0.089	−0.584	−1.229	0.493	0.59
SO	−0.197	−0.547	−1.178[d] / −1.190	1.190	0.61
SO_2	−0.148	−0.441	−1.506	1.282	0.51
CO	−0.241	−0.541	−1.012	0.403	0.52

a) At 32 °C. b) Errors estimated to be within 0.004 ppm. c) Errors estimated to be within 0.005. d) Proton at the higher field gives a larger Δ_c value (Fig. 1).

are summarized in Table 3. As the substituent becomes more electron-withdrawing, the association seems to prevail. This is also in line with the view that the principal cause of this interaction should be hydrogen bonding to the α-methylene protons.[19]

The changes of chemical shift can be attributed mainly to the effect of electrostatic field originating at halide ion. The electrostatic field at the hydrogen atom is a function of the anion–hydrogen distance, and the limiting shift (Δ_c) is a function of distance and the angle. This can be seen from the simple approximation in terms of Buckingham's equation for the electrostatic field produced by the point charge:[20]

$$\Delta_c = -A(1/r_{HX}^2)\cos\theta - B(1/r_{HX}^4), \quad (7)$$

where r_{HX} is the distance from the anion center to the hydrogen nucleus, and θ is the angle between the C–H and H–anion vector.

Thus, the location of the halide ion can be inferred from the value of Δ_c. In each compound the absolute values of Δ_c decrease in the order α-$CH_2 \gg$ *ortho* > *meta*, suggesting that the chloride ion is located in a close neighborhood of α-methylene protons.

Linear Free Energy Relationship. For equilibrium constant of the complex formation (K), a linear Hammett relationship holds in every series of compounds, the positive ρ values being obtained. The results are given in Table 3. Positive ρ values indicate that substituted chloromethanes act as a hydrogen bond donor. Electron-withdrawing substituents enhance the acidity and the donor capacity of a proton.

Table 4. Arrhenius parameters for the formation of complex [p-NO_2-Ph-X-CH_2Cl + Cl^-]

X	$\Delta H°$[a] (kcal mol^{-1})	$\Delta S°$[b] (eu)
NONE	−4.88	−18.6
S	−1.75	−7.19
SO	−1.40	−4.18
SO_2	−1.22	−3.82
CO	−5.31	−21.0

a) Errors estimated to be within 0.5 kcal mol^{-1}. b) At 20 °C. Errors estimated to be within 2.0 eu.

Arrhenius Parameters for the Formation of Complex. Equilibrium constants were determined at temperatures 0—30 °C. Arrhenius parameters of formation for the anion-substrate complex are given for p-nitrophenyl derivatives as the representative in Table 4. Both the enthalpy of formation ($\Delta H°$) and the entropy of formation ($\Delta S°$) give negative values, which are in a reasonable range for the hydrogen bonding equilibria.[17,19] Negative values of $\Delta H°$ indicate that a stabilization can be attained to some extent by complex formation. The order of stabilization ($-\Delta H°$), [$-\Delta H_X^\circ$ for $ArXCH_2Cl$: $-\Delta H_{SO_2}^\circ < -\Delta H_{SO_2}^\circ < -\Delta H_S^\circ < -\Delta H_{NONE}^\circ < -\Delta H_{CO}^\circ$] is not in agreement with the order of the magnitude of K. It is in contrast to the fact that in most hydrogen bonding equilibria there is a coincidence between the order of magnitude of K and of $-\Delta H°$.[21] Negative values of $\Delta S°$ are found as is often the case with a bimolecular association. In the present case, the stabilization of the complex is counterbalanced by the entropy loss, giving rise to a K smaller than unity or close to unity. As will be suggested later from the study of proton relaxation time, it seems that the freezing of intramolecular motion plays an important role in decreasing $\Delta S°$.

Effect of the Complex Formation on Proton Spin-lattice Relaxation Time (T_1). Recently, T_1 measurements have been applied to the investigation of interactions between or within organic molecules.[22,23] The T_1 value is very sensitive to the change of environmental factors. In the present case T_1 gives unique indication of the interaction between the anionic nucleophile and the substrate.

Each proton of substituted chloromethanes shows an appreciable increase in relaxation rate ($1/T_1 = R_1$) on addition of the nucleophilic anion (Cl^-). Perchlorate ion gives no significant effect on T_1, reflecting its poor ability as a hydrogen bond acceptor (Table 5). This suggests that the influence of the increasing viscosity of the acetonitrile solution caused by the addition of ammonium salt is not detrimental under the present experimental conditions. It has also been established that the chlorine atom (from tetraethylammonium chloride), with its small gyromagnetic moment, can give no noticeable contribution to the nuclear magnetic relaxation.[25,26] Thus, one possible mechanism remains operative in altering T_1 on complexing. That is the change of the rotational correlation time (τ_c), caused by the retardation of the intramolecular rota-

TABLE 5. EFFECT OF COMPLEXING ON T_1[a)]

X[b)]	$R_1^0(CH_2)$[c)] / $R_1^0(meta)$	$R_1^c(CH_2)$[c)] / $R_1^c(meta)$	$\tau_c^0(CH_2)$[d)] / $\tau_c^0(meta)$	$\tau_c^c(CH_2)$[d)] / $\tau_c^c(meta)$	$\tau_c^c/\tau_c^0(CH_2)$ / $\tau_c^c/\tau_c^0(meta)$
NONE	0.12_2	0.33_9[f)]	4.5_4	$12._6$	2.7_8
	(0.12_8)[e)]	(0.31_3)	(4.7_7)	($11._7$)	(2.4_5)
	0.06_2	0.26_2	$17._3$	$70._7$	4.0_9
	(0.06_5)	(0.24_0)	($18._2$)	($67._0$)	(3.6_9)
S	0.18_3	1.15_7	6.7_9	$43._0$	6.3_3
	0.07_0	0.13_1	$19._6$	$36._6$	1.8_6
SO	0.26_0	0.78_8[g)]	9.6_9	$29._3$	3.0_2
	0.07_3	0.09_2	$20._4$	$25._7$	1.2_6
SO_2	0.23_6	0.64_9	8.7_8	$24._1$	2.7_4
	0.07_5	0.08_8	$21._0$	$24._4$	1.1_6
CO	0.40_5	1.93_6	$15._1$	$72._0$	4.7_7
	0.05_8	0.34_1	$16._2$	$95._0$	5.8_6

a) At 25 °C. b) p-NO_2-Ph-X-CH_2Cl. c) s^{-1}. d) ps. e) Values in parentheses are the data where $TEAClO_4$ (0.8 M) was added to the standard solution to detect the influence of viscosity. f) For α-d_1, at 30 °C, $R_1^0(CHD)/R_1^0(CH_2)=0.02^2/0.09^4=0.23^4$, $R_1^c(CH_2)/R_1^0(CH_2)=3.8_3$, $R_1^c(CHD)/R_1^0(CHD)=4.3_5$. g) Proton at the higher field gives greater R_1^c. $R_1^c(CH_2)=\{R_1^c(CH_2-l)+R_1^c(CH_2-h)\}/2=\{0.417+1.158\}/2$; CH_2-h and CH_2-l denote methylene proton at the higher field and the lower field (*cf.* Fig. 1).

tion in the complexed substrate.[27)]

For the relaxation of the α-methylene protons of substituted chloromethanes, only a single H–H distance corresponding to geminal protons should be considered, since aromatic protons are situated in too remote a position to contribute significantly to the relaxation of α-methylene protons (the interaction contributing to the spin-lattice relaxation of protons diminishes rapidly with increase in the interproton distance, as expressed by Eq. 4). The postulate is verified by the deuteruim labelling experiment. Substitution of one of the methylene protons with deuterium causes a striking increase in T_1.[26)] Similarly, for relaxation of the protons on benzene ring (*para* substituted), only a single H–H distance between the nearest neighbor, vicinal protons, needs to be considered.

Consequently, as a first approximation, T_1 can be correlated with rotational correlation time (τ_c), as expressed by Eq. 4, where 1.78 Å is taken to be the quantity r_{HH} for α-methylene protons and 2.49 Å for vicinal protons on benzene ring. Variations in the proton spin-lattice relaxation rate ($R_1=1/T_1$) and τ_c of α-methylene proton and meta proton on complexing are shown for substituted chloromethanes having a p-nitro group on the phenyl ring in Table 5. The postulate seems to be reasonable, since the τ_c^c value calculated is shoter at a more mobile α-methylene group than at a less mobile aromatic ring.

Change of T_1 (or τ_c) furnishes additional evidence that nucleophilic chloride ion interacts with the chloromethanes. The substrates studied can be classified into two groups, one group of compounds (X=S, SO, SO_2) which show little change in $\tau_c(meta)$ but a significant change in $\tau_c(CH_2)$, and the other (X=NONE, CO) in which both the ring proton and the α-methylene proton show significant change in the rate of relaxation. Such tendency is in line with that of the enthalpy and entropy of the formation of complex and with the temperature coefficient of the limiting shift ($\partial\Delta_c/\partial T$).[28)]

The former group shows small negative enthalpy and entropy of formation of the complex, their limiting shift being hardly affected at all by the change in temperature.[28)] This tendency of the parameters suggests that the nature of the association is of hydrogen bonding. On complexing, the substrate moiety becomes "rigid", the intramolecular rotation about the chloromethyl group being frozen considerably to bring about a common τ_c^c for both the ring proton and the methylene proton. Such a τ_c^c may correspond to the molecular motion of the complex as a whole. In this class of compounds, $\tau_c(meta)$ may be taken as a measure of the molecular motion of the substrate as a whole mass, since the rotation around the pheyl ring—X axis is considered to have little effect upon the relaxation of both the *ortho* and/or *meta* proton.[27)]

Thus, a reasonable explanation can be presented for the compounds of the former group. The data indicate that the important part of the loss of entropy can be attributed to the freezing of the internal rotation at the complexed species.

The latter group of compounds (X=NONE, CO) show an extensive change in τ_c (and/or R_1) for both the α-methylene and the ring proton(s). The two compounds show significant enthalpy and entropy of formation of the complex, their limiting shifts showing a significant dependency on temperature. The behavior implies that some interaction other than hydrogen bonding can be operative in the complexing of these substrates.[19,20a,20b)]

(p-Nitrophenyl)chloromethane shows a change in $\tau_c(CH_2)$ comparable to that found for the former group of compounds, however, change in $\tau_c(meta)$ is anomalously large. A tentative explanation is that some other kind of relaxation mechanism is operative for the ring proton(s), the former proposition for the relaxation being not valid for the complex derived from this substrate. Another explanation is that the complexing brings about a particular conformation in which another dipole-dipole interaction is possible between the α-methylene and the ring proton(s). A

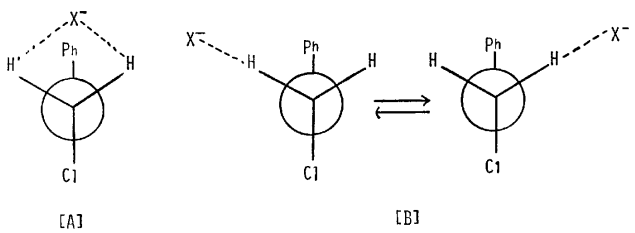

Fig. 2. Modes of coordination of halide ion to substituted chloromethanes.

reasonable change in $\tau_c(CH_2)$ for the deuterated substrate (α-d_1) seems to suggest the first possibility. An interaction between the chlorine and the phenyl ring may be responsible for the additional relaxation.

2-Chloro-1-(*p*-nitrophenyl)ethanone indicates an extensive interaction with chloride ion. Characteristic implication for this compound is that an uncomplexed substrate shows a common τ_c° at both the α-methylene and the ring proton. This suggests that intramolecular rotation is already hindered about the chloromethyl moiety. On the formation of the complex, the substrate seems to become "rigid", otherwise some additional mechanism seems to be operating. An interaction between the chloride ion and the carbonyl group was suggested in the change of CMR shift caused by the addition of chloride.[29] Such an interaction between the nucleophile and the carbonyl group is postulated in the S_N2 reactions of α-halo ketones.[30]

Mode of complexing. The data obtained seem to be indicative of the array of nucleophile and the substrate moiety in this complex. Changes of chemical shift induced by the formation of the complex (Δ_c) are much larger for α-methylene protons than for aromatic protons. There is an apparent parallelism in the magnitude of the equilibrium constant (K) and the order of the electron deficiency at the α-methylene (K_X for $ArXCH_2Cl$; $K_S < K_{SO} < K_{SO_2}$). It seems that the major site of coordination upon complexing with nucleophile is the α-methylene protons. The changes of T_1 upon complexing also are in line with the view that the major site of coordination is the α-methylene protons.

Two typical modes of coordination of nucleophile to the α-methylene protons, shown in Fig. 2, are (A) a rear side coordination of the nucleophile to the chlorine bonded to carbon, and (B) a rapidly exchanging system, where the nucleophile coordinates to one of the protons at a time, collinear to a C–H bond. These two possibilities are indistinguishable in a rapidly exchanging system as observed in the present PMR studies. However, taking into account the electrostatic repulsion between the halide ion and the chlorine atom on the substrate, (A) seems to be more feasiblle. In the case of the complex formation between β-glucopyranosyl derivatives and a halide ion, the nucleophile seems to be located between the H-1 and the H-5 (and not far from H-3) of the pyranose ring in a similar way to mode (A) in Fig. 2.[3]

It is concluded that the substrate-nucleophile complex should exist in the Finkelstein reaction mixture, and that the nucleophilic anion is located in the close neighborhood of the rear side of carbon to chlorine bond, whichever mode [(A) or (B)] of coordination is operative. Such a coordination resembles that in the transition state of S_N2 reactions. Recent MO calculation also suggests that the deep energy minimum is formed which corresponds to a strong hydrogen bonding interaction in the reaction of monofluoroethane and fluoride ion.[31]

The authors wish to express their thanks to Dr. Kazuyuki Akasaka for the discussion on the interpretation of the proton relaxation study. This work is supported by a Grant-in-Aid for Scientific Research from the Ministry of Education (No. 83151, 84076, 748167).

References

1) J. Hayami, N. Tanaka, S. Kurabayashi, Y. Kotani, and A. Kaji, *Bull. Chem. Soc. Jpn.*, **44**, 3091 (1971).
2) J. Hayami, N. Tanaka, and A. Kaji, *Bull. Chem. Soc. Jpn.*, **46**, 954 (1973).
3) J. S. Martin, J. Hayami, and R. U. Lemieux, *Can. J. Chem.*, **46**, 3263 (1968).
4) R. D. Green and J. S. Martin, *J. Am. Chem. Soc.*, **90**, 3659 (1968).
5) M. K. Chantooni, Jr., and I. M. Kolthoff, *J. Am. Chem. Soc.*, **92**, 7025 (1970).
6) I. M. Kolthoff and M. K. Chantooni, Jr., *J. Am. Chem., Soc.* **91**, 4621 (1969).
7) The positions of the substituent on benzene ring is denoted as follows. *para*-C$_6$H$_4$-X-CH$_2$Cl (*meta*, *ortho*)
8) R. L. Scott, *Recl. Trav. Chim. Pays-Bas.*, **75**, 787 (1956).
9) H. A. Benesi and J. H. Hildebrand, *J. Am. Chem. Soc.*, **71**, 2703 (1949).
10) R. P. Taylor and I. D. Kuntz, Jr., *J. Am. Chem. Soc.*, **94**, 7963 (1972).
11) G. W. Stockton and J. S. Martin, *J. Am. Chem. Soc.*, **94**, 6921 (1972).
12) K. Akasaka, T. Imoto, S. Shibata, and H. Hatano, *J. Magn. Reson.*, **18**, 328 (1975).
13) H. Strehlow and J. Frahm, *Ber. Bunsenges.*, **79**, 57 (1957).
14) T. C. Farrar and E. D. Becker, "Pulse and Fourier Transform NMR, Introduction to Theory and Methods," Academic Press, New York, N. Y. (1971).
15) An interpretation for the higher K of the tetrabutylammonium (TBA) bromide or the TBA iodide is to assume the lower degree of ion pair dissociation in the concentrated solution of these two ammonium salts in acetonitrile.

At a low concentration of the salt (<0.3 M), the observed complexing shift is almost equal for both the TBA and tetraethylammonium (TEA) bromide on complexing with chloromethyl sulfones. On increasing the halide ion concentration, the observed down-field shift becomes definitely greater for TEA than for TBA salt. Upon Scott-Benesi-Hildebrand analysis, such a difference gives rise to a larger K for TBA. As the single K (Δ_c) is expected for Br^- ("effective" Br^-), one should assume a lower degree of dissociation for TBA than that for TEA bromide. Similarly, lower degree of dissociation gives rise to high apparent K for the TBA iodide.

Such a treatment is against the ion pair phenomena in a very dilute solution where TBA shows greater dissociation

than TEA does. One of the referees has pointed out this controversy. He suggested that the difference in K can be accounted for by postulating the higher degree of dissociation for TBA and that only the dissociated bromide ion is responsible for the complexing. This treatment seems to be attractive and is sound in principle. However, it should predict much smaller down-field shift for TEA bromide, compared to TBA bromide, especially on going from dilute to concentrated soultion of the ammonium salt. This is just contrary to the case.

For a compromise to both points of view, it could be proposed that the complexing (and neccssarily the bimolecular displacement in acetonitrile) proceeds by the intervention of the ion-paired nucleophile instead of the free dissociated halide ion.

However, the controversy remains unsettled.

16) Y. Kondo, T. Kato, and N. Tokura, *Bull. Chem. Soc. Jpn.*, **48**, 285 (1975).

17) a) S. Y. Lam and R. L. Benoit, *J. Am. Chem. Soc.*, **98**, 1156 (1976); b) A. Allerhand and P. von R. Schleyer, *J. Am. Chem. Soc.*, **85**, 1233, 1715 (1963); c) E. M. Arnett, L. Joris, E. Mitchell, T. S. S. R. Murty, T. M. Gorrie, and P. von R. Schleyer, *J. Am. Chem. Soc.*, **92**, 2365 (1970).

18) TEA chloride can easily be purified, and is not very hygroscopic but sufficiently soluble in acetonitrile. With chloride ion, the observed complexing shift is greater then that with other halide ions studied. TEA fluoride attacks most of the substrates. (*cf.* J. Hayami, N. Ono, and A. Kaji, *Tetrahedron Lett.*, **1968**, 1385).

19) One of the referees suggested that value of $\Delta - H^\circ$ for (*p*-nitrophenyl)chloromethane and for 2-chloro-1-(*p*-nitrophenyl)ethanone is too large to be ascribed to a simple hydrogen bonding to carbon bound hydrogen. The peculiar behavior of the two compounds is also observed in the change of relaxation rate upon complexing and in the temperature coefficient of the limiting shift ($\partial\Delta_c/\partial T$). The tendencies in $\partial\Delta_c/\partial T$ suggest some interactions other than hydrogen bonding can be operative in the two compounds.[23] (This criterion is circumstantial, however, and one cannot rule out the view that some additional interaction is operative for the three other classes of compounds studied.) However, since the linear Hammett relationship holds in each class of the compounds studied, with respect to the XCH_2Cl group as the reference position, and in view of the analogy to the other example of substrate-nucleophile association reported,[3,4] the hydrogen bonding to the α-methylene proton can be postulated as the major driving force for the association.

20) a) A. D. Buckingham, *Can. J. Chem.*, **38**, 300 (1960); b) N. Muller and R. C. Reiter, *J. Chem. Phys.*, **42**, 326 (1965); c) Ref. 4.

21) D. Gurka and R. W. Taft, *J. Am. Chem. Soc.*, **91**, 4794 (1969).

22) H. H. Mantsch, H. Saito, L. C. Leith, and I. C. P. Smith, *J. Am. Chem. Soc.*, **96**, 256 (1974).

23) R. S. Norton and A. Allerhand, *J. Am. Chem. Soc.*, **98**, 1007 (1976).

24) Slight increase in R_1 was observed by the addition of TEA perchlorate to the solution of the substrate in acetonitrile. However, the change in rate was within experimental error (±10%) inherent in the measurement of T_1 and was ignored.

25) A. Carrington and A. D. McLachlan, "Introduction to Magnetic Resonance," Harper and Row, New York, N. Y. (1967).

26) In a similar way to Eq. 4, direct dipole-dipole interaction of chloride ion contributes to the rate of relaxation as shown by

$$R_1^{H\text{-}Cl} = (15/2)\hbar^2\gamma_H^2\gamma_{Cl}^2\tau_c/r_{HCl}^6 \quad (4a)$$

where γ_{Cl} is the gyromagnetic ratio of chlorine and r_{HCl} is the distance between chloride ion and the proton in question.

When one uses the values

$\gamma_H = 26753$ rad s^{-1} G^{-1} (the gyromagnetic ratio of proton)

$\gamma_{Cl} = 2516$ rad s^{-1} G^{-1} (weighted mean of the gyromagnetic ratio for ^{35}Cl and for ^{37}Cl)

$r_{HH} = 1.78$ Å (distance between geminal protons of methylene group),

one obtains, from Eqs. 4 and 4a, $R_1^{H\text{-}H}/R_1^{H\text{-}Cl} = 174$ for $r_{HCl} = 2.5$ Å (This is 0.5 Å shorter than the sum of the atomic and ionic radii, a typical hydrogen bonding distance)[3] and $R_1^{H\text{-}H}/R_1^{H\text{-}Cl} = 3.2_8$ for $r_{HCl} = 1.3$ Å (the covalent bond distance for hydrogen chloride).

These values suggest that, in the former case, the contribution of the direct interaction of the chloride ion is less than 1% of the contribution of the geminal protons. Even at the covalent bond distance, the contribution of the chloride ion is about 23% of the contribution of the geminal proton. One might assume that, at a reasonable hydrogen bond distance, the direct interaction of the chloride ion plays no important role in the spin-lattice relaxation process.

Results of the study with (*p*-nitrophenyl)chloromethane-α-d_1 support this postulate. Data from Table 5 [footnote f)] give $R_1^c(CHD)/R_1^c(CH_2) = 0.26_6$. The significantly slow relaxation of monodeuterated compound indicates that any one of the following conceivable factors does not contribute more than 30% of the spin-lattice relaxation of normal undeuterated substrate: 1) direct dipole-dipole interaction of chloride ion, 2) relaxation by the contribution of the nuclear quadrupole of the chloride ion, 3) long range interaction between methylene proton and the ring protons.

27) The observed rate of relaxation was almost identical, within experimental error, for the vicinal protons on the same phenyl ring. Thus τ_c(*meta*) and τ_c(*ortho*) calculated were almost equal. The intramolecular rotation about the axis of the phenyl-X bond is considered to be ineffective for the relaxation of the ortho and meta proton nuclei. Thus the τ_c(*meta*) can be regarded as a measure of the correlation time of molecular motion as the whole mass. There are examples where difference in τ_c is ascribed to difference in an intramolecular rotation. *Cf.* a) A. Suggett, *J. Solution Chemistry*, **5**, 33 (1976); b) E. Breitmaier, K-H Spohn, and S. Berger, *Angew. Chem. Int. Ed. Engl.*, **14**, 144 (1975).

28) As Muller has pointed out,[20b] some indication is given as to the nature of the solute-solute interaction from the temperature coefficient of $\partial\Delta_c/\partial T$. Generally, when a strong hydrogen bonding is operative, hydrogen bonding shift in PMR is little affected by the changes in temperature. In an association where significant stabilization is found with a significant $\partial\Delta_c/\partial T$, some (additional) interaction other than hydrogen bonding can be operative.

$\partial\Delta_c/\partial T$(ppm deg^{-1}) for p-NO_2PhXCH_2Cl: 1.2×10^{-2} (X=NONE), 2.0×10^{-2} (X=CO), 0.6×10^{-2} (X=S), 0.4×10^{-2} (X=SO), 0.2×10^{-2} ($X=SO_2$).

29) $Ph^{13}COCH_2Cl$ showed limiting CMR shift 5.0 ppm on complexation with chloride ion while no such a shift was observed for $Ph^{13}CH_2Cl$.

30) J. W. Thorpe and J. Warkentin, *Can. J. Chem.*, **51**, 927 (1973), and references cited therein.

31) J. J. Dannenberg, *J. Am. Chem. Soc.*, **98**, 6261 (1976).

Nucleoside Analogs. 5. Synthesis of Carbocyclic Pyrimidine Nucleoside Analogs

Kin-ichi TADANO, Sumio HORIUCHI, and Tetsuo SUAMI*

Department of Applied Chemistry, Faculty of Engineering, Keio University, Hiyoshi, Yokohama 223

(Received July 18, 1977)

Six carbocyclic analogs of uridine and thymidine in which the pentofuranosyl groups are replaced by a carbocyclic cyclopentane system have been synthsized. Their biological activities were determined against *HeLa* S3 cells.

In connection with the preceding papers,[1-4] a report is given on the synthesis of carbocyclic analogs of uridine and thymidine in which the pentofuranosyl groups are replaced by a cyclopentane derivative.

1-β-D-Arabinofuranosylthymine (Ara-T),[5] which has been found in nature, has antiviral activity against 2DNA viruses, herpes virus and vaccinia virus in *HeLa* cell culture.[6]

Since 1-β-D-arabinofuranosylcytosine (Ara-C)[7] is a well known carcinostatic agent,[8] a carbocyclic analog of pyrimidine nucleoside might exhibit antineoplastic activity.

In the present study, three uridine and three thymidine analogs have been prepared and their biological activities are tested against *HeLa* cells.

Three stereoisomers of 5-amino-1,2,3,4-cyclopentanetetrol[3] **1**, **2**, and **3** were treated with nitrourea and subsequently acetylated by the conventional method to give corresponding 1,2,3,4-tetra-*O*-acetyl-5-ureido-1,2,3,4-cyclopentanetetrols **4**, **5**, and **6**, respectively.

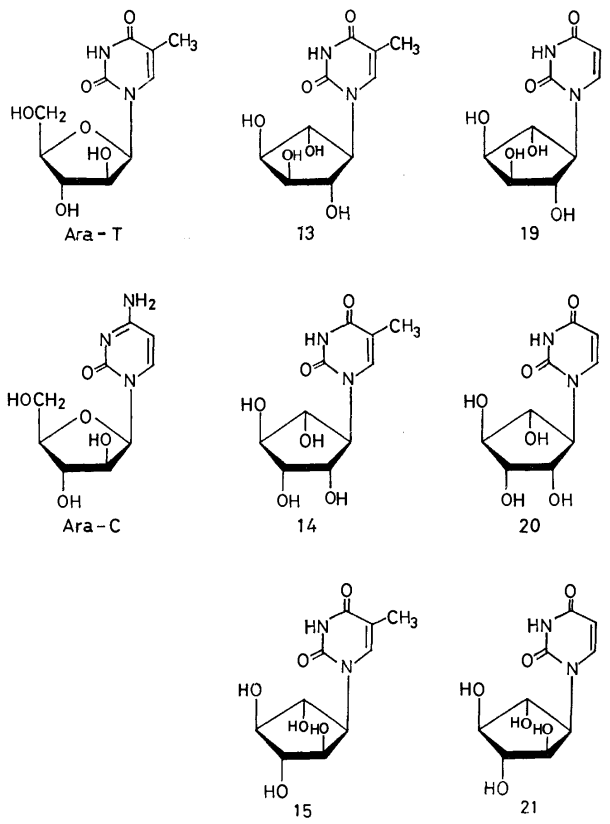

Scheme 1.

When **4**, **5**, and **6** were treated with 3-methoxy-2-methylacryloyl chloride[9] in pyridine by an analogous method described by Naito *et al.*,[10] 1,2,3,4-tetra-*O*-acetyl-5-[*N'*-(3-methoxy-2-methylacryloyl)ureido]-1,2,3,4-cyclopentanetetrols **7**, **8**, and **9** were obtained. In their ^{1}H NMR spectra, a doublet at δ 9.21—9.31 (1H, J=8—9 Hz) is attributable to NH linked to the cyclopentane ring, a singlet at δ 8.56—8.86 (1H) being ascribed to NH where the 3-methoxy-2-methylacryloyl group is attached. This indicates that the 3-methoxy-2-methylacryloyl group is attached to the terminal amino group of **4**, **5**, and **6**.

Ring closure of **7**, **8**, and **9** in aqueous ammonia afforded 1-(2,3,4,5-tetrahydroxycyclopentyl)thymines **13** **14**, and **15**. Their successful ring closure was demonstrated by measuring their UV spectra at different pH.[11] Their *O*-acetyl derivatives **16**, **17**, and **18** were prepared by the usual acetylation.

On the other hand, when the ureido derivatives **4**, **5**, and **6** reacted with 3-ethoxyacryloyl chloride [12] by an analogous method described by Bobeck and Farkas,[13] 1,2,3,4-tetra-*O*-acetyl-5-*N'*-(3-ethoxyacryloyl) ureido-1,2,3,4-cyclopentanetetrols **10**, **11**, and **12** were obtained. Their structures were confirmed by means of ^{1}H NMR spectra.

Ring closure of **10**, **11**, and **12** in aqueous ammonia afforded 1-(2,3,4,5-tetrahydroxycyclopentyl)uracils **19**, **20**, and **21**. Their *O*-acetyl derivatives **22**, **23**, and **24** were also prepared.

Compounds **13**, **14**, **15**, **19**, **20**, and **21** showed no biological activity against *HeLa* S3 cells.

Experimental

Melting points were determined in capillary tubes and are uncorrected. Acetylation was carried out in the usual way with acetic anhydride in pyridine. Solutions were concentrated under reduced pressure at 40—50 °C. Silica gel (Wakogel C-300, Wako Pure Chemical Industries Ltd.) was used for column chromatography and TLC was performed on silica gel (Wakogel B-5FM) plates in 5:1 (v/v) benzene-ethanol system. ^{1}H NMR spectra were recorded at 60 MHz with a Varian A-60D spectrometer, peak positions being given in δ values. UV spectra were measured with a Hitachi-Perkin Elmer UV-VIS 139 spectrometer.

*1,2,3,4-Tetra-*O*-acetyl-(1,4/2,3,5)-5-ureido-1,2,3,4-cyclopentanetetrol (4).* A mixture of (1,4/2,3,5)-5-amino-1,2,3,4-cyclopentanetetrol[3] (**1**, 536 mg) and nitrourea (455 mg) in water (25 ml) was stirred at room temperature overnight. The solution was concentrated and the residue was acetylated. The solution was poured into ice-cold water (120 ml) and extracted with chloroform repeatedly. After being dried over Na_2SO_4, the chloroform extract was concentrated to dryness.

* To whom correspondence should be addressed.

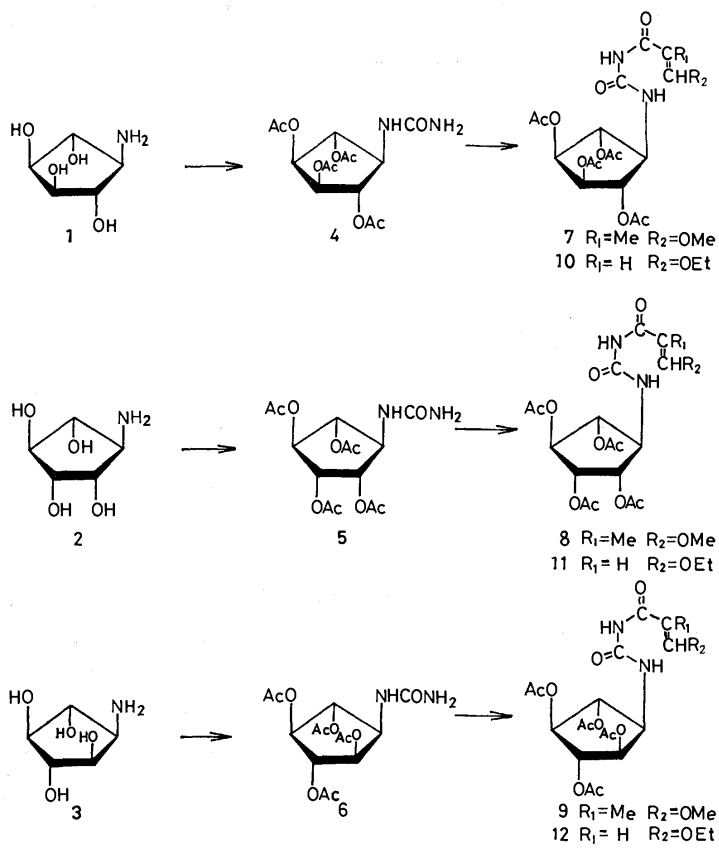

Scheme 2.

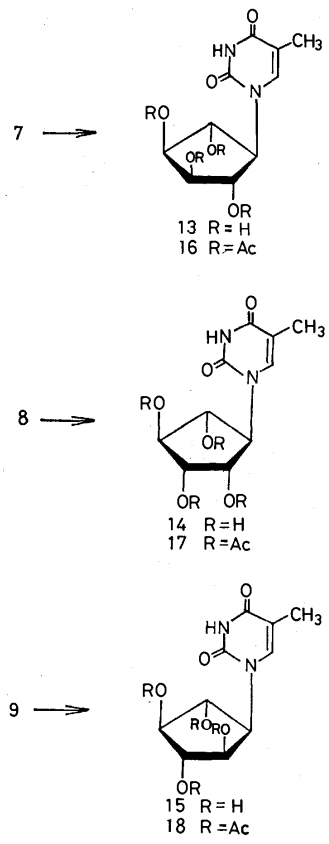

Scheme 3.

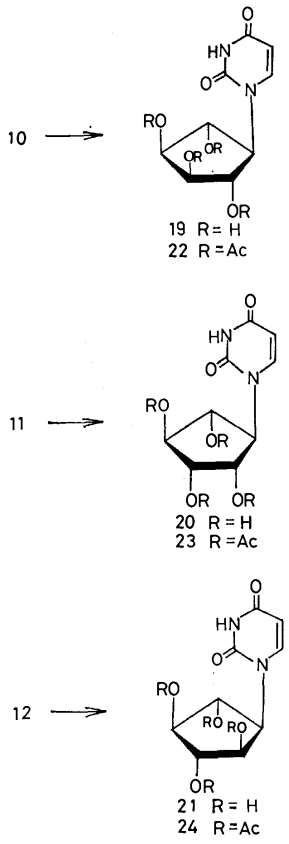

Scheme 4.

The residue was recrystallized from ethanol to give 823 mg (64%) of **4** as needles, mp 196—197 °C. ^{1}H NMR (DMSO-d_6): δ 2.02 (s, 12, 4×OAc), 3.28 (s, 2, NH_2), 6.42 (d, 1, J=9 Hz, NH).

Found: C, 47.00; H, 5.46; N, 7.77%. Calcd for $C_{14}H_{20}N_2O_9$: C, 46.67; H, 5.60; N, 7.77%.

*1,2,3,4-Tetra-O-acetyl-*DL*-(1,2,4/3,5)-5-ureido-1,2,3,4-cyclopentanetetrol (**5**).* A mixture of DL-(1,2,4/3,5)-5-amino-1,2,3,4-cyclopentanetetrol[3] (**2**, 1.23 g) and nitrourea (1.30 g) in water (60 ml) was heated under reflux for 3 h. Subsequent treatment was analogous to that described in the preparation of **4**. An oily residue was crystallized from ethyl acetate–petroleum ether to give 1.84 g (62%) of **5**, mp 165—166 °C.

Found: C, 46.51; H, 5.52; N, 7.53%. Calcd for $C_{14}H_{20}N_2O_9$: C, 46.67; H, 5.60; N, 7.77%.

*1,2,3,4-Tetra-O-acetyl-*DL*-(1,3,5/2,4)-5-ureido-1,2,3,4-cyclopentanetetrol (**6**).* 1,2,3,4-Tetra-*O*-acetyl-DL-(1,3,5/2,4)-5-acetamido-1,2,3,4-cyclopentaneterol[14] (3.26 g) was heated under reflux in 6 M hydrochloric acid (50 ml) for 1.5 h and the solution was concentrated to dryness. An aqueous solution of the residue was neutralized with Amberlite IRA-400(OH^-) resin and was concentrated. The residue was recrystallized from ethanol to give 1.25 g (93%) of DL-(1,3,5/2,4)-5-amino-1,2,3,4-cyclopentanetetrol (**3**), mp 142—144 °C.

Found: C, 39.97; H, 7.52; N, 8.66%. Calcd for $C_5H_{11}NO_4 \cdot 1/2H_2O$: C, 39.99; H, 7.93; N, 8.48%.

A mixture of **3** (1.00 g) and nitrourea (1.24 g) in water (50 ml) was heated under reflux for 4 h. The mixture was worked up as in the preparation of **4**. The crude product was recrystallized from ethanol to give 2.03 g (84%) of **6** as needles, mp 203—204 °C. ^{1}H NMR ($CDCl_3$–DMSO-d_6, 5 : 1): δ 2.08 (s, 6, 2×OAc), 2.10 (s, 3, OAc), 2.17 (s, 3, OAc), 5.57 (s, 2, NH_2), 6.46 (d, 1, J=9 Hz, NH).

Found: C, 46.64; H, 5.52; N, 7.87%. Calcd for $C_{14}H_{20}N_2O_9$: C, 46.67; H, 5.60; N, 7.77%.

*1,2,3,4-Tetra-O-acetyl-(1,4/2,3,5)-5-[N′-(3-methoxy-2-methylacryloyl)ureido]-1,2,3,4-cyclopentanetetrol (**7**).* A mixture of **4** (1.50 g), 3-methoxy-2-methylacryloyl chloride[9] (0.90 g), pyridine (5 ml) and chloroform (5 ml) was agitated at ambient temperature for 2 days. The solution was concentrated to dryness and the residue was dissolved in water (30 ml). The aqueous solution was extracted 3 times with chloroform (30 ml). After being dried over Na_2SO_4, the combined chloroform extract was concentrated. The residue was recrystallized from ethanol to give 1.31 g (68%) of **7**, mp 138—139 °C. ^{1}H NMR ($CDCl_3$): δ 1.78 (d, 3, J=1 Hz, C–CH_3), 2.07 (s, 6, 2×OAc), 2.08 (s, 6, 2×OAc), 3.86 (s, 3, C–OCH_3), 7.33 (q, 1, J=1 Hz, acryloyl CH), 8.56 (s, 1, N′H), 9.31 (d, 1, J=9 Hz, NH).

Found: C, 49.86; H, 5.68; N, 6.05%. Calcd for $C_{19}H_{26}N_2O_{11}$: C, 49.78; H, 5.72; N, 6.11%.

*1,2,3,4-Tetra-O-acetyl-*DL*-(1,2,4/3,5)-[N′-(3-methoxy-2-methylacryloyl)ureido]-1,2,3,4-cyclopentanetetrol (**8**).* A mixture of **5** (1.00 g), 3-methoxy-2-methylacryloyl choride[9] (1.12 g), pyridine (5 ml) and chloroform (5 ml) was stirred at ambient temperature for 40 h. The solution was worked up as in the preparation of **7**. A product was recrystallized from ether to give 0.59 g (47%) of **8**, mp 167—168 °C. ^{1}H NMR ($CDCl_3$): δ 1.79 (d, 3, J=1 Hz, C–CH_3), 2.04 (s, 3, OAc), 2.06 (s, 3, OAc), 2.08 (s, 6, 2×OAc), 3.87 (s, 3, C–OCH_3), 7.35 (q, 1, J=1 Hz, acryloyl CH), 8.86 (s, 1, N′H), 9.21 (d, 1, J=8 Hz, NH).

Found: C, 49.88; H, 5.74; N, 5.86%. Calcd for $C_{19}H_{26}N_2O_{11}$: C, 49.78; H, 5.72; N, 6.11%.

*1,2,3,4-Tetra-O-acetyl-*DL*-(1,3,5/2,4)-5-[N′-(3-methoxy-2-methylacryloyl)ureido]-1,2,3,4-cyclopentanetetrol (**9**).* A mixture of **6** (1.00 g), 3-methoxy-2-methylacryloyl chloride[9] (0.56 g), pyridine (5 ml) and chloroform (10 ml) was stirred for 38 h. The solution was worked up as in the preparation of **7**. A product was recrystallized from ether-petroleum ether to give 0.43 g (34%) of **9**, mp 130—131 °C. ^{1}H NMR ($CDCl_3$): δ 1.77 (s, 3, J=1 Hz, C–CH_3), 2.07 (s, 3, OAc), 2.08 (s, 3, OAc), 2.10 (s, 3, OAc), 2.16 (s, 3, OAc), 3.87 (s, 3, C–OCH_3), 7.34 (q, 1, J=1 Hz, acryloyl CH), 8.78 (s, 1, N′H), 9.22 (d, 1, J=8 Hz, NH).

Found: C, 49.48; H, 5.66; N, 5.79%. Calcd for $C_{19}H_{26}N_2O_{11}$: C, 49.78; H, 5.72; N, 6.11%.

*1,2,3,4-Tetra-O-acetyl-(1,4/2,3,5)-5-[N′-(3-ethoxyacryloyl)ureido]-1,2,3,4-cyclopentanetetrol (**10**).* A mixture of **4** (1.50 g), 3-ethoxyacryloyl chloride[12] (1.05 g), pyridine (7 ml) and chloroform (7 ml) was stirred overnight. The solution was poured into water (50 ml) and extracted with chloroform repeatedly. After being dried over Na_2SO_4, the chloroform extract was concentrated. The residue was purified on a silica gel column (110 g, 30 × 410 mm) using 10:1 (v/v) benzene–ethanol as eluent. Fractions showing a single spot on TLC (R 0.44) were combined and concentrated. The residue was recrystallized from ethyl acetate-petroleum ether to give 677 mg (35%) of **10**, mp 148—149 °C. ^{1}H NMR ($CDCl_3$): δ 1.36 (t, 3, J=7 Hz, C–$OCH_2C\underline{H}_3$), 2.08 (s, 12, 4 × OAc), 4.00 (q, 2, J=7 Hz, C–$OC\underline{H}_2CH_3$), 5.34 (d, 1, J=12 Hz, acryloyl CH), 7.60 (d, 1, J=12 Hz, acryloyl CH), 9.21 (d, 1, J=8 Hz, NH), 9.49 (s, 1, N′H).

Found: C, 49.89; H, 5.86; N, 5.90%. Calcd for $C_{19}H_{26}N_2O_{11}$: C, 49.78; H, 5.72; N, 6.11%.

*1,2,3,4-Tetra-O-acetyl-*DL*-(1,2,4/3,5)-5-[N′-(3-ethoxyacryloyl)ureido]-1,2,3,4-cyclopentanetetrol (**11**).* A mixture of **5** (0.40 g), 3-ethoxyacryloyl chloride[12] (0.50 g) and pyridine (5 ml) in chloroform (5 ml) was stirred for 13 h. The mixture was worked up as in the preparation of **10**. The product was recrystallized from ethanol to give 123 mg (24%) of **11**, mp 147—148 °C. ^{1}H NMR ($CDCl_3$): δ 1.35 (t, 3, J=7 Hz, C–$OCH_2C\underline{H}_3$), 2.06 (s, 3, OAc), 2.08 (s, 3, OAc), 2.09 (s, 3, OAc), 2.10 (s, 3, OAc), 3.98 (q, 2, J=7 Hz, C–$OC\underline{H}_2CH_3$), 5.35 (d, 1, J=12 Hz, acryloyl CH), 7.62 (d, 1, J=12 Hz, acryloyl CH), 9.11 (d, 1, J=8 Hz, NH), 9.78 (s, 1, N′H).

Found: C, 49.83; H, 5.70; N, 5.96%. Calcd for $C_{19}H_{26}N_2O_{11}$: C, 49.78; H, 5.72; N, 6.11%.

*1,2,3,4-Tetra-O-acetyl-*DL*-(1,3,5/2,4)-5-[N′-(3-ethoxyacryloyl)ureido]-1,2,3,4-cyclopentanetetrol (**12**).* A mixture of **6** (1.14 g), 3-ethoxyacryloyl chloride[12] (1.27 g) and pyridine (5 ml) in chloroform (5 ml) was worked up as in the preparation of **10**. A product was recrystallized from ethyl acetate-petroleum ether to give 589 mg (41%) of **12**, mp 132—135 °C. ^{1}H NMR ($CDCl_3$): δ 1.37 (t, 3, J=7 Hz, C–$OCH_2C\underline{H}_3$), 2.06 (s, 3, OAc), 2.09 (s, 6, 2×OAc), 2.15 (s, 3, OAc), 4.00 g (q, 2, J=7 Hz, C–$OC\underline{H}_2CH_3$), 5.33 (d, 1, J=12 Hz, acryloyl CH), 7.61 (d, 1, J=12 Hz, acryloyl CH), 9.11 (d, 1, J=9 Hz, NH), 9.52 (s, 1, N′H).

Found: C, 49.81; H, 5.88; N, 6.20%. Calcd for $C_{19}H_{26}N_2O_{11}$: C, 49.78; H, 5.72; N, 6.11%.

*1-[(1,3,4/2,5)-2,3,4,5-Tetrahydroxycyclopentyl]thymine (**13**).* A solution of **16** (741 mg) in methanol (20 ml) saturated with ammonia was stirred at ambient temperature for 15 h. The solution was concentrated, and the residue was recrystallized from ethanol to give 447 mg (99%) of **13**, mp 241—245 °C. UV: $\lambda_{max}^{0.1M\ HCl}$ 272 nm (ε=1.0×10^4), $\lambda_{max}^{H_2O}$ 273 nm (ε=0.99 ×10^4), $\lambda_{max}^{0.1M\ NaOH}$ 272 nm (ε=0.76×10^4).

Found: C, 46.61; H, 5.52; N, 10.64%. Calcd for $C_{10}H_{14}N_2O_6$: C, 46.51; H, 5.46; N, 10.85%.

*1-[*DL*-(1,3/2,4,5)-2,3,4,5-Tetrahydroxycyclopentyl]thymine (**14**).* A solution of **8** (580 mg) in 3.5% aqueous ammonia (12 ml)

was heated at 80 °C for 5 h with agitation. The solution was concentrated to dryness and the residue was recrystallized from ethanol to give 298 mg (91%) of **14**, mp 248—252 °C (dec). UV: $\lambda_{max}^{0.1M\ HCl}$ 272 nm ($\varepsilon=0.94\times10^4$), $\lambda_{max}^{H_2O}$ 272 nm ($\varepsilon=0.95\times10^4$), $\lambda_{max}^{0.1M\ NaOH}$ 272 nm ($\varepsilon=0.72\times10^4$).

Found: C, 46.53; H, 5.46; N, 10.96%. Calcd for $C_{10}H_{14}N_2O_6$: C, 46.51; H, 5.46; N, 10.85%.

*1-[DL-(1,2,4/3,5)-2,3,4,5-Tetrahydroxycyclopentyl]thymine (**15**).* A solution of **9** (295 mg) in 3.5% aqueous ammonia (10 ml) was heated at 80 °C for 5 h with agitation. The solution was concentrated to *ca.* 1 ml and the residue was stored in a refrigerator overnight to give 129 mg (77%) of **15**, mp 285—288 °C (dec). UV: $\lambda_{max}^{0.1M\ HCl}$ 272 nm ($\varepsilon=1.0\times10^4$), $\lambda_{max}^{H_2O}$ 271 nm ($\varepsilon=1.0\times10^4$), $\lambda_{max}^{0.1M\ HCl}$ 270 nm ($\varepsilon=0.8\times10^4$).

Found: C, 46.64; H, 5.53; N, 10.95%. Calcd for $C_{10}H_{14}N_2O_6$: C, 46.51; H, 5.46; N, 10.85%.

*1-[(1,3,4/2,5)-2,3,4,5-Tetraacetoxycyclopentyl]thymine (**16**).* A solution of **7** (1.20 g) in 3.5% aqueous ammonia (20 ml) was heated at 80 °C for 5 h with agitation. The solution was concentrated to dryness and the residue was acetylated. The product was recrystallized from ethanol to give 961 mg (86%) of **16**, mp 193—194 °C. ^1H NMR ($CDCl_3$): δ 1.96 (d, 3, $J=1$ Hz, C-CH_3), 2.07 (s, 6, 2×OAc), 2.11 (s, 6, 2×OAc), 7.10 (q, 1, $J=1$ Hz, pyrimidine CH), 9.45 (s, 1, pyrimidine NH).

Found: C, 50.65; H, 5.23; N, 6.42%. Calcd for $C_{18}H_{22}N_2O_{10}$: C, 50.70; H, 5.20; N, 6.57%.

*1-[DL-(1,3/2,4,5)-2,3,4,5-Tetraacetoxycyclopentyl]thymine (**17**).* Compound **14** (51 mg) was acetylated and the product was recrystallized from ethanol to give 74 mg (87%) of **17**, mp 207—208 °C. ^1H NMR ($CDCl_3$): δ 1.93 (d, 3, J 1 Hz, C-CH_3), 2.07 (s, 6, 2×OAc), 2.11 (s, 6, 2×OAc), 6.93 (q, 1, $J=1$ Hz, pyrimidine CH), 9.37 (s, 1, pyrimidine NH).

Found: C, 50.44; H, 5.15; N, 6.50%. Calcd for $C_{18}H_{22}N_2O_{10}$: C, 50.70; H, 5.20; N, 6.57%.

*1-[DL-(1,2,4/3,5)-2,3,4,5-Tetraacetoxycyclopentyl]thymine (**18**).* Compound **15** (161 mg) was acetylated and the product was recrystallized from ethanol to give 246 mg (93%) of **18**, mp 177—179 °C. ^1H NMR ($CDCl_3$): δ 1.92 (d, 3, $J=1$ Hz, C-CH_3), 2.02 (s, 3, OAc), 2.07 (s, 3, OAc), 2.09 (s, 6, 2×OAc), 7.10 (q, 1, $J=1$ Hz, pyrimidine CH), 9.55 (s, 1, pyrimidine NH).

Found: C, 50.89; H, 5.19; N, 6.48%. Calcd for $C_{18}H_{22}N_2O_{10}$: C, 50.70; H, 5.20; N, 6.57%.

*1-[(1,3,4/2,5)-2,3,4,5-Tetrahydroxycyclopentyl]uracil (**19**).* A solution of **22** (101 mg) in methanolic ammonia (5 ml) was stirred overnight at ambient temperature. The solution was concentrated to dryness and the residue was recrystallized from ethanol to give 54 mg (90%) of **19**, mp 237—240 °C. UV: $\lambda_{max}^{0.1M\ HCl}$ 267 nm ($\varepsilon=1.06\times10^4$), $\lambda_{max}^{H_2O}$ 267 nm ($\varepsilon=1.06\times10^4$), $\lambda_{max}^{0.1M\ NaOH}$ 267 nm ($\varepsilon=0.78\times10^4$).

Found: C, 44.66; H, 5.06; N, 11.44%. Calcd for $C_9H_{12}N_2O_6$: C, 44.26; H, 4.96; N, 11.47%.

*1-[DL-(1,3/2,4,5)-2,3,4,5-Tetrahydroxycyclopentyl]uracil (**20**).* A solution of **11** (110 mg) in 3.5% aqueous ammonia (5 ml) was heated at 80 °C for 5 h with agitation. The solution was concentrated to *ca.* 1 ml and the residue was stored in a refrigerator overnight to give 36 mg (62%) of **20**, mp 231—234 °C. UV: $\lambda_{max}^{0.1M\ HCl}$ 267 nm ($\varepsilon=1.0\times10^4$), $\lambda_{max}^{H_2O}$ 267 nm ($\varepsilon=1.0\times10^4$), $\lambda_{max}^{0.1M\ NaOH}$ 266 nm ($\varepsilon=0.72\times10^4$).

Found: C, 44.51; H, 5.09; N, 11.81%. Calcd for $C_9H_{12}N_2O_6$: C, 44.26; H, 4.96; N, 11.47%.

*1-[DL-(1,2,4/3,5)-Tetrahydroxycyclopentyl]uracil (**21**).* A solution of **24** (100 mg) in methanolic ammonia (5 ml) was stirred at ambient temperature overnight. The solution was concentrated to dryness and the residue was recrystallized from ethanol to give 56 mg (94%) of **21**, mp 255—257 °C. UV: $\lambda_{max}^{0.1M\ HCl}$ 267 nm ($\varepsilon=1.2\times10^4$), $\lambda_{max}^{H_2O}$ 266 nm ($\varepsilon=1.2\times10^4$), $\lambda_{max}^{0.1M\ NaOH}$ 266 nm ($\varepsilon=0.81\times10^4$).

Found: C, 44.38; H, 4.94; N, 11.36%. Calcd for $C_9H_{12}N_2O_6$: C, 44.26; H, 4.96; N, 11.47%.

*1-[(1,3,4/2,5)-2,3,4,5-Tetraacetoxycyclopentyl]uracil (**22**).* A solution of **10** (544 mg) in 3.5% aqueous ammonia (20 ml) was heated at 80 °C for 5 h with agitation. The solution was concentrated to dryness and the residue was acetylated. The product was recrystallized from ethanol to give 460 mg (94%) of **22**, mp 229—231 °C. ^1H NMR (DMSO-d_6): δ 2.10 (s, 6, 2×OAc), 2.15 (s, 6, 2×OAc), 5.84 (d, 1, $J=8$ Hz, pyrimidine CH), 7.97 (d, 1, $J=8$ Hz, pyrimidine CH), 7.34—8.54 (broad, 1, pyrimidine NH).

Found: C, 49.33; H, 4.83; N, 6.63%. Calcd for $C_{17}H_{20}N_2O_{10}$: C, 49.52; H, 4.89; N, 6.79%.

*1-[DL-(1,3/2,4,5)-2,3,4,5-Tetraacetoxycyclopentyl]uracil (**23**).* Compound **20** (53 mg) was acetylated and the product was recrystallized from ethanol to give 87 mg (97%) of **23**, mp 219—221 °C. ^1H NMR (DMSO-d_6): δ 2.09 (s, 3, OAc), 2.13 (s, 3, OAc), 2.15 (s, 6, 2×OAc), 5.85 (d, 1, $J=8$ Hz, pyrimidine CH), 8.06 (d, 1, $J=8$ Hz, pyrimidine CH), 8.16 (s, 1, pyrimidine NH).

Found: C, 49.39; H, 4.96; N, 6.56%. Calcd for $C_{17}H_{20}N_2O_{10}$: C, 49.52; H, 4.89; N, 6.79%.

*1-[DL-(1,2,4/3,5)-2,3,4,5-Tetraacetoxycyclopentyl]uracil (**24**).* A solution of **12** (582 mg) in 3.5% aqueous ammonia (20 ml) was heated at 80 °C for 5 h with agitation. The solution was concentrated to dryness and the residue was acetylated. The product was purified on a silica gel column (70 g, 30×270 mm) using 5 : 1 (v/v) benzene-ethanol as an eluent. Fractions showing a single spot on TLC (R_f 0.66) were combined and concentrated to dryness. The residue was recrystallized from ethyl acetate-ethanol to give 345 mg (73%) of **24**, mp 187—188 °C. ^1H NMR (DMSO-d_6): δ 2.02 (s, 3, OAc), 2.08 (s, 3, OAc), 2.11 (s, 6, 2×OAc), 5.80 (d, 1, $J=8$ Hz, pyrimidine CH), 8.00 (d, 1, $J=8$ Hz, pyrimidine CH), 8.19 (s, 1, Pyrimidine NH).

Found: C, 49.66; H, 4.97; N, 6.67%. Calcd for $C_{17}H_{20}N_2O_{10}$: C, 49.52; H, 4.89; N, 6.79%.

We thank Mr. Saburo Nakada for carrying out elemental analyses.

References

1) T. Suami, Y. Sato, Y. Fukai, and Y. Sakota, *J. Heterocycl. Chem.*, **6**, 663 (1969).
2) T. Suami, Y. Fukai, Y. Sakota, M. Karimoto, N. Takoi, and Y, Tsukamoto, *Bull. Chem. Soc. Jpn.*, **44**, 1965 (1971).
3) T. Suami, S. Nishiyama, K. Tadano, and F. W. Lichtenthaler, *Bull. Chem. Soc. Jpn.*, **46**, 2562 (1973).
4) K. Tadano, Y. Emori, M. Ayabe, and T. Suami, *Bull. Chem. Soc., Jpn.* **50**, 1572 (1977).
5) W. Bergmann and B. J. Feeney, *J. Am. Chem. Soc.*, **72**, 2809 (1950).
6) J. de Rudder and M. Privat de Garilhe, *Antimicrob. Agents Chemother.*, **1965**, 578.
7) E. R. Walwick, W. K. Roberts, and C. A. Dekker, *Proc. Chem. Soc.*, **1959** 84.
8) R. J. Suhadolnik, "Nucleoside Antibiotics," Wiley Interscience, New York (1970), pp. 156—165.
9) L. L. Bieber, *C. R. Acad. Sci.*, **233**, 655 (1961); G. Shaw and R. N. Warrener, *J. Chem. Soc.*, **1958**, 153.
10) T. Naito, M. Hirata, T. Kawasaki, and M. Sano, *Chem. Pharm. Bull.*, **9**, 703 (1961).
11) K. C. Murdock and R. B. Angier, *J. Am. Chem. Soc.*, **84**, 3748 (1962).
12) A. E. Tschitschibabin, *J. Prakt. Chem.*, **73**, 326 (1906); N. C. Deno, *J. Am. Chem. Soc.*, **69**, 2233 (1947).
13) M. Bobeck and J. Farkas, *Collect. Czech. Chem. Commun.*, **34**, 1684 (1969).
14) T. Suami, K. Tadano, S. Nishiyama, and F. W. Lichtenthaler, *J. Org. Chem.*, **38**, 3691 (1973).

The Formation of Alkyl Acetate in the Reaction of Trialkylborane with Lead(IV) Acetate or Phenyliodoso Acetate*

Yuzuru MASUDA and Akira ARASE

Department of Applied Chemistry, Kitami Institute of Technology, Kitami, Hokkaido 090

(Received August 8, 1977)

In the reaction of trialkylborane with lead(IV) acetate or phenyliodoso acetate in benzene, about two thirds of the alkyl groups of trialkylborane were converted to the corresponding alkyl acetate without any isomerization of the alkyl group. Lead(IV) acetate reacted preferentially with the secondary alkyl group, while phenyliodoso acetate reacted only with the primary alkyl group. In either reaction, one mole of oxidizing agent was consumed for the formation of one mole of alkyl acetate.

Synthetic reactions using organoborane[1] can be roughly classified into two types by their reaction products.[2] One is the combination of the alkyl group to the carbon atom, and the other is the combination of the alkyl group to the hetero atom. We are interested in the latter reaction and have studied the severance of the carbon-boron linkage of trialkylborane by oxidation with a metal compound, followed by the combination of the resulting alkyl group with the ligand of the metal compound.

Recently we reported that trialkylborane gave the corresponding alkyl chloride or alkyl bromide in the reaction with aqueous iron(III) chloride[3] or copper(II) bromide,[3] and also gave alkyl thiocyanate or alkyl selenocyanate in the reaction with aqueous iron(III) thiocyanate[3,5] or iron(III) selenocyanate[4,5] (Eq. 1).

$$R_3B \xrightarrow{Fe^{3+} \text{ or } Cu^{2+},\ X^-} 2\,RX + RB(OH)_2 \qquad (1)$$

X=Cl, Br, SCN, and SeCN

In these reactions, the reduction of Fe(III) to Fe(II) or Cu(II) to Cu(I) occurred; the reactions seemed to proceed in ligand-transfer oxidation by metal compounds for the alkyl radical generated from trialkylborane.[6]

Kochi described that the oxidation of alkyl radical by copper(II) acetate and lead(IV) acetate involved an electron-transfer mechanism, and now, by the former reagent,[7] olefin was formed as the major product by the elimination of hydrogen from the alkyl radical, while by the latter reagent, substitution product,[8] RX (X=H, OAc, and R′, derived from the solvent) was characteristically produced.

On the other hand, Suzuki and his co-workers[9] found that alkyl acetate was formed by an anodic oxidation of trialkylborane in an acetic acid–sodium acetate solution.

Thus, we studied the reaction of trialkylborane with lead(IV) acetate in the hope that alkyl acetate might be formed from trialkylborane.

Results and Discussion

Reaction of Trialkylboranes with Lead(IV) Acetate. As a preliminary examination, trihexylborane, prepared by the hydroboration of 1-hexene with borane in tetrahydrofuran, was subjected to a reaction with the benzene solution of lead(IV) acetate. A relatively slow reaction occurred. The reaction mixture was worked up, and then distilled to give two compounds in a ratio of 10 : 1. These compounds were identified as hexyl acetate (the major one) and 1-methylpentyl acetate (the minor one) by direct comparisons with authentic samples. When the tetrahydrofuran was taken off before the addition of lead(IV) acetate, the amount of hexyl acetates increased remarkably. Accordingly, the subsequent reactions were conducted in the absence of tetrahydrofuran.

To obtain optimum reaction conditions, the reaction was carried out using varying amounts of lead(IV) acetate under several temperatures. Some results are presented in Table 1.

In the reaction at 55 °C for 24 h, the best results were obtained giving 7.8 mmol of hexyl acetate and 0.8 mmol of 1-methylpentyl acetate from 5 mmol of trihexylborane. On the oxidation of the reaction mixture with an aqueous hydrogen peroxide solution, under weakly basic conditions, 7.8 mmol of hexyl acetate, 0.8 mmol of 1-methylpentyl acetate, 6.3 mmol of hexyl alcohol, and a trace amount of 1-methylpentyl alcohol were obtained. A characteristic feature of the reaction is revealed by these results. That is, two thirds of the alkyl group of trialkylborane can participate in the reaction, giving alkyl acetate almost exclusively, without any isomerization of the alkyl group. This characteristic is worthy of remark because, in the reaction of valeric acid with the lead(IV) acetate butyl

TABLE 1. REACTION[a] OF TRIHEXYLBORANE WITH LEAD(IV) ACETATE

Exp. no.	React. temp, °C	$Pb(OAc)_4$ mmol	Products, mmol[b]	
			Hexyl acetate	1-Methylpentyl acetate
1	20	15	0.8	0.3
2	40	15	5.5	0.6
3	55	15	7.8	0.8
4	75	15	6.0	0.8
5	55	10	7.2	0.8
6	55	5	4.7	0.3
7	55	2.5	2.2	0.2

a) The reaction was carried out in benzene for 24 h by using 5 mmol of trihexylborane, prepared from 1-hexene by hydroboration. b) Determined by GLPC, using PEG 20 M as the liquid phase.

* A preliminary report of this work was presented at the 36th National Meeting of the Chemical Society of Japan, Osaka, April, 1977.

$$\text{Valeric acid} \xrightarrow[\text{benzene}]{Pb(OAc)_4} \underset{25\%}{\text{butane}} + \underset{2\%}{\text{1-butene}} + \underset{1.1\%}{\text{2-butene}} + \underset{20.6\%}{\text{butylbenzene}} + \underset{2\%}{\text{butyl acetate}} + \underset{2\%}{\text{1-methylpropyl acetate}}$$

Scheme 1.

radical, initially formed by decarboxylation, several reaction products were given by electron-transfer oxidation[8] (Scheme 1). In the present reaction, only trace amounts of hexane, hexene, and hexylbenzene were detected.

As is shown in Exp. 6 and 7, one mole of lead(IV) acetate is consumed in the formation of one mole of hexyl acetate, suggesting that two electrons take part in the formation of one molecule of hexyl acetate. Thus, the reaction may be written stoichiometrically as follows:

$$R_3B + 2Pb(OAc)_4 \longrightarrow 2\ ROAc + RB(OAc)_2 + 2Pb(OAc)_2. \quad (2)$$

The results of the reactions of several trialkylboranes with lead(IV) acetate under the optimum reaction conditions are presented in Table 2.

Similar results were obtained in all the reactions examined. For example, 5 mmol of tri-*exo*-2-norbornylborane gave 8.5 mmol of *exo*-2-norbornyl acetate.

Another important feature of the reaction is the fact that the secondary alkyl group reacts in preference to the primary one in the case of the mixed trialkylborane, which contains primary and secondary alkyl groups on the same boron atom. That is, dicyclohexylhexylborane gave mostly cyclohexyl acetate. Further, although one third of the hexyl group still remained on the boron atom, almost all of the 1-methylpentyl group[10] was converted to 1-methylpentyl acetate in the reaction of trihexylborane. Bis(1,2-dimethylpropyl)hexylborane (**1**) and bis(2-methylcyclohexyl)hexylborane (**2**) gave only trace amounts of products, and, on oxidation with an aqueous hydrogen peroxide solution, under weakly basic conditions, the corresponding alcohols were formed quantitatively. Although, in both cases, no detailed study has been

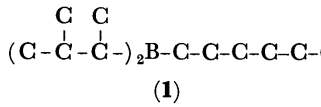

(**1**)

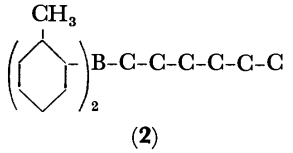

(**2**)

made, the large steric hindrance on the boron atom seems to prevent any interaction between trialkylborane and lead(IV) acetate.

When 5 mmol of tricyclohexylborane was allowed to react with lead(IV) acetate in chloroform, 1.6 mmol of cyclohexyl acetate and 2.2 mmol of cyclohexyl chloride were formed. This fact strongly suggests that an alkyl

Table 2. Reaction[a] of trialkylboranes with lead(IV) acetate

R_3B (5 mmol)	Product	Yield,[b] mmol
$(1\text{-Me-propyl})_3B$	1-Me-propyl-OAc	7.5
$(Hexyl)_3B$	Hexyl-OAc	7.8 (7.5)[c]
	1-Me-pentyl-OAc	0.8 (0.7)[c]
$(Cyclohexyl)_3B$	Cyclohexyl-OAc	7.7 (7.1)[c]
$(Octyl)_3B$	Octyl-OAc	5.7 (5.5)[c]
	1-Me-heptyl-OAc	0.6 (0.5)[c]
$(Cyclooctyl)_3B$	Cyclooctyl-OAc	6.0 (6.0)[c]
$(Norbornyl)_3B$	*exo*-Norbornyl-OAc	8.5 (8.4)[c]
$(Cyclohexyl)_2B\text{-hexyl}$	Cyclohexyl-OAc	6.2
	Hexyl-OAc	0.5

a) Carried out at 55 °C for 24 h by using 15 mmol of $Pb(OAc)_4$ and 25 ml of benzene. b) Determined by GLPC. c) Isolated by distillation.

radical has an important role in the reaction. Although describing the reaction mechanism in detail is not the main purpose of this report, these results may be explained by the following reaction scheme:

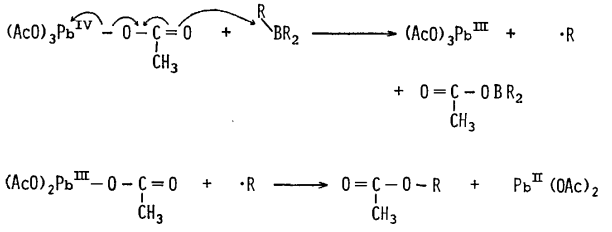

Scheme 2.

Many reactions of organoborane with oxidizing agents have been studied, and in many cases characteristic products for each reaction have been obtained.[11–14] The present reaction gave alkyl acetate characteristically. On the other hand, synthetic methods of alkyl carboxylate from olefin have also been reported.[9,15] Except for the reaction cited in Ref. 9, though, they are all "Markownikoff addition" reactions of carboxylic acid to olefin. The present reaction is a practically applicable one-pot synthesis of primary alkyl acetate from α-olefin by means of the "Anti-Markownikoff addition" reaction.

Reaction of Trialkylborane with Phenyliodoso Acetate. Next, we examined the reaction of trialkylborane with phenyliodoso acetate, which is known to act in almost the same manner as lead(IV) acetate in oxidation reactions.[16] The results are presented in Table 3.

In contrast to the oxidation with lead(IV) acetate, phenyliodoso acetate converted only the primary alkyl group to primary alkyl acetate. For example, 5 mmol of dicyclohexylhexylborane gave only 4.4 mmol of hexyl acetate; on the oxidation of the reaction mixture with the aqueous hydrogen peroxide solution, under weakly basic conditions, 4.4 mmol of hexyl acetate, 10 mmol of cyclohexyl alcohol, and 0.4 mmol of hexyl alcohol were obtained. In the case of trihexylborane, hexyl acetate was formed, uncontaminated with 1-methylpentyl acetate. Thus, the reaction provides a more excellent method than that of lead(IV) acetate for the synthesis of primary alkyl acetate from α-olefin.

Table 3. Reaction[a] of trialkylboranes with phenyliodoso acetate

R_3B (5 mmol)	Product	Yield,[b] mmol
$(Hexyl)_3B$	Hexyl-OAc	9.3 (9.2)[e]
	1-Me-pentyl-OAc	trace (trace)[e]
	Hexyl-OAc	4.5[c]
		2.4[d]
$(Cyclohexyl)_3B$	Cyclohexyl-OAc	no reaction
$(Octyl)_3B$	Octyl-OAc	7.2 (7.0)[e]
	1-Me-heptyl-OAc	trace (trace)[e]
$(Cyclohexyl)_2B$-hexyl	Hexyl-OAc	4.4
	Cyclohexyl-OAc	0

a) Carried out at 55 °C for 8 h by using 10 mmol of phenyliodoso acetate and 20 ml of benzene. b) Determined by GLPC. c) Phenyliodoso acetate, 5 mmol. d) Phenyliodoso acetate, 2.5 mmol. e) Isolated by column chromatography.

As has been shown in the reaction of trihexylborane, one mole of phenyliodoso acetate was consumed for the formation of one mole of hexyl acetate, and a comparable amount of iodobenzene was formed (Eq. 3):

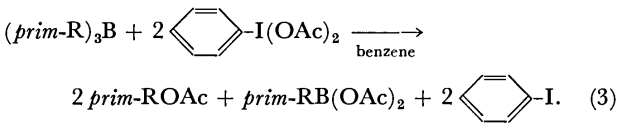

$$(prim\text{-}R)_3B + 2\,C_6H_5\text{-}I(OAc)_2 \xrightarrow[\text{benzene}]{} 2\,prim\text{-}ROAc + prim\text{-}RB(OAc)_2 + 2\,C_6H_5\text{-}I \quad (3)$$

The yield of alkyl acetate was not reduced in the presence of tetrahydrofuran. Moreover, no alkyl chloride was formed in the reaction conducted in chloroform. These facts seem to show that, in contrast to the case of lead(IV) acetate, the alkyl radical is not involved in the reaction. Pelter et al. described that, in the nucleophilic migration of the alkyl group of the trialkylborane cyanate complex, the primary alkyl group is more labile than the secondary one.[17] Thus, in the reaction of trialkylboranes with phenyliodoso acetate, it is probable that the nucleophilic attack of the alkyl group on the iodonium cation is involved. The following reaction scheme may be proposed:

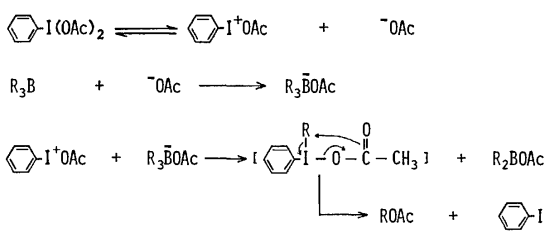

Scheme 3.

As has been described previously, lead(IV) acetate converts preferentially the secondary alkyl group, while phenyliodoso acetate converts only the primary one. Thus, both reactions, compensating for each other, may provide a new method of synthesizing alkyl acetates from a variety of olefins.

Experimental

Instruments. GLPC was performed using a NEVA Model 1400. The PMR spectra were obtained on a Hitachi Model R-20A spectrometer. The infrared spectra were recorded on a Shimadzu 27G spectrometer. The mass spectra were obtained on a Hitachi Model M-52 mass spectrometer.

Materials. Commercial 1-hexene, 1-octene, cyclohexene, cyclooctene, benzene, and tetrahydrofuran were dried with lithium aluminium hydride and used after distillation under an argon atmosphere. Commercial 2-norbornene and 2-butene were used without any purification. The chloroform was dried over phosphorus pentaoxide and was used after distillation under an argon atmosphere.

The tetrahydrofuran solution of borane was prepared by the method described in the literature.[11]

The lead(IV) acetate was prepared by the method described in the literature,[18] its purity was above 98%.[19]

The phenyliodoso acetate was prepared by the method described in the literature;[20] mp 157—158 °C (lit, 158 °C).

Reaction of Trialkylborane with Lead(IV) Acetate. The following procedure is representative. A dry, 50-ml, round-bottomed flask, equipped with a gas inlet, a magnetic stirring bar, a septum inlet, a reflux condenser, and a dropping funnel, was flushed with argon. In the flask 5.63 ml (15 mmol) of 1-hexene was hydroborated with 5 mmol of borane in tetrahydrofuran, and then the tetrahydrofuran was removed under reduced pressure at 40 °C. In an argon atmosphere, 6.65 g (15 mmol) of lead(IV) acetate in 25 ml of benzene was added, drop by drop, to the trihexylborane through the dropping funnel, after which the solution was stirred at 55 °C for 24 h. The lead(II) acetate was precipitated as a white solid with the progress of reaction. In the analytical experiment, the solution, to which an internal standard substance has been added, was analysed by GLPC (PEG 20M, supported on Diasolid M, was used as the liquid phase). In the preparative experiment, 10 ml of water was added to the solution to destroy any residual lead(IV) acetate. Then the mixture was saturated with sodium chloride, and the lower aqueous layer was separated and extracted with pentane several times. The combined upper organic layer and pentane extracts were washed with a saturated aqueous sodium chloride solution, and dried over anhydrous sodium sulfate. On distillation at 170 °C/757 mmHg, 1.15 g of a mixture containing 7.5 mmol of hexyl acetate and 0.7 mmol of 1-methylpentyl acetate was obtained. The IR, PMR, and mass spectra of all the alkyl acetates, except for norbornyl acetate, were consistent with those obtained from authentic samples.

exo-*2-Norbornyl Acetate*: The IR spectrum showed a strong band at 1730 cm^{-1}. The mass spectrum (20 eV) was completely consistent with the standard spectrum[21] of 2-norbornyl acetate (m/e=154, M^+). PMR (CCl_4, TMS) spectrum; δ=0.95–1.95 (m, 4H, H-3,5,6,7), 1.88 (s, 3H), 2.24 (br, s, 2H, H-1,4), 4.48 (dd, 2H, $J_{H\text{-}2\,end\text{-}H\text{-}3\,exo}$=2 Hz and $J_{H\text{-}2\,end\text{-}H\text{-}3\,end}$=9 Hz.)

Reactions of Trialkylboranes with Phenyliodoso Acetate. To trialkylborane, prepared in the same manner as in the reaction with lead(IV) acetate, a 3.22-g portion (10 mmol) of phenyliodoso acetate in 20 ml of benzene was added, drop by drop, after which the mixture was stirred at 55 °C for 8 h. A yellowish homogeneous solution resulted. In the analytical experiment, the solution, into which an internal standard substance has been added, was analysed by GLPC (PEG 20M, supported on Diasolid M, was used as the liquid phase). In the preparative experiment, the solvent was removed under reduced pressure and the products were separated by column chromatography (silica gel). Iodobenzene, formed by the reduction of phenyliodoso acetate, was effectively removed by elution with hexane, and then the alkyl acetate was eluted with benzene.

References

1) (a) G. M. L. Cragg, "Organoboranes in Organic

Synthesis," Dekker, New York (1973); (b) H. C. Brown, "Organic Syntheses via Boranes," Wiley, New York (1975).
2) A. Suzuki, *Kagaku*, **30**, 919 (1975).
3) A. Arase, Y. Masuda, and A. Suzuki, *Bull. Chem. Soc. Jpn.*, **47**, 2511 (1974).
4) A. Arase and Y. Masuda, *Chem. Lett.*, **1976**, 785.
5) A. Arase and Y. Masuda, *Chem. Lett.*, **1976**, 1115.
6) (a) J. K. Kochi and R. V. Subramanian, *J. Am. Chem. Soc.*, **87**, 1508 (1965); (b) C. L. Jenkins and J. K. Kochi, *ibid.*, **94**, 856 (1971); (c) C. L. Jenkins and J. K. Kochi, *J. Org. Chem.*, **36**, 3095 (1971).
7) J. K. Kochi, *J. Am. Chem. Soc.*, **85**, 1958 (1963).
8) J. K. Kochi, *J. Am. Chem. Soc.*, **87**, 3609 (1965).
9) T. Taguchi, Y. Takahashi, M. Itoh, and A. Suzuki, *Chem. Lett.*, **1974**, 1021.
10) The 1-methylpentyl group in trihexylborane is considered to exist as $(hexyl)_2B(1\text{-methylpentyl})$ and $(hexyl)B(1\text{-methylpentyl})_2$ by anology with tripentylborane. A. Arase, Y. Masuda, M. Itoh, M. Itoh, and A. Suzuki, *Nippon Kagaku Kaishi*, **1972**, 395.
11) Oxidation by alkaline hydrogen peroxide yields alcohol. G. Zweifel and H. C. Brown, *Org. React.*, **13**, 1 (1963).
12) Oxidation by molecular oxygen yields alkylborane peroxide. See, for example, S. B. Mirbiss, *J. Am. Chem. Soc.*, **83**, 3051 (1961).
13) Oxidation by amine oxide yields alkyl borate. See, for example, R. Köster and Y. Morita, *Angew. Chem, Int. Ed. Engl.*, **5**, 580 (1966).
14) Oxidation by chromic acid yields carbonyl compound. See, for example, H. C. Brown and C. P. Corg, *J. Am. Chem. Soc.*, **83**, 2951 (1961).
15) (a) T. J. Thomson and G. J. Leuck, *J. Am. Chem. Soc.*, **44**, 2894 (1922); (b) A. L. McCloskey, G. S. Fonken, R. Wikluiber, and W. S. Johnson, *Org. Synth.*, Coll. Vol. IV, 261 (1963); (c) R. E. Strabe, *ibid.*, IV, 417 (1963); (d) W. S. Johnson, A. L. McCloskey, and D. A. Dunnigen, *J. Am. Chem. Soc.*, **72**, 516 (1950).
16) R. Criegee and H. Beucker, *Ann.*, **1938**, 541, 218.
17) A. Pelter, M. G. Hutchings, and K. Smith, *J. Chem. Soc., Chem. Commun.*, **1973**, 186.
18) J. C. Bailar, Jr., *Inorg. Synth.*, Vol. 1, 47 (1939).
19) L. F. Fieser and M. Fieser, "Reagent for Organic Synthesis," Wiley, Vol. 1, New York (1967), p. 537.
20) K. H. Pausacker, *J. Chem. Soc.*, **1953**, 107.
21) E. Stenhagen, S. Abrahamsson, and F. W. McLafferty, "Registry of Mass Spectral Data," Wiley, Vol. 1, New York (1974), p. 429.

Photochemical Reactions of 2-(Alkoxycarbonyl)-, 2-Cyano-, and 2-(Phenylthio)-cycloalkanones in Alcoholic Solution. Formation of ω-Substituted Esters

Masao TOKUDA, Yasuyuki WATANABE, and the late Mitsuomi ITOH

Department of Chemical Process Engineering, Hokkaido University, Sapporo 060

(Received August 17, 1977)

Photochemical reaction of ethyl 2-oxo-1-cyclohexanecarboxylate (**3**) in methanol gave ethyl methyl heptanedioate, *trans*- and *cis*-ethyl 7-oxo-2-heptenoate, and ethyl 7-oxo-3-heptenoate in 25, 7, 8, and 21% yields, respectively. Photochemical reactions of **3** in ethanol, isopropyl alcohol, and *t*-butyl alcohol gave the corresponding ω-alkoxycarbonyl esters. Other 2-(alkoxycarbonyl)-cyclopentanones and -cycloheptanone underwent similar reactions to give the corresponding ω-alkoxycarbonyl esters. Photochemical reactions of 2-cyanocyclohexanones in methanol similarly gave ω-cyano esters and ω-formyl α,β-unsaturated nitriles. However, photochemical reactions of 2-(phenylthio)- and 2-(methylthio)cyclohexanones in methanol did not give the corresponding ω-phenylthio or ω-methylthio carboxylic acid esters, products resulting from a preferential cleavage of a carbon-sulfur bond being obtained.

Photochemical reactions of cycloalkanones have been extensively studied.[1] Cycloalkanones undergo the Norrish Type I cleavage to give acyl alkyl biradical, which is then transformed in alcoholic solution into carboxylic acid ester *via* a ketene intermediate,[2] unsaturated aldehyde[2,3] and cyclic ether[4] as the main paths. Of these the transformation into carboxylic acid esters is of interest as regards synthesis since the employment of cycloalkanones with appropriate substituents at α-position would produce ω-substituted esters. In contrast to the photochemical reactions of 2-alkyl-substituted cycloalkanones,[1] those of other cycloalkanones substituted with alkoxycarbonyl, cyano,[5] or alkylthio groups[6] have received little attention. We have studied the photochemical reactions of such substituted cyclopentanones, cyclohexanones and cycloheptanones in alcohol solvent with emphasis placed on the ester forming reactions. Photochemical reactions of aliphatic β-keto esters undergo intermolecular hydrogen abstraction or α-cleavage to give various photoproducts.[7]

Results and Discussion

Photochemical Reaction of 2-(Alkoxycarbonyl)cycloalkanones. When a 0.16 M solution of ethyl 2-oxo-1-cyclohexanecarboxylate (**3**) in methanol was irradiated for 10 h with a 500 W high pressure mercury vapor lamp, cyclohexanone **3** was almost entirely consumed and ethyl methyl heptanedioate (**8a**), ethyl *trans*-7-oxo-2-heptenoate (**11**), ethyl *cis*-7-oxo-2-heptenoate (**12**), ethyl 7-oxo-3-heptenoate (**13**), and dimethyl heptanedioate (**14**) were produced in 25, 7, 8, 21, and 5% yields, respectively. It was confirmed that the dark reaction of **3** in methanol for 7 days gives no products. Irradiation of ethyl 2-oxo-1-cyclopentanecarboxylate (**1**), methyl 2-oxo-1-cyclopentanecarboxylate (**2**), ethyl 2-oxo-1-cycloheptanecarboxylate (**4**) and **3** in various alcohols gave the corresponding ω-alkoxycarbonyl esters (**6**—**9**) and ω-formyl unsaturated esters. We have been particularly interested in the ester forming reactions leading to products such as **6**—**9**. The yields of these products and the conversion of 2-(alkoxycarbonyl)-

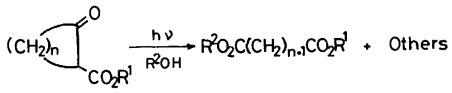

1 : n=3, $R^1=C_2H_5$ 6 : n=3, $R^1=C_2H_5$ a, $R^2=CH_3$
2 : n=3, $R^1=CH_3$ 7 : n=3, $R^1=CH_3$ b, $R^2=C_2H_5$
3 : n=4, $R^1=C_2H_5$ 8 : n=4, $R^1=C_2H_5$ c, $R^2=CH(CH_3)_2$
4 : n=5, $R^1=C_2H_5$ 9 : n=5, $R^1=C_2H_5$ d, $R^2=C(CH_3)_3$

cycloalkanones are summarized in Table 1. We see that the ring size has no significant effect on the ester forming reaction, although the photochemical reaction of cyclohexanone **3** seems to be relatively slow. A large difference in conversion is seen in the photochemical reaction of **3** by employing different alcohols, but none in **1** probably due to its higher reactivity than **3**. Substitution of the alkyl group at 1-position has little effect on the yield of ω-alkoxycarbonyl ester. Irradiation of ethyl 1-methyl-2-oxo-1-cyclopentanecarboxylate (**5**) in methanol for 70 h gave dimethyl 2-methylhexanedioate (**10**) in a 29 % yield.

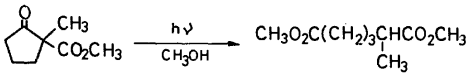

5 10

All the products obtained were probably formed *via* an intermediate acyl(alkoxycarbonyl)alkyl biradical, which is then transformed into ω-alkoxycarbonyl ketene or ω-formyl α,β-unsaturated ester. The ketene was converted into ω-alkoxycarbonyl ester such as **6**—**9** in alcoholic media. Decreasing conversion of cycloalkanones in methanol, ethanol, isopropyl alcohol to *t*-butyl alcohol may be due to the increase in viscosity of the latter alcohols. In more viscous alcohols such as *t*-butyl alcohol, recombination of an intermediate birad-

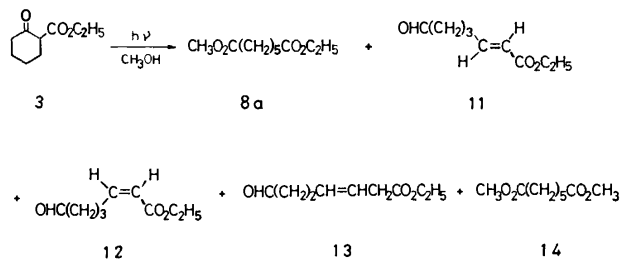

3 8a 11 12 13 14

Table 1. Photochemical reactions of 2-(alkoxycarbonyl)cycloalkanones and 2-cyanocycloalkanones in alcohols[a]

Substrate	Alcohol R^2	Product	Yield of products (%)[b]	Conversion of cycloalkanones (%)
1	CH_3	**6a**	28	95
1[c]	CH_3	**6a**	25	92
1	C_2H_5	**6b**	22	95
1	$(CH_3)_2CH$	**6c**[e]	—	95
1	$(CH_3)_3C$	**6d**[e]	—	95
2	CH_3	**7a**	32	95
2[c]	CH_3	**7a**	29	93
3	CH_3	**8a**	25	71
3	C_2H_5	**8b**	16	43
3	$(CH_3)_2CH$	**8c**	14	33
3	$(CH_3)_3C$	**8d**	4	25
4	CH_3	**9a**	28	91
5	CH_3	**10**	29	95
15	CH_3	**17a**	28	60
15[d]	C_2H_5	**17b**	14	77
16	CH_3	**18**	16	89

a) Externally irradiated with a 500 W high pressure mercury vapor lamp for 70 h. b) Based on 2-(alkoxycarbonyl)- or 2-cyanocycloalkanones consumed. c) Externally irradiated with a Pyrex filtered high pressure mercury vapor lamp for 70 h. d) Externally irradiated with a 500 W high pressure mercury vapor lamp for 90 h. e) Not isolated.

ical giving the starting cycloalkanone would occur to some extent. ω-Formyl β,γ-unsaturated ester **13** is produced by a photochemical deconjugation of ω-formyl α,β-unsaturated ester (**11**→**12**→**13**). This is seen from the results in which the decrease in the yields of **11** and **12** is accompanied by an increase in the yield of **13** with the prolongation of irradiation time. Facile photochemical isomerization of α,β-unsaturated ester to β,γ-unsaturated isomer has been studied.[8]

The UV absorption spectra of 2-(alkoxycarbonyl)cycloalkanones show a high intensity absorption of the enol tautomer in the region 255—263 nm and a low intensity absorption of the keto tautomer in the region 280—300 nm.[9] Although the latter is usually masked by the former, the non-enolizable cycloalkanones such as **5** have a low intensity absorption at 295 nm in ethanol solution, assigned to n,π^* transition of the keto tautomer. Irradiation of cycloalkanones **1**—**4** with a Pyrex filtered light (>280 nm) gave almost the same yields of ω-alkoxycarbonyl esters **6**—**9** as those with an ordinary high pressure lamp, whereas no reaction occurred when the irradiation was carried out with a 253.7 nm light. These photochemical reactions are not greatly effected by the addition of oxygen, 1,3-pentadiene,

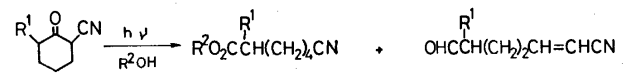

15 : R^1=H
16 : R^1=CH_3

17a: R^1=H, R^2=CH_3
17b: R^1=H R^2=C_2H_5
18 : R^1=R^2=CH_3

19 : R^1=H
20 : R^1=CH_3

or naphthalene. The present photochemical reactions of 2-(alkoxycarbonyl)cycloalkanones leading to ω-alkoxycarbonyl esters might proceed mainly *via* the excited n,π^* singlet of the keto tautomers.

Photochemical Reaction of 2-Cyanocycloalkanones. Photochemical reactions of 2-cyanocycloalkanones in alcohol solvent undergo similar reactions to those of 2-(alkoxycarbonyl)cycloalkanones. Irradiation of 2-oxo-1-cyclohexanecarbonitrile (**15**) and 3-methyl-2-oxo-1-cyclohexanecarbonitrile (**16**) in alcohols gave the corresponding ω-cyano esters **17** and **18** and ω-formyl α,β-unsaturated nitrile **19** and **20**. Yields and conversion in these photochemical reactions are given in Table 1.

The irradiation of 1-methyl-2-oxo-1-cyclohexanecarbonitrile in methanol has been reported to produce ω-cyano ester and ω-formyl α,β-unsaturated nitrile in a 1:13 ratio,[5] but in the present photochemical reaction of **16** they were obtained in a 2:3 ratio. In the photochemical reaction of **16**, an abstraction of tertiary hydrogen at 3-position by α-cyanoalkyl radical moiety of the intermediate biradical would occur to a considerable extent as compared with that of secondary hydrogen at 6-position by acyl radical moiety. No products resulting from the alternative cleavage of the bond between C-2 and C-3 were detected.

Photochemical Reaction of 2-(Phenylthio)cyclohexanone. Irradiation of 2-methylthiocyclohexanone (**21**) in methanol, benzene, or ether gave polymeric products. Small amounts of cyclohexanone and dimethyl disulfide were detected by GLPC analysis. Irradiation of 2-phenylthiocyclohexanone (**22**) in methanol also gave polymeric products besides a small amount of cyclohexanone. However, irradiation of **22** in benzene for 70 h gave cyclohexanone, cyclohexenone, diphenyl disulfide, diphenyl sulfide and thiophenol in the yields 34, 2, 5, 3, and 3 %, respectively. All the products obtained resulted from a preferential cleavage of a carbon–sulfur bond. Diphenyl disulfide might be formed by a combination of phenylthio radical or further photolysis of thiophenol.[6] As a result, no cleavage of Norrish Type I occurred in these photochemical reactions of 2-(phenylthio)- or 2-(methylthio)cyclohexanones.

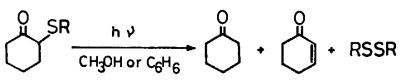

21 : R=CH_3
22 : R=C_6H_5

+ RSSR + RSR + RSH

Experimental

Gas-liquid chromatographic analyses were carried out with a Hitachi K-53 and a Hitachi 063, the preparative work being done with a Varian Autoprep 700. A SE-30 column supported on Diasolid L was mainly used in GLPC analyses. Other liquid phases were unsatisfactory because the starting 2-(alkoxycarbonyl)cycloalkanones were often decomposed in GLPC columns. Infrared spectra were obtained with a Hitachi EPI-G22, and nuclear magnetic resonance spectra were measured with a JEOL 3H-60 and a Hitachi R-22 using tetramethylsilane as an internal standard. Mass spectra were obtained with a Hitachi RM-50 GC. Quantitative GLPC analyses were carried out by an internal standard

method.

General Procedure for Irradiation. The starting cycloalkanone in alcoholic solvent (0.16 M) in a quartz tube was cooled in water and externally irradiated with a 500 W high pressure mercury vapor lamp for 70 h. Nitrogen gas was allowed to pass through the mixture during the course of irradiation. An immersion apparatus was employed for preparation. Quantitative experiments in different alcohols were carried out with a merry-go-round procedure for irradiation.

Preparations of 2-Substituted Cycloalkanones. Ethyl 2-oxo-1-cyclopentanecarboxylate (**1**), bp 107 °C/18 mmHg, was prepared from diethyl adipate and metal sodium by the method of Pinkney.[10] Methyl 2-oxo-1-cyclopentanecarboxylate (**2**), bp 105 °C/17 mmHg, was also prepared by a similar method. Ethyl 2-oxo-1-cyclohexanecarboxylate (**3**), bp 103.5 °C/12 mmHg, was prepared by the method of Snyder *et al.*[11] from cyclohexanone and diethyl oxalate. Ethyl 2-oxo-1-cycloheptanecarboxylate (**4**), bp 136 °C/22 mmHg, was prepared by the method of Krapcho *et al.*[12] from cycloheptanone and diethyl carbonate. Methyl 1-methyl-2-oxo-1-cyclopentanecarboxylate (**5**) was prepared by methylation of **2**.[13] 2-Oxo-1-cyclohexanecarbonitrile (**15**), bp 138—140 °C/15 mmHg, was prepared by the method of Satoda *et al.*[15] or Meyer[16] from 2-chlorocyclohexanone[14] and sodium cyanate. 3-Methyl-2-oxo-1-cyclohexanecarbonitrile (**16**), bp 95—96 °C/3 mmHg, was prepared by the method of Kuehne[17] from 3-methyl-2-pyrrorydino-1-cyclohexene, bp 117 °C/20 mmHg, and cyanogen chloride. 2-Methylthiocyclohexanone (**21**), bp 98—100 °C/15 mmHg, was prepared by the method of Truce *et al.*[18] from 2-chlorocyclohexanone and sodium methanethiolate. 2-Phenylthiocyclohexanone (**22**), bp 115—117 °C/3 mmHg, was prepared by the method of Seebach *et al.*[19] from cyclohexanone and diphenyl disulfide or by the method of Wilputte *et al.*[20] from 2-chlorocyclohexanone and sodium benzenethiolate. All the 2-substituted cycloalkanones were purified by a distillation or a preparative GLPC.

Photochemical Reaction of Ethyl 2-Oxo-1-cyclohexanecarboxylate (3). A mixture of 6.8 g of **3** and 250 ml of dry methanol (0.16 M) was irradiated for 10 h with an immersion apparatus using a 500 W high pressure mercury vapor lamp. After removal of the solvent, distillation gave 4.7 g of crude product; bp 60.0—85.0 °C/1 mmHg. The distillate was separated into four principal components by preparative GLPC using a SE-30 column. The second component was identified as unreacted ester **3**. The fourth component was identified as ethyl methyl hexanedioate (**8a**): IR (CCl_4) 1735 cm^{-1}; NMR (CCl_4) δ 1.22 (t, 3H), 3.59 (s, 3H), 4.05 (q, 2H), 1.62 (m, 6H), 2.22 ppm (t, 4H); *m/e* (rel intensity) 171 (M^+-OCH_3, 40), 157 ($M^+-OC_2H_5$, 48), 88 (49), 55 (100). Found: C, 59.60; H, 9.06%. Calcd for $C_{10}H_{18}O_4$: C, 59.38; H, 8.97%. The first component was further separated into two products by preparative GLPC using a CW-20 M column. One was identified as ethyl *cis*-7-oxo-2-heptenoate (**12**): IR (CCl_4) 2820, 2720, 1720, 1645 cm^{-1}; NMR (CCl_4) δ 1.30 (t, 3H), 1.77 (qi, 2H), 2.48 (t, 2H), 2.73 (q, 2H), 4.17 (q, 2H), 5.78 (dm, 1H, J=10.5 Hz), 6.24 (dt, 1H, J=10.5 Hz, J=7.5 Hz), 9.85 ppm (s, 1H); *m/e* (rel intensity) 170 (M^+, 3), 142 (16), 127 (42), 125 (50), 114 (100), 99 (93), 86 (72), 81 (83), 68 (92). Found: C, 63.20; H, 8.30%. Calcd for $C_9H_{14}O_3$: C, 63.51; H, 8.29%. The other product was identified as ethyl 7-oxo-3-heptenoate (**13**): IR (CCl_4) 2820, 2720, 1735 cm^{-1}; NMR (CCl_4) δ 1.26 (t, 3H), 2.5 (m, 4H), 3.00 (m, 2H), 4.12 (q, 2H), 5.60 (m, 2H), 9.81 ppm (s, 1H); *m/e* (rel intensity) 170 (M^+, 8), 142 (51), 127 (12), 125 (33), 124 (47), 99 (37), 97 (82), 96 (70), 79 (76), 67 (100), 55 (83). Found: C, 63.73; H, 8.21%. Calcd for $C_9H_{14}O_3$: C, 63.51; H, 8.29%. The third component was further separated into two products by preparative GLPC using a CW-20M column. One was identified as dimethyl heptanedioate (**14**) by comparison with an authentic sample, the other as ethyl *trans*-7-oxo-2-heptenoate (**11**): IR (CCl_4) 2820, 2720, 1725, 1655 cm^{-1}; NMR (CCl_4) δ 1.27 (t, 3H), 1.80 (qi, 2H), 2.24 (q, 2H), 2.48 (t, 2H), 4.17 (q, 2H), 5.80 (d, 1H, J=16.0 Hz), 6.88 (dt, 1H, J=16.0 Hz, J=6.5 Hz), 9.83 ppm (s, 1H); *m/e* (rel intensity) 170 (M^+, 2), 142 (10), 127 (36), 125 (50), 114 (82), 99 (72), 81 (100), 68 (77), 55 (53). Found: C, 63.35; H, 8.20%. Calcd for $C_9H_{14}O_3$: C, 63.51; H, 8.29%. GLPC analysis showed that the conversion of **3** was 91% and yields of **8a**, **11**, **12**, **13**, and **14** were 25, 7, 8, 21, and 5%, respectively.

When a sample of 0.16 M **3** in methanol in a quartz tube was externally irradiated for 70 h, **8a** was obtained in 25% yield.

Irradiation of **3** in ethanol for 70 h gave diethyl heptanedioate (**8b**) in 16% yield as the major product. **8b** was identified by comparison with an authentic sample.

Irradiation of **3** in isopropyl alcohol for 70 h gave ethyl isopropyl heptanedioate (**8c**) in 14% yield: IR (CCl_4) 1735 cm^{-1}; NMR (CCl_4) δ 1.18 (d, 6H), 1.24 (t, 3H), 1.65 (m, 6H), 2.20 (t, 4H), 4.05 (q, 2H), 4.90 ppm (m, 1H); *m/e* (rel intensity) 230 (M^+, 6), 185 (26), 171 (72), 143 (80), 125 (81), 101 (78), 69 (78), 55 (89), 41 (100). Found: C, 62.70; H, 9.60%. Calcd for $C_{12}H_{22}O_4$: C, 62.58; H, 9.63%.

Irradiation of **3** in *t*-butyl alcohol for 70 h gave *t*-butyl ethyl heptanedioate (**8d**) in 4% yield: IR (CCl_4) 1735 cm^{-1}; NMR (CCl_4) δ 1.23 (t, 3H), 1.40 (s, 9H), 1.55 (m, 6H), 2.13 (t, 2H), 2.22 (t, 2H), 4.06 ppm (q, 2H); *m/e* (rel intensity) 171 (28), 143 (27), 125 (27), 57 (100). Found: C, 63.63; H, 9.70%. Calcd for $C_{13}H_{24}O_4$: C, 63.90; H, 9.90%.

When a 0.08 M solution of **3** in methanol was irradiated for 42 h with a 15 W low pressure mercury vapor lamp, products such as **8a**, **11**, **12**, **13**, and **14** were not obtained. Irradiation of a 0.16 M solution of **3** in methanol in the presence of oxygen, 0.1—0.5 M 1.3-pentadiene or 0.16 M naphthalene gave **8a** in almost the same yields with nearly the same conversion.

Photochemical Reaction of Ethyl 2-Oxo-1-cyclopentanecarboxylate (1). Irradiation of a 0.16 M solution of **1** in methanol for 70 h gave ethyl methyl hexanedioate (**6a**) in 28% yield: IR (CCl_4) 1735 cm^{-1}; NMR (CCl_4) δ 1.24 (t, 3H), 1.62 (m, 4H), 2.25 (m, 4H), 3.63 (s, 3H), 4.07 ppm (q, 2H); *m/e* (rel intensity) 188 (M^+, 2), 157 (36), 143 (32), 115 (52), 111 (60), 59 (57), 55 (100). Found: C, 57.35; H, 8.50%. Calcd for $C_9H_{16}O_4$: C, 57.43; H, 8.57%.

Irradiation of a 0.16 M solution of **1** in ethanol for 70 h gave diethyl hexanedioate (**6b**) in 22% yield. **6b** was identified by comparison with an authentic sample.

Photochemical Reaction of Methyl 2-Oxo-1-cyclopentanecarboxylate (2). Irradiation of a 0.16 M solution of **2** in methanol for 70 h gave dimethyl hexanedioate (**7a**) in 32% yield. **7a** was identified by comparison with an authentic sample.

Photochemical Reaction of Ethyl 2-Oxo-1-cycloheptanecarboxylate (4). Irradiation of a 0.16 M solution of **4** in methanol for 70 h gave ethyl methyl octanedioate (**9a**) in 28% yield: IR (CCl_4) 1735 cm^{-1}; NMR (CCl_4) δ 1.24 (t, 3H), 1.6 (m, 8H), 2.25 (t, 4H), 3.65 (s, 3H), 4.08 ppm (q, 2H); *m/e* (rel intensity) 185 (M^+-OCH_3, 43), 171 (90), 143 (62), 138 (100), 129 (76), 97 (72), 88 (59), 83 (60), 69 (93), 55 (83). Found: C, 61.09; H, 9.28%. Calcd for $C_{11}H_{20}O_4$: C, 61.09; H, 9.32%.

Photochemical Reaction of Methyl 1-Methyl-2-oxo-1-cyclopentanecarboxylate (5). Irradiation of a 0.16 M solution of **5** in methanol for 70 h gave dimethyl 2-methylhexanedioate

(**10**) in 29% yield: IR (CCl_4) 1735 cm^{-1}; NMR (CCl_4) δ 1.15 (d, 3H), 1.62 (m, 4H), 2.25 (t, 2H), 2.45 (m, 1H), 3.64 ppm (s, 6H); *m/e* (rel intensity) 157 (M^+-OCH_3, 17), 156 (30), 128 (48), 127 (40), 124 (47), 96 (60), 95 (59), 94 (70), 69 (100), 67 (98).

*Photochemical Reaction of 3-Methyl-2-oxo-1-cyclohexanecarbonitrile (**16**).* Irradiation of a 0.16 M solution of **16** in methanol gave three principal products. These were separated by preparative GLPC using a SE-30 column. From spectral data, the first was identified as *cis*-6-methyl-7-oxo-2-heptenenitrile (*cis*-**20**): IR (CCl_4) 2710, 2810, 2220, 1725 cm^{-1}; NMR (CCl_4) δ 1.18 (d, 3H), 1.3—2.1 (m, 2H), 2.50 (q, 2H), 2.5 (m, 1H), 5.36 (m, 1H, J=11.0 Hz), 6.47 (dt, 1H, J=11.0 Hz, J=7.5 Hz), 9.85 ppm (s, 1H), *m/e* (rel intensity) 137 (M^+), 122 (2), 108 (8), 94 (14), 81 (28), 80 (30), 67 (100), 58 (42). The second was identified as *trans*-6-methyl-7-oxo-2-heptenenitrile (*trans*-**20**): NMR (CCl_4) δ 1.14 (d, 3H), 1.3—2.0 (m, 2H), 2.27 (q, 2H), 2.54 (m, 1H), 5.37 (m, 1H, J=17.0 Hz), 6.68 (dt, 1H, J=17.0 Hz, J=7.0 Hz), 9.82 ppm (s, 1H). IR and mass spectra of *trans*-**20** were almost identical with those of *cis*-**20**. The third was identified as methyl 6-cyano-2-methylhexanoate (**18**): IR (CCl_4) 2250, 2230, 1735 cm^{-1}; NMR (CCl_4) δ 1.15 (d, 3H), 1.51 (m, 6H), 2.30 (t, 2H), 2.45 (m, 1H), 3.66 ppm (s, 3H); *m/e* (rel intensity) 138 (M^+-OCH_3, 13), 109 (47), 88 (100), 69 (44), 55 (29). Found: C, 63.75; H, 8.90; N, 8.12%. Calcd for $C_9H_{15}NO_2$: C, 63.88; H, 8.94; N, 8.28%. GLPC analysis showed that the yields of *cis*-**20**, *trans*-**20**, and **18** were 5, 19, and 16%, respectively.

*Photochemical Reaction of 2-Oxo-1-cyclohexanecarbonitrile (**15**).* Irradiation of a 0.16 M solution of **15** in methanol for 70 h gave methyl 6-cyanohexanoate (**17a**) in 28% yield: IR (CCl_4) 2230, 1735 cm^{-1}; NMR (CCl_4) δ1.58 (m, 6H,) 2.31 (t, 2H), 2.32 (t, 2H), 3.66 ppm (s, 3H); *m/e* (rel intensity) 124 (M^+-OCH_3, 42), 96 (40), 74 (100), 69 (27), 59 (26), 55 (25). Found: C, 62.22; H, 8.39; N, 9.18%. Calcd for $C_8H_{13}NO_2$: C, 61.91; H, 8.44; N, 9.03%. Although product **19** was not isolated, its presence in the irradiated mixture was shown by GC-mass spectroscopy.

*Photochemical Reaction of 2-Methylthiocyclohexanone (**21**).* When a 0.16 M solution of **21** in methanol was irradiated for 70 h, the solution turned red-brown with precipitation of a solid. Removal of solvent gave tar. A slight formation of cyclohexanone was detected by GLPC analysis. Irradiation in ether or benzene afforded similar results.

*Photochemical Reaction of 2-Phenylthiocyclohexanone (**22**).* When a 0.16 M solution of **22** in methanol was irradiated for 70 h, the solution turned red-brown with precipitation of a solid. GLPC analysis showed that 76% of **22** was consumed, a slight amount of cyclohexanone being produced. Similar irradiation in benzene produced cyclohexanone, cyclohexenone, diphenyl disulfide, diphenyl sulfide, and thiophenol in 34, 2, 5, 3, and 3% yields, respectively. The conversion of **22** was 94%.

References

1) (a) N. J. Turro, J. C. Dalton, K. Dawes, G. Farrington, R. Hantola, D. Morton, M. Niemczyk, and N. Schore, *Acc. Chem. Res.*, **5**, 92 (1972); (b) O. L. Chapman and D. S. Weiss, "Organic Photochemistry," ed by O. L. Chapman, Marcel Dekker, Inc., Vol. 3, New York, N. Y. (1973), p. 197; (c) W. M. Horspool, "Photochemistry," ed by D. Bryce-Smith, The Chemical Society, Vol. 6, London (1975), p.316.

2) G. Quinkert, *Angew. Chem., Int. Ed. Engl.*, **4**, 211 (1965).

3) R. Srinivasan, "Advances in Photochemistry," ed by W. A. Noyes, Jr., G. S. Hammond, and J. N. Pitts, Jr., Interscience, Vol. 1, New York (1963), p. 83.

4) (a) G. Quinkert, G. Cimbollek, and G. Buhr, *Tetrahedron Lett.*, **1966**, 4573; (b) N. J. Turro and R. M. Southam, *ibid.*, **1967**, 545; (c) D. R. Morton, E. L. Ruff, R. M. Southam, and N. J. Turro, *J. Am. Chem. Soc.*, **92**, 4349 (1970); (d) D. R. Morton and N. J. Turro, *ibid.*, **95**, 3947 (1973).

5) G. K. Chip and T. R. Lynch, *Can. J. Chem.*, **52**, 2249 (1974).

6) J. R. Collier and J. Hill, *Chem. Commun.*, **1968**, 700.

7) (a) M. Tokuda, M. Hataya, J. Imai, M. Itoh, and A. Suzuki, *Tetrahedron Lett.*, **1971**, 3133; (b) V. V. Chung, M. Tokuda, A. Suzuki, and M. Itoh, *Bull. Chem. Soc. Jpn.*, **49**, 341 (1976).

8) (a) M. Itoh, M. Tokuda, K. Kihara, and A. Suzuki, *Tetrahedron*, **24**, 6591 (1968); (b) M. Itoh, M. Tokuda, K. Seguchi, K. Taniguchi, and A. Suzuki, *Kogyo Kagaku Zasshi*, **72**, 219 (1969); (c) M. J. Jorgenson, *Chem. Commun.*, **1965**, 137; (d) R. R. Rando and W. von E. Doering, *J. Org. Chem.*, **33**, 1671 (1968); (e) M. J. Jorgenson and L. Gundel, *Terahedron Lett.*, **1968**, 4991; (f) J. A. Barltrop and J. Wills, *ibid.*, **1968**, 4987; (g) M. J. Jorgenson and S. Patumtevapibal, *ibid.*, **1970** 489.

9) S. J. Rhoads, J. C. Gilbert, A. W. Decora, T. R. Garland, R. J. Spangler, and M. J. Urbigkit, *Tetrahedron*, **19**, 1625 (1963).

10) P. S. Pinkney, *Org. Synth.*, Coll. Vol. II, 116 (1943).

11) H. R. Snyder, L. A. Brooks, and S. H. Shapiro, *Org. Synth.*, Coll. Vol. II, 531 (1943).

12) A. P. Krapcho, J. Diamanti, C. Cayen, and R. Bingham. *Org. Synth.*, Coll. Vol. V, 198 (1973).

13) M. S. Newman, M. D. Farbman, and H. Hipsher, *Org. Synth.*, Coll. Vol. III, 188 (1955).

14) I. Satoda, T. Fukui, and K. Mori, *J. Pharm. Soc. Jpn.* **79** 961 (1959).

15) R. E. Meyer, *Helv. Chim. Acta*, **16**, 1291 (1933).

16) M. E. Kuehne, *J. Am. Chem. Soc.*, **81**, 5400 (1959).

17) W. E. Truce and R. H. Knospe, *J. Am. Chem. Soc.*, **77**, 5063 (1955).

18) D. Seebach and M. Teschner, *Tetrahedron Lett.*, **1973**, 5113.

19) R. Wilputte and R. H. Martin, *Bull. Soc. Chim. Belg.*, **65**, 874 (1956); *Chem. Abstr.*, **51** 6588h (1957).

The Syntheses of [3]- and [4]Ruthenocenophanes

Shin-ichi KAMIYAMA,[1] Toshishige M. SUZUKI, Tetsuo KIMURA, and Akira KASAHARA*

Government Industrial Research Institute Tohoku, Nigatake, Haranomachi, Sendai 983

**Department of Applied Chemistry, Faculty of Engineering, Yamagata University, Yonezawa 992*

(Received August 25, 1977)

[3]- and [4]ruthenocenophanes as well as other ruthenocene derivatives were synthesized. The preparation of ruthenocenes in this experiment required more forced reaction conditions than those of the corresponding ferrocenes. Two cyclopentadienyl rings of these ruthenocenophanes are found to tilt mutually, and the degree of the ring-tilting of [3]ruthenocenophane is greater than that of the [4] homolog.

A large number of heteroannularly bridged ferrocenes, designated [m]ferrocenophanes, have played important roles in the investigations of the physical and chemical properties of the ferrocene molecule.[2] On the other hand, there have been only a few investigations of [m]ruthenocenophanes or of other ruthenocene derivatives.[3] Recently, the first synthesis of [5]ruthenocenophanes has been reported.[4] This paper will be concerned with the syntheses and characterizations of several new [3]- and [4]ruthenocenophanes. The introduction of a heteroannularly bridged carbon chain into a ruthenocene molecule will cause a distortion of the cyclopentadienyl rings from their normal parallel geometry. The degree of the tilting of two cyclopentadienyl rings and of the conformational flexibility of linking chains is expected to depend on the length of the carbon chain and on the steric circumstances. These steric effects will be discussed on the basis of proton magnetic resonance, infrared and electronic spectra.

Results and Discussion

Synthesis of [3]Ruthenocenophan-1-one (V) and [3]Ruthenocenophane (VI). The introduction of a three-carbon interannular bridge into a ruthenocene molecule was achieved by the cyclization of 3-ruthenocenylpropionic acid (IV) to V. Compound IV was prepared from formylruthenocene (II). Bublitz *et al.* have previously reported that, in the presence of $POCl_3$, the reaction of ruthenocene (I) with *N*-methylformanilide in chlorobenzene led to the formation of II in only a 8% yield.[5] However, we have found that II is formed in a reproducibly good yield (46%) by the reaction of I with *N*-methylformanilide without any solvent in the presence of $POCl_3$. The condensation of II with malonic acid afforded 3-ruthenocenylacrylic acid (III). The hydrogenation of III in ethanol over PtO_2 gave IV quantitatively. An intramolecular Friedel-Crafts-type reaction of IV with trifluoroacetic anhydride required a longer reaction time (two weeks) in refluxing cyclohexane than that needed in the case of the ferrocene derivative.[6] This difference in the reaction conditions of cyclization may be because ruthenocenes are generally less reactive and because the distance between two cyclopentadienyl rings of a ruthenocene is longer than that of a ferrocene.[7,8] Compound VI was prepared by the reduction of V with lithium aluminum hydride-aluminum trichloride in the usual manner.

Synthesis of [4]Ruthenocenophan-2-one (VII) and [4]Ruthenocenophane (IX). In a mixture of methanol and ether, the reaction of V and diazomethane led to the formation of VII, accompanied by a small amount of [4]ruthenocenophan-1-one (VIII), while the reduction of VII with lithium aluminum hydride-aluminum trichloride gave a good yield of IX (Scheme 1).

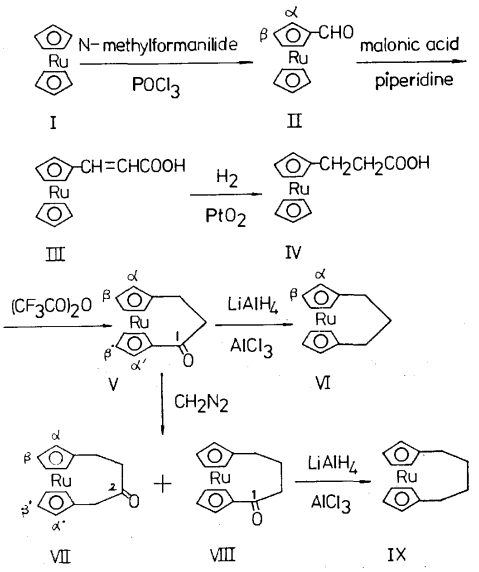

Scheme 1. Syntheses of ruthenocenophanes.

Proton Magnetic Resonance Spectra. The details of the ^1H NMR spectra of ruthenocenes, together with the reported spectra of ferrocenes,[9] are summarized in Table 1. The assignments of the signals of ruthenocene derivatives are based on those of the corresponding ferrocenes and multibridged ferrocenophanes.[10] It has previously been reported that, in the ^1H NMR spectra of ferrocene derivatives, alkyl substituents do not cause a noticeable difference in the chemical shift between α- and β-protons of the cyclopentadienyl rings to which they are attached.[9] The most striking manifestation of the ring tilt in [m]ferrocenophanes with different bridge lengths is the variation in the cyclopentadienyl ring proton patterns.[9] In the case of VI, the protons of cyclopentadienyl rings appear as two unsymmetrical triplets separated by 0.23 ppm, corresponding to an A_2B_2 system where vicinal and cross-ring coupling constants are approximately equal and considerably smaller than the chemical shift difference between unlike protons.[9] Compound IX also shows two triplets separated by 0.11 ppm. On the basis of the ^1H NMR spectrum, Rinehart *et al.*[11] have suggested that the tilting rings of [3]ferrocenophane serve to bring the α-protons of the rings closer to the Fe atom

TABLE 1. ^{1}H NMR CHEMICAL SHIFTS OF

Compound	Cyclopentadienyl proton				
	H_α	H_β	$\lvert H_\beta - H_\alpha \rvert$	$H_{\alpha'}$	$H_{\beta'}$
Formylruthenocene (II)	4.85^{t} [d] (J=1.8 Hz)	5.08^{t} (J=1.8 Hz)	0.23	4.65^{s} [a]	
3-Ruthenocenylacrylic acid (III)	4.71^{t} (J=1.8 Hz)	4.99^{t} (J=1.8 Hz)	0.28	4.55^{s}	
3-Ruthenocenylpropionic acid (IV)	4.4—4.7^{m} [e]		—	4.4—4.7^{m}	
[3]Ruthenocenophan-1-one (V)	4.60^{t} (J=1.4 Hz)	4.86^{t} (J=1.4 Hz)	0.26	5.10^{t} (J=1.4 Hz)	4.97^{t} (J=1.4 Hz)
[3]Ruthenocenophane (VI)	4.37^{t} (J=1.8 Hz)	4.60^{t} (J=1.8 Hz)	0.23	—	—
[4]Ruthenocenophan-2-one (VII)	4.46^{t} (J=1.6 Hz)	4.67^{t} (J=1.6 Hz)	0.21	4.67^{t} (J=1.6 Hz)	4.46^{t} (J=1.6 Hz)
[4]Ruthenocenophane (IX)	4.46^{t} (J=1.5 Hz)	4.57^{t} (J=1.5 Hz)	0.11	—	—
1,1,2,2-Tetramethyl-[2]ferrocenophane[f]	3.98^{t}	4.52^{t}	0.54	—	—
[3]Ferrocenophane[f]	3.87^{t}	4.01^{t}	0.14	—	—
[4]Ferrocenophane[f]	3.93^{s}		0.00	—	—
[3]Ferrocenophan-1-one[f]					
[4]Ferrocenophan-2-one[f]					

a) Singlet. b) Broad singlet. c) Doublet. d) Triplet. e) Multiplet. f) Ref. 9.

TABLE 2. THE CARBONYL STRETCHING FREQUENCIES OF RUTHENOCENE AND FERROCENE DERIVATIVES (cm^{-1})

Compound	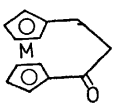	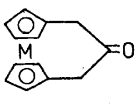	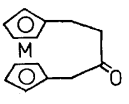	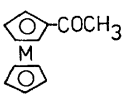
M				
Ru	1656[a]		1710[a]	1658[b]
Fe	1681[c]	1703[d]	1706[c]	1658[b]

a) In a KBr pellet and a Nujol mull. b) Ref. 7; in a KBr pellet. c) Ref. 6. d) Ref. 12; in CCl_4.

than the β-protons, therefore, the former experience a greater shielding influence. Extending this hypothesis, the larger splitting of the ring proton resonance of VI implies a greater dihedral angle of the two rings compared to the [4] homolog (IX). Barr and Watts have reported that the singlet resonance of [4]ferrocenophane is in accord with an undistorted ferrocene nucleus.[9] On the other hand, the splitting of the ring proton resonance of IX seems to suggest that the rings are mutually inclined to some extent, in contrast to the case of [4]ferreocenophane. This difference might be due to the distance between the two cyclopentadienyl rings of a ruthenocene being longer by 1.1 Å than that of a ferrocene.[8] Since the peak separation of VI is greater than that of IX, furthermore, the rings of the former might be tilted more than those of the latter.

The bridging methylene protons of VI and IX appear as one broad singlet and two multiplets respectively. In the case of V and VII, again, bridging methylene protons appear as two triplets and as two triplets and one singlet respectively. On the other hand, the methylene protons of [3]ferrocenophan-1-one and [4]ferrocenophan-2-one appear as sharp singlets, and Barr and Watts have suggested that facile conformational interconversion within the bridge is clearly indicated by the appearance of the bridging methylene protons as sharp singlets in the ^{1}H NMR spectra of [3]- and [4]ferrocenophane classes.[9] These results, therefore, seem to indicate that [3]- and [4]ruthenocenophanes (V, VII) have a smaller conformational flexibility than the corresponding ferrocenophanes.

Infrared Spectra. The values of the carbonyl-stretching absorptions of ruthenocenes, together with the reported values of the corresponding ferrocenes,[6,7,12] are given in Table 2. The absorption bands of the ruthenocene series are located at positions similar to those of the corresponding ferrocenes except for [3]ruthenocenophan-1-one (V). The difference in the carbonyl-stretching frequencies of V and acetylruthenocene is only 2 cm^{-1}, while that of [3]ferrocenophan-1-one and acetylferrocene is 23 cm^{-1}. In view of the following three factors: (i) the distance between two cyclopentadienyl rings of a ruthenocene is longer than that of a ferrocene,[8] (ii) the ^{1}H NMR chemical shift difference between the α- and β-protons of the cyclopentadienyl rings in ruthenocenophanes is larger than that in the corresponding ferrocenophanes, and (iii) the IR absorption bands of acetylruthenocene, acetylferrocene and V, in which π-orbitals of carbonyl groups can effectively conjugate with π-systems of cyclopentadienyl rings, are located at lower frequencies than those of [4]ruthenocenophan-2-one (VII), [4]ferrocenophan-2-one, and [3]ferrocenophan-1-one,[6,13] though these spectra should have been measured in dilute solutions, it is assumed that the cyclopentadienyl rings of ruthenocenophanes are more inclined than those of the corresponding ferrocenophanes.

Electronic Spectra. The details of the electronic spectra of ruthenocene derivatives are listed in Table 3. Figure 1 shows the electronic spectra of VI and IX, along with that of ruthenocene (I) in ethanol. The

RUTHENOCENE AND FERROCENE DERIVATIVES (δ).

Bridged Methylene Proton				Substituent	
H_1	H_2	H_3	H_4		
—	—	—	—	9.71[s] (-CHO)	
—	—	—	—	5.95, 7.21[d c)]	(J=15.6 Hz, *trans* olefinic protons)
—	—	—	—	2.55[bs b)]	(methylene protons)
—	2.74[t] (J=3.6 Hz)	2.82[t] (J=3.6 Hz)	—	—	
1.76[bs]	1.76[bs]	—	—	—	
3.24[s]	—	2.66[t] (J=8.4 Hz)	2.76[t] (J=9.6 Hz)	—	
2.1—2.6[m]	1.3—1.8[m]	—	—	—	
—	—	—	—	—	
1.95[s]	1.95[s]	—	—	—	
1.4—1.5[m]	1.0—1.2[m]	—	—	—	
—	2.99[s]	2.99[s]	—	—	
3.30[s]	—	2.77[s]	2.77[s]	—	

TABLE 3. ELECTRONIC SPECTRA OF RUTHENOCENE DERIVATIVES[a)]

Compound	λ_{max} (nm) (ε)		
Ruthenocene (I)		274 (286)	324 (268)
Formylruthenocene (II)		251 (13100)	344 (1460)
3-Ruthenocenylacrylic acid (III)	226 (5000)[sh b)]	268 (8020)	346 (1380)
3-Ruthenocenylpropionic acid (IV)			300 (731)
[3]Ruthenocenophan-1-one (V)		251 (4900)	292 (1020)[sh], 332 (697)[sh]
[3]Ruthenocenophane (VI)		265 (384)[sh]	325 (603)
[4]Ruthenocenophan-2-one (VII)		269 (1120)[sh]	
[4]Ruthenocenophane (IX)			317 (302)

a) In absolute EtOH. b) Shoulder.

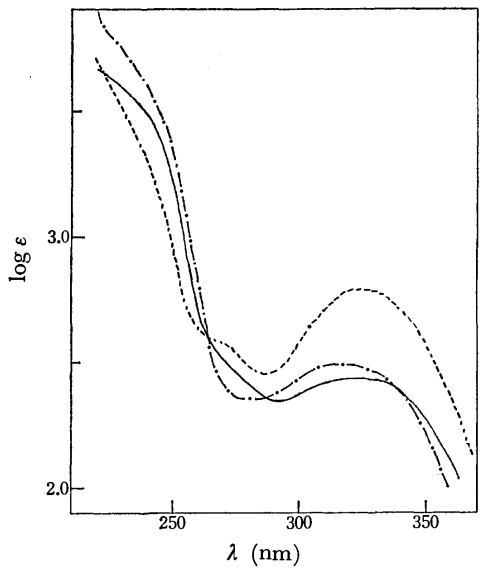

Fig. 1. The electronic spectra, taken in abs. ethanol: (——) ruthenocene (I), (----) [3]ruthenocenophane (VI) and (—·—·—) [4]ruthenocenophane (IX).

electronic spectra of d^6 metallocene including I have been thoroughly studied.[14] According to the earlier band assignments, the absorption peak in the 320—330 nm region for each compound corresponds to the spin-allowed d-d transitions (two $^1A_{1g}\rightarrow{}^1E_{1g}$ and one $^1A_{1g}\rightarrow{}^1E_{2g}$), and the intense band at *ca.* 240 nm is associated with the charge transfer transitions of metal to ligand and ligand to metal. Although the spin-allowed d-d bands of I, VI and IX are located at similar positions, the band intensity of VI is much higher than that of I or IX. On the contrary, the intensity of the charge transfer bands of VI is lower than that of I or IX. The intensity of the spin-allowed d-d bands of IX is slightly higher than that of I, though their over-all spectra resemble each other. The cyclopentadienyl rings are distorted from their normal sandwich geometry when they are connected by short chains. The ^1H NMR study suggested that the cyclopentadienyl rings of VI are more inclined than those of IX. Thus, the ring-tilting will bring about an increase in the intensity of the spin-allowed d-d bands and a depression in the intensity of the charge transfer bands. The inclination of the cyclopentadienyl rings upon the introduction of bridging chains seems to alter the degree

of the overlap between the metal d-orbitals and the p-orbitals of cyclopentadienyl rings. Furthermore, the ligand-field strength is changed with a distortion of rings from their normal parallel geometry. These effects might change the spectra of the present ruthenofcene derivatives.

Experimental

Materials. All the melting points are uncorrected. Ruthenocene (I) was prepared according to the method described by Hofer and Schlögl.[3]

Measurements. The ^1H NMR spectra were obtained with a JEOL JNM-PMX-60 spectrometer (60 MHz) at room temperature. All the chemical shifts are expressed in δ (ppm; downfield from internal Me_4Si). The IR spectra were measured in KBr pellets with a Hitachi Model 285 infrared spectrometer. The electronic spectra were recorded with a Shimadzu Double 40-R spectrophotometer at room temperature.

Formylruthenocene (II). Into a flask containing 8.0 g (0.035 mol) of ruthenocene (I), we vigorously stirred three portions of 12.46 g (0.092 mol) of *N*-methylformanilide and 8.82 g (0.057 mol) of phosphoryl chloride every 2 h at 90 °C under a nitrogen atmosphere. After the addition of 86.4 g of sodium acetate trihydrate in 400 ml of water, the solution was refluxed for 1 h, and then stirred overnight at room temperature. The solution was extracted three times with ether which had been washed successively with a hydrochloric acid solution (1 M), water, saturated sodium hydrogencarbonate, and finally brine, and then dried over anhydrous sodium sulfate. The ether extract, concentrated to 100 ml, was shaken with a solution of 36 g of sodium hydrogensulfite in 400 ml of water. The hydrogensulfite addition compound was washed with ether and then dried. The hydrogensulfite addition compound was taken up in 200 ml of a sodium hydroxide solution (2 M), and the liberated aldehyde was extracted into ether. The combined ether extract was washed with brine and then dried over anhydrous sodium sulfate. After the removal of the solvent, the sublimation of the crude product gave 4.2 g (46%) of formylruthenocene (II); mp 103—104 °C(hexane-dichloromethane), (lit,[3] 86—87 °C). IR(KBr) 1649 cm^{-1} (C=O). Found: C, 50.92; H, 3.85%. Calcd for $C_{11}H_{10}RuO$: C, 50.97; H, 3.89%.

3-Ruthenocenylacrylic Acid (III). The aldehyde (II) (5.5 g), malonic acid (5.5 g), and piperidine (1.3 ml) were dissolved in pyridine (100 ml), and the mixture was heated at 100 °C for 2 h under a nitrogen atmosphere. The cooled solution was diluted with water and extracted with chloroform. The chloroform extract was washed with dilute hydrochloric acid and water, and then extracted with a 2 M sodium hydroxide solution. The acidification of the aqueous layer precipitated 3-ruthenocenylacrylic acid (III) (5.4 g; 85%); mp 228—229 °C (dioxane-water). IR(KBr) 1666 (C=O) and 1612 cm^{-1} (C=C). Found: C, 51.71; H, 4.18%. Calcd for $C_{13}H_{12}RuO_2$: C, 51.83; H, 4.02%.

3-Ruthenocenylpropionic Acid (IV). The hydrogenation of 4.0 g (0.013 mol) of III in 400 ml of ethanol over 50 mg of PtO_2 gave 4.0 g (98%) of 3-ruthenocenylpropionic acid (IV); mp 99—100 °C (petroleum ether). IR(KBr) 1824 cm^{-1} (C=O). Found: C, 51.68; H, 4.61%. Calcd for $C_{13}H_{14}RuO_2$: C, 51.49; H, 4.65%.

[3]Ruthenocenophan-1-one (V). A solution of 3.00 g (0.0099 mol) of IV and 50 g (0.238 mol) of trifluoroacetic anhydride in 800 ml of cyclohexane was refluxed for 2 weeks under a nitrogen atmosphere. The cooled solution was poured into a saturated sodium hydrogencarbonate solution, extracted three times with ether which had been washed to neutrality, and then dried over anhydrous sodium sulfate. The removal of the solvent left 2.26 g (80%) of the crude product; mp 175—176 °C (acetone-water). Found: C, 54.74; H, 4.12%. Calcd for $C_{13}H_{12}RuO$: C, 54.74; H, 4.24%.

[3]Ruthenocenophane (VI). An ether solution (150 ml) of V (1.0 g) was added to a suspension of litihum aluminum hydride (0.2 g) and aluminum trichloride (0.8 g) in ether (50 ml). After refluxing for 4 h, the excess reagent was decomposed with moist ether and then with water. The resulting reaction mixture was extracted three times with ether which had been washed with water, saturated sodium hydrogencarbonate and finally brine, and then dried over anhydrous sodium sulfate. The removal of the solvent left 0.84 g (90%) of the crude product; mp 123—124 °C (hexane). Found: C, 57.30; H, 5.23%. Calcd for $C_{13}H_{14}Ru$: C, 57.56; H, 5.20%.

[4]Ruthenocenophan-2-one (VII) and [4]Ruthenocenophan-1-one (VIII). To a solution of 2.0 g (0.0070 mol) of V in 100 ml of methanol and 150 ml of ether, we added 100 ml of an etheral solution containing 0.050 mol of diazomethane. The solution was kept at 0 °C in the dark for 10 h, and then evaporated *in vacuo*. The residue was column-chromatographed over silica gel. The first band, eluted with benzene, yielded 1.5 g (71%) of [4]ruthenocenophan-2-one (VII); mp 165—166 °C (hexane-dichloromethane). Found: C, 56.12; H, 4.78%. Calcd for $C_{14}H_{14}RuO$: C, 56.19; H, 4.72%.

The second band, eluted with benzene-ethyl acetate (4 : 1), yielded a small amount of [4]ruthenocenophan-1-one (VIII) which was not isolated in the pure state.

[4]Ruthenocenophane (IX). This compound was prepared in a 73% yield under the same conditions as VI; mp 73—74 °C (benzene). Found: C, 58.89; H, 5.88%. Calcd for $C_{14}H_{16}Ru$: C, 58.94; H, 5.65%.

References

1) To whom correspondence should be addressed.
2) G. B. Shul'pin and M. I. Rybinskaya, *Usp. Khim.*, **43**, 1524 (1974) and the references cited therein.
3) O. Hofer and K. Schlögl, *Tetrahedron Lett.*, **1967**, 3485; *J. Organomet. Chem.*, **13**, 443 (1968).
4) A. N. Nesmeyanov, G. B. Shul'pin, D. V. Zagorevskii, and M. I. Rybinskaya, *Dokl. Akad. Nauk SSSR*, **229**, 881 (1976).
5) D. E. Bublitz, W. E. MacEwen, and J. Kleinberg, *J. Am. Chem. Soc.*, **84**, 1845 (1962).
6) M. Rosenblum, A. K. Banerjee, N. Danieli, R. W. Fish, and V. Schlatter, *J. Am. Chem. Soc.*, **85**, 316 (1963).
7) M. D. Rausch, E. O. Fischer, and H. Grubert, *J. Am. Chem. Soc.*, **82**, 76 (1960).
8) E. A. Siebold and L. E. Sutton, *J. Chem. Phys.*, **23**, 1967 (1955); J. D. Dunitz, L. E. Orgel, and A. Rich, *Acta Crystallogr.*, **9**, 373 (1956); R. K. Bohn and A. Haaland, *J. Organomet. Chem.*, **5**, 470 (1966); G. L. Hardgrove and D. H. Templeton, *Acta Crystallogr.*, **12**, 28 (1959).
9) T. H. Barr and W. E. Watts, *Tetrahedron*, **24**, 6111 (1968).
10) M. Hisatome, T. Sakamoto, and K. Yamakawa, *J. Organomet. Chem.*, **107**, 87 (1976).
11) K. L. Rinehart, Jr., A. K. Frerichs, P. A. Kittle, L. F. Westman, D. H. Gustafson, R. L. Pruett, and J. E. McMahon, *J. Am. Chem. Soc.*, **82**, 4111 (1960).
12) W. Mock and J. H. Richard, *J. Org. Chem.*, **27**, 4050 (1962).
13) T. H. Barr and W. E. Watts, *Tetrahedron*, **24**, 3219 (1968).
14) Y. S. Sohn, D. N. Hendrickson, and H. B. Gray, *J. Am. Chem. Soc.*, **93**, 3603 (1971).

The Chlorination of Hydrocarbons. XIV. The Chlorination of Vinyl Compounds[1)]

Kiyonori SHINODA

Toyama Technical College, Hongo, Toyama 930-11

(Received September 5, 1977)

The competitive chlorination of various vinyl compounds was carried out in order to elucidate the effect of the structure on the addition rate of chlorine to a double bond. A linear free-energy relationship was found to exist between the reactivities in the presence of oxygen and Taft's σ^* constants. The ρ^* value was calculated to be -1.20. On the other hand, the plot deviated slightly from a straight line; this shows the Taft relationship between the reactivities for the photochlorination and σ^* values, known as an extra acceleration due to the hyperconjugation of the alkyl group.

Paraffin hydrocarbons have been photochlorinated in the liquid phase by Migita and his co-workers.[2,3)] The gas-phase photochlorination of several chloroethanes has also been performed by Mack.[4)] Both groups of workers found Taft's $\rho^*\sigma^*$ relationship to be obeyed. While there have been such extensive studies of the substitutional chlorination, though only a little is known about the addition of chlorine to a double bond.

The effect of the structure on the rate of chlorination was investigated by carrying out competitive reactions with various vinyl compounds.

Experimental

Reagents. All the reagents used in this work were purchased from the Tokyo Kasei Kogyo Co. except for the carbon tetrachloride and hydroquinone, which were obtained from Wako Pure Chemical Industries. They were all of a G.R. or E.P. grade and were not purified further. The chlorine and oxygen were taken from commercial cylinders and were passed through a sulfuric acid trap before use.

Photochemical Procedure. The chlorination was carried out in 100-ml, flat, cylindrical, semibatch Pyrex reactor.[5)] A mixture of two vinyl compounds (both 0.1 mol), hydroquinone (0.001 mol) and hexachloroethane (0.002 mol) in 50 ml of carbon tetrachloride was added to the reactor. Hexachloroethane was useful as the standard material of gas chromatography.

The reactor was immersed in a thermostat at 30 °C and illuminated with a 100-W mercury lamp (Ushio UM-102) placed 5.0 cm above the reaction vessel. The chlorine was fed into the reactor at the rate of 0.1 mol/h. After a period required for the attainment of steady conditions, the irradiation was started. At regular time intervals, 1-ml samples were taken from the reacting solution and analyzed by means of gas chromatography (Shimadzu GC-5, SDC 550 or PEG 6000).

Dark Chlorination Procedure in the Presence of Oxygen. The dark chlorination procedure was the same as that used in the photochemical reaction except for the use of the oxygen. The chlorine and oxygen gases were led from the cylinders through a mixer to the reactor at the rates of 0.1 and 0.04 mol/h respectively.

Results

It is well known that the liquid-phase chlorination of linear olefins gives predominantly addition products, while the chlorination of olefins with branching at the double bond gives predominantly allylic substitution products.[6)] These vinyl compounds were found to give predominantly addition products, accompanied by minor amounts of allylic substitution products. In all the runs, two vinyl compounds were competitively chlorinated in order to keep the effect of the induction period and the concentration of chlorine constant

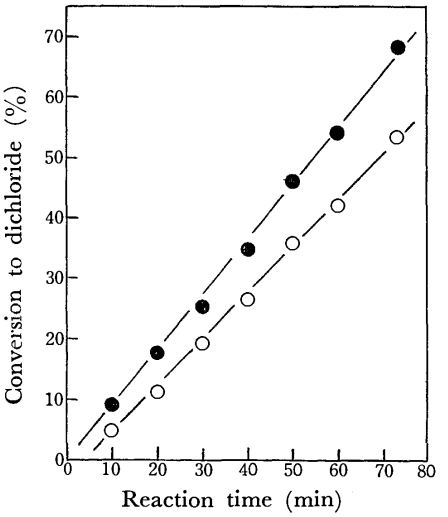

Fig. 1. Competitive photochlorination of allyl chloride and 3-chloro-1-butene at 30 °C.
○: Allyl chloride, ●: 3-chloro-1-butene.

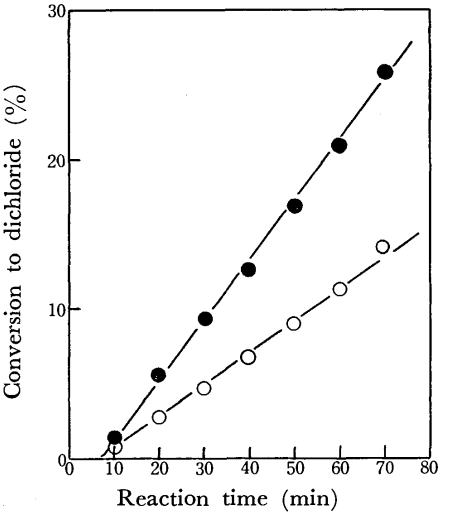

Fig. 2. Competitive chlorination of allyl chloride and 3-chloro-1-butene in the presence of oxygen at 30°C.
○: Allyl chloride, ●: 3-chloro-1-butene.

TABLE 1. RELATIVE RATE CONSTANTS (k/k_0) AND POLAR SUBSTITUENT CONSTANTS (σ^*)

CH_2=CH-R	Substituent R	k/k_0 Radical	k/k_0 Ionic	σ^*[8]
	-CN	0.138	0.00109	3.64[a]
	-COOH	0.283	0.00197	2.94[a]
	$-COOCH_3$	0.383	0.0181	2.00
	$-COCH_3$	—	0.0352	1.65
	$-CH_2CN$	0.601	0.215	1.300
	$-CH_2Cl$	1.00 (standard)	1.00 (standard)	1.050
	$-CH_2Br$	1.57	1.40	1.000
	$-CHClCH_3$	1.17	2.06	0.950[a]
	$-CH_2I$	1.73	1.63	0.85
	$-C_6H_5$	1.99	2.00	0.600
	$-CH_2COCH_3$	3.09	—	0.60
	$-CH_2C_6H_5$	1.90	—	0.215
	$-CH_2CH_2CH_2CH_3$	7.01	26.9	−0.130
	$-CH_2CH(CH_3)_2$	9.44	35.9	−0.210
	$-C(CH_3)_3$	7.72	—	−0.300

a) M. Kosugi, T. Migita, and Y. Nagai, *Nippon Kagaku Zasshi*, **92**, 477 (1971).

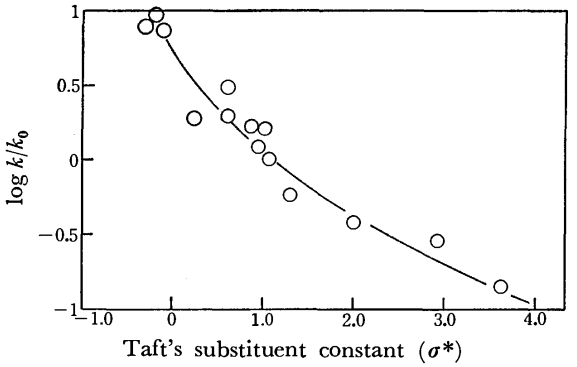

Fig. 3. Taft's plot for photochlorination of vinyl compounds at 30 °C.

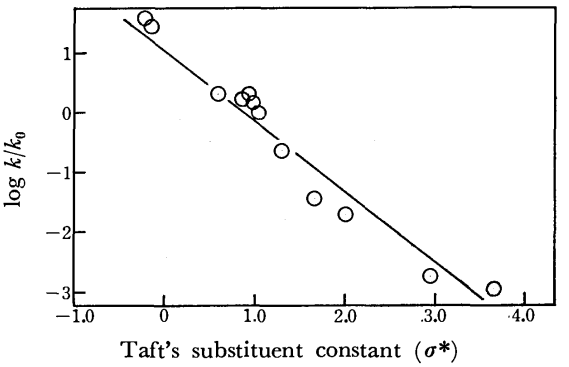

Fig. 4. Taft's plot for chlorination of vinyl compounds in the presence of oxygen at 30 °C.

throughout an experiment. The plots of the conversion of vinyl compounds into the addition products against the reaction time are found to be linear, as is shown in Figs. 1 and 2. Figure 1 shows the competitive photochlorination of allyl chloride and 3-chloro-1-butene as typical experimental data. The results of the competitive chlorination of these compounds for a dark run with oxygen are shown in Fig. 2. The values of the relative rate constants were calculated from the slopes of these straight lines, obtained according to the previous paper.[7] These relative rate constants are given in the first two columns of Table 1.

Discussion

As can be seen from Table 1, the rate of chlorination was increased by the electron-releasing substituent group and decreased by the electron-withdrawing group. Since the reactivity seemed to be affected by the polar nature of the substituent, Taft's equation was applied to this chlorination:

$$\log k/k_0 = \rho^*\sigma^*, \quad (1)$$

where k/k_0 is the relative rate constant with respect to the standard reaction (allyl chloride in this case).

The logarithms of the relative rate constants for the photochemical chlorination of vinyl compounds are plotted against Taft's substituent constants, σ^* (Fig. 3). Figure 4 shows also Taft's $\rho^*\sigma^*$ plot for the dark chlorination in the presence of oxygen. It is said that the chlorination of unsaturated compounds in nonpolar media proceeds according to the polar and radical pathways.[9] Then, the competitive chlorinations of methyl acrylate and cyclohexane were carried out in order to confirm that either pathway is predominant. The procedure was the same as has been described in the Experimental section. The results of such experiments are summarized in Fig. 5. A dark chlorination under oxygen produced mainly methyl 2,3-dichloropropionate, while chlorocyclohexane was detected in a trace amount. On the other hand, chlorocyclohexane was formed by the substitutive chlorination of cyclohexane for a photochemical reaction, The attack on

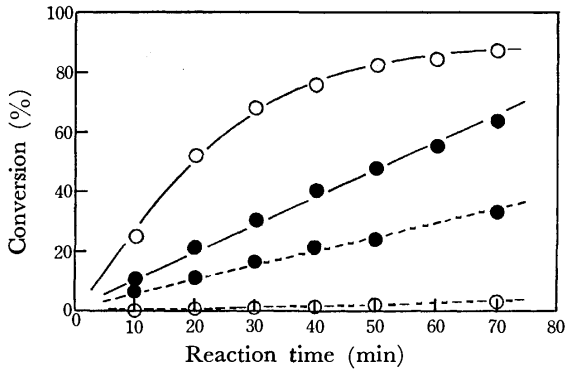

Fig. 5. Competitive chlorination of methyl acrylate and cyclohexane at 30 °C.
○: Chlorocyclohexane from cyclohexane, ●: methyl 2,3-dichloropropionate from methyl acrylate.
——: Illuminated, ----: darkness.

the completely saturated substrate, cyclohexane, is compelling evidence for the presence of free radical chains. The photochlorination took place more rapidly than the dark chlorination in the presence of oxygen, as can be seen by comparing Fig. 1 with 2. This phenomenon is also observed in Fig. 5. In general, the reaction under oxygen became just slow enough to allow a pale yellow color to appear in a solution during the chlorine addition. For a series of dark runs under oxygen, the chlorination of a substrate with an electron-withdrawing group was fairly slow (Table 1).

It has been reported that terminal and linear olefins followed the radical pathway, whereas olefins with carbon-chain branching at the double bond followed the polar pathway.[9] The polar pathway was also described to be favored by the dilution of the olefin at low olefin concentrations for the dark runs, but this effect could be counteracted with light.[10]

Therefore, it was concluded that the chlorination of these vinyl compounds at higher concentrations under illuminated conditions proceeded predominantly according to the radical pathway. The photochlorination is a radical reaction, while the dark chlorination under oxygen is an ionic one since oxygen acts as a radical inhibitor. The reactivity pattern of the chlorine atom toward vinyl compounds is similar to that of the chlorine molecule, as is shown in Figs. 3 and 4.

A linear free-energy relationship might be found to exist between the relative rate constants of the ionic reaction and Taft's σ^* constants. The ρ^* value was calculated to be -1.20. On the other hand, in the case of the radical reaction, the relative rate constants were slightly more dependent on Taft's σ^* constants than those of the dark runs and the plot seemed to deviate from a straight line, making a concave curve. This phenomenon has been known in connection with the photochlorination of chloroethanes as an extra acceleration by the hyperconjugation effects of the alkyl group.[2] Accordingly, it may be thought that the hyperconjugation of the alkyl group is similarly pronounced during the photochlorination of vinyl compounds.

In α-olefin, the electron displacement produced by the electron-releasing alkyl group renders the terminal carbon susceptible to attack by positive chlorine:

$$R\rightarrow CH=CH_2 \longleftrightarrow R-\overset{\oplus}{C}H-\overset{\ominus}{\underset{\cdot\cdot}{C}}H_2. \quad (1)$$

On the contrary, nitrile group of acrylonitrile is electron-withdrawing, and the electron displacement causes the unsubstituted carbon atom to become more positive, as is indicated in Formula (a) by a curved arrow.

$$H\equiv C-CH=CH_2 \longleftrightarrow \overset{\ominus}{\underset{\cdot\cdot}{N}}=C=CH-\overset{\oplus}{C}H_2 \quad (2)$$

(a) (b)

Owing to the electron displacement, the unsubstituted carbon atom carries a positive charge and is particularly inaccessible to the electrophilic agents (b).

The dark chlorination of vinyl compounds in the presence of the radical inhibitor oxygen proceeds through ionic intermediates. Taft[6] has suggested that these intermediates can explain an ionic-type mechanism for which the rate-determining step is the addition of a positive chlorine ion to form a carbonium ion and a negative chlorine ion. Therefore, the relative rate constants for the chlorination of various vinyl compounds under oxygen supported an electrophilic attack by the chlorine molecule.

The reactions of chlorine atom with ring-substituted toluenes[11,12] as well as chloroethanes[2,4] have been studied, and the chlorine atom might be thought of as an electrophilic radical.

Both reactions are electrophilic and have negative values of ρ^*. The negative values of ρ^* indicate that the electron-donating substituents increase the addition rate of chlorine to the double bond, in agreement with the previous data indicating that the hydrogen abstraction by a chlorine atom is an electrophilic reaction.

References

1) Part XIII of this series: K. Shinoda, *Chem. Lett.*, **1975**, 219.
2) T. Migita, M. Kosugi, and Y. Nagai, *Bull. Chem. Soc. Jpn.*, **40**, 920 (1967).
3) M. Kosugi, K. Takeuchi, and T. Migita, *Bull. Chem. Soc. Jpn.*, **42**, 3354 (1969).
4) W. Mack, *Tetrahedron Lett.*, **49**, 4993 (1967).
5) K. Shinoda, *Nippon Kagaku Kaishi*, **1973** 536.
6) R. W. Taft, Jr., *J. Am. Chem. Soc.*, **70**, 3364 (1948).
7) K. Shinoda, *Nippon Kagaku Kaishi*, **1973**, 542.
8) M. S. Newman, "Steric Effects in Organic Chemistry," John Wiley & Sons, New York (1956), p. 618.
9) M. L. Poutsma, *Science*, **157**, 997 (1967).
10) M. L. Poutsma, *J. Am. Chem. Soc.*, **87**, 2161 (1965).
11) C. Walling and B. Miller, *J. Am. Chem. Soc.*, **79**, 4181 (1957).
12) G. A. Russell and R. C. Williamson, *J. Am. Chem. Soc.*, **86**, 2357 (1964).

^{13}C NMR Chemical Shifts and Cationic Reactivity of Linear Conjugated Dienes

Kan-ichi HASEGAWA, Ryuzo ASAMI, and Kensuke TAKAHASHI

Department of Synthetic Chemistry, Nagoya Institute of Technology, Gokiso-cho, Showa-ku, Nagoya 466

(Received October 5, 1977)

The chemical shifts of the C_1 and C_2 of *trans*-1-alkyl-1,3-butadienes were correlated with Taft's σ^*, the proportionality constants being -35.9 and 12.3 ppm/σ^*, respectively. The values 6.2 and -43.6 ppm/σ^* were obtained for the C_1 and C_2 of 2-alkyl-1,3-butadienes, respectively. The observed chemical shifts of disubstituted butadienes roughly agreed with the values estimated from those of monosubstituted butadienes by means of additivity relationship. The cationic reactivity of linear conjugated dienes should be determined by the magnitude of the steric restriction of substituents and that of the stability of the resulting cation.

The cationic polymerizability of linear conjugated dienes has been discussed in preceding papers,[1-8] with particular attention given to the relation between the structure and the reactivity of the monomers. The relative reactivity of the monomers toward a styryl cation has been explained in terms of the magnitude of both the stability of the resulting cation and the steric hindrance between substituents.[4-8]

In general, an electrophilic reagent attacks on the carbon in butadienyl framework in the mode of forming the most stable cation. Its position is considered to be that of the carbon of the highest electron density in the conjugated double bonds. Thus, knowledge of electron distribution in the ground state of the dienes is helpful for understanding the chemical reactivities of conjugated dienes.

This paper deals with the polarization of conjugated dienes in relation to their reactivity. ^{13}C NMR measurements have been made for both alkyl-1,3-butadienes and phenyl-1,3-butadienes. A discussion is given on whether ^{13}C NMR chemical shifts of the dienes, accepted as an index of the electronic distribution of monomers in the ground state, are correlative to the relative reactivity of the dienes.

Experimental

1- and 2-phenyl-1,3-butadienes,[1,2] methyl and phenyl-substituted 1,3-butadienes,[6] 1- and 2-alkyl-1,3-butadienes,[7] and dimethyl-1,3-butadienes[8] were prepared as described previously.

^{13}C NMR spectrum was measured at 10 MHz on a Hitachi R-26 spectrometer. ^{13}C chemical shifts were determined for neat liquids by using benzene as an internal reference (10% by volume) and then converted into δ_c values (TMS reference) by using $\delta(C_6H_6) = 128.7$ ppm.

Theoretical Calculation

Quantum chemical calculations were carried out by the CNDO/2 method[9] and parametrization without further modification. Convergence was judged from the energy level criterion of 1.0×10^{-3} eV in all the orbital energies. The atomic coordinates of the butadienes were determined from the following bond distances and bond angles: –C=C–, 1.34 Å; =C–C=, 1.48 Å; =C–H, 1.08 Å; –C–H, 1.09 Å; =C–C–, 1.51 Å; –C–C–, 1.54 Å; C=C (aromatics), 1.39 Å; C–C_6H_5, 1.51 Å; ∠C–C–C, ∠C–C–H, 109°28′; ∠C=C–C, ∠C=C–H, 120°. Computations were made on a FACOM 230—75 Computer at the Data Processing Center of Kyoto University.

Results

^{13}C NMR Chemical Shifts of Alkyl-1,3-butadienes. The signals for alkyl-1,3-butadienes in the ^{13}C NMR spectra were assigned by means of off-resonance proton-decoupling and additivity relationship.[10,11] The chemical shifts obtained for alkyl-1,3-butadienes are given in Table 1. The signals for butadiene skeleton appeared over a span of 50 ppm in the range 107—157 ppm. Introduction of an alkyl group on C_1 of butadiene caused the signal for C_4 in the highest field among the four butadiene carbon signals.

In the case of *trans*-isomers, the chemical shift of the substituted carbon moved toward lower field by 16—30 ppm and its neighbor carbon absorption toward higher field by 6—10 ppm. Although the magnitude for the γ effect was small, the signal for the C_3 nucleus showed an upfield shift of 0.6—1.0 ppm. The signal for the C_4 was shifted to higher field by 2 ppm regardless of the kind of alkyl substituent. Alkyl substituents such as methyl, ethyl, and *t*-butyl groups deshielded the C_1 nuclei by 16.6, 19.7, and 29.2 ppm, and shielded the C_2 nuclei by 7.7, 6.3, and 10.4 ppm, respectively.

The alkyl substitution of the corresponding ethylenes also produced consistent changes such as 10.3, 17.4, and 25.6 ppm for the C_α shielding in downfield shift and 7.8, 10.0, and 14.4 ppm for the C_β shielding in upfield shift, respectively.[12,13] The deshielding effect of the alkyl group on the C_α is greater in 1-alkyl-1,3-butadienes than in 1-alkenes, the reverse being true for the shielding effect of the alkyl group on the C_β. The signals for the butadienyl carbons of the *cis* isomers appeared at higher field than those of their *trans* isomers except for the C_4 nucleus.

In the ^{13}C NMR spectra of 2-alkyl-1,3-butadienes, the signal for the C_1 appeared at the highest field. The signals for the C_1 and C_4 nuclei moved to higher field in comparison with those of butadiene. The reverse was true for both the C_2 and C_3 nuclei. The difference between C_1 and C_2 chemical shifts increased with an increase in the bulkiness of alkyl group. Introduction of an alkyl group such as methyl, ethyl, isopropyl, and *t*-butyl groups on the C_2 of butadiene gives rise to the deshielding of the C_2 nuclei by 5.7, 11.1, 16.0, and 20.0 ppm and the shielding of the C_1 nuclei by 3.2, 3.7,

Table 1. ^{13}C Shieldings of alkyl-1,3-butadienes[a)]

Compound	Chemical shift (ppm)[b)]					
	C_1	C_2	C_3	C_4	C_5	C_6
Butadiene (BD)[c)]	116.6	137.2	137.2	116.6		
trans-1-Methyl-BD	133.2	129.5	137.8	114.4	17.2	
cis-1-Methyl-BD	130.9	126.4	132.5	116.5	12.8	
trans-1-Ethyl-BD	136.3	130.9	137.7	114.5	25.9	13.4
cis-1-Ethyl-BD	134.0	129.5	132.7	116.6	21.2	14.1
trans-1-Isopropyl-BD	142.0	128.7	137.9	114.8	31.2	22.2
cis-1-Isopropyl-BD	139.9	127.9	132.9	116.8	27.0	22.9
trans-1-*t*-Butyl-BD	145.8	126.8	138.2	114.9	43.4	29.9
Isoprene	113.4	142.9	140.3	116.4	17.6	
2-Ethyl-BD	112.9	148.3	139.6	114.7	24.6	12.6
2-Isopropyl-BD	112.4	153.2	139.1	112.7	29.1	22.1
2-*t*-Butyl-BD	107.6	157.2	137.6	114.9	35.2	29.8
1,2-Dimethyl-BD[d)]	127.1	135.5	142.1	110.3	11.1	13.6
1,3-Dimethyl-BD[e)]	125.1	135.1	142.2	114.5	18.8	18.3
1,4-Dimethyl-BD	126.2	132.8	132.8	126.2	17.5	
2,3-Dimethyl-BD	113.0	143.8	143.8	113.0	20.3	

a) $\overset{6}{C}-\overset{5}{C}-\overset{1}{C}=\overset{2}{C}-\overset{3}{C}=\overset{4}{C}$, $\overset{1}{C}=\overset{2}{C}-\overset{3}{C}=\overset{4}{C}$ neat sample, room temperature. b) Downfield from TMS. c) See Ref. 10.

$\overset{5}{C}-\overset{6}{C}$

d) $\overset{1}{C}=\overset{2}{C}-\overset{3}{C}=\overset{4}{C}$ (with $\overset{5}{C}$ and $\overset{6}{C}$) e) $\overset{1}{C}=\overset{2}{C}-\overset{3}{C}=\overset{4}{C}$ (with $\overset{5}{C}$ and $\overset{6}{C}$)

4.2, and 9.0 ppm, respectively, in comparison with those of butadiene. These changes of the chemical shifts of the C_1 and C_2 of 2-alkyl-1,3-butadiene were smaller than those of either 1-alkyl-1,3-butadienes or 1-alkenes.

The signal due to the central carbon of the alkyl group in the neighborhood of butadiene skeleton moved to lower field by 4—12 ppm for the substitution of an α-hydrogen by methyl group, *i.e.*, $-C-H \rightarrow -C-CH_3$. This deshielding effect was larger in 1-alkyl-1,3-butadiene than in 2-alkyl-1,3-butadiene.

The chemical shifts of dimethyl-1,3-butadienes roughly agreed with the values estimated from the data of both 1,3-pentadiene and isoprene by means of the additivity relationship. The difference between the observed and the estimated values was the largest for the chemical shift of 1,2-dimethyl-1,3-butadiene. The chemical shifts of the C_4 nuclei in dimethyl-1,3-butadienes moved to higher field in the order 2,4-hexadiene < 1,3-dimethyl-1,3-butadiene < 2,3-dimethyl-1,3-butadiene < 1,2-dimethyl-1,3-butadiene.

^{13}C NMR Chemical Shifts of Phenyl-1,3-butadienes. The ^{13}C chemical shifts of phenyl-1,3-butadienes are summarized in Table 2. A certain uncertainty is inevitable in the assignment of closely spaced signals within *ca.* 1 ppm. Introduction of a phenyl group on either the C_1 or C_2 of butadiene gives rise to a deshielding of the C_4 nucleus by 1 ppm. The chemical shifts of the C_1 and C_2 of 1-phenyl-1,3-butadiene moved 16.5 ppm to downfield and 7.5 ppm to upfield relative to those of butadiene, respectively. In the case of styrene, these values have been reported to be 13.9 ppm and 9.6 ppm, respectively.[14)] The chemical shift of the C_3 was not affected by introduction of 1-phenyl group. On comparing the data for 2-phenyl-1,3-butadiene with butadiene, we find a change of 11.6 ppm for the C_2 and 0.7—1.5 ppm for the C_1, C_3, and C_4. The chemical shifts of the C_1 and C_4 of 2-phenyl-1,3-butadiene were the same as that of the C_4 of 1-phenyl-1,3-butadiene.

Table 2. ^{13}C Shieldings of phenyl-1,3-butadienes[a)]

Compound	Chemical shift (ppm)[b)]				
	C_1	C_2	C_3	C_4	C_5
1-PB[c)]	133.1	129.7	137.4	117.6	
1-Methyl-1-PB	143.2	117.1	133.7	113.7	16.2
2-Methyl-1-PB	130.7	135.6	142.4	115.8	20.5
3-Methyl-1-PB	131.8	129.2	142.0	117.5	17.9
trans-4-Methyl-1-PB	129.7	129.7	132.5	130.3	17.9
cis-4-Methyl-1-PB	132.5	124.3	125.1	130.3	13.2
2-PB[c)]	117.3	148.8	138.7	117.7	
1-Methyl-2-PB	131.9	142.1	127.2	117.7	13.8
3-Methyl-2-PB	117.8	144.3	151.8	114.1	21.7

a) Neat sample, room temperature. b) Downfield from TMS. c) 1-PB=1-phenyl-1,3-butadiene, 2-PB=2-phenyl-1,3-butadiene.

The substituent effect on the shieldings of the butadienyl skeleton of methyl and phenyl-substituted 1,3-butadienes can also be estimated by means of the additivity relationship. An application of the additivity relationship for the chemical shift of methyl and phenyl-substituted 1,3-butadiene was shown to be more relevant than that of dimethyl-1,3-butadienes. Methyl substitution on the C_1 position of 1-phenyl-1,3-butadiene

Table 3. Electron densities of 1,3-butadienes calculated by using CNDO/2 method

Substituent	Total electron density[a]				π-Electron density[a]			
	C_1	C_2	C_3	C_4	C_1	C_2	C_3	C_4
H	4.0431	3.9853	3.9853	4.0431	1.0179	0.9821	0.9821	1.0179
trans-1-Methyl-	3.9930	4.0116	3.9848	4.0498	0.9858	1.0239	0.9765	1.0302
cis-1-Methyl-	3.9911	4.0111	3.9852	4.0484	0.9851	1.0252	0.9787	1.0272
2-Methyl-[b]	4.0631	3.9475	3.9922	4.0431	1.0529	0.9584	0.9862	1.0156
trans-1-Ethyl-	3.9908	4.0201	3.9831	4.0524	0.9782	1.0376	0.9748	1.0346
1,2-Dimethyl-	4.0120	3.9729	3.9926	4.0474	1.0181	0.9990	0.9842	1.0231
1-Phenyl-	4.0072	4.0032	3.9873	4.0447	0.9993	1.0001	0.9794	1.0221

a) Electron unit. b) Transoid.

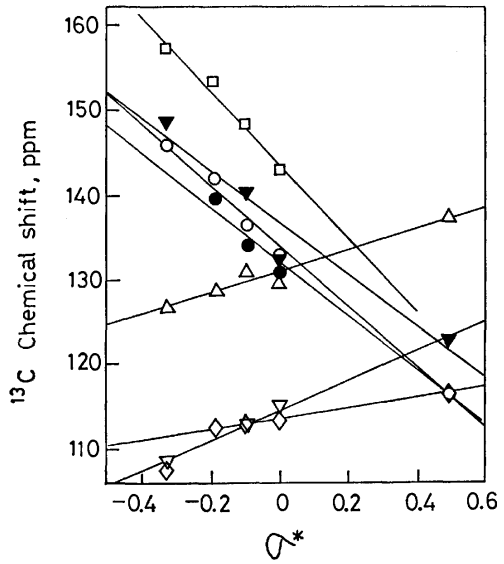

Fig. 1. Hammett plots of the ^{13}C chemical shifts of alkyl-1,3-butadienes and 1-alkenes against Taft's σ*: *trans*-1-alkyl-1,3-butadienes; ○, C_1 ($\rho^* = -35.9 \pm 1.7$ ppm/σ*); △, C_2, ($\rho^* = 12.3 \pm 1.7$ ppm/σ*); *cis*-1-alkyl-1,3-butadienes; ●, C_1, ($\rho^* = -32.3 \pm 3.3$ ppm/σ*); 2-alkyl-1,3-butadienes; ◇, C_1 ($\rho^* = 6.2 \pm 0.3$ ppm/σ*) □, C_2 ($\rho^* = -43.6 \pm 5.0$ ppm/σ*), 1-alkenes; ▽, C_1 ($\rho^* = 17.4 \pm 0.8$ ppm/σ*); ▼, C_2 ($\rho^* = -30.7 \pm 4.9$ ppm/σ*).

gives rise to the upfield shift of the C_2 as known for its β-effect. The signal for the C_4 also shifted to higher field than that estimated by means of the additivity relationship. The chemical shift of the C_4 of 1-phenyl-1,3-butadiene was not affected by introduction of a methyl group on the C_3. In 1-phenyl-1,3-pentadiene, the C_4 was no longer the most electron-rich carbon in the butadienyl framework. The signal for the C_4 of 1-methyl-1-phenyl-1,3-butadiene appeared at the highest field among the butadienyl groups of these nine phenyl-1,3-butadienes.

Discussion

Sensitivity Constants for the ^{13}C Chemical Shifts of Alkyl-1,3-butadienes. Figure 1 shows the Hammett plots of the chemical shifts of both alkyl-1,3-butadienes and 1-alkenes against Taft's σ*. A slope of −35.9 ppm/σ* was obtained from the correlation of the C_1 chemical shifts of *trans*-1-alkyl-1,3-butadienes with σ*. The value is slightly more negative than that for the C_2 chemical shifts of 1-alkenes whereas the reverse is true for the C_2 chemical shifts. No linear correlation with σ* was found for the C_3 and C_4 shieldings of 1-alkyl-1,3-butadienes; the signals for the C_3 and C_4 showed a downfield shift of 0.5—1.0 ppm and an upfield shift of 2 ppm, respectively, regardless of the kind of alkyl group.

Thus, the 1-alkyl group caused the shielding of both the C_2 and C_4 and the deshielding of both the C_1 and C_3 in the butadiene framework. The results suggest that the substituent effect is transmitted on the conjugated framework by alternation in a mode of decaying. On the ^{13}C chemical shifts along the conjugated framework of *trans*-1-substituted-1,3-butadiene, Kajimoto and Fueno[15] also concluded that the substituent effect in conjugated dienes is transmitted mainly through its π-framework by successive polarization of the –CH=CH– groups involved. However, the polarization of conjugated double bonds by the alkyl group was so small that the chemical shifts of the C_3 and C_4 were not correlated with Taft's σ*. The rearrangement of a charge caused by the introduction of an alkyl group was mainly the polarization between the C_1 and C_2 rather than a net transfer of charge from the alkyl group to the butadienyl framework, as shown in the results of CNDO/2 calculation of 1,3-pentadiene (Table 3).

In 2-alkyl-1,3-butadienes, linear correlations with σ* were found for both the C_1 chemical shifts excluding that of 2-*t*-butyl-1,3-butadiene and the C_2 chemical shifts. The ρ* value obtained for the C_1 shielding, 6.2 ppm/σ*, was smaller than that for the C_1 of the corresponding 1-alkenes. The ρ* value of −43.6 ppm/σ* obtained for the C_2 chemical shifts is 1.4 times as negative as that for the C_2 of the 1-alkenes. No correlation is found between the C_4 and σ*.

Hyperconjugation, polarization through π- and σ-bonds, and a field effect directly operative through space are seen in transmitting the substituent effect of alkyl group in 2-alkyl-1,3-butadienes. The results showing that the shielding of the C_4 approaches that of the C_1 in the order methyl<ethyl<isopropyl might be explained in terms of the field effect of the alkyl group. Unexpected values of the C_1 and C_4 chemical shifts of 2-*t*-alkyl-1,3-butadiene were observed since this compound cannot take a coplanar transoid form owing

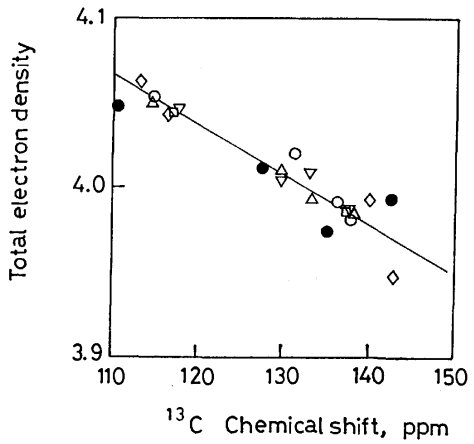

Fig. 2. Correlation of the ^{13}C chemical shifts of 1,3-butadienes with the total electron densities calculated by using the CNDO/2 method: ○, *trans*-1,3-hexadiene; △, *trans*-1,3-pentadiene; □, 1,3-butadiene; ▽, *trans*-1-phenyl-1,3-butadiene; ◇, isoprene; ●, 1,2-dimethyl-1,3-butadiene.

to the steric hindrance.[16]

Correlation of ^{13}C Chemical Shift with Total Electron Density. Figure 2 shows a correlation of ^{13}C chemical shift of 1,3-butadienes with the total electron density of carbon. Proportionality constant 340 ppm/e was obtained; this is about twice as large as the generally accepted value of 160 ppm/e for the π-electron densities in aromatics. The electron density of the butadienyl carbon can be estimated by means of its ^{13}C chemical shift.

Position Attacked by a Carbonium Ion. In general, propagating ends attack on the C_4 of 1-alkyl-1,3-butadienes and mainly the C_1 of 2-alkyl-1,3-butadienes.[6] These selective positions are due to both the carbon of the greatest electron density in the butadienyl framework and the highest stability of the resulting cation. These factors can be applied to the determination of the attacked position of dimethyl-1,3-butadienes. An attack of styryl cation on the most electron-rich carbon in the conjugated double bonds results in the highest stable cation. In nine phenyl-1,3-butadienes (Table 2), however, the positions of *trans*/*cis*-4-methyl-1-phenyl-1,3-butadienes and 1-methyl-2-phenyl-1,3-butadiene attacked by a styryl cation coincide not with that of the carbon of the highest electron density in the conjugated double bonds but the position forming the highest stable cation. Thus, the latter is the predominant factor in determining the position attacked by a carbonium ion.

Reactivity of Linear Conjugated Dienes. The relative reactivity of linear conjugated dienes toward a styryl cation is given in Table 4. The reactivities of 1- and 2-alkyl-1,3-butadienes decrease with an increase of the bulkiness of alkyl group.[7] The chemical shift of the C_4 of 1-alkyl-1,3-butadienes is unaffected whereas that of the C_1 of 2-alkyl-1,3-butadienes moves to higher field with an increase of the inductive effect of alkyl group. Thus, the order of reactivity of the alkyl-1,3-butadienes is related not to the electron density of the carbon in the ground state but to the magnitude of the steric hindrance between the monomer and an attacking cation.

Table 4. Reactivity of conjugated dienes toward a styryl cation[a]

Substituents	$1/r_1$[b]	Relative reactivity[c]	Chemical shift[d] (ppm)
1-Methyl-	0.97	0.58	114.4
1-Ethyl-	0.66	0.40	114.5
1-Isopropyl-	0.58	0.35	114.8
1-*t*-Butyl-	0.41	0.25	114.9
2-Methyl-	0.88	0.53	113.4
2-Ethyl-	0.57	0.34	112.9
2-Isopropyl-	0.54	0.32	112.4
2-*t*-Butyl-	0.50	0.30	107.6
1,2-Dimethyl-	1.64	0.98	110.3
1,3-Dimethyl-	1.82	1.09	114.5
1,4-Dimethyl-	0.85	0.51	126.2
2,3-Dimethyl-	1.30	0.78	113.0
1-Phenyl-	1.67	1.00	117.6
1-Methyl-1-phenyl-	33	19.8	113.7
2-Methyl-1-phenyl-	1.49	0.89	115.8
3-Methyl-1-phenyl-	40	24.0	117.5
4-Methyl-1-phenyl-	1.15	0.69	130.3
2-Phenyl-	0.59	0.35	117.3
1-Methyl-2-phenyl-	0.95	0.57	131.9
3-Methyl-2-phenyl-	0.63	0.38	117.8

a) Using $SnCl_4$·TCA in methylene chloride at −78 °C. b) Styrene (M_1)-diene (M_2). c) Relative reactivity for 1-phenyl-1,3-butadiene. d) ^{13}C shielding of the butadienyl carbon, attacked by a styryl cation, downfield from TMS.

The reactivity of dimethyl-1,3-butadiene can be explained not in terms of the electron density of either the C_4 or the C_1 in the ground state but the stability of the resulting allylic cation. In the case of dimethyl-1,3-butadienes, no steric hindrance in transition state on the electrophilic reaction needs to be taken into consideration except for 2,4-hexadiene.

When steric hindrance in the propagation of phenyl-1,3-butadiene series toward a styryl cation is of minor importantance or almost the same, the reactivity of the monomer increases with an increase in the stability of the resulting cation rather than in the electron density of the carbon attacked by cation. The methyl group introduced on either the β- or the δ-carbon, numbered from the terminal carbon attacked by the cation, enhances the reactivity to the extent of about 15—20, whereas methyl substitution on the γ-carbon produces a small increase or decrease in the reactivity up to the extent of 1.1.

The relative reactivity of linear conjugated dienes toward an electrophilic reagent can be determined by both the magnitude of the steric restriction of substituents and that of the stability of the resulting cation. Thus, for a detailed discussion on the reactivity of the butadienes, the above factors should be taken into consideration in addition to the information on ^{13}C NMR spectra.

The authors wish to express their gratitude to Mr. Kunimi Fujieda for the measurements of ^{13}C NMR spectra.

References

1) R. Asami, K. Hasegawa, and T. Onoe, *Polym. J.*, **8**, 43 (1976).
2) R. Asami and K. Hasegawa, *Polym. J.*, **8**, 53 (1976).
3) R. Asami and K. Hasegawa, *Polym. J.*, **8**, 67 (1976).
4) R. Asami, K. Hasegawa, N. Asai, I. Moribe, and A. Doi, *Polym. J.*, **8**, 74 (1976).
5) K. Hasegawa and R. Asami, *Polym. J.*, **8**, 276 (1976).
6) K. Hasegawa, R. Asami, and T. Higashimura, *Macromolecules*, **10**, 585 (1977).
7) K. Hasegawa, R. Asami, and T. Higashimura, *Macromolecules*, **10**, 592 (1977).
8) K. Hasegawa and R. Asami, *J. Polym. Sci., Polym. Chem. Ed.*, in press.
9) J. A. Pople and G. A. Segal, *J. Chem. Phys.*, **44**, 3289 (1966).
10) G. B. Savitsky and K. Namikawa, *J. Phys. Chem.*, **68**, 1956 (1964).
11) D. M. Grant and E. G. Paul, *J. Am. Chem. Soc.*, **86**, 2984 (1964).
12) R. A. Friedel and H. L. Retcofsky, *J. Am. Chem. Soc.*, **85**, 1300 (1963).
13) G. B. Savitsky, P. D. Ellis, K. Namikawa, and G. E. Maciel, *J. Chem. Phys.*, **49**, 2395 (1968).
14) K. S. Dhami and J. B. Stothers, *Can. J. Chem.*, **43**, 510 (1965).
15) O. Kajimoto and T. Fueno, *Tetrahedron Lett.*, **1972**, 3329.
16) R. T. Hobgood and J. H. Goldstein, *J. Mol. Spectrosc.*, **12**, 76 (1964).

The Reaction of 2,4,6-Trimethylbenzonitrile *N*-Oxide with Polysubstituted *p*-Benzoquinones

Shinsaku SHIRAISHI, Satoru IKEUCHI, Manabu SENŌ, and Teruzo ASAHARA
Institute of Industrial Science, The University of Tokyo, Roppongi, Minato-ku, Tokyo 106
(Received November 4, 1977)

The reaction of 2,4,6-trimethylbenzonitrile *N*-oxide with various di- and tetrasubstituted *p*-benzoquinones and the structures of the products were studied. All of the tetrasubstituted quinones gave dioxazole derivatives through addition at the carbonyl site, whereas the disubstituted quinones gave dioxazoles or isoxazoline derivatives depending on the substituents. The reactivity of the quinone carbonyl toward the nitrile oxide varies with the substituents and with the substitution pattern; this phenomenon is discussed in terms of the resonance and inductive effects of the substituents.

Nitrile *N*-oxide is known to be a typical 1,3-dipole and to undergo 1,3-dipolar cycloaddition reaction with various unsaturated compounds to give heterocycles. *p*-Benzoquinones have two kinds of potential reactive sites, *i.e.*, two C=C and two C=O bonds. Cycloaddition with unsubstituted *p*-benzoquinone is known to occur at the C=C bond to give isoxazoline derivatives, which are then oxidized to isoxazoles.[1] In general, C=C bonds are more reactive than C=O bonds toward 1,3-dipoles, and so cycloaddition preferentially takes place at a C=C bond.[2] In a previous paper,[3] however, we reported that tetrahalo-*p*-benzopuinones (*p*-haloanils) make C=O addition with aromatic nitrile *N*-oxides to form dioxazole derivatives. Recently, cyclobutenediones have been reported to undergo this type of addition with mesitonitrile *N*-oxide.[4] The carbonyl addition has also been reported in the reaction of diazomethane with *p*-benzoquinones having all of the hydrogens replaced by electronegative groups.[5] 2,6-Dimethoxy-*p*-benzoquinone has also been shown to make carbonyl addition with diazomethane.[6] The dependence of the addition site on the substituents and the substitution pattern of the quinone will give a certain clue to the consideration of the exact nature of the cycloaddition reaction. In this respect, the reactions of mesitonitrile *N*-oxide with various polysubstituted *p*-benzoquinones were investigated; the results will be discussed in this paper. The effects of substituents on the reactivity of quinone carbonyls will also be discussed in terms of both inductive and resonance effects.

Results and Discussion

Mesitonitrile *N*-oxide (2,4,6-trimethylbenzonitrile *N*-oxide, MNO) was allowed to react with tetramethyl-*p*-benzoquinone (DQ), tetramethoxy-*p*-benzoquinone (TMOQ), 2,5-dichloro-3,6-dimethoxy-*p*-benzoquinone (25DCMOQ), 2,6-dichloro-3,5-dimethoxy-*p*-benzoquinone (26DCMOQ), 2,6-dibromo-3,5-dimethoxy-*p*-benzoquinone (26DBMOQ), 2,3-dichloro-5,6-dicyano-*p*-benzoquinone (DDQ), 2,3-dichloro-1,4-naphthoquinone (23DCNQ), 2,6-dimethyl-*p*-benzoquinone (26DMQ), 2,5-dimethyl-*p*-benzoquinone (25DMQ), 2,6-dimethoxy-*p*-benzoquinone (26DMOQ), 2,5-dimethoxy-*p*-benzoquinone (25DMOQ), and 2,6-dichloro-*p*-benzoquinone (26DCQ) in chloroform at room temperature.

All of the tetrasubstituted quinones gave 1 : 1-carbonyl addition products, some of which added another MNO to give 1 : 2-adducts. The PMR spectrum of the 1 : 1-adduct from DQ and MNO (**1**) shows two singlets, at 1.92 and 2.10 ppm(δ), with a relative area corresponding to each six protons due to methyl groups on the quinone moiety, and that of the 1 : 2-adduct (**2**) shows a singlet resonance signal, at 1.98 ppm, with a relative area corresponding to twelve protons due to four methyl groups on the quinone residue. The IR spectrum of the latter has no absorption band in the $\nu_{C=O}$ region (1650—1750 cm^{-1}). TMOQ gave a 1 : 1-adduct (**3**) and no 1 : 2-adduct because of its very low reactivity. The adduct **3** has two singlet resonance signals in its PMR spectrum due to methoxyl groups on the quinone moiety. 25DCMOQ gave one 1 : 1-adduct and one 1 : 2-adduct. The PMR and IR spectroscopic aspects are substantially similar to those of the corresponding adducts from DQ. Thus, the

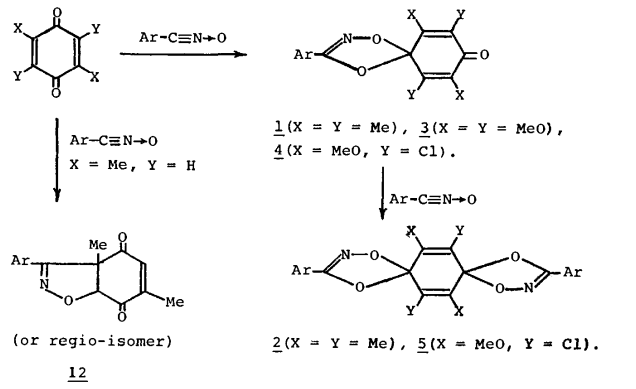

Scheme 1.

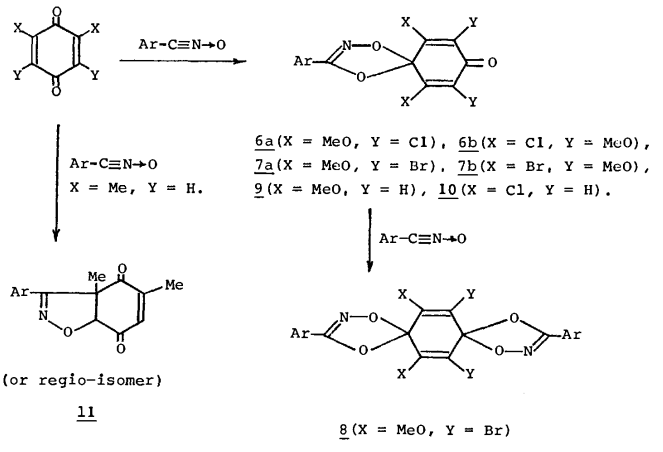

Scheme 2.

Table 1. The reaction products of aromatic nitrile *N*-oxides with substituted *p*-benzoquinones

Product	Compd. No.	Reactants mole ratio[a]	React. time, h	Yield %	Mp, °C[b]	Anal. Found (Calcd) C	H	N	IR, $\nu_{C=O}$ cm^{-1}	MS, *m/e*
C=O adducts										
DQ·MNO	**1**	1/1	20 days	50[c]	98.5—101	74.08 (73.82	6.90 7.12	4.05 4.30)	1675	325(M^+), 164, 161
DQ·MNO_2	**2**	1/2	30 days	51[d]	199—202	84.17 (83.92	6.96 7.04	5.51 5.76)	—	
TMOQ·MNO	**3**	1/1	20 days	82	152—154	61.79 (61.69	5.72 5.95	3.83 3.60)	1655 1675	
25DCMOQ·MNO	**4**	1/1	100	66	176—179	54.70 (54.29	4.48 4.30	3.79 3.52)	1690	
25DCMOQ·MNO_2	**5**	1/2	120	90	182—184	60.32 (60.11	4.75 5.04	5.15 5.01)	—	560, 558(M^+), 397, 236, 208, 193, 161
26DCMOQ·MNO	**6a**	1/1	24	47	116—120	54.08	4.33	3.70	1680	
	6b			11	142—145	54.52 (54.29	4.56 4.30	3.43 3.52)	1680	
26DBMOQ·MNO	**7a**	1/1	24	21	128—130	44.46	3.54	2.73	1680	489, 487, 489(M^+), 324, 296, 281, 253, 225, 161
	7b			13	150—152[e]	44.45 (44.38	3.60 3.52	2.84 2.88)	1680	
26DBMOQ·MNO_2	**8**	1/2	70	75	171—174	51.68 (51.87	4.57 4.35	4.42 4.32)	—	
26DMOQ·MNO	**9**	1/1.1	24	82	169—172	65.36 (65.64	5.76 5.81	4.02 4.25)	1695	329(M^+), 168, 161
26DCQ·MNO	**10**	1/1	15	77	139—141	56.60 (56.83	3.98 3.87	3.96 4.14)	1670	339, 337(M^+), 178, 176, 161
26DCQ·DNO[g]	**17**	1/1	15	78	135—141	58.04 (57.97	4.40 4.29	3.86 3.98)	1680	
26DCQ·BNO	**18**	1/1.2[h]	6	36	168—171	53.00 (52.73	2.51 2.38	4.56 4.73)	1690	
DDQ·MNO	**13**	1/1	6	73	116—119[f]	55.39 (55.69	2.69 2.86	11.09 10.82)	1710	
DDQ·MNO_2	**14**	1/2	10	75	165—169[f]	61.54 (61.21	4.22 4.04	10.48 10.20)	—	
23DCNQ·MNO	**15**	1/1	15	76	149—152	61.67 (61.87	4.08 3.89	3.88 3.61)	1675	
23DCNQ·MNO_2	**16**	1/2	20	83	182—184	65.71 (65.58	4.71 4.76	5.10 5.10)	—	
C=C adducts										
26DMQ·MNO	**11**	1/1	15	33[i]	116—118	73.08 (73.34	6.69 6.59	4.91 4.71)	1680	297(M^+), 282, 254, 202, 186, 161
25DMQ·MNO	**12**	1/1	15	30[i]	59— 62	73.12 (73.34	6.82 6.59	4.88 4.71)	1670	

a) All of the reactions were conducted in chloroform at room temperature, unless otherwise cited. b) All of the products were purified by recrystallization from hexane, unless otherwise noted. c) Unreacted starting materials were recovered. The yields based on the reacted starting materials were almost quantitative. d) The 1 : 1-adduct **1** was also obtained in a 32% yield based on DQ. e) Recrystallized from methanol. f) Recrystallized from a mixture of hexane and chloroform. g) DNO means 2,3,5,6-teramethylbenzonitrile *N*-oxide. h) See the experimental section. i) This reaction gave a complicated mixture of products. Attempts to separate and characterize the other products were not successful.

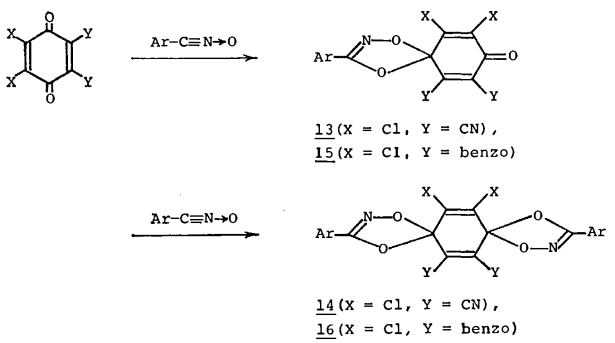

Scheme 3.

quinones with two carbonyls with equal structural surroundings gave only one 1 : 1-adduct, as is shown in Schemes 1 and 3. On the other hand, some of the quinones with two carbonyls with different structural surroundings, such as 26DCMOQ and 26DBMOQ, gave two 1 : 1-adducts, which then gave the same 1 : 2-adduct upon the addition of another MNO. The addition site of the 1 : 1-adduct was determined by PMR spectroscopy, as will be discussed later. All of the 1 : 2-adducts obtained here may be mixtures of *cis* and *trans* isomers, as was observed for the 1 : 2-adduct from chroranil and MNO.[3] Attempts to separate them, however, have not yet been successful.

Disubstituted quinones also gave 1 : 1-adducts; their structures were also determined to be those of carbonyl addition products except for those from dimethylquinones, 25DMQ and 26DMQ, which gave isoxazoline derivatives as the main products and some other unisolable by-products. Between the C=O and C=C addition products, a distinct difference is observed in their PMR spectra. The resonance signal due to 2- and 6- methyls on the mesityl residue of the C=O adduct appears as a single peak at a lower field than that due to 4-methyl protons, which always appears around 2.3 ppm, independently of the substitution patterns of the starting quinones. On the other hand, the resonance signal of the C=C adduct appears at a higher field than that of 4-methyl, which also appears at about 2.3 ppm. The upper-field shift of the 2- and 6-methyl signals can be interpreted in terms of their increased shielding by the magnetic anisotropy of the carbonyl in the C=C addition product, where the two methyls are located in the vicinity of the carbonyl group and where one methyl is above, and the other below, the plane of the group. Furthermore, some differences are observed in the spectra of the quinone moieties. For example, the methoxyl and methine on the quinone moiety of the adduct from 26DMOQ (**9**) resonate at 3.80 and 5.48 ppm respectively, each as one singlet, whereas those of the adduct from 26DMQ (**11**) each appear at two different positions. This can reasonably be explained only by considering that **9** is a spiro-dioxazole derivative and **11** is an isoxazoline derivative, as is shown in Scheme 2. The two singlets, each with relative areas corresponding to three protons in the PMR spectrum of **11**, are due to aliphatic and olefinic methyls respectively, while the other two singlets, each corresponding to one proton, are due to angular and olefinic hydrogens respectively. The structure of the C=C addition products may be considered to be that shown in Schemes 1 and 2, judging from the chemical shifts of the angular methyl and methine

Table 2. PMR Spectral data of the addition products δ, ppm, in $CDCl_3$ (relative area)

Compound No. of the products	Mesityl residue			Quinone residue	
	2,6-Me	4-Me	3,5-H		
C=O addition					
1	2.46 (6)	2.30 (3)	6.93 (2)	1.92 (6)	2.10 (6)
2	2.46 (12)	2.29 (6)	6.91 (4)	1.98 (12)	
3	2.39 (6)	2.30 (3)	6.89 (2)	3.80 (6)	4.11 (6)
4	2.42 (6)	2.29 (3)	6.92 (2)	3.97 (3)	4.26 (3)
5	2.44 (12)	2.30 (6)	6.92 (4)	4.09 (6)	
6a	2.40 (6)	2.29 (3)	6.92 (2)	4.23 (6)	
6b	2.46 (6)	2.29 (3)	6.89 (2)	3.95 (6)	
7a	2.40 (6)	2.30 (3)	6.93 (2)	4.20 (6)	
7b	2.52 (6)	2.29 (3)	6.91 (2)	3.96 (6)	
8	2.40 (6) 2.53 (6)	2.29 (6)	6.87 (4)	4.04 (6)	
9	2.39 (6)	2.29 (3)	6.89 (2)	3.80 (6)	5.48 (2)
10	2.47 (6)	2.30 (3)	6.92 (2)	6.49 (2)	
15	2.47 (6)	2.28 (3)	6.91 (2)	7·78 (4) m	
16	2.45 (12)	2.27 (6)	6.91 (4)	7.70 (4) m	
C=C addition					
11	2.15 (9) [a]	2.27 (3)	6.88 (2)	1.69 (3) 4.26 (1)	[2.15] 6.62 (1)
12	2.16 (6)	2.29 (3)	6.89 (3) [b]	1.70 (3) 4.35 (1)	1.98 (3) [6.89]

a) Overlapping with the signal due to a methyl on the quinone residue. b) Overlapping with the signal due to olefinic methine proton on the quinone residue.

protons of the adducts. The characterization data for all of the addition products are summarized in Table 1, and the PMR data, in Table 2.

The structures of the 1 : 1-carbonyl addition products from such quinones as are shown in Scheme 2, the carbonyls of which have different structural surroundings, were determined by means of their PMR spectra, as will be described below. A comparison of the chemical shifts of the 2- and 6-methyls on the mesityl residue among the six 1 : 1-adducts, **3**, **6a**, **6b**, **9**, **10**, and the 1 : 1-adduct from MNO and chloranil,[3] reveals that the adduct from chloranil, **6b**, and **10** have the same chemical shift of 2.46—2.47 ppm, while the others have one of 2.39—2.40. This fact can be explained by assuming that the methyls of the former adducts interract with the chlorine atoms on the quinone moieties, and those of the latter, with the methoxyl groups. Thus the structures of the **6a**, **6b**, **9**, and **10** adducts were determined to be such as are shown in Scheme 2. As to the two isomereric adducts from MNO and 26DBMOQ ,the **7a** isomer, the signal due to the 2- and 6-methyls of which appears at 2.40 ppm, is determined to be formed by the addition of MNO to the carbonyl with methoxyl substituents on its α and α' positions, and the **7b** isomer, the signal of which is at 2.52 ppm, by such an addition to the carbonyl on the other side. This assignment was made by the comparison of the chemical shift of the corresponding methyl groups of the adduct from MNO and bromanil, the signal of which appears at 2.53 ppm.[3] This is supported by the fact that **7a** and **7b** gave the same 1 : 2-adduct upon the addition of another MNO and that the 1 : 2-adduct shows two signals, at 2.40 and 2.53 ppm, due to the 2- and 6-methyls on the mesityl residues attached to the two sides.

The structure determination presented above reveals the following facts: 26DMOQ and 26DCQ added MNO at more sterically hindered carbonyl, and made no further addition. DQ gave a 1 : 2-adduct with MNO, but TMOQ gave only a 1 : 1-adduct. 26-DCMOQ and 26DBMOQ gave two isomers of the 1 : 1-adducts, and the major products were those formed by addition to the carbonyls on the methoxyl-substituted side.

These results imply that the carbonyl addition is governed by the resonance and inductive effects of the quinone substituents. The resonance effect reduces the reactivity of the carbonyl on its meta-position, while the positive inductive effect enhances the reactivity of the carbonyl. This conclusion is very qualitative, but it can explain the facts described above and also the fact that the reactivity of tetrasubstituted quinones decreases in the order of; DDQ, tetrahalo-*p*-benzoquinones, 26DCMOQ, and 26DBMOQ. A marked reduction in the reactivity by the resonance effect is clearly seen in the facts that 25DMOQ does not react at all with MNO under the given reaction conditions and that the reactivity of 25DCMOQ is much less than that of 26DCMOQ.

Experimental

All the melting points cited are uncorrected. The characterization data for the products are given in Table 1. The PMR spectra were recorded with a Hitachi R-20A or a R-22 spectrometer. The Mass spectra were determined with a Hitachi RMU-7L high-resolution mass spectrometer.

Materials. The 2,6-dichloro-*p*-benzoquinone (26DCQ) 2,3-dichloro-5,6-dicyano-*p*-benzoquinone (DDQ), and 2,3-dichloro-1,4-naphthoquinone (23DCNQ) were commercially obtained and were used after recrystallization. The 2,5- and 2,6-dimethyl-*p*-benzoquinones (25 and 26DMQ) were prepared from 2,5- and 3,5- dimethylphenols respectively.[7] The 2,6-dimethoxy-*p*-benzoquinone (26DMOQ) was prepared by the nitric acid oxidation of pyrogallol trimethyl ether, which had itself been obtained by the methylation of pyrogallol with dimethyl sulfate.[8] The 2,6-dichloro- and 2,6-dibromo-3,5-dimethoxy-*p*-benzoquinones (26DCMOQ and 26DBMOQ) were prepared from 26DMOQ by chlorination and bromination respectively.[8] The tetramethoxy-*p*-benzoquinone (TMOQ) was synthesized by treating 26-DBMOQ with sodium methoxide.[8] The tetramethyl-*p*-benzoquinone (DQ) was prepared from durene,[9] and the 2,5-dichloro-3,6-dimethoxy-*p*-benzoquinone (25DCMOQ), from chloranilic acid.[10]

Reaction of Quinones with Mesitonitrile N-*Oxide (MNO).* The reactions were conducted by dissolving the reactants in chloroform in a concentration of about 5 mmol/300 ml and by then allowing the mixture to react at ambient temperatures for a given period. After the reaction, the solvent was evaporated and the residue was treated by means of column chromatography on silica gel (Wako gel C-100), with a benzene or chloroform eluent. The reaction conditions and the results are tabulated in Table 1. Some typical examples follow.

*6,10-Dichloro-3-mesityl-1,4-dioxa-2-azaspiro[4.5]deca-2,6,9-trien-8-one (**10**)*: A solution of 1.00 g (5.65 mmol) of 26DCQ and 0.910 g (5.65 mmol) of MNO in 300 ml of chloroform was stirred for 15 h at room temperature. Then, the solvent was evaporated under a reduced pressure, and the residue was treated with column chromatography on silica gel with benzene. The elute was recrystallized from hexane to give the title compound, which weighed 1.47 g (77%).

*7,9-Dibromo-3-mesityl-6,10-dimethoxy-1,4-dioxa-2-azaspiro[4.5]-deca-2,6,9-trien-8-one (**7a**) and 6,10-Dibromo-3-mesityl-7,9-dimethoxy-1,4-dioxa-2-azaspiro[4.5]deca-2,6,9-trien-8-one (**7b**)*: A solution of 1.60 g (4.91 mmol) of 26DBMOQ and 0.790 g (4.91 mmol) of MNO in 300 ml of chloroform was stirred for 24 h at room temperature. The solvent was then evaporated to complete dryness under a reduced pressure, without heating, to give a reddish brown solid. The solid was treated with hot hexane to separate the hexane-soluble part from the insoluble one. Cooling the hot solution gave 0.50 g (21%) of the crystals of **7a**. The subsequent evaporation of the filtrate gave 1.40 g of the residue, most of which was determined to be **7a**. The hexane-insoluble part weighed 0.30 g (13%) and was recrystallized from methanol to give 0.13 g of **7b**. The PMR spectrum of the reddish-brown solid above showed that the reaction was almost completed; the product composition ratio of **7a** to **7b** was estimated to be about 7 : 1 by a comparison of the intensities of the signals at 4.20 and 3.96, which are due to the methoxyl groups on the quinone moieties of **7a** and **7b** respectively.

*6,14-Dibromo-3,11-dimesityl-7,13-dimethoxy-1,4,9,12-tetraoxa-2,10-diazadispiro[4.2.4.2]tetradeca-2,6,10,13-tetraene (**8**)*: A solution of 1.60 g (4.91 mmol) of 26DBMOQ and 1.58 g

(9.82 mmol) of MNO in 300 ml of chloroform was stirred at room temperature for 70 h. The subsequent evaporation of the solvent and recrystallization of the residue from hexane gave 2.39 g (75%) of the title compound.

*3-Mesityl-6,7,9,10-tetramethyl-1,4-dioxa-2-azaspiro[4.5]deca-2,6,9-trien-8-one (**1**)*: A solution of 1.00 g (6.1 mmol) of DQ and 1.00 g (6.2 mmol) of MNO in 200 ml of chloroform was allowed to stand at an ambient temperature for 20 days, after which the solvent was evaporated to give a yellow viscous oil, which was subsequently treated by means of column chromatography on silica gel with benzene. MNO, DQ, and the title compound were eluted out in that order. The product weighed 1.0 g (50%), and the recovered MNO and DQ weighed 0.5 g each.

*3,11-Dimesityl-6,7,13,14-tetramethyl-1,4,9,12-tetraoxa-2,10-diazadispiro[4.2.4.2]tetradeca-2,6,10,13-tetraene (**2**)*: A reaction of 0.82 g (5.1 mmol) of MNO with 0.40 g (2.5 mmol) of DQ in 150 ml of chloroform at an ambient temperature for 30 days gave 0.62 g (51%) of the title compound and 0.26 g (32%) of the 1 : 1-adduct, **1**, upon the column chromatography of the reaction products.

*3-Mesityl-3a,5(or 6,7a)-dimethyl-3a,4,7,7a-tetrahydrobenzisoxazole-4,7-dione (**11**)*: A solution of 0.70 g (5.1 mmol) of 26DMQ and 0.82 g (5.1 mmol) in 200 ml of chloroform was let stand at room temperature for 15 h; solvent was then evaporated to leave a tan yellow solid, which was washed with hexane to remove the hexane-highly soluble part. The residue was recrystallized from hexane to give 0.50 g (33%) of the title compound. Several components were observed in the hexane washing by TLC, but all attempts at their separation have not yet been successful.

Reaction of Benzonitrile N*-Oxide (BNO) with 26DCQ. 6,10-Dichloro-3-phenyl-1,4-dioxa-2-azaspiro[4.5]deca-2,6,9-trien-8-one (**18**)*: Into a solution of 0.55 g (3.53 mmol) of benzhydroxamoyl chloride in 20 ml of tetrahydrofuran (THF), was added, drop by drop, a solution of 0.36 g (3.54 mmol) of triethylamine in 10 ml of THF at a temperature below 0 °C. The triethylammonium chloride thus precipitated was removed by filtration, and the filtrate was added to a solution of 0.48 g (2.71 mmol) of 26DCQ in 30 ml of THF. The mixture was allowed to react with stirring at room temperature for 6 h, and then the solvent was removed by evaporation. The residue was treated with column chromatography on silica gel with benzene to give 0.10 g (24% based on the starting benzhydroxamoyl chloride) of 3,4-diphenyl-1,2,5-oxadiazole 2-oxide (diphenylfuroxan), 0.40 g of an unidentified oil, and 0.33 g (36% based on the quinone) of the title compound.

References

1) A. Quilico and G. Stagno D'Alcontres, *Gazz. Chim. Ital.*, **80**, 140 (1950); T. Sasaki and T. Yoshioka, *Bull. Chem. Soc., Jpn.*, **41**, 2206 (1968).

2) Ch. Grundmann and P. Grünanger, "The Nitrile Oxides," Springer Verlag, Berlin (1971), pp. 95, 103; R. Huisgen, *Angew. Chem.*, **75**, 741 (1963).

3) S. Shiraishi, S. Ikeuchi, M. Senō, and T. Asahara, *Bull. Chem. Soc. Jpn.*, **50**, 910 (1977).

4) N. G. Argyropoulos, N. E. Alexandron, and D. N. Nicolaides, *Tetrahedron Lett.*, **1976**, 83.

5) B. Eistert, H. Fink, and A. Müller, *Chem. Ber.*, **95**, 2403 (1976).

6) B. Eistert, H. Fink, K. Pfleger, and G. Kaeffner, *Justus Liebigs Ann. Chem.*, **735**, 145 (1970).

7) L. I. Smith, J. W. Opie, S. Wawzonek, and W. W. Prichard, *J. Org. Chem.*, **4**, 318 (1939).

8) R. Robinson and C. Vasey, *J. Chem. Soc.*, **1941**, 660.

9) L. I. Smith and R. O. Denyes, *J. Am. Chem. Soc.*, **58**, 304 (1936); L. I. Smith, *Org. Synth.*, Coll. Vol. 2, 254 (1943).

10) C. Graube, *Ann.*, **340**, 244 (1905).

Abnormal Wallach Rearrangement of 4-Alkylazoxybenzenes

Ichiro SHIMAO and Shigenori MATSUMURA

Department of Industrial Chemistry, Faculty of Engineering, Toyama University, Takaoka-shi, Toyama 933

(Received June 20, 1977)

The major product in the reaction of 4-alkylazoxybenzenes with sulfuric acid is not 4-(*p*-alkylphenylazo)phenol, which is regarded as the usual product of Wallach rearrangement. The following azophenols were obtained as major products; 2-alkyl-5-(phenylazo)phenol (R : Me), 2-alkyl-4-(phenylazo)phenol (R : Et), and 4-(phenylazo)phenol (R : *i*-Pr and *t*-Bu).

In a previous paper,[1] the present authors reported abnormal Wallach rearrangement for 4,4'-dialkylazoxybenzenes. For example, it was found that, in the reaction of 4,4'-dimethylazoxybenzene, the hydroxyl group was mainly introduced into the meta position of the azo group, and that reactions of 4,4'-dialkylazoxybenzenes take place more rapidly than does that of azoxybenzene.

On the other hand, it was reported that, when α-4-methylazoxybenzene was treated with concentrated sulfuric acid, the main product is 4-(*p*-tolylazo)phenol.[2,3] In order to evaluate the effect of the alkyl group, it appears important to investigate the rearrangement of 4-alkylazoxybenzenes (**1**). It was found that the main rearrangement product of 4-methylazoxybenzene (**1a**) differs from that described in the literature.[2,3] Furthermore, in the present paper, the reactions of some 4-alkylazoxybenzenes are discussed.

Results and Discussion

4-Alkylazoxybenzenes were treated with 85% sulfuric acid at 50 °C. The reaction products were separated by column chromatography in most cases.

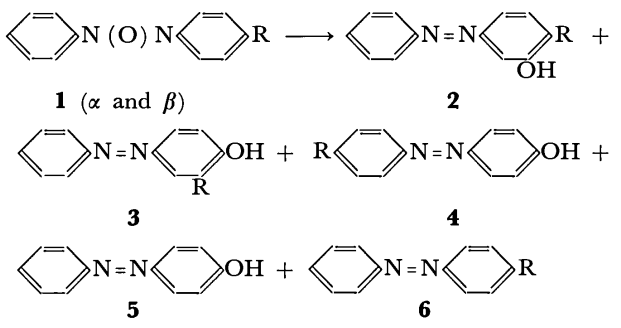

1 (α and β) **2**

3 **4**

5 **6**

1—4, 6	R
a	Me
b	Et
c	*i*-Pr
d	*t*-Bu

Table 1 shows the results for the reactions of *p*-tolyl-NNO-azoxybenzene (**1aα**) and *p*-tolyl-ONN-azoxybenzene (**1aβ**). Both **1aα** and **1aβ** gave 2-methyl-5-(phenylazo)phenol (**2a**) as the major rearrangement product. The structure of **2a** was confirmed in the following way. This compound (**2a**) was acetylated using a conventional method. The acetate was identified by comparison with a sample obtained by condensation of 3-acetoxy-4-methylaniline and nitrosobenzene. Contrary to earlier reports,[2,3] 4-(*p*-tolylazo)-phenol (**4a**) was obtained only as a minor product.

The α isomer of **1a** reacted somewhat faster than the β isomer. This agrees with the results of kinetic studies reported by Hahn, *et al.*[4] The mp and IR spectra of the recovered azoxy compounds were identical with those the respective starting materials. Consequently, **1aα** and **1aβ** do not rapidly isomerize with each other under the reaction conditions. Furthermore, **1aα** and **1aβ** gave similar proportions of reaction products.

Since the α and β isomers of **1** were not separately available, excepting **1a**, mixtures of α and β isomers of **1** were used. These were prepared by hydrogen peroxide oxidation of the corresponding 4-alkylazobenzene (**6**). It has been reported that the oxidation of asymmetrical azobenzenes give a mixture of azoxybenzene isomers (the isomer ratio is about 1 : 1), excepting azobenzenes having special substituents in the ortho position.[5] The results for the reaction of **1** (in a mixture of the α and β isomers) are also shown in Table 1.

In the reaction of **1b**, the main rearrangement product was 2-ethyl-4-(phenylazo)phenol (**3b**), and azophenols, **2b**, **4b**, and **5**, were also formed. 4-Isopropyl- and 4-*t*-butyl-azoxybenzenes, **1c** and **1d**, gave mainly **5**. The reaction products varies with the type of alkyl group. Except for the formation of **4**, the effect of the alkyl group on the distribution of reaction products is similar to that in reactions of 4,4'-dialkylazoxybenzenes.[6] Gaschromatographic analysis of the reaction products showed that a small amount of a 2-hydroxyazo compound was formed in each case. However, it could not be determined whether the azophenol was 5-alkyl-2-(phenylazo)phenol or 2-(*p*-alkylphenylazo)phenol.

The formation of various azophenols may be interpreted by the mechanism shown in Scheme 1. Normal Wallach rearrangement is generally explained by a dicationic intermediate mechanism,[7] which consists of

Table 1. Reaction of 4-alkylazoxybenzenes with sulfuric acid

	Yield (%)					
	1	**2**	**3**	**4**	**5**	**6**
1aα	26	37	6	7		7
1aβ	60	24	3	4		2
1a[a]	22	41	7	8		8
1b[a]	24	10	28	3	7	9
1c[a]	25		1		42	8
1d[a]	26				57	10

a) A mixture of α and β isomers.

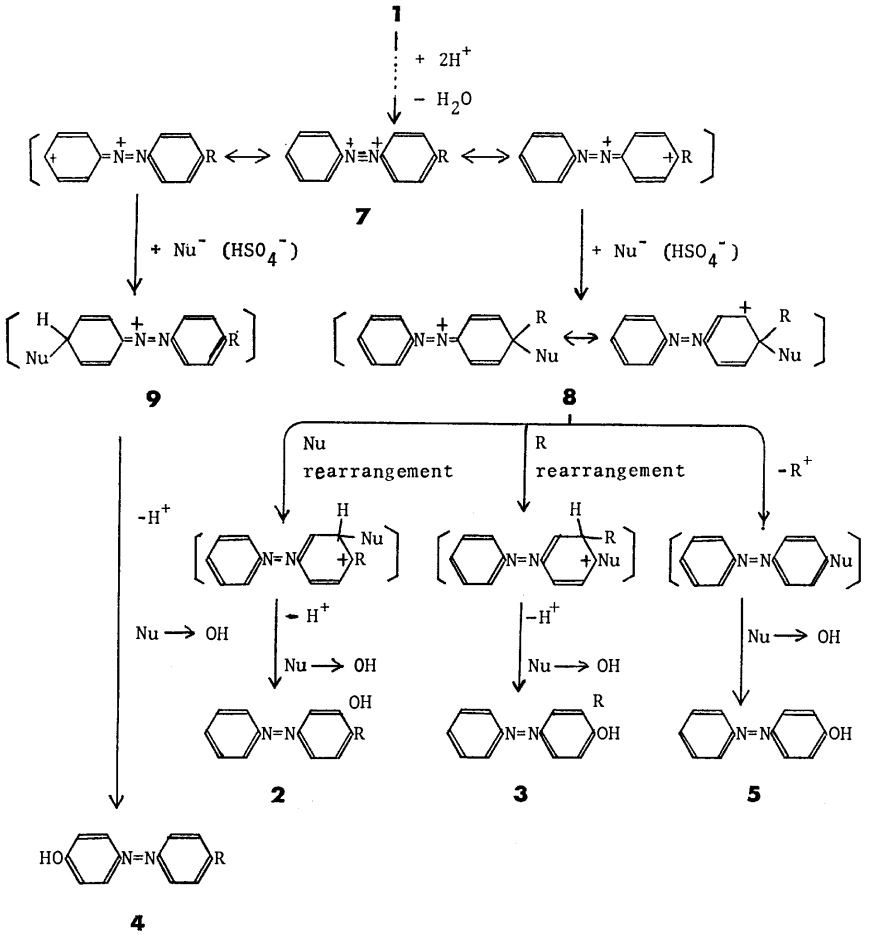

Scheme 1.

the formation and the nucleophilic attack of dicationic intermediate (**7**), followed by the deprotonation of **9**, and the conversion of the nucleophilic group into a hydroxyl group to give **4**. The following explanations involve some modification of the dicationic mechanism.

The dicationic intermediate (**7**) is formed by the diprotonation and subsequent dehydration of **1**. Subsequently, when the nucleophile, probably HSO_4^-, attacks the carbon atom having an alkyl group in **7**, the intermediate ion (**8**) is formed. The routes for the formation of azophenols, **2**, **3**, and **5**, from **8** are similar to those proposed previously for the Wallach rearrangement of 4,4'-dialkylazoxybenzenes.[1]

It is generally stated that 4-substituted 4'-hydroxyazobenzenes are the main products of Wallach rearrangement of 4-monosubstituted azoxybenzenes.[2,3,8] However, **1a** and **1b** gave only small amounts of **4**, that is, the reactions proceed weakly along this route in the case of **1**. The benzene ring having an alkyl group of **7** is preferentially attacked by a nucleophile yielding **8**, because of the electron-releasing effect of the alkyl group.

Similarly, in the reaction of an azoxybenzene with an electron-releasing group at its meta position, a hydroxyl group was found to be introduced mainly into the benzene ring having the substituent. For example, 3-methylazoxybenzene (a mixture of the α and β isomers) gave 2-methyl-4-(phenylazo)phenol (yield 30%) and only a 2% yield of 4-(*m*-tolylazo)-phenol,[9] while 3-methoxyazoxybenzene (a mixture of the α and β isomers) gave 2-methoxy-4-(phenylazo)-phenol (yield 26%).

In all case, substituted azobenzenes were also formed. Furthermore, **1d** gave **6a** in a 5% yield, namely, the *t*-butyl group was replaced by a methyl group. The mechanism of azobenzene formation is still unknown. Although the pathway from **7** to **6** is obscure, it appears likely that a methyl group in the *t*-butyl group migrates to the carbon atom of the benzene ring in **7** and then the isopropyl moiety is eliminated.

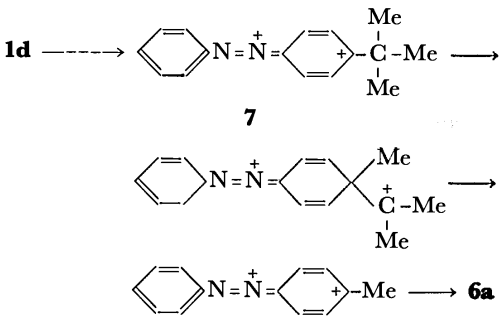

Experimental

The IR spectra were recorded with a JASCO IRA-1 spectrophotometer. The NMR spectra were obtained with a JEOL MH-100 spectrometer using TMS as the internal standard. The gas-chromatographic analysis was carried out

using a Shimadzu GC-2C apparatus on a 0.75 m × 3 mm column packed with 2% Silicone OV-225. The high-speed liquid-chromatographic analysis was carried out using a JASCO-FLC 150 apparatus on a 0.5 m × 2.1 mm column packed with JASCODAC SV-02 (the solvent was methanol-water), JASCOSIL WC-01 (the solvent was hexane-chloroform), or WC-03 (the solvent was hexane). All melting points are uncorrected.

Azoxybenzenes. 4-Methylazoxybenzenes, **1a**α and **1a**β, were prepared using methods described in the literature. **1a**α, mp 50.5—51.5 °C (lit,[10] 50—51 °C). **1a**β, mp 62—64 °C (lit,[5] 63.5—64 °C). Compounds **1a**—**1d** were obtained by oxidation of the corresponding azobenzenes with hydrogen peroxide.[11] The products were recrystallized from hexane, or subjected to chromatography on an alumina column (the solvent was benzene), yield: 85%. It was shown by a comparison of their NMR spectra with those of **1a**α and **1a**β that the products were mixtures of the α and β isomers. However, the isomer ratios, α/β, could not be determined. **1a**, mp 30—36 °C (lit,[12] 30—35 °C). **1b**, oil, Found: C, 74.48; H, 6.40; N, 12.34%. Calcd for $C_{14}H_{14}N_2O$: C, 74.31; H, 6.24; N, 12.38%. **1c**, mp 36—45 °C. Found: C, 75.05; H, 6.83; N, 11.59%. Calcd for $C_{15}H_{16}N_2O$: C, 74.97; H, 6.71; N, 11.66%. **1d**, mp 25—36 °C. Found: C, 75.40; H, 7.00; N, 11.15%. Calcd for $C_{16}H_{18}N_2O$: C, 75.56; H, 7.13; N, 11.02%.

4-Alkylazobenzenes. Compounds **6a**—**6d** were prepared by the condensation of nitrosobenzene and the corresponding 4-alkylaniline in acetic acid.[13] The products were purified by chromatography on alumina column (the solvent was benzene) and by recrystallization from ethanol. **6a**, mp 66—67 °C (lit,[14] 66—67 °C). **6b** (yield, 71%), mp 26—27 °C. Found: C, 79.69; H, 6.84; N, 13.33%. Calcd for $C_{14}H_{14}N_2$: C, 79.96; H, 6.71; N, 13.32%. **6c** (yield, 76%), mp 46.5—47.5 °C. Found: C, 80.15; H, 7.44; N, 12.54%. Calcd for $C_{15}H_{16}N_2$: C, 80.32; H, 7.19; N, 12.49%. **6d** (yield, 70%) mp 48—49 °C. Found: C, 80.82; H, 7.60; N, 11.70%. Calcd for $C_{16}H_{18}N_2$: C, 80.63; H, 7.61; N, 11.76%.

The Reactions of 4-Alkylazoxybenzenes with Sulfuric Acid. A solution of **1** (0.005 mol) in 85% sulfuric acid (25 ml) was heated at 50 °C for 30 min. The reaction mixture was poured into cold water and then extracted with chloroform. The organic phase was washed with water, and dried over anhydrous sodium sulfate. After removal of the solvent, the residue was subjected to chromatography on a silica gel (Wakogel C-200) column using benzene as the solvent.

First fraction. This fraction was a mixture of **1**, **6** and small amounts of 2-hydroxy-4-(or 4'-)alkylazobenzenes which were analyzed using gas chromatography. Furthermore, the mixture was again subjected to chromatography on an alumina column using hexane-benzene (2:1) as the solvent. Fraction 1 gave **6** and fraction 2 gave **1**. In the case of **1d**, fraction 2 upon rechromatography gave **6a**, mp 66.5—67 °C, and fraction 3 gave **1d**. The mp and IR spectra of azobenzenes **6a**—**6d** and of the recovered **1a**α and **1a**β were in good agreement with those of respective authentic samples. Other recovered **1a**—**1d** were identified by comparing their IR spectra and GC retention times with those of the corresponding starting materials.

Second fraction. Recrystallization from benzene gave 2-alkyl-5-(phenylazo)phenol (**2**). **2a**, mp 153.5—154.5 °C. Found: C, 73.49; H, 5.61; N, 13.40%. Calcd for $C_{13}H_{12}N_2O$: C, 73.56; H, 5.70; N, 13.20%. **2b**, mp 136—137 °C. Found: C, 74.35; H, 6.19; N, 12.29%. Calcd for $C_{14}H_{14}N_2O$: C, 74.31; H, 6.24; N, 12.38%.

Azophenol **2a** and **2b** were acetylated with acetic anhydride and pyridine. The products were recrystallized from hexane. The acetate of **2a**, mp 73—73.5 °C (yield 70%). The acetate of **2b**, mp 29—30 °C (yield 75%). The mp and IR spectra of both acetates were identical with those of respective authentic samples.

Third fraction. Recrystallization from hexane or ethanol-water gave 2-alkyl-4-(phenylazo)phenol (**3**). **3a**, mp 130—131.5 °C. **3c**, mp 126.5—128 °C. Since the **3b** was impure, crude **3b** was acetylated with acetic anhydride in pyridine. The product was recrystallized form hexane to yield acetate of **3b**, mp 47—48 °C. These compounds were identified by comparing their mp and IR spectra with those of authentic samples.

Fourth fraction. In the case of **1a**, recrystallization from ethanol-water gave **4a**, mp 154—155 °C. In the case of **1b**, this fraction was found by high-speed liquid-chromatographic analysis to be a mixture of **4b** and **5**. The mixture was acetylated with acetic anhydride and pyridine, and the resulting acetate was also analyzed by high-speed liquid-chromatography. In the cases of **1c** and **1d**, recrystallization from benzene gave **5**, mp 155—156 °C (lit,[15] 152 °C).

The Reactions of 3-Methyl- and 3-Methoxy-azoxybenzenes with Sulfuric Acid. The azoxy compounds were treated with sulfuric acid using the procedure described above. 3-Methylazoxybenzene gave 3-methylazobenzene (yield 6.5%) and a mixture of 2-methyl-4-(phenylazo)phenol (yield 30%) and 4-(*m*-tolylazo)phenol (yield 2%) which was analyzed by high-speed liquid-chromatography. 3-Methoxyazoxybenzene gave 3-methoxyazobenzene (yield 12%) and 2-methoxy-4-(phenylazo)phenol, mp 69—70 °C (lit,[16] 70.5—71.5 °C).

Preparation of Authentic Samples. Azophenols, **3** and **4**, were prepared by diazo-coupling of the corresponding phenols and diazonium salts.[17] The products were subjected to chromatography on a silica gel column (the eluent was benzene), and then recrystallized from hexane-benzene. **3a**, mp 132—133 °C (lit,[18] 129—130 °C) (yield 55%). **3b**, mp 89—89.5 °C (yield 40%). Found: C, 74.37; H, 6.44; N, 12.55%. Calcd for $C_{14}H_{14}N_2O$: C, 74.31; H, 6.24; N, 12.38%. **3c**, mp 127.5—128 °C (yield 30%). Found: C, 74.97; H, 6.72; N, 11.63%. Calcd for $C_{15}H_{16}N_2O$: C, 74.97; H, 6.71; N, 11.66%. **4a**, mp 154—154.5 °C (lit,[19] 152 °C). Compounds **4b**, **4c**, and **4d** have been repotred previously.[1]

3-Ethyl-4-acetoxyazobenzene, the acetate of **3b**, was prepared by the acetylation of **3b** with acetic anhydride and pyridine, and then recrystallized from hexane (yield 86%), mp 48—49 °C. Found: C, 71.43; H, 5.94; N, 10.66%. Calcd for $C_{16}H_{16}N_2O_2$: C, 71.62; H, 6.01; N, 10.44%.

3-Acetoxy-4-alkylazobenzenes, the acetate of **2a** and **2b**, were prepared by condensation of 3-acetoxy-4-alkylaniline and nitrosobenzene according to the method given in a previous report.[1] The acetate of **2a**, mp 72.5—73.5 °C from hexane (yield 21%). Found: C, 71.10; H, 5.51; N, 11.28%. Calcd for $C_{15}H_{14}N_2O_2$: C, 70.85; H, 5.55; N, 11.02%. The acetate of **2b**, mp 29—30 °C from hexane (yield 28%). Found: C, 71.90; H, 6.09; N, 10.63%. Calcd for $C_{16}H_{16}N_2O_2$: C, 71.62; H, 6.01; N, 10.44%.

We wish to express our thanks to Professor Syuzi Hirooka for valuable suggestions and encouragement.

References

1) I. Shimao and S. Matsumura, *Bull. Chem. Soc. Jpn.*, **49**, 2294 (1976).

2) S. Oae, T. Fukumoto, and M. Yamagami, *Bull. Chem. Soc. Jpn.*, **36**, 601 (1963).

3) J. Yamamoto and K. Furuya, *Yuki Gosei Kagaku*

Kyokai Shi, **30**, 179 (1972).
4) C. S. Hahn, K. W. Lee, and H. H. Jaffé, *J. Am. Chem. Soc.*, **89**, 4975 (1967).
5) M. A. Berwick and R. E. Rondeau, *J. Org. Chem.*, **37**, 2409 (1972).
6) Ref. 1. It was found upon reinvestigation of previous work that 4,4'-dimethylazoxybenzene also gives 2-methyl-4-(*p*-tolylazo)phenol in a 1.5% yield.
7) R. A. Cox and E. Buncel, "The Chemistry of the Hydrazo, Azo and Azoxy Groups," ed by S. Patai, John Wiley & Sons, New York (1975), p. 808, and references cited therein.
8) a) C. S. Hahn and H. H. Jaffé, *J. Am. Chem. Soc.*, **84**, 946 (1962); b) P. H. Gore, *Chem. Ind.*, **1959**, 191.
9) T. Parsons and J. C. Bailar, *J. Am. Chem. Soc.*, **58**, 268 (1936). They did not describe the formation of 4-(*m*-tolylazo)phenol.
10) T. E. Stevens, *J. Org. Chem.*, **29**, 311 (1964).
11) B. T. Newbold, *J. Org. Chem.*, **27**, 3919 (1962).
12) I. Shimao, *Nippon Kagaku Kaishi*, **1974**, 1151.
13) K. H. Schundehütte, "Houben-Weyl Methoden der Organischen Chemie," Band 10, Teil 3, Georg Thieme Verlag, Stuttgart (1965), p. 332.
14) W. Lischke, *Ann.*, **303**, 637 (1898).
15) O. Wallach and L. Kiepenheuer, *Ber.*, **14**, 2617 (1881).
16) P. Jacobson, M. Jaenicke, and F. Meyer, *Ber.*, **29**, 2685 (1896)
17) Ref. 13, p. 263.
18) E. Nölting and O. Kohn, *Ber.*, **17**, 363 (1884).
19) W. McPherson and G. W. Stratton, *J. Am. Chem. Soc.*, **37**, 912 (1915).

New Methods for the Preparation of 3-Substituted Furans[1)]

Katsuhiko INOMATA, Shin-ichi AOYAMA, and Hiroshi KOTAKE
Department of Chemistry, Faculty of Science, Kanazawa University, Kanazawa 920
(Received September 12, 1977)

It was found that ethyl 4,4-dimethoxy-2-(phenylthio)butyrate and 3-tosylpropanal ethylene acetal are useful starting materials for the preparation of 3-substituted furans. Several 3-substituted furans, including dendrolasin [3-(4,8-dimethyl-3,7-nonadienyl)-furan], were prepared by the reaction of these compounds with alkyl halides in good yields.

It is known that a number of furan derivatives occurring in nature are 3-substituted furans such as dendrolasin [3-(4,8-dimethyl-3,7-nonadienyl)-furan]. Although some methods for the preparation of 3-substituted furan derivatives were recently reported,[2)] they require many steps or considerably complicated pathways with low overall yields. In this paper we wish to describe new convenient methods for the preparation of 3-substituted furans in three steps starting from ethyl 4,4-dimethoxy-2-(phenylthio)butyrate (Method A) and 3-tosylpropanal ethylene acetal (Method B).

Method A. The starting material, ethyl 4,4-dimethoxy-2-(phenylthio)butyrate (**3**), was readily prepared by the reaction of sodium salt of ethyl (phenylthio)acetate (**1**) with 2-bromoacetaldehyde dimethyl acetal (**2**).

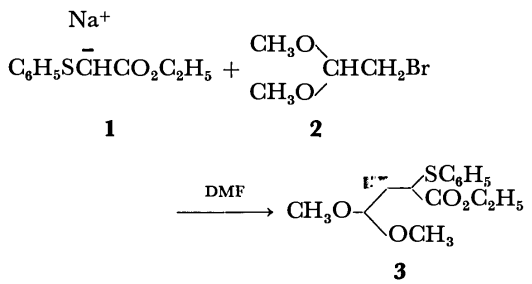

1 **2** **3**

The desired 3-substituted furans were synthesized from **3** and alkyl halide **4** according to the following scheme.

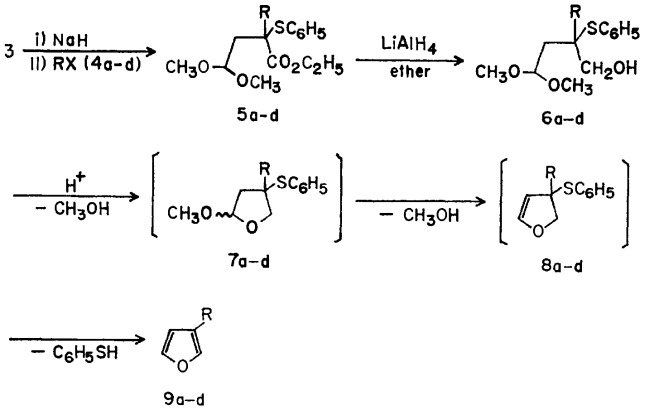

5a-d **6a-d** **7a-d** **8a-d** **9a-d**

In the first place the sodium salt of **3** was allowed to react with alkyl halide in DMF at 60 °C to give the alkylated ester **5**, which was then reduced to alcohol **6** by the reaction with lithium aluminium hydride in ether at room temperature in almost quantitative yield. Finally, a benzene solution of **6** was refluxed in the presence of a catalytic amount of *p*-toluenesulfonic acid for 2 h to give the expected 3-alkylfuran **9** in good yield.

Preparation of 3-benzylfuran (**9a**), 3-octadecylfuran (**9b**), 3-geranylfuran (**9c**, nordendrolasin), and dendrolasin (**9d**) was carried out by this method (Table 1).

From the fact that the cyclic intermediate **7a** was isolated by the reaction of **6a** with an acidic catalyst at room temperature, the conversion of **6** into the corresponding 3-alkylfurans **9** appears to proceed as follows. First the cyclic intermediate **7** is formed by elimination of one molecule of methanol. By increasing temperature, another methanol is eliminated to form 3-alkyl-3-(phenylthio)dihydrofuran **8**, which has a labile phenylthio group at an allylic position and is finally converted into 3-alkylfuran **9** by elimination of benzenethiol.

Consequently, the method can be characterized by the formation of the intermediate, 4-hydroxybutanal dimethyl acetal derivative **6** having phenylthio group on C-3 as a leaving group, which is an important precursor of 3-substituted furan. This consideration provided an alternate method for the preparation of 3-substituted furans starting from crystalline 3-tosylpropanal ethylene acetal (**10**) which is accessible from acrylaldehyde, ethylene glycol, and *p*-toluenesulfinic acid.[3)]

Method B. The reduction process in Method A is not required as shown in the following scheme.

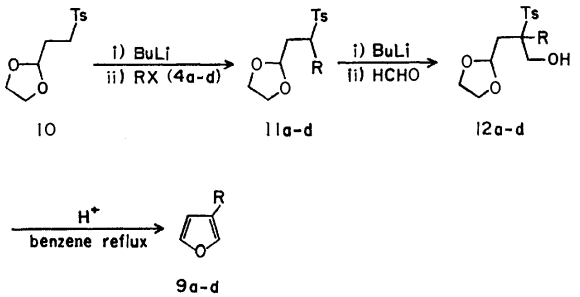

10 **11a-d** **12a-d** **9a-d**

The readily available **10** was converted into lithium salt by stirring with an equimolar amount of butyllithium in tetrahydrofuran at −78 °C for 10 min under nitrogen atmosphere. Treatment of the salt with alkyl halide at −78 °C and then at room temperature gave the alkylation product **11**. Similar lithiation of **11** in tetrahydrofuran and subsequent reaction with formaldehyde gave alcohol **12** corresponding to the key intermediate **6** in Method A. In a similar way to that for **6**, a benzene solution of **12** was refluxed in the presence of a catalytic amount of *p*-toluenesulfonic acid for 3.5 h to afford 3-alkylfuran **9** in good yield. The results are given in Table 2.

Table 1. Synthesis of 3-substituted furans by method A

RX	Isolated yield (%) 5a—d	9a—d
4a, $C_6H_5CH_2Br$	82	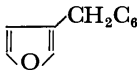 89
4b, $CH_3(CH_2)_{17}I$	82	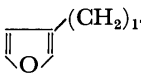 83
4c, 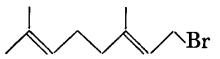	78	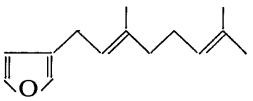 83
4d, 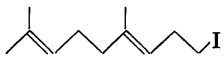	79	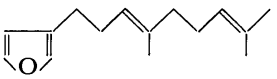 81

Table 2. Synthesis of 3-substituted furans by method B

RX	Isolated yield (%) 11a—d	12a—d	9a—d
4a, $C_6H_5CH_2Br$	88	86	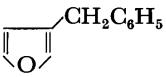 88
4b, $CH_3(CH_2)_{17}I$	82	80	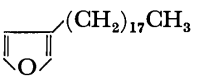 85
4c, 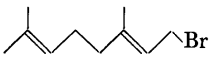	88	81	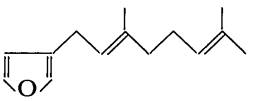 85
4d, 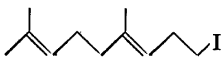	85	83	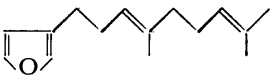 86

Experimental

All the melting points were taken with a micro melting point apparatus (Yanagimoto-Seisakusho) and are uncorrected. The proton NMR spectra were recorded on a JEOL JNM-MH 60 spectrometer. Chemical shifts are reported in terms of the δ scale relative to TMS as an internal standard. The IR spectra were taken with a JASCO IRA-1 diffraction grating infrared spectrometer.

Materials. All the solvents were distilled according to general methods and were stored over molecular sieves or sodium metal as a drying agent. Homogeranyl iodide (4,8-dimethyl-3,7-nonadienyl iodide, **4d**, bp 58—61 °C/0.002 Torr [lit,[4] bp *ca.* 80 °C/0.04 Torr]) and 3-tosylpropanal ethylene acetal (**10**, recrystallized from ethanol. mp 83—84 °C [lit,[3] mp 83—85 °C]) were prepared by the reported procedures,[3,4] respectively. Butyllithium (about 15% in hexane) was obtained from Wako Pure Chemical Industries Co. Thin-layer chromatography (TLC) was performed on Merck's Kieselgel 60 PF_{254} (Art. 7749) using a mixture of benzene and ethyl acetate as an eluent, unless otherwise stated.

*Ethyl 4,4-Dimethoxy-2-(phenylthio)butyrate (**3**).* To a suspension of sodium hydride (33 mmol) in DMF (20 ml) was added dropwise a DMF solution (10 ml) of ethyl (phenylthio)acetate (6.10 g, 31 mmol) at room temperature under nitrogen atmosphere. After 15 min, a solution of 2-bromoacetaldehyde dimethyl acetal (**2**, 5.41 g, 32 mmol) in DMF (10 ml) was added at 60 °C. The reaction mixture was then allowed to stand at 60 °C for 3.5 h. Precipitates were removed by filtration and the filtrate was concentrated under reduced pressure. The residue was treated with a pH 7.2 buffer solution, followed by extraction with ethyl acetate. The organic extract was dried over Na_2SO_4, concentrated, and distilled, giving 6.10 g (69%) of **3**: Bp 138—141 °C/1 Torr; IR 1720, 1145, 1115, 1060 cm^{-1}; NMR (CCl_4) δ 1.15 (t, 3H), 2.02 (dd, 2H), 3.23 (s, 6H), 3.63 (t, 1H), 4.04 (q, 2H), 4.42 (t, 1H), 7.24 (m, 5H).

*Ethyl 2-Benyl-4,4-dimethoxy-2-(phenylthio)butyrate (**5a**).* To a suspension of sodium hydride (1.25 mmol) in DMF (3 ml) was added dropwise a DMF solution (1 ml) of **3** (299 mg, 1.05 mmol) at 60 °C under nitrogen atmosphere. After 5 min, a solution of benzyl bromide (**4a**, 180 mg, 1.06 mmol) in DMF (1 ml) was added at 60 °C. The reaction mixture was allowed to stand at 60 °C for 3 h and then worked up according to the above procedure. The resulting residue was separated by preparative TLC to afford **5a** (322 mg, 82%) as an oil: IR 1718, 1182, 1115, 1070, 1040 cm^{-1}; NMR ($CDCl_3$) δ 1.17 (t, 3H), 2.14 (d, 2H), 3.27 (s, 2H), 3.31 (s, 3H), 3.37 (s, 3H), 4.03 (q, 2H), 4.88 (t, 1H), 7.32 (m, 10H).

In a similar way, the corresponding alkylation products **5b**, **5c**, and **5d** were obtained by the reaction of **3** with octadecyl iodide (**4b**), geranyl bromide [(*E*)-3,7-dimethyl-2,6-octadienyl bromide, **4c**], and homogeranyl iodide [(*E*)-4,8-dimethyl-3,7-nonadienyl iodide, **4d**], respectively. Spectral data of the products are as follows.

5b: Oil, IR 1725, 1145 cm^{-1}; NMR ($CDCl_3$) δ 1.17 (t, 3H), 1.22 (s, 37H), 2.03 (d, 2H), 3.21 (s, 6H), 4.01 (q, 2H), 4.67 (t, 1H), 7.23 (m, 5H).

5c: Oil, IR 1720, 1180, 1120, 1090, 1075, 1040 cm^{-1};

NMR ($CDCl_3$) δ 1.17 (t, 3H), 1.57 (s, 6H), 1.66 (s, 3H), 2.04 (m, 6H), 2.41 (d, 2H), 3.17 (s, 6H), 4.00 (q, 2H), 4.60 (t, 1H), 5.04 (broad, 1H), 5.32 (t, 1H), 7.23 (m, 5H).

5d: Oil, IR 1720, 1180, 1120, 1095, 1060, 1045 cm^{-1}; NMR ($CDCl_3$) δ 1.22 (t, 3H), 1.60 (s, 3H), 1.64 (s, 3H), 1.66 (s, 3H), 2.00 (m, 10H), 3.28 (s, 6H), 4.09 (q, 2H), 4.75 (t, 1H), 5.06 (m, 2H), 7.34 (m, 5H).

*3-Benzyl-4-hydroxy-3-(phenylthio)butanal Dimethyl Acetal (**6a**).* The ester **5a** (390 mg, 1.04 mmol) was reduced with lithium aluminium hydride (38 mg, 1.00 mmol) in ether (7 ml) at room temperature for 30 min followed by treatment with concd NaOH. The ethreal extract dried over Na_2SO_4 was evaporated and the residue was separated by preparative TLC to afford **6a** (338 mg, 98%) as an oil: IR 3460, 1112, 1038 cm^{-1}; NMR ($CDCl_3$+D_2O) δ 1.78 (d, 2H), 2.90 (s, 2H), 3.12 (s, 6H), 3.35 (s, 2H), 4.77 (t, 1H), 7.14 (m, 10H).

In other cases, the reduction products **6b**—**d** were not isolated. The crude products were used in the subsequent cyclization reaction.

*3-Benzylfuran (**9a**).* A benzene solution of **6a** (332 mg, 1 mmol) was refluxed in the presence of a catalytic amount of *p*-toluenesulfonic acid (*ca.* 5 mg) for 2 h. The reaction mixture was washed with 1 M NaOH and dried over Na_2SO_4. After removal of the solvent, the residue was separated by preparative TLC using hexane as an eluent to afford **9a** (143 mg, 91%) as an oil: IR 1578, 870 cm^{-1}; NMR ($CDCl_3$) δ 3.61 (s, 2H), 6.08 (m, 1H), 7.05 (m, 1H), 7.07 (s, 5H), 7.16 (t, 1H).

In a similar way, other 3-alkylfurans **9b**—**d** were prepared from **6b**—**d**. Their spectral data are as follows.

9b: Melts at near 35 °C, IR 1555, 865 cm^{-1}; NMR ($CDCl_3$) δ 0.88 (t, 3H), 1.25 (s, 32H), 2.32 (t, 2H), 6.15 (m, 1H), 7.12 (m, 1H), 7.23 (t, 1H).

9c: Oil, IR 1555, 863 cm^{-1}; NMR ($CDCl_3$) δ 1.62 (s, 3H), 1.67 (s, 6H), 2.08 (m, 4H), 3.17 (d, 2H), 5.25 (broad, 1H), 5.39 (t, 1H), 6.33 (m, 1H), 7.28 (m, 1H), 7.42 (t, 1H).

9d: Oil, The following spectra are almost identical with the published ones.[5] IR 1560, 870 cm^{-1}; NMR ($CDCl_3$) δ 1.56 (s, 6H), 1.66 (s, 3H), 1.98 (m, 4H), 2.34 (m, 4H), 4.8—5.3 (m, 2H), 6.18 (m, 1H), 7.12 (m, 1H), 7.22 (t, 1H).

*4-Benzyl-2-methoxy-4-(phenylthio)oxolane (**7a**).* A benzene solution (20 ml) of **6a** (200 mg, 0.6 mmol) was stirred in the presence of a catalytic amount of *p*-toluenesulfonic acid for 30 min at room temperature. The reaction mixture was neutralized with Na_2CO_3, washed with water, and dried over Na_2SO_4. After evaporation of the solvent, the residue was separated by preparative TLC to afford **7a** (168 mg, 93%) as an oil: IR 1100, 1025 cm^{-1}; NMR ($CDCl_3$) δ 1.9—2.2 (m, 2H), 2.85 and 2.99 (s, 2H, *ca.* 1 : 3), 3.18 and 3.21 (s, 3H, *ca.* 1 : 3), 3.79 and 3.86 (s, 2H, *ca.* 3 : 1), 4.7—5.1 (m, 1H), 7.15 (m, 10H).

*3-Benzyl-3-tosylpropanal Ethylene Acetal (**11a**).* 3-Tosylpropanal ethylene acetal (**10**, 1.31 g, 5.00 mmol) was coverted into lithium salt by stirring with an equimolar amount of butyllithium in tetrahydrofuran (25 ml) at −78 °C for 10 min under nitrogen atmosphere. After treatment of the salt with benzyl bromide (**4a**, 0.86 g, 5.02 mmol) at −78 °C and then at room temperature, the mixture was concentrated on evaporation of the solvent under reduced pressure. The residue was treated with a pH 7.2 buffer solution, followed by extraction with ethyl acetate. The organic extract was dried over Na_2SO_4 and evaporated to dryness. Recrystallization from ethanol gave **11a** (1.55 g, 88%): Mp 97—99 °C, IR 1300, 1285, 1140 cm^{-1}; NMR ($CDCl_3$) δ 2.00 (m, 2H), 2.34 (s, 3H), 2.99 (m, 2H), 3.56 (m, 5H), 4.76 (t, 1H), 7.07 (m, 5H), 7.23 (d, 2H), 7.71 (d, 2H). Found: C, 65.80; H, 6.50%. Calcd for $C_{19}H_{22}O_4S$: C, 65.88; H, 6.40%.

Products **11b**—**d** were prepared in a similar way, except that **11c**, **d** were separated by preparative TLC. Physical properties and analytical data of the products are as follows.

11b: Mp 82—83 °C, IR 1300, 1285, 1140 cm^{-1}; NMR ($CDCl_3$) δ 0.87 (t, 3H), 1.23 (s, 36H), 2.45 (s, 3H), 3.16 (m, 1H), 3.84 (m, 4H), 4.97 (t, 1H), 7.31 (d, 2H), 7.74 (d, 2H), Found: C, 70.80; H, 10.44%. Calcd for $C_{30}H_{52}O_4S$: C, 70.83; H, 10.30%.

11c: Oil, IR 1300, 1290, 1280, 1130 cm^{-1}; NMR ($CDCl_3$) δ 1.51 (s, 3H), 1.54 (s, 3H), 1.62 (s, 3H), 1.90 (m, 6H), 2.34 (s, 3H), 2.46 (m, 2H), 3.17 (m, 1H), 3.17 (m, 4H), 4.92 (m, 3H), 7.23 (d, 2H), 7.67 (d, 2H).

11d: Oil, IR 1305, 1295, 1285, 1140 cm^{-1}; NMR (CCl_4) δ 1.55 (s, 6H), 1.65 (s, 3H), 1.93 (m, 10H), 2.40 (s, 3H), 3.10 (m, 1H), 3.74 (m, 4H), 4.85 (m, 3H), 7.21 (d, 2H), 7.60 (d, 2H).

*3-Benzyl-4-hydroxy-3-tosylbutanal Ethylene Acetal (**12a**).* 3-Benzyl-3-tosylpropanal ethylene acetal (**11a**, 352 mg, 1 mmol) was converted into lithium salt in tetrahydrofuran (10 ml) according to the above procedure. Gaseous formaldehyde (generated by heating paraformaldehyde) was bubbled through a solution of the salt at −78 °C. The reaction mixture was brought to room temperature for 30 min and then concentrated on evaporation of the solvent under reduced pressure. The residue was treated with a pH 7.2 buffer solution, followed by extraction with ethyl acetate. The organic extract was dried over Na_2SO_4 and concentrated. The resulting residue was separated by preparative TLC to afford **12a**, which was further recrystallized from ethanol to give pure **12a** (328 mg, 86%): mp 61—62 °C, IR 3520, 1280, 1140 cm^{-1}; NMR ($CDCl_3$ +D_2O) δ 2.03 (t, 2H), 2.39 (s, 3H), 3.14 (dd, 2H), 3.72 (m, 4H), 3.84 (dd, 2H), 4.98 (t, 1H), 7.15 (m, 5H), 7.23 (d, 2H), 7.71 (d, 2H). Found: C, 63.66; H, 6.70%. Calcd for $C_{20}H_{24}O_5S$: C, 63.82; H, 6.43%.

Products **12b**—**d** were prepared in a similar way. Physical properties and analytical data of the products are as follows.

12b: mp 57—59 °C, IR 3470, 1290, 1280, 1130 cm^{-1}; NMR ($CDCl_3$) δ 0.87 (t, 3H), 1.22 (s, 34H), 2.13 (d, 2H), 2.42 (s, 3H), 3.85 (m, 7H), 5.12 (t, 1H), 7.27 (d, 2H), 7.67 (d, 2H). Found: C, 69.19; H, 10.30%. Calcd for $C_{31}H_{54}O_5S$: C, 69.11; H, 10.10%.

12c: Oil, IR 3500, 1290, 1280, 1125 cm^{-1}; NMR ($CDCl_3$) δ 1.55 (s, 3H), 1.57 (s, 3H), 1.66 (s, 3H), 1.98 (m, 6H), 2.38 (s, 3H), 2.54 (m, 2H), 3.83 (m, 6H), 5.17 (m, 3H), 7.28 (d, 2H), 7.73 (d, 2H).

12d: Oil, IR 3500, 1295, 1280, 1130 cm^{-1}; NMR ($CDCl_3$) δ 1.55 (m, 9H), 1.95 (m, 10H), 2.36 (s, 3H), 3.21 (broad s, 1H), 3.79 (m, 6H), 4.7—5.3 (m, 3H), 7.24 (d, 2H), 7.67 (d, 2H).

Cyclization of **12a**—**d** to the corresponding 3-alkylfurans **9a**—**d** was performed according to the procedure described for 3-benzylfuran (**9a**).

References

1) Preliminary Communication: H, Kotake, K. Inomata, S. Aoyama, and H. Kinoshita, *Chem. Lett.*, **1977**, 73.

2) (a) J. E. McMurry and S. F. Donovan, *Tetrahedron Lett.*, **1977**, 2869; and references cited therein; (b) A. Zamojski and T. Kozluk, *J. Org. Chem.*, **42**, 1089 (1977); (c) J. A. Turner and W. Herz, *J. Org. Chem.*, **42**, 1900 (1977).

3) G. K. Cooper and L. J. Dolby, *Tetrahedron Lett.*, **1976**, 4675.

4) E. J. Corey and M. Jautelat, *Tetrahedron Lett.*, **1968**, 5787.

5) T. Sakai, K. Nishimura, and Y. Hirose, *Bull. Chem. Soc. Jpn.*, **38**, 381 (1965).

NOTES

BULLETIN OF THE CHEMICAL SOCIETY OF JAPAN, VOL. 51 (3), 933—934 (1978)

Critical Micelle Concentration Reduction of Aqueous Sodium Dodecyl Sulfate Solutions upon the Addition of Alcohols

Kohji HAYASE and Shigeo HAYANO

Institute of Industrial Science, The University of Tokyo, Roppongi, Minato-ku, Tokyo 106

(Received July 27, 1977)

Synopsis. Linear relations were found between the critical micelle concentration (CMC) reduction and the carbon number of the alcohols added both at 313.15 K and 328.15 K. The slopes of the CMC reduction against the carbon number of the alcohols are almost the same at 298.15, 313.15, and 328.15 K.

It is well known that upon the addition of alcohols to surfactant micellar solutions, the critical micelle concentration (CMC) decreases.[1-5] Flockhart[4] has reported the effect of temperature on the CMC of sodium dodecyl sulfate (SDS) in water and in aqueous ethanol solutions. Shirahama and Kashiwabara[5] have already discussed the CMC reduction effects due to alcohols (C_2—C_4) on aqueous SDS solutions at 298.15 K.

The present authors have already reported the CMC reduction of SDS upon the addition of 1-butanol, 1-pentanol, 1-hexanol and 1-heptanol, and the distribution coefficients of the alcohols between the aqueous and micellar phases.[6] The relation between the CMC reduction, the distribution coefficients and the standard free energy changes of penetration of the alcohols has been discussed thermodynamically.[7] An important factor which governs the CMC reduction effects is the molar fraction of the alcohol in the micellar phase, because the molar fraction of the alcohol in the micellar phase has a great influence on the chemical potential of the mixed micelle.[7]

Since these results were obtained only at 298.15 K, further work is required at various other temperatures. In this paper, experimental work on the CMC reduction due to the addition of alcohols to the aqueous SDS solutions at 313.15 and 328.15 K is reported.

Experimental

Method. The CMC was determined using the electric conductivity method at 313.15 and 328.15 K. Details of the procedures have been described in a previous paper.[6]

Materials. SDS for biochemical use (Wako Pure Chemical Industries, Ltd.) was recrystallized twice from ethanol, and was carefully dried in vacuo for 50 h. 1-Butanol, 1-pentanol, 1-hexanol, and 1-heptanol of high purity (higher than 99%) were used. The water used was passed through Milli-Q2 Systems (Nihon Millipore Co.) until its specific conductivity fell below $10^{-7}\ \Omega^{-1}\ cm^{-1}$.

Results and Discussion

The CMC of aqueous SDS solutions containing 1-butanol, 1-pentanol, 1-hexanol, and 1-heptanol at 313.15 and 328.15 K are shown in Table 1. The more hydrophobic and the more concentrated the alcohols added, the more marked becomes the reduction in the CMC. These results follow the same trend as the results for 298.15 K.[6] Also at 313.15 and 328.15 K, the penetration of the alcohols into the micelle from the aqueous phase decreases the chemical potentials of the micelles and, therefore, decreases the CMC. To discuss the standard free energy changes of penetration of the alcohols from the aqueous to micellar phases at 313.15 and 328.15 K, these CMC data will be useful.

Table 1. CMC values for SDS to which a small amount of alcohol was added

	313.15 K		328.15 K	
	Alcohol concn (mmol/dm³)	CMC (mmol/dm³)	Alcohol concn (mmol/dm³)	CMC (mmol/dm³)
Pure water		8.47		9.57
1-Butanol	43.01	7.18	41.16	8.62
	78.24	6.53	77.70	7.24
	122.94	5.45	116.57	6.46
1-Pentanol	12.71	7.30	14.55	8.29
	26.08	6.47	25.77	7.43
	38.24	5.49	40.01	6.45
1-Hexanol	3.731	7.60	5.121	8.13
	7.375	6.59	9.683	6.93
	11.267	6.01	14.095	6.12
1-Heptanol	1.041	7.92	1.559	8.49
	2.117	6.89	2.303	7.87
	3.126	6.30	3.068	7.45

Table 2. CMC decrease upon the addition of alcohol

$\ln(-d\ln CMC/dY_a)$

	298.15 K[6]	313.15 K	328.15 K
1-Butanol	5.36	5.24	5.12
1-Pentanol	6.45	6.33	6.30
1-Hexanol	7.57	7.56	7.55
1-Heptanol	8.54	8.51	8.38

The limiting values of $\ln(-d\ln CMC/dY_a)$ at $Y_a=0$ (Y_a is the molar fraction of alcohol in the aqueous phase) were computed using the second-degree least-square method and are shown in Table 2. There are linear relations between $\ln(-d\ln CMC/dY_a)$ and the temperature for each alcohol, as illustrated in Fig. 1. Their slopes are -8.0×10^{-3}, -5.1×10^{-3}, -8.2×10^{-4}, and $-5.4\times10^{-3}\ K^{-1}$ for 1-butanol, 1-pentanol, 1-

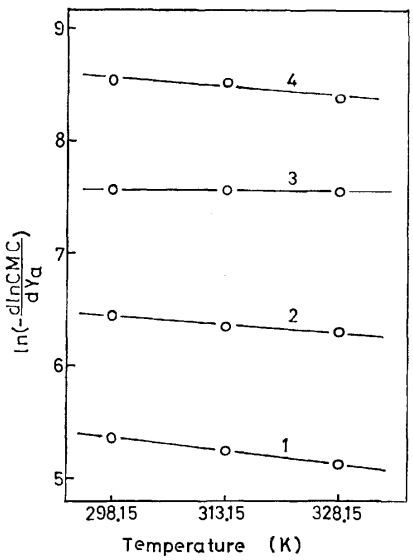

Fig. 1. $\ln(-\mathrm{dlnCMC}/\mathrm{d}Y_a)$ as a function of temperature.
(1) 1-Butanol, (2) 1-pentanol,
(3) 1-hexanol, (4) 1-heptanol.

hexanol, and 1-heptanol, respectively. For 1-butanol, 1-pentanol, and 1-hexanol, the slopes decreases with increasing carbon number of the alcohols, but for 1-heptanol the slope is higher than expected. The reason for this is still not clear.

Linear relations between the $\ln(-\mathrm{dlnCMC}/\mathrm{d}Y_a)$ and the carbon number of the alcohols are found again at 298.15, 313.15, and 328.15 K. The following equations were obtained using the first-degree least-squares method, thus

$$\ln(-\mathrm{dlnCMC}/\mathrm{d}Y_a) = 1.07n + 1.11 \quad \text{at } 298.15\,\mathrm{K}, \quad (1)^{7)}$$

$$\ln(-\mathrm{dlnCMC}/\mathrm{d}Y_a) = 1.10n + 0.84 \quad \text{at } 313.15\,\mathrm{K}, \quad (2)$$

$$\text{and } \ln(-\mathrm{dlnCMC}/\mathrm{d}Y_a) = 1.10n + 0.77 \quad \text{at } 328.15\,\mathrm{K}, \quad (3)$$

where n is the carbon number of the alcohol.

In the papers of Shirahama and Kashiwabara[5] and of Hayase and Hayano,[7] the relation between $\ln(-\mathrm{dlnCMC}/\mathrm{d}Y_a)$ and n were discussed combining the distribution coefficients of the alcohols between the aqueous and micellar phases. Accordingly, it was shown the relation is between $\ln(-\mathrm{dlnCMC}/\mathrm{d}Y_a)$, instead of $\ln(-\mathrm{dCMC}/\mathrm{d}Y_a)$, and n, although a linear relation does exist between $\ln(-\mathrm{dCMC}/\mathrm{d}Y_a)$ and n.

In Eqs. 1, 2, and 3 the slopes are almost same (1.1) for the three temperatures. Namely, the CMC reduction effect of the methylene group is the same for the temperature range studied. But, the higher the temperature, the less the CMC reduction effect of each alcohol. Equations 1, 2, and 3 can be rewritten in the following equation,

$$\ln(-\mathrm{dlnCMC}/\mathrm{d}Y_a) = An + B, \quad (4)$$

where A is independent of the temperature, and B is dependent on the temperature.

Accordingly, the CMC reduction effect can be divided into an alcohol carbon number dependent part (the first term) and a temperature dependent part (the second term). Though the physical meaning of Eq. 4 is not clear at present, it is of interest to measure the validity of the equation for other surfactants and additives.

References

1) K. Shinoda, *Bull. Chem. Soc. Jpn.*, **26**, 101, (1953).
2) K. Shinoda, *J. Phys. Chem.*, **58**, 1136 (1954).
3) N. Nishikido, Y. Moroi, H. Uehara, and R. Matuura, *Bull. Chem. Soc. Jpn.*, **47**, 2634 (1974).
4) B. D. Flockhart, *J. Colloid Sci.*, **12**, 557 (1957).
5) K. Shirahama and T. Kashiwabara, *J. Colloid Interface Sci.*, **36**, 65 (1971).
6) K. Hayase and S. Hayano, *Bull. Chem. Soc. Jpn.*, **50**, 83 (1977).
7) K. Hayase and S. Hayano, *J. Colloid Interface Sci.*, in press.

BULLETIN OF THE CHEMICAL SOCIETY OF JAPAN, VOL. 51 (3), 935—936 (1978)

The Crystal and Molecular Structure of 4-(1-Hydroxy-2,6,6-trimethyl-2-cyclohexenyl)-3-buten-2-one

Hideo UEDA,* Chuji KATAYAMA, and Jiro TANAKA

Department of Chemistry, Faculty of Science, Nagoya University, Chikusa, Nagoya 464

(Received August 26, 1977)

Synopsis. The crystal and molecular structure of a hydroxy derivative of α-ionone, 4-(hydroxy-2,6,6-trimethyl-2-cyclohexenyl)-3-buten-2-one, was studied by means of X-ray analysis. The atoms including the conjugated double bond in the side chain and those around the double bond in the ring form planes orthogonal to each other.

4-(1-Hydroxy-2,6,6-trimethyl-2-cyclohexenyl)-3-buten-2-one is an important derivative of (—)-α-ionone in its correlation to the structure of abscisic acid. Oritani and Yamashita have synthesized the optical active compounds[1-3] and provided us with crystals for X-ray analysis. The structure is interesting from the view point of CD analysis of α-ionone and abscisic acid.

Experimental

The space group of the crystal determined from the oscillation and Weissenberg photographs. The unit-cell parameters were determined by the least-squares method, using 12 reflections carefully measured on Hilger & Watts four-circle diffractometer with Ni-filtered Cu $K\alpha$ radiation(λ=1.5418 Å). Crystal data: $C_{13}H_{20}O_2$, $M.W.$=208.30, orthorhombic $P2_12_12_1$, a=12.359(1), b=13.018(1), c=7.738(1) Å, Z=4, D_m=1.109, D_c=1.111 g·cm^{-3}, μ=5.84 cm^{-1} (for Cu $K\alpha$ radiation). The intensity data were collected on a diffractometer with 2θ-ω scanning mode($2\theta \leqq 72°$). The size of the crystal used was 0.3×0.3×0.3 mm. An isotropic extinction correction was made by the method of Hamilton.[4]

Determination and Refinement of the Structure

The structure was determined by the direct method with the program MULTAN[5] using 127 reflections with $|E| \geqq 1.50$. An E map computed from the phase set with the highest figures of merit (FOM=1.21) revealed all the atoms except those of hydrogen. Refinement of the structure was performed by the block-diagonal least-squares method with 1152 independent reflections of $|F^\circ| \geqq 3\sigma$. The final refinement was carried out with anisotropic thermal parameters for non-hydrogen atoms and isotropic thermal factors for hydrogen atoms. The R-index converged to 0.053 with an equal weight for each reflection. The atomic scattering factors were taken from the International Tables for X-ray Crystallography.[6] Part of the computation was performed at the Nagoya University Computation Center. The observed and calculated structure factors are given in Table 1.[7]

* Present address: Central Research Laboratory, Ube Industries Ltd., Nishihon-machi, Ube, Yamaguchi 755.

TABLE 2. ATOMIC COORDINATES AND THEIR STANDARD DEVIATIONS

	x	y	z
C (1)	0.0536 (3)	0.8926 (3)	0.9609 (4)
C (2)	0.1308 (3)	0.8007 (3)	0.9945 (5)
C (3)	0.2411 (4)	0.8216 (4)	0.9133 (6)
C (4)	0.2932 (3)	0.9186 (4)	0.9788 (6)
C (5)	0.2147 (3)	1.0037 (4)	1.0023 (5)
C (6)	0.1081 (3)	0.9941 (3)	0.9993 (5)
C (7)	0.0828 (5)	0.7009 (4)	0.9167 (8)
C (8)	0.1466 (4)	0.7864 (4)	1.1909 (6)
C (9)	0.0338 (4)	1.0853 (4)	1.0305 (6)
C (10)	0.0217 (3)	0.8979 (3)	0.7726 (5)
C (11)	−0.0794 (3)	0.9023 (3)	0.7125 (5)
C (12)	−0.1001 (3)	0.9092 (3)	0.5239 (5)
C (13)	−0.2165 (4)	0.9079 (5)	0.4670 (6)
O (1)	−0.0271 (3)	0.9173 (3)	0.4205 (3)
O (2)	−0.0450 (2)	0.8810 (2)	1.0569 (3)
H (O2)	−0.038 (3)	0.889 (3)	1.141 (5)
H (C3a)	0.237 (3)	0.822 (3)	0.796 (5)
H (C3b)	0.300 (3)	0.759 (3)	0.934 (5)
H (C4a)	0.319 (4)	0.903 (4)	1.093 (7)
H (C4b)	0.346 (4)	0.951 (4)	0.888 (7)
H (C5)	0.255 (4)	1.073 (3)	1.010 (6)
H (C7a)	0.081 (3)	0.701 (3)	0.794 (6)
H (C7b)	0.133 (4)	0.630 (4)	0.948 (7)
H (C7c)	−0.014 (4)	0.706 (4)	0.943 (7)
H (C8a)	0.071 (3)	0.760 (3)	1.246 (6)
H (C8b)	0.173 (4)	0.849 (4)	1.246 (7)
H (C8c)	0.206 (4)	0.729 (4)	1.205 (7)
H (C9a)	−0.031 (4)	1.088 (4)	0.936 (7)
H (C9b)	−0.013 (4)	1.064 (4)	1.156 (7)
H (C9c)	0.078 (5)	1.166 (4)	1.023 (8)
H (C10)	0.091 (3)	0.902 (3)	0.685 (5)
H (C11)	−0.154 (4)	0.897 (3)	0.791 (6)
H (C13a)	−0.226 (4)	0.923 (3)	0.354 (6)
H (C13b)	−0.253 (4)	0.835 (4)	0.487 (7)
H (C13c)	−0.278 (5)	0.946 (4)	0.551 (8)

Results and Discussion

The structure is shown in Fig. 1. The atomic coordinates for all atoms are given in Table 2. Intramolecular distances and bond angles are all normal. The atoms of side chain, C(10), C(11), C(12), C(13), and O(1), are on the plane $0.0300X-0.9961Y-0.0829Z+1.075=0$, where the maximum deviation is 0.03 Å. The double bonds C(10)=C(11) and C(12)=O(1) take a *cis* conformation. The atoms around the C(5)=C(6) double bond in the ring also form a plane given by $0.0157X+0.2309Y-0.9789Z-1.801=0$, where the

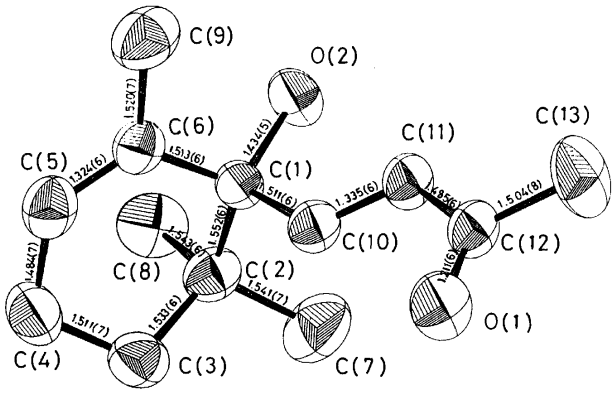

Fig. 1. The atomic labelings of (−)-1′-hydroxy-α-ionone.
Carbon and oxygen atoms are represented as thermal ellipsoids of a size such that the vibrating atoms have a 50% probability of being found within them. The absolute configuration of the melecule was drawn to be in conformity with the established configuration by a chemical correlation method.

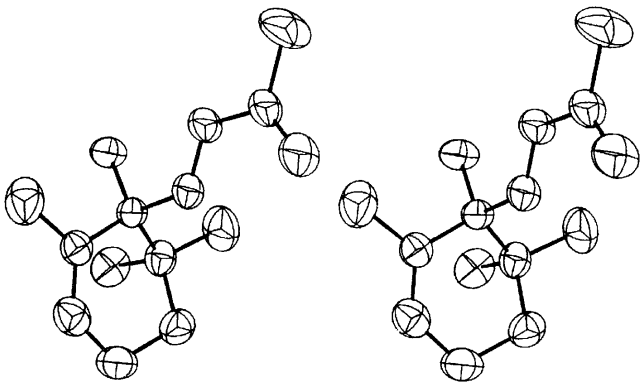

Fig. 2. A stereoscopic view of (−)-1′-hydroxy-α-ionone.
The absolute configuration and the criterion to the thermal ellipsoids of carbon and oxygen atoms are the same as in Fig. 1.

maximum deviation is 0.02 Å. These planes are at an angle of 97° to each other. A stereoscopic view of

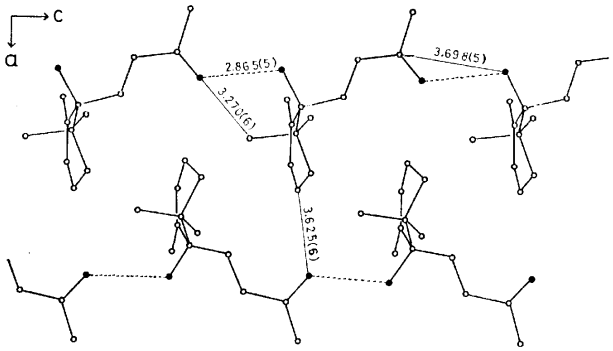

Fig. 3. The projection of molecules along the b axis.
Carbon atoms are depicted as open circles and oxygen atoms as filled circles. Hydrogen bonds are represented with broken lines. The configuration is the same as in Fig. 1.

the molecule is shown in Fig. 2, and the projection of molecules in the crystal in Fig. 3. Hydrogen bonding exists between the oxygen atoms of the carbonyl group of the side chain and the hydroxyl group of the adjacent molecule. All the other interatomic contacts are normal.

The authors are grateful to Dr. Takayuki Oritani, Tohoku University, for supply of the sample.

References

1) T. Oritani and K. Yamashita, *Agric. Biol. Chem.*, **36**, 885(1972).
2) T. Oritani and K. Yamashita, *Tetrahedron Lett.*, **1972**, 2521.
3) T. Oritani and K. Yamashita, *Agric. Biol. Chem.*, **37**, 1115(1973).
4) W.C. Hamilton, *Acta Crystallogr.*, **10**, 629(1957).
5) G. Germain, P. Main, and M. M. Woolfson, *Acta Crystallogr., Sect. A*, **27**, 368(1971).
6) "International Tables for X-Ray Crystallography," Birmingham, Vol III, Kynoch Press (1968), p. 201.
7) Table 1 is kept at the Chemical Society of Japan, Kanda, Surugadai, Chiyoda-ku, Tokyo (Document No. 7808).

BULLETIN OF THE CHEMICAL SOCIETY OF JAPAN, VOL. 51 (3), 937—938 (1978)

Fluorescence of the Hindered Phenoxyl Radical*

Tadashi OKAMURA** and R. W. YIP

Division of Chemistry, National Research Council Canada, Ottawa, Canada K1A 0R6

(Received November 7, 1977)

Synopsis. Fluorescence and excitation spectra of the 2,4,6-tritertiarybutylphenoxyl radical which is stabilized by a steric hindrance have been measured in benzene at room temperature. The emitting state seems to correspond with a state visualized in the excitation spectrum.

Absorption spectra of the phenoxyl radical and its alkyl derivatives were extensively investigated by means of flash photolysis method.[1,2] The 2,4,6-tritertiarybutylphenoxyl has an almost identical spectrum with that of the phenoxyl.[1] The emissions of these free radicals have not yet been analyzed, while those of the benzyls which have the same number of conjugated π-electrons as the phenoxyls have been investigated[3-7] closely in detail. It is very interesting to study the emitting processes of these radicals comparing with that of the benzyl, in order to examine the electronic spectra of aromatic free radicals more systematically.

2,4,6-Tritertiarybutylphenol and benzene were Analytical Reagent (Aldrich Chemical) and of spectrograde, respectively. This parent material of the radical was purified by repeated recrystallizations. The 2,4,6-tritertiarybutylphenoxyl was prepared from 2,4,6-tritertiarybutylphenol dissolved in benzene at 5×10^{-2} M concentration by the addition of PbO_2 (3 g of PbO_2 in 25 ml of solution). The oxidization of the phenol was carried out under nitrogen saturated condition at room temperature. After producing the radical, the solution was transferred to a sample cell and degassed. A Farrand Mark I spectrofluorometer was used for the measurements. Bandwidth was set at 5 nm.

Fluorescence emission and excitation spectra observed are shown in Fig. 1. The radical was stable enough to be measured these spectra by the usual static method at room temperature. High stability of this radical has been reported.[8] It was suggested that tertiarybutyl substituents prevent the recombination reactions of the radicals to form quinone type products.

The excitation spectrum shows distinct peaks at 404 and 386 nm which correspond well with the reported absorption data: at 401 and 383 nm in CCl_4, and 400 and 382 nm in hexane.[2] Therefore, the emission spectrum observed by the excitation at 390 nm shown in Fig. 1 can reasonably be assigned to be the fluorescence from the 2,4,6-tritertiarybutylphenoxyl radical. The fluorescence spectrum shows a peak at 425 nm and has no distinct vibrational structure.

The first absorption bands of the phenoxyl radicals are substantially blue-shifted and stronger compared with those of the benzyl radical, and fluorescence spectra of the benzyl radicals in rigid glass are more structured than that of the radical observed. The essential difference between these two types of radicals is that the phenoxyl has a heteroatom bearing two lone pairs which may decrease electron repulsion. This repulsion is possibly considered to lower the energy of the first electronic transition. Furthermore, the lone pairs on the oxygen atom of the phenoxyl give rise to $n\rightarrow\pi^*$ transitions in the electronic spectra. Calculations of the doublet states of the phenoxyl by P-P-P[9] and CNDO/S[10] methods were reported. In both calculations, one or two low energy states in visible region which carry low or no oscillator strength were predicted, other than the observed states in near ultraviolet region. Considering these theoretical results also, one may expect the presence of a hidden emitting state in the visible region. However, the fluorescence spectrum measured in this work indicates that the emitting state possibly corresponds to a state visualized in the absorption and excitation spectra around 400 nm, because a fluorescence peak in the observed spectrum is not much separated from the absorption one. It is also possible that there exists unknown emitting state of which absorption is weaker and hidden in the apparent absorption around 400 nm.

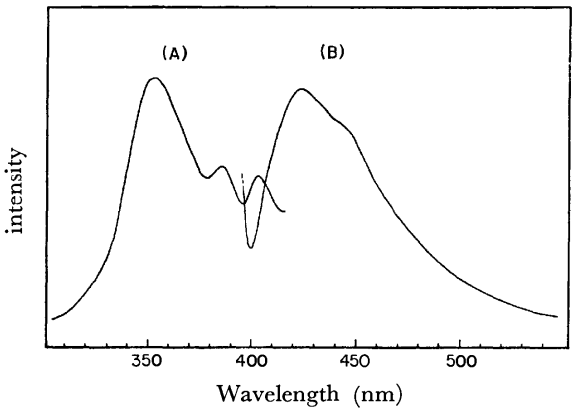

Fig. 1. Fluorescence emission and excitation spectra of 2,4,6-tritertiarybutylphenoxyl radical in benzene at room temperature.
(A) and (B) are the excitation spectrum monitored at 430 nm and the fluorescence spectrum excited at 390 nm, respectively.

The above results represent one of the few reported fluorescence from a free radical at ambient temperature in solution.

References

1) E. J. Land, G. Porter, and E. Strachan, *Trans. Faraday Soc.*, **57**, 1885 (1961).

2) E. J. Land and G. Porter, *Trans. Faraday Soc.*, **59**, 2016 (1963).

* Issued as NRCC No. 16512.

** N.R.C.C. Research Associate, 1975—1976. Present address: Department of Chemistry, Tokyo Institute of Technology, Ohokayama, Meguro-ku, Tokyo.

3) C. Cossart-Magos and S. Leach, *J. Chem. Phys.*, **56**, 1534 (1972).
4) D. M. Friedrich and A. C. Albrecht, *J. Chem. Phys.*, **58**, 4766 (1973).
5) T. Okamura, K. Obi and I. Tanaka, *Chem. Phys. Lett.*, **20**, 90 (1973).
6) T. Okamura, K. Obi and I. Tanaka, *Chem. Phys. Lett.*, **26**, 218 (1974).
7) T. Okamura and I. Tanaka, *J. Phys. Chem.*, **79**, 2728 (1975).
8) C. D. Cook, C. B. Depatie, and E. S. English, *J. Org. Chem.*, **24**, 1356 (1959).
9) A. Hinchliffe, R. E. Stainbank, and M. A. Ali, *Theor. Chim. Acta*, **5**, 95 (1966).
10) H. M. Chang, H. H. Jaffe, and C. A. Masmanidis, *J. Phys. Chem.*, **79**, 1118 (1975).

BULLETIN OF THE CHEMICAL SOCIETY OF JAPAN, VOL. 51 (3), 939—940 (1978)

A Synthesis of 2-Substituted 2-Cyclopenten-1-ones

Junya IDE, Kiyoshi SAKAI, and Yasuo YURA

Central Research Laboratories, Sankyo Co., Ltd, 1-2-58 Hiromachi, Shinagawa-ku, Tokyo 140

(Received October 25, 1976)

Synopsis. 2-Substituted 2-cyclopenten-1-ones, *i.e.*, 2-(6-methoxycarbonylhexyl)-2-cyclopentene-1-on and 2-butyl-2-cyclopenten-1-one were synthesized by cyclization of the corresponding 4-oxo-1-pentanals, which were obtained from 3-substituted 1,1-dimethoxy-2,4-pentadiones through several steps.

Recently a large amount of research has been devoted to developing synthetic routes to substituted 2-cyclopenten-1-ones. This has been due to the fact that many natural products possess this moiety as their major structural feature.[1] Particularly, 2-(6-carboxyhexyl)-2-cyclopenten-1-one and its esters[2] are valuable intermediates to 11-deoxyprostanoids[3] which possess potential pharmacological activities. We wish to report a new synthetic route to 2-alkyl-2-cyclopenten-1-ones.

Catalytic hydrogenation of 1,1-dimethoxy-3-(6-methoxycarbonylhexyl)-2,4-pentadione (**1a**),[4] prepared from 1,1-dimethoxy-2,4-pentadione and methyl 7-iodoheptanoate, over platinum in methanol afforded two epimeric keto alcohols **2a** and **epi-2a** in a ratio of 95 : 5 in 98% yield. Analogously, catalytic reduction of 3-butyl-1,1-dimethoxy-2,4-pentadione (**1b**) gave two epimeric alcohols **2b** and **epi-2b** in a ratio of 93 : 7 in 86% yield.[5] Treatment of the keto alcohols **2a** and **2b** with dicyclohexylcarbodiimide and a catalytic amount of copper(I) chloride in ether[6] gave the α,β-unsaturated ketones **3a** and **3b** in 81 and 92% yields, respectively. The ketone **3** was also obtained by treatment of the p-toluenesulfonate of the alcohol **2** with potassium acetate in aqueous *N,N*-dimethylformamide at 100 °C for 2.5 h in 60 and 55% yields, respectively. Hydrogenation of the α,β-unsaturated ketone **3** over 5% Pd–C in methanol gave the saturated ketones **4a** and **4b** in 85 and 88% yields, respectively.

Treatment of **4** with a slight excess of benzyl mercaptan and zinc chloride in dioxane at 50 °C for 1 h afforded bis(benzylthio)-derivatives **5a** and **5b** in 74 and 78% yields, respectively. Dethioacetalization of **5** was effected with mercury(II) chloride and cadmium carbonate in aqueous acetonitrile at 40 °C for 2 h to give the corresponding aldehyde **6**[7] in good yield. Cyclization of the keto aldehydes **6a** and **6b** with potassium carbonate in methanol afforded the 2-substituted 2-cyclopenten-1-ones **7a** and **7b** in 36 and 35% yields, respectively.

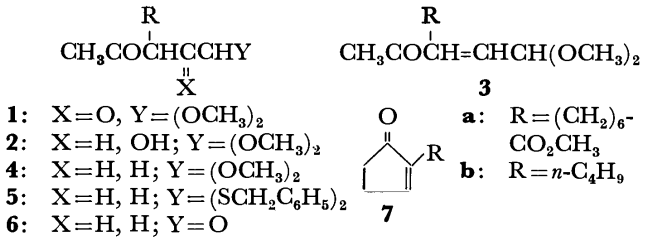

Scheme 1.

Experimental

NMR spectra were recorded on a Varian A-60 spectrometer using TMS as an internal standard in deuterio chloroform, IR spectra were taken on a Hitachi EPI-G3 in liquid films, and the results of NMR spectra and elemental analyses are shown in Table 1.

*Catalytic Hydrogenation of **1a** and **1b**.* A solution of **1a** (633 mg, 2.11 mmol) and PtO_2 (60 mg) in MeOH (35 ml) was hydrogenated under ordinary pressure. The solution was concentrated *in vacuo* to give an oily residue (622 mg), which was chromatographed (SiO_2, 10 g, hexane–benzene, 2:1) to afford the major alcohol **2a** (590 mg, 93% yield); IR: ν 3460, 1740, 1717 and 1700 cm^{-1}. Further elution with hexane–benzene–ether (1:2:0.4) gave the minor alcohol **epi-2a** (30 mg, 4.7% yield); IR: ν 3470, 1743 and 1710 cm^{-1}.

Similar hydrogenation of **1b** (2.16 g, 10 mmol) afforded the major alcohol **2b** (1.8 g, 83% yield); IR: ν 3450 and 1705 cm^{-1}, and the minor alcohol **epi-2b** (120 mg, 5.5% yield); IR: ν 3500 and 1714 cm^{-1}.

*Dehydration of **2a** and **2b**.* A solution of **2a** (20 g, 66 mmol), DCCI (16.3 g, 79 mmol) and copper(I) chloride (300 mg) in ether (230 ml) was heated under reflux for 20 h. The mixture was filtered and washed with ether. After the filtrate was evaporated *in vacuo*, the residue (25.2 g) was chromatographed (SiO_2, 250 g, benzene) to afford **3a**, (15.2 g, 81% yield), bp 140—150 °C/0.3 Torr (bath temp); IR: ν 1743, 1680, and 1650 cm^{-1}.

Similar procedure of **2b** (44.7 g, 0.204 mol) gave **3b** (35 g, 85.5% yield), bp 96—98 °C/2 Torr; IR: ν 1680 and 1655 cm^{-1}.

*Dehydration of **2a** via Its p-Toluenesulfonate.* The *p*-toluenesulfonate of **2a**, prepared from **2a** (2.1 g, 6.9 mmol) and *p*-toluenesulfonyl chloride (1.35 g, 7.1 mmol) in pyridine, were heated with potassium acetate (4.0 g) in DMF (20 ml) and H_2O (4 ml) at 100 to 110 °C for 2.5 h. The mixture was worked up as usual and the residue (1.7 g) was chromatographed (SiO_2, 17 g) to give **5a** (1.2 g, 60.1% yield).

*Catalytic Hydrogenation of **3a** and **3b**.* A solution of **3a** (7 g, 0.024 mol) in THF (70 ml) was hydrogenated over Pd-$CaCO_3$ (5 g) under ordinary pressure. After usual work-up, an oily residue (7.05 g) was distilled *in vacuo* to afford **4a** (5.7 g, 81% yield), bp 145—155 °C/0.3 Torr; IR: ν 1745 and 1720 cm^{-1}.

Analogous hydrogenation of **3b** (10 g, 0.05 mol) afforded **4b** (8.7 g, 87% yield), bp 100—110 °C/5 Torr (bath temp); IR: ν 1716 cm^{-1}.

*Benzylthioacetalization of **4a** and **4b**.* To a solution of **4a** (3.45 g, 12 mmol), benzyl mercaptan (3.47 g, 28 mmol) and Na_2SO_4 (4 g) in dioxane (15 ml) was added powdered anhyd. $ZnCl_2$ (8 g) at room temp. The mixture was stirred at 50 °C for 1 h, and poured into cold water. The aqueous solution was extracted with ether and the extracts were washed with H_2O and dried. After evaporation of the solvent *in vacuo*, the residue was chromatographed (SiO_2, 50 g, benzene–ether, 95 : 5) to afford **5a** (4.18 g, 74.1% yield); IR: ν 1743 and 1717 cm^{-1}.

Table 1. NMR spectra and elemental analyses[a)]

Compound	NMR ($CDCl_3$) in ppm	Obsd(%) C	Obsd(%) H	Calcd(%) C	Calcd(%) H
2a	(+D_2O): 2.19(3, s, $COCH_3$), 2.8(1, dt, J=3.1 and 7 Hz, COCH), 3.4 and 3.41(6, two s, OCH_3), 3.66(1, dd, J=4 and 3.1 Hz, CHOH), 4.21 (1, d, J=4 Hz, CHOMe)	59.37	8.97	59.19	9.27
epi-2a	(+D_2O): 2.22(3, s, $COCH_3$), 2.8(1, dt, J=7 and 3.5 Hz, COCH), 3.38 and 3.5(6, two s, OCH_3), 3.7(1, dd, J=3.5 and 4.2 Hz, CHOH), 4.25 (1, d, J=4.2 Hz, CHOMe)	59.01	9.45	59.19	9.27
2b	2.19(3, s, $COCH_3$), 2.8(1, dt, J=7 and 3 Hz, COCH), 3.7(1, dd, J=3 and 4 Hz, CHOH)	60.37	10.08	60.52	10.16
epi-2b	2.22(3, s, $COCH_3$), 2.8(1, dt, J=3.5 and 7 Hz, COCH), 3.71(1, dd, J=3.5 and 4 Hz, CHOH), 4.25(1, d, J=4 Hz, CHOMe)	60.74	9.87	60.52	10.16
3a	2.22(3, s, $COCH_3$), 3.38(6, s, OCH_3), 5.16(1, d, J=6.5 Hz, CHOMe), 6.43(1, d, J=6.5 Hz, =CH)	62.88	9.23	62.91	9.15
3b	2.31(3, s, $COCH_3$), 3.34(6, s, OCH_3), 6.35(1, d, J=6.5 Hz, =CH)	65.86	10.21	65.97	10.07
4a	2.15(3, s, $COCH_3$), 3.31(6, s, OCH_3), 4.32(1, t, J=5.5 Hz, CHOMe)	62.35	9.96	62.47	9.79
4b	2.13(3, s, $COCH_3$), 3.3(6, s, OCH_3), 4.29(1, t, J=5.5 Hz, CHOMe)	65.18	10.80	65.31	10.96
5a	1.94(3, s, $COCH_3$), 3.38(1, q, J=6 and 8 Hz, COCH), 3.73 and 3.78 (4, two s, SCH_2)	68.51	7.78	68.60	7.67
5b	1.94(3, s, $COCH_3$), 3.38(1, q, J=6 and 8 Hz, COCH), 3.73 and 3.78(4, two s, SCH_2)	71.41	7.58	71.45	7.82
6a	2.18(3, s, $COCH_3$), 9.66(1, t, J=1 Hz, CHO)	64.61	9.03	64.44	9.15
6b	2.18(3, s, $COCH_3$), 9.67(1, t, J=1 Hz, CHO)	68.95	10.21	69.19	10.32
7a	0.98—1.73(3, m), 1.9—2.7(8, m), 7.13(1, m, CH=)				
7b	0.93(3, t, CH_3), 1.37(4, m, CH_2CH_2), 2.2(4, m, CH_2CH=), 2.5(2, m, CH_2CO), 7.14(1, m, CH=)	78.38	10.13	78.21	10.21

a) The NMR spectra data of the substituent "R" in compounds 2 to 7 are not described.

Similar procedure of **4b** (300 mg, 1.5 mmol) gave **5b** (447 mg, 78% yield); IR:ν 1716 cm^{-1}.

Cyclization of ***5a*** *and* ***5b***. A solution of **5a** (4.72 g, 10 mmol), $HgCl_2$ (10 g) and $CdCO_3$ (5.4 g) in CH_3CN (50 ml) and H_2O (10 ml) was stirred under N_2 atmosphere at room temp. for 3 h. After removal of inorganic substances, the filtrate was washed with H_2O and dried. The solvent was evaporated *in vacuo* to give a crude aldehyde **6a** (2.2 g, 90% yield), which was practically usable; IR:ν 2730, 1745, 1725 and 1715 cm^{-1}. A solution of the crude **6a** (2.2 g) and anhyd. K_2CO_3 (7 g) in MeOH (100 ml) was stirred at room temp for 20 h. The mixture was neutralized with aq. AcOH and extracted with ether. The extracts were washed with H_2O and dried. After evaporation of the solvent *in vacuo*, the residue was chromatographed (SiO_2, 20 g, hexane-benzene, 2:1) to afford **7a**[2)] (720 mg, 36% yield); IR:ν 1745, 1706 and 1635 cm^{-1}.

Similar cyclization of **5b** (3.1 g, 8 mmol) gave **7b** (565 mg, 41% yield); IR:ν 1708 and 1637 cm^{-1}.

References

1) For recent reviews on the synthesis of 3-oxocyclopentenes and jasmoniods: see R. A. Ellison, *Synthesis*, **1973**, 397: T. L. Ho, *Synth. Commun.*, **4**, 265 (1974).

2) B. M. Trost and S. Kuroizumi, *Tetrahedron Lett.*, **1974**, 1929; K. Kondo and D. Tsunemoto, *Tetrahedron Lett.*, **1975**, 1397.

3) N. Finch, J. J. Fitt, and I. H. Hsu, *J. Org. Chem.*, **40**, 206 (1975).

4) J. Ide, K. Sakai, and Y. Yura, *Synth. Commun.*, **6**, 299 (1976).

5) In this reduction no regioisomeric alcohol **8** was found. Therefore, this hydrogenation interestingly occurred regio- and stereoselectively.

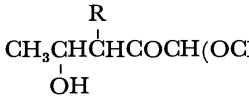

9

6) E. J. Corey, N. H. Andersen, R. M. Carlson, J. Paust, E. Vedejs, I. Vlattas and R. E. K. Winter, *J. Am. Chem. Soc.*, **90**, 3245 (1968).

7) Deacetalization of **4** to the aldehyde with various kinds of acids was unsuccessful. Treatment of **4** with concd. hydrochloric acid in acetone resulted in the furan derivatives **9** (**9a**: 52%, **9b**: 58% yield). Treatment of **4b** with 75% aqueous acetic acid containing catalytic amount of sulfuric acid gave the furan derivative **10b** (50.4% yield) along with a trace amount of the keto aldehyde **6**.

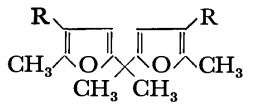

9

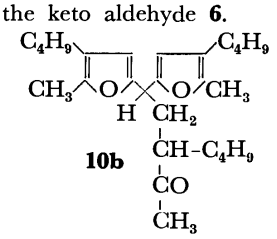

10b

BULLETIN OF THE CHEMICAL SOCIETY OF JAPAN, VOL. 51 (3), 941—942 (1978)

A-Substituted 5β-Steroids. IX. Preparation of 5β-Cholest-1-ene and 2-ene from 2β-Bromo-5β-cholestan-3-one[1]

Kanji ABE* and J. Yasuo SATOH

Department of Chemistry, Faculty of Science, Rikkyo University, Nishi-Ikebukuro, Toshima-ku, Tokyo 171

(Received June 7, 1977)

Synopsis. 5β-Cholest-1-ene has been prepared from 2β-bromo-5β-chloestan-3-one. An alternative route to 5β-cholest-2-ene has also been developed by use of bromoketone. These olefins are less stable, being oxidized gradually by air to 5β-cholest-1-en-3-one at room temperature.

In a previous paper[2] a report was given on the preparation of 5β-cholest-2-ene (**2**) by the treatment of 2β,3-bis(methylsulfonyloxy)-5β-cholestane, obtained from 2β-acetoxy-5β-chloestan-3-one *via* 5β-cholestane-2β,3-diols, with sodium iodide in boiling cyclohexanone. The process is tedious as compared with the one-step preparation from 3-substituted 5β-cholestanes[3] although undesirable contamination of 5β-cholest-3-ene can be reduced. 2β,4β-Dibromo-5β-cholestan-3-one, on treatment with chromium(II) acetate, is reduced to 2β-bromo-5β-cholestan-3-one (**3**), which is further converted into 5β-cholest-1-en-3-one (**4**) on reaction with calcium carbonate and *N*,*N*-dimethylformamide.[4] In this paper we describe the preparation of 5β-cholest-1-ene (**1**) and 2-ene (**2**) from **3**, and give some observations on the oxygenation of these olefins on exposure to air at room temperature.

The procedures for the preparation of **1** and **2** are summarized in the Scheme.

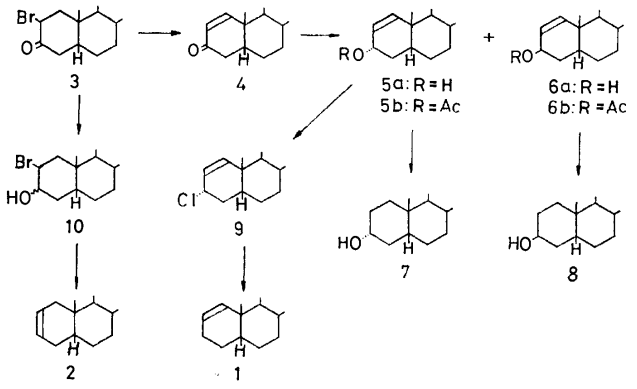

Scheme. Pathway to 5β-cholest-1-ene and 2-ene.

The reduction of **4** with lithium aluminium hydride readily gave a mixture of allyl alcohols. The major product, obtained by crystallization from acetone, was characterized as 5β-cholest-1-en-3α-ol (**5a**) on the basis of its transformation into 5β-cholestan-3α-ol (**7**) on hydrogenation in cyclohexane in the presence of palladium catalyst. Concentration of the mother liquor and crystallization several times from ether–methanol gave a small amount of the isomeric allyl alcohol, which was determined to be 5β-cholest-1-en-3β-ol (**6a**) by catalytic reduction to 5β-cholestan-3β-ol (**8**). Treatment of **5a** with thionyl chloride gave a chloro compound in 73% yield. The compound is regarded as 3α-chloro-5β-cholest-1-ene (**9**) by a comparison of its NMR spectrum with those of **5a** and **6a**: In the NMR spectrum of **9**, the signals at δ 4.50 showed double-doublet couplings, the constants (J=7.0, 10.0 Hz) of which were similar to those of the signals at δ 4.16 (J=5.0, 8.2 Hz) due to 3β-H in **5a**, but quite distinct from those of the multiplet signals at δ 3.98 ($W/2$= 8.5 Hz) due to 3α-H in **6a**. 5β-Cholest-1-ene (**1**) was obtained by the reduction of **9** with lithium aluminium hydride.

5β-Cholest-2-ene (**2**) was obtained from **3** by the method used for the preparation of 5α-cholest-2-ene.[5]

The olefins were relatively less stable at room temperature. **1** and **2** remained unchanged for a long time at room temperature. However, these olefins were gradually oxidized by air (see Table). 5β-Cholest-1-en-3-one (**4**) was mainly obtained from the samples of **1** and **2** which had been preserved for about a year at room temperature.[6] On the other hand, oxygenation scarcely took place in the samples of **1** and **2** preserved in a refrigerator kept below 5 °C. The results indicate that the oxygenation of the olefins is promoted by light and temperature. However, the mechanism of oxygenation has not been clarified because of complex factors participating in the reaction.

TABLE. OXYGENATION PRODUCTS OF THE OLEFINS AGED FOR A YEAR

Olefin	Temperature	Yield(%)	
		Recovered olefin	5β-Cholest-1-en-3-one
5β-Cholest-1-ene	r. t.[a]	15	80
	<5 °C	100	—
5β-Cholest-2-ene	r. t.[a]	20	79
	<5 °C	100	—

a) Room temperature.

Experimental

All melting points are uncorrected. IR spectra were determined with a Hitachi Model 215 grating instrument. NMR spectra were measured with a Hitachi Perkin-Elmer Model R-20A spectrometer in carbon tetrachloride with reference to tetramethylsilane as an internal standard.

Lithium Aluminium Hydride Reduction of 5β-Cholest-1-en-3-one (4). Lithium aluminium hydride (0.5 g) was added to a solution of **3**[4] (2.5 g) in dry ether (100 ml) at temperature below 0 °C. The mixture was allowed to warm to room temperature. The excess hydride was then decomposed with acetone and dil sulfuric acid. The organic layer was washed with aq sodium hydrogencarbonate and water, dried and

* Present address: Special Reference Laboratories, Inc., Nishiki, Nerima-ku, Tokyo 176.

evaporated. Crystallization from acetone gave 5β-cholest-1-en-3α-ol (**5a**, 1.6 g) as needles, melting at 122—124 °C. IR (KBr): 3300, 3020, 1650, 1065, 1047, 760, and 738 cm^{-1}; NMR δ: 0.65 (3H, s, 18-CH_3), 1.00 (3H, s, 19-CH_3), 4.16 (1H, dd, J=5.0, 8.2 Hz, 3β-H), and 5.50 (2H, s, $W/2$=3.0 Hz). Found: C, 83.80; H, 12.05%. Calcd for $C_{27}H_{46}O$: C, 83.87; H, 11.99%.

Acetylation of **5a** with pyridine–acetic anhydride gave 3α-acetate (**5b**), melting at 113—115 °C. IR (KBr): 1735, 1240, 1025, 770, and 735 cm^{-1}; NMR δ: 0.66 (3H, s, 18-CH_3), 1.02 (3H, s, 19-CH_3), 1.98 (3H, s, 3α-OAc), 5.28 (1H, t, J=9.0 Hz, 3β-H), 5.39 (1H, d, J=9.5 Hz, 2-H), and 5.67 (1H, d, J=9.5 Hz, 1-H). Found: C, 80.66; H, 10.94%. Calcd for $C_{29}H_{48}O_2$: C, 81.25; H, 11.29%.

5β-Cholest-1-en-3β-ol (**6a**, 60 mg) was obtained as plates from the mother liquor by repeated crystallization from ether–methanol. Mp 114—118 °C; IR (KBr): 3020, 1650, 1040, 1010, and 780 cm^{-1}; NMR δ: 0.65 (3H, s, 18-CH_3), 1.03 (3H, s, 19-CH_3), 3.98 (1H, m, $W/2$=8.5 Hz, 3α-H), and 5.63 (2H, s with shoulder). Found: C, 84.56; H, 12.65%. Calcd for $C_{27}H_{46}O$: C, 83.87; H, 11.99%.

Acetylation of **6a** with pyridine-acetic anhydride gave 3β-acetate (**6b**), melting at 67—69 °C. IR (KBr): 3020, 1720, 1250, 1020, 850, and 770 cm^{-1}; NMR δ: 0.67 (3H, s, 18-CH_3), 1.09 (3H, s, 19-CH_3), 1.98 (3H, s, 3β-OAc), and 4.92—5.92 (3H, complex signals). Found: C, 81.24; H, 10.65%. Calcd for $C_{29}H_{48}O_2$: C, 81.25; H, 11.29%.

*Hydrogenation of 5β-Cholest-1-en-3α-ol (**5a**) and 3β-ol (**6a**).* A mixture of **5a** (100 mg), 5% palladium–charcoal (50 mg), and cyclohexane (20 ml) was stirred vigorously under hydrogen atmosphere at room temperature for 1 h. The solution was filtered and evaporated under reduced pressure. Crystallization of the residue from ether–methanol gave 5β-cholestan-3α-ol (**7**, 45 mg) as fine needles, melting at 108—111 °C (lit,[7] mp 107—109 °C).

Similar hydrogenation of **6a** (10 mg) gave 5β-cholestan-3β-ol **8**, 6 mg) as needles, melting at 100—102 °C (lit,[7] mp 96—98 °C).

*3α-Chloro-5β-cholest-1-ene (**9**).* Thionyl chloride (1.0 ml) was added to a solution of **5a** (313 mg) in benzene (10 ml), and the mixture was stirred at room temperature for 3 h, poured into water containing ice, and extracted with ether. The organic layer was washed with aq sodium hydrogencarbonate and saline, dried and evaporated. Crystallization of the oil from acetone afforded **9** (240 mg) as fine needles. Mp 74—76 °C; IR (KBr): 3020, 1640, 775, and 665 cm^{-1}; NMR δ: 0.65 (3H, s, 18-CH_3), 1.02 (3H, s, 19-CH_3), 4.50 (1H, dd, J=7.0, 10.0 Hz, 3β-H), and 5.50 (2H, s, $W/2$=4.5 Hz). Found: C, 80.12; H, 11.18%. Calcd for $C_{27}H_{45}Cl$: C, 80.05; H, 11.20%.

*5β-Cholest-1-ene (**1**).* Lithium aluminium hydride (3.0 g) was added to a solution of **9** (5.5 g) in dry ether (500 ml), and the mixture was refluxed for 22 h. After the excess hydride had been decomposed with dil sulfuric acid, the ethereal layer was washed with aq sodium hydrogencarbonate and water, dried and evaporated. Crystallization of the oil from acetone gave **1** (3.7 g) as needles, melting at 48—51 °C. IR (KBr): 3020, 1650, 718, and 706 cm^{-1}; NMR δ: 0.65 (3H, s, 18-CH_3), 0.99 (3H, s, 19-CH_3), and 5.47 (2H, s, $W/2$=2.0 Hz). Found: C, 87.15; H, 12.85%. Calcd for $C_{27}H_{46}$: C, 87.49; H, 12.51%.

*Sodium Borohydride Reduction of 2β-Bromo-5β-cholestan-3-one (**3**).* Sodium borohydride (0.36 g) was added with stirring to a suspension of **3** (4.0 g) in absolute ethanol (160 ml). The mixture was stirred for 60 min and then concentrated under reduced pressure. The residue was dissolved in ether, and the solution was washed with water repeatedly and dried over anhydrous sodium sulfate. Evaporation of the solvent under reduced pressure gave 2β-bromo-5β-cholestan-3ξ-ol (**10**, 4.0 g) as a colorless oil, which resisted crystallization from various solvents. IR (NaCl): 3420 cm^{-1}.

*5β-Cholest-2-ene (**2**).* Zinc dust (36.0 g) was added to a solution of the bromohydrin mixture (**10**, 3.7 g) in acetic acid (40 ml), and the mixture was refluxed for 90 min. After the zinc dust had been filtered off, the filtrate was diluted with water and extracted with ether. The organic layer was neutralized with aq sodium hydrogencarbonate, washed with saline, dried and evaporated. The product (3.2 g) was chromatographed over silica gel, and the fractions eluted with hexane were collected and crystallized from acetone, giving **2** as needles (1.3 g), melting at 46—48 °C (lit,[2] mp 47—48 °C). IR (KBr): 3020, 1655, and 660 cm^{-1}; NMR δ: 0.64 (3H, s, 18-CH_3), 0.95 (3H, s, 19-CH_3), and 5.49 (2H, s, $W/2$=4.5 Hz.)

*Gas Chromatography of the Oxygenation Products of 5β-Cholest-1-ene (**1**) and 2-ene (**2**).* A Hitachi Model 063 instrument was used for gas chromatography. Oxygenation products were analyzed with use of a 2 m×5 mm column packed with 5% OV-17 on Chromosorb W (80—100 mesh) operating at 250 °C. Olefins (**1**) and (**2**) in glass tubes equipped with a screw cap were preserved for *ca.* a year at room temperature and at temperature below 5 °C.

In both samples of **1** and **2** aged at room temperature, most of the olefins were converted into **4**. On the other hand, no oxygenated product was present in **1** or **2** aged at temperature below 5 °C.

References

1) K. Abe, Thesis, Rikkyo University (1976).

2) T. Takahashi, Y. Satoh, H. Toda, and A. Hagitani, *Nippon Kagaku Zasshi*, **90**, 1267 (1969).

3) D. D. Evans and C. W. Shoppee, *J. Chem. Soc.*, **1953**, 540; R. J. Bridgewater and C. W. Shoppee, *ibid.*, **1953**, 1709; G. Bellucci, F. Macchia, and V. Malaguzzi, *Tetrahedron Lett.*, **1966**, 4973.

4) J. Y. Satoh, K. Misawa, T. T. Takahashi, M. Hirose, C. A. Horiuchi, S. Tsuji, and A. Hagitani, *Bull. Chem. Soc. Jpn.*, **46**, 3155 (1973).

5) L. F. Fieser and X. A. Dominguez, *J. Am. Chem. Soc.*, **75**, 1704 (1953).

6) Similar oxygenation was observed in 5β-cholest-3-ene, which was completely oxidized to cholest-4-en-3-one in six months on exposure to air at room temperature.

7) W. G. Dauben, R. A. Michell, and J. F. Eastham, *J. Am. Chem. Soc.*, **74**, 3852 (1952).

BULLETIN OF THE CHEMICAL SOCIETY OF JAPAN, VOL. 51 (3), 943—944 (1978)

A Quinone and a Phenol from a Myrsinaceae Plant

Takenori KUSUMI, Hiroshi KAKISAWA,* Yuh-Pan CHEN,* Jing-Ing LYN,* and Hong-Yen HSU*

Department of Chemistry, University of Tsukuba, Sakura-mura, Niihari-gun, Ibaraki 300-31

**Brion Research Institute of Taiwan, 116, Chung-Ching South Rd., Sec. 3, Taipei, Taiwan*

(Received June 18, 1977)

Synopsis. Ardisianone and ardisianol isolated from *Ardisia quinquegona* Blume were determined to be 2-(2-acetoxypentadecyl)-6-methoxy-1,4-benzoquinone and 4-acetoxy-2-(2-acetoxypentadecyl)-6-methoxyphenol, respectively.

In the course of our studies on constituents of Chinese herbal drugs, a yellow pigment and a phenol, designated as ardisianone and ardisianol, respectively, were found from *Ardisia quinquegona* Blume. The plants of Myrsinaceae species are known to contain many benzoquinoid pigments.[1-4] All of these quinones have been proved to possess 2-alkyl-3,6-dihydroxy(or methoxy)-1,4-benzoquinone chromophores. In contrast to these pigments, the present new pigment has been found to have 2-alkyl-6-methoxy-1,4-benzoquinone group.

The UV absorption maxima (268 and 363 nm) of ardisianone, $C_{24}H_{38}O_5$, appeared in shorter wave length than those of 2-hydroxy-5-methoxy-,[1] 2-hydroxy-6-methoxy-,[5] and 5-alkyl-3-hydroxy-2-methoxy-1,4-benzoquinones,[5] and coincided with those of 3-,[5] 5-,[5] and 6-methoxy-2-alkyl-1,4-benzoquinones.[5] The presence of the methoxybenzoquinone group was supported by the appearance of characteristic fragments[6] **a** and **b** in the mass spectrum. The PMR spectrum

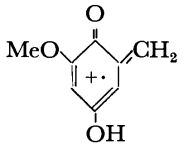

a

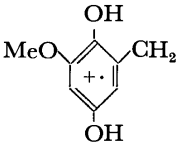

b

showed a pair of doublets at δ 5.84 (J=2 Hz) and 6.83 (J=2 Hz) assignable to 5- and 3-protons of 2-alkyl-6-methoxy-1,4-benzoquinone from the coupling constant. The latter doublet was broadened by coupling with methylene protons (δ 2.63) at 2-position. The PMR spectrum showed the signals of methoxyl (δ 3.80) and acetoxyl (δ 1.98) groups, in addition to a broad singlet (24 H) at δ 1.28 and a deformed triplet (3 H) at δ 0.88, which could be assigned to methylene and methyl protons of tridecyl group, respectively. Decoupling experiments revealed that two nonequivalent protons observed at δ 2.63 is coupled to a proton at δ 4.95 with J=8 and 4 Hz, and also to a quinoid proton at δ 6.83 with J= 0.5 Hz, showing the presence of Ar–CH_2–CH(OAc)– moiety. Irradiation at δ 2.63 changed the multiplet at δ 4.95 into a broad triplet and the broad doublet at δ 6.83 into a sharp doublet. From these facts the structure of ardisianone was assigned to **1**.

Ardisianol, $C_{26}H_{42}O_6$, showed UV maxima at 230 and 283 nm, which shifted to 258 and 298 nm by addition of aqueous potassium hydroxide. Its IR spectrum exhibited the absorption bands at 3400 (OH) and 1770 cm^{-1} (phenyl acetate). These spectral properties indicated that ardisianol is a phenol possessing an acetoxyl group on the aromatic ring. The intense absorptions at 2925 and 1720 cm^{-1} suggested the presence of an alkyl chain bearing another acetoxyl group. The PMR spectrum of ardisianol partly resembled that of **1**, and the presence of methoxyl and 2-acetoxypentadecyl groups was easily deduced from the signals at δ 3.81 (3H, s), 1.90 (3H, s), 2.80 (2H, ABX), 5.05 (1H, m), 1.26 (24H, bs), and 0.90 (3H, t). A sharp singlet (3H) at δ 2.20 was assignable to an acetoxyl group of phenyl acetate. The aromatic protons of ardisianol appeared as a broad singlet at δ 6.41 (2H). These facts indicated that ardisianol was tetrasubstituted (OMe, OH, OAc, and 2-acetoxypentadecyl)benzene, but the positions of these substituents were not clarified from the spectral data.

Hydrogenation of **1** over platinum catalyst in acetic anhydride followed by addition of sodium acetate afforded a colorless monoacetyl product without formation of the diacetate. The monoacetylated product was found to be identical with ardisianol. The monoacetate was further converted into the diacetate (**3**) under rather forced reaction conditions. The monoacetyl group was first incorporated at C_4–OH group by steric effect, and hence the structure of ardisianol was represented by 4-acetyldihydroardisianone (**2**). The PMR spectrum of the diacetate (**3**) showed an AB quartet centered at δ 6.54 due to aromatic protons. The coupling constant (J=2 Hz) is well consistent with the 2,6-disubstituted hydroquinone of the structure (**3**).

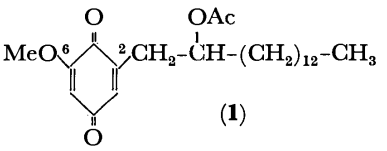

(**1**)

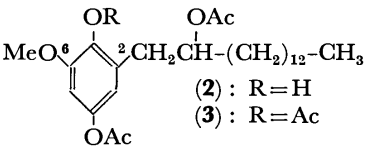

(**2**): R=H
(**3**): R=Ac

Experimental

The melting points are uncorrected. PMR spectra were recorded on a Hitachi H-60 instrument, TMS being used as an internal standard (δ, ppm). IR spectra were taken on a Hitachi EPS-3T spectrometer. Mass spectra were obtained with a Hitachi RMU-6M spectrometer.

*Isolation of Ardisianol (**2**).* The dried and pulverized stems and leaves (720 g) of *Ardisia quinquegona* Blume (Myrsinaceae) were extracted with hot hexane three times. The

combined hexane extracts were concentrated under vacuum, and the dark brown solid residue (20 g) was chromatographed on a column of silica gel (Merck, Kieselgel 60, Art, 7734, 1 Kg). Elution of the column with hexane-ethyl acetate (8 : 1) yielded a white solid, which on crystallization from hexane gave ardisianol (260 mg) as colorless needles; mp 82—84 °C. Found: C, 68.44; H, 9.39%. Calcd for $C_{26}H_{42}O_6 \cdot 1/3H_2O$: C, 68.38; H, 9.42%. UV (EtOH): 230sh (logε, 3.74) and 283 nm (3.52). IR (KBr): 3400, 2925, 2850, 1770, 1720, 1630, 1600, 1500, 1470, 1440, 1380, 1265, and 1230 cm^{-1}. MS *m/e* (rel intensity): 450 (M^+, 0.5), 422 (4), 408 (0.5), 390 (3), 380 (4), 362 (13), 348 (19), 320 (100), 154 (19), and 153 (18).

*Isolation of Ardisianone (**1**).* Further elution with hexane-ethyl acetate (8 : 1) furnished a yellow solid, which on crystallization from ethanol yielded ardisianone (350 mg) as yellow needles; mp 49—54 °C. Found: C, 70.82; H, 9.69%. Calcd for $C_{24}H_{38}O_5$: C, 70.90; H, 9.42%. UV (EtOH); 268 (logε, 4.12) and 363 nm (3.01). IR (KBr): 2925, 2850, 1730, 1690, 1655, 1625, 1605, 1470, 1380, 1330, 1240, and 1050 cm^{-1}. MS *m/e* (rel intensity): 408 (0.5), 407 (0.5), 406 (M^+, 0.5), 364 (7), 346 (27), 194 (21), 153 (20), and 152 (18).

Ardisianol from Ardisianone. A mixture of ardisianone (1; 17 mg) and platinum oxide (7 mg) in acetic anhydride (0.2 ml) was stirred under hydrogen atmosphere at room temperature. After 5 min, yellow color of the mixture disappeared. Sodium acetate (20 mg) was then added, and the mixture was stirred under hydrogen overnight. The product was taken up into ether. The ethereal solution was washed with water and brine, and dried over sodium sulfate. Evaporation of the ether yielded pale yellow crystals (17 mg). Recrystallization from hexane gave rise to white crystalline powder (mp 84—86 °C), the IR spectrum (KBr) of which was superimposable over that of ardisianol.

*1,4-Diacetoxy-3-methoxy-5-(2-acetoxypentadecyl)benzene (**3**).* A solution of ardisianol (14 mg) in pyridine (0.1 ml) and acetic anhydride (0.1 ml) was warmed at 45 °C in a sealed tube overnight. The reaction mixture was poured into water, and extracted with ether. After being washed with water, the ethereal layer was evaporated, affording colorless crystals. Recrystallization from hexane yielded ardisianol acetate (**3**); mp 60.5—62 °C. Found: C, 67.63; H, 8.94%. Calcd for $C_{22}H_{44}O_5 \cdot 1/3H_2O$: C, 67.46; H, 9.03. IR(KBr): 1750 and 1730 cm^{-1}. PMR (δ, CCl_4): 0.91 (3H, t), 1.28 (24H, bs), 1.98 (3H, s), 2.24 (3H, s), 2.30 (3H, s), 2.70 (2H, ABX, $J_{AB}=13$, $J_{AX}=6$, $J_{BX}=7$ Hz), 3.79 (3H, s), 4.75 (1H, m), and 6.55 (2H, AB, $J_{AB}=2$ Hz).

References

1) H. Ogawa and S. Natori, *Phytochemistry*, **7**, 773 (1968).
2) C. B. Rao and V. Venkateswarlu, *J. Org. Chem.*, **26**, 4529 (1942).
3) M. Hiramoto, *Yakugaku Zasshi*, **59**, 671 (1937), **62**, 460, 464 (1942).
4) H. Ogawa, S. Sakaki, K. Yoshihira, and S. Natori, *Tetrahedron Lett.*, **1968**, 1387.
5) R. H. Thomson, "Naturally Occuring Quinones," Academic Press, New York (1971), Chap. 3.
6) H. Ogawa and S. Natori, *Chem. Pharm. Bull.*, **16**, 1709 (1968).

BULLETIN OF THE CHEMICAL SOCIETY OF JAPAN, VOL. 51 (3), 945—946 (1978)

Uptake of Ammine-Cobalt(III) Complexes into *Escherichia Coli* Cells

Kiyoshi TANABE, Kitao FUJIWARA, and Keiichiro FUWA

Department of Chemistry, Faculty of Science, The University of Tokyo, Bunkyo-ku, Tokyo 113

(Received July 27, 1977)

Synopsis. The uptake of Co into *E. coli* cells was studied in various Co(III) ammine complexes. It was found to be independent of the incubating temperature and existence of Mg^{2+} ion, but dependent on the ligands, the uptake of Co being in the following order. $[Co(NH_3)_4(OH_2)_2]_2(SO_4)_3 > [Co(NH_3)_5(OH_2)]Cl_3 > [Co(NH_3)_6]Cl_3 \gg [Co(en)_3]Cl_3 > [Co(OH_2)_6]Cl_2$

Wide attention has been given to the activities or properties of various inorganic complexes of transition metals in biological fields. For example, it was found that *cis*-dichlorodiamineplatinum(II) suppresses the division of *E. coli* cells by inhibiting DNA synthesis.[1,2] Chromium, palladium, and rhodium complexes also have a similar function.[3,4] Several reports suggest that these complexes might become useful anti-cancer drugs by controlling the propagation of cancer cells in consequence of interaction between DNA molecule and the complexes.[5]

The effect of several cobalt(III) complexes which induce filamentous growth or inhibit the respiration of *E. coli* has also been reported.[6] On the assumption of quantitative estimation for the biological function of these complexes, the locomotion and distribution of the complexes in the bioorganism have not been fully elucidated. The uptake of several cobalt(III) complexes into the *E. coli* cells is given in this report.

Experimental

Escherichia coli B (ATCC 11246) was used as the test organism, which was grown in minimum nutrient media: K_2HPO_4(40 mM), KH_2PO_4(22 mM), $(NH_4)_2SO_4$ (7.6 mM), disodium citrate (2.1 mM), $MgSO_4$(0.8 mM), and glucose (27.8 mM) were dissolved in distilled water. Cobalt(III) complexes $[Co(NH_3)_6]Cl_3$, $[Co(en)_3]Cl_3$, $[Co(NH_3)_5(OH_2)]Cl_3$, and $[Co(NH_3)_4(OH_2)_2]_2(SO_4)_3$ were prepared by the usual methods.

E. coli was preincubated twice and incubated in 200 ml media at 30 °C with shaking. When turbidity of media become O.D. 0.7, the cobalt(III) complexes were added to make cobalt concentration 30 ppm. *E. coli* cells incubated with complexes for 1 h were harvested by centrifugation (5000×g 8 min), washed twice with 0.9% sodium chloride solution, dried at 105 °C until weights of harvest became constant within 0.3 mg, and ashed at 600 °C in an electric furnace. After the ashed cells had been dissolved in hydrochloric acid, the amount of cobalt was determined by atomic absorption analysis using a Hitachi 207 atomic absorption spectrophotometer.

Results and Discussion

Many mechanisms concerning the uptake of metal ions have been reported. For example, the uptake of the cobalt(II) into *E. coli* is an active transport linked with the energy metabolism,[7,8] and is suppressed in the presence of Mg^{2+} as shown in Table 1.

The uptake of cobalt(III) complexes is independent of the presence of Mg^{2+}. The amount of complexes taken up into the cell is found to be almost unchanged with incubation temperature. The results indicate that the uptake of these complexes depends on the physical adsorption on the cell surface, but not on the biological activity. This can be supported by the fact that it is difficult for hydrophilic ions to pass the biological membrane without active transport system.

Ease of uptake of the cobalt(III) complexes is in the following order: $[Co(NH_3)_4(OH_2)_2]_2(SO_4)_3 > [Co(NH_3)_5(OH_2)]Cl_3 > [Co(NH_3)_6]Cl_3 \gg [Co(en)_3]Cl_3 > [Co(OH_2)_6]Cl_2$. The amounts of taken-up complexes seem to be dominated by the number of aqua ligands. From the fact that $[Co(NH_3)_6]Cl_3$ is taken up about three times more than $[Co(en)_3]Cl_3$, the hydrophilicity of ligands seems also important in the uptake of complexes. The results indicate that the formation of hydrogen bond with cell surface *via* the hydrogen atom of ligands of the complex plays an important role in the uptake of the cobalt(III) complexes.

The authors are indebted to Dr. Shozo Toda for his useful suggestions.

References

1) J. P. Macquet and T. Theophanides, *Inorg. Chim. Acta*, **18**, 189 (1976).

2) J. J. Roberts and J. M. Pascoe, *Nature*, **235**, 282 (1972).

TABLE 1. UPTAKE OF COBALT(III) COMPLEXES (μg Co/100 mg dried weight)

Temperature	3 °C	11 °C	20 °C	25 °C	30 °C	30 °C ($-Mg^{2+}$)
$[Co(NH_3)_6]Cl_3$	65.0	74.9	70.4	72.7	75.0	62.8
$[Co(NH_3)_5(OH_2)]Cl_3$	67.0	95.5	78.5	85.3	—	75.0
$[Co(NH_3)_4(OH_2)_2]_2(SO_4)_3$	111.0	154.6	121.0	77.5	—	109.4
$[Co(en)_3]Cl_3$	19.9	30.2	30.7	24.2	22.4	27.6
$[Co^{II}(OH_2)_6]Cl_2$	7.7	18.7	11.8	16.2	8.9	49.2

The content of cobalt in the whole cells of *E. coli* which were incubated with the ammine complexes at various temperatures between 3 and 30 °C.

3) A. Theodotou, R. J. Stretton, A. H. Norburg, and A. G. Massey, *Bioinorg. Chem.*, **5**, 253 (1976).
4) M. J. Cleare and J. D. Hoeschele, *Bioinorg. Chem.*, **2**, 187 (1973).
5) B. Rosenberg, L. Van Champ, J. E. Trosko, and V. H. Mansour, *Nature*, **222**, 385 (1960).
6) B. J. Crawford, D. E. Talburt, and D. A. Johnson, *Bioinorg. Chem.*, **3**. 121 (1974).
7) D. L. Nelson and E. P. Kennedy, *J. Biol. Chem.*, **246**, 3042 (1971).
8) K. Fujiwara, M. Iwamoto, S. Toda, and K. Fuwa, *Agric. Biol. Chem.*, **41**, 313 (1977).

BULLETIN OF THE CHEMICAL SOCIETY OF JAPAN, VOL. 51 (3), 947—948 (1978)

An ESR Study of *N*-Sulfonylaminyls[1]

Yozo MIURA, Yuji NAKAMURA, and Masayoshi KINOSHITA

Department of Applied Chemistry, Faculty of Engineering, Osaka City University, Sumiyoshi-ku, Osaka 558

(Received September 9, 1977)

Synopsis. *N*-(3,5-Di-*t*-butylphenyl)-*N*-sulfonylaminyls, 3,5-*t*-$Bu_2C_6H_3$-$\dot{N}$-SO_2-R, were investigated by means of ESR spectroscopy. The a_N values are 7.8 G, and the a_H values due to the *N*-phenyl ring protons are 5.6 (*o*-H) and 7.6 G (*p*-H). However, no couplings due to the protons in R have been detected. From these results, it is concluded that the unpaired electron is located on the nitrogen atom and the *N*-phenyl ring, negligibly delocalized onto the sulfonyl group.

N-Sulfonylaminyls have been of considerable interest as intermediates in chemical and photochemical reactions.[2] However, the radicals have little been investigated by means of ESR spectroscopy.[3] Recently, we have examined some nitrogen-centered free radicals in which one or two divalent sulfur atoms are adjacent to the central nitrogen.[1] Sulfonylaminyls are also of interest in comparison with the nitrogen-centered free radicals from the point of view of ESR spectroscopy. In this paper we will report an ESR study of *N*-(3,5-di-*t*-butylphenyl)-*N*-sulfonylaminyls (**2**).

The radicals **2** were generated in benzene by hydrogen-abstraction from sulfonamides, **1**, by *t*-butoxyl which

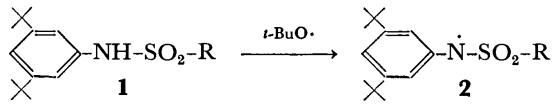

was obtained on the pyrolysis of di-*t*-butyl diperoxyoxalate.[4] The ESR parameters for **2** are listed in Table 1, and a typical ESR spectrum is illustrated in Fig. 1. As can be seen from the figure, well-resolved spectra were recorded in any case by this procedure. However, some peaks in the signals were gradually broadened with the passage of time (*ca.* 1 h). This may be caused by the occurrence of a secondary radical which could not be identified.

The ESR parameters for **2** are quite different from those reported for sulfonyl nitroxides, $RN(O\cdot)SO_2R'$, ruling out the possibility that **2** are nitroxides.[5]

The a_H values of **2** are considerably large and are constant within the limits of experimental error, regardless of the sulfonyl groups. On the other hand, no couplings due to the sulfonyl protons have ever been detected. From these results, it is obvious that the unpaired electron is located on the nitrogen and the *N*-phenylring, negligibly delocalized onto the sulfonyl group. The *g*-values for **2** are 2.0033, which is approximately equal to that for a typical nitrogen-centered free radical, diphenylaminyls (2.0032)[6] or 3,4-dihydro-2,4,6-triphenyl-2*H*-1,2,4,5-tetrazin-1-yl (2.0033).[7] In contrast, the *g*-value (2.0059) of the *N*-(arylthio)aminyl, **3**, is considerably larger than those of **2**.[8]

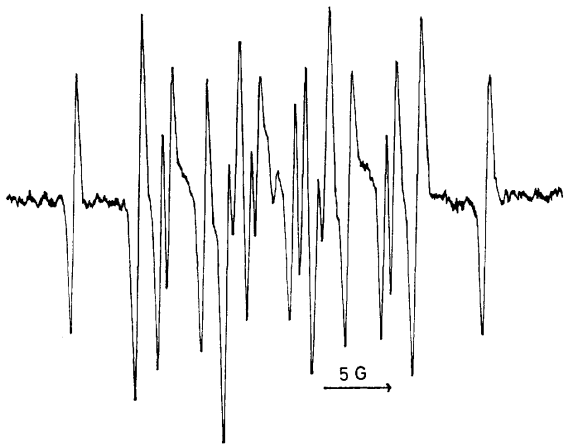

Fig. 1. An ESR spectrum of **2a** in benzene at room temperature.

The results obtained for **2** are consistent with those for the sulfonyl-conjugated radicals, $\cdot CR_1R_2SO_2R_3$,[9] in which the unpaired electron is not delocalized onto the sulfonyl group. In the case of **3**,[8] on the other hand, the unpaired electron is delocalized to some extent onto the *S*-phenyl ring.

On the basis of the results and discussion, it is concluded that sulfonyl groups have not ability to delocalize the unpaired electron in *N*-sulfonylaminyls, much as in the case of the sulfonyl-conjugated carbon radicals.[9]

Experimental

All the melting points are uncorrected. The IR spectra were run on a JASCO IR-G Spectrometer, while the NMR

TABLE 1. THE ESR PARAMETERS FOR *N*-(3,5-DI-*t*-BUTYLPHENYL)-*N*-SULFONYLAMINYLS (**2**)[a]

	Radical[b]	a_N[c]	$a_{o\text{-}H}$[c,d]	$a_{p\text{-}H}$[c,d]	*g*-Value
2a	R-$\dot{N}$-SO_2-C_6H_5	7.75	5.63	7.56	2.0033
2b	R-$\dot{N}$-SO_2-$C_6H_4CH_3$-*p*	7.79	5.64	7.62	2.0033
2c	R-$\dot{N}$-SO_2-CH_3	7.79	5.59	7.57	2.0033
3[e]	R-$\dot{N}$-S-C_6H_4Cl-*p*	9.58	3.70	4.42	2.0059

a) In benzene at room temperature. b) R: 3,5-Di-*t*-butylphenyl. c) In gauss. d) Due to the *N*-phenyl ring protons. e) The a_H value due to the *S*-phenyl ortho-protons: 0.75 G; see Ref. 8.

spectra were recorded with a Hitachi-Perkin Elmer R-20 Spectrometer, using TMS as the internal standard. 3,5-Di-*t*-butylaniline[10] and di-*t*-butyl diperoxyoxalate[4] were prepared by the reported methods.

Preparation of Sulfonamides. A solution of sulfonyl chloride (0.010 mol), 3,5-di-*t*-butylaniline (0.0097 mol), and triethylamine (0.011 mol) in dry ether (200 ml) was stirred for two days at room temperature. After the reaction mixture was filtered, ether was removed by evaporation and the resulting residue was subjected to column-chromatography [Mallinckrodt, silica gel (100 mesh), eluent: benzene/hexane: 15/1], followed by recrystallization from appropriate solvents.

N-*(3,5-Di-*t*-butylphenyl)benzenesulfonamide (**Ia**).* Colorless prisms with a mp of 144—145 °C (from benzene/hexane: 1/5, then hexane). Yield: 80%. IR (KBr): 3200 (NH) and 1170 cm^{-1} (SO_2). NMR ($CDCl_3$): δ 1.20 (s, *t*-Bu, 18H) and 6.82—7.85(m, C_6H_3 and C_6H_5, 8H). Found: C, 69.94; H, 7.51; N, 3.98%. Calcd for $C_{20}H_{27}NO_2S$: C, 69.52; H, 7.88; N, 4.05%.

N-*(3,5-Di-*t*-butylphenyl)-*p*-toluenesulfonamide (**Ib**).* Colorless prisms with a mp of 173—175 °C (from benzene/hexane: 1/10, then hexane). Yield: 82%. IR (KBr): 3200 (NH) and 1150 cm^{-1} (SO_2). NMR ($CDCl_3$): δ 1.20 (s, *t*-Bu, 18H), 2.35 (s, CH_3, 3H), and 6.85—7.76 (m, C_6H_3 and C_6H_4, 7H). Found: C, 70.22; H, 8.20; N, 3.90%. Calcd for $C_{21}H_{29}NO_2S$: C, 70.15; H, 8.13; N, 3.90%.

N-*(3,5-Di-*t*-butylphenyl)methanesulfonamide (**Ic**).* Colorless needles with a mp of 134—136 °C (from hexane). Yield 56%. IR (KBr): 3300 and 3200 (NH) and 1160 and 1140 cm^{-1} (SO_2). NMR ($CDCl_3$): δ 1.30 (s, *t*-Bu, 18H), 2.98 (s, CH_3, 3H), 6.95 (bs, NH, 1H), and 7.05—7.27 (m, C_6H_3, 3H). Found: C, 63.87; H, 8.67; N, 5.00%. Calcd for $C_{15}H_{25}NO_2S$: C, 63.56; H, 8.89; N, 4.94%.

ESR Spectra. Sulfonamide (20 mg), di-*t*-butyl peroxyoxalate (30 mg), and benzene (0.4 ml) were placed in an ESR tube, after which the solution was degassed by three freeze-and-thaw cycles, then sealed. The ESR signals were recorded at room temperature (*ca.* 21 °C) on a JES-ME-3X Spectrometer with an X-band microwave unit and 100 KHz field modulation.

References

1) Part VI of this series "ESR Studies of Nitrogen-centered Free Radicals," for Part V, see Y. Miura, H. Asada, and M. Kinoshita, *Bull. Chem. Soc. Jpn.*, **50**, 1855 (1977).

2) For a review, see R. S. Neale, *Synthesis*, **1971**, 1.

3) R. Istratoiu, I. Pascaru, and A. T. Balaban, *Z. Naturforsch., Teil B*, **28**, 543 (1973).

4) P. D. Bartlett, E. P. Benzing, and R. E. Pincock, *J. Am. Chem. Soc.*, **82**, 1762 (1960).

5) *E.g.*, the values reported for $PhSO_2N(O\cdot)Ph$ are 11.5 (a_N), 1.68 ($a_{o\text{-}H}$ and $a_{p\text{-}H}$), and 0.74 G ($a_{m\text{-}H}$); N. Negoita, R. Baican, F. Domsa, and A. T. Balaban, *Rev. Roum. Chim.*, **18**, 995 (1973).

6) F. A. Neugebauer and S. Bamberger, *Chem. Ber.*, **107**, 2362 (1974).

7) R. Kuhn and H. Trischmann, *Monatsh. Chem.*, **95**, 457 (1964).

8) Y. Miura, Y. Katsura, and M. Kinoshita, *Chem. Lett.*, **1977**, 409.

9) P. M. Carton, B. C. Gilbert, H. A. H. Laue, R. O. C. Norman, and R. C. Sealy, *J. Chem. Soc., Perkin Trans. 2*, **1975**, 1245.

10) N. L. Allinger, H. M. Blatter, L. A. Freiberg, F. M. Karkowiki, *J. Am. Chem. Soc.*, **88**, 2999 (1966).

BULLETIN OF THE CHEMICAL SOCIETY OF JAPAN, VOL. 51 (3), 949—950 (1978)

Alicyclic Terpenoids from Cyclocitryl Phenyl Sulfides. VI.[1] Syntheses of β-Ionone Derivatives

Sigeru TORII,* Kenji UNEYAMA, and Ichiro KAWAHARA
Department of Industrial Chemistry, School of Engineering, Okayama University, Okayama 700

(Received September 11, 1977)

Synopsis. 4-(2,6,6-Trimethyl-3-oxo-1-cyclohexenyl)-3-buten-2-one and 4-(2,6,6-trimethyl-1,3-cyclohexadienyl)-3-buten-2-one were efficiently synthesized by alkylation of 2,4,4-trimethyl-3-(phenylsulfonylmethyl)-2-cyclohexen-1-ol and 1-(phenylsulfonylmethyl)-2,6,6-trimethyl-1,3-cyclohexadiene with propylene oxide followed by oxidation and elimination of sulfonyl group, respectively.

In connection with studies on the synthesis of terpenoids, we demonstrated a simple preparation of cyclocitryl phenyl sulfone (**1**) and its use as a synthon for cyclocitral.[2] The sulfone **1** was also converetd to β-ionone, deoxytrisporone,[3] and vitamin A acid methyl esters.[4] Here, we describe a convenient preparation of 1-phenylsulfonylmethyl-2,6,6-trimethylcyclohexa-1,3-diene (**4**) from **1**, as well as syntheses of 4-(2,6,6-trimethyl-3-oxo-1-cyclohexenyl)-3-buten-2-one (**5**), a tea aroma substance[5,6] and 4-(2,6,6-trimethyl-1,3-cyclohexadienyl)-3-buten-2-one (**6**), a tobacco flavor constituent,[7,8] from **2** and **4**, respectively.

Oxidation of **1** with 1.5 equiv of SeO_2 in dioxane at 80 °C for 1.5 h gave the alcohol **2** (74%) and the starting material **1** (23%). On treatment of **2** with PBr_3 in dry ether at 0 °C,[9] the alcohol **2** was converted smoothly to the corresponding bromo compound **3**, which was dehydrobrominated by the action of 1.5 equiv of LiCl in DMF at 100 °C for 2 h, affording **4** in 92% yield.

The reaction of **2** with 2 equiv. of BuLi in THF at −70 °C, followed by reaction with propylene oxide at room temperature for 20 hours, provided the diol **7** in 86% yield. The alcohol **7** was easily purified by column chromatography (SiO_2) and was homogeneous by TLC, but the NMR was unexpectedly complex, presumably due to intramolecular hydrogen bonding between the hydroxyl group and sulfonyl oxygen and/or the presence of diastereomers on C-2 and C-4. On oxidation with Jones reagent, **7** was converted to the corresponding diketone in 92% yield, whose NMR spectrum was in agreement with the structure **8**.

Treatment of **8** with MeONa in *t*-BuOH-EtOH at room temperature afforded **5** in 78% yield.[11]

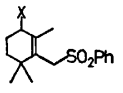

1 X=H
2 X=OH
3 X=Br

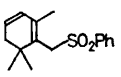

4

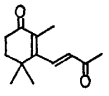

5

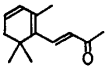

6

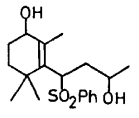

7

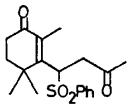

8

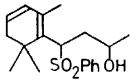

9

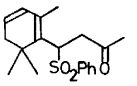

10

Alkylation of **4** with propylene oxide was performed similarly with 1 equiv. of BuLi, affording **9** in 95% yield. Oxidation of **9** was attempted with both Jones and Collins reagents, but the yield of the ketone **10** was unsatisfactory. However, when **9** was oxidized with pyridinium chlorochromate in anhydrous dichloromethane at room temperature as described by Corey,[12] the ketone **10** was obtained in 82% yield. Then, **10** was subjected to the base-promoted elimination of sulfonyl group with MeONa in *t*-BuOH–EtOH at room temperature to give **6** in 88% yield. The IR and NMR spectra of **6** are consistent with those reported.[7]

Experimental

Melting points are uncorrected. IR spectra were determined with a Jasco IRA-1 infrared spectrometer. NMR spectra were obtained at 60 MHz with a Hitachi R-24 spectrometer and the chemical shift values are expressed in δ value (ppm) relative to Me_4Si in $CDCl_3$.

*2,4,4-Trimethyl-3-phenylsulfonylmethyl-2-cyclohexen-1-ol (**2**).* A mixture of **1** (102 mg, 0.37 mmol) and SeO_2 (62 mg, 0.56 mmol) in 1 ml of dioxane was stirred at 80 °C for 1.5 h. After removing the precipitate with centrifuge and evaporating the solvent *in vacuo*, the residue was chromatographed (SiO_2, benzene/hexane=5/1) to give **2** (82 mg, 74%) together with **1**(24 mg, 23%): Mp 94—95 °C (benzene/hexane =1/10); IR (Nujol) 3500 (OH), 1632 (C=C), 1302, 1137 (SO_2) cm^{-1}; NMR ($CDCl_3$) δ 8.02—7.42 (5H, m, ArH), 3.98 (2H, s, CH_2SO_2), 3.80—4.10 (1H, m, CHOH), 2.98 (1H, s, OH), 1.84 (3H, s, CH_3C=), 1.12—2.22 (4H, m, CH_2), 1.08 (3H, s, CH_3), 1.01 (3H, s, CH_3).

Found: C, 65.42; H, 7.53%. Calcd for $C_{16}H_{22}O_3S$: C, 65.29; H, 7.53%.

*2,6,6-Trimethyl-1-(phenylsulfonylmethyl)-3-bromocyclohexene (**3**).* Into a solution of **2** (372 mg, 1.26 mmol) in 1.2 ml of dry ether and 0.8 ml of dry THF was added dropwise phosphorus tribromide (344 mg, 1.27 mmol) at 0 °C and the mixture was stirred for 2.5 h. After addition of saturated $NaHCO_3$, the organic substances were extracted with AcOEt. The extracts were washed with brine, dried (Na_2SO_4), and concentrated *in vacuo* to give **3** as pale colored crystals (450 mg, 100%): Mp 129—130 °C (AcOEt/hexane=1/10); IR(Nujol)

1305, 1145 (SO_2) cm^{-1}; NMR ($CDCl_3$) δ 7.45—8.02 (5H, m, ArH), 4.58—4.75 (1H, m, CHBr), 3.96 (2H, s, CH_2SO_2), 2.07—2.26 (2H, m, CH_2), 1.86 (3H, s, CH_3), 1.27—1.68 (2H, m, CH_2), 1.06 (3H, s, CH_3), 1.03 (3H, s, CH_3).

Found: C, 53.68; H, 5.99%. Calcd for $C_{16}H_{21}O_2SBr$: C, 53.79; H, 5.93%.

*2,6,6-Trimethyl-1-(phenylsulfonylmethyl)-1,3-cyclohexadiene (**4**).* A mixture of **3** (450 mg, 1.26 mmol) and LiCl (80 mg, 1.89 mmol) in dry DMF was stirred under N_2 at 100 °C for 2 h. After addition of 5 ml of water, the organic substances were extracted with ether. The extracts were washed with brine, dried (Na_2SO_4), and concentrated *in vacuo* to yield 351 mg of crystals, which was chromatographed (SiO_2, AcOEt/hexane=1/5) to give **4** (323 mg, 93%): Mp 58—60 °C (benzene/hexane=1/10); IR (Nujol) 1305, 1145 (SO_2) cm^{-1}; NMR ($CDCl_3$) δ 7.38—8.04 (5H, m, ArH), 5.78 (2H, br s, CH=CH), 4.01 (2H, s, CH_2SO_2), 2.07 (2H, d, J=4 Hz, CH_2C=), 1.62 (3H, s, CH_3C=), 1.11 (6H, s, CH_3).

Found: C, 69.43; H, 7.42%. Calcd for $C_{16}H_{20}O_2S$: C, 69.55; H, 7.30%.

*4-Phenylsulfonyl-4-(2,6,6-trimethyl-3-hydroxy-1-cyclohexenyl)-2-butanol (**7**).* Into a solution of **2** (103 mg, 0.35 mmol) in 1.5 ml of dry THF, was added ethereal solution of BuLi (0.8 mmol) at −50 °C under N_2. After stirring for 15 min, propylene oxide (0.2 ml) was added to the mixture, which was stirred at room temperature for additional 20 h. The reaction mixture was quenched with saturated NH_4Cl and extracted with AcOEt. The extracts were washed with brine, dried (Na_2SO_4), and concentrated *in vacuo* to yield a viscous liquid, which was chromatographed (SiO_2, benzene/AcOEt=1/1) to give **7** (106 mg, 86%): IR (neat) 3407 (OH), 1291, 1137 (SO_2) cm^{-1}; NMR ($CDCl_3$) δ 7.34—8.00 (5H, m, ArH), 3.39—4.46 (3H, m, CHOH, $CHSO_2$), 2.42—3.00 (2H, m, OH), 2.08 (3H, s, CH_3C=), 1.39—2.40 (6H, m, CH_2), 0.67—1.32 (9H, m, CH_3).

Found: C, 64.92; H, 8.09%. Calcd for $C_{19}H_{28}O_4S$: C, 64.75; H, 8.01%.

*4-Phenylsulfonyl-4-(2,6,6-trimethyl-3-oxo-1-cyclohexenyl)-2-butanone (**8**).* Into a solution of **7** (46 mg, 0.13 mmol) in 0.5 ml of CH_2Cl_2, was added Jones reagent[13] (0.2 ml, 0.52 mmol) under ice-cooling and the mixture was stirred at 5 °C for 1 h. After addition of 0.5 ml of water, the organic substances were extracted with $CHCl_3$. The extracts were washed with saturated $NaHCO_3$ and water, dried (Na_2SO_4), and concentrated *in vacuo* to yield 45 mg of dark brown crystals, which were chromatographed (SiO_2, benzene/AcOEt=2/1) to give **8** (41 mg, 92%): Mp 128—129 °C (benzene/hexane=1/10); IR (Nujol) 1717 (C=O), 1658 (C=C), 1297, 1148 (SO_2) cm^{-1}; NMR ($CDCl_3$) δ 7.35—7.93 (5H, m, ArH), 4.95 (1H, dd J=6.6 and 2.4 Hz, $CHSO_2$), 3.91 (1H, dd J=6.6 and 19.2 Hz, CH_2CSO_2), 2.73 (1H, dd J=2.4 and 19.2 Hz, CH_2CSO_2), 2.28—2.52 (2H, m, CH_2), 2.10 (3H, s, CH_3), 2.07 (3H, s, CH_3), 1.64—2.00 (2H, m, CH_2), 1.17 (3H, s, CH_3), 0.97 (3H, s, CH_3).

Found: C, 65.59; H, 7.04%. Calcd for $C_{19}H_{24}O_4S$: C, 65.50; H, 6.94%.

*4-Phenylsulfonyl-4-(2,6,6-trimethyl-1,3-cyclohexadienyl)-2-butanol (**9**).* The alcohol **9** could be prepared in 95% yield under similar reaction conditions to the procedure described for **7**: IR (neat) 3493 (OH), 1303, 1143 (SO_2) cm^{-1}; NMR ($CDCl_3$) δ 7.31—8.02 (5H, m, ArH), 5.62—5.86 (2H, m, CH=CH), 4.21—4.56 (1H, m, $CHSO_2$), 3.46—4.06 (1H, m, CHOH), 1.56—2.36 (7H, m, CH_2, OH), 1.99 (3H, s, CH_3), 0.78—1.40 (9H, m, CH_3).

Found: C, 68.37; H, 7.98%. Calcd for $C_{19}H_{26}O_3S$: C, 68.24; H, 7.84%.

*4-Phenylsulfonyl-4-(2,6,6-trimethyl-1,3-cyclohexadienyl)-2-butanone (**10**).* Into a solution of pyridinium chlorochromate (74 mg, 0.34 mmol) in 1 ml of dry CH_2Cl_2, was added the alcohol **9** (58 mg, 0.17 mmol) dissolved in 0.5 ml of dry CH_2Cl_2 under N_2 and the mixture was stirred at room temperature for 8 h. After addition of 1 ml of water, the organic substances were extracted with $CHCl_3$. The extracts were washed with brine, dried (Na_2SO_4), and concentrated *in vacuo* to yield a dark brown oil, which was chromatographed (SiO_2, benzene/AcOEt=10/1) to give **10** (47 mg, 82%) as a colorless liquid: IR (CCl_4) 1721 (C=O), 1646 (C=C), 1302, 1145 (SO_2) cm^{-1}; NMR ($CDCl_3$) δ 7.35—8.00 (5H, m, ArH), 5.74 (2H, br s, CH=CH), 4.95 (1H, dd J=6.6 and 4.8 Hz, $CHSO_2$), 3.71 (1H, dd J=6.6 and 18.6 Hz, CH_2CSO_2), 2.79 (1H, dd J=4.8 and 18.6 Hz, CH_2CSO_2), 2.05 (3H, s, CH_3), 2.01 (3H, s, CH_3), 1.80—2.20 (2H, m, CH_2), 0.94 (3H, s, CH_3), 0.82 (3H, s, CH_3).

Found: C, 68.88; H, 7.37%. Calcd for $C_{19}H_{24}O_3S$: C, 68.66; H, 7.28%.

*4-(2,6,6-Trimethyl-3-oxo-1-cyclohexenyl)-3-buten-2-one (**5**).* A solution of **8** (74 mg, 0.21 mmol) in 4 ml of dry *t*-BuOH was added into 50 mg of MeONa under N_2 and the mixture was stirred at room temperature for 5 h. The reaction mixture was quenched with saturated NH_4Cl and extracted with ether. The ether extracts were washed with brine, dried (Na_2SO_4), and concentrated *in vacuo* to yield a dark brown oil, which was chromatographed (SiO_2, benzene/AcOEt=7/1) to give **5** (34 mg, 78%) as crystals.

*4-(2,6,6-Trimethyl-1,3-cyclohexadienyl)-3-buten-2-one (**6**).* The compound **6** could be prepared in 78% yield under similar reaction conditions to the procedure described for **5**.

References

1) S. Torii, K. Uneyama, and H. Hamada, *Bull. Chem. Soc. Jpn.*, **50**, 2503 (1977).

2) S. Torii, K. Uneyama, and M. Ishihara, *Chem. Lett.*, **1975**, 479.

3) K. Uneyama and S. Torii, *Tetrahedron Lett.*, **1976**, 443.

4) K. Uneyama and S. Torii, *Chem. Lett.*, **1977**, 39.

5) Isolation of **5**: (a) K. Ina and H. Eto, *Agr. Biol. Chem.*, **35**, 962 (1971); (b) V. Prelog and H. L. Meier, *Helv. Chim. Acta*, **33**, 1276 (1950).

6) Synthesis of **5**: (a) P. Karrer and C. H. Eugster, *Helv. Chim. Acta*, **34**, 1400 (1951); (b) H. B. Henbest, *J. Chem. Soc.*, **1951**, 1074; (c) K. Ina and H. Eto, *Agric. Biol. Chem.*, **36**, 1091 (1972).

7) Isolation of **6**: E. Demole and D. Berthet, *Helv. Chim. Acta*, **55**, 1866 (1972).

8) Synthesis of **6**: (a) H. B. Henbest, *Nature*, **161**, 481 (1948); (b) G. Büchi, K. Seitz, and O. Jeger, *Helv. Chim. Acta*, **32**, 39 (1949): (c) Ref. 6a; (d) Ref. 6b; (e) M. Mousseron-Canet, J. C. Mani, and J. P. Dalle, *C. R. Acad. Sci., Ser. C*, **262**, 1397 (1966); (f) J. A. Findlay and W. D. Mackay, *Can. J. Chem.*, **49**, 2369 (1971); (g) W. Skorianetz and G. Ohloff, *Helv. Chim. Acta*, **57**, 2439 (1975).

9) P. A. Grieco and Y. Masaki, *J. Org. Chem.*, **39**, 2135 (1974).

10) M. Julia and D. Arnould, *Bull. Soc. Chim. Fr.*, **1973**, 746.

11) The IR and NMR spectra of **5** are consistent with those reported.[5a]

12) E. J. Corey and J. W. Suggs, *Tetrahedron Lett.*, **1975**, 2647.

13) C. Djerassi, R. R. Engle, and A. Bowers, *J. Org. Chem.*, **21**, 1547 (1956).

BULLETIN OF THE CHEMICAL SOCIETY OF JAPAN, VOL. 51 (3), 951—952 (1978)

Synthesis of 4-(D-Alanylamino)-2-amino-2,4-dideoxy-D-xylose*

Hassan Akhtar KHAN,** Hironobu HASHIMOTO, and Juji YOSHIMURA

Laboratory for Chemistry of Natural Products, Faculty of Science, Tokyo Institute of Technology, Nagatsuta-machi, Midori-ku, Yokohama, 227

(Received September 22, 1977)

Synopsis. A prumycin diastereomer having D-configuration, 4-(D-alanylamino)-2-amino-2,4-dideoxy-D-xylose, was first synthesized from L-arabinose *via* benzyl 2,3-anhydro-4-azido-α-D-lyxopyranoside.

Prumycin, 4-(D-alanylamino)-2-amino-2,4-dideoxy-L-arabinose, is an antifungal antibiotic[2] and was synthesized independently by three Japanese groups.[3,4,5] In the course of study for the relationship between structures and biological activities, we have also synthesized prumycin and its diastereomers having L-configuration except L-lyxo one.[1] In the present paper, we would like to report the first synthesis of a prumycin diastereomer in D-series using the method developed by us for the synthesis of prumycin.[4] L-Arabinose was used as starting material instead of D-xylose, which was used for the synthesis of L-stereoisomers. 2,3,4-Tri-*O*-mesylate(**1**) of benzyl β-L-arabinopyranoside was subjected to azidolysis to give the corresponding 4-azido derivative(**2**) in excellent yield. Treatment of **2** with sodium methoxide in methanol gave a mixture of benzyl 2,3-anhydro-4-azido-α-D-lyxo(**3**) and -α-D-ribo-pyranoside (**4**), which were separated easily on a silica gel column. The yields of these epoxides depend on the reaction conditions, especially on the concentration of the bases and on the reaction times. As the rates of formation and ring opening reaction of **3** are apparently slower than those of **4**, higher base concentration and longer reaction time facilitate the predominant formation of **3**. In the optimal conditions the both epoxides were formed in 60% yield. By treatment of **2** with 0.7 M sodium methoxide in methanol under reflux for 6—7 h **3** and **4** were obtained in 20 and 15% yields, respectively. The structures of these epoxides were ascertained by the $J_{1,2}$ and $J_{3,4}$ values in their NMR spectra.[6]

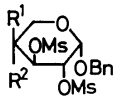

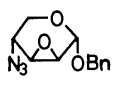

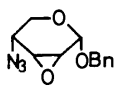

1 R^1=OMs, R^2=H **3** **4**
2 R^1=H, R^2=N_3

Ammonolysis of **3** gave benzyl 2-amino-4-azido-α-D-xylopyranoside(**5**) predominantly, which was obtained in 65% yield after chromatographic separation from its ring opening isomer(**6**). The structures of these products were determined by their NMR data, especially by the coupling constants of ring protons as shown in the Experimental. Then, **5** was treated with *t*-butyl azidoformate to give the *N*-*t*-butoxycarbonylated derivative(**7**). The azido group of **7** was hydrogenated selectively in the presence of platinum oxide and condensed with *N*-benzyloxycarbonyl-D-alanine *p*-nitrophenyl ester successively as reported for the synthesis of prumycin. The condensation product(**9**) was converted into 4-(D-alanylamino)-2-amino-2,4-dideoxy-D-xylose hydrochloride(**10**) in good yield by treatment with formic acid, followed by hydrogenolysis under acidic conditions in the presence of palladium-carbon. The biological activities of **10** will be presented elsewhere.

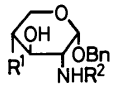

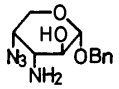

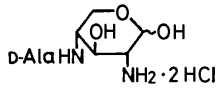

5 R^1=N_3, R^2=H **6** **10**
7 R^1=N_3, R^2=*t*-BOC
8 R^1=NH_2, R^2=*t*-BOC
9 R^1=*N*-Cbz-D-Ala,
R^2=*t*-BOC

Experimental

^{1}H NMR spectra were recorded with a JNM-PS-100 spectrometer at 100 MHz in deuteriochloroform containting tetramethylsilane as an internal standard. IR spectra were taken with a Hitachi Model EPI-GS grating spectrometer. Optical rotations were measured in chloroform(C) or methanol (M) in a 0.5 dm tube with a Carl Zeiss LEP-AL polarimeter. Chemical shifts and coupling constants were recorded in δ and Hz units, and IR frequencies in cm^{-1}.

*Benzyl 2,3,4-Tri-O-mesyl-β-L-arabinopyranoside (**1**).* Benzyl β-L-arabinopyranoside[7] (50 g) was mesylated with mesyl chloride (100 g) in pyridine(400 ml) in the usual manner. Yield 75—80%. mp 100—102 °C, $[\alpha]_D$ +71.2° (*c* 1.0, C); NMR: 5.21 (d, H_1, $J_{1,2}$=3.8), 4.90 (dd, H_2, $J_{2,3}$=11.0), 5.12 (dd, H_3, $J_{3,4}$=3.3), 2.92 and 3.15 (s, 3 and 6H, OMs); IR(KBr): 1180 and 1360 (SO_2). Found: C, 38.21; H, 4.63; S, 19.91%. Calcd for $C_{15}H_{22}O_{11}S_3$: C, 37.96; H, 4.67; S, 20.27%.

*Benzyl 4-Azido-4-deoxy-2,3-di-O-mesyl-α-D-xylopyranoside (**2**).* A solution of **1**(50 g), sodium azide(8 g) and urea(1.5 g) in *N*,*N*-dimethylformamide(370 ml) containing water(40 ml) was heated at 110 °C for 24 h. The reaction mixture was evaporated, and the residue was extracted with chloroform. The extract was washed with water, dried with anhydrous sodium sulfate, and evaporated to give a syrup in 81% yield. The syrup was purified on a silica gel column (Wako gel C-200); $[\alpha]_D$ +123.5° (*c* 0.85, C); NMR: 5.15 (d, H_1, $J_{1,2}$=3.6), 4.91 (dd, H_2, $J_{2,3}$=9.5), 4.59 (dd, H_3, $J_{3,4}$=6.0), 2.95 and 3.13 (s, 3H each, OMs); IR(NaCl): 2110 (N_3), 1180 and 1360 (SO_2). Found: C, 40.16; H, 4.73; N, 9.69; S, 15.42%. Calcd for $C_{14}H_{19}N_3O_8S_2$: C, 39.90; H, 4.54; N, 9.97; S, 15.22%.

*Benzyl 2,3-Anhydro-4-azido-4-deoxy-α-D-lyxopyranoside (**3**)* and *-ribopyranoside (**4**).* A 4—5% solution of **2** in methanol containing *ca.* 6 equimolar sodium was refluxed for 6—7 h, until the most of **2** has disappeared. Methanol was evapo-

* Aminosugars XXX. For part XXIX, see Ref. 1.
** UNESCO fellow 1975—1976.

rated and the residue was dissolved in benzene. The benzene layer was washed with water, dried, and evaporated to give a syrup, which was fractionated on a silica gel column by elution with benzene to obtain at first an oily **3** and secondly **4**, in 20% and 15% yields, respectively. **3**: $[\alpha]_D$ +101.4° (*c* 1.2, M); NMR: 4.96 (s, H_1, $J_{1,2}$=0.5), 3.13 and 3.30 (dd, H_2 and H_3, $J_{2,3}$=3.3, $J_{3,4}$=0.5); IR(NaCl): 2100 (N_3). Found: C, 58.79; H, 5.26; N, 17.01%. Calcd for $C_{12}H_{13}N_3O_3$: C, 58.29; H, 5.30; N, 17.00%. **4**: $[\alpha]_D$ +181° (*c* 1.0, M); NMR: 4.94 (d, H_1, $J_{1.2}$=2.7); IR (NaCl): 2100 (N_3). Found: C, 58.61; H, 5.21; N, 16.82 %. Calcd for $C_{12}H_{13}N_3O_3$: C, 58.29; H, 5.30; N, 17.00%.

*Benzyl 2-Amino-4-azido-2,4-dideoxy-α-D-xylopyranoside (**5**) and Benzyl 3-Amino-4-azido-3,4-dideoxy-α-D-arabinopyranoside (**6**).* A methanol solution of **3**(3.5 g) was saturated with ammonia at 0 °C, and then heated in a sealed glass tube at 90 °C for 24 h. After complete evaporation of the solvent, the crystalline product obtained(3.5 g) was fractionated on a silica gel column by elution with benzene containing 5% 2-pronanol (v/v). The faster-eluting component was **5** (2.2 g, 61%) followed by the isomeric 3-amino derivative (**6**: 0.8 g, 23%). **5**: Mp 95—96 °C, $[\alpha]_D$ +184.6° (*c* 1.0, M); NMR: 4.78 (d, H_1, $J_{1,2}$=3.5), 2.69 (dd, H_2, $J_{2,3}$=9.3) and $J_{3,4}$ was found to be 9.4 Hz with the aid of $Eu(FOD)_3$. IR(KBr): 2100 (N_3), 3300 and 3350 (NH_2 and OH). Found: C, 54.40; H, 6.24; H, 21.39%. Calcd for $C_{12}H_{16}N_4O_3$: C, 54.54; H, 6.06; N, 21.21%. **6**: Mp 110—111° C, $[\alpha]_D$ −45.1° (*c* 1.0, M); NMR: 4.23 (d, H_1, $J_{1,2}$=6.9), 3.35 (dd, H_2, $J_{2,3}$=9.2), 2.81 (dd, H_3, $J_{3,4}$=3.9), 3.66 (m, H_4), 3.50 and 4.00 (dd each, H_5 and $H_{5'}$, $J_{4,5}$ and $J_{4,5'}$: 1.2 and 2.4); IR(KBr): 2100 (N_3), 2280 and 2320 (NH_2 and OH). Found: C, 54.92; H, 6.15; N, 21.51%. Calcd for $C_{12}H_{16}N_4O_3$: C, 54.54; H, 6.10; N, 21.21%.

*Benzyl 4-Azido-2-(t-butoxycarbonylamino)-2,4-dideoxy-α-D-xylopyranoside (**7**).* A solution of **5** (1.5 g), *t*-butyl azidoformate (2 g) and triethylamine(1.8 g) in dioxane (15 ml) was heated at 60—70 °C for 3—4 h. The crude product obtained was passed through a column of silica gel by elution with benzene. The first fraction was collected to give **7** (1.8 g), which was recrystallized from methanol. Mp 119—120 °C, $[\alpha]_D$ +191° (*c* 0.7, M); NMR; 4.87 (d, H_1, $J_{1,2}$=1.8) and 1.46 (s, 9H, *t*-Bu); IR(KBr): 2100 (N_3) and 1685 (urethane). Found; C, 55.78; H, 6.66; N, 15.59%. Calcd for $C_{17}H_{24}N_4O_5$: C, 56.08; H, 6.64; N, 15.38%.

*Benzyl 4-Amino-2-(t-butoxycarbonylamino)-2,4-dideoxy-α-D-xylopyranoside (**8**).* Hydrogenation of **7** (1.7 g) in methanol was carried out in the presence of platinum oxide to give **8** (1.3 g); mp 172—175 °C, $[\alpha]_D$ +157° (*c* 1.1, M); NMR (DMSO-d_6): 4.90 (d, H_1, $J_{1,2}$=3.0) and 1.46 (s, 9H, *t*-Bu); IR (KBr): 1685 (urethane) and 3370 (NH_2 and OH). Found: C, 59.81; H, 7.67; N, 8.66%. Calcd for $C_{17}H_{26}N_2O_5$: C, 60.34; H, 7.74; N, 8.28%.

*Benzyl 4-(N-Benzyloxycarbonyl-D-alanylamino)-2-(t-butoxycarbonylamino)-2,4-dideoxy-α-D-xylopyranoside (**9**).* The compound **8** was coupled with *N*-benzyloxycarbonyl-D-alanine *p*-nitrophenyl ester in *N,N*-dimethylformamide in the usual manner to give **9** in 60% yield. Mp 145—147 °C, $[\alpha]_D$ +2.3° (*c* 1.0, M), IR(KBr): 1710 and 1690 (urethane), *1650 and 1520 (amide) and 3320 (NH and OH).* Found: C, 61.92; H, 6.50; N, 7.51%. Calcd for $C_{28}H_{37}N_3O_8$: C, 61.87; H, 6.81; N, 7.73%.

*4-(D-Alanylamino)-2-amino-2,4-dideoxy-D-xylose Dihydrochloride (**10**).* Compound **9** was treated with 98% formic acid for removal of *t*-butoxycarbonyl group and then hydrogenated with palladium-charcoal (10%) in 0.1 N in 50% aqueous ethanol to give **10** in 80% yield, mp 170—175 °C (dec), $[\alpha]_D$ +76.3° (*c* 1.0, M). Found: C, 32.50; H, 6.40; N, 14.09%. Calcd for $C_8H_{19}Cl_2N_3O_4$: C, 32.88; H, 6.55; N, 14.39%.

We thank Mr. Matsumoto for measuring the NMR spectra, and the members of our organic analysis laboratory for microanalysis.

References

1) H. Hashimoto, F. Chiba, K. Araki, and J. Yoshimura, *Carbohydr. Res.* (submitted).

2) T. Hata, S. Omura, M. Katagiri, K. Atsumi, J. Awaya, S. Higashikawa, K. Yasui, H. Terada, and S. Kuyama, *J. Antibiot.*, **24**, 900 (1971).

3) H. Kuzuhara and S. Emoto, *Tetrahedron Lett.* **1975**, 1853.

4) J. Yoshimura, H. Hashimoto, and T. Nishide, *Chem. Lett.*, **1976**, 201.

5) A. Hasegawa, N. Aritake, and M. Kiso, *Carbohydr. Res.*, **52**, 137 (1976).

6) O. Achmatowicz, Jr. and B. Szechner, *Carbohydr. Res.*, **50**, 23 (1976).

7) L. E. Ballou, *J. Am. Chem. Soc.*, **79**, 165 (1957).

BULLETIN OF THE CHEMICAL SOCIETY OF JAPAN, VOL. 51 (3), 953—954 (1978)

Formation of 5-Phenyltetrazole from N^2-Benzoyl-N^4-(phenylsulfonyl)benzohydrazide Hydrazone

Suketaka Ito, Yumo Tanaka, Akikazu Kakehi, and Mikio Kawahata

Department of Industrial Chemistry, Faculty of Engineering, Shinshu University, Wakasato, Nagano 380

(Received October 28, 1977)

Synopsis. 5-Phenyltetrazole is obtained in a moderate yield by the mercury(II) oxide oxidation of the title hydrazidine prepared from *N*-(phenylsulfonyl)benzohydrazonoyl chloride and benzohydrazide. The tetrazole formation is interpreted in terms of an intramolecular S_N2 type process of the intermediate formazan with the removal of benzenesulfinic acid. In the absence of oxidizing agents, the hydrazidine gives 2,5-diphenyl-1,3,4-oxadiazole and 3,5-diphenyl-4-phenylsulfonylamino-4*H*-1,2,4-triazole.

In a previous paper[1] we reported a method for preparing 2,5-disubstituted tetrazoles by the reaction of *N*-(phenylsulfonyl)benzohydrazonoyl chloride(**1**) with arylhydrazines, in which the hydrazines act as a nucleophile in the initial reaction step. This method using hydrazine is, however, not applicable to the preparation of 5-monosubstituted tetrazoles, since hydrazine acts as a base to lead to the formation of 3,6-diphenyl-1,4-bis(phenylsulfonyl)-1,4-dihydro-1,2,4,5-tetrazine. The present paper deals with the formation of 5-phenyltetrazole and other two azoles from **1** and benzohydrazide(**2**).

When a solution of **1** and two equivalent amounts of **2** in THF was stirred for 18—20 h at room temperature, the reaction mixture turned slightly acidic with the precipitation of benzohydrazide hydrochloride. Work-up gave N^2-benzoyl-N^4-(phenylsulfonyl)benzohydrazide hydrazone(**3**) or its tautomer in 92% yield together with a trace amount of 2,5-diphenyl-1,3,4-oxadiazole(**4**) and 3,5-diphenyl-4-phenylsulfonylamino-4*H*-1,2,4-triazole(**5**).

The hydrazidine(**3**) afforded 5-phenyltetrazole(**6**) in 56% yield along with *S*-phenyl benzenethiosulfonate and benzoic acid, when treated with mercury(II) oxide (yellow)–potassium carbonate.[2] With potassium carbonate alone,[3] the yield of **6** decreased to 32%.

The recrystallization of **3** from methanol or THF–hexane resulted in a partial conversion of **3** into **4**, and at higher temperature the formation of **5** from **3** was also observed. Heating compound **3** at its melting point without solvent gave **5** almost quantitatively. Prolonged stirring or refluxing the mixture of **1** and **2** in THF, without the isolation of **3** formed intermediately, brought about an increase in the yields of **4** and **5** along with the formation of benzenesulfonohydrazide and 1-benzoyl-2-phenylsulfonylhydrazine (see Experimental section).

The sequence of reactions is summarized as follows (Scheme 1):

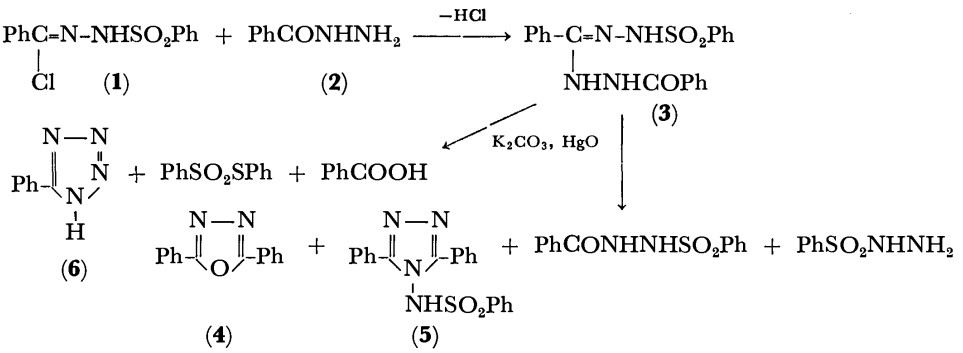

Scheme 1.

The formation of **6** from **3** can be formulated as follows (Scheme 2):[4]

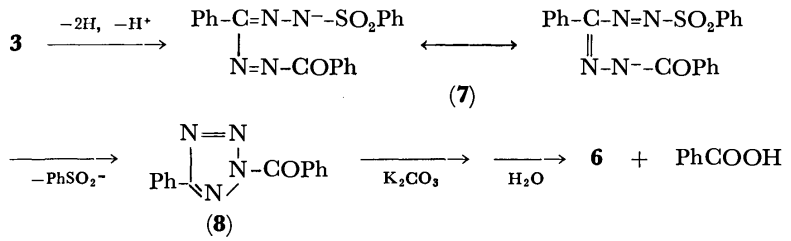

Scheme 2.

For the step **7**→**8**, two mechanisms are possible: one involves the Bamford-Stevens type α-elimination of benzenesulfinic acid followed by the 1,5-dipolar cyclization of the resulting (benzoylazo)diazomethane(Scheme 3), and the other an intramolecular S_N2 type displacement of benzenesulfinate ion by the benzoylamino-anion part of **7**.

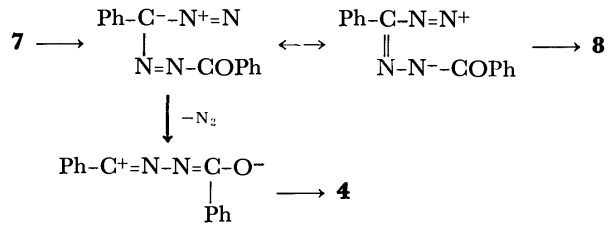

Scheme 3.

However, the azodiazomethane is also the source of **4**[5] as shown in Scheme 3. From the fact that **4** could not be obtained in this tetrazole-formation reaction, the direct displacement mechanism may be reasonable.[6] The precursor of the *S*-phenyl benzenethiosulfonate is benzenesulfinic acid[8] removed from **7**.

The formation of **4** and **5** can be easily explained in terms of an intramolecular cyclization of **3** with the removal of benzenesulfonohydrazide and water, respectively. 1-Benzoyl-2-phenylsulfonylhydrazine should be the hydrolyzed product of **3**.

Experimental

Melting points were determined with a Yanagimoto micro-melting point apparatus Model MP-S3 and are uncorrected. The microanalysis was performed on a Perkin-Elmer elemental analyzer Model 240, and the IR spectra were recorded with a JASCO DS-301 spectrometer. The products were identified by means of their analytical and spectral data and by comparison with authentic specimens prepared by other synthetic methods.

Preparation of N^2*-Benzoyl-*N^4*-(phenylsulfonyl)benzohydrazide Hydrazone (3).* A solution of **1**[1] (10 mmol) and **2**(20 mmol) in THF (40 ml) was stirred for 18—20 h at room temperature. After the removal of precipitated benzohydrazide hydrochloride by filtration, the filtrate was concentrated below 40 °C and extracted with chloroform. The chloroform extract was washed with water, dried(Na_2SO_4), and then concentrated, giving fairly pure **3**(92%) as an amorphous solid, which was purified by recrystallization from methanol or by re-precipitation from THF-hexane, mp 205—207 °C (dec).[9] IR(KBr, cm^{-1}):[10] 3270, 3205(ν_{NH}); 1640(ν_{CO}); 1300(asym ν_{SO_2}); 1162(sym ν_{SO_2}). Found: C, 61.01; H, 4.49; N, 14.45%. Calcd for $C_{20}H_{18}N_4O_3S$: C, 60.90; H, 4.60; N, 14.20%.

Oxidation of 3 with Mercury(II) Oxide(yellow). A mixture of **3**(0.395 g, 1 mmol), HgO(0.324 g, 1.5 mmol), K_2CO_3 (0.4 g, 3 mmol), $CaSO_4$(0.4 g, 3 mmol), and dioxane(15 ml) was stirred for 20 h at room temperature. The reaction mixture was filtered and washed with dioxane(20 ml), and then with water(50 ml). The filtrate combined with the washings(dioxane) was concentrated to give crude *S*-phenyl benzenethiosulfonate(0.096 g), which was purified by recrystallization from ethanol, mp 43—44 °C(lit,[11] 45 °C). The water-washings were acidified with dil. HCl, saturated with NaCl, and then extracted with ether. Chromatographic treatment (silica gel, benzene-ethanol) of the ether extract gave benzoic acid(0.072 g, 59%) and **6**(0.075 g, 56%): Mp 213—214 °C (dec)(lit,[5a] 214—215 °C, dec).

Oxadiazole(4) and Aminotriazole (5). A THF solution of **1** and **2**(1 : 2 mole ratio) was refluxed for 4 h or stirred for 5 d at room temperature. The resulting precipitates were separated by filtration and washed with water, giving almost pure **5**: mp 312—315 °C(dec)(acetone).[12]

The THF layer was concentrated, extracted with chloroform, and washed with water, After the removal of the solvent, the residue was chromatographed(silica gel, benzene-ether-ethanol), giving **4** (mp 138—139 °C; lit,[5a] 137—138 °C), 1-benzoyl-2-phenylsulfonylhydrazine(mp 197—198 °C; lit,[13] 199 °C), and benzenesulfonohydrazide, which was confirmed as acetone phenylsulfonylhydrazone: Mp 143—144 °C. IR(KBr, cm^{-1}): 3189(ν_{NH}); 1332, 1162(ν_{SO_2}). Found: C, 51.04; H, 5.71; N, 13.04%. Cacld for $C_9H_{12}N_2O_2S$: C, 50.94; H, 5.70; N, 13.20%. The results are summarized in Table 1.

Table 1. Oxadiazole(**4**) and aminotriazole(**5**)

Reaction Conditions[a]	Yield(%) of products[b]			
	4	**5**	$PhCONHNHSO_2Ph$	$PhSO_2NHNH_2$
I	37	30	27	26
II	40	13	32	40

a) I: Refluxing for 4 h. II: Stirring for 5 d at room temperature. b) Yield as mole per cent based on **1**.

The present work was partially supported by a Grant-in-Aid for Scientific Research from the Ministry of Education(Grant No. 165196).

References

1) S. Ito, Y. Tanaka, and A. Kakehi, *Bull. Chem. Soc. Jpn.*, **49**, 762 (1976).
2) No formation of **4** and **5** was observed in this case.
3) The mixture(in dioxane) was stirred for 5 d.
4) In the absence of mercury(II) oxide, the oxidation of **3** to formazan proceeds probably *via* the autoxidation with atmospheric oxygen catalyzed by potassium carbonate.
5) a) R. Huisgen, J. Sauer, H. J. Sturm, and J. H. Markgraf, *Chem. Ber.*, **93**, 2106 (1960).
b) R. M. Herbst, *J. Org. Chem.*, **26**, 2372 (1961).
6) This intramolecular displacement process may be well represented by the interaction of the lone-pair orbital of the benzoylazo α-nitrogen(or the benzoylamino nitrogen) with the σ* orbital of the $PhSO_2$-N bond in the planar quasi-aromatic configuration of **7**.[1,7]
7) S. Ito, Y. Tanaka, A. Kakehi, and K. Kondo, *Bull. Chem. Soc. Jpn.*, **49**, 1920 (1976).
8) J. L. Kice and K. W. Bowers, *J. Am. Chem. Soc.*, **84**, 605 (1962).
9) Compound **3** alters to **5** without complete melting when heated gradually, while it shows its clear melting point, giving **5**, when placed on a pre-heated metal plate.
10) Absorption peaks of the crystalline **3**. Compound **3** in the amorphous state exhibits absorption peaks at 3275^{sh}, 3252(ν_{NH}), 1609(ν_{CO}), 1330(asym ν_{SO_2}), and 1166(sym ν_{SO_2}): This difference is probably due to the tautomerism or the molecular association.
11) E. Knoevenagel and A. Römer, *Ber.*, **56B**, 215 (1923).
12) S. Ito, Y. Tanaka, A. Kakehi, and T. Matsuno, *Bull. Chem. Soc. Jpn.*, **50**, 327 (1978).
13) P. Grammaticakis, *Bull. Soc. Chim. Fr.*, **1953**, 86.

COMMENTS

BULLETIN OF THE CHEMICAL SOCIETY OF JAPAN, VOL. 51 (3), 955 (1978)

The Condensation of Nitromethane with Ketoses

Gerhardus J. LOURENS

Adcock-Ingram Research, P. O. Box 5932, Johannesburg 2000, Republic of South Africa

(Received December 16, 1977)

A recent paper,[1] published in *Bull. Chem. Soc. Japan* and describing an alleged new synthesis of branched-chain deoxy nitro and amino sugars, has prompted this reply. It seems quite unlikely that the author, in carrying out a proper scientific literature search, could have overlooked my original paper on this matter, as it is well documented in the chemical literature[2,3] and has been reviewed.[4]

In any event, the unusual identity of the two papers[1,3] points to the fact that Abdel-Rahman must have been in possession of the paper published in *Carbohydrate Research*. In comparing the two papers it is quite clear that most of the sentences in the entire paper were copied exactly. Furthermore, both papers describe the addition of nitromethane to 1,2-*O*-isopropylidene-5-*O*-trityl-α-D-*erythro*-pentafuranos-3-ulose in nitromethane as the solvent, and in the presence of sodium hydride at −20 °C, as well as subsequent reactions carried out on the product obtained.

In addition, the yields, melting points, optical rotations, infrared and NMR data correspond exactly with those given in the original paper,[3] which is quite unusual. If the yields given by Abdel-Rahman, which are the same as given in the *Carbohydrate Research* paper, are recalculated on the basis of the changed quantities used, one finds:

Compound	Yield recalculated	Given[1]	Literature[3]
2	71.6%	76%	76%
5	53.3%	58%	58%
6	75.3%	82%	82%

These figures speak for themselves.

In the changed description of the preparation of Compound **3**, the author did not realise that the chromatography step, as described, was absolutely necessary in order to purify the product from the less polar triphenylmethane formed in the reaction. Perhaps the most unbelievable feature about this paper is the fact that Abdel-Rahman was able to obtain a correct elementary carbon, hydrogen and nitrogen analysis of $C_{12}H_{16}NO_9$, which is in fact the M^+-15 mass for Compound **3**; in my paper[3] an accurate determination of the mass was done on the base peak of M^+-15, which calculated for $C_{12}H_{16}NO_9$.

Finally, no literature references other than those listed[5] in the original article,[3] were included; this shows that more recent literature had not been searched. Several similar additions with nitromethane, though, have been described in recent years.[6]

References

1) M. M. A. Abdel-Rahman, *Bull. Chem. Soc. Jpn.*, **50**, 1619 (1977).

2) G. J. Lourens, *Tetrahedron Lett.*, **1969**, 3733; *Chem. Abstr.*, **72**, 21890s (1970).

3) G. J. Lourens, *Carbohydr. Res.*, **17**, 35 (1971); *Chem. Abstr.*, **74**, 142252 (1971).

4) "Carbohydrate Chemistry," Vol. 3, Senior Reporter R. D. Guthrie, The Chemical Society, London (1970), p. 122.

5) Omitted: H. P. Albrecht and J. G. Moffatt, *Tetrahedron Lett.*, **1970**, 1063, which appeared simultaneously with the original communication.[1]

6) S. W. Gunner, R. D. King, W. G. Overend, and N. R. Williams, *J. Chem. Soc., C*, **1970**, 1954; A. Rosenthal and K. -S. Ong, *Can. J. Chem.*, **48**, 3034 (1970); J. Yoshimura, K. Kobayashi, K. Sato, and M. Funabashi, *Bull. Chem. Soc. Jpn.*, **45**, 1806 (1972); J. Yoshimura, K. Sato, K. Kobayashi, and C. Shin, *ibid.*, **46**, 1515 (1973); A. Rosenthal and G. Schöllnhammer, *Can. J. Chem.*, **50**, 1780 (1972); W. P, Blackstock, C. C. Kuenzle, and C. N. Eugster, *Helv. Chim. Acta*, **57**, 1003 (1974).

A copy of the comment of Lourens was sent to Abdel-Rahman in December 1977, but his reply does not arrive yet.
The Editors

Reaction of Hydrogen Atoms with Acrylaldehyde

Seiichiro KODA, Kazumoto NAKAMURA, Takashi HOSHINO, and Tsutomu HIKITA

Department of Reaction Chemistry, Faculty of Engineering, The University of Tokyo, Hongo, Bunkyo-ku, Tokyo 113

(Received May 27, 1977)

The reaction of hydrogen atoms with acrylaldehyde was investigated in a fast flow reactor equipped with a time-of-flight type mass spectrometer under reduced pressure. Main reaction products were carbon monoxide, ethylene, ethane, methane, and propanal. Consideration of the distributions of the reaction products under various reaction conditions showed that hydrogen atoms attacked the C=C double bond, especially its inner carbon side under reduced pressure. Resulting hot radicals caused subsequent reactions. The relative value of the apparent bimolecular rate constant of the reaction against that of *trans*-2-butene with hydrogen atoms was 1.6±0.2, which supported the above-mentioned initial reaction.

Hydrogen atoms add to C=C double bonds forming vibrationally excited alkyl radicals. These excited radicals can undergo unimolecular dissociation or be collisionally stabilized. On the other hand, the weak aldehydic hydrogen of saturated aldehydes is known to be abstracted by hydrogen atoms. The reaction of hydrogen atoms with simple monoolefins and aldehydes were already well elucidated, and data on respective reaction rates have also been fully reviewed.[1,2] By contrast the reactions of conjugated double bond systems with hydrogen atoms in gas phase seem not to have been fully studied. One known example is H+butadiene.[1,3] The reason for the remarkably high rate constant for this reaction seems to be still uncertain.

Acrylaldehyde is an interesting compound because it contains a conjugated double bond system, as well as a weakly bound aldehydic hydrogen. Though the reaction with oxygen atoms has been studied,[4,5] that with hydrogen atoms has never been investigated.

From the viewpoint of environmental science, acrylaldehyde is a noteworthy compound because of its possible role in photochemical smog and its strong toxicity. Only one study on the potential of smog formation of acrylaldehyde has so far been published.[6] Thus, the investigation of the reaction sequences in the mixture of acrylaldehyde with the simplest species, atomic hydrogen, will contribute to our understanding of the role of acrylaldehyde in photochemical smog.

Experimental

The experimental apparatus is illustrated in Fig. 1, which is almost similar to the apparatus of Arrington *et al.*[7] Hydrogen atoms were produced by a 2450 MHz microwave discharge in a mixture of hydrogen and argon, and were introduced into a Pyrex reaction tube (inner diam, 1.28 cm). Acrylaldehyde was added to the flow *via* an inner tube (outer diam, 0.32 cm) which was movable in order to control the reaction time. A part of the reaction mixture was directly introduced into a time-of-flight type mass spectrometer (Hokushin Denki Co., Ltd., Bendix Model) through a pin-hole (diam, 0.01 cm) positioned at the end of the reaction tube.

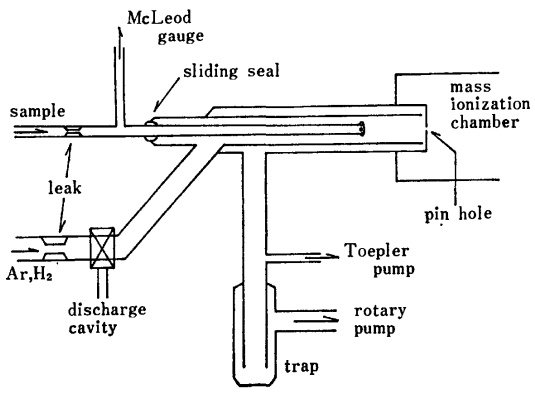

Fig. 1. Apparatus.

The reactions were carried out at room temperature (298± 5 °C). The pressure in the reaction tube (around 0.3 Torr) was measured by a McLeod gauge. The pressure drop along the reaction tube between the point of addition of acrylaldehyde and the pin-hole (maximum distance, 10 cm) was found to be negligibly small.

The mass flow velocity of each gas was calculated from the pressure drop with time in a standard volume. The linear flow velocity (about 3 m/s) was calculated from the total volume flow rate, the reactor pressure and the cross-sectional area of the reaction tube. The reaction time was calculated by dividing the length between the point of addition of acrylaldehyde and the pin-hole to the mass spectrometer by the linear flow velocity. The reaction time was varied between 3 and 33 ms by the change of the position of the inner tube.

The concentration of hydrogen atoms was determined through titration with ethylene. A similar method was adopted by Halstead *et al.*[8] The concentration of hydrogen atoms was usually around 3×10^{-7} mol/l, and that of acrylaldehyde was $(1—10)\times10^{-7}$ mol/l. The total concentration of gases was around 1.5×10^{-5} mol/l.

The major products were identified by analysis of the ionization efficiency curves of the respective parent mass peaks. The quantitative analyses were carried out based on the fragmentation patterns and relative sensitivities of standard samples.

In some experiments, a part of the reaction mixture was pumped by a Toepler pump into a gas sampler and was analyzed by means of gas chromatography with columns of Molecular Sieve 5A (for CO), Porapak Q and 3,4-dimethylsulforane (for hydrocarbons), and Polyethylene glycol 1500 (for aldehydes).

Purest hydrogen and argon (both 99.99%) obtained commercially were passed through traps cooled at liquid nitrogen temperature, and then introduced to the discharge region through leaks. Commercially obtained acrylaldehyde was purified gas-chromatographically with a column of Tritolyl phosphate. The resultant purity was at least 99%.

Results

Figure 2 shows the yields of the products estimated by use of mass spectrometry at the reaction time of

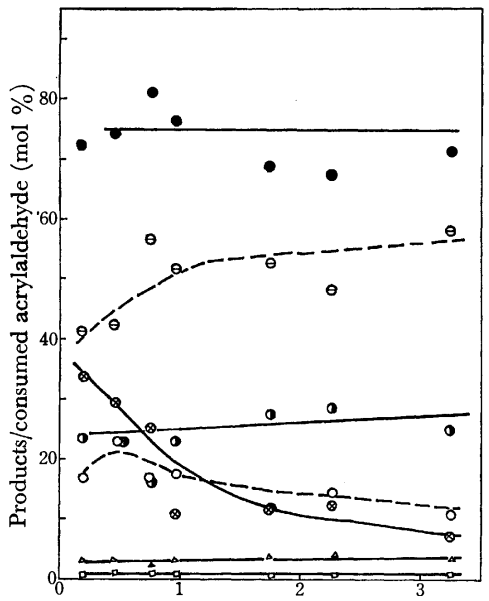

Fig. 2. The distribution of products at various different $[A]_0/[H]_0$.
Reaction conditions: total pressure, 0.38 Torr (Ar, 1.7 $\times 10^{-5}$ mol/l, H_2, 3.9×10^{-6} mol/l); $[H]_0$, 4.0×10^{-7} mol/l; $[A]_0$, 1.0×10^{-7} — 1.3×10^{-6} mol/l; reaction time, 22 ms.
Products: ● CO, ⊖ C_2H_4, ◑ C_2H_5CHO, ⊗ CH_4, ○ C_2H_6, △ CH_3CHO, □ C_3H_8.

TABLE 1. THE RESULTS OF GAS CHROMATOGRAPHIC ANALYSES

Product (mol %)	Initial concn of acrylaldehyde	
	1.1×10^{-6} mol/l	2.2×10^{-7} mol/l
Carbon monoxide	77	77
Ethylene	67	58
Propanal	15	9.8
Ethane	13	16
Methane	14	16
Acetaldehyde	1.7	2.6
Others	trace	5.4 (propane)
		2.4 (propylene)
		0.4 (acetylene)

The figures are the mole percent of the product divided by the consumed acrylaldehyde. Because the amounts of the consumed acrylaldehyde could not be measured, the equivalent concentration of the consumed acrylaldehyde was calculated from mass balance considerations, on the assumption that no products were missed. Reaction conditions: total pressure, 0.50 Torr ([Ar]= 2.6×10^{-5} mol/l, $[H_2]=6.0\times 10^{-7}$ mol/l), the initial concentration of hydrogen atoms, 1.75×10^{-7} mol/l.

22 ms. The analytical results are shown in Table 1. These two results agree with each other, though allowance should be made for the different reaction conditions and the very different time for analyses. The relatively low yield of propanal (Table 1) may be attributed to its probable adsorption in the analysis system for gas chromatography.

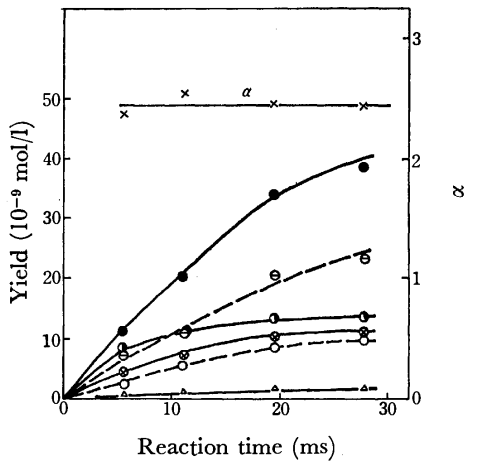

Fig. 3. Product growth curves with reaction time.
Reaction conditions: total pressure, 0.38 Torr (Ar, 1.7 $\times 10^{-5}$ mol/l, H_2, 3.9×10^{-6} mol/l); $[H]_0$, 2.3×10^{-7} mol/l; $[A]_0$, 1.0×10^{-7} mol/l.
Products: ● CO, ⊖ C_2H_4, ◑ C_2H_5CHO, ⊗ CH_4, ○ C_2H_6, △ CH_3CHO.
α(×): in this estimation, 1.5 mol of hydrogen atoms was assumed to be consumed for 1 mol production of CO, see text.

Figure 3 shows the growth of each product and the change of the stoichiometric ratio α with reaction time. Here, α is the ratio of the amount of the consumed hydrogen atoms to that of the consumed acrylaldehyde.

$$\alpha = ([H]_0-[H])/([A]_0-[A]) \quad \text{(i)}$$

[A], $[A]_0$ are the concentrations of acrylaldehyde, and [H], $[H]_0$, those of hydrogen atoms, at the reaction time t and at the initial time, respectively.

The amount of the consumed hydrogen atoms was calculated on the assumption that they were either trapped in the products (such as ethylene, methane, ethane, and propanal), or converted to hydrogen molecules. In the former case, the amount of the trapped hydrogen atoms was estimated from the yields of the products. In the latter case, carbon monoxide was produced simultaneously. The amount of the consumed hydrogen atoms ($-\Delta[H]$) was estimated to be about 1.5 times as large as the amount of the produced carbon monoxide ($\Delta[CO]$) from consideration of the hydrogen mass balance in an experiment where the initial hydrogen atoms were almost completely consumed within 33 ms. The experimental condition of the reaction were: The initial concn of the hydrogen atoms, 4.0×10^{-7} mol/l, $[A]_0/[H]_0$, 0.5. The reaction was found to be completed in about 30 ms. Because the amounts of the hydrogen atoms trapped in the products other than CO could be calculated, the ratio, $-\Delta[H]/\Delta[CO]$ could be easily estimated from the hydrogen mass balance. The ratio might depend on the initial conditions and change with reaction time, but we were obliged to adopt the constant value 1.5 in the estimation of α.

The value α was shown to be roughly constant throughout the reaction (Fig. 3). This fact allows to calculate the apparent bimolecular reaction rate constant of the reaction (ii) by the following simple

procedure.

$$\text{acrylaldehyde} + H \longrightarrow \text{products} \quad \text{(ii)}$$

The rate equation (iii) is integrated to result in (iv).

$$d[A]/dt = k_{ap}[A][H] \quad \text{(iii)}$$

$$k_{ap}t = [1/([H]_0-[A]_0)] \ln ([A]_0[H]/[A][H]_0)$$
$$= [1/([H]_0-[A]_0)] \ln [[A]_0([H]_0-\alpha([A]_0-[A]))/[A][H]_0] \quad \text{(iv)}$$

The right hand side of the above equation could be calculated from the data of $[H]_0$, $[A]_0$, $[A]$, and α. The resultant values are plotted against the reaction time t in Fig. 4. The slope of the straight line gave the bimolecular rate constant.

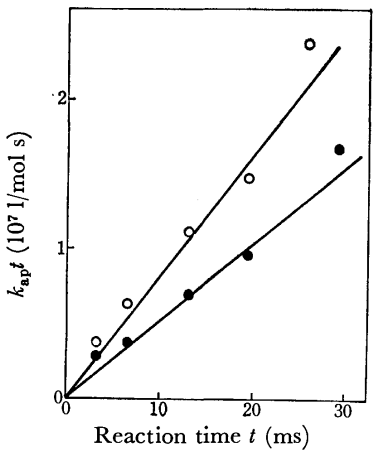

Fig. 4. The relationship between $k_{ap}t$ *vs.* reaction time. Reaction conditions: total pressure, 0.29 Torr (Ar, 1.4 $\times 10^{-6}$ mol/l, H_2, 1.4×10^{-5} mol/l); $[H]_0$, 2.84×10^{-7} mol/l, $[A]_0$ and [*trans*-2-butene]$_0$, 1.60×10^{-7} mol/l.
-●-: For reaction of *trans*-2-butene (α=2.8),
-○-: for reaction of acrylaldehyde (α=2.4).

k_{ap} for acrylaldehyde = $(8.1\pm 0.8)\times 10^8$ l/mol s

The reaction of *trans*-2-butene with hydrogen atoms was studied in the same apparatus as a reference. The apparent bimolecular rate constant was obtained similarly (Fig. 4) to be,

k_{ap} for *trans*-2-butene = $(5.1\pm 0.5)\times 10^8$ l/mol s.

Thus the relative rate constant of the reaction of acrylaldehyde, k_{ap}(for acrylaldehyde)/k_{ap}(for *trans*-2-butene), was calculated from the above absolute rate constants to be 1.6 ± 0.2. The possible incomplete mixing of the reactants and the diffusion of hydrogen atoms along the reaction tube make the exact estimation of the reaction time difficult. Thus the relative value might be more reliable than the absolute one, though it is worth nothing that the absolute constant for *trans*-2-butene agrees well with the value reported by Daby *et al.*[9]

Discussion

Reaction Mechanism. In the experiments where the initial rate $[A]_0/[H]_0$ is less than 1, the low yield of ethylene is compensated by the relatively high yields of ethane and methane, as shown in Fig. 2. This should be due to the occurrence of the secondary reactions of the product ethylene with hydrogen atoms to some extent to yield methane and ethane. The apparent reaction rate constant of ethylene with hydrogen atoms was reported by Michael *et al.* to be 0.9×10^8 l/mol s in 0.96 Torr Ar,[10] whereas our value in a similar apparatus is 0.4×10^8 l/mol s in 0.5 Torr Ar,[11] and is much smaller than that of acrylaldehyde, 8.1×10^8 l/mol s as described previously; thus the consumption of the primary product ethylene is expected to occur to any appreciable extent only when hydrogen atoms still remain after acrylaldehyde is almost completely consumed.

On the other hand, in the experiments where the ratio $[A]_0/[H]_0$ is kept larger than 1, the yield of each product is relatively constant and does not depend on that ratio. The observed product distribution should then reflect the primary reaction sequences of acrylaldehyde with hydrogen atoms.

Addition of hydrogen atoms to aldehydic CO bond has not been observed to proceed to any appreciable extent.[1] Hydrogen atoms may then either add to the C=C double bond or abstract the aldehydic hydrogen from acrylaldehyde. The rate of the reaction of saturated aldehydes with hydrogen atoms is known to be smaller than the addition to simple monoolefins by a factor of around 10. Then the abstraction of the aldehydic hydrogen is not expected to be the main reaction in the case of acrylaldehyde. This idea is supported by the experimental observation that acetylene was produced only in a negligibly small yield. Acetylene should have been produced in a relatively high yield through subsequent reactions, if the abstraction was the main primary process. The following reaction sequence is expected to follow the abstraction:

$$CH_2{=}CHCHO + H \longrightarrow CH_2{=}CH\dot{C}O + H_2$$
$$CH_2{=}CH\dot{C}O + H \longrightarrow CH{\equiv}CH + CO + H_2,\ CH_2{=}\dot{C}H + CHO$$
$$CH_2{=}\dot{C}H + H \longrightarrow CH{\equiv}CH + H_2.$$[12-14]

of course, we cannot deny the following possibility completely, based on the absence of acetylene among the reaction products.

$$CH_2{=}CHCHO + H \longrightarrow CH_2{=}CHCO + H_2$$
$$CH_2{=}CHCO + H \longrightarrow CH_2{=}CH_2 + CO$$

Thus the primary processes are considered to be the additions (1a) and (1b).

$$CH_2{=}CHCHO + H \rightleftarrows \dot{C}H_2CH_2CHO^* \ (I_a^*) \quad \text{(1a, -1a)}$$
$$\rightleftarrows CH_3\dot{C}HCHO^* \ (I_b^*) \quad \text{(1b, -1b)}$$

Here, the asterisk means that the species possesses some excess energy.

The resulting hot alkyl-like radicals I_a^* and I_b^* may either decompose unimolecularly or be stabilized.

$$I_a^* \longrightarrow CH_2{=}CH_2 + CHO \quad \text{(2)}$$
$$I_a^* + M \longrightarrow I_a + M \quad \text{(3a)}$$
$$I_b^* + M \longrightarrow I_b + M \quad \text{(3b)}$$

Though no thermochemical or structural data on the radicals I_a and I_b are known, we expect that I_a^* may behave like the hot *n*-propyl radical and I_b^* like the hot isopropyl radical produced in the reaction of

propylene with hydrogen atoms.[15,16] I_b* is assumed not to decompose because it does not seem to lead to any favorable dissociation reactions. By the analogy to the hydrogen atom-propylene system, the possible subsequent reactions are summarized as follows:

$$I_a, I_b + H \longrightarrow CH_3CH_2CHO^* \quad (4)$$

$$CH_3CH_2CHO^* + M \longrightarrow CH_3CH_2CHO + M \quad (5)$$

$$CH_3CH_2CHO^* \longrightarrow CH_3CH_2 + CHO \quad (6)$$

$$CH_3CH_2 + H \longrightarrow C_2H_6, 2CH_3 \quad (7)$$

$$CH_3 + H + M \longrightarrow CH_4 + M \quad (8)$$

$$CHO + H \longrightarrow CO + H_2 \quad (9)$$

Considerations of the fact that relatively complex radicals react with hydrogen atoms very rapidly† and of the fact that the concentration of hydrogen atoms is much higher than the possible concentrations of these radicals in the present study guarantee the neglect of any reactions other than those described above for the radicals, I_a, I_b, and C_2H_5. But for the radicals, CH_3 and CHO, radical-radical reactions may be as important as radical-atomic hydrogen reactions, because the latter reactions are not expected to be rapid enough under reduced pressure. The rate constant of Reaction 9 seems to be still uncertain,[18,19] but if a probable value of around 1×10^9 l/mol s is adopted, the reactions such as 10 and 11[19,20] cannot be neglected.

$$CHO + CHO \longrightarrow H_2 + 2CO \quad (10)$$

$$CHO + CH_3 \longrightarrow CH_4 + CO \quad (11)$$

The Reaction 12 may not be neglected, similarly.

$$CH_3 + CH_3 \longrightarrow C_2H_6 \quad (12)$$

The occurrence of Reactions 10 and 11 is expected to result in lowering the ratio, $-\Delta[H]/\Delta[CO]$, below 2. If the Reactions are limited to (1)—(9), the ratio should be 2. In fact, we have found the ratio 1.5, as described before.

According to the preceding discussions, we propose the reactions (1a, −1a) and (1b, −1b) followed by (2) through (12) as the main reaction sequence of the system of acrylaldehyde with hydrogen atoms under the reaction conditions of reduced pressure and also of $[A]_0/[H]_0\approx1$.

The net fraction of the hydrogen atom addition to the inner side of the C=C double bond is defined by Eq. v.

$$p = \frac{k_{1a}\times\dfrac{k_2+k_{3a}[M]}{k_{-1a}+k_2+k_{3a}[M]}}{k_{1a}\times\dfrac{k_2+k_{3a}[M]}{k_{-1a}+k_2+k_{3a}[M]}+k_{1b}\times\dfrac{k_{3b}[M]}{k_{-1b}+k_{3b}[M]}} \quad (v)$$

On the other hand, the following relation can be derived through a simple mass balance treatment.

$$([C_2H_5CHO]+[C_2H_6]+0.5[CH_4])/[C_2H_4] \text{ (defined as } R)$$
$$= \frac{k_{1a}k_{3a}[M]/(k_{-1a}+k_2+k_{3a}[M])+k_{1b}k_{3b}[M]/(k_{-1b}+k_{3b}[M])}{k_{1a}k_2/(k_{-1a}+k_2+k_{3a}[M])} \quad (vi)$$

We can expect $k_2\gg k_{-1a}$, assuming that the hot radical I_a* is similar to usual hot alkyl radicals, which undergo the C–C bond cleavage predominantly.[21] Moreover, the relatively low pressure of the present work allows to assume $k_2>k_{3a}[M]$. Then the following approximations results:

$$p \approx k_{1a}/(k_{1a}+k_{1b}k_{3b}[M]/(k_{-1b}+k_{3b}[M])) \quad (vii)$$

$$R \approx k_{1b}k_{3b}[M]/k_{1a}(k_{-1b}+k_{3b}[M]) \quad (viii)$$

Thus the net fraction p is related to the value R by the following equation.

$$p \approx 1/(1+R) \quad (ix)$$

We have got the value of R as 0.7 from the data shown in Fig. 2. The net fraction of the hydrogen addition to the inner side of the C=C double bond was then estimated to be about 0.60 ($=1/(1+0.7)$) under the present conditions.

Relative Reaction Rate. We wish to find out a quantum-chemical measure with which the reaction rate of the addition of the hydrogen atoms to each carbon atom among various C=C double bonds can be predicted and to know whether the addition of the atoms to acrylaldehyde is similar to the addition to simple olefins, or not.

Yang[22] showed that the activation energy of the addition to olefins were related to the corresponding localization energy. But this measure cannot be used to show the reactivity of individual carbon atom. Daby *et al.*[9] related the relative rate to the free valence. Though they got some success, they had to classify monoolefins into two groups; inner olefins and α-olefins. Thus we suspected if the atomic population might be an adequate measure for our present purpose, considering that atomic hydrogen seems to behave as an electrophilic reagent to some extent.[23]

In fact, we could find a good linear relationship between the atomic population of each carbon atom of C=C double bond of simple olefins and the logarithm of the relative rate constant (data are taken from Cvetanović *et al.*[1,24]) as shown in Fig. 5. The atomic populations were calculated by CNDO/2 for stable configurations (Table 2). In the case of symmetric olefins (*trans*- and *cis*-2-butenes and ethylene), the experimentally obtained rate constants were divided by 2; these olefins are considered to possess two equivalent reaction centers. In the case of propylene, 1-butene and 2-methylpropene, the experimental relative rate constants were plotted against the higher values of atomic population; those of terminal sides. This is reasonable because of the large difference in the atomic populations between the terminal and inner carbons. It is known that the percentage of the addition to the inner side is very small.[25]

The apparent reaction rate constant of acrylaldehyde is described by Eq. x according to the previously given reaction sequence.

$$k_{ap} = k_{1a}(k_2+k_{3a}[M])/(k_{-1a}+k_2+k_{3a}[M]) + k_{1b}k_{3b}[M]/(k_{-1b}+k_{3b}[M]) \quad (x)$$

By adopting the previous assumption, $k_2\gg k_{-1a}$, we get

$$k_{ap} \approx k_{1a} + k_{1b}k_{3b}[M]/(k_{-1b}+k_{3b}[M]) \approx k_{1a}(1+R) \quad (xi)$$

† For example, the values, 3.6×10^{10} l/mol s by Kurylo *et al.*[17] and 2×10^{10} l/mol s by Michael *et al.*[10] were reported as the rate constant of the reaction, $H+C_2H_5$, under reduced pressure.

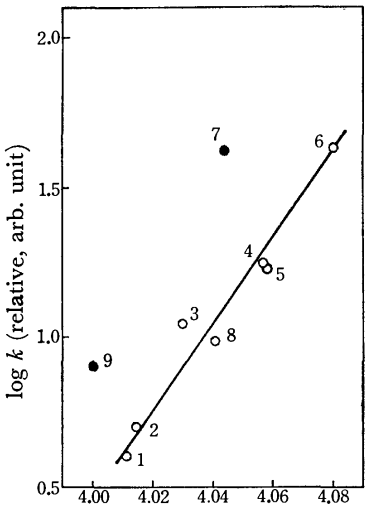

Fig. 5. The relationship between log (relative rate constant) and the atomic population.
1: *cis*-2-Butene, 2: *trans*-2-butene, 3: ethylene, 4: 1-butene, 5: propylene, 6: 2-methylpropene, 7: butadiene, 8: the inner carbon of acrylaldehyde (*vs.* k_{1a}), 9: the terminal carbon of acrylaldehyde (*vs.* $k_{1b}k_{3b}[M]/(k_{-1b}+k_{3b}[M])$).

TABLE 2. ATOMIC POPULATIONS BY CNDO/2

Substrate	C_1	C_2
$C_1=C_1$	4.0296	—
$C_1=C_2-C$	4.0573	3.9764
$C_1=C_2-C-C$	4.0568	3.9804
$C_1=C_2(-C)-C$	4.0794	3.9389
cis-$C-C_1=C_1-C$	4.0112	—
trans-$C-C_1=C_1-C$	4.0144	—
$C_1=C_2-C_2=C_1$	4.0434	3.9839
$C_1=C_2-C=O$	4.0000	4.0405

The calculations are for stable configurations. The computation program was taken from Ref. 26.

The relative rate constant, k_{ap} (for acrylaldehyde)/k_{ap}(for *trans*-2-butene) was 1.6 as described before. By adoptating 0.7 for R in Eq. xi, we estimated the value of k_{1a}(for acrylaldehyde)/k_{ap}(for *trans*-2-butene) to be 0.94. The apparent rate constant k_{ap} for *trans*-2-butene does not change over a wide pressure range, and should be equal to the primary addition rate constant, which was adopted in Ref. 24.[9] By use of this rate constant for *trans*-2-butene as a common reference, the constant k_{1a}(for acrylaldehyde) was compared with the rate constant for olefins in Fig. 5 (point 8). This point is on the line derived from the data of monoolefins. Thus the atomic population is a good quantum-chemical measure in the case of the addition to the inner carbon side of acrylaldehyde as well as in the case of monoolefins.

In spite of the reasonable relationship between the relative rate constant and the corresponding atomic population for monoolefins, the rate constant of butadiene is much higher than is predicted from its atomic population. Similarly, the rate constant k_{1b} in the case of acrylaldehyde seems to be much higher than expected. The point 9 in Fig. 5 is the lower limit of the relative value of k_{1b} against the atomic population of the terminal carbon of the C=C bond. The point indicates the relative value of $k_{1b}k_{3b}[M]/(k_{-1b}+k_{3b}[M])$ $(=k_{ap}-k_{1a})$ and should be the lower limit of k_{1b}. In these cases, the addition of atomic hydrogen results in production of stable π-allyl type radicals, and their stability should be the cause of the rapidness of the addition. It is expected that the individual atomic population can not be a good measure in this case.

Conclusion

1) Hydrogen atoms add mainly to the C=C double bond of acrylaldehyde, though some other possibilities are not completely eliminated.

2) Under reduced pressure, the net attacking position of hydrogen atoms is mainly (about 60% under the pressure of the present work, 0.3 Torr) the inner carbon side of the C=C double bond. Under higher pressures, the fraction of the addition to the terminal carbon may increase.

3) The rate of the addition to the inner carbon side can be explained by its atomic population as a quantum-chemical measure in a similar fashion as in monoolefins.

4) The subsequent reactions are regarded as unimolecular decompositions and collisional stabilizations of the resulting hot radicals in a similar fashion as in olefin-atomic hydrogen systems.

We are grateful to Professor Soji Tsuchiya, the Univ. of Tokyo, for his encouragement throughout this work. The reaction apparatus was originally constructed by him. We also acknowledge the Grant-in-Aid of the Ministry of Education given to this work.

References

1) W. E. Jones, S. D. Macknight, and L. Teng, *Chem. Rev.*, **73**, 407 (1973).
2) H. G. Wagner and J. Wolfrum, *Angew. Chem. Int. Ed. Engl.*, **10**, 604 (1971).
3) S. Koda and T. Hikita, *Bull. Chem. Soc. Jpn.*, **44**, 2888 (1971).
4) R. D. Cadle, S. S. Lin, and R. F. Hausman, Jr., *Chemosphere*, **1**, 15 (1972).
5) J. S. Gaffney, R. Atkinson, and J. N. Pitts, Jr., *J. Am. Chem. Soc.*, **97**, 5049 (1975).
6) B. Dimitriades and T. C. Wesson, *J. Air Poll. Control Assoc.*, **22**, 33 (1972).
7) C. A. Arrington, W. Brennen, G. P. Glass, J. V. Michael, and H. Niki, *J. Chem. Phys.*, **43**, 525 (1965).
8) M. P. Halstead, D. A. Leathard, R. M. Marshall, and J. H. Purnell, *Proc. R. Soc. London, Ser. A*, **316**, 575 (1970).
9) E. E. Daby, H. Niki, and B. Weinstock, *J. Phys. Chem.*, **75**, 1601 (1971).
10) J. V. Michael, D. T. Osborne, and G. N. Suess, *J. Chem. Phys.*, **58**, 2800 (1973).
11) Our unpublished results.
12) G. G. Volpi and F. Zocchi, *J. Chem. Phys.*, **44**, 4010 (1966).
13) J. V. Michael and H. Niki, *J. Chem. Phys.*, **46**, 4969 (1967).
14) W. A. Payne and L. J. Stief, *J. Chem. Phys.*, **64**, 1150

(1976).
15) W. E. Falconer, B. S. Rabinovitch, and R. J. Cvetanović, *J. Chem. Phys.*, **39**, 40 (1963).
16) M. J. Lexton, R. M. Marshall, and J. H. Purnell, *Proc. R. Soc. London, Ser. A*, **324**, 433 (1971).
17) M. J. Kurylo, N. C. Peterson, and W. Braun, *J. Chem. Phys.*, **53**, 2776 (1970).
18) W. R. Brennen, I. D. Gay, G. P. Glass, and H. Niki, *J. Chem. Phys.*, **43**, 2569 (1965).
19) B. A. Ridley, J. A. Davenport, L. J. Stief, and K. H. Welge, *J. Chem. Phys.*, **57**, 520 (1972).
20) M. J. Yee Quee and J. C. J. Thynne, *Trans. Faraday Soc.*, **63**, 1656 (1967).
21) B. S. Rabinovitch and D. W. Setser, *Adv. Photochem.*, **3**, 1 (1964).
22) K. Yang, *J. Am. Chem. Soc.*, **84**, 3795 (1962).
23) J. A. Kerr and M. J. Parsonage, "Evaluated Kinetic Data on Gas Phase Addition Reactions," Butterworths (1972), p. 370.
24) R. J. Cvetanović and L. C. Doyle, *J. Chem. Phys.*, **50**, 4705 (1969).
25) W. E. Falconer and W. A. Sunder, *Int. J. Chem. Kinetics*, **3**, 395 (1971).
26) G. A. Segal, "Quantum Chemistry Program Exchange," No. 91, Department of Chemistry, Indiana University, Bloomington, Ind., 47401, 1966.

Intramolecular Hydrogen Bond between Hydroxyl Group and π-Base in 2-Hydroxybiphenyl

Yoshikazu Ioki, Hiroko Kawana,* and Kichisuke Nishimoto*

Biophysics Division, National Cancer Center Research Institute, Tokyo 104

**Department of Chemistry, Faculty of Science, Osaka City University, Osaka 558*

(Received July 20, 1977)

In order to clarify the nature of the intramolecular hydrogen bond between the hydroxyl group and the π-electron system in 2-hydroxybiphenyl, MO calculation based on the CNDO/2 MO method has been carried out. The total electronic energy of the molecule has been divided into one- and two-atomic terms. It was found that the resonance term mainly contributes to the intramolecular hydrogen bond formation. Contribution of other terms is discussed.

Since Wulf *et al.*[1] reported the doublet of the first overtone of the O–H stretching vibration in 2-hydroxybiphenyl, many workers[2–19] have studied the nature of the hydrogen bond with π-base, such as aromatic hydrocarbons and olefins. This type of hydrogen bond might play some role in the physico-chemical properties and chemical reactivity of the molecule. By adopting the theory of Mulliken's charge-transfer complex, some workers have concluded that charge-transfer interaction makes important contribution to this type of hydrogen bond formation.[11,13,19] However, they did not make clear whether it is the main contribution, since no comparison of various terms in the interaction energies was made.

This paper describes an attempt to analyze the intramolecular hydrogen bond energy of 2-hydroxybiphenyl by the calculation based on the CNDO/2 method.[20] 2-Hydroxybiphenyl, having antiseptic activity, is a typical molecule with intramolecular interaction of H···π type. The electron correlation is not taken into account in the CNDO/2 SCF method, and the calculated value of total electronic energy is not highly reliable. However, our object is to calculate the energy difference between the non-bonded and the hydrogen bonded systems. Since the effect of electron correlation might be mostly cancelled out we have used the simple semi-empirical MO method, CNDO/2. The total energy is divided into one- and two-atomic terms, the two-atomic term being further divided into resonance, exchange, and Coulomb terms. So far energy decomposition studies on intramolecular hydrogen bond with π-electron system do not seem to have been reported. Recently a study on the intermolecular hydrogen bonds of some small systems has been made by Kitaura and Morokuma,[21] but their method can not be applied directly to the intramolecular hydrogen bond problem.

Procedure

Geometry. 2-Hydroxybiphenyl is assumed to be twisted around the central single bond (Fig. 1) because of the repulsions among non-bonded ring hydrogens. For biphenyl, the dihedral angle between phenyl planes was estimated to be *ca.* 40°.[22] There is an additional steric hindrance between the hydroxyl group and phenyl ring in 2-hydroxybiphenyl. Ōki *et al.* assumed that the dihedral angle of the present molecule

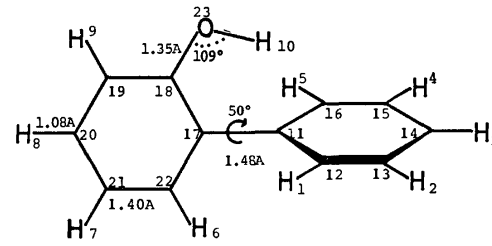

Fig. 1. Geometry and numbering adopted for the molecular orbital calculations.

is 50°.[13]

In order to confirm the validity of the assumed conformation, we have carried out SCF-MO-CI calculation by the P-P-P method[23] using variable β approximation and N-gamma for two-center electron repulsion integrals. This method provides satisfactory results for $\pi\rightarrow\pi^*$ transitions.[24] The calculated results for 2-hydroxybiphenyl are summarized in Table 1 with experimental values. The calculated and experimental results agree satisfactorily.

Table 1. Calculated transition energies and oscillator strengths of 2-hydroxybiphenyl

Calcd		Obsd	
ΔE(eV)	f	ΔE(eV)	$\varepsilon\times10^{-3}$
4.38	0.11	4.36	6
5.26	0.51	5.06	12
5.70	0.31		
6.05	0.33	6.00[sh]	23
6.15	0.81		
6.25	0.41		

Interaction Energies. The intramolecular hydrogen bond energy of 2-hydroxybiphenyl is given by the difference of total energies between hydrogen bonded structure **I** and non-bonded structure II shown in Fig. 2. The total energy can be expressed by the sum of one- and two-atomic terms:[20]

$$E_{\text{total}} = \sum_{A} E_A + \sum_{A<B} E_{AB}, \tag{1}$$

where

$$E_A = \sum_{\mu}^{A} P_{\mu\mu} U_{\mu\mu} + \frac{1}{2}\sum_{\mu}^{A}\sum_{\nu}^{A}\left(P_{\mu\mu}P_{\nu\nu} - \frac{1}{2}P_{\mu\nu}^2\right)\gamma_{AA}, \tag{2}$$

$$E_{AB} = \sum_{\mu}^{A}\sum_{\nu}^{B} 2P_{\mu\nu}\beta_{AB}^{\circ}S_{\mu\nu} - \sum_{\mu}^{A}\sum_{\nu}^{B}\frac{1}{2}P_{\mu\nu}^2\gamma_{AB} + (Z_A - P_{AA})(Z_B - P_{BB})\gamma_{AB}. \tag{3}$$

We refer to the first, second, and third terms of two-atomic term (Eq. 3) as resonance, exchange, and Coulombic interaction energies, respectively. The difference in these energy terms between bonded and non-bonded structures, is used for discussing the nature of the hydrogen bond.

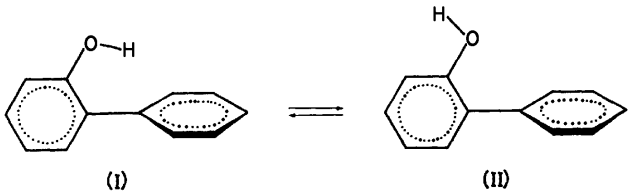

(I) (II)

Fig. 2. Assumed geometry of 2-hydroxybiphenyl.

Results and Discussion

The calculated results for each term are summarized in Tables 2, 3, and 4. Intramolecular hydrogen bond energy ($\Delta E=E(\mathbf{I})_{\text{total}}-E(\text{II})_{\text{total}}$) of the present molecule calculated by the CNDO/2 method is −0.193 eV, which is larger than the experimental value for

Table 3. Calculated total energies associated with two-atomic terms (in eV)

	Structure I	Structure II	$E(\mathbf{I})-E(\text{II})$
$\sum_{A<B}E_{AB}$	−710.4209	−710.2212	−0.1997
$\sum_{A}E_{HA}$ [a)]	−20.4851	−20.0014	−0.4837
Resonance	−20.4196	−19.8876	−0.5320
Exchange	−6.1496	−6.2813	0.1317
Coulomb	6.0841	6.1675	−0.0834

a) See Table 4.

Table 2. Calculated one-atomic terms of 2-hydroxybiphenyl (in eV)

Atom	Structure I	Structure II	Atom	Structure I	Structure II	Atom	Structure I	Structure II
1	−12.29295	−12.31117	9	−12.20039	−12.24681	17	−143.12038	−143.04830
2	−12.29397	−12.30978	10	−11.11982	−11.22776	18	−141.97950	−141.99221
3	−12.28841	−12.30532	11	−142.66898	−142.67655	19	−143.56136	−143.63519
4	−12.29552	−12.30903	12	−143.36160	−143.36896	20	−143.22607	−143.21155
5	−12.30162	−12.28555	13	−143.27698	−143.26206	21	−143.42328	−143.41195
6	−12.30627	−12.28959	14	−143.34993	−143.33280	22	−143.22066	−143.24660
7	−12.29422	−12.29170	15	−143.25843	−143.25778	23	−476.31951	−476.17039
8	−12.28768	−12.29543	16	−143.35772	−143.32587			

$\sum E_A(\mathbf{I})-\sum E_A(\text{II}) = 0.00709$ eV

Table 4. Calculated two-atomic terms (E_{HA}) associated with the hydroxyl hydrogen and other atoms (in eV)

Atom	Resonance I	Resonance II	Exchange I	Exchange II	Coulomb I	Coulomb II	$E_{HA}(\mathbf{I})-E_{HA}(\text{II})$
1	0	0	0	0	−0.0011	−0.0017	0.0006
2	0	0	0	0	−0.0009	−0.0013	0.0004
3	0	0	0	0	−0.0006	−0.0011	0.0005
4	−0.0002	0	0	0	−0.0014	−0.0016	−0.0001
5	−0.0784	−0.0022	−0.0033	−0.0002	0.0371	−0.0005	−0.0416
6	0.0004	−0.0001	−0.0003	−0.0005	−0.0019	−0.0006	−0.0005
7	0	0	0	0	−0.0008	−0.0007	−0.0001
8	−0.0001	0.0004	−0.0005	−0.0003	−0.0005	−0.0010	−0.0003
9	−0.0002	−0.0627	0	−0.0040	0.0063	0.0190	0.0539
11	−0.3423	−0.0038	−0.0165	−0.0005	0.1186	0.0290	−0.2649
12	−0.0004	−0.0001	−0.0001	0	−0.0091	−0.0064	−0.0031
13	0.0001	0	−0.0001	−0.0001	0.0013	0.0012	0
14	0.0010	0	−0.0006	0	−0.0089	−0.0046	−0.0039
15	−0.0121	0	−0.0003	−0.0001	0.0048	0.0018	−0.0093
16	−0.7574	−0.0016	−0.0537	−0.0001	0.1131	−0.0050	−0.6913
17	0.1490	−0.0929	−0.0140	−0.0248	0.0210	−0.0011	0.2748
18	−0.1856	−0.2469	−0.0038	−0.0044	0.3917	0.3805	0.0732
19	−0.0939	0.0966	−0.0260	−0.0115	−0.0346	−0.0180	−0.2216
20	0.0017	−0.0025	−0.0007	−0.0002	0.0037	0.0049	0.0025
21	−0.0001	−0.0002	−0.0001	−0.0001	−0.0144	−0.0122	−0.0021
22	−0.0044	0.0016	−0.0004	−0.0005	0.0059	0.0028	−0.0028
23	−19.0967	−19.5732	−6.0292	−6.2340	5.4548	5.7841	0.3520
ΣE_{HA}	−20.4196	−19.8876	−6.1496	−6.2813	6.0841	6.1675	−0.4837

X–H···π type interaction (<3 kcal/mol).[25] Since the CNDO/2 method usually gives larger binding energies,[26] the present result seems to be reasonable. The change of one-atomic term ($\Delta\sum E_A$) due to the formation of intramolecular hydrogen bond is quite small due to cancellation of one-atomic terms (ΔE_A) (Table 2). However, the two-atomic terms considerably stabilize the system, showing that energy of the hydrogen bond comes mostly from the two-atomic terms (Table 3). It should be noted that the interaction energy (ΔE_{HA}) between the hydrogen of hydroxyl group and the other atoms is remarkably large, more than double the value of $E(\mathbf{I})_{AB}-E(\mathrm{II})_{AB}$ (last column, Table 3). This shows that ΔE_{HA} greatly stabilizes the hydrogen bond, but some of the other two-atomic terms cause destabilization. The stabilization energy comes from the resonance (−0.532 eV) and Coulomb (−0.083 eV) terms. The exchange term (0.132 eV) plays the role of destabilization. The calculated result shows a decrease of O–H bond energy (atom 23 in Table 4), in line with the observed infrared spectral shift due to O–H vibrational lower frequency. Both the resonance and exchange terms of O–H bond energy decrease (−0.477 eV and −0.205 eV respectively), though the Coulomb term increases (0.329 eV).

It is evident that the hydrogen bond is formed mainly from resonance energy between the hydroxyl group and carbon atoms 11 (−0.339 eV) and 16 (−0.756 eV). For the sake of clarification, we have given the values of the term $P_{\mu\nu}S_{\mu\nu}$ between 1s orbital of the hydrogen of hydroxyl group and the valence orbitals of carbon atoms 11 and 16 as a measure of contribution to the resonance terms (Table 5). The amount associated with $2p_z$ orbital of carbon atom 16 is the largest (0.014), those associated with other orbitals not being small.

Table 5. Overlap integral ($S_{\mu\nu}$), bond order ($P_{\mu\nu}$), and their product ($P_{\mu\nu}S_{\mu\nu}$) between 1s orbital of hydroxyl hydrogen and valence orbitals of atoms 11 and 16

Orbital		$S_{\mu\nu}$	$P_{\mu\nu}$	$P_{\mu\nu}S_{\mu\nu}$
C_{11}	2s	0.1043	0.0318	0.0033
	$2p_x$	−0.0277	−0.0142	0.0004
	$2p_y$	0.0804	0.0309	0.0025
	$2p_z$	0.0958	0.0545	0.0052
C_{16}	2s	0.1390	0.0474	0.0066
	$2p_x$	−0.0961	−0.0433	0.0042
	$2p_y$	0.0155	0.0071	0.0001
	$2p_z$	0.1357	0.1061	0.0144

It is of interest to investigate the potential energy of O–H···π bonded system. We have calculated the total energies as a function of O–H distance, where only the position of the hydrogen of hydroxyl group is varied, all the other atoms keeping their positions unchanged. The result is shown in Fig. 3. The potential curve has a minimum at 1.04 Å of O–H distance. In the case of the non-bonded one, the calculated equilibrium O–H distance is 1.03 Å. This lengthening of O–H distance due to hydrogen bond formation leads to a decrease in the force constant, reflecting the lower shift of O–H vibrational frequency as observed in the infrared spectra.[13] The charge density on oxygen atom is minimum at 1.2 Å, increasing considerably with the O–H distance (Table 6). The charge densities of carbon atoms 11 and 16 decrease monotonously with increase in distance. This suggests that the charge-transfer structure $(O–H)^-\cdots C^+$ contributes to the intramolecular hydrogen bond formation to some extent. The present calculation shows that, when the O–H distance increases beyond 1.4 Å, the contribution of another type of charge-transfer structure $O^-\cdots(H–C)^+$ increases (Table 6). Thus double minimums in line with the experiment of infrared spectroscopy might be expected, though the CNDO/2 calculation gives no confirmation.

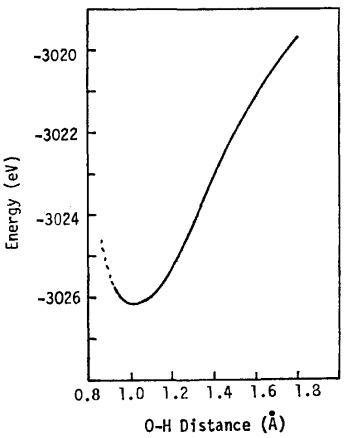

Fig. 3. Total energy of 2-hydroxybiphenyl in hydrogen bonded form as a function of O–H distance.

Table 6. Charge density on atoms in hydrogen bonded structure of 2-hydroxybiphenyl *vs.* O–H distance (Å)

O–H distance	Charge density				
	O_{23}	H_{10}	C_{16}	C_{11}	C_{12}
0.96	6.2594	0.8478	4.0215	3.9581	4.0160
0.98	6.2573	0.8502	4.0214	3.9579	4.0160
1.0	6.2554	0.8526	4.0213	3.9578	4.0161
1.2	6.2447	0.8726	4.0189	3.9547	4.0164
1.4	6.2525	0.8833	4.0141	3.9486	4.0176
1.6	6.2842	0.8796	4.0077	3.9387	4.0207
1.8	6.3669	0.8479	3.9962	3.9132	4.0254

Conclusion

Although hydrogen bonds of X–H···π type have been extensively studied, few investigations have been made on the changes of energy terms of all the atoms in the molecule due to the formation of the hydrogen bond. In the present work, we have tried to clarify the nature of X–H···π hydrogen bond and have obtained the following results. i) The contribution of one-atomic terms to the hydrogen bond in 2-hydroxybiphenyl is quite small. ii) The interaction between the hydrogen of hydroxyl group with the other atoms mainly contributes to stabilization of the hydrogen bonded conformation. However, considerable contribution to the instability comes from interactions among the other

atoms. iii) Most of the stabilization energy comes from resonance terms of the interaction between 1s orbital of the hydrogen of hydroxyl group and orbitals of carbon atom 16, mainly of its $2p_z$ orbital. iv) Exchange interaction between the hydrogen of hydroxyl group and the other atoms destabilizes the hydrogen bond. It should be noted that if we consider only the interacting hydrogen moiety, we obtain more than double the hydrogen bond energy (Table 3). v) The calculated result of charge densities as a function of O–H distance indicates the involvement of charge-transfer structures in the hydrogen bonded formation.

The results verify at least qualitatively that the resonance term including charge-transfer is the main one to stabilize intramolecular hydrogen bond of O–H$\cdots\pi$ type. Although it was discussed that charge-transfer interaction made important contribution, this fact was not revealed concretely. The present result forms a contrast with the ordinary hydrogen bond of X–H$\cdots$n type where Coulombic interaction also makes significant contribution to the stability. This characteristic of X–H$\cdots\pi$ type is considered to be due to the neutrality of the proton acceptor benzene-ring and delocalization of the electrons. The present treatment provides a method which is convenient for clarifying the nature of intramolecular hydrogen bonds of large molecles.

References

1) O. R. Wulf, U. Liddel, and S. B. Hendricks, *J. Am. Chem. Soc.*, **58**, 2287 (1936).
2) R. E. Richards and H. W. Thompson, *J. Chem. Soc.*, **1947**, 1260.
3) W. Luttke and R. Mecke, *Z. Elektrochem.*, **53**, 241 (1949).
4) W. Luttke and R. Mecke, *Z. Physik. Chem.*, **195**, 53 (1950).
5) V. von Keussler and G. Rossmy, *Z. Elektrochem.*, **60**, 136 (1956).
6) A. W. Baker and A. T. Shulgen, *J. Am. Chem. Soc.*, **80**, 5358 (1958).
7) H. Musso and S. von Grunelius, *Chem. Ber.*, **92**, 3101 (1959).
8) P. von R. Schleyer, D. S. Trifan, and R. Bacskai, *J. Am. Chem. Soc.*, **80**, 6691 (1958).
9) W. Beckering, *J. Phys. Chem.*, **65**, 206 (1961).
10) A. W. Baker and A. T. Shulgin, *Spectrochim. Acta*, **19**, 1161 (1963).
11) Z. Yoshida and E. Ōsawa, *J. Am. Chem. Soc.*, **87**, 1467 (1965).
12) W. F. Baitinger, Jr., P. von R. Schleyer, and K. Mislow, *J. Am. Chem. Soc.*, **87**, 3168 (1965).
13) M. Ōki and H. Iwamura, *J. Am. Chem. Soc.*, **89**, 576 (1967).
14) M. Ōki, H. Iwamura, T. Onoda, and M. Iwamura, *Bull. Chem. Soc. Jpn.*, **24**, 1905 (1968) and the proceeding papers of this series.
15) E. M. Arnett, L. Joris, E. Mitchell, T. S. S. R. Murty, T. M. Gerrie, and P. von R. Schleyer, *J. Am. Chem. Soc.*, **92**, 2365 (1970).
16) A. S. N. Murthy, S. N. Bhat, and C. N. R. Rao, *J. Chem. Soc., A*, **1970**, 1251.
17) J. E. Del Bene and F. T. Marchese, *J. Chem. Phys.*, **58**, 926 (1973).
18) J. R. Sabin, *Theor. Chim. Acta*, **27**, 69 (1972).
19) C. N. R. Rao, P. C. Dwivedi, H. Ratajczak, and W. J. Orville-Thomas, *J. Chem. Soc., Faraday Trans. 2*, **1975**, 955.
20) J. A. Pople and G. A. Segal, *J. Chem. Phys.*, **44**, 3289 (1966).
21) K. Kitaura and K. Morokuma, *Int. J. Quant. Chem.*, **10**, 325 (1976).
22) O. Bastiansen, *Acta Chem. Scand.*, **4**, 926 (1950).
23) R. G. Parr, "Quantum Theory of Molecular Electronic Structure," W. A. Benjamin, New York-Amsterdam (1963).
24) K. Nishimoto, *Theor. Chim. Acta*, **7**, 207 (1967).
25) M. Ōki, H. Iwamura, and Y. Urushibara, *Bull. Chem. Soc. Jpn.*, **31**, 669 (1958); M. Ōki, H. Iwamura, T. Onoda, and M. Nishida, *Bull. Chem. Soc. Jpn.*, **39**, 809 (1966).
26) J. A. Pople and D. L. Beveridge, "Approximate Molecular Orbital Theory," McGraw-Hill, New York (1970).

Application of Infrared ATR Spectroscopy to Liquid Crystals. II.[1] Surface-induced Orientation of Nematic MBBA and Reorientation in Electric Fields

Aritada HATTA, Hideaki NOHARA, and Wataru SUĒTAKA

Laboratory of Interface Science of Metals, Faculty of Engineering, Tohoku University, Aramaki Aoba, Sendai 980

(Received August 3, 1977)

A polarized infrared ATR technique was used to demonstrate the orientation of a nematic liquid crystal, *N*-(*p*-methoxybenzylidene)-*p*-butylaniline (MBBA), due to the walls of the electrode and an externally applied DC electric field. Polarized ATR spectra were obtained as a function of the field strength on liquid films 15 μm thick between a silicon ATR prism and a brass plate serving as electrodes. The observed infrared dichroism revealed the average orientation of molecules in boundary layers about 1 μm thick on the Si electrode surface. The ordering or packing of molecules before application of the field affects the response of molecules to the electric field in a striking manner. Molecular orientations on the Si electrode are discussed in some detail.

In recent years, dramatic developments were seen in the application of liquid crystals to electro-optical display devices.[2] For example, a dynamic scattering effect[3] has now proven to be most valuable in the application of nematic liquid crystals. Another important effect of electric field on liquid crystals is the change in orientation due to the anisotropy of the dielectric constants of the liquid crystal molecule.[4]

Heilmeier and Zanoni[5] have successfully obtained color switching using a nematic liquid crystal containing dissolved pleochroic dye molecules. This method is based on the guest-host interaction[6,7] by which the orientation of the guest dye is controlled by the orientation of its nematic host in an applied electric field. For practical applications of this effect, however, a high response to the electric field is essential to the liquid crystal. However, it has been pointed out that the interaction between liquid crystal molecules and electrode surfaces may often lower the response of the liquid crystal. Despite this limitation, the field-induced orientation is very interesting for several aspects of application.[2]

On the other hand, infrared spectroscopy is a powerful tool for obtaining information about the orientational behavior of liquid crystals. In this regard, therefore, it seems interesting to observe field-induced orientation using infrared techniques. Indeed, the molecular orientation of nematic *N*-(*p*-methoxybenzylidene)-*p*-cyanoaniline in DC electric fields has been investigated by Neff, Gulrich, and Brown[8] using a transmission method. However, no other infrared study of field-induced orientation has yet appeared. This is probably due to the fact that extremely thin films are required for obtaining accurate intensity data because of the high absorption of liquid crystals, as is generally the case. This difficulty is removed when the ATR method[9] is used, because the observed intensities are determined by the electric-field penetration of infrared radiation a few microns into the sample and are independent of the sample thickness.[10] The most significant advantage of using the ATR method is that electric fields of electromagnetic radiation exist in all three spatial directions at the reflecting interface. Therefore, this technique can be used to obtain information about any orientation of the liquid crystal.

For the above reasons, the infrared ATR technique was first applied to the study of the orientation of MBBA liquid crystals, and quantitative data which enabled the determination of the orientation pattern and its degree of order were obtained.[1] The present report describes the infrared ATR spectra of MBBA under the application of DC electric fields.

Experimental

The liquid crystal cell used for the ATR measurements has already been described in a previous paper.[1] In brief, the liquid crystal was sandwiched between a silicon ATR prism and a conducting plate, which were held apart by a polyester spacer. The Si prism and the substrate plate served as electrodes; a DC electric field was applied normal to the liquid layer 15 μm thick. The Si prism served as the positive electrode. The liquid crystal was maintained at a constant temperature by an electric heater placed in a brass box in contact with the substrate plate.

The ATR spectra were measured by placing the liquid crystal cell in the sample beam of a double-beam ATR attachment, at an angle of incidence of 40 °. In order to account for the absorption of the sample prism itself, a similar Si prism was placed in the reference beam. The infrared radiation was polarized using a AgCl polarizer.

A brass plate polished to a high degree of flatness was used as an electrode opposite the Si prism. The electrode plate and Si prism were subjected to ultrasonic cleaning for 30 min in ethyl alcohol followed by rinsing in acetone. Guaranteed-grade MBBA reagent from a commercial source was used without further purification.

Results and Discussion

Infrared Dichroism from Polarized ATR Spectra. A detailed description has already been given of an approximate method of determining the orientation pattern of a liquid crystal from measured amounts of the dichroic ratio.[1] Therefore, little will be given here concerning the method itself.

An ATR spectrum is essentially the reflection loss due to the interaction of an evanescent wave with an absorbing medium. According to Flournoy and Schaffers,[11] the reflectivities of radiation having the electric vector polarized perpendicular and parallel to the plane of incidence are given respectively by

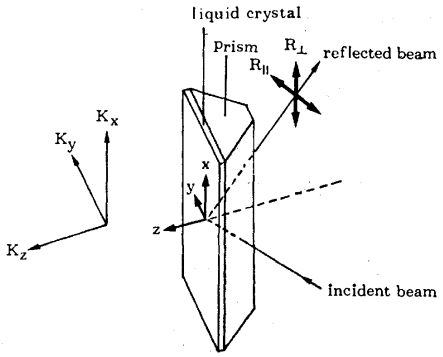

Fig. 1. Coordinate system showing the attenuated total reflection (ATR) from anisotropic absorbing liquid crystal. K_x, K_y, and K_z are the components of the absorption coefficient along the prism-fixed axes. $R_\parallel$ and $R_\perp$ indicate the reflectivities of the radiation polarized parallel and perpendicular to the plane of incidence, respectively.

$$\ln R_\perp = -pK_x$$

and

$$\ln R_\parallel = -qK_y - rK_z, \tag{1}$$

where p, q, and r are functions of the refractive indices of the absorbing medium and of the internal reflection prism, and the angle of incidence. Furthermore, K_x, K_y, and K_z are the components of the absorption coefficient along the prism-fixed axes shown in Fig. 1. In Fig. 1, the sample of the liquid crystal is assumed to be much thicker than the effective penetration depth of the evanescent wave.[10] The dichroic ratio D for a given vibration band can be written as

$$D = \frac{\log (R_\parallel^\circ/R_\parallel)}{\log (R_\perp^\circ/R_\perp)} = \frac{q}{p}\left(\frac{K_y}{K_x}\right) + \frac{r}{p}\left(\frac{K_z}{K_x}\right), \tag{2}$$

where $R_\parallel^\circ$ and $R_\perp^\circ$ are the background reflectivities measured with the radiation polarized parallel and perpendicular to the plane of incidence, respectively.

In order to calculate coefficients p, q, and r, it is desirable to know accurately the birefringence, $\Delta n = n_e - n_o$, in the infrared region for MBBA, where the extraordinary index n_e and ordinary index n_o correspond to the directions parallel and perpendicular to the optical axis of the director, respectively. In Eq. 2, the n_o contribution to the coefficients, q/p and r/p, is much smaller than the Δn contribution.[11] Therefore, n_o is conveniently assumed to be 1.54 in accordance with the value observed in the visible region,[12] as before.[1] On the other hand, the Δn for well oriented MBBA has been suggested to be 0.05—0.1 in the infrared region,[1] which is much less than 0.22 in the visible region.[12] Such a small birefringence change would, however, require a highly accurate measurement on the same system. Hence, the contribution from the birefringence was omitted in Eq. 2. Since birefringence is obviously related to the degree of order, its omission may result in an overestimation of the degree of order by about 10% for a sample of high structural order (if $\Delta n = 0.1$ in the infrared). For a less ordered sample, however, the error caused by the omission is negligibly small. Using the isotropic index of 1.54 assumed for MBBA and 3.42 for Si,[13] the coefficients were calculated for an incident angle of 40° and for one reflection at the Si-MBBA interface. The results are $p = 1.700$, $q = 1.215$, and $r = 2.384$. Upon substituting these values into Eq. 2, the observed dichroic ratio can be used to estimate the degree of anisotropy of the absorption coefficients.

This procedure can be simplified by assuming uniaxial symmetry for the nematic liquid crystals as follows. For example, if molecules in the liquid film are oriented normal to the Si prism surface (homeotropic), one finds $K_x = K_y$ from Fig. 1 and then Eq. 2 reduces to

$$D = 0.72 + 1.40\left(\frac{K_z}{K_x}\right). \tag{3}$$

If the molecules are oriented parallel, for instance, to the x axis which is perpendicular to the plane of incidence (uniformly homogeneous), one obtains

$$D = 2.12\left(\frac{K_z}{K_x}\right). \tag{4}$$

In particular, if the molecules are randomly oriented, *i.e.*, if $K_x = K_y = K_z$, the dichroic ratio becomes 2.12, regardless of the vibration type.

On the other hand, the degree of orientation order, S, is conveniently defined with respect to the orientation of the long axis of the molecule relative to the optical axis of the liquid crystal.[14] In this case the degree of order is given by

$$S = \frac{1}{2}(3\cos^2\alpha - 1) = \frac{(d-1)}{S_\beta(d+2)}, \tag{5}$$

with

$$S_\beta = \frac{1}{2}(3\cos^2\beta - 1),$$

where α is the angle between the long axis of the molecule and the optical axis of the uniaxial liquid crystal, and β is the angle between the long axis and the direction of the vibrational transition moment, as is shown in Fig. 2. In Eq. 5, $d = K_\parallel/K_\perp$, where $K_\parallel$ and $K_\perp$ are the absorption coefficients parallel and perpendicular to the optical axis, respectively, as is shown in Fig. 2. Accordingly, d is given by K_z/K_x for the homeotropic case, whereas it is given by K_x/K_z for the uniformly homogeneous case (if the preferred axis is x). Hence, the magnitude of K_z/K_x in the above examples acts as the measure for evaluating the orientation type and its

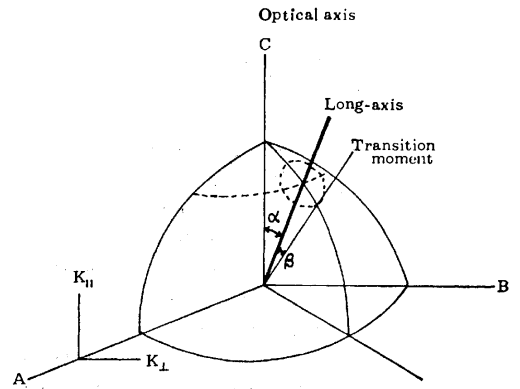

Fig. 2. Uniaxial orientation of the long-axis of the molecule around the optical axis and of the transition moment about the long-axis of the molecule. $K_\parallel$ component is taken to be parallel to the optical axis.

degree of order.

In terms of the d defined above, the degree of order S changes from 0 to 1, corresponding to a change from isotropic orientation or perfect orientation with $\alpha=54°44'$ to perfect orientation with $\alpha=0°$. It should, however, be mentioned that Eq. 5 is valid only when the molecules are packed as if they are allowed to rotate freely about their own long axes.

Based on Eq. 5, the β values of several important vibrations of MBBA were determined to within an accuracy of $\pm 10\%$ for highly-ordered homeotropic and uniformly-homogeneous liquids.[1] This fact demonstrates that Eq. 5 is a good approximation to the degree of order in terms of the orientation of the long axis of the molecule.

Orientation of Molecules at Electrode Surfaces. When a static electric field of rather low strength is applied to the liquid crystal, the primary effect of the field is the interaction with the dielectric tensor of the liquid so that the molecules tend to be oriented with their axes of maximum dielectric constant parallel to the field.[15] The reorientation is, however, often restrained by the surface orientation of the molecules at electrodes.[2] On the other hand, if the DC field is sufficiently high to produce hydrodynamic scattering, a greatly disordered texture is expected to be observed. In order to elucidate the electric-field effect on liquid crystals, it is necessary to know the original orientation produced by the electrode surfaces.

Because in the present work the Si ATR prism also served as an electrode, it is necessary to discuss the orientation of the MBBA molecules present on the Si prism surface. For this purpose, polarized ATR spectra were obtained for a thin liquid film of MBBA having an estimated thickness of 0.2 μm. The vaporized sample was deposited onto the reflection surface of the Si prism for nine internal reflections.

The observed ATR spectra are shown in Fig. 3. The absorption band assignments[1,16] and the observed D values are listed in Table 1, together with the β values[1] corresponding to these vibrations. On the other hand, when polarized infrared light was passed through the plane of the sample film at normal incidence, the spectrum was identical irrespective of the orientation of the electric field of the incident radiation. This demonstrates that the transition moments of the molecule are randomly oriented about the direction normal to the Si surface; the equality of K_x and K_y holds in the present case. Therefore, the dichroism observed from ATR spectra should be interpreted in terms of the uniaxial orientation of molecules about the z axis, which is perpendicular to the Si surface. On the basis of the assumption that the long axes of the molecules are uniaxially aligned with respect to the z axis, S values were calculated from the observed dichroic ratios[18] and the β values. The resulting S values are given in Table 1.

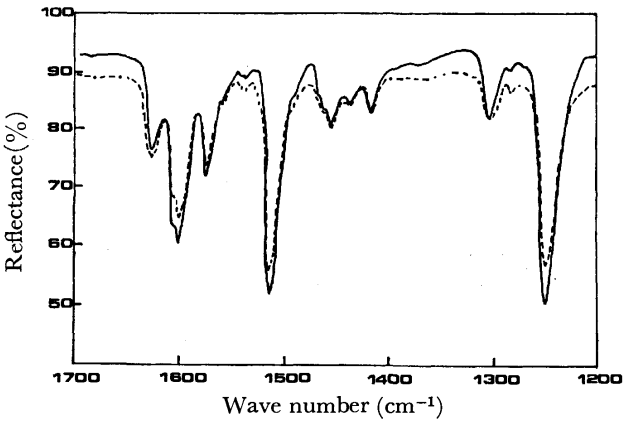

Fig. 3. Infrared polarized ATR spectra of thin MBBA liquid film (0.2 μm) at 25 °C deposited from vapor. Solid and broken lines refer to the orientation of the electric vectors of radiation parallel and perpendicular to the plane of incidence, respectively.

Thus, on the Si surface, MBBA molecules tend to be oriented with their long axes parallel to that surface in agreement with results based on other methods.[19] Nevertheless, the resulting S value for the 1630 cm^{-1} band is much larger than that for other vibration bands. This fact suggests anomalous structure of the thin film such that the molecules may not have complete freedom of rotation about the long axes of the molecules in the film. Assuming uniaxial alignment of the long axes with respect to the z axis, as mentioned above, and no molecular rotation about the long axes, the distribution of the transition moments can be calculated using the simple relation,

$$2\tan^2\gamma = \frac{K_z}{K_x}, \tag{6}$$

where γ is the angle that the transition moment makes with the surface plane. The γ values thus obtained are also given in Table 1.

Table 1. Fundamental data[18] obtained from polarized infrared ATR spectra for a thin liquid film of MBBA at 25 °C

(Thickness-0.2 μm)

Wave number (cm^{-1})	Assignment	β[17] (degrees)	D	K_z/K_x	S	γ (degrees)
1630	C=N str.	32.1	1.21	0.27	0.82	20
1600	phenyl-ring str.	21.5	1.37	0.41	0.40	24
1578	phenyl-ring str.	10.5	1.26	0.32	0.44	22
1520	phenyl-ring str.	20.3	1.28	0.33	0.49	22
1250	C–O–C asym. str.	20.8	1.33	0.38	0.43	24
1160	phenyl C–H in-plane def.	15.9	—	—	—	—
1030	CH_3–O str. (C–O–C sym. str.)	43.0	—	—	—	—

While the film treated above is too thick for the determination of the orientation of the molecules adsorbed on or present near the Si surface, a "quasi-fixed" orientation may be supposed, because the orientation mechanism in thin films primarily involves the epitaxy.[20] In this connection, it appears important to examine the existence of "quasi-fixed" orientation in thick films. For this reason, we now consider the case where a voluminous sample of MBBA comes in contact with the Si surface.

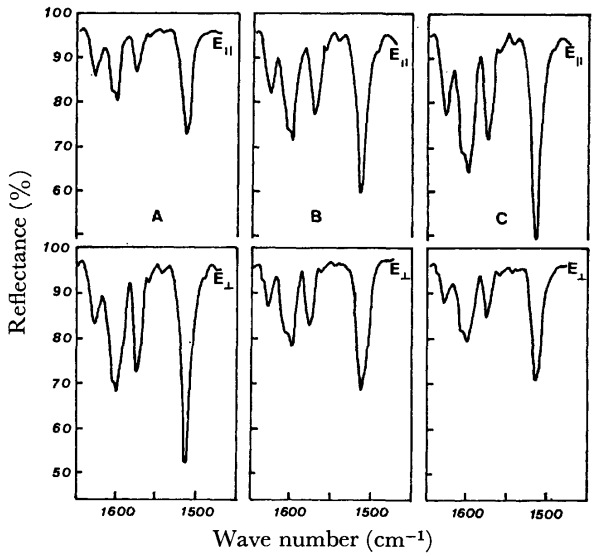

Fig. 4. Infrared polarized ATR spectra of MBBA (thickness: 2 mm).
$E_{\parallel}$ and $E_{\perp}$ refer to the polarized radiation used. A: original spectra (nematic; T=25 °C), B: spectra recorded 72 h later (nematic; T=25 °C), C: spectra of isotropic state (T=50 °C).

Figure 4 shows the polarized ATR spectra of MBBA liquid having a thickness of 2 mm. It must be mentioned here that each spectrum (A—C) appeared with the liguid layer about 1 μm thick at the Si-MBBA interface, depending upon experimental conditions. Accordingly, the three orientations that can be deduced from these spectra occur with the liquid having this thickness.

A brass plate was used as an opposite substrate. Since the substrate is very far from the Si prism surface, any possible orientation due to the substrate probably gives no contribution to the molecular orientation near the Si surface. Spectra (A) of Fig. 4 exhibit strong perpendicular dichroism, indicating that the preferred direction of the long molecular axes is parallel to the x axis, which is perpendicular to the plane of incidence, *viz.*, uniformly homogeneous orientation (see Fig. 1). This orientation almost disappears at an isotropic temperature of 50 °C, as is seen from spectra (C), but reappears upon lowering the temperature to the nematic temperature of 25 °C. The dichroic ratios taken from spectra (A) and (C) are given in Table 2.

The D values for spectra (C) are close to the value expected for isotropic orientation, but a difference of about 10% on the average is noticed between them. Since this discrepancy is greater than the limits of experimental error, the isotropic liquid may be influenced by the Si surface in contact with it.

Based on the dichroic ratios from spectra (A) and with the β values, the values of S were determined using Eqs. 3 and 5. The resulting S values are given in Table 2. As is seen in Table 2, the S values are indicative of a highly-ordered uniformly homogeneous orientation. The mechanism of the uniformly-homogeneous texture is, however, not understood in detail, but it is quite likely that the orientation is due to material flow[21] along the Si wall surface. Spectra (A) remained almost unchanged generally for as long as 24 h, but changed into spectra (B) after 72 h. The dichroic ratios taken from spectra (B) are given in Table 2.

The magnitude of the dichroic ratios is well explained by assuming a randomly-homogeneous orientation with poor order, as is shown in Table 2. Thus, the orientation pattern arising from the flow orientation is regarded as about the same as that for a liquid 0.2 μm thick, as mentioned above. In the present case, however, the "quasi-fixed" structure is greatly quenched. This fact shows that the "quasi-fixed" structure is confined to the vicinity of the Si surface and that its degree of order decreases with increasing film thickness.

Orientation Behavior of Molecules in an Electric Field. In what follows we shall deal with a relatively thin liquid layer (15 μm) contained between a Si prism and a conducting substrate plate.

Since the liquid-crystal orientation near the surface extends into the bulk, the above mentioned "asymmetric-electrode" cell would give rise to an orientation distortion at the interface of different orientations from the electrodes. However, if the opposite electrode material interacts much more strongly with the molecules than does the Si electrode, a predominant orientation probably develops over large areas and, consequently, it would overcome the flow orientation or weakly-bound

TABLE 2. POLARIZED INFRARED ATR DATA FOR LIQUID MBBA (for a thickness of 2 mm)
A-flow orientation (25 °C), B-randomly homogeneous orientation (25 °C), and C-isotropic orientation (50 °C).

Wave number	A			B			C		
	D	K_z/K_x	S	D	K_z/K_x	S	D	K_z/K_x	S[a]
1630	0.82	0.39	0.59	1.53	0.58	0.34	2.01	0.92	0.05
1600	0.53	0.25	0.63	1.49	0.55	0.27	1.90	0.84	0.07
1578	0.43	0.20	0.60	1.47	0.54	0.23	1.91	0.85	0.06
1520	0.48	0.23	0.64	1.49	0.55	0.26	1.88	0.83	0.08

a) Calculated assuming that $K_x=K_y$.

orientation at the Si surface mentioned above. In fact, this is always the case provided the opposite electrode surface is specially treated to give a birefringent texture.[1] In other words, this means that the "quasi-fixed" orientation at the Si surface cannot exert any important role on the type of birefringent orientation.

To examine the DC electric-field effect on the orientation of MBBA, a brass plate was used as the opposite electrode. The surface of the brass electrode was coated with a very thin film of lecithin in order to obtain a uniform homeotropic texture in the absence of any field. Because MBBA has a negative dielectric anisotropy,[22] the molecules should be aligned perpendicular to the electric-field direction.

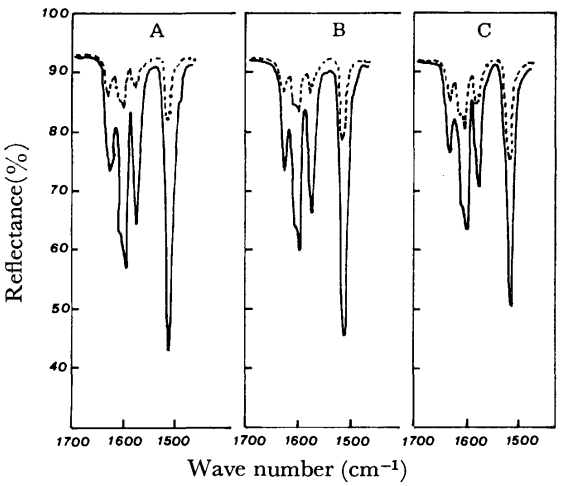

Fig. 5. Polarized infrared ATR spectra of nematic MBBA (25 °C); the opposite electrode: lecithin coated brass plate; thickness: 15 μm. Solid and broken lines refer to the electric vectors of radiation polarized parallel and perpendicular to the plane of incidence, respectively. The three sets of spectra correspond to different applied voltage; A: 0 V; B: 15 V rms; C: 30 V rms.

The polarized ATR spectra from a liquid 15 μm thick at 25 °C for different applied voltages are shown in Fig. 5. The dichroism of the vibration bands in the absence of any field indicates good homeotropic orientation of the sample. The average value of S deduced was 0.54. The dichroism of the vibration bands decreased with step increases in the voltage, indicating deformation of the homeotropic orientation. The S value can serve as an indicator of the extent of deformation.

The S value, which was obtained by averaging S over all vibration bands measured, is plotted as a function of the applied field in Fig. 6. As is shown in Fig. 6, the S value slightly decreased with increasing voltage up to 10 kV/cm and decreased more rapidly with subsequent increases in the electric field. Upon the removal of the field, the original arrangement was restored. The S value increased by 0.03, probably due to relaxation to a more stable form. Because dielectric reorientation always precedes dynamic scattering, the initial decrease in S probably arises from dielectric reorientation, whereas the second decrease in S is attributed to dynamic scattering. It is, however, significant that voltages applied above the threshold for

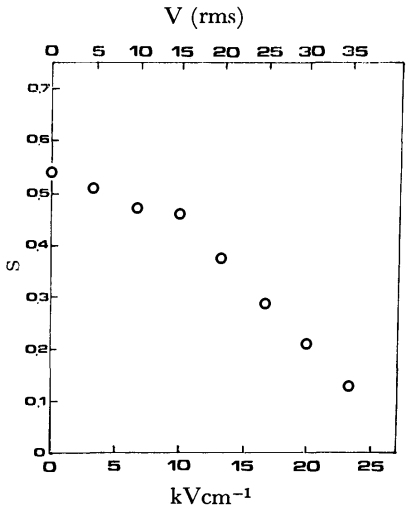

Fig. 6. The degree of order (S) of homeotropic orientation as a function of applied DC voltage.

dielectric orientation[15] produce no appreciable deformation of the homeotropic structure.

In this connection, it has generally been assumed that molecules near the electrodes are maintained in place by the boundaries in an electric field.[23] This idea is probably based on the interaction between the liquid-crystal molecules and the electrode surfaces. However, since the same result was obtained when the Si-prism surface was coated with lecithin, the above limited electric-field response is, probably, ascribed to the strong aligning force of the lecithin which aligns the molecules perpendicular to the surface. In Fig. 6, the S value decreases as the applied voltage is increased, which indicates that dynamic scattering becomes more pronounced with increasing voltage. However, it is important to note that homeotropy of the liquid is still present even at high voltages.

In the light of these results, subsequent experiments were carried out using a new brass plate as the opposite electrode. The original texture observed was a flow orientation. The polarized ATR spectra recorded are depicted in Fig. 7(A). The S value obtained for that alignment was 0.59 on the average. The flow orientation remained for long periods of time. To attain sample stabilization, the liquid cell was permitted to stand for 15 hours and was maintained at 25 °C. The results of the ATR measurements are shown in Fig. 7(B). The parallel dichroism of the spectra is indicative of the tendency for the molecules to orient themselves perpendicular to the electrodes.

Based on the foregoing discussion, it is thought that the spontaneous homeotropy arises from the brass electrode surface. The values of K_z/K_x and of S calculated from the experimental D values are given in Table 3. The generally low S value is an indication of the rather weak aligning force of the brass electrode. However, a marked difference in S is seen between the 1630 and 1030 cm^{-1} bands, suggesting poor nematic-type packing of the molecules. To establish the average initial orientation, the values of γ were calculated from the K_z/K_x values using Eq. 6. The results of γ are given in Table 3 and the molecular orientation deduced is

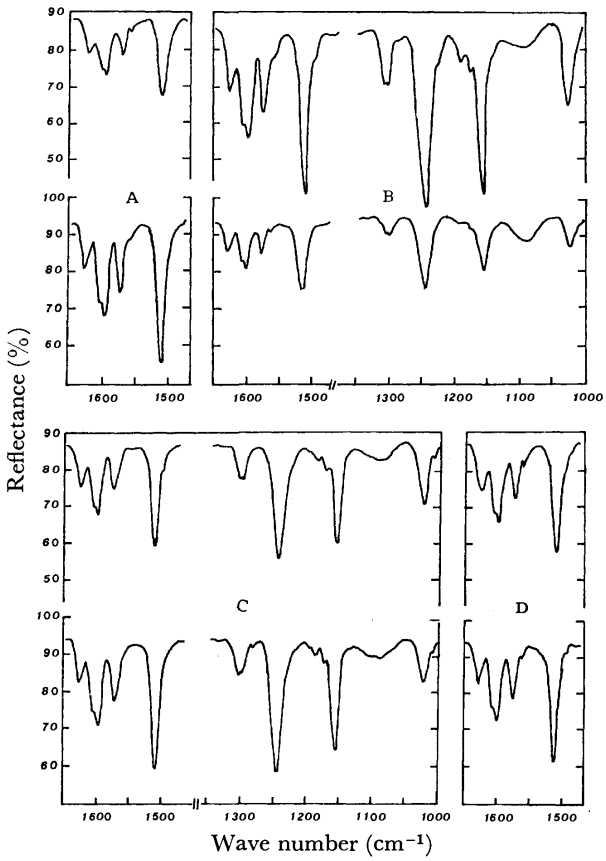

Fig. 7. Polarized infrared ATR spectra of nematic MBBA (25 °C) depending upon applied DC voltage. Upper and lower spectra were measured with the radiation polarized parallel and perpendicular to the plane of incidence, respectively. A: Initial flow orientation; B: homeotropic orientation appeared 15 h later in field-off; C: DC 5 V applied on B; D: DC 9 V applied on B.

depicted in Fig. 9(a).

A sharp change in dichroism was observed when a DC electric field was applied to this texture. In order to follow the sequence of spectral change in detail, measurements were carried out for driving voltages from 0 to 9 volts. For comparison, the polarized ATR spectra recorded at field strengths of 5 and 9 volts are reproduced in Figs. 7(C) and (D), respectively.

The dichroic ratios of the observed ATR spectra are plotted *versus* the external DC field in Fig. 8. As is

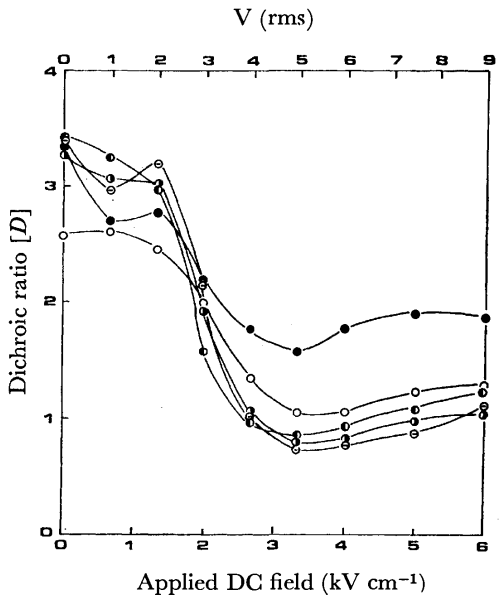

Fig. 8. Dichroic ratio (D) of various vibration bands as a function of applied DC voltage. ○: 1630 cm^{-1}; ⊖: 1578 cm^{-1}; ◑: 1520 cm^{-1}; ◐: 1250 cm^{-1}; ●: 1030 cm^{-1} band. The vibration assignments for these bands are presented in Table 1.

shown in the figure, reorientation begins at about 2 V and saturates at 5 V. Since the applied voltage exceeds 5 V, the dichroic ratios gradually decrease, probably due to domain formation[15] and the subsequent dynamic scattering, both of which interfere with the alignment.

The reorientation behavior mentioned above is in accord with that of the dielectric permittivity observed for relatively thick liquid MBBA by Ikeno *et al.*[24] Assuming the orientation at 5 V to be randomly homogeneous, the S values shown in Table 3 are obtained. The scattered values of S given in the table suggest that the molecules are packed in such a way that the rotation of the molecules about their own long axes is limited. Therefore, the γ values were calculated assuming uniaxial orientation of the long axis of the molecule, as before. The resulting values of γ are given in Table 3. Generally the change in γ with applied DC field appears to depend upon β. For example, the maximum change is found for the 1578 cm^{-1} band, whereas the minimum change is for the 1030 cm^{-1} band. Such behavior is understandable as a consequence of the negative

TABLE 3. POLARIZED INFRARED ATR DATA FOR LIQUID MBBA (for thickness of 15 μm) AT 25 °C
A-homeotropic orientation and B-randomly homogeneous orientation at a DC potential of 5 V.

Wave number	A				B			
	D	K_z/K_x	S	γ (degrees)	D	K_z/K_x	S	γ (degrees)
1630	2.59	1.33	0.17	39	1.06	0.24	0.88	19
1600	3.22	1.78	0.26	43	0.84	0.09	0.96	12
1578	3.43	1.93	0.25	45	0.79	0.05	0.90	9
1520	3.27	1.83	0.26	44	0.82	0.07	1.00	11
1250	3.41	1.92	0.29	44	0.93	0.15	0.80	15
1160	4.08	2.39	0.36	48	0.99	0.19	0.66	17
1030	3.34	1.88	0.75	44	1.78	0.75	0.33	32

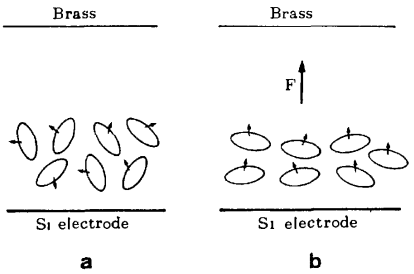

Fig. 9. Schematic representation of the molecular orientation of nematic MBBA before (a) and after (b) the application of DC electric field. Arrows indicate the dipole moments.

anisotropy of the molecule.

The molecular orientation in the DC electric field is drawn schematically in Fig. 9(b).

On the other hand, when the voltage was switched off, the sample exhibited a greatly improved homeotropy. An S value of 0.50, on the average, was obtained for this texture. This change is considered to be caused by the disturbance due to the applied field up to 9 V, as mentioned above.

When the 5 V DC voltage was subsequently applied, no appreciable dielectric distortion was observed: an average S value of 0.40 was obtained. Failure to produce a molecular reorientation comparable to that previously produced at the same voltage is consistent with the increased ordering or denser packing of the molecules before field application. Thus, the structure of the liquid film affects the response of molecules to the external electric field in a striking manner.

In conclusion, this ATR method affords three-dimensional information about the static and dynamic orientation behavior of liquid crystals in thin films. However, it must be emphasized that the surface influences of the electrodes are always important for interpreting observed results. This study will be extended to *N*-(*p*-ethoxybenzylidene)-*p*-cyanoaniline. The results for this compound will be published in the near future.

References

1) Part I, A. Hatta, *Bull. Chem. Soc. Jpn.*, **50**, 2522 (1977).

2) G. W. Gray and P. A. Winsor, "Liquid Crystals and Plastic Crystals," Vols. I and II, John Wiley & Sons, New York (1974).

3) G. H. Heilmeier, L. A. Zanoni, and L. A. Barton, *Proc. IEEE*, **56**, 1162 (1968); G. H. Heilmeier, L. A. Zanoni, and L. A. Barton, *IEEE. Trans.*, **ED-17**, 22 (1970); W. Helfrich, *J. Chem. Phys.*, **51**, 4092 (1969).

4) E. F. Carr, *J. Chem. Phys.*, **39**, 1979 (1963); E. F. Carr, *ibid.*, **42**, 738 (1965); E. F. Carr, *ibid.*, **43**, 3905 (1965); M. Schadt and W. Helfrich, *Appl. Phys. Lett.*, **18**, 127 (1971); A. Boller, M. Scherrer, M. Schadt, and P. Wild, *Proc. IEEE*, **60**, 1002 (1972); W. Maier and G. Meier, *Z. Elektrochem.*, **65**, 556 (1961); W. Maier and G. Meier, *Z. Naturforsch., Teil A*, **16**, 470 (1961); G. Meier and A. Saupe, *Mol. Cryst.*, **1**, 515 (1966).

5) G. H. Heilmeier and L. A. Zanoni, *Appl. Phys. Lett.*, **13**, 91 (1968).

6) E. Sackmann, *Chem. Phys. Lett.*, **3**, 253 (1969); E. Sackmann, *J. Am. Chem. Soc.*, **90**, 3569 (1968); G. P. Ceasar and H. B. Gray, *ibid.*, **91**, 191 (1969).

7) R. A. Levenson, H. B. Gray, and G. P. Ceasar, *J. Am. Chem. Soc.*, **92**, 3653 (1970).

8) V. D. Neff, L. W. Gulrich, and G. H. Brown, *Mol. Cryst.*, **1**, 225 (1966).

9) N. J. Harrick, *J. Phys. Chem.*, **64**, 1110 (1960); J. Fahrenfort, *Spectrochim. Acta*, **17**, 698 (1961).

10) N. J. Harrick, "Internal Reflection Spectroscopy," Interscience, New York (1967).

11) P. A. Flournoy and W. J. Schaffers, *Spectrochim. Acta*, **22**, 5 (1966).

12) I. Haller, H. A. Huggins, and M. J. Freiser, *Mol. Cryst. Liq. Cryst.*, **16**, 53 (1972); G. Labrunie and S. Valette, *Appl. Optics*, **13**, 1802 (1974); R. Chang, *Mol. Cryst. Liq. Cryst.*, **34L**, 65 (1976).

13) M. Herzberger and C. D. Salzberg, *J. Opt. Soc. Am.*, **52**, 420 (1962).

14) A. Saupe and W. Maier, *Z. Naturforsch., Teil A*, **16**, 816 (1961); A. Saupe, *ibid., Teil A*, **19**, 161 (1964).

15) W. Helfrich, *Mol. Cryst. Liq. Cryst.*, **21**, 187 (1973).

16) G. Vergoten, G. Fleury, R. N. Jones, and A. Nadeau, *Mol. Cryst. Liq. Cryst.*, **36**, 327 (1976).

17) The average values of β obtained from homeotropic and uniformly homogeneous samples of MBBA (Ref. 1).

18) In this case, the film is much thinner than the penetration depth of the evanescent wave and hence Eq. 1 is no longer valid for the calculation of the reflectivities. Instead, the calculation of the electric field amplitudes of the evanescent wave was carried out based on approximate equations applicable to the present case.[10] For the present case, the dichroic ratio is expressed as $D=0.90+1.14\,K_z/K_x$. The S values in Table 1 were calculated using this relation.

19) H. Onagawa and K. Miyashita, *Oyo Buturi*, **42**, 133 (1973).

20) M. Ashida, A. Hamada, and T. Watanabe, *Bull. Chem. Soc. Jpn.*, **45**, 2312 (1972); N. Uyeda, Y. Murata, T. Kobayashi, and E. Suito, *J. Cryst. Growth*, **26**, 267 (1974); J. C. Buchholz and G. A. Somorjai, *J. Chem. Phys.*, **66**, 573 (1977).

21) W. Helfrich, *J. Chem. Phys.*, **50**, 100 (1969); Ch. Gähwiller, *Phys. Rev. Lett.*, **28**, 1554 (1972); R. Chang, *Mat. Res. Bull.*, **7**, 267 (1972).

22) F. Rondelez, D. Diguet, and F. Durand, *Mol. Cryst. Liq. Cryst.*, **15**, 183 (1971).

23) E. J. Kahn, *Appl. Phys. Lett.*, **20**, 199 (1972).

24) S. Ikeno, M. Yokoyama, and H. Mikawa, *Mol. Cryst. Liq. Cryst.*, **36**, 89 (1976).

Magnetic Study of α- and β-Diamminecopper(II) Chlorides and Bromides

Takeshi Asai, Hiroshi Saheki,* Kayako Hori,** and Ryôiti Kiriyama

The Institute of Scientific and Industrial Research, Osaka University, Yamadakami, Suita 565

(Received August 13, 1977)

The magnetic susceptibilities, χ, of α- and β-$Cu(NH_3)_2X_2$(X=Cl, Br) were measured from 4.2 to 360 K. Those of β-$Cu(NH_3)_2X_2$ obeyed the Curie-Weiss law above 50 K. The Weiss constants and effective Bohr magneton numbers are $-3.5(\pm1)$ K and $1.75(\pm0.01)$ for X=Cl, and -9.7 K and 1.82 for X=Br. α-$Cu(NH_3)_2Cl_2$ showed a rounded maximum for χ at 30 K. A linear Heisenberg model with the parameters, $J=-23.5(\pm1)$ K and $g=2.03(\pm0.03)$, gave good agreement with observations. α-$Cu(NH_3)_2Br_2$ had a peak for χ at $47(\pm2)$ K. This temperature is probably a Neèl temperature. The strong magnetic interaction of the α-form compounds is related to the compressed coordination octahedron of $[Cu(NH_3)_2X_4]^{2-}$. All samples used were solid solutions of $Cu(NH_3)_2X_2$ and NH_4X. An analysis of χ suggests that the Cu^{2+} cations in α-$Cu(NH_3)_2Cl_2$ are distributed inhomogeneously over a short range. A similar inhomogeneity was also found for the β-$Cu(NH_3)_2X_2$ samples. In this sense, the β-form may be better described as a solid solution of α-$Cu(NH_3)_2X_2$ and NH_4X rather than as a dimorph.

Diamminecopper(II) chloride and bromide have interesting stereochemical features. The copper(II) cation of these halides is situated at the center of a compressed $[Cu(NH_3)_2X_4]^{2-}$ (X=Cl, Br) octahedron, whereas in many copper(II) compounds the copper(II) cation is in an elongated octahedral environment. Studies have been made on the crystal structures of these compounds,[1-3] and their IR and optical absorption,[4] and ESR spectra.[4] Similarly, these compounds diluted with NH_4X[5] and ammonium halides doped with copper(II) ions[6-10] have also been studied. In the present study, the magnetic susceptibilities of α- and β-$Cu(NH_3)_2X_2$ were measured in order to learn the effect of a particular coordination on a magnetic property.

However, these halides are dimorphous. One of them has a chain structure of the coordination octahedra, $[Cu(NH_3)_2X_4]^{2-}$, while the other consists of isolated octahedra. Since both dimorphs exist at room temperature, it is questionable whether they are a thermodynamically-stable phase. In analyzing the magnetic susceptibility of α-$Cu(NH_3)_2Cl_2$, information on the distribution of copper(II) cations was obtained. From this information the phase relationship will be discussed.

Experimental

Preparation. Preparation of α- and β-$Cu(NH_3)_2X_2$ (X=Cl, Br) samples followed a known method.[1] The process always resulted in precipitates containing NH_4X. Moreover, the precipitates of the α-form partially transformed into the β-form during washing with an NH_4X aqueous solution. This partial transformation was prevented by washing the precipitate with acetone immediately after the parent solution had been filtered off. Ammonium halides contaminating precipitates were separated by decantation from acetone. This separation was repeated until the X-ray diffraction powder pattern of the sample indicated the disappearance of diffraction lines from NH_4X or indicated that the intensity ratio of several strong lines no longer varied.

* Present address: Mitsui Aluminum Co., Ltd., 80 Yotsuyama-cho, Omuta 836.

** Present address: Department of Chemistry, Faculty of Science, Ochanomizu University, Otsuka, Bunkyo-ku, Tokyo 112.

Magnetic Measurements. The magnetic susceptibilities were measured from 4.2 to 360 K on a Faraday balance. The apparatus was calibrated for $CoHg(SCN)_4$.[11] Corrections were made for diamagnetism (-1.21 and -1.46 mm^3 mol^{-1} for the chlorides and bromides, respectively)[12] and for Van Vleck paramagnetism (0.75 mm^3 mol^{-1}).[13]

Results

The results of chemical analysis of the samples are given in Table 1. All samples obtained in this study contain more N and X than their stoichiometric composition of $Cu(NH_3)_2X_2$ (X=Cl, Br). Considering the caution exercised in their preparation, these samples are not a mixture of $Cu(NH_3)_2X_2$ and NH_4X, but are a solid solution of these two compounds. These preparations always gave solid solutions with no pure $Cu(NH_3)_2X_2$.

Table 1. Results of chemical analysis and the molar fractions of $Cu(NH_3)_2X_2$ deduced therefrom

Compound	Mass fraction[a]				Molar fraction of $Cu(NH_3)_2X_2$
	Cu	N	H	X	
α-$Cu(NH_3)_2Cl_2$	0.3520	0.174	0.041	0.4334	0.814
β-$Cu(NH_3)_2Cl_2$	0.2392	0.206	0.052	0.5069	0.353
α-$Cu(NH_3)_2Br_2$	0.2243	0.112	0.026	0.6375	0.792
β-$Cu(NH_3)_2Br_2$	0.1836	0.119	0.031	0.6662	0.525

a) Calcd for $Cu(NH_3)_2Cl_2$: Cu 0.3771, N 0.1663, H 0.0359, Cl 0.4208; for $Cu(NH_3)_2Br_2$: Cu 0.2469, N 0.1088, H 0.0235, Br 0.6208.

The magnetic susceptibilities are shown in Figs. 1—4. Throughout this paper, values of the magnetic susceptibility, χV_m, are given for one mole of copper(II) cations.

For both compounds having β-form, the magnetic susceptibility decreased monotonically with increasing temperature and obeyed the Curie-Weiss law above 50 K. The Weiss constants, θ, and effective Bohr magneton numbers, n_μ, deduced therefrom are given in Table 2.

In contrast to the features of the β-form compounds, the magnetic susceptibilities of the α-form compounds

Table 2. Weiss constants θ and effective Bohr magneton numbers n_μ obtained by application of the Curie-Weiss law

Compound	θ/K[a)]	n_μ[b)]
α-$Cu(NH_3)_2Cl_2$	−36	1.85
α-$Cu(NH_3)_2Br_2$	−70	1.95
β-$Cu(NH_3)_2Cl_2$	−3.5	1.75
β-$Cu(NH_3)_2Br_2$	−9.7	1.82

a) Maximum e.s.d. is ±2 K. b) Maximum e.s.d. is ±0.02.

clearly indicate that strong magnetic interaction occurs among copper(II) cations. The magnetic susceptibility of the α-form chloride compound exhibits a round maximum at 30 K. Combined with the crystal structure (Fig. 5), this suggests the magnetic interaction to be of a one-dimensional character. The temperature dependence agreed well with that of the linear Heisenberg spin system[14] having the parameters, $J=-23.5(\pm1)$ K and $g=2.03(\pm0.03)$. Fitting to the equation for a linear Ising spin system was unsuccessful.

Since the above-mentioned analysis neglected the fact that the sample was a solid solution, the following model was checked by taking the $Cu(NH_3)_2Cl_2$ molar fraction into account. If the cations are distributed randomly, a linear chain of $[Cu(NH_3)_2Cl_4]^{2-}$ octahedra is cut into smaller chains and the proportion of each smaller chain is determined by the $Cu(NH_3)_2Cl_2$ molar fraction. Assuming that the Heisenberg-type interaction operates only between the nearest neighbor cations in a chain and that the values of parameters J and g are the same for all types of chains, the magnetic susceptibility of the system was calculated as the statistical sum of that of each component. It indicated, however, no maximum, in contrast with the data. Therefore, this model is not applicable to the present case.

The magnetic susceptibility of α-$Cu(NH_3)_2Br_2$ showed a peak at 47(±2) K, and not a round maximum. This suggests that 47 K is a Neèl temperature and that below this temperature copper(II) spins are ordered antiferromagnetically. In support of this, the reduced magnetic

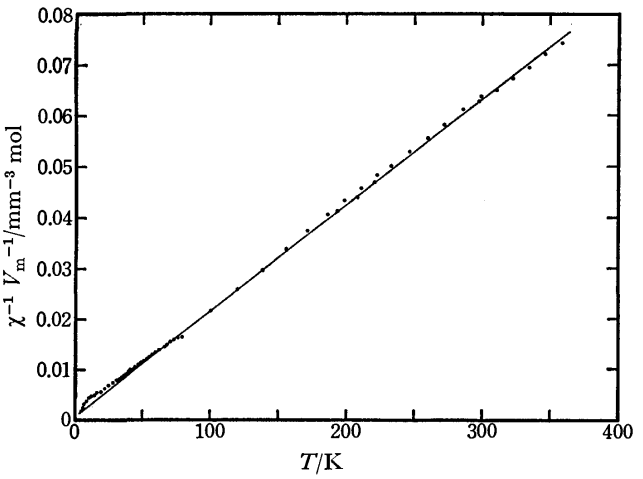

Fig. 1. Temperature dependence of the reciprocal susceptibility of β-$Cu(NH_3)_2Cl_2$. The solid line shows a Curie-Weiss relation.

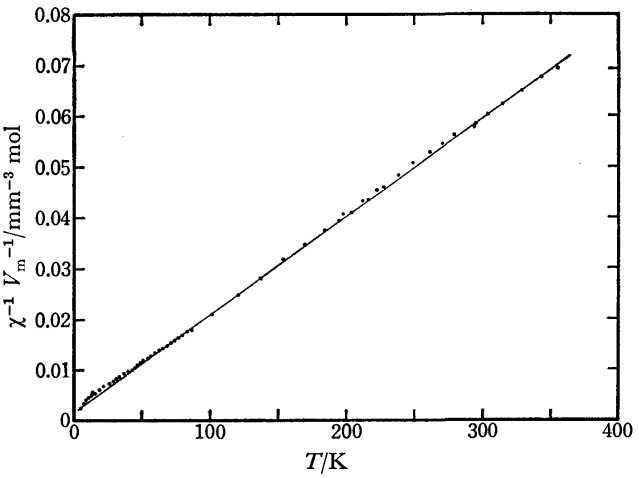

Fig. 2. Temperature dependence of the reciprocal susceptibility of β-$Cu(NH_3)_2Br_2$. The solid line shows a Curie-Weiss relation.

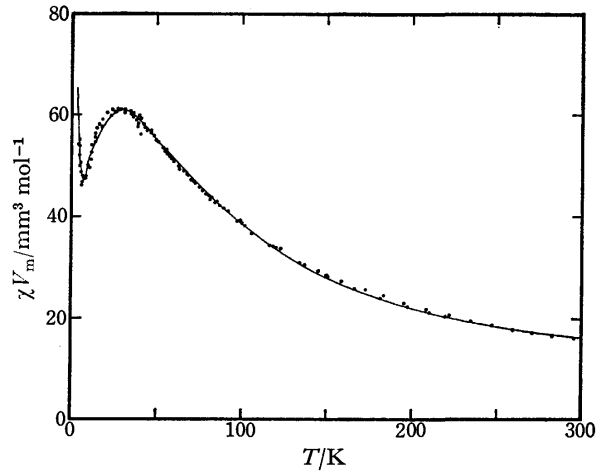

Fig. 3. Temperature dependence of the susceptibility of α-$Cu(NH_3)_2Cl_2$. The solid line shows a calculated one with contributions from a linear Heisenberg model ($J=-23.5$ K, $g=2.03$) and another paramagnetic term. The latter was included to explain the dependence below 10 K and was calculated by the relation of $\chi_p V_m$/mm^3 mol^{-1}=16.7/(T/K−3.3).

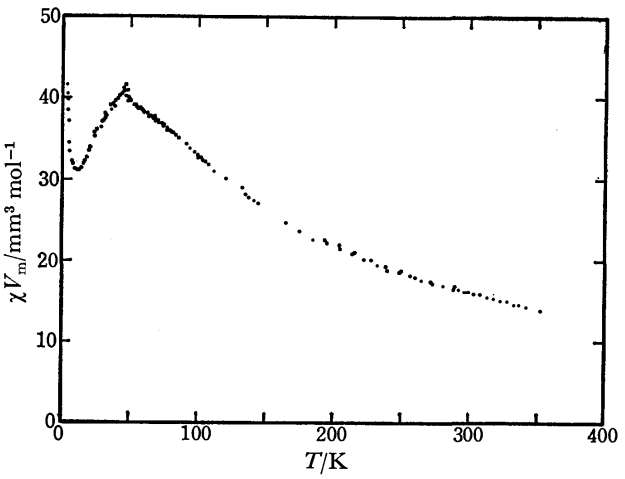

Fig. 4. Temperature dependence of the susceptibility of α-$Cu(NH_3)_2Br_2$.

susceptibility $\chi(T)/\chi(T_N)$ below T_N agreed well with that predicted by simple molecular field theory,[18] although the theory was not applicable to the data over the entire temperature range measured.

For both α-form compounds, the values of parameters θ and n_μ were deduced from data above 110 K for the chloride and above 190 K for the bromide. They are given in Table 2.

Discussion

Crystal Structure. Diamminecopper(II) chloride and bromide are dimorphous.[1] The crystal structures of β-$Cu(NH_3)_2Br_2$[1] and β-$Cu(NH_3)_2Cl_2$ are isomorphous and belong to the cubic system (Fig. 5). The arrangement of the NH_3 molecules and halogen anions is of the CsCl type. The copper(II) cations are situated at the face-centered sites of the anion lattice, forming a $[Cu(NH_3)_2X_4]^{2-}$ compressed octahedron. These copper sites are occupied only with a small probability of 1/6 and the orientation of the octahedron is random along the three crystallographic axes.

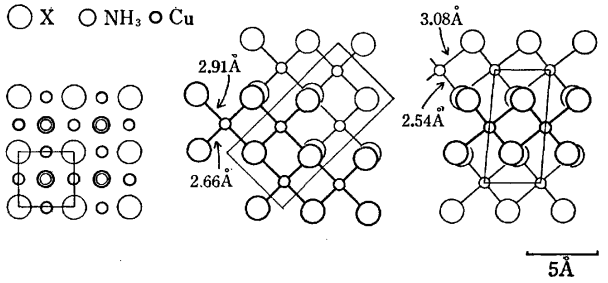

(a) β-$Cu(NH_3)_2X_2$ (b) α-$Cu(NH_3)_2Cl_2$ (c) α-$Cu(NH_3)_2Br_2$

Fig. 5. Projection of crystal structure. Atoms at $z'=0$ is shown by a thin line and those at $z'=1/2$ by a thick one, where z' is a positional parameter along the axis perpendicular to the sheet of the paper. A nitrogen atom in α-forms is situated above and below a Cu atom and omitted for simplicity. Chlorine atoms overlapping each other in the α-chloride are shifted for easy view.

The crystal structures of the α-form result from ordering of the octahedron found in the structure of the β-form. This ordering brings about deformation of the lattice and the coordination octahedron itself. The deformation of the octahedron is such that short and long Cu–X distances are distinguished as is often seen in many halo-copper(II) complexes, $CuX_2 \cdot 2L$ (L= H_2O or organic molecules containing an N atom).[15] In α-$Cu(NH_3)_2Br_2$,[2] the coordination octahedron shares two opposite Cl–Cl edges to form an infinite linear chain like that in $CuCl_2 \cdot 2H_2O$ whereas, in α-$Cu(NH_3)_2Cl_2$,[3] zigzag chains result from the sharing of two adjacent Cl–Cl edges of the octahedron.

Magnetic Properties. For the β-forms, the observed magnetic susceptibilities show mainly the behavior expected for an isolated copper(II) ion (Figs. 1 and 2). This observation is compatible with the crystal structure together with a large dilution of NH_4X molecules (Table 1). However, deviation from the Curie-Weiss law was observed below 50 K and the Weiss constants have a non-zero value. This means that the copper(II) ions in these compounds are not fully isolated. This is discussed further below.

The magnetic susceptibility of α-$Cu(NH_3)_2Cl_2$ agrees well with a one-dimensional Heisenberg spin system having a J value of −23.5 K. Thus, an antiferromagnetic interaction must occur along the zigzag chain. Since the separation between copper(II) ions exceeds 3.9 Å, the direct interaction of copper(II) spins should be negligible. A copper(II) cation has four Cu^{2+} neighbors in a chain and two types of paths along which the superexchange interaction are possible. One of the paths passes the short (2.61 Å) and long (2.91 Å) Cu–Cl bonds between two nearest neighbor cations, whereas the other passes the two long Cu–Cl bonds between two alternate neighboring cations. Since the latter includes only long Cu–Cl bonds, only the former should be effective in this compound. This view is consistent with the result obtained from the ESR study of a doped copper ion in NH_4Cl at 4.2 K[8,10] for which a superhyperfine interaction was detected only between a copper spin and two nearest Cl nuclei in the center of the $[Cu(H_2O)_2Cl_4]^{2-}$ with orthorhombic symmetry. The value of J obtained is about twice that of a typical one-dimensional chloro-complex of $CuCl_2 \cdot 2C_5H_5N$ (J= −13.6 K).[16] The accuracy in the structural analysis of α-$Cu(NH_3)_2Cl_2$, however, is not enough to permit a discussion of the difference in the J values.

The magnetic susceptibility of α-$Cu(NH_3)_2Br_2$ indicates a three-dimensional ordering of copper(II) spins below 47 K. Therefore, a magnetic interaction must occur between linear chains, as well as within a chain. On inspection of the crystal structure, it appears that $NH_3 \cdots Br$ hydrogen bonds probably play the principal role in the interchain interaction. There are four such paths with an N···Br distance of 3.51 Å. Boettcher and Spaeth have shown that in the paramagnetic center of $[Cu(NH_3)_2Cl_4]^{2-}$ in NH_4Cl, an ammonia molecule reorients about the Cu–N bonding axis at 4.2 K.[10] The situation is probably the same in α-$Cu(NH_3)_2Br_2$ and hence the hydrogen bonding is weak. In $K_2CuCl_4 \cdot 2H_2O$, copper(II) cations interact through $H_2O \cdots Cl$ hydrogen bonding the magnitude of the interaction being of the order of 0.1 K.[17] On the other hand, Cu–Br chemical bonding plays a role in the intrachain interaction. Therefore, in α-$Cu(NH_3)_2Br_2$, the intrachain interaction should be stronger than the interchain interaction. The ratio of their magnitudes was estimated to be 1×10^{-1} from T_N and θ by application of molecular field theory.[18] This value is very large compared with the usual values of the order of 10^{-3} or less.[19] Furthermore, the value of the ratio T_N/θ, which is 0.67 for α-$Cu(NH_3)_2Br_2$, is much greater than the corresponding values, which are less than 0.2, for typical antiferromagnetic Heisenberg chains, and is close to values of 0.7—0.8 for three-dimensional Heisenberg magnets.[19] These facts indicate that the interchain interaction is very strong in α-$Cu(NH_3)_2Br_2$.

Strong magnetic interaction was observed in the α-form compounds. This is the result of the particular coordination of the copper(II) cation. As the coordination octahedron $[Cu(NH_3)_2X_4]^{2-}$ is compressed along the Cu–N bonding axis,[1] the unpaired electron of the

copper(II) cation occupies the $3d_{x^2-y^2}$ orbital.[4-10] Because the lobes of this orbital point to four chlorine neighbors, stronger magnetic interaction is expected in this case than in the case in which the unpaired electron occupies the $3d_{z^2}$ orbital in the elongated octahedral coordination.

Phase Relationship. The samples in this study were all solid solutions. However, the magnetic susceptibility of the α-$Cu(NH_3)_2Cl_2$ sample cannot be explained on the assumption that the copper(II) cations are distributed randomly and that the magnetic interaction between them is isotropic. A calculation based on this assumption showed that the maximum magnetic susceptibility χ_{max} is much larger for small chains than for an infinite chain; *e.g.* the χ_{max} of a tetramer, which is the most predominant species in the case of random distribution, is greater by 26.5% than that of the infinite chain. Therefore, the fact that the observed magnetic susceptibility agree well with an infinite linear Heisenberg model strongly suggests that the sample is not homogeneous over a short range. The copper(II) cations group together and form a chain long enough to exhibit the magnetic feature of an infinite chain.

In this connection, Tomlinson and Hathaway[4] have published an interesting observation for β-$Cu(NH_3)_2X_2$. They observed an isotropic ESR spectrum for the chloride and no signal for the bromide. They explained this by the effect of exchange coupling between the copper(II) cations. Because the occupancy factor of the copper site is only 1/6, their ESR results indicate that their samples of the β-form are inhomogeneous over a short range like the present sample of α-$Cu(NH_3)_2Cl_2$. On the contrary, the magnetic susceptibility of the β-form in the present study has primarily the character of that of an isolated copper(II) ion. The difference may be due to a greater local inhomogeneity in their samples than in the present ones. Local inhomogeneity is suggested also for the present samples due to small Weiss constants and deviation from the Curie-Weiss law below 50 K.

The preparation data[1] support this view. When a concentrated NH_4X solution was used as a solvent, the precipitate was of the β-form and remained stable. When a dilute NH_4X solution was used, the first precipitate was also of the β-form, which then transformed into the α-form. This means that, for a high concentration of copper, the system is more stabilized by clustering than by random distribution of the cations. The latter situation is probably stable only at very low copper concentrations. Thus, the local inhomogeneity needs to be taken into consideration for certain physical measurements on samples of the β-form, although a statistical distribution of copper(II) ions has been derived from X-ray analysis.[20] Together with the similarity between the crystal structures of β-$Cu(NH_3)_2X_2$ and NH_4X, the β-form may be better described as a solid solution of α-$Cu(NH_3)_2X_2$ and NH_4X rather than as one of dimorphs.

References

1) F. Hanic and I. A. Cakajdova, *Acta Crystallogr.*, **11**, 610 (1958).
2) F. Hanic, *Acta Crystallogr.*, **12**, 739 (1959).
3) L. Zsoldos, *Magy. Fiz. Foly.*, **10**, 189 (1962).
4) A. A. G. Tomlinson and B. J. Hathaway, *J. Chem. Soc. A*, **1968**, 2578.
5) D. E. Billing, B. J. Hathaway, and A. A. G. Tomlinson, *J. Chem. Soc., A*, **1971**, 2839.
6) N. J. Trappeniers and S. H. Hagen, *Physica*, **31**, 122, 251 (1965); S. H. Hagen and N. J. Trappeniers, *ibid.*, **47**, 165 (1970); *ibid.*, **66**, 166 (1973).
7) J. R. Pilbrow and J. M. Spaeth, *Phys. Status Solidi*, **20**, 225, 237 (1967).
8) B. Bechtle, F. Boettcher, and J. M. Spaeth, *Phys. Status Solidi B*, **43**, K169 (1971).
9) P. A. Narayana and K. V. L. N. Sastry, *J. Chem. Phys.*, **57**, 3266 (1972); *ibid.*, **58**, 769 (1973).
10) F. Boettcher and J. M. Spaeth, *Phys. Status Solidi B*, **61**, 465 (1974); *ibid.*, **62**, 65 (1974).
11) B. N. Figgis and R. S. Nyholm, *J. Chem. Soc.*, **1958**, 4190.
12) Landolt-Börnstein Zahlenwerte und Funktionen, [6], II. Band, 10 Teil, Springer Verlag, Berlin (1962); *ibid.*, Neue Serie, Gruppe II, Band II, Springer Verlag, Berlin (1966).
13) B. N. Figgis and R. L. Martin, *J. Chem. Soc.*, **1956**, 3837.
14) J. C. Bonner and M. E. Fisher, *Phys. Rev.*, **135**, A640 (1964).
15) R. Colton and J. H. Canterford, "Halides of the First Row Transition Metals," Wiley-Interscience, London (1969), Chap. 9.
16) K. Takada, S. Matsukawa, and T. Haseda, *J. Phys. Soc. Jpn.*, **30**, 1330 (1971).
17) T. Okuda and M. Data, *J. Phys. Soc. Jpn.*, **28**, 308 (1970).
18) A. H. Morrish, "The Physical Principles of Magnetism," John Wiley, New York (1965), pp. 447—453.
19) L. J. de Jongh and A. R. Miedema, *Adv. Phys.*, **23**, 1 (1974), Tables 2, 5—7, and 12.

20) The idea of local inhomogeneities is not contrary to the result of X-ray analysis. Ususal X-ray analysis gives information on the average structure. Local inhomogeneities, if present, yield a large temperature factor. Hanic and Cakajdova give a large value for the temperature factor (Ref. 1). The inhomogeneities discussed here may contribute to this in some degree.

^{14}N Nuclear Quadrupole Resonance of Some Heterocyclic Compounds *via* Nuclear Double Resonance

Takuya MARUIZUMI, Yukio HIYAMA, Noriyuki WATANABE, and Eiji NIKI

Department of Industrial Chemistry, Faculty of Engineering, The University of Tokyo, Bunkyo-ku, Tokyo 113

(Received August 29, 1977)

Using proton-nitrogen double resonance in the laboratory frame, the ^{14}N nuclear quadrupole resonances (NQR) of 2,4(1*H*,3*H*)-pyrimidinedione[uracil], 2,3-dihydro-2-thioxo-4(1*H*)-pyrimidinone[2-thiouracil], 2,4-(1*H*,3*H*)-pyrimidinedithione[2,4-dithiouracil], and 1,3-dihydro-2*H*-benzimidazole-2-thione[2-mercaptobenzimidazole] have been measured at room temperature. The NQR parameters of uracil and its sulfur-substituted compounds are interpreted by using the Townes and Dailey theory.

Because of pharmacological interest, many studies of sulfur-substituted pyrimidines and purines have been performed by various spectroscopic means, but not by the nuclear quadrupole resonance (NQR). In this paper we report the observation of NQR of ^{14}N in 2,4(1*H*,3*H*)-pyrimidinedione[uracil], 2,3-dihydro-2-thioxo-4(1*H*)-pyrimidinone[2-thiouracil], 2,4(1*H*,3*H*)-pyrimidinedithione[2,4-dithiouracil], and 1,3-dihydro-2*H*-benzimidazole-2-thione[2-mercaptobenzimidazole]. These data yield information about the electron density on the nitrogen nucleus and hence about the chemical bonding of these molecules.

Spin 1 nuclei such as ^{14}N have three quadrupole states in an electric field gradient, and three transitions can occur between these three states. The frequencies are given by[1]

$$\nu_{\pm} = \frac{3}{4}e^2Qq\left(1 \pm \frac{\eta}{3}\right), \quad (1)$$

$$\nu_0 = \nu_+ - \nu_- = \frac{1}{2}\eta e^2Qq, \quad (2)$$

where e^2Qq is the ^{14}N quadrupole coupling constant and η is the asymmetry parameter.

Nuclear magnetic double resonance (NMDR) in the laboratory frame was employed to detect the NQR transitions. NMDR methods —as first introduced by Hartmann and Hahn[2] and later by Lurie and Slichter[3]— facilitate observation of ^{14}N NQR whose transition frequency often lies in the region 0.3—3 MHz and is thus not accessible by conventional continuous wave techniques.

Experimental

Samples. The samples were all polycrystalline chemicals.

NMDR in the Laboratory Frame. The details of NMDR were described by Slusher and Hahn.[4] In brief, the sample is first magnetized in a high d.c. magnetic field H_0 (about 6 kG here) for a high-field spin-lattice relaxation time and then adiabatically demagnetized to zero field [(a) to (b) in Fig. 1]. The spin order of the abundant spins [protons here] is now very high but a suitably phase or pulse modulated radio frequency field H_{1B} which resonates a rare spin [^{14}N here] quadrupole transition will continuously break the spin order of the abundant spins. The loss may be observed by adiabatically remagnetizing the sample [(c) to (d)] and observing a decrease of the majority spins' nuclear magnetic signals with the help of a 90° pulse. By sweeping the frequency ν_B of the phase or pulse modulated field [in 10 kHz steps here] the entire quadrupole resonance spectrum may be recorded. In this study ν_B was swept from 450 kHz to 4 MHz. Most parts of the NMDR apparatus built in this laboratory were based on the design of Slusher and Hahn.[4]

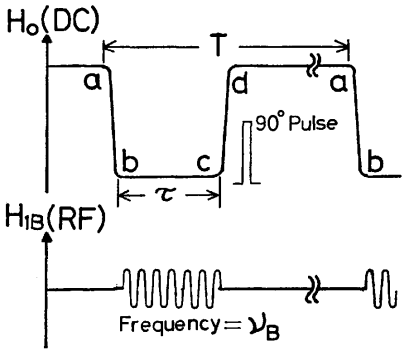

Fig. 1. Nuclear double resonance sequence.

Results and Discussion

Using the high-field and zero-field spin-lattice relaxation times for each molecule, the cycle time T [see Fig. 1] and zero field time τ were determined before performing the double resonance experiment. These data are collected in Table 1.

Table 1. High-field and zero-field spin-lattice relaxation times at room temperature and experimental conditions

Substance	T_1[a]	T_{1D}[b]	T_{1N}[c]	$[T-\tau]$[d]
Uracil	60	8	56	[90—3]
2-Thiouracil	52	3	20	[100—2]
2,4-Dithiouracil	107	8	30	[120—3]
2-Mercapto-benzimidazole	43	5	104	[60—3]

a) T_1 is the high-field spin-lattice relaxation time which is measured by 90°-τ-90° method. b) T_{1D} is the short zero-field relaxation time constant. c) T_{1N} is the long relaxation time. d) Cycle time T and zero field time τ. All the times in this table are in sec.

Figure 2 shows the zero-field proton spin-lattice relaxation, where the proton signal at first decreases quickly and later more slowly with time. This slow decay of proton magnetization is caused by the remagnetization of the proton system by cross interaction with the ^{14}N system, which has a long spin-lattice relaxation time.

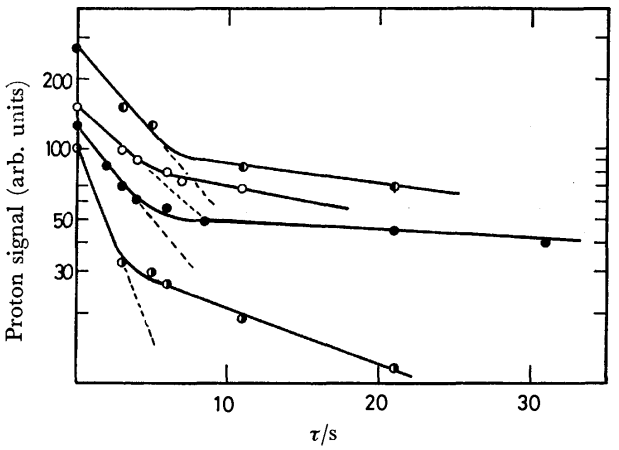

Fig. 2. Zero-field proton spin-lattice relaxation.
◐: Uracil, ◑: 2-thiouracil, ○: 2,4-dithiouracil, ●: 2-mercaptobenzimidazole.

Table 2. Observed ^{14}N NQR transition frequencies (kHz), coupling constants e^2Qq (kHz), asymmetry parameters η, and experimental temperature T (K)

Substance	[ν_+,	ν_-,	ν_0]	e^2Qq	η	T
Uracil	[2300,	1640,	660]	2630	0.502	294
2-Thiouracil	[2060,	1250,	810]	2207	0.734	300
	[2110,	1430,	680]	2360	0.580	300
2,4-Dithiouracil	[2030,	not obsd,	850]	2140	0.794	301
	[1970,	not obsd,	730]	2140	0.682	301
2-Mercapto-benzimidazole	[2340,	1790,	550]	2750	0.40	299

The observed transition frequencies, quadrupole coupling constants e^2Qq, and asymmetry parameters η are collected in Table 2. Though the two sets of lines corresponding to the two nitrogen atoms in uracil were observed at 77 K,[5] they could not be resolved at room temperature. In dithiouracil there remains some uncertainty when the ν_+ line is paired with the ν_0 line, since ν_- lines have not been observed. By comparing the absorption intensities of the two lines in each absorption band [ν_+ or ν_0], the pairing given in Table 2 was made. Figure 3 shows the chart recorder output of the ν_+ and ν_0 lines in the NQR spectrum of ^{14}N in dithiouracil. In the ν_0 [or ν_+] band, the dip of the resonance (a) [or (a')] is smaller than that of (b) [or (b')]. For the uracil group, the quadrupole coupling constant tends to decrease and the asymmetry parameter tends to increase as oxygen atoms are replaced by sulfur atoms. For uracil and its sulfur-substituted compounds it is very difficult to give the definitive assignment of one set of observed lines to one particular site within each molecule.

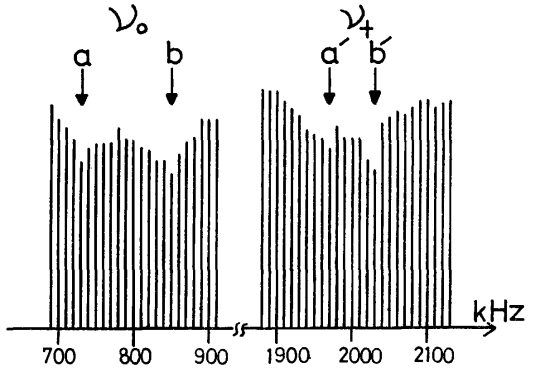

Fig. 3. Chart recorder output of the ν_+ and ν_0 lines in the NQR spectrum of ^{14}N in 2,4-dithiouracil.

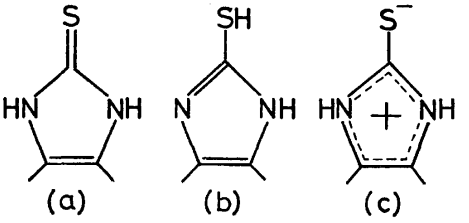

Fig. 4. Structural forms of 2-mercaptobenzimidazole.
(a) Thione, (b) thiol, (c) ionic.

Mercaptobenzimidazole can be represented by the three different structural forms illustrated in Fig. 4. When the thiol form is the predominant tautomer in the solid, we can expect two different ^{14}N NQR transitions. According to the X-ray analysis of the solid by Form *et al.*,[6] the molecule exists in the thione form with *mm* symmetry. This means the two nitrogen atoms are equivalent; our results are consistent with such a structural analysis.

The NQR parameters of uracil and its sulfur-substituted compounds are analyzed by the following formulae, (3) and (4),[1] which are used for pyrrole-type nitrogen:

$$(e^2Qq/e^2Qq_0)\left[1+\frac{\eta}{3}\right] = L - \bar{B}, \tag{3}$$

$$(e^2Qq/e^2Qq_0)\eta = \frac{3}{2}(A-\bar{B})(1-\cot^2\gamma). \tag{4}$$

Here L is the pi population, A is the N–H sigma population, $\bar{B}$ is the averaged N–C sigma population, 2γ is the CNC angle, and e^2Qq_0 is the coupling constant of an electron in a 2p orbital of nitrogen. In order to estimate L and $\bar{B}$, we assume that A is 1.33[7] and e^2Qq_0 is 7.4 MHz.[5,8] For uracil the averaged value of the two CNC angles[10] is used for 2γ. As the X-ray analysis of thiouracil has not been published, we assume 2γ is 122°. For dithiouracil the experimental values[9] are used. The results are given in Table 3. From uracil to dithiouracil, the lone pair population L is monotonically decreasing. This decrease of lone pair population suggests the increase of the ionic term $-^+NH{=}C(-S^-)-$ in the resonance structures.

Table 3. The orbital occupation numbers for nitrogen in uracil and its sulfur-substituted compounds

Substance	L (lone pair)	$\bar{B}$ (N–C)	[η][a]
Uracil	1.58	1.16	[0.502]
2-Thiouracil	1.49	1.12	[0.734]
	1.53	1.15	[0.580]
2,4-Dithiouracil	1.47	1.11	[0.794]
	1.49	1.14	[0.682]

a) The asymmetry parameters are used to distinguish the two nitrogen sites in each molecule.

References

1) E. A. C. Lucken, "Nuclear Quadrupole Coupling Constants," Academic Press, London and New York (1969).
2) S. R. Hartmann and E. L. Hahn, *Phys. Rev.*, **128**, 2042 (1962).
3) F. M. Lurie and C. P. Slichter, *Phys. Rev.*, **A133**, 1108 (1964).
4) R. E. Slusher and E. L. Hahn, *Phys. Rev.*, **166**, 332 (1968).
5) D. T. Edmonds, *J. Magn. Reson.*, **6**, 265 (1972).
6) G. R. Form, E. S. Raper, and T. C. Downie, *Acta Crystallogr., Sect. B*, **32**, 345 (1976).
7) M. T. Weiss and M. W. P. Strandberg, *Phys. Rev.*, **83**, 567 (1951).
8) L. Krause and M. A. Whitehead, *Mol. Phys.*, **25**, 99 (1973).
9) E. Shefter and H. G. Mautner, *J. Am. Chem. Soc.*, **89**, 1249 (1967).
10) R. F. Stewart, *Acta Crystallogr.*, **23**, 1102 (1967).

Study of the Chemisorption and Hydrogenation of Propylene on Platinum by Temperature-Programmed Desorption

Susumu TSUCHIYA, Masami NAKAMURA,* and Norihiko YOSHIOKA**

Department of Industrial Chemistry, Faculty of Engineering, Yamaguchi University, Tokiwadai, Ube 755

(Received September 2, 1977)

The temperature-programmed desorption (TPD) chromatograms of propylene from platinum black comprised four peaks: A, B, C, and D, with peak maxima at about 260, 380, 570, and higher than 720 K respectively. Peaks A and B were identified as the mixtures of propylene and propane. Peaks C and D were methane formed from chemisorbed propylene by decomposition as the temperature was raised during the subsequent TPD. The reactivities of various types of chemisorbed hydrogen previously detected by TPD were also investigated with regard to the hydrogenation of propylene. Two types of chemisorbed hydrogen, presumed to be present on the surface in the form of hydrogen atoms chemisorbed on top of platinum atoms and in the bridge form of molecular hydrogen, were found to react with propylene.

Four different types of chemisorbed hydrogen (α, β, γ, and δ) were previously found on the platinum surface, with the temperature-programmed desorption (TPD) peak maxima at about 170, 250, 360, and 570 K respectively.[1] Their participation in the H_2–D_2 exchange reaction was also examined;[2] only α and γ, were found to readily undergo surface exchange at low temperatures.

The present work has been carried out in order to obtain more information on the differences in the reactivities of the forms of chemisorbed hydrogen, and on the chemisorption and hydrogenation of propylene.

Experimental

Apparatus. The apparatus used for the present study was essentially the same as that used previously,[2] except for minor modifications. It consisted basically of two parts: an adsorption and reaction system, in which the adsorption and reaction were measured in a conventional manner, and a TPD system, in which adsorbed gas was later desorbed into a carrier-gas stream (N_2 or He) by means of the programmed heating of the catalyst. The concentration of the desorbed gas was measured and recorded by means of a thermal conductivity detector. When the ambient gas consisted of hydrocarbons, a gas chromatograph equipped with a thermal conductivity detector instead of a Pirani gauge was employed to estimate the pressure. A mercury manometer and a McLeod gauge were occasionally used to calibrate the detector, but they were then isolated from the reaction system by means of a stopcock to avoid the contamination of the catalyst by mercury vapor. An oil-diffusion pump behind the rotary oil pump was used for the evacuation of the system.

Materials. The catalyst used in the present investigation was a platinum black obtained from Wako Pure Chemical Industries, Ltd., it was pressed into tablets about 2-mm thick and 4 mm in diameter. Atomic absorption spectrophotometric analysis showed that the largest metallic impurity was Fe (130 ppm), followed by Rh (80 ppm) and Pd (20 ppm). The catalyst was first reduced in a hydrogen stream at atmospheric pressure for 35 h at 520 K, and then for 5 h at 720 K. Its surface area, as estimated by the BET method, was 3.2×10^3 cm^2/g.

Cylinder hydrogen (99.975%) supplied by the Osaka Hydrogen Co. was stored in a reservoir for use as a reactant after having been passed over platinized silica at 720 K and then through a liquid nitrogen trap. The same cylinder hydrogen could also be fed through to the reactor for the reduction of the catalyst. Matheson's deuterium (99.5%) passed through a liquid nitrogen trap was also used as a reactant. Propylene obtained from Takachiho Chemical Industry Co., Ltd., was purified by repeated distillation with liquid nitrogen traps; its gas chromatographic analysis indicated a purity of 99.9%. High-purity helium (99.995%) and high-purity nitrogen (99.999%), obtained from the Seitetsu Kagaku Co., Ltd., were used as carrier gases for TPD after having been passed through a molecular sieve trap cooled in liquid nitrogen.

Procedure. Before each run, the catalyst was treated with hydrogen for 4 h at 680 K and under atmospheric pressure, and then heated up to 820 K in the stream of carrier gas; all the hydrogen chemisorbed on the catalyst was removed by this desorption. The catalyst was then cooled to a selected temperature in the carrier gas, and the reactor was evacuated for 30 min, unless otherwise stated, using the oil-diffusion pump to remove the carrier gas. The catalyst activity fell at first, but became reasonably stable after about fifty runs. All the data reported here were obtained with the stabilized catalyst.

In a typical experiment on propylene, a known amount of propylene was adsorbed for 15 min at the experimental temperature. The reactor was then cooled to 238 K with the propylene present in the gas phase, and kept for 15 min. Following this, the carrier gas, helium, was diverted from the bypass into the reactor in order to remove the propylene in the gas phase, and then after 5 min, the catalyst was heated in a programmed manner. Before heating, hydrogen was sometimes admitted to react the adsorbed propylene after the helium had been removed by five minutes' evacuation. The reaction time in these cases was 30 min.

TPD chromatograms were obtained on the recorder chart and showed peaks due to the gas desorbed from the catalyst at different temperatures. A more detailed desorption of the TPD method has been given elsewhere.[3] The heating was stopped at about 800 K, after which the catalyst was kept in the helium stream for 20 min at the same temperature before cooling. Reproducible results were usually obtained by this procedure. When the results were not reproducible, however, the catalyst was treated with 20 to 30 kPa of oxygen for 1 h at about 770 K to oxidize any organic contamination, and was then again reduced by hydrogen as has been described above. This treatment improved the reproducibility considerably.

In the hydrogenation of propylene, various types of chemisorbed hydrogen were first prepared by the TPD technique described previously,[1,2] and then propylene was admitted to

* Present address: Central Glass Co., Ltd., Ube 755.

** Present address: Shikoku Paper Mfg. Co., Ltd., Kumagaya 360-01.

the reaction system to start the reaction. Before the propylene was admitted, however, ten minutes' evacuation was done and the α-hydrogen weakly adsorbed on the surface was removed. Helium was added to dilute the propylene when the circulating pump in the reaction system was operated. After the reaction, all the system except for the reactor was evacuated through a liquid nitrogen trap to collect any condensable hydrocarbons, which were transferred to a sampler for analysis. The carrier gas was then diverted into the reactor, and any materials adsorbed on the catalyst were removed by TPD.

Analysis. The reactants, the reaction mixtures, and the desorption products were identified by gas chromatography. The deuterio-hydrocarbons obtained after the reaction were analyzed by means of a JEOL JMS D-100 mass spectrometer. Before subjecting the reaction mixture to mass-spectrometric analysis, they were separated gas chromatographically to avoid any mutual interference of the mass spectra.

Results and Discussion

Temperature-Programmed Desorption. Figure 1 shows some typical TPD chromatograms taken after the propylene had been adsorbed on the platinum black in the absence or presence of hydrogen as indicated, with helium used as the carrier gas. The pressure of the propylene or hydrogen admitted was 6.1×10^2 Pa, and the reaction temperature was 238 K. These four TPD chromatograms resemble each other, characteristically being composed of four peaks appearing at about 260, 380, 570, and higher than 720 K. These peaks are referred to as A, B, C, and D in the order of appearance with increase in the temperature. By gas chromatographic analysis, Peaks A and B were identified as the mixtures of propylene and propane, while Peaks C and D were methane. It is suggested that the propane was formed by the self-hydrogenation of chemisorbed propylene, where hydrogen was absent. The methane may be formed by decomposition from the chemisorbed propylene heated by TPD, as was previously suggested[4] for the ethylene-platinum system. In order to observe the desorbing hydrogen more clearly, nitrogen was used as the carrier gas for the TPD; only δ-hydrogen was observed in the TPD chromatogram. The other form of hydrogen may have been removed from the surface when propylene was admitted, probably by the displacement in the adsorption and/or in the surface hydrogenation to propane. On the surface, accordingly, only the admitted propylene along with δ-hydrogen was adsorbed in the form of propylene and/or propane. The results suggest that propylene is more strongly adsorbed on platinum than hydrogen.

It is not very clear at this stage whether the propane in the Peaks A and B, where hydrogen was present, is a result of the self-hydrogenation, or of the desorption of propane formed by hydrogenation, or both.

Table 1. Hydrogenation of propylene on platinum black[a]

Series	Surface reactant: Type of chemisorption and estimated amount[b] (cm³, STP) β	γ	δ	Gas-phase reactant: Pressure of propylene (10^2 Pa)	Propane formed (cm³, STP)
A	—	—	—	6.7	0.0022
B1	—	—	0.0358	6.5	0.0035
B2	—	—	0.0467	6.5	0.0046
C1	—	0.0383	0.0334	6.6	0.0314
C2	—	0.0383	0.0334	6.5	0.0296
D1	0.0078	0.0441	0.0332	6.5	0.0400
D2	0.0045	0.0246	0.0371	6.0	0.0196

a) Catalyst weight, 2.53 g. Reaction temp, 246 K, and reaction time, 20 min. b) Estimated from TPD chromatograms in comparable experiments.

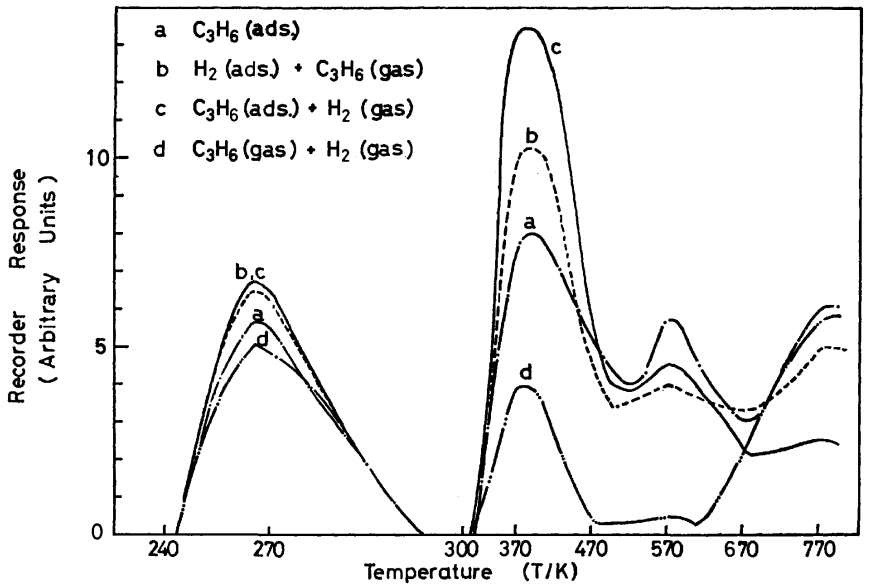

Fig. 1. TPD chromatograms of propylene on platinum. (a) C_3H_6 only was adsorbed. (b) H_2 was preadsorbed and C_3H_6 was subsequently admitted. (c) C_3H_6 was preadsorbed and H_2 was subsequently admitted. (d) C_3H_6 and H_2 were simultaneously admitted.

TABLE 2. HYDROGENATION OF PROPYLENE WITH LABELED HYDROGEN CHEMISORBED ON PLATINUM[a)]

Type of surface used	Amounts of hydrogen preadsorbed[b)] (mm^3, STP)			Pressure of C_3H_6 (10^2 Pa)	Deuteriopropanes formed (mm^3, STP)				
	β	γ	δ		d_0	d_1	d_2	d_3	d_4
H–H–D	15.4	11.3	2.8	6.1	16.8	—	—	—	—
H–D–H	27.7	31.9	5.1	6.1	12.5	8.6	2.7	1.1	0.6
D–H–D	26.5	30.6	4.8	6.1	24.3	1.8	—	—	—
D–H–D	15.9	13.1	3.8	6.5	14.0	2.7	—	—	—
D–D–H	16.9	12.6	2.8	6.7	9.1	4.2	1.3	0.5	0.5

a) Catalyst weight, 1.80 g. Reaction temp, 238 K, and reaction time, 30 min. b) Estimated from TPD chromatograms in comparable experiments.

Reactivity of Chemisorbed Hydrogen. Table 1 shows the results of the surface hydrogenation experiments with hydrogen preadsorbed on the platinum black in various forms (the surface reactant), and with gaseous propylene subsequently admitted into the reaction system (the gas-phase reactant). The amounts of propane formed in Series B with δ-hydrogen agreed approximately with those in Series A, in which propane was formed by a self-hydrogenation reaction. Apparently, δ-hydrogen hardly reacts with the gas-phase reactant under the present experimental conditions.

In Series C, with δ- and γ-hydrogen preadsorbed on the surface, however, relatively larger amounts of propane were produced than in Series B. The amounts of propane formed agreed with those of the preadsorbed γ-hydrogen. In the TPD chromatogram obtained after propylene was admitted to the preadsorbed hydrogen, where nitrogen was used as the carrier gas, the γ-hydrogen disappeared, while δ-hydrogen was still present in almost the same amount. It is, therefore, clear that γ-hydrogen is involved in the hydrogenation.

In Series D, in which β-, γ-, and δ-hydrogen were preadsorbed, the amounts of propane formed were again in approximate agreement with those of γ-hydrogen, suggesting that only preadsorbed γ-hydrogen reacted. The contribution of β-hydrogen to the hydrogenation, however, could not be observed, because the amounts of preadsorbed β-hydrogen were much smaller than those of γ-hydrogen. It was, accordingly, not clear at this stage whether or not only γ-hydrogen participates in the hydrogenation.

To elucidate the point, the preadsorbed hydrogen was partially displaced by deuterium before propylene was introduced, and the deuteropropanes formed by hydrogenation were then analyzed. The participation of the different types of chemisorbed hydrogen was consequently elucidated. For the sake of simplicity, the word "hydrogen" in the present paper will hereafter stand for both isotopes, protium and deuterium, and, where necessary, the individual isotopes will be designated as H and D. The types of surface used were as follows: (1) δ-Hydrogen was displaced by deuterium, and γ- and β-hydrogen were protium (H–H–D); (2) δ- and β-hydrogen were deuterium, and γ-hydrogen was protium (D–H–D); (3) δ- and β-hydrogen were protium, and γ-hydrogen was deuterium (H–D–H); (4) δ-hydrogen was protium, and β- and γ-hydrogen were deuterium (D–D–H). The method of preparation was described previously;[5)] the isolation of different types of chemisorbed hydrogen was confirmed by separate TPD experiments.

Table 2 shows the results of hydrogenation: the amounts of hydrogen preadsorbed and those of the individual deuteriopropanes formed by the hydrogenation are shown. The reactions were carried out at 238 K for 30 min. In the mass spectra of propylene, the reactant, the $m/e>42$ could not be observed, the ^{13}C contribution having been corrected.

Obviously, propylene is deuterated to deuteriopropane over the H–D–H, D–H–D, and D–D–H surface, but not over the H–H–D surface. These results agree quite well with the above suggestions that δ-hydrogen does not, and γ-hydrogen does, participate in the hydrogenation. The results also suggest the participation of β-hydrogen, which was not detected before. The total amount of deuteropropanes formed over the H–D–H surface was larger than that over the D–H–D surface under similar experimental conditions, and it seems that γ-hydrogen is more reactive than β-hydrogen. Over the D–D–H surface, propane-d_0 was formed, suggesting that the self-hydrogenation of propylene took place even when hydrogen was present.

On the mechanism of the hydrogenation of olefins, extensive studies have previously been reported.[6)] It is premature at present to discuss the matter on the basis of our results and to add further conclusions to other than those already reported.

It has previously been presumed that γ-hydrogen is present on the surface in the form of hydrogen atoms chemisorbed on top of platinum atoms, and that β-hydrogen is molecular hydrogen chemisorbed in a bridge form.[1)] The difference in the reactivity may, accordingly, be due to the chemisorbed state, whether or not the H–H bond has been split. In the H_2–D_2 exchange reaction, β-hydrogen is not reactive, but it is reactive in the hydrogenation of propylene. It is, accordingly, probable that a different tendency would be shown depending upon the sort of reaction; the explication of the other reactions awaits further investigations.

The authors are grateful to Mr. Shizuo Fujisaki of this faculty for obtaining the mass spectra, and also to Professor Tatsuaki Yashima and Dr. Nobuo Takahashi of Tokyo Institute of Technology for the atomic absorption spectrophotometric analysis of the catalyst. The work was supported by a Grant-in-Aid for Scientific Research from the Ministry of Education, for which the authors' thanks are due.

References

1) S. Tsuchiya, Y. Amenomiya, and R. J. Cvetanović, *J. Catal.*, **19**, 245 (1970).
2) S. Tsuchiya, Y. Amenomiya, and R. J. Cvetanović, *J. Catal.*, **20**, 1 (1971).
3) R. J. Cvetanović and Y. Amenomiya, *Adv. Catal.*, **17**, 103 (1962).
4) R. Komers, Y. Amenomiya, and R. J. Cvetanović, *J. Catal.*, **15**, 293 (1969).
5) N. Yoshioka, M. Nakamura, and S. Tsuchiya, *Chem. Lett.*, **1977**, 445.
6) G. C. Bond, "Catalysis by Metals," Academic Press, New York (1962), p. 229.

The Crystal Structure of a Stable Benzocyclobutene. II. 2,7-Di-*t*-butyl-10,10,11,11-tetracyano-4,5,9,12-tetraphenyltetracyclo-[6.4.0.0^{3,6}.0^{9,12}]dodeca-1(8),2,4,6-tetraene

Harumichi TSUKADA, Hirotaka SHIMANOUCHI, and Yoshio SASADA

Laboratory of Chemistry for Natural Products, Tokyo Institute of Technology, Ookayama, Meguro-ku, Tokyo 152

(Received September 10, 1977)

As the first step in the investigation of the reaction mechanism of a benzocyclobutene derivatives, the title compound has been determined by the X-ray diffraction method. The crystals are monoclinic; space group $P2_1/n$; $a=28.117(3)$, $b=11.148(1)$, $c=13.167(1)$ Å, and $\beta=97.26(1)°$. The asymmetric unit contains one molecule of the title compound and acetonitrile. The structure was solved by the direct method and refined by the block-diagonal least-squares method to a final R factor of 0.088 for 5456 observed reflections. The molecular framework consists of a planar ten-membered ring from benzodicyclobutene and a slightly folded four-membered ring formed by the addition of tetracyanoethylene (TCNE). Calculation has been undertaken for the non-bonded interaction energy of possible modes of approach between benzodicyclobutene and TCNE. The results are in qualitative agreement with the folding of the four-membered ring.

The Diels-Alder reactions of a benzodicyclobutene derivative (**1**)[1] with some dienophiles may be classified into three types: i) Tetracyanoethylene (TCNE) attacks the C(4)–C(5) double bond to give a "linear" adduct (**2**);[2] ii) bridged compounds across the central six-membered ring are obtained by means of a reaction with *trans*-1,2-dicyanoethylene (DCNE) and also as by-products of the reaction with TCNE,[3] and iii) some other dienophiles are added to C(1)–C(10) to produce "angular" adducts.[4] The diversity of the reactions of the molecule (**1**) should be studied stereochemically as well as electronically.

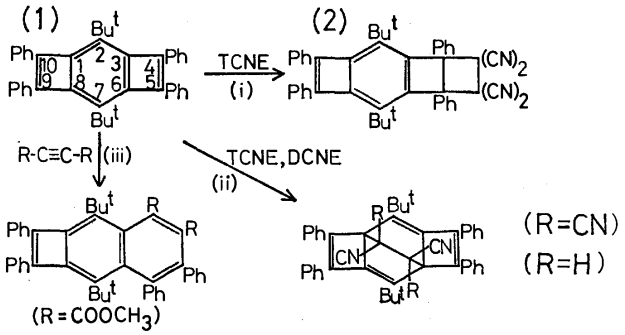

The present paper will deal with the X-ray analysis of the title compound (**2**), one of the linear adducts, as the first step in the investigation of the reaction route.

Experimental

Crystals suitable for structure determination were provided by Professor Fumio Toda of Ehime University. The crystals were orange prisms. Weissenberg photographs showed the systematic absences; $(h0l)$, $h+l\neq 2n$, and $(0k0)$, $k\neq 2n$, indicating that the space group was $P2_1/n$. Accurate unit-celldimensions and intensity data were obtained on a Rigaku automated four-circle diffractometer using graphite-monochromated Mo $K\alpha$ radiation. The crystal data are listed in Table 1. A total of 7404 independent reflections ($2\theta\leqq 50°$) were obtained, in which 5456 had intensities greater than $3\sigma(I)$. Lorentz and polarization corrections were made as usual.

TABLE 1. CRYSTAL DATA

2,7-Di-*t*-butyl-10,10,11,11-tetracyano-4,5,9,12-tetraphenyltetracyclo[6.4.0.0^{3,6}.0^{9,12}]dodeca-1(8),2,4,6-tetraene: acetonitrile.

$C_{48}H_{38}N_4$: C_2H_3N	
$F.W.$	711.9
Crystal system	monoclinic
Space group	$P2_1/n$
a	28.117(3) Å
b	11.148(1)
c	13.167(1)
β	97.26(1)°
U	4094(1) Å^3
Z	4
D_m	1.157 g cm^{-3}
D_x	1.155

Structure Determination

The structure was solved by the direct method.[5] Fourier synthesis using 545 normalized structure factors ($|E|\geqq 1.7$) clearly revealed 55 non-hydrogen atoms, including those in acetonitrile. The atomic parameters were refined by the block-diagonal least-squares method. The thermal parameters of acetonitrile became twice as large as those of the other atoms. All the hydrogen atoms except for those of acetonitrile were located on a difference map. In spite of the quite large thermal parameters, the bond lengths of acetonitrile are rather reasonable. Moreover, the difference synthesis showed no large peak near the position of these atoms. Therefore, there were no difficulties in determining the occupancy of acetonitrile. At the final stage of the refinement, anisotropic temperature factors were introduced for all the non-hydrogen atoms.

The weighting scheme was $w=1/\{1+0.2(10-|F_o|)\}$ for $|F_o|<10$, $w=1$ for $10\leqq|F_o|\leqq 30$, and $w=1/\{1+0.8(|F_o|-30)\}$ for $|F_o|>30$, so as to make the average of $w(|F_o|-|F_c|)^2$ almost equal over all the range of $|F_o|$ values. The final R factor was 0.088 for the non-zero reflections and 0.14 for all the reflections.* The atomic scattering factors were taken from *International Tables*

Table 2. Final positional ($\times 10^4$) and thermal ($\times 10^3$) parameters

The temperature factor has this form:

$$\exp[-2\pi^2(U_{11}h^2a^{*2}+U_{22}k^2b^{*2}+U_{33}l^2c^{*2}+2U_{12}hka^*b^*+2U_{13}hla^*c^*+2U_{23}klb^*c^*)].$$

Atom	x	y	z	U_{11}	U_{22}	U_{33}	U_{12}	U_{13}	U_{23}
C(1)	1636(1)	704(3)	3216(2)	33(2)	37(2)	35(2)	−2(1)	−1(1)	4(1)
C(2)	2133(1)	1038(3)	3464(2)	33(2)	35(2)	41(2)	−5(1)	3(1)	3(1)
C(3)	2321(1)	430(3)	4317(2)	30(2)	42(2)	44(2)	−6(1)	−2(1)	0(1)
C(4)	2773(1)	177(3)	5084(3)	38(2)	49(2)	45(2)	−3(2)	−7(1)	3(2)
C(5)	2535(1)	−584(3)	5620(3)	41(2)	53(2)	44(2)	−1(2)	−5(1)	5(2)
C(6)	2068(1)	−389(3)	4896(2)	41(2)	44(2)	35(2)	−2(1)	−2(1)	5(1)
C(7)	1592(1)	−679(3)	4699(2)	40(2)	45(2)	34(2)	−4(1)	5(1)	2(1)
C(8)	1386(1)	−43(3)	3795(2)	32(2)	38(2)	35(2)	−1(1)	0(1)	−3(1)
C(9)	906(1)	111(3)	3124(2)	28(1)	45(2)	39(2)	−2(1)	2(1)	−1(1)
C(10)	596(1)	1219(3)	3454(2)	35(2)	47(2)	43(2)	1(1)	3(1)	−1(2)
C(11)	926(1)	2137(3)	2916(2)	42(2)	43(2)	42(2)	0(2)	0(1)	−1(2)
C(12)	1196(1)	1010(3)	2465(2)	31(2)	39(2)	37(2)	−1(1)	3(1)	5(1)
C(13)	1154(1)	830(3)	1336(2)	42(2)	37(2)	39(2)	−8(1)	2(1)	4(1)
C(14)	1541(1)	388(3)	886(3)	54(2)	45(2)	49(2)	2(2)	8(2)	1(2)
C(15)	1494(2)	108(4)	−149(3)	81(3)	69(3)	53(2)	−3(2)	19(2)	−9(2)
C(16)	1051(2)	233(5)	−744(3)	98(3)	93(4)	43(2)	−20(3)	4(2)	−10(2)
C(17)	662(2)	617(5)	−302(3)	71(3)	90(3)	48(2)	−11(2)	−13(2)	0(2)
C(81)	707(1)	913(4)	728(3)	53(2)	70(3)	44(2)	−5(2)	−7(2)	1(2)
C(19)	662(1)	−1000(3)	2655(2)	37(2)	45(2)	40(2)	−7(1)	0(1)	3(2)
C(20)	940(1)	−1767(3)	2141(3)	57(2)	49(2)	64(2)	−8(2)	10(2)	−7(2)
C(21)	754(2)	−2849(4)	1732(4)	87(3)	61(3)	89(3)	−7(2)	9(3)	−21(3)
C(22)	285(2)	−3147(4)	1825(4)	97(4)	53(3)	107(4)	−23(3)	−16(3)	−16(3)
C(23)	9(2)	−2400(4)	2341(4)	59(3)	66(3)	110(4)	−22(2)	−14(2)	13(3)
C(24)	192(1)	−1324(4)	2757(3)	42(2)	57(2)	67(2)	−9(2)	−3(2)	10(2)
C(25)	3286(1)	537(3)	5300(2)	37(2)	59(2)	40(2)	−3(2)	−8(1)	9(2)
C(26)	3639(1)	−235(4)	5063(3)	47(2)	78(3)	67(3)	10(2)	−5(2)	−10(2)
C(27)	4120(1)	28(5)	5388(4)	44(2)	134(5)	71(3)	23(3)	−2(2)	−12(3)
C(28)	4241(1)	1052(5)	5928(3)	42(2)	132(4)	65(3)	−21(3)	−7(2)	−6(3)
C(29)	3896(2)	1826(5)	6154(4)	60(3)	93(4)	100(4)	−21(3)	−14(3)	−23(3)
C(30)	3414(1)	1577(4)	5847(4)	49(2)	74(3)	91(3)	−2(2)	−10(2)	−23(3)
C(31)	2708(1)	−1266(4)	6553(3)	43(2)	59(2)	50(2)	−4(2)	−4(2)	14(2)
C(32)	2920(2)	−2369(4)	6488(4)	109(4)	65(3)	68(3)	20(3)	−5(3)	12(2)
C(33)	3112(2)	−2980(5)	7374(4)	131(5)	86(4)	88(4)	27(4)	−11(3)	31(3)
C(34)	3093(2)	−2495(6)	8314(4)	108(4)	116(5)	75(3)	13(4)	−19(3)	44(3)
C(35)	2885(2)	−1395(6)	8386(4)	127(5)	148(6)	51(3)	24(4)	−16(3)	15(3)
C(36)	2695(2)	−760(5)	7509(3)	100(4)	96(4)	56(3)	23(3)	−15(2)	4(3)
C(37)	2422(1)	1938(3)	2896(3)	41(2)	47(2)	55(2)	−11(2)	4(2)	8(2)
C(38)	2118(1)	2706(4)	2085(3)	59(2)	53(2)	60(2)	−10(2)	0(2)	17(2)
C(39)	2807(1)	1246(4)	2392(4)	51(2)	71(3)	93(3)	−6(2)	30(2)	14(2)
C(40)	2677(1)	2819(4)	3693(3)	65(3)	57(3)	74(3)	−27(2)	−10(2)	11(2)
C(41)	1354(1)	−1558(4)	5369(3)	46(2)	62(2)	47(2)	−7(2)	4(2)	19(2)
C(42)	822(1)	−1756(4)	5034(3)	53(2)	93(3)	67(3)	−25(2)	5(2)	29(2)
C(43)	1614(2)	−2758(4)	5377(5)	85(3)	61(3)	139(5)	−6(3)	23(3)	39(3)
C(44)	1403(2)	−1053(5)	6470(3)	79(3)	138(5)	40(2)	−33(3)	8(2)	10(3)
C(45)	677(1)	2973(3)	2177(3)	45(2)	48(2)	62(2)	7(2)	7(2)	3(2)
C(46)	1231(1)	2869(3)	3669(3)	52(2)	49(2)	54(2)	−3(2)	12(2)	−6(2)
C(47)	100(1)	1302(3)	2931(3)	40(2)	49(2)	62(2)	5(2)	9(2)	2(2)
C(48)	597(1)	1387(3)	4563(3)	47(2)	55(2)	51(2)	0(2)	14(2)	0(2)
N(1)	499(1)	3626(3)	1581(3)	64(2)	74(2)	88(3)	20(2)	10(2)	28(2)
N(2)	1459(1)	3461(3)	4242(3)	77(2)	71(2)	77(2)	−13(2)	1(2)	−24(2)
N(3)	−274(1)	1386(3)	2509(3)	38(2)	82(3)	90(3)	7(2)	−3(2)	7(2)
N(4)	610(1)	1496(4)	5420(3)	90(3)	92(3)	53(2)	7(2)	21(2)	−8(2)
C(49)	694(3)	4696(6)	6280(7)	160(7)	93(5)	201(8)	8(5)	81(6)	1(5)
C(50)	261(3)	5446(5)	6204(5)	192(7)	83(4)	111(5)	−38(4)	71(5)	−17(4)
N(5)	−79(3)	6063(5)	6144(5)	207(6)	105(4)	140(5)	−8(4)	75(5)	−24(4)

for X-Ray Crystallography.[6] The final atomic parameters are listed in Table 2,* while the crystallographic numbering scheme is shown in Fig. 1.

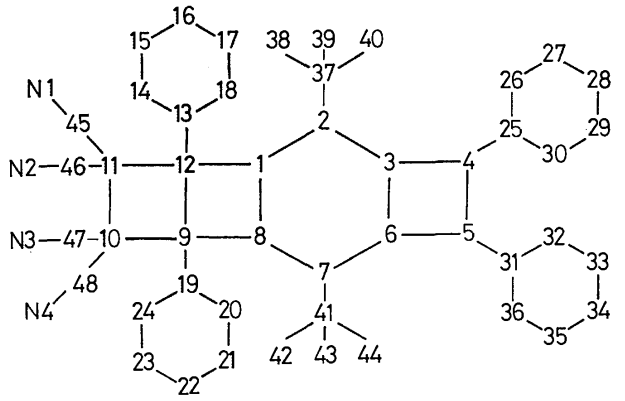

Fig. 1. Crystallographic numbering scheme.

Results and Discussion

The crystal structure is shown in Fig. 2, the molecular framework is shown in Fig. 3, and the bond lengths and angles are listed in Table 4. Ten atoms of the molecular framework, which are originally the skeleton of **1**, are nearly coplanar (Table 3). By the addition of TCNE, a new cyclobutane ring is formed, which makes a dihedral angle (109.0°) with the ten-membered ring. The corresponding dihedral angle of perchloro-3, 4,7,8-tetramethylenetricyclo[4.2.0.0^{2,5}]octane[7] is 115°. In the cyclobutane ring, all the bond lengths exceed 1.60 Å, considerably longer than the usual C(sp^3)–C(sp^3) lengths. Such an elongation effect of the four-membered ring may be attributed to the strong repulsion between the non-bonded atoms. For example, the C–C bond length is 1.56 Å in cyclobutane and 1.583 Å in *cis*-3,4-dichloro-1-cyclobutene.[8] Also elongated is that in the

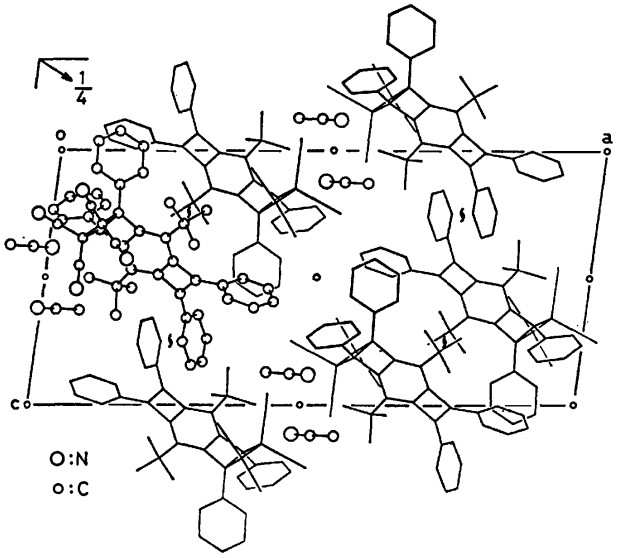

Fig. 2. Crystal structure projected along the b axis.

* The tables of structure factors and the atomic parameters of the hydrogen atoms are kept as Document No. 7809 at the Chemical Society of Japan.

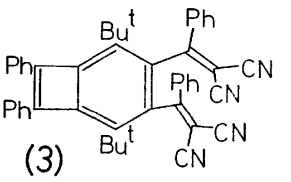

Table 3. Deviations (*l*/Å) from the plane through the ten-membered ring

C(1)*	−0.040
C(2)*	0.011
C(3)*	0.008
C(4)*	0.010
C(5)*	−0.005
C(6)*	−0.009
C(7)*	0.001
C(8)*	0.003
C(9)*	0.016
C(12)*	0.005
C(10)	1.489
C(11)	1.556
C(37)	0.074
C(41)	−0.008
C(25)	0.044
C(31)	0.007

Asterisks are used to define the best plane.

Table 4a. Bond lengths (*l*/Å)
Standard deviations are given in parentheses.

C(1)–C(2)	1.442(4)	C(19)–C(20)	1.390(5)
C(1)–C(8)	1.381(4)	C(19)–C(24)	1.392(5)
C(1)–C(12)	1.522(4)	C(20)–C(21)	1.394(6)
C(2)–C(3)	1.360(5)	C(21)–C(22)	1.381(7)
C(2)–C(37)	1.543(5)	C(22)–C(23)	1.374(8)
C(3)–C(4)	1.548(5)	C(23)–C(24)	1.390(7)
C(3)–C(6)	1.435(5)	C(25)–C(26)	1.379(6)
C(4)–C(5)	1.336(5)	C(25)–C(30)	1.387(6)
C(4)–C(25)	1.488(5)	C(26)–C(27)	1.399(8)
C(5)–C(6)	1.536(5)	C(27)–C(28)	1.365(8)
C(5)–C(31)	1.475(5)	C(28)–C(29)	1.360(8)
C(6)–C(7)	1.370(5)	C(29)–C(30)	1.391(7)
C(7)–C(8)	1.442(5)	C(31)–C(32)	1.374(7)
C(7)–C(41)	1.529(5)	C(31)–C(36)	1.384(7)
C(8)–C(9)	1.526(5)	C(32)–C(33)	1.399(8)
C(9)–C(10)	1.604(5)	C(33)–C(34)	1.358(9)
C(9)–C(12)	1.612(5)	C(34)–C(35)	1.368(9)
C(9)–C(19)	1.509(5)	C(35)–C(36)	1.401(9)
C(10)–C(11)	1.605(5)	C(37)–C(38)	1.540(5)
C(10)–C(47)	1.479(5)	C(37)–C(39)	1.547(6)
C(10)–C(48)	1.471(5)	C(37)–C(40)	1.546(6)
C(11)–C(12)	1.619(5)	C(41)–C(42)	1.519(6)
C(11)–C(45)	1.461(5)	C(41)–C(43)	1.523(7)
C(11)–C(46)	1.472(5)	C(41)–C(44)	1.545(7)
C(12)–C(13)	1.490(5)	C(45)–N(1)	1.139(5)
C(13)–C(14)	1.393(5)	C(46)–N(2)	1.136(5)
C(13)–C(18)	1.406(5)	C(47)–N(3)	1.130(5)
C(14)–C(15)	1.387(6)	C(48)–N(4)	1.131(6)
C(15)–C(16)	1.391(7)	C(49)–C(50)	1.471(12)
C(16)–C(17)	1.370(7)	C(50)–N(5)	1.172(10)
C(17)–C(18)	1.386(7)		

Table 4b. Bond angles (ϕ/°)

Standard deviations are given in parentheses.

C(2)–C(1)–C(8)	125.3	(3)	C(12)–C(13)–C(18)	120.8	(3)
C(2)–C(1)–C(12)	140.7	(3)	C(14)–C(13)–C(18)	118.1	(3)
C(8)–C(1)–C(12)	93.7	(3)	C(13)–C(14)–C(15)	121.0	(3)
C(1)–C(2)–C(3)	108.8	(3)	C(14)–C(15)–C(16)	119.8	(4)
C(1)–C(2)–C(37)	127.8	(3)	C(15)–C(16)–C(17)	119.9	(5)
C(3)–C(2)–C(37)	123.4	(3)	C(16)–C(17)–C(18)	120.8	(5)
C(2)–C(3)–C(4)	146.3	(3)	C(13)–C(18)–C(17)	120.4	(4)
C(2)–C(3)–C(6)	126.1	(3)	C(9)–C(19)–C(20)	116.8	(3)
C(4)–C(3)–C(6)	87.6	(3)	C(9)–C(19)–C(24)	124.1	(3)
C(3)–C(4)–C(5)	92.0	(3)	C(20)–C(19)–C(24)	119.0	(3)
C(3)–C(4)–C(25)	140.5	(3)	C(19)–C(20)–C(21)	121.0	(4)
C(5)–C(4)–C(25)	127.5	(3)	C(20)–C(21)–C(22)	119.3	(5)
C(4)–C(5)–C(6)	91.7	(3)	C(21)–C(22)–C(23)	120.2	(5)
C(4)–C(5)–C(31)	129.2	(3)	C(22)–C(23)–C(24)	120.8	(5)
C(6)–C(5)–C(31)	139.1	(3)	C(19)–C(24)–C(23)	119.7	(4)
C(3)–C(6)–C(5)	88.8	(3)	C(4)–C(25)–C(26)	119.7	(4)
C(3)–C(6)–C(7)	126.0	(3)	C(4)–C(25)–C(30)	120.4	(4)
C(5)–C(6)–C(7)	145.2	(3)	C(26)–C(25)–C(30)	119.5	(4)
C(6)–C(7)–C(8)	108.7	(3)	C(25)–C(26)–C(27)	119.8	(4)
C(6)–C(7)–C(41)	122.1	(3)	C(26)–C(27)–C(28)	120.2	(5)
C(8)–C(7)–C(41)	129.2	(3)	C(27)–C(28)–C(29)	120.4	(5)
C(1)–C(8)–C(7)	125.0	(3)	C(28)–C(29)–C(30)	120.4	(5)
C(1)–C(8)–C(9)	95.0	(3)	C(25)–C(30)–C(29)	119.8	(4)
C(7)–C(8)–C(9)	140.0	(3)	C(5)–C(31)–C(32)	120.7	(4)
C(8)–C(9)–C(10)	113.6	(3)	C(5)–C(31)–C(36)	120.3	(4)
C(8)–C(9)–C(12)	84.9	(2)	C(32)–C(31)–C(36)	118.9	(4)
C(8)–C(9)–C(19)	117.9	(3)	C(31)–C(32)–C(33)	120.6	(5)
C(10)–C(9)–C(12)	89.8	(2)	C(32)–C(33)–C(34)	120.7	(6)
C(10)–C(9)–C(19)	120.6	(3)	C(33)–C(34)–C(35)	119.1	(6)
C(12)–C(9)–C(19)	121.6	(3)	C(34)–C(35)–C(36)	121.2	(6)
C(9)–C(10)–C(11)	90.4	(2)	C(31)–C(36)–C(35)	119.5	(5)
C(9)–C(10)–C(47)	115.8	(3)	C(2)–C(37)–C(38)	114.7	(3)
C(9)–C(10)–C(48)	115.7	(3)	C(2)–C(37)–C(39)	108.9	(3)
C(11)–C(10)–C(47)	108.6	(3)	C(2)–C(37)–C(40)	108.1	(3)
C(11)–C(10)–C(48)	115.4	(3)	C(38)–C(37)–C(39)	109.8	(3)
C(47)–C(10)–C(48)	109.8	(3)	C(38)–C(37)–C(40)	106.6	(3)
C(10)–C(11)–C(12)	89.5	(2)	C(39)–C(37)–C(40)	108.6	(3)
C(10)–C(11)–C(45)	116.4	(3)	C(7)–C(41)–C(42)	114.3	(3)
C(10)–C(11)–C(46)	112.1	(3)	C(7)–C(41)–C(43)	108.8	(4)
C(12)–C(11)–C(45)	117.3	(3)	C(7)–C(41)–C(44)	108.3	(4)
C(12)–C(11)–C(46)	114.7	(3)	C(42)–C(41)–C(43)	109.2	(4)
C(45)–C(11)–C(46)	106.5	(3)	C(42)–C(41)–C(44)	107.0	(4)
C(1)–C(12)–C(9)	86.3	(2)	C(43)–C(41)–C(44)	109.1	(4)
C(1)–C(12)–C(11)	103.4	(3)	C(11)–C(45)–N(1)	177.2	(4)
C(1)–C(12)–C(13)	125.0	(3)	C(11)–C(46)–N(2)	178.1	(4)
C(9)–C(12)–C(11)	89.6	(2)	C(10)–C(47)–N(3)	178.0	(4)
C(9)–C(12)–C(13)	118.2	(3)	C(10)–C(48)–N(4)	177.9	(4)
C(11)–C(12)–C(13)	119.2	(3)	C(49)–C(50)–N(5)	178.7	(8)
C(12)–C(13)–C(14)	120.3	(3)			

unsaturated four-membered ring of the benzocyclobutene derivative (**3**),[9] a compound formed by the heat isomerization of the present compound. Our results, however, show much longer values than these compounds, indicating that the elongation effect is fortified by the bulky substituents. This suggests that this cyclobutane ring is easily cleaved. The bond between the *t*-butyl group and the skeleton is also affected by the repulsion. The averaged value, 1.54 Å, is comparable to that of the **3** molecule. The contraction of the C(1)–C(2)–C(37) and C(3)–C(2)–C(37) angles is 4.4°, and the C(1)–C(2)–C(3) angle is 108.8°. The corresponding values of the **3** molecule are 7 and 109° respectively. Although **2** and **3** are different about the cleaved ring, the resemblance in conformation of the *t*-butyl groups between **2** and **3** shows that the steric effects of the surrounding substituents are similar to each other. A detailed comparison indicates that, in **2**, one of the

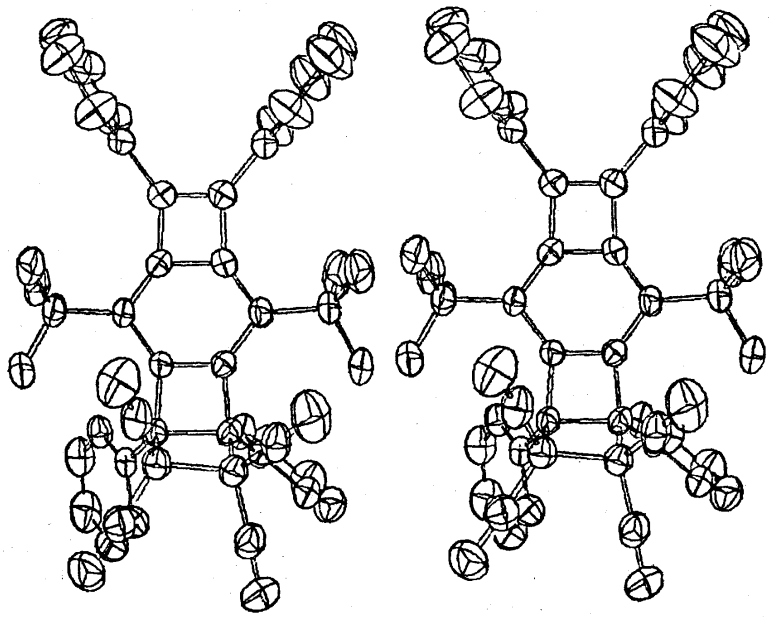

Fig. 3. A stereoscopic view perpendicular to the tenmembered ring.

methyl groups of the *t*-butyl group lies close to the skeletal plane. This is quite reasonable because, in the case of **3**, the cyano and phenyl groups jamming the in-plane methyl groups from both sides of the skeletal plane may have more freedom in their conformation than in the case of **2**. Phenyl groups attached to the unsaturated four-membered ring are rotated around the connecting bonds in both **2** and **3** molecules. The rotation angles of **2** are 80.2 and 91.7°, greater than those of **3**, 61 and 74°. These relatively large values, which may be attributed to the steric effect of the out-of-plane methyl groups, will serve to protect the reaction of one more TCNE to the unsaturated four-membered ring.

The central six-membered ring of the **2** molecule takes a shallow boat form, whereas the **3** molecule has a flattened crown conformation in which atoms deviate alternately from the plane. The four-membered rings annelated to the central six-membered ring are almost co-planar in **2**. However, the cyclobutane ring formed by the addition of TCNE is significantly non-planar. The dihedral angle between the C(9)–C(10)–C(11) and C(9)–C(12)–C(11) planes is 8.5°. The torsion angle C(9)–C(10)–C(11)–C(12) is 6.6°. This small, but significant, non-planarity may be regarded as a result of the steric effect of the bulky substituents. This effect, which also causes the elongation and distortion of some bond lengths and angles presented above, may play an intermediate role in the addition reaction as well. Therefore, we have calculated the non-bonded interaction energy for all the possible modes of approach between the **1** molecule and TCNE.

First, it was assumed that, in the stable conformation of the **1** molecule, four phenyl groups are rotated by 60° around the connecting bonds. This assumption is supported by the observation that some compounds with many phenyl groups have similar conformations; that of hexaphenylbenzene is 67.2°, for example.[10] Second, it was assumed that the plane of TCNE is parallel to that of the cyclobutene ring of **1** and that the center of the former approaches through the normal, passing the midpoint of the reactive double bond of the latter so as to make the overlap of the π-orbitals the maximum. For energy calculation, the distance between the double bonds and also the relative orientation were taken as variables. The former was varied from 4.0 to 3.4 Å, which is the van der Waals contact. The latter was every 10° of rotation up to 180° around the axis through the midpoints of both the double bonds. Some possible conformational changes of **1** in the reaction were

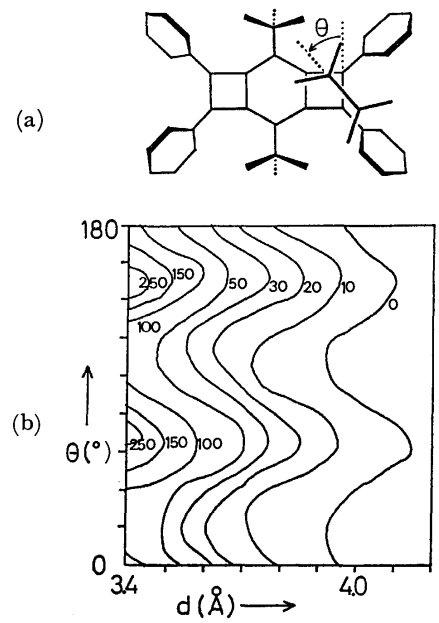

Fig. 4. (a) Relative orientation of the two molecules. (b) Two dimensional map of the non-bonded interaction energy (kcal mol^{-1}).

excluded from these calculations so as to reduce the number of parameters. For the same reason, the non-parallel approach of the two molecules was not considered. The potential functions used were those of Giglio.[11] The results are shown in Fig. 4. There are two potential grooves at the torsion angles of 20 and 110°, the former having a large overlap of the π-orbital. Therefore, the former mode of approach is preferable in the addition reaction. When the new cyclobutane is formed, strong intramolecular repulsion may modify the structure of **2** from the assumed one. However, the distortion of this cyclobutane ring, expressed in terms of the interedge angle (6.6°), is in qualitative agreement with the probable mode of approach. This indicates that such a calculation of the intermolecular interaction may be useful for the investigation of the reaction route of the **1** molecule with some dienophiles. The analyses of the other Diels-Alder adducts are in progress.

The authors are grateful to Professor Fumio Toda of Ehime University for supplying the sample and also for his valuable suggestions.

References

1) F. Toda and M. Ohi, *J. Chem. Soc., Chem. Commun.*, **1975**, 506.
2) F. Toda and N. Dan, *J. Chem. Soc., Chem. Commun.*, **1976**, 30.
3) F. Toda, private communication.
4) F. Toda and K. Tanaka, *J. Chem. Soc., Chem. Commun.*, **1976**, 177.
5) J. Karle and I. L. Karle, *Acta Crystallogr.*, **21**, 849 (1966).
6) "International Tables for X-Ray Crystallography," Vol. IV, The Kynoch Press, Birmingham (1974), pp. 72—98.
7) A. Furusaki, *Bull. Chem. Soc. Jpn.*, **40**, 758 (1967).
8) O. Bastiansen and J. L. Derissen, *Acta Chem. Scand.*, **20**, 1089 (1966).
9) H. Tsukada, H. Shimanouchi, and Y. Sasada, *Acta Crystallogr., Sect. B*, **33**, 2951 (1977).
10) J. C. J. Bart, *Acta Crystallogr., Sect. B*, **24**, 1277 (1968).
11) E. Giglio, *Nature*, **222**, 339 (1969).

ESR Studies of Oxygen, Sulfur Oxide, and Sulfur Radicals Adsorbed on NaX Zeolite

Natsuko KANZAKI and Iwao YASUMORI

Department of Chemistry, Tokyo Institute of Technology, O-okayama, Meguro-ku, Tokyo 152

(Received September 12, 1977)

The states of O_2 and SO_2 adsorbed on NaX zeolite were investigated by means of ESR. No oxygen anion radicals were formed thermally on NaX up to 773 K. The adsorption of O_2 on γ-irradiated NaX in a vacuum, however, resulted in an ESR spectrum due to O_2^-. Several kinds of O_2^- species and O_3^- were found to be formed on NaX by γ-irradiation in the presence of O_2. These oxygen anion radicals showed different reactivities with N_2O, ethylene and propylene, and transferred electrons to SO_2 to form SO_2^-. The SO_2^- radical was also produced on NaX by raising the temperature from 298 to 573 K after the introduction of SO_2. This reacted with O_2 to form a radical, like SO_4^-, but upon evacuating the O_2, the reaction was reversed to give the original SO_2^-. When the temperature of NaX was further raised to 773 K in the presence of SO_2, a spectrum assigned to a polyatomic sulfur radical appeared indicating that SO_2 decomposition occurred at high temperature. This polymer radical was stable in an O_2 atmosphere at room temperature.

It has been verified using ESR that O_2^- and other oxygen anion radicals are formed on partially reduced oxides of molybdenum, titanium, zinc, vanadium and chromium containing trapped electrons.[1-5] It has also been found that SO_2^- is formed on these surfaces by introducing SO_2 at room temperature.[4-7] The reaction of SO_2^- with O_2 was also investigated. On magnesium oxide, this reaction produced SO_3^-.[8] SO_4^- was formed in the case of vanadium oxide.[7] A diamagnetic ion was mainly produced by a reaction on partially reduced titanium oxide.[6] These investigations are helpful for determining the intermediates in the oxidation of SO_2 on solid surfaces.

On the other hand, it is known that the O_2^- radical is produced on various cation exchanged Y-type zeolites when subjected to γ-irradiation.[9-12] Ono *et al.* have found thermal formation of SO_2^- on Y-type zeolites and have reported that SO_2^- on decationated Y zeolite reacts with O_2 to give O_2^-.[13] This finding appears rather unusual in view of the higher electron affinity of SO_2 as compared with that of O_2. On X-type zeolites, however, the adsorbed state of SO_2 has not yet been studied, and oxygen was examined only for cerium- and lanthanum-exchanged zeolites.[14] In this paper, the formation of these radicals on NaX and their reactivities are reported in some detail to obtain insight into the electron-donating power of zeolite.

Experimental

The NaX zeolite used was Linde type 13X which has a unit cell composition of $Na_{88}[(AlO_2)_{88}(SiO_2)_{104}]$. This sample was soaked in an aqueous solution of sodium acetate, supplied by the Wako Pure Chemical Ind., Ltd., to remove impurity cations and to avoid decationation.[15] Then the sample was washed thoroughly with ion-exchanged water and dried at 383 K. About 0.1 g of the sample was placed in a quartz sample tube with a breakable seal and heated under vacuum up to 823 K at a rate of 150 K/h. After degassing for 6 h at 823 K, the sample was cooled to room temperature and was exposed to the respective gases at 5—20 Torr at room temperature.

Unless otherwise noted, the ESR measurements were made at 77 K using a JES-3BS-X spectrometer with 100 kHz field modulation and a TE_{012} mode cavity. After evacuating the NaX sample at 823 K, a negligibly weak singlet signal was observed at $g=2.002$. γ-Irradiation was carried out at room temperature using a ^{60}Co γ-ray source with a total dosage of 12 Mrads. The irradiated sample was transferred into one end of the sample tube and the measuring end of the tube was heated with a flame to remove color centers generated in the wall during γ-irradiation. The gases used were of high purity and were obtained from the Takachiho Chemical Co.

Results and Discussion

Oxygen Radicals on NaX. An NaX sample was treated with O_2 at various temperatures between 298 and 773 K. No ESR spectrum, except a background, was observed. However, the ESR spectrum shown in Fig. 1(a) was observed when the sample was irradiated

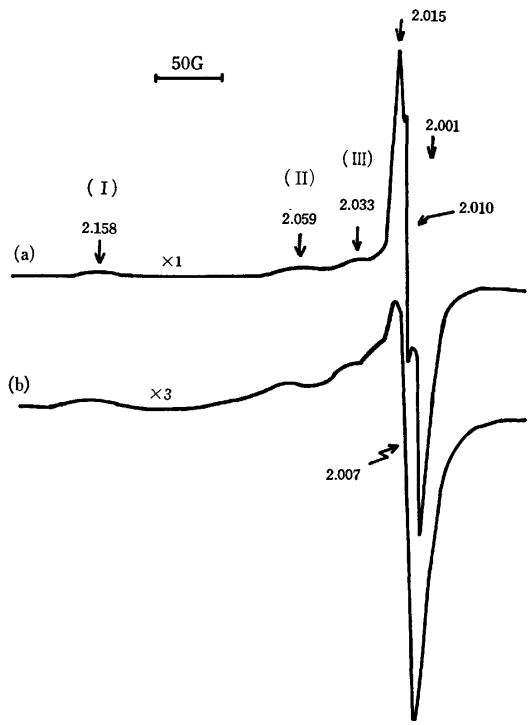

Fig. 1. ESR spectra of (a) NaX γ-irradiated in the presence of O_2 and (b) the same sample followed by N_2O addition.

in the presence of O_2. The high-field side of this signal (g_z=2.015, g_y=2.010, and g_x=2.001) is assigned to O_3^- from a comparison with ESR spectra due to various kinds of oxygen radicals.[1,11,16–22] The shape of this spectrum did not change upon evacuation at room temperature, but the intensities of all lines (the I, II, III, and O_3^- signals) were reduced to from 3/4 to 2/3 of the original values.

When N_2O was introduced into this sample after evacuation at room temperature, the spectrum due to O_3^- disappeared and a typical O_2^- spectrum[1,11,14,19] was clearly observed, as is shown in Fig. 1(b). This indicates that O_3^- is unstable compared with O_2^- and is affected by N_2O which is an efficient electron acceptor.[22] Several low-field lines correspond to O_2^- having different g_z values (g_z(I)=2.158, g_z(II)=2.059, and g_z(III)=2.033 in Fig. 1(b)) because of various crystal-field environments.[11] The lines corresponding to different g_x and g_y are superposed on each other to some extent. The spectrum in Fig. 1(b) was also obtained by heating the NaX sample at 373 K; the O_3^- signal disappeared above 373 K, while those for O_2^-(I), (II), and (III) remained up to 423, 523, and 473 K, respectively, upon heating.

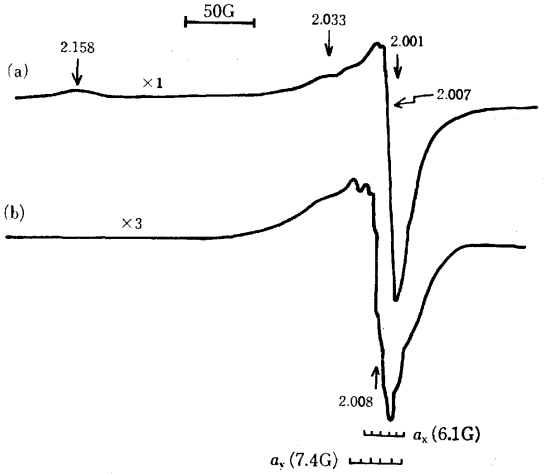

Fig. 2. ESR spectra obtained from NaX γ-irradiated in the presence of O_2 and exposed to (a) ethylene and (b) 1-butene or propylene.

Ethylene, propylene, and 1-butene were introduced in order to investigate the reactivities of the oxygen radicals. When the irradiated sample was exposed to ethylene at room temperature, the signals due to O_3^- and O_2^-(II) disappeared and the spectrum shown in Fig. 2(a) was obtained. This fact indicates that the O_3^- and O_2^-(II) can react with ethylene. For propylene and 1-butene addition, all the oxygen radicals except O_2^-(III) reacted and their ESR signals disappeared (Fig. 2(b)). A line shape characteristic of O_2^-(III) was clearly observed after this reaction, that is, g_z=2.033, g_y=2.008, and g_x=2.002. This spectrum appeares to show superhyperfine lines due to ^{27}Al (I=5/2), although they are not clearly resolved. The splittings ($|a_x|$=6.1 G, $|a_y|$=7.4 G) coincide well with those for O_2^- adsorbed on other zeolites.[10,12]

Upon further addition of oxygen (150 Torr) to the

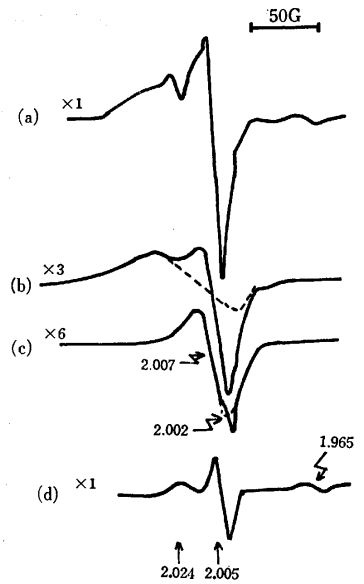

Fig. 3. ESR spectra of γ-irradiated NaX (a) under vacuum, (b) after N_2O addition, and (c) after heated at 423 K. (d) ESR spectrum obtained by subtracting (b) from (a).

sample, the spectrum due to O_2^-(III) was observed only because of the broadening of other lines. All the spectra recovered upon evacuation of the oxygen. This broadening effect indicates that O_2^-(III) exists in the sodalite unit or hexagonal prism, while O_3^-, O_2^-(I) and O_2^-(II) occur in the supercage.[11,15]

The ESR spectrum shown in Fig. 3(a) was obtained after NaX had been irradiated in a vacuum. The introduction of N_2O gradually changed this spectrum. Fig. 3(b) shows the result observed after exposure to N_2O for 24 h. This spectrum is converted to that shown in Fig. 3(c) upon heating the sample to 423 K after evacuation of the N_2O. The dotted line in Fig. 3(b) was obtained by subtracting spectrum (c) from spectrum (b). Similarly, Fig. 3(d) shows the difference between spectra (a) and (b). These spectra indicate that spectrum (a) is composed of a broad singlet signal (g=2.010, the dotted line in Fig. 3(b)), isotropic signals (g=2.007, 2.002, and 1.965, in Figs. 3(c) and (d)), and an anisotropic signal ($g_{//}$=2.024, $g_{\perp}$=2.005, in Fig. 3(d)). A comparison of the g values and the line shapes of these signals with those obtained by γ-irradiation of other samples[10,11,16,23] leads to the conclusion that the isotropic signals (g=2.007 and 2.010) and the anisotropic signal can be attributed to V centers, while the other signals (g=2.002 and 1.965) are due to F centers.

When O_2 was introduced into the NaX which had been subjected to γ-irradiation under vacuum, the signals due to the V and F centers disappeared and a new signal (g_z=2.027, g_y=2.008, and g_x=2.001, in Fig. 4), which can be assigned to O_2^-, was obtained.[11,16] It is known that the trapped electron at an anion vacancy reacts with O_2 to form O_2^-.[11,24] The spin concentration of the O_2^- formed on irradiated NaX was several times larger than those of the V and F centers of the original NaX sample, as estimated from ESR signals. This result suggests the presence of other kinds of trapped

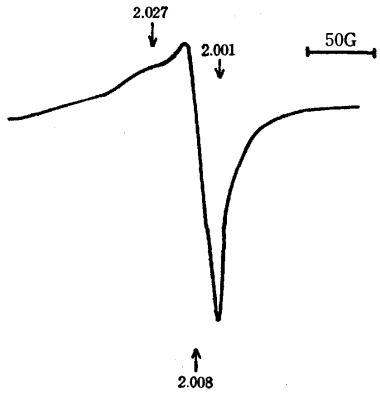

Fig. 4. ESR spectrum obtained from NaX γ-irradiated and exposed to O_2.

TABLE 1. g VALUES OF OXYGEN ANION RADICALS PRODUCED ON NaX

		g_1	g_2	g_3
γ-Irradiation in the presence of O_2	O_2^-	2.158	2.007—2.008	2.001
	O_2^-	2.059	2.007	2.002
	O_2^-	2.033	2.008	2.003
	O_3^-	2.015	2.010	2.001
Exposure to O_2 after γ-irradiation	O_2^-	2.027	2.008	2.001

electrons which are not ESR active. Table 1 summarizes the g values of the oxygen anion radicals formed on NaX after γ-irradiation. Details of the absorption sites of these O_2^- species will be discussed in a subsequent paper.

Reaction of Oxygen Radicals with SO_2. The introduction of SO_2, which has a higher electron affinity than does O_2,[6] to NaX irradiated in the presence of O_2 removes the signals due to O_3^-, O_2^-(I) and O_2^-(II), resulting in the spectrum shown in Fig. 5(a). The spectrum is composed of the O_2^-(III) signal and a new signal with principal g values of $g_{//}=2.008$ and $g_{\perp}=2.001$. This result was confirmed by the ESR spectra

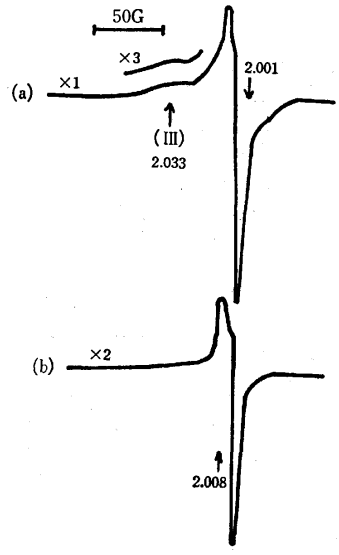

Fig. 5. ESR spectra obtained from NaX γ-irradiated in the presence of O_2 and exposed to SO_2, recorded at (a) 77 K and (b) room temperature.

obtained at room temperature, since the signal due to O_2^-(III) was broadened at this temperature and a new signal was clearly observed (Fig. 5(b)). This new signal can be attributed to SO_2^-, since the g components and the shape coincide well with those for the radical.[4,6,7] The formation of SO_2^- on NaX which was not γ-irradiated was negligibly small at room temperature. Therefore, the SO_2^- formation is considered to be caused by charge transfer from O_2^- to SO_2 (1), or electron capture from an F center (2), thus

$$O_2^- + SO_2 \longrightarrow SO_2^- + O_2 \quad (1)$$

or

$$SO_2 + e^- \longrightarrow SO_2^-. \quad (2)$$

It was found that the introduction of SO_2 into NaX irradiated under vacuum also produced an SO_2^- signal which had the same g components as that for NaX irradiated in the presence of O_2. This SO_2^- radical is formed by the capture of an electron from an F center and the amount of the radical formed is about 50% of that of the O_2^- produced on NaX upon γ-irradiation in the presence of O_2. This shows that the number of F centers produced on NaX by γ-irradiation in an O_2 atmosphere is small, since most of the electrons would be trapped by O_2 to form O_2^-. Moreover, reaction (1) appears to occur easily since the electron affinity of SO_2 is higher than that of O_2. From these points of view, it can be concluded that the transfer of an electron from O_2^- to SO_2 occurs predominantly on NaX γ-irradiated in the presence of O_2. The spin concentration of the SO_2^- produced on this NaX was found to be about 50% of that of the O_2^- which disappeared upon the introduction of SO_2. This indicates that the reaction of SO_2 with O_2^- leads partly to the formation of diamagnetic compounds.[6]

Sulfur Oxide and Sulfur Radicals on NaX. Upon heating NaX from 298 to 573 K after the introduction of SO_2, the intensity of ESR spectrum attributed to SO_2^- was found to increase. This spectrum is exactly the same as that obtained for γ-irradiated NaX. When the temperature was further raised to 673 K, the SO_2^- signal was attenuated and a new anisotropic signal appeared at low field (Fig. 6(a), $g\approx2.030$). This signal became distinct after heating to 773 K (Fig. 6(b)). It is evident that a polyatomic sulfur biradical is present on the surface from a comparison of this spectrum ($g_z=2.048$, $g_y=2.030$, $g_x=2.002$) with those obtained

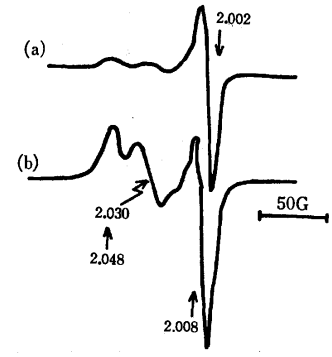

Fig. 6. ESR spectra obtained from NaX after heat treatment at 673 K (a) and 773 K (b) in the presence of SO_2.

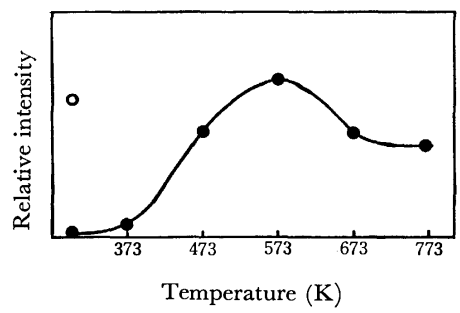

Fig. 7. Temperature dependence of SO_2^- formation on NaX (●). The radical formed on NaX γ-irradiated under vacuum at room temperature is also shown in the figure (○).

by the photolysis of solid COS,[25] sublimed sulfur[26] and sulfur-saturated zeolites 3A, 4A, and 5A.[27] The line corresponding to the smallest g value, $g=2.002$, overlaps with the spectrum of SO_2^-. Figure 7 shows the temperature dependence of the SO_2^- formation. The relative intensity for the radical produced on γ-irradiated NaX is also plotted in the figure.

It is known that both SO_2^- and O_2^- are formed on partially-reduced oxides soon after the introduction of SO_2 and O_2.[1-7] On the other hand, the amount of SO_2^- formed was small on NaX without heating in an SO_2 atmosphere and no O_2^- was formed without γ-irradiation. These results indicate that NaX is a rather weak electron donor compared with partially-reduced oxides. This fact can be attributed to the difference in the electron-donating centers on the respective surfaces: for the oxides, the center consists of low-valent metal cations, while $[AlO_{4/2}]^-$ is suggested as the center for the zeolites.[13]

When O_2 was introduced at room temperature onto NaX which was treated at 573 K in the presence of SO_2, the observed spectrum of SO_2^- after cooling to 77 K showed an appreciable change, as is shown in Fig. 8(a). In the spectrum recorded at room temperature (Fig. 8(b)), however, the SO_2^- signal with decreased intensity due to the reaction is distinguished from the new broadened signal at this temperature. The spectrum shown in Fig. 8(c) was obtained by subtracting this SO_2^- signal from the spectrum shown in Fig. 8(a). After evacuation at room temperature, the new signal almost disappeared and the intensity of the SO_2^- signal was restored.

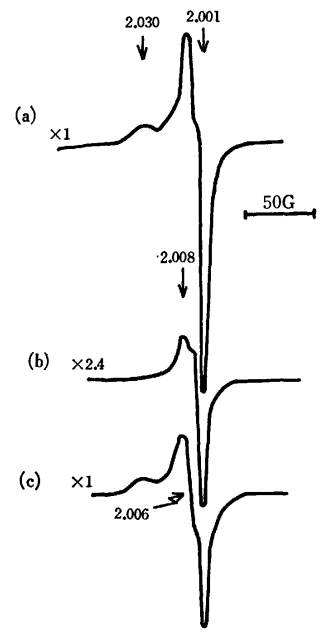

Fig. 8. ESR spectra after reaction of SO_2^- with O_2 recorded at (a) 77 K and (b) room temperature. (c) The spectrum obtained by subtracting the signal due to SO_2^- from (a).

The g_y value of the new signal was estimated to be 2.006, although the superposed SO_2^- signal decreased the accuracy of the measured value. Rao *et al.* have reported that SO_2^- adsorbed on vanadium oxide reacts with O_2 forming SO_4^-.[7] The g values of the radical obtained in the present work ($g_z=2.030$, $g_y=2.006$, $g_x=2.001$) are similar to those for SO_4^-.[7,28-30] Since the SO_2^- signal intensity was restored by evacuation, the new radical formed on NaX by the reaction of SO_2^- with O_2 appears to be a complex which has an SO_4^--like structure, although SO_2^- combines rather weakly with O_2, thus

$$SO_2^- \underset{-O_2}{\overset{+O_2}{\rightleftharpoons}} SO_4^- \ (SO_2^- \cdot O_2).$$

It is suggested that SO_2^- on decationated zeolites transfers electrons to O_2 to form O_2^-.[13] However, this formation of O_2^- appears to be difficult on NaX since no O_2^- is formed by only thermal treatment. Even with γ-irradiation, the O_2^- radicals obtained have different g tensors from this signal (Table 1). In addition, O_2 has a lower electron affinity compared with that of SO_2.[6,31,32] Thus, an electron transfer reaction, such as

$$O_2 + SO_2^- \longrightarrow O_2^- + SO_2,$$

is difficult to proceed, although the reverse reaction can easily occur.

On the other hand, when O_2 was introduced into this NaX sample, the decrease in the total SO_2^- spin reached about 65% and was accompanied by the appearance of an SO_4^--like signal. This means that the reaction of SO_2^- with O_2 also leads to the formation of diamagnetic compounds as in the case of the reaction of O_2^- with SO_2. However, when O_2 was introduced onto NaX which had been heated to 773 K in the presence of SO_2, the signals due to the existing SO_2^- and polysulfur radicals were scarcely affected. This result indicates that the state of SO_2^- is different from that of the radical formed on NaX heated below 573 K. SO_2^- may exist in the sodalite unit since the radical does not react with O_2, which is held in the supercage at room temperature,[15] while, below 573 K, SO_2^- is formed in the supercage. The SO_2 molecule must be able to penetrate into the sodalite unit at high temperature as well as does O_2.[15]

The presence of polysulfur radicals indicates that SO_2 on NaX decomposes above 673 K. As the intensity of the radical increases, the SO_2^- radicals decrease in number (Fig. 7) and exist only inside the sodalite unit.

The SO_2^- in the supercage may be converted to a polysulfur radical, while the SO_2^- in the sodalite unit may not change into this radical because the cavity is too small for polymeric formation.

References

1) I. D. Mikheikin, A. I. Mashchenko, and V. B. Kazanskii, *Kinet. Katal.*, **8**, 1363 (1967).
2) J. H. Lunsford and J. P. Jayne, *J. Chem. Phys.*, **44**, 1487 (1966).
3) V. A. Shvets, M. E. Sarichev, and V. B. Kasansky, *J. Catal.*, **11**, 378 (1968).
4) V. M. Vorotyntsev, V. A. Shvets, and V. B. Kazanskii, *Kinet. Katal.*, **12**, 1249 (1971).
5) L. K. Przheval'skaya, V. A. Shvets, and V. B. Kazanskii, *Kinet. Katal.*, **15**, 180 (1974).
6) A. I. Mashchenko, G. B. Pariiskii, and V. B. Kazanskii, *Kinet. Katal.*, **9**, 151 (1968); *ibid.*, **8**, 704 (1967).
7) K. V. S. Rao and J. H. Lunsford, *J. Phys. Chem.*, **78**, 649 (1974).
8) Y. B. Turrit and J. H. Lunsford, *J. Phys. Chem.*, **77**, 1365 (1973).
9) P. H. Kasai, *J. Chem. Phys.*, **43**, 3322 (1965).
10) K. M. Wang and J. H. Lunsford, *J. Phys. Chem.*, **73**, 2069 (1969).
11) K. M. Wang and J. H. Lunsford, *J. Phys. Chem.*, **74**, 1512 (1970).
12) K. M. Wang and J. H. Lunsford, *J. Phys. Chem.*, **75**, 1165 (1971).
13) Y. Ono, H. Tokunaga, and T. Keii, *J. Phys. Chem.*, **79**, 752 (1975).
14) S. Krzyzanowski, *J. Chem. Soc., Faraday Trans. 1*, **72**, 1573 (1976).
15) T. Imai and H. W. Habgood, *J. Phys Chem.*, **77**, 925 (1973).
16) J. C. Vedrine, A. Abou-Kais, J. Massardier, and G. Dalmai-Imelik, *J. Catal.*, **29**, 120 (1973).
17) C. Naccache, *Chem. Phys. Lett.*, **11**, 323 (1971).
18) R. D. Iyengar, M. Codell, J. S. Karra, and Turkevich, *J. Am. Chem. Soc.*, **88**, 5055 (1966).
19) M. Setaka and T. Kwan, *Bull. Chem. Soc. Jpn.*, **43**, 2727 (1970).
20) N. Wong and J. H. Lunsford, *J. Chem. Phys.*, **56**, 2664 (1972).
21) S. Schlick, *Chem. Phys. Lett.*, **4**, 421 (1969).
22) A. J. Tench, T. Lawson, and J. F. J. Kibblewhite, *J. Chem. Soc., Faraday Trans. 1*, **68**, 1169 (1972).
23) J. C. Vedrine and C. Naccache, *J. Phys. Chem.*, **77**, 1606 (1973).
24) A. J. Tench and P. J. Holroyd, *Chem. Commun.*, **1968**, 471.
25) D. A. Stiles, R. Kewley, O. P. Strausz, and H. E. Gunning, *Can. J. Chem.*, **43**, 2442 (1965).
26) H. E. Radford and F. O. Rice, *J. Chem. Phys.*, **33**, 774 (1960).
27) Z. Dudzik and K. F. Preston, *J. Colloid Interface Sci.*, **26**, 374 (1968).
28) P. W. Atkins, J. A. Brivati, A. Horsfield, M. C. R. Symons, and P. A. Tevalion, *Int. Symp. Free Radicals, 6th*, (1963).
29) J. R. Morton, D. M. Bishop, and M. Randic, *J. Chem. Phys.*, **45** 1885 (1966).
30) K. Aiki and K. Fukuda, *J. Phys. Soc. Jpn.*, **22**, 663 (1967).
31) L. G. Christophorou, "Atomic and Molecular Radiation Physics," John Wiley & Sons, New York (1971), p. 565.
32) H. O. Pritchard, *Chem. Rev.*, **52**, 529 (1953).

Polarized Electronic Absorption Spectra and Assignment of Fluorene and Biphenyls

Tetsutaro YOSHINAGA, Hiroshi HIRATSUKA, and Yoshie TANIZAKI

Department of Chemistry, Tokyo Institute of Technology, Meguro-ku, Tokyo 152

(Received September 22, 1977)

The divided electronic spectra polarized parallel to the long and short axes of molecules of biphenyl, THP (4,5,9,10-tetrahydropyrene), fluorene, and DHPH (9,10-dihydrophenanthrene) were determined by dichroism analysis using the stretched PVA film method. The experimental results are in good agreement with the ones calculated by the LCAO MO SCF CI method. Every compound has a very weak absorption ($f \approx 10^{-4}$) as the first band in the region of 32000—35000 cm^{-1}, which is electronically allowed and polarized parallel to the short axis. The intense band (34000—44000 cm^{-1}) of biphenyl consists of a relatively strong (39100 cm^{-1}) band and a weak (40500 cm^{-1}) band: the former is polarized parallel to the long axis and the latter to the short. Both fluorene and DHPH show five well corresponding electronic bands in the region below 45000 cm^{-1}.

The assignment of the electronic spectrum of fluorene has been studied[1-5] from the viewpoint of a biphenyl derivative. For fluorene itself, there have been few studies done in terms of the three fundamental factors: the transition energy, the polarization direction, and the oscillator strength. The agreement between the calculated and experimental results seems especially unsatisfactory for the very weak first band. On the other hand, there are a great many studies for the biphenyl spectrum, both theoretical and experimental.[6-11] These studies may be grouped into two types: the comformation and the assignment. From the conformational study, the dihedral angle of the biphenyl has been determined in crystal state (0°), in solution (20—30°) and in vapor (≈45°). As for the assignment of the biphenyl spectrum, however, no detailed experimental study in terms of the above three factors has yet been made.

In the present study, we determined the polarized absorption spectra of biphenyl, fluorene, 9,10-dihydrophenanthrene, and 4,5,9,10-tetrahydropyrene[12] in the stretched PVA [poly(vinyl alcohol)] film, and divided the spectra into two components, which are polarized along the long and short axes of the molecule, by means of the dichroism analysis.[13] And then, comparing the component spectra with the calculated results, we assigned the spectra of fluorene and the biphenyl with respect to the three fundamental factors stated above.

Experimental

Material. Commercially available biphenyl (E.P.: extra pure reagent, >99% G.C.), fluorene (U.P.: ultra pure reagent, zone refined), 9,10-dihydrophenanthrene (G.R.: guaranteed reagent; abbrev. DHPH), and 4,5,9,10-tetrahydropyrene (G. R.: abbrev. THP) were obtained from Tokyo Kasei Kogyo Co., Ltd. Biphenyl was purified by repeated recrystallization from water containing ethanol. THP was furthermore refined using a special treatment at Tokyo Kasei Kogyo Co., Ltd., at our request. PVA powder, which was used for the preparation of film, was obtained commercially (Koso Chemical Co., Ltd.) and was used without further purification.

Polarized Spectra. The polarized absorption spectra of samples in the stretched PVA films were measured with a Shimadzu QV-50 Spectrophotometer equipped with a calcite polarizer of the Glan-Thompson type and a rotation apparatus for the polarizer.

The method of dichroism analysis using the stretched PVA film has already been reported.[13] The notations cited here are as follows: R_S is the stretch ratio of the PVA film, $D_{\parallel}$ and $D_{\perp}$ are the optical densities of the sample in a stretched film for the incident light polarized parallel and perpendicular to the stretching direction, respectively, and R_d is the dichroic ratio and is defined as $D_{\parallel}/D_{\perp}$. The orientation angle θ, which was computed theoretically using the R_S and R_d values, is indicated along the R_d curve in the figure. It means the angle of the transition moment with respect to an orientation direction associated with the molecular axis.

We divided the absorption spectrum observed in the non-streched PVA film into the component spectra along the long and short axes of the molecule, according to the method already described.[13] In the present case, we chose the angle for the greatest R_d value as the orientation angle of the long axis transition, since the sum of the apparent orientation angles for the maximum and minimum R_d values is smaller than a right angle. [The reason for such a selection has been described in detail in Refs. 12 and 13.]

The experimental oscillator strength f^{exp} was determined from the divided spectra by the following formula:

$$f^{exp} = 4.32 \times 10^{-9} \int \varepsilon_\sigma d\sigma,$$

where ε_σ is the molar extinction coefficient at wave number σ and the ε_σ value in ethanol was used instead of that in PVA, since it was confirmed experimentally that the ε_σ value in PVA is nearly equal to that in ethanol.

Calculation

In the MO calculation, the LCAO ASMO SCF CI method (PPP approximation[14,15]) was employed. The one- and two-center electron repulsion integrals were evaluated by the Pariser-Parr[14] and Nishimoto-Mataga equations.[16] Substituent effects of methylene groups were taken into consideration as the conjugative effect.[17] All the molecules were assumed to be planar and the geometry of THP is shown in Fig. 1(a) as the representative of the biphenyl. The C–C bond lengths in benzene rings were taken as 1.395 Å and the bond angles $\angle CCC = 120°$. Other bond lengths were taken as $(C_4\text{–}C_5) = (C_9\text{–}C_{10}) = 1.480$ and $(C{=}H_2) = 0.900$ Å. The resonance integrals were taken as $\beta(C_9\text{–}C_{10}) = \beta(C_{10}\text{–}C_{11}) = -2.00$, $\beta(C{=}H_2) = -5.30$, and $\beta(C{=}C) = -2.236$ eV. The geometry of fluorene shown in Fig. 1(b) was assumed as follows with reference to the crystal structure.[2] The C–C bond lengths in the six-

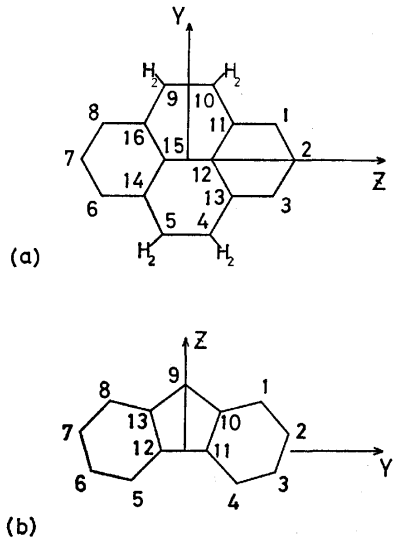

Fig. 1. Geometries of the THP (4,5,9,10-tetrahydropyrene) and fluorene molecules.

membered rings were taken as 1.400 Å and the bond angles $\angle CCC=120°$, and for the five-membered ring: $(C_{10}-C_{11})=(C_{12}-C_{13})=1.400$, $(C_{11}-C_{12})=1.480$, $(C_9-C_{10})=(C_9-C_{13})=1.460$ Å, and $\angle C_{10}C_{11}C_{12}=\angle C_{11}C_{12}C_{13}=108°$.

Results and Discussion

Dichroic Spectra and Divided Spectra. Figure 2 shows the dichroic spectra of biphenyl, fluorene, DHPH, and THP in the stretched PVA film. The spectra of these compounds are quite similar to one another, except that both the fluorene and DHPH spectra have additional bands at about 300 nm which are missing in those of biphenyl and THP.

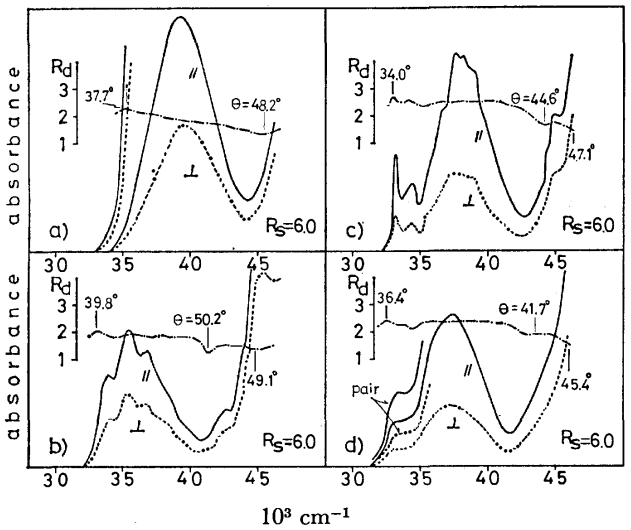

Fig. 2. Dichroic spectra and R_d curves for (a) biphenyl, (b) THP (4,5,9,10-tetrahydropyrene), (c) fluorene, and (d) DHPH (9,10-dihydrophenanthrene) in the stretched PVA films. The solid and broken lines indicate the absorbances ($D_{\parallel}$ and $D_{\perp}$) for the incident light polarized parallel and perpendicular to the stretching direction, respectively. R_d(chain line) is the dichroic ratio defined by $D_{\parallel}/D_{\perp}$.

The R_d curve of each compound has the maximum around the long wavelength side of the first absorption band and it clearly decreases toward longer wavelengths. The decrease of the R_d curve was confirmed by the dichroic spectra of the more concentrated sample films. This indicates that a weak band polarized parallel to the short axis is hidden in the longest wavelength region of the strong band polarized parallel to the long axis.

In order to reveal the two component spectra polarized parallel to the long and short axes of the molecule, we divided the spectra of the samples in the non-stretched PVA films. The divided spectra are shown in Fig. 3. The spectrum of THP shown in Fig. 3(b), which have already been reported,[12] are reproduced for the comparison with those of other samples, especially with that of biphenyl.

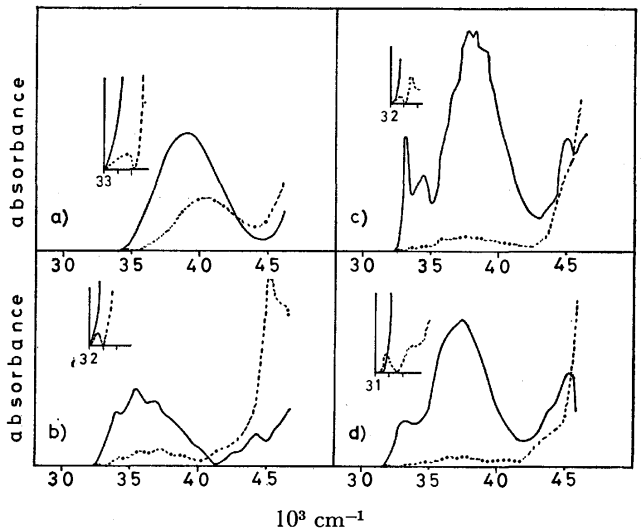

Fig. 3. Divided (component) spectra of (a) biphenyl, (b) THP (4,5,9,10-tetrahydropyrene), (c) fluorene, and (d) DHPH (9,10-dihydrophenanthrene) in the non-stretched PVA films. The solid and broken lines are long and short axis component spectra, respectively.

Figure 3(a) shows the component spectra of biphenyl. In the main absorption region of 34000—44000 cm^{-1}, there are two bands at 39100 and 40500 cm^{-1}: the former is polarized parallel to the long axis and the latter to the short. A very weak band polarized parallel to the short axis appears at 34600 cm^{-1}. In the region higher than 42000 cm^{-1}, two relatively strong bands exist, which are polarized perpendicularly to each other.

That the first absorption band (34000—44000 cm^{-1}) of biphenyl is composed of three electronic transitions has been inferred by Berlman from the investigation of the luminescence of biphenyl and its analogs.[10] These three transitions may correspond to the 34600, 39100, and 40500 cm^{-1} bands of the present work. As for the position of the very weak band (34600 cm^{-1}) of biphenyl, there are many experimental data[7] and most of them fall in the range 33000—34000 cm^{-1}.

Figures 3(c) and (d) show the component spectra of

fluorene and DHPH, respectively. These are quite similar to each other except that the vibrational structure is revealed in the fluorene spectra. Both of the component spectra also show a very weak band at about 32000 cm^{-1}, which corresponds to those of biphenyl (34600 cm^{-1}) and THP (32800 cm^{-1}).

Popov *et al.*[5] determined the dichroic spectra of fluorene in the poly(vinyl butyral) film. The dichroism clearly shows an abrupt dropping toward the corresponding wavelength region of the weak band. This dropping suggests the existence of a hidden band of a short axis polarized transition, though they did not point it out.

Both of the component spectra of fluorene and DHPH have a band of long axis polarization in the region of 32000—35000 cm^{-1}. Since this band is missing in the biphenyl and THP spectra, it is considered as an additional characteristic band for fluorene and DHPH. The appearance of this band may have some relations with the partial loss of symmetry (D_{2h}—C_{2v}).[4]

Comparison of Experimental and Calculated Results. The experimental and calculated results are compared in Tables 1—4 for biphenyl, THP, fluorene, and DHPH, respectively. The first absorption bands of all the sample molecules are extraordinarily weak and have the polarization parallel to the short axis. The experimental oscillator strengths are the order of 10^{-4} and correspond well to the calculated ones. As for the intensity of this band of biphenyl, for instance, usually zero values of the oscillator strengths have been computed, except in the calculation by Momicchioli *et al.*[3] This could be attributed to a disregard of the off-diagonal terms of the transition density matrix.[18]

As is seen from Fig. 3, only biphenyl shows very smooth component spectra, while the other samples have fine structure or a shoulder. Therefore, we could estimate experimentally, all the 0-0 transition energies except for that of biphenyl. As is shown in Tables 2—4, the experimental energies agree well with the calculated ones for the allowed transitions lower than 45000 cm^{-1} of THP, fluorene, and DHPH. For the case of biphenyl (Table 1), however, the experimental energy (39100 cm^{-1}) of the main band (the second), for example, was considerably higher than the calculated one (36400 cm^{-1}, the third transition), because we had to take the energy at the band maximum as the experimental one.

We have already pointed out that the main intense band 34000—44000 cm^{-1}) of biphenyl (Fig. 3(a)) consists of two subbands. One (39100 cm^{-1}) of these, which is polarized parallel to the long axis, could be assigned as the third transition (36400 cm^{-1}) of the calculated results. But the other band, which is polarized to the short axis and has the maximum at 40500 cm^{-1}, cannot be assigned to any allowed transition calculated (Table 1). The calculated results shown in Table 1, however, have been obtained by assuming that biphenyl

Table 1. Comparison of calculated and experimental results for biphenyl (D_{2h})

Transtn. No.	Transition energy		Oscillator strength		Polarization		Symmetry
	Calcd 10^3 cm^{-1} (nm)	Obsd 10^3 cm^{-1} (nm)	Calcd[a]	Obsd	Calcd	Obsd	
I	34.63 (289)	34.6 (289)	3.1×10^{-4}	6×10^{-5}	y	short	B_{2u}
II	35.09 (285)						B_{3g}
III	36.40 (275)	39.1 (256)	0.8471	0.293	z	long	B_{1u}
IV	46.50 (215)	[40.5] [247][b]		[0.120][b]		[short][b]	B_{3g}
V	47.82 (209)						A_g
VI	48.85 (205)	>46	0.8868		y	short	B_{2u}
VII	48.87 (205)						A_g
VIII	49.66 (201)	>46	1.0832		z	long	B_{1u}

a) All terms of the transition density matrix were included. b) To be assigned as an allowed transition (B_3) provided that biphenyl belongs to the point group D_2.

Table 2. Comparison of calculated and experimental results for 4,5,9,10-tetrahydropyrene (THP) [D_{2h}]

Transtn. No.	Transition energy		Oscillator strength		Polarization		Symmetry
	Calcd 10^3 cm^{-1} (nm)	Obsd 10^3 cm^{-1} (nm)	Calcd[a]	Obsd	Calcd	Obsd	
I	33.56 (298)	32.8 (305)	1.9×10^{-4}	4.4×10^{-4}	y	short	B_{2u}
II	34.03 (294)	[34.2] [292][b]				[short][b]	B_{3g}
III	35.03 (286)	33.9 (295)	0.7290	0.298	z	long	B_{1u}
IV	43.96 (228)						B_{3g}
V	45.90 (218)						A_g
VI	46.71 (214)	[41.4] [242][c]	1.1858		y	short	B_{2u}
VII	47.28 (212)	[42.6] [235][c]	1.1358		z	long	B_{1u}

a) See footnote a) in Table 1. b) To be assigned as an electronically forbidden band or an intensity borrowing band. c) In the previous paper, 45200 and 46000 cm^{-1} were used as the observed transition energies of VI and VII, respectively. (See Ref. 12).

Table 3. Comparison of calculated and experimental results for fluorene (C_{2v})

Transtn. No.	Transition energy		Oscillator strength		Polarization		Symmetry
	Calcd 10^3 cm^{-1} (nm)	Obsd[b] 10^3 cm^{-1} (nm)	Calcd[a]	Obsd	Calcd	Obsd	
I	33.95 (295)	32.6 (307)	5.4×10^{-3}	1.0×10^{-4}	z	short	A_1
II	34.62 (289)	33.1 (302)	0.0600	0.0623	y	long	B_2
III	35.76 (280)	36.0 (278)	0.5636	0.377	y	long	B_2
IV	45.09 (222)	43.6 (229)	0.2466		y	long	B_2
V	46.71 (210)	45.0 (220)	0.0902		z	short	A_1
VI	48.42 (207)		0.7992		z		A_1
VII					y		B_2

a) See footnote a) in Table 1. b) An other broad weak band, which is considered to be an intensity borrowing band, was observed in the region of 33000—42000 cm^{-1}.

Table 4. Comparison of calculated and experimental results for 9,10-dihydrophenanthrene (DHPH) (C_{2v})

Transtn. No.	Transition energy		Oscillator strength		Polarization		Symmetry
	Calcd 10^3 cm^{-1} (nm)	Obsd[b] 10^3 cm^{-1} (nm)	Calcd[a]	Obsd	Calcd	Obsd	
I	34.15 (293)	31.7 (315)	2.2×10^{-4}	2.0×10^{-4}	z	short	A_1
II	34.59 (289)	33.2 (301)	0.0063	0.0369	y	long	B_2
III	35.86 (279)	36.0 (278)	0.7731	0.296	y	long	B_2
IV	45.33 (221)	43.6 (229)	0.1035		y	long	B_2
V	46.54 (215)	44.0 (227)	0.2880		z	short	A_1
VI	48.15 (208)		0.7607		z		A_1
VII	48.52				y		B_2

a) See footnote a) in Table 1. b) See footnote b) in Table 3.

belongs to the point group D_{2h}. But, in order to explain the extra band at 40500 cm^{-1}, it is necessary to consider that the real biphenyl molecule in the PVA substrate has some non-zero dihedral angle, *i.e.*, it belongs to the point group D_2. Thus the $B_{3g}\leftarrow A_g$ transition in Table 1 should be altered to $B_3\leftarrow A$ transition which becomes an allowed transition. Moreover, strictly speaking, the statement "the polarization in the short axis direction" should be changed to "the polarization direction perpendicular to the long axis of molecule," because in dichroism analysis we cannot distinguish the difference in the two directions of the out of plane transition and the in-plane short axis transition. For that reason, the extra band (40500 cm^{-1}) of biphenyl can be explained as an allowed transition.

The other samples also show the respective extra bands in the region 33000—42000 cm^{-1}. However, the intensities are much weaker than the extra band of biphenyl. This may be attributed to some electronically forbidden transition or to intensity borrowing.

References

1) a) E. Merkel and C. Wiegand, *Z. Naturforsch., Teil B*, **3**, 93 (1948); E. Merkel, *Ber. Bunsenges. Phys. Chem.*, **69**, 716 (1965); b) J. Platt, *J. Chem. Phys.*, **19**, 101 (1951); c) E. M. Layton, Jr., *J. Mol. Spectrosc.*, **5**, 181 (1960); d) G. Hohlneicher, F. Dörr, N. Mika, and S. Schneider, *Ber. Bunsenges. Phys. Chem.*, **72**, 1144 (1968); e) C. A. Pinkham and S. C. Wait, Jr., *J. Mol. Spectrosc.*, **27**, 326 (1968); f) T. Keumi, N. Mochinaga, and Y. Oshima, *Nippon Kagaku Kaishi*, **1974**, 2243.

2) D. M. Burns and J. Iball, *Proc. R. Soc. London, Ser. A*, **227**, 200 (1955).

3) F. Momicchioli and A. Rastelli, *J. Chem. Soc., B*, **1970**, 1353.

4) T. Hoshi, H. Inoue, J. Shiraishi, and Y. Tanizaki, *Bull. Chem. Soc. Jpn.*, **44**, 1743 (1971).

5) K. R. Popov, L. V. Smirnov, V. L. Grebneva, and L. A. Nakhimovskaya, *Opt. Spectrosk.*, **31**, 363 (1971). [*Opt. Spectrosc.*, **31**, 195 (1971).]

6) a) H. Suzuki, *Bull. Chem. Soc. Jpn.*, **27**, 597 (1954); *ibid.*, **32**, 1340, 1350, 1357 (1959); b) K. Mislow, M. A. W. Glass, H. B. Hopps, E. Simon, and G. H. Wall, Jr., *J. Am. Chem. Soc.*, **86**, 1710 (1964); c) L. O. Edward and W. T. Simpson, *J. Chem. Phys.*, **52**, 4237 (1970); d) A. Gamba, G. F. Tantardini, and M. Simonetta, *Spectrochim. Acta, Part A*, **28**, 1877 (1972); e) B. Norden, R. Hakanson, and M. Sundbom, *Acta Chem. Scand.*, **26**, 429 (1972); f) D. Perahia and A. Pullman, *Chem. Phys. Lett.*, **19**, 73 (1973); g) T. G. McLaughlin, *Diss. Abstr. Int.*, **B33**, 3581 (1973); h) R. M. Hochstrasser, R. D. McAlpine, and J. D. Whiteman, *J. Chem. Phys.*, **58**, 5078 (1973); i) K. Razinaqvi, J. Donatsch, and U. P. Wil, *Chem. Phys. Lett.*, **34**, 285 (1975).

7) Y. Gondo, *J. Chem. Phys.*, **41**, 3928 (1964).

8) A. Unaue and P. Bothorel, *Bull. Soc. Chim. Fr.*, **1965**, 1640.

9) E. C. Lim and Y. H. Li, *J. Chem. Phys.*, **52**, 6416 (1970).

10) I. B. Berlman and O. Steingraber, *J. Chem. Phys.*, **43**, 2140 (1965); *ibid.*, **52**, 5616 (1970).

11) F. Momicchioli, M. C. Bruni, and I. Baraldi, *J. Phys. Chem.*, **76**, 3983 (1972).

12) T. Yoshinaga, H. Hiratsuka, and Y. Tanizaki, *Bull. Chem. Soc. Jpn.*, in press. (pyrene and hydropyrenes).

13) Y. Tanizaki and S. Kubodera, *J. Mol. Spectrosc.*, **24**, 1 (1967); H. Hiratsuka, Y. Tanizaki, and T. Hoshi, *Spectrochim. Acta, Part A*, **28**, 2375 (1972).
14) R. Pariser and R. G. Parr, *J. Chem. Phys.*, **21**, 466, 767 (1953).
15) J. A. Pople, *Proc. Phys. Soc. London, Ser. A*, **68**, 81 (1955).
16) N. Mataga and K. Nishimoto, *Z. Phys. Chem. N. F.*, **13**, 13 (1957).
17) T. Morita, *J. Chem. Phys.*, **25**, 1290 (1956); *Bull. Chem. Soc. Jpn.*, **31**, 322 (1958); *ibid.*, **33**, 1486 (1960).
18) T. Yoshinaga, H. Hiratsuka, and Y. Tanizaki, *Bull. Chem. Soc. Jpn.*, in press. (oscillator strengths).

The Reflection Spectra of the Crystalline Electron Donor-Acceptor Complexes of TCNQ

Masashi TANAKA

Department of Chemistry, Faculty of Science, Nagoya University, Chikusa, Nagoya 464

(Received September 27, 1977)

The polarized reflection spectra were measured on the crystals of TCNQ complexes with phenothiazine, anthracene, pyrene, acenaphthene, carbazole, hexamethylbenzene, and 1,10-phenanthroline. The crystalline absorption spectra were obtained by the K-K transformation of the reflection spectra. The charge-transfer degree and the stabilization energy in the ground state were estimated for each complex by analysing the charge-transfer bands in the solid state. The charge-transfer degree of the TCNQ–phenothiazine complex is 19.6%, while those of the TCNQ–carbazole, anthracene, and hexamethylbenzene complexes are 12.0, 10.5, and 8.0% respectively. Furthermore, those values for TCNQ–1,10-phenanthroline, acenaphthene, and pyrene are about 5%. The relationship between the charge-transfer excitation energy and the ionization potential of a series of the donor molecules is also discussed.

7,7,8,8-Tetracyanoquinodimethane (TCNQ) is a strong electron-acceptor and forms molecular complexes with various electron donors. Investigation has been carried out extensively to elucidate the nature of the intermolecular interaction in these molecular complexes. The appearance of the charge-transfer (CT) band, absent from the constituent free molecules, is characteristic of these complexes; the correlation of the electronic states of the complexes with the absolute absorption intensity of the CT band was discussed by Tanaka.[1] That is, the charge-transfer degree in the ground state can be obtained by measuring the absorption intensity of the CT band; it can thus be found to what extent the charge-transfer structures contribute to the stabilization of the electron donor-acceptor complex in the ground state.

In this paper, the author will present the crystal reflection spectra of TCNQ complexes with phenothiazine, anthracene, pyrene, acenaphthene, carbazole, hexamethylbenzene, and 1,10-phenanthroline. These reflection spectra will then be transformed into the absorption spectra by the Kramers-Kronig (K-K) method. The transformed absorption spectra will enable us to discuss the charge-transfer degrees of a series of complexes with a common acceptor (TCNQ) and the stabilization energies in the ground state.

Experimental

Single crystals of TCNQ complexes were crystallized after hot euimolar solutions of the components had been mixed and allowed to cool very slowly.

The reflection spectra at the normal incidence have been measured over the range of 5000—40000 cm^{-1} by means of a reflection spectrophotometer made in our laboratory, while the absorption spectra have been obtained by the K-K transformation. The oscillator strength along the α axis of the crystal may be evaluated by using the following equation,

$$f^{\alpha} = 4.32\times10^{-9}\int n_{\alpha}(\sigma)\varepsilon_{\alpha}(\sigma)\mathrm{d}\sigma,$$

where the integration is effected over the whole band, where σ is the wavenumber, and where n_{α} and ε_{α} are the α components of the refractive index and the molar absorption coefficient.

Theoretical

The analysis of the electronic states of the CT complexes was discussed by Tanaka[1] and so will be only briefly summarized here.

TCNQ complexes form a configuration of the ADA type in the crystal. Then, the ground state can be described by a wavefunction,

$$\Psi_0 \simeq \Phi(\mathrm{ADA}) + \sum_i b_i\{\Phi_i(\mathrm{AD^+A^-}) + \Phi_i(\mathrm{A^-D^+A})\}/\sqrt{2},$$

where $\Phi(\mathrm{ADA})$ represents a non-bonding, and $\Phi_i(\mathrm{AD^+A^-})$ and $\Phi_i(\mathrm{A^-D^+A})$, the i-th CT configurations. The charge-transfer degree and the stabilization energy in the ground state are given as $\sum_i b_i^2$ and $\Delta E=\sum_i b_i^2 E_{\mathrm{CT}}^i$. The wavefunction $\Psi_{\mathrm{CT}}^i(-)$ for the optically allowed i-th excited state is given by

$$\Psi_{\mathrm{CT}}^i(-) \simeq \{\Phi_i(\mathrm{AD^+A^-}) - \Phi_i(\mathrm{A^-D^+A})\}/\sqrt{2},$$

and the oscillator strength is defined as follows:

$$f_i = 3\times1.085\times10^{11}E_{\mathrm{CT}}^i b_i^2|\boldsymbol{R}_{\mathrm{AD}}|^2,$$

where $\boldsymbol{R}_{\mathrm{AD}}$ is the vector between the acceptor and donor molecules in units of cm and E_{CT}^i is the excitation energy in cm^{-1}. Accordingly, by comparing the experimental and theoretical oscillator strengths, we can obtain the magnitude values of b_i^2 and also information about the electronic states of the CT complexes.

The b_i coefficient can be correlated to the so-called transfer integral, $t_{\mathrm{A}k,\mathrm{D}l}$, as follows:

$$\begin{aligned} b_i &= \sqrt{2}(\Phi(\mathrm{ADA})|H|\Phi_i(\mathrm{AD^+A^-}))/E_{\mathrm{CT}}^i, \\ &= 2(\phi_{\mathrm{A}}^k|F|\phi_{\mathrm{D}}^l)/E_{\mathrm{CT}}^i, \\ &\equiv 2t_{\mathrm{A}k,\mathrm{D}l}/E_{\mathrm{CT}}^i, \end{aligned}$$

where $\phi_{\mathrm{A}}{}^k$ is the k-th molecular unoccupied orbital of the acceptor, and $\phi_{\mathrm{D}}{}^l$, the l-th molecular occupied orbital of the donor. The transfer integral, $t_{\mathrm{A}k,\mathrm{D}l}$, may be approximated by the use of the overlap integral, $S_{\mathrm{A}k,\mathrm{D}l}$

$$t_{\mathrm{A}k,\mathrm{D}l} = -KS_{\mathrm{A}k,\mathrm{D}l} = -K(\phi_{\mathrm{A}}^k|\phi_{\mathrm{D}}^l).$$

Here, K is the constant taken as 15.0 eV and the overlap integral can be estimated by a method shown before.[2] Therefore, the comparison between the observed and calculated values of b_i^2 makes it possible to assign the character of the CT band. The molecular orbital is represented by taking the long axis of the molecule

as the y axis and the short axis as the z axis, except in the case of the hexamethylbenzene molecule. In hexamethylbenzene, the z axis is taken as the normal to the molecular plane.

All of the above-mentioned computations were carried out on a FACOM 230-75 computer at the Nagoya University Computation Center.

Results

TCNQ-Phenothiazine Complex. The complex of TCNQ-phenothiazine crystallizes in the form of needles elongated along the a axis, and the space group is C2/c.[3] TCNQ and phenothiazine molecules are stacked alternately in infinite columns parallel to the a axis. The interplanar distance is 3.44 A, and the distance between centers parallel to the a axis, R_{AD}, is 3.52 A. The mode of overlapping is shown in Fig. 1. The

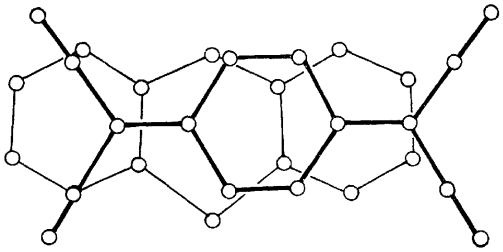

Fig. 1. The molecular overlap of the TCNQ–phenothiazine complex.

reflection spectra are observed for the polarizations parallel and perpendicular to the a axis on the (010) face, and the absorption spectra are obtained by the K-K transformation of the reflection spectra, as is shown in Figs. 2 and 3.

The a-axis reflection spectrum shows three separate bands. The first band peak occurs at 6200 cm^{-1}, with a reflectivity of 31.6%, while the second peak occurs at 17800 cm^{-1}, with 6.6% reflectivity. The third band, in the region of 29000 cm^{-1}, has a reflectivity of 6.9%. The $a_\perp$ spectrum for (010) shows no clear structure in the region of the first a axis band at 6200 cm^{-1}. The

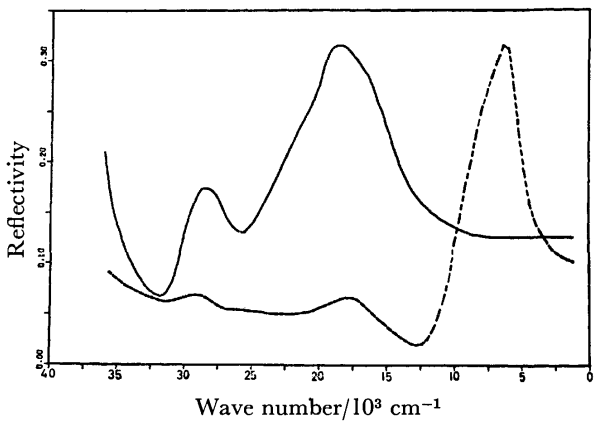

Fig. 2. The a(dashed line) and $a_\perp$(solid line) axes reflection spectra obtained on the (010) face of the crystal of TCNQ-phenothiazine complex.

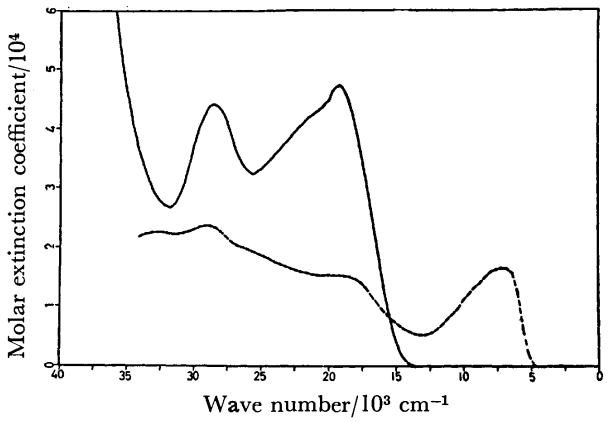

Fig. 3. The a(dashed line) and $a_\perp$(solid line) axes absorption spectra obtained by the K-K transformation of the reflection spectra of the crystal of TCNQ-phenothiazine complex.

intense band at 18500 cm^{-1} has a reflectivity of 31.5%, and the 28400 cm^{-1} band has a 17.4% reflectivity.

In the absorption spectra, the 6200 cm^{-1} band is exclusively polarized along the a axis and can be

TABLE 1. THE CT TRANSITION ENERGIES (E_{CT} IN 10^3 cm^{-1}), THE CHRGE-TRANSFER DEGREES (b_i^2 IN %), AND THE STABILIZATION ENERGIES (ΔE IN kcal) IN THE GROUND STATE OF THE CRYSTALS OF TCNQ COMPLEXES

Donors	E_{CT}	I_p(eV)[17]	C(eV)	P(eV)	I_c(eV)[17]	Obsd f_i	Obsd R_{AD}(A)	Obsd b_i^2	Calcd $S_{Ak,Dl}$	Calcd b_i^2	ΔE
Phenothiazine	7.1	7.14	2.36	1.10	4.36	0.549	3.52	19.2	0.0121	17.0	3.89
Anthracene	12.8	7.4	2.32	0.69	5.6	0.189	3.50	3.7	0	0.0	1.34
	21.4					0.583	3.50	6.8	0.0190	4.6	4.16
(total)								(10.5)		(4.6)	(5.50)
Pyrene	13.2	7.55	2.28	0.83	5.8	0.212	3.57	3.9	0.0072	1.7	1.46
	19.5					0.091	3.57	1.1	{0.0051 0.0039}	{0.4 0.2}	0.61
(total)								(5.0)		(2.3)	(2.07)
Acenaphthene	14.3	7.66	2.36	0.73		0.271	3.37	5.1	0.0123	4.3	2.04
Carbazole	14.6		2.40			0.637	3.34	12.0	0.0246	16.6	5.00
Hexamethylbenzene	16.0	7.85	2.30	0.77		0.765	4.28	8.0	0.0163	6.1	3.66
1,10-Phenanthroline	20.5		2.34			0.407	3.41	5.2	0.0078	0.8	3.06

assigned to the CT transition from the highest occupied orbital ($\phi_D^8(b_1)$) of the phenothiazine molecule to the lowest unoccupied orbital ($\phi_A^9(b_{1g})$) of the TCNQ molecule. The oscillator strength of this band is 0.549, and the observed charge-transfer degree (19.2%) is in good agreement with the calculated value of 17.0%, as is shown in Table 1. The 18500 and 29000 cm^{-1} bands are strongly polarized along the $a_\perp$ axis. The inclination of the long axis of the molecule with respect to the stacking a axis is 75° on the (010) face, and the long-axis transitions of the TCNQ and phenothiazine molecules should be more intensely observed in the $a_\perp$ axis spectrum. Therefore, the 18500 cm^{-1} band may be regarded as due to the long-axis transition (LE_1) of the TCNQ molecule,[4] and the 29000 cm^{-1} band, as due to the long-axis transition of the phenothiazine molecule. The LE_1 band of TCNQ is 6400 cm^{-1} red-shifted from the peak occurring at 24900 cm^{-1} in the chloroform-solution spectrum. This large shift seems to be due to the large charge-transfer degree (*ca.* 19%) in the ground state of the crystal of the TCNQ-phenothiazine complex. The 29000 cm^{-1} band corresponds to the 31300 cm^{-1} band of the phenothiazine molecule in the ehtanol solution.

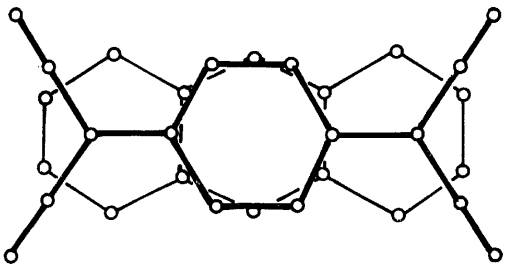

Fig. 4. The molecular overlap of the TCNQ–anthracene complex.

TCNQ–Anthracene Complex. The complex of TCNQ–anthracene forms a monoclinic crystal with a space group of C2/m,[5] and the structure consists of infinite columns of alternate TCNQ and anthracene molecules stacked in columns parallel to the c axis of the unit cell, with the mean molecular planes perpendicular to this axis. The mode of molecular overlap is such that the long axes of each molecule are parallel and their centers are superimposed, as is shown in Fig. 4. Therefore, the interplanar distance takes the same value (3.50A) as the intermolecular distance, R_{AD}. The reflection spectra are observed for the polarizations parallel and perpendicular to the c axis on the (010) face, and the absorption spectra are obtained by the K-K transformation of the reflection spectra, as is shown in Figs. 5 and 6. These spectra coincide with the spectra measured by Eckhardt and Pennelly.[6]

The c-axis reflection spectrum shows two bands. The first band, at 11800 cm^{-1}, has a reflectivity of 7.3%, while the second band occurs at 20800 cm^{-1}, with a 5.3% reflectivity. The $c_\perp$ spectrum for (010) consists of one intense peak at 23200 cm^{-1} and one shoulder at 35300 cm^{-1}. The 23200 cm^{-1} band has a reflectivity of 35.6%.

In the absorption spectra, as there is no mixing between the CT band and the locally excited $\pi \rightarrow \pi^*$

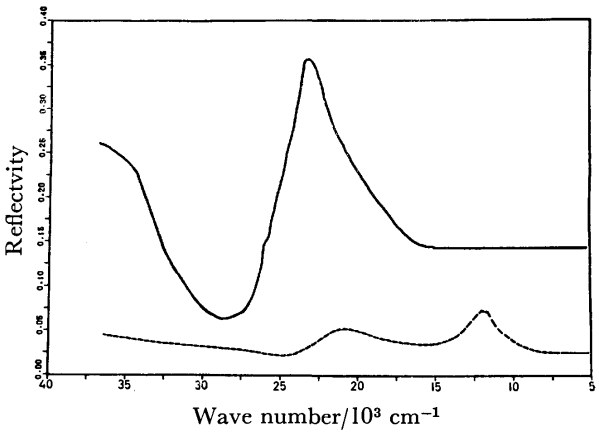

Fig. 5. The c(dashed line) and $c_\perp$(solid line) axes reflection spectra obtained on the (010) face of the crystal of TCNQ–anthracene complex.

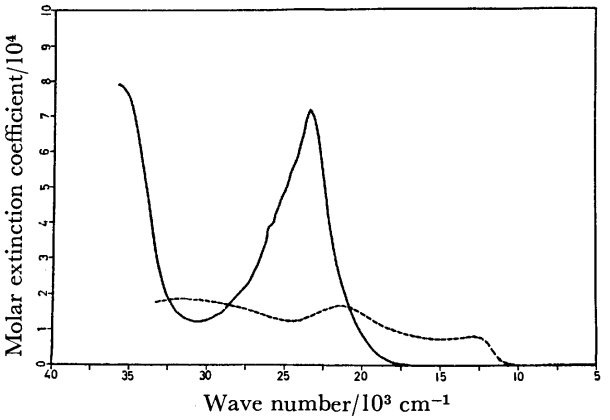

Fig. 6. The c(dashed line) and $c_\perp$(solid line) axes absorption spectra obtained by the K-K transformation of the reflection spectra of the crystal of TCNQ–anthracene complex.

bands of each molecule in the complex with a D_{2h} symmetry, the c-axis polarized band can be assigned to the charge-transfer band. Therefore, the two CT bands are observed at 12800 and 21400 cm^{-1}; it should be noted that the second CT band, at 21400 cm^{-1}, becomes more intense than the first CT band, at 12800 cm^{-1}. The oscillator strengths of these CT bands are 0.189 and 0.583, and the contributions (b_i^2) to the charge-transfer degree in the ground state are 3.7 and 6.8% respectively. According to the molecular overlap shown in Fig. 4 and the overlap integrals given in Table 1, the transition from the highest occupied anthracene orbital ($\phi_D^7(b_{2g})$) to the lowest unoccupied TCNQ orbital ($\phi_A^9(b_{1g})$) is forbidden, but the CT transition can be allowed from the third occupied anthracene orbital ($\phi_D^5(b_{1g})$) to the lowest unoccupied TCNQ orbital ($\phi_A^9(b_{1g})$). Accordingly, the weak CT band at 12800 cm^{-1} may be assigned to the $\phi_D^7(b_{2g}) \rightarrow \phi_A^9(b_{1g}$ transition, and the intense CT band at 21400 cm^{-1}, to the $\phi_D^5(b_{1g}) \rightarrow \phi_A^9(b_{1g})$ transition. The calculated charge-transfer degree supports these assignments strongly, as is shown in Table 1. The $c_\perp$ absorption spectrum has two intense bands. The first band, at 23400 cm^{-1}

corresponds to the LE_1 band of the TCNQ molecule and the second band, in the region of 35000 cm^{-1}, to the β band of the anthracene molecule, which is polarized along the long axis of the anthracene molecule.[7]

TCNQ-Pyrene Complex. The crystal of the TCNQ-pyrene complex was obtained as very dark green needles by the slow evaporation of a tetrahydrofuran solution; the space group is $P2_1/b$.[8] The crystal structure is built up from isolated TCNQ and pyrene molecules alternating in plane-to-plane stacks, and the stacking axis is the crystalline a axis (the needle axis).

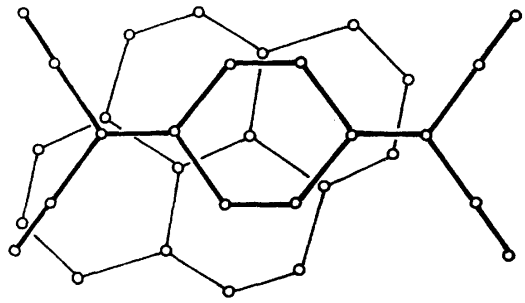

Fig. 7. The molecular overlap of the TCNQ-pyrene complex.

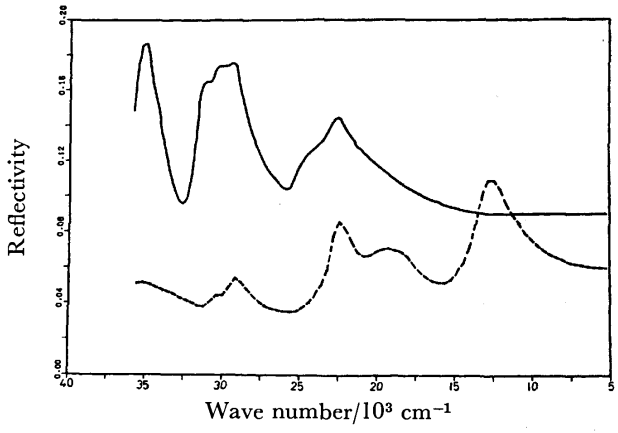

Fig. 8. The a(dashed line) and $a_\perp$(solid line) axes reflection spectra obtained on the (011) face of the crystal of TCNQ-pyrene complex.

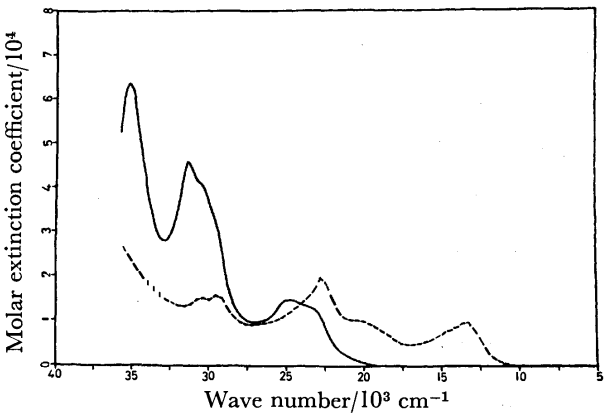

Fig. 9. The a(dashed line) and $a_\perp$(solid line) axes absorption spectra obtained by the K-K transformation of the reflection spectra of the crystal of TCNQ-pyrene complex.

The mean perpendicular separation between the planes of adjacent donor and acceptor components is 3.50 A, and the intermolecular distance along the stacking axis, R_{AD}, is 3.57 A. The molecular overlap, as viewed in the direction perpendicular to the mean molecular planes, is shown in Fig. 7. The reflection spectra are observed for the polarizations parallel and perpendicular to the a axis on the (011) face, and the absorption spectra are obtained by the K-K transformation of the reflection spectra, as is shown in Figs. 8 and 9.

The a axis reflection spectrum has five bands at 12600, 19300, 22400, 29200, and 35200 cm^{-1}. The reflectivity of the first band at 12600 cm^{-1} is 10.9%, while the broad second band at 19300 cm^{-1} has its reflectivity of 7.1%. The third band occurs at 22400 cm^{-1}, with an 8.6% reflectivity; the higher energy bands have lower reflectivities. The $a_\perp$-axis reflection spectrum shows no clear structure in the region of the first two bands in the a-axis spectrum. The first peak appears at 22400 cm^{-1}, with a reflectivity of 14.4%, while the 29400 and 35000 cm^{-1} bands have reflectivities of 17.5 and 18.7% respectively.

In the absorption spectra, the two bands at 13200 and 19500 cm^{-1} are active for the light polarized parallel to the a axis and may reasonably be assigned to the CT bands. The oscillator strengths of these two bands are 0.212 and 0.091, and the contributions (b_i^2) to the charge-transfer degree in the ground state are 3.9 and 1.1% respectively. Judging from the overlap integrals shown in Table 1, the first CT band seems to be due to the transition from the highest occupied pyrene orbital ($\phi_D^8(b_{2g})$) to the lowest unoccupied TCNQ orbital ($\phi_A^9(b_{1g})$), while the second CT band consists of nearly degenerate transitions from the third and fourth highest occupied pyrene orbital ($\phi_D^6(b_{3u})$ and $\phi_D^5(a_u)$). The third band, in the region of 24000 cm^{-1}, has the same magnitude as the absorption intensities in the a- and $a_\perp$-axes spectra. The (011) projection shows that the long axis of the TCNQ molecule is at an angle of 55° to the a axis, and the absorption intensities of the LE_1 band must be comparable for the a- and $a_\perp$-axes spectra. Therefore, the 24000 cm^{-1} band may be assigned to the LE_1 band of the TCNQ molecule. On the other hand, the long axis of the pyrene molecule is at an angle of 78° to the a axis, and the higher energy bands at 31400 and 35200 cm^{-1} should have stronger absorption intensities in the $a_\perp$-axis spectrum than in the a-axis spectrum. Therefore, the 31400 and 35200 cm^{-1} bands

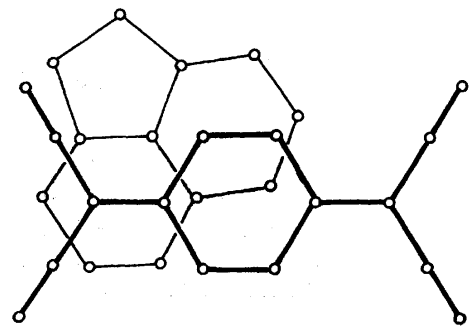

Fig. 10. The molecular overlap of the TCNQ-acenaphthene complex.

may be attributed to the long-axis transitions (p and β bands of the pyrene molecule[9] respectively).

TCNQ-Acenaphthene Complex. The complex of TCNQ-acenaphthene forms a triclinic crystal of a space group of $P\bar{1}$,[10] and TCNQ and acenaphthene are stacked alternately in infinite columns parallel to the a-axis. The intermolecular distance along the stacking axis, R_{AD}, is 3.37 A, and the molecular overlap is as is depicted in Fig. 10. The reflection spectra are observed for the polarizations parallel and perpendicular to the a-axis on the (011) face, and the absorption spectra are obtained by the K-K transformation of the reflection spectra, as is shown in Figs. 11 and 12.

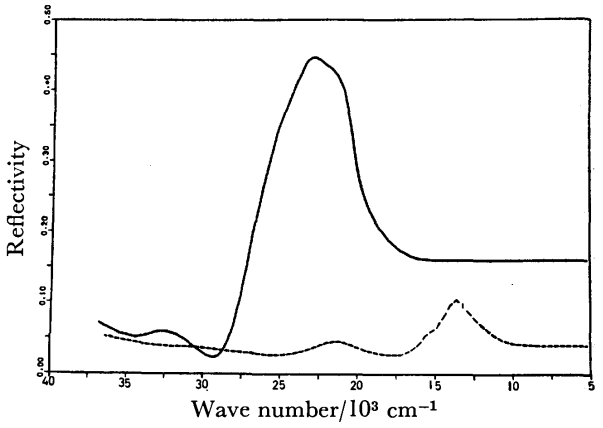

Fig. 11. The a(dashed line) and $a_\perp$(solid line) axes reflection spectra obtained on the (011) face of the crystal of TCNQ-acenaphthene complex.

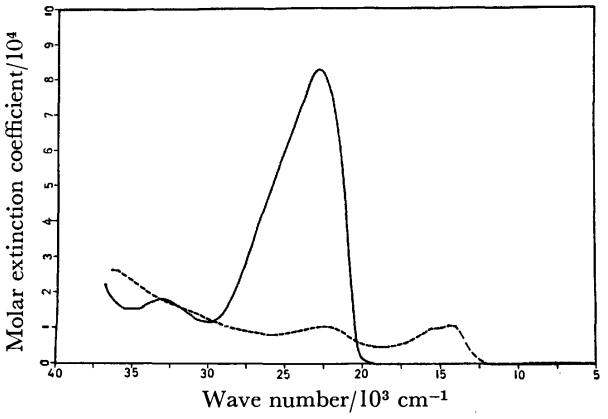

Fig. 12. The a(dashed line) and $a_\perp$(solid line) axes absorption spectra obtained by the K-K transformation of the reflection spectra of the crystal of TCNQ-acenaphthene complex.

The a-axis reflection spectrum shows two separate bands. The first band peak occurs at 13600 cm^{-1}, with a reflectivity of 10.4%, and the second band appears at 21200 cm^{-1}, with a 4.6% reflectivity. The $a_\perp$-axis reflection spectrum shows no clear structure in the first a-axis band. The intense band occurs at 23000 cm^{-1}, with a reflectivity of 44.6%, and the weak band, at 32600 cm^{-1}, with a 6.0% reflectivity.

In the absorption spectra, the first band at 14300 cm^{-1} is active for the light parallel to the a axis and may be due to the CT transition from the highest occupied acenaphthene orbital ($\phi_D{}^5(a_2)$) to the lowest unoccupied TCNQ orbital ($\phi_A{}^9(b_{1g})$). The oscillator strength of the band is 0.271, and the charge-transfer degree in the ground state is 5.1%, as is shown in Table 1. The second band, at 22800 cm^{-1}, is more strongly polarized along the $a_\perp$-axis direction than alone the a axis. The inclination of the long axis of the molecule with respect to the stacking a axis is 85°, and the long-axis transitions of the TCNQ and acenaphthene molecules should be more intensely observed in the $a_\perp$-axis spectrum than in the a-axis. Therefore, the second band may be regarded as the LE_1 band of the TCNQ molecule. The third weak band, in the region of 33000 cm^{-1}, can be assigned to the α band of the acenaphthene molecule.[11]

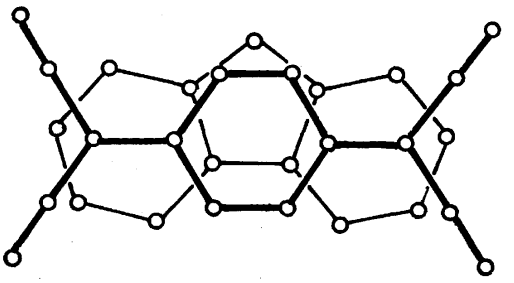

Fig. 13. The molecular overlap of the TCNQ-carbazole complex.

TCNQ-Carbazole Complex. The crystals of the TCNQ-carbazole complex are orthorhombic, and the space group is Immm.[12] The structure consists of infinite columns of alternate TCNQ and carbazole molecules, and the column is parallel to the c-axis. The molecular planes are perpendicular to the c-axis, and the long axes of each molecule are parallel to the a-axis. The molecular overlap is shown in Fig. 13. The intermolecular distance, R_{AD}, is the same as the mean perpendicular separation (3.34 A) between the molecular planes. The reflection spectra are observed for the polarizations parallel and perpendicular to the c-axis on the (010) face, and the absorption spectra are obtained by the K-K transformation of the reflection spectra, as is shown in Figs. 14 and 15.

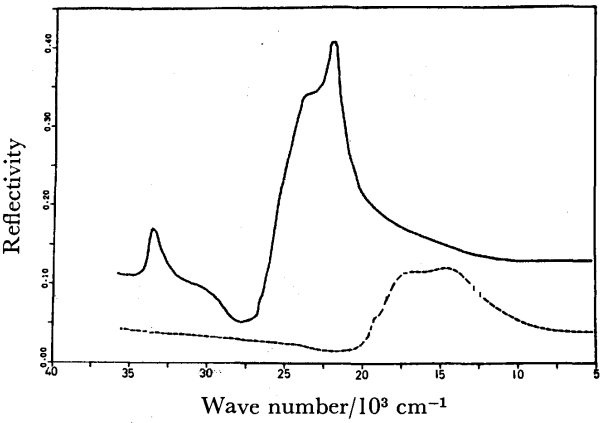

Fig. 14. The c(dashed line) and a(solid line) axes reflection spectra obtained on the (010) face of the crystal of TCNQ-carbazole complex.

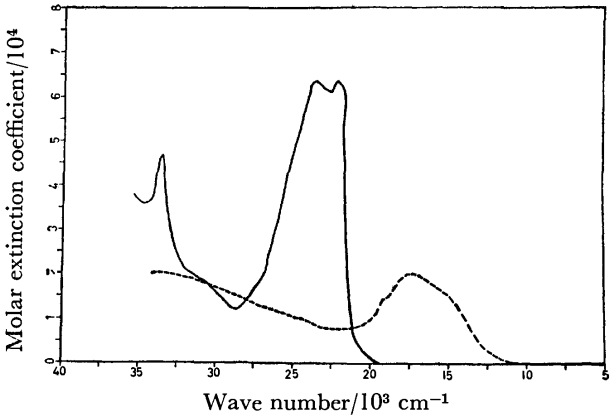

Fig. 15. The c(dashed line) and a(solid line) axes absorption spectra obtained by the K-K transformation of the reflection spectra of the crystal of TCNQ-carbazole complex.

The c-axis reflection spectrum has a band with a 12.0% reflectivity which splits into doublets at 14600 and 16600 cm^{-1}. The a-axis reflection spectrum consists of two bands. The intense band occurs at 21800 cm^{-1}, with a reflectivity of 40.6%, while the sharp band occurs at 33600 cm^{-1}, with a 17.0% reflectivity.

In the absorption spectra, the first band at 14600 cm^{-1} is active for the light parallel to the c-axis and can be assigned to the CT transition from the highest occupied carbazole orbital ($\phi_D^7(a_2)$) to the lowest unoccupied TCNQ orbital ($\phi_A^9(b_{1g})$). The oscillator strength of the CT band is 0.637, and the charge-transfer degree in the ground state is 12.0%. The second and third bands, at 22200 and 33600 cm^{-1}, are polarized along the a-axis, which is parallel to the long-axis of each molecule. Therefore, the 22200 cm^{-1} band can be regarded as the LE_1 band of TCNQ, and the 33600 cm^{-1} band as corresponding to the 34100 cm^{-1} band (α^* band) of the carbazole molecule in an ethanol solution.[13]

TCNQ-Hexamethylbenzene Complex. The crystals of the complex of TCNQ-hexamethylbenzene are monoclinic, and the space group is I2/m.[14] The structure consists of infinite columns of alternate molecules, and the column is parallel to the *a*-axis. The mean molecular separation is 3.55 A, and the intermolecular distance parallel to the a axis, R_{AD}, is 4.28 Å. The molecular overlap is illustrated in Fig. 16. The reflection spectra are obtained for the polarizations

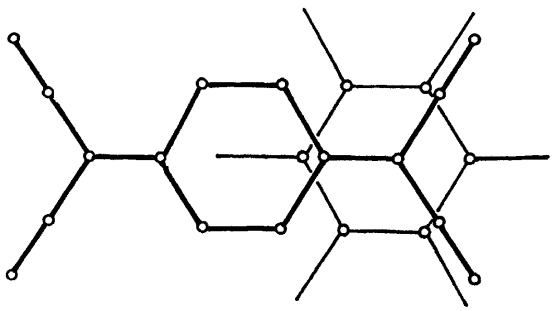

Fig. 16. The molecular overlap of the TCNQ-hexamethylbenzene complex.

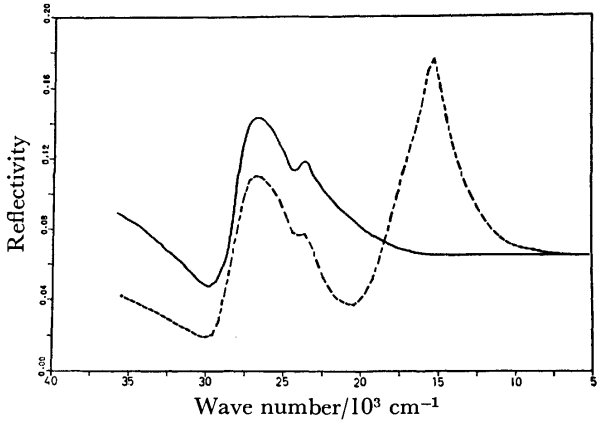

Fig. 17. The a(dashed line) and $a_\perp$(solid line) axes reflection spectra obtained on the (010) face of the crystal of TCNQ-hexamethylbenzene complex.

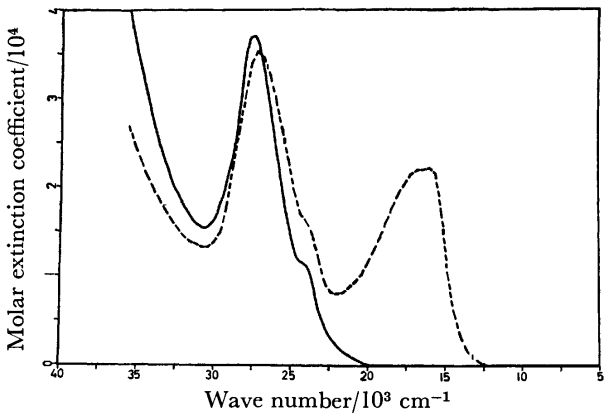

Fig. 18. The a(dashed line) and $a_\perp$(solid line) axes absorption spectra obtained by the K-K transformation of the reflection spectra of the crystal of TCNQ-hexamethylbenzene complex.

parallel and perpendicular to the a-axis on the (010) face. The absorption spectra are obtained by the K-K transformation of the reflection spectra, as is shown in Figs. 17 and 18.

The a-axis reflection spectrum has two bands. The first band occurs at 15200 cm^{-1}, with a reflectivity of 17.6%. The second band has the 0-0 transition at 23600 cm^{-1}, and the band peak appears at 26800 cm^{-1}, with an 11.0% reflectivity. The $a_\perp$-axis reflection spectrum shows no clear structure in the first a-axis band. The band corresponding to the second a-axis band has its first peak at 23600 cm^{-1}, while the main peak is located at 26800 cm^{-1}, with a reflectivity of 14.3%.

In the absorption spectra, the first band at 16000 cm^{-1} is polarized along the a-axis and may be assigned to the CT transition from one of the highest occupied hexamethylbenzene orbitals ($\phi_D^2(e_{1g})$) to the lowest unoccupied TCNQ orbital ($\phi_A^9(b_{1g})$). The oscillator strength of the CT band is 0.765, and the charge-transfer degree in the ground state is 8.0%. The second band at 27400 cm^{-1} has the same magnitude of absorption intensities in the a- and $a_\perp$-axes spectra. The (010) projection shows that the long-axis of the TCNQ

molecule is inclined at an angle of 56° to the stacking axis and indicates that the long-axis transition should be observed with the comparable absorption intensities for the a and $a_\perp$ axes spectra. Therefore, the 27000 cm^{-1} band can be attributed to the LE_1 transition of the TCNQ molecule.

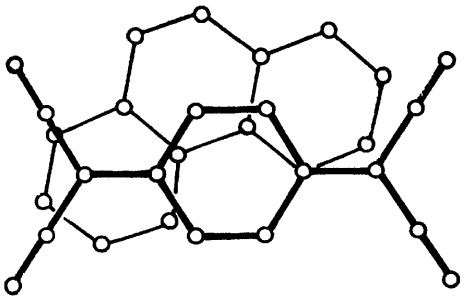

Fig. 19. The molecular overlap of the TCNQ–1,10-phenanthroline complex.

TCNQ-1,10-Phenanthroline Complex. The complex of TCNQ-1,10-phenanthroline forms a monoclinic crystal with a space group of $P2_1/n$.[15] The TCNQ and 1,10-phenanthroline molecules are packed in continuous mixed stacks usually, and the stacking axis is the c-axis. The mean interplanar donor-acceptor distance, R_{AD}, is 3.41 Å. The molecular overlap is shown in Fig. 19. The reflection spectra are observed for the polarizations parallel and perpendicular to the c-axis on the (010) face. The absorption spectra are obtained by the K-K transformation of the reflection spectra, as is shown in Figs. 20 and 21.

The c-axis reflection spectrum has a broad band at 18000 cm^{-1}, with a reflectivity of 4.6%. The $c_\perp$-axis reflection spectrum has two intense bands, at 22800 and 36800 cm^{-1}, with reflectivities of 26.7 and 19.8%.

In the absorption spectra, the first band at 20500 cm^{-1} is active for the light parallel to the c-axis and can be assigned to the CT transition from the highest occupied 1,10-phenanthroline orbital ($\phi_D^7(b_1)$) to the lowest unoccupied TCNQ orbital ($\phi_A^9(b_{1g})$). The oscillator strength of the CT band is 0.407, and the charger-transfer degree in the ground state is 5.2%.

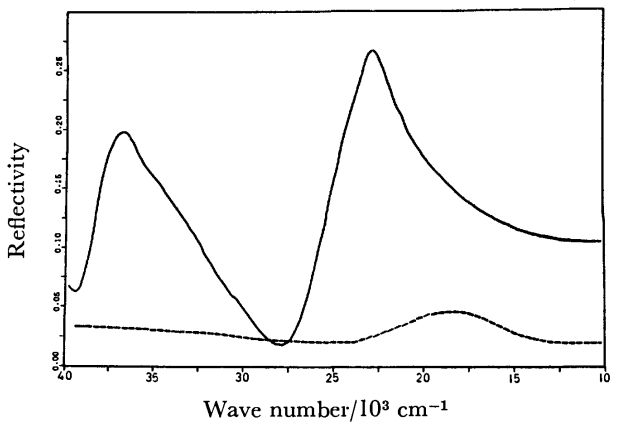

Fig. 20. The c(dashed line) and $c_\perp$(solid line) axes reflection spectra obtained on the (010) face of the crystal of TCNQ–1,10-phenanthroline complex.

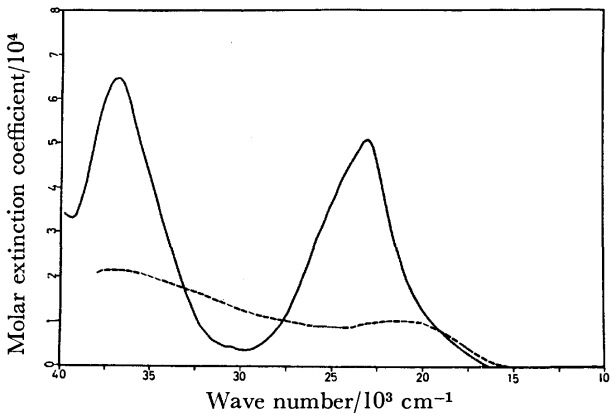

Fig. 21. The c(dashed line) and $c_\perp$(solid line) axes absorption spectra obtained by the K-K transformation of the reflection spectra of the crystal of TCNQ–1,10-phenanthroline.

The second and third bands at 23000 and 36800 cm^{-1} are polarized along the $c_\perp$-axis. The (010) projection shows that the long axes of the TCNQ and 1,10-phenanthroline molecules are nearly perpendicular to the a-axis. Therefore, the 23000 cm^{-1} band can be attributed to the LE_1 band of TCNQ, and the 36800 cm^{-1} band, to the long-axis transition of 1,10-phenanthroline.

Discussion

The energy of the CT transition, E_{CT}, is given approximately by the equation

$$E_{CT} = I_p - E_A - C - P,$$

where I_P is the ionization potential of the donor; E_A, the electron affinity of the acceptor; C, the Coulombic interaction between donor and acceptor molecules, and P, the polarization energy. That is, the observed energies (E_{CT}) of the charge-transfer transitions maintain a linear relation with the ionization potentials (I_P) of the donor molecules, as is shown in Table 1. The first CT band of the TCNQ–phenothiazine complex is located in the lowest energy region, and the CT bands of TCNQ–anthracene, pyrene, acenaphthene, and hexamethylbenzene are observed in the order of increasing energy, in the same manner as that of the ionization potential. The Coulomb energy of the first band can be estimated by the use of the Nishimoto-Mataga approximation, and the electron affinity of the TCNQ molecule was determined to be 2.80 eV by Klots, Compton, and Raaen.[16] Then, the polarzation energy, P, can be deduced as is shown in Table 1. It should be noted that the crystal of the TCNQ–phenothiazine complex has a large polarization energy (P=1.10 eV) although those of the other complexes are 0.7—0.8 eV. This extraordinary size of the crystal of the TCNQ–phenothiazine complex was also observed in the phenothiazine crystal.[17] The vertical ionization energy of a molecular crystal, I_C, is related to the ionization energy, I_P, of the corresponding gaseous molecule by the relation: $I_P = I_C + P$. Therefore, the values of $I_P - I_C$ are equal to the polarization energy, P, in the solid state; it is shown in Table 1 that the phenothiazine

crystal has a larger value of the polarization energy $P(=I_P-I_C)$ than the other compounds.

The stabilization energies in the ground state are determined by means of the equation: $\Delta E=\sum_i b_i^2 E_{CT}^i$, and are shown in Table 1. According to Table 1 and the molecular overlaps, the crystals of the complexes forming a configuration of a high symmetry like the TCNQ-anthracene and carbazole systems are more strongly stabilized by the charge-transfer force, although this seems not to be a general rule.

References

1) M. Tanaka, *Bull. Chem. Soc. Jpn.*, **50**, 2881 (1977).
2) M. Tanaka, *Bull. Chem. Soc. Jpn.*, **50**, 3194 (1977).
3) H. Kobayashi, *Acta Crystallogr., Sect. B*, **30**, 1010 (1974).
4) R. R. Pennelly and C. J. Eckhardt, *Chem. Phys.*, **12**, 89 (1976).
5) R. M. Williams and S. C. Wallwork, *Acta Crystallogr., Sect. B*, **24**, 168 (1968).
6) C. J. Eckhardt and R. R. Pennelly, *J. Am. Chem. Soc.*, **98**, 2034 (1976).
7) L. B. Clark and M. R. Philpott, *J. Chem. Phys.*, **53**, 3790 (1970).
8) C. K. Prout, I. J. Tickle and J. D. Wright, *J. Chem. Soc., Perkin Trans. 2*, **1973**, 528.
9) J. Tanaka, *Bull. Chem. Soc. Jpn.*, **38**, 86 (1965).
10) I. J. Tickle and C. K. Prout, *J. Chem. Soc., Perkin Trans. 2*, **1973**, 727.
11) M. Tanaka, *Bull. Chem. Soc. Jpn.*, **49**, 2315 (1976).
12) H. Kobayashi, *Bull. Chem. Soc. Jpn.*, **46**, 2675 (1973).
13) M. Tanaka, *Bull. Chem. Soc. Jpn.*, **49**, 3382 (1976).
14) R. H. Colton and D. E. Henn, *J. Chem. Soc., B*, **1970**, 1532.
15) I. Goldberg and U. Shmueli, *Cryst. Struct. Commun.*, **2**, 175 (1973).
16) C. E. Klots, R. N. Compton, and V. F. Raaen, *J. Chem. Phys.*, **60**, 1177 (1974).
17) F. Gutmann and L. E. Lyons, "Organic Semiconductors," John Wiley and Sons, New York (1967), pp. 351, 667.

Bond Orbital Calculations on the Methane and Silane Molecules. II. Vertical Transition Energies of the Lower Singlet-Excited States of CH_4

Shigeyoshi KATAGIRI and Susumu KOHDA-SUDOH

Department of Chemistry, Faculty of Science, Hirosaki University, Hirosaki 036

(Received July 6, 1977)

The vertical singlet-transition energies of CH_4 were calculated using the BO method. Two types of basis sets, minimal and extended, were employed. The vertical transition energy of the lowest singlet state of CH_4 was found to be 9.1 eV using the extended-basis set. This transition is assigned to a Rydberg-type transition in agreement with experiments. The other lower excited-states of CH_4 may also be assigned to Rydberg transitions. The main features of the present BO calculations do not differ greatly from those of other extended-basis MO calculations. The total energy of the ground state is discussed briefly.

In previous bond orbital (BO) calculations[1] for the methane and silane molecules, the total energies of the ground states were calculated in this, as well as the ordinary SCF-LCAO-MO, method and the polarization parameters were approximately equal to those of the O–H and N–H bonds in the water[2] and ammonia[3] molecules, respectively. It appears interesting to investigate how well excited states are expressed by the BO method. Among the many properties of the excited molecular states our interest here is mainly in the lowest vertical transition energies for the present BO calculations. The total energy of the ground state of CH_4 will be discussed briefly.

Recently, extended-basis MO calculations are frequently carried out on the electronic structure and spectra of medium-sized molecules using Gaussian-type orbitals (GTO) as atomic orbitals (AO).[4-12] These calculations have succeeded in explaining the electronic spectra of organic molecules, especially Rydberg-type transitions. The present authors have already calculated the vertical transition energies of CH_4 using the MO method,[13] and found that the lowest excited state of CH_4 can be assigned to a transition of an electron from the $1t_2$ to the 3s-like Rydberg MO's in agreement with the electron-impact experiments of Harshbarger and Lassetre.[14] Here BO calculations for the vertical transition energies of methane obtained using two basis sets (*i.e.*, minimal and extended-basis sets) are presented. BO-type calculations have already been performed by Klessinger and McWeeny[15] using the group-function method with minimal Slater-type AO (STO) as the basis set. They discussed only two excited states, A_1 and T_2, which were described by linear combinations of four locally-excited configurations (excitons), with the results not in quantitative agreement with experiment.

In this study other excited states which can also be constructed from other types of electron promotion (*vide infra*) were investigated. The molecular geometry is assumed to be T_d and the bond distance is fixed at R(C–H)=2.05 a.u.[16] The STO are used as the basis AO, with the orbital exponents:

$$\delta_{1s}(C) = 5.7,\ \delta_{2s}(C) = \delta_{2p}(C) = 1.625,$$
$$\delta_{3s}(C) = \delta_{3p}(C) = 0.4388,\ \text{and}\ \delta_{1s}(H) = 1.2.$$

These values were obtained from Slater's rules, except for $\delta_{1s}(H)$. All molecular integrals were calculated on the HITAC 8800/8700 Computer at the University of Tokyo Computer Centre, using the library program written by Taketa (Y4TC/AD05; Molecular Integrals over CGTO), where the molecular integrals were calculated over the composite GTO's.[17] The CI calculations were carried out on the NEAC 2200 Model 700 Computer at the Tohoku University Computer Centre.

Method of Calculations

In previous BO studies, the original non-orthogonal basis set,

$$\mathbf{a} = (1s, 2s, 2p_x, 2p_y, 2p_z, H_1, H_2, H_3, H_4), \quad (1)$$

where H_i is the ith hydrogen 1s AO, was transformed into the orthonormalized basis set,

$$\mathbf{b} = (1s, b_1, h_1, b_2, h_2, b_3, h_3, b_4, h_4), \quad (2)$$

using the procedure of McWeeny and Ohno.[2] That is, all the valence orbitals were Schmidt-orthogonalized to the carbon inner shell (1s), the carbon 2s′ and 2p orbitals were tetrahedrally hybridized, and finally all the orbitals obtained were orthonormalized according to Löwdin's method. The orthonormalized orbitals, b_i and h_i, were used to construct the bond orbitals (BO) for the ith bond, thus

$$B_i = \lambda^2 h_i + \sqrt{1-\lambda^2}\, b_i, \quad (3)$$

where λ is a variational parameter. Now we assume the following antibonding BO (A_i) for constructing the excited state of CH_4,

$$A_i = \mu^2 b_i - \sqrt{1-\mu^2}\, h_i. \quad (4)$$

In order to maintain orthogonality between the ground and excited states, we make the assumption that the variational parameters, λ and μ, in Eqs. 3 and 4 are identical, such that $\lambda^2=\mu^2=0.46$, the optimum value for the ground state of CH_4, throughout the present calculations.[1] The number, and types of electron promotion taken into account will be discussed below in detail.

Extended-basis Calculations: The extra-valence AO, the 3s and 3p orbitals of the carbon atom, were added to the minimal-basis set. In the calculations, the following suppositions were made. First, the bonding BO are the same as those of the minimal-basis calculations. Second, the pseudo-antibonding BO are expressed by only the

extra-valence AO, thus

$$A_i = \frac{1}{2}(3s \pm 3p_x \pm 3p_y \pm 3p_z), \quad (5)$$

where the 3s and 3p AO are orthonormalized to the inner and valence shell AO of the C atom using the Schmidt procedure, and the signs are chosen to form directed hybridized orbitals toward to the ith H atom, as in the case of b_i in Eqs. 3 and 4. Finally, we neglect the overlap integrals between the A_i and the hydrogen 1s AO, *i.e.*, $S(A_i, B_i)=0$,[20] to insure orthogonality for the A_i and B_i. The form of the pseudo-antibonding orbitals is of great advantage to constructing symmetry adapted basis functions, and should be regarded as virtually equivalent orbitals.

Wavefunctions of the Excited States: We can consider many types of electron promotion from the bonding orbitals (B_i) to the antibonding or pseudo-antibonding orbitals (A_i). The excited electronic configurations arising from one- and two-electron promotion are taken into account in the CI calculations. The types of electron promotion actually considered are

$$\{(B_i)^2\} \longrightarrow \{(B_t)(A_j)\}, \quad (16)$$
$$\{(B_i)^2\} \longrightarrow \{(A_j)^2\}, \quad (16)$$
$$\{(B_i)^2\} \longrightarrow \{(A_t)(A_j)\}, \quad i \neq j, \quad (12)$$
$$\{(B_i)^2\} \longrightarrow \{(A_k)(A_l)\}, \quad i \neq k \neq l, \quad (12)$$
$$\{(B_i)^2(B_j)^2\} \longrightarrow \{(B_i)(B_j)(A_i)^2\}, \quad i \neq j, \quad (12)$$

and

$$\{(B_k)^2(B_l)^2\} \longrightarrow \{(B_k)(B_l)(A_i)^2\}, \quad i \neq k \neq l, \quad (12)$$

where an electron promotion, such as $\{(B_i)^2(B_j)^2\} \rightarrow \{(B_i)(B_j)(A_i)^2\}$ means that two electrons in the bonding BO, B_i and B_j, are excited to the vacant antibonding or pseudo-antibonding BO (A_i) at the same time and the other doubly-occupied orbitals remain unchanged. The numbers in parenthesis are the possible ways of exciting the electron from four bonding BO to four antibonding or pseudo-antibonding BO.

The symmetry-adapted basis functions of the excited states are easily obtained by taking appropriate linear combinations of the above excited configurations. From the fact that the direct product $(A_1+T_2)\otimes(A_1+T_2)$ is $2A_1+E+T_1+3T_2$, for example, we can take the following combinations of four singly-excited configurations as one of the CI basis functions for the states A_1 and T_2

$$\Psi(A_1 \text{ or } T_2) = c_1\psi(B_1 \rightarrow A_1) + c_2\psi(B_2 \rightarrow A_2) + c_3\psi(B_3 \rightarrow A_3) + c_4\psi(B_4 \rightarrow A_4), \quad (6)$$

where the symbol A is used to denote both the symmetry species and pseudo-antiboding BO, although being careful to avoid confusion. The final excited-state wavefunction will be expressed as a linear combination of these symmetry-adapted basis functions.

Results and Discussion

The vertical transition energies of the lower excited states are given in Table 1, along with other MO calculations and experimental results. The total enrgy of the ground state of CH_4 is improved considerably by the configuration interaction. The results of the CI are shown in Table 2, where the results indicate the extent that individual excited configurations contribute to the improvement of the total energy. In the minimal-basis calculations, the doubly-excited configurations, such as $(B_i)^2 \rightarrow (A_j)^2$, are most affected by the CI calculations. Especially, the energy lowering due only to local configurations, *i.e.*, $(B_i)^2 \rightarrow (A_i)^2$ is calculated to be -0.0535 a.u., which amounts to about 88% of the entire energy decrease. This results from inclusion of intra-bond electron correlation. This can be compared with the result (0.0517 a.u.) of previous modified BO calculations,[1] where electron correlation between orbitals of two different spins (different orbitals for different spins) were included. In the extended-basis calculations, on the other hand, the singly-excited configurations make exclusively dominant contributions to the decrease of the total energy. As for the results of the minimal-basis calculations, the energy decrease due only to local configurations, *i.e.*, $(B_i)^2 \rightarrow (B_iA_i)$, is very great ($-0.0323$ a.u.), which amounts to about 86% of the total energy decrease.

TABLE 2. ENERGY DECREASE DUE TO CI (a.u.)

Excited configuration	Minimal basis	Extended basis
$(B_t)^2 \rightarrow (B_tA_j)$	-0.0026	-0.0376
$(B_t)^2 \rightarrow (A_j)^2$	-0.0550	-0.0001
Others	-0.0035	-0.0000
Total	-0.0611	-0.0377
Total energy	-40.1658	-40.1451

Turning our attention now to the predicted excited states, the symmetry of the calculated lowest excited-state, as seen from Table 1, is T_2 in all cases except for the minimal-basis MO calculations. In spite of the

TABLE 1. VERTICAL TRANSITION ENERGIES (eV)

State	Minimal basis				Extended basis					Obsd[f]	
	(I)[a]	(II)[b]	MO[c]	GF[d]	(I)	(II)	MO[c]	EOM[e]	CI[e]		
$1T_2$	20.52	17.43	23.78	21.11	9.37	9.11	11.62	10.24	10.76	9.7	10.3
E	21.97	22.56	21.93		13.37	13.28	12.49	11.72	12.40		
$2T_2$	26.08	26.49	24.08		13.44	13.29	12.50	11.68	12.47	11.7	
$1A_1$	27.40	27.79	27.65	28.11	14.52	14.36	13.06	12.38	13.55		
T_1	27.67	29.26	21.50		18.89	18.89	12.54	11.77	12.43		
$3T_2$	33.47	33.76			21.95	21.63	23.67				
$2A_1$	36.21	36.04			23.50	23.38	27.25				

a) Single-excitation CI. b) Double-excitation CI. c) See Ref. 13. d) See Ref. 15. e) See Ref. 11. f) See Ref. 18.

fact that the T_2 state participates in an electronically-allowed transition, the vertical transition energies calculated using the minimal-basis set are too high in comparison with the experimental results, and moreover exceed the ionization potential.[18] This is common for non-empirical calculations using the minimal-basis set.[10,15] The situation, however, is changed drastically by introducing into the basis set the extra-valence AO of the C atom. The lowest excited state is calculated to be 9.4 and 9.1 eV above the ground state for cases (I) and (II), respectively (see footnotes to Table 1). The symmetry of this state is that of the dipole-allowed T_2 state for both calculations. The agreement with experiment is fairly good. Williams and Poppinger have calculated the transition energies of CH_4 using the CI and EOM methods, for which they also used the extra-valence 3s and 3p AO of the C atom as bases.[11] As is seen from Table 1, their results show almost the same tendency as the present BO calculations with respect to the transition energies, but there are some differences for the relative ordering of the calculated excited states. The BO results do not differ in main features from the MO results, although it is of note that the BO lowest T_1 state is considerably higher than that for the MO calculations.

In the extended-basis BO calculations, the results of CI with both singly- and doubly-excited configurations give lower transition energies than do those including only single excitations. For the minimal-basis BO calculations, on the other hand, inverse results are obtained, except for only two states ($1T_2$ and $2A_1$). This appears to conflict with the conventional SCF-LCAO-MO CI results that the doubly-excited CI give higher vertical transition energies than do the singly-excited CI, because of the improvement of the ground-state total energy for the former CI calculations. This may be understood from the BO-CI results shown in Table 2.

It is interesting to examine the nature of the lowest excited state. It has already been shown, for MO calculations,[13] that the lowest vacant MO ($3a_1$) resembles the 3s AO of the C atom which is orthogonalized to the 2s and 1s AO using Schmidt procedure, and the lowest singlet excited-state is assigned to the Rydberg transition, *i.e.*, from the triply degenerate $2t_2$ MO to the above 3s-like MO. In the present BO calculations, this T_2 state is expressed as

$$\begin{aligned}{}^1\Psi(T_2) = {} & 0.212\{\psi(B_1\rightarrow A_1)+\psi(B_2\rightarrow A_2) \\ & -\psi(B_3\rightarrow A_3)-\psi(B_4\rightarrow A_4)\} \\ & +0.173\{\psi(B_1\rightarrow A_2)+\psi(B_2\rightarrow A_1) \\ & -\psi(B_3\rightarrow A_4)-\psi(B_4\rightarrow A_3)\} \\ & +0.294\{\psi(B_1\rightarrow A_3)+\psi(B_2\rightarrow A_4) \\ & -\psi(B_3\rightarrow A_1)-\psi(B_4\rightarrow A_2)\} \\ & +0.294\{\psi(B_1\rightarrow A_4)+\psi(B_2\rightarrow A_3) \\ & -\psi(B_3\rightarrow A_2)-\psi(B_4\rightarrow A_1)\} \\ & +\text{doubly-excited configurations},\end{aligned}$$

where the $\psi(B_i\rightarrow A_j)$ denote the excited singlet configurations arising from one-electron promotion from the B_i to the A_j orbitals. The lowest excited state is not expressed only by local excitation. The contribution of the doubly-excited configurations to this state is small.

It is seen that the lower excited states of CH_4 are not explained by the valence-shell transitions using the minimal-basis calculations, but can be understood to be Rydberg-type transitions obtained using the extended-basis calculations. This agrees with the results of the extended-basis MO calculations.[13] Here, no consideration was made of the interaction between the Rydberg and valence-shell transitions. However, more extended-basis MO calculations will be presented elsewhere,[19] in which the mixing of the above two types of transitions will be discussed.

The authors wish to express their thanks to Professor Hiroshi Taketa of Kyushu University for helpful communications regarding the use of the molecular integral program (Y4TC/AD05; library program at the University of Tokyo Computer Centre).

References

1) S. Kohda and S. Katagiri, *Bull. Chem. Soc. Jpn.*, **46**, 1428 (1973).
2) R. McWeeny and K. Ohno, *Proc. R. Soc. London, Ser. A*, **255**, 367 (1960).
3) A. Tsuchida and K. Ohno, *J. Chem. Phys.*, **39**, 600 (1963).
4) R. Ditchfield, W. J. Hehre, and J. A. Pople, *J. Chem. Phys.*, **54**, 724 (1971).
5) P. J. Bruna, S. D. Peyerimhoff, and R. J. Buenker, *Chem. Phys.*, **3**, 35 (1974).
6) R. J. Buenker and S. D. Peyerimhoff, *J. Chem. Phys.*, **53**, 1368 (1970).
7) W. J. Hehre and W. A. Lathan, *J. Chem. Phys.*, **56**, 5255 (1972).
8) S. Rothenberg, R. H. Young, and H. F. Schaefer, *J. Am. Chem. Soc.*, **92**, 3243 (1970).
9) B. Roos and P. Siegban, *Theoret. Chem. Acta*, **17**, 199 (1970).
10) F. Pauzat, J. Ridard, and B. Levy, *Mol. Phys.*, **23**, 1163 (1972).
11) G. R. J. Williams and D. Poppinger, *Mol. Phys.*, **30**, 1005 (1975).
12) T. Nomura, A. Tanaka, H. Tatewaki, T. Noro, T. Takada, H. Kashiwagi, F. Sasaki, and K. Ohno, Symposium on the Molecular Structure at Tokyo (1976).
13) S. Katagiri and S. Sudoh, Symposium on the Molecular Structure at Nagoya (1975).
14) W. R. Harshbarger and E. N. Lassettre, *J. Chem. Phys.*, **58**, 1505 (1973).
15) M. Klessinger and R. McWeeny, *J. Chem. Phys.*, **37**, 601 (1962).
16) R. M. Pitzer, *J. Chem. Phys.*, **46**, 4871 (1967).
17) K. O-ohata, H. Taketa, and S. Huzinaga, *J. Phys. Soc. Jpn.*, **21**, 2306 (1966). In this work, s-type STO (1s, 2s, 3s, and hydrogen 1s) were all expanded using 8-terms GTO, and p-type STO (2p and 3p) using 6-terms GTO.
18) H. H. Brongersma and L. J. Oosterhoff, *Chem. Phys. Lett.*, **3**, 437 (1969).
19) The 4s and 4p AO are taken into account in the basis set.
20) The overlap integral between the pseudo-antibonding A_i orbital and the hydrogen 1s AO is calculated to be 0.1534, but the overlap integral between the A_i and the B_i orbitals (with $\lambda^2=0.46$) is 0.075.

Study of Solutions of Tetraalkylammonium Salts in Acetone by Vapor Pressure Osmometry and Conductometry

Ha Chung LEE and Yutaka MIYAHARA

Department of Chemical Engineering, Faculty of Engineering, Nagoya University, Chikusaku, Nagoya 464

(Received July 12, 1977)

Vapor pressure depressions at 40.3 °C and electric conductivities at 25 and 40.3 °C have been measured for Bu_4NCl, Bu_4NBr, Bu_4NI, and Pr_4NI in acetone. Experiments were carried out with the greatest care to minimize the contact of salts and their solutions with air. A new representation of activity coefficients has been proposed for the undissociated species. Analysis by means of the representation gives better agreement between the dissociation constants and those obtained from electric conductivities. The very small dissociation constant of Bu_4NCl found previously has been corrected.

A number of papers[1,4,6,8] have appeared on the study of solutions of electrolytes in nonaqueous solvents by means of electric conductivity measurement. The dissociation of electrolyte salts is not complete in nonaqueous solvents. The dissociation constants have been determined by several authors. The activities in nonaqueous solutions of alkali halides[2] and tetraalkylammonium salts[3] were measured with a vapor pressure osmometer (VPO), and the dissociation constants of salts were estimated.

However, the dissociation constants of tetraalkylammonium salts were not in good agreement with those[4,8] determined conductometrically.

The present experiments have been undertaken in order to compare the dissociation constants obtained by two methods. The study of solutions of tetraalkylammonium salts, Bu_4NCl, Bu_4NBr, Bu_4NI, and Pr_4NI, in acetone by means of VPO has been repeated, measurements of the electric conductivities of the same solutions also being carried out.

In the calculation of dissociation constants from the VPO data, the activity coefficient of undissociated molecules has been taken into account.

Theoretical

It is well known that the tetraalkylammonium salts, MX, dissociate in acetone as

$$MX \rightleftarrows M^+ + X^-. \quad (1)$$

Thus, the Gibbs-Duhem equation gives

$$N_1 \,d\ln a_1 + m_2 \,d\ln a_2 + m_3 \,d\ln a_3 + m_4 \,d\ln a_4 = 0, \quad (2)$$

where a_2, a_3, and a_4 are the activities of MX, M^+, and X^-, respectively, and a_1 is the activity of the solvent. N_1 is the moles of 1 kg of the solvent ($=1000/M_1$: M_1 the molecular weight of the solvent), and m_2, m_3, and m_4 are the molalities of MX, M^+, and X^-, respectively. Integration of Eq. 2 gives

$$\ln a_1 = -\frac{1}{N_1}\left(m_2 + 2m_4 + \int_0^{m_4} m_2 \,d\ln\gamma_2 + 2\int_0^{m_4} m_4 \,d\ln\gamma_4\right). \quad (3)$$

We assume that the activity coefficients of ions M^+ and X^- obey the Debye-Huckel (D-H) limiting law.[3] The integration of the last term of the right-hand side of Eq. 3 is, then, given by

$$2\int_0^{m_4} m_4 \,d\ln\gamma_4 = -\frac{4.606A(\sqrt{m_4 d_0})^3}{3d_0}\sigma(X) - 2\left\{m_4 - \frac{\ln(1+0.001m_4M_2)}{0.001M_2}\right\}, \quad (4)$$

$$X = Ba_0\sqrt{m_4 d_0},$$

$$\sigma(X) = \frac{3}{X^3}\left\{(X+1) - \frac{1}{X+1} - 2\ln(X+1)\right\},$$

where A and B are the constants in the D-H equation (see Eq. 9), and d_0 the density of the solvent. The second term in the right-hand side of Eq. 4 was omitted in Eq. 10 of the previous paper.[3]

The form of activity coefficient of the undissociated molecules, γ_2, should be duly considered. In the theory of Fuoss-Onsager, it has been assumed to be unity. We have attempted to determine the dissociation constant from the concentration dependence of the activity of the solvent by means of the curve-fitting. We start from the following two assumptions with respect to γ_2.

$$\text{I} \quad \ln\gamma_2 = 0 \quad (5)$$

$$\text{II} \quad \ln\gamma_2 = -\beta_2 m_2 + (\beta_3 m_2^2 + \cdots).$$

Integration of the third term in the right-hand side of Eq. 3 leads to

$$\int_0^{m_4} m_2 \,d\ln\gamma_2 = -\frac{\beta_2}{2}m_2^2 + \left(\frac{2\beta_3}{3}m_2^3 + \cdots\right). \quad (6)$$

Assumption II shows that the deviation of γ_2 from unity caused by various unknown factors is compensated by introducing a parameter β_2.

A function h defined by

$$h = \frac{N_1 \ln a_1}{m} + 1 \quad (7)$$

was used for the analysis of the experimental results, where m is the molality of salt.

Experimental

Material. Tetraalkylammonium salts, Bu_4NCl, Bu_4NBr, Bu_4NI, and Pr_4NI, and acetone (guaranteed grade, Nakarai Chemical Co., Ltd.) were used. Before use, the salts were dried for five days in a vacuum oven at 50 °C with molecular sieves 3 Å (1/8-in. pellets). Fresh molecular sieves were used each day. Acetone was dried with anhydrous calcium sulfate and distilled in the presence of the molecular sieves. The water content was confirmed to be less than 0.01 wt % by the Karl-Fischer analysis. The molecular sieves and anhydrous calcium sulfate were dried, before use, over a period of 12 h in

an electric oven at 360 and 250 °C, respectively. KCl was dried by a similar way to that for the tetraalkylammonium salts. The conductivity water was prepared by the usual method by passing dried nitrogen gas. Great care was taken to minimize the contact of the salts and their solutions with air. A dry box filled with nitrogen gas was used.

Vapor Pressure Osmometer. A vapor pressure osmometer Hitachi-Perkinelmer 115 was used. The experimental procedures were reported.[2] The temperature of measurement was 40.3 °C.

Conductometry. The conductometer, a model CM-1DB, Toa Denpa Co., Ltd., was calibrated with a Wheatstone Bridge, Type BD-30 of Shimadzu Co., Ltd. The cell constants were determined with KCl solutions in the usual way. Temperature of measurements were 25 and 40.3 °C.

Results and Discussion

Vapor Pressure Osmometry. Proportionality constants K_s, of the apparatus obtained for several compounds of known molecular weight is given in Table 1. The plots of Δr, the change of resistance of a bridge in the apparatus, against the concentration, m, for the tetraalkylammonium salts in acetone, are given in Fig. 1. The values of h, calculated from Eq. 7 are given in Table 2. The profile of plots of h against the concentration clearly shows the existence of a dissociation equilibrium in the solutions.[3]

Table 1. Proportionality constant of VPO in acetone solutions at 40.3 °C

	Molecular weight	$-K_s \times 10^{-4}$
Biphenyl	154.2	5.75
Hexamethylbenzene	162.3	5.75
Benzil	210.2	5.83
1-Octadecanol	270.5	5.83
Glycerol tribenzoate	404.4	5.83

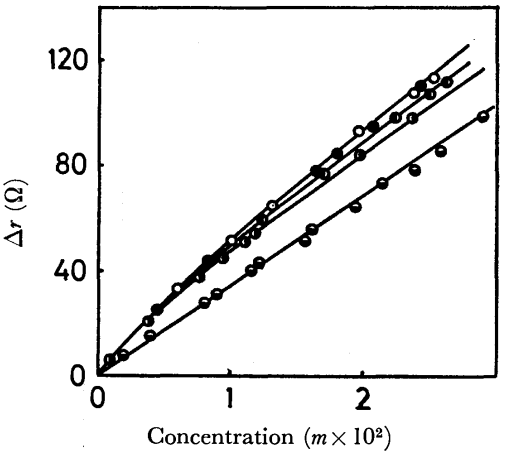

Fig. 1. Relationships between Δr and m for benzil and tetraalkylammonium salts at 40.3 °C.
◑: Bu_4NCl, ◐: Bu_4NBr, ○: Bu_4NI, ●: Pr_4NI, ◒: benzil.

Numerical analysis of function h was carried out. Two parameters, K_d and β_2, were determined on assumptions I and II by the method of least-squares. A HITAC 10 computer was used for the curve fitting of function h. The best values of K_d and β_2 and their standard deviations, σ, are given in Table 3. The difference between assumptions I and II is not highly

Table 2. h values of tetraalkylammonium salts in acetone at 40.3 °C

	Concentration $m \times 10^3$	h	Concentration $m \times 10^3$	h	Concentration $m \times 10^3$	h
Bu_4NCl	0.4824	-0.899_3	0.9741	-0.790_3	1.0234	-0.761_8
	3.915	-0.600_5	4.128	-0.546_8	7.604	-0.457_6
	8.026	-0.417_9	9.388	-0.404_2	11.100	-0.366_0
	11.842	-0.345_2	19.702	-0.257_1	23.641	-0.219_0
Bu_4NBr	1.0490	-0.802_9	1.2291	-0.827_6	2.1590	-0.765_8
	2.3396	-0.793_9	3.9354	-0.652_5	4.224	-0.623_3
	4.389	-0.629_9	8.302	-0.488_2	8.588	-0.459_3
	8.805	-0.480_4	12.188	-0.406_6	12.300	-0.422_6
	13.264	-0.379_4	16.479	-0.352_4	16.992	-0.332_4
	17.858	-0.337_3	18.729	-0.325_7	21.779	-0.297_4
	22.321	-0.296_4	24.190	-0.283_0	24.908	-0.268_5
Bu_4NI	1.3526	-0.857_4	1.5432	-0.781_2	2.3971	-0.750_9
	2.9316	-0.713_9	5.0524	-0.626_3	6.005	-0.579_9
	8.817	-0.538_6	9.976	-0.508_1	10.551	-0.495_8
	12.618	-0.461_7	12.803	-0.472_9	17.299	-0.401_1
	17.505	-0.389_6	19.588	-0.389_7	19.800	-0.373_3
	21.154	-0.365_1	22.959	-0.351_8	23.787	-0.334_5
	25.000	-0.340_4	25.163	-0.334_4		
Pr_4NI	1.0792	-0.807_6	1.2115	-0.903_0	1.9850	-0.741_9
	2.1886	-0.701_6	4.5469	-0.612_1	8.3093	-0.533_1
	8.8329	-0.522_5	9.1678	-0.521_7	13.039	-0.448_5
	13.717	-0.443_6	15.948	-0.412_2	16.415	-0.397_3
	17.958	-0.380_9	20.609	-0.352_4	20.757	-0.367_0
	24.271	-0.323_7	24.315	-0.329_9		

Table 3. Dissociation constants obtained by VPO at 40.3 °C (in terms of molality)

	Assump. I		Assump. II		
	$K_d \times 10^3$	σ	$K_d \times 10^3$	β_2	σ
Bu_4NCl	2.88	0.054	3.33	12.5	0.040
Bu_4NBr	4.32	0.062	7.10	41.7	0.036
Bu_4NI	6.33	0.041	10.00	41.7	0.023
Pr_4NI	6.00	0.044	9.07	38.9	0.031

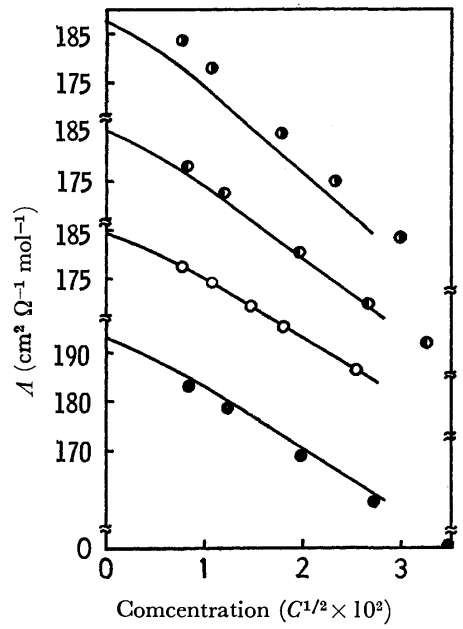

Fig. 2. Relationships between Λ and $\sqrt{C}$ for tetraalkylammonium salts at 25 °C. Lines show the results in literature.[4]
◑: Bu_4NCl, ◐: Bu_4NBr, ○: Bu_4NI, ●: Pr_4NI.

significant, but the values obtained from assumption II seem more favorable.

Conductometry. The concentration dependence of the conductivities obtained at 25 °C by the present measurements is compared in Fig. 2 with that found in literature.[4] The results obtained were analyzed by means of the Fuoss-Onsager theory.[5] The parameters in the Fuoss-Onsager equation where C is the concentration in molarity scale, were determined by the method of least squares.[9]

$$\Lambda = \Lambda_0 - S(C\alpha)^{1/2} + EC\alpha \log_{10}(C\alpha) + JC\alpha - K_A f_\pm^2 C\alpha\Lambda, \quad (8)$$

$$\ln f_\pm^2 = -\frac{4.606A\sqrt{C\alpha}}{1+Ba_0\sqrt{C\alpha}}. \quad (9)$$

The values of conductivity parameters, K_A, a_0 (ion-size parameter), and Λ_0 at 25 °C obtained are given in Table 4, the values in literature[4,8] being given for comparison. The physical constants of acetone used in the present calculation are as follows.

t/°C	d_0/(g cm^{-3})	η/(g cm^{-1} s^{-1})	ε
25	0.7844	0.00303[4]	20.56[4]
40.3	0.7667[6]	0.00263_6[6]	19.24[6]

Analysis of the conductivity data at 40.3 °C was made by the same procedure. However, the values of a_0 used were those obtained at 25 °C (Table 4) for the sake of consistency. If the value of a_0 is determined independently by curve-fitting the best value contains some ambiguity and is not unique. The temperature change of a_0 seems to be negligible. The value of a_0 for Pr_4NI at 25 °C, 3.28 Å, was lower than the other values. Thus, the value 5.24 Å in literature was used in this case. The data of the concentrations up to 1×10^{-3} mol/dm^3 were analyzed by the Fuoss-Onsager equation. The results are shown in Table 5. The data of concentrations up to 20×10^{-3} mol/dm^3 were analyzed by the Fuoss-Hisa Equation.[7] The results are shown in Fig. 3. No tendency of the formation of poly-ions at high concentrations was observed.

Table 4. Conductivity parameters of tetraalkylammonium salts in acetone at 25 °C (Å=0.1 nm)

	This research			Literature[4,8]		
	K_A	a_0(Å)	Λ_0	K_A	a_0(Å)	Λ_0
Bu_4NCl	437.4	5.69	193.4	430.0	5.7	187.6[4]
Bu_4NBr	309.0	5.78	186.9	285.0	5.0	185.3[4]
Bu_4NI	164.4	5.61	184.7	155.0	5.1	184.4[4]
Pr_4NI	138.5	3.28	191.3	174.0	5.1	193.1[4]
				164.2	5.24	190.7[8]

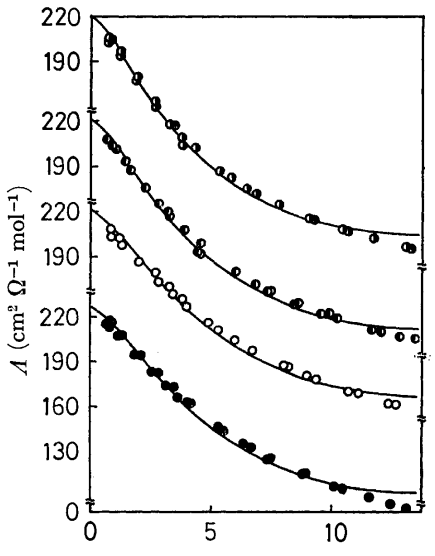

Fig. 3. Relationships between Λ and $\sqrt{C}$ to very high concentration for tetraalkylammonium salts at 40.3 °C. Lines show the values calculated from Fuoss-Hisa equation.
◑: Bu_4NCl, ◐: Bu_4NBr, ○: Bu_4NI, ●: Pr_4NI.

Comparison of VPO and Conductometry. In a previous work,[3] the dissociation constants of the tetraalkylammonium salts in acetone obtained by VPO were compared with those found in literature. The agreement between them was not satisfactory. The results of the present study are summarized in Table 5, where the dissociation constants were obtained (1) by VPO on the assumption II, and (2) by conductometry

Table 5. Comparison of dissociation constants by VPO and conductometry at 40.3 °C (in terms of molality)

	VPO	Conductometry	VPO[3]
	Assump. II	up to 1×10^{-3} mol/dm^3	Our previous work
Bu_4NCl	3.33×10^{-3}	2.50×10^{-3}	0.55×10^{-3}
Bu_4NBr	7.10×10^{-3}	3.56×10^{-3}	4.5×10^{-3}
Bu_4NI	10.00×10^{-3}	7.39×10^{-3}	4.0×10^{-3}
Pr_4NI	9.07×10^{-3}	5.97×10^{-3}	4.4×10^{-3}

using the Fuoss-Onsager equation from the data of concentrations less than 1×10^{-3} mol/dm^3 at 40.3 °C. The previous data are also given for the sake of comparison. Concentrations in terms of molality were used. The agreement is satisfactory.

The difference between the results obtained by assumptions I and II was not serious (Tables 3 and 5). However, introduction of parameter β_2 seems reasonable, since it compensates various errors due to the assumption of ideality.

References

1) G. S. Darbari and S. Petrucci, *J. Phys. Chem.*, **74**, 268 (1970).
2) H. Nomura, M. Ando, and Y. Miyahara, *Nippon Kagaku Zasshi*, **91**, 840 (1970).
3) M. Imura, H. Nomura, F. Kawaizumi, and Y. Miyahara, *Bull. Chem. Soc. Jpn.*, **47**, 2559 (1974).
4) D. F. Evans, J. Thomas, J. A. Nadas, and S. M. A. Matesich, *J. Phys. Chem.*, **75**, 1714 (1971).
5) R. M. Fuoss and F. Accasciana, "Electrolytic Conductaece," Interscience Publishers, Inc., New York, N. Y. (1959).
6) W. A. Adams and K. J. Laidler, *Can. J. Chem.*, **46**, 1977 (1968).
7) R. M. Fuoss and K. L. Hisa, *Proc. Natl. Acad. Sci. U.S.A.*, **57**, 1550 (1967).
8) M. J. McDowell and C. A. Kraus, *J. Am. Chem. Soc.*, **73**, 3293 (1951).
9) R. L. Kay, *J. Am. Chem. Soc.*, **82**, 2099 (1960).

Radiation Chemical Reactions in Carbon Dioxide–Propane System. III. Formation of Oxygen Containing Products

Yasumasa IKEZOE and Shoichi SATO

Japan Atomic Energy Research Institute, Tokai-mura, Ibaraki 319-11

(Received August 10, 1977)

The G value of water and 2-propanol as well as that of carbon monoxide decreased with decrease in propane concentration below 0.5%, the value of acetone remaining constant. Considering the effects of dose rate and irradiation temperature on the product yields, the results indicate that the formation of water and 2-propanol competes with the back reaction, or the reoxidation of carbon monoxide. A clustered negative ion, $O^-(CO_2)_n$ seems to be the oxidizing species responsible both for the back reaction and the formation of water and 2-propanol. The G value of $O^-(CO_2)_n$ was estimated to be 1.3. The formation of acetone is independent of the back reaction.

In the radiolysis of carbon dioxide, reoxidation of carbon monoxide, or the back reaction, is of great interest.[1] The back reaction in the carbon dioxide–propane system was studied at a low propane concentration,[2] and found to be accelerated by raising the total pressure or lowering the dose rate.

In order to clarify the relation between the two reactions and the properties of the oxidizing species present in the reaction system, we have examined the formation of oxygen containing products at the low propane concentration, where the back reaction competes with the formation of oxygen containing products.

Experimental

Carbon dioxide (Takachiho Chemical, pure gas, stated 99.99% up) and propane (Takachiho Chemical, research grade, stated 99.7% up) were used after uncondensable gas had been removed with a liquid nitrogen trap. Pyrex ampoules (160 and 64 ml) were washed with distilled water thoroughly. The reactant gas was introduced into the ampoules connected to a vacuum line, their pressure being measured with a stainless steel Bourdon gauge. Irradiation of the ampoules by ^{60}Co γ-rays and the dosimetry were carried out as described previously.[2] High temperature irradiation was carried out in an electric furnace, in which the temperature was controlled to an accuracy of ± 2 °C.

The irradiated gas was analyzed by means of mass spectrometry and gas chromatography. Three columns were used to separate eleven products; column I (molecular sieve 5A, 70 cm, 30 °C) was used to analyze carbon monoxide and methane, column II (Porapak R, 1.5 m, 120 °C) 2-propanol and hexanes,[3] column III (Porapak T; 2 m+Porapak T coated with 0.5% polyethylene glycol; 5 cm, 120 °C) water, acetone, propylene oxide, isobutane, butane, isopentane and pentane. The analysis of a small amount of water ($\approx 10^{-7}$ mol) required particular attention because of its adsorption on the wall surface of the analytical vacuum line. The effect of adsorption was minimized by conditioning the wall surface with the irradiated gas before its introduction. Details were described elsewhere.[4]

Results

Effect of Propane Concentration. The effects of propane concentration below 1.1% on the G values of various products are shown in Figs. 1 and 2. The G values were obtained at a constant dose 6.7 Mrad, total pressure 1.88×10^5 Pa, temperature 308 K and exposure rate 0.95 MR/h. The maximum G(CO) value

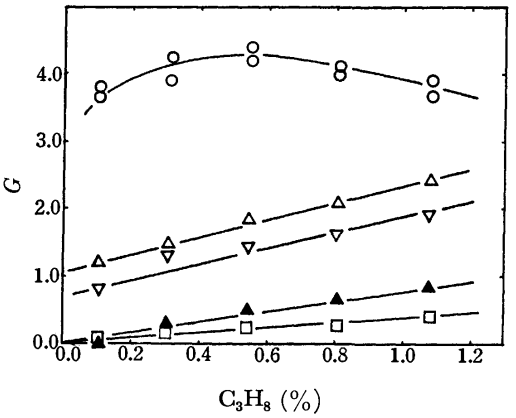

Fig. 1. Effect of propane concentration, I. 160 ml glass ampoule, $CO_2+C_3H_8$; 1.88×10^5 Pa, γ exposure rate; 0.95 MR/h, absorbed dose; 6.7 Mrad. ○; CO, △; $H_2\times3$, △; $CH_4\times3$, ▲; (hexanes) $\times5$, □; (isopentane) $\times5$.

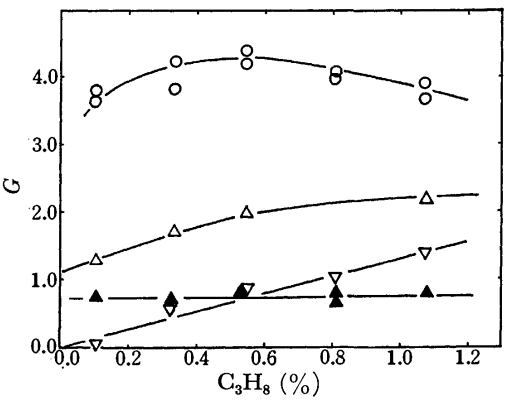

Fig. 2. Effect of propane concentration, II. ○; CO, △; H_2O, ▽; i-PrOH $\times10$, ▲; (acetone) $\times10$.

4.3 ± 0.1 and the concentration of propane 0.5% at which the maximum G(CO) value was obtained agree with our previous results within experimental error.[2] The decrease in G(CO) value with the reduction of propane concentration less than 0.5% is attributed to the back reaction.

The occurrence of the back reaction should necessarily lead to a variation in the G values of the products in this reaction system. The G values of hydrogen and methane (Fig. 1) decreased linearly with the reduction

in propane concentration, but their extrapolated values at the propane concentration of zero per cent did not reach zero. The values of isopentane and hexanes were small (<0.2), apparently converging to zero.

The effect of propane concentration on the formation of oxygen containing products is directly related to the reaction of the oxidizing species responsible for the back reaction. In the range of propane concentration investigated, formation of oxygen containing products competes with the back reaction.

Three oxygen containing products, water, 2-propanol and acetone, besides carbon monoxide were identified and measured. The G value of water (1—3) was the largest of the three. The G values of 2-propanol and acetone were of the same order of magnitude (0.1—0.2), those of other oxygen containing products, such as methanol, ethanol and propylene oxide, being smaller than 0.03. Neither propanal nor 1-propanol was detected. From the material balance of oxygen, it is obvious that unidentified oxygen containing products, not detected by the analytical procedures employed, still remain.

The G value of acetone did not decrease with decrease in propane concentration, remaining constant (0.08 ± 0.01) in the whole range of propane concentration investigated (Fig. 2). This indicates that acetone is formed by the reaction of an oxidizing species not responsible for the back reaction.

The G values of water and 2-propanol decreased with decrease in propane concentration. The G value of 2-propanol decreased linearly and converged to zero at zero per cent propane, while the G value of water did not converge to zero. This suggests that both water and 2-propanol are formed by the reaction of the oxidizing species responsible for the back reaction, but the mechanisms of their formations differ.

Effects of Dose Rate and Temperature. For the propane concentration 0.27%, the back reaction and its suppression are dynamically balanced. The back reaction has been found to be retarded by raising the dose rate, resulting in an apparent increase in G(CO) value.[2] The formation of the oxygen containing products seems to depend on the dose rate.

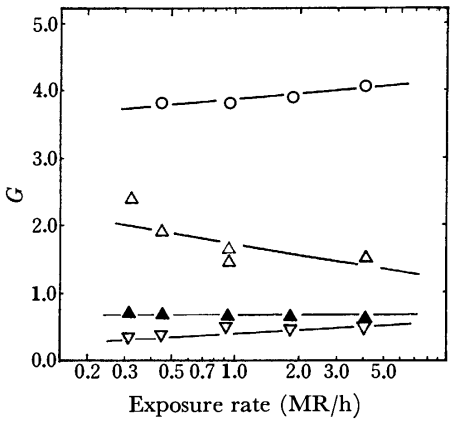

Fig. 3. Effect of dose rate. 160 ml glass ampoule, $CO_2+C_3H_8$; 1.12×10^5 Pa, C_3H_8; 0.27%, absorbed dose; 6.7 Mrad. ○; CO, △; H_2O, ▽; *i*-PrOH×10, ▲; (acetone)×10.

The effect of dose rate at 0.27% propane on the G value of carbon monoxide, water, 2-propanol, and acetone is shown in Fig. 3. The G values of other products such as hydrogen, methane, isopentane, and hexanes were also examined. They remained constant in the whole range of dose rate investigated.

The G(CO) value increased with the dose rate in agreement with the previous result.[2] The G value of water decreases with the rate, that of acetone remaining constant (0.07 ± 0.01). The G value of 2-propanol at 0.27% propane was very small (<0.05), increasing slightly with dose rate. The retardation of the back reaction by the rise in dose rate is accompanied by a decrease in the formation of water and a slight increase in the formation of 2-propanol.

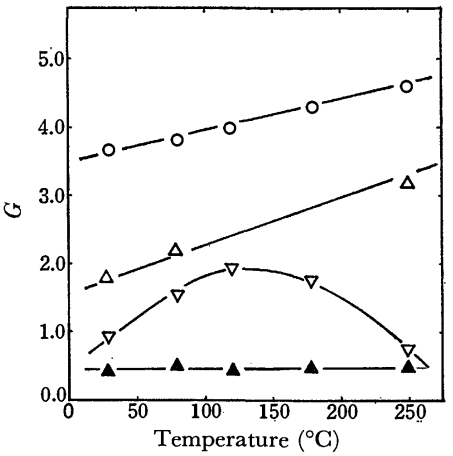

Fig. 4. Effect of irradiation temperature. 64 ml glass ampoule, $CO_2+C_3H_8$; 4.58 mg/ml, C_3H_8; 1.1%, γ exposure rate; 0.45 MR/h, absorbed dose; 6.7 Mrad. ○; CO, △; H_2O, ▽; *i*-PrOH×5, ▲; (acetone)×5.

The effect of irradiation temperature on the G values of carbon monoxide, water, 2-propanol and acetone is shown in Fig. 4. Conditions were as follows: irradiation temperature 30—250 °C, with the other conditions constant; gas density 4.58 mg/ml, propane concentration 1.1%, exposure rate 0.45 MR/h, and absorbed dose 6.7 Mrad. We see from Figs. 1 and 2 that at 1.1% propane the formation of oxygen containing products predominates over the back reaction. The mechanism of their formation seems to be the same as that at 0.27% propane.

The G value of 2-propanol shows an interesting behavior. At first, it increased from 0.2 to 0.4 with the rise in temperature from 30 to 120 °C, decreasing to 0.15 at 250 °C. That of acetone remained constant (0.1 ± 0.01).

The G values of carbon monoxide and water increased steadily with the irradiation temperature. This is in constrast to the effect of the dose rate on the G values (Fig. 3).

Discussion

Oxygen Containing Products and the Back Reaction. The formation of oxygen containing products results from the reactions of the same oxidizing species respon-

sible for the back reaction. The following reactions were proposed for the mechanism of such reactions.[2]

$$X^- + CO \longrightarrow CO_2 + Y^- + Z_1 \quad (1)$$

$$X^- + C_3H_8 \longrightarrow Y^- + Z_2 \quad (2)$$

$$X^- + R^+ \longrightarrow mCO_2 + Z_3 \quad (3)$$

$$Y^- + R^+ \longrightarrow nCO_2 + Z_4 \quad (4)$$

In these reactions, X^- denotes a clustered negative ion containing an oxygen atom or molecule, Y^- an electron or a negative ion other than X^-, R^+ any possible positive ion, and Z a neutral product.

Reactions 2 and 3 contribute to the formation of oxygen containing products. Reaction 3 contributes not only to the formation of oxygen containing products but also to the back reaction, depending on the identity of R^+.[5] Reaction 2, the scavenging of X^- by propane, leads to the formation of oxygen containing products other than carbon monoxide, competing with Reactions 1 and 3. The yield of the product in Reaction 2 becomes low with decrease in propane concentration.

Oxygen containing products are formed by reactions of the oxidizing species other than X^-. An oxygen atom (ground and excited) and the positive ion containing an oxygen atom or molecule[7] are conceivable. They are expected to react preferentially with propane even at the reduced concentration of propane, because of their high reactivity with propane. In this case propane concentration has little effect on the yield of the oxygen containing products.

Water and 2-Propanol. The results show that the G values of water and 2-propanol, as well as of carbon monoxide depend in a complicated way on propane concentration, dose rate, and irradiation temperature, indicating that there is a certain relation between the back reaction and the formation of water and 2-propanol.

It is impossible to determine the exact mechanism of the formation of water and 2-propanol which explains all the experimental results. However, the following reactions seem plausible for qualitative explanation.

ionic mechanism of water formation

$$O^-(CO_2)_n + C_3H_8 \longrightarrow (OH)^-(CO_2)_n + C_3H_7 \quad (2')$$

$$(OH)^-(CO_2)_n + C_3H_8 \longrightarrow H_2O + nCO_2 + C_3H_7 + e^- \quad (5)$$

radical mechanism of water formation

$$O + C_3H_8 \longrightarrow OH + C_3H_7 \quad (6)$$

$$OH + C_3H_8 \longrightarrow H_2O + C_3H_7 \quad (7)$$

mechanism of 2-propanol formation

$$(OH)^-(CO_2)_n + C_3H_7 \longrightarrow i\text{-PrOH} + nCO_2 + e^- \quad (8)$$

Water should be formed by at least two processes, ionic and radical. In the former, other ionic species such as $O_2^-(CO_2)_n$, $O^+(CO_2)_n$ and $O_2^+(CO_2)_n$, have been considered, in addition to $O^-(CO_2)_n$, to be the probable oxidizing species in pure carbon dioxide.[8] However, in the present reaction system, $O_2^-(CO_2)_n$ seems to be negligible since the formation of oxygen is inhibited by propane. The contribution of $O^+(CO_2)_n$ and $O_2^+(CO_2)_n$ was neglected because of their low yields.[5,7] On the other hand, O^- (and $O^-(CO_2)_n$) can be formed by the dissociative attachment of an electron to carbon dioxide.[9]

By the above mechanism, the yield of water by the ionic process will depend on the concentration of propane because of the competing back reaction 1. On the other hand, the yield by the radical process will not depend on it, since O atom preferentially reacts with propane. The G value of water which is due to the radical process, $G(H_2O)_r$, can be approximated by the extrapolated G value 1.1 of water to zero per cent propane (Fig. 1). The G value of water due to the ionic process, $G(H_2O)_i$, could be estimated by subtracting $G(H_2O)_r$ from the experimental G value of water. The maximum $G(H_2O)_i$ thus obtained is 1.1.

Formation of 2-propanol seems to be due to the ionic process (Reactions 2′ and 8). The rate of Reaction 8 should depend on the dose rate more strongly than that of Reaction 5, since the concentration of C_3H_7 is a function of dose rate, but not that of propane. Thus, the above mechanism satisfies qualitatively the experimental effect of dose rate on the formation of water and 2-propanol (Fig. 3). Reaction 8 is expected to depend on the irradiation temperature.[10]

If the above mechanism holds for the formation of water and 2-propanol, the G value of $O^-(CO_2)_n$ can be estimated by

$$G(O^-(CO_2)_n) \approx G(H_2O)_i + G(i\text{-PrOH}) = 1.3. \quad (9)$$

Acetone. The G value of acetone is costant irrespective of the reduction in propane concentration (Fig. 2). Consequently, the oxidizing species, $O^-(CO_2)_n$, responsible for the back reaction in the present reaction system, is excluded from the precursor of acetone. Moreover it kept a constant value irrespective of the variation in dose rate and irradiation temperature (Figs. 3 and 4). The results suggest that acetone is a product of a reaction of highly excited species formed by the direct action of the ionizing radiations on carbon dioxide, having a high reactivity with propane.

Excited oxygen atoms and atom ions are known to be formed in quantity in the primary process in the radiolysis of carbon dioxide.[12] Among them, $O(^1D)$ reacts with paraffins to form ketone.[13,14]

$$O(^1D) + RH \longrightarrow H_2 + \text{ketone} \quad (10)$$

The formation of acetone could be explained by an analogous reaction of $O(^1D)$ with propane, if Reaction 10′ were independent of the propane concentration and irradiation temperature.

$$O(^1D) + C_3H_8 \longrightarrow CH_3COCH_3 + H_2 \quad (10')$$

However, in the reaction system investigated, $O(^1D)$ would preferentially react with carbon dioxide and be deactivated to the ground state, $O(^3P)$.[15] The rate of Reaction 10′ should depend on the concentration of propane. Reaction 10′ for the formation of acetone is thus not compatible with the experimental result (Fig. 2). This is confirmed by the lack of 1-propanol formation, since 1-propanol is formed in a greater amount than 2-propanol[16] and probably acetone,[14] when $O(^1D)$ reacts with propane. The formation of acetone should be ascribed to the excited species other

than O(^{1}D). So far the precursor of acetone can not be identified further.

The precursor of acetone differs from the oxidizing species which is responsible for the back reaction in the present reaction system. However, the possibility that the highly excited species responsible for the formation of acetone plays a role in the back reaction in pure carbon dioxide cannot be excluded. The back reaction in pure carbon dioxide is probably not identical to that in the carbon dioxide–propane system even at very low propane concentration.

References

1) A. R. Anderson and D. A. Dominey, *Radiat. Res. Rev.*, **1**, 269 (1968).

2) Y. Ikezoe and S. Sato, *Bull. Chem. Soc. Jpn.*, **51**, 33 (1978).

3) A mixture of 2-methylpentane and 2,3-dimethylbutane.

4) S. Sato, Y. Ikezoe, S. Shimizu, H. Nakajima, and T. Kobayashi, JAERI-M 7316 (1977).

5) The most abundant positive ions in the reaction system seem to be $(C_3H_8)^+(CO_2)_n$ and $(C_3H_7)^+(CO_2)_n$, the reaction of which with X^- probably contributes to the formation of oxygen containing products. $(CO_2)^+(CO)(CO_2)_n$ and $(CO_2)^+(CO_2)_n$ are also conceivable positive ions. The reaction of $(CO_2)^+(CO)(CO_2)_n$ with X^- contributes to the back reaction, and that of $(CO_2)^+(CO_2)_n$ with X^- only to neutralization.

6) Y. Ikezoe and S. Sato, *J. Nucl. Sci. Technol.*, **13**, 503 (1976).

7) In pure carbon dioxide, $(CO_2)^+(CO_2)_n$, $O^+(CO_2)_n$, and $O_2^+(CO_2)_n$ are major positive ions.[8] But in the present reaction system, the positive charge is expected to be concentrated on propane and its fragments, because of the low ionization potential of propane (11.1 eV) as compared with those of carbon dioxide (13.9 eV), an oxygen atom (13.6 eV), and oxygen (12.1 eV).

8) D. A. Parkes, *J. Chem. Soc., Faraday Trans. 1*, **69**, 198 (1973).

9) D. A. Parkes, *J. Chem. Soc., Faraday Trans. 1*, **68**, 627 (1972).

10) When the temperature is raised, clustered ions become less clustered.[11] Under such conditions, 2-propanol, even if formed by Reaction 8, would at once be decomposed by the excess heat of reaction.

11) H. W. Ellis, R. Y. Pai, I. R. Gatland, and E. W. McDaniel, *J. Chem. Phys.*, **64**, 3935 (1976).

12) C. Willis and A. W. Boyd, *Int. J. Radiat. Phys. Chem.*, **8**, 71 (1976).

13) R. K. M. Jayantry, R. Simonaitis, and J. Heicklen, *Int. J. Chem. Kinet.*, **8**, 107 (1976).

14) A. J. Colussi and R. J. Cvetanovic, *J. Phys. Chem.*, **79**, 1891 (1975).

15) G. Paraskevopoulos and R. J. Cvetanovic, *J. Am. Chem. Soc.*, **91**, 7572 (1969).

16) H. Yamazaki and R. J. Cvetanovic, *J. Chem. Phys.*, **41**, 3703 (1964).

A New Expression for Excess Volumes of Binary Mixtures

Masanao KATO and Nobuo SUZUKI

Department of Chemistry, Faculty of Science, Tohoku University, Sendai 980

(Received September 26, 1977)

A new expression for excess volumes of binary mixtures is derived. This equation contains four adjustable but physically-meaningful parameters: two non-randomness factors and two partial molar volumes at infinite dilution. The applicability of this equation is tested against data in the literature for several non-ideal mixtures, and it is found that this equation successfully expresses the experimental curves of excess volume, V^E, over the entire concentration range. Furthermore, it is demonstrated that the non-randomness factors used in the excess volume expression can be used to estimate the excess Gibbs energy, G^E, of binary mixtures based on the Wilson equation.

The excess volume is one of the fundamental thermodynamic quantities of liquid mixtures and an enormous amount of data has been obtained for this quantity.[1,2] Systematic attempts to describe quantitatively the properties of liquid mixtures have been based on current solution theories, *i.e.*, the Flory theory,[3] the cell model of Prigogine and co-workers,[4] regular solution theory,[5] the corresponding state theory,[6] *etc.*[7,8] These theories are almost successful in expressing the excess thermodynamic functions of non-polar binary mixtures, but only quantitative agreement has been obtained for polar binary mixtures.

Recently, Wilson and Scatchard[9] proposed an expression for G^E, H^E, and S^E, which is in excellent agreement with experimental results. Following Wilson, Prausnitz and his collaborators[10-12] introduced some equations for G^E based on the idea of a local mole or segment fraction. Unfortunately, these equations do not include terms involving pressure as a variable, so that they cannot be used to express V^E.

In this study, a new equation for V^E is derived by introducing the idea of non-random mixing. This new expression contains two measurable and two adjustable, but physically-meaningful, parameters, *i.e.*, two partial molar volumes at infinite dilution and two non-randomness factors. The applicability of the equation will be examined for several binary mixtures in the literature.

Derivation of the New Equation

As the general model of a binary mixture, we take into account non-random mixing of two components as introduced into two liquid models proposed by Scott[6] and extended by Renon and Prausnitz.[10] We assume that the probability of finding molecules of one type (i molecules) in the vicinity of a central molecule (j molecule) can be represented by the local mole fraction in a solvation sphere. Furthermore, we assume that the excess functions are determined by the local mole fraction of the first solvation sphere. We denote the local mole fraction of the component i adjacent to the central molecule j by x_{ij}, which is equal to $1-x_{jj}$.

When $x_{11}=1$, the volume occupied by one mole of the first component is equal to its molar volume in the pure state, V_1^*. For the state for which $x_{21}=1$, the volume occupied by one mole of the first component is denoted by V_{21}. Accordingly, the volume occupied by one mole of the first component in a mixture is $(V_1^*x_{11}+V_{21}x_{21})$. Similarly, the volume occupied by the second component can be represented by $(V_2^*x_{22}+V_{12}x_{12})$ in a mixture. Consequently, the molar volume of the liquid mixture can be represented by

$$V_{mix} = x_1(V_1^*x_{11}+V_{21}x_{21}) + x_2(V_2^*x_{22}+V_{12}x_{12}), \quad (1)$$

where x_1 and x_2 are the mole fractions of the first and second components, respectively. Therefore, the excess volume of the binary mixture is

$$\begin{aligned} V^E &= V_{mix} - V_{ideal} \\ &= x_1x_{21}(V_{21}-V_1^*) + x_2x_{12}(V_{12}-V_2^*). \end{aligned} \quad (2)$$

Now, we introduce the non-randomness factor, Λ_{ij}, which relates the local mole fraction to the overall mole fraction by

$$\frac{x_{ij}}{x_{jj}} = \Lambda_{ij}\frac{x_i}{x_j} \quad (x_{ij}+x_{jj}=1). \quad (3)$$

The non-randomness factor has been independently defined by different authors as follows:

$$\Lambda_{ij} = \exp\frac{-\alpha_{ij}(g_{ij}-g_{jj})}{RT} \quad \text{(by Renon and Prausnitz)} \quad (4)$$

and

$$\Lambda_{ij} = \frac{V_i^*}{V_j^*}\exp\frac{-(\lambda_{ij}-\lambda_{jj})}{RT} \quad \text{(by Wilson)}, \quad (5)$$

where g_{ij} and λ_{ij} are the parameters corresponding to the interaction energy between the i and j molecules and α_{ij} is the parameter characteristic of the reciprocal of the coordination number of lattice. These two definitions for Λ have similar physical meanings. Wilson's definition includes the fixed volume term V_i^*/V_j^*, so that it cannot be applied to the calculation of V^E. The definition of the non-randomness factor used here is

$$\Lambda_{ij} = \exp\frac{-(\lambda_{ij}-\lambda_{jj})}{RT}, \quad (6)$$

since the local mole fraction is used. Recently, Huggins[13] pointed out that the parameters, g_{ij} and λ_{ij}, are of ambiguous units. So, the value of the non-randomness factors themselves were estimated, as Wilson did, although it is possible to express the non-randomness factors as a function of $(\lambda_{ij}-\lambda_{jj})/R$.

From Eq. 3, x_{ij} can be represented as

$$x_{ij} = \frac{x_i\Lambda_{ij}}{x_j+x_i\Lambda_{ij}}, \quad (7)$$

where $\Lambda_{jj}=\Lambda_{ii}=1$. By substitution of Eq. 7 into Eq. 2, the equation for a binary mixture is obtained, thus,

$$V^E = x_1x_2\left\{\frac{\Lambda_{21}}{x_1+x_2\Lambda_{21}}(V_{21}-V_1^*)+\frac{\Lambda_{12}}{x_1\Lambda_{12}+x_2}(V_{12}-V_2^*)\right\}. \quad (8)$$

This equation can be partially differentiated with respect to x_1, according to the relations, $(\partial V^E/\partial x_1)_{x_1=0}=(V_1^\infty-V_1^*)$ and $-(\partial V^E/\partial x_1)_{x_1=1}=(V_2^\infty-V_2^*)$, where V^∞ is the partial molar volume at infinite dilution. From this procedure, we obtain

$$V^E = x_1x_2\left\{\frac{x_2\Lambda_{21}(V_1^\infty-V_1^*)+x_1\Lambda_{12}(V_2^\infty-V_2^*)}{(x_1+x_2\Lambda_{21})(x_2+x_1\Lambda_{12})}\right\}. \quad (9)$$

Equation 9 shows that if the partial molar volumes at infinite dilution and, at least, two measured values of V^E are accurately obtained, the two non-randomness factors, Λ_{21} and Λ_{12}, can be calculated.

The advantage of this analysis is that the parameters in this expression are physically meaningful and the non-randomness factors thus obtained can be used to estimate the excess Gibbs energy by combination with the Wilson equation.[9] In this case, the Wilson equation must be transformed to

$$\frac{G^E}{RT} = -x_1\ln\left(x_1+\frac{V_2^*}{V_1^*}\Lambda_{21}x_2\right)-x_2\ln\left(\frac{V_1^*}{V_2^*}\Lambda_{12}x_1+x_2\right). \quad (10)$$

Applicability of the New Equation

Figure 1 shows some typical examples of theoretical curves of V^E. For curves 1, 3, and 5, the non-randomness factors are assumed to be constant and equal to 1. When $V_1^\infty-V_1^*=V_2^\infty-V_2^*$, the curve is symmetrical, but when $V_1^\infty-V_1^*\neq V_2^\infty-V_2^*$, a skewed curve is obtained. Especially, when $V_1^\infty-V_1^*>0>V_2^\infty-V_2^*$, the curve has an S-shape. Curves 2, 4, 6, and 7 show cases of non-randomness factors of different magnitudes. Curve 2 differs in flatness from curve 1. For curve 4, the mole fraction corresponding to $V^E=0$ is shifted to the left in comparison with curve 3. For curves 5, 6, and 7, the mole fractions giving maximum V^E values differ from

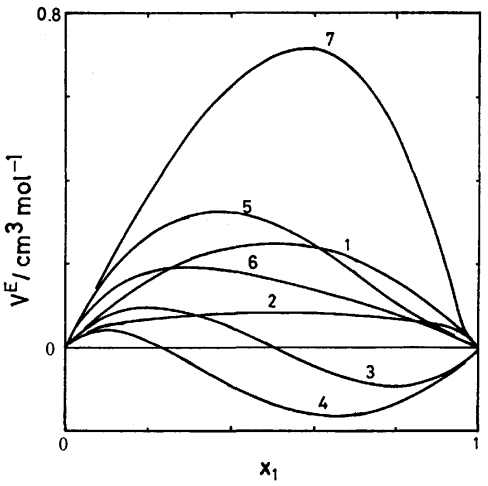

Fig. 1. Dependence of V^E curves on the value of parameters.

Curve	Λ_{21}	Λ_{12}	$V_1^\infty-V_1^*$ / cm^3 mol^{-1}	$V_2^\infty-V_2^*$ / cm^3 mol^{-1}
1	1.0	1.0	1.0	1.0
2	0.1	0.1	1.0	1.0
3	1.0	1.0	1.0	−1.0
4	0.3	1.0	1.0	−1.0
5	1.0	1.0	2.0	0.4
6	0.2	0.2	2.0	0.4
7	5.0	0.2	2.0	0.4

Table 1. Volume parameters and standard deviation at 298.15 K

Components		Parameters				$\sigma/10^{-4}$ cm^3 mol^{-1} [a]		
First	Second	$V_1^\infty-V_1^*$ / cm^3 mol^{-1}	$V_2^\infty-V_2^*$ / cm^3 mol^{-1}	Λ_{21}	Λ_{12}	Eq. 9	Polyn.	Literature
Methanol	1-Butanol	0.1671	0.5788	0.628	0.408	2	3	14
1-Butanol	1-Octanol	0.1552	0.2144	1.088	0.136	5	5	14
1-Butanol	1-Hexanol	0.0502	0.0692	0.255	0.408	4	4	14
1-Butanol	1-Decanol	0.3020	0.4356	0.574	0.366	4	4	14
Methanol	1-Octanol	0.1901	2.3321	0.283	0.183	20	11	14
Ethanol	1-Octanol	0.1110	0.7798	0.211	0.192	4	3	14
1-Propanol	1-Octanol	0.1846	0.3532	0.449	0.304	4	3	14
1-Hexanol	1-Octanol	0.0343	0.0499	0.290	0.630	3	3	14
Benzene	*o*-Xylene	0.8848	1.1398	1.292	0.926	8	8	15
Benzene	*m*-Xylene	0.9627	1.4015	1.060	0.945	21	22	15
Benzene	*p*-Xylene	0.7256	0.9934	0.249	0.705	9	9	15
Methanol	Benzene	0.356	−0.468	0.225	0.161	30	16	16
Water[b]	2-Butoxyethanol	−1.9074	−4.8736	0.276	0.421	280	289	17
Ethanol	Toluene	1.045	−1.164	0.164	0.352	45	30	18
Ethanol	*o*-Xylene	1.527	−0.818	0.157	0.479	63	40	18
Ethanol	*m*-Xylene	1.664	−0.359	0.199	0.799	77	37	18
Ethanol	*p*-Xylene	1.153	−0.930	0.198	0.359	35	17	18

a) $\sigma=\sqrt{\frac{\Sigma(V^E_{calcd}-V^E_{obsd})^2}{N-2,}}$, the standard deviation, where N is the number of data points. V^E_{calcd} and V^E_{obsd} denote the calculated and observed values of V^E, respectively. b) At 300.15 K.

each other. It is found that the shape of the V^E curve is primarily determined by the signs and magnitudes of $V_1^\infty - V_1^*$ and $V_2^\infty - V_2^*$.

These theoretical results were tested against data from the literature for 20 binary mixtures. As stated previously, two non-randomness factors can be readily calculated from accurately measured values of V^E. For this purpose, the V^E data at $x_1=0.3$ and $x_1=0.7$ obtained using a reported smoothing equation were used. The calculated non-randomness factors are listed in Table 1 with the standard deviations of the smoothing and the theoretical curves.

The agreement between the present equation and experiment is quite satisfactory. Typical examples are shown in Fig. 2. As is shown in Table 1, the standard deviations of V^E calculated from the smoothing equation and the new equation are of the same order for systems have V^E curves of simple shape. For systems having S-shaped V^E curves, such as the benzene+methanol system, however, the standard deviation calculated from the new equation is larger than that for the smoothing equation. This is probably due to the uncertainty in the $V_i^\infty - V_i^*$ value. Generally, for systems having S-shaped V^E curves, the $V_i^\infty - V_i^*$ calculated using the new equation appear to be larger than those using the smoothing equation. Small $|V_i^\infty - V_i^*|$ values produce small maximum or minimum values of the V^E curves. For systems having S-shaped V^E curves, very good estimates of V^E can be made utilizing the alternative equation with four adjustable parameters: two non-randomness factors and two partial molar volumes.

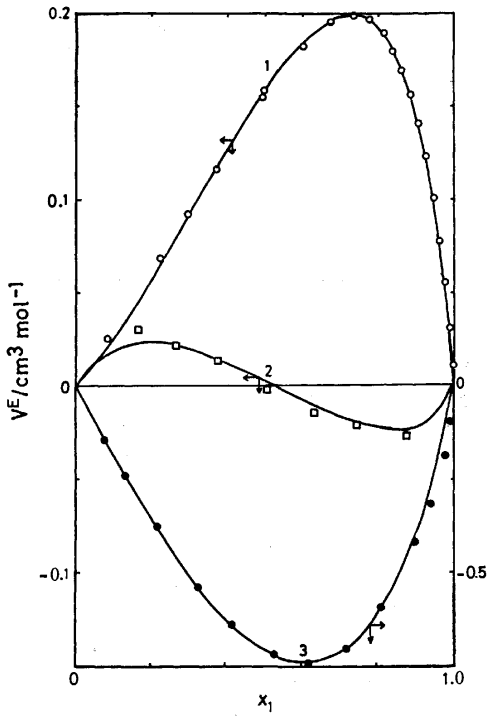

Fig. 2. The examples of the test of new equation for binary systems. Curve 1 corresponds to methanol+1-octanol system; curve 2, methanol+benzene; curve 3, water+2-butoxyethanol.

For systems containing nitroethane, the temperature dependence of V^E has been investigated by Handa *et al.*[19] It is of interest to apply the new equation to those systems. The estimated non-randomness factors are listed in Table 2. In Table 2, the system containing 2-methylpentane at 298.15 K is qualitatively fitted by Eq. 9, because of the S-shaped V^E curve. As is shown, the non-randomness factors tend to increase with temperature, which means that the mixture becomes ideal. This tendency is consistent with the expected behavior for normal mixtures. However, the temperature dependence of the non-randomness factors is larger than that predicted from either definition by Wilson and Scatchard[9] or by Renon and Prausnitz.[10] It is assumed that the molecular distribution adjacent to the central molecule is determined by two factors, *i.e.*, a combinatorial factor depending on the molecular size and shape, and a residual factor depending on the molecular interaction energy, and that the non-randomness factors account for these two factors. Furthermore, we have no method to separate the excess volume into two factors. Thus, it appears difficult to exactly express the temperature dependence.

The non-randomness factors calculated from the V^E data are not necessarily consistent with those defined in the Wilson equation, which are calculated from G^E data. Nevertheless, the G^E values for several binary mixtures calculated by applying the present non-randomness factors to the Wilson equation are in qualitative agreement with the observed value. As is shown in Fig. 3, the calculated G^E values for the benzene+*m*-xylene[20] and for the methanol+benzene[16] systems are in relatively good agreement with the observed values, while the calculated G^E values for the water+2-

Table 2. The dependence of volume parameters on the temperature for systems containing nitroethane as the first component

Second component	Temperature / K	$V_1^\infty - V_1^*$ / cm^3 mol^{-1}	$V_3^\infty - V_2^*$ / cm^3 mol^{-1}	Λ_{21}	Λ_{12}	σ[a] / cm^3 mol^{-1}
2-Methylpentane	298.15	2.285	−0.503	0.214	0.193	0.011_2
	303.15	3.065	−0.403	0.159	0.244	0.005_9
	313.15	2.861	−0.497	0.193	0.394	0.004_5
2,3-Dimethylbutane	298.15	2.341	−0.671	0.156	0.254	0.004_7
	313.15	2.644	−0.768	0.179	0.348	0.006_4
2,2-Dimethylbutane	298.15	1.739	−1.735	0.147	0.426	0.009_9
	313.15	1.722	−1.968	0.224	0.607	0.004_3

a) The standard deviation is $\sigma=\sqrt{\frac{\Sigma(V^E_{calcd}-V^E_{obsd})^2}{N-2}}$, where N is the number of data points.

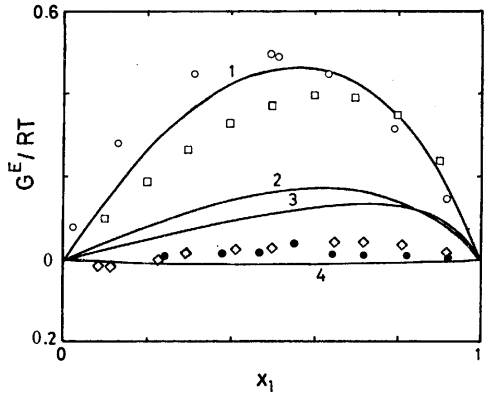

Fig. 3. Application of nonrandomness factor to Wilson equation. Curve 1 and ○ correspond to methanol+benzene system; curve 2 and □, water+2-butoxyethanol; curve 3 and ◇, methanol+1-butanol; curve 4 and ●, benzene+*m*-xylene.

butoxyethanol[17] and for the methanol+1-butanol[21] systems are in only qualitative agreement with the observed values. Recalling that the accuracy of the V^E data sensitively affect the reliability of the non-randomness factors, the poor agreement between the latter two systems is partly due to the uncertainty in the non-randomness factors.

Conclusion

The new equation with only two parameters successfully fits the excess volumes of binary mixtures to the same order as the smoothing equation. These two parameters have exact physical meanings, contrary to the traditional smoothing equation parameters. At the present stage, the G^E calculated from V^E data are in qualitative agreement with observed values.

The authors wish to thank Mr. H. Watarai for helpful discussions throughout this study.

References

1) J. Timmermans, "The Physico-Chemical Constants of Binary Systems in Concentrated Solution," Interscience, Vols. 1 and 2, New York, N. Y. (1959); Vols. 3 and 4 (1960).
2) R. Battino, *Chem. Rev.*, **71**, 5 (1971).
3) P. J. Flory, R. A. Orwoll, and A. Vrij, *J. Am. Chem. Soc.*, **86**, 3507 (1964).
4) I. Prigogine, "The Molecular Theory of Solutions," North-Holland Pub. Co. (1957).
5) J. H. Hildebrand, J. M. Prausnitz, and R. L. Scott, "Regular and Related Solutions," van Nostrand-Reinhold Co. (1970).
6) R. L. Scott, *J. Chem. Phys.*, **25**, 193 (1956).
7) J. Winnick and J. M. Prausnitz, *Chem. Eng. J.*, **2**, 241 (1971).
8) M. L. Huggins, *J. Phys. Chem.*, **80**, 1317 (1976).
9) G. M. Wilson and G. Scatchard, *J. Chem. Soc.*, **86**, 127 (1964).
10) H. Renon and J. M. Prausnitz, *AIChE J.*, **14**, 135 (1968).
11) D. S. Abrams and J. M. Prausnitz, *AIChE J.*, **21**, 1 (1975).
12) A. Fredenslund, R. L. Jones, and J. M. Prausnitz, *AIChE J.*, **21**, 1086 (1975).
13) M. L. Huggins, *J. Phys. Chem.*, **74**, 371 (1970).
14) H. D. Pflug and G. C. Benson, *Can. J. Chem.*, **46** 287 (1968).
15) J. Singh, H. D. Pflug, and G. C. Benson, *Can. J. Chem.*, **46**, 1939 (1968).
16) G. Scatchard, S. E. Wood, and J. M. Mochel, *J. Am. Chem. Soc.*, **68**, 1960 (1946).
17) G. Scatchard and G. M. Wilson, *J. Am. Chem. Soc.*, **86**, 133 (1964).
18) F. Pardo and H. C. van Ness, *J. Chem. Eng. Data*, **10**, 163 (1965).
19) Y. P. Handa, C. M. Knobler, and R. L. Scott, *J. Chem. Thermodyn.*, **9**, 451 (1977).
20) T. Boublík and G. C. Benson, *Can. J. Chem.*, **47**, 539 (1969).
21) J. Polák, S. Murakami, V. T. Lam, H. D. Pflug, and G. C. Benson, *Can. J. Chem.*, **48**, 2457 (1970).

Viscoelastic Behavior of Some Di(normal alkyl) Phthalates

Noriyuki KINJO* and Tsurutaro NAKAGAWA

Department of Polymer Science, Faculty of Science, Hokkaido University, Sapporo 060

(Received September 28, 1977)

The viscoelastic behavior of a homologous series of di-*n*-alkyl phthalates varying in alkyl chain length from methyl- to nonyl- was studied by means of torsional braid analysis (TBA). The glass transition temperatures, T_g, were determined as the temperature at loss maximum. The T_g decreases with increasing alkyl chain length in the di-*n*-alkyl phthalates, up to dibutyl. Thereafter, the T_g increases gradually with further increase in the alkyl chain length. This behavior can be explained by taking into account two factors which determine the T_g, the molecular weight and the intermolecular interaction. The increase in the number of methylene groups in the phthalates brings about two effects: first, the T_g is increased with increasing molecular weight and, second, the T_g is decreased owing to shielding of the interaction between polar carbonyl groups due to the presence of non-polar methylene groups. When the number of methylene groups is four, the two effects counterbalance each other and the T_g of dibutyl phthalate is the lowest of the di-*n*-alkyl phthalate series.

It is generally recognized that the glass transition temperatures (T_g) of polymers or oligomers can vary with the chain length, and a number of studies have been reported which are concerned with the relationship between the T_g and the molecular weight of polymers and, moreover, the factors affecting the dependence of the T_g on the molecular weight.[1-6] It may be pointed out that several factors affect the T_g-molecular weight relation: these include the crystallinity, the molecular weight distribution, the complexity of the backbone chain, such as the stiffness or flexibility, the polarity, and the end-group or chain association effect.[5,6,11] In spite of its importance, the mutual relation of these factors is not clear at present. In particular, it is likely that no attention was paid to the association effect caused by end-groups, since the effect is very slight compared with that of the molecular weight.[4] It is guessed that this end-group effect is appreciable only when the chain length is very short, that is, when the molecular weight is low. It is the purpose of the present work to clarify the effectiveness of the end-groups on the T_g-molecular weight relation.

However, the relaxation behavior of low molecular-weight glassy substances was more recently noted in analogy to that of polymers.[7-10] Secondary dispersions have already been observed for 1-alkanols and lactones, and were discussed in relation to the molecular motions of methylene sequences.[7-9] It is the aim of the present paper to report whether similar behavior due to methylene sequences appears in di-*n*-alkyl phthalates.

Experimental

Samples. The samples used in this study were various di-*n*-alkyl phthalates: dimethyl phthalate (DMP), diethyl phthalate (DEP), dipropyl phthalate (DPrP), dibutyl phthalate (DBP), dipentyl phthalate (DPeP), dioctyl phthalate (DOP), and dinonyl phthalate (DNP). These phthalates received from commercial souces were washed in water, dried on molecular sieves, and then distilled *in vacuo*. The conditions were as follows: DMP −132 °C/666 Pa, DEP −141 °C/666 Pa, DPrP −158 °C/666 Pa, DBP −182 °C/666 Pa, DPeP −170 °C/66.6 Pa, DOP −165 °C/13.3 Pa, DNP −184 °C/13.3 Pa.

Measurements. The viscoelastic behavior of di-*n*-alkyl phthalates was studied using the torsional braid analysis (TBA) method at a frequency of 0.5 Hz. After dipping a glass braid used as the supporting substrate into liquid samples, these sample-braid composite systems were mounted on the torsional pendulum apparatus, quickly immersed in liquid nitrogen, and then damping measurements were made for an increasing temperature rate of 0.5 °C/min.

Using the TBA method, the elastance of sample-glass braid composite system is obtained, and not the elasticity of the samples themselves. Since it was previously confirmed that the glass braid shows no dispersion in this temperature region, the observed dispersion behavior is considered to be due to the impregnating sample itself.[12,13]

Results and Discussion

The viscoelastic behavior of di-*n*-alkyl phthalates is shown in Figs. 1 and 2. The storage elastance rapidly decreases in the temperature region in which the maximum of the loss elastance occurs. For damping measurements, the glass transition temperature (T_g) is customarily taken as the temperature of maximum loss elastance. The T_g values, which lower than the melting points by 30—60 °C, are summarized in Table 1 together with the melting points of the phthalates. T_g determined using the DTA have been reported by Garfield and Petrie[14] to be −85 °C for diethyl phthalate and −87 °C for dioctyl phthalate. This is in good agreement with the present data, taking into account the frequency of 0.5 Hz of the present TBA method.[16]

In the case of dimethyl and dioctyl phthalates, the viscoelastic behavior differs somewhat from that of the other phthalates. In the present experiments, the samples were quickly cooled down to glass form and then the temperature was gradually raised. The storage elastance first decreases near the T_g value. A subsequent increase in storage elastance is observed and may be attributed to crystallization, because, generally speaking, substances can be crystallized only in the supercooled liquid state at temperatures between the T_g and the melting point. With further increase in the temperature the storage elastance finally decreases again due to fusion. The temperature of the final decrease in storage elastance approximately coincides with the melting

* Present address: Hitachi Research Laboratory, Hitachi Ltd., 4026 Kuji-cho, Hitachi, Ibaraki, 319-12.

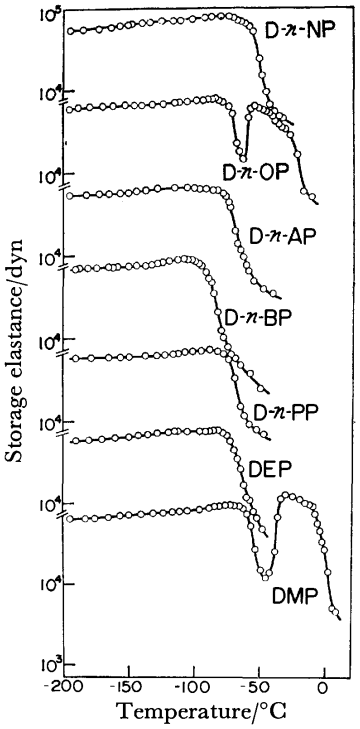

Fig. 1. Temperature dependence of storage elastance for di-*n*-alkyl phthalate-braid composite systems.
D-*n*-NP: di-*n*-nonyl phthalate, D-*n*-OP: di-*n*-octyl phthalate, D-*n*-AP: di-*n*-amyl phthalate, D-*n*-BP: di-*n*-butyl phthalate, D-*n*-PP: di-*n*-propyl phthalate, DEP: diethyl phthalate, DMP: dimethyl phthalate.

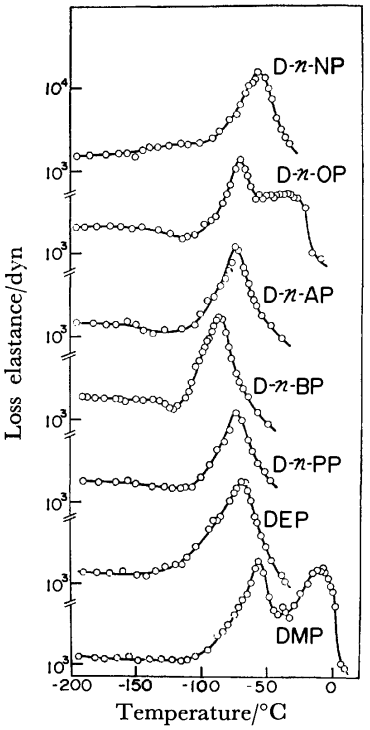

Fig. 2. Temperature dependence of loss elastance for di-*n*-alkyl phthalate-braid composite systems.
D-*n*-NP: di-*n*-nonyl phthalate, D-*n*-OP: di-*n*-octyl phthalate, D-*n*-AP: di-*n*-amyl phthalate, D-*n*-BP: di-*n*-butyl phthalate, D-*n*-PP: di-*n*-propyl phthalate, DEP: diethyl phthalate, DMP: dimethyl phthalate.

Table 1. Glass transition temperatures and melting points of the di-*n*-alkyl phthalates studied

Substance	T_g / °C		T_m [b] / °C
	TBA method	DTA method[a]	
Dimethyl phthalate	−57	—	0 or 5.5[c]
Diethyl phthalate	−69	−85	−40.5 or 40[c]
Dipropyl phthalate	−75	—	−31
Dibutyl phthalate	−84	—	−35 or −40[c]
Dipentyl phthalate	−75	—	—
Dioctyl phthalate	−70	−87	−25
Dinonyl phthalate	−60	—	—

a) Quoted from Ref. 14. b) Melting points quoted from Ref. 15. c) Two data are reported.

point of −25 °C for dioctyl phthalate and of 0 °C for dimethyl phthalate. Corresponding to the above-mentioned behavior, the loss elastance *vs.* temperature curves show two maxima. The other phthalates may not crystallize as do the dioctyl and dimethyl phthalates, and each shows a single dispersion due to the glass transition.

It is well established that the T_g of polymers becomes higher with increasing molecular weight.[1-3] Recently, Cowie has studied the dependence of the T_g on the molecular weight for a number of oligomers and polymers.[6] The change in T_g with increasing molecular weight is more marked in the oligomeric region than in the polymeric region.

Figure 3 shows the T_g values of di-*n*-alkyl phthalates as a function of the alkyl chain length, ***n***. Compared with the case of usual polymers or oligomers, the change in the T_g with chain length is particularly interesting in the case of the di-*n*-alkyl phthalate series. The T_g decreases with increasing alkyl chain length up to dibutyl. Thereafter, the T_g increases gradually with a further increase in the alkyl chain length. This behavior is not satisfactorily explained by the conventional concept of the T_g-molecular weight relation. It is necessary to consider that there exist two factors which determine the T_g: (1) the molecular weight or chain length and (2) the intermolecular interaction. The increase in the number of methylene groups in the di-*n*-alkyl phthalates brings about two effects: first, the T_g becomes higher with increasing molecular weight and, second, the T_g decreases due to shielding of the interactions between the polar carbonyl groups and/or the aromatic rings due to the presence of non-polar methylene groups. When the number of methylene groups is four, the two effects counterbalance each other and the T_g of the dibutyl phthalate is the lowest of the di-*n*-alkyl phthalate series.

Figure 3 also shows the two sets of series of T_g *vs.* alkyl chain length plots for 1-alkanols[9] and lactones.[8] In this case, each has a different polar end-group, one having an –OH group and the other a –COO– group, respectively. An identical trend is also observed for

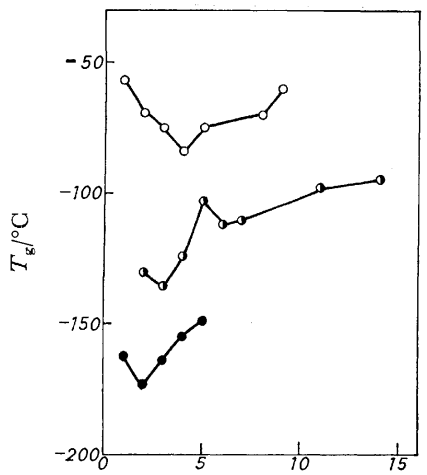

Fig. 3. Glass transition temperature T_g of di-*n*-alkyl phthalates, 1-alkanols,[9] and lactones[8] as a function of n, where n is the number of methylene groups.
○: Di-*n*-alkyl phthalates.

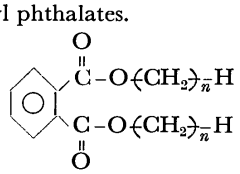

◑: Lactones.[8]

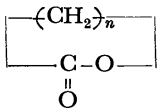

●: 1-Alkanols.[9]

$H(CH_2)_nOH$

these two series. In the 1-alkanol series, a pronounced minimum T_g value is observed for ethyl alcohol, that is, $n=2$. On the other hand, in the lactone series, the minimum T_g value is situated at $n=3$, that is, γ-butyrolactone.

It is believed that the n-value which shows the minimum T_g value in a given series having methylene groups depends on the mutual interaction strength of the end-groups. The stronger the interaction between the attractive groups in molecules, the larger the n-value, since longer methylene sequences are required in order to shield the attractive force which brings about a higher T_g. Such a concept appears to be reasonable from the results shown in Fig. 3.

With regard to the secondary dispersions of low molecular-weight substances, several investigators have observed dispersions at temperatures below the T_g for 1-alkanols,[7,9] lactones,[8] glucose pentaacetate, *etc.*[10] Some were not observed in dielectric loss measurements and were assigned to molecular motions of alkyl chains. However, for the di-*n*-alkyl phthalates reported here, no secondary dispersion was observed at all, as is shown in Fig. 2. Further experiments on other systems will be necessary in order to elucidate this very interesting problem.

The authors wish to express their thanks to Professor T. Komatsu and Dr. K. Nakamura of Hokkaido University for helpful discussions. The present work was supported in part by a Grant for Scientific Research from the Ministry of Education.

References

1) T. G. Fox, Jr., and P. J. Flory, *J. Appl. Phys.*, **21**, 581 (1950).
2) T. G. Fox and P. J. Flory, *J. Polym. Sci.*, **14**, 315 (1954).
3) K. Ueberreiter and G. Kanig, *J. Colloid Sci.*, **7**, 569 (1952).
4) J. A. Faucher, *Polym. Lett.*, **3**, 143 (1965).
5) R. F. Boyer, *Macromolecules*, **7**, 142 (1974).
6) J. N. G. Cowie, *Eur. Polym. J.*, **11**, 297 (1975).
7) K. H. Illers, *Rheol. Acta*, **3**, 185 (1964).
8) J. V. Koleske and R. D. Lundberg, *J. Polym. Sci., A-2*, **10**, 323 (1972).
9) J. A. Faucher and J. V. Koleske, *Phys. Chem. Glasses*, **7**, 203 (1966).
10) J. V. Koleske and J. A. Faucher, *J. Chem. Ed.*, **43**, 254 (1966).
11) E. Alfthan and A. Ruvo, *Polymer*, **14**, 329 (1973).
12) N. Kinjo and T. Nakagawa, *Polym. J.*, **5**, 316 (1973).
13) N. Furusho, T. Komatsu, and T. Nakagawa, *Nippon Kagaku Zasshi*, **1973**, 1164.
14) L. J. Garfield and S. E. Petrie, *J. Phys. Chem.*, **68**, 1750 (1964).
15) Beilsteins Handbuch der Organischen Chemie, 4 Auflage, Brittes Ergänzungs Werk, Band IX, Springer Verlag, Berlin (1971).
16) J. A. Prins, Ed., "Physics of Non-Crystalline Solids," North-Holland, Amsterdam (1965), pp. 320—332.

Kinetics of the Reaction at the Silver Sulfide-Liquid Sulfur Interface

Jun SASAKI, Junichiro MIZUSAKI, and Kazuo FUEKI

Department of Industrial Chemistry, Faculty of Engineering, The University of Tokyo, Hongo, Bunkyo-ku, Tokyo 113

(Received October 17, 1977)

The reaction rate, v, at the $Ag_2S/S(l)$ interface was determined as a function of the silver activity a_{Ag} in Ag_2S utilizing a solid-state electrochemical cell, $Ag/AgI/Ag_2S/Pt$. The rate equation was found to be expressed by $v=k(a_{Ag})^2-k'$. On the basis of the theory by Kobayashi and Wagner, the rate-controlling step of the $Ag_2S/S(l)$ interface reaction is concluded to be $S^-(ad)+e\rightarrow S^{2-}(ad)$. The overall reaction rate of silver sulfidization by liquid sulfur can be well explained by the mixed control of a three-step reaction; the $Ag_2S/S(l)$ interface reaction, the diffusion of silver ions in Ag_2S, and the Ag/Ag_2S interface reaction.

Alpha-AgI is an ionic conductor, the conductivity of which is as high as that of aqueous ionic solutions. This extraordinarily high conductivity is due to the special crystal structure. Also, silver chalcogenides, Ag_2X, have high ionic and electronic conductivities due to their structure and non-stoichiometry. Therefore, several electrochemical investigations have been carried out using α-AgI as an electrolyte and silver chalcogenides as electrodes. The silver activity in solid Ag_2X can be determined by emf measurements using an electrochemical cell, $Ag/AgI/Ag_2X$. Conversely, when a constant voltage is applied to the cell, the silver ions flow through AgI and the electrons, through the outer circuit. As a result, silver atoms are transferred from Ag to Ag_2X or in the reverse direction, the rate of silver transfer can be measured as the electric current. When the equilibrium is established between Ag and Ag_2X under an applied constant voltage, the silver activity in Ag_2X has a constant value corresponding to the applied voltage. Therefore, the silver activity in Ag_2X can be controlled by the voltage applied to the cell.

So far, various thermodynamical and kinetic measurements have been done by means of the Ag/AgI Ag_2X cell. For example, the non-stoichiometric ranges and phase relations of Ag–S,[1,2] Ag–Se[3,4] and Ag–Te[5] systems have been investigated by the coulometric titration technique, and kinetic studies have been carried out on solid-solid[6,7] and gas-solid[8–11] interface reactions.

Electrochemical methods in which the $Ag/AgI/Ag_2X$ cell is employed give interesting results which cannot be obtained by other methods for the investigation of solid-state reactions. The present work aims to study the $Ag_2S/S(l)$ interface reaction kinetically using the $Ag/AgI/Ag_2S$ cell.

Experimental

Materials. A silver rod was prepared by melting silver powder (99.99% purity) and casting it in a silica tube, 10 mm in inner diameter. The rod was cut into pellets 10 mm thick, and a hole, 1.5 mm in diameter, was drilled along the axis of each pellet. Silver sulfide was prepared by the sulfidization of silver with liquid sulfur. One end of a glass tube, 10 mm in outer diameter and 8 mm in inner diameter, was finished as flat as possible, placed in contact with a silver pellet, and pressed by a weight. Then, sulfur purified by vacuum distillation was dropped into the glass tube to react the sulfur with silver at 200 °C. Since the lower end of the tube was so flat that leakage of liquid sulfur could be avoided. Silver sulfide grown in the glass tube was taken out and sliced into pellets 2—3 mm thick. Each pellet was pressed under a pressure of 5 t/cm² and polished to a thickness of about 1 mm. Silver iodide pellets, 10 mm thick were prepared by pressing AgI powder under a pressure of 5 t/cm².

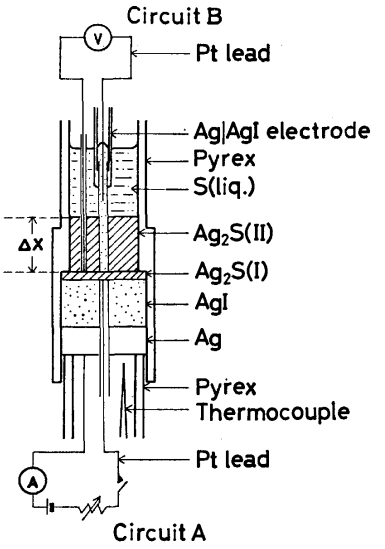

Fig. 1. Apparatus for the measurement of the rate of $Ag_2S/S(l)$ interface reaction.

Kinetic Study on the $Ag_2S/S(l)$ Interface Reaction. The apparatus and technique employed in the present study were generally similar to those used by Mizusaki and his co-investigators[12] for their investigation of the $Ag_2Se/Se(l)$ interface reaction. However, an improvement was made in the apparatus, since the dissociation pressure of Ag_2S is higher than that of Ag_2Se.[13] As is shown in Fig. 1, two glass tubes, one of which was 13 mm in inner diameter, the other being 10 mm in inner diameter, were joined. Three pellets of Ag, AgI, and $Ag_2S(I)$, 10 mm in diameter, were assembled and pressed with the joined glass tube. Since AgI tends to deform plastically, the pressing resulted in a close contact between the AgI pellet and the inner wall of the glass tube. Thus, the vaporization of sulfur from Ag_2S could be prevented. The end surface of the glass tube was finished as flat as possible so that liquid sulfur could be held in the tube without leakage when the end was placed in contact with the $Ag_2S(I)$ pellet. The Ag/AgI electrode in a small alumina tube, 1.5 mm in outer diameter, was placed in the glass tube so that the tip could be brought to contact with the surface of the $Ag_2S(I)$ pellet. The reaction rate was measured as an electric current flowing through the outer circuit A, by means of an ammeter, while the poten-

tial difference between the $Ag_2S(I)$ pellet and Ag was determined by means of potentiometer.

Rate Measurement of the Reaction between Silver and Liquid Sulfur. The same apparatus and technique as used by Mizusaki and his co-investigators[12] were employed for the measurement. A silver cylinder, 8 mm in diameter, and a Ag_2S pellet, 10 mm in diameter, were assembled and pressed with a glass tube, 10 mm in outer diameter. Then, sulfur was dropped into the glass tube, and the change in the thickness of the Ag_2S pellet was followed with time by means of a cathetometer.

Observation of the Ag_2S Surface with SEM. After the sulfidization, the liquid sulfur was poured out and the residual sulfur on the surface of Ag_2S was dissolved with CS_2. The surface of the Ag_2S thus obtained was examined by means of an SEM.

Results and Discussion

Observation on the Ag_2S Surface by Means of SEM. Observation of the surface of Ag_2S by means of SEM revealed that the surface of Ag_2S is always compact, regardless of the experimental conditions, as is shown in Fig. 2.

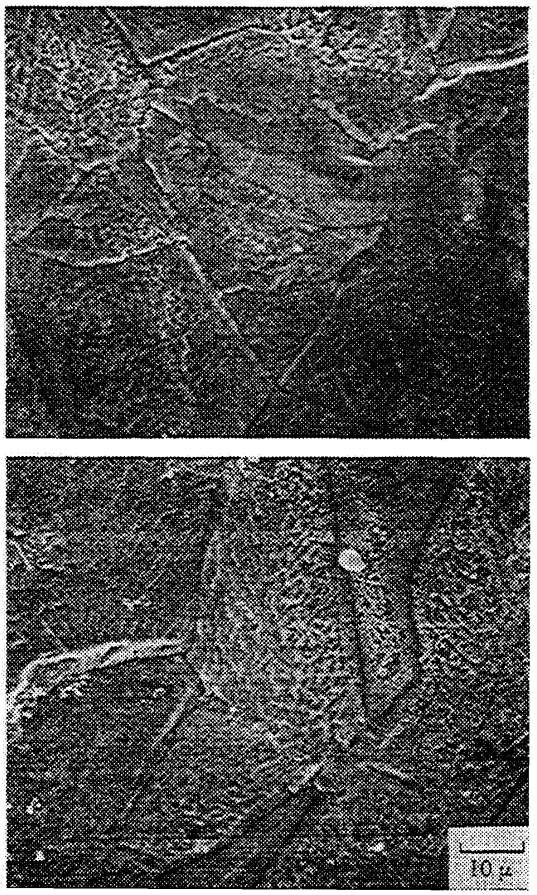

Fig. 2. SEM photographs of the surface of Ag_2S at the $Ag_2S/S(l)$ interface. (185 °C)
(a): $I\,A^{-1}=1080$ mA cm^{-2} (b): $I\,A^{-1}=192$ mA cm^{-2}

Results of a Kinetic Study of the $Ag_2S/S(l)$ Interface Reaction. When the circuit A is open, $Ag_2S(I)$ is in equilibrium with the liquid sulfur, and the potential difference, $E°$, appearing in the circuit B gives the standard free energy formation of Ag_2S by means of the following relation,

$$E° = -\Delta G°/2F, \tag{1}$$

where F is Faraday's constant. If metallic silver is taken as the standard state, the silver activity, a^*_{Ag}, in Ag_2S equilibrated with liquid sulfur is represented by the equation

$$a^*_{Ag} = \exp(-F\cdot E°/R\cdot T). \tag{2}$$

When the switch is turned on and a constant current, I, is allowed to flow in, the silver ions are transported from the Ag electrode to the $Ag_2S(I)/S(l)$ interface through AgI and $Ag_2S(I)$, while the electrons flow from the Ag electrode to the $Ag_2S/S(l)$ interface through the outer circuit and $Ag_2S(I)$. The silver ions and electrons arriving at the $Ag_2S(I)/S(l)$ interface react with liquid sulfur to form $Ag_2S(II)$ in the glass tube at a constant rate. Accordingly, the Ag/AgI electrode used for the measurement of the potential difference is buried in the $Ag_2S(II)$ layer. If the area of the $Ag_2S/S(l)$ interface is represented by A, the reaction at the $Ag_2S/S(l)$ interface proceeds at a rate of $I/2F\cdot A$ and a potential difference is produced at the $Ag_2S(II)/S(l)$ interface. If the silver activity in $Ag_2S(II)$ at the $Ag_2S/S(l)$ interface and that in $Ag_2S(I)$ at the tip of Ag/AgI electrode are designated by a'_{Ag} and a_{Ag} respectively, and if the thickness of $Ag_2S(II)$ layer is Δx, the following relations are obtained:

$$E' - E = \frac{I\cdot\Delta x}{\sigma_{Ag^+}\cdot A}, \tag{3}$$

$$E' = -\frac{2.303R\cdot T}{F}\log a'_{Ag}, \tag{4}$$

$$E = -\frac{2.303R\cdot T}{F}\log a_{Ag}, \tag{5}$$

where σ_{Ag^+} is the ionic conductivity of Ag^+ ions in Ag_2S. In Eq. 3, σ_{Ag^+} is assumed to be independent of the silver activity in Ag_2S.[14]

Figure 3 shows the plot of E *vs.* Δx at 200 °C. Since $I/\sigma_{Ag^+}A$ is constant under a constant current, I, E' is determined from the intercepts of the ordinate with the

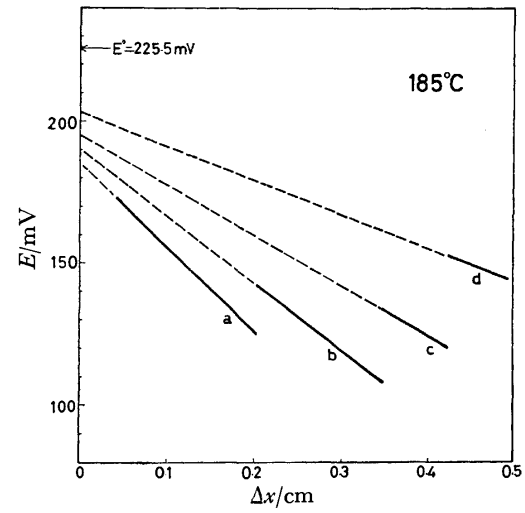

Fig. 3. Plots of E *vs.* Δx.
a: $I\,A^{-1}=1080$ mA cm^{-2}, b: $I\,A^{-1}=880$ mA cm^{-2},
c: $I\,A^{-1}=660$ mA cm^{-2}, d: $I\,A^{-1}=440$ mA cm^{-2}.

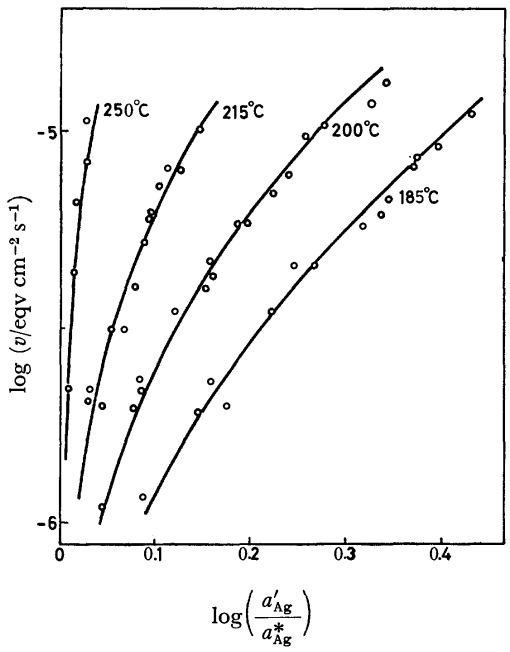

Fig. 4. Plots of log v *vs.* $\log(a'_{Ag}/a^*_{Ag})$.

extrapolated lines. The $E°$ measured in the present work is shown by an arrow. It is in good agreement with that obtained by Kiukkola and Wagner.[5] The potential difference, $E°-E'$, gives the driving force of the Ag_2S/S(l) interface reaction.

Figure 4 shows the relationship between the reaction rate and a'_{Ag}/a^*_{Ag}. The logarithm of a'_{Ag}/a^*_{Ag} is equivalent to $(E°-E')/2.303\ R\cdot T$.

Kinetics of the Ag_2S/S(l) Interface Reaction. Kobayashi and Wagner[8] studied the kinetics of the reduction of Ag_2S by H_2 and found that the rate of reduction at the gas-solid interface depends not only on the partial pressure of the reacting gases, but also on the activity of the reacting chemical species in solid. A similar dependence of the surface reaction rate on the activity of the reacting chemical species was observed in redox reactions between CO_2 or CO and metal oxides, such as FeO,[15,16] Fe_3O_4,[15] and CoO,[17] and in redox reactions between H_2S or H_2 and metal sulfides.[18,19] From these results, it is concluded that the dependence of the reaction rate on the activity of the reacting chemical species in solids would be like that for the gas-solid interface reactions. In the case of the Ag_2S/S(l) interface reaction, the reaction rate was found to depend on the silver activity of Ag_2S at the Ag_2S/S(l) interface, as is shown in Fig. 4. So, it is expected that a mechanism similar to that of the gas-solid interface reaction would be operative in the present interface reaction.

According to Gee's[20] study, the molecular species of liquid sulfur are S_8 and S_6 with a cyclic structure and polymeric sulfur in the temperature range of the present investigation. They are in equilibrium with each other. At the Ag_2S(II)/S(l) interface, S_x molecule would adsorb and dissociate in the following way:

$$S_x(l) = xS(ad). \tag{6}$$

Since the density of liquid sulfur is several thousand times that of sulfur vapor, it is considered that the surface of Ag_2S is saturated with adsorbed sulfur and that the surface concentration of S(ad) is constant.

The process whereby S(ad) is reduced to S^{2-}(ad) must be

$$S(ad) + e \longrightarrow S^-(ad), \tag{7}$$

$$S^-(ad) + e \longrightarrow S^{2-}(ad). \tag{8}$$

Since S(ad) is in equilibrium with S(l), $a_s(ad)$ is equal to $a_s(l)$. Moreover, it is assumed that S^{2-}(ad) is in equilibrium with the S^{2-} ion in Ag_2S and that equilibria are established among chemical species, Ag, Ag^+, e, S, S^-, and S^{2-}, in Ag_2S. As the activity of Ag^+, a_{Ag^+} is constant regardless of the composition of Ag_2S,[1] the activity of the respective species depends on a'_{Ag} as follows:

$$a_e \propto a'_{Ag}, \tag{9}$$

$$a_{Ag^+},\ a_{S^{2-}} = \text{const.} \tag{10}$$

a) If Reaction 7 is rate-controlling,

$$v_1 = \vec{k}_1 a_S(ad) a_e - \overleftarrow{k}_1 a_{S^-}(ad). \tag{11}$$

The $a_s(ad)$ activity is equal to $a_s(l)$ and is independent of a'_{Ag}. Since a preliminary equilibrium is established in Eq. 8,

$$\frac{a_{S^{2-}}(ad)}{a_{S^-}a_e} = K_2, \tag{12}$$

that is

$$a_{S^-} = \frac{a_{S^{2-}}(ad)}{K_2}(a_e)^{-1}. \tag{13}$$

The $a_{S^{2-}}(ad)$ activity is equal to $a_{S^{2-}}$ in the Ag_2S bulk; therefore,

$$a_{S^-} \propto a'^{-1}_{Ag}. \tag{14}$$

Thus, Eq. 11 can be rewritten in the form

$$v_1 = k_1 a'_{Ag} - k_{-1}(a'_{Ag})^{-1}. \tag{15}$$

b) If Reaction 8 is rate-controlling,

$$v_2 = \vec{k}_2 a_{S^-}(ad) a_e - \overleftarrow{k}_2 a_{S^{2-}}(ad). \tag{16}$$

Assuming that equilibrium is kept for Reaction 7, we obtain

$$\frac{a_{S^-}(ad)}{a_S(ad)a_e} = K_1. \tag{17}$$

Thus,

$$a_{S^-}(ad) = K_1 a_S(ad) a_e \propto a'_{Ag}. \tag{18}$$

Accordingly,

$$v_2 = k_2(a'_{Ag})^2 - k_{-2}. \tag{19}$$

As may be noticed from Eqs. 15 and 19, the rate equations have the general expression,

$$v = \vec{k}(a'_{Ag})^m - \overleftarrow{k}(a'_{Ag})^{-n}, \tag{20}$$

where $m=1$ and $n=1$ when the S(ad) + e → S^-(ad) reaction is slow, and $m=2$ and $n=0$ when the S^-(ad) + e → S^{2-}(ad) reaction is slow. When the equilibrium is established between Ag_2S and liquid sulfur, v in Eq. 20 is zero; therefore,

$$\vec{k}(a^*_{Ag})^m = \overleftarrow{k}(a^*_{Ag})^{-n}. \tag{21}$$

The insertion of Eq. 21 into Eq. 20 gives

$$v = \vec{k}(a^*_{Ag})^m \left\{ \left(\frac{a'_{Ag}}{a^*_{Ag}}\right)^m - \left(\frac{a'_{Ag}}{a^*_{Ag}}\right)^{-n} \right\}$$
$$= k \left\{ \left(\frac{a'_{Ag}}{a^*_{Ag}}\right)^m - \left(\frac{a'_{Ag}}{a^*_{Ag}}\right)^{-n} \right\}. \quad (22)$$

A curve-fitting calculation using data for 185 °C and 200 °C in Fig. 4 showed that a set of $m=2$ and $n=0$ gives a better agreement between the calculated and observed values than a set of $m=1$ and $n=1$. It is concluded that the $S^-(ad)+e \rightarrow S^{2-}(ad)$ reaction is rate-controlling for the $Ag_2S/S(l)$ interface reaction.

In the case of $m=2$ and $n=0$, Eq. 22 is rewritten as

$$v = k \left\{ \left(\frac{a'_{Ag}}{a^*_{Ag}}\right)^2 - 1 \right\}. \quad (23)$$

Figure 5 shows the plot of log v *vs.* log $\{(a'_{Ag}/a^*_{Ag})^2-1\}$. The data for each temperature fall on a straight line. From the intercept of the ordinate with the plotted lines, we can calculate the rate constant, k. Figure 6 shows the Arrhenius plot for k. The Arrhenius equation is

$$k = 1.22 \times 10^7 \exp\left(\frac{-26900}{RT}\right) \quad (\text{eqv cm}^{-2}\,\text{s}^{-1}) \quad (24)$$

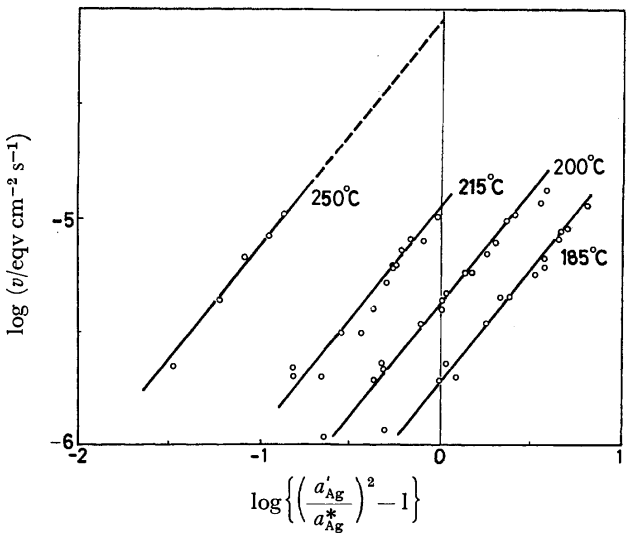

Fig. 5. Plots of log v *vs.* $\log\{(a'_{Ag}/a^*_{Ag})^2-1\}$.

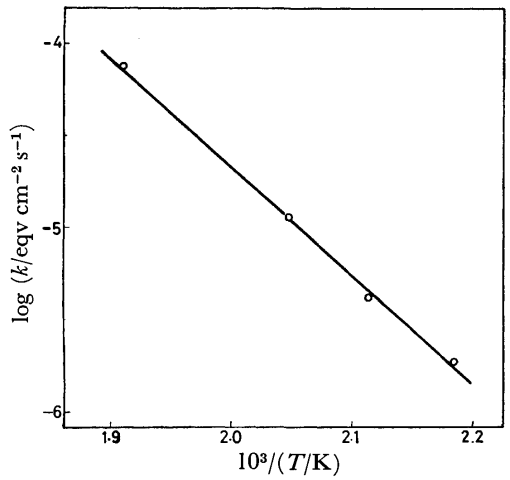

Fig. 6. Arrhenius plot of k.

Driving Forces of the Three Steps of Silver Sulfidization. The reaction of metal tarnishing consists of three elementary steps:

1) Reaction at the metal/scale interface,
2) diffusion of electrons and ions through the growing scale, and
3) reaction at the gas (or liquid)/scale interface.

If one of these steps is rate-controlling, the driving force, that is, the difference in the silver chemical potential of the step, is equal to that of the over-all reaction. If two or three steps are simultaneously slow, the driving force of the over-all reaction is divided into two or three parts.

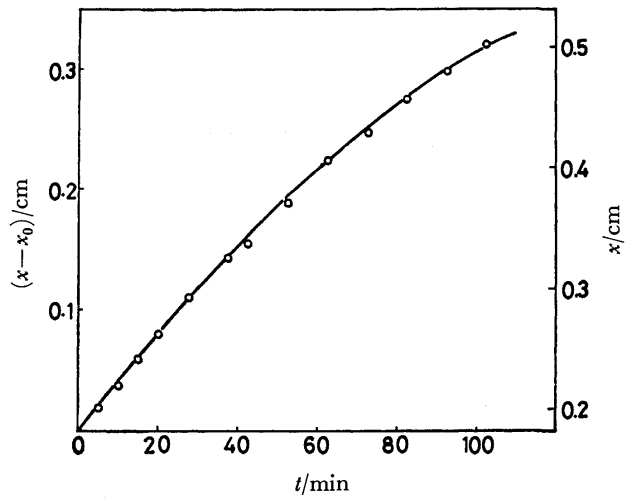

Fig. 7. Plot of x or $x-x_0$ *vs.* time.

Mizusaki and his co-investigators[12] have determined the distribution of the chemical potential of silver in a growing Ag_2Se layer in the selenization of silver, and have found that Ag_2Se and Se(l) are actually in chemical equilibrium during the reaction. In the present study, the difference in the silver chemical potential across the $Ag_2S/S(l)$ interface was observed during the sulfidization. This finding suggests that the sulfidization of silver is mixed-controlling. Therefore, the driving force for each reaction step was calculated from the sulfidization curve given in Fig. 7. In this figure, x is the total thickness of the Ag_2S layer and $x-x_0$ is the increase in the thickness of the Ag_2S layer. The over-all reaction rate is calculated by the graphical differentiation of the curve. The ionic conductivity of Ag_2S is calculated from Eq. 3 and the gradient of the straight lines in Fig. 2. Thus,

$$\sigma \cdot T = 3.8 \times 10^4 \exp\left(\frac{-2900}{RT}\right) \quad (\text{ohm}^{-1}\,\text{cm}^{-1}\,\text{K}). \quad (25)$$

The value agrees with the result obtained by means of the four-probe conductivity measurement.[21]

If the silver activity of Ag_2S at the Ag/Ag_2S interface is denoted by a''_{Ag}, the logarithm of silver activity ratio (a'_{Ag}/a''_{Ag}) is

$$\log\left(\frac{a'_{Ag}}{a''_{Ag}}\right) = \frac{I \cdot xF}{\sigma_{Ag^+} \cdot A \cdot R \cdot T}$$
$$= \frac{vx \cdot F^2}{\sigma_{Ag^+} \cdot R \cdot T}. \quad (26)$$

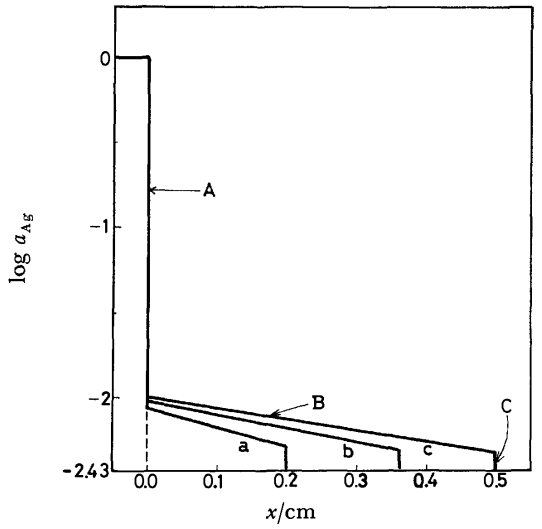

Fig. 8. Distribution of log a_{Ag} during the reaction at 200 °C.
a: $t=0$ min. b: $t=50$ min. c: $t=100$ min.
A: Potential difference at Ag/Ag_2S interface.
B: Potential difference in Ag_2S layer.
C: Potential difference at $Ag_2S/S(l)$ interface.

The activity ratio (a'_{Ag}/a^*_{Ag}) at the $Ag_2S/S(l)$ interface is obtained from the relation of v *vs.* log (a'_{Ag}/a^*_{Ag}) in Fig. 4. Since the reaction rate, v, can be obtained from Fig. 7, and since log a^*_{Ag} is calculated by means of Eq. 2, the distribution of the chemical potential of silver in the Ag_2S layer during the sulfidization can be drawn. Figure 8 shows the plots of log a_{Ag} against x. Evidently, the over-all reaction is mixed-controlling by means of three reaction steps. From Fig. 8 we can estimate the chemical potential difference at the Ag/Ag_2S interface during the reaction. The result is in good agreement with the result of the electrochemical measurement carried out by Mizusaki and his co-investigators.[7]

Summary

(1) The $Ag_2S/S(l)$ interface reaction was investigated kinetically. The rate equation was found to be represented by

$$v = 1.22\times10^{7}\exp\left(\frac{-26900}{RT}\right)\left\{\left(\frac{a'_{Ag}}{a^*_{AG}}\right)^2-1\right\}.$$

(eqv cm^{-2} s^{-1})

It was also concluded that the reaction step,

$$S^-(ad) + e \longrightarrow S^{2-}(ad),$$

is rate-controlling.

(2) The driving forces of the $Ag_2S/S(l)$ interface reaction and the diffusion of the silver ions in Ag_2S were quantitatively determined. In the initial stage of sulfidization, the over-all reaction was mixed-controlled by means of three step reactions: $Ag_2S/S(l)$ interface reaction, diffusion, and Ag/Ag_2S interface reaction.

References

1) C. Wagner, *J. Chem. Phys.*, **21**, 1819 (1953).
2) H. Rickert, V. Sattler, and Ch. Wedde, *Z. Phys. Chem., N. F.*, **98**, 339 (1975).
3) T. Takahashi and O. Yamamoto, *J. Electrochem. Soc.*, **118**, 1051 (1971).
4) N. Valverde, *Z. Phys. Chem., N. F.*, **70**, 113 (1970).
5) K. Kiukkola and C. Wagner, *J. Electrochem. Soc.*, **104**, 379 (1957).
6) H. Rickert and C. D. O'Briain, *Z. Phys. Chem., N. F.*, **31**, 71 (1962).
7) J. Mizusaki, K. Fueki, and T. Mukaibo, *Bull. Chem. Soc. Jpn.*, **46**, 1663 (1973).
8) H. Kobayashi and C. Wagner, *J. Chem. Phys.*, **26**, 1609 (1957).
9) E. Bechtold and U. Schwabe, *Z. Phys. Chem., N. F.*, **81**, 230 (1972).
10) H. Rickert and K.-H. Tostmann, *Werkst. Korros.*, **21**, 965 (1970).
11) H. Rickert, *Z. Elektrochem.*, **65**, 463 (1961).
12) J. Mizusaki, K. Fueki, and T. Mukaibo, *Bull. Chem. Soc. Jpn.*, **47**, 2851 (1974).
13) J. Hladik, Ed., "Physics of Electrolyte," Academic Press, Vol. 2, London (1972), pp. 519—538.
14) S. Miyatani, *J. Phys. Soc. Jpn.*, **24**, 328 (1968).
15) H. J. Grabke, *Ber. Bunsenges.*, **60**, 48 (1965).
16) S. Kurihara, K. Fueki, T. Mukaibo, and Y. Wada, *Bull. Chem. Soc. Jpn.*, **43**, 2761 (1970).
17) F. Pettit and J. B. Wagner, Jr., *Acta Metall.*, **12**, 41 (1964).
18) M. Katsumoto, K. Fueki, and T. Mukaibo, *Bull. Chem. Soc. Jpn.*, **46**, 3641 (1973).
19) M. Katsumoto, K. Fueki, and T. Mukaibo, *Bull. Chem. Soc. Jpn.*, **47**, 54 (1974).
20) G. Gee, *Trans. Faraday Soc.*, **48**, 515 (1952).
21) H. Okazaki, *J. Phys. Soc. Jpn.*, **23**, 355 (1967).

Absorption Spectra of Inter- and Intramolecular Exciplex Systems of Pyrene and *N,N*-Dimethylaniline in Alcoholic Solutions

Junji HINATU, Hiroshi MASUHARA, Noboru MATAGA,* Yoshiteru SAKATA,** and Soichi MISUMI**

Department of Chemistry, Faculty of Engineering Science, Osaka University, Toyonaka, Osaka 560
***The Institute of Scientific and Industrial Research, Osaka University, Suita, Osaka 565*

(Received October 22, 1977)

Absorption spectra of inter- and intramolecular exciplex systems of pyrene and *N,N*-dimethylaniline in alcoholic solution were obtained by means of ns laser photolysis. The spectra of intermolecular systems can be reproduced by the superposition of bands of the pyrene anion and the *N,N*-dimethylaniline cation. Similar results were obtained with intramolecular systems of P_1 and P_2, where P_n is (1-pyrenyl)-$(CH_2)_n$-(*p*-dimethylaminophenyl). The absorption band of P_3 exciplex is structureless and very broad, the position of the maximum remaining unchanged. From the relation between absorption spectra and conformation of intramolecular systems, it is concluded that the broad band is due to the sandwich type of structure of the donor cation and the acceptor anion. Anomalous behavior of intermolecular exciplexes in alcoholic solutions is discussed on the basis of their absorption spectra.

The measurement of the absorption spectra of excited molecules in solution has become possible by application of lasers. The absorption spectra of exciplex systems have been measured by several workers[1-5] and the following problems have been discussed: (a) The back CT transition from the anionic moiety to the cationic one. The absorption band due to this transition can be observed in addition to the absorption bands ascribed to the transitions localized in anion as well as cation. (b) Dependence of spectra upon solvent, which has its origin in fluorescence studies on exciplexes.[6] (c) The relation between absorption spectra of exciplexes and their geometrical conformation. We have examined these problems comparing the results of inter- and intramolecular exciplex systems in the same solvent.

The other subject of the present work is to study the exciplexes in alcohols by means of their absorption spectra. The behavior of exciplexes is very sensitive towards environments, some anomalies in alcohols being pointed out as follows. (i) According to the results on the intermolecular exciplex system composed of pyrene (Py) and *N,N*-dimethylaniline (DMA) in aprotic solvents,[7,8] quantum yield and lifetime of exciplex fluorescence decrease with increase in solvent polarity. When dielectric constant is *ca.* 12 the yield decreases sharply, ionic dissociation occurring in place of fluorescent exciplex formation.[9] However, the exciplex fluorescence in alcoholic solutions shows smaller red shift, higher quantum yield and longer lifetime as compared to the results in aprotic solvents with the same value of dielectric constant.[3,10] The experimental values in various alcohols show dependence upon solvent dielectric constant in a similar manner to that in the case of aprotic solvents. In other words, the results in protic solutions correspond to those in aprotic ones with lower value of dielectric constant. (ii) The ionic dissociation to free cation and anion was investigated in polar solvents and empirical equations representing the relationship between dissociation yield and the solvent dielectric constant were proposed.[11] Although the same type of equation is satisfied in both cases of alcohols and aprotic solvents, the parameters in the equation differ from each other.

In the present work absorption spectra of inter- and intramolecular exciplex systems of Py and DMA were observed in some alcohols by means of ns laser photolysis. The intramolecular systems of P_n, (n=1, 2, 3),

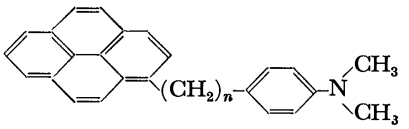

were examined in order to clarify the relation between spectra and geometrical conformation. Absorption spectra of intermolecular exciplex were observed in 1-pentanol, 2-propanol, and ethanol. The dynamics of exciplex in alcohols are discussed on the basis of these spectra.

Experimental

Laser Photolysis Apparatus. The details of our ns laser photolysis apparatus are essentially the same as those reported.[12] Improvement was made on the wiring of photomultiplier HTV 1P28 for improving S/N ratio.[13] Examined voltage larger than the standard value is supplied to 1—5 dynodes, the signal current being withdrawn from the 6th dynode with 50 Ω resistor. Negative value of 50 V was supplied to the remainder of dynodes in order to obtain correct time-response. The breeder current of the last two dynodes is 30 mA. A series of capacitors are set between successive dynodes. The linearity of an output signal was checked, the sum of intensity of fluorescence and monitoring flash lamp being confirmed to be measured correctly.

Improvement was also made by setting a simple and convenient monitoring device for exciting pulse intensity. The 347 nm pulse is partially reflected, scattered with MgO and lead to a pin photodiode HP 5082 4220. The signal is deformed to a pulse, whose height is a few volt and decay time is 10 ms, by use of a peak hold circuit.[14] Relative intensity of an exciting pulse is digitally given on solid state display, which holds the value until the next laser shot is given. This device was checked with an oscilloscope-photomultiplier system and also by a thermopile (HADRON 100).[15]

Linearity between the Intensity of an Exciting Laser Pulse and Measured Optical Density. Besides nonlinear effect due to high intensity laser excitation, geometrical correlation between exciting beam and monitoring light sometimes leads to a

*To whom all correspondence should be addressed.

deviation from linearity between the intensity of an exciting pulse and measured optical density.[16] This can be ascribed to the contribution of stray light from an exciting pulse to monitoring light, or to inhomogeneous spatial distribution of an exciting pulse. The linearity was confirmed by measuring the T-T absorption spectra of anthracene in ethanol and the bands of anions produced through the ionic dissociation of Py–DMA and 1,2,4,5-tetracyanobenzene–toluene systems in acetonitrile.

Absorption spectra of the exciplex systems were obtained by use of oscillograms at various wavelength. The fluctuation of an excitation intensity was ±6%.

Materials. Py, DMA, and P_n's are the same as used previously.[4,17] The GR grade 2-propanol, 1-pentanol and ethanol were used without purification. The concentration of solution was adjusted so that the optical density at 347 nm is about unity. This corresponds to the order of 10^{-3} and 10^{-5} M in the cases of inter- and intramolecular systems, respectively. The concentration of DMA in the former system was determined so as to quench the Py fluorescence more than 95%. All the solutions were degassed by the usual freeze-pump-thaw method.

Results

Since the exciplex consisting of aromatic hydrocarbon and amine has a large dipole moment, its electronic structure is considered to be an ion-pair of the donor cation and the acceptor anion. The absorption spectra may be similar to the sum of bands of the donor cation and the acceptor anion. The back CT transition from the anion to the cation is also expected to appear.[1,3,18] Usually the reference spectra used for the assignment of the exciplex absorption spectra are those of an anion produced by alkaline metal reduction of hydrocarbon and of a cation produced by γ-irradiation. The difference of measuring apparatus and of environments of ions lead to some ambiguity in discussing the spectral shape. The transient spectra of intermolecular Py–DMA system in acetonitrile are referred to, since their measurements can be made by the same laser photolysis apparatus and in the fluid solution. It is well known that the ionic dissociation to the Py anion and the DMA cation is the main deactivation process in acetonitrile, and its quantum yield is about 0.8.[19] Since no chemical species other than ions and triplet Py is detected, these spectra are the best reference for assigning the $S_n \leftarrow S_1$ spectra of exciplexes. The result is given in Fig. 1. The bands at about 24000 cm^{-1} and at 20100 cm^{-1} are ascribed to the triplet Py and to the Py anion, respectively. The shoulder at 22000 cm^{-1} is due to the superposition of bands of both ions. These bands are in agreement with those in literatue.[20] At a long delay the ion bands decrease and the triplet Py increases. The band shape in the region from 18000—23000 cm^{-1} is independent of delay time. Therefore, the bands in this region are mainly ascribed to the sum of the Py anion and the DMA cation, the concentration ratio of both ions being unity.

The time-resolved spectra of the intermolecular Py–DMA system in 2-propanol and 1-pentanol are given in Figs. 2 and 3. Since the decay of short-lived component agrees with that of exciplex fluorescence, the

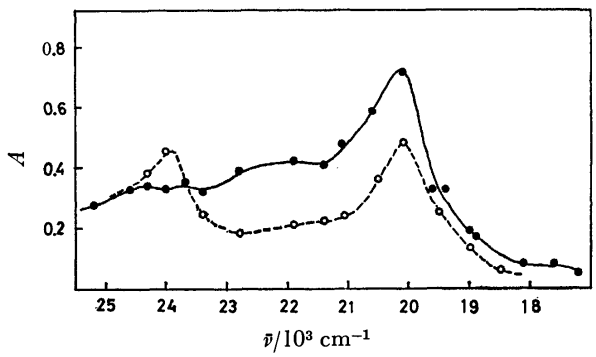

Fig. 1. Transient absorption spectra of intermolecular Py–DMA system in acetonitrile (See text).
-●- 30 ns after the beginning of laser oscillation. (In the present paper the delay time is given in this manner.), -○-150 ns.

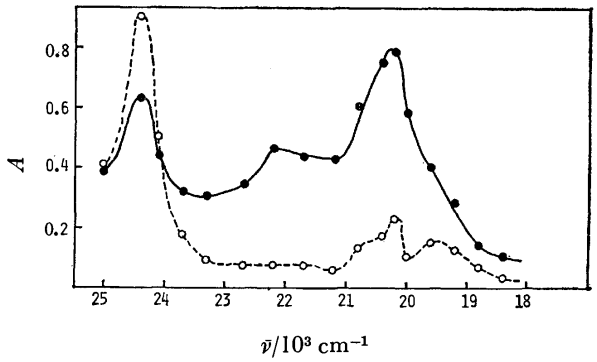

Fig. 2. Transient absorption spectra of intermolecular Py–DMA system in 2-propanol.
-●- 50 ns, -○- 400 ns.

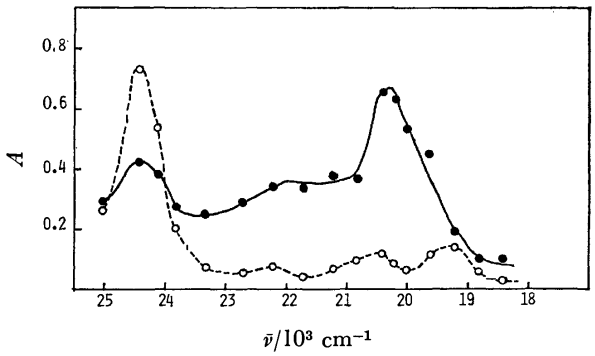

Fig. 3. Transient absorption spectra of intermolecular Py–DMA system in 1-pentanol.
-●- 50 ns, -○- 400 ns.

spectra obtained at the short delay is tentatively ascribed to the exciplex. These two spectra agree with those given in Fig. 1 except for the contribution of the triplet Py. As the bands at 20200 and 22200 cm^{-1} decrease, the triplet Py increases. Similar results were obtained also in ethanol.

Observed spectra of P_1 and P_2 in 2-propanol are given in Figs. 4 and 5. The rise of the short-lived components is too fast to be analyzed, their decays being identical with those of exciplex fluorescence. As

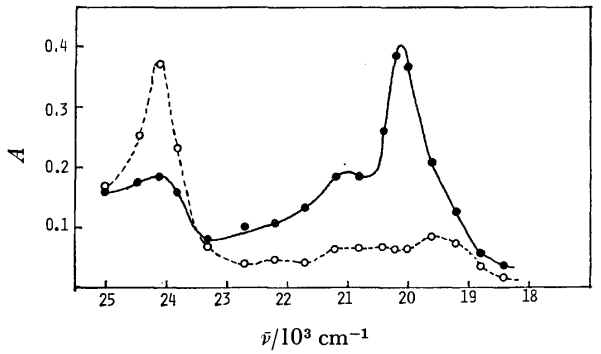

Fig. 4. Transient absorption spectra of P_1 in 2-propanol. -●- 15 ns, -○- 150 ns.

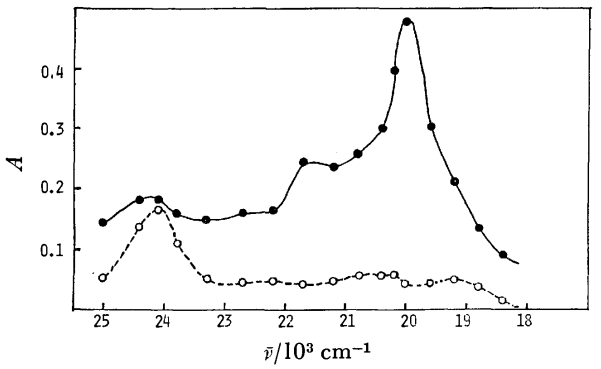

Fig. 5. Transient absorption spectra of P_2 in 2-propanol. -●- 25 ns, -○- 250 ns.

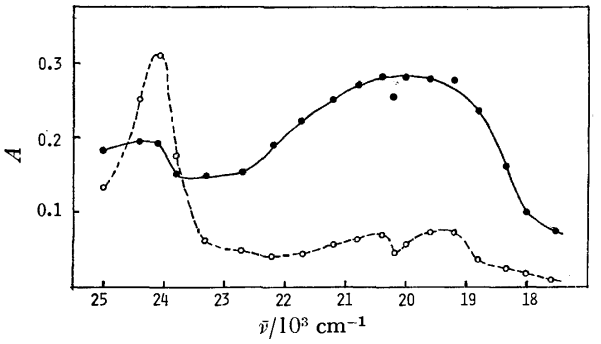

Fig. 6. Transient absorption spectra of P_3 in 2-propanol. -●- 35 ns, -○- 350 ns.

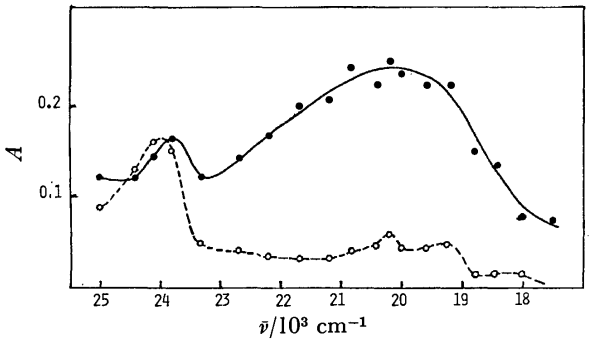

Fig. 7. Transient absorption spectra of P_3 in acetone. -●- 35 ns, -○- 350 ns.

compared with the bands of intermolecular systems the shoulder at the higher wave number side of the Py anion band is shifted to red, its intensity relative to that of the Py anion band (20000 cm^{-1}) increasing. At a long delay, only the triplet Py is identified, its characteristic peak being observed at 24100 cm^{-1}.

The absorption spectra of P_3 are very broad, the band maximum being almost at the same position as that of P_1 or P_2, as shown in Fig. 6. The half-width is about 4000 cm^{-1}. Since ionic dissociation is prohibited in the case of intramolecular compounds, exciplex is formed also in acetone in spite of its high polarity. The absorption spectra of P_3 in the latter solvent are similar to those in alcohol (Fig. 7). The absorption band due to the triplet Py of P_3 shows a peak at 24100 cm^{-1} just as in the case of P_1 and P_2.

The present results can be summarized as follows. (i) The spectra of intermolecular systems can be reproduced approximately by the superposition of bands of the acceptor anion and the donor cation. (ii) Although similar spectra are observed in the cases of P_1 and P_2, the shoulder at higher wave number side of the Py anion band is shifted to the red compared with the case of intermolecular system. (iii) P_3 exciplex shows a characteristic broad band. (iv) The T-T spectra of intramolecular systems are independent of the number of the methylene chain, the characteristic band lying at 24100 cm^{-1}. On the other hand, the triplet Py of intermolecular system shows an absorption peak at 24400 cm^{-1}.

Discussion

Absorption Spectra and Geometrical Conformation of Intramolecular Exciplex Systems. The relation between absorption spectra and geometrical conformation has been studied in detail in the case of 1,2,4,5-tetracyanobenzene complexes in the excited state.[18] However, information on exciplex is scarce.[4] Compounds P_1 and P_2 cannot take the structure of sandwich type, the distance between donor and acceptor moieties being rather long. On the other hand, both stretched and stacked forms are possible for P_3. The dipole moment of all these exciplexes is quite large.[7,8] Exciplexes can be considered approximately to be a kind of ion-pair consisting of donor cation and acceptor anion. In the cases of P_1 and P_2, the interaction between both ions seems to be rather small and the absorption spectra can be reproduced by the superposition of bands of their component ions. Similar spectra can be expected if the exciplex of P_3 is of stretched form. However, a quite broad band is observed, so that P_3 exciplex seems to take the geometry, which is impossible in the cases of P_1 and P_2. Presumably, it is a structure of sandwich type where the donor and the acceptor are in the stacked form and distance between two moieties is rather short.

The present spectra of P_3 are similar to those of intermolecular Py–*N*,*N*-diethylaniline (DEA) system in nonpolar solvents.[5] The following interpretations might be possible with respect to this broad band.

(a) The overlap between MO's of both ions causes the back CT transition from the anion to the cation.

The sum of the latter transitions and the local excitation of the Py anion leads to the broadening of the band at 20000 cm^{-1}. Since the transition moment between the CT and locally excited configurations is zero as a first approximation, the intensity of the back CT transition comparable to that of ion bands should be due to rather strong mixing of both configurations in the fluorescent state, which is inconsistent with the experimental[7,8] and theoretical[21] results indicating large dipole moment of the exciplex. An alternative interpretation may be the mixing in the higher excited state, to which the transition occurs.

(b) The electrostatic interaction between both ions may be rather strong in the case of P_3, which seems to produce the spectral broadening. This interpretation has been suggested in studies on the electronic spectra of ion-pairs produced in rigid matrix.[22]

Although correct interpretation is beyond our present knowledge, the spectral change due to the differences in distance and orientation between two moieties is demonstrated.

Intermolecular Exciplex Systems in Alcoholic Solutions. The fluorescence quantum yield of exciplex is higher and its lifetime longer in alcohols than in aprotic solvents with similar dielectric constant. This can be ascribed to high viscosity and long dielectric relaxation time of alcohols. The electron transfer from DMA to the excited Py is not followed by the solvation to free ions, which can be attributed to network structure of solvent due to hydrogen bonding. The resulting exciplex in alcohols has the same structure and property as those in nonpolar aprotic solvents. This is not in line with the results on the transient absorption spectra. The spectra of Py–DMA intermolecular system in 2-propanol and 1-pentanol are in agreement with the superposition of bands of the Py anion and the DMA cation and are similar to the spectra of P_1 and P_2 in 2-propanol, but they differ a great deal from the spectra of intermolecular Py–DEA in nonpolar solvents and of P_3 in 2-propanol.

A possible explanation is to assume the role of geminate ion-pair, introduced by Goodall *et al.*[23] It is postulated that the exciplexes in these alcohols are produced through the recombination of a geminate ion-pair or they are in equilibrium with the geminate ion-pair.[3,23,24] If the geminate ion-pair is the main chemical species which exists during the observed exciplex fluorescence lifetime, the spectra measured should be reproduced by the superposition of bands of the Py anion and the DMA cation. The excess energy corresponding to an energy gap between the encounter complex and the geminate ion-pair permits diffusional motion, which leads to a longer distance than that of the stretched P_3. However, the produced pair cannot be completely separated from each other since they are captured in the network of hydrogen bond, leading to the exciplex formation due to recombination.

In order to elucidate these problems magnetic field modulations of the Py triplet and Py anion concentrations formed through quenching of singlet excited Py molecules by amines in polar solvents have been recently investigated.[24,25] In the case of Py–DEA–methanol system, magnetic field modulation has been actually observed. The effect has been interpreted to be due to a magnetic field dependent triplet production in the geminate radical ion-pair induced by hyperfine interaction of the unpaired electrons. Thus, in this case, the existence of the geminate ion-pair is confirmed and the geminate pair as well as the dissociated radical ions can be the main product of the fluorescence quenching reaction.[25] However, in the case of Py–DEA–2-propanol system no magnetic field dependence of the triplet as well as the ion radical concentrations was observed. Thus, exciplex is a predominating species instead of a geminate ion-pair. Since the same conclusion is expected in both Py–DEA and Py–DMA systems, the main transient is exciplex, which gives the above transient absorption spectra of Py–DMA–2-propanol system.

The structure of the P_3 exciplex in 2-propanol differs from that of the Py–DMA intermolecular exciplex in the same solvent. The latter might have a more loose structure owing to the more extensive solvation as compared with the former of the sandwich type structure. The present result indicates that the structure of the exciplex is affected considerably by the properties of solvent.

References

1) R. Potashnik, C. R. Goldschmidt, M. Ottolenghi, and A. Weller, *J. Chem. Phys.*, **55**, 5344 (1971).

2) E. J. Land, J. T. Richards, and J. K. Thomas, *J. Phys. Chem.*, **76**, 3805 (1972).

3) N. Orbach and M. Ottolenghi, *Chem. Phys. Lett.*, **35**, 175 (1975).

4) N. Mataga, T. Okada, H. Masuhara, N. Nakashima, Y. Sakata, and S. Misumi, *J. Lumin.*, **12/13**, 159 (1976).

5) H. Fujiwara, N. Nakashima, and N. Mataga, *Chem. Phys. Lett.*, **47**, 185 (1977).

6) N. Mataga, T. Okada, and N. Yamamoto, *Bull. Chem. Soc. Jpn.*, **39**, 2562 (1966); *Chem. Phys. Lett.*, **1**, 119 (1967).

7) N. Mataga, "Exciplex," ed by M. Gordon and W. R. Ware, Academic Press, New York (1975), p. 113; N. Orbach and M. Ottolenghi, *ibid.*, p. 75; M. Ottolenghi, *Acc. Chem. Res.*, **6**, 153 (1973).

8) T. Okada, Thesis, Osaka University, Osaka (1976).

9) Y. Taniguchi, Y. Nishina, and N. Mataga, *Bull. Chem. Soc. Jpn.*, **45**, 764 (1972).

10) T. Hino, Mc Thesis, Osaka University, Osaka (1975).

11) H. Masuhara, T. Hino, and N. Mataga, *J. Phys. Chem.*, **79**, 994 (1975).

12) H. Masuhara, M. Shimada, N. Tsujino, and N. Mataga, *Bull. Chem. Soc. Jpn.*, **44**, 3310 (1971).

13) J. W. Hunt and J. K. Thomas, *Radiat. Res.*, **32**, 149 (1967).

14) K. Sakurai, "Mini-kon Gijutsu Nyumon," Kyoritsu, Tokyo (1974), p. 106.

15) It has been pointed out that the smooth ns pulse shape detected with a photodiode sometimes consists of many ultra-short pulses. This was confirmed by examining the relation between intensity obtained with a photodiode and that with a thermopile since the latter gives the correct energy output. The linear relation between the digital value and an output of a thermopile suggests that ultra-short pulse does not contribute mainly to the present exciting power. See G. Makkes van der Deijl, J. Dousma, S. Speiser, and J. Kommandeur, *Chem. Phys. Lett.*, **20**, 17 (1973).

16) C. R. Goldschmidt, in "Lasers in Physical Chemistry and Biophysics," ed by J. Joussot-Dubien, Elsevier Scientific Publishing Co., Amsterdam-Oxford-New York (1975).
17) T. Okada and N. Mataga, *Bull. Chem. Soc. Jpn.*, **49**, 2190 (1976).
18) H. Masuhara and N. Mataga, *Z. Phys. Chem. N. F.*, **80**, 113 (1972); H. Masuhara, N. Tsujino, and N. Mataga, *Bull. Chem. Soc. Jpn.*, **46**, 1088 (1973); N. Tsujino, H. Masuhara, and N. Mataga, *Chem. Phys. Lett.*, **21**, 301 (1973); H. Masuhara and N. Mataga, *ibid.*, **22**, 305 (1973).
19) H. Schomburg, Thesis, Göttingen (1975); This value was recently confirmed in this laborartory (H. Masuhara and N. Mataga, to be published).
20) T. Shida and S. Iwata, *J. Am. Chem. Soc.*, **95**, 473 (1973); J. Jagur-Grodzinski, M. Feld, S. L. Yang, and M. Szwarc, *J. Phys. Chem.*, **69**, 628 (1965); E. J. Land and G. Porter, *Trans. Farady Soc.*, **59**, 2027 (1963); J. Langelaar, J. Weddam-Van Beek, H. Ten Brink, and J. D. W. van Voorst, *Chem. Phys. Lett.*, **7**, 368 (1970).
21) H. Beens, Thesis, Free University, Amsterdam (1969).
22) K. Kimura, S. Katsumata, and K. Sawada, *J. Phys. Chem.*, **76**, 639 (1972).
23) D. M. Goodall, N. Orbach, and M. Ottolenghi, *Chem. Phys. Lett.*, **26**, 365 (1974).
24) K. Schulten, H. Staerk, A. Weller, H.-J. Werner, and B. Nickel, *Z. Phys. Chem. N. F.*, **101**, 371 (1976).
25) R. Haberkorn and M. E. Michel-Beyerle, *Z. Naturforsch.*, **31a**, 499 (1976); M. E. Michel-Beyerle, R. Haberkorn, W. Bube, E. Steffens, H. Schröder, H. J. Neusser, E. W. Schlag, and H. Seidlitz, *Chem. Phys.*, **17**, 139 (1976).

Diffusional and Conductive Membrane Permeabilities to Ions in Liquid Membrane-Aqueous Inorganic Electrolyte System

Kazuo NOMURA, Akira MATSUBARA, and Hideo KIMIZUKA*

Laboratory of Chemistry, College of General Education, Kyushu University 01, Ropponmatsu, Fukuoka 810

**Department of Chemistry, Faculty of Science, Kyushu University 33, Hakozaki, Fukuoka 812*

(Received November 4, 1977)

Utilizing a liquid membrane-aqueous inorganic electrolyte system, the membrane permeability to ion α estimated from the conductance and potential data, P_α, and that at zero electric current estimated from the salt flow and potential data, P_α^0, were determined. A solution of calcium hexadecyl sulfate dissolved in 1-octanol and calcium chloride were used as the liquid membrane and the inorganic electrolyte, respectively. The results showed that $P_{Ca}^0/P_{Cl}^0 \approx P_{Ca}/P_{Cl} \approx 10$ and $P_{Cl}^0 \approx P_s^0$, where subscript s refers to the salt. The latter result indicates that the diffusion of a salt through the membrane is governed by the co-ion permeation. It was shown that P_α^0 is smaller than P_α and that P_α decreases with increase in the concentration of external calcium chloride solution while P_α^0 is nearly independent of the concentration. The difference between P_α and P_α^0 can be explained in terms of the elements of permeability and conductance matrices estimated from the electrical and salt flow data.

Liquid membranes have been extensively investigated by analytical chemists, because of their high selectivity to a particular ion.[1] They have also drawn the attention of investigators working with biological membranes as a model for a carrier transport.[2] In spite of numerous experimental works, theories proposed for ion transport through liquid membrane are not as many as those for fixed site membranes. The theory of Eisenman *et al.*[3-6] is widely used to analyze the ion transport phenomena through liquid membranes, but it is derived on the basis of the Nernst-Plank equation.

A theory based on nonequilibrium thermodynamics was presented in a previous paper.[7] It was shown[8] that the equations describing the membrane phenomena for a fixed site membrane is applicable to a liquid membrane with mobile site.

We have carried out an electrochemical study utilizing a cation-exchange liquid membrane containing calcium hexadecyl sulfate for the experimental presentation of the theory.

Experimental

Materials. Calcium hexadecyl sulfate was prepared from sodium hexadecyl sulfate according to the method of Lottermoser and Püschel.[9] Sodium hexadecyl sulfate was prepared from purified 1-hexadecanol obtained by fractional distillation of a commercial sample.[10] All other reagents were of guranteed grade and used without further purification.

Apparatus. The cell assembly is schematically shown in Fig. 1. Two compartments are separated by a liquid membrane supported on a Teflon millipore film (Fluoro Pore, No. EP100, pore size 1.0 μm, thickness 50 μm, from Sumitomo Electric Ind., Ltd.). The liquid membrane was prepared by dissolving calcium hexadecyl sulfate in water-saturated 1-octanol at a concentration of 2.5×10^{-3} mol/dm^3. The diffusional area of the membrane was 0.2 cm^2. Small cells (1.5 cm^3) were used. The concentration of $CaCl_2$ in the internal solution (compartment II) was kept at 4×10^{-3} mol/dm^3, that of the external one (compartment I) being varied from 4×10^{-4} to 10^{-1} mol/dm^3. The whole assembly was thermostated at 25 ± 0.02 °C and the solution in each compartment was stirred with magnetic stirrer at a rate of 200 rpm. The small solubility of calcium hexadecyl sulfate in aqueous solution, an order of 10^{-6} mol/dm^3, was obtained at 25 °C.[11] The dissolution of calcium hexadecyl sulfate in the aqueous phase may be ignored. This was also confirmed by the constancy of the conductance of aqueous calcium chloride solution in contact with the liquid membrane.

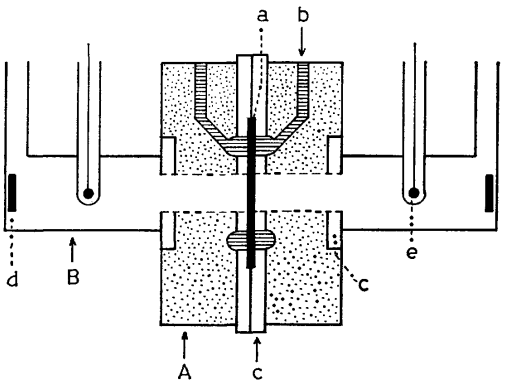

Fig. 1. Schematic diagram of the experimental cell assembly.
A; The holder of the liquid membrane made of two polyethylene-boards. B; The half glass cell. a; The liquid membrane supported on a Teflon millipore film. b; The liquid membrane was retained in the circumference of the supporting film. c; The silicon rubber-packing. d; The magnetic spin bar. e; A pair of platinized platinum electrodes.

Salt Flow Measurement. The salt flow was studied by measuring the change in the concentration of the solution. Concentration changes were followed by the electric conductance of the external and internal solutions measured by means of the two Pt-Pt electrodes connected to the Yanagimoto conductivity outfit Model MY-7. The solutions were replaced with fresh ones several times, until a steady membrane resistance was obtained. It took more than 24 h on some occasions to attain a steady salt flow.

A theory for the liquid membrane has been presented[8] by assuming 1) steady state, 2) absence of the flow of water as well as organic solvent, 3) the dissociation equilibrium for the mobile site-counter ion binding within the liquid membrane, and 4) presence of the mobile site only within the liquid membrane. It has been shown that the equations describing transport phenomena for the fixed site membrane[7] is equally applicable to the system with a mobile site membrane.

The membrane permeability to ion α, P^0_α, as well as that to salt, P^0_s, at zero electric current can be estimated by using the equations[7] for the flux, J^0_α and the salt flux, J_s:

$$J^0_\alpha = \nu_\alpha J_s = -P^0_\alpha \Delta\bar{a}_\alpha = -P^0_\alpha\{a^{II}_\alpha \exp(Z_\alpha \Phi_0/2) - a^I_\alpha \exp(-Z_\alpha\Phi_0/2)\}, \quad (1)$$

and

$$J_s = -P^0_s \Delta a_s = -P^0_s(a^{II}_s - a^I_s), \quad (2)$$

where

$$\Phi_0 = FV_0/RT, \quad (3)$$

ν, Z, F, α, V_0, R, and T denote the stoichiometric coefficient, the charge number, Faraday constant, the activity, the membrane potential at zero electric current, gas constant and absolute temperature, respectively. Superscripts I and II refer to compartments I and II, respectively, and subscripts α and s to ion α and salt s, respectively.

Membrane Potential and Conductance Measurements. The membrane potential was measured by means of two calomel electrodes connected to the Orion digital pH meter Model 701. The calomel electrode was connected to each compartment through an agar bridge. In experiments at lower concentrations, the solutions were replaced by fresh ones several times in order to avoid contamination with KCl diffusing from the agar bridge.

The membrane resistance was measured by means of the two Pt-Pt electrodes connected to the same conductivity outfit as used for the salt flow measurement. The membrane resistance was obtained by subtracting the solution resistance from the total one. After the steady state was attained, the membrane resistance remained constant. Errors inherent to the measurement of the membrane resistance were 4—5 percent.

The membrane permeability to ion α, P_α, is related to ion conductance, g_α, by[7]

$$g_\alpha = t_\alpha G_m = \frac{(Z_\alpha F)^2}{RT} P_\alpha (a^I_\alpha a^{II}_\alpha)^{1/2} \frac{\sinh Z_\alpha(\Phi_0 - \Phi_\alpha)/2}{Z_\alpha(\Phi_0 - \Phi_\alpha)/2}, \quad (4)$$

where

$$\Phi_\alpha = FV_\alpha/RT, \quad (5)$$

and t_α denotes the apparent transport number, G_m the membrane conductance, and V_α the equilibrium membrane potential for the ion α.

Results and Discussion

The membrane potential, V_0, the membrane conductance, G_m, and the salt flow, J_s, are plotted against the mean activity of $CaCl_2$ in the external solution ($a^I_\pm$) in Fig. 2. The apparent transport number, t_{Ca}, estimated from the potential *vs.* logarithm of mean activity relation was nearly constant, 0.96, within the range of concentration studied.

Membrane permeability at zero electric current, P^0_{Ca}, P^0_{Cl} and P^0_s, can be estimated from the potential and salt flow data according to Eqs. 1 and 2. P_{Ca} and P_{Cl} can be estimated from the potential and conductance data according to Eq. 4. The results are shown in Fig. 3.

We see that $P^0_{Ca} > P^0_{Cl}$, $P_{Ca} > P_{Cl}$, $P^0_{Ca} < P_{Ca}$, and $P^0_{Cl} \approx P^0_s < P_{Cl}$. Since the membrane is a cation exchanger, the results $P^0_{Ca} > P^0_{Cl}$ and $P_{Ca} > P_{Cl}$ are as expected. The ratio of P^0_{Ca} to P^0_{Cl} and that of P_{Ca} to P_{Cl} are both about ten. The result, $P^0_{Cl} \approx P^0_s$, indicates that the diffusion of salt through the liquid membrane is governed by co-ion permeation.

P_{Ca} and P_{Cl} decrease with the increase in the geometric mean of the activities of external and internal solutions as shown in Fig. 3. On the other hand, P^0_{Ca}, P^0_{Cl}, and P^0_s show no appreciable concentration dependence. P^0_α, P_α and P^0_α/P_α can respectively be expressed as functions of the elements of permeability matrix $P_{\alpha\beta}$'s and of conductance matrix $g_{\alpha\beta}$'s ($\alpha \neq \beta$) as follows.

$$P^0_\alpha = (P_{\alpha\alpha}P_{\beta\beta} - P_{\alpha\beta}P_{\beta\alpha})/P_\beta, \quad (6)$$

$$P_\alpha = P_{\alpha\alpha} + Z_\beta P_{\beta\alpha}/Z_\alpha, \quad (7)$$

and

$$\frac{P^0_\alpha}{P_\alpha} = 1 - \frac{Z_\beta P_{\beta\alpha}}{Z_\alpha P_\alpha} - \frac{Z_\alpha P_{\alpha\beta}}{Z_\beta P_\beta} = 1 - g_{\alpha\beta}\left(\frac{1}{g_\alpha} + \frac{1}{g_\beta}\right). \quad (8)$$

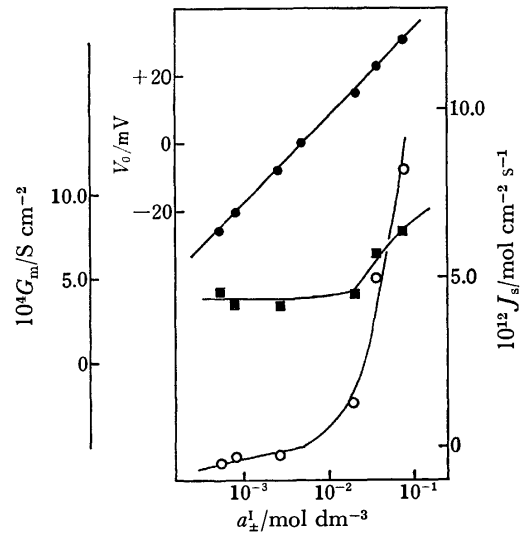

Fig. 2. The membrane potential (●), the membrane conductance (■), and the salt flow (○), each as a function of the mean activity of external solution. The concentration of the internal solution was kept at 4×10^{-3} mol/dm^3.

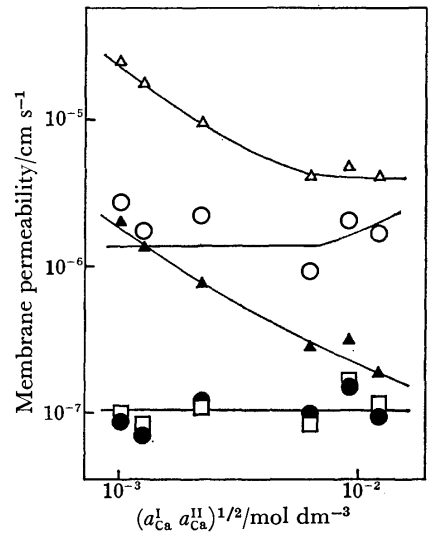

Fig. 3. The membrane permeabilities as a function of the geometric mean of the activity of external and internal solutions. △; P_{Ca}, ▲; P_{Cl}, ○; P^0_{Ca}, ●; P^0_{Cl} □; P^0_s. The solid lines indicate the values of P^0_α and P_α calculated from $P_{\alpha\beta}$ (Fig. 5) according to Eqs. 6 and 7, respectively.

$P_{\alpha\beta}$ is related to an element of conductance matrix $g_{\alpha\beta}$:

$$g_{\alpha\beta} = \frac{Z_\alpha Z_\beta F^2}{RT} P_{\alpha\beta}(a_\beta^{\mathrm{I}} a_\beta^{\mathrm{II}})^{1/2} \frac{\sinh Z_\beta(\Phi_0 - \Phi_\beta)/2}{Z_\beta(\Phi_0 - \Phi_\beta)/2}, \quad (9)$$

and $g_{\alpha\beta}$ can be estimated according to the equation

$$g_{\alpha\beta} = g_{\beta\alpha} = G_{\mathrm{m}} t_\alpha t_\beta - \frac{(Z_\alpha \nu_\alpha F)^2 P_{\mathrm{s}}^0 \Delta a_{\mathrm{s}}}{\nu_{\mathrm{s}} \Delta\mu_{\mathrm{s}}}, \quad (10)$$

where

$$\nu_{\mathrm{s}} = \nu_\alpha + \nu_\beta,$$

and $\Delta\mu_{\mathrm{s}}$ denotes the chemical potential difference of salt across membrane. The diagonal elements of conductance matrix, $g_{\alpha\alpha}$ and $g_{\beta\beta}$, are given by

$$g_{\alpha\beta} = g_\alpha - g_{\alpha\alpha} = g_\beta - g_{\beta\beta}. \quad (11)$$

The value of $g_{\alpha\beta}$ was evaluated by means of Eq. 10 where the activity data of calcium chloride in phases I and II were taken from Handbook of Chemistry (Chemical Society of Japan). The other elements $g_{\alpha\alpha}$ and $g_{\beta\beta}$ were calculated by means of Eq. 11. These elements were plotted against the mean activity of calcium chloride in phase I as shown in Fig. 4. The elements of permeability matrix were estimated by means of Eq. 9 and the results are shown in Fig. 5.

The ratio P_α^0/P_α may be calculated from Eq. 8 by using the elements of the permeability matrix. A comparison of the observed values with calculated ones is given in Fig. 6. The agreement is satisfactory.

The full lines in Fig. 3 represent P_α^0 and P_α calculated by means of Eqs. 6 and 7, respectively. We see that the agreement between theory and experiment is satisfactory.

P_α^0 can be expressed by

$$\frac{1}{P_\alpha^0} = \frac{1}{P_\alpha^0(\mathrm{I})} + \frac{1}{P_\alpha^0(\mathrm{m})} + \frac{1}{P_\alpha^0(\mathrm{II})}, \quad (12)$$

where (I) and (II) refer to the boundary layers in phases I and II, respectively, and (m) denotes the membrane phase.[7] Since the system is close to equilibrium with respect to calcium ions, we can put

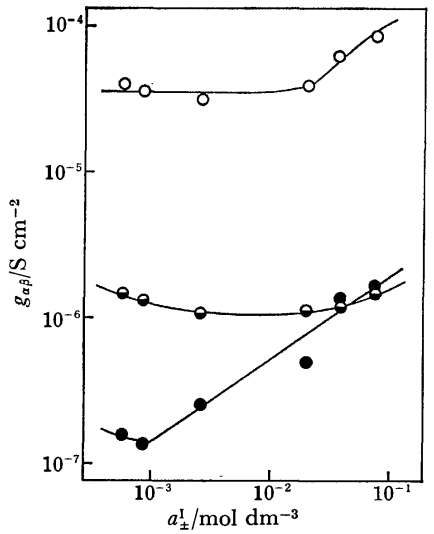

Fig. 4. The elements of the conductance matrix as a function of the mean activity of external solution. The concentration of internal solution was kept at 4×10^{-3} mol/dm^3. ○; $g_{\mathrm{Ca.Ca}}$, ◒; $g_{\mathrm{Ca.Cl}}$, ●; $g_{\mathrm{Cl.Cl}}$.

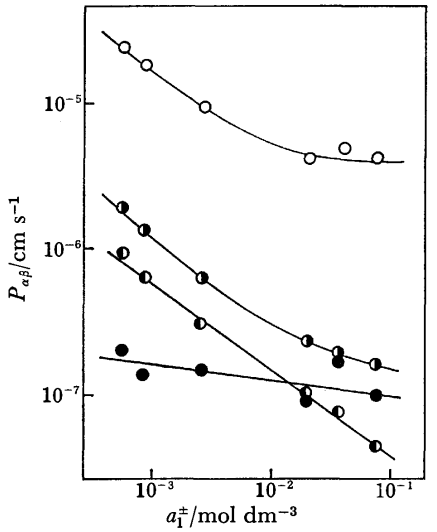

Fig. 5. The elements of the permeability matrix as a function of the mean activity of external solution. The concentration of internal solution was kept at 4×10^{-3} mol/dm^3. ○; $P_{\mathrm{Ca.Ca}}$, ◑; $-P_{\mathrm{Cl.Ca}}$, ◐; $-P_{\mathrm{Ca.Cl}}$, ●; $P_{\mathrm{Cl.Cl}}$.

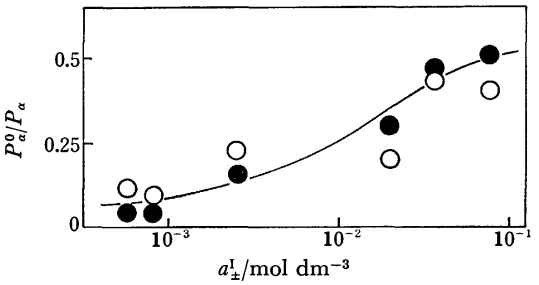

Fig. 6. The ratio P_α^0/P_α as a function of the mean activity of external solution. The concentration of internal solution was kept at 4×10^{-3} mol/dm^3. ○; $P_{\mathrm{Ca}}^0/P_{\mathrm{Ca}}$, ●; $P_{\mathrm{Cl}}^0/P_{\mathrm{Cl}}$. The solid line was calculated from $P_{\alpha\beta}$ according to Eq. 8.

$$\frac{1}{P_{\mathrm{Ca}}^0(\mathrm{I})} = \frac{l(\mathrm{I})}{D_{\mathrm{Ca}}(\mathrm{I}) \cdot C_{\mathrm{Ca}}(\mathrm{I})} (a_{\mathrm{Ca}}^{\mathrm{I}} a_{\mathrm{Ca}}^{\mathrm{II}})^{1/2} \quad (13)$$

and

$$\frac{1}{P_{\mathrm{Ca}}^0(\mathrm{II})} = \frac{l(\mathrm{II})}{D_{\mathrm{Ca}}(\mathrm{II}) \cdot C_{\mathrm{Ca}}(\mathrm{II})} (a_{\mathrm{Ca}}^{\mathrm{I}} a_{\mathrm{Ca}}^{\mathrm{II}})^{1/2}, \quad (14)$$

where l, D, and C denote the boundary layer thickness, the diffusion coefficient in boundary layer and the concentration, respectively. Assuming that the thickness of boundary layers to be 100 μm, the values of $1/P_{\mathrm{Ca}}^0$ (I) and $1/P_{\mathrm{Ca}}^0$ (II) were found to be in the order of 10^3 cm^{-1} s, while $1/P_{\mathrm{Ca}}^0$ was the order of 10^5—10^6 cm^{-1} s, *i.e.*,

$$P_{\mathrm{Ca}}^0 \approx P_{\mathrm{Ca}}^0(\mathrm{m}). \quad (15)$$

It can be concluded that the transport process is the membrane control. Since the membrane resistance was obtained by subtracting part of the solution resistance from the total one, we have

$$P_{\mathrm{Ca}} \approx P_{\mathrm{Ca}}(\mathrm{m}). \quad (16)$$

The theory based on the Nernst-Plank equation can not differentiate P_α from P_α^0.[7] Thus an explanation for the transport phenomena should be made on the basis of nonequilibrium thermodynamics.

This research has been supported in part by a Grant-in-Aid for Scientific Research from the Ministry of Education.

References

1) R. A. Durst, Ed., "Ion Selective Electrode," Dept. of Commerce, National Bureau of Standards Special Publication 314, Washington, D. C. (1969), Chaps. 1 and 2.
2) G. M. Shean and K. Sollner, *Ann. N. Y. Acad. Sci.*, **137**, 759 (1966).
3) F. Conti and G. Eisenman, *Biophys. J.*, **6**, 227 (1966).
4) J. L. Walker and G. Eisenman, *Biophys. J.*, **6**, 513 (1966).
5) J. P. Sandblom, G. Eisenman, and J. L. Walker, *J. Phys. Chem.*, **71**, 3862 (1967).
6) J. L. Walker, G. Eisenman, and J. P. Sandblom, *J. Phys. Chem.*, **72**, 978 (1968).
7) H. Kimizuka and K. Kaibara, *J. Colloid Interface Sci.*, **52**, 516 (1975).
8) A. Yamauchi, T. Minematsu, and H. Kimizuka, *Membrane*, **2**, 69 (1977).
9) A. Lottermoser and F. Püschel, *Kolloid-Z.*, **63**, 175 (1933).
10) R. Matuura, H. Kimizuka, S. Miyamoto, and R. Shimozawa, *Bull. Chem. Soc. Jpn.*, **31**, 532 (1958).
11) A. Matsubara, K. Nomura, and H. Kimizuka, *Mem. Fac. Sci. Kyushu Univ. Ser. C*, **10**, 111 (1977).

Polarized Absorption Spectra of Single Crystals of Tetrathiafulvalenium Salts

Tadashi SUGANO, Kyuya YAKUSHI, and Haruo KURODA

Department of Chemistry, Faculty of Science, The University of Tokyo, Hongo, Tokyo 113

(Received November 8, 1977)

The polarized absorption spectra over the range, 5000—37000 cm^{-1}, were observed on the single crystals of the highly-conductive, mixed-valence tetrathiafulvalenium salts, (TTF)$Br_{0.71}$, (TTF)$I_{0.71}$, and (TTF)$(SCN)_{0.57}$, by using a microspectrophotometer. The spectra of these crystals were very similar to each other. The observed spectra were successfully interpreted in terms of the localized model, considering the charge transfer transitions between TTF species and the local excitations associated with the intramolecular transitions of the molecule and ion of TTF. The spectrum of the (TTF)(ClO_4) crystal were also studied to aid the interpretations of the spectra of the mixed-valence TTF salts.

The crystal of the charge-transfer salt of tetrathiafulvalene (TTF) with tetracyano-*p*-quinodimethane (TCNQ) is composed of the segregated stacks of TTF and TCNQ. A variety of evidences[1-8] indicate that an incomplete charge transfer is taking place between TTF and TCNQ in this salt, so that the TTF and TCNQ stacks are of mixed-valence characters. In the case of (TTF)(TCNQ), both the TTF and TCNQ stacks are contributing to the metal-like behaviors displayed by this salt.[9,10] This situation causes considerable complexities in analysing the physical properties of (TTF)-(TCNQ).[7,8,11-13] There are a group of the mixed-valence TTF salts which display high electrical conductivities almost comparable to (TTF)(TCNQ). These are (TTF)$Br_{0.71-0.76}$,[14] (TTF)$I_{0.71}$,[14-16] (TTF)-$(SCN)_{0.54-0.58}$[16-18] and (TTF)$(SeCN)_{0.54-0.58}$.[16,17] These mixed-valence TTF salts are almost isomorphous with each other,[16-22] having nearly the same one-dimensional stack of TTF, and the metal-like electrical conductivities as well as other physical properties of these salts, are primarily determined by the nature of the mixed-valence TTF stack. Thus these salts can be regarded as the suitable model compounds for the purpose to study the electronic behaviors of the mixed-valence, one-dimentional TTF stack.

The electrical and magnetical properties of the TTF salts mentioned above have been studied by several authors.[14-18,23,24] As regards their optical properties, the observations of reflection spectra were reported on (TTF)$Br_{0.76}$,[22,25] (TTF)$I_{0.71}$[26] and (TTF)$(SeCN)_{0.54}$,[17] but no direct observation of the absorption spectra of single crystals have been hitherto reported.

In the present work, we have studied the polarized absorption spectra of small single crystals of (TTF)$Br_{0.71}$, (TTF)$I_{0.71}$ and (TTF)$(SCN)_{0.57}$, over the range of 5000—37000 cm^{-1} (0.6—4.5 eV), by use of a microspectrophotometer. For the sake of comparison, we have also studied the absorption spectrum of (TTF)-(ClO_4).

Experimental

TTF was synthesized by the method reported by Melby *et al.*,[27] recrystallized from the cyclohexane solution, and finally purified by repeating sublimation in vacuum. The mixed-valence halides, (TTF)$Br_{0.71}$ and (TTF)$I_{0.71}$, were prepared by the procedures described in our previous paper.[24,28] (TTF)(ClO_4) was prepared by the method reported by Hünig *et al.*[29] (TTF)$(SCN)_{0.57}$[18] was kindly provided by Dr. H. Kobayashi of Toho University.

The polarized absorption spectra of single crystals were measured at room temperature by means of a microspectrophotometer, Olympus MS-A-IV. In order to observe absorption spectrum, it is necessary to obtain a crystal of the size and thickness suitable for the measurement of absorption spectrum by the microspectrophotometer. We dissolved each salt in the deairated dry hot acetonitrile, dropped a small amount of the hot solution on a quartz plate, and allowed for the solvent to evaporate leaving small crystals of the salt on the quartz plate. We examined the crystals thus formed on the quartz plate, by a polarization microscope to select out a suitable crystal. The crystal habit was also checked by the observation under the polarization microscope. The sizes of the crystals used in the present study of absorption spectra were less than 1 μm in thickness, 5—20 μm in width and 20—50 μm in length.

Results and Discussion

(TTF)(ClO_4), a Simple Cation Radical Salt. (TTF)(ClO_4) is expected to be a salt composed of $(TTF)^+$ and $(ClO_4)^-$. Fig. 1 shows the infrared spectra of (TTF)(ClO_4) and (TTF)(DDQ),[30] measured by the Nujol-mull method. The infrared spectrum of (TTF)-(DDQ) shows all absorption bands characteristic of $(DDQ)^-$, which appear in the infrared spectrum of $Li^+(DDQ)^-$,[31] and exhibits no band attributable to DDQ molecule. Thus, (TTF)(DDQ) can be concluded to be a salt composed of $(TTF)^+$ and $(DDQ)^-$. We can attribute all of the residual bands in the infrared spectrum of (TTF)(DDQ) to those arising from $(TTF)^+$. When the infrared spectrum of (TTF)(ClO_4) is compared with that of (TTF)(DDQ), we can see that all bands in the former spectrum correspond to the ones which have been attributed to $(TTF)^+$ in the latter case, there being no band attributable to TTF molecule. This fact proves that (TTF)(ClO_4) is indeed the salt composed of $(TTF)^+$ and $(ClO_4)^-$.

From the Weissenberg photographs, it was found that the crystal of (TTF)(ClO_4) is orthorhombic, with the space group Pbca(D_{2h}^{15}), the approximate lattice constants being $a=16.7$, $b=20.6$, and $c=12.8$ Å. It crystallizes from the acetonitrile solution as thin crystals elongated along the a-axis with the developed face (001). We measured the polarized absorption spectra

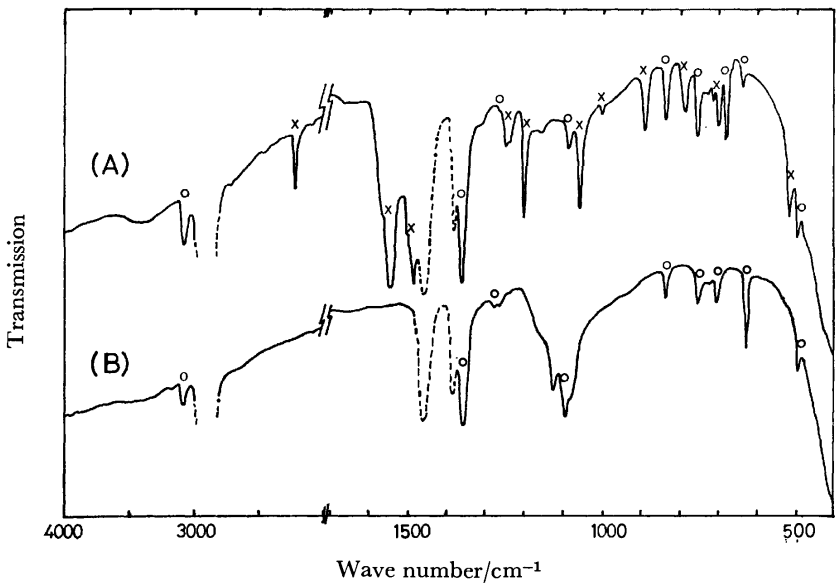

Fig. 1. Infrared spectra of TTF–DDQ(A) and TTF–ClO_4(B). The bands due to $(TTF)^+$ are indicated with a open circle and those due to $(DDQ)^-$ with a cross. The dashed line represent the absorption by Nujol.

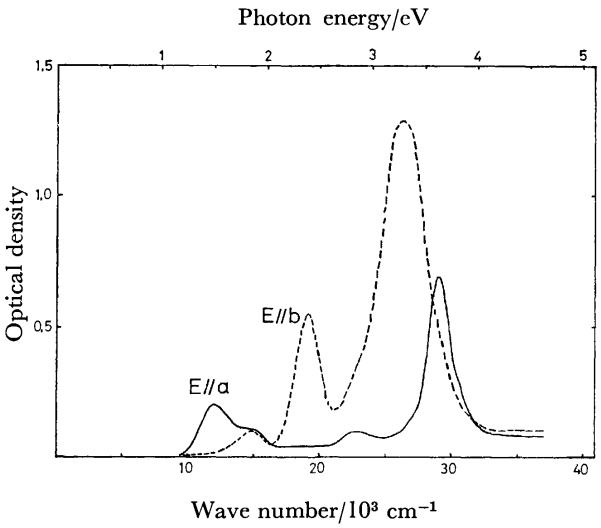

Fig. 2. Polarized absorption spectra observed on the (001) plane of a single crystal of $(TTF)(ClO_4)$.

on the (001) plane of $(TTF)(ClO_4)$ crystal, with the light polarizations, parallel to a- and b-axes respectively, and obtained the spectra shown in Fig. 2.

In the region below 17×10^3 cm^{-1}, the a-axis spectrum exhibits an absorption maxium at 12.0×10^3 cm^{-1} with a shoulder at about 15×10^3 cm^{-1}, while the b-axis spectrum shows a maxium at 15.0×10^3 cm^{-1}. Seemingly there are two absorption bands; the one is at 12.0×10^3 cm^{-1}, completely polarized in the a-axis direction, and the other is at 15.0×10^3 cm^{-1} with a transition moment in the direction inbetween the a- and b-axes. In these regions, we can not expect any local-excitation (LE) band associated with an intramolecular transition of $(TTF)^+$. Thus the observed absorption bands must be the ones arising from the charge transfer between $(TTF)^+$ ions. The fact that the first CT band (at 12.0×10^3 cm^{-1}) is completely polarized in the a-axis direction, indicates that $(TTF)^+$ ions are stacked on each other along the a-axis. The origin of the second CT band (at 15.0×10^3 cm^{-1}) is not clear. Presumably, there are two different types of the overlap between the neighboring $(TTF)^+$ ions in the crystal, and the first CT band arises from the one with the closest overlap and the second CT band arises from the other type of overlap.

TABLE 1. WAVE NUMBERS AND RELATIVE INTENSITIES (given in the parentheses)[a] OF LOCAL EXCITATION BANDS OF $(TTF)^+(ClO_4)^-$ AND THOSE OF THE SOLUTION SPECTRUM OF THE $(TTF)^+$ ION

Transition	Transition in $(TTF)^+$ (calcd)[b]			Transition in $(TTF)^+$ (exp.)[c]	$(TTF)^+(ClO_4)^-$	
	Assignment	Polarization	$\bar{\nu}$(10^3 cm^{-1})	$\bar{\nu}$(10^3 cm^{-1})	$\bar{\nu}$(10^3 cm^{-1})	Polarization
LE_1	$b_{1u}\leftarrow b_{2g}$	x	16.8(0.48[d])	17.3(0.27[e])	19.2(0.28[f])	b-axis
LE_2	$b_{3g}\leftarrow b_{1u}$	y	17.8(0.21)	20.3(sh.)	22.8(0.03)	(a-axis)
LE_3	$b_{2g}\leftarrow b_{1u}$	x	19.5(1.00)	23.0(1.00)	26.4(1.00)	b-axis
LE_4	$b_{1u}\leftarrow b_{3g}$	y	23.7(0.52)	29.6(0.32)	29.1(0.34)	(a-axis)

a) Relative to the intensity of the LE_3 band. b) See Ref. 32. The x-axis is chosen for the long axis of molecule. c) See Ref. 29. d) Relative oscillator strengths. e) Relative absorption coefficients. f) Relative peak heights (correspond to absorption coefficients).

In the region above 17×10^3 cm^{-1}, both the a-axis and b-axis spectra show two absorption bands. The wave numbers and relative intensities of these bands are listed in Table 1. The absorption spectrum of the $(TTF)^+$ ion in the solution shows four absorption bands in the corresponding region, the maxima of which are located at 17.3×10^3, 23.0×10^3, and 29.6×10^3 cm^{-1}, respectively.[29] According to the semi-empirical limited-CIS-CF-MO calculation,[32] the lowest four allowed transitions of $(TTF)^+$ are associated respectively with the following electronic excitations between π-orbitals, $b_{1u}\leftarrow b_{2g}$ (x polarized), $b_{3g}\leftarrow b_{1u}$ (y polarized), $b_{2g}\leftarrow b_{1u}$ (x polarized) and $b_{1u}\leftarrow b_{3g}$ (y polarized), where x and y stand for the long and short axes of the ion, respectively. The predicted energies and oscillartor strengths of these transitions well correspond to the four absorption bands observed in the solution spectrum, as shown in Table 1. By comparing the spectra of $(TTF)(ClO_4)$ with the solution spectrum of $(TTF)^+$, we can conclude that the 19.2×10^3 and 26.4×10^3 cm^{-1} bands of the b-axis spectrum are the local-excitation (LE) bands associated with the 17.3×10^3 and 23.0×10^3 cm^{-1} transitions of $(TTF)^+$. Note that the intensity ratio of the above two bands are in good agreement with the intensity ratio of the corresponding bands in the solution spectrum. We will call the 19.2×10^3 and 26.4×10^3 cm^{-1} bands of $(TTF)(ClO_4)$ as LE_1 and LE_3, respectively.

The 29.1×10^3 cm^{-1} band in the a-axis spectrum is likely to be the LE band associated with the 29.6×10^3 cm^{-1} transition of $(TTF)^+$. Since the LE band associated with the 20.3×10^3 cm^{-1} transition of $(TTF)^+$ should appear in the spectrum of $(TTF)(ClO_4)$ in the region of $20—24\times10^3$ cm^{-1} with the same polarization as the above LE band, we can attribute the weak absorption band at 22.8×10^3 cm^{-1} in the a-axis spectrum, to this LE band. The intensity ratio of the two absorption bands of the a-axis spectrum is consistent with this interpretation. We will call the 20.3×10^3 and 29.1×10^3 cm^{-1} bands of $(TTF)(ClO_4)$ as LE_2 and LE_4, respectively.

The LE_1, LE_2, and LE_3 bands have been shifted to higher energy by about 2×10^3 cm^{-1} as compared with the corresponding absorption bands of the solution spectrum of $(TTF)^+$. This is just the magnitude of the shift that is often found in the crystal where the intermolecular charge-transfer interaction is taking place between the constituent radical ions. According to the above interpretation of the observed spectra, the LE bands associated with the long-axis polarized transitions of $(TTF)^+$ appear only in the b-axis spectrum, showing that they have no components of the transition moments in the a-axis direction. This fact implies that the long axis of $(TTF)^+$ is in the bc plane of the $(TTF)(ClO_4)$ crystal.

Mixed-valence TTF Salts. The TTF sublattices of $(TTF)Br_{0.71}$,[19] $(TTF)I_{0.71}$,[20,21] and $(TTF)(SCN)_{0.57}$[18] are very similar to each other as illustrated in Table 2, where the unit cell of $(TTF)(SCN)_{0.57}$ has been transformed from a tetragonal simple lattice to a C-centered lattice in order to facilitate the comparison with the halides. In all of the three salts, TTF molecules (or ions)

Table 2. TTF Sublattices of $(TTF)Br_{0.71}$, $(TTF)I_{0.71}$, and $(TTF)(SCN)_{0.57}$

	a(Å)	b(Å)	c(Å)	β(deg)
$(TTF)Br_{0.71}$[a]	15.62	15.63	3.57	91.2
$(TTF)I_{0.71}$[b]	16.01	16.04	3.55	91.3
$(TTF)(SCN)_{0.57}$[c]	15.77	15.77	3.61	90.0

a) See Ref. 19. b) See Refs. 20 and 21. c) See Ref. 18. The tetragonal unit cell is changed to a C-centered unit cell.

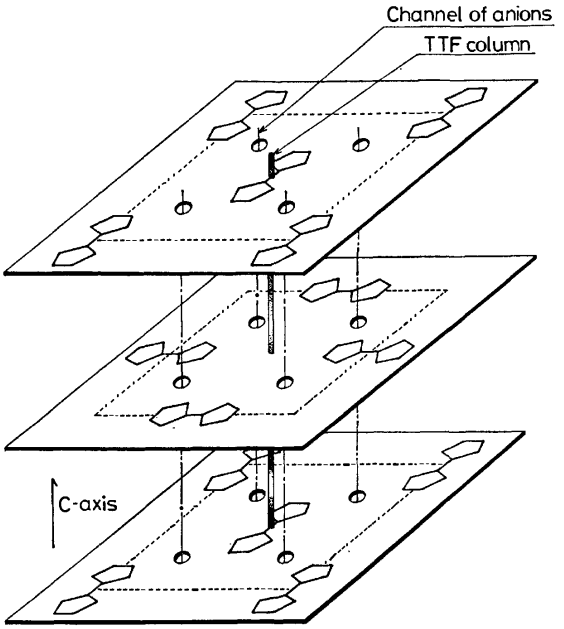

Fig. 3. Schematic picture of the TTF sublattice found for the mixed-valence TTF salts. About eight times enlarged in the c-axis direction.

are stacked along the c-axis with an eclipsed overlap, making their molecular planes almost perpendicular to the c-axis (see Fig. 3). All three salts crystallize from the hot acetonitrile solutions as crystals elongated along the a-axis with the developed face (100). The absorption spectra were measured on the (100) planes of these crystals with the light polarizations, parallel to the b- and c-axis respectively. The observed spectra are

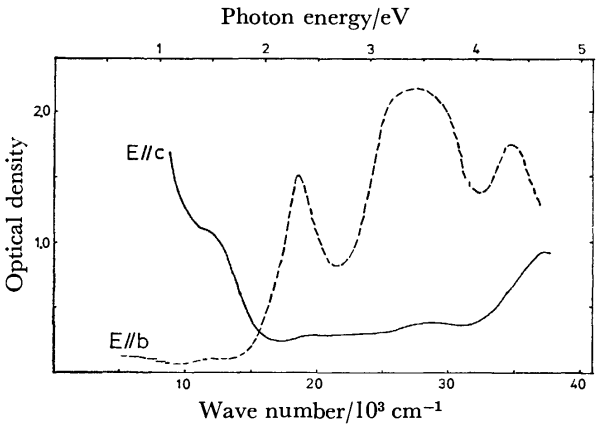

Fig. 4. Polarized absorption spectra observed on the (100) plane of a single crystal of $(TTF)Br_{0.71}$.

TABLE 3. WAVE NUMBERS OF ABSORPTION BANDS IN THE SPECTRA OF THE MIXED-VALENCE TTF SALTS

Transition character	c-axis spectra $\bar{\nu}(10^3\ cm^{-1})$			b-axis spectra $\bar{\nu}(10^3\ cm^{-1})$			Intramolecular transitions[a]	
	Bromide	Iodide	Thiocyanate	Bromide	Iodide	Thiocyanate	TTF^+	TTF^0
CT band								
$(TTF)^+(TTF)^0 \rightarrow (TTF)^0(TTF)^+$	<9.0	<7.5	<8.0					
$(TTF)^+(TTF)^+ \rightarrow (TTF)^0(TTF)^{2+}$	12.5	12.4	11.0					
LE band								
$(TTF)^+$ LE_1				18.5	18.4	17.6	17.3 (5030) 20.3 (sh)	
LE_3+LE_4				27.5	27.0	27.7	23.0 (18600) 29.6 (5970)	22.4 (263) 28.0 (sh)
$(TTF)^0$				34.9	33.0	34.5		32.5 (12200)
Unknown	≈37	≈35	≈37					

a) See Ref. 29. Absorption coefficient is given in the parenthesis.

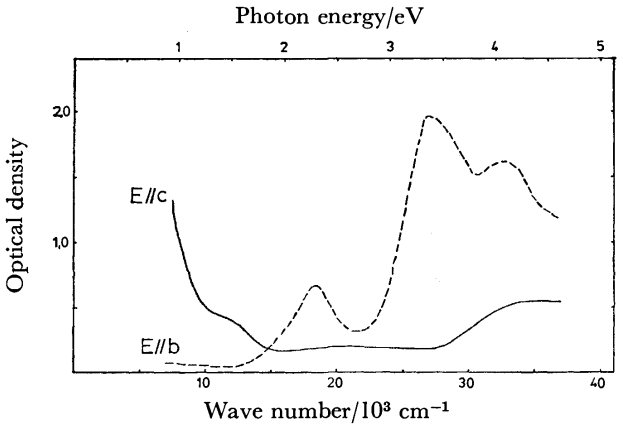

Fig. 5. Polarized absorption spectra observed on the (100) plane of a single crystal of $(TTF)I_{0.71}$.

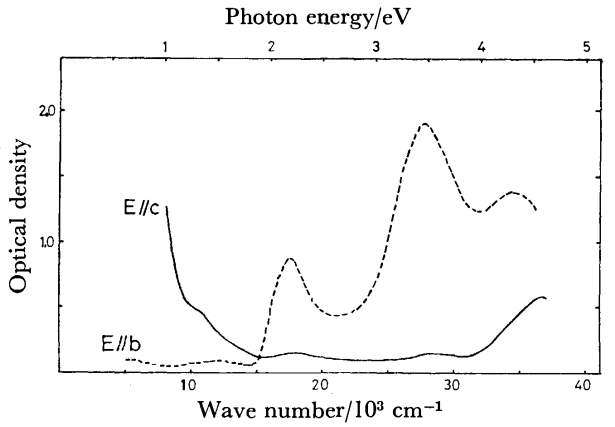

Fig. 6. Polarized absorption spectra observed on the (100) plane of a single crystal of $(TTF)(SCN)_{0.57}$.

shown in Figs. 4, 5, and 6. The wave numbers and relative intensities of the observed bands are listed in Table 3.

One can easily see from the arrangement and orientation of TTF in these salts that an absorption band associated with the intermolecular charge transfer along the TTF stack should appear exclusively in the c-axis spectrum, while the LE bands associated with the intramolecular transitions of $(TTF)^+$ ion and/or TTF molecule, both the long-axis and short-axis polarized ones, should appear only in the b-axis spectrum.

The spectra observed of the three salts are very similar to each other. The c-axis spectrum of each salt exhibit a strong absorption band in the region below $15\times10^3\ cm^{-1}$, and the b-axis spectrum shows three absorption maxima in the region above $15\times10^3\ cm^{-1}$. The former must be due to the intermolecular charge transfer and the latter must be due to the local excitations.

Let us first examine the LE bands which appear in the b-axis spectra. All salt exhibit three absorption maxima located at about 18×10^3, 27×10^3, and 34×10^3 cm^{-1}, respectively. Since the solution spectrum of TTF molecule exhibits no absorption band in the region below $22\times10^3\ cm^{-1}$, the first maximum at about $18\times10^3\ cm^{-1}$ cannot be due to the TTF neutral molecule. We can attribute it to the LE band associated with the $17.3\times10^3\ cm^{-1}$ transition of $(TTF)^+$. The second maximum is very strong, suggesting that it is associated with some strong transitions in the TTF molecule or $(TTF)^+$ ion. Although the TTF molecule has two transitions (at 22.4×10^3 and $28.0\times10^3\ cm^{-1}$) in the corresponding region, both of them are of very low oscillator strength, and cannot be taken as the origin of the observed strong absorption maximum. The possible origins of the second absorption maximum which is commonly observed in the b-axis spectra of the three mixed-valence salts, would be the 23.0×10^3 or $29.6\times10^3\ cm^{-1}$ transitions of $(TTF)^+$. It should be noted that the positions of the second absorption maxima observed for the three TTF salts are very close to that of the LE_3 band of $(TTF)(ClO_4)$, but the observed band shapes are considerably broader as compared with the latter. Seemingly, the local excitation bands associated with the 23.0×10^3 and $29.6\times10^3\ cm^{-1}$ transitions of $(TTF)^+$ are superimposed on each other to give a broad absorption maximum. TTF molecule has a srtong transition at $32.5\times10^3\ cm^{-1}$.[29,33,34] The third absorp-

tion maximum which is located at 33—35 $\times 10^3$ cm^{-1} in the b-axis spectra, is most likely to be the LE band associated with the above transition of TTF molecule.

As we have described above, all absorption bands observed in the b-axis spectra of the three salts can be interpreted either as a LE band associated with a transition of $(TTF)^+$ or that associated with a transition of $(TTF)^0$. If positive holes are completely delocalized through the TTF stack to give the same fractional charge on every TTF molecule, the TTF stack will exhibits an absorption spectrum composed of the bands which cannot be simply correlated with the transitions of $(TTF)^+$ and $(TTF)^0$. The fact that the observed spectra can be well interpreted in terms of the intramolecular transitions of $(TTF)^+$ and $(TTF)^0$, suggests that, as regards the optical properties, the TTF stack behaves as if it is composed of ions and molecules of TTF in spite of the metal-like high electrical conductivity through the TTF stack.

According to the interpretations of the spectra mentioned above, the intensity ratio of the first and third bands in the b-axis spectrum of each salt must be related to the ratio of $(TTF)^+$ and $(TTF)^0$. Using the molar extinction coefficient of the 17.3 $\times 10^3$ cm^{-1} band of the solution spectrum of $(TTF)^+$ and that of the 32.5 $\times 10^3$ cm^{-1} band of the solution spectrum of $(TTF)^0$, we estimated the ionized fraction of TTF from the observed intensity ratio. The ionized fraction of TTF thus obtained is 0.67, 0.58, and 0.62 for $(TTF)Br_{0.71}$, $(TTF)I_{0.71}$, and $(TTF)(SCN)_{0.57}$, respectively. These are very rough values since we have to expect various sources of error in the procedures of obtaining them from the observed crystal spectra. Nevertheless the results are quite reasonable. In particular, it is interesting to see that the ionized fraction is estimated to be appreciably lower in $(TTF)I_{0.71}$ than in $(TTF)Br_{0.71}$. Recently, we showed[5] that the S 2p peaks of the X-ray photoelectron spectra of mixed-valence TTF salts can be well reproduced by superimposing the S 2p peak characteristic of $(TTF)^0$ and that characteristic of $(TTF)^+$, assuming an appropriate intensity ratio. From the above analyses of the observed S 2p peaks we concluded that the ionized fraction of TTF is 0.71 and 0.52 in $(TTF)Br_{0.71}$ and $(TTF)I_{0.71}$, respectively, thus an incomplete charge transfer must be taking place in $(TTF)I_{0.71}$ while a complete charge transfer is taking place in $(TTF)Br_{0.71}$. The results obtained in the present study from the analyses of the intensity ratio of the LE bands are consistent with the above conclusion from the X-ray photoelectron spectra.

As shown in Figs. 4, 5, and 6, the c-axis spectra of these salts exhibit a strong absorption band extending to the infrared region. Because of the low-energy limit of our microspectrophotometer, we were not able to determine the wave number of the low-energy absorption maximum. The maximum was reported to be at 5000 cm^{-1} in the case of $(TTF)Br_{0.76}$.[22,35] Probably, the maximum is located in the same region also in the cases of the TTF salts studied here. This low-energy band can be safely assigned to an intermolecular CT transition.

There is a shoulder in the tail of the strong band mentioned above. This shoulder is located at 12.5 $\times 10^3$, 12.4 $\times 10^3$, and 11.0 $\times 10^3$ cm^3 cm^{-1} in $(TTF)Br_{0.71}$, $(TTF)I_{0.71}$, and $(TTF)(SCN)_{0.57}$, respectively. Seemingly, this is the second CT band. Since the ionized fraction of TTF is 0.5—0.7 in the three salts, we can expect two types of CT transition. The one is associated with the charge transfer from a $(TTF)^+$ ion to another $(TTF)^+$ ion, and the other is associated with that from a TTF molecule to a $(TTF)^+$ ion. The latter CT transition is expected to be considerably lower in energy than the former one. As we have shown in Fig. 2, the CT band of $(TTF)(ClO_4)$ appears at 12.0 $\times 10^3$ cm^{-1}, which has been attributed to the charge transfer between $(TTF)^+$ ions. The position of the shoulder observed in the spectra of the mixed-valence TTF salts is almost the same as the above CT band of $(TTF)(ClO_4)$. This fact strongly suggests that the observed shoulder is associated with the charge transfer from a $(TTF)^+$ ion to the neighboring $(TTF)^+$ ion within a TTF stack. Then the strong, low-energy band can be attributed the charge transfer from a TTF molecule to a $(TTF)^+$ ion. We will call the latter CT band as the CT(I) and the former as CT(II). The natures of these two CT transitions can be schematically expressed as follows:[6-8]

$$\text{CT(I)};\ (TTF)^+(TTF)^0 \longrightarrow (TTF)^0(TTF)^+$$

$$\text{CT(II)};\ (TTF)^+(TTF)^+ \longrightarrow (TTF)^0(TTF)^{2+}$$

If we assume the localized model with a strong electronic correlation, we could expect that TTF ions in the mixed valence TTF stack will be separated from each other by TTF molecule. Thus, when the ionized fraction is nearly one half, the following type of arrangement of ions and molecules will be dominant in the TTF stack.

$$\cdots (TTF)^+(TTF)^0(TTF)^+(TTF)^0 \cdots$$

This means that the probability of finding $(TTF)^+$-$(TTF)^+$ pairs in the TTF stack is very small as compared with the probability of finding $(TTF)^+(TTF)^0$ pairs in the salt where the ionized fraction is 0.5—0.7, so that the intensity of the CT(II) band must be very much lower than that of the CT(I) band in the cases of the mixed-valence salts studied here. This is in agreement with the observations.

In the c-axis spectra of the three mixed-valence salts, there is an absorption band with the maximum at 35—37 $\times 10^3$ cm^{-1}. This cannot be due to acceptor since neither the halogen ions (or atom), nor the $(SCN)^-$ ion, have any absorption band in the corresponding region.[36] The origin of this band is not clear at present. A possible origin would be a π-σ^* or σ-π^* transition of TTF with the transition dipole perpendicular to the molecular plane.

Summary and Conclusion

The polarized absorption spectra over the range of 5000—37000 cm^{-1} were observed on the small single crystals of the mixed-valence TTF salts, $(TTF)Br_{0.71}$, $(TTF)I_{0.71}$, and $(TTF)(SCN)_{0.57}$, which are known to be quasi-one-dimensional conductors. By comparing the observed spectra with the solution spectra of the molecule and monopositive ion of TTF and with the

spectrum of the $(TTF)^{+}(ClO_4)^{-}$ crystal, we have concluded that the observed spectra can be satisfactorily interpreted in terms of the model which assumes a strong charge localization. The observed spectra also indicate that the ionized fraction of TTF is appreciably smaller in $(TTF)I_{0.71}$ than in $(TTF)Br_{0.71}$. These features are consistent with the conclusion derived from the analyses of the X-ray photoelectron spectra of the mixed-valence TTF salts.

Thus one may conclude that the charges are strongly localized in the TTF stacks of these mixed-valence TTF salts, so that TTF molecules can be considered as being not in the fractionally-charged state, but either in the singly-charged state or in the neutral state, in spite of the metal-like high electrical conductivities displayed by these salts.

References

1) G. Shirane, S. M. Shapiro, R. Comès, A. F. Garito, and A. J. Heeger, *Phys. Rev. B*, **14**, 2325 (1976).
2) S. Kagoshima, T. Ishiguro, and H. Anzai, *J. Phys. Soc. Jpn.*, **41**, 2061 (1976).
3) W. D. Grobman, R. A. Pollak, D. E. Eastman, E. T. Maas, Jr., and B. A. Scott, *Phys. Rev. Lett.*, **32**, 534 (1974).
4) S. F. Lin, W. E. Spicer, and B. H. Schechtman, *Phys. Rev. B*, **12**, 4148 (1975).
5) I. Ikemoto, T. Sugano, and H. Kuroda, *Chem. Phys. Lett.*, **49**, 45 (1977).
6) J. B. Torrance, B. A. Scott, and F. B. Kaufman, *Solid State Commun.*, **17**, 635 (1975).
7) J. Tanaka, M. Tanaka, T. Kawai, T. Takabe, and O. Maki, *Bull. Chem. Soc. Jpn.*, **49**, 2358 (1976).
8) J. B. Torrance, Proc. Conf. Organic Conductors and Semiconductors, Siofok, Hungary, Aug., 1976, to be published.
9) A. J. Heeger and A. F. Garito, "Low-Dimensional Cooperative Phenomena," ed by H. J. Keller Plenum Press, New York (1974), p. 89.
10) D. M. Chaikin, J. F. Kwak, R. L. Greene, S. Etemad, and E. M. Engler, *Solid State Commun.*, **19**, 1201 (1976).
11) E. F. Rybaczewski, L. S. Smith, A. F. Garito, A. J. Heeger, and B. G. Silbernagel, *Phys. Rev. B*, **14**, 2746 (1976).
12) Y. Tomkiewicz, A. R. Taranko, and J. B. Torrance, *Phys. Rev. B*, **15**, 1017 (1977).
13) J. B. Torrance, Y. Tomkiewicz, and B. D. Silverman, *Phys. Rev. B*, **15**, 4738 (1977).
14) R. J. Warmack, T. A. Callcott, and C. R. Watson, *Phys. Rev. B*, **12**, 3336 (1975).
15) R. B. Somoano, A. Gupta, V. Hadek, T. Datta, M. Jones, R. Deck, and A. M. Herman, *J. Chem. Phys.*, **63**, 4970 (1975).
16) F. Wudl, D. E. Schafer, W. M. Walsh, Jr., L. W. Rupp, F. J. DiSalvo, J. V. Waszczak, M. L. Kaplan, and G. A. Thomas, *J. Chem. Phys.*, **66**, 377 (1977).
17) R. B. Samoano, A. Gupta, V. Hadek, M. Novotny, M. Jones, T. Datta, R. Deck, and A. M. Herman, *Phys. Rev. B*, **15**, 595 (1977).
18) H. Kobayashi and K. Kobayashi, *Bull. Chem. Soc. Jpn.*, **50**, 3127 (1977).
19) S. J. LaPlaca, P. W. R. Corfield, R. Thomas, and B. A. Scott, *Solid State Commun.*, **17**, 635 (1975).
20) J. J. Daly and F. Sanz, *Acta Crystallogr., Sect. B*, **31**, 620 (1975).
21) C. K. Johnson and C. R. Watson, Jr., *J. Chem. Phys.*, **64**, 2271 (1976).
22) B. A. Scott, S. J. LaPlaca, J. B. Torrance, B. D. Silverman, and B. Walber, *J. Am. Chem. Soc.*, **99**, 6631 (1977).
23) G. A. Thomas, F. Wudl, F. DiSalvo, W. M. Walsh, Jr., L. W. Rupp, and D. E. Schafer, *Solid State Commun.*, **20**, 1009 (1976).
24) T. Sugano and H. Kuroda, *Chem. Phys. Lett.*, **47**, 92 (1977).
25) J. B. Torrance, B. A. Scott, B. Welber, and F. B. Kaufman, *Bull. Am. Phys. Soc.*, **22**, 424 (1977).
26) R. J. Warmack and T. A. Callcott, *Phys. Rev. B*, **14**, 3238 (1976).
27) L. R. Melby, H. D. Hartzler, and W. A. Sheppard, *J. Org. Chem.*, **39**, 2456 (1974).
28) Both the iodide and the bromide obtained here correspond to the ordered mixed-valence phases described in the paper by Scott *et al.* (Ref. 22).
29) S. Hünig, G. Kiesslich, H. Quast, and D. Scheutzow, *Liebigs Ann. Chem.*, **1973**, 310.
30) DDQ; 2,3-dichloro-5,6-dicyano-*p*-benzoquinone.
31) R. Knoesel, *Bull. Soc. Chim. Fr.*, **1967**, 4300.
32) R. Zahradník, P. Čársky, S. Hünig, G. Kiesslich, and D. Scheutzow, *Int. J. Sulfur Chem.*, **C6**, 109 (1971).
33) D. L. Coffen, J. Q. Chambers, D. R. Williams, P. E. Garrett, and N. D. Canfield, *J. Am. Chem. Soc.*, **93**, 2258 (1971).
34) T. Sugano and K. Yakushi, unpublished work on the crystals, and data in stretched polyethylene film had been given in R. Gleiter, E. Schmidt, D. O. Cowan and J. P. Ferraris, *J. Electron Spectrosc., Rel. Phenom.*, **2**, 207 (1973).
35) B. A. Scott, J. B. Torrance, S. J. LaPlaca, P. Corfield, D. C. Green, and S. Etemad, *Bull. Am. Phys. Soc.*, **21**, 496 (1976).
36) C. K. Jørgensen "Halogen Chemistry," ed by V. Gutmann, Academic, London (1967), p. 265.

Kinetics of Oxidation of 4-Hydroxy-4-methyl-2-pentanone by Sodium *N*-Chloro-*p*-toluenesulfonamide

K. V. UMA and S. M. MAYANNA
Department of Chemistry, Central College, Bangalore University, Bangalore 560001, India
(Received May 6, 1977)

The kinetics of oxidation of 4-hydroxy-4-methyl-2-pentanone (diacetone alcohol) by sodium *N*-chloro-*p*-toluenesulfonamide (Chloramine-T, RNClNa) in presence of hydrochloric acid (0.05—0.6 M) has been studied at 30 °C. The reaction follows first order kinetics with respect to chloramine-T. The reaction rate depends on the square of the [H^+] and independent of the alcohol concentration. The energy and entropy of activation have been found to be 65.56 kJ mol^{-1} and -73.81 JK^{-1} respectively. The rate of reaction has been affected by the addition of potassium chloride and dioxane to the reaction mixture. A mechanism has been proposed involving diacetone alcohol and H_2OCl^+ formed by the hydrolysis of chloramine-T. Applying steady state condition to RNHCl, a rate expression has been given to account for the observed results. Kinetic data have been used in the analytical estimation of diacetone alcohol in acidic medium.

Sodium *N*-chloro-*p*-toluenesulfonamide (chloramine-T) acts as an oxidising agent in both acidic and alkaline media with two electron change per mole. The oxidative properties of chloramine-T have been recently applied in the analytical estimations of variety of organic compounds in relatively low acidic and basic media.[1-3] Chloramine-T decomposes slightly in concentrated mineral acid solutions.[4] Kinetics of oxidations of α-hydroxy acids,[5] ketones[6] and allyl alcohol[7,8] have been studied. 4-Hydroxy-4-methyl-2-pentanone (diacetone alcohol) as a lacquer solvent finds a number of industrial applications. Kinetics of oxidation of diacetone alcohol by Co^{3+} and H_2O_2 have been reported.[9,10] A review of literature shows that diacetone alcohol can be estimated by brominating agent,[11] colorimetric,[12] gas[13] and column[14] chromatographic techniques. However, these methods are indirect and less accurate. The present paper deals with the kinetics of oxidation and analytical estimation of diacetone alcohol by chloramine-T.

Experimental

Chloramine-T (E. Merck) was purified according to the method of Morris *et al.*[15] Diacetone alcohol (BDH, bp 164 °C, η_D—1.4300) and all acids (AR) except perchloric acid were distilled and used. Dioxane (BDH) was purified by Riche and Milas' method,[16] potassium chloride was of analytical grade. All solutions were prepared from freshly distilled water. KCl–HCl buffers were used for the pH range 1—2. An approximately decinormal solution of chloramine-T was prepared and standardized by iodometric method.[17] The required quantity of the alcohol was accurately weighed and dissolved in the proper solvent to give nearly 0.2 M solution. Several samples were made up for each run in iodine flasks, from stock solutions prepared at reaction temperature (30± 0.1 °C). Reactions were timed from the addition of diacetone alcohol. Samples were analyzed for chloramine-T by iodometric method. The reaction was studied up to 90%. Duplicate runs agreed with each other within 3%.

Stoichiometry

Reaction mixture containing excess chloramine-T over diacetone alcohol were kept at 30 °C in presence of 0.2 M HCl for 24 h. Estimation of the unchanged chloramine-T showed that one mole of diacetone alcohol consumed one mole of chloramine-T.

$$(CH_3)_2C(OH)CH_2COCH_3+RNClNa+H_2O \longrightarrow CH_3COCH_2COCH_3+CH_3OH+RNH_2+NaCl$$

2,4-Pentanedione and methanol in the reaction mixture were identified by dimethyldiacetylpyridinediol and formaldehyde tests[18] respectively.

Results

Kinetic Data. Oxidation of diacetone alcohol (DAA) by chloramine-T (CAT) was carried out at different initial concentrations of the reactants in presence of 0.2 M HCl at 30 °C. In presence of excess of alcohol, plot of $\log[CAT]_0/[CAT]_t$ against time was

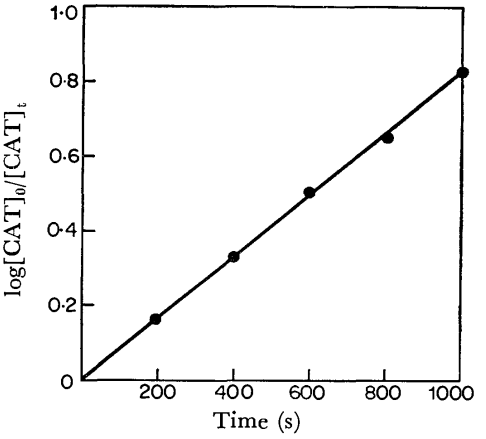

Fig. 1. Variation of the concentration of chloramine-T with time.

TABLE 1. KINETICS OF OXIDATION OF 4-HYDROXY-4-METHYL-2-PENTANONE BY SODIUM *N*-CHLORO-*p*-TOLUENESULFONAMIDE
Temp 30±0.1 °C. [H^+]=0.2 M.

$[CAT]_0$	$[DAA]_0$	10^3 *K* (s^{-1})	$[CAT]_0$	$[DAA]_0$	10^3 *K* (s^{-1})
0.005	0.100	6.70	0.0025	0.100	6.78
0.005	0.200	6.73	0.0050	0.100	6.73
0.005	0.300	6.74	0.0065	0.100	6.75
0.005	0.500	6.71	0.0050[a]	0.100	6.70

a) In presence of excess of *p*-toluenesulfonamide.

TABLE 2. EFFECT OF [H+] ON THE REACTION RATES
$[CAT]_0=0.005M$, $[DAA]_0=0.1M$
Temp=30±0.1 °C.

[H+]	0.05	0.1	0.2	0.3	0.4	0.5	0.6
$10^2 K$ (s^{-1})	0.0387	0.153	0.675	1.380	2.530	3.915	5.555
$\frac{10K}{[H^+]^2}$	1.550	1.530	1.543	1.588	1.581	1.565	1.543

linear (Fig. 1) passing through the origin showing that the order with respect to chloramine-T was unity. The first order rate constant was found to be independent of [DAA] (Table 1).

The kinetics of oxidation was studied at different concentrations of HCl (0.05—0.6 M). The rate constant increased with increase in [H+] (Table 2). A plot of log k *vs.* log [H+] gave a straight line with slope of two.

TABLE 3. EFFECT OF TEMPERATURE ON THE REACTION RATE
$[CAT]_0=0.005M$, $[DAA]_0=0.10M$,
$[H^+]=0.2M$

Temperature (K)	293	303	313	323
$10K$ (s^{-1})	2.787×10^{-3}	6.75×10^{-3}	1.635×10^{-2}	3.846×10^{-2}

Oxidation was also carried out at different temperatures (20—50 °C) in presence of 0.2 M HCl. From the corresponding data (Table 3) at 20, 30, 40, and 50 °C, the Arrhenius activation energy and entropy of activation were found to be 65.26 kJ mol^{-1} and −73.81 J K^{-1} respectively.

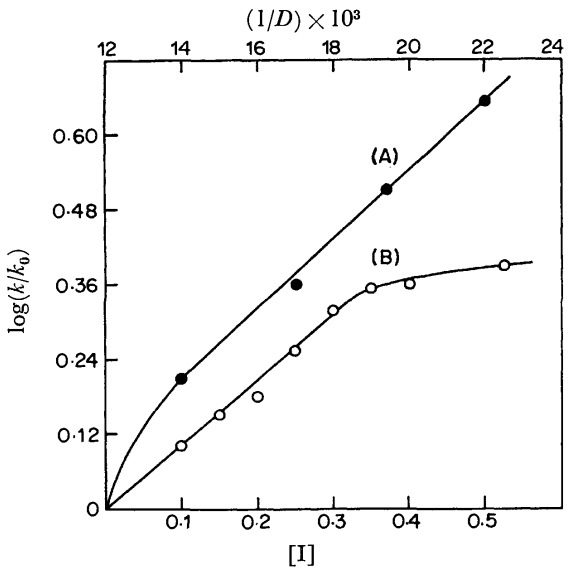

Fig. 2. Variation of rate constant with deilectric constant of the medium (B) and concentration of potassium chloride (A).

In presence of 0.2 M HCl, the effect of potassium chloride on the reaction rate at 30 °C up to ionic strength (I) 0.5 was investigated, the results of which are shown in Fig. 2. The line A shows the variation of log k/k_0 (k and k_0 are the rate constants with and without salt) with I for potassium chloride. The reaction rate was accelarated by the addition of potassium chloride.

Solvent effect on the reaction rate was studied. A series of kinetic runs were made in water–dioxane mixture of various compositions (10—40% dioxane by volume) at 30 °C in presence of 0.2 M HCl. Even in the mixture of dioxane and water, the reaction follows first order kinetics. The line B (Fig. 2) gives the variation of log k/k_0 (k and k_0 are the constants with and without dioxane respectively) with $1/D$ (D, the dielectric constant of the medium). The rate constant increased on increasing the amount of dioxane in the mixture. However, the variation is linear up to 30% dioxane in the mixture.

Analytical Data. Preliminary Studies: Known amounts of diacetone alcohol solution in the proper solvent were added to a known excessive volume (10—20%) of chloramine-T in an iodine flask placed in a thermostat at 30 °C. The reaction mixture was set aside for various intervals of time with occasional shaking. Then the excess of chloramine-T was determined by back titration.

Table 4 gives a typical set of results for the extent of oxidation of diacetone alcohol in 30 min at 30 °C by an excess of chloramine-T. It is seen that oxidation is slow in media other than hydrochloric acid. The rate of oxidation increases gradually as the concentra-

TABLE 4. EXTENT OF OXIDATION OF 4-HYDROXY-4-METHYL-2-PENTANONE BY SODIUM *N*-CHLORO-*p*-TOLUENESULFONAMIDE

Medium	CAT used (mol) / Alcohol taken (mol)	Medium	CAT used (mol) / Alcohol taken (mol)
pH 2.0[a)]	0.164	0.5N HCl	0.202
pH 1.0[a)]	0.170	1.0N HCl	0.216
0.2N HCl	0.185	1.0N CH_3COOH	0.124
0.2N H_2SO_4	0.160	2.0N HCl	0.230
0.2N $HClO_4$	0.170	2.5N HCl	0.320
0.3N HCl	0.185	3.0N HCl	0.504
0.4N HCl	0.188	4.0N HCl	0.765

a) KCl–HCl buffer. Alcohol taken, 5 mmol; CAT taken, 10 mmol; Time, 30 min; Temp, 30 °C.

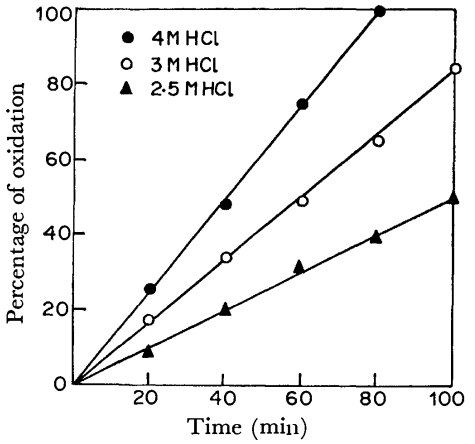

Fig. 3. Percentage of oxidation of diacetone alcohol by chloramine-T at 30 °C, at different time intervals with various concentrations of hydrochloric acid.

tion of hydrochloric acid increases, but the increase become rapid at or above 4 N acid. The extent of oxidation above 2 N hydrochloric acid is a function of time interval. Figure 3 shows the variation of extent of oxidation of diacetone alcohol with time at different concentrations of hydrochloric acid.

Recommended Procedure. Prepare an aqueous solution of diacetone alcohol (0.1 M). Add an aliquot containing 0.1—2.5 mM to a measured excessive (10—20%) volume of 0.1 N chloramine-T containing enough hydrochloric acid to make the overall acid concentration 4 N. Shake the mixture and keep it in a thermostat at 30 °C for 2 h. Add 20 ml of 10% potassium iodide solution and 10 ml of 2 N sulfuric acid and titrate with 0.1 N sodium thiosulfate. Run a blank with chloramine-T solution containing 4 N acid keeping for 2 h. The amount (mgs) of diacetone alcohol in the experimental solution is given by

$$X = 58Y(V_1 - V_2),$$

where Y is the normality of the thiosulfate, V_1 is the blank titration and V_2 the volume of thiosulfate used to titrate the excess of chloramine-T after oxidation of diacetone alcohol.

Detailed study of diacetone alcohol has brought out the following facts; (i) Foreign ions such as NO_3^-, ClO_4^-, and SO_4^{2-} have no influence up to ionic strength 0.25. (ii) Potassium chloride has slight effect on the rate of oxidation. (iii) The stoichiometry is unaffected by a reversal of the order of addition of oxidant and diacetone alcohol. (iv) The reaction rate is slightly retarded in sulfuric acid and perchloric acid (*cf.* Table 4).

Some typical results of analysis of diacetone alcohol in aqueous solutions are given in Table 5. The values obtained are accurate within 1.5%.

Table 5. Estimation of 4-hydroxy-4-methyl-2-pentanone by sodium *N*-chloro-*p*-toluenesulfonamide

Alcohol taken (mg)	Alcohol found (mg)	Alcohol taken (mg)	Alcohol found (mg)
2.90	2.94	26.10	26.23
5.80	5.87	31.90	32.14
8.70	8.78	37.70	37.93
11.60	11.71	41.70	42.12
14.50	14.64	47.70	48.05
20.30	20.46	53.50	53.76

Discussion

Chloramine-T in aqueous solution undergoes dissociation[19]

$$RNClNa \rightleftharpoons RNCl^- + Na^+ \qquad (1)$$

$RNCl^-$ in acidic solution gives chloronium ion (Cl^+) which reacts with water to give H_2OCl^+. The following consecutive steps have been proposed[8] for the formation of H_2OCl^+ from $RNCl^-$:

$$H^+ + RNCl^- \underset{k_1}{\overset{k_{-1}}{\rightleftharpoons}} RNHCl \quad \text{slow} \qquad (2)$$

$$RNHCl + H^+ \xrightarrow{k_2} RNH_2 + Cl^+ \quad \text{still slower(rds)} \qquad (3)$$

$$Cl^+ + H_2O \xrightarrow{k_3} H_2OCl^+ \quad \text{fast} \qquad (4)$$

H_2OCl^+ attacks diacetone alcohol in a fast step as follows:

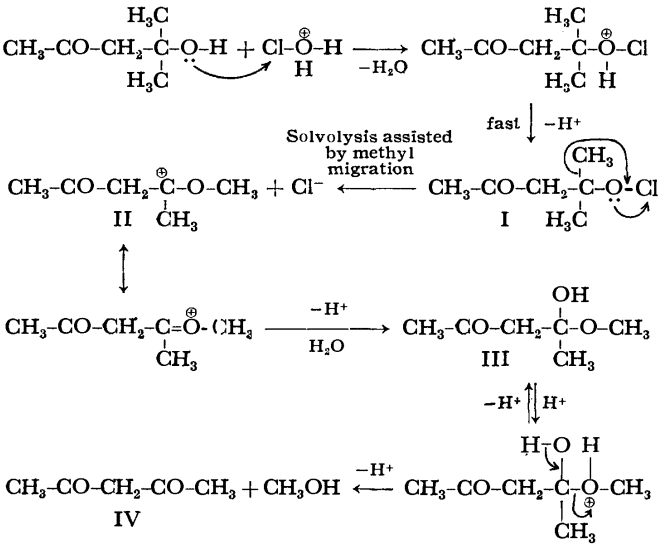

The attack of the electrophile Cl^+ on an unshared pair of electros on the oxygen of the alcohol and the elimination of H^+ produces the alkyl hypochlorite (I) in a fast step. The weak O–Cl bond may be expected to break readily by solvolytic attack by water is assisted by methyl migration to produce a stabilized carbonium ion. The attack by water produces a hemiacetal (III) which is readily hydrolysed to the diketone (VI). The key step of methyl migration to electron deficient oxygen is similar to Baeyer-Villiger oxidation of ketones.[20] In this case also, formation of a discrete oxene is unlikely and the departure of Cl^- ion and migration of methyl group is concerted.

Applying steady state conditions for RNHCl, one could derive the rate equation

$$\frac{-d[CAT]}{dt} = \frac{k_1k_2[CAT][H^+]^2}{k_1 + k_2[H^+]},$$

when $k_{-1} \gg k_2[H^+]$ the above equation reduces to

$$\frac{-d[CAT]}{dt} = \frac{k_1k_3}{k_{-1}}[CAT][H^+]^2.$$

This is in agreement with the experimental results. The increase of rate constant by the presence of potassium chloride and in dioxane–water mixture (Fig. 2) is in support of the rate determining step involving an ion and a neutral molecule[21,22] step (3).

Negative entropy of activation perhaps indicate the complex nature of the oxidation of diacetone alcohol by chloramine-T.

The authors are grateful to Dr. D. S. Mahadevappa, Professor of Chemistry, University of Mysore and Dr. V. R. Dani, of our department, for helpful discussions. One of us (K.V.U.) thanks Professor M. Shadaksharaswamy, Head of the Dept. of Chemistry, Central College, Bangalore University, Bangalore and Professor

P. S. Ambikadevi, Principal, Maharanis Science College, Bangalore, for their kind encouragement.

References

1) A. Berka, J. Vulterin, and J. Zyka, "Newer Redox Titrants," Pergamon press, New York (1965), p. 37.
2) G. Aravamudan and D. Venkappayya, *Talanta*, **15**, 704 (1968).
3) D. S. Mahadevappa and N. M. Madegowda, *Talanta*, **22**, 771 (1975).
4) V. R. S. Rao, D. Venkappayya, and G. Aravamudan, *Talanta*, **17**, 772 (1970).
5) S. P. Mushran, M. C. Agarwal, and B. Prasan, *J. Chem. Soc., B*, **1971**, 1712.
6) S. P. Mushran, R. Sanahi, and M. C. Agarwal., *Z. Naturforsch, Teil B*, **27**, 1161 (1972).
7) D. S. Mahadevappa and H. M. K. Naidu, *Aust. J. Chem.*, **27**, 1203 (1974).
8) D. S. Mahadevappa and H. M. K. Naidu, *Aust. J. Chem.*, **28**, 899 (1975).
9) A. Meenakshi and M. Santappa, *Indian J. Chem.*, **8**, 467 (1970).
10) Devtschi Akademie der Wissenschaften zu Berlin, Brit. Pat. 937.165, 18 September (1963).
11) N. G. Polyankie, V. S. Markavich, and N. E. Shitvel, *Zh. Anal. Khim.*, **19**, 1132 (1964).
12) T. Bota, D. Sireteanu, M. Panaitesu, and J. Herscovici, *Rev. Chim.*, **16**, 337 (1965).
13) P. Fore sara and H. P. Dupay, *J. Gas Chromatogr.*, **6**, 522 (1968).
14) Holybecher, Zavis, and Praze, *Anal. Chem.*, **5**, 45 (1969),
15) J. C. Morris, J. A. Salazan, and M. A. Wineman, *J. Am. Chem. Soc.*, **70**, 2036 (1948).
16) Weissberger, "Techniques of Organic Chemistry," Vol. VII, Interscience Publishers, Inc. New York (1955), p. 372.
17) K. Bottger and W. Bottger, *Z. Anal. Chem.*, **70**, 225 (1927).
18) F. Fiegal, "Spot Tests in Organic analysis," VII, Elsevier, New York (1966), pp. 413, 446.
19) E. Bishop and V. F. Jennings, *Talanta*, **1**, 197 (1958).
20) C. M. Hassal in "Organic Reactions," ed by Adams *et al.* Vol. IX, John Wiley and Sons, Inc., New York (1957), p. 73.
21) A. A. Frost and R. G. Pearson, "Kinetics and Mechanism," Wiley Eastern PVT Ltd., New Delhi (1970), p. 152.
22) K. J. Laidler and Eyring, *Ann. N, Y. Acad Sci.*, **39**, 303 (1940).

Pure Nuclear Quadrupole Resonance of *Ionic* Halides. I. ^{79}Br-NQR Investigation of the Hydrogen Bonding, the ^{1}H–^{2}D Isotope Effect, and the "Order-Disorder" Transition in the Anilinium Bromides $C_6H_5NH_3^{\oplus}Br^{\ominus}$, $C_6H_5ND_3^{\oplus}Br^{\ominus}$, and $C_6D_5NH_3^{\oplus}Br^{\ominus}$*,†

Wolfgang PIES and Alarich WEISS

Institut für Physikalische Chemie, Technische Hochschule Darmstadt, D-6100 Darmstadt, Germany

(Received June 30, 1977)

The ^{79}Br-NQR spectra of anilinium bromide, $C_6H_5NH_3^{\oplus}Br^{\ominus}$, of anilinium-$d_3$ bromide, $C_6H_5ND_3^{\oplus}Br^{\ominus}$, and of anilinium-$d_5$ bromide, $C_6D_5NH_3^{\oplus}Br^{\ominus}$, have been investigated in the temperature range $77 \leq T/K \leq 350$. The three compounds show an order-disorder phase transition near room temperature. The respective transition temperatures have been determined as 296.9 K ($C_6H_5NH_3^{\oplus}Br^{\ominus}$), 291.5 K ($C_6H_5ND_3^{\oplus}Br^{\ominus}$), and 297.6 K ($C_6D_5NH_3^{\oplus}Br^{\ominus}$). The large value of the ^{79}Br-NQR frequency ($\nu = 17.780$ MHz at 77 K for $C_6H_5NH_3^{\oplus}Br^{\ominus}$) and the large ^{1}H–^{2}D isotopic shift of this frequency ($\approx$400 kHz at 77 K by deuteration of the $NH_3^{\oplus}$-group) have been interpreted in terms of hydrogen bonding N–H···Br$^{\ominus}$. The state of order in the high temperature modification is discussed in the light of the ^{79}Br-NQR spectrum. The ^{79}Br-NQR frequency of the Br$^{\ominus}$ ion in the low temperature modification is related to the change in the monoclinic angle β and to the temperature dependence of the order parameter $s \propto \{(T_c - T)/T_c\}^{1/3}$.

In the course of an X-ray study of anilinium bromide, $C_6H_5NH_3^{\oplus}Br^{\ominus}$, Taguchi[1] noticed that "Weissenberg photographs prepared at different seasons of the year, using one and the same crystal, showed differences in detail." This remarkable behavior led to the discovery of the phase transition of anilinium bromide. According to him,[1] $C_6H_5NH_3^{\oplus}Br^{\ominus}$ is orthorhombic (modification **I**, D_{2h}^{10}-Pnaa, $Z=4$) above, and monoclinic (modification **II**, C_{2h}^{5}-P2$_1$/a, $Z=4$) below the transition temperature, given as $T_{II,I}=300.7$ K. The transformation was studied as well by calorimetry, DTA, and dilatometry showing a typical lambda type behavior of the heat capacity and an abnormal thermal expansion below $T_{II,I}=295$ K.[2] The X-ray diffraction analysis of the high temperature modification **I** by Nitta *et al.*[3] led to the determination of the positional parameters (hydrogen excluded). The crystal symmetry requires that the principal axis of the anilinium ion (N–C$_1$···C$_4$ axis) lies on a twofold symmetry axis. On the other hand, it is reasonable to assume a pyramidal configuration (C_{3v}) of the $-NH_3^{\oplus}$-group. The lack of correspondence between the symmetry of this group (threefold axis) and the point-group symmetry of the anilinium cation (twofold axis) indicates that there must be either a static orientational disorder of the $-NH_3^{\oplus}$-group or a rotation about the C$_1$–N bond as a "free" rotation or fast reorientation of the ammonium group. In the monoclinic structure of the low temperature modification **II** the requirement of the twofold symmetry imposed on the C$_4$···C$_1$–N axis is lost. An infrared study by Cabana and Sandorfy[4] corroborates the implications of the X-ray work.

We became interested in the phase transition of anilinium bromide in the course of ^{35}Cl-, ^{79}Br-, ^{127}I-NQR studies on chloroanilinium salts[5,6a] and on other possibly hydrogen bonded iodides and bromides (*e.g.* guanidinium halides[6b,c]). For $C_6H_5NH_3^{\oplus}Br^{\ominus}$ (**I**) one expects a ^{79}Br-NQR signal, to be observable with a nonpulse technique only if in the time scale of the NQR experiment (some 10^{-7} s) there is the same ordered arrangement of neighbors around each of the crystallographically equivalent Br$^{\ominus}$ ions. The NQR experiment, therefore, may be helpful to decide between a static orientational disorder of the $NH_3^{\oplus}$-group on the one hand, and a "free" rotation or a fast reorientation of this group on the other.

Experimental

Materials. Anilinium bromide, $C_6H_5NH_3^{\oplus}Br^{\ominus}$, and anilinium-$d_5$ bromide, $C_6D_5NH_3^{\oplus}Br^{\ominus}$, were prepared by adding freshly distilled aniline or aniline-d_5 (Merck, 99% D) to an excess of an aqueous solution of hydrobromic acid. The precipitated salts were recrystallized from aqueous HBr and dried over P_2O_5 in a desiccator. The identity of the colorless crystal powders was proven by chemical analyses [Calcd (found) for C_6H_8BrN: C, 41.41 (41.32), H, 4.63 (4.69), N, 8.05% (8.10%); for $C_6H_3D_5BrN$: C, 40.26 (40.14); ^{2,1}H: 4.50 (4.50), N: 7.81% (7.83%)]. The compounds are free of water of crystallization. $C_6H_5NH_3^{\oplus}Br^{\ominus}$ decomposes at 292 °C. The degree of deuteration of $C_6D_5NH_3^{\oplus}Br^{\ominus}$ was checked by high resolution ^{1}H-NMR to be 95% or better. Anilinium-d_3 bromide, $C_6H_5ND_3^{\oplus}Br^{\ominus}$, was prepared by dissolving $C_6H_5NH_3^{\oplus}Br^{\ominus}$ in excess D_2O (98% D) and removing the water with P_2O_5 in a desiccator system. This process was repeated twice. Again the degree of deuteration was checked by ^{1}H-NMR to be 95% or better. This last result has also been strengthened by the NQR spectra of this compound.

NQR Measurements. The ^{79,81}Br-NQR spectra were observed on polycrystalline samples with a Decca-Radar-NQR-spectrometer, using Zeeman modulation and side band suppression. The spectrometer was, in general, operated with a time constant of 10 s. The internal marker system, used for the determination of the resonance frequencies, was checked by frequent comparisons with a Rhode & Schwarz WIK BN 4421 frequency meter and a Rhode & Schwarz FEG 3 frequency counter. Additionally, the marker unit was

* Partly presented at the 76. Hauptversammlung der Deutschen Bunsengesellschaft für Physikalische Chemie, Braunschweig, Germany, May 1977.

† Part of a Dr.-Ing. thesis, to be submitted by W. Pies to the Technische Hochschule Darmstadt (D 17).

proved to be correct by giving the literature values for the ^{35}Cl-NQR frequency of α-paradichlorobenzene as described earlier.[7] The measured NQR frequencies are considered to be accurate to at least ±0.005 MHz.

Temperature Measurements. The sample temperature was achieved either by thermostating the sample holder with a Lauda Kryostat TUK 30D (temperature range $245 < T/K < 350$) or by immersing the sample holder into different slush baths[8] (for $T < 245$ K) or into liquid nitrogen ($T = 77$ K).

The temperature measurement units, each consisting of an iron-constantan thermocouple and a Metrawatt Symmetra D millivoltmeter, were calibrated in the temperature range $280 \leqq T/K \leqq 310$ (that is, within the vicinity of the transition points) with a standardized mercury thermometer with 0.1° graduation before and after use. The calibration of the thermocouple was done as well at the liquid nitrogen boiling point. During the NQR measurements the thermocouple was placed inside the sample holder very close to the sample tube. It was checked in separate runs that the temperature measured with this thermocouple and at this position, within the reading accuracy (0.1 K) of the instrument, was identical with the temperature inside the sample measured with the second thermocouple under the conditions of the NQR experiments. This condition was fulfilled, at least in the temperature range $280 \leqq T/K \leqq 310$. At $T = 77$ K, the difference between both thermocouples in their respective positions was not larger than 0.5 K, which is rather unimportant for the NQR measurements on the anilinium bromides investigated here, since the temperature coefficient of the ^{79}Br-NQR frequency drops down to $|\Delta\nu/\Delta T| \leqq 1$ kHz K^{-1} at 77 K. The temperature measurements are therefore considered to be accurate to ±0.1 K at $280 \leqq T/K \leqq 310$, and to ±0.5 K, or better, outside this range.

Results

Two NQR signals have been observed for anilinium bromide in the frequency range $7 \leqq \nu/MHz \leqq 30$ at $T = 273$ K (modification **II**) and at $T = 303$ K (modification **I**) as well. Both resonances have been ascribed to the $Br^{\ominus}$ ion as the frequency ratio is identical with the ratio of the quadrupole moments of the bromine isotopes $Q(^{79}Br)/Q(^{81}Br) = 1.1970$. This NQR spectrum gives evidence that there is only one bromide ion in the asymmetric unit of the crystallographical unit cell, in accordance with the results of the X-ray work.[1,3] In Table 1 the ^{79}Br-NQR frequencies of the investigated anilinium bromide samples are listed for $T = 77$ K, for a second temperature just below, and for a third just above the respective transition temperatures of the different species. Well defined NQR signals have been observed in both the low temperature modification **II** and the high temperature modification **I**. No change in the line shapes could be seen in passing through the

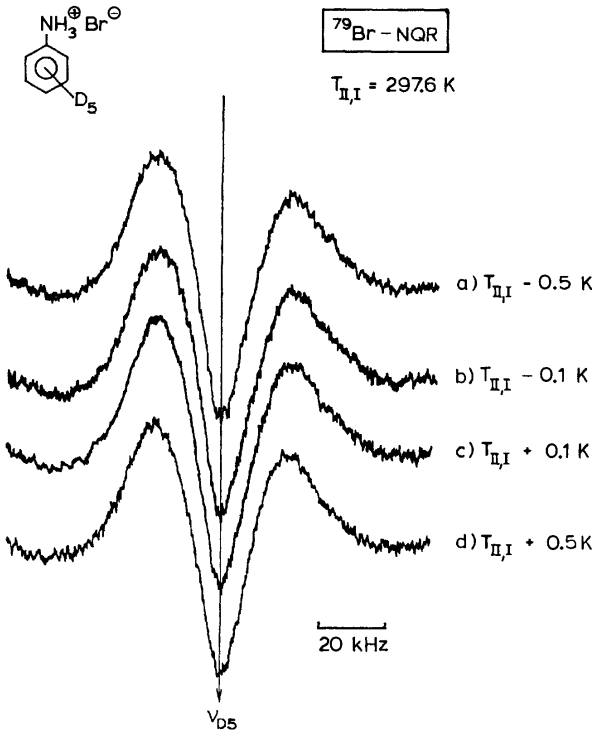

Fig. 1. ^{79}Br-NQR signal of anilinium-d_5 bromide in passing the phase transition point. The signals at four different temperatures near $T_{II,I}$ are shifted relative to each other in such a way that the center of the signals, ν_{D5}, falls together. The experimental (unshifted) results are: a) $T = 297.1$ K: $\nu_{D5} = 16.458$ MHz; b) $T = 297.5$ K: $\nu_{D5} = 16.447$ MHz; c) $T = 297.7$ K: $\nu_{D5} = 16.443$ MHz; d) $T = 298.1$ K: $\nu_{D5} = 16.441$ MHz.

TABLE 1. ^{79}Br-NQR FREQUENCIES OF ANILINIUM BROMIDES[a]

Sample	Symbol	Modification II, $T = 77$ K: ν_{exp}/MHz	S/N	$\Delta\nu_{1/2}$/kHz	Modification II, $T < T_{II,I}$: T/K	ν_{exp}/MHz	S/N	$\Delta\nu_{1/2}$/kHz	Modification I, $T > T_{I,II}$: T/K	ν_{exp}/MHz	S/N	$\Delta\nu_{1/2}$/kHz
$C_6H_5NH_3^{\oplus}Br^{\ominus}$	ν_H	17.780	16	19	294.2	16.557	24	15	298.7	16.471	27	13
$C_6H_5ND_3^{\oplus}Br^{\ominus}$	ν_{D3}	17.390	5	17	290.4	16.118	22	17	298.7	16.055	24	16
$C_6D_5NH_3^{\oplus}Br^{\ominus}$	ν_{D5}	17.688	20	17	294.2	16.538	22	15	298.8	16.437	22	15
$C_6H_5NH_3^{\oplus}Br^{\ominus}/C_6D_5NH_3^{\oplus}Br^{\ominus}$ [b]	ν_H	17.780	6.5	17	294.2	16.561	(5.5)	(13)	298.7	16.473	9	14
	ν_{D5}	17.689	6.5	14		16.541	(4)	(9)		16.438	9	13
$(C_6H_5NH_3^{\oplus})_{1-x}(C_6D_5NH_3^{\oplus})_x Br^{\ominus}$ [c] $(x=0.5)$	ν_{SS}	no ^{79}Br-NQR signal			294.2	16.553	6	18	298.7	16.457	5	19
$C_6H_5NH_{3(1-x)}D_{3x}^{\oplus}Br^{\ominus}$ [c] $(x=0.5)$	—	no ^{79}Br-NQR signals at $T = 77$ K and at room temperature observed										

a) Estimated error in ν: $< \pm 0.005$ MHz: S/N = signal-to-noise ratio; $\Delta\nu_{1/2}$ = half width. For $T_{II,I}$ see Table 2.
b) Mechanical mixture. c) Solid solution.

transition point (Fig. 1). Deuteration of the ammonium group has a very pronounced effect on the ^{79}Br-NQR signal of the $Br^{\ominus}$ ion. The frequency is shifted by about 400 kHz or more to lower values for both modifications. In contrast, the shift of the NQR line caused by deuteration of the benzene nucleus is smaller by about an order of magnitude near room temperature, but it is at first sight unexpectedly large (92 kHz) at $T=77$ K. Again the resonance frequency is lowered. The mechanical mixture of anilinium bromide and anilinium-d_5 bromide exhibits the ^{79}Br-NQR signals of the crystalline components with reduced signal-to-noise ratio. Figure 2 demonstrates the relative frequency shift due to the ring deuteration. In the solid solution $(C_6H_5NH_3^{\oplus})_{1-x}(C_6D_5NH_3^{\oplus})_xBr^{\ominus}$ there is a statistical distribution of fully protonated and ring-deuterated anilinium cations. Therefore the electric field gradient varies statistically at the bromine nucleus. The extreme values of the EFG may be taken to be those of the pure components of the solid solution. For $T=294$ K and $T=299$ K the difference between the resonance frequencies of $C_6H_5NH_3^{\oplus}Br^{\ominus}$ and $C_6D_5NH_3^{\oplus}Br^{\ominus}$ is small, some 30 kHz at most. Consequently, one observes a single broadened ^{79}Br-NQR line, for the solid solution with $x=0.5$ approximately centered in the middle of the lines of the pure components (Figs. 2i and 2ii). At $T=77$ K the ^{79}Br-NQR signal of the solid solution is spread over $\approx$90 kHz, and in this case no signal has been found using a conventional superregenerative oscillator (Fig. 2iii). As one may expect from the large separation of the ^{79}Br-NQR signals of $C_6H_5NH_3^{\oplus}Br^{\ominus}$ and $C_6H_5ND_3^{\oplus}Br^{\ominus}$, no signal could be found for the solid solution of the anilinium bromide and anilinium-d_3 bromide, $C_6H_5NH_{3(1-x)}D_{3x}^{\oplus}Br^{\ominus}$ ($x=0.5$). In addition to the ^{1}H-NMR analysis, this result proves that the degree of deuteration of the anilinium-d_3 bromide sample is fairly high.

The temperature dependence of the ^{79}Br-NQR frequency of anilinium bromide and its two deuterated derivatives, $C_6H_5ND_3^{\oplus}Br^{\ominus}$ and $C_6D_5NH_3^{\oplus}Br^{\ominus}$, has been investigated in the temperature range $77 \leqq T/K \leqq 350$. (The crystal structure determination[3] of the high temperature modification was done at $T=343$ K.) As usual in NQR spectroscopy, the resonance frequency decreases with increasing temperature, but, moreover, the frequency *versus* temperature curves of all three species show the following peculiar behavior. At $T=$ 77 K the absolute value of the temperature coefficient $|\Delta\nu/\Delta T|$ is less than 1 kHz K^{-1}. It increases progres-

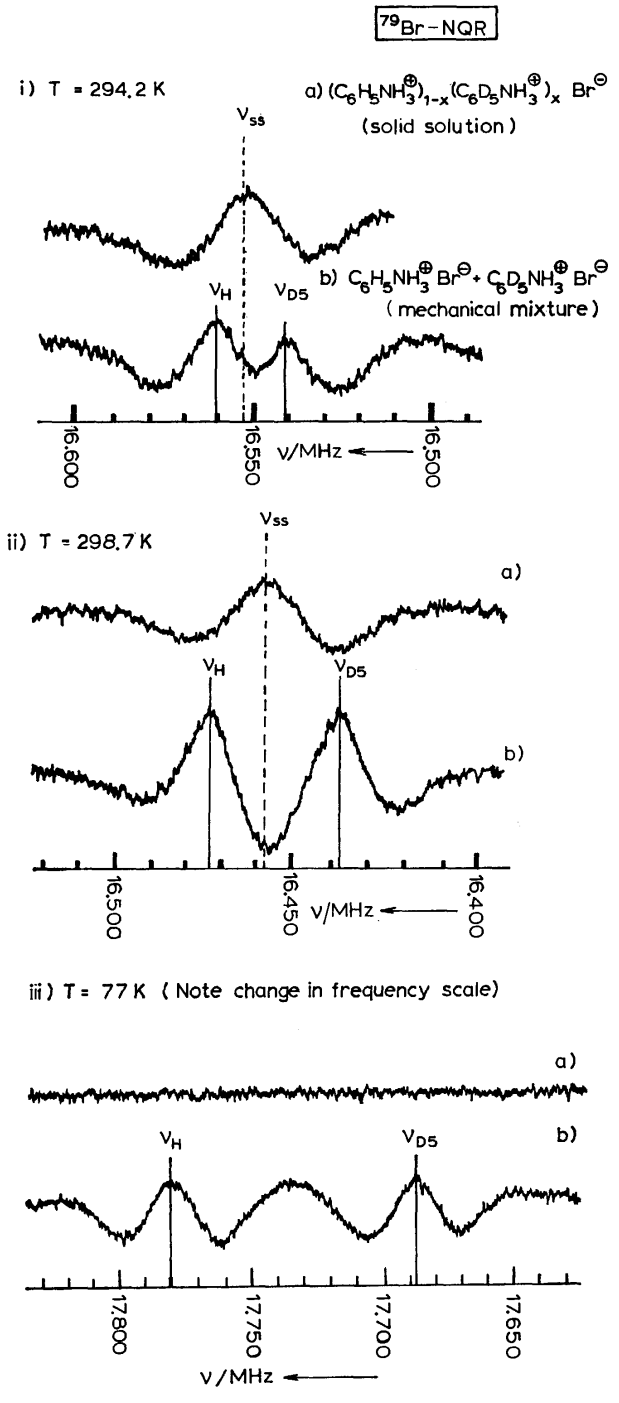

Fig. 2. ^{79}Br-NQR signals of a) the solid solution of anilinium bromide and anilinium-d_3 bromide ($x=0.5$) and of b) the mechanical mixture of an equal amount of the pure components: i) at a temperature just below the resp. $T_{II,I}$, ii) at a temperature just above the resp. $T_{II,I}$, iii) at $T=77$ K [frequency scale condensed compared with i) and ii)].

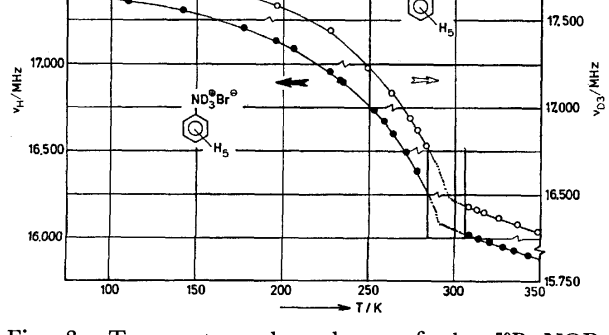

Fig. 3. Temperature dependence of the ^{79}Br-NQR frequencies of anilinium bromide (open circles: ○) and anilinium-d_3 bromide (full circles: ●) in the temperature range $77 \leqq T/K \leqq 350$. The area around the transition point is enlarged in Fig. 4.

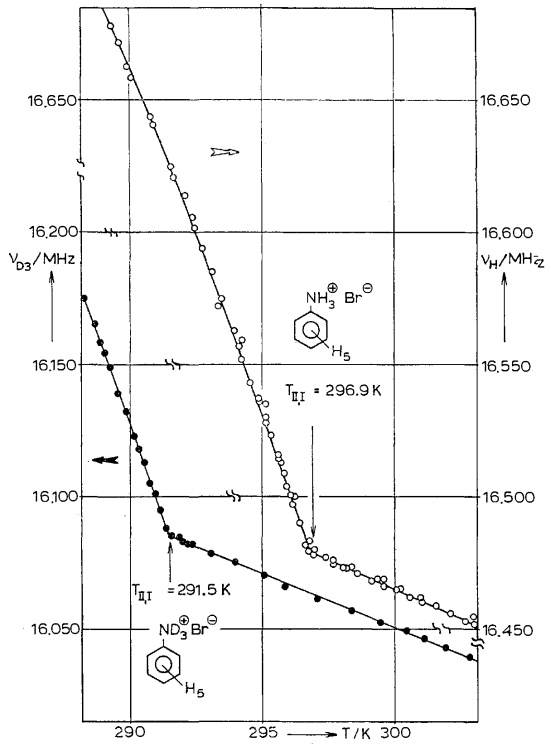

Fig. 4. Temperature dependence of the ^{79}Br-NQR frequencies of anilinium bromide (open circles: ○), and of anilinium-d_3 bromide (full circles: ●) in the close vicinity of the transition points.

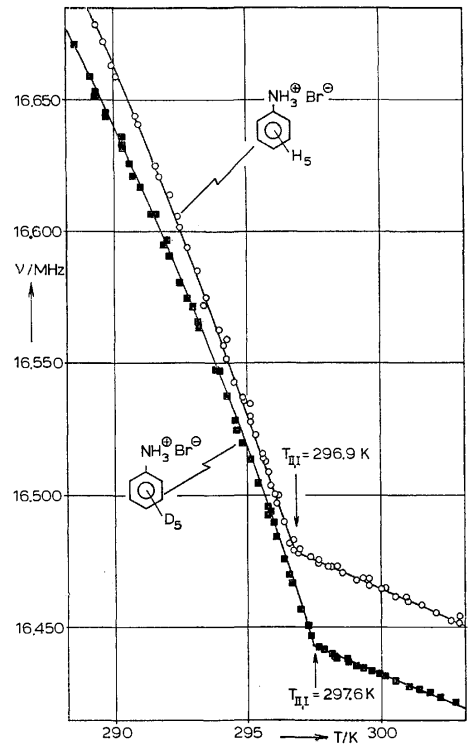

Fig. 5. Temperature dependence of the ^{79}Br-NQR frequencies of anilinium bromide (open circles: ○), and anilinium-d_5 bromide (full squares: ■) in the close in the close vicinity of the transition points.

sively with increasing temperature, reaching a maximum value of $|\Delta\nu/\Delta T| \approx 30$ kHz K^{-1}. At a certain critical temperature, which is considered to be the transition temperature $T_{II,I}$ of the respective species, each frequency *versus* temperature curve changes abruptly in slope. Above this critical temperature $|\Delta\nu/\Delta T|$ has a much lower value, approximately 4 kHz K^{-1}. The temperature dependence of the ^{79}Br-NQR frequencies of $C_6H_5NH_3^{\oplus}Br^{\ominus}$ and $C_6H_5ND_3^{\oplus}Br^{\ominus}$ is graphically displayed in Fig. 3 for the whole temperature range investigated. $\nu(T)$ of the ring-deuterated compound $C_6D_5NH_3^{\oplus}Br^{\ominus}$ has been omitted, since its respective frequencies have only been measured at $T=$ 77 K and at $247 \leqq T/K \leqq 345$; they would be nearly indistinguishable from those of the fully protonated anilinium bromide in the scale used in Fig. 3. The close similarity of the ν–T-curves is clearly seen. For $T < T_{II,I}$ the curvature is quite similar to that of the monoclinic angle β *versus* temperature in the special case of anilinium bromide.[1] More generally, $\nu(^{79}Br) = f(T)$ resembles a function "order parameter$=f(T)$" near the critical temperature. Figures 4 and 5 show sections of the $\nu(T)$-graphs in close vicinity of the transition points of the three species. Regarding the frequency scale and the strongly expanded temperature scale, the scatter of the points on these curves is rather small. For anilinium bromide and anilinium-d_5 bromide, the $\nu(^{79}Br) = f(T)$ data were collected from at least two different samples of each compound in several $\nu = f(T)$ runs. $C_6H_5ND_3^{\oplus}Br^{\ominus}$ has been studied in only one sample in a single temperature run.

In addition to the large frequency shift due to the ammonium deuteration, also the transition tempera-

TABLE 2. TEMPERATURE DEPENDENCE OF ^{79}Br-NQR FREQUENCIES OF ANILINIUM BROMIDE, ANILINIUM-d_3 BROMIDE, AND ANILINIUM-d_5 BROMIDE IN THE VICINITY OF THE TRANSITION TEMPERATURES $T_{II,I}$: $\nu_{calcd}(^{79}Br) \pm \sigma = a_0 + a_1 T + a_2 T^2$

Compound	σ/MHz	a_0/MHz	$10^2 a_1$/MHz K^{-1}	$10^5 a_2$/MHz K^{-2}	Z[a]	Temperature range	$T_{II,I}$/K[b]
$C_6H_5NH_3^{\oplus}Br^{\ominus}$	0.0023	−26.6195	+32.0881	−59.1864	40	$288 \leqq T/K \leqq 296.5$	296.9±0.1
	0.0009	+18.6045	−1.0152	+1.0073	27	$297.5 \leqq T/K \leqq 348.5$	
$C_6H_5ND_3^{\oplus}Br^{\ominus}$	0.0008	−32.7306	+36.5000	−67.7667	19	$286 \leqq T/K \leqq 291$	291.5±0.1
	0.0007	+18.2308	−1.0578	+1.1031	21	$292 \leqq T/K \leqq 343$	
$C_6D_5NH_3^{\oplus}Br^{\ominus}$ [c]	0.0015	−28.2405	+33.0538	−60.6156	46	$288.5 \leqq T/K \leqq 297.5$	297.6±0.1
	0.0006	+18.4613	−0.9737	+0.9920	35	$298 \leqq T/K \leqq 345$	

a) σ=standard deviation; Z=Number of experimental points in the least-squares fit. b) Determined as intersection of the respective polynomials in the temperature range $290 \leqq T/K \leqq 300$K. c) For $246.5 \leqq T/K \leqq 297.5$: $\nu_{D5} = -265.1364 + 428.9561 \cdot 10^{-2} T - 2441.3889 \cdot 10^{-5} T^2 + 618.3218 \cdot 10^{-7} T^3 - 589.6038 \cdot 10^{-10} T^4$, where ν is in MHz and T in K. σ=0.0016 MHz; Z=76.

ture $T_{II,I}$ is affected strongly by the isotopic exchange in being lowered by as much as 5.4 K (see Fig. 4). However, the critical temperature of $C_6D_5NH_3^{\oplus}Br^{\ominus}$ is only slightly elevated (by 0.7 K) as compared with that of $C_6H_5NH_3^{\oplus}Br^{\ominus}$ (see Fig. 5). The transition temperatures $T_{II,I}$ of the three anilinium species have been determined as the intersection of the respective ν-T-curves of the ^{79}Br-resonances. For this reason, the function $\nu(^{79}Br)=f(T)$ have been described in a polynomial form for both modifications **I** and **II** of the three species. Table 2 gives the coefficients a_i of the polynomials

$$\nu = \sum a_i \cdot T^i \qquad (1)$$

for each of the three anilinium bromide species. Three coefficients (parabolic approximation: a_0, a_1, a_2) were found to describe $\nu(T)$ reasonably well in the given temperature range. Additionally, the standard deviation σ, the number of experimental points used in the least squares fit and the transition temperatures determined are listed. It was not possible to describe the ^{79}Br-NQR frequencies of the low temperature modification **II** analytically for the whole temperature range from 77 K to $T_{II,I}$ by either a simple Bayer-type function[9]

$$\nu = a - \frac{b}{e^{c/T}-1} \qquad (2)$$

or in a polynomial form with a reasonable number of parameters.

Discussion

In the first section we discuss the significance of the value of the ^{79}Br-NQR frequency of anilinium bromide with regard to the question of hydrogen bonding in this compound. In the second part this question will be dealt with in the light of the hydrogen-deuterium isotope effect. Then the state of order of the high temperature modification is discussed and the fourth section treats the temperature dependence of the ^{79}Br-NQR frequencies and its relation to the order parameter of the low temperature modification.

The Origin of the Finite Electric Field Gradient at the Site of the Ion $Br^{\ominus}$ in $C_6H_5NH_3^{\oplus}Br^{\ominus}$. The detection of a Br-NQR signal in anilinium bromide is interesting in itself. The charge distribution of a free bromide ion is spherically symmetric, therefore, the electric field gradient (EFG) vanishes, whereby e^2qQ/h and ν are zero. A non-zero EFG at the site of the bromine nucleus in $Br^{\ominus}$ can be created by its incorporation into a crystal lattice at a site with non-cubic point symmetry, it is considered to be small in purely ionic crystals. Additional interactions such as covalent bonding and hydrogen bonding may enlarge the EFG and thereby the resonance frequency.

The question arises, whether the rather high value of the ^{79}Br-NQR frequency in anilinium bromide is in itself a proof for N–H$^{\oplus}$···Br$^{\ominus}$ hydrogen bonding in this solid. For comparison we shall discuss briefly the ^{79}Br-frequencies of other bromides (Table 3). Having $Na^{\oplus}$ ions as next nearest neighbors of $Br^{\ominus}$ substitutionally incorporated into KBr, Andersson[10] found for $^{79}Br^{\ominus}$ $e^2qQ/h=14.03$ MHz. This shows that $\nu(^{79}Br)$-values of up to 7 MHz can be caused by a non-cubic point symmetry. Larger ^{79}Br-NQR frequencies are found for $BaBr_2$, $PbBr_2$, and $PBr_4^{\oplus}Br^{\ominus}$, compounds in which some interatomic distances metal-to-bromine and bromine-to-bromine, respectively, are smaller than the commonly accepted ionic radii sum.[11,12] Interpreting this as a sign for a small covalent bond character the high $^{79}Br^{\ominus}$-NQR frequencies of these three compounds are understandable.

In the tetragonal phase NH_4Br(**III**), where hydrogen bonding is undoubtedly present, the ^{79}Br quadrupole coupling constant does not exceed 6 MHz[13] because the hydrogen bonds are arranged in a nearly regular tetrahedron around $Br^{\ominus}$ resulting in a charge distribution which is close to spherosymmetry. This is lost if one or more of the hydrogens in the $NH_4^{\oplus}$ group are substituted by alkyl groups. For seven alkylammonium bromides Frausto da Silva and Vilas Boas[14] found ^{79}Br-NQR signals in the frequency range of $12<\nu/\text{MHz}<19$ at $T=306$ K. They claim that the distortion of the symmetry of the electron cloud of the halide ions "is so pronounced that it cannot be originated only by second order lattice effects in a 100% ionic structure" but by the formation of N–H$^{\oplus}$···X$^{\ominus}$ hydrogen bonds. These bonds had been postulated before from X-ray and IR studies.[15] Hydrogen bonding has been proposed to be present in anilinium bromide as well.[1-4] The rather high ^{79}Br-NQR frequency of anilinium bromide

Table 3. ^{79}Br nuclear quadrupole coupling data of bromide ions $Br^{\ominus}$ in different inorganic and organic solids

Compound	Method[a]	T/K	$\nu(^{79}Br)$/MHz	Remarks	Reference
$C_6H_5NH_3^{\oplus}Br^{\ominus}$	PQR	77	17.780	Modification **II**	This work
$K_{1-x}Na_xBr$ ($x\ll 1$)	NMR	RT	7.015	$Na^{\oplus}$ in shell {1,0,0}	10
$BaBr_2$	PQR	77	26.01	—	29
			14.59		
$PbBr_2$	PQR	77	33.305	Orthorhombic modification	36, 37
			24.741		
$PBr_4^{\oplus}Br^{\ominus}$	PQR	77	22.25[b]	Assigned to $Br^{\ominus}$	38
$NH_4^{\oplus}Br^{\ominus}$	NMR	≈80	2.83	Tetragonal modification	13
		≈230	≈0.5		
$CH_3NH_3^{\oplus}Br^{\ominus}$	PQR	306	12.88	—	14

a) NMR=quadrupole splitting of wide line Br-NMR; PQR=pure Br-NQR.
b) Four NQR frequencies near 240 MHz are ascribed to the ^{79}Br in $PbBr_4^{\oplus}$[38,39].

Table 4. Hydrogen-deuterium isotope effect on the ^{35}Cl, ^{79}Br, and ^{127}I-NQR frequencies of simple and complex halides[a)]

Compound	Nucleus	T/K	ν_H/MHz	$\frac{\nu_H-\nu_D}{kHz}$	$10^2\frac{\nu_H-\nu_D}{\nu_H}$	Comments	Reference
Anilinium bromide	^{79}Br	77	17.780	+390	+2.19	$T<T_{II,I}$	This work
$C_6H_5NH_3^{\oplus}Br^{\ominus}$		289.8	16.664	+533	+3.20		
$C_6H_5ND_3^{\oplus}Br_{\ominus}$		298.7	16.471	+416	+2.53	$T>T_{II,I}$	
Anilinium bromide	^{79}Br	77	17.780	+92	+0.52	$T<T_{II,I}$	This work
$C_6H_5NH_3^{\oplus}Br^{\ominus}$		294.2	16.557	+19	+0.11		
$C_6D_5NH_3^{\oplus}Br^{\ominus}$		298.7	16.471	+34	+0.21	$T>T_{II,I}$	
3-Chloroanilinium iodide	^{127}I	77	24.359	+817	+3.35	$\nu(5/2\rightleftharpoons3/2)$	6a
3-$ClC_6H_4NH_3^{\oplus}I^{\ominus}$			24.620	+598	+2.43	$\nu(3/2\rightleftharpoons1/2)$	
3-$ClC_6H_4ND_3^{\oplus}I^{\ominus}$		298	26.544	+832	+3.13	$\nu(5/2\rightleftharpoons3/2)$	
			24.934	+728	+2.92	$\nu(3/2\rightleftharpoons2/2)$	
	^{35}Cl	77	34.995	−11	−0.03	Cl at benzene ring	
		298	34.738	−10	−0.03		
Guanidinium iodide	^{127}I	300	27.235	+449	+1.65	$\nu(5/2\rightleftharpoons3/2)$ site A; $\eta_A=0$	6b
$[C(NH_2)_3]^{\oplus}I^{\ominus}$			13.614	+221	+1.63	$\nu(3/2\rightleftharpoons1/2)$	
$[C(ND_2)_3]^{\oplus}I^{\ominus}$			25.018	+499	+1.99	$\nu(5/2\rightleftharpoons3/2)$ site B; $\eta_B=0$	
			12.510	+251	+2.01	$\nu(3/2\rightleftharpoons1/2)$	
4-Chloropyridinium hexachlorostannate(IV)	^{35}Cl	298	17.521	+8	+0.05	Cl in $SnCl_6^{2\ominus}$	This work
$(4\text{-}ClC_5H_4NH^{\oplus})_2SnCl_6^{2\ominus}$			17.322	+11	+0.06		
$(4\text{-}ClC_5H_4ND^{\oplus})_2SnCl_6^{2\ominus}$			14.982	−35	−0.23		
			35.928	−4	−0.01	Cl at pyridine ring	
Tris(sarcosine)calcium chloride	^{35}Cl	292	2.160	+40	+1.85	paraelectric phase: "N–H···$Cl^{\ominus}$"-bonding	22
$(CH_3N^{\oplus}H\cdots CH_2COO^{\ominus})_3\cdot CaCl_2$							
$(CH_3N^{\oplus}D\cdots CH_2COO^{\ominus})_3\cdot CaCl_2$							
Barium dibromide dihydrate	^{79}Br	77	4.57	−40	−0.88	—	29
$BaBr_2\cdot2H_2O$							
$BaBr_2\cdot2D_2O$							
Sodium tetrachloroaurate(III) dihydrate	^{35}Cl	273	28.83±1	0	0		
$NaAuCl_4\cdot2H_2O$			28.44±1	≈+10 ±10	(≈+0.04 ±0.04)		
$NaAuCl_4\cdot2D_2O$			27.46±1	0	0		30
			25.67±1	≈+30 ±10	≈+0.12 ±0.04	"O–H···Cl–Au"-bonding	
2,2-Dichloropropane	^{35}Cl	77	34.883	+23	+0.07	No H-bonding	40
$CH_3CCl_2CH_3$							
$CD_3CCl_2CD_3$							

a) The subscripts H and D mark the value for the protonated and the deuterated form respectively. The error in ν is ±0.005 MHz or less for the first five compounds. The error in $\nu_H-\nu_D$ is ±0.002 MHz or less for the ^{35}Cl-NQR frequencies of 3-chloroanilinium iodide and 4-chloropyridinium hexachlorostannate(IV) and for the ^{79}Br-NQR frequencies of anilinium bromide/anilinium-d_5 bromide around room temperature (see Fig. 2).

found (17.780 MHz at $T=77$ K) supports the assumption of a hydrogen-bridged bromide ion. However, the frequency value alone may not be sufficient as a reliable proof of N–$H^{\oplus}\cdots Br^{\ominus}$ hydrogen bonding.

^1H–^2D Isotope Effect. The substitution of D for H in the ammonium group of anilinium bromide was undertaken to gain some more definite NQR evidence about the hydrogen bridge N–$H^{\oplus}\cdots Br^{\ominus}$ in this compound. In case there is no hydrogen bonding N–$H^{\oplus}\cdots Br^{\ominus}$, the ion $Br^{\ominus}$ is isolated and therefore not affected by this isotopic exchange in the first approximation. If at all, only a slight shift of the resonance frequency to higher values is expected because of the reduced torsional amplitudes of the N–D modes.

In case of a hydrogen bond N–$H^{\oplus}\cdots Br^{\ominus}$, the effect of deuteration can be followed along the lines given by Coulson[16] for the isotope effect on an asymmetric O–H···O bond. In a normal isolated O–H bond, replacement of hydrogen by deuterium leads to a small shortening of the interatomic distance due to the anharmonicity of the O–H vibration. In an O–H···O hydrogen bonding system a decrease of the distance r_{O-H} causes an increase of the distance R_{O-O}[17,18,19a)]. Therefore, if $r_{O-D}<r_{O-H}$, as in the isolated bond, the O–O distance is enlarged by deuteration, $(R_{O-O})_D>(R_{O-O})_H$ (the subscripts H and D stand for the hydrogen and deuterium bond respectively). This indeed has been found experimentally for short and intermediate asymmetric O–H···O hydrogen bonds (Ubbelohde effect)[20,18b,21)]. By analogy, for the bond N–$H^{\oplus}\cdots Br^{\ominus}$ in anilinium

bromide, $r_{N-D}<r_{N-H}$ and $(R_{N-Br})_D>(R_{N-Br})_H$ is expected. Deuteration moves the bromide ion farther away from the nitrogen and the hydrogen atoms and $Br^{\ominus}$ approaches somewhat more the state of an isolated, non-hydrogen bonded ion. The ^{79}Br-NQR frequency should decrease upon deuteration and the frequency shift should be positive:

$$\Delta\nu_{H-D} = \nu_H(^{79}Br) - \nu_D(^{79}Br) > 0. \quad (3)$$

This has been found here for the anilinium bromides $C_6H_5NH_3^{\oplus}Br^{\ominus}$ and $C_6H_5ND_3^{\oplus}Br^{\ominus}$ (Tables 1 and 4). Also the magnitude of the H–D isotope effect support the assumption of hydrogen bonding in anilinium bromide. For $X^{\ominus}=I^{\ominus}$, $Cl^{\ominus}$, an analogous ^{1}H–^{2}D effect on the halogen NQR frequencies of the halide ions has been found in 3-chloroanilinium iodide,[6a] guanidinium iodide,[6b] and tris(sarcosine)calcium chloride[22] as well. Table 4 shows that the NQR frequency shifts due to deuteration, $\Delta\nu_{H-D}$, range from +1.5% to +3.5%.

The ability of complex ions like $SnCl_6^{2-}$ to form hydrogen bonds is strongly reduced compared with that of $X^{\ominus}=Cl^{\ominus}$, $Br^{\ominus}$, $I^{\ominus}$. This is seen on the infrared spectra of the corresponding guanidinium salts,[23] pyrimidinium salts,[24,25] and pyridinium salts.[26] Hydrogen bonding in 4-chloropyridinium hexachlorostannate(IV) is proposed in ^{35}Cl-NQR and X-ray work[27,28] and should be rather weak. Deuteration, therefore, has only a small influence on the ^{35}Cl frequencies of the complex ion. A frequency shift toward a more isolated $SnCl_6^{2-}$ ion is expected. Accordingly, the lowest ^{35}Cl-NQR signal attributed to the hydrogen-bonded-chlorines should move to higher frequencies and the two other signals to lower frequencies. This view is supported by experimental results.

Examples for deuteration shifts presumably caused by other effects than hydrogen bonding are also found in Table 4: the isotope effects on the NQR frequencies of the meta-Cl in 3-chloroanilinium iodide, of the *para*-Cl in 4-chloropyridinium hexachlorostannate(IV), and, as a reference, of the chlorine atoms in 2,2-dichloropropane. All these chlorines show small but definite positive or negative isotopic shifts.

The ^{1}H–^{2}D isotope effect on the ^{79}Br-NQR signal in $BaBr_2\cdot 2H_2O$[29] and on the ^{35}Cl-NQR signals of $NaAuCl_4\cdot 2H_2O$[30] does not follow the lines developed above for hydrogen bonded halides. This is not surprising in the case of the barium salt, since its bromine frequency is well within the limits of a purely ionic $Br^{\ominus}$, and the $Br^{\ominus}$ may not be hydrogen bonded at all in $BaBr_2\cdot 2H_2O$. In $NaAuCl_4\cdot 2H_2O$ the O–H···Cl bond[30–32] is a rather debatable one, the shortest O–Cl distance (3.42 Å[33]) is appreciably longer than the sum of the usually accepted van der Waals radii (3.20 Å[19b]). Here Gallagher's[20] proposal may be followed that deuteration strengthens very weak hydrogen bonds. Fryer and Smith[30] explained in this way the isotopic shift of the lowest ^{35}Cl-NQR signal, but stressed the fact that other solid state effects may also be responsible for the small H–D effect in $NaAuCl_4\cdot 2H_2O$.

The shift of the ^{79}Br-NQR frequency of the $Br^{\ominus}$ by deuteration of the benzene ring of anilinium bromide remains to be discussed. It is in the order of an effect of lattice dynamics at room temperature and above it, but quite large at liquid nitrogen temperature. The reason for this is not clear to us yet. It might be that this strong shift is due to hindered oscillations of the anilinium ion around its longest axis. Indications of such oscillations have been found by Nitta *et al.*[3] for the high temperature phase and the close similarity of the structures may allow such a behavior in the low temperature phase as well. An investigation of partially deuterated anilinium bromides, as $4\text{-}DC_6H_4NH_3^{\oplus}Br^{\ominus}$ and $2,3,5,6\text{-}D_4C_6HNH_3^{\oplus}Br^{\ominus}$, could probably be helpful in finding an explanation for this large isotope effect.

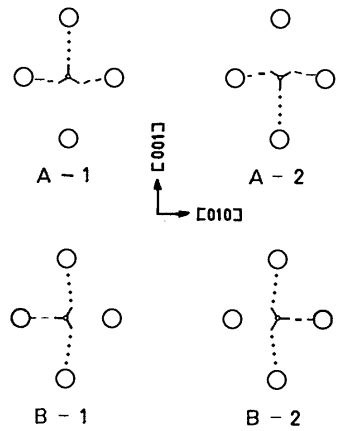

Fig. 6. Energetically favored orientations of the $-NH_3^{\oplus}$ group with respect to neighboring bromide ions $Br^{\ominus}$ according to Ref. 3. Short hydrogen bonds (R_{N-Br}= 3.30 Å) are hyphenated, long hydrogen bonds (R_{N-Br}= 3.48 Å) are dotted. ○=Br; =NH_3.

State of Order in the High Temperature Modification. The apparent discrepancy between the symmetry of the anilinium ion in the crystal (diagonal axis through $N\text{–}C_1\cdots C_4$) and the symmetry of the $-NH_3^{\oplus}$ group (threefold axis) disappears, when the three hydrogen atoms bound to the nitrogen atom "occupy statistical positions by some means."[1,3] There are two limiting cases shown by Taguchi[1] and Nitta *et al.*:[3] a static statistical distribution (model **a**) and a dynamic statistical distribution (model **b**). In both models an orientationl disorder of the $NH_3^{\oplus}$ group with respect to the four neighboring bromide ions is assumed. Four orientations of the $NH_3^{\oplus}$ group are energetically favored as shown in Fig. 6 (taken from Ref. 3). In the orientations A-1 and A-2 there are two strong and one weak hydrogen bond between the nitrogen atoms and the bromide ions. Both, A-1 and A-2, are equally probable in the high temperature modification, whereas in the monoclinic low temperature phase one of these orientations would be stabilized. Additionally, there may be a further arrangement B characterized by one strong and two weak hydrogen bonds, also with two equally probable orientations B-1 and B-2. "Static statistically distributed" means that the ammonium hydrogens occupy the positions given by A-1 and A-2 (or by A-1, A-2, B-1, and B-2) randomly in space. They remain in these position for a time, long compared to the time scale of the respective technique (here the NQR spectro-

scopy, that is the residence time is longer than about 10^{-7} s). Model **b** (dynamic statistical distribution) assumes randomness in time, that is a short correlation time (less than 10^{-8} s). The $-NH_3^{\oplus}$ group is "flipping among different orientations"[1] or even rotating freely (as incorporated into the X-ray structure factor calculations by Nitta *et al.*[3]). Model **a** fulfills the demand of the space group for a twofold symmetry along the principal axis of the anilinium ion by averaging in space, model **b** by averaging in time.

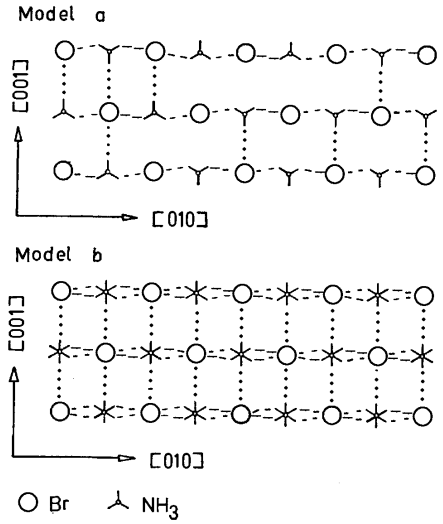

Fig. 7. Schematic representation of a static statistical distribution (random in space: model **a**) and dynamical statistic distribution (random in time: model **b**) of the hydrogen atoms of the $-NH_3^{\oplus}$ group. Only the orientations A-1 and A-2 are considered. Short hydrogen bonds are hyphenated, long hydrogen bonds are dotted. The local symmetry at the bromide ions is different in model **a**, whereas it is identical at each $Br^{\ominus}$ in model **b**.

The surrounding of the bromide ions (all $Br^{\ominus}$ are crystallographically equivalent) is shown in Fig. 7 for model **a**, representing a part of the projection of the structure of $C_6H_5NH_3^{\oplus}Br^{\ominus}$ on the plane (100). Dashed lines symbolize the strong hydrogen bonds (R_{N-Br}= 3.30 Å) and dotted lines the weak ones (R_{N-Br}=3.48 Å). The $-NH_3^{\oplus}$ groups are oriented randomly in space (only the arrangements A-1 and A-2 are considered). This distribution results in different surroundings for the $Br^{\ominus}$ which average in space to the twofold axis of symmetry for the $Br^{\ominus}$ and the ammonium nitrogen, as observed by X-ray diffraction. However, in a microscopic observation such as NQR, which observes mainly the immediate surroundings of an atom, the different arrangements around each $Br^{\ominus}$ cause different electric field gradients at each bromine nucleus due to divergent contributions of the crystal field. A broadening of the ^{79}Br-NQR line, if not separate bromine signals, should be observed, most likely suppressing the signal beyond the noise level in observing with a non-pulse technique. Since a clear, definite ^{79}Br-NQR signal has been found in the high temperature modification of anilinium bromide and since no broadening of the line could be observed within the limits of the superregenerative detection in passing through the transition point (Fig. 1), it is concluded that a static statistical distribution is incompatible with the results of ^{79}Br-NQR spectroscopy. This conclusion is emphasized by the fact that no bromine signal could be found in the solid solution $C_6H_5NH_{3(1-x)}D_{3x}^{\oplus}Br^{\ominus}$ (x=0.5), where the hydrogen and deuterium atoms are distributed "static statistically" among the ammonium nitrogens and where the surroundings of the bromide ions are random with regard to the hydrogen isotope.

The second limiting case, dynamic statistical distribution (model **b**), is also represented in Fig. 7. Here an identical surrounding is given for each $Br^{\ominus}$ also in the microscopic picture by averaging in time. This is in accord with a single, unbroadened ^{79}Br-NQR line in the high temperature phase. The dynamic disorder can be produced by i) a free rotation of the $-NH_3^{\oplus}$ group or ii) by a rapid reorientation of this group. Hydrogen bonding between $NH_3^{\oplus}$ and $Br^{\ominus}$ implies that there is no free rotation of the $-NH_3^{\oplus}$ group. X-Ray diffraction (the distance N–Br is shorter than the van der Waals distance[3]), infrared spectroscopy (low frequency of the stretching vibration and enlarged line width[4]), and ^{79}Br-NQR spectroscopy (high frequency of the NQR signal and large isotope effect $^1H \leftrightarrow ^2D$, see preceding discussion) all indicate a hydrogen bond between the anilinium nitrogen and the bromide ion. Free rotation is therefore ruled out. The only model for the disorder in the high temperature modification of anilinium bromide compatible with all experimental results is that of a $-NH_3^{\oplus}$ group which reorients rapidly in a multiple well potential with equilibrium positions given by the hydrogen bonding to the bromide ions.

Temperature Dependence and Order Parameter. In most cases the temperature dependence of NQR frequencies is adequately described in its salient features by the Bayer theory:[9a] the average internal EFG at the nucleus decreases with increasing temperature because of the increase in the amplitude of the thermal vibrations. This theory describes only the isochorus part of the temperature dependence, $(\partial\nu/\partial T)_V$. It fails in describing $\nu=f(T)$ at constant pressure if the last term in Eq. 4,

$$\left(\frac{\partial\nu}{\partial T}\right)_P = \left(\frac{\partial\nu}{\partial T}\right)_V - \frac{\alpha}{\chi}\left(\frac{\partial\nu}{\partial T}\right)_T \qquad (4)$$

(α=thermal expansion coefficient, χ=compressibility) is not negligible compared with the Bayer term $(\partial\nu/\partial T)_V$. Kushida *et al.*[9b] have shown that the volume expansion affects the temperature dependence of the EFG in ionic or nearly ionic crystals appreciably.

For the high temperature modification of anilinium bromide the temperature dependence of the $\nu(^{79}Br)$ is weak. ν decreases with increasing temperature as predicted by the Bayer theory, $\nu(T)$ being practically linear. The order of magnitude found for $(\partial\nu/\partial T)_P$ of $Br^{\ominus}$ in $C_6H_5NH_3^{\oplus}Br^{\ominus}$ (**I**) is expected from a normal increase of the thermal vibrations and a "normal" volume expansion.

The temperature variation of the ^{79}Br-NQR frequency is by far more pronounced in the low temperature modifications, especially in approaching the transition point (Figs. 3—5). In this temperature region (235≦

T/K≦303), Suga[2] found an anomalous expansion coefficient. Therefore, it is not surprising that in the low temperature modification $\nu(T)$ cannot be described with a Bayer type function (Eq. 2). At least one additional temperature dependent term has to be considered, which takes the anomalous volume expansion into account. The curvature of $\nu(T)$ reminds of the temperature dependence of an order parameter $s(T)$ near T_c (*e.g.* Ref. 34). The continuous character of the phase transition in $C_6H_5NH_3Br$ and the temperature dependence of the monoclinic deformation β strengthens this analogy. Taguchi[1] considers the monoclinic deformation as a shear, which displaces with respect to the $Br^{\ominus}$ site the nearest neighbors of the bromide ion (the nitrogen and the hydrogen atoms) in the direction of the c-axis. This displacement is proportional to $\tan \Delta\beta$, where $\Delta\beta=\beta-90°$, with $\beta=90°$ at $T=T_{II,I}$. Since $\Delta\beta<2°$ (at $T=163$ K: $\Delta\beta=1°22'$[1]), $\tan \Delta\beta \approx \Delta\beta$, and the change of the N–Br distance with the monoclinic deformation is proportional to the square of $\Delta\beta$:

$$\Delta R_{N-Br} \propto (\Delta\beta)^2. \quad (5)$$

The same proportionality holds for the $\Delta R_{H\cdots Br}$. The maximum component of the electric field gradient, eq, depends on r^{-3}. Assuming that the change in eq is mainly caused by the change in the distance of the nearest neighbors to the ion $Br^{\ominus}$, one can show that e^2qQ/h of $Br^{\ominus}$ in the monoclinic phase depends on $(\Delta\beta)^2$. Neglecting the change in the asymmetry parameter, which for $I=3/2$ affects the resonance frequency only weakly, one finds

$$\Delta\nu(^{79}Br) \propto (\Delta\beta)^2 \quad (6)$$

in the region just below the transition point, where the monoclinic deformation governs the structural changes with temperature. Figure 8 shows that the expected proportionality (Eq. 6) is well fulfilled in the temperature range 288 K$<T<T_{II,I}$. It is not expected that Eq. 6 holds outside a small temperature range just below the transition point.

Suga[2] showed that an order-disorder theory analogous to that of Bragg and Williams describes fairly well main features of the phase transition of anilinium bromide such as transition entropy, anomalous thermal expansion, and the function $\Delta\beta=f(T)$. According to Suga, $\Delta\beta$ is proportional to the order parameter s.

$$\Delta\beta \propto s \quad (7)$$

It has been shown that the order parameter s is described by a power law

$$s \propto \varepsilon^n \quad (8)$$

($\varepsilon=(T_c-T)/T_c$; T_c=critical temperature, n=critical exponent). Far from T_C the critical exponent is 1/2 (Landau theory), while it changes (*e.g.* for perovskite-type crystals) down to 1/3 for $\varepsilon<0.1$ in analogy with magnetic and fluid systems[34,35]. Combining the proportionalities (6), (7), and (8), it follows

$$\Delta\nu(^{79}Br) \propto \varepsilon^{2n}, \quad (9)$$

and close to the transition point, assuming $n=1/3$,

$$\Delta\nu(^{79}Br) \propto (T_c-T)^{2/3}. \quad (10)$$

Although the once-hoped-for universality of the values for the critical exponent n had to be abandoned,[34] it is rather satisfying that the ^{79}Br-NQR frequency in $C_6H_5NH_3^{\oplus}Br^{\ominus}$ follows this proportionality (Eq. 10) in the temperature range 295≦T/K≦260 with T_C=

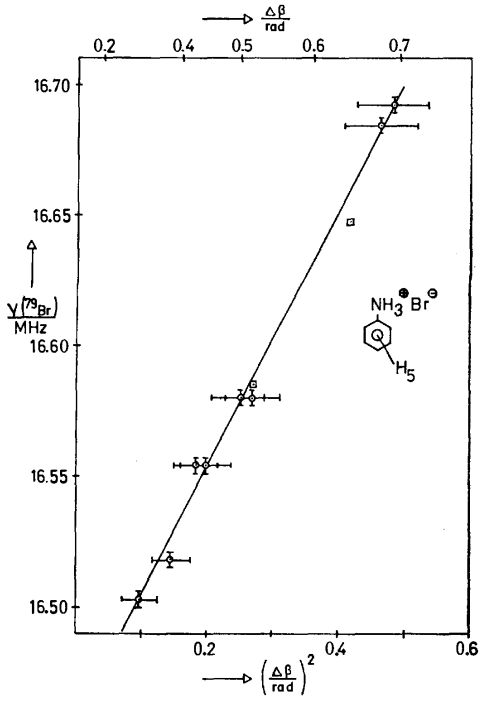

Fig. 8. ^{79}Br-NQR frequency of the low temperature modification of anilinium bromide as a function of $(\Delta\beta)^2=(\beta-90°)^2$. β=monoclinic angle of the low temperature modification **II**. Circles (⊙): the value of $\Delta\beta$ including the limits of error as taken from Fig. 3 in Ref. 1. Squares (⊡): $\Delta\beta$ as taken from Fig. 2 in Ref. 1, no limits of error are given in this case.

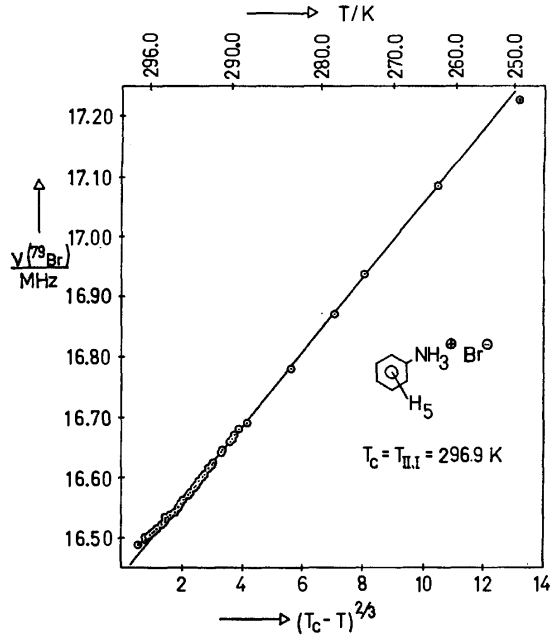

Fig. 9. ^{79}Br-NQR frequency of the low temperature modification of anilinium bromide as a function of the deviation of the temperature from the critical temperature T_c. The power of (T_c-T) indicates a non-classical critical exponent of $n=1/3$ (see text).

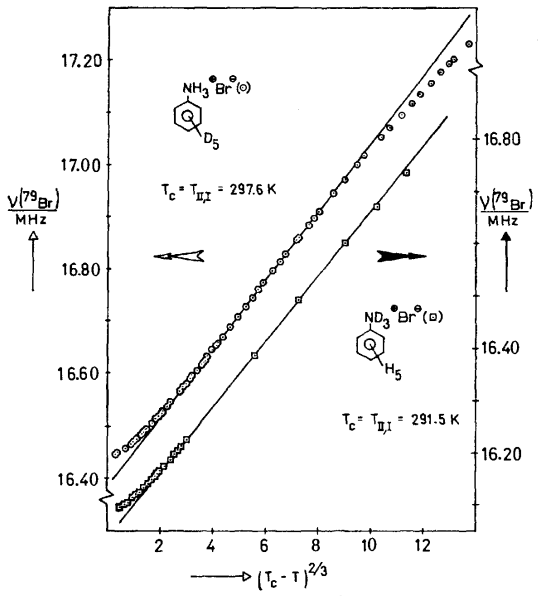

Fig. 10. ^{79}Br-NQR frequencies of the low temperature modification of anilinium-d_3 bromide and anilinium-d_5 bromide as a function of $(T_c-T)^{2/3}$. The power of (T_c-T) indicates a non-classical critical exponent of $n=1/3$ (see text).

$T_{II,I}$=296.9 K (Fig. 9). In this region the formation of the ordered monoclinic low temperature phase, expressed by the structural displacement parameter $\Delta\beta$ acting as an order parameter, governs the temperature dependence of the ^{79}Br-NQR frequency. There may be a second region, $225<T/K<260$, where $\nu(^{79}Br)$ is proportional to (T_c-T), that is, $n=1/2$, but the experimental data are too scarce to be definite in this case. Relation 10 holds also for both deuterated anilinium bromides, $C_6H_5ND_3^{\oplus}Br^{\ominus}$ and $C_6D_5NH_3^{\oplus}Br^{\ominus}$ within a range of some 30 K below $T_{II,I}$ (Fig. 10).

From this it is clear that a simple Bayer-type function (Eq. 2) or a polynomial with a small number of coefficients a_i (Eq. 1) must fail in the description of $\nu(T)$ of anilinium bromide **II**. The temperature dependence of the resonance frequency is in this case a superposition of at least three effects: i) the normal volume independent temperature dependency caused by the increase of the amplitudes of thermal vibrations with increasing temperature (Bayer-term), ii) a strong volume dependent term (second term in Eq. 4), which comes into play through the anomalous thermal expansion below $T_{II,I}$, and iii) a strong variation of the asymmetry parameter η with temperatures just below $T_{II,I}$ not allowing to disregard the η-dependency of the resonance frequency. Such a strong variation of η with temperature has been observed in the (probably isotypic) anilinium iodide below its critical temperature ($T_{II,I}$= 241 K).[6a] The description of contribution ii) is additionally complicated by the fact that a change from a Landau-type behavior (critical exponent $n=1/2$) to a non-classical behavior ($n\neq 1/2$) may occur for $\varepsilon=(T_c-T)/T_c<0.1$.

Résumé

The investigation of the ^{79}Br-NQR spectra of anilinium bromide and its partially deuterated derivatives has lead to the following conclusions:

1. The rather large ^{79}Br-NQR frequency of the $Br^{\ominus}$ ion can be explained by assuming N–H$^{\oplus}$···Br$^{\ominus}$ hydrogen bonds and, vice versa, $\nu(^{79}Br)$ of this order of magnitude can serve as an argument for hydrogen bonding in the respective solid.

2. The large frequency shift on deuteration corroborates the model of a hydrogen bonded ion $Br^{\ominus}$. The direction of the ^{1}H–^{2}D shift can be explained by assuming that deuteration enlarges the hydrogen bond length in asymmetric hydrogen bonds (Ubbelohde effect).

3. The high temperature modification of anilinium bromide can be described by a model which considers a rapid (faster than $\approx 10^{-8}$ s) reorientating $NH_3^{\oplus}$ group.

4. The strong temperature dependence of the ^{79}Br-NQR frequency found immediately below the transition point can be rationalized by a model which interprets a structural displacement parameter (in this case: $\Delta\beta$) as an order parameter. The non-classical critical exponent is 1/3 in this region for the temperature dependence of the order parameter.

We are grateful to Prof. J. L. Ragle, University of Massachusetts, and to Dr. W. Weyrich, Technische Hochschule Darmstadt, for interesting discussions. We also enjoyed the privilege of a conversation with Prof. D. Nakamura, Nagoya University, Nagoya. We wish to thank Dr. W. Weyrich and Mr. P. Bachmann, THD, for help in the least-squares calculations.

This work was supported by the Deutsche Forschungsgemeinschaft and by the Fonds der Chemischen Industrie. We are grateful to the Chemische Fabrik Kalk GmbH., Köln-Kalk, for the supply of hydrobromic acid.

References

1) I. Taguchi, *Bull. Chem. Soc. Jpn.*, **34**, 392 (1961).
2) H. Suga, *Bull. Chem. Soc. Jpn.*, **34**, 426 (1961).
3) I. Nitta, T. Watanabe, and I. Taguchi, *Bull. Chem. Soc. Jpn.*, **34**, 1405 (1961).
4) A. Cabana and C. Sandorfy, *Can. J. Chem.*, **40**, 622 (1961).
5) a) W. Pies and A. Weiss, *Z. Naturforsch.*, **26b**, 555 (1971); b) N. Nowak, W. Pies, and A. Weiss, *Proc. 2nd Intern. Symp. NQR Spectroscopy*, Viareggio **1973**, (Publ.1975), 165.
6) a) W. Pies and A. Weiss, *J. Magn. Reson.*, in press. b) H. M. Maurer, W. Pies, and A. Weiss, *Ber. Bunsenges. Phys, Chem.*, **80**, 1242 (1976); c) W. Pies and A. Weiss, *Chem. Ber.*, **111**, 335 (1978).
7) W. Pies and A. Weiss, *J. Magn. Reson.*, **21**, 377 (1976).
8) A. E. Rondeau, *J. Chem. Eng. Data*, **11**, 124 (1966).
9) a) H. Bayer, *Z. Phys.*, **130**, 227 (1951); b) T. Kushida, G. B. Benedek, and N. Bloembergen, *Phys. Rev.*, **104**, 1364 (1956).
10) L. O. Andersson, *Ark. Fysik*, **40**, 71 (1969).
11) R. L. Sass, E. B. Brackett, and T. E. Brackett, *J. Phys. Chem.*, **67**, 2863 (1963).
12) W. A. Gabes and K. Olie, *Acta Crystallogr., Sect. B*, **26**,

443 (1970); M. van Driel and C. H. MacGillavry, *Recl. Trav. Chim. Pays-Bas*, **60**, 869 (1941).
13) J. Itoh and Y. Yamagata, *J. Phys. Soc. Jpn.*, **17**, 481 (1962); K. R. Jeffrey, A. G. Brown, and R. L. Armstrong, *Phys. Rev.*, **B8**, 3071 (1973).
14) J. J. R. Frausto da Silva and L. F. Vilas Boas, *Rev. Port. Quim.*, **14**, 115 (1972).
15) a) B. Chenon and C. Sandorfy, *Can. J. Chem.*, **36**, 1181 (1958); C. Brisette and C. Sandorfy, *ibid.*, **38**, 34 (1960); b) F. Jellinek, *Acta Crystallogr.*, **11**, 626 (1958).
16) C. A. Coulson, *Research* **10**, 149 (1957).
17) K. Nakamoto, M. Margoshes, and R. E. Rundle, *J. Am. Chem. Soc.*, **77**, 6480 (1955).
18) W. C. Hamilton and J. A. Ibers, "Hydrogen Bonding," W. A. Benjamin, New York (1968); a) p. 53; b) p. 104.
19) G. C. Pimentel and A. L. McClellan, *Ann. Rev. Phys. Chem.*, **22**, 347 (1971); a) p. 356; b) p. 355.
20) K. J. Gallagher, in: "Hydrogen Bonding," ed by D. Hadzi, Pergamon Press, New York (1959), p. 45, and references therein.
21) I. Olovsson and P.-G. Jönsson, in "The Hydrogen Bond," ed by P. Schuster *et al.*, North Holland, Amsterdam (1976), p. 420.
22) R. Blinc, M. Mali, R. Osredkar, and J. Seliger, *J. Chem. Phys.*, **63**, 35 (1975).
23) R. Mecke and W. Kutzelnigg, *Spectrochim. Acta*, **16**, 1225 (1960).
24) R. Foglizzo and A. Novak, *Spectrochim. Acta*, **26A**, 2281 (1970).
25) A. Novak, *Structure Bonding*, **18**, 177 (1974).
26) D. Cook, *Can. J. Chem.*, **39**, 2009 (1961).
27) T. B. Brill and W. A. Welsh, *J. Chem. Soc., Dalton Trans.*, **1973**, 357.
28) R. C. Gearhart, T. B. Brill, W. A. Welsh, and R. H. Wood, *J. Chem. Soc., Dalton Trans.*, **1973**, 359.
29) A. F. Volkov and N. I. Smirnov, *Dokl. Akad. Nauk SSSR*, **211**, 1377 (1973); *Dokl. Phys. Chem. USSR (Engl. Transl.)*, **211**, 677 (1973).
30) C. W. Fryer and J. A. S. Smith, *J. Chem. Soc., A*, **1970**, 1029.
31) K. Ichida, Y. Kuroda, D. Nakamura, and M. Kubo, *Bull. Chem. Soc. Jpn.*, **44**, 1996 (1971).
32) A. Sasane, T. Matuo, D. Nakamura, and M. Kubo, *J. Magn. Reson.*, **4**, 257 (1971).
33) M. Bonamico, G. Dessy, and A. Vaciago, *Atti Accad. Nazl. Lincei, Rend., Classe Sci. Fis., Mat. Nat.*, **39**, 504 (1965).
34) H. E. Stanley, "Introduction to Phase Transitions and Critical Phenomena," Clarendon Press, Oxford (1971), p. 4.
35) F. Borsa, "Local Properties at Phase Transitions," ed by K. A. Müller and A. Rigamonti, Proc. Int. School of Phys. "Enrico Fermi," Course LIX, 9-21 July, 1973, Varenna sul Lago di Como, Italy, North-Holland, Amsterdam (1976), p. 255.
36) T. J. Bastow and H. J. Whitfield, *Aust. J. Chem.*, **27**, 1397 (1974).
37) a) G. K. Semin, T. A. Babushkina, and G. G. Yakobson, "Nuclear Quadrupole Resonance in Chemistry," *(Engl. Transl.)*, Halsted Press, New York (1975), p. 501; b) A. F, Volkov and G. K. Semin, *Izv. Akad. Nauk SSSR, Ser. Khim.* **1969** (7), 1634 (*Engl. Transl.*, p. 1522).
38) E. A. Kravchenko, O. M. Ivanova, and E. G. Il'in, *Zh. Neorg. Khim.*, **20**, 2556 (1975); *Russ. J. Inorg. Chem. (Engl. Transl.)*, **20**, 1416 (1975).
39) S. L. Segel and R. G. Barnes, "Catalog of Nuclear Quadrupole Interactions and Resonance Frequencies in Solids. Part I: Elements and Inorganic Compounds," US At. Energy Comm. IS-520 (1962), p. 26.
40) J. L. Ragle and K. L. Sherk, *J. Chem. Phys.*, **50**, 3553 (1969).

The Interaction Potential Surfaces for Alkali-trimers

S. Noor MOHAMMAD
Department of Physics, Indian Institute of Technology, Kharagpur, West Bengal, India
(Received August 27, 1977)

Semi-empirical potential energy surfaces for some alkali-trimer complexes have been calculated using the simplest form of London equation. In the calculations use has been made of two new exponential potentials for the singlet and triplet states of diatomic molecules. The calculated potential surfaces at small internuclear distances show shallow well extending into the entrance and exit valleys without an energy barrier. The complexes are seen to be stable over all configurations; they are most stable however in the linear symmetric configuration. The force constants corresponding to bending and stretching deformations have been calculated for homonuclear trimers only. It has been observed that unlike stretching, the bending deformations do not sensitively affect the energy variation of the ground state.

The alkali atom-alkali dimer exchange reaction

$$L' + L_2 \longrightarrow L'L + L, \quad (1)$$

where L and L′ are same or different atoms, are believed to be important in determining the energy transfer and condensation in supersonic alkali nozzle beams[1] and in determining nuclear relaxation times observed in the NMR of alkali dimers in optically bumped alkali vapours.[2] Recently some molecular beam reaction scattering has been measured[3] for $Na+Cs_2$, Rb_2, K_2, and $K+Rb_2$. A knowledge of potential energy surfaces of the trimer complexes formed therein is of considerable importance in order to help resolve the reaction dynamics, to determine the reaction cross-section and isotope effects, and to provide theoretical interpretation of the reactive scattering data.

Alkali trimers are intermediate of alkali atom-dimer exchange reaction. The experimental observation of Foster *et al.*[4] indicates only that they are stable molecules and suggests nothing about their binding energy and geometry. A diatomics-in-molecules calculation[5] for Li_3 shows it to be a stable molecule bound approximately by 9 kcal/mol with respect to $Li+Li_2$. The recent *ab initio* calculation[6] of Davies *et al.*, on the other hand, suggests that linear Li_3 is bound 3 kcal/mol lower in energy with respect to the same reactants. Pseudopotential calculations[7] on Na_3 and K_3 indicate that they are unbound with respect to atom-dimer dissociation. Semi-empirical valence bond calculations,[8] however, show that linear trimers are stable molecules in the ground state.

In the present study our aim is to determine semi-empirically the potential energy surfaces of some alkali trimer complexes and to obtain thereform their binding energies, equilibrium geometries and equilibrium vibrational force constants.

Method of Calculation

A non-ionic valence bond method has been used in the present calculation. Only the ns valence electron of each alkali atom is explicitly taken into consideration. All the trimers are thus reduced to three-electron three-orbital systems. The Hamiltonian operator for such systems in atomic units is

$$H = \sum_i[-\nabla_i^2/2 - \sum_a Z_a/r_{ai} + \sum_{i>j} 1/r_{ij}] + \sum_{a>b} Z_a Z_b/R_{ab}, \quad (2)$$

where the subscripts i, j, *etc.* refer to electrons and a, b, *etc.* to nuclei. There are two linearly independent canonical structures ϕ_1 and ϕ_2 coresponding to the bonding scheme (a—b,c) and (a,b—c) respectively. If one assumes that the orbitals a,b, and c are mutually orthogonal, the secular determinant written in terms of the Hamiltonian matrix elements H_{ij} and the overlap matrix elements S_{ij} will yield

$$E_\pm = Q_{ab} + Q_{bc} + Q_{ca} \pm 2^{-1/2}[(J_{ab}-J_{bc})^2 + (J_{bc}-J_{ca})^2 + (J_{ca}-J_{ab})^2]^{1/2}. \quad (3)$$

Here Q and J are the diatomic Coulomb and exchange integrals respectively. These integrals have been evaluated at the three internuclear distances R_{ab}, R_{bc}, and R_{ca}. This equation is known as London equation.[9] In Eq. 3 the zero of the energy refers to the separated atoms and since Q and J are both negative quantities E_- refers to the binding energy of more stable state. However, the diatomic integrals Q and J are more difficult to evaluate for alkali diatomics. In order to circumvent this difficulty, we adopt the semi-empirical method of Cashion and Herschbach,[10] and obtain from identical valence bond approximation

$$E_\pm = Q \pm J, \quad (4)$$

where E_+ and E_- refer to $^1\Sigma_g$ and $^3\Sigma_u$ states respectively. If these potential curves are known independently Q and J can be evaluated as

$$Q = \frac{1}{2}[E(^1\Sigma) + E(^3\Sigma)], \quad (5)$$

and

$$J = \frac{1}{2}[E(^1\Sigma) - E(^3\Sigma)]. \quad (6)$$

The problem thus reduces to obtaining accurate potential energy curves for the $^1\Sigma_g$ and $^3\Sigma_u$ electronic states of alkali diatomics.

Diatomic Potential Curves

Singlet Potential. Whitehead and Grice,[8] in their studies of atom-dimer exchange reaction of lithium and sodium, made use of *ab initio*[11-15] and RKR[16] curves for Li_2, LiNa, and Na_2. Due to lack of similar data on the other dimers of alkali atoms, it is not possible to extend their method to the trimers involving atoms other than Li and Na. Recently the classical turning

points for the vibrational levels of the $^1\Sigma_g$ state of K_2, Rb_2, and Cs_2 have also been derived.[17] One major disadvantage of these curves is that these are constructed only in the region for which sufficient spectroscopic data exist. For Li_2, data for the higher vibrational levels being not available, Krupenie *et al.*[16] fitted its RKR curve to the Lippincott potential[18-21] to get extrapolation at large internuclear distances. Another disadvantage of this method is that it gives only numerical values of the curve at a series of points, and not a suitable analytical form for the same. Further, these curves are not available for the heteronuclear diatomics of the present series. Recently Sannigrahi *et al.*[22] have used Morse[23] and Rydberg[24] potentials for the $^1\Sigma_g$ state. But in case of alkali dimers it can be seen[25] that the Morse potential predicts too much attraction at large internuclear distances. Though the Rydberg potential is much better than the Morse, in many cases it deviates greatly from the RKR curves, and on the average, predicts α_e within -3.2% and $\omega_e x_e$ within 11.74% for the fifty diatomic molecules studied.[26] In our recent study[26] of the interatomic potentials for the bound states of diatomic molecules we have proposed a new potential,

$$U_2(R) = D_e\left\{\left(\frac{R_e}{R}\right)^{2n}\exp\left[-2\alpha(R^2-R_e^2)\right] - 2\left(\frac{R_e}{R}\right)^{n}\exp\left[-\alpha(R^2-R_e^2)\right]\right\}, \quad (7)$$

where

$$\alpha = (\Delta^{1/2}-n)/2R_e^2, \quad (8)$$

$$n = 0.324 + 0.313\Delta^{1/2} + 0.01\Delta \quad \text{for } 0 \lesssim \Delta^{1/2} \lesssim 3.2$$
$$= 1.3637 - 0.206\Delta^{1/2} + 0.004\Delta \quad \text{for } 3.2 \lesssim \Delta^{1/2} < \infty, \quad (9)$$

and

$$\Delta = R_e^2 k_e/2D_e.$$

$-D_e$ is the minimum value of $U_2(R)$, R_e is the value of R at which $U_2(R)=-D_e$ and k_e is the measure of curvature of the potential curve at $R=R_e$. A detailed investigation shows that this is perhaps the best three-parameter potential over an extended region of R. It predicts α_e and $\omega_e x_e$ and other spectroscopic constants such as higher order vibrational force constants n_e and o_e almost exactly for a large number of molecules. This is, in fact, a generalisation of the Vershni III potential.[27] In Fig. 1 we have compared this potential with the corresponding Varshni III, RKR and *ab initio* curves for Li_2, LiNa, and Na_2. The curves of this figure shows that the present potential is equally applicable to the other alkali dimers also. We use this potential for the $^1\Sigma$ ground state.

Triplet Potential. Except for a long range van der Waals attraction the $^3\Sigma_u^+$ excited electronic state is a repulsive one and no experimental information is available for this. We are, therefore, to depend for this on a reliable theoretical calculation. Since the interaction of two alkali metal atoms is qualitatively similar to the interaction of two hydrogen atoms whose theoretical curve can be accurately constructed by the perturbation method of Dalgarno and Lynn,[28] Davies *et al.*[6] in their calculations of collision integrals, used the same to predict the triplet curves for alkali metal diatomics. These are given by $60.70\exp(-1.37\,R)$, $105\exp(-1.51\,R)$, $211\exp(-1.45\,R)$, $170\exp(-1.34\,R)$, and $173\exp(-1.27\,R)$ for Li_2, Na_2, K_2, Rb_2, and Cs_2 respectively. The main defect of this method is that it gives an individual potential for each dimer. Krupenie *et al.* used a method originally suggested by Keyes[29] to estimate the $^3\Sigma_u^+$ potential of Li_2. He simply changed the sign in the exchange term of the double exponential function representing the $^1\Sigma_g^+$ potential. When compared with the *ab initio* curve, this is seen to lie too high by a factor of 2 to 4.

In connection with some classical trajectory studies of alkali atom-dimer exchange reactions Whitehead[30] has recently proposed a Porter-Karplus[31] type anti-Morse potential for Li_2, LiNa, and Na_2. This is given by

$$U_w^{(3)}(R) = D_e^{(3)}[(x+1)^2-1], \quad (10)$$

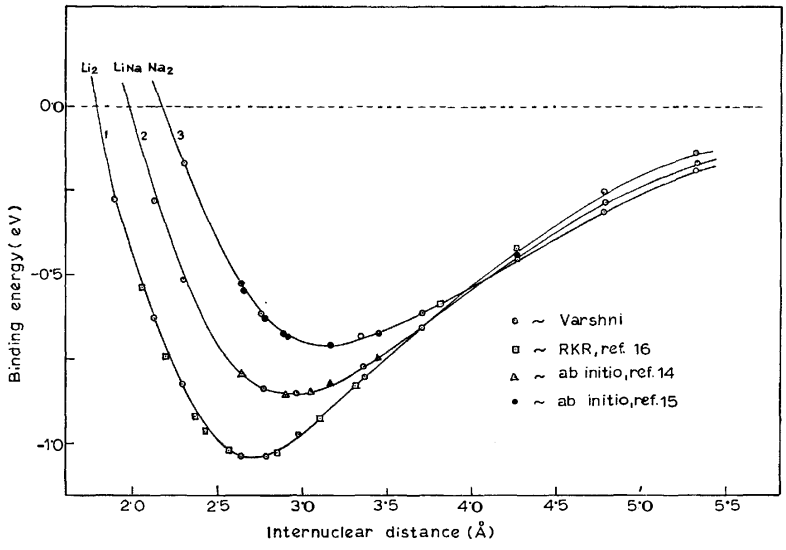

Fig. 1. Comparison of potential energy curves for the ground state of Li_2, LiNa, and Na_2.

where

$$x = \exp[-\beta^{(3)}(R-R_e)]. \quad (11)$$

$D_e^{(3)}=3.30$, 3.09, and 3.30 kcal/mol and $\beta^{(3)}=1.240$, 1.254, and 1.230 Å^{-1} for Li_2, LiNa, and Na_2 respectively. Equation 10 has been obtained by fitting to the *ab initio* data. The main objection to $U_w^{(3)}(R)$ is that it requires an independent knowledge of the triplet state potential data which uptill now are available only for Li_2, LiNa and Na_2. Consequently its applicability is limited to these dimers only.

With a view to devising a triplet potential of general validity we change the sign of the repulsive part of Eq. 7 and then fit it to the *ab initio* data[12-15] to get

$$U_2^{(3)}(R) = 0.50D_e\left\{\left(\frac{R_e}{R}\right)^{2n}\exp[-2\alpha(R^2-R_e^2)] + 0.05\left(\frac{R_e}{R}\right)^{n}\exp[-\alpha(R^2-R_e^2)]\right\}. \quad (12)$$

Like its singlet counterpart it is expected to show correct limiting behaviour at large internuclear distances. We tried to construct the triplet potential corresponding to the Varshni also and it is interesting to see that it comes out as the same as Eq. 12 with $n=1$. The identifying feature of these potentials is that they can be expressed in terms of the ground state potential parameters for which sufficient informations are available for the present systems. In Fig. 2 we have compared Eq. 12 with the corresponding Varshni (triplet) and *ab initio* curves for Li_2, LiNa and Na_2. It can be seen from this figure that the said potential agrees quite well with the latter curves. Since alkali dimers behave quite ideally with respect to semi-empirical parametrisation, we believe that this potential (which has been obtained only for the specific cases of Li_2, LiNa and Na_2) might also be useful for the rest of the diatomics in the series. We use this potential for the triplet state.

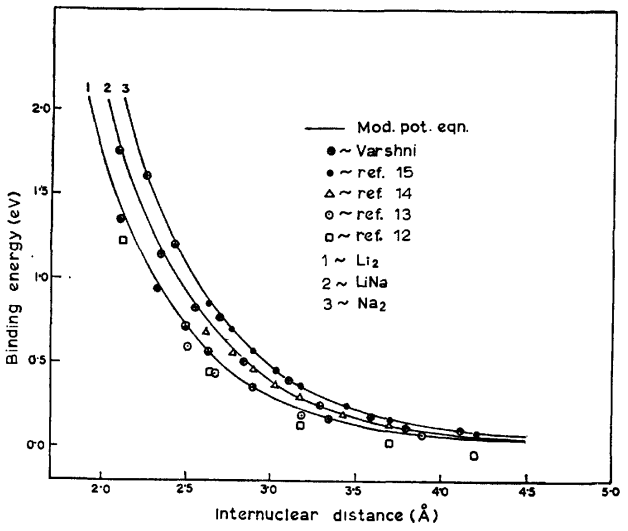

Fig. 2. Comparison of potential energy curves for the triplet state of Li_2, LiNa, and Na_2.

Results

The potential parameters D_e, R_e, and K_e needed to evaluate Eqs. 7 to 12 are given in Table 1. All these data are taken from Herzberg[32] and from the summary of Evans *et al.*[33] Using Eq. 3 potential energy surfaces consisting of a series of contour lines of constant energy are now constructed for all the triatomic complexes for both Varshni III and our own potential model. Such surfaces for the linear configuration of Li_3, LiLiNa and, NaLiNa are shown in Figs. 3 to 5. Potential energy surfaces of other trimers, which are not shown in the figure are similar to those of Li_3, LiLiNa, and NaLiNa. These surfaces are very much important in the sense that can provide useful informations towards detailed rate calculation by the solution of classical equation of motion. All these surfaces exhibit shallow potential well at small internuclear distances which extends into the entrance and exit valleys without an energy barrier.

Table 1. Ground state potential parameters for alkali-dimers

Dimer	$-D_e$(eV)[e]	r_e(Å)[e]	k_e(mdyn/Å)[e]
Li_2	1.05	2.672	0.256
Na_2	0.74	3.08	0.174
K_2	0.52	3.923	0.099
Rb_2	0.493[a]	4.127[a]	0.081
Cs_2	0.453[a]	4.465[a]	0.069
LiNa	0.88[c]	2.911[b]	0.195[d]
LiK	0.739[c]	3.238[c]	0.149
NaK	0.61	3.476[c]	0.129
NaRb	0.57	3.565	0.122

a) Taken from Ref. 33. b) Taken from Ref. 14.
c) Determined by the formula $x_{ab}=(x_{aa}\,x_{bb})^{1/2}$, where all x_{aa} are taken from Refs. 32 and 33.
d) Calculated from the observed vibrational frequency, see Ref. 32. e) All these data except those taken from a, b, c, and d are from Ref. 32. The vibrational force constants are calculated from the observed vibrational frequency given in this reference.

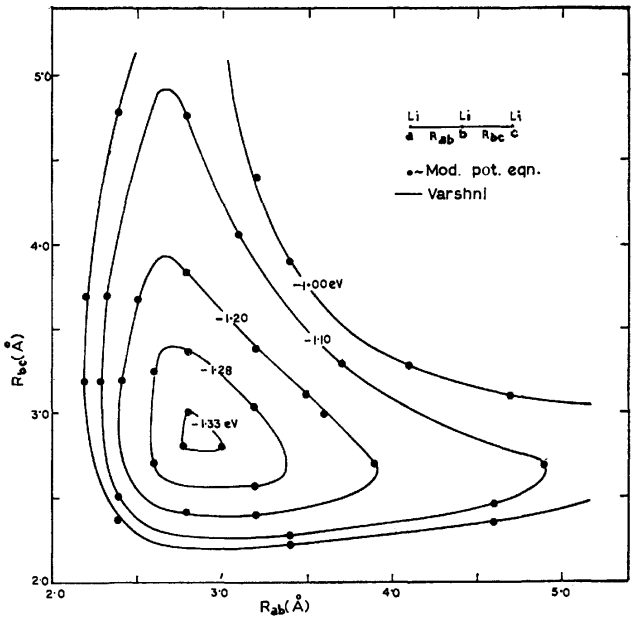

Fig. 3. Potential energy surfaces of Li_3 for linear configuration.

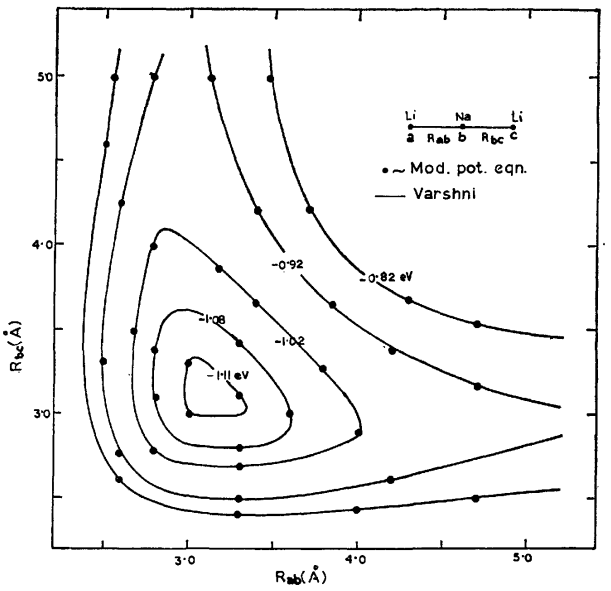

Fig. 4. Potential energy surfaces of LiNaLi for linear configuration.

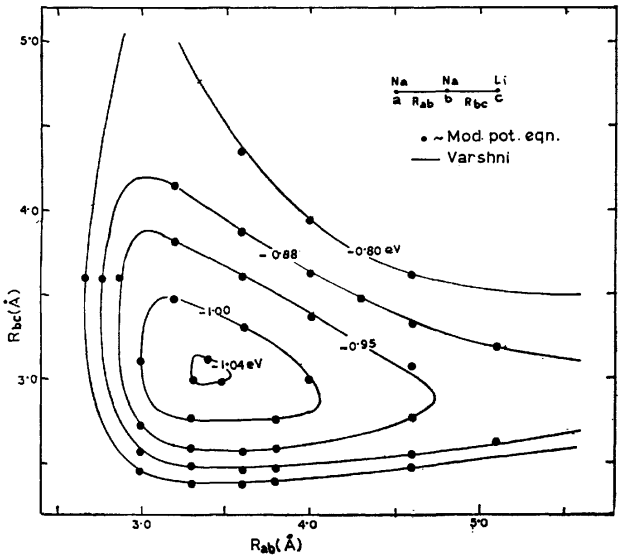

Fig. 5. Potential energy surfaces of NaNaLi for linear configuration.

The reacting atom, coming along the entrance valley is first reflected back and forth at the sides of the basin and undergoes a continual conversion of translational into vibrational energy and vice versa. As a result, the atom wanders about the potential basin until it either passes out through the gap into the exit valley which means reaction has taken place or it returns to the valley whence it entered. The depths of the potential wells are defined to be the binding energy of trimers. These binding energies in the case of symmetric trimers are found to decrease in the order $Li_3 > Na_3 > K_3 > Rb_3 > Cs_3$ in line with the bond energy values of the corresponding dimers. However, in the mixed alkali cases the potential well is deepest when the lighter alkali occupies the central position. The variation

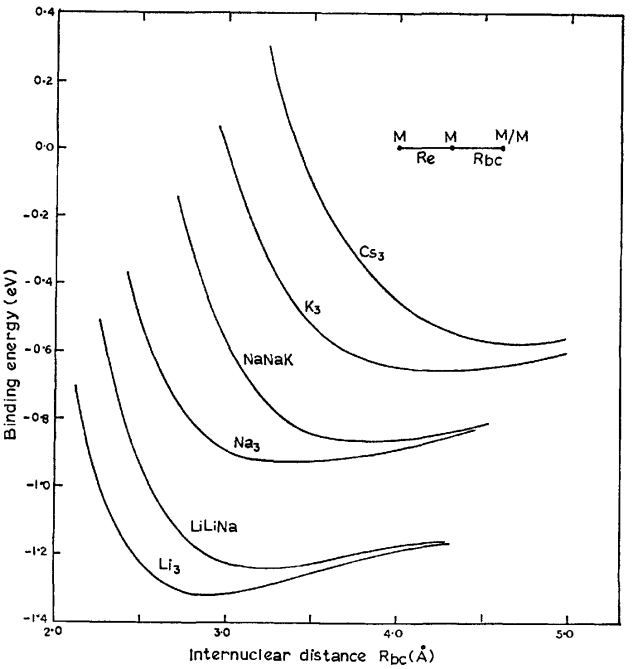

Fig. 6. Energy curves for approach of M (or M′) to M_2 fixed at M_2 equilibrium internuclear distances in the linear configuration for Li_3, LiLiNa, Na_3, NaNaK, K_3, and Cs_3.

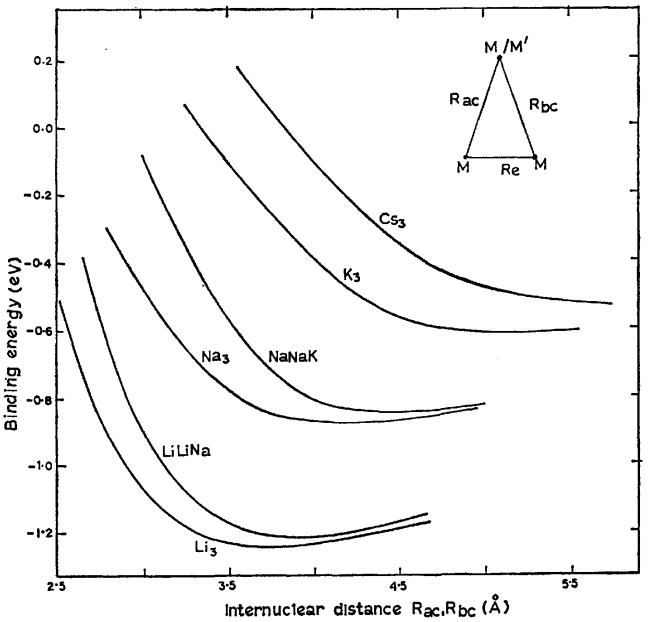

Fig. 7. Energy curves for approach of M (or M′) to M_2 fixed at M_2 equilibrium internuclear distances in the isosceles triangular configuration for Li_3, LiLiNa, Na_3, NaNaK, K_3, and Cs_3.

of binding energy of Li_3, Na_3, LiLiNa, NaNaK, K_3, and Cs_3 with bond length are shown in Figs. 6 and 7 for collinear and isosceles triangular configurations respectively. In each case the reacting alkali dimer is kept fixed at its equilibrium internuclear distance R_e, and binding energy is plotted as a function of the reactant alkali distance. Calculated values of binding energy and bond length are given in Table 2. It can

be seen from this table that the symmetric alkali trimers are most stable in the linear symmetric configuration. The bond length of a trimer is in general greater than the bond length of the corresponding dimer.

Table 2. Calculated values of binding energies (Δ) and bond lengths (r_{ab}, r_{bc}) for alkali trimers in linear symmetric and isosceles triangular configurations

$M'+M_2$ $\rightarrow$(M'MM) $\rightarrow$M'M+M	$-\Delta$ (kcal/mol)[a] Δ_r	Δ_p	r_{ab}(Å)	r_{bc}(Å)
$Li+Li_2$	6.58	6.58	2.85	2.85
$\rightarrow$(LiLiLi)	4.50	4.50	3.68	2.67
$\rightarrow Li_2+Li$				
$Na+Na_2$	4.70	4.70	3.27	3.27
$\rightarrow$NaNaNa	3.18	3.18	4.21	3.08
$\rightarrow Na_2+Na$				
$K+K_2$	3.46	3.46	4.05	4.05
$\rightarrow$KKK	2.24	2.24	5.08	3.923
$\rightarrow K_2+K$				
$Rb+Rb_2$	3.23	3.23	4.28	4.28
$\rightarrow$RbRbRb	2.12	2.12	5.50	4.127
$\rightarrow Rb_2+Rb$				
$Cs+Cs_2$	2.93	2.93	4.68	4.68
$\rightarrow$CsCsCs	1.96	1.96	5.83	4.465
$\rightarrow Cs_2+Cs$				
$Na+Li_2$	4.61	8.53	3.30	2.80
$\rightarrow$NaLiLi	3.81	7.72	3.89	2.672
$\rightarrow$NaLi+Li				
$Na+Li_2$	1.73	5.65	3.12	3.12
$\rightarrow$LiNaLi	—	—	—	—
$\rightarrow$LiNa+Li				
$Li+Na_2$	7.03	3.81	2.97	3.40
$\rightarrow$LiNaNa	3.75	0.52	4.10	3.08
$\rightarrow$LiNa+Na				
$Li+Na_2$	8.88	5.65	3.15	3.15
$\rightarrow$NaLiNa	—	—	—	—
$\rightarrow$NaLi+Na				
K+Li	3.16	10.33	3.60	2.68
$\rightarrow$KLiLi	3.16	10.33	4.20	2.672
$\rightarrow$KLi+Li				
$K+Li_2$	—	4.68	3.44	3.44
$\rightarrow$LiKLi	—	—	—	—
$\rightarrow$LiK+Li				
$Li+K_2$	7.30	2.25	3.26	3.52
$\rightarrow$LiKK	3.46	—	3.48	3.923
$\rightarrow$LiK+K				
$Li+K_2$	9.73	4.68	3.45	3.45
$\rightarrow$KLiK	—	—	—	—
$\rightarrow$KLi+K				
$K+Na_2$	3.04	6.04	3.84	3.22
$\rightarrow$KNaNa	2.61	5.60	4.37	3.08
$\rightarrow$KNa+Na				
$K+Na_2$	0.88	3.87	3.70	3.70
$\rightarrow$NaKNa	—	—	—	—
$\rightarrow$NaK+Na				
$Na+K_2$	4.73	2.65	3.67	4.32
$\rightarrow$NaKK	2.61	0.53	4.70	3.923
$\rightarrow$NaK+K				
$Na+K_2$	5.95	3.87	3.64	3.64
$\rightarrow$KNaK	—	—	—	—
$\rightarrow$KNa+K				
$Rb+Na_2$	2.61	6.53	3.84	3.17
$\rightarrow$RbNaNa	2.42	6.34	4.65	3.08
$\rightarrow$RbNa+Na				
$Rb+Na_2$	—	3.59	3.80	3.80
$\rightarrow$NaRbNa	—	—	—	—
$\rightarrow$NaRb+Na				
$Na+Rb_2$	4.34	2.56	3.78	4.41
$\rightarrow$NaRbRb	4.22	0.67	4.98	4.127
$\rightarrow$NaRb+Rb				
$Na+Rb_2$	—	3.61	3.83	3.83
$\rightarrow$RbNaRb	—	—	—	—
$\rightarrow$RbNa+Rb				

a) Δ_r and Δ_p correspond to potential well depths with respect to reactants and products respectively. The upper and lower result in each row corresponds to linerar and isosceles triangular configurations respectively.

The ground (linear symmetric) state of alkali trimers can be further characterised by the force constants of its stretching and bending deformations. If R_{01} and R_{02}, and E_0 stand respectively for the internuclear distances and energy of the minimum energy intermediate state, then variation of energy around this state, to the lowest order is given by [34]

$$2(E-E_0) = A_{11}q_1^2 + A_{22}q_2^2 + A_{33}q_3^2, \tag{13}$$

where the terms q_i are defined as

$$q_1 = \frac{1}{2}[R_{ab}+R_{bc}-(R_{01}+R_{02})],$$

$$q_2 = \frac{1}{4}[(R_{01}+R_{02})^2-R_{bc}^2]^{1/2}, \tag{14}$$

and

$$q_3 = \frac{1}{2}(R_{ab}-R_{bc}),$$

q_1 describes a symmetrical stretching, q_2 a bending, and q_3 an asymmetric stretching motion. The coefficients

$$A_{ii} = \frac{\partial^2(E_0-E_i)}{\partial q_i^2} \tag{15}$$

are the corresponding force constants. As an illustration, we have calculated these force constants for the homonuclear trimers. These are given in Table 3.

Table 3. Calculated values of force for the ground state of homonuclear trimers

Trimer	A_{11} (mdyn/Å) sym. stretching	$A_{22}\times 10$(mdyn/Å) asym. stretching	$A_{33}\times 10^3$(mdyn/Å) bending
Li_3	0.1293	0.3658	0.1264
Na_3	0.0857	0.2589	0.0406
K_3	0.0614	0.1415	0.0131
Rb_3	0.0486	0.1166	0.0119
Cs_3	0.0360	0.0995	0.0067

It can be seen from this table that the symmetric stretching force constants of the trimers are about half the magnitude of the force constants of the corresponding dimer. Again the asymmetric force constant which is important primarily in regard to "tunneling corrections" is almost one-fourth the magnitude of the symmetric force constant of an alkali trimer. Very low values of the bending force constant which determines the size of the (L, L_2) exchange cross-section near the threshold indicates that the rate of increase of potential

energy as a complex is bent from the collinear conformation is very small.

Conclusion

For lack of experimental data on alkali trimers it is not possible to test the validity of the present calculation. However, because of the semi-empiricism of the method employed certain errors are likely to enter the calculations. The omission of three-centre integrals in London equation may be a possible source of error. Pedersen and Porter[35] have shown that the three-centre integrals in the calculation of H_3 complexes almost insignificantly contribute near the collinear saddle point. Similar trend may be expected to be followed also in the case of alkali complexes. Since in alkali atoms the np valence orbital is very close to the ns orbital we should have considered their effects in the calculations. However, the use of diatomic potential curves in the calculation of Coulomb and exchange integrals includes their effects to a certain extent. Whitehead and Grice considered the inclusion of overlap integral in their calculations of Q and J, and have shown that it increases the binding energy by about 2 kcal/mol. The inclusion of this integral effectively in the London equation seems not to be theoretically consistent. We have not, therefore, studied the same in the present calculations.

The most distinguishing feature of the present calculation is that only with the knowledge of three spectroscopic constants of a dimer one can now construct its potential energy surface with much less labour and computational expenses.

I am grateful to Professor H. N. Bose for his kind interests in the work.

References

1) R. J. Gordon, Y. T. Lee, and D. R. Hirschbach, *J. Chem. Phys.*, **54**, 2293 (1971).
2) R. Gupta, W. Harper, G. Roe, and W. Park, *Phys. Rev. Lett.*, **32**, 574 (1974).
3) J. C. Whitehead and R. Grice, *Faraday Discuss. Chem. Soc.*, **55**, 320, 374 (1973).
4) P. J. Foster, R. E. Leckenby, and E. J. Robbins, *J. Phys. B*, **2**, 478 (1969).
5) A. L. Companion, D. J. Steible, and A. J. Starshak, *J. Chem. Phys.*, **49**, 3637 (1968).
6) D. W. Davies and G. del Conde, *Faraday Discuss. Chem. Soc.*, **55**, 369 (1973).
7) B. T. Pickup and W. B. Brown, *Mol. Phys.*, **23**, 1189 (1972).
8) J. C. Whitehead and R. Grice, *Mol. Phys.*, **26**, 267 (1973).
9) F. London, *Z. Electrochim.*, **35**, 552 (1929). See also S. Glasstone, K. J. Laidler, and H. Eyring, "Theory of Rate Processes," McGraw Hill Book Co. Inc., New York (1941), p. 77.
10) J. K. Cashion and D. R. Herschbach, *J. Chem. Phys.*, **40**, 2358 (1964); **41**, 2199 (1964).
11) W. Demtroder, M. McClintock, and R. N. Zare, *J. Chem. Phys.*, **51**, 5495 (1969).
12) C. Manneback, *Physica*, **29**, 769 (1963).
13) A. C. Wahl, Unpublished calculations, 1970.
14) P. J. Bertoncini, G. Das, and A. C. Wahl, *J. Chem. Phys.*, **52**, 5112 (1970).
15) P. J. Bertoncini and A. C. Wahl, Unpublished calculations, 1972.
16) P. H. Krupenie, E. A. Mason, and J. T. Vanderslice, *J. Chem. Phys.*, **39**, 2399 (1963).
17) R. H. Davies, E. A. Mason, and R. J. Munn, *Phys. Fluids*, **8**, 444 (1965).
18) E. R. Lippincott, *J. Chem. Phys.*, **23**, 1131 (1955); *J. Am. Chem. Soc.*, **78**, 5171 (1956); *J. Phys. Chem.*, **61**, 921 (1957).
19) E. R. Lippincott and M. O. Dayhoff, *Spectrochim. Acta*, **16**, 397 (1960); E. R. Lippincott, *J. Chem. Phys.*, **26**, 1678 (1957).
20) E. R. Lippincott, D. Steele, and P. Caldwell, *J. Chem. Phys.*, **35**, 123 (1961).
21) D. Steele and E. R. Lippincott, *J. Chem. Phys.*, **35**, 2065 (1961).
22) A. B. Sannigrahi and S. N. Mohammad, *Indian J. Pure Appl. Phys.*, **13**, 154 (1975).
23) P. M. Morse, *Phys. Rev.*, **34**, 57 (1929).
24) R. Rydberg, *Z. Phys.*, **73**, 376 (1931); **80**, 514 (1933).
25) O. Sinanoglu and K. S. Pitzer, *J. Chem. Phys.*, **31**, 960 (1959).
26) S. N. Mohammad (to be published).
27) Y. P. Varshni, *Rev. Mod. Phys.*, **29**, 664 (1957).
28) A. Dalgarno and N. Lynn, *Proc. Phys. Soc. (London), Ser, A*, **89**, 821 (1956).
29) R. W. Keyes, *J. Chem. Phys.*, **29**, 523 (1958).
30) J. C. Whitehead, *Mol. Phys.*, **29**, 177 (1975).
31) R. N. Porter and M. Karplus, *J. Chem. Phys.*, **40**, 1105 (1964); see also S. Sato, *Bull. Chem. Soc. Jpn.*, **28**, 450 (1955).
32) G. Herzberg, "Spectra of Diatomic Molecules," Van Nostrand Co., Inc. New York (1950). For ω_e of LiNa see M. N. Hessel, *Phys. Rev. Lett.*, **26**, 215 (1971).
33) R. H. Evans, R. Jacobson, T. R. Munson, and D. D. Wagman, *J. Res. Natl. Bur Std. (U.S.)*, **55**, 83 (1955).
34) F. E. Harris, D. A. Micha, and H. A. Pohl, *Ark. Phys.*, **30**, 259 (1965).
35) L. Pedersen and R. N. Porter, *J. Chem. Phys.*, **47**, 4751 (1967).

Preparation of Nickel(II) Complexes with 2,3-Butanediamines and Their Thermal Octahedral-Square Planar Transformation

Hideyuki NISHIMOTO, Tadatsugu YOSHIKUNI, Akira UEHARA, Eishin KYUNO,* and Ryokichi TSUCHIYA

Department of Chemistry, Faculty of Science, Kanazawa University, Kanazawa 920
**Department of Pharmaceutical Science, School of Pharmacy, Hokuriku University, Kanazawa 920*

(Received July 4, 1977)

The following nickel(II) complexes with *meso*- or *dl*-2,3-butanediamine (abbreviated to *meso*-bn and *dl*-bn, respectively) were prepared: $[Ni(meso\text{-bn})_3]X_2\cdot 2H_2O$, $[Ni(meso\text{-bn})_2]X_2$ and $[Ni(H_2O)_2(dl\text{-bn})_2]X_2$ (X=Cl, Br). It was found from the changes in the absorption spectra and magnetic susceptibilities that $[Ni(meso\text{-bn})_3]X_2\cdot 2H_2O$ complexes, when heated to 188 (X=Cl) and to 233 °C (X=Br), respectively, undergo transformations from octahedral to square planar structures with the loss of two moles of lattice water and one mole of coordinated *meso*-bn. $[Ni(H_2O)_2(dl\text{-bn})_2]X_2$ complexes were similarly found to transform from octahedral to square planar structures at 120 (X=Cl) and at 110 °C (X=Br), respectively with the evolution of two moles of coordinated water. After this transformation, the resulting complexes underwent the inverse transformation from square planar to octahedral structure at 170 °C, without any weight change. The effect of the configurational difference between *meso*- and *dl*-bn on the formation of tris and bis(2,3-butanediamine) complexes is also discussed.

Nickel(II) ions form complexes of various structures, *e.g.*, octahedral, tetrahedral and square planar structures, depending upon the ligands, with mutual transformations often occurring among them.[1] Tsuchiya *et al.* have reported structural transformations of $[Ni(H_2O)_2(NN\text{-deen})_2]X_2$, where *NN*-deen is *N,N*-diethylethylenediamine and X is a halide ion;[2] the chloride, upon heating, evolved two moles of coordinated water accompanied by the anation of chloride ions with the retention of the original octahedral structure, whereas the bromide transformed from an octahedral to a square planar structure without anation of bromide ions after the liberation of water molecules.

The structural transformation of nickel(II) complexes upon heating in solid phase is characterized by a change in the coordination number from six to four, as is seen for the above bromide. On the other hand, an interesting thermal equilibrium has been reported on the basis of spectral measurements that the structure of bis(*N,N*-diethylethylenediamine)copper(II) tetrafluoroborate, perchlorate and nitrate changes to square planar as the temperature is lowered, but to octahedral as the temperature is raised.[3] Tsuchiya *et al.* also recently found a novel example of a transformation from square planar to octahedral structure in the benzimidazole complex, $[Ni(bimd)_4](NO_3)_2\cdot 2.5C_2H_5OH$, in the solid phase.[4]

In addition to nickel(II) complexes containing N-substituted diamine, the thermal behavior of complexes with the C-substituted diamines, 2-methyl-1,2-propanediamine and 1,2-diphenylethylenediamine, have been studied in the solid phase by Farago *et al.*[5] and by Lifschitz *et al.*,[6] respectively. Transformations from octahedral to square planar structure are observed in these examples.

The present study was undertaken to prepare various types of the nickel(II) complexes containing *meso*- and *dl*-2,3-butanediamines, as C-substituted ethylenediamines, and to investigate thermal transformations in the solid phase and steric effects due to alkyl substitution.

Experimental

Preparation and Identification of 2,3-Butanediamines. A solution containing a mixture of *meso*- and *dl*-2,3-butanediamines (*meso*-bn and *dl*-bn, respectively) was obtained by the method described in Ref. 7. From the solution, *meso*-bn and *dl*-bn were separated as dihydrochlorides by the addition of hydrochloric acid, and were identified from IR and NMR spectra.[8]

The yields were about 20% for *meso*-bn and 9% for *dl*-bn.

*Preparation of the Complexes. Tris(*meso*-2,3-butanediamine)nickel(II) Halide Dihydrates, [Ni(*meso*-bn)$_3$]Cl$_2\cdot 2H_2O$ (I) and [Ni(*meso*-bn)$_3$]Br$_2\cdot 2H_2O$ (II).* A methanolic solution of nickel chloride or bromide was added to a solution of excess amounts of the free *meso*-diamine obtained by adding KOH to the diamine dihydrochloride. The resulting solution was allowed to stand for about three days in a refrigerator, with a bluish-violet *meso*-bn complex obtained. Recrystallization was carried out from ethanol.

*Bis(*meso*-2,3-butanediamine)nickel(II) Halides, [Ni(*meso*-bn)$_2$]Cl$_2$ (III) and [Ni(*meso*-bn)$_2$]Br$_2$ (IV).* These complexes were prepared in a manner similar to that used for complexes I and II, except for ligand molar ratios of 2: 1. A mixture of methanol and water (1: 1) was used as a solvent, and yellow plates were obtained.

*Diaquabis(*dl*-2,3-butanediamine)nickel(II) Halides, [Ni(H$_2$O)$_2$(*dl*-bn)$_2$]Cl$_2$ (V) and [Ni(H$_2$O)$_2$(*dl*-bn)$_2$]Br$_2$ (VI).* By a method similar to that used for complexes III and IV, blue crystals were obtained by recrystallization from water.

Analytical data for all the complexes obtained are summarized in Table 1.

Measurements. Derivatograms for thermal reactions of the complexes, electronic spectra and magnetic susceptibilities were measured in the manner previously reported.[2,4]

Results and Discussion

Derivatography. The derivatograms for complexes I and II are shown in Fig. 1. The former chloride shows a 28.6% mass loss in the TG curve in the temperature range from 50 to 188 °C, which just corresponds to the total liberation of two moles of lattice water and one mole of *meso*-bn. On the other hand, in the latter

TABLE 1. ANALYTICAL DATA FOR NICKEL(II) COMPLEXES WITH *meso*- AND *dl*-2,3-BUTANEDIAMINES

Complex	C%		H%		N%	
	Found	Obsd	Found	Obsd	Found	Obsd
(I) $[Ni(meso\text{-bn})_3]Cl_2\cdot 2H_2O$	33.65	33.51	9.71	9.37	18.84	19.54
(II) $[Ni(meso\text{-bn})_3]Br_2\cdot 2H_2O$	27.70	27.77	8.16	7.77	16.22	16.19
(III) $[Ni(meso\text{-bn})_2]Cl_2$	31.49	31.41	8.16	7.91	17.85	18.31
(IV) $[Ni(meso\text{-bn})_2]Br_2$	24.20	24.34	6.16	6.13	14.15	14.19
(V) $[Ni(H_2O)_2(dl\text{-bn})_2]Cl_2$	27.31	28.10	8.34	8.25	16.21	16.39
(VI) $[Ni(H_2O)_2(dl\text{-bn})_2]Br_2$	22.30	22.29	6.55	6.56	13.00	12.41

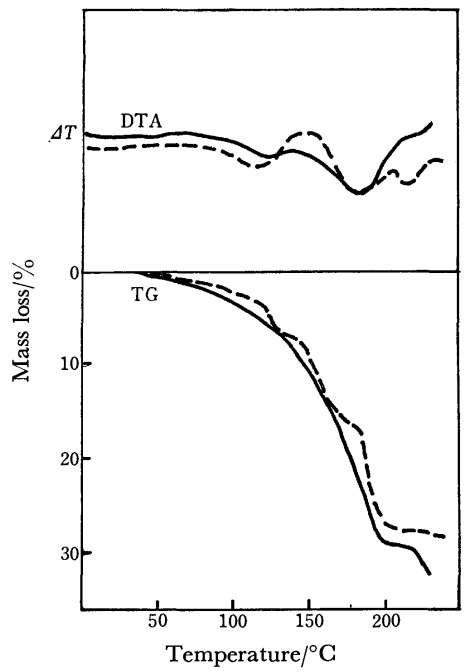

Fig. 1. Derivatograms of $[Ni(meso\text{-bn})_3]Cl_2\cdot 2H_2O$(——) and $[Ni(meso\text{-bn})_3]Br_2\ 2H_2O\cdot$(——).

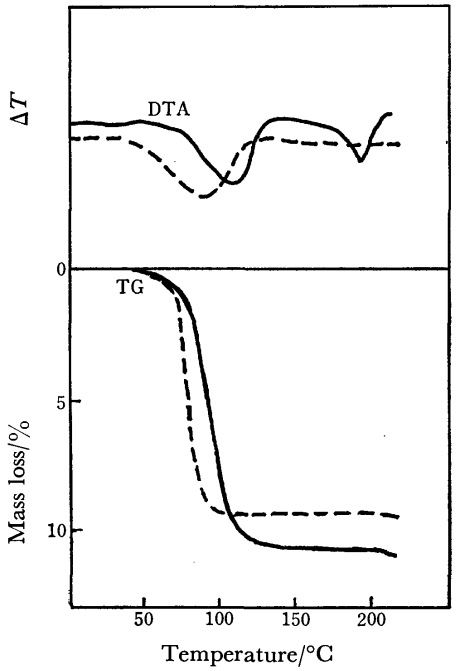

Fig. 2. Derivatograms of $[Ni(H_2O)_2(dl\text{-bn})_2]Cl_2$ (——) and $[Ni(H_2O)_2(dl\text{-bn})_2]Br_2$ (——).

bromide, three steps due to mass losses corresponding to the successive liberation of two moles of lattice water, that of a half mole of *meso*-bn and that of another half mole were found at 122, 192, and 233 °C, respectively.

The derivatograms for complexes V and VI are shown in Fig. 2. The former chloride shows a 10.4% mass loss in the TG curve between 70 and 120 °C. This mass loss matches the liberation of two moles of coordinated water. It is worth noting that an endothermic peak appears at 170 °C without any change in the TG and DTG curves, which is the basis of new information described in a later section.

For complex VI, a 8.4% mass loss was found in the range from 35 to 100 °C. This corresponds to the liberation of two moles of coordinated water. The endothermic peak was, however, not as distinctly observed as for complex V.

Electronic Spectra. Color changes of the complexes in each heating step are summarized in Table 2. This table also includes the magnetic moments which will be discussed in a later section.

The electronic spectral changes corresponding to these color changes were measured in the solid state. The diffuse reflection spectra of complex I, the sample

TABLE 2. COLOR AND MAGNETIC MOMENT OF THE COMPLEXES IN EACH HEATING STEP

Complex	Color	Magnetic moments (μ_{eff} B.M.)		Color	Magnetic moments (μ_{eff} B.M.)		Color	Magnetic moments (μ_{eff} B.M.)
(I) $[Ni(meso\text{-bn})_3]Cl_2\cdot 2H_2O$	bluish violet	3.33	50—188 °C →	yellow	diamag.			
(II) $[Ni(meso\text{-bn})_3]Br_2\cdot 2H_2O$	bluish violet	3.24	122—223 °C →	yellow	diamag.			
(V) $[Ni(H_2O)_2(dl\text{-bn})_2]Cl_2$	blue	3.39	70—120 °C →	yellow	diamag.	180 °C →	green	3.11
(VI) $[Ni(H_2O)_2(dl\text{-bn})_2]Br_2$	blue	3.28	35—110 °C →	yellow	diamag.	170 °C →	gray	3.44

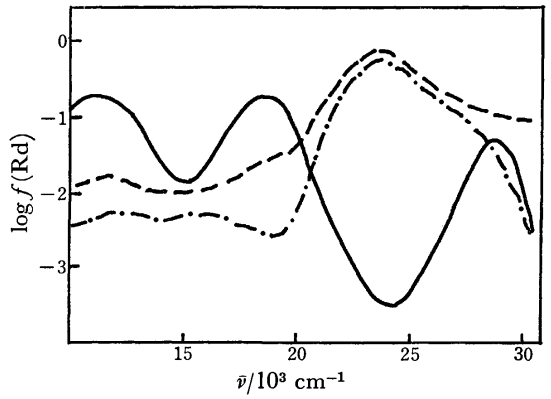

Fig. 3. Electronic spectra of $[Ni(meso\text{-bn})_3]Cl_2 \cdot 2H_2O$ (——), the sample obtained by heating it at 180 °C (– – –) and of $[Ni(meso\text{-bn})_2]Cl_2$ prepared in aqueous solution.

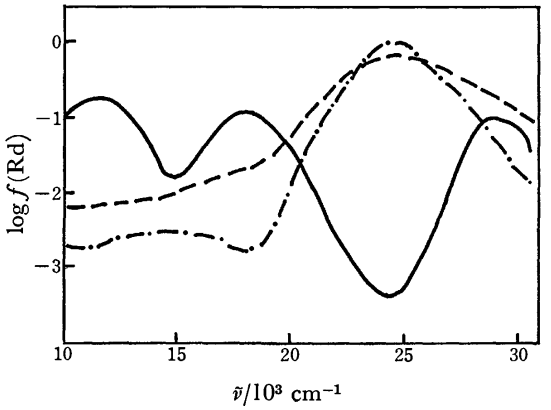

Fig. 4. Electronic spectra of $[Ni(meso\text{-bn})_3]Br_2 \cdot 2H_2O$ (——), the sample obtained by heating it at 220 °C (– – –) and of $[Ni(meso\text{-bn})_2]Br_2$ prepared in aquous solution.

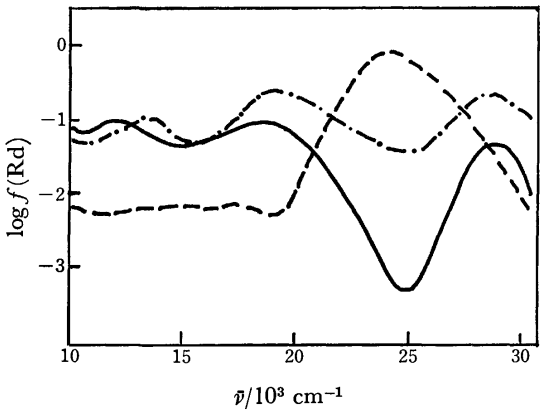

Fig. 5. Electronic spectra of $[Ni(H_2O)_2(dl\text{-bn})_2]Cl_2$ (——), the samples obtained by heating it at 120 °C (– – –) and at 180 °C (-·-·-).

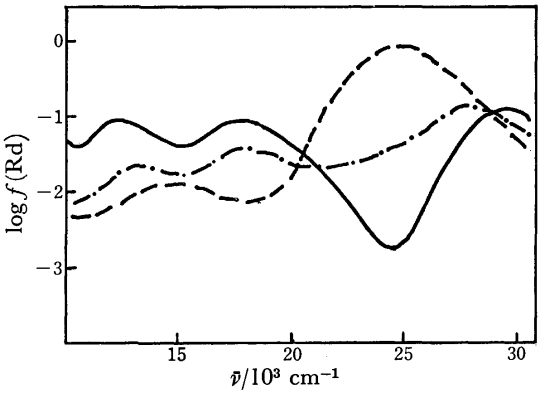

Fig. 6. Electronic spectra of $[Ni(H_2O)_2(dl\text{-bn})_2]Br_2$ (——), the samples obtained by heating it at 110 °C (– – –) and at 170 °C (-·-·-).

obtained by heating complex I to 180 °C, and of complex III are compared in Fig. 3, and the corresponding spectra of complex II, the sample obtained by heating complex II to 220 °C, and of complex IV in Fig. 4. Complexes I and II gave three characteristic maxima at 11, 18, and 28×10^3 cm^{-1}, which are assignable to the $^3A_{2g} \rightarrow {}^3T_{2g}$, $^3A_{2g} \rightarrow {}^3T_{1g}(F)$, and $^3A_{2g} \rightarrow {}^3T_{1g}(P)$ transitions in the octahedral nickel(II) complex at room temperature. After heating, these absorption bands were almost quenched and one strong band appeared at 24×10^3 cm^{-1}, which was assigned to the $^1A_{1g} \rightarrow {}^1A_{2g}$ transition in the square planar nickel(II) complex.[9]

The spectra of complex V and the samples obtained by heating this complex to 120 and 180 °C are shown in Fig. 5. At 120 °C, a new strong absorption band due to the formation of the square planar structure appears after the disappearance of the three absorption bands attributed to the octahedral structure, as was observed for complexes I and II. It is notable, however, that when heated to 180 °C, the three original absorption bands reappear after the disappearance of the strong band observed at 120 °C. This suggests the occurrence of a second thermal transformation from square planar to octahedral structure, an exceptional change for nickel(II) complexes.

The spectra of complex VI and the samples obtained by heating it to 110 and 170 °C are shown in Fig. 6. In a manner similar to that for complex V, the three original absorption bands disappear and one strong band appears upon heating at 110 °C, showing that the transformation from octahedral to square planar structure occurs. On the other hand, above 170 °C, the three absorption bands weakly reappear. Partial transformation from square planar to octahedral structure appears to occur.

Magnetic Moments. The magnetic moments at room temperature for complexes I, II, V, and VI and the samples obtained by heating them to each temperature at which a transformation occurs are listed in Table 2. For complexes I and II, the paramagnetic species change to diamagnetic species. By combining these results with the spectral changes due to heating, it is concluded that the change in the structure from octahedral to square planar occurs during the thermal reaction.

On the other hand, for complexes V and VI, the paramagnetic species change to diamagnetic species with the first heating step in a manner similar to that for complexes I and II. In the second heating step, however, the paramagnetism is recovered. Although the

tetrahedral nickel(II) complex is paramagnetic, it is known that its magnetic moment (3.7 B.M.) is significantly larger than that for the octahedral complex (3.3 B.M.).[10] A stepwise structural transformation, octahedral→square planar→octahedral, is concluded to occur in complex V.

On the other hand, in complex VI having a magnetic moment of 3.44 B. M. and the three weak absorption bands when heated above 170 °C, the partial transformation from square planar to either octahedral or tetrahedral structure is presumed to take place in a second heating step. It is to be noted that such a novel transformation including the subsequent inverse change from square planar to octahedral structure was found.

Relationship between the Conformation of 2,3-bn Coordinated and Ease of Complex Formation. In the present study, diaquabis(*dl*-bn)nickel(II) complexes were prepared, but the corresponding *meso*-bn complexes could not be prepared. This difference is probably due to the difference in the conformational structures of the coordinated 2,3-bn.

The conformations of *dl*-bn and *meso*-bn coordinated to the nickel ion are depicted below.

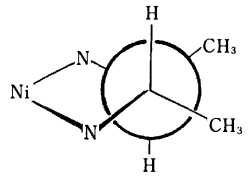

dl-bn

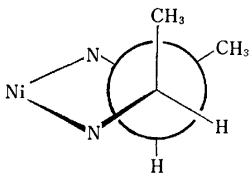

meso-bn

In complexes containing two moles of *dl*-bn in a square planar structure, the four methyl groups are all equatorial and the apical positions will admit the coordination of water molecules easily forming diaquabis(*dl*-bn)nickel(II) complexes easily.

For complexes containing two *meso*-bn, on the other hand, two of the four methyl groups are axial and, therefore, the water molecules are not easily coordinated in the apical positions. This may be the principal reason why diaquabis(*meso*-bn)nickel(II) complexes could not be prepared.

References

1) G. W. Everett, Jr., and R. H. Holm, *J. Am. Chem. Soc.*, **87**, 2118 (1965).

2) R. Tsuchiya, S. Joba, A. Uehara, and E. Kyuno, *Bull. Chem. Soc. Jpn.*, **46**, 1454 (1973).

3) A. B. P. Lever, E. Mantovani, and J. C. Donini, *Inorg. Chem.*, **10**, 2424 (1971).

4) R. Tsuchiya, E. Kyuno, A. Uehara, S. Joba, and S. Ohba, *Chem. Lett.*, **1976**, 911.

5) K. E. Farago, J. M. James, and V. C. G. Trew, *J. Chem. Soc. A*, **1968**, 48.

6) I. Lifschitz, J. C. Bos, and K. M. Dijkema, *Z. Anorg. Allg. Chem.*, **242**, 97 (1939).

7) F. H. Dickey, W. Fikett, and H. J. Lucas, *J. Am. Chem. Soc.*, **74**, 944 (1952).

8) L. M. Jackman, "Applications of Nuclear Magnetic Resonance Spectroscopy in Organic Chemistry," Pergamon Press, London (1959), p. 119.

9) S. Arakawa, T. Nozawa, and M. Hatano, *Bull. Chem. Soc. Jpn.*, **47**, 2643 (1974).

10) F. A. Cotton, O. D. Faut, and D. M. L. Goodgame, *J. Am. Chem. Soc.*, **83**, 344 (1961).

Multidentate Ligand Kinetics. II. The Ligand Substitution Reactions of the Triethylenetetraminecadmium(II) Ion and the Tetraethylenepentaminecadmium(II) Ion with the Ethylenediaminetetraacetatocuprate(II) Ion

Tetsuo KATSUYAMA and Toshihiko KUMAI

Department of Basic Technology, Faculty of Engineering, Yamagata University, Yonezawa, Yamagata 992

(Received August 4, 1977)

The kinetics and mechanism of the ligand-substitution reactions of triethylenetetraminecadmium(II) ion (Cd(II)-trien) and tetraethylenepentaminecadmium(II) ion (Cd(II)-tetren) with ethylenediaminetetraacetatocuprate(II) ion (Cu(II)-edta) were studied spectrophotometrically at I=0.2 M (1 M=1 mol dm^{-3}) and at 25.0 °C. The ligand-substitution reactions were catalyzed by traces of either edta or the polyamine (triethylenetetramine and tetraethylenepentamine). The substitution reactions were shown to proceed by means of a chain reaction mechanism where the chain-propagating steps are the reactions of the metal complexes with the free ligands. Each chain-propagating step was investigated. The ligand-substitution reactions of Cd(II)-trien and Cd(II)-tetren with edta were studied by the use of the chain reactions in the pH range of 8.8—10.2. The rate law is expressed as: $-d[CdR^{2+}]/dt=k_L[CdR^{2+}][edta^{4-}]+k_{HL}[CdR^{2+}][Hedta^{3-}]$, where R refers to trien or tetren. The rate constants, k_L and k_{HL}, were determined at 25.0 °C and I=0.2 M as: $k_L=(1.3\pm0.2)\times10^6$ M^{-1} s^{-1} and $k_{HL}=(6.5\pm1.5)\times10^4$ M^{-1} s^{-1} for Cd(II)-trien, and $k_L=(3.6\pm0.4)\times10^5$ M^{-1} s^{-1} and $k_{HL}=(1.0\pm0.2)\times10^4$ M^{-1} s^{-1} for Cd(II)-tetren.

Ligand-substitution reactions between two multidentate ligand complexes have been studied by Margerum *et al.*[1-4] A coordination chain reaction mechanism was proposed for the substitution reactions, where the chain-propagating steps are the reactions of the metal complexes with the free ligands.

These coordination chain reactions are useful for analytical purposes.[5-7] To widen their analytical application, though, it seemed worthwhile to find other coordination chain-reaction systems and to compare them with each other. In a previous paper,[8] the ligand-substitution reaction between the ethylenediaminetetraacetatocuprate(II) ion (Cu(II)-edta) and the triethylenetetraminezinc(II) ion (Zn(II)-trien) was studied; this reaction was found to proceed by means of a coordination chain reaction mechanism. In the present study, the ligand-substitution reaction of Cu(II)-edta with the triethylenetetraminecadmium(II) ion (Cd(II)-trien), and that with the tetraethylenepentaminecadmium(II) ion (Cd(II)-tetren) were investigated:

$$Cuedta^{2-} + CdR^{2+} \rightleftharpoons CuR^{2+} + Cdedta^{2-}, \quad (R1)$$

where R represents triethylenetetramine (trien) or tetraethylenepentamine (tetren). The results were compared with those of the other systems, which were found to proceed by means of a coordination chain-reaction mechanism. The coordination chain reactions of the present systems provide a useful method for the study of the ligand substitutions of Cd(II)-trien and Cd(II)-tetren with edta.

Experimental

Reagents. Guaranteed reagent-grade cadmium(II) oxide was dissolved in perchloric acid. Twice-recrystallized sodium carbonate was added to the solution to obtain cadmium carbonate. A cadmium(II) perchlorate solution was then prepared by dissolving the cadmium carbonate in a perchloric acid solution. GR grade trien and tetren were purified by distillation under reduced pressure. The polyamine was dissolved in water, and its concentration was determined by the use of a standard copper nitrate solution.

Solutions of Cd(II)-trien and Cd(II)-tetren were prepared by the following procedure. The cadmium(II) perchlorate was added stoichiometrically to a solution containing the ligand, after while a slight excess of the cadmium(II) perchlorate was added to the solution. The excess cadmium(II) of the solutions of Cd(II)-trien and Cd(II)-tetren was precipitated as hydroxide at about pH 9.7 and 10.0 respectively. The precipitate was filtered off, and the solution's pH was then adjusted to about 7 for storage. The concentrations of the Cd(II)-polyamine solutions were determined by a method reported previously.[8]

The way of preparing the Cu(II)-edta solution was described previously.[8] GR-grade sodium perchlorate and sodium chloride were recrystallized from its aqueous solution. The other chemicals used were of a GR grade.

Apparatus and Kinetic Measurements. The Cu(II)-polyamines are stronger complexes than Cu(II)-edta, while the opposite is true for cadmium ion, so that the ligand exchange between Cu(II)-edta and Cd(II)-polyamine goes to completion, while the reverse reaction can be neglected in the kinetic study. The kinetics was studied in the presence of a large excess of Cu(II)-edta and small amounts of edta. In the kinetic measurements, a stopped-flow technique was employed with a Hitachi Model RSP2 Rapid Scanning Spectrophotometer. After the two reactant solutions had been mixed, the reaction was followed automatically, the transmittance of the reaction system at 550 nm (in the Cd(II)-trien system) or 575 nm (in the Cd(II)-tetren system) being recorded as a function of the time. The molar absorption coefficients of Cu(II)-trien, Cu(II)-tetren, and Cu(II)-edta are as follows: ε(Cu(II)-trien)=138 M^{-1} cm^{-1} (1 M=1 mol dm^{-3}), ε(Cu(II)-edta)=5 M^{-1} cm^{-1} at 550 nm, ε(Cu(II)-tetren)=111 M^{-1} cm^{-1}, ε(Cu(II)-edta)=11 M^{-1} cm^{-1} at 575 nm, which were measured with a Hitachi 139 spectrophotometer. Cd(II)-trien, Cd(II)-tetren, and Cd(II)-edta do not absorb light in the visible region.

A mannitol–boric acid–sodium borate or sodium borate–sodium hydroxide buffer system was used to control the pH of the solution. All the pH values were measured with a Toa Electronics Model HM-15A digital pH-meter. The

ionic strength was adjusted to 0.2 M with sodium perchlorate or sodium chloride (at pH 9.0—10.2 in the Cd(II)-trien system). All the measurements were made in a thermostated room. The reaction temperature was controlled at 25.0 °C within ±0.1 °C using a thermoelectric circulating bath. Several calculations were performed with the aid of a TOSBAC 40 computer.

Results

Ligand-substitution Reaction between Cu(II)-edta and Cd(II)-trien. At pH's from 9.0 to 10.2 the rate equation can be expressed as

$$-\frac{d[Cdtrien^{2+}]}{dt} = k'_{o,1}[Cdtrien^{2+}], \quad (1)$$

where $k'_{o,1}$ is the conditional rate constant involving the concentrations of edta and hydrogen ions. The rate plots of $\log(A_\infty - A)$ *vs.* t, where A and A_∞ denote, respectively, the absorbances at time t and infinity, were linear for over 80% of the reaction. Then the conditional rate constant, $k'_{o,1}$, was determined from the slope of the straight line. The values of the conditional rate constant, $k'_{o,1}$, were found to be linearly related to the added free edta concentration: $[edta]_a$($[edta]_a = \sum_{i=0}^{4}[H_iedta^{(4-i)-}]$) in the region above a threshold value of b, provided that all the other experimental conditions were kept constant (Fig. 1). Thus, the conditional rate constant, $k'_{o,1}$, is expressed by

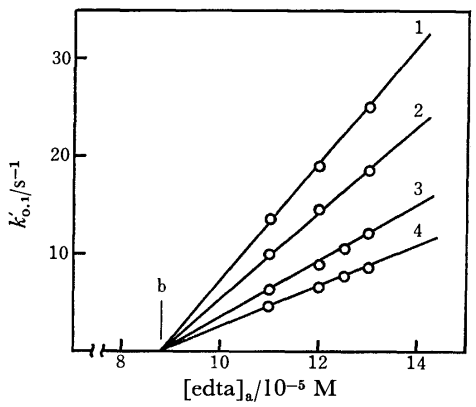

Fig. 1. $k'_{o,1}$ as a function of the concentration of added free edta.
Conditions: $[Cuedta^{2-}]=2.50\times10^{-2}$ M, $[Cdtrien^{2+}]=1.50\times10^{-3}$ M, I=0.2 M, 25.0 °C.
1: pH=10.15, 2: pH=9.89, 3: pH=9.70, 4: pH=9.44.

$$k'_{o,1} = k_{o,1}([edta]_a - b). \quad (2)$$

The values of $k_{o,1}$ determined at various pH's are plotted against the pH in Fig. 4.

On the other hand, at lower pH's from 7.5 to 8.5 the reaction was of the zeroth-order with respect to Cd(II)-trien. Thus, the rate law is given by

$$-\frac{d[Cdtrien^{2+}]}{dt} = k'_{o,0}, \quad (3)$$

where $k'_{o,0}$ is the conditional zeroth-order rate constant involving the Cu(II)-edta, the added free edta, and the hydrogen-ion concentration. The plots of A *vs.* t were linear for over 80% of the reaction. Thus, the

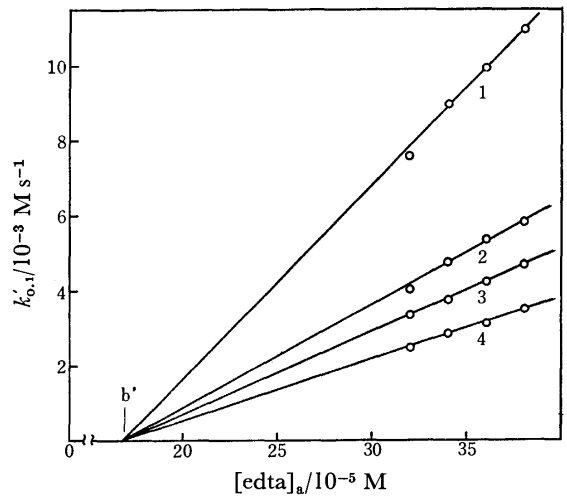

Fig. 2. $k'_{o,0}$ as a function of the concentration of added free edta.
Conditions: $[Cuedta^{2-}]=2.50\times10^{-2}$ M, $[Cdtrien^{2+}]=1.50\times10^{-3}$ M, I=0.2 M, 25.0 °C.
1: pH=8.10, 2: pH=7.81, 3: pH=7.70, 4: pH=7.50.

conditional zeroht-order rate constant, $k'_{o,0}$ was calculated from the slope of the straight line. The values of $k'_{o,0}$ at constant concentrations of the Cu(II)-edta and the hydrogen ion are linearly related to the added free edta concentration $[edta]_a$ in the region above the threshold value of b' (Fig. 2). Thus, the conditional rate constant, $k'_{o,0}$, is expressed by

$$k'_{o,0} = k_{o,0}([edta]_a - b'). \quad (4)$$

The values of the $k_{o,0}$ slope were obtained at various pH's.

Ligand-substitution Reaction between Cu(II)-edta and Cd(II)-tetren. At pH's from 8.2 to 9.7 the reaction was of the first-order with respect to Cd(II)-tetren. The rate plots of $\log(A_\infty - A)$ *vs.* t were linear for over 80% of the reaction. Then the conditional first-order rate constant, k'_o, was determined from the slope of the straight line. The conditional rate constant, k'_o, was independent of the concentration of Cu(II)-tetren. From these results, the following rate equation is derived:

$$-\frac{d[Cdtetren^{2+}]}{dt} = k'_o[Cdtetren^{2+}]. \quad (5)$$

In addition, the values of the conditional rate constant, k'_o, at a constant pH are linearly related to the added free edta concentration in the region above the threshold value of b''. Thus, the conditional rate constant, k'_o, is expressed by

$$k'_o = k_o([edta]_a - b''). \quad (6)$$

The values of k_o determined at various pH's are plotted against pH in Fig. 5.

Discussion

Reaction Mechanism. The following chain-reaction mechanism was proposed for the ligand-substitution reactions of Cd(II)-trien and Cd(II)-tetren with Cu(II)-edta:

$$\mathrm{Cuedta^{2-}} + \mathrm{R'} \underset{k_{-2}}{\overset{k_2}{\rightleftharpoons}} \mathrm{CuR^{2+}} + \mathrm{edta'}, \qquad \text{(R2)}$$

$$\mathrm{CdR^{2+}} + \mathrm{edta'} \underset{k_{-3}}{\overset{k_3}{\rightleftharpoons}} \mathrm{Cdedta^{2-}} + \mathrm{R'}, \qquad \text{(R3)}$$

where edta′ and R′ represent the sums of the uncomplexed species of edta and polyamine (trien or tetren) respectively. On the basis of the proposed mechanism, the following rate law was derived:

$$-\frac{d[CdR^{2+}]}{dt} = \frac{(k_2k_3[Cuedta^{2-}][CdR^{2+}] - k_{-2}k_{-3}[Cdedta^{2-}][CuR^{2+}])[L']}{k_2[Cuedta^{2-}] + k_{-2}[CuR^{2+}] + k_3[CdR^{2+}] + k_{-3}[Cdedta^{2-}]}, \qquad (7)$$

where [L′] is the total concentration of free ligands, edta and polyamine ([edta′]+[R′]). The rate law is derived from a steady-state treatment with the assumptions that all of the exchange is carried out by means of Reactions R2 and R3, and that the concentrations of the free ligands, edta and polyamine, remain constant throughout the exchange.

In this discussion it is necessary to calculate the conditional equilibrium constants of Reactions R2 and R3, ([CuR²⁺][edta′]/[Cuedta²⁻][R′] and [Cdedta²⁻]-[R′]/[CdR²⁺][edta′]). The conditional equilibrium constants can be calculated from the stability constants of the related complexes and the protonation constants of the related ligands.[9] The conditional equilibrium constants calculated are plotted against the pH in Fig. 3.

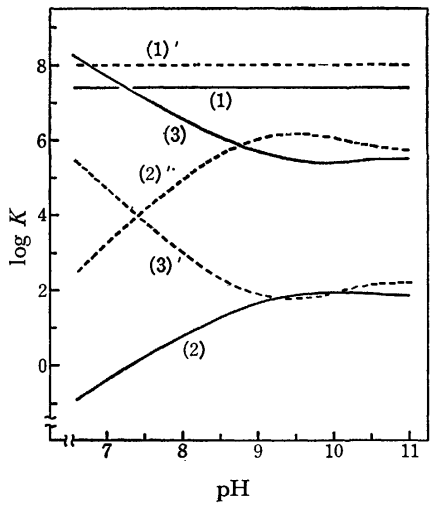

Fig. 3. Dependence of conditional equilibrium constants of reactions (R1), (R2), and (R3) on pH at 25.0 °C and I=0.2 M.
1,1′: (R1), 2,2′: (R2), 3,3′: (R3).
The full lines show the constants of the Cd(II)-trien system and the dotted lines show that of the Cd(II)-tetren system.

Cd(II)-trien System. In the Cd(II)-trien system, Equilibrium R3 much favors the right, so it appears reasonable to assume $k_3 \gg k_{-3}$. Therefore, Eq. 7 can be simplified to

$$-\frac{d[Cdtrien^{2+}]}{dt} = \frac{k_2k_3[Cuedta^{2-}][Cdtrien^{2+}][L']}{k_2[Cuedta^{2-}] + k_{-2}[Cutrien^{2+}] + k_3[Cdtrien^{2+}]}. \qquad (8)$$

The following approximation seems reasonable from Figs. 3 and 4, as will be shown later. In the denominator of Eq. 8, the k_2[Cuedta²⁻] term becomes predominant and the other terms may be neglected for the reaction with a large excess of Cu(II)-edta at pH 9.0—10.2. Thus, Eq. 8 becomes

$$-\frac{d[Cdtrien^{2+}]}{dt} = k_3[Cdtrien^{2+}][L']. \qquad (9)$$

If free metal ions (*e.g.*, metal impurity) are present in the system, the metal ions will react very rapidly with the added free edta. Consequently, the concentration of free ligands ([L′]) in the solution is written as

$$[L'] = [edta]_a - [M], \qquad (10)$$

where [M] is the concentration of free metal ions (*e.g.*, the metal impurity). Thus, Eq. 9 becomes

$$-\frac{d[Cdtrien^{2+}]}{dt} = k_3([edta]_a - [M])[Cdtrien^{2+}]. \qquad (11)$$

As has been stated above, Eq. 1 can be rewritten as

$$-\frac{d[Cdtrien^{2+}]}{dt} = k'_{o,1}[Cdtrien^{2+}] = k_{o,1}([edta]_a - b)[Cdtrien^{2+}]. \qquad (12)$$

Therefore, k_3 and [M] in Eq. 11 should correspond to $k_{o,1}$ and b respectively. In Fig. 4, the value of k_3 determined at various pH's is plotted against the pH.

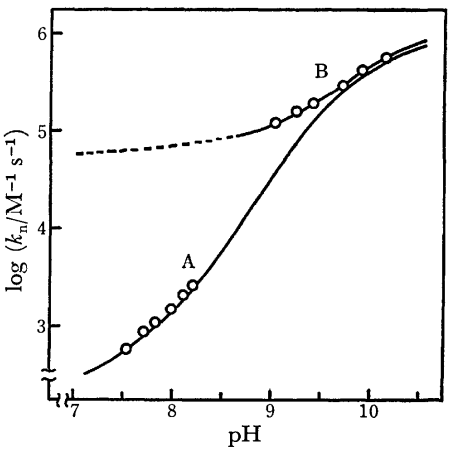

Fig. 4. Dependence of the conditional rate constants k_2 and k_3 ($=k_{o,1}$) of the Cd(II)-trien system on pH at 25.0 °C and I=0.2 M.
A: k_2, B: k_3 ($=k_{o,1}$). The lines A and B are the curves calculated with the aid of the individual rate constants. ——: Extrapolated by Eq. 21.

On the other hand, in the denominator of Eq. 8, the k_3[Cdtrien²⁺] term becomes predominant and the other terms may be neglected for pH 7.5—8.5; this can be shown to be valid from Figs. 3 and 4. Thus, Eq. 8 becomes

$$-\frac{d[Cdtrien^{2+}]}{dt} = k_2[Cuedta^{2-}][L']. \qquad (13)$$

For a large excess of Cu(II)-edta, k_2[Cuedta^{2-}] is constant during the reaction, so that Eq. 13 becomes

$$-\frac{d[Cdtrien^{2+}]}{dt} = (const)([edta]_a - [M]). \quad (14)$$

Equation 3 can be rewritten as

$$-\frac{d[Cdtrien^{2+}]}{dt} = k_{o,0}([edta]_a - b'). \quad (15)$$

Therefore, Eq. 14 agrees with the rate equation derived experimentally at lower pH's. Thus, k_2 can be calculated from the value of $k_{o,0}$. The value of k_2 thus obtained is plotted against the pH in Fig. 4. The conditional rate constant, k_2, thus obtained agrees with the conditional rate constant of the reaction of Cu(II)-edta with trien which was determined previously.[8]

Cd(II)-tetren System. In the Cd(II)-tetren system, the R2 equilibrium much favors the right, so that the $k_2 \gg k_{-2}$ inequality can be considered to hold. Therefore, Eq. 7 can be simplified to

$$-\frac{d[Cdtetren^{2+}]}{dt} = \frac{k_2 k_3[Cuedta^{2-}][Cdtetren^{2+}][L']}{k_2[Cuedta^{2-}] + k_3[Cdtetren^{2+}] + k_{-3}[Cdedta^{2-}]}. \quad (16)$$

The conditional rate constant, k_2, was calculated from the rate constants of the reaction of Cu(II)-edta with tetren which had been determined by Margerum *et al.*[10] The value of k_2 thus calculated is plotted against the pH in Fig. 5. The following approximation seems reasonable from Figs. 3 and 5. In the denominator of Eq. 16, the k_2[Cuedta^{2-}] term becomes predominant and the other terms may be neglected under the present experimental conditions. Consequently, Eq. 16 becomes

$$-\frac{d[Cdtetren^{2+}]}{dt} = k_3[Cdtetren^{2+}][L'] = k_3([edta]_a - [M])[Cdtetren^{2+}]. \quad (17)$$

Equation 5 can be rewritten as

$$-\frac{d[Cdtetren^{2+}]}{dt} = k_o([edta]_a - b'')[Cdtetren^{2+}]. \quad (18)$$

Therefore, Eq. 17 agrees with the rate equation derived experimentally. Then k_3 is equal to k_o. The value of k_3 thus determined is plotted against the pH in Fig. 5.

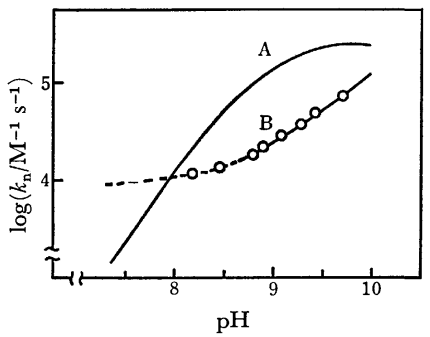

Fig. 5. Dependence of the conditional rate constants k_2 and k_3 ($=k_o$) of the Cd(II)-tetren system on pH at 25.0 °C and I=0.2 M.
A: k_2, B: k_3 ($=k_o$). The lines A and B are the curves calculated with the aid of the individual rate constants.
----: Extrapolated by Eq. 21.

Resolution of the Conditional Rate Constant, k_3. The following relation can be derived from a steady-state consideration of Reactions R2 and R3 on the assumption that the concentrations of the free ligands remain constant:

$$\frac{[edta']}{[R']} = \frac{k_2[Cuedta^{2-}] + k_{-3}[Cdedta^{2-}]}{k_{-2}[CuR^{2+}] + k_3[CdR^{2+}]} \approx \frac{k_2[Cuedta^{2-}]}{k_{-2}[CuR^{2+}] + k_3[CdR^{2+}]}. \quad (19)$$

The inequality k_2[Cuedta^{2-}]$\gg k_{-2}$[CuR^{2+}]$+k_3$[CdR^{2+}] holds under the present experimental conditions in the Cd(II)-trien and Cd(II)-tetren systems. Consequently, [edta']$\gg$[R']. Thus, [L']=[edta']+[R']$\approx$[edta']. In the pH 8.8—10.2 range, the dominant species of edta are Hedta^{3-} and edta^{4-}. Thus, the following relationship can be derived:

$$k_3[L'][CdR^{2+}] = k_3[edta'][CuR^{2+}] = k_L[edta^{4-}][CdR^{2+}] + k_{HL}[Hedta^{3-}][CdR^{2+}], \quad (20)$$

where k_L and k_{HL} are the rate constants for the following reactions

$$\begin{array}{ccc} edta^{4-} & \xrightarrow{k_L} & Cdedta^{2-} + R \\ CdR^{2+} + \uparrow\downarrow & & \\ Hedta^{3-} & \xrightarrow{k_{HL}} & Cdedta^{2-} + HR^{+} \end{array} \quad (R4)$$

With the protonation constant of Hedta^{3-}, Eq. 20 is rewritten as

$$k_3(K_1[H^+]+1) = k_{HL}K_1[H^+] + k_L, \quad (21)$$

where K_1 is the protonation constant. The plots of the left-hand side of Eq. 21 *vs.* K_1[H$^+$] give a straight line in the Cd(II)-trien and Cd(II)-tetren systems, as is shown in Figs. 6 and 7. The slopes and intercepts correspond to the k_{HL} and k_L rate constants respectively. The rate constants obtained in the two systems are summarized in Table 1.

The concentrations of the hydrogen and hydroxide complexes[9] of CdR^{2+} are negligibly small at high pH values (9—10); for example, the concentration of CdHtrien^{3+} is 0.06% of [Cd(II)-trien]$_{total}$ at pH 9.6. It seems reasonable to neglect the contribution of the hydrogen and hydroxide complexes of CdR^{2+} to the total reaction in the present pH region. Using the

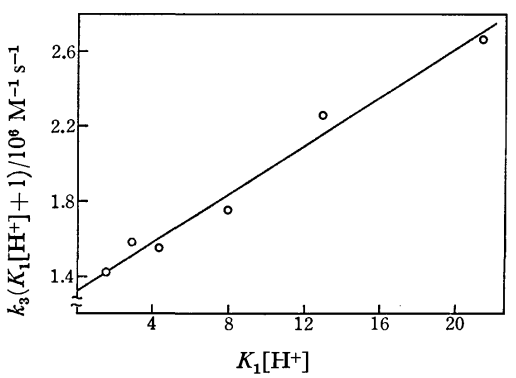

Fig. 6. Relation between $k_3(K_1[H^+]+1)$ and K_1[H$^+$] in the Cd(II)-trien system.

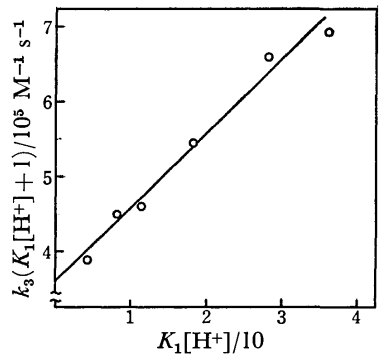

Fig. 7. Relation between $k_3(K_1[H^+]+1)$ and $K_1[H^+]$ in the Cd(II)-tetren system.

TABLE 1. RATE CONSTANTS FOR THE LIGAND-SUBSTITUTION REACTION OF THE Cd(II)-POLYAMINE COMPLEX WITH edta AT 25.0 °C AND I=0.2 M

	$\frac{k_L}{M^{-1}\,s^{-1}}$	$\frac{k_{HL}}{M^{-1}\,s^{-1}}$
Cd(II)-trien[a]	$(1.3\pm0.2)\times10^6$	$(6.5\pm1.5)\times10^4$
Cd(II)-tetren[b]	$(3.6\pm0.4)\times10^5$	$(1.0\pm0.2)\times10^4$

a) I=0.2 M(NaCl), b) I=0.2 M($NaClO_4$).

resolved rate constants, the conditional rate constant, k_3, can be calculated from Eq. 21 at pH 8.8—10.2. The values calculated for the Cd(II)-trien and Cd(II)-tetren systems are shown in Figs. 4 and 5 respectively. In Figs. 4 and 5, the dotted lines show the estimates calculated from Eq. 21.

Mechanism of the Substitution Reactions of Cd(II)-polyamine Complexes with edta. The following reaction mechanism was proposed for the ligand-substitution reactions of Cd(II)-trien and Cd(II)-tetren with edta

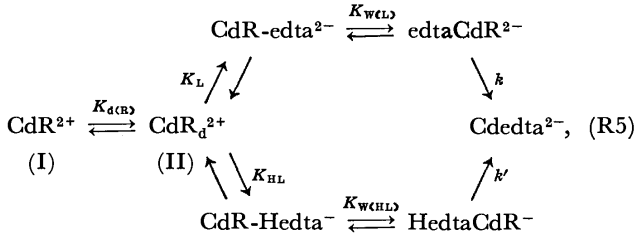

where $K_{d(R)}$ refers to the dissociation constant of the complex CdR^{2+} to the partially dissociated complex CdR_d^{2+}, K_L and K_{HL} are the formation constants of the outer-sphere complexes, CdR-edta^{2-} and CdR-Hedta$^-$ respectively, and $K_{W(L)}$, the equilibrium constant between CdR-edta^{2-} and the mixed ligand intermediate edtaCdR^{2-} (inner-sphere complex). According to the proposed mechanism, the rate equation of the substitution of the Cd(II)-polyamine complexes with edta can be written as

$$\begin{aligned}\frac{d[Cdedta^{2-}]}{dt} &= k[edtaCdR^{2-}] + k'[HedtaCdR^-]\\ &= K_dK_LK_{W(L)}k[CdR^{2+}][edta^{4-}]\\ &\quad + K_dK_{HL}K_{W(HL)}k'[CdR^{2+}][Hedta^{3-}]\\ &= k_L[CdR^{2+}][edta^{4-}]\\ &\quad + k_{HL}[CdR^{2+}][Hedta^{3-}]. \qquad (22)\end{aligned}$$

The estimation of the k/k' ratio is interesting. From Eq. 22 the following relationship is derived

$$\frac{k_L}{k_{HL}} = \frac{K_LK_{W(L)}k}{K_{HL}K_{W(HL)}k'} \qquad (23)$$

The release of a water molecule from the outer-sphere complex is the rate-determining step in the formation of a metal complex.[11] Therefore, the rate of the formation of edtaCdR^{2-} from CdR-edta^{2-} is expected to be equal to that of HedtaCdR$^-$ from CdR-Hedta$^-$. Further, the rate of the dissociation of edta^{4-} from edtaCdR^{2-} to the outer-sphere complex does not seem to differ from that of Hedta^{3-} from HedtaCdR$^-$. Thus, it appears reasonable to assume that $K_{W(L)}\approx K_{W(HL)}$. K_L and K_{HL} can be calculated according to the Fuoss equation.[12,13] Then, with the calculated values of K_L and K_{HL}, and the rate constants of k_L and k_{HL}, the k/k' ratio can be estimated. The ratios obtained at I=0.2 M and 25 °C are 3.1 and 5.6 for the Cd(II)-trien and Cd(II)-tetren systems respectively. In other words, the formation rate of Cdedta^{2-} from edtaCdR^{2-} is larger than that from HedtaCdR$^-$. The dipolar-ion (zwitter-ion) form of edta is known to be unreactive in the formation of many metal complexes because the NH$^+$ group of edta prevents chelation.[14] Therefore, in the formation of Cdedta^{2-} from HedtaCdR$^-$, the NH$^+$ group of the edta seems to prevent the chelation. Consequently, k' can be expected to be less than k. Thus, the coordination of the second nitrogen atom to the central metal in the mixed ligand intermediates, HedtaCdR$^-$ and edtaCdR^{2-}, is probably rate-determining.

The reaction mechanisms of the two systems (Cd(II)-trien and Cd(II)-tetren) seem to be similar except that the dissociation of the (I) complex to the partially dissociated complex (II) is different. Further, the $K_{d(Cdtrien)} > K_{d(Cdtetren)}$ inequality can be expected to hold, because the formation constant of Cd(II)-tetren is greater than that of Cd(II)-trien. Therefore, the rate of the reaction of Cd(II)-trien with edta can be expected to be faster than that of the Cd(II)-tetren system. This agrees with the experimental results.

Comparison of Chain-reaction Systems. The coordination chain-reaction systems use Cu(II)-edta as one reactant, while the other reactant consists of metal(II)-polyamine complexes. It is interesting to compare the reaction rates of the coordination chain-reaction systems. The reaction rates under the same conditions can be compared by means of the conditional rate constant, k_3, when the reaction is of the first-order with respect to the metal(II)-polyamine complex. The conditional

TABLE 2. CONDITIONAL RATE CONSTANTS FOR THE LIGAND-SUBSTITUTION REACTIONS OF THE METAL(II)-POLYAMINE COMPLEXES WITH edta AT A CERTAIN pH AT 25.0 °C AND AT I=0.2 M

	$\frac{k_3}{M^{-1}\,s^{-1}}$	pH		$\frac{k_3}{M^{-1}\,s^{-1}}$	pH
Cd(II)-trien	2.14×10^5	9.5	Cd(II)-tetren	2.52×10^4	9.0
Zn(II)-trien[8]	9.33×10^5		Zn(II)-tetren[15]	5.13×10^2	
Ni(II)-trien[5]	$1.6\times10^{3a)}$		Ni(II)-tetren[3]	$1.2^{a)}$	

a) I=0.1 M

Table 3. The lower limit of the pH region where the first-order reaction proceeds in the presence of a 15-fold excess of Cu(II)-edta

	pH		pH
Cd(II)-trien	9.44	Cd(II)-tetren	7.80
Zn(II)-trien	9.90	Zn(II)-tetren	7.30
Ni(II)-trien	7.8	Ni(II)-tetren	5.9

rate constants, k_3, of various systems at a certain pH are summarized in Table 2. Table 2 shows that the reaction rates of the cadmium and zinc systems are greater than that of the nickel system, and that the reaction rate of the trien system is greater than that of the tetren system. In fast reactions, kinetic measurements can be easily repeated using the stopped-flow technique. Therefore, in analytical applications, using the fast-coordination chain reaction, rapid analysis may be achieved by handling the results statistically with an on-line computer.

The pH region where the first-order reaction takes place can be estimated approximately from the conditional rate constants and the experimental conditions. In Table 3, the lower limits of the pH region in the presence of a 15-fold excess of Cu(II)-edta are tabulated. It may be seen from Tables 2 and 3 that the greater the value of k_3, the greater is the lower limit of the pH region. In general, the first-order reaction takes place without an excess of Cu(II)-edta when $k_2 \gg k_3$. However, a large excess of Cu(II)-edta is required for the first-order reaction when the $k_2 \gg k_3$ inequality is not satisfied.

References

1) D. C. Olson and D. W. Margerum, *J. Am. Chem. Soc.*, **84**, 680 (1962).
2) D. C. Olson and D. W. Margerum, *J. Am. Chem. Soc.*, **85**, 297 (1963).
3) D. W. Margerum and J. D. Carr, *J. Am. Chem. Soc.*, **88**, 1639 (1966).
4) J. D. Carr and D. W. Margerum, *J. Am. Chem. Soc.*, **88**, 1645 (1966).
5) D. W. Margerum and R. K. Steinhaus, *Anal. Chem.*, **37**, 222 (1965).
6) R. H. Stehl, D. W. Margerum, and J. J. Latterll, *Anal. Chem.*, **39**, 1346 (1967).
7) D. W. Margerum and R. H. Stehl, *Anal. Chem.*, **39**, 1351 (1967).
8) T. Katsuyama and T. Kumai, *Bull. Chem. Soc. Jpn.*, **48**, 3581 (1975).
9) L. G. Sillén and A. E. Martell, "Stability Constants of Metal-ion Complexes," The Chemical Society, London (1964).
10) J. D. Carr, R. A. Libby, and D. W. Margerum, *Inorg. Chem.*, **6**, 1083 (1967).
11) M. Eigen and K. Tamm, *Z. Electrochem.*, **66**, 107 (1962).
12) R. M. Fuoss, *J. Am. Chem. Soc.*, **80**, 5059 (1958).
13) G. G. Hammes and M. L. Morell, *J. Am. Chem. Soc.*, **86**, 1497 (1964).
14) J. C. Cassatt and R. G. Wilkins, *J. Am. Chem. Soc.*, **90**, 6045 (1968).
15) T. Katsuyama and T. Kumai, Abstr. No. 3M13, 32th National Meeting of the Chemical Society of Japan, Tokyo, April 1975.

Japanese Tea Leaves: A Possible Biological Standard Reference Material

Keiichiro FUWA, Kenji NOTSU, Kin-ichi TSUNODA, Hideaki KATO, Yuko YAMAMOTO,* Kensaku OKAMOTO,* Yukiko DOKIYA,** and Shozo TODA**

Department of Chemistry, Faculty of Science, The University of Tokyo, Hongo, Bunkyo-ku, Tokyo 113
**National Institute for Environmental Studies, Yatabe, Ibaraki 300-21*
***Department of Agricultural Chemistry, Faculty of Agriculture, The University of Tokyo, Yayoi, Bunkyo-ku, Tokyo 113*

(Received September 1, 1977)

Japanese Tea Leaves, prepared by pulverizing with an agate ball mill and sieving with a Saran fiber sieve (50 mesh) were assessed as a possible biological standard reference material for elemental analysis. The metal content of the tea leaves was determined independently at two laboratories using atomic absorption and flame emission spectrometry. Neutron activation analysis was also performed to determine the content (21 elements) of Tea Leaves. For some elements the result from the various methods were compared. The characteristics of Tea Leaves are discussed and the elemental composition is compared to that of Orchard Leaves (NBS SRM, 1571). The most significant characteristic of Tea Leaves was the high manganese content.

The need for standard reference materials in elemental analysis is steadily increasing, due primarily to the ever-increasing demand for elemental data in many scientific fields.

Standard reference materials were first prepared in 1904 by NBS.[1] They were metal samples such as cast iron in chip form. United States Geological Survey (USGS) prepared in 1955 standard rock samples, G 1 and W 1, which were distributed to analytical laboratories throughout the world.[2]

After 1960 many studies concerned with standard reference materials have taken place. Bowen's[3] study on "kale powder" began in 1960 and in this study, 42 elements were determined at many laboratories using 11 different analytical methods. Vallee[4] has studied the metal content of bone ash standard sample. Jones,[5] a member of Bowen's group has studied eight grass samples by direct-reading emission spectrometry. The present authors have determined the metal content of these grass samples by atomic absorption spectrometry.[6] Sideman's[7] work on serum samples was concerned only with Ca and involved participation by 31 laboratories. Yamagata's[8] work on Cd in rice was brought about from environmental Cd contamination resulting in abnormally high Cd level in rice production. The work by NBS research group[1,9] has been the most detailed and of the most practical use.

Recently, trace element analyses of various types of biological and/or environmental samples have been performed so extensively that it has become necessary to prepare new biological standard materials. As part of a co-operative study with NBS for the development of new biological standard materials, Japanese Tea Leaves were investigated as a possible standard reference materials. The sample was prepared on a small scale and analysis using two analytical methods, atomic absorption spectrometry and neutron activation analysis, was performed at the University of Tokyo and the National Institute for Environmental Studies.

Experimental and Results

Preparation of Tea Leaves. Three kinds of tea leaves were obtained from National Research Institute for Tea. They were (1) "Sen-cha", a middle grade green tea(Tea B), (2) old tea leaves which are not suitable for drinking(Tea C) and (3) powdered tea leaves(Tea D). The weight of the original tea samples was about 1 kg.

TABLE 1. METAL DISTRIBUTION IN TEA LEAVES (μg/g)

Sample	K	Ca	Mg	Mn	Fe	Zn
B Powder	23300	2320	1770	610	142	66
Part retained under sieve	27000	3260	1840	660	104	59
C Powder	10700	6870	1350	2650	241	19
Part retained under sieve	10200	7130	1300	2310	160	16

Tea samples B and C were pulverized with an agate ball mill and passed through a sieve made of Saran(50 mesh). The rigid parts of the leaves such as leafstalks were retained by the sieve and for both tea samples(B and C) the amount retained was approximately 100 g. Elemental analysis of both parts indicated that more Ca and less Fe were contained in the unpowdered part retained on the sieve. The powdered part which passed through the sieve was used for the further elemental analysis.

Tea D, a homogenized powder was analysed directly.

Preservation of the Samples. The powdered samples were stored in a desiccator containing silica gel and weighed periodically to determine whether the weight changed during storage. Standard materials should be preserved without any change for long periods. The results, summarized in Table 2, indicate that the dry weight did not alter significantly within 6 months.

TABLE 2. CHANGE OF WATER CONTENT DURING STORAGE OF TEA POWDER IN DESICCATOR (Silica Gel)

Sample	Water content (%)	
	Nov., 1975	May, 1976
Tea B	5.4	6.0
Tea C	7.2	6.6
Tea D	7.4	5.9

Water content was measured after 24 h drying at 90 °C.

Homogeniety of the Sample. To determine whether the powdered samples were homogeneous, the Fe content of 18 randomlly selected portions (0.5 g) of Tea C was determined

Table 3. Fe content in tea powder C

		Fe(μg/g)
Bottle 1	262	
	240	
	249	av. 250
Bottle 2	246	
	228	
	237	av. 237
Bottle 3	253	
	241	
	235	av. 243
Bottle 4	244	
	240	
	236	av. 240
Bottle 5	243	
	247	
	234	av. 241
Bottle 6	241	
	250	
	250	av. 247

average 243,
range 228—262,
c.v. 3.5%.

by atomic absorption spectrometry. Portions (0.5 g) of sample (C) were taken from three parts of every six bottles of Tea C. The tea powder was contained in six sample bottles and each sample bottle was sub-divided in three equal parts before the portions were selected. The results of the analysis of the 18 sub samples are shown in Table 3, and indicate that the homogeniety of the tea sample is similar to that of Orchard Leaves.

Table 4. Experimental conditions for atomic absorption measurement

	National Institute for Environ. Studies	The University of Tokyo
Desiccation	105 °C upto constant	90 °C, 24 h
Sample amount	1 g	0.5 g
Ashing Wet:	HNO_3 (4 ml) + H_2O_2 (3 ml) 100 ml flask with cooler and trap	HNO_3 (4 ml) + H_2O_2 (3 ml) 50 ml Kjeldahl flask
Dry:	450 °C 15 h	
Atomic absorption Instrument		
Flame:	Hitachi 508	Jarrell-Ash AAI-Mark 2, Seiko SAS 721
Flameless:	Perkin-Elmer 503 +HGA 2000	Varian-Techtron AA 1000+CRA 63
Standard solution, Metal	in 0.1 N HNO_3	Metal in Matrix (K 200, Ca 50, Mg 20, P 20, Na 17, Al 10, Mn 10 μg/ml)

Determination of Mn, Fe, Zn, and Pb by Atomic Absorption Spectrometry. Atomic absorption determination of Mn, Fe, Zn, and Pb was performed by two laboratories, independently. The experimental conditions employed by the two laboratories are shown in Table 4. In the work, different sample pretreatments were adopted and different standard solutions were used. At the National Institute for Environmental Studies, standard metal ion solution containing nitric acid(0.1 M) was used while at the University of Tokyo, a a matrix solution which contained the particular metal ion as well as other major elements in the tea leaves was used. At the University of Tokyo, the optimum conditions of flame atomic absorption measurement for each element was decided using the response-surface plot method, details of which have been described elsewhere.[10]

Table 5. Fe, Mn and Zn contents in tea leaf samples and orchard leaves

		National Inst for Environ. Studies		The Univ. of Tokyo	(Certified value)
Fe	Tea B	135[a]	137[b]	142	
	Tea C	242	226	241	
	Tea D	375	438	423	
	Orchard leaves	268	239	281	300±20
Mn	Tea B	626	620	605	
	Tea C	2760	2690	2650	
	Tea D	977	984	1010	
	Orchard leaves	91	91	95	91±4
Zn	Tea B	59	61	66	
	Tea C	20	19	19	
	Tea D	95	85	90	
	Orchard leaves	25	29	32	25±3

(μg/g) a) Wet ashing. b) Dry ashing.

Table 6. Pb contents in tea leaf samples and orchard leaves

	National Inst. for Environ. Studies		The Univ. of Tokyo	(Certified value)
Tea B	2.9[a]	3.4[b]	1.8	
Tea C	5.6	5.5	2.9	
Tea D	4.0	3.4	2.0	
Orchard Leaves	43.3	16.1		45±3

(μg/g) a) Wet ashing. b) Dry ashing.

The results for Mn, Fe, and Zn are shown in Table 5 and indicate that the date for the two laboratories agree within 10% in most cases and that there is no significant difference between the data obtained by wet ashing and those by dry ashing. Concentrations of Pb determined by carbon rod furnace atomic absorption spectrometry at the two laboratories do not agree. This is shown in Table 6. This discrepancy may be caused by the difference in the background correction system adopted by the two laboratories and/or by the chemical interference from the matrix elements. This is presently under investigation.

Neutron Activation Analysis. In addition to atomic absorption and flame emission spectrometry mentioned above, 21 elements including Mn, Fe, Zn, K, Ca, and Mg were determined by conventional non-destructive neutron activation analysis. Neutron irradiation were carried out in 100 KW TRIGA Mark II Reactor of Rikkyo University. Each tea sample (almost 100 mg) was irradiated under a thermal neutron flux of 5×10^{11} for 5 min. A 4048 channel pulse height analyzer coupled with a Ge(Li) detector was used to detect the γ-rays which were emitted from the radioactive nuclides. Al, V, Cu, Ca, and Mg were determined after 1 to 2 min irradiation, while Cl, Mn, K, and Na were determined after 1 to 2 h irradiation. The samples were further irradiated under a thermal neutron flux of 5×10^{11} n cm^{-1} s^{-1} for 30 h and As, Br, La, Sm, Ba, Rb, and Cr were determined after 5 to 6 days. Finally Fe, Sb, Se, Zn, and Co were determined after about 100 days. In this work,

Table 7. Elementary composition of tea leaf samples and orchard leaves (μg/g)

	Tea B[a)]	Tea C[a)]	Tea D[a)]	Orchard Leaves	
				Found[a)]	Certified
K	24000±8000	11000±4000	22000±7000	13000±3000	14700±300
Ca	2500±400	4200±900	1900±400	20000±500	20900±300
Mg	1300±400	5100±2400	1000±600	7100±1100	6200±200
Cl	1700±100	1200±100	1100±100	910±50	(700)
Mn	530±4	2300±10	890±8	102±1	91±4
Al	420±10	2000±40	660±20	385±5	
Fe	280±150	360±210	440±230	290±40	300±20
Zn	55±8	13±3	65±9	20±2	25±3
Na	33±4	30±20	20±5	87±5	82±6
Rb	29±6	8±2	44±9	11±1	12±1
Cu	15±8	59±37	27±15	19±4	12±1
Br	13.0±0.2	25.0±0.3	7.8±0.1	11.7±0.4	(10)
Ba	2.3±0.8	5.1±0.8	1.3±0.8	46±9	
Cr	1.1±0.3	1.2±0.3	0.8±0.2	2.8±0.3	(2.3)
Se	1.0±0.2	1.8±0.3	1.2±0.2		
As	0.42±0.23	0.20±0.05	0.31±0.12		10±1
V	0.2±0.1		0.4±0.1	0.82±0.07	
La	0.19±0.01	1.60±0.03	0.26±0.01	1.3±0.1	
Sb	0.15±0.06	0.14±0.08	0.11±0.06	3.0±0.1	
Co	0.10±0.02	0.16±0.02	0.18±0.02	0.19±0.04	(0.2)
Sm	0.023±0.002	0.23±0.01	0.032±0.003	0.13±0.01	

a) Determined by neutron activation analysis. Errors correspond to the statistical errors on counting radioactivities.

elemental standards and Orchard Leaves were irradiated together with the tea samples.

The results for the three tea leaf samples(B, C, D) are shown in Table 7, together with those for Orchard Leaves. Errors cited in this table correspond to the statistical errors on counting radioactivities. The elemental composition of Orchard Leaves determined in this work compares favorably with that reported by NBS[9)]. The results for V, Cu, Na, and and K which were determined at short irradiation time (5 min) have large errors. This was due to the relatively large amount of Mn in the tea leaves which resulted in the over-production of ^{56}Mn at long irradiation time.

Discussion

Of the elements determined by neutron activation analysis, Mn, Fe, Mg, and Zn were also determined by atomic absorption spectrometry and K and Ca by flame emission spectrometry. A comparison of the data for Zn, Mn, and Ca is shown in Figs. 1—3, respectively. These results indicate that the metal

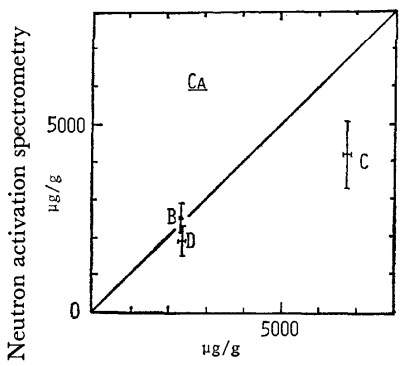

Fig. 1. Comparison of calcium content determined by activation analysis and flame emission spectrometry.

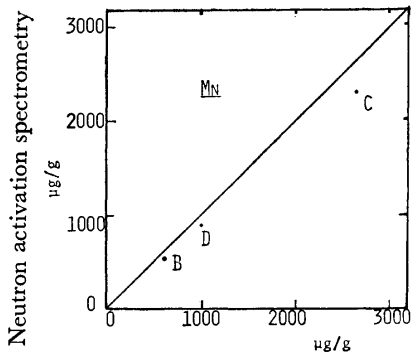

Fig. 2. Comparison of manganese content determined by activation analysis and atomic absorption spectrometry.

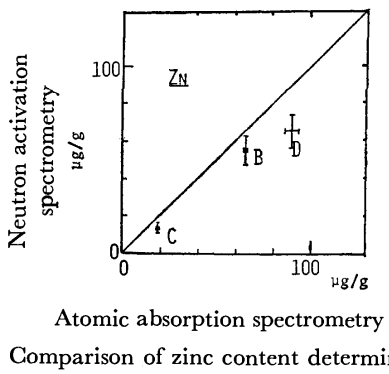

Fig. 3. Comparison of zinc content determined by activation analysis and atomic absorption spectrometry.

contents determined by activation analysis are slightly lower than those for emission or absorption spectrometry. The results also agree with the comment of Bowen:[3] "the differences (in analytical results) between techniques were usually larger than the differences between individual laboratories in which the same technique was used." In our case, the difference in analytical data for the two laboratories by the same technique (atomic absorption spectrometry) is smaller than that by the different techniques (atomic absorption or flame emission spectrometry and neutron activation analysis).

To decide whether the tea leaf samples are suitable as a new biological reference material, the results obtained must be assessed. The prerequisites for a standard reference material might be listed as follows:

1. Availability in large amount.
2. Availability at low cost.
3. Preservation for a long period.
4. Safety for transportation.
6. Appropriate elemental composition.

Point 1 and 2 are met since there is a supply of tea leaves at low cost. Tea leaf samples were shown to be preserved for at least six months. In the case of biological samples, the alteration caused by activities of microbes should be considered as well as the chemical alteration. Irradiation of the samples by ^{60}Co, as was the case in preparing Orchard leaf samples at NBS,[11] is one of the most powerful techniques to prevent biological alteration. For tea leaf samples, a steaming procedure used in commercial processing of raw tea may be a suitable sterilization process.

One of the most important criteria for a standard reference material is homogeniety. The tea leaf samples prepared in this work were shown to be homogeneous (Fe determined in 18 randomly selected sub-samples of Tea C).

As a new biological standard, the elemental composition must also be characteristic compared with other similar kinds of standard materials produced in the past. In Figs. 4—6 and in Table 7, a comparison of the elemental composition between Orchard Leaves and Tea B, Tea C, and Tea D is shown.

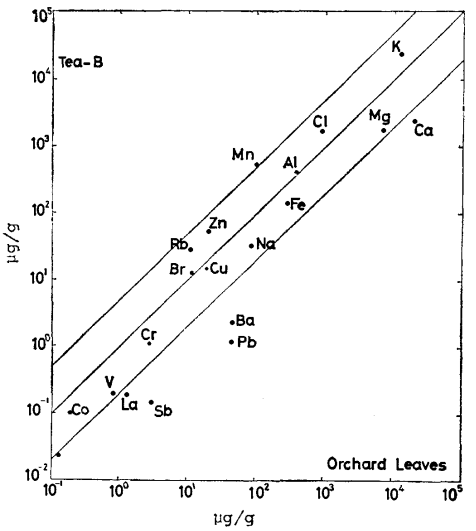

Fig. 4. Elementary compositions of Tea B and Orchard Leaves.

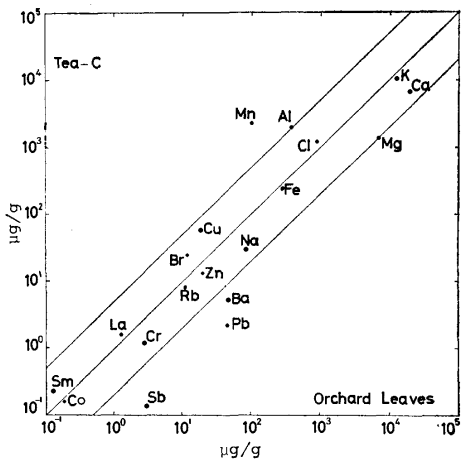

Fig. 5. Elementary compositions of Tea C and Orchard Leaves.

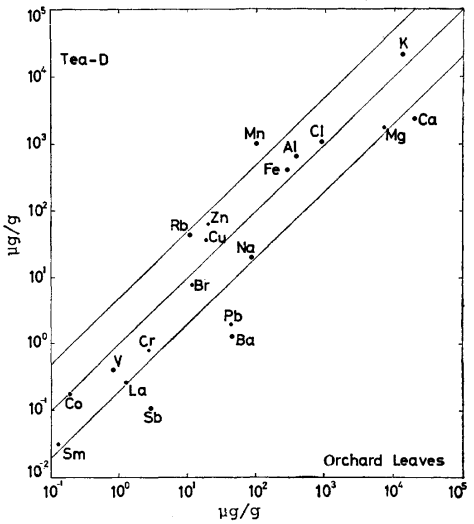

Fig. 6. Elementary compositions of Tea D and Orchard Leaves.

The characteristic features of the elemental compositions are summarized as follows:

1. The Mn content of the tea leaf samples is much higher than for Orchard Leaves.
2. The Ca and Ba contents are lower in the tea leaf samples.
3. As for the other elements, the content in the tea leaf samples is similar to that of Orchard Leaves.

Growth of the tea plant in acid soil may reflect the high content of Mn in the tea leaf samples. The high level of Mn might make tea leaf samples to be preferred as a standard reference material when acid-resistant plants such as rice, are analysed. In addition, it is necessary to eliminate contamination during the preparation procedure even if the homogeniety of the contaminant elements is certified. For example, the Pb content in Orchard Leaves is relatively greater than for most other edible plant products. This suggests that the Pb levels in Orchard Leaves may partly arise from contamination from sources such as pesticides. The low recovery of Pb in Orchard Leaves by ashing

compared to that for tea leaf samples may indicate that a certain part of Pb in Orchard Leaves is in an inorganic form which may behave differently from inert Pb at the ashing step (Table 6).

Practically, it would be difficult to eliminate contamination from foreign elements in the preparation process, but further work may resolve this and improve the sample product.

To summarize, tea leaf samples may be a candidate for a new biological standard reference material.

The authors wish to express their heartly thanks to Dr. Masayuki Nakagawa of National Research Institute of Tea, for his help in getting the raw material and to Dr. Kenji Tomura of Rikkyo University for his help in utilizing the reactor.

This work is supported partially by Japan-U.S. Cooperative Project between JSPS and NSF No. 6R023.

References

1) J. P. Cali, *Anal. Chem.*, **48**, 802 A (1976).
2) H. W. Fairbairn, *Geochim. Cosmochim. Acta*, **4**, 143 (1953).
3) H. J. M. Bowen, *Analyst*, **92**, 124 (1967).
4) B. L. Vallee, personal communication.
5) J. B. Jones, Proceedings of Pittsburg Conference on Anal. Chem. and Apple. Spec. (1967).
6) Y. Dokiya, S. Aizawa, K. Fuwa, and M. Shirashi, Proceedings of Annul Meeting, Jpn. Soc. Anal. Chem. (Fukuoka) (1973).
7) L. Sideman, *Clin. Chem.*, **16**, 597 (1970).
8) N. Yamagata, *Bunseki Kagaku*, **20**, 515 (1971).
9) Certificate for Orchard Leaves, U. S. Dept. of Commerce, NBS (1970).
10) K. Fujiwara, H. Haraguchi, and K. Fuwa, *Anal. Chem.*, **47**, 743 (1975).
11) P. D. LaFleur, Anal. Div. NBS-USA personal communication.

Trimethylenediamine Complexes. IV.* Kinetics and Mechanism of Acid and Base Hydrolysis of Tetranitro(ethylenediamine)- and Tetranitro(trimethylenediamine)cobaltates(III)

Yoshiaki Ito and Shinichi Kawaguchi

Department of Chemistry, Faculty of Science, Osaka City University, Sumiyoshi-ku, Osaka 558

(Received September 6, 1977)

Hydrolysis of $Co(NO_2)_4(AA)^-$ (AA=en or tn) was studied in acidic and basic aqueous solutions by the spectrophotometric method. In faintly acidic solution (6>pH>4) the aquation proceeds reversibly to attain an equilibrium with $Co(NO_2)_3(H_2O)(AA)$, K_{eq} being $(1.71\pm0.03)\times10^{-2}$ and $(3.55\pm0.06)\times10^{-2}$ mol·l^{-1} for AA=en and tn, respectively, at 25.0 °C and $\mu=0.1$. With increasing concentration of hydrogen ion the acid-catalyzed pathway becomes increasingly important. In basic solution (12.2>pH>9.5) $Co(NO_2)_3(OH)(AA)^-$ was formed irreversibly as the first product. Kinetic data of these hydrolysis reactions are interpreted in terms of the dissociative mechanism involving a five-coordinate intermediate $Co(NO_2)_3(AA)$. The rates of nitrite release from $Co(NO_2)_4(tn)^-$ ($(9.27\pm0.03)\times10^{-4}$ s^{-1}) and deaquation from $Co(NO_2)_3(H_2O)(tn)$ ($(3.95\pm0.12)\times10^{-4}$ s^{-1}) are several times greater than those for the corresponding ethylenediamine complexes ($(2.08\pm0.01)\times10^{-4}$ and $(5.46\pm0.10)\times10^{-5}$ s^{-1}, respectively.

Although the trans structure of Erdmann's salt $NH_4[Co(NO_2)_4(NH_3)_2]$ was confirmed by X-ray analysis,[1] two geometrical isomers are expected to exist in equilibrium in solution. Kyuno prepared analogous Erdmann-type complexes by replacing the ammine ligands with ethylenediamine and propylenediamine.[2a] The tetranitrodiammine- and tetranitro(ethylenediamine)cobaltates(III) were further used for preparation of dinitrodianionodiammine and related cobalt(III) complexes.[2b] Usually *cis*-dinitrobis(ethylenediamine)cobalt(III) nitrite is prepared by the reaction of hexanitrocobaltate(III) with ethylenediamine,[3] intermediacy of the tetranitro(ethylenediamine)cobaltate(III) complex in the series of reaction being postulated by Kettle.[4] The reaction of sodium hexanitrocobaltate(III) with diamine afforded $[Co(NO_2)_2(AA)_2][Co(NO_2)_4(AA)]$, where AA stands for ethylenediamine or trimethylenediamine.

Tetranitro(diamine)cobaltate(III) anions are interesting complexes in preparative coordination chemistry. Kinetic and equilibrium studies of the nitrite displacement have been performed in order to clarify the reaction mechanism. The effect of ring size in the ethylenediamine and trimethylenediamine chelates on the rates and equilibria has also been investigated. The acid-catalyzed aquation of the tetranitrodiamminecobaltate(III) ion was reported by Malik and McAuley.[5]

Experimental

Preparation of Complexes. Dinitrobis(diamine)cobalt(III) Tetranitro(diamine)cobaltate(III), $[Co(NO_2)_2(AA)_2][Co(NO_2)_4(AA)]$: To a cold solution (100 ml) of sodium hexanitrocobaltate(III) (20 g, 49.5 mmol) was added with stirring a 50% aqueous solution of an equimolar amount of ethylenediamine(en) or trimethylenediamine(tn). Orange yellow crystallites separated were washed with water and dried over silica gel in a desiccator. The yield was 20% (*ca.* 6 g). The results of elemental analysis correspond to the composition of $Co_2(NO_2)_6(AA)_3$, suggesting that they are complex salts of the type $[Co(NO_2)_2(AA)_2][Co(NO_2)_4(AA)]$. The ethylenediamine complex was obtained by Kyuno by the reaction of $Co(NO_2)_4(NH_3)_2^-$ with ethylenediamine and identified as a less soluble trans isomer.[2a] Found: C, 12.34; H, 4.56; N, 27.76; Co, 20.58%. Calcd for $Co_2(NO_2)_6(en)_3$: $C_6H_{24}N_{12}O_{12}Co_2$: C, 12.55; H, 4.21; N, 29.27; Co, 20.53%. Found: C, 17.38; H, 5.05; N, 26.53; Co, 19.10%. Calcd for $Co_2(NO_2)_6(tn)_3$: $C_9H_{30}N_{12}O_{12}Co_2$: C, 17.54; H, 4.91; N, 27.28; Co, 19.12%.

Potassium Tetranitro(ethylenediamine)cobaltate(III), $K[Co(NO_2)_4(en)]$ and Potassium Tetranitro(trimethylenediamine)cobaltate(III) Hemihydrate, $K[Co(NO_2)_4(tn)]\cdot1/2H_2O$: These compounds were prepared with a solution of potassium tricarbonatocobaltate(III) as the starting material,[6] and recrystallized twice from methanol–water (1:1 by volume). The yields were 40 and 46%, respectively. Found: C, 7.30; H, 2.67; N, 23.41%. Calcd for $K[Co(NO_2)_4(en)]$: $C_2H_8N_6O_8CoK$: C, 7.02; H, 2.36; N, 24.56%. Found: C, 9.95; H, 3.36; N, 22.74%. Calcd for $K[Co(NO_2)_4(tn)]\cdot1/2H_2O$: $C_3H_{11}N_6O_{8.5}CoK$: C, 9.87; H, 3.04; N, 23.01%.

Isolation in Solution of Trinitroaqua(diamine)cobalt(III), $Co(NO_2)_3(H_2O)(AA)$: About 0.3 g of potassium tetranitro(diamine)cobaltate(III) was dissolved in 20 ml of water. To the resulting solution was added 15 ml of 0.04 mol·l^{-1} sodium hydroxide and the mixture was stirred for about 30 min at 40—50 °C (AA=en) or room temperature (AA=tn). The solution was then acidified to pH 2—3 with perchloric acid, and poured into a 20 cm column of 2 cm diameter containing a mixture of equal amounts of a sodium type cation exchange resin (Dowex 50WX8, 50—100 mesh) and a perchlorate type anion exchanger (Dowex 1X8, 50—100 mesh). The column was kept cold with ice water. The trinitro complex, the product of hydrolysis, is electrically neutral, running through the column. The effluent was kept cold with ice–water and protected against light. The solution was subjected to determination of the acid dissociation constant, the cobalt(III) content being determined by the photochemical reduction to cobalt(II) followed by photometric analysis of the latter as a tetraisothiocyanatocobaltate(II) complex.[7] In order to confirm the reproducibility, the isolation and determination of the trinitroaqua(diamine) complexes were repeated three times, respectively.

Measurements. The hydrogen ion activity in solution was determined with a Beckman "Century" SS-1 pH meter with a Beckman 39301 glass electrode and a Beckman 39400 calomel electrode, and converted into the hydrogen ion concentration by virtue of the activity coefficient $f_H=0.83$ at 25 °C and $\mu=0.1$.[8] The method is applicable to solutions in which

*Part III: H. Kawaguchi and S. Kawaguchi, *Bull. Chem. Soc. Jpn.*, **46**, 3453 (1973).

10^{-3} mol·l^{-1}>[H$^+$]>10^{-11} mol·l^{-1}, and the hydrogen ion concentration in more acidic solutions was determined by titration. Absorption spectra were recorded on Hitachi EPS-3T and 139 spectrophotometers.

Determination of the Acid Dissociation Constants of the Trinitroaqua(diamine)cobalt(III) Complexes: Buffer solutions were prepared with use of potassium dihydrogen phosphate–sodium hydroxide (pH 5.68—7.16), borax–perchloric acid (pH 7.97—9.28) and borax–sodium hydroxide (pH 9.47—10.29) systems. A given quantity of the effluent solution of the trinitroaqua(diamine)cobalt(III) complex was poured into a measuring flask containing a buffer solution, and the ionic strength was adjusted to μ=0.1 with a solution of sodium perchlorate. Thus solutions with various pH were prepared at 0 °C and the spectra were recorded promptly at 2 °C.

Kinetic Studies: The desired amount of a buffer solution was placed in a dark measuring flask and kept in a thermostat. Solid K[Co(NO$_2$)$_4$(en)] (0.040 g) or K[Co(NO$_2$)$_4$(tn)]·1/2H$_2$O (0.050 g) was poured into the solution by means of thermostated pure water to make up 100 ml of the reaction mixture. The complex was readily dissolved by agitation, and the reaction started. Aliquots were pipetted at appropriate time intervals and subjected to specrtal measurement. Perchloric acid was used for the preparation of acidic solutions. Since hydrolysis was very fast in acidic solutions where [H$^+$]≥0.65 mol·l^{-1}, a Union Giken Stopped-flow, Rapid-Scan Spectrophotometer RA 1300 was used for measuring spectra in the 355—505 nm region.

Results

Acid Dissociation Constants of the Trinitroaqua(diamine)cobalt(III) Complexes. The spectra of Co(NO$_2$)$_3$(H$_2$O)(AA) complexes in aqueous solution change with pH showing an isosbestic point at 502 nm (AA=en) or 506 nm (AA=tn). The following dissociation equilibria (Eq. 1) are responsible for the spectral behavior, the limiting spectra (Fig. 1) being assigned to aqua and hydroxo complexes.

$$\underset{\mathbf{2}}{\mathrm{Co(NO_2)_3(H_2O)(AA)}} \rightleftharpoons \mathrm{H^+} + \underset{\mathbf{3}}{\mathrm{Co(NO_2)_3(OH)(AA)^-}} \quad (1)$$

The spectra at various hydrogen ion concentrations were analyzed by means of the equation

$$\log\{(A-\varepsilon_3 c_M)/(\varepsilon_2 c_M - A)\} = \mathrm{p}K_a + \log[\mathrm{H^+}], \quad (2)$$

where c_M is the total concentration of the cobalt(III) complexes, A is the optical density of a solution at a given wave length, and ε_2 and ε_3 denote the molar extinction coefficients at the same wave length of the aqua (**2**) and hydroxo (**3**) complexes, respectively. For the ethylenediamine complexes ε_2 and ε_3 are 328 and 204 l·mol^{-1}·cm^{-1}, respectively, at 410 nm where the separation of spectra is the highest, and ε_2=279 and ε_3=146 l·mol^{-1}·cm^{-1} at 420 nm in the case of the trimethylenediamine complexes.

The plots of $\log\{(A-\varepsilon_3 c_M)/(\varepsilon_2 c_M - A)\}$ against pH gave straight lines with a slope of −1.0 in either case, the pK_a values being 8.40±0.04 and 8.21±0.03 for the ethylenediamine and trimethylenediamine complexes, respectively, at 2 °C and μ=0.1.

Aquation of the Tetranitro(diamine)cobaltate(III) Complexes. In weakly acidic solutions (6>pH>4) the tetranitro complex is hydrolyzed to produce the trinitroaqua complex. The reaction is reversible, the backward anation being effected by addition of excess nitrite ions.

$$\underset{\mathbf{1}}{\mathrm{Co(NO_2)_4(AA)^-}} + \mathrm{H_2O} \rightleftharpoons \underset{\mathbf{2}}{\mathrm{Co(NO_2)_3(H_2O)(AA)}} + \mathrm{NO_2^-} \quad (3)$$

In the presence of more than ten times excess of sodium nitrite, aquation of the tetranitro complex proceeds as a pseudo first order reaction to attain an equilibrium, revealing an isosbestic point at 480 (AA=en) or 487 nm (AA=tn).

$$-\mathrm{d}\ln([\mathrm{Co(NO_2)_4(AA)^-}]_t - [\mathrm{Co(NO_2)_4(AA)^-}]_{eq})/\mathrm{d}t = k_{obsd}$$

$$\ln\{(A_0-A_{eq})/(A_t-A_{eq})\} = k_{obsd}t \quad (4)$$

Subscripts 0, t, and eq refer to the time zero, t, and the equilibrium state, respectively. The reaction was followed by measuring the absorbance A at 430 (AA=en) or 440 nm (AA=tn). The plot $\ln\{(A_0-A_{eq})/(A_t-A_{eq})\}$ *vs.* t gave straight lines over two to three half lives. The values of the pseudo first order rate constant k_{obsd} at various hydrogen and nitrite ion concentrations are summarized in Table 1.

The equilibrium constant of Reaction 3 is related to the nitrite concentration by

$$K = [\mathrm{Co(NO_2)_3(H_2O)(AA)}]_{eq}[\mathrm{NO_2^-}]_{eq}/[\mathrm{Co(NO_2)_4(AA)^-}]_{eq} = [\mathbf{2}]_{eq}[\mathrm{NO_2^-}]_{eq}/[\mathbf{1}]_{eq}$$

$$(A_{eq}-A_2)/(A_1-A_{eq}) = [\mathrm{NO_2^-}]_{eq}/K, \quad (5)$$

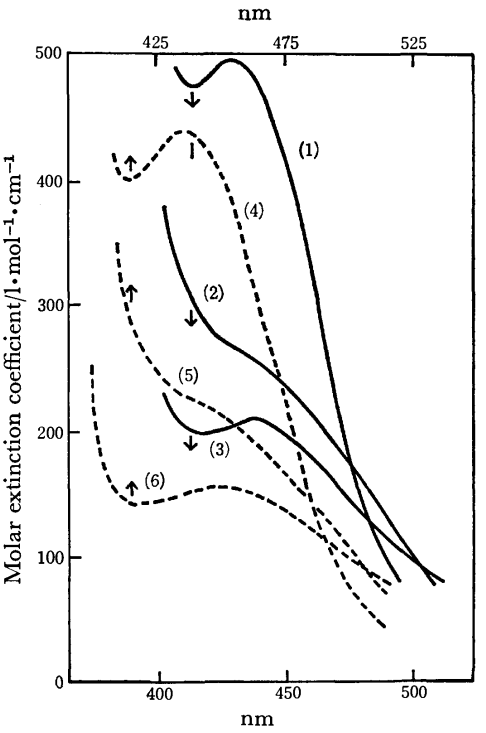

Fig. 1. Absorption spectra in the 400—500 nm region of Co(NO$_2$)$_4$(en)$^-$ (1), Co(NO$_2$)$_3$(H$_2$O)(en) (2), Co(NO$_2$)$_3$(OH)(en)$^-$ (3), Co(NO$_2$)$_4$(tn)$^-$ (4), Co(NO$_2$)$_3$(H$_2$O)(tn) (5), and Co(NO$_2$)$_3$(OH)(tn)$^-$ (6) in aqueous solution.

Table 1. Pseudo first order rate constants of aquation of the tetranitro(diamine)cobaltate(III) complexes at 25.0 °C and $\mu=0.1$, c_M being 1.169×10^{-3} and 1.369×10^{-3} mol·l^{-1} for the ethylenediamine and trimethylenediamine complexes, respectively

pH	$10^3\,c_{NO_2}$ / mol·l^{-1}	$10^5\,k_{obsd}$ / s^{-1}
Ethylenediamine complex		
5.42	11.99	8.19
5.52	12.00	7.33
5.60	19.99	6.65
5.77	39.98	6.39
5.81	40.00	6.21
5.68	59.97	5.88
5.72	59.97	5.85
5.71	79.96	5.95
5.77	79.96	6.01
5.71	99.95	5.88
5.72	100.0	5.46
5.36	20.00	6.55
5.28	20.00	6.53
5.22	20.00	6.81
5.14	20.00	6.99
5.01	20.00	6.59
4.92	20.00	6.74
Trimethylenediamine complex		
5.52	19.99	63.8
5.62	20.00	65.7
5.62	29.98	58.3
5.72	39.98	56.4
5.88	40.00	54.7
5.68	39.98	52.7
5.76	59.97	51.4
5.81	60.00	52.0
5.92	80.00	47.3
5.92	80.00	51.3
5.82	99.95	51.4
5.73	40.00	55.7
5.59	40.00	57.0
5.49	40.00	56.7
5.38	40.00	56.0
5.02	40.00	58.0
4.72	40.00	56.0

where **2** and **1** denote the trinitroaqua and tetranitro complexes, respectively, and $A_2=\varepsilon_2 c_M$ and $A_1=\varepsilon_1 c_M$. The molar extinction coefficients were determined as $\varepsilon_2=268$ and $\varepsilon_1=483$ l·mol^{-1}·cm^{-1} at 430 nm in the case of AA=en, and $\varepsilon_2=233$ and $\varepsilon_1=432$ l·mol^{-1}·cm^{-1} at 440 nm for AA=tn. Since the pK_a of nitrous acid lies around 2.95($\mu=0.25$)—3.15($\mu=0$) at 25 °C[9] and protonation of the nitrite ion is negligible at the present conditions (pH=4.7—6.0), the value of $[NO_2^-]_{eq}$ was calculated by

$$[NO_2^-]_{eq} = c_{NO_2} + c_M(A_1-A_{eq})/(A_1-A_2), \quad (6)$$

where c_{NO_2} denotes the concentration of nitrite ions added.

As shown in Fig. 2 the plots of the left side term of Eq. 5 against $[NO_2^-]_{eq}$ give straight lines through the origin. From the slope of each straight line the equilibrium constant of aquation of the tetranitro complex (Eq. 3) at 25.0 °C and $\mu=0.1$ was determined to be $(1.71\pm0.03)\times10^{-2}$ and $(3.55\pm0.06)\times10^{-2}$ mol·l^{-1} for AA=en and tn, respectively.

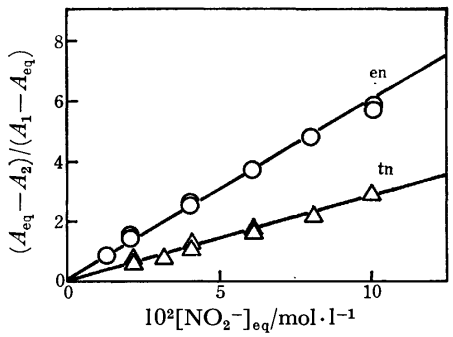

Fig. 2. The linear plot of Eq. 5 in order to determine the equilibrium constant of aquation of $Co(NO_2)_4(AA)^-$ at 25.0 °C and $\mu=0.1$. The absorbance was determined at 430 nm (AA=en) or 440 nm (AA=tn).

Acid-Catalyzed Aquation of Tetranitro(diamine)cobaltate(III) Complexes. In more acidic solutions, aquation of the tetranitro(diamine)cobaltate(III) complexes becomes fast with increasing hydrogen ion concentration. In the 2.5>pH>1.0 region, the first-order rate law holds for about two half lives. After this the spectra begin to deviate from the isosbestic point indicating the contribution of the succeeding aquation step. The observed pseudo first order rate constants are plotted against the hydrogen ion concentration in Fig. 3 to afford straight lines in line with Eq. 7.

$$k_{obsd} = k_0 + k_a[H^+] \quad (7)$$

At 25.0 °C and $\mu=0.1$, $k_0=(2.8\pm0.4)\times10^{-4}$ s^{-1} and $k_a=(2.2\pm0.1)\times10^{-2}$ l·mol^{-1}·s^{-1} for $Co(NO_2)_4(en)^-$ and $k_0=(8.6\pm1.0)\times10^{-4}$ s^{-1} and $k_a=(5.5\pm0.2)\times10^{-2}$ l·mol^{-1}·s^{-1} for $Co(NO_2)_4(tn)^-$.

In order to gain insight into the acid-catalyzed aquation (the second term in Eq. 7), rapid reactions in more acidic solutions (1.0 mol·l^{-1}>[H$^+$]>0.65 mol·l^{-1})

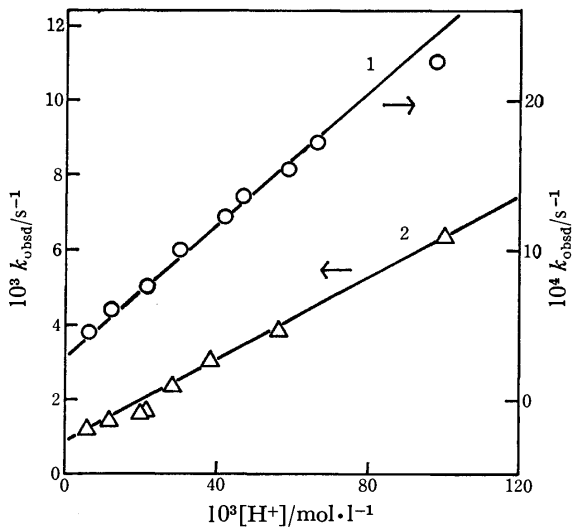

Fig. 3. The pseudo first order rate constants of aquation of $Co(NO_2)_4(AA)^-$ at various hydrogen ion concentrations (AA=en (1) and tn (2)).

were examined by following the spectral change in the 355—505 nm region with a rapid-scan spectrophotometer. For either of the ethylenediamine and trimethylenediamine complexes, the isosbestic point was maintained up to 50 s after commencement of the reaction. The pseudo first order rate constant was obtained by the Guggenheim method.[10] The result shows a linear dependence on the hydrogen ion concentration even in these highly acidic solutions, giving $k_a=1.9\times10^{-2}$ and 3.6×10^{-2} l·mol^{-1}·s^{-1} for AA=en and tn, respectively, at 25.0 °C, $\mu=2.0$ mol·l^{-1} ($NaClO_4$). These values are less accurate than but close to those obtained in the 2.5>pH>1.0 region at $\mu=0.1$.

Base Hydrolysis of the Tetranitro(diamine)cobaltate(III) Complexes. The base hydrolysis reaction of the tetranitro complex proceeds irreversibly to produce the trinitrohydroxo complex.

$$\underset{\mathbf{1}}{Co(NO_2)_4(AA)^-} + OH^- \longrightarrow \underset{\mathbf{3}}{Co(NO_2)_3(OH)(AA)^-} + NO_2^- \qquad (8)$$

When a buffer solution was employed to maintain a constant hydroxide ion concentration, the reaction followed the first order rate law (Eq. 9) during the course of two half lives.

$$\ln\{(A_0-A_\infty)/(A_t-A_\infty)\} = k'_{obsd}t, \qquad (9)$$

where $A_\infty=\varepsilon_3 c_M$, the absorbance being determined at 430 and 440 nm for AA=en and tn, respectively.

Beyond this the plot of the left side term of Eq. 9 against time begins to deviate from the straight line. Concurrently the absorption spectra begin to deviate from the isosbestic point (Fig. 4). The successive base hydrolysis of the trinitrohydroxo complex seems to contribute to the overall kinetics.

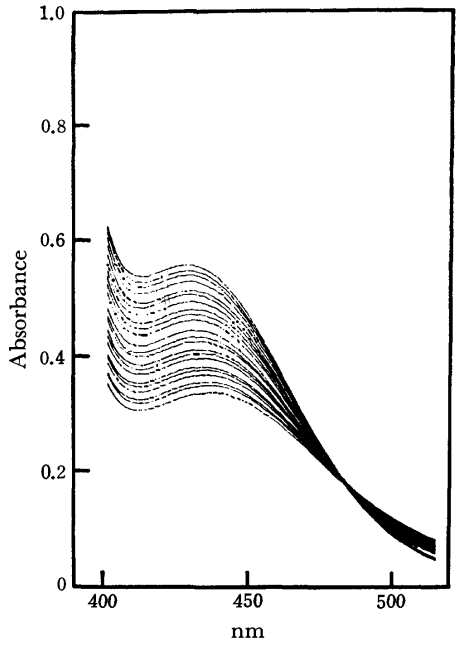

Fig. 4. The spectral change during the initial 100 min (about two half-lives) in the base hydrolysis of $Co(NO_2)_4(en)^-$ at 25.0 °C, $\mu=0.1$ and pH=11.94 with $c_M=1.169$ mmol·l^{-1}.

Table 2. Pseudo first order rate constants of the base hydrolysis of the tetranitro(diamine)cobaltate-(III) complexes at 25.0 °C and $\mu=0.1$, c_M being 1.169×10^{-3} and 1.369×10^{-3} mol·l^{-1} for the ethylenediamine and trimethylenediamine complexes, respectively

pH	$10^3 c_{NO_2}$ / mol·l^{-1}	$10^4 k'_{obsd}$ / s^{-1}	Buffer solution
Ethylenediamine complex			
9.76	0	2.03	Borax–NaOH
10.00	0	2.03	
10.65	0	2.06	
11.34	0	2.05	Na_2HPO_4–NaOH
11.80	0	2.04	
11.94	0	2.07	
10.67	20.00	2.11	Borax–NaOH
10.64	28.00	2.19	
10.67	40.00	2.10	
10.66	50.00	2.07	
Trimethylenediamine complex			
9.55	0	9.37	
9.76	0	9.48	Borax–NaOH
9.98	9.985	9.19	
10.03	20.00	9.25	
10.03	30.00	8.98	
10.04	0	9.37	
10.08	40.01	8.98	
10.38	0	9.37	
11.32	0	9.40	Na_2HPO_4–NaOH
11.39	0	9.17	Borax–NaOH
11.79	0	9.14	Na_2HPO_4–NaOH
11.94	0	9.29	
12.23	20.00	9.48	NaOH

Table 3. Pseudo first order rate constants of the base hydrolysis of the tetranitro(diamine)cobaltate(III) complexes at several temperature at 25.0 °C, $\mu=0.1$, pH=9.77 (BORAX-NaOH), $c_{NO_2}=0$, $c_M=1.181\times10^{-3}$ (en) and 1.369×10^{-3} (tn) mol·l^{-1}

Temp / °C	$10^4 k'_{obsd}$ / s^{-1}	ΔH^* / kcal·mol^{-1}	ΔS^* / cal·deg^{-1}·mol^{-1}
Ethylenediamine complex			
19.8	0.875±0.022	27.2±0.7	15.9±2.0
25.0	2.08 ±0.01		
30.1	4.41 ±0.04		
35.2	9.52 ±0.16		
Trimethylenediamine complex			
15.1	1.97 ±0.04	26.0±0.4	14.9±1.2
20.1	4.45 ±0.05		
25.0	9.27 ±0.03		
30.1	18.0 ±0.08		

The pseudo first order rate constants k'_{obsd} of Reaction 8 at 25.0 °C and other temperatures are given in Tables 2 and 3, respectively. The Eyring plots of these data give the following activation parameters: $\Delta H^*=27.2\pm0.7$ (en) and 26.0 ± 0.4 (tn) kcal·mol^{-1}, and $\Delta S^*=15.9\pm2.0$ (en) and 14.9 ± 1.2 (tn) cal·deg^{-1}·mol^{-1}.

Discussion

Although the nitrite ion can coordinate to a metal ion as a unidentate ligand through either the nitrogen or oxygen atom, the N-bonded nitro isomer is usually more stable than the O-bonded nitrito isomer.[11] The *trans*-$Co(NO_2)_4(NH_3)_2^-$ salts[1,12] and $K[Co(NO_2)_4(en)]$[13] were confirmed by X-ray analysis to be nitro complexes. $K[Co(NO_2)_4tn]\cdot 1/2H_2O$ may also be presumed to contain the Co–N bonding.

Two geometrical isomers, facial and meridional, are conceivable for the hydrolysis products $Co(NO_2)_3(H_2O)(AA)$ and $Co(NO_2)_3(OH)(AA)^-$. Distinct isosbestic points were observed in the spectral change during the course of acid and base hydrolysis reactions of $Co(NO_2)_4(AA)^-$. The spectra of $Co(NO_2)_3(H_2O)(AA)$ at various pH's also manifest isosbestic points. The results can be satisfactorily understood on the assumption that only one of the geometrical structures is realized by both of the trinitro complexes. However, no isolation and characterization of the trinitro complexes as solid specimen have been achieved, the stereochemistry of hydrolysis reactions of the tetranitro complexes remaining unclarified.

Mechanism of the Hydrolysis Reactions. The kinetic data of the acid and base hydrolysis of $Co(NO_2)_4(AA)^-$ are satisfactorily explained on the basis of the dissociative (**D**) mechanism including the pentacoordinate intermediate, $Co(NO_2)_3(AA)$.

$$Co(NO_2)_4(AA)^- \underset{k_{NO_2}}{\overset{k_{-NO_2}}{\rightleftharpoons}} Co(NO_2)_3(AA) + NO_2^- \quad (10)$$

$$Co(NO_2)_3(AA) + H_2O \underset{k_{-H_2O}}{\overset{k_{H_2O}}{\rightleftharpoons}} Co(NO_2)_3(H_2O)(AA) \quad (11)$$

$$+H^+ \uparrow\downarrow -H^+ \text{ (fast)}$$

$$Co(NO_2)_3(AA) + OH^- \xrightarrow{k_{OH}} Co(NO_2)_3(OH)(AA)^- \quad (12)$$

In basic solution the reaction proceeds irreversibly to afford the hydroxotrinitro complex, and the reverse anation reaction need not be considered. If we assume a steady state for the pentacoordinate intermediate, the pseudo first order rate constant is given by

$$k'_{obsd} = k_{-NO_2}(k_{H_2O}+k_{OH}[OH^-])/(k_{NO_2}[NO_2^-]+k_{H_2O}+k_{OH}[OH^-]). \quad (13)$$

The observed pseudo first order rate constant is independent of pH in the 9.5—12.2 region and also of the added nitrite concentration (Table 2). The calculated k'_{obsd} in Eq. 13 can be reconciled with the experimental results only when

$$k_{OH}[OH^-] \gg k_{NO_2}[NO_2^-] + k_{H_2O}, \quad (14)$$

resulting in

$$k'_{obsd} = k_{NO_2}. \quad (15)$$

Thus the spontaneous dissociation of a nitrite ligand is the rate determining step in the base hydrolysis of $Co(NO_2)_4(AA)^-$.

The base hydrolysis of octahedral metal complexes usually follows the S_N1CB or $\mathbf{D}_{cb}$ mechanism (dissociative mechanism with respect to the conjugate base).[14] If this is the case for $Co(NO_2)_4(AA)^-$, pK_a of the complex should be much smaller than 10 in order for the deprotonation equilibrium (Eq. 16) to be completely shifted to the right rendering the rate of hydrolysis independent of pH.

$$Co(NO_2)_4(AA)^- + OH^- \rightleftharpoons Co(NO_2)_4(AA-H)^{2-} + H_2O \quad (16)$$

Such a high acidity seems unreasonable for the negative diamine complexes even if the electron attracting property of the nitro ligands is taken into account, since pK_a of $Co(NH_3)_6^{3+}$ and $Co(en)_3^{3+}$ is estimated to be larger than 14.[15] Furthermore, if the conjugate base were the predominant species in basic solution of $Co(NO_2)_4(AA)^-$, the spectrum should differ significantly from that in acidic solution. No change with pH was observed in spectra of the tetranitro complexes at 2 °C, denying the appreciable deprotonation of $Co(NO_2)_4(AA)^-$ in basic solution. Thus $\mathbf{D}_{cb}$ mechanism is not operative and **D** mechanism (Eq. 10—12) seems to be favorable for the base hydrolysis of $Co(NO_2)_4(AA)^-$.

In weakly acidic solution (6>pH>4) the pseudo first order rate constant of hydrolysis k_{obsd} is smaller than that in basic solution, being independent of pH in this region (Table 1). Since the hydroxide ion concentration is very low in this case ($<10^{-8}$ mol·l^{-1}), path 12 can be neglected to derive the rate equation

$$-d\ln([Co(NO_2)_4(AA)^-]_t - [Co(NO_2)_4(AA)^-]_{eq}) = k_{obsd} = (k_{-NO_2}k_{H_2O}+k_{NO_2}k_{-H_2O}[NO_2^-])/(k_{H_2O}+k_{NO_2}[NO_2^-]), \quad (17)$$

which is transformed into

$$\frac{1}{k_{-NO_2}-k_{obsd}} = \frac{1}{k_{-NO_2}-k_{-H_2O}} + \frac{(k_{H_2O}/k_{NO_2})}{k_{-NO_2}-k_{-H_2O}}\cdot\frac{1}{[NO_2^-]}. \quad (18)$$

Since k_{-NO_2} is obtained by measurements in basic solutions (Eq. 15), the left side term in Eq. 18 can be calculated for various nitrite concentrations. As is seen in Fig. 5, the plot of $(k_{-NO_2}-k_{obsd})^{-1}$ *vs.* $[NO_2^-]^{-1}$ gives rise to a straight line, the intercept and slope of which afford k_{-H_2O} and k_{H_2O}/k_{NO_2}, thus enabling calculation of the equilibrium constant of aquation (3).

$$K = k_{-NO_2}k_{H_2O}/k_{NO_2}k_{-H_2O} \quad (19)$$

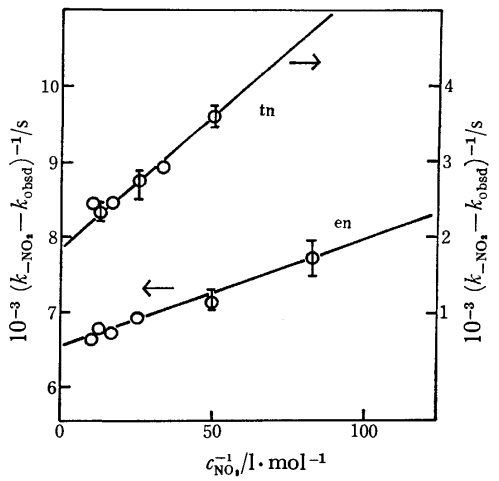

Fig. 5. Linear plots (Eq. 18) of rate data for the aquation of $Co(NO_2)_4(AA)^-$ at 25.0 °C and μ=0.1.

Table 4. Rate and equilibrium data at 25.0 °C and μ=0.1 of the hydrolysis of $Co(NO_2)_4(AA)^-$

AA	en	tn
k_{-NO_2}/s^{-1}	$(2.08\pm0.01)\times10^{-4}$	$(9.27\pm0.03)\times10^{-4}$
k_{OH}/k_{NO_2}	$\gg5\times10^3$	$\gg5\times10^3$
k_{-H_2O}/s^{-1}	$(5.46\pm0.10)\times10^{-5}$	$(3.95\pm0.12)\times10^{-4}$
$\frac{k_{H_2O}/k_{NO_2}}{mol\cdot l^{-1}}$	$(2.15\pm0.14)\times10^{-3}$	$(1.79\pm0.13)\times10^{-2}$
$K_{kin}/mol\cdot l^{-1}$ a)	$(8.19\pm0.72)\times10^{-3}$	$(4.20\pm0.45)\times10^{-2}$
$K_{eq}/mol\cdot l^{-1}$ b)	$(1.71\pm0.03)\times10^{-2}$	$(3.55\pm0.06)\times10^{-2}$

a) Calculated by Eq. 19. b) Calculated by Eq. 5.

The spontaneous aquation and anation reactions of cationic cobalt(III) complexes usually follow the dissociative interchange ($\mathbf{I}_d$) mechanism.[14] However, several anionic cobalt(III) complexes such as $Co(SO_3)_2(en)_2^-$ and $Co(CN)_5(H_2O)^{2-}$ are known to follow the **D** mechanism,[16] $Co(NO_2)_4(AA)^-$ becoming a new example. The rate and equilibrium constants are summarized in Table 4. The values of equilibrium constants calculated by Eq. 19 nearly coincide with those determined directly (Eq. 5). From these data the relative nucleophilicity of H_2O, NO_2^-, and OH^- toward the pentacoordinate intermediate $Co(NO_2)_3(AA)$ is calculated as the ratio $k_{H_2O}/[H_2O]$: k_{NO_2}: k_{OH}, and found to be $1:2.6\times10^4:\gg1.3\times10^8$ for AA=en, and $1:3.1\times10^3:\gg1.6\times10^7$ for AA=tn. The nucleophilicity order coincides with the basicity order of these reagents, reflecting the hard character of $Co(NO_2)_3(AA)$.

With increasing hydrogen ion concentration the acid-catalyzed aquation of $Co(NO_2)_4(AA)^-$ becomes increasingly important, which may proceed *via* the following two steps.

$$Co(NO_2)_4(AA)^- + H^+ \overset{K_H}{\rightleftharpoons} Co(NO_2)_3(HNO_2)(AA) \quad (20)$$

$$Co(NO_2)_3(HNO_2)(AA) \xrightarrow{k_{-HNO_2}} Co(NO_2)_3(AA) + HNO_2 \quad (21)$$

In acidic solutions where pH<2, free nitrite ions are mostly protonated and the reverse step of Eq. 10 can be neglected, giving the rate law

$$k_{obsd} = (k_{-NO_2}+k_{-HNO_2}K_H[H^+])/(1+K_H[H^+]). \quad (22)$$

In the acidity region examined the simple two term rate law (Eq. 7) holds, indicating that $K_H[H^+]\ll1$, giving rise to

$$k_0 = k_{-NO_2} \text{ and } k_a = k_{-HNO_2}K_H. \quad (23)$$

The values of k_0 obtained from the intercepts of straight lines in Fig. 3 nearly coincide with those of k_{-NO_2} given in Table 4. Thus the doubly protonated species $Co(NO_2)_2(HNO_2)_2(AA)$ need not be considered. The value of k_{-HNO_2} can not be obtained independently of K_H, but seems to be much greater than 10^{-2} s^{-1}.

The acid-catalyzed aquation of nitrocobalt(III) complexes has been investigated,[17] the pseudo first order rate constant of aquation of *trans*-$Co(NO_2)_2(tn)_2^+$ in a 1.09 mol·l^{-1} sulfuric acid solution at 25.0 °C having been reported[18] to be 6.9×10^{-5} s^{-1}. As compared with this the present k_{-HNO_2} value is astonishingly larger. A similar situation is noticed in the rate of spontaneous aquation. Staples[19] stated that no aquation of *cis*- and *trans*-$Co(NO_2)_2(en)_2^+$ occurs in neutral or faintly acidic solutions. On the contrary, $Co(NO_2)_4(en)^-$ is hydrolyzed spontaneously at a fairly fast rate of $(2.08\pm0.01)\times10^{-4}$ s^{-1} at 25.0 °C, indicating that the Co–NO_2 bond in the tetranitro(diamine) complexes is remarkably weaker than that in the dinitrobis(diamine) complexes. Similar results were also obtained for $Co(NO_2)_4(NH_3)_2^-$, k_0 being reported[5] to be 1.7×10^{-4} s^{-1} at 25 °C and μ= 2.5 mol·l^{-1}.

As to the mechanism of the acid-catalyzed aquation of $CoNO_2(NH_3)_5^{2+}$ in sulfuric acid, Harris *et al.*[20] postulated from the results of ^{18}O tracer experiments that the proton-assisted nitrosonium ion release occurred, leaving $CoOH(NH_3)_5^{2+}$ which maintains one oxygen atom of the nitrite ligand. A similar N–O bond fission mechanism is also suggested for the acid-catalyzed replacement of nitro-ligand from some dinitrodiamine platinum(II) complexes.[21] It is not certain whether an analogous mechanism is operative or a simple release of nitrous acid occurs in the acid-catalyzed aquation of $Co(NO_2)_4(AA)^-$.

Kinetic Chelate Ring Size Effect. The ligand substitution rates of trimethylenediamine complexes have been compared in several instances with those of the corresponding ethylenediamine complexes. Although *trans*-$CoCl_2(tn)_2^+$ and *trans*-$CoBr_2(tn)_2^+$ aquate 1500 times and 680 times as fast as the corresponding en complexes, respectively,[22] the acid-catalyzed aquation of *trans*-$Co(NO_2)_2(tn)_2^+$ is only a few times faster than that of *trans*-$Co(NO_2)_2(en)_2$.[+18,23] The aquation rate of $CoCO_3(tn)_2^+$ is similar to that of $CoCO_3(en)_2$,[+24] while the rate of carbonate exchange of the tn complex is smaller than that of the en complex.[25] In the present case the rate of nitrite release from $Co(NO_2)_4(tn)^-$ is 4.5 times and the rate of aqua ligand release from $Co(NO_2)_3(H_2O)(tn)$ 7.2 times larger than those of the corresponding en complexes (Table 4).

Trimethylenediamine forms a six-membered chelate ring whose conformation is usually of chair form in crystals.[26] In solution, however, the energy difference between chair and skew-boat conformers is small,[27] and 30% of Δ-$Co(tn)_3^{3+}$ and *ca.* 9% of $Ni(tn)(H_2O)_4^{2+}$ are in the skew-boat form in aqueous solutions at 20 and 27 °C, respectively.[28,29] Couldwell and House[30] presumed that the tn rings of *trans*-$CoCl_2(tn)_2^+$ can adopt the skew-boat configuration and steric interaction between the central methylene protons and the chloro ligands may be responsible for the exceptionally rapid aquation.

Holmes and Williams determined the thermodynamic functions of the copper(II) and nickel(II) complexes of en and tn.[31] The difference in the enthalpy of formation of $M(en)(H_2O)_4^{2+}$ and $M(tn)(H_2O)_4^{2+}$ amounts to 1.43 ± 0.18 kcal·mol^{-1} for Cu(II) and 2.01 ± 0.14 kcal·mol^{-1} for Ni(II). It appears that if the enthalpies of free en and tn are similar to each other, the five-membered en ring has stronger bonds than the six-membered tn ring by 13 and 28% for the Cu(II) and Ni(II) complexes, respectively. The enthalpy of activation for the nitrite release from $Co(NO_2)_4(tn)^-$ is smaller by 1.2 kcal·mol^{-1} than that for $Co(NO_2)_4(en)^-$

(Table 3). The difference seems to stem from the energy difference at the ground state, and both complexes may have similar enthalpies at the transition state where the steric strain is released by dissociation of one nitrite ligand. The positive entropy of activation is also in line with the proposed **D** mechanism.

The authors are grateful to Mr. J. Gohda for the elemental analysis. Financial aid from the Ministry of Education is acknowledged.

References

1) Y. Komiyama, *Bull. Chem. Soc. Jpn.*, **30**, 13 (1957).
2) (a) E. Kyuno, *Nippon Kagaku Zasshi*, **78**, 1494 (1957); (b) E. Kyuno, *ibid.*, **80**, 724 (1959).
3) J. C. Bailar, Jr., *Inorg. Synth.*, Vol. 4, 177 (1953).
4) S. F. A. Kettle, "Coordination Compounds," Nelson, London (1969), Chap. 3.
5) M. N. Malik and A. McAuley, *J. Chem. Soc., A*, **1969**, 917.
6) M. Shibata, M. Mori, and E. Kyuno, *Inorg. Chem.*, **3**, 1573 (1964).
7) R. G. Hughes, J. F. Endicott, M. Z. Hoffman, and D. A. House, *J. Chem. Ed.*, **46**, 440 (1969).
8) J. Kielland, *J. Am. Chem. Soc.*, **59**, 1675 (1937).
9) L. G. Sillén and A. E. Martell, Ed., "Stability Constants of Metal-Ion Complexes. Supplement No. 1," The Chemical Society, London (1971), p. 91.
10) A. A. Frost and R. G. Pearson, "Kinetics and Mechanism," 2nd ed, Wiley, New York (1961), p. 49.
11) J. L. Burmeister, *Coord. Chem. Rev.*, **3**, 225 (1968); A. H. Norbury and A. I. P. Sinha, *Quart. Rev.*, **24**, 69 (1970).
12) Y. Komiyama, *Bull. Chem. Soc. Jpn.*, **29**, 300 (1956).
13) Y. Kushi, M. Kuramoto, S. Yamamoto, and H. Yoneda, *Inorg. Nucl. Chem. Lett.*, **12**, 629 (1976).
14) T. W. Swaddle, *Coord. Chem. Rev.*, **14**, 217 (1974).
15) F. Basolo and R. G. Pearson, "Mechanism of Inorganic Reactions," 2nd ed, Wiley, New York (1967), p. 33.
16) J. E. Byrd and W. K. Wilmarth, *Inorg. Chim. Acta Rev.*, **5**, 7 (1971).
17) P. J. Staples, *Coord. Chem. Rev.*, **11**, 277 (1973).
18) P. D. Grosse and P. J. Staples, *J. Inorg. Nucl. Chem.*, **31**, 1443 (1969).
19) P. J. Staples, *J. Chem. Soc.*, **1964**, 2534.
20) A. D. Harris, R. Stewart, D. Hendrickson, and W. L. Jolly, *Inorg. Chem.*, **6**, 1052 (1967).
21) D. Humphreys and P. J. Staples, *J. Inorg. Nucl. Chem.*, **39**, 1185 (1977).
22) I. R. Jonasson, R. S. Murray, D. R. Stranks, and J. K. Yandell, Proc. XII ICCC, 1969, p. 32.
23) D. G. Lambert and J. G. Mason, *J. Am. Chem Soc.*, **88**, 1637 (1966).
24) V. S. Sastri and G. M. Harris, *J. Am. Chem. Soc.*, **92**, 2943 (1970).
25) J. E. Boyle and G. M. Harris, *J. Am. Chem. Soc.*, **80**, 782 (1958).
26) T. Nomura, F. Marumo, and Y. Saito, *Bull. Chem. Soc. Jpn.*, **42**, 1016 (1969); K. Matsumoto, S. Ooi, and H. Kuroya, *ibid.*, **43**, 1903 (1970); E. Yasaki, I. Oonishi, H. Kawaguchi, S. Kawaguchi, and Y. Komiyama, *ibid.*, **43**, 1354 (1970); K. Matsumoto, M. Yonezawa, H. Kuroya, H. Kawaguchi, and S. Kawaguchi, *ibid.*, **43**, 1269 (1970); R. J. Gene and M. R. Snow, *J. Chem. Soc., A*, **1971**, 2981 H. V. F. Schousboe-Jensen, *Acta Chem. Scand.*, **26**, 3413 (1972); K. Matsumoto, H. Kawaguchi, H. Kuroya, and S. Kawaguchi, *Bull. Chem. Soc. Jpn.*, **46**, 2424 (1973).
27) L. J. DeHayes and D. H. Busch, *Inorg. Chem.*, **12**, 1505 (1973).
28) P. G. Beddoe, M. J. Harding, S. F. Mason, and B. J. Peart, *Chem. Commun.*, **1971**, 1283.
29) J. E. Sarneski and C. N. Reilley, *Inorg. Chem.*, **13**, 977 (1974).
30) M. C. Couldwell and D. A. House, *Inorg. Chem.*, **11**, 2024 (1972).
31) F. Holmes and D. R. Williams, *J. Chem. Soc., A*, **1967**, 1702.

Application of a Coagulated Mixture Prepared from Finely Divided Cation and Anion Exchange Resins to the Enrichment of Copper(II)

Masutaro ABE, Kunio OHZEKI, and Tomihito KAMBARA

Department of Chemistry, Faculty of Science, Hokkaido University, Sapporo 060

(Received September 16, 1977)

Mutual coagulation takes place, when a suspension of finely divided cation exchanger is added to that of anion exchanger. The resulting mixed resin is bulky and easily separated from the solution by filtration. A rapid and selective collection of a trace amount of copper(II) ion was carried out by the combined use of mixed resin and 8-quinolinol-5-sulfonic acid (H_2qs). The copper(II) collected on the mixed resin in the form of $[Cu(qs)_2]^{2-}$ was brought into solution from the resin with ethylenediaminetetraacetate, converted into copper(II)–diethyldithiocarbamate, extracted into methyl isobutyl ketone, and determined by atomic absorption spectrometry. The method was satisfactorily applied to the determination of a trace amount of copper(II) in well water.

Finely divided ion exchange resin particles can collect ions from solutions much more rapidly than beads of the conventional size, since the rate of ion exchange reaction is inversely proportional to the square of the radius of the resin particles.[1] One of the characteristics of such a fine resin is coagulation caused by the addition of suspensions of oppositely charged resin particles.[2] The use of the coagulated resin for rapid ion removal has been demonstrated by Pinfold and Karger.[2]

We have examined the analytical utilization of the mixed resin of finely divided cation and anion exchangers. A rapid and selective concentration of a trace amount of copper(II) ion is reported.

Experimental

Reagents. A copper(II) standard solution was prepared from nitrate and standardized against EDTA. A 10^{-2} M (mol dm^{-3}) 8-quinolinol-5-sulfonate (Hqs^-) solution was prepared by dissolving the acid (H_2qs, Wako Pure Chemicals Inc.,), in an alkaline solution. The Dotite 4 NA (Dojindo Lab.) was dissolved to give ethylenediaminetetraacetic acid tetrasodium salt (Na_4edta) solution. Sodium diethyldithiocarbamate for atomic absorption spectrometry (Naddtc, Wako) was used in a 5 w/v% aqueous solution. Methyl isobutyl ketone (MIBK) and other reagents of guaranteed grade were used. Deionized-redistilled water was used.

Apparatus. A Hitachi 508 atomic absorption spectrometer with a Fe–Co–Ni–Cu–Cr–Mn multielement hollow cathode lamp was used for the determination of copper(II) in MIBK extract under the following conditions: wavelength 324.8 nm, lamp current 10 mA, slit width 0.18 mm, acetylene flow rate 1.5 l min^{-1} at 0.5 kg cm^{-2}, and air flow rate 13 l min^{-1} at 1.8 kg cm^{-2}. A Toyo KG 25 filter holder (Toyo Roshi Co., Ltd.) was used.

Ion Exchange Resin. Macroreticular type Amberlyst 15 and A-26 (both Rohm and Haas Co.) in RSO_3Na and $RN(CH_3)_3Cl$ forms, respectively, were used. The dry cation exchange resin was washed with ethanol until the washings became colorless, and then cleaned and recycled several times between hydrogen and sodium forms. The chloride form of the anion exchange resin was regulated as usual. The wet resin was crushed into a slurry which was then diluted to a suspension. The suspension was then filtered through a 3G3 glass filter to remove resin particles larger than 30 μm. The particle sizes of the resins in the resulting stock suspension were in the range 0.2—30 μm. The lower limit was confirmed by the fact that the resin particles in the suspension could not pass a millipore filter of 0.2 μm pore size.

The ion exchange capacity of the resin in the suspension was determined as follows. In the case of the cation exchanger, the solid particles in a known amount of the suspension were collected onto a millipore filter, and the sodium ion on the resin was eluted with hydrochloric acid solution and determined by atomic absorption spectrometry. For the anion exchange resin, the chloride ion on the resin was eluted with sodium nitrate solution and determined absorptiometrically by the mercury(II) thiocyanate method.[3] The exchange capacities thus obtained were 0.031 meq ml^{-1} for the cation exchange resin suspension (CRS) and 0.030 meq ml^{-1} for the anion exchange resin suspension (ARS), respectively.

Results and Discussion

Coagulation. The mutual coagulation of the finely divided cation and anion exchangers was examined first. A 5.0-ml portion of CRS was taken into a 50-ml stoppered measuring cylinder and varying amounts of ARS were added. After adjusting the total volume to 50 ml with water, the mixture was shaken vigorously for 5 min and allowed to stand for 5 min. The coagulated material thus obtained was removed by filtration with a 3G3 glass filter. The extent of coagulation was estimated from the turbidity of the resulting filtrate.

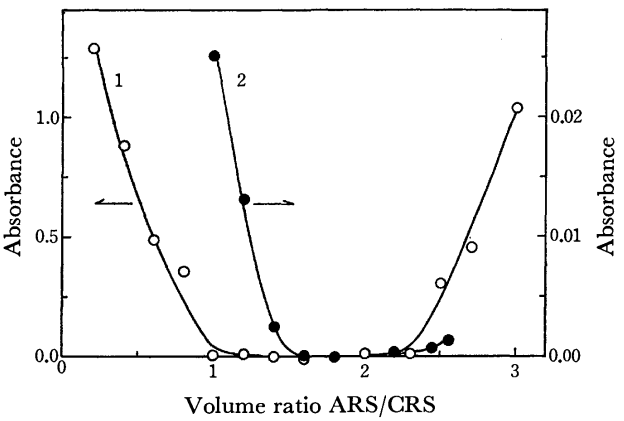

Fig. 1. Coagulation of cation and anion exchangers. Amounts of CRS involved in 50 ml of the mixtures: ●; 1.0 ml, ○; 5.0 ml.

As a measure of turbidity, the absorbance of the solution was determined in a 1-cm cell at an arbitrary wavelength of 500 nm against water. The results are shown in Fig. 1. The turbidity of the filtrate due to the remaining CRS decreased with increasing amount of ARS, almost complete coagulation being attained when 6—10 ml of ARS was added to 5.0-ml portion of CRS (curve 1, Fig. 1). With further addition of ARS, the solution became turbid due to excess ARS. The 1.0-ml portion of CRS was most satisfactorily deposited from the solution with addition of 1.6—1.8 ml of ARS (curve 2, Fig. 1).

Exchange Capacity of the Coagulated Resin. The number of ion exchange sites consumed for the association of 5.0 ml of CRS with 8.0 ml of ARS was estimated by determining the sodium and chloride ions expelled from both resins as a result of mutual coagulation. The proportions of the ion exchange sites taking part in the coagulation to the total ion exchange sites in CRS and ARS were found to be 3.7 and 5.3%, respectively. The exchange capacities of cation and anion exchangers decrease only a little by coagulation.

Effect of Concentration of Sodium Chloride on Coagulation. A 1.0-ml portion of CRS and 1.6 ml of ARS were added to 250 ml of a solution containing various amounts of sodium chloride. The mixture was shaken for 10 min. The resins coagulated on being left to stand for 10 min from a 0.1 M sodium chloride solution. With increasing concentration of sodium chloride, it took a longer time to obtain sufficient coagulation. No satisfactory coagulation was attained in the solution containing sodium chloride (0.5 M) even after long standing.

Adsorption of Copper(II). The adsorption of copper(II) ion onto the coagulated resin was investigated in the presence of calcium and chloride ions which are most commonly present in natural water. A 1.0-ml portion of CRS and 1.6 ml of ARS were taken into an eggplant type flask, and 5 μg of copper(II) and varying amounts of calcium chloride solution were then added. The mixture was diluted to *ca.* 40 ml with water and shaken for 30 min. The resulting coagulated resin was removed by filtration. The copper(II) in the filtrate was extracted as copper(II)–ddtc complex into MIBK and determined by atomic absorption spectrometry.

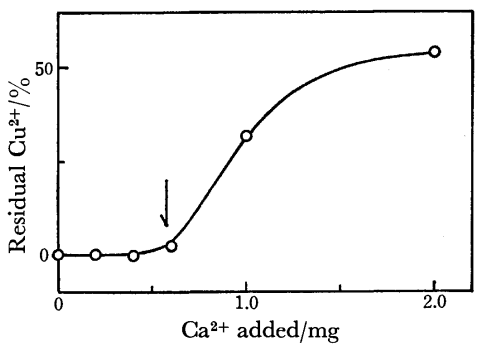

Fig. 2. Recovery of 5.0 μg of copper(II) from 40 ml of solutions containing varying amounts of calcium chloride onto the coagulated resin prepared from 1.0 ml of CRS and 1.6 ml of ARS. Arrow indicates the amount of calcium ion corresponding to the exchange capacity of CRS.

As shown in Fig. 2, copper(II) was quantitatively collected onto the mixed resin until the exchange capacity of the cation exchanger in the mixed resin was satisfied by the calcium ion. Thereafter, the amount of non-fixed copper(II) in the solution increased with increasing amount of calcium ion.

Choice of Chelating Agent. The utilization of complexation in ion exchange analysis was described by Ringbom.[4] Recently, the use of ion exchange resins in combination with chelating agents, such as 8-quinolinol-5-sulfonic acid[5] and a sulfonic acid derivative of dithizone[6] has been reported. In order to enhance the selectivity of the mixed resin for copper(II), ethylenediamine (en) and Hqs^- were examined as chelating agents. The former combined with copper(II) to form the complex cation while the latter formed the complex anion. Both complexes could be more strongly fixed onto the resin than simple ions. In the presence of 3 μmol of en, 15 μg of copper(II) were quantitatively collected from a solution containing 2 mg of calcium ion onto the coagulated resin prepared from 1.0 ml of CRS and 1.6 ml of ARS under the optimal conditions. The effect of en is obvious. However, better results were obtained by use of Hqs^-.

Effect of Hqs^-. In the presence of 2 μmol of Hqs^-, 5 μg of copper(II) were collected from 40 ml of a calcium chloride solution containing 20 mg of calcium ion onto the coagulated resin prepared from 1.0 ml of CRS and 1.6 ml of ARS (curve 1, Fig. 3).By combination of 2.5 ml of CRS and 4.0 ml of ARS, copper(II) was effectively collected onto the mixed resin in the presence of 50 mg of calcium ion (curve 2, Fig. 3).

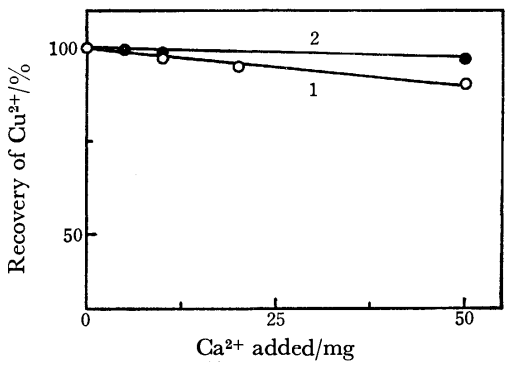

Fig. 3. Recovery of 5.0 μg of copper(II) from 40 ml of solutions containing varying amounts of calcium chloride in the presence of 2 μmol of Hqs^- onto the mixed resin: ○; 1.0 ml of CRS and 1.6 ml of ARS, and ●; 2.5 ml of CRS and 4.0 ml of ARS.

Adsorption of the Chelate. The recovery of copper(II) increased with increasing concentration of Hqs^- until the mole ratio of the reagent to copper content reached 2: 1, and thereafter, copper(II) was quantitatively collected as shown in Fig. 4. The results indicate that the copper(II) was fixed onto the resin in the form of $[Cu(qs)_2]^{2-}$. The recovery of copper(II) was retarded when the amount of the chelating agent increased beyond the exchange capacity of the anion exchanger in the coagulated resin. This is attributable to competition between anions of copper(II)–qs complex and the

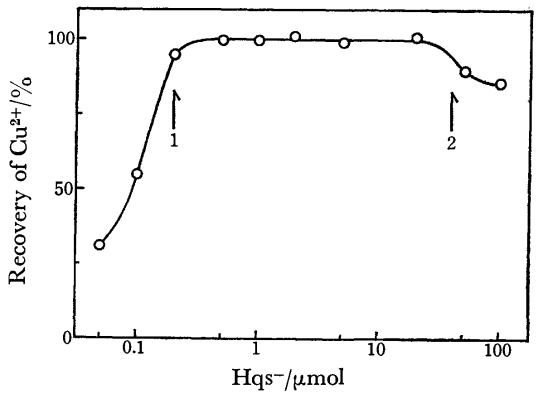

Fig. 4. Effect of the amount of Hqs^- on the recovery of 5.0 μg of copper(II) from 40 ml solutions containing 20 mg of calcium ion onto the coagulated resin prepared from 1.0 ml of CRS and 1.6 ml of ARS. Arrow 1 indicates the point where mole ratio of copper(II) to Hqs^- reached to 1 to 2, and arrow 2 shows the amount of Hqs^- corresponding to the exchange capacity of ARS in the mixed resin.

excess chelating agent for anion exchange sites in the mixed resin. Even if a molecular adsorption of the complex onto the resin matrix might exist,[7] it seems to be much less effective than the ion exchange.

Effect of pH. As shown in Fig. 5, copper(II) was quantitatively collected onto the mixed resin from the solution over the pH range 4—12. The optimal pH range confirmed was much wider than that of 3.5—6.0 observed in the liquid-liquid ion-association extraction system in which an ion-pair of $[Cu(qs)_2]^{2-}$ with quaternary ammonium cation, zephiramine, was extracted into chloroform.[8]

Shaking and Standing Times. A 5-μg portion of copper(II) in 250 ml of a sample solution containing 1.0 ml of CRS, 1.6 ml of ARS, and 2 μmol of Hqs^- was

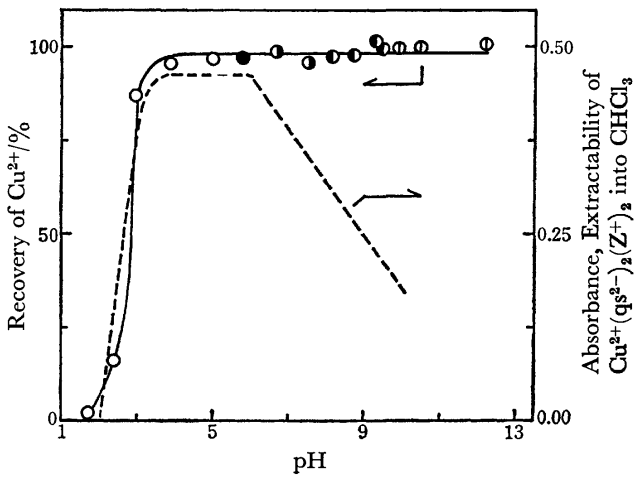

Fig. 5. Effect of pH on the recovery of 5.0 μg of copper(II) from 40 ml of solutions containing 20 mg of calcium ion and 2 μmol of Hqs^- onto the coagulated resin prepared from 1.0 ml of CRS and 1.6 ml of ARS. Dashed line indicates the results obtained in ion-association extraction system.
Buffer systems: ○; NaOAc–HCl, ●; unbuffered, ◑; γ-collidine–HCl, ◐; NH_3–NH_4Cl, ⓘ; Borax–NaOH.

well fixed onto the anion exchanger when the mixture was shaken for more than 5 min. The appreciable coagulation of the resins occurred on standing for 10 min. The resulting mixed resin was easily separated by filtration.

Elution of Copper(II) Fixed on the Resin. Of the eluting agents studied, EDTA tetrasodium salt solution was the most satisfactory. Copper(II) fixed on the resin was quantitatively eluted with 20 ml of 0.1—0.2 M of EDTA tetrasodium salt solutions at an eluting rate of 1.0—2.0 ml min^{-1}.

Extraction of Copper(II) from the Eluate. The copper(II)–edta complex in the eluate was converted into the copper(II)–ddtc complex and extracted into MIBK. The organic extract was sprayed into the flame of an atomic absorption spectrometer, resulting in the sensitivity for copper by *ca.* 4 times that obtained by spraying an aqueous solution.[9]

Established Procedure. A 50—500-ml sample solution containing 0.5—5 μg of copper(II) is taken into a separatory funnel. The pH of solution is adjusted to 4—12 with sodium hydroxide solution. Then 2 ml of a 1.0×10^{-3} M Hqs^- solution, 1.0 ml of CRS and 1.6 ml of ARS are added. After shaking for 10 min, the mixture is allowed to stand for several minutes until the coagulated resin settles. The mixed resin is separated by filtration with suction from the solution onto a filter paper (Toyo Roshi No. 2). The copper(II) species on the resin are then eluted with 20 ml of a 0.2 M EDTA tetrasodium salt solution into another separatory funnel. Five ml of 5% Naddtc solution is added and the resulting copper(II)–ddtc complex is extracted into 5.0 ml of MIBK, and the organic extract is then subjected to atomic absorption spectrometry.

Blank Value. Several blank tests were carried out according to the established procedure using 250-ml portions of deionized-redistilled water. The recorder response corresponding to *ca.* 0.2 μg of copper was found.

Effect of Foreign Ions. The concentration procedure was tested with a synthetic sample solution, the components of which are given in Table 1. The effects of iron(III) and aluminum(III) were also examined by adding various amounts to 250-ml portions of the

Table 1. Effect of various ions on the recovery of copper(II)

Composition (μg ml^{-1})		Cu^{2+} found (μg)	Recovery[a] (%)
A:	Na^+ 33, K^+ 7.8, Ca^{2+} 10, Mg^{2+} 2.4, Cl^- 57, HCO_3^- 36, SO_4^{2-} 9.6, SiO_2 7.5	5.1	102
		5.1	102
		4.9	98
B[b]: A+Fe^{3+}	0.08	5.3	106
	0.4	5.1	102
	2.0	5.1	102
C[c]: A+Al^{3+}	0.08	4.8	96
	0.4	4.8	96
	2.0	4.8	96

a) Cu^{2+} 5.0 μg, Sample 250 ml. b) Fe^{3+} added as ammonium iron(III) sulfate. c) Al^{3+} added as aluminum(III) potassium sulfate.

synthetic sample solution. Recovery of copper(II) was not affected by each addition up to 0.5 mg.

It was also found that good recovery of 5 μg of copper(II) contained in 50—500 ml of the sample solution (composition A, Table 1) can be made.

Analysis. The above developed method was applied to the determination of copper(II) in well water taken from our University campus. The standard addition method was employed using 250-ml portions of sample solution. The blank test was carried out using a 250-ml portion of deionized-redistilled water. The linear least-squares regression equation for recorder response of atomic absorption spectrometry, y cm, as a function of added amount of copper(II), x μg, is

$$y = 2.69\ x + 2.50,$$

where y is corrected for the blank value. The F-factor for regression analysis is 4918, highly significant to $F(1, 3: 0.01)=34.1$. The 95% confidence limits are 3.72 ± 0.063 ng ml^{-1}, the value for the coefficient of variation being 5.3%.

This work was supported in part by a Grant-in-Aid for Scientific Research from the Ministry of Education.

References

1) G. E. Boyd, A. W. Adamson, and L. S. Meyers, *J. Am. Chem. Soc.*, **69**, 2836 (1947).
2) T. A. Pinfold and B. L. Karger, *Sep. Sci.*, **5**, 183 (1970).
3) JIS K 0101 (1966).
4) A. Ringbom, "Complexation in Analytical Chemistry," Interscience Publishers, New York/London (1963), Chap. 6.
5) H. Akaiwa, H. Kawamoto, N. Nakata, and Y. Ozeki, *Chem. Lett.*, **1975**, 1049.
6) H. Tanaka, M. Chikuma, A. Harada, T. Ueda, and S. Yube, *Talanta*, **23**, 489 (1976).
7) R. L. Gustafson and J. A. Lirio, *Ind. Eng. Chem., Prod. Res. Dev.*, **7**, 116 (1968).
8) T. Kambara, M. Maeyama, and K. Hasebe, *Bunseki Kagaku*, **20**, 1249 (1971).
9) J. E. Allan, *Spectrochim. Acta*, **17**, 467 (1961).

The Stereochemistry of Copper(II) Complexes Containing *N,N'*-Di-8-quinolylethylenediamine and Its Optically Active Derivatives

Toshishige M. SUZUKI, Shin-ichi KAMIYAMA, and Tetsuo KIMURA

Government Industrial Research Institute, Tohoku Nigatake, Haranomachi, Sendai 983

(Received October, 3, 1977)

Copper(II) complexes of a series of quadridentate ligands, *N,N'*-di-8-quinolylethylenediamine (dqen), (*R*)-*N,N'*-di-8-quinolylpropylenediamine {(*R*)-dqpn}, and (*R,R*)-*N,N'*-di-8-quinolyl-1,2-cyclohexanediamine {(*R,R*)-dqchxn}, have been prepared. Their d-d absorption spectra, magnetic moments, and molar conductivities indicate that the complexes have a five-coordinated structure, in which one of the quinoline groups of the ligands occupies an apical position. The circular dichroism (CD) spectra of the optically active ligands and their complexes exhibit exiton couplets in the ligand's $\pi^* \leftarrow \pi$ transition region. From the signs of the couplets, the preferable configurations of the (*R*)-dqpn and (*R,R*)-dqchxn complexes are assigned to Δ.

A number of papers have been published on metal complexes with 8-aminoquinoline and its derivatives.[1] Nielsen and Dahl prepared copper(II) complexes of *N,N'*-di-8-quinolylalkanediamines (dqdiamine), but conclusive evidence for the structure of the complexes is lacking.[1d] These quadridentate ligands are interesting in their intermediate character between aliphatic and aromatic systems, and also in the variety of stereochemistry of their metal complexes. The dqdiamines are structurally similar to quadridentate Schiff base-type ligands such as *N,N'*-disalicylideneethylenediamine (salen). Although stereochemical studies of the complexes with such Schiff bases have been extensively done,[2] none of bqdiamine complexes are known thus far.

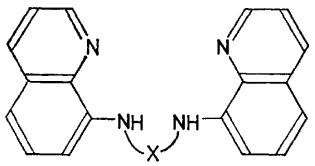

X = CH_2CH_2 : dqen
= $CH_2\underset{CH_3}{CH}$: dqpn
= $\underset{}{CH}\text{-}\underset{}{CH}$: dqchxn

This paper will deal with the stereochemistry of copper(II) complexes of dqen and optically active (*R*)-dqpn and (*R,R*)-dqchxn. Molecular models predict that the steric interaction between 2 and 2' protons of the dqdiamine would prevent the formation of square-planar complexes. The deviation from co-planarity of the two coordinated quinoline nuclei will bring about a dissymmetric configuration about the metal ion. The ligands derived from optically active diamines are expected to coordinate to metal ions with sterically preferred configurations because of the conformational requirements of the diamine chelate rings.

Experimental

N,N'-*Di-8-quinolylethylenediamine (dqen).* This was prepared according to the method described in the literature.[1b] Recrystallization from ethanol gave prismatic tan crystals; mp 162—163 °C.

(R)-N,N'-*Di-8-quinolylpropylenediamine* {(R)-*dqpn*}. Racemic propylenediamine (pn) was resolved by the method of Dwyer *et al.*[3] *R*-pn was obtained by the neutralization of its tartrate (3 mol, 67.27 g) with barium hydroxide. After the filtration of barium tartrate, the filtrate was used directly for the next condensation process. To the filtrate in a 2-dm^3 three-necked flask fitted with a mechanical stirrer, a condenser, and a thermometer, were added 8-hydroxyquinoline (0.6 mol, 87.10 g) and sodium disulfite (0.6 mol, 114.13 g), after which the mixture was gently refluxed for 7 days with stirring. The reaction mixture was made alkaline with a 50% aqueous sodium hydroxide solution at 60 °C, and after cooling the mixture was extracted with benzene. The extract was washed with water and dried over anhydrous potassium carbonate. After the removal of the solvent, 40.64 g of a pale brown oil was obtained. The crude oil (10 g) was purified as a hexane solution through an Al_2O_3 column. Pale yellow small plates (6.56 g) were obtained after the removal of the solvent, and recrystallized from hexane; mp 96.3—97.0 °C.

(R,R)-*Di-8-quinolylcyclohexanediamine* {(R,R)-*dqchxn*}. This was prepared according to a method similar to that for (*R*)-dqpn, using *R,R*-cyclohexanediamine[4] (chxn) in place of R-pn. Recrystallization from benzene gave yallow needles; mp 174—174.5 °C.

[$CuCl_2$(*dqen*)]. Copper(II) chloride dihydrate (0.85 g in 20 cm^3 of ethanol) and dqen (1.6 g in 100 cm^3 of ethanol) were mixed, and the resulting green solution was stored in a refrigerator overnight. The green crystals deposited were filtered off, washed with ethanol and ether, and air-dried; 1.2 g.

[$CuCl_2$(R)-*dqpn*]·*1/2*H_2O. This was prepared by a method similar to that used for [$CuCl_2$(dqen)].

[$CuCl_2$(R,R)-*dqchxn*]. Copper(II) chloride dihydrate (0.85 g in 100 cm^3 of ethanol) and (*R,R*)-dqchxn (20 cm^3 of benzene) were mixed. The resultant dark green solution was evaporated to about 50 cm^3 and stored in a refrigerator. The dark green crystals thus deposited were filtered, washed with ethanol, and ether, and air-dried; 0.65 g.

Measurements. Electronic absorption spectra were recorded on a Shimadzu Double 40-R spectrophotometer. The circular dichroism spectra were recorded on Jasco J-20 and Jasco J-20A spectropolarimeters. The magnetic measurements were carried out at room temperature (24—25 °C) by the Gouy method, using distilled water as the calibrant. The conductivities were determined on a TOA CM-6A conductometer at 25 °C.

Results and Discussion

Optically active ligands of the type, *N,N'*-di-8-

Table 1. Elemental analysis and some properties of ligands and complexes

Compound	Found (Calcd %) C	H	N	Magnetic moments and conductances μ_{eff} (B.M.)	(Λ_M, Ω^{-1} cm^2 mol^{-1}) H_2O	CH_3OH
dqen	76.61 (76.40)	5.94 (5.77)	18.61 (17.85)			
(*R*)-dqpn	75.54 (76.81)	5.96 (6.14)	17.32 (17.06)			
(*R,R*)-dqchxn	78.58 (78.23)	6.58 (6.56)	15.20 (15.20)			
[$CuCl_2$(dqen)]	52.92 (53.22)	4.32 (4.04)	12.44 (12.49)	1.99	248	101
[$CuCl_2${(*R*)-dqpn}]1/2H_2O	53.34 (53.46)	4.74 (4.48)	11.64 (11.87)	2.00	221	92
[$CuCl_2${(*R,R*)-dqchxn}]	55.02 (55.34)	5.09 (5.03)	9.80 (10.25)	1.97	217	118

quinolylalkanediamine, and their complexes are described for the first time. The results of the elemental analysis and other properties of the ligands and their copper(II) complexes are presented in Table 1.

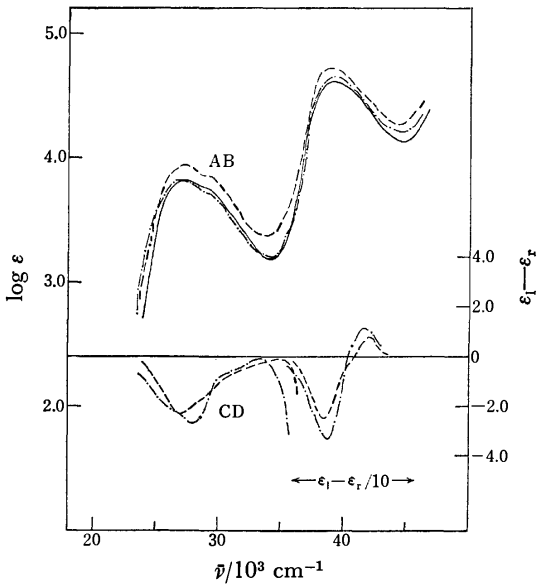

Fig. 1. Absorption(AB) and circular dichroism(CD) spectra of (——) dqen, (– – –) (*R*)-dqpn and (-·-·-) (*R,R*)-dqchxn in methanol.

Ligands. The electronic absorption and CD spectra of the ligands in methanol are shown in Fig. 1. Their band locations and intensities are summarized in Table 2. The substitution of propylenediamine or cyclohexanediamine for the ethylenediamine moiety of dqen produces little change in the absorption spectra. The two main absorption bands, centered at about 27000 and 40000 cm^{-1}, are due to the $\pi^*\leftarrow$n and $\pi^*\leftarrow\pi$ transitions of the quinoline nuclei.[5] A negative-positive CD couplet[6] (from lower to higher energy), centered at *ca.* 40000 cm^{-1}, is observed for the optically active ligands. The strong Cotton effects do not usually arise from the vicinal induction of assymmetric carbons. These CD patterns should arise from exiton splitting of the transitions of the quinoline nuclei. Similar coupled CD spectra have been reported for the optically active Schiff bases containing conjugated systems, such

Table 2. Absorption (AB) and circular dichroism (CD) data in 10^3 cm^{-1}, (log ε) and ($\varepsilon_l-\varepsilon_r$)

Compound	AB	CD
dqen	27.03 (3.81)	
	sh 29.41 (3.72)	
	39.06 (4.61)	
(*R*)-dqpn	27.03 (3.93)	27.40 (− 2.37)
	sh 28.99 (3.85)	
	39.37 (4.70)	38.46 (−26.10)
		42.02 (+ 7.11)
(*R,R*)-dqchxn	27.03 (3.80)	27.76 (− 2.76)
	sh 28.99 (3.71)	
	39.06 (4.58)	38.76 (−32.20)
		41.67 (+11.50)
[$CuCl_2$(dqen)]	sh 11.11 (1.43)	
	15.15 (1.86)	
	31.75 (3.98)	
	33.33 (4.01)	
	43.48 (4.74)	
[$CuCl_2${(*R*)-dqpn}]· 1/2H_2O	sh 11.11 (1.53)	
	15.63 (2.05)	14.71 (+ 0.81)
	31.75 (3.97)	31.75 (− 2.42)
	33.33 (4.00)	
		40.65 (− 9.44)
	43.48 (4.69)	43.48 (+38.4)
[$CuCl_2${(*R,R*)-dqchxn}]	sh 11.11 (1.73)	12.50 (− 0.02)
	16.13 (2.15)	15.63 (+ 0.72)
	31.75 (3.95)	32.26 (+ 4.85)
	33.56 (3.98)	
		41.32 (−16.60)
	43.48 (4.70)	43.10 (+24.92)

as (*R*)-*N,N'*-disalicylidenepropylenediamine and (*R,R*)-*N,N'*-disalicylidenecyclohexanediamine.[2a-2c,2g] Figure 2 shows the three possible conformations of (*R*)-dqpn (a, b, c) and the only possible conformation of (*R,R*)-dqchxn (d). Of the three possible conformations of (*R*)-dqpn, (a) and (b) should give rise to strong optical activity, since in (c) the two quinoline nuclei are *trans*-parallel, resulting in inactive coupling. The pattern and intensities in the CD spectrum of the (*R*)-dqpn are quite similar to those of (*R,R*)-dqchxn, which necessarily has the (d) conformation, regulated by the fused cyclohexane ring. This result indicate that the most stable conformation of (*R*)-dqpn is the (a) conformer in

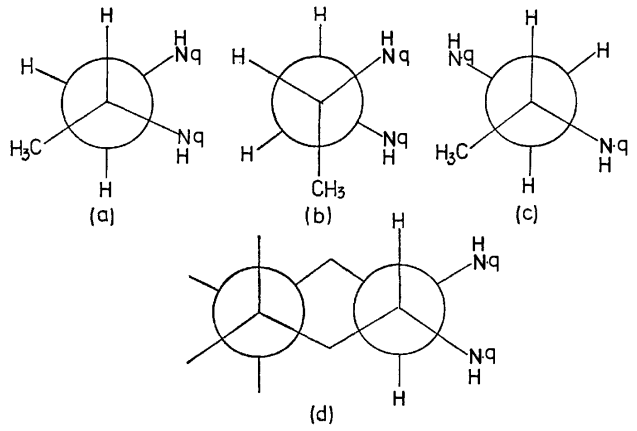

Fig. 2. Conformations of (*R*)-dqpn (a, b, c) and the only possible conformation of (*R,R*)-dqchxn (d); q denotes quinoline nuclei.

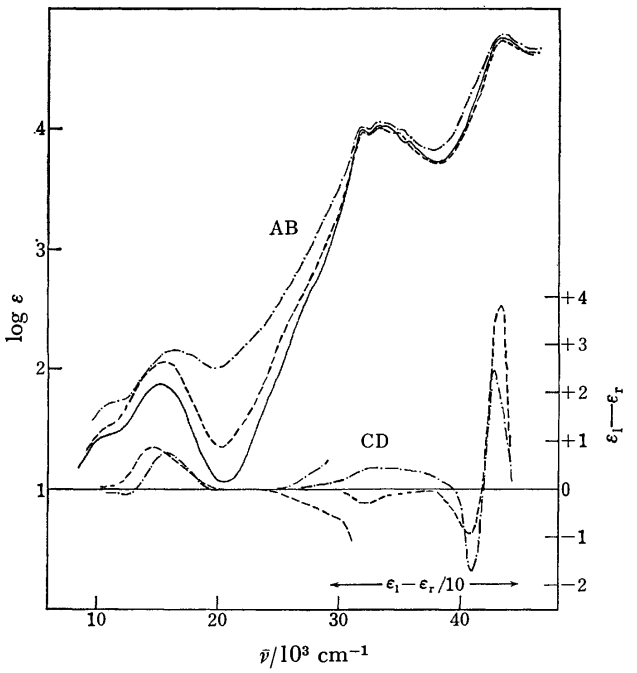

Fig. 3. Absorption (AB) and circular dichroism (CD) spectra of (——) [CudqenCl$_2$], (----) [Cu(*R*)-dqpnCl$_2$] and [Cu(R,R)-dqchxnCl$_2$] in H_2O.

methanol.

Copper(II) Complexes. Figure 3 shows the electronic absorption and CD spectra of the series of copper(II) complexes in water. The absorption bands in the 10000—20000 cm^{-1} region are due to the d–d transitions. Each complex gives a shoulder at *ca.* 11000 cm^{-1} and a main peak at *ca.* 15000 cm^{-1}. It is known that for many copper(II) complexes, a shoulder appears at about 11000 cm^{-1} as a result of ligation along the tetragonal axis.[7-9] It might be difficult for the present ligands to take square-planar arrangements in the copper(II) complexes because of the steric hindrance between 2 and 2′ quinoline protons. The weak shoulders at *ca.* 11000 cm^{-1} suggest the apical ligation of one or two quinoline group(s) of the ligands that is, a *cis* type coordination of dqdiamine to the copper(II) ion. Although the *cis* complexes have two different geometrical arrangements, *cisα* and *cisβ*, the present complexes are probably *cisβ* (Fig. 4), since the steric interaction between the bulky terminal chelate moiety and the substituents of the central diamine chelate ring might be greater in *cisα* than in *cisβ*.[10] The magnetic moments of the three complexes (Table 1) are within the range of those reported for the five-coordinated or octahedral complexes,[1g] and higher than those of planar complexes (μ_{eff}; 1.8—1.9 B. M.).[11] The molar conductivities indicate that all the complexes are 1 : 1 electrolytes in methanol, and 1 : 2 electrolytes in an aqueous solution.[12] These results imply that the complexes have five-coordinated structure, [CuCl(dqdiamine)]Cl in the solid state, and that they dissociate into [CuCl(dqdiamine)]$^+$ and Cl$^-$ ions in methanol. When the complexes are dissolved in water, the coordinated Cl$^-$ ion will be replaced by the H_2O molecule to give bivalent complex cation, *i.e.*, [Cu(H_2O)(dqdiamine)]$^{2+}$.

The cyclohexanediamine bridge of (*R,R*)-dqchxn will exclusively take the λ-gauche[13] conformation upon coordination, because it has a *trans*-fused chelate ring. In the (*R*)-dqpn complex, however, a conformational inversion of the propylenediamine chelate moiety is possible wherein the C-methyl group is axial for the δ, and equatorial for the λ conformation. Since the overall CD pattern of the (*R*)-dqpn complex is similar to that of the (*R,R*)-dqchxn complex, the central chelate conformation and the absolute configuration of the (*R*)-dqpn complex must be the same as those of the (*R,R*)-dqchxn complex. Thus, the preferred conformation of the propylenediamine chelate moiety should be λ with the methyl group being equatorial.

The (*R*)-dqpn and (*R,R*)-dqchxn complexes give positive main Cotton effects in the d-d region. Unfortunately, the absolute configurations of the complexes cannot be known at present from the Cotton effects in this region. Sharp couplet CD components (negative and positive from lower to higher energy) centered at 42000 cm^{-1}, corresponding to the ligand $\pi^* \leftarrow \pi$ absorption bands, are seen for both complexes. The observation of a CD couplet with opposite-signed components corresponding to the ligand $\pi^* \leftarrow \pi$ transitions indicates that the two quinoline nuclei take a dissymmetric arrangements as has been mentioned. Since the CD pattern in the $\pi^* \leftarrow \pi$ couplet of the ligands did not change upon complexation, the dissymmetric arrangement of the free ligands must be maintained in their complexes. Figure 4 shows schematic drawings of the

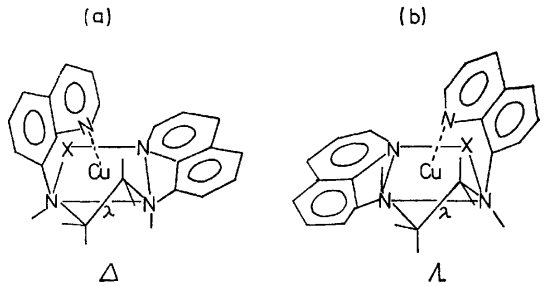

Fig. 4. Schematic structures of (a) Δ-*cisβ*[CuX(λ-dqdiamine)]$^+$, (b) Λ-*cisβ*[CuX(λ-dqdiamine)]$^+$ ions.

Δ-cisβ and *Λ-cisβ* forms of [CuX(λ-dqdiamine)]$^+$ (X= Cl^-). It is clear that the dissymmetric arrangement of the ligand does not change on complexation in the case of the *Δ-cisβ* form. The steric interaction between alkyl protons of the central chelate bridge and the π-electron cloud of the apically ligated quinoline nuclei seems to be greater in *Λ-cisβ* than in *Δ-cisβ*. Therefore, the *Δ-cisβ* might be more probable than the *Λ-cisβ* in the present complexes. Such behavior is in agreement with the exiton coupling theory. As defined by Bosnich,[14] when the configuration is *Λ*, the negative component of the $\pi^* \leftarrow \pi$ couplet will lie at higher energy, while it will lie at a lower energy when the chirality is *Δ*, the latter corresponding to the present complexes.

The authors wish to express their thanks to Dr. Yoichi Sasaki for his helpful discussions. We also would like to thank Dr. Hiroshi Yokoi for the magnetic measurements.

References

1) a) R. Nast, H. Bier, and J. Grimm, *Z. Anorg. Allg. Chem.*, **309**, 289 (1961); b) K. A. Jensen and P. H. Nielsen, *Acta Chem. Scand.*, **18**, 1 (1964); c) J. C. Fanning and L. T. Taylor, *J. Inorg. Nucl. Chem.*, **27**, 2217 (1965); d) P. H. Nielsen and O. Dahl, *Acta Chem. Scand.*, **20**, 1113 (1966); e) M. R. Litzow, L. F. Power, and A. M. Tait, *J. Chem. Soc., A*, **1970**, 275; f) M. R. Litzow, L. F. Power, and A. M. Tait, *ibid.*, **1970**, 2908; g) M. R. Litzow, L. F. Power, and A. M. Tait, *ibid.*, **1970**, 3226.

2) a) B. Bosnich, *J. Am. Chem. Soc.*, **90**, 627 (1968); b) R. S. Downing and F. L. Urbach, *ibid.*, **90**, 5344 (1968); c) R. S. Downing and F. L. Urbach, *ibid.*, **91**, 5977 (1969); d) R. S. Downing and F. L. Urbach, *ibid.*, **92**, 5861 (1970); e) R. L. Farmer and F. L. Urbach, *Inorg. Chem.*, **11**, 2562 (1970); f) Y. Fujii, T. Isago, M. Sano, N. Yamagishi, S. Hirasawa, and S. Takahashi, *Bull. Chem. Soc. Jpn.*, **49**, 3509 (1976); g) A. Pashini, M. Gullotti, and R. Ugo, *J. Chem. Soc., Dalton Trans.*, **1977**, 346.

3) F. P. Dowyer and F. L. Shulman, *J. Am. Chem. Soc.*, **81**, 290 (1959).

4) F. M. Jaeger and L. Bijkerk, *Z. Anorg. Allg. Chem.*, **233**, 101 (1937).

5) E. S. Stern and C. J. Timmons, "Electronic Absorption Spectroscopy in Organic Chemistry," 3rd ed, Edward Arnold, London (1970), p. 142.

6) J. A. Schellman, *Acc. Chem. Res.*, **1**, 144 (1968).

7) T. Murakami, T. Nozawa, and M. Hatano, *Bull. Chem. Soc. Jpn.*, **46**, 2456 (1973).

8) F. A. Cotton and G. Wilkinson, "Advanced Inorganic Chemistry," 2nd ed, Interscience Publishers, New York (1966), p. 906.

9) T. Murakami and M. Hatano, *Bull. Chem. Soc. Jpn.*, **49**, 3037 (1976).

10) a) M. Goto, M. Saburi, S. Yoshikawa, *Inorg. Chem.*, **8**, 358 (1969); b) R. G. Asperger, *ibid.*, **8**, 2127 (1969); c) B. Bosnich and W. R. Kneen, *ibid.*, **9**, 2191 (1970); d) J. Cragel, Jr., and G. R. Brubaker, *ibid.*, **11**, 303 (1972).

11) J. Lewis and R. A. Walton, *J. Chem. Soc., A*, **1965**, 1559.

12) A. D. Westland, *J. Chem. Soc.*, **1965**, 3060.

13) (*δ,λ*) and (*Δ,Λ*) refer to the chelate-ring conformations and the absolute configurations about a metal ion respectively, as defined in *Inorg. Chem.*, **9**, 1 (1970).

14) B. Bosnich, *Acc. Chem. Res.*, **2**, 266 (1969).

Reaction between Vanadium Trichloride Oxide and Hydrogen Sulfide

Akimasa YAJIMA, Ryoko MATSUZAKI, and Yuzo SAEKI

Research Laboratory of Resources Utilization, Tokyo Institute of Technology, 4259, Nagatsuta-cho, Midori-ku, Yokohama 227

(Received October 3, 1977)

The details of the reaction between vanadium trichloride oxide and hydrogen sulfide were examined at 20 and 60 °C. The main products by the reaction were vanadium dichloride oxide, sulfur, and hydrogen chloride. In addition to these products, small amounts of vanadium trichloride, vanadium tetrachloride, disulfur dichloride, and sulfur dioxide were formed. The formations of the above-mentioned reaction products can be explained as follows: The first stage is the reaction between vanadium trichloride oxide and hydrogen sulfide, $2VOCl_3(l)+H_2S(g)\rightarrow 2VOCl_2(s)+S(s)+2HCl(g)$. Then the resulting sulfur reacts with the unreacted vanadium trichloride oxide, $2VOCl_3(l)+2S(s)\rightarrow 2VOCl_2(s)+S_2Cl_2(l)$. The resulting disulfur dichloride subsequently reacts with the unreacted vanadium trichloride oxide, $2VOCl_3(l)+S_2Cl_2(l)\rightarrow 2VCl_4(l)+S(s)+SO_2(g)$. The resulting vanadium tetrachloride reacts with the sulfur formed during the reaction, $2VCl_4(l)+2S(s)\rightarrow 2VCl_3(s)+S_2Cl_2(l)$, and also reacts with hydrogen sulfide, $2VCl_4(l)+H_2S(g)\rightarrow 2VCl_3(s)+S(s)+2HCl(g)$.

As regards the reaction between vanadium trichloride oxide ($VOCl_3$) and hydrogen sulfide, Ehrlich and Siebert[1] have briefly reported that $VOCl_3$ reacts with hydrogen sulfide to form vanadium dichloride oxide ($VOCl_2$), sulfur, and hydrogen chloride. Also, there have been patents which report that the precipitate formed by the reaction between the $VOCl_3$ dissolved in titanium tetrachloride and hydrogen sulfide consists of vanadium sulfide,[2] and that the precipitate contains vanadium chiefly in the forms of vanadium trichloride (VCl_3) and $VOCl_2$.[3]

In this study, the details of the reaction between $VOCl_3$ and hydrogen sulfide were examined.

Experimental

Materials. The sample of $VOCl_3$ used was prepared by the chlorination of divadium pentaoxide, which had been obtained by the thermal decomposition of guaranteed reagent ammonium metavanadate, in the presence of carbon at 300 °C.[4] Disulfur dichloride(S_2Cl_2) was prepared by the chlorination of guaranteed reagent sulfur.[5] Vanadium tetrachloride(VCl_4) was prepared by the chlorination of high purity vanadium(V 99.8% up) at 500 °C.[6]

Experimental Procedures. The apparatus used for this experiment consisted of a Pyrex reaction vessel of 21 mm inner diameter and 70 mm height with a water-cooled condenser which was connected to a gas absorption unit. 8—9 g of $VOCl_3$ was poured into the reaction vessel and held at 20 or 60 °C in an argon atmosphere. Then pre-dried hydrogen sulfide was introduced into the reaction vessel at a flow-rate of 10 ml/min for a specified period with stirring.

The gaseous hydrogen chloride which formed was absorbed in water. The unreacted $VOCl_3$ containing the liquid product was separated from the solid product by distillation under reduced pressure at room temperature. The solid, liquid, and gaseous products were examined by chemical analysis and X-ray diffractometry.

The possible reactions which were considered to occur on the basis of the above-mentioned experiments, $VOCl_3+S$, $VOCl_3+S_2Cl_2$, VCl_4+S, and VCl_4+H_2S, were examined in the manner described above.

Throughout this work, all the chlorides and chloride oxides were handled in an argon atmosphere or in vacuo to prevent any contamination with moisture.

Analytical. X-Ray analysis of the solid product was performed using Ni filtered Cu radiation. The part of the diffractometer containing the sample was designed to be maintained in a dry nitrogen atmosphere, in order to prevent contamination of the sample with moisture during the irradiation.

Chemical analysis of the sample was performed as follows: The sample was hydrolyzed with dilute nitric acid and filtered. The vanadium content in the filtrate was determined by chelatometric titration,[7] while the chlorine and sulfur contents in the filtrate were gravimetrically determined as AgCl and $BaSO_4$, respectively. The filtered residue, solid sulfur, was dissolved in acetone and determined by titration with 0.05 N sodium cyanate solution.[8]

The gaseous hydrogen chloride which formed was determined gravimetrically as AgCl. The gaseous sulfur dioxide which formed was determined by iodometry after being absorbed in an iodine–potassium iodide solution.

Results and Discussion

Reaction Products for $VOCl_3$ and Hydrogen Sulfide. The reaction between $VOCl_3$ and hydrogen sulfide was examined with special attention given to the reaction product which formed. The variations of the amount of the solid product formed by the reaction between $VOCl_3$ and hydrogen sulfide with the reaction time

Table 1. Experimental results for the reaction between $VOCl_3$ and H_2S

Temp (°C)	$VOCl_3$ used (g)	Product: Solid: Amount (g)	Solid: $VOCl_2$ (%)	Solid: VCl_3 (%)	Solid: S (%)	Liquid: VCl_4 (g)	Liquid: S_2Cl_2 (g)	Gas HCl (g)	Note
20	8.62	5.98	84	6	10	0.05	0.00_8	1.36	Unreacted $VOCl_3$ 1.74 g
60	8.50	6.31	82	8	10	0.04	0.00_5	1.41	Unreacted $VOCl_3$ 1.18 g

were examined at 20 and 60 °C. Using these preliminary experimental results, the reaction products obtained by passing hydrogen sulfide through $VOCl_3$ for 4 h at 20 °C and 3 h at 60 °C were examined. The amounts of the solid products obtained at 20 and 60 °C are shown in Table 1.

The X-ray diffraction diagrams of the solid products obtained at 20 and 60 °C showed them to be a mixture of $VOCl_2$,[9] VCl_3,[10] and sulfur(orthorhombic),[11] as shown in Fig. 1. Chemical analysis gave V 33.0, Cl 47.2, S 10.0% for the product obtained at 20 °C, and V 32.9, Cl 47.6, S 10.0% for the product obtained at 60 °C. The percentages of $VOCl_2$, VCl_3, and S in the solid products, which were calculated from the chemical analysis (Cl base), are shown in Table 1. From these results, it was observed that the constituents of the solid products were almost the same regardless of the reaction temperature.

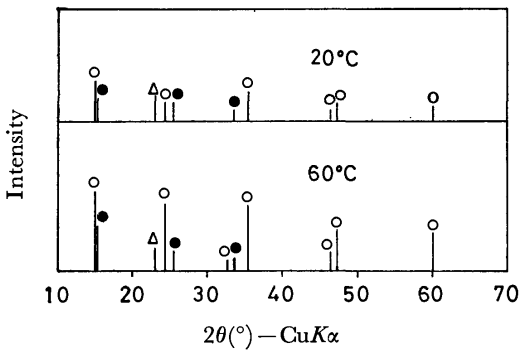

Fig. 1. X-Ray diffraction diagrams of the solid products obtained by the reaction between $VOCl_3$ and H_2S.
○: $VOCl_2$, ●: VCl_3, △: S.

Chemical analysis of the $VOCl_3$ containing the liquid product obtained at 20 and 60 °C gave V 29.1, Cl 61.5, S 0.2%. In the course of the chemical analysis of the sample, a liberation of sulfur was observed on dissolving the sample in dilute nitric acid. This indicated that the $VOCl_3$ contained S_2Cl_2[12] as a reaction product. The atomic ratio of the V content to the Cl content obtained by subtracting the Cl content corresponding to the S_2Cl_2 from the total Cl content was calculated to be $1:3.0_3$. This ratio is lower than the calculated value, 1: 3.00, for $VOCl_3$. The only vanadium chloride in the liquid state at room temperature is VCl_4, except for $VOCl_3$ itself. From these reasons, it was considered that VCl_4 was formed in addition to S_2Cl_2. The amounts of VCl_4, S_2Cl_2, and unreacted $VOCl_3$ are shown in Table 1.

The amounts of gaseous hydrogen chloride which formed during the reaction are also shown in Table 1. In addition, it was observed that a small amount of sulfur was deposited inside the glass line outside the reaction vessel. This fact indicated that sulfur dioxide was formed and reacted with hydrogen sulfide to form sulfur according to the reaction, $SO_2+2H_2S\rightarrow 3S+2H_2O$.[12]

The calculations to obtain the moles of the above-mentioned reaction products, based on the amounts shown in Table 1, showed that $VOCl_2$, sulfur, and hydrogen chloride were the main products and that the molar ratio of $VOCl_2$: S: HCl was approximately 2: 1: 2. From this result, the main reaction which occurred by passing hydrogen sulfide through $VOCl_3$ was found to be the following:

$$2VOCl_3(l) + H_2S(g) \longrightarrow 2VOCl_2(s) + S(s) + 2HCl(g). \quad (1)$$

The formations of small amounts of VCl_4, sulfur dioxide, and S_2Cl_2 were observed as mentioned above. Considering this observation and the description[13] that $VOCl_3$ reacts with sulfur to form VCl_4, SO_2, and $VOCl_2$, it seemed to be probable that the formations of VCl_4, SO_2, and S_2Cl_2 were due to the following reactions, which occurred during the reaction between the unreacted $VOCl_3$ and the sulfur which had formed:

$$2VOCl_3(l) + 2S(s) \longrightarrow 2VOCl_2(s) + S_2Cl_2(l),$$

$$2VOCl_3(l) + S_2Cl_2(l) \longrightarrow 2VCl_4(l) + S(s) + SO_2(g).$$

In addition to the above-mentioned reaction products, VCl_3 was also formed. The formation of VCl_3 was considered to be due to the reactions between the VCl_4 and the sulfur to form VCl_3 and S_2Cl_2, and between the VCl_4 and hydrogen sulfide to form VCl_3, sulfur, and hydrogen chloride.[1]

Side Reactions during the Reaction between $VOCl_3$ and Hydrogen Sulfide. In order to confirm the side reactions which were considered to occur during the reaction between $VOCl_3$ and hydrogen sulfide, experiments on these reactions: $VOCl_3+S$, $VOCl_3+S_2Cl_2$, VCl_4+S, and VCl_4+H_2S, were carried out at 20 °C for 4 h and at 60 °C for 3 h. Solid products were determined by X-ray diffractometry and chemical analysis. Liquid products were determined by chemical analysis in the same manner as described in the previous paragraph.

Experimental conditions and results for the reaction between $VOCl_3$ and sulfur are shown in Table 2.

Table 2. Experimental results for the reaction between $VOCl_3$ and S

Temp (°C)	$VOCl_3$ used (g)	S used (g)	Product: Solid $VOCl_2$ (g)	Product: Liquid S_2Cl_2 (g)	Product: Liquid VCl_4 (g)	Product: Gas SO_2 (g)
20	8.13	1.14	0.06	0.03_1	0.01	0.00_2
60	7.86	1.32	0.07	0.03_7	0.01	0.00_2

From the experimental results described later, the formations of small amounts of VCl_4 and sulfur dioxide may be due to the reaction between the unreacted $VOCl_3$ and the S_2Cl_2 which formed during the reaction. From these results, $VOCl_3$ would seem to react gradually with sulfur to form $VOCl_2$ and S_2Cl_2, as follows:

$$2VOCl_3(l) + 2S(s) \longrightarrow 2VOCl_2(s) + S_2Cl_2(l). \quad (2)$$

The experimental results for the reaction between $VOCl_3$ and S_2Cl_2 are shown in Table 3.

From these results, $VOCl_3$ reacts gradually with S_2Cl_2 to form VCl_4, sulfur, and sulfur dioxide, as

TABLE 3. EXPERIMENTAL RESULTS FOR THE REACTION BETWEEN $VOCl_3$ AND S_2Cl_2

Temp (°C)	$VOCl_3$ used (g)	S_2Cl_2 used (g)	Product: Solid S (g)	Product: Liquid VCl_4 (g)	Product: Gas SO_2 (g)
20	8.43	3.24	0.00_7	0.08	0.01_2
60	8.67	3.13	0.01_0	0.12	0.01_7

follows:

$$2VOCl_3(l) + S_2Cl_2(l) \longrightarrow 2VCl_4(l) + S(s) + SO_2(g). \quad (3)$$

It was also found that the formation of a small amount of sulfur dioxide during the reaction between $VOCl_3$ and hydrogen sulfide, described in the previous paragraph, was due to the reaction between $VOCl_3$ and S_2Cl_2.

Experimental results for the reactions between VCl_4 and sulfur and between VCl_4 and hydrogen sulfide are shown in Tables 4 and 5, respectively.

TABLE 4. EXPERIMENTAL RESULTS FOR THE REACTION BETWEEN VCl_4 AND S

Temp (°C)	VCl_4 used (g)	S used (g)	Product: Solid VCl_3 (g)	Product: Liquid S_2Cl_2 (g)
20	7.78	1.29	5.37	2.30_9
60	7.79	1.30	5.64	2.42_3

TABLE 5. EXPERIMENTAL RESULTS FOR THE REACTION BETWEEN VCl_4 AND H_2S

Temp (°C)	VCl_4 used (g)	Product: Solid VCl_3 (g)	Product: Solid S (g)	Product: Liquid S_2Cl_2 (g)	Product: Gas HCl (g)
20	7.97	5.45	0.41_1	0.21_5	1.15
60	7.86	5.90	0.42_3	0.24_4	1.23

The results shown in Table 4 confirm that the reaction between VCl_4 and sulfur proceeds at an appreciable rate to form VCl_3 and S_2Cl_2, as follows:

$$2VCl_4(l) + 2S(s) \longrightarrow 2VCl_3(l) + S_2Cl_2(l). \quad (4)$$

From the result of the reaction between VCl_4 and sulfur, the small amount of S_2Cl_2 formed during the reaction between VCl_4 and hydrogen sulfide may be due to the reaction between the unreacted VCl_4 and the sulfur which formed. These results confirm that the reaction between VCl_4 and hydrogen sulfide proceeds at an appreciable rate to form VCl_3, sulfur, and hydrogen chloride, as follows:

$$2VCl_4(l) + H_2S(g) \longrightarrow 2VCl_3(s) + S(s) + 2HCl(g). \quad (5)$$

As described in the previous paragraph, $VOCl_2$, sulfur, and hydrogen chloride were formed as the main products by the reaction between $VOCl_3$ and hydrogen sulfide. In addition to these products, small amounts of VCl_3, VCl_4, S_2Cl_2, and sulfur dioxide were formed.

From the above-mentioned experimental results, the formations of the reaction products mentioned above can be explained as follows: The first stage is the reaction between $VOCl_3$ and hydrogen sulfide to form $VOCl_2$, sulfur, and hydrogen chloride according to Reaction 1. Then the resulting sulfur reacts with the unreacted $VOCl_3$ to form $VOCl_2$ and S_2Cl_2 according to Reaction 2. The resulting S_2Cl_2 subsequently reacts with the unreacted $VOCl_3$ to form VCl_4, sulfur, and sulfur dioxide according to Reaction 3. The resulting VCl_4 reacts with the sulfur formed during the reaction to form VCl_3 and S_2Cl_2 according to Reaction 4, and also reacts with hydrogen sulfide to form VCl_3, sulfur, and hydrogen chloride according to Reaction 5.

Consequently, the amonts of VCl_4, VCl_3, S_2Cl_2, and sulfur dioxide are small. Also, since Reactions 4 and 5 proceed at appreciable rates, the amount of VCl_4 is smaller than that of VCl_3.

References

1) P. Ehrlich and W. Siebert, *Z. Anorg. Allg. Chem.*, **302**, 275 (1959).
2) B. De Witt, U. S. Patent., 2370525 (1945).
3) F. Ferrero and G. Sironi, Ger. Offen., 1925291 (1969).
4) Y. Saeki, T. Ōno, and R. Matsuzaki, *Kogyo Kagaku Zasshi*, **74**, 828 (1971).
5) G. Brauer, "Handbuch der Präparativen Anorganishen Chemie," Ferdinand Enke Verlag, Stuttgart (1954), p. 287.
6) C. Starr, F. Bitter, and A. R. Kaufmann, *Phys. Rev.* **58**, 977 (1940).
7) J. Krtil, *Z. Anal. Chem.*, **219**, 412 (1966).
8) D. A. Skoog and J. K. Bartlett, *Anal. Chem.*, **27**, 369 (1955).
9) R. J. Sime, *Z. Krist.*, **124**, 238 (1967).
10) Joint Committee on Powder Diffraction Standards, Powder Diffraction File, 15-382.
11) ASTM Powder Diffraction File, 8-247.
12) R. C. Brasted, "Comprehensive Inorganic Chemistry," Vol. VIII, P. Van Nostrand Co., Inc., Princeton (1961), pp. 43, 92.
13) G. W. Watt and U. Kask, *J. Inorg. Nucl. Chem.*, **27**, 1925 (1965).

Synthesis and Properties of Metal Complexes with 2-Thiophenealdehyde Oxime

Hiro KUMA, Kyoji MOTOBE, and Shoichiro YAMADA

Institute of Chemistry, College of General Education, Osaka University, Toyonaka, Osaka 560

(Received October 17, 1977)

Cobalt(II), nickel(II), copper(II), zinc(II), and manganese(II) complexes with 2-thiophenealdehyde oxime have been prepared and characterized mainly on the basis of electronic spectra and magnetic data. The cobalt(II) and nickel(II) complexes isolated are of the general formulae: (A) $MX_2(oxime)_4$ (X=Cl, Br); (B) $M(NCS)_2(oxime)_2$. These compounds and $ZnCl_2(oxime)_4$ are all six-coordinated, and the complexes (B) are probably multinuclear. Copper(II) and manganese(II) form complexes of the formula $MX_2(oxime)_2$ (X=Cl, Br). Possible structures for these complexes are also discussed. 2-Thiophenealdehyde oxime is unidentate in all these complexes, being coordinated through the nitrogen atom.

In the course of studies on metal complexes with oximes,[1] the present authors happened to obtain cobalt(II), nickel(II), and zinc(II) complexes with 2-thiophenealdehyde oxime, which had composition different from that of previously reported complexes with this ligand.[2] Reinvestigation, therefore, was undertaken in order to examine these and related complexes in more detail. The present paper describes synthesis and characterization of 3d transition metal complexes with 2-thiophenealdehyde oxime, which is abbreviated as tox in the present paper.

Experimental

Materials. 2-Thiophenealdehyde oxime was prepared as reported previously.[3]

Analytical data of the metal complexes prepared in the present work are given in Table 1.

Dihalogenotetrakis(2-thiophenealdehyde oxime)cobalt(II), $CoX_2(tox)_4$ (X=Cl, Br). Cobalt(II) halide hexahydrate (0.01 mol) was added to a solution of 2-thiophenealdehyde oxime (0.04 mol) in ethanol (100 ml) at 65—70 °C. The reaction was continued with stirring under reflux for about two hours. The solution was filtered and allowed to stand overnight at room temperature. Yellow-brown (X=Cl) or brown (X=Br) crystals were collected by filtration and recrystallized from methanol.

$Co(NCS)_2(tox)_2$ was prepared in a manner analogous to the dihalogeno-complexes. A yellow-brown crystalline precipitate was washed with chloroform. The compound is insoluble in common organic solvents.

Dihalogenotetrakis(2-thiophenealdehyde oxime)nickel(II). *$NiX_2(tox)_4$ (X=Cl, Br)* were prepared as yellow-green crystals in a manner similar to the corresponding cobalt(II) complexes. Recrystallization was carried out from methanol.

$Ni(NCS)_2(tox)_2$. 2-Thiophenealdehyde oxime (0.03 mol) was added to a solution of $Ni(NCS)_2$ (0.01 mol) in ethanol (100 ml). The reaction was continued with stirring under reflux for about 2 h at 65—70 °C. A pale green crystalline precipitate was washed with chloroform. The compound is almost insoluble in common organic solvents.

Dichlorotetrakis(2-thiophenealdehyde oxime)zinc(II) was prepared as colorless microcrystals by a method similar to the correspoding cobalt(II) complex.

$CuX_2(tox)_2$ (X=Cl, Br) were obtained as yellow-brown (X=Cl) and brown (X=Br) crystals in a manner analogous to $CoX_2(tox)_4$. The product was recrystallized from methanol.

$MnCl_2(tox)_2$ was obtained as pale-yellow crystals in a manner analogous to the corresponding copper(II) complex. Recrystallization was carried out from methanol.

$MnBr_2(tox)_2$ was prepared as pale-yellow microcrystals in a manner similar to the chloride analogue.

Measurements. Electronic absorption spectra of the complexes were measured on a Shimadzu MPS-50L spectrophotometer. Infrared spectra were recorded as Nujol mulls using a Hitachi EPI-S2 infrared spectrophotometer and a Hitachi 215 infrared spectrophotometer.

Magnetic mesurements were carried out at room temperature by the Gouy method. Powder X-ray diffraction patterns were obtained with a Rigakudenki 4001-A2 diffractometer using Co K_α radiation and an iron filter.

TABLE 1. ANALYTICAL DATA OF METAL COMPLEXES WITH 2-THIOPHENEALDEHYDE OXIME

Compound	Found, %			Calcd, %			μ
	C	H	N	C	H	N	
$NiCl_2(tox)_4$	37.33	3.50	8.68	37.63	3.16	8.78	3.21
$NiBr_2(tox)_4$	32.90	2.95	8.02	33.05	2.77	7.71	3.15
$Ni(NCS)_2(tox)_2$	33.48	2.42	13.25	33.60	2.35	13.31	3.22
$CoCl_2(tox)_4$	37.26	3.35	8.64	37.61	3.15	8.78	5.14
$CoBr_2(tox)_4$	32.63	3.06	7.76	33.04	2.77	7.71	5.15
$Co(NCS)_2(tox)_2$	33.38	2.38	13.28	33.58	2.35	13.06	4.95
$ZnCl_2(tox)_4$	36.94	3.26	8.91	37.28	3.13	8.70	dia
$CuCl_2(tox)_2$	30.99	2.54	7.12	30.89	2.59	7.20	1.92
$CuBr_2(tox)_2$	25.15	2.26	5.86	25.15	2.11	5.86	1.85
$MnCl_2(tox)_2$	31.72	2.85	7.44	31.59	2.65	7.37	6.05
$MnBr_2(tox)_2$	25.60	2.15	6.01	25.61	2.15	5.98	5.96

μ: BM at room temperature

Results and Discussion

Nickel(II) Complexes. A compound of composition $NiCl_2(tox)_2$ was reported previously.[2] In the present work, however, this complex could not be isolated, but instead complexes of the formula $NiX_2(tox)_4$, X being Cl and Br, were obtained.

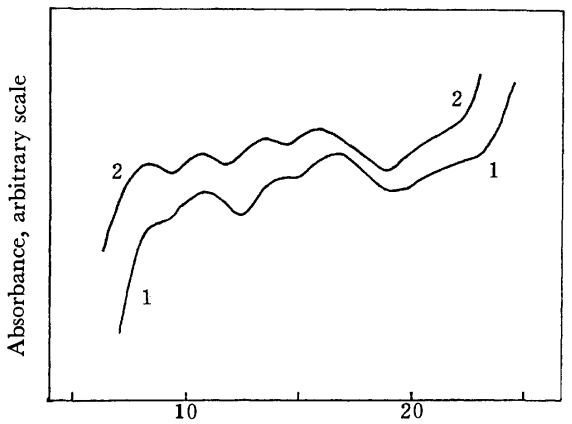

Fig. 1. Electronic absorption spectra of *trans*-dihalogenotetrakis(2-thiophenaldehyde oxime)nickel(II), *trans*-$[NiX_2(tox)_4]$, in Nujol: 1, X=Cl; 2, X=Br.

These nickel(II) complexes prepared are paramagnetic and of a high spin type (Table 1). The electronic absorption spectrum of $NiCl_2(tox)_4$ is very similar to those of *trans*-$NiCl_2(acox)_4$ and *trans*-$NiCl_2(bzox)_4$,[1] where acox and bzox denote acetaldehyde oxime and benzaldehyde oxime, respectively (Fig. 1). It is presumed that $NiCl_2(tox)_4$ has a similar structure to that of *trans*-$NiCl_2(acox)_4$, namely a six-coordinate *trans*-dichloro-structure, in which the oxime molecules are bound as unidentate ligands with the nickel(II) ion through the nitrogen atom.[1,4] It is also concluded that $NiBr_2(tox)_4$ has a six-coordinate *trans*-dibromo-structure, since its powder X-ray diffraction pattern is very similar to that of $NiCl_2(tox)_4$. In agreement with this, electronic absorption spectrum of $NiBr_2(tox)_4$ bears a close resemblance to that of *trans*-$NiBr_2(acox)_4$ (Fig. 1).[1] It is thus found that in these dihalogeno-nickel(II) complexes the ligands tox are bound with the nickel(II) ion as unidentate ligands through their nitrogen atom.

TABLE 2. BAND SPLITTING AND CRYSTAL FIELD PARAMETERS OF *trans*-$[NiX_2(tox)_4]$ IN 10^3 cm^{-1}

	X=Cl	X=Br
ν ($^3E_g^a \leftarrow {}^3B_{1g}$)	8.7	8.2
ν ($^3B_{2g} \leftarrow {}^3B_{1g}$)	10.8	10.7
ν ($^3A_{2g} \leftarrow {}^3B_{1g}$)	14.3	13.4
ν ($^3E_g^b \leftarrow {}^3B_{1g}$)	16.6	16.0
Dq^{xy}	1.08	1.07
Dq^z	0.66	0.57
Dt	0.24	0.29
Ds	0.43	0.49

The approximate symmetry of *trans*-$NiX_2(tox)_4$ is D_{4h}. Six-coordinate nickel(II) complexes of O_h symmetry show three spin-allowed d-d bands, each of which is split into two components as the symmetry of the complexes changes from O_h to D_{4h}. The band splitting observed in the spectra of $NiX_2(tox)_4$ is so remarkable that it is possible to obtain the components of the two main d-d bands from the magnitude of the splitting. The maxima of the components are shown in Table 2. From these data and using expressions derived on the basis of crystal field approximation,[5,6] values for Dq^{xy}, Dq^z, Ds, and Dt were estimated and shown in Table 2.

Comparison of the results with previous data[1,5,6] gives the following order as to the in-plane crystal field parameter: py>tox>acox>bzal$\gg$tu, where py and tu denote pyridine and thiourea, respectively. It is thus found that tox, acox, and bzox are close to py and much higher than tu in the spectrochemical series. A marked difference between tox and tu seems to be in agreement with the assumption that tox is coordinated as a unidentate ligand through its nitrogen atom with the nickel(II) ion; tu is known to be coordinated through the sulfur atom.

TABLE 3. ABSORPTION MAXIMA (in 10^3 cm^{-1}) OF METAL-(II) COMPLEXES WITH 2-THIOPHENEALDEHYDE OXIME IN NUJOL

Compound	ν
$Ni(NCS)_2(tox)_2$	8.7, 16.4
$Ni(NCS)_2(acox)_2$	8.6, 16.5
$CoCl_2(tox)_4$	8.8, 15.3 sh, 18.6
$CoBr_2(tox)_4$	8.7, 14.8 sh, 18.3
$Co(NCS)_2(tox)_2$	9.1, 15.5 sh, 18.7

sh: shoulder. Band assignment may be made as previously reported in Ref. 1 in the text.

The complex $Ni(NCS)_2(tox)_2$ is paramagnetic with a moment of 3.2 BM, and its electronic absorption spectrum is typical of the six-coordinate nickel(II) complex (Table 3). This complex shows infrared ν(C–N) and ν(C–S) vibration at 2120 and 770 cm^{-1}, respectively. These values, which are close to those of $Ni(NCS)_2(acox)_2$, lie in the range expected for the bridging NCS group.[7] It is most likely that $Ni(NCS)_2(tox)_2$ has a similar structure to that of $Ni(NCS)_2(acox)_2$, which was concluded to have a multinuclear structure with six-coordinate nickel(II) ions and bridging NCS ions.[1]

Just as in the nickel(II) complexes with acetaldehyde oxime and benzaldehyde oxime,[1] the dihalogeno-nickel-(II) complexes with 2-thiophenealdehyde oxime show hydrogen-bonded OH stretching vibrations at about 3180—3200 cm^{-1}, while $Ni(NCS)_2(tox)_2$ shows a sharp OH band at a much higher frequency, indicative of the presence of the non-hydrogen-bonded NOH group.

Cobalt(II) and Zinc(II) Complexes. Previously reported $CoCl_2(tox)_2$ and $ZnCl_2(tox)_2$[2] were not isolated, but only $CoX_2(tox)_4$ and $ZnCl_2(tox)_4$, X being Cl and Br, were obtained in the present work. The complexes $CoX_2(tox)_4$ are paramagnetic with magnetic

moments of about 5.1 BM, which are in the range expected for the six-coordinate cobalt(II) complexes. Their electronic absorption spectra are also typical of the six-coordinate cobalt(II) complexes (Table 3).

The powder X-ray diffraction patterns of $CoCl_2(tox)_4$ and $CoBr_2(tox)_4$ are very similar to those of the corresponding dichloro- and dibromo-nickel(II) analogues, respectively. Therefore, the complexes $CoX_2(tox)_4$ have a six-coordinate *trans*-dihalogeno-structure, in which the ligands tox are coordinated as unidentate ligands to the metal ion through the nitrogen atom, the sulfur atom in tox not being bound to the metal ion.

In a similar way $ZnCl_2(tox)_4$ has a *trans*-dihalogeno-structure, since its powder X-ray diffraction pattern is very similar to those of $CoCl_2(tox)_4$ and $NiCl_2(tox)_4$.

The complex $Co(NCS)_2(tox)_2$ shows a powder X-ray diffraction pattern, which is very similar to that of $Ni(NCS)_2(tox)_2$. Therefore, the cobalt(II) complex probably has a similar structure to that of the nickel(II) analogue, namely a multinuclear structure, in which the metal ions assume six-coordination with the NCS groups as bridges, just as in $Ni(NCS)_2(acox)_2$.[1] The cobalt(II) complex $Co(NCS)_2(tox)_2$ is paramagnetic with a magnetic moment of 4.95 BM, which lies in the range expected for the six-coordinate cobalt(II) complex. Its electronic spectrum is also in agreement with the six-coordinate stereochemistry. Its infrared ν(C–N) and ν(C–S) vibrations appear at 2110 and 775 cm^{-1}, respectively. The values indicate the presence of the bridging NCS group on the basis of the previously proposed criteria.[7]

Exactly like the corresponding nickel(II) complex, $CoX_2(tox)_4$ exhibit hydrogen-bonded OH stretching vibrations at about 3190—3200 cm^{-1}, while $Co(NCS)_2(tox)_2$ shows a sharp OH band at a much higher frequency, suggesting the presence of the non-hydrogen-bonded NOH group. This finding is similar to that of the corresponding complexes with acox and bzox.[1]

Copper(II) and Manganese(II) Complexes. Two copper(II) complexes $CuX_2(tox)_2$ were obtained in the present work, X being Cl and Br. One of them (X=Cl) had been reported previously.[2] In view of the results on the corresponding cobalt(II) and nickel(II)complexes, it may be reasonable to assume that tox is coordinated as a unidentate ligand through its nitrogen atom in the complexes $CuX_2(tox)_2$. Billing and Underhill[8] examined correlation between electronic absorption spectra and stereochemistry of complexes of the type CuX_2L_2, L being pyridine and its derivatives. On the basis of their conclusions, the stereochemistry of $CuX_2(acox)_2$ and $CuX_2(bzox)_2$ was discussed in a previous paper.[1]

The electronic spectra of $CuX_2(tox)_2$ have the first d-d band at about 14.3×10^3 cm^{-1}. The maxima are close to those of the multinuclear complexes $CuX_2(acox)_2$, $CuX_2(bzox)_2$, and $CuX_2(py)_2$.[1,8] According to the criteria reported previously,[1,8] and in view of the present finding that tox lies close to acox, bzox, and py in the spectrochemical series, the electronic spectra seem to indicate that $CuX_2(tox)_2$ most probably have a structure similar to that of the multinuclear forms of $CuX_2(acox)_2$, $CuX_2(bzox)_2$, and $CuX_2(py)_2$, in which the copper(II) ions are six-coordinated with halide ions as bridges.

The powder X-ray diffraction patterns of $MnCl_2(tox)_2$ and $MnBr_2(tox)_2$ are very similar to those of the corresponding dichloro- and dibromo-copper(II) analogues, respectively. It is most likely that the complexes $MnX_2(tox)_2$ may have a structure similar to that of the multinuclear $CuX_2(tox)_2$, the manganese(II) ions being in the six-coordinated environment with the halide ions as bridges. A similar structure was reported previously for $MnX_2(py)_2$.[9]

Table 4. Maxima of main d-d absorption bands and of some infrared bands of copper(II) complexes with 2-thiophenealdehyde oxime

Compound	d-d band, 10^3 cm^{-1}	Infrared bands, cm^{-1}	
		ν (M–L)	ν (M–X)
$CuCl_2(tox)_2$	14.3	272	310, 223
$CuBr_2(tox)_2$	14.3	262	221, 203
$CuCl_2(acox)_2$	14.8	272	296, 235
$CuBr_2(acox)_2$	14.8	259	243, 208
$CuCl_2(py)_2$	14.5	268	294, 235[a]
$CuBr_2(py)_2$	14.6	269	255, 202[a]
$MnCl_2(tox)_2$		213	232
$MnBr_2(tox)_2$		210	<200
$MnCl_2(py)_2$		212	233[a]
$MnBr_2(py)_2$		212	<200[a]

a) Infrared data are taken from Ref. 9 in the text.

Their infrared ν(M–X) and ν(M–L) bands also seem to correspond well to those of multinuclear $CuX_2(py)_2$, $CuX_2(acox)_2$, and $MnX_2(py)_2$ (Table 4).

The present authors are grateful to Professor Masayoshi Obashi for powder X-ray diffraction patterns.

References

1) H. Tanaka, H. Kuma, and S. Yamada, *Bull. Chem. Soc. Jpn.*, **50**, 3259 (1977).
2) M. P. Coakley and M. E. Casey, *J. Inorg. Nucl. Chem.*, **34**, 1937 (1972).
3) A. Biedermann, *Ber.*, **19**, 1854 (1886).
4) M. E. Stone, B. E. Robertson, and E. Stanley, *J. Chem. Soc., A*, **1971**, 3632.
5) A. B. P. Lever, *Coord. Chem. Rev.*, **3**, 119 (1968).
6) C. R. Hare and C. J. Ballhausen, *J. Chem. Phys.*, **40**, 788 (1964).
7) S. M. Nelson and T. M. Shepherd, *J. Inorg. Nucl. Chem.*, **27**, 2123 (1965).
8) D. E. Billing and A. E. Underhill, *J. Inorg. Nucl. Chem.*, **30**, 2147 (1968).
9) R. J. H. Clark and C. S. Williams, *Inorg. Chem.*, **4**, 350 (1965).

The Crystal Structure of Iron Particles Dispersed in a Glasslike Carbon Matrix

Mamoru OMORI,* Toshio HIRAI,* and Seishi YAJIMA
The Oarai Branch, The Research Institute for Iron, Steel and Other Metals, Tohoku University, Oarai, Ibaraki 311-13
(Received October 24, 1977)

Ultra-fine iron particles were dispersed in a glasslike carbon matrix by the heat treatment of acetylferrocene-furfural resins. The dispersed iron particles were investigated by means of X-ray and electron diffraction analyses and by means of electron microscopy. In resins heat-treated at 400 °C, iron particles of varying diameters were observed by means of electron microscopy. The crystal structure of the iron particles was analyzed by means of X-ray and electron diffractions. Finely subdivided iron particles were identified as hexagonal, close-packed (hcp) and expanded, body-centered cubic (bcc) irons. The hcp iron is the high-pressure phase of iron metal. The ultra-fine iron particles were coagulated to larger particles by heat treatment above 400 °C. The size of their unit cell was the same as that of standard bcc iron.

Considerable interest is being devoted to the study of ultra-fine particles of metals and metal compounds because many of their properties are essentially different from those in the bulk state. Fine particles are prepared by means of the evaporation and condensation of metal in an inert gas at a low pressure. In the fine particles of chromium (>100 Å), a new class of crystals has been observed.[1,2] As the particle size of ferromagnetic material is reduced to a diameter of 10—100 Å, it shows a ferromagnetic-to-superparamagnetic transition. By the use of ferromagnets dispersed in glass and zeorite matrices, their superparamagnetic behavior has been investigated.[3-7] Ultra-fine particles of iron and cobalt, less than about 30 Å in diameter, which have been prepared by electrodeposition onto mercury, are superparamagnetic.[8,9] Superparamagnetic cobalt particles (<14 Å) are prepared by precipitation into Cu–2%Co alloy.[10,11] Ultra-fine nickel particles (<50 Å) are reduced from $Ni(NO_3)_2$ in a silica gel and are superparamagnetic.[12,13] Ferrite particles whose diameters are less than about 100 Å have superparamagnetic properties.[14,15] Moreover, atomic metals have been prepared in the matrices of inert gas from the vapour of metals at the temperature of liquid helium.[16-18]

As has been reported in previous papers, ultra-fine iron particles have been prepared in a glasslike carbon matrix by the heat treatment of acetylferrocene–furfural resins.[19-21] Their particle size varies with the iron content in the resin. The dispersion of iron particles is markedly related to the resin structure. The ultra-fine particles are not prepared by the heat treatment of ferrocene–phenol resin, which is different in structure from the acetylferrocene–furfural resin.[22] The glasslike carbon is stable at elevated temperatures, and does not show any strong peaks in X-ray and electron diffractions. Its absorption coefficient for X-rays and an electron beam is small, since it is an amorphous compound consisting of carbon, hydrogen, and oxygen. Therefore, the iron particles dispersed in the glasslike carbon matrix are favorable for the X-ray and electron diffraction analyses and for electron-microscopic observations.

In the present investigation, the crystal structure and size of iron particles dispersed in the glasslike carbon matrix were studied in detail. The iron atoms were liberated from ferrocene skeletons in the acetylferrocene-furfural resin by heat treatment at 400 °C. The liberated iron coagulated to ultra-fine iron particles of various sizes. The ultra-fine iron particles were coagulated in the glasslike carbon matrix by the irradiation of the electron beam and by heat treatment above 400 °C. The crystal structure of these iron particles was then analyzed by means of X-ray and electron diffractions. The size and shape of the particles were observed by means of an electron microscope.

Experimental

Preparation and Pyrolysis of Resins. The synthesis of acetylferrocene–furfural resin was described in a previous paper.[23] When the molar ratio of furfural (F) to acetylferrocene (A) in the starting material exceeded the F/A ratio of 15, the resin was not obtained. Acetone was added to the starting material containing furfural a more than the F/A ratio of 15. The furfural (1 mol) was mixed with 0.2 mol of acetylferrocene and acetone. To the mixture, concentrated sulfuric acid was then added until it amounted to 4 wt% of the total weight of furfural, acetylferrocene, and acetone. The subsequent treatment to get the resin was done in the way reported previously.[23] The resin was heated in an electric furnace under a vacuum as follows: 100—350 °C, 3.5 h; 350—400 °C, 2 h; 400—1500 °C, 100 °C/h. The heating was stopped at the desired maximum temperature. The heat-treated resin was then cooled to room temperature in an electric furnace. The heat-treated resin in a vacuum container was placed in the glovebox replaced with argon gas. The following operating procedures were carried out in the glovebox. The heat-treated resin was ground to powder using an agate mortar and a pestle. For X-ray diffraction measurements, the fine powdered sample, which had been passed through a 325-mesh screen, was loaded into a thin glass capillary and then sealed with silicone grease. The powdered sample for electron-microscopic measurements was placed in a glass tube filled with anhydrous hexane and then sealed with a rubber cap.

Elemental Analysis and Measurement of Properties. The determination of the iron was carried out with a Hitachi-207 atomic absorption spectrophotometer. The apparent densities were calculated from the weight and size of the resins.

* Present address: The Research Institute for Iron, Steel and Other Metals, Tohoku University, Sendai 980.

Table 1. Polycondensation of acetylferrocene and furfural

	Molar concentration			Elemental analysis (wt %)			Density (g/cm^3)
	Acetylferrocene	Furfural	Acetone	Fe	C	H	
2-Resin	1	2	0	12.2	64.98	4.29	1.43
5-Resin	1	5	0	9.08	64.01	3.77	1.43
10-Resin	1	10	0	7.51	62.50	3.95	1.02
20-Resin	1	20	3	3.14	63.56	4.01	0.976
30-Resin	1	30	5	2.26	63.65	3.91	0.968
40-Resin	1	40	7	1.67	62.16	3.49	0.973
100-Resin	1	100	19	0.81	63.16	3.62	0.947
Furan resin	0	5	1	0	63.04	3.11	0.946

The X-ray diffraction patterns were recorded on a Rigaku Geigerflex diffractometer using a Debye-Scherrer camera, Fe $K\alpha$ radiation, and a Mo filter. Electron-microscopic observation was carried out by using a JEM-100B transmission electron microscope at a direct magnification of 150000.

Results and Discussion

The synthetic results for acetylferrocene–furfural resins are summarized in Table 1. The structure of acetylferrocene–furfural resin has already been elucidated.[23] Ferrocene skeletones form a main chain in the structure. It is evident that the resin is stable above 300 °C, since the IR spectrum of resin does not change up to 300 °C. Upon heating the resin at 400 °C, though, all the absorption bands in the IR spectrum disappear.[23] Therefore, the resin can be concluded to be destroyed and converted into a glasslike carbon containing iron. It seems likely that the iron atom in the ferrocene skeleton is liberated and then forms an iron metal or its compound. When ferrocene is pyrolyzed above 400 °C, the iron metal is liberated from it. The liberated iron does not react with carbon, since iron carbides are not detected in the pyrolyzed product.[24] Moreover, body-centered cubic (bcc) iron is the only product when a graphite–$FeCl_3$ intercalate compound is heated at 950 K for 3 h.[25] Therefore, iron carbides are not produced from the liberated iron in the heat-treated resin. In addition, the formation of iron oxides has to be taken into account, since the glasslike carbon contains oxygen. It is well known that an iron monoxide is reduced with carbon at 350 °C *in vacuo*.[26] Therefore, it was considered that the liberated iron did not react *in vacuo* with the oxygen contained in the glasslike carbon. In the heat-treated resins, 10-Resin heat-treated at 400 °C [10-Resin (400 °C)] was pyrophoric on exposure to air. However, the pyrophoric phenomenon was not observed in the resin heat-treated above 400 °C. As is shown in Table 2, the quantity of hydrogen and oxygen in heat-treated resins decreased with an increase in the heat-treatment temperature, in a manner analogous to that of heat-treated glasslike carbons.[27] The iron contents of heat-treated resins increased with an increase in the heat-treatment temperatures (400—1200 °C). However, the iron contents of resins (1500 °C) decreased compared with those of resins (1200 °C). The decrease in the iron content was due to the higher vapour pressure of iron metal than that of carbon at high temperatures.[28]

Electron-microscopic Observation. The transmission electron micrographs of resins (400 °C) are shown in Photo. 1: Micrographs (1-1 and 1-2) correspond to the bright-field image of 2-Resin (400 °C); 1-3, 1-4, 1-5, 1-6, and 1-7, to the bright-field images of 10-, 10-, 30-, 40-, and 100-Resins (400 °C) respectively. The transmission electron micrograph (1-8) is based on Furan resin (400 °C). In the micrograph (1-1), iron particles 10—25 Å in diameter were uniformly dispersed, while larger iron particles (30—150 Å) were only thinly scattered. These iron particles coagulated upon irradiation by a strong electron beam, as is shown in Photo. 1-2. The coagulation of iron particles was due to the heat generated by the irradiation of the electron beam. In the case of 5-Resin (400 °C), the uniform dispersion of iron particles (10—25 Å) was similar to that of 2-Resin (400 °C). This uniform dispersion can be observed in

Table 2. Elemental analysis of heat-treated resins (wt %)

Sample	Heat treatment (°C)											
	400			800			1200			1500		
	Fe	C	H	Fe	C	H	Fe	C	H	Fe	C	H
2-Resin	13.20	69.07	3.68	19.1	76.01	0.61	21.2	76.43	0.15	19.1	80.49	0.06
5-Resin	10.60	71.08	3.22	13.8	80.54	0.63	15.6	81.31	0.33	15.9	83.27	0.07
10-Resin	7.96	72.01	3.58	12.1	81.01	0.50	12.9	81.90	0.29	11.7	87.96	0.09
20-Resin	3.65	73.33	3.65	4.47	87.01	0.71	6.45	88.20	0.31	5.87	93.55	0.02
30-Resin	2.54	75.06	3.77	4.13	87.31	0.51	4.45	90.12	0.16	3.32	95.77	0.03
40-Resin	2.06	76.36	3.69	3.41	87.87	0.66	3.50	91.40	0.21	2.90	96.23	0.09
100-Resin	1.00	77.14	3.78	1.10	89.90	0.61	1.82	93.28	0.31	0.98	98.43	0.10

the micrograph (1-3) of 10-Resin (400 °C). However, iron particles of irregular sizes (10—150 Å) were dispersed in the other part of the 10-Resin (400 °C), as is shown in Photo. 1-4. Since the density of 10-Resin was less than that of 2- and 5-Resins, the coagulation of iron must be greatly affected by the small difference in the heating temperature in the resin. Iron particles of irregular sizes (10—100 Å) were also observed in the glasslike carbon matrix of 30-Resin (400 °C). However, the number of iron particles in it was less than in 10-Resin (400 °C). No iron particles were found in the glasslike carbon of 40-Resin (400 °C), as is shown in Photo. 1-6. This indicates that the iron particles are subdivided into finer particles less than about 10 Å in diameter and which cannot be detected by means of the electron microscope. In the case of 100-Resin (400 °C), the iron particles were similarly less than about 10 Å in diameter. The transmission electron micrographs of 40- and 100-Resins (400 °C) were the same as that of Furan resin (400 °C). The size of the iron particles, as observed by means of the electron microscope, is shown in Table 3. The iron

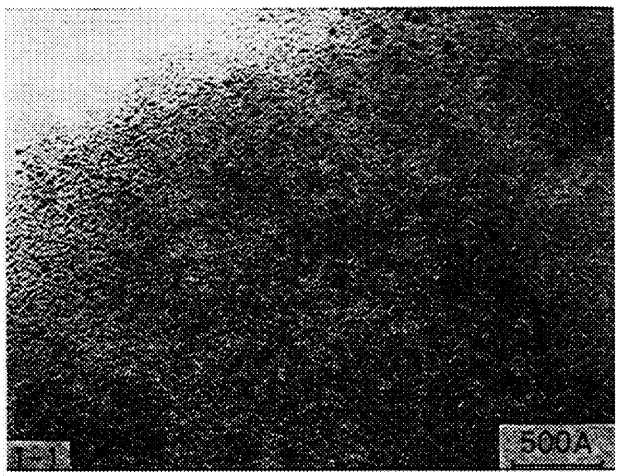

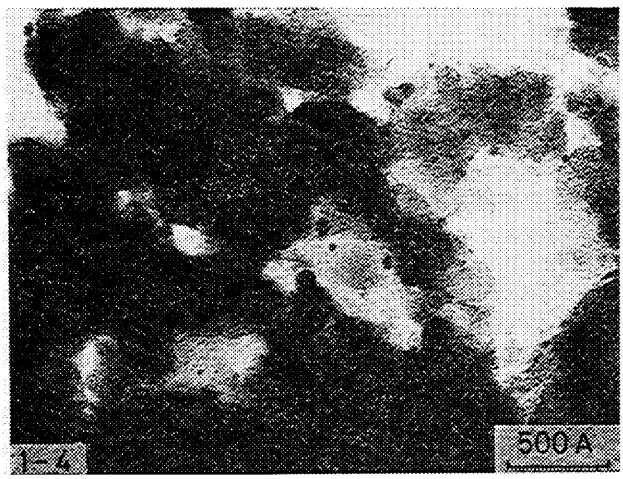

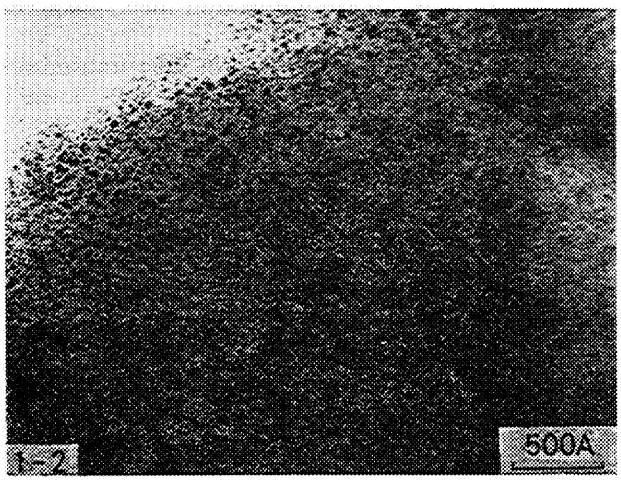

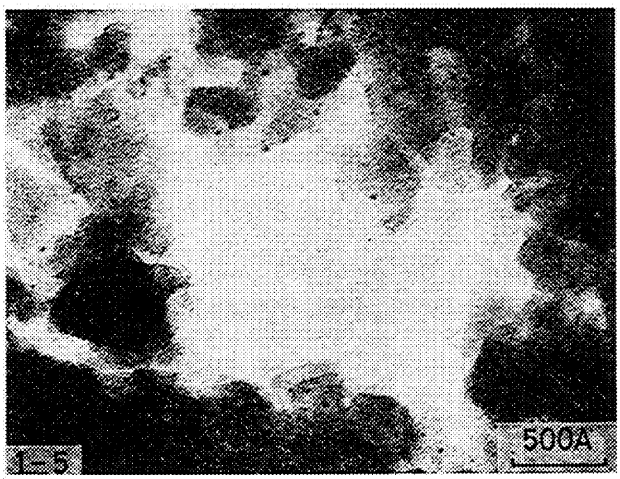

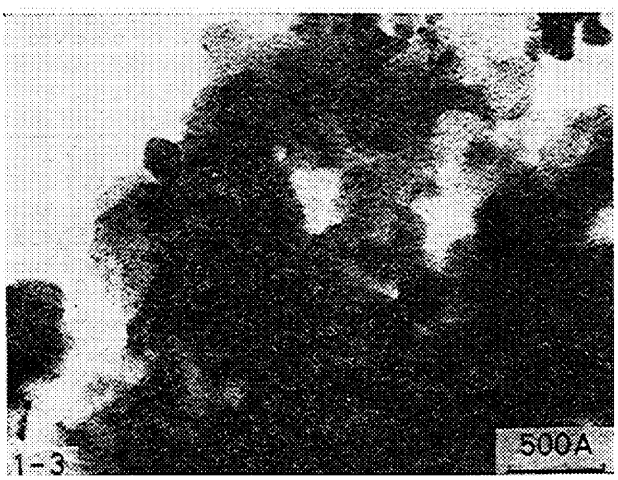

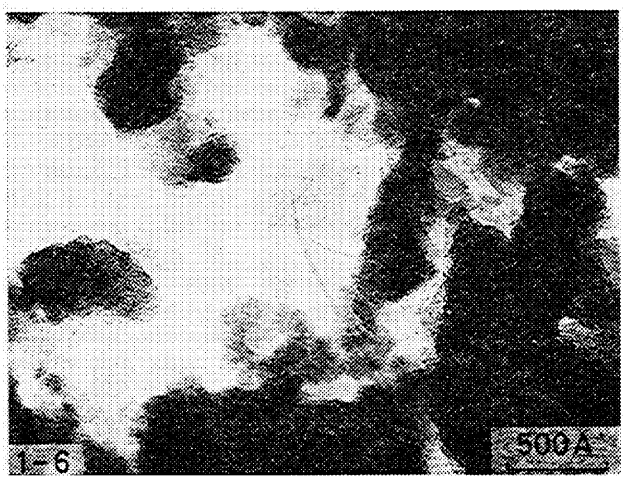

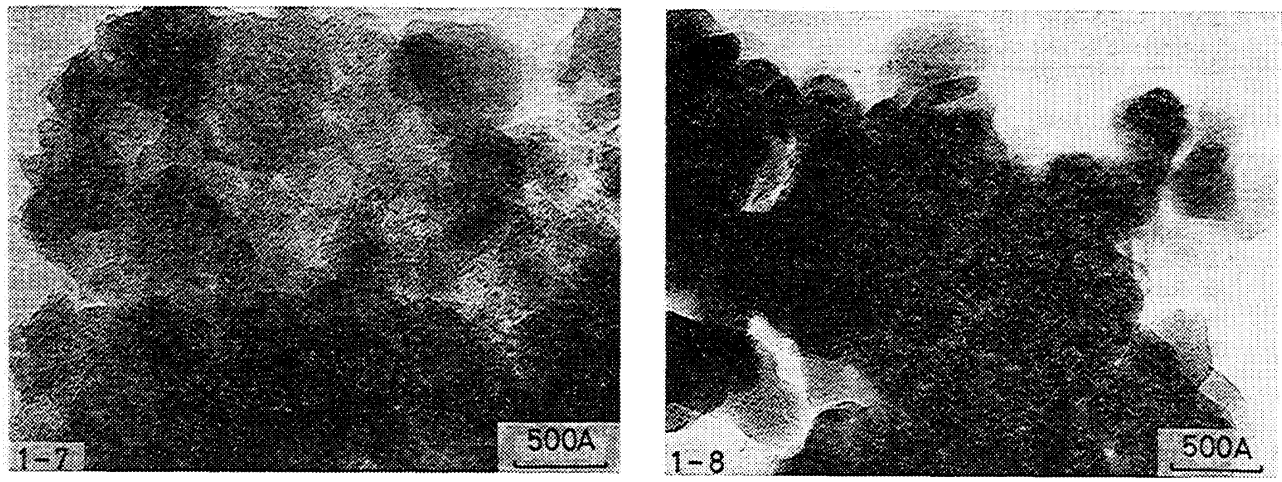

Photo. 1. Transmission electron micrographs of resins heat-treated at 400 °C. (1-1): 2-Resin, (1-2): 2-Resin irradiated with electron beam, (1-3): 10-Resin, (1-4): 10-Resin, (1-5): 30-Resin, (1-6): 40-Resin, (1-7): 100-Resin, (1-8): Furan resin.

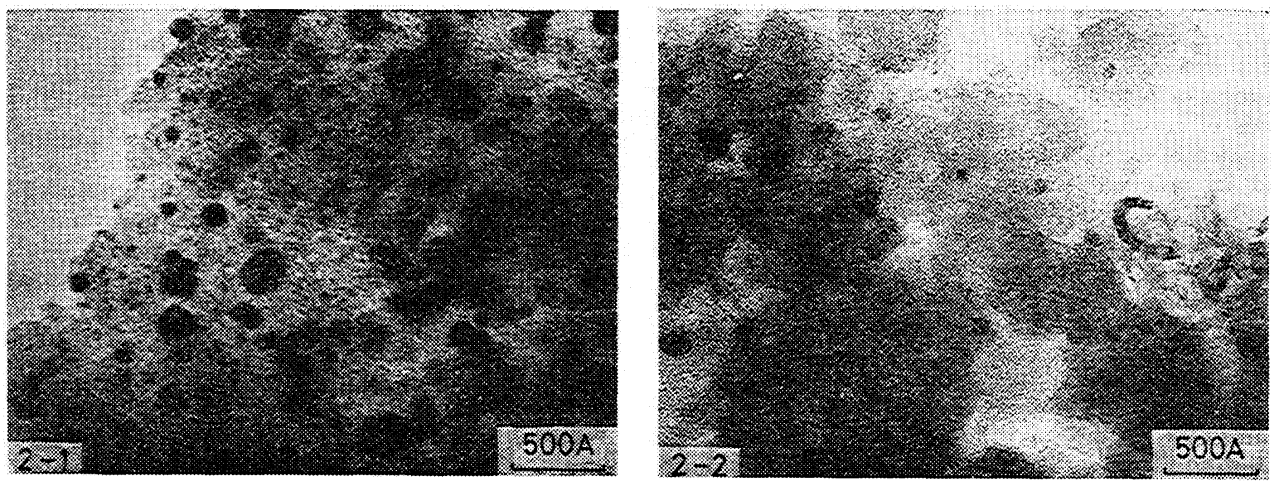

Photo. 2. Transmission electron micrographs of resins heat-treated at 800 °C. (2-1): 2-Resin, (2-2): 100-Resin.

particles in resins (400 °C) did not coagulate to large particles, and their diameters were less than about 200 Å, as is shown in Table 3. Transmission electron micrographs of 2-Resin (800 °C) and 100-Resin (800 °C) are shown in Photo. 2 (2-1, 2-2). The iron particles which were not detected in 100-Resin (400 °C) were observed in 100-Resin (800 °C) as particles 30—200 Å in diameter. The uniformly dispersed iron particles (10—25 Å) coagulated to larger ones with a diameter of more than about 30 Å in 2- to 10-Resins (800 °C). The iron particles of the resins became larger in size than those of the resins, as is shown in Table 3. The pyrophoric phenomenon was due to the presence of the ultra-fine particles less than 200 Å in diameter. The reason for the pyrophoric phenomenon of 10-Resin was explained by the density being lower than those of 2- and 5-Resins and the iron content being higher than those of 20- to 100-Resins. The number of iron particles observed in 30- to 100-Resins (800 °C) was small, but was greater than that of iron particles (30—200 Å) in 2- to 30-Resins (400 °C). The size of the iron particles increased with an increase in the heat-treatment temperature from 1200 to 1500 °C, as is shown in Table 3. The largest iron particles, with a diameter of about 1000 Å, were observed in 10- and 30-Resins (1500 °C). In another resin (1500 °C), the iron particles were not able to coagulate to such large particles. The smallest particles of 2- to 5-Resins (1200 and 1500 °C) were less than those of other resins (1200 and 1500 °C), despite their high iron contents. These results show that the iron particles are finely subdivided in a glasslike carbon matrix, even at high temperatures. The dense glasslike carbon prepared from 2- to 5-Resins was

Table 3. Size of iron particles in heat-treated resins (Å)

Sample	Heat treatment (°C)			
	400	800	1200	1500
2-Resin	10—150	30—200	50—250	50—600
5-Resin	10—200	30—400	50—400	50—500
10-Resin	10—150	30—500	100—600	100—1000
30-Resin	10—100	30—100	100—600	100—1000
40-Resin	<10	30—100	100—500	100—500
100-Resin	<10	30—200	100—200	100—500

Table 4. X-Ray analysis of iron particles dispersed in the glasslike carbon matrix

Sample	Heat treatment (°C)			
	400	800	1200	1500
2-Resin	$\alpha'+\varepsilon$	α	α	α
5-Resin	$\alpha'+\varepsilon$	α	α	α
10-Resin	$\alpha'+\varepsilon$	α	α	α
20-Resin	—	α	α	α
30-Resin	—	—	α	α
40-Resin	—	—	α	α
100-Resin	—	—	α	α

α': expanded bcc Fe, $a_0=2.95$. α: bcc Fe, $a_0=2.86$—2.87. ε: hcp Fe, $a_0=3.30$, $c_0=5.21$.

excellent in its dispersion of iron particles. The observed iron particles were nearly spherical. No characteristic shape related to the crystal structure was found.

Structural Analysis. The crystal structure of iron particles dispersed in the glasslike carbon matrix was analyzed using the X-ray diffraction data. The results are summarized in Table 4. In the X-ray diffraction patterns of 2- to 10-Resins (400 °C), lines based on two kinds of crystals were observed. One of the crystals consisted of expanded, body-centered cubic (bcc) iron, and its unit cell was $a_0=2.95$, larger than that of standard bcc iron (Ref. 29, $a_0=2.8664$). The other crystal consisted of hexagonal, close-packed (hcp) iron. The hcp iron is a high-pressure phase.[30] In the X-ray diffraction of the high-pressure-phase iron, the six diffraction lines are interpreted as being 101, 100, 110, 112, 002, and 103.[31] As is shown in Table 5, these lines

Table 5. X-ray diffraction data of the ultra-fine iron particle in 2- to 10-resins (400 °C)

d(Å)	(hkl)
2.85	(100)
2.61	(002)
2.51	(101)
1.61	(110)
1.48	(103)
1.39	(112)
1.30	(004)
1.10	(203)

were also observed in the X-ray diffraction pattern of ultra-fine iron. Moreover, two extra lines in it corresponded to the 004 and 203 lines. In the diffraction pattern of the 2- to 10-Resins (400 °C), the 110 line of hcp iron overlapped with the 200 line of the expanded bcc iron. The size of the unit cell of the high-pressure phase varies with the pressure: $a=2.465$, $c=4.050$, $c/a=1.643$ at 150 kbars; $a=2.421$, $c=3.828$, $c/a=1.580$ at 400 kbars.[31] At an atmospheric pressure of 1, the hcp phase of the binary Fe–C alloy has been prepared by means of a splat quenching; $a_0=2.502$, $c/a=1.643$.[32] The unit-cell size of ultra-fine hcp iron was $a_0=3.30$ and $c_0=5.21$ ($c/a=1.58$). The unit cell of ultra-fine iron was larger than those of the high-pressure phase and the binary alloy. However, the c/a ratio was similar to those of these hcp phases. For 20- to 100-Resins (400 °C), no diffraction lines were observed except for a broad line in the vicinity of $2\theta=50°$. The broad line was thought to be due to the glasslike carbon, since the same line was observed in Furan resin (400 °C). The few iron particles (10—150 Å) that were observed in 20- to 30-Resins (400 °C) did not contribute to the X-ray diffraction line. The line due to the bcc phase was observed in 2- to 20-Resins (800 °C). Its unit-cell size was $a_0=2.86$—2.87, equal to that of the standard bcc iron. While the iron particle was observed in 30- to 100-Resins (800 °C), the diffraction line of the iron particles was not obtained. The iron particles did not coagulate enough to give an X-ray diffraction pattern in these resins. The broad line due to the glasslike carbon was, however, present in these resins (800 °C). X-ray diffraction confirmed the presence of standard bcc iron in 2- to 100-Resins (1200° and 1500 °C), although the iron content of 100-Resin (1500 °C) was lower than 1%. In these resins the iron particles coagulated to become a large iron particle which was adequate for the X-ray diffraction. In 2- to 10-Resins (400 °C), the number of iron particles (30—200 Å) was less than that of 30- to 100-Resins (800 °C). It is most likely that the iron particles (30—200 Å) in 2- to 10-Resins (400 °C) do not reveal any diffraction lines. Therefore, the hcp and expanded bcc irons are interpreted as being iron particles with diameters 10—25 Å. According to the similarity in crystal structure, it is reasonable to imagine that the iron particles grow in this order; the hcp iron, the expanded bcc iron, and the standard bcc iron.

Table 6. Electron-diffraction analysis of iron particles dispersed in heat-treated resins

Sample	Heat treatment (°C)			
	400	800	1200	1500
2-Resin	R+S	R+S	R+S	R+S
5-Resin	R+S	R+S	R+S	R+S
10-Resin	—	R+S	R+S	R+S
20-Resin	—	R+S	R+S	R+S
30-Resin	—	R+S	R+S	R+S
40-Resin	—	R+S	R+S	R+S
100-Resin	—	R+S	R+S	R+S

R: diffraction ring. S: diffraction spot.

The results of the electron-diffraction analysis are shown in Table 6. In the electron-diffraction profiles of 2- and 5-Resins (400 °C), diffraction rings of both hcp iron and expanded bcc iron were observed. Both rings consisted of diffraction spots. The precise dimensions of the unit cell could not be calculated from the diffraction ring. The appearance of spots suggested that the hcp and expanded bcc irons were a single crystal or a polycrystalline. Since their crystal size was less than 25 Å, it was concluded that the polycrystalline could not be formed. In 10- to 100-Resins (400 °C), there existed only a broad ring instead of the diffraction ring

based on the hcp and expanded bcc irons. The broad ring was due to the glasslike carbon. In 30- to 100-Resins (800 °C), the crystal structure of ultra-fine iron particles which were not clarified by the X-ray diffraction analysis was identified as that of the standard bcc iron. The diffraction rings and spots due to the standard bcc iron were observed in all resins (800 to 1500 °C), as is shown in Table 6.

These results lead to the following conclusions. The ultra-fine iron particles are prepared by the heat treatment of acetylferrocene-furfural resin *in vacuo*. The hcp and expanded bcc irons are identified in the ultra-fine iron particles prepared at 400 °C. The unit cell of hcp iron was larger than that of iron metal under a high pressure. Upon heating, both hcp and expanded bcc iron particles coagulate to larger particles to form the standard bcc iron.

The authors would like to thank Mr. Tsutomu Shoji and Mrs. Hide Arai, Tohoku University, for their cooperation in the iron and CH analyses. Thanks are also due to Messrs. Haruo Yotsumoto and Eiichi Watanabe of the Japan Electron Optics Laboratory for their assistance in the electron-microscopic observation.

References

1) K. Kimoto, I. Nishida, and R. Uyeda, *J. Phys. Soc. Jpn.*, **20**, 1963 (1965).
2) K. Kimoto and I. Nishida, *J. Phys. Soc. Jpn.*, **22**, 744 (1967).
3) C. R. Bamford, *Phys. Chem. Glasses*, **3**, 54 (1962).
4) M. O'Horo and R. Steinitz, *Mater. Res. Bull.*, **3**, 117 (1968).
5) L. N. Mulay, D. W. Collins, and W. Fisher, Jr., *Jpn. J. Appl. Phys.*, **6**, 1342 (1967).
6) D. W. Collins and L. N. Mulay, *J. Am. Ceram. Soc.*, **53**, 74 (1970).
7) R. W. J. Wedd, B. V. Liengme, J. C. Scott, and J. R. Sams, *Solid State Commun.*, **7**, 1091 (1969).
8) W. Henning and E. Vogt, *J. Phys. Rad.*, **20**, 277 (1959).
9) F. E. Luborsky and P. E. Lawrence, *J. Appl. Phys.*, **32**, 231S (1961).
10) L. Weil and L. Gruner, *C. R. Acad. Sci.*, **243**, 1629 (1956).
11) J. J. Becker, *Trans. Am. Inst. Metal. Eng.*, **209**, 59 (1957).
12) D. Schultze, *Naturwissenschaften*, **6**, 128 (1960).
13) C. R. Abeledo and P. W. Selwood, *J. Appl. Phys.*, **32**, 229S (1961).
14) A. E. Berkowitz and W. J. Schuele, *J. Appl. Phys.*, **30**, 134S (1959).
15) W. J. Schuele and V. D. Deetscreek, *J. Appl. Phys.*, **32**, 235S (1961).
16) T. K. McNab, H. Micklitz, and P. H. Barrett, *Phys. Rev. B*, **4**, 3787 (1971).
17) H. Micklitz and P. H. Barrett, *Phys. Rev. B*, **5**, 1704 (1972).
18) H. Micklitz and P. H. Barrett, *Phys. Rev. Lett.*, **28**, 1547 (1972).
19) S. Yajima and M. Omori, *Chem. Lett.*, **1972**, 843.
20) S. Yajima and M. Omori, *Chem. Lett.*, **1974**, 277.
21) S. Yajima and M. Omori, *Nature*, **267**, 823 (1977).
22) M. Omori, K. Nagashima, and S. Yajima, *Bull. Chem. Soc. Jpn.*, **50**, 1157 (1977).
23) M. Omori, M. Kurono, and S. Yajima, *Bull. Chem. Soc. Jpn.*, **48**, 1291 (1975).
24) B. Ya, Andreev, L. M. Dyagileva, and G. I. Feklisov, *Dokl. Akad. Nauk SSSR*, **158**, 1348 (1964).
25) M. J. Tricker, E. L. Evans, P. Cadman, N. C. Davies, and B. Bach, *Carbon*, **12**, 499 (1974).
26) A. M. Aksay, "Vacuum Metallurgy," ed by R. F. Bunshah, Reinhold Publishing Co., New York (1958).
27) H. Honda, Y. Sanada, T. Furuta, and H. Teranishi, *Tanso*, No. 46, 2 (1966).
28) D. R. Stull, *Ind. Eng. Chem.*, **39**, 517 (1947).
29) ASTM Powder Diffraction File, No. 6-0696.
30) E. P. Bundy, *J. Appl. Phys.*, **36**, 616 (1965).
31) R. L. Clendenen and H. G. Drickamer, *J. Phys. Chem. Solids*, **25**, 865 (1964).
32) R. C. Ruhl and M. Cohen, *Trans. Met. Soc. AIME*, **245**, 241 (1969).

Pyrolytic Sulfurization Gas Chromatography. II.[1] Simple Determination of the Correction Factors Using Five Standard Compounds

Tadashi HARA, Kaoru FUJINAGA, and Katsuya TSUJI

Department of Applied Chemistry, Faculty of Engineering, Doshisha University, Karasuma Imadegawa, Kamigyo-ku, Kyoto 602

(Received September 12, 1977)

An improvement has been made in the pyrolytic sulfurization gas chromatographic method, by which the atomic ratio between C, H, O, and N in a sample can be simultaneously determined. Analysis was carried out by use of the correction factors instead of calibration curves. Correction factors were obtained by use of five standard compounds, naphthalene, thiourea, cyanoguanidine, sucrose, and amidosulfuric acid. The method is simple, accurate, and applicable to various compounds.

In order to establish a new elemental analysis method by which several elements can be simultaneously determined, a combustion technique in sulfur (S) vapor instead of the conventional one in oxygen (O) atmosphere was proposed.[1] The individual elements in a sample were converted as follows: carbon (C) to carbon dioxide (CO_2), carbonyl sulfide (COS), and carbon disulfide (CS_2), hydrogen (H) to hydrogen sulfide (H_2S), O to CO_2 and COS and nitrogen (N) to nitrogen molecule (N_2). The products were determined by gas chromatography. The chemical composition of the original compound was estimated by dividing each peak area of N_2, C-, and O-containing compounds by the peak area of H_2S, and by applying the calibration curves between H and C or O or N to the quotients. In order to find the sum of individual peak areas of C- and O-containing compounds, the relation between the peak areas of CO_2, COS, and CS_2 and their mole numbers was used, the correction factors of CO_2, COS, and CS_2 being obtained from the reaction between carbon monoxide (CO) and S.

Since the chemical composition was determined by the calibration curves obtained from four compounds and the correction factors obtained by the reaction between pure CO and S, the method was not always simple and convenient.

The present method is much more convenient as compared with the previous one. Five compounds, naphthalene, thiourea, cyanoguanidine, sucrose, and amidosulfuric acid were chosen as standard and the correction factors of the individual products to H_2S were obtained on the assumption that each peak area of the products corresponds to their mole numbers in the original compound. The method is characterized by obtaining all the correction factors by five times of analysis and by estimating the weight ratio of each atom by a simple calculation using the correction factors. The method is applicable to various compounds and reasonable results are obtained.

Experimental

Apparatus and Reagents. The sampler and displacement apparatus were similar to those previously used. A transparent quartz tube, 2.5 mm i.d., 3.5 mm o.d., and 110 mm long, was used after treatment similar to that in the previous procedure. Gas chromatograms were taken on Shimadzu GC-4B and GC-4C. Naphthalene, thiourea, sucrose, and cyanoguanidine were of reagent grade for elemental analysis, and the other reagents were of analytical grade.

Procedure. The procedure was similar to that given in the previous paper except for placing the sample in a reaction tube and keeping it in a desiccator overnight.

Detection of water as a product could not be carried out by combination of the silica gel column and the molecular sieve 5A column in the previous experiment. However, it could be achieved by connecting a 0.25 m Chromosorb 104 (80—100 mesh) column with a 1.75 m Porapak Q (80—100 mesh) column in series and by raising temperature at a rate of 20 °C/min over 80—185 °C. Under these conditions, N_2, CO_2, H_2S, COS, H_2O, SO_2, and CS_2 were separated satisfactorily. Though the separation of CO from N_2 was difficult, it was found that the amount of CO evolved was negligible.

Results and Discussion

Correction Factors. The relationship between the constituent atoms of standard compounds and the products by the reaction is as follows: Naphthalene (C, H) to CS_2 and H_2S; thiourea and cyanoguanidine (C, H, N) to CS_2, H_2S, and N_2; sucrose (C, H, O) to CS_2, H_2S, CO_2, and COS; amidosulfuric acid (N, H, O) to H_2S, N_2, H_2O, and SO_2. Assuming that each peak area of the compounds corresponds to their mole numbers in the original compound, we obtain

$$\left(\frac{C}{H}\right)_t = \frac{K(CS_2)A(CS_2)}{2K(H_2S)A(H_2S)} = \frac{K(CS_2)A(CS_2)}{2A(H_2S)}, \quad (1)$$

$$\left(\frac{N}{H}\right)_t = \frac{K(N_2)A(N_2)}{K(H_2S)A(H_2S)} = \frac{K(N_2)A(N_2)}{A(H_2S)}, \quad (2)$$

$$\left(\frac{C}{H}\right)_t = \frac{K(CO_2)A(CO_2)+K(COS)A(COS)+K(CS_2)A(CS_2)}{2K(H_2S)A(H_2S)}, \quad (3)$$

$$\left(\frac{O}{H}\right)_t = \frac{2K(CO_2)A(CO_2)+K(COS)A(COS)}{2K(H_2S)A(H_2S)}, \quad (4)$$

$$\left(\frac{N}{H}\right)_t = \frac{K(N_2)A(N_2)}{K(H_2S)A(H_2S)+K(H_2O)A(H_2O)}, \quad (5)$$

$$\left(\frac{O}{H}\right)_t = \frac{2K(SO_2)A(SO_2)+K(H_2O)A(H_2O)}{2[K(H_2S)A(H_2S)+K(H_2O)A(H_2O)]}, \quad (6)$$

where $A(CS_2)$, $A(H_2S)$, $A(N_2)$, $A(CO_2)$, $A(COS)$, $A(SO_2)$, and $A(H_2O)$ are referred to the individual peak area and $(C/H)_t$, $(N/H)_t$, and $(O/H)_t$ to the theoretical atomic ratios in individual compounds. Each correction factor was obtained on the basis of $K(H_2S)=1.00$.

Table 1. Correction factors

Standard compound	Correction factor						
	$K(N_2)$	$K(CO_2)$	$K(H_2S)$	$K(COS)$	$K(H_2O)$	$K(SO_2)$	$K(CS_2)$
Naphthalene			1.00				0.609
Thiourea	1.26		1.00				0.600
Cyanoguanidine	1.18		1.00				0.601
Sucrose		1.10	1.00	0.712			
Amidosulfuric acid			1.00		2.33	0.816	
Average	1.22	1.10	1.00	0.712	2.33	0.816	0.603

Table 2. Calculation of the content of C, H, O, and N

Element	Product	Mole ratio	Weight ratio	Content %
N	N_2	$K(N_2)A(N_2)=1.22A(N_2)$	$M(N_2)K(N_2)A(N_2)=28.014[1.22A(N_2)]$	Obtained from Eq. 7
C	CO_2	$K(CO_2)A(CO_2)=1.10A(CO_2)$	$M(CO_2)K(CO_2)A(CO_2)=44.009[1.10A(CO_2)]$	
	COS	$K(COS)A(COS)=0.712A(COS)$	$M(COS)K(COS)A(COS)=28.010[0.712A(COS)]$	Obtained from Eq. 8
	CS_2	$K(CS_2)A(CS_2)=0.603A(CS_2)$	$M(CS_2)K(CS_2)A(CS_2)=12.011[0.603A(CS_2)]$	
H	H_2S	$K(H_2S)A(H_2S)=1.00A(H_2S)$	$M(H_2S)K(H_2S)A(H_2S)=2.016A(H_2S)$	Obtained from Eq. 9
	H_2O	$K(H_2O)A(H_2O)=2.33A(H_2O)$	$M(H_2O)K(H_2O)A(H_2O)=18.015[2.33A(H_2O)]$	
O	CO_2	$1.10A(CO_2)$	$44.009[1.10A(CO_2)]$	
	COS	$0.712A(COS)$	$28.010[0.712A(COS)]$	Obtained from Eq. 10
	H_2O	$2.33A(H_2O)$	$18.015[2.33A(H_2O)]$	
	SO_2	$K(SO_2)A(SO_2)=0.816A(SO_2)$	$M(SO_2)K(SO_2)A(SO_2)=31.998[0.816A(SO_2)]$	

The correction factor of CS_2, $K(CS_2)$, was calculated by Eq. 1 from the results of naphthalene, thiourea, and cyanoguanidine, and that of N_2 similarly by Eq. 2 from the results of thiourea and cyanoguanidine. $K(CO_2)$ and $K(COS)$ were obtained by Eqs. 3 and 4 from the results of sucrose, and $K(H_2O)$ and $K(SO_2)$ by Eqs. 5 and 6 from the results of amidosulfuric acid. All the correction factors (Table 1) were used in the following analysis.

Determination of the Atomic Ratio of Compounds. The atomic ratio between C, H, O, and N was calculated by use of the chromatogram data (Table 2). The mole ratios between the individual products were found by multiplying the correction factors by the peak areas. The weight ratios between the individual products were obtained by multiplying the above mole ratios by the molecular weights obtained by substracting the weight of S from the molecular weight of the products, the weight ratios of the individual products to all the products being found.

As seen from Eqs. 7—10, the weight ratios between the individual elements were obtained by multiplying the weight ratio of the desired element in the products by the weight ratios and by summing them up.

$$N_{wt\%}=\left[\frac{2E(N)}{M(N_2)}\frac{M(N_2)K(N_2)A(N_2)}{n}\right]\times 100=\left[28.014\frac{1.22A(N_2)}{n}\right]\times 100, \tag{7}$$

$$\begin{aligned}C_{wt\%}&=\left[\frac{E(C)}{M(CO_2)}\frac{M(CO_2)K(CO_2)A(CO_2)}{n}+\frac{E(C)}{M(COS)}\frac{M(COS)K(COS)A(COS)}{n}\right.\\&\quad\left.+\frac{E(C)}{M(CS_2)}\frac{M(CS_2)K(CS_2)A(CS_2)}{n}\right]\times 100\\&=\left[12.011\times\frac{1.10A(CO_2)+0.712A(COS)+0.603A(CS_2)}{n}\right]\times 100,\end{aligned} \tag{8}$$

$$\begin{aligned}H_{wt\%}&=\left[\frac{2E(H)}{M(H_2S)}\frac{M(H_2S)K(H_2S)A(H_2S)}{n}+\frac{2E(H)}{M(H_2O)}\frac{M(H_2O)K(H_2O)A(H_2O)}{n}\right]\times 100\\&=\left[2.016\times\frac{A(H_2S)+2.33A(H_2O)}{n}\right]\times 100,\end{aligned} \tag{9}$$

$$\begin{aligned}O_{wt\%}&=\left[\frac{2E(O)}{M(CO_2)}\frac{M(CO_2)K(CO_2)A(CO_2)}{n}+\frac{E(O)}{M(COS)}\frac{M(COS)K(COS)A(COS)}{n}\right.\\&\quad\left.+\frac{E(O)}{M(H_2O)}\frac{M(H_2O)K(H_2O)A(H_2O)}{n}+\frac{2E(O)}{M(SO_2)}\frac{M(SO_2)K(SO_2)A(SO_2)}{n}\right]\times 100\\&=\left[\frac{2[1.10A(CO_2)]+0.712A(COS)+2.33A(H_2O)+2[0.816A(SO_2)]}{n}\times 15.999\right]\times 100,\end{aligned} \tag{10}$$

TABLE 3. ANALYTICAL RESULTS OF AMINO ACIDS AND CARBOXYLIC ACIDS

Sample	C wt%			H wt%			O wt%			N wt%		
	Theor.	Exptl.	Error	Theor.	Exptl.	Erorr	Theor.	Exptl.	Error	Theor.	Exptl.	Error
Glycine	32.00	32.68	0.68	6.71	6.76	0.05	42.63	41.86	−0.77	18.66	18.70	0.04
γ-Aminobutyric acid	46.59	46.59	0	8.80	9.02	0.22	31.03	30.99	−0.04	13.58	13.40	−0.18
L-Phenylalanine	65.43	65.08	−0.35	6.71	6.71	0	19.37	19.58	0.19	8.48	8.63	0.15
L-Tryptophan	64.69	64.12	−0.57	5.92	5.63	−0.29	15.67	16.23	0.56	13.72	14.02	0.30
L-Citrulline	41.14	41.71	0.57	7.48	7.39	−0.09	27.40	27.18	−0.22	23.99	23.72	−0.27
L-Methionine[a)]	51.26	51.20	−0.06	9.46	9.41	−0.05	27.31	27.55	0.24	11.96	11.83	−0.13
L-Aspartic acid	36.10	36.12	0.02	5.30	5.19	−0.11	48.08	47.77	−0.31	10.52	10.92	0.40
L-Glutamic acid	40.82	41.10	0.28	6.17	5.93	−0.24	43.50	43.82	0.32	9.52	9.15	−0.37
L-Homoserine	40.33	40.73	0.40	7.62	7.42	−0.20	40.29	39.47	−0.82	11.76	12.38	0.62
Malonic acid	34.63	34.67	0.04	3.87	3.74	−0.13	61.50	61.59	0.09			
Fumaric acid	41.39	40.88	−0.51	3.47	3.43	−0.04	55.14	55.69	0.55			
Succinic acid	40.68	40.59	−0.09	5.12	4.98	−0.14	54.20	54.43	0.23			
Suberic acid	55.16	54.75	−0.41	8.10	8.13	0.03	36.74	37.12	0.38			
Lauric acid	71.95	71.98	0.03	12.08	12.05	−0.03	15.97	15.97	0			
Myristic acid	73.63	73.07	−0.56	12.36	12.64	0.28	14.01	14.28	0.27			
Palmitic acid	74.94	74.12	−0.82	12.58	12.73	0.15	12.48	13.14	0.66			
Stearic acid	75.99	75.14	−0.85	12.76	13.08	0.32	11.25	11.78	0.53			
Terephthalic acid	57.84	57.61	−0.23	3.64	3.52	−0.12	38.52	38.87	0.35			

a) Since S atom could not be determined, it was neglected in the composition of methionine.

where n is referred to the sum of the weight ratios, $M(N_2)$, $M(CO_2)$, $M(COS)$, $M(H_2S)$, $M(H_2O)$, $M(SO_2)$, and $M(CS_2)$ to the molecular weight of each compound, and $E(N)$, $E(C)$, $E(H)$, and $E(O)$ to the atomic weight of each element.

Analysis of Various Compounds. Various amino acids and carboxylic acids were analyzed (Table 3). The accuracy of the present method is similar to that of the former. However, an erroneous result is obtained when the carbon content is high. This seems to be due to the tailing phenomena with an increasing amount of CS_2 and the subsequent and incorrect reading of the chromatogram. The former method is applicable only to compounds containing H, but the present method is applicable even to H-free inorganic compounds.

Compounds other than amino acids and carboxylic acids were analyzed (Table 4). In the previous experiment, the compounds containing nitro group and phenols gave erratic results owing to the formation of water. However, in the present experiment, good results were obtained which agree with the theoretical values. This is due to the fact that no water is formed. It was concluded that the difference resulted from the different oxygen uptake of the two chromatographs, Shimadzu GC-4B and GC-4C, and the oxygen uptake by an apparatus from air took place during charge of the next sample after completion of analysis. It is remarkable in a new apparatus. The oxygen uptake by a new apparatus is minimized by treating a stainless steel tube with an aqueous solution of water glass or disodium

TABLE 4. ANALYTICAL RESULTS OF THE OTHER COMPOUNDS

Sample	C wt%			H wt%			N wt%			O wt%		
	Theor.	Exptl.	Error	Theor.	Exptl.	Error	Theor.	Exptl.	Error	Theor.	Exptl.	Error
meso-Erythritol	39.34	39.19	−0.15	8.25	8.44	0.19	52.41	52.37	−0.04			
Dimethylglyoxime	41.37	40.87	−0.50	6.94	6.92	−0.02	27.56	27.31	−0.25	24.13	24.89	0.76
Diphenylglyoxime	69.99	69.61	−0.38	5.03	5.28	0.25	13.32	13.34	0.02	11.66	11.77	0.11
p-Dimethylamino-benzaldehyde	72.46	71.67	−0.79	7.43	7.88	0.45	10.72	10.93	0.21	9.39	9.53	0.14
Benzophenone	85.69	84.80	−0.89	5.53	5.87	0.34	8.78	9.33	0.55			
Benzil	79.98	79.55	−0.43	4.80	4.79	−0.01	15.22	15.65	0.43			
2,2′-Bipyridine	76.90	76.11	−0.79	5.16	5.26	0.10				17.94	18.63	0.69
Myristyl alcohol	78.43	77.58	−0.85	14.11	14.91	0.80	7.46	7.51	0.05			
2,2′,3,3′,4,4′,5,5′,6-Nonamethyldiphenylmethane	89.73	89.11	−0.62	10.27	10.89	0.62						
2,6-Dimethylphenol	78.65	79.18	0.53	8.25	8.33	0.08	13.10	12.49	−0.61			
8-Quinolinol	74.47	73.71	−0.76	4.86	4.99	0.13	11.02	11.16	0.14	9.65	10.14	0.49
m-Nitroaniline	52.17	51.59	−0.58	4.38	4.42	0.04	23.17	23.29	0.12	20.28	20.71	0.43

Table 5. Analytical results of acetates

Sample	Structural formula	C wt%			H wt%			O wt%		
		Theor.	Exptl.	Error	Theor.	Exptl.	Error	Theor.	Exptl.	Error
Sodium acetate	CH_3COONa	40.68	40.31	−0.37	5.12	5.02	−0.10	54.19	54.67	0.47
Potassium acetate	CH_3COOK	40.68	40.34	−0.34	5.12	5.23	0.11	54.19	54.43	0.24
Magnesium acetate	$Mg(CH_3COO)_24H_2O$	25.27	27.89	2.62	7.42	7.64	0.22	67.31	64.48	−2.83
Calcium acetate	$Ca(CH_3COO)_2H_2O$	35.30	35.85	0.55	5.92	5.68	−0.24	58.78	58.47	−0.31
Strontium acetate	$Sr(CH_3COO)_21/2H_2O$	37.80	38.32	0.52	5.55	5.27	−0.28	56.65	56.41	−0.24
Barium acetate	$Ba(CH_3COO)_2$	40.68	40.86	0.18	5.12	5.02	−0.10	54.19	54.12	−0.07

hydrogenphosphate.

The analytical results of sodium 1-naphthalenesulfonate did not agree with the theoretical values as in the previous work. This is attributed to the purity of a sample judging from the results of gravimetric analysis of sodium and sulfur.

The accuracy in the determination of C, H, O, and N is shown by the following standard deviation: σ_C= 0.46, σ_H=0.24, σ_O=0.39, and σ_N=0.36%. Though five compounds were chosen as standard, they could be reduced to three if accuracy of the analysis including the reading of the chromatogram is improved.

Analysis of Acetates. The acetates of alkali and alkaline earth metal were analyzed (Table 5). No analysis could be carried out for lithium acetate since the reaction tube containing lithium acetate exploded during the course of reaction. Of the alkaline earth metal acetates, magnesium acetate gave a considerable error. This shows that magnesium, differing from other alkaline earth metals, has a larger affinity to oxygen than to sulfur. This is understandable if we take into consideration $\Delta G°$=49.16kJ/mol at 1200 K for the formation of magnesium sulfide.[2]

References

1) K. Tsuji, K. Fujinaga, and T. Hara, *Bull. Chem. Soc. Jpn.*, **50**, 2292 (1977). Part 1.

2) I. Barin and O. Knacke, "Thermochemical Properties of Inorganic Substances," Springer-Verlag, Berlin (1973), p. 441.

The Stereochemistry of 3-Hydroxy-2-methylbutyric Acid

Akira TAI and Motomasa IMAIDA

Division of Organic Chemistry, Institute for Protein Research, Osaka University, Yamada-kami, Suita, Osaka 565

(Received May 13, 1977)

Four stereoisomers of methyl 3-hydroxy-2-methylbutyrate (I), (+)-*threo*-I, (−)-*threo*-I, (+)-*erythro*-I, and (−)-*erythro*-I, were prepared, and their absolute configurations were determined. The configurations of (+)-*threo*-I, $[\alpha]_D^{20}$ +36.80° (*c* 5, methanol) and (+)-*erythro*-I, $[\alpha]_D^{20}$ +14.32° (*c*, 5, methanol) were assigned to (2*S*, 3*S*) and (2*S*, 3*R*) respectively.

The present work was undertaken in connection with two other studies. One is the study of the stereo-differentiating (asymmetric) hydrogenation of methyl 2-methyl-3-oxobutyrate (III) into methyl 3-hydroxy-2-methylbutyrate (I) over an asymmetrically modified nickel catalyst.[1] In this study, the determinations of $[\alpha]_D$ and the absolute configuration of each stereoisomer of I are essential for the evaluation of the reaction. The other is the study of the stereochemistry of the CH_3–CH(OH)–CH(CH_3)– group of sex pheromones of sawflies.[2]

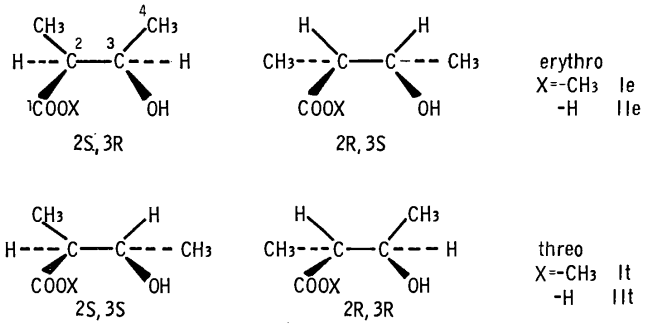

Fig. 1.

The configurations of four stereoisomers of I are shown in Fig. 1. The pair of (2*R*, 3*R*)- and (2*S*, 3*S*)-I was conventionally designated as the *threo* isomer (It), and that of (2*R*, 3*S*)- and (2*S*, 3*R*)-I, as the *erythro* isomer (Ie). Optically active I ($[\alpha]_D$+22°) was first isolated from the degradation product of tetrin B by Rinehart and co-workers.[3] The configuration at C-3 of this compound was assigned to *S*, but that at C-2 was not made clear. Masken and Polgar reported that each diastereomer of I showed a different retention time in GLC and assigned the diastereomer with long retention time to Ie based on the NMR and IR spectroscopic analyses.[4] However, neither the optical resolution of Ie and It nor the determination of the absolute configurations of optically active Ie and It has been reported.

Results and Discussion

Diastereoisomeric I consisting of Ie and It in a ratio of 6 to 4 was obtained by the hydrogenation of methyl 2-methyl-3-oxobutyrate (III) over DL-tartaric acid-modified Raney nickel.[5] It is better to use modified Raney nickel for this hydrogenation, since unmodified Raney nickel is easily corroded by III and often loses its catalytic activity in the course of the hydrogenation.[6]

After the hydrolysis of I into 3-hydroxy-2-methylbutyric acid (II), II was converted to cyclohexylammonium salt. The recrystallization of the cyclohexylammonium salt from ethanol gave one of the diastereomers of II in a pure state. GLC and NMR analyses of its methyl ester indicated that the resulting isomer corresponded to the *erythro* isomer (IIe) assigned by Masken and Polgar. The cyclohexylammonium salt in the combined mother liquid was converted to sodium salt by treatment with sodium hydroxide. The recrystallization of the sodium salt from a methanol–acetone mixture gave the other diastereomer, IIt, in a pure state.

The optical resolution of each diastereomer was accomplished in the usual manner. The resulting isomer and resolving reagent were as follows: (+)-IIe and (+)-IIt by quinine, (−)-IIe by quinidine, and (−)-IIt by cinchonidine.

All the isomers of II were converted to their methyl ester (I) by the treatment of diazomethane. Thus, (+)-IIe was converted to (+)-Ie, (−)-IIe to (−)-Ie, (+)-IIt to (+)-It, and (−)-IIt to (−)-It. The configuration at the C-2 position of I was correlated to that of (+)-(*S*)-methyl 2-methylbutyrate (IV).[7] The conversion of I to IV was carried out in two steps:

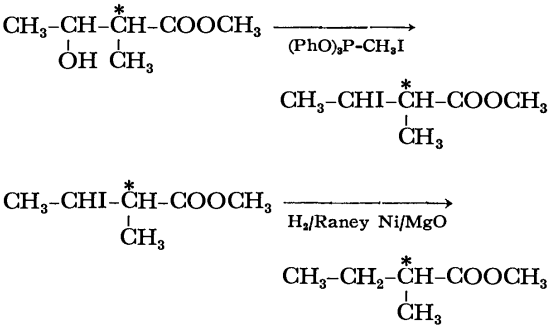

From (+)-Ie and (−)-It, (+)-(*S*)-IV and (−)-(*R*)-IV were obtained respectively. Therefore, the configurations at the C-2 position of (+)-Ie and (+)-It are *S* while those of (−)-Ie and (−)-It are *R*.

The configuration at the C-3 position of I was determined by Horeau's method.[8] When an excess amount of (±)-2-phenylbutyric anhydride was treated with (+)-Ie, (+)-(*S*)-2-phenylbutyric acid was recovered. It was empirically demonstrated that when the configuration of I was that shown in Scheme 1, the recovered 2-phenylbutyric acid (V) had the (+)-(*S*)-enantiomer in excess. Therefore, the configuration at the C-3

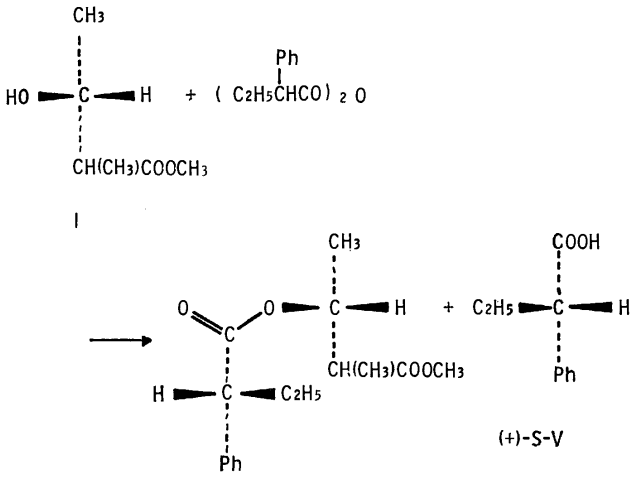

Scheme 1.

position of (+)-Ie could be assigned to *R*. In the same manner, the reactions with both (+)-It and (−)-Ie gave (−)-(*R*)-V. Thus, the configurations at 3-C of (+)-It and (−)-Ie were assigned to *S*.

Table 1. Absolute configuration and optical rotation of methyl 3-hydroxy-2-methylbutyrate (I)

Isomer[a]	Absolute configuration	$[\alpha]_D^{20}$ (*c* 5, methanol)
(+)-*threo*-I	(2*S*,3*S*)	+36.80°
(−)-*thero*-I	(2*R*,3*R*)	
(+)-*erythro*-I	(2*S*,3*R*)	+14.32°
(−)-*erythro*-I	(2*R*,3*S*)	

a) The sign of each isomer shows the direction of α_D^{20} observed in neat.

The configuration and optical rotation of each isomer are listed in Table 1. The relative configurations at C-2 and C-3 assigned by Masken are consistent with the present results.

Experimental

The analytical GLC was carried out with a Shimadzu GC-4A gas chromatograph using a 3-m, 5-mm o.d. glass column packed with 5% NPGS on Chromosorb W at stated temperatures. The preparative GLC was carried out with a Shimadzu GC-3HA instrument using a 3-m, 8-mm o.d. stainless column packed with the same packing.

The optical rotations were measured with a Perkin Elmer 241 polarimeter at 20 °C under the stated conditions.

The NMR spectra were taken with a Hitachi R-24 spectrometer at 60 MHz. The IR spectra were taken with a Shimadzu IR-27G spectrometer. All the chemicals except as stated below were obtained from commercial sources and were used without further purification.

Methyl 2-Methyl-3-oxobutyrate (III). This was prepared from methyl acetoacetate and methyl iodide, bp 75—78 °C. GLC (at 90 °C) indicated a 98% purity; retention time, 9.1 min. Also there was 2% of methyl 2,2-dimethyl-3-oxobutyrate; retention time, 7.9 min.

Diastereoisomeric Methyl 3-Hydroxy-2-methylbutyrate (I). In an autoclave (1000 ml capacity), 300 g of III and 23 g of Raney nickel modified with DL-tartaric acid were placed. Hydrogen was added until the pressure reached 110 kg/cm², and then heating was commenced. After the temperature of the reaction mixture had become 65 °C, this temperature was maintained until the end of the reaction; after 24 h there was no fall in the pressure. After the removal of the catalyst, the distillation of the product gave 271 g of crude I, bp 79—81 °C/18 mmHg. GLC (at 90 °C) indicated that the products consisted of 39% of It (retention time 12.8 min), 58% of Ie (retention time 14.1 min), and 4% of unidentified impurities (retention times 11.0 and 15.2min).

Separation of threo-*I (It) and* erythro-*I (Ie).* The crude I (271 g) was saponified with 30% aqueous sodium hydroxide (300 ml) at room temperature. Most of the water was evaporated under reduced pressure, and the residue was acidified with 12M hydrochloric acid (120 ml) and they extracted with three 300 ml portions of ether. The evaporation of the ether from the combined extract gave 224 g of crude 3-hydroxy-2-methylbutyric acid (II). This was dissolved in 350 ml of ethanol and mixed with 180 g of cyclohexylamine under nitrogen. On cooling the solution overnight, a part of the salt was crystallized. Two successive recrystallizations of the crystalline part from 95% ethanol gave 166 g of cyclohexylammonium salt of IIe, mp 148 °C, Found: C, 59.74; H, 10.81; N, 6.34%. Calcd for $C_{11}H_{23}NO_3 \cdot (1/4)H_2O$: C, 59.56; H, 10.68; N, 6.31%. The attempts to eliminate the water from the sample resulted in failure, since the salt was decomposed with the evolution of cyclohexylamine on heating *in vacuo*. Small portions of the salt were acidified, and the liberated acid was converted to methyl ester with diazomethane. The GLC (at 90 °C) of the ester showed a single peak corresponding to the *erythro*-isomer; retention time, 14.3 min.

The mother liquids of the original crystallization and the first recrystallization were combined and concentrated to dryness. The residue was dissolved in 150 ml of 30% aqueous sodium hydroxide and washed with two 150 ml portions of ether. After reducing the water from the aqueous layer on a rotatory evaporator, the remaining dense sirup (*ca.* 70 ml) was mixed with 1100 ml of a methanol–acetone (1 : 5) mixture and crystallized at 0 °C. Two successive recrystallizations from methanol gave 48 g of sodium salt of IIt, mp 210—215 °C. The salt was too hygroscopic for the elemental analysis to be performed with a completely dried sample. The results of the elemental analysis were as follows; Found: C, 41.51; H. 6.52%. Calcd for $C_5H_9O_3Na \cdot (1/4) \cdot H_2O$: C, 41.52; H, 6.62, GLC (at 90 °C) of methyl ester derived from the sample showed a single peak of the *threo-isomer*; retention time, 12.5 min.

Optical Resolution of IIe. When a solution of cyclohexylammonium salt of IIe (150 g) in 1500 ml of water was passed through a column packed with 500 ml of Amberlite IR-120 (H^+ type), 2000 ml of an acidic eluate were collected. To the eluate 220 g of quinine was added, after which the mixture was stirred until the added base was completely dissolved. After the decoloration of the solution with activated charcoal, it was evaporated to dryness under reduced pressure to give crude quinine salt. Ethanol was added to the crude salt in portions at the boiling temperature until the salt was completely dissolved (*ca.* 180 ml of ethanol was required); on cooling, crystals of the quinine salt were precipitated. Recrystallization from ethanol was carried out in the manner described above. The progress of resolution was followed by the measurement of the optical rotation of the sodium salt derived from a small portion of quinine salt by treatment with aqueous sodium hydroxide. After three recrystallizations, the rotation reached a steady value, are unchanged by two further recrystallizations. The quinine salt of IIe

obtained amounted to 50 g; mp 140—141 °C, $[\alpha]_D^{20}$ −134 °C (*c* 1, H_2O). This was dissolved in 100 ml of water and treated with 5% aqueous sodium hydroxide with stirring until the pH of the mixture became 10. The removal of the liberated quinine by filtration and the evaporation of the filtrate gave a dense sirup, which was then dissolved in 50 ml of ethanol. After removing the insoluble matter by filtration, the filtrate was mixed with 250 ml of acetone to give 15 g of (−)-sodium salt of IIe as crystals, $[\alpha]_D^{20}$ −7.20 ° (*c* 10, H_2O), +13.61 ° (*c* 5, 3 M HCl).

The sodium salt (98 g), $[\alpha]_D^{20}$ +2.0 (*c* 10, H_2O), recovered from the combined mother liquids of the first and second crystallizations was dissolved in 1500 ml of water, after which the solution was passed through a column packed with 500 ml of Amberlite IR-120 (H^+ type). Into the acidic eluate (1700 ml), a 280-g portion of quinidine was added, and the mixture was stirred until all the base had dissolved. After removing the insoluble matter, the solution was evaporated to dryness to give crude quinidine salt. Four successive recrystallizations of the salt from acetone gave 110 g of quinidine salt of optically pure IIe; $[\alpha]_D^{20}$ 172 ° (*c* 10, H_2O), mp 100 °C. This was then converted to (+)-sodium salt of IIe in a yield of 30 g; $[\alpha]_D^{20}$ +7.53 ° (*c* 10, H_2O), −13.74 ° (*c* 10, 3M HCl).

(+)-Methyl erythro *3-Hydroxy-2-methylbutyrate (Ie).* The acid liberated from 10 g of (−)-sodium salt of IIe by treatment with 24 ml of 10 M HCl was extracted with three 30-ml portions of ether, and the combined extract was dried over anhydrous magnesium sulfate. After the solvent had been reduced, a slight excess of ethereal diazomethane was added to solution at 5 °C, and the mixture was kept at room temperature for 20 min. After the excess of diazomethane had then been decomposed with HCl, the solution was washed with water, dried over magnesium sulfate, and concentrated. The distillation of the condensate under reduced pressure gave 8.5 g of (+)-Ie, bp 75 °C/15 mmHg; α_D^{20} +11.30 ° (neat); GLC (at 90 °C); single peak; retention time, 14.0 min; NMR ($CDCl_3$, TMS), δ 1.18 (3H, d, J=6.4 Hz), 1.19 (3H d, J=7.0 Hz), 2.46 (1H, broad signal), 2.51 (1H, m), 3.70 (3H, s), 4.06 (1H, m), IR (neat) 3550, 2990, 2940, 1730, 1200, 1085, 1032 cm^{-1}. This product contains *ca.* 1% of water, as estimated from the results of the elemental analysis. A-2g portion of the product was boiled in 30 ml of dry benzene in order to remove the water as the benzene azeotrope and was then distilled at atmospheric pressure to give an analytical sample; bp 183 °C/763 mmHg; Found; C, 54.60; H, 9.46%. Calcd for $C_6H_{12}O_3$: C, 54.53; H, 9.15%. $[\alpha]_D^{20}$ +14.32 (*c* 5, CH_3OH), −4.04 (*c* 5, $CHCl_3$). The GLC, NMR, and IR data of the sample were identical with those listed above.

(−)-Methyl erythro *3-Hydroxy-2-methylbuthyrate (Ie).* By the same procedure mentioned before, 10 g of (+)-sodium salt of IIe was converted into (−)-Ie in a yield of 8.5 g, α_D^{20} −11.39° (neat). The bp, water content, retention time in GLC, and NMR and IR spectra were identical with those of the (+)-isomer.

Optical Resolution of IIt. A solution of sodium salt of IIt (98 g) in 1000 ml of water was passed through a column packed with 500 ml of Amberlite IR-120 (H^+ type). The acidic eluate (1700 ml) was mixed with 230 g of quinine and stirred until it was completely dissolved. The solution was then concentrated to 200 ml and allowed to stand overnight at 5 °C to give 137 g of quinine salt as crystals. After recrystallizing three times from water, the resulting 30-g portion of the salt (mp 154 °C, $[\alpha]_D^{20}$ −163 °(*c* 2, 50% ethanol)) was converted into (+)-sodium salt of IIt in a yield of 23 g, $[\alpha]_D^{20}$ +10.6 °(*c* 10, H_2O), +26.5 ° (*c* 5, 3M HCl).

The sodium salt (70 g, $[\alpha]_D^{20}$ −4.5 ° (*c* 10, H_2O)) recovered from the mother liquid was dissolved in 800 ml of water and treated with Amberlite IR-120 (H^+ type). The acid thus liberated was subjected to further resolution by the recrystallization of its cinchonidine salt from a mixture of acetone and 2-propanol (4 to 1). After recrystallizing five times, the salt was converted into (−)-sodium salt of IIt in a yield of 10 g, $[\alpha]_D^{20}$ −10.20 ° (*c* 10, H_2O), −26.30 ° (*c* 10, 3M HCl).

(+)- and (−)-Methyl 3-Hydroxy-2-methylbutyrate (It). (+)- and (−)-salt of IIt were converted into the methyl ester by the method described above.

From 10 g of (+)-sodium salt of IIt, 8.7 g of (+)-It were obtained; bp 83 °C/18 mmHg, water content, *ca.* 0.5%, α_D^{20} +34.80° (neat), GLC (at 90 °C), single peak; retention time, 13.0 min; NMR ($CDCl_3$, TMS) δ 1.18 (3H, d, J=7.2 Hz), 1.22 (3H, d, J=6.3 Hz), 1.19 (1H, broad signal), 2.47 (1H, m), 3.71 (3H, s), 3.82 (1H, m), IR (neat) 3550, 2990, 2960, 1730, 1200, 1100, 1045 cm^{-1}. The dehydrated analytical sample was prepared by the method described before; bp 181 °C/764 mmHg, Found: C, 54.51; H, 9.43%. Calcd for $C_6H_{12}O_3$: C, 54.53; H, 9.15%, $[\alpha]_D^{20}$ +36.80° (*c* 5, CH_3OH), +32.51° (*c* 5, $CHCl_3$). The GLC, NMR, and IR data of this sample were identical with those listed above.

From 10 g of (−)-sodium salt of IIt, 8.6 g of (−)-It were obtained; water content, *ca.* 1%, α_D^{20} −34.72° (neat). The GLC, NMR, and IR data of this compound were identical with those of the (+)-isomer.

Methyl 3-Iodo-2-methylbutyrate. Partially resolved (+)-Ie (5g, α_D^{20} +7.08° (neat)) was mixed with methyl tris-(phenoxy)phosphonium iodide prepared from 15 g of triphenyl phosphite and 4.3 g of methyl iodide. The mixture was then stirred at 50 °C overnight. As the product we extracted four 20-ml portions of hexane. The combined extract was washed with a 30-ml portion of water, dried over anhydrous sodium sulfate, and concentrated to one tenth of its original volume under reduced pressure. The distillation of the condensate gave 1.2 g of a diastereomeric mixture of methyl 3-iodo-2-methylbutyrate, bp 98—102 °C/12 mmHg. GLC (at 130 °C) indicated a 97.5% purity as a diastereomeric mixture (retention times 6.2 and 6.7 min) and 2.5% of an unidentified impurity (retention time 5.7 min). The NMR spectra (CCl_4, TMS) showed those signals; δ 1.32 and 1.33 (d, J=7.1) for the $C\underline{H}_3$–CH–$COOCH_3$ of each diastereomer, 1.90 and 1.98 (d, J=6.4) for the $C\underline{H}_3$–CHI– of each diastereomer, 2.5 (m) for –$C\underline{H}(CH_3)$–, 3.75 (s) for –O–$C\underline{H}_3$, and 4.05 (m) for –CHI–. The spectra were consistent with the structure of methyl 3-iodo-2-methylbutyrate. The IR spectra did not show any OH stretching, indicating the absence of the starting material in the product.

Partially resolved (−)-It (5 g, α_D^{20} −19.1° (neat)) was converted into methyl 3-iodo-2-methylbutyrate (1.1 g) by the method discribed before. The GLC, NMR, and IR data of the product were identical with those of the product derived from (+)-Ie.

Hydrogenolysis of Methyl 3-Iodo-2-methylbutyrate. Into an atmospheric pressure hydrogenation vessel which had been filled with hydrogen, methyl 3-iodo-2-methylbutyrate derived from (+)-Ie (0.8 g), magnesium oxide (0.5 g), and a Raney nickel catalyst (1.8 g in 10 ml of methanol) were introduced. The mixture was shaken at 45 °C for 48 h under an atmospheric pressure of hydrogen. After the removal of the insoluble matter by filtration, the filtrate was subjected to flash distillation at 50 mmHg. The distillate collected in a cold trap was transferred into an evaporator fitted with a Snyder column and was concentrated to 1.5 ml on heating under atmospheric pressure. GLC (at 50 °C) indicated that the condensate consisted of methyl 2-methylbutyrate and methanol

in a ratio of 1 to 10, with an accompanying trace amount of a high-boiling substance. The preparative GLC (at 40 °C) of the condensate gave pure methyl 2-methylbutyrate (IV), $[\alpha]_D^{20}$ +14.4° (*c* 4, methanol). The GLC, NMR, and IR data of the product were identical with those of the authentic compound prepared from racemic 2-methylbutyric acid (Tokyo Kasei Kogyo Co., Ltd.)

In the same manner as has been presented before, methyl 3-iodo-2-methylbutyrate was converted into IV, $[\alpha]_D^{20}$ −11.7° (*c* 4, methanol). The GLC, NMR, and IR data of the product were identical with those of an authentic compound.

Kinetic Resolution of (±)-2-Phenylbutyric Anhydride with I. A solution of (±)-2-phenylbutyric anhydride (0.6), (+)-Ie (0.1 g), and pyridine (2 g) in 10 ml of benzene was kept at room temperature for 12 h and then a 15-ml portion of water was added. The mixture was stirred for 30 min, a 30-ml portion of dilute hydrochloric acid was added, and the new mixture was extracted with 50 ml of ether. The ether layer was washed with water and extracted with a 50-ml portion of a 5% aqueous sodium hydrogencarbonate solution. The aqueous extract was acidified with dilute hydrochloric acid, followed by extraction with ether. The ether extract was dried over anhydrous magnesium sulfate and then evaporated to dryness to give 0.16 g of 2-phenylbutyric acid, which had α_D^{20} +0.80° in 2 ml of benzene.

The reactions of (−)-Ie and (+)-It with 2-phenylbutyric anhydride were carried out as before. The values of α_D^{20} (0.16 g of a sample in 2 ml of benzene) of the recovered 2-phenylbutyric acid were −0.73° for (−)-Ie and −0.96° for (+)-It. The NMR and IR spectra of each acid were identical with those of an authentic compound (Wako Pure Chemical Industries, Ltd.).

The authors wish to express their thanks to Professor Yoshiharu Izumi and Dr. Tadao Harada for their helpful suggestions. They also wish to thank Mmes. Aiko Kobatake and Mihoko Yamamoto for their elemental analysis. This work was supported in part by a Scientific Research Grant from the Ministry of Education, Japan (110308).

References

1) Y. Izumi, *Angew. Chem. Int. Ed. Engl.*, **10**, 871 (1971).
2) D. M. Jewett, F. Matsumura, and H. C. Coppel, *Science*, **192**, 51 (1976).
3) R. C. Pandy, V. F. German, Y. Nishikawa, and K. L. Rinehart, *J. Am. Chem. Soc.*, **93**, 3738 (1971).
4) K. Masken and N. Polgar, *J. Chem. Soc., Perkin Trans. 1*, **1973**, 109.
5) Y. Izumi, T. Harada, T. Tanabe, and K. Okuda, *Bull. Chem. Soc. Jpn.*, **44**, 1418 (1971).
6) Y. Izumi, *Proc. Jpn. Acad.*, **53**, 38 (1977).
7) J. A. Mills and W. Klyne, *Progr. Stereochem.*, **1**, 177 (1954).
8) (a) A. Horeau, *Tetrahedron Lett.*, **1961**, 506;
(b) A. Horeau and H. B. Kagan, *Tetrahedron*, **20**, 2431 (1964).

Structural Studies of the Interaction between Indole Derivatives and Biologically Important Aromatic Compounds. I. The Crystal and Molecular Structure of the Indole-3-acetic Acid–Nicotinamide (1: 1) Complex

Masatoshi INOUE, Toshimasa SAKAKI, Takaji FUJIWARA,* and Ken-ichi TOMITA*

Osaka College of Pharmacy, Kawai, Matsubara-City, Osaka 580

**Faculty of Pharmaceutical Sciences, Osaka University, Yamadakami, Suita, Osaka 565*

(Received June 8, 1977)

The title complex crystallizes in the monoclinic space group $P2_1/c$. The unit-cell dimensions are $a=11.287(5)$, $b=5.110(3)$, $c=26.391(3)$ Å, and $\beta=107.07(2)°$. The crystal structure was solved by a direct method. By block-diagonal least-squares refinements, the R-value dropped to 0.069. All the nitrogen and oxygen atoms in the complex participate in the hydrogen bonding. No prominent overlapping between pyridine and indole rings is observed in the crystal. Both molecules are hydrogen-bonded to form infinite-layered structures perpendicular to the c-axis; those structures are held together by van der Waals contacts.

Pullman and Pullman[1] showed that the indole moiety of tryptophan was the best electron donor in amino acids, and Isenberg and Szent-Györgyi[2] presented evidence of charge-transfer interaction in the complex of tryptophan and NAD. Since then, a number of investigations have been undertaken to establish the precise mechanism of such interactions as indole derivatives and NAD or FAD as a model for protein-coenzyme interaction,[3–7] and indole derivatives and nucleic acid or its constituent as a model for protein-nucleic acid interaction.[8–12] As a result, it has been suggested that one of the main factors controlling these interactions is a charge-transfer force between the indole ring and the aromatic ring.[13] Recently, Herriott *et al.*[14] determined the crystal structure of 1-[2-(3-indolyl)ethyl]-3-carbamoylpyridinium chloride as a model of tryptophan–NAD interaction and observed the overlapping of the indole ring and the cationic pyridinium ring. To investigate to what extent a protonation is actually important for the interaction of the indole ring and the pyridinium ring, we tried to crystallize the molecular complex, with indole-3-acetic acid (IAA) as a donor and nicotinamide (NA) or *N*-methylnicotinamide as an acceptor. The crystal size of the IAA: *N*-methylnicotinamide complex is not suitable for X-ray analysis at present. We wish to report here the crystal structure of a 1: 1 molecular complex of NA and IAA.

Experimental

Equimolar amounts of NA and IAA were dissolved in a 99.5% ethanol solution. After evaporation at room temperature, light-brown, plate-shaped crystals were obtained. The melting point of the crystals is 138—139 °C. Preliminary oscillation and Weissenberg photographs showed the crystals to be monoclinic and the space group to be $P2_1/c$, judging from the systematic absent spectra.

The crystallographic data are shown in Table 1. The density was measured by the floatation method in a benzene–carbon tetrachloride mixture. Three-dimensional intensity data were collected with a computer-controlled four-circle diffractometer with Ni-filtered Cu $K\alpha$ radiation. By means of the $\omega/2\theta$ scan technique, a total of 1918 independent reflections were collected within $\sin\theta/\lambda$ less than 0.54 Å^{-1}. The intensities were corrected for the Lorentz and polarization factors, but not for the absorption. The intensities of three standard reflections measured for every 50 reflections of the data set showed no decrease in intensity during the run. The scan speed was 4°/min, and 5-s background measurements were performed at each terminus of the scan. All the numerical calculations were carried out on an NEAC 2200-700 computer of the Computation Center of Osaka University using "UNICS" programs (1973).[15] Atomic scattering factors in "International Tables for X-Ray Crystallography," Vol. 4 (1974)[16] were used.

TABLE 1. CRYSTAL DATA

$C_6H_6ON_2 \cdot C_{10}H_9O_2N$	
$a=11.287$ (5) Å	$F.W.$ 297.31
$b=5.110$ (3)	Space group $P2_1/c$
$c=26.391$ (3)	$Z=4$
$\beta=107.07$ (2)°	$V=1455.1$ Å^3
$D_m=1.353$ g cm^{-3}	μ(Cu $K\alpha$)$=9.21$ cm^{-1}
$D_x=1.357$	

Determination and Refinement of the Structure

The structure was solved by the direct method with the "MULTAN" program[17] using 443 reflections with $|E|\geqq 1.20$. An E-map computed with the phase set of the highest figure of merit, 1.302, revealed the positions of all the non-hydrogen atoms. After least-squares refinement, a difference map revealed the positions of all fifteen hydrogen atoms (peak height: 0.3—0.5 e Å^{-3}), which were included in all subsequent refinements with isotropic temperature factors.

The final least-squares refinement was made with a weighting scheme of this form: $w=0.15$ for $F_o=0$, $w=1.0$ for $0<F_o\leqq 34.0$, and $w=\{1+0.776(|F_o|-34.0)\}^{-1}$ for $F_o>34.0$. In the last cycle of refinement, none of the positional parameters shifted more than one-third of the estimated standard deviation. The final R-value including $F_o=0$ is 0.069. The observed and calculated structure factors are listed in Table 2.[18]

Results and Discussion

A perspective view of the NA and IAA molecules projected on each ring plane is presented in Fig. 1,

Table 3. Atomic coordinates ($\times 10^4$) and their standard deviations of heavy atoms

Atom	x	y	z
NN1	5296(2)	4156(6)	721(1)
NC2	4079(3)	4036(6)	486(1)
NC3	3249(2)	5789(6)	597(1)
NC4	3695(3)	7754(6)	966(1)
NC5	4965(3)	7866(7)	1213(2)
NC6	5711(3)	6048(7)	1083(2)
NC7	1899(3)	5405(6)	338(1)
NN8	1181(2)	7508(5)	258(1)
NO9	1478(2)	3177(4)	214(1)
IN1	1026(2)	−3312(6)	2340(1)
IC2	−59(3)	−3385(8)	1928(1)
IC3	−16(3)	−1569(8)	1564(1)
IC4	1744(4)	1812(8)	1568(2)
IC5	2924(4)	2541(8)	1864(2)
IC6	3524(4)	1310(9)	2334(2)
IC7	2975(3)	−691(8)	2531(1)
IC8	1791(3)	−1424(6)	2239(1)
IC9	1153(3)	−251(7)	1752(1)
IC10	−989(4)	−1030(10)	1048(1)
IC11	−2058(3)	602(7)	1082(1)
IO12	−2849(2)	1109(6)	613(1)
IO13	−2239(2)	1307(6)	1484(1)

Table 4. Anisotropic thermal parameters ($\times 10^4$) and their standard deviations of heavy atoms

The anisotropic temperature factors are expressed in this form: $\exp\{-(B_{11}h^2+B_{22}k^2+B_{33}l^2+B_{12}hk+B_{13}hl+B_{23}kl)\}$.

Atom	B_{11}	B_{22}	B_{33}	B_{12}	B_{13}	B_{23}
NN1	63(2)	426(13)	21(1)	54(9)	13(2)	24(4)
NC2	66(3)	347(14)	16(1)	42(10)	16(2)	16(5)
NC3	62(3)	247(11)	15(1)	00(9)	15(2)	11(4)
NC4	82(3)	303(13)	20(1)	−11(11)	9(2)	−7(5)
NC5	88(3)	366(15)	24(1)	−38(12)	−4(2)	−20(6)
NC6	67(3)	446(17)	25(1)	−31(12)	−1(2)	38(6)
NC7	64(3)	267(12)	13(1)	7(9)	16(2)	−1(4)
NN8	64(2)	226(10)	24(1)	29(8)	16(2)	0(4)
NO9	67(2)	226(8)	20(1)	6(6)	10(1)	−10(3)
IN1	92(3)	419(13)	17(1)	30(10)	17(2)	26(4)
IC2	86(3)	543(18)	17(1)	31(13)	20(2)	7(6)
IC3	87(3)	618(19)	13(1)	185(13)	21(2)	−8(5)
IC4	182(5)	486(18)	20(1)	174(16)	75(3)	53(6)
IC5	195(6)	480(19)	29(1)	−93(18)	97(4)	−5(7)
IC6	138(4)	591(21)	26(1)	−142(16)	57(3)	−43(7)
IC7	97(3)	561(19)	19(1)	7(14)	21(2)	−7(6)
IC8	88(3)	347(14)	15(1)	79(11)	26(2)	11(5)
IC9	108(3)	403(15)	14(1)	152(12)	40(2)	26(5)
IC10	108(4)	1076(31)	14(1)	382(19)	15(2)	2(7)
IC11	69(3)	500(16)	14(1)	47(12)	17(2)	2(5)
IO12	93(2)	921(18)	15(1)	249(11)	16(2)	35(4)
IO13	89(2)	720(15)	17(1)	177(10)	7(2)	−65(4)

along with the atomic numbering. The atomic coordinates and thermal parameters, with their estimated standard deviations for non-hydrogen atoms are given in Tables 3 and 4 respectively. The coordinates and isotropic thermal parameters for hydrogen atoms are given in Table 5.

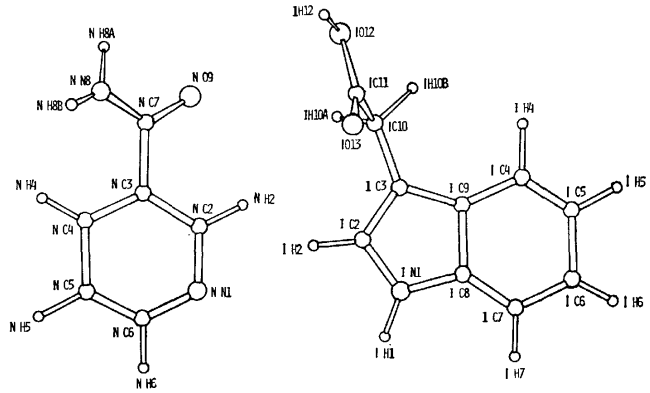

Fig. 1. The perspective view of NA and IAA molecules with the atomic numbering.

Table 5. Hydrogen atom coordinates ($\times 10^3$) and isotropic temperature factors, with their standard deviations

Atom	x	y	z	B(Å^2)
NH2	376(3)	255(8)	20(1)	3.8(9)
NH4	307(3)	909(8)	108(1)	4.3(9)
NH5	532(3)	940(8)	152(1)	4.3(9)
NH6	669(3)	608(7)	126(1)	3.6(8)
NH8A	28(3)	729(8)	10(1)	3.8(9)
NH8B	146(4)	919(10)	28(2)	8.1(14)
IH1	121(4)	−450(8)	268(2)	5.4(10)
IH2	−78(3)	−478(8)	192(1)	4.0(9)
IH4	127(4)	287(8)	121(2)	5.4(10)
IH5	335(4)	408(9)	171(2)	5.5(11)
IH6	439(4)	192(8)	253(2)	5.1(10)
IH7	342(3)	−156(8)	289(1)	4.7(10)
IH10A	−132(4)	−274(10)	87(2)	7.6(13)
IH10B	−62(3)	2(8)	78(2)	4.6(9)
IH12	−359(4)	223(8)	66(2)	5.6(10)

Table 6. Bond lengths and their standard deviations

	NA		
NN1–NC2	1.332(4)Å	NN1–NC6	1.341(5)Å
NC2–NC3	1.388(4)	NC3–NC4	1.387(5)
NC3–NC7	1.489(4)	NC4–NC5	1.391(5)
NC5–NC6	1.364(6)	NC7–NN8	1.325(4)
NC7–NO9	1.240(4)		
	IAA		
IN1–IC2	1.380(5)	IN1–IC8	1.372(4)
IC2–IC3	1.347(6)	IC3–IC9	1.434(5)
IC3–IC10	1.504(6)	IC4–IC5	1.382(7)
IC4–IC9	1.408(6)	IC5–IC6	1.379(7)
IC6–IC7	1.374(6)	IC7–IC8	1.384(5)
IC8–IC9	1.409(5)	IC10–IC11	1.492(6)
IC11–IO12	1.323(5)	IC11–IO13	1.192(5)

The Molecular Structure. Tables 6 and 7 show the bond lengths and angles, with their standard deviations.

NA Molecule: The NC5–NC6 bond length, 1.364 Å, is apparently smaller than the averaged C–C bond length in the pyridine ring;[19] this tendency is also observed in the crystal structures of 3,3′-dicarbamoyl-1,1′-trimethylenedipyridinium dichloride monohy-

TABLE 7. BOND ANGLES AND THEIR STANDARD DEVIATIONS

NA	
NC2–NN1–NC6	117.5(3)°
NC2–NC3–NC4	119.2(3)
NC4–NC3–NC7	122.0(3)
NC4–NC5–NC6	118.7(4)
NC3–NC7–NN8	117.5(3)
NN8–NC7–NO9	122.3(3)
NN1–NC2–NC3	122.6(3)
NC2–NC3–NC7	118.8(3)
NC3–NC4–NC5	118.1(3)
NC5–NC6–NN1	123.9(4)
NC3–NC7–NO9	120.2(3)
IAA	
IC2–IN1–IC8	109.2(3)
IC2–IC3–IC9	107.4(3)
IC9–IC3–IC10	125.6(4)
IC4–IC5–IC6	121.5(4)
IC6–IC7–IC8	117.5(4)
IC7–IC8–IN1	130.0(3)
IC8–IC9–IC3	106.7(3)
IC3–IC9–IC4	135.5(4)
IC10–IC11–IO12	112.8(3)
IO12–IC11–IO13	122.0(3)
IN1–IC2–IC3	109.5(3)
IC2–IC3–IC10	127.0(4)
IC5–IC4–IC9	118.9(4)
IC5–IC6–IC7	121.5(4)
IC7–IC8–IC9	122.9(3)
IN1–IC8–IC9	107.1(3)
IC8–IC9–IC4	117.8(3)
IC3–IC10–IC11	115.8(4)
IC10–IC11–IO13	125.2(4)

TABLE 8. DEVIATIONS OF ATOMS FROM THE LEAST-SQUARES PLANES

Equations of the best planes with the $m_1X+m_2Y+m_3Z=d$ formula in an orthogonal space.

Plane	m_1	m_2	m_3	d
Pyridine ring	0.3342	0.6048	−0.7229	1.7750
Amide group	0.4199	0.1155	−0.9002	0.3345
Indole ring	−0.5644	0.6652	0.4889	2.1097
Carboxyl group	0.5459	0.8368	−0.0430	−1.6023

Deviations (in Å) from the best planes

NA		IAA	
Pyridine ring		Indole ring	
NN1*	−0.006	IN1*	−0.020
NC2*	0.001	IC2*	0.002
NC3*	0.003	IC3*	0.021
NC4*	−0.002	IC4*	−0.015
NC5*	−0.002	IC5*	−0.005
NC6*	0.007	IC6*	0.010
NC7	0.092	IC7*	0.012
NH2	−0.006	IC8*	−0.007
NH4	0.049	IC9*	0.003
NH5	0.034	IC10	0.080
NH6	0.007	IH1	−0.063
Amide group		IH2	0.033
NC3*	0.002	IH4	−0.072
NC7*	−0.007	IH5	−0.003
NN8*	0.003	IH6	0.018
NO9*	0.003	IH7	−0.017
NH8A	0.022	Carboxyl group	
NH8B	−0.185	IC10*	−0.005
		IC11*	0.017
		IO12*	−0.005
		IO13*	−0.007
		IH12	−0.004

Atoms with asterisks define the plane.

drate,[20] 3-carbamoyl-1-methylpyridinium 9-adenylacetate dihydrate[21] and 3-carbamoyl-1-methylpyridinium picrate, chloride, and iodide.[22]

The bond angles are reasonable compared with those of the other pyridine derivatives.[23–27] The dimensions of the amide group are similar to those cited by Bracher and Small.[28] The planarity of the NA molecule is given in Table 8. The NC7 atom deviates slightly from the pyridine-ring plane (0.09 Å). The amide group is almost planar, and the dihedral angle between the amide group and the pyridine-ring plane is 30.6°. The conformation of NA in the complex is different from that of the isolated molecule.[24]

The torsion angle, τ(NC2–NC3–NC7–NO9), is 29.3° in this complex and 155.9° in the isolated molecule, and they are in opposite directions to each other. The torsional angles found in the pyridine derivatives can be grouped into three angles: 150, 35, and 0°. A theoretical calculation of the conformation of the NA molecule[29] predicts that the most stable conformation has the torsional angle, τ, at 150°, and the next one, at 35°. The conformation of the present NA molecule belongs to the second stable conformation.

IAA Molecule: The bond lengths and angles are similar to those reported for IAA[30–32] and indole derivatives.[33] The planar carboxyl group is not in a resonance state because the IC11–IO13 bond has a strong double-bond character (1.192 Å). The IC10 atom is slightly out of the indole-ring plane (0.08 Å), contrary to 5-methoxyindole-3-acetic acid[31] and the isolated IAA.[30] The dihedral angle between the carboxyl group and the indole ring is 104.9°.

The torsion angle, χ(IC2–IC3–IC10–IC11), is 80.4° in this complex, 97.7° in the isolated IAA, and 113.4° in the 5-methoxytryptamine: IAA complex,[32] while the torsional angle, Ψ(IC3–IC10–IC11–IO13), is −6.4° in this complex, −11.7° in the isolated IAA, and −29.4° in the 5-methoxytryptamine: IAA complex. These facts show that such a conformation of the IAA molecule would be most stable regardless of the environmental changes in the crystal.

The Crystal Structure. Figure 2 shows the packing diagram viewed down the b-axis, where the dotted lines represent the hydrogen bonds (see Table 9). All the nitrogen and oxygen atoms in the complex participate in hydrogen bonding. The neighboring NA molecules related by a center of symmetry form a hydrogen-bonded dimer (NN8···NO9=2.913 Å, NN8–NN8HA···NO9=179.4°), similar to that found in a number of amide compounds,[34] but not in the isolated NA. The NN8

Table 9. Hydrogen bonds and short contacts less than 3.5 Å

Superscribed numbers represent symmetry operators.

Hydrogen bonds				
Donor	Acceptor	Distance D···A	H···A	Angle D–H···A
IO12[1)]	NN1[2)]	2.691(4)Å	1.64(4)Å	176(4)°
IN1[1)]	IO13[7)]	3.008(4)	2.22(4)	131(3)
NN8[1)]	NO9[4)]	2.913(3)	1.93(4)	179(3)
NN8[1)]	NO9[5)]	2.922(3)	2.04(5)	161(5)

Short contacts		
IC11[1)]	NN1[2)]	3.385(5)Å
IO13[1)]	NN1[2)]	3.261(4)
IO13[1)]	IC7[8)]	3.328(5)
NC7[1)]	IO12[4)]	3.493(4)
IO12[1)]	NC3[4)]	3.473(4)
IC4[1)]	IN1[5)]	3.462(5)
NC5[1)]	IO13[6)]	3.498(5)
NC6[1)]	IO12[6)]	3.471(5)
NO9[1)]	IC10[8)]	3.394(6)
IO12[1)]	NC6[2)]	3.425(5)
IO13[1)]	NC6[2)]	3.303(5)
IO13[1)]	IC8[3)]	3.457(4)
NN8[1)]	IO12[4)]	3.446(4)
IC4[1)]	IC2[5)]	3.492(6)
IC5[1)]	IN1[5)]	3.499(6)
NC6[1]	IC11[6)]	3.429(5)
NC6[1)]	IO13[6)]	3.502(5)

Symmetry code			
Superscript	Symmetry operator		
1)	x	y	z
2)	$-1+x$	y	z
3)	$-x$	$0.5+y$	$0.5-z$
4)	$-x$	$1-y$	$-z$
5)	x	$1+y$	z
6)	$1+x$	$1+y$	z
7)	$-x$	$-0.5+y$	$0.5-z$
8)	$-x$	$-y$	$-z$

atom is also hydrogen-bonded to the NO9 atom of the NA molecule, translated to the b-axis by one unit. Therefore, these hydrogen bonds form a network system connecting the NA molecules on the ab-plane, as is shown in Fig. 3.

On the other hand, the IO12 atom of the IAA molecule participates in a strong hydrogen bond[35)] with the NN1 of the NA molecule, with a distance of 2.691 Å and the IO12–IO12H···NN1 angle of 176.3°; then, the IO13 atom is hydrogen-bonded to the IN1 atom of the neighboring indole ring, related by a diad screw axis with a distance of 3.008 Å. The hydrogen bonds and short contacts of less than 3.5 Å found in the crystal are listed in Table 9. Many short contacts were found between the carboxyl group in IAA and the pyridine ring in the neighboring NA molecule.

As a whole, both NA and IAA molecules are hydrogen-bonded to form infinite-layered structures perpendicular to the c-axis, structures which are held together by van der Waals contacts. The prominent overlapping between the pyridine and indole rings was

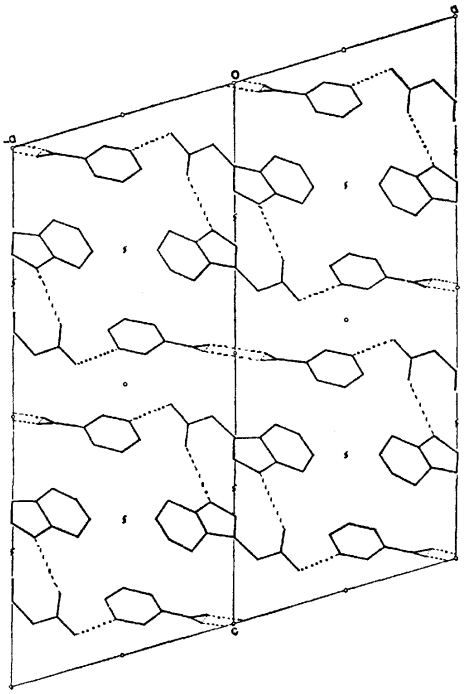

Fig. 2. Molecular packing of IAA–NA viewed down the b-axis. The dotted lines represent the possible hydrogen bonds.

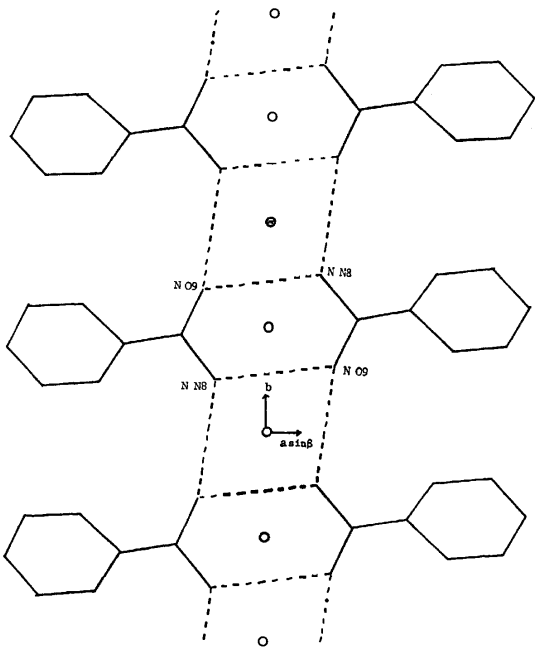

Fig. 3. The hydrogen bond network connected the NA molecules on the ab-plane.

not observed in this crystal, contrary to our expectations, but Ash *et al.*[36)] recently found a prominent overlapping between the pyridinium and indole rings, arising from the π-π interactions in the crystal of the 3-carbamoyl-1-methylpyridinium *N*-acetyl-*l*-tryptophanate complex. This fact may indicate that the quaternary nitrogen atom in 1-methylnicotinamide, similar to NAD^+, is a necessity in the case of a specific charge-transfer interaction between the indole ring and the pyridine ring.

References

1) B. Pullman and A. Pullman, *Proc. Natl. Acad. Sci. U.S.A.*, **44**, 1197 (1958).
2) I. Isenberg and A. Szent-Györgyi, *Proc. Natl. Acad. Sci. U.S.A.*, **45**, 1229 (1959).
3) G. Cilento and P. Tedeschi, *J. Biol. Chem.*, **236**, 907 (1961).
4) S. Shifrin, *Biochim. Biophys. Acta*, **81**, 205 (1964).
5) M. Shinitzky, *Israel J. Chem.*, **6**, 525 (1968).
6) H. Umeyama, A. Imamura, and C. Nagata, *J. Theor. Biol.*, **46**, 1 (1974).
7) J. F. Pereira and G. Tollin, *Biochim. Biophys. Acta*, **143**, 79 (1967).
8) C. Hélène, *Photochem. Photobiol.*, **18**, 255 (1973).
9) J. L. Dimicoli and C. Hélène, *J. Am. Chem. Soc.*, **95**, 1036 (1973).
10) F. Morita, *Biochim. Biophys. Acta*, **343**, 674 (1974).
11) R. Mathur-De Vré and A. J. Bertinchamps, *Rad. Environm. Biophys.*, **11**, 135 (1974).
12) F. Brun, J. J. Toulmé, and C. Hélène, *Biochemistry*, **14**, 558 (1975).
13) M. A. Slifkin, "Charge Transfer Interactions of Biomolecules," Academic Press, London and New York (1971), pp. 97—117.
14) J. R. Herriott, A. Camerman, and D. A. Deranleau, *J. Am. Chem. Soc.*, **96**, 1585 (1974).
15) The Universal Crystallographic Computing System (Library Programs in the Computing Center of Osaka University, 1973), The Crystallographic Society of Japan.
16) "International Tables for X-Ray Crystallography," Vol. 4, Kynoch Press, Birmingham (1974).
17) G. Germain, P. Main, and M. M. Woolfson, *Acta Crystallogr., Sect. A*, **27**, 368 (1971).
18) Table 2 is kept at the Chemical Society of Japan, Kanda, Surugadai, Chiyoda-ku, Tokyo 101(Document No. 7810).
19) V. Schomaker and L. Pauling, *J. Am. Chem. Soc.*, **61**, 1769 (1939).
20) J. K. Frank, N. N. Thayer, and I. C. Paul, *J. Am. Chem. Soc.*, **95**, 5386 (1973).
21) D. Voet, *J. Am. Chem. Soc.*, **95**, 3763 (1973).
22) G. R. Freeman and C. E. Bugg, *Acta Crystallogr., Sect. B*, **30**, 431 (1974).
23) W. B. Wright and G. S. D. King, *Acta Crystallogr.*, **6**, 305 (1953).
24) W. B. Wright and G. S. D. King, *Acta Crystallogr.*, **7**, 283 (1954).
25) T. Takano, Y. Sasada, and M. Kakudo, *Acta Crystallogr.*, **21**, 514 (1966).
26) B. Bak, L. Hansen, and J. Rastrup-Andersen, *J. Chem. Phys.*, **22**, 2013 (1954).
27) P. F. Durant, P. Piret, and M. V. Meerssche, *Acta Crystallogr.*, **22**, 52 (1967).
28) B. H. Bracher and R. W. H. Small, *Acta Crystallogr.*, **23**, 410 (1967).
29) J. L. Coubeils, B. Pullman, and Ph. Courrière, *Biochem. Biophys. Res. Commun.*, **44**, 1131 (1971).
30) I. L. Karle, K. Britts, and P. Gum, *Acta Crystallogr.*, **17**, 496 (1964).
31) T. Sakaki, A. Wakahara, T. Fujiwara, and K. Tomita, *Bull. Chem. Soc. Jpn.*, **48**, 536 (1975).
32) T. Sakaki, A. Sogo, A. Wakahara, T. Kanai, T. Fujiwara, and K. Tomita, *Acta Crystallogr., Sect. B*, **32**, 3235 (1976).
33) A. Wakahara, Dissertation, Faculty of Pharm. Sci., Osaka Univ., (1974), p. 124.
34) L. Leiserowitz and G. M. J. Schmidt, *J. Chem. Soc., A*, **1969**, 2372.
35) J. Donohue, *J. Phys. Chem.*, **56**, 502 (1952).
36) R. P. Ash, J. R. Herriott, and D. A. Deranleau, *J. Am. Chem. Soc.*, **99**, 4471 (1977).

Structural Studies of the Interaction between Indole Derivatives and Biologically Important Aromatic Compounds. II. The Crystal and Molecular Structure of the Tryptamine-Phenylacetic Acid (1:1) Complex

Masatoshi INOUE, Toshimasa SAKAKI, Takaji FUJIWARA,* and Ken-ichi TOMITA*

Osaka College of Pharmacy, Kawai, Matsubara-City, Osaka 580

**Faculty of Pharmaceutical Sciences, Osaka University, Yamadakami, Suita, Osaka 565*

(Received June 8, 1977)

The title complex crystallizes in the monoclinic space group of $P2_1/c$. The unit-cell dimensions are $a=6.673(4)$, $b=19.017(8)$, $c=13.394$ (7) Å, and $\beta=110.54(2)°$. The crystal structure was solved by a direct method. By block-diagonal least-squares refinements, the R-value converged to 0.062. In this complex, a salt bridge is found between the anionic carboxyl group of phenylacetic acid (PAA) and the cationic amino group of tryptamine (TPA). All the hydrogen atoms attached to the nitrogen atoms participate in the hydrogen bonding. The two complex molecules are hydrogen-bonded around a center of symmetry to form one unit, which is held together by van der Waals contacts in the b- and c-directions. Each unit is also stabilized by forming a hydrogen bond with the unit of the neighboring cell translated in the a-direction.

The 1:1 molecular complex of tryptamine (TPA) and phenylacetic acid (PAA) was crystallized, and its structure was determined in order to investigate the interaction between the benzene and indole rings, because the existence of interaction between tyrosine and tryptophan residue has been indicated by fluorescence studies.[1-4]

Experimental

Equimolar amounts of TPA and PAA were dissolved in a 50% ethanol aqueous solution. After evaporation at room temperature, transparent platelet crystals were obtained. Preliminary oscillation and Weissenberg photographs indicated the crystal to be monoclinic and the space group to be $P2_1/c$, judging from the systematic absent spectra.

TABLE 1. CRYSTAL DATA

$C_8H_8O_2 \cdot C_{10}H_{12}N_2$	
$a=6.673(4)$Å	*F.W.* 296.35
$b=19.017(8)$	Space group $P2_1/c$
$c=13.394(7)$	$Z=4$
$\beta=110.54(2)°$	$V=1591.7$Å^3
$D_m=1.230$ g cm^{-3}	μ(Cu $K\alpha$)$=7.61$ cm^{-1}
$D_x=1.237$	

The crystallographic data are shown in Table 1. The density was measured by the floatation method in a benzene-carbon tetrachloride mixture. The three-dimensional intensity data were collected with a computer-controlled four-circle diffractometer using Ni-filtered Cu $K\alpha$ radiation. By means of the ω-2θ scan technique, the intensities of a total of 2108 independent reflections within $\sin\theta/\lambda$ less than 0.54 Å^{-1} were collected and corrected for the Lorentz and polarization factors, but not for the absorption. Standard reflections measured for every 50 reflections of the data set showed no decrease in intensity during the run. The scan speed was 4°/min, and the backgrounds were measured in 5 s. All the numerical calculations were carried out on an NEAC 2200-700 computer of the Computation Center of Osaka University using the "UNICS" program (1973).[5] The atomic scattering factors used were in "International Tables for X-Ray Crystallography," Vol. 4 (1974).[6]

Determination and Refinement of the Structure

The phases of 331 reflections ($E\geqq1.2$) were determined by the symbolic addition method, and the following three-dimensional E-map revealed reasonable peaks corresponding to the heavy atoms.

The structure was refined by the least-squares method, and a difference map revealed the positions of all twenty hydrogen atoms (peak height: 0.35—0.45 e Å^{-3}). The final least-squares refinement, including hydrogen atoms with isotropic temperature factors, was performed with a weighting scheme of this form: $w=1.26$ for $F_o=0$, $w=1.0$ for $0<F_o\leqq28$, and $w=\{1.0+2.0(F_o-28.0)\}^{-1}$ for $F_o>28.0$. In the last cycle of refinement, no parameters shifted more than one-fifth of the estimated deviation. The final R-value was 0.062, including $F_o=0$.

The residual fluctuations in the difference Fourier map were within the range from −0.3 to 0.3 e Å^{-3}. The observed and final calculated structure factors are listed in Table 2.[7]

Results and Discussion

The perspective view of the component molecule with the atomic numbering and the a-axis projection

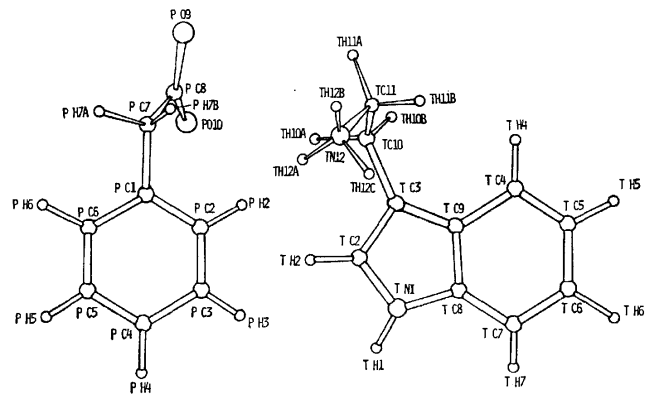

Fig. 1. The perspective view of PAA and TPA molecules with the atomic numbering.

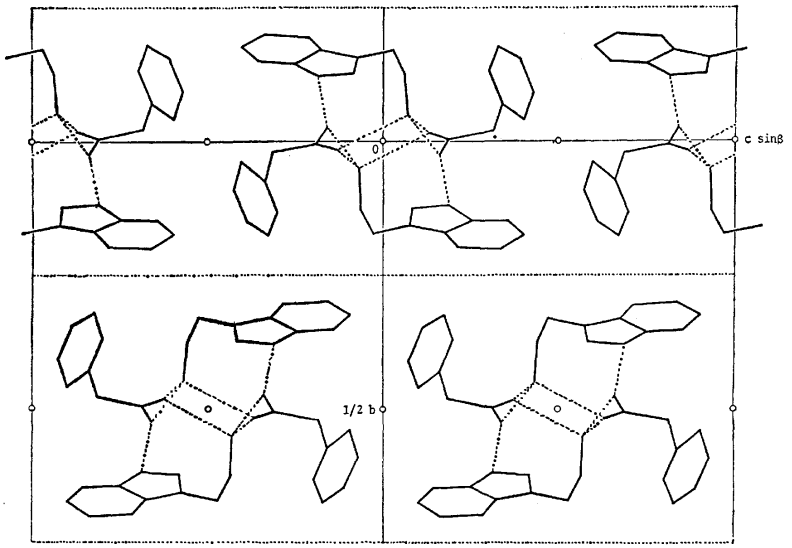

Fig. 2. Molecular packing of TPA–PAA viewed down the a-axis.

of the molecular packing are presented in Figs. 1 and 2 respectively, where the dotted lines indicate the hydrogen bonds. The atomic coordinates and thermal parameters, with their estimated standard deviations for non-hydrogen atoms, are given in Tables 3 and 4. The coordinates with isotropic thermal parameters for hydrogen atoms are shown in Table 5.

The Molecular Structure. Tables 6 and 7 show the bond lengths and angles, with their standard deviations. The equations of the least-squares planes for the benzene ring, the carboxyl group, the indole ring, and the aminoethyl group, and the deviations of the individual atoms from these planes are listed in Table 8.

PAA Molecule: The planarity of the benzene ring including the PC7 atom is good, and the bond lengths within the benzene ring are in the range of 1.377 to 1.387 Å (average value: 1.380 Å), significantly shorter than in the standard aromatic ring (1.395±0.003 Å)[8] as well as the smaller PC1–PC7 bond length (1.509 Å). The carbon-oxygen bond lengths in the carboxyl group are both short, but are nearly identical, and the PC7–PC8 bond length (1.521 Å) is close to that of the normal $C(sp^3)$–$C(sp^2)$ single bond.[9] The torsional angles, χ(PC2–PC1–PC7–PC8) and ϕ(PC1–PC7–PC8–PO9), are 64.8° and −168.1° respectively. As these values are similar to those in β-phenethylamine (χ=72.6°, ϕ=−171.1°),[10] the precursor of PAA in a living body, both conformations might be fixed in their metabolic

TABLE 3. ATOMIC COORDINATES (×10⁴) AND THEIR STANDARD DEVIATIONS OF HEAVY ATOMS

Atom	x	y	z
PC1	1681(4)	660(1)	6640(2)
PC2	2023(5)	1351(1)	6990(2)
PC3	3469(5)	1769(2)	6737(2)
PC4	4577(5)	1508(2)	6121(2)
PC5	4203(5)	827(2)	5752(3)
PC6	2776(5)	408(1)	6011(2)
PC7	105(4)	202(2)	6919(2)
PC8	664(4)	39(1)	8097(2)
PO9	−776(3)	−234(1)	8363(1)
PO10	2499(3)	171(1)	8732(1)
TN1	4106(4)	1205(1)	1870(2)
TC2	3888(4)	1277(1)	820(2)
TC3	5661(4)	1574(1)	729(2)
TC4	9170(4)	1969(2)	2225(2)
TC5	10138(5)	2005(2)	3308(3)
TC6	9087(5)	1782(2)	3984(2)
TC7	7056(5)	1500(1)	3594(2)
TC8	6083(4)	1456(1)	2490(2)
TC9	7108(4)	1690(1)	1795(2)
TC10	5979(5)	1741(1)	−298(2)
TC11	7526(4)	1265(1)	−572(2)
TN12	6822(3)	516(1)	−667(2)

TABLE 4. ANISOTROPIC THERMAL PARAMETERS (×10⁴) AND THEIR STANDARD DEVIATIONS OF HEAVY ATOMS

Atom	B_{11}	B_{22}	B_{33}	B_{12}	B_{13}	B_{23}
PC1	215(7)	27(1)	46(2)	−6(4)	50(5)	11(2)
PC2	338(9)	28(1)	61(2)	−4(4)	123(7)	2(2)
PC3	413(10)	26(1)	75(2)	−40(5)	105(8)	4(2)
PC4	322(9)	36(1)	88(2)	−36(5)	132(8)	23(3)
PC5	353(10)	35(1)	107(3)	12(5)	231(9)	16(3)
PC6	322(9)	26(1)	80(2)	6(4)	156(7)	7(2)
PC7	214(7)	40(1)	58(2)	−43(4)	57(6)	9(2)
PC8	184(6)	21(1)	62(2)	−4(3)	111(5)	−3(2)
PO9	235(5)	35(1)	84(1)	−41(3)	181(5)	−8(2)
PO10	204(5)	39(1)	53(1)	−52(3)	48(4)	13(1)
TN1	259(6)	30(1)	95(2)	−40(4)	187(6)	−14(2)
TC2	202(7)	29(1)	82(2)	−12(4)	105(6)	−19(2)
TC3	208(7)	21(1)	68(2)	7(4)	105(6)	2(2)
TC4	225(7)	29(1)	93(2)	−27(4)	93(7)	−9(2)
TC5	300(9)	37(1)	95(3)	−14(5)	30(8)	−17(3)
TC6	435(11)	33(1)	75(2)	37(5)	30(8)	−13(2)
TC7	470(11)	24(1)	77(2)	33(5)	190(8)	1(2)
TC8	279(8)	19(1)	71(2)	1(4)	139(6)	−2(2)
TC9	198(6)	18(1)	70(2)	−3(3)	104(6)	0(2)
TC10	331(9)	28(1)	73(2)	16(4)	128(7)	14(2)
TC11	266(8)	30(1)	73(2)	−27(4)	145(7)	7(2)
TN12	189(5)	29(1)	58(1)	−12(3)	104(5)	1(2)

Table 5. Hydrogen atom coordinates ($\times 10^3$) and isotropic temperature factors, with their standard deviations

Atom	x	y	z	B(Å)
PH2	119(5)	154(2)	743(2)	3.8(7)
PH3	380(5)	228(2)	704(3)	4.8(8)
PH4	564(5)	183(2)	593(2)	4.0(7)
PH5	507(5)	64(2)	527(3)	5.0(8)
PH6	256(5)	−11(2)	569(2)	4.0(7)
PH7A	−8(5)	−28(2)	649(2)	4.2(7)
PH7B	−139(5)	43(2)	665(3)	5.1(8)
TH1	298(6)	90(2)	193(3)	6.1(9)
TH2	254(5)	113(2)	16(2)	3.4(7)
TH4	1008(5)	214(2)	176(3)	5.3(8)
TH5	1174(5)	221(2)	366(2)	4.5(7)
TH6	986(5)	180(2)	486(3)	4.7(8)
TH7	628(5)	135(2)	408(2)	4.3(7)
TH10A	447(4)	171(2)	−93(2)	3.2(6)
TH10B	661(5)	223(2)	−23(3)	4.7(8)
TH11A	768(4)	140(2)	−130(2)	2.9(6)
TH11B	900(4)	129(2)	3(2)	3.1(6)
TH12A	528(5)	41(2)	−98(2)	4.3(7)
TH12B	763(5)	23(2)	−99(2)	3.6(7)
TH12C	716(5)	28(2)	8(2)	3.9(7)

Table 6. Bond lengths and their standard deviations

	PAA		
PC1–PC2	1.387(4)Å	PC1–PC6	1.381(4)Å
PC1–PC7	1.509(4)	PC2–PC3	1.381(5)
PC3–PC4	1.379(5)	PC4–PC5	1.377(5)
PC5–PC6	1.377(5)	PC7–PC8	1.521(4)
PC8–PO9	1.248(3)	PC8–PO10	1.247(3)
	TRP		
TN1 –TC2	1.369(4)	TN1 –TC8	1.375(4)
TC2 –TC3	1.355(4)	TC3 –TC9	1.432(4)
TC3 –TC10	1.497(4)	TC4 –TC5	1.368(5)
TC4 –TC9	1.396(4)	TC5 –TC6	1.392(5)
TC6 –TC7	1.378(5)	TC7 –TC8	1.393(4)
TC8 –TC9	1.407(4)	TC10–TC11	1.512(4)
TC11–TN12	1.491(3)		

process.[11]

The dihedral angle between the benzene ring and the carboxyl group is 110.1°.

TPA Molecule: Three hydrogen atoms found in the difference map are tetrahedrally bound to the nitrogen atom of the aminoethyl side chain, indicating the amino group to be in a cationic form, $-NH_3^+$.

The bond length of TC11–TN12, 1.491 Å, is similar to the normal values reported previously.[12–14] The bond lengths and angles of the indole moiety are normal, in the range found in the crystal structures of indole derivatives.[11] The planarity of the indole ring is better than those of the other tryptamine derivatives.[12,13,15]

The TH1 atom deviates significantly from the indole ring plane, causing the TN1–TN1H···PO9 angle to be 163.0°. The conformation of the tryptamine molecule found in this complex, (χ(TC2–TC3–TC10–TC11)= 107.2° and ϕ(TC3–TC10–TC11–TN12)=−59.8°), is a stable one according to the energy calculation by Pullman *et al.*[16]

Table 7. Bond angles and their standard deviations

PAA	
PC2–PC1–PC6	118.4(3)°
PC6–PC1–PC7	121.0(2)
PC2–PC3–PC4	120.5(3)
PC4–PC5–PC6	120.6(3)
PC1–PC7–PC8	115.8(2)
PC7–PC8–PO10	119.4(2)
PC2–PC1–PC7	120.6(2)
PC1–PC2–PC3	120.6(3)
PC3–PC4–PC5	119.0(3)
PC5–PC6–PC1	120.9(3)
PC7–PC8–PO9	116.6(2)
PO9–PC8–PO10	123.9(2)
TRP	
TC2 –TN1 –TC8	108.6(2)
TC2 –TC3 –TC9	106.2(2)
TC9 –TC3 –TC10	128.3(2)
TC4 –TC5 –TC6	121.1(3)
TC6 –TC7 –TC8	117.2(3)
TC7 –TC8 –TC9	121.9(3)
TC8 –TC9 –TC3	107.2(2)
TC3 –TC9 –TC4	133.8(3)
TC10–TC11–TN12	111.8(2)
TN1 –TC2 –TC3	110.7(3)
TC2 –TC3 –TC10	125.5(3)
TC5 –TC4 –TC9	119.1(3)
TC5 –TC6 –TC7	121.7(3)
TC7 –TC8 –TN1	130.8(3)
TN1 –TC8 –TC9	107.3(2)
TC8 –TC9 –TC4	119.0(3)
TC3 –TC10–TC11	115.2(3)

Although it is influenced by the various crystal-packing forces, it is noteworthy that a similar conformation is also found in the tryptamine hydrochloride[15] and tryptamine picrate[13] crystals, suggesting that this conformation is intrinsic and the most probable one for the tryptamine molecule. The dihedral angle between the indole ring and the aminoethyl group is 77.8°

The Crystal Structure. In the TPA-PAA complex, a salt bridge is formed between the anionic carboxyl group of PAA and the cationic amino group of TPA. The possible hydrogen bonds and the short contacts less than 3.5 Å are given in Table 9. All the hydrogen atoms attached to either an oxygen or nitrogen atom participate in the hydrogen bondings, forming infinite chains along the a-axis, as is shown in Fig. 3. There is no possibility of indole ring-benzene ring interaction, the dihedral angle between these planes being 119.3°.

However, the carboxyl plane of PAA lies fairly parallel to the plane of the indole ring of TPA (dihedral angle, 9.4°), with a 3.52 Å separation on the average, as is shown in Fig. 4. Even though these contact distances are slightly longer than the van der Waals separation, the possibility can not be discarded of the interaction

TABLE 8. DEVIATIONS OF ATOMS FROM THE LEAST-SQUARES PLANES

Equations of the best planes with the $m_1X+m_2Y+m_3Z=d$ formula in an orthogonal space

Plane	m_1	m_2	m_3	d
Benzene ring	0.4760	−0.3310	0.8226	5.5000
Carboxyl group	−0.3829	0.9116	0.1494	2.8673
Indole ring	0.4094	−0.9123	0.0129	−1.3037
Aminoethyl group	0.1825	−0.1360	0.9738	−0.0603

Deviations (in Å) from the best planes

PAA		TRP	
Benzene ring		Indole ring	
PC1*	−0.010	TN1*	0.006
PC2*	0.008	TC2*	0.006
PC3*	0.000	TC3*	−0.009
PC4*	−0.008	TC4*	0.000
PC5*	0.006	TC5*	0.012
PC6*	0.002	TC6*	−0.007
PC7	−0.004	TC7*	−0.005
PH2	0.032	TC8*	0.001
PH3	−0.043	TC9*	−0.004
PH4	−0.001	TC10	−0.030
PH5	0.009	TH1	0.225
PH6	0.021	TH2	0.009
Carboxyl group		TH4	0.026
PC7*	0.001	TH5	0.025
PC8*	−0.005	TH6	0.015
PO9*	0.002	TH7	−0.043
PO10*	0.002	Aminoethyl group	
PC1	−0.287	TC10*	0.0
		TC11*	0.0
		TN12*	0.0
		TC3	1.171

Atoms with asterisks define the plane.

TABLE 9. HYDROGEN BONDS AND SHORT CONTACTS LESS THAN 3.5Å

Superscribed numbers represent symmetry operators.

Hydrogen bonds

Donor	Acceptor	Distance D···A	Distance H···A	Angle D–H···A
TN1[1)]	PO9[5)]	2.821(3)Å	1.87(4)Å	163(3)°
TN12[1)]	PO9[4)]	2.784(3)	1.83(3)	175(3)
TN12[1)]	PO10[2)]	2.788(3)	1.81(3)	168(3)
TN12[1)]	PO10[3)]	2.793(3)	1.75(3)	174(3)

Short contacts

TC2[1)]	PO10[2)]	3.359(3)Å
TN12[1)]	PO9[3)]	3.326(3)
TN12[1)]	PC8[3)]	3.424(3)
TC2[1)]	PO9[5)]	3.323(3)

Symmetry code

Superscript	Symmetry operator		
1)	x	y	z
2)	x	y	$-1+z$
3)	$1-x$	$-y$	$1-z$
4)	$1+x$	y	$-1+z$
5)	$-x$	$-y$	$1-z$

between the polarizable π-electron system and the polar carbonyl group being similar to those in serotonin

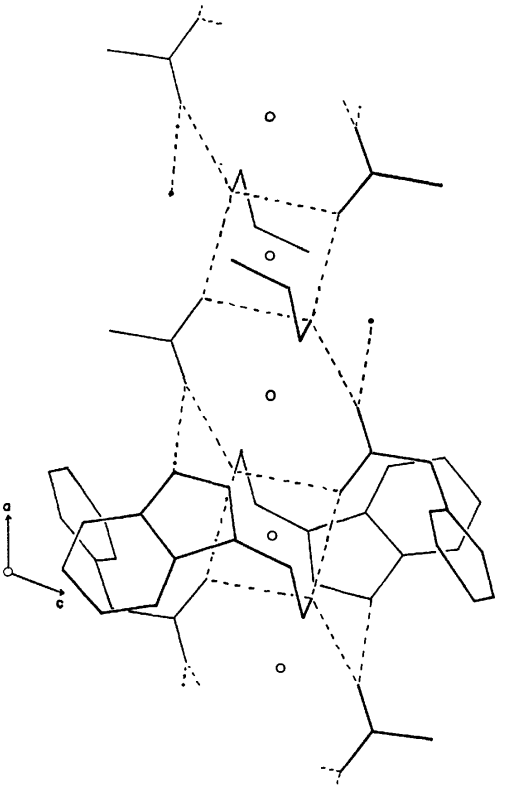

Fig. 3. The hydrogen bond network on the ac-plane found in this complex.

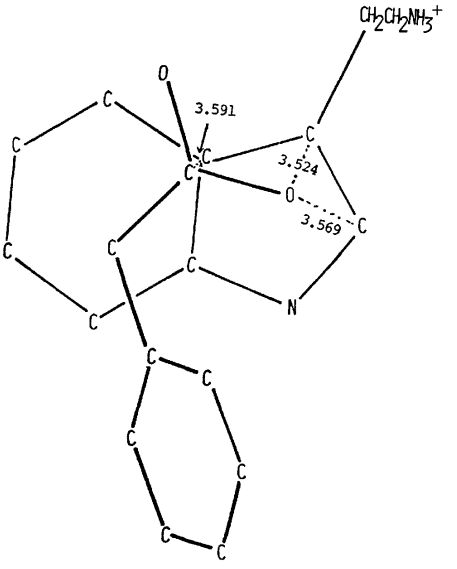

Fig. 4. Geometry of the stacked indole ring and carboxyl group projected to the indole ring plane.

picrate,[14] tryptophan picrate, and tryptamine picrate.[13] As a whole, each of the two complex molecules is hydrogen-bonded around a center of symmetry to form one unit (two TPA and two PAA), and each is stabilized by forming a hydrogen bond with the unit of the neighboring cell, translated in the a-direction (see Figs. 2 and 3), a structure which is held together by van der Waals contact in the b- and c-directions.

In this hydrogen-bonding mode, as a complex of 5-methoxytryptamine–5-methoxyindole-3-acetic acid

and 5-methoxytryptamine-indole-3-acetic acid,[12] one of the carboxyl oxygen atoms forms two hydrogen bonds with two neighboring NH_3^+-groups. The other participates in two hydrogen bonds with a neighboring NH_3^+-group and a nitrogen atom in the indole ring, which may strengthen the hydrogen bond between anionic COO^- and cationic NH_3^+.

References

1) I. Weinryb and R. F. Steiner, *Biochemistry*, **9**, 135 (1970).
2) J. A. D'Anna, Jr., and G. Tollin, *Biochemistry*, **10**, 57 (1971).
3) J. W. Longworth, *Photochem. Photobiol.*, **7**, 587 (1968).
4) T. Tamaki, *Bull. Chem. Soc. Jpn.*, **46**, 2527 (1973).
5) The Universal Crystallographic Computing System (Library Programs in the Computing Center of Osaka University, 1973).
6) "International Tables for X-Ray Crystallography," Vol. 4, Kynoch Press, Birmingham (1974).
7) Table 2 is kept at the Chemical Society of Japan, Kanda, Surugadai, Chiyoda-ku, Tokyo 101 (Document No. 7811).
8) "International Tables for X-Ray Crystallography," Vol. 3, Kynoch Press, Birmingham (1968), p. 276.
9) M. Sundaralingam and E. F. Putkey, *Acta Crystallogr., Sect. B*, **26**, 790 (1970).
10) P. G. Tsoucaris, *Acta Crystallogr.*, **14**, 909 (1961).
11) A. Wakahara, Dissertation, Faculty of Pharm. Sci., Osaka Univ. (1974).
12) T. Sakaki, A. Sogo, A. Wakahara, T. Kanai, T. Fujiwara, and K. Tomita, *Acta Crystallogr., Sect. B*, **32**, 3235 (1976).
13) G. L. Gartland, G. R. Freeman, and C. E. Bugg, *Acta Crystallogr., Sect. B*, **30**, 1841 (1974).
14) U. Thewalt and C. E. Bugg, *Acta Crystallogr., Sect. B*, **28**, 82 (1972).
15) A. Wakahara, T. Fujiwara, and K. Tomita, *Bull. Chem. Soc. Jpn.*, **46**, 2481 (1973).
16) B. Pullman, Ph. Courriére, and H. Berthod, *J. Med. Chem.*, **17**, 439 (1974).

A Study of the Mass Spectrum of Phenazine

Shizuko EGUCHI

Department of Chemistry, Faculty of Science, Hiroshima University, Higashisenda-machi, Hiroshima 730

(Received June 27, 1977)

The mass spectrum of phenazine, a nitrogen-containing aromatic compound, was investigated in detail using a combination of ion kinetic energy spectroscopy and defocusing technique. In the fragmentation of the singly charged ions the molecular ion lost H· in the first stage to give an $[M-1]^+$ or $[M-2]^+$ ion, which was degraded *via* the expulsion of CN· or C_2H_2 in the next stage and of HCN or C_2H_3· in a later stage. Doubly charged ions also appeared in considerable intensity, and the fragmentation sequence differed significantly from that of the singly charged ions.

Although there are some reports[1-4] about the mass spectra of phenazine and substituted phenazines, it cannot be said that the fragmentation mechanism has been fully clarified, because the investigations have usually been carried out in applying mass spectrometry to the analysis of bacterial metabolites. In the present paper, the mass spectrum of phenazine was investigated in detail by determining the elemental compositions of all the fragment ions using high resolution mass spectrometry and by sorting out the metastable ions using a combination of ion kinetic energy spectroscopy and the defocusing technique. Thus, many points which need to be corrected were found in the fragmentation pathway already reported for the phenazine nucleus.

Results and Discussion

In the ordinary mass spectrometry, phenazine, a nitrogen-containing aromatic compound, exhibited a simple spectrum which consisted of weak fragment peaks, except for the intense molecular peak at *m/e* 180, as shown in Fig. 1. For the purpose of determining the multiplicity of the peaks and the elemental composition of each ion, the high resolution mass spectrum was measured with a computer on-line system and/or with a pen-recording system under the conditions of slower magnetic scanning and narrower widths of entrance and collector slits. Seventeen fragment peaks, listed in Table 1, were confirmed to be constituted of two or three ions.

On the other hand, the IKE spectrum[5,6] of phen-

TABLE 1. MULTIPLICITY OF THE SPECTRAL PEAKS AND ELEMENTAL COMPOSITION OF EACH FRAGMENT ION IN THE MASS SPECTRUM OF PHENAZINE

m/e	Elemental composition	%	*m/e*	Elemental composition	%
180	$C_{12}H_8N_2$ (1)	100	100	C_8H_4 (28)	100
179	$C_{12}H_7N_2$ (2)	100	99	C_8H_3 (29)	100
178	$C_{12}H_6N_2$ (3)	100	90	$C_6H_4N_1$ (30)	100
154	$C_{10}H_6N_2$ (4)	42	89	$C_6H_3N_1$ (31)	50
	$C_{11}H_8N_1$ (5)	58		C_7H_5 (32)	50
153	$C_{10}H_5N_2$ (6)	30	78	$C_5H_4N_1$ (33)	75
	$C_{11}H_7N_1$ (7)	70		C_6H_6 (34)	25
152	$C_{11}H_6N_1$ (8)	94	77	$C_5H_3N_1$ (35)	59
	$C_{12}H_8$ (9)	6		C_6H_5 (36)	41
151	$C_{11}H_5N_1$ (10)	100	76	$C_5H_2N_1$ (37)	15
140	$C_{10}H_6N_1$ (11)	100		C_6H_4 (38)	85
129	$C_8H_5N_2$ (12)	54	75	$C_5H_1N_1$ (39)	23
	$C_9H_7N_1$ (13)	46		C_6H_3 (40)	77
128	$C_8H_4N_2$ (14)	trace	74	C_6H_2 (41)	100
	$C_9H_6N_1$ (15)	52	64	$C_4H_2N_1$ (42)	67
	$C_{10}H_8$ (16)	48		C_5H_4 (43)	33
127	$C_9H_5N_1$ (17)	68	63	C_5H_3 (44)	100
	$C_{10}H_7$ (18)	32	62	C_5H_2 (45)	100
126	$C_9H_4N_1$ (19)	20	56	C_4H_8 (46)	100
	$C_{10}H_6$ (20)	80	53	$C_3H_3N_1$ (47)	100
125	$C_9H_3N_1$ (21)	7	52	$C_3H_2N_1$ (48)	24
	$C_{10}H_5$ (22)	93		C_4H_4 (49)	76
103	$C_7H_5N_1$ (23)	100	51	C_4H_3 (50)	100
102	$C_7H_4N_1$ (24)	73	50	C_4H_2 (51)	100
	C_8H_6 (25)	27			
101	$C_7H_3N_1$ (26)	50			
	C_8H_5 (27)	50			

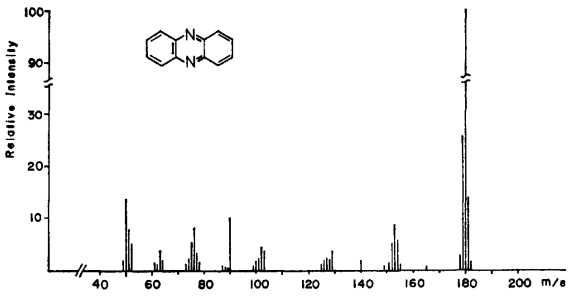

Fig. 1. Ordinary mass spectrum of phenazine.

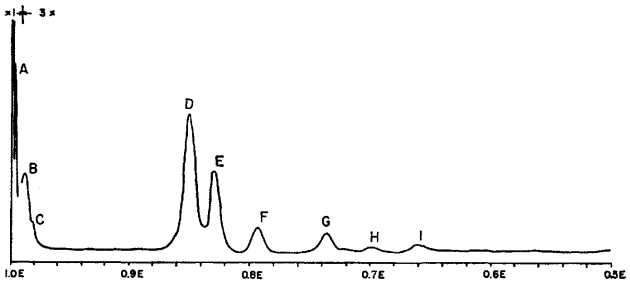

Fig. 2. IKE spectrum of phenazine from $E/2$ to E.

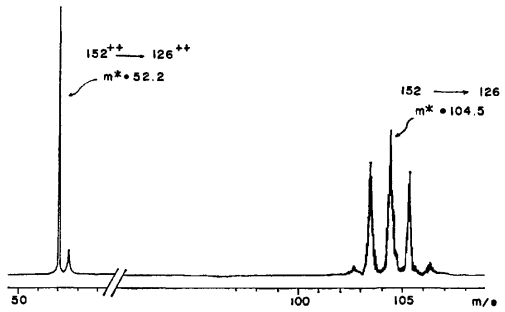

Fig. 3. Metastable ion spectrum at $0.8290E$.

azine was taken over a range of electric sector voltage from $1.0E$ to $0.5E$ (Fig. 2), and then the range corresponding to the width of each peak in this spectrum was searched with magnetic current scanning at $0.0005E$ intervals of the electric sector voltage to determine the number of metastable ions. If some metastable ions are included in a certain peak of the IKE spectrum, they appear in general as separated peaks in the metastable ion specra, such as that shown in Fig. 3. Since each of these metastable peaks, however, slightly varies in the intensity and m/e value depending upon the electric sector voltage used, the reading of the m/e value of a certain metastable ion at the maximum intensity was determined as the mass unit of this metastable ion.[7,8] Based on such analysis, peak E in the IKE spectrum of phenazine was determined to include four metastable ions, at m/e 103.5, 104.5, 105.4, and 52.2, for each of which one or several transitions were listed in Table 2. These transitions were assigned from the elemental compositions of singly and doubly charged ions which are listed in Tables 1 and 4. As shown in Table 2, the observed metastable ion value contained several metastable ions because a metastable ion value could not measured with an accuracy better than 1000 ppm in the present work. Accordingly, a few possible transitions were proposed for the observed metastable ion value; similar results had been reported in the mass spectrum of *N*-cyclohexylguanidine.[9] Similar analyses were also carried out on the other peaks (A—D, F—I) of the IKE spectrum.

Thus, peaks A, B, and C of the IKE spectrum, which were very close to the main beam ion, were characterized as the expulsion of H· or H_2 from the main beam ion and the remaining peaks, from D to I, as the expulsion of C_2H_2, CN·, C_2H_3·, or HCN from the molecular ion or several fragment ions, as listed in Table 3. Among them, transitions due to the loss of a hydrogen molecule such as 180→178+2 and 153→151+2, have not yet been reported in the mass spectra of phenazine and substituted phenazines, nor in those of other nitrogen-containing aromatic compounds. However, no metastable ions, which would correspond to the direct expulsion of fragments such as C_2H_2, CN·, C_2H_3·, or

Table 2. Exact masses of the metastable ions included in peak E of IKE spectrum and transition assignment

Transition				Calcd $\gamma=E_1/E$	Calcd m^*	Obsd m^*
153		127				
$C_{10}H_5N_2^+$ (30%)	→	$C_9H_5N_1^+$ (68%)	+ CN·	0.8300 (9)	105.46	
$C_{11}H_7N_1^+$ (70%)	↗	$C_9H_5N_1^+$	+ C_2H_2	0.8300 (2)	105.45	105.4
	↘	$C_{10}H_7^+$ (32%)	+ CN·	0.8301 (1)	105.47	
152		126				
$C_{11}H_6N_1^+$ (94%)	↗	$C_9H_4N_1^+$ (20%)	+ C_2H_2	0.8289 (0)	104.47	
	↘	$C_{10}H_6^+$ (80%)	+ CN·	0.8289 (8)	104.49	104.5
$C_{12}H_8^+$ (6%)	→	$C_{10}H_6^+$	+ C_2H_2	0.8289 (2)	104.48	
$C_{12}H_8^{2+}$ (100%)	→	$C_{10}H_6^{2+}$ (100%)	+ C_2H_2	0.8289 (1)	52.24	52.2
151		125				
$C_{11}H_5N_1^+$ (100%)	↗	$C_9H_3N_1^+$ (7%)	+ C_2H_2	0.8277 (5)	103.49	103.5
	↘	$C_{10}H_5^+$ (93%)	+ CN·	0.8278 (4)	103.51	

Table 3. Exact masses of the metastable ions in the IKE spectrum and the transition assignment

Peak in IKE spectrum	Transition $m_1 \rightarrow m_2 + (m_1 - m_2)$	Lost element. comp.	Obsd m^*
A	$180^+ \rightarrow 179^+ + 1$	H	178.0
	$179^+ \rightarrow 178^+ + 1$	H	177.0
	$154^+ \rightarrow 153^+ + 1$	H	152.0
	$153^+ \rightarrow 152^+ + 1$	H	151.0
	$152^+ \rightarrow 151^+ + 1$	H	150.0
B	$180^+ \rightarrow 178^+ + 2$	H_2	176.0
	$153^+ \rightarrow 151^+ + 2$	H_2	149.0
	$77^+ \rightarrow 76^+ + 1$	H	75.0
	$76^+ \rightarrow 75^+ + 1$	H	74.0
	$75^+ \rightarrow 74^+ + 1$	H	73.0
C	$51^+ \rightarrow 50^+ + 1$	H	49.0
D	$179^+ \rightarrow 153^+ + 26$	C_2H_2 or CN	130.8
	$178^+ \rightarrow 152^+ + 26$	C_2H_2 or CN	129.8
	$180^{2+} \rightarrow 152^{2+} + 28$	N_2	64.2
E	$153^+ \rightarrow 127^+ + 26$	C_2H_2 or CN	105.4
	$152^+ \rightarrow 126^+ + 26$	C_2H_2 or CN	104.5
	$151^+ \rightarrow 125^+ + 26$	C_2H_2 or CN	103.5
	$152^{2+} \rightarrow 126^{2+} + 26$	C_2H_2	52.2
F	$126^+ \rightarrow 100^+ + 26$	C_2H_2	79.4
	$125^+ \rightarrow 99^+ + 26$	C_2H_2 or CN	78.4
	$128^+ \rightarrow 101^+ + 27$	C_2H_3 or HCN	79.7
	$126^{2+} \rightarrow 100^{2+} + 26$	C_2H_2	39.7
G	$103^+ \rightarrow 76^+ + 27$	C_2H_3 or HCN	56.1
	$102^+ \rightarrow 75^+ + 27$	C_2H_3 or HCN	55.1
H	$90^+ \rightarrow 63^+ + 27$	C_2H_3 or HCN	44.1
I	$77^+ \rightarrow 50^+ + 27$	C_2H_3 or HCN	32.5
	$152^{2+} \rightarrow 100^{2+} + 52$	C_4H_4	32.8

HCN from the molecular ion, could be detected. From the above observation, it may be concluded that the major fragmentation of phenazine undergoes nuclear cleavage not directly, as described by other workers,[1-4] but after the loss of H· or H_2.

On the basis of the elemental composition of the fragment ions and the transition assignment of the metastable ions, the significant fragmentation sequence of the singly charged ion in phenazine was deduced as shown in Scheme 1. The loss of H· from the molecular ion (1) yielded a $C_{12}H_7N_2$ ion (*m/e* 179) (2) as the most abundant fragment ion in the spectrum. The ion (2) gave two kinds of *m/e* 153 ions, $C_{10}H_5N_2$ (6) and $C_{11}H_7N$ (7), in a ratio of 30: 70 under expulsion of C_2H_2 and CN·, respectively. The ion (6) produced C_9H_5N (*m/e* 127) (17) under expulsion of CN·, and the ion (7) subsequently lost C_2H_2, CN·, or H_2 to be degraded to C_9H_5N (*m/e* 127, 68%) (17), $C_{10}H_7$ (*m/e* 127, 32%) (18), or $C_{11}H_5N$ (*m/e* 151) (10). There are two pathways for the C_9H_5N ion (17), but the route *via* the $C_{11}H_7N$ (7) was thought to be predominant from the above-mentioned relative intensity of the intermediate ions.

The molecular ion was further degraded *via* the second pathway, including successive losses of H_2 and CN·, to give a $C_{11}H_6N$ ion (*m/e* 152) (8), which was then degraded to a C_8H_4 ion (*m/e* 100) (28) *via* a C_9H_4N (*m/e* 126) (19) and a $C_{10}H_6$ (*m/e* 126) (20) in a ratio of 20: 80, and which lost H· to give an ion of $C_{11}H_5N$ (*m/e* 151) (10). In the formation of $C_{12}H_8$ ion (*m/e* 152, 6%) (9) which was degraded to $C_{10}H_6$ (*m/e* 126, 20%) (20) under expulsion of C_2H_2, the metastable ion corresponding to the transition from molecular ion to the ion (9) was not detected.

Furthermore, the ion (10) which was formed by loss of H_2 from the ion (7) and of H· from the ion (8) degraded to C_8H_3 (*m/e* 99) (29) *via* a C_9H_3N (*m/e* 125) (21) and a $C_{10}H_5$ ion (*m/e* 125) (22) in a ratio of 7: 93.

In the smaller fragment range of the ordinary mass

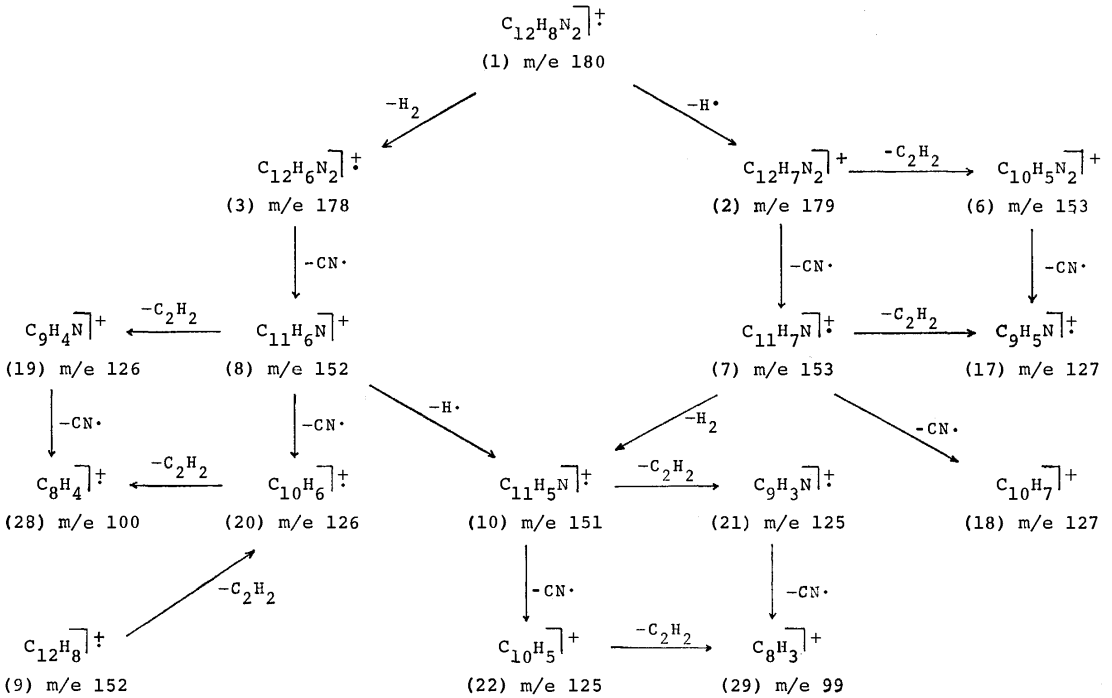

Scheme 1. Fragmentation sequence of singly charged ions of phenazine supported by metastable ion.

Table 4. Elemental compositions of doubly charged ions of phenazine

Obsd mass m/e	Mass of biradical ion $m/e \times 2$	Calcd for elemental composition	$\Delta m.u.$ (1×10^{-3})	Elemental composition
90.0344	180.0688	180.0687	0.1	$C_{12}H_8N_2$
76.0290	152.0580	152.0624	4.4	$C_{12}H_8(M-N_2)$
63.0219	126.0438	126.0468	3.0	$C_{10}H_6(M-C_2H_2N_2)$
50.0155	100.0310	100.0312	0.2	$C_8H_4(M-C_4H_4N_2)$

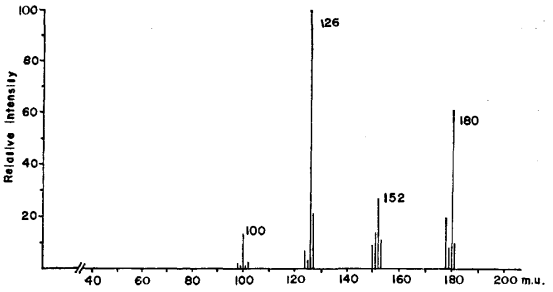

Fig. 4. $2E$ doubly charged ion spectrum of phenazine.

spectrum of phenazine, two ions appeared at m/e 90 and 63, and also the metastable ion corresponding to the transition between both ions could be detected at m/e 44.1 by the above-mentioned analysis of the IKE spectrum. However, the aromatic structure of phenazine and the fact that the metastable ion was far too weak (peak H in Fig. 2) compared with the intensities of the precursor and daughter ions in the ordinary mass spectrum were expected that doubly charged ions existed in the mass spectrum of phenazine. For these reason, the $2E$ doubly charged ion spectrum was taken by setting the electric sector voltage at twice the value used for accelerating.[6,10-12] This exhibited the characteristic ions shown in Fig. 4, whose elemental compositions were determined from the exact masses accordingly to a procedure[12] reported previously (Table 4). These observations revealed that m/e 90, 76, 63, and 50 ions in the ordinary spectrum were partly composed of doubly charged ions of 180, 152, 126, and 100 mass units respectively. The major fragmentation sequence of the doubly charged ions of phenazine was thus deduced to be Scheme 2.

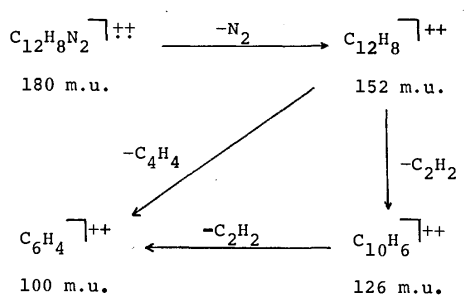

Scheme 2. Fragmentation sequence of doubly charged ions of phenazine.

Ion kinetic energy spectra of organic molecules show peaks corresponding to ions having energies in excess of that of the main beam ion. It has been shown that the peaks correspond to charge-exchange reactions of

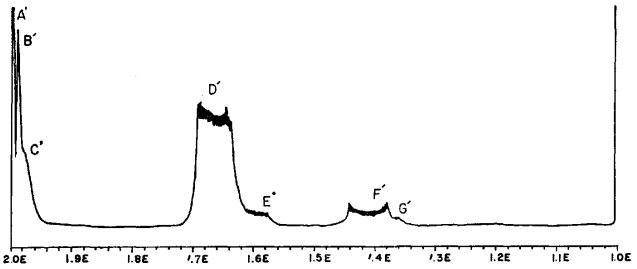

Fig. 5. High energy IKE spectrum from E to $2E$.

doubly charged ions or to decompositions of metastable clusters of ions in high energy IKE spectra of aromatic hydrocarbons.[11] The above reactions were expected from the existence of the doubly charged ions detected in the phenazine, and therefore the high energy IKE spectrum was measured over the range from E to $2E$ (Fig. 5). Peaks that appear between E to $2E$ in the high energy IKE spectrum may be due to one of two separate processes including doubly charged ions: collision-induced charge transfers and charge separation reactions. Peak A', which appears exactly at $2.0E$, is

Table 5. Transitions assignment of high energy IKE spectrum of phenazine

Peak in IKE spectrum	Transition $m_1 \rightarrow m_2 + (m_1 - m_2)$	Calcd γ[a]
A'	$180^{2+} \rightarrow 180^+$	2.0
	$179^{2+} \rightarrow 179^+$	2.0
	$178^{2+} \rightarrow 178^+$	2.0
	$153^{2+} \rightarrow 153^+$	2.0
	$152^{2+} \rightarrow 152^+$	2.0
	$151^{2+} \rightarrow 151^+$	2.0
	$150^{2+} \rightarrow 150^+$	2.0
	$127^{2+} \rightarrow 127^+$	2.0
	$126^{2+} \rightarrow 126^+$	2.0
	$102^{2+} \rightarrow 102^+$	2.0
	$100^{2+} \rightarrow 100^+$	2.0
B'	$180^{2+} \rightarrow 179^+$	1.989
	$153^{2+} \rightarrow 152^+$	1.987
	$152^{2+} \rightarrow 151^+$	1.987
	$126^{2+} \rightarrow 125^+$	1.984
C'	$180^{2+} \rightarrow 178^+$	1.974
	$152^{2+} \rightarrow 150^+$	1.974
D'	$180^{2+} \rightarrow 152^+ + 28^+$	1.689
	$178^{2+} \rightarrow 150^+ + 28^+$	1.685
	$152^{2+} \rightarrow 126^+ + 26^+$	1.685
	$150^{2+} \rightarrow 124^+ + 26^+$	1.653
E'	$126^{2+} \rightarrow 100^+ + 26^+$	1.587
F'	$178^{2+} \rightarrow 126^+ + 52^+$	1.416
G'	$126^{2+} \rightarrow 87^+ + 39^+$	1.381

a) γ: Electric sector voltage ratio, E_1/E.

due to the collision-induced reaction in which doubly charged ions are converted to singly charged ions without loss of any mass units. Peak B′ is due to a reaction in which a doubly charged ion not only loses a charge but also a fragment of one mass unit:

$$m_1^{2+} \xrightarrow{\text{collision}} m_1^{+} \longrightarrow (m-1)^{+}$$

or

$$m_1^{2+} \longrightarrow (m-1)^{2+} \xrightarrow{\text{collision}} (m-1)^{+}$$

But these two processes cannot be distinguished in the present work. Similarly, peak C′ is due to a reaction in which two hydrogen atoms with one charge are lost. Other peaks, D′ to G′, were constituted of some broad dish-topped peaks which were known to be attributable to $m_1^{2+} \rightarrow m_2^{+} + (m_1 - m_2)^{+}$ type decompositions of the doubly charged ions.[13] Mass analyses of the above-mentioned peaks were carefully carried out with a interval of $0.0005E$ in the electric sector voltage to determine metastable ions. The resulted assignments of reactions and transitions are listed in Table 5.

Conclusion

The metastable ion transition, which occurred in the first free region of the mass spectrometer, was analyzed in detail by utilizing the ion kinetic energy spectroscopy and the defocusing technique. It was clarified that the molecular ion of phenazine lost H· or H_2 in the first stage of the fragmentation to give $[M-H]^+$ or $[M-H_2]^+$ ion, which was degraded step by step *via* expulsion of CN· or C_2H_2 and successive expulsion of HCN or C_2H_3·.

Doubly charged ions were also confirmed to occur to a certain extent in the mass spectrum of phenazine. The metastable transition of these ions was similarly analyzed and a fragmentation sequence was proposed.

Experimental

The high resolution mass spectra were taken using an on-line system which combined a HITAC-10 computer with a Hitachi RMU-7L double focusing mass spectrometer: ionizing energy 70 eV, ionizing current 80 μA, and accelerating voltage 3.2 kV. For determining multiplicity of peaks and elemental composition of ions, singly changed ion spectra were taken at 10 and 8 μm widths of entrance and collector slits respectively (normally 20 and 17 μm). The IKE and metastable ion spectra were examined on the RMU-7L modified with a metastable defocusing attachment.

On the other hand, the $2E$ doubly charged ion spectrum was taken at an electric sector voltage twice as large as the normally used accerating voltage, under 5×10^{-6} Torr of source pressure. For analysis of the transition from a $2E$ doubly charged ion to two singly charged ions, the high energy IKE spectrum was taken over the sector voltage from E, at which the main beam of stable ion was transmitted, to $2E$, and the mass units of the metastable ions were determined under the condition of the $2E$ spectrum measurment.

The author wishes to express her hearty gratitude to Prof. Shûichi Hayashi and Asst. Prof. Mitsuru Nakayama, Faculty of Science, Hiroshima University, for suggesting this investigation and for the constant guidance in the course of this study. Thanks are also given to Prof. Hisao Nakata, Aichi Kyoiku University, for his helpful discussions.

References

1) Y. Morita, *Chem. Pharm. Bull.*, **14**, 426 (1966).
2) F. G. Holliman, R. A. W. Johnstone, and B. J. Millard, *J. Chem. Soc., C*, **1967**, 2351.
3) H. Budzikiewicz, C. Djerassi, and D. H. William, "Mass Spectrometry of Organic Compounds," Holden-Day, San Francisco (1967), p. 584.
4) Q. N. Porter and J. Baldas, "Mass Spectrometry of Heterocyclic Compounds," Wiely-Interscience, New York (1971), p. 497.
5) J. H. Beynon, R. M. Caprioli, and W. F. Baitinger, *Chem. Commun.*, **1969**, 723.
6) J. H. Beynon, R. M. Caprioli, W. F. Baitinger, and J. W. Amy, *Int. J. Mass Spectrom. Ion Phys.*, **3**, 313 (1969).
7) E. Tajima and J. Seibl, *Int. J. Mass Spectrom. Ion Phys.*, **3**, 245 (1969).
8) M. Nakayama, S. Eguchi, A. Matsuo, and S. Hayashi, *Shitsuryobunseki*, **21**, 101 (1973).
9) J. H. Beynon, J. A. Hopkinson, and A. E. Williams, *Org. Mass Spectrom.*, **1**, 169 (1968).
10) T. Ast, J. H. Beynon, and R. G. Cooks, *Org. Mass Spectrom.*, **6**, 749 (1972).
11) J. H. Beynon, R. M. Caprioli, W. F. Baitinger, and J. W. Amy, *Org. Mass Spectrom.*, **3**, 455 (1970).
12) S. Eguchi, M. Nakayama, and S. Hayashi, *Org. Mass Spectrom.*, **11**, 574 (1976).
13) R. G. Cooks, J. H. Beynon, R. M. Caprioli, and G. R. Lester, "Metastable Ions," Elsevier, Amsterdam(1973), p. 192.

^{13}C Spin-lattice Relaxation and Molecular Structure. II.[1] The Application of ^{13}C Spin-lattice Relaxation Times (T_1) to Assignments of Signals in the Proton-decoupled ^{13}C NMR Spectrum of 5-Ethyl-5*H*-dibenzophosphole

Teruyuki HAYASHI and Hiroshi NAKANISHI

National Chemical Laboratory for Industry, Hon-machi, Shibuya-ku, Tokyo 151

(Received July 4, 1977)

The spin-lattice relaxation times (T_1) of the ^{13}C nuclei in 5-ethyl-5*H*-dibenzophosphole (**1**) were studied. The ^{13}C NMR signals of the quarternary carbons of **1** in the aromatic region, whose assignments are very difficult by other techniques, were successfully assigned by means of the spin-lattice relaxation method. The dipolar relaxation terms and their reciprocal values were calculated by the use of the internuclear-distances between the carbon nuclei and hydrogen or phosphorus ones, and were compared with the observed T_1 values. It was found by studying the observed T_1's of the ethyl group in **1** that the rotation around the C–P bond is more strongly restricted than that around the C–C single bond.

As the recent development of the FT method in NMR spectroscopy has facilitated the measurement of ^{13}C spin-lattice relaxation times (T_1), the application of the T_1 method to the study of molecular geometries and motions is a recently developing field.[1-3] Moreover, the T_1 method has become a useful method for the assignment of signals in the ^1H-decoupled ^{13}C NMR spectra of various organic molecules.[4]

In the study of the catalytic hydroformylation of olefins by rhodium- or cobalt-tertiary phosphine complexes, dibenzophospholyl derivatives have been revealed to be efficient catalyst ligands.[5] In the course of the spectroscopic elucidation of the effectiveness of the catalysts, it was necessary to assign the ^{13}C NMR signals of the dibenzophospholes.[5] Moreover, the signal assignments of ring carbons are important for the study of the aromaticity of phospholes.[6] However, it is very difficult to assign the signals of quaternary carbons in dibenzophospholes by techniques such as those employing the chemical shifts and the coupling patterns of J_{CH} in the ^1H-undecoupled ^{13}C spectrum. In addition, the coupling constants between the carbon and phosphorus nuclei (J_{CP}) cannot give us fully conclusive information about the signal assignments, as will be described later. In the view of these factors, the spin-lattice relaxation method is expected to be useful to overcome the difficulty.

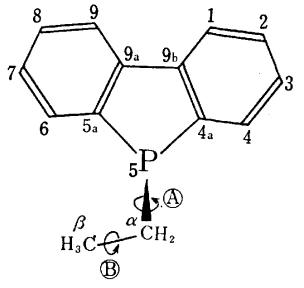

In this report, we will describe the first application of the T_1 method to the ^{13}C NMR signal assignments of a tertiary phosphine, choosing 5-ethyl-5*H*-dibenzophosphole (**1**) as an example. The internal rotation of the ethyl group of **1** will also be discussed briefly.

Experimental

Materials. The 5-ethyl-5*H*-dibenzophosphole (**1**) and ethyldiphenylphosphine (**2**) were prepared according to a procedure similar to that used for 5-benzyl-5*H*-dibenzophosphole[7] in a pure nitrogen atmosphere. **1** and **2** were NMR spectroscopically pure.

Spectral Measurements. The ^{13}C NMR spectra were recorded on a NEVA NV-14 spectrometer operating at 15.087 MHz with a Varian 620/L computer (16 K) for a pulse FT method. The T_1's were determined by the usual 180°-τ-90° pulse-sequence method. The pulse-delay time was set at five times greater than the longest T_1 to be measured. Free induction decays were accumulated for from 40 to 400 times. The spectral width was 1000 Hz for the aromatic carbon signals and 600 Hz for the alkyl carbon signals. In order to avoid the oxidation of the phosphine and the influence of the dissolved oxygen on the T_1 value of each nucleus, the sample containing degassed 20 vol% of acetone-d_6 was sealed under pure nitrogen. The T_1 values were evaluated by means of the least-squares method, using from 6 to 8 data points. The errors of the T_1 values thus obtained are smaller than *ca.* 10%.

Results and Discussion

The ^1H-decoupled ^{13}C spectrum of **1** is shown in Fig. 1. The peaks are alphabetically labelled from the lowest field as is shown in Fig. 1. Although **1** has eight kinds of carbons, the ^1H-decoupled ^{13}C spectrum consists of fourteen peaks due to various couplings (J_{CP}) between carbon-13 and phosphorus nuclei. The usual and easiest way to assign these signals is to obtain the information by investigating the coupling constants, J_{CH} in a ^1H- and ^{31}P-undecoupled ^{13}C spectrum or J_{CP} in a ^1H-decoupled ^{31}P-undecoupled ^{13}C spectrum. In the former technique, however, full information cannot be obtained because of the considerable overlapping of peaks in the aromatic region,* although in the alkyl region, the higher-field peaks of M and N can be assigned to the methyl carbon based on their coupling patterns. On the other hand, in the latter technique, it was expected that the assignment might be made by

* It can only be said that the A—D peaks are assigned to quarternary carbons at the 4a(5a) and 9a(9b) positions.

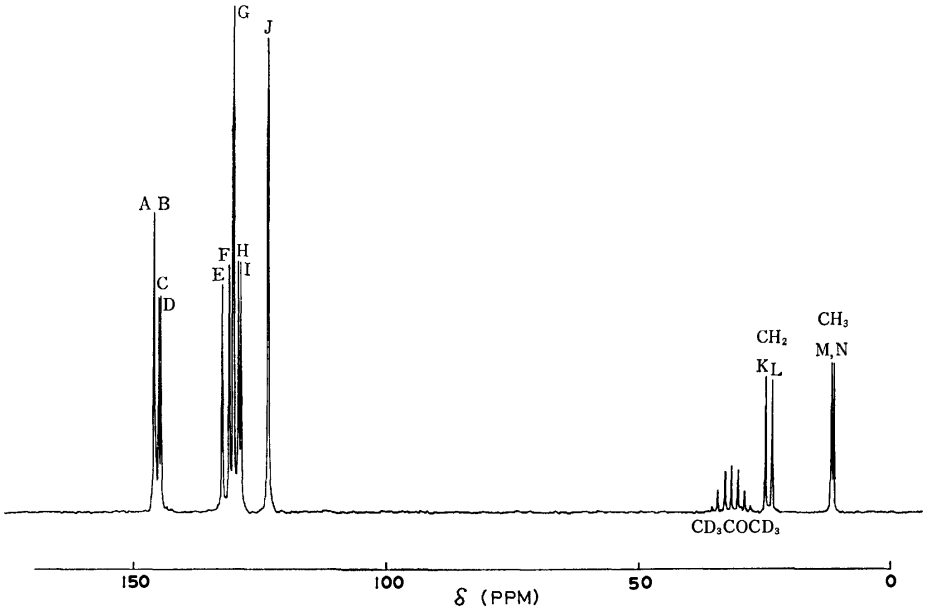

Fig. 1. The ^{1}H decoupled ^{31}P undecoupled ^{13}C NMR spectrum of **1** (at 15.087 MHz, spectrum width: 3300 Hz, pulse width: 35 μs, pulse delay: 25 s, accumulation: 3200 times, sensitivity enhancement: 0.2 s, ^{2}D lock).

considering the differences in the values of the coupling constants between the phosphorus and carbon nuclei at the α, β, γ, and δ positions. Unfortunately, however, the coupling constant between α-carbon and the phosphorus nuclei ($^{\alpha}J_{CP}$) is not always larger than that between β-carbon and the phosphorus nuclei ($^{\beta}J_{CP}$).[8,9] In addition, it was found that the order in the coupling constants of methylene and methyl carbons ($^{\alpha}J_{CP}$ and $^{\beta}J_{CP}$) is reversed in **1** and in ethyldiphenylphosphine (**2**), as is shown in Table 1. Therefore, the straightforward assignment of, for example, quarternary carbons at 4a(5a) and 9a(9b) cannot be made from the J_{CP} coupling constants.

Table 1. The coupling constants[a] between the phosphorus and α- and β-carbon nuclei of the ethyl group in **1** and **2**

Compound	$^{\alpha}J_{CP}(CH_2)$ Hz	$^{\beta}J_{CP}(CH_3)$ Hz
1	19.0	6.6
2[b]	10.9	16.9

a) The signs of these coupling constants are not taken into account. b) The values reported in Ref. 8 are the reverse of our data. Probably, the literature data is somehow a mistake.

The third method for the assignment is the comparison of chemical shifts of **1** with those of structurally analogous compounds, for example, **2**. Since the five-membered ring in **1** is strained because of the deviations of the bond angles at the sp^2 carbon and phosphorus atoms from 120 and 109.5° respectively, and since the aromaticity[6] in the ring of **1** may make the situation more complex, the chemical shifts of C(4a), C(5a), C(9a), and C(9b) in **1** cannot be directly compared with those in **2**.

Therefore, the spin-lattice relaxation method was employed to overcome these difficulties, since T_1 is a quantity closely related to molecular structures and motions.

As the ^{13}C NMR spectrum of **1** in this study is a ^{1}H-decoupled and ^{31}P-undecoupled ^{13}C spectrum, its spin system contains spin-spin couplings (J_{CP}). It is generally considered[10–16] that the T_1's in such a spin system with spin-spin coupling as **1** are complex and different from those in a spin system without spin-spin couplings, because the presence of cross-correlation phenomena between the coupling nuclei may influence the T_1 values. For example, the longitudinal components (T_1 components) of the magnetic moments in the former spin system do not show simple exponential decays by a dipole-dipole relaxation mechanism, whereas in the latter spin system (*e.g.*, in a ^{1}H- and ^{31}P-decoupled ^{13}C spectrum of **1**) they show simple exponential decays. In our case, however, the cross-correlation is expected to be negligibly small because of the extremely remote resonances of carbon-13 and the phosphorus nuclei: $|J_{CP}|/(\omega_P-\omega_C) \ll 1$, ($|J_{CP}| \leqq 21.3$ Hz, and $\omega_P-\omega_C=9.2$ MHz at 15.1 MHz for ^{13}C nuclei). If this is not the case, the decay curves of the longitudinal components of the magnetic moments in the ^{13}C nuclei of **1** cannot be described by a single exponential decay.[11] Actually, the experimentally obtained decay curves unambiguously show straight lines in all peaks of **1**. The decay curves of Peaks A—D are shown in Fig. 2 as examples. Moreover, if the cross-correlation effect is large, the T_1 value of one peak in the doublet signal in **1** must be different from that of the other peak.[10–11] However, the obtained "apparent" T_1 value** of one peak in the doublet is almost the same as that of the other counter-peak, within the limits of experimental error, as is

** T_1 values which are evaluated by means of the usual method used for a decoupled spin system.

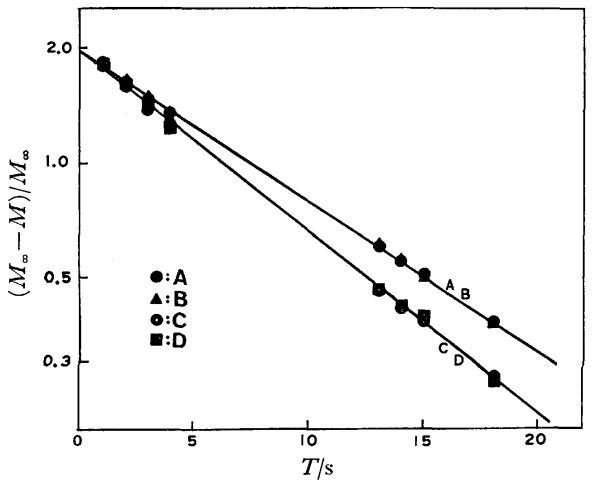

Fig. 2. The semi-log plot of $(M_\infty - M)/M_\infty$ versus pulse delay time (T) of the peaks A—D in the ^1H decoupled ^{31}P undecoupled ^{13}C NMR spectrum of **1**.

TABLE 2. THE CHEMICAL SHIFTS (δ, FROM TMS INTERNAL), COUPLING CONSTANTS ($|J_{CP}|$), T_1 VALUES, AND ASSIGNMENTS OF THE PEAKS IN **1**

Peak	δ / ppm	$\lvert J_{CP}\rvert$ / Hz	T_1 / s	Carbon
A, B	144.7	1.5	10.9, 11.3	9a, 9b
C, D	143.6	6.7	9.3, 9.2	4a, 5a
E, F	130.6	21.3	0.45, 0.44	
G	129.1	0	0.41	
H, I	127.9	7.4	0.40, 0.39	
J	122.1	0	0.44	
K, L	22.5	19.0	0.56, 0.49	$\alpha(CH_2)$
M, N	9.5	6.6	1.8, 1.9	$\beta(CH_3)$

shown in Table 2. Thus, these results indicate that, in the case of **1**, the "true" T_1 values should be almost the same as the "apparent" T_1 values of the doublet peaks of the carbon-13 signals. From now on, for convenience, in this paper we will refer to the "apparent" T_1 values as T_1 values.

Although ^{13}C nuclei can be relaxed by four mechanisms (dipole-dipole, spin-rotation, chemical shift anisotropy, and scalar mechanisms), the latter three mechanisms can be excluded in the case of **1**, because **1** is a considerably large molecule and the obtained T_1's are relatively small (<12 s). The T_1 by the dipole-dipole mechanism is described as the following equation:

$$\frac{1}{T_1^{dd}} = \hbar^2\gamma_C^2\left\{\gamma_H^2\sum_i\frac{N_i}{r_i(CH)^6} + \gamma_P^2\frac{1}{r(CP)^6}\right\}\tau_c, \quad (1)$$

where γ_C, γ_H, and γ_P are the gyromagnetic ratio of carbon-13, hydrogen, and phosphorus respectively, N is the number of equivalent nuclei, r is the internuclear distance, and τ_c is the correlation time. It can be assumed, considering the molecular shape, that an isotropic (or pseudoisotropic) overall tumbling motion

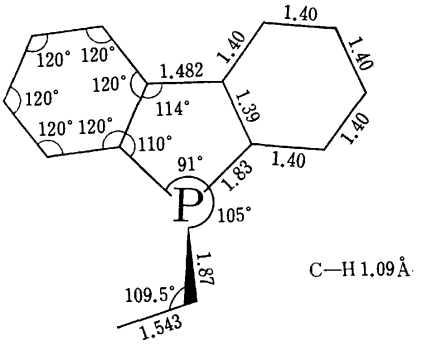

Fig. 3. The assumed bond lengths and bond angles of **1**.

occurs in **1**. Thus, the common correlation time τ_c, may be adopted for carbons in the dibenzophospholyl moiety, but for the ethyl carbons the τ_c's by both the tumbling motion and the internal rotation must be considered.

The molecular geometry of **1** was assumed to be as is shown in Fig. 3. The bond lengths and bond angles described in Fig. 3 were assumed by analogy with ethane, benzene, triphenylphosphine,[17] benzylphosphole,[18] and a metal complex of **1**.[19] According to Eq. 1, the value of the dipolar term, $[\sum_j\hbar^2\gamma_C^2\gamma_{X(j)}^2(\sum_i N_i/r_i^6)]$ (X(j): nuclei which relax the carbon-13 nucleus), and its reciprocal, $[T_1\cdot\tau_c]$, were calculated*** using the internuclear-distances, r_{CH} and r_{CP}, evaluated from these data. The results are shown in Table 3.

TABLE 3. THE CALCULATED DIPOLAR TERMS[a] AND THEIR RECIPROCAL ($T_1\cdot\tau_c$) VALUES OF THE CARBONS IN **1**

Carbon	Dipolar term / 10^{10} s^{-2}	$T_1\cdot\tau_c$ / 10^{-11} s^2
1, 9	2.18	4.59
2, 8	2.22	4.50
3, 7	2.22	4.50
4, 6	2.19	4.57
4a, 5a	0.0568	176
9a, 9b	0.0428	234
$\alpha(CH_2)$	4.41	2.27
$\beta(CH_3)$	6.51	1.54

a) $\equiv\sum_j\hbar^2\gamma_C^2\gamma_{X(j)}^2\left(\sum_i\frac{N_i}{r_i^6}\right)$.

Quarternary Carbons. C(4a) mainly relaxes by one β-hydrogen, four γ-hydrogen, and one α-phosphorus nuclei, while C(9a) mainly relaxes by one β-hydrogen, three γ-hydrogen, and one β-phosphorus nuclei. The calculations show that the contribution to the relaxation by δ-positioned nuclei is negligibly small. The differences in the number and position of the counter-atoms for relaxation cause the deviation of the dipole-dipole relaxation times of the carbons with a common tumbling

*** The deviation of the assumed bond-length from the real one is expected to be not more than the amount whose contribution is estimated to be less than 5% of the $T_1\cdot\tau_c$ value, judging from the X-ray analylsis data of triphenylphosphine,[17] benzylphosphole,[18] and the metal complex of **1**.[19]

motion. The observed T_1 values of Peaks A—D are much greater than those of Peaks E—J. This indicates that Peaks A—D must be assigned to the quarternary carbons, 4a(5a) and 9a(9b). In comparison with the observed T_1 and calculated $T_1 \cdot \tau_c$ values (see Tables 2 and 3), Peaks A and B are assigned to carbons 9a and 9b, and Peaks C and D, to carbons 4a and 5a. The observed T_1 ratio between C(9a) and C(4a) is in excellent agreement with the calculated T_1 ratio: $T_1(9a)^{obsd}/T_1(4a)^{obsd}=1.2$ and $T_1(9a)^{calcd}/T_1(4a)^{calcd}=1.3$. This means that the few assumptions made in this investigation are sufficiently valid.

Aromatic CH Carbons. All the calculated $T_1 \cdot \tau_c$ values of aromatic CH carbons are almost the same. Although the numbers and positions of the counter-atoms for the relaxation are different from each other in the aromatic CH carbons, the contribution to the relaxation by the α-hydrogen nuclei is overwhelmingly large. The observed T_1 values are almost the same, within the limits of experimental error (0.39—0.45 s). The equality in the observed T_1's of four kinds of aromatic CH carbons and the same calculated $T_1 \cdot \tau_c$ values indicate that all these carbons have a common correlation time, τ_c; an isotropic tumbling motion occurs in **1**. Therefore, we cannot obtain any information about the assignment of the aromatic CH carbons in **1** by means of the T_1 technique.

Ethyl Carbons. As has been described before, Peaks K and L were assigned to the methylene carbon, and Peaks M and N, to the methyl carbon, judging from their coupling patterns in ^{1}H-undecoupled ^{13}C spectrum. As the methylene carbon is bonded to two hydrogen (H) atoms and one phosphorus atom as the counter-atoms for the dipolar relaxation, and the methyl carbon, to three H atoms, the T_1's of these carbons may be expected to be different from each other. The calculated $T_1 \cdot \tau_c$ values are 2.27×10^{-11} s^2 for CH_2 and 1.54×10^{-11} s^2 for CH_3. However, the observed T_1's are the opposite; 0.53 s for CH_2 and 1.8 s for CH_3. The results indicate that the correlation times (τ_c) of the methylene and methyl carbons are quite different from each other, and the observed T_1's show that the rate of the internal rotation of the methyl group (B) is much faster than that of the internal rotation of the ethyl group (A) (*cf.* Eq. 1). This is an unexpected result, for the rotation around the C(sp^3)–C(sp^3) bond is known to be more strongly restricted than that around the C–P bond. For example, it is known from microwave spectroscopy that the rotational barrier around the C–C bond in isobutane is higher than that around the C–P bond in trimethylphosphine,[20] and that the barrier in ethane[21] is higher than that in methylphosphine,[22] as is shown below: V/(kcal/mol); $(CH_3)_3CH$: 3.9,[20] $(CH_3)_3P$: 2.6,[20] CH_3-CH_3: 3.0,[21] and CH_3PH_2: 1.96.[22] This interesting fact, that the A roration in **1** is more strongly restricted than the B rotation, may be explained by considering that the substituent at the phosphorus atom (*i.e.*, the *o,o'*-biphenylene group) is much bulkier than that at the β-carbon atom (*i.e.*, three hydrogen atoms); this steric repulsion effect may mainly raise the barrier to rotation around this C–P bond, although the bond-length (1.87 Å) between C_α and P atoms is considerably longer than that (1.54 Å) between C_α and C_β atoms.

The authors wish to express their hearty thanks to Drs. Ikuei Ogata, Masato Tanaka, and Osamu Yamamoto of this Laboratory for their help in this study.

References

1) Part I: H. Nakanishi and O. Yamamoto, *Chem. Phys. Lett.*, **35**, 407 (1975).
2) G. C. Levy, *Acc. Chem. Res.*, **6**, 161 (1973).
3) "Topics in Carbon-13 NMR Spectroscopy," ed by G. C. Levy, Vol. 2, John Wiley and Sons, New York (1976).
4) F. W. Wehrli, in Ref. 3, p. 343.
5) M. Tanaka, T. Hayashi, Y. Kawabata, and I. Ogata, Abstracts of 26th International Congress of Pure and Applied Chemistry, Part 1, p. 125, Tokyo (1977).
6) There are arguments over the existence of aromaticity in phosphole ring. a) A. N. Hughes and D. Kleemola, *J. Heterocycl. Chem.*, **13**, 1 (1976), and the references cited therein; b) W. Schäfer, A. Schweig, and F. Mathey, *J. Am. Chem. Soc.*, **98**, 407 (1976); c) N. D. Epiotis and W. Cherry, *ibid.*, **98**, 4365 (1976).
7) B. R. Ezzell and L. D. Freedman, *J. Org. Chem.*, **34**, 1777 (1969).
8) B. E. Mann, *J. Chem. Soc., Perkin Trans. 2*, **1972**, 30.
9) G. A. Gray and S. E. Cremer, *J. Chem. Soc., Chem. Commun.*, **1974**, 451, and the references cited therein.
10) I. Solomon, *Phys. Rev.*, **99**, 559 (1955).
11) H. Shimizu and S. Fujiwara, *J. Chem. Phys.*, **34**, 1561 (1961).
12) E. L. Mackor and C. Maclean, *J. Chem. Phys.*, **42**, 4254 (1965).
13) R. Freeman and S. Wittekoek, *J. Chem. Phys.*, **52**, 1529 (1970).
14) C. L. Mayne, D. W. Alderman, and D. M. Grant, *J. Chem. Phys.*, **63**, 2514 (1975).
15) P. E. Fagerness, D. M. Grant, K. L. Kuhlman, C. L. Mayne, and R. E. Parry, *J. Chem. Phys.*, **63**, 2524 (1975).
16) A. D. Bain and R. M. Lynden-Bell, *Mol. Phys.*, **30**, 325 (1975).
17) J. J. Daly, *J. Chem. Soc.*, **1964**, 3799.
18) P. Coggon, J. F. Engel, A. T. McPhail, and L. D. Quin, *J. Am. Chem. Soc.*, **92**, 5779 (1970).
19) H. M. Powell, D. J. Watkin, and J. B. Wilford, *J. Chem. Soc., A*, **1971**, 1803.
20) D. R. Lide, Jr., and D. E. Mann, *J. Chem. Phys.*, **29**, 914 (1958).
21) J. P. N. Brewer, I. F. Eckhard, H. Heaney, and B. A. Marples, *J. Chem. Soc., C*, **1968**, 664.
22) T. Kojima, E. L. Breig, and C. C. Lin, *J. Chem. Phys.*, **35**, 2139 (1961).

α,β-Unsaturated Carboxylic Acid Derivatives. XIV. The Synthesis and Reduction of Diels-Alder Adducts from Ethyl 3-Nitro-2-alkenoates and Cyclopentadiene[1]

Chung-gi SHIN,* Yasuhiro KOSUGE, Masanori YAMAURA, and Juji YOSHIMURA**

Laboratory of Organic Chemistry, Faculty of Technology, Kanagawa University, Rokkakubashi, Kanagawa-ku, Yokohama 221

***Laboratory of Chemistry for Natural Products, Faculty of Science, Tokyo Institute of Technology, Ōkayama, Meguro-ku, Tokyo 152*

(Received July 19, 1977)

The Diels-Alder reactions of cyclopentadiene with ethyl (*E*)- and (*Z*)-3-nitrocrotonate were carried out to give only the (2+4)-nitro adduct as a mixture of three diastereomers, while that of the diene with ethyl (*Z*)-3-nitrocinnamate gave two kinds of cycloaddition products, (2+2)- and (2+4)-nitro adducts. All the nitro adducts were reduced with aluminum-amalgam to give the corresponding mono- and dihydroxyamino compounds, in which vicinal *endo*-ethoxycarbonyl-*endo*-hydroxyamino derivatives cyclized readily to give tricyclic compounds containing isoxazolidinone ring. The stereochemistry of all the new compounds were established on the basis of IR and NMR spectroscopic analyses.

In previous papers, we reported the stereospecific formation of ethyl 3-nitro-2-alkenoate (**1**) by the elimination reaction of 2-acetoxy- or 2-chloro-3-nitroalkanoate with a base[2] and the assignment of the geometric configuration of the olefinic compounds by the photoisomerization of the (*E*)-isomer into the (*Z*)-isomer and by the their NMR analysis.[3] Although ethyl 3-nitrocinnamate (**1b**) could not be isomerized, we have recently reported on (*Z*)-geometry as a convenient configurational determination of **1b** by the application of the Diels-Alder reaction.[4]

In this paper, we wish to report further chemical proof of the configuration of ethyl (*E*)- and (*Z*)-3-nitro-2-crotonate (**1a**) by a similar method, together with a detailed description of that of (*Z*)-**1b**; *i.e.*, the cycloaddition products of **1a** with cyclopentadiene were examined to determine whether or not they form an isoxazolidinone ring between vicinal ethoxycarbonyl and hydroxyamino groups after reduction with aluminum–amalgam (Al–Hg). The structures and stereochemistry of all the new products were established on the basis of IR and NMR spectroscopic data as well as the results of elemental analyses.

Results and Discussion

Reaction of 1 with Cyclopentadiene. According to the method reported previously by Umezawa *et al.*,[5,6] a solution of **1b** and cyclopentadiene in benzene was heated in a sealed tube at 100 °C for 1 h to give a semi-solid substance. Its subsequent chromatographic separation on a silica gel column, using benzene and acetone as eluents, gave two kinds of cycloaddition products (**2** and **3**) in fairly good yields. Similarly, the reaction of (*Z*)-**1a** with cyclopentadiene gave an adduct (**10**) in a 75.5% yield. Furthermore, that of (*E*)-**1a** with cyclopentadiene in benzene with stirring at room temperature for 24 h was carried out to give two kinds of adducts (**8** and **9**) in 64.2 and 15.0% yields respectively. All the products were obtained as colorless crystals.

The IR spectrum of all the new cycloaddition products showed a strong band at 1720—1730 due to an ethoxycarbonyl group, strong bands at 1535—1550 and 1340—1360 due to a nitro group, and a weak band in the

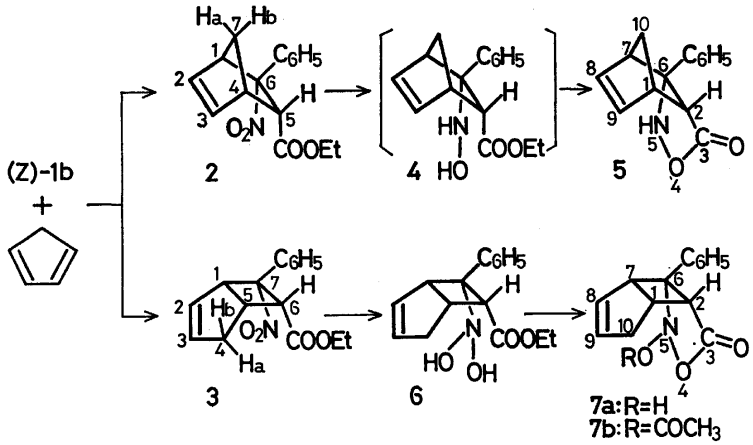

Scheme 1.

* To whom all correspondence should be addressed.

1630—1655 cm^{-1} region due to a ring carbon-carbon double bond. Moreover, from a comparison of the NMR spectra, it was found that the spectral pattern of **3** was considerably different from those of the other products (**2**, **8**, **9**, and **10**). The chemical shifts and coupling constants were assigned as shown in Table 3 by means of the double-resonance method. In the NMR spectrum of **3** (Table 3), the signals at δ 2.12 (d, 1H, $J_{4b,5}$=2.0 Hz), 2.66 (dd, 1H, $J_{4a,4b}$=18.0 Hz), 3.86 (d, 1H, $J_{5,6}$=8.3 Hz), 3.88 (m, 1H, 5-H) and 5.60 (d, 1H, $J_{1,5}$=8.3 Hz) are attributable to geminal protons at the 4-position and *cis*-protons at the 6-, 5-, and 1-positions respectively, while, in those of **2**, **8**—**10**, the signals of the 7- and 5-protons appeared at δ 1.42—2.08 (d, 2H, $J_{7a,7b}$=9.0—9.5 Hz) and at 3.30—4.13 (d, 1H, $J_{4,5}$=2.5—3.0 Hz) respectively. In general, (2+4)-cycloaddition products such as norbornenes and (2+2)-cycloaddition products such as bicyclo[3.2.0]heptenes can be readily distinguished from each other by means of the coupling constants between their geminal protons at the 4- and 7-positions, which have been reported to range from 8 to 10 Hz in the former adduct[5-8] and from 15 to 20 Hz in the latter.[9-11] Accordingly, **3** was identified as a (2+2)-nitro adduct. Moreover, from the *cis*-addition principle and the *endo*-rule in the Diels-Alder reaction, and the absence of any long-range coupling between the 7- and 5-protons, which are out of the *W*-letter relationship, it is reasonable to conclude that Compounds **2**, **9** and **10** are 5-*endo*-ethoxycarbonyl-6-*endo*-nitro-6-*exo*-phenylbicyclo[2.2.1]hept-2-ene, 5-*endo*-ethoxycarbonyl-6-*exo*-nitro-6-*endo*-methylbicyclo[2.2.1]-hept-2-ene, and 5-*endo*-ethoxycarbonyl-6-*endo*-nitro-*exo*-methylbicyclo[2.2.1]hept-2-ene respectively. On the other hand, from the presence of the long-range coupling (d, $J_{5,7a}$=3.0 Hz) which was collapsed by the irradiation of 5- or 7a-proton, the configuration of **8** was determined to be 5-*exo*-ethoxycarbonyl-6-*endo*-nitro-6-*exo*-methylbicyclo[2.2.1]hept-2-ene. Since the two J values between *cis* protons on cyclobutane ring are equal, Compound **3** was concluded to be 6-*endo*-ethoxycarbonyl-7-*endo*-nitro-7-*exo*-phenylbicyclo[3.2.0]hept-2-ene. These results indicate that the reaction of (*Z*)-**1b** proceeds stereospecifically to form only an *endo*-adduct and that those of (*E*)- and (*Z*)-**1a** follow the *endo*-rule unambiguously (see Table 1), because the *exo*-isomer, 5-*exo*-ethoxycarbonyl-6-*exo*-nitro-6-*endo*-methylbicyclo[2.2.1]hept-2-ene (**11**), could not be obtained.

The thermal (2+2)-cycloaddition of **1b** to diene seems to be rare, although many photochemical cycloadducts from diene and dienophiles have been reported in the literature.[9,12] However, interestingly, it was found that neither the (2+2)- nor the (2+4)-cycloaddition of **1** to the diene proceeded photochemically.

Reduction of the Nitro Adducts with Al–Hg. The *cis* stereochemistry of the nitro and ethoxycarbonyl groups of Compounds **2**, **10** (5-*endo*-6-*endo*), and **3** (6-*endo*-7-*endo* structure) were further substantiated by the facts that they were reduced to give the corresponding mono- or dihydroxyamino derivatives, which were immediately cyclized between vicinal ethoxycarbonyl and hydroxyamino groups to give tricyclic isoxazolidinone derivatives.

Although Compounds **8** and **9** were treated with Al–Hg in ether to give the corresponding 6-hydroxyamino derivatives (**12** and **13** respectively), a similar reduction of **2** and **10** readily gave 6-*exo*-phenyl- and methyl-*endo*-4-oxa-5-azatricyclo[5.2.1.$0^{2,6}$]dec-8-en-3-one (**5** and **15**) respectively *via* unstable intermediates, the corresponding 6-*endo*-hydroxyamino derivatives (**4** and **14**), in which **4** could not be isolated purely. Moreover, the treatment of **14** with *N*-bromosuccinimide (NBS) in chloroform gave the *N*-bromo derivative of **15** (**16**), which could not be derived from **15** and NBS. Surprisingly, the similar reduction of **3** gave stable colorless

Table 1. Physical data and IR spectra of bicyclo[2.2.1]- and [3.2.0]heptene derivatives

Compd No.	Yield (%)	Mp, °C (Bp, °C/mmHg)	Formula	Found (Calcd), % C	H	N	IR spectrum, cm^{-1} in KBr NHOH (OH)	COOEt	C=C	NO_2
2	47.3[a]	84—85	$C_{16}H_{17}NO_4$	66.63 (66.88)	5.93 (5.96)	4.78 (4.88)		1725	1640, 1540,	1360
3	31.5[a]	90—91	$C_{16}H_{17}NO_4$	66.92 (66.88)	5.95 (5.96)	4.86 (4.88)		1735	1620, 1550,	1350
6	48.8[b]	97—98	$C_{16}H_{19}NO_4$	66.35 (66.42)	6.63 (6.62)	4.78 (4.84)	(3450), (3225),	1738	1640	
8	64.2[c]	98—99	$C_{11}H_{15}NO_4$	58.65 (58.67)	6.71 (6.67)	6.20 (6.22)		1720	1650, 1540,	1350
9	15.0[d]	41—43 (92—98/0.2)	$C_{11}H_{15}NO_4$	58.39 (58.67)	6.69 (6.67)	6.31 (6.22)		1725	1655, 1535,	1355
10	75.5[d]	38—40 ((98—99/0.2)	$C_{11}H_{15}NO_4$	58.76 (58.67)	6.77 (6.67)	6.30 (6.22)		1735	1635, 1535,	1355
12	74.7[a]	133—134	$C_{11}H_{17}NO_3$	62.54 (62.54)	7.98 (8.11)	6.25 (6.63)	3250,	1730	1640	
13	22.0[e]	137—138	$C_{11}H_{17}NO_3$	62.62 (62.54)	7.99 (8.11)	6.58 (6.63)	3250,	1730	1630	
14	15.0[f]	137—138	$C_{11}H_{17}NO_3$	62.70 (62.54)	8.18 (8.11)	6.63 (6.63)	3250,	1725	1630	

a) Colorless needles from ethanol. b) Colorless fibers from benzene. c) Colorless prisms from ethanol. d) Colorless needles from hexane. e) Colorless needles from cyclohexane–ethanol. f) Colorless needles from carbon tetrachloride.

Table 2. Physical data and IR spectra of tricyclo[5.2.1.$0^{2,6}$]- and [5.3.0.$0^{2,6}$]decene derivatives

Compd No.	Yield (%)	Mp °C	Formula	Found (Calcd), % C	H	N	IR spectrum, cm^{-1} in KBr NH (OH)	Lactone	C=C
5	31.6[a]	112—113	$C_{14}H_{13}NO_2$	73.89 (73.99	5.82 5.77	6.14 6.16)	3240,	1765,	1640
7	52.5[b]	118—119	$C_{14}H_{13}NO_3$	68.72 (69.12	5.39 5.39	5.75 5.76)	(3340),	1745,	1620
7b	48.5[c]	107—108	$C_{16}H_{15}NO_4$	67.33 (67.36	5.11 5.30	5.03 4.91)	1775, acetyl	1755,	1630
15	24.0[d]	95—96	$C_9H_{11}NO_2$	65.77 (65.44	6.75 6.71	8.45 8.48)	3250,	1760,	1660
16	43.0[a]	102—103	$C_9H_{10}NO_2Br$	44.42 (44.28	4.21 4.13	5.61 5.74)		1640,	1620

a) Colorless needles from ethanol. b) Colorless prisms from hexane. c) Colorless prisms from ethanol. d) Pink prisms from carbon tetrachloride.

Table 3. Chemical shifts (δ) and coupling constants (Hz) of bicyclo[2.2.1]- and [3.2.0]heptenes

Compound No.	H^1	H^2	H^3	H^4	H^5	H^6	C_6H_5 [CH_3]	H^{7a} [H^{4a}	H^{7b} H^{4b}]	OH [NHOH]
2	4.07(bs)	6.10(dd) $J_{2,3}$=5.7 $J_{1,2}$=3.0	6.73(dd) $J_{3,4}$=3.0	3.18(bs)	3.62(d) $J_{4,5}$=3.0		7.40— 7.85(m)	1.67(d) $J_{7a,7b}$=9.2	1.46(dd) $J_{1,7b}$=2.0 $J_{4,7b}$=2.0	
3	5.60(d) $J_{1,5}$=8.3	5.95(dd) $J_{2,3}$=5.7	6.08(dd)		3.88(m)	3.86(d) $J_{5,6}$=8.3	7.30— 7.94(m)	[2.66(dd) $J_{4a,4b}$=18.0	2.12(d)] $J_{4b,5}$=2.0	
6	5.66(d) $J_{1,5}$=8.0	5.88(dd) $J_{2,3}$=6.0	6.04(dd) $J_{3,4}$=3.0		3.46(m)	3.64(d) $J_{5,6}$=8.0	7.40(m)	[2.77(dd) $J_{4a,4b}$=17.5	2.41(dd)] $J_{4b,5}$=2.0	2.05—3.00 7.20—7.70
8	3.21(dd) $J_{1,2}$=3.0	6.05(dd) $J_{2,3}$=6.0	6.34(dd) $J_{3,4}$=3.0	3.09(bs)	3.35(d) $J_{4,5}$=3.0 $J_{5,7a}$=3.0		[1.85(s)]	2.80(d) $J_{7a,7b}$=9.5	1.69(d)	
9	3.46(dd) $J_{1,2}$=3.0	6.15(dd) $J_{2,3}$=6.0	6.66(dd) $J_{3,4}$=3.0	3.18(bs)	4.13(d) $J_{4,5}$=3.0		[1.51(s)]	1.54(d) $J_{7a,7b}$=9.0	1.42(d)	
10	3.14(bs) $J_{1,2}$=2.5	6.03(dd) $J_{2,3}$=6.0	6.55(dd) $J_{3,4}$=2.5	3.14(bs)	3.30(d) $J_{4,5}$=2.5		[2.03(s)]	1.67(bd) $J_{7a,7b}$=9.5	2.03(bd)	
12	2.80(bs)	6.31(bs)		2.97(bs)	1.83(d) $J_{4,5}$=3.0 $J_{5,7a}$=3.0		[1.40(s)]	2.30(dd) $J_{7a,7b}$=9.5	1.82(d)	[5.50(bs)]
13	2.80(bs)	6.01—6.34(m)		2.94(bs)	2.61(d) $J_{4,5}$=3.0		[1.11(s)]	1.76(d) $J_{7a,7b}$=9.0	1.44(d)	[5.62(bs)]

Measured in $CDCl_3$.

Table 4. Chemical shifts (δ) and coupling constants (Hz) of tricyclo[5.2.1.$0^{2,6}$]- and [5.3.0.$0^{2,6}$]decenes

Compound No.	H^1	H^2	5-NH[OH]	6-C_6H_5[CH_3]	H^7	H^8	H^9	H^{10a}	H^{10b}
5	3.76(m)	3.76(d) $J_{1,2}$=4.0	6.14(bs)	7.43(m)	3.48(m)	6.43(dd) $J_{8,9}$=5.5	6.56(dd) $J_{1,9}$=3.0	1.70(d) $J_{10a,10b}$=9.0	1.54(dd) $J_{1,10b}$=2.0 $J_{7,10b}$=2.0
7a	3.43(m)	3.74(d) $J_{1,2}$=8.0	[7.20—7.70]	7.40(m)	5.64(d) $J_{1,7}$=8.0	5.79(dd) $J_{7,8}$=3.0 $J_{8,9}$=6.0	6.12(dd) $J_{9,10}$=3.0	2.74(dd) $J_{10a,10b}$=18.0 $J_{1,10a}$=8.0	2.38(d) $J_{1,10b}$=2.5
7b	3.40(m)	3.85(d) $J_{1,2}$=8.1		7.45—7.69(m)	5.73(d) $J_{1,7}$=8.1	5.95(dd) $J_{7,8}$=3.5	6.12(dd) $J_{9,10}$=3.0	2.80(dd) $J_{10a,10b}$=17.8 $J_{1,10a}$=8.1	2.46(d) $J_{1,10b}$=2.0
15	2.86(bs)	3.02(d) $J_{1,2}$=5.0	3.33(bs)	[1.58(s)]	2.86(bs)	6.31(dd) $J_{7,8}$=2.5 $J_{8,9}$=6.0	6.45(dd) $J_{9,10}$=2.5	1.77(d) $J_{10a,10b}$=9.5 $J_{1,10b}$=2.5	1.62(d) $J_{1,10b}$=2.5

Measured in $CDCl_3$.

crystals of unexpected 6-*endo*-ethoxycarbonyl-7-*endo*-dihydroxyamino-7-*exo*-phenylbicyclo[3.2.0]hept-2-ene (**6**), which was subsequently heated in dry benzene at 50 °C to give the expected 5-hydroxy-6-*exo*-phenyl-*cis*-*cisoid*-*cis*-4-oxa-5-azatricyclo[5.3.0.$0^{2,6}$]dec-8-en-3-one (**7a**) in a 52.5% yield. In order to prove the presence of the hydroxy group, **7a** was acetylated by the usual procedure, using acetic anhydride and pyridine at room temperature, to give the corresponding 5-acetoxy derivative (**7b**) in a 48.5% yield.

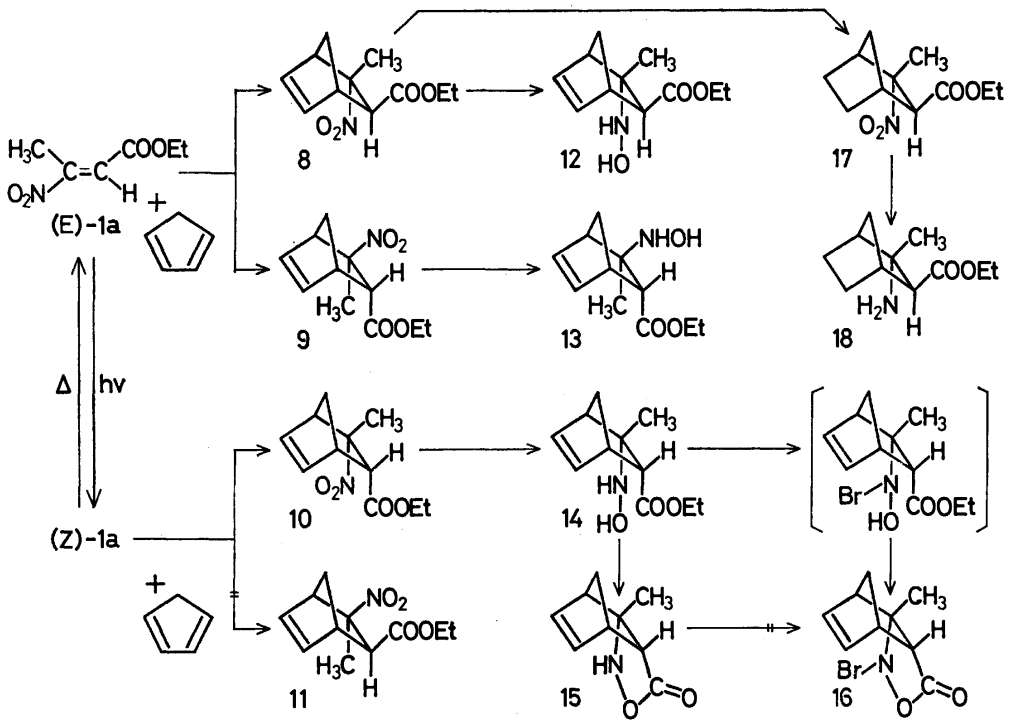

Scheme 2.

The structures of all the new reduction products and tricyclic compounds were characterized spectroscopically (see Tables 3 and 4) and gave satisfactory elemental analyses (see Tables 1 and 2), although the attempt at the measurement of the NMR spectrum of **14** was unsuccessful.

On the other hand, the catalytic reduction of **8** with Raney-nickel in ethanol at room temperature was carried out to give the corresponding 6-nitronorbornene (**17**) in the initial step; the further reduction of **17** gave the corresponding 6-aminonorbornene (**18**) in an almost quantitative yield.

In the IR spectrum, all the hydroxyamino and the tricyclic compounds showed a weak band in the 1630—1640 cm^{-1} region due to a ring double bond. Particularly, the IR spectra of **6** and **7a** showed the strong absorption bands of hydroxyl groups at 3450 and 3225, and 3340 cm^{-1}, respectively. The disappearance of the hydroxyl absorption and the appearance of a carbonyl band at 1775 cm^{-1} upon the acetylation of **7a**, and the presence of a molecular peak (*m/e* 244 (M^+)) in the mass spectrum of **7a**, supported the presence of an *N*-hydroxyisoxazolidinone ring in **7a**.

In the NMR spectra of **12** and **13**, the signals of the two protons at δ 5.50 and 5.62 are both attributable to the hydroxyamino group, while, in that of **6**, the broad signals of two protons of dihydroxyamino groups appeared in the δ 2.05—3.00 and 7.20—7.70 regions. It seemed that the chemical shift in the lower field is due to a hydrogen bond between one of the hydroxyl groups and the ethoxycarbonyl groups.

In conclusion, the cycloaddition reaction and reduction sequences are generalized for the chemical determination of the configurations of β-nitro olefinic acids.

Experimental

All the boiling and melting points are uncorrected. The IR spectra were recorded with a Hitachi EPI-G3 Spectrometer. The NMR spectra were measured with a JNM-PS 100 Spectrometer (Japan Electron Optics Laboratory Co., Ltd.), using tetramethylsilane as the internal standard.

Starting Materials. The (*E*)- and (*Z*)-isomers of **1a** and the (*Z*)-isomer of **1b** were prepared and confirmed by a method previously reported.[2-4]

Preparation of 2 and 3. A solution of (*Z*)-**1b** (2.9 g, 9 mmol) and cyclopentadiene (0.9 g, 14 mmol) in dry benzene (20 ml) was heated in a sealed tube at 100 °C for 1 h. After the removal of the benzene under reduced pressure, the residual semi-solid thus obtained was chromatographed on a silica gel column, using benzene–acetone (50: 1, V/V) as the eluent, to give two fractions. After each of the fractions had been concentrated under reduced pressure, the first one gave **2** and the second one gave **3** both as colorless crystals.

Preparation of 10. In an analogous manner, a reaction mixture of (*Z*)-**1a** (8.0 g, 50 mmol) and cyclopentadiene (4.0 g, 60 mmol) in benzene (100 ml) was worked up to give a viscous syrup, which gradually solidified to give only colorless crystalline **10**.

Preparation of 8 and 9. A solution of (*E*)-**1a** (8.0 g, 50 mmol) and cyclopentadiene (4.0 g, 60 mmol) in dry benzene (100 ml) was stirred overnight at room temperature. After the removal of the benzene under reduced pressure, a pale yellow semi-solid was obtained. The residue was recrystallized from ethanol to give colorless crystalline **8.** Subsequently, the mother liquor was evaporated to give a residual syrup. The yellowish residue was distilled under reduced pressure to give a viscous syrup, which gradually solidified to give colorless crystalline **9**.

Preparation of 5. A solution of **2** (2.9 g, 10 mmol) in ether (10 ml) was vigorously stirred into a suspension of Al–Hg (made from Al (1.5 g) and $HgCl_2$ (1.5 g))[13] in ether (50 ml)

at room temperature. After a few minutes, the ether began to reflux. During the addition of the above solution, a few drops of water were added at 20-min intervals to maintain refluxing. After the addition of the solution of **2** had been completed, the stirring was continued for 4 h. The mixture was then extracted thoroughly several times with ether (200 ml) and finally twice with ethyl acetate (60 ml). The combined extracts were dried over anhydrous magnesium sulfate and then evaporated to give colorless crystalline **5**.

Preparation of ***6***. In an analogous manner, a reaction mixture of **3** (1.5 g, 5 mmol) with Al–Hg (from Al (1.0 g) and $HgCl_2$ (1.0 g)) in ether (30 ml) was worked-up to give colorless crystalline **6**, after stirring for 3 h.

Preparation of ***12***. A mixture of **8** (4.5 g, 20 mmol) and Al–Hg (from Al (4 g) and $HgCl_2$ (4 g)) in ether (100 ml) was stirred for 6 h; there after a similar work-up gave **12**, 5-*exo*-ethoxycarbonyl-6-*endo*-hydroxyamino-6-*exo*-methylbicyclo-[2.2.1]hept-2-ene, as colorless crystals.

Preparation of ***13***. Similarly, Compound **9** was treated with Al–Hg in ether to give **13**, 5-*endo*-ethoxycarbonyl-6-*exo*-hydroxyamino-6-*endo*-methylbicyclo[2.2.1]hept-2-ene, as colorless crystals.

Preparation of ***14*** *and* ***15***. Similarly, Compound **10** was treated with Al–Hg in ether, giving colorless crystals (**14**), 5-*endo*-ethoxycarbonyl-6-*endo*-hydroxyamino-6-*exo*-methylbicyclo[2.2.1]hept-2-ene. The crystals obtained were gradually converted to **15** by refluxing in carbon tetrachloride for 1 h.

Preparation of ***16***. Into a solution of **14** (1.1 g, 5 mmol) in chloroform (20 ml) we stirred NBS (0.7 g, 5 mmol), portion by portion below 10 °C. After stirring for 1 h, the resulting solution was washed once with water and then dried over anhydrous magnesium sulfate. The solution was evaporated to give **16**, 5-bromo-6-*exo*-methyl-4-oxa-5-azatricyclo[5.2.1.$0^{2,6}$]-dec-8-en-3-one, as colorless crystals.

Preparation of ***7a***. A solution of **6** (0.3 g, 1 mmol) in dry benzene (10 ml) was refluxed for 5 min. After the removal of the benzene under reduced pressure, a residual syrup was obtained. The syrup was dissolved in hexane (5 ml), and then the hexane solution was allowed to stand at room temperature to give colorless crystalline **7a**.

Preparation of ***7b***. The acetylation of **7a** (0.12 g, 0.5 mmol) was carried out by the usual procedure using acetic anhydride (10 ml) and pyridine (3 ml) at room temperature; it gave colorless crystalline **7b**, 5-acetoxy-6-*exo*-phenyl-*cis*-*oid*-*cis*-4-oxa-5-azatricyclo[5.3.0.$0^{2,6}$]dec-8-en-3-one.

Preparation of ***17***. To a suspension of a Raney-nickel catalyst (3 ml) in ethanol (200 ml) we added **8** (6 g, 26.7 mmol). The mixture was shaken under a hydrogen atmosphere at room temperature for 24 h. After the removal of the catalyst by filtration, the resulting solution was evaporated under reduced pressure to give a residue. The residual syrup was distilled under reduced pressure to a colorless oil, which gradually crystallized to give **17**, 5-*exo*-ethoxycarbonyl-6-*endo*-nitro-6-*exo*-methylbicyclo[2.2.1]heptane, as colorless crystals. Yield, 5.7 g (97.4%); bp 118—120 °C/1 mmHg, mp 34.5—36.5 °C. NMR ($CDCl_3$): δ 1.25—2.25 (6H, m, 2-, 3- and 7-H), 1.66 (3H, s, 6-CH_3), 2.60 (2H, m, 1- and 4-H), 3.64 (1H, d, $J_{5,7b}$=2.8 Hz, 5-H). IR (KBr): 1745 (ester), 1550 and 1360 (NO_2) cm^{-1}. Found: C, 57.99; H, 7.56; N, 6.12%. Calcd for $C_{11}H_{17}NO_4$: C, 58.13; H, 7.54; N, 6.61%.

Preparation of ***18***. In an analogous manner, a mixture of **17** (5.7 g, 26.0 mmol) and Raney-nickel (3 ml) in ethanol (200 ml) was worked-up to give a colorless oil, 6-*endo*-amino-5-*exo*-ethoxycarbonyl-6-*exo*-methylbicyclo[2.2.1]heptane (**18**). Yield, 4.9 g (95.7%); bp 90—91 °C/0.7 mmHg. NMR ($CDCl_3$): δ 1.16 (2H, s, 6-NH_2), 1.25—2.25 (6H, m, 2-, 3- and 7-H), 1.54 (3H, s, 6-CH_3), 1.90 (1H, m, 4-H), 2.03 (1H, d, $J_{5,7b}$=2.3 Hz, 5-H), 2.40 (1H, m, 1-H). IR (KBr): 3350 (NH_2), 1735 (ester) cm^{-1}. Found: C, 66.78; H, 9.67; N, 7.10%. Calcd for $C_{11}H_{19}NO_2$: C, 66.97; H, 9.71; N, 7.10%.

References

1) Part XIII: C. Shin, M. Hayakawa, N. Suzuki, A. Ohtsuka, and J. Yoshimura, *Bull. Chem. Soc. Jpn.*, **51**, 550 (1978).

2) C. Shin, Y. Yonezawa, H. Narukawa, K. Nanjo, and J. Yoshimura, *Bull. Chem. Soc. Jpn.*, **45**, 3595 (1972).

3) C. Shin, Y. Yonezawa, and J. Yoshimura, *Nippon Kagaku Kaishi*, **1974**, 718.

4) C. Shin, H. Narukawa, M. Yamaura, and J. Yoshimura, *Tetrahedron Lett.*, **1977**, 2147.

5) S. Umezawa, M. Kinoshita, and H. Yanagisawa, *Bull. Chem. Soc. Jpn.*, **40**, 209 (1967).

6) M. Kinoshita, H. Yanagisawa, S. Doi, E. Kaji, and S. Umezawa, *Bull. Chem. Soc. Jpn.*, **42**, 209 (1969).

7) W. E. Noland, B. A. Langager, J. W. Manthey, A. G. Zacckei, D. L. Petrak, and G. L. Eian, *Can. J. Chem.*, **45**, 2969 (1967).

8) L. D. Hall, *J. Org. Chem.*, **29**, 297 (1964).

9) L. A. Hull and P. D. Bartlett, *J. Org. Chem.*, **40**, 824 (1975).

10) B. D. Kramer and P. D. Bartlett, *J. Am. Chem. Soc.*, **94**, 3934 (1972).

11) G. L. Lange, M. A. Huygins, and E. Heidert, *Tetrahedron Lett.*, **1976**, 4409.

12) O. Chapman, A. Griswold, E. Hoganson, G. Lenz, and J. Reasoner, *Pure Appl. Chem.*, **9**, 584 (1964).

13) C. Shin, M. Masaki, and M. Ohta, *Bull. Chem. Soc. Jpn.*, **43**, 3219 (1970).

Polyelectrolyte Complexes of Chitosan with Sodium Carboxymethyldextran

Hiroshi FUKUDA and Yasuo KIKUCHI*

Faculty of Home Economics, Hiroshima Women's University, Uzina-machi, Hiroshima 734
**Faculty of Engineering, Hiroshima University, Senda-machi, Hiroshima 730*

(Received July 27, 1977)

Mixing of chitosan with sodium carboxymethyldextran having opposite charge gave rise to the formation of novel water-insoluble precipitates. The mole ratios of N/COO^- in the polyelectrolyte complexes thus prepared were estimated to be 0.248—1.658. It was found that pH, mole ratio of N/Na and the order of mixing play an important role in determining the composition ratio of N/COO^- in the polyelectrolyte complexes. IR spectroscopic studies, blood clotting test, elementary analyses, the color reaction with Toluidine Blue and studies on solubility of polyelectrolyte complexes revealed that there is no noticeable interactions between –COOH groups and –OH groups. However, the $-NH_3^+$ groups in chitosan participate in the binding with carboxymethyldextran, probably through its $-COO^-$ groups, in the polyelectrolyte complexes. It seems that the number of binding sites between $-NH_3^+$ and $-COO^-$ groups in the polyelectrolyte complexes at pH 3.0 is smaller than those prepared at pH 6.5. Both the polyelectrolyte complexes prepared at pH 3.0 and 6.5 suppressed the coagulation of blood. This anti-thrombogenic property should be related to elution of anti-thrombogenic carboxymethyldextran.

A solution of charged polyelectrolyte reacts with one of oppositely charged polyelectrolyte to form a water-insoluble hydrous complex whose composition, in general, is sensitive to the composition of reaction mixture, order of mixing and the polyion concentration. Reports in this field have been given by some investigators.[1,2]

The mechanism of polyion interaction, the probable structure of the polyelectrolyte complex (PEC), and their properties have been investigated in detail by Michaels *et al.*[3,4] However, only a few papers[5] deal with the polyion interaction between polysaccharides, or polysaccharide and synthetic macromolecules, in spite of its importance concerning biological system, membranes and industrial and biomedical application.[6]

We have reported on chemical reactions of chitosan with dextran[7,8] and of [2-(diethylamino)ethyl] dextran with dextran.[9] This paper deals with a novel chemical reaction of chitosan with sodium carboxymethyldextran (CMD) and the results of our studies on the polyelectrolyte complex thus prepared.

Experimental

Chitosan (Tokyo Kasei Co., Ltd., nitrogen content 7.65%) and CMD (Meito Sangyo Co., Ltd., sodium content 7.38%; degree of substitution 0.70/A.G.U.; viscosity of its 1% aqueous solution 970 centipoise at 20 °C) were used. Chitosan was purified by reprecipitation from its acidic solution with 20% sodium hydroxide solution; CMD was used without purification.

When the pH of solution is below 2 no precipitate is formed by mixing chitosan with CMD and when the pH of chitosan solution is higher than 6.5, chitosan remains insoluble. Thus, the reactions were carried out at pH 3.0 and pH 6.5, respectively. Purified chitosan was dissolved in 0.1% hydrochloric acid solution. The pH of solution was then adjusted to 3.0 and 6.5 with sodium hydroxide solution. CMD was dissolved in water (pH 6.5), and the solution was adjusted to pH 3.0 with hydrochloric acid solution. These chitosan solutions were added dropwise to CMD solutions, adjusted to the same pH as those of chitosan solutions, respectively, with stirring under the conditions given in Table 1. Water-insoluble precipitate (PEC) was thus obtained. After being left to stand for a half hour, the precipitate was washed with 0.01 M hydrochloric acid solution, water and methanol, and then separated by centrifugation, dried *in vacuo* for a week, until a constant weight was attained.

The blood clotting test was carried out according to the procedure of Imai and Nose.[10] 160 mg PEC was pressed (5 t/4.5 cm^2) with poly (vinyl chloride) powder, a reinforcing agent, in a vacuum for 10 min. The blood (Red Cross Hospital Blood Center) was kept in a thermostat at 4—6 °C for one or two months. The ACD blood was prepared by adding the blood to an anticoagulant citrate dextrose solution consisting of sodium citrate, citric acid and dextrose.

Elementary analyses of the PEC were performed at the Institute of Physical and Chemical Research, the infrared spectra being taken by the KBr method. Purple coloration appears by the reaction of CMD with a solution containing Toluidine Blue.[11] This is utilized for the demonstration of CMD elution from PEC.

Results and Discussion

Experimental conditions, yield and elementary analyses for the PEC are given in Tables 1 and 2, respectively. The yield of PEC becomes smaller with an increase in the mole ratio N/Na of the reaction mixture. The nitrogen content in PEC prepared at pH 6.5 (B series) is greater than that prepared at pH 3.0 (A series), while the nitrogen content in PEC of A-2 and B-2, prepared in the mixing order, CMD to chitosan, is greater than that of PEC prepared in the reverse order, chitosan to CMD. The nitrogen content in the PEC becomes greater with increase in the mole ratio N/Na of the reaction mixture.

The data on the infrared spectra and elementary analyses suggest that the $-NH_3^+$ groups in chitosan participate in the binding with CMD, probably through its $-COO^-$ group in PEC. Thus, the mole numbers of $-COO^-$ groups in PEC were calculated from its nitrogen content. The mole ratios of N/COO^- in PEC were determined (Table 2), by assuming that the sodium or chlorine content in PEC is approximately zero. The mole ratios of N/COO^- in PEC, A-1 to B-4, were estimated to be 0.248 to 1.658. The pH value, the mole ratio of N/Na in the reaction mixture and the order of mixing, play an important role in determining the

Table 1. Conditions and yields in the preparation of polyelectrolyte complexes[a)]

Sample code	Volume of chitosan solution (ml)	Volume of CMD solution (ml)	Mixing order	Mole ratio of N/Na in the reaction mixture	Yield (mg/100ml chitosan solution)
A-1[b)]	100	170	Chitosan to CMD	1.0	364
A-2[b)]	100	170	CMD to chitosan	1.0	386
A-3[b)]	25	212.5	Chitosan to CMD	0.2	1323
A-4[b)]	200	68	Chitosan to CMD	5.0	78
B-1[c)]	100	170	Chitosan to CMD	1.0	441
B-2[c)]	100	170	CMD to chitosan	1.0	302
B-3[c)]	25	212.5	Chitosan to CMD	0.2	392
B-4[c)]	200	68	Chitosan to CMD	5.0	126

a) Concentration of chitosan and sodium carboxymethyldextran (CMD): 2.0 g/l. b) Both solutions adjusted to pH 3.0. c) Both solutions adjusted to pH 6.5.

Table 2. Elementary analyses and composition of polyelectrolyte complexes

Sample code	Nitrogen[a)] content (%)	Sodium[b)] content (%)	Chlorine[b)] content (%)	Mole ratio of N/COO^- in the polyelectrolyte complex
A-1[c)]	1.45	0.055	0.085	0.397
A-2	2.12	/	/	0.648
A-3	0.98	/	/	0.248
A-4	1.72	/	/	0.491
B-1[d)]	2.69	0.065	0.210	0.914
B-2	3.81	/	/	1.658
B-3	2.33	/	/	0.740
B-4	3.49	/	/	1.406

Sample codes correspond to those in Table 1.
a) Nitrogen analysis carried out according to Kjeldahl method. b) Analyses performed at the Institute of Physical and Chemical Research. c) Carbon content: 40.09%, hydrogen content: 6.05%. d) Carbon content: 38.19%, hydrogen content: 6.23%.

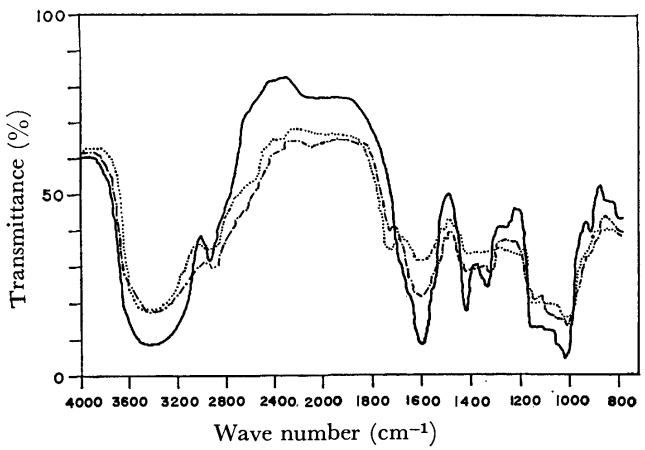

Fig. 1. IR spectra of polyelectrolyte complexes and polymer blend of chitosan with sodium carboxymethyldextran.
——: Polymer blend of chitosan with sodium carboxymethyl-dextran (mole ratio of N/Na=1.0), ·····: polyelectrolyte complex of A-1, -·-·-: polyelectrolyte complex of B-1.
Sample codes, A-1 and B-1, correspond to those in Table 1.

ratio of the reactive group of CMD to that of chitosan in the PEC. The mole ratios of N/COO^- in the PEC of series A were smaller than those of series B. Only the PEC of series A, A-1, A-2, and A-4, having not more than 0.5 of the mole ratio N/COO^-, gave slight purple coloration with Toluidine Blue. It seems that the number of binding sites between $-NH_3^+$ and $-COO^-$ groups in the PEC of series A is smaller than those of series B, and CMD in the PEC of series A should be liable to detach itself from the PEC chain.

The IR spectra of PEC are roughly similar to those of a mixture of CMD and chitosan, differing from each other in detail. PEC has an absorption band around 1740 cm^{-1}, [12] assigned to -COOH group. This is absent in the mixture of CMD and chitosan. The smaller the ratio of N/Na in the reaction mixture, or the smaller the nitrogen content in PEC, the stronger the absorption band around 1740 cm^{-1}. The absorption band in the PEC of A-2 and B-2 prepared in the mixing order, CMD to chitosan, is stronger than the band prepared in the reverse mixing order, chitosan to CMD. The stronger the absorption band around 1740 cm^{-1}, the weaker the absorption band around 1600 cm^{-1}. Though neither the shift in absorption band around

Table 3. Solubilities of polyelectrolyte complexes

Sample code	Ternary[a)] solvent-I		Ternary[b)] solvent-II		Formic acid		Dimethyl sulfoxide	
	R	H	R	H	R	H	R	H
A-1	△	△	△	△	△	○	×	×
A-2	△	△	△	△	△	○	×	△
A-3	△	△	△	△	△	○	×	△
A-4	△	△	△	△	△	○	×	△
B-1	△	△	△	△	△	○	×	×
B-2	△	△	△	△	△	○	△	△
B-3	△	△	△	△	△	○	△	△
B-4	△	△	△	△	△	○	△	△

Sample codes correspond to those in Table 1. All the polyelectrolyte complexes were insoluble, even on heating, in *N,N*-dimethylformamide. R: Room temperature, H: Heating. ○: Almost soluble, △: Partially soluble, ×: Insoluble. a) Aceton/potassium bromide/water (20: 20: 60 wt%). b) Hydrochloric acid/dioxane/water (45: 50: 5 wt%).

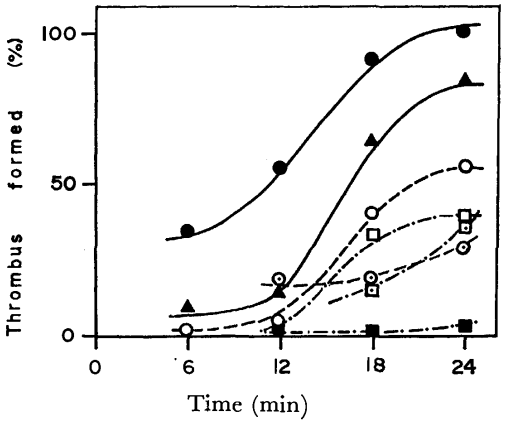

Fig. 2. Percentage of thrombus formed on polyelectrolyte complexes compared with that on glass.
●: Glass, ▲: polyvinyl chloride, ⊙: B-2, ○: B-4, ⊡: A-1, □: A-2, ■: A-2 (without reinforcing agent). Sample codes A-1, A-2, B-2, and B-4 correspond to those in Table 1.

3500 cm^{-1} assigned to –OH groups nor the change in its absorption intensity about PEC were observed appreciably in the mixture of CMD and chitosan blended in the same ratio as that of the PEC composition, there would be no appreciable interaction between the –OH group and other reactive groups, especially carboxyl group. On the other hand, there is no absorption around 1500 cm^{-1}, which is assigned to $-NH_3^+$ group,[13] in the mixture of CMD and chitosan. The sodium and chlorine contents in the PEC are distinctly smaller than those in CMD or chitosan. The results suggest that the $-NH_3^+$ groups in chitosan participate in the binding with CMD through its $-COO^-$ groups.

PEC are insoluble or hardly soluble in dimethyl sulfoxide or *N,N*-dimethylformamide, partially soluble in a ternary solvent mixture, and soluble in formic acid on heating (Table 3). The difference in solubility between the PEC of series A and those of series B is hardly discernible. However, the PEC of series B is soluble in dimethyl sulfoxide.

The blood clotting test was performed for the PEC (Table 1) by gravimetric measurement[10] of the amount of thrombus at appropriate time intervals, after addition of calcium chloride solution (0.1 M, 0.02 ml) to ACD blood (0.2 ml) which had been in contact with samples. PEC has an anti-thrombogenic character; it suppresses the coagulation of blood. The amount of thrombus on the PEC is 20—50% of that on glass (Fig. 2). The difference in anti-thrombogenic behavior between the PEC of series A and that of series B is hardly discernible. The elution of anti-thrombogenic CMD from PEC into the blood might be related to our results.

References

1) E. Tsuchida and T. Osada, *Kobunshi Kagaku*, **22**, 384 (1973).
2) H. Noguchi, *Kobunshi Kagaku*, **22**, 402 (1973).
3) A. S. Michaels and R. G. Miekke, *J. Phys. Chem.*, **65**, 1765 (1961).
4) A. S. Michaels and N. S. Schneider, *J. Phys. Chem.*, **69**, 1477 (1965).
5) K. Shinoda and A. Nakajima, "Summary of Paper in 23th Polymer Symposium," (Tokyo, Japan), 1974, p. 21.
6) A. Nakajima, *Kagaku To Kogyo*, **27**, 746 (1974).
7) Y. Kikuchi and H. Fukuda, *Makromol. Chem.*, **175**, 3593 (1974).
8) H. Fukuda and Y. Kikuchi, *Makromol. Chem.*, **178**, 2895 (1977).
9) Y. Kikuchi and H. Fukuda, *Nippon Kagaku Kaishi*, **1977**, 1051.
10) Y. Imai and Y. Nose, *J. Biomed. Mater. Res.*, **6**, 165 (1972).
11) Y. Ishizuka, *Biochemistry*, **27**, 173 (1955).
12) K. Nakanishi, "IR Absorption Spectroscopy," Nankōdō, Tokyo (1965), p. 56.
13) Y. Kikuchi and H. Fukuda, *Nippon Kagaku Kaishi*, **1976**, 1505.

Photo-Induced Friedel-Crafts Acylation of Anthracene with Aroyl Chlorides

Takashi TAMAKI

Research Institute for Polymers and Textiles, Sawatari 4-1, Kanagawa-ku, Yokohama 221

(Received July 28, 1977)

The photo-excitation of anthracene (**1**) in the presence of benzoyl chloride and its *p*- or *m*-substituted compounds (**2**) gave the corresponding 2- and 9-aroylanthracenes. No isomeric 1-aroylanthracenes (**3**) were detected. The aroyl chlorides (**2**) were found to quench the fluorescence of **1**. The quenching constants obtained increased with increasing electron-withdrawing ability of the substituents and are in agreement with those independently obtained from the quantum yield determinations. The efficiency of the photoaroylation was dependent on the solvent polarity. The results suggest a plausible photochemical mechanism, which involves a CT complex formed from **1** in the excited singlet state and **2** in the ground state. This complex formation is supported by the positional selectivity exhibited in the product distribution.

Few papers concerning photo-induced Friedel-Crafts reactions have been published.[1-5] The photochemical mechanisms differ from case to case. For the photoacetylation of benzene with trifluoroacetic acid, an ionic intermediate was assumed.[1b] The photoalkylation of the phenyl nucleus with chloroacetyl derivatives occurs through a radical reaction,[2] while, in the presence of metallic halides, electrophilic substitution prevails.[3] Recently, positional selectivity was reported for the photobenzoylation of anthracene (**1**) with benzoyl chloride (**2d**): substitution on the aromatic ring preferentially occurs at positions 2 and 9, but scarcely at position 1.[5] This paper describes further results for photoaroylation and discusses the photochemical mechanisms.

Continuing attention has been focused on the exciplex formation between electron-rich aromatics and compounds containing an activated C–Cl or similar bond.[6] It is supposed for these systems that the chemical reactivity of the C–Cl bond plays an important role in the quenching process, although CT interaction is primarily responsible for association of an exciplex. The quenching mechanisms may be related to the case described here.

Results

Photoaroylation. The absorption spectra of a mixed solution of anthracene (**1**) and benzoyl chloride (**2d**) are shown in Fig. 1a. No new absorption bands are seen before irradiation. The solution was exposed to 365 nm mercury light in a nitrogen atmosphere. The irradiating light was absorbed by **1**, but not by the aroyl chlorides (**2**), the absorbance of **2** being negligible

Table 1. Characteristics of the products formed from the photoaroylation of anthracene

Product	Yield[a] (%)	Mp (°C)	ν_{max}[d] (cm^{-1})	δ[e] (ppm)	Coloration[f] with H_2SO_4	Emission in EtOH (λ_{max} in nm)
4a	29	189—190		3.9(3H)	P	502
4b	23	183—185		2.4(3H)	P	498
4c	27	158—159		2.4(3H)	P	520
4d	19	169—171[b]			P	523
4e	30	211—213			P	523
4f	30	140—142		3.8(3H)	P	522
4g	28	200—202			P	510
4h	29	223—224			P	538
4i	24	198—199	2220(CN)		V	544
4j	19	191—193	2220(CN)		V	560
5a	30	185—186		3.75(3H)	V	—[g]
5b	53	125—126		2.9(3H)	PB	—
5c	36	131—133		2.25(3H)	G	—
5d	47	145—146[c]			PB	—
5e	37	162—163			PB	—
5f	51	155—158		3.7(3H)	G	—
5g	34	186—188			PB	—
5h	58	139—141			PB	—
5i	56	155—157	2230(CN)		PB	—
5j	11	217—218	2220(CN)		G	—

a) Relative to anthracene loss (60% conversion). b) Lit,[29] 175 °C. c) Lit,[28] 148 °C. d) 1650—1670 cm^{-1} (C=O), except as noted. e) 8.4—8.5 (2H, Ar) and 7.0—8.4 (Ar) for a series of compounds of **3**; 8.5—8.7 (1H, Ar) and 6.8—8.3 (Ar) for a series of compounds of **4**, except as noted. f) P, purple; V, violet; PB, Prussian blue; G, green. g) No emission.

above 340 nm. The major products obtained were identified, by comparison with anthentic species, to be 2- (**4d**) (19% in benzene and 24% in acetonitrile based on the amount of **1** consumed) and 9-benzoylanthracene (**5d**) (47% in benzene and 57% in acetonitrile). No isomeric 1-benzoylanthracene (**3d**) was detected. Other aroyl chlorides (**2a**—**c** and **e**—**j**) gave the corresponding products under appropriate conditions. The product yields were 20—30% for **4**, 30—60% for **5**, as listed in Table 1, and trace or nil amounts for **3**.

Besides the ketonic compounds, anthracene photodimer was also formed with less yields (10—20%) than that in the absence of **2**. Added dry hydrogen chloride prevented photoaroylation and caused the chlorination of **1**. In an oxygen stream, photoaroylation was repressed (**4d**, 5%; **5d**, 10%) and anthraquinone was formed as a major product (40%).

In the case of **2d** in acetonitrile, irradiation was also performed with the 254 nm light, which was absorbed by all starting materials. The same ketonic products, **4d** (5%) and **5d** (40%), and in addition 9,10-dibenzoylanthracene (15%) were formed. The yield of **4d** is remarkably small compared with that for 365 nm light irradiation.

Reaction Pathway. In order to elucidate the reaction pathway of the photoaroylation, the extinction

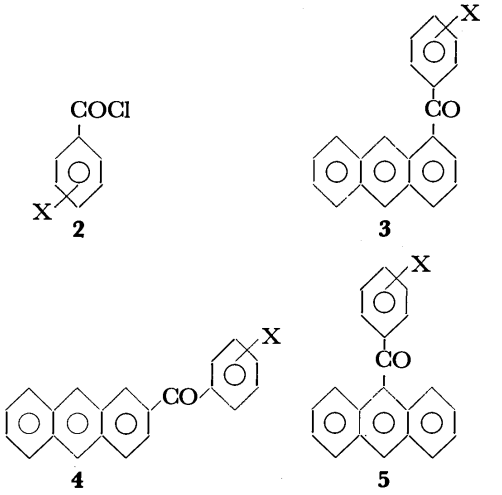

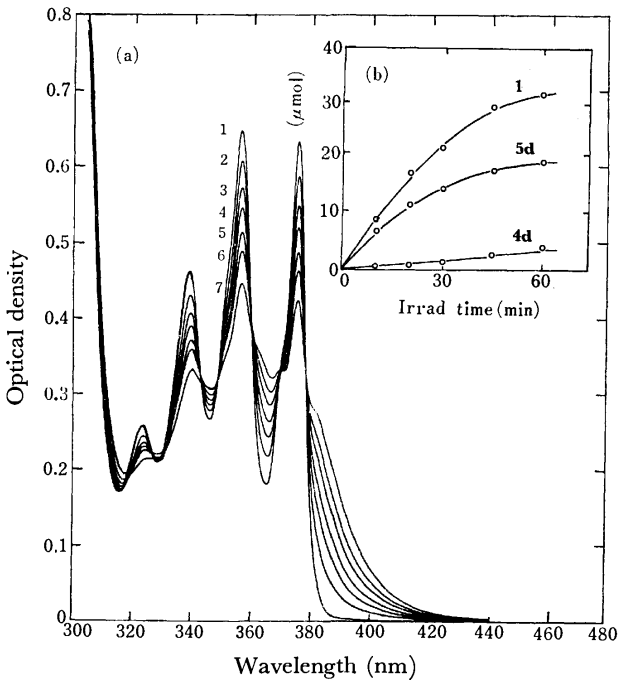

Fig. 1. (a) Absorption spectra during irradiation: (1) 0, (2) 10, (3) 20, (4) 30, (5) 45, (6) 60, (7) 90 min, (b) Conversion curves based on the spectral changes on the assumption that anthracene (**1**), 2-, (**4d**), and 9-benzoylanthracene (**5d**) are responsible for the spectra.

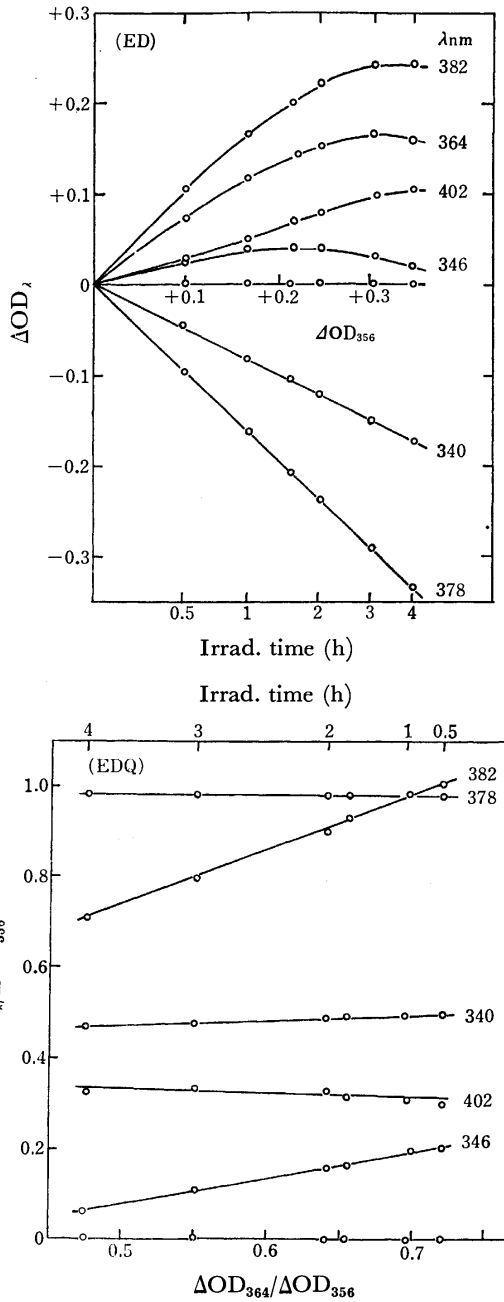

Fig. 2. Extinction difference (ED) and extinction difference quotient (EDQ) diagrams of the absorption spectra.

difference (ED) and extinction difference quotient (EDQ) diagrams[7] are plotted in Fig. 2, using the spectral data shown in Fig. 1a. The ED diagram shows linear curves at all wavelengths until about one-half of the starting amounts of **1** had been consumed. These linear relations suggest that the photoreaction proceeds only *via* a one-step reaction, *i.e.*, **1**+**2**→one product or products with a constant yield ratio. Since both isomeric ketones, **4d** and **5d**, are formed immediately after irradiation, as is shown in Fig. 1b, it can be concluded that these compounds are simultaneously produced by a bimolecular reaction of **1** and **2**. The product yield ratio of **4d** to **5d** is *ca.* 0.1 at the initial stage of the photoreaction, as is shown in Fig. 1b.

For more prolonged irradiation periods, the ED plots deviate from linear relations, particularly at wavelengths of the **5d** peak maxima (346, 364, and 382 nm). However, all the EDQ plots remain linear up to nearly complete consumption of **1**. This indicates that **5d** formed undergoes a subsequent chemical change, while **4d** unchanges. In a preliminary experiment, it was found that irradiation of **5d** in benzene gave none of the isomeric ketones, but gave a photodimer analogous to those derived from **1** or its meso substituted compounds.[8] Consequently, the photodimerization may be mainly responsible for the loss of **5** during the course of photoaroylation. The possibility of the isomerization reaction can be excluded.

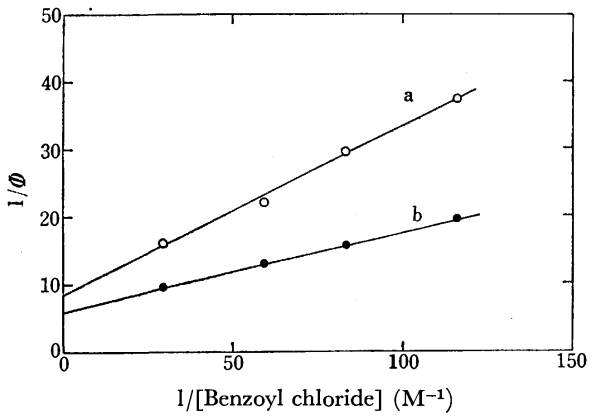

Fig. 3. Concentration dependency of the quantum yield for the loss of anthracene: (a) in benzene and (b) in acetonitrile.

Quantum Yields. The loss of **1** is dependent on the aroyl chloride concentration, as is shown in Fig. 3, where the reciprocals of the quantum yields for the disappearance of **1** are plotted against the reciprocals of the benzoyl chloride concentrations. Values of the products of the limiting quantum yield and the quenching constant, $k_q\tau$ (the ratio of intercept to slope), are listed in Table 2. Although the values of the limiting quantum yield are about the same for most reactions of **2** in benzene, they become much more enhanced in acetonitrile for the aroyl chlorides which have an electron-withdrawing substituent. On the contrary, the electron-repelling substituents relatively depress the quantum yield in acetonitrile.

Table 2. The limiting quantum yields and quenching constants in the photo-aroylation of anthracene

Aroyl chloride		Solvent: Benzene Φ_∞[a]	Benzene $k_q\tau$[b] (M^{-1})	Acetonitrile Φ_∞[a]	Acetonitrile $k_q\tau$[b] (M^{-1})
p-CH_3O	(**2a**)	0.12	11	<0.03[c]	c
p-CH_3	(**2b**)	0.15	30	0.11	40
m-CH_3	(**2c**)	0.13	39	0.12	69
H	(**2d**)	0.12	35	0.16	62
p-F	(**2e**)	0.13	40	0.15	74
m-CH_3O	(**2f**)	d	d	d	d
p-Cl	(**2g**)	0.13	39	0.21	98
m-Cl	(**2h**)	0.12	48	0.31	75
m-CN	(**2i**)	<0.03[c]	c	0.18	89
p-CN	(**2j**)	<0.01[c]	c	0.06	170

a) The limiting quantum yield determined from the intercept in the $1/\Phi$ *vs.* 1/[Q] plots. b) Determined from the ratio of intercept to slope. c) Not determined to good precision due to less reactivity. d) Not determined due to internal filter effect of *m*-methoxybenzoyl chloride.

Table 3. Fluorescence quenching data

Aroyl chloride		Solvent: Benzene $k_q\tau$[a] (M^{-1})	Benzene $10^{-9}k_q$[b] ($M^{-1}s^{-1}$)	Acetonitrile $k_q\tau$[a] (M^{-1})	Acetonitrile $10^{-10}k_q$[b] ($M^{-1}s^{-1}$)
p-CH_3O	(**2a**)	15	3.1	61	1.2
p-CH_3	(**2b**)	29	5.9	68	1.3
m-CH_3	(**2c**)	35	7.1	71	1.4
H	(**2d**)	38	7.8	78	1.5
p-F	(**2e**)	38	7.8	78	1.5
m-CH_3O	(**2f**)	38	7.8	71	1.4
p-Cl	(**2g**)	46	9.4	82	1.6
m-Cl	(**2h**)	48	9.7	88	1.7
m-CN	(**2i**)	56	11	95	1.8
p-CN	(**2j**)	62	13	110	2.1

a) The slope of the Stern-Volmer plots for an excitation wavelength of 380 nm. b) Determined from the singlet lifetime of anthracene: τ 4.9 ns in benzene and 5.3 ns in acetonitrile (Ref. 10).

Fluorescence Quenching. The Stern-Volmer plots were linear for most quenchers, **2**, while upward curvature was observed for **2i** and **j**. No new emission was detected in the presence of **2**. The values of $k_q\tau$ as determined from the initial slope and of the quenching rate constant, k_q, are listed in Table 3. The values of $k_q\tau$ obtained are in agreement with those obtained from the quantum yield determinations (Table 2) to within experimental errors. The k_q increases with increasing electron-withdrawing ability of the substituent and ultimately approaches the diffusion rate canstant, k_{diff}, which is equal to 1×10^{10} $M^{-1}s^{-1}$ in benzene and 1.8×10^{10} $M^{-1}s^{-1}$ in acetonitrile, as calculated using the Debye expression.[9] The upward curvatures in the

Table 4. Quantum yields for direct photolysis of aroyl chlorides

Aroyl chloride		Quantum yield
p-CH_3O	(**2a**)	0.046
H	(**2d**)	0.038
m-Cl	(**2h**)	0.029
m-CN	(**2i**)	0.016
p-CN	(**2j**)	0.033

Stern-Volmer plots and the large k_q values suggest that a ground-state complex is formed from **1** and the aroyl chlorides, the substituent of which is strongly electron-withdrawing (*vide infra*).

Direct Photolysis of Aroyl Chlorides. The quantum yields are listed in Table 4. The data indicate that **2** becomes more photostable when an electron-withdrawing substituent is introduced into the aroyl system. The trend of the substituent effect is distinctly different from that for photoaroylation. Furthermore, it is noteworthy that the quantum yields for direct photolysis are much smaller than the limiting quantum yields of the photoaroylation (the fourth column in Table 2).

Discussion

The agreement between the quenching constants obtained independently from the fluorescence and photochemical measurements indicates that the photoreaction occurs in the excited singlet state of **1**. As is shown in Fig. 1a, only a very weak absorption band of **2** overlaps with the fluorescence of **1**, the long wavelength absorption maxima of **2** lying in much higher energy regions (*ca.* 100 kcal/mol) than that of **1** (76 kcal/mol).[10] Therefore, it is difficult to consider that the excitation energy would be transferred to the quencher through classical mechanisms, such as trivial or resonance energy transfer.[11] If these mechanisms were operating, the photoaroylation efficiencies would be related to those for direct photolysis of the quenchers, because these quenching processes lead to the formation of excited quenchers. However, the substitution dependence of the two photoreactions is exactly opposite.

On the other hand, the increase in the quenching constant with increasing electron-abstracting ability of the aroyl system suggests that the quenching process involves an exciplex formed from the excited aromatic hydrocarbon and the quencher. The exciplex mechanism is well established for electron-donor-acceptor pairs, for which the energy transfer appears to be strongly endothermic.[12] This mechanism is favored for explaining the positional selectivity observed, as is discussed below.

Consequently, the photoreaction may conform to the following reaction scheme, which was postulated for singlet quenching by electron transfer,[13] thus

$$\underset{\mathbf{1}}{{}^1\mathrm{An}^*} + \underset{\mathbf{2}}{\mathrm{Q}} \underset{k_{-q}}{\overset{k_{diff}}{\rightleftarrows}} \underset{\mathbf{6}}{[{}^1\mathrm{An}^* \cdots \mathrm{Q}]} \xrightarrow{k_e} \underset{\mathbf{7}}{[\mathrm{An}^{\delta+} \cdots \mathrm{Q}^{\delta-}]^*}$$

$$\underset{\text{Products}}{\overset{k_r}{\swarrow}} \qquad \underset{\mathrm{An} + \mathrm{Q},}{\overset{k_d}{\downarrow}} \qquad (1)$$

where An and ^{1}An* denote **1** in the ground and excited singlet states, respectively, Q denotes the aroyl chlorides, [^{1}An*···Q] is a proximate pair in a solvent cage, [$An^{\delta+}$···$Q^{\delta-}$]* denotes an exciplex, and the k are rate constants. The exciplex is either deactivated through radiationless decay or transformed into a radical ion pair and/or a zwitterionic intermediate, **8**, which yields products by the elimination of hydrogen chloride.

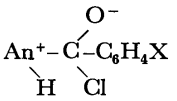

8

The validity of an exciplex is substantiated by the fact that the yield of **4d** decreased when the reaction solution was irradiated with the 254 nm light. Under these conditions, the fraction of the incident light which is absorbed by **1** is relatively small, the quencher being able to absorb extensive amounts of the light. Therefore, substitution through an exciplex may compete with that through an aroyl radical generated by direct photolysis of the quencher. The latter photoreaction predominantly gives **5d**, because the carbon atom at the meso position of **1** has the greatest reactivity. It appears likely that the inefficient formation of **4d** is a response to the decrease in the probability for exciplex formation.

Furthermore, the quenching effect by oxygen may support the existence of long-lived intermediates. Judging from the fact that the photooxidation of **1** is rather inefficient in benzene[14,15] and that the singlet lifetime of **1** is very short, especially under the reaction conditions, added oxygen would not be expected to interfere by quenching ^{1}An*, but to become involved by quenching long-lived exciplex and/or radical ions.

The solvent dependence of the photoreaction is consistent with the mechanisms proposed. The higher quantum and product yields in acetonitrile *vs.* benzene are due to a greater degree of solvent stabilization for the polar exciplex in a high polarity solvent than in a poor polarity solvent. In this respect, it appears surprising that **2i** and **2j** are rather inactive in the photoaroylation, in spite of their great efficiency for fluorescence quenching. This may be the consequence of the rapid formation of solvated radical ions, since they are strong electron acceptors.

This scheme leads to the modified Strern-Volmer equation,

$$\phi_f^\circ/\phi_f = 1 + k_q\tau[\mathrm{Q}], \qquad (2)$$

where

$$k_q = \frac{k_{diff}k_e}{k_{-q}+k_e}, \qquad (3)$$

ϕ_f and ϕ_f° are the fluorescence quantum yield in the presence and absence of the quencher, respectively, k_{diff} and k_{-q} are the rate constants for diffusive formation and for separation of a proximate pair (**6**), respectively, and k_e is the rate constant for electron transfer. The quantum yield of the photoreaction, Φ, is given by

$$\Phi = \frac{k_q\tau[\mathrm{Q}]}{1+k_q\tau[\mathrm{Q}]}\,\frac{k_r}{k_r+k_d}, \qquad (4)$$

where the first term on the right-hand side is the prob-

ability for exciplex formation, the second term is the fraction of the exciplex which gives the photoproducts, and k_r and k_d are the rate constants for chemical transformation and for degradation to the starting materials, respectively. The limiting quantum yield refers to the rate-constant ratio, $k_r/(k_r+k_d)$. The data are summarized in Tables 2 and 3.

It is assumed in the reaction scheme that an exciplex is formed irreversibly. This assumption is convenient for the quenching reaction which occurs with a nearly diffusion-controlled rate.[16] Since CT interaction is mainly responsible for exciplex binding,[12] a definite relation between the k_q values measured and the Hammett substituent constant, σ, is expected. Although the k_q values given in Table 3 cannot be linearly correlated with σ, probably owing to the levelling effect, it appears possible to apply the kinetic treatment developed by Evans to the nearly diffusion-controlled quenching process.[13] On the assumption that the rate constant for the diffusive separation of a proximate pair, k_{-q}, is a constant parameter which is determined only by the properties of the solvent,[13] a linear free-energy relation is derived from Eq. 3, thus

$$\ln \frac{k_q}{k_{diff}-k_q} = \ln \frac{k_e}{k_{-q}} \propto \Delta G^{\ddagger}, \qquad (5)$$

where $\Delta G^{\ddagger}$ is the free energy of activation for the electron-transfer process.

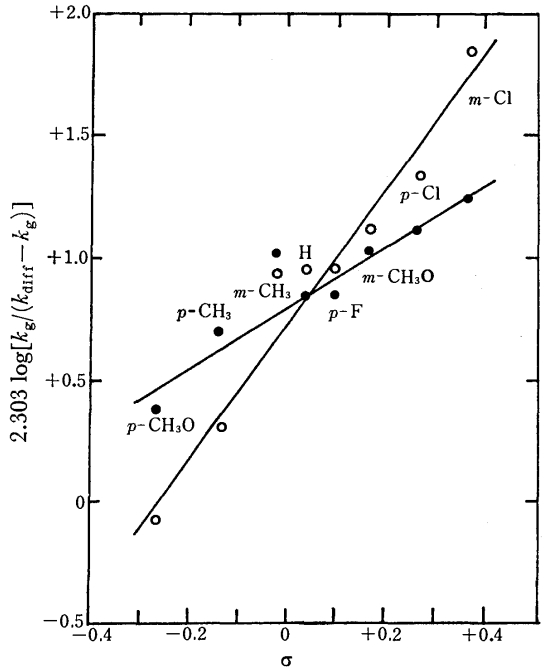

Fig. 4. Linear free-energy relation of the quenching constant: (○) in benzene and (●) in acetonitrile.

As is shown in Fig. 4, a linear relation is obtained between σ and the function, 2.303 $\log[k_q/(k_{diff}-k_q)]$, which was determined from the measured values of k_q and the calculated values of k_{diff}. The ρ values are 2.8 in benzene and 1.3 in acetonitrile. These positive ρ values strongly support CT interaction, in which electron transfer occurs from ^{1}An* to **2** in the ground state. The correctly linear relations shown in Fig. 4 confirm the validity of the reaction scheme proposed.

One should take account of a few possibilities for positional selectivity. First, there is the possibility that isomerization of the products gives rise to apparent positional selectivity. In fact, it is known that a variety of product distributions are produced in the thermal Friedel-Crafts acetylation of **1**, depending on the experimental conditions.[17] Substitution occurs prevalently at the meso position under mild conditions, whearas the acetyl group first attached at the meso position rapidly migrates to outer-ring positions under slightly drastic conditions and/or for prolonged reaction times. In contrast with the thermal reactions, the ketonic products in this system are formed from a bimolecular reaction of **1** and **2** without isomerization. Thus, the product-formation behavior is different from that in the ground-state reaction.

Second, the reactivity of the aromatic nucleus should be taken into account. As is known, low-lying excited singlet states of **1** consist of the ^1L_a and ^1L_b states, the former being much more abundant and slightly lower in energy than the latter.[18] The singlet-state reaction is, in general, expected to occur in the ^1L_a state. An MO calculation allowing for configuration interaction suggests that the increase in the reactivity of **1** upon photoexcitation is positionally dependent.[19] The reactivity sequences predicted by the free-valence index are 9> 1>2 for the ^1L_a state and 9>2>1 for the ^1L_b state. If the ^1L_a state is active, photoaroylation would be expected to form three position isomers in yields following the same order as those of the reactivity sequences. However, the product distribution given was contrary to the theoretical expectation, appearring severly selective at the outer-ring positions.

The discrepancies between the theory and experiment may be partly explained by the steric effect. But this is not conclusive, since there is no reason why meso substitution should be predominant.

Third, these considerations result in the tentative conclusion that the exciplex is important in determining positional selectivity. It appears likely that the exciplex interaction leads to considerable changes in the electronic structure of ^{1}An*, resulting in a different enhancement of the chemical reactivity from that of the original molecule. Based on strong selectivity between the positions of the outer ring, it may be supposed that the electronic structure of ^{1}An* would change increasingly, particularly when the quencher approaches the outer ring. At this time, if the CT interaction occurs along the long axis of **1**, then it would cause greater stabilization of the longitudinally polarized ^1L_b state than of the transverse-polarized ^1L_a state.

The inversion of the electronic state is intramolecularly established in the aromatic compounds into which a powerful substituent is introduced. It is well-accepted that the substituent primarily shifts toward the red and intensifies an electronic transition band lying in the same direction as that of the extending conjugation.[18,20] In this connection, it should be noted that the absorption spectra of **3d** and **4d** are quite different from that of the parent **1**, while the absorption spectrum of **5d**

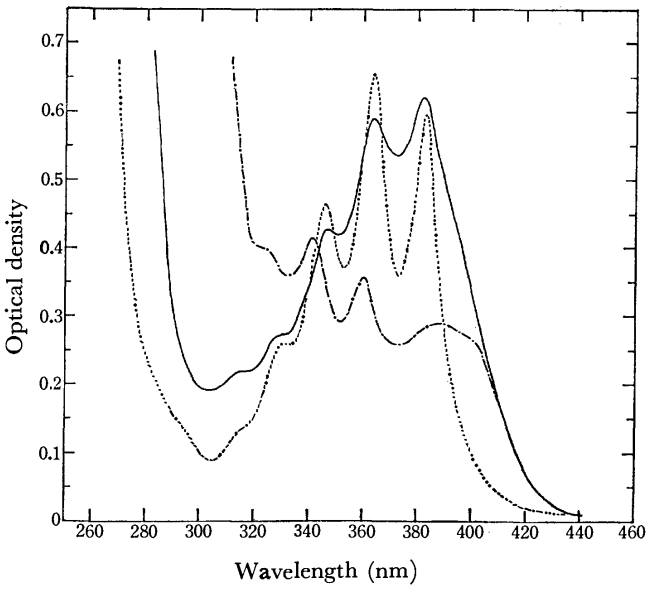

Fig. 5. Absorption spectra of 1-benzoylanthracene (solid line), 2-benzoylanthracene (broken line), and 9-benzoylanthracene (dotted line) in acetonitrile (10^{-4} M).

is similar in general shape and intensity to that of **1**, except for a slight shift to longer wavelengths, as is shown in Fig. 5. The spectral information implies that the electronic conjugation of the transition bands of the aromatic ring and benzoyl group is greatly enhanced when the substituent is introduced into the outer ring. The spectral deformation of 2-substituted **1** is known to be due to the result that the ^1L_b band emerges on the low-energy side of the ^1L_a band.[21] Such intramolecular interactions may be related to the intermolecular interaction of **1** with **2**.

Finally, ground-state complex formation will be considered. The Stern-Volmer treatment gave upward curvatures for **2h**—**j** with increasing concentration up to 2 M. This indicates that a contact complex is formed

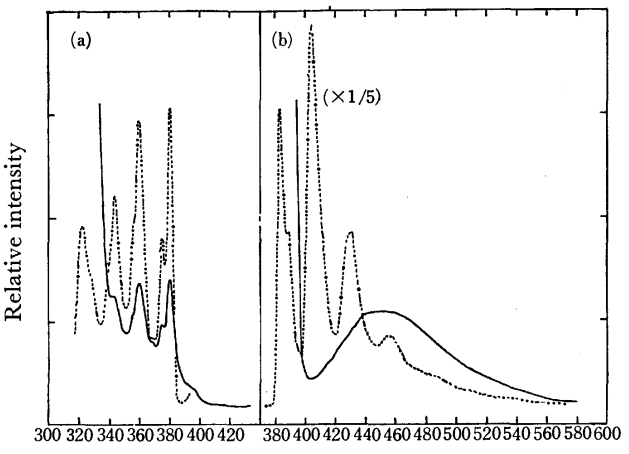

Fig. 6. Emission and excitation spectra of a mixture of anthracene (5×10^{-5} M) and *p*-chlorobenzoyl chloride (2 M) in a solid ether solution at 77 K: (a) excitation spectra for monitoring at 470 nm (solid line) and at 400 nm (dotted line); (b) emission spectra for excitation at 390 nm (solid line) and at 360 nm (broken line).

in the ground state,[22] although no change was observed in the absorption spectra, except for a slight red-shift due to the increasing dielectric constant of the solvent. A glassy ether solution containing **1** and **2g** or **h** at 77 K showed structureless fluorescence when excited at 390 nm. The corresponding absorption band was seen as a shoulder of the longest wavelength band of **1** in the excitation spectrum (Fig. 6). These spectra were confirmed to be different from those derived from anthracene aggregates,[23] since only the monomer bands were seen in the absence of the quencher. Therefore, the low-temperature emission is also indicative of the formation of CT complex related to that of the anthracene–trimesitinoyl chloride system reported by Briegleb.[24] Although very weak or no CT fluorescence was detected for the other aroyl chlorides, **2a**—**f**, which have less electron-withdrawing substituents, it appears likely that complex formation becomes feasible upon photo-excitation of the donor, since electronic excitation leads to a decrease in the ionic potential.[25]

Experimental

Reagents. Benzoyl chloride was purified by washing with cold 5% aqueous sodium hydrogencarbonate followed by fractional distillation. The other aroyl chlorides available commercially or produced by ordinary procedures using the corresponding acids and thionyl chloride, were distilled twice *in vacuo* to eliminate hydrogen chloride. Anthracene was recrystallized three times from benzene. Benzene was washed with concentrated sulfuric acid and water, dried over calcium chloride, and then distilled over sodium. Acetonitrile was dried by shaking with silica gel and diphosphorus pentaoxide, and purified by fractional distillation over diphosphorus pentaoxide.

Irradiation. Benzene was used as the solvent in a series of preparative runs, since all the starting materials and products were largely soluble in it. The 365-nm light was isolated from a 500-W medium-pressure mercury lamp equipped with a filter combination composed of Corning 7-60 and Toshiba UV-35 filters and a cupric sulfonate solution. A reaction mixture (50 ml) of **1** (1×10^{-2} M in benzene and 3×10^{-3} M in acetonitrile) and **2** (0.1—0.13 M) in a Pyrex flask was exposed to the light in a nitrogen atmosphere at about 25 °C. Irradiation was carried out for 16 h. In most cases, the loss of **1** was about 60% of the starting quantities. In the cases of **2a**, **i**, and **j**, more prolonged irradiation periods (*ca.* 40 h) were required to accomplish the same conversion. After removal of the remaining **2** with aqueous sodium hydrogencarbonate and evaporation of the solvent, the products were subjected to chromatography on a silica column. Elution with a 4: 1 cyclohexane benzene solution gave two major and several minor products. The major products were characterized by their UV, IR, and NMR spectra, coloration with concentrated sulfulic acid, and emissive behavior in ethanol, as listed in Table 1. The anthracene dimer was obtained as a precipitate in the eluting solvent.

Irradiation using the 254-nm light was performed using an 8-W low-pressure mercury lamp without any filter. An acetonitrile solution (80 ml) of **1** (3×10^{-3} M) and **2d** (0.14 M) in a quartz flask was exposed to the light in nitrogen. The procedures for product isolation were the same as those noted above.

Photoreaction of 9-Benzoylanthracene. A benzene solution was exposed to a 500-W medium-pressure lamp. After irra-

diation, the solvent was evaporated and the residues were extracted with methanol to remove the remaining monomer. A white powder was obtained and was recrystallized from benzene. The product was identified as the dimer and decomposed at 217 °C to recover the monomer. It was also found that crystalline **5d** dispersed in water gave the dimer upon irradiation in air. Although it has been reported that crystalline **5d** undergoes autooxidation in the presence of light giving anthraquinone,[26] no photooxidation was observed under the present conditions.

Quantum Yield Determinations. A low concentration of **1** (3×10^{-4} M) was employed to avoid photodimerization and to insure simple kinetics. At this concentration, the loss of **1** in the absence of the quencher was very small as compared with that in its presence. The amounts of **1** consumed in the presence of various concentrations of **2** (8×10^{-3}—3×10^{-2} M) were followed using a spectrophotometer at time intervals during the progress of the photoreaction and were subtracted from those in the absence of **2**. Since the photoproducts absorb increasing amounts of the incident light, resulting in a decrease in the photoreaction rate (see Fig. 1a), the quantum yields are based on the initial slopes of the conversion curves. Chemical changes in the dark were negligible. The incident and transmitted light intensities were monitored using potassium trioxalatoferrate(III) actinometry or an Eppley thermopile.

Errors were inevitable in determining the quantum yields. In the cases of **2i** and **j**, the conversion of **1** could not be precisely estimated, since the photoreaction rates were very slow under these conditions. A least-squares calculation was made to determine the values of the slope and the intercept in the plots of $1/\phi$ *vs.* 1/[Q]. The maximum error is $\pm30\%$.

Direct Photolysis of Aroyl Chlorides. Acetonitrile solutions of **2a, d,** and **h**—**j** (7—9×10^{-3} M) in quartz cells were exposed to an 8-W low-pressure lamp in nitrogen. The light intensity was determined using potassium trioxalatoferrate(III) actinometry. The aroyl chloride loss was estimated using the iron (III) hydroxamate method.[27] The molar absorptivities (λ_{max}) of the iron(III) hydroxamates derived from the aroyl chlorides are as follows: 1.64×10^3 (550 nm) for **2a**, 1.47×10^3 (540 nm) for **2d**, 1.62×10^3 (530 nm) for **2h**, 1.54×10^3 (525 nm) for **2i**, and 1.61×10^3 (520 nm) for **2j**.

Fluorescence Measurements. The quenching measurements were made using a Hitachi MPF-2A spectrofluorometer at 20 °C. Samples were prepared in quartz cells constructed from 1-cm square tubing. The concentrations employed for **2** were in the same range as that for the quantum-yield determinations. Sample solutions containing **1** (10^{-4} M) and **2** were deoxygenated by purging with argon for 5 min before measurement. Since the unquenched spectral distribution was the same as that in the absence of the quencher, the relative fluorescence intensity was determined by estimating the height of the peak maximum. The quenching constant was calculated from the initial slope of the Stern-Volmer plots. The error is $\pm10\%$.

The emission and excitation spectra at 77 K were measured with a low-temperature cell compartment. The spectra are uncorrected. Upon careful cooling, a transparent solid glass solution was formed from an ether solution of **1** (5×10^{-5} M) and **2** (2 M), except for **2i** and **j**, for which measurements could not be made because of precipitation upon cooling resulting in cracks in the glassy solution. The emission measurements were made for excitation at 360 and 390 nm, for which the phosphorescence of **2** was negligible. On the other hand, the phosphorescence of **2** contributed largely to the shorter-wavelength side of the excitation spectra monitored at 470 nm, while only excitation spectra attributable to **1** were observed when monitored at 400 nm.

Preparation of the Authentic Compounds. 9-Benzoylanthracene **5d** was prepared according to the thermal Friedel-Crafts method using aluminum chloride as a catalyst.[26] Mp 144—145 °C (lit,[28] 148 °C)

Found: C, 90.08; H, 4.99%. Calcd for $C_{21}H_{14}O$: C, 89.23; H, 5.00%.

The other isomeric ketones, **3d** and **4d**, were prepared using the Grignard reaction of phenylmagnesium bromide with the corresponding cyanoanthracenes. To 4.4 g of 1-anthracenecarboxylic acid were added 3.6 g of *p*-toluenesulfonamide and 8.7 g of phosphorus pentachloride and the mixture was warmed in a hot-air bath. The temperature was gradually raised to 200 °C and the volatile products were distilled out. The cooled reaction mixture was treated with 8 ml of pyridine and gently warmed. To this solution was cautiously added 40 ml of water and the solid was collected. After washing with water and a 5% sodium hydroxide, the dried products were purified using silica-column chromatography with a benzene eluent. The 1-cyanoanthracene obtained was recrystallized from ethanol: yield, 90%; mp 142 °C (lit,[29] 144.5 °C).

Found: C, 89.51; H, 4.33; N, 6.72%. Calcd for $C_{15}H_9N$; C, 88.64; H, 4.46; N, 6.89%.

2-Cyanoanthracene was prepared in a similar manner: yield, 95%; mp 195 °C (lit,[29] 200 °C).

Found: C, 88.44; H, 4.28; N, 6.79%.

To 0.3 g of cyanoanthracene in 20 ml of benzene was added an equimolar amount of phenyl magnesium bromide in ether. The reaction mixture was warmed and ether was distilled out. The residual benzene solution was refluxed for 2 h. After treatment with ammonium chloride, the ketimine was extracted with aqueous acetic acid (1:1) and hydrolyzed under reflux for 1 h. The addition of a mineral acid, such as hydrogen chloride, was important for hydrolysis of the *l*-isomer. Yellow products were extracted with benzene and purified by silica-column chromatography. Elution with benzene gave the corresponding ketones.

1-Benzoylanthracene **3d**: yield, 58%; mp 138—139 °C (lit,[29] 141 °C).

Found: C, 89.52; H, 5.04%.

2-Benzoylanthracene **4d**: yield, 86%, mp 178 °C (lit,[29] 175 °C)

Found: C, 90.07, H, 4.95%.

References

1) (a) D. Bryce-Smith, R. Deshpande, A. Gilbert, and J. Grzonka, *Chem. Commun.*, **1970**, 561; (b) D. Bryce-Smith, G. B. Cox, and A. Gilbert, *ibid.*, **1971**, 914.

2) O. Yonemitsu and S. Naruto, *Tetrahedron Lett.*, **1969**, 2387.

3) Y. Izawa, T. Ishihara, and Y. Ogata, *Tetrahedron*, **28**, 211 (1972).

4) J. Martens, K. Praefcke, and U. Schulze, *Synthesis*, **1976**, 532.

5) T. Tamaki, *J. Chem. Soc., Chem. Commun.*, **1976**, 335.

6) F. H. Quina, Z. Hamlet, and F. A. Carroll, *J. Am. Chem. Soc.*, **99**, 2240 (1977) and references cited therein.

7) H. Mauser, *Z. Naturforsh.*, **23b**, 1025 (1968).

8) E. Heller and G. M. J. Schmidt, *Isr. J. Chem.*, **9**, 449 (1971).

9) A. A. Lamola, "Energy Transfer and Organic Photochemistry," Interscience Publishers, New York, N. Y. (1969), p. 34.

10) S. L. Murov, "Handbook of Photochemistry," Marcel Dekker, New York (1973), p. 3.

11) Ref. 9, pp. 18—44.

12) A. Weller, *Pure Appl. Chem.*, **16**, 115 (1968).

13) T. R. Evans, *J. Am. Chem. Soc.*, **93**, 2081 (1971).
14) (a) R. M. Hochstrasser and G. B. Porter, *Quart. Rev.*, **14**, 146 (1960); (b) E. J. Bowen and D. W. Tanner, *Trans. Faraday Soc.*, **51**, 475 (1955).
15) It was confirmed that the photooxidation of anthracene was inefficient in benzene, the photodimerization being predominant even in an oxygen stream. The yield of anthraquinone was very poor (*ca.* 3%), contrary to that in the pressence of benzoyl chloride.
16) F. D. Lewis and C. E. Hoyle, *J. Am. Chem. Soc.*, **97**, 5950 (1975).
17) P. H. Gore, *Chem. Rev.*, **55**, 229 (1955).
18) H. H. Jaffe and M. Orchin, "Theory and Application of Ultraviolet Spectroscopy," John Wiley and Sons, New York, N. Y. (1962), pp. 316—321.
19) N. Mataga, *Bull. Chem. Soc. Jpn.*, **31**, 463 (1958).
20) R. N. Jones, *J. Am. Chem. Soc.*, **67**, 2127 (1945).
21) S. Suzuki and H. Baba, *Bull. Chem. Soc. Jpn.*, **37**, 519 (1964).
22) C. Lewis and W. R. Ware, *Mol. Photochem.*, **5**, 261 (1973).
23) E. A. Chandross, J. Ferguson, and E. G. McRae, *J. Chem. Phys.*, **45**, 3546 (1966).
24) G. Briegleb,"Electronen-Donator-Acceptor-Komplexe," Springer-Verlag, Berlin (1961), pp. 82—88.
25) J. B. Birks, "Photophysics of Aromatic Molecules," John Wiley and Sons, New York, N. Y. (1970), pp. 420—421.
26) P. H. Gore and J. A. Hoskins, *J. Chem. Soc.*, **1964**, 5666.
27) R. F. Goddu, N. F. LeBlanc, and C. M. Wright, *Anal. Chem.*, **27**, 1251 (1955).
28) J. W. Cook, *J. Chem. Soc.*, **1962**, 1281.
29) H. Waldman and A. Oblath, *Ber. B*, **71**, 366 (1938).

Oxidative Degradation of Polymers. V. Ozonization of Polypropylene and Polystyrene in Carbon Tetrachloride

Tsuneo SAITO, Etsuo NIKI,* Takeo SHIONO, and Yoshio KAMIYA

Department of Reaction Chemistry, Faculty of Engineering, The University of Tokyo, Hongo, Tokyo 113

(Received August 1, 1977)

The rates and products of ozonization of atactic polypropylene and polystyrene were studied in carbon tetrachloride at 30 and 70 °C. Atactic polypropylene underwent cleavage statistically by ozone to give oxygenated products. The molecular weight of polypropylene decreased with the progress of ozonization. Most chain ends of ozonized polypropylene were suggested to be carboxylic acids. Ozonization of polystyrene brought about crosslinking as well as chain scission, giving rise to broadening of molecular weight distribution. The major product from polystyrene was carboxylic acid.

Plastics and rubber deteriorate in the presence of ozone because of its powerful oxidizing action.[1] Ozonization of organic compounds, especially olefins, has been studied extensively.[2,3] The ozonization of polyethylene is reported to give peroxide, carbonyl and carboxylic compounds,[4–8] while polystyrene becomes brittle and discolored.[6,9] Razumovskii *et al.* found peroxide, carbonyl and carboxylic groups on the surface of ozonized polystyrene.[9] Both atactic and isotactic polypropylene films are also ozonized at ambient temperatures without induction period.[10] The attack of ozone on polymers was observed to result in chain scission.[11–13] However, the results so far obtained are qualitative and the arguments are speculative. More information is needed in order to clarify the nature of ozonization of polymers. In the course of our study on the oxidative degradation of polymers, we have studied the ozonization of atactic polypropylene and polystyrene in carbon tetrachloride.

Experimental

Materials. Polypropylene, kindly supplied by Mr. Fujita, Mitsui Petrochemical Ind. Co. was purified as follows. 92 g of chopped polypropylene was first soaked in 500 ml benzene at room temperature for about a week. The insoluble fraction was separated by filtration and the soluble fraction was repeatedly precipitated from the benzene solution by addition to excess methanol. It was finally dried in a vacuum at room temperature. The infrared spectrum of the purified polypropylene showed little absorption at 997 cm^{-1} but strong absorption at 975 cm^{-1}, indicating that little isotactic polypropylene was present. The intrinsic viscosity at 45 °C in carbon tetrachloride and the number average molecular weight of the purified atactic polypropylene were found to be 0.213 dl/g and 1.2×10^4, respectively.

Commercial polystyrene was purified by the conventional method using benzene and methanol as solvent and precipitant, respectively. The polystyrene solution was then washed successively with acid, water, alkali and water. Finally its 2% solution in chloroform was introduced slowly into excess methanol under vigorous stirring to give white powder polystyrene, which was dried in a vacuume at room temperature. The purified polystyrene dissolved completely into methyl ethyl ketone, indicating that it is atactic. The intrinsic viscosity at 45 °C in carbon tetrachloride was found to be 0.770 dl/g. The number average molecular weight was calculated as 2.1×10^5 by means of following equation obtained from the standard mono-dispersed polystyrenes.

$$[\eta] = 1.34 \times 10^{-4} \bar{M}_n^{0.706} \quad (1)$$

Carbon tetrachloride was treated with ozone prior to the oxidation reaction. Ozone was produced in a standard ozone generator, Nippon Ozone Co., Ltd. Model O-3-2, by charging pure oxygen dried with silica gel. The concentration of ozone in the feed gas determined by iodometric titration was 2—4%.

Procedures. Oxidation was carried out in a *ca.* 100 ml vessel equipped with a condenser. The oxidation was started by bubbling O_3–O_2 gas through the reaction mixture which was stirred vigorously with a magnetic stirrer. The amount of ozone consumed was calculated from the difference of the ozone concentration in the exhaust gases in the absence and the presence of substrate.

The reaction mixture was analyzed as follows. Viscosity was measured at 45 °C in carbon tetrachloride using a modified Ostwald viscosimeter. The molecular weight distribution was measured at 40 °C by gel permeation chromatography (DuPont-Shimadzu Model 830). Various types of crosslinked polystyrene gel columns (Shimadzu) were employed according to the molecular weight measured. Tetrahydrofuran (THF) was used as a carrier liquid at a speed of 1 ml/min. Both refractive index and ultraviolet absorption were used as a detector device. The calibration curve for the molecular weight of polystyrene was prepared by using standard, monodispersed polystyrenes; it was corrected for polypropylene with the Q-values given by Ouano and Mercier.[14]

Low-boiling products were determined by gas liquid chromatography. The conditions are given in Table 1.

Total amount of peroxides and acids formed was determined by iodometric and neutralization titrations, respectively. The

TABLE 1. GAS LIQUID CHROMATOGRAPHIC ANALYSIS

Column	Temp, °C	Carrier gas	Detector
Porapak-Q, 2 m, 50/80 mesh	100, 140, 170	N_2	FID
15 wt % Apiezon-L, 5m, on 80/100 mesh Uniport B	80, 140, 160	He	TCD
20 wt % PEG 20M, 7m, on 80/100 mesh Uniport B	75, 84	He	TCD
Chromosorb 101, 3m, 60/80 mesh	80	He	TCD

* To whom correspondence should be made.

oxidized polymers were analyzed by IR, UV, and ^1H NMR spectra and also by elemental analysis. Low molecular weight acids were determined by isotachophoretic analysis. An aqueous solution of 0.01 M gultamic acid was used as the terminal solution, and an aqueous solution containing 0.01 M L-histidine and 0.01 M L-histidine hydrochloride as the leading solution.

Results and Discussion

Ozonization of Polypropylene. The results of ozonization of polypropylene are summarized in Table 2. Although the initial solution of polypropylene in carbon tetrachloride was colorless, it became pale yellow after about 30 min. Discoloration increased with increase in reaction time. The change in molecular weight can best be visualized by the analysis of gel permeation chromatography. Figure 1 shows an example of the gel permeation chromatogram of the ozonized polypropylene. The molecular weight of polypropylene decreases markedly with the progress of ozonization (Fig. 1 and Table 2). The molecular weight decreased from 12000 to 500 in 10 h. The absorption at 260 nm also increased with increase in reaction time, stronger absorption being observed for lower molecular weight fractions (Fig. 1). The infrared spectrum of the product solution showed the formation of hydroxyl (3400 cm^{-1}) and carbonyl (1710 cm^{-1}) groups. Formation of methanol, acetone, acetaldehyde and acetic acid, observed by gas liquid chromatographic analysis, was very slight except for acetic acid at high conversion: acetic acid accounts for not more than 20% of total acid observed. Acetic acid was also observed by isotachophoretic analysis.

The total number of chain ends calculated from the initial weight of polypropylene and its final average molecular weight are given in Table 2. The results would underestimate the total number of chain ends as expected from the molecular weight distribution shown in Fig. 1. However, they correspond remarkably well with those of observed acid, indicating that much of the chain ends of the ozonized polypropylene is carboxylic acid.

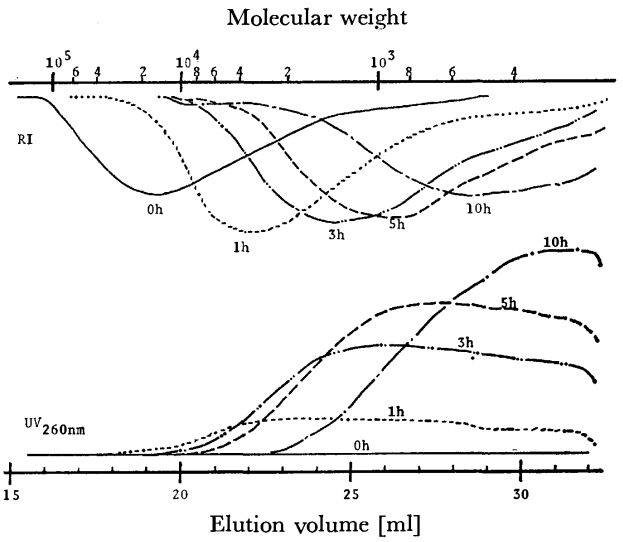

Fig. 1. Gel permeation chromatograms of polypropylene ozonized at 30 °C in carbon tetrachloride (Run No.5).

The results of elemental analysis for initial and ozonized polypropylenes are summarized in Table 3. It was confirmed that ozonized polypropylene contains no chlorine. This suggests that polymer carbon radical reacts with oxygen immediately before it attacks carbon tetrachloride and abstracts chlorine atom. Tables 2 and

TABLE 2. OZONIZATION OF ATACTIC POLYPROPYLENE AT 30 °C IN 50 ml CARBON TETRACHLORIDE

Run No.	1	2	3	4	5
APP,[a] mmol	47.5	47.8	12.0	12.5	11.9
Time, h	1	4	2	9	10
O_3 supplied/APP, mol/mol	0.16	0.62	1.23	5.31	6.25
Molecular weight by GPC at time t (h)					
t=0	12000	12000	12000	12000	12000
0.5		9000	6200		
1	7000	6800	3400	4400	3400
2		5400	1900	2000	
3		3000		1700	1300
4		2400		1400	
5				1100	900
7				800	
9				700	
10					500
Total number of chain ends, mmol	0.57	1.68	0.53	1.50	2.01
Total acid, mmol	0.70	1.9		1.9	2.1
Peroxide, mmol	0.68	2.6		0.42	0.49
Low boiling products, mmol					
Methanol		trace		trace	trace
Acetaldehyde		trace		trace	trace
Acetone	trace	small		small	small
Acetic acid	trace	trace		0.09	0.37

a) By monomer unit.

Table 3. Elemental analysis of initial and ozonized polypropylene

Run No.	Initial		1	2	3
	Calcd	Found			
Molecular weight		12000	7000	2400	1900
C, %	85.63	85.53	81.29	78.08	75.74
H, %	14.37	14.95	14.02	13.52	12.15
O,[a] %	0		4.69	8.40	12.11
H/C	2.00	2.08	2.05	2.06	1.99
$\Delta O/C_3H_6$	0		0.13	0.24	0.36
Peroxidic oxygen,[b] %	0		1.6		
Carboxylic oxygen,[c] %	0		0.4		

a) By difference. b) Determined by iodometric titration. c) Determined by neutralization titration.

3 show that the lower the molecular weight, the higher the content of oxygen and that the ratio of carbon to hydrogen atoms remains constant. Oxygen is incorporated not only as carboxylic acid but also as other functional groups such as hydroperoxide, alcohol and ketone.

The ^1H NMR analysis showed new peaks at 6.2 ppm and 5.0 ppm for ozonized polypropylene. However, they were not identified. The formation of carbon dioxide was confirmed by the formation of white precipitate when the exhaust gas was passed through the aqueous barium hydroxide solution.

Ozonization of Polystyrene. The ozonization of polystyrene was performed in a similar way to that for polypropylene. Distinct results were obtained. Discoloration of the reaction mixture to pale yellow was also observed for polystyrene. A white gummy substance was precipitated with the progress of ozonization. The substance was insoluble in carbon tetrachloride but partly soluble in acetone and tetrahydrofuran.

The pertinent results of the ozonization of polystyrene are summarized in Table 4. The effect of temperature was found to be small. Figure 2 shows an example of the gel permeation chromatograms of ozonized polystyrene. Broadening of molecular weight distribution was observed in each reaction, both lower and higher molecular weight fractions being formed. Since the column we used can not separate polymers with molecular weight higher than 10^6, the formation of crosslinked polymers, is indicated in Fig. 2.

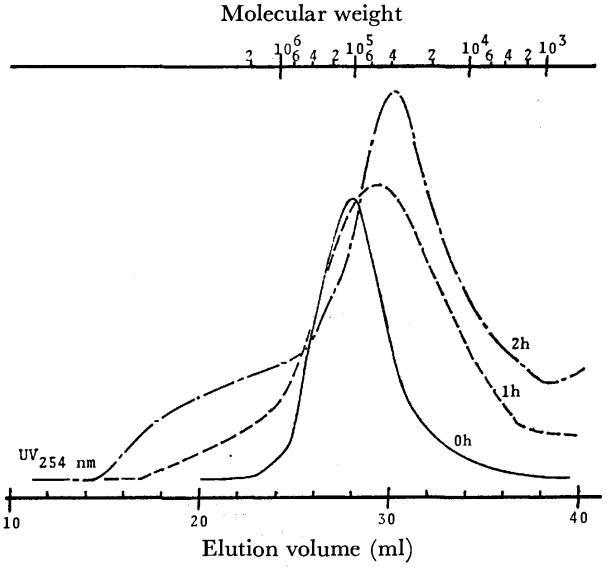

Fig. 2. Gel permeation chromatograms of polystyrene ozonized at 70 °C in carbon tetrachloride (Run No. 7).

Figure 3 shows the infrared spectra of the reaction mixture and the production of hydroxyl (3400 cm^{-1})

Table 4. Ozonization of polystyrene in 50 ml carbon tetrachloride

Run No.	Initial	6	7	8	9	10
PS,[a] mmol		9.62	9.62	9.61	9.60	4.82
Temperature, °C		70	70	70	30	30
Time, h		1	2	4	1.5	2
O_3 supplied/PS, mol/mol		0.63	1.54	2.87	1.08	3.07
Peroxide,mmol					0.83	
Acid, mmol					3.22	
Elemental analysis of ozonized polystyrene						
C, %	92.26		74.44	68.40	84.66	72.94
H, %	7.74		6.18	5.69	7.29	6.31
O,[b] %	0		(19.38)[c]	(25.91)[c]	8.05	20.75
H/C	1.00		0.99	0.99	1.02	1.03
$\Delta O/C_8H_8$					0.57	1.71
Peroxidic oxygen, %			1.1	0.9	0.3	
Carboxylic oxygen, %			4.9	3.9	3.6	

a) Polystyrene by monomer unit. b) By difference. c) Containing some chlorine due to incomplete removal of carbon tetrachloride.

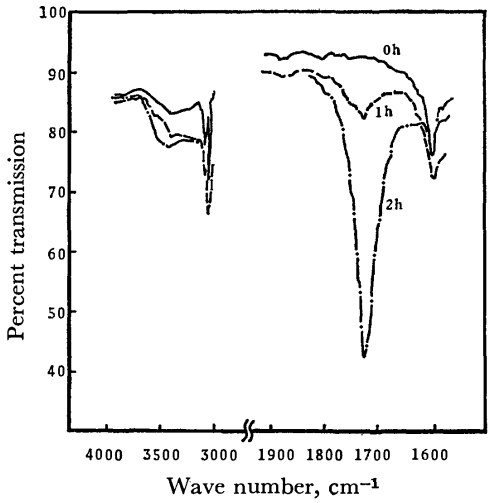

Fig. 3. Infrared spectra of ozonized polystyrene (Run Nos. 6 and 7).

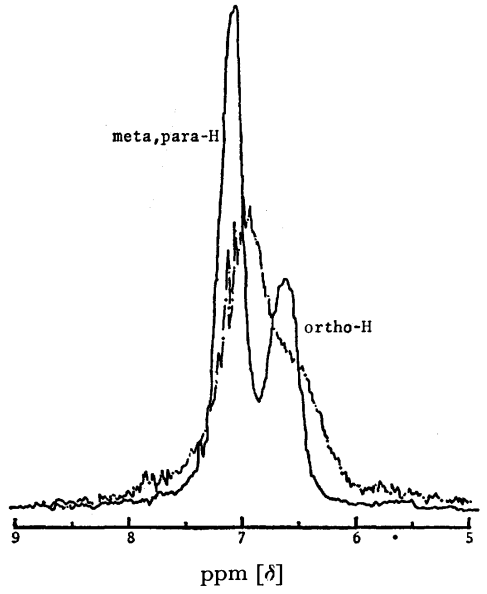

Fig. 4. NMR spectra of initial and ozonized polystyrene (Run No. 8).
——: Initial,
-·-·-: ozonized, 70 °C, 4 h.

and carbonyl (1730 cm^{-1}) groups. The UV spectrum showed the formation of a new band at 283 nm.

The results of elemental analyses, summarized in Table 4, show that much oxygen is incorporated into the polymer chain. Major products are carboxylic acid. Much of the chain ends should be acid.

Figure 4 shows the ^1H NMR spectra of initial and ozonized polystyrenes. The spectra of 6.63 and 7.10 ppm correspond respectively to *ortho* hydrogen and *meta*- and *para*-hydrogens of aromatic ring. The ratio is 2 to 3. The spectrum of ozonized polystyrene indicates the cleavage of aromatic ring. It was found by isotachophoretic analysis that formic acid was formed from polystyrene.

The results show that polypropylene is cleaved by ozone at ambient temperature to give dibasic acids as major products, polystyrene being both crosslinked and cleaved.

It has not yet been established how the initiation reactions proceed in the ozonization of saturated hydrocarbons.[15] It appears that the ozonization of carbon-hydrogen bond involves a hydrotrioxide, but the exact mode of formation of this intermediate and how it is converted into products has not been clarified. Hellman and Hamilton[16] postulated a scheme in which the ozonization of carbon-hydrogen bond proceeds through carbon radical and/or carbonium ion. The formation of 1-chloro- and 1-bromoadamantane in the ozonization of adamantane in the presence of bromotrichloromethane[17] suggests the presence of carbon radical. However, high ratio of retention of stereoregularity in the ozonization of saturated hydrocarbons[17,18] implies that this radical is not entirely free. The important role of ozone in the ozonization of polypropylene should be in the initial production of free radicals, which is supported experimentally by ESR analyses.[19,20] The adventitious impurities involved in polypropylene such as hydroperoxide, alcohol and carbonyl compounds might also contribute in the initiation reactions. Since polypropylene is relatively reactive toward oxygen, these impurities might be formed inevitably during the course of processing and storing.

After the initial production of radicals, the ozonization should resemble oxidation by molecular oxygen, where peroxyl and alkoxyl radicals are important chain carrying species.[21] The reported kinetic isotope effect and relative reactivities observed in the ozonization of aliphatic hydrocarbons[16,22] suggest the preferential attack of ozone on tertiary carbon-hydrogen bond of polypropylene to yield tertiary polypropylene radical. The characteristic feature of ozonization, when compared with autoxidation by molecular oxygen, is the rapid cleavage of polymer chain and high yield of carboxylic acid. It is not clear whether ozone is effective in direct scission of the carbon-carbon sigma bond. Carbon-carbon double bond is cleaved quite rapidly by ozone. Since the molecular weight of polypropylene decreases monotonously as the ozonization proceeds, the contribution of residual double bond involved in the initial polypropylene, if any, should be small. Since not much double bond should be formed in the autoxidation of polypropylene under sufficient oxygen, we assume that chain scission arises mostly from the β-scission of polypropylene alkoxyl radical. Primary alcohol is easily oxidized to aldehyde, which is then oxidized to carboxylic acid by ozone.

It is not clear why polystyrene behaves quite differently from polypropylene toward ozone. Ozone may attack either tertiary benzylic hydrogen or aromatic ring of polystyrene. The reactivity of the tertiary hydrogen of polystyrene is much lower than that of corresponding model compounds and polypropylene.[23] The crosslinking is not so important in the oxidation of polystyrene in solution by molecular oxygen as in the ozonization. Therefore, the cleavage of the aromatic ring should play a key role in the formation of crosslinked polystyrene. The ozonization of aromatic

compounds has been examined by many investigators, most extensively by Wibaut and his colleagues.[24] Ozone is able to function as a 1,3-dipole, an electrophile, or as a nucleophile, but it behaves primarily as an electrophilic reagent in its reactions with aromatic compounds.[24] In fact, the relative ozonization rates correlate well with the electron donating properties of alkyl substituted benzenes.[25] Thus the zwitter ion may play an important role and might be responsible for the crosslinking. The detailed mechanism of the crosslinking is now being studied with model compounds. It may be worth noting that the ozonization of simple aromatic compounds such as benzene, toluene and phenol gives insoluble polymeric materials.

The authors are grateful to Shimadzu Seisakusho for the use of the isotachophoretic analyzer.

References

1) J. F. Rabek, "Comprehensive Chemical Kinetics," ed by C. H. Bamford and C. F. H. Tipper, Vol. 14, Degradation of Polymers, Elsevier (1975), p. 516.
2) P. S. Bailey, *Chem. Rev.*, **58**, 925 (1958).
3) R. W. Murray, *Acc. Chem. Res.*, **1**, 313 (1968); R. Criegee, *Angew. Chem. Int. Ed. Engl.*, **14**, 745 (1975).
4) G. D. Cooper and M. Prober, *J. Polym. Sci.*, **44**, 397 (1960).
5) F. H. Winslow, W. Matreyek, A. M. Trozzolo, and R. H. Hansen, *Polym. Prepr., Am. Chem. Soc., Div. Polym. Chem.*, **9**, 377 (1968).
6) A. A. Kefeli, S. D. Razumovskii, and G. E. Zaikov, *Vysokomol. Soedin., Ser. A*, **13**, 803 (1971).
7) Yu. A. Pentin, B. N. Tarasevich, and B. S. El'tsefon, *Zh. Fiz. Khim.*, **46**, 2116 (1972); *Chem. Abstr.*, **77**, 152760 (1972).
8) L. Rektorikova and P. Svoboda, *Plasty Kauc.*, **11**, 333 (1974); *Chem. Abstr.*, **82**, 86789 (1975).
9) S. D. Razumovskii, O. N. Karpukhin, A. A. Kefeli, T. V. Pokholok, and G. E. Zaikov, *Vysokomol. Soedin., Ser. A*, **13**, 782 (1971).
10) J. Vsiansky, *Chem. Vlakna*, **21**, 64 (1971); *Chem. Abstr.*, **77**, 20499 (1972).
11) G. Geisler and H. Wergin, *J. Prakt. Chem.*, **25**, 135, 141, 150 (1964).
12) D. J. Priest, *J. Polym. Sci., Part. A-2*, **9**, 1777 (1971).
13) S. D. Razumovskii, A. A. Kefeli, and G. E. Zaikov, *Eur. Polym. J.*, **7**, 275 (1971).
14) A. C. Ouano and P. L. Mercier, *J. Polym. Sci., Part. C*, **21**, 309 (1968).
15) S. W. Benson, *Adv. Chem. Ser.*, **77**, 74 (1968).
16) T. M. Hellman and G. A. Hamilton, *J. Am. Chem. Soc.*, **96**, 1530 (1974).
17) M. C. Whiting, A. J. N. Bolt, and J. H. Parish, *Adv. Chem. Ser.*, **77**, 4 (1968).
18) G. A. Hamilton, B. S. Ribner, and T. M. Hellman, *Adv. Chem. Ser.*, **77**, 15 (1968).
19) T. V. Pokholok, R. M. Vikhlyaev, O. N. Karupukhin, and S. D. Razumovskii, *Vysokomol. Soedin., Ser. B*, **11**, 692 (1969).
20) A. Yamaoka, J. Yamauchi, and K. Ikemoto, 15th ESR Symposium, October, 1976, Kumamoto, p. 55.
21) E. Niki, C. Decker, and F. R. Mayo, *J. Polym. Sci. Polym. Chem. Ed.*, **11**, 2813 (1973).
22) D. G. Williamson and R. J. Cvetanovic, *J. Am. Chem. Soc.*, **92**, 2949 (1970).
23) E. Niki and Y. Kamiya, *J. Org. Chem.*, **38**, 1403 (1973); *J. Chem. Soc., Perkin Trans. 2*, **1975**, 1221.
24) J. P. Wibaut and F. L. J. Sixma, *Rec. Trav. Chim.*, **71**, 761 (1952).
25) T. W. Nakagawa, L. J. Andrews, and R. M. Keefer, *J. Am. Chem. Soc.*, **82**, 269 (1960).

Metal-Assisted Terpenoid Synthesis. V.[1] The Catalytic Trimerization of Isoprene to *trans*-β-Farnesene and Its Synthetic Applications for Terpenoids

Susumu AKUTAGAWA, Takanao TAKETOMI, Hidenori KUMOBAYASHI, Kiyoshi TAKAYAMA, Taichi SOMEYA, and Sei OTSUKA*

Central Research Laboratory, Takasago Perfumery Co. Ltd., 31-36, 5-Chome, Kamata, Ohta-ku, Tokyo 144

**Department of Chemistry, Faculty of Engineering Science, Osaka University, Toyonaka, Osaka 560*

(Received August, 5, 1977)

Isoprene oligomerization was effected with a catalyst system Ni(OR)(η^3-C_3H_5)PPh(NEt_2)$_2$ (R=*n*-$C_{11}H_{23}$, *n*-$C_{15}H_{31}$) to give a linear trimer fraction above 70% yield. The major component of the trimer fraction is (*E*)-7,11-dimethyl-3-methylene-1,6,10-dodecatriene (*trans*-β-farnesene) (**1**). The minor constituents of the fraction are (*E*)-2,6-dimethyl-10-methylene-1,6,11-dodecatriene. As slightly higher boiling point fractions, two cyclic trimers 1,5,9-trimethyl-1,5,9-cyclododecatriene and 1,5,10-trimethyl-1,5,9-cyclododecatriene were detected. Factors that influence the reaction path leading to **1** were discussed. Sesqui- and diterpenoids, including farnesyl acetate, farnesylacetone and isophytol were synthesised starting from **1**. A regioselective tail to tail coupling of **1** was achieved with a palladium catalyst to give the dimer $C_{30}H_{48}$ which, upon catalytic hydrogenation, gave perhydrosqualene in 85% yield.

The synthesis of natural terpenoids based on isoprene has attracted the interest of organic chemists,[2] extensive investigations being made to effect selective oligomerization of isoprene with transition metal catalysts.[3] Such attempts have been less rewarding than the case of 1,3-butadiene; only a few attempts were successful for the catalytic synthesis of natural terpenoids. Until recently only monoterpenoids, 2,6-dimethyl-1,3,6- and 1,3,7-octatriene, were obtained in reasonable yields.[4] The selective linear oligomerization of isoprene[5] to give higher terpenoids appears to be difficult.

Trans-β-farnesene (**1**) and its double bond isomer, (*E*)-2,6-dimethyl-10-metflylene-1,6,11-dodecatriene (**2**) can be produced catalytically.[6] Doubtless **1** is a useful intermediate for the synthesis of sesqui- and diterpenoids. For example, farnesyl acetate, farnesylacetone, isophytol and squalane could readily be derived in good yields from **1**. This paper describes the selective linear trimerization of isoprene and the synthetic applications of **1**.

Results and Discussion

Catalytic Oligomerization. The isoprene oligomerization was effected with a nickel alkoxide catalyst, Ni(OR)(η^3-C_3H_5)L [L=PPh(NEt_2)$_2$] (*vide infra*). Conversion reaches about 45% after 8 h at 70 °C. First, the catalyst was deactivated with methanol. A mixture of the dimers and trimers (79.5% based on reacted isoprene) was then isolated by vacuum distillation. As the results of analytical GLC show (Figure), the dimer fraction contains four components and the trimer fraction consists of six isomers in the ratio **1**/**2**/**3**/**4**/**5**/**6**= 87/4/3/2/1/3. Thus the linear oligomers constitute the major components. Under appropriate reaction conditions using a nickel complex as catalyst, it is possible to obtain **1** with a selectivity approaching as high as 87% of the trimer fraction (60% based on the total oligomers produced).

By the conventional fractional distillation, the crude products were separated into three fractions, *viz.*, the dimer, linear and cyclic trimers. Each fraction was then subjected to preparative GLC to isolate the isomers. All the dimer components (**a**—**d**) are readily identified by comparing the retention times with those of authentic samples.

The structural assignments of **1** and **2** have been reported.[6] Compounds **3** and **4** were identified on the basis of the catalytic hydrogenation and their spectro-

Table 1. Spectral data of linear trimers

Linear trimer	NMR[a] (δ)	IR[b] (cm^{-1})	UV[c] (nm)
1	1.59 (3H, s), 1.62—1.79 (6H, s), 1.90—2.18(8H, m), 4.60 (2H, s), 5.10 (4H, m), 6.27 (1H, t)	3080, 1772, 1601 908, 892	241 (ε 2.3×10^4)
2	1.50 (3H, m), 1.59 (3H, s), 1.68 (3H, s), 1.90 (4H, m), 2.18 (4H, m), 4.60 (2H, s), 4.92 (2H, s), 5.10 (3H, m), 6.26 (1H, t)	3082, 1770, 1604 906, 895	240 (ε 2.2×10^4)
3	1.15 (3H, d), 1.25 (3H, m), 1.59 (3H, s), 1.68 (3H, s), 2.15 (2H, q), 2.19 (2H, d), 4.60 (2H, s), 5.10 (3H, m), 5.60—7.01 (2H, m, J=16.0 Hz), 6.25 (1H, t)	3085, 1770, 1602 915, 892	232 (ε 2.0×10^4)
4	1.25 (2H, m), 1.59 (3H, s), 1.68 (6H, s), 2.15 (4H, t), 4.60 (4H, s), 5.10 (1H, t), 5.60—7.01 (2H, m, J=15.8 Hz)	3080, 1772, 1605 895	231 (ε 1.9×10^4)

a) 60 MHz, in CCl_4, s: singlet, d: doublet, t: triplet, q: quartet, m: multiplet. b) Neat. c) Measured in ethanol.

scopic properties (Table 1). Upon catalytic hydrogenation, **3** and **4** absorbed 4 mol of hydrogen producing 2,6,10-trimethyldodecane and 2,6,11-trimethyldodecane, respectively. Their ^{1}H NMR and IR spectra are in line with the assignment of **3** as (3*E*)-2,6,10-trimethyl-1,3,6,11-dodecatetraene and of **4** as (3*E*)-2,7,11-trimethyl-1,3,6,11-dodecatetraene. Although the spectral data available do not allow unambiguous determination of the double bond geometries at C-6 in **3** and **4**, it is likely, in view of the established structures of **1** and **2**,[6] that these double bonds are of *E*-configuration. In line with this inference, the chemical shift (δ, 1.59 ppm) of the singlet signal of the inner allyl methyl protons of **3** and **4** coincides with that of the corresponding signal of **1** or **2**.

Cyclic trimers **5** and **6** can be further purified by crystallization from hexane. Isomer **5** forms less soluble crystals, mp 43.5 °C. Upon ozonization and subsequent treatment of the ozonide with dimethyl sulfide, **5** yield 4-ketopentanal as the sole product, while the mother liquid containing **5** and **6** (1/3) gives a mixture of 1,4-butanedial, 4-oxopentanal and acetonylacetone in a ratio 1/1.5/1. The structures of **5** and **6** are thus assigned as 1,5,9- and 1,5,10-trimethyl-1,5,9-cyclododecatriene, respectively. The full assignment of isoprene cyclotrimers, in spite of numerous studies on cyclotrimerizations of 1,3-butadiene, has not been established.[3c,5] Although the double bond geometries of these oligomers remain to be elucidated, the all trans configuration is tentatively assigned to isomer **5** of higher melting point.

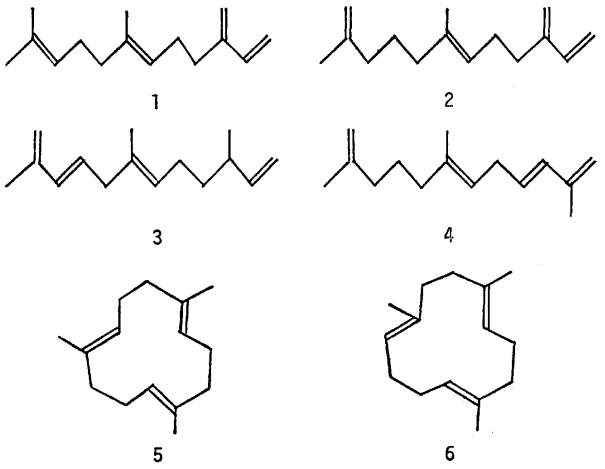

The neutral auxiliary ligand (L) plays a role of paramount importance in the nickel mediated catalysis.[6] $[NiX(\eta^3\text{-}C_3H_5)]_2$ alone gave the linear trimers in a very low yield. The presence of electron-donating phosphines or arsine such as $PPh(NEt_2)_2$ or $As(i\text{-}C_3H_7)_3$ is necessary for efficient catalysis. Various catalysts or their precursors were prepared by use of the following mixture: (1) 1:1 $Ni(\eta^3\text{-}C_3H_5)_2$ and $PPh(NEt_2)_2$, (2) 1:1:3 $Ni(acac)_2$, $PPh(NEt_2)_2$, and $AlEt_3$, and (3) 1:1:1.2 $[NiX(\eta^3\text{-}C_3H_5)]_2$, $PPh(NEt_2)_2$ or $As(i\text{-}C_3H_7)_3$, and NaOR (R=long chain alkyl). Representative results obtained have been given.[6] Qualitatively the relative catalytic activities are (1)$\simeq$(3)$<$(2).

The anionic ligand also influences the catalysis.

Table 2. Trimerization of isoprene[a]

No.	Base[b]	Conversion (%)	Dimers (%)	Trimers (%)[c]	Highers (%)[d]	Content (%) of **1** in Trimers
1	—	0	—	—	—	—
2	MeONa	35.1	42.1	35.2	22.7	30.6
3	$n\text{-}C_4H_9ONa$	41.5	29.5	46.1	24.4	62.2
4	$n\text{-}C_{15}H_{31}ONa$	40.5	21.2	71.6	20.5	87.3
5	$n\text{-}C_{15}H_{31}ONa$[e]	30.7	30.5	51.0	18.5	71.0
6	$LiNEt_2$	15.6	75.2	3.5	11.3	0

a) The mol ratio of isoprene/$[NiBr(\eta^3\text{-}C_3H_5)L]$ (**7**) is 100/1, at 70 °C for 7 h. b) The ratio of **7**/base was 1.2 unless otherwise stated. c) Contains all trimers (**1**—**6**). d) Based on the reacted isoprene. e) The ratio of **7**/base was 1/2.4.

Mononuclear halide complexes, $[NiXL(\eta^3\text{-}C_3H_5)]_2$ (X= Cl, Br), were found ineffective. The halide ligand may be replaced by the diethylamino group. However, the trimer yield was much lower (Table 2). Use of acetate or thiolate anions for X completely killed the catalytic activity. When the halide X is replaced by an alkoxide, in particular by a long-chain alkoxide (recipe 3), the oligomerization occurs smoothly producing the two linear trimers (**1** and **2**) with high selectivities (>75%). Recipe (2) also gives a high selectivity for the trimers. A conspicuous difference between recipe (2) and (3) is the ratio **1**/**2**. The former gives **2** as the major trimer, the latter predominantly **1**.

The alkoxide catalyst (recipe 3) is the only nickel system so far which gives natural β-farnesene as the major product. The effect of the anionic ligand is therfore noteworthy. Both the selectivity for trimers (**1**+**2**) and the ratio **1**/**2** were found to increase in the order: $CH_3O < n\text{-}C_4H_9O < n\text{-}C_{15}H_{31}O$ (Table 2).

In view of the conspicuous tendency of related alkoxide nickel complexes $[Ni(OR)(\eta^3\text{-}C_3H_5)]_2$ to disproportionate into $Ni(\eta^3\text{-}C_3H_5)_2$ and "$Ni(OR)_2$"[7] and of the facile β-hydrogen elimination of alkoxide Pd(II) or Pt(II) compounds,[8] it is unlikely that compound **8** remains under the reaction conditions.

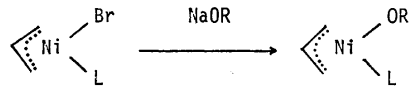

7 8

It was difficult to follow **8** under the reaction conditions and attempts to identify the active catalyst species were unsuccessful. However, the marked controlling effect of the alkoxide anion suggests that the anion is involved in the active species producing the linear trimers.

The linear oligomerization is always accompanied to some extent by cyclo-oligomerization. This side reaction seems to occur with a "naked" Ni(0) or Ni(0)-L species containing no alkoxide anion, as established by Jolly and Wilke for the Ni(0)-catalyzed cyclooligomerization.[3c] The Ni(0) species could be produced directly from disproportionation[7] of **8** or from reductive elimination[8]

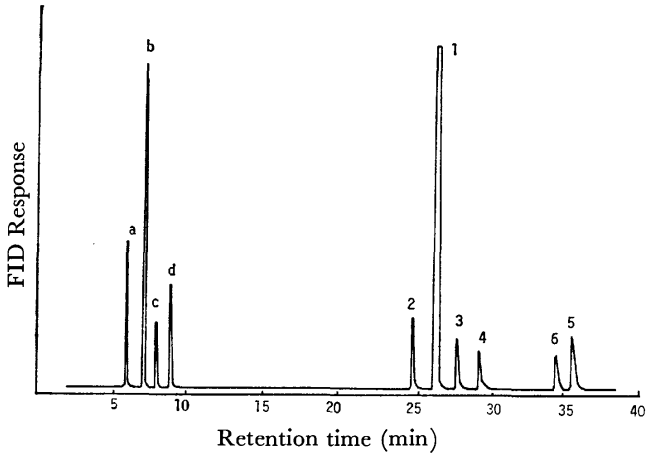

Fig. 1. Gas chromatogram[1] of the dimer and trimer fractions of the isoprene oligomerization.[2]
1) Column C, 130 °C; 2) Run 4 in Table 1 as representative example; **a**, 1,5-dimethyl-5-vinyl-1-cyclohexene; **b**, dipentene; **c**, 1,6-dimethyl-1,5-cyclooctadiene; **d**, 1,5-dimethyl-1,5-cyclooctadiene; **1**, *trans*-β-farnesene; **2**, (*E*)-2,6-dimethyl-10-methylene-1,6,11-dodecatriene; **3**, (3*E*)-2,6,10-trimethyl-1,3,6,11-undecateraene; **4**, (3*E*)-2,7,11-trimethyl-1,3,6,11-dodecateraene; **5**, 1,5,9-trimethyl-1,5,9-cyclododecatriene; **6**, 1,5,10-trimethyl-1,5,9-cyclododecatriene.

of **8**. It is inferred that although the major active species is the alkoxide-containing species (*vide infra*), the present catalyst systems also contains a minor amount of the "naked" Ni(0) species. The latter is responsible for the formation of the cyclotrimers.

A reaction scheme was proposed on the basis of a Ni(0)-L species.[6] Methyl hydrogen migration is assisted by an electron-donating ligand L. The hydrogen migration pathway was established by deuterium distribution studies on the trimer product **2** from 1,1,4,4-tetradeuterated isoprene. Key intermediates **9** and **10** were postulated to account for the formation of **1** and **2** (Eqs. 1 and 2).

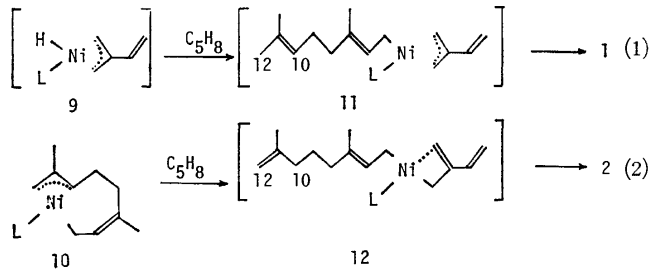

The present catalyst systems are ineffective for the isomerization of **2** to **1** suggesting two separate routes leading to the double bond isomers **1** and **2**. Intermediate **10** would lead to **12** whose dimer ligand contains a terminal double bond, since a nucleophilic hydride attack would occur at the secondary carbon in the η^3-allyl part of **10** rather than at the terminal carbon which is more anionic. Since **10** is unlikely to be a precursor of **11**, the formation of **1** is best accounted for by isoprene insertion into a Ni–H bond in the postulated intermediate **9**. The marked effect of a long chain alkoxide ligand (Table 2) invokes an intermediacy of an alkoxide complex like **13** which can not be detected.

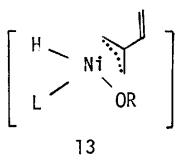

Recipe (2) might give predominantly **12**, which in turn is derived from the dimer complex **10**. Compound **10** has been isolated by Barnett *et al.*[9] The formation of **10** does not require the methyl hydrogen migration. It appears that one role of the alkoxide is to assist hydrogen abstraction to form a hydride species NiH(OR) involved in **13**. It is also possible that the large alkoxide group stabilizes the NiH(OR) species. The increased coordination number in **13** as compared to **9** is in line with the increased formal oxidation state. We tentatively postulate a reaction scheme essentially similar to the previous one for the formation of **1** and **2**. Regarding the minor isomeric products **3** and **4**, several routes involving the dimer intermediates **10** or its σ-π valence isomer are conceivable for the formation.

Derivative Chemistry. Purification of **1** can be achieved by repeated fractional distillation of the linear trimer fraction, but with a substantial loss due to polymerization. The crude product containing over 80% **1** was found to be satisfactory for most synthetic purposes. No further purification was necessary since many functionalization reactions occur preferentially at the 2-substituted 1,3-diene terminus of **1** and **2** rather than at the 1-substituted 1,3-diene part of **3** and **4**. The isolation of products, *e.g.* oxygen-containing terpenoids, is often achieved by distillation through a short fractionation column.

The high reactivity of the terminal group of **1** facilitates regio-selective introduction of a functional group useful for further extension of the carbon chain. Some representative examples are shown below.

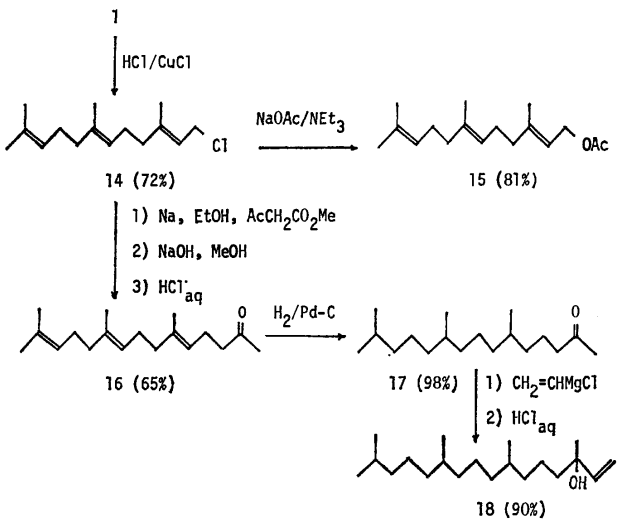

These derivations[10] do not require further comment. Yield and selectivity for each process are satisfactory.

Since the starting material **1** is contaminated with a few percent of **2**, farnesyl chloride **14** or acetate **15** contains 1—3% of the corresponding double bond isomer (2,6,11-triene). Both *E* and *Z* geometries were found for the newly formed trisubstituted double bond at C-2. In the above scheme the *Z*-form is not shown for the sake of clarity.

It is known that a regioselective tail to tail coupling of isoprene molecules can be achieved by a palladium catalyst.[11] A modified palladium catalyst consisting of palladium nitrate, triphenylphosphine, and sodium *o*-methoxyphenolate (molar ratio; 1/2/4) was found to have much higher activity and excellent regioselectivity. More than one mol of **1** could be dimerized at the terminal carbon (**19**) by 1 m gram atom of palladium in 92% selectivity. Squalane (**20**) is obtained quantitatively from **19**.

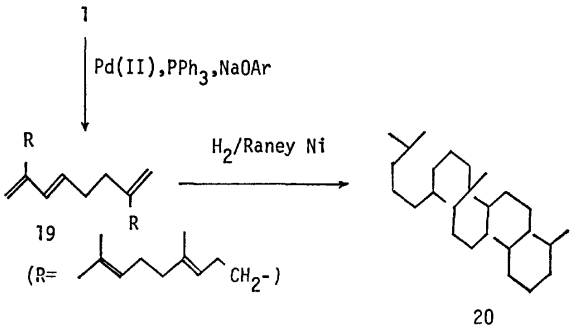

Experimental

Nuclear magnetic resonance spectra were measured on a JEOL Model C-60HL (60 MHz), mass spectra on a Hitachi 6M-GC gas chromatogram-mass spectrometer, and infrared spectra on a JASCO-IRG. Analytical gaschromatograms were obtained with a Hitachi 063 instrument with a flame ionization detector using the following columns: A (20% Carbowax 20 M on Chromosorb W, 3 m×3 mm), B (7% SE-30 silicone rubber on Chromosorb W, 2 m×3 mm), **C** (Capillary, R-45, 45 m×0.5 mm), and D (Capillary, PEG 4000, 45 m×0.25 mm). Preparative separation was made on Shimadzu GC-1C gas chromatograph with a 2 m×1.5 cm column of 20% Carbowax 20 M on 60—80 Celite 545.

Bis(diethylamino)phenylphosphine (bp 145 °C/2 Torr) was prepared by treating phenylphosphonous dichloride with an excess of diethylamine. η^3-Allylnickel bromide was prepared from nickel carbonyl and allyl bromide. Isoprene was distilled over calcium hydride under nitrogen. Solvents were distilled and kept over Molecular Sieves 5A. Other reagent-grade chemicals were used without further purification. Manipulation of organometallics was performed under nitrogen atmosphere.

Preparation of Bromo(η^3-allyl)[bis(diethylamino)phenylphosphine]-nickel(I) (7). To a benzene solution of bromo(η^3-allyl)-nickel(I) (5.1 g, 28.3 mmol) was added bis(diethylamino)-phenylphosphine (7.6 g, 30 mmol) at 10 °C. After being stirred at 20 °C for 10 h, the mixture was evaporated *in vacuo* to leave a black solid. Recrystallization from hexane gave 10.3 g of **7** as violet needles, mp 215 °C (dec), in 81.5% yield based on the nickel complex; NMR (C_6D_6) 0.48 (d, J=3, $\underline{CH_2}$=CH–), 0.57 (t, $\underline{CH_3}$–CH_2–), 1.67 (d, J=6, $\underline{CH_2}$=CH–), 2.80 (q, N–$\underline{CH_2}$–), 4.32 (m, CH_2=$\underline{CH}$–) and 6.58 (s, $\underline{C_6H_5}$–). Found: C, 47.1; H, 6.7; N, 6.8%; Ni, 12.9% (chelatometric titration). Calcd for $C_{17}H_{30}N_2PBrNi$: C, 47.3; H, 7.0; N, 6.5; Ni, 13.6%.

General Procedure for Isoprene Oligomerization. To an isoprene (50 mmol) suspension of a base (1.2 mmol) was added a benzene solution of **7** (1.0 mmol) at 0 °C. The brown solution was heated at 70 °C for 7 h. The reaction product, after deactivation with 1 ml of methanol, was distilled to give a mixture of dimers and trimers (bp 60 °C/30 Torr to 85 °C/3 Torr) and residues. The mixture of dimers and trimers was then analyzed by GLC on column C.

Preparation of Isoprene Trimers in Large Scale. Isoprene (1.36 kg, 20 mol), *n*-$C_{15}H_{31}ONa$ (120 g, 0.48 mol) and a benzene solution of **7** (96 g, 0.4 mol) were charged in this order in a 5-litre stainless steel autoclave. Autoclaving was carried out to let the temperature rise from 20 to 80 °C over a period of 5.5 h. After the autoclave had been cooled, 50 ml of methanol was added to deactivate the catalyst. The unreacted isoprene (740 g) was recovered by distilling directly from the autoclave to a trap chilled at −20 °C, leaving 835 g of crude products. The reaction products were poured into ice–water (1 litre), extracted with ether (3×1 litre), and the ether solution was washed with 1% hydrogen peroxide solution (2×100 ml), 2 M hydrochloric acid (2×100 ml), saturated sodium hydrogencarbonate solution (2×200 ml) and saturated brine. The solvent was evaporated *in vacuo*, the crude liquid products weighing 621 g. Fractional distillation of the liquid products with a 70 cm Widmer column gave the dimer fraction, 103 g (21.2% based on reacted isoprene), bp 70—95 °C/30 Torr, the linear trimer fraction, 349 g (71.6%), bp 97—105 °C/3 Torr, and the cyclic trimer fraction, 35 g (7.2%), bp 107—110 °C/3 Torr, leaving a residue, 125 g (20.5%). Each fraction was analyzed by GLC on column C.

Separation of Cyclic Trimer. A hexane solution of the cyclic trimer fraction (25 g) was cooled at −30 °C and kept at this temperature overnight. The resulting crystals were rapidly filtered at this temperature and washed with chilled hexane (3×5 ml); needle (10.7 g), mp 43.5 °C. The GLC analysis on column C exhibits one peak, the retention time of which coincides with that of **5**. NMR ($CDCl_3$), 1.91 (s, $\underline{CH_3}$–C=), 2.29 (m, –$\underline{CH_2}$–C=) and 5.45 (t, J=16.0, C=$\underline{CH}$–); mass, *m/e* 204 (3.5%, M^+).

Ozonolysis of Cyclic trimers. A stream of ozone-containing (3.2%) oxygen was introduced into a solution of **5** (7.5 g) in dichloromethane (150 ml) at −10 °C for 5 h. The ozonide was decomposed by adding dimethyl sulfide (20 ml) at −15 °C and subsequent heating at 50 °C for 4 h. The mixture was then poured into ice–water (100 ml), extracted with dichloromethane (3×50 ml). The usual work-up gave a yellow oil (6.2 g), bp 72 °C/12 Torr. The oil was homogeneous on GLC (column D) and identical with an authentic sample of 4-oxopentanal in IR and NMR.

The ozonolysis of a mixture of cyclic trimers 5.5 g (the mother liquid, a 1/3 mixture of **5** and **6**) was carried out similarly to give a mixture of 1,4-butanedial (28.6%), 4-oxopentanal (42.8%) and 2,5-hexanedione (26.1%).

Attempted Isomerization of Linear Trimers. A 71.5/28.5 mixture of **1** and **2** (3.5 g) was heated in the presence of **7** (0.96 g) and *n*-$C_{15}H_{31}ONa$ (1.2 g) at 80 °C for 7 h. After adding methanol (1 ml), the mixture was worked up as usual to give 2.1 g of a mixture of **1** and **2**, bp 101 °C/3 Torr and a polymeric residue (1.4 g). The ratio of recovered **1** and **2** was the same as that of starting material.

Hydrogenation of Linear Trimers. A mixture of linear trimers (2.0 g) was hydrogenated (Pd–C, 0.1 g, H_2, 10 kg/cm² at 25 °C) to give two saturated hydrocarbons in the ratio 93.7/6.3. The abundant isomer was identical with an authentic sample of 2,6,10-trimethyldodecane in the retention time

of GLC (column C) and mass spectra. The other isomer was identified as 2,6,11-trimethyldodecane, which was prepared by reaction of 3,7-dimethyloctylmagnesium chloride with 3-methylbutanal and subsequent dehydration and hydrogenation.

Hydrochlorination of Linear Trimers. Hydrogen chloride was introduced to a solution of linear trimers (300 g) in dichloromethane (300 ml) containing a catalytic amount of copper(I) chloride (3 g) at 0 °C for 5 h (weight increase, 45 g). The mixture was neutralized with 10% aqueous sodium carbonate, the organic layer being extracted with dichloromethane (2× 200 ml). The combined extracts were washed with saturated salt solution and evaporated *in vacuo* to give **14** (341 g) as a light yellow oil; NMR ($CDCl_3$), 3.46 (d, J=8.0, $-\underline{CH_2}Cl$). Found: Cl, 12.1% (titration method) Calcd for 87.3% content of $C_{15}H_{25}Cl$: Cl, 12.9%.

Synthesis of Farnesyl Acetate (15). A mixture of **14** (137 g, 0.5 mol), anhydrous sodium acetate (49.2 g, 0.6 mol) and triethylamine (6 ml) was stirred at 60 °C for 5 h. The reaction mixture was poured into ice–water (200 ml), extracted with ether (3× 150 ml), and the ether solution was washed with 2 M hydrochloric acid (2× 30 ml), 5% aqueous sodium hydrogen carbonate (3× 50 ml) and saturated brine, dried and evaporated to give a slightly yellow oil (135 g). The fractional distillation of the crude products with a 20 cmWidmer column gave a mixture of **3** and **4** (17.8 g), bp 91 °C/2 Torr and a mixture of stereoisomers of **15** (112 g), bp 105—107 °C/2 Torr (58.9% yield based on **1**). The ratio of stereoisomers was 65/35 for (2*E*,6*E*)- and (2*Z*,6*E*)-farnesyl acetate. The products were identified by comparison with authentic samples as regards retention times of GLC and mass spectra.

Synthesis of Farnesylacetone (16). To a solution of sodium ethoxide prepared by dissolving 2.5 g (0.11 g atom) of sodium in ethanol (100 ml) was added methyl acetoacetate (12.8 g, 0.11 mol) and **14** (27.4 g, 0.1 mol). After being refluxed for 5 h with stirring, the mixture was poured into ice–water (100 ml) and extracted with ether and worked up as usual to give an oil (39.1 g). A methanol solution of 1 M sodium hydroxide (120 ml) was added to the oil and the mixture was heated at 50 °C for 3 h. After the solvent had been evaporated, the whole mixture was poured into ice–water (100 ml) and acidified with 1 M hydrochloric acid and extracted with ether (3× 100 ml). The ether solution was worked up as usual to give an oil (29.3 g). The fractional distillation of the oil with a 20 cm Widmer column gave a mixture of **3** and **4** (3.6 g), bp 90 °C/2 Torr and a mixture of stereoisomers of farnesylacetone (**16**) (19.8 g), bp 105—107 °C/2 Torr, in 47.1% yield based on **1**. The ratio of stereoisomers, (5*E*,9*E*)- and (5*Z*,9*E*)-farnesylacetone, was 72/28. They were identified by comparison with authentic samples as regards retention times of GLC (column A) and in mass spectra.

Synthesis of Isophytol (18). A sample (15 g) of **16** was hydrogenated (Pd–C, 1.0 g in 30 ml 2-propanol, H_2, 70 kg/cm² at 100 °C for 3 h) to give **17** (14.9 g), bp 103 °C/1 Torr, semicarbazone, mp 85.1 °C (lit, 85.1 °C).

To a THF solution of vinylmagnesium chloride (12 ml, 0.012 mol), prepared from magnesium and vinyl chloride in THF, was added a THF (10 ml) solution of **17** (2.72 g, 0.01 mol) at 5 °C. After being stirred for 5 h at 25 °C, the mixture was poured into ice–water (50 ml) and acidified with 1 M hydrochloric acid and extracted with ether (3× 50 ml). The ether solution was worked up as usual to give **18** (2.85 g), bp 115 °C/1 Torr in 87.7% yield based on **17**. The GLC analysis (column A) of **17** and **18** showed a 95.2 and 94.1%, respectively, purity.

Dimerization of trans-*β-Farnesene.* A mixture of palladium nitrate (0.14 g, 1.0 mmol), triphenylphosphine (0.52 g, 2.0 mmol) and sodium *o*-methoxyphenolate (0.58 g, 4.0 mmol) and the linear trimers (102 g, 0.5 mol) in 2-propanol (100 ml) was heated at 60 °C for 12 h with stirring. After 2-propanol had been distilled off *in vacuo*, the residual mixture was extracted with ether (3× 100 ml). The usual work up of the extract gave an oil (101 g) which was distilled to give a mixture of **3** and **4** (13.2 g), bp 90 °C/3 Torr, and farnesene dimer (**19**), 80.1 g, bp 95 °C/0.005 Torr (90.5% based on **1**). For 19: IR, 1800, 1640, 973, 890, and 835 (cm^{-1}); NMR (CCl_4), 1.18 (s, $\underline{CH_3}$–C=), 1.50 (m, $-CH_2-$), 2.18 (m, =C–$\underline{CH_2}-$), 4.60 (s, $-\underline{CH_2}$=C), 5.15 (t, J=7, $-\underline{CH}$=C) and 5.52 (m, $-\underline{CH}$=C); *m/e* 408 (2.5%, M^+).

Synthesis of Perhydrosqualene (squalane) (20). The hydrogenation of **19** (20 g) in the presence of Raney nickel (W-4, 1.0 g) under H_2 (80 kg/cm² at 100 °C) gave **20** (20.1 g) quantitatively, bp 102 °C/0.01 Torr; *m/e* 422 (15.2%, M^+). The GLC analysis on column B showed a main peak (91%) retention time of which was identical with that of an authentic sample of squalane.

References

1) For part IV see S. Akutagawa, *Bull. Chem. Soc. Jpn.*, **49**, 3646 (1976).

2) For reviews see: J. Tanaka, T. Katagiri, and K. Takabe, *Yuki Gosei Kagaku Kyokai Shi*, **28**, 41 (1970); A. Watanabe and K. Suga, *Yukagaku*, **23**, 653 (1974); A. Watanabe and K. Suga, *Koryo*, **N/19**, 110 (1975).

3) For reviews see: a) R. Baker, *Chem. Rev.*, **73**, 487 (1973); b) P. Heimbach, *Yuki Gosei Kagaku Kyokai Shi*, **31**, 299 (1973); c) P. W. Jolly and G. Wilke, "The Organic Chemistry of Nickel," Vol. II, Academic Press, New York, N. Y. (1975); d) J. Tsuji, *Acc. Chem. Res.*, **6**, 8 (1973).

4) a) A. Misono, Y. Uchida, K. Furuhata, and S. Yoshida, *Bull. Chem. Soc. Jpn.*, **42**, 2303 (1969); b) Y. Uchida, K. Furuhata, and S. Yoshida, *ibid.*, **44**, 1966 (1971); c) A. Misono, Y. Uchida, K. Furuhata, and S. Yoshida, *ibid.*, **42**, 1383 (1969); d) Y. Uchida, K. Furuhata, and H. Ishiwatari, *ibid.*, **44**, 1118 (1971).

5) For reviews see: S. Otsuka and S. Akutagawa, "Oligomer," ed by M. Ookawara, T. Saegusa, and T. Higashimura, Kodansha, Tokyo (1976), pp. 59—144.

6) S. Akutagawa, T. Taketomi, and S. Otsuka, *Chem. Lett.*, **1976**, 485.

7) U. Birkenstock, H. Bönnemann, B. Bogdanović, D. Walter, and G. Wilke, "Homogeneous Catalysis," Advances in Chemistry Series 70, *Am. Chem. Soc.*, (1968), p. 250.

8) T. Yoshida and S. Otsuka, *J. Am. Chem. Soc.*, **99**, 2134 (1977).

9) B. Barnett, B. Büssemeier, P. Heimbach, P. W. Jolly, C. Krüger, I. Tkatchenko, and G. Wilke, *Tetrahedron Lett.*, **1972**, 1457.

10) For the synthesis of common terpenoids, *cf.* O. Isler and P. Schudel, "Advances in Organic Chemistry," ed by R. A. Raphael *et al.*, Vol. 4, Interscience, New York (1963), pp. 115—224; A. F. Thomas, "The Total Synthesis of Natural Products," ed by J. ApSimon, Wiley, Vol. 2, New York (1973), pp. 1—107.

11) a) A. D. Josey. *J. Org. Chem.*, **39**, 139 (1974); b) K. Takahashi, G. Hata and A. Miyake, *Bull. Chem. Soc. Jpn.*, **46**, 600 (1973); c) J. Berger, Ch. Duscheck, and H. Reichel, *J. Prakt. Chem.*, **315**, 1077 (1973); d) M. Anteunis and A. De Smet, *Synthesis*, **1974**, 800.

The Relative Rates of Ene Reaction of Benzyne with Cyclic Olefins: The Stereochemical Course†

Masahiko KATO, Yukio OKAMOTO,* Takeji CHIKAMOTO, and Toshio MIWA
Faculty of Science, Osaka City University, Sugimoto-cho, Sumiyoshi-ku, Osaka 558
**Wakayama Technical College, Gobo, Wakayama 644*
(Received August 16, 1977)

The benzyne reaction of cyclic olefins, in competition with that of cyclohexene has been studied. The relative reactivities for ene reaction and the stereoselectivity of the reaction with 4-*t*-butylcyclohexene, which afforded *trans*-5-*t*-butyl-3-phenylcyclohexene and *cis*-3-*t*-butyl-6-phenylcyclohexene, are consistent with the stereochemical requirements along the reaction pathway.

The reaction of benzyne with cyclic olefins has been attracting interest in connection with the stereochemical course of the reaction.[1-4]

The addition of benzyne to cyclic dienes falls into three categories: [2+2]-, [2+4]-cycloaddition reactions, and ene reaction. The former is believed to be a stepwise reaction and the latter two are mostly concerted reactions.[2] Stephenson has discussed the stereochemistry of the ene reaction, which proceeded in general in a concerned manner, as depicted in Fig. 1.[5]

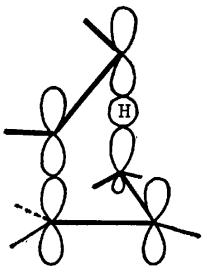

Fig. 1.

As cyclic olefins of medium-sized rings have rather mobile molecular frameworks within the limited conformations, the geometry of approach of benzyne toward cyclic olefins will be, in some cases, somewhat strained, and hence the geometry which can achieve a better overlapping of the correlated molecular orbitals in the transition state will be reflected in the reactivities for the ene reaction.

However, there is no report on the study of relative reactivities for ene reaction of olefins against benzyne, so we investigated the competition reaction of cyclic olefins in the presence of one equivalent of cyclohexene. For cyclic olefins, we chose simple ones: *i.e.*, cyclopentene (**1**), 4-*t*-butylcyclohexene (**2**), cycloheptene (**3**), *cis*-cyclooctene (**4**), and 1,2-cyclononadiene (**5**), to avoid the complexity arising from steric hindrance by substituents.

Identification of Products. Reaction with (a) Cyclopentene: From the 1: 1 addition mixture, **6** and **7** were detected as products. The fact that **6** showed no olefinic proton signal in the NMR spectrum, in addition to an integral ratio (4: 2: 6) of aromatic, benzylic, and aliphatic proton signals and to a A_2B_2 symmetry of aromatic signals, supported the [2+2]-structure. The NMR spectrum of **7** indicated that it was a phenyl substituted cyclopentene with two non-equivalent olefinic protons, which defined unequivocally the structure as 3-phenylcyclopentene.

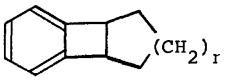

(**6**) $n=1$
(**9**) $n=3$
(**11**) $n=4$

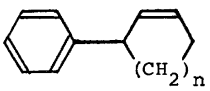

(**7**) $n=1$
(**8**) $n=2$
(**10**) $n=3$
(**12**) $n=4$

Scheme 1.

(b) Cyclohexene: 3-Phenylcyclohexene (**8**)[6] was obtained as the sole product and identified on the basis of IR and NMR spectra.

(c) Cycloheptene: Compounds **9** and **10** were separated using preparative GLC and characterized on the basis of their spectral data. The former was identified with a sample obtained by hydrogenation of a [2+2]-cycloaddition product of benzyne to cycloheptatriene.[7,8]

(d) cis-*Cyclooctene*: Because the 1: 1 addition products could not be separated using preparative GLC, the product mixture dissolved in ethyl acetate was hydrogenated over 10% Pd on carbon. GLC analysis of the hydrogenation products allowed us to estimate that the original mixture contained **11** and **12** in a ratio of 1: 7.7 by weight;[9] this result was also obtained from the examination of the PMR integral ratio of the original mixture.

(e) 1,2-Cyclononadiene: The products were separated using GLC, and were identified as **13** and **14** on the basis of the spectral data.[1]

*(f) 4-*t*-Butylcyclohexene*: The 1: 1 addition products were separated into two components, **15** and **16**, in a ratio of 1: 1.2; these were carefully investigated. Catalytic hydrogenation (Pd–C) of **15** gave thermodynamically unstable *trans*-3-*t*-butyl-1-phenylcyclohexane, which was transformed to a known *cis*-isomer by treatment with potassium *t*-butoxide in DMSO. Hydrogenation of **16** over PtO_2 gave *cis*-4-*t*-butyl-1 phenylcyclohexane,[10] which was treated under the same conditions of base to give exclusively the known *trans*-isomer. The position of the double bond in **15** and **16** was determined on the basis of their spectral data. The absence of intense absorption bands near 250 nm in UV

† Parts of this work were presented at the 36th Spring Meeting of the Japan Chemical Society, April 1—4, 1977 (Osaka). See the Abstracts II (1977), p. 1092.

TABLE 1. RELATIVE REACTION RATES OF CYCLIC OLEFINS WITH BENZYNE

Olefins	Relative rates [ene]	Relative rates [2+2]	θ_1	θ_1'	Preferred conformations
Cyclopentene	1.25[a]	0.19[a]	30°	30°	planar[11]
			17°	40°	envelope[12]
Cyclohexene	1.00	0	4—13°	47—56°	half-chair[12-14]
Cycloheptene	0.62	0.22	32—40°	80—88°	chair[12,15]
cis-Cyclooctene	0.88	0.11	20—56°	64—81°	twist[12,16]
4-*t*-Butyl-cyclohexene	0.89 (0.49+0.40)	0	4—13°	47—56°	half-chair[14]
1,2-Cyclo-nonadiene	7.54 (17.55)[b]	1.63 (4.40)[b]	35°	83°	rigid

a) Dichloromethane was used as solvent. b) Acetonitrile was used as solvent.

spectra of **15** and **16** eliminates phenyl-conjugated cyclohexene structures. That they showed two olefinic proton signals strongly coupled with benzylic proton signals in NMR spectra defined the structures.

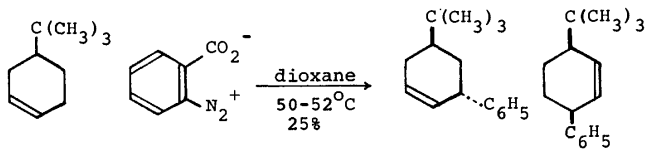

(**15**) 1: 1.2 (**16**)

Scheme 2.

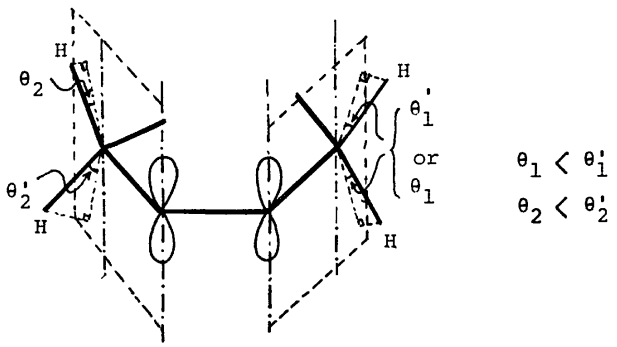

Fig. 2.

Competition Reaction with Cyclohexene. A mixture of an olefin, cyclohexene, and benzenediazonium-*o*-carboxylate in a molar ratio of 1: 1: 2 suspended in dioxane was stirred and heated at 50—52 °C. The hydrocarbon products were separated and carefully examined with the use of GLC. The results are collected in Table 1.

TABLE 2.

Cyclic olefins	Ratios of ene/[2+2]	θ_1	θ_2
cis-Cyclononene[18]	∞	0°	0°
Cyclohexene[19]	∞	13°	13°
cis-Cyclooctene[9]	8	0°	34—46°
1,2-Cyclononadiene[1]	6.2	0°	45°
Cycloheptene[7]	2.6	24°	39°
1,3,5-Cycloheptatriene[7]	2.3	36°	36°
trans-Cyclononene[17]	0.9	60°	30°
trans-Cyclooctene[9]	0	55°	65°

Results and Discussion

In 1973, Crews noticed that the product ratio of ene/[2+2] reaction of benzyne for cyclic olefins varies as an angle θ_1 changes (Fig. 2): the ratio and θ_1 values (in parentheses) are ∞ (4°), 3 (5°), 0.8 (33°), 0.07 (37°).[17] We had reached a similar conclusion when we studied the reaction with cycloheptatriene and cycloheptene.[7] Table 2 shows the data[7b] and includes additional values. The dihedral angles (θ_1, θ_1', θ_2, θ_2') between the axis of each *p*-orbital and the corresponding adjacent methylene C–H bonds are taken as shown in Fig. 2 and measured by the examination of the molecular models. If the molecular model is mobile, θ_2 was obtained after θ_1 was fixed by making it as small as possible. From this table, it is clear that the ene reaction becomes of no account compared to [2+2] cycloaddition when θ_1 (or θ_2) becomes an angle exceeding 55°.

Arnold and co-workers have demonstrated that the hydrogen abstraction occurs regioselectively in the ene reaction of β-pinene with benzyne. This experiment supports the assertion that the reaction proceeds in concerted mechanism.[20]

Accordingly, it is expected that the more close to zero degrees the dihedral angle (θ_1) between a relevant C–H bond and the adjacent olefinic *p*-orbital is (Fig. 2), the more smoothly the ene reaction of benzyne will proceed.

In the case of cyclohexene, however, the ene/[2+2] ratio is reported to be infinite.[6] We could not be convinced either that the [2+2] reaction with benzyne proceeded at similar rates for every olefin or that the ene reaction with cyclohexene advanced at an extraordinary rate. In order to obtain further knowledge about the transition state for the ene reaction of benzyne, we examined the reaction with a cyclohexene having a rather fixed conformation, *i.e.*, 4-*t*-butylcyclohexene. From the knowledge of conformational analysis, we need not consider a conformation of **2** keeping *t*-butyl group in axial position. If the most stable half-chair conformation of cyclohexene ring could easily flip into a half-boat form having an equatorial *t*-butyl group during the reaction (Scheme 3), *cis*-5-*t*-butyl-3-phenylcyclohexene (**17**) might be formed by way of path c. This was not the case. It is clear that the ene reaction involving a quasi-equatorial C–H bond with dihedral angle 47—56°

has not taken place, while the one involving an quasi-axial C–H bond with 4—13° has occurred. These results show undoubtedly that the transition states a and b are practically important.

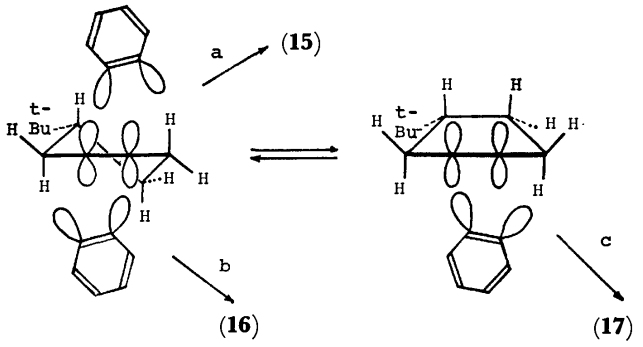

Scheme 3.

In the competition reaction between 4-*t*-butylcyclohexene and cyclohexene, formation of **15** is somewhat retarded in comparison with the formation of **16**, the rate of which is almost comparable to a half of the formation of 3-phenylcyclohexene from cyclohexene. From this fact, it is assumed that cyclic olefins react with benzyne, with high probabilities, in their most thermodynamically stable conformations, which, except *cis*-cyclooctene,[16] have a plane or an axis of symmetry intersecting the middle point of the C=C double bond. Therefore, to analyze the ene reaction, it will be enough to compare the conformation of one of the two methylene groups adjacent to the double bond. The angles θ_1 and θ_1' are obtained from measurements on the molecular models.

In the electronic spectra of conjugated ketones with steric hindrance of conjugation, it is claimed that the degree of conjugation is proportional to a directly excited molecular fraction r, or a ratio of molecular extinction coefficients of hindered to unhindered ketone, $\varepsilon/\varepsilon_0$, which is approximately given by $\cos^2\theta$ (θ: dihedral angle).[21] If we suppose that the ene reaction proceeds readily in harmony with the degree of hyperconjugation between an allylic hydrogen and the double bond, the plots of relative rates as a function of $\cos^2\theta_1+\cos^2\theta_1'$ given in Fig. 3 must have some clear feature. (In case of θ_1' 55°, $\cos^2\theta_1'$ is neglected). The approximately linear relationship in them is in line with the stereochemical course of ene reaction discussed above.

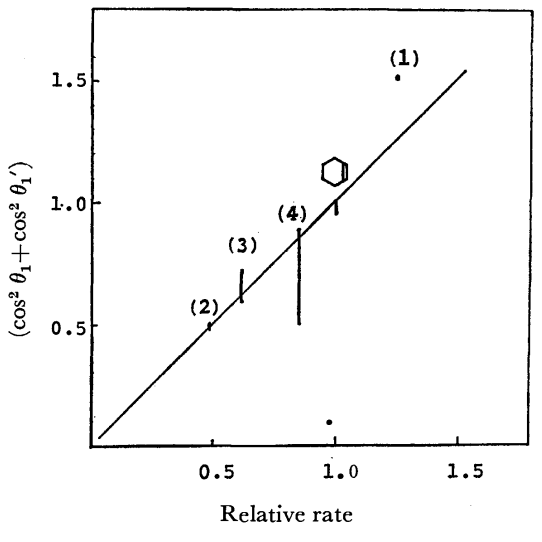

Fig. 3. Plot of relative rates against $\cos^2\theta_1+\cos^2\theta_1'$ for ene reaction of benzyne.

In the case of cyclopentene, if we were to choose either a planar[11] or an envelope conformation,[12] the plots deviate above the line.

In the case of *cis*-cyclooctene, the molecular framework is so labile that there are some preferable conformations,[12,16] of which the one with the smallest θ_1 satisfies the linearity.

On the other hand, at first sight, it seemed that there is no regularity between the reactivities of [2+2]-cycloaddition and the conformations of cyclic olefins. But it is interesting to note that the [2+2]-reaction proceeded in similar rates for cyclopentene and cycloheptene, while the relative rate for *cis*-cyclooctene fell to approximately a half of that for cycloheptene. This suggests that either above or below the sp^2-sp^2 plane of cyclooctene happens to be blocked from any attack of benzyne with the intramolecular methylene group, owing to the mobility of the molecular structure. We could not find any reason to justify the absence of the [2+2] product when cyclohexene was used as a substrate.

The relative rates for both ene and [2+2] reaction with 1,2-cyclononadiene are exceptional, as compared with the other olefins. The extraordinary enhancement of both reaction rates suggests a process of a different mechanism, that is, the ionic process[22] shown in Scheme 4, in addition to the ring strain. This seems to be supported by an increase in relative reactivities when the reaction was carried out in a more polar solvent such as acetonitrile. Further studies on the reactivities of allenes are now in progress.

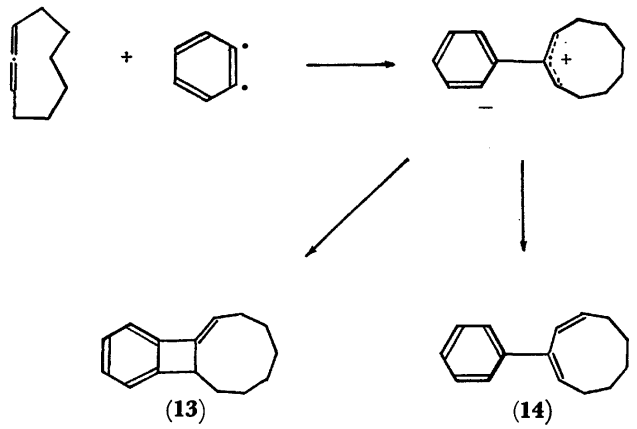

Scheme 4.

Experimental

The NMR spectra were obtained on a JEOL Model PS-100 spectrometer with carbon tetrachloride as a solvent and TMS as an internal standard. The chemical shifts are expressed in ppm from TMS. The IR was recorded on a JASCO Model

IRE spectrometer. GLC analysis was carried out on a Varian Aerograph Model 90P gas chromatograph under quoted conditions.

Reaction of Cyclopentene with Benzyne. Solid benzenediazonium-*o*-carboxylate, prepared from 20 mmol of anthranilic acid,[23] was suspended in dichloromethane (100 ml) containing cyclopentene (1.36 g, 20 mmol) and stirred at 37 °C for 3 h. The resulting solution was washed successively with water, aq sodium bicarbonate, and water, then dried (anhyd sodium sulfate). The residue (2.06 g) from the organic layer, dissolved in benzene, was chromatographed on Silicic Acid (Mallinckrodt, 100 g) and eluted with the same solvent. The hydrocarbon fraction (1.33 g, light brown liquid) from the eluate was rechromatographed on Silicic Acid (50 g). Fraction 1—10 (417 mg) contained **6** and **7** in a ratio of 0.26: 1 and fractions 11—20 (225 mg) contained **7**. GLC separation of the samples (see below) gave pure samples of them. The physical data of **6** and **7**: **6** NMR δ: 1.1—2.1 (6H, m), 3.78 (2H, broad d), 6.75—7.2 (4H, A_2B_2 type). Found: C, 91.63; H, 8.49%. IR ν(liq. film): 3060, 2930, 2850, 1460, 1350, 1290, 1205, 1112, 1003, 997, 820, 763, 743. **7** NMR δ: 1.5—2.0 (1H, m), 2.2—2.4 (3H, m), 3.68—4.0 (1H, m), 5.6—6.0 (2H, m), 6.9—7.4 (5H, m). IR ν(liq. film): 3060, 2940, 2850, 1602, 1496, 1455, 1360, 1080, 1032, 1012, 917, 760, 730, 700. Found: C, 91.57; H, 8.46%. Calcd for $C_{11}H_{12}$: C, 91.61; H, 8.39%.

Reaction of 4-t-Butyl-1-cyclohexene with Benzyne. Solid benzenediazonium-*o*-carboxylate, prepared from 20 mmol of anthranilic acid,[23] was suspended in dioxane (100 ml) containing 4-*t*-butyl-1-cyclohexene (2.76 g, 20 mmol) and stirred under heating at 50—52 °C for 3 h. The solvent was evaporated and the residue, taken in dichloromethane, was washed successively with 5% aq sodium bicarbonate and water. After drying the organic solution, the residue, taken in benzene, was chromatographed on Silicic Acid (50 g). The yellow liquid obtained by elution with benzene was rechromatographed on Silicic Acid (50 g) with hexane–ether (90: 10 v/v) as solvent. The 1: 1 addition products (1.07 g, 25% yield) were obtained as a pale yellow oil, which was separated using preparative GLC [10% Silicone DC-QF-1 on Chromosorb WAW; 1/4 inch×3 m; Helium flow rate, 20 ml/min; column temperature, 150 °C; retention times: **15**, 15.3 min; **16**, 19.7 min]. Physical data: **15** NMR δ: 0.76 (9H, s), 0.9—2.3 (5H, m); 3.54 (1H, broad S), 5.6—6.1 (2H, m), 7.0—7.3 (5H, m); IR (liq. film) ν: 3020, 2945, 2870, 1600, 1498, 1480, 1452, 1400, 1370, 1238, 1078, 1032, 880, 785, 760, 720, 702. **16** NMR δ: 0.96 (9H, s), 1.1—2.1 (5H, m), 2.06 (s, impurity), 3.2—3.5 (1H, m), 5.6—6.1 (2H, m), 7.0—7.3 (5H, m). IR (liq. film) ν: 3020, 2940, 2860, 1600, 1495, 1480, 1452, 1398, 1370, 1226, 1075, 1032, 1020, 990, 890, 850, 818, 767, 756, 730, 700.

*Characterization of **15**.* **15** (60 mg), dissolved in ethyl acetate (5 ml) was hydrogenated over 10% Pd–C as a catalyst to give *trans*-1-*t*-butyl-3-phenylcyclohexane (**18**) (54 mg) as the sole product. **18** NMR δ: 0.87 (9H, s), 0.9—2.0 (7H, m), 2.0—2.5 (2H, m), 2.95—3.3 (1H, broad s), 6.9—7.4 (5H, m). IR (liq. film) ν: 2930, 2850, 1600, 1500, 1470—1480, 1450, 1400, 1370, 1230, 1030, 780, 757, 728, 700.

18 (20 mg), dissolved in DMSO (6 ml), was treated with potassium *t*-butoxide (100 mg) at 120—130 °C for 1.5 h under nitrogen atmosphere to give *cis*-isomer[10] of **18** (5 mg). An authentic *cis*-isomer was synthesized from 4-*t*-butyl-2-phenyl-1-cyclohexanone by Wolff-Kischner reduction (KOH–hydrazine hydrate in diethylene glycol) in 74% yield and identified. *cis*-1-*t*-Butyl-3-phenylcyclohexane NMR δ: 0.89 (9H, s), 0.9—2.1 (9H, m), 2.2—2.8 (1H, m), 6.9—7.3 ((5H, m). IR (liq. film) ν: 3030, 2930, 2850, 1602, 1500, 1480, 1450, 1400, 1370, 1240, 1072, 1032, 762, 701. Found: C, 88.89; H, 11.39%. Calcd for $C_{16}H_{24}$; C, 88.82; H, 11.18%.

*Characterization of **16**.* Catalytic hydrogenation of **16** (20 mg) over platinum oxide (5 mg), dissolved in ethyl acetate, gave *cis*-1-*t*-butyl-4-phenylcyclohexane (**19**) as a colorless liquid. **19** NMR δ: 0.81 (9H, s), 0.9—2.0 (7H, m), 2.0—2.42 (2H, broad d), 3.02 (1H, broad s), 6.95—7.4 (5H, m). IR (liq. film) ν: 2930, 2850, 1602, 1500, 1480, 1452, 1400, 1370, 1028, 802, 760, 730, 700. Found: C, 88.89; H, 11.29%. Calcd for $C_{16}H_{24}$: C, 88.82; H, 11.18%.

When 10% Pd–C was used as a catalyst in place of platium oxide, some *trans*-1-*t*-butyl-4-phenylcyclohexane was formed along with **19**. Isomerization of **19** to the *trans*-isomer was carried out (DMSO/*t*-butoxide) as described above for that of **18**.[10] *trans*-Isomer of **19**: mp 40.5—41 °C. NMR δ: 0.87 (9H, s), 0.9—2.1 (9H, m), 2.1—2.6 (1H, m), 6.9—7.3 (5H, m). IR (liq film) ν: 2930, 2840, 1600, 1498, 1480, 1450, 1400, 1370, 1230, 1018, 898, 760, 700. This compound was identified with an authentic sample.[10]

A Competitive Benzyne Reaction of a Representative Olefin with Cyclohexene. Solid benzenediazonium-*o*-carboxylate, prepared from 20 mmol of anthranilic acid,[23] suspended in dioxane (100 ml) containing 10 mmol each of cyclohexane and an olefin, was stirred under heating at 50—52 °C until the gas evolution had ceased. After the usual work-up (see above experiment on 4-*t*-butylcyclohexene), the product mixture was roughly chromatographed on Silicic Acid (100 g) using benzene as solvent. The hydrocarbon fraction was rechromatographed on Silicic Acid (50 g) with the use of hexane as solvent. The products were estimated and separated into their components with use of GLC. For GLC separation, two kinds of columns, *i.e.*, a 10% polyethylene glycol succinate on Chromosorb WAW, 1/4 inch×2 m (Column 1), and a 10% silicone DC-QF-1 on Chromosorb WAW, 1/4 inch×3 m (Column 2), were used. The retention times are: On column 1: (column temp 140 °C; Helium flow rate, 30 ml/min) **6**, 2.68; **7**, 3.6; **8**, 6.0 min; (column temp 130 °C; He, 20 ml/min) **9**, 12.4, **10**, 14.9 min; (column temp 150 °C; He, 20 ml/min) **12**, 12.4; **8**, 4.95 min. On column 2: (column temp 180 °C; He, 20 ml/min) **14**, 9.5; **13**, 11.3 min; (column temp 150 °C; He, 20 ml/min) **15**, 6.2; **16**, 7.5; **8**, 3.45 min.

The authors are grateful to Mr. Jun-ichi Goda for the analytical data.

References

1) H. H. Wasserman and L. S. Keller, *Chem. Commun.*, **1970**, 1483.
2) G. Mehta and B. P. Singh, *Tetrahedron Lett.*, **1974**, 4297.
3) G. Mehta and B. P. Singh, *Tetrahedron*, **30**, 2409 (1974).
4) H. H. Wasserman and L. S. Keller, *Tetrahedron Lett.*, **1974**, 4355.
5) L. M. Stephenson and D. L. Mattern, *J. Org. Chem.*, **41**, 3614 (1976).
6) H. E. Simmons, *J. Am. Chem. Soc.*, **83**, 1657 (1961): L. Friedman and P. W. Rabideau, *Tetrahedron Lett.*, **1968**, 5735.
7) (a) M. Kato, T. Sawa, and T. Miwa, *Chem. Commun.*, **1971**, 1635; (b) T. Sawa, M. D. Thesis, Osaka City University, (1973), p. 18.
8) L. Lombardo and D. Wege, *Tetrahedron Lett.*, **1971**, 3981.
9) R. G. Gassman and H. P. Benecke, *Tetrahedron Lett.*, **1969**, 1089.
10) E. W. Garbisch, Jr., *J. Am. Chem. Soc.*, **85**, 3228 (1963).
11) G. V. Smith and H. Kriloff, *J. Am. Chem. Soc.*, **85**, 2016 (1963); O. L. Chapman, *ibid.*, **85**, 2014 (1963).

12) P. Foulani and C. Clement, *Bull. Soc. Chim. Fr.*, **1971**, 3444.
13) J. E. Chiang and S. H. Bauer, *J. Am. Chem. Soc.*, **91**, 1898 (1969).
14) Y. Senda and S. Imaizumi, *Tetrahedron*, **30**, 3813 (1974).
15) M. St-Jacques and C. Vaziri, *Can. J. Chem.*, **51**, 1192 (1973).
16) R. Pauncz and D. Ginsburg, *Tetrahedron*, **9**, 40 (1960).
17) P. Crews and J. Beard, *J. Org. Chem.*, **38**, 529 (1973).
18) G. Mehta, *Indian J. Chem.*, **10**, 592 (1972).
19) G. Ahlgren and B. Akermark, *Tetrahedron Lett.*, **1970**, 3047.
20) V. Garsky, D. F. Koster, and R. T. Arnold, *J. Am. Chem. Soc.*, **96**, 4207 (1974).
21) E. A. Braude, "Determination of Organic Structures by Physical Methods," ed by E. A. Braude and F. C. Nachod, Academic Press, New York and London (1955), pp. 169—174.
22) M. Stiles, R. G. Miller, and U. Burckhardt, *J. Am. Chem. Soc.*, **85**, 1792 (1963).
23) M. Kato, Y. Okamoto, and T. Miwa, *Tetrahedron*, **27**, 4013 (1971).

Reactions of Tetramethylbenzenedicarbonitriles and Tetramethylbenzonitriles with Fuming Nitric Acid. A New Route to Some Substituted Phthalides and 1,3-Dihydroisobenzofuran-1-imines[1]

Hitomi SUZUKI, Mamie KOGE, Akiyoshi INOUE, and Terukiyo HANAFUSA

Department of Chemistry, Faculty of Science, Hiroshima University, Higashi-sendamachi, Hiroshima 730

(Received August 31, 1977)

The reaction of tetramethylbenzenedicarbonitriles and tetramethylbenzonitriles with fuming nitric acid (d=1.5) has been investigated at room temperature in the dark. 2,4,5,6-Tetramethylbenzene-1,3-dicarbonitrile and 2,3,5,6-tetramethylbenzene-1,4-dicarbonitrile gave, after aqueous work-up, 4-cyano-5,6,7-trimethyl- and 5-cyano-4,6,7-trimethylphthalides, respectively, in high yields, while 3,4,5,6-tetramethylbenzene-1,2-dicarbonitrile produced appreciable amounts of two cyanonitro-3-cyclohexen-1-ones in addition to 7-cyano-4,5,6-trimethylphthalide. Similarly, 2,3,4,6- and 2,3,5,6-tetramethylbenzonitriles afforded 4-nitro-5,6,7-trimethyl- and 5-nitro-4,6,7-trimethylphthalides, respectively, along with the expected nitro compounds. In contrast, 2,3,4,5-tetramethylbenzonitrile underwent normal nitration, giving 6-nitro derivative as the sole product. The phthalide formation was found to proceed through 1,3-dihydroisobenzofuran-1-imines presumably derived from the initially formed *o*-cyanobenzyl nitrates. The reaction appears to provide potential utility in the synthesis of some substituted phthalides and 1,3-dihydroisobenzofuran-1-imines.

Pentamethylbenzonitrile reacts with nitric acid regiospecifically at the *ortho* side-chain to give 6-cyano-2,3,4,5-tetramethylbenzyl nitrate in high yield, which on acid hydrolysis is easily converted into 4,5,6,7-tetramethylphthalide.[2] This reaction appears interesting, since it provides a new route to some substituted phthalides of pharmaceutical interest. We therefore undertook an investigation of the scope of the reaction using as substrate a series of tetramethylbenzenedicarbonitriles (**1a—c**) and tetramethylbenzonitriles (**1d—f**). Simple phthalides are usually prepared by the hydrolysis of *o*-(halomethyl)benzoic acid and its derivatives, reduction of phthalic anhydride and related compounds, or oxidation of appropriate benzene derivatives containing oxidizable adjacent carbon chains.

Tetramethylbenzenedicarbonitriles. Dinitriles **1a—c** were nearly inert toward the action of nitric acid in dichloromethane solution and were recovered almost

Table 1. Physical properties of some polysubstituted phthalides and 1,3-dihydroisobenzofuran-1-imines[a]

Compound		R	R^1	R^2	Mp (°C)	PMR spectra (δ)	IR spectra (cm^{-1})
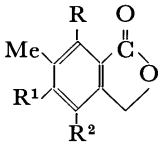 7	**7a**	CN	Me	Me	286—287	2.35(Me), 2.37(Me), 2.60(Me), 5.23(CH_2)	2220, 1765, 1115, 1050
	7b	Me	Me	CN	213—214	2.32(Me), 2.61(Me), 2.72(Me), 5.31(CH_2)	2235, 1763, 1121, 1018
	7c	Me	CN	Me	262—264	2.50(Me), 2.59(Me), 2.67(Me), 5.21(CH_2)	2230, 1757, 1126, 1024
	7h	Me	Me	NO_2	191—194	2.37(Me), 2.59(Me), 2.77(Me), 5.38(CH_2)	1765, 1530, 1350, 1120, 1015
	7i	Me	NO_2	Me	203—205	2.23(Me), 2.27(Me), 2.69(Me), 5.21(CH_2)	1775, 1535, 1355, 1290, 1115, 1015
	7j	Me	Me	NH_2	235—245 (dec)	2.20(Me), 2.26(Me), 2.57(Me), 5.03(CH_2)	3500, 3420, 1740, 1650, 1310, 1135, 1010,
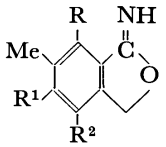 6	**6a**	CN	Me	Me	—[b]	2.30(Me), 2.33(Me), 2.58(Me), 5.21(CH_2)	3250, 2225, 1660, 1290, 1225, 1040, 1005, 945
	6b	Me	Me	CN	197—199[c] (dec)	2.32(Me), 2.59(Me), 2.79(Me), 5.29(CH_2)	3280, 2230, 1680, 1295, 1240, 1030, 960, 900
	6c	Me	CN	Me	200—202[c] (dec)	2.43(Me), 2.56(Me), 2.71(Me), 5.15(CH_2)	3300, 2240, 1670, 1290, 1210, 1020, 950
	6h	Me	Me	NO_2	183—185[c] (dec)	2.38(Me), 2.56(Me), 2.84(Me), 5.38(CH_2)	3300, 1680, 1530, 1350, 1265, 1015, 955
	6i	Me	NO_2	Me	195—200[c] (dec)	2.16(Me), 2.24(Me), 2.73(Me), 5.13(CH_2)	3320, 1670, 1535, 1365, 1290, 1270, 1215, 1025, 955

a) Satisfactory elemental analyses were obtained for all new phthalides and 1,3-dihydroisobenzofuran-1-imines. b) Not determined. c) The melting ranges of the 1,3-dihydroisobenzofuran-1-imines vary depending on the rate of heating.

Table 2. Physical properties of isomeric nitrotetramethylbenzonitriles

Compound	Mp[a] (°C)	PMR spectra (δ)	IR spectra (cm^{-1})
6-Nitro-2,3,4,5-tetramethylbenzonitrile (**1g**)	175—176	2.25 (2 Me), 2.34 (Me), 2.54 (Me)	2225, 1535, 1275, 830
5-Nitro-2,3,4,6-tetramethylbenzonitrile (**1h**)	159—161	2.26 (Me), 2.28 (Me), 2.46 (Me), 2.57 (Me)	2225, 1535, 855
4-Nitro-2,3,5,6-tetramethylbenzonitrile (**1i**)	195—198	2.20 (2 Me), 2.56 (2 Me)	2225, 1535, 830

a) These compounds begin to sinter at around 135—150 °C and melt with partial sublimation.

unchanged under the conditions successfully employed for the reaction of pentamethylbenzonitrile. Thus, dinitriles were dissolved in fuming nitric acid (d=1.5) itself and the mixture was allowed to stand at room temperature for several days. When the reaction mixture from **1b** or **1c** was diluted with water, rather surprisingly, little precipitate was obtained. However, when the slightly turbid solution thus obtained was set aside overnight, a white crystalline solid separated out and was readily identified as cyanotrimethylphthalide (**7b**—**c**) on the basis of elemental analysis, molecular weight (m/e 201 (M^+)), and spectral data, as summarized in Table 1.

Of the three isomeric tetramethylbenzenedicarbonitriles, 3,4,5,6-tetramethylbenzene-1,2-dicarbonitrile (**1a**) was the least reactive member and behaved somewhat differently. However, by keeping it in contact with the nitrating agent for a week or longer, an appreciable amount of two cyanonitro-3-cyclohexen-1-ones (**8b** and **10**) was obtained in addition to the expected phthalide (**7a**). The structure proof for these nitro ketones and a possible mode of their formation will be the subject of the accompanying paper.

When the reaction mixture was diluted with cold water and the aqueous filtrate was immediately neutralized with sodium hydrogencarbonate, a yellow solid was obtained and crystallized from ethanol to pale yellow fine needles. Its mass spectral data (m/e 200 (M^+)) and elemental analysis were consistent with the formula $C_{12}H_{12}N_2O$. The PMR spectrum showed absorptions due to three methyl groups (δ 2.30—2.84), one methylene group (δ 5.15—5.38), and one imino proton (δ *ca.* 4—5; exchangeable with D_2O). The IR spectrum exhibited absorption bands due to the imino group at 3250—3300 and 1660—1680 cm^{-1}, in addition to the expected absorptions characteristic for a cyano group (2220—2235 cm^{-1}) and unsaturated cyclic ether (1015—1040 and 1210—1290 cm^{-1}). On acid hydrolysis it was converted into phthalide (**7a**—**c**). On the basis of the spectral evidence and the chemical transformation, the compound was identified as cyanotrimethyl-1,3-dihydroisobenzofuran-1-imine (**6a**—**c**). Few cyclic imidates of this type have been described previously, and most of these were obtained in unspecified yields by heating *o*-(halomethyl)benzamides at high temperatures.[3]

The isolation of imidate **6** provides a reasonable mechanism for the conversion of polymethylbenzonitriles into phthalides (Scheme 2). Nitronium ion makes an *ipso* attack at the site *meta* to the cyano group in **1** to form the arenium ion (**2**), which releases a proton from the activated methyl group *para* to the site of attack to give the triene (**3**), which is then transformed into the benzyl nitrate (**4**). In moderately strong protogenic acidic media, the nitrate **4** undergoes intramolecular ring closure through nucleophilic attack of the ester oxygen on the neighboring electron-deficient carbon of the nitrilium ion (**5**), giving **6** as a water-soluble salt.

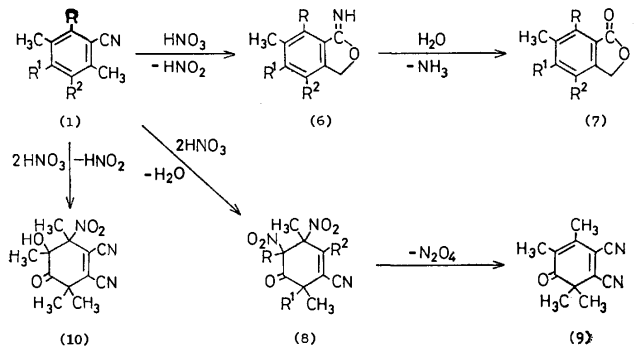

	R	R^1	R^2
a	CN	Me	Me
b	Me	Me	CN
c	Me	CN	Me
d	H	Me	Me
e	Me	Me	H
f	Me	H	Me
g	NO_2	Me	Me
h	Me	Me	NO_2
i	Me	NO_2	Me
j	Me	Me	NH_2

Scheme 1.

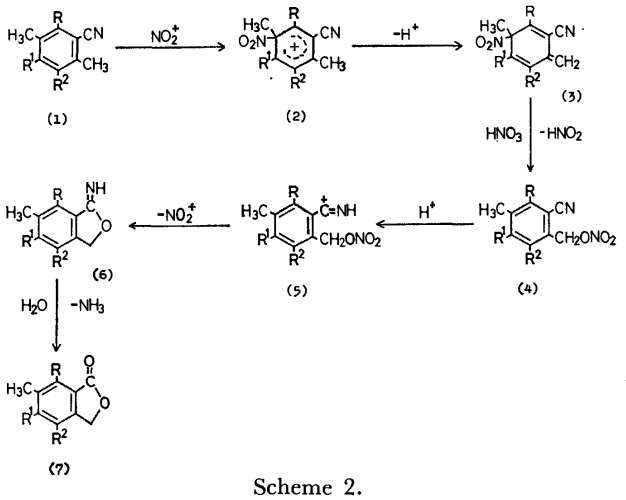

Scheme 2.

Formation of 1,3-dihydroisobenzofuran-1-imines is thus limited to those nitriles having at least one pair of methyl groups *para* to each other; others are simply nitrated on the ring or recovered unchanged. In contrast to the nitration of polymethylbenzenes in acetonitrile, in which *N*-(polymethylbenzyl)acetamides are obtained,[4] no Ritter-type reaction leading to 2,3-dihydro-1-isoindolones[5] was observed. To our knowledge, the formation reaction seems to be the first example in which the electrophilic carbon of the nitrilium ion displaces the acyl component on the ester oxygen, giving imidates as stable products.

Tetramethylbenzonitriles. The reaction of nitriles **1e—f** with fuming nitric acid proceeded with more ease, giving after the usual work-up a mixture of the corresponding nitrotrimethylphthalide (**7h—i**) and nitrotetramethylbenzonitrile (**1h—i**). In addition, a nitro ketone (**8d**) was obtained as a minor product from **1f**. When the reaction mixture was quenched with water and the aqueous filtrate was immediately neutralized with sodium hydrogencarbonate, nitrotrimethyl-1,3-dihydroisobenzofuran-1-imine (**6h—i**) was obtained. In sharp contrast, 2,3,4,5-tetramethylbenzonitrile (**1d**) was simply nitrated on the ring, giving 6-nitro-2,3,4,5-tetramethylbenzonitrile (**1g**) under the same conditions.

As a further extension of the present work, three isomeric trimethylbenzenetricarbonitriles were prepared and similarly treated with fuming nitric acid. However, the combined deactivating effect of three cyano groups surpassed the activating effect of three methyl groups and no reaction could be observed.

Although a limited number of cases have been investigated, it seems likely that many nitriles of the type **1** will yield phthalides and 1,3-dihydroisobenzofuran-1-imines in acceptable yields when appropriately treated with fuming nitric acid. Thus, the present reaction provides a simple direct route to some substituted phthalides and 1,3-dihydroisobenzofuran-1-imines for which no convenient preparative procedures have been available.

Experimental

All melting points were obtained on a hot-stage apparatus and are uncorrected. IR spectra were run as Nujol mulls on a Hitachi 215 spectrophotometer and only prominent peaks are recorded. PMR spectra were measured in deuteriochloroform with a Varian T-60 spectrometer using TMS as an internal standard. Mass spectra (MS) were obtained on a Hitachi RMS-4 mass spectrometer with 70 eV ionizing current.

Materials. Tetramethylbenzenedicarbonitriles and tetramethylbenzonitriles were prepared by allowing the corresponding iodoarenes to react with copper(I) cyanide in phosphoric tris(dimethylamide). The following typical example illustrates the general procedure used in the synthesis of the nitriles.

*2,3,5,6-Tetramethylbenzonitrile (**1f**).* A mixture of iododurene (11.7 g; 45 mmol),[6] copper(I) cyanide (5.2 g; 58 mmol), and phosphoric tris(dimethylamide) (15 ml) was heated with stirring at 90—100 °C for 2 h, and then poured into aqueous iron(III) chloride solution to decompose the complex. The light tan solid was collected by filtration and washed successively with water, aqueous sodium hydrogensulfite, and water. It was sucked as dry as possible and then placed in a filter thimble and extracted with light petroleum using a Soxhlet extractor. The extract was evaporated and the residue was crystallized from ethanol to give **1f** as fine needles: yield, 5.1 g (73%); mp 76—77 °C. PMR: δ 2.20 (s, 6H), 2.37 (s, 6H), and 6.97 (s, 1H); IR: 2205, 1010, and 890 cm^{-1}.

The above procedure applied to other iodo- and diiodotetramethylbenzenes gave the corresponding benzonitriles and benzenedicarbonitriles in 48—75% yields.

*2,3,4,5-Tetramethylbenzonitrile (**1d**)*: Mp 76—77 °C. PMR: δ 2.23 (s, 3H), 2.27 (s, 6H), 2.42 (s, 3H), and 7.17 (s, 1H).

*2,3,4,6-Tetramethylbenzonitrile (**1e**)*: Mp 66—67 °C. PMR: δ 2.17 (s, 3H), 2.28 (s, 3H), 2.44 (s, 6H), and 6.87 (s, 1H).

*3,4,5,6-Tetramethylbenzene-1,2-dicarbonitrile (**1a**)*: Mp 230—231 °C. PMR: δ 2.54 (s, 6H) and 2.35 (s, 6H).

*2,4,5,6-Tetramethylbenzene-1,3-dicarbonitrile (**1b**)*: Mp 178—180 °C. PMR: δ 2.26 (s, 3H), 2.56 (s, 6H), and 2.71 (s, 3H).

*2,3,5,6-Tetramethylbenzene-1,4-dicarbonitrile (**1c**)*: Mp 208—210 °C. PMR: δ 2.52 (s, 12H).

Reaction of Tetramethylbenzenedicarbonitriles with Fuming Nitric Acid. The procedure used in each of the reactions described in the text was identical; therefore, only a typical example of these reactions will be reported in detail.

*2,4,5,6-Tetramethylbenzene-1,3-dicarbonitrile (**1b**).* To stirred fuming nitric acid (d=1.5; 10 g) cooled at −10 — −5 °C, **1b** (0.60 g; 3.26 mmol) was added in portions, and the mixture was allowed to stand at room temperature (25—30 °C) for several days, during the course of which the initial dark brown color faded to light yellow. The mixture was diluted with water (≈100 ml) and the resulting somewhat turbid solution was filtered and set aside overnight. The crystalline deposit was collected by filtration and crystallized from aqueous methanol to furnish *4-cyano-5,6,7-trimethylphthalide (**7b**)* as fine prisms, mp 213—214 °C. Yield, 0.63 g (96%). MS: *m/e* 201 (M^+), 172 (base peak), 144, and 115. Found: C, 71.4; H, 5.4; N, 7.0%. Calcd for $C_{12}H_{11}NO_2$: C, 71.6; H, 5.5; N, 7.0%.

When the above aqueous solution was immediately neutralized with sodium hydrogencarbonate, *4-cyano-5,6,7-trimethyl-1,3-dihydroisobenzofuran-1-imine (**6b**)* was obtained as a pale yellow precipitate, mp 197—199 °C (dec). MS: *m/e* 200 (M^+), 172, 145, 130, and 115. Found: C, 71.9; H, 6.1; N, 13.9%. Calcd for $C_{12}H_{12}N_2O$: C, 72.0; H, 6.0; N, 14.0%.

By a similar treatment, dinitriles **1a** and **1c** were converted into the corresponding phthalides **7a** and **7c**, or 1,3-dihydroisobenzofuran-1-imines **6a** and **6c**, respectively, in 18—76% yield. The former dinitrile produced appreciable amounts of 3-cyclohexen-1-one derivatives **8b** and **10** in addition.

Reaction of Tetramethylbenzonitriles with Fuming Nitric Acid. The general procedure is illustrated below with the reaction of *2,3,4,6-tetramethylbenzonitrile (**1e**)*.

A solution of **1e** (1.59 g; 10 mmol) in fuming nitric acid (20 g) was allowed to stand at room temperature for several days, after which the mixture was poured onto crushed ice to give *5-nitro-2,3,4,6-tetramethylbenzonitrile (**1h**)* as a yellow solid (0.62 g). The aqueous part was filtered and set aside overnight to give a further deposit, which was collected by filtration and recrystallized from aqueous methanol, giving *4-nitro-5,6,7-trimethylphthalide (**7h**)* as fine needles, mp 191—194 °C. Yield, 0.70 g (53%). MS: *m/e* 221 (M^+), 205, and 177. Found: C, 60.0; H, 5.2; N, 6.3%. Calcd for $C_{11}H_{11}NO_4$: C, 59.7; H, 5.0; N, 6.3%.

On being neutralized with sodium hydrogencarbonate, the acid solution gave *4-nitro-5,6,7-trimethyl-1,3-dihydroisobenzofuran-1-imine (**6h**)*, mp 183—185 °C. Yield, 0.50 g (23%). MS: *m/e* 220 (M^+), 203, 175, 160, and 147. Found: C, 59.8; H, 5.5; N, 12.4%. Calcd for $C_{11}H_{12}N_2O_3$: C, 60.0; H, 5.5; N, 12.7%.

When **6h** in methanol was treated with hydrogen in the presence of Pd/C catalyst at room temperature, *4-amino-5,6,7-trimethylphthalide (7j)* was obtained, which on heating sintered and decomposed at around 235—245 °C. MS: *m/e* 191 (M^+), 176, 162, 146, and 134. Found: C, 69.4; H, 6.8; N, 7.5%. Calcd for $C_{11}H_{13}NO_2$: C, 69.1; H, 6.9; N, 7.3%.

The same procedure applied to nitrile **1f** gave *4-nitro-2,3,-5,6-tetramethylbenzonitrile* (**1i**; 8—40%), *5-nitro-4,6,7-trimethylphthalide* (**7i**; 10—23%), and a nitro ketone (**8d**; 4—9%), or *5-nitro-4,6,7-trimethyl-1,3-dihydroisobenzofuran-1-imine (6i)* as a precursor of **7i**.

2,3,4,5-Tetramethylbenzonitrile (1d). A solution of **1d** in fuming nitric acid was left to stand at room temperature for several days. The usual work-up of the reaction mixture, followed by crystallization of a solid product from ethanol, gave *6-nitro-2,3,4,5-tetramethylbenzonitrile (1g)* as the sole product; pale yellow needles, mp 175—176 °C. Found: C, 64.8; H, 6.0; N, 13.7%. Calcd for $C_{11}H_{12}N_2O_2$: C, 64.7; H, 5.9; N, 13.7%.

We are grateful to the Ministry of Education and the Saneyoshi Scientific Foundation for financial support of this work.

References

1) The reaction of polysubstituted aromatics. Part XLVII; Part XLVI: H. Suzuki and M. Shinoda, *Synthesis*, **1977**, 640. A preliminary account has been published: H. Suzuki, M. Koge, and T. Hanafusa, *J. Chem. Soc. Chem. Commun.*, **1977**, 341.

2) H. Suzuki and T. Hanafusa, *Bull. Chem. Soc. Jpn.*, **46**, 3607 (1973). For a general review of non-conventional processes which occur as a consequence of *ipso* attack, see S. R. Hartshorn, *Chem. Soc. Rev.*, **3**, 167 (1974); B. Moodie and K. Schofield, *Acc. Chem. Res.*, **9**, 287 (1976); H. Suzuki, *Synthesis*, **1977**, 217.

3) S. Gabriel, *Ber.*, **20**, 2235 (1887); S. Gabriel and W. Landsberger, *ibid.*, **31**, 2732 (1898); G. Berti, *Gazz. Chim. Ital.*, **87**, 707 (1957); L. M. Yagupol'ski and R. V. Belinskaya, *Zhur. Obshch. Khim.*, **36**, 1414 (1966). The alternative route involves the reaction of *o*-lithiobenzonitrile with ketone; W. E. Parham and L. D. Jones, *J. Org. Chem.*, **41**, 1187 (1976).

4) E. Hunziker, J. R. Penton, and H. Zollinger, *Helv. Chim. Acta*, **54**, 2043 (1971); H. Suzuki and T. Hanafusa, *Bull. Chem. Soc. Jpn.*, **46**, 3607 (1973).

5) L. I. Krimen and D. J. Cota, *Org. React.*, **17**, 213 (1969).

6) H. Suzuki, *Org. Synth.*, **51**, 94 (1971).

Formation of Cyanonitro-3-cyclohexen-1-ones in the Reaction of Tetramethylbenzonitriles with Fuming Nitric Acid[1]

Hitomi SUZUKI, Akiyoshi INOUE, Mamie KOGE, and Terukiyo HANAFUSA

Department of Chemistry, Faculty of Science, Hiroshima University, Higashi-sendamachi, Hiroshima 730

(Received August 31, 1977)

The reaction of 3,4,5,6-tetramethylbenzene-1,2-dicarbonitrile with fuming nitric acid at room temperature yielded appreciable amounts of 3,4-dicyano-5,6-dinitro-2,2,5,6-tetramethyl-3-cyclohexen-1-one and 3,4-dicyano-6-hydroxy-5-nitro-2,2,5,6-tetramethyl-3-cyclohexen-1-one in addition to the expected side-chain substitution products. 2,3,5,6-Tetramethylbenzonitrile similarly gave 3-cyano-5,6-dinitro-2,2,4,5-tetramethyl-3-cyclohexen-1-ones as minor products. The structures of these nitro ketones have been assigned by spectral methods and a probable mechanistic pathway to their formation is presented.

Nuclear oxidation of polyalkylbenzenes and their derivatives with concentrated nitric acid usually leads to the formation of cross-conjugated cyclic ketones (2,5-cyclohexadien-1-ones), while linearly conjugated cyclic ketones (2,4-cyclohexadien-1-ones) are rarely formed.[2] With some moderately deactivated polyalkylbenzene derivatives, however, the latter type of oxidation seems to occur more often than has ever been considered. In the preceding paper, we have reported the isolation of nitro carbonyl compounds as side products from the reaction of tetramethylbenzonitriles with fuming nitric acid. We describe herein the structural assignments of these carbonyl compounds and a probable mechanistic pathway to their formation.

Reaction of 3,4,5,6-tetramethylbenzene-1,2-dicarbonitrile (**1**) with fuming nitric acid (d=1.5) at room temperature for several days gave appreciable amounts of two carbonyl compounds, which melted at 116—117 °C and 150—152 °C, respectively, in addition to the expected benzyl nitrate (**4**) and phthalide (**12**).

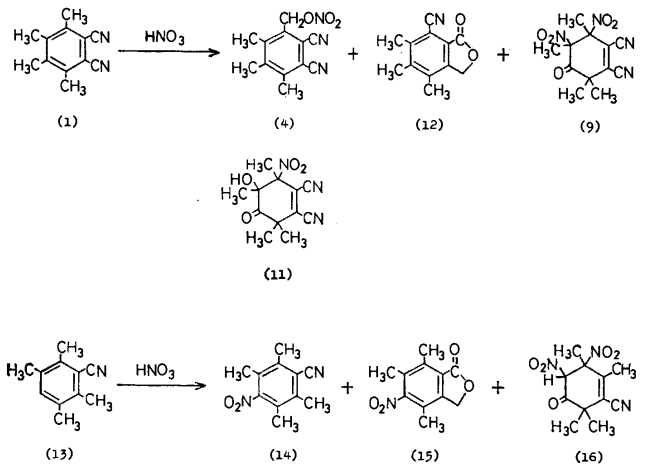

Scheme 1.

The *low-melting compound (9)* had the formula $C_{12}H_{12}N_4O_5$; its mass spectrum showed peaks at m/e 292 (M^+), 246 (M^+-NO_2), 200 (M^+-2NO_2), 185 ($M^+-2NO_2-CH_3$), 172 (M^+-2NO_2-CO), 157 (base peak; $M^+-2NO_2-CO-CH_3$), and 142 ($M^+-2NO_2-CO-2CH_3$). Its IR spectrum suggested the formation of an unsaturated nitro carbonyl compound with absorption bands due to a nitro group (1560 and 1330 cm^{-1}), a carbonyl group (1745 cm^{-1}), and the carbon-carbon double bond (1635 cm^{-1}). Its PMR spectrum with four singlets at δ 2.27, 2.05, 1.26, and 1.22 indicated the presence of four methyl groups intact. The possibility of the conjugated carbonyl compound was ruled out by the absence of an UV maximum above 220 nm.

This nitro carbonyl compound was thermally unstable and, when heated gently in ligroin, it readily released nitrogen dioxide and was converted into another new ketone (**8**), $C_{12}H_{12}N_2O$, mp 83—84 °C. Its mass spectrum was quite similar to that of the parent compound **9**, except for the lack of two minor peaks at m/e 292 and 246. The high carbon-to-hydrogen ratio of the empirical formula points to an unsaturated cyclic structure. The IR spectrum showed the presence of the cyano group (2210 cm^{-1}) and the conjugated carbonyl group (1670 and 1625 cm^{-1}), but absorptions due to the nitro group were no longer observed. An intense band at 315 nm ($\log \varepsilon$=3.61) in the UV spectrum and a characteristic mass pattern with peak clusters at m/e 102—107, 88—93, and 77—79 were in accord with the presence of a 2,4-cyclohexadien-1-one system. The PMR spectrum consisted of three singlets at δ 2.19, 2.06, and 1.44, with relative areas 1 : 1 : 2. The signal at δ 1.44 obviously represented the *gem*-dimethyl grouping, but exhibited a significant downfield shift as compared to the normal positions of this grouping, δ 1.11—1.28.[3] If we make a reasonable assumption that the vicinal disposition of the two cyano groups in **1** remains intact during the course of reaction, the *gem*-methyl groups should be placed next to the *vic*-dicyano grouping. These data were consistent with the formulation of this compound as 4,5-dicyano-2,3,6,6-tetramethyl-2,4-cyclohexadien-1-one (**8**). The original nitro carbonyl compound was, therefore, formulated as 3,4-dicyano-5,6-dinitro-2,2,5,6-tetramethyl-3-cyclohexen-1-one (**9**). This structural assignment was further substantiated by the CMR spectrum, which indicated the presence of four methyls (δ 18.6, 18.6, 23.2, and 23.5), two cyano groups (δ 110.8 and 112.0), a carbonyl carbon (δ 200.7), two olefinic carbons (δ 122.1 and 144.1), two sp^3 carbons attached to nitrogen (δ 70.0 and 87.5), and a sp^3 carbon in non-hetero atom function (δ 51.8).

The *high-melting compound (11)* was a slightly water-soluble, crystalline solid, which was obtained by extracting with ether the aqueous solution from which **4** and **12** separated out. Elemental analysis and mass spectrum established its molecular composition to be

$C_{12}H_{13}N_3O_4$, suggesting an unsaturated cyclic structure similar to **9**. The IR spectrum showed absorptions due to the hydroxyl and carbonyl groups at 3470 and 1720 cm^{-1}, respectively, in addition to those for the cyano group (2230 cm^{-1}), the carbon-carbon double bond (1640 cm^{-1}), and the nitro group (1570, 1340, and 850 cm^{-1}). A moderate fall of the carbonyl stretching frequency as compared to that in **9** suggested the location of the hydroxyl group in the vicinity of the carbonyl group. The PMR spectrum exhibited resonances for four methyl groups (δ 1.18, 1.30, 1.88, and 2.00). The CMR spectrum (in $CDCl_3/(CD_3)_2SO$ (5: 1)) indicated the presence of four methyls (δ 17.2, 18.0, 22.5, and 22.5), two cyano groups (δ 111.1 and 112.0), a carbonyl carbon (δ 200.3), two olefinic carbons (δ 120.2 and 138.7), two sp^3 carbons adjacent to nitrogen and oxygen (δ 68.9 and 94.3, respectively), and a sp^3 carbon in non-hetero atom function (δ 48.6). The UV spectrum showed no maximum above 220 nm, ruling out the possibility of a conjugated ketone. On the basis of the spectral data and reasoning similar to that used to arrive at the structures **8** and **9**, the compound was assigned the structure, 3,4-dicyano-6-hydroxy-5-nitro-2,2,5,6-tetramethyl-3-cyclohexen-1-one (**11**).

On a similar treatment, 2,3,5,6-tetramethylbenzonitrile (**13**) gave a nitro ketone (**16**) along with the expected ring and side-chain products (**14** and **15**).

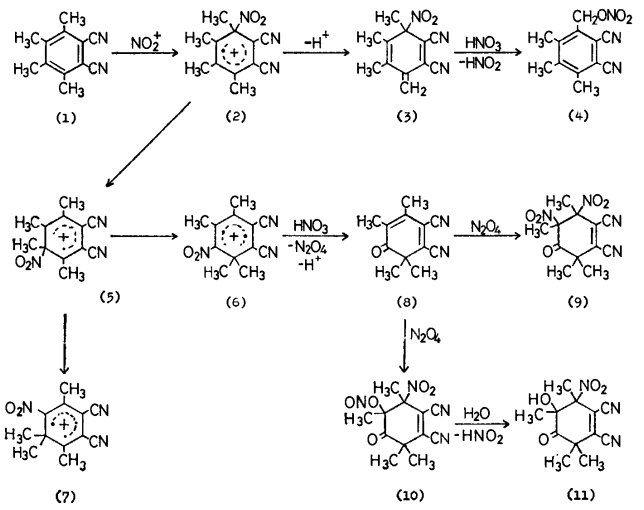

Scheme 2.

Formation of these nitro ketones can be explained by a sequence of reactions involving addition-elimination and alkyl migration, as exemplified by the conversion of **1** to **9** and **11** (Scheme 2). Thus, electrophilic attack of nitronium ion on **1** will occur at C-3 position to form the arenium ion (**2**), which could react in either of the two competing pathways: proton release from the activated methyl group in **2** to form the triene intermediate (**3**) will give the nitrate (**4**), whereas the 1,2-migration of nitro group in **2** followed by the 1,2-migration of the *ipso* methyl group in ion (**5**) to form ion (**6**) will lead to the formation of the carbonyl compounds **9** and **11**.[4] In the latter path, methyl migration in **5** will occur in one preferred direction to yield **6**, since the latter ion would be more effectively stabilized by the substituent groups than that (**7**) formed by the migration in the other direction. Capture of **6** by nitric acid or nitrate ion will lead to unstable *gem*-nitro nitrate, from which nitrogen dioxide is eliminated to yield the ketone **8**. Addition of nitrogen dioxide to **8** will give **9** as the final product. The alternative mode of the addition of nitrogen dioxide to **8** will produce an unstable adduct (**10**), which on hydrolysis will give the ketone **11**.

Experimental

All melting points were taken on a hot stage apparatus and are uncorrected. The IR, PMR, and mass spectra were obtained using the same procedures and apparatus described in the preceding paper, unless otherwise stated. The CMR spectra were determined on a Hitachi R-26 spectrometer by Dr. M. Mishima of Kyushu University. The UV spectra were recorded on a Hitachi 124 spectrophotometer in methanol solutions.

Reaction of Tetramethylbenzonitriles with Fuming Nitric Acid.

a) 3,4,5,6-Tetramethylbenzene-1,2-dicarbonitrile (1). Dinitrile **1** (1.10 g; 6 mmol) was dissolved in fuming nitric acid (d=1.5; 20 g) and the mixture was allowed to stand at room temperature (20—30 °C) for several days, during the course of which the solution became dark red and nitrogen dioxide was liberated. On diluting with water, a yellow pasty precipitate (0.84 g) was obtained, which was dissolved in a minimum amount of dichloromethane and fractionally precipitated by dropwise addition of pentane. A nitro carbonyl compound was obtained as an early precipitate (0.48 g; 28%) and a nitrate (0.21 g; 14%) was also obtained from the mother liquor. These products were identified as *3,4-dicyano-5,6-dinitro-2,2,5,6-tetramethyl-3-cyclohexen-1-one (9)* and *5,6-dicyano-2,3,4-trimethylbenzyl nitrate (4)*, respectively, on the basis of elemental analyses and spectral data. **9**: Mp 116—117 °C. Found: C, 49.9; H, 4.2; N, 18.9%. Calcd for $C_{12}H_{12}N_4O_5$: C, 49.3; H, 4.1; N, 19.2%. **4**: Mp 105—106 °C. PMR: δ 2.45 (s, 3H), 2.57 (s, 3H), 2.57 (s, 3H), and 5.52 (s, 2H); IR: ν_{max} 2220 (CN), 1640, 1280, and 840 cm^{-1} (ONO_2). Found: C, 58.5; H, 4.3; N, 17.4%. Calcd for $C_{12}H_{11}N_3O_3$: C, 58.8; H, 4.5; N, 17.1%.

Heating the ketone **9** in ligroin readily eliminated nitrogen dioxide, giving a new ketone melting at 83—84 °C; this was identified as *4,5-dicyano-2,3,6,6-tetramethyl-2,4-cyclohexadien-1-one (8)*. Found: C, 71.8; H, 6.3; N, 13.6%. Calcd for $C_{12}H_{12}N_2O$: C, 72.0; H, 6.0; N, 14.0%.

The aqueous part was set aside overnight and afforded a white precipitate (0.23 g; 19%), which was collected by filtration and crystallized from aqueous ethanol to give *7-cyano-4,5,6-trimethylphthalide (12)*, mp 286—287 °C (sublim.).[5] Found: C, 71.3; H, 5.4; N, 7.4%. Calcd for $C_{12}H_{11}NO_2$: C, 71.6; H, 5.5; N, 7.0%.

The mother liquor was further extracted with ether and the combined extract was washed successively with aqueous sodium hydrogencarbonate and water, and evaporated *in vacuo* to yield a yellow syrup (0.38 g), from which *3,4-dicyano-6-hydroxy-5-nitro-2, 2, 5, 6-tetramethyl-3-cyclohexen-1-one (11)* slowly separated out as fine needles, mp 150—152 °C. Found: C, 54.6; H, 5.0; N, 16.0%. Calcd for $C_{12}H_{13}N_3O_4$: C, 54.8; H, 5.0; N, 16.0%.

b) 2,3,5,6-Tetramethylbenzonitrile (13). A solution of nitrile **13** (1.59 g; 10 mmol) in fuming nitric acid (d=1.5; 21 g) was stirred at 30 °C for 3 days, after which the mixture was poured onto crushed ice to give a yellow oily substance (0.99 g). This was triturated with small amounts of cold

dichloromethane and the white powder obtained was crystallized from ligroin, giving *3-cyano-5,6-dinitro-2,2,4,5-tetramethyl-3-cyclohexen-1-one (**16a**)* as fine needles (0.13 g; 4.9%), mp 150—151 °C. The dichloromethane solution was evaporated and the residue was fractionally crystallized from benzene/cyclohexane, giving another nitro ketone (**16b**; 0.1 g; 3.8%) isomeric with **16a**, mp 144—147 °C, and *4-nitro-2,3,5,6-tetramethylbenzonitrile* (**14**; 0.17 g; 8.3%), mp 195—198 °C.[5] **16a**: MS: *m/e* 267 (M^+), 221, 205, 191, 175 (base peak), 160, and 147; PMR ($(CD_3)_2SO$): δ 1.15 (s, 3H), 1.37 (s, 3H), 2.15 (s, 3H), 2.33 (s, 3H), and 6.10 (s, H); IR: ν_{max} 2230 (CN), 1700 and 1220 (C=O), 1570, 1360, and 1340 cm^{-1} (NO_2); UV: no maximum above 220 nm. Found: C, 49.2; H, 4.9; N, 15.5%. Calcd for $C_{11}H_{13}N_3O_5$: C, 49.4; H, 4.9; N, 15.7%. **16b**: MS: *m/e* 267 (M^+), 221, 205, 191, 175, 160, and 147; PMR ($(CD_3)_2SO$): δ 1.13 (s, 3H), 1.18 (s, 3H), 1.93 (s, 3H), 2.47 (s, 3H), and 6.07 (s, 1H); IR: ν_{max} 2240 (CN), 1710 and 1225 (C=O), 1560 and 1340 cm^{-1} (NO_2); UV: no maximum above 220 nm. Found: C, 49.1; H, 4.9; N, 15.2%. Calcd for $C_{11}H_{13}N_3O_5$: C, 49.4; H, 4.9; N, 15.7%.

The aqueous part from which **14** and **16** separated out was set aside overnight, giving *5-nitro-4,6,7-trimethylphthalide (**15**)* as a crystalline precipitate (0.23 g; 10.4%).[5] Mp 203—205 °C. Found: C, 60.0; H, 5.2; N, 6.5%. Calcd for $C_{11}H_{11}NO_4$: C, 59.7; H, 5.0; N, 6.3%.

Acknowledgement is made to the Ministry of Education and the Saneyoshi Scientihc Foundation for financial support.

References

1) The reaction of polysubstituted aromatics. Part XLVIII; Part XLVII: H. Suzuki, M. Koge, A. Inoue, and T. Hanafusa, *Bull. Chem. Soc. Jpn.*, **51**, 1168 (1978).

2) For a review of nuclear oxidation which occurs as a consequence of *ipso* nitration, see H. Suzuki, *Synthesis*, **1977**, 217; B. Moodie and K. Schofield, *Acc. Chem. Res.*, **9**, 287 (1976).

3) Polymethyl-2,4-cyclohexadien-1-ones are known to have PMR peaks for 2-methyl at δ 1.83—1.88, 3-methyl at δ 1.02—1.25, 4-methyl at δ 1.86—1.88, 5-methyl at δ 1.74—1.83, and 6-methyl at δ 1.11—1.28, respectively: H. Hart, P. M. Collins, and A. J. Waring, *J. Am. Chem. Soc.*, **88**, 1005 (1966); A. J. Waring, M. R. Morris, and M. M. Islam, *J. Chem. Soc., C*, **1971**, 3274.

4) An interesting example of a multi-step migration of a methyl group has recently been observed in the nitration of pentamethylbenzene with nitric acid in fluorosulfuric acid, and a possible intervention of the electron-transfer process has been suggested for the nuclear oxidation of alkyl aromatics: A. N. Detsina, V. I. Mamatyuk, and V. A. Koptyug, *Zhur. Org. Khim.*, **13**, 130 (1977).

5) Spectral data are given in the preceding paper of this series.

Oxidation of 2-Aryl-4*H*-1-benzopyrans with Potassium Permanganate

Kazu KUROSAWA and Yoshihiro ASHIHARA

Department of Chemistry, Faculty of Science, Kumamoto University, Kurokami, Kumamoto 860

(Received September 2, 1977)

The oxidation of twelve 2-aryl-4*H*-1-benzopyrans with potassium permanganate in acetone gave the corresponding flavones in excellent yields.

Flavones can be synthesized from 2'-hydroxychalcones[1] or from flavanones[2] or they can be synthesized from *o*-(benzoyloxy)acetophenones by the Baker-Venkataraman rearrangement followed by cyclization[3] or from *o*-hydroxyacetophenone and aromatic acid anhydride by Allan-Robinson condensation.[4] Flavones can also be formed in reactions with flavylium chloride.[5] In a previous publication,[6] Ashihara *et al.* have reported that the oxidation of 2-aryl-2*H*-1-benzopyrans with potassium permanganate in acetone gives the corresponding flavones in moderate yields. The oxidation of twelve 2-aryl-4*H*-1-benzopyrans with potassium permanganate which produce flavones in 17—81% yields, are also reported by these authors. This procedure provides a simple method for the preparation of flavones.

The 2-aryl-4*H*-1-benzopyrans (Ia—i) were prepared by lithium aluminium hydride reduction[7] of 2-aryl-1-benzopyrylium chlorides. The structures of the new 2-aryl-4*H*-1-benzopyrans were confirmed by examining their NMR spectra and by elemental analysis.

When 7-methoxy-2-(*p*-methoxyphenyl)-4*H*-1-benzopyran (Ig) was oxidized in acetone with potassium permanganate for molar ratios of 1:3, 1:4, and 1:5 (entries 7, 8, and 9 in Table 1), 4',7-dimethoxyflavone (IIg) was obtained in 74, 81, and 72% yields, respectively. Therefore, the oxidation of other 2-aryl-4*H*-1-benzopyrans was carried out for molar ratios of 1:4 until all the potassium permanganate added had been consumed. When the oxidation of Ig was carried out in pyridine or in *t*-butyl alcohol (entries 10 and 11), poor yields were observed (61% in pyridine and 65% in *t*-butyl alcohol). The oxidation of Ig in acetic acid (entry 12) gave *p*-anisic acid (III). Jurd[8] has reported that hydrolysis of Ig with aqueous acetic acid gives 3-(2-hydroxy-4-methoxyphenyl)-4'-methoxypropiophenone (IV). This indicates that Ig is unstable under the reaction conditions and, in fact, upon treatment of Ig with acetic acid containing a trace of water, IV was obtained. It appears that Ig was hydrolyzed under the reaction conditions to give IV, which was then oxidized with potassium permanganate to *p*-anisic acid (III). With 5,7-dimethoxy-2-(*p*-methoxyphenyl)-4*H*-1-benzopyran (Ik), the yield of IIk was low (17%, entry 16) accompanied by many unidentified products. For the oxidation of 2-aryl-2*H*-1-benzopyran[6] with potassium permanganate, it was observed that the methoxyl group at position 2' causes a decrease in the yield of flavone and this is ascribed to the steric hindrance of the methoxyl group towards the attacking reagent. It appears that a similar steric effect could also explain the low yield of IIk: the methoxyl group at position 5 may hinder the approach of the reagent to the methylene group in Ik. An unsuccessful attempt was made to isolate products which could be formed by the attack of the reagent at position 2 or 3.

2-*p*-Tolyl-4*H*-1-benzopyran (Ie) gave 4'-methylflavone (IIe) (entry 5), indicating that the reaction can be adapted to the preparation of alkylated flavones.

TABLE 1. OXIDATION OF 2-ARYL-4*H*-1-BENZOPYRANS (I) WITH POTASSIUM PERMANGANATE

Entry	Substrate	Reaction conditions			Product (% yield)
		Molar ratio of I: $KMnO_4$	Time (h)	Solvent	
1	Ia[13]	1:4	1	acetone	IIa[18] (64)
2	Ib	1:4	1.5	acetone	IIb[5] (78)
3	Ic	1:4	3	acetone	IIc[19] (67)
4	Id[14]	1:4	2	acetone	IId[20] (72)
5	Ie	1:4	2.5	acetone	IIe[21] (64)
6	If[15]	1:4	2	acetone	IIf[22] (77)
7	Ig[16]	1:3	0.25	acetone	IIg[23] (74)
8	Ig	1:4	2.5	acetone	IIg (81)
9	Ig	1:5	10	acetone	IIg (72)
10	Ig	1:4	6	pyridine	IIg (61)
11	Ig	1:4	2.5	*t*-butyl alcohol	IIg (65)
12	Ig	1:4	7	acetic acid	III (97)
13	Ih	1:4	2	acetone	IIh[24] (77)
14	Ii	1:4	2	acetone	IIi (63)
15	Ij	1:4	3	acetone	IIj (71)
16	Ik[17]	1:4	1	acetone	IIk[26] (17)
17	Il	1:4	3	acetone	III[27] (74)

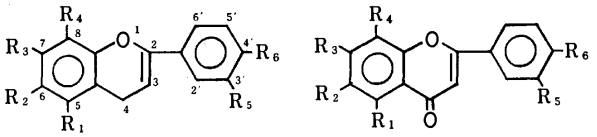

Ia—II IIa—III

a $R_1=R_2=R_3=R_4=R_5=R_6=H$
b $R_1=R_3=R_4=R_5=R_6=H$, $R_2=OCH_3$
c $R_1=R_2=R_4=R_5=R_6=H$, $R_3=OCH_3$
d $R_1=R_2=R_3=R_4=R_5=H$, $R_6=OCH_3$
e $R_1=R_2=R_3=R_4=R_5=H$, $R_6=CH_3$
f $R_1=R_3=R_4=R_5=H$, $R_2=R_6=OCH_3$
g $R_1=R_2=R_4=R_5=H$, $R_3=R_6=OCH_3$
h $R_1=R_2=R_4=R_5=H$, $R_3=OCH_3$, $R_6=OCH_2Ph$
i $R_1=R_2=R_3=R_5=H$, $R_4=R_6=OCH_3$
j $R_1=R_2=R_3=R_4=H$, $R_5=R_6=OCH_3$
k $R_2=R_4=R_5=H$, $R_1=R_3=R_6=OCH_3$
l $R_1=R_2=R_4=H$, $R_3=R_5=R_6=OCH_3$

Fig. 1.

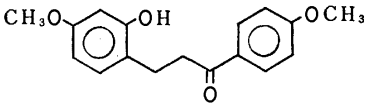

Fig. 2.

The oxidation of 2-(*p*-benzyloxyphenyl)-7-methoxy-4*H*-1-benzopyran (Ih) also gave the corresponding flavone (IIh) (entry 13). This suggests that a hydroxylated flavone can be synthesized by debenzylation of IIh.

It should be noted that the oxidation of 2-aryl-4*H*-1-benzopyran with potassium permanganate is also interesting in connection with the biogenetic type transformations of the 2-aryl-2*H*-1-benzopyrans into 3-flavanols,[9,10] 4-flavanols,[11,12] 3,4-flavandiols,[10,11] and 3,4-epoxyflavans.[10]

Experimental

All ^1H NMR spectra were recorded with a Hitachi R 24 NMR spectrometer with TMS as an internal standard. The IR spectra were recorded with a JASCO grating spectrometer. The UV spectra were recorded with a Hitachi EPS-3T spectrophotometer. Melting points were determined on a Yanagimoto micro hot-stage and are uncorrected.

Preparation of 2-Aryl-4H-1-benzopyrans (Ib,c,e,h,i,j, and l). A typical preparation of a 2-aryl-4*H*-1-benzopyran was carried out as follows. A mixture of 2-aryl-1-benzopyrylium chloride (10 mmol) (2-aryl-1-benzopyrylium chloride was prepared by condensing a *o*-hydroxybenzaldehyde and an acetophenone in ethyl acetate with dry hydrogen chloride), lithium aluminium hydride (0.7 g), and anhydrous ether (100 ml) was stirred at 0 °C until the color of the 2-aryl-1-benzopyrylium chloride disappeared (3—5 h). After the removal of the ether, the resulting solid was triturated with benzene and the benzene solution was then filtered through a short silica gel column. The filtrate was evaporated *in vacuo* to give 2-aryl-4*H*-1-benzopyran as crystals which were recrystallized from methanol. The 2-aryl-4*H*-1-benzopyrans were somewhat unstable compounds and colored on exposure to air at room temperature, but could be stored for a long time in a refrigerator.

6-Methoxy-2-phenyl-4H-1-benzopyran (Ib): Mp 104—105 °C, 74% yield, IR ($CHCl_3$) 1695 cm^{-1} (C=C), UV (MeOH) λ_{max} (ε) 245 (23800) and 296 nm (4460), NMR (CCl_4) δ=3.50 (2H, d, J=3.5 Hz, $-CH_2-$), 3.69 (3H, s, OCH_3), 5.30 (1H, t, J=3.5 Hz, $H_{(3)}$), 6.54 (1H, d, J=2.5 Hz, $H_{(5)}$), 6.55 (1H, dd, J=9.0 and 2.5 Hz, $H_{(7)}$), 6.86 (1H, d, J=9.0 Hz, $H_{(8)}$), and 7.2—7.7 (5H, m, Ph). Found: C, 80.49; H, 5.83%. Calcd for $C_{16}H_{14}O_2$: C, 80.64; H, 5.92%.

7-Methoxy-2-phenyl-4H-1-benzopyran (Ic): Mp 65—66 °C, 61 % yield, IR ($CHCl_3$) 1695 cm^{-1} (C=C), UV (MeOH) λ_{max} (ε) 237 (19100) and 279 nm (5550), NMR (CCl_4) δ=3.49 (2H, d, J=3.7 Hz, $-CH_2-$), 3.75 (3H, s, OCH_3), 5.42 (1H, t, J=3.7 Hz, $H_{(3)}$), 6.49 (1H, dd, J=9.5 and 2.5 Hz, $H_{(6)}$), 6.49 (1H, d, J=2.5 Hz, $H_{(8)}$), 6.87 (1H, m, $H_{(5)}$), and 7.2—7.7 (5H, m, Ph). Found: C, 79.13; H, 5.79%. Calcd for $C_{16}H_{14}O_2 \cdot 1/4\ H_2O$: C, 79.15; H, 6.02%.

2-p-Tolyl-4H-1-benzopyran (Ie): Mp 90—91 °C, 56% yield, IR ($CHCl_3$) 1695 cm^{-1} (C=C), UV (MeOH) λ_{max} (ε) 244 (21900) and 281 nm (5310), NMR (CCl_4) δ=2.36 (3H, s, CH_3), 3.53 (2H, d, J=3.5 Hz, $-CH_2-$), 5.36 (1H, t, J=3.5 Hz, $H_{(3)}$), 6.7—7.3 (6H, m, $H_{(3')}$, $H_{(5')}$, and $H_{(5-8)}$), and 7.53 (2H, m, $H_{(2')}$ and $H_{(6')}$). Found: C, 86.16; H, 6.37%. Calcd for $C_{16}H_{14}O$: C, 86.45; H, 6.35%.

2-(p-Benzyloxyphenyl)-7-methoxy-4H-1-benzopyran (Ih): Mp 138—139 °C, 71% yield, IR ($CHCl_3$) 1690 cm^{-1} (C=C), UV (MeOH) λ_{max} (ε) 249 (24500) and 277 nm (12100), NMR ($CDCl_3$) δ=3.47 (2H, d, J=3.8 Hz, $-CH_2-$), 3.76 (3H, s, OCH_3), 5.08 (2H, s, $-CH_2-$), 5.36 (1H, t, J=3.8 Hz, $H_{(3)}$), 6.58 (1H, dd, J=9.0 and 2.5 Hz, $H_{(6)}$), 6.58 (1H, d, J=2.5 Hz, $H_{(8)}$), 6.98 (3H, m, $H_{(5)}$, $H_{(3')}$, and $H_{(5')}$), 7.40 (5H, m, Ph), and 7.58 (2H, m, $H_{(2')}$ and $H_{(6')}$). Found: C, 80.07; H, 5.85%. Calcd for $C_{23}H_{20}O_3$: C, 80.21; H, 5.85%.

8-Methoxy-(p-methoxyphenyl)-4H-1-benzopyran (Ii): Mp 91—92 °C, 49% yield, IR ($CHCl_3$) 1697 cm^{-1} (C=C), UV (MeOH) λ_{max} (ε) 251 (22600) and 279 nm (9670), NMR (CCl_4) δ=3.48 (2H, d, J=3.5 Hz, $-CH_2-$), 3.72 (3H, s, OCH_3), 3.81 (3H, s, OCH_3), 5.31 (1H, t, J=3.5 Hz, $H_{(3)}$), 6.4—7.4 (3H, m, $H_{(5)}$, $H_{(6)}$, and $H_{(7)}$), 6.74 (2H, m, $H_{(3')}$ and $H_{(5')}$), and 7.53 (2H, m, $H_{(2')}$ and $H_{(6')}$). Found: C, 75.85; H, 6.07%. Calcd for $C_{17}H_{16}O_3$: C, 76.10; H, 6.01%.

2-(3,4-Dimethoxyphenyl)-4H-1-benzopyran (Ij): Mp 107—108 °C, 35% yield, IR ($CHCl_3$) 1696 cm^{-1} (C=C), UV (MeOH) λ_{max} (ε) 249 (17400) and 287 nm (8060), NMR (CCl_4) δ 3.54 (2H, d, J=3.5 Hz, $-CH_2-$), 3.80 (3H, s, OCH_3), 3.86 (3H, s, OCH_3), 5.27 (1H, t, J=3.5 Hz, $H_{(3)}$), 6.6—7.3 (7H, m, aromatic). Found: C, 75.80; H, 5.95%. Calcd for $C_{17}H_{16}O_3$: C, 76.10; H, 6.01%.

2-(3,4-Dimethoxyphenyl)-7-methoxy-4H-1-benzopyran (Il): Mp 128—129 °C, 66% yield, IR ($CHCl_3$) 1695 cm^{-1} (C=C), UV (MeOH) λ_{max} (ε) 249 (15600) and 280 (10100), NMR ($CDCl_3$) δ=3.46 (2H, d, J=3.5 Hz, $-CH_2-$), 3.77 (3H, s, OCH_3), 3.88 (3H, s, OCH_3), 3.92 (3H, s, OCH_3), 5.36 (1H, t, J=3.5 Hz, $H_{(3)}$), and 6.5—7.4 (6H, m, aromatic). Found: 72.28; H, 6.11%. Calcd for $C_{18}H_{18}O_4$: C, 72.46; H, 6.08%.

Oxidation of 2-Aryl-4H-1-benzopyrans with Potassium Permanganate. A typical oxidation of a 2-aryl-4*H*-1-benzopyran with potassium permanganate was carried out as follows. A mixture of a 2-aryl-4*H*-1-benzopyran (1 mmol), potassium permanganate (3—5 mmol), and an appropriate solvent (30 ml) was stirred at room temperature until the color of the potassium permanganate disappeared (the time required is shown in the table). The 2-aryl-4*H*-1-benzopyran was also consumed within that time, as confirmed by TLC. The reaction mixture was filtered and the manganese dioxide formed was washed with chloroform. The combined filtrate was then evaporated and the resulting solid was recrystallized to give II. In the case of Ik, products were separated on TLC by eluting with chloroform and then recrystallized. The yields are based on the amount 2-aryl-4*H*-1-benzopyran used. IIa, mp 97 °C (benzene–light

petroleum) (lit,[18] mp 97 °C); IIb, mp 160—161 °C (MeOH) (lit,[5] mp 162 °C); IIc, mp 109—110 °C (MeOH) (lit,[19] mp 110—111 °C); IId, mp 153—154 °C (benzene–light petroleum) (lit,[20] mp 157—158 °C); IIe, mp 112—113 °C (aq MeOH) (lit,[21] mp 116 °C); IIf, mp 204—205 °C (MeOH) (lit,[22] mp 194—195 °C); IIg, 150—151 °C (MeOH) (lit,[23] mp 144 °C); IIh, mp 192—193 °C (MeOH) (lit,[24] mp 194 °C); IIi, mp 138—139 °C (MeOH), IR ($CHCl_3$) 1648 cm^{-1} (C=O), UV (MeOH) $\lambda_{max}(\varepsilon)$ 231 (19400), 270 (16300), and 324 nm (28000), NMR ($CDCl_3$) $\delta=3.88$ (3H, s, OCH_3), 4.00 (3H, s, OCH_3), 6.70 (1H, s, $H_{(3)}$), 7.00 (2H, m, $H_{(3')}$ and $H_{(5')}$), 7.15 (1H, dd, $J=9.0$ and 2.5 Hz, $H_{(7)}$), 7.30 (1H, t, $J=9.0$ Hz, $H_{(6)}$), 7.38 (1H, dd, $J=9.0$ and 2.5 Hz, $H_{(5)}$), and 7.91 (2H, m, $H_{(2')}$ and $H_{(6')}$) (Found: C, 72.16; H, 5.02%. Calcd for $C_{17}H_{14}O_4$: C, 72.33; H, 5.00%); IIj, mp 151—152 °C(MeOH) (lit,[25] mp 155 °C); IIk, mp 155—156 °C (MeOH) (lit,[26] mp 156 °C); IIl, mp 174—175 °C (MeOH) (lit,[27] mp 176 °C).

*Hydrolysis of 7-Methoxy-2-(*p*-methoxyphenyl)-4*H*-1-benzopyran (Ig)(3-(2-Hydroxy-4-methoxyphenyl)-4'-methoxypropiophenone(IV))*.

A mixture of Ig (134 mg) and acetic acid (15 ml) containing a drop of water was stirred at room temperature for 2 h. After the removal of the acetic acid *in vacuo*, the resulting liquid was separated on a silica gel plate by eluting with chloroform. The crude material was recrystallized from aqueous methanol to give IV (109 mg, 73%), mp 77—78 °C (lit,[8] mp 78 °C).

References

1) H. S. Mahal and K. Venkataraman, *J. Chem. Soc.*, **1936**, 569.
2) A. Löwenbein, *Ber.*, **57**, 1515 (1924).
3) W. Baker, *J. Chem. Soc.*, **1933**, 1381.
4) J. Allan and R. Robinson, *J. Chem. Soc.*, **125**, 2192 (1924).
5) D. W. Hill and R. R. Melhuish, *J. Chem. Soc.*, **1935**, 1161.
6) Y. Ashihara, Y. Nagata, and K. Kurosawa, *Bull. Chem. Soc. Jpn.*, **50**, 3298 (1977).
7) K. G. Marathe, E. M. Philbin, and T. S. Wheeler, *Chem. Ind. (London)*, **1962**, 1793.
8) L. Jurd, *Tetrahedron*, **23**, 1057 (1967).
9) J. W. Clark-Lewis and E. J. McGarry, *Aust. J. Chem.*, **26**, 809 (1973).
10) J. W. Clark-Lewis, E. J. McGarry, and A. H. Ilsley, *Aust. J. Chem.*, **27**, 865 (1974).
11) J. W. Clark-Lewis and E. J. McGarry, *Aust. J. Chem.*, **26**, 2447 (1973).
12) J. W. Clark-Lewis and M. I. Baig, *Aust. J. Chem.*, **24**, 2581 (1971).
13) K. Freudenberg and K. Weinges, *Liebigs Ann, Chem.*, **590**, 140 (1954).
14) A. B. Kulkarni and R. C. Shah, *Current Sci. (India)*, **22**, 339 (1953). *Chem. Abstr.*, **48**, 6999e (1954).
15) E. Merck, A.-G. Neth. Appl. 6,408,925 (Cl. C 07d) March 1, 1965. *Chem. Abstr.*, **63**, 9919d (1965).
16) L. Jurd, *Chem. Ind. (London)*, **1966**, 1683.
17) F. E. King, J. W. Clark-Lewis, and W. F. Forbes, *J. Chem. Soc.* **1955**, 2948.
18) W. Feuerstein and St. v. Kostanecki, *Ber.*, **31**, 1760 (1898).
19) T. Emilewicz and St. v. Kostanecki, *Ber.*, **32**, 312 (1899).
20) K. v. Auwers and L. Anschütz, *Ber.*, **54**, 1558 (1921).
21) F. D. Cramer and G. H. Elschnig, *Chem. Ber.*, **89**, 1 (1956).
22) A. T. M. Dunne, J. E. Gowan, J. Keane, B. M. O'Kelly, D. O'Sullivan, M. M. Roche, P. M. Ryan, and T. S. Wheeler, *J. Chem. Soc.*, **1950**, 1252.
23) J. Tambor, *Ber.*, **49**, 1710 (1916).
24) T. H. Simpson and L. Garden, *J. Chem. Soc.*, **1952**, 4638.
25) J. Berstein, C. Fraschina, and St. v. Kostanecki, *Ber.*, **38**, 2180 (1905).
26) J. Czajkowski, St. v. Kostanecki, and J. Tambor, *Ber.*, **33**, 1991 (1900).
27) G. W. K. Cavill, F. M. Dean, A. McGookin, B. M. Marshall, and A. Robertson, *J. Chem. Soc.*, **1954**, 4573.

Sulfur-Carbonyl Interaction in Rigid β-Keto Sulfides

Iwao TABUSHI, Yoshinao TAMARU, and Zen-ichi YOSHIDA
Department of Synthetic Chemistry, Kyoto University, Sakyo-ku, Kyoto 606
(Received September 3, 1977)

The electron donating ability of sulfur to a positively charged center through space was examined by means of ultraviolet spectroscopy. 7-Thiabicyclo[2.2.1]heptan-2-one and -2,5-dione exhibited finely separated charge transfer band (from divalent sulfide to carbonyl) at 260 nm in UV spectra, the longest wave-length for S–Cco charge transfer band so far reported. The assignment of these CT bands was confirmed by comparison with relevant reference compounds.

Recently it has been reported that the sulfur-bridge greatly accelerates the solvolysis of 2-*endo*-chloro-7-thiabicyclo[2.2.1]heptane, while it decelerates the solvolysis of 2-*exo*-chloro isomer (the former solvolyzed 4.7×10^9 times faster than the latter).[1] Spectroscopic examination of the sulfur-carbonyl interaction might give more insight into this sulfur participation. Although the interaction between sulfur (donor) and carbonyl (acceptor) has been observed in UV and IR spectroscopy,[2,3] little effort has been done to confirm under what conditions, steric and electronic, sulfur-carbonyl interaction, sulfur-positive center interaction, becomes most efficient. For this purpose, more model systems are required, especially the rigid sulfur-containing molecules of known geometry.

The aim of the present study is to examine the nature of the sulfur-carbonyl interaction in β-keto sulfides, taking 7-thiabicyclo[2.2.1]heptan-2-one (**4**),[4] 7-thiabicyclo[2.2.1]heptane-2,5-dione (**7**), and the related compounds as sterically and spacially fixed models.

Results and Discussion

Syntheses of 7-Thiabicyclo[2.2.1]heptan-2-one (4) and 7-Thiabicyclo[2.2.1]heptane-2,5-dione (7); Oxidation of Hydroxy Sulfides 3 and 6 to Oxo Sulfides 4 and 7. 7-Thiabicyclo[2.2.1]heptan-2-one (**4**), 7-thiabicyclo-[2.2.1]heptane-2,5-dione (**7**) and the corresponding sulfones (**9** and **11**) were prepared according to Scheme 1. Controlled acetolysis of 2,5-*endo-endo*-dichloro-7-thiabicyclo[2.2.1]heptane (**1**)[5] gave a mixture of 2-*endo*-acetoxy-5-*endo*-chloro-7-thiabicyclo[2.2.1]heptane (**2**) and 2,5-*endo-endo*-diacetoxy-7-thiabicyclo[2.2.1]-heptane (**5**). After separation of **2** and **5** by means of column chromatography, **2** was reduced with $NaBH_4$ to give 2-*endo*-hydroxy-7-thiabicyclo[2.2.1]heptane (**3**). 2,5-*endo-endo*-Dihydroxy-7-thiabicyclo[2.2.1]heptane (**6**) was obtained by the hydrolysis of **5**. The key step in Scheme 1 consists of the selective oxidation of hydroxyl group to ketone in the presence of the sulfide linkage highly susceptible to oxidation. The oxidation of **3** to **4** was performed by chromium trioxide-pyridine complex[6] in good yield (83%) without appreciable oxidation of sulfur. Similar oxidation of **6** gave **7** in 35% yield together with 5-*endo*-hydroxy-7-thiabicyclo[2.2.1]heptan-2-one in 35% yield. This indicates that the latter considerably resists further oxidation[7] (see Experimental). On the other hand the oxidation of **3** to **4** with Jone's reagent[8] was not successful, mainly affording a mixture of sulfoxides (2-*endo*-hydroxy-7-thiabicyclo-[2.2.1]heptane 7-oxides; a mixture of 38 and 62% of *syn* and *anti* sulfoxides, respectively) in *ca.* 60% yield and the expected keto sulfide **4** only in a low yield (*ca.* 10%).[9] Attempted Oppenauer oxidation of **3** and **6** with aluminium isopropoxide and cyclohexanone in refluxing toluene[10] was not successful. 7-Thiabicyclo-[2.2.1]heptan-2-one 7,7-dioxide (**9**) was prepared in good yield by the oxidation with Jone's reagent from 2-*endo*-hydroxy-7-thiabicyclo[2.2.1]heptane 7,7-dioxide (**8**), which was prepared from **3** by oxidation with hydrogen peroxide in acetic acid. 7-Thiabicyclo[2.2.1]-heptane-2,5-dione 7,7-dioxide (**11**) was also prepared in good yield by oxidation with Jone's reagent from **10**, which was prepared from **6** by oxidation with perbenzoic acid in chloroform. **11** decomposed readily to give hydroquinone and sulfur dioxide in the presence of acid.[11]

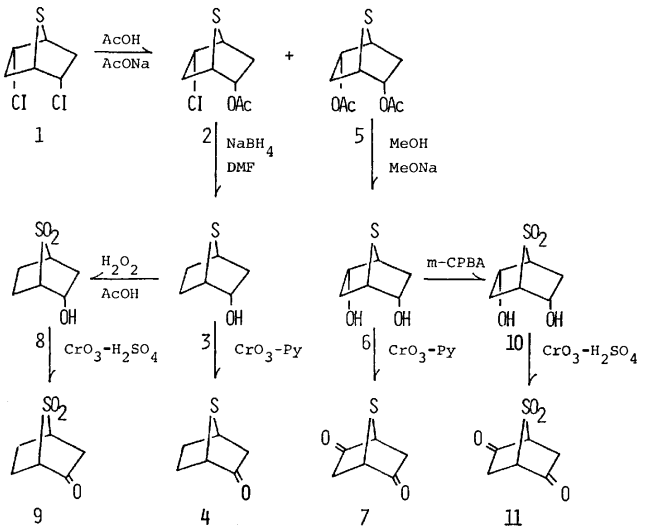

Scheme 1.

It seems worthwhile to note some characteristics in NMR spectra of **4** and **7** from the viewpoint of structural confirmation. For **4** the introduction of ketonic carbonyl group caused upfield shift of the bridge-head proton α to carbonyl by 0.08 ppm, while the bridge-head proton β to carbonyl shifted to downfield by 0.15 ppm as compared with 7-thiabicyclo[2.2.1]heptane (**12**) (Fig. 1). This upfield shift of bridge-head proton α to carbonyl is quite the reverse of that anticipated from the inductive effect and magnetic anisotropy of carbonyl.[12] Corey and his co-workers[13] first pointed out a similar abnormality concerning the NMR spectrum of norbornanone, *viz.*, the bridge-head proton α to carbonyl shifted down

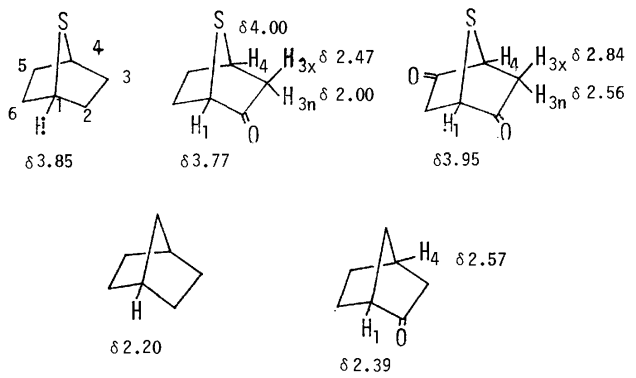

Fig. 1. Influence of carbonyl group to the bridge-head protons of bicyclo[2.2.1]heptane system.

field only by 0.19 ppm, and the bridge-head proton β to carbonyl by 0.37 ppm as compared with norbornane. The assignment was confirmed by Farnum and Mehta[14] by deuterium labeling experiments.

As a result of the substitution of methylene bridge for sulfur atom, the NMR spectra of bicyclo[2.2.1]-heptane system became simplified and well resolved.[15] The assignments were confirmed by using a shift reagent (europium dipivaloylmethanate), coupled with spin-decoupling experiments (see Experimental). The bridge head protons of **7** resonated in midway between the peaks of H_1 and H_4 of **4**. The following coupling constants were obtained by spin-decoupling experiments for **7**; $J_{H_1,H_{3x}}=1.5$ Hz, $J_{H_{3x},H_{3n}}=18$ Hz, $J_{H_4,H_{3x}}=3.5$ Hz, and $J_{H_4,H_{3n}}=0.75$ Hz. The computer simulation, with use of these values and $J_{H_1,H_4}=0$ Hz, gave a result almost superimposable on the spectrum of **7** (Fig. 2).

Transannular Sulfur-Carbonyl Interaction in the Ultraviolet Spectroscopy. The ultraviolet spectra of **4**, **7** and

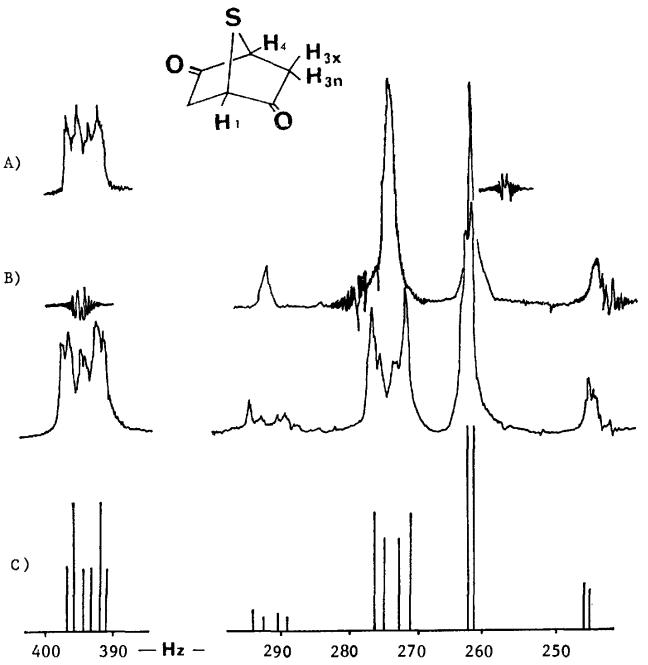

Fig 2. NMR spectra of **7** (100 MHz).
A) Saturation of H_{3n}.
B) Saturauion of $H_{1,4}$.
C) Computer simulation.

related compounds were measured in solvents of various polarities. The absorption maxima and extinction coefficients are summarized in Table 1. The keto sulfide **4** and **7** exhibited three separated absorptions at about 220, 260 and 300 nm as shown in Fig. 3. The strong absorption at about 220 nm, similar to that of 7-thiabicyclo[2.2.1]heptane (**12**), can be assigned to n, σ*,[16] although the intensity is smaller than that of

Table 1. Ultraviolet spectra[a]

Compound	Assignment	Hexane	Acetonitrile	Ethanol	Water
7-Thiabicyclo[2.2.1]heptan-2-one (**4**)	n, σ*	222.5 (902)	221.6 (718)	223 (1060)	—[b]
	CT	255 (191)	257.5 (273)	259.5 (233)	257.5 (210)
		260 (185)			
	n, π*	289 (168)	296 (286)	304 (360)	300 (393)
		298 (231)	304 (324)		
		308 (247)	315 (216)		
		319 (147)			
7-Thiabicyclo[2.2.1]heptan-2,5-dione (**7**)	n, σ*	238.6 (652)	238.5 (733)	238.5 (722)	240 (644)
	CT	258 (220)	261.5 (261)	261.5 (300)	262 (306)
	n, π*	289 (288)	296 (466)	298 (566)	300 (666)
		299 (402)	305 (514)	305 (583)	
		309 (413)	315 (342)		
		321 (233)			
7-Thiabicyclo[2.2.1]heptan-2-one 7,7-dioxide (**9**)	n, π*			288 (54)	293 (68)
				297 (60)	
				307 (51)	
				319 (23)	
7-Thiabicyclo[2.2.1]heptane	n, σ*	213 (4078)		211 (2970)	
		249 (36.2)		248 (40.9)	
Bicyclo[2.2.1]heptan-2-one	n, π*	293 (22)		290 (26)	

a) λ_{max} was measured in nm. Molar extinction coefficient is given in parentheses. b) This band was observed as an inflection at longer wavelength side (*ca.* 220 nm) of the main absorption band.

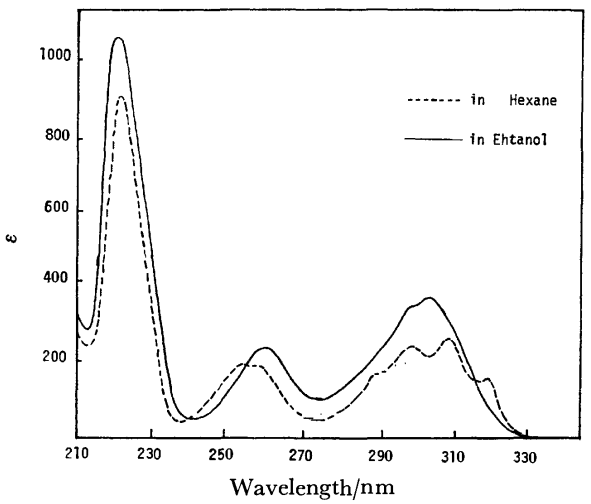

Fig. 3. Ultraviolet spectra of **4** in hexane and ethanol.

12 by a factor of three or four.[17] No absorption was observed around this region in the ultraviolet spectra of the corresponding sulfone **9**[18] or 7-thiabicyclo[2.2.1]-heptane 7,7-dioxide.

The absorption at *ca.* 300 nm, with a fine structure at intervals of *ca.* 1080 cm^{-1} for **4** and *ca.* 1130 cm^{-1} for **7** in hexane, showed a small but steady blue shift on changing the solvent from non-polar to polar. The large extinction coefficients observed for **4** (393 in water) and for **7** (666 in water) suggest that the band is due to n, π^* transition with the strong homoconjugation between sulfur and carbonyl.[19] The anomalously intense n, π^* absorption has been reported for dehydronorcamphor skeleton and was attributed to the homoconjugation between carbonyl and double bond.[20] The keto sulfides (**4** and **7**) seem to satisfy the geometrical requirements for S–CO interaction proposed by Wladislaw *et al.*[19b,19c] They suggested that of the four rotational isomers, A or C is favorable for S–CO interaction. The extinction coefficient of **7** is approximately twice as large as that of **4**.

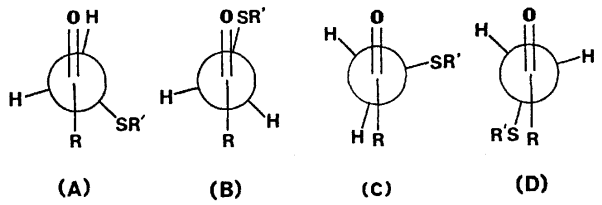

The two bands n, σ^* and n, π^* could be assigned regarding **4** (and **7**) as a composite of 7-thiabicyclo-[2.2.1]heptane and norbornanone, but the band at 260 nm can not be explained in such a manner. The band was assigned to the charge transfer band from divalent sulfur to carbonyl based on the following. (a) The band shows a small but appreciable red shift on increasing the polarity of solvent. (b) It disappears on the oxidation of **4** to sulfone **9**. This indicates lone pair electrons on sulfur participate in the CT transition. The charge transfer band at 260 nm seems to be the longest ever reported.[21] The canonical form in the charge transfer excited state of **4** can be expressed in **13**,[2,3] which *a priori* seems to have some connection to the anchimerically assisted species by sulfur in the formation of incipient carbonium ion in solvolysis.[1]

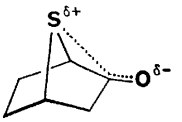

13

In order to correlate the CT band and the ability of anchimeric assistance by sulfur, more examples of well separated CT bands are requested.

Experimental

Melting points (sealed capillary) are uncorrected. The elemental analyses were performed either at the Microanalysis Center of Kyoto University or at the Faculty of Pharmaceutical Science of Kyushu University. Infrared spectra were measured with a Hitachi Model EPI-G3 grating spectrophotometer, NMR spectra with a Varian T 60 or HA-100 spectrometer, mass spectra with a Hitachi Model RMU 6C mass spectrometer, and ultraviolet spectra with a Hitachi EPS-3T recording spectrophotometer.

Preparation and structural determination of 2-*endo*-acetoxy-5-*endo*-chloro-7-thiabicyclo[2.2.1]heptane (**2**), 2-*endo*-hydroxy-7-thiabicyclo[2.2.1]heptane (**3**), and 2,5-*endo*-*endo*-diacetoxy-7-thiabicyclo[2.2.1]heptane (**5**) have been reported.[1]

Oxidation of 3 with Jone's Reagent. Cold Jone's reagent, prepared from 114 mg (1.14 mmol) of CrO_3, 186 mg of concd H_2SO_4 and 0.5 ml of distilled water, was added dropwise with ice cooling and stirring to a solution of 174 mg (1.34 mmol) of **3** in 1.5 ml of acetone. The color of the reaction mixture turned from red to green. After being stirred for 30 min at 0 °C, the reaction mixture was diluted with 2 ml of water and extracted with 2 portions of 5 ml of dichloromethane. The combined dichloromethane extracts were dried over magnesium sulfate and condensed to 60 mg of colorless oil.

On the basis of NMR, IR, and VPC analyses, the oily product was found to consist of *ca.* 30% of 7-thianorbornan-2-one (**4**), *ca.* 50% of **3** and 20% of sulfoxide. The water layer was neutralized with sodium hydrogencarbonate and allowed to stand at room temperature to evaporate water. The solid residue was washed twice with 15 ml of acetone. Acetone extracts were evaporated and adsorbed on silica gel. Elution was benzene (10)–ethanol (2) afforded 70 mg of a *syn* and *anti* mixture of 2-*endo*-hydroxy-7-thiabicyclo[2.2.1]heptane 7-oxides. The structures of these products were confirmed by a comparison of spectra (NMR, IR) with those of sulfoxides derived from **3** by oxidation with equimolar amount of *m*-chloroperbenzoic acid. Further structural confirmation was given by the oxidation of a mixture of sulfoxides with H_2O_2 in acetic acid to give 2-*endo*-hydroxy-7-thiabicyclo[2.2.1]heptane 7,7-dioxide **8** as a sole product.

ν_{max}^{KBr} (*syn*, *anti* mixture) 3330 cm^{-1} (S), 2930 cm^{-1} (M), 1072 cm^{-1} (sh), 1030 cm^{-1} (v.s., ν_{S-O} and ν_{C-O}), and 1005 cm^{-1} (sh). $\delta_{CDCl_3}^{TMS}$ (*syn*, *anti* mixture) 5.06 (multiplet, α proton to OH of *syn*-sulfoxide, area intensity 8), 4.20 (double triplets, $J=10$ and 4 Hz, α proton to OH of *anti*-sulfoxide, 13), 3.6 (narrow multiplet, bridgehead protons and OH, 67) and 2.5—1.3 (multiplet, methylene and ethylene protons, 113). The composition ratio of *anti* to *syn* was determined on the basis of area intensities of α protons[22] to OH to be *ca.* 1.6.

2-endo-Hydroxy-7-thianorbornane 7-Oxide. *m*-Chloroperbenzoic acid (156 mg, 0.77 mmol, 85% assay) was added at room temperature to a solution of 100 mg (0.77 mmol) of **3** in 10 ml of dichloromethane. After being stirred for 1 day, the solvent was removed and the solid residue was washed with two portions of 1 ml of water to transfer sulfoxides to the water layer. Evaporation of water gave transparent solid, which was adsorbed on silica gel. Elution with benzene (10)–ethanol (2) gave 102 mg of a mixture of sulfoxides. The composition ratio of *anti*- to *syn*-sulfoxide determined by NMR spectroscopy was *ca.* 1.0.

*Oxidation of **3** with Chromium Trioxide-Pyridine Complex.* Chromium trioxide (280 mg, 2.8 mmol) was added in portions to 2.5 ml of dry pyridine with stirring in a 10 ml flask fitted with a KOH drying tube. To a yellow suspension of chromium trioxide-pyridine complex was added in one portion a solution of 150 mg (1.15 mmol) of **3** in 2.0 ml dry pyridine at room temperature. The solution was allowed to stand overnight and then poured into 50 ml of ether. The filtrate was washed with dilute hydrochloric acid and then with water saturated with NaCl. Evaporation of ether through a 10 cm Vigreux column under atmospheric pressure left 122 mg (82.5 %) of 7-thiabicyclo[2.2.1]heptan-2-one (**4**) as a white waxy solid, which was purified by preparative VPC, followed by sublimation (80 °C/760 mmHg). 7-Thiabicyclo[2.2.1]heptan-2-one (**4**): Mp 115.8—116.6 °C (in a sealed tube). $\delta^{TMS}_{CCl_4}$ 4.00 (broad singlet, H_4, 1H), 3.77 (broad singlet, H_1, 1H), 2.47 (double doublets, $J=16$ and 4 Hz, H_{3x}, 1H), 2.00 (doublet, $J=16$ Hz, H_{3n}, 1H) and 2.03 (multiplet, H_5, H_6, 4H).

To a solution of 12 mg of **4** in 0.5 ml of CCl_4 was added europium dipivaloylmethanate progressively. The downfield shifts observed were: for H_1, by 0.50 and 1.16 ppm (for 4.5 mg and 9.0 mg of dipivaloylmethanate, respectively); H_{3x}, by 0.56 and 1.16 ppm; H_{3n}, 0.53 and 1.10 ppm; H_4, by 0.16 and 0.36 ppm; H_5, H_6, by *ca.* 0.2 and 0.43 ppm.

Saturation of H_4 proton resulted in the collapse of proton H_{3x} to a doublet ($J=16$ Hz). ν^{KBr}_{max} 1745 cm^{-1} (S), 1060 cm^{-1} (M) and 446 cm^{-1} (M). *m/e*; 128 (M^+, 36), 100 (18), 85 (88), 71 (8), 67 (100), 58 (20) and 55 (35).

Found: C, 56.30; H, 6.00%. Calcd for C_6H_8OS: C, 56.22; H, 6.29%.

*2,5-endo-endo-Dihydroxy-7-thiabicyclo[2.2.1]heptane (**6**).* 11.5 g (50 mmol) of **5** and 50 mg of sodium were dissolved in 200 ml of absolute methanol under nitrogen. After being refluxed overnight, methanol and methyl acetate were distilled off to give a white solid. Recrystallization from benzene gave 6.95 g (95%) of white crystals of **6**. The physical and spectral properties are the same as those in the literature.[5]

*Thiabicyclo[2.2.1]hepthane-2,5-dione (**7**).* To a yellow suspension of chromium trioxide-pyridine complex (30 mmol) in 20 ml of dry pyridine was added 1.0 g (6.85 mmol) of solid **6** at room temperature. After being stirred overnight at room temperature, the reaction mixture was poured into 100 ml of ether. After the inorganic materials had been filtered off the ether extract was washed with dilute hydrochloric acid. Evaporation of ether gave 710 mg of a colorless waxy solid. The solid was adsorbed on silica gel and eluted with benzene (5)–ethanol (1) to give 350 mg of **7** and 330 mg of 5-*endo*-hydroxy-7-thiabicyclo[2.2.1]heptan-2-one. Prolonged reaction time did not affect the product ratio significantly. Dioxo sulfide **7** was recrystallized from benzene–hexane–dichloromethane: Mp 130.0—131.0 °C. $\delta^{TMS}_{CDCl_3}$ (100 MHz) 3.94 (triple doublets, $J=3.5$ and 1.5 Hz, H_1 and H_4, 2H), 2.79 (double quartets, $J=18$, 3.5 and 1.5 Hz, H_{3x} and H_{6x}, 2H) and 2.57 (double doublets, $J=18$ and 0.75 Hz, H_{3n} and H_{6n}, 2H).

ν^{KBr}_{max} 1765 cm^{-1} (sh), 1742 cm^{-1} (S), 1720 cm^{-1} (sh), 1414 cm^{-1} (M), 1200 cm^{-1} (S), 1053 cm^{-1} (M), 941 cm^{-1} (M), 901 cm^{-1} (M), 540 cm^{-1} (S), and 428 cm^{-1} (M). *m/e* 142 (M^+, 33), 114 (6) 100 (10), 98 (9), 86 (25), 72 (13), 59 (20), 58 (20), 55 (100) and 45 (30).

Found: C, 50.58; H, 4.48; O, 22.39. Calcd for $C_6H_6O_2S$: C, 50.68; H, 4.25; O, 22.50%.

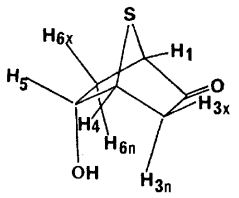

14

*5-endo-Hydroxy-7-thiabicyclo[2.2.1]heptan-2-one (**14**):* $\delta^{TMS}_{CDCl_3}$ 4.76 (double triplets, $J=10$ and 3.5 Hz, H_5, 1H) 3.93 (singlet, OH, 1H), 3.9—3.6 (multiplet, H_1 and H_4, 2H), 3.00 (doublet, $J=17$ Hz, H_{3n}, 1H), 2.43 (double doublets, $J=17$ and 4 Hz, H_{3x}, 1H), 2.8—2.4 (multiplet, H_{6x}, 1H) and 1.63 (double doublets, $J=15$ and 3.5 Hz, H_{6n}, 1H). ν^{KBr}_{max} 3420 cm^{-1} (S), 1742 cm^{-1} (sh), 1728 cm^{-1} (S), 1118 cm^{-1} (W), 1096 cm^{-1} (W), 1051 cm^{-1} (M), 1032 cm^{-1} (M), and 1000 cm^{-1} (W). *m/e* 144 (M^+, 73), 57 (100).

*2-endo-Hydroxy-7-thiabicyclo[2.2.1]heptane 7,7-Dioxide (**8**).* With water cooling and stirring, 1.5 ml (13 mmol) of 30% hydrogen peroxide was added dropwise to a solution of 297 mg (2.28 mmol) of **3** in 2 ml of acetic acid. The mixture was then heated at 70—80 °C overnight. After cooling, methyl mercaptan was introduced at moderate speed into this reaction mixture until peroxide test became negative (KI-starch). Evaporation of the solvent gave 330 mg of a waxy solid. Column chromatography on silica gel eluted with benzene (10)–ethanol (1) gave 290 mg (79.5%) of **8**: Mp 227.5—229.0 °C (in a sealed tube). $\delta^{TMS}_{CDCl_3}$ 4.80 (double triplets, $J=9$ and 3 Hz, 1H), 3.03 (narrow multiplet, 2H) 2.6 (singlet, 1H), 2.7—1.9 (multiplet, 5H) and 1.50 (double doublets, $J=14$ and 2.5 Hz, 1H). ν^{KBr}_{max} 3485 cm^{-1} (S), 1297 cm^{-1} (VS), 1161 cm^{-1} (S), 1126 cm^{-1} (S), 1043 cm^{-1} (M), and 514 cm^{-1} (M).

*7-Thiabicyclo[2.2.1]heptan-2-one 7,7-Dioxide (**9**).* To a solution of 100 mg (0.62 mmol) of **8** in 2 ml of acetone chilled with ice and stirred was added dropwise Jone's reagent prepared from 470 mg (4.7 mmol) of chromium trioxide, 760 mg of concd H_2SO_4 and 1.5 ml of distilled water. After completion of addition stirring was continued for 40 min in ice and then at room temperature for 40 min. The excess oxidizing reagent was treated with 2-propanol with ice cooling. The reaction mixture was extracted with three portions of 20 ml of dichloromethane and the combined dichloromethane extracts were washed with 5 ml of water saturated with NaCl. Evaporation of the solvent gave 74 mg (74%) of white solid **9**. Recrystallization from CCl_4–hexane and sublimation under reduced pressure gave 50 mg of pure **9**; mp *ca.* 229 °C (dec in a sealed tube). $\delta^{TMS}_{CDCl_3}$ 3.53 (narrow multiplet, 2H), 3.20 (double doublets, $J=18.0$ and 3.5 Hz, 2H), 2.66 (doublet, $J=18.0$ Hz, 1H), 2.7—1.9 (multiplet, 4H). *m/e* 160 (M^+, 32), 96 ($M^+ - SO_2$, 80). 68 (100), 64 (62), and 55 (85).

Found: C, 44.91; H, 5.15; S, 19.84; O, 29.75%. Calcd for $C_6H_8SO_3$: C, 44.99; H, 5.03; S, 20.02; O, 29.96%.

*2,5-endo-endo-Dihydroxy-7-thianorbornane 7,7-Dioxide (**10**).* To a solution of 5.0 g (34.2 mmol) of **6** in 1250 ml of $CHCl_3$ was added dropwise a solution of 11.3 g (81.9 mmol) of perbenzoic acid in 150 ml of $CHCl_3$ at room temperature with stirring. After the completion of addition (3 h), the reaction mixture was refluxed for 5—6 h and then allowed to stand overnight at room temperature. After filtration of transparent

crystalline precipitate (5.30 g) of **10**, the solution was condensed to *ca.* 200 ml and into this residue was passed methyl mercaptan vigorously to destroy the excess peroxide. The mixture was cooled with ice to give additional 0.38 g of **10**: Mp 277 °C (dec, in a sealed tube) $\delta^{TMS}_{pyridine\text{-}d_5}$ 6.44 (singlet, 2H), 5.00 (quintet, J=4 Hz, 2H), 3.2 (narrow multiplet, 2H) and 2.6 (narrow multiplet, 4H). ν^{KBr}_{max} 3570 (S), 1295 (M), 1160 (S), 920 (M), and 860 cm^{-1} (M).

Found: C, 40.53; H, 5.64%. Calcd for $C_6H_{10}SO_4$: C, 40.44; H, 5.66%.

*7-Thiabicyclo[2.2.1]heptane-2,5-dione 7,7-Dioxide (**11**).* To a 1.5 ml of aqueous solution of 200 mg (1.12 mmol) of **10** chilled with ice and stirred was added dropwise Jone's reagent prepared from 7.52 mmol of chromium trioxide, 1.2 g of concd H_2SO_4 and 3.2 ml of distilled water. After completion of addition (30 min), stirring was continued for 1 h in ice and then at room temperature for 4 h. The reaction mixture was extracted with four portions of 10 ml of dichloromethane and the combined extracts were dried over calcium chloride. Evaporation of the solvent gave 90 mg of crystals. Yellow crystals of hydroquinone sublimed at the neck of the flask. Recrystallization from chloroform gave 74 mg of **11**: Mp 160 °C (dec in a sealed tube). $\delta^{TMS}_{CDCl_3}$ 4.10 (quartet, J=4.5 and 1.5 Hz, 2H), 3.44 (double quartets, J=1.5, 4.5, and 19 Hz, 2H) and 2.84 (doublet, J=19 Hz, 2H). ν^{KBr}_{max} 3000 (M), 1760 (S), 1416 (M), 1322 (S), 1218 (M), 1118 (S), 586 (S), 586 (S), and 450 cm^{-1} (M).

Found: C, 41.47; H, 3.74; S, 18.45%. Calcd for $C_6H_6SO_4$: C, 41.38; H, 3.47; S, 18.41%.

References

1) I. Tabushi, Y. Tamaru, Z. Yoshida, and T. Sugimoto, *J. Am. Chem. Soc.*, **97**, 2886 (1975).

2) N. J. Leonard, T. W. Milligan, and T. L. Brown, *J. Am. Chem. Soc.*, **82**, 4075 (1960).

3) L. A. Paquette and L. D. Wise, *J. Am. Chem. Soc.*, **89**, 6659 (1967).

4) The molecular geometry of 7-thiabicyclo[2.2.1]heptane has been determined by gas electron diffraction. T. Fukuyama, K. Kuchitsu, Y. Tamaru, Z. Yoshida, and I. Tabushi, *J. Am. Chem. Soc.*, **93**, 2799 (1971).

5) E. J. Corey and E. Block, *J. Org. Chem.*, **31** 1663 (1966).

6) (a) H. H. Sisler, J. D. Bush, and O. E. Accountius, *J. Am. Chem. Soc.*, **70**, 3827 (1948); (b) G. I. Poos, G. E. Arth, R. E. Beyler, and L. H. Sarett, *J. Am. Chem. Soc.*, **75**, 422 (1953); (c) J. L. Baas, A. D. Davies-Fidder, and H. O. Huisman, *Tetrahedron*, **22**, 259 (1966); (d) L. A. Paquette, G. V. Meehan, and L. D. Wise, *J. Am. Chem. Soc.*, **91**, 3231 (1969).

7) A. K. Awasthy, J. Rocek, and R. M. Moriarty, *J. Am. Chem. Soc.*, **89**, 5400 (1967).

8) (a) K. Bowder, E. A. Braude, E. R. H. Jones, and B. C. L. Weedon, *J. Chem. Soc.*, **1946**, 45; (b) L. A. Paquette and R. W. Houser, *J. Am. Chem. Soc.*, **91**, 3807 (1969).

9) Sheehan and Brandt reported that aldehyde-sulfide could be transformed with Jones' reagent in to carboxylic acid-sulfide in high yield. J. C. Sheehan and K. G. Brant, *J. Am. Chem. Soc.*, **87**, 5468 (1965).

10) T. Komeno, M. Kishi and K. Nabeyama, *Tetrahedron*, **27**, 1503 (1970).

11) A similar behavior was observed for **9** at an elevated temperature. I. Tabushi, Y. Tamaru and Z. Yoshida, *Tetrahedron Lett.*, **1976**, 3957.

12) L. M. Jackman and S. Sternhell, "Application of Nuclear Magnetic Resonance Spectroscopy in Organic Chemistry," Pergamon Press Ltd. Headington Hill Hall, Oxford, 2nd ed, (1969), pp. 88—92.

13) E. J. Corey, J. Casanova, Jr., P. A. Vatakencherry, and R. Winter, *J. Am. Chem. Soc.*, **85**, 169 (1963).

14) D. G. Farnum and G. Mehta, *J. Am. Chem. Soc.*, **91**, 3256 (1969).

15) E. I. Synder and B. Franzus, *J. Am. Chem. Soc.*, **86**, 1166 (1964). For a review on long range coupling, see S. Sternhell, *Rev. Pure and Appl. Chem.*, **14**, 15 (1964).

16) (a) E. A. Fehnel and M. Carmack, *J. Am. Chem. Soc.*, **71**, 84 (1949); (b) H. P. Koch, *J. Chem. Soc.*, **1949**, 387; (c) R. E. Davis, *J. Org. Chem.*, **23**, 1380 (1958).

17) H. Labhart and G. Wagniere, *Helv. Chem. Acta*, **42**, 2219 (1959).

18) 7-Thiabicyclo[2.2.1]heptane-2,5-dione 7,7-dioxide (**11**) decomposed at room temperature in water or methanol to sulfur dioxide and hydroquinone during the course of UV measurement.

19) (a) C. Ganter and J. F. Moser, *Helv. Chim. Acta*, **51**, 300 (1969); (b) B. Wladislaw, H. Viertler, F. A. C. Andrade, and E. B. Demant, *Int. J. Sulfur Chem.*, **A**, **2**, 161 (1972); (c) B. Wladislaw, H. Viertler, and E. B. Demant, *J. Chem. Soc., B*, **1971**, 565.

20) (a) R. C. Cookson and W. S. Wariyar, *J. Chem. Soc.*, **1956**, 2302; (b) A. Moscowitz, K. Mislow, M. A. W. Glass, and C. Djerassi, *J. Am. Chem. Soc.*, **84**, 1945 (1962); (c) P. G. Gassman, D. H. Aue, and D. S. Patton, *J. Am. Chem. Soc.*, **80**, 4211 (1964); (d) L. N. Ferguson and J. C. Nnadi, *J. Chem. Educ.*, **42**, 529 (1965).

21) (a) A. Padwa, A. Battisti, and E. Shefter, *J. Am. Chem. Soc.*, **91**, 4000 (1969); (b) A. Padwa and A. Battisti, *ibid*, **93**, 1304 (1971); (c) A. Padwa and A. Battisti, *ibid.*, **94**, 521 (1972).

22) M. Kishi and T. Komeno, *Tetrahedron Lett.*, **1971**, 2641.

Asymmetric Reactions. III. The Asymmetric Synthesis of Methyl 2-Phenylpropionate in the Presence of Chiral Polymers

Tetsushi YAMASHITA, Hiroshi YASUEDA, Noriyuki NAKATANI, and Nobuo NAKAMURA

Department of Chemistry, Faculty of Science, Osaka City University, Sumiyoshi-ku, Osaka 558

(Received September 14, 1977)

The asymmetric addition of methanol to phenylmethylketene was carried out in the presence of a chiral polymer obtained by the co-polymerization of *N*-benzyl-2-pyrrolidinylmethyl acrylate with methyl acrylate. The products obtained for the above co-polymer showed a correlation between log k_R/k_S and $1/T$ deviating from linearity, while those for poly(*N*-benzyl-2-pyrrolidinylmethyl acrylate) exhibited a linear relationship. *N*-Benzyl-2-pyrrolidinylmethyl butyrate, hexanoate, and stearate were also used as catalysts; they showed asymmetric efficiencies intermediate between those of *N*-benzyl-2-pyrrolidinylmethyl propionate and poly(*N*-benzyl-2-pyrrolidinylmethyl acrylate). The use of several high- and low-molecular-weight catalysts derived from cinchonine was similarly attempted in order to examine the polymer effect with regard to the stereoselectivity.

Several chiral polymers[1-2] derived from optically active amino alcohols have been used for the study of polymer effects in the asymmetric addition of methanol to phenylmethylketene (PMK):

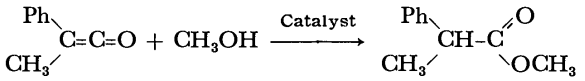

In previous papers,[1-2] poly(*N*-benzyl-2-pyrrolidinylmethylacrylate (PA) yielded optically rotational products with a sign opposite to that of products for its corresponding monomeric model compound (*N*-benzyl-2-pyrrolidinylmethyl propionate; Al).

The products obtained for PA showed a linear correlation between log k_R/k_S and $1/T$, while those for Al exhibited only a non-linear relationship. (k_R and k_S: the rate constants for the *R* and *S*-isomers respectively).

The results obtained with PA were interpreted in terms of the effect of molecular immobility;[2-3] the steric bulkiness of the back-bone of the polymer increases the degree of conformational rigidity of the molecules in the side chain.

In the present work, several *N*-benzyl-2-pyrrolidinylmethanol derivatives were used to clarify these observations more precisely.

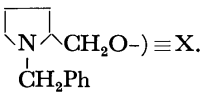

$CH_3(CH_2)_n$-CO-X Al[2], $n=1$
A2 $n=2$
A3 $n=4$
A4 $n=16$

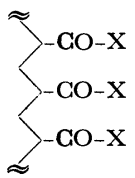

(PA)[2]

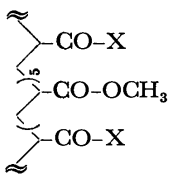

(CPA)

The asymmetric addition of methanol to PMK was carried out in a manner similar to that reported earlier.[1-2]

Figure 1 shows the log k_R/k_S-$1/T$ relation of the addition products obtained for the above catalysts.

A soluble co-polymer (CPA) was obtained by the co-polymerization of one molar equivalent amount of *N*-benzyl-2-pyrrolidinylmethyl acrylate with five molar equivalent amounts of methyl acrylate. The products

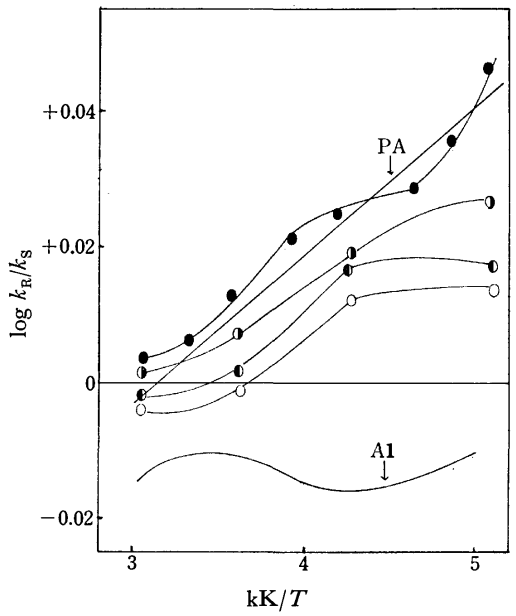

Fig. 1. Plots of log k_R/k_S against $1/T$ in case of A2 (○), A3 (◐), A4 (◑) and CPA (●).

from CPA reveal a relationship deviating somewhat from linearity (see Fig. 1). CPA decreases the degree of conformational rigidity of the molecules in the side chain in comparison with PA. The optically active molecules (X) of CPA are more mobile than those of PA because of the larger distance among the chiral pendants (X) of CPA.

A2, A3, and A4 were derived through the reaction of *N*-benzyl-2-pyrrolidinylmethanol with butyryl, hexanoyl, and stearoyl chloride respectively.

Figure 1 shows that the action of low-molecular-weight catalysts gradually became similar to that of polymeric catalysts with the increase in the length of the carbon chain in the acyl group.

Figure 2 indicates the plots of the optical yields of the addition products obtained for the *N*-benzyl-2-pyrrolidinylmethanol catalysts at −78 °C.

Al gave a product with an excess of *S*-enantiomer in a 1% optical yield, and CPA yielded a product with an excess of *R*-enantiomer in the highest optical yield (5.3%).

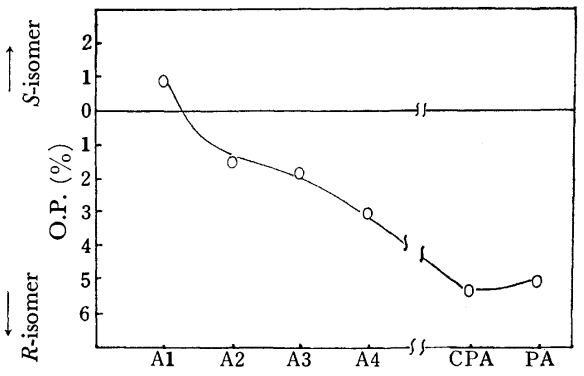

Fig. 2. The optical purities (O.P.) of the esters obtained with *N*-benzyl-2-pyrrolidinylmethanol catalysts at −78 °C.

Let us also describe the use of several cinchonine catalysts in order to examine this sort of polymer effect more clearly.

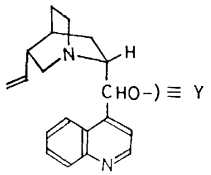

$CH_3(CH_2)_n$-CO-Y B1,[2] n= 0
B2,[2] n= 1
B3, n= 2
B4, n= 4
B5, n=16

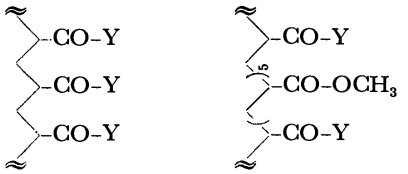

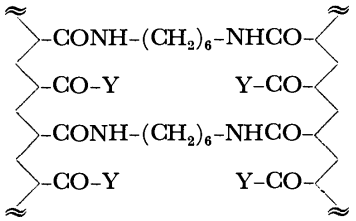

(CPB-2)[2]

B3, B4, and B5 were obtained by the reaction of cinchonine with butyryl, hexanoyl, and stearoyl chloride respectively. CPB-1 (soluble co-polymer) was derived through the co-polymerization of one molar equivalent amount of *o*-acryloylcinchonine[2] with five molar equivalent amounts of methyl acrylate. PB and CPB-2 were prepared according to the method reported previously.[2]

Figure 3 shows plots of log k_R/k_S against $1/T$ in the case of the above cinchonine catalysts.

Figure 3 shows that low-molecular-weight catalysts (B3, B4, and B5) gave the addition products of an *R*-configuration predominantly at higher reaction temperatures, and yielded the products of an *S*-configuration preferentially at lower temperatures. Figure 3 also indicates that polymeric catalysts (CPB-1, PB and

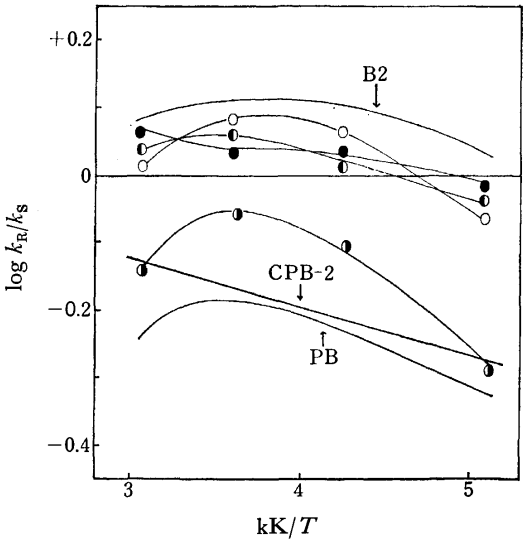

Fig. 3. Plots of log k_R/k_S against $1/T$ in case of B3 (●), B4 (◐), B5 (○) and CPB-1 (◑).

CPB-2) provided the addition products of an *S*-configuration preferably in the present range of reaction temperatures (−78 °C—+50 °C). CPB-2, in which the mobility of the chiral pendants (Y) is most strongly restricted by the cross-linking of the polymer, yielded addition products showing linear plots between log k_R/k_S and $1/T$.

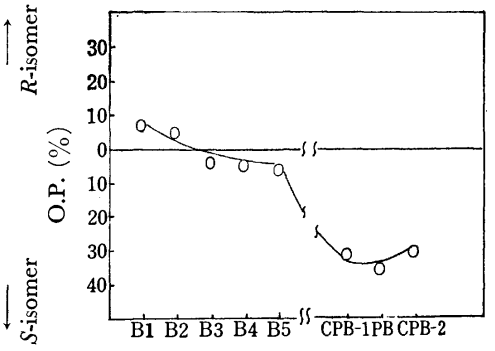

Fig. 4. The optical purities (O.P.) of the esters obtained with cinchonine catalysts at −78 °C.

Figure 4 shows the plots of the optical yields of the addition products given for cinchonine catalysts at −78 °C.

The preferable configuration of the addition products obtained for low-molecular-weight catalysts changed from *R* to *S* with an increase in the length of the carbon chain in the acyl group. Polymeric catalysts gave the addition products of an *S*-configuration predominantly; the maximum optical yield (35%) of the addition product was given in the case of PB.

Figures 3 and 4 reveal that cinchonine catalysts gave results similar to those obtained for *N*-benzyl-2-pyrrolidinylmethanol catalysts.

Experimental

N-Benzyl-2-pyrrolidinylmethyl Butyrate (A2). A solution of *N*-benzyl-2-pyrrolidinylmethanol (1 g), butyryl chloride (0.55 g), and triethylamine (0.53 g) in dry dichloromethane (100 ml) was stirred at room temperature. After 24 h, the solution was poured into water (100 ml). The organic layer thus separated out was washed with saturated sodium hydrogencarbonate and water, and dried over anhydrous sodium sulfate. After the removal of the solvent, the residue was distilled to give a colorless oil. Yield, 70%. Bp 180—190 °C at 2 mmHg. $[\alpha]_D^{20}=-28°$ (*c* 1.4, benzene). Found: C, 73.18; H, 8.92; N, 4.99%. Calcd for $C_{16}H_{23}NO_2$; C, 73.56; H, 8.81; N, 5.36%.

N-Benzyl-2-pyrrolidinylmethyl Hexanoate (A3). Yield, 80%. Bp 180—190 °C at 1 mmHg. $[\alpha]_D^{20}=-26°$ (*c* 1, benzene). Found: C, 74.81; H, 9.44; N, 4.61%. Calcd for $C_{18}H_{27}NO_2$: C, 74.74; H, 9.34; N, 4.84%.

N-Benzyl-2-pyrrolidinylmethyl Stearate (A4). Yield, 70%. Mp 43—45 °C. $[\alpha]_D^{15}=-19°$ (*c* 1.6, benzene). Found: C, 78.71; H, 11.50; N, 2.74%. Calcd for $C_{30}H_{51}NO_2$: C, 78.77; H, 11.15; N, 3.06%.

o-Stearoylcinchonine (B5). A solution of cinchonine (1.5 g), stearoyl chloride (1.6 g), and triethylamine (0.8 g) in dry benzene (100 ml) was stirred under refluxing. After 20 h, the solution was cooled to room temperature and poured into water (100 ml). The organic layer thus separated out was washed with saturated sodium hydrogencarbonate and water, and then dried over anhydrous sodium sulfate.

After the removal of the solvent, the residue was recrystallized from ether. Yield, 71%. Mp 37 °C. $[\alpha]_D^{20}=+57°$ (*c* 2, chloroform). Found: C, 79.13; H, 10.23; N, 4.83%. Calcd for $C_{37}H_{56}N_2O_2$: C, 79.28; H, 10.00; N, 5.00%.

o-Butyrylcinchonine (B3) was similarly obtained as an oily material in a 79% yield. $[\alpha]_D^{20}=+97°$ (*c* 2, chloroform).

o-Hexanoylcinchonine (B4) was also given as a syrup in a 76% yield. $[\alpha]_D^{20}=+87°$ (*c* 2, chloroform).

The TLC of B3 (B4) gave only one spot for several solvent systems and showed it to be a single material.

Poly(N-benzyl-2-pyrrolidinylmethyl acrylate-methyl acrylate) (CPA). A mixture of *N*-benzyl-2-pyrrolidinylmethyl acrylate (0.588 g) and methyl acrylate (1.03 g) containing azobisisobutyronitrile (10 mg) was polymerized without any solvents in a sealed tube at 80 °C for 24 h, and then cooled to room temperature. The product was dissolved in a small amount of dry benzene and then poured into ether. A sticky precipitate was given in an 85% yield. $[\alpha]_D^{12}=-9.7°$ (*c* 1, benzene). Mol wt 4840 (benzene).

Poly(o-acryloylcinchonine-methyl acrylate) (CPB-1). A solution of *o*-acryloylcinchonine[2] (1 g), methyl acrylate (1.2 g), and azobisisobutyronitrile (10 mg) in dry benzene (10 ml) was refluxed with stirring in an argon atmosphere. After 20 h, the solution was cooled to room temperature and poured into ether. A precipitate (CPB-1) was filtered off and washed thoroughly with ether. Yield, 70%. $[\alpha]_D^{20}=+38°$ (*c* 2, chloroform). Mol wt 12500 (dichloromethane).

The Addition of Methanol to PMK. Freshly distilled PMK (330 mg) and CPA (17 mg) were added to 25 ml of dry toluene at −78 °C in an argon atmosphere. After the addition of methanol (82 mg), the mixture was stirred at the same temperature. After 10 h, the end point of the reaction was confirmed by the absence of the yellow color of PMK. The toluene solution was then poured into dilute hydrochloric acid and filtered off. The organic layer thus separated out was washed with saturated sodium hydrogencarbonate and water, and dried over anhydrous sodium sulfate. After the removal of the solvent, the residue was distilled to give an oil in an 80% yield. $[\alpha]_D^{20}=-5.8°$ (*c* 10, toluene).

The TLC and GLC of the product showed it to be a single material. The IR and NMR spectra of the product were completely in agreement with those of authentic methyl-2-phenylpropionate. The use of other basic catalysts was similarly attempted at various reaction temperatures.

In those experiments, a Jasco IRA-1 (IR) apparatus, a JEOL-60 MC (NMR) apparatus, a Varian M920 (GLC) apparatus, a Rex-automatic polarimeter (optical rotation; 10-cm cell), and a Knauer vapor-pressure osmometer (molecular weight) were used for the measurement of the samples.

References

1) T. Yamashita, H. Yasueda, and N. Nakamura, *Chem. Lett.*, **1974**, 585.

2) T. Yamashita, H. Yasueda, Y. Miyauchi, and N. Nakamura, *Bull. Chem. Soc. Jpn.*, **50**, 1532 (1977).

3) a) H. Pracejus and G. Kohl, *Ann. Chem.*, **722**, 1 (1969). b) H. Pracejus and H. Matje, *J. Prakt. Chem.*, **24**, 195 (1964).

Synthesis of Indole Derivatives by Cu_2O-Catalyzed Cyclization of *o*-(α-Cyanoalkyl)phenyl Isocyanides and *o*-[α-(Methoxycarbonyl)alkyl]phenyl Isocyanides

Yoshihiko Ito, Yoshinori Inubushi, Toru Sugaya, Kazuhiro Kobayashi, and Takeo Saegusa

Department of Synthetic Chemistry, Faculty of Engineering, Kyoto University, Kyoto 606

(Received September 29, 1977)

o-(Cyanomethyl)phenyl isocyanide and *o*-(methoxycarbonylmethyl)phenyl isocyanide were heated with a catalytic amount of Cu_2O in benzene to give 3-cyanoindole and 3-(methoxycarbonyl)indole in 86 and 92% yields, respectively. Lithiations of *o*-(cyanomethyl)phenyl isocyanide and *o*-(methoxycarbonylmethyl)phenyl isocyanide with butyllithium at −78 °C followed by the reaction with alkyl halides such as methyl iodide, allyl bromide, butyl bromide, benzyl bromide and methyl α-bromoacetate afforded the corresponding *o*-(α-cyanoalkyl)phenyl isocyanides and *o*-[α-(methoxycarbonyl)alkyl]phenyl isocyanides. *o*-(α-Cyanoalkyl)phenyl isocyanides and *o*-[α-(methoxycarbonyl)alkyl]phenyl isocyanides thus obtained were also cyclized by Cu_2O catalyst producing 3-alkyl-3-cyano-3*H*-indoles and 3-alkyl-3-(methoxycarbonyl)-3*H*-indoles, respectively, in moderate yields.

In the continuation of our studies[1] on synthetic reactions caused by Cu_2O-isonitrile complex, it has been found that the so-called active methylene compounds such as malonate, acetoacetate and cyclopentadiene were reacted with Cu_2O in the presence of isonitrile to produce organocopper(I) isonitrile complexes, which undergo an isonitrile insertion into their copper-carbon bonds.[2] On the basis of the isonitrile insertion of organocopper(I) isonitrile complexes, some heterocycle syntheses have been already reported.[3] Herein, we wish to report a new synthetic method of indole derivatives by the Cu_2O-catalyzed reactions of *o*-(cyanomethyl)phenyl isocyanide (**1a**) and *o*-(methoxycarbonylmethyl)phenyl isocyanide (**1b**),[4] in which intermediacy of the corresponding organocopper(I) isonitrile complexes (**2**) may by assumed.

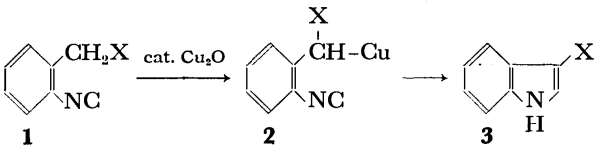

1 **2** **3**

a: X=CN
b: X=CO_2CH_3

Results and Discussion

Isocyanides (**1a** and **1b**) were heated with a catalytic amount of Cu_2O to give 3-cyanoindole (**3a**)[5] and 3-(methoxycarbonyl)indole (**3b**)[6] in high yields, respectively. For example, a mixture of **1a** (2 mmol) and Cu_2O (0.025 mmol) in 2 ml of benzene was heated at 55 °C for 6 h with stirring. The progress of reaction was monitored by IR absorption band ($\nu_{N\equiv C}$=2150 cm^{-1}) characteristic of the starting isocyanide. After the insoluble copper catalyst was removed by filtration, the filtrate was evaporated and then subjected to column chromatography to give 3-cyanoindole (**3a**) in 86% yield.

o-(α-Cyanoalkyl)phenyl isocyanide (**4a**) and *o*-[α-(methoxycarbonyl)alkyl]phenyl isocyanide (**4b**), which were readily prepared *via* the lithiation of **1a** and **1b** followed by the reaction with alkyl halides (Table 1), were also cyclized by Cu_2O catalyst producing 3-alkyl-3-cyano-3*H*-indole (**5a**) and 3-alkyl-3-(methoxycarbonyl)-3*H*-indole (**5b**), respectively, in moderate yields. Results are summarized in Table 2.

Table 1. Alkylations of *o*-(cyanomethyl)phenyl isocyanide (**1a**) and *o*-(methoxycarbonylmethyl)phenyl isocyanide (**1b**)[a,b]

Starting phenyl isocyanide (**1**)	Alkyl halide	Product (**4**) (%)
1a	CH_3I	**4a-i** (76)
	i-C_3HBr	**4a-ii** (44)
	CH_2=$CHCH_2Br$	**4a-iii** (94)
	$C_6H_5CH_2Br$	**4a-iv** (83)
	$BrCH_2CO_2CH_3$	**4a-v** (57)
1b	CH_3I	**4b-i** (88)
	CH_2=$CHCH_2Br$	**4b-ii** (52)
	C_4H_9Br	**4b-iii** (51)

a) Alkylations of **1a** were performed by the lithiation of **1a** (5 mmol) with butyllithium (5 mmol) in 10 ml of THF at −78 °C followed by addition of alkyl halide (6 mmol). b) Alkylations of **1b** were performed by the lithiation of **1b** (1.5 mmol) with butyllithium (1.5 mmol) in 4 ml of diglyme and 1 ml of HMPA at −78 °C followed by addition of alkyl halide (2.0 mmol).

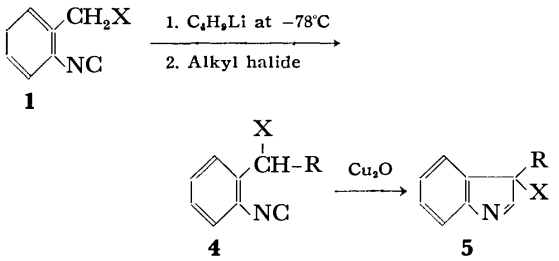

1 **4** **5**

a: X=CN
b: X=CO_2CH_3

The following scheme involving organocopper(I) isonitrile complex (**2**) may be assumed for the present Cu_2O-catalyzed indole synthesis. The first step is the formation of **2**, in which an acidic hydrogen at the benzylic position of **1** is replaced by copper. The organocopper(I) isonitrile complex (**2**) subsequently undergoes an intramolecular isonitrile insertion to give a cyclic

Table 2. Indole synthiesis by Cu_2O-catalyzed cyclizations of *o*-(α-cyanoalkyl)phenyl isocyanides and *o*-[α-(methoxycarbonyl)alkyl]-phenyl isocyanides

o-(α-Cyanoalkyl)-phenyl isocyanide and *o*-[α-(methoxycarbonyl)-alkyl]phenyl isocyanide	Reaction[a] Temp (°C)	Time (h)	Product (**3**) and (**5**) (%)
1a	55	6	**3a** (86)
1b	55	6	**3b** (92)
4a-i	70	10	**5a-i** (71)
4a-ii	80	18	**5a-ii** (61)
4a-iii	80	13	**5a-iii** (60)
4a-iv	80	25	**5a-iv** (62)
4a-v	80	6	**5a-v** (43)
4b-i	80	30	**5b-i** (80)
4b-ii	80	30	**5b-ii** (71)
4b-iii	80	30	**5b-iii** (88)

a) Cyclizations of **1** (and **4**) were performed by heating **1** (or **4**) (2 mmol) and Cu_2O (0.025 mmol) in 2 ml of benzene.

organocopper(I) intermediate (**6**). The abstraction of the acidic hydrogen of **1** by **6** produces indole derivative (**3**) regenerating **2** which initiates the next cycle of reaction.

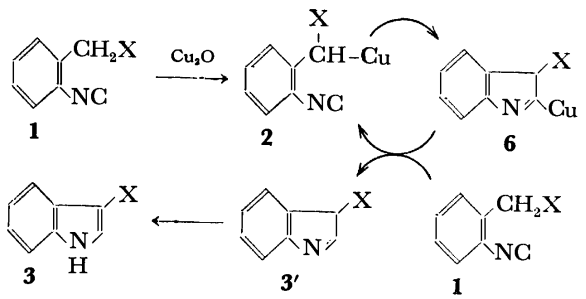

Scheme 1.

The present indole synthesis is interestingly compared with the previously reported indole synthesis *via* the selective lithiation at the benzylic position of the alkyl group in *o*-alkylphenyl isocyanide and the subsequent cyclization.[4] The Cu_2O-catalyzed synthesis of indole is only applicable to *o*-alkylphenyl isocyanides which bear a benzylic hydrogen activated by cyano and ester groups. However, in view of the feasibility of the reaction conditions (a catalytic amount of Cu_2O and reaction temperature), the present method which complements our earlier procedure[4] is practically useful for the preparation of 3-cyano- and 3-(alkoxycarbonyl)indole derivatives.

Experimental

Materials. Cu_2O was commercially available and dried *in vacuo* prior to use. Alkyl halides and organic solvents all purified by distillation under nitrogen. *o*-(Cyanomethyl)phenyl isocyanide (mp 66 °C) (**1a**) was prepared in 78% yield according to the Ugi's procedure[7] from *o*-(formylamino)phenylacetonitrile which was prepared by formylation of *o*-aminophenylacetonitrile[8] with acetic formic anhydride.[9] *o*-(Methoxycarbonylmethyl)phenyl isocyanide (**1b**), bp 95 °C (0.6 Torr), was prepared in 69% yield by the reaction of *o*-(lithiomethyl)phenyl isocyanide with methyl chloroformate.[4]

Cu_2O Catalyzed Cyclization of o-*(Cyanomethyl)phenyl Isocyanide (**1a**).* A mixture of 284 mg (2 mmol) of *o*-(cyanomethyl)-phenyl isocyanide (**1a**), 3.6 mg (0.025 mmol) of Cu_2O and 2 ml of benzen was heated at 55 °C for 6 h with stirring under nitrogen. After the reaction mixture was filtered, the filtrate was distilled *in vacuo*. The residue was subjected to column chromatography (silica gel–chloroform) giving 3-cyanoindole (**3a**) in 86% yield. **3a** was identified by comparing the spectral data with those of the authentic sample.[5]

Cyclization reaction of *o*-(methoxycarbonylmethyl)phenyl isocyanide (**1b**) was carried out in a similar way. The product of 3-(methoxycarbonyl)indole (**3b**) (92% yield) was identified by comparing the spectral data with those of the authentic sample.[6]

Reaction of o-*(Cyanomethyl)phenyl Isocyanide (**1a**) with Methyl Iodide.* To a mixture of 710 mg (5 mmol) of *o*-cyanomethylphenyl isocyanide and 10 ml of THF cooled at −78 °C with stirring under nitrogen, butyllithium (5 mmol, 1.8 M hexane solution) was added. After 15 min, 0.37 ml (6 mmol) of methyl iodide was added dropwise to the mixture, which was then allowed to warm up to room temperature. The reaction mixture was filtered to remove insoluble inorganic salts and evaporated *in vacuo*. The residue was subjected to column chromatography on silica gel eluting with benzene–chloroform (5: 1) to yield *o*-(α-cyanoethyl phenyl)isocyanide (**4a-i**) (76% yield). Product of **4a-i** was identified by IR and NMR spectra.

Other alkylations of **1a** were carried out according to the procedure mentioned above.

Reaction of o-*(Methoxycarbonylmethyl)phenyl Isocyanide (**1b**) with Allyl Bromide.* To a mixture of 263 mg (1.5 mmol) of *o*-(methoxycarbonylmethyl)phenyl isocyanide (**1b**), 4 ml of diglyme and 1 ml of HMPA cooled at −78 °C, butyllithium (1.5 mmol, 1.8 M hexane solution) was added. After 15 min, 242 mg (2 mmol) of allyl bromide was added to the mixture and stirred for 1 h at −78 °C, which was then allowed to warm up to room temperature. The reaction mixture was poured into ether and washed with water, and dried over Na_2SO_4. The ether solution was evaporated *in vacuo* and subjected to column chromatography on silica gel eluting with chloroform to give 57% yield of *o*-[1-(methoxycarbonyl)-3-butenyl]phenyl isocyanide (**4b-ii**). Product of **4b-ii** was identified by IR and NMR spectra.

Other alkylations of **1b** were carried out according to the procedure mentioned above.

General Procedure for Cu_2O Catalyzed Cyclization of o-*(α-Cyanoalkyl)phenyl Isocyanide (**4a**) and* o-*[α-(Methoxycarbonyl)alkyl]phenyl Isocyanide (**4b**).* A mixture of 312 mg (2 mmol) of *o*-(α-cyanoethyl)phenyl isocyanide (**4a-i**), 3.6 mg (0.025 mmol) of Cu_2O and 2 ml of benzene was heated at 70 °C for 10 h with stirring under nitrogen. The reaction mixture was filtered, and the filtrate was subjected to vacuum distillation to afford 3-cyano-3-methyl-3*H*-indole (**5a-i**) in 71% yield, bp 95 °C (0.8 Torr). **5a-i**: IR (neat) 2225, 1605 cm^{-1}; NMR (CCl_4 with Me_4Si) δ 1.68 (s, 3H), 7.3—7.8 (m, 4H), 7.98 (s, 1H). Found: C, 76.72; H, 5.20; N, 17.68%. Calcd for $C_{10}H_8N_2$: C, 76.90; H, 5.16; N, 17.94%.

According to the above procedure, other *o*-(α-cyanoalkyl)-phenyl isocyanides (**4a**) and *o*-[α-(methoxycarbonyl)alkyl]-phenylisocyanides (**4b**) were cyclized.

*3-Cyano-3-isopropyl-3*H*-indole (**5a-ii**)*: Bp 105—108 °C (1 Torr), IR (neat) 2220, 1600 cm^{-1}; NMR ($CDCl_3$ with Me_4Si) δ 1.10 (d, 6H), 2.40 (m, 1H), 7.20—8.00 (m, 4H), 7.19 (s,

1H). Found: C, 78.41; H, 6.65; H, 15.03%. Calcd for $C_{12}H_{12}N_2$: C, 78.23; H, 6.57; N, 15.21%.

*3-Cyano-3-allyl-3*H*-indole (**5a-iii**)*: Bp 110—112 °C (1 Torr), IR (neat) 2220, 1640, 1600 cm^{-1}; NMR (CCl_4 with Me_4Si) δ 2.71 (d, 2H), 5.18 (m, 1H), 5.45 (m, 1H), 6.00 (m, 1H), 7.30—8.00 (m, 4H), 8.15 (s, 1H). Found: C, 79.32; H, 5.77; N, 15.45%. Calcd for $C_{12}H_{10}N_2$: C, 79.09; H, 5.53; N, 15.38%.

*3-Cyano-3-benzyl-3*H*-indole (**5a-iv**)*: was isolated by column chromatography on silica gel (benzene). **5a-iv**: IR (Neat) 2220, 1600 cm^{-1}; NMR ($CDCl_3$ with Me_4Si) δ 3.19 (s, 2H), 7.00—7.90 (m, 9H), 7.10 (s, 1H). Found: C, 82.93; H, 5.01; N, 12.28%. Calcd for $C_{16}H_{12}N_2$: C, 82.73; H, 5.21; N, 12.06%.

*3-Cyano-3-(methoxycarbonylmethyl)-3*H*-indole (**5a—v**)*: was isolated by column chromatography on silica gel (chloroform). **5a—v**: IR (neat) 2210, 1740, 1600 cm^{-1}: NMR (CCl_4 with Me_4Si) δ 2.27 (s, 1H), 2.92 (s, 1H) 3.73 (s, 3H), 7.20—7.75 (m, 4H), 8.25 (s, 1H). Found: C, 67.51; H, 4.88; N, 12.91%. Calcd for $C_{12}H_{10}N_2O_2$: C, 67.28; H, 4.71; N, 13.08%.

*3-(Methoxycarbonyl)-3-methyl-3*H*-indole (**5b-i**)*: was isolated by column chromatography on silica gel (chloroform). **5b-i**: IR (neat) 1730. 1600 cm^{-1}; NMR (CCl_4 with Me_4Si) δ 1.58 (s, 3H), 3.55 (s, 3H), 6.90—7.50 (m, 4H), 7.90 (s, 1H). Found: C, 69.58; H, 5.72; N, 7.28%. Calcd for $C_{11}H_{11}NO_2$: C, 69.82; H, 5.86; N, 7.40%.

*3-(Methoxycarbonyl)-3-allyl-3*H*-indole (**5b-ii**)*: was isolated by column chromatography on silica gel (1:4 ethyl acetate–chloroform). **5b-ii**: IR (neat) 1730, 1640, 1600 cm^{-1}; NMR (CCl_4 with Me_4Si) δ 2.70 (m, 2H), 3.64 (s, 3H), 5.0—5.6 (m, 3H), 6.80—7.50 (m, 4H), 7.95 (s, 1H). Found: C, 72.80; H, 6.11; N, 6.73%. Calcd for $C_{13}H_{13}NO_2$: C, 72.54; H, 6.09; N, 6.51%.

*3-(Methoxycarbonyl)-3-butyl-3*H*-indole (**5b-iii**)*: was isolated by column chromatography on silica gel (chloroform). **5b-iii**: IR (neat) 1730, 1590 cm^{-1}; NMR ($CDCl_3$ with Me_4Si) δ 0.83 (t, 3H), 1.20—1.50 (m, 4H), 2.00 (m, 2H), 3.68 (s, 3H). 7.00—7.60 (m, 4H), 8.18 (s, 1H). Found: C, 72.88; H, 7.59; N, 5.92%. Calcd for $C_{14}H_{17}NO_2$: C, 72.70; H, 7.41; N, 6.06%.

References

1) Y. Ito and T. Saegusa, *Synthesis*, 291 (1975).
2) Y. Ito, T. Konoike, and T. Saegusa, *J. Organomet. Chem.*, **85**, 395 (1975).
3) T. Saegusa, Y. Ito, H. Kinoshita, and S. Tomita, *J. Org. Chem.*, **36**, 3316 (1971).
4) Y. Ito, K. Kobayashi, and T. Saegusa, *J. Am. Chem. Soc.*, **99**, 3532 (1977).
5) H. M. Blatter, H. Lukaszewski, and G. de Stevens, *Org. Synth.*, Coll. Vol. 5, 656 (1973).
6) F. Milich and E. I. Becker, *J. Org. Chem.*, **23**, 1096 (1958).
7) I. Ugi and R. Meyr, *Angew Chem.*, **60**, 702 (1958).
8) V. Rousseau and H. G. Lindwall, *J. Am. Chem. Soc.*, **72**, 3047 (1950).
9) M. Fieser and L. F. Fieser, "Reagents for Organic Synthesis," Vol. 2, 10 (1969).

Stereochemistry of Nucleophilic Addition Reactions. 5. Formation of Stabilized Ylides from Methyl 4,6-*O*-Benzylidene-2,3-dideoxy-3-nitro-β-D-*erythro*-hex-2-enopyranoside with Some *S*-Ylides; An Important Role of the Nitro Group for Stabilization of the Ylides[1]

Tohru SAKAKIBARA, Rokuro SUDOH, and Toshio NAKAGAWA*

Department of Chemistry, Faculty of Science, Tokyo Institute of Technology, Ookayama, Meguro-ku, Tokyo 152

**Department of Chemistry, Yokohama City University, Mutsuura-cho, Kanazawa-ku, Yokohama 236*

(Received October 14, 1977)

Treatment of methyl 4,6-*O*-benzylidene-2,3-dideoxy-3-nitro-β-D-*erythro*-hex-2-enopyranoside (**1**) with dimethyloxosulfonium methylide and dimethylsulfonium α-methylphenacylide afforded cyclopropane derivatives, whereas similar reactions with dimethylsulfonium phenacylide and dimethylsulfonium ethoxycarbonylmethylide gave stabilized ylides. In all cases the *S*-ylides enter the C-2 position of **1** from the side trans to the anomeric methoxyl group. The ylide structures were determined from IR and NMR data and confirmed by transformation into the desulfurized products. Anomalous stability of these ylides are attributed to the delocalization of the negative as well as positive charge over the carbonyl and the nitro group, respectively.

Only one example[2] is known of the reactions of nitro olefin with *S*-ylides (dimethyloxosulfonium methylide), in which cyclopropane derivatives are exclusively formed. Our studies[3] on the nucleophilic addition reaction to methyl 4,6-*O*-benzylidene-2,3-dideoxy-3-nitro-β-D-*erythro*-hex-2-enopyranoside (**1**) and its α-anomer and related subjects[4] strongly suggest that under kinetically controlled conditions nucleophiles approach from the equatorial side in the β-series,[5] but predominantly from the axial side in the α-series. In order to confirm the surmise we have carried out the reactions of **1** and its α-anomer with some *S*-ylides; these seem to be controlled kinetically.[6] We wish to report the reactions of **1** with *S*-ylides in this paper.

Results and Discussion

Treatment of **1** with dimethyloxosulfonium methylide in DMSO at room temperature for 1 h gave methyl (2*R*,3*R*)-4,6-*O*-benzylidine-2,3-dideoxy-2,3-*C*-methylene-3-nitro-β-D-*erythro*-hexopyranoside (**2**) in 75% yield. The configuration of **2** was assigned from the values of $J_{1,2}=0$ Hz, indicating that the conformation of **2** is similar to that of methyl 2,3-anhydro-4,6-*O*-benzylidene-3-nitro-β-D-allopyranoside.[7,4a]

On the other hand, when **1** was treated with dimethylsulfonium phenacylide in THF at room temperature for 18 h, methyl 4,6-*O*-benzylidene-2,3-dideoxy-2-*C*-[α-(dimethylsulfuranylidene)phenacyl]-3-nitro-β-D-glucopyranoside (**3**) was obtained in 78% yield instead of a cyclopropane derivative. The structure of **3** was determined by the following data: i) molecular ion peak *m/e* 473 was observed, ii) its IR spectrum (KBr) showed absorption bands due to a characteristic carbonyl group of ylide species[8] at 1505 cm^{-1} and due to a nitro group at 1555 cm^{-1}, iii) the NMR spectrum revealed the presence of a α-(dimethylsulfuranylidene)-phenacyl group (5-H of phenyl and 6-H of SMe_2) and *gluco* configuration for **3** ($J_{1,2}=7.5$ and $J_{2,3}=J_{3,4}=10$ Hz), iv) catalytic desulfurization over Pd/C afforded quantitatively methyl 4,6-*O*-benzylidene-2,3-dideoxy-3-nitro-2-*C*-phenacyl-β-D-glucopyranoside (**5**), accompanied by the odor of dimethyl sulfide, whose *gluco* configuration was deduced from the values of $J_{1,2}=7.5$ and $J_{2,3}=J_{3,4}=10$ Hz.

A similar stabilized ylide **4** was prepared in 75% yield by treating **1** with dimethylsulfonium ethoxycarbonylmethylide in THF at room temperature for 18 h. The results of elemental analysis fit the formula $C_{20}H_{27}NO_8S$, which is confirmed by the molecular ion peak *m/e* 441.

Table 1. Chemical shifts (δ) at 100 MHz in chloroform-*d* (Me_4Si as internal standard)

Compd.	H-1	H-2	H-3	H-4	H-5	H-6a	H-6e	H–C[a]	H–C′[a]
2	4.52(s)	2.28(t)		4.96(d)	2.99(six)	3.75(t)	4.23(q)	2.28(t)[b]	1.64(t)[c]
3	5.37(d)	2.60(q)	6.20(t)	←	4.4—3.7		→	—	—
4	4.96(d) 4.71(d)	3.6—3.5 (m)	5.81(t) 5.40(t)	4.09(t)	4.06(six)	3.74(t)	4.40(q)	—	—
5	4.82(d)	2.68(m)	5.23(q)	4.18(t)	3.62(six)	3.83(t)	4.36(q)	3.24(d)	3.07(d)
6	4.65(d)	2.7—2.3 (m)	5.02(t)	4.15(t)	3.52(six)	3.82(t)	4.37(q)	← 2.3—2.7 →	
7	5.77(d)	2.57(d)	—	4.64(d)	3.15(six)	3.68(t)	4.24(q)	—	—
9	5.13(s)	—	2.64(q)	3.52(q)	3.41(six)	3.68(t)	4.24(q)	2.34(d)	—

a) The methine or methylene proton(s) of a chain or cyclopropane moiety. b) Exo proton of the cyclopropane ring, assigned by the presence of long range coupling ($J_{exo.4}=1.2$ Hz) due to "W-orientation." c) Endo proton of the cyclopropane ring.

TABLE 2. FIRST-ODER COUPLING CONSTANTS (Hz) MEASURED AT 100 MHz IN CHLOROFORM-*d*

Compd	$J_{1,2}$	$J_{2,3}$	$J_{3,4}$	$J_{4,5}$	$J_{5,6a}$	$J_{5,6e}$	$J_{6a,6e}$	
2	0	—	—	10	10	5.0	10	$J_{2,c}=J_{2,c'}=J_{c,c'}=6.0$
3	7.5	10	10					
4	7.5	10	10	10	10	5.0	10	
5	8.4	11.6	10	8.8	10	4.4	10	$J_{2,c}=J_{2,c'}=4.4$
6	7.5	10	10	10	10	5.0	10	
7	1.3	—	—	10	10	5.0	10	
9	0	—	1.5	9.4	9.4	4.4	9.4	$J_{3,c}=6.9$

The IR spectrum (KBr) showed the presence of an ester carbonyl group of ylide species[8] (1615 cm^{-1}) and a nitro group (1560 cm^{-1}). Catalytic desulfurization of **4** to **6** also supports the structure of **4**. The NMR spectrum of **4** shows a pattern quite different from that of **3**, indicating that compound **4** consists of two geometrical isomers (Fig. 1), formed by the restricted rotation about the C(ylide)–C(carbonyl) bond, in an approximately 1 : 1 ratio; the appearance of two doublets (at δ 4.96 and 4.71) and two triplets (at δ 5.81 and 5.40) due to H-1 and H-3, respectively, at 20 °C in $CDCl_3$. With respect to the sugar moiety, they have the same *gluco* configuration with the same $^4C_1$ conformation because of the same values for their coupling constants, $J_{1,2}=7.5$ and $J_{2,3}=J_{3,4}=10$ Hz, as well as the exclusive formation of **6** from **4**. The equilibrium of the isomers was studied by examining the temperature dependence of the NMR spectrum: At 90 °C the two doublets (H-1) and two triplets (H-3) collapse into broad singlets centered at δ 4.75 and 5.60, respectively. At 115 °C the former appears at δ 4.77 as a doublet and the latter at δ 5.48 as a triplet. A similar phenomenon was reported by Casanova, Jr. and Rutolo, Jr. concerning dimethylsulfonium methoxycarbonylmetflylide;[9] in NMR spectra, the methine proton signal, a sharp singlet at 45 °C, becomes a broad singlet at 0 °C and two singlets at −45 °C.

The formation of the different products according to the ylides used might be explained as follows. An intermediate zwitterion arising from the nucleophilic addition of the anionic center of the ylide to the C-2 position of the nitro olefin **1** should collapse to cyclopropane. However, if an acidic hydrogen atom was present on the ylide carbon atom, the proton shift predominates over the cyclopropanation giving the stabilized ylides. In fact the reaction of **1** with dimethylsulfonium α-methylphenacylide, bearing no available hydrogen atom, afforded the cyclopropane **7** in 71% yield. The cyclopropane structure for **7** was determined by comparison of its IR and NMR spectra with those of **2**. From the steric ground the benzoyl group on the cyclopropane ring seems to occupy the exo position and the methyl the endo position. However, no definite assignment has been established.

Ylides **3** and **4** are extremely stable as compared with the usual ylides having one anion stabilizing group such

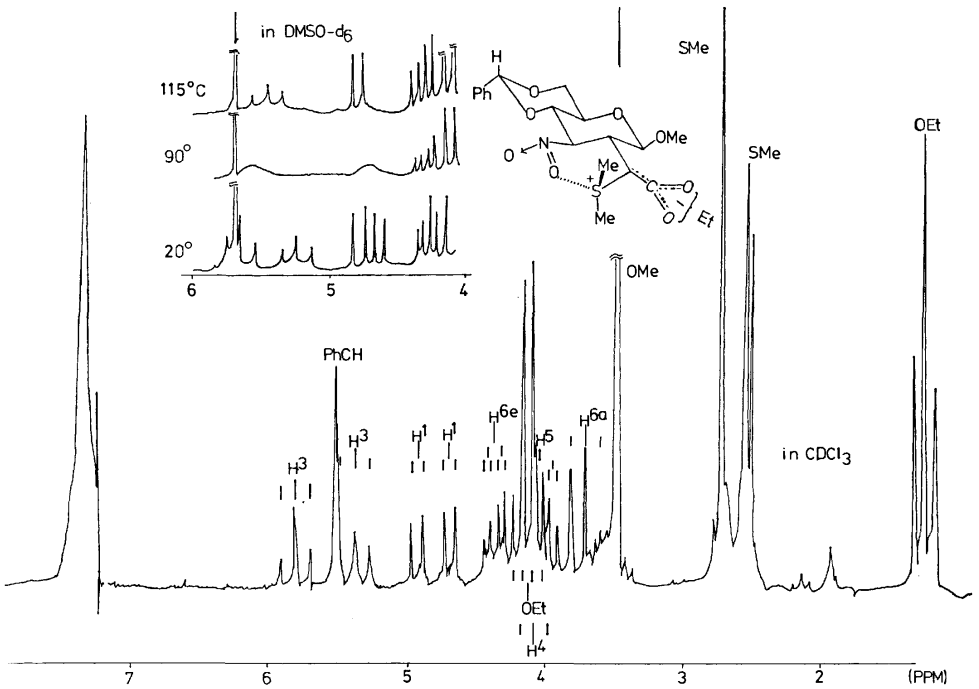

Fig. 1. The NMR spectrum of the stabilized ylide **4** (in $CDCl_3$, 100 MHz), the partial NMR spectra of **4** under the elevated temperature (in DMSO-d_6, 100 MHz), and the most plausible structure of **4**.

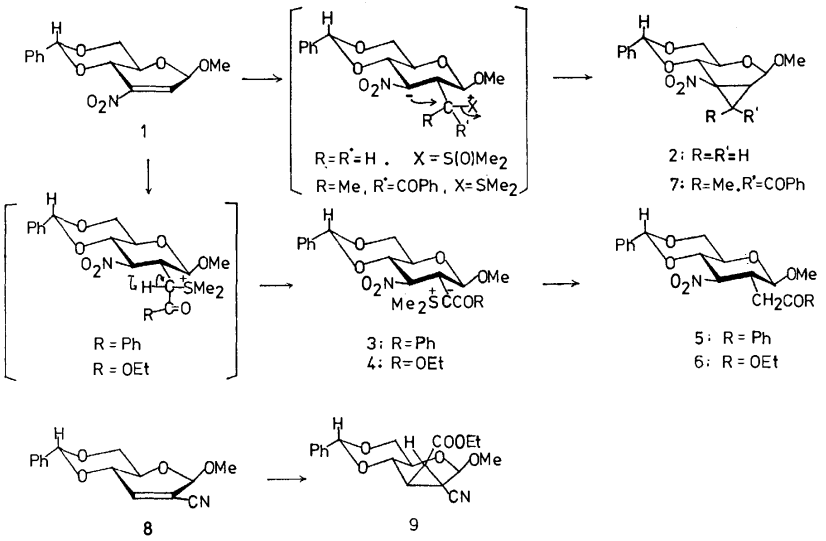

as carbonyl; *e.g.* the molecular ion peaks appear in EI-mass spectra, no change being observed on keeping the samples in open vessels at room temperature for 2 years or on treatment with silica gel column chromatograph. The anomalous stability of ylides **3** and **4** cannot be explained only in terms of the delocalization of negative charge over a ethoxycarbonyl or a carbonyl group. The most satisfactory explanation is based on the delocalization of the positive charge on the sulfur atom over the nitro group orientated in a suitable position to form the π_d–π_p bond with the sulfur atom through a stable six-membered ring system (Fig. 1).

This surmise was chemically supported. The reaction of methyl 5-*O*-benzoyl-2,3-dideoxy-3-nitro-β-D-*glycero*-pent-2-enofuranoside[10] with dimethylsulfonium ethoxycarbonylmethylide afforded complicated results, the isolation of products being unsuccessful. However, the NMR spectrum of the crude reaction mixture showed the absence of dimethylsulfonium moiety, indicating no formation of a stabilized ylide corresponding to **4**. This is reasonable if the formation of a stabilized ylide requires the delocalization of both the negative and positive charges, the latter being sterically impossible in the 2,3-*trans* furanose system. The reaction of methyl 4,6-*O*-benzylidene-2-cyano-2,3-dideoxy-β-D-*erythro*-hex-2-enopyranoside (**8**)[3,4c] with dimethylsulfonium ethoxycarbonylmethylide afforded a mixture of three compounds,at least, from which the cyclopropane derivative **9** and the starting material **8** were isolated in 23 and 10% yield, respectively. During column chromatography on silica gel, generation of dimethyl sulfide was detected by its smell, suggesting the formation of a ylide corresponding to **4** and its much less stability as compared with that of **4**. Such an interaction of the linear cyano group with the sulfur atom of the ylide is stericall difficult. The cyclopropane structure for **8** was determined from the results of elemental analsysis, IR (CN at 2250 and CO at 1725 cm^{-1}) and NMR spectra (presence of cyclopropane ring protons at δ 2.34 and 2.64; $J_{3,4}$= 1.6 Hz).

Experimental

Melting points were determined in capillaries and are uncorrected. IR spectra were recorded on KBr discs for crystals and on NaCl plates for syrup. NMR spectra were determined for solutions in chloroform-*d* (tetramethylsilane as internal standard) with a JNM-4H-100 (JEOL) spectrometer. Solutions were evaporated under reduced pressure.

*Methyl (2*R*,3*R*)-4,6-O-Benzylidene-2,3-dideoxy-2,3-C-methylene-3-nitro-β-*D-erythro-*hexopyranoside (2).* A solution of the ylide was prepared from 440 mg of sodium hydride (over 55% purity), 2.64 g (12 mmol) of trimethyloxosulfonium iodide and 6 ml of DMSO.[11] A solution of 2.93 g (10 mmol) of **1**[12] in 10 ml of DMSO was added with stirring. The mixture was stirred at room temperature for 1 h and poured into 50 ml of cold water. The precipitate was separated and washed with water and recrystallized from ethanol to give 2.3 g (72%) of **2**: Mp 147.5—148.0 °C; $[\alpha]_D^{20}$ −44.2° (*c* 1, $CHCl_3$); IR 1550 (NO_2) cm^{-1}.

Found: C, 58.63; H, 5.74; N, 4.72%. Calcd for $C_{15}H_{17}NO_6$: C, 58.63; H, 5.58; N, 4.56%.

Methyl 4,6-O-Benzylidene-2,3-dideoxy-2-C-[α-(dimethylsulfuranylidene)phenacyl]-3-nitro-β-D-glucopyranoside (3). To a solution of **1** (293 mg, 1 mmol) in distd THF (15 ml) was added dimethylsulfonium phenacylide[13] (270 mg, 1.5 mmol) at 0 °C. The mixture was kept for 18 h, the organic solvent being evaporated. The remaining solid was washed with water and recrystallized from ethanol–acetone to give 383 mg (78%) of yellow-green crystals of **3**: Mp 157—158 °C; $[\alpha]_D^{20}$+28.8° (*c* 1, $CHCl_3$); IR 1555 (NO_2) and 1505 (CO) cm^{-1}.

Found: C, 59.03; H, 5.88; N, 2.82; S, 6.79%. Calcd for $C_{24}H_{27}NO_7S \cdot H_2O$: C, 58.64; H, 5.95; N, 2.85; S, 6.52%.

Methyl 4,6-O-Benzylidene-2,3-dideoxy-2-C-[dimethylsulfuranylidene)ethoxycarbonylmethyl]-3-nitro-β-D-glucopyranoside (4). To a solution of **1** (586 mg, 2 mmol) in distd THF (15 ml) was added dimethylsulfonium ethoxycarbonylmethylide[14] (592mg, 4 mmol) at 0 °C. The mixture was stirred at the same temperature for 4 h, the organic solvent being evaporated. The remaining solid was washed with water and recrystallized from ethanol to give 661.5 mg (75%) of yellow-green crystals of **4**: Mp 165.5—166.0 °C; $[\alpha]_D^{20}$ +39.0° (*c* 1, $CHCl_3$); IR 1615 (COOEt) and 1560 (NO_2) cm^{-1}.

Found: C, 54.34; H, 6.12; N, 3.01; S, 7.24%. Calcd for $C_{20}H_{27}NO_8S$: C, 54.41; H, 6.16; N, 3.17; S, 7.26%.

Methyl 4,6-O-Benzylidene-2,3-dideoxy-3-nitro-2-C-phenacyl-β-D-glucopyranoside (5). A solution of **4** (316 mg, 0.64 mmol) in methanol (20 ml) was hydrogenated in the presence of 10% Pd/C (200 mg). After 17 h, the catalyst was filtered off and the filtrate was evaporated and the residue was recrystallized from ethanol to give 250 mg (94%) of cotton-like, colorless crystals of **5**: Mp 173—174 °C; $[\alpha]_D^{20}$ −27.5° (*c* 1, $CHCl_3$); IR 1685 (CO) and 1550 (NO_2) cm^{-1}.

Found: C, 63.74; H, 5.75; N, 3.65%. Calcd for $C_{22}H_{23}NO_7$: C, 63.91%; H, 5.61; N, 3.39%.

Methyl 4,6-O-Benzylidene-2,3-dideoxy-2-C-ethoxycarbonylmethyl-3-nitro-β-D-glucopyranoside (6). A solution of **4** (441 mg, 1 mmol) in methanol (20 ml) was hydrogenated in the presence of 10% Pd/C (250 mg). After 2 days, the catalyst was filtered off and the filtrate was evaporated. The residue was recrystallized from ethanol to afford 343 mg (90%) of colorless crystals of **6**: Mp 146—146.5 °C; $[\alpha]_D^{20}$ −46.6° (*c* 1, $CHCl_3$); IR 1730 (COOEt) and 1555 (NO_2) cm^{-1}.

Found: C, 56.65; H, 5.84; N, 3.94%. Calcd for $C_{18}H_{23}NO_8$: C, 56.68; H, 6.08; N, 3.67%.

*Methyl (2R,3S)-2,3-C-(1-Benzoylethylidene)-4,6-O-benzylidene-2,3-dideoxy-3-nitro-β-D-*erythro*-hexopyranoside (7).* Dimethylsulfonium α-methylphenacylide (640 mg, 3.3 mmol), prepared according to a similar method to that for the preparation of dimethylsulfonium ethoxycarbonylmethylide, was added to a solution of **1** (879 mg, 3 mmol) in distd THF (20 ml) at room temperature. The mixture was kept for 9 h and the solvent was evaporated, affording crystalline residue, which was recrystallized from ethanol–acetone to give 906 mg (71%) of colorless crystals of **7**: Mp 143—144 °C; $[\alpha]_D^{20}$ −68.0° (*c* 1, $CHCl_3$); IR 1690 and 1675 (CO) and 1550 (NO_2) cm^{-1}.

Found: C, 65.04; H, 5.47; N, 3.12%. Calcd for $C_{23}H_{23}NO_7$: C, 64.93; H, 5.45; N, 3.29%.

*Methyl (2R,3R)-4,6-O-Benzylidene-2-cyano-2,3-C-(ethoxycarbonylmethylene)-2,3-dideoxy-β-D-*erythro*-hexopyranoside (9).* To a solution of **8**[3,4c] (400 mg, 1.47 mmol) in THF (10 ml) was added dimethylsulfonium ethoxycarbonylmethylide (245 mg, 1.66 mmol) at room temperature with stirring. The mixture was stirred for 4 h and the solvent was evaporated to give a syrup, which was washed with water. The NMR spectrum of the crude product revealed the presence of two products at least in an approximately 1.5: 1 ratio. After separation of starting material **8** (40 mg, 10% recovery), the syrup was chromatographed on silica gel (C-300, Wakogel) with benzene to afford 121.5 mg (23%) of **9**, whose NMR spectrum agreed with that of the major product: Mp 129—129.5 °C; $[\alpha]_D^{20}$ −72.3° (*c* 1, $CHCl_3$) IR 2250 (CN) and 1725 (COOEt) cm^{-1}.

Found: C, 63.58; H, 5.98; N, 4.10%. Calcd for $C_{19}H_{21}NO_6$: C, 63.50; H, 5.89; N, 3.90%.

Smell of dimethyl sulfide was detected during the course of column chromatography on silica gel. This suggests that the ylide formed corresponding to **4** was not stable in chromatographic separation.

References

1) Preliminary results: T. Sakakibara, T. Takamoto, R. Sudoh, and T. Nakagawa, *Chem. Lett.*, **1972**, 1219.

2) J. Asunkis and H. Shechter, *J. Org. Chem.*, **33**, 1164 (1968).

3) T. Sakakibara and R. Sudoh, *J. Org. Chem.*, **42**, 1746 (1977), and references cited therein.

4) a) H. H. Baer and W. Rank, *Can. J. Chem.*, **49**, 3192 (1971); b) *ibid.*, **52**, 2257 (1974); c) H. Paulsen and W. Greve, *Chem. Ber.*, **107**, 3013 (1974).

5) An exception is reported; H. H. Baer and F. Kienzle, *J. Org. Chem.*, **34**, 3848 (1969), and explanation for this is presented in Ref. 3.

6) B. M. Trost and L. S. Melvin, Jr., "Sulfur Ylides," Academic Press, New York (1975), pp. 88—91.

7) T. Sakakibara, S. Kumazawa, and T. Nakagawa, *Bull. Chem. Soc. Jpn.*, **43**, 2655 (1970).

8) B. M. Trost and L. S. Melvin, Jr., "Sulfur Ylides," Academic Press, New York (1975), pp. 23—24.

9) J. Casanova, Jr., and Rutolo, Jr., *Chem. Commun.*, **1967**, 1224.

10) T. Takamoto, H. Tanaka, and R. Sudoh, *Chem. Lett.*, **1972**, 1125.

11) E. J. Corey and M. Chaykovsky, *J. Am. Chem. Soc.*, **87**, 1353 (1965).

12) H. H. Baer and T. Neilson, *Can. J. Chem.*, **43**, 840 (1965).

13) B. M. Trost, *J. Am. Chem. Soc.*, **89**, 138 (1967).

14) G. B. Payne, *J. Org. Chem.*, **32**, 3351 (1967).

Stereochemistry of Nucleophilic Addition Reactions. 6. Synthesis of Isoxazoline *N*-Oxide Derivatives from Methyl 4,6-*O*-Benzylidene-2,3-dideoxy-3-nitro-α-D-*erythro*-hex-2-enopyranoside with Some *S*-Ylides[1]

Tohru SAKAKIBARA and Rokuro SUDOH

Department of Chemistry, Faculty of Science, Tokyo Institute of Technology, Ookayama, Meguro-ku, Tokyo 152

(Received October 14, 1977)

In the reactions of dimethyloxosulfonium methylide, dimethylsulfonium ethoxycarbonylmethylide, and dimethylsulfonium phenacylide with the title compound, axial attack predominates over equatorial attack, particularly in the case of dimethylsulfonium phenacylide equatorial attack being no longer observed. Axial attack afforded exclusively 1,4-addition products (isoxazoline *N*-oxide derivatives), whereas equatorial attack gave only 1,2-addition products (cyclopropane and stabilized ylide, respectively). Discussion is given on such high selectivities.

In a previous paper[2] a report was given on the reactions of methyl 4,6-*O*-benzylidene-2,3-dideoxy-3-nitro-β-D-*erythro*-hex-2-enopyranoside with some *S*-ylides, where equatorial attack occurs selectively to give cyclopropane derivatives or new stabilized ylides depending on the ylide used. In order to obtain information on the stereochemistry of Michael type reaction of α-glycoside series,[3] we have carried out the reaction of methyl 4,6-*O*-benzylidene-2,3-dideoxy-3-nitro-α-D-*erythro*-hex-2-enopyranoside (**1**) with *S*-ylides and have found that axial attack predominates over equatorial attack, the former affording 1,4-addition product and the latter 1,2-addition product, exclusively.

Results and Discussion

Treatment of **1** with dimethyloxosulfonium methylide in DMSO at room temperature for 1.5 h afforded a mixture of methyl (2*R*,3*R*)-4,6-*O*-benzylidene-2,3-dideoxy-2,3-*C*-methylene-3-nitro-α-D-*erythro*-hexopyranoside (**2**) and (methyl 4,6-*O*-benzylidene-2,3-dideoxy-α-D-*erythro*-hexopyranosido)[3,2-*c*]isoxazoline *N*-oxide (**3**) in a 1:3.5 ratio as determined by NMR spectroscopy. After separation of **2** by crystallization, compound **3** was isolated by column chromatography on silica gel. The results of elemental analysis of both compounds correspond to the formula $C_{15}H_{17}NO_6$. The cyclopropane structure for **2** was determined from its IR (presence of NO_2 but absence of C=N absorption band) and NMR spectra (presence of cyclopropane ring protons at δ 2.61, 2.18, and 1.98). The configuration of **2** was determined from the value $J_{1,2}$=6.2 Hz[4] and long range coupling ($J_{4,exo}$=1.0 Hz) owing to "W-orientation." The IR spectrum of **3** revealed no absorption band for a nitro but a C=N group (1640 cm^{-1}). The complicated NMR spectrum of **3** due to overlap of ring protons was not completely assigned. However, the structure of **3** was deduced by comparison of its IR and NMR spectra with those of **5** and supported by conversion into hydroxyimino derivative **9**.

Reaction of **1** with dimethylsulfonium ethoxycarbonylmethylide in THF at 0 °C gave a mixture of the stabilized ylide **4** (*ca.* 22%) and isoxazoline *N*-oxide **5** (55%). After separation of crystalline compound **5**, stabilized ylide **4** was separated as a syrup by means of column chromatography on silica gel. Although **4** was not completely purified, the ylide structure for **4** was determined from its IR (the characteristic absorption band of an ester carbonyl group of the ylide species at 1630 cm^{-1} and that of a nitro group at 1560 cm^{-1}) and NMR spectra (two methyl signals for SMe_2 at δ 2.76 and 2.65).[2] Assignment of the *gluco* configuration to **4** was based on the values $J_{1,2}$=3.5, $J_{2,3}$=12.5, and $J_{3,4}$=10 Hz. The structure of **4** was confirmed by desulfurization into methyl 4,6-*O*-benzylidene-2-*C*-(ethoxycarbonylmethyl)-2,3-dideoxy-3-nitro-α-D-glucopyranoside (**6**); $J_{1,2}$=3.1 and $J_{2,3}$=$J_{3,4}$=11.1 Hz. The structure of **5** was determined on the basis of its elemental analysis (molecular formula $C_{18}H_{21}NO_8$) and IR spectra (absence of NO_2 but presence of COOEt and C=N absorption bands at 1720 and 1645 cm^{-1}, respectively). The isoxazoline *N*-oxide structure was supported by the fact that treatment of **5** with triphenylphosphine in boiling benzene for 15 h afforded isoxazoline **7** in 91% yield. Thus with the isoxazoline ring fused at C-2 and C-3, compound **5** should have the *arabino* configuration existing in a boat form or the *ribo* configuration existing in a chair form. The signals of H-1 and H-7 (the ring proton of the isoxazoline nucleus), which overlap, were clearly resolved into two doublets having spacings 6.0 and 7.0 Hz by addition of shift reagent, $Eu(DPM)_3$. The reagent probably undergoes complexation with the *N*-oxide group or the ethoxycarbonyl group, resulting in displacement of the H-7 signal to much lower field than that of the H-1 signal. The value of $J_{1,2}$=6.0 Hz suggests that **5** has the *arabino* configuration existing in a boat form. This was confirmed chemically. Catalytic hydrogenation of **5** over Raney nickel afforded a mixture of two products at least in an approximately 3:1 ratio as determined by NMR spectroscopy, from which the major product **8** was isolated in 35% yield. The IR spectrum revealed the presence of a hydroxyl (3380), an amino (3310), and an ester carbonyl group (1735 and 1700 cm^{-1}). The *altro* configuration of **8** was determined from its coupling-constant data ($J_{1,2}$=0, $J_{2,3}$=1.3, and $J_{3,4}$=3.8 Hz), the values being confirmed with the aid of spin decoupling; irradiation at δ 2.41 (H-2) and at δ 3.49 (H-3).

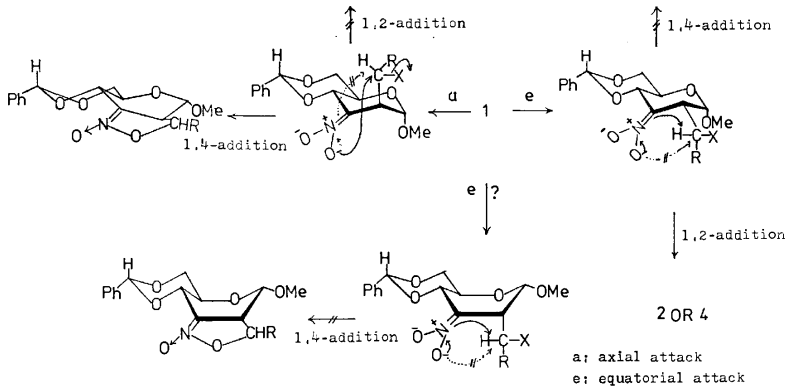

Hydrogenation of **3** and **5** over 10% Pd/C afforded hydroxyimino derivative **9** and **10**, respectively. The results of elemental analysis and IR and NMR spectra fit the hydroxyimino structures.

A similar reaction of **1** with dimethylsulfonium phenacylide in THF at room temperature afforded 5-benzoyl-(methyl 4,6-*O*-benzylidene-2,3-dideoxy-α-D-*erythro*-hexopyranosido)[3,2-*c*]isoxazoline *N*-oxide (**11**) in 89.9% yield, no evidence being detected for formation of stabilized ylide corresponding to **4**.[2] The structure of **11** was deduced by comparison of spectral data with those of **5**. When this reaction was carried out on a larger scale, another product was formed.

The ratio of axial attack, which affords the isoxazoline *N*-oxide **3**, **5**, and **11**, increased according to the sequence $Me_2SOCH_2 < Me_2SCHCOOEt < Me_2SCHCOPh$. The ratios of **5** to **4** were 1.6: 1 in THF at room temperature, 3.2: 1 in THF at 0 °C, and 5.3: 1 in DMSO at 0 °C. The results could be attributed to steric hindrance between incoming ylide and the glycosidic methoxyl group.

In general, conjugate addition of *S*-ylide with carbon-carbon double bond activated by electron-withdrawing substituent(s) gives preferentially a three-membered ring product. However, exceptions are reported, in which an unfavorable five-membered ring product predominates. This is explained in terms of formation of unusually stable cisoid intermediate.[5] However, the intermediary nitronate has no such cis or trans form. Thus, the explanation can not be applied to the observed high selectivity, *i.e.*, axial attack gave the 1,4-addition products, equatorial attack the 1,2-addition products. The following rationalization seems to be likely. If the ylide approaches from the axial side, an intermediary nitronate should have a chairlike transition state in which the carbon atoms at C-3 and C-2 move up and down, respectively, to afford a product. Molecular models indicate that, during this movement interaction between the oxygen atom of the nitro group and the carbon atom (C-7) bearing the sulfur atom is more efficient than that between the C-3 and C-7 carbon atom to give the isoxazoline derivative. On the other hand, when the ylide comes from the equatorial side, the orginal half-chair conformation changes into a boatlike transition state, where the incoming ylide approaches from the stereoelectronically acceptable axial direction. Although the alternative chairlike transition state is unfavorable for stereoelectronic control[6] and $A^{1,3}$ strain,[7] the transition state also seems to be possible because of the favorable anomeric effect.[8] The relationship between C-3 and C-7 in the boatlike transition state resembles that in the chairlike transition state derived by axial attack, indicating the preferred formation of 1,4-adduct. However, experimental results show selective formation of 1,2-addition products. Thus the chairlike transition state even in the case of equatorial attack is more likely, in which the favorable interaction between C-3 and C-7 carbon atoms is predicted by molecular models.

It is noteworthy that epoxidation of **1** with hydrogen peroxide in a weakly alkaline medium exclusively afforded 1,2-addition product, *i.e.*, methyl 2,3-anhydro-4,6-*O*-benzylidene-3-*C*-nitro-α-D-mannopyranoside.[3d] Though in this reaction intermediary nitronate should have a similar structure derived by axial attack of the ylides, molecular models suggest that the C-3 carbon atom is orientated in a more suitable position than the oxygen atom of the nitro group to make the displacement of hydroxide ion take place. Such a difference can be attributed to the shorter bond length of the C–O as compared with the C–C bond.

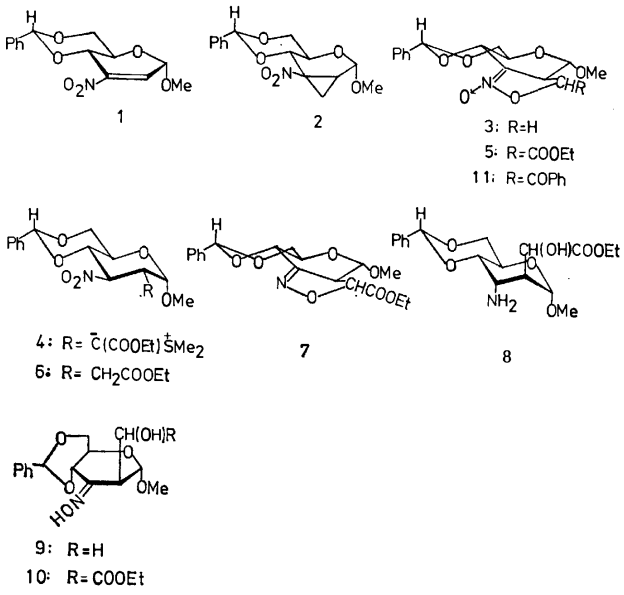

Experimental

Melting points were determined in capillaries and are uncorrected. IR spectra were recorded by use of KBr discs

and NMR spectra were determined with solutions in chloroform-*d* (tetramethylsilane as internal standard) with a JNM-4H-100 (JEOL) spectrometer. Solutions were evaporated under reduced pressure. Column chromatography was performed on silica gel (C-300, Wakogel, Japan).

*Treatment of **1** with Dimethyloxosulfonium Methylide.* To a solutions of dimethyloxosulfonium methylide, prepared from trimethyloxosulfonium iodide (770 mg) and sodium hydride (over 55% purity, 154 mg) in DMSO (7 ml), was added 6 ml of DMSO solution of **1**[9] (1.03 g, 3.5 mmol) at 0 °C. The mixture was kept at 0 °C for 30 min and for 1 h at room temperature and then poured into 70 ml of water. The precipitate was collected and washed with water. Its NMR spectrum revealed that it is a mixture consisting of **2** and **3** in the ratio 1:3.5. Recrystallization from ethanol–diisopropyl ether gave 150 mg of **2**: Mp 131—132 °C; $[\alpha]_D^{20}+35.0°$ (*c* 1, $CHCl_3$); IR 1550 cm^{-1} (NO_2); NMR $\delta=5.81$ (s, 1, PhCH), 5.04 (d, 1, H-1, $J_{1,2}=6.3$ Hz), 4.92 (d, 1, H-4, $J_{4,5}=9.4$, $J_{4,exo}=1.0$ Hz), 4.28 (q, 1, H-6e, $J_{5,6e}=5.0$, $J_{5,6a}=10$ Hz), 3.37 (six, 1, H-5), 3.37 (s, 3, OMe), 2.61 (oct, 1, H-2, $J_{2,exo}=11.3$, $J_{2,endo}=8.1$ Hz), 2.18 (oct, 1, H_{exo}, $J_{exo,\,endo}=6.3$ Hz), and 1.98 (q, 1, H_{endo}).

Found: C, 58.60; H, 5.61; N, 4.44%. Calcd for $C_{15}H_{17}NO_6$: C, 58.63; H, 5.58; N, 4.56%.

The combined mother liquors were evaporated and chromatographed with benzene as eluent. The fast running fraction was **2** (28 mg, total yield 16.5%) and the slow running fraction was **3**, which was recrystallized from ethanol–diisopropyl ether to give 607 mg (56.2%) of **3**: Mp 178.5—179.5 °C; $[\alpha]_D^{20}-139.2°$ (*c* 1, $CHCl_3$); IR 1640 cm^{-1} (C=N); NMR $\delta=5.69$ (s, 1, PhCH), 4.73 (d, 1, H-1, $J_{1,2}=6.0$ Hz), 3.41 (s, 3, OMe), and 4.8—3.8 (7-H).

Found: C, 58.57; H, 5.65; N, 4.57%. Calcd for $C_{15}H_{17}NO_6$: C, 58.63; H, 5.58; N, 4.56%.

*Treatment of **1** with Dimethylsulfonium Ethoxycarbonylmethylide.* To a solution of **1** (293 mg, 1 mmol) in THF (7 ml) was added the ylide (163 mg, 1.1 mmol) at 0 °C. The mixture was kept at 0 °C for 30 min and then at room temperature for 16 h and evaporated. The residue crystallized from ethanol to give 138 mg of **5**: Mp 151.5—152 °C; $[\alpha]_D^{20}-121°$ (*c* 1, $CHCl_3$); IR 1720 (COOEt) and 1645 (C=N) cm^{-1}; NMR $\delta=5.72$ (s, 1, PhCH), 4.95 (d, 1, H-7, $J_{2,7}=7.0$ Hz), 4.89 (d, 1, H-1, $J_{1,2}=6.0$ Hz), 3.45 (s, 3, OMe), 1.31 (t, 3, OEt), and 4.55—3.85 (7-H).

Found: C, 57.32; H, 5.65; N, 3.64%. Calcd for $C_{18}H_{21}NO_8$: C, 56.99; H, 5.58; N, 3.65%.

The mother liquor was evaporated and chromatographed on a column with benzene–ethanol (20:1, v/v) as eluent. The fast running fraction was **5** (70 mg, total yield 55%) and the slow running fraction was a light yellow syrup of **4** (80 mg). Attempts for purification by preparative TLC were unsuccessful. The syrup was hydrogenated without further purification. The syrup (143 mg) was dissolved in methanol and hydrogenated over 10% Pd/C (200 mg). After 2 days the catalyst was removed by filtration. The filtrate was evaporated to give a syrup, which crystallized from ethanol to afford 100 mg (81%) of **6**: Mp 91.5—92.0 °C; $[\alpha]_D^{20}+72°$ (*c* 1, $CHCl_3$); IR 1720 (COOEt) and 1550 (NO_2) cm^{-1}; NMR $\delta=5.55$ (s, 1, PhCH), 4.93 (d, 1, H-1, $J_{1,2}=3.1$ Hz), 4.78 (t, 1, H-3, $J_{2,3}=J_{3,4}=11.3$ Hz), 3.35 (s, 3, OMe), and 1.23 (t, 3, OEt).

Found: C, 56.55; H, 6.01; N, 3.94%. Calcd for $C_{18}H_{23}NO_8$: C, 56.68; H, 6.08; N, 3.67%.

A similar treatment in THF at room temperature or in DMSO (5 ml) at 0 °C for 30 min and then 1 h at room temperature afforded a mixture consisting of **5** and **4** in the ratios 1.6:1 and 5.3:1, respectively, as determined by NMR spectroscopy.

*5-Ethoxycarbonyl-(methyl 4,6-O-benzylidene-2,3-dideoxy-α-D-erythro-hexopyranosido)[3,2-c]isoxazoline (**7**).* To a solution of **5** (57 mg, 0.15 mmol) was added triphenylphosphine (39.3 mg, 0.15 mmol). The mixture was heated under reflux for 15 h and evaporated to give a syrup, which was chromatographed on a column with carbon tetrachloride–ethyl acetate (10:1, v/v) to afford 51 mg of **7**. Recrystallization from ethanol gave 44 mg (81%) of **7**: Mp 159—160 °C; $[\alpha]_D^{20}-120°$ (*c* 0.5, $CHCl_3$); IR 1758 (COOEt) and 1620 (C=N) cm^{-1}; NMR $\delta=5.66$ (s, 1, PhCH), 4.8—4.7 (q, 2. H-1 and H-7, overlap), 3.82 (t, 1, H-6a, $J_{5,6a}=J_{6a,6e}=10$ Hz), 3.42 (s, 3, OMe), and 1.31 (t, 3, OEt).

Found: C, 59.77; H, 5.94; N, 3.98%. Calcd for $C_{18}H_{21}NO_7$: C, 59.49; H, 5.83; N, 3.86%.

*Methyl 3-Amino-4,6-O-benzylidene-2-C-[(ethoxycarbonyl)hydroxymethyl]-2,3-dideoxy-α-D-altropyranoside (**8**).* A solution of **5** (64 mg, 0.17 mmol) in ethyl acetate (10 ml) was hydrogenated in the presence of Raney nickel (80 mg) at room temperature. After 7 days the catalyst was filtered off and washed thoroughly with chloroform. The filtrate was evaporated to give a solid, the NMR spectrum of which showed the presence of two compounds. Recrystallization from acetone afforded 21.7 mg (35%) of **8**. The signals of its NMR spectrum corresponded to those of the major product: Mp 167—168 °C; $[\alpha]_D^{20}+64.2°$ (*c* 1, $CHCl_3$); IR 3380 (OH), 3310 (NH), and 1735 and 1700 (COOEt) cm^{-1}; NMR $\delta=5.62$ (s, 1, PhCH), 4.73 (s, 1, H-1), 4.24 (q, 2, OEt), 4.22 (d, 1, H-7, $J_{2,7}=7.5$ Hz), 3.49 (broad s, 1, H-3, $J_{2,3}=1.3$, $J_{2,4}=3.8$ Hz), 3.36 (s, 3, OMe), 2.41 (broad d, 1, H-2), and 1.30 (t, 3, OEt).

Found: C, 58.75; H, 6.85; N, 3.76%. Calcd for $C_{18}H_{25}NO_7$: C, 58.84; H, 6.86; N, 3.81%.

*Methyl 4,6-O-Benzylidene-2,3-dideoxy-2-C-hydroxymethyl-3-hydroxyimino-α-D-arabinohexopyranoside (**9**).* A solution of **3** (240 mg, 0.78 mmol) in THF (10 ml) was hydrogenated in the presence of 10% Pd/C (200 mg) at room temperature. After 20 h the catalyst was removed by filtration and the filtrate was evaporated to give a white powder. Recrystallization from ethanol gave 176 mg (73%) of **9**: Mp 170.5—171.5 °C; $[\alpha]_D^{20}-68.6°$ (*c* 1, $CHCl_3$); IR 3450 and 3250 (OH) cm^{-1}; NMR $\delta=5.62$ (s, 1, PhCH), 4.73 (d, 1, H-1, $J_{1,2}=4.7$ Hz), 4.52 (q, 1, H-4, $J_{2,4}=1.0$, $J_{4,5}=9.4$ Hz), 3.38 (s, 3, OMe), and 2.90 (m, 1, H-2).

Found: C, 58.34; H, 6.24; N, 4.47%. Calcd for $C_{15}H_{19}NO_6$: C, 58.24; H, 6.19; N, 4.53%.

*Methyl 4,6-O-Benzylidene-2-C-[(ethoxycarbonyl)hydroxymethyl]-2,3-dideoxy-3-hydroxyimino-α-D-arabinohexopyranoside (**10**).* A similar treatment of **5** (139 mg, 0.37 mmol) with 10% Pd/C (100 mg) in THF (10 ml) afforded **10**. Recrystallization from ethanol gave 113 mg (81%) of **10**: Mp 163.5—164.5 °C; $[\alpha]_D^{20}-68.4°$ (*c* 1, $CHCl_3$); IR 3400 (OH) and 1720 (COOEt) cm^{-1}; NMR $\delta=5.58$ (s, 1, PhCH), 4.92 (d, 1, H-1 or H-7, $J_{1,2}=5.6$ or $J_{2,7}=5.6$ Hz), 4.49 (d, 1, H-4, $J_{4,5}=8.8$ Hz), 4.35 (d, 1, H-7 or H-1, $J_{2,7}=3.1$ or $J_{1,2}=3.1$ Hz), 3.75 (t, 1, H-6a, $J_{5,6a}=J_{6a,6e}=9.4$ Hz), 3.40 (s, 3, OMe), 3.34 (q, 1, H-2), and 1.21 (t, 3, OEt).

Found: C, 57.06; H, 6.23; N, 3.55%. Calcd for $C_{18}H_{23}NO_8$: C, 56.68; H, 6.08; 3.67%.

*5-Benzoyl-(methyl 4,6-O-benzylidene-2,3-dideoxy-α-D-erythro-hexopyranosido)[3,2-c]isoxazoline N-Oxide (**11**).* To a solution of **1** (58.6 mg, 0.2 mmol) in THF (3 ml) was added dimethylsulfonium phenacylide (45 mg, 0.25 mmol) at room temperature. The mixture was stirred for 3 h and then poured into ice-water. Extraction with chloroform and evaporation of the solvent afforded a NMR-spectroscopically pure solid (74 mg, 89.9%). Analytical sample was prepared by recrystallization from ethanol: Mp 162.5—163.0 °C; $[\alpha]_D^{20}-227°$ (*c* 1, $CHCl_3$); IR 1705 (COPh) and 1638 (C=N) cm^{-1}; NMR

δ=5.59 (s, 1, PhCH), 5.58 (d, 1, $J_{2,7}$=6.3 Hz), 4.88 (d, 1, H-1, $J_{1,2}$=6.0 Hz), and 3.37 (s, 3, OMe).

Found: C, 64.14; H, 5.21; N, 3.32%. Calcd for $C_{22}H_{21}NO_7$: C, 64.22; H, 5.15; N, 3.40%.

References

1) Preliminary results of this work have been published: T. Sakakibara and R. Sudoh, *J. Chem. Soc., Chem. Commun.*, **1977**, 7.

2) T. Sakakibara, R. Sudoh, and T. Nakagawa, *Bull. Chem. Soc. Jpn*, **51**, 1189 (1978).

3) a) T. Sakakibara and R. Sudoh, *J. Org. Chem.*, **40**, 2823 (1975); b) T. Sakakibara and R. Sudoh, *Carbohydr. Res.*, **50**, 191 (1976); c) *ibid*, **58**, 31 (1977); d) H. H. Baer and W. Rank, *Can. J. Chem.*, **49**, 3192 (1971); e) *ibid*, **52**, 2257 (1974).

4) E. L. Albano, D. Horton, and J. H. Lauterbach, *Chem. Commun.*, **1968**, 357; W. Meyer zu Reckendorf and U. Kamprath-Scholtz, *Angew. Chem.*, **1968**, 152.

5) B. M. Trost and L. S. Melvin, Jr., "Sulfur Ylides," Academic Press, New York (1975), pp. 77—107.

6) E. L. Eliel, N. L. Allinger, S. J. Angyal, and G. A. Morrison, "Conformational Analysis," Interscience, New York N. Y. (1965), pp 307—317; E. Toromanoff, *Top. Stereochem.*, **2**, 157 (1969).

7) F. Johnson, *Chem. Rev.*, **68**, 375 (1968).

8) P. L. Durette and D. Horton, *Adv. Carbohydr. Chem. Biochem.*, **26**, 49 (1971).

9) H. H. Baer and F. Kienzle, *Can. J. Chem.*, **45**, 983 (1967).

The Effect of Macrocyclic Polyethers on the Alkylation of Sodium 2-Naphtholate

Sadatoshi AKABORI and Hiroyuki TUJI

Department of Chemistry, Faculty of Science, Tōho University, Funabashi, Chiba 274

(Received October 18, 1977)

The alkylation of sodium 2-naphtholate, in the presence of benzo-18-crown-6 or 4,7,13,16,21,24-hexaoxabicyclo[8.8.8]hexacosane is found to give high ratios of $O/O+C$ alkylation when conducted in THF, in benzene, and in water. The striking increase in the product ratio is attributed to a specific complexation of the macrocyclic polyethers, which facilitate the dissociation of the ion-pair aggregate of the sodio-derivative which exists in benzene or THF. The polyethers may act as phase-transfer catalysts when the reaction is run in water. In support of this conclusion, the reaction in DMF or acetonitrile, in which the dissociation of sodium 2-naphtholate takes place, fails to show any effect of the macrocyclic polyethers on the product ratio.

It is well known[1] that the 2-naphthoxide ion is an ambident anion capable of forming a covalent bond at either the oxygen or carbon atom on alkylation. Kornblum *et al.*[2] found that, whereas sodium 2-naphtholate (I) could be alkylated with benzyl bromide, propyl bromide, and methyl iodide, the solvent plays a decisive role in determining the reaction course of the ambident anion. For example, when sodium 2-naphtholate is treated with benzyl bromide in a dimethyl sulfoxide solution, benzyl 2-naphthyl ether (II) is produced in a 95% yield, whereas in water the main product is 1-benzyl-2-naphthol (III) (84% yield).

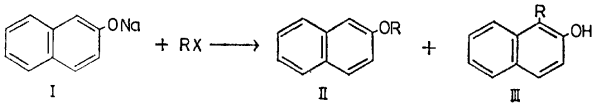

I II III

In recent years it has been generally accepted that quaternary ammonium halides and crown ethers can be used as phase-transfer catalysts[3] in two-phase ionic reactions. In addition, crown ethers possess a unique ability to fill the coordination sites of cations[4] and to convert contact ion-pairs into separated ions.[5] The combination of these two effects may affect the alkylation of sodium 2-naphtholate in a serious manner. Therefore, we have investigated the effect of benzo-18-crown-6 (IV) and 4,7,13,16,21,24-hexaoxabicyclo-[8.8.8]hexacosane (V)[6] on the reaction of alkyl and benzyl halides with sodium 2-naphtholate in various solvents.

Results and Discussion

The following reactions of sodium 2-naphtholate with benzyl and alkyl halides were run in several solvents with or without added macrocyclic polyethers (IV and V). The reactions were carried out by stirring sodium 2-naphtholate in a given solvent with benzyl bromide in the presence or absence of a small quantity of a macrocyclic polyether (IV or V). After the usual work-up, the products were analyzed by GLC.

We first investigated the homogeneous benzylation of sodium 2-naphtholate in aprotic solvents with relatively high or low dielectric constants. The yields of the *O*- and *C*-alkylation products are listed in Table 1 (Runs 10—15). As the data show, the reaction of benzyl

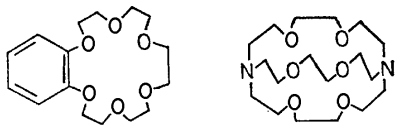

IV V

bromide with sodium 2-naphtholate in DMF and acetonitrile yields the *O*-alkylation product, whereas in the THF solvents, which have relatively a low dielectric constant, the *C*-alkylation occurs to a substantial extent. The addition of IV or V to the reaction mixture did not affect the product ratio in acetonitrile and DMF, but caused a remarkable increase in the ratios of *O*-alkylation to *C*-alkylation for the reaction in THF. In THF, sodium 2-naphtholate exists as ion pairs and higher aggregates.[2] Therefore, in the reaction of sodium 2-naphtholate with benzyl bromide (Run 4), the $O/O+C$ alkylation product ratio is rather low;[2] however, in the presence of IV or V (Runs 5 and 6) a reaction under similar conditions gave a high yield of the ether (II), together with a small % of the *C*-alkylation product. In this reaction, clearly, the ion-pair separating ability of the macrocyclic polyether accounts for this dramatic effect; it is known[5,7] that an equimolar amount of a crown ether suffices to convert ion-pairs into separated ions. In contrast, in a solvent with a high dielectric constant, such as acetonitrile or DMF, it is conceivable that the alkylation reaction involves free 2-naphthoxide ions (or loose ion pairs). Therefore, the polyethers fail to affect the products of alkylation.

Phase-transfer Reactions. The results are summarized in Table 1 (Runs 1—3 and 7—9). While it was difficult for the reaction of benzyl bromide with sodium 2-naphtholate to proceed in benzene (Runs 7—9), it proceeded smoothly in the presence of V to afford alkylation products totalling a 77% yield, showing that V was effective in solubilizing sodium 2-naphtholate in benzene. In the absence of the macrocyclic polyether, because of the low solubility of sodium 2-naphtholate in benzene and the low dielectric constant of benzene, a heterogeneous (solid-liquid) reaction occurred to give 1-benzyl-2-naphthol in a low yield as the main product. This result was consistent with the observation by Kornblum[8] that the heterogeneous alkylation of sodium phenolate proceeded through the

Table 1. Reaction of alkyl halides with sodium 2-naphtholate[a)]

Run No.	Alkyl halide	Solvent	Catalyst	Reaction time (h)	Products (%)		$\frac{O}{O+C}$ ratios
					O-Alkylated	*C*-Alkylated[b)]	
1	$PhCH_2Br$	H_2O		24	12	73	0.14
2	$PhCH_2Br$	H_2O	IV	24	60	18	0.77
3	$PhCH_2Br$	H_2O	V	24	77	8	0.91
4	$PhCH_2Br$	THF		24	51	30	0.63
5	$PhCH_2Br$	THF	IV	24	65	2	0.97
6	$PhCH_2Br$	THF	V	24	73	1	0.99
7	$PhCH_2Br$	C_6H_6		24	1	9	0.10
8	$PhCH_2Br$	C_6H_6	IV	24	58	12	0.83
9	$PhCH_2Br$	C_6H_6	V	24	76	1	0.99
10	$PhCH_2Br$	DMF		2	87	0	1.00
11	$PhCH_2Br$	DMF	IV	2	89	0	1.00
12	$PhCH_2Br$	DMF	V	2	90	0	1.00
13	$PhCH_2Br$	CH_3CN		42	63	4	0.94
14	$PhCH_2Br$	CH_3CN	IV	42	60	4	0.94
15	$PhCH_2Br$	CH_3CN	V	42	58	3	0.95
16	CH_3I	H_2O		48	27	15	0.64
17	CH_3I	H_2O	IV	48	65	10	0.87
18	CH_3I	H_2O	V	48	97	3	0.97
19	CH_3I	THF		3	79	8	0.91
20	CH_3I	THF	IV	3	94	4	0.96
21	CH_3I	THF	V	3	51	4	0.93
22	CH_3I	C_6H_6		120	0	0	
23	CH_3I	C_6H_6	IV	120	14	10	0.58
24	CH_3I	C_6H_6	V	120	7	6	0.54
25	CH_3I	CH_3CN		3	86	9	0.91
26	CH_3I	CH_3CN	IV	3	87	8	0.92
27	CH_3I	CH_3CN	V	3	71	6	0.92
28	CH_3I	DMF		3	90	0	1.00
29	CH_3I	DMF	IV	3	89	0	1.00
30	CH_3I	DMF	V	3	91	0	1.00

a) All the reactions were conducted at 25 °C. b) This yield includes any alkylated products arising from the further alkylation of 1-benzyl-2-naphthol or 1-methyl-2-naphthol.

C-alkylation process. In contrast, in the presence of IV or V, the reactivity of the oxygen site became enhanced relative to that of the carbon site of the ambident anion: these results may be interpreted by thinking that sodium 2-naphtholate is solubilized in a benzene solution to produce highly reactive naked anions to cause a reaction with benzyl bromide in the homogeneous phase. Obviously the crown ether functioned as a solid-liquid phase-transfer agent. The most pronounced effect on the ratio of *O*-alkylation to *C*-alkylation was found in water. The reaction of an aqueous solution of sodium 2-naphtholate with benzyl bromide in the absence of IV or V gave a 12% yield of the *O*-alkylation product (II) and a 73% yield of the *C*-alkylation product. The explanation for this result is that strong proton donors such as water in the absence of IV or V solvated the anionic oxygen atom and thereby suppressed the *O*-alkylation. In sharp contrast, in the presence of IV or V in water, the $O/O+C$ ratios of the alkylation products markedly increased. When IV or V was added to the reaction mixture, the ambident anion produced in water could be transported into the organic layer (benzyl bromide) as a loosely separated ion pair, with a cryptated cation as an escort; the *O*-alkylation now occurred. The results are completely consistent with a phase-transfer mechanism.[9] Similar results were found in the reactions of sodium 2-naphtholate with methyl iodide in aprotic solvents and water.

Experimental

Analysis. The products were generally analyzed on a Hitachi 023 gas chromatograph equipped with a flame-ionization detector with a 1 m×3 mm column packed with 60—80 mesh Chromosorb W (washed with acid and treated with dimethyldichlorosilane) and coated with 20% Carbowax 20 M (for the analysis of benzylated products at *ca.* 240 °C) or with a 3 m×3 mm column packed with 80—100 mesh Chromosorb W (washed with acid and treated with dimethyldichlorosilane) and coated with 3% Silicone OV-17 (for the analysis of methylated products at *ca.* 210 °C).

Materials. Benzo-18-crown-6[4] and 4,7,13,16,21,24-hexaoxa-1,10-diazabicyclo[8.8.8]hexacosane[6] were prepared according to the procedures described in the literature. Authentic samples (1-benzyl-2-naphthol,[10] benzyl 2-naphthyl ether,[2] 1,1-dibenzyl-2-naphthalenone,[11] 1-methyl-2-naphthol,[12] methyl 2-naphthyl ether,[2] and methyl 1-methyl-2-naphthyl ether[2]) were also prepared according to the procedures

described in the literature. The sodium 2-naphtholate was prepared as has been described by Kornblum *et al.*,[2] while the alkyl halides (commercial samples) were used directly provided that the physical constants agreed with the reported values. The solvents used were purified by distillation.

General Procedure. The typical procedures for the reaction of alkyl halides with sodium 2-naphtholate are as follows.

Reaction of Benzyl Bromide with Sodium 2-Naphtholate. In Water: A magnetic stirring bar was placed in a 10-ml vial, after which sodium 2-naphtholate (1.06 mmol), benzo-18-crown-6 (0.3 mmol), and 4 ml of water were introduced. The mixture was stirred for 0.5 h at 25 °C. Benzyl bromide (1.2 mmol) was then added all at once, after which the mixture was stirred for a further 2.5 h. The resulting mixture was poured into 10 ml of water, acidified with 18% hydrochloric acid at 0 °C, and extracted with benzene four times. The extracts were combined and concentrated to a 5-ml volume. GLC analyses revealed the presence of four components, which were identified as 2-naphthol (17%), benzyl 2-naphthyl ether (60%), 1-benzyl-2-naphthol (9%), and 1,1-dibenzyl-2-naphthalenone (9%); the relative retention times of these components were 1.00: 2.11: 9.00: 16.6.

In Tetrahydrofuran: A mixture of sodium 2-naphtholate (0.92 mmol), benzo-18-crown-6 (0.2 mmol), and 4 ml of THF was stirred for 30 min at 25 °C. Benzyl bromide (1.0 mmol) was added all at once, after which the mixture was stirred for a further 65 h. The work-up and analysis were performed as has been described above. The analysis by GLC revealed the presence of 2-naphthol (25%), benzyl 2-naphthyl ether (65%), 1-benzyl-2-naphthol (1%), and 1,1-dibenzyl-2-naphthalenone (1%).

Reaction of Methyl Iodide with Sodium 2-Naphtholate. In Tetrahydrofuran: A mixture of sodium 2-naphtholate (6.01 mmol), benzo-18-crown-6 (0.32 mmol), and 10 ml of anhydrous THF was stirred for 30 min at 25 °C. Methyl iodide (7.2 mmol) was then added all at once, after which the mixture was stirred for a further 20 h. The resulting mixture was poured into 20 ml of water, acidified with 18% aq hydrochloric acid, and extracted with benzene. The benzene extract was washed with 10% aqueous sodium hydroxide and with water. Analysis by GLC identified the neutral fraction as consisting of methyl 2-naphthyl ether (94%) and methyl 1-methyl-2-naphthyl ether (4%); the relative retention times of these two components were 1.00: 2.26. The alkali and water extracts were combined and acidified with 18% aq hydrochloric acid at 0 °C, and then extracted with benzene. The subsequent analysis of the product by GLC indicated the presence of 2-naphthol (1%) and 1-methyl-2-naphthol (1%), whose retention times were 1.26 times that of 2-naphthol.

In Water: A mixture of sodium 2-naphtholate (6.01 mmol), benzo-18-crown-6 (0.32 mmol), and 10 ml of water was stirred for 30 min at 25 °C. Methyl iodide (7.2 mmol) was then added all at once, after which the mixture was stirred for a further 48 h. The work-up and analysis were performed as has been described above.

The authors wish to express their gratitude to Professor Michinori Ōki, the University of Tokyo, for his valuable discussion and suggestions.

References

1) For example, J. March, "Advanced Organic Chemistry. Reactions, Mechanisms, and Structure," McGraw-Hill, New York (1968), p. 298.
2) N. Kornblum, R. Seltzer, and P. Haberfield, *J. Am. Chem. Soc.*, **85**, 1148 (1963).
3) E. V. Dehmlow, "New Synthetic Methods," Vol. 1, Verlag Chemie (1975), p. 18.
4) C. J. Pedersen, *J. Am. Chem. Soc.*, **89**, 7017 (1967).
5) K. H. Wong, G. Konizer, and J. Smid, *J. Am. Chem. Soc.*, **92**, 666 (1970).
6) B. Dietlich, J. M. Lehn, and J. P. Sauvage, *Tetrahedron Lett.*, **1969**, 2885, 2889.
7) J. Amly, D. C. Garwood, and D. J. Cram, *J. Am. Chem. Soc.*, **92**, 4321 (1970); J. N. Roitan and D. J. Cram, *J. Am. Chem. Soc.*, **93**, 2231 (1971).
8) N. Kornblum and A. P. Lurie, *J. Am. Chem. Soc.*, **81**, 2705 (1959).
9) C. M. Starks, *J. Am. Chem. Soc.*, **93**, 195 (1971).
10) L. Claisen, *Ann.*, **442**, 243 (1925).
11) D. Y. Curtin, R. C. Tuites, and D. H. Dybvig, *J. Org. Chem.*, **25**, 155 (1960).
12) K. Fries and E. Hubner, *Ber.*, **39**, 442 (1906).

Photolyses of *S,S*-Dimethyl-*N*-(ethoxycarbonyl)sulfimide in Hydrocarbons and in Oxygen Compounds

Noboru TORIMOTO, Tadao SHINGAKI,* and Toshikazu NAGAI*

Science Education Institute of Osaka Prefecture, Karita-cho, Sumiyoshi-ku, Osaka 558

**College of General Education, Osaka University, Toyonaka, Osaka 560*

(Received October 19, 1977)

The behavior of ethoxycarbonylnitrene (**3**), generated photochemically from *S,S*-dimethyl-*N*-(ethoxycarbonyl)-sulfimide (**1**), upon insertion into the C–H bonds and the O–H bonds was compared with that of **3** generated from ethyl azidoformate (**2**). Ethoxycarbonylnitrene generated from **1** was inserted preferentially into the α C–H bonds of cyclic ethers. The relative reactivity toward **3** of the primary, secondary, and tertiary C–H bonds in 2,4-dimethylpentane is in the ratio of 1 : 9 : 35. The insertion of **3** into the tertiary C–H bonds of *cis*- and *trans*-1,4-dimethylcyclohexanes proceeded stereospecifically. The reaction of **3** with alcohols gave the O–H insertion products. These results show that the insertion of **3** generated from **1**, as well as that of the nitrene from **2**, into the hydrocarbon C–H bonds and the O–H bonds proceeds only for the singlet.

The decomposition of some amidates or sulfimides is known to be a method of generating a nitrene intermediate. For example, *N*-trimethylammoniododecanesulfonamidate was thermolyzed to give a sulfonylnitrene,[1] *S,S*-dimethyl-*N*-benzoylsulfimide was photolyzed to give benzoylnitrene,[2] and *S,S*-dimethyl-*N*-(ethoxycarbonyl)-sulfimide was photolyzed to give ethoxycarbonylnitrene.[3] Ethoxycarbonylnitrene, generated by the photolysis of *S,S*-dimethyl-*N*-(ethoxycarbonyl)sulfimide (**1**),[3] gave a product distribution similar to that resulting photochemically from the azide[4] in the reaction with cyclohexene. On the other hand, the nitrene from **1** was produced largely (more than 50%) in triplet form,[3] although the photodecomposition of the azide showed that one-fourth of the nitrene formed was in the triplet state,[4] in addition to *cis*- and *trans*-4-methyl-2-pentenes. As for C–H insertion, ethoxycarbonylnitrenes, generated by the photochemical[5] and thermal[6] decompositions of ethyl azidoformate or by the α-elimination of *N*-(*p*-nitrophenylsulfonyloxy)urethane,[5] showed nearly the same regioselectivities. It has not been reported, however, whether or not the ethoxycarbonylnitrene generated from the ylide shows, on insertion into C–H bonds, behavior similar to that of the nitrene generated from the other precursors.

In this paper, the regioselectivity and the stereospecificity of **3** derived from the precursors **1** and ethyl azidoformate (**2**) in the insertion into C–H bonds will be described.

Results and Discussion

Photolysis of 1 in Hydrocarbons and in Ethers. A solution of *N*-carbethoxyiminodimethylsulfurane (**1**) in cyclic ether or in a mixture of hydrocarbon and 1,2-dichloroethane was irradiated by the light (mainly 2537 Å) of a low-pressure mercury arc at 0 °C with stirring under an atmosphere of nitrogen. The insertion products (**4**) of **3** into the C–H bonds were obtained, accompanied by an abstraction product, urethane. The yields are listed in Table 1.

The insertion took place preferentially at the C–H bonds of the α-position of the ethers. The preferential formation of the α C–H insertion products in the ethers was also observed in the photolyses of **2**.[7–9] The reaction with 2,4-dimethylpentane gave three isomeric insertion products, resulting from an attack on all the primary (1°), secondary (2°), and tertiary (3°) C–H bonds.

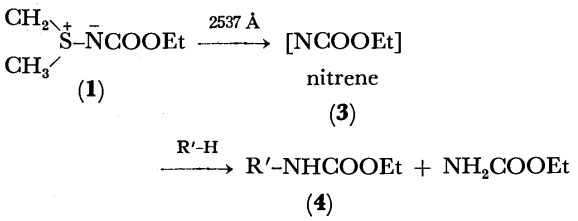

(**1**) (**3**) (**4**)

(R′: hydrocarbon residue or ether residue)

Relative Reactivity. From the yields of the insertion products of **1** with 2,4-dimethylpentane, the relative reactivities of the 1, 2, and 3° C–H bonds toward **3** was calculated to be in the ratio of 1 : 9 : 35. On the other hand, **3**, generated by the photolysis of **2**, reacted with the 1, 2, and 3° C–H bonds of 2-methylbutane in the ratio of 1 : 9 : 34.[4] The values resulting from these two experiments are in remarkably good agreement, though the substrate hydrocarbons employed are not the same.

Stereochemistry. In order to investigate the stereospecificity in the C–H insertion of **3**, generated from **1**, **1** was photolyzed in *cis*- and *trans*-1,4-dimethylcyclohexanes. The results are displayed in Table 2, compared with those of **3** generated from **2**.[10]

The reaction of **3** generated from **1** with either *cis*- or *trans*-1,4-dimethylcyclohexane gave only one tertiary urethane, accompanied by urethane and two kinds of secondary urethanes; the reaction was virtually completely stereospecific. In this respect, it has the same tendency as the reaction of **3** generated from **2**.[10] Therefore, the results show that the ethoxycarbonylnitrene generated from **1** is inserted into the C–H bonds of hydrocarbon only in the singlet state, like the nitrene from the azide.

Dilution Effect. It is well known that, in the nitrene reaction, dilution with such inert solvents as dichloromethane and dibromomethane promotes the singlet-triplet intersystem crossing of nitrenes. For example, cyanonitrene, generated thermally from cyanogen azide, was inserted stereospecifically into the C–H bonds of *cis*- and *trans*-1,2-dimethylcyclohexanes in

Table 1. Photolysis of **1** in hydrocarbons and in ethers

Substrate	Product (%)[a]	
	4	H_2NR[b]
(**a**)	(**a**) 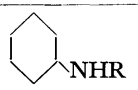	
	18.1	27.0
	(**b$_1$**) $(CH_3)_2CCH_2CH(CH_3)_2$ (NHR)	
(**b**) $(CH_3)_2CHCH_2CH(CH_3)_2$	14.1	
	(**b$_2$**) $(CH_3)_2CHCHCH(CH_3)_2$ (NHR)	71.4
	3.6	
	(**b$_3$**) $(CH_3)_2CHCH_2CHCH_3$ (CH_2NHR)	
(**c**)	2.4	
	(**c**) 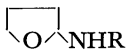	
	23.8	27.6
(**d**)	(**d**) 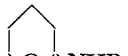	
	20.0	39.5
(**e**)	(**e**) 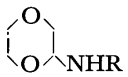	
	24.1	7.5

a) Calculated on the basis of the ylide used. b) R: $COOC_2H_5$

Table 2. Photolysis of **1** in 1,4-dimethylcyclohexanes

Mole ratio	Product (%)[a]			
	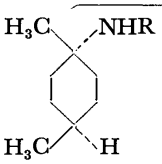 (*cis*-**4**)	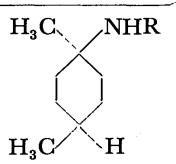 (*trans*-**4**)	*cis*-**5**[c] or *trans*-**5**[c]	H_2NR[b]
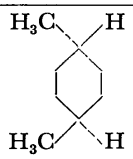 $C_2H_4Cl_2$ *trans*				
1 : 2	ND[d]	13.1	16.3	34.5
	(ND)	(11.0)	(11.7)	(16.0)
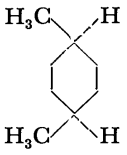 *cis*				
1 : 2	8.4	ND	8.7	27.7
1 : 4	5.2	ND	5.0	37.3
1 : 20	3.9	ND	4.8	80.4
	(14.0)	(ND)	(12.8)	(18.0)

( ) Indicates the values resulting from the photolysis of **2** without dilution.[10] a) b) See Table 1, footnotes. c) Total yields of the secondary urethanes. d) ND: not detected.

the absence of the inert solvents. However, the insertion of the nitrene with the cyclohexanes diluted with the inert solvents proceeded non-stereospecifically, giving a mixture of *cis* and *trans* isomeric products.[11] That is, triplet cyanonitrene, produced from the decay of a singlet, is also inserted into the C–H bonds of hydrocarbons. On the other hand, the insertion of ethoxycarbonylnitrene, generated by the photochemical and the thermal decompositions of the azide or by the α-elimination of *N*-(*p*-nitrophenylsulfonyloxy)urethane, proceeded completely stereospecifically toward the C–H bond of optically active 3-methylhexane diluted with dichloromethane.[12]

As can be seen in Table 2, the insertion of **3** into the tertiary C–H bond proceeded completely stereospecifically, even at about a 5 mol % dilution with 1,2-dichloroethane. Therefore, it may be concluded that the ethoxycarbonylnitrene generated from *S,S*-dimethyl-*N*-(ethoxycarbonyl)sulfimide behaves just like those generated from the other precursors in stereochemistry as well as in the selectivity of the insertion into the C–H bonds of hydrocarbons, and that triplet ethoxycarbonylnitrene, unlike triplet cyanonitrene, can not be inserted into C–H bonds. The difference in behavior between the triplet ethoxycarbonyl and cyano-nitrenes may be explained as follows: the HN̈CN radical, produced through hydrogen abstraction by the triplet nitrene, is much more resonance-stabilized than the HN̈COOEt radical, permitting combination with the radicals derived from substrates.

Table 3. Photolysis of **1** and **2** in alcohols

Alcohol	Product (%)[a]					
	Insertion into O–H bond			Abstraction (H_2NR^b)		
	1	**2**		**1**	**2**	
		Direct	Sensitized		Direct	Sensitized
C_2H_5OH	9.1	11.0	ND[c]	63.0	71.0	64.6
n-C_3H_7OH	11.0	15.0	ND	61.8	46.0	80.5
n-C_4H_9OH	6.2	27.0	ND	52.4	47.0	74.9

a) b) See Table 1, footnotes. c) ND: not detected.

*Photolysis of **1** in Alcohols.* The behavior toward alcohols of the **3** generated from **1** was similar to that of the **3** derived by the direct photolysis of **2**, although the insertion-abstraction ratio decreased in the present precursor (**1**) compared with that in the **2** precursor, as is shown in Table 3. The photolyses of **1**, as well as the direct photolyses of **2**, gave products for nitrene insertion into the O–H bonds, while the sensitized photolyses gave no such insertion products.[8] The insertion in the direct photolyses has been concluded to proceed *via* the formation of O–N ylide intermediate resulting from the singlet nitrene.[8] Consequently, the O–H insertion in the photolyses of **1** is also thought to involve O–N ylide formation, as is shown in the following scheme:

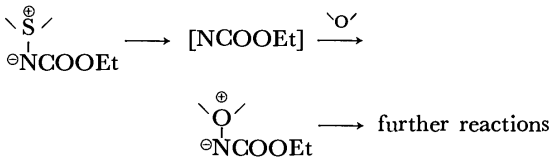

Scheme 1.

Experimental

The equipment and techniques have been described previously.[7]

Materials. The preparation of *cis*- and *trans*-1,4-dimethylcyclohexanes has been described previously.[13] The *S,S*-dimethyl-*N*-(ethoxycarbonyl)sulfimide (**1**) was prepared by the method of Whitfield *et al.*[14] The tetrahydrofuran, tetrahydropyran, 1,4-dioxane, cyclohexane, 2,4-dimethylpentane, 1,2-dichloroethane, ethanol, 1-propanol, and 1-butanol were used after the commercial reagents had been purified according to the published directions.[16]

Authentic Samples. The preparation of authentic samples of *N*-cyclohexylurethane (**4a**), *N*-(*cis*-1,4-dimethylcyclohexyl)urethane (*cis*-**4**), and *N*-(*trans*-1,4-dimethylcyclohexyl)urethane (*trans*-**4**) has been described previously.[13] The authentic samples of *N*-(1-isopropyl-2-methylpropyl)-urethane (**4b**$_2$) and *N*-(2,4-dimethylpentyl)urethane (**4b**$_3$) were prepared from ethyl chloroformate and the corresponding amines, which was themselves previously been prepared by the method of Breslow.[15] **4b**$_2$: IR (neat, cm^{-1}): 3350 (NH), 1710 (C=O), 1250 (C–O). NMR (CCl_4, τ): 5.42 (NH, 1H, bs), 5.95 (OCH_2, 2H, q), 6.51—7.02 (NCH, 1H, m), 7.93—8.60 (2CH, 2H, m), 8.78 (ester-CH_3, 3H, t), 9.09 ($2CH_3$, 6H, d), 9.14 ($2CH_3$, 6H, d). **4b**$_3$: IR (neat, cm^{-1}): 3350 (NH), 1710 (C=O), 1255 (C–O). NMR (CCl_4, τ): 5.10 (NH, 1H, bs), 6.00 (OCH_2, 2H, q), 6.92—7.27 (NCH_2, 2H, m), 8.04—9.02 (2CH and CH_2, 4H, m), 8.81 (ester-CH_3, 3H, t), 9.13 (CH_3, 3H, d), 9.16 ($2CH_3$, 6H, d).

*Photolyses of **1** in Hydrocarbons and in Ethers.* A solution of **1** (450 mg, 3 mmol) in ethre (0.6 mol) or in a mixture of hydrocarbon (0.4 mol) and 1,2-dichloroethane (19.8 g, 0.2 mol) was irradiated by the light (mainly 2537 Å) of a low-pressure mercury arc at 0 °C with stirring under an atmosphere of nitrogen untill the NMR signal at τ 7.30 due to the *gem*-dimethyl group of **1** has disappeared. Then, the excess substrate was evaporated under reduced pressure and the residue was analyzed by VPC.

In Hydrocarbons: In cyclohexane, **4a** (95 mg) was isolated. In 2,4-dimethylpentane, *N*-(1,1,3-trimethylbutyl)urethane (**4b**$_1$, 79 mg), **4b**$_2$ (20 mg), and **4b**$_3$ (13 mg) were isolated. **4b**$_1$: IR (neat, cm^{-1}): 3350 (NH), 1710 (C=O), 1260 (C–O). NMR (CCl_4, τ): 5.49 (NH, 1H, bs), 6.05 (OCH_2, 2H, q), 8.02—8.60 (CH and CH_2, 3H, m), 8.77 ($2CH_3$, 6H, s), 8.83 (ester-CH_3, 3H, t), 9.10 ($2CH_3$, 6H, d). Found: C, 63.98; H, 11.26; N, 7.35%. Calcd for $C_{10}H_{21}O_2N$: C, 64.13; H, 11.30; N, 7.48%. The IR and the NMR spectral data and VPC retention times of **4a**, **4b**$_2$, and **4b**$_3$ were identical with those of the authentic samples. In *cis*-1,4-dimethylcyclohexane, *cis*-**4** (50 mg) and a mixture of two kinds of secondary urethanes (*cis*-**5**, 52 mg) were isolated. The mixture of the secondary urethanes did not separate into two parts on the columns employed. The IR and the NMR spectral data and the VPC retention time of *cis*-**4** were identical with those of the authentic sample. *N*-(*cis*-2,5-Dimethylcyclohexyl)urethane (*cis*-**5**, a mixture of the isomers): IR (neat, cm^{-1}): 3320 (NH), 1700 (C=O), 1240 (C–O). NMR (CCl_4, τ): 5.2 (NH), 5.76 (OCH_2), 7.50—9.23 (ring-CH and

CH_2, ring-side CH_3, ester-CH_3). Found: C, 65.99; H, 10.48; N, 6.98%. Calcd for $C_{11}H_{21}O_2N$: C, 66.29; H, 10.62; N, 7.03%. In *trans*-1,4-dimethylcyclohexane, *trans*-**4** (66 mg) and two kinds of secondary urethane (*trans*-$\mathbf{5}_1$ and *trans*-$\mathbf{5}_2$, 70 mg), which were subsequently cleanly separated into individual isomers by VPC, were isolated. The analytical data of *trans*-**4** were identical with those of the authentic sample. One isomer of *N*-(*trans*-2,5-dimethylcyclohexyl)urethanes (*trans*-$\mathbf{5}_1$): IR (neat, cm^{-1}): 3350 (NH), 1700 (C=O), 1240 (C–O). NMR (CCl_4, τ): 5.22 (NH, 1H, bs), 5.86 (OCH_2, 2H, q), 7.93—9.30 (ring-CH and CH_2, 9H, m), 8.73 (ester-CH_3, 3H, t), 9.07 ($2CH_3$, 6H, d). Found: C, 66.11; H, 10.49; N, 7.10%. The other (*trans*-$\mathbf{5}_2$): IR (neat, cm^{-1}): 3320 (NH), 1690 (C=O), 1270 (C–O). NMR (CCl_4, τ): 5.20 (NH, 1H, bs), 5.86 (OCH_2, 2H, q), 7.60—9.36 (ring-CH and CH_2, 9H, m), 8.74 (ester-CH_3, 3H, t), 9.05 ($2CH_3$, 6H, d). Found: C, 66.41; H, 10.58; N, 6.09%.

In Ethers: In tetrahydrofuran, tetrahydropyran, and 1,4-dioxane, *N*-(2-tetrahydrofuryl)urethane (**4c**, 113 mg), *N*-(2-tetrahydropyranyl)urethane (**4d**, 104 mg), and *N*-(1,4-dioxan-2-yl)urethane (**4e**, 126 mg) were isolated respectively. The IR and the NMR spectral data of **4c**, **4d**, and **4e** have been given in previous papers.[7,8]

In cis-*1,4-Dimethylcyclohexane Diluted with Dichloroethane*: The reaction of **1** (450 mg, 3 mmol) in a solation of *cis*-1, 4-dimethylcyclohexane (14 g, 0.12 mol) and 1,2-dichloroethane (48 g, 0.48 mol) gave 31 mg of *cis*-**4** and 30 mg of *cis*-**5**. When a solution of 0.03 mol of *cis*-1,4-dimethylcyclohexane and 0.6 mol of 1,2-dichlroethane were used, the reaction gave 23 mg of *cis*-**4** and 29 mg of *cis*-**5**.

Photolyses of **1** *in Alcohols*. A solution of **1** (3 mmol) in alcohol (0.6 mol) was irradiated by the light (mainly 2537 Å) of a low-pressure mercury arc at 0 °C with stirring in an atmosphere of nitrogen. The reaction mixture was treated by the procedures described for the reaction in hydrocarbons and in ethers.

In ethanol, 1-propanol, and 1-butanol, *N*-ethoxyurethane (36 mg), *N*-propoxyurethane (48 mg), and *N*-butoxyurethane (30 mg) were isolated respectively. The IR and the NMR spectral data and elemental analyses of these products have been given in a previous paper.[8]

The authors are particulary indebted to Dr. Hisao Arakawa and Dr. Akira Matsumoto of the Science Education Institute of Osaka Prefecture for help in the peparation of this paper and for many useful suggestions.

References

1) P. Robson and P. R. H. Speakman, *J, Chem. Soc., B*, **1968**, 463.
2) U. Lerch and J. G. Moffatt, *J. Org. Chem.*, **36**, 3391 (1971).
3) Y. Hayashi and D. Swern, *Tetrahedron Lett.*, **1972**, 1921.
4) W. Lwowski and F. W. Mattingly, *J. Am. Chem. Soc.*, **87**, 1947 (1965).
5) W. Lwowski and T. J. Maricich, *J. Am. Chem. Soc.*, **87**, 3630 (1965).
6) D. S. Breslow, T. J. Prosser, A. F. Marcantonio, and C. A. Genge, *J. Am. Chem. Soc.*, **89**, 2384 (1967).
7) N. Torimoto, T. Shingaki, and T. Nagai, *Bull. Chem. Soc. Jpn.*, **49**, 2572 (1976).
8) N. Torimoto, T. Shingaki, and T. Nagai, *Bull. Chem. Soc. Jpn.*, **50**, 1517 (1977).
9) H. Nozaki, S. Fujita, H. Takaya, and R. Noyori, *Tetrahedron*, **23**, 45 (1967).
10) T. Shingaki, M. Inagaki, N. Torimoto, and M. Takebayashi, *Chem. Lett.*, **1972**, 155.
11) A. G. Anastassiou, *J. Am. Chem. Soc.*, **89**, 3184 (1967).
12) J. M. Simon and W. Lwowski, *J. Am. Chem. Soc.*, **91**, 5107 (1969).
13) N. Torimoto, T. Shingaki, and T. Nagai, *J. Org. Chem.*, in press.
14) G. F. Whitfield, H. S. Beilan, D. Saika, and D. Swern, *Tetrahedron Lett.*, **1970**, 3543.
15) D. S. Breslow, E. I. Edwards, E. C. Linsay, and H. Omura, *J. Am. Chem. Soc.*, **98**, 4268 (1976).
16) J. A. Riddic and W. B. Bunger, "Organic Solvents," in "Techniques of Chemistry," Vol. VII, ed by A. Weissberger, Wiley-Interscience, New York, N. Y. (1970).

The Benzannelated Annulenones. Syntheses and Properties of 10-Methylbenzo[*d*]-6,8-bisdehydro[15]annulenone and 12-Methylbenzo[*f*]-8,10-bisdehydro[15]annulenone

Jūro Ojima* and Yūji Shiroishi

Department of Chemistry, Faculty of Science, Toyama University, Gofuku, Toyama 930

(Received October 20, 1977)

Synthesis of two methylated monobenzannelated bisdehydro[15]annulenones is described. It was found by means of ^{1}H-NMR spectra that the protonated annulenones are diatropic.

The effect of benzannelation on a conformationally fixed, potentially diatropic bisdehydro[15]annulenone was studied for compounds fused by cyclohexene and benzene rings by Weavers *et al.*[1] It was shown that the monobenzannelated annulenone **1** is atropic, protonated **1** showing diatropic nature. On the other hand, we have shown that the monobenzannelated bisdehydro[13] **2** and [17]annulenone **3** are paratropic themselves.[2] It was therefore decided to prepare the methylated monobenzobisdehydro[15]annulenones **7** and **12**, as well as

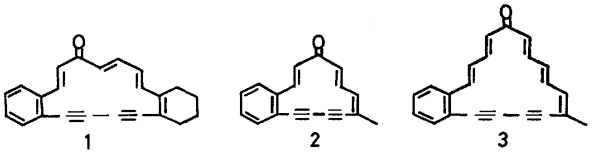

the respective protonated species **8** and **13**. As reported by Sondheimer *et al.*, the methyl substituent should be more desirable as compared with cyclohexene moiety for the study of ring current effects.[3] Information on the conjugative effects between the annulenone ring and the benzene nucleus can be obtained from these isomeric compounds, since **7** and **12** have similar geometry and planarity. The present paper deals with the synthesis and properties of two monobenzobisdehydro[15]annulenones, *viz.*, 10-methylbenzo[*d*]-6,8-bisdehydro[15]annulenone **7** and 12-methylbenzo[*f*]-8,10-bisdehydro[15]annulenone **12**.

Synthesis. Aldol condensation of the ketone **4**[4] and the dienyne aldehyde **5**[2c] by means of methanolic potassium hydroxide gave the acyclic ketone **6** in 49% yield. Oxidative coupling of **6**, under Eglinton's conditions using copper(II) acetate monohydrate in pyridine,[5] afforded the desired annulenone **7** as yellow crystals in 31% yield. The condensation of the dienyne ketone **9**[6] and the aldehyde **10**,[7] under the same conditions gave acyclic ketone **11** in 68% yield. Oxidation of **11** with copper(II) acetate monohydrate as before gave the annulenone **12** as yellow crystals in 27% yield. Treatment of **7** or **12** with trifluoroacetic acid gave the corresponding protonated species, **8** (purple; λ_{max} 272 sh, 332 sh, 367, 468 sh, 498, 559 sh, 599 nm) or **13** (red purple; λ_{max} 271, 346, 368 sh, 507 sh, 539 nm), respectively. Quenching of **8** and **13** with aqueous sodium hydrogencarbonate resulted in regeneration of **7** and **12**, respectively.

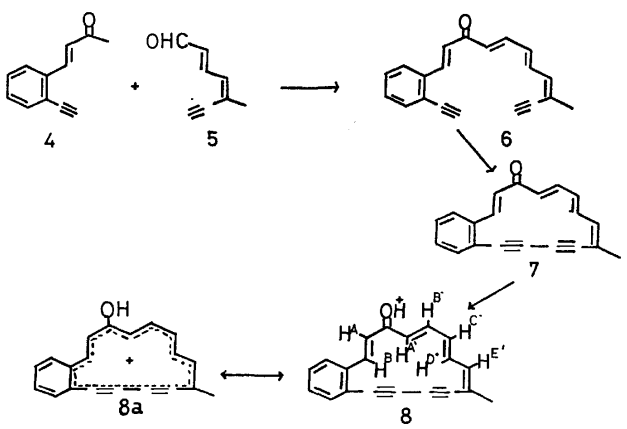

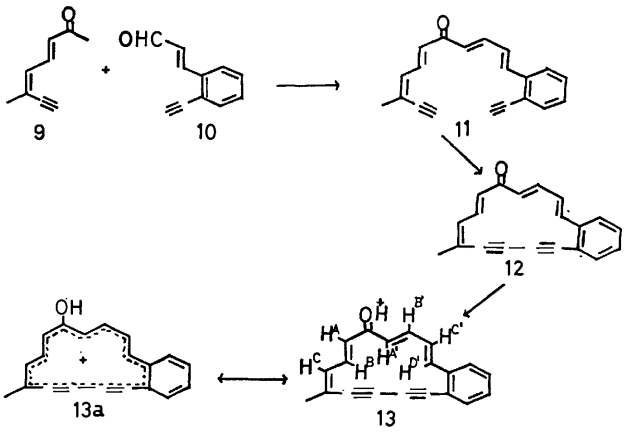

Properties. Electronic absorption maxima of **7** and **12** are given in Table 1. Little difference in these spectra seems to suggest that a difference in the annelated-position of benzene gives no essential change on the conjugative effects between the benzene nucleus and bisdehydro[15]annulenone skeleton. The NMR spectra indicate that both **7** and **12** are atropic, since not much shifts were observed for the resonances of the olefinic protons of **7** and **12** except for the slightly low field shift of methyl protons, as compared with those of the corresponding acyclic ketone **6** and **11**, respectively(see Experimental). The NMR data of the protonated

Table 1. Electronic absorption maxima of **7** and **12** in ether; λ_{max} (ε, in parentheses)

7	**12**
223 (18700)	228 (25200)
262 sh (13200)	256 (18700)
278 sh (18200)	274 sh (21600)
299 (22100)	302 (28900)
377 (8130)	372 sh (8210)

* Author to whom inquiries should be addressed.

Table 2. ^{1}H-NMR parameters of **8** and **13** in CF_3COOD at 90 MHz
(τ-Values; internal standard, TMS; J values in Hz in parentheses).

Proton	**8**	**13**
$H^{A'}$	5.55 d (16)[a]	4.91 d (15.5)[c]
$H^{D'}$	5.43 dd (16, 12)	4.87 d (15.5)[c]
H^{B}	4.75 d (16)[a]	4.80 dd (15.5, 12)
H^{A}	1.92 d (16)	2.60 d (15.5)
$H^{B'}$	1.35 dd (16, 7)[b]	
$H^{C'}$	2.55 dd (16, 7)[b]	
H^{C}	——	1.90—2.35 (m, 6H)
$H^{E'}$	2.17d (12)	
Benzenoid H	1.96—2.08 (m, 3H)	
Benzenoid H	1.32—1.42 (m, 1H)	1.58—1.70 (m, 1H)
$-CH_3$	7.47 s	7.40 s

a), b), c) These are tentative assignments and may be reversed in each group, but most probable values are given in Table 2 referring to the chemical shifts of the related compounds.[1]

monobenzobisdehydro[15]annulenones **8** and **13** (in CF_3COOD) are given in Table 2. Compounds **8** and **13** are diatropic, as indicated by the relative chemical shifts of the inner and outer protons, as well as the low field methyl resonances. We expected that annulenones **7** and **12** would also exhibit the diatropic nature corresponding to the paratropic [13] **2** and [17]annulenone **3**. However, it was found that the protonated species **8** and **13** are diatropic and can be represented by delocalized formulae **8a** and **13a**, respectively. This result is in line with that obtained by Weavers *et al.*[1]

Experimental

Freshly deoxygenated ether and 20% methanolic potassium hydroxide solutions were prepared and used as reported previously.[2b,c] All melting points are uncorrected. Brockmann alumina (Act. II—III) was used for column chromatography. The ^{1}H-NMR, IR, UV, and mass spectra were taken with the instruments Varian EM-930 or Varian XL-100, Hitachi EPI-S2, Hitachi-124, and JEOL-MS-OI-SG-2, respectively. Shoulders in UV spectra are denoted by sh. Wavelength of absorption maximum is recorded in nm and ε-values are given in parentheses. Chemical shifts are given in τ-values with respect to TMS as an internal standard, while the coupling constants (J) are given in Hz.

1-(o-Ethynylphenyl)-9-methyl-1,4,6,8-undecatetraen-10-yn-3-one **6**. To a mixture of the dienyne aldehyde (**5**, 1.00 g, 8.32 mmol) and the ketone (**4**, 1.84 g, 10.8 mmol) in ether (35 ml) was added a 20% methanolic potassium hydroxide solution (3.3 ml) with stirring at −5—0 °C. The mixture was then stirred for 3.5 h at the same temperature under nitrogen atmosphere. Neutralization with acetic acid (4 ml) followed by pouring into water (100 ml) and extraction with benzene gave an organic extract which was worked up as usual. The residue obtained by evaporation of the solvent was chromatographed on alumina (150 g) with light petroleum ether −ethyl ether (20: 80) to give the ketone (**6**, 1.12 g, 49%) as yellow needles from benzene-hexane, mp *ca.* 75 °C (dec), MS: *m/e* 272 (M^+, 100); mol wt, 272.3; IR (KBr disk): 3270, 3240 (−C≡CH), 2100 (−C≡C−), 1670, 1625, 1600 (C=O, C=C), 1005 cm^{-1} (*trans* C=C); UV (ether): λ_{max} 227 (17100), 250 sh (13800), 255 (14400), 277 (10400), 292 (11100), 356 nm (30800); NMR (90 MHz, $CDCl_3$): 1.97 (d, 16, 1H, olefinic H), 2.30—3.80 (m, 10H, olefinic and benzenoid H), 6.53 (s, 2H, −C≡CH), 8.05 (s, 3H, $-CH_3$). Found: C, 88.34; H, 6.00%. Calcd for $C_{20}H_{16}O$: C, 88.20; H, 5.92%.

10-Methylbenzo[d]-*6,8-bisdehydro*[*15*]*annulenone* **7**. A solution of **6** (600 mg, 2.20 mmol) in pyridine (46 ml) was added with stirring over a period of 15 min to a solution of copper(II) acetate monohydrate (9.1 g) in pyridine (30 ml) at 50 °C; the mixture was stirred for 3 h at 63 °C. The mixture was then chilled, diluted with benzene (100 ml), and filtered through Hyflo Super-Cel. The precipitates formed were washed with benzene (100 ml×4). The filtrate was washed with dilute hydrochloric acid until it turned slightly acidic. It was then worked up in the usual way. The residual red liquid, after solvent removal, was chromatographed on alumina (150 g) with light petroleum ether-ethyl ether (80: 20—35: 65) to give **7** (185 mg, 31%). Recrystallization from benzene gave yellow needles, mp *ca.* 140 °C (dec); MS: *m/e* 270 (M^+, 45), 269 (100); mol wt, 270.3; IR (KBr disk): 2150 (−C≡C−), 1650, 1620, 1600 (C=O, C=C), 970 cm^{-1} (*trans* C=C); NMR (100 MHz, $CDCl_3$): 1.98—2.05 (m, 1H, benzenoid H), 2.65—3.54 (m, 10H, olefinic and benzenoid H), 7.90 (s, 3H, $-CH_3$); UV: see Table 1. Found: C, 88.59; H, 4.96%. Calcd for $C_{20}H_{14}O$: C, 88.86; H, 5.22%.

1-(o-Ethynylphenyl)-9-methyl-1,3,6,8-undecatetraen-10-yn-5-one **11**. A mixture of ketone (**9**, 0.98 g, 7.30 mmol) and aldehyde (**10**, 1.65 g, 10.6 mmol) in ether (30 ml) was treated with a 20% methanolic potassium hydroxide (3 ml) under nitrogen atmosphere at 0 °C, and stirred at −8—−4°C for 4 h. After addition of acetic acid (4 ml), the mixture was worked up as in the preparation of **6**, giving a red liquid. Chromatography of the liquid over alumina (180 g) with light petroleum ether–ethyl ether (75: 25—70: 30) gave the desired ketone (**11**, 1.35 g, 68%) as a partly crystalline, orange liquid, which formed yellow needles from hexane–benzene, mp 97.0—98.6 °C; MS: *m/e* 272 (M^+, 100); mol wt, 272.3; IR (KBr disk): 3300, 3250 (−C≡CH), 2100 (−C≡C−), 1660, 1600 (C=O, C=C), 1000 cm^{-1} (*trans* C=C); UV (ether): λ_{max} 228 sh (17300), 233 (17500), 255 (16300), 263 sh (15400), 295 sh (11200), 352 nm (33000); NMR (100 MHz, $CDCl_3$): 2.14—3.61 (m, 11H, olefinic and benzenoid H), 6.45 (s, 1H, −C≡CH), 6.60 (s, 1H, −C≡CH), 7.95 (s, 3H, $-CH_3$). Found: C, 87.94; H, 5.91%. Calcd for $C_{20}H_{16}O$: C, 88.20; H, 5.92%.

12-Methylbenzo[f]-*8,10-bisdehydro*[*15*]*annulenone* **12**. A solution of **11** (1.34 g, 4.92 mmol) in pyridine (50 ml) was added dropwise to a stirred solution of copper(II) acetate monohydrate (20.3 g) in pyridine (68 ml) for 15 min at 50 °C, and the reaction mixture was stirred for 3 h at 63 °C. The mixture was then worked up as in the preparation of **7**, affording a dark red liquid. The liquid was chromatographed on alumina (180 g) and annulenone (**12**, 359 mg, 27%) was eluted with light petroleum ether–ethyl ether (40: 60—30: 70). Recrystallization from benzene-hexane gave yellow needles, mp 176 °C (dec); MS: *m/e* 270 (M^+, 70), 241 (100); mol wt, 270.3; IR (KBr disk): 2150 (−C≡C−), 1645, 1615, 1600 (C=O, C=C), 985 cm^{-1} (*trans* C=C); NMR (100 MHz, $CDCl_3$): 2.12—2.23 (m, 1H, benzenoid H), 2.36—3.64 (m, 10H, olefinic and benzenoid H), 7.87 (s, 3H, $-CH_3$); UV: see Table 1. Found: C, 88.89; H, 5.09%. Calcd for $C_{20}H_{14}O$: C, 88.86; H, 5.22%.

The authors wish to thank Drs. S. Akiyama and F. Ogura, and Prof. M. Nakagawa, Osaka University, for the measurement of the NMR spectra at 100 MHz. One of the authors (J. O.) is grateful to the Ministry

of Education for financial support of this investigation through a Grant-in-Aid (054103, 1975) for Scientific Research.

References

1) R. T. Weavers, R. R. Jones, and F. Sondheimer, *Tetrahedron Lett.*, **1975**, 1043.

2) a) J. Ojima, M. Ishiyama, A. Kimura, and Y. Yokoyama, *Tetrahedron Lett.*, **1975**, 1909; b) J. Ojima, Y. Yokoyama, and M. Enkaku, *Bull. Chem. Soc. Jpn.*, **50**, 1522 (1977); c) J. Ojima, M. Ishiyama, and A. Kimura, *Bull. Chem. Soc. Jpn.*, **50**, 1584 (1977).

3) a) R. L. Wife and F. Sondheimer, *Tetrahedron Lett.*, **1974**, 195; b) T. M. Cresp, J. Ojima, and F. Sondheimer, *J. Org. Chem.*, **42**, 2130 (1977); Although no decision was made on the tropicity of bis(cyclohexene)-annelated bisdehydro[13]annulenone in an early study (P. D. Howes, E. LeGoff, and F. Sondheimer, *Tetrahedron Lett.*, **1972**, 3691), it seems that the compound is paratropic in analogy with the result on the dimethyl analogue (Ref. 3b).

4) J. Ojima, T. Yokomachi, and A. Kimura, *Bull. Chem. Soc. Jpn.*, **49**, 2840 (1976).

5) G. Eglinton and A. R. Galbraith, *Chem. Ind. (London)*, **1956**, 737; *J. Chem. Soc.*, **1959**, 889.

6) J. Ojima, T. Katakami, G. Nakaminami, and M. Nakagawa, *Bull. Chem. Soc. Jpn.*, **49**, 292 (1976).

7) J. Ojima, A. Kimura, Y. Yokoyama, and T. Yokoyama, *Bull. Chem. Soc. Jpn.*, **48**, 367 (1975).

Synthesis of 2,3 : 7,8-Bis(polymethylene)-4*H*,9*H*-benzo[1,2-*b* : 4,5-*b*']dipyrans and Their Oxidation to the Corresponding Benzodilactones[1)]

Jaswant Rai MAHAJAN and Maria Beatriz MONTEIRO

Departamento de Química, Universidade de Brasília, 70.000, Brasília, DF, Brasil

(Received June 27, 1977)

Four members of a new series of the title benzodipyrans have been synthesized through the alkylation of the pyrolidine-enamines of 6,7,8- and 12-membered cycloalkanones with 2,5-bis(dimethylaminomethyl)hydroquinone, followed by hydrolysis and subsequent cyclization of the intermediate products. Oxidation of these benzodipyrans with *m*-chloroperbenzoic acid (MCPBA) afforded the corresponding benzodilactones in 10—65% yield, the rest of the material being a mixture of hydroxylated carbonyl compounds.

We have recently reported the synthesis of several medium ring and macrocyclic keto lactones (**2, 4, 6, 9**) by the intramolecular reverse Dieckmann reaction of 2,2-dialkyl-5,5-dimethyl-1,3-cyclohexanediones (**1**) as well as by various oxidative procedures, as shown in Chart 1.[2)] Although these synthetic keto lactones have only a distant resemblance with the natural antibiotic macrolides,[3)] yet it is noteworthy that a majority of these compounds as well as some of the synthetic intermediates have shown *in vitro* biological activity against one or the other of the following microorganisms: *Staphylococcus aureus*, *Escherichia coli*, *Bacillus megatherium*, *Candida albicans*, and *Leptomonas pessoai*.[4)] These promising bioassays encouraged us to explore the synthesis of symmetrical benzodilactones (**16**) from the title compounds (**15**), by procedures successfully developed in the case of benzo- and naphtho-fused keto lactones **6**.[2c)] We now report the results of this investigation.

As the literature search in the ring index[5)] and chemical abstracts revealed that 4*H*,9*H*-benzo[1,2-*b*: 4,5-*b*']dipyran as well as its derivatives have not been described, we patterned the synthesis of the title compounds **15** after a successful route developed in the case of benzo- and naphthopyrans (**5a,b**), through the enamine alkylation of the Mannich bases derived from phenol and 2-naphthol.[2c,6a)] In contrast to the use of mono *o*-phenolic Mannich bases for the above purpose, there is no mention of the use of *bis* Mannich bases, derived from dihydric phenols, for the preparation of the corresponding dipyrans.[6)] We hereby describe that 2,5-bis(dimethylaminomethyl)hydroquinone[7)] (**10**) can be successfully employed for the synthesis of the title compounds **15**, as shown in Chart 2.

Although condensation between the Mannich base **10** and the enamine (**11**; n=4) could not be carried out in dioxane, according to the original method of Von Strandtmann,[6a)] the desired reaction could be successfully conducted in *N*,*N*-dimethylformamide (DMF).[2c)] The duration of reaction as well as its temperature had to be carefully controlled to obtain optimal results for

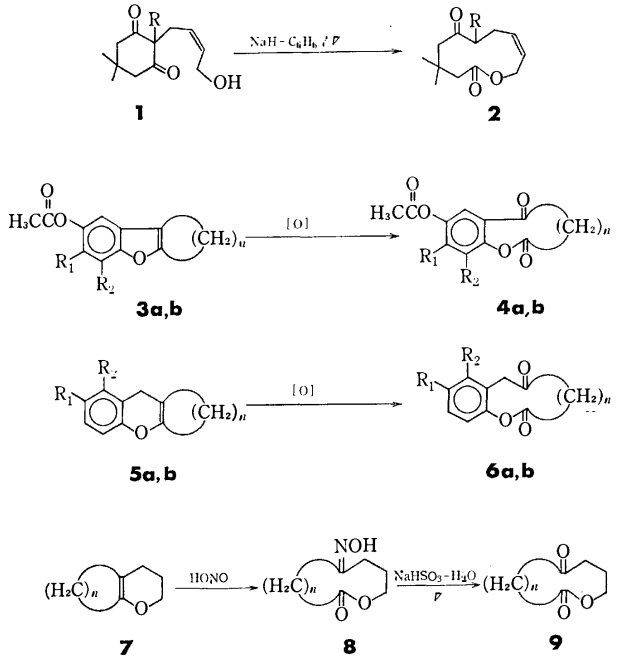

a: R_1=R_2=H, b: R_1=R_2=$(CH=CH)_2$,; n=4,5,6,10

Chart 1.

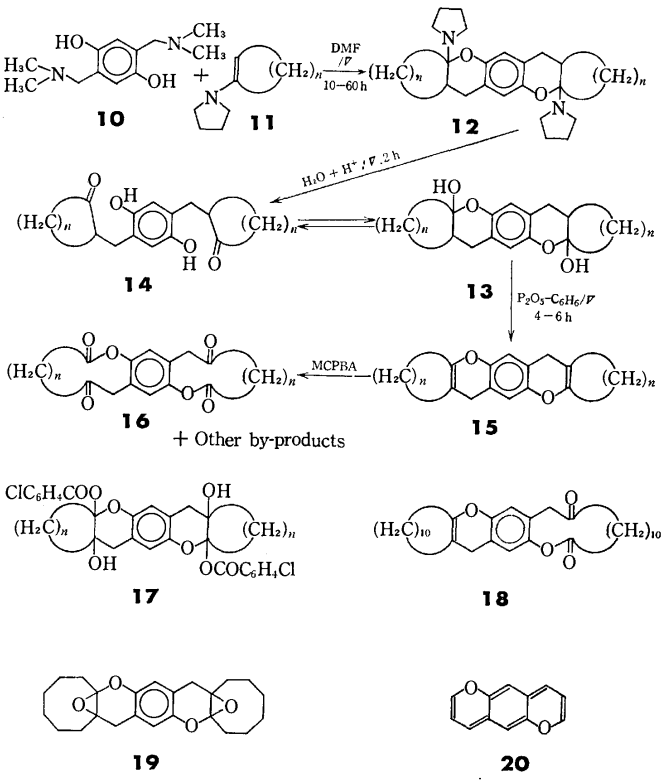

n=4,5,6,10

Chart 2.

each enamine. In most of the cases, the intermediate amino compound (**12**) was not isolated and was hydrolyzed *in situ* at the end of first step. However, in the case of enamine derived from cyclododecanone (**11**; $n=10$), the intermediate adduct (**12**; $n=10$) precipitated from the reaction mixture and was obtained as a coarse powder in 57% yield. Its hydrolysis in a two phase system containing benzene, water, and acetic acid, furnished the product (**14**; $n=10$) in 95% yield. On the other hand, the same product (**14**; $n=10$) could be obtained, in a slightly lower yield of an inferior quality, by direct hydrolysis of the reaction mixture.

Attempted extension of the present condensation to enamine derived from acetophenone[8] resulted in an intractable mixture of products.

One would expect an equilibrium between the cyclic form (**13**) and the acyclic form **14**. Moreover, the former could form diastereoisomers. In fact, only one of these compounds was present, in the solid state, entirely in the cyclic form (**13**; $n=4$), as evidenced by the absence of carbonyl absorption in its infrared spectrum, while the rest of the compounds ($n=5$, 6, 10) showed strong absorptions both in the OH and CO regions. The carbonyl absorption in these compounds (1681—1695 cm^{-1}) is shifted to lower wave numbers due to hydrogen bonding.[9] Attempted dehydration of these compounds in refluxing dioxane, containing catalytic amount of *p*-toluenesulfonic acid or phosphorus pentaoxide, proceeded in poor yield and was unsatisfactory. However, dehydration in benzene employing 2 molar equivalent of phosphorus pentaoxide furnished the desired benzodipyrans (**15**; $n=4$—6, 10) in 60—90% yield. The characteristic infrared absorption of these compounds (1692—1706 cm^{-1}) is in agreement with that observed in the corresponding benzopyran series.[2c]

One particular difficulty encountered in the present work was the poor solubility of most of the compounds described here, in the common organic solvents. Moreover, these compounds, especially the benzodipyrans **15**, suffer autoxidation while in solution. Therefore, crystallization of **14** and **15** was carried out in solutions containing catalytic amount of hydroquinone. Even so, mother liquors of benzodipyran (**15**; $n=10$) afforded, after silica gel column chromatography, a small quantity of a pure product which was characterized as keto lactone **18**, on the bases of its infrared (1751, 1712, 1695 cm^{-1}), and mass spectra. Similar autoxidations have already been observed in the benzo- and naphthopyran **5a,b** series.[2c]

As *m*-chloroperbenzoic acid (MCPBA) had proved to be the best reagent for the preparation of keto lactones **6a,b** from the corresponding benzo- and naphthopyrans **5a,b**[2c] the same reagent was used, with moderate success, in the present series. However, as the benzodipyrans **15** have two sites of reaction, the half oxidized and several other expected by-products, such as hydroxy ester (**17**), the corresponding tetrol, and combinations thereof become possible.[10] This made the isolation and purification of the desired products rather difficult in the present work. Under careful conditions, the desired dilactones **16** were obtained in 10—65% yields; the rest of the material being a mixture of products, showing both hydroxyl and carbonyl absorptions in the infrared spectrum.

Mechanistic considerations on the oxidation of cyclic enol ethers by MCPBA suggest that for optimal results, competitive reactions of the intermediate epoxide with *m*-chlorobenzoic acid and water be avoided.[10] Borowitz has attained this objective by employing 50% excess of the peracid in a limited volume of the solvent (CH_2Cl_2), the *m*-chlorobenzoic acid precipitates out of the reaction mixture as formed, because it is much less soluble than the corresponding peracid.[10] In an attempt to improve the present procedure, we treated benzodipyran (**15**; $n=6$) with MCPBA in the presence of potassium carbonate[11] and obtained the corresponding diastereoisomeric bis-epoxides (**19**; TLC, IR, NMR) as the exclusive products ($\approx$100%). Attempted posterior cleavage of this epoxide with MCPBA[10] or periodic acid in tetrahydrofuran[12] resulted in a complex mixture of products from which the isolation of the desired keto lactone appeared difficult (TLC).

Similarly, while the dipyran (**15**; $n=10$) was recovered unchanged from an attempted oxidation with potassium permanganate in acetone at room temperature, it gave complex mixture of products when ozonolyzed[2b,c] or oxidized with ruthenium tetraoxide ($RuCl_3$–$NaIO_4$) in dichloromethane–water.[13]

Due to poor solubility in most of the organic solvents, we could not obtain the NMR spectra of benzodilactones **16**. However, these products have been fully characterized by their elemental analysis, infrared and mass spectra. The molecular and fragmentation ions of these compounds are in accord with their structure, but the details of mass spectral studies will be reported elsewhere, along with other related series.

Experimental

Melting points (°C) are uncorrected and were determined on a Kofler block or, when mentioned, in capillary tube sealed under reduced pressure. The latter mps are sharper and more reproducible. The infrared (IR) spectra were taken as KBr discs on a Perkin Elmer 137 instrument and the absorption maxima (ν_{max}) are reported in wave numbers (cm^{-1}). ^1H NMR spectra were recorded on a Varian A60-D (60 MC) spectrometer and the reported values (δ ppm) are relative to internal TMS. As usual, s=singlet, m=multiplet, *etc.* The mass spectra were obtained on a Varian CH-7-spectrometer and the details will be published elsewhere; only the molecular ions (M^+) are reported here.

Progress of reaction was followed by thin layer chromatography (TLC) on silica gel G plates run in benzene, containing 5—10% ethanol. 2,5-Bis(dimethylaminomethyl)hydroquinone was prepared according to the procedure described by Caldwell and Thompson.[7] Enamines of cycloalkanones were prepared by the azeotropic method described by Stork *et al.* and in other literature references.[14] Nomenclature and numbering of the heterocyclic compounds is based on that described for the benzo[1,2-*b*: 4,5-*b'*]dipyran (**20**) in the Ring Index[5] and the Chemical Abstracts.[15]

*Condensation of 2,5-Bis(dimethylaminomethyl)hydroquinone (**10**) with Enamines (**11**; n=4,5,6,10).* General Procedure: A solution of the Mannich base (**10**; 10 mmol) and the desired

enamine (20 mmol) in *N,N*-dimethylformamide (40 ml) was heated in an oil bath (130—140 °C) during 10—60 h, while a slow stream of nitrogen was bubbled through the reaction mixture. At the end of the reaction, when the evolution of dimethylamine became neglegible, hot water (20 ml) was added, pH of the medium adjusted to 5—6 with 1 M hydrochloric acid and the heating continued another 1—2 h. The cooled reaction mixture was elaborated as described under individual compound.

*2,7-Dihydroxy-3,4,8,9-tetrahydro-2,3 : 7,8-bis(tetramethylene)-2*H,7H-*benzo*[*1,2*-b: *4,5*-b']*dipyran* (**13**: n=*4*). The reaction between the Mannich base (**10**) and enamine (**11**; *n*=4) was complete in 10—12 h. The final product precipitated from the reaction mixture during the hydrolysis step and was filtered off. It was sparingly soluble in the common organic solvents: methanol, ethanol, 1-propanol, acetone, ethyl acetate, chloroform, carbon tetrachloride, benzene, ether, tetrahydrofuran, dioxane, glyme, *etc.* It was purified by refluxing in benzene–ethanol and filtering hot to obtain a faintly yellow powdery solid (80% yield), mp 221—223 °C (dec); ν_{max} 3436 and small absorption at 1672. Analytical sample was prepared by dissolving a small quantity in a large excess of hot 1,2-dichloroethane–ethanol and filtering hot. The filtrate was concentrated on a rotary evaporator till turbidity appeared, when it was allowed to crystallize affording white fine crystals, mp 232—234 °C (dec), with softening ≈226 °C; ν_{max} 3448; no absorption in the CO region. TLC of this compound (one spot only) revealed it to be most probably a single diastereomer. Found: C, 72.53; H, 8.08%. Calcd for $C_{20}H_{26}O_4$: C, 72.70; H, 7.93%.

2,5-Bis[*(2-oxocycloheptyl)methyl*]*hydroquinone* (**14**; n=*5*). Enamine (**11**; *n*=5) and the Mannich base (**10**) were allowed to react for 30 h. After hydrolysis, the cooled reaction mixture was extracted with chloroform and work-up as usual to obtain a solid (60%), which was crystallized from 1,2-dichloroethane–ethanol yielding shiny plates, mp 232—235 °C (dec); ν_{max} 3448, 1686. Found: C, 73.63; H, 8.43%. Calcd for $C_{22}H_{30}O_4$: C, 73.71; H, 8.44%.

2,5-Bis[*(2-oxocyclooctyl)methyl*]*hydroquinone* (**14**; n=*6*), was obtained in a manner just described above. Crystallization from benzene–ethanol afforded the pure product (47%) as fine white crystals, mp 228—230 °C (dec); ν_{max} 3436, 1681. Found: C, 74.46; H, 8.92%. Calcd for $C_{24}H_{34}O_4$: C, 74.58; H, 8.87%.

2,5-Bis[*(2-oxocyclododecyl)methyl*]*hydroquinone* (**14**; n=*10*), separated as an oily-solid from the reaction mixture. The supernatant was decanted and the product washed with water, followed by petroleum ether (40—60 °C). The residue was dissolved in benzene and treated with petroleum ether (40—60 °C) to afford a fine crystalline solid (50%). Further purification in the same solvent system furnished fine white crystals, mp 206—209 °C (dec); ν_{max} 3509, 1695. Found: C, 76.95; H, 10.09%. Calcd for $C_{32}H_{50}O_4$: C, 77.06; H, 10.10%.

*2,7-Di(1-pyrrolidinyl)-3,4,8,9-tetrahydro-2,3:7,8-bis(decamethylene)-2*H,7H-*benzo*[*1,2*-b: *4,5*-b']*dipyran* (**12**; n=*10*). After ≈12 h of reaction between the Mannich base (**10**) and the enamine (**11**; *n*=10), a solid began to separate. At the end of reaction (60 h), the hydrolysis step was omitted. The reaction mixture was cooled, filtered and the product washed with benzene. On refluxing in a mixture of benzene–ethanol and filtering hot, the pure amino-adduct (**12**; *n*=10) was obtained as a coarse powder (57%), mp 200—206 °C (dec); ν_{max} 2959, 1497, 1458. This product (1 mmol) was refluxed (N_2) in a mixture of water (10 ml), acetic acid (2 ml) and benzene (20 ml), containing catalytic amount of hydroquinone. After ≈2 h, a solid began to float in the benzene layer. After a reflux of 6 h, the reaction mixture was cooled, the product filtered and washed successively with water and ethanol. The dry product (95%), mp 206—209 °C (dec) had infrared spectrum identical with the product (**14**; *n*=10) described above.

*Preparation of 2,3: 7,8-Bis(polymethylene)-4*H,9H-*benzo*[*1,2*-b: *4,5*-b']*dipyranes* (**15**; n=*4,5,6,10*). A suspension of diol **13** (*n*=4) (10 mmol) or a solution of the hydroxy ketones **14** (*n*=5,6,10) (10 mmol) in benzene (300—600 ml), containing phosphorus pentaoxide (20 mmol) and hydroquinone (50 mg), was refluxed (N_2) 2—6 h, till there was no more of the starting material (TLC). The cooled reaction mixture was decanted and allowed to stand over sodium carbonate decahydrate for 1 h, when the solvent was evaporated to obtain the desired product: **15** (*n*=4) was crystallized from benzene–ethanol to obtain faintly yellow, shiny plates (63%), mp 205—207 °C (dec); ν_{max} 1706; δ (CS_2) 1.5—2.4 (m, $8CH_2$), 3.1 (s, benzylic $2CH_2$), 6.3 (s, 2H aromatic). Found: C, 81.73; H, 7.54%. Calcd for $C_{20}H_{22}O_2$: C, 81.60; H, 7.53%.

15 (*n*=5) was obtained as yellowish shinyl plates (85%) from the same solvent system, mp 212—217 °C (dec); 234—235 °C (dec) in a sealed capillary tube; ν_{max} 1704. Due to its sparing solubility in $CHCl_3$, CCl_4, CS_2, and acetone, it was not possible to obtain its NMR spectrum. Found: C, 82.14; H, 7.88%. Calcd for $C_{22}H_{26}O_2$: C, 81.95; H, 8.13%.

15 (*n*=6) was also crystallized from the same solvents affording (61%) faintly yellow needles, mp 172—180 °C (dec); 188—190 °C in a sealed capillary tube; ν_{max} 1701; δ (CS_2) 1.4—1.8 (m, $8CH_2$), 1.9—2.4 (m, allylic $4CH_2$), 3.2 (s, benzylic $2CH_2$), 6.3 (s, 2H aromatic). Found: C, 82.45; H, 8.67%. Calcd for $C_{24}H_{30}O_2$: C, 82.24; H, 8.63%.

15 (*n*=10) was crystallized from chloroform to furnish (90%) shinyl cottony needles, mp 180—195 °C (dec); 212—213 °C in a sealed capillary tube; ν_{max} 1692; δ (CS_2) 1.2—1.8 (m, $16CH_2$), 1.9—2.4 (m, allylic $4CH_2$), 3.2 (s, benzylic $2CH_2$), 6.3 (s, 2H aromatic). Found: C, 83.04; H, 10.06%. Calcd for $C_{32}H_{46}O_2$: C, 83.06; H, 10.02%.

The hydroquinone derivatives **14** and the benzodipyranes **15** undergo autoxidation during prolonged heating while in solution. Consequently, these compounds were recrystallized as quickly as possible and in solutions containing catalytic amount of hydroquinone. Even so an oxidized product was isolated from the mother liquors of benzodipyran **15** (*n*=10), as described below.

Isolation of Benzopyran Lactone (**18**). Mother liquors of benzodipyran **15** (*n*=10) (1.3 g) were chromatographed on a silica gel (Merck; 80 g) column, eluted with benzene containing successively increasing amount (0—3%) of ethanol. 25 fractions of 20 ml were collected and fractions 10—15 combined on the basis of TLC examination. Recrystallization from absolute ethanol gave off-white, fluffy solid (≈15 mg), mp 158—160 °C; ν_{max} 1751, 1712, 1695; *m/e* 494 (M^+).

Oxidation of Benzodipyrans (**15**) *to Benzodilactones* (**16**). To obtain consistent results, the *m*-chloroperbenzoic acid (MCPBA) bought from the Aldrich Chemical Company (85%) was dried over $CaCl_2$, under reduced pressure, while the peracid bought from BDH was used without any further treatment. The following oxidation procedure is illustrative for the series.

Dilactone **16** (n=*4*): The solid benzodipyran (**15**; *n*=4; 147 mg, 0.5 mmol) was added, in small portions during 15—20 min, to a stirred solution of MCPBA (3 mmol, 0.52 g) in dichloromethane (6 ml), kept around 15—20 °C by a cold water bath and protected by a drying tube. Soon a white solid began to separate and stirring was continued till (1 h) all the starting material had been consumed (TLC). The reaction mixture was filtered and the solids washed with

carbon tetrachloride. The filtrate was evaporated to dryness and triturated with absolute ethanol to dissolve the soluble products, leaving an insoluble portion (96 mg). Similar treatment of the filter-cake gave 20 mg of an insoluble product. Both these insoluble residues were combined (116 mg) on the bases of their IR spectra, TLC, and mp 215—220 °C (dec). This product was sparingly soluble in common organic solvents. It was purified by a short reflux in a mixture of 1,2-dichloroethane–ethanol and filtering while hot, affording shiny plates (96 mg; 54%), mp 218—221 °C (dec). An analytical sample was prepared by recrystallization of a small portion from a large excess of the same solvent mixture, yielding thin plates, mp 224—231 °C (dec); 191—194 °C (dec) in a sealed capillary tube; ν_{max} ≈3448 (overtones), 1754, 1706; *m/e* 358 (M^+). Found: C, 66.89; H, 6.15%. Calcd for $C_{20}H_{22}O_6$ (358): C, 67.02; H, 6.19%.

Dilactone ***16*** *(n=5)*, was obtained in a similar manner to afford white needles (60%), mp 251—254 °C (dec), with softening ≈247 °C; ν_{max} ≈3472 (overtones), 1738, 1706; *m/e* 386 (M^+). Found: C, 68.14; H, 6.68%. Calcd for $C_{22}H_{26}O_6$ (386): C, 68.38; H, 6.78%.

Dilactone ***16*** *(n=6)*, was obtained as shiny white needles (65%), mp 260—261 °C (dec), with softening ≈233 °C; ν_{max} ≈3472 (overtones), 1745, 1709; *m/e* 414 (M^+). Found: C, 69.37; H, 7.32%. Calcd for $C_{24}H_{30}O_6$ (414): C, 69.55; H, 7.30%.

Dilactone ***16*** *(n=10)*, was obtained as white needles (10%) from absolute ethanol, mp 238—239 °C (dec); ν_{max} ≈3484 (overtones), 1754, 1712; *m/e* 526 (M^+). Found: C, 73.18; H, 8.96%. Calcd for $C_{32}H_{46}O_6$ (526): C, 72.97; H, 8.80%.

*Preparation of the Bis-epoxide (**19**).* To a suspension of MCPBA (2 mmol) and anhydrous potassium carbonate (10 mmol) in dichloromethane (5 ml) was added slowly a suspension of the benzodipyran (**15**; *n*=6) (116 mg, 0.33 mmol) in the same solvent (2 ml), with stirring at room temperature. After 6 h the reaction mixture was filtered and the solids washed with carbon tetrachloride. The filtrate was washed with water, dried over anhydrous sodium sulfate and evaporated to afford a crystalline product (116 mg), mp 129—135 °C; ν_{max} 2941, 1513, 1464; $\delta(CDCl_3)$ 1.2—2.6 (m, 12-CH_2), 3.0—3.6 (two superimposed broad AB quartets, benzylic 2CH_2; separated due to the two forms of the bis-epoxide), 6.5 (s, 2H aromatic). Attempted recrystallization of this product resulted in the opening of the epoxides (TLC, IR).

The above experiment repeated in the presence of a limited quantity of potassium carbonate (1.33 mmol), gave only the above epoxides.

*Attempted Further Oxidation of the Epoxide (**19**) with MCPBA.* A solution of the epoxide (64 mg, 0.15 mmol) in dichloromethane (2 ml) was added to a solution of the per acid (0.5 mmol) in the same solvent (2 ml). The reaction mixture was stirred at room temperature for 2 h, when it was diluted with chloroform and washed successively with 0.5 M sodium hydroxide and water. Drying and evaporation furnished a solid (55 mg) consisting of a complex mixture of products (TLC).

Similarly, attempted oxidation of the epoxide mixture (**19**) with periodic acid in tetrahydrofuran resulted in a complex mixture of products.

We thank Drs. O. E. Edwards and H. Séguin of the NRC, Ottawa, Canada, for some of the elemental analysis and H. B. Machado of the IE-UFMG, Belo Horizonte, Brazil, for the mass spectra of benzodilactones.

References

1) A major part of this work was presented by M. B. Monteiro as M. Sc. Thesis to the University of Brasilia, 1976.

2) a) J. R. Mahajan, *Synthesis*, **1976**, 110; b) J. R. Mahajan and H. C. Araújo, *Synthesis*, **1975**, 54; c) J. R. Mahajan and H. C. Araújo, *ibid*, **1976**, 111; d) J. R. Mahajan, G. A. L. Ferreira, and H. C. Araújo, *J. Chem. Soc., Chem. Commun.*, **1972**, 1078.

3) W. Keller-Schierlein, *Fortschr. Chem. Org. Naturst.*, **30**, 313 (1973); M. Binder and C. Tamm, *Angew, Chem.*, **85**, 369 (1973); *Angew. Chem. Int. Ed. Engl.*, **12**, 370 (1973).

4) I. Roitman, J. R. Mahajan, L. H. S. Corrêa, J. B. Calixto, H. C. Araújo, G. A. L. Ferreira, and B. J. Nunes, Anais do V Congresso Brasileiro de Microbiologia, 1974, resumo 9, p. 186, and our unpublished data.

5) A. M. Patterson, L. T. Capell, and D. F. Walker, "The Ring Index," 2nd ed, American Chemical Society, Washington, D.C. (1960), p. 460.

6) a) M. von Strandtmann, M. P. Cohen, and J. Shavel, Jr., *J. Heterocyclic Chem.*, **7**, 1311 (1970); b) M. Tramontini, *Synthesis*, **1973**, 703; c) F. F. Blickem, *Org. React.*, **1**, 303 (1942); d) J. H. Brewster and E. L. Eliel, *ibid.*, **7**, 99 (1953).

7) W. T. Caldwell and T. R. Thompson, *J. Am. Chem. Soc.*, **61**, 765 (1939).

8) K. Taguchi and F. H. Westheimer, *J. Org. Chem.*, **36**, 1570 (1971).

9) K. Nakanishi, "Infrared Absorption Spectroscopy," Holden-Day, Inc., San Francisco and Nankodo Company Limited, Tokyo (1962), p. 42; R. N. Jones, P. Humphries, F. Herling, and K. Dobriner, *J. Am. Chem. Soc.*, **74**, 2820 (1952).

10) I. J. Borowitz, G. J. Williams, L. Gross, and R. Rapp, *J. Org. Chem.*, **33**, 2013 (1968); I. J. Borowitz, G. Gonis, R. Kelsey, R. Rapp, and G. J. Williams, *ibid.*, **31**, 3032 (1966).

11) J. K. Crandall, D. B. Banks, R. A. Colyer, R. J. Watkins, and J. P. Arrington, *J. Org. Chem.*, **33**, 423 (1968).

12) L. Fieser and M. Fieser, "Reagents for Organic Synthesis," Vol. 1, John Wiley, New York (1967), p. 817.

13) R. L. Augustine, Ed., "Oxidation," Vol. 1, Marcel Dekker, New York (1969), p. 17; S. Wolfe, S. K. Hasan, and J. R. Campbell, *Chem. Commun.*, **1970**, 1420.

14) G. Stork, A. Brizzolara, H. Landesman, J. Szmulszkovicz, and R. Terrell, *J. Am. Chem. Soc.*, **85**, 207 (1963); R. D. Burpitt and J. G. Thweatt, *Org. Synth.* Coll. Vol. 5, 277 (1973); K. C. Brannock, R. D. Burpitt, V. W. Goodlett, and J. G. Thweatt, *J. Org. Chem.*, **28**, 1462 (1963); M. E. Kuehne, *J. Am. Chem. Soc.*, **81**, 5400 (1959).

15) *Chem. Abstr.*, Index Guide, **75**, 213G (1971).

Semi-Empirical Configuration Interaction Studies on the π-Electron Spectra of Nonbenzenoid Molecules

N. K. Das Gupta* and F. W. Birss

Theoretical Chemistry Division, Chemistry Department, University of Alberta, Edmonton, Canada

(Received October 26, 1976)

A modification of the method of Yamaguchi *et al.* has been used to predict the π-electronic spectra of a number of nonbenzenoid molecules containing five- and seven-membered rings. Good correlation of the theoretical and experimental transition energies is found. The calculated intensities are also reasonably consistent with experiment, to the extent of raising questions as to the source of intensity in the bands of some molecules.

Semi-empirical self-consistent-field calculations have been applied to many molecules with π-electrons with considerable success in reproducing the electronic spectra and ground state properties such as heat of atomization and sites of reactivity.[1,2] The choice of parameters in the semi-empirical context is critical in some of these predictions. In particular, the value of β, the two-centre resonance integral, has a different range of values according to whether it is electronic spectra or heats of atomization that are to be predicted by the calculation.[1]

In the case of electronic spectra, there persist discrepancies between observed and calculated frequencies and oscillator strengths, even with an apparently adequate choice of β. In this paper we therefore report attempts to improve upon the predictions of spectra for some molecules for which we have recently given the results of self-consistent-fields calculations,[3,36,38] now using configuration interaction.

In such work, three primary variations in method can occur: the choice of formula for the two-centre resonance integral, the choice of formula for the two-centre two-electron repulsion integrals and the configurations to be included in the interaction study.

A computer programme was developed which was capable of generating all configurations arising from all possible one- and two-electron excitations involving all of the occupied and unoccupied orbitals obtained in a prior molecular orbital calculation. It was found that an adequate fit of the experimental spectra could be obtained using only those configurations arising from one-electron excitations, provided the orbitals were the self-consistent-field set, and that such a choice frequently gave a better fit than did the use of the full one- and two-electron excitation set. Therefore all of this work is on the basis of configurations arising from one-electron excitations involving orbitals obtained in a prior self-consistent-field calculation. In the case of the larger molecules studied in this work, even this restricted basis is unnecessarily large since many of the configurations which, within the orbital approximation, represent excitation beyond the ionization limit, contribute very little to the functions of interest: those with energies lying within about eight electron volts of the ground state. For such molecules a restricted number of the highest occupied orbitals and the lowest unoccupied orbitals were involved in excitations to form the configurations used as basis.

In the recent literature, two methods of calculating two-centre, two-electron repulsion integrals, γ_{ij}, have been much used: the formulae of Ohno[4] and of Nishimoto and Mataga.[5] The former has been used very successfully in the context of self-consistent-field studied toward obtaining heats of atomization and resonance energies.[1,2,6] We have also found it to be good for use for similar studies directed toward obtaining electronic spectra predictions.[3,36,38] In the present work, on the other hand, we have found that the Nishimoto-Mataga formula,

$$\gamma_{ij} = 14.397/(1.293+r_{ij}). \quad \text{(eV)} \qquad (1)$$

with r_{ij} the internuclear separation (Å), yields superior fitting between the observed spectra and those calculated using the configuration interaction method. In this formula the parameter value, 1.293, is chosen so that the one-centre two-electron repulsion integral, γ_{ij}, has the value 11.134 eV, equal to the difference between the sp^2 valenece state ionization energy (11.16 eV) and electron affinity (0.026 eV) for carbon.[7] In the self-consistent-field calculation, the γ_{ij} between neighbouring atoms were varied at each interaction on the basis of the internuclear separation, r_{ij}, calculated from the bond order (p_{ij})—bond length relation[8]

$$r_{ij} = 1.520 - 0.186p_{ij}. \quad \text{(Å)} \qquad (2)$$

The γ_{ji} integrals between non-neighbouring atoms were based upon a particular choice of molecular geometry and were not varied throughout the calculation. For the benzenoid systems the choice was with all bond lengths equal to 1.40 Å, all bond angles equal to 120°. For azulene,[9] aceheptylene,[10a] pentaleno[*def*]heptalene[10b] and acepleiadylene,[11] the structures reported in the literature were used. For the other molecuels, whose experimental structures were not available reasonable geometries[3,6,36,38] were selected.

The formula used for evaluation of the two-centre resonance integral between neighbouring centres was that of Yamaguchi *et al.*,[8a]

$$\beta_{ij} = \beta_0 \exp[1.7(1.397-r_{ij})], \qquad (3)$$

with the internuclear distance, r_{ij}, calculated as described above and varied at each self-consistent-field interaction. The parameter β_0 was chosen to depend upon the number of rings[8b] in the molecule under investigation, on the basis of fitting the spectra of benzenoid systems. For benzene, $\beta_0 = -2.38$ eV, for naphthalene and azulene, $\beta_0 = -2.28$ eV, and for larger molecules, $\beta_0 = -2.15$ eV were used. Results for these

* On leave of absence from Department of Chemistry, Visva-Bharati University, Santiniketan, West Bengal, India.

Table 1. $\pi^* \leftarrow \pi$ transitions and oscillator strengths, f

Molecule	Sym-metry	Experimental		Present work		Other work							
		eV	log ε (or f)	eV	f[c]	eV	f	eV	f	eV	f	eV	f[a]
I		Ref. 18				Ref. 14		Ref. 39		Ref. 40			
(10)[b]	B_{2u}	4.8		4.89	0	4.880		5.28	0	4.71	0		
	B_{1u}	6.2	0.1	6.19	0	5.760		5.90	0	6.01	0		
	E_{1u}	6.7	0.9	7.01	1.203	6.972		7.30	2.50	6.83	1.167		
II		Ref. 19				Ref. 14		Ref. 8		Ref. 40			
(26)	B_{3u}	4.0	0.002	4.02	0.001	4.033	0	4.18	0	4.02	0		
	B_{2u}	4.5	0.18	4.55	0.183	4.419	0.200	4.68	0.20	4.52	0.204		
	A_g			5.54	0	5.461	0	5.76	0				
	B_{3u}	5.6	1.70	5.61	1.901	5.582	1.960	5.77	1.96	5.66	1.949		
	B_{1g}			5.79	0	5.648	0	5.97	0				
	B_{1g}			6.10	0	5.993	0	6.29	0				
	B_{2u}	6.5	0.20	6.11	0.628	6.073	0.579	6.30	0.65	6.15	0.615		
	A_g			6.92	0	6.861	0						
				7.08	0	6.987	0						
	B_{1g}			7.58	0	7.536	0						
				7.65	0	7.603	0						
	B_{2u}	7.4	0.6	7.71	0.926	7.626	0.953						
III		Ref. 19				Ref. 14		Ref. 40		Ref. 41			
(26)	B_{3u}			3.46	0.003					3.58	0		
	B_{2u}	3.3	0.10	3.54	0.242	3.484	0.317	3.58	0.274	3.59	0.313		
						3.604	0						
	B_{1g}			4.62	0	4.656	0			4.50	0		
				4.63	0	4.677	0			4.79	0		
	A_g			4.70	0	4.814	0			4.81	0		
	B_{3u}	4.8	2.28	4.79	2.616	4.831	2.522	4.97	2.745	4.84	2.523		
										5.19	0.044		
	B_{2u}			5.30	0	5.264	0			5.36	0		
	B_{2u}	5.6	0.28	5.62	0.231	5.850	0.221	5.903	0.087	5.87	0.604		
	B_{3u}			5.72	0								
	B_{2u}			5.74	0.169	5.916	0.560						
	A_g			5.98	0	6.059	0						
				6.17	0	6.206	0			6.21	0		
				6.51	0	6.574	0						
	B_{1g}			6.65	0								
	B_{2u}	6.7	0.65	6.75	1.065								
IV		Ref. 20				Ref. 14		Ref. 39		Ref. 40			
(26)	A_1	3.8	0.003	3.61	0	3.630	0	4.00	—	3.75	0		
	B_2	4.2	0.18	4.19	0.244	4.157	0.322	4.15	0.30	4.28	0.311		
				4.45	0.006	4.615	0						
		4.9	1.09	4.88	1.564	4.922	1.486	4.73	1.78	5.03	1.541		
	A_1			4.99	0.544	4.978	0.540	5.04	1.09	5.12	0.572		
				5.18	0.002	5.249	0	5.17	—				
				5.44	0.270	5.497	0.330						
	B_2			5.73	0	5.757	0	5.23	—				
	A_1			5.75	0.001	5.820	0						
	B_2	5.8	0.60	5.89	0.283	5.950	0.265	5.85	0.24	5.67	0.303		
				6.03	0.099	6.071	0.200						
	A_1			6.43	0.001	6.445	0						
	B_2			6.44	0.002	6.468	0						
	A_1	6.6	0.59	6.53	0.455	6.657	0.446	6.32	0.26	6.15	0.263		
	B_2			6.58	0.162	6.763	0.125	6.74	0.47				
V		Ref. 21				Ref. 14		Ref. 40		Ref. 41			
(26)	B_{2u}	3.3	2.41	3.35	0	3.470	0	3.36	0	3.49	0		
	B_{3u}	3.7	4.74	3.64	0.629	3.556	0.680	3.68	0.701	3.64	0.675		
	B_{1g}			4.30	0	4.271	0			4.10	0		
	B_{1g}			4.38	0	4.306	0			4.27	0		

TABLE 1. (Continued)

Molecule	Sym-metry	Experimental eV	Experimental log ε (or f)	Present work eV	Present work f[c]	Other work eV	Other work f	Other work eV	Other work f	Other work eV	Other work f	Other work eV	Other work f[a]
	B_{2u}	4.6	4.73	4.73	0.099	4.703	0.948	4.84	0.956	4.77	0.954		
	A_g			4.86	0	4.832	0			4.90	0		
	B_{1g}			4.98	0	4.946	0			5.00	0		
	B_{3u}	5.2	4.94	5.14	1.612	5.207	1.468	5.38	1.616	5.25	1.485		
	A_g			5.21	0	5.199	0			5.08	0		
				5.27	0	5.266	0			5.33	0		
				5.95	0	5.939	0			5.98	0		
	B_{2u}	6.0	4.68	5.96	0.001	5.985	0						
	B_{1g}			6.02	0	5.997	0						
				6.04	0	6.040	0						
	B_{3u}	6.3	4.59	6.37	1.034	6.319	0.940			6.47	1.046		
VI		Refs. 20 and 22				Ref. 31		Ref. 32					
(82)	B_u	3.4	2.301	3.43	0.001	3.22	0.15	3.47	0.003				
	B_u	3.8	3.785	3.82	0.408	4.24	0.45	3.91	0.28				
	B_u	4.6	4.813	4.55	2.073	4.60	0.46	4.93	2.81				
	B_u			4.94	0.097								
	B_u			4.98	0.550								
	B_u			5.42	0.001								
	B_u	5.6	4.155	5.52	0.267	5.78	0.07	5.36	1.14				
	B_u			6.06	0.256								
	B_u	6.4	4.025	6.47	0.265	6.34	0.95						
	B_u	6.7	4.699	6.68	0.935								
VII		Ref. 23				Ref. 14		Ref. 8		Ref. 3b			
(26)	B_2	2.0	0.009	1.94	0.023	1.918	0.0221	2.05	0.025	2.28	0.13		
	A_1	3.4	0.08	3.42	0.005	3.370	0.005	3.53	0.005	3.63	0.85		
	B_2			4.26	0.132	4.221	0.117	4.41	0.13				
	A_1	4.5	1.10	4.65	1.827	4.616	1.818	4.78	1.88	4.10	0.47		
	B_2	5.2	0.38	5.50	0.392	5.499	0.443	5.68	0.41	5.05	0.28		
	A_1			5.83	0.010	5.806	0.022	6.03	0.010				
	B_2			6.19	0.188	6.147	0.118	6.41	0.19				
	A_1	6.4	0.65	6.51	0.387	6.439	0.402	6.72	0.39	6.17	0.22		
	B_2			6.80	0.744	6.791	0.782						
VIII		Ref. 16				Ref. 16		Ref. 15		Ref. 33			
(37)	B_2	2.7	1.4	3.05	0.014	2.75	0.04	2.614	0.041	2.796		2.74[49]	0.04
	B_2	3.7	3.7	3.63	0.124	3.75	0.31	3.699	0.243	3.744		3.72	0.30
	A_1	3.8	4.0	3.77	0.236	3.83	0.22	3.934	0.156	3.817		3.76	0.20
	A_1	4.5	3.5	4.59	0	4.75	0	4.551	0.044	4.824		4.74	0.002
	B_2	5.4	4.7	5.24	1.239	5.56	1.21	5.629	1.076	5.572		5.52	1.21
	A_1	≈6.14[49]		6.18	1.355								
IX		Ref. 24				Ref. 17		Ref. 13		Ref. 3b			
(37)	B_2	1.8		1.58	0.003	1.73	0.003	1.65	0	1.67	0.03		
	A_1	2.6	2.94	2.65	0.001	2.91	0.001						
	A_1	3.2	3.33					3.02	0	2.95	0.18		
	A_1	3.4	3.21	3.38	0.049	3.64	0.073			3.80	0.86		
	B_2	3.8	4.80	3.58	0.089	3.86	0.11	3.74	0.036	3.59	0.49		
	A_1							3.85	0.094				
	B_2	4.7	4.65	4.49	0.384	4.79	0.39	5.23	0.778	4.17	0.46		
	A_1			4.66	1.505								
X		Refs. 42 and 34				Ref. 36a		Ref. 31		Ref. 34			
(50)	B_{2u}	2.90		2.98	0.043			2.77	0.49				
		3.04											
		3.06								3.23	0.048		
		3.22				3.25	0.09	3.15	0.15				
	B_{3u}	3.64		3.52	0.276	3.51	0.65						
	B_{2u}	3.73		3.78	0.145	3.69	0.85	3.64	0.24	3.75	0.33		
		3.80								4.09	0.18		

Table 1. (Continued)

Molecule	Sym-metry	Experimental		Present work		Other work							
		eV	log ε (or f)	eV	f[c]	eV	f	eV	f	eV	f	eV	f[a]
	B_{2u}	5.23		5.07	0.00	5.28	0.44	5.04	0.37	5.41	0.008		
	B_{3u}	5.69		5.56	0.26	5.54	0.60	5.67	0.37	5.99	2.18		
	B_{2u}			5.62	2.002								
XI		Ref. 25				Ref. 36a		Ref. 15		Ref. 31			
(50)	B_2	2.22	2.05			2.52	0.20	2.173	0.065	2.774	0.08	2.33[49]	0.06
		2.92	2.58	2.81	0.036								
		3.23	3.20										
		3.35	3.68										
	A_1	3.49	3.85	3.49	0.352	3.51	0.70	3.359	0.334	3.454	0.67	3.34	0.41
	B_2	3.64	3.90	3.55	0.058					3.539	0.01	3.68	0.10
		4.20	3.95			3.94	0.48	3.910	0.051				
	A_1	4.35	3.95	4.49	0.001							4.46	0.003
	B_2	4.59	3.87			4.60	0.68	4.286	0.015				
	B_2	4.98	4.49	4.95	0.602	5.10	0.67			4.900	0.44	5.10	0.85
	A_1	5.06		5.11	0.161	5.21	0.25	5.089	0.022	5.168	0.07	5.14	0.52
	B_2	5.39	4.42	5.25	0.390	5.23	0.44			5.368	0.05	5.53	0.07
				5.34	0.019								
	A_1	≈5.77[49]		5.65	0.901							5.82	0.85
	B_2	5.93	4.60	5.83	0.534	6.08	0.29						
	A_1			5.91	0.544								
XII		Ref. 24				Ref. 17		Ref. 13		Ref. 3b			
(50)	B_2	1.6	2.108	1.45	0.012	1.52	0.014	1.56	0.01	1.68	0.07		
	A_1	2.9	2.81	2.66	0.005	2.89	0.009	3.09	0.038	3.29	0.17		
	B_2	3.3	4.09	3.26	0.279	3.47	0.30	3.46	0.16	3.28	0.70		
	A_1	4.0	4.0	4.26	0.531	3.82	0.14	4.06	0.087	4.13	0.53		
	B_2			4.16	0.013	4.48	0.019			4.25	0.35		
	A_1	4.8		5.10	0.321	4.57	0.53						
	B_2	4.9		4.64	1.438	4.95	1.44	4.94	0	5.20	0.07		
XIII		Ref. 51				Ref. 16		Ref. 15		Ref. 36a		Ref. 51	
(65)	B_2	3.07	0.012	3.40	0.002	3.32	0.01	3.331	0.023	3.44	0.24	3.57	0.005
	A_1	3.41	0.17	3.51	0.372	3.51	0.52	3.583	0.640	3.57	0.81	3.69	0.43
	B_2	3.84	0.05	3.68	0.051	3.93	0.08	4.094	0.068	4.03	0.52	3.91	0.06
	A_1	4.30	0.55	4.26	0.214	4.48	0.22	4.697	0.199			4.50	0.22
	A_1	4.70	(0.14)[d]	4.75	0.020	5.08	0.01			4.83	0.53	5.03	0.02
	B_2	4.73	(0.08)	4.98	0.069	5.13	0.05	5.196	0.028	4.96	0	5.19	0.06
	A_1			5.06	0.517	5.26	0.60			5.18	0.20		
	B_2	5.23	0.44	5.12	1.078	5.39	1.28	5.252	0.003	5.57	0.01	5.34	1.16
	A_1	5.39	(0.13)	5.53	0.829							5.31	0.58
	A_1	5.73	0.26	5.90	0.012							5.80	0.81
	B_2	6.08	(?)	6.07	0.241							6.17	0.01
XIV		Refs. 12 and 25				Ref. 3a		Ref. 15		Ref. 34			
(65)	A_1	2.5	3.6	2.82	0.259			2.504	0.002	2.98	0.28		
								2.553	0.056				
	B_2	3.0		2.95	0.013	2.9	0.26	2.986	0.115	3.15	0.026		
				3.09	0.059	3.1	0.31						
						3.3	0.98			3.32	0.066		
	B_2	3.8	4.6	3.54	0.017	3.9	0.43	3.998	1.715	3.87	0.025		
	A_1			4.25	0.642	4.2	0.39	4.187	0.207	4.50	0.96		
				4.35	0.365	4.4	0.51			4.67	0.16		
						4.6	0.0						
	B_2	4.8	4.3	4.79	0.798	4.7	0.01			5.09	0.87		
						5.0	0.0						
	A_1			4.90	0.032					5.13	0.010		
	A_1			5.27	0.027	5.34[g]	0.44			5.26	0.021		
	B_2			5.29	0.375	5.35[g]	0.23						
	B_2					5.4	0.01						

TABLE 1. (Continued)

Molecule	Sym-metry	Experimental eV	Experimental log ε (or f)	Present work eV	Present work f[c]	Other work eV	Other work f	Other work eV	Other work f	Other work eV	Other work f	Other work eV	Other work f[a]
	B_2			5.67	0.111								
	A_1									5.64	0.021		
	B_2	5.8		5.84	0.665	5.84[g]	0.31			5.68	0.40		
	A_1			5.91	1.043								
XV		Refs. 12 and 26				Ref. 3a		Ref. 15		Ref. 12			
(65)		2.2	2.8	2.36	0.080	2.6	0.46	1.803		2.10	0.08		
		3.0	3.4	3.04	0.068	2.9	0.24	2.792		2.89	0.3		
				3.47	0.054			3.496					
		3.6	3.9	3.65	0.182	3.7	0.73	3.722		3.61	0.6		
						3.8	0.35						
		4.0		4.04	0.051	4.1	0.49	4.153		3.90	0.1		
						4.2	0.18						
										4.31	0.2		
				4.66	0.223								
		4.6	4.5	4.70	0.623	4.7	0.42			4.51	1.3		
XVI		Refs. 12 and 27				Ref. 3a		Ref. 15		Ref. 12			
(65)		2.4	2.9	2.44	0.107			1.949		2.23	0.1		
						2.8	0.24						
		2.9	3.8	3.08	0.095	2.9	0.77	2.746		2.90	0.5		
		3.4		3.41	0.092	3.5	0.21	3.674					
				3.75	0.160					3.78	0.3		
				4.12	0.071	3.9	0.56	3.910		3.83	0.07		
		4.3	4.5	4.52	0.234	4.3	0.49	4.118		4.18	1.2		
						4.4	0.16			4.37	0.8		
				4.57	0.494	4.6	0.32						
		4.9	4.8	4.73	0.913	5.0	0.11			4.61	0.4		
						5.2	0.37						
XVII						Ref. 3b		Ref. 12					
(26)	B_2			0.54	0.029	0.77	0.09	0.22	0.01				
	A_1			2.29	0.092	2.37	0.27	1.98	0.2				
	A_1			2.36	0.135	2.49	0.19	2.22	0.03				
	B_2			2.98	0.006			3.39	0.004				
	B_2			3.29	0.019	3.37	0.48	3.45	0.02				
	B_2			4.05	0.353	3.77	0.85	3.90	1.6				
	A_1			4.08	0.158	4.26	0.47						
	B_2			4.16	0.009	4.21	0.09						
						4.23	0.00						
	A_1			4.36	0.125	4.48	0.09						
	B_2			4.80	2.321								
	A_1			5.09	0.766								
	A_1			5.48	0.076								
XVIII		Refs. 12 and 28				Ref. 3a		Ref. 12					
(65)		1.8	2.1	1.65	0.006			1.81	0.004				
		2.2	3.1	2.18	0.009	2.2	0.016	2.38	0.05				
		2.8	3.8	2.96	0.056	2.9	0.21	3.11	0.3				
				3.11	0.076	3.0	0.55	3.20	0.09				
		3.4		3.58	0.101	3.4	0.53	3.66	1.1				
				3.95	0.074	3.8	0.37	4.07	0.9				
				4.17	0.522	4.1	0.31	4.30	0.2				
		4.3		4.43	1.665	4.3	0.22	4.43	1.1				
		4.9		4.84	0.277	5.0	0.20						
XIX		Ref. 29				Ref. 3b		Ref. 12		Ref. 35			
(26)	B_{1g}	(1.61)	(1—1.65)	1.67	0	1.83	0	1.82	0	1.81	Forb.		
	B_{2u}	2.6	4.11	2.41	0.139			2.54	0.2	2.62	0.163		
	A_g			2.98	0			3.05	0	3.19	Forb.		
	B_{3u}	3.0	2.92	3.21	0.010	3.27	0.74	3.20	0.1	3.46	0.015		

Table 1. (Continued)

Molecule	Sym-metry	Experimental eV	Experimental log ε (or f)	Present work eV	Present work f[c]	Other work eV	Other work f	Other work eV	Other work f	Other work eV	Other work f	Other work eV	Other work f[a]
	B_{2u}	3.6	4.13	3.86	0.048	3.51	0.73	3.91	0.0004				
	B_{3u}	4.2	4.32	3.98	0.678	4.07	0.23	3.72	1.7				
	B_{2u}	4.6	5.03	4.70	0.987	4.59	0.59	4.18	2.1	4.19	0.51		
XX		Ref. 43				Ref. 12		Ref. 3b		Ref. 35		Ref. 43	
(65)	B_{1g}	1.74	0.002	1.61	0	1.84	0	1.72	0	1.85	0	1.88	0
	B_{2u}	2.47	0.04	2.40	0.205	2.64	0.5			2.68	0.254	2.54	0.24
	A_g	2.93	0.002	2.95	0	2.93	0	3.08	0	3.21	0	2.85	0
	B_{3u}	3.19	0.09	3.19	0.025	3.20	0.2	3.25	1.27	3.47	0.058	3.21	0.16
		3.22											
	B_{2u}	3.60	0.09	3.64	0.004	3.47	0.4	3.57	0.63	3.93	0.007	3.66	0.09
	B_{1g}			3.87	0			3.84	0				
	B_{3u}	3.87	0.26	4.08	0.619			3.87	0.61			4.41	0.45
	B_{2u}	4.33	1.2	4.49	2.810	4.01	2.5	4.00	0.97			4.74	3.25
	B_{3u}	4.65		5.18	0.486							5.38	0.43
	B_{1g}	5.02		5.22	0							5.51	0
	A_g	5.27		5.25	0							5.56	0
	A_g	5.52		5.53	0								
XXI		Ref. 30				Ref. 3b		Ref. 35					
(82)	B_2	1.2	1.74	1.03	0.012	1.41	0.01	1.19	0.017				
	A_1	2.1	2.44	2.08	0.006	2.57	0.04	2.29	0.005				
	B_2			2.93	0.049			3.18	0.191				
	A_1	3.1	3.67	3.07	0.114	3.21	0.01	3.36	0.117				
	A_1			3.26	0.146			3.54	0.208				
	B_2	3.7	3.88	3.64	0.236	3.76	0.14						
	B_2			3.83	0.054								
	B_2	4.2	4.88	4.10	1.221	4.26	0.78						
	A_1			4.78	1.205								
	B_2			5.20	0.726								
	A_1	5.32	4.40	5.34	0.468	5.17	0.01						
XXII						Ref. 34		Ref. 31		Ref. 36a			
(82)	B_{1g}			2.07	0	2.15	0			1.70	0		
	B_{3u}			2.93	0.006			2.628	0.59	3.25	0.33		
	B_{2u}			3.07	0.527	3.13	0.014	3.096	0.01	3.16	1.00		
	B_{3u}			3.42	0.113	3.30	0.60	3.449	0.15	3.48	0.38		
	B_{2u}					3.69	0.15						
	A_g			4.16	0	4.51	0			4.41	0		
	B_{3u}			4.38	0.036			4.519	0.03	4.45	0.58		
	A_g			4.52	0	4.94	0			4.79	0		
	B_{2u}			4.94	0.989	4.70	0.091	5.111	1.08	4.95	1.00		
	B_{3u}			5.11	1.304	5.30	1.17						
	B_{1g}			5.34	0	5.46	0						
	B_{2u}			5.69	1.072	5.49	1.71			5.25	0.44		
XXIII		Ref. 50				Ref. 36a		Ref. 50					
(82)	B_2	1.45≃3.00		1.99	0.089	1.98	0.28	1.52					
	A_1	2.46	2.00										
	A_1	2.86	4.00	3.06	0.417	3.21	1.03	2.93					
	B_2	3.29		3.39	0.086			3.45					
	A_1	3.61	3.60	3.97	0.004	3.83	0.37	3.82					
	B_2	4.09		3.78	0.090	3.88[e]	0.15	3.66					
	A_1	4.25		4.31	0.643	4.33	0.95	3.87					
	B_2	4.45≃4.30		4.78	0.354	4.74	0.65	4.28					
	A_1	4.77≃4.30		4.82	1.019			4.80					
	B_2			4.95	0.297								
	A_1			4.96	0.171	5.06	0.07	4.88					
	B_2	5.13≃4.30		5.25	0.013	5.19[e]		5.18					
	A_1			5.45	0.082			5.33					

TABLE 1. (Continned)

Molecule	Sym-metry	Experimental eV	Experimental log ε (or f)	Present work eV	Present work f[c]	Other work eV	Other work f	Other work eV	Other work f	Other work eV	Other work f	Other work eV	Other work f[c]
	B_2			5.55	0.084								
	B_2	5.75	4.48	5.79	0.960			5.64					
XXIV		Ref. 45				Ref. 36a		Ref. 52					
(82)		3.40	3.96	3.12	0.064	3.25	0.27	3.26	0.06				
		3.54	3.99	3.44	0.380	3.26	0.78	3.60	0.48				
		4.13	3.58	4.02	0.241	4.18	0.52	4.13	0.03				
		4.59	3.96	4.57	0.017	4.55	0.71	4.55	0.23				
				4.75	0.435			4.74	0.07				
				4.97	0.813			4.96	0.22				
		5.20	4.54	5.17	0.751	5.27	0.43	5.31	0.41				
		5.39	4.58	5.39	0.299	5.36	0.26	5.39	0.17				
								5.53	0.85				
XXV						Ref. 36a		Ref. 44					
(82)	B_2			2.40	0.002	2.05	0.01	2.01					
								3.15					
	A_1			3.24	0.446	3.35	0.88	3.20					
	B_2			3.83	0.099	3.90	0.84	3.87					
								4.62					
	A_1			4.78	0.550	4.63	0.02	4.75					
	A_1			5.18	0.423	5.20	0.51	5.11					
	B_2			5.49	1.404	5.42	0.37	5.48					
XXVI		Ref. 46				Ref. 36a							
		1.84	3.20										
(82)	B_2	1.91	3.17	2.11	0.093	2.26	0.34	1.98[53),f)]					
		2.01	3.14										
	A_1			2.28	0.164			2.21					
	B_2	3.29	4.69	3.08	0.033	3.22	0.30	3.24					
	A_1	3.43	4.51	3.62	1.709	3.52	0.70	3.59	>0.2				
	A_1	3.91	4.04[53),f)]	3.79	0.137			3.76					
								3.80	<0.02				
								3.81					
	B_2	4.23	4.25	4.12	0.035	4.04	0.39	4.27	<0.02				
	B_2	4.38	4.23	4.59	0.672	4.29	0.05	4.33					
	A_1	5.17	4.23	5.09	0.548	4.98	0.02						
	A_1	5.46	4.32	5.24	0.165	5.52	0.45						
	A_1			5.52	0.211								
XXVII						Ref. 36a							
(82)				2.92	0.320	2.97	0.35						
				2.95	0.123								
				3.35	0.027	3.13	0.97						
				3.50	0.084	3.43	0.31						
				3.94	0.187	3.79	0.38						
				4.30	0.088								
				4.35	0.679	4.41	0.55						
				4.43	0.222	4.49	0.32						
				4.80	0.114								
				4.89	0.870	4.84	0.40						
				5.09	0.338								
				5.46	0.153	5.41	0.41						
XXVIII		Ref. 47				Ref. 36a		Ref. 37		Ref. 31			
(82)	B_{3u}	3.02	4.55	3.13	0.696	3.24	1.08	3.06		2.779	1.20		
	B_{2u}	3.38	3.98	3.28	0.035					4.434	0.02		
		3.55	3.58			3.78	0						
	B_{3u}	4.24	5.10	4.21	0.436	4.20	0.89	3.98		4.003	0.07		
	B_{3u}	4.72	4.53	4.85	0.997	4.86	0.62			4.645	0.32		
	B_{2u}	4.90	4.56	4.96	0.260	5.04	1.00	4.85		4.825	0.16		

Table 1. (Continued)

Molecule	Sym-metry	Experimental eV	Experimental log ε (or f)	Present work eV	Present work f[c]	Other work eV	Other work f	Other work eV	Other work f	Other work eV	Other work f	Other work eV	Other work f[a]
XXIX		Ref. 48				Ref. 38							
(82)	B_{3u}	3.22	4.19	3.16	0.718	3.22	0.97						
	B_{3u}	4.26	4.09	4.42	0.001	4.14	0.56						
	B_{2u}	5.07	4.30	4.88	0.509	5.31	0.24						
	B_{3u}			5.11	0.082								
	B_{2u}	5.52	4.72	5.55	1.438	5.52	0.93						

a) f-Values quoted in column 8 were not included in Ref. 3a (molecules XIV—XVI and XVIII). b) Figure in the parentheses in the first column indicates the number of configurations. c) Figures in fourth column are f-values for molecules I—IV and VII and others they correspond to log ε. d) Values in parentheses in third column refer to shoulder. e) Not included in the Ref. 36a. f) f-Values not shown lie between 0.02 to 0.2. g) Not included in the Ref. 3a.

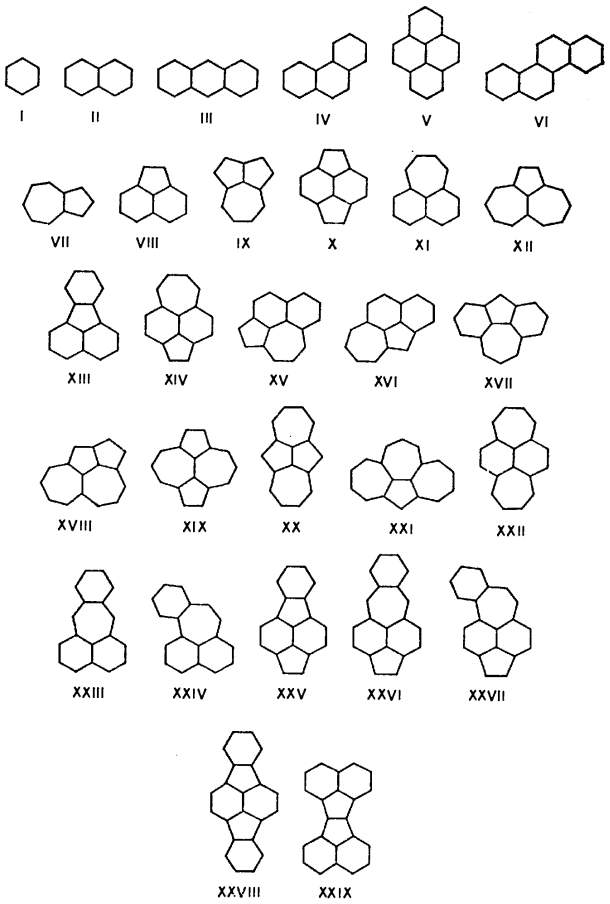

Fig. 1. Molecules studied.
I: Benzene, II: naphthalene, III: anthracene, IV: phenanthrene, V: pyrene, VI: chrysene, VII: azulene, VIII: acenaphthylene, IX: aceazulylene, X: pyracylene, XI: pleiadiene, XII: acheptylene, XIII: fluoranthene, XIV: acepleiadylene, XV: naphth[*cde*]-azulene, XVI: cyclohept[*bc*]acenaphthylene, XVII: cyclohept[*def*]fluorene, XVIII: pentaleno[*def*]heptalene, XIX: azupyrene, XX: dicyclohepta[*cd,gh*]-pentalene, XXI: azuleno[8,8a,1,2-*def*]heptalene, XXII: dipleiadadiene, XXIII: benzopleiadiene, XXIV: benzo[4,5]cyclohepta[1,2,3-*de*]naphthalene, XXV: acefluoranthylene, XXVI: benzo[6,7]acepleiadylene, XXVII: benzo[5,6]acepleiadylene, XXVIII: indeno[1,2,3-*cd*]fluoranthene, XXIX: acenaphth[1,2-*a*] acenaphthylene.

standardization molecules are included in Table 1.

Results and Discussion

The calculated electronic spectra are given in Table 1, along with any available experimental data and other theoretical predictions. The standard deviation of the differences between observed and calculated transition energies for the bands chosen for the standardization of β_0 is 0.08 eV. For these benzenoid systems the agreement between theory and experiment is generally very good, with an overall fit as good as, or better than, that achieved by other workers. The results of azulene, a subsidiary test molecule, are also of good quality.

We have reported elsewhere[3,36,38] and included here for comparison, the predicted transitions for some non-benzenoid hydrocarbons (molecules VII to XXIX) using a different parameterization and the self-consistent field method. In almost all cases the present results achieved a consistently better correlation with experiment. The comparison with the results of other workers[8,12,17,31,33–35,37] yields the same general conclusion.

In most cases there is not only reasonable agreement for the transition energies but also a definite, if rough, agreement in the trends followed by the intensities. There are, however, notable exceptions, when the theoretical intensity is reasonably large. Examples of this are the 4.5 eV transition of acenaphthylene and the 3.8 eV transition of acepleiadylene. An experimental study of such transitions to determine whether their intesity may be due to vibronic coupling would be worthwhile.

In recent years Michl *et al.*[49–53] studied the electronic structure of the excited states of some of the molecules studied here (VIII, XI, XIII, XX, XXIII, XXIV, and XXVI). If we consider single excitations then it would be clear from the table that our results are in better agreement with the experiment than those of Michl *et al.*

Conclusion. It has been found that by slight modification of the method of Yamaguchi *et al.* by making the value of β_0 dependent on the size of the molecules $\pi^* \leftarrow \pi$ spectral transitions of a large number of conjugated systems can be predicted with reasonably

good accuracy.

We are grateful to the National Research Council for a grant in aid to this research, both for computing funds and for a fellowship for N. K. Das Gupta. The use of the facilities of the Computing Services of the university is acknowledged with pleasure.

References

1) A. L. H. Chung and M. S. J. Dewar, *J. Chem. Phys.*, **42**, 756 (1965).
2) a) D. H. Lo and M. A. Whitehead, *Can. J. Chem.*, **46**, 2027 (1968); b) M. J. S. Dewar and C. DeLlano, *J. Am. Chem. Soc.*, **91**, 789 (1969); c) M. J. S. Dewar and A. J. Harget, *Proc. R. Soc., Ser A*, **315**, 443 (1970).
3) a) F. W. Birss and N. K. Das Gupta, *Can. J. Chem.*, **49**, 2840 (1971); b) A. Das Gupta and N. K. Das Gupta, *Can. J. Chem.*, **52**, 155 (1974); **53**, 915 (1975).
4) K. Ohno, *Theor. Chem. Acta*, **2**, 219 (1964).
5) N. Mataga and K. Nishimoto, *Z. Phys. Chem.*, **13**, 140 (1957).
6) A. Das Gupta and N. K. Das Gupta, *Tetrahedron*, **28**, 3587 (1972).
7) J. Hinze and H. H. Jaffé, *J. Am. Chem. Soc.*, **84**, 540 (1962).
8) a) H. Yamaguchi, T. Nakajima, and T. L. Kunii, *Theor. Chem. Acta*, **12**, 349 (1968); b) K. Nishimoto and R. Fujishiro, *Bull. Chem. Soc. Jpn.*, **37**, 1660 (1964).
9) J. M. Robertson, H. M. M. Shearer, G. A. Sim, and D. G. Watson, *Acta Crystallogr.*, **15**, 1 (1962).
10) a) R. Quasba, F. Brandl, W. Hoppe, and R. Huber, *Acta Crystallogr., Ser B*, **25**, 1189 (1969); b) H. J. Lindner, *Chem. Ber.*, **102**, 2456 (1969).
11) A. W. Hansen, *Acta Crystallogr.*, **13**, 215 (1960); **21**, 97 (1966).
12) P. Baumgartner, E. Weltin, G. Wagniere, and E. Heilbronner, *Helv. Chim. Acta*, **48**, 751 (1965).
13) N. K. Das Gupta and M. A. Ali, *Theor. Chim. Acta*, **4**, 101 (1966).
14) K. Nishimoto and L. S. Forster, *Theor. Chim. Acta*, **3**, 407 (1965).
15) J. Koutecky, P. Hochman, and J. Michl, *J. Chem. Phys.*, **40**, 2439 (1964).
16) E. Heilbronner and J. P. Weber, J. Michl, and R. Zahradnik, *Theor. Chim. Acta (Berl.)*, **6**, 141 (1966).
17) H. Yamaguchi, T. Terasaka, and T. Nakajima, *Theor. Chim. Acta*, **18**, 255 (1970).
18) J. N. Murrell, "The Theory of the Electronic Spectra of Organic Molecules," Chapman and Hall Ltd., London (1971), p. 127.
19) *Ibid*, p. 120.
20) H. B. Klevens and J. R. Platt, *J. Chem. Phys.*, **17**, 470 (1949).
21) "UV Atlas of Organic Compounds," Vol. II, Butterworths, (1966), p. E6/5.
22) *Ibid*, Vol. III, (1967), p. E5/1.
23) E. Heilbronner, "Nonbenzenoid Aromatic Compounds," ed by D. Ginsberg, Interscience Publishers, Inc., N. Y. (1959), p. 196; R. Pariser, *J. Chem. Phys.*, **25**, 1112 (1956); G. R. Hunt and I. G. Ross, *J. Mol. Spectrosc.*, **9**, 52 (1962).
24) K. Hafner and J. Schneider, *Liebigs Ann. Chem.*, **624**, 37 (1959).
25) V. Bockelheide and G. K. Vick, *J. Am. Chem. Soc.*, **78**, 653 (1956).
26) P. D. Gardner, C. E. Wulfman, and C. L. Osborn, *J. Am. Chem. Soc.*, **80**, 143 (1958).
27) D. H. Reid, W. H. Stafford, and J. P. Ward, *J. Chem. Soc.*, **1955**, 1193.
28) K. Hafner, R. Fleischer, and K. Fritz, *Angew. Chem. Int. Ed. Engl.*, **4**, 69 (1965).
29) A. G. Anderson, Jr., A. A. MacDonald, and A. F. Montana, *J. Am. Chem. Soc.*, **90**, 2993 (1968).
30) K. Hafner, G. Hafner-Schneider, and F. Baur, *Angew. Chem. Int. Ed. Engl.*, **7**, 808 (1968).
31) G. Fuvini, A. Gamba, M. Simonetta, *Theor. Chim. Acta*, **13**, 175 (1969).
32) N. S. Ham and K. Rudenberg, *J. Chem. Phys.*, **25**, 13 (1956).
33) P. Hochman, R. Zahradnik, and V. Kvasnicka, *Collect. Czech. Commun.*, **33**, 3478 (1968).
34) H. Yamaguchi and T. Nakajima, *Bull. Chem. Soc. Jpn.* **44**, 682 (1971).
35) A. Toyota and T. Nakajima, *Bull. Chem. Soc. Jpn.*, **46**, 2284 (1973).
36) a) A. Das Gupta and N. K. Das Gupta, *Tetrahedron*, **33**, 169 (1977); b) *Can. J. Chem.*, **54**, 3227 (1976).
37) N. K. Ray and K. K. Sharma, *Indian J. Chem.*, **10**, 668 (1972).
38) A. Das Gupta and N. K. Das Gupta, *J. Mol. Struct.*, **27**, 113 (1975).
39) E. Weltin, J. P. Weber, and E. Heilbronner, *Theor. Chim. Acta*, **2**, 114 (1964).
40) J. E. Bloor, B. R. Gilson, and N. Brearley, *Theor. Chim. Acta*, **8**, 35 (1967).
41) K. Nishimoto, *Theor. Chim. Acta*, **7**, 207 (1967).
42) B. M. Trost, G. M. Brigt, C. Frihart, and D. Britelli, *J. Am. Chem. Soc.*, **93**, 737 (1971).
43) V. Cratochvil, J. Kolc, and J. Michl, *J. Mol. Spectrosc.*, **57**, 436 (1975).
44) R. Zahradnik, "Nonbenzenoid Aromatics," ed by J. P. Snyder, Academic Press, (1971), p. 57.
45) J. M. Muller, D. Cogniant, and P. Cogniant, *Tetrahedron Lett.*, **1971**, 45; J. T. Craig, K. W. Tan, and A. D. Woolhouse, *Tetrahedron Lett.*, **1971**, 3209.
46) M. P. Cava and R. H. Schlessinger, *J. Am. Chem. Soc.*, **85**, 835 (1963); *Tetrahedron*, **21**, 3051 (1965).
47) H. W. D. Stubbs and S. H. Tucker, *J. Chem. Soc.*, **1951**, 2936.
48) R. L. Letsinger and J. A. Gilpin, *J. Org. Chem.*, **29**, 243 (1964).
49) E. W. Thulstrup and J. Michl, *J. Am. Chem. Soc.*, **98**, 4533 (1976); J. Kolc and J. Michl, *ibid.*, **98**, 4540 (1976).
50) J. Kolc, J. W. Downing, A. P. Manzara, and J. Michl, *J. Am. Chem. Soc.*, **98**, 930 (1976).
51) J. Kolc, E. W. Thulstrup, and J. Michl, *J. Am. Chem. Soc.*, **96**, 7188 (1974).
52) J. F. Muller, D. Cagniant, O. Chavlet, D. Lavalette, J. Kole and J. Michl, *J. Am. Chem. Soc.*, **96**, 5038 (1974).
53) J. Kolc and J. Michl, *J. Am. Chem. Soc.*, **95**, 7391 (1973).

The Codimerization of Styrene and Butadiene with Three-Component Catalysts Consisting of Palladium Salt, Lewis Acid, and Tertiary Phosphine

Takehiko Ito and Yasuo Takami

National Chemical Laboratory for Industry, 1-1, Honmachi, Shibuya-ku, Tokyo 151

(Received September 29, 1977)

The reaction of styrene and butadiene in the presence of a three-component catalyst consisting of a palladium salt, a Lewis acid, and a tertiary phosphine was investigated. As the three-component catalyst, combinations of such palladium(II) salts as $(\pi\text{-}C_3H_5PdCl)_2$, $(PdCl_2\cdot C_6H_5CH{=}CH_2)_2$ and $Pd(acac)_2$, such Lewis acids as BF_3 and $AlCl_3$, and such tertiary phosphines as Ph_3P and Bu_3P were adopted. From the reaction, 1-phenyl-1,4-hexadiene (a straight-chain codimer) was obtained as the main product, together with small amounts of branched-chain codimers. The ratio of the 1-phenyl-1,4-hexadiene to the branched-chain codimers was varied to some extent by changing the molar ratio of styrene to butadiene. With an increase in the molar ratio the ratio of 1-phenyl-1,4-hexadiene to the branched-chain codimers decreased. A reaction mechanism for the selective formation of 1-phenyl-1,4-hexadiene which involves the addition of butadiene, in preference to styrene, to a palladium hydride is proposed.

Recently dimerizations and codimerizations of olefins catalyzed by organometallic complexes have attracted much attention because of the utility of the reaction products and the novelty of the type of reaction, and a number of studies have been reported. However, the codimerization between two olefins such as butadiene and styrene, both of which coordinate strongly to catalyst metals, is very difficult; only the cotrimerization of two moles of butadiene with one mole of styrene has been reported.[1]

In the course of our study of a three-component catalyst system[2] consisting of a palladium salt, a Lewis acid, and a tertiary phosphine, we have found that the codimerization of styrene with butadiene proceeds smoothly by the use of this catalyst system, thus affording 1-phenyl-1,4-hexadiene.[3] In the present paper, details of the codimerization, which is the first example of the catalytic synthesis of 1-phenyl-1,4-hexadiene, will be reported.

Experimental

Reagents. Palladium complexes and a 1:1 adduct of boron trifluoride and triphenylphosphine ($BF_3\cdot Ph_3P$) were synthesized according to the methods described in the literature. $BF_3\cdot Ph_3P$: mp 176 °C (lit,[4] mp 175 °C). The nitrobenzene was used after drying with diphosphorus pentaoxide. The other reagents were used after drying and purification according to the usual manners.

Synthesis of 1-Phenyl-1,4-hexadiene. Into a 100-ml stainless-steel autoclave cooled in a ethanol–Dry Ice bath, 30 ml (345 mmol) of butadiene, 20 ml (170 mmol) of styrene, 10 ml of dichloromethane, and a solution of 0.6 mmol of $BF_3\cdot Ph_3P$ and 0.3 mmol of di-μ-chlorobis(π-allyl)dipalladium ($(\pi\text{-}C_3H_5PdCl)_2$) in 10 ml of dichloromethane were introduced under a nitrogen atmosphere. The mixture was then stirred for 1 h at 100 °C. The unreacted butadiene was purged after cooling, and then a small amount of an aqueous solution of sodium carbonate was added to decompose the catalyst. After the precipitate has been removed by filtration, the reaction mixture was distilled, and a fraction with a bp of 95—100 °C/4 mmHg was collected. GLC analysis of this fraction showed that it contained 11.2 g (71 mmol) of 1-phenyl-1,4-hexadiene. From this fraction, 1-phenyl-1,4-hexadiene (*trans,trans*-isomer 88%, *cis,trans*-isomer 12%) (bp 94 °C/5 mmHg (lit[5], 122 °C/21 mmHg)) was easily separated by distillation using a spinning-band column (length, 50 cm).

Codimerization under Various Reaction Conditions. The codimerization reactions shown in Tables 1—4 were carried out in a manner similar to that described above. After the decomposition of the catalyst, the reaction products were analyzed in the following way.

Analysis of the Reaction Products. To the reaction mixture, biphenyl was added as an internal standard. A small amount of aliquots of the reaction mixture and its catalytic hydrogenation product with palladium–charcoal was analyzed by GLC. From the results of the GLC analysis, the yields of 1-phenyl-1,4-hexadiene, individual dimers of butadiene and styrene, and the trimer of butadiene and the composition of the skeleton isomers of the codimer were determined.

The codimers were analyzed using a Golay column after removing the nitrobenzene used as a solvent and the high-boiling products by means of a precut column. Golay column: Silicone DC 550, 45 m × 0.25 mmϕ, 130 °C. Carrier gas: N_2 1 ml/min. Precut column: PEG 9000, 40 cm × 3 mmϕ. The high-boiling products were analyzed by using a column (Silicone KF 45, 10% Diasolid M, 3 m × 3 mmϕ) at 230 °C.

Structure Determination of the Reaction Products. A typical gas chromatogram of the products in the presence of $(\pi\text{-}C_3H_5PdCl)_2$–$BF_3\cdot Ph_3P$ catalyst is shown in Fig. 1. The main components of the reaction products were separated by a combination of fractional distillation and preparative GLC, and their structures were determined by means of IR, NMR, *etc.*

Peak 1: 1,3,6-Octatriene.

Peak 2: 5-Phenyl-1,3-hexadiene. IR; 1002 cm^{-1}, 898 cm^{-1}, 1648 cm^{-1} ($H_2C{=}CH{-}CH{=}CH{-}$). Hydrogenation gave 2-phenylhexane.

Peak 3: 1-Phenyl-3-methyl-1,4-pentadiene. IR; 912 cm^{-1}, 993 cm^{-1} ($-CH{=}CH_2$), 965 cm^{-1}, 1635 cm^{-1} (*trans*-CH=CH–). Hydrogenation gave 1-phenyl-3-methylpentane.

Peak 4: From the fact that hydrogenation gave dodecane, it was presumed to be dodecatetraene (a trimer of butadiene).

Peaks 5, 6: Since hydrogenation gave 1-phenylhexane, they were presumed to be 1-phenylhexadiene.

Peak 7: *trans, trans*-1-Phenyl-1,4-hexadiene. IR; 963 cm^{-1}, 1650 cm^{-1} (*trans*-CH=CH–). NMR; 1.65 ppm (3H, m,

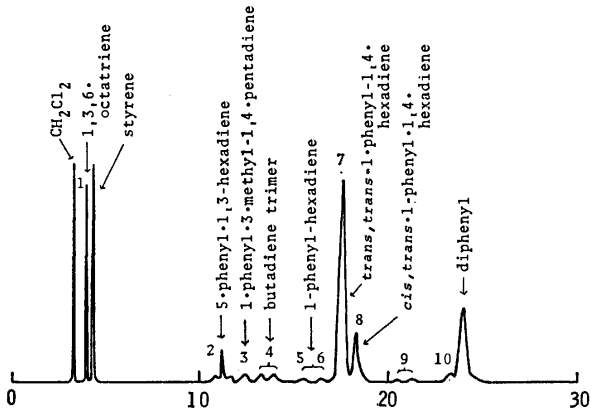

Fig. 1. Gas chromatogram of the compounds obtained by the reaction of butadiene and styrene in the presence of the catalyst consisting of $(\pi\text{-}C_3H_5PdCl)_2$–$BF_3\cdot Ph_3P$. ($(\pi\text{-}C_3H_5PdCl)_2$ 0.15 mmol, $BF_3\cdot Ph_3P$ 0.3 mmol, CH_2Cl_2 20 ml, styrene 170 mmol, butadiene 170 mmol, reaction time 1 hr, reaction temperature 100 °C). (Column. Golay column 45 m, temperature 120 °C)

CH_3–C=), 2.8 ppm (2H, m, =C–CH_2–C=), 5.2—6.3 ppm (4H, m, olefin proton), 7.25 ppm (5H, m, ring proton). Hydrogenation gave 1-phenylhexane.

Peak 8: *cis,trans*-1-Phenyl-1,4-hexadiene. IR; 963 cm^{-1}, 710 cm^{-1}, 1650 cm^{-1}. Hydrogenation gave 1-phenylhexane.

The constitutions of the products under the conditions adopted in Fig. 1 were approximately as follows: Peak 2, 6%; Peak 3, 2%; Peak 4, 4%; Peak 5+Peak 6, less than 1%; Peak 7, 77%; Peak 8, 11%; Peak 9+Peak 10, less than 1%. The constitutions of the alkylbenzene obtained by hydrogenation of the codimers formed in the above reaction were: 1-phenylhexane 89%, 2-phenylhexane 8%, 1-phenyl-3-methylpentane 3%.

Reaction of $(\pi\text{-}C_3H_5PdCl)_2$, $BF_3\cdot Ph_3P$ and Styrene. To a solution of 1.51 mmol of $(\pi\text{-}C_3H_5PdCl)_2$ and 3.03 mmol of $BF_3\cdot Ph_3P$ in 7 ml of nitrobenzene, 33.4 mmol of styrene and 1.586 mmol of decane (as an internal standard) were added under a nitrogen atmosphere, after which the mixture was stirred for 15 min at 40 °C. The resulting mixture was hydrogenated under hydrogen pressure, using palladium–charcoal in ethanol. From the GLC analysis of the hydrogenation product, the formation of 1.32 mmol of 1-phenylpentane and 0.16 mmol of 2-phenylpentane was detected.

Results and Discussion

Reaction Catalyzed by $(\pi\text{-}C_3H_5PdCl)_2$–$BF_3\cdot Ph_3P$. As the catalyst systems consisting of a palladium salt, a Lewis acid, and a tertiary phosphine, various combinations are possible. In the previous papers[2] we have reported on various combinations which are active for the codimerization of butadiene with a monoolefin such as ethylene and propylene or for the codimerization of styrene with a monoolefin. In the present study, a catalyst system consisting of a combination of $(\pi\text{-}C_3H_5PdCl)_2$ and $BF_3\cdot Ph_3P$ has been mainly used because this catalyst system is comparatively soluble in many solvents.

Composition and Structure of Reaction Products. A gas chromatogram of the products of the reaction of styrene and butadiene in the presence of a typical catalyst system, $(\pi\text{-}C_3H_5PdCl)_2$–$BF_3\cdot Ph_3P$ (molar ratio=1:2), is shown in Fig. 1. 1-Phenyl-1,4-hexadiene was obtained as the main product; the sum of its *trans,trans*-isomer and *cis,trans*-isomer reached about 88 mol % of the C_{12}-compounds consisting of a codimer of butadiene with styrene and a butadiene trimer, showing the high selectivity of 1-phenyl-1,4-hexadiene. As reaction products, the respective dimers and trimers of butadiene and styrene were also obtained along with the codimer. However, 1-phenyldecatriene, which is known to be the main product of the reaction of styrene and butadiene catalyzed by nickel-containing catalysts,[1] was scarcely obtained at all. This is of interest as a difference resulting from the metal species of the catalysts.

Effect of the Molar Ratio of Styrene to Butadiene: In the present reaction, 1-phenyl-1,4-hexadiene, which has a straight-chain structure, is obtained as the main product. As one of the factors which dominate the structure of the reaction products, the coordination strength of the olefins used can be considered. In a reaction of ethylene and styrene using the same catalyst, as in the present

Table 1. Effect of the molar ratio of styrene to butadiene on the codimerization of styrene and butadiene with the $(\pi\text{-}C_3H_5PdCl)_2$–$BF_3\cdot Ph_3P$ catalyst

(Nitrobenzene, 20 ml; $(\pi\text{-}C_3H_5PdCl)_2$, 0.15 mmol; $BF_3\cdot Ph_3P$, 0.3 mmol; 100 °C, 1 h)

Run No.	Butadiene	Styrene	1-Phenyl-1,4-hexadiene		Styrene dimer	Styrene recovd.	Butadiene dimer	Butadiene trimer	Oligomer[b]	Composition of hydrogenated codimer[c]		
	mmol	mmol	mmol	(*trans* %)[a]	mmol	mmol	mmol	mmol	g	1-Ph-Hex[d] %	2-Ph-Hex[e] %	1-Ph-3-Me-Pent[f] %
1	170	540	77	(88)	42	288	8	1	14	86	11	2.6
2	170	350	55	(87)	16	231	10	1	7	88	9	2.7
3	170	170	36	(87)	4	116	15	2	3	90	7	3.0
4	350	170	31	(87)	2	114	25	3	2	91	6	3.1
5	510	170	25	(89)	1	140	36	3	5	92	5	3.1
6	230	150[g]	35	(87)	3	80	22	6	3	92	5	3.0

a) Amount (%) of the *trans, trans*-isomer in the total 1-phenyl-1,4-hexadiene. b) Amount of the distillation residue obtained by the distillation of the reaction products at 180 °C (bath temp)/4 mmHg. c) Composition of the product obtained by the hydrogenation of the with codimer the palladium–charcoal catalyst. d) 1-Phenylhexane. e) 2-Phenylhexane. f) 1-Phenyl-3-methylpentane. g) Styrene was introduced into the reaction mixture at the rate of 0.2 ml/min throughout the reaction.

study, we have previously reported that no dimerization of ethylene occurs and that the codimers derived from the addition of ethylene to the α-position of styrene are obtained, because styrene coordinates to the catalyst in preference to ethylene.[2c] In the present reaction, both styrene and butadiene have a strong coordination ability, so it is of interest which olefin coordinates preferentially to the catalyst and, consequently, how the reaction proceeds. Therefore, the effects of the molar ratio of styrene to butadiene on the reaction were investigated. The results are shown in Table 1.

When the molar ratio was varied from 3/1 to 1/3, the yield of 1-phenyl-1,4-hexadiene decreased with the decrease in the amount of styrene or with the increase in the amount of butadiene. However, the effect of the variation in the amount of butadiene was less than that of the amount of styrene. This appears to show that butadiene coordinates to the catalyst in preference to styrene and that, hence, the effect of the concentration of butadiene is smaller than that of styrene. With the decrease in the amount of styrene relative to butadiene, the formation of the styrene dimer was greatly reduced. This also shows the preferential coordination of butadiene. When distilled, the amount of the residue increased with an increase in the amount of styrene used, and the residue is thought to be composed mainly of an oligomer of styrene.

As for the composition of the alkylbenzene obtained by the hydrogenation of the codimer, with the variation in the molar ratio of butadiene to styrene from 1/3 to 3/1 1-phenylhexane increased from 86 to 92%, and 1-phenyl-3-methylpentane slightly increased from 2.6 to 3.1%, whereas 2-phenylhexane decreased from 11 to 5%. These facts suggest that 1-phenylhexane and 1-phenyl-3-methylpentane are formed by analogous mechanisms, but 2-phenylhexane is formed by a different mechanism. It can be said that the influence of the competitive coordination of styrene and butadiene is revealed as a variation of the composition of the hydrogenation products.

The ratio of the *trans,trans* isomer to *cis,trans*-1-phenyl-1,4-hexadiene is thought to be in equilibrium, and the ratio was approximately constant, not depending upon the butadiene/styrene ratio.

Effects of Reaction Conditions: The effects of the solvent, the reaction time, the reaction temperature, and the catalyst composition upon the reaction were investigated. The results of the experiments using nitrobenzene as a solvent are shown in Table 2, while those of the experiments using dichloromethane are shown in Table 3. As is clear from the comparison of the results of Run 7 and Run 17, or the results of Run 4 and Run 18, both the yield and the composition of the codimer are little affected by the type of solvent used. However, the separation of nitrobenzene from the reaction products is troublesome because its boiling point is close to those of the products. Therefore, the use of dichloromethane is preferable, and its separation from the products is much easier than that of nitrobenzene.

A greatly increased yield of 1-phenyl-1,4-hexadiene was obtained by the elongation of the reaction time from 1 to 2 h at 100 °C (Runs 7, 8), but by the elongation from 2 to 4 h the yield of 1-phenyl-1,4-hexadiene, the amount of styrene recovered, and the amount of the distillation residue were little affected (Run 9). On the other hand, when the reaction using double amounts of styrene and butadiene was carried out for 4 h, approximately double amounts of 1-phenyl-1,4-hexadiene were obtained (Run 10). Therefore, the results of Run 9 seem to suggest the existence of some coordination equilibrium between the reaction products and monomers and that, because of the equilibrium, the reaction does not proceed.

The codimerization occurred at 70 °C and proceeded smoothly above 100 °C. The reaction between styrene and ethylene, as we have reported in a previous paper,[2-c] proceeds easily at 30 °C; on the contrary, the present codimerization does not proceed at 40 °C, showing the influence of the strong coordination of butadiene.

As for the effect of the molar ratio of $BF_3 \cdot Ph_3P/(\pi\text{-}C_3H_5PdCl)_2$, when the ratio is below 2 (*i.e.*, P/Pd atomic ratio$<$1) the yield of 1-phenyl-1,4-hexadiene decreases

Table 2. Codimerization of styrene and butadiene with the $(\pi\text{-}C_3H_5PdCl)_2$–$BF_3 \cdot Ph_3P$ catalyst under various reaction conditions

(Nitrobenzene, 20 ml; $(\pi\text{-}C_3H_5PdCl)_2$, 0.15 mmol; styrene, 170 mmol; butadiene, 170 mmol)

Run No.	React. temp °C	React. time h	$BF_3 \cdot Ph_3P$: Pd ratio[g]	1-Phenyl-1,4-hexadiene		Styrene dimer	Butadiene dimer	Butadiene trimer	Oligomer[b]	Composition of hydrogenated codimer[c]		
				mmol	(*trans* %)[a]	mmol	mmol	mmol	g	1-Ph-Hex[d] %	2-Ph-Hex[e] %	1-Ph-3-Me-Pent[f] %
7	100	1	1	36	(87)	4	15	2	3	90	7	3
8	100	2	1	52	(86)	8	12	3	7	91	6	3
9	100	4	1	57	(86)	7	11	3	7	91	6	3
10[h]	100	4	1	108	(88)	10	33	6	5	90	7	3
11	40	1	1	0.5		—	—	—	1	—	—	—
12	70	1	1	7	(88)	1	5	—	1	87	10	3
13	120	1	1	52	(85)	7	10	3	7	91	6	3
14	100	1	0.75	33	(87)	4	12	2	3	90	7	3
15	100	1	0.5	21	(87)	2	9	2	2	90	7	3

a)—f) The same as in Table 1. g) The ratio of $BF_3 \cdot Ph_3P$ to monomeric $(\pi\text{-}C_3H_5PdCl)$ (=P/Pd atomic ratio).
h) Three hundred and fifty millimoles of styrene and 350 mmol of butadiene were used.

TABLE 3. CODIMERIZATION OF STYRENE AND BUTADIENE WITH THE (π-$C_3H_5PdCl)_2$–$BF_3\cdot Ph_3P$ CATALYST IN DICHLOROMETHANE

(Dichloromethane, 20 ml; (π-$C_3H_5PdCl)_2$, 0.15 mmol; $BF_3\cdot Ph_3P$, 0.3 mmol; reaction temp, 100 °C)

Run No.	Butadiene mmol	Styrene mmol	React. time h	1-Phenyl-1,4-hexadiene mmol	(*trans* %)[a]	Styrene dimer mmol	Styrene recovd. mmol	Butadiene dimer mmol	Butadiene trimer mmol	Oligomer[b] g	Composition of hydrogenated codimer[c] 1-Ph-Hex[d] %	2-Ph-Hex[e] %	1-Ph-3-Me-Pent[f] %
16	170	350	1	61	(87)	25	175	7	1	7	88	9	3
17	170	170	1	37	(87)	4	99	16	2	4	90	7	3
18	350	170	1	32	(88)	2	124	22	2	2	91	6	3
19	170	170	2	49	(87)	5	80	14	3	5	90	6	3
20[g]	170	170	2	34	(89)	4	104	8	1	4	91	7	2
21[h]	170	170	2	33	(88)	4	113	10	2	3	88	9	3
22[i]	170	170	2	44	(88)	11	42	7	2	11	89	9	2
23[j]	170	170	2	0.1		—	134	0.5	—	1	—	—	—
24[k]	170	170	2	0.5[l]		—	161	0.3	—	0.5	—	—	—

a)—f) The same as in Table 1. g) (($PdCl_2\cdot PhCH{=}CH_2)_2$ 0.15 mmol+$BF_3\cdot Ph_3P$ 0.3 mmol) was used as a catalyst. h) ($Pd(acac)_2$ 0.3 mmol+$BF_3\cdot Ph_3P$ 0.3 mmol) was used as a catalyst. i) A double amount of $BF_3\cdot Ph_3P$ (0.6 mmol) was used. j) ((π-$C_3H_5PdCl)_2$ 0.15 mmol+$BF_3\cdot Ph_3P$ 0.3 mmol+Ph_3P 0.3 mmol) was used as a catalyst. k) ($PdCl_2\cdot PhCH{=}CH_2)_2$ (0.3 mmol) was used alone as a catalyst. l) Scarcely no formation of 1-phenyl-1,4-hexadiene was observed, but a compound which seemed to be phenylcyclohexene was formed just as the case in the absence of a catalyst.

with the decrease in $BF_3\cdot Ph_3P$ (Table 2), but even if 2 mol of $BF_3\cdot Ph_3P$ per atom of Pd are used, the yield does not increase (Table 3, Run 22). These results indicate that (π-$C_3H_5PdCl)_2$ is activated by 1 mol of $BF_3\cdot Ph_3P$ per atom of Pd. When triphenylphosphine is added to a (π-$C_3H_5PdCl)_2$–$BF_3\cdot Ph_3P$ catalyst system with an atomic ratio of Pd: P: B=1: 1: 1, the resulting catalyst system (Pd: P: B=1: 2: 1) has no activity (Run 23). It can be considered that excess phosphine coordinates strongly to palladium and inhibits the coordination of olefins.

Palladium compounds other than (π-$C_3H_5PdCl)_2$ can be used as catalyst components. The results obtained by using the ($PdCl_2\cdot C_6H_5CH{=}CH_2)_2$–$BF_3\cdot Ph_3P$ and $Pd(acac)_2$–$BF_3\cdot Ph_3P$ catalyst systems are given in Table 3 (Runs 20, 21). ($PdCl_2\cdot C_6H_5CH{=}CH_2)_2$ alone is ineffective as a catalyst, yielding only a small amount of a codimer (Run 24).[6] This is believed to be due to the formation of a stable complex of the palladium salt with butadiene.

Reaction with a Catalyst Consisting of Palladium Salt, Aluminum Chloride, and Tertiary Phosphine. As a Lewis acid, aluminum chloride can be used instead of boron trifluoride. The results obtained by using a (π-$C_3H_5PdCl)_2$–$AlCl_3$–R_3P catalyst system are shown in Table 4. Both the activity of the catalyst and the composition of the reaction products are not very different from those obtained by a (π-$C_3H_5PdCl)_2$–$BF_3\cdot Ph_3P$ catalyst system, though it is preferable, when aluminum chloride is used, to employ nitrobenzene as the solvent in order to carry out the reaction in a homogeneous state.

When the atomic ratio of Al/P or Al/Pd was increased from 1 to 2 by changing the quantities of palladium salt and phosphine and by using approximately constant amounts of aluminum chloride, the amounts of the

TABLE 4. CODIMERIZATION OF STYRENE AND BUTADIENE WITH THE (π-$C_3H_5PdCl)_2$–$AlCl_3$–R_3P CATALYST

(Nitrobenzene, 20 ml; reaction temp, 100 °C; 1 h)

Run No.	Butadiene mmol	Styrene mmol	Catalyst Pd:$AlCl_3$:R_3P ratio[g]	R_3P (mmol)	R	1-Phenyl-1,4-hexadiene mmol	(*trans* %)[a]	Styrene dimer mmol	Butadiene dimer mmol	Butadiene trimer mmol	Oligomer[b] g	Composition of hydrogenated codimer[c] 1-Ph-Hex[d] %	2-Ph-Hex[e] %	1-Ph-3-Me-Pent[f] %
25	170	170	1:1:1	(0.52)	Ph-[h]	51	(85)	5	15	4	4	90	7	3
26	170	170	1:1.5:1	(0.30)	Ph-	36	(86)	4	12	2	3	90	7	3
27	170	170	1:2:1	(0.21)	Ph-	25	(86)	1	10	2	5	91	6	3
28	350	170	1:1:1	(0.47)	Ph-	39	(86)	2	23	3	1	91	6	3
29	170	350	1:1:1	(0.51)	Ph-	58	(86)	15	9	1	4	89	8	3
30[j]	170	170	1:1:1	(0.48)	Ph-	34	(85)	4	13	2	2	90	7	3
31	170	170	1:1:1	(0.44)	Bu-[i]	16	(89)	1	6	0	1	90	5	5
32	170	350	1:1:1	(0.50)	Bu-	27	(89)	4	5	0	1	90	5	5

a)—f) The same as in Table 1. g) Pd means monomeric (π-C_3H_5PdCl). The ratio is equal to the atomic ratio of Pd: Al: P. h) Triphenylphosphine. i) Tributylphosphine. j) Reaction time, 1/2 h.

distillation residue (oligomer) per palladium atom were increased, but the yields of 1-phenyl-1,4-hexadiene per palladium atom were not increased very much (Runs 25—27). Therefore, it seems to be appropriate to use an approximately equal mole of aluminum chloride to phosphine.

The effects of the molar ratio of styrene to butadiene were similar to those of the case using a $(\pi\text{-}C_3H_5PdCl)_2$–$BF_3\cdot Ph_3P$ catalyst system. By increasing the molar ratio, the yield of 1-phenyl-1,4-hexadiene was increased and the proportion of 2-phenylhexane was also increased.

When tributylphosphine was used instead of triphenylphosphine, the yield of 1-phenyl-1,4-hexadiene decreased and the proportion of 1-phenyl-3-methylpentane to the total hydrogenated codimers increased, suggesting that butadiene tends somewhat to react in the form of under the influence of tributylphosphine.[7]

Reaction Path. For the codimerization of styrene and ethylene using the same catalyst system as in the present codimerization, we have proposed a reaction mechanism which involves the formation of a palladium hydride as an active species of the catalyst system.[2c] In the present codimerization, the active species of the catalyst system is believed to be essentially the same as that described above. As has already been mentioned with regard to the composition of the alkylbenzene obtained by the hydrogenation of codimers, 1-phenylhexane and 1-phenyl-3-methylpentane increased with an increase in the amount of butadiene employed, while 2-phenylhexane and styrene dimer increased with an increase in the amount of styrene (Table 1). In Fig. 1, as a compound which gives 2-phenylhexane by hydrogenation, only 5-phenyl-1,3-hexadiene has a structure capable of giving 2-phenylhexane.

From these facts, it can be considered that 1-phenylhexane and 1-phenyl-3-methylpentane are formed according to Eqs. 1 and 2 respectively, and that 2-phenylhexane is formed according to Eq. 3.

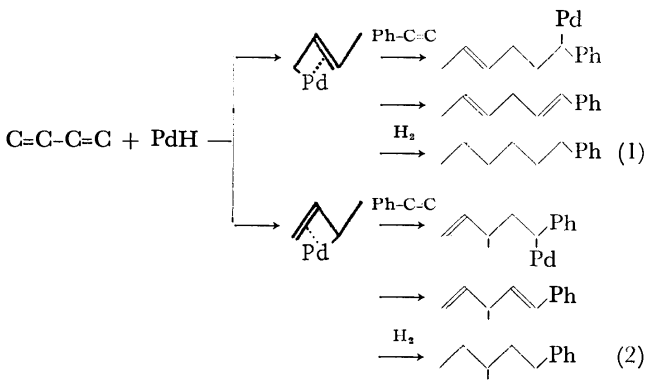

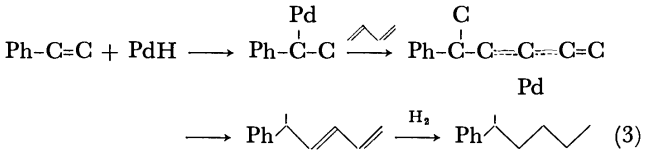

However, when the reaction of styrene with allyl groups coordinating to palladium was carried out by adding excess amounts of styrene to a solution of $(\pi\text{-}C_3H_5PdCl)_2$ and $BF_3\cdot Ph_3P$ in a molar ratio of 1 : 2, and when the resulting reaction mixture was hydrogenated, phenylpentanes (*ca.* 50 mol % based on the $(\pi\text{-}C_3H_5PdCl)_2$ used) were obtained; GLC analysis showed that the phenylpentanes consisted of 1-phenylpentane (89%) and 2-phenylpentane (11%). Therefore, it seems necessary to consider the participation of the following pathway (Eq. 4) for the formation of 2-phenylhexane:

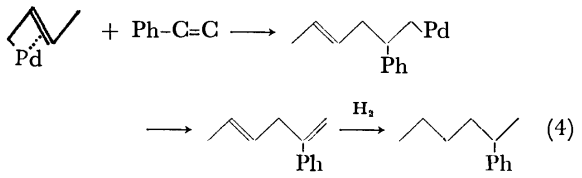

References

1) H. Müller, D. Wittenberg, H. Seibt, and E. Scharf, *Angew. Chem.*, **77**, 318 (1965).

2) a) T. Ito, T. kawai, and Y. Takami, *Tetrahedron Lett.*, **1972**, 4775; b) T. Ito, T. Kawai, and Y. Takami, *Chem. Lett.*, **1972**, 1047; c) T. Ito, K. Takahashi, and Y. Takami, *Nippon Kagaku Kaishi*, **1974**, 1097.

3) A part of this work has been presented in a preliminary communication: T. Ito, K. Takahashi, and Y. Takami, *Tetrahedron Lett.*, **1973**, 5049.

4) Fr. Hein, and H. L. Pruefer, *Monatsber, Deut. Akad. Wiss. Berlin*, **7/8**, 381 (1961); *Chem. Abstr.*, **57**, 16649 (1961).

5) G. Descotes, M. Fournier, and R. Mugnier, *Bull. Soc. Chim. Fr.*, **1968**, 3346.

6) In the case of the reaction of styrene and ethylene, $(PdCl_2\cdot C_6H_5CH{=}CH_2)_2$ is effective as a catalyst by itself.[2c]

7) In the oligomerization of olefins with complex catalysts containing phosphine compounds, it has been established that the structure of the oligomer formed often varies with the difference in the type of phosphine employed; B. Bogdanovic, B. Henc, H. G. Karman, H. G. Nüssel, and G. Wilke, *Ind. Eng. Chem.*, **62**, No. 12, 34 (1970).

NOTES

BULLETIN OF THE CHEIMCAL SOCIETY OF JAPAN, VOL. 51 (4), 1225—1226 (1978)

The Oxidation Mechanism of Copper in Nitrogen Oxide

Yoshio TAKASU and Yoshiharu MATSUDA

Faculty of Engineering, Yamaguchi University, Tokiwadai, Ube, Yamaguchi 755

(Received August 22, 1977)

Synopsis. The rate-determining step of the oxidation of copper in nitrogen oxide was proposed to be the dissociation of the adsorbed nitrogen oxide on the surface of the oxide film.

Although many studies have been made of the high-temperature oxidation of metals, few investigations of reactions in nitrogen oxide are recorded.[1,2] The present authors have reported in an earlier paper[3] that the oxidation of copper in nitrogen oxide (700—820 °C, 3.5—14 Torr) followed a linear rate law, suggesting that the rate-determining step is the reaction at the gas/oxide interface. Moreover, the following total reaction was proposed for the reaction;

$$2Cu + NO(g) = Cu_2O + 1/2N_2(g),$$

with an apparent activation energy of ≈113 kJ/mol. In this study, the oxidation of copper in nitrogen oxide was examined at higher pressures (20 and 30 Torr). The oxidation mechanism is discussed in the light of the present results and those from earlier studies.[3]

The experimental procedure was the same as that described previously.[3] The oxidation process was followed in a conventional high-vacuum system. The polycrystalline specimens (99.999% Cu) were 10×5 mm in area and had a thickness of 0.5 mm. The samples were annealed in a vacuum at 700 °C for 2 h, electropolished, and then heated in a hydrogen atmosphere at 700 °C for 1 h prior to the oxidation measurements. High-purity nitrogen oxide in a glass cylinder (Takachiho Co.) was used without further purification.

Figure 1 shows the oxidation curves for copper under various pressures of nitrogen oxide at 700 °C. The data obtained from this study at 20 and 30 Torr also obeyed the linear rate law in the early stage of the oxidation. The rate at these two pressures decreased later, however,

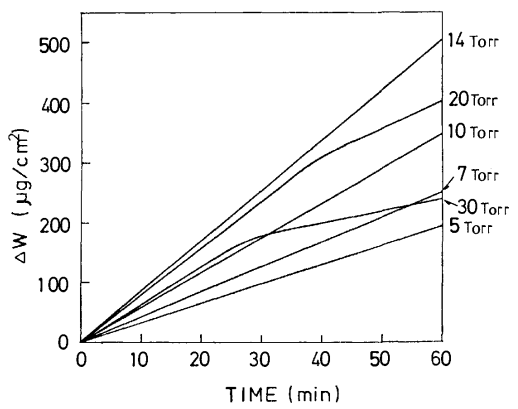

Fig. 1. Oxidation curves of copper in various pressures of nitrogen oxide at 700 °C.

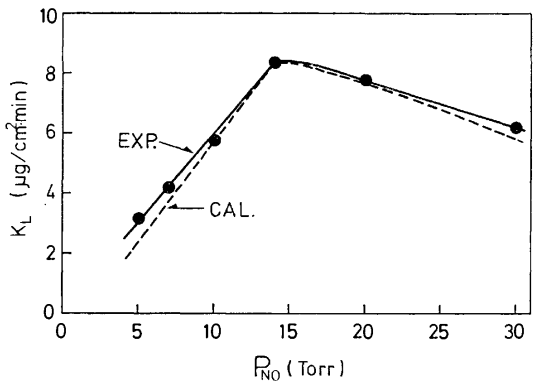

Fig. 2. The relation between the pressure of nitrogen oxide and the linear rate constant for the oxidation of copper at 700 °C. Dashed curve: theoretical result using Eq. 11 and normalized to maximum rate constant at $p=14$ Torr.

showing evidence for two stages of oxide growth. The pressure dependence of the rate constant, K_L, in the early stage of the oxidation is shown in Fig. 2. At first the rate increased with the pressure, read a maximum around 14 Torr, and then decreased. This behaviour suggests that the rate-determining step of the oxidation is to be found in the dissociation of the absorbed nitrogen oxide on the surface of the oxide film. As has been discussed by Ritchie and Hunt[4] for the oxidation in oxygen, the surface reaction sequences for the NO–Cu system could be given as follows:

$$NO(g) + S = NO(a), \quad (1)$$

$$NO(a) + S = N(a) + O(a), \quad (2)$$

$$2N(a) = N_2(a) + S, \quad (3)$$

$$N_2(a) = N_2(g) + S, \quad (4)$$

$$O(a) = O^-(a) + \oplus, \quad (5)$$

$$O^-(a) = O^{2-}(a) + \oplus, \quad (6)$$

$$O^{2-}(a) = O^{2-}(\text{Lattice}) + S, \quad (7)$$

where (g) denotes the gaseous species; (a), the adsorbed species; S, the vacant adsorption site, and ⊕, the electron hole. If we consider Step 2 to be rate-determining, then

$$K_1 = \frac{[NO(a)]}{p[S]}, \quad (8)$$

$$r = k_2[S][NO(a)], \quad (9)$$

$$G = [S] + [NO(a)], \quad (10)$$

where K_1 denotes the equilibrium constant for Step 1; p, the pressure of nitrogen oxide; r, the oxidation rate; k_2, the rate constant for Step 2, and G, the total number

of adsorption sites.

From Eqs. 8, 9, and 10 we obtain

$$r = \frac{k_2 K_1 G^2 p}{(1+K_1 p)^2}. \quad (11)$$

Equation 11 shows that r is proportional to the pressure of nitrogen oxide if $K_1 p \ll 1$, but that r is inversely proportional to the pressure if $K_1 p \gg 1$. The decrease in the reaction rate in the higher-pressure range can thus be attributed to a decrease in the number of vacant adsorption sites as a result of the adsorption of nitrogen oxide. The calculated values for the rate constant at 700 °C based on Eq. 11 are also plotted in Fig. 2, whereby the curve is normalized to the maximum rate constant at $p=14$ Torr.

The authors are grateful to Dr. A. M. Bradshaw of the Fritz-Haber-Institut, Berlin, for helpful discussion and critical reading of the manuscript.

References

1) M. Farber, A. J. Darnell, and D. M. Ehrenberg, *J. Electrochem. Soc.*, **102**, 446 (1955).

2) Y. Takasu, Y. Matsuda, S. Maru, and N. Hayashi, *Nature*, **255**, 544 (1975).

3) Y. Takasu, M. Takagi, and Y. Matsuda, *Chem. Lett.*, **1977**, 1043.

4) I. M. Ritchie and G. L. Hunt, *Surface Sci.*, **15**, 524 (1969).

BULLETIN OF THE CHEMICAL SOCIETY OF JAPAN, VOL. 51 (4), 1227—1228 (1978)

Unusual Products of the Leuckart Reaction of 1-Acenaphthenone

Jiro TATSUGI, and Michio OKUMURA

Department of Applied Chemistry, Aichi Institute of Technology, Yakusa, Toyoda 470-03

(Received June 22, 1977)

Synopsis. In the reaction between formamide and 1-acenaphthenone, 1,1′-biacenaphthenyliden-2-one was obtained instead of 1-acenaphthenamine which is expected to be formed by the Leuckart reaction. When formic acid was incorporated in the reaction, besides 1,1′-biacenaphthenyliden-2-one two new nitrogen-containing compounds were isolated; their structures were identified to be acenaphtho[1,2-*d*]pyrimidine and diacenaphtho[1,2-*b*: 1′,2′-*d*]pyridine by independent syntheses.

The reaction of 1-acenaphthenone (**1**) with formamide or ammonium formate gave exclusively a nitrogen-free product (**2**) (75% yield). When **1** was treated with a mixture of formamide and anhydrous formic acid, two new products (**3**) and (**4**) were obtained along with the liberation of CO_2 (Table 1). When using 80% formic acid in place of the anhydrous acid, the yield of **2** increased and those of **3** and **4** were reduced. The nitrogen-free product **2** decolorized bromine and permanganate solutions, suggesting the presence of unsaturated bonds. The IR spectrum of **2** showed the presence of a carbonyl group and its NMR spectrum showed a singlet at 4.70 ppm which is assignable to allylic methylene protons. This compound was identified to be the structure shown in the scheme by independent synthesis of the compound by the aldol condensation of **1** in the presence of caustic alkali.

Table 1. Reaction of 1-acenaphthenone with the mixture of formamide and anhydrous formic acid

1-Acenaphthenone **1** mol	$HCONH_2$ mol	HCOOH mol	Temp (°C)	Time (h)	Yields (%) **2**	**3**	**4**
0.02	0.46	none	150	3	75	—	—
0.01	0.23	0.23	150	3	31	28	9
0.01	0.23	0.18[a)]	150	3	69	9	1
0.01	0.23	0.23	55	18	—	—	—
0.01	0.23	0.23	100	3	6	trace	—
0.01	0.23	0.23	110	3	13	6	—
0.01	0.23	0.23	125	3	26	10	2

a) *ca.* 80% HCOOH.

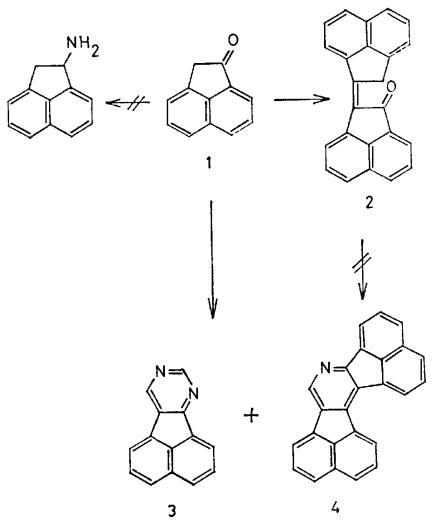

Fig. 1.

The compound **3** has an experimental formula of C_7H_4N; the structure is suggested to have a pyrimidine nucleus by the IR spectrum. Furthermore, the NMR spectrum in $CDCl_3$ is well interpreted to be acenaphtho[1,2-*d*]pyrimidine. The authentic acenaphtho[1,2-*d*]-pyrimidine was independently prepared by the reaction of 2-formyl-1-acenaphthenone (**1a**) with formamidine (Fig. 2).

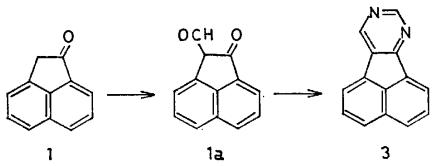

Fig. 2.

The admixture of **3** with the authentic sample showed no melting point depression and the R_f values of both compounds were the same.

The compound **4** was identified as diacenaphtho[1,2-*b*: 1′,2′-*d*]pyridine on the basis of its IR, UV, and mass spectra and elementary analysis. The independent synthesis of **4** was accomplished by converting 2-(ethoxymethylidene)-1-acenaphthenone into 2-(aminomethylidene)-1-acenaphthenone by dry ammonia and then condensing it with **1**. The authentic compound showed the same R_f value as that of **4** isolated from the Leuckart reaction products.

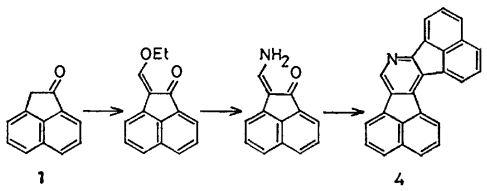

Fig. 3.

Recently, pyrimidine derivatives were isolated from the Leuckart reaction mixture in thiophene derivatives by Hill and Loev,[1)] and Srinivasan and Rampal,[2)] though the formation of the pyridine derivatives has not yet been reported.

The above mentioned **3** and **4** are new compounds which have not yet been reported in the literature.

In the reaction of **1** with formamide, which took place exclusively as an aldol condensation and showed no Leuckart reaction, formamide seemed to perform the

role of a protic solvent. In the presence of formic acid, however, the Leuckart reaction is in competition with the aldol reaction and gives **2**, **3**, and **4**, but no normal Leuckart reaction products. It may be assumed that **3** and **4** might result *via* an intermediate of the Leuckart reaction. It is worthy to note that **4** might be produced by the condensation of **2** with formamide as shown in Fig. 1. This can be ruled out since no **4** was isolated from the reaction mixture of **2** and formamide.

When 80% formic acid was used, the yield of **2** increased and those of **3** and **4** decreased. It is reasonable to consider that the presence of water favors the enolization of **1** and accelerates the aldol condensation by the dissociation of formic acid. Further experiments are necessary, however, to consider the reaction route of the formation of **3** and **4** in the Leuckart reaction conditions. This is now in progress.

Experimental

The melting points were determined on a Yanaco MP-type apparatus and are uncorrected. The IR spectra were taken in potassium bromide pellets on a Hitachi 215 grating spectrometer. The UV spectra were recorded on a Hitachi EPS-3T spectrophotometer. The NMR spectra were obtained on a JEOL JNM-C-60H spectrometer using TMS as internal standard.

Reaction of 1-Acenaphthenone ***1*** *with Formamide.* A mixture of **1** (3.36 g, 0.02 mol) and formamide (19.0 ml, 0.46 mol) was heated at 150 °C for 3 h. After cooling the reaction mixture, the precipitate was filtered and washed with methanol. The unchanged **1** was recovered from the methanol washing (13% recovery). Recrystallization of the crude product (2.53 g) from 300 ml of benzene (or chloroform) gave 2.38 g (75%) of **2**, yellow needles, mp 259—260 °C (lit, 262,[3] 258 °C[4]). IR (KBr): 1690 cm^{-1} (C=O). NMR ($CDCl_3$): δ=4.70 (2H, s) and 7.61—8.31 (12H, m). The mixed melting point with an authentic sample synthesized by Graebe's method[3] showed no depression.

The reaction of **1** with ammonium formate at 190 °C for 10 h gave a similar result.

Reaction of ***1*** *with Formamide and Formic Acid.* A mixture of **1** (1.68 g, 0.01 mol), formamide (9.5 ml, 0.23 mol), and anhydrous formic acid (8.5 ml, 0.23 mol) was heated at 150 °C for 3 h. In about 10 minutes evolution of carbon dioxide and precipitation of a colored product were observed. After heating at 150 °C for 30 min, the reaction mixture showed the presence of four spots (**1**, **2**, **3**, and **4**) on thin-layer chromatography (TLC). The colored product was separated by filtration and washed with methanol and then with ether. 0.66 g of yellow solid (two spots on TLC) was obtained. It was chromatographed by means of SiO_2 with chloroform as eluent. The first fraction collected was recrystallized from benzene to afford 0.50 g (31%) of **2**. The second fraction was recrystallized from dioxine to give 0.15 g (9%) of **4**, yellow needles, mp>300 °C, IR (KBr): 1582, 1510, 1430, and 1358 cm^{-1}. UV (dioxane) max: 332.5 nm (log ε 4.63). Found: C, 91.63; H, 4.00; N, 4.20%. Calcd for $C_{25}H_{13}N$: C, 91.72; H, 4.00; N, 4.28%. MS *m/e*: 327. The filtrate was extracted with chloroform. The chloroform layer was washed with H_2O and dried over $MgSO_4$, and then the chloroform was evaporated. The residue was recrystallized from acetone to give 0.58 g (28%) of **3**, pale yellow needles, mp 154—155 °C. IR (KBr): 1582, 1542, 1425, and 1378 cm^{-1}. UV (EtOH) max: 234 nm (log ε 4.44). NMR ($CDCl_3$) δ=9.36 (1H, s), 9.32 (1H, s), and 7.75—8.57 (6H, m). Found: C, 82.55; H, 4.02; N, 13.77%. Calcd for $C_{14}H_8N_2$: C, 82.33; H, 3.95; N, 13.72%. Picrate: yellow needles, mp 210—212 °C.

2-Formyl-1-acenaphthenone ***1a.*** A 100-ml three necked flask was equipped with a stirrer and a reflux condenser to which is attached a drying tube containing soda lime. 1-Acenaphthenone **1** (1.68 g, 0.01 mol), ethyl formate (3 ml, 0.04 mol), dioxane (40 ml), and an ethanolic solution of sodium ethoxide prepared by dissolving sodium (1.0 g, 0.04 mol) in 10 ml of absolute ethanol were added to the flask and stirred at 0 °C under nitrogen atomosphere for 12 h. The precipitate was separated by filtration and dissolved in water. The water-insoluble part **2** was filtered off. The filtrate was extracted by ether to remove the unreacted **1**. The aqueous layer was acidified with 1 M-HCl to precipitate **1a**, which was filtered, washed thoroughly with water, and dried. Recrystallization from benzene gave the purified product, 1.57 g (80%), mp 179—180 °C (lit, 180—182 °C[5]).

*Acenaphtho[1,2-*d*]pyrimidine* ***3.*** A solution of **1a** (0.98 g, 0.005 mol) and formamidine acetate (0.73 g, 0.007 mol) in 20 ml of ethanol was heated to reflux for 13 h and then the solvent was evaporated using a rotary evaporator. The residue was dissolved in 50 ml of chloroform, washed with 1M-sodium hydroxide solution, and dried over anhydrous sodium sulfate. Evaporation of chloroform gave a pale yellow residue, which was recrystallized from THF to yield 0.8 g (79%) of authentic **3**, mp 154—155 °C.

*Diacenaphtho[1,2-*b*: 1′,2′-*d*]pyridine* ***4.*** A mixture of **1** (1.68 g, 0.01 mol) and triethyl orthoformate (2.0 g, 0.014 mol) was mixed with 30 ml of acetic anhydride and heated to reflux for 12 h with stirring. The reaction mixture was then poured into ice-water and stirred at room temperature to decompose the acetic anhydride and then extracted with chloroform. The chloroform layer was washed with water and dried over anhydrous sodium sulfate. After removal of the solvent, the residue was extracted with hexane. The hexane extract was evaporated and dried *in vacuo*. The residue was dissolved in absolute ethanol and then treated with dry ammonia. The ethanol solution was evaporated to dryness. The residue and **1** (0.84 g, 0.005 mol) and were dissolved into HMPA (10 ml). The solution was heated at 150 °C for 5 h under nitrogen atmosphere. It was cooled to room temperature to precipitate a solid product, which was filtered, washed with ethanol, and recrystallized from dioxane to give purified **4**.

Attempted Reaction of ***2*** *with Formamide.* A mixture of **2** (0.795 g, 0.0025 mol) and formamide (9.5 ml, 0.23 mol) was heated at 150 °C for 3 h. After cooling the reaction mixture, the precipitate was filtered and washed with methanol. 0.771 g (97%) of the unchanged **2** was recovered. The expected product **4** was not formed.

We are grateful to Prof. Y. Yukawa of Osaka University and Prof. S. Okumura for helpful discussions.

References

1) Daivid T. Hill and Bernard Loev, *J. Org. Chem.*, **38**, 2102 (1973).
2) M. Srinivasan and J. B. Rampal, *Tetrahedron Lett.*, **1974**, 2883.
3) Von C. Graebe and J. Jequier, *Ann. Chem.*, **290**, 202 (1896).
4) K. Dziewonski and T. Litynski, *Ber.*, **58**, 2539 (1925).
5) Elisa Ghigi, Anna Maria Drusiani, and Laura Plessi, *Ann. Chim. (Rome)*, **53**, 266 (1963).

BULLETIN OF THE CHEMICAL SOCIETY OF JAPAN, VOL. 51 (4), 1229—1230 (1978)

Micellar Effects on Base-Catalyzed Isomerization of Prostaglandin A_1 and Prostaglandin A_2

Kaneto UEKAMA, Fumitoshi HIRAYAMA, and Shyukou YAMASAKI

Faculty of Pharmaceutical Sciences, Kumamoto University, Oe-honmachi, Kumamoto 862

(Received August 25, 1977)

Synopsis. Micellar effects on base-catalyzed isomerization of A-type prostaglandins to B-type prostaglandins were studied. Cationic and non-ionic micellar systems increased the rate of isomerization, but anionic systems either decreased or had negligible effects on the rate constants. Incorporation of the prostaglandins into the hydrophobic interior of the micelles was suggested by circular dichroism spectra.

The enone moiety of A-type prostaglandins (PGA) is susceptible to isomerization in alkaline conditions to form B-type prostaglandins (PGB),[1] which consequently elicites the loss of biological activity.[2] It is well known that micellar systems influence the rate of various kinds of organic reactions, providing useful information about the reaction mechanism.[3] Thus, micellar effects on base-catalyzed isomerization of prostaglandin A_1 (PGA_1) and prostaglandin A_2 (PGA_2) were examined to better understand the nature of rearrangement reactions through substrate-surfactant interactions. The effect of surfactants on the circular dichroism (CD) spectra of PGA were also investigated, anticipating an incorporation of PGA into the hydrophobic interior of the micelles.

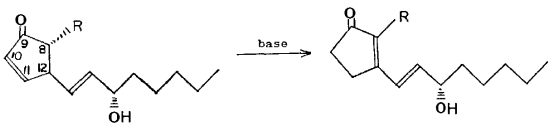

PGAs PGAs

PGA_1, PGB_1: $R=(CH_2)_6COOH$

PGA_2, PGB_2: $R=CH_2CH=CH(CH_2)_3COOH$

Experimental

Materials. The prostaglandins used were donated by the Ono Pharmaceutical Co., Ltd. Hexadecyltrimethylammonium chloride (CTAC), dodecyltrimethylammonium chloride (DTAC), sodium hexadecyl sulfate (NaCS), sodium dodecyl sulfate (NaLS), and poly(oxyethylene) dodecyl ether (Brij-35) were commercially obtained and purified using the usual methods.[4] All other materials and solvents were of analytical reagent grade.

Measurements. The CD and UV spectra were measured at 25 °C using a Jasco J-40 AS spectropolarimeter and a Shimadzu spectrophotometer, respectively, in a 0.1 M sodium phosphate buffer solution (pH 6.0). The CD spectra are expressed in terms of molar ellipticity, $[\theta]$. The critical micelle concentration (CMC) of the surfactants was determined spectrophotometrically[5] at 60 °C and at pH 11.2.

Kinetic Studies. The isomerization of PGA (3.8×10^{-5} M) in the presence and in the absence of surfactants was followed spectrophotometrically by measuring the apparence of PGB (284 nm) at 60 °C. The first-order dependence of the rate constants on the hydroxide ion concentration was ascertained for both PGA_1 and PGA_2, for an activation energy of 18.7 kcal/mol at pH 12.0.[6] The pH profile of the logarithm of the rate constant (k_{obsd}) for both PGA_1 and PGA_2 is linear with a slope of 0.75 from pH 9.5 to 12.0. No appreciable change in the slope was observed even in the presence of surfactants.

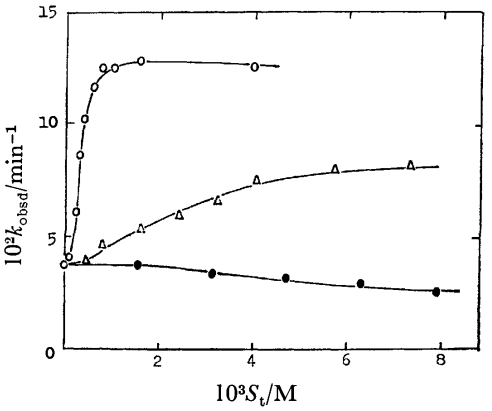

Fig. 1. The plots of observed rate constants for isomerization of PGA_1 *vs.* surfactant concentration, S_t, in phosphate buffer (pH=11.2, μ=0.2) at 60°.
-○-: CTAC, -●-: NaLS, -△-: Brij-35.

Results and Discussion

As is shown in Fig. 1, cationic and non-ionic surfactants enhanced the isomerization rates, but anionic surfactants either decreased or had negligible effects on the rate constants above the CMC values. The results for ionic micellar systems suggest the development of an anionic charge on the cyclopentanone ring of PGA during the rate-determining step. It was also noted that activation of the base (toward C–H proton abstraction) in cationic micelles becames greater with increasing hydrophobic chain length of the surfactant. The observed rate constant (k_{obsd}) as a function of surfactant concentration was quantitatively evaluated[7] to yield the non-micellar (k_o) and micellar (k_m) rates, and the K/N value of the PGA-micelle complex. As is shown in Table 1, the K/N values of the PGA_1 system are larger than those of the PGA_2 system. This may be due to the greater hydrophobic tendency of PGA_1 compared to PGA_2, as is expected from their partition coefficients.[8]

Figure 2 shows the CD spectra of the PGA_1–CTAC system, as an example, where PGA_1 exhibits a strong positive band at 238 nm ($[\theta]=6.10\times10^4$) and a weak negative band at 314 nm ($[\theta]=-9.21\times10^3$) due to the π-π^* and n-π^* transitions of the enone chromophore, respectively.[9] When CTAC micelles were introduced into the PGA_1 solution, the positive peak was shifted to shorter wavelengths (by about 3 nm) and the negative

Table 1. Kinetic parameters for micellar effect on isomerization of PGA at pH 11.2 and at 60 °C

Substrate			Micellar system			
	Partition[a] coefficient	k_o (min^{-1})		CMC ($\times 10^3$ M)	k_m (min^{-1})	K/N[b] (M^{-1})
			CTAC	0.12	0.15	5000
			DTAC	1.7	0.12	590
PGA_1	80.8	0.038	NaCS	0.14	0.034	—[c]
			NaLS	2.1	0.011	110
			Brij-35	0.75	0.12	220
			CTAC		0.17	3900
			DTAC		0.14	470
PGA_2	69.4	0.044	NaCS		0.041	—[c]
			NaLS		0.012	97
			Brij-35		0.14	190

a) Determined between chloroform and 0.1 M phosphate buffer of pH 6.0 at 25 °C. b) K: association constant of PGA-micelle complex, N: aggregation number of micelle. c) Could not be determined due to a small change in the rate constant.

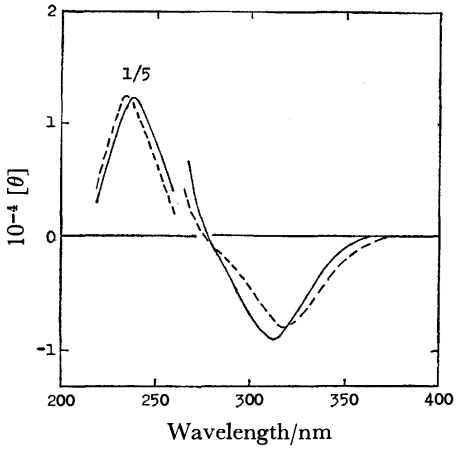

Fig. 2. The CD spectra of PGA_1 in the presence (——) and absence (——) of CTAC (1.0×10^{-3} M) in 0.1 M phosphate buffer (pH=6.0, μ=0.2) at 25°.

peak was shifted to longer wavelengths (by about 8 nm). The effect of other surfactants on the CD spectra of PGA are similar to that of the PGA_1–CTAC system, for which the magnitude and direction of the spectral changes appears to be correlated with the association constants of PGA-micelle complexes. Similar spectra changes were also observed when PGA were dissolved in less polar solvents, such as ethanol-buffer and dioxane-buffer solutions. This type of spectral shift, the bathochromic shift of the π-π^* transition and the hypsochromic shift of the n-π^* transition with decreasing solvent polarity, is a well-known solvent effect in CD spectroscopy. Thus, the above results indicate that the chromophore of the PGA may be located in the hydrophobic circumstances of the micelles.

The rate enhancement observed for non-ionic micellar systems, however, cannot be interpretable soley on the basis of hydrophobic interactions. It was found that α- and β-cyclodextrins increase the isomerization rate with almost the same order of magnitude as dose Brij-35 in alkaline conditions,[10] for which the catalytic effects of cyclodextrins may be ascribed mainly to conformational changes of the substrate within the hydrophobic cavity of cyclodextrins and/or to alternations in the structure of the surrounding water.[11] An analogous situation is proposed for PGA-non-ionic micellar systems.

References

1) N. H. Andersen, *J. Lipid Res.*, **10**, 320 (1968).
2) T. O. Oesterling, W. Morozowichi, and T. J. Roseman, *J. Pharm. Sci.*, **61**, 1861 (1972).
3) J. H. Fendler and E. J. Fendler, "Catalysis in Micellar and Macromolecular System," Academic Press, New York (1975).
4) D. G. Herries, W. Bishop, and F. M. Richards, *J. Phys. Chem.*, **68**, 1842 (1964).
5) F. M. Menger and C. E. Portnoy, *J. Am. Chem. Soc.*, **89**, 4698 (1967).
6) D. C. Monkhous, L. Van Campen, and A. J. Aguiar, *J. Pharm. Sci.*, **62**, 576 (1973).
7) E. J. Fendler, R. R. Liechti, and J. H. Fendler, *J. Org. Chem.*, **35**, 1658 (1970).
8) K. Uekama, F. Hirayama, K. Ikeda, and K. Inaba, *J. Pharm. Sci.*, **66**, 706 (1977).
9) M. J. Cho, W. C. Krueger, and T. O. Oesterling, *J. Pharm. Sci.*, **66**, 149 (1977).
10) K. Uekama, F. Hirayama, K. Ikeda, and K. Inaba, The 97th Annual Meeting of the Pharmaceutical Society of Japan, Tokyo, April 1977 (Pref. Abst., p. IV-194).
11) S. Tanaka, K. Uekama, and K. Ikeda, *Chem. Pharm. Bull.*, **24**, 2825 (1976).

BULLETIN OF THE CHEMICAL SOCIETY OF JAPAN, VOL. 51 (4), 1231—1232 (1978)

Analysis of the NMR Line Shape Dually Modulated by the Chemical Exchange and by the Scalar Coupling Relaxation. ^{13}C NMR Spectrum of the Trimethylaluminum Dimer

Osamu YAMAMOTO and Masaru YANAGISAWA

National Chemical Laboratory for Industry, Honmachi, Shibuya-ku, Tokyo 151

(Received September 12, 1977)

Synopsis. ^{13}C methyl signals of the trimethylaluminum dimer, broadened by the chemical exchange and the scalar coupling interaction with ^{27}Al, were analyzed in order to obtain the rates of the bridge-terminal exchange of the methyl groups. The exchange rates were compared with those obtained from the ^{1}H resonance, and a good agreement was obtained. A brief discussion is given of some advantages and difficulties of the analysis.

It is well known that the alkyl groups of the trialkylaluminum dimer undergo a rapid exchange between the bridge and the terminal positions at ambient temperature. This exchange in the trialkylaluminum dimer has been studied extensively by ^{1}H and ^{13}C NMR spectroscopies, and the Arrhenius parameters for the exchange have been calculated.[1,2] In a previous paper[3] we have shown that, even within the slow-exchange limits, the ^{13}C signals of the methyl groups in the trimethylaluminum (TMA) dimer are broadened by the scalar coupling between the ^{13}C and ^{27}Al nuclei, which is modulated by the rapid quadrupole relaxation of the Al nucleus. By analyzing the line shape of the ^{13}C signals and using the relaxation time of ^{27}Al, we were able to obtain the scalar coupling constant between ^{13}C and ^{27}Al (J_{C-Al}) within the slow-exchange limits. In this exchanging system, under the rapid and intermidiate exchange conditions, the signals of the ^{13}C nuclei directly bonded to Al are dually modulated by two time-dependent effects, *i.e.*, the chemical exchange and the scalar coupling with ^{27}Al, in which situation the analysis of the NMR line shape is rather complicated. However, if one of the effects of the interactions on the line shape could be accurately known, we would have the possiblity of obtaining information on the other interaction by analyzing the line shape. In the present note, as an example of the line-shape analysis under such circumstances, the methyl carbon signal of TMA is studied to obtain exchange rates at various temperatures, with the ^{27}Al relaxation rates and J_{C-Al} known, and the exchange rates thus obtained are compared with those obtained from the ^{1}H resonance.

The ^{1}H and ^{13}C spectra were recorded on a NEVA NV-14 spectrometer at 60 and 15.1 MHz respectively. The sample concentration is *ca.* 10% of TMA in cyclopentane-d_{10}. The other experimental details are the same as those reported in a previous paper.[3]

The expressions for the NMR intensities at the frequency of ω under the influence of the chemical exchange and the scalar coupling relaxation have the same form,[4] both given by

$$I(\omega) = Re[\mathbf{W}\cdot\mathbf{A}^{-1}\cdot\mathbf{1}], \quad (1)$$

where the vector $\mathbf{W}$ has components proportional to the populations, $\mathbf{1}$ is a unit column vector, and *Re* means the real part. For the methyl signals of TMA undergoing the bridge-terminal exchange, $\mathbf{A}$ has the form:

$$\mathbf{A} = i(\mathbf{\Omega}-\omega\mathbf{E}) + \mathbf{Q} + \mathbf{K}, \quad (2)$$

in which $\mathbf{\Omega}$ is the diagonal matrix whose elements are the chemical shifts of each site, and $\mathbf{E}$, the unit matrix. $\mathbf{Q}$ and $\mathbf{K}$ are the matrices representing the effects of the scalar coupling relaxation and the chemical exchange respectively, and are further decomposed as

$$\mathbf{Q}+\mathbf{K} = \begin{pmatrix} \mathbf{Q}^{b}+\mathbf{K}_1{}^{b} & \mathbf{K}_2{}^{b} \\ \mathbf{K}_2{}^{t} & \mathbf{Q}^{t}+\mathbf{K}_1{}^{t} \end{pmatrix}, \quad (3)$$

where the superscripts b and t refer to the bridge and the terminal positions respectively. $\mathbf{Q}^{b}$, $\mathbf{K}_1{}^{b}$, *etc.* are also matrices whose components are referred to the ^{13}C lines which would be split by ^{27}Al if the scalar relaxation mechanism were absent. The detailed expressions for $\mathbf{Q}^{b}$, $\mathbf{Q}^{t}$ and $\mathbf{W}$ of TMA were presented in the previous paper.[3] $\mathbf{Q}$ contains information about the J_{C-Al} and ^{27}Al relaxation times, conversely, if the two quantities are known, the line shape of ^{13}C under the influence of the scalar relaxation can be calculated.

$\mathbf{K}_1{}^{b}$ and $\mathbf{K}_1{}^{t}$ are simple diagonal matrices whose diagonal elements are $-1/\tau_b$ and $-1/\tau_t$ respectively. τ_b and τ_t are the life-time of the methyl group at the bridge and the terminal positions respectively, and $2\tau_b=\tau_t$, since the population at the bridge position is one-half of that of the terminal. $\mathbf{K}_2{}^{b}$ and $\mathbf{K}_2{}^{t}$ correspond to the off-diagonal parts of the kinetic transfer matrix, $\mathbf{A}$, in the usual expression for the exchanging system. In constructing $\mathbf{K}_2{}^{b}$ and $\mathbf{K}_2{}^{t}$, we assume that the exchange process is "intramolecular"[2] and one bridge bond is broken during the exchange. Thus, the methyl carbon at the terminal position which sees the ^{27}Al spin state of, say, $\left|\frac{5}{2}\right>$ goes to the bridge position at which the methyl carbon coupled with two Al nuclei, and sees one of the six composite ^{27}Al spin states; $\left|\frac{5}{2}\right>\left|\frac{5}{2}\right>$, $\left|\frac{5}{2}\right>\left|\frac{3}{2}\right>$, ... $\left|\frac{5}{2}\right>\left|-\frac{5}{2}\right>$. Thus, the elements of the corresponding column in the corresponding row of $\mathbf{K}_2{}^{t}$ have the values of $1/6\tau_t$, and the other elements of the row are 0. The bridge carbon, after exchange, goes to a site which corresponds to one of the spin states of ^{27}Al with which the bridge carbon couples before exchange. (For example, from the site of $\left|\frac{5}{2}\right>\left|\frac{3}{2}\right>$ to either $\left|\frac{5}{2}\right>$ or $\left|\frac{3}{2}\right>$ but from the site of $\left|\frac{5}{2}\right>\left|\frac{5}{2}\right>$ only to the site of $\left|\frac{5}{2}\right>$.) Consequently, $\mathbf{K}_2{}^{b}$

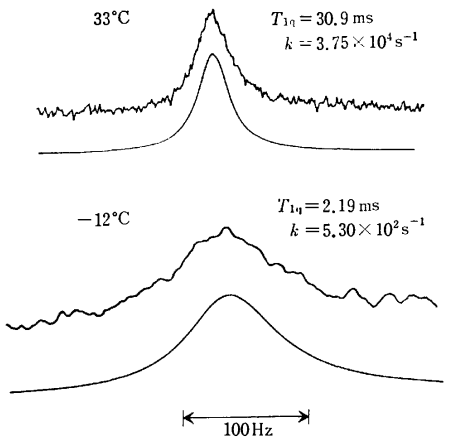

Fig. 1. Observed and calculated ^{13}C spectra of TMA at various temperature. The chemical shift difference between the bridge and the terminal carbons is 60 Hz at 15.1 MHz.

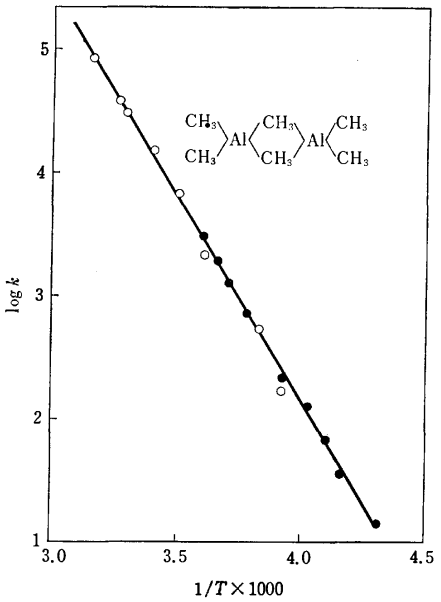

Fig. 2. Arrhenius plot of the exchange rates in TMA. ● from the ^{1}H resonance and ○ from the ^{13}C resonance. The straight line was obtained by the least squares fit of only the ^{1}H resonance data. The Arrhenius parametrs obtained from both ^{1}H and ^{13}C data are $E_a=15.2\pm0.8$, $\Delta H^*=14.6\pm0.8$, $\Delta G^*=11.6\pm0.1$ kcal /mol, and $\Delta S^*=10.0\pm2.0$ e.u. at 25 °C. These are in good agreement with literature valaues.[1,2]

has the elements $1/\tau_t$, $1/2\tau_t$ or 0. In this way, the matrices $\mathbf{K}_2{}^b$ and $\mathbf{K}_2{}^t$ can be easily constructed.

The rate constant for the exchange $k=1/\tau_b$ can be calculated from Eq. 1 by a visual fitting of the observed spectra with the calulated ones in a try-and-error method if the coupling constant, J_{C-Al}, and the ^{27}Al relaxation time, T_{1q}, are known. The J_{C-Al}'s in TMA were found to be 19 and 110 Hz for the bridge and the terminal carbons respectively, and the ^{27}Al relaxation time, T_{1q}, were obtained from the line-widths of the ^{27}Al resonance lines.[3]

The results obtained are shown in Figs. 1 and 2. The exchange rates were also obtained from the ^{1}H resonance, for which the usual line-shape analyses were carried out. It can be seen from Fig. 2 that the exchange rates obtained from the ^{13}C resonance fit well with the straight line which is obtained from the ^{1}H resonance, particularly in the higher temperature range. Thus, the procedure presented here, though complicated in its calculation, can be successfully used to obtain the exchange rates with an accuracy comparable with that of the usual line-shape analysis when the latter method cannot be employed. The results obtained in this work also provide a cross-check on the validity of the method and the accuracy in the values of the J_{C-Al}'s in TMA reported in the previous paper.[3]

A difficulty in the line-shape analysis mentioned above arises from the different NOE-enhancement factors for the bridge and the terminal carbons in the ^{1}H decoupled ^{13}C spectra. The intensity ratio of the terminal to the bridge carbons is about 1.8 at −70 °C (at the slow-exchange limit). This indicates that the NOE factor for the bridge carbon is larger than that of the terminal. Since the J_{C-Al} is smaller in the bridge than in the terminal carbon, the contribution of the scalar coupling mechanism to the relaxation rate of ^{13}C is smaller, and thus that of the dipole-dipole interaction is larger, in the bridge carbon than in the terminal, which leads to the larger NOE factor in the bridge carbon. Therefore, the spectra calculated without taking account of the difference in the NOE factor will not agree with the observed one.

Indeed, this is the case for the spectra with intermediate and slow exchange rates (below *ca.* −30 °C). However, the difference in the NOE factor can be assumed to be negligible provided that the exchange rate is much faster than the ^{13}C relaxation rates, because the redistribution of the spin population among the various energy levels, which causes the NOE factors to be different, does not occur during the short life-time at each site. Thus, Eq. 1 can be safely employed in the high-temperature range.

Note that, in the ^{1}H resonance, the line-widths at temperatures of 10 °C or higher are too narrow to obtain accurate values of the exchange rates. In the ^{13}C resonance, however, the line-widths are sufficiently wide at room temperature because of the scalar coupling interaction, and accurate values are obtained in the high-temperature range, in which the ^{1}H resonance cannot be applied for the TMA system. This is another advantage of the present method.

References

1) K. C. Ramey, J. F. O'Brien, I. Hasegawa, and A. E. Bochert, *J. Phys. Chem.*, **69**, 3418 (1965).
2) O. Yamamoto, K. Hayamizu, and M. Yanagisawa, *J. Organometal. Chem.* **73**, 17 (1974), and references cited therein.
3) O. Yamamoto, *J. Chem. Phys.*, **63**, 2988 (1975).
4) A. Abragam, "The Principles of Nuclear Magnetism," Clarendon Press, Oxford (1962), Chap. XI.

BULLETIN OF THE CHEMICAL SOCIETY OF JAPAN, VOL. 51 (4), 1233—1234 (1978)

The Reactions of the $(ZrO)_2P_2O_7$-NiO System and the ZrP_2O_7-NiO System

Makio KINOSHITA, Saburo BABA,* Akira KISHIOKA, and Michio AMAGASA**

Department of Chemistry, Faculty of Science and Technology, Sophia University, Kioicho, Chiyoda-ku, Tokyo 102

(Received July 1, 1977)

Synopsis. The reaction between $(ZrO)_2P_2O_7$ and NiO at elevated temperatures up to 1340 °C yielded $Ni_3(PO_4)_2$ and ZrO_2 over the whole composition. The reaction between ZrP_2O_7 and NiO yielded $NiO \cdot 4ZrO_2 \cdot 3P_2O_5$ and $Ni_3(PO_4)_2$ in the molar ratios up to equimolarity.

The ternary ZrO_2–CaO–P_2O_5 system was investigated by Bremser,[1] who reported the formation of $CaZr(PO_4)_2$ in the reaction of ZrP_2O_7 with $CaCO_3$. Recently, Šljukić *et al.* obtained the compound $M^{I}M_2'^{IV}(PO_4)_3$ (M=alkali metal and M'=Zr, Ti, Th, and U) by reacting the quadrivalent metal oxide with the alkali metal phosphate in the presence of B_2O_3 flux and investigated these compounds crystallographically.[2] They found that only $NaTh_2(PO_4)_3$ among these compounds showed piezoelectricity.[3] More recently, Allulli *et al.* prepared $ZrM(PO_4)_2 \cdot 4H_2O$ ($M=Mn^{II}$, Co^{II}, NiO^{II}, Cu^{II}, and Zn^{II}) by treating ionexchangeable $ZrHNa(PO_4)_2 \cdot 5H_2O$ with bivalent metal ions and obtained anhydrous phosphates $MZr(PO_4)_2$ by heating the resultant phosphates at higher temperature. These phosphates showed X-ray diffraction patterns similar to those of $CaZr(PO_4)_2$.[4]

However, few studies have been reported concerning the reaction of $(ZrO)_2P_2O_7$ and ZrP_2O_7 with other metal oxides, so the investigation of these reactions will be of interest.

Experimental

Materials. ZrP_2O_7 was prepared by a method similar to that used by Amphlett *et al.*[5] Zirconium phosphate gel was precipitated by adding 1.0 mol dm^{-3} H_3PO_4 to 0.4 mol dm^{-3} $ZrO(NO_3)_2$ solution containing 0.1 mol dm^{-3} HNO_3, the molar ratio of PO_4/Zr being 2.5. The gel was calcined at 1050 °C for 5 h. $(ZrO)_2P_2O_7$ was obtained by calcining ZrP_2O_7 at about 1600 °C for 1 h in a propane-oxygen furnace.

The calcined powder of ZrP_2O_7 and $(ZrO)_2P_2O_7$ was separately pulverized to particles under 74 μm in diameter with an agate ball mill. The purity of these materials was 99.5 wt% or more.

NiO was prepared by calcining nickel hydroxide, which was obtained by mixing 0.5 mol dm^{-3} $Ni(NO_3)_2$ solution with an excess of 0.5 mol dm^{-3} NaOH solution. The nickel hydroxide was calcined at 300 and 600 °C for 3 h.

Reactions at the Contact Surface of One-paired Tablets. The specimen powder was pressed into a tablet of 20 mm in diameter by about 5 mm in thickness under a pressure of 500 kg cm^{-2}. The NiO-tablet was placed on a $(ZrO)_2P_2O_7$-tablet and was heated for 24 h at 1200 °C in a SiC-furnace. After these tablets were removed from the furnace, the reaction products in the surface layers of the tablets were scraped off and examined by X-ray powder diffractometry. ZrP_2O_7 and NiO tablets were similarly heated at 1000 °C for 24 h.

Reactions in the Mixtures of Various Concentrations. The mixture of $(ZrO)_2P_2O_7$ and NiO or that of ZrP_2O_7 and NiO was wet with acetone and thoughly mixed for 30 min in an agate mortar. Then the mixture was pressed under a pressure of 500 kg cm^{-2} to form tablets weighing 0.3 g (10 mm in diameter and about 1.5 mm in thickness). The molar fraction of NiO in both systems was varied from 0.1 up to 0.9 at intervals of 0.1. The tablets were heated at 1200 °C for 24 h. The reaction products in the samples were determined by X-ray diffraction analysis.

Equimolar powder mixtures of both systems were subjected to DTA (heating rate: 10 °C/min, in air).

Isolation and Chemical Analysis of the Reaction Product Insoluble in HCl. The equimolar mixture of ZrP_2O_7 and NiO was heated at 1100 °C for 24 h and for an additional hour at 1400 °C. After $Ni_3(PO_4)_2$ was dissolved by boiling with 6 mol dm^{-3} HCl for 1 h, ZrO_2 in the insoluble residue was removed by flotation with 0.04 mol dm^{-3} sodium lauryl sulfate solution. The final residue thus obtained could not be identified from the known data. The P_2O_5, ZrO_2, and NiO in this unknown product were gravimetrically determined as $Mg_2P_2O_7$,[6] ZrO_2,[7] and bis(dimethylglyoximato)nickel(II)[8] respectively.

Results

Products. In the products of all systems, $Ni_3(PO_4)_2$ and monoclinic ZrO_2 were found. Nickel orthophosphate agreed with the compound existing in the NiO–P_2O_5 binary phase diagram.[9] The chemical formula of the unknown product was $NiO \cdot 4ZrO_2 \cdot$

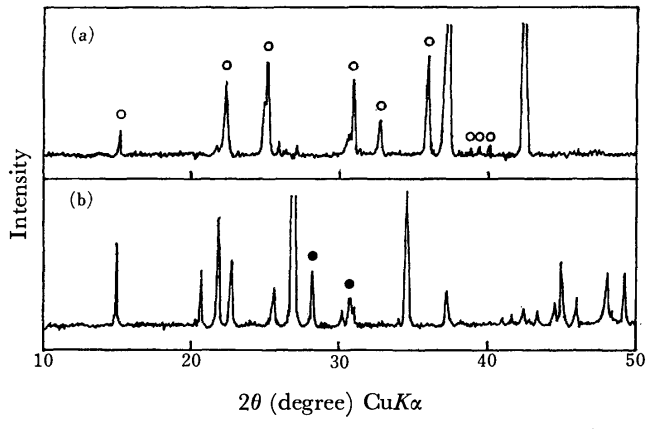

Fig. 1. X-Ray powder diffraction patterns of the surface layer of (a) NiO and (b) $(ZrO)_2P_2O_7$ tablet. (1200 °C). (a) ○: $Ni_3(PO_4)_2$, no mark: NiO, (b) ●: ZrO_2 (monoclinic), no mark: $(ZrO)_2P_2O_7$.

* Present address: Torio Co., Ltd., Aobadai, Meguro-ku, Tokyo 153.

** Present address: Zengyo, Fujisawa-shi, Kanagawa 251.

$3P_2O_5$ or $NiZr_4(PO_4)_6$ (Found: NiO, 7.77; ZrO_2, 48.88; P_2O_5, 43.77 wt %. Calcd: NiO, 7.52; ZrO_2, 49.60; P_2O_5, 42.88 wt %). The color of this substance was purple-red. The X-ray powder diffraction pattern of this substance was quite different from that of $NaZr_2(PO_4)_3$ or $CaZr(PO_4)_2$.[10]

Reactions at the Contact Surface of One-paired Tablets. $(ZrO)_2P_2O_7$–NiO System: X-Ray diffraction patterns of the surface layers of pair of NiO–$(ZrO)_2P_2O_7$ tablets are shown in Fig. 1. The $Ni_3(PO_4)_2$ was formed in the surface layer of the NiO-tablet and ZrO_2 in that of the ZrP_2O_7-tabelt. Hence, the reaction in each tabelt can be represented by the following equations:

$$(ZrO)_2P_2O_7 \longrightarrow 2ZrO_2 + P_2O_5, \quad (1)$$

$$3NiO + P_2O_5 \longrightarrow Ni_3(PO_4)_2. \quad (2)$$

This result is similar to that for the MgO–$Mg_2P_2O_7$ system reported by Jagisch and Bengtson, that is, $Mg_3(PO_4)_2$ was formed in the surface layer of the MgO-tablet by the cross diffusion of P_2O_5.[11]

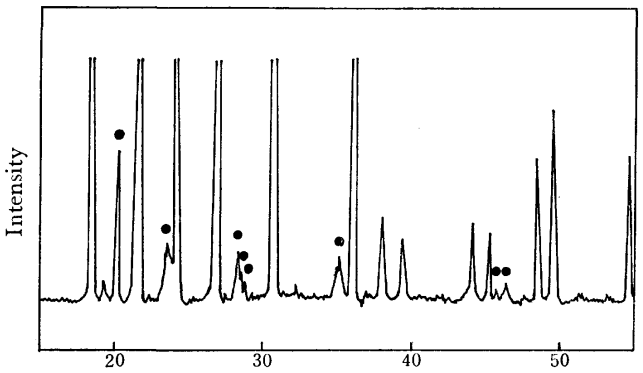

Fig. 2. X-ray diffraction pattern of the surface layer of ZrP_2O_7 tablet. (1000 °C).
●: $NiO \cdot 4ZrO_2 \cdot 3P_2O_5$, no mark: ZrP_2O_7.

ZrP_2O_7–NiO System: X-Ray diffraction pattern of the surface layer of the ZrP_2O_7-tablet is shown in Fig. 2. In the surface layer of the NiO-tablet, $Ni_3(PO_4)_2$ was formed as shown in Fig. 1(a). The $NiO \cdot 4ZrO_2 \cdot 3P_2O_5$ was formed in the surface layer of the ZrP_2O_7-tablet. Accordingly, this reaction proceeded *via* inter-diffusion. The reaction in each tablet can be represented by the following equations:

$$4ZrP_2O_7 + NiO \longrightarrow NiO \cdot 4ZrO_2 \cdot 3P_2O_5 + P_2O_5, \quad (3)$$

$$3NiO + P_2O_5 \longrightarrow Ni_3(PO_4)_2. \quad (4)$$

Reactions in the Mixtures of Various Concentrations. In the $(ZrO)_2P_2O_7$–NiO system, $Ni_3(PO_4)_2$ and ZrO_2 were formed over the whole composition, although the maximum in the formation of these products were found at the $NiO/(ZrO)_2P_2O_7$ ratio of 3. In the ZrP_2O_7–NiO system, the formation of $NiO \cdot 4ZrO_2 \cdot 3P_2O_5$ increased with the increasing molar ratio up to unity. When the ratio of NiO/ZrP_2O_7 exceeded one, $NiO \cdot 4ZrO_2 \cdot 3P_2O_5$ was not formed, but $Ni_3(PO_4)_2$ and ZrO_2 were formed. In the reaction of the equimolar mixture, $NiO \cdot 4ZrO_2 \cdot 3P_2O_5/Ni_3(PO_4)_2$ was nearly equal to unity. Accordingly, the reaction can be represented by the following equation:

$$4ZrP_2O_7 + 4NiO \longrightarrow NiO \cdot 4ZrO_2 \cdot 3P_2O_5 + Ni_3(PO_4)_2 \quad (5)$$

DTA thermograms of both systems of the equimolar mixture showed a broad exothermic peak ranging between 800 and 1150 °C and a sharp endothermic peak at 1340 °C. The former was attributed to the formation of certain reaction products and the latter to the elutectic point[9] of $Ni_3(PO_4)_2$ and NiO. A small endothermic peak at 300 °C in the ZrP_2O_7–NiO system was due to the structural conversion[12] of ZrP_2O_7 from cubic to tetragonal.

References

1) A. H. Bremser, Ph. D. Thesis, University of Illinois, Urbana, 1967.
2) M. Šljukić, B. Matković, B. Prodić, and S. Ščavničar, *Croat. Chem. Acta*, **39**, 145 (1967).
3) M. Topić, B. Prodić, and M. Šljukić, *Czech. J. Phys.* **19**, 1295 (1969).
4) S. Allulli, C. Ferragina, A. L. Ginestra, M. A.Massucci, N. Tomassini, and A. A. G. Tomlinson, *J. Chem. Soc. Dalton Trans.*, **1976**, 2115.
5) C. B. Amphlett, L. A. McDonald, and M. J. Redman, *J. Inorg. Nucl. Chem.*, **6**, 220 (1958).
6) M. Ishibashi, "Teiryo Bunseki Jikkenho," Fuzanbo, Tokyo (1962), pp. 134—136.
7) G. E. F. Lundell and H. B. Knowles, *J. Am. Chem. Soc.*, **41**, 1801 (1919).
8) S. Takagi, "Teiryo Bunseki No Jikken To Keisan," Nanjyo Shoten, Vol. 1, Tokyo (1949), pp. 224—246.
9) J. F. Saver, *Trans, Brit. Ceram. Soc.*, **65**, 191 (1966).
10) C. Bettinli, A. La Ginestra, and M. Valigi, *Atti Acc. Nazl. Lincei, Classe Sci. Fis. Mat. Nat.*, **33**, 472 (1962).
11) R. Jagisch and B. Bengtson, *Arkiv Kemi, Mineral. Geol.*, **22 A**, 1 (1945).
12) D. E. Harrison, H. A. Mckinstry, and F. H. Hummel, *J. Am. Ceram. Soc.*, **37**, 277 (1954).

BULLETIN OF THE CHEMICAL SOCIETY OF JAPAN, VOL. 51 (4), 1235—1236 (1978)

The Anodic Voltammetry of Deoxyribonucleic Acid at a Glassy Carbon Electrode

Toshio YAO, Tamotsu WASA, and Soichiro MUSHA

Department of Applied Chemistry, College of Engineering, University of Osaka Prefecture, Mozuumemachi, Sakai 591

(Received July 6, 1977)

Synopsis. Deoxyribonucleic acid was oxidized in two steps at a glassy carbon electrode. The peak currents had the characteristics of adsorption currents, but if the surface of the electrode was not fully covered by the adsorbed polynucleotide molecule the peak currents had rather the characteristics of diffusion-controlled currents.

Electrochemical methods have been used for the investigation of the chemical and physical properties of solutions of deoxyribonucleic acids (DNA). It has been established that two of the four bases usually found in every DNA, adenine and cytosine, are reducible at the dropping mercury electrode, both in a free form[1-3] and bound to the nucleotide chain.[4-6] However, the two reducible bases are reduced only in a pH range where they are converted to the protonated form,[7] and their half-wave potentials are very close.

A few studies of the electrochemical oxidation of the purine bases were done at the pyrolytic graphite electrode[8-10] and the glassy carbon electrode (GCE).[11] Guanine and adenine, which are constituent bases of DNA, were voltammetrically oxidized at different potentials over the pH range of 0—14. In the present work, the electrochemical oxidation of DNA and its adsorption behavior on the electrode surface were investigated by means of a linear-sweep voltammetry using a stationary GCE.

Experimental

Chemicals. The herring-sperm DNA used throughout this work was obtained from the Wako Pure Chemical Co. All the other reagents were of a reagent grade.

Apparatus. The anodic voltammograms were recorded using a Yanagimoto P-8 type Polarograph at a scan rate of 3.3 mV/s. A three-electrode voltammetric cell maintained at (20±0.1) °C was used for all the experiments. An aqueous saturated calomel electrode (SCE) was used as the reference electrode, and a platinum wire served as the counter electrode. The working electrode was constructed from a glassy carbon rod 3 mm in diameter (Grade GC-20, Tokai Electrode Co.). The rod was cut into a length of 10 mm and was sealed in one end of a glass tube 3 mm in diameter with epoxy cement. The end of the glass tube-carbon rod assembly was polished with 400-grade emery paper until it was quite smooth.

Voltammetric Procedure. In order to obtain reproducible results, a standard pretreatment procedure was applied before recording each voltammogram. The GCE was polished for 30 s with 1500-grade emery paper, and then for 60 s with a paste of sedimented calcium carbonate. The surface of the electrode was washed with a fine spray of distilled water. Any water remaining on the electrode surface was then removed by touching the surface very gently with a piece of soft absorbent paper. The test solutions were not deaerated. The GCE was inserted into the test solutions, and then the solutions were stirred gently for a few seconds. The voltage scan was commenced after quiescency for 20 s at the starting potential (always 0.0 V *vs.* SCE). At least three replicate voltammograms were recorded for each test solution.

Results and Discussion

Figure 1 shows the typical anodic voltammograms of DNA obtained at the stationary GCE. The voltammetric oxidation of DNA took place in two steps; the first and second peaks can be attributed to the oxidation of the guanine and adenine contained in the DNA molecules. The half-peak potentials ($E_{P/2}$) of the voltammetric oxidation peaks shifted linearly towards negative potentials with an increase in the pH; $E_{P/2}$(*vs.* SCE)/V= 1.06−0.060 pH for the first peak and $E_{P/2}$(*vs.* SCE)/V= 1.41−0.065 pH for the second peak over the pH range of 2—12. The peak current (i_P) did not change much with the pH.

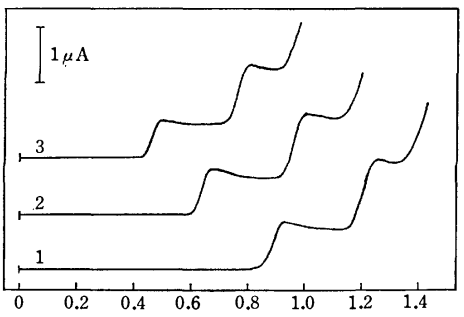

Fig. 1. Anodic voltammograms of DNA at different pH values. pH(Britton-Robinson buffer): curve 1; pH 3.02, curve 2; pH 6.98, curve 3; pH 10.03.
DNA concentration; 0.4 mg/ml, GCE geometric area; 7.1 mm², scan rate; 3.3 mV/s.

As is shown in Fig. 2, the peak current reached a limiting value as the DNA concentration was increased, but in the concentration range below 0.8 mg/ml a linear relationship was observed between the peak current and the concentration. This behavior is probably connected with the coverage of the GCE surface by polynucleotide molecules. Also, the peak potentials for both peaks were dependent on the DNA concentration and shifted slightly to more positive values with the increase in the concentration. Over the concentration range of 0.1—1 mg/ml this shift was about 30—50 mV for both peaks.

In order to study the adsorption of DNA on the GCE surface, the effect of the voltage scan rate on the peak

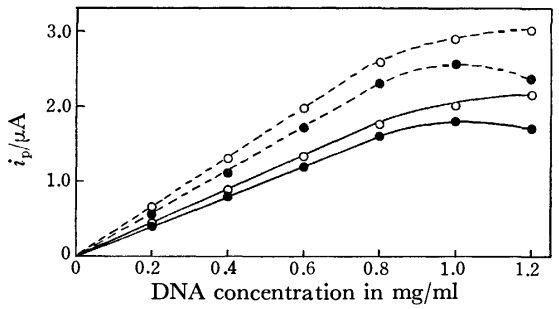

Fig. 2. Peak current-concentration curves for the voltammetric oxidation of DNA at the stationary GCE.
——; First peak, ——; second peak.
pH(Britton-Robinson buffer): ○; pH 3.02, ●; pH 7.00. GCE geometric area; 7.1 mm², scan rate; 3.3 mV/s.

current was examined. The electrochemical oxidation of DNA was irreversible; cyclic voltammetric experiments have shown that no cathodic peak corresponding to the rereduction of the oxidation product was observed at any scan rate. For a linear diffusion-controlled irreversible peak, the peak current function, $i_P/ACV^{1/2}$, should be a constant,[12] and a plot of this function *vs.* $V^{1/2}$ should be a straight line parallel to the $V^{1/2}$ axis, where A is the area of the electrode surface; C, the bulk concentration of the depolarizer, and V, the scan rate. At the various pH values, the peak current functions of both peaks were almost independent of the scan rate. However, at DNA concentrations higher than 1.0 mg/ml the peak current functions of the two peaks of DNA clearly increased with the increase in the scan rate. This behavior is typical of an electrode process where the reactant is adsorbed on the electrode.[13]

These effects of the concentration and the scan rate on the peak current imply that the voltammetric oxidation of DNA takes place in the adsorbed state on the surface of the electrode. The peak currents of DNA have the characteristics of adsorption currents when the surface of GCE is fully covered by adsorbed polynucleotide molecules. However, if the surface is not fully covered, the peak currents have rather the characteristics of diffusion-controlled currents.

In the DNA molecule, the number of guanine equals the number of cytosine, while the number of adenine equals that of thymine (Chargaff's rule). Thus, the ratio of the sum of the voltammetrically active groups of adenine and guanine to the sum of the nonactive groups of cytosine and thymine is approximately one. The herring-sperm DNA contained 14.5% (mass fraction) of guanine and 16.7% of adenine. The value of the diffusion coefficient of guanine was 1.22×10^{-5} cm²/s. The value of the diffusion coefficient of DNA, which was determined from the peak current of the guanine contained in DNA, was 7.3×10^{-7} cm²/s. Also, the value of the diffusion coefficient of DNA, computed with the aid of the Einstein-Stokes law, was 3.6×10^{-7} cm²/s,[4] from the presumed value of the molecular weight of 1×10^{6}.

References

1) D. L. Smith and P. J. Elving, *J. Am. Chem. Soc.*, **84**, 1412 (1962).
2) G. Dryhurst and P. J. Elving, *Talanta*, **16**, 855 (1969).
3) B. Janik and P. J. Elving, *J. Electrochem. Soc.*, **116**, 1087 (1969).
4) P. Valenta and P. Grahmann, *J. Electroanal. Chem.*, **49**, 41 (1974).
5) V. Brabec, *J. Electroanal. Chem.*, **50**, 235 (1974).
6) H. W. Nürnberg and P. Valenta, *J. Electroanal. Chem.*, **57**, 125 (1974).
7) V. Brabec and E. Palecek, *Biophysik*, **6**, 290 (1970).
8) G. Dryhurst and P. J. Elving, *J. Electrochem. Soc.*, **115**, 1014 (1968).
9) G. Dryhurst and G. F. Pace, *J. Electrochem. Soc.*, **117**, 1259 (1970).
10) G. Dryhurst, *Talanta*, **19**, 769 (1972).
11) T. Yao, T. Wasa, and S. Musha, *Bull. Chem. Soc. Jpn.*, **50**, 2917 (1977).
12) R. S. Nicholson and I. Shain, *Anal. Chem.*, **36**, 706 (1964).
13) R. H. Wopschall and I. Shain, *Anal. Chem.*, **39**, 1514 (1967).

BULLETIN OF THE CHEMICAL SOCIETY OF JAPAN, VOL. 51 (4), 1237—1238 (1978)

The Nitrogen Oxide Complex of the Iron(II) Protoporphyrin IX Dimethyl Ester

Tetsuhiko YOSHIMURA

The Environmental Science Institute of Hyogo Prefecture, Suma-ku, Kobe, Hyogo 654

(Received July 22, 1977)

Synopsis. A nitrogen oxide complex of the iron(II) protoporphyrin IX dimethyl ester was synthesized and characterized by means of its infrared spectrum and electron paramagnetic resonance (EPR) spectra at the X- and Q-band frequencies. The EPR spectra in the glass state and in the polycrystalline powder state distinctly indicated the existence of three *g*-values, showing a rhombic symmetry.

Since the nitrogen oxide molecule has an unpaired electron and coordinates to iron(II) hemoproteins, it has been widely used as a probe for investigating the symmetry around the heme iron and the electronic structure of the heme group.[1] The nitrogen oxide complex of the iron(II) protoporphyrin IX dimethyl ester, ONFe(PPDME), is an interesting model compound in relation to such nitrosylhemoproteins.

TABLE 1. IR DATA OF ONFe(PPDME) (in cm^{-1})

Method or solvent	Dielectric constant	Strteching frequency	
		CO (ester)	NO
Nujol mull		1739	1656
KBr disk		1735	1655
CCl_4	2.24	1743	1684
Benzene	2.28	1741	1672
Toluene	2.38	1739	1673
$CHCl_3$	4.81	1732	1675
CH_2Cl_2	7.77	1735	1669
$ClCH_2CH_2Cl$	10.7	1737	1665
N-Methyl imidazole		1735	1616

Table 1 shows the infrared stretching frequencies of the NO (ν_{NO}) and carbonyl groups (ν_{CO}) at the porphyrin periphery for ONFe(PPDME). The ν_{NO} values, measured by the KBr disk technique, are smaller than those for nitrosyltetraphenylporphinatoiron(II), ONFe(TPP),[2] and nitrosyloctaethylporphinatoiron(II)[3] (1670 and 1671 cm^{-1} respectively). In addition, the ν_{NO} value in *N*-methylimidazole (NMIm), which occupies an axial position *trans* to the nitrosyl group, is smaller than that (1625 cm^{-1}) for ONFe(TPP)(NMIm),[4] while it is nearly identical with that (1615 cm^{-1}) for nitrosylhemoglobin (NOHb),[5] in which the imidazole group of proximal histidine is a *trans* axial ligand. Thus, differences in substituents on the porphyrin periphery affect the NO stretching mode for the nitrosyl porphyrin Fe(II) complex. As is shown in Table 1, the ν_{CO} and ν_{NO} values are sensitive to the solvent. Contrary to the case of the ν_{CO} value, the ν_{NO} value shifts essentially to a lower frequency with an increase in the polarity of the solvent, in agreement with the results of Maxwell and Caughey.[5] Such a solvent effect may reflect a considerable degree of polarization in ONFe(PPDME) resulting from the delocalization of the unpaired electron of the nitrosyl group and the d_π–p_π back bonding.[6]

The X-band EPR spectra in the acetone, dichloromethane, and toluene glass states distinctly indicate the existence of three *g*-values, suggesting a bending of the Fe–N–O unit and rhombic symmetry (Fig. 1 and Table 2). In chloroform glass and polycrystalline powder states, the three *g*-values can not be estimated from the X-band spectra, but they can from the Q-band spectra (Fig. 2). As is shown in Table 2, the *g*-values in the glass state for ONFe(PPDME) are comparable to those for ONFe(TPP),[7] while the coupling constants of the ^{14}N hyperfine splitting (hfs) for the former are slightly smaller than those for the latter. From the facts that the observed g_3-value is essentially equal to the free spin value and that the hfs of NO nitrogen is clearly

TABLE 2. EPR PARAMETERS OF ONFe(PPDME)

	State	Temp[a]	g_{iso}	g_1	g_2	g_3	A_{iso}	A_1	A_2	A_3 (G)
ONFe(PPDME)	powder	RT(Q)		2.093	2.04	2.009				
		LNT(Q)		2.099	2.02	2.006				
	in toluene	RT	2.052				15.8			
		LNT		2.102	2.058	2.010		13	16	16.7
	in $CHCl_3$	RT	2.052				15.8			
		LNT		2.08		2.010				16.6
		LNT(Q)		2.09	2.06	2.010				
	in CH_2Cl_2	RT	2.052				16.1			
		LNT		2.098	2.059	2.010		14	16	16.5
	in acetone	RT	2.051				16.1			
		LNT		2.111	2.061	2.010		12.8	16.4	16.5
ONFe(TPP)[7]	in toluene	RT	2.051				16.3			
		−140 °C		2.103	2.064	2.010		12.6	17.2	17.3

a) RT, room temp; LNT, liquid nitrogen temp; Q, measured at the Q-band freq.

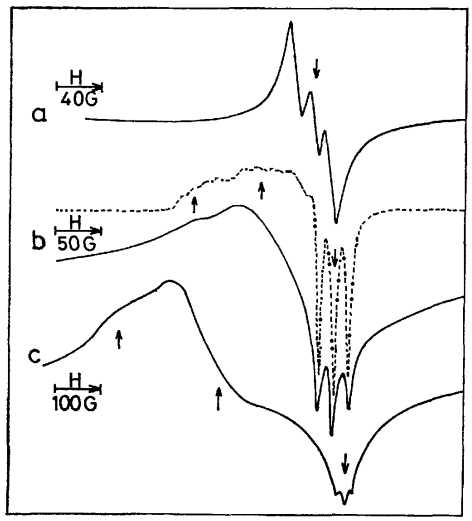

Fig. 1. EPR spectra for ONFe(PPDME) in $CHCl_3$ (——) and in acetone (——): (a) X-band spectra at room temp (soln); (b) X- and (c) Q-band spectra at liq N_2 temp (frozen glass).

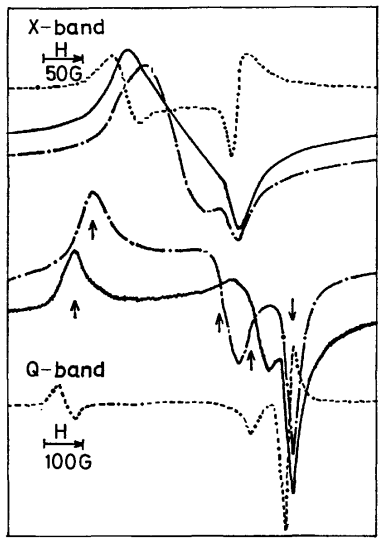

Fig. 2. X- and Q-band EPR spectra for ONFe(PPDME) in polycrystalline powder state at room temp (-•••-, lst derivative) and at liq N_2 temp (——, lst derv.;----, 2nd derv.).

resolved at g_3 absorption, it may be inferred that the g_3 absorption is to be assigned to the g_z absorption and that the unpaired electron of the nitrosyl group is considerably delocalized to the iron d_{z^2} orbital. The g-values for ONFe(PPDME) are found to vary with the experimental conditions, such as the temperature and the powder or solution states, and, among the rest, the g_2-value is especially highly sensitive to such conditions. The g_y-value for NO-protoheme complexes with different nitrogenous bases has been reported to be particularly sensitive to the kind of base.[6] The g_y-value for the $(d_{z^2})^1$ configuration is dependent on the energy separation between d_{z^2} and d_{xz} orbitals and the electron population in each orbital.[8] Thus, the energy and the electron population of the d_π orbital can be expected to be sensitive to environments around Fe–N–O unit in the nitrosylprotoheme complexes.

It has been found that, upon the addition of inositol hexaphosphate (IHP) to NOHb, the hfs from imidazole ^{14}N of proximal histidine (N_ε) is weakened and that from ^{14}NO is intensified.[9] The coupling constant (16.5 G) and the g-value (about 2.0) of the central peak for the ^{14}NO triplet in IHP-treated NOHb are nearly identical with those of ONFe(PPDME) in the glass state, showing that the structure of the nitrosylprotoheme in IHP-treated NOHb is similar to that of ONFe(PPDME). These EPR results suggest that the Fe–N_ε bond in IHP-treated NOHb is stretched or cleaved.[5]

Experimental

Synthesis. ONFe(PPDME) was synthesized by a procedure analogous to that used for ONFe(TPP).[2] One gram of ClFe(PPDME) was added to a chloroform(10 ml)–dry pyridine(1 ml) mixture. The solution thus obtained was deoxidized by bubbling pure N_2 for 10 min. Nitrogen oxide, passed through a KOH column to free it of higher nitrogen oxides, was bubbled into the solution for an hour, and then the excess nitrogen oxide was removed by bubbling N_2 through the solution. Methanol, distilled from Mg, was added to the solution until crystals began to precipitate. The products were filtered off, washed with methanol, and recrystallized from chloroform-methanol, to obtain dark purple crystals of ONFe(PPDME). Calcd for $FeC_{36}H_{36}N_5O_5$: C, 64.10; H, 5.38; N, 10.38; Fe, 8.28%. Found: C, 63.85; H, 5.47; N, 10.35; Fe, 8.22%. The analytical results and the IR spectrum confirmed the absence of pyridine in the product. The procdut was handled in a dry box filled with nitrogen.

Measurements. The IR absorption spectra were recorded on Jasco DS-402G and IR-G IR grating spectrophotometers. The EPR measurements were carried out using a JES-ME-3X (X-band) spectrometer and a JES-PE-3Q (Q-band) spectrometer, both with 100 KHz field modulation. The second derivative display was obtained by the use of the 80 Hz field modulation. As a standard, DPPH powder and MgO powder doped with Mn^{2+} were used. All the solvents were spectrograde reagents and were deoxidized by bubbling pure N_2 prior to use.

References

1) H. Kon, *J. Biol. Chem.*, **243**, 4350 (1968); T. Yonetani, H. Yamamoto, J. E. Erman, J. S. Leigh, and G. H. Reed, *J. Biol. Chem.*, **247**, 2447 (1972); Y. Henry and R. Banerjee, *J. Mol. Biol.*, **73**, 469 (1973); A. Szabo and L. D. Barron, *J. Am. Chem. Soc.*, **97**, 660 (1975).

2) W. R. Scheidt and M. E. Frisse, *J. Am. Chem. Soc.*, **97**, 17 (1975).

3) L. D. Spaulding, C. C. Chang, N-T. Yu, and R. H. Felton, *J. Am. Chem. Soc.*, **97**, 2517 (1975).

4) W. R. Scheidt and P. L. Piciulo, *J. Am. Chem. Soc.*, **98**, 1914 (1976).

5) J. C. Maxwell and W. S. Caughey, *Biochemistry*, **15**, 388 (1976).

6) H. Kon and N. Kataoka, *Biochemistry*, **8**, 4757 (1969).

7) B. B. Wayland and L. W. Olson, *J. Am. Chem. Soc.*, **96**, 6037 (1974).

8) A. H. Maki, N. Edelstein, A. Davidson, and R. H. Holm, *J. Am. Chem. Soc.*, **86**, 4580 (1964).

9) H. Rein, O. Ristau, and W. Scheler, *FEBS Lett.*, **24**, 24 (1972).

BULLETIN OF THE CHEMICAL SOCIETY OF JAPAN, VOL. 51 (4), 1239—1240 (1978)

The Concentration and Separation of a Trace Amount of Cobalt(II) in Sea Water as Its 1-Nitroso-2-naphtholate by Extraction Chromatography

Takaharu Honjo, Shuhei Abe, and Toshiyasu Kiba

Department of Chemistry, Faculty of Science, Kanazawa University, Kanazawa, Ishikawa 920

(Received August 16, 1977)

Synopsis. The behavior of a trace amount of cobalt(II) in extraction and back extraction has been examined with 1-nitroso-2-naphthol in carbon tetrachloride, and the results have also been applied to the concentration and separation of a trace amount of cobalt(II) in sea water as its 1-nitroso-2-naphtholate by extraction chromatography.

Extraction chromatography has been proved to be a powerful technique in the mutual separation of various metals,[1] because the extraction and back extraction may repeatedly accompany it during the process in the chromatographic column. However, this technique has not yet been applied to the concentration and separation of trace amounts of metals in natural waters. In this investigation, the behavior of a trace amount of cobalt(II) in extraction and back extraction with 1-nitroso-2-naphthol in carbon tetrachloride has been examined in detail, and the results have also been applied to the concentration and separation of a trace amount of cobalt(II) in sea water by using a Kel-F column, with 1-nitroso-2-naphthol in carbon tetrachloride as the stationary phase.

Experimental

The experimental procedures for the liquid-liquid extraction and the extraction chromatography were the same as have previously been described.[2,3] 1-Nitroso-2-naphthol was purified by recrystallization from cold petroleum ether. The behavior of cobalt(II) in extraction and extraction chromatography was checked by using a ^{60}Co tracer. The chromatographic column was prepared as follows: to 6.0 g of Kel-F powder of 42—80 mesh, a 15-ml portion of a solution containing 10^{-2} M 1-nitroso-2-naphthol in carbon tetrachloride was added. The mixture was then stirred until it became homogeneous. After having then stood for one night, the mixture was poured into a column which had been filled with a pre-equilibrated eluting solution of pH 3.8. The chromatographic column bed thus prepared (20—22 cm in height) was washed with 50—200 ml of the eluting solution of pH 3.8 at the flow rate of 1.0 ml/min in order to eliminate the excess organic solution. A solution containing a trace amount of cobalt(II) ($<10^{-5}$ M) with the ^{60}Co tracer was then poured onto the column, and the cobalt was collected on the column by passing through an aqueous solution of pH 3.8 at a flow rate of 0.6—4.0 ml/min. The cobalt was strongly held in the stationary phase, but was finally washed down as cobalt chelate in carbon tetrachloride by passing 30 ml of acetone through the column, because the cobalt was not eluted even with a concentrated HCl solution.

Results and Discussion

First of all, the behavior of a trace amount of cobalt(II) in extraction and back extraction has been studied with 10^{-5}—10^{-2} M of various chelating agents in carbon tetrachloride. The results (Fig. 1) revealed that 1-nitroso-2-naphthol gave rise to an extraction behavior of cobalt(II) similar to that of STTA;[4] that is, the back extraction of the cobalt chelate extracted did not occur at all even when the organic phase was shaken with an aqueous solution of 12 M HCl and of 1 M NaOH, by both of which other interfering ions, such as iron(III), nickel(II), and copper(II), and the free ligand could be stripped out from the organic phase. This abnormal behavior of cobalt chelates seems to be caused by the formation of certain inert complexes such as trivalent cobalt chelates.[5] The quantitative extractability of cobalt(II) (trace—10^{-4} M) is attained in about one minute's shaking, and the volume of the initial aqueous solution seems to have no effect on the extraction recovery of cobalt(II), even at a fourteen-fold volume of the organic phase (Fig. 2). On the basis of the experimental results described above, the chromatographic behavior of a trace amount of cobalt(II) was

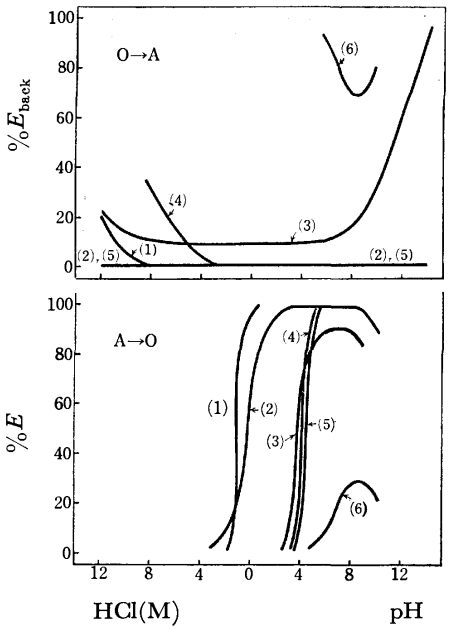

Fig. 1. Effect of pH or HCl(M) on the extraction and the back extraction of a trace amount of cobalt(II). 10^{-5}—10^{-2}M chelating agents–carbon tetrachloride system.
Chelating agents: (1) 10^{-2}M NaDDTC (sodium diethyldithiocarbamate), (2) 10^{-2}M 1-nitroso-2-naphthol, (3) 10^{-2}M cupferron, (4) 10^{-4}M dithizone, (5) 10^{-3}M STTA, (6) 10^{-2}M TTA
Shaking time: 30 min, O→A: Back extraction, A→O: Extraction

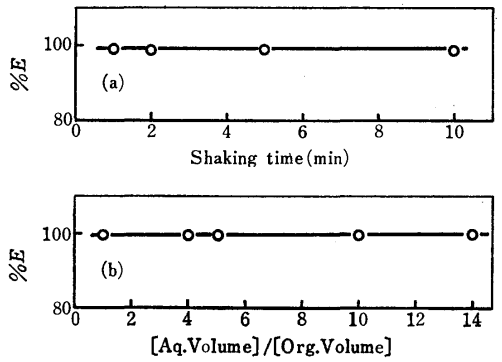

Fig. 2. (a) Effect of shaking time. (b) Effect of the volume of the aqueous phase.
Co(II): Trace—10^{-4}M, 1-nitroso-2-naphthol: 10^{-2}M, solvent: carbon tetrachloride, pH 4.0

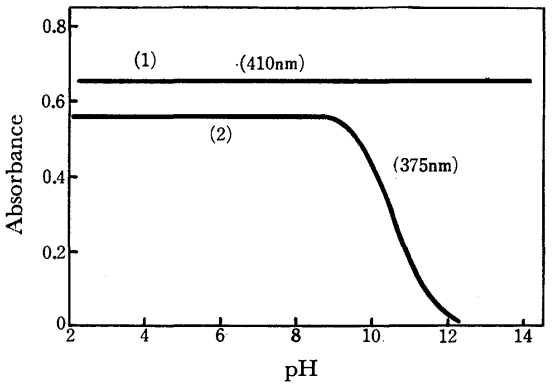

Fig. 3. Back-washing of 1-nitroso-2-naphthol and its cobalt chelate in carbon tetrachloride with an aqueous solution of different pH/acidity.
(1): 2×10^{-5}M Cobalt chelate, (2) 10^{-4}M 1-nitroso-2-naphthol.

studied by means of the Kel-F column, which consists of 8.3 ml of 1-nitroso-2-naphthol in carbon tetrachloride as the stationary phase and of 3.8 ml of an eluting solution as the mobile phase; it was loaded with 50 ml of a pre-equilibrated test solution of pH 3.8 at the flow rate of 0.6—4.0 ml/min, followed by 50—1000 ml of acidified sea water of pH 3.0—4.0 containing a trace amount of cobalt(II) with a ^{60}Co tracer at the flow rate of 0.6—2.0 ml/min. When the sea water was passed through the column, it turned the upper side of the column bed pink, and the length of the band expanded to 5 cm for 400 ml of the effluent, 8 cm for 600 ml of the effluent, and 11 cm for 800 ml of the effluent. It was found that 30—40% of 1-nitroso-2-naphthol in the stationary phase flowed down for about 400—500 ml of the effluent. This fact—that is, the loss of 1-nitroso-2-naphthol from the stationary phase during the chromatographic process—is a weak point in extraction chromatography and may decrease the usefulness of the column for the concentration of a trace amount of cobalt(II) in sea water. In all cases, the cobalt in about 1000 ml of sea water and a distilled water was collected quantitatively with the use of the Kel-F

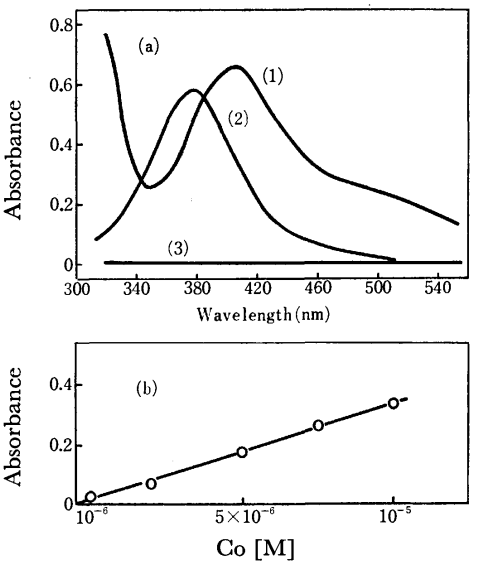

Fig. 4. (a) Absorption spectra of 1-nitroso-2-naphthol and its cobalt chelate in carbon tetrachloride after back washing of the organic phase with a solution of 1M NaOH. (1): 2×10^{-5}M Cobalt chelate after back washnig, (2): 10^{-4}M 1-nitroso-2-naphthol before washing, (3): 1-nitroso-2-naphthol of (2) after back washing.
(b) Working curve for cobalt(II) at 410 nm.

column and was not eluted, not even with a concentrated HCl solution, as could have been predicted from the extraction behavior. The cobalt was finally washed down as metal chelates, together with the excess 1-nitroso-2-naphthol in carbon tetrachloride, by passing 30 ml of acetone through the column. When the organic phase was shaken with a 1 M NaOH solution, the excess of the free 1-nitroso-2-naphthol was almost entirely transferred into an aqueous solution, leaving only the cobalt chelate in the organic phase (Fig. 3). The cobalt chelate with 1-nitroso-2-naphthol could be determined selectively by measuring its absorbance in carbon tetrachloride at 410 nm with a 1 cm quartz cell (Fig. 4), as has briefly been pointed out in a previous short communications on the determination of cobalt(II) in sea water.[6] The recovery of cobalt(II) was about 97—99% under the conditions of this investigation.

References

1) T. Braun and G. Ghersini, "Extraction Chromatography," Elsevier Scientific Publishing Company, Amsterdam (1975).
2) T. Honjo, M. Horiuchi, and T. Kiba, *Bull. Chem. Soc. Jpn.*, **47**, 1176 (1974).
3) T. Honjo and T. Kiba, *Bull. Chem. Soc. Jpn.*, **46**, 1694 (1973).
4) T. Honjo and T. Kiba, *Bull. Chem. Soc. Jpn.*, **45**, 185 (1972).
5) N. Suzuki and H. Yoshida, *Nippon Kagaku Zasshi*, **80**, 1008 (1959).
6) E. Kentner and H. Zeitlin, *Anal. Chim. Acta*, **49**, 587 (1970).

BULLETIN OF THE CHEMICAL SOCIETY OF JAPAN, VOL. 51 (4), 1241—1242 (1978)

Synthesis and Spectral Studies of Dichloroacetates of Lanthanoids

Megh SINGH, M. P. BHUTRA, P. P. VAISHNAVA, and S. N. MISRA
Department of Chemistry and Physics, University of Jodhpur, Jodhpur, India

(Received May 30, 1977)

Synopsis. Dichloroacetates of lanthanoids (Pr, Nd, Sm, Ho, and Er) have been synthesized and characterized by elemental analysis, absorption and IR spectral data, and the X-ray power patterns. Magnetic moments of these derivatives have been measured. Molecular weights determined ebullioscopically in acetic acid showed them to be dimeric.

The halogen substituted acetates of d transition elements have been extentively studied.[1,2,6,7] However, there has been only a very limited effort made in the study of halogen substituted acetates of lanthanoids.[3,4] The trihydrated dichloroacetates (DCA) separate out from the reaction of lanthanoids carbonates and dichloroacetic acid. These can be made anhydrous by keeping in a vacuum desiccator over P_2O_5 for 4 days or heating at 60 °C for 6 h at 0.01 Torr pressure.

Experimental

Crystalline lanthanoids dichloroacetates were prepared by adding slight excess lanthanoids carbonates to dichloroacetic acid (Fluka).

Absorption spectra were measured on Carl Zeiss VSU-2 Spectrophotometer in water and infrared spectra of the KBr pellets were run on a Perkin-Elmer 521 Spectrophotometer.

X-Ray diffraction patterns were obtained using a Phillips diffractometer with nickel filtered Cu$K\alpha$ radiation. Magnetic properties of the compounds were measured by Gouy method at 295 K. The molar susceptibilities were corrected for the diamagnetism of the constituent atoms by means of Pascal's constant.[5] Molecular weights were determined in acetic acid by Gallenkemp semimicro ebulliometer with thermistor ensing.

Results and Discussion

Stretching frequencies $\gamma_s COO^-$ in acetates have been found to be sensitive to both coordination to a metal and substitution in acetate group.[6,7] During the complex formation $\gamma_s COO^-$ shifts to higher frequency, while $\gamma_a COO^-$ shifts in opposite direction. Comparing the values of $\gamma_a COO^-$ in sodium dichloroacetate,[8] Cu(II)[2] and lanthanoids dichloroacetates we have observed that the $\gamma_a COO^-$ values lie inbetween highly ionic sodium dichloroacetate and covalent Cu(II) dichloroacetate. In the lower lanthanoids (Pr and Nd) the values are closer to sodium analogue, while in the higher lanthanoids (Ho and Er) dichloroacetates the values lie closer to copper analogue. This appears well in the conformity of lanthanoids contraction. The $\gamma_a COO^-$ of lanthanoids dichloroacetates, a strong band occuring at 1615—1622 cm^{-1} shows a decrease as compared to sodium analogue, which can be interpreted in terms of dimeric COO^- group, as parallel behavior was observed in the case of Cu(II) dichloroacetate[2]. The existence of dimeric nature of dichloroacetate group is also supported by our mol wt data which point toward dimeric units for dichloroacetate thus involving both bidentate and dimeric dichloroacetate grouping.

C–Halogen Stretching. In lanthanoids dichloroacetates we find high C–halogen and weak low C–halogen stretching frequencies pointing towards the existence of both trans and gauche conformation on the line suggested by Spinner.[8] In general, we find high C–halogen stretching frequencies generally increase with

TABLE 1. ANALYTICAL, MAGNETIC SUSCEPTIBILITY AND MOLECULAR WEIGHT DATA FOR DICHLOROACETATES OF LANTHANOIDS

Compound	Elementary analysis[a] Metal (%)	Cl (%)	C (%)	H (%)	Molar susceptibility $\chi'^{coor}_m \times 10^6$ cgs units	Magnetic moment μ_{eff} in B.M.	Mol wt (Found)
$Pr(CHCl_2COO)_3 \cdot 3H_2O$	24.23 (24.34	36.71 36.75	12.49 12.45	1.51 1.56)	5069	3.47	—
$Nd(CHCl_2COO)_3 \cdot 3H_2O$	24.59 (24.78	36.43 36.54	12.31 12.38	1.43 1.55)	5548	3.63	—
$Sm(CHCl_2COO)_3 \cdot 3H_2O$	25.62 (25.58	36.12 36.15	12.16 12.24	1.52 1.54)	1766	2.04	—
$Ho(CHCl_2COO)_3 \cdot 3H_2O$	27.17 (27.36	35.14 35.28	11.75 11.95	1.50 1.50)	45264	10.37	—
$Er(CHCl_2COO)_3 \cdot 3H_2O$	27.73 (27.64	35.03 35.15	11.96 11.90	1.41 1.49)	38134	9.52	—
$Pr(CHCl_2COO)_3$	26.81 (26.85	40.43 40.53	13.60 13.73	0.51 0.57)	—	—	1007 (524.73)
$Nd(CHCl_2COO)_3$	27.14 (27.31	40.21 40.28	13.51 13.64	0.43 0.57)	—	—	1002 (528.06)
$Er(CHCl_2COO)_3$	30.42 (30.35	38.50 38.59	12.89 13.07	0.46 0.54)	—	—	1087 (551.08)

a) Figures in parentheses indicate the calculated values.

Table 2. Characteristic COO⁻, C–halogen stretchings frequencies and low frequency IR absorption of dichloroacetates (DCA)

Sodium[8] DCA	Cu[10] DCA	Pr DCA	Nd DCA	Sm DCA	Ho DCA	Er DCA	Assignments
1660 m	1689 s	1515 s	1615 s	1615 s	1622 s	1625 s	ν_{asym} COO⁻
1640 vs	1582 s	1580 s	1580 s	1580 s	1595 ms	1595 s	
1399 s	1435 sh	1410 ms	1410 ms	1415 m	1416 ms	1416 m	ν_{sym} COO⁻
	1415 vs	1380 m	1375 ms	1380 s	1386 s	1380 s	
821	835 sh	830 w	829 w	827 sh	840 w	834 w	
807 R	825 vs	822 s	817 s	820 s	822 s	827 s	ν_{asym} C–Cl_2
779 R	807 w	792 m	794 m	794 m	802 m	794 w	
738	761 w	726 w	759 w	755 w	747 w	742 w	ν_{sym} C–Cl_2
	502 w	462 w	456 w	456 w	456 w	457 w	
	482 vw	433 w	436 w	433 w	428 w	430 w	β_{asym} C–Cl_2
	463 sh	425 w	421 w	416 w	408 w	412 w	
	442 w						
	408 w	398 w	396 w	392 w	379 w	384 w	β_{sym} C–Cl_2

R=Raman, β=deformation.

the rise of atomic number of lanthanoids, again in conformity with the lanthanoids contraction. Absorption in 500—350 cm^{-1} of dichloroacetates probably arises from C–halogen bending vibrations. Faniran and Patel[2] reported four bands for Cu(II) dichloroacetate, while in lanthanoids dichloroacetates we observe three bands. The higher frequency band in dichloroacetates can be identified with antisymmetric motion, while those at lower frequencies are attributed to the symmetrical deformations.

Table 3. Nephelauxetic ratio (β), covelency parameter (δ) and bonding parameter ($b^{1/2}$) of the DCA of lanthanoids

Compound	β	δ (%)	$b^{1/2}$
Pr DCA	0.99230	+0.7761	0.06205
Nd DCA	0.99467	+0.5358	0.05162
Sm DCA	0.99887	+0.1131	0.02377
Ho DCA	1.0052	−0.5174	—
Er DCA	1.0051	−0.5173	—

Karraker[9] showed that the symmetry coordination number of a lanthanoids could be predicted from the shape, intensity and wavelength of its hypersensitive transitions in the visible absorption spectrum. The shape of the hypersensitive transition of Nd dichloroacetate ($^4I_{9/2}\rightarrow{}^4G_{5/2}$, $^2G_{7/2}$) in water is quite identical with the bands of the nonacoordinated $Nd(BrO_3)_3\cdot 9H_2O$ in water as well as in solid.[9] The similarlity among the spectra indicate that in these solutions at least the dichloroacetates are most likely nonaccordinated. It is, of course, risky to transfer conclusions from solution measurement to solid compounds, but we feel that the evidence in hand suggests that these compounds are most likely nonacoordinated in solid state as well.

The values of nephelauxetic ratio (β) which are less than one, and covalency parameters (δ) which are positive indicate thereby that the nature of bonding

Table 4. Power X-ray diffraction data of DCA of lanthanoids

Pr		Nd		Sm		Ho		Er	
d(Å)	I/I_0	d(Å)	I/I_0	d(Å)	I/I_0	d(Å)	I/I_0	d(Å)	I/I_0
11.8565	100	11.4710	100	11.7770	100	11.6220	100	11.7770	100
3.7909	20	3.7509	12	3.7660	26	3.8968	18	5.7860	5
2.9377	24	2.9144	28	2.9330	17	2.9190	38	3.8801	37
2.6724	8	2.7040	3	2.6649	6	2.3362	3	2.9190	60
2.3010	19	2.3421	21	2.3480	12			2.3962	8
1.9632	13	1.9513	13	1.9938	7			1.9473	6
								1.9012	1

between metal and ligand is covalent as compared to lanthanoids aqua ions. Like Sinha[10] we find negative values for δ in case of Ho and Er, which he interpreted in terms of ionic characters in the complexes as compared to respective aqua ions. This behavior is quite surprising in view of the highly coordinated nature of the dichloroacetate grouping. The smaller values of bonding parameter $b^{1/2}$ [11] suggests that 4f orbitals are very slightly involved in bonding in lanthanoids dichloroacetates. The magnetic susceptibilities of Pr, Nd, Sm, Ho, and Er dichloroacetates have been measured and the values of magnetic moments of these derivatives have been found to be quite closer to the values reported by earlier workers.[12–15] X-Ray diffraction studies indicate the compounds to be isomorphous within a group by virtue of similar interplanar spacing d and the line intensities.

References

1) M. Melnik, *Acta Facultatis. Pharmaceuticae.*, **25**, 37 (1974), (and references cited therein); *Acta Chem. Scand.*, **25**, 3777 (1971).

2) K. S. Patel and J. A. Faniran, *J. Inorg. Nucl. Chem.*, **38**, 352 (1976), **38**, 1001 (1976); **36**, 2261 (1974).

3) G. P. Tilley and J. E. Roberts, *Inorg. Chem.*, **2**, 745 (1963).

4) R. C. Paul, G. Singh, and J. S. Ghotra, *Indian J. Chem.*, **11**, 294 (1973).

5) A. Earnshaw, "Introduction to Magnetochemistry," Academic Press, London (1968), pp. 5—6.

6) A. V. R. Warrier and P. S. Narayanan, *Spectrochim. Acta*, **23A**, 1061 (1967).

7) A. V. R. Warrier and R. S. Krishnan, *Spectrochim. Acta, Part A*, **27**, 1243 (1971).

8) E. Spinner, *J. Chem. Soc.*, **1964**, 4217.

9) D. G. Karraker, *Inorg. Chem.*, **6**, 1863 (1967); *J. Chem. Educ.*, **47**, 424 (1970).

10) S. P. Sinha, *J. Inorg. Nucl. Chem.*, **33**, 2205 (1971).

11) D. E. Henrie and G. R. Choppin, *J. Chem. Phys.*, **49**, 477 (1968).

12) F. Hund, *Z. Phys.*, **33**, 855 (1925).

13) J. H. Van Vleck and Frank, *Phys. Rev.*, **34**, 1499, 1625 (1929).

14) M. S. Ansari and N. Ahmad, *J. Inorg. Nucl. Chem.*, **37**, 2099 (1975); **38**, 1232 (1976).

15) T. Moeller and E. P. Horwitz, *J. Inorg. Nucl. Chem.*, **12**, 49 (1959).

BULLETIN OF THE CHEMICAL SOCIETY OF JAPAN, VOL. 51 (4), 1243—1244 (1978)

An Investigation on the Effect of Structural Variation on Thermal Decomposition of Rare Earth Chromates(V)

Ajoy Roy, M. Chaudhury, and K. Nag

Department of Inorganic Chemistry, Indian Association for the Cultivation of Science, Calcutta 700032, India

(Received July 22, 1977)

Synopsis. Non-isothermal decomposition kinetics of $LaCrO_4$, $PrCrO_4$, and $NdCrO_4$ have been investigated. In each case, first order decomposition takes place. The energy of activation, E_a^* has been evaluated by applying five different computational procedures based on the data of TG, DTA, and DTG. These values are fairly in good agreement with each other and the average activation energies per mole of the compounds are : $LaCrO_4$: 240 kcal, $PrCrO_4$: 180 kcal and $NdCrO_4$: 170 kcal. The above trend in E_a^* has been rationalized by taking into consideration the packing of atoms in rare earth chromates(V).

In previous publications[1-3] we have shown that rare earth (Ln) trisoxalato complexes, $LnM(C_2O_4)_3 \cdot nH_2O$ (M=Fe(III), Co(III), and Cr(III)) serve as excellent precursors for the corresponding rare earth perovskites, $LnMO_3$. Rare earth trisoxalatochromates(III) are additionally interesting because not only the rare earth orthochromites but also the rare earth chromates(V), $LnCrO_4$ can be obtained from them.[3] An important feature of the rare earth chromates(V) is the variation of structure in the series. While $LaCrO_4$ is monoclinic and $NdCrO_4$ and other higher members are tetragonal, $PrCrO_4$ is dimorphic.[4] We have been intrigued therefore, to see how variation on structure of these compounds influence the activation energies of their thermal decomposition. While the present work was in progress Doyle and Pryde have reported[5] isothermal decomposition kinetics of several rare earth chromates(V). The present study intends to report the activation energies for the decomposition of $LaCrO_4$, $PrCrO_4$, and $NdCrO_4$ from TG, DTA, and DTG under nonisothermal condition by applying several computational procedures. The results obtained here are significantly at variance with those reported by Doyle and Pryde.

Experimental

$LnCrO_4$ were prepared[3] by heating $LnCr(C_2O_4)_3 \cdot nH_2O$ at 520 °C for 2 h. The purity of the products were checked by chemical analysis and from their X-ray powder patterns.[4] Thermal analysis were carried out in a MOM Derivatograph. The sample size was *ca.* 750 mg and the particle size was *ca.* 200 mesh. The samples were heated in air and the heating rate was maintained to 6 °C/min. The enthalpy change was evaluated in a way described earlier.[6]

Results and Discussion

The sole feature of the decomposition reaction

$$LnCrO_4 \longrightarrow LnCrO_2 + 1/2O_2$$

is the endothermic evolution of oxygen in the temperature range 700—800 °C. The observed weight losses are in good agreement with the expected values showing the purity of the compounds. The first order decomposition behavior of these compounds has been established by applying five different computational procedures.[7-11] Table 1 summarizes the E_a^* values for each of the compounds obtained from these methods. The results show that for each compounds, the E_a^* values are fairly in good agreement, the variation is within 10%. The average values of E_a^* for these compounds are: $LaCrO_4$, 240 kcal; $PrCrO_4$, 180 kcal; $NdCrO_4$, 170 kcal. In Table 1 the values reported by Doyle and Pryde[5] are also shown for comparison. It may be noted that activation energies reported by Doyle and Pryde are quite low compared to our values. While the present study shows that the decreasing order of the activation energies are $LaCrO_4 > PrCrO_4 > NdCrO_4$, the trend observed by Doyle and Pryde is $PrCrO_4 > LaCrO_4 > NdCrO_4$.

The trend in E_a^* observed by us can be rationalized if the structures of rare earth chromates are taken into consideration. It may be pointed out that $LaCrO_4$ is isostructural to the monoclinic modification of $CePO_4$ whose crystal structure has been determined.[12] $CePO_4$ structure may be described by a space-filling network in which the cation has an irregular coordination of eight oxygen. For each Ce atom, four short bonds, given as 2.37 Å extend to the corner of four different phosphate groups. Four longer bonds 2.66 Å, connect to the edges of two additional tetrahedra. On the other hand, $NdCrO_4$ is isostructural to zircon, $ZrSiO_4$. In zircon, Si–O bond length is 1.62 Å within the SiO_4 tetrahedra and Zr–O distance is 2.05 Å within the longer ZrO_4 tetrahedra.[13] Buisson *et al.*[14] have shown that in $YCrO_4$, the shortest Cr–O distance is 1.66 Å and the shortest Y–O bond length is 2.44 Å. The stereoscopic models of $CePO_4$ and $ZrSiO_4$ reveal that $CePO_4$ is having a much more close packed structure than $ZrSiO_4$.

Inasmuch as the thermal energy required to activate

Table 1. Activation energies of $LnCrO_4$

Method used	E_a^* (kcal/mol)		
	$NdCrO_4$	$PrCrO_4$	$LaCrO_4$
Freeman-Carroll[a]	167	169	220
Horowitz-Metzger[a]	170	181	244
Coats-Redfern[a]	157	165	225
Borchardt-Daniel[b]	171	177	261
Dave-Chopra[c]	170	202	251
Average E_a^*	170	180	240
Doyle-Pryde[d]	59	84	73
ΔH	4.1	3.9	3.9

a) From TG. b) From DTA. c) From DTG.
d) The values reported in Ref. 5.

a compound having tight packing of atoms will be more than a compound having less packed structure, the activation energy for $LaCrO_4$, therefore, is expected to be greater than $NdCrO_4$. Although $PrCrO_4$ is dimorphic, powder diffraction pattern reveals that the lines due to the tetragonal phase are much abundant. It is reasonable therefore to expect that the activation energy for $PrCrO_4$ will be closer to $NdCrO_4$ rather than $LaCrO_4$. Table 1 shows such is actually the case.

The enthalpy change involved in the decomposition of the rare earth chromates are almost same for each of the compounds and is about 4 kcal/mol.

References

1) K. Nag and A. Roy, *J. Inorg. Nucl. Chem.*, **38**, 1983 (1976).
2) K. Nag and A. Roy, *Thermochim. Acta*, **17**, 247 (1976).
3) A. Roy and K. Nag, *J. Inorg. Nucl. Chem*, in press.
4) H. Schwarz, *Z. Anorg. Allg. Chem.*, **322**, 1, 15, 129, 137 (1963).
5) W. P. Doyle and I. J. Pryde, *J. Inorg. Nucl. Chem.*, **38**, 487 (1976).
6) G. S. Sanyal and K. Nag, *J. Inorg. Nucl. Chem.*, **39**, 1127 (1977).
7) E. S. Freeman and B. Carroll, *J. Phys. Chem.*, **62**, 394 (1958).
8) H. H. Horowitz and G. M. Metzger, *Anal. Chem.*, **35**, 1454 (1963).
9) A. W. Coats and J. P. Redfern, *Nature*, **201**, 68 (1964).
10) H. J. Borchardt and F. Daniels, *J. Am. Chem. Soc.*, **79**, 41 (1957).
11) N. G. Dave and S. K. Chopra, *Z. Phys. Chem. (N.F.)*, **48**, 257 (1966).
12) R. C. L. Mooney-Slater, *Z. Krist.*, **117**, 371 (1962).
13) R. G. Wykoff, "Crystal Structure," Vol. 3, 2nd ed, Interscience Publishers (1960), p. 16.
14) G. Buisson, F. Bertant, and J. Mareschal, *C. R. Acad. Sci., Paris*, **259**, 411 (1964).

BULLETIN OF THE CHEMICAL SOCIETY OF JAPAN, VOL. 51 (4), 1245—1246 (1978)

Manganese Dioxide Oxidation of Thioureas

T. C. SHARMA, N. S. SAHNI, and Amba LAL
School of Studies in Chemistry, Vikram University, Ujjain 456010, India

(Received June 6, 1977)

Synopsis. Manganese dioxide oxidation of thioureas in chloroform at room temperature gave the corresponding ureas.

The oxidation of thiourea and its derivatives has received wide attention due to its potential importance in the biological activity of these compounds. The oxidation of these compounds is reported to give rise to a variety of products, depending upon the nature of the oxidant and the reaction conditions. Thus, thiourea and its alkyl and aryl derivatives have been oxidized to the corresponding disulfide with potassium bromate in sulfuric acid medium,[1] whereas *N,N'*-dialkylthioureas are readily oxidized to the corresponding carbodiimides by alkaline hypochlorites.[2] Carbodiimides have also been prepared by the desulfurization of *N,N'*-disubstituted thioureas with various metal oxides such as mercury(II) oxide,[3] lead oxide,[4,5] and arsenic oxide.[6] However, thiourea, when oxidized with potassium permanganate, gave urea.[7] In the oxidation of thioureas with bromine or thionyl chloride, bis(*N*-substituted amidino) disulfides were isolated as hydrobromide salts.[8–13]

In this laboratory we have oxidized thioureas to ureas by manganese dioxide, a very mild and selective reagent. The reactions have been completed at room temperature by shaking a mixture of the oxidant and the substrate in chloroform. In every case, the corresponding urea has been obtained as the end product, identified by its melting point, elemental analysis, and IR spectrum. The IR spectra of these compounds showed intense absorption in the 1655—1670 cm^{-1} region due to carbonyl stretching.

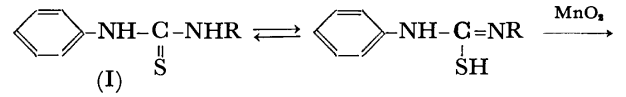

(I)

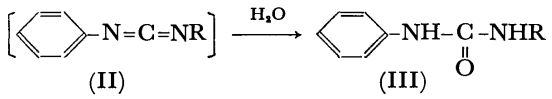

(II) (III)

(a) R=H (b) R=C_6H_5
(c) R=$C_6H_4CH_3$(*p*-) (d) R=C_6H_4Cl(*p*-)
(e) R=$C_6H_4OCH_3$(*p*-) (f) R=C_6H_4Cl(*m*-)

A probable mechanism for this reaction may involve the initial formation of carbodiimide(II) which reacts with water, under the experimental conditions, to afford the corresponding urea (III).

Experimental

Starting Materials. Active manganese dioxide was prepard from manganese sulfate dihydrate and potassium permanganate according to the literature method.[14] All thioureas were prepared by mixing phenyl isothiocyanate and corresponding anilines in molecular ratio in ethanol and heating the mixture.

Oxidation of Phenylthiourea. A mixture of phenylthiourea (2 g), manganese dioxide (10 g) and chloroform (150 ml) was shaken at room temperature for 5 h. The mixture was filtered and the oxide was washed with chloroform. The combined filtrate and washings were evaporated to afford a residue (1.1 g), which on crystallization from benzene gave colorless crystals of phenylurea (IIIa), mp 148 °C (lit,[15] mp 147 °C). (Found: C, 61.7; H, 5.8; N, 20.4%. Calcd for $C_7H_8N_2O$: C, 61.8; H, 5.9; N, 20.6%). λ_{max} (KBr); 3435, 3315, 1670, 1625, 1605, 1565, 1507, 1460, 1365, 1295, 1265, 755, and 705 cm^{-1}.

The other products of this series obtained similarly are listed in Table 1. These compounds have been crystallized from benzene.

The authors thank Professor M. M. Bokadia for providing laboratory facilities.

References

1) B. Singh, B. Chand, and M. S. Saran, *Bull. Chem. Soc. Jpn.*, **38**, 43 (1965).
2) E. Schmidt, M. Seefelder, R. S. Jennen, W. Striewsky, and M. Von Martius, *Ann.*, **571**, 83 (1951).
3) W. Weith, *Ber.*, **6**, 1389 (1873).
4) I. W. Herzog, *Z. Angew. Chem.*, **33**, 140 (1940).

TABLE 1. VARIOUS UREAS OBTAINED

Compound No	Mp °C		Yield %	Formula		C%	H%	N%
IIIb	236	(lit,[16] mp 237—237.5)	65	$C_{13}H_{12}N_2O$	Calcd	73.6	5.6	13.2
					Found	73.4	5.6	13.1
IIIc	217	(lit,[17] mp 218)	62	$C_{14}H_{14}N_2O$	Calcd	74.3	6.2	12.4
					Found	74.2	6.0	12.2
IIId	237	(lit,[18] mp 237—238)	64	$C_{13}H_{11}N_2OCl$	Calcd	63.5	4.4	11.3
					Found	63.3	4.4	11.1
IIIe	190	(lit,[19] mp 186—190)	70	$C_{14}H_{14}N_2O_2$	Calcd	69.4	5.8	11.6
					Found	69.3	5.6	11.3
IIIf	184	(lit,[20] mp 183—184)	68	$C_{13}H_{11}N_2OCl$	Calcd	—	—	11.3
					Found	—	—	11.0

5) E. Schmidt, W. Striewsky, and F. Hitzler, *Ann.*, **560**, 222 (1948).
6) R. F. Coles, *Chem. Abstr.*, **54**, 24464 (1960).
7) E. A. Werner, *J. Chem. Soc.*, **115**, 1168 (1919).
8) P. K. Srivastava and Y. R. Rao, *J. Indian Chem. Soc.*, **40**, 803 (1963).
9) P. K. Srivastava, *Indian J. Chem.*, **1**, 434 (1963); **2**, 154 (1964).
10) P. Klatsmanyi-Gabor, T. Meisel, and L. Erdey, *Acta Chim. Acad. Sci. Hung.*, **40**, 99 (1964).
11) F. Kurzer and P. M. Sanderson, *J. Chem. Soc.*, **1957**, 4461; **1959**, 1058; **1963**, 3336.
12) G. Barnikow and J. Bodeker, *Chem. Ber.*, **100**, 1394 (1967).
13) P. K. Srivastava and M. Saleem, *Tetrahedron Lett.*, **1968**, 2725.
14) E. F. Pratt and T. P. McGovern, *J. Org. Chem.*, **29**, 1540 (1964).
15) T. L. Davis and K. C. Blanchard, *J. Am. Chem. Soc.*, **45**, 1816 (1923).
16) J. R. Scott and J. B. Cohen, *J. Chem. Soc.*, **121**, 2034 (1922).
17) C. K. Ingold, *J. Chem. Soc.*, **125**, 87 (1924).
18) C.-H. Kao, H.-Y. Fang, and Peter P. T. Sah, *J. Chinese Chem. Soc.*, **3**, 137 (1935); *Chem. Abstr.*, **29**, 6173 (1935).
19) C. Naegeli, A. Tyabji, and L. Conrad, *Helv. Chim. Acta*, **21**, 1127 (1938); *Chem. Abstr.*, **33**, 541 (1939).
20) R. P. Lastovskiĭ, *Zh. Obshch. Khim.*, **18**, 921 (1948); *Chem. Abstr.*, **43**, 170 (1949).

BULLETIN OF THE CHEMICAL SOCIETY OF JAPAN, VOL. 51 (4), 1247—1248 (1978)

Asymmetric, Partial Acetylation of *dl*-1-Phenylethanol by Means of Chiral Polymers

Tetsushi YAMASHITA, Hiroshi YASUEDA, and Nobuo NAKAMURA

Department of Chemistry, Faculty of Science, Osaka City University, Sumiyoshi-ku, Osaka 558

(Received June 20, 1977)

Synopsis. The partial esterification of *dl*-1-phenylethanol with acetic anhydride was carried out in the presence of poly(*O*-acryloylquinine), poly(*N*-benzyl-2-pyrrolidinylmethylacrylate), and poly(*O*-acryloyl-*N*-benzylephedrine). The propionyl esters of quinine, *N*-benzyl-2-pyrrolidinylmethanol and *N*-benzylephedrine were also used as low molecular weight catalysts. The above polymeric and monomeric catalysts showed poor, asymmetric efficiencies for this esterification.

Several synthetic polymers[1,2] derived from optically active amino alcohols have been used for the study of polymeric effects and asymmetric reactions. Some polymeric catalysts have yielded products with higher optical yields than their corresponding monomeric catalysts.

This report describes the use of poly(*O*-acryloylquinine)[2] (P-1), poly(*N*-benzyl-2-pyrrolidinylmethyl acrylate)[2] (P-2), and poly(*O*-acryloyl-*N*-benzylephedrine)[1] (P-3) in the asymmetric, partial acetylation[3-5] of *dl*-1-phenylethanol. The use of *O*-propionylquinine[2] (A-1), *N*-benzyl-2-pyrrolidinylmethyl propionate[2] (A-2), and *O*-propionyl-*N*-benzylephedrine[1] (A-3) was also examined. The acetylation was carried out in a manner similar to that reported by Wegler.[3]

$$2\ \mathrm{Ph{-}\underset{\underset{CH_3}{|}}{CH}{-}OH} + (CH_3CO)_2O \xrightarrow[\text{Catalyst}]{} \mathrm{Ph{-}\underset{\underset{CH_3}{|}}{CH}{-}OH} + \mathrm{Ph{-}\underset{\underset{CH_3}{|}}{CH}{-}OCOCH_3}$$

Two equivalent amounts of *dl*-1-phenylethanol were allowed to react with one equivalent amount of acetic anhydride in the presence of one equivalent amount of a catalyst. The molar equivalent amount of the polymeric catalyst was calculated on the basis of that of the monomer used in the polymerization (*e.g.*, 100 mg of P-1 corresponds to 100 mg of A-1).

TABLE 1. THE OPTICAL YIELDS AND CONFIGURATIONS OF α-METHYLBENZYL ACETATE

Catalyst	O.Y.[a] (%)	Conf.[b]
A-1	1.12	*S*
P-1	0.21	*S*
P-1[c]	0.74	*S*
P-1[d]	1.13	*S*
A-2	0.14	*R*
P-2	0.08	*R*
A-3	0.09	*S*
P-3	0.00	—

a) The O.Y. (optical yield, %) was calculated with respect to the value for optically pure (*S*)-α-methylbenzyl acetate,[6] $[\alpha]_D^{28} = -118°$ in benzene. b) The configuration of the predominant isomer. c) P-1/acetic anhydride=5. d) P-1/acetic anhydride=10.

Table 1 shows the optical yields and configurations of α-methylbenzyl acetate obtained with these catalysts.

Table 1 indicates that asymmetric acetylation was carried out more effectively with monomeric than with polymeric catalysts.

Ten equivalent amounts of P-1 to one equivalent amount of acetic anhydride were required to obtain α-methylbenzyl acetate in a 1.13% optical yield, while one equivalent amount of A-1 was needed to obtain acetylated alcohol with the same value of optical yield. These results suggest that no favorable polymer effect with regard to stereoselectivity is observed for this esterification.

Dumont *et al.*[7] have also reported that a chiral polymeric rhodium complex catalyzed the asymmetric hydrogenation of olefins with a lower efficiency than did the corresponding monomeric complex.

Experimental

(A). To a solution of A-1 (2.28 g) and *dl*-1-phenylethanol (1.46 g) in 10 ml of carbon tetrachloride was added acetic anhydride (0.61 g). The mixture was stirred under reflux for 15 h. After removal of the solvent, the residue was dissolved in ether. The ethereal solution was washed with 1 M-hydrochloric acid to remove A-1, successively with saturated sodium hydrogencarbonate and water, and dried. The solution was evaporated to dryness under reduced pressure. The residue was distilled to give a colorless oil (1.50 g). Bp 90 °C at 13 mmHg. $[\alpha]_D^{17} = -0.604°$ (*c* 50, benzene). GLC and TLC of this oil showed it to be composed of two materials. The mixture was subjected to column chromatography on alumina (2×30 cm, 200 mesh, neutral).

Elution with hexane gave 0.73 g of acetylated alcohol. $[\alpha]_D^{13} = -1.32°$ (*c* 25, benzene). Further elution with ether gave 0.61 g of unreacted 1-phenylethanol. $[\alpha]_D^{16} = +0.65°$ (*c* 25, benzene).

The above acetylated and unreacted alcohols were distilled and their optical rotations were measured again. α-Methylbenzyl acetate, bp 105—108 °C at 15 mmHg. $[\alpha]_D^{15} = -1.34°$ (*c* 20, benzene). 1-Phenylethanol, bp 93 °C at 12 mmHg. $[\alpha]_D^{15} = +0.67°$ (*c* 20, benzene). The structure of acetate and unreacted alcohol was confirmed by NMR and IR.

(B). To a solution of P-1 (2.28 g) and *dl*-1-phenylethanol (1.46 g) in 10 ml of carbon tetrachloride was added acetic anhydride (0.61 g), and the mixture was refluxed with stirring. After 15 h, the solution was evaporated to dryness *in vacuo*. Ether was added to the residue, and a precipitate of P-1 was filtered off. The filtrate was evaporated to give a mixture of acetate and unreacted alcohol in a 90% yield. After having been distilled, the mixture was separated into 1-phenylethanol and α-methylbenzyl acetate by column chromatography in a manner similar to that described in (A). The use of other monomeric and polymeric catalysts was attempted according to methods similar to those described in (A) and (B).

The optical rotations of l-phenylethanol and α-methylbenzyl acetate were measured by means of a JASCO DIP-4 automatic polarimeter (10 cm cell, *c* 20—50, benzene).

A JASCO IRA-1 (IR), a JEOL-60 MC (NMR) and a Varian M 920 (GLC) were used for the measurement of the samples in this experiment.

References

1) T. Yamashita, H. Yasueda, and N. Nakamura, *Chem. Lett.*, **1974**, 585.
2) T. Yamashita, H. Yasueda, Y. Miyauchi, and N. Nakamura, *Bull. Chem. Soc. Jpn.*, **50**, 1532 (1977).
3) R. Wegler, *Ann. Chem.*, **506**, 77 (1933).
4) C. W. Bird, *Tetrahedron*, **18**, 1 (1962).
5) S. Mitsui and Y. Kudo, *Tetrahedtron*, **23**, 4271 (1967).
6) H. R. Snyder and J. H. Brewster, *J. Am. Chem. Soc.*, **71**, 291 (1949).
7) W. Dumont, J. C. Poulin, T. P. Dang, and H. B. Kagan, *J. Am. Chem. Soc.*, **95**, 8295 (1973).

BULLETIN OF THE CHEMICAL SOCIETY OF JAPAN, VOL. 51 (4), 1249—1250 (1978)

Conformational Analysis of 9,14-Dihydrotribenzo[*a,c,f*]cyclooctene and Its Derivatives

Yasuo SHIGEMITSU, Masayoshi JURO, Yuji MUKUNO, and Yoshinobu ODAIRA

Department of Petroleum Chemistry, Faculty of Engineering, Osaka University, Suita, Osaka 565

(Received August 16, 1977)

Synopsis. 9,14-Dihydrotribenzo[*a,c,f*]cyclooctene, 9,14-dihydrotribenzo[*a,c,f*]cycloocten-9-one, and 9,14-dihydrotribenzo[*a,c,f*]cyclooctene-9,14-dione, which are all new bridged aromatics containing a biphenyl moiety, have been prepared. Saddle conformations have been suggested for all of them on the basis of the spectra data.

The chemistry of bridged aromatics containing three or more benzene rings has received increasing interest in recent years. There have been a number of reports on the synthesis and conformational analysis of 10,15-dihydro-5*H*-tribenzo[*a,d,g*]cyclononene and its derivatives.[1] Little attention, however, has been paid to the chemistry of 9,14-dihydrotribenzo[*a,c,f*]cyclooctene derivatives, which are new bridged aromatics containing a biphenyl moiety. We wish to report here the preparation and conformational determination of 9,14-dihydrotribenzo[*a,c,f*]cyclooctene (**2**), 9,14-dihydrotribenzo[*a,c,f*] cycloocten-9-one (**3**), and 9,14-dihydrotribenzo[*a,c,f*]-cyclooctene-9,14-dione (**4**).[2]

The hydrocarbon **2** was prepared by the acid-catalyzed cycloalkylation of benzene with 2,2′-bis-(hydroxymethyl)biphenyl (**1**) in almost quantitative yield.[1d,1e,3] Oxidation of **2** with sodium dichromate in acetic acid under reflux gave **3** in 62% yield.[1c,1e] The monoketone **3** resisted further oxidation under the same conditions, but could be oxidized with chromic anhydride in acetic acid under reflux to give **4** in 17% yield.

The PMR spectrum of **2** showed the benzylic protons as a singlet at δ 3.65, indicating that **2** takes a flexible conformation. On lowering the temperature the singlet began to split and at about −40 °C it separated into a distinct AB quartet at δ 3.59 and 3.74 (J=15.0 Hz). The UV absorption spectrum of **2** was the same in shape and band position as that of 2,2′-dimethylbiphenyl.[4] This result suggests that the two benzene rings of the biphenyl moiety in **2** would be twisted by about 70°.[5] A molecular model of **2** shows that the two benzene rings of the biphenyl moiety are nearly coplanar in the crown form, while they are quite twisted in the saddle form. These facts allow assignment of a saddle conformation for **2**. The hydrocarbon **2** undergoes inversion between the two possible saddle forms **2a** and **2b** at normal temperatures, but is frozen in one form at lower temperatures. The free energy of activation ($\Delta F^{\ddagger}$) for the inversion process is calculated to be 15.3 kcal/mol at 25 °C in CD_2Cl_2.[6]

The monoketone **3**, on the other hand, is a rigid molecule at room temperature, since its PMR spectrum showed the benzylic protons as an AB quartet at δ 3.7 and 4.1 (J=14.3 Hz). On raising the temperature the two doublets were observed to broaden and finally at 84 °C to coalesce into a broad singlet, thus permitting calculation of $\Delta F^{\ddagger}$ for the inversion: 17.5 kcal/mol at 84 °C in C_7D_8. The band position of the carbonyl absorption at 1643 cm^{-1} for **3** is approximately the same as that for benzophenone (1647 cm^{-1}), suggesting that the carbonyl group of **3** would conjugate strongly with a benzene ring. A molecular model of **3** reveals that in a crown conformation such a strong conjugation may not be possible because of the non-coplanarity of the carbonyl group with the benzene rings. The alternative assignment of a saddle conformation to **3** would be more compatible with its UV spectrum, which showed a much more intense band at long wavelength (>310 nm) than that of an open chain model compound, *o*-benzylbenzophenone (**5**).[7] This intense band indicates the presence of a longer conjugative system in **3** than in **5**. If the carbonyl group is coplanar with the benzene ring A, the angle of the twist in the biphenyl moiety should be as large as that of 2,2′-disubstituted biphenyl (≈70°). In this case the UV spectrum of **3** should be more similar to that of **5**. On the other hand, if the carbonyl group is coplanar with the benzene ring B, the twist in the biphenyl moiety would be small enough for the benzene rings B and C to be conjugated. Based on the spectral data and the above considerations, we would like to propose that the monoketone **3** may possess the saddle conformation in which the carbonyl group is coplanar with the benzene ring of the biphenyl moiety.

The ^{13}C NMR spectrum of **4** showed a carbonyl carbon resonance at 200.7 ppm and its IR spectrum showed a carbonyl band at 1670 cm^{-1}, indicating that the two carbonyl groups would take the same conformation. The carbonyl stretching frequency for **4** is 12 cm^{-1} higher than that for the open chain compound, *o*-dibenzoylbenzene (**6**) (1658 cm^{-1}). The carbonyl bond force constant for **4**, calculated by using the equation proposed by Halford,[8] is greater by 0.12 than that for **6**.[9] This result suggests that the two carbonyl groups of **4** would not lie in the plane of any benzene ring, but would make a certain angle with the benzene rings. The angle, however, would not be so large as to impede completely the conjugation of the carbonyl group with the benzene ring, since the UV spectrum of **4** showed a much more intense band at 330 nm (ε 641) than that for **6** (ε 269). This intense band, compared with that of **6**, may be explained in terms of the conjugation of the two carbonyl groups with the benzene ring. Thus the UV data are inconsistent with the assignment of a crown conformation for **4**, because the crown conformation would lead to inhibition of the conjugation due to the orthogonality of the carbonyl groups with the benzene rings. Consequently, we feel that it is reasonable to assign a saddle conformation for **4**, although the

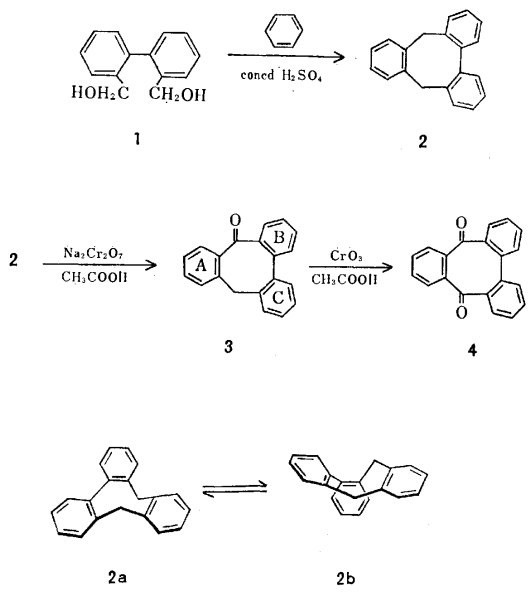

present spectral data are not sufficient to confirm the definitive structure of **4**.

Experimental

All melting points are uncorrected. The IR spectra were obtained on a JASCO IR-G spectrophotometer or a Hitachi Perkin-Elmer 225 grating infrared spectrophotometer in a potassium bromide pellet. The PMR spectra were recorded on a JEOL JNM-PS-100 spectrometer using tetramethylsilane as an internal standard. The ^{13}C NMR spectra were recorded on a JEOL PS 100-EC 100 spectrometer. The mass spectra were taken on a Hitachi RMU-6E mass spectrometer and the UV spectra on a Hitachi two-wavelength double beam spectrophotometer 356. 2,2′-Bis(hydroxymethyl)biphenyl (**1**) (mp 110—111 °C, lit,[10] 112 °C) was prepared from dimethyl diphenate according to the procedure of Kakis *et al.*[10]

9,14-Dihydrotribenzo[a,c,f]*cyclooctene (2).* The hydrocarbon **2** was prepared according to the procedure of Dagan and Rabinovitz.[1e,3] The crude product was recrystallized from petroleum ether–benzene to give pure **2** as colorless plates, mp 137—139 °C. IR: 3060, 3030, 2920, 1475, 1430, 775, 745 cm^{-1}; MS: *m/e* 256 (M^+, base peak); PMR (CD_2Cl_2): δ 3.65 (s, 4H), 7.16 (bs, 4H), 7.32 (bs, 8H); UV: $\lambda_{max}^{95\%EtOH}$ 233 (ε 7970), 263 (1130), 272 nm (733). Found: C, 93.54; H, 6.22%. Calcd for $C_{20}H_{16}$: C, 93.71; H, 6.29%.

9,14-Dihydrotribenzo[a,c,f]*cyclooctene-9-one (3).* The hydrocarbon **2** (423 mg, 1.65 mmol) and sodium dichromate (2.8 g, 9.4 mmol) in acetic acid (140 ml) and water (25 ml) were refluxed for 53 h. The reaction mixture was poured into ice–water and the product was collected by filtration, washed successively with aqueous sodium hydrogencarbonate and water, and then chromatographed on a silica gel column. Elution with petroleum ether recovered the unreacted **2** (113 mg). Elution with benzene–petroleum ether (2:3) afforded the monoketone **3** (213 mg, 62%) which was recrystallized from methanol to give colorless prisms, mp 131—133 °C. IR: 1643 cm^{-1}; MS: *m/e* 270 (M^+, base peak); PMR ($CDCl_3$): δ 3.7 (d, 1H, J=14.3 Hz), 4.1 (d, 1H, J=14.3 Hz), 7.1—7.5 (m, 11H), 7.9 (bd, 1H), ^{13}C NMR ($CDCl_3$): δ 40.0 (>CH_2), 200.0 ppm (>C=O); UV: $\lambda_{max}^{95\%EtOH}$ 235 (ε 16750), 255 sh (8710), 295 sh (1380), 335 sh nm (367). Found: C, 88.76; H, 5.07%. Calcd for $C_{20}H_{14}O$: C, 88.86; H, 5.22%.

9,14-Dihydrotribenzo[a,c,f]*cyclooctene-9,14-dione (4).* An acetic acid solution (20 ml) of **3** (350 mg, 1.3 mmol) and chromic anhydride (1.2 g. 12 mmol) was refluxed for 44 h. The same workup as that described above and purification by column chromatography on silica gel gave the unreacted monoketone **3** (110 mg) and the desired diketone **4** (36 mg, 17%). Recrystallization from methanol gave pure **4** as colorless needles, mp 201—203 °C. IR: 1670 cm^{-1}; MS: *m/e* 284 (M^+), 255 (base peak); PMR ($CDCl_3$): δ 6.94—7.74 (m); ^{13}C NMR (C_6D_6): δ 200.7 ppm (>C=O); UV: $\lambda_{max}^{95\%EtOH}$ 230 (ε 29400), 285 sh (2840), 330 sh nm (641). Found: C, 84.57; H, 4.30%. Calcd for $C_{20}H_{12}O_2$: C, 84.49; H, 4.25%.

The authors wish to thank Professor M. Ogawa and Dr. Y. Ishii of Kansai University for the measurements of the ^{13}C NMR spectra.

References

1) a) A. S. Lindsey, *J. Chem. Soc.*, **1965**, 1685; b) A. Goldup, A. B. Morrison, and G. M. Smith, *ibid.*, **1965**, 3864; c) R. C. Cookson, B. Halton, and I. D. R. Stevens, *J. Chem. Soc., B*, **1968**, 767; d) T. Sato, K. Uno, and M. Kainosho, *J. Chem. Soc., Chem. Commun.*, **1972**, 579; e) T. Sato and K. Uno, *J. Chem. Soc., Perkin Trans. 1*, **1973**, 895.

2) Recently the parent ring system, 2,5,7-cyclooctatriene-1,4-dione has been synthesized: M. Oda, Y. Kayama, H. Miyazaki, and Y. Kitahara, *Angew. Chem. Int. Ed. Engl.*, **14**, 418 (1975).

3) During the course of our study, synthesis of **2** by the same procedure has been reported independently: A. Dagan and M. Rabinovitz, *J. Am. Chem. Soc.*, **98**, 8268 (1976). The spectral properties of **2** were identical with those of the hydrocarbon reported, although the mp of **2** (137—139 °C) was somewhat higher than that reported. The reason for this difference in mp is not clear.

4) G. H. Beaven, D. M. Hall, M. S. Lesslie, E. E. Turner, and G. R. Bird, *J. Chem. Soc.*, **1954**, 131.

5) H. H. Jaffé and M. Orchin, "Theory and Applications of Ultraviolet Spectroscopy," John Wiley & Sons, Inc., New York, N. Y. (1962), p. 389.

6) H. Kessler, *Angew. Chem. Int. Ed. Engl.*, **9**, 219 (1970).

7) K. R. Huffmann, M. Loy, and E. F. Ullmann, *J. Am. Chem. Soc.*, **87**, 5417 (1965).

8) J. O. Halford, *J. Chem. Phys.*, **24**, 830 (1956).

9) The difference in the bond force constants was calculated by assuming that the internal C–CO–C bond angles of **4** and **6** are not varied.

10) F. J. Kakis, M. Fetizon, N. Douchkine, M. Golfier, P. Mourgues, and T. Prange, *J. Org. Chem.*, **39**, 523 (1974).

BULLETIN OF THE CHEMICAL SOCIETY OF JAPAN, VOL. 51 (4), 1251—1252 (1978)

Synthesis of 4-Methyl-1,2-oxathiin 2,2-Dioxide

Tetsuo AKIYAMA, Masaki SUGIHARA, Takeshi IMAGAWA, and Mituyosi KAWANISI

Department of Industrial Chemistry, Faculty of Engineering, Kyoto University, Yoshida, Sakyo-ku, Kyoto 606

(Received September 3, 1977)

Synopsis. The reaction of isoprene with the SO_3–DMF complex afforded isoprene δ-sultone (**3**) in a 48% yield. The addition of bromine to **3** gave a dibromo product (**4**) and successive treatment of **4** with triethylamine in benzene and with triethylamine in the presence of silver tetrafluoroborate gave 4-methyl-1,2-oxathiin 2,2-dioxide in an 18% yield.

A δ-sultone, 1,2-oxathiin 2,2-dioxide is a structurally interesting compound since it is equivalent to 2-pyrone, the C=O group of which is replaced by a sulfonyl group (SO_2). In addition, 1,2-oxathiin 2,2-dioxides, which readily release sulfur dioxide to give furans,[1] can be regarded as potential starting materials for the synthesis of furan derivatives. From the viewpoint of synthesis, the 1,2-oxathiin 2,2-dioxides which have one substituent at the 4 or 5 position appear to be useful in the preparation of 3-substituted furans.[2] In the present paper, the first synthesis of 4-methyl-1,2-oxathiin 2,2-dioxide (**1**) is reported.

Up to the present time, no preparations of 1,2-oxathiin 2,2-dioxide and its monosubstituted derivatives, except the 6-substituted derivative[3] have been reported. Even in this case, the detailed method of preparation was not reported. The reaction sequence is depicted in the following scheme.

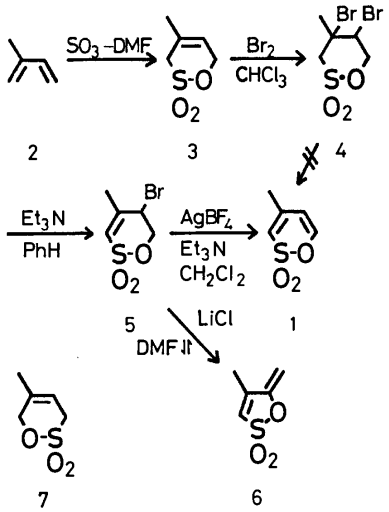

Scheme 1.

To the best of the authors' knowledge, only a few cases of successful formation of six-membered δ-sultones by way of the cycloaddition of SO_3 with a 1,3-diene are known,[4] although the reactions between SO_3 and olefinic compounds have been widely investigated.[5]

The reaction of isoprene (**2**) with the SO_3-*N*,*N*-dimethylformamide (DMF) complex[4a] was attempted and isoprene δ-sultone (**3**) was obtained as the sole product, in a 48% yield. The structure of **3** was differentiated from that of the alternate, **7**, in view of the fact that the methylene protons adjacent to the SO_2 group exhibited a broad singlet peak and did not couple with the olefinic proton in the ^{1}H-NMR spectra. This was further confirmed by chemical transformation (*vide infra*).

Similarly, 2,3-dimethyl-1,3-butadiene gave a δ-sultone (18% yield), but none of these products was formed in the case of 1,3-butadiene, 1,3-pentadiene and 1,3-cyclohexadiene. The reaction between SO_3 and 1,3-butadiene following a published procedure[5b] gave a δ-sultone, but the yield was extremely low.

The addition of bromine to isopren δ-sultone (**3**) in a chloroform solution afforded the corresponding dibromo derivative (**4**: 91%). Treatment of **4** with triethylamine in benzene induced monodehydrobromination giving **5** (95%). The additional treatment of **5** with bases, such as pyridine or potassium *t*-butoxide, in addition to triethylamine failed to produce a dienic compound. However, dehydrobromination of **5** by means of lithium chloride and calcium carbonate in refluxing *N*,*N*-dimethylformamide afforded a dienic compound in a 60% yield the structure of which was found to be 4-methyl-5-methylene-1,2-oxathiole 2,2-dioxide (**6**) from elemental analysis and spectral data. The formation of the ring-contracted product (**6**) is intriguing, but the true mechanism is not known as yet.

The following procedure gave the target compound, (**1**). Thus, treatment of **5** with triethylamine in dichloromethane in the presence of silver tetrafluoroborate gave **1** in an 18% yield. Support for this structural assignment comes from ^{1}H- and ^{13}C-NMR spectra. The signals of protons at C_5 and C_6 in the ^{1}H-NMR spectra display a typical AX pattern (J=5.9 Hz) and the ^{13}C-NMR spectra show that three olefinic carbons at the 3, 5, and 6 positions attach to one proton, respectively. The reaction appears to proceed as in the following scheme.

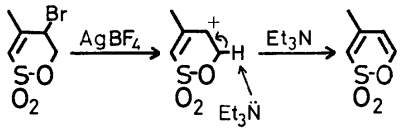

Scheme 2.

Experimental

All temperatures are uncorrected. The IR spectra were obtained on a Shimadzu IR-27 spectrometer. The mass spectra were taken using a Hitachi RMS-4 mass spectrometer. The NMR spectra were obtained on Varian EM-360 and CFT-20 spectrometers, TMS being chosen as the internal standard.

Isoprene δ-Sultone (3). To a solution of SO_3 (13.3 g; 0.166 mol) in 60 ml of DMF were added 10.0 g (0.147 mol) of isoprene all at once at room temperature. After the slightly exothermic reaction subsided within about one-half hour, the reaction mixture was stirred for 24 h at room temperature and neutralized with cold $NaHCO_3$ aq and extracted with benzene. The extract was washed with water to remove DMF and dried (Na_2SO_4). After removal of the solvent *in vacuo*, the residue slowly crystallized. Recrystallization from EtOH gave 10.5 g (48.0%) of 4-methyl-3,6-dihydro-1,2-oxathiin 2,2-dioxide (**3**), mp 35—36 °C; MS: *m/e* 148 (M^+, 21%); IR (Nujol): 1180, 1360 cm^{-1}; ^{1}H-NMR ($CDCl_3$): δ 5.54 (m, 1H, –CH=), 4.83 (m, 2H, OCH_2), 3.58 (broad s, 2H, CH_2SO_2), 1.83 ppm (broad s, 3H, CH_3); ^{13}C-NMR ($CDCl_3$): δ 128.2 (>C=), 117.2 (=CH–), 71.5 (CH_2O), 50.1 (CH_2SO_2), and 22.5 ppm (CH_3). Found: C, 40.55; H, 5.54%. Calcd for $C_5H_8SO_3$: C, 40.52; H, 5.44%.

2,3-Dimethyl-1,3-butadiene δ-Sultone. In a similar manner, the reaction of 2,3-dimethyl-1,3-butadiene with the SO_3–DMF complex gave 3,4-dimethyl-3,6-dihydro-1,2-oxathiin 2,2-dioxide in an 18% yield; ^{1}H-NMR ($CDCl_3$): δ 4.70 (broad s, 2H, OCH_2), 3.55 (broad s, 2H, CH_2SO_2) and 1.77 ppm (two s, 6H, $2CH_3$): ^{13}C-NMR ($CDCl_3$): δ 122.8 and 119.6 (2>C=), 74.5 (CH_2O), 50.0 (CH_2SO_2), 19.1 and 13.8 ppm ($2CH_3$).

Dibromo δ-Sultone (4). A solution of 1.13 g (7.6 mmol) of **3** and 1.22 g (8.0 mmol) of bromine in chloroform (20 ml) was stirred at room temperature for 24 h. The reaction mixture was treated with $NaHSO_3$ aq to remove excess bromine. Extraction with chloroform and evaporation of the solvent followed by distillation gave 2.14 g (91%) of 4,5-dibromo-4-methyl-1,2-oxathiane 2,2-dioxide (**4**), bp 130 °C/5 mmHg, mp 99—100 °C; MS: *m/e* 227, 229 (M^+—Br, 40%); IR: 1170, 1360 cm^{-1}; ^{1}H-NMR ($CDCl_3$): δ 5.1—4.4 (m, 3H, OCH_2-CHBr), 3.87 (s, 2H, CH_2SO_2) and 2.17 ppm (s, 3H, CH_3); ^{13}C-NMR ($CDCl_3$): δ 71.5 (OCH_2), 58.8 (CH_2SO_2), 57.6 (–C–Br), 52.8 (>CHBr), and 30.2 ppm (CH_3). Found: C, 19.41; H, 2.60%. Calcd for $C_5H_8Br_2SO_3$: C, 19.50; H, 2.62%,

Bromo δ-Sultone (5). A solution of 231 mg (0.75 mmol) of **4** and 1 ml of triethylamine in benzene (20 ml) was heated under reflux for 2 h. After filtration of triethylamine hydrobromide and evaporation of the solvent, distillation gave 163 mg (94.7%) of 5-bromo-4-methyl-5,6-dihydro-1,2-oxathiin 2,2-dioxide (**5**); bp 180 °C/16 mmHg, mp 129—130 °C, MS: *m/e* 226, 228 (M^+, 7%), 147 (M^+—Br, 100%); ^{1}H-NMR ($CDCl_3$): δ 6.10 (broad s, 1H, –CH=), 5.2—4.3 (m, 3H, OCH_2CHBr) and 2.15 ppm (d, 3H, CH_3); ^{13}C-NMR: δ 131.3 (>C=), 122.4 (–CH=), 73.9 (CH_2O), 41.7 (CHBr), and 21.6 ppm (CH_3). Found: C, 26.66; H, 3.08%. Calcd for $C_5H_7BrSO_3$: C, 26.45; H, 3.11%.

4-Methyl-5-methylene-1,2-oxathiole 2,2-Dioxide (6). To a solution of 680 mg (3 mmol) of **5** in *N,N*-dimethylformamide was added 127 mg (3 mmol) of lithium chloride and the reaction mixture was refluxed for 6 h. After the addition of water, the reaction mixture was extracted with benzene. The extract was washed with water to remove DMF and dried (Na_2SO_4). After removal of the solvent *in vacuo*, the residue crystallized. Recrystallization from ethanol gave 263 mg (60%) of **6**; mp 51—52 °C; MS: *m/e* 146 (M^+, 43%), 82 (M^+—SO_2, 14%); IR: 1650, 1600, 1440, 1330, 1180, 880, and 750 cm^{-1}; ^{1}H-NMR ($CDCl_3$): δ 6.63 (broad s, 1H, –CH=), 4.87—5.22 (m, 2H, $=CH_2$) and 2.17 ppm (d, 3H, CH_3); ^{13}C-NMR: δ 152.2 and 142.7 (2 >C=), 121.1 (–CH=), 94.4 ($=CH_2$) and 12.2 ppm (CH_3); Found: C, 40.86; H, 4.36%. Calcd for $C_5H_6SO_3$: C, 41.15; H, 4.14%.

4-Methyl-1,2-oxathiin 2,2-Dioxide (1). To a solution of 1.05 g (4.6 mmol) of **5** and 1.3 ml of triethylamine in dichloromethane (20 ml) was added 0.90 g (4.6 mmol) of silver tetrafluoroborate. The reaction mixture was stirred for 48 h at room temperature. Removal of silver bromide by filtration and isolation by column chromatography on silica gel gave 125 mg (18.5%) of **1**; bp 120—125 °C/20 mmHg; MS: *m/e* 146 (M^+, 100%), 82 (M^+—SO_2, 20%); ^{1}H-NMR ($CDCl_3$): δ 6.96 (d, 1H, =CH–O), 6.38 (broad s, 1H, =CH–SO_2), 5.85 (d, 1H, –CH=), and 2.08 ppm (d, 3H, CH_3); ^{13}C-NMR: δ 145.8 (=CH–O), 145.6 (>C=), 116.4 (=$CHSO_2$), 109.3 (–CH=), and 21.6 ppm (CH_3). Found: C, 40.98; H, 4.28%. Calcd for $C_5H_6SO_3$: C, 41.15; H, 4.14%.

References

1) Th. Morel and P. E. Verkade, *Recl. Trav. Chim. Pays-Bas*, **70**, 35 (1951).

2) The significance of the substituted furans, particularly of the 3-substituted furans, has been noted recently; for a leading reference, see J. E. McMurry and S. F. Donovan, *Tetrahedron Lett.*, **1977**, 2869 and references cited therein.

3) W. E. Barnett, M. G. Newton, and J. A. McCormack, *J. Chem. Soc., Chem. Commun.*, **1972**, 264.

4) a) F. G. Bordwell, R. D. Chapman, and C. E. Osborne, *J. Am. Chem. Soc.*, **81**, 2002 (1959); b) E. Jongejan, H. Steinberg, and Th. J. de Boer, *Tetrahedron Lett.*, **1976**, 397.

5) For leading references, see. a) M. Nagayama, O. Okumura, S. Noda, and A. Mori, *J. Chem. Soc., Chem. Commun.*, **1973**, 841, and b) M. D. Robbins, and C. D. Broaddus, *J. Org. Chem.*, **39**, 2459 (1974).

BULLETIN OF THE CHEMICAL SOCIETY OF JAPAN, VOL. 51 (4), 1253—1254 (1978)

Gas Phase Photochemical Reactions of Nitrogen Dioxide. Effect of Oxygen on the Conversion of Benzene into Nitrobenzene

Kazuo WATANABE, Hiroshi ISHIKAWA, and Wataru ANDO

Department of Chemistry, The University of Tsukuba, Niiharigun, Ibaraki 300-31

(Received September 3, 1977)

Synopsis. Gas phase photochemical nitration of benzene with nitrogen dioxide in the presence of oxygen was studied. Conversion of benzene into nitrobenzene was drastically accelerated by oxygen.

Vapor phase nitration of benzene with nitrogen dioxide to produce nitrobenzene has been studied to some extent under thermal and photochemical conditions in oxygen free systems,[1] but no examination has been reported on the effect of oxygen. From the viewpoint that the role of oxygen is significant in photoreaction, studies were carried out in the gas phase photochemical reaction of hydrocarbons with nitrogen dioxide in the presence and absence of oxygen. We would like to report that addition of oxygen remarkably causes a high conversion of benzene into nitrobenzene in gas phase nitration.

A cylindrical reaction vessel made of Pyrex glass (350 ml) and equipped with Teflon stopcocks and silicon rubber septum was used. Commercial benzene was dried completely and distilled, first and last fractions being rejected until it became gas chromatographically pure. Nitrogen dioxide dried over phosphorus pentaoxide was purified by repeated trap to trap distillation in a vacuum. Extra pure dry nitrogen and oxygen (Nihon Tokusyu Gas Co.) were used. Known amounts of benzene and nitrogen dioxide were admitted to the reaction vessel under reduced pressure, and diluted with either dry nitrogen or oxygen. Samples were irradiated externally for period of 2 h with a 400 W high-pressure mercury lamp at the temperature of running water. The irradiated products were extracted with dry dichloromethane and analyzed with a Hitachi 163 flame ionization detector with a 20 m OV-101 capillary glass column. Gas chromatographic peaks were identified by comparison of their retention times and of mass spectra with those of authentic samples.

Results and Discussion

A solution of 5.48×10^{-4} mol of benzene and 22.3×10^{-4} mol of nitrogen dioxide was introduced into the reaction vessel with a syringe and irradiated for 2 h. The irradiated mixture was extracted with dry dichloromethane and analyzed by GLC. Nitrobenzene was obtained in 28% yield on the basis of starting benzene. Neither phenol nor nitrophenol was obtained in a detectable yield.[2]

The same reaction was carried out in the presence of oxygen. Irradiation of a mixture of 5.48×10^{-4} mol of benzene and 22.3×10^{-4} mol of nitrogen dioxide and 22.3×10^{-4} mol of oxygen afforded nitrobenzene in 55% yield. The presence of oxygen increases the yield of nitrobenzene. The yield of nitrobenzene on the photolysis of nitrogen dioxide and benzene with a variable concentration of oxygen was examined. The results are given in Table 1. We see a remarkable increase in the yield of nitrobenzene in the presence of oxygen. Although we did not measure the absolute rate of reaction, results show that oxygen accelerates the conversion rate into nitrobenzene in the vapor phase photochemical reactions.

Table 1. Yields of nitrobenzene in C_6H_6–NO_2–O_2 system[a]

Run	Reaction conditions			Yields of nitrobenzene (%)
	NO_2 (mol)	O_2 (mol)	N_2 (mol)	
1	4.1×10^{-4}	0	0	trace
2	4.1×10^{-4}	22.3×10^{-4}	0	3
3	4.1×10^{-4}	0	22.3×10^{-4}	trace
4	4.1×10^{-4}	44.6×10^{-4}	0	21
5	4.1×10^{-4}	0	44.6×10^{-4}	1
6	22.3×10^{-4}	0	0	28
7	22.3×10^{-4}	11.2×10^{-4}	0	50
8	22.3×10^{-4}	22.3×10^{-4}	0	55
9	22.3×10^{-4}	33.5×10^{-4}	0	71
10	22.3×10^{-4}	44.6×10^{-4}	0	82
11	22.3×10^{-4}	66.9×10^{-4}	0	85
12	22.3×10^{-4}	0	44.6×10^{-4}	11

a) 5.48×10^{-4} mol of benzene was used in each run.

The following scheme might account for the formation of nitrobenzene. Oxygen atom, generated by photodissociation of nitrogen dioxide, adds benzene ring to produce biradical [A], which reacts with nitrogen

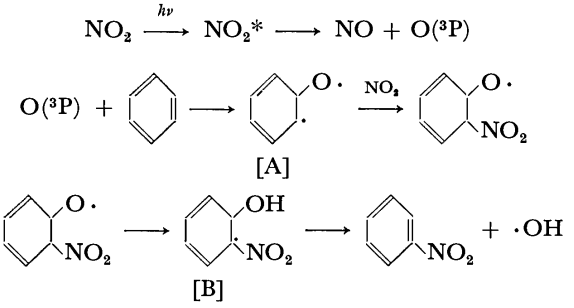

Scheme 1.

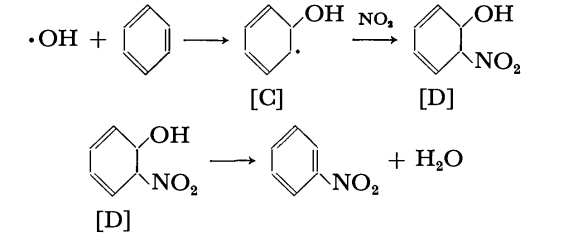

Scheme 2.

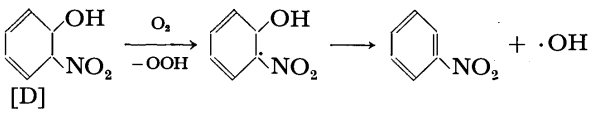

[D]

$$\cdot OOH + NO \longrightarrow \cdot OH + NO_2$$

$$2NO + O_2 + M \text{ (surface of wall)} \longrightarrow 2NO_2 + M$$

Scheme 3.

dioxide to produce adduct [B] with concomitant migration of hydrogen atom (intramolecular hydrogen abstraction by oxyl radical). Here, monoradical species [B] should smoothly eliminate hydroxy radical to produce nitrobenzene (Scheme 1). Hydroxy radical generated herein effectively undergoes addition to benzene ring to produce [C], which reacts with nitrogen dioxide to produce 6-nitro-2,4-cyclohexadiene-1-ol [D]. The formation of nitrobenzene by direct dehydration from [D] might be expected (Scheme 2). The mechanisms indicate that nitrobenzene formation is significantly affected by oxygen. In the presence of oxygen, there are two additional routes for the efficient formation of nitrobenzene. The first mechanism assumes the effective conversion of nitric oxide into nitrogen dioxide by oxygen, keeping the high concentration of nitrogen dioxide in the system. An alternative route on the participation of oxygen involves the formation of hydroperoxy radical from [D] which will oxidize nitric oxide to form nitrogen dioxide and hydroxy radical. These ideas are summarized in Scheme 3. Reproduction of nitrogen dioxide would be important for increasing the yield of nitrobenzene.

References

1) D. L. Bunbury, *Can. J. Chem.*, **43**, 1714 (1965), and references cited therein.

2) In low concentration (0.1—1 ppm) of nitrogen dioxide, phenol and *o*-nitrophenol were obtained as main products.

BULLETIN OF THE CHEMICAL SOCIETY OF JAPAN, VOL. 51 (4), 1255—1256 (1978)

New Synthetic Methods for Benzyloxycarbonyl-L-arginine-*p*-nitroanilide, Benzoyl-L-arginine-*p*-nitroanilide, and Acetyl-L-arginine-*p*-nitroanilide*

Oyin SOMORIN,** Norio NISHI, and Junzo NOGUCHI

Department of Polymer Science, Faculty of Science, Hokkaido University, Kita-ku, Sapporo 060

(Received September 5, 1977)

Synopsis. The optically active substrates for two peptidases, benzoyl-L-arginine-*p*-nitroanilide hydrochloride (L-BAPA·HCl) and acetyl-L-arginine-*p*-nitroanilide(L-AAPA·HCl), were readily prepared through the synthesis of benzyloxycarbonyl-L-arginine-*p*-nitroanilide hydrochloride(L-ZAPA·HCl). Benzyloxycarbonyl-L-arginine and *p*-nitroaniline were directly coupled without any racemization. The product, L-ZAPA·HCl, was quantitatively debenzyloxycarbonylated with hydrogen chloride in glacial acetic acid at 50 °C to L-arginine-*p*-nitroanilide dihydrochloride(L-APA·2HCl) which gave, on benzoylation or acetylation, L-BAPA·HCl or L-AAPA·HCl respectively.

N^{α}-Acylated arginine-*p*-nitroanilides are well known to be suitable substrates for trypsin and papain.[1,2] The low basicity of the amino group of *p*-nitroaniline makes it difficult for it to couple with the carboxyl group of arginine activated by the DCCI-, azide-, or active ester-method. The activation of the amino group of *p*-nitroaniline seems to be necessary to facilitate coupling with the carboxyl group of arginine. Hence, in our previous papers on the syntheses of L-BAPA·HCl[3] and other acylated L-arginine-*p*-nitroanilides,[4] the amino group of *p*-nitroaniline was activated by converting it to the isocyanate and the guanidino group of arginine was masked with the nitro group. The synthetic routes reported previously,[3,4] however, are complicated because of the several reaction steps involved.

Convenient syntheses of L-ZAPA·HCl, L-BAPA·HCl, and L-AAPA·HCl have now been achieved, as is shown in Scheme 1. L-ZAPA·HCl was prepared by the direct coupling of N^{α}-benzyloxycarbonyl-L-arginine and *p*-nitroaniline using a modification of the procedure of Erlanger *et al.*[5] for the synthesis of DL-BAPA·HCl. As it had been expected, there was no racemization in the synthesis of L-ZAPA·HCl, unlike as in the case of the benzoyl analog. In the modified coupling procedure, only one equivalent mole of the tertiary amine was used, since two equivalent moles as in the procedure of Erlanger *et al.*[5] caused a decrease in the yield of L-ZAPA·HCl. The order of the addition of reagents affected the yield of L-ZAPA·HCl. The optimum yield was obtained by the following procedure: a mixture of triethylamine and *p*-nitroaniline in diethyl phosphite was added to a solution of phosphorus pentoxide in diethyl phosphite. A solution of benzyloxycarbonyl-L-arginine containing phosphoric acid in diethyl phosphite was then added to the above mixture. The addition of reagents in this order is consistent with the mechanism of reaction proposed by Schramm and Wissmann.[6] L-ZAPA·HCl was successfully debenzyloxycarbonylated to L-APA·2HCl with hydrogen chloride in acetic acid at 50 °C. The yield of L-APA·2HCl was quantitative, and its melting point and its specific optical rotation were identical with those previously reported.[4] L-AAPA·HCl and L-BAPA·HCl have the same physical constants (melting points and specific optical rotations) as those reported by Nishi *et al.*[4]

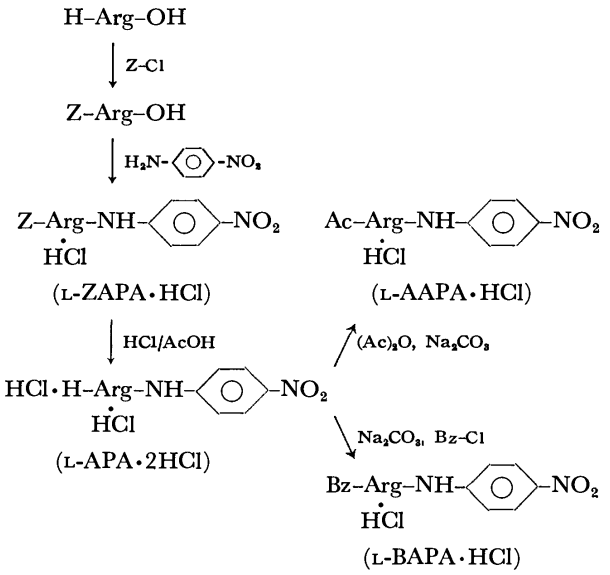

Scheme 1. Improved and simplified synthetic routes for benzoyl-L-arginine-*p*-nitroanilide hydrochloride (L-BAPA·HCl) and acetyl-L-arginine-*p*-nitroanilide hydrochloride (L-AAPA·HCl). Z: Benzyloxycarbonyl, Ac: acetyl, Bz: benzoyl.

From the result of the enzymatic hydrolysis of L-ZAPA·HCl by trypsin, the new substrate, L-ZAPA·HCl seems to be more excellent than L-BAPA·HCl and tosyl-L-arginine-*p*-nitroanilide hydrochloride (L-TAPA·HCl) because it can be prepared easily and because of its higher solubility in water and higher susceptibility to tryptic hydrolysis, as is shown in Fig. 1. The details of L-ZAPA·HCl as a substrate for peptidases are under investigation.

Experimental

The ultraviolet and visible absorption spectra were measured with a Hitachi 323 Automatic Spectrophotometer. The optical rotations were measured with a Yanagimoto Automatic

* This work was presented at the 14th Meeting of the Hokkaido Branch of the Biochemical Society of Japan, July 1977.

** Japan Society for the Promotion of Science Visiting Scholar from Chemistry Department, University of Lagos, Nigeria.

Recording Polarimeter, Model OR-1. The elemental analyses were carried out by means of a Yanagimoto CHN Corder, Model MT-2; the results for the known products agreed with the theoretical values. The melting points for samples over 220 °C were determined with a Mitamura hot-stage apparatus.

*N^{α}-Benzyloxycarbonyl-*L*-arginine-*p*-nitroanilide Hydrochloride (*L*-ZAPA·HCl).* Solution A, containing *p*-nitroaniline(4.14 g, 0.03 mol) and triethylamine(4.2 ml, 0.03 mol) in diethyl phosphite(15 ml), was added to Solution B, containing phosphorus pentaoxide(8.55 g, 0.06 mol) in diethyl phosphite(30 ml). A solution of N^{α}-benzyloxycarbonyl-L-arginine(9.24 g, 0.03 mol) containing 85% phosphoric acid (2.1 ml, 0.03 mol) in diethyl phosphite(30 ml) was then added to the mixture of Solution A and B. The reaction mixture was heated on a water bath with stirring for 2 h in a well-ventilated hood. Diethyl phosphite was removed *in vacuo*, and the residual oil dissolved in 300 ml of 1 M HCl after heating at 85 °C for about 5 min. After the solution had stood in the refrigerator overnight, a semisolid oil was precipitated. This semisolid oil was separated by decanting off the acid solution, washed with cold water, and then dried. The oily product which crystallized on triturating with ethyl acetate was filtered and washed with small quantities of ethyl acetate and cold acetone. The crystalline product was recrystallized by dissolving it in hot water, and after it had been cooled to about 50 °C, an equal volume of 1M HCl was added After the solution had stood at 4 °C overnight, an almost colorless crystalline product was obtained. Yield, 7.2 g (50%); mp 181—182 °C; $[\alpha]_D^{20}$ −16.0° (*c* 1, ethanol) Found: C, 51.62; H, 5.29; N, 18.05; Cl, 7.59%. Calcd for $C_{20}H_{25}N_6O_5Cl$: C, 51.64; H, 5.42; N, 18.08; Cl, 7.64%.

L-Arginine-p-nitroanilide Dihydrochloride(L-APA·2HCl). A solution of L-ZAPA·HCl (5 g) in pure glacial acetic acid (200 ml) was saturated with dry hydrogen chloride at 50 °C for 90 min. The reaction mixture was then evaporated *in vacuo* to a small volume, and the crystalline product was precipitated with dry ether. The product was recrystallized from water/acetone. Yield, 3.55 g (90%); mp 245 °C; $[\alpha]_D^{20}$ +80.6° (*c* 1, water)

Benzoyl-L-arginine-p-nitroanilide Hydrochloride(L-BAPA·HCl) and Acetyl-L-arginine-p-nitroanilide Hydrochloride(L-AAPA·HCl). L-BAPA·HCl and L-AAPA·HCl were prepared from L-APA·2HCl by the procedures reported by Nishi and Noguchi.[4] The melting points and specific optical rotations were identical with those previously reported.[4]

The Absorption Spectra and Tryptic Digestion of L-ZAPA·HCl and Other L-Arginine-p-nitroanilides. The wavelength of maximum absorption, λ_{max}, for L-ZAPA·HCl at a concentration of 7.8×10^{-5} M was 315 nm with a molar extinction coefficient of 1.41×10^4. The enzymatic hydrolyses of L-ZAPA·HCl, L-BAPA·HCl, and L-TAPA·HCl are shown in Fig. 1; they were determined by the measurement of *p*-nitroaniline at 410 nm, at which wavelength neither the L-ZAPA·HCl nor any of the other L-arginine-*p*-nitroanilides[4] has any absorbance.

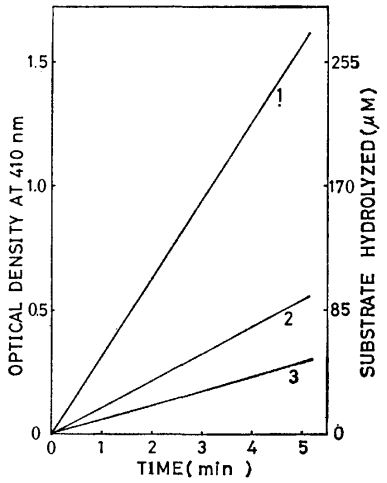

Fig. 1. Tryptic hydrolyses of 1. L-ZAPA·HCl, 2. L-BAPA·HCl, and 3. L-TAPA·HCl as a function of time. Initial concentration of *p*-nitroanilide substrate: 10^{-3}M in 0.05M tris-HCl buffer (pH 8.2) containing 0.02M $CaCl_2$ and 1% dimethylformamide. Trypsin concentration was 10 μg/ml and incubation period was 300 s at 25 °C.

The financial assistance of the Japan Society for the Promotion of Science is gratefully acknowledged.

References

1) S. Tokura, N. Nishi, and J. Noguchi, *J. Biochem.*, **69**, 599 (1971).
2) H. Nakata and S. Ishii, *Biochem. Biophys. Res. Commun.*, **41**, 393 (1970).
3) N. Nishi, S. Tokura, and J. Noguchi, *Bull. Chem. Soc. Jpn.*, **43**, 2900 (1970).
4) N. Nishi and J. Noguchi, *Bull. Chem. Soc. Jpn.*, **46**, 572 (1973).
5) B. F. Erlanger, N. Kokowsky, and W. Cohen, *Arch. Biochem. Biophys.*, **95**, 271 (1961).
6) G. Schramm and H. Wissmann, *Chem. Ber.*, **91**, 1073 (1958).

BULLETIN OF THE CHEMICAL SOCIETY OF JAPAN, VOL. 51 (4), 1257—1258 (1978)

Synthetic Photochemistry. XII.[1] The Sensitized Photooxidation Reaction of Some Spirocyclic Derivatives of Vinylcyclopropanes

Hitoshi TAKESHITA, Toshihide HATSUI, Ryuta IWABUCHI, and Shinji ITOH
Research Institute of Industrial Science, 86, Kyushu University, Hakozaki, Fukuoka 812

(Received September 8, 1977)

Synopsis. The dye-sensitized photooxidation of the Diels-Alder adducts prepared from 2-substituted tropones and spiro[2.4]hepta-4,6-diene was caried out. A marked difference in the reactivities was observed between the two structural types of adducts; 3,3-ethylene derivatives gave nor-epoxides, but 5,5-ethylene derivatives resulted in the recovery of the starting materials.

Previously, we have reported[2] the occurrence of a novel degradation process to form an epoxy norolefin, **B**, by the singlet oxygen oxidation of **A**, a spirocyclic vinylcyclopropane, in addition to the splitting into a dialdehyde, **C**. In considering this new process, we wanted to extend the reaction to other spiro olefins in order to ascertain its applicability and limitations. Looking for suitable substrates, we noticed a report by Tanida *et al.*[3] which described the Diels-Alder reaction of spiro[2.4]hepta-4,6-diene (**1**) with tropone (**2**) to form two *endo*-(4+2)π-adducts (**3** and **4**); we ourselves repeated the experiments to obtain some analogues from 2-chlorotropone (**5**) and 2-methoxytropone (**6**). Tropolone (**7**) was unreactive under similar conditions. We will herein describe the results of the photo-sensitized oxygenation of the adducts.

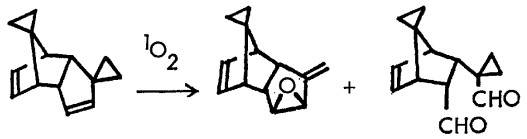

(**A**) (**B**) (**C**)

Diels-Alder Reaction of Troponoids and Spiroheptadiene (1). Slightly modifying Tanida's conditions, we have carried out the reaction with **5** and **6** and have confirmed the formation of similar types of adducts (**8**, **9**, **12**, and **13**), together with new 1 : 2-adducts (**10** and **14**). In addition, an *exo*-(4+2)π-adduct, **11**, was obtained from **1** and **5**.[4]

Sensitized Photooxidation of the Adducts. When a chloroform solution of **3** was irradiated by means of a 500 W tungsten lamp in the presence of Methylene Blue for 86 h, a single compound, colorless crystals (**15**), was obtained in a 79% yield. The NMR [δ: 2.73 (2H, br s), 3.31 (1H, d, J=2.5 Hz), 3.45 (2H, m), 3.60 (1H, d, J=2.5 Hz), 5.24 (1H, br s), 5.41 (1H, d, J=2 Hz), 5.64 (1H, dd, J=11, 2.5 Hz), 5.97 (1H, t, J=8 Hz), 6.31 (1H, t, J=8 Hz), and 7.13 (1H, dd, J=11, 9 Hz)] spectrum revealed the formation of an epoxy group and a terminal ethylene group, suggesting an oxidative fragmentation product related to **B**. Thus, the carbonyl group in the molecule suppressed the formation of a dialdehyde.

On the other hand, the isomer (**4**) afforded no product when similarly irradiated for 144 h.

When a chloroform solution of **8** and Methylene Blue was similarly irradiated for 77 h, the sole product (**16**), also a vinyloxirane, was obtained in a 64% yield. The NMR [δ: 3.03 (2H, br s), 3.45 (1H, dd, J=9, 8 Hz), 3.54 (1H, d, J=3 Hz), 3.75 (1H, d, J=3 Hz), 3.82 (1H, d, J=8 Hz), and 7.50 (1H, d, J=9 Hz)] and the IR [ν: 925, 880 cm^{-1}] spectra indicated the structure of **16**. **9** was inert against the oxygenation.

Similarly, **12** afforded only **17** in an 89% yield, but **13** was inert. The NMR [δ: 2.95 (2H, br s), 3.50 (3H, s), 3.38—3.72 (4H, m), 5.25 (1H, br s), 5.45 (1H, br s), 5.95 (1H, dd, J=9, 8 Hz), 6.17 (1H, dm, J=10 Hz), and 6.38 (1H, t, J=8 Hz)] and IR [ν: 930, 890 cm^{-1}] spectra of **17** indicated the structure.

The continuous exposure of the adducts to oxygen in the dark caused no reaction; thus, the formation of vinyloxiranes is photochemical. Meanwhile, we have recently shown[6] that, during the oxygenation of **A**, a quenching of singlet oxygen by sodium azide has resulted in the complete suppression of both **B** and **C**, with the alternative production of free radical products. Therefore, the vinyloxiranes must be related to the singlet-oxygen oxidation,[7] and the location of the carbonyl group in the spirocyclic vinylcyclopropanes controlled the whole oxidation reaction. We have to admit that, compared to the reaction with a hydrocarbon, **A**, the reaction with the present series has revealed a critical rate decrease for usual singlet-oxygen oxidation, but this might be explained in terms of a quenching effect by the carbonyl group, as has already been described in connection with the photooxidation of tropinone derivatives.[8] Together with this quenching

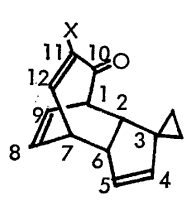

3: X=H
8: X=Cl
12: X=OMe

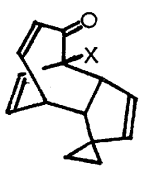

4: X=H
9: X=Cl
13: X=OMe

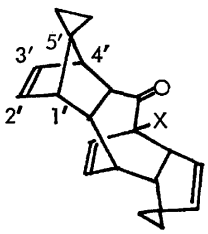

10: X=Cl
14: X=OMe

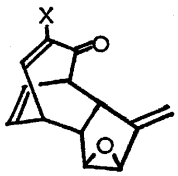

15: X=H
16: X=Cl
17: X=OMe

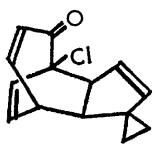

11

effect, the observed change in the product controle is probably also attributable to the carbonyl group, but these remote effects are not fully understandable at the present stage.

Experimental

Addition Reaction of Tropone (2) and Spiro[2.4]hepta-4,6-diene (1). A mixture of **2** (355 mg) and **1** (0.4 g) were heated in a sealed tube at 110—115 °C for 72 h, with a slight modification of the reported conditions.[3] A work-up of the mixture gave **3** (232 mg (35%)), and **4** (185 mg (28%)).

Addition Reaction of 2-Chlorotropone (5) and 1. **1** (2.5 ml) and **5** (1.00 g) were mixed in a sealed tube and then heated at 130—135 °C for 72 h. Repeated chromatography of the mixtures with benzene to benzene-ether afforded **8** (741 mg, 44%) as colorless needles; mp 133—135 °C (from benzene)[Found: C, 72.45; H, 5.62%. Calcd for $C_{14}H_{13}OCl$: C, 72.26; H, 5.63%. δ: 0.5—0.9 (4H, m), 2.61 (1H, dd, J=9, 2 Hz), 3.46 (1H, dddm, J=9.5, 8, 2 Hz), 3.52 (1H, ddm, J=2, 1 Hz), 3.74 (1H, dq, J=9, 2 Hz), 5.17 (1H, dd, J=5.5, 2 Hz), 5.37 (1H, dd, J=5.5, 2 Hz), 6.10 (1H, tt, J=8, 1 Hz), 6.40 (1H, tm, J=8 Hz), and 7.45 (1H, d, J=9.5 Hz); ν: 1680 cm^{-1}; λ_{max}^{MeOH}: 237 nm (ε: 3100), 273 (2200)], **9** (303 mg, 18%); pale yellow needles, mp 67—68 °C (from ethanol)[Found: C, 72.42; H, 5.70%. δ: 0.5—1.0 (4H, m), 2.93 (1H, dd, J=8.5, 2 Hz), 2.94 (1H, td, J=8, 2 Hz), 3.65 (1H, dt, J=8.5, 2 Hz), 5.29 (1H, dd, J=5.5, 2 Hz), 5.85 (1H, dd, J=5.5, 2 Hz), 5.94 (1H, dd, J=11, 0.7 Hz), 6.08 (1H, dt, J=9, 0.7 Hz), 6.36 (1H, ddm, J=9, 8 Hz), and 7.04 (1H, dd, J=11, 8 Hz); ν: 1680 cm^{-1}], **11** (16.8 mg, 1%); a pale yellow oil[Found: *M. W.*, 232.0645 (M$^+$). Calcd for $C_{14}H_{13}OCl$: 232.0655. δ: 0.76 (4H m). 2.71 (1H, dd, J=10, 5 Hz), 3.27 (1H, dddm, J=8, 7.5, 5 Hz), 4.02 (1H, dt, J=10, 2 Hz), 5.26 (1H, dd, J=6, 2 Hz), 5.63 (1H, dd, J=6, 2 Hz), 5.92 (1H, d, J=11 Hz), 6.07 (1H, d, J=9 Hz), 6.42 (1H, dd, J=9, 7.5 Hz), and 6.96 (1H, dd, J=11, 8 Hz); ν: 1690 cm^{-1}], and **10** (as a mixture with **8**), 78.3 mg.

Isolation of 10. A mixture (75 mg) of **8** and **10** was dissolved in chloroform (20 ml) and was then irradiated by means of a tungsten lamp in the presence of Methylene Blue (20 mg) under an oxygen stream. The mixture was then chromatographed on a silica gel column to give **10** as colorless needles; mp 150—151 °C, 21 mg (0.9% overall from **5**) [Found: *M. W.*, 324.1295. Calcd for $C_{21}H_{21}OCl$: 324.1281. δ: 0.3—0.9 (8H, m), 2.12 (1H, br s), 2.26 (1H, ddm, J=8, 2.5 Hz), 2.75 (1H, dt, J=9, 2.5 Hz), 2.88 (1H, dm, J=4 Hz), 2.98 (1H, ddm, J=9, 2.5 Hz), 3.28 (1H, dd, J=9, 4 Hz), 3.78 (1H, dt, J=9, 1.5 Hz), 5.36 (1H, dd, J=6, 1.5 Hz), 5.37 (1H, d, J=9.5 Hz), and 5.8—6.2 (4H, m, 3-H, 12-H, 2′-H, and 3′-H); ν: 1710 cm^{-1}; λ_{max}^{MeOH}: 225 nm (ε: 5000, sh), 254 (1800)].

Addition Reaction of 2-Methoxytropone (6) with 1. A mixture of **1** (2.5 ml) and **6** (1.00 g) was heated in a sealed tube at 130—135 °C for 94 h. The mixture thus formed, a dark brownish oil, was fractionated by chromatography using silica gel to give **12**, 395 mg (23.5%) of a pale yellow oil[Found: C, 77.12; H, 6.98%. Calcd for $C_{15}H_{16}O_2$: C, 78.92; H, 7.06%. δ: 0.50—0.90 (4H, m), 2.62 (1H, dm, J=9 Hz), 3.35—3.82 (3H, m), 3.56 (3H, s), 5.16 (1H, dd, J=6, 2 Hz), 5.40 (1H, dd, J=6, 2 Hz), 6.00 (1H, t, J=8 Hz), 6.17 (1H, d, J=9 Hz), and 6.43 (1H, t, J=8 Hz); ν: 1670 cm^{-1}, λ_{max}^{MeOH}: 234 nm (ε: 9200), 282 (8050)], **13**, 160 mg (9.5%), pale yellow needles, mp 123—125 °C (from ethanol) [Found: C, 78.72; H, 7.12%. δ: 0.50—0.80 (4H, m), 2.82 (1H, dd, J=9, 2 Hz), 2.99 (1H, ddm, J=9, 7 Hz), 3.59 (3H, s), 3.66 (1H, dt, J=9, 2 Hz), 5.24 (1H, dd, J=6, 2 Hz), 5.66 (1H, dd, J=6, 2 Hz), 5.80 (1H, d, J=11 Hz), 6.01 (1H, dm, J=9 Hz), 6.37 (1H, dd, J=9, 7 Hz), and 7.00 (1H, dd, J=11, 9 Hz); ν: 1680 cm^{-1}; λ_{max}^{MeOH}: 225 nm (δ: 7800), 250 (6500)], and **14**, 246 mg (10.5%), colorless needles, mp 148—150 °C (from ethanol) [Found: *M. W.*, 230. δ: 0.20—0.90 (8H, m), 2.08 (1H, tm, J=3 Hz), 2.24 (1H, ddm, J=8, 3 Hz), 2.66 (1H, dt, J=10, 3 Hz), 2.84 (1H, dd, J=4, 3 Hz), 2.89 (1H, dm, J=10 Hz), 3.13 (1H, dd, J=10, 4 Hz), 3.38 (3H, s), 3.88 (1H, dt, J=10, 2Hz), 5.19 (1H, d, J=9 Hz), 5.32 (1H, dd, J=6, 2 Hz), 5.63 (1H, dd, J=6, 2 Hz), 5.91 (1H, dd, J=9, 8 Hz), 5.94 (1H, dd, J=6, 3 Hz), and 6.10 (1H, dd, J=6, 3 Hz); ν: 1710 cm^{-1}].

An Attempted Addition Reaction of Tropolone (7) and 1. **7** (214 mg) and **1** (0.6 ml) were mixed in a sealed tube and heated for 72 h at 130—135 °C. The mixture was then treated with acetic anhydride (0.5 ml) and evaporated *in vacuo*; the residual mass was chromatographed through a silica gel column with benzene. Only **7** as the acetate (203 mg (93%)), and the dimer of **1** (355 mg) were obtained.

Sensitized Photooxidation of 3. **3** (690 mg) was dissolved in chloroform (40 ml), and was irradiated by a 500-W tungsten lamp in the presence of Methylene Blue (20 mg) under oxygen bubbling. After 86 h, the mixture was chromatographed to give colorless needles (**15**) (mp 82—83 °C (from methanol); 386 mg (79%) [Found: C, 77.67; H, 6.07%. Calcd for $C_{13}H_{12}O_2$: C, 77.98; H, 6.04%]), together with **3** (195 mg). Inspections of every chromatographic fraction confirmed the absence of any other product.

Sensitized Photooxidation of 8. **8** (600 mg) and Methylene Blue (20 mg) were dissolved in chloroform (30 ml), and the mixture was irradiated by means of a 500-W tungsten lamp for 77 h, with a continuous bubbling of oxygen, at −5—0 °C. The mixture was then fractionated by chromatography to give **16** (colorless needles, mp 125—126 °C (from ethanol), 150 mg (64%) [Found: *M. W.*, 234.0474 (M$^+$). Calcd for $C_{13}H_{11}O_2Cl$: 234.0448. ν: 1680 cm^{-1}]), along with only **8** (365 mg).

Sensitized Photooxidation of 12. **12** (609 mg) and Methylene Blue (20 mg) were dissolved in chloroform (30 ml), and the mixture was irradiated by means of a 500-W tungsten lamp for 204 h with a bubbling oxygen stream at −5—0 °C. After a chromatography, the mixture gave a pale yellow oil, **17** (446 mg (89%) [Found: C, 73.55; H, 6.61%. Calcd for $C_{14}H_{14}O_3$: C, 73.02; H, 6.13%. ν: 1680 cm^{-1}]), together with **12** (110 mg). No other product was detectable.

References

1) Part XI: H. Takeshita, A. Mori, N. Yamamoto, and T. Fujita, *Kyushu Daigaku Seisan Kagaku Kenkyusho Hokoku*, **66**, 9 (1977).

2) H. Takeshita, T. Hatsui, and H. Kanamori, *Tetrahedron Lett.*, **1973**, 1697.

3) H. Tanida, T. Yano, and M. Ueyama, *Bull. Chem. Soc. Jpn.*, **45**, 946 (1972).

4) The formation of an *exo*-(4+2)π-adduct in the Diels-Alder reaction of **5** and cyclopentadiene has been recognized; *cf.* S. Itô, K. Sakan, and Y. Fujise, *Tetrahedron Lett.*, **1969**, 775.

5) S. Itô, H. Takeshita, and Y. Shoji, *Tetrahedron Lett.*, **1969**, 1815.

6) T. Hatsui and H. Takeshita, *Chem. Lett.*, **1977**, 603.

7) An irradiation of **A** using a high-pressure mercury lamp without the sensitizer under an oxygen atmosphere produced no isolable product other than the starting material.

8) M. H. Fisch, J. C. Gramain, and J. A. Oleson, *Chem. Commun.*, **1970**, 13.

BULLETIN OF THE CHEMICAL SOCIETY OF JAPAN, VOL. 51 (4), 1259—1260 (1978)

The Reaction of Decaborane with Carbonyl Compounds

Toyosuke TANAKA, Tsuneo MATSUDA, Katsunori KIMIJIMA, and Yuichi IWASAKI

Faculty of Engineering, Saitama University, Shimoohkubo, Urawa, Saitama 338

(Received September 12, 1977)

Synopsis. Decaborane formed adducts with cyclohexanones, 2-octanone, acetaldehyde, or acetone, which were cleft in the presence of water into alcohols, boric acid, and hydrogen. Olefins and boroxins as secondary products were identified.

Several addition compounds[1] of decaborane, $B_{10}H_{14}$,[2] have been studied since Stock's first observation[3] of $B_{10}H_{14}\cdot(NH_3)_6$, formed by the evaporation of a liquid ammonia solution of decaborane. In this study, new reactions of decaborane with carbonyl compounds, such as acetaldehyde, acetone, 2-octanone, cyclohexanone, 2-methylcyclohexanone, 3-methylcyclohexanone, and 4-methylcyclohexanone, were carried out.

When solid decaborane was treated with a carbonyl compound ($RCH_2R'CO$) in the range from room temperature to 120 °C, the 1 : 1 adduct from both reactants was formed in a pasty mass of the reaction mixture. Though the adduct could not be isolated because of its unstability for oxygen or moisture, its parent peak in the mass spectra and the lack of any absorption associated with the carbonyl group in IR observed in the adduct.

$$B_{10}H_{14} + RCH_2R'CO \longrightarrow RCH_2R'CO\cdot B_{10}H_{14}.$$

The addition of water as an additional reactant to decaborane and a carbonyl compound accelerated both adduct formation and their decomposition into alcohol, boric acid, and H_2. Based upon the measured molar yields of the products, the primary decomposition of the adduct may be stoichiometrically expressed as follows

$$RCH_2R'CO\cdot B_{10}H_{14} + 30\,H_2O \longrightarrow RCH_2R'CHOH + 10\,H_3BO_3 + 21\,H_2.$$

Beside the primary decomposition products, olefins and boroxin compounds were observed in the reaction. The formation of olefins may be brought about by the dehydration of the alcohols primarily yielded:

$$RCH_2R'CHOH \longrightarrow RCH{=}CHR' + H_2O.$$

Just after the reaction of decaborane with acetone in H_2O, three compounds, 2-propanol and boric acid in a pasty mass, and H_2, were found. Tri(isopropoxy)-boroxin, however, was identified in the pasty mixture after the mixture was put aside without any treatment for 24 h. Thus, the boroxine may be formed by the condensation of alcohol and metaboric acid resulting from the dehydration of boric acid as the first product. No formation of boroxine from alcohol with boric acid was proven.

$$3\,H_3BO_3 \longrightarrow H_3B_3O_6 + 3\,H_2O,$$

$$3\,RCH_2R'CHOH + H_3B_3O_6 \longrightarrow (RCH_2R'CHO\text{-}\underset{|}{B}\text{-}O\text{-})_3 + 3\,H_2O.$$

The yields of the alcohols and olefins, together with their isomers as the main reaction products from decaborane with carbonyl compounds, are summarized in Table 1.

TABLE 1. ALCOHOL AND OLEFIN FROM THE REACTION OF DECABORANE WITH CARBONYL COMPOUNDS

Carbonyl compd	Alcohol,[a] %		Olefin,[a] %		Conditions
Cyclohexanone	Cyclohexanol	72.0	Cyclohexene	18.7	90 °C, in the absence of H_2O
Cyclohexanone	Cyclohexanol	15.4	Cyclohexene	80.0	Room temp, in the presence of H_2O
Cyclohexanone	Cyclohexanol	60.5	Cyclohexene	32.5	120 °C, in the absence of H_2O
2-Methylcyclohexanone	*cis*-2-Methylcyclohexanol	4.0	1-Methylcyclohexene	4.7	The same as above
	trans-2-Methylcyclohexanol	7.8	3-Methylcyclohexene	44.2	
3-Methylcyclohexanone	*cis*-3-Methylcyclohexanol	15.8	3-Methylcyclohexene	2.3	The same as above
	trans-3-Methylcyclohexanol	6.4	4-Methylcyclohexene	48.1	
4-Methylcyclohexanone	*cis*-4-Methylcyclohexanol	4.8	4-Methylcyclohexene	49.7	The same as above
	trans-4-Methylcyclohexanol	25.8			
2-Octanone	2-Octanol	8.6	1-Octene	4.7	50 °C, in the absence of H_2O
			cis-2-Octene	21.7	
			trans-2-Octene	65.2	
2-Octanone	2-Octanol	26.0	Octenes	traces	Room temp, in the presence of H_2O
Acetaldehyde	Ethanol	26.0			The same as above
Acetone	2-Propanol	90.0			The same as above

a) The yields of alcohol and olefin were calcd based on decaborane.

Experimental

The decaborane, supplied by the Callery Chem. Co., U.S.A., was purified by recrystallization from hexane. The other liquid reagents were distilled before the reaction. The experiments were performed in an atmosphere of dry nitrogen or of argon. The products were examined with an infrared spectrometer, a mass spectrometer, and by gas chromatography, In the gas-chromatographic analysis a Molecular sieve 5A column was used for H_2, with He as the carrier gas. A didecyl phthalate column was also used for the liquid products.

Reaction of Decaborane with Cyclohexanone. A solution of 1.227 g (0.01 mol) of decaborane and 0.980 g (0.01 mol) cyclohexanone in 17 g of cyclohexane was kept at 80—83 °C for 4 h. The subsequent removal of the solvent and the excess constituents *in vacuo* gave 2.11 g of a pasty solid; IR (in CS_2) 1338, 1360 cm^{-1} (B–O); mass spectrum *m/e* 222 (M^+ $B_{10}H_{14}COC_5H_{10}$).

The pasty solid product decomposes mainly into boric acid and cyclohexanol, upon filtration, drying, and so on.

Reaction of Decaborane with Cyclohexanone in the Presence of Water. The mixture from 0.086 g (0.71 mmol) of decaborane 1.3 g (13 mmol) of cyclohexanone and 0.3 g (17 mmol) of water was stirred at room temperature for 15 min. During the reaction, the 156-ml portion (760.8 mmHg, 17 °C) of gas evolved was put in a gas receiver and was analyzed by gas chromatography; the gas was found to be a mixture of H_2 (99.0%) and N_2(1.0%).

The liquid portion of the reaction mixture was distilled off under reduced pressure. The liquid distillate, which weighed 0.14 g, was then subjected to gas-chromatographic analysis. Four constituents—cyclohexanone recovered (35%), cyclohexanol (8%), cyclohexene (30%), and an unknown compound (10%)—were found.

The mixture remaining after evacuation was extracted with light petroleum, after which the solvent was evaporated; this gave a residue which, on recrystallization from benzene-light petroleum, yielded 0.02 g of tris(cyclohexyloxy)boroxin. The mp and mixed mp with an authentic sample[4] was 166—167 °C; IR 720, 735 cm^{-1} (out-of-plane boroxin skeletal vibration) 1338, 1360 cm^{-1} (stretch B–O); mass spectrum *m/e* 378.

Found: B, 8.58%. Calcd for $C_{18}H_{33}O_6B_3$: B, 8.58%.

The remainder after extraction with light petroleum gave 0.3 g boric acid. The mp and mixed mp with an authentic sample was 184—185 °C.

Found: B, 17.16%. Calcd for H_3BO_3: B, 17.48%.

Reaction of Decaborane with Acetone in the Presence of Water. To a mixture of 0.37 g (3 mmol) of decaborane and 3.48 g (60 mmol) of acetone we added 1.80 g (100 mmol) of H_2O. A reaction took place, and 1425 ml (776.5 mmHg, 20 °C) (60.5 mmol) of hydrogen were evolved. The rectification of the reaction mixture gave a liquid distillate which was determined by gas chromatography to contain 0.16 g (2.7 mmol) of 2-propanol. The recrystallization of the solid residue with aqueousethanol yielded 0.18 g (29 mmol) of boric acid, which was identical in its mp and IR spectrum with the authentic sample.

Boroxin Formation from Decaborane, Acetone, and Water. A mixture of 0.32 g (2.6 mmol) of decaborane, 2.6 g (45 mmol) of acetone, and 0.35 g (10.5 mmol) of H_2O was allowed to stand for 24 h at room temperature. The subsequent removal of the liquid portion and the recrystallization of the resulting solid residue by using light petroleum and benzene-petroleum gave 1.0 g of tris(isopropyl)boroxin, mp 45—46 °C; IR (in CS_2) 720, 735 cm^{-1} (B–O in boroxin skeleton); mass spectrum *m/e* 258 (M^+).

Found: B, 12.60%. Calcd for $C_9H_{21}B_6O_3$: B, 12.58%.

References

1) a) W. H. Hilland and M. S. Johnson, *Anal. Chem.*, **27**, 1300 (1955); b) S. J. Fitch and A. W. Laubengayer, *J. Am. Chem. Soc.*, **80**, 5911 (1958); c) H. C. Beachell and D. E. Hoffman, *ibid.*, **84**, 180 (1962).

2) a) A. Stock "Hydrides of Boron and Silicon," Cornell University Press, Ithaca, New York (1933); b) E. L. Muetterties "Boron Hydride Chemistry," Academic Press, New York (1975); c) W. N. Lipscomb, *Science*, **196**, 1047 (1977).

3) A. Stock and E. Pohland, *Ber.*, **62B**, 90 (1929).

4) K. G. O'Brien, *Aust. J. Chem.*, **16**, 915 (1963).

BULLETIN OF THE CHEMICAL SOCIETY OF JAPAN, VOL. 51 (4), 1261—1262 (1978)

New Synthesis of γ-Hydroxyglutamic Acid

Takenori KUSUMI, Hiroshi KAKISAWA, Shinnichiro SUZUKI, Kaoru HARADA, and Choji KASHIMA*

Department of Chemistry, University of Tsukuba, Sakura-mura, Niihari-gun, Ibaraki 300-31

(Received September 16, 1977)

Synopsis. γ-Hydroxyglutamic acid was prepared easily via 3-ethoxycarbonyl-5-methoxycarbonyl-2-isoxazoline, which was the 1,3-dipolar adduct of methyl acrylate and ethyl cyanoformate *N*-oxide.

It has been reported that γ-hydroxy α-amino acids occur in some kinds of plants.[1a,b,c] γ-Hydroxyglutamic acid (**1**) has been found in the green parts of the plants, *Phlox decussa*[2] and *Linaria vulgaris*.[3] By enzymatic decarboxylation, this γ-hydroxyglutamic acid gives 4-amino-2-hydroxybutyric acid (**2**), which is known to accelarate the activity of antibiotics such as kanamycin.[4,5] γ-Hydroxyglutamic acid (**1**) is expected to have the biological activity.

(**1**) (**2**)

In this paper, we describe the new synthesis of **1**, *via* the 1,3-dipolar addition of ethyl cyanoformate *N*-oxide (**3**) and acrylic esters.

Glycine ethyl ester hydrochloride was treated with sodium nitrite to give ethyl chloro(hydroxyimino)acetate (**4**). It was reported that chloro oxime (**4**) smoothly yielded nitrile oxide (**3**) by the treatment with bases such as triethylamine.[6] Therefore, **4** was slowly added to a mixture of triethylamine and methyl acrylate in chloroform at room temperature. After standing for 2 days, the products were purified by distillation giving an oil. From the spectral properties, the product was found to be 3-ethoxycarbonyl-5-methoxycarbonyl-2-isoxazoline (**5a**) (71% yield). Another expected compound (**6**) was not detected.

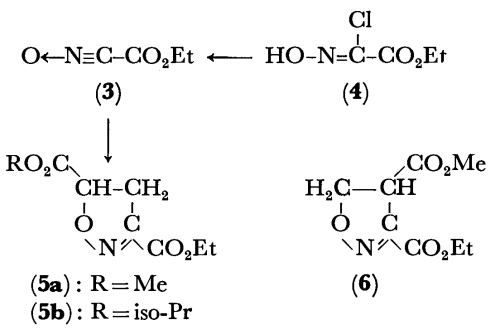

(**3**) (**4**)

(**5a**): R=Me
(**5b**): R=iso-Pr

(**6**)

For the cleavage of N–O bond, **5a** was hydrogenated over platinum in the presence of 1 equivalent of hydrochloric acid. By the direct hydrolysis of the reduced product (**7**) with 20% hydrochloric acid, a disatereomeric mixture of lactam, lactone and free amino acid forms of γ-hydroxyglutamic acid was obtained. The reaction mixture was dissolved in a small volume of water, and the solution was saturated with hydrogen chloride at 0 °C. The precipitate, which was assigned to the *threo*-γ-hydroxyglutamic acid lactone (**8a**) hydrochloride[7] was obtained in 40% yield. By the ion exchange chromatography of the filtrate, the free *erythro*-γ-hydroxyglutamic acid (**1b**)[7] was isolated in 20% yield. Also the mixture of lactams, (**9a**) and (**9b**), was eluted. However, *erythro* lactone (**8b**) could not be isolated from the reaction mixture.

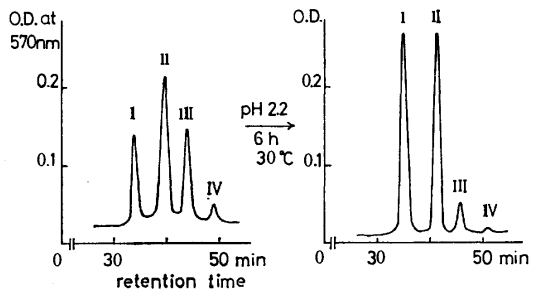

Fig. 1. Amino acid analysis of hydrolyzed product of **7**. Column: Yanagimoto SCX-1001; temp: 55 °C; elution buffer: citrate buffer, pH 3.25.

The product ratio of the amino acid and its lactone was determined by amino acid analyzer. In the amino acid chromatogram (Fig. 1), the reaction mixture showed four peaks (I—IV). After the buffered solution (sodium citrate buffer, pH 2.2) of the mixture was kept at room temperature for 6 hours, the peaks III and IV remarkably decreased, and the peaks I and II increased. When the solution of **8a** was allowed to stand in similar conditions, the peak III of **8a** gradually decreased, while the peak I increased. The peak II was found to correspond to **1b**. Thus, these four peaks (I—IV) were assigned to the compounds (**1a**), (**1b**), (**8a**), and (**8b**), respectively. After the peaks III and IV were diminished, the ratio of **1a** and **1b** was evaluated as 4: 6 from the

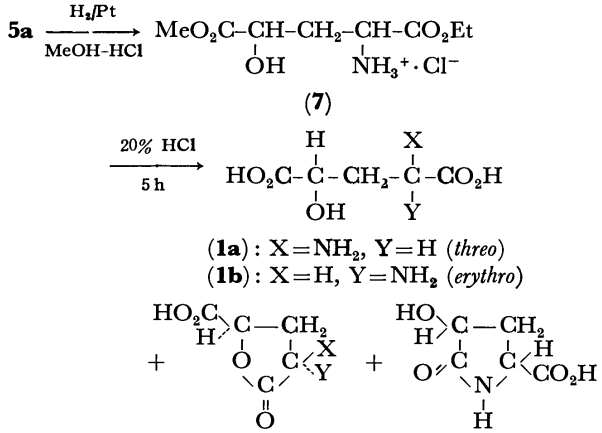

(**7**)

(**1a**): X=NH_2, Y=H (*threo*)
(**1b**): X=H, Y=NH_2 (*erythro*)

(**8a**): X=NH_2, Y=H (*threo*) (**9a**), (**9b**)
(**8b**): X=H, Y=NH_2 (*erythro*)

result of amino acid analysis.

In the hydrogenation on platinum, the isoxazolines are expected to change the ratio of the diastereomers by a bulky group on C-5 position. Therefore, 3-ethoxycarbonyl-5-isopropoxycarbonyl-2-isoxazoline (**5b**) was synthesized from isopropyl acrylate and the nitrile oxide (**3**). After hydrogenation and hydrolysis as described above, the ratio of **1a** and **1b** was determined as 4: 6. The isopropoxycarbonyl group has no effect on the ratio of the diastereomers. The lack of specificity of the hydrogenation must be due to facile rapture of the N–O bond prior to the reduction of the C=N bond.

In conclusion, the method described above is considered to have the general utility in the γ-hydroxyamino acid synthesis. This method for the γ-hydroxyamino acid synthesis is in progress.

Experimental

The melting points and boiling points are uncorrected. PMR spectra were recorded on a Hitachi R-24A instrument, TMS being used as an internal standard (δ, ppm). IR spectra were taken on a Hitachi EPI-S2 spectrometer. The amino acid chromatograms were recorded on a Yanagimoto amino acid analyzer LC-5S.

3-Ethoxycarbonyl-5-methoxycarbonyl-2-isoxazoline (5a). A solution of ethyl chloro(hydroxyimino)acetate[6] (**4**; 6.73 g) in dry chloroform (150 ml) was added to a solution of methyl acrylate (15 ml) and triethylamine (30 ml) in chloroform (50 ml) during 2.5 h at room temperature. The slightly brown solution was stirred at room temperature for two days, and the solution was washed with dilute hydrochloric acid and water. After drying over magnesium sulfate, the chloroform was evaporated under vacuum affording a brown liquid. Fractional distillation produced **5a** as a pale yellow liquid: Bp 107—121 °C/3 mmHg (7.0 g); NMR ($CDCl_3$): 1.35 (1H, t, J=7 Hz), 3.51 (2H, d, J=8 Hz), 3.78 (3H, s), 4.34 (2H, q, J=7 Hz), and 5.18 (1H, t, J=8 Hz); IR (film): 1740, 1600, 1260, 1120, 1020, and 920 cm^{-1}. Found: C, 47.77, H, 5.51, N, 6.84%. Calcd for $C_8H_{11}NO_5$: C, 47.76, H, 5.51, N, 6.96%.

Hydrogenation of 5a and Subsequent Hydrolysis. The isoxazoline (**5a**) (3.02 g) was hydrogenated over platinum oxide (0.30 g) in methanol (100 ml)–3M hydrochloric acid (5 ml) at room temperature for 24 hr. The catalyst was filtered away, and the filtrate was concentrated to a colorless oil. The oil was refluxed in 20% hydrochloric acid (130 ml) for 5 h, and the yellow solution was treated with charcoal. After the charcoal was removed by filtration, the filtrate was concentrated giving a pale green oil (3.0 g), which partyl crystallized on standing. The oil (3.0 g) was dissolved in water (1.2 ml), and the solution was saturated with hydrogen chloride at 0 °C. The resulting mixture was allowed to stand in a refrigerator for two days. The precipitated *threo*-γ-hydroxyglutamic acid lactone hydrochloride (**8a**) (736 mg) was collected by filtration: Mp 228—230 °C (dec) [lit,[7] 228—230 °C (dec)]. IR (KBr): 3600—2400 (br), 1785, 1755, 1200, 1045 cm^{-1}; MS *m/e* 145 (M^+−HCl), 101 (145−CO_2), 100 (145−CO_2H), 84 (101−NH_3), 83 (100−NH_3), 72 (100−CO), 56 (100−CO_2), and 55 (83−CO).

The filtrate was concentrated, and a small volume of water was added. The solution was again saturated with hydrogen chloride. The second crop (343 mg) of **8a**, mp 225 °C (dec), was collected by filtration. The filtrate was concentrated producing a yellow oily residue (1.5 g), which was chromatographed on a cation exchange (Dowex-50, 100 g). Elution with water afforded a pale green oil (360 mg), from which the diastereomeric mixture of the lactams (**9a** and **9b**) was separated as semisolid by trituration (200 mg): IR (KBr): 3700—2300 (br), 1730, 1685, and 1100 cm^{-1}. This mixture afforded *threo* and *erythro* γ-hydroxyglutamic acid (by amino acid analysis) when it was heated with 6M hydrochloric acid at 100 °C for one day.

Further elution with 15% trimethylamine solution afforded a light yellow oil (1.05 g). The oil (965 mg) was dissolved in water (0.5 ml). Hydrochloric acid (3M) was added in small portions until the pH of the solution reached 3. The precipitated *erythro*-γ-hydroxyglutamic acid was collected by filtration (417 mg), mp 165—166 °C (dec) [lit,[7] 166 °C (dec)]. Analytical sample was obtained by recrystallization from water–ethanol. (Found: C, 36.82; H, 5.49; N, 8.67%. Calcd for $C_5H_9NO_5$: C, 36.81; H, 5.56; N, 8.59%).

3-Ethoxycarbonyl-5-isopropoxycarbonyl-2-isoxazoline (5b). In a 100-ml flask was placed isopropyl acrylate (1.96 g) in dry chloroform (5 ml), and to this mixture was added triethylamine (5 ml). A solution of the chloro oxime (**4**) (1.9 g) in chloroform (10 ml) was added to the mixture with stirring during 1 h at room temperature. The mixture was stirred at room temperature for 20 h, and diluted with chloroform. The solution was washed with several portions of water, and dried over sodium sulfate. The solution was concentrated affording a light brown oil, which was distilled under vacuum (1.63 g); bp 130—134 °C/3 mmHg. NMR ($CDCl_3$): 1.39 (6H, d, J=7 Hz), 1.43 (3H, t, J=7 Hz), 3.43 (2H, d, J=10 Hz), 4.32 (2H, q, J=7 Hz), 5.10 (1H, t, J=10 Hz), and 5.05 (1H, heptet, J=7 Hz). Found: C, 52.18; H, 6.67; N, 6.01%. Calcd for $C_{10}H_{15}O_5N$: C, 52.39; H, 6.60; N, 6.11%.

References

1) a) J. A. Bakhuis, *Nature*, **180**, 713 (1957); b) L. Fowden, *ibid.*, **209**, 807 (1966); c) P. Linko and A. I. Virtanen, *Acta Chem. Scand.*, **12**, 68 (1958).

2) L. Benoiton, M. Winitz, S. M. Birnbaum, and J. P. Greenstein, *J. Am. Chem. Soc.*, **79**, 6192 (1957).

3) S. Hatanaka, *Acta. Chem. Scand.*, **16**, 513 (1962).

4) T. Naito, S. Toda, K. Fujikawa, Y. Miyaki, H. Koshiyama, H. Ohkuma, and T. Kamiyama, *J. Antibiot.*, **26**, 297 (1973).

5) H. Sato, T. Kusumi, K. Imaye, and H. Kakisawa, *Bull. Chem. Soc. Jpn.*, **49**, 2815 (1976).

6) G. S. Skinner, *J. Am. Chem. Soc.*, **46**, 731 (1924).

7) T. Kaneko, Y. K. Lee, and T. Hanafusa, *Bull. Chem. Soc. Jpn.*, **35**, 875 (1962).

BULLETIN OF THE CHEMICAL SOCIETY OF JAPAN, VOL. 51 (4), 1263—1264 (1978)

Formation of (4*S*,5*R*)-4-(Nitrovinyl)-2-phenyl-1,3-dioxan-5-yl Formate from Methyl 4,6-*O*-Benzylidene-2-deoxy-2-nitro-β-D-glucopyranoside

Tohru SAKAKIBARA and Rokuro SUDOH

Department of Chemistry, Faculty of Science, Tokyo Institute of Technology, Ookayama, Meguro-ku, Tokyo 152

(Received September 19, 1977)

Synopsis. Acetylation of methyl 4,6-*O*-benzylidene-2-deoxy-2-nitro-β-D-glucopyranoside with acetic anhydride–pyridine afforded a mixture of the expected 3-*O*-acetate and the title compound in a *ca.* 1: 1 ratio; the structure of the latter compound was confirmed by conversion into an adduct with hydrazoic acid.

Acetylation of the nitro alcohol **1** with acetic anhydride–sodium acetate gave the corresponding 3-*O*-acetate **2** in 70% yield,[1] but treatment of **1** with acetic anhydride–pyridine unexpectedly gave the title compound **3** besides the acetate **2**. In this paper we wish to report on the structural determination of **3**.

Treatment of **1** with acetic anhydride and pyridine at room temperature for 4 h gave a mixture of **2** and **3** in a ratio of *ca.* 1: 1 as determined by NMR spectroscopy. Both compounds were isolated by fractional crystallization. The results of elemental analysis of **3** correspond to the formula $C_{13}H_{13}NO_6$, confirmed by the appearance of the molecular ion peak at *m/e* 279, and its IR spectrum shows the presence of a carbonyl (1715) and nitro olefin (1660 and 1515 cm^{-1}) group but the absence of a hydroxyl and an *O*-acetyl group. The NMR spectrum revealed that the product had lost the glycosidic methoxyl group but retained the benzylidene group. One proton singlet at δ 8.08 was assigned to the formyl proton, its chemical shift agreeing with that of (4*S*,5*R*)-4-nitromethyl-2-phenyl-1,3-dioxan-5-yl formate (**5**).[2] The signals of olefinic protons (H-1 and H-2) overlapped to give a singlet at δ 7.24 with two proton intensity. In order to confirm the structure, the nitro olefin **3** was treated with hydrazoic acid to give the adduct **4**, the IR spectrum of which showed the presence of azide (2170), formyl (1725), and nitro (1560 cm^{-1}) groups, and NMR spectrum exhibited a singlet at δ 8.06 (–OCHO) but no signal at δ 7.24 region due to olefinic protons. Although all the signals expected for **4** were observed and their assignments were verified by double-resonance experiments, the configuration at C-2 position has not been determined.

When acetylation was carried out at 0 °C and stopped after 20 min, the acetate **2** was formed almost exclusively. From this result and the fact[3] that hydration or the addition of acetic acid occurs readily to methyl 4,6-*O*-benzylidene-2,3-dideoxy-3-nitro-β-D-*erythro*-hex-2-enopyranoside in aqueous pyridine or in pyridine–acetic acid solution the following route seems to be reasonable. Under the reaction conditions, elimination of methnol followed by the addition of acetic acid should give rise to the diacetate **6**,[4] which would be converted into the unstable nitro alcohol **7** during the course of isolation process. The C_1–C_2 bond cleavage of **7** facilitated by the nitro group[2] and the subsequent elimination of acetic acid should afford the nitro olefin **3**.

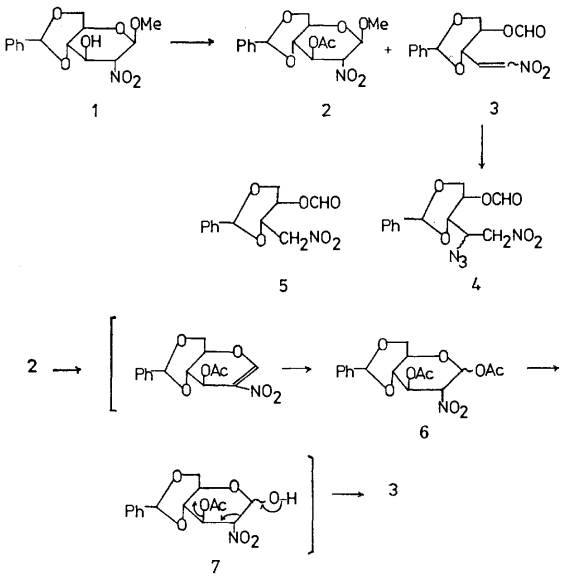

Experimental

Melting points were determined in capillaries and are uncorrected. IR spectra were recorded for KBr discs and NMR spectra for solutions in $CDCl_3$ (tetramethylsilane as internal standard) with a JNM-4H-100 (JEOL). Commercial acetic anhydride and pyridine were used without purification.

Acetylation of Methyl 4,6-O-Benzylidene-2-deoxy-2-nitro-β-D-glucopyranoside (1) with Acetic Anhydride–Pyridine. To a solution of the nitro alcohol **1** (1.02 g) in pyridine (8 ml) was added acetic anhydride (4 ml) at room temperature. The mixture was kept for 4 h and poured into 100 ml of ice water. The precipitate was filtered and washed thoroughly with water to give 964 mg of a crude product. The IR and NMR spectra indicated it to be a mixture of **2** and **3** (approximately 1: 1). The crude product was recrystallized from ethyl acetate; the first crop was colorless crystals of **3** (410 mg): Mp 137.0—137.5 °C; $[\alpha]_D^{20}$ 0° (*c* 1, $CHCl_3$); IR 1715 (CO), 1660 and 1515 cm^{-1} (C=C–NO_2); NMR δ=8.08 (s, 1, CHO), 7.24 (s, 2, H-1 and H-2), 5.60 (s, 1, PhCH), 4.93 (sex, 1, H-4, $J_{3,4}$=10.0, $J_{4,5e}$=5.6, $J_{4,5a}$=10.0 Hz), 4.58 (d, 1, H-3), 4.51 (q, 1, H-5e, $J_{5a,5e}$=10.0 Hz), 3.71 (t, 1, H-5a), and 7.42 (broad s, 5, Ph).

Found: C, 56.11; H, 4.65; N, 4.92%. Calcd for $C_{13}H_{13}NO_6$: C, 55.91; H, 4.70; N, 5.02%.

The second crop (430 mg) was **2** containing small amounts of **3** as judged by its IR spectrum. Recrystallization from ethyl acetate gave pure **2** (380 mg), identical with an authentic sample.[1]

Addition of Hydrazoic Acid to the Nitro Olefin 3. To a solution of **3** (45 mg) in THF (3 ml) was added a chloroform solution containing hydrazoic acid (*ca.* 1.6 N, 0.15 ml). The mixture was stirred for 3 h at room temperature and then

evaporated *in vacuo* to give a crystalline residue (52 mg). The NMR spectrum showed the presence of two products in a ratio of approximately 5: 1. The major product crystallized from ethanol was 34.8 mg of **4**: Mp 137.5—138.0 °C; $[\alpha]_D^{20}$ +0.31° (*c* 0.6, $CHCl_3$); IR 2170 (N_3), 1725 (CHO), and 1560 cm^{-1} (NO_2); NMR δ=8.06 (s, 1, CHO), 7.38 (broad s, 5, Ph), 5.48 (s, 1, PhCH), 5.28 (sex, 1, H-4, $J_{3,4}$=9.7, $J_{4,5e}$=5.0, $J_{4,5a}$=10.0 Hz), 4.66 (d, 1, H-1, $J_{1,2}$=8.8 Hz), 4.65 (d, 1, H-1′, $J_{1',2}$=5.0 Hz), 4.51 (q, 1, H-5e, $J_{5e,5a}$=11.3 Hz), 4.21 (oct, 1, H-2, $J_{2,3}$=2.2 Hz), 4.01 (q, 1, H-3), and 3.68 (t, 1, H-5a).

Found: C, 48.62; H, 4.34; N, 17.51%. Calcd for $C_{13}H_{14}N_4O_6$: C, 48.45; H, 4.38; N, 17.39%.

References

1) T. Sakakibara and R. Sudoh, *Carbohydr. Res.*, **50**, 197 (1976).

2) T. Sakakibara, T. Takamoto, and T. Nakagawa, *Bull. Chem. Soc. Jpn.*, **44**, 865 (1971).

3) T. Sakakibara and R. Sudoh, unpublished results.

4) Elimination of acetic acid appears to predominate that of methanol; the former should reversible but not the latter, resulting in the formation of the diacetate **6**.

BULLETIN OF THE CHEMICAL SOCIETY OF JAPAN, VOL. 51 (4), 1265—1266 (1978)

The Reaction of Benzeneseleninic Acid with Olefins in Acetic Acid. A New Method of Acetoxyselenation

Noritaka MIYOSHI, Yoshitsugu TAKAI, Shinji MURAI, and Noboru SONODA*

Department of Petroleum Chemistry, Faculty of Engineering, Osaka University, Suita, Osaka 565

(Received October 4, 1977)

Synopsis. The reaction of benzeneseleninic acid with olefins in acetic acid gave 2-acetoxyalkyl phenyl selenides in good yields.

During the course of studies on oxyselenation,[1,2] a new and convenient method was found for the synthesis of 2-acetoxyalkyl phenyl selenides by use of benzeneseleninic acid.[3] The acetoxyselenation was carried out

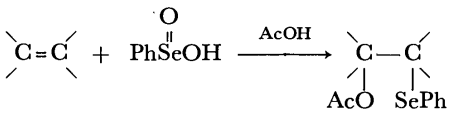

(1)

by heating in acetic acid an equimolar mixture of olefin and benzeneseleninic acid, prepared from diphenyl diselenide by the procedure of Ayrey *et al.*[4] Acetoxyselenated products, 2-acetoxyalkyl phenyl selenides (**1**), were easily isolated by distillation under reduced pressure in good yields. The results of acetoxyselenation of cyclohexene, styrene, 1-hexene, and 1-octene are given in Table 1. The structure of (**1**) was determined by spectroscopic methods and elemental analyses. The

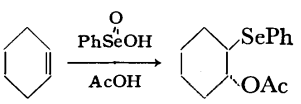

(2)

(**1a**)

reaction of cyclohexene with benzeneseleninic acid in acetic acid at 80 °C gave *trans*-2-acetoxycyclohexyl phenyl selenide (**1a**) as the sole product (Eq. 2). In the acetoxyselenation of styrene, addition of the phenylseleno group occurred selectively at the terminal methylene carbon atom to give 2-acetoxy-2-phenylethyl phenyl selenide (**1b**), whereas a similar reaction of aliphatic terminal olefin such as 1-hexene or 1-octene gave two isomers, the primary selenide as a major product and the secondary selenide as shown below.

TABLE 1. REACTION OF BENZENESELENINIC ACID WITH OLEFINS IN ACETIC ACID

Olefin	Acetoxyselenated product (**1**)		Yield (%)
Cyclohexene	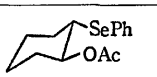 **1a**		81
Styrene	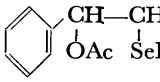 **1b**		80
1-Hexene	n-$C_4H_9CH(OAc)CH_2SePh$ **1c** n-$C_4H_9CH(SePh)CH_2OAc$ **1d**	[82:18]	87
1-Octene	n-$C_6H_{13}CH(OAc)CH_2SePh$ **1e** n-$C_6H_{13}CH(SePh)CH_2OAc$ **1f**	[86:14]	86

* To whom correspondence should be addressed.

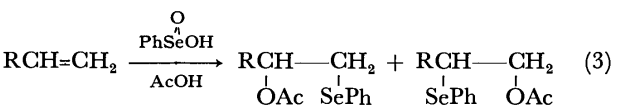

(3)

It is likely that the attack of phenylselenenyl acetate (PhSeOAc)[5] to olefinic double bond takes place judging from the cationic mode of addition of phenylseleno group observed in the present acetoxyselenation. The destiny of the oxygen atom which was originally bonded to the selenium atom of the seleninic acid is not clear. However, evolution of a considerable amount of carbon dioxide (one fifth moles per one mole of the seleninic acid used) was observed in all cases. Oxidation of the solvent seems likely to take place concurrently.

Considerable interest has developed in the chemistry of selenoxide,[6] the syn elimination of phenyl selenoxide having recently been found to be a convenient and high-yield method for the preparation of various olefinic compounds.[7] The present oxyselenation may provide a useful procedure for the preparation of the precursor of an allyl acetate[8] from olefin.

Experimental

Materials. Commercial olefins (styrene, 1-hexene and 1-octene) were purified by distillation before use. Cyclohexene was prepared by the dehydration of cyclohexanol.[9] Benzeneseleninic acid was prepared from diphenyl diselenide according to the procedure of Ayrey *et al.*[4]

Apparatus. IR spectra were measured with a Shimalzu Model IR-27C grating infrared spectrometer, proton NMR spectra with a JEOL Model JNM-3H-60 and JNM-PS-100 using tetrachloromethane as a solvent and tetramethylsilane-(TMS) as an internal standard, and mass spectra with a Hitachi Model RM-60 mass spectrometer operating at 70 eV.

Reaction of Cyclohexene with Benzeneseleninic Acid. A solution of cyclohexene(10 mmol, 0.82g) and benzeneseleninic acid(10 mmol, 1.90 g) in acetic acid (30 ml) was heated at 80 °C for 24 h under stirring. After completion of the reaction, evaporation of acetic acid gave a dark orange oil, which was purified by distillation to give 2-acetoxycyclohexyl phenyl selenide(**1a**, 2.41 g, 81%), bp 137—138 °C/1 Torr; Found: 56.52; H, 6.26%. Calcd for $C_{14}H_{18}O_2Se$: C, 56.57; H, 6.10%. IR (neat), 1740 cm^{-1} ($\nu_{c=o}$). MS *m/e*, 298 (M^+), 238 (M^+—AcOH). NMR (100 MHz) δ 1.92 (3H, s, OC(=O)C<u>H</u>$_3$), 1.36—2.06 (8H, m, ring methylene), 3.12 (1H, d-t, J=4.1 and 9.2 Hz, C<u>H</u>SePh), 4.72 (1H, d-t, J=4.1 and 9.2 Hz, C<u>H</u>OAc), 7.15—7.40 (3H, m, phenyl), 7.40—7.56 (2H, m, phenyl).

Reaction of Styrene with Benzeneseleninic Acid. A solution of styrene (10 mmol, 1.04 g) and benzeneseleninic acid (10 mmol, 1.90 g) in acetic acid (30 ml) was heated at 80° for 24 h under stirring. Removal of the solvent gave a dark orange oil, which was purified by distillation to give 2-acetoxy-2-phenylethyl phenyl selenide (**1b**, 2.56 g, 80%), bp 166—167 °C/0.5

Torr; Found: C, 59.89; H, 5.19%. Calcd for $C_{16}H_{16}O_2Se$: C, 60.19; H, 5.05%. IR (neat), 1748 cm^{-1}. MS *m/e* 320 (M^+), 260 (M^+-AcOH). NMR (60 MHz) δ 1.96 (3H, s, OC(=O)C$\underline{H}_3$), 3.16 (1H, d-d, J=6 Hz, C$\underline{H}_2$SePh), 3.22 (1H, d, J=7.5 Hz, C$\underline{H}_2$SePh), 5.83 (1H, d-d, J=6 and 7.5 Hz, C$\underline{H}$OAc), 7.14—7.55 (10H, m, phenyl).

Reaction of 1-Hexene with Benzeneseleninic Acid. A solution of 1-hexene (10 mmol, 0.84 g) and benzeneseleninic Acid (10 mmol, 1.90 g) in acetic acid (30 ml) was heated at 80 °C for 24 h under stirring. Removal of the solvent by distillation gave a dark orange oil, which was distilled under reduced pressure to give a mixture of isomeric acetoxyselenated products (2.60 g) [Table 1], bp 122—134 °C/0.6 Torr; MS *m/e* 300 (M^+), 240 (M^+-AcOH). Found: C, 55.92; H, 6.75%. Calcd for $C_{14}H_{20}O_2Se$: C, 56.19; H, 6.74%. The NMR spectrum of the distillate showed the presence of two isomers. 2-Acetoxyhexyl phenyl selenide (**1c**) was isolated by repeated distillation of the mixture. Attempts to isolate **1d** were unsuccessful. NMR (CCl_4) of **1c**; δ 1.92 (3H, s, OC(=O)C$\underline{H}_3$), 0.70—0.90 (9H, m, *n*-$C_4\underline{H}_9$), 2.99 (2H, d, J=6 Hz, C$\underline{H}_2$SePh), 4.90—5.15 (1H, quintet centered at δ 4.93, J=6 Hz, C$\underline{H}$OAc). 2-(Phenylseleno)hexyl acetate (**1d**) was characterized by analysis of the NMR spectrum of a mixture of **1c** and **1d**. The methine (CHSePh) and methylene (CH_2OAc) signals of **1d** were observed at δ 3.32—3.60 (m, 1H) and δ 4.00—4.40 (m, 2H), respectively. The amount of **1d** in the mixture of two isomers was estimated from the NMR spectrum of the mixture by comparison of the integrated peak area of methylene of **1c** (d, δ 2.99, C$\underline{H}_2$SePh) with that of **1d** (m, δ 4.00—4.40, C$\underline{H}_2$OAc). The NMR spectrum of the mixture of two isomers (**1c** and **1d**) showed the ratio of **1c**: **1d** to be 82: 18.

Reaction of 1-Octene with Benzeneseleninic Acid. A solution of 1-octene (10 mmol, 1.02 g) and benzeneseleninic acid (10 mmol, 1.90 g) in acetic acid (30 ml) was heated at 80 °C for 24 h under stirring. Removal of the solvent by distillation gave a dark orange oil, which was distilled under reduced pressure to give a mixture of isomeric acetoxyselenated products (2.82 g) [Table 1], bp 135—148 °C/0.8 Torr; MS *m/e* 328 (M^+), 268 (M^+-AcOH). Found: C, 58.54; H, 7.67%. Calcd for $C_{16}H_{24}O_2Se$: C, 58.71; H, 7.39%. The NMR spectrum of the distillate showed the presence of two isomers. 2-Acetoxyoctyl phenyl selenide (**1e**) was isolated by repeated distillation of the mixture. Attempts to isolate **1f** were unsuccessful. NMR (CCl_4) of **1e**; δ 1.93 (3H, s, OC(=O)C$\underline{H}_3$), 0.90—2.15 (13H, m, *n*-$C_6\underline{H}_{13}$), 2.98 (2H, d, J=6 Hz, C$\underline{H}_2$SePH), 4.70—5.15 (1H, quintet centered at δ 4.92, C$\underline{H}$OAc), 7.11—7.50 (5H, m, phenyl). 2-(Phenylseleno)octyl acetate (**1f**) was characterized on the basis of the NMR spectrum of a mixture of **1e** and **1f**. The methine (C$\underline{H}$SePh) and methylene (C$\underline{H}_2$OAc) signals of **1f** were observed at δ 3.30—3.70 (m, 1H) and δ 4.00—4.40 (m, 2H), respectively. The amount of **1f** in the mixture of two isomers was estimated from the NMR spectrum of the mixture by comparison of the integrated peak area of methylene of **1e** (d, δ 2.98, C$\underline{H}_2$SePh) with that of **1f** (m, δ 4.00—4.40, C$\underline{H}_2$OAc). The NMR spectrum of the mixture of two isomers (**1e** and **1f**) showed the ratio of **1e**: **1f** to be 86: 14.

References

1) N. Miyoshi, S. Furui, S. Murai, and N. Sonoda, *J. Chem. Soc., Chem. Commun.*, **1975**, 293.

2) N. Miyoshi, S. Murai, and N. Sonoda, *Tetrahedron Lett.*, **1977**, 851.

3) Presented at the 30th National Meeting of the Chemical Society of Japan held in Osaka, April 1974: *cf.* Preprint of the Meeting, III, p. 1287 (1974); At almost the same time as our presentation, Sharpless and Lauer reported briefly on the reaction of cyclohexene with benzeneseleninic acid: see K. B. Sharpless and R. F. Lauer, *J. Org. Chem.*, **39**, 429 (1974).

4) G. Ayrey, D. Barnard, and D. T. Woodbridge, *J. Chem. Soc.*, **1962**. 2089.

5) G. Holzle and W. Jenny, *Helv. Chim. Acta*, **41**, 593 (1958); W. Jenny, *ibid.*, **36**, 1278 (1953).

6) K. B. Sharpless, K. M. Gordon, R. F. Lauer, D. W. Patrick, and M. W. Young, *Chem. Scripta*, **8A**, 9 (1975); H. J. Reich, J. M. Renga, and I. L. Reich, *J. Am. Chem. Soc.*, **97**, 5434 (1975).

7) K. B. Sharpless, M. W. Young, and R. F. Lauer, *Tetrahedron Lett.*, **1973**, 1979; H. J. Reich, I. L. Reich, and J. M. Renga, *J. Am. Chem. Soc.*, **95**, 5813 (1973); D. L. Clive, *J. Chem. Soc., Chem. Commun.*, **1973**, 695.

8) K. B. Sharpless and R. F. Lauer, *J. Org. Chem.*, **39**, 429 (1974); K. B. Sharpless and R. F. Lauer, *J. Am. Chem. Soc.*, **95**, 2697 (1973); D. L. Clive, *J. Chem. Soc., Chem. Commun.*, **1974**, 100.

9) A. E. Osterberg, *Org. Synth.*, Coll. Vol. I, 185 (1941).

BULLETIN OF THE CHEMICAL SOCIETY OF JAPAN, VOL. 51 (4), 1267—1268 (1978)

Preparation of Aroyl and Arenesulfonyl Fluorides from the Corresponding Chlorides Using Zinc Fluoride–Pyridine System

Akira SEKIYA and Nobuo ISHIKAWA

Department of Chemical Technology, Tokyo Institute of Technology, Ookayama, Meguro-ku, Tokyo 152

(Received December 17, 1977)

Synopsis. Convenient preparation of aroyl and arenesulfonyl fluorides in high yields was achieved by the reaction of the corresponding chlorides with zinc fluoride in pyridine.

A number of methods for the conversion of carboxylic acid chlorides or bromides into fluorides have been reported. In earlier days, various metal fluorides such as SbF_3,[1a,b] AsF_3, AgF,[1a] KF, KHF_2,[1c] HgF_2,[1d] and ZnF_2[1e] were used for this purpose, although they do not give satisfactory results. In recent years, more complex fluorides, such as Na_2SiF_6,[2] potassium fluorosulfinate,[3] triethylammonium fluoride,[4] hexafluoroacetone-KF adduct[5] or morpholinosulfur trifluoride[6] have been reported as fluorinating reagents.

In our earlier paper[7] it was mentioned that smooth formation of a ketone from (heptafluoro-1-methylethyl)-zinc iodide and benzoyl chloride was induced in the zinc fluoride–pyridine system, in which an in situ conversion of benzoyl chloride into fluoride was recognized. Further investigation has revealed that zinc fluoride is surprisingly effective in pyridine for the conversion of not only aroyl chlorides but also arenesulfonyl chlorides into the corresponding fluorides under mild conditions.

Several decades ago, the reaction of zinc fluoride with acetyl chloride (no solvents) for three days[8] and the reaction of zinc fluoride with organic sulfonyl chlorides in water were reported,[9] the results being, however, unsatisfactory yields of the corresponding fluorides. We describe here a practically useful method for the preparation of aroyl and arenesulfonyl fluorides by reaction in the zinc fluoride–pyridine system.

After addition of benzoyl chloride to an equimolar amount of zinc fluoride in pyridine at room temperature (25 °C), tracing of the reaction by ^{19}F NMR analyses revealed rapid conversion of the chloride into fluoride, which was completed quantitatively within 20 min. However, on using a half-molar amount of zinc fluoride the reaction was much slower, and 73 and 88% conversions after 40 min and 12 h respectively were observed.

Replacement of zinc fluoride by potassium fluoride, or of pyridine by other tertiary amines (Et_3N, $PhNMe_2$, or *N*-methylpiperidine) or by other solvents (DMSO, DMF, MeCN, or THF) gave no satisfactory results, showing almost no occurrence of conversion. The exclusive effectiveness of pyridine is presumably due

Table 1. Preparation of aroyl and arenesulfonyl fluorides

$$ArCOCl\ (or\ ArSO_2Cl) + ZnF_2 \xrightarrow[r.t.]{Pyr.} ArCOF\ (or\ ArSO_2F) + ZnClF$$

ArCOF or $ArSO_2F$	Preparation			Bp[c] (°C/mmHg)	Mp[c] (°C)	^{19}F NMR[d] COF or SO_2F
	Method[a]	Time (min)	Yield[b] (%)			
p-$MeOC_6H_4COF$	A	40	83	74/5[e]	——	−93.3 (neat)
p-MeC_6H_4COF	A	20	84	110/94 (90—91/25)[f]	——	−94.8 (neat)
C_6H_5COF	A	20	82	101/130 (154—155)[g(i)]	——	−94.8 (neat)
p-ClC_6H_4COF	B	20	82	——	59—60[h]	−96.0 (CCl_4)
p-$NO_2C_6H_4COF$	B	20	100	——	138—139 (144—146)[i]	−97.6 (C_6H_6)
p-$MeC_6H_4SO_2F$	B	120	80	——	42.5—43.5 (43—44)[g(ii)]	−144.3 (CCl_4)
$C_6H_5SO_2F$	B	120	82	62—65/2 (203—204)[g(iii)]	——	−144.6 (neat)
p-$ClC_6H_4SO_2F$	B	120	90	——	53—54 (48—49)[i]	−142.0 (MeCN)
p-$BrC_6H_4SO_2F$	B	120	94	——	66—67 (65—66)[k]	−142.0 (MeCN)

a) See experimental section. b) Yields are those of the products actually isolated. c) Values in the literature are shown in parentheses. d) Chemical shifts in the solvents in parentheses are shown in δ ppm from ext. CF_3CO_2H. e) Calcd, C, 62.34%; H, 4.58%; Found, C, 61.68%; H, 4.55%. f) N. Ishikawa and S. Sasaki, *Chem. Lett.*, **1976**, 1407. g) "Dictionary of Organic Compounds" 4th ed, Eyre and Spottiswoode Pub. Ltd., (1965), (i) Vol. 1, p. 359; (ii) Vol. 1, p. 330; (iii) Vol. 5, p. 3072. h) Calcd, C, 53.02%; H, 2.54%; Found, C, 53.21%; H, 2.61%. i) L. N. Markovskij, V. E. Pashinnik, and A. V. Kirsanov, *Synthesis*, **1973**, 787. j) M. Kulka, *J. Am. Chem. Soc.*, **72**, 1215 (1950). k) M. E. Aberlin and C. A. Bunton, *J. Org. Chem.*, **35**, 1825 (1970).

to its ability to weaken the Zn–F linkage through an appropriate coordination to the zinc atom.

The reaction was extensively studied using aroyl chlorides with varied substituents. As summarized in Table 1, the corresponding fluorides were obtained in sufficiently high yields in all the runs. However, when phenylacetyl chloride, an aliphatic acid chloride, was employed, the yield of fluoride was only 57% (^{19}F NMR analysis) even after 4 h's reaction.

Conversion of arenesulfonyl chlorides into fluorides was also examined in a similar manner. For example, conversion of benzenesulfonyl chloride into the fluoride occurred quantitatively after 2 h (^{19}F NMR). Results of experiments with several other arenesulfonyl chlorides are shown in Table 1.

Experimental

Anhydrous Zinc Fluoride. Anhydrous zinc fluoride was easily prepared as follows. An aqueous solution of zinc chloride (two molar equiv.) was added to an aqueous solution of potassium fluoride and the precipitates obtained were collected by filtration, washed thoroughly with water and dried over phosphorus pentaoxide at 180 °C in vacuo. Yield was almost quantitative.

General Procedures for Fluorination. To a solution of zinc fluoride (0.03 mol) in pyridine (30 ml) aroyl chloride or arenesulfonyl chloride (0.03 mol) was added with stirring at room temperature (25 °C). Stirring was continued until the reaction was completed (checked by ^{19}F NMR) then treated by either method (A) or (B), as follows:

(A) In the case of low-boiling products resistant to hydrolysis; the reaction mixture was poured into ice-cold 25% hydrochloric acid. The liberated aroyl fluoride was extracted with ether and the ethereal solution was washed with water and dried over magnesium sulfate. Evaporation of ether gave the aroyl fluoride, which was purified by distillation under reduced pressure.

(B) The reaction mixture was concentrated under reduced pressure and the resulting residue was extracted with warm hexane or benzene. Evaporation of the solvent gave crude aroyl fluoride or arenesulfonyl fluoride which was purified by distillation under reduced pressure or by recrystallization.

References

1) a) M. M. Meslans, *Compt. Rend.*, **114**, 1020 (1892); b) F. Swarts, *Bull. Soc. Chim.*, **15**, 1134 (1896); c) M. A. Borodin, *C. R. Acad. Sci.*, **55**, 553 (1862); d) O. Ruff and G. Bahlau, *Ber.*, **51**, 1758 (1919); e) M. M. Meslans, *Ann. Chim. Phys.*, **1**, 411 (1894).

2) J. Dahlmos, *Angew. Chem.*, **71**, 274 (1959).

3) F. Seel and J. Langer, *Chem. Ber.*, **91**, 2553 (1958).

4) I. L. Knunyants, Yu. A. Cheburkov, and M. D. Bargamova, *Izv. Akad. Nauk SSSR, Ser. Khim.*, **1963**, 1393.

5) A. G. Pittman and D. L. Sharp, *J. Org. Chem.*, **31**, 2316 (1966).

6) L. N. Markoviski, V. E. Pashinnik, *Synthesis*, **1975**, 801.

7) A. Sekiya and N. Ishikawa, *Chem. Lett.*, **1977**, 81.

8) F. F. Blicke, *J. Am. Chem. Soc.*, **46**, 1515 (1924).

9) W. Davies and J. H. Dick, *J. Chem. Soc.*, **1931**, 2104.

TEA CO_2 Laser Induced Photoreactions of Ethylene, Chloroethylenes and Chloroethanes

Keiichi NAGAI and Mikio KATAYAMA

Department of Pure and Applied Sciences, College of General Education, The University of Tokyo, Komaba, Meguro-ku, Tokyo 153

(Received June 15, 1977)

TEA CO_2 laser induced chemical reactions of ethylene, chloroethylenes and chloroethanes have been investigated. Since these compounds have absorptions at wavelengths of 10.6 or 9.6 μm band of the CO_2 laser, strong excitation of the molecular vibration gives rise to an infrared photochemical reaction. In chlorine derivatives, the cleavage of the C–Cl bond by the laser irradiation appears to initiate decompositions of these materials. The final products were mainly brought about by molecular elimination of HCl, H_2, or Cl_2. The present results demonstrate that the CO_2 laser induced reactions differ form their thermal reactions.

Since the development of infrared lasers, a considerable number of investigations on infrared photochemical reactions induced by continuous wave (CW) or transverse excited atomospheric (TEA) CO_2 laser irradiation have been reported.[1-4] Braun and Tsang[5] have observed TEA CO_2 laser induced chemical reactions for isobutyl and ethyl chlorides, bromides and iodides. For all except the iodides the reaction took place *via* the molecular elimination of hydrogen halides. With respect to the iodides, cleavage of the C–I bond competed with the elimination of hydrogen halide. The infrared photochemical reactions of ethylene, chloroethylenes, chloroethanes and mixtures of these compounds with SF_6 or H_2 induced by TEA CO_2 laser irradiation have been observed. In those cases, the vibrationally excited molecules took direct part in chemical reactions. Irradiation by infrared laser pulse gives rise to an elevation of the specific vibrational temperature of molecule, keeping the translational temperature almost unchanged. Therefore, in this respect the infrared laser induced reactions differ from the thermally induced ones, although the reaction products are similar.

Experimental

The TEA CO_2 laser constructed and used was a double discharge type with three pairs of Rogowski electrodes of 60 cm length each.[6] The cavity length was about 200 cm, being formed by a 20 m radius aluminum-coated concave mirror and a flat uncoated germanium output ethalon. Under ordinary conditions, the simultaneous oscillation of multiple lines of multi-modes was observed, and the strongest line was P(20) of the 10.6 μm band. The oscillations of P(14)—P(22) and R(16) of this band with less than 1/10 of the intensity of the P(20) line were also observed. The power output was about 1 J with a pulse duration of 100 ns; its repetition rate was about 1 Hz. The absorption cell of about 3 cm length was inserted into the laser cavity for a selective oscillation of appropriate lines of the laser. When SF_6 gas of 150 Torr was introduced into the cell, the oscillation of the 9.6 μm band was accomplished, and its power output was slightly less than that of the 10.6 μm band. The oscillation of R branch of the 9.6 μm band was obtained by using C_2H_3Cl gas of about 150 Torr.

Reaction cells made of duralmine were used. One had the dimensions of 100 mm length and inner diameter of 30 mm, and the other was 50 mm length and 20 mm diameter. The reaction cell was closed by two KCl windows permitting passage of the laser beam. The sample gas in the reaction cell was irradiated by the laser pulse focused with germanium lens of f=5 cm; the diameter of the focal spot was ≈0.5 mm. The peak power of the laser at the focus was more than 1 GW/cm², but its irradiation did not show any appreciable temperature elevation of the sample gas. The products of the infrared photoreaction were examined by infrared absorption. No appreciable differences of products were found with changing cell dimensions.

Results and Discussion

For a pressure of sample gas higher than 50 Torr, the irradiation by high power laser gives rise to a dielectric breakdown. This produces an avalanche of electrons, and the reactions caused by the breakdown have been shown to be the same as those initiated by an electric discharge.[8] Therefore, the infrared laser induced reactions have been observed in the pressure range of 10—50 Torr, where the reaction was mainly infrared-photochemical. Although the dielectric breakdown was unobserved at these pressures, the emission of visible luminescence was observed around the focus of the lens.

Typical results, including the experimental conditions, are presented in Table 1. The products listed in this table were obtained after an irradiation of 30—60 min. A more detailed examination of the results is now given.

Ethylene. The reaction product of C_2H_4 was C_2H_2 and the yield was proportional to the pressure of ethylene in the range of 10—50 Torr. The reaction is one of elimination of the H_2 molecule. When the mixture of C_2H_4 and H_2 (20 Torr: 20 Torr) was irradiated, the partial pressure of the product C_2H_2 was found to be 1.5 Torr, which is almost the same order of magnitude as that of the pure C_2H_4. The addition of H_2 did not produce any detectable change in the rate of decomposition of ethylene.

Chloroethylene. The main reaction of the chloroethylenes was the elimination of hydrogen chloride from the initial reagent. Under the irradiation conditions, C_2H_3Cl at 22 Torr produced C_2H_2 at 2.2 Torr. The presence of C_2HCl was not detected in the products, indicating the difficulty of eliminating H_2 compared with that of HCl. It is reasonable to predict this since the energy required for the elimination of H_2 is estimated to be 75 kcal/mol from the energies of C–H and H–H bonds, while the energy required for the elimina-

TABLE 1. PRODUCTS OF CO_2 LASER INDUCED PHOTOCHEMICAL REACTIONS

Reagents, pressures	Reaction products, partial pressures	Irradiation conditions
C_2H_4 (20 Torr)	C_2H_2 (1.8 Torr)	10.6 μm P, 3000 shots
C_2H_3Cl (22 Torr)	C_2H_2 (2.2 Torr)	10.6 μm P, 3000 shots
$CCl_2=CH_2$ (10 Torr)	C_2HCl (1.5 Torr) C_2H_2 (0.5 Torr)	9.6 μm P+R, 1500 shots[a]
C_2HCl_3 (18 Torr)	C_2Cl_2 (5 Torr) C_2HCl (0.5 Torr)	10.6 μm P, 3000 shots
C_2HCl_3 (20 Torr) $+H_2$ (20 Torr)	C_2H_2 (2.7 Torr) $CCl_2=CH_2$ (0.7 Torr) C_2HCl (0.1 Torr)	10.6 μm P, 3000 shots
C_2H_5Cl (20 Torr)	C_2H_4 (5 Torr) C_2H_2 (1 Torr)	10.6 μm P, 3000 shots
$CHCl_2$-CH_3 (10 Torr)	C_2H_2Cl (1.7 Torr) C_2H_2 (1 Torr)	10.6 μm P, 1500 shots[a]
$CHCl_2$-CH_3 (10 Torr)	C_2H_3Cl (4.4 Torr) C_2H_2 (1.4 Torr)	9.6 μm P, 1500 shots[a]
$CHCl_2$-CH_3 (10 Torr) $+SF_6$ (1 Torr)	C_2H_3Cl (1.5 Torr)	10.6 μm P, 1500 shots[a]
CH_2Cl-CH_2Cl (20 Torr)	C_2H_3Cl (<0.1 Torr)	10.6 μm P, 3000 shots
CH_3-CCl_3 (20 Torr)	$Cl_2C=CH_2$ (<0.1 Torr)	10.6 μm P, 3000 shots
$CHCl_2$-CH_2Cl (11 Torr)	$Cl_2C=CH_2$ (1.1 Torr) CHCl=CHCl (*trans*) (0.3 Torr) CHCl=CHCl (*cis*) (0.5 Torr)	10.6 μm P, 3000 shots

a) A smaller reaction cell was used.

tion of HCl is about 50 kcal/mol.[5,7] Since this molecule absorbs at a wavelength of 9.6 μm, the 9.6 μm laser photochemical reaction was also observed. However, the production of C_2H_2 was slightly less than that by the 10.6 μm irradiation.

The ν_8 vibrational mode of $Cl_2C=CH_2$ is infrared active and the absorption can be observed at the 9.6 μm R branch of the CO_2 laser. Hence, the reaction was induced by the irradiation of the TEA CO_2 laser with the R branch of 9.6 μm radiation. The reaction products were C_2HCl and C_2H_2 at a ratio 5:1. The following processes may be suggested for the production of the C_2H_2 molecule.

1) The infrared laser irradiation brings about a cleavage of the C–Cl bond and creates a $ClC=CH_2$ radical.

2) The transfer of an H atom produces a HClC=CH radical.

3) The cleavage of the C–Cl bond of the radical HClC=CH by the laser irradiation yields the C_2H_2 molecule.

The process assumed above is equivalent to the elimination of a Cl_2 molecule, following the scrambling of the H atom.

Since $Cl_2C=CH_2$ has no absorption at the wavelength of 10.6 μm TEA CO_2 laser, its irradiation produced no reaction in the pure sample. However, the SF_6 sensitized reaction of $Cl_2C=CH_2$ was induced by the 10.6 μm laser irradiation, but the quantity of products was too small for complete identification. The results of the direct and sensitized reactions are listed in Table 2. The absorption coefficients of the mixture of $Cl_2C=CH_2$ and SF_6 (14 Torr: 1 Torr) were measured by using the laser with 4 mJ output. The observed value at 10.6 μm was 5 times as large as the absorption coefficient at 9.6 μm. Although the irradiated laser power of 10.6 μm was about 1.5 times as large as the power of 9.6 μm band, the reaction rate of the direct process was larger by an order of magnitude. In the mixture of SF_6 and $Cl_2C=CH_2$, the ν_3 mode of SF_6 was excited successively to its higher vibrational levels by the incident 10.6 μm laser. The vibrational energies of SF_6 transfered to the vibrationally excited levels of $Cl_2C=CH_2$, giving rise to the dissociation of this molecule. It should be noted that any decomposition of SF_6 molecule in the present mixture was not detected. The observed results in Table 2 indicate that the direct laser excitation of the ν_6 vibration of $Cl_2C=CH_2$ (CH rocking mode) accelerates the reaction rate significantly.

TABLE 2. TEA CO_2 LASER INDUCED CHEMICAL REACTION OF $Cl_2C=CH_2$

	Direct excitation	SF_6 sensitized reaction
Sample	$Cl_2C=CH_2$ (14 Torr)	+ SF_6 (1 Torr)
Laser line	9.6 μm R	10.6 μm P
Relative laser power	1	≈1.5
Relative absorption coefficient (4 mJ)	1	≈5
Reaction rate	>6	1

In a previous paper the TEA CO_2 laser induced isomerization and decomposition of ClHC=CHCl has been reported.[8] The observed reactions promoted by the direct excitation or SF_6 sensitization using TEA CO_2 laser are listed in Table 3. The absorption coefficient of the mixture of ClHC=CHCl (*trans*) and SF_6 (10 Torr: 1 Torr) at 10.6 μm is 50 times as large as that of the pure substance, but the reaction rate of the sensitized excitation is only 6 times as fast as the rate of the direct excitation. Although the main reaction was the *trans-cis* isomerization in both cases, the production of C_2H_2 and C_2HCl were also observed in the

TABLE 3. TEA CO_2 LASER INDUCED CHEMICAL REACTION OF ClHC=CHCl (*trans*)

	Direct excitation	SF_6 sensitized reaction
Sample	ClHC=CHCl (10 Torr)	ClHC=CHCl (10 Torr) + SF_6 (1 Torr)
Laser line	10.6 μm P	10.6 μm P
Relative absorption coefficient (4 mJ)	1	≈50
Relative reaction rate	1	6
Ratio of products C_2H_2/C_2HCl	0.6	0

case of direct excitation. In the SF_6 sensitized reaction, only the C_2HCl molecule was obtained, indicating that the reaction resembles the pyrolysis of ClHC=CHCl.[9] The infrared photoreaction induced by the direct excitation of ClHC=CHCl differs then from the thermal one.

The frequency of the ν_{12} vibrational mode of ClHC=CCl_2 coincides with the 10.6 μm TEA laser, and the irradiation of 3000 shots produced 5 Torr of C_2Cl_2 and 0.5 Torr of C_2HCl from 18 Torr of this molecule. The ratio of the products, C_2Cl_2 and C_2HCl, may be given by the activation energies of the elimination of HCl and Cl_2 molecules. Goodall and Howlett reported that the thermal reaction products of $ClHC=CCl_2$ were C_6Cl_6 and HCl.[10] Although the presence of C_2Cl_2 molecules has not been detected in the pyrolysis of $ClHC=CCl_2$, the C_6Cl_6 molecule may be formed at higher translational temperatures from activated C_2Cl_2 molecules, which are presumably produced by the elimination of hydrogen chloride from the parent molecules. Appreciable amounts of C_6Cl_6 were not detected in the laser induced reaction products, suggesting that elevation of the translational temperature is insufficient to allow the reaction $3\ C_2Cl_2 \rightarrow C_6Cl_6$. It is evident from our observation that the infrared laser induced reaction of $ClHC=CCl_2$ is significantly different from that of the pyrolysis. Furthermore, in the 10.6 μm laser induced reaction of the mixture of $ClHC=CCl_2$ and H_2 (20 Torr : 20 Torr) the products were C_2H_2 of 2.7 Torr, $Cl_2C=CH_2$ of 0.7 Torr and C_2HCl less than 0.1 Torr, but C_2Cl_2 was not detected in contrast to the case of pure $ClHC=CCl_2$. The major products obtained from the 10.6 μm laser irradiated mixture of $ClHC=CCl_2$ and D_2 were $CHD=CCl_2$, $CD_2=CCl_2$, and $H_2C=CCl_2$. The productions of C_2D_2, C_2HD, and a trace of C_2H_2 were also observed. These results seem to indicate that the CO_2 laser irradiation gives rise to a cleavage of C–Cl bond of $ClHC=CCl_2$ molecule.

Chloroethanes. The reaction products of C_2H_5Cl at 25 Torr were C_2H_4 and C_2H_2 with partial pressure of 5 and 1.5 Torr respectively. At less than 25 Torr, the quantities of the products were proportional to the initial pressures of the samples. When increased to 40 Torr, the partial pressures of the products, C_2H_4 and C_2H_2, reached 6 and 3 Torr respectively. Assuming that the infrared laser irradiated C_2H_5Cl gives rise to the production of C_2H_4 alone and the reaction product C_2H_2 of the present experiment is brought about by the irradiation of C_2H_4 by the same laser, then the partial pressure of C_2H_2 must be less than 1/5 of the really observed value. Therefore, we may conclude that the major part of C_2H_2 must be directly, and almost simultaneously, produced from C_2H_5Cl by the CO_2 laser irradiation. Barton and Howlett have reported that the pyrolysis of this material gives rise to the production of C_2H_4 but not to noticeable amounts of C_2H_2.[11] These experimental results demonstrate that the mechanism in both reactions is different.

Infrared absorption of $Cl_2HC–CH_3$ was observed at wavelengths of the 9.6 μm P, R and 10.6 μm R bands of the CO_2 laser, but not at the 10.6 μm P band. Hence, the irradiation of the R branch of 10.6 μm laser pulse produced C_2H_3Cl of 1.7 Torr and C_2H_2 of 1 Torr from 10 Torr of $Cl_2HC–CH_3$. The irradiated products with the P branch of the 9.6 μm band were C_2H_3Cl of 4.4 Torr and C_2H_2 of 1.4 Torr. Since the production of C_2H_2 is almost of the same order as that of C_2H_3Cl, only a small part of C_2H_2 may be assumed to be produced by the laser induced reaction of C_2H_3Cl which is given from $Cl_2HC–CH_3$ by the 9.6 or 10.6 μm R infrared photodissociation. This is because the yield of C_2H_2 from the laser induced reaction of C_2H_3Cl is less than 10% of the parent molecule. The 9.6 μm R laser irradiation produced 1.2 Torr of C_2H_3Cl and 0.3 Torr of C_2H_2 from 10 Torr of $Cl_2HC–CH_3$. Since the C_2H_3Cl molecule does not absorb in the 9.6 μm R line, C_2H_2 in the present observation must be directly produced from $Cl_2HC–CH_3$ by the 9.6 μm R laser irradiation. The experimental results obtained by Barton and Howlett indicate that C_2H_2, the thermal decomposition product of $Cl_2HC–CH_3$, is only 3% of the major pyrolysis product C_2H_3Cl,[11] suggesting the different mechanisms between the pyrolysis and the infrared laser induced reaction.

The infrared photochemical decomposition of $CHCl_2–CH_2Cl$ was also investigated. The decomposition products were *cis*- and *trans*-CHCl=CHCl and $CCl_2=CH_2$ in a concentration ratio of 0.5:0.3:1.1. The pyrolysis of $CHCl_2–CH_2Cl$ has been investigated by Williams[12] and by Teramoto *et al.*,[13] and they have proposed both processes—radical chain and unimolecular reactions—for the decomposition. The ratio of the decomposition products $H_2C=CCl_2$ and ClHC=CHCl was found to be 0.7. Teramoto *et al.* have also confirmed that the product $H_2C=CCl_2$ decreased when the radical chain reaction was inhibited. In the infrared laser induced reaction, we obtained a value 1.4 for the ratio of the products, $H_2C=CCl_2$ and ClHC=CHCl. From our experimental results it may be concluded that the infrared laser induced reaction of $CHCl_2–CH_2Cl$ is mainly promoted by the radical reaction.

Translational and Vibrational Temperatures. Recently the impulsive opto-acoustic effect has been reported. This gives rise to a temperature change in a certain gas by the absorption of the CO_2 laser pulse.[14] When the infrared laser pulse is absorbed by the gas, the population of relevant vibrational levels deviates from the thermal equilibrium for the short duration of the laser pulse. The energy supplied by the laser pulse as an increment of the vibrational energy is finaly transformed into translational energy of the molecule by the vibrational-translational relaxation, giving rise to elevation of the translational temperature. When the pressure of gas is 20 Torr, about 10 ms after irradiation the translational temperature of the molecules decreases to the initial value. This is caused by the dissipation of the translational energy to the cell wall or other surroundings.

In the present study of the laser induced reaction, the translational temperature increase of sample gas may be observed only in a short duration of about 10 ms. Ambartzumian *et al.*[15] have estimated that the temperature increase of ClHC=CHCl by the TEA CO_2 laser

irradiation was less than 350 °C which gave the maximum temperature of the gas at about 650 °C. Furthermore, they observed that the gas was kept at around 650 °C only for a short duration of 10^{-4} s. Under these conditions thermal reaction was assumed to be negligible. The same discussion may be applied in our case. In the present study, the temperature increase of sample gas by the irradiation of 3000 laser pulses was assumed to be negligible. Therefore, the energy supplied by the laser provided the elevation of vibrational temperature which gave rise to the infrared photochemical reaction. The experimental results support the present assumption that the thermal and infrared laser reactions are not the same.

The infrared laser dissociation of SF_6 molecules was understood on the assumption that the molecules are excited to the true continuum of the levels above the dissociation limit through the exciattion of quasicontinuum of the vibrational levels. From the measurement of dissociation thresholds of SF_6, almost 20 photons/molecule were deposited by the ultrashort laser pulse, implying a vibrational temperature of $T=1800$ K.[16]

The numbers of photons needed for dissociation of molecules in the present investigation are in the order of 20—40, which depends upon the molecules. Since the threshold power for molecular dissociation was unobserved in the present case, the vibrational temperature at the threshold could not be determined, even if it could be defined. However, the number of normal modes and the process of the laser dissociation may be almost the same as those of SF_6. The vibrational temperature at around the dissociation threshold may be an order of 2000 K.

Conclusion

The TEA CO_2 laser induced chemical reactions of ethylene, chloroethylenes and chloroethanes have been observed. The results demonstrate that the reactions are caused by multiple steps or multiple absorptions of the infrared photons, following the elimination of hydrogen or hydrogen chloride molecules, or by the cleavage of the C–Cl bond. Furthermore, the experimental results indicate that the products and the reaction mechanisms are somewhat different from those of thermal reactions. It is rather difficult to elucidate the complete mechanism of the infrared laser induced photoreaction from the present observations, since its mechanism seems to vary with molecules. However, the detailed studies on the reaction of the individual substances will give information on the reactions of molecules whose vibrations of a certain mode are highly excited.

This research was supported partly by the Grant-in-Aid from the Ministry of Education.

References

1) N. G. Basov, E. P. Markin, A. N. Oraevskii, A. V. Pankratov, and A. N. Skachkov, *JETP Lett.*, **14**, 165 (1971).
2) A. Yogev, R. M. J. Loewenstein, and D. Amar, *J. Am. Chem. Soc.*, **94**, 1091 (1972).
3) M. P. Freeman, D. N. Travis, and M. F. Goodman, *J. Chem. Phys.*, **60**, 231 (1974).
4) A. Yogev and R. M. J. Loewenstein, *J. Am. Chem. Soc.*, **95**, 8487 (1973).
5) W. Braun and W. Tsang, *Chem. Phys. Lett.*, **49**, 354 (1976).
6) H. J. Seguin, K. Manes, and J. Tulip, *Rev. Sci. Instr.* **43**, 1134 (1972).
7) L. Pauling, "The Nature of Chemical Bond," Cornell Univ. Press, Ithaca, N. Y. (1960).
8) K. Nagai and M. Katayama, *Chem. Phys. Lett.*, **51**, 329 (1977).
9) A. M. Goodall and K. E. Howlett, *J. Chem. Soc.*, **1956**, 2640; *ibid.*, **1956**, 3092.
10) A. M. Goodall and K. E. Howlett, *J. Chem. Soc.*, **1954**, 2640.
11) D. H. R. Barton and K. E. Howlett, *J. Chem. Soc.*, **1949**, 165.
12) R. J. Williams, *J. Chem. Soc.*, **1953**, 113.
13) K. Teramoto, M. Kitabatake, and T. Onouchi, *Kogyo Kagaku Zasshi*, **67**, 50 (1964).
14) T. Aoki and M. Katayama, *Jpn. J. Appl. Phys.*, **10**, 1303 (1971); H. Aung, K. Nagai, and M. Katayama, *J. Phys. Soc. Jpn.*, **37**, 186 (1974).
15) R. V. Ambartzumian, N. V. Chekalin, V. S. Doljikov, V. S. Letokhov, and V. N. Lokman, *J. Photochem.*, **6**, 55 (1976—1977).
16) J. G. Black, E. Yablonovitch, N. Bloembergen, and S. Mukamel, *Phys. Rev. Lett.*, **38**, 1131 (1977).

Bromine-81 Nuclear Quadrupole Resonance and Aluminum-27 Nuclear Magnetic Resonance in $AlBr_3$ Complexes

Tsutomu OKUDA, Hideta ISHIHARA, Koji YAMADA, and Hisao NEGITA

Department of Chemistry, Faculty of Science, Hiroshima University, Hiroshima 730

(Received July 7, 1977)

The Zeeman effect on ^{81}Br NQR and the quadrupole effect on ^{27}Al NMR in $L \cdot AlBr_3$ complexes (L=KBr, $POBr_3$, and H_2S) were studied at room temperature. It was found that the ^{27}Al quadrupole-coupling constant for these complexes decreases with decreasing coupling constant of the ^{81}Br atom in $-AlBr_3$ and that the atomic arrangement about the Al atom has C_{3v} symmetry in $POBr_3 \cdot AlBr_3$ and $H_2S \cdot AlBr_3$. In the latter complex, H_2S molecule is reorientated at room temperature. The amount of charge transfer in these complexes was estimated on the basis of the Townes-Dailey theory and the bond angle $\angle$Br–Al–Br was found to depend on the amount of the charge transfer. The temperature dependence of the ^{81}Br NQR frequencies was observed in order to obtain information about molecular motion in $H_2S \cdot AlBr_3$ and $POBr_3 \cdot AlBr_3$.

For $L \cdot AlBr_3$ molecular complexes (L=ligand), the charge distribution of the acceptor molecule can be determined on the basis of the Townes-Dailey theory which is relatively simple but appears to still be valuable.[1,2] In order to estimate the charge distribution using this procedure, it is necessary to determine the $\angle$Br–Al–Br bond angles and the quadrupole-coupling constants for both Al and Br atoms. Some research employing NQR has already been reported on $L \cdot AlBr_3$ molecular complexes.[3-5] All, however, was performed on polycrystalline samples. Therefore, an attempt was made to observe the Zeeman effect on ^{81}Br NQR and the quadrupole effect on ^{27}Al NMR using single crystals.

Experimental

$KBr \cdot AlBr_3$ and $POBr_3 \cdot AlBr_3$ were prepared by mixing equimolar amounts of the relevant compounds. $H_2S \cdot AlBr_3$ was prepared by passing hydrogen sulfide through a carbon disulfide solution of aluminum bromide.[6] The single crystals were grown employing the Bridgman-Stockbarger method. The melting points of these complexes are as follows: 191 °C for $KBr \cdot AlBr_3$, 181 °C for $POBr_3 \cdot AlBr_3$, and 83 °C for $H_2S \cdot AlBr_3$. The bromine content was determined using the Fajans method. Found: Br, 83.6%. Calcd for $KBr \cdot AlBr_3$: Br, 82.9%. Found: Br, 87.5%. Calcd for $POBr_3 \cdot AlBr_3$: Br, 86.6%. Found: Br, 78.5%. Calcd for $H_2S \cdot AlBr_3$: Br, 79.7%.

The NQR spectrometer was a self-quenching super-regenerative oscillator with frequency modulation and the resonance lines were displayed on an oscilloscope. The Zeeman effect on ^{81}Br NQR was studied using the zero-splitting cone method. A magnetic field of *ca.* 250 G was applied by means of a Helmholtz coil. ^{81}Br NQR frequencies were observed at various temperatures which were attained in a Dewar vessel by cooling petroleum ether with liquid nitrogen or heating liquid paraffin with an electric heater.

^{27}Al NMR was observed using a broad-line NMR spectrometer (Model JES-ME 1) from the Japan Electron Optics Lab. Co., Ltd. The resonance frequency was fixed at 13.00 MHz and the magnetic field was varied to obtain the resonance.

Results and Discussion

^{81}Br NQR. The NQR frequencies of ^{81}Br atoms at room temperature are listed in Table 1. For $H_2S \cdot AlBr_3$, only one ^{81}Br NQR line was observed. This is consistent with the results of X-ray analysis,[6] that is, the bromine atoms of the complex are situated at equivalent positions in the crystal. For $POBr_3 \cdot AlBr_3$, two ^{81}Br NQR lines were observed. Although its crystal structure is not known at present, the formation of the O–Al bond is obvious from infrared spectroscopic studies.[7] Therefore, the structure of the complex is assumed to be Br_3P–O–$AlBr_3$. Consequently, the lower and higher resonance lines can be assigned to the Br atoms linked to the Al and P atoms, respectively, referring to the ^{81}Br NQR frequencies of Al_2Br_6 and $POBr_3$ in their pure states.[8,9] For $KBr \cdot AlBr_3$, four ^{81}Br NQR lines were observed. The average frequency was in the same range as those of $LiAlBr_4$ and $NaAlBr_4$ and was considerably lower than that of the terminal ^{81}Br atoms of KAl_2Br_7.[10] One of the constituents of the complex was assumed to be a distorted tetrahedral ion, $AlBr_4^-$.

Table 1. NQR parameters for ^{81}Br at room temperature

Compound		Frequency (MHz)	η (%)	$e^2Qq_{zz}h^{-1}$ (MHz)
$H_2S \cdot AlBr_3$		81.69	8.1±0.8	163.20
$POBr_3 \cdot AlBr_3$	ν_a	78.70	1.9±0.7	157.39
	ν_b	211.07	2.6±0.6	422.09
$KBr \cdot AlBr_3$	ν_a	76.31	3.1±0.3	152.60
	ν_b	77.56	24.4±0.7	153.60
	ν_c	78.27	10.8±0.7	156.23
	ν_d	79.91	7.5±0.7	159.66

The zero-splitting patterns were obtained from the Zeeman effect at room temperature and are shown in Figs. 1—3. The bond angles $\angle$Br–M–Br (M=Al and P) can be deduced, if the principal z axis of the ^{81}Br EFG tensor is assumed to be parallel to the direction of the M–Br bond. The results thus obtained are listed in Table 2.

For $H_2S \cdot AlBr_3$, X-ray analysis of the powder sample shows that there is only one type of $AlBr_3$ unit in the crystal, and three zero-splitting patterns are expected.[6] However, six zero-splitting patterns were obtained, as is shown in Fig. 1. Accordingly, it is evident that there are two kinds of $AlBr_3$ units which differ only in the orientation in the crystal. More precise X-ray analysis is necessary in order to clarify the crystal structure of this complex.

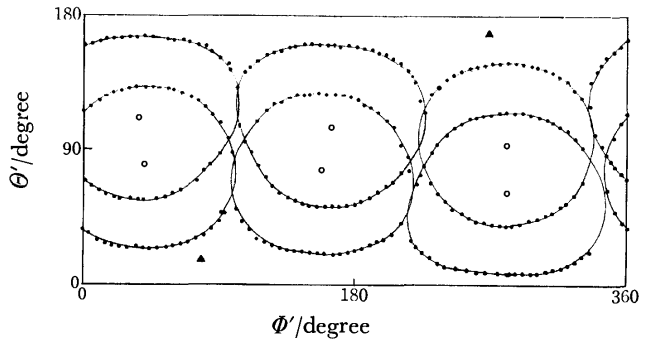

Fig. 1. Zero-splitting patterns of ^{81}Br Zeeman lines in $H_2S \cdot AlBr_3$. The direction of the three-fold axis is indicated by ▲. Θ' and Φ' are polar and azimuthal angles, respectively, in the coordinate fixed to the sample.

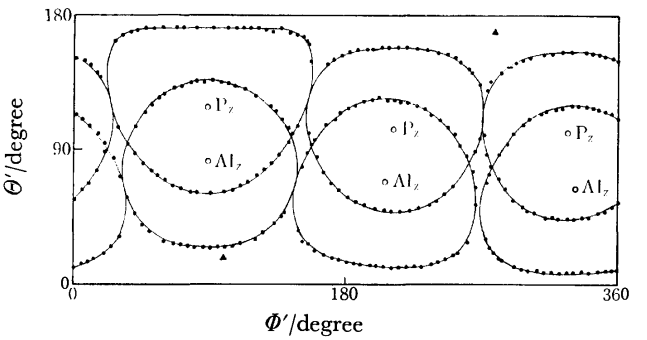

Fig. 2. Zero-splitting patterns of ^{81}Br Zeeman lines in $POBr_3 \cdot AlBr$. The direction of the principal z axes of the EFG tensors at the ^{81}Br atoms linked to the Al and P atom are indicated by Al_z and P_z, respectively. The direction of the three-fold axis is indicated by ▲. Θ' and Φ' are polar and azimuthal angles, respectively, in the coordinate fixed to the sample.

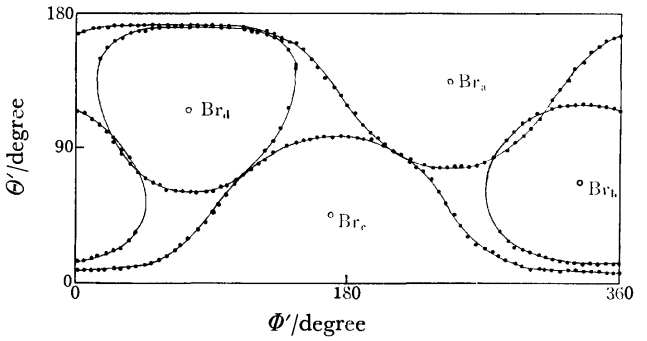

Fig. 3. Zero-splitting patterns of ^{81}Br Zeeman lines in $KBr \cdot AlBr_3$. The subscripts correspond to those of the resonance lines. Θ' and Φ' are polar and azimuthal angles, respectively, in the coordinate fixed to the sample.

For $POBr_3 \cdot AlBr_3$, the three-fold axis is found to be parallel to the P–O–Al bond which has a bond angle of 180.0±0.7°, because the three-fold axis of $AlBr_3$ is parallel to that of $POBr_3$ to within 0.7° from the result of the Zeeman effect. The configuration of $AlBr_3$ relative to $POBr_3$ is eclipsed, as is shown in Fig. 2. In $KBr \cdot AlBr_3$, the atomic arrangement about the Al atom is approximately tetrahedral, as is shown in Table 2, and the average bond angle is 109.5°.

Table 2. Bond angles ∠Br-M-Br

Compound	M	∠Br-M-Br (degree)	
$H_2S \cdot AlBr_3$	Al	112.7±0.4	
$POBr_3 \cdot AlBr_3$	Al	111.8±0.7	
	P	109.4±0.5	
$KBr \cdot AlBr_3$[a)]	Al	105.8±0.4	108.2±0.3
		109.4±0.5	110.1±0.3
		111.7±0.3	111.8±0.1

a) Six bond angles can be determined because four bromine atoms are nonequivalent.

The value of the asymmetry parameter, η, was determined using the following equation,[11]

$$\sin^2\Theta = 2/(3-\eta\cos 2\Phi), \quad (1)$$

where Θ and Φ are the polar and azimuthal angles of the Zeeman magnetic field with respect to the principal coordinates of the EFG tensor at the resonating nucleus. Consequently, the quadrupole-coupling constant, e^2Qq_{zz}/h, of the ^{81}Br atom was calculated using

$$\nu = (e^2Qq_{zz}/2h)(1+\eta^2/3)^{1/2}, \quad (2)$$

where ν is the ^{81}Br NQR frequency. The value of η and e^2Qq_{zz}/h thus obtained are listed in Table 1.

^{27}Al NMR. Only one central resonance line ($m=+1/2 \leftrightarrow m=-1/2$), which was affected by the second-order quadrupole interaction, was observed for both $H_2S \cdot AlBr_3$ and $POBr_3 \cdot AlBr_3$. The rotation patterns of the central line were obtained by measuring the shift, ΔH, from the magnetic field H_L corresponding to a Larmor frequency ν_L of 13.00 MHz, when the sample was rotated about the rotation axis perpendicular to the external magnetic field. The results are shown in Fig. 4. The frequency shift, $\Delta\nu$, can be represented in terms of the magnetic field by the following equation:[12]

$$\Delta\nu = -\nu_L(\Delta H/H_L^2)(\Delta H+H_L). \quad (3)$$

Since the components >S–$AlBr_3$ in $H_2S \cdot AlBr_3$ and –O–$AlBr_3$ in $POBr_3 \cdot AlBr_3$ have C_{3v} symmetry, respectively, the frequency shift of the central line was analyzed using the following equation derived from second-order perturbation theory with $\eta=0$,[13]

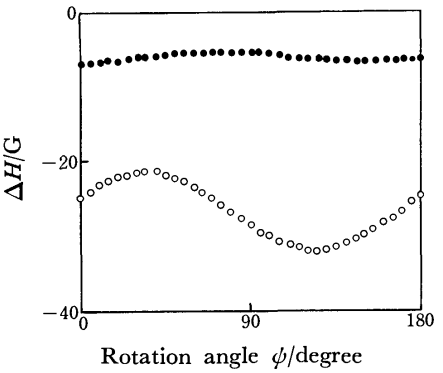

Fig. 4. Rotation patterns of ^{27}Al NMR central lines. $H_2S \cdot AlBr_3$ (○) for $\delta=10.5°$ and $\phi_0=35.0°$. $POBr_3 \cdot AlBr_3$ (●) for $\delta=8.5°$ and $\phi_0=70.0°$.

$$\Delta\nu = -(\nu_Q^2/16\nu_L)(a-3/4)(1-\mu^2)(9\mu^2-1), \quad (4)$$

where $\nu_Q=3e^2Qq/2I(2I-1)h$, $a=I(I+1)$, and $\mu=\sin\delta\cos(\psi-\psi_0)$. δ is the angle between the rotation axis and the principal z axis of the ^{27}Al EFG tensor. ψ is the rotation angle and ψ_0 is the value when the principal z axis lies in the plane formed by the rotation axis and the magnetic field.

Neither first- nor second-order splitting of ^{27}Al NMR spectra in $KBr\cdot AlBr_3$ were observed, so that the ^{27}Al quadrupole-coupling constant is estimated to be less than 1.3 MHz from the line width of the spectrum in the polycrystalline sample.

The ^{27}Al quadrupole-coupling constants thus obtained are as follows: 9.1±0.1 MHz for $H_2S\cdot AlBr_3$, 4.2±0.1 MHz for $POBr_3\cdot AlBr_3$, and less than 1.3 MHz for $KBr\cdot AlBr_3$. It was found that the ^{27}Al quadrupole-coupling constants for these complexes decrease with decreasing coupling-constant of the ^{81}Br atom in the $-AlBr_3$ components. A similar relation has been obtained by Tong[14] between the NQR frequencies of ^{69}Ga and ^{35}Cl atoms in L–$GaCl_3$ molecular complexes (L=ligand).

The Bond Character. The amount of charge transfer in these molecular complexes were estimated according to the Townes-Dailey theory. Supposing C_{3v} symmetry for hybrid orbitals centered at the Al atom, the four orthonormal hybrid wavefunctions can be expressed by[2]

$$\begin{aligned}
\psi_1 &= s_1\phi_s + (1-s_1^2)^{1/2}\phi_{p_z},\\
\psi_2 &= s_2\phi_s + (1-s_2^2)^{1/2}\{\phi_{p_z}\cos\theta-\phi_{p_x}\sin\theta\},\\
\psi_3 &= s_2\phi_s + (1-s_2^2)^{1/2}\{\phi_{p_z}\cos\theta+(1/2)\phi_{p_x}\sin\theta\\
&\qquad -(\sqrt{3}/2)\phi_{p_y}\sin\theta\},
\end{aligned} \quad (5)$$

and

$$\psi_4 = s_2\phi_s + (1-s_2^2)^{1/2}\{\phi_{p_z}\cos\theta+(1/2)\phi_{p_x}\sin\theta + (\sqrt{3}/2)\phi_{p_y}\sin\theta\},$$

where θ is the angle ∠Br–Al–L (L=ligand). s_1^2 and s_2^2 represent the fractional s character of the Al–L and Al–Br bonds, respectively. The population of orbital ψ_1, which is directed toward the ligand, is denoted by a_{Al} and the population of orbitals ψ_2, ψ_3, and ψ_4, which are directed toward the Br atoms, by b_{Al}. Then, the total electric field gradient of the Al atom is given by

$$q_{zz}(^{27}Al) = (b_{Al}-a_{Al})\{3-2/\sin^2\theta\}q_{at}. \quad (6)$$

It is evident that from the spherical triangle that there exists a relation such that $\cos^2\theta=(2\cos\alpha+1)/3$, where α is the ∠Br–Al–Br angle. Considering the increase in the EFG due to positive ionization of the Al atom, the quadrupole-coupling constant is given by

$$e^2Qq_{zz}/h(^{27}Al) = (b_{Al}-a_{Al})\{-3\cos\alpha/(1-\cos\alpha)\} \times (1+\varepsilon_{Al}\rho_{Al})e^2Qq_{at}/h(^{27}Al). \quad (7)$$

On the other hand, the ^{81}Br quadrupole-coupling constant is given by[2]

$$e^2Qq_{zz}/h(^{81}Br) = \{(1-s^2)(2-b_{Br})/(1+\varepsilon_{Br}\rho_{Br})\} \times e^2Qq_{at}/h(^{81}Br), \quad (8)$$

where s^2 is the fractional s character of the Br–Al σ orbital and b_{Br} is the population of this orbital. In Eqs. 7 and 8, $e^2Qq_{at}/h(^{27}Al)$ and $e^2Qq_{at}/h(^{81}Br)$ are the atomic quadrupole-coupling constants, the ε are parameters which correct for the ionization, and ρ_{Al} and ρ_{Br} are the positive and negative charges, respectively. The ρ are related to the population numbers by $\rho_{Al}=3-(3b_{Al}+a_{Al})$ and $\rho_{Br}=b_{Br}-1$. It is assumed that $b_{Al}+b_{Br}=2$ and $b_{Al}>a_{Al}$. Furthermore, s and ε the were chosen such that $s^2=0.15$, $\varepsilon_{Br}=0.13$, and $\varepsilon_{Al}=0.27$.[15]

Table 3. Population numbers a_{Al}, b_{Al}, and b_{Br}

Compound	a_{Al}	b_{Al}	b_{Br}
$H_2S\cdot AlBr_3$	0.13	0.33	1.67
$POBr_3\cdot AlBr_3$	0.22	0.31	1.69
$KBr\cdot AlBr_3$	0.30	0.30	1.70
	0.31	0.31	1.69
	0.31	0.31	1.69
	0.32	0.32	1.68

The values of a_{Al}, b_{Al}, and b_{Br} can be calculated from Eqs. 7 and 8, using the values of the bond angles and the quadrupole-coupling constants. The results are listed in Table 3. For $KBr\cdot AlBr_3$, a_{Al} is assumed to be equal to b_{Al}, because it cannot be specifield which bromine atom participate in the coordinate ion. Then it is evident that the donor powers of the ligands increase in the order $H_2S<POBr_3<Br^-$, provided that a_{Al} is regarded as a measure of the amount of charge transfer. In this connection, both ^{81}Br and ^{27}Al quadrupole-coupling constants in $-AlBr_3$ decrease with increasing a_{Al} or increasing degrees of charge transfer. In addition, it is seen that the bond angle approaches the tetrahedral angle with increasing a_{Al}. Therefore, in consideration of the results of the molecular-orbital calculation shown below, it appears that as the $AlBr_3$ in the complex approaches the tetrahedral arrangement, the strength of the donor-acceptor bond increases.

For BCl_3 and BF_3, the effect of reorganization has been explained using the results of CNDO/2 molecular-orbital calculations.[16] In the present investigation, an extended Hückel method for $AlBr_3$ was carried out.[17] The calculated lowest unoccupied virtual-orbital energy, E(LUMO), and the total electronic energy, E(ELEC), are presented as a function of the bond angle ∠Br–Al–Br in Fig. 5. This figure shows that E(LUMO) decreases with the reorganization of the planar molecule to the pyramidal form, in other words, the electron affinity of $AlBr_3$ increases with the reorganization, resulting in the formation of a stronger donor-acceptor bond. Meanwhile, the energy required to reorganize the planar molecule to the pyramidal form has been estimated by Cotton and Leto[18] to be 27.9 kcal/mol for $AlBr_3$, and this cannot be explained by only the change in E(ELEC) upon reorganization, as is shown in Fig. 5.

Upon the formation of a complex, the reorganization of a ligand is also considered to play an important role. According to the Zeeman effect on ^{81}Br NQR, the bond angle ∠Br–P–Br in $POBr_3\cdot AlBr_3$ is greater than that in $POBr_3$. Analogously, the H–H distance in H_2S is found from the results of the ^{1}H NMR studies to become larger upon the formation of $H_2S\cdot AlBr_3$, as is shown below. The second moment of the ^{1}H

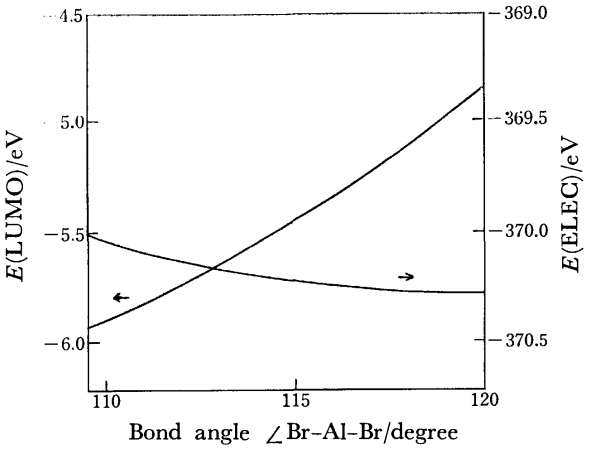

Fig. 5. Calculated energies for E(LUMO) and E(ELEC) as a function of the bond angle ∠Br-Al-Br.

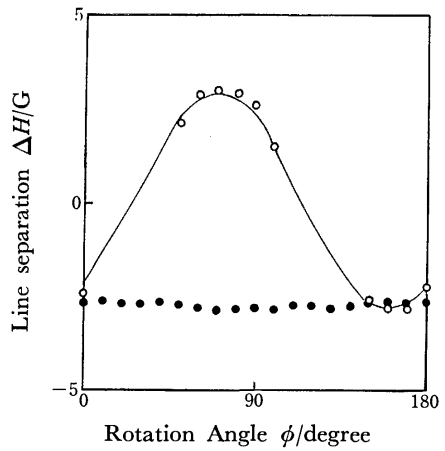

Fig. 6. Line separations in ^{1}H NMR spectra for $H_2S \cdot AlBr_3$. Sample A (○) for $\delta' = 22.8°$ and $\phi_0' = 71.4°$ Sample B (●) for $\delta' = 79.5°$ and $\phi_0' = 160.0°$.

NMR spectrum for the polycrystalline sample is 1.8—2.5 G[2] over the temperature range from 108 to 300 K and this suggests that reorientation of a proton pair takes place. The rotation patterns of the line separation of the ^{1}H NMR spectrum for two different single crystals were observed at room temperature and are shown in Fig. 6. Since the reorientation is considered to take place about the apparent three-fold axis along the S–Al bond, the line separation was analyzed according to[19]

$$\Delta H = (3/2)\mu r^{-3}\{3\cos^2\delta' \cos^2(\phi' - \phi_0') - 1\} \, |(3\cos^2\gamma - 1)|, \quad (9)$$

where the notations are the same with those used by Rangarajan and Ramakrishna. From this analysis, the reorientation axis was found to be consistent with the three-fold axis to within 3° and it was found that $|(3/2)\mu r^{-3}(3\cos^2\gamma - 1)| = 2.27$ G. Using this value and a Gaussian component line chosen by Pake,[20] $S(H - H_0) = \exp\{-(H - H_0)^2/2\beta^2\}$ with $\beta = 0.8$ G, the spectrum for the polycrystalline sample at room temperature can be reproduced. If the H–H line is assumed to be perpendicular to the apparent three-fold axis, the H–H distance is estimated to be 2.1 Å, which is larger than 1.88 Å from the result of NMR for H_2S in the solid phase.[21]

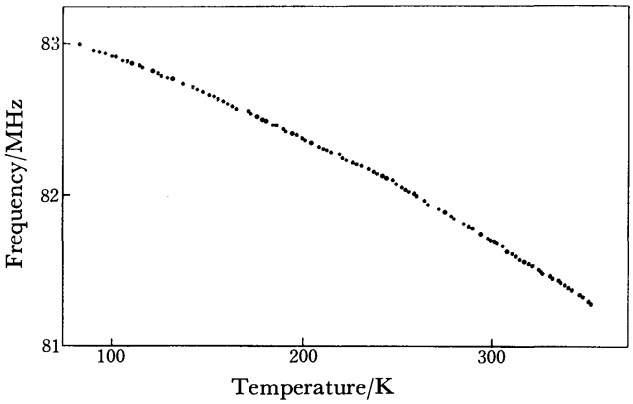

Fig. 7. Temperature dependence of ^{81}Br NQR frequency in $H_2S \cdot AlBr_3$.

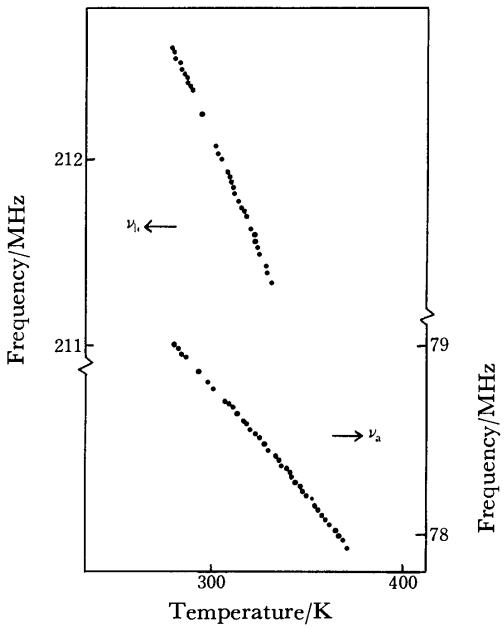

Fig. 8. Temperature depences of ^{81}Br NQR frequencies, ν_a and ν_b in $POBr \cdot AlBr_3$.

Temperature Dependence of the ^{81}Br NQR Frequencies. For $H_2S \cdot AlBr_3$, one ^{81}Br NQR line was observed at temperatures from 77 K to the melting point and the frequency decreases monotonically with increasing temperature, as is shown in Fig. 7. For $POBr_3 \cdot AlBr_3$, upon cooling, both ^{81}Br NQR lines of $AlBr_3$ and $POBr_3$ fade out around 273 K, whereas upon warming, the resonance lines of $AlBr_3$ and $POBr_3$ fade out at around 373 and 333 K, respectively, as is shown in Fig. 8. The fading out in the high temperature range may be caused by reorientation about the three-fold axis. Similar behavior has been observed for $POCl_3 \cdot GaCl_3$,[22] although the resonance lines fade out at temperatures different from those for $POBr_3 \cdot AlBr_3$. The reason for the fading out at a lower temperature, 273 K, is not apparent at the present time.

We wish to express our gratitude to Dr. Masaru

Ohsaku and Mr. Norihisa Bingo of Hiroshima University for the molecular-orbital calculations.

References

1) E. A. C. Lucken, *Fortschr. Chem. Forsh.*, **30**, 155 (1972).
2) T. Deeg and A. Weiss, *Ber. Bunsenges. Phys. Chem.*, **79**, 497 (1975).
3) L. A. Lobanova, E. N. Gur'yanova, A. F. Volkov, and R. R. Shifrina, *Zh. Obshch. Khim.*, **45**, 1857 (1975).
4) Yu. K. Maksyutin, E. V. Bryukhova, G. K. Semin, and E. N. Gur'yanova, *Izv. Akad. Nauk SSSR, Ser. Khim.*, **1968**, 2658.
5) T. Deeg and A. Weiss, *Ber. Bunsenges. Phys. Chem.*, **80**, 2 (1976).
6) A. Weiss, R. Plass, and A. Weiss, *Z. Anorg. Allg. Chem.*, **283**, 390 (1956).
7) W. Van der Veer and F. Jellinek, *Recl. Trav. Chim. Pay-Bas.*, **89**, 833 (1970). Von E. W. Wartenberg and J. Goubeau, *Z. Anorg. Allg. Chem.*, **329**, 269 (1964).
8) T. Okuda, H. Terao, O. Ege, and H. Negita, *J. Chem. Phys.*, **52**, 5489 (1970).
9) T. Okuda, K. Hosokawa, K. Yamada, Y. Furukawa, and H. Negita, *Inorg. Chem.*, **14**, 1207 (1975).
10) K. Yamada, *J. Sci. Hiroshima Univ., Ser. A*, **41**, 77 (1977).
11) C. Dean, *Phys. Rev.*, **96**, 1053 (1954).
12) M. Kasahara and I. Tatsuzaki, *J. Phys. Soc. Jpn.*, **36**, 786 (1974).
13) M. H. Cohen and F. Reif, *Solid State Physics*, **5**, 321 (1957).
14) D. A. Tong, *Chem. Commun.*, **1969**, 790.
15) B. P. Dailey and C. H. Townes, *J. Chem. Phys.*, **23**, 118 (1955).
16) D. F. Shriver and B. Swanson, *Inorg. Chem.*, **10**, 1354 (1971).
17) This calculation was carried out using the parameters which were the same as those used by Hastie and Margrave. J. W. Hastie and J. L. Margrave, *J. Phys. Chem.*, **73**, 1105 (1969). The off-diagonal terms were approximated using the equation $H_{ij}=KG_{ij}(H_{ij}+H_{ij})/2$ and $K=1.75$. Aluminum-bromine distances were fixed at 2.25 Å and calculations were carried out with sp-basis orbitals.
18) F. A. Cotton and J. R. Leto, *J. Chem. Phys.*, **30**, 993 (1959).
19) G. Rangarajan and J. Ramakrishna, *J. Chem. Phys.*, **49**, 5536 (1968).
20) G. E. Pake, *J. Chem. Phys.*, **16**, 327 (1948).
21) D. C. Look and I. J. Lowe, *J. Chem. Phys.*, **44**, 3441 (1966).
22) J. W. Jost and R. F. Schneider, *J. Phys. Chem. Solids*, **36**, 349 (1975).

Static and Kinetic Studies of the Interaction of Toluidine Blue with Chondroitin-4-sulfate

Kojiro TAKAHASHI,* Zengo HORIUCHI, and Tatsuya YASUNAGA

Department of Chemistry, Faculty of Science, Hiroshima University, Higashi-Senda Machi, Hiroshima 730

(Received August 12, 1977)

The binding of Toluidine Blue to chondroitin-4-sulfate was investigated by absorption spectra, titration curves, and temperature-jump relaxation spectra. The results were well interpreted by a basic model of binding to a linear lattice, where the cooperative interaction is restricted to the nearest-neighbor binding sites. The parameters g (number of binding sites per disaccharide repeating unit), K (cooperative binding constant), and q (strength factor of cooperativity) in 0.015 M phosphate buffer (pH 7.0) were determined to be 2, 1.02×10^5 M^{-1}, and 270 $\pm$60, respectively. The fastest process of the three relaxations observed in the system of Toluidine Blue-chondroitin-4-sulfate, could be interpreted as the aggregation process for cooperative binding. The rate constant $\tilde{k}_R$ was determined to be 1.6×10^8 M^{-1} s^{-1} at 28 °C.

The cooperative binding of dye to linear biopolymer has been well known as the aggregation of dye molecules on the charged polymer.[1] Schwarz's theory has well interpreted the static and dynamic phenomena of the cooperative binding of dye molecules to such polymers as polyglutamic acid, polyacrylic acid, and polyphosphate.[2-6] Recently, an extensive model for competitive cooperative bindings has been derived theoretically and has been applied to the investigations on the mechanisms of proflavin binding to poly(A) and DNA.[7,8]

The interactions of dyes with glucosaminoglycans, which have been known to adopt helical conformations in the solid state,[9-13] have been studied by the measurements of absorption spectra, optical rotatory dispersion, and circular dichroism.[14-18] One approach employing such measurements and using cationic dye has been performed as a probe of the glucosaminoglycan conformation in dilute aqueous solution. However, the kinetics of the conformational changes of glucosaminoglycans and the interactions of dyes with polymers have not been examined.

In the present paper, the first kinetical attempt to explain the interaction of dye with polysaccharide will be made systematically in the system of Toluidine Blue–chondroitin-4-sulfate by referring to a basic model of cooperative binding of a small ligand to a linear polymer.

Experimental

Chondroitin-4-sulfate (Ch4-S) from whale cartilage was purchased from Seikagaku Kogyo Co., Ltd. (Tokyo). The molecular weight was determined to be 24000 by means of an intrinsic viscosity measurement in 0.015 M phosphate buffer (pH 7.0) containing 0.2 M NaCl at 25 °C, using the following relation:[19]

$$(\eta) = 3.1\times10^{-4} M_W^{0.74},$$

where η is the intrinsic viscosity and M_w is the weight-average molecular weight. Toluidine Blue (TB) was purchased from Chroma Gesellschaft and was purified by washing with chloroform until the chloroform was colorless. Solutions of TB were made fresh for each experiment. The polymer-dye complex was prepared by adding TB to Ch4-S solutions with stirring. The pH was adjusted by the addition of NaOH or HCl. The measurements of the pH dependencies of the absorption spectra and the titration curves were performed without controlling the ionic strength. All sample solutions except those used for these two measurements were prepared with 0.015 M phosphate buffer solution (pH 7.0 and constant ionic strength (μ=0.06)). The concentration of Ch4-S (C_p) was calculated as the mole concentration of disaccharide repeating units. The weighing-in concentration of TB (C_A°) was checked by the measurement of absorbance at 630 nm. The pH values of solutions were measured with a Hitachi-Horiba Type F-5 pH meter. The absorption spectra were observed with a Union Giken SM 401 spectrophtometer. The extinction coefficient (ε) in the solution was obtained from E(absorbance)/C_A°. The extinction coefficients of pure monomer (ε_A) and pure dimer (ε_D) in TB were 4.2×10^4 and 0.13×10^4 M^{-1} cm^{-1} at 630 nm, respectively.

Titrations were performed in a closed 500-ml flask. After the addition of a very small amount of the standardized HCl titrant, a solution of 10 ml was removed for pH measurement. The percent protonation of Ch4-S as a function of pH was computed from the amount of added titrant minus the solvent blank volume.

Details of the Joule-heating temperature-jump apparatus have already been described elsewhere.[20] A temperature-jump of 8 °C was produced by a 20 kV capacitor discharge, giving a heating time of about 50 μs. All static experiments were performed at 25$\pm$0.5 °C.

Results

Static Studies. The absorption spectra of Ch4-S–TB complexes under the various polymer-to-dye ratios ($P/D=C_p/C_A^\circ$) at pH 7.0 are shown in Fig. 1. The solid line at P/D=0 exhibits two peaks, around 630 nm (due to the monomer of TB molecular) and 600 nm (due to the dimer). By adding Ch4-S to TB solution, a new band appears around 550 nm. The metachromatic effect becomes prominent with increasing P/D. The metachromatic band shift, however, is not observed within the range of P/D=5—50. With a P/D above 50, the band shifts to the longer wavelength side. The negative metachromatic effect may be attributed to the occurrence of isolated dye molecules from the polymer–dye complexes.

Figure 2 shows that the pH values of TB are approxi-

* Present address: Mitsubishi-Kasei Institute of Life Sciences, 11 Minamiooya, Machida, Tokyo 194.

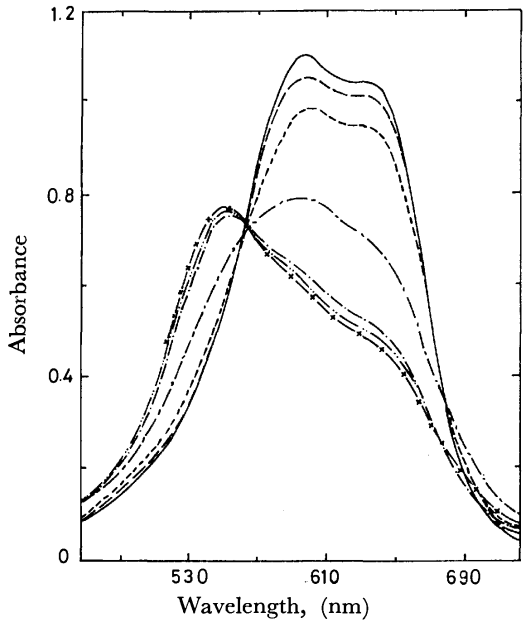

Fig. 1. P/D dependence of absorption spectra of the TB-Ch4-S complex in 0.015 M phosphate buffer (pH 7.0) at 25 °C and $C_A^\circ = 8\times10^{-5}$ M: (——) $P/D=0$; (— —) $P/D=0.1$; (---) $P/D=0.2$; (—·—) $P/D=0.5$; (—·—) $P/D=1$; (—··—) $P/D=3$; (—×—) $P/D=6$.

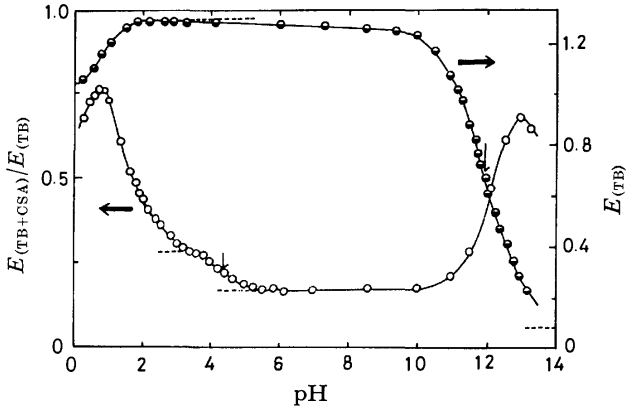

Fig. 2. pH dependencies of absorbances of TB and TB-Ch4-S at 630 nm, where E means the total absorbance: (◒) $C_A^\circ = 4\times10^{-5}$ M; (○) $C_A^\circ = 4\times10^{-5}$ M, $C_P = 2\times10^{-4}$ M.

mately 12 and 1, and that a small shoulder appears over the pH range of 3.5—5.5 in the Ch4-S–TB system. The titration curves of the Ch4-S and Ch4-S–TB complexes are demonstrated in Fig. 3 by plots of (pH—log $\alpha/(1-\alpha)$) against α, where α denotes the degree of ionization of the acid. The titration curve (a) suggests that there exist three conformations of Ch4-S in solution at least.** The titration curve (b), however, presents more simple features than Ch4-S alone. The extrapolated lines from the higher α values of the two curves give the pK values of 3.38 for (a) and 4.25 for (b). Their

** The analysis of the corresponding titration curve has been reported in the paper of the potentiometric titration study for the helix-coil transition of polyglutamic acid by M. Nagasawa *et al.*[22]

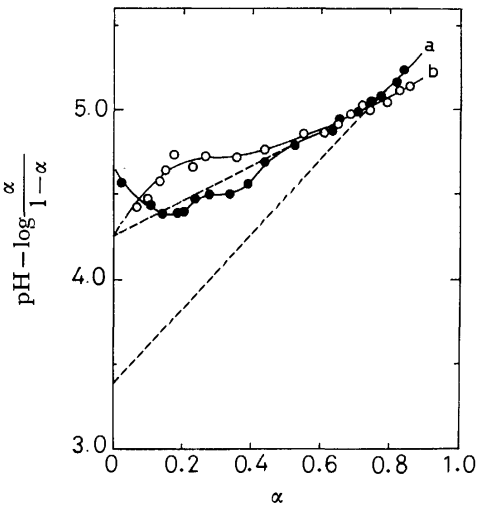

Fig. 3. Titration curves of Ch4-S and TB-Ch4-S complex at 25 °C: (●) $C_P = 2\times10^{-4}$ M; (○) $C_A^\circ = 4\times10^{-5}$ M, $C_P = 2\times10^{-4}$ M. The solid lines are the smooth curves between the experimental points. The dashed lines are the extrapolated lines from the higher α values.

values are in good agreement with the one obtained in 0.1 M NaCl solution by M.B. Mathews[21] for the former and with the one estimated from the pH dependency of the absorbance in Fig. 2 for the latter.

The representations of both measured and interpolated extinction coefficients at 630 nm in the solutions of TB and TB–Ch4-S can be found in Fig. 4. The curve at $P/D=0$ means that the aggregation of dye molecules causes the monomer concentration to decrease: the extinction coefficients (ε) in the variable solutions approach to the (ε_D) of the pure dimer from the (ε_A) of the pure monomer. Such smooth curves, however, do not appear upon adding Ch4-S in TB solution. The reversely sigmoid curves may occur by the cooperative binding of TB to Ch4-S. In the binding process where the cooperative interaction of nearest neighbor binding sites can be considered, there exist at least two different types of intrinsic binding processes:[2]

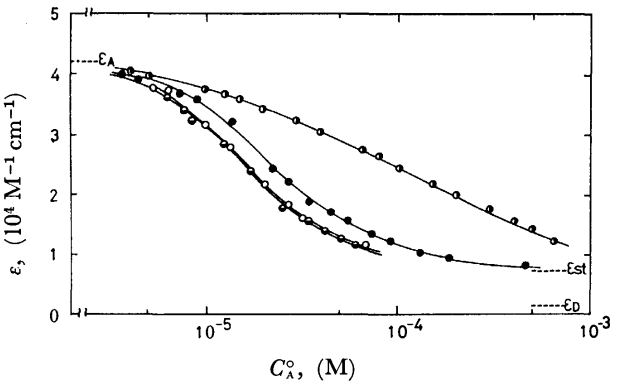

Fig. 4. Plots of molar extinction of TB solutions against C_A° in 0.015 M phosphate buffer (pH 7.0) at 630 nm: (◑) $P/D=0$; (●) $P/D=0.55$; (◒) $P/D=5.85$; (○) $P/D=55.2$.

I: an initial nucleation of binding $uuu + A \overset{K^*}{\rightleftharpoons} uau$,

II: the aggregation (or growth) process

$$uau + A \overset{K}{\rightleftharpoons} uaa,$$

where A, u, and a are the free monomeric ligand, the unoccupide binding site, and the binding site occupied by ligand, respectively. The binding constant for the initial nucleation process is defined to be $K^*=\overline{C}_{uau}/(\overline{C}_A\cdot\overline{C}_{uuu})$, while the cooperative binding constant is $K=\overline{C}_{uaa}/(\overline{C}_A\cdot\overline{C}_{uau})$. In order to analyse quantitatively the cooperative binding process, some constants should be estimated from the curves of Fig. 4. First, the dimerization constant K_d of TB in the absence of Ch4-S was calculated by using the following equation:

$$[(\varepsilon_A-\varepsilon)/C_A^\circ]^{1/2} = (2K_d/\Delta\varepsilon)^{1/2}[\Delta\varepsilon-(\varepsilon_A-\varepsilon)], \quad (1)$$

where $\Delta\varepsilon=(\varepsilon_A-\varepsilon_D)$. The value of $K_d=6.1\times10^3$ M^{-1} at pH 7.0 and 25 °C is in agreement with that estimated by H. Ushio *et al.*[6] It is also necessary to obtain the extinction coefficient ε_{st} of the dye molecules stacked on the Ch4-S molecules. The extinction coefficient is expressed by the following relation:

$$\varepsilon = \bar{\gamma}_A\varepsilon_A + 2K_dC_A^\circ\bar{\gamma}_A^2\varepsilon_D + \bar{\theta}\,gp\varepsilon_{st}, \quad (2)$$

where $\bar{\gamma}_A$ is the fraction of free monomeric dye, $\bar{\theta}$ is the fraction of occupied sites of polymer, g is the number of binding sites per disaccharide repeating unit of Ch4-S, and $p=P/D$. With the reduced version of mass conservation

$$\bar{\gamma}_A + 2K_dC_A^\circ\bar{\gamma}_A^2 + \bar{\theta}gp_{st}=1, \quad (3)$$

the transformation of Eq. 2 gives the following equation:

$$\varepsilon = \varepsilon_{st} + (\varepsilon_A-\varepsilon_{st})\bar{\gamma}_A + (\varepsilon_D-\varepsilon_{st})2K_dC_A^\circ\bar{\gamma}_A^2. \quad (4)$$

Quantitative estimations show that the last term of Eq. 4 can be practically neglected. By further introducing the cooperative binding constant K and the variable S $(=\overline{C}_{uaa}/\overline{C}_{uau}=K\overline{C}_A=KC_A^\circ\bar{\gamma}_A)$ for the calculation of equilibrium concentrations of any desired binding state, the following equation is obtained:

$$\varepsilon = \varepsilon_{st} + (\varepsilon_A-\varepsilon_{st})(S/K)C_A^{\circ-1}. \quad (5)$$

The plots of ε *versus* $C_A^{\circ-1}$ are shown in Fig. 5. If the parameter S becomes almost constant with respect to changes of C_A° at strong cooperativity and medium p, the plots should eventually result in the straight lines. Linear relationships do occur obviously for the smaller values of $C_A^{\circ-1}$. Extrapolation of $C_A^{\circ-1}\to0$ yields $\varepsilon_{st}=0.7\times10^4$ M^{-1} cm^{-1}.

For obtaining the value of g, Eq. 3 can be rewritten as the following relation:[3]

$$1-\bar{\theta}gp = \bar{\gamma}_A(1+2K_dC_A^\circ\bar{\gamma}_A) \equiv \gamma_A^*, \quad (6)$$

where γ_A^* is the total fraction of free dye. The values of γ_A^* calculated by using Eq. 5 and $\bar{\gamma}_A=(S/K)C_A^{\circ-1}$ are plotted against the P/D at constant C_A° in Fig. 6. The intercept on the P/D axis of the common limiting straight line for small P/D (<0.5) yields $g=2.0$. From the value of γ_A^* of the intersection point of the experimental curve and an auxiliary straight line with half

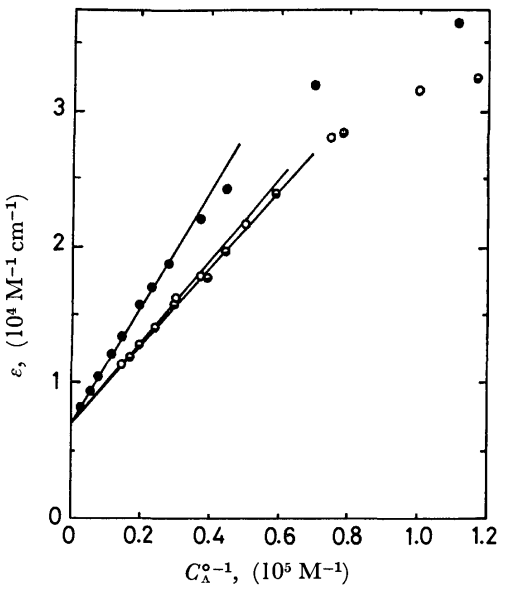

Fig. 5. Plots of molar extinction of TB solutions against $C_A^{\circ-1}$: (●) $P/D=0.55$; (○) $P/D=5.85$; (◒) $P/D=55.2$.

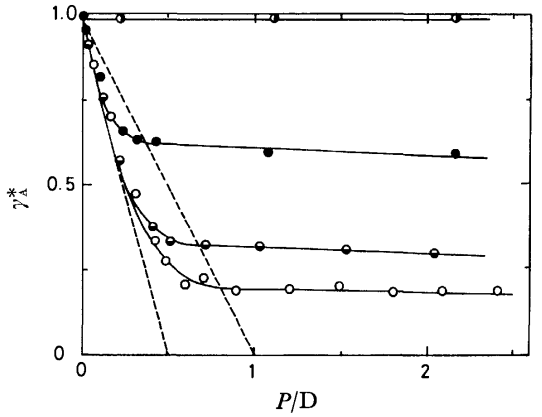

Fig. 6. Plots of total fraction of free dye against various P/D in 0.015 M phosphate buffer (pH 7.0) at 25 °C: (◑) $C_A^\circ=9.2\times10^{-6}$ M; (●) $C_A^\circ=1.9\times10^{-5}$ M; (◒) $C_A^\circ=3.9\times10^{-5}$ M; (○) $C_A^\circ=6.7\times10^{-5}$ M.

the slope of the first one in the figure, the value of K was determined to be 1.02×10^5 M^{-1} by

$$K = (\overset{\circ}{\gamma}_A^*\cdot C_A^\circ)^{-1} + 2K_d, \quad (7)$$

where $\overset{\circ}{\gamma}_A^*$ denotes the γ_A^* at the intersection point.[3] Since the values of $\bar{\theta}$ at the various initial concentrations of dye are easily accessible from Eq. 6 at constant P/D, the cooperativity parameter $(q=K/K^*)$ was calculated by the following relation:[2]

$$[1-2\bar{\theta}/\{\bar{\theta}(1-\bar{\theta})\}^{1/2}]\cdot\overline{C}_A^{1/2} = (g/K)^{1/2} - (gK)^{1/2}\overline{C}_A. \quad (8)$$

The average value of q was estimated to be 270±60 from the two straight lines shown in Fig. 7.

Using the values of ε_A, ε_D, ε_{st}, and K_d obtained above, the concentrations of stacked dye molecules $\overline{C}_{st}$ were estimated by using the following relation:

$$E = \varepsilon_A\overline{C}_A + 2\varepsilon_D\overline{C}_D + \varepsilon_{st}\overline{C}_{st}, \quad (9)$$

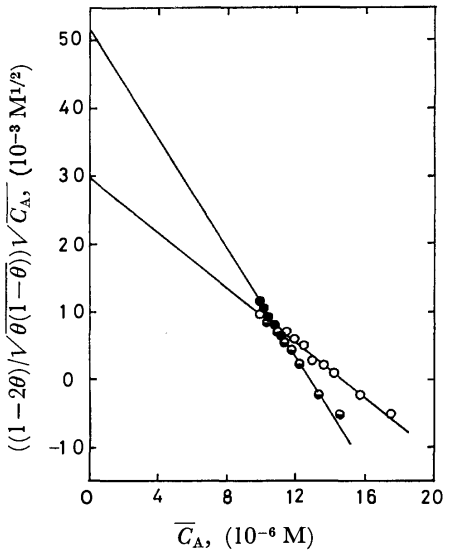

Fig. 7. Plots to determine cooperative parameter q for the TB-Ch4-S system: (●) $C_A^\circ = 1.9\times10^{-5}$ M; (◒) $C_A^\circ = 3.9\times10^{-5}$ M; (○) $C_A^\circ = 6.7\times10^{-5}$ M.

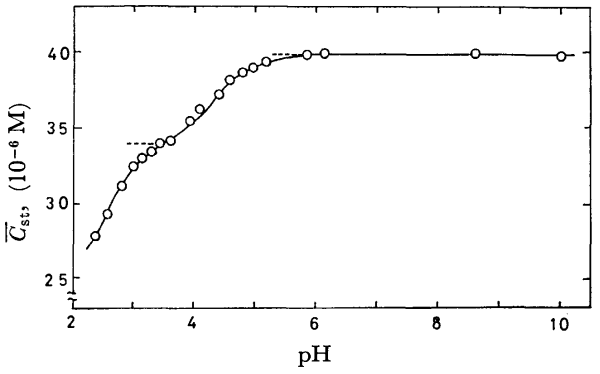

Fig. 8. pH dependence of the concentration of stacked dye molecule $\overline{C}_{st}$ in the TB-Ch4-S system at $C_A^\circ = 4\times10^{-5}$ M, $C_p = 2\times10^{-4}$ M and 25 °C.

where E denotes the total absorbance of the solution. The pH dependency of $\overline{C}_{st}$ is demonstrated in Fig. 8. The two-step saturation curve implies the existence of two interactions involving ionizing groups, that is, TB interacts with a sulfuryl group and a carboxyl group of Ch4-S.

Kinetic Studies. Some typical relaxation curves are shown in Fig. 9. At the metachromatic band (550 nm), a fast single relaxation spectrum was observed with the relaxation time of 10^{-4} s order, as shown in Fig. 9(a), while at 630 nm due to monomeric dye a faster change of absorbance was followed by two slower changes with the relaxation times of the order of 10^{-2} and 10^{-1} s, as shown in Fig. 9(b). This faster change appears to be relaxation with the same order of rate as the one observed at 550 nm. The relaxation amplitude, however, was very small and could not be analyzed. The dichroic effect due to optical anisotropy, which is caused by the induced orientation of the macromolecules in the direction of the electric field, was checked by two observations. At 550 and 630 nm, no change of relaxation amplitudes was observed by using

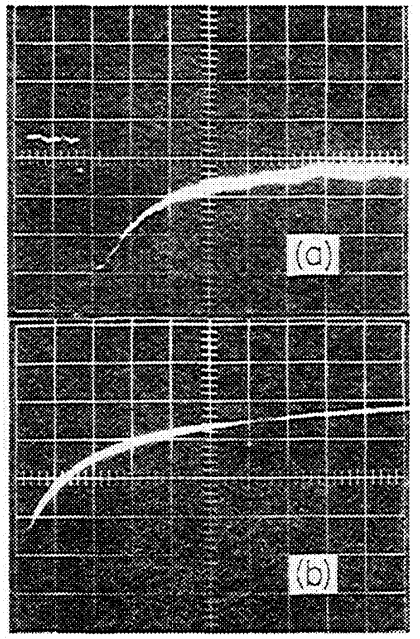

Fig. 9. Typical relaxation curves of the TB-Ch4-S system in 0.015 M phosphate buffer (pH 7.0) at 28 °C: $C_A^\circ = 4\times10^{-5}$ M, $P/D = 5.1$; (a) 550 nm, sweep of 0.2 ms, vertical scale of 0.1 V/div.; (b) 630 nm, sweep of 50 ms, vertical scale of 0.1 V/div.

a polarizer and no relaxation spectrum was detected at any isosbestic point. Furthermore, a more rapid change was observed at 630 nm in the dye solution. The absorbance change, however, was smaller than the fastest one observed at 630 nm in the presence of Ch4-S and was completed within the heating time of the apparatus. This change probably corresponds to a monomer-dimer reaction of the dye which appears under a certain ionic strength (μ=0.06 in the present work). In the presence of Ch4-S, however, the contribution to the monomer-dimer reaction of free dye was within the experimental error of the spectrum change shown in Fig. 9(b). From the variety of observations described above, the faster relaxation at the metachromatic band was analysed quantitatively as the chemical relaxation due to the equilibrium shift between the monomeric dye and the stacked dye molecules. In the present paper, two slower relaxations at 630 nm which may be interpreted by the conformational changes of TB–Ch4-S complex are not treated; this problem will be reported later.

According to the theory of cooperative binding, the binding of dye to linear polymers consists of the following two elementary steps:[2,4]

$$\text{auu} + \text{A} \underset{k_D}{\overset{k_R}{\rightleftharpoons}} \text{aau} \qquad (k_R/k_D = K), \tag{10}$$

$$\text{auuu} + \text{A}_2 \underset{k_{D'}}{\overset{k_{R'}}{\rightleftharpoons}} \text{aaau} \qquad (k_{R'}/k_{D'} = K^2/K_d). \tag{11}$$

The mean relaxation time τ_b^* of the binding process is[2,4]

$$1/\tau_b^* = 2\tilde{k}_R(g/q^{1/2})\{\bar{\theta}(1-\bar{\theta})\}^{1/2}\cdot p\cdot C_A^\circ, \tag{12}$$

where

$$\tilde{k}_R = \beta k_R + (1-\beta)k_{R'}, \tag{13}$$

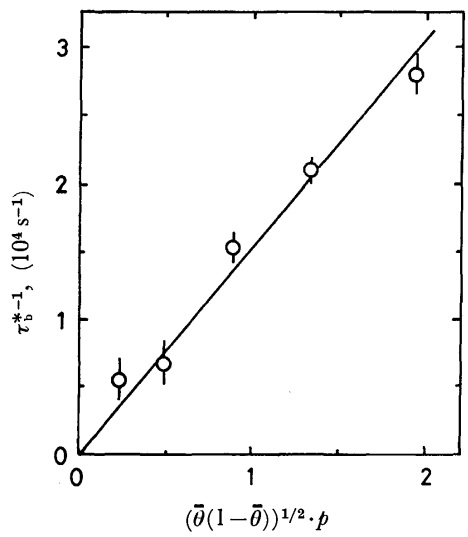

Fig. 10. Plot of the reciprocal mean relaxation time of cooperative binding τ_b^{*-1} against $\{\bar{\theta}(1-\bar{\theta})\}^{1/2}\cdot p$: $C_A^\circ = 4\times10^{-5}$ M.

$$\beta = 1/(1+4K_d\bar{C}_A) \simeq K/(K+4K_d). \quad (14)$$

The plot of τ_b^{*-1} againt $\{\bar{\theta}(1-\bar{\theta})\}^{1/2}\cdot p$ at constant C_A° value is shown in Fig. 10. From the slope of the straight line traversing the origin, $\tilde{k}_R$ was calculated to be 1.6×10^8 M^{-1} s^{-1}. By using the obtained K and K_d values, the β value was found to be approximately 0.8.

Discussion

The nature of the conformations of Ch4-S, which are known to adopt helical states in the solid state,[9,12] has not been estabilshed yet in solution. Chondroitin-6-sulfate, which has two ordered structures containing single helixes,[11,13] forms two states, flexible coil and rigid rod, in solution at a certain ionic strength.[23] As shown in Fig. 3, the titration curve of Ch4-S may imply that Ch4-S has three conformations in solution at least (for example: rigid rod, flexible coil, and random coil). The titration curve in the presence of TB may also imply that the transition between helical conformations (rigid rod$\rightleftharpoons$flexible coil) of Ch4-S is disturbed by masking the ionizing groups of Ch4-S with TB. Above pH 6, however, the deprotonations of Ch4-S are perhaps completed and the conformation of Ch4-S may be random coil in either the absence or the presence of TB. Therefore, the interaction of Ch4-S with TB at pH 7.0 would be also interpreted by a basic model of the cooperative binding of dye to linear biopolymer.

The number of binding sites per disaccharide repeating unit of Ch4-S was estimated to be $g=2.0$. Apparently the disaccharide repeating unit does not have specific binding sites for TB molecules. The unit of Ch4-S is electrically negative due to the carboxyl and sulfuryl groups and the TB molecule is electrically positive. Starting from the negative charges of the unit, it may be easily explained that the polymer chain only serves as a template favoring the formation of stacked aggregates by reducing the electrostatic repulsion between the positive charges of TB ions. On the other hand, the concentration of $\bar{C}_{st}$ increases with ionizations of sulfuryl and carboxyl groups. From these results, the binding of TB to Ch4-S is considered to be essentially an electrostatic interaction.

The cooperative binding constant K contains the contributions of two binding processes, the nucleation process (denoted by K^*) and the growth process (denoted by q). With a value of $q=270$ the average number of ligands in a stacked aggregate*** is 17.4 at $S=1$ and $\bar{\theta}=1/2$. This value is smaller than the total number of binding sites on one polymer chain (about 100). This may imply that a basic model of binding to a linear polymer can also be applied to a relatively shorter chain such as Ch4-S. On the other hand, the binding constant of the nucleation process K^*, which can be calculated with the relation $K^*=K/q$, is about 380 M^{-1}. The value is the same order of magnitude as K^* in the proflavine–polyglutamic acid system.[5] This means that the binding of isolated (*i.e.*, unstacked) TB molecules to Ch4-S is an electrostatic binding.

The obtained value of the rate constant for the growth process $\tilde{k}_R$ is reasonable considering the ionic strength used in the present work, because it is of the same order of magnitude as those obtained in the systems of acridine orange-polyglutamic acid[4] and proflavine–polyacrylic acid.[5] Since the value of β is about 0.8, it may be suggested qualitatively that the binding of free monomeric dye is approximately 80% in the aggregation process, under the assumption that k_R is the same order of magnitude as $k_{R'}$.

On the basis of the above considerations of the static and kinetic data, it is confirmed that the binding of TB to Ch4-S is essentially an electrostatic interaction but consists of a strong cooperative interaction ($K \gg K^*$), and that the recombination of dye molecules with binding sites in the immediate neighborhood of already occupied sites is a diffusion controlled process.

References

1) D. F. Bradley and M. K. Wolf, *Proc. Nat. Acad. Soc. U. S.*, **45**, 944 (1959).
2) G. Schwarz, *Eur. J. Biochem.*, **12**, 442 (1970).
3) G. Schwarz, S. Klose, and W. Balthasar, *Eur. J. Biochem.*, **12**, 454 (1970).
4) G. Schwarz and W. Balthasar, *Eur. J. Biochem.*, **12**, 461 (1970).
5) G. Schwarz and S. Klose, *Eur. J. Biochem.*, **29**, 249 (1972).
6) H. Ushio, T. Yasunaga, T. Sano, and Y. Tsuji, *Biopolymers*, **15**, 187 (1976).
7) M. Dourlent, *Biopolymers*, **14**, 1717 (1975).
8) M. Dourlent and J. F. Hogrel, *Biopolymers*, **15**, 29 (1976).
9) F. A. Bettelheim, *Biochim. Biophys. Acta*, **83**, 350 (1964).
10) E. D. T. Atkins, C. F. Phelps, and J. K. Sheehan,

*** The average number of ligands in a stacked aggregate is generally calculated by the following relation:[2]

$$m_a^\infty = \lambda_0(g/s)^{1/2}\cdot\{\bar{\theta}/(1-\bar{\theta})\}^{1/2},$$

where

$$\lambda_0 = 1 + (\sigma s)^{1/2}\cdot\{\bar{\theta}/(1-\bar{\theta})^{1/2}, \qquad \sigma = 1/q.$$

Biochem. J., **128**, 1255 (1972).
11) E.D.T. Atkins, R. Gaussen, D. H. Issac, V. Nandanwar, and J. K. Sheehan, *Polym. Lett.*, **10**, 863 (1972).
12) E. D. T. Atkins and T. C. Laurent, *Biochem. J.*, **133**, 605 (1973).
13) S. Arnott, J. M. Guss, D. W. L. Hukins, and M. B. Mathews, *Science*, **180**, 743 (1973).
14) M. D. Schoenberg and R. S. Moore, *Biochim. Biophys. Acta*, **83**, 42 (1964).
15) E. J. Eyring, H. Kraus, and J. T. Yang, *Biopolymers*, **6**, 703 (1968).
16) D. M. Power, J. S. Moore, G. O. Phillips, and J. V. Davies, *Int. J. Radiat. Biol.*, **20**, 111 (1971).
17) K. Nakajima and G. Matsumura, *Biopolymers*, **12**, 2539 (1973).
18) M. K. Salter, W. B. Rippon, and E. W. Abrahamson, *Biopolymers*, **15**, 1213 (1976).
19) M. B. Mathews, *Arch. Biochim. Biophys.*, **61**, 367 (1956).
20) T. Yasunaga and S. Harada, *Bull. Chem. Soc. Jpn.*, **42**, 2165 (1969).
21) M. B. Mathews, *Biochim. Biophys. Acta*, **35**, 9 (1959).
22) M. Nagasawa and A. Holtzer, *J. Am. Chem. Soc.*, **86**, 538 (1964).
23) M. Nakagaki and M. Ikeda, *Bull. Chem. Soc. Jpn.*, **41**, 555 (1968).

Isotope Effect in Thermal Ionic Reactions of Isomeric Transition-Activated ^{80}Br and ^{82}Br in the HBr–CH_4 System

Kenjiro KONDO and Masuo YAGI

Laboratory of Nuclear Science, Faculty of Science, Tohoku University, Kanayama, Tomizawa, Sendai 982

(Received August 26, 1977)

The reactions of isomeric-transition activated ^{82}Br were studied in the gaseous $H^{82m}Br$–CH_4(HBr/CH_4= 0.1±0.01) system. $CH_3{}^{82}Br$ and $CH_2{}^{82}BrBr$ were identified as the reaction products; their absolute yields were 0.8% for $CH_3{}^{82}Br$ and 3.7% for $CH_2{}^{82}BrBr$ respectively. The results were compared with those obtained in the $H^{80m}Br$–CH_4 and $^{80m}Br_2$ (or $^{82m}Br_2$)–CH_4 systems. The effect of Kr and Xe additives showed that these products were formed only through kinetic energy-independent (thermal-ionic) reactions, as opposed to the results obtained in the $^{80m}Br_2$ (or $^{82m}Br_2$)–CH_4 system. This difference was explained on the basis of the kinetic energies initially acquired by the bromine atoms in the molecular-explosion process. In addition, an outstanding isotope effect resulting from the difference in the decay schemes of ^{80m}Br and ^{82m}Br was observed between the I. T.-activated ^{80}Br and ^{82}Br reactions in the $H^{80m}Br$–CH_4 and $H^{82m}Br$–CH_4 systems, and it was pointed out from the analysis of the ^{80m}Br-data that the two successive internal conversions in the ^{80m}Br decay were responsible for this isotope effect. It was considered that the second internal conversion started in a liquid-like condition such as ion-clusters containing the ^{80}Br in the intermediate state; this idea is supported by the experimental results obtained in the condensed phase.

There is a definite difference between the decay schemes of ^{80m}Br and ^{82m}Br.[1] ^{80m}Br($t_{1/2}$=4.38 h) is de-excited to the ground state of ^{80}Br through the intermediate state with a half-life of 7.4 ns, whereas ^{82m}Br ($t_{1/2}$=6.1 min) is de-excited by a one-stage transition. The first transition of ^{80m}Br and the single transition of ^{82m}Br are fully converted (≈100%), while the second transition of ^{80m}Br is partly converted (≈61%). These internal conversions are followed by the Auger-electron emission, and the resulting atom is left with a high positive charge.[2–4] Furthermore, the intramolecular electron transfer between the highly positively charged bromine and the remainder in a source molecule results a molecular explosion; consequently, the bromine atom acquires an appreciable kinetic energy.

So far it has been reported that both the kinetic energy and the positive charge of the I. T.-activated ^{80}Br and ^{82}Br play very important roles in determining the chemical reactions of these atoms in the $^{80m}Br_2$ and/or $^{82m}Br_2$–CH_4 systems.[5–9] However, the present authors have previously pointed out that the ^{80m}Br undergoes only kinetic energy-independent (thermal-ionic) reactions in the $H^{80m}Br$–CH_4 system,[10] in which the kinetic energy imparted to the ^{80}Br is 0.75 eV[11] on an average, being greatly different from the kinetic energy (40.3 eV)[12] for the $^{80m}Br_2$. In order to elucidate further the roles of the kinetic energy and the charge in the recombination reactions, the I. T.-activated ^{82}Br reactions were studied in this work by using $H^{82m}Br$ as a source molecule in gaseous CH_4.

On the other hand, several experimental evidences have been accumulated for the isotope effect in the reactions of ^{80}Br and ^{82}Br activated by the isomeric transition in the CH_4[13] and CH_3Br[14b] systems. Previously Tachikawa has reported that the isotope effect resulting from the difference of the above decay modes appears in the energetic process to form CH_3Br, but not in the thermal process in the gaseous CH_4 system, using Br_2 as a source molecule.[13] Similarly, it is very interesting to examine an isotope effect by using $H^{80m}Br$ and $H^{82m}Br$ as source molecules in gaseous CH_4. The chief purpose of this paper is to search for a possible isotope effect, especially between thermal ionic reactions in the two systems. Furthermore, the mechanisms of the formation of individual products were examined by the addition of HCl and $CH_2{=}CH_2$ to the system instead of inert gases, and discussed on the basis of ion-molecule reactions involving $^{82}Br^+$.

Experimental

Materials. All the gaseous reagents used, supplied by the Takachiho Chemical Co., were used directly without additional purification. The listed purities were 99.95% for CH_4, Kr, and HCl, 99.8% for $CH_2{=}CH_2$, and 99.9% for Xe respectively. All the other reagents were of an extremely pure grade, purchased from the Junsei Chemical Co., Ltd.

Preparation of $H^{80m}Br$ and $H^{82m}Br$. $H^{80m}Br$ was synthesized from the $^{80m}Br_2$, obtained by the thermal decomposition of palladium bromide irradiated by the bremsstrahlung which was produced by the impact of a 40—60 MeV electron on a Pt converter in the linear-electron accelerator of Tohoku University. The details of preparation have been shown in previous papers.[10,14a] On the other hand, $H^{82m}Br$ was prepared by the thermal neutron irradiation of liquid HBr, sealed in a thin quartz ampoule. Thermal neutron irradiations were performed for 1—2 min by using the pneumatic tube No. 3 of the Kyoto University Reactor at a neutron flux of 3×10^{13} n cm^{-2} s^{-1}, with a concomitant gamm-ray dose rate of about 10^6 R h^{-1}. A trace amount of bromine, produced by the radiation-induced decomposition of HBr, was observed. In order to remove the Br_2 thus formed, the irradiated ampoule was broken by a mechanical shock in the vacuum line, and then the $H^{82m}Br$ purified was distilled into a storage bulb through a Dry Ice trap. The $H^{80m}Br$ produced at the same time by thermal-neutron irradiations was used in several runs to find out if there is a difference between the yields in the two experiments using HBr prepared by the above two different methods.

Sample Preparation. The quantities of CH_4, HBr (^{80m}Br or ^{82m}Br labeled), and other additive gases required were measured with a mercury manometer. These gases were introduced into cylindrical Pyrex glass ampoules (50, 100, and 200 ml in capacity) with a long neck of capil-

lary tubing cooled at the temperature of liquid nitrogen, and then sealed off. All these procedures were carried out by using a vacuum line composed of greaseless stop-cocks and joints. A quick sample preparation was requested to provide as many ^{82m}Br as possible for the isomeric transition experiments because of the short-life of ^{82m}Br($t_{1/2}$=6.1 min). The volatilization of the reaction mixtures by immersing the ampoule into hot water was done just 6 minutes after the end of irradiation; about 60% of the ^{82m}Br remained, provided for the I.T-induced reaction. The ratio of HBr to CH_4 and the total pressure were kept constant at 0.1±0.01 and 660±30 mmHg, respectively, throughout the series of gas-phase experiments. On the other hand, in the solid-phase experiment using $H^{80m}Br$ as a source molecule, reaction mixtures of HBr(65 cmHg), CH_4(130 cmHg), and/or HCl (130 cmHg) were solidified at the temperature of liquid nitrogen. The CH_4 deposited on the wall of the reaction vessel was thawed and mixed well with HBr and/or HCl by shaking, and then the mixture was solidified again at the bottom of the vessel.

Extraction, Activity Measurement, and Yield Determination. The radioactive bromine was separated into organic and inorganic layers by solvent extraction after the reaction mixture has been allowed to stand for more than 2 h in a dark place at 40 °C. The solvent extraction procedure was the same as that in the earlier experiments.[10,14a] A portion of the organic fraction was submitted to a gas chromatograph, while the product analysis was carried out by the use of a column (75 cm in length, 3 mm in diameter) filled with 60—80 mesh Celite 545, and coated with silicon oil (20% in weight). The fraction of each product was collected in glass tubes cooled in a Dry Ice ethanol bath at the outlet of the column. The radioactivity of each fraction was counted with a NaI(Tl) scintillation counter and/or a Ge(Li) semiconductor detector. Thus, the relative yields of the individual products were determined.

On the other hand, given volumes of organic and inorganic fractions were pipetted to test tubes. The photopeaks of 0.618 MeV from the ^{80}Br and/or 0.554 MeV from the ^{82}Br in both fractions were counted with a high resolution Ge(Li) semiconductor detector connected to a multichannel pulse-height analyser. In the ^{82m}Br-experiments, the solvent extraction and the activity measurement were performed after the ^{80m}Br had completely decayed out. The activities of both the inorganic and organic fractions were corrected for the separation time.

The organic yields were determined as the ratio (in percentage) of the activity of the organic fraction to the total activity, while the individual product yield was obtained by simply multiplying the relative yield of each product by the organic yield. For the several runs in the $H^{82m}Br$–CH_4 system, the individual product yields were determined directly by the radio-gas chromatograph technique adopted by Tachikawa *et al.* in the ^{80m}BrBr–CH_4 system.[5] However, there was no difference between the yields in the two methods, as well as the result previously obtained in the $H^{80m}Br$ experiments.[10]

The experimental errors arising from the standard deviation due to statistical fluctuations in the counting and chemical procedures were 7—15% for the ^{80m}Br-experiments and less than 10% for the ^{82m}Br.

Results

From the product analysis using a radio-gas chromatograph, we identified the $CH_3{}^{82}Br$ and $CH_2{}^{82}BrBr$ in the $H^{82m}Br$–CH_4 system, as well as the early observations obtained in the $H^{80m}Br$–CH_4 system.[10] The effect of Kr and Xe additives on the yield distribution is shown in Table 1 and depicted graphically in Fig. 1, together with the results in the $H^{80m}Br$–CH_4 system.[10,14a] The $H^{80m}Br$ prepared by thermal-neutron irradiations was used in several runs to find out if the results are different from those previously obtained by using the $H^{80m}Br$ prepared by the (γ, n) reaction.[10,14] However, no difference in the yields was observed between them. The $CH_3{}^{82}Br$ and $CH_2{}^{82}BrBr$ yields were 0.8% and

Table 1. Percentage of ^{82}Br stabilized in organic combiantions in a gaseous mixture of an additive and CH_4
(HBr/CH_4=0.1±0.1; total pressure: 660±30 mmHg)

Mole fraction additive (mf)		CH_3Br (%)	CH_2Br_2 (%)	Organic yield (%)
Kr	Xe			
0	0	0.8±0.1	3.7±0.2	4.5±0.2
0	0	0.8±0.1	3.8±0.2	4.6±0.2
0	0	0.7±0.1	3.8±0.3	4.5±0.2
0.10	0	0.7±0.1	3.7±0.3	4.4±0.3
0	0.20	0.9±0.1	3.9±0.4	4.8±0.4
0.25	0	0.8±0.1	3.7±0.2	4.5±0.2
0	0.30	0.9±0.1	3.3±0.2	4.2±0.2
0.40	0	0.6±0.1	3.6±0.3	4.2±0.3
0.45	0	0.7±0.1	3.8±0.3	4.5±0.3
0	0.50	0.7±0.1	3.6±0.3	4.3±0.3
0.60	0	0.7±0.1	3.4±0.3	4.1±0.3
0.70	0	0.6±0.1	3.8±0.3	4.4±0.3
0.80	0	0.5±0.1	4.5±0.4	5.0±0.3
0.85	0	0.7±0.1	4.8±0.5	5.5±0.4
0.90	0	0.8±0.1	5.3±0.4	6.1±0.4

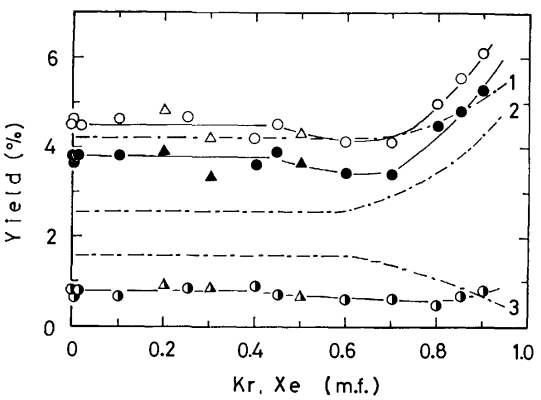

Fig. 1. Effect of Kr and Xe additives on the yield distributions.
($H^{82m}Br$(or $H^{80m}Br$)/CH_4=0.1±0.01)
Kr additive Xe additive
-○- -△-: organic yield
-●- -▲-: $CH_2{}^{82}BrBr$
-◑- -▲-: $CH_3{}^{82}Br$
The dashed lines were those previously obtained in the $H^{80m}Br$–CH_4 system.[10]
Line 1: organic yield, line 2: $CH_2{}^{80}BrBr$, line 3: $CH_3{}^{80}Br$.

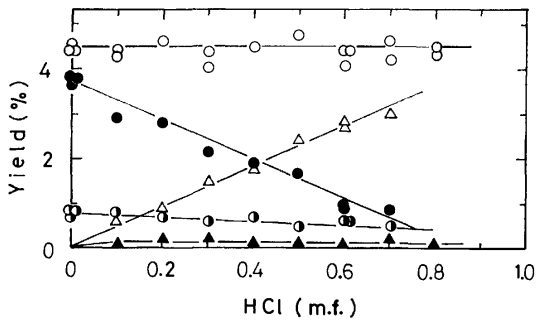

Fig. 2. Effect of HCl additive on the yield distributions.
($H^{82m}Br/CH_4=0.1\pm0.01$).
-○-: Organic yield, -△-: $CH_2{}^{82}BrCl$, -●-: $CH_2{}^{82}BrBr$, -▲-: $CH_3CH^{82}BrCl$, -◑-: $CH_3{}^{82}Br$.

3.7%, respectively, at 0 mf of additives. The $CH_2{}^{82}BrBr$ yield was much greater than the $CH_3{}^{82}Br$ yield over the whole range of additive concentrations, contrary to the results in the I.T.-experiments of the $^{80m}Br_2$ and/or the $^{82m}Br_2$–CH_4 system.[13]

The organic yields were slightly greater in the $H^{82m}Br$–CH_4 than in the $H^{80m}Br$–CH_4 system, and no change in the yield distributions upon the addition of Kr and Xe was observed in the range of 0—0.5 mf. The additional formation of $CH_2{}^{82}BrBr$ was observed in additive concentrations over about 0.6 mf, as well as in the early findings reported by the present authors and Tachikawa *et al.* in the $H^{80m}Br$–CH_4[10] and $^{80m}Br_2$–CH_4[16,17] systems respectively.

The outstanding difference between the results in the $H^{82m}Br$–CH_4 and $H^{80m}Br$–CH_4 systems was found in the distribution of individual products, as can be seen in Fig. 1. The yield ratio of $CH_3{}^{82}Br$ to $CH_2{}^{82}BrBr$ was 0.22, very different from the value of 0.59 obtained in the $H^{80m}Br$–CH_4 system. Obviously there is an isotope effect between the reactions of I.T.-activated ^{80}Br and ^{82}Br in the $H^{80m}Br$ and/or $H^{82m}Br$–CH_4 systems. The effect of the HCl additive instead of inert gases was also examined in the $H^{82m}Br$–CH_4 system; the results are shown in Fig. 2. The $CH_2{}^{82}BrCl$ and $CH_3CH^{82}BrCl$ were observed to be other than the $CH_3{}^{82}Br$ and $CH_2{}^{82}BrBr$ from its radio-gas chromatogram. The organic yield was almost constant in 0—0.7 mf of HCl, and the decrease in $CH_3{}^{82}Br$ and $CH_2{}^{82}BrBr$ yields almost offset the increase in $CH_2{}^{82}BrCl$ and $CH_3CH^{82}BrCl$ yields. The results suggested that these products were formed through the reactions of the same precursor.

In addition, the $CH_3CH_2{}^{82}Br$ was observed in the experiment using $CH_2{=}CH_2$ additive other than the $CH_3{}^{82}Br$ and $CH_2{}^{82}BrBr$, much as in the findings obtained in the $H^{80m}Br$–CH_4–$CH_2{=}CH_2$ system.[10]

The relative yield ratio of each product to the $CH_2{}^{80}BrBr$ obtained in the solid phase are shown in Table 3. The yield ratios of $CH_3{}^{80}Br$ to $CH_2{}^{80}BrBr$ were about 1.2 for the $H^{80m}Br$–CH_4 and 1.6 for the $H^{80m}Br$–CH_4–HCl system, different from the value of 0.22 for the gas-phase experiment in the $H^{82m}Br$–CH_4 system.

Discussion

Contribution of Charge and the Kinetic Energy to the I.T.-Induced ^{80}Br and ^{82}Br Reactions. The most convenient method of differentiating the energetic reaction from thermal ionic reactions is through the addition of inert gas as an energy sink of the energetic bromine atom. Especially, Kr moderates most effectively the kinetic energy of the bromine atom, since the mass of Kr is almost equal to that of bromine. In addition, Kr, and Xe, used in the present experiment, are chemically inert; also, the charge transfer from the Br^+ ion to the inert gas molecules seems not to be important, judging from the ionization potentials of the Br atom (11.8 eV) and the inert gases (Kr: 13.9 eV, Xe: 12.1 eV). Therefore, if the organic yields decrease upon the addition of Kr and Xe, it must be due to the removal of ^{82}Br kinetic energy; the rest, insensitive to these inert-gas additives, must be derived from thermal ionic reactions.

As Fig. 1 shows, the addition of Kr and Xe did not cause any changes in either the organic or the individual product yields in the concentration of 0—0.5

Table 2. Percentage yields of organic products due to kinetic and thermal-ionic processes in the I. T. and (n,γ)-experiments (HBr (or Br_2)/CH_4=0.1±0.01)

System		$H^{82m}Br$–CH_4[a]	$H^{80m}Br$–CH_4[b]	$Br^{82m}Br$–CH_4[c]	$Br^{80m}Br$–CH_4[c]	(n,γ)-activated[d]* $^{82m}Br_2$–CH_4
E_{max} (eV)		1.3	1.3	158	158	417
Org. yield (%)		4.5	4.25	6.1	4.7	13.8
Kinetic process	CH_3Br (%)	0	0	4.5	3.0	11.4
	CH_2Br_2 (%)	0	0	0	0	1.0
Thermal-ionic process	CH_3Br (%)	0.8	1.60	0.5	0.5	0.9
	CH_2Br_2 (%)	3.7	2.65	1.1	1.1	0.5

a) Present work. b) Ref. 10. c) Ref. 13. d) Ref. 15. *) $Br_2/CH_4=0.2$—0.03.

Table 3. The yield ratios of products to CH_2Br_2 in the solid $H^{80m}Br$–CH_4 and $H^{80m}Br$–CH_4–HCl systems

System	CH_3Br	CH_2BrCl	CH_2Br_2	$CH_3CHBrCl$	CH_3CHBr_2	CH_2BrCH_2Br	$CHBr_3$
$H^{80m}Br$–CH_4	1.2	—	1	—	0.90	0.18	0.34
$H^{80m}Br$–CH_4–HCl	1.6	0.96	1	0.51	0.79	—	<0.1

These are all average values of three runs.

mf. This fact is indicative that the I.T.-activated ^{82}Br enters the organic chemical combination only through a thermal ionic process in the $H^{82m}Br$–CH_4 system, much as in the early findings obtained in the $H^{80m}Br$–CH_4 system.[10] The thermal ionic yields were 0.8% for CH_3Br and 3.7% for CH_2Br_2. The present results are summarized in Table 2, together with those previously obatined in the I.T.-[10,13] and (n,γ)-experiments[15] in gaseous CH_4. As is shown in Table 2, the recombination reactions of I.T.-activated ^{80}Br and ^{82}Br in both $H^{80m}Br$–CH_4 and $H^{82m}Br$–CH_4 systems are greatly different from those in other systems, in which the reaction proceeds mainly through kinetic energy dependent reactions. This difference can be explained on the basis of the kinetic energies initially acquired by the Br atom, which depend on the nature of the source molecule. In the case of the isomeric transition of ^{80m}Br and ^{82m}Br, the kinetic energy of the bromine atom ranges from 0 eV to maximum (E_{max}) of 1.3 and 158 eV respectively for the HBr and Br_2 used as source molecules, the most probable energies being 0.75 and 37 eV.[11] On the other hand, the ^{80}Br born from the (n,γ) activation has kinetic energy spectrum ranging from 0 to 417 eV.[11] The thermal ionic yields increase with a decrease in E_{max}, while, on the contrary, the kinetic energy-dependent yields tend to increase with an increase in E_{max}.

Previously it has been pointed out that the thermal ionic yield depends largely on the probability of the bromine ion reaching the thermal energy region by escaping from the charge neutralization.[10] From a comparison of the cross-sections for the charge-transfer reaction of bromine ions and for the formation of a capture-collision complex as a function of the velocity of the Br^+ ion, it was indicated that the charge neutralization takes place predominantly in the high-energy region over than about 1 eV, while the capture-collision complex is formed favourably at the energies below 1 eV.[10,17] Therefore, it is considered that most of the $^{80}Br^+$ and $^{82}Br^+$ produced by the (n,γ) reaction and the I.T. in Br_2 lose their charges before they reach the energy region in which the collision complex formation occurs preferentially. Thus, in these systems, the reactions are thought to be mainly due to a kinetic (hot) process involving neutral bromine atoms. On the other hand, it is considered that the formation of complex ions, such as ^{80}Br and/or ^{82}Br labeled CH_4Br^+ and $HBrBr^+$, proceeds at first in the I.T.-induced reaction in HBr; even if the charge neutralization takes place, the Br atom thus formed cannot undergo kinetic energy-dependent reactions because its kinetic energy is not sufficient for the Br to replace directly the H atom of CH_4. As has been mentioned in the following section, the CH_4Br^+ is considered to be a precursor of the formation of individual products.

Isotope-Effects in the Reactions of I.T.-Activated ^{80}Br and ^{82}Br. There have been several studies relating to the isotope effects (differences in organic yields) of (n,γ)- and I.T.-activated bromine reactions in the condensed and gas phases. Tachikawa[13] and Helton *et al.*[18] observed the kinetic-energy isotope effects of I.T.-and (n,γ)-activated bromine reactions in gaseous $^{80m}Br_2$ (or $^{82m}Br_2$)–CH_4 and Br_2–CH_3F systems respectively; these results were explained on the basis of the average number of possible collisions of the energetic bromine atom in the E_1—E_2 reactive region,[19] in which the energetic (hot) reactions take place. However, thus far no thermal ionic isotope effect has been reported in the bromine reactions induced by unclear transformations. As Fig. 1 shows, obviously there is the isotope effect between thermal ionic reactions in the $H^{80m}Br$–CH_4 and $H^{82m}Br$–CH_4 systems; also the yield distributions in the system of the HCl additive shown in Fig. 2 were greatly different from those previously obtained in the $H^{80m}Br$–CH_4–HCl system.[10]

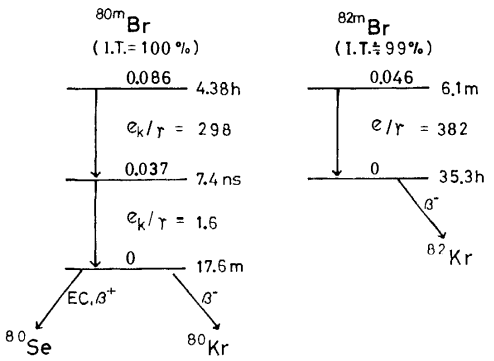

Fig. 3. Decay schemes of ^{80m}Br and ^{82m}Br.

Since the mass difference between ^{80}Br and ^{82}Br can not be considered to be responsible for the above isotope effect, this isotope effect may be brought about by the difference in the decay schemes of ^{80m}Br and ^{82m}Br,[1] shown in Fig. 3. The ^{80m}Br is de-excited in two stages through the intermediate state with a half-life of 7.4 ns; the first stage is a M3 transition of 49 keV, and the second, an El transition of 37 keV. From the internal conversion coefficients, the first transition is internally almost 100% converted, while the second is only 61% converted. On the other hand, the isomer of ^{82}Br is de-excited in a single stage by means of a M3 transition with an internal conversion coefficient of 382 (fully converted, $\approx$100%). Since the M3 transitions in ^{80m}Br and ^{82m}Br are essentially the same, the charge and kinetic-energy distribution on the excited ^{80}Br should be identical with those on the ^{82}Br. However, the excited ^{80}Br has a successive transition to the ground state. 61% of the excited ^{80}Br is de-excited through the second internal conversion process, while the remaining 39% undergoes de-excitation to the ground state by means of 37 keV γ-ray emission. However, even if the ^{80}Br is in a chemical combination, the chemical consequence resulting from this γ-emission is considered to be negligible since the kinetic energy achieved on the ^{80}Br is of an order of 10^{-2} eV, which is not sufficient to break any bond in the molecule, only enough to produce a little excitation of it. From these considerations, the reaction processes of isomeric transition-activated ^{80}Br can be classified into the following two types:

Process (A): 39%

internal conversion+37 keV γ-ray emission

(no chemical effect)

Process (B): 61%
internal conversion+internal conversion

Since the chemical effect resulting from Process (A) is essentially identical to those in the $H^{82m}Br$–CH_4 system, the yields due to Process (A) is equal to 39% of that obtained in the $H^{82m}Br$–CH_4 system. Therefore, the yield due to Process (B) is provided by subtracting that due to Process (A) from the organic yield in the $H^{80m}Br$–CH_4 system. The organic yields due to Process (B) were calculated by means of the following equation (I); they are depicted in Figs. 4 and 5, where the yields have been normalized by multiplying them by the factor of 100/61=1.64:

Yield (%) due to Process (B)

$$= \frac{100}{61}(^{80m}\text{Br-Yield} - 39\% \text{ of } ^{82m}\text{Br-Yield}) \qquad \text{(I)}$$

As Fig. 4 shows both the $CH_3{}^{80}Br$ and $CH_2{}^{80}BrBr$ yields were constant in 0—0.6 mf of Kr; this indicates that these products due to Process (B) are also formed through reactions independent of the kinetic energy of the ^{80}Br. The yield ratio of CH_3Br to CH_2Br_2 in Process (B) was 1.14, very different from the value of 0.22 for Process (A). This fact indicates that the $CH_3{}^{80}Br$ is formed more preferentially in Process (B) than in Process (A). Similarly, the $CH_3CH^{80}BrCl$ was found to be formed mainly in Process (B) in the $H^{80m}Br$–CH_4–HCl system, and the yield ratio of CH_3Br to CH_2Br_2 was close to unity over a wide range of HCl concentration, as can be seen in Fig. 5. Thus, there is a striking difference between the yield distributions of individual products for Process (A) and Process (B), and it is evident that Process (B) is responsible for the above isotope effect.

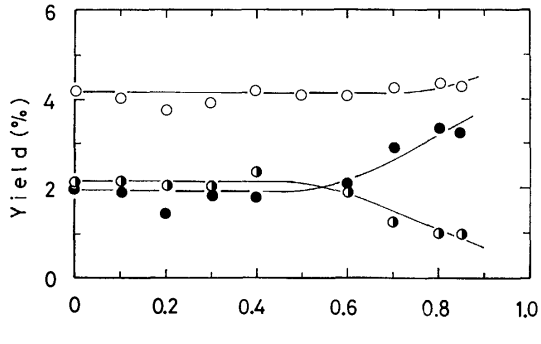

Fig. 4. Normalized yields due to the process (B) in the system of Kr and Xe additives.
-○-: Organic yield, -◐-: $CH_3{}^{80}Br$, -●-: $CH_2{}^{80}BrBr$.

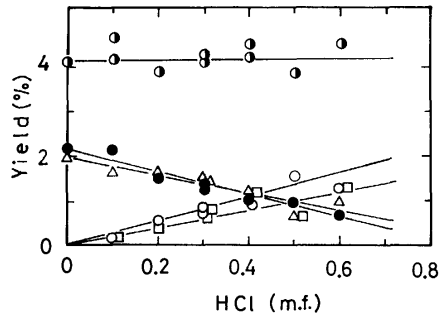

Fig. 5. Normalized yields due to the process (B) in the system of HCl additive.
-◑-: Organic yield, -●-: $CH_3{}^{80}Br$, -△-: $CH_2{}^{80}BrBr$, -○-: $CH_2{}^{80}BrCl$, -□-: $CH_3CH^{80}BrCl$.

If the life-time of the intermediate of ^{80m}Br(1.1×10^{-8} s) is too short for the excited bromine atom to undergo chemical reactions prior to the transition to the ground state, the successive transition will result in only an additional build-up of the charge on the free atom, and this process will not give any kinetic energy to the ^{80}Br. In this case, no isotope effect will appear. The existence of an isotope effect, therefore, supports the idea that its life-time is long enough for the bromine atom to undergo chemical reactions prior to the second transition. However, this does not necessarily mean that all of the excited ^{80}Br react with surroundings to enter into certain chemical combinations within its life-time.

As has been stated in the previous section, the kinetic energy of ^{80}Br freed *via* the molecular explosion following the second internal conversion is very much dependent on the remainder of the molecule containing the excited ^{80}Br. However, both the $CH_3{}^{80}Br$ and the $CH_2{}^{80}BrBr$ due to Process (B) are formed only through kinetic energy-independent reactions. This fact may be suggestive that the second molecular explosion occurs from such chemical species as $H^{80}Br$, $H^{80}Br^+$, and $H_2{}^{80}Br^+$,[20] but if so, its chemical consequence will also be identical to the one due to Process (A) and no isotope effect will appear between them. From these considerations, it seems to be more likely that, even if the excited ^{80}Br is in certain chemical combinations, the environment surrounding the ^{80}Br is different from that in Process (A).

From an energy standpoint, it is considered that the $^{82}Br^+$ and $^{80}Br^+$ ions undergo at first ion-molecule reactions to form the capture collision complexes, $CH_4{}^*Br^+$ and HBr^*Br^+, since generally no activation energy is required for these reactions (Eqs. 1 and 2);

$$^*Br^+ + CH_4 \rightarrow CH_4{}^*Br^+, \qquad (1)$$

$$^*Br^+ + HBr \rightarrow HBr^*Br^+. \qquad (2)$$

(Here, the Br^+ with a star sign shows the $^{82}Br^+$ and/or excited $^{80}Br^+$.)

So far the presence of sticky collision complexes of such a type has been confirmed by using a mass-spectrometer in the various alkyl halide and hydrocarbon systems.[21–23] Further, it is expected, from a rough calculation by using the equation proposed by Magee *et al.*,[24] that the life-times of complex ions are at least longer than that of the ^{80}Br intermediate state (1.1×10^{-8} s).[10] Therefore, these complex ions have an ample opportunity to collide with surroundings prior to the successive transition in Process (B), since the collision time is about 10^{-9} s under the present experimental conditions. In the study of the radiation chemistry in the gas phase, Lind has suggested that thermal ions have a big chance to form an ion-cluster containing several molecules before they give the final products.[25] The attractive force considered here is that arising between the ion and the ion-induced dipole or

dipole moment on the molecule; also, it is generally known that thermal ions at high pressures form, more preferentially, ion-clusters.[26-28] In the present experiment, it is thought that the $CH_4{}^{80}Br^+$ and $HBr^{80}Br^+$ complex ions interact with surrounding molecules to form the ion-cluster before the second isomeric transition occurs. Therefore, the chemical effect due to Process (B) is considered to be very similar to that in the condensed phase. This idea was confirmed by the fact that the yield distributions of CH_3Br and CH_2Br_2 in the solid phase were very similar to those due to Process (B). That is, the yield ratios of CH_3Br to CH_2Br_2 obtained in the solid phase experiments were 1.2 for the $H^{80m}Br$–CH_4 and 1.6 for the $H^{80m}Br$–CH_4–HCl system, as is shown in Table 3; these values are very close to those obtained in Process (B). Thus, this ion-cluster model is qualitatively supported by the fact that the $CH_3{}^{80}Br$ is formed more preferentially than the $CH_2{}^{80}BrBr$ in the condensed phase. The large amount of energy evolved from the second molecular explosion is considered to be dissipated readily to the rigid sphere of the cluster and spent in the formation of ions, radicals, and excited species, which contribute directly or indirectly to the individual product formation.

Thus, the isotope effect found in the thermal ionic reactions of I.T.-activated ^{80}Br and ^{82}Br can be qualitatively explained by introducing the idea that the ion-cluster containing the ^{80}Br in Process (B) is formed in the intermediate state. However, the details of the reactions in such a field must await until further experiments.

The Formation of $CH_3{}^{82}Br$ and $CH_2{}^{82}BrBr$ via Thermal Ionic Reactions. As a possible explanation for the formation of $CH_2{}^{80}BrBr$ *via* the thermal ionic process in the I.T.-experiment on the $^{80m}BrBr$–CH_4 system, Tachikawa has previously suggested that the $CH_4{}^{80}Br^+$ complex ion undergoes charge neutralization following its decomposition to such fragments as $CH_3{}^{80}Br$, and $CH_2{}^{80}Br$, and that the $CH_2{}^{80}Br$ radical thus formed can be easily scavenged by Br_2 to form the $CH_2{}^{80}BrBr$.[13] However, the present authors previously pointed out that the $CH_2{}^{80}Br$ and $CH^{80}Br$ radicals would not be present in the $H^{80m}Br$–CH_4 as precursors for the formation of $CH_2{}^{80}BrBr$.[10,14]

Similarly, it was confirmed experimentally in this work that the precursors responsible for the formation of $CH_2{}^{82}BrBr$ were not the $CH_2{}^{82}Br$ and $CH^{82}Br$ radicals. That is, if the $CH_2{}^{82}Br$ is present in the system, the radical reacts with HBr to form $CH_3{}^{82}Br$ more preferentially than to form $CH_2{}^{82}BrBr$, since the reaction leading to the $CH_3{}^{82}Br$ is more exothermic by about 18 kcal/mol than that giving the $CH_2{}^{82}BrBr$. Similarly, the $CH_2{}^{82}Br$ radical reacts with HCl to form the $CH_3{}^{82}Br$ more preferentially than to form the $CH_2{}^{82}BrCl$ in the system of the HCl additive. However, as Figs. 1 and 2 show, the $CH_2{}^{82}BrBr$ yields were greater than those of $CH_3{}^{82}Br$ over the entire range of additive concentrations; further, the $CH_2{}^{82}BrCl$ yields increased with an increase in the HCl concentration in the system of the HCl additive. Furthermore, if the $CH^{82}Br$ is present in the system, it is considered that the radical reacts readily with $CH_2{=}CH_2$ to give ^{82}Br labeled-bromocyclopropane and/or aryl bromide in the system of the $CH_2{=}CH_2$ additive,[24] but no radioactive peak corresponding to these products was observed on the radio-gas chromatograms, as is shown in Table 4. Thus, the radicals such as $CH_2{}^{82}Br$ and $CH^{82}Br$ are not considered to be the precursors leading to the formation of $CH_2{}^{82}BrBr$ *via* a thermal-ionic process.

Table 4. Effect of $CH_2{=}CH_2$ additive on the yield distributions ($H^{82m}Br/CH_4 = 0.1 \pm 0.01$)

$CH_2{=}CH_2$ mf	Organic yield (%)	CH_3Br (%)	CH_3CH_2Br (%)	CH_2Br_2 (%)
0.1	40.3	0.8	39.3	0.2
0.3	49.3	0.4	48.9	<0.1

Although there are no precise information on the ion-molecule reactions leading to the $CH_3{}^{82}Br$ and $CH_2{}^{82}BrBr$ in Process (A) because of lack of knowledge concerning the chemical behaviour of complex ions under high pressures, the possibility of the formation of these products by the ion-molecule reactions involving $CH_4{}^{82}Br^+$ was evaluated from a thermodynamical point of view. Most ion-molecule reactions of $^{82}Br^+$, $CH_4{}^{82}Br^+$, and $HBr^{82}Br^+$ with additives, leading directly to the formation of $CH_3{}^{82}Br$ and $CH_2{}^{82}BrBr$, are not favoured because of their high endothermicities. However, the H^+-transfer reaction from $CH_4{}^{82}Br^+$ to CH_4 and/or HBr are considered to be the principal reactions for the formation of $CH_3{}^{80}Br$, since Reactions 3 and 4 are roughly exothermic by 47 and 63 kcal/mol respectively for the $^{82}Br^+$ ground state:[10]

$$CH_4{}^{82}Br^+ + CH_4 \rightarrow CH_3{}^{82}Br + CH_5^+ \quad (3)$$

$$CH_4{}^{82}Br^+ + HBr \rightarrow CH_3{}^{82}Br + H_2Br^+ \quad (4)$$

On the other hand, among the various types of ion-molecule reactions involving the $^{82}Br^+$, $CH_4{}^{82}Br^+$, and $HBr^{82}Br^+$, only the following reactions, 5 and 6, are conceivable as steps in the reaction routes leading to the formation of $CH_2{}^{82}BrBr$ and $CH_2{}^{82}BrCl$, since these reactions are exothermic by about 45 and 28 kcal/mol respectively:[10]

$$CH_4{}^{82}Br^+ + HBr \rightarrow CH^{82}BrBr^+ + 2H_2 \quad (5)$$

$$CH_4{}^{82}Br^+ + HCl \rightarrow CH^{82}BrCl^+ + 2H_2 \quad (6)$$

As was pointed out in a previous paper,[10] it is considered that these ions lose their charges through charge-transfer reactions with impurities present in the system or with the wall of the reaction vessel, and that the radicals thus formed undergo H-abstraction from surrounding molecules to give $CH_2{}^{82}BrBr$ and $CH_2{}^{82}BrCl$ respectively. The details of these reactions will be revealed by accumulating data concerning ion-molecule reactions of these ions under high pressures.

The additional formation of $CH_2{}^{82}BrBr$ in concentrations of Kr and Xe over than 0.5 mf might be explained by ion-molecule reactions involving such ions as $Kr^{82}Br^+$ (or $Xe^{82}Br^+$), as well as by the explanation previously proposed in the $H^{80m}Br$–CH_4 system.[10] However, the answer to this problem must await more information concerning the ion-molecule reactions of Br^+ with inert gases and the reactivities of these complex

ions containing an inert molecule.

The authors wish to thank the staff members of the Hot Laboratory of the Kyoto University Reactor for their pneumatic-tube operations in neutron irradiations and the Linac crew of the Laboratory of Nuclear Science of Tohoku University for their accelerator operations.

References

1) C. M. Lederer, J. M. Hollander, and I. Perlman, "Table of Isotopes," John Wiley & Sons, New York (1968), pp. 215, 217.
2) S. Wexler and T. Davis, *J. Chem. Phys.*, **18**, 376 (1965).
3) S. Wexler and G. Anderson, *J. Chem. Phys.*, **33**, 850 (1960).
4) S. Wexler, *J. Chem. Phys.*, **36**, 1992 (1962).
5) E. Tachikawa and T. Kahara, *Bull. Chem. Soc. Jpn.*, **43**, 1293 (1970).
6) M. Yagi, K. Kondo, and T. Kobayashi, *Bull. Chem. Soc. Jpn.*, **44**, 580 (1971).
7) J. B. Nicholas and E. P. Rack, *J. Chem. Phys.*, **48**, 4085 (1968).
8) E. Tachikawa, *Bull. Chem. Soc. Jpn.*, **42**, 2304 (1970).
9) E. Tachikawa and J. Okamoto, *Radiochim. Acta*, **13**, 159 (1970).
10) K. Kondo and M. Yagi, *Bull. Chem. Soc. Jpn.*, **51**, 372 (1978).
11) M. E. Berg, W. H. Grauer, R. H. Helton, and E. P. Rack, *J. Phys. Chem*,. **79**, 1327 (1975).
12) A. R. Kazanjian and W. F. Libby, *J. Chem. Phys.*, **42**, 277 (1965).
13) E. Tachikawa, *Bull. Chem. Soc. Jpn.*, **43**, 63 (1970).
14) a) M. Yagi, K. Kondo, and T. Kobayashi, *Res. Rep. Lab. Nucl. Sci., Tohoku University*, **6**, 129 (1973). b) M. Yagi and K. Kondo, presented at the 24th National Meeting of the Chemical Society of Japan, Osaka, 1971, Abstr. p. 688.
15) M. Saeki, K. Numakura, and E. Tachikawa, *Bull. Chem. Soc. Jpn.*, **45**, 1715 (1972).
16) K. Numakura, M. Saeki, and E. Tachikawa, *Bull. Chem. Soc. Jpn.*, **46**, 1 (1973).
17) M. Yagi, K. Kondo, and T. Kobayashi, *Res. Rep. Lab. Nucl. Sci., Tohoku University*, **6**, 129 (1973).
18) R. W. Helton, M. Yoong, and E. P. Rack, *J. Phys. Chem.*, **75**, 2072 (1971).
19) P. J. Estrup and R. Wolfgang, *J. Am. Chem. Soc.*, **82**, 2661 (1960).
20) If the second molecular explosion takes place in the molecules containing carbon and/or bromine atoms, the kinetic energy imparted to the ^{80}Br is considered to be higher than the threshold energy for the energetic reactions.
21) R. F. Pottie and W. F. Hamill, *J. Phys. Chem.*, **63**, 877 (1957).
22) C. E. Melton and P. S. Rudolph, *J. Chem. Phys.*, **32**, 1128 (1960).
23) C. D. Wagner, P. A. Wadworth, and D. P. Stevenson, *J. Chem. Phys.*, **28**, 517 (1958).
24) J. L. Magee and M. Burton, *J. Chem. Soc.*, **56**, 842 (1952).
25) S. C. Lind, "The Chemical Effects of Alpha Particles and Electrons," Chemical Catalog Co., New York (1928), p. 663.
26) "Ion-Molecule Reactions," ed by J. L. Franklin, Vol. 1, Plenum Press, New York (1972), p. 315.
27) J. L. Magee and L. Funabashi, *Radiat. Res.*, **10**, 622 (1959).
28) S. Bloom and H. Margenau, *Phys. Rev.*, **85**, 670 (1952).
29) J. M. Rodriguez, J. M. Lo, and C. M. Wai, *Radiochem. Radional. Lett.*, **20**, 353 (1975).

Generation of Olefin Metathesis Catalysts from $W(CO)_6$ and Group IVa Metal Halides under Photochemical Conditions[1)]

Megumu NAGASAWA, Kiyoshi KIKUKAWA, Makoto TAKAGI, and Tsutomu MATSUDA

Department of Organic Synthesis, Faculty of Engineering, Kyushu University, Hakozaki, Higashi-ku, Fukuoka 812

(Received September 5, 1977)

Irradiation of a solution of $W(CO)_6$ and group IV_a metal halides in benzene by UV light gave the olefin metathesis catalysts, of which the combination $W(CO)_6$–$TiCl_4$ was the most effective. Association of the coordinatively unsaturated $W(CO)_5$ and $TiCl_4$ was suggested to be a key step in the formation of a catalytically active complex. A survery was also made for other $W(CO)_6$–MX_n combinations for photo-generation of metathesis catalyst.

Much effort has been made in search for the olefin metathesis catalysts and elucidation of the reaction mechanism.[2,3)] A mechanism involving intermediate formation of carbene complex has been strongly suggested.[3)] However, in view of catalyst preparation, most of the effective catalysts appear to consist of W or Mo compounds in their medium oxidation states. A combination such as WCl_6–R_nAlCl_{3-n} is typical, where the former component is partially reduced by the latter during the course of preparation. As a new access to metathesis-active W species of medium oxidation state, photochemical energy can be used to activate the otherwise inactive combination between W compounds and the cocatalytic oxidizing or reducing components. Two possible combinations can be considered: i) $W(CO)_6$–MX_n, where MX_n is a transition metal halide in high oxidation state, and ii) WCl_6–ML_n, where ML_n stands for the metal complex in low oxidation state. The latter photosystem has so far been unsuccessful, but the former gave a number of new metathesis catalysts, the results of which are given in the present communication. A metathesis catalyst from photosystem has recently been reported by Krausz *et al.*[4)] and by Agapiou and McNelis,[5)] in which $W(CO)_6$–CCl_4 was irradiated.

Results

A solution of $W(CO)_6$ and MX_n, each 4.3×10^{-3} M in benzene, was irradiated by a high pressure mercury lamp at room temperature for 1 h. To the resulting solution was added 260 fold molar amount of 1-octene, and the mixture was stirred at 30 °C in the dark. The product was found to be a mixture of straight-chain internal olefins of carbon number between 3 and 14. It is obvious that the catalysts effected both isomerization and metathesis of the substrate olefin. The result of the analysis of the product after 18—20 h reaction is summarized in Table 1. The yields of C_3 to C_7 olefins are not included, since the determination of these olefins was less reliable under our experimental conditions. $TiCl_4$ was the most effective cocatalyst, followed by $ZrCl_4$ and $HfCl_4$. No metathesis catalyst from $W(CO)_6$-group IVa metal halides has so far been reported. The catalyst mixture before the addition of olefin was brownish and homogeneous for $TiCl_4$, but it was slightly turbid for $ZrCl_4$ and $HfCl_4$ because of their low solubility in benzene. In each case, the turbidity gradually increased in the reaction with olefin. The catalyst activity of $W(CO)_6$–$TiCl_4$ was roughly comparable to that of $W(CO)_6$–CCl_4, the major side reactions being the isomerization of olefin in the former and the addition of CCl_3–Cl component to olefin in the latter system.[6)] It should be emphasized that all these MX_n compounds either alone or as combined with $W(CO)_6$ showed no activity for metathesis unless the mixture with $W(CO)_6$ was irradiated. Among other MX_n compounds tested, $AlCl_3$, $SnCl_4$ and $TaCl_5$ were found effective, but the activity of the resulting catalyst was slight at room temperature. The metal salts, $MoCl_5$, $NbCl_5$, $VOCl_3$, VCl_4, $(C_5H_5)_2TiCl_2$, $FeCl_3$, $ZnCl_2$, and $AgClO_4$ were totally inactive under comparative reaction conditions.

The $W(CO)_6$–WCl_6 system was studied in some detail. Due to the strong Lewis acidity of WCl_6, this photosystem gave only C_8-substituted benzenes (Friedel-Crafts alkylation, 74%) and oligomers from 1-octene (22%) under the standard conditions. Alkylation of the aromatic solvent was also the major reaction in the absence of irradiation. Even under irradiation, a proper selection of parameters, such as the concentration of catalyst or olefin, was required to suppress the alkylation and to make the metathesis activity ob-

TABLE 1. CATALYSIS OF PHOTOSYSTEM $W(CO)_6$–MX_n IN THE METATHESIS OF 1-OCTENE[a)]

	Yield of olefins, %[b)]					
MX_n	C_9	C_{10}	C_{11}	C_{12}	C_{13}	C_{14}
$TiCl_4$	12	2	2	4	10	11
$ZrCl_4$	9	1	1	1	5	9
$HfCl_4$	4	tr	tr	tr	tr	2
WCl_6[c)]	24	tr	tr	2	6	7

a) Catalyst solution: Unless otherwise noted, 4.3×10^{-3} M $W(CO)_6+4.3\times10^{-3}$ M MX_n in benzene was irradiated for 1 h by high pressure mercury lamp through a pyrex filter at 20—25 °C. Metathesis reaction: $W(CO)_6$/1-octene (mol ratio)=260, 18—20 h at 30 °C in the dark after addition of olefin.
b) Yield: (mol product/mol 1-octene added to catalyst solution)×100; tr, trace. C_n : linear internal olefins in trans coefiguration with n carbon atoms. c) $[W(CO)_6]=4.3\times10^{-3}$ M. $W(CO)_6$: WCl_6 : 1-octene=1 : 0.5 : 260. The reaction mixture was refluxed for 4 h after addition of olefin.

servable. Low $WCl_6/W(CO)_6$ ratio (<0.5) combined with high concentration of olefin appeared to favor metathesis. No alkylation was observed under conditions of the run given in Table 1. A competition between alkylation and metathesis depending on the catalyst concentrations as well as on the olefin concentration has been reported by Hocks *et al.*[7] The general trends observed in the present system were similar to those reported. The effect of irradiation time was not critical in our conditions so far as the irradiation time of 40—70 min was adopted. Low pressure mercury lamp could be used instead of the high pressure lamp, but this introduced the formation of hydrogen chloride, and the products became more complex.[8]

In order to reduce the complexity due to isomerization of the terminal olefin, 3-heptene was subjected to metathesis with $W(CO)_6$–TiX_4 catalyst under conditions similar to those in Table 1. The effect of the isomerization could not be eliminated, the products containing the olefins derived from 2-heptene in addition to those from 3-heptene. Figure 1 illustrates a typical conversion-time profile. The reaction is seen to reach some "equilibrium" olefin composition after 6 h. The yields of complementary olefins, *e.g.*, hexene and octene, were in 1 : 1 molar ratio. Similar conversion-time profiles are shown for various catalyst compositions in Fig. 2, where only the combined yields of hexenes and octenes are indicated. The combination, $W(CO)_6$–$TiCl_4$, was more effective than $W(CO)_6$–$TiBr_4$. A change in the ratio $TiCl_4/W(CO)_6$ exerted considerable influence on the rate of metathesis reaction. With the optimum ratio at 1.0, both the increase and decrease in the ratio resulted in lowering the catalyst activity. A similar behavior was also confirmed in the reaction of 1-octene. The increase in the total catalyst concentration increased the reaction rate as expected, but in a complicated manner. The catalyst underwent a considerable temperature effect, the reaction not proceeding below 15 °C. The selectivity of the catalyst defined as per cent molar ratio of the combined yield of octenes and hexenes to the amount of the substrate heptene consumed was dependent on

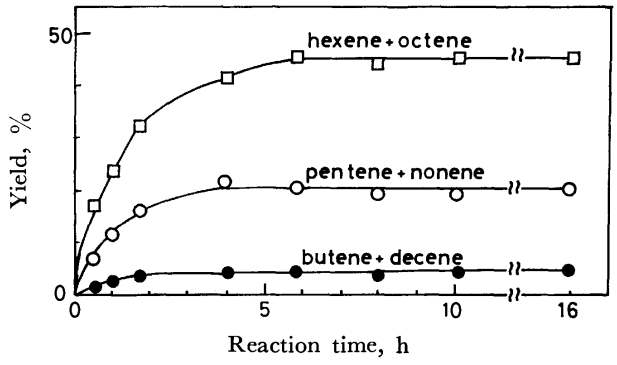

Fig. 1. Metathesis of 3-heptene by photosystem $W(CO)_6$–$TiCl_4$. Reaction conditions are similar to those in Table 1.
$[W(CO)_6]=4.3\times10^{-3}$ M; W : Ti : 3-heptene = 1 : 1 : 260; yield (%), (combined molar yield of complementary olenfins/mol 3-heptene added to the catalyst solution) × 100.

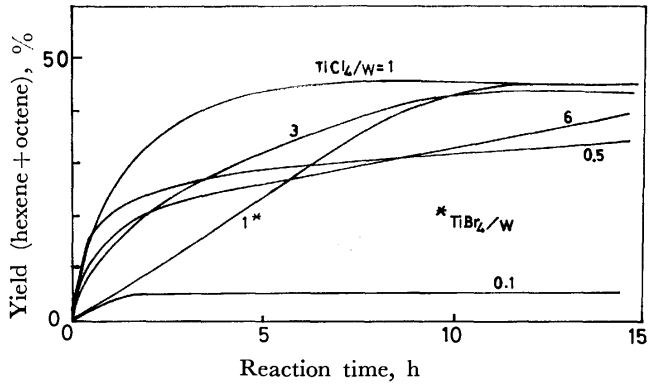

Fig. 2. Effect of catalyst composition on the rate of metathesis. Conditions are similar to those in Fig. 1 and Table 1.
$[W(CO)_6]=4.3\times10^{-3}$ M, 3-heptene/W = 260.

Ti/W ratio. The selectivity increased with the increase in Ti/W ratio, the effect being slight: $TiCl_4/W(CO)_6$ ratio, % selectively; 0.5, 57; 1, 63; 3, 72; 6, 71; 1 ($TiBr_4$ in place of $TiCl_4$), 60.

Discussion

One CO molecule dissociates from $W(CO)_6$ to from coordinatively unsaturated $W(CO)_5$ on irradiation by UV light.[9] Examination with a high pressure mercury lamp indicates that exactly one mole of carbon monoxide is evolved per mole of $W(CO)_6$ irrespective of the combination $W(CO)_6$–WCl_6 or $W(CO)_6$–$TiCl_4$. Since no further gas evolution was observed on prolonged irradiation, it is most probable that $W(CO)_5$ is the species involved in the formation of metathetically active complex. The observation that the maximum metathetic activity is obtained for the photosystem with $TiCl_4/W(CO)_6$ ratio of 1 suggests that 1 : 1 molar reaction of $TiCl_4$ and $W(CO)_5$ is essential for the formation of the caralyst. The catalyst solution was also prepared by adding $TiCl_4$ to the irradiated solution of $W(CO)_6$ in benzene, the activity being considerably lower than that by the standard procedure. Krausz *et al.* reported that the reaction of $W(CO)_5$ with CCl_4 produces $W(CO)_5Cl$ and this complex is an essential intermediate in the photochemically induced olefin metathesis (Reaction 1).[4] In our system, the over-all process may be delineated as in reaction 2, since the CO gas escapes out of the system. In reaction 1 the zero-valent tungsten complex $W(CO)_6$ was oxidized by CCl_4 to $W(CO)_5Cl$, in which tungsten is formally in +1 oxidation state. The oxidation state of tungsten in the association complex $W(CO)_5TiCl_4$ in Reaction 2 might be in +1.

$$W(CO)_6 \xrightarrow{h\nu} W(CO)_5 + CO \xrightarrow{CCl_4} W(CO)_5Cl + COCl_2 + \text{other products} \quad (1)$$

$$W(CO)_6 \xrightarrow{h\nu} W(CO)_5 \xrightarrow{TiCl_4} W(CO)_5TiCl_4 \quad (2)$$

If $W(CO)_5X$ species can be a potential precursor

for the metathesis catalyst, several other routes to the catalytically active systems can be envisaged. The reaction of $W(CO)_6$ in benzene with halogens (I_2, ICl, ICl_3, and Br_2) in the presence or in the absence of light failed to produce the catalyst. The solution of $W(CO)_6$ in various halogenated organic solvents was irradiated as a possible extension of the photosystem $W(CO)_6$–CCl_4. Tetrachloroethylene, trichloroethylene and chlorobenzene[10] were found to give the catalyst of varying activity and selectivity depending on the irradiation conditions. *In situ* generation of the catalyst in which a $W(CO)_6$–MX_n–olefin mixture in benzene was irradiated, sometimes proved to be much more effective than the standard procedure. This suggests a possibility of improving the catalytic activity by proper selection of irradiation conditions and the catalytic cofactors which trap the photo-generated intermediate such as $W(CO)_5$.

Experimental

Materials. $W(CO)_6$ was purified by vacuum sublimation. Contaminations in WCl_6 were removed by sublimation at 200 °C. Commercial metal halides were used. 1-Octene and 3-heptene were distilled from sodium, and organic solvents were purified by standard methods. All these reagents were kept and handled under dry nitrogen.

Catalyst Solutions. Irradiation of benzene solution containing appropriate catalyst precursor ($W(CO)_6+MX_n$) was achieved either by a 100 W immersion-type high pressure mercury lamp (Riko UVL-100HA) equipped with a water-jacketted pyrex cell of 100 ml content or by an 80 W coil-type low pressure mercury lamp (Ushio UL1-8HQ) with a jacketted quartz cell of 100 ml content which was placed inside the coiled lamp. Eighty milliliters of the solution was utilized. After irradiation the required amount of olefin was added under stirring. Often, aliquots of the catalyst solution were transfered from the photo-cell to another reaction vessel, and the subsequent reaction was conducted in the latter. All the manipulations were carried out under dry nitrogen. Irradiation of the benzene solution containing both olefin and metal compounds, though effective for metathesis reaction, was not employed as a standard procedure, since it sometimes introduced more complexity in the product.

Metathesis Products. The progress of the reaction was monitored by GLC, using octadecane or octane as an internal standard. Metathesis products were isolated from the final reaction mixture and identified by the conventional spectroscopic method as well as by comparison with standard samples of saturated hydrocarbon after the products had been hydrogenated. All of the internal olefins showed a strong IR band at 960 cm^{-1} indicating *trans* configuration. In the work-up of the reaction mixture from 3-heptene, most of the solvent (benzene) had to be removed by refrigeration followed by filtration, before the products were subjected to preparative GLC.

References

1) Presented at the 36th National Meeting of the Chemical Society of Japan, Higashi-Osaka, April, 1977.

2) R. J. Haines, *Chem. Soc. Rev.*, **14**, 155 (1975).

3) a) J. McGinnis, T. J. Katz, and S. Hurwitz, *J. Am. Chem. Soc.*, **98**, 605 (1976); b) T. J. Katz, J. McGinnis, and C. Altus, *J. Am. Chem. Soc.*, **98**, 606 (1976); c) C. P. Casey, H. E. Tuinstra, and M. C. Saeman, *J. Am. Chem. Soc.*, **98**, 608 (1976).

4) P. Krausz, F. Garnier, and J. E. Dubois, *J. Am. Chem. Soc.*, **97**, 437 (1975); *J. Organomet. Chem.*, **108**, 197 (1976).

5) A. Agapiou and E. McNelis, *J. Chem. Soc., Chem. Commun.*, **1975**, 187.

6) Detailed metathesis study with the photosystem $W(CO)_6$–CCl_4 is not available.[4,5] In the present study, $W(CO)_6$–CCl_4 system, in which the latter component was employed either as solvent or as an additive in benzene solution, was irradiated in a manner similar to that described for $W(CO)_6$–MX_n (see Experimental). The conditions were thus different from those reported. The addition of CCl_4 to olefin, which under our conditions proceeded to a comparable extent to metathesis in the reaction of 1-octene, was not described in the literature.[4,5]

7) a) L. Hocks, A. J. Hubert, and Ph. Teyssie, *Tetrahedron Lett.*, **1973**, 2719; b) L. Hocks, A. Noels, A. Hubert, and P. Teyssie, *J. Org. Chem.*, **41**, 1631 (1976).

8) In the following study, the high pressure lamp could be replaced by the low pressure lamp whenever the former proved to be effective, but the nature of the resulting catalyst was generally more complex.

9) M. Wrighton, *Chem. Rev.*, **74**, 401 (1974).

10) The reaction in chlorobenzene was possible only under irradiation with a low pressure lamp.

Metal-ion Complexation of Noncyclic Poly(oxyethylene) Derivatives. II. PMR Studies of the Complexation with Alkali and Alkaline-earth Metal Cations*

Shozo YANAGIDA, Kazutomo TAKAHASHI, and Mitsuo OKAHARA

Department of Applied Chemistry, Faculty of Engineering, Osaka University, Yamadakami, Suita, Osaka 565

(Received September 21, 1977)

The complexation of homogeneous polyethylene glycols and their dimethyl ethers(glymes) with alkali and alkaline-earth metal cations was studied by PMR spectroscopy on the basis of a comparison with crown ethers. The ethylene proton signal of octaethylene glycol in methanol-d_4 was split into three lines by the addition of a potassium, rubidium, caesium, strontium, or barium cation. The latter two cations also caused large downfield shifts of the signals, which are quite comparable with those of 15-crown-5 and 18-crown-6 caused by the same metal cations. As for heptaethylene glycol, a splitting was observed in the presence of a strontium ion or an alkali metal cation except for a lithium ion. A large downfield shift was also observed in the presence of a strontium or barium ion. As for hexaethylene glycol, the signal was split only by a sodium ion, and the optimal interaction with a calcium ion was confirmed on the basis of the downfield shift. In methanol-d_4, lithium and magnesium ions did not cause any change in the PMR spectra of either the crown ethers or the glycols. The PMR downfield-shift method also disclosed the metal-ion complexation of the glycols in water. The terminal hydroxyl groups play an important role in the complexation.

In the preceding paper,[1] we clarified, by solvent extraction, that acyclic poly(oxyethylene)(POE) derivatives with at least seven oxyethylene units complex fairly well with alkali metal ions in water and that their extracting power is comparable with that of 18-crown-6. In the cases of alkaline-earth metal ions, however, the solvent-extraction method was found inadequate to evaluate their complexation because of the poor solubility of the complexes in dichloromethane.

Of the instrumental methods used for the evaluation of the metal-ion complexation of organic ligands, NMR spectroscopy has proven to be the most facile and informative under various conditions.[2-8] In general, complexation with metal cations or the ion pairs leads to a change in the conformation of the ligands and, as a result, the splitting or broadening of the absorption signals. When the charged complex and the anion are separately solvated and the ion pairing is negligible, which means the absence of an anion effect, a downfield shift can be exclusively expected due to the increased electronegativity of the donor atoms in the ligands. Thus, the change in the PMR spectra can be a qualitative measure of the extent of the complexation in a series of ligands.

With these facts in mind, we have undertaken the present studies to ascertain the complexation of relatively short but homogeneous polyethylene glycols (PEG) and their dimethyl ethers(glymes) with alkali and alkaline-earth metal cations in methanol and in water. The thiocyanates again turned out to be convenient salts for these studies because of their high solubility in methanol.

Experimental

Materials. RuSCN, CsSCN, and $Sr(SCN)_2$ were prepared according to the method reported for $Ba(SCN)_2$.[9] $LiSCN \cdot 2H_2O$ was obtained from Mitsuwa Pure Chemicals. The other salts were the same materials as in the preceding paper. The anhydrous thiocyanates were prepared by vacuum dehydration at 100 °C. The following chemicals were obtained in the highest available purity from the sources indicated: methanol-d_4 and deuterium oxide(CEA products through Nakarai Chemicals, Ltd.); ethylene glycol(EO1), ethylene glycol dimethyl ether(glyme)(MeEO1Me), diethylene glycol(EO2), and triethylene glycol(EO3)(Wako Pure Chemicals Industries, Ltd.); diethylene glycol dimethyl ether(diglyme)(MeEO2Me) (Yoneyama Chemical Industries Ltd.); triethylene glycol dimethyl ether (triglyme)(MeEO3Me)-(Nakarai Chemicals, Ltd.); tetraethylene glycol (EO4) (Japan Catalytic Chemical Industry, Ltd.); tetraethylene glycol dimethyl ether(tetraglyme)(MeEO4Me)(Tokyo Kasei Kogyo Co., Ltd.) and 12-crown-4(Bokusui Brown Co., Ltd.). They were all used after distillation.

Penta-, hexa-, hepta-, and octaethylene glycols(EO5—EO8) were prepared according to the method reported previously;[10] bp(°C/mmHg) EO5, 165—168/0.2; EO6, 180—189/0.3; EO7, 210—212/0.35; EO8, 214—218/0.27. Their dimethyl ethers, *e.g.*, penta-, hexa-, hepta-, and octaglymes (MeEO5Me, MeEO6Me, MeEO7Me, and MeEO8Me) were prepared similarly the from sodium salt of EO1 monomethyl ether and the dichloride of EO3, from the sodium salt of EO2 monomethyl ether and the dichloride of EO2, from the sodium salt of EO2 monomethyl ether and the dichloride of EO3, and the from sodium salt of EO2 monomethyl ether and the dichloride of EO4, respectively; bp(°C/mmHg): MeEO5Me, 120—123/0.25; MeEO6Me, 145—148/0.1; MeEO7Me, 175—180/0.5; MeEO8Me, 215—218/0.45. Hexaethylene glycol monomethyl ether(137—141/0.05) and octaethylene glycol monomethyl ether (MeEO8)(212—216/0.16) were prepared from EO2 chloroethyl methyl ether and the sodium salt of EO3, and that of EO5, respectively.

Measurment of PMR Spectra. The PMR spectra were obtained using a JEOL LMN-PS-100 spectrometer on an expanded scale(sweep width, 270 Hz), with 8% dioxane in benzene as the external reference. The chemical shifts are expressed in Hz downfield, without any bulk magnetic susceptibility correction. The differences in the chemical shifts of the main oxyethylene protons and methyl protons were determined by the successive measurement of the signals of

* A preliminary report of this work was presented at the 36th National Meeting of the Chemical Society of Japan, Higashi Osaka, April 1977.

a plain 1% POE solution and those of 1% POE solution containing metal salt(0.04—0.05 mol/kg). The molar ratio of the salt to POE ranged from about 2 to 7, depending on the molecular weight of the POE. For the measurement in deuterium oxide, the salt concentration was increased to 0.2 mol/kg.

Results and Discussion

Downfield Shifts for Crown Ethers in the Presence of Alkali or Alkaline-earth Thiocyanates. In Table 1 we summarize the downfield shifts for 15-crown-5 and 18-crown-6 caused by the presence of alkali and alkaline-earth metal thiocyanates. Alkali and ammonium ions caused small downfield shifts in methanol, but all alkaline-earth metal ions except the magnesium ion caused downfield shifts which are large enough to be a measure of metal-ion complexations both in methanol and in water. These facts are consistent with the recent observations made using 220 MHz PMR spectroscopy.[7]

On the other hand, lithium and magnesium ions did not bring about any observable shifts in methanol-d_4, not even for 12-crown-4.

Recently, Izatt *et al.*[11] have reported the association constants for the reactions of several crown ethers with alkali and alkaline-earth metal cations in water and in aqueous methanol. Compared with the log K values, the downfield shifts are not necessarily proportional to the corresponding log K values; also, surprisingly, the calcium ion induced larger downfield shifts for both the crown ethers than would be expected from the respective log K values. Further, the shift induced by the calcium ion for 18-crown-6 is larger than that for 15-crown-5 both in methanol and in water, and the barium ion caused a larger shift for 15-crown-5 than for 18-crown-6. These facts are quite in conflict with the ion radius cavity concept.[13,14] The ioslation of some stable calcium ion-crown ethers complexes[15,16] substantiates the strong interaction with the crown ethers as well as the large downfield shifts. The interaction of the crown ethers with the calcium ion seems to have been underestimated thus far.[17]

Interaction of Polyethylene Glycols(PEG) and Their Dimethyl Ethers (Glymes) with Alkali Metal and Ammonium Ions in Methanol. The downfield shift in the 60 MHz PMR spectra of PEG in the presence of potassium iodide was too small to draw any decisive conclusion on their interaction.[3] A reinvestigation of the high resolution PMR spectroscopy(100 MHz) using various thiocyanate salts has, however, revealed the following facts: (1) the downfield shifts are all quite small, just as for the crown ethers(Table 2); (2) the spectrum of hexaethylene glycol was changed into two partially resolved peaks in the presence of sodium thiocyanate (Table 2, Fig. 1); (3) the sharp signal of heptaethylene glycol was split into two or three peaks by all alkali metal thiocyanates except lithium thiocyanate (Table 2, Fig. 1); (4) the sharp signal of octaethylene glycol was changed into three partially resolved peaks, accompanied by small downfield shifts in the presence of potassium, rubidium, and caesium thiocyanates (Table 2, Fig. 1); (5) the potassium ion caused downfield shifts for glymes which are proportional to the log K values (Table 3); (6) in the presence of ammonium

Table 1. Association constants and cation-induced downfield shifts for crown ether complexes in methanol and in water

Metal ions	Ionic radius (Å)[a]	15-Crown-5			18-Crown-6			
		Log K[b]	Downfield shift (Hz)[c]		Log K		Downfield shift (Hz)[c]	
		in H_2O	in CD_3OD (Concn)[d]	in D_2O (Concn)[d]	in 70 wt% CH_3OH[e]	in H_2O[b]	in CD_3OD (Concn)[d]	in D_2O (Concn)[d]
Li^+		—	0.5 (0.07)	—	—	—	—	—
Na^+	0.95	0.7	2.6 (0.04)	—	2.76 (4.32[f])	0.80	−0.7 (0.05)	—
K^+	1.33	0.74	−0.2 (0.04)	—	4.33 (6.10[f])	2.03	0.3 (0.04)	0.9 (0.18)
NH_4^+	1.48	1.71	0.3 (0.04)	—	—	1.23	3.7 (0.05)	—
Rb^+	1.48	0.62	0.7 (0.04)	—	3.46	1.56	0.4 (0.05)	—
Cs^+	1.69	0.8	0.8 (0.05)	—	2.84 (4.62[f])	0.99	−0.3 (0.05)	—
Mg^{2+}	0.78	—	0.7 (0.05)	—	—	—	1.7 (0.05)	—
Ca^{2+}	1.06	—	19.2 (0.05)	8.6 (0.20)	2.51	<0.5	21.7 (0.05)	11.4 (0.19)
Sr^{2+}	1.27	1.95	23.4 (0.05)	13.0 (0.20)	5.0	2.72	22.6 (0.05)	17.8 (0.20)
Ba^{2+}	1.43	1.71	24.3 (0.05)	16.6 (0.19)	6.0	3.87	18.8 (0.05)	13.1 (0.18)

a) 1Å=0.1 nm. b) Determined at 25 °C. See Ref. 11a. c) Minus means upfield shift. Measured at 23 °C. d) mol/kg. e) Determined at 25 °C. See Ref. 11b. f) Determined in methanol at 25 °C. See Ref. 12.

TABLE 2. ALKALI METAL ION-INDUCED DOWNFIELD SHIFTS FOR HOMOGENEOUS PEG IN METHANOL-d_4

Metal ions	Downfield shifts (Hz)[a]			
	EO5 (Concn)[b]	EO6 (Concn)[b]	EO7 (Concn)[b]	EO8 (Concn)[b]
Li^+	−0.4 (0.05)	−0.1 (0.05)	—	—
Na^+	0.3 (0.0)	2.8, 1.8 (0.05)	1.7, 0.7 (0.05)	2.4 (0.04)
K^+	—	0.1 (0.05)	2.8, 0.8 (0.05)	4.1, 3.1 0.8(0.04)
NH_4^+	—	1.6 (0.05)	1.9 (0.04)	2.1 (0.04)
Rb^+	—	−0.1 (0.04)	1.3, 0.3 (0.04)	6.1, 4.9 3.1(0.05)
Cs^+	—	0.6 (0.05)	0.2, −0.6 (0.05)	4.9, 3.8 2.7(0.04)

a) Measured at 23 °C. Minus means upfield shift.
b) mol/kg.

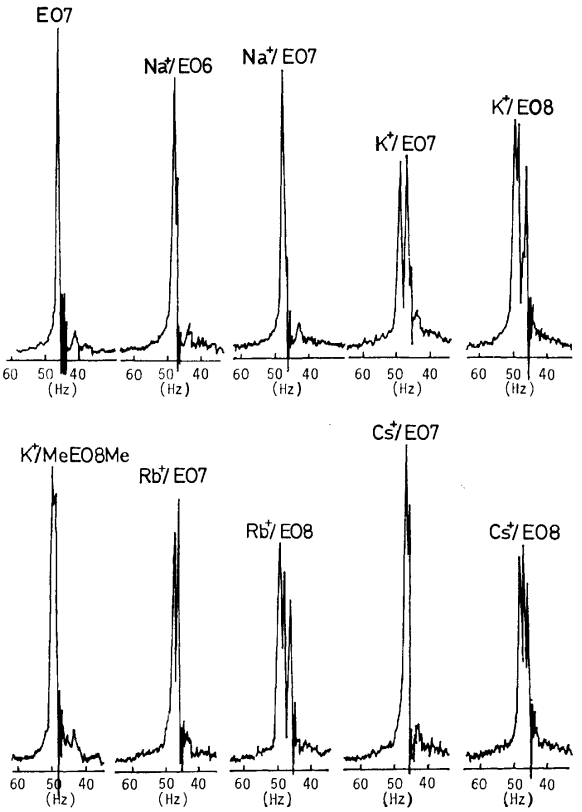

Fig. 1. NMR signals in methanol-d_4 of oxyethylene protons of the homogeneous PEG and glymes in the absence or the presence of alkali metal cation.

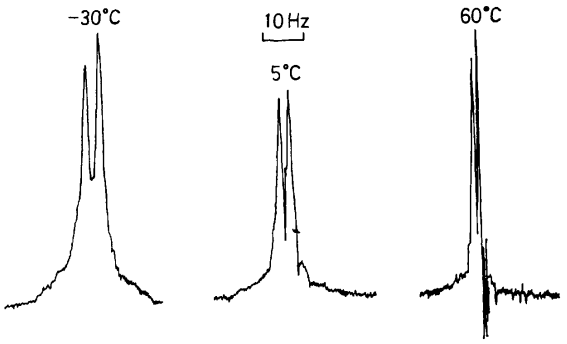

Fig. 2. PMR signals at various temperature of Hexaethylene glycol with KSCN in methanol-d_4.

thiocyanate, small shifts were observed for the higher glycols as well as for the crown ethers(Table 2); (7) the potassium ion caused partial splitting in octaglyme (Table 3, Fig. 1), and (8) the resolved spectrum of heptaethylene glycol in the presence of potassium thiocyanate was identical with that observed in the presence of potassium iodide and showed a tendency to coalesce with the elevation of the temperature (Fig. 2).

Liu[3] also reported the partial splitting for heptaethylene glycol in the presence of potassium iodide. However, the splitting was strangely ascribed to the drastic conformational change which originally exists rather than to that provoked by the interaction with potassium iodide.[19] On the other hand, Reinhoudt *et al.*[8] recently noted the splitting of the PMR signal of the alkali metal ion-crown ether complexes, in which the size of the crown ether cavity is more than sufficient to accommodate the cation. Considering these facts and the similar phenomena caused by some alkaline-earth metal ions (Fig. 6), the splitting of the signals in the presence of metal cations can be ascribed to the strong complexation with the metal cations. Therefore, it can be concluded that, in methanol, the complexation with the sodium ion becomes significant for hexaethylene glycol, while those with potassium, rubidium, or caesium are significant for heptaethylene glycol.

Complexation of PEG and Glymes with Alkaline-earth Metal Cations in Methanol. As expected, calcium, strontium, and barium ions caused appreciable downfield shifts for PEG and glymes, while the magnesium ion did not. In Figs. 3, 4, and 5, their shifts are plotted as a function of the number of oxyethylene units(n).

The calcium ion caused the maximum downfield shift for hexaethylene glycol, which is comparable with that of 15-crown-5. In the cases of hexaglyme and heptaglyme, small shifts were recorded, indicating their

TABLE 3. POTASSIUM ION-INDUCED DOWNFIELD SHIFTS FOR GLYMES AND ASSOCIATION CONSTANTS IN METHANOL

Glymes	Downfield shifts (Hz)[a]				
	MeEO3Me	MeEO5Me	MeEO6Me	MeEO7Me	MeEO8Me
Oxyethylene protons	1.3	1.9	2.7	3.2	4.1, 3.4
Methyl protons	1.8	2.9	3.4	4.2	4.1
log K in CH_3OH[b]	—	2.20	2.55	2.87	

a) Concentration of KSCN is 0.04 mol/kg. b) See Ref. 18.

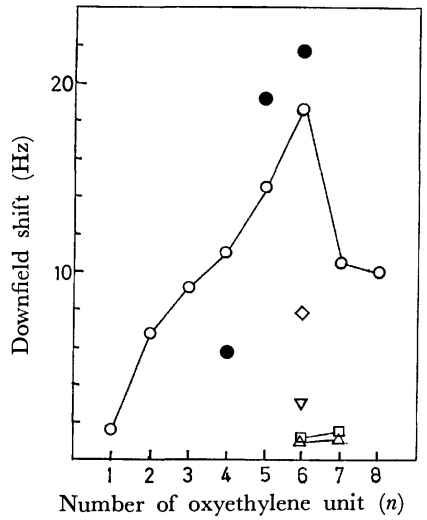

Fig. 3. Calcium-ion induced Downfield shifts for homogeneous poly(oxyethylene) derivatives in methanol-d_4.
●, Oxyethylene protons of the crown ethers; ○, oxyethylene protons of the PEG; □, oxyethylene protons of the glymes; ◇, oxyethylene protons of hexaethylene glycol monomethyl ether; △, methyl protons of the glymes; ▽, methyl protons of hexaethylene glycol monomethyl ether.

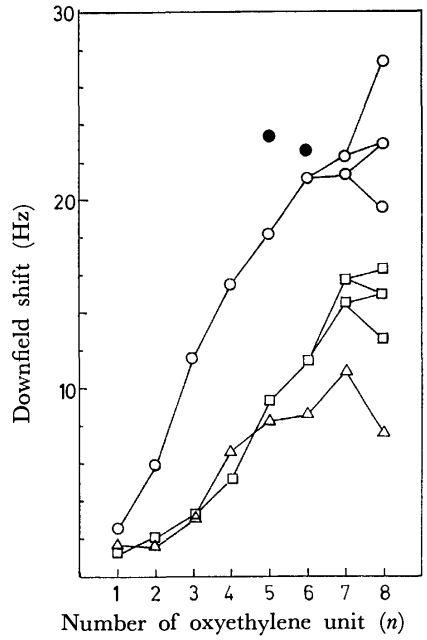

Fig. 4. Strontium-ion induced downfield shifts for homogeneous poly(oxyethylene) derivatives in methanol-d_4.
●, Oxyethylene protons of the crown ethers; ○, oxyethylene protons of the PEG; □, oxyethylene protons of the glymes; △, methyl protons of the glymes.

weak interaction. On the other hand, hexaethylene glycol monomethyl ether showed a medium shifts, accompanied by the splitting of the main signal. These facts suggest that the terminal hydroxyl groups play an important role in the complexation with the calcium ion in methanol (Fig. 3).

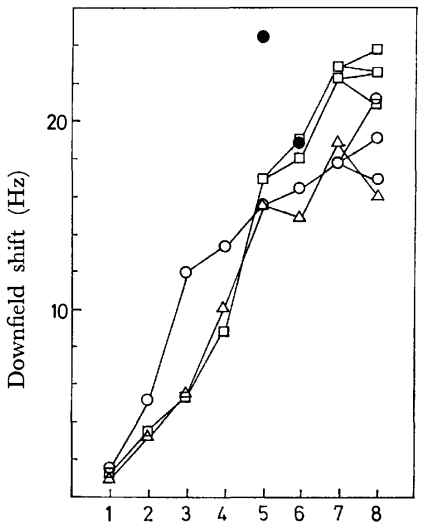

Fig. 5. Barium-ion induced Downfield shifts for the homogeneous poly(oxyethylene) derivatives in D_2O.
●, Oxyethylene protons of the crown ethers; ○, oxyethylene protons of the PEG; □, oxyethylene protons of the glymes; △, methyl protons of the glymes.

In the case of the strontium ion (Fig. 4), the interaction becomes significant above triethylene glycol and the complexing tendency increases remarkably with the number of oxyethylene units. Interestingly, the downfield shifts for hepta- and octaethylene glycols are quite comparable with those for the crown ethers, and their signals are split into two or three peaks respectively (Fig. 6). Heating at 60 °C led to the coalescence of the split signal of heptaethylene glycol with a slight upfield shift. (The difference between the chemical shifts with and without the strontium ion was found to be 21 Hz.) Since it was reported that the splitting due to the conformational change for heptaethylene glycol in a nonpolar solvent does not disappear easily with an increase in the temperature,[19] the easy coalescence supports the cation-induced splitting.

Glymes with more than four oxyethylene units also interact strongly with the strontium ion, and the averaged downfield shifts for hepta- and octaglymes and the shifts for their methyl protons indicate that the heptaglyme attain the optimal interaction. Judging from the differences in the downfield shifts between PEG and glymes, the terminal hydroxyl groups are important to some extent in creating effective interaction with the strontium ion.

With regard to the barium ion (Fig. 5), the series of PEG and glymes showed quite similar downfield shifts, which turned out to be more than that of 18-crown-6 when they have more than seven oxyethylene units. The main signal of pentaglyme broadened and those of hexaglyme and heptaglyme split into two peaks, while that of heptaethylene glycol resulted in broadening, and that of octaethylene glycol, in three resolved lines(Fig. 6). The rather large shifts and splitting for glymes imply that the terminal hydroxyl groups do not already play a characteristic role in the

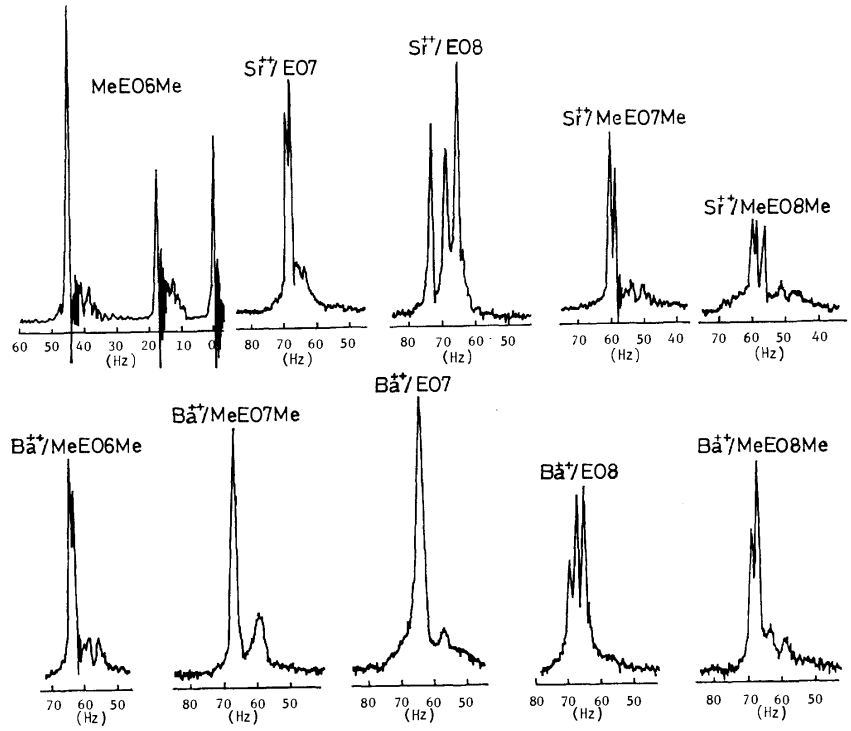

Fig. 6. NMR signals in methanol-d_4 of oxyethylene protons of the homogeneous PEG and glymes in the absence or the presence of alkaline-earth metal cation.

complexation with the barium ion in methanol.

It is interesting to note that one of the three split lines for octaethylene glycol in the presence of the strontium or barium ion was observed upfield (Fig. 6). The eighth oxyethylene unit may not be utilized in complexation, probably because of the crowding in the complexed ion.

Metal-ion Complexation of PEG in Water. Hitherto, no one has succeeded in observing by PMR the metal-ion complexation of acyclic POE derivatives in water.[3] As is shown in Table 1, we found that calcium strontium, and barium ions caused appreciable downfield shifts of the crowns' proton signals even in water, while the potassium ion did not.

In the presence of calcium thiocyanate, hexaethylene glycol, which showed the maximum interaction with the calcium ion in methanol, gave partially resolved peaks in water with a slight downfield shift (Fig. 7). The signal of heptaethylene glycol was shifted 5.6 Hz downfield by the strontium ion(0.12 mol/kg) and 7.9 Hz downfield by the barium ion (0.02 mol/kg). In view of the larger shift by the barium ion, the shifts for a series of polyethylene glycols were determined; they are plotted as a function of the oxyethylene units(n)

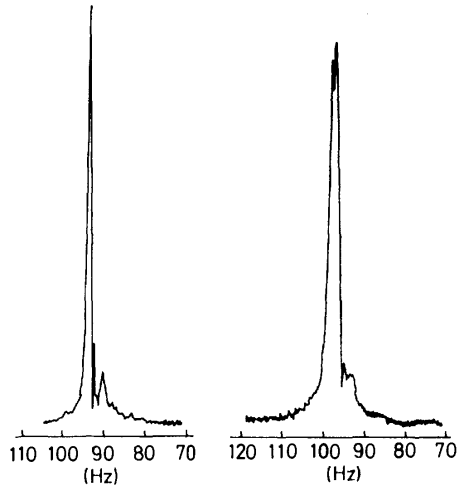

Fig. 7. PMR signals in D_2O of hexaethylene glycol in the absence (the left) and the presence (the right) of calcium thiocyanate.

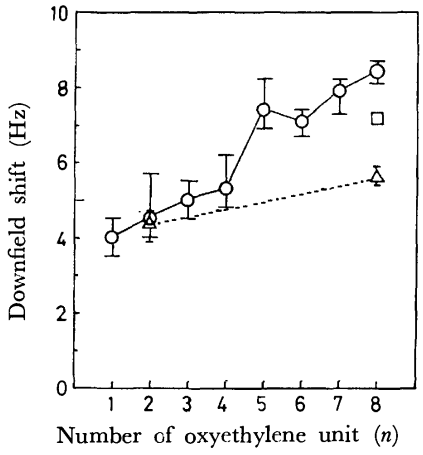

Fig. 8. Barium-ion induced downfield shifts for the homogeneous poly(oxyethylene) derivatives in D_2O. ○, Oxyethylene protons of the PEG; △, oxyethylene protons of the glymes; □, oxyethylene protons of the octaethylene glycol monomethyl ether.

in Fig. 8. The downfield shifts increased rapidly at pentaethylene glycol and then gradually with the increase in the number of oxyethylene units. The shift for monomethyl octaethylene glycol is reduced slightly, but the shift for octaglyme dropped to the extent of that for tetraethylene glycol. It is apparent that the terminal hydroxyl group is important in obtaining a high complexation in water. The smaller downfield shifts for PEG than those for the crown ethers, however, imply that the topology control, *e.g.*, the macrocyclic effect, plays a much more important role in the complexation in water.

Conclusion. It is now clear that polyethylene glycols show a strong ion-dipole binding affinity in methanol, especially toward the potassium, rubidium, caesium, calcium, strontium and barium ions, in spite of the absence of the topology control based on the ionic radius and the cavity size. In addition, there seem to be an optimum number of oxyethylene units in the glycols for a given cation; *e.g.*, the sodium and calcium ions are for six oxyethylene units; the potassium, rubidium, caesium, and strontium ions, for seven oxyethylene units, and the barium ion, for five or seven oxyethylene units.

The conformation of the oxyethylene unit in PEG has recently been clarified to favor the TGT conformation, even in an aqueous medium.[20] Such a conformation is apparently convenient to form stable five-membered ring chelates.[14] The optimal arrangement of the repeating oxyethylene units with the TGT conformation would work cooperatively and would lead to effective complexation with alkali and alkaline-earth cations. In other words, the energetically favorable TGT conformation and entropically favorable[21] oxyethylene chain must be the origins of the chelating ability of POE.

The isolation of some homogeneous PEG–metal cation complexes substantiating the PMR studies will be disclosed in a subsequent paper.

The authors wish to express their thanks to Mrs. Yoko Miyaji for her kind performance of the elaborative PMR measurment. They also wish to acknowledge the generous gift of the tetraethylene glycol used in this work by Mr. Naotsugu Kurata of the Japan Catalytic Chemical Industry, Ltd.

References

1) S. Yanagida, K. Takahashi, and M. Okahara, *Bull. Chem. Soc. Jpn.*, **50**, 1386 (1977).
2) a) D. Nicholls and M. Szwarc, *J. Phys. Chem.*, **71**, 2727 (1967); b) E. Schaschel and M. C. Day, *J. Am. Chem. Soc.*, **90**, 504 (1968).
3) K. Liu, *Macromolecules*, **1**, 308 (1968).
4) a) K. H. Wong, G. Konizer, and J. Smid, *J. Am. Chem. Soc.* **92**, 666 (1970); b) L. L. Chan, K. H. Wong, and J. Smid, *ibid.*, **92**, 1955 (1970).
5) a) J-M. Lehen, J. P. Saurage, and B. Dietrich, *J. Am. Chem. Soc.*, **92**, 2916 (1970); b) B. Dietrich, J. M. Lehn, and J. P. Sauvage, *Tetrahedron*, **29**, 1647 (1973).
6) a) E. Pretsch, M. Vasak, and W. Simon, *Helv. Chim. Acta*, **55**, 1098 (1972); b) R. Büchi, E. Pretsch, and W. Simon, *ibid.*, **59**, 2327 (1976); c) R. Büchi, E. Pretsch, and W. Simon, *Tetrahedron Lett.*, **1976**, 1709.
7) D. Live and S. I. Chan, *J. Am. Chem. Soc.*, **98**, 3769 (1976).
8) D. N. Reinhoudt, R. T. Gray, F. DeJong, and C. J. Smit, *Tetrahedron*, **33**, 563 (1977).
9) K. M. Herstein, *Inorg. Synth.*, Vol. III, 24 (1950).
10) R. Fordyce, E. L. Lovell, and H. Hibbert, *J. Am. Chem. Soc.*, **61**, 1905 (1939).
11) a) R. M. Izatt, R. E. Terry, B. L. Haymore, L. D. Hansen, N. K. Dalley A. G. Avondet, and J. J. Christensen, *J. Am. Chem. Soc.*, **98**, 7620 (1976); b) R. M. Izatt, R. E. Terry, D. P. Nelson, Y. Chan, D. J. Eatough, J. S. Bradshaw, L. D. Hansen, and J. J. Christensen, *ibid.*, **98**, 7626 (1976).
12) H. K. Frenshorf, *J. Am. Chem. Soc.*, **93**, 600 (1971).
13) C. J. Pedersen and H. K. Frensdorf, *Angew. Chem. Int. Ed. Engl.*, **11**, 16 (1972).
14) J-M. Lehn, *Struct. Bonding(Berlin)*, **16**, 1 (1973).
15) J. D. Dunitz and P. Seiler, *Acta Crystallogr., Sect. B*, **30**, 2750 (1974).
16) During the PMR measurments, the complex of 12-crown-4 with $Ca(SCN)_2$ was precipitated. The composition was found to be 12-crown-4·$Ca(SCN)_2$·H_2O. Unpublished work.
17) R. M. Izatt, D. J. Eatough, and J. J. Christensen, *Struct. Bonding(Berlin)*, **16**, 161 (1973).
18) G. Chaput, G. Jeminet, and J. Jullard, *Can. J. Chem.*, **53**, 2240 (1975).
19) K. Liu, *Macromolecules*, **1**, 213 (1968).
20) a) P. G. Assarsson, P. S. Leung, and G. J. Safford, *Polymer Reprints*, **10**, (2), 1241 (1969); b) T. M. Connor and K. A. Melauchlan, *J. Phys. Chem.*, **69**, 1888 (1965); c) K. Liu and J. L. Parsons, *Macromol. Chem.*, **94**, 194 (1966); d) J. L. Koenig and A. C. Angood, *J. Polym. Sci., Part A-2*, **8**, 1787 (1970).
21) J. Smid, *Angew. Chem. Int. Ed. Engl.*, **11**, 112 (1972).

The Kinetics of the Radiation-induced Chain Dechlorination of Hexachloroethane in Alcohols

Takeshi SAWAI, Naoki OHARA, and Toshinari SHIMOKAWA

Tokyo Metropolitan Isotope Research Center, Fukazawa, Setagaya, Tokyo 158

(Received September 24, 1977)

The kinetics of the radiation-induced dechlorination of hexachloroethane was investigated in deoxygenated alcohol solutions. The major products were hydrogen chloride, pentachloroethane, 1,1,2,2-tetrachloroethane, tetrachloroethylene, and aldehydes or acetone. No 1,1,1,2-tetrachloroethane was observed. The radiation-chemical yields of these products and the disappearance of hexachloroethane were quite high; these facts indicate that a chain reaction is involved in these processes. After the hexachloroethane had effectively dechlorinated down to tetrachloro compounds, there were no marked changes in the lower chlorinated compound upon continuous irradiation. Tetrachloroethane was formed *via* pentachloroethane, but tetrachloroethylene was produced by means of $C_2Cl_5 \rightarrow C_2Cl_4 + Cl$ reaction and the yield was paticularly high in methanol compared with the other alcohols. The chain length of the dechlorination from hexachloroethane to pentachloroethane and from pentachloroethane to tetrachloroethane increased in the order of 2-propanol > ethanol > methanol. The $G(-C_2Cl_6)$ and G(products) were proportional to (dose rate)$^{-1/2}$, and the ratio of $G(C_2HCl_5)$ to $G(C_2Cl_4)$ was a constant in each alcohol solution, regardless of the dose rate. The α-hydroxy alkyl radical is the chain carrier for the dechlorination reaction of hexachloroethane in alcohol solutions. The relative rates of the dechlorination were found to be 1, 3, and 14 for $\dot{C}H_2OH$, $CH_3\dot{C}HOH$, and $(CH_3)_2\dot{C}OH$, respectively. The order in the rate is in agreement with that of the redox potential of these radicals. The effect of the irradiation temperature on the products yields was also examined.

Halocarbons are important for examining the fundamental processes in radiation chemistry because of their high electron affinity, and the main reaction of the radiolysis is dehalogenation.[1] It is known that the radiation-induced chain dehalogenation of some organic halocompounds proceeds in aqueous solutions containing a small amount of alcohol[2,3] and in the solutions of alcohols[4-6] or cyclohexane.[7-11] Sherman *et al.* showed that tetrachloromethane[4] and 1,1,1-trichloro-2,2-bis(*p*-chlorophenyl)ethane (DDT)[5] were dechlorinated to trichloromethane and 1,1-dichloro-2,2-bis-(*p*-chlorophenyl)ethane (DDE) by a relatively short chain reaction in γ-irradiated 1- and 2-propanol solutions at room temperature. Rajbenbach *et al.* indicated that the chain-dechlorination process was induced by the γ-irradiation of dilute cyclohexane solutions of chloroethanes at temperatures of 25—250 °C.[7-11] The dechlorination yield was not so high at room temperature (for example, $G(HCl) \approx 100$ in 0.1 M hexachloroethane), and a relatively high temperature was required for a high G-value.

On the other hand, it is known that a chain dechlorination reaction took place upon the γ-irradiation of dilute alkaline 2-propanol solutions of alkyl halides,[12] polychlorinated biphenyls[13,14] and of penta and trichlorobenzene[15] at room temperature (for instance, $G(Cl^-) \approx 6500$ in a 0.2 M KOH-2-propanol solution of 0.07 M pentachlorobenzene). These substances were changed to the lower chlorinated compounds, producing potassium chloride and acetone. The chain reaction is probably caused by the $(CH_3)_2\dot{C}O^-$ formed by the reaction of the hydroxide ion with the $(CH_3)_2\dot{C}OH$ radical. On the other hand, no marked chain dechlorination occurred in alkaline methanol and ethanol solutions or in neutral simple aliphatic alcohols.

The purpose of this study is to investigate the kinetics of the radiation-induced chain dechlorination in simple, neutral aliphatic alcohol solutions of hexachloroethane with a half-wave potential lower than tetrachloromethane, DDT, and pentachlorobenzene.

Experimental

Materials. The methanol, ethanol, and 2-propanol (Dojin Chemical's spectrophotometric reagent or super special grade) were used as received. The chloroethanes and tetrachloroethylene used were special reagent grade from the Tokyo Kasei Co., Ltd.

Procedure. Aliquots(4 ml) of freshly prepared alcohol solutions of $1—2 \times 10^{-2}$ M hexachloroethane in a 12-mm OD Pyrex tube equipped with a stopper were irradiated with ^{60}Co γ-rays at room temperature after having been deoxygenated by flushing the solutions for about 30 min with pure nitrogen gas. The dose rate was determined by means of a ferrous sulfate dosimeter, and the absorbed dose in the samples was calculated by correcting for the electron density of the solutions. Irradiation was performed at the dose rate of $5.25 \times 10^{17}—2.80 \times 10^{19}$ eV/g h. The irradiation under a constant temperature was carried out in a water bath with a regulator.

Analysis. The hydrochloric acid was analysed by titration with a 0.02 M sodium hydroxide solution and with a 0.01 M silver nitrate solution. The determination of the other substances was carried out by means of a Shimadzu 4B gas chromatograph equipped with a flame-ionization detector. Chloroethanes (hexa-, penta-, and tetra chloroethane) were determined at 80 °C by the use of a 3-m glass column filled with silicon OV-17 on chromosorb. For tetrachloroethylene and aldehydes, a 2-m glass column packed with polyethylene glycol-200 was used. The acetone was measured at 50 °C by using a 2-m glass column of polyethylene glycol-20M. These substances were quantitatively determined by a comparison of their peak heights with those of authentic samples. A formalin solution(about 37%) was used as a standard for formaldehyde, and the concentration was measured in advance by iodometry. All the products except hydrochloric acid were identified by the use of a gas chromatograph-mass spectrometer(Nihondenshi Model JMS-D100).

Results and Discussion

Yield-dose Curve in Alcohol Solutions of Hexachloroethane. The products identified in the radiolysis of deoxygenated alcohol solutions of hexachloroethane were hydrogen chloride, pentachloroethane(C_2HCl_5), 1,1,2,2-tetrachloroethane($C_2H_2Cl_4$), tetrachloroethylene(C_2Cl_4), and some carbonyl compounds. No 1,1,1,2-tetrachloroethane was observed.

2-Propanol Solution: Figure 1 shows the concentrations of C_2Cl_6, HCl, C_2HCl_5, $C_2H_2Cl_4$, and C_2Cl_4 as functions of the dose. The chloride ion increased with a very high yield up to about 7×10^{17} eV/g, and then showed an almost constant value above 1.5×10^{18} eV/g. The hexachloroethane decreased rapidly with the dose until most of it disappeared at about 3×10^{17} eV/g. On the other hand, the C_2HCl_5 increased with the decrease in C_2Cl_6, and the concentration of C_2HCl_5 was practically comparable to that of the C_2Cl_6 consumption. Further irradiation caused a rapid decrease in C_2HCl_5 and a concomitant increase in $C_2H_2Cl_4$. The concentrations of $C_2H_2Cl_4$ formation and C_2HCl_5 consumption were almost equal in the dose range from 0.58 to 1.8×10^{18} eV/g, and above 2×10^{18} eV/g there were also no marked change in the concentration of $C_2H_2Cl_4$, which was a half of that of the chloride ion and was equal to the initial concentration of C_2Cl_6. Only a tetrachloroethylene was observed in the whole dose region. The radiation-chemical yields(*G*-values) at the dose of 3.42×10^{17} eV/g are calculated to be 2300, 1700, 60, and 2000 for the chloride ion, C_2HCl_5, C_2Cl_4, and, $-C_2Cl_6$ respectively. It was confirmed in other experimental series that the yield of acetone was almost equivalent to that of the chloride ion. These results suggest that C_2Cl_6 in the deoxygenated 2-propanol solution is effectively dechlorinated by a chain reaction to $C_2H_2Cl_4$ via C_2HCl_5, thus forming hydrochloric acid and acetone.

Methanol Solution: The yield-dose plots in methanol solution of C_2Cl_6 are shown in Fig. 2. The concentrations of HCl, $C_2H_2Cl_4$, C_2Cl_4, and formaldehyde increased monotonously with the decrease in C_2Cl_6 up to about 1.3×10^{19} eV/g; on the other hand, C_2HCl_5 decreased very slowly with the dose above $\approx6\times10^{18}$ eV/g. These *G*-values, which were calculated from the linear portions of these curves in Fig. 2, were 540, 110, 200, 290, and 320 for HCl, C_2HCl_5, C_2Cl_4, $-C_2Cl_6$, and formaldehyde.

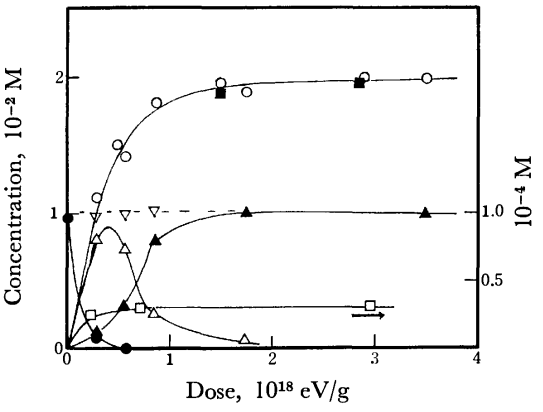

Fig. 1. Product yields as a function of dose from 9.6×10^{-3} M C_2Cl_6 in 2-propanol.
Dose rate, 1.71×10^{18} eV/g h.
○: Cl^-, ■: H^+, ●: C_2Cl_6, △: C_2HCl_5, ▲: $C_2H_2Cl_4$, □: C_2Cl_4, ▽: sum of C_2Cl_6, C_2HCl_5, $C_2H_2Cl_4$, and C_2Cl_4.

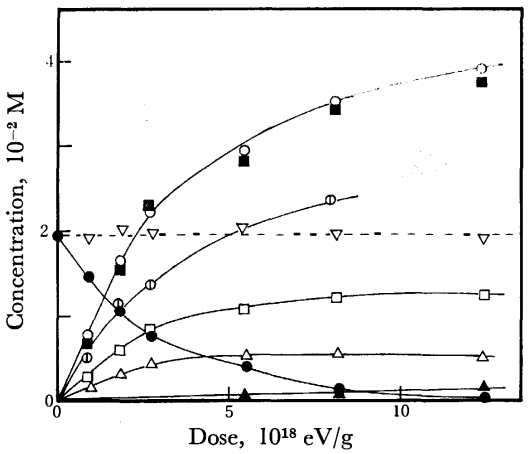

Fig. 2. Product yields as a function of dose from 1.96×10^{-2} M C_2Cl_6 in methanol.
Dose rate, 5.43×10^{18} eV/g h.
○: Cl^-, ■: H^+, ●: C_2Cl_6, △: C_2HCl_5, ▲: $C_2H_2Cl_4$, □: C_2Cl_4, ⓘ: HCHO, ▽: sum of C_2Cl_6, C_2HCl_5, $C_2H_2Cl_4$, and C_2Cl_4.

The largest differences in comparison with the results for 2-propanol solutions are found to be as follows:

a. All the *G*-values in the methanol except $G(C_2Cl_4)$ are much lower than those of 2-propanol.

b. $G(-C_2Cl_6)$ is considerably lower than $G(Cl^-)$ and, on the contrary, is about three times as high as $G(C_2HCl_5)$.

c. $G(C_2Cl_4)$ is two times as high as $G(C_2HCl_5)$.

d. A considerable amount of formaldehyde is produced instead of acetone in the 2-propanol, and the concentration of formaldehyde is remarkably lower than that of the chloride ion.

e. After almost all of the C_2Cl_6 has disappeared (above 8×10^{18} eV/g), the decrease of C_2HCl_5 with the dose is only a little.

The effect of the initial concentration of C_2Cl_6 on the *G*-values is given in Table 1. These values increased with the initial concentration.

Ethanol Solution: The relationship between the concentrations of products and the dose was relatively similar to the result for 2-propanol, as is shown in Fig.

Table 1. Effects of the concentration of C_2Cl_6 in methanol on the *G*-values

C_2Cl_6 10^{-2} M	*G*-value				
	Cl^-	$-C_2Cl_6$	C_2HCl_5	C_2Cl_4	HCHO
0.54	161	90	29	58	93
1.96	542	288	109	218	320
4.91	730	445	147	277	490

Dose rate : 5.43×10^{18} eV/g h.

3. Further irradiation suppressed the C_2HCl_5 completely, and the concentrations of the chloride ion and $C_2H_2Cl_4$ reached an almost constant value. At that time, the concentration of $C_2H_2Cl_4$ was equivalent to the initial C_2Cl_6 concentration and was one half of the chloride ion.

As can be seen in Figs. 1, 2, and 3, the fact that the sums of the concentrations of C_2Cl_6, C_2HCl_5, C_2Cl_4, and $C_2H_2Cl_4$ observed in the irradiated solutions were always correspondent to the initial concentration of C_2Cl_6 indicates that the production of other chlorinated compounds can be ignored.

Dechlorination of C_2HCl_5, $C_2H_2Cl_4$, and C_2Cl_4 in Alcohol Solutions. The results in the methanol and 2-propanol solutions of 1×10^{-2} M C_2HCl_5 are given in Fig. 4. In the 2-propanol, the concentrations of the chloride ion, $-C_2HCl_5$, and acetone were almost equal to $G\approx700$. This fact shows that C_2HCl_5 is also dechlorinated by the chain reaction to form $C_2H_2Cl_4$, the chloride ion, and acetone. On the other hand, the $G(Cl^-)$ in the methanol was merely 24, and no C_2Cl_4 was observed in either solution.

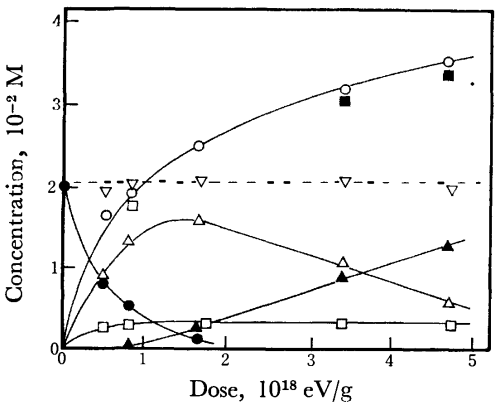

Fig. 3. Product yields as a function of dose from 2.01 $\times10^{-2}$ M C_2Cl_6 in ethanol.
Dose rate, 1.68×10^{18} eV/g h.
○: Cl^-, ■: H^+, ●: C_2Cl_6, △: C_2HCl_5, ▲: $C_2H_2Cl_4$, □: C_2Cl_4, ▽: sum of C_2Cl_6, C_2HCl_5, $C_2H_2Cl_4$, and C_2Cl_4.

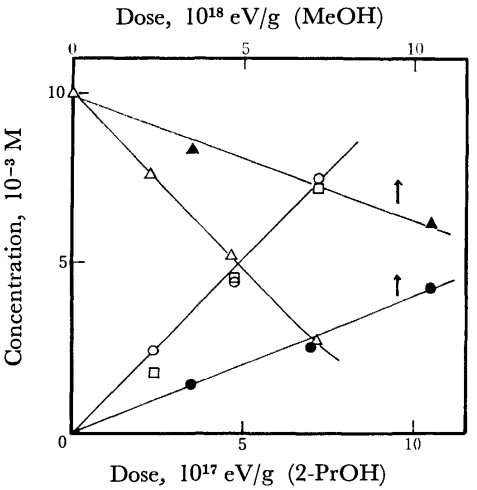

Fig. 4. Product yields as a function of dose from 1.0 $\times10^{-2}$ M C_2HCl_5 in methanol and in 2-propanol.
Dose rate, 5.22×10^{18} eV/g h in methanol (closed symbol), 1.43×10^{18} eV/g h in 2-propanol (open symbol).
○, ●: Cl^-, △, ▲: C_2HCl_5, □: $C_2H_2Cl_4$.

Upon irradiating the solutions of 1×10^{-2} M $C_2H_2Cl_4$ and C_2Cl_4, the hydrochloric acid increased linearly with the dose. The *G*-values in the $C_2H_2Cl_4$ solutions were 4.3, 4.2 (dose rate, 1.1×10^{19} eV/g h), and 3.5 (dose rate, 7.6×10^{18} eV/g h) for 2-propanol, ethanol, and methanol. For C_2Cl_4, these values were 6 in 2-propanol (dose rate, 2.1×10^{19} eV/g h) and 2.2 in methanol (dose rate, 1.1×10^{19} eV/g h). Therefore, it is found that $C_2H_2Cl_4$ and C_2Cl_4 are not dechlorinated by the chain reaction any longer. These findings are in good agreement with the results for C_2Cl_6 solutions presented in Figs. 1, 2, and 3.

Effect of the Dose Rate on the G-values in 2×10^{-2} M C_2Cl_6 Solutions. The effects of the dose rate on

Table 2. Effects of the dose rate on the *G*-values

Solution	Dose rate 10^{18} eV/g h	*G*-value							
		Cl^-	$-C_2Cl_6(a)$	$C_2HCl_5(b)$	$C_2Cl_4(c)$	R_1R_2CO	$a+c$	$b+c$	b/c
2-Propanol	0.525	8000	7700	7000	140	7500	7840	7140	50
	0.855	6800	6000	5900		5100			
	1.70	5100	4900	4600	100	5100	5000	4700	46
	2.76	4900	4400	4600		4600			
	5.32	3500	3000	3000		3300			
	6.71	3100	2900	3000	65	3000	2965	3065	46
	11.9	2500			55				
Ethanol	0.855	2600	2200	2000	220		2420	2220	9.1
	1.70	2200	1800	1700	180		1980	1880	9.4
	5.21	1800	1400	1200	150		1550	1350	8.0
Methanol	0.585	1200	700	210	400	660	1100	610	0.52
	1.71	750	410	150	290		700	440	0.52
	5.48	540	290	110	220	320	510	330	0.50
	11.2	340	220	58	140	260	360	198	0.42
	28.0	250	150	45	98	190	248	143	0.46

$C_2Cl_6=2.0\times10^{-2}$ M, R_1,R_2 : CH_3 or H.

the G-values are summarized in Table 2. All the G-values, except $G(C_2Cl_4)$, decreased with an increase in the dose rate and, at the same dose rate, became lower in the order of 2-propanol, ethanol, and methanol. On the G-values shown in Table 2, the following relations can be seen, within the limits of experimental error;

a. $G(Cl^-)$ equals the sum of $G(-C_2Cl_6)$ and $G(C_2Cl_4)$.

b. $G(-C_2Cl_6)$ is approximately correspondent to $G(R_1R_2CO)$, and also to $G(C_2HCl_5)$ plus $G(C_2Cl_4)$.

c. The ratio of $G(C_2HCl_5)/G(C_2Cl_4)$ is a constant for each solution and decreases in the order of 2-propanol, ethanol, and methanol.

Dechlorination of C_2Cl_6 in Alkaline Solutions of 2-Propanol and Methanol. In the irradiation of deoxygenated alkaline(KOH) alcohol solutions of C_2Cl_6, potassium chloride precipitated much as in the alkaline 2-propanol solutions of polychlorinated biphenyls[13,14] and chlorobenzenes.[15] The yield of the chloride ion increased with the dose, as is shown in Table 3. The initial $G(Cl^-)$s were $\gtrsim$13000 and $\gtrsim$1900 for the 2-propanol and methanol respectively. These values are found to be considerably higher than those of the neutral solutions at the same dose rate in Table 2. Moreover, in the neutral solutions, the percentage of the dechlorination did not exceed 33% within this dose range, but in the alkaline solutions it did so at a relatively low dose and the chloride ion was still produced with a fairly high yield. Thus, the $G(Cl^-)$s were calculated to be 230 and 50 at the doses between 0.90 and 4.5×10^{18} eV/g in the 2-propanol, and between 2.6 and 19.2×10^{18} eV/g in the methanol respectively. The product analysis by gas chromatography was not carried out, but these high G-values indicate that C_2Cl_6 may be more dechlorinated by the chain reaction to the lower chlorinated compound than to tetrachloro compound in the alkaline solutions.

Dechlorination Reaction of Chloroethanes in Alcohols. The hexachloroethane in the solutions of methanol, ethanol, and 2-propanol was dechlorinated to form hydrochloric acid, C_2HCl_5, C_2Cl_4, and aldehydes or acetone. These high G-values (see Table 2) show that all the products are produced by a chain-reaction mechanism. Sherman *et al.* proposed the following radical chain reaction for the dechlorinations of tetrachloromethane[4] and DDT[5] to trichloromethane and DDE in the 2-propanol solutions:

Initiation

$$(CH_3)_2CHOH \xrightarrow{\sim\sim} X \text{ (radicals, } e^-_{solv.}) \quad (1)$$

$$X + RCl_n \longrightarrow XCl + \dot{R}Cl_{n-1} \quad (2)$$

(where RCl_n is CCl_4 or DDT)

Propagation

$$\dot{R}Cl_{n-1} + (CH_3)_2CHOH \longrightarrow RCl_{n-1}H + (CH_3)_2\dot{C}OH \quad (3)$$

$$(CH_3)_2\dot{C}OH + RCl_n \longrightarrow (CH_3)_2CO + HCl + \dot{R}Cl_{n-1} \quad (4)$$

If the chain dechlorination of C_2Cl_6 in the alcohol solutions follows the above mechanisms, the $G(HCl)$ should be in agreement with $G(-C_2Cl_6)$, $G(C_2HCl_5)$, and $G(R_1R_2CO)$; moreover, C_2Cl_4 should not be found as a product. On the other hand, the results in Table 2 do not apparently support the above findings because of the large discrepancy among G-values, especially in the methanol, and also the formation of a considerable amonut of C_2Cl_4. Therefore, some additional reaction may be required for the direct formation of C_2Cl_4 from C_2Cl_6, since C_2Cl_4 was observed immediately after irradiation (Figs. 1, 2, and 3) and was not formed from C_2HCl_5 (Fig. 4).

Horowitz *et al.* showed that HCl, C_2HCl_5, monochlorocyclohexane, and C_2Cl_4 were produced in high yields by the γ-radiolysis of C_2Cl_6 in cyclohexane at 24—100 °C; for example, $G(HCl)$ and $G(C_2Cl_4)$ reached to $\approx$4000 in a 0.1 M C_2Cl_6 solution at 100 °C. They suggested that these high G-values arose from sequence of reactions:[7]

$$2\,c\text{-}C_6H_{12} \xrightarrow{\sim\sim} 2\,c\text{-}\dot{C}_6H_{11} + H_2 \quad (5)$$

$$c\text{-}\dot{C}_6H_{11} + C_2Cl_6 \longrightarrow c\text{-}C_6H_{11}Cl + \dot{C}_2Cl_5 \quad (6)$$

$$\dot{C}_2Cl_5 + c\text{-}C_6H_{12} \longrightarrow C_2HCl_5 + c\text{-}\dot{C}_6H_{11} \quad (7)$$

$$\dot{C}_2Cl_5 \longrightarrow C_2Cl_4 + Cl \quad (8)$$

$$Cl + c\text{-}C_6H_{12} \longrightarrow HCl + c\text{-}\dot{C}_6H_{11} \quad (9)$$

Assuming that C_2Cl_4 is formed by Reaction 8 in the alcohol solutions, the following correlation can be expected to hold for the G-values in Table 2 on the bases of Reactions 1, 2, 3, 4, 8, and 9′:

$$Cl + R_1R_2CHOH \longrightarrow HCl + R_1R_2\dot{C}OH \quad (9')$$

a. $G(HCl)$ equals the sum of $G(-C_2Cl_6)$ and $G(C_2Cl_4)$.

b. $G(-C_2Cl_6)$ is equal to the sum of $G(C_2HCl_5)$ and $G(C_2Cl_4)$, and also to $G((CH_3)_2CO)$ or $G(HCHO)$. As can be seen in Tables 1 and 2, the above correlations

Table 3. The chloride-ion yield as a function of the dose in 0.2 M KOH alkaline solutions of 2.0×10^{-2} M C_2Cl_6

Solution	Dose 10^{18} eV/g						
	0.10	0.90	1.75	2.60	4.25	7.70	19.2
2-Propanol	3.1	4.1			5.4		
Methanol		2.7	3.8	4.1		4.5	5.4

Cl^- yield : $\times10^{-2}$ M,
Dose rate : 8.35×10^{17} eV/g h in 2-propanol
5.22×10^{18} eV/g h in methanol.

hold within the limits of experimental error. Therefore, the chain-dechlorination reaction of C_2Cl_6 in alcohol solutions can be described as follows:

Initiation

$$R_1R_2CHOH \rightsquigarrow X,\ e^-_{solv.} \quad (10)$$

(where R_1 and R_2 are CH_3 or H)

$$X + R_1R_2CHOH \longrightarrow XH + R_1R_2\dot{C}OH \quad (11)$$

$$e^-_{solv.} + C_2Cl_6 \longrightarrow \dot{C}_2Cl_5 + Cl^- \quad (12)$$

Propagation

$$R_1R_2\dot{C}OH + C_2Cl_6 \longrightarrow R_1R_2CO + \dot{C}_2Cl_5 + HCl \quad (13)$$

$$\dot{C}_2Cl_5 + R_1R_2CHOH \longrightarrow C_2HCl_5 + R_1R_2\dot{C}OH \quad (14)$$

$$\dot{C}_2Cl_5 \longrightarrow C_2Cl_4 + Cl \quad (15)$$

$$Cl + R_1R_2CHOH \longrightarrow HCl + R_1R_2\dot{C}OH \quad (16)$$

The steady-state treatment for Reactions 14 and 15 leads to the following expression:

$$G(C_2HCl_5) = k_{14}[R_1R_2CHOH]/k_{15} \times G(C_2Cl_4) \quad (I)$$

Thus, $G(C_2HCl_5)$ should be proportional to $G(C_2Cl_4)$. The relationship between the two G-values is given in Fig. 5 for the methanol, ethanol, and 2-propanol solutions. From the slopes in Fig. 5, k_{14}/k_{15} is obtained as 0.02, 0.59, and 3.1 for methanol, ethanol, and 2-propanol respectively. These results show that Reaction 14 is more predominant in the 2-propanol than in the methanol. Thus, the ratio of $G(C_2Cl_4)$ to $G(C_2HCl_5)$ was very low in the former solution, but, on the contrary, was quite high in the latter solution. The values of k_{14}/k_{15} show that hydrogen abstraction from 2-propanol by the C_2Cl_5 radical is much faster than that from methanol and ethanol. The order of the hydrogen abstraction from alcohols is in agreement with that by the CF_3,[3] OH,[16] and H[17] radicals.

If the termination of the chain involves a reaction between two alcohol radicals ($2k_{17}=1-3\times10^9$ M^{-1} s^{-1}):[18-23]

$$2\,R_1R_2\dot{C}OH \begin{cases} \longrightarrow R_1R_2CHOH + R_1R_2CO & (17a) \\ \longrightarrow R_1R_2COH \\ \quad\quad\quad R_1R_2COH & (17b) \end{cases}$$

the G-values shown in Table 2 are given by following expressions under steady irradiation:

$$G(-C_2Cl_6) = G(\dot{C}_2Cl_5) = G(X) + 10k_{13}[C_2Cl_6](G(X)/k_{17}I)^{1/2} \quad (II)$$

$$G(C_2HCl_5) = G(\dot{C}_2Cl_5)k_{14}[R_1R_2CHOH]/k_{15} \quad (III)$$

$$G(C_2Cl_4) = G(\dot{C}_2Cl_5)k_{15}/k_{14}[R_1R_2CHOH] \quad (IV)$$

$$G(HCl) = G(-C_2Cl_6) + G(C_2Cl_4) = G(\dot{C}_2Cl_5)(1+k_{15}/k_{14}[R_1R_2CHOH]) \quad (V)$$

where I is the dose rate.

It is known that the ratio of the combination reaction 17b to the disproportionation 17a depends on the nature of the R_1R_2COH radical. For the CH_2OH radical, the ratio of 17b to 17a is 10; in contrast, $(CH_3)_2\dot{C}OH$ more probable results in acetone.[24] Assuming that the production of acetone by Reaction 17a can be neglected in comparison with that by Reaction 13, $G((CH_3)_2CO)$ can be also expressed by Equation II. The predicated linear dependence of the G-values on $I^{-1/2}$ is in agreement with the experimental data (Figs. 6 and 7). From the slopes of $G(-C_2Cl_6)$ *vs.* $I^{-1/2}$, the ratio of k_{13} for methanol, ethanol, and 2-propanol is obtained to be 1 : 3 : 14 by using $2k_{17}=2.7\times10^9$,[22] 2.0×10^9,[19] and 1.4×10^9 M^{-1} s^{-1} [20] for $\dot{C}H_2OH$, $CH_3\dot{C}HOH$, and $(CH_3)_2\dot{C}OH$, respectively.

It is very interesting that the dechlorination yield is dependent on the kinds of chloroethanes and solvents. Sherman showed that the following charge-transfer process seems most likely to be involved in the dechlorination of CCl_4:[4]

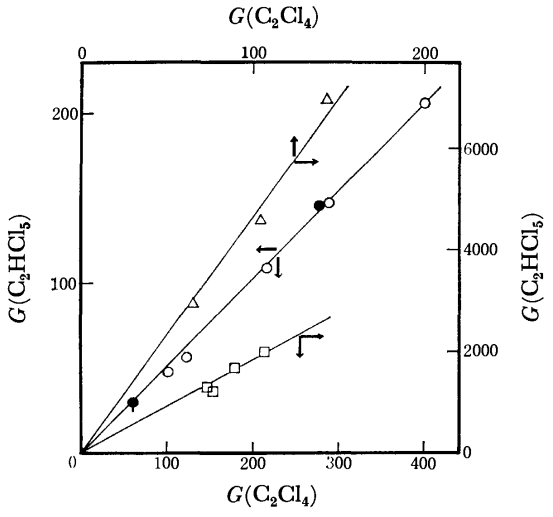

Fig. 5. $G(C_2HCl_5)$ as a function of $G(C_2Cl_4)$ in the solutions of 2.0×10^{-2} M C_2Cl_6.
△: 2-Propanol, □: ethanol, ○, ●: methanol, ●: 4.9×10^{-2} M C_2Cl_6, ●: 0.54×10^{-2} M C_2Cl_6.

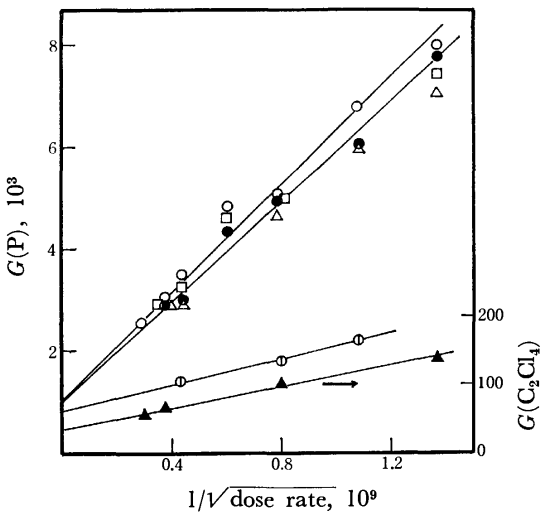

Fig. 6. G-values as a function of (dose rate)$^{-1/2}$ from 2×10^{-2} M C_2Cl_6 in 2-propanol and in ethanol.
○: Cl^-, ●: $-C_2Cl_6$, △: C_2HCl_5, ▲: C_2Cl_4, □: $(CH_3)_2CO$, ⊙: $-C_2Cl_6$ in ethanol.

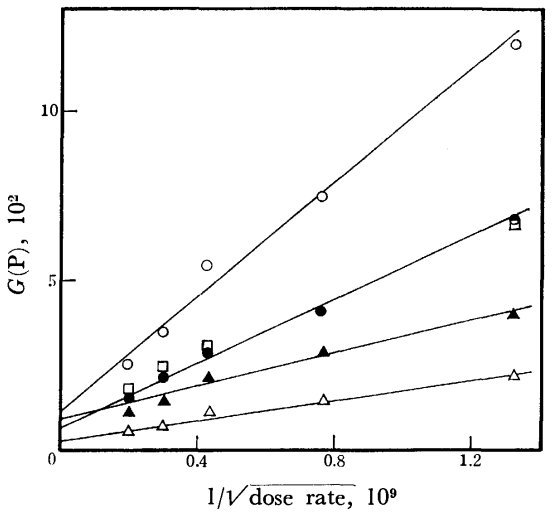

Fig. 7. G-values as a function of (dose rate)$^{-1/2}$ from 2×10^{-2} M C_2Cl_6 in methanol.
○: Cl^-, ●: $-C_2Cl_6$, △: C_2HCl_5, ▲: C_2Cl_4, □: HCHO.

$$(CH_3)_2\dot{C}OH + CCl_4 \longrightarrow (CH_3)_2C{=}OH^+ + \dot{C}Cl_3 + Cl$$

$$(CH_3)_2C{=}OH^+ + \text{solvent} \longrightarrow (CH_3)_2CO + H^+$$

In the investigation of the dehalogenation of aliphatic halogen compounds, such as bromoacetic acid, by an aliphatic free radical in aqueous solutions, Andar *et al.* also indicated that the dehalogenation was due to a charge-transfer mechanism rather than halogen abstraction and that the reactivity of charge-transfer followed the sequence of $(CH_3)_2\dot{C}OH > CH_3\dot{C}HOH > \dot{C}H_2OH$ for simple aliphatic alcohol radicals. For instance, the $G(Br^-)$s were 9.5, 61, and >350 for methanol, ethanol, and 2-propanol in the aqueous solutions of 1×10^{-3} M bromoacetic acid containing 5M alcohol. The reactivity of halogen compounds toward the radical, on the other hand, increased in this order: $ClCH_2COOH < BrCH_2COOH < CBr_3COOH$.[2]

It is also known that the α-hydroxy alkyl radical acts as a reducing agent.[25] The $RH+A\rightarrow R+A^-+H^+$ reaction occurs at an appreciable rate whenever the redox potential (E) of A(acceptor molecule) is lower than that of RH(donor radical), and the electron-transfer reaction is dependent on the difference of the E between RH and A.[26] In our case, A and RH correspond to C_2Cl_6 and $R_1R_2\dot{C}OH$. The redox potential is generally proportional to the half-wave potential ($E_{1/2}$) of polarography($E=E_{1/2}+0.244$).[26] The values for C_2Cl_6, $\dot{C}H_2OH$, $CH_3\dot{C}HOH$, and $(CH_3)_2\dot{C}OH$ are known to be −0.66,[27] −0.98, −1.18, and −1.30 V.[28] Therefore, the dechlorination of C_2Cl_6 occurs significantly in all solutions; therefore, the finding that $G(-C_2Cl_6)$ was highest in the 2-propanol is reasonable.

It is clear that $C_2H_2Cl_4$ is formed by the dechlorination of C_2HCl_5 from the change in the concentrations of the chloride ion, C_2HCl_5, and $C_2H_2Cl_4$ after consuming C_2Cl_6 (Figs. 1 and 3), and from the correlation of $G(Cl^-)=G(-C_2HCl_5)=G(C_2H_2Cl_4)$(Fig. 4). The G-value of $-C_2HCl_5$ was about 600 in the 2-propanol and 24 in the methanol(Fig. 4). For the ethanol, a mean G-value between the 2-propanol and methanol should be obtainable by judging from the decrease in C_2HCl_5 shown in Fig. 3. The chain dechlorination of C_2HCl_5 in alcohol solutions seems to proceed in the same way as the reaction of C_2Cl_6. The large difference in $G(-C_2HCl_5)$ for the 2-propanol and the methanol may be due to the difference in their redox potentials between C_2HCl_5 and $R_1R_2\dot{C}OH$. On the other hand, C_2Cl_4 and $C_2H_2Cl_4$ were not dechlorinated by the chain reaction any longer. This is because their half-wave potentials are apparently higher than those of $R_1R_2\dot{C}OH$ ($C_2Cl_4\approx-1.8$ V, $C_2H_2Cl_4\approx-2$ V).[27]

On the other hand, it is known that the α-hydroxy alkyl radical behaves as either an acid or a base[28] and that the half-wave potentials in the basic form are ≈-1.8 and −2.2 V for $\dot{C}H_2O^-$ and $(CH_3)_2\dot{C}O^-$.[25,29]

$$R_1R_2\dot{C}OH \rightleftharpoons R_1R_2\dot{C}O^- + H^+ \qquad (pK\approx12)$$

In this case, the potentials in the basic form are apparently higher than those in the basic form; moreover, the potentials of $(CH_3)_2\dot{C}O^-$ and $\dot{C}H_2OH$ are higher than, or almost equal to, those of $C_2H_2Cl_4$ and C_2Cl_4. Therefore, in the alkaline alcohols, the initial $G(Cl^-)$ was higher than that in the neutral solutions; C_2Cl_6 might thus be more easily dechlorinated to the lower chlorinated compound than the tetrachloro compound.

Effect of Temperature on the Product Yields. The yields of products are shown in Table 4 upon irradiating $1.6-1.7\times10^{-2}$ M C_2Cl_6 in solutions of methanol and

Table 4. Effect of the temperature on the product yields

Solution	Temp (°C)	Concentration, 10^{-2} M								
		Cl^-	$-C_2Cl_6(a)$	$C_2HCl_5(b)$	$C_2Cl_4(c)$	$C_2H_2Cl_4(d)$	Σ	b/c	$a+c$	$b+c$
Methanol	0	0.70	0.45	0.21	0.18	0	1.54	1.2	0.63	0.39
	25	1.84	1.01	0.34	0.66	0.01	1.60	0.52	1.67	1.0
	50	2.87	1.51	0.25	1.15	0.03	1.52	0.22	2.67	1.4
2-Propanol	0	2.29	1.69	1.38	0.05	0.31	1.75		2.05[a]	1.74[b]
	25	2.86	1.70	0.66	0.09	1.03	1.78		2.82[a]	1.75[b]
	50	3.40	1.70	0.04	0.18	1.59	1.81		3.47[a]	1.81[b]

Methanol : 1.6×10^{-2} M C_2Cl_6, 1.6×10^{18} eV/g,
2-propanol : 1.7×10^{-2} M C_2Cl_6, 0.8×10^{18} eV/g,
Σ, a) $a+c+d$, b) $b+c+d$.

2-propanol at 0, 25, and 50° C. The chloride ion increased with the temperature, and the total concentration of chlorocompounds observed in the irradiated solutions was a constant(=the initial concentration of C_2Cl_6) in both the solutions.

In the methanol, the concentrations of the chloride ion and $-C_2Cl_6$ were correspondent to those of $-C_2Cl_6$ plus C_2Cl_4, and C_2HCl_5 plus C_2Cl_4, respectively at each temperature. On the other hand, in the 2-propanol, the above correlations were not found because almost all of the C_2Cl_6 disappeared, to be followed by the formation of a considerable amount of $C_2H_2Cl_4$. However, taking into consideration the fact that all the $C_2H_2Cl_4$ was produced from C_2HCl_5, the sum of $-C_2Cl_6$ C_2Cl_4, and $C_2H_2Cl_4$ equals the concentration of the chloride ion(last column in Table 4). Therefore, the dechlorination reaction is likely to be the same at temperatures of 0—50 °C. The decrease in the ratio of C_2HCl_5 to C_2Cl_4 in the methanol with the temperature may be caused by the fact that Reaction 14 was much more promoted than Reaction 15 at high temperatures.

The authors are indebted to Dr. Kinji Anda and Mr. Masao Usui, Tokyo Metropolitan Industrial Technic Institute, for making available their gas chromatograph-mass spectrometer.

References

1) "The Chemistry of the Carbon-Halogen Bond," Part 2, ed by S. Patai, Chap. 12 of "The Radiation Chemistry of the Carbon-Halogen Bond," John Wiley & Sons (1973).
2) M. Anbar and P. Neta, *J. Chem. Soc. A*, **72**, 837 (1967).
3) G. Bullock and R. Coopen, *Trans. Faraday Soc.*, **66**, 2055 (1970).
4) C. Radlowski and W. V. Sherman, *J. Phys. Chem.*, **74**, 3043 (1970).
5) R. Evans, E. Nesyto, C. Radlowski, and W. V. Sherman *J. Phys. Chem.*, **75**, 2762 (1971).
6) H. Ogura, T. Fujimura, T. Unnai, and M. Kondo, *Bull. Chem. Soc. Jpn.*, **48**, 1613 (1975).
7) A. Horowitz and L. A. Rajbenbach, *J. Phys. Chem.*, **74**, 678 (1970).
8) M. G. Katz, A. Horowitz, and L. A. Rajbenbach, *Trans. Faraday Soc.*, **67**, 2354 (1971).
9) R. Aloni, M. G. Katz, and L. A. Rajbenbach, *Int. J. Chem. Kinetics*, **7**, 699 (1975).
10) M. G. Katz, G. Baruch, and L. A. Rajbenbach, *J. Chem. Soc., Faraday Trans. 1*, **72**, 1903 (1976).
11) M. G. Katz, G. Baruch, and L. A. Rajbenbach, *J. Chem. Soc., Faraday Trans. 1*, **72**, 2462 (1976).
12) W. V. Sherman, *J. Phys. Chem.*, **72**, 2287 (1968).
13) T. Sawai and Y. Shinozaki, *Chem. Lett.*, **1972**, 865; T. Sawai, T. Shimokawa, and Y. Shinozaki, *Bull. Chem. Soc. Jpn.*, **47**, 1889 (1974).
14) S. Arai, M. Matsui, I. Moriguchi, and M. Imamura, *Reports Inst. Phys. Chem. Res.*, **48**, 185 (1972).
15) T. Sawai, T. Shimokawa, T. Sawai, I. Hosoda, and M. Kondo, *J. Nucl. Sci. Tech.*, **12**, 502 (1975); T. Shimokawa and T. Sawai, *ibid.*, **14**, 731 (1977).
16) L. M. Dorfman and G. E. Adams, NSRDS-NBS-46 (1973).
17) M. Anbar, Farhatazi, and A. B. Ross, NSRDS-NBS-51 (1975).
18) I. A. Taub and L. M. Dorfman, *J. Am. Chem. Soc.*, **84**, 4053 (1962).
19) W. A. Seddon and A. O. Allen, *J. Phys. Chem.*, **71**, 1914 (1967).
20) M. Simic, P. Neta, and E. Hayon, *J. Phys. Chem.*, **73**, 3794 (1969).
21) J. W. Fletcher, P. J. Richards, and W. A. Seddon, *Can. J. Chem.* **48**, 3765 (1970).
22) D. W. Johnson and G. A. Salmon, *J. Chem. Soc., Faraday Trans. 1*, **71**, 583 (1975).
23) J. Rabani, W. A. Mulac, and M. S. Matheson, *J. Phys. Chem.*, **81**, 99 (1977).
24) J. Teply, *Radiat. Res. Rev.*, **1**, 361 (1969).
25) E. Hayon and M. Simic, *Acc. Chem. Res.*, **7**, 114 (1974).
26) P. S. Rao and E. Hayon, *J. Am. Chem. Soc.*, **96**, 1287 (1974).
27) K. Schwabe, "Polarographie und Chemishe Konstitution Organischer Verbindungen," Akademie-Verlag, Berlin (1957), p. 306.
28) K. D. Asmus, A. Hengline, A. Wigger, and G. Beck, *Ber. Bunsenges Phys. Chem.*, **70**, 756 (1966).
29) V. J. Lilie, G. Beck, and A. Hengline, *Ber. Bunsenges Phys. Chem.*, **75**, 458 (1971).

Conductometric Studies on the Ion-pair Formations of $[Cr(NH_3)_6]^{3+}$, $[Co(NH_3)_6]^{3+}$, $[Cr(en)_3]^{3+}$, and $[Co(en)_3]^{3+}$ with Several Anions in Aqueous Solutions

Tatsuo Takahashi and Takefumi Koiso

Department of Chemistry, Fukushima Technical College, Iwaki 970

(Received September 24, 1977)

The thermodynamic ion-association constants (K) of $[Cr(NH_3)_6]^{3+}$, $[Co(NH_3)_6]^{3+}$, $[Cr(en)_3]^{3+}$, and $[Co(en)_3]^{3+}$ with several anions in aqueous solutions were determined using the conductometric method. The log K values obtained at 25.0 °C are 1.1_7 for $[Cr(NH_3)_6]^{3+}$–SCN^-, 1.3_4 for $[Cr(en)_3]^{3+}$–SCN^-, 1.3_0 for $[Co(NH_3)_6]^{3+}$–SCN^-, 1.3_4 for $[Co(en)_3]^{3+}$–SCN^-, 1.6_8 for $[Co(en)_3]^{3+}$–Br^-, 1.4_6 for $[Co(en)_3]^{3+}$–I^-, 1.3_7 for $[Co(en)_3]^{3+}$–ClO_4^-, 3.2_0 for $[Cr(NH_3)_6]^{3+}$–$C_2O_4^{2-}$, and 2.9_7 for $[Cr(en)_3]^{3+}$–$C_2O_4^{2-}$. The results indicate that the SCN^- ion has less of a tendency to associate with the complex cations than do other univalent anions, the K values of SCN^- being of the same order of magnitude as those of ClO_4^-, and that the K values of chromium(III) complex cations with several anions are slightly smaller than those of the corresponding cobalt(III) complex cations.

In order to clarify the factors that influence the extent to which ions associate in aqueous solutions, the ion-association constants of ion-pairs have been determined by various researchers[1–10] using various methods. In previous papers,[11,12] Takahashi *et al.* have reported that the ion-association constants determined using the conductometric and spectrophotometric methods were not very different from each other, and that the electrostatic interaction between ions is the dominant influence.

Also, it was found that the internal conjugate base (ICB) effect[13] should be considered in ion-pair formation.

In the present paper, conductometric studies of the ion-pairs, $[Co(en)_3]^{3+}$–X^- (X=SCN, Br, I, ClO_4), $[Cr(NH_3)_6]^{3+}$–SCN^-, $[Cr(en)_3]^{3+}$–SCN^-, $[Co(NH_3)_6]^{3+}$–SCN^-, $[Cr(NH_3)_6]^{3+}$–$C_2O_4^{2-}$, and $[Cr(en)_3]^{3+}$–$C_2O_4^{2-}$ are presented. Some factors are briefly discussed from the viewpoint given in previous papers.[11,12]

Experimental

The compounds used in this study were prepared according to procedures described in the literature. Each compound was carefully purified by triple recrystallization from redistilled water. The purity was examined using conventional chemical analysis of the components; the results are in very good agreement with the theoretical values. Solutions of different concentrations were carefully prepared using conductivity water having an electrolytic conductivity lower than 4×10^{-7} S cm^{-1}. The electrolytic conductivities were measured with the same apparatus and using the same procedures previously described.[11,12]

Results and Discussion

The relations between the molar conductivities, Λ, of the complexes and the ionic strength (I) are shown in Figs. 1—3; the broken lines indicate the theoretical Onsager lines for the fully ionized electrolyte. The molar conductivities of the oxalates shown in Fig. 3 have large deviations, indicating that there is strong ion-association between $[Cr(NH_3)_6]^{3+}$ or $[Cr(en)_3]^{3+}$ and $C_2O_4^{2-}$.

Table 1 presents the limiting molar conductivity, $\Lambda°$, of each complex determined by the Onsager extrapolation method,[14] and also the limiting molar conductivity, $\lambda°$, of each complex cation calculated from the $\Lambda°$ value. However, the $\Lambda°$ (1/6 M_2 $(C_2O_4)_3$) was assumed to be equal to the sum of the $\lambda°$ (1/3 M^{3+}) value for the corresponding complex cation obtained in this study and in previous studies[11,12] and the value (74.2 S cm^2 mol^{-1}) for $\lambda°$ (1/2 $C_2O_4^{2-}$), because the Onsager method was not considered to be appropriate for higher-valent electrolytes; the $\Lambda°$ (1/6 $[Cr(NH_3)_6]_2(C_2O_4)_3\cdot5H_2O$) and $\Lambda°([Cr(en)_3]_2(C_2O_4)_3)$ values thus estimated are 172.6 and 147.8 S cm^2 mol^{-1}, respectively.* The so-called Stokes radii, r_s, of these complex cations

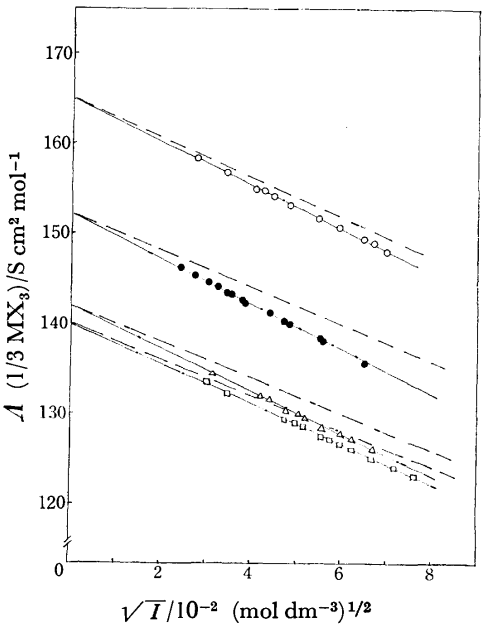

Fig. 1. The Onsager plots of hexaamminechromium(III) thiocyanate (-○-), tris(ethylenediamine)cobalt(III) iodide (-●-), tris(ethylenediamine)cobalt(III) perchlorate (-△-), and tris(ethylenediamine)-chromium(III) thiocyanate (-□-) in aqueous solutions at 25.0 °C.

* When Onsager's method for determining the $\Lambda°$ values is applied to the conductivities of the oxalates, the approximate $\Lambda°(1/6[Cr(NH_3)_6]_2(C_2O_4)_3\cdot5H_2O)$ and $\Lambda°(1/6[Cr(en)_3]_2(C_2O_4)_3$ values are 173 and 148 S cm^2 mol^{-1}, respectively.

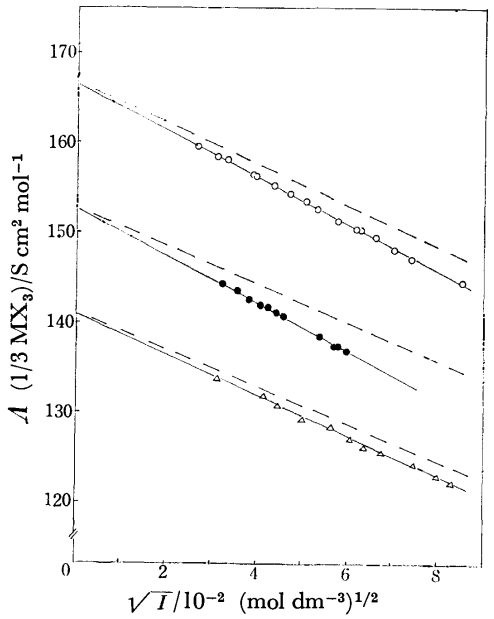

Fig. 2. The Onsager plots of hexaamminecobalt(III) thiocyanate (-○-), tris(ethylenediamine)cobalt(III) bromide (-●-), and tris(ethylenediamine)cobalt(III) thiocyanate (-△-) in aqueous solutions at 25.0 °C.

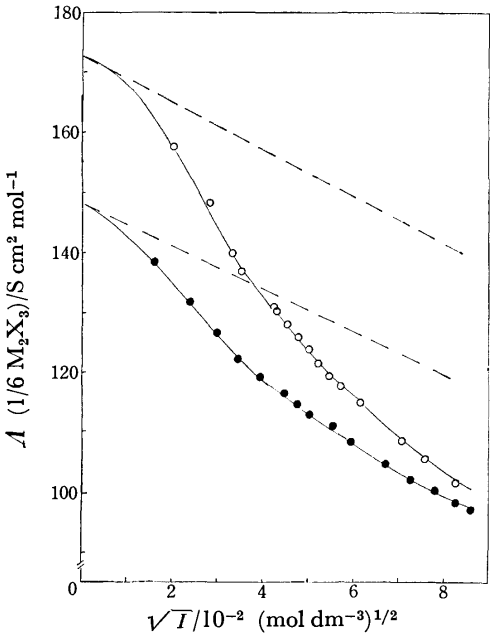

Fig. 3. The Onsager plots of hexaamminechromium(III) oxalate (-○-) and tris(ethylenediamine)chromium(III) oxalate (-●-) in aqueous solutions at 25.0 °C.

determined from the conductivity data of this study are summarized in Table 2, in which the results reported previously are also presented. The degrees of dissociation of the possible ion-pairs were determined according to the successive approximation method described by Jenkins and Monk[1] and, then, the thermodynamic ion-association constants, K, were calculated from both the degree of dissociation obtained and the activity coefficients of the ions as estimated from the Debye-Hückel limiting equation. In the present calculation, the limiting conductivities of the ion-pairs

Table 1. The limiting molar conductivity of chromium(III) and cobalt(III) complexes (MX_3), and the complex cations (M^{3+}) in aqueous solutions at 25.0 °C

Complex	Molar conductivity (S cm² mol⁻¹)	
	Λ° (1/3MX_3)	λ°(1/3M^{3+})
$[Cr(NH_3)_6](SCN)_3$	164.6	98.1
$[Cr(en)_3](SCN)_3$	139.7	73.2
$[Co(NH_3)_6](SCN)_3$	165.7	99.2
$[Co(en)_3](SCN)_3$	140.7	74.2
$[Co(en)_3]Br_3$	152.1	74.0
$[Co(en)_3]I_3 \cdot H_2O$	151.4	74.6
$[Co(en)_3](ClO_4)_3$	141.4	74.0

Table 2. The limiting molar conductivity and the Stokes radius, r_S, of complex cations aqueous solutions at 25.0 °C

Complex cations	λ°(1/3M^{3+}) (S cm² mol⁻¹)	r_S (Å)
$[Cr(NH_3)_6]^{3+}$	98.1	2.81
	98.5[11]	2.80[11]
	98.5[12]	2.80[12]
$[Cr(en)_3]^{3+}$	73.2	3.76
	73.4[11]	3.75[11]
	74.1[12]	3.72[12]
$[Co(NH_3)_6]^{3+}$	99.2	2.78
	99.2[1]	2.78[1]
	99.0—99.7[4,7]	2.78—2.76[4,7]
$[Co(en)_3]^{3+}$	74.2	3.71
	74.7[1]	3.69[1]

was estimated from the relations,

$$\frac{\lambda^\circ(1/2M^{3+}X^-)}{\lambda^\circ(1/3M^{3+})} = \frac{2}{3}$$

and

$$\frac{\lambda^\circ(M^{3+}C_2O_4^{2-})}{\lambda^\circ(1/3M^{3+})} = \frac{1}{3}.$$

The results are given in Table 3, together with those which have been determined by various researchers using various methods.

If the closest approach of the two ions of the ion-pair is assumed to be equal to the sum of their Stokes radii, the K value can be estimated from the Bjerrum theory.[15] Table 4 shows the log K values calculated theoretically.

On the basis of the results given in Table 3, it appears reasonable to conclude that the K values of chromium(III) complex cations with several anions are a little smaller than those of the corresponding cobalt(III) complex cations. A similar conclusion has been drawn in previous studies.[11,12] Although the detailed comparison of the K values obtained using the same method on a given ion-pair was limited, it was also likely that the K values for $[M(NH_3)_6]^{3+}$ (M=Cr, Co) with such ions as ClO_4^-, NO_3^-, $C_2O_4^{2-}$, and SO_4^{2-} are a little larger than those for $[M(en)_3]^{3+}$ with the respective anions. Since the Stokes radii of $[M(en)_3]^{3+}$ are larger

TABLE 3. LOGARITHMIC ASSOCIATION CONSTANTS FOR INFINITE DILUTION AT 25.0 °C

Ion-pair	log (K/mol^{-1} dm^3)	Method[a)]	Investigators	Ref.
$[Cr(NH_3)_6]^{3+}$-ClO_4^-	1.1_8	cond	Takahashi, Koiso, and Tanaka (1974)	11
	1.0_0[c)]	sp	Takahashi, Koiso, and Tanaka (1974)	11
$[Co(NH_3)_6]^{3+}$-ClO_4^-	1.4_0	cond	Katayama and Tamamushi (1968)	7
$[Cr(en)_3]^{3+}$-ClO_4^-	1.0_2	cond	Takahashi, Koiso, and Tanaka (1974)	11
$[Cr(en)_3]^{3+}$-ClO_4^-	1.2_0[c)]	sp	Takahashi, Koiso, and Tanaka (1974)	11
	0.9_0[c)]	sp	Takahashi and Koiso (1976)	12
$[Co(en)_3]^{3+}$-ClO_4^-	1.3_7	cond	Present study	
$[Cr(NH_3)_6]^{3+}$-SCN^-	1.1_7	cond	Present study	
$[Co(NH_3)_6]^{3+}$-SCN^-	1.3_0	cond	Present study	
$[Cr(en)_3]^{3+}$-SCN^-	1.3_4	cond	Present study	
$[Co(en)_3]^{3+}$-SCN^-	1.3_4	cond	Present study	
$[Cr(NH_3)_6]^{3+}$-I^-	1.2_9	cond	Takahashi, Koiso, and Tanaka (1974)	11
	1.3_4	sp	Takahashi, Koiso, and Tanaka (1974)	11
$[Co(NH_3)_6]^{3+}$-I^-	1.3_8	cond	Katayama and Tamamushi (1968)	7
$[Cr(en)_3]^{3+}$-I^-	1.4_2	cond	Takahashi, Koiso, and Tanaka (1974)	11
	1.3_3	sp	Takahashi, Koiso, and Tanaka (1974)	11
$[Co(en)_3]^{3+}$-I^-	1.4_6	cond	Present study	
$[Cr(NH_3)_6]^{3+}$-Cl^-	1.3_7	cond	Takahashi and Koiso (1976)	12
$[Co(NH_3)_6]^{3+}$-Cl^-	1.4_9	cond	Jenkins and Monk (1951)	1
	1.5	cond	Tamamushi, Isono, and Katayama (1967)	4
$[Cr(en)_3]^{3+}$-Cl^-	1.5_8	cond	Takahashi and Koiso (1976)	12
	1.6_5	sp	Takahashi and Koiso (1976)	12
$[Co(en)_3]^{3+}$-Cl^-	1.7_2	cond	Jenkins and Monk (1951)	1
$[Cr(NH_3)_6]^{3+}$-Br^-	1.5_7	cond	Takahashi and Koiso (1976)	12
$[Co(NH_3)_6]^{3+}$-Br^-	1.6_5	cond	Katayama and Tamamushi (1968)	7
$[Cr(en)_3]^{3+}$-Br^-	1.5_0	cond	Takahashi and Koiso (1976)	12
	1.4_6	sp	Takahashi and Koiso (1976)	12
$[Co(en)_3]^{3+}$-Br^-	1.6_8	cond	Present study	
$[Cr(NH_3)_6]^{3+}$-NO_3^-	1.5_3	cond	Takahashi and Koiso (1976)	12
$[Co(NH_3)_6]^{3+}$-NO_3^-	1.6_3	cond	Katayama and Tamamushi (1968)	7
$[Cr(en)_3]^{3+}$-NO_3^-	1.4_9	cond	Takahashi and Koiso (1976)	12
$[Cr(NH_3)_6]^{3+}$-SO_4^{2-}	3.1_4[b*)]	pol	Tanaka, Ogino, and Satô (1966)	3
	3.1_5[b*)]	chron	Tanaka and Yamada (1967)	6
$[Co(NH_3)_6]^{3+}$-SO_4^{2-}	3.2_1[b*)]	pol	Tanaka, Ogino, and Satô (1966)	3
	3.5_6	cond	Jenkins and Monk (1951)	1
	3.3_0[b*)]	chron	Tanaka and Yamada (1967)	6
	3.2_6[b**)]	sp	Tanaka, Kobayashi, and Kamada (1967)	5
$[Cr(en)_3]^{3+}$-SO_4^{2-}	2.9_9[b*)]	chron	Tanaka and Yamada (1967)	6
$[Co(en)_3]^{3+}$-SO_4^{2-}	3.4_5	cond	Jenkins and Monk (1951)	1
	3.1_0[b**)]	sp	Tanaka, Kobayashi, and Kameda (1967)	5
	3.2_2[b*)]	chron	Tanaka and Yamada (1967)	6
$[Cr(NH_3)_6]^{3+}$-$C_2O_4^{2-}$	3.2_0	cond	Present study	
$[Co(NH_3)_6]^{3+}$-$C_2O_4^{2-}$	3.2_5	cond	Katayama and Tamamushi (1968)	7
$[Cr(en)_3]^{3+}$-$C_2O_4^{2-}$	2.9_7	cond	Present study	

a) Methods of measurement: cond—conductivity, sp—spectrophotometry, pol—polarography, and chron—chronopotentiometry. b) The values calculated from concentration constants obtained at I=0.10(*) (mol dm^{-3}) and I=0.07(**) (mol dm^{-3}). c) These values were determined indirectly.[11,12]

than that of $[M(NH_3)_6]^{3+}$, this view is to be expected so far as the ion-association is assumed to depend only on Coulombic interaction between the ions. Therefore, it appears appropriate to state that the electrostatic interaction between ions is the dominant influence among various factors in the process of ion-pair formation of the complex cation with oxoacid anions, such as ClO_4^-, NO_3^-, $C_2O_4^{2-}$, and SO_4^{2-}. Furthermore, Table 2 also indicates that the K values of the complex cations with SCN^- are smaller than those with other univalent anions, except for ClO_4^-. That is, the extent of association is about the same in the perchlorate and thiocyanate systems. The smaller tendency of the complex cations to associate with SCN^- is probably due to the fact that the SCN^- is not only of low charge and large size, but also that it is a linear ion. Thus, the SCN^- ion may possess rotational entropy which would be lost on ion-association.[16]

TABLE 4. LOGARITHMIC ASSOCIATION CONSTANTS CALCULATED FROM BJERRUM'S THEORY OF THE ION-PAIRS IN AQUEOUS SOLUTIONS AT 25.0 °C

Ion-pair	log (K/mol^{-1} dm^3)
$[Cr(NH_3)_6]^{3+}$-SCN^-	1.7_6
$[Cr(en)_3]^{3+}$-SCN^-	1.6_3
$[Co(NH_3)_6]^{3+}$-SCN^-	1.7_7
$[Co(en)_3]^{3+}$-SCN^-	1.6_4
$[Co(en)_3]^{3+}$-Br^-	1.6_7
$[Co(en)_3]^{3+}$-I^-	1.6_7
$[Co(en)_3]^{3+}$-ClO_4^-	1.6_4
$[Cr(NH_3)_6]^{3+}$-$C_2O_4^{2-}$	3.0_8
$[Cr(en)_3]^{3+}$-$C_2O_4^{2-}$	2.9_0

The authors express their thanks to Professor Nobuyuki Tanaka (Department of Chemistry, Faculty of Science, Tohoku University) for his valuable and kind assistance throughout the course of this work.

References

1) I. L. Jenkins and C. B. Monk, *J. Chem. Soc.*, **1951**, 68.
2) S. H. Laurie and C. B. Monk, *J. Chem. Soc.*, **1963**, 3343.
3) N. Tanaka, K. Ogino, and G. Satô, *Bull. Chem. Soc. Jpn.*, **39**, 366 (1966).
4) R. Tamamushi, T. Isono, and S. Katayama, *Bull. Chem. Soc. Jpn.*, **40**, 334 (1967).
5) N. Tanaka, Y. Kobayashi, and M. Kamada, *Bull. Chem. Soc. Jpn.*, **40**, 2839 (1967).
6) N. Tanaka and A. Yamada, *Z. Anal. Chem.*, **224**, 117 (1967).
7) S. Katayama and R. Tamamushi, *Bull. Chem. Soc. Jpn.*, **41**, 606 (1968).
8) N. Tanaka, H. Kaneko, and T. Shirakashi, *Nippon Kagaku Zasshi*, **92**, 957 (1971).
9) S. Katayama, *Bull. Chem. Soc. Jpn.*, **46**, 106 (1973).
10) H. Yokoyama and H. Yamatera, *Chem. Lett.*, **1973**, 337.
11) T. Takahashi, T. Koiso, and N. Tanaka, *Nippon Kagaku Kaishi*, **1974**, 65.
12) T. Takahashi and T. Koiso, *Bull. Chem. Soc. Jpn.*, **49**, 2784 (1976).
13) D. B. Rorabacher, *Inorg. Chem.*, **5**, 1891 (1966).
14) L. Onsager, *Physik. Z.*, **28**, 277 (1927).
15) N. Bjerrum, *Kgl. Danske videnskab.*, **7**, No.9 (1926).
16) A. L. Phipps and R. A. Plane, *J. Am. Chem. Soc.*, **79**, 2458 (1957).

N,N-Disubstituted 1,3-Dithiolan-2-iminium–TCNQ^{-} Salts: Effect of the Substituents on the Nitrogen Atom on the Composition and the Electrical Conductivity

Shingo Araki and Toshio Tanaka

Department of Applied Chemistry, Faculty of Engineering, Osaka University, Suita, Osaka 565

(Received September 27, 1977)

Following 10 simple and complex salts of TCNQ^{-} with *N,N*-disubstituted 1,3-dithiolan-2-iminium cations; $(CH_2)_2\langle S \rangle C{=}\overset{+}{N}R^1R^2 \cdot (TCNQ)_n^{-}$ (n=1 when R^1=R^2=*n*-Pr, *n*-C_6H_{13}, *n*-C_8H_{17}, Ph, and R^1=Me and R^2=Ph; n=2 when R^1= R^2=*n*-Pr, *n*-Bu, Ph, and R^1=Me and R^2=Ph), and $[(CH_2)_2\langle S \rangle C{=}\overset{+}{N}(n\text{-}C_{10}H_{21})_2]_2 \cdot (TCNQ)_3^{2-}$ were prepared. Of these, simple salt $(CH_2)_2\langle S \rangle C{=}\overset{+}{N}(n\text{-}C_8H_{17})_2 \cdot TCNQ^{-}$ was obtained in two different crystalline forms; unstable violet needles and green plates. All the salts as compacted samples displayed semi-conducting behaviors in the 20—90 °C range. Electrical resistivities of the 1:2 complex salts fell in the range of 5—90 ohm cm at 25 °C, while the simple and 2:3 complex salts showed much large resistivities (the order of 10^3—10^9 ohm cm). The measurements of electronic absorption spectra and magnetic susceptibilities indicated that the simple salts in the solid state involve dimeric $(TCNQ)_2^{2-}$, except for the green salt of $(CH_2)_2\langle S \rangle C{=}\overset{+}{N}(n\text{-}C_8H_{17})_2 \cdot TCNQ^{-}$ which consists of the iminium cation and discrete TCNQ^{-} radical anion. Electronic spectra of the 1 : 2 and 2 : 3 complex salts also are discussed in comparison with analogous TCNQ^{-} salts reported so far.

In the previous paper,[1] we reported the preparation and electrical resistivity of some simple and complex salts formed between *N,N*-dialkyl-1,3-dichalcogenacycloalkan-2-iminium cations and 7,7,8,8-tetracyanoquinodimethane (TCNQ) radical anion; $(CH_2)_n\langle Y \rangle C{=}\overset{+}{N}R_2 \cdot TCNQ^{-}$ and $(CH_2)_n\langle Y \rangle C{=}\overset{+}{N}R_2 \cdot (TCNQ)_2^{-}$ (n=2, 3; Y=S, Se; R=Me, Et; but not all combinations). The resistivities of the simple salts as compacted samples fell in the 10^4—10^5 ohm cm range at 25 °C with the activation energies of 0.27—0.37 eV. The complex salts (compacted samples) exhibited the resistivities of 2.4 to 4.0 ohm cm with very small activation energies (0.018—0.087 eV); there was no appreciable difference of the resistivity between the *N,N*-dimethyl- and *N,N*-diethyliminium–$(TCNQ)_2^{-}$.

The present work was undertaken to study the effect of the *N*-substituents of the iminium cations on the composition and electrical resistivity of the TCNQ^{-} salts. This paper reports the preparation and electrical resistivity of a series of simple and complex salts of TCNQ^{-} radical anion with *N,N*-disubstituted 1,3-dithiolan-2-iminium cations, $(CH_2)_2\langle S \rangle C{=}\overset{+}{N}R^1R^2$ (R^1=R^2=*n*-Pr, *n*-Bu, *n*-C_6H_{13}, *n*-C_8H_{17}, *n*-$C_{10}H_{21}$, Ph, and R^1=Me and R^2=Ph). The resistivity is discussed in terms of stacking of TCNQ^{-} on the basis of electronic absorption spectra and magnetic susceptibilities in the solid state.

Experimental

Materials. Bis(*N,N*-disubstituted 1,3-dithiolan-2-iminium) tetrabromodimethylstannate(IV), $[(CH_2)_2\langle S \rangle C{=}\overset{+}{N}R_2]_2 \cdot [SnBr_4Me_2]^{2-}$, was synthesized by reaction of bis(*N,N*-disubstituted dithiocarbamato)dimethyltin(IV), $Me_2Sn(S_2CNR_2)_2$, with 1,2-dibromoethane by a manner similar to the *N,N*-dimethyliminium analog.[2] R=*n*-Pr, mp 143.5—145.5 °C. Found: C, 27.28; H, 4.73; N, 3.32%. Calcd for $C_{20}H_{42}N_2S_4Br_4Sn$: C, 27.38; H, 4.84; N, 3.19%. R=*n*-Bu, mp 121—122.5 °C. Found: C, 30.74; H, 5.38; N, 3.02%. Calcd for $C_{24}H_{50}N_2S_4Br_4Sn$: C, 30.88; H, 5.41; N, 3.00%. R=*n*-C_6H_{13}, mp 86—87 °C. Found: C, 36.54; H, 6.28; N, 2.78%. Calcd for $C_{32}H_{66}N_2S_4Br_4Sn$: C, 36.76; H, 6.38; N, 2.68%. R=*n*-C_8H_{17}, mp 86—88 °C. Found: C, 41.31; H, 7.10; N, 2.48%. Calcd for $C_{40}H_{82}N_2S_4Br_4Sn$: C, 41.49; H, 7.15; N, 2.42%. R=*n*-$C_{10}H_{21}$, mp 88—91 °C. Found: C, 45.07; H, 7.79; N, 2.24%. Calcd for $C_{48}H_{98}N_2S_4Br_4Sn$: C, 45.39; H, 7.79; N, 2.21%. R=Ph, mp 153—157 °C. Found: C, 37.47; H, 3.37; N, 2.74%. Calcd for $C_{32}H_{34}N_2S_4Br_4Sn$: C, 37.93; H, 3.39; N, 2.77%.

N-Methyl-*N*-phenyl-1,3-dithiolan-2-iminium trichlorodimethyl-stannate(IV), $(CH_2)_2\langle S \rangle C{=}\overset{+}{N}MePh \cdot [SnCl_3Me_2]^{-}$,[2] was prepared as described in the literature.

*N,N-Disubstituted 1,3-Dithiolan-2-iminium–TCNQ Simple Salts, $(CH_2)_2\langle S \rangle C{=}\overset{+}{N}R^1R^2 \cdot TCNQ^{-}$ (R^1=R^2=n-Pr (**1**), n-C_6H_{13} (**2**), n-C_8H_{17} (**3**), Ph (**4**), and R^1=Me and R^2=Ph (**5**).)* To a solution of Li^+TCNQ^{-} (2.4 mmol) in hot ethanol was added a hot ethanol solution of $[(CH_2)_2\langle S \rangle C{=}\overset{+}{N}(n\text{-}Pr)_2]_2 \cdot [SnBr_4Me_2]^{2-}$ (1.2 mmol). The mixture was filtered. The filtrate was allowed to stand in a refrigerator overnight to afford **1**, which was recrystallized from acetonitrile, 71% yield. Other four simple salts were similarly prepared by reaction of TCNQ^{-} with the appropriate iminium cation in ethanol, 70—83% yields. Of these salts, **3** was obtained as a mixture of violet crystals (**3a**) and green ones (**3b**). These were separated by fractional crystallization from ethanol.

*N,N-Disubstituted 1,3-Dithiolan-2-iminium–TCNQ Complex Salts, $(CH_2)_2\langle S \rangle C{=}\overset{+}{N}R^1R^2 \cdot (TCNQ)_2^{-}$ (R^1=R^2=n-Pr (**6**), Ph (**8**), and R^1=Me and R^2=Ph (**9**)).* To a hot acetonitrile solution of **1** obtained as above (1.5 mmol) was added neutral TCNQ (1.5 mmol) in hot acetonitrile. After filtration, the mixture was allowed to stand in a refrigerator overnight to afford **6**, 73% yield. Complex salts **8** and **9** were similarly prepared by reaction of **4** or **5** with TCNQ at the mole ratio of 1:1 in acetonitrile, 75 and 78% yields respectively.

Table 1. Properties and analytical data of the $TCNQ^{-}$ salts

No.	Compound		Mp (dec) °C	%C Found (Calcd)	%H Found (Calcd)	%N Found (Calcd)
1	$[^{-}_{S}\!\!>\!C\!=\!\overset{+}{N}(n\text{-Pr})_2\cdot TCNQ^{-}$	Purple needles	131—133	61.32 (61.73)	5.29 (5.44)	17.06 (17.14)
2	$[^{-}_{S}\!\!>\!C\!=\!\overset{+}{N}(n\text{-}C_6H_{13})_2\cdot TCNQ^{-}$	Purple needles	>110	65.41 (65.80)	6.80 (6.97)	14.52 (14.22)
3a	$[^{-}_{S}\!\!>\!C\!=\!\overset{+}{N}(n\text{-}C_8H_{17})_2\cdot TCNQ^{-}$	Violet needles	97— 98	67.98 (67.83)	7.59 (7.73)	12.90 (12.76)
3b	$[^{-}_{S}\!\!>\!C\!=\!\overset{+}{N}(n\text{-}C_8H_{17})_2\cdot TCNQ^{-}$	Green plates	97— 98	68.01 (67.83)	7.64 (7.73)	12.87 (12.76)
4	$[^{-}_{S}\!\!>\!C\!=\!\overset{+}{N}Ph_2\cdot TCNQ^{-}$	Dark-purple needles	>140	67.18 (68.04)	3.63 (3.81)	14.84 (14.70)
5	$[^{-}_{S}\!\!>\!C\!=\!\overset{+}{N}MePh\cdot TCNQ^{-}$	Purple needles	>170	63.23 (63.74)	3.67 (3.90)	16.92 (16.90)
6	$[^{-}_{S}\!\!>\!C\!=\!\overset{+}{N}(n\text{-Pr})_2\cdot(TCNQ)_2^{-}$	Black needles	>212	64.58 (64.68)	4.04 (4.29)	20.85 (20.58)
7	$[^{-}_{S}\!\!>\!C\!=\!\overset{+}{N}(n\text{-Bu})_2\cdot(TCNQ)_2^{-}$	Black plates	>196	65.83 (65.59)	4.28 (4.73)	20.42 (19.68)
8	$[^{-}_{S}\!\!>\!C\!=\!\overset{+}{N}Ph_2\cdot(TCNQ)_2^{-}$	Black plates	>195	68.59 (68.80)	2.91 (3.26)	18.23 (18.52)
9	$[^{-}_{S}\!\!>\!C\!=\!\overset{+}{N}MePh\cdot(TCNQ)_2^{-}$	Black needles	>222	65.87 (65.99)	3.02 (3.26)	20.38 (20.38)
10	$\left[^{-}_{S}\!\!>\!C\!=\!\overset{+}{N}(n\text{-}C_{10}H_{21})_2\right]_2\cdot(TCNQ)_3^{2-}$	Dark-purple needles	88— 90	69.65 (69.64)	7.44 (7.43)	13.61 (13.87)

N,N-Dibutyl- and N,N-Didecyl-1,3-dithiolan-2-iminium-TCNQ Complex Salts, $(CH_2)_2\langle^{S}_{S}\!\!>\!C\!=\!\overset{+}{N}(n\text{-Bu})_2\cdot(TCNQ)_2^{-}$ (7) and $[(CH_2)_2\langle^{S}_{S}\!\!>\!C\!=\!\overset{+}{N}(n\text{-}C_{10}H_{21})_2]_2\cdot(TCNQ)_3^{2-}$ (10). The reaction of $Li^{+}TCNQ^{-}$ (2.4 mmol) with $[(CH_2)_2\langle^{S}_{S}\!\!>\!C\!=\!\overset{+}{N}(n\text{-Bu})_2]_2\cdot[SnBr_4Me_2]^{2-}$ (1.2 mmol) in hot ethanol was carried out as described in **1**, giving **7**, which was recrystallized from acetonitrile, 65% yield based on $Li^{+}TCNQ^{-}$. Similarly, $Li^{+}TCNQ^{-}$ reacted with $[(CH_2)_2\langle^{S}_{S}\!\!>\!C\!=\!\overset{+}{N}(n\text{-}C_{10}H_{21})_2]_2\cdot[SnBr_4Me_2]^{2-}$ at the mole ratio of 2:1 in ethanol to afford **10**, 63% yield based on $Li^{+}TCNQ^{-}$.

Elemental analyses and properties of the simple and complex salts obtained are listed in Table 1.

Physical Measurements. Electrical resistivities, electronic absorption and infrared spectra, and magnetic susceptibilities were measured as described previously.[1]

Results and Discussion

Synthesis and Electrical Properties. The reaction of *N,N*-dibutyl- and *N,N*-didecyl-1,3-dithiolan-2-iminium cations with $TCNQ^{-}$ radical anion gave the 1 : 2 and 2 : 3 complex salts, **7** and **10**, respectively, irrespective of the mole ratio of the reactants. These results are analogous to the reaction of the *N,N*-diethyliminium cation with $TCNQ^{-}$.[1] There are two possible oxidizing agents in the reaction mixture. One is the iminium cation, because the cation easily undergoes a nucleophilic attack on the carbon atom at the 2, 4, or 5 position.[3] The other is the $[SnBr_4Me_2]^{2-}$ anion which may be reduced to give any Sn(II) species. However, no reduced product has been obtained in the present study. On the other hand, the other iminium cations used here reacted with $TCNQ^{-}$ to give simple salts **1**—**5**, of which **3** was obtained in two crystalline forms with different colors; violet needles (**3a**) and green plates (**3b**). Crystals **3a** slowly changed in color to green at room temperature irreversibly, suggesting that **3a** is in a metastable state. This color change occurred instantly on heating **3a** at 70 °C. Simple salts **1**, **4**, and **5** further reacted with an equimolar amount of neutral TCNQ to yield complex salts **6**, **8**, and **9**, respec-

Table 2. Electrical resistivity (ρ) and activation energy (E_a) of the $TCNQ^{-}$ salts

Compound	$\rho_{25°C}$ [a] / ohm cm	E_a / eV
Simple salt		
1	2.2×10^{5}	0.20
2	1.3×10^{7}	0.54
3b	1.9×10^{9}	1.3
4	4.4×10^{3} (5.0×10^{3})	0.16
5	8.2×10^{5}	0.29
Complex salt		
6	6.9×10	0.061
7	9.0×10	0.099
8	3.4×10 (3.3×10)	0.12
9	5.4	0.059
10	6.3×10^{6}	0.53

a) The values in parentheses were obtained by the four-probe method.

tively. On the other hand, **2** and **3** were only recovered in their reactions with neutral TCNQ in acetonitrile.

The electrical resistivities (ρ) of simple and complex salts at 25 °C and the activation energies (E_a) calculated from the equation $\rho=\rho_0\exp(E_a/kT)$ are listed in Table 2. The resistivity of **3a** has not been measured for its thermal instability as described above. All the simple and complex salts show typical semi-conducting behavior in the temperature range measured. The resistivity of **9** is low in the same degree as those of the corresponding *N,N*-dimethyl- and *N,N*-diethyliminium salts, $(CH_2)_2\langle^{S}_{S}\rangle C{=}\overset{+}{N}R_2\cdot(TCNQ)_2^-$ (3.8 and 3.3 ohm cm for R=Me and Et, respectively).[1] Other 1 : 2 complex salts obtained here showed about 10 times higher resistivities than **9** as well as the *N,N*-dimethyl- and *N,N*-diethyliminium analogs. This result seems to indicate that the electrical resistivity of the 1 : 2 complex salts increases by introducing bulky substituents on the iminium nitrogen.

Electronic Spectra and Magnetic Susceptibilities. Figure 1 shows the electronic absorption spectra of **1** and **2** in the solid state. These spectral patterns closely resemble those of analogous simple salts, $(CH_2)_n\langle^{S}_{S}\rangle C{=}\overset{+}{N}Me_2\cdot TCNQ^-$ (n=2 or 3) and $(CH_2)_2\langle^{Se}_{Se}\rangle C{=}\overset{+}{N}Me_2\cdot TCNQ^-$, which have been reported to involve dimeric $(TCNQ)_2^{2-}$.[1] The existence of the $(TCNQ)_2^{2-}$ dimer in **1** and **2** is also suggested from their diamagnetic properties in the solid state ($\chi_M=-3.4\times10^{-4}$ and -4.5×10^{-4} emu mol^{-1}, respectively). Many TCNQ⁻ simple salts reported so far exhibit a band in the 8000—10000 cm^{-1} region, which has been assigned to the charge-transfer (CT) transition between TCNQ⁻ radical anions.[1,4,5] It is noted that the CT band of **2** was fairly blue-shifted compared with **1**. This fact may be correlated with the higher electrical resistivity and the larger activation energy of **2** than **1**. Simple salts **4** and **5** in the solid state exhibited electronic absorption spectra similar to that of **1**, as shown in Table 3. They also showed diamagnetic properties at room temperature. These facts confirm that dimeric $(TCNQ)_2^{2-}$ also exists in solid **4** and **5**.

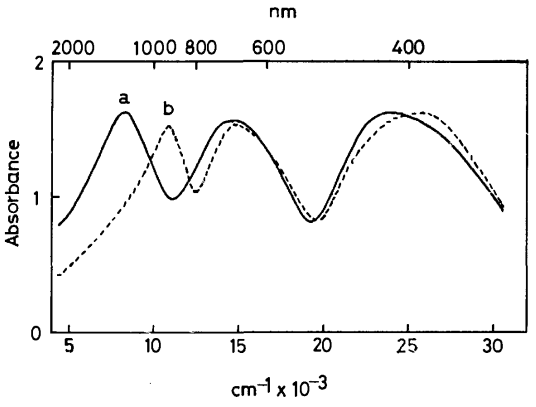

Fig. 1. Absorption spectra of **1** (a) and **2** (b) in Nujol mulls.

Table 3. Absorption maxima of the electronic spectra of the TCNQ⁻ salts in Nujol mulls

Compound	cm$^{-1}\times10^{-3}$ a)					
1		8.4			14.7	23.8
2		10.9			14.9	26.0
3a		9.1			14.9	24.1
3b			11.2	13.0		22.2—25.6
4		8.6			14.5	23.8
5		8.8			14.9	23.8
6			10.4	11.6	(17)	25.3
7			9.8	11.1	(17)	25.0
8			9.6	11.0	(17)	24.4
9			10.0	11.4	(17)	26.3
10	5.3	11.2			17.7	24.4 26.3

a) Shoulders in parentheses.

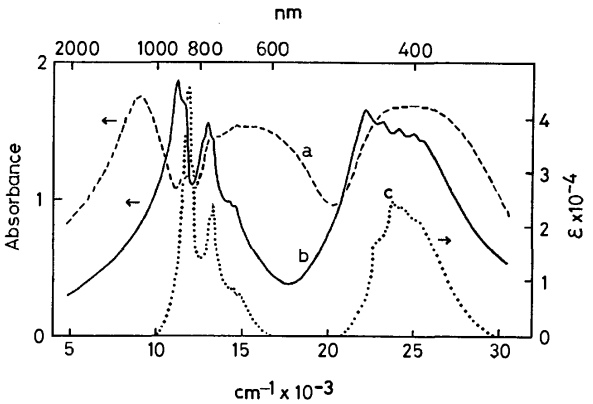

Fig. 2. Absorption spectra of **3a** (a) **3b** (b) in Nujol mulls, and of **3a** or **3b** in acetonitrile (c).

Figure 2 illustrates the electronic absorption spectra of **3a** and **3b** in the solid state and in acetonitrile. Solid **3a** exhibited three absorptions, and the spectral pattern resembles that of **1** shown in Fig. 1, suggesting that the stacking of TCNQ⁻ in **3a** can be described in terms of a dimeric pair. On the other hand, solid **3b** displayed a quite different spectrum from those of other simple salts; the spectrum of **3b** is rather similar in appearance to that of **3a** or **3b** in acetonitrile, where the salt is expected to dissociate into the iminium cation and TCNQ⁻ radical anion.[1] This observation shows that solid **3b** essentially consists of the iminium cation and the discrete TCNQ⁻ radical anion. This is also supported from the observation that **3b** exhibited a large paramagentic susceptibility ($\chi_M=1.2\times10^{-3}$ emu mol^{-1}) in the solid state at room temperature, while **3a** showed a diamagentic property ($\chi_M=-5.7\times10^{-4}$ emu mol^{-1}). This result is consistent with high electrical resistivity and large activation energy of **3b** compared with other simple salts (Table 2).

Figure 3 shows the electronic absorption spectra of complex salts **8** and **10** in the solid state. The spectrum of **8** resembles not only those of the *N,N*-dimethyl- and *N,N*-diethyliminium analogs[1] but also the reflectance spectra of several TCNQ⁻ complex salts such as with $MePh_3P^+$ and *N*-propylquinolinium$^+$.[4] Similar spectra were observed in other 1 :2 complex salts, **6**, **7**, and

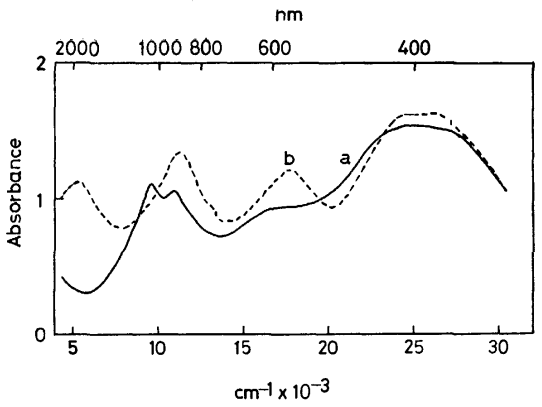

Fig. 3. Absorption spectra of **8** (a) and **10** (b) in Nujol mulls.

9 (Table 3). Furthermore, complex salts **6**—**9** exhibited the CT band between $TCNQ^{-}$ and TCNQ in the 3400—2700 cm^{-1} range in the infrared spectra, as the *N,N*-dimethyl- and *N,N*-diethyliminium analogs[1] and $MePh_3P^{+}(TCNQ)_2^{-}$[4] did.

The spectrum of 2:3 complex salt **10** in the solid state showed four absorption bands (Table 3). Except for the lowest energy band at 5300 cm^{-1}, the appearance of the spectrum roughly resembles those of the simple salts except for **3b**, suggesting the existence of dimeric $(TCNQ)_2^{2-}$. This is compatible with the diamagnetism of **10** ($\chi_M = -5.2 \times 10^{-4}$ emu mol^{-1}). The lowest energy band may tentatively be assigned to the CT transition between $TCNQ^{-}$ and TCNQ. The spectral features of **10** are nearly coincident with those of the reflectance spectra of $(Cs^{+})_2(TCNQ)_3^{2-}$ and $(morpholinium^{+})_2(TCNQ)_3^{2-}$.[4] Complex salt **10** is therefore suggested to have a stacking of TCNQ moiety similar to the Cs^{+} and $morpholinium^{+}$ salts, whose X-ray structure analyses revealed that interplanar separations of the TCNQ moieties are short enough to cause a CT interaction, while there exists the unit consisting of two $TCNQ^{-}$ radical anions and one neutral TCNQ.[6,7]

References

1) S. Araki, H. Ishida, and T. Tanaka, *Bull. Chem. Soc. Jpn.*, **51**, 407 (1978).
2) T. Tanaka and T. Abe, *Inorg. Nucl. Chem. Lett.*, **4**, 569 (1968); T. Tanaka, K. Tanaka, and T. Yoshimitsu, *Bull. Chem. Soc. Jpn.*, **44**, 112 (1971).
3) T. Nakai and M. Okawara, *Tetrahedron Lett.*, **1967**, 3835.
4) Y. Iida, *Bull. Chem. Soc. Jpn.*, **42**, 71, 637 (1969).
5) J. Tanaka, M. Tanaka, T. Kawai, T. Takabe, and O. Maki, *Bull. Chem. Soc. Jpn.*, **49**, 2358 (1976).
6) C. J. Fritchie, Jr. and P. Arthur, Jr., *Acta. Crystallogr.*, **21**, 139 (1966).
7) T. Sundaresan and S. C. Wallwork, *Acta Crystallogr., B*, **28**, 491 (1972).

Electrostatic Force Study with Floating Wave Function. Comparative Study on the Origins of the Molecular Shapes of CH_3^+ and NH_3

Hiroshi NAKATSUJI, Kazuo MATSUDA, and Teijiro YONEZAWA

Department of Hydrocarbon Chemistry, Faculty of Engineering, Kyoto University, Kyoto 606

(Received October 7, 1977)

The force and density origins of the molecular shapes of CH_3^+ and NH_3 are studied comparatively on the basis of the floating wave functions which satisfy the Hellmann-Feynman theorem for the forces acting on the terminal protons. It is confirmed quantitatively that the previous concepts of the electrostatic force (ESF) theory correctly grasp the origins of the molecular shapes. Namely, the *density-guiding rule* which states that the nuclei are pulled in the direction of the electron-cloud reorganization (*i.e.*, the electron-cloud preceding and incomplete following), is verified as the density origin. The force origin which is the AD and EC forces reflects and quantifies the density origin. The roles of the other forces are also easily predicted by the ESF theory.

It is now well established that the force concept based on the Hellmann-Feynman (H-F) theorem[1] gives a quite intuitive basis for the understandings of various chemical phenomena.[2–13] Though such approaches had been thought to have a difficulty in the reliability of the *calculated* H-F force,[14] it is well known that if we use the floating wave function[15–17] the H-F theorem is satisfied, so that the intuitive force concept gains also a sufficient reliability, which is the same as in the conventional energetics.[18] In this series of papers,[19] we investigate quantitatively the force and density origins of some molecular geometries and chemical reactions on the basis of the floating wave functions. A purpose of this series is to give a sufficient quantitative basis for the force theoretic approach. This is an urgent necessary step in comparison with the conventional energetics, and moreover such studies will give a basis to investigate more complex phenomena than those studied so far by this approach. Another purpose of this series (especially in the first few ones) lies in the verification of the concepts of the electrostatic force (ESF) theory[8–11] from a purely theoretical *ab initio* point of view. Though the success of the ESF theory, especially in the field of molecular geometry[8] (*i. e.*, the theory has predicted the geometries of various molecules *without* calculations in agreement with *experiments*), is itself a strong proof for the validity of the ESF concepts, we aim in these studies a more direct verification.

Due to the H-F theorem[1] the force acting on a nucleus is determined solely by the electron density $\rho(\boldsymbol{r})$ (the nuclear part is trivial). It is one of the basic observables in quantum mechanics, and due to Hohenberg and Kohn's theorem,[20] it includes all of the informations of the system. Therefore, we can express the origins of various molecular processes with either the force or the density behaviors along the processes.[21] The density origin is the reorganization of the electron density along the process,[7,9] which is characterized generally as the electron-cloud preceding or the electron cloud incomplete following which works respectively to accelerate or resist the process.[9] In other words, *the nuclei are pulled in the direction of the electron-cloud reorganization.* This simple rule constitutes a guiding principle for nuclear rearrangement processes on the basis of the behaviors of the electron density alone,[8b,9] and may be called a *density guide* or *density-guiding rule.* The force origin reflects and quantifies this origin. The partitioning of the H-F force into the atomic dipole (AD), exchange (EC), and extended gross charge (EGC) forces[8] gives a way to study quantitatively the regional role of the electron density. They are parallel with the chemical concepts like lone pair, bond, and gross charge, respectively.[8] The AD and EC forces are of particular importance since the electron-cloud preceding and incomplete following manifest themselves mainly in the AD and EC forces.[9] This is a reason[9] why these forces have played such important roles in the ESF theory applied to molecular geometries,[8b,9] chemical reactions, [10]and long-range forces.[11]

When the ESF concepts are applied to the AH_3 molecules, the origins of their shapes are expected as follows.[8,9] Namely, when the molecule is bent slightly from the planar form, the electron density in the atomic (A and H) and overlap (A–H) regions will precede (in the pyramidal molecules) or incompletely follow (in the planar molecules) the nuclear bending displacement. The constituent nuclei will therefore be pulled by the AD and EC forces in the bending or planarizing direction, respectively, and will move in the direction to the equilibrium geometry. Though we tried to verify this picture in the previous paper,[9b] it was insufficient since the wave function used there did not satisfy the H-F theorem. Here, we want to examine this picture quantitatively on the basis of the floating wavefunctions.

In the previous communication of this series,[19] we have reported a simpler way of obtaining the floating wave function. Namely, if we limit ourselves to the force $\boldsymbol{F}_A$ acting on a special nucleus A of the system, it is sufficient that only the AO's belonging to the atom A be floated and their centers be determined variationally. The resultant wave function gives a reliable H-F force $\boldsymbol{F}_A$ which satisfies the H-F theorem. Based on this fact, we have studied quantitatively the force and density origins of the molecular shape of H_2O, limiting ourselves to the transverse force acting on the terminal protons. It has been confirmed that the ESF picture as described in the preceding paragraph correctly grasps the origin of the bent geometry of H_2O.[19] In this paper, we will examine further such ESF concept of the origins of the molecular shapes of CH_3^+ and NH_3. We will again limit ourselves to the transverse force acting on the terminal protons and investigate

the behaviors of the electron density in the A–H region during the out-of-plane bending process. It will give a comparative basis for the origins of the molecular shapes of planar and pyramidal molecules.

We note that in the previous extensive applications of the ESF theory to various molecular geometries,[8] we have mostly concerned with the force acting on the central nucleus (*e.g.* the nucleus A in the AH_3 molecule). It is clear from these studies that such method is easier and more fruitful for constructing a predictive theory of molecular geometries without calculations.[8] However, for the AH_3 molecules, the calculations of the floating wave functions become more elaborate for the force $\boldsymbol{F}_A$ than for the force $\boldsymbol{F}_H$, since the numbers of the basis AO's are smaller for H than for the heavier atom A. Therefore, we will postpone the *ab initio* study of $\boldsymbol{F}_A$ in the subsequent paper. We remark however that for general molecules (*e.g.* AX_n molecules) the floating wave function is more easily obtained for $\boldsymbol{F}_A$ than for $\boldsymbol{F}_X$, in contrast to the AH_3 molecules.

Floating Wave Functions for CH_3^+ and NH_3

The SCF-MO calculations have been carried out with the use of the minimal STO-3G bases[22] with the standard exponents reported by Hehre *et al.*[23] We have used the modified version of the Gaussian 70 Program. In obtaining the floating wave function, we have adopted a simpler procedure noted previously.[19] Namely, we have floated only the 1s AO's on the terminal protons and the other AO's on carbon and nitrogen, which are the 1s, 2s, $2p_x$, $2p_y$, and $2p_z$ AO's were kept fixed on the nuclei. Therefore, the present wave functions satisfy the H-F theorem for the forces acting on the terminal protons. The C–H and N–H lengths of CH_3^+ and NH_3 were kept fixed at, respectively, 1.120 and 1.033 Å which are the lengths optimized by the STO-3G calculations.[24] The experimental N–H length is 1.012 Å.[24] We have calculated the transverse force acting on the terminal protons and also the behaviors of the electron density in the A–H region at various out-of-plane bending angles θ. Several quantities pertinent to the present analysis are defined in Fig. 1.

Tables 1 and 2 give the variationally best positions of the $1s_H$ floating AO's (FAO's) of CH_3^+ and NH_3, respectively, and the effects of floating on the SCF energy and the H-F transverse force $\boldsymbol{F}_{H\perp}$ acting on the terminal protons. The H-F force is partitioned

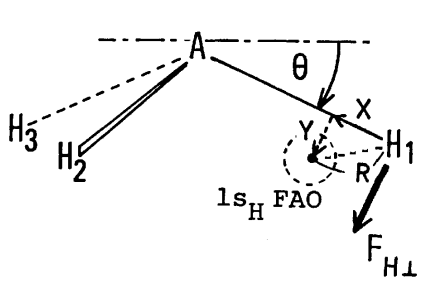

Fig. 1. Definitions of the out-of-plane bending coordinate θ, the centers of the $1s_H$ FAO's and the transverse force acting on the terminal protons $\boldsymbol{F}_{H\perp}$ for the AH_3 molecules.

into the atomic dipole (AD), exchange (EC), and extended gross charge (EGC) forces with a slight modification of the previous ones used for the non-floating wave function.[8,25] The values in parentheses are those obtained from the non-floating wave functions. The distance R of the FAO center from the proton is about 0.04 Å for CH_3^+ and about 0.02 Å for NH_3. It was about 0.03 Å for H_2O.[19] They are all in the same order of magnitude as those reported previously for H_2 by Shull and Ebbing.[26] Though the FAO center of CH_3^+ lies outside of the pyramid ($Y<0$), that of NH_3 lies inside of the pyramid ($Y>0$). For both cases, the distance Y is sensitive to the bending angle θ, though the distance X is insensitive. (The latter would be sensitive to the stretching mode). As will be seen later, these behaviors of the FAO's are closely related with the manners of the electron-cloud reorganization during the out-of-plane bending processes. The floating of the AO's gives a freedom in the wave function to describe such behaviors of the electron density especially in the atomic regions.

The floating of the $1s_H$ AO's was not effective to improve the SCF energy, as studied earier by Shull and Ebbing for the hydrogen molecule.[26] The energy lowering obtained by the floating is about 0.008 a.u. (5 kcal/mol) for CH_3^+ and 0.003 a.u. (2 kcal/mol) for NH_3. They are very small in comparison with those obtained by the other ways of improving the wave function. For example, the addition of the polarization function on hydrogen, which also describes the polarization of the electron density in the atomic region, lowers the SCF energy of NH_3 by 0.058 a.u. in the similar calculations of the STO-3G level[10b] and by 0.039 a.u. in the calculations of double-zeta accuracy.[27] However, in contrast to the floating method, it is generally difficult in such procedures to assure the complete satisfaction of the H-F theorem, so long as the basis set is incomplete.

Though the effect of floating is quite small for the SCF energy, it is very large and important for the H-F force. As seen from Tables 1 and 2, the errors for the H-F theorem are essentially zero in the floating wave functions, though they are large in the non-floating wave functions especially for NH_3. The small non-zero errors still remaining in the floating wave functions of CH_3^+ are the numerical errors in determining the optimal FAO centers. These error values have been obtained by calculating directly the error term for the H-F theorem, *i.e.*, the term $\langle \partial\Psi/\partial \boldsymbol{R}_A | H | \Psi\rangle + \langle \Psi | H | \partial\Psi/\partial \boldsymbol{R}_A\rangle$, by the method developed by Moccia *et al.*[28] Thus, it is confirmed that the present floating wave function satisfies the H-F theorem for the force acting on the terminal protons.

As seen from Table 1, the equilibrium shape of CH_3^+ is calculated to be planar from both the floating and non-floating wave functions. The planar geometry of CH_3^+ is well established by the previous studies.[24,29] The out-of-plane bending force constant calculated from the H-F force is 0.93 md/Å with the floating wave function and 0.82 md/Å with the non-floating wave function. The former should of course be identical with the result obtained from the SCF energy

Table 1. Center of $1s_H$ FAO and the effects of floating on the SCF energy E and the H-F force $F_{H\perp}$ for CH_3^+

θ (Deg)	FAO Center (Å)			$-\Delta E \times 10^3$ (au)	$F_{H\perp} \times 10^2$ (au)[a]					
	X	Y	R		Total H-F	Error	AD	EC(H-C)	EC(H--H)[b]	EGC
0 (Eq)	0.041	0.0	0.041	8.1	0.0 (0.0)	0.0 (0.0)	0.0 (0.0)	0.0 (0.0)	0.0 (0.0)	0.0 (0.0)
5	0.041	−0.0006	0.041	8.1	−1.10(−0.97)	−0.07(−0.19)	−0.08(0.0)	−0.69(−0.70)	−0.08(−0.07)	−0.24(−0.21)
10	0.041	−0.0018	0.041	8.0	−2.34(−1.95)	0.00(−0.38)	−0.27(0.0)	−1.35(−1.40)	−0.17(−0.14)	−0.55(−0.41)
15	0.040	−0.0033	0.040	7.9	−3.60(−2.96)	0.05(−0.57)	−0.44(0.0)	−2.04(−2.12)	−0.28(−0.23)	−0.85(−0.62)
24.3	0.039	−0.0042	0.039	7.6	−5.93(−5.02)	−0.07(−1.09)	−0.63(0.0)	−3.42(−3.52)	−0.55(−0.47)	−1.32(−1.03)

a) The values in parentheses are obtained from the non-floating wave functions. b) This value is the sum of the two identical EC(H--H) forces.

Table 2. Center of $1s_H$ FAO and the effects of floating on the SCF energy E and the H-F force $F_{H\perp}$ for NH_3

θ (Deg)	FAO Center (Å)			$-\Delta E \times 10^3$ (au)	$F_{H\perp} \times 10^2$ (au)[a]					
	X	Y	R		Total H-F	Error	AD	EC(H-N)	EC(H--H)[b]	EGC
0	0.019	0.0	0.019	2.3	0.0 (0.0)	0.0 (0.0)	0.0 (0.0)	0.0 (0.0)	0.0 (0.0)	0.0 (0.0)
10	0.020	0.009	0.022	2.9	1.24(−0.96)	0.00(2.11)	1.60(0.0)	0.68(0.93)	−0.17(−0.29)	−0.87(−1.60)
15	0.020	0.012	0.023	3.3	1.30(−1.55)	0.00(2.79)	2.08(0.0)	0.71(1.05)	−0.29(−0.45)	−1.20(−2.15)
24.3(Eq)	0.020	0.012	0.023	3.6	0.00(−3.12)	0.00(3.12)	2.29(0.0)	−0.07(0.31)	−0.62(−0.80)	−1.59(−2.63)
40	0.021	0.008	0.022	3.6	−6.35(−8.55)	0.00(2.09)	1.63(0.0)	−3.66(−3.36)	−1.68(−1.79)	−2.64(−3.40)

a) The values in parentheses are obtained from the non-floating wave functions. b) This value is the sum of the two identical EC(H--H) forces.

curve. On the other hand, for NH_3 (Table 2), the effect of the floating on the H-F force is essential even for the qualitative calculation of the equilibrium shape. With the non-floating wave function, the shape is calculated to be planar! This is because the minimal STO-3G basis fixed on the nuclei is far from complete and can not describe the polarization of the electron density in the atomic region near the proton (see below). However, with the floating wave function, NH_3 is calculated to be pyramidal with $\theta_{eq}=24.3°$ ($\angle HNH=104.2°$) which is just the same as the STO-3G geometry.[24] The experimental value is $\theta_{eq}=22.1°$ ($\angle HNH=106.7°$).[24]

The partitioning of the H-F force into the AD, EC, and EGC forces clarifies the details how the floating of the $1s_H$ AO's improves the H-F force. As seen in Tables 1 and 2, the largest effect of the floating occurs for the AD force. It improves most of the errors included in the non-fioating H-F force (50—80% for CH_3^+ and 70—80% for NH_3). This is because the H-F force is most sensitive to the errors in the region near the nucleus. In the non-floating wave function, the AD force was always zero since the present basis AO's do not include the polarization functions on the hydrogen atom. In the floating wave function, it arises because the $1s_H$ AO density floating apart from the proton pulls it in the direction of the floating. For CH_3^+, Y is negative so that the induced AD force is negative, while for NH_3, Y is positive so that the AD force is positive. In both cases, the distance Y and the AD force are parallel. The second largest effect of the floating occurs for the EGC force. For CH_3^+ the floating enlarges the repulsive EGC force, whereas for NH_3 it diminishes: in CH_3^+ the outward floating ($Y<0$) of the $1s_H$ AO makes its proton more bare so that the repulsion increases, while in NH_3 the AO floated inward of the proton ($Y>0$) shields it more effectively from the repulsion with the other protons. These "self-shielding" effects have arisen from the modification of the partitioning as given in Ref. 25. The effect of floating is smallest for the EC force as expected from the small distance Y in comparison with the bond distance. The effect is smaller for CH_3^+ than for NH_3 since Y is smaller for CH_3^+.

Origin of the Molecular Shape

In this section we study quantitatively the force and density origins of the molecular shapes of CH_3^+ and NH_3. We investigate the behaviors of the electron density and the induced forces acting on the terminal protons during the out-of-plane bending process. Since the present floating wave function satisfies the H-F theorem, we can examine quantitatively the concepts developed previously in the ESF theory.

First, we study the density and force origins of the planar geometry of CH_3^+. Figure 2 shows the change in the electron density of CH_3^+ when it is bent by 15° from the planar form. The density at $\theta=0°$, which is symmetric with respect to the CH_3 plane, was subtracted from that at $\theta=15°$ with superposing the C–H_1 axis on the right hand side.[30] This figure is then meaningful only in the region near the C–H_1 axis. The real and dotted lines show respectively the increase and decrease in the electron density. From this figure, we see that the reorganization of the C–H bond density of CH_3^+ shows a typical feature of the electron-cloud incomplete following in the out-of-plane bending process. Namely, as seen from the increase and the decrease in the regions above and below the C–H_1 axis, respectively, the C–H bond density at $\theta=15°$ does not lie on the C–H axis, but follows with lag the out-of-plane bending displacement of the C–H axis. The bond density, following back of the C–H axis, will pull the terminal proton in the reverse direction to θ, so that the molecule will be restored again to the planar form: i.e., the equilibrium geometry of CH_3^+ is expected to be planar in accordance with the previous studies.[29] This is the result of the density-guiding rule applied to the geometry of CH_3^+.

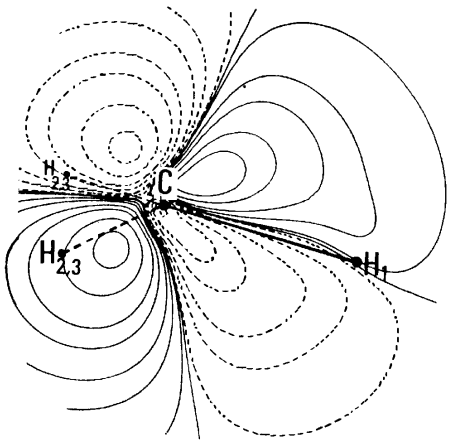

Fig. 2. Electron-cloud reorganization in CH_3^+ at $\theta=15°$ in the C-H_1 region. The density at $\theta=0°$ was subtracted from that at $\theta=15°$ with superposing the C-H_1 axes. The contours are at 0.0, ±0.001, ±0.005, ±0.01, +0.015, −0.02, +0.025, ±0.04, ±0.07, ±0.1, and ±0.15 au (real lines ≥0, dashed lines <0).

The above density origin is verified from Fig. 3 which shows the analysis of the transverse force $\boldsymbol{F}_{H\perp}$ acting in CH_3^+ during the bending process. The dotted line shows the SCF energy curve. Throughout the bending process, the protons of CH_3^+ receive the planarizing forces; *i.e.*, the molecule is calculated to be planar. In CH_3^+ all of the force components are cooperative to make the molecule planar. Among these, the dominant force origin is the EC(H–C) force. It arises from the incomplete following of the C–H bond density as depicted in Fig. 2. [If the C–H bond density always lies on the C–H axis (complete following), it does not induce the *transverse* EC(H–C) force.] The electron-cloud incomplete following in the atomic region manifests itself in the AD force. It has arisen through the floating of the $1s_H$ AO's. The behaviors of the $1s_H$ FAO's seen from the distance Y given in Table 1 clearly show the occurrence of the electron-cloud incomplete following in the atomic region. The sum of the EC (H–C) force and the AD force accounts most (≈70%) of the total planarizing force.

Thus, we conclude that the density origin of the

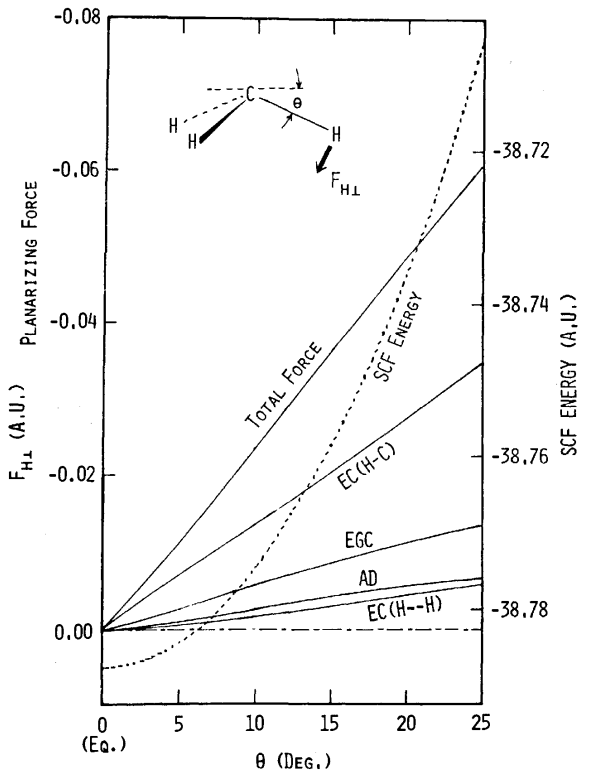

Fig. 3. The transverse force $\boldsymbol{F}_{H\perp}$ and the SCF energy *vs.* the out-of-plane bending angle θ for CH_3^+.

planar shape of CH_3^+ lies in the occurrence of the electron-cloud incomplete following of the C–H bond density during the out-of-plane bending process. We have confirmed that the electron-cloud incomplete following as depicted in Fig. 2 occurs over the all angular range studied here ($0°<\theta<24.3°$) and that the extent increases with the increase in the bending angle θ. The force origin, which is the EC(H–C) and AD forces (mostly the EC(H–C) force), reflects and confirms this density origin.

In Fig. 3, the other minor force components, *i.e.*, the EGC and EC(H--H) forces are also cooperative to make CH_3^+ planar. We note that the roles of these forces are also naturally understood. Namely, in CH_3^+, the net gross charges of the terminal hydrogens are positive, so that the EGC force which represents the interaction between the shielded protons would be repulsive. The EC(H--H) force would also be repulsive since it arises from the exchange interaction between the doubly occupied C–H bond orbitals. Among these, the origin of the EC(H--H) force may be included in the electron-cloud incomplete following as has been discussed previously for the similar interaction during the internal rotation of ethane.[8]

We next investigate the density and force origins of the pyramidal shape of NH_3. In Fig. 4 we have depicted the electron-cloud reorganizations in NH_3 at the bending angles $\theta=15$, 24.3 (calculated equilibrium), and 40°. They are defined similarly to Fig. 2.[30,31] As seen from Fig. 4, the electron-cloud reorganization in NH_3 is quite different from that in CH_3^+. At $\theta=15°$ (Fig. 4(A)), the behavior of the N–H bond density of NH_3 shows a typical feature of the electron-

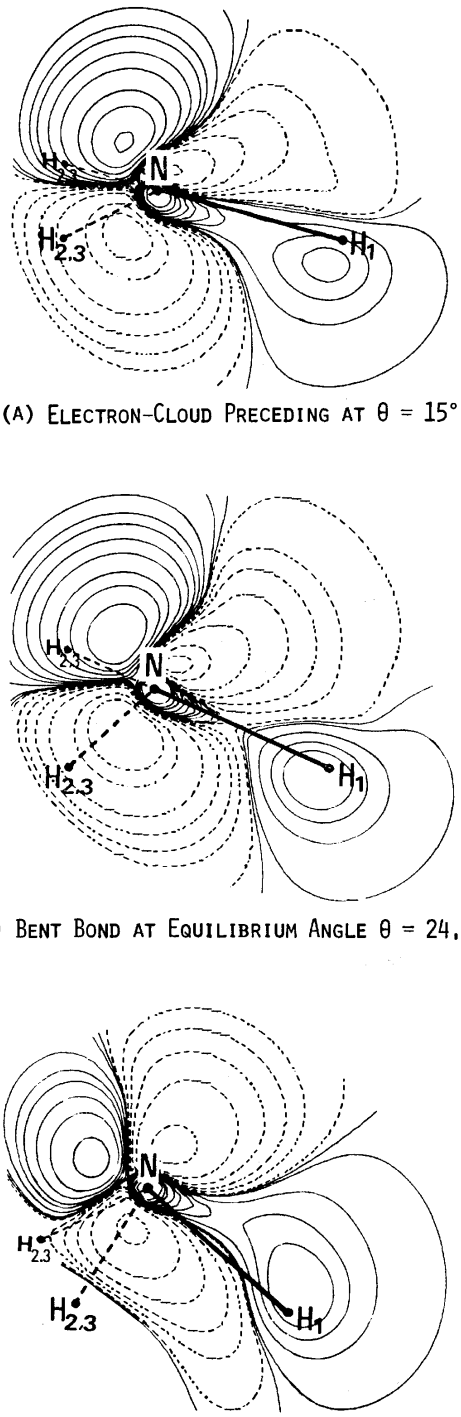

Fig. 4. Electron-cloud reorganization in NH_3 in the $N\text{-}H_1$ region during the out-of-plane bending process. (A) $\Delta\rho(15°)=\rho(15°)-\rho(0°)$, (B) $\Delta\rho(24.3°)=\rho(24.3°)-\rho(0°)$, (C) $\Delta\rho(40°)=\rho(40°)-\rho(24.3°)$. In subtracting the reference density, the $N\text{-}H_1$ axes were superposed. The levels of the contours are the same as those given in Fig. 2.

cloud preceding.[9] Namely, the increase and the decrease in the electron density in the regions below and above the $N\text{-}H_1$ axis, respectively, shows that the N–H bond density does not lie on the N–H axis, but

bends more than the N–H axis. The N–H density, preceding ahead of the bending movement of the N–H axis, will pull the terminal proton in the bending direction, so that the bending process will be accelerated further. Therefore, the stable shape of NH_3 is expected to be pyramidal in agreement with the experiment. When the molecule reaches the equilibrium angle (θ=24.3°), such preceding character almost vanishes as seen in Fig. 4(B). The bond electron density becomes almost symmetric with respect to the N–H axis in order to keep the terminal proton in an electrostatic equilibrium with respect to the transverse force. A small preceding character seen especially in the atomic region near H shows an inward bent bond which is necessary to cancel with the interproton repulsions at the equilibrium geometry.[9b] When the molecule is bent further from the equilibrium angle, the N–H bond density again dispart from the N–H axis, and the electron-cloud incomplete following occurs as seen in Fig. 4(C). This behavior is just reverse to that seen at θ=15° (Fig. 4(A)). The N–H bond density, following back of the N–H axis, will pull the terminal proton upwards so that the molecule will be restored again to the equilibrium angle. In summary, the electron-cloud reorganization in NH_3 during the out-of-plane bending process is characterized by the electron-cloud preceding in the region $0°<\theta<24.3°$ and the electron-cloud incomplete following in the region $\theta>24.3°$. From the density guide, we may expect the equilibrium angle at about 24.3° where the density behavior turns reverse from the preceding to the incomplete following.

In Fig. 5 we have shown the analysis of the transverse force $\boldsymbol{F}_{H\perp}$ in NH_3 during the out-of-plane bending process. By virtue of the floating, the equilibrium angle calculated from the H-F force agrees with that obtained from the SCF energy curve. Among the force components shown in Fig. 5, only the AD and EC(H–N) forces work to accelerate the bending process in the range $0°<\theta<\theta_{eq}$. Therefore, the force orgin of the pyramidal shape of NH_3 is the AD and EC(H–N) forces which reflect the electron-cloud preceding in the atomic and overlap regions, respectively. The other forces, *i.e.*, the EGC and EC(H--H) forces, work to resist the bending process by the same reason as explained for CH_3^+. This fact clearly confirms the importance of the electron-cloud preceding in the region $0°<\theta<\theta_{eq}$. Without it, the pyramidal shape of NH_3 can not be realized. At the equilibrium angle (24.3°), the repulsive EGC and EC(H--H) forces are canceled out by the AD force. The EC(H–N) force is almost zero at this angle. This means that the inward bent bond character at the equilibrium geometry, which is necessary to cancel the interproton repulsions, occurs mostly in the atomic region near the proton (see Fig. 4(B)). In the angular region $\theta>\theta_{eq}$, the force on the proton works to restore the molecule again to the equilibrium angle. It arises from the EC(H–N), EGC, and EC(H–H) forces. The AD force contributes to the restoring force by diminishing its bending role. Among these, the slope of the EC(H–N) force is steepest so that it becomes the most important component of the restoring force. It reflects the electron-cloud incomplete following depicted in Fig. 4(C) at θ=40°. Thus, it is confirmed that the density guide applied to the geometry of NH_3 certainly grasps the most important factors of the force components. The dominant force origin, which is the AD and EC(H–N) forces, reflects and confirms the density origin summarized in the preceding paragraph.

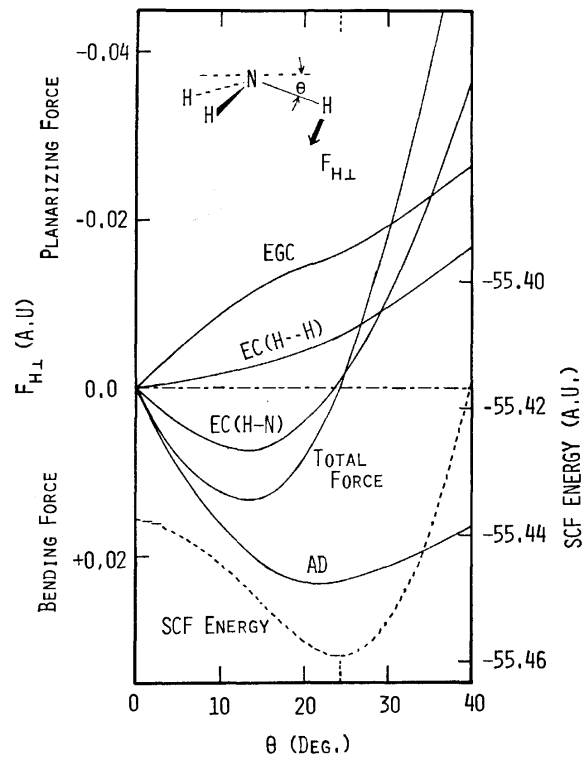

Fig. 5. The transverse force $\boldsymbol{F}_{H\perp}$ and the SCF energy *vs.* the out-of-plane bending angle θ for NH_3.

It is interesting to note that the density and force origins of the pyramidal shape of NH_3 are quite similar to those of the bent geometry of H_2O reported previously.[19] On the basis of the generality of the density-guiding rule as discussed in the previous paper,[9] we believe that this similarlity in the force and density origin is actually a more general one which is correct at least for any kind of AH_2, AH_3, and related substituted molecules having bent or pyramidal geometries. By the same reason, the force and density origins shown here for CH_3^+ would also be common to the above types of molecules having linear or planar geometries.

It would also be worthwhile to remark that for both CH_3^+ and NH_3, the curves for the EC(H–A) forces cross the zero line at about the equilibrium angle; *i.e.*, at θ=0° for CH_3^+ and at θ=23° for NH_3. The same is also true for H_2O; *i.e.*, just at $\theta=\theta_{eq}$ (=40°) (see Fig. 3 in Ref. 19). If this is true more generally, we can estimate the equilibrium angle only from the EC(H–A) force, and furthermore, since the effect of the floating is small for the EC(H–A) force, this procedure would be possible *even* with the *non*-floating wave functions. Actually, such procedure with the use of the non-floating wave function gives the equilibrium angle 0° for CH_3^+, 25° for NH_3 (see Tables 1 and 2), and 40° for H_2O. These values agree surprisingly well

with those obtained from the floating wave functions which are 0, 24.3, and 40°, respectively. The experimental values are 0, 22.1, and 37.8°, respectively.[24]

Density Behavior Reflected in the Potential Energy Curve

It is well known that the energy is an explicit function of not only the electron density $\rho(\boldsymbol{r})$ but also the off-diagonal first-order density matrix $\rho(\boldsymbol{r}|\boldsymbol{r}')$ and the second-order density matrix $\Gamma(\boldsymbol{r}_1, \boldsymbol{r}_2)$.[32] The latter two functions are much more complicated than the electron density. On the other hand, the H–F theorem states that the force acting on a nucleus is determined solely by the electron density $\rho(\boldsymbol{r})$ surrounding the nucleus. The nuclear repulsion term is trivial. Therefore, if we integrate the H-F force along the process, we can obtain the potential energy curve solely from the dynamic behavior of the electron density during the nuclear rearrangement process. Though this is trivial, the underlying concept of this procedure is simpler and more visual than that of the conventional energetics. A condition for the (numerical) equivalence between the conventional energetics and the *integrated* H-F force approach is the holdness of the H-F theorem, which the present floating wave function satisfies. Then, we examine here such idea for CH_3^+ and NH_3 by integrating the force curves given in Figs. 3 and 5.

Figures 6 and 7 show the enrgy curves for CH_3^+ and NH_3, respectively, obtained by the direct integration of the H-F force curves given in Figs. 3 and 5. By virtue of the floating, the curves of the integrated

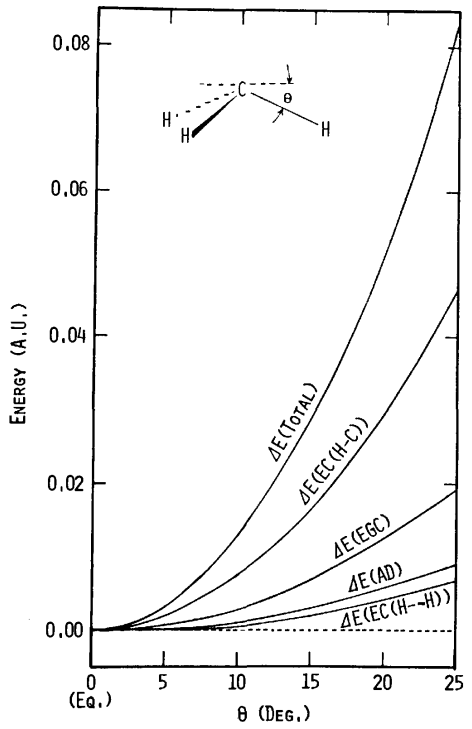

Fig. 6. Partitioning of the potential energy curve into the force theoretic terms for CH_3^+.

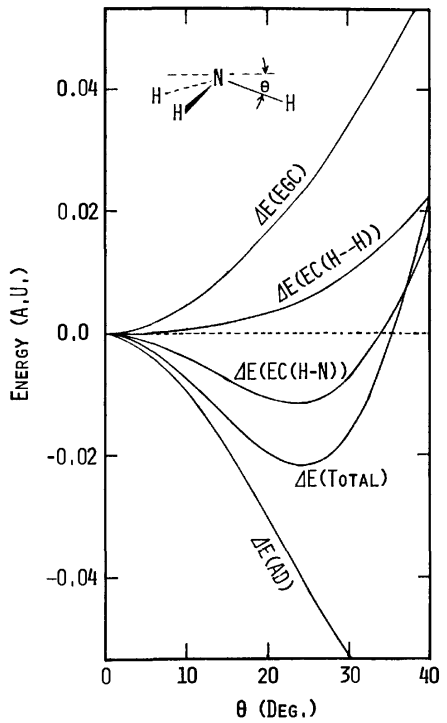

Fig. 7. Partitioning of the potential energy curve into the force theoretic terms for NH_3.

H-F forces (denoted as ΔE(Total)) are just superposable with the SCF energy curves shown in Figs. 3 and 5. The partitioning of the ΔE(Total) curve into the force theoretic terms given in Figs. 6 and 7 helps to analyze the potentical energy curve in terms of the regional roles of the electron-cloud reorganization during the bending process. The electron-cloud incomplete following in CH_3^+ shown in Fig. 2 works to destabilize the system as seen in the ΔE(EC(H–C)) and ΔE(AD) curves given in Fig. 6. It is the main origin of the potential energy curve ΔE(Total). For NH_3, the electron-cloud preceding in the atomic and overlap regions works to stabilize the molecule as seen from the ΔE(AD) and ΔE(EC(H–N)) curves in the angular region $0°< 0<\theta_{eq}$. In the region $\theta>\theta_{eq}$, the electron-cloud incomplete following works to destabilize the system as seen in the ΔE(EC(H–N)) curve. For both CH_3^+ and NH_3, the parallelism between the ΔE(EC(H–A)) curve and the total curve is surprising. The same trend was also seen previously for H_2O.[19] Thus, it is confirmed that the density-guiding rule certainly shows the path along which the energy becomes lower most effectively.

Concluding Remarks

In this paper, we have studied the force and density origins of the molecular shapes of CH_3^+ and NH_3 on the basis of the floating wavefunctions which satisfy the H-F theorem for the force acting on the terminal protons. The present results may be summarized as follows:

1) The floating of the AO's gives a freedom in the wave function to describe an appropriate behavior of

the electron density especially in the atomic region. The direction and the extent of the floating of the FAO's accord with those expected from the general behaviors of the electron density, *i.e.*, the electron-cloud preceding and incomplete following. The effect of the floating on the H-F force is largest for the AD force.

2) For the floating wave function, the simple and pictorial concepts of the force theory holds in a sufficient accuracy. On this basis, we have confirmed that the previous concepts of the ESF theory correctly grasp the origins of the molecular shapes. The density-guiding rule based on the behaviors of the electron density is verified as the rule for the density origin. The force origin which is the AD and EC(H–A) forces reflects and quantifies the density origin. The roles of the other forces are also easily predicted by the ESF theory.

Lastly, it would be important to remark about an interpretation why the electron-cloud preceding or the incomplete following occurs in the A–H bond region under the bending process. Recently, Deb has given a postulate that the highest occupied molecular orbital (HOMO) would be most responsible for these behaviors since the HOMO is most weakly bound to the nuclear framework.[13] He has tried to systematize various molecular geometries on the basis of the "HOMO postulate."[12,13] Though this idea is interesting, this assumption seems to feel difficulty for larger molecules since they have many levels in the vicinity of the HOMO. The electron-cloud preceding and the incomplete following, which should be the density origin even for larger molecules,[9] are the behaviors of the *total* electron density. On the other hand, when we focus our attention on the force acting on the central atom (*e. g.* the atom A of the AH_3), we can easily predict the behaviors of the electron density on the basis of the chemically transferable concepts like lone pair, bond, gross charge, and the various effects on them (*e. g.* substituent effect), as has been shown previously in the ESF theory.[8] Therefore, we believe that for predictive applications, it is easier and more fruitful to focus our attention to the force acting on the central atom, except for the problems of the internal rotation barrier.[8] An *ab initio* verification of this approach will be given in the succeeding paper.

The authors would like to thank Dr. S. Yamabe, Dr. K. Kitaura, and Professor K. Morokuma for the use of the modified version of the Gaussian 70 Program, and Mr. S. Kanayama for the assistance of some computations. This study has been supported partially by the Scientific Research Grants from the Ministry of Education and by the Japan-U.S. Cooperative Science Program from the Japan Society for the Promotion of Science.

References

1) H. Hellmann, "Einführung in die Quantenchemie," Deuticke, Vienna (1937), p. 285; R. P. Feynman, *Phys. Rev.*, **56**, 340 (1939).

2) An exaustive review for the force concepts in chemistry has been given in a) B. M. Deb, *Rev. Mod. Phys.*, **45**, 22 (1973). and will appear in b) B. M. Deb, Ed., "The Force Concept in Chemistry," Macmillan, Bombay, in press. The Japanese readers may also refer to the following reviews written in Japanese; c) H. Nakatsuji, *Kagaku*, **28**, 17, 108 (1973); d) H. Nakatsuji, *Kagaku No Ryoiki*, **30**, 881 (1976).

3) T. Berlin, *J. Chem. Phys.*, **19**, 208 (1951).

4) R. F. W. Bader, W. H. Henneker, and P. Cade, *J. Chem. Phys.*, **46**, 3341 (1967), and the succeeding papers.

5) R. F. W. Bader and A. K. Chandra, *Can. J. Chem.*, **46**, 953 (1968).

6) J. O. Hirschfelder and M. A. Eliason, *J. Chem. Phys.*, **47**, 1164 (1967).

7) R. F. W. Bader and A. D. Bandrauk, *J. Chem. Phys.*, **49**, 1666 (1968); R. F. W. Bader, I. Keaveny, and G. Runtz, *Can. J. Chem.*, **47**, 2308 (1969).

8) a) H. Nakatsuji, *J. Am. Chem. Soc.*, **95**, 345, 354, 2084 (1973); b) H. Nakatsuji and T. Koga, Chap. 4 of Ref. 2b.

9) a) H. Nakatsuji, *J. Am. Chem. Soc.*, **96**, 24 (1974); b) *ibid.*, **96**, 30 (1974).

10) a) H. Nakatsuji, T. Kuwata, and A. Yoshida, *J. Am. Chem. Soc.*, **95**, 6894 (1973); b) H. Nakatsuji, T. Koga, K. Kondo, and T. Yonezawa, *J. Am. Chem. Soc.*, **100**, 1029 (1978).

11) H. Nakatsuji and T. Koga, *J. Am. Chem. Soc.*, **96**, 6000 (1974); T. Koga and H. Nakatsuji, *Theoret. Chim. Acta*, **41**, 119 (1976).

12) B. M. Deb, *J. Am. Chem. Soc.*, **96**, 2030 (1974); B. M. Deb, P. N. Sen, and S. K. Bose, *ibid.*, **96**, 2044 (1974).

13) B. M. Deb, *J. Chem. Educ.*, **52**, 314 (1975); B. M. Deb, S. K. Bose, and P. N. Sen, *Indian J. Pure Appl. Phys.*, **14**, 444 (1976).

14) L. Salem and E. B. Wilson, Jr., *J. Chem. Phys.*, **36**, 3421 (1962); L. Salem and M. Alexander, *ibid.*, **39**, 2994 (1963).

15) A. C. Hurley, *Proc. R. Soc. London, Ser. A*, **226**, 170, 179, 193 (1954); A **235**, 224 (1956); C. A. Coulson and A. C. Hurley, *J. Chem. Phys.*, **37**, 448 (1962).

16) A. C. Hurley, "Molecular Orbitals in Chemistry, Physics, and Biology," ed by P.-O. Löwdin and B. Pullman, Academic, New York (1964), p. 161.

17) G. G. Hall, *Phil. Mag.*, **6**, 249 (1961).

18) J. O. Hirschfelder, W. Byers Brown, and S. T. Epstein, *Adv. Quantum Chem.*, **1**, 255 (1964).

19) H. Nakatsuji, K. Matsuda, and Yonezawa, *Chem. Phys. Lett.*, **54**, 347 (1978).

20) P. Hohenberg and W. Kohn, *Phys. Rev.*, **136**, B864 (1964).

21) E. B. Wilson, Jr., *J. Chem. Phys.*, **36**, 2232 (1962); see also A. A. Frost, *ibid.*, **37**, 1147 (1962); S. T. Epstein, A. C. Hurley, R. E. Wyatt, and R. G. Parr, *ibid.*, **47**, 1275 (1967); H. Nakatsuji and R. G. Parr, *ibid.*, **63**, 1112 (1975).

22) The STO-3G expansion coefficients and exponents used here are those included in the Gaussian 70 Program.

23) W. J. Hehre, R. F. Stewart, and J. A. Pople, *J. Chem. Phys.*, **51**, 2657 (1969).

24) W. A. Lathan, L. A. Curtiss, W. J. Hehre, J. B. Lisle, and J. A. Pople, *Prog. Phys. Org. Chem.*, **11**, 175 (1974).

25) The explicit formulas for the AD, EC, and EGC forces used in the present calculations are the same as those given in Ref. 8b, except that the net-exchange force integral is modified as

$$\langle \chi_{rA} | (f_A)_0 | \chi_{sB} \rangle \equiv \langle \chi_{rA} | f_A | \chi_{sB} \rangle - \frac{1}{2} S_{rAsB} \times \{ \langle \chi_{rA} | f_A | \chi_{rA} \rangle + \langle \chi_{sB} | f_A | \chi_{sB} \rangle \},$$

where the first term in the brace was added here. It vanishes for the non-floating wave function.

26) H. Shull and D. Ebbing, *J. Chem. Phys.*, **28**, 866 (1958).
27) B. Roos and P. Siegbahn, *Theoret. Chim. Acta*, **17**, 199 (1970).
28) R. Moccia, *Theoret. Chim. Acta*, **8**, 8 (1967); P. Pulay, *Mol. Phys.*, **17**, 197 (1969).
29) S. D. Peyerimhoff, R. J. Buenker, and L. C. Allen, *J. Chem. Phys.*, **45**, 734 (1966); R. E. Kari and I. G. Csizmadia, *ibid.*, **50**, 1443 (1969); G. V. Bünau, G. Diercksen, and H. Preuss, *Int. J. Quantum Chem.*, **1**, 645 (1967).
30) Though the electron-cloud preceding and incomplete following are the behaviors of the *total* electron density, they are more visually depicted when an appropriate reference density is introduced. Since we are concerned here only in the electron density in the A–H region, we have introduced as the reference density the one obtained at $\theta=0°$ since it is symmetric with respect to the A–H axis. Therefore, the present difference density maps show chiefly the electron-cloud reorganization induced by the out-of-plane bending displacements.
31) At $\theta=40°$ we have used as the difference density the density obtained at $\theta=24.3°$ (calculated equilibrium), since there the transverse force is zero and the N–H bond density is almost symmetric with respect to the N–H axis. These two features are common to the planar form used as the reference at $\theta=15$ and 24.3°.
32) P.-O. Löwdin, *Phys. Rev.*, **97**, 1474 (1955).

Vibrational Spectra of Dimethylaminosulfonyl Chloride and Its *C*-Deuterated Derivative

Yukiko TANAKA, Yoshimasa TANAKA, Yutaka SAITO, and Katsunosuke MACHIDA*

Faculty of Pharmaceutical Sciences, Okayama University, Tsushima-Naka Okayama 700

**Faculty of Pharmaceutical Sciences, Kyoto University, Sakyo-ku Kyoto 606*

(Received October 15, 1977)

The infrared and Raman spectra of dimethylaminosulfonyl chloride and its *C*-deuterated derivative have been recorded in the liquid state. The fundamental frequencies have been assigned by referring to the band intensities, Raman depolarization ratios and isotopic frequency shifts. A normal coordinate analysis based on a planar C_s molecular model has been carried out by using a simple Urey-Bradley force field for stretching and bending coordinates and a valence force field for torsional coordinates. The calculated frequencies based on a refined set of force constants agree well with the observed ones.

Infrared and Raman spectra of dimethylaminosulfonyl chloride, $(CH_3)_2NSO_2Cl$, have been reported by Bürger *et al.*[1] and Schneider *et al.*[2] The latter authors have also carried out a normal coordinate analysis for the simplified 7 body model, C_2NSO_2Cl. There seems to remain, however, much ambiguity on assignments of several skeletal vibrations which are expected to couple with the methyl group modes. The present work has been undertaken to clarify this point by referring to the spectral change on deuterating the two methyl groups, and to compare the related force constants with those of other sulfonyl compounds. A normal coordinate analysis has been carried out for the complete molecular model including the motion of the hydrogen atoms. By using a refined set of 25 force constants, the observed frequencies of both the isotopic compounds have been reproduced satisfactorily.

Experimental

Materials. Dimethylaminosulfonyl chloride, DMSCl, was prepared by the reaction between sulfuryl chloride and dimethylamine hydrochloride (reagent grade).[3] Dimethyl-d_6-aminosulfonyl chloride, DMSCl-d_6, was synthesized by the same reaction with the use of dimethyl-d_6-amine hydrochloride (Merck AG., 98% deuterated), and distilled twice under reduced pressure (bp 83—85 °C at 25 mmHg). The isotopic purity of the product was estimated to be more than 98% by NMR spectra.

Measurements. The infrared spectra were measured in the liquid state on a JASCO DS 403G grating spectrophotometer. The absorption frequencies were calibrated by the standard absorptions of polystyrene, indene and water vapor. The Raman spectra were measured for the liquid samples sealed in 1 mm unheparinized haematocript tubes on a JEOL S-1 laser Raman spectrophotometer. The 488.0 nm line of a Coherent 52G Ar^+ laser was used as the excitation source.

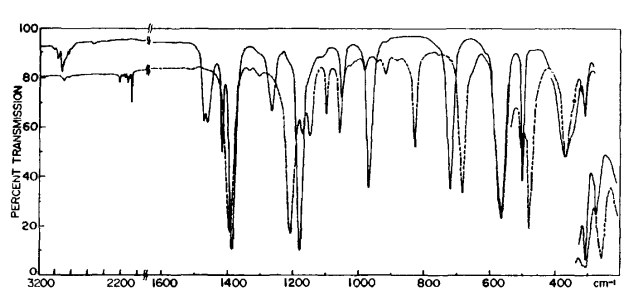

Fig. 1. Infrared spectra of DMSCl(——) and DMSCl-d_6 (----).

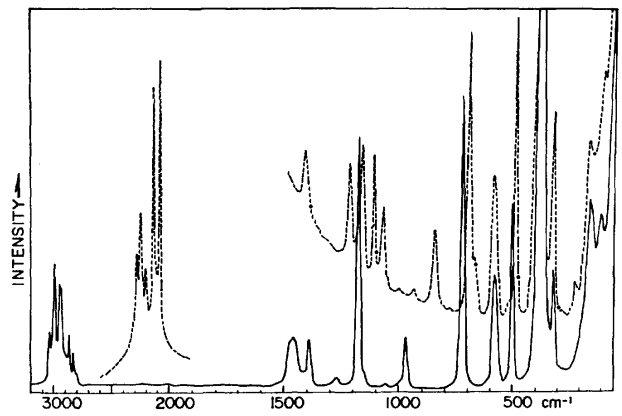

Fig. 2. Raman spectra of DMSCl (——) and DMSCl-d_6 (----).

The infrared spectra are shown in Fig. 1 and the Raman spectra in Fig. 2. The observed frequencies are listed in Table 1 together with approximate band intensities and assignments.

Vibrational Assignments

The fundamental frequencies of dimethylaminosulfonyl chloride were given rough assignments by Bürger *et al.*[1] and Schneider *et al.*[2] on the assumption that the vibrations of the methyl hydrogen atoms were virtually independent of the skeletal vibrations of the molecule. The spectral change on the *C*-deuteration of the methyl groups in this work revealed, however, that there are considerable vibrational couplings between the methyl groups and the other part of the molecule. The infrared bands at 1470 and 1459 cm^{-1} and the Raman band at 1456 cm^{-1} are assigned clearly to the CH_3 asymmetric deformation vibrations and the infrared band at 1416 cm^{-1} to the CH_3 symmetric deformation. On the *C*-deuteration, these bands disappear and the corresponding bands due to the CD_3 groups appear around 1150, 1100, and 1060 cm^{-1}. At the same time the strong infrared and Raman bands at 1177 cm^{-1} due certainly to the SO_2 symmetric stretching vibration shift to 1207 cm^{-1}. In the infrared spectrum no appreciable change in relative intensity is observed with these fre-

Table 1. Observed frequencies and assignments

$(CH_3)_2NSO_2Cl$			$(CD_3)_2NSO_2Cl$		
IR[a]	Raman[a,b]	Assignments[c]	IR[a]	Raman[a,b]	Assignments[c]
2970 vw	2970 s, p 2950 s, p	$\nu_aCH_3(a',a'')$	2230 vw	2241 m, p	$\nu_aCD_3(a',a'')$
			2070 vw	2115 s, p 2075 s, p	$\nu_sCD_3(a',a'')$
2860 vw	2860 m, p	$\nu_sCH_3(a',a'')$			
1470 m	—	$\delta_aCH_3(a',a'')$	1395 vs	1400 m, dp	$\nu_aSO_2(a'')$
1459 m	1456 wb, p	$\delta_aCH_3(a',a'')$	1207 vs	1207 m, p	$\nu_sSO_2+\nu_sCNC(a')$
1416 m	—	$\delta_sCH_3(a',a'')$	1173 m	—	$\nu_aCNC+\delta_sCD_3(a'')$
1385 vs	1387 m, dp	$\nu_aSO_2(a'')$	1153 m	1155 m, p	$\nu_sSO_2+\delta_sCD_3+\nu_sCNC(a')$
1264 m	1270 vw, p?	$\nu skel+\rho CH_3(a')$	1099 w	1102 m, p	$\delta_sCD_3+\nu SN(a')$
1177 vs	1177 s, p	$\nu_sSO_2(a')$ $\nu_aCNC+\rho CH_3(a'')$	1057 m	1065 m, p	$\delta_aCD_3(a',a'')$
			982 w	990 vw, dp	$\delta_aCD_3+\delta_sCD_3(a'')$
1115 vw	—	$\rho CH_3(a')$	919 w	920 vw, p	$\rho CD_3(a')$
1049 m	1053 vw, ?	$\rho CH_3(a'')$	827 m	835 vw, dp	$\rho CD_3(a'')$
966 s	967 w, p	$\rho CH_3+\nu_sCNC(a')$ $\rho CH_3+\nu_aCNC(a'')$	755 vw	760 vw, ?	$\rho CD_3+\nu skel(a')$ $\rho CD_3+\nu_aCNC(a'')$
716 s	718 vs, p	$\nu SN+\nu_sCNC(a')$	682 s	684 s, p	$\nu SN+\nu_sCNC(a')$
562 s	576 s, p	$\beta SO_2+\nu SCl(a')$	561 s	575 m, p	$\beta SO_2+\nu SCl(a')$
—	—	$\delta skel+\rho SO_2(a'')$	505 m	510 sh, ?	$\delta skel+\rho SO_2(a'')$
500 s	504 s, p	$\omega SO_2+\nu SCl(a')$	478 m	480 m, p	$\omega SO_2+\nu SCl(a')$
369 m	374 vs, p	$\nu SCl+\omega SO_2(a')$ $\delta skel(a')$	369 m	374 vs, p	$\nu SCl+\omega SO_2(a')$
			318 sh	—	$\delta skel(a')$
309 w	315 w, dp	$tSO_2(a'')$	309 w	315 w, dp	$tSO_2(a'')$
276 w	—	$\delta skel(a')$	257 w	—	$\delta skel(a')$
—	—	$\rho SO_2+tCNC(a'')$	—	218 vw, dp	$\rho SO_2+tCNC(a'')$
—	153 m, p	$\delta skel(a')$	—	150 m, p	$\delta skel(a')$
—	105 w, ?	$\tau SN(a'')$	—	95 w, ?	$\tau SN(a'')$

a) vs, very strong; s, strong; m, medium; w, weak; vw, very weak; b, broad; sh, shoulder. b) p, polarized; dp, depolarized. c) ν, stretching; β, bending; δ, deformation; ρ, rocking; ω, wagging; t, twisting; τ, torsion.

quency shifts, while in the Raman spectrum the intensity of the 1177 cm^{-1} band of DMSCl seems to be partitioned among the 1207, 1155, and 1102 cm^{-1} bands of DMSCl-d_6. This result suggests that the SO_2 symmetric stretching vibration of DMSCl-d_6 couples strongly with the CD_3 deformation vibrations. On the contrary, the SO_2 asymmetric stretching band around 1390 cm^{-1} undergoes only a slight isotope shift in both the infrared and Raman spectra. The infrared band at 1264 cm^{-1} assigned previously to the CH_3 rocking vibration[1,2] proved to disappear on the *C*-deuteration. According to the calculated normal modes, the contribution of the skeletal stretching vibrations to this band is also important. The infrared bands at 1115, 1049, and 966 cm^{-1} vanishing on the *C*-deuteration were assigned to the CH_3 rocking vibrations and were classified into the a′ and the a″ species by referring to the depolarization ratios of the corresponding Raman bands and the results of a preliminary calculation. The 1049 and the 966 cm^{-1} bands were assigned to the skeletal stretching vibrations by the previous authors.[1,2] Similarly, the infrared bands at 919, 827, and 755 cm^{-1} of DMSCl-d_6 newly appearing on the *C*-deuteration were assigned to the CD_3 rocking vibrations. The infrared band at 716 cm^{-1} of DMSCl shifts to 682 cm^{-1} on the *C*-deuteration and can be assigned to the S–N stretching vibration in agreement with the assignment of Bürger *et al.*[1] According to the calculated normal modes, the S–N stretching vibration contributes also to the infrared bands at 1264, 1177 and 966 cm^{-1} of DMSCl and at 1207, 1153, 1099, and 755 cm^{-1} of DMSCl-d_6.

The polarized Raman band at 374 cm^{-1} is extremely strong and remains unshifted on the *C*-deuteration. This band is assigned certainly to the S–Cl stretching vibration from analogy with the spectra of CH_3SO_2Cl and CD_3SO_2Cl.[4] The previous authors assigned this band to the C–N–C deformation vibration,[1,2] but such a strong band is missing in the Raman spectrum of $(CH_3)_2NSO_2NH_2$.[5] On the *C*-deuteration of DMSCl, the infrared bands at 562 and 309 cm^{-1} remain unshifted but those at 500 and 276 cm^{-1} shift to lower frequencies by about 20 cm^{-1}. By referring to the Raman depolarization ratios and the assignments of the related compounds,[4,6-9] the 562, 500, and 309 cm^{-1} bands were assigned to the SO_2 bending, wagging and twisting vibrations, respectively, and the 276 cm^{-1} band to the skeletal deforamtion vibration. The present as-

Table 2. Product and modified sum rules

	Product rule ratios[a]		Modified sum rule[c]
	Obsd[b]	Calcd	
a′	19.693	20.634	1.5534×10^7 $(cm^{-1})^2$
a″	19.760	19.828	1.5492×10^7 $(cm^{-1})^2$

a) $\prod(\nu_i DMSCl/\nu_i' DMSCl\text{-}d_6)$. b) The calculated frequencies were used in place of the unobserved frequencies. c) $\Sigma(\nu_i DMSCl)^2-\Sigma(\nu_i' DMSCl\text{-}d_6)^2$.

TABLE 3. FORCE CONSTANTS (in mdyn/Å)

K(SO)	9.723_1	K(SN)	3.010_3	K(SCl)	1.439_9	K(CN)	2.580_3	K(CH)	4.573[a]
H(OSO)	1.099_3	H(OSN)	0.115_6	H(OSCl)	0.141_0	H(NSCl)	0.213[a]	H(SNC)	0.243_1
H(CNC)	0.091_2	H(NCH)	0.357_4	H(HCH)	0.457_9	F(OSO)	-0.581_4	F(OSN)	1.657_4
F(OSCl)	0.402[a]	F(NSCl)	0.200[a]	F(SNC)	0.685_1	F(CNC)	0.703[a]	F(NCH)	0.372_8
F(HCH)	-0.037_0	κ(S)[b]	0.022[a]	κ(C)[b]	-0.048_8	τ(SN)[c]	0.279_4	τ(CN)[c]	0.090[a]

a) Assumed. b) in mdyn Å. c) Torsional constant in mdyn Å/rad².

signments of the SO_2 deformation vibration are considerably different from those of the previous authors.[1,2] An infrared band at 505 cm^{-1} and a Raman band at 218 cm^{-1} of DMSCl-d_6 newly appearing on the *C*-deuteration are assignable to the a″ skeletal deformation and the SO_2 rocking vibrations, respectively. The corresponding bands of DMSCl seem to be overlapped by the neighboring bands at the higher frequency side. The weak Raman band at 105 cm^{-1} of DMSCl is assigned to the S–N torsional vibration since the observed shift to 95 cm^{-1} on the *C*-deuteration is too small for the CH_3 torsion. No bands assignable to the CH_3 or the CD_3 torsional vibrations were observed.

Normal Coordinate Analysis

Following Schneider *et al.*,[2] we assumed that dimethylaminosulfonyl chloride takes the C_s structure in which each SO bond is at the trans position of a CH_3–N bond. In this model, the normal modes of DMSCl are classified as 18a′+15a″. The structure parameters used in the calculation are shown in Fig. 3. The bond lengths and the valence angles related to the C_2NS skeleton were taken from tetramethylsulfuric diamide[10] and those related to the SO_2 group from sulfuryl chloride.[11] The tetrahedral angle was assumed for the methyl group. The local symmetry coordinates were constructed in the usual form[12] and the redundant coordinate associated with the $-SO_2-$ group was eliminated numerically on diagonalizing the G matrices. The torsional coordinates were those defined by Miyazawa and Fukushima.[13]

A simple Urey-Bradley force field including 25 force constants was employed for the stretching and the bending coordinates and a valence force field for the torsional coordinates. Initially, the force constants for the $(CH_3)_2N-$ group were transferred from methylamine,[14] those for the $-SO_2Cl$ group from sulfuryl chloride[7] and those around the S–N bond from sulfuric diamide.[9] The torsional force constants τ(C–N) and τ(S–N) were assumed to be equal to the constants for the C–C and the C–S torsional coordinates of dialkyl disulfide,[15] respectively. On refining the force constants, the observed frequencies were taken mostly from the infrared

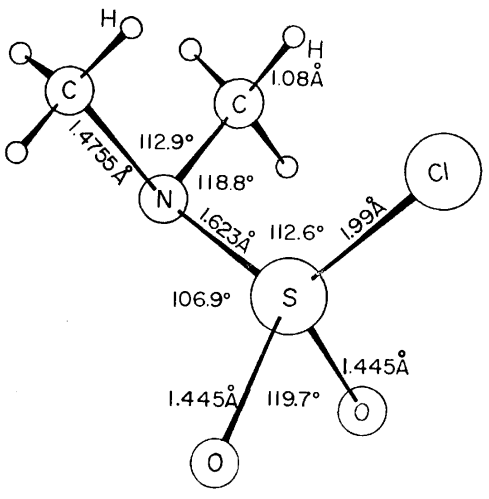

Fig. 3. Molecular structure and structural parameters.

TABLE 4. FUNDAMENTAL FREQUENCIES OF DMSCl AND DMSCl-d_6

	DMSCl		DMSCl-d_6	
	Obsd	Calcd	Obsd	Calcd
a′	2970	2981	2230	2222
	2970	2979	2230	2215
	2860	2849	2070	2053
	1470	1476	1207	1228
	1459	1471	1153	1159
	1416	1440	1099	1107
	1264	1238	1057	1053
	1177	1166	1057	1029
	1115	1109	919	888
	966	960	755	792
	716	725	682	665
	562	563	561	559
	500	505	478	490
	369	369	369	364
	369	365	318	335
	276	290	257	267
	—	196	—	140
	153[a]	117	150[a]	108
a″	2970	2980	2230	2217
	2970	2979	2230	2215
	2860	2848	2070	2050
	1470	1467	1395	1391
	1459	1462	1173	1175
	1416	1430	1057	1055
	1385	1390	1057	1041
	1177	1163	982	1019
	1049	1057	827	813
	966	992	755	793
	—	512	505	483
	309	305	309	302
	—	252	218[a]	235
	—	200	—	144
	105[a]	105	95[a]	94

a) Raman frequency.

data. These frequencies satisfied the isotopic product rule[16] and the modified sum rule[17] fairly well as shown in Table 2. The force constants were refined first by referring to the Jacobian matrix elements, and then by the method of least squares. The final set of the force constants is listed in Table 3, and the calculated frequencies are compared with the observed ones in Table 4.

In support of the empirical assignments given in the preceding section, the observed shifts of the skeletal frequencies below 750 cm^{-1} on the *C*-deuteration were reproduced well by the calculation. The stretching constant K(SN) is appreciably smaller than the corresponding constants of $NH_2SO_2NH_2$[9] and $CH_3SO_2NH_2$,[6] probably because the electron drawing effect of the chlorine atom tends to reduce the S–N bond order. The constant K(SCl) is also smaller than that of $ClSO_2Cl$[7] but is comparable with that of CH_3SO_2Cl.[4] The value of K(SO) is close to the average of those of $NH_2SO_2NH_2$[9] and $ClSO_2Cl$,[7] reflecting well the intermediate structure, NSO_2Cl, of DMSCl. Regarding K(SO), it may be also pointed out that $CH_3SO_2NH_2$,[6] $CH_3SO_2CH_3$[8] and $NH_2SO_2NH_2$[9] are all alike while DMSCl resembles CH_3SO_2Cl.[4] Thus, the effect of the NR_2(R=H or CH_3) group on the S–O bond order is similar to that of the CH_3 group, and in this respect the SO_2 group differs markedly from the C=O group as pointed out by Bellamy and Williams.[18]

The authors wish to express their sincere gratitude to Professor Toyozo Uno of Kyoto University for his encouragement throughout this work and to Mr. Akimasa Iwado of Okayama University for the measurement of the NMR spectra. The calculation in this work was performed on FACOM 230 series computers at Data Processing Center, Kyoto University and on a NEAC 2200/500 computer at Okayama University Computer Center.

References

1) H. Bürger, K. Burczyk, A. Blaschette, and H. Safari, *Spectrochim. Acta*, **27A**, 1073 (1971).
2) W. Schneider, G. Kessler and H.-A. Lehmann, *Z. Anorg. Allgem. Chem.*, **356**, 239 (1968).
3) N. C. Hansen, *Acta Chem. Scand.*, **17**, 2141 (1963).
4) K. Hanai, T. Okuda, and K. Machida, *Spectrochim. Acta*, **31A**, 1227 (1975).
5) Y. Tanaka, Y. Saito, and K. Machida, unpublished data.
6) K. Hanai, T. Okuda, and K. Machida, *Spectrochim. Acta*, **31A**, 1217 (1975).
7) H. Toyuki and K. Shimizu, *Bull. Chem. Soc. Jpn.*, **39**, 2364 (1966).
8) T. Uno, K. Machida, and K. Hanai, *Spectrochim. Acta*, **27A**, 107 (1971).
9) T. Uno, K. Machida, and K. Hanai, *Spectrochim. Acta*, **22**, 2065 (1966).
10) T. Jordan, H. W. Smith, L. Lohr, Jr., and W. N. Lipscomb, *J. Am. Chem. Soc.*, **85**, 846 (1963).
11) K. J. Palmer, *J. Am. Chem. Soc.*, **60**, 2360 (1938).
12) T. Shimanouchi, *Nat. Stand. Ref. Data Ser., Bur. Stand.*, **6**, (1967).
13) T. Miyazawa and K. Fukushima, *J. Mol. Spectrosc.*, **15**, 308 (1967).
14) E. L. Wu, G. Zerbi, S. Califano, and B. Crawford, Jr., *J. Chem. Phys.*, **35**, 2060 (1961).
15) H. Sugeta, *Spectrochim. Acta.*, **31A**, 1729 (1975).
16) O. Redlich, *Z. Phys. Chem.*, **B28**, 371 (1935).
17) K. Machida, *J. Chem. Phys.*, **38**, 1360 (1963).
18) L. J. Bellamy and R. L. Williams, *J. Chem. Soc.*, **1957**, 863.

Light Scattering Study of Local Structure in Solution. Double-Layered Structure Formation in Chloroform Solution of Surfactant

Tadashi KATO and Tsunetake FUJIYAMA

Department of Chemistry, Faculty of Science, Tokyo Metropolitan University, Fukazawa, Setagaya-ku, Tokyo 158

(Received October 17, 1977)

Light scattering spectra have been observed for binary solutions of chloroform–tetrabutylammonium chloride (TBACl) and chloroform–hexadecyltrimethylammonium chloride (HTACl) at various concentrations. The Rayleigh intensities have been reduced to concentration fluctuations. The observed concentration dependence of the concentration fluctuation was explained in terms of the existence of aggregates which were composed of a few surfactant molecules and several decades of chloroform molecules. Using the infrared data, the structures of the aggregates were demonstrated to be double-layered. In HTACl solution, a singular concentration dependence of concentration fluctuation was observed in the concentration range below 0.004 mole fraction.

In previous reports,[1,2] quantitative analysis of the infrared absorption intensities of some water soluble surfactants in chloroform solutions has been reported. In these reports it has been postulated that those surfactants dissolve in chloroform by forming hydrogen bonds with several solvent chloroform molecules. As the hydrogen bonds were not of the 1 : 1 type, an investigation to elucidate the structure of these complexes was undertaken.

Recently, a method has been reported for determining the local structures existing in binary solutions by observing the concentration fluctuation at different concentrations. This has been applied to various liquid mixtures.[3–7] In the present study, the light scattering method has been applied in chloroform solutions of the surfactants. Hexadecyltrimethylammonium chloride (HTACl) and tetrabutylammonium chloride (TBACl) were chosen since their specific refractive index incriments are large enough to measure the concentration fluctuation accurately and reliable infrared data are available for thier chloroform solutions. Elucidation of the double-layered structures may be determined by the complementary use of vibration spectra and light scattering spectra for these solutions. The experimental part of the light scattering study on HTACl–chloroform solution has been published already.[8]

Experimental

All chemicals used in the present study were commercial products. Chloroform was purified by column chromatography on alumina in order to eliminate water and ethanol. HTACl and TBACl were dried over P_2O_5 under vacuum for several days. The sample solutions were made dust-free by the use of a millipore filter FG of 0.2 μm pore size.

Light scattering spectra were observed by the use of a spectrometer designed and constructed in the laboratory.[3] The refractive indices of the sample solutions were measured by means of an Abbe refractometer (Atago). All the measurements were performed at 24±0.5 °C for CTACl solution and 21±0.5 °C for TBACl solution.

Results and Discussion

Light Scattering Spectra and Concentration Fluctuation. Figure 1 illustrates the light scattering spectra for chloroform solutions of TBACl in the concentration range of 0—0.036 mole fractions (for the spectra of HTACl, see Ref. 8). After separating the Rayleigh part from the observed spectra, the Rayleigh intensity was expressed relative to the Rayleigh intensity of pure chloroform. Then, the concentration fluctuation of the surfactants, $N\langle(\Delta x)^2\rangle$, was calculated from the equation[4]

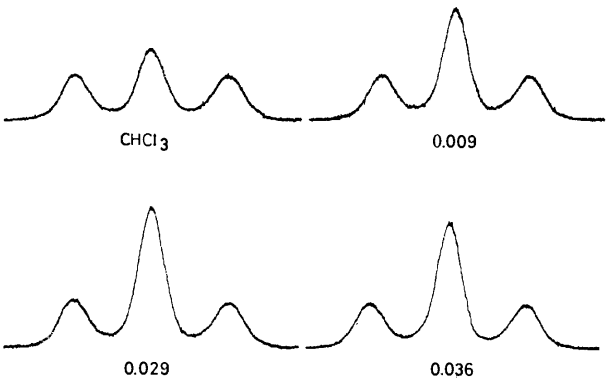

Fig. 1. Observed light scattering spectra for TBACl–chloroform system at 21 °C. Concentration is expressed in terms of mole fraction of TBACl.

$$N\langle(\Delta x)^2\rangle = \frac{RT^2}{M(\partial n/\partial x)^2_{P,T}}\left[\frac{S}{S_0}\left(\frac{n_0}{n}\right)^2\frac{\rho}{\rho_0}\frac{(\partial n_0/\partial T)^2_{P,x}}{C_{Pg^0}} - \frac{(\partial n/\partial T)^2_{P,x}}{C_{Pg}}\right], \quad (1)$$

where R is the gas constant, M the mean molecular weight, T the absolute temperature, n the refractive index, ρ the density, C_{P_g} the specific heat per gram, N the total number of molecules of the field within which the concentration fluctuation is considered, and (S/S_0) is the intensity ratio of Rayleigh lines. The suffix zero specifies quantities related to pure chloroform.

In Fig. 2, the concentration fluctuation thus obtained was plotted as a function of mole fraction, $\bar{x}$, of the surfactants. The broken line in Fig. 2 corresponds to the concentration fluctuation expected for an ideal binary solution. From the figure the observed concentration flutuation is seen to take larger values than those of an ideal binary solution at low concentration and smaller values as the concentration increases. Therefore, the concentration fluctuation of each system has a maximum value. The concentration at which the concentration fluctuation of TBACl takes a maximum value is higher than that of HTACl. In the region

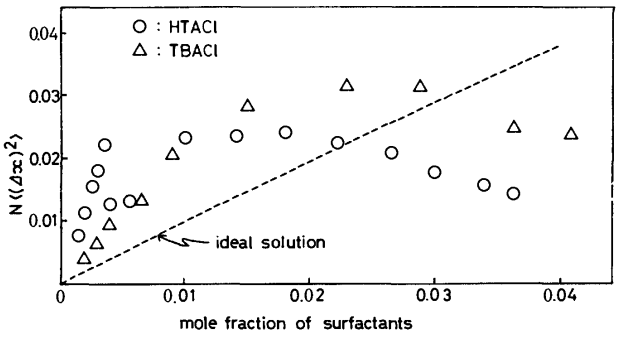

Fig. 2. Observed concentration fluctuation for TBACl-chloroform system.

where $\bar{x}$ is smaller than 0.004, the concentration fluctuation of HTACl increases rapidly with increasing $\bar{x}$, and decreases sharply at $\bar{x}=0.004$. In the concentration range of $\bar{x}>0.004$, it again increases gradually with increasing $\bar{x}$. The concentration flutuaction of TBACl, however, does not exhibit such singular concentration dependence in the low concentration region. These results suggest that the surfactant molecules aggregate with each other, in addition to the aggregation with chloroform molecules. The infrared data, on the other hand, suggests that these surfactant molecules form strong hydrogen bonds with chloroform molecules. Therefore, it is expected that an aggregate of the type A_lB_{ln} exist in these solutions, where l is the aggregation number of surfactants and n is the solvation number of chloroform per one surfactant molecule, where A and B refer to surfactant and chloroform molecules, respectively.

Analysis of $N\langle(\Delta x)^2\rangle$. Analysis of the observed concentration fluctuation employed the so-called association complex model.[5,6] From the discussion in the preceding paragraph, it may be assumed that an aggregate of the type A_lB_{ln} and a free chloroform molecule, B_1, behave as independent molecules in the solution. Aggregates of the type A_l may be assumed negligible since the analysis of infrared absorption intensity has shown that all surfactant molecules form hydrogen bonds with chloroform molecules in this concentration range. Aggregates of the type B_l may be assumed negligible since the hydrogen bonding between chloroform molecules is very weak in comparison with that between chloroform and surfactant molecules.[9]

Assuming that A_lB_{ln} and B_1 behave as independent molecules in the solution, the probability, $f(N_A)$, of finding N_A numbers of A molecules within the region which contains a constant number, N, of molecules may be expressed as[6]

$$f(N_A)=\frac{(N_1+N_2)!}{N_1!N_2!}P^{N_1}(1-P)^{N_2}, \tag{2}$$

with

$$N_1 = N - nN_A$$
$$N_2 = N_A/l$$
$$P = \bar{N}_1/(\bar{N}_1+\bar{N}_2)$$

where N_1 and N_2 are molecular numbers of aggregates, B_1 and A_lB_{ln}, respectively. Then, the number fluctuation of A molecules in the region considered may be calculated thus

$$\langle(\Delta N_A)^2\rangle_N = \frac{-1}{(\partial^2 \ln f(\bar{N}_A)/\partial \bar{N}_A{}^2)_N}$$
$$= \frac{\bar{N}_A}{N^2}[N-(n+1)\bar{N}_A] \times [lN-\{l(n+1)-1\}\bar{N}_A]. \tag{3}$$

Therefore, the concentration fluctuation may be expressed as:

$$N\langle(\Delta x_A)^2\rangle = \bar{x}_A[1-(n+1)\bar{x}_A] \times [l-\{l(n+1)-1\}\bar{x}_A]. \tag{4}$$

Figure 3 demonstrates the concentration dependence of the concentration fluctuation calculated from Eq. 4 for $l=2$ and for various n-values, together with the observed concentration fluctuation values for TBACl solution. The figure demonstrates that the concentration fluctuation decreases in magnitude as n increases. The theoretical curve for $n=10$ best explains the curve in the sence that the concentration fluctuation takes a maximum value at $\bar{x} \approx 0.03$. Figure 4 demonstrates the concentration dependence of the concentration fluctuation calculated from Eq. 4 for $n=10$ and various l-values. The figure demonstrates that the concentration fluctuation increases in magnitude as l increases

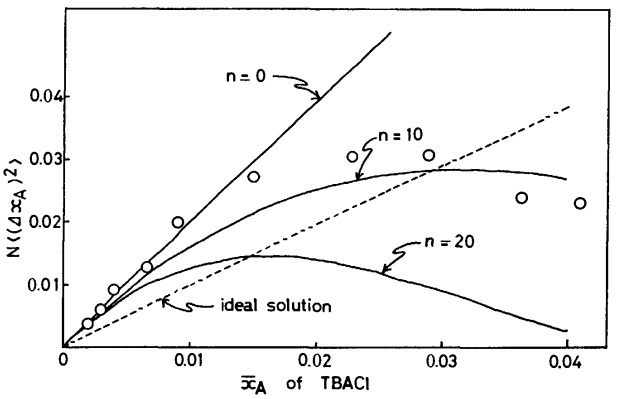

Fig. 3. Theoretical values of concentration fluctuation calculated from Eq. 4 for $l=2$ and $n=0$, 10, and 20. The open circles correspond to observed values for TBACl-chloroform system.

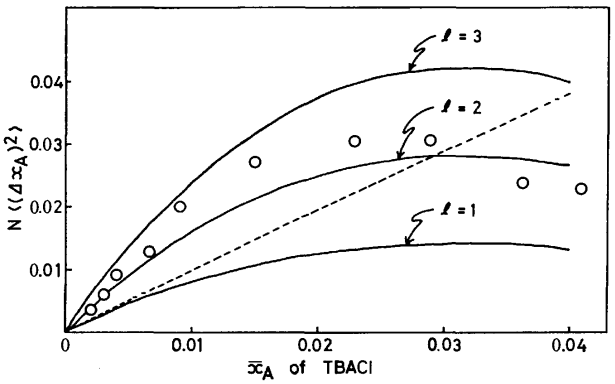

Fig. 4. Theoretical values of concentration calculated from Eq. 4 for $n=10$, and $l=1$, 2, and 3.

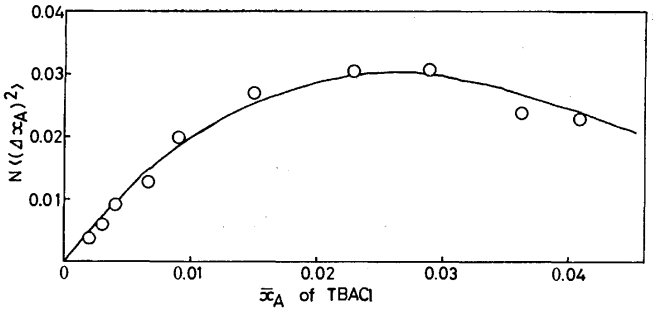

Fig. 5. Final results of theoretical calculation for TBACl-chloroform system ($l=2.6$, $n=12$).

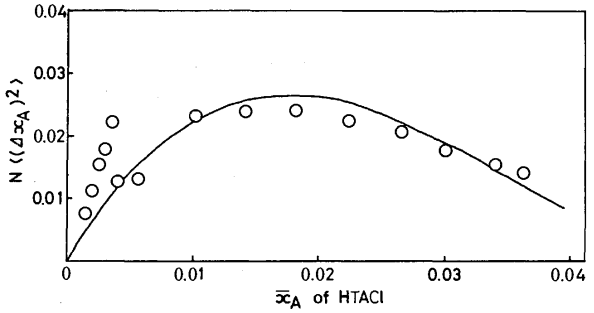

Fig. 6. Final results of theoretical calculation for HTACl-chloroform system ($l=3.4$, $n=18$).

without change in function, *i.e.*, the concentration at which the concentration fluctuation takes a maximum value is almost independent of l-values. The best fit between the calculated and the observed concentration fluctuation curves was obtained by setting $l=2.6$ and $n=12$ for TBACl solution and $l=3.4$ and $n=18$ for HTACl solution. The theoretical calculations are shown in Figs. 5 and 6.

Local Structure in the Solution. The present results may be summarized as follows. The surfactants studied dissolve in chloroform by forming an aggregate which is made up of a few surfactant molecules and several decades of chloroform molecules. This conclusion is in apparent contrast to the conclusion drawn from the infrared analysis, in that there, the indication is that the surfactants dissolve in chloroform by forming complexes which are made up of several chloroform molecules and one surfactant molecule.[1] Table 1 shows the value of l and n obtained from the present study, together with the n-values obtained from the infrared study, n_{IR}. It was to be expected that the n and n_{IR} values would not agree and the difference is thought to be real. From the intensity ratio of the infrared absorption bands corresponding to the free and the bonded chloroform molecules, the number ratio of free and bonded chloroform molecules may be determined. Therefore, the infrared result affords rigorous information about the number of chloroform molecules which are directly attached to the surfactant molecules by hydrogen bonds. In the light scattering study, however, the molecular aggregate which behaves as a single molecule in solution is important, since concentration fluctuation is determined by the spatial distribution of component molecules in solution.

Table 1. l and n values obtained in the present study and n_{IR} values obtained from the infrared absorption study for chloroform solutions of TBACl and HTACl

	TBACl	HTACl
l	2—3	3—4
n	12	18
n_{IR}[a)]	2	4—4.5

a) See Ref. 1.

Combining results obtained from these light scattering and infrared absorption studies indicate a double-layered aggregate structure formed in the solutions; l numbers of surfactant molecules make a core of the aggregate and the core is surrounded by $(l\times n)$ numbers of chloroform molecules. Among the $(l\times n)$ numbers of chloroform molecules in one aggregate, $(l\times n_{IR})$ numbers of chloroform molecules form hydrogen bonds directly with the surfactant molecules and make a first shell. The remaining $l(n-n_{IR})$ numbers of chloroform molecules envelope the first shell by weak intermolecular interactions.

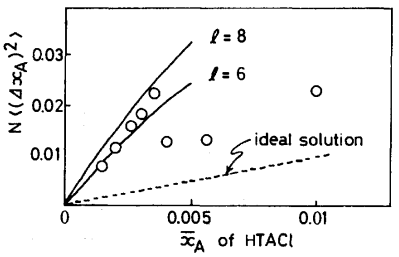

Fig. 7. Observed and calculated concentration fluctuation for HTACl-chloroform system in the region of $x_A \leq 0.01$.

The singular behavior of the concentration fluctuation observed for HTACl solution at low concentration is of some interest. Figure 7 shows the observed and calculated concentration fluctuation in the region where $\bar{x}_A$ is smaller than 0.01. As can be seen from Eq. 4, concentration fluctuation is only marginally affected by n for small values of $\bar{x}_A$, that is, it is largely dependent on l. Therefore, a dummy number of 18 was set for the n-value in the theoretical calculation. From the figure the number of the surfactant molecules making an aggregate was determined to be 6—8 for HTACl. In TBACl solution, on the other hand, such singular concentration dependence of concentration fluctuation was not observed. This difference may arise from the molecular structure of HTACl which favors the aggregation of HTACl in chloroform.[10]

This work was partly supported by a research grant from the Ministry of Education.

References

1) M. Okazaki, I. Hara, and T. Fujiyama, *J. Phys. Chem.*, **80**, 64 (1976).
2) M. Okazaki, I. Hara, and T. Fujiyama, *J. Phys. Chem.*, **80**, 1586 (1976).
3) K. Iwasaki, M. Tanaka, and T. Fujiyama, *Bunko*

Kenkyu, **25**, 134 (1976).

4) K. Iwasaki, M. Tanaka, and T. Fujiyama, *Bull. Chem. Soc. Jpn.*, **49**, 2719 (1976).

5) K. Iwasaki, Y. Katayanagi, and T. Fujiyama, *Bull. Chem. Soc. Jpn.*, **49**, 2988 (1976).

6) T. Kato and T. Fujiyama, *J. Phys. Chem.*, **80**, 2771 (1976).

7) K. Iwasaki and T. Fujiyama, *J. Phys. Chem.*, **81**, 1908 (1977).

8) T. Kato and T. Fujiyama, *J. Phys. Chem.*, **81**, 1560 (1977).

9) The validity of this assumption has been discussed on the model system, $CHCl_3$–EtOH and CCl_4–EtOH: T. Kato, S. Hyodo, and T. Fujiyama, *J. Phys. Chem*, in press.

10) The refree's comment has been against the experimental result itself. It says that this singular behavior of the concentration fluctuation may arise from the existence of "impurity" in the observed system. We think this may or may not be so, because we could not recognize the existence of any impurities by the use of our experimental technique. We feel it is more important to report the fact that the *l*-value of 6—8 was obtained from our experimental result and from our theoretical analysis, because it suggests the fact that the aggregation number in the low concentration range is larger than that in the high concentration range.

The Reactions of Dichlorotriazinyl Reactive Dyes with Cellulose and Simultaneous Diffusion in Cellulose

Hiromi MOTOMURA and Zenzo MORITA

Department of Textiles and Polymer Science, Faculty of Engineering, Tokyo University of Agriculture and Technology, Koganei, Tokyo 184

(Received October 17, 1977)

The diffusion coefficients and rate constants of the reactions of C. I. Reactive Yellow 4, Orange 1, and Red 1 were measured at 30 °C by means of a cylindrical cellophane film roll. The diffusion coefficients of the three hydrolyzed dyes were nearly constant at all the pH values examined. The apparent diffusion coefficients of all the active species of Orange 1 and Red 1 except Yellow 4 were gradually decreased with an increase in the pH of the dyebath; this decrease was due to the hydrolysis of the active species in the cellulose substrate. The rate constants of the reactions with cellulose were of a pseudo-first-order; *i.e.*, the second-order rate constants of reactions with cellulose were constant up to a certain pH, and thereafter they decreased with an increase in the pH of the dyebath. The pH dependence of the reactivity with cellulose was similar to that of the hydrolysis reported previously. The concentration profiles of the removed and immobilized species in cellulose dyed from a weakly alkaline dyebath agreed with the theoretical profiles of active and reacted species respectively. From a highly alkaline dyebath, those of the immobilized species agreed with the theoretical profiles of reacted species, while those of the removed ones did not agree with theoretical profiles of active species because of hydrolysis.

Only a few works on the reaction of reactive dyes with cellulose have been reported,[1-3] though there have been many studies of the mechanisms on the reactive dyeing.[4,5] The reactivities of mono- and dichlorotriazinyl reactive dyes have been examined through reactions with water[6-15] and with alcohols as a model for cellulose.[1,7,10-13] The rate of the reaction of reactive dyes with cellulose must be derived from the theory of the diffusion with a simultaneous reaction in solid cellulose. Preston and Fern have obtained the diffusion coefficients and the rate constants of reactions with cellulose from Danckwart's equation by measuring the total amount of reactive dye on the substrate.[1]

In a previous paper, the theoretical equations which described the concentration profile of the immobilized species of reactive dyes in the substrate were derived from the diffusion equation with a chemical reaction of the first-order or pseudo-first-order.[3] A new method by which the reaction-rate constants of dye with cellulose could be obtained from the concentration profiles of reactive dyes was presented, though the basic diffusion equation used was the same as that of Preston and Fern. The profiles were measured from the cylindrical-film-roll method, where, after the diffusion, the immobilized profile was experimentally obtained by removing the active and hydrolyzed species by scouring; it corresponded to the theoretical distribution of reactive dyes fixed by the chemical reaction with cellulose.

In the present paper, the reaction-rate constants of dichlorotriazinyl reactive dyes will be obtained from the concentration profiles of the immobilized species by using the same method as in the previous paper[3] and will be discussed in comparison with those of hydrolysis and alcoholysis.[6-15] The diffusion coefficients of active and hydrolyzed species will also be measured.

Experimental

Films. Cellophane films (#300, Tokyo Cellophane Sheet Co., Ltd.) were cut 5 cm wide and 60 cm long and scoured several times in boiling water for 2 h. The thickness of a swollen film was measured to be 3.68×10^{-3} cm. The cylindrical film roll was made by the usual method.

Reactive Dyes and Reactive Dyeing. Three reactve dyes manufactured and supplied by the Nippon Kayaku Co., Ltd., were used, and the dyeing was performed at 30 °C under the dyebath conditions shown in Table 1. The reagents for the buffer solutions used in order to adjust the pH of the dyebath were KH_2PO_4 and $Na_2B_4O_7$ from pH 6.8 to 9.0, $Na_2B_4O_7$ and Na_2CO_3 from 9.2 to 11.0, and Na_2HPO_4 and NaOH at pH 12. NaCl was added to adjust the ionic strength of the dyebath.

In order to exclude the influence of the hydrolyzed species in the dyebath, a constant feed of the stock solutions of both the reactive dye and the buffer was carried out by the use of a quantitative pump, and the same amount of solutions used as feed was allowed to overflow. A cylindrical cellophane roll was dipped into the dyebath for a prescribed time. After the dyeing, it was immediately opened and the layers from the surface were cut off in halves. One film cut off was promptly scoured in boiling water for 20 min to remove the unreacted dye with cellulose and was dried after scouring. The other one was also dried, but without scouring.

TABLE 1. DYEING CONDITIONS

C. I. Reactive	Mikacion dyes	Ionic strength	Concentration of dyebath (mol/dm³)	Concentration of dyebath (g/dm³)	Dyeing time (h)
Yellow 4	Yellow RS	0.15	1.93×10^{-4}	0.15	1—12
		0.15	3.86×10^{-4}	0.30	
Orange 1	Brilliant Orange GS	0.15	5.36×10^{-4}	0.60	1— 6
Red 1	Brilliant Red 2BS	0.15	6.45×10^{-4}	1.0	1— 4
		0.50	6.45×10^{-4}	1.0	

Dyeing with Hydrolyzed Dyes at Various pHs and with Reactive Dyes at pH 6.8. As the reactions with cellulose were not observed, the diffusion coefficients of the reactive dye at pH 6.8 and those of the hydrolyzed one at various pHs were measured by the Sekido-Matsui method using a cylindrical cellophane film roll, as the concentration profiles in this case were Fickian.[16] The concentration profiles obtained in these experiments or the dyes adsorbed could be completely removed by the scouring of the films dyed with the hydrolyzed species and the active ones at pH 6.8. A purified sample of the hydrolyzed species was prepared by the hydrolysis of the reactive dyes and by salting-out with sodium acetate.[3]

Concentration Profiles of Immobilized and Removed Dyes and Determination of Reaction-Rate Constants, k. The concentrations of the dyes in the films were obtained by measuring the optical densities at the wavelength of the maximum absorption of the dye by means of a Shimadzu 40S spectrophotometer. The calibration curves of the reactive dyes in the film were made with the hydrolyzed and purified dye as the reference in molar concentration. The concentration profile of the immobilized dyes was obtained from the scoured film after dyeing, and that of the removed dyes, from the difference between the concentrations of the scoured and unscoured films at each layer. The former corresponds to the concentration of reactive dye reacted with cellulose, and the latter, theoretically to the active species not yet reacted with cellulose if there were no or little reaction with water in cellulose. The dyes reacted with cellulose were not removed, as was confirmed by no coloration of the renewed scouring solution and by no hydrolysis of the dye-fiber bond under all the dyeing conditions.

The reaction rate-constant, k, was approximately determined from the relation between k and the ratio of the fixed dye to the total dye in the first layer (*cf.* Ref. 3, Fig. 6). The surface concentration, C_o, could be obtained by the extrapolation of the profile of the removed dye. The diffusion coefficients, D, k, and C_o, obtained above were modified so as to fit the experimental profile to the theoretical one by means of a trial-and-error method with a computer. Under highly alkaline conditions, they were obtained from the fitting of the experimental profile for the immobilized species to the theoretical one. In order to avoid the contrary modification of C_o and obtain a highly reliable value of C_o, several experiments were carried out for different dyeing times under certain dyebath conditions. The most satisfactory values of C_o, k, and D especially were evaluated from the experimental profiles for different dyeing times.

Results and Discussion

Diffusion of Reactive Dyes. Some experimental profiles of the immobilized and removed species in cellulose are shown in Figs. 1—3. As has been mentioned previously, the concentration profiles of immobilized and active species for reactive dyes in cellulose could be described by theoretical equations derived from the diffusion equation with a chemical reaction of a pseudo-first-order:

$$\frac{\partial C}{\partial t} = D\frac{\partial^2 C}{\partial x^2} - kC, \qquad (1)$$

where C(mol/kg) was the concentration of active species, t(min) was the time, x(cm) was the distance, and k (min^{-1}) was the pseudo-first-order rate constant of the reaction with cellulose, provided that the diffusion coefficient, D(cm^2/min), of the active species was constant. This equation was solved under the conditions of an infinite dyebath, *i.e.*, a constant surface concentration, C_o.[3] The theoretical profiles of the fixed and active species are also shown in the figures.

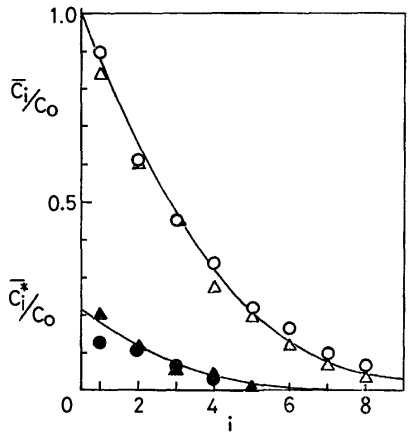

Fig. 1. Concentration profiles of the active (○, △) and immobilized species (●, ▲) of C. I. Reactive Red 1 at pH 7.6 (I=0.5), 30 °C and for 2 h. Results from two experiments under the same condition are shown. The lines in figure are the theoretical ones for $D=8.2\times10^{-7}$ cm^2/min and $k=2.0\times10^{-3}$ min^{-1}.

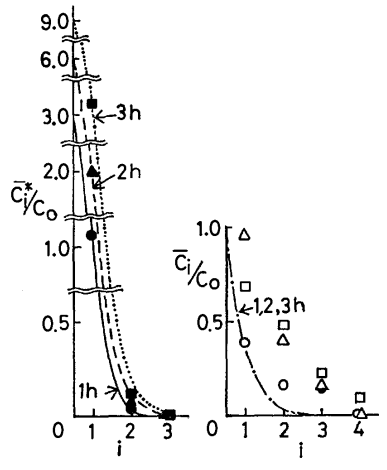

Fig. 2. Concentration profiles of the active (○ at 1 h, △ at 2 h, and □ at 3 h) and immobilized species (● at 1 h, ▲ at 2 h, and ■ at 3 h) of C. I. Reactive Orange 1 at pH 11.6 (I=0.15) and 30 °C. The lines in figure are the theoretical ones for $D=1.0\times10^{-7}$ cm^2/min and $k=5.0\times10^{-2}$ min^{-1}.

The concentration profiles obtained experimentally are classified into three types by comparing them with the theoretical profiles of the immobilized and active species. Type 1 consists of profiles dyed from a weakly alkaline dyebath; a typical example is shown in Fig. 1, where the agreements between the experimental profiles of the immobilized and removed species and the theoretical profiles of fixed and active species, and their reproducibility are fairly good. Type 2 consists of profiles dyed from a moderately alkaline dyebath; it is shown in Fig. 2, where the experimental immobilized profiles for different diffusion times are in agreement

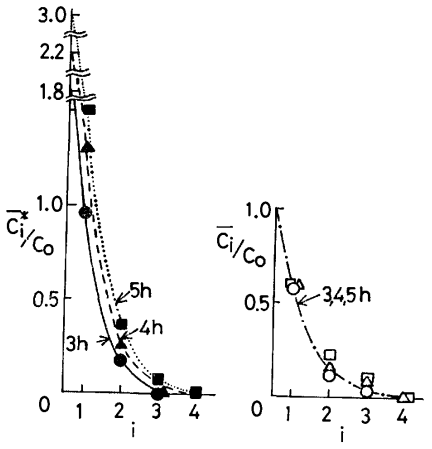

Fig. 3. Concentration profiles of the active (○ at 3 h, △ at 4 h, and □ at 5 h) and immobilized species (◐ at 3 h, ▲ at 4 h, and ■ at 5 h) of C. I. Reactive Yellow 4 at pH 9.2 (I=0.15) and 30 °C. The lines on figure are theoretically described by Eqs. 7 and 8 of Ref. 3 (D=9.0×10^{-8} cm^2/min, k=1.0×10^{-2} min^{-1}).

with the theoretical profiles for the fixed species, but the removed ones are not in agreement with that for the active species. Type 3 is intermediate between them and is shown in Fig. 3, where the profiles of the immobilized species for different diffusion times are in agreement with the theoretical profiles of the fixed species, but the experimental profiles of the removed species penetrated more deeply than the theoretical ones. The theoretical profiles for the active species shown in Figs. 2 and 3 are asymptote and show that no active species can penetrate more deeply than the line. Theoretically, all the active species adsorbed from the dyebath are reacted with cellulose, and the distribution of active species is in the equilibrium state. The experimental profiles of the removed species shown in Fig. 2, however, penetrated the more deeply, the longer the diffusion times. As the penetrations of fixed and active species must be theoretically in agreement with each other,[3] there should be inactive or hydrolyzed species in cellulose during diffusion. There would be other reasons for the minor possibility that the hydrolyzed dyes in the alkaline dyebath were also adsorbed, though the concentration of active species in the dyebath was kept constant and the surface concentration of active species was not varied during the dyeing, or that the species immobilized by the reaction with cellulose were mobilized again by the hydrolysis of the dye-fiber bond. The last possibility was experimentally confirmed to be so small that the reaction-rate constant, k, was not practically influenced at 30 °C below pH 12.0 under the experimental conditions of the present study.

Because of the agreement between the experimental and theoretical profiles for the immobilized species, and because of the disagreement between the removed or experimental profile and the active or theoretical one under highly alkaline conditions, the D and k of active species were determined from the immobilized profiles. The D and C_0 at various pHs are compared with those

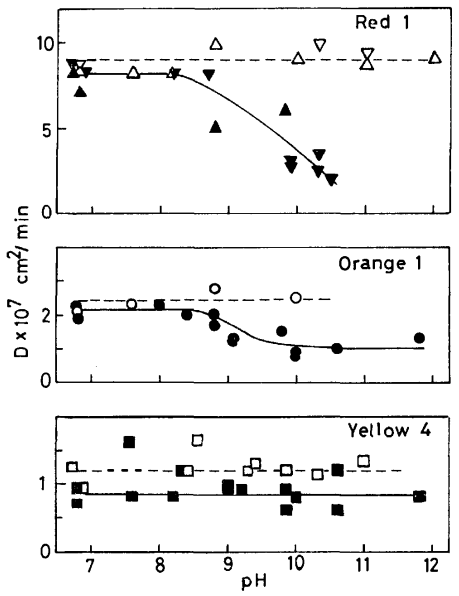

Fig. 4. Apparent diffusion coefficients of the active (solid symbols) and hydrolyzed species (open symbols) at 30 °C and I=0.15. In the case of Red 1, results for I=0.15 (▽ and ▼) and for I=0.5 (△ and ▲) are shown.

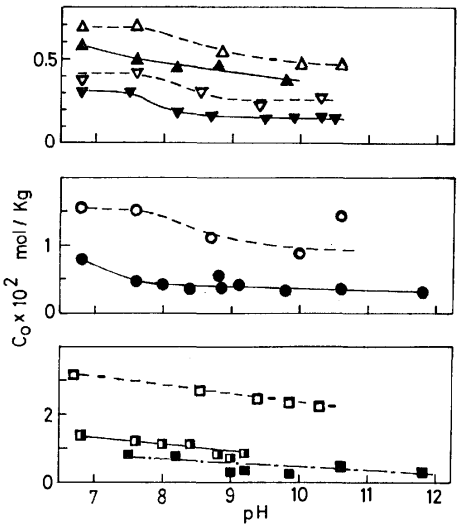

Fig. 5. Surface concentrations of the active and hydrolyzed species at 30 °C.

Dye	Species	Symbol	Ionic strength I	Concentration (mol/dm^3)	Concentration (g/dm^3)
Red 1	H	△	0.50	8.14×10^{-4}	(0.5)
		▽	0.15	1.63×10^{-3}	(1.0)
	A	▲	0.50	6.45×10^{-4}	(1.0)
		▼	0.15		
Orange 1	H	○	0.15	8.64×10^{-4}	(0.5)
	A	●	0.15	5.36×10^{-4}	(0.6)
Yellow 4	H	□	0.15	1.56×10^{-3}	(0.9)
	A	◨	0.15	3.86×10^{-4}	(0.3)
		■	0.15	1.93×10^{-4}	(0.15)

H=Hydrolyzed, A=Active.

of hydrolyzed species in Figs. 4 and 5. Though the C_0 of the hydrolyzed species were slightly decreased with an increase in the pH, the C_0's of the active species were almost constant under the alkaline conditions above pH 8. This shows that C_0 can actually be kept constant at a highly alkaline pH if a sufficient amount of electrolytes is added to the dyebath. Sumner and Taylor have reported, after using the dye base and diamino derivatives of three Procion dyes, the complicated findings that the affinities of Yellow 4 were constant over the whole pH range between 8 and 13, while those of Red 1 were constant up to pH 10 and then decreased slightly with an increase in the pH.[17] Although the standard affinities of reactive dyes for cellulose could not be calculated, as no alkaline adsorption by cellulose was measured in the present study, the adsorption behavior of the active and hydrolyzed species for the three reactive dyes used all appeared to have the same pH dependence.

At pH 6.8, the D values of the hydrolyzed species for the three dyes were slightly larger than those of the active species (Fig. 4). Sumner and Taylor also observed that the D values of the dye bases for three Procion dyes were larger than those of diamino derivatives and estimated that those of active species were intermediate.[17] Although they reported the complicated diffusional behavior of three Procion dyes at various pH values between 8 and 13, the D values of the hydrolyzed species for the three reactive dyes used in the present study appeared to be constant over the whole pH range examined (Fig. 4). However this behavior for Yellow 4 appeared to be in accordance with their results.

On the other hand, the D values of the active species for Orange 1 and Red 1, as estimated from the diffusion profiles of the immobilized species, apparently decreased with an increase in the pH, and that for Yellow 4 was nearly constant over the whole pH range examined. The decreasing tendency of the D for Red 1 was larger than that for Orange 1. As was mentioned in the previous paper (*cf.* Ref. 3, Fig. 1), some combinations of D and k described theoretically the concentration

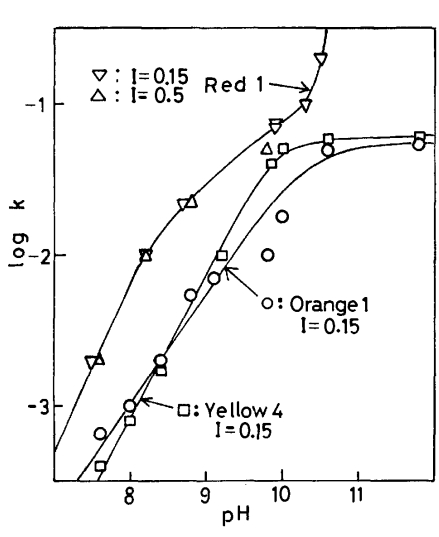

Fig. 6. Effect of pH on the rate constants of reaction with cellulose at 30 °C.

profiles of the immobilized and active species obtained from a diffusion experiment. Because the k values of active species could be estimated by various methods, because their obtained values coincided with each other, and because the pH dependence of k was similar to that of the rate constants of hydrolysis (*cf.* Fig. 6), the values of k obtained can be considered reasonable. If the D of an active species was estimated from the profile of the immobilized species with the value of k obtained above, however, it was smaller than the D of the hydrolyzed species under highly alkaline conditions. It is notable that the dyes with larger D values of the active species have a larger decreasing tendency than those with smaller ones do. It has been also shown in the previous paper that the larger the D of the active species and the smaller the k, the deeper was the penetration of immobilized and active species of reactive dyes into the substrate.[3] Thus, the dyes with larger k values are hindered in penetrating into the substrate. In spite of the fact that the D in the present study was estimated considering this effect, a cosiderably large rate of reaction with water in cellulose would be expected under highly alkaline conditions if the D of active species was constant over the whole pH range and was equal to that at pH 6.8. However, the detailed studies of the mechanism of the pH dependence for D and of the differences among the reactive dyes are now under way.

Reaction with Cellulose. The reaction-rate constants, k, determined from the immobilized profiles at various pHs are shown as relationships between log k and pH in Fig. 6. The relationships were similar to that of hydrolysis measured by Ingamells *et al.* at 20 °C.[7] They observed two kinds of relations between the rate of hydrolysis and the pH. Such a relation is also found in Fig. 6; *i.e.*, the effect of the pH on the reactivity for Yellow 4 and Orange 1 is different from that for Red 1. In the cases of Yellow 4 and Orange 1, log k had a constant slope up to pH 11. The rate constants of the hydrolysis for Yellow 4 and Red 1 were measured to be 0.016 and 0.060 min^{-1} respectively by Sumner and Vickerstaff at pH 11 and 30 °C.[18] According to Dawson *et al.*, they were 0.0175 min^{-1} for Yellow 4 and 0.055 min^{-1} for Red 1.[6] Comparing the rate constants of the reaction with cellulose for Yellow 4 in the present study with those of hydrolysis quoted above, the former value was about 5 times larger than the latter at pH 11, though the ionic strength and the kind of buffer solution were different. Although the k of Red 1 at pH 11 was too large to be obtained by measuring the optical densities of the immobilized species on cellophane, it was estimated by extrapolation of the k-pH relationship in Fig. 6 and thus found to have the value of 0.6—1.0 min^{-1}, 10—17 times larger than that of the hydrolysis. The rate constants of the reaction with cellulose for Red 1 measured by Preston and Fern at 20 °C were 25—11 times larger than those of the hydrolysis over the pH range between 9.5 and 12.8.[1] The ratio of the constants of the reaction with cellulose to those of hydrolysis may differ with the kind of reactive dye. On the other hand, the effect of the ionic strength on the rate of reaction with

cellulose for Red 1 was investigated by changing the salt concentration added to the dyebath. As is shown in Fig. 6, no influences on the rate constants by the ionic strength were observed within the range of experimental error.

The authors would like to thank the Nippon Kayaku Co., Ltd., for the assistance of its staff in the preparation of this paper.

References

1) C. Preston and A. S. Fern, *Chimia*, **15**, 177 (1961).
2) I. D. Rattee, *Endevour*, **20**, 154 (1961).
3) H. Motomura and Z. Morita, *J. Appl. Polym. Sci.*, **21**, 487 (1977).
4) W. F. Beech, "Fibre-Reactive Dyes," Logos Press, London (1970).
5) K. Venkataraman, Ed., "The Chemistry of Synthetic Dyes," Vol. VI, Reactive Dyes, Academic Press, New York (1972).
6) T. L. Dawson, A. S. Fern, and C. Preston, *J. Soc. Dyers Colour.*, **76**, 210 (1960).
7) W. Ingamells, H. H. Sumner, and G. Williams, *J. Soc. Dyers Colour.*, **78**, 274 (1962).
8) S. Horrobin, *J. Chem. Soc.*, **1963**, 4130.
9) J. R. Aspland and A. Johnson, *J. Soc. Dyers Colour.*, **81**, 425, 477 (1965).
10) P. Rys and H. Zollinger, *Helv. Chim. Acta*, **49**, 749 (1966).
11) A. Datyner, P. Rys, and H. Zollinger, *Helv. Chim. Acta*, **49**, 755 (1966).
12) P. Rys and H. Zollinger, *Helv. Chim. Acta*, **49**, 761 (1966).
13) P. Rys, *Textilveredlung*, **2**, 95 (1967).
14) I. D. Rattee and K. S. Murthy, *J. Soc. Dyers Colour.*, **85**, 368 (1969).
15) M. Komaki, T. Kaneda, M. Hayashi, M. Hida, and A. Yabe, *Sen'i Gakkaishi*, **29**, T-546 (1973).
16) M. Sekido and K. Matsui, *Sen'i Gakkai Shi*, **20**, 778 (1964).
17) H. H. Sumner and B. Taylor, *J. Soc. Dyers Colour.*, **83**, 445 (1967).
18) H. H. Sumner and T. Vickerstaff, *Melliand Textilber.*, **42**, 1161 (1961).

The Effects of Halide Ions on the Radiation-induced Decoloration of Azo and Anthraquinone Dyes in N_2O-saturated Aqueous Solutions

Nobutake SUZUKI, Okihiro TOKUNAGA, and Masamitsu WASHINO

Japan Atomic Energy Research Institute, Takasaki Radiation Chemistry Research Establishment, Takasaki, Gunma 370-12

(Received November 18, 1977)

The radiation-induced decoloration of azo and anthraquinone dyes was studied in N_2O-saturated aqueous solutions containing halide ions. In the N_2O-saturated solutions, the decoloration yield, $G(-\text{Dye})$, increased markedly upon the addition of Br^- and I^-, which are efficient scavengers of the OH radical. In the nitrogen-saturated solutions, however, the $G(-\text{Dye})$ decreased upon the addition of Br^- and I^-. Such an increase in the $G(-\text{Dye})$ upon the addition of Br^- and I^- in the N_2O-saturated solutions is mainly attributable to the attacks of the halide radical anions, Br_2^- and I_2^-, on the ring structure of the dyes. On the other hand, the $G(-\text{Dye})$ was not changed upon the addition of Cl^- in the N_2O-saturated solution. This may be attributable to the very slow rate of the formation of Cl_2^- in a neutral solution.

In a preceding paper,[1] we studied the effect of NCS^- on the radiation-induced decoloration of Acid Red 265 (azo dye) and Acid Blue 40 (anthraquinone dye) in N_2O-saturated aqueous solutions and found that the $G(-\text{Dye})$ increased markedly upon the addition of NCS^-, which is an efficient scavenger of the OH radical; we concluded that such an increase in the $G(-\text{Dye})$ was mainly attributable to the attack of the radical anion $(NCS)_2^-$, which is formed through Reactions 1 and 2, on the ring structure of the dyes;

$$NCS^- + OH \longrightarrow NCS + OH^-, \quad (1)$$

$$NCS + NCS^- \rightleftarrows (NCS)_2^-. \quad (2)$$

It is known that, in analogy with NCS^-,[2,3] in pulse-irradiated N_2O-saturated solutions halide ions, X^-, react rapidly and quantitatively with the OH radicals to form halide radicals, following the formation of halide radical anions, X_2^-:[3-7]

$$X^- + OH \xrightarrow{k_3} X + OH^-, \quad (3)$$

$$X + X^- \rightleftarrows X_2^-. \quad (4)$$

An effect similar to that of NCS^- on the radiation-induced decoloration of dyes may, therefore, be expected in the N_2O-saturated solutions containing halide ions. In this paper, the effects of Cl^-, Br^-, and I^- on the radiation-induced decoloration of azo and anthraquinone dyes were investigated in order to demonstrate the reaction scheme of inorganic radical anions with the dyes more clearly.

Experimental

The experimental procedures were the same as in the preceding work.[1,8,9] The dye solutions were prepared by dissolving recrystallized Acid Red 265 (C. I. 18129)[8] or Acid Blue 40 (C. I. 62125)[9] in triply distilled water. The dye solutions were bubbled with N_2O for 20 min prior to irradiation and were then irradiated with cobalt-60 gamma rays at room temperature. In some experiments, nitrogen was bubbled in for 30 min prior to irradiation.

The absorption spectra were measured with a Shimadzu UV-200 spectrophotometer. The decoloration yield, $G(-\text{Dye})$, was determined by measuring the optical density at 542 nm for Acid Red 265 and at 610 nm for Acid Blue 40.

Results and Discussion

N_2O-saturated Acid Blue 40 Solutions. The $G(-\text{Dye})$ for the N_2O-saturated 0.1 mM Acid Blue 40 solutions containing halide ions (Cl^-, Br^-, and I^-) (initial pH 6.1—6.8) is shown as a function of the halide ion concentrations in Fig. 1. In the solutions containing Br^- and I^-, the $G(-\text{Dye})$ increased steeply with an increase in the Br^- and I^- concentrations up to about 4 mM Br^- and 0.4 mM I^-; then it increased gradually above about 4 mM Br^- and 0.4 mM I^-. The $G(-\text{Dye})$ increased up to 2.07 (at 10 mM Br^-) and 1.84 (at 1 mM I^-) upon the addition of halide ions from 0.51 for the N_2O-saturated solution without halide ions. In the N_2O-saturated solution containing Cl^-, however, the $G(-\text{Dye})$ was almost equal to that (0.51) for the N_2O-saturated solution without halide ions, even upon the addition of 20 mM Cl^-. It is noteworthy that the tendency of the $G(-\text{Dye})$—Br^- and I^--concentration curves is similar to that of the $G(-\text{Dye})$—NCS^--concentration curve, shown in Fig. 2 in our preceding paper.[1] The increase in the G-

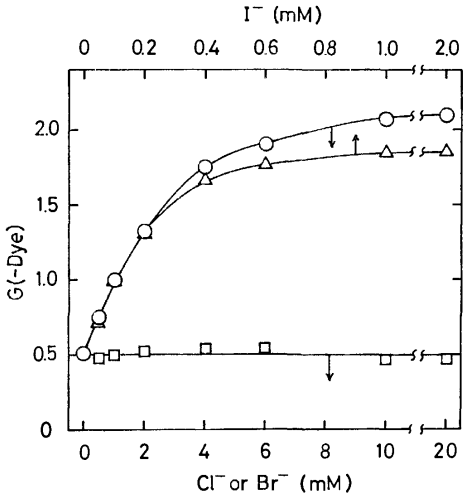

Fig. 1. Effect of halide ions on $G(-\text{Dye})$ in the N_2O-saturated Acid Blue 40 solutions.
Dye concentration: 0.1 mM. Dose: 1.8×10^4 rad.
Cl^- (□), Br^- (○), and I^- (△).

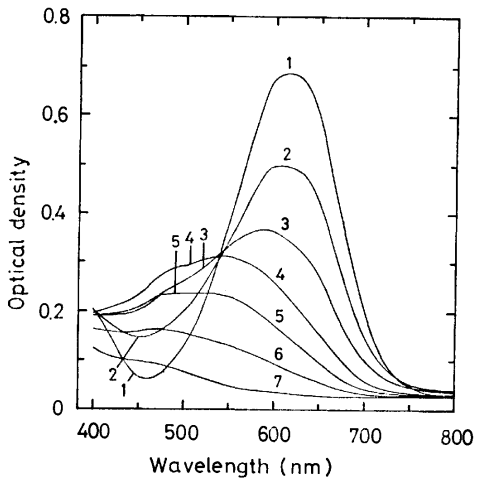

Fig. 2. Absorption spectra of unirradiated and irradiated N_2O-saturated Acid Blue 40 solutions containing 10 mM Br^-.
Dye concentration: 0.1 mM. Doses (rad): 0 (Curve 1), 1.8×10^4 (Curve 2), 3.7×10^4 (Curve 3), 5.5×10^4 (Curve 4), 1.1×10^5 (Curve 5), 2.2×10^5 (Curve 6), and 3.9×10^5 (Curve 7).

(—Dye) upon the addition of halide ions was in the order of $I^->Br^->Cl^-$ at the same concentrations. This order almost corresponds to the order of the rate constants for the reactions of halide ions with OH radicals in neutral solutions[10,11] (the rate constant for Cl^- was referred to the value at pH 9). The absorption spectrum of an unirradiated N_2O-saturated solution did not change upon the addition of halide ions. Also, scarcely no new absorption bands appeared in the wavelength range of 400 to 800 nm upon the irradiation of the N_2O-saturated Cl^-, Br^-, and I^- solutions without the dye. On the other hand, the G(—Dye) in the nitrogen-saturated solutions decreased to 0.10 (at 10 mM Br^-) and 0.07 (at 1 mM I^-) upon the addition of halide ions from 0.18 for the nitrogen-saturated solution without halide ions. In the nitrogen-saturated solution containing Cl^-, the G(—Dye) was almost equal to that (0.18) for the nitrogen-saturated solution without halide ions, even upon the addition of 20 mM Cl^-.

The radiation-induced decoloration scheme of Acid Blue 40 in the nitrogen-saturated solution has been presented in a preceding paper[9] as follows:

$$AB + OH \xrightarrow{k_5} ABOH \longrightarrow \text{decolored product}, \quad (5)$$

$$AB + OH \longrightarrow ABOH' \longrightarrow \text{colored product}, \quad (6)$$

$$AB + e^-_{aq} \longrightarrow AB_{red} \text{ (decolored product)}, \quad (7)$$

$$AB + e^-_{aq} \longrightarrow AB'_{red} \text{ (colored product)}, \quad (8)$$

where AB, ABOH, and AB_{red} are Acid Blue 40, its OH adduct, and its reduction product by the attack of the hydrated electron respectively. In the N_2O-saturated solution, however, the hydrated electrons are converted into the OH radicals by Reaction 9:[12]

$$N_2O + e^-_{aq} \longrightarrow OH + OH^- + N_2. \quad (9)$$

In such systems, the rate constants of the hydrated electron with N_2O and Acid Blue 40 are $8.7\times10^9\ M^{-1}\ s^{-1}$ at pH 7[13] and $1.5\times10^{10}\ M^{-1}\ s^{-1}$ at pH 5.1—6.3[9] respectively. In the N_2O-saturated 0.1 mM Acid Blue 40 solution, since the N_2O concentration (about 3×10^{-2} M) is about 300 times larger than the dye concentration, a large portion of the hydrated electrons are converted into the OH radicals, because $(8.7\times10^9\ M^{-1}\ s^{-1})\times(3\times10^{-2}\ M)\gg(1.5\times10^{10}\ M^{-1}\ s^{-1})\times(1\times10^{-4}\ M)$. In the N_2O-saturated solution, therefore, Acid Blue 40 is decolored only by Reaction 5.

In the N_2O-saturated 0.1 mM Acid Blue 40 solutions containing Br^- and I^-, most of the OH radicals react rapidly with Br^- and I^- to form the Br and I radicals above about 2 mM Br^- and 0.2 mM I^-, because k_3 $(1.2\times10^9\ M^{-1}\ s^{-1}$ at pH 7 for Br^-[10]$)\times[Br^-]$ and k_3 $(1.02\times10^{10}\ M^{-1}\ s^{-1}$ at neutral for I^-[10]$)\times[I^-]$ are larger than k_5 $(6.6\times10^9\ M^{-1}\ s^{-1}$ at pH 5.1—6.3[9]$)\times$ [Dye], following the formation of the halide radical anions, Br_2^- and I_2^-, by Reactions 3 and 4.[3,5-7] In a neutral solution containing Cl^-, however, the rate of the formation of Cl_2^- by Reactions 3 and 4 is very slow.[4,10,14]

In our preceding paper,[1] we concluded that the increase in the G(—Dye) upon the addition of NCS^- in the N_2O-saturated solution was mainly attributable to the attack of the radical anion $(NCS)_2^-$ formed through Reactions 1 and 2 on the ring structure of the dye as follows:

$$AB + (NCS)_2^- \longrightarrow (AB(NCS)_2)^- \longrightarrow \text{decolored product}, \quad (10)$$

$$AB + (NCS)_2^- \longrightarrow (AB(NCS)_2)^{-\prime} \longrightarrow \text{colored product}. \quad (11)$$

According to the earlier studies of the radiation-induced inactivation of lysozyme in the N_2O-saturated solutions containing halide ions,[14,15] the inactivation was caused by a reaction between lysozyme and the halide radical anion:

$$\text{lysozyme} + X_2^- \longrightarrow \text{inactive product}. \quad (12)$$

Adams *et al.*[14,15] suggested the possibility that the site of the X_2^- attack is the ring structure of tryptophan in lysozyme; that is, the reaction with X_2^- is a direct addition to the ring structure of tryptophan (T):

$$T + X_2^- \longrightarrow (TX_2)^-. \quad (13)$$

Consequently, it may be concluded from these facts that the increase in the G(—Dye) upon the addition of Br^- and I^- in the N_2O-saturated solutions is mainly attributable to the attacks of the halide radical anions, Br_2^- and I_2^-, formed through Reactions 3 and 4 on the Acid Blue 40 molecule as follows:

$$AB + Br_2^- \text{ (or } I_2^-) \longrightarrow (ABBr_2)^- \text{ (or } (ABI_2)^-) \longrightarrow \text{decolored product}, \quad (14)$$

$$AB + Br_2^- \text{ (or } I_2^-) \longrightarrow (ABBr_2)^{-\prime} \text{ (or } (ABI_2)^{-\prime}) \longrightarrow \text{colored product}. \quad (15)$$

The Acid Blue 40 molecule has two kinds of reaction sites for Reactions 14 and 15: (a) the anthraquinone ring, and (b) the substituted benzene ring, not conjugated to the carbonyl group in the anthraquinone ring. The attack of the halide radical anions, Br_2^- and I_2^-, on Site b is independent of the decoloration

reaction. The increase in the $G(-\text{Dye})$ in Fig. 1 indicates that the halide radical anions, Br_2^- and I_2^-, destroy the dye chromophore more efficiently than does the OH radical. As has already been described, the $G(-\text{Dye})$ was not changed upon the addition of Cl^- in the N_2O-saturated solution. This may be attributable to the very slow rate of the formation of Cl_2^- in a neutral solution.[4,10,14]

The absorption spectra for the unirradiated and irradiated N_2O-saturated solutions containing 10 mM Br^- and 1 mM I^- are shown in Figs. 2 and 3 respectively. The absorption band at 610 nm in both the solutions disappear with an increase in the dose; at the same time, a new absorption band near 460—490 nm seems to appear slightly at a higher dose (Curves 4—7 in Figs. 2 and 3). This new absorption band scarcely appeared at all in the N_2O-saturated solutions without halide ions, however, as may be seen in Fig. 4 in the preceding paper.[1] The absorption band near 460—490 nm coincides approximately with that for the reduction products of Acid Blue 40 formed by the attacks of the hydrated electron and the alcohol radical on the carbonyl group in the anthraquinone ring.[9] The new absorption band which appeared in the solutions containing Br^- and I^- was also similar to that which appeared in the solution containing NCS^-, as may be seen in Fig. 3 in our preceding paper.[1] Consequently, it may be assumed that a part of the Acid Blue 40 is reduced by the attack of the halide radical anions, Br_2^- and I_2^-, on the carbonyl group in the anthraquinone ring, thus forming the reduction product as follows:

$$AB + Br_2^- \text{ (or } I_2^-) \longrightarrow AB_{red} \text{ (decolored product at 610 nm)}. \quad (16)$$

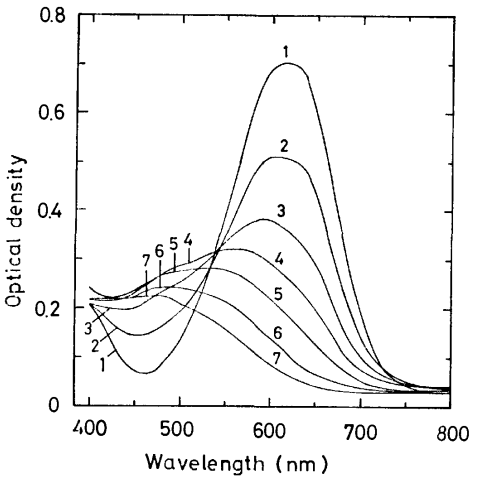

Fig. 3. Absorption spectra of unirradiated and irradiated N_2O-saturated Acid Blue 40 solutions containing 1 mM I^-.
Dye concentration: 0.1 mM. The number of the curves is the same with Fig. 2.

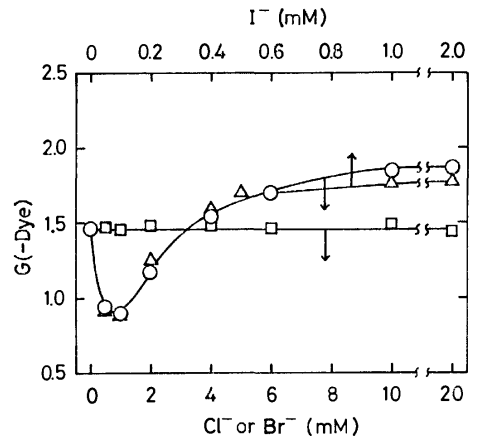

Fig. 4. Effect of halide ions on $G(-\text{Dye})$ in the N_2O-saturated Acid Red 265 solutions.
Dye concentration: 0.1 mM. Dose: 1.8×10^4 rad.
Cl^- (□), Br^- (○), and I^- (△).

On the other hand, the $G(-\text{Dye})$ for the nitrogen-saturated solutions decreased upon the addition of Br^- and I^-, as has already been described, in contrast to that for the N_2O-saturated solutions. This phenomenon was similar to that for the nitrogen-saturated solution containing NCS^-.[1] Reactions 17 and 18 may be considered as the reactions responsible for the decrease in the $G(-\text{Dye})$ upon the addition of Br^- and I^- in the nitrogen-saturated solution,[5,13] that is, the reactions of the hydrated electron with the halide radical anions, X_2^-, and the halide radicals, X, decreasing the X_2^- concentration:

$$X_2^- + e_{aq}^- \longrightarrow 2X^-, \quad (17)$$

$$X + e_{aq}^- \longrightarrow X^-. \quad (18)$$

Under the conditions of this study, the contribution of Reaction 17 to the decrease in the $G(-\text{Dye})$ is very large and that of Reaction 18 is very small, because the X and hydrated electron concentrations are negligibly small compared with the X^- concentration and the rate constants of the reactions of X with X^- [3,5] and of the hydrated electron with X_2^- [13] are very large.

N_2O-saturated Acid Red 265 Solutions. The $G(-\text{Dye})$ for the N_2O-saturated 0.1 mM Acid Red 265 solutions containing halide ions (Cl^-, Br^-, and I^-) (initial pH 6.4—6.9) is shown as a function of the halide ion concentrations in Fig. 4. In the solutions containing Br^- and I^-, the $G(-\text{Dye})$ decreased at first to 0.90 (at 1 mM Br^-) and 0.88 (at 0.1 mM I^-) upon the addition of halide ions, and then it increased with an increase in the Br^- and I^- concentrations up to about 10 mM Br^- and 1 mM I^-, in contrast to the results for the Acid Blue 40 solution in Fig. 1. The $G(-\text{Dye})$ increased up to 1.85 (at 10 mM Br^-) and 1.76 (at 1 mM I^-) upon the addition of halide ions from 1.46 for the N_2O-saturated solution without halide ions. In the N_2O-saturated solution containing Cl^-, however, the $G(-\text{Dye})$ was almost equal to that (1.46) for the N_2O-saturated solution without halide ions, even upon the addition of 20 mM Cl^-, analogous with the results for the Acid Blue 40 solution in Fig. 1. It is noteworthy that the tendency of the $G(-\text{Dye})$ —$Br^-$and I^- concentrations curves is similar to that of the $G(-\text{Dye})$—NCS^- concentration curve, shown in Fig. 5 in our preceding paper[1]. The absorption spectrum of an unirradiated N_2O-saturated solution was not changed upon the addition of halide ions. On the other hand,

the $G(-\text{Dye})$ in the nitrogen-saturated solution decreased to 0.25 (at 10 mM Br^-) and 0.27 (at 1 mM I^-) upon the addition of halide ions from 1.00 for the nitrogen-saturated solution without halide ions. In the nitrogen-saturated solution containing Cl^-, the $G(-\text{Dye})$ was almost equal to that (1.00) for the nitrogen-saturated solution without halide ions, even upon the addition of 20 mM Cl^-.

The radiation-induced decoloration scheme of Acid Red 265 in the nitrogen-saturated solution has been presented in a preceding paper[8] as follows:

$$AR + OH \longrightarrow AROH \longrightarrow \text{decolored product}, \quad (19)$$

$$AR + OH \longrightarrow AROH' \longrightarrow \text{colored product}, \quad (20)$$

where AR and AROH are Acid Red 265 and its OH adduct respectively.

In the N_2O-saturated Acid Red 265 solutions containing Br^- and I^-, the increase in the $G(-\text{Dye})$ is also mainly attributable to the attack of the halide radical anions, Br_2^- and I_2^-, formed through Reactions 3 and 4 on the Acid Red 265 molecule as follows:

$$AR + Br_2^- \text{ (or } I_2^-) \longrightarrow (ARBr_2)^- \text{ (or } (ARI_2)^-) \longrightarrow \text{decolored product}, \quad (21)$$

$$AR + Br_2^- \text{ (or } I_2^-) \longrightarrow (ARBr_2)^{-\prime} \text{ (or } (ARI_2)^{-\prime}) \longrightarrow \text{colored product}. \quad (22)$$

The Acid Red 265 molecule has two kinds of reaction sites for Reactions 21 and 22: (a) the aromatic rings connected directly to the azo group, and (b) the substituted benzene ring, not conjugated to the azo group. The attack of the halide radical anions, Br_2^- and I_2^-, on Site b is independent of the decoloration reaction. It is difficult for the direct attack of the halide radical anions, Br_2^- and I_2^-, on the azo group to take place because the azo group is stabilized by the hydrogen bonding with an adjacent OH group in a naphthalene ring.[8] Furthermore, the masking of the azo group can be expected because of the steric effect of the adjacent SO_3Na and CH_3 groups.[8]

The decrease in the $G(-\text{Dye})$ upon the addition of Br^- (up to 1 mM) and I^- (up to 0.1 mM) in Fig. 4 may be explained as follows.[1] At low Br^- and I^- concentrations, the halide radicals formed by Reaction 3 react with Acid Red 265 rather than with the halide ions to form mainly the colored product as in Reaction 23:

$$AR + X \longrightarrow ARX' \longrightarrow \text{colored product}, \quad (23)$$

thus decreasing the $G(-\text{Dye})$. As the Br^- and I^- concentrations increase, the halide radicals react with the halide ions rather than with Acid Red 265 to form the halide radical anions as in Reaction 4, thus increasing the $G(-\text{Dye})$. On the other hand, the decrease in the $G(-\text{Dye})$ upon the addition of Br^- and I^- was not observed in the N_2O-saturated Acid Blue 40 solution (Fig. 1). This may be attributable to the formation of both the decolored and colored products by the reaction of the halide radicals with Acid Blue 40 as in Reactions 24 and 25:

$$AB + X \longrightarrow ABX \longrightarrow \text{decolored product}, \quad (24)$$

$$AB + X \longrightarrow ABX' \longrightarrow \text{colored product}. \quad (25)$$

References

1) N. Suzuki and H. Hotta, *Bull. Chem. Soc. Jpn.*, **50**, 1441 (1977).
2) G. E. Adams, J. W. Boag, J. Currant, and B. D. Michael, "Pulse Radiolysis," Proceedings of the International Symposium held at Manchester, April, 1965, Academic Press, London (1965), pp. 117—129.
3) J. H. Baxendale, P. L. T. Bevan, and D. A. Stott, *Trans. Faraday Soc.*, **64**, 2389 (1968).
4) M. Anbar and J. K. Thomas, *J. Phys. Chem.*, **68**, 3829 (1964).
5) H. C. Sutton, G. E. Adams, J. W. Boag, and B. D. Michael, "Pulse Radiolysis," Proceedings of the International Symposium held at Manchester, April, 1965, Academic Press, London (1965), pp. 61—81.
6) B. Čerček, M. Ebert, C. W. Gilbert, and A. J. Swallow, "Pulse Radiolysis," Proceedings of the International Symposium held at Manchester, April, 1965, Academic Press, London (1965), pp. 83—98.
7) J. K. Thomas, *Trans. Faraday Soc.*, **61**, 702 (1965).
8) N. Suzuki, T. Nagai, H. Hotta, and M. Washino, *Bull. Chem. Soc. Jpn.*, **48**, 2158 (1975).
9) N. Suzuki, T. Nagai, H. Hotta, and M. Washino, *Bull. Chem. Soc. Jpn.*, **49**, 600 (1976).
10) L. M. Dorfman and G. E. Adams, NSRDS-NBS 46 (1973).
11) I. Kraljić and N. C. Trumbore, *J. Am. Chem. Soc.*, **87**, 2547 (1965).
12) F. S. Dainton and S. R. Logan, *Trans. Faraday Soc.*, **61**, 715 (1965).
13) M. Anbar, M. Bambenek, and A. B. Ross, NSRDS-NBS 43 (1973).
14) G. E. Adams, J. E. Aldrich, R. H. Bisby, R. B. Cundall, J. L. Redpath, and R. L. Willson, *Radiat. Res.*, **49**, 278 (1972).
15) G. E. Adams, *Adv. Radiat. Chem.*, **3**, 125 (1972).

Linear Response Polarizability Theory of the UV, ORD, and CD Bandshapes of Helical Biopolymers. Single- and Double-Stranded Polyadenylic Acids

Hirotoshi Ito, Yasumasa J. I'Haya, and Toshiyuki Eri

Department of Materials Science, The University of Electro-Communications, Chofu-shi, Tokyo 182

(Received November 24, 1977)

The UV, ORD, and CD spectral bandshapes of polyadenylic acid (poly A) have been investigated theoretically in order to challenge the problems of whether discrimination of the single- and double-stranded poly A's is computationally possible and of what structure poly A holds in a neutral solution. A linear response polarizability theory is applied to the derivation of UV, ORD, and CD bandshape functions of a polymer composed of N identical monomers. Using the observed and/or assumed values for the spectral bandshape of the adenine monomer, the UV, ORD, and CD spectra of both single- and double-stranded poly A's are calculated by changing geometrical parameters. The single-stranded poly A at neutral pH is assumed to have a regular helical structure which is regarded as a counterpart of the double helix form of the double-stranded poly A. This model leads to the chain-length (N) effect which in turn suggests that the structure of poly A in a neutral solution is very flexible and is such that it can be approximated as a random assembly of adenine dimers and/or trimers, when the theoretical spectra of both the single- and double-stranded poly A's are compared.

Amalgamation of the UV, ORD, and CD spectra in large molecules and molecular aggregates provides valuable information on conformation and property of the system, by which we are often able to disentangle the knots of incoherent prefiguration that has been attained from other experimental and/or theoretical sources in advance. In order to make good use of such an operation, however, a reliable theory is needed for a simultaneous analysis of these spectral bandshapes, in which working formulas for theoretical prediction of the bandshapes should be put together on an equal footing of approximations with one another. The case of helical biopolymers certainly falls under this category.

Recently, toward the analysis of the ORD and CD spectral curves of the single-stranded polyadenylic acid (poly A), we have demonstrated the promising reliability and wide applicability of the linear response polarizability theory[1] which is essentially a unified theory of the Fano-DeVoe model[2-5] with Applequist's polarizability theory of optical rotation[6]. As a closely equivalent treatment to ours, Cech *et al.*[7] have shown that DeVoe's all-orders-coupled oscillator polarizability model[3,4] successfully reproduces the CD spectrum of poly A. However, in contrast to such an extensive application of DeVoe's model, we like to point out that our model for the UV, ORD, and CD spectral bandshapes has a more convenient merit in correlating and explaining the molecular properties of biopolymers in terms of a small number of parameters; *i.e.*, transition energies, oscillator strengths, directions of transition moments, and half-widths of the absorption spectra of constituent monomer molecules.

The observed ORD and CD spectra of poly A are entirely different in acid (pH 4.6) and neutral solutions, indicating the existence of conformations of different kinds.[8-10] Optical absorption spectra,[8,10] viscosity measurement,[8] and X-ray analysis[11] offer an evidence that poly A shapes into the single-stranded helix in neutral solution and into the double-stranded helix in low pH solution, at room temperature. A possible explanation for such difference in conformation is a matter of main concern in the present paper. We therefore carry out comparative calculations of the UV, ORD, and CD spectral bandshapes of poly A by making use of the linear response theory, and show how the molecular conformations are reflected in these spectral bandshapes computed by varying the necessary molecular geometrical parameters. Afterward, we will discuss a problem of whether the discrimination of the single- and double-stranded poly A's can be made on the basis of the theoretical prediction of spectral bandshapes.

In the following, we first define a polarizability tensor of a homopolymer, and next outline the derivation of the UV, ORD, and CD bandshape functions by making use of the polarizability tensor. We then mention the geometrical properties of a helical polymer, by which we compute the bandshapes under a variety of conditions.

Polymer Polarizability Tensor

Let us consider the matrix elements of the polarizability tensor, $\boldsymbol{\alpha}^{P}_{mn}(\bar{\nu})$, of a polymer composed of N identical monomers (N-mer). The polymer polarizability tensor can be bulit up from the polarizability tensors, $\boldsymbol{\alpha}^{M}_{mn}(\bar{\nu})$, of individual monomers by making use of the Green's function method, when we know the unperturbed monomer polarizability tensor,

$$\begin{aligned}\boldsymbol{\alpha}^{M}_{mn}(\bar{\nu}) &= \boldsymbol{\alpha}^{M}_{mn}(\bar{\nu})\delta_{mn} = \boldsymbol{\alpha}^{M}_{m}(\bar{\nu}) \\ &= +(hc)^{-1}\sum_{\lambda}\boldsymbol{\mu}^{(m)}_{0\lambda}\boldsymbol{\mu}^{(m)}_{\lambda 0}[(\bar{\nu}-\tilde{\nu}^{(m)}_{\lambda 0}+i\eta_{\lambda})^{-1} \\ &\qquad -(\bar{\nu}+\tilde{\nu}^{(m)}_{\lambda 0}-i\eta_{\lambda})^{-1}], \qquad (1)\end{aligned}$$

where

$$\boldsymbol{\mu}^{(m)}_{0\lambda} = \langle 0^{(m)}|\sum_{i} e(\mathbf{r}_i-\mathbf{r}_m)|\lambda^{(m)}\rangle \equiv \langle 0^{(m)}|\boldsymbol{\mu}_m|\lambda^{(m)}\rangle. \qquad (2)$$

$\boldsymbol{\mu}^{(m)}_{0\lambda}\boldsymbol{\mu}^{(m)}_{\lambda 0}$ is a dyadic product of the transition moment between the λth excited state $|\lambda^{(m)}\rangle$ and the ground state $|0^{(m)}\rangle$ of the mth monomer; $\mathbf{r}_i$ and $\mathbf{r}_m$ are the vectors going from the origin of the system to the ith electron of the mth monomer and to the center of the mth monomer, respectively; η_{λ} is a positive and infinitesimally small quantity. $\boldsymbol{\alpha}^{M}_{m}(\bar{\nu})$ is given in units of cm^3 when $(\boldsymbol{\mu}^{(m)}_{\lambda 0}/e)$ is measured in units of cm, $\bar{\nu}$ is in units of cm^{-1}, and $e^2/(hc)=1.1614093\times10^{-3}$. Note

that the plus sign before $(hc)^{-1}$ of Eq. 1 defines the sign convention for the polarizability adopted in the present paper, which is different from the usual one. Hereafter, the superscripts, (1), (2), ···, denote the successive numbers of residues.

In the treatment mentioned above, the excited states of the polymer system is actually regarded as perturbed excited states of a hypothetically non-interacting molecular aggregate of N identical monomers, which are created by the intermolecular Coulomb interaction upon excitation. We do not consider the intermolecular exchange of electrons. Now, let us calculate the Coulomb interaction V_{mn} between the mth and nth monomers by the dipole-dipole approximation. It is then convenient to expand the Coulomb interaction V_{mn} in terms of the dipole operators $\boldsymbol{\mu}_m$ and $\boldsymbol{\mu}_n$ and the unit dipole interaction tensor $\mathbf{U}_{mn}$;

$$V_{mn} = \sum_{i\in m}\sum_{j\in n}(e^2/r_{ij}) \approx \sum_i e(\mathbf{r}_i-\mathbf{r}_m)\cdot\mathbf{U}_{mn}\cdot\sum_j e(\mathbf{r}_j-\mathbf{r}_n) = \boldsymbol{\mu}_m\cdot\mathbf{U}_{mn}\cdot\boldsymbol{\mu}'_n. \tag{3}$$

Instead, we use the following notation for V_{mn} hereafter;

$$\{V(\mathbf{r},\mathbf{r}')\}_{mn} \approx e(\mathbf{r}-\mathbf{r}_m)\cdot\mathbf{U}_{mn}\cdot e(\mathbf{r}'-\mathbf{r}'_n), \tag{4}$$

where

$$\mathbf{U}_{mn} = (1/r_{mn}^3)(\mathbf{1}_{mn}-3\mathbf{r}_{mn}\mathbf{r}_{mn}/r_{mn}^2) = -(3/r_{mn}^5)\begin{pmatrix} x_{mn}^2-(r_{mn}^2/3) & x_{mn}y_{mn} & x_{mn}z_{mn} \\ y_{mn}x_{mn} & y_{mn}^2-(r_{mn}^2/3) & y_{mn}z_{mn} \\ z_{mn}x_{mn} & z_{mn}y_{mn} & z_{mn}^2-(r_{mn}^2/3)\end{pmatrix}. \tag{5}$$

In Eqs. 3 and 4, the single dot denotes the single contraction and $\mathbf{r}_{mn}$ is a vector for intermolecular distance,

$$\mathbf{r}_{mn} = \mathbf{r}_n - \mathbf{r}_m = x_{mn}\hat{\mathbf{i}} + y_{mn}\hat{\mathbf{j}} + z_{mn}\hat{\mathbf{k}}. \tag{6}$$

The polarizability tensor is derived from the polarization propagator[5] $G(\mathbf{r},\mathbf{r}';E)$, which describes the propagation of the electronic density fluctuation, the propagator of the mth monomer being given by

$$G_m^{\mathrm{M}}(\mathbf{r},\mathbf{r}';E) = G_{mn}^{\mathrm{M}}(\mathbf{r},\mathbf{r}';E)\delta_{mn} = \sum_\lambda\left(\frac{\langle 0^{(m)}|\rho(\mathbf{r})|\lambda^{(m)}\rangle\langle\lambda^{(m)}|\rho(\mathbf{r}')|0^{(m)}\rangle}{E-E_{\lambda 0}^{(m)}+i\eta_\lambda} - \frac{\langle 0^{(m)}|\rho(\mathbf{r}')|\lambda^{(m)}\rangle\langle\lambda^{(m)}|\rho(\mathbf{r})|0^{(m)}\rangle}{E+E_{\lambda 0}^{(m)}-i\eta_\lambda}\right)\delta_{mn}, \tag{7}$$

with

$$\rho(\mathbf{r}) = \sum_i \delta([\mathbf{r}-\mathbf{r}_m]-\mathbf{r}_i), \qquad \rho(\mathbf{r}') = \sum_i \delta([\mathbf{r}'-\mathbf{r}_n]-\mathbf{r}_i), \tag{8}$$

where $E=hc\tilde{\nu}$ and $E_{\lambda 0}^{(m)}=hc\tilde{\nu}_{\lambda 0}^{(m)}$.

The electronic density disturbance and fluctuation induced by the external light source are accompanied with the transition dipole moment, the measure of which defines the polarizability. Then, the monomer polarizability tensor can naturally be defined by

$$\boldsymbol{\alpha}_{mn}^{\mathrm{M}}(E) = \int_m \mathrm{d}^3\mathbf{r}\int_n \mathrm{d}^3\mathbf{r}' e(\mathbf{r}-\mathbf{r}_m)G_{mn}^{\mathrm{M}}(\mathbf{r},\mathbf{r}';E)e(\mathbf{r}'-\mathbf{r}'_n), \tag{9}$$

where m and n close by the integral signs denote the integration only over such domains that $\mathbf{r}$ and $\mathbf{r}'$ lie in the mth and nth monomers, respectively. From Eq. 7, $\langle 0^{(m)}|\rho(r)|\lambda^{(m)}\rangle$ is obviously found to be the transition density, so that Eq. 2 is rewritten as

$$\boldsymbol{\mu}_{0\lambda}^{(m)} = \int \mathrm{d}^3\mathbf{r} e(\mathbf{r}-\mathbf{r}_m)\langle 0^{(m)}|\rho(\mathbf{r})|\lambda^{(m)}\rangle. \tag{10}$$

In the zeroth order, the polarization propagator for the polymer is hypothetically assumed to be

$$\{G^{\mathrm{HP}}(\mathbf{r},\mathbf{r}';E)\}_{mn} = G_m^{\mathrm{M}}(\mathbf{r},\mathbf{r}';E)\delta_{mn}. \tag{11}$$

It is then preferable to write down the higher order terms in the following manner:[5]

$$G^{\mathrm{P}}(\mathbf{r},\mathbf{r}';E) = G^{\mathrm{HP}}(\mathbf{r},\mathbf{r}';E) + \int \mathrm{d}^3\mathbf{r}''\int \mathrm{d}^3\mathbf{r}''' G^{\mathrm{HP}}(\mathbf{r},\mathbf{r}'';E)V(\mathbf{r}'',\mathbf{r}''')G^{\mathrm{P}}(\mathbf{r}''',\mathbf{r}';E), \tag{12}$$

or in its matrix element representation,

$$G_{mn}^{\mathrm{P}}(\mathbf{r},\mathbf{r}';E) = G_m^{\mathrm{M}}(\mathbf{r},\mathbf{r}';E)\delta_{mn} + \int_m \mathrm{d}^3\mathbf{r}''\int_n \mathrm{d}^3\mathbf{r}''' G_m^{\mathrm{M}}(\mathbf{r},\mathbf{r}'';E)\{V(\mathbf{r}'',\mathbf{r}''')\}_{mn}\cdot G_n^{\mathrm{M}}(\mathbf{r}''',\mathbf{r}';E) + \cdots \tag{13}$$

Finally, we have the following expression for the polymer polarizability tensor:

$$\boldsymbol{\alpha}_{mn}^{\mathrm{P}}(\tilde{\nu}) = \int_m \mathrm{d}^3\mathbf{r}\int_n \mathrm{d}^3\mathbf{r}' e(\mathbf{r}-\mathbf{r}_m)G_{mn}^{\mathrm{P}}(\mathbf{r},\mathbf{r}';hc\tilde{\nu})e(\mathbf{r}'-\mathbf{r}'_n) = \boldsymbol{\alpha}_m^{\mathrm{M}}(\tilde{\nu})\delta_{mn} + \boldsymbol{\alpha}_m^{\mathrm{M}}(\tilde{\nu})\cdot\mathbf{U}_{mn}\cdot\boldsymbol{\alpha}_n^{\mathrm{M}}(\tilde{\nu}) + \sum_l \boldsymbol{\alpha}_m^{\mathrm{M}}(\tilde{\nu})\cdot\mathbf{U}_{ml}\cdot\boldsymbol{\alpha}_l^{\mathrm{M}}(\tilde{\nu})\cdot\mathbf{U}_{ln}\cdot\boldsymbol{\alpha}_n^{\mathrm{M}}(\tilde{\nu}) + \cdots \tag{14}$$

UV, ORD, and CD Bandshape Functions of an N-mer

In the present paper, optical rotation of a helical polymer is ragarded as optical rotation induced conformationally by the regular aggregation of achiral residues in the absorption region of the residues. This means that the optical activity is derived from the electronic interaction among the achiral residues. In fact, it is known that the magnitudes of conformationally induced optical rotation of natural and synthetic polynucleotides are much larger than those of intrinsic optical rotation of isolated mononucleotides having chrial structures.[8] In order to predict optical activity of polynucleotides in the present formalism, chiral residues such as mononucleotides can therefore be approximated by achiral residues such as nucleic acid bases, neglecting the sugar-phosphate backbones. In the following, we also derive a scalar representation for the polarizability of such polymers, which is rather convenient for practical computations of UV spectral bandshapes compared with Eq. 14.

The total dipole moment of the polymer induced by the applied external field $\mathbf{E}(\mathbf{r}_n)$ is given by

$$\boldsymbol{\mu}^{\mathrm{P}}(\tilde{\nu}) = \sum_m^{\mathrm{N}}\boldsymbol{\mu}_m^{\mathrm{P}}(\tilde{\nu}) = \sum_m^{\mathrm{N}}\sum_n^{\mathrm{N}}\boldsymbol{\alpha}_{mn}^{\mathrm{P}}(\tilde{\nu})\cdot\mathbf{E}(\mathbf{r}_n) = \sum_m^{\mathrm{N}}\sum_n^{\mathrm{N}}\boldsymbol{\alpha}_{mn}^{\mathrm{P}}(\tilde{\nu})\cdot[\mathbf{E}(0)+\mathbf{r}_n\cdot\nabla\mathbf{E}(0)], \tag{15}$$

where the second line is obtained by Taylor's expansion of $\mathbf{E}(\mathbf{r}_n)$ about the origin of the polymer coordinate system. Taking the average over all orientations with

respect to the laboratory-fixed coordinate system, we obtain the following relationship, which is the same as that derived by Applequist:[6]

$$\langle \boldsymbol{\mu}^{\mathrm{P}}(\tilde{\nu})\rangle_{\mathrm{av}} = (1/3)\sum_{m}^{\mathrm{N}}\sum_{n}^{\mathrm{N}}[\mathrm{tr}\,\boldsymbol{\alpha}^{\mathrm{P}}_{mn}(\tilde{\nu})]\mathbf{E}(0) + (1/6)\sum_{m}^{\mathrm{N}}\sum_{n}^{\mathrm{N}}\mathbf{r}_n\cdot(\boldsymbol{\alpha}^{\mathrm{P}}_{mn}(\tilde{\nu}):\boldsymbol{\varepsilon})\nabla\times\mathbf{E}(0) = \sum_{m}^{\mathrm{N}}\sum_{n}^{\mathrm{N}}\bar{\alpha}^{\mathrm{P}}_{mn}(\tilde{\nu})\mathbf{E}(0) + \beta(\tilde{\nu})\,\mathrm{Rot}\,\mathbf{E}(0), \quad (16)$$

where $\boldsymbol{\varepsilon}$ is the isotropic third order tensor. The double-dot product of the two tensors in the parentheses reduces to

$$\boldsymbol{\alpha}^{\mathrm{P}}_{mn}(\tilde{\nu}):\boldsymbol{\varepsilon} = [\alpha^{\mathrm{Pxy}}_{mn}-\alpha^{\mathrm{Pyz}}_{mn}]\hat{\mathbf{i}} + [\alpha^{\mathrm{Pxz}}_{mn}-\alpha^{\mathrm{Pzx}}_{mn}]\hat{\mathbf{j}} + [\alpha^{\mathrm{Pyx}}_{mn}-\alpha^{\mathrm{Pxy}}_{mn}]\hat{\mathbf{k}}, \quad (17)$$

where the superscripts zy, yz, *etc.* indicate the tensor components. $\bar{\alpha}^{\mathrm{P}}_{mn}(\tilde{\nu})$ in the second line of Eq. 16 defines the scalar polarizability of the polymer. The coefficient before Rot $\mathbf{E}(0)$ in Eq. 16 is the molecular rotatory parameter $\beta(\nu)$ which measures the rotation of the electric field vector of the light wave passing through the medium at the point $\mathbf{r}_n$ measured from the origin;

$$\begin{aligned}\beta(\tilde{\nu}) &= (1/6)\sum_{m}^{\mathrm{N}}\sum_{n}^{\mathrm{N}}\mathbf{r}_n\cdot(\boldsymbol{\alpha}^{\mathrm{P}}_{mn}(\tilde{\nu}):\boldsymbol{\varepsilon})\\ &= -(1/6)\sum_{m}^{\mathrm{N}}\sum_{n}^{\mathrm{N}}\mathbf{r}_m\cdot(\boldsymbol{\alpha}^{\mathrm{P}}_{mn}(\tilde{\nu}):\boldsymbol{\varepsilon})\\ &= (1/12)\sum_{m}^{\mathrm{N}}\sum_{n}^{\mathrm{N}}\mathbf{r}_{mn}\cdot(\boldsymbol{\alpha}^{\mathrm{P}}_{mn}(\tilde{\nu}):\boldsymbol{\varepsilon})\\ &= (1/12)\sum_{m}^{\mathrm{N}}\sum_{n}^{\mathrm{N}}\{x_{mn}(\alpha^{\mathrm{Pzy}}_{mn}(\tilde{\nu})-\alpha^{\mathrm{Pyz}}_{mn}(\tilde{\nu}))\\ &\qquad + y_{mn}(\alpha^{\mathrm{Pxz}}_{mn}(\tilde{\nu})-\alpha^{\mathrm{Pzx}}_{mn}(\tilde{\nu}))\\ &\qquad + z_{mn}(\alpha^{\mathrm{Pyx}}_{mn}(\tilde{\nu})-\alpha^{\mathrm{Pxy}}_{mn}(\tilde{\nu}))\}. \end{aligned} \quad (18)$$

Here, it should be noticed that in the third line the factor (1/2) is introduced by combining the first line with the second one. The minus sign before the second line follows from Eq. 17, by interchanging suffixes m and n and also by allowing for the fact that $\boldsymbol{\alpha}^{\mathrm{P}}_{mn}$ is equal to the transposed element of $\boldsymbol{\alpha}^{\mathrm{P}}_{mn}$.

By relating β to the macroscopic quantities, molar rotation and ellipticity,[1] one obtains the bandshape functions $[\Psi(\tilde{\nu})]$ and $[\Xi(\tilde{\nu})]$ of the ORD and CD spectra, respectively;

$$[\Psi(\tilde{\nu})] = -288\pi^2 N_{\mathrm{A}}\tilde{\nu}^2(1/N)\,\mathrm{Re}\,\beta(\tilde{\nu}) \quad (\mathrm{deg\,cm^2\,dmol^{-1}}), \quad (19)$$

$$[\Xi(\tilde{\nu})] = -288\pi^2 N_{\mathrm{A}}\tilde{\nu}^2(1/N)\,\mathrm{Im}\,\beta(\tilde{\nu}) \quad (\mathrm{deg\,cm^2\,dmol^{-1}}), \quad (20)$$

where N_{A} is Avogadro's number.

The bandshape function of the UV absorption spectrum is derived from the coefficient of $\mathbf{E}(0)$ in the first term of Eq. 16. The wave number-dependent molar extinction coefficient[12] is then computed by

$$\varepsilon(\tilde{\nu}) = -(8\pi^2 N_{\mathrm{A}}/2302.6)\tilde{\nu}[(1/N)\sum_{m}^{\mathrm{N}}\sum_{n}^{\mathrm{N}}\mathrm{Im}\,\bar{\alpha}^{\mathrm{P}}_{mn}(\tilde{\nu})], \quad (\mathrm{l\,mol^{-1}\,cm^{-1}}). \quad (21)$$

Note that the factor (1/3) is involved in $\bar{\alpha}^{\mathrm{P}}_{mn}(\tilde{\nu})$.

For a model polymer composed of translationally and/or helically arranged equivalent monomers,[13] neglecting an end effect, we can derive

$$\sum_{m}^{\mathrm{N}}\sum_{n}^{\mathrm{N}}\bar{\alpha}^{\mathrm{P}}_{mn}(\tilde{\nu}) = (1-\sum_{m}^{\mathrm{N}}\overline{U}_{nm}\bar{\alpha}^{\mathrm{M}}_{n}(\tilde{\nu}))^{-1}\sum_{m}^{\mathrm{N}}\sum_{n}^{\mathrm{N}}\bar{\alpha}^{\mathrm{M}}_{n}(\tilde{\nu})\delta_{nm} = N\bar{\alpha}^{\mathrm{M}}_{n}(\tilde{\nu})(1-\sum_{m}^{\mathrm{N}}\overline{U}_{nm}\bar{\alpha}^{\mathrm{M}}_{m}(\tilde{\nu}))^{-1}, \quad (22)$$

which involves the dipole-dipole interactions to infinite orders. $\overline{U}_{nm}$ is the scalar interaction potential between unit dipoles,

$$\overline{U}_{nm} = \mathbf{e}_n\cdot\mathbf{e}_m/r^3_{nm} - 3(\mathbf{e}_n\cdot\mathbf{r}_{nm})(\mathbf{e}_m\cdot\mathbf{r}_{nm})/r^5_{nm}, \quad (23)$$

where the unit vector $\mathbf{e}_m$ is defined by

$$\boldsymbol{\mu}^{(m)}_{0\lambda} = |\boldsymbol{\mu}^{(m)}_{0\lambda}|\mathbf{e}_m. \quad (24)$$

Equation 22 is a scalar representation for the polymer polarizability, which is convenient for the evaluation of UV spectral bandshapes. However, we do not employ Eq. 22 in actual computations, because we want to compute UV, ORD, and CD bandshapes altogether on the same approximate grounds. Therefore, we use Eq. 14, in which terms higher than the third terms are truncated, for all the bandshape calculations.

For the calculations of Eqs. 19—21, which reduce to those of the real and imaginary parts of $\boldsymbol{\alpha}^{\mathrm{M}}_{m}(\tilde{\nu})$, the necessary formulas[1,13] are obtained as follows:

$$\begin{aligned}\mathrm{Im}\,\boldsymbol{\alpha}^{\mathrm{M}}_{m}(\tilde{\nu}) &= -\pi(hc)^{-1}\sum_{\lambda}\boldsymbol{\mu}^{(m)}_{0\lambda}\boldsymbol{\mu}^{(m)}_{\lambda 0}\{\delta(\tilde{\nu}-\tilde{\nu}^{(m)}_{\lambda 0}) + \delta(\tilde{\nu}+\tilde{\nu}^{(m)}_{\lambda 0})\}\\ &= -(hc)^{-1}\sum_{\lambda}\boldsymbol{\mu}^{(m)}_{0\lambda}\boldsymbol{\mu}^{(m)}_{\lambda 0}\{\eta_\lambda[(\tilde{\nu}-\tilde{\nu}^{(m)}_{\lambda 0})^2+\eta^2_\lambda]^{-1}\\ &\qquad +\eta_\lambda[(\tilde{\nu}+\tilde{\nu}^{(m)}_{\lambda 0})^2+\eta^2_\lambda]^{-1}\}, \end{aligned} \quad (25)$$

and

$$\begin{aligned}\mathrm{Re}\,\boldsymbol{\alpha}^{\mathrm{M}}_{m}(\tilde{\nu}) &= -(\mathcal{P}/\pi)\int_{-\infty}^{\infty}dE\,\mathrm{Im}\,\boldsymbol{\alpha}^{\mathrm{M}}_{m}(E)\,\mathrm{sign}\,(E)(\tilde{\nu}-E)^{-1}\\ &= +(hc)^{-1}\sum_{\lambda}\boldsymbol{\mu}^{(m)}_{0\lambda}\boldsymbol{\mu}^{(m)}_{\lambda 0}\{(\tilde{\nu}-\tilde{\nu}^{(m)}_{\lambda 0})[(\tilde{\nu}-\tilde{\nu}^{(m)}_{\lambda 0})^2+\eta^2_\lambda]^{-1}\\ &\qquad -(\tilde{\nu}+\tilde{\nu}^{(m)}_{\lambda 0})[(\tilde{\nu}+\tilde{\nu}^{(m)}_{\lambda 0})^2+\eta^2_\lambda]^{-1}\}, \end{aligned} \quad (26)$$

both of which represent features of the Lorentzian bandshape.

In this computation, the damping factor $\eta_\lambda=(1/2)$ (half-width) is treated as an empirical parameter, with the condition $\eta_\lambda \ll \tilde{\nu}^{(m)}_{\lambda 0}$. From Eqs. 21 and 25, we can derive the approximate working formula for estimating η_λ (in $\mathrm{cm^{-1}}$) from the experimental values for the molar extinction coefficient ε^{M} and the oscillator strength $f_{\lambda 0}$ of the monomer molecule;

$$[\varepsilon^{\mathrm{M}}(\tilde{\nu}^{(m)}_{\lambda 0})]_{\max} \approx 7.37126\times 10^7(f_{\lambda 0}/\eta_\lambda), \quad (27)$$

when the second term of Eq. 25 is neglected (this is justified because the second term is usually much smaller than the first term in Eq. 25). By substituting these approximate η_λ's into Eqs. 25 and 26, real and imaginary parts of the monomer polarizability tensor are computed.

It should finally be noted that the sum rule[1,13] holds for the UV, ORD, and CD spectral intensities. In the present scheme, it is clearly understood that the total polarizability tensor given in Eq. 14 for the conformationally induced optically active polymer becomes a 3×3 antisymmetric matrix which is derived from the monomer 3×3 (diagonal and/or symmetric) polariz-

ability tensors. In other words, the absorption spectrum is given by the diagonal terms of the polymer polarizability tensor, while the optical activity is determined by the off-diagonal terms.

Geometrical Properties for a Helical Polymer

In the computational work, it is necessary to know the geometrical properties of the regular polymers such as single- and double-stranded poly A's.

(i) For a single-stranded helical homopolymer, let the origin of the whole system be the center of the circle cut off perpendicularly to the helix axis, in which the center of one of the monomers (called the first monomer) is involved. The unit vector $\hat{\mathbf{i}}$ is taken perpendicularly to the helix axis to the center of the first monomer (radial), $\hat{\mathbf{j}}$ perpendicular to $\hat{\mathbf{i}}$ (tangential to the helix), both in the plane of the section, and $\hat{\mathbf{k}}$ along the helix axis (Figs. 1 and 2). Then the vector $\mathbf{r}_n$ going from the origin to the center of the nth monomer is expressed by

$$\mathbf{r}_n = a\cos(n\phi)\hat{\mathbf{i}} + a\sin(n\phi)\hat{\mathbf{j}} + nL\hat{\mathbf{k}}, \tag{28}$$

where a is the radius of the sectional circule, L the pitch of the helix (the advance parallel to the helix axis), and ϕ is the angle of rotation transferring a given monomer, n say, to the next nearest one, $n+1$. The distance vector between the mth and nth monomers is then defined by Eq. 6. By making use of the rotational operator, $\mathbf{R}((n-1)\phi)$, we can relate the polarizability tensor of the nth monomer to that of the first monomer;

$$\boldsymbol{\alpha}_n^{\mathrm{M}}(\bar{\nu}) = \mathbf{R}((n-1)\phi)\cdot\boldsymbol{\alpha}_1^{\mathrm{M}}(\bar{\nu})\cdot\mathbf{R}(-(n-1)\phi), \tag{29}$$

since

$$\boldsymbol{\mu}_{0\lambda}^{(n)} = [\mathbf{R}(\phi)]^{n-1}\cdot\boldsymbol{\mu}_{0\lambda}^{(1)} = \mathbf{R}((n-1)\phi)\cdot\boldsymbol{\mu}_{0\lambda}^{(1)}$$
$$\equiv \begin{pmatrix} \cos((n-1)\phi) & -\sin((n-1)\phi) & 0 \\ \sin((n-1)\phi) & \cos((n-1)\phi) & 0 \\ 0 & 0 & 1 \end{pmatrix} \begin{pmatrix} [\mu_{0\lambda}^{(1)}]_{\hat{\mathbf{i}}} \\ [\mu_{0\lambda}^{(1)}]_{\hat{\mathbf{j}}} \\ [\mu_{0\lambda}^{(1)}]_{\hat{\mathbf{k}}} \end{pmatrix}, \tag{30}$$

where $[\mu_{0\lambda}^{(1)}]_{\hat{\mathbf{i}}}$ *etc.* are the components of the transition moment of the first monomer in the directions of $\hat{\mathbf{i}}$ (ridial), $\hat{\mathbf{j}}$ (tangential), and $\hat{\mathbf{k}}$ fixed as the center of the first monomer.

(ii) For a double-stranded helical homopolymer like (poly A)·(poly A), we assign the odd integers $\{2m'-1, 2n'-1\}$ for the numberings of the positions of the residues (placed in the x'y'-plane of Fig. 3 or displaced translationally along the helix axis) in one of the strands and the even numbers $\{2m', 2n'\}$ for those (in the x″y″-plane) in another strand.

Let us obtain the intermolecular distances in the double-stranded polymers. The position vectors for the double-strands are now given by

$$\mathbf{r}_{2m'-1} = a\cos(m'\phi)\hat{\mathbf{i}} + a\sin(m'\phi)\hat{\mathbf{j}} + m'L\hat{\mathbf{k}}, \tag{31}$$

$$\mathbf{r}_{2m'} = a\cos(m'\phi+\gamma')\hat{\mathbf{i}} + a\sin(m'\phi+\gamma')\hat{\mathbf{j}} + (m'L+L')\hat{\mathbf{k}}, \tag{32}$$

where a translation L' along the helix axis followed by

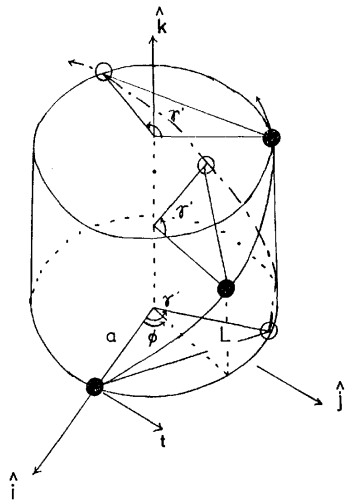

Fig. 1. Double-stranded helix and its geometrical parameters (a, ϕ, L, γ', L'). Solid circles represent the residues on one of the strands and open circles those on the other strand. $\hat{\mathbf{i}}$, $\hat{\mathbf{j}}$ and $\hat{\mathbf{k}}$ are the unit vectors in the Cartesian coordinate, $\hat{\mathbf{k}}$ being along the helical axis.

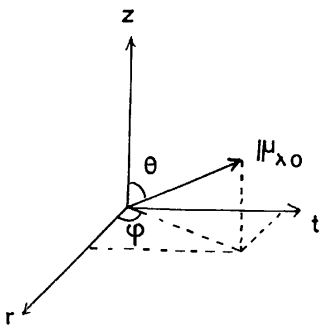

Fig. 2. Coordinate system for transition moment of a residue. r is the radial direction and t is tangential to the helix, z being along the helical axis.

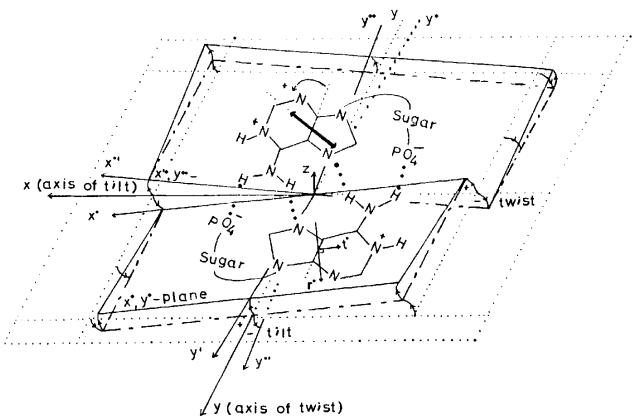

Fig. 3. Perspective drawing of a hydrogen-bonded base pair in the double-stranded polyadenylic acid. The bold arrow represents the direction of the transition moment. r' and t' are, respectively, the radial and tangential directions of the residue on the x',y'-plane. As for the other notations, see the text.

a rotation γ' about the axis brings about either of strands onto another strand as shown in Fig. 1. The vector for the intermolecular distance is again calculated from Eq. 6.

The following relationships produced by the screw operation in this polymer system also make it easy to carry out the actual computation. For one of the strands, we can relate the $(2n'+1)$th monomer with the first monomer in the following manner:

$$\boldsymbol{\mu}_{0\lambda}^{(2n'+1)} = \mathbf{R}(n'\phi)\cdot\boldsymbol{\mu}_{0\lambda}^{(1)}, \tag{33}$$

$$\boldsymbol{\alpha}_{2m'+1,2n'+1}^{M}(\tilde{\nu}) = \mathbf{R}(m'\phi)\cdot\boldsymbol{\alpha}_{11}^{M}(\tilde{\nu})\cdot\mathbf{R}(-n'\phi). \tag{34}$$

For the other strand, we also have similar relationships;

$$\boldsymbol{\mu}_{0\lambda}^{(2n'+2)} = \mathbf{R}(n'\phi)\cdot\boldsymbol{\mu}_{0\lambda}^{(2)}, \tag{35}$$

$$\boldsymbol{\alpha}_{2m'+2,2n'+2}^{M}(\tilde{\nu}) = \mathbf{R}(m'\phi)\cdot\boldsymbol{\alpha}_{22}^{M}(\tilde{\nu})\cdot\mathbf{R}(-n'\phi). \tag{36}$$

From Eqs. 34 and 36, we can derive

$$\boldsymbol{\alpha}_{2m'+2,2n'+2}^{M}(\tilde{\nu}) = \mathbf{R}(\gamma')\cdot\boldsymbol{\alpha}_{2m'+1,2n'+1}^{M}(\tilde{\nu})\cdot\mathbf{R}(-\gamma'), \tag{37}$$

since

$$\boldsymbol{\mu}_{0\lambda}^{(2)} = \mathbf{R}(\gamma')\cdot\boldsymbol{\mu}_{0\lambda}^{(1)} \equiv \mathbf{R}_z(-\gamma')\cdot\boldsymbol{\mu}_{0\lambda}^{(1)}, \tag{38}$$

where $\mathbf{R}_z$ denotes an operator defined by the rotation of the coordinate system about the helix axis.

(iii) Since the two planes which involve one adenine molecule each, the x',y',- and x'',y''-planes in Fig. 3, are inclined each other, it is not very easy to specify relative positions of the monomer transition moments by a polar coordinate fixed at each monomer position so as to fit the X-ray data. Instead, one can easily relate the components of these moments, $[\mu_{0\lambda}^{(m)}]\hat{\mathrm{i}}$ *etc.*, to those described by the Cartesian coordinate system fixed at the adenine molecule (the X-axis is taken along the central C_4–C_5 bond, the X, Y-axes being in the molecular plane), specifying the following five angles as shown in Fig. 3 (let the plane perpendicular to the helix axis be the x,y-plane): An angle of rotation about the y-axis (*twist*); an angle of rotation about the x-axis (tilt); an angle between the x-axis and the original radial direction $\mathbf{r}$ $(\widehat{\mathrm{xr}})$; an angle between the molecular X-axis and the radial direction $\mathbf{r}$ $(\widehat{\mathrm{Xr}})$; an angle between the x'-axis and the radial direction $\mathbf{r}'$ on the x',y'-plane $(\widehat{\mathrm{x'r'}})$. Values of the latter three angles are estimated from the observed values for the original x, y-plane.[11] A plus sign of the rotation angle is defined to be counterclockwise with respect to the right-handed coordinate system. Then we have

$$\begin{pmatrix} [\mu_{0\lambda}^{(1)}]_{\hat{\mathrm{r}}} \\ [\mu_{0\lambda}^{(1)}]_{\hat{\mathrm{j}}} \\ [\mu_{0\lambda}^{(1)}]_{\hat{\mathrm{k}}} \end{pmatrix} = \mathbf{R}_z(\widehat{xr})\cdot\mathbf{R}_y(-twist)\cdot\mathbf{R}_{x'}(-tilt)\cdot \mathbf{R}_{z'}(-\widehat{x'r'})\cdot\mathbf{R}_{z'}(\widehat{Xr}) \begin{pmatrix} [\mu_{0\lambda}^{(1)}]_X \\ [\mu_{0\lambda}^{(1)}]_Y \\ [\mu_{0\lambda}^{(1)}]_Z \end{pmatrix}, \tag{39}$$

where

$$\mathbf{R}_{x'}(-tilt) = \begin{pmatrix} 1 & 0 & 0 \\ 0 & \cos(-tilt) & \sin(-tilt) \\ 0 & -\sin(-tilt) & \cos(-tilt) \end{pmatrix}, \tag{40}$$

$$\mathbf{R}_y(-twist) = \begin{pmatrix} \cos(-twist) & 0 & -\sin(-twist) \\ 0 & 1 & 0 \\ \sin(-twist) & 0 & \cos(-twist) \end{pmatrix}, \tag{41}$$

and

$$\mathbf{R}_\zeta(Q) = \begin{pmatrix} \cos Q & \sin Q & 0 \\ -\sin Q & \cos Q & 0 \\ 0 & 0 & 1 \end{pmatrix} \tag{42}$$

for $\mathbf{R}_z(\widehat{xr})$, $\mathbf{R}_{z'}(-\widehat{x'r'})$, and $\mathbf{R}_{z'}(\widehat{Xr})$. These relationships are convenient for actual calculation of the polymer polarizability.

The transition moment of the second monomer can be related to that of the first one by

$$\mu_{0\lambda}^{(2)} = \mathbf{R}(180°)\cdot\mu_{0\lambda}^{(1)}, \tag{43}$$

where the definition of $\mathbf{R}(180°)$ follows Eq. 30.

Results and Discussion

The spectral parameters necessary for computations of the UV, ORD, and CD spectral bandshapes are listed in Table 1. These are the observed and/or assumed transition energies, oscillator strengths, damping factors, and directions of the transition moments of the adenine monomer. The damping factors are determined as described above so that a starting UV absorption bandshape function for adenine can reproduce roughly well the observed spectrum of adenine.

It is known experimentally that poly A in neutral solution takes a flexibly stacked conformation of single strand, while at low pH it becomes a protonated structure like

$$2(\text{poly A}) + 2H^+ \rightleftharpoons (\text{poly A}^+\text{H})\cdot(\text{poly A}^+\text{H}).$$

In this case, the base-pairing illustrated in Fig. 3 forms a rigid double-stranded helix (Fig. 1) for which we assume a parallelly interwound structure analyzed by Rich *et al.*;[11] pitch 3.8 Å at 45° rotation, a=2.97 Å, *tilt*=+4°, *twist*=+10°, $\widehat{Xr}$=−23.2°, $\widehat{x'r'}$=−117.4°. A number of model calculations are carried out by chang-

Table 1. Spectroscopic parameters for adenine taken from experimental data

pH	Energy[a] $hc\,\tilde{\nu}_{\lambda 0}^{(m)}$ (eV)	Oscillator strength $f_{\lambda 0}$	Damping[b] factor η_λ (eV)	Direction of transition moment[c] θ (°)
7	4.76	0.27[d]	0.184	+ 3
	5.99	0.40	0.158	−92
	6.53	0.26	0.184	+ 3
2.5	4.72	0.27[e]	0.187	+ 3
	6.18	0.26	0.119	−92
	6.51	0.40	0.236	+ 3

a) D. Voet, W. B. Gratzer, R. A. Cox, and P. Doty, *Biopolymers*, **1**, 193 (1963). b) Estimated from $hc\,\tilde{\nu}_{0\lambda}^{(m)}$, ε^M, and $f_{\lambda 0}$. The molar extinction coefficients, ε^M, are taken from a) above. c) A. F. Fucaloro and L. S. Forster, *J. Am. Chem. Soc.*, **93**, 6443 (1971); note that the signs are opposite to those of Fucaloro and Forster who follow the DeVoe-Tinoco convention. d) M. Tanaka and S. Nagakura, *Theor. Chim. Acta*, **6**, 320 (1966). e) Assumed from the UV absorption spectrum of adenine hydrochloride observed by H. H. Chen and L. B. Clark, *J. Chem. Phys.*, **58**, 2593 (1973).

Table 2. Figure index[a]

Fig. No.	Strand	*tilt* (°)	*twist* (°)	$\widehat{x'r'}$ (°)	Helix radius (Å)	*N*
4	Single	−4.0	0.0	0.0	2.97	2, 3, 8, 10, 12, 14
5	Single	4.0	10.0	−117.4	2.97, 5.0, 7.0	8
6	Single	−4.0	10.0	−27.4	2.97	8
		−2.0	0.0	−27.4	2.97	8
		4.0	10.0	−117.4	2.97	8
7[b]	Double	4.0	10.0	−117.4	2.97	8

a) Helical pitch: $L=3.8$Å, $\phi=45°$. $\widehat{Xr}=-23.2°$ is used for all calculations. b) $\gamma'=180°$.

ing values of the parameters from those for the reference structure cited above. In Table 2 are listed the values of these parameters and the figure numbers in which the predicted UV, ORD, and CD spectra are drawn. For convenience, it is assumed that the model for the single-stranded helix is not a flexibly and/or randomly stacked but has a regularly and rigidly stacked structure; in other words, it is regarded as a counterpart of the double helix (*vide infra*).

We show the bandshapes computed for the single-stranded poly A in Figs. 4—6 and those for the double-stranded poly A in Fig. 7. First of all, the effect of the chain-length (N) of the single-stranded poly A on bandshapes is examined in Fig. 4. Here we set $\widehat{x'r'}=0°$ (*i.e.*, the *tilt* axis is taken along the radial direction and the *twist* axis along the tangential direction), *tilt*$=-4.0°$, and *twist*$=0°$. It is to be noted that a helical structure appears to begin even in the *dimer* ($N=2$) and *trimer* models ($N=3$), as can be seen in Fig. 4. With an increase of N, the UV, ORD, and CD bandshapes are likely to converge to respective certain shapes (Fig. 4), the trend being pointed out before by Tinoco *et al.* in the treatment of the exciton theory.[14] In comparison with the monomer UV bandshapes, a large hypochromism appears in the 260 nm region of all the polymer UV bandshapes in the pH 7 model calculations (Figs. 4—7), which is well compared with the UV absorption spectrum of poly A observed by Michelson,[15] and Beers and Steiner.[16] As for the ORD and CD bandshapes as well, the calculated curves are qualitatively in accord with those observed.[8-10]

The intensities of the ORD and CD spectra decrease and the UV bandshapes look like that of the free adenine molecule as the radius (a) of the helix increase, as can be seen in Fig. 5 where the X-ray data of the double-stranded poly A are used for the $N=8$ single-stranded poly A model calculations. The parameters, $\widehat{x'r'}=-27.4°$, *twist*$=+10°$, and *tilt*$=-4°$, in the $N=8$ model predict well the observed ORD[8], CD[9], and UV[10,15,16] spectral shapes (see Fig. 6), while the parameters taken from the X-ray data of the double-stranded poly A, $\widehat{x'r'}=-117.4°$, *twist*$=+10°$, and *tilt*$=+4°$, do not produce reasonable ORD and CD curves (a figure is not shown). This is particularly true for ORD and CD spectral features in the 230 nm region; the latter param-

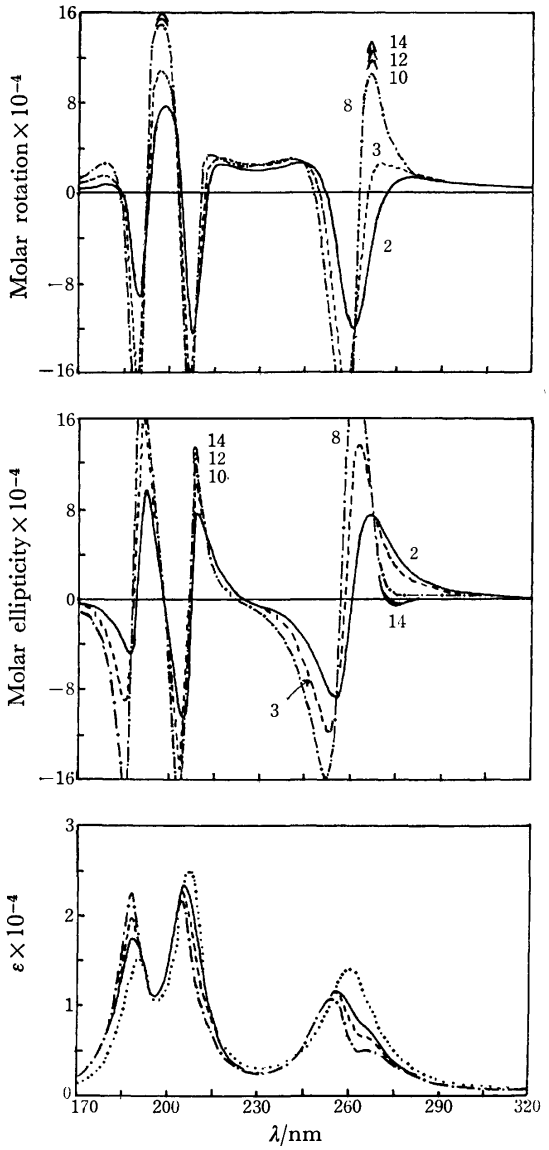

Fig. 4. The chain-length dependence ($N=2$, 3, 8, 10, 12, 14) of the ORD (top), CD (middle), and UV (bottom) bandshapes of the singlestranded polyadenylic acid ($a=2.97$Å, *tilt*$=-4.0°$, *twist*$=0°$, $\widehat{x'r}=0°$). The dotted line (·····) in the bottom shows the observed UV absorption spectrum of adenine.

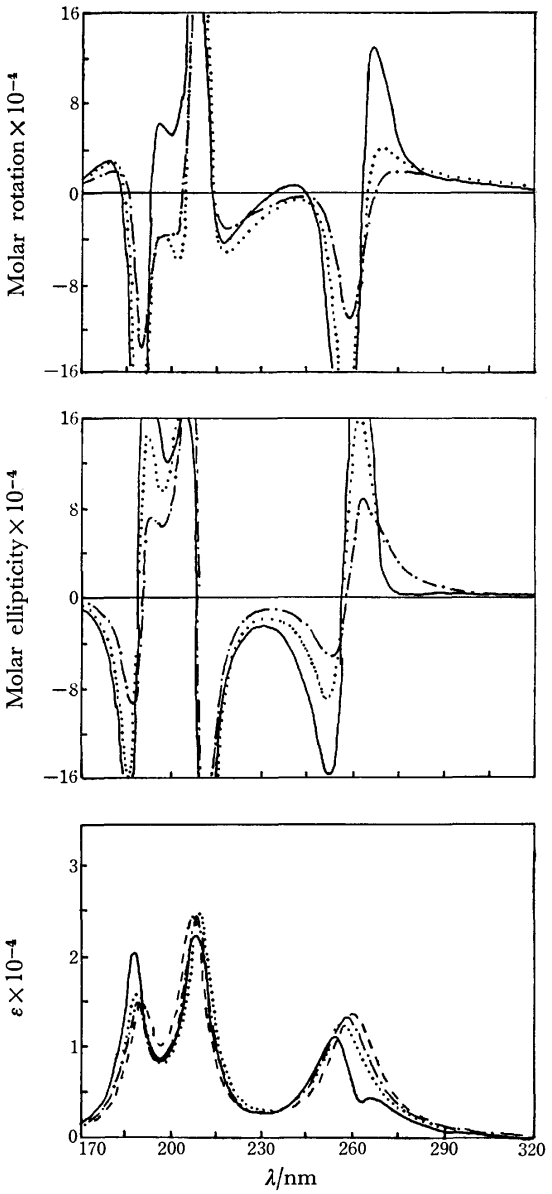

Fig. 5. Dependence of the ORD (top), CD (middle), and UV (bottom) bandshapes of the single-stranded polyadenylic acid on the radius (a) of the helix ($N=8$, $a=2.97$Å, $tilt=4°$, $twist=+10°$, $\widehat{Xr}=-23.2°$, $\widehat{x'r'}=-117.4°$). (——): $a=2.97$Å, (……): $a=5.0$Å; (—·—): $a=7.0$Å. The broken line (- - -) in the bottom shows the observed UV absorption spectrum of adenine.

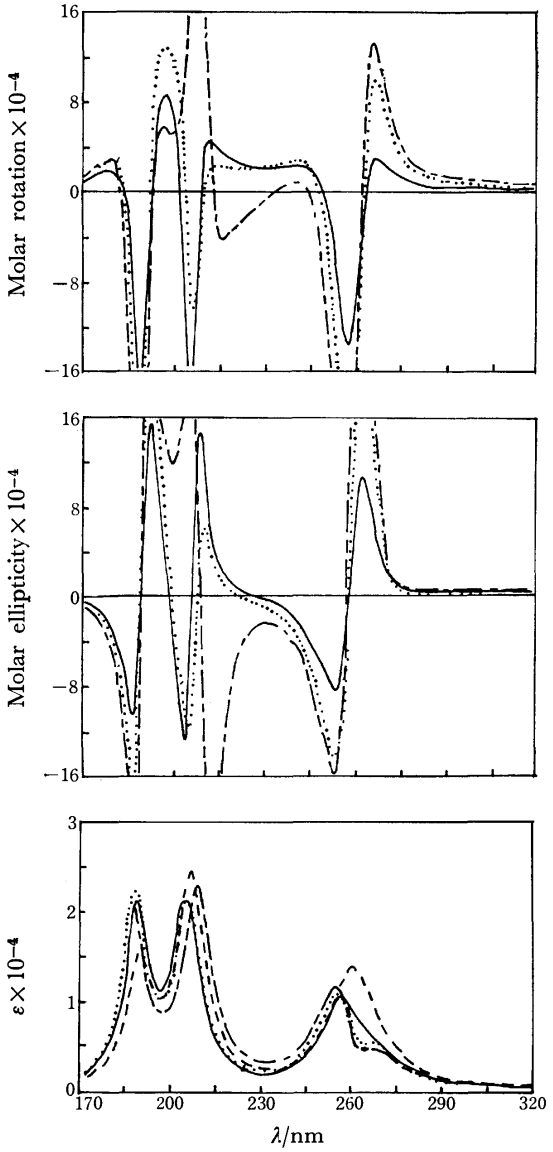

Fig. 6. Comparison of the selected theoretical ORD (top), CD (middle), and UV (bottom) bandshapes of the single-stranded polyadenylic acid in the $N=8$ model. (——): $tilt=-4°$, $twist=+10°$, $\widehat{x'r'}=-27.4°$; (……): $tilt=-2°$, $twist=0°$, $\widehat{x'r'}=-27.4°$; (—·—): $tilt=+4°$, $twist=+10°$, $\widehat{x'r'}=-117.4°$. The broken line (- - -) in the bottom shows the observed UV absorption spectrum of adenine.

eters bring about a too small peak in the ORD 230 nm region and no positive peak in the CD 220 nm region. This is probably due to the assumption of the orderly arranged rigid structure for the single-stranded poly A which may be considered to have a considerably flexible structure in nature. The predicted ORD and CD curves are therefore slightly stronger in intensity at their peaks and troughs and the predicted UV spectral shapes show rather strong hypochromism, compared with the observed spectra to which rather loose conformations of poly A may contribute; the model can be considered to be in between the real single- and double-stranded poly A's.

In Fig. 7 are compared the bandshapes of the double-stranded poly A, one calculated with the spectral parameters for the pH 7 adenine and the other with those for the pH 2.5 adenine. This is because the ORD and CD spectra of the double-stranded poly A have been measured around pH 4.5, while the spectroscopic data for the pH 4.5 free adenine molecule are not available. The molecular geometries are taken from the X-ray data in either case. As a matter of course, the predicted UV, ORD, and CD spectral bandshapes markedly

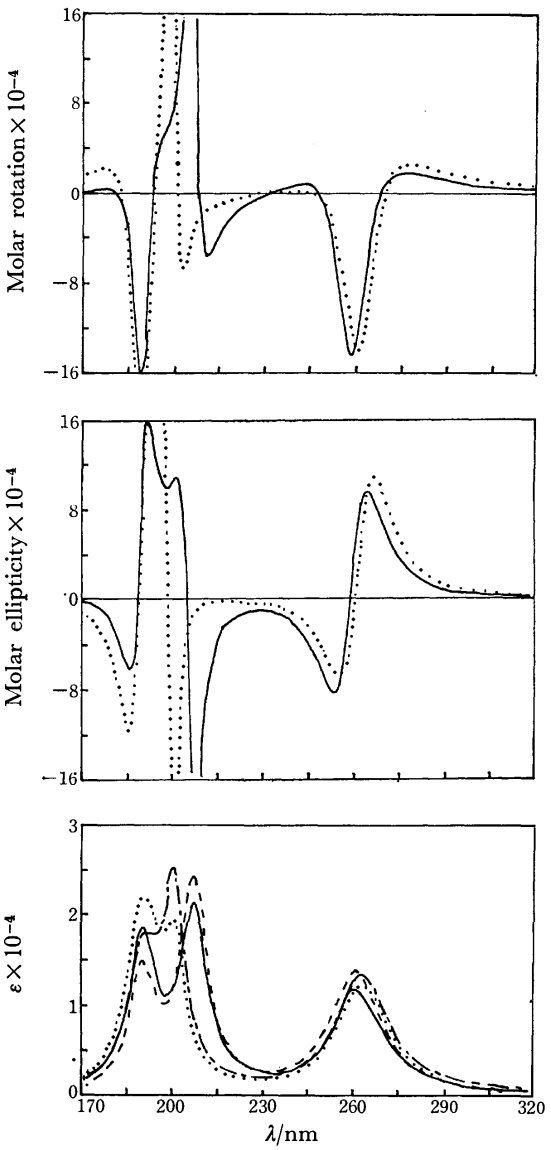

Fig. 7. Predicted ORD (top), CD (middle), and UV (bottom) bandshapes of the double-stranded polyadeylic acid ($N=8$, $a=2.97$Å, $titl=+4°$, $twist=+10°$, $\widehat{x'r'}=-117.4°$). (——): Calculated with the spectral parameters for pH=7 adenine; (·····): Calculated with the spectral parameters for pH=2.5 adenine. The broken line (- - -) in the bottom shows the observed UV absorption spectrum of adenine.

depend upon the pH values. In contrast with Fig. 6, the ORD and CD spectra turn out to be broader when the double-stranded helix is formed, which features agree in general with experiment.

Going into detail however, the predicted UV, ORD, and CD spectral intensities are in direct opposition to observations; in the observed spectra, the UV hypochromicity at the longer wavelength side enhances, and the ORD peak at 280 nm and the trough at 250 nm and the CD peak at 260 nm all gain their intensities at low pH, the CD trough at 240 nm being unchanged.

We now try to explain this discrepancy. The chain-length effect is notable as shown in Fig. 4, but it is to be recalled that a model for the single-stranded poly A adopted there corresponds to a counterpart of the double-stranded poly A. An actual structure of poly A in neutral solution is considered to be not so rigid as the present model but flexible to a certain extent. In fact, only small chain-length effect has been observed for poly A in neutral solution.[17] If we approximate a structure of poly A in the pH 7 solution as the dimer model ($N=2$ in Fig. 4), the relation between the UV hypochromicities and also the ORD and CD spectral intensities of the single- and double-stranded poly A's can be explained without difficulty. In other words, we may speculate that the structure of poly A in neutral solution is such that it can be approximated as an assembly of adenine dimer and/or trimer.

In alternative way of looking is possible. As Fig. 6 shows, the UV, ORD, and CD bandshapes of the single-stranded poly A approach those of free adenine as the position of the residues (a) gets away from the helix axis, simply because the relative distance between the two monomers located nearly on a level surface becomes larger and hence $\mathbf{U}_{mn}$ becomes smaller. Even when one does not throw over the rigid single-stranded model therefore, one only has to give larger values for a in order to get out of the above-mentioned dilemma.

An experimental fact must be mentioned to judge which view is right. Blake and Peacocke[18] observed a distinct Cotton effect around 440 nm due to proflavine bound to poly A in acid solution but no optical activity for the same system in neutral solution. This probably comes from the fact that in the poly A–proflavine complex the dyes are regularly arranged around the poly A double-helices in acid solution, while they are not because poly A does not take a regular helical structure in neutral solution.

The present treatment must await further improvements on quantitative description of spectral bandshapes of helical and non-helical biopolymers. We have not undertaken calculations with finer parametrization, since the spectral data available for the residue and the polymer in different pH solutions seem to be far from perfect. Nevertheless, we believe that the present theory and results provide a useful step for the understanding of the many-body aspect and the determination of conformations of helical biopolymers.

References

1) H. Ito, T. Eri, and Y. J. I'Haya, *Chem. Phys. Lett.*, **39**, 150 (1976); *ibid.*, **45**, 610 (1977).
2) U. Fano, *Phys. Rev.*, **118**, 451 (1960).
3) H. DeVoe, *J. Chem. Phys.*, **41**, 393 (1964).
4) H. DeVoe, *J. Chem. Phys.*, **43**, 3199 (1965).
5) A. Herzenberg and A. Modinos, *Proc. Phys. Soc.*, **87**, 597 (1966).
6) J. Applequist, *J. Chem. Phys.*, **58**, 4251 (1973).
7) C. L. Cech, W. Hug, and I. Tinoco, Jr., *Biopolymers*, **15**, 131 (1976).
8) D. N. Holcomb and I. Tinoco, Jr., *Biopolymers.*, **3**, 121 (1965).
9) J. Brahms, *Nature*, **202**, 797 (1964).
10) J. Brahms, A. M. Michelson, and K. E. Van Holde, *J. Mol. Biol.*, **15**, 467 (1966).

11) H. A. Rich, D. R. Davies, F. H. Crick, and J. D. Watson, *J. Mol. Biol.*, **3**, 71 (1961).
12) W. Kauzmann, "Quantum Chemistry," Academic Press, New York (1967), p. 579.
13) H. Ito, T. Eri, and Y. J. I'Haya, *Chem. Phys.*, **8**, 68 (1975); *ibid.*, **10**, 497 (1975).
14) I. Tinoco, Jr., R. W. Woody, and D. F. Bradle, *J. Chem. Phys.*, **38**, 1317 (1963).
15) A. M. Michelson, *J. Chem. Soc.*, **1959**, 1371.
16) R. F. Beers, Jr. and R. F. Steiner, *Nature*, **179**, 1076 (1957).
17) D. Poland, J. N. Vournakis, and H. A. Scheraga, *Biopolymers*, **4**, 223 (1966).
18) A. Blake and A. R. Peacocke, *Biopolymers*, **5**, 383 (1967).

ESR Study of Hot Ions in Solid Solutions of $K_2[(Zn,Cd,Hg)(CN)_4]$

Henryk KOZLOWSKI,* Jun-ichi ISOYA, and Shizuo FUJIWARA
Department of Chemistry, Faculty of Science, The University of Tokyo, Hongo, Bunkyo-ku, Tokyo 113
(Received July 19, 1977)

The ESR spectra of Cd(I) hot ions produced in solid solutions of $K_2[(Zn, Cd, Hg)(CN)_4]$ indicate that there are paramagnetic species of hot-ion molecules characteristic of the single phase of $K_2[Zn(CN)_4]$ and of the solid solution. The total contribution from the s and p orbitals to the spin density of the Cd(I) hot ions is constant, although the relative contributions from these two orbitals vary. It is shown that the mother lattice surrounding the hot ions determines the electronic structure and stability of the hot ions. These results suggest that the investigation of hot ions in a solid solution is useful for the study of microstructure of the solid solution.

Electron spin resonance (ESR) is useful for the investigation of the "hot ions"[1] which are produced by the X-ray or γ-ray irradiation of diamagnetic complexes. A large number of investigations have been carried out on various species of central metal ions.[2-5] An unpaired electron in a hot-ion molecule of Zn(I), Cd(I), Hg(I) can be described in terms of a ground state with a large s-orbital character. As a matter of fact, a considerable contribution of the s-orbital to the ground state of the metal ions has been experimentally evidenced by the large isotropic hyperfine coupling constants.[3-6]

This paper will report on the effect of a "solid solution" on the character of hot ions. It will be shown how the mother lattice of hot ions affects the electronic state of the latter, particularly with respect to their stabilities. Two different kinds of metal ions were mixed together, thus being made into cyanide complexes, where each of the metal ions produces hot ions with the unpaired electron in the s-orbital. By the γ-ray irradiation of the cyanide complexes, hot ions were produced therein. ESR was observed in the products. The ESR spectra thus obtained were compared to those of the hot ions produced in the complex compound of one of the composing metal ions (which will be referred to, hereafter, as the single-phase compound). It was found that the solid-solution sample presented new lines besides the lines of the latter which were found in the single-phase compound. This result seems to refer to the fact that the components of the sample of a solid solution are not homogenous with respect to the distribution of the components; rather each component exists in two forms, one surrounded by the metal ions of the same kind, and the other, by those of other species. The lifetimes of the hot ions differ from each other according to the type. The observed results will be discussed in correlation with the electronic structures of the hot ions.

Experimental

Samples of the cyanides of the mixed metal ions were prepared by the evaporation of a mixed aqueous solution of $K_2[M(CN)_4]$ and $K_2[M'(CN)_4]$, where M and M' are one of three combinations; Zn and Cd, Zn and Hg, and Cd and Hg. The samples were sealed *in vacuo* (10^{-6} mmHg) and irradiated by γ-rays from a ^{60}Co source at the temperature of liquid nitrogen. After the irradiation, the ESR spectra of the samples were recorded with a JELCO 3BSX spectrometer at the temperature of liquid nitrogen.

* On leave from Institute of Chemistry, University of Wroclaw, Wroclaw, Poland.

Results

The ESR spectra of the γ-ray irradiated solid solutions are shown in Figs. 1—4. All the spectra were almost symmetrical with respect to the center of $g=2$, presenting a structure of very large hyperfine coupling constants. (In order to save space, each figure shows only half of each spectrum.) The ratios which can be seen in the figures refer to the compositions of the mother solutions, not to the compositions of the solid samples. However, we assume that this fact will not disturb any of the discussions to be given below. In the case of the $K_2[(Zn,Cd)(CN)_4]$ system (Fig. 1), one can distinguish three lines, I, II, and III. All these lines are

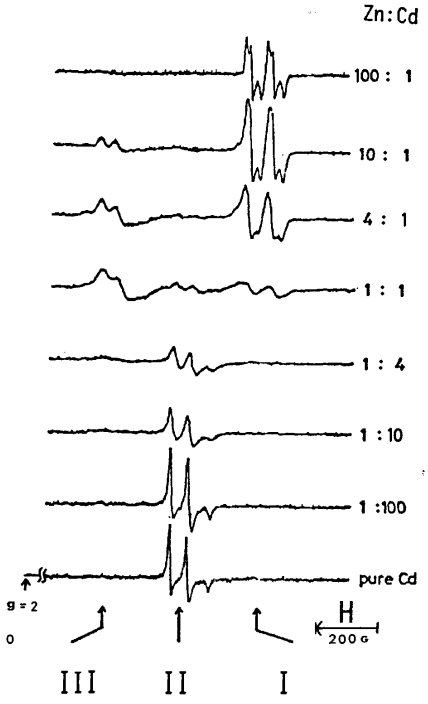

Fig. 1. ESR spectra of the Cd(I) hot ion in the $K_2[Zn(CN)_4]$-$K_2[Cd(CN)_4]$ solid solution. ($F=0$, $m_F=0$) ($F=1$, $m_F=+1$) transition for the ^{111}Cd and ^{113}Cd isotopes. The spectrum in the figure represents a half of the lower-field side of the hfs of Cd(I).

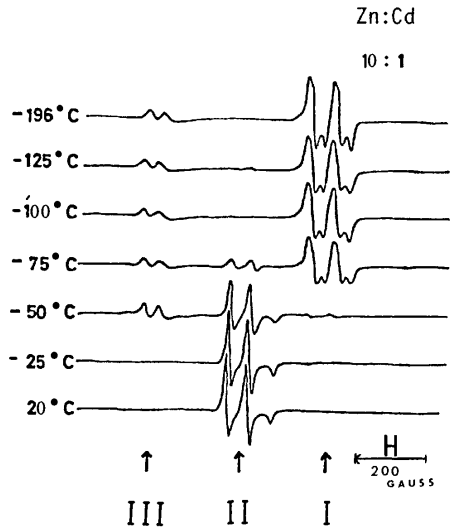

Fig. 2. ESR spectra of the Cd(I) hot ion in the $K_2[Zn(CN)_4]$-$K_2[Cd(CN)_4]$ solid solution with the molar ratio of 10 : 1. The spectra were measured at 77 K after the solution has been annealed at the temperatures indicated in the figure.

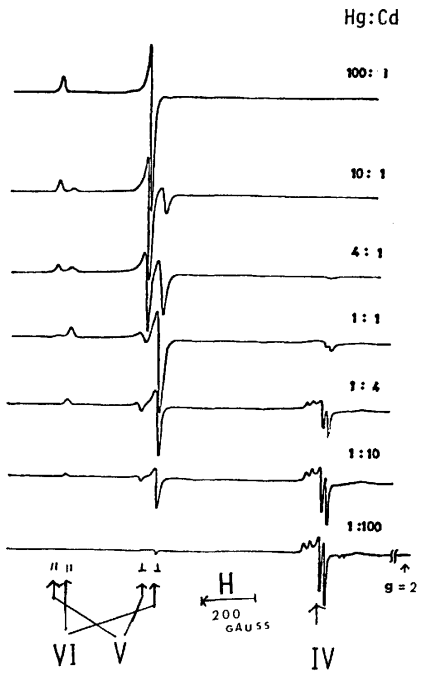

Fig. 3. ESR spectra ($(F=1, m_F=-1)$ $(F=1, m_F=0)$) of the Cd(I) (high field) and Hg(I) hot ions in the $K_2[Hg(CN)_4]$-$K_2[Cd(CN)_4]$ solid solution. Only the high-field side of the hf line is shown.

formed of two lines which have already been recognized as those of Cd(I) in the single-phase compound of cadmium. Those two lines are attributable to the isotopes of ^{111}Cd and ^{113}Cd. Each of the two lines shows a composite structure attributable to the contribution of the anisotropic nature of the electron. A comparison of the spectrum of Fig. 1 to that of the Cd(I) hot ion in the single-phase compound shows that Line II is attributable to Cd(I), which is surrounded by Cd(I), whereas Lines I and III are new lines of Cd(I)

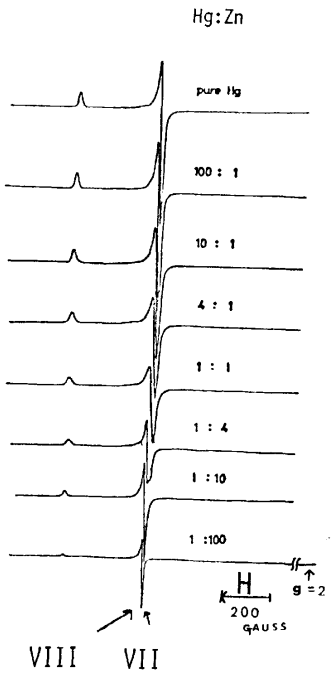

Fig. 4. ESR spectra of the Hg(I) hot ion in the $K_2[Hg(CN)_4]$-$K_2[Zn(CN)_4]$ solid solution. $(F=1, m_F=-1)$, $(F=1, m_F=0)$ transition of the ^{199}Hg isotope.

which have appeared in the solid-solution sample. Both of them are stable at the temperature of liquid nitrogen. However, they show an appreciable temperature dependence when they are annealed for 15 min at some elevated temperature and then cooled to the temperature of liquid nitrogen for the performance of the ESR measurements. Figure 2 shows the spectra at the temperature of liquid nitrogen after annealing at different temperatures. Lines I and III vanish with the elevation of the temperature. It is remarkable that the intensity of II increases parallel with the decreses in I and III. This seems to suggest that the unpaired electrons in I and III are transferrable to II. As may be seen in Fig. 3, similar results are also observed with the system of $K_2[(Cd,Hg)(CN)_4]$, where the lines of VI refer to Hg(I), characteristic of a solid-solution system; the V lines, to Hg(I) in $K_2[Hg(CN)_4]$, and the IV lines, to Cd(I) in $K_2[Cd(CN)_4]$. In the case of $K_2[(Zn,Hg)(CN)_4]$, it is noted that the position of Line VIII, which can be assigned to Hg(I) in the solid solution, is close to that of Hg(I) in the single-phase compound, VII (*cf.* Fig. 4). The solid-solution signals of Hg(I) in $K_2[(Cd,Hg)(CN)_4]$ become observable upon slight warming, even if they cannot be detected immediately just after irradiation. The observed results can be summarized as follows: 1) the hot ions are produced in the γ-ray irradiated mixed solid solutions, $K_2[(M,M')(CN)_4]$; 2) they are classified into two types, one characteristic of the mixed solution (Signals I, III in Fig. 1, VI in Fig. 3, and VIII in Fig. 4), and the other the same as that produced in the single-phase compound (to be referred to as the pure sample hereafter), $K_2[M(CN)_4]$ (II in Fig. 1, IV and V in Fig. 3, and VII in Fig. 4). Spin Hamiltonian parameters

TABLE 1. ESR PARAMETERS FOR Cd(I) IONS IN THE $K_2[Zn(CN)_4]$ LATTICE

T [K]	Isotope	A (G)	g
liq N_2	113	$A_z=1815$	$g_1=1.978$
		$A_y=1745$	$g_2=1.996$
		$A_x=1718$	$g_3=1.998$
		$A_{av}=1759$	$g_{av}=1.990$
	111	$A_z=1735$	$g_1=1.979$
		$A_y=1668$	$g_2=1.995$
		$A_x=1642$	$g_{av}=1.990$
143	113	$A_{av}=1790$	$g_{av}=1.991$
	111	$A_{av}=1714$	$g_{av}=1.990$
163	113	$A_{av}=1811$	$g_{av}=1.991$
	111	$A_{av}=1731$	$g_{av}=1.991$
183	113	$A_{av}=1833$	$g_{av}=1.992$
	111	$A_{av}=1745$	$g_{av}=1.992$
Pure salt : Cd(I) in the $K_2[Cd(CN)_4]$ lattice			
liq N_2	113	$A_{av}=1510$	$g_{av}=1.989$
	111	$A_{av}=1440$	

were obtained for the Cd(I) hot ions, Species I in the $K_2[Zn(CN)_4]$ lattice, and Species II in the $K_2[Cd(CN)_4]$ lattice. All these results are shown in Table 1.

Discussion

The aforementioned results refer to the effect of a solid solution—that the hot ions differ depending on their surroundings, whether they are embedded in a lattice of metal ions of same kind or in one of ions of a different kind. The difference in the electronic natures of these two cases can be derived from the ESR parameters below.

A $K_2[Cd(CN)_4]$ molecule has a Td symmetry. Assuming that the Cd(I) hot ion still holds the position of Cd(II) in the mother lattice, the ground state may be expressed as

$$\phi^\circ = c_i\phi_{ns} + \sum_j K_j\phi_{j,lig}, \quad (1)$$

where ϕ_{ns} is the s-orbital of the metal ion and where $\phi_{j,lig}$ are the wave functions of the ligand; the symmetry of this state is A_1. In Cd(I) hot ions, however, the symmetries of the g and A tensors are C_{3v} in the pure salt[3] and orthorhombic in the $K_2[Zn(CN)_4]$ lattice. Therefore, the contribution from the np and the nd orbitals must be added to the ground state in the case of Cd(I) hot ions. The energy of the nd orbitals is assumed to be much higher than that of ns. Hence, it seems reasonable to represent a ground-state function as

$$\phi^\circ = c_1\phi_{ns} + c_2\phi_{np_z} + \sum_j K_j\phi_{j,lig}. \quad (2)$$

The np_z orbital is assumed to have an A_1 symmetry as ns. Accordingly, the two orbitals of np_z and ns are assumed to be able to mix with each other. The spin-orbit interaction between the ground state and the np_x and np_y orbitals contributes to the g anisotropy. Neglecting the overlap integrals with ligands, the g-shift at the axial component is given by

$$\Delta g = -\frac{2\xi_{np}}{\Delta E}c_2^2, \quad (3)$$

where ξ_{np} is a spin-orbit coupling constant and where ΔE is the energy difference between the ground state and the $np_{x,y}$ orbitals.[7] This equation enables us to estimate the contribution of the p_z orbital to the ground state.

Using these values: $\xi_{np}=1000$ and $4000\ cm^{-1}$, and $\Delta E=33000$ and $40000\ cm^{-1}$ for Cd(I) and Hg(I) ions respectively,[8] the values of c_2^2 for the pure salt are obtained, with the use of the g-values reported in a previous paper,[3] to be as shown in parentheses in

TABLE 2a. MOLECULAR ORBITAL PARAMETERS FOR HOT ION AT THE TEMPERATURE OF LIQUID NITROGEN

Type of hot ion	c_1^2	c_2^2	$c_1^2+c_2^2$
Species II of			
Cd(I)	0.33	0.24(0.23)[a]	0.57
Hg(I)	0.38	0.19(0.21)[a]	0.57

a) Values in parentheses were obtained from the Δg values.

TABLE 2b. TEMPERATURE DEPENDENCE OF THE MOLECULAR ORBITAL OF THE SPECIES I OF Cd(I), Cd(I) IN $K_2[Zn(CN)_4]$

T	c_1^2	c_1^2	$c_1^2+c_2^2$
liq N_2	0.38	0.18	0.56
143 K	0.39		
183 K	0.40		

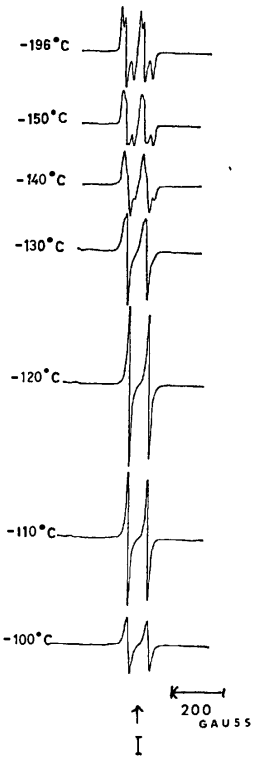

Fig. 5. Temperature dependence of the ESR spectra of the Cd(I) hot ion (Species I) in the $K_2[Zn(CN)_4]$ lattice.

Table 2. With the use of the A tensor components, the contributions from the s-orbital, c_1^2, and those of the p orbital, c_2^2, to the graund state are also calculated (*cf.* Table 2). The good agreement between the two c_2^2 values obtained from the g and A tensors justifies the formerly presented assumption that the overlap integral is negligible. In Fig. 5, the temperature dependence of the ESR spectra of Species I is presented. The spectra in the figure were measured at the temperatures cited. For the Cd(I) hot ion (Species I) in the $K_2[Zn(CN)_4]$ lattice, the values of c_1^2 and c_2^2 can be evaluated from the values of the A tensor, as is shown in Table 2. From the axial spectra at rather high temperatures, only c_1^2 can be determined. This value increases with the temperature; the averaged g value also increases slightly. From Table 2 it can be seen that, for the Cd(I) ion, the total contribution from the s and p_z orbitals is almost constant in all the cases examined, even if the relative contributions from the s and p_z orbitals vary. This may also refer to the fact that all of the ESR spectra arise from the same chemical species, which are little different with respect to the nature of the symmetry of the ion. The magnitude of the ratio of the s- and p-orbital contributions may serve as a measure of the distortion of the symmetry. The increase in the c_1^2 and g values suggests that the symmetry of the molecule becomes higher with an increase in the temperature. For a better understanding of this dynamic phenomenon, though, a further study of the ESR on a single crystal is necessary.

From a comparison between the pure salt and the solid-solution data for the Cd(I) ion, it is concluded that the symmetry of the hot ion in the $K_2[Zn(CN)_4]$ lattice (Species I) is higher than that of any other species in the pure salts.

In order to interpret the fact that Species II appear along with the decay of Species I and III (*cf.* Fig. 2), we have to assume that some aggregates of the Cd(II)-ion molecules exist in the sample. When Species I and III dacay, excess electrons are transferred to those aggregates and produce Cd(I) hot ions in the lattice of $K_2[Cd(CN)_4]$, which has been produced locally. As a result, this kind of species is relatively stable and can be observed even at higher temperatures. As to the exact nature of Species III, a further investigation of the single-crystal sample will be needed.

References

1) S. Fujiwara, T. Watanabe, and H. Tadano, *J. Coord. Chem.*, **1**, 195 (1971).

2) S. Fujiwara, MPT Report, Ser. II, Vol. 4, "Magnetic Resonance," ed. by McDowell (1974), and references included therein.

3) J. Isoya and S. Fujiwara, *Bull. Chem. Soc. Jpn.*, **45**, 2182 (1972).

4) R. S. Eachus, M. C. R. Symons, and J. K. Yandell, *Chem. Commum.*, **1970**, 979.

5) R. S. Eachus and M. C. R. Symons, *J. Chem. Soc., A*, **1970**, 3080.

6) J. Isoya, Ph. D. Thesis, Tokyo University, 1974.

7) A. Abragam and B. Bleaney, "Electron Paramagnetic Resonance of Transition Ions," Clarendon Press (1970).

8) L. B. Knight and W. Weltner, *J. Chem. Phys.*, **55**, 2061 (1971).

Preparation and Isomerization of Three Isomers of L-Histidinato-iminodiacetatocobalt(III) Complex

Masatoshi WATABE, Masayuki ZAMA, and Sadao YOSHIKAWA*

General Education Department of Kogakuin University, Hachioji, Tokyo 193

**Department of Synthetic Chemistry, Faculty of Engineering, The University of Tokyo, Hongo, Bunkyoku, Tokyo 113*

(Received July 6, 1977)

Three isomers of L-histidinatoiminodiacetatocobalt(III) complex have been prepared and characterized on the basis of their absorption, circular dichroism and proton magnetic resonance spectra. These isomers isomerized mutually in water at 80 °C. The equilibrium mole fractions of these isomers in water were found for *cisN*, *transN* and *fac* to be 0.91, 0.04, and 0.05, respectively.

In previous papers,[1,2] the preparation and the isomer distribution at equilibrium in water in the presence of active carbon were studied for the mixed cobalt(III) complexes with D-aspartate and L-2,4-diaminobutyrate ions. The distribution in favor of one isomer was found. In the present paper, the preparation of mixed cobalt(III) complexes containing iminodiacetate (=ida) and L-histidinate (=his) ions will be reported. Their absorption, PMR, and CD spectra are discussed. These isomers were found to isomerize in water in the absence of active carbon as in the case of [Co(L-prolinato)$_3$].[3] The relative rate constants for the isomerizations were determined by using a network analysis.[4]

Experimental

Preparations. Iminodiacetic acid (1.33 g) and L-histidine (1.55 g) were dissolved in 15 cm^3 of water. To this solution was added 1M-sodium hydroxide until the pH of the solution became *ca.* 9. To this mixture was added a solution (20 cm^3) of $CoCl_2 \cdot 6H_2O$ (2.38 g) containing 5 cm^3 of 10% H_2O_2. The mixture was stirred at 80 °C for 30 min and filtered to remove the small amount of precipitate. The filtrate was passed through a colum (30×500 mm) containing strong cation exchange resin, Dowex 50WX8 (100—200 mesh, sodium form). Elution with water produced a violet band followed by a red band. The violet eluate was condensed to about 10 cm^3 and allowed to stand at room temperature for one week. Violet crystals (M1) and a gray violet powder (M2) appeared and were separated by a spatula. The product in the third red eluate isomerized with ease at room temperature, and consequently was kept in a refrigerator. Only a small amount of crystals were obtained (M3). Found M1: C, 34.82; H, 3.72; N, 16.10%. Calcd for $CoC_{10}H_{13}N_4O_6$: C, 34.95; H, 3.81; N, 16.30%. Found M2: C, 33.85; H, 3.89; N, 15.72%. Calcd for $CoC_{10}H_{13}N_4O_6 \cdot 0.5H_2O$: C, 34.06; H, 4.00; N, 15.89%. Found M3: C, 33.33; H, 4.00; N, 15.41%. Calcd for $CoC_{10}H_{13}N_4O_6 \cdot H_2O$: C, 33.21; H, 4.18; N, 15.49%.

Isomerization. A solution containing one isomer was stirred and maintained at 80 °C in a temperature-controlled reaction vessel. The concentrations of M1, M2, and M3 were determined as follows. Initially, the concentrations of the M3 isomer (*fac*) was determined using high speed liquid chromatography and optical density. The concentrations of the M1 and M2 isomers could not be determined by chromatography since their bands overlaped. These were determined by measuring molar rotations [ϕ] at 454 and 500 nm. The values of the isomers are as follows.

	454 nm	500 nm
M1	4706	0
M2	0	−3029
M3	2066	3214

The concentrations of the M1 and M2 isomers were calculated using the following equation

$$[\phi]_{M1}x+[\phi]_{M2}y+[\phi]_{M3}(1-x-y)=\alpha[\text{molecular weight}]/cl,$$

where $[\phi]_{M1}$, $[\phi]_{M2}$, and $[\phi]_{M3}$ are the molar rotations, x and y are the concentrations of the M1 and M2 isomers, respectively. c is the initial concentration of the isomer, α the observed rotation expressed in degrees, and l the cell length. Since the concentration loss of the complexes due to reactions other than the isomerization was less than 2 percent, the concentration of the complex was assumed to be constant throughout the experiment. The isomerization of M3 was not attempted because of its insufficient yield.

Measurements. The electronic absorption spectra and optical rotatory dispersion curves were measured with a JASCO ORD-UV-5 spectrometer. The CD spectra were measured with a JASCO J-20 spectrometer, and the PMR spectra (60 MHz) in D_2O with a JEOL MH-60 spectrometer using sodium 2,3-dimethyl-2-silapentane-5-sulfonate as an internal reference.

Results and Discussion

Figure 1 shows the possible isomers of [Co(ida)(L-his)]. The two meridional isomers (a and b) are denoted by *cisN* and *transN* (the nitrogen atom of ida is cis or trans to the amine nitrogen atom of L-his). Figure 2 shows the absorption spectra of the three isomers of [Co(ida)(L-his)] and the numerical data are listed in Table 1. Zompa assigned the configurations of the three isomers of [Co(L-his)$_2$]$^+$ [5] by comparing their absorption spectra with those of the three isomers of [Co(L-2,4-dba)$_2$]$^+$ [6] (dba=diaminobutyrate ion). From previous spectroscopic studies,[7] it appears that the nitrogen atom of imidazole and that of ammine occupy nearly the same positions in the spectrochemical series. Since the nitrogen atom of amine lies at a higher position in the spectrochemical series than that of ammine, the nitrogen (Nα) attached to the α-carbon atom of L-his lies at a higher position than that of the imidazole ring (Ni). Yamatera's parameters[8] concerning the first band were estimated from the absorption maxima of the $[Co(NH_3)_6]^{3+}$,[9] $[Co(ox)_3]^{3-}$ [10] and *trans*(*N*)-K$[Co(ida)_2]^-$,[11] complexes ($\delta(NH_3\text{-ox})=4500$ and $\delta(N\alpha\text{-ox})=7400$ cm^{-1}). The estimated positions

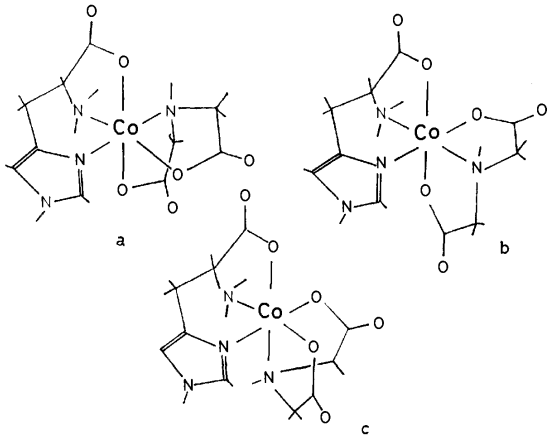

Fig. 1. The three possible geometrical isomers of the [Co(ida)(L-his)] complexes, a: *mer-cisN*, b: *mer-transN*, c: *fac*. The isomers are named by considering 5-membered N and O atoms.

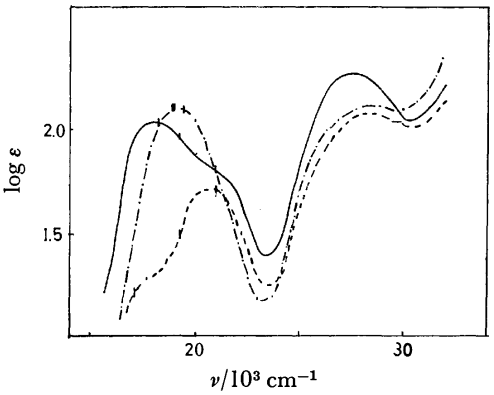

Fig. 2. Visible absorption spectra of [Co(ida)(L-his)]. *cisN* (——) *transN* (- - -), and *fac* (—·—·).

of the first absorption bands of the isomers are illustrated in Fig. 2. The isomer(M1) having a shoulder at the highest wave number in the first absorption band region can be assigned to the *cisN* isomer and one(M2) having a shoulder at the lowest wave number to the *transN* isomer.

PMR Spectra. Figure 3 shows the PMR spectra of [Co(ida)(L-his)]. We have reported that when X is an oxygen atom in the moity –CH–NH_2–Co(III)–X

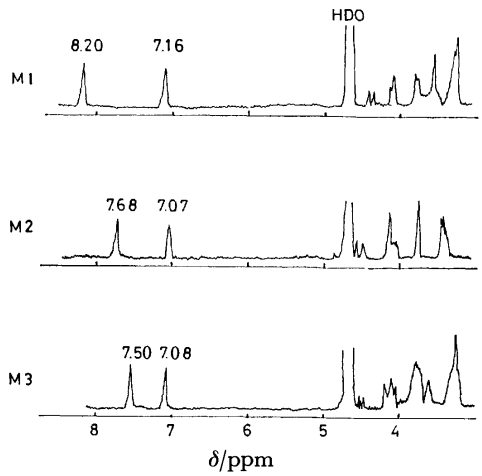

Fig. 3. PMR spectra of M1 (*cisN*), M2 (*transN*), and M3 (*fac*).

(X is trans to NH_2), the methine proton signals appear at a slightly higher magnetic field strength than in the case when X is a nitrogen atom. The sharp peaks in the low magnetic field region may be due to the imidazole protons attached to the 2-carbon (Fig. 3). This assings the *cisN* isomer for M1 and the *transN* for M2, since the sharp peak for M1 is located in a lower magnetic field than those for M2 and M3.

CD Spectra. Figure 4 shows the CD spectra of the isomers of [Co(ida)(L-his)]. The configurational effect of the complexes having one or two optically active tridentate ligands can not be well classified in terms of Δ and Λ chirality. These are for example $[Co(L\text{-}asp)_2]^-$,[12] *mer*-$[Co(dien)_2]^{3+}$,[13] (dien=diethylenetriamine), $[Co(L\text{-}2,4\text{-}dba)_2]^+$,[6] $[Co(L\text{-}2,3\text{-}dpa)_2]^+$[14] (dpa = diaminopropionate ion), and [Co(ida)(L-asp)]$^-$.[15] The complication of their CD spectra may be chiefly attributed to the vicinal effect due to the branch from the α-carbon atom. If such a vicinal effect can be eliminated from the CD curves, the calculated CD spectra may be compared with those of the known simple complexes. The assumption that the vicinal and the configurational effects is additive leads to the following additivity formulae:

$$\Delta\varepsilon(M1) = \Lambda(5\text{—}5) + \Lambda(5\text{—}5) + \Lambda(5\text{—}6) + L$$
$$\Delta\varepsilon(M2) = \Lambda(5\text{—}5) + \Lambda(5\text{—}6) + L$$
$$\Delta\varepsilon(M3) = \Lambda(5\text{—}5) + \Lambda(5\text{—}6) + \Lambda(5\text{—}6) + L$$

Table 1. Absorption and CD data of [Co(ida)(L-his)]

Complex	I band				II band			
	Aasorption		CD		Absorption		CD	
	$\bar{\nu}$ max[a]	log ε	$\bar{\nu}$ max	Δε	$\bar{\nu}$ max	log ε	$\bar{\nu}$ max	Δε
M1 (*cisN*)	18.0	2.05	17.2	0.69	27.0	2.28	27.0	0.73
	20.8	1.81	20.2	−1.02				
M2 (*transN*)	17.7	1.28	17.2	1.08	28.2	2.09	27.0	0.50
	20.6	1.72	20.4	−0.70				
M3 (*fac*)	19.1	2.12	17.9	−0.95	28.2	2.11	27.8	−0.13
			20.0	0.48				

a) Wave numbers are given in 10^3 cm^{-1}.

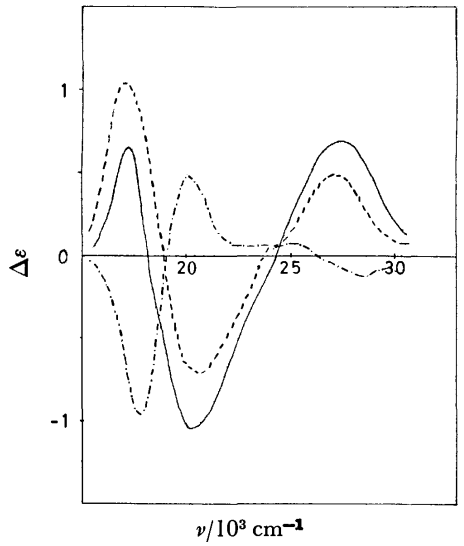

Fig. 4. CD spectra of three isomers of [Co(ida)(L-his)]. *cisN* (——), *transN* (- - -), and *fac* (—•—•).

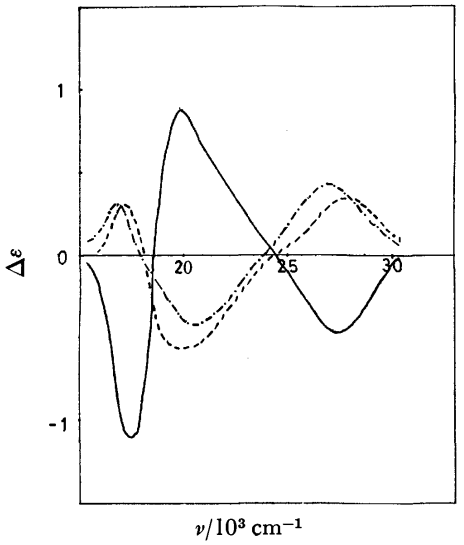

Fig. 5. Curve analysis of [Co(ida)(L-his)]. L(—•—•), Δ(5—5) (——), and Δ(5—6) (- - -).

where Δ(5—5) means the configurational effect between 5- and 5-membered chelate rings and L the vicinal effect due to L-his. It is reasonably assumed that $\Delta(5—5)+\Delta(5—5)=0$ and $\Delta(5—6)+\Delta(5—6)=0$. Then $\Delta(5—5)=\Delta\varepsilon(M3)-L$, $\Delta(5—6)=\Delta\varepsilon(M1)-L$. The calculated curves of Δ(5—5) and Δ(5—6) are shown in Fig. 5. The sign of Δ(5—5) in the lower wave number side of the first absorption band is negative and that of Δ(5—6) positive. The intensity of the Δ(5—6) ($=-\Delta(5—6)$) is smaller than that of Δ(5—5). The decrease in the intensity appears to correspond to the change in the CD intensity between $[Co(en)_3]^{3+}$ and $[Co(tn)_3]^{3+}$ [16] (tn=trimethylenediamine). The configurational curve, Δ(5—5) compare favorably with those for Δ-*cis*(*N*)-$[Co(ida)_2]^-$ [17] and Δ-*cis*(*N*)-$[Co(L\text{-}alama)_2]^-$ [18] (alama=alanine-*N*-acetate ion) though its intensity is small. The above results show that the structures of all the isomers may be assigned

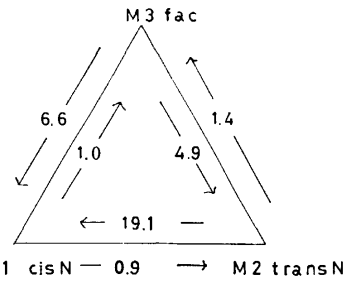

Fig. 6. The network of the isomerzation system.

on the basis of their CD spectra.

Isomerization. The three isomers of [Co(ida)(L-his)] isomerized in water without any catalysis. The mole fractions of these three isomers at equilibrium were 0.91 for *cisN*, 0.04 for *transN*, and 0.05 for *fac*. Such a distribution in favor of the *cisN* isomer is remarkable. The free energy differences at 25 °C are as follows; $\Delta G_{12}=G(M1)-G(M2)=-RT\ln(91/4)=-7.7$kJ and $\Delta G_{13}=-7.2$kJ. Figure 6 shows the relative rate constants calculated by means of the same method as that in the previous paper.[2] The molecular model concept suggests that the five-membered chelate rings of the coordinated ida can twist to some extent. The nearest atoms between the two coordinated ligands are the 2-proton of the imidazole and one of the methylene protons of ida for *cisN*, and the 2-proton of the imidazole and the imino proton of ida for *transN*. However, these distances do not appear to cause steric hindrance. In the case of the *fac* isomer, the distance between the one proton of L-his and the imino proton of ida is nearly 2.3—2.5 Å. This may cause some steric hindrance between these two ligands. However, the large free energy differences obtained are not reasonably accounted for by steric hindrance only. The electronic effect which is transmitted through the bonds may explain this distribution although this can not be deduced from the data.

References

1) M. Watabe, K. Onuki, and S. Yoshikawa, *Bull. Chem. Soc. Jpn.*, **48**, 687 (1975).
2) M. Watabe, S. Kawaai, and S. Yoshikawa, *Bull. Chem. Soc. Jpn.*, **49**, 1845 (1976).
3) R. G. Denning and T. S. Piper, *Inorg. Chem.*, **5**, 1056 (1965).
4) M. Boudart, "Kinetics of Chemical Processes," Prentice Hall, In., Englewood Clifts, Newjersey (1968).
5) L. J. Zompa, *Chem. Commun.*, **1969**, 783.
6) W. A. Freeman and C. F. Liu, *Inorg. Chem.*, **9**, 1191 (1970).
7) W. Eilbeck, F. Holmes, A. Underhill, *J. Chem. Soc., A*, **1967**, 757.
8) H. Yamatera, *Bull. Chem. Soc. Jpn.*, **31**, 95 (1958).
9) H. Siebert, C. Siebert, and K. Wieghardt, *Z. Anorg. Allg. Chem.*, **380**, 30 (1971).
10) *Inorg. Synth.* **1**, 37.
11) J. Hidaka, Y. Shimura, and R. Tsuchida, *Bull. Chem. Soc. Jpn.*, **35**, 567 (1962).

12) S. Yamada, J. Hidaka, and B. E. Douglas, *Inorg. Chem.*, **10**, 2187 (1971).
13) Y. Yoshikawa and K. Yamasaki, *Bull. Chem. Soc. Jpn.*, **45**, 179 (1972).
14) W. A. Freeman and C. F. Liu, *Inorg. Chem.*, **7**, 764 (1968).
15) J. Hidaka, S. Yamada, and B. E. Douglas, *J. Coord. Chem.*, **2**, 123 (1972).
16) P. G. Beddoe and S. F. Mason, *Inorg. Nucl. Chem. Lett.*, **4**, 433 (1968).
17) C. W. Van Saun and D. W. Cooke, *Inorg. Chem.*, **8**, 1145 (1969).
18) K. Okamoto, J. Hidaka, and Y. Shimura, *Bull. Chem. Soc. Jpn.*, **44**, 1601 (1971).

Phase Equilibria in the Lu_2O_3–V_2O_3–V_2O_5 System at 1200 °C

Kenzo KITAYAMA and Takashi KATSURA

Department of Chemistry, Tokyo Institute of Technology, Ookayama, Meguro-ku, Tokyo 152

(Received July 11, 1977)

The phase equilibria in the Lu_2O_3–V_2O_3–V_2O_5 system were established at 1200 °C. In this system, Lu_2O_3, $LuVO_3$, $LuVO_4$, V_2O_3, V_3O_5, V_4O_7, V_5O_9, V_6O_{11}, V_7O_{13}, and three new compounds $Lu_7V_3O_{16}$, $Lu_2V_2O_7$, and LuV_4O_8 are stable. $LuVO_4$, V_2O_3, VO_2, $Lu_7V_3O_{16}$, $Lu_2V_2O_7$, and LuV_4O_8 have non-stoichiometric compositions. The relationships between the composition and the $-\log P_{O_2}$ values of the solid solutions were obtained from the thermogravimetric results. On the basis of the phase equilibria, the standard Gibbs free energies of several reactions were determined. The spacings, relative intensities, and densities of new compounds were also determined.

In a previous paper,[1] the authors have established the phase equilibria in the Sm_2O_3–V_2O_3–V_2O_5 system at 1200 °C. In this system, we reported the existence of three ternary compounds, $Sm_{10}V_2O_{20}$ ($5Sm_2O_3 \cdot V_2O_5$), $SmVO_3$, and $SmVO_4$, and the homologous series of V_nO_{2n-1} of n=2—7. They also determined the standard Gibb energies of formation referred to reactions, $SmVO_3+1/2O_2=SmVO_4$ and $4Sm_2O_3+2SmVO_3+2O_2=Sm_{10}V_2O_{20}$, and the standard Gibbs energies of oxidation of the vanadium oxides found in the system.

In this paper, we choose Lu_2O_3 as one of the rare earth sesquioxides in the Lu_2O_3–V_2O_3–V_2O_5 system because its ionic radius is the smallest of the lanthanoid elements. The precise phase equilibria in the Lu_2O_3–V_2O_3 system have not yet been investigated, but the existence of orthorhombic $LuVO_3$ as a ternary compound in the system is well known, and its crystallographic properties have been reported.[2]

Recently, Brusset *et al.*[3] have studied the Lu_2O_3–V_2O_5 system in the temperature range from 600 to 1500 °C. They showed the existence of $4Lu_2O_3 \cdot V_2O_5$ together with a well-known tetragonal $LuVO_4$ phase, although the stable temperature range was not clear. As for the crystallographic properties of $4Lu_2O_3 \cdot V_2O_5$, they showed a simple X-ray diffraction diagram with only three peaks 2θ by Cu $K\alpha$(about 29.5, 31.9, and 32.3). However, the possibility of the existence of $4Lu_2O_3 \cdot V_2O_5$ was so ambiguous that they said that the diagram was incomplete.

The objectives of the present study are:(1) to establish the detailed phase equilibria in the Lu_2O_3–$V_2O_3 \cdot V_2O_5$ system at 1200 °C by changing the oxygen partial pressure; (2) to calculate the thermochemical properties based on the phase equilibria; and (3) to ascertain, upon the completion of the studies of the Ln–V–O system, whether or not the relationship between related standard Gibbs free energies of reaction and the ionic radii of rare earth ions as in the Ln–Fe–O system.[4]

Experimental

Analytical grades of Lu_2O_3(99.9%) and V_2O_5, which was obtained by heating the guaranteed grade of NH_4VO_3 at 500 °C in air for 24 h, have been employed as the starting materials. The desired ratios of Lu_2O_3/V_2O_5 were obtained by mixing thoroughly in an agate mortar under ethyl alcohol. The mixtures thus obtained were treated by the procedures described previously.[1]

The apparatus and procedures for controlling the oxygen partial pressure, keeping at a constant temperature, the method of thermogravimetry, the criterion for equilibrium establishment, the method of identifying solid phases after quenching, the method of lattice constant determination, the method of measuring the actual oxygen partial pressures, and the method of wet chemical analysis are the same as those discussed in previous papers.[1,5-7]

The oxygen partial pressure of $10^{-12.00}$ atm was chosen as the reference weight standard as was determined in the Sm_2O_3–V_2O_3–V_2O_5 system.

Results and Discussion

Phase Equilibria. Eleven samples with the different Lu_2O_3/V_2O_5 compositions of 0.1111, 0.2500, 0.3333, 0.4286, 0.5385, 1.0000, 1.500, 1.857, 2.333, and 4.000 were prepared. In Fig. 1, the relationships between the oxygen partial pressures and the compositions, W_{O_2}/W_T, of the samples with Lu_2O_3/V_2O_5 compositions of 0.1111, 0.2500, 0.4286, 1.500, 2.333, and 4.000 are shown as representative, where W_{O_2} is the weight gain from the reference weight standard, and W_T the toal weight gain of the samples as if the $V_2O_3+O_2=V_2O_5$ reaction were to be completed. In Table 1, the results of the identification of phases are shown; in the first column are the compositions of the starting material; in the second column, the experimental con-

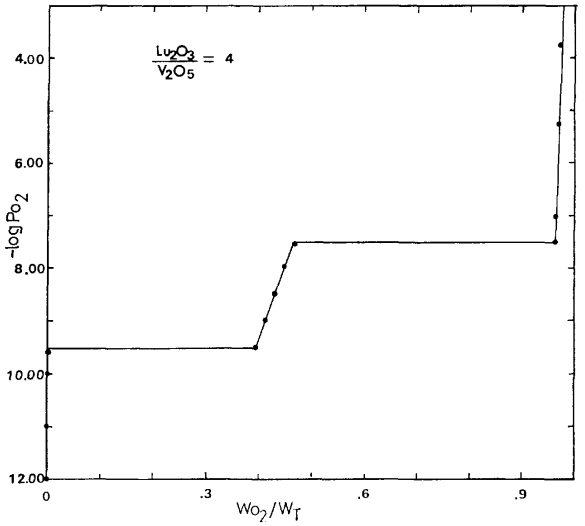

Fig. 1-1. The relationship between $-\log P_{O_2}$ and weight gains of the sample, $Lu_2O_3/V_2O_5=4$.

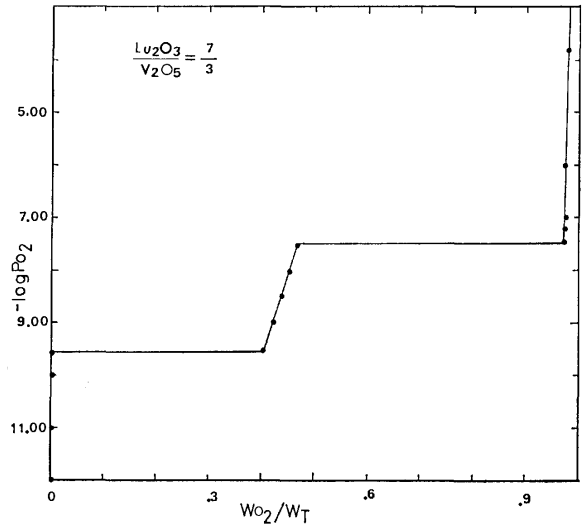

Fig. 1-2. The relationship between $-\log P_{O_2}$ and weight gains of the sample, $Lu_2O_3/V_2O_5=7/3$.

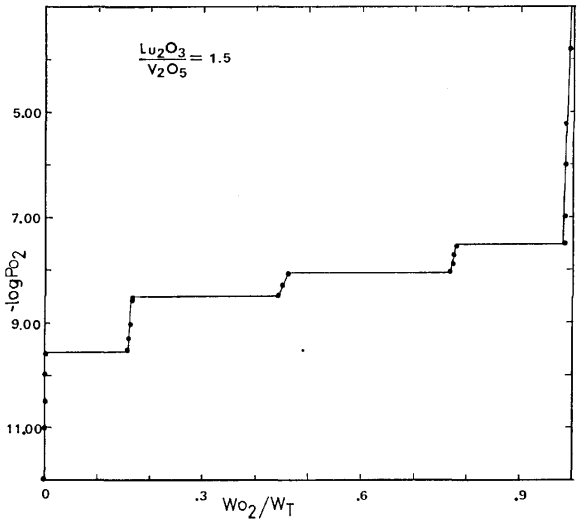

Fig. 1-3. The relationship between $-\log P_{O_2}$ and weight gains of the sample, $Lu_2O_3/V_2O_5=1.5$.

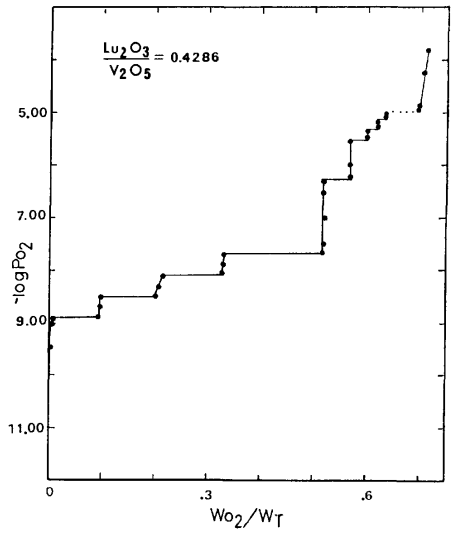

Fig. 1-4. The relationship between $-\log P_{O_2}$ and weight gains of the sample, $Lu_2O_3/V_2O_5=0.4286$.

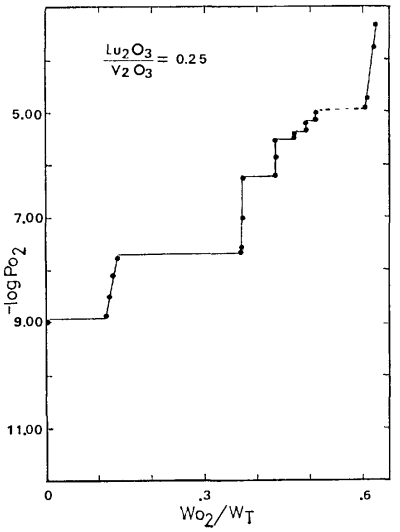

Fig. 1-5. The relationship between $-\log P_{O_2}$ and weight gains of the sample, $Lu_2O_3/V_2O_5=0.25$.

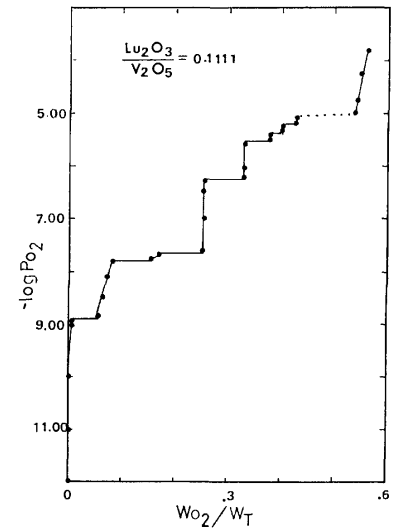

Fig. 1-6. The relationship between $-\log P_{O_2}$ and weight gains of the sample, $Lu_2O_3/V_2O_5=0.1111$.

ditions of log P_{O_2}, and in the third, the experimental time duration. Based on the experimental results of the thermogravimetry and the identification of the phases, the phase diagram shown in Fig. 2 was obtained. Following phases are stable under the present experimental conditions; Lu_2O_3(R), $LuVO_4$(B), $LuVO_3$(C), V_2O_3(D), V_3O_5(E), V_4O_7(F), V_5O_9(G), V_6O_{11}(H), V_7O_{13}(I), VO_2(J), and three new compounds, $Lu_2V_2O_7$(K), $Lu_7V_3O_{16}$(L), and LuV_4O_8(M). The letters in parentheses are the abbreviations of the compounds. $4Lu_2O_3 \cdot V_2O_5$, which has been reported by Brusset *et al.*,[3] did not appeared under the present experimental conditions. From the present results and Brusset's, $4Lu_2O_3 \cdot V_2O_5$ seems not to be stable, at least below 1500 °C.

Lu_2O_3 was stable under the present experimental conditions, as has already pointed out by Sekine and Katsura[8]. $LuVO_4$, $Lu_2V_2O_7$, $Lu_7V_3O_{16}$, LuV_4O_8, V_2O_3, and VO_2 have apparent deviations from the

TABLE 1. IDENTIFICATION OF PHASES

Starting materials (mol%)		$-\log P_{O_2}$ (atm)	Time (h)	Phase
Lu_2O_3	V_2O_5			
80	20	12.00	7	$Lu_2O_3+LuVO_3$
		9.00	64	$Lu_2O_3+Lu_7V_3O_{16}$
		7.90	71	$Lu_2O_3+Lu_7V_3O_{16}$
		7.00	70	$Lu_2O_3+LuVO_4$
		0.68	120	$Lu_2O_3+LuVO_4$
60	40	12.00	7	$Lu_2O_3+LuVO_3$
		9.00	64	$LuVO_3+Lu_7V_3O_{16}$
		8.30	123	$Lu_2V_2O_7+Lu_7V_3O_{16}$
		7.90	71	$LuVO_4+Lu_7V_3O_{16}$
		7.00	70	$Lu_2O_3+LuVO_4$
		3.80	82	$Lu_2O_3+LuVO_4$
35	65	8.70	52	$LuVO_3+LuV_4O_8$
		8.00	71	$LuVO_4+LuV_4O_8$
30	70	12.00	7	$V_2O_3+LuVO_3$
		9.00	64	$V_2O_3+LuVO_3$
		8.30	49	$Lu_2V_2O_7+LuV_4O_8$
		7.90	71	$LuVO_4+LuV_4O_8$
		7.60	49	$V_3O_5+LuVO_4$
		7.00	70	$V_3O_5+LuVO_4$
		5.80	57	$V_4O_7+LuVO_4$
		5.50	62	$V_5O_9+LuVO_4$
		5.30	62	$V_6O_{11}+LuVO_4$
		5.10	80	$V_7O_{13}+LuVO_4$
		3.79	82	VO_2+LuVO_4
10	90	12.00	7	$V_2O_3+LuVO_3$
		9.00	64	$V_2O_3+LuVO_3$
		8.70	52	$V_2O_3+LuV_4O_8$
		7.90	53	$V_2O_3+LuV_4O_8$
		7.70	50	$V_3O_5+LuV_4O_8$
		7.00	70	$V_3O_5+LuVO_4$
		5.80	57	$V_4O_7+LuVO_4$
		5.50	62	$V_5O_9+LuVO_4$
		5.30	62	$V_6O_{11}+LuVO_4$
		5.10	80	$V_7O_{13}+LuVO_4$
		3.80	82	VO_2+LuVO_4

TABLE 2. THE RELATIONSHIP BETWEEN THE COMPOSITIONS AND OXYGEN PARTIAL PRESSURES OF THE SOLID SOLUTIONS

$N_o/N_d = a+b\log P_{O_2}+c(\log P_{O_2})^2$

d	a	b	c
$Lu_7V_3O_{16}$	1.22	0.107	0
$Lu_2V_2O_7$	0.971	0.127	0
$LuVO_4$	4.20×10^{-3}	2.16×10^{-3}	0
LuV_4O_8	0.824	0.101	0
V_2O_3	1.76	0.363	0.0187

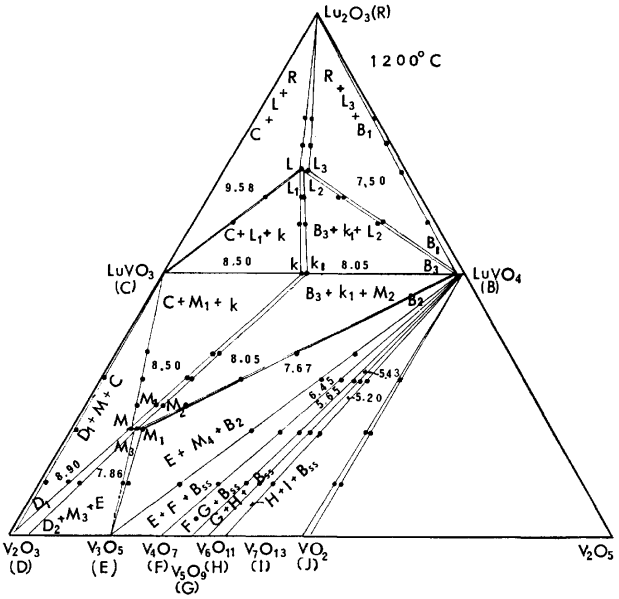

Fig. 2. Phase equilibria in the Lu_2O_3-V_2O_3-V_2O_5 system at 1200 °C. Numerical values in three solid phases regions are the oxygen partial pressures in $-\log P_{O_2}$ in equilibrium. Abbreviations are same as those in Table 3.

TABLE 3. COMPOSITIONS, STABILITY RANGES IN OXYGEN PARTIAL PRESSURES, AND ACTIVITIES IN SOLID SOLUTIONS

Component	Composition	Symbol	$-\log P_{O_2}$	$\log a_i$
$LuVO_4$	$LuVO_{4.00}$	B	0.68[a]—1.94[b]	0.0201
	$LuVO_{3.99}$	B_1	7.50	0.00346
	$LuVO_{3.99}$	B_2	7.67	0.00243
	$LuVO_{3.99}$	B_3	8.05	0
$LuVO_3$	$LuVO_{3.00}$	C	9.50—12.00[c]	0
V_2O_3	$V_2O_{3.00}$	D	9.98—12.00[c]	0
	$V_2O_{3.01}$	D_1	8.90	−0.00085
	$V_2O_{3.07}$	D_2	7.86	−0.0180
$Lu_2V_2O_7$	$Lu_2V_2O_{6.89}$	K	8.50	0
	$Lu_2V_2O_{6.95}$	K_1	8.05	0.0180
$Lu_7V_3O_{16}$	$Lu_7V_3O_{16.2}$	L	9.58	0
	$Lu_7V_3O_{16.3}$	L_1	8.50	−0.137
	$Lu_7V_3O_{16.4}$	L_2	8.05	−0.212
	$Lu_7V_3O_{16.4}$	L_3	7.50	−0.319
LuV_4O_8	$LuV_4O_{7.93}$	M	8.90	0
	$LuV_4O_{7.97}$	M_1	8.50	0.0109
	$LuV_4O_{8.01}$	M_2	8.05	0.0136
	$LuV_4O_{8.03}$	M_3	7.86	0.0116
	$LuV_4O_{8.05}$	M_4	7.67	0.00786

a) The stability range in $\log P_{O_2}$ may be higher than −0.68. b) This value was obtained by extrapolation by using the experimental values. c) The stability range in $\log P_{O_2}$ may be lower than −12.00.

stoichiometric composition, judging from the results of thermogravimetry. The relationship between the N_o/N_d and the $\log P_{O_2}$ of the solid solutions is obtained by using the results of the thermogravimetry and by the method of the least squares with the general quadratic equation; $N_o/N_d=a+b\log P_{O_2}+c(\log P_{O_2})^2$. Here, N_o/N_d indicates the deviation of the oxygen atoms from the stoichiometric compound d.[6] The factors used to obtain a, b, and c, for each solid solution are given in Table 2. As for the V_2O_3 solid solution, previous data[1] were used to obtain a, b, and c. In Table 3, the compositions, the stability ranges in the oxygen partial pressures, and the abbreviations of the compounds are tabulated. The deviations from the

Table 4. Spacing and relative intensities of $Lu_7V_3O_{16}$ and LuV_4O_8

$Lu_7V_3O_{16}$				LuV_4O_8			
d	I/I_0	d	I/I_0	d	I/I_0	d	I/I_0
5.702	20	1.7022	16	5.041	20	2.1656	49
5.106	7	1.6793	21	4.852	59	2.0805	20
4.234	3	1.6094	22	4.570	14	2.0459	20
3.501	3	1.5941	24	4.416	61	2.0412	20
3.397	4	1.5823	6	3.899	28	1.9912	11
3.347	2	1.5667	12	3.581	11	1.9544	10
3.164	100	1.5518	24	3.439	26	1.9418	12
3.021	97	1.5107	12	3.372	18	1.9063	14
2.996	26	1.4817	14	3.010	20	1.8801	11
2.855	46	1.4615	12	2.950	34	1.7913	41
2.669	34	1.4284	13	2.776	29	1.7554	20
2.5978	61	1.3633	8	2.670	24	1.7243	10
2.5534	17	1.3153	5	2.6505	67	1.7066	22
2.1869	20	1.2996	8	2.6208	100	1.6622	17
2.1186	19	1.2899	8	2.5923	22	1.6462	28
2.0737	12	1.2755	5	2.5429	18	1.5257	11
2.0188	7	1.2588	5	2.5068	20	1.5082	17
1.9227	50	1.2520	11	2.4787	12	1.4746	17
1.9014	21	1.2382	6	2.4349	39	1.4398	17
1.8330	7	1.2306	10	2.3650	11	1.4075	11
1.7801	26			2.3264	10	1.3931	14

stoichiometric composition of $LuVO_4$ extended up to $LuVO_{3.99}$ at $\log P_{O_2}=-8.05$. $Lu_2V_2O_7$ has the composition ranges from $Lu_2V_2O_{6.89}$ at $\log P_{O_2}=-8.50$ to $Lu_2V_2O_{6.95}$ at $\log P_{O_2}=-9.58$ to $Lu_7V_3O_{16.4}$ at $\log P_{O_2}=-7.50$, and LuV_4O_8 from $LuV_4O_{7.93}$ at $\log P_{O_2}=-8.90$ to $LuV_4O_{8.05}$ at $\log P_{O_2}=-7.67$.

The relative intensities, spacings, assignments of indices, and density of $Lu_2V_2O_7$ have already been reported.[10] Recently, Bazuev *et al.*[11] reported the existence of $Lu_2V_2O_7$. According to them, $Lu_2V_2O_7$ was prepared from a mixture of Lu_2O_3 and VO_2 using the ceramic technique and had a ferromagnetic property. The lattice constant, 9.932±0.001 Å, is in very good agreement with ours, 9.934±0.001 Å.

In this study, we did not succeed in assigning the indices for new compounds, $Lu_7V_3O_{16}$ and LuV_4O_8. The relative intensities and spacings are given in Table 4. The sample powders of $Lu_7V_3O_{16}$ and LuV_4O_8 which were used in the X-ray diffraction and in the measurement of the density were prepared at an oxygen partial pressure of $\log P_{O_2}=-8.30$ and for 72 h and 92 h heating respectively. The densities of $Lu_7V_3O_{16}$ and LuV_4O_8 were determined to be 8.63 and 6.66 g/cm^3 respectively, using the powder picnometric method; they are given in Table 5, together with the powder color. The values in the second column in Table 5 imply the oxygen partial pressures at which the samples were prepared.

Table 5. Densities and colors of new compounds

Compound	$-\log P_{O_2}$ (atm)	Density (g/cm^3)	Color
$Lu_7V_3O_{16}$	8.30	8.63	dark brown
$Lu_2V_2O_7$	8.30	7.64	black
LuV_4O_8	8.20	6.66	black

The lattice constants of $LuVO_4$ and $LuVO_3$ are given in Table 6, together with the previous data.[2,3,12] Both data are in good agreement with the previous data, and neither depends on the oxygen partial pressure at which the samples were prepared.

The results and discussion of the V–O system have been presented in a previous paper.[1]

Calculation of Standard Gibbs Engergies of Reactions.

On the basis of the phase equilibria, the standard Gibbs energies of reaction, referred to the equations in Table 7, can be calculated from the equation; $\Delta G^\circ=-RT\ln K$, where R is the gas constant; T the absolute temperature, and K the equilibrium constant of each reaction. The activity of each component, $LuVO_4$, V_2O_3, $Lu_2V_2O_7$, $Lu_7V_3O_{16}$, and LuV_4O_8, in each solid solution at the compositions of B_3, D, K, L, and M may be set equal to unity. The activity of each component in the solid solution can readily be calculated by means of the Gibbs-Duhem equation on the basis of the experimental results presented in Table 2. A detailed calculation method has been described in a paper of Kimizuka and Katsura.[13] Activities which are necessary to calculate the standard Gibbs energies of the reaction are listed in the fifth column in Table 3. As an example, we will calculate the standard Gibbs energy of the reaction

$$2Lu_2O_3 + 3LuVO_3 + 1/2O_2 = Lu_7V_3O_{16}. \quad (1)$$

The equilibrium constant of Reaction 1 is represented as follows:

$$K(1) = a_{Lu_7V_3O_{16}}/(a_{Lu_2O_3}\cdot a^3_{LuVO_3}\cdot P^{-1/2}_{O_2}) = P^{-1/2}_{O_2}.$$

Here, $a_{Lu_2O_3}$ and a_{LuVO_3} are unity and $a_{Lu_7V_3O_{16}}$ may

TABLE 6. UNIT-CELL DIMENSIONS OF $LuVO_4$ AND $LuVO_3$

Sample	$-\log P_{O_2}$	a(Å)	b(Å)	c(Å)	V(Å)[3]
$LuVO_4$	0.68	7.022±0.001		6.230±0.001	307.2±0.1
	7.00	7.024±0.001		6.230±0.001	307.4±0.1
		7.0243[12]		6.2316	
		7.025±0.002[3]		6.233±0.002	
$LuVO_3$	10.00	5.210±0.001	5.568±0.001	7.527±0.001	218.3±0.1
	12.00	5.212±0.001	5.565±0.001	7.526±0.001	218.3±0.1
		5.214±0.002[2]	5.561±0.002	7.530±0.002	218.3±0.05

TABLE 7. STANDARD GIBBS FREE ENERGIES OF REACTIONS

	Equation	$-\log P_{O_2}$ (atm)	$-\Delta G^\circ$ (kcal)
(1)	$2Lu_2O_3+3LuVO_3+1/2O_2=Lu_7V_3O_{16}$	9.58±0.02	32.3±0.1
(2)	$Lu_7V_3O_{16}+O_2=3LuVO_4+2Lu_2O_3$	7.50±0.10	52.8±0.8
(3)	$2LuVO_3+1/2O_2=Lu_2V_2O_7$	8.50±0.02	28.6±0.1
(4)	$Lu_2V_2O_7+1/2O_2=2LuVO_4$	8.05±0.02	27.0±0.1
(5)	$LuVO_3+1/2O_2=LuVO_4$		27.8±0.2
(6)	$2LuVO_3+3V_2O_3+1/2O_2=2LuV_4O_8$	8.90±0.10	29.8±0.4
(7)	$LuV_4O_8+1/2O_2=V_3O_5+LuVO_4$	7.67±0.02	25.8±0.1

be set as equal to unity, as has been described above. Using the above equation, $\Delta G^\circ=-RT\ln K=1/2\,P_{O_2}$, $\Delta G^\circ(1)=-32.3$ kcal/mol is obtained, where P_{O_2} implies the equilibrium oxygen partial pressure of Reaction 1. The standard Gibbs energies of reaction, referred to Eqs. 1 to 7, are summarized in Table 7. The values of Reaction 5 are obtained by using the values of Reactions 3 and 4.

References

1) K. Kitayama and T. Katsura, *Bull. Chem. Soc. Jpn.*, **50**, 889 (1977).
2) G. J. McCarthy, C. A. Sipe, and K. E. McIlvried, *Mater. Res. Bull.*, **9**, 1279 (1974).
3) H. Brusset, F. Madaule-Aubry, B. Blanck, J. P. Glaziou, and J. P. Laude, *Can. J. Chem.*, **49**, 3700 (1971).
4) T. Katsura, K. Kitayama, T. Sugihara, and N. Kimizuka, *Bull. Chem. Soc. Jpn.*, **48**, 1809 (1975).
5) T. Katsura and H. Hasegawa, *Bull. Chem. Soc. Jpn.*, **40**, 561 (1967).
6) N. Kimizuka and T. Katsura, *J. Solid State Chem.*, **13**, 176 (1975).
7) T. Katsura and A. Muan, *Trans. Soc. Min. Eng. AIME*, **230**, 77 (1964).
8) T. Sekine and T. Katsura, *J. Solid State Chem.*, **17**, 49 (1976).
9) L. S. Darken and R. W. Gurry, *J. Am. Chem. Soc.*, **67**, 1398 (1945).
10) K. Kitayama and T. Katsura, *Chem. Lett.*, **1976**, 815.
11) G. W. Bazuev, O. V. Makarova, V. Z. Oboldin, and G. P. Shveikin, *Dokl. Akad. Nauk SSSR*, **230**, 869 (1976).
12) X-Ray powder data, Card 17-880, A. S. T. M.
13) N. Kimizuka and T. Katsura, *J. Solid State Chem.*, **15**, 151 (1975).

Analysis of Tin Corrosion Products Using Conversion Electron Mössbauer Spectroscopy, Transmission Mössbauer Spectroscopy, and X-Ray Diffractometry

Mamoru SHIBUYA, Kazutoyo ENDO, and Hirotoshi SANO

Department of Chemistry, Faculty of Science, Tokyo Metropolitan University, Fukazawa, Setagaya, Tokyo 158

(Received September 2, 1977)

Tin plates corroded by various acids were nondestructively analyzed by a ^{119}Sn conversion electron Mössbauer spectroscopy, a transmission Mössbauer spectroscopy, and an X-ray diffractometry. The conversion electron method was shown to be useful for analysis of some corrosion products which could not be easily observed by the transmission method. By using both the Mössbauer spectroscopy and the X-ray diffractometry, the corrosion products formed by 6.7M-HNO_3, 5.7M-HCl, and 9.0M-H_2SO_4 were determined to be $SnO_2 \cdot nH_2O$, $Sn_4(OH)_6Cl_2$, and $SnSO_4$, respectively.

Since Swanson and Spijkerman reported Mössbauer spectra of thin foil of ^{57}Fe by a conversion electron method,[1] the potential of this technique has been explored and its practical use has been recognized in such investigations as oxidation products,[2-4] corrosion products,[5] ion implantations,[6-8] and metallurgy.[9] The measurement is performed by detecting conversion electrons and Auger electrons. Although a transmission measurement gives information on the total bulk of a sample, the method has the restriction that the sample should be thin. However, the conversion electron method can provide information on the surface layers of a bulky sample because of the limited penetration range of the electrons. In a thick sample, which can be neither destroyed nor transformed in shape, most Mössbauer spectroscopic analyses have been so far made in a reflection geometry by detecting the scattered X- or γ-rays associated with the resonance of nuclei.[10,11] However, the conversion electron method is available for analysis of the chemical compositions and structures in thinner surface layers than can be studied with the scattered X- or γ-ray methods.

In the present paper, we describe the systematic studies of tin metals corroded by a variety of acids by means of the conversion electron method and the transmission method. An X-ray diffractometry was also applied to complement the Mössbauer spectroscopic analysis. Model compounds were synthesized in separate experiments in order to identify the corroded products.

Experimental

In order to detect conversion electrons, we constructed a gas-flow type proportional counter, which is essentially the same as that designed by Swanson and Spijkerman.[1] Our counter is made of a 2 mm thick brass plate and is rectangular in shape, $15 \times 20 \times 15$ cm^3. The anode consists of two tungsten wires of 0.00254 cm diameter which are 7.5 cm apart from each other and symmetrically located with respect to the centerline. The top plate is removable to facilitate placing the sample inside the counter and varying the number and the location of the anode wires.

Conversion electron Mössbauer spectra were determined at room temperature by placing a sample inside the counter. During accumulation of the spectra the anode was kept at a positive potential of 1370V with respect to the grounded brass plate and a helium-methane gas(*e.g.* Q gas) was passed through the counter at the flow-rate of *ca.* 10 cm^3/min. Transmission spectra were recorded by using a NaI(Tl) scintillation counter mounted behind the proportional counter. Both the Mössbauer spectra were measured against a 2 mCi $Ca^{119m}SnO_3$ source moving in a constant acceleration mode at room temperature. X-Ray diffraction data were obtained by using Rigakudenki No. 2001.

Samples studied were prepared by corroding 1 mm thick tin plates in various acid solutions at room temperature and by drying them at room temperature.

Results and Discussion

Mössbauer Spectra. Figure 1 shows Mössbauer spectra of a tin plate corroded by 6.7M-HNO_3 for 5 min. A transmission spectrum (a) gives two peaks, the isomer shift(I. S.) values of which are 0.00 mm/s and 2.56 mm/s with respect to calcium stannate. A conversion electron spectrum (b) consists of only one peak, which corresponds to the less intense line observed in the transmission spectrum. The main peak found in the transmission spectrum is assigned to β-Sn from its peak position. The peak of 0.00 mm/s isomer shift is assigned to the corrosion species formed on the tin

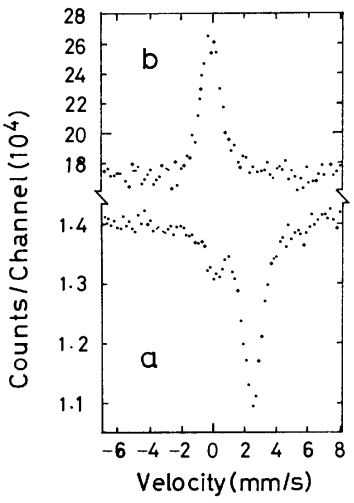

Fig. 1. Mössbauer spectra of a tin plate corroded by 6.7 M-HNO_3 for 5 min. a) Transmission spectrum, b) conversion electron spectrum.

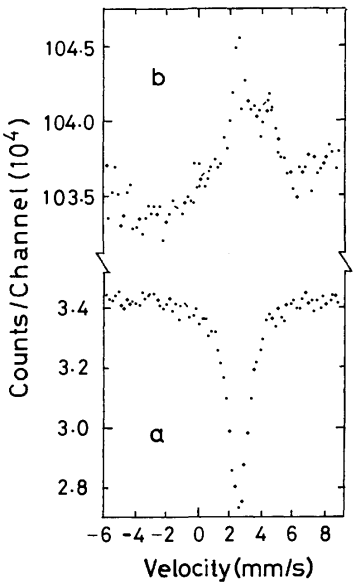

Fig. 2. Mössbauer spectra of a tin plate corroded by 5.7 M-HCl for 6.5 h. a) Transmission spectrum, b) conversion electron spectrum.

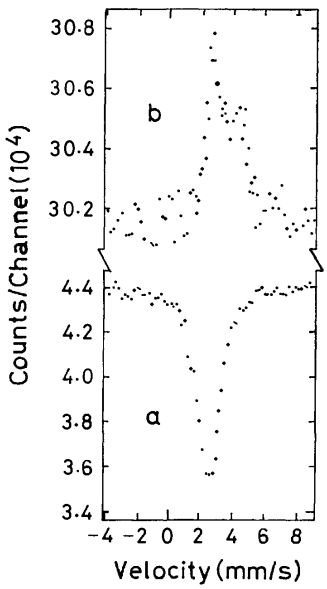

Fig. 3. Mössbauer spectra of a tin plate corroded by 9.0 M-H_2SO_4 for 3.8 d. a) Transmission spectrum, b) conversion electron spectrum.

plate surface by reacting with 6.7M-HNO_3 because the spectrum of an uncorroded tin plate reveals only one peak, with the I. S. value of 2.56 mm/s.

Mössbauer spectra obtained from a tin plate corroded by 5.7M-HCl for 6.5 h are shown in Fig. 2. The transmission spectrum(a) gives a single peak assigned to β-Sn. The conversion electron spectrum(b) shows two peaks, the I. S. values of which are 4.44 mm/s and 2.56 mm/s; the latter peak has a shoulder at the I. S. value of nearly 0.00 mm/s.

As seen in Fig. 3, the transmission spectrum(a) of a tin plate corroded by 9.0M-H_2SO_4 for 3.8 d consists of a single peak, while the conversion electron Mössbauer spectrum(b) gives another peak around 4.40 mm/s.

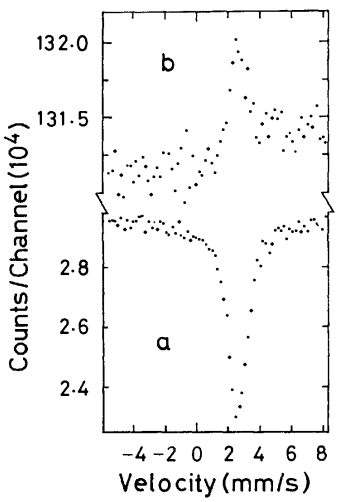

Fig. 4. Mössbauer spectra of a tin plate corroded by 27.0 M-HF for 6.2 d. a) Transmission spectrum, b) conversion electron spectrum.

The conversion electron spectrum of a tin plate corroded by 27.0M-HF for 6.2 d (Fig. 4 b) shows an intensive peak corresponding to β-Sn; no other peak can be clearly observed.

Thickness of Corrosion Layers. It was found from the experimental results that the line width of the substrate observed for the scattered electron is narrower than that for the γ-ray transmission method. For example, the comparsion of the β-Sn peaks observed in the two detection methods for the sample treated by sulfuric acid shows that the line width (fwhm) is 0.85 mm/s for the scattered electron method and 1.56 mm/s for the transmission method. This narrowing is quantitatively explained in terms of the decreased range of the electrons in the substrate, β-Sn. The electrons emitted from the substrate, β-Sn, are scattered through the corroded layers. If the corrosion layers exceed the effective range of the scattered electrons, the peak assinged to the substrate cannot be observed in the conversion electron spectrum. Therefore, it is concluded that corrosion layers for the sample treated by nitric acid nearly exceed the effective range of the conversion electrons. In order to determine the thickness of the corrosion layers, we estimated the effective range of the resonantly scattered electrons from ^{119}Sn for typical inorganic compounds; SnO_2, $CaSnO_3$, and $BaSnO_3$. The line width of a γ-ray transmission spectrum is proportional to an effective thikness, T, which is represented as

$$T = n\sigma tf. \quad (1)$$

Here n is the concentration of ^{119}Sn atoms in a unit volume; σ, the resonance cross-section; t, the absorber thickness; and f, the recoilless fraction. The experimental line width increases linearly with the increase in the concentration of the resonance atoms. In a previous communication, we demonstrated that the relation between the experimental line width and the effective thickness for γ-rays can be roughly applicable to the scattered electron method.[12] The

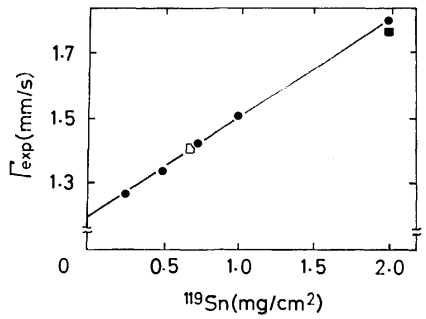

Fig. 5. Experimental line width *vs.* the apparent thickness of ^{119}Sn for SnO_2 by γ-ray transmission method (●). The line width observed by the scattered electron method (□) for the same sample as those by the γ-ray transmission method (■).

thickness dependence of the experimental line width in the γ-ray transmission method is shown in Fig. 5, together with the experimental line width obtained for the scattered electron method. For SnO_2 of 2.0 mg $^{119}Sn/cm^2$, the line width found in the γ-ray transimssion method is 1.79 mm/s and that found in the scattered electron method is 1.41 mm/s. The apparent thickness for the electron method obtained graphically from Fig. 5 is 0.72 mg/cm^2 in SnO_2. The value of apparent thickness for each sample is shown in the second column on Table 1. Electrons interact with surrounding atoms and ionize them during their passages. The Bethe's approximated equation concerning the energy loss of electrons shows that the stopping power of materials for electrons is proportional to the atomic number(Z) and inversely to the atomic weight(A) of the interacting atom. By assuming that the value of Z/A is nearly constant for each element concerned, the apparent effective thickness obtained from Fig. 5 is listed in the third column of Table 1. The values are in good agreement with each other, and do not depend on the kind of compounds with which the electrons interact. In the comparison of the line width of the scattered electron spectra with those of the γ-ray transmission spectra, it is found that the apparent cross-section is not identical for the two different kinds of detection methods. The apparent cross-section for emission of conversion electrons is approximately greater than that of γ-ray radiations by a conversion coefficient, α. The values shown in the third column in Table 1 must be divided by the conversion coefficient, 5.12, since the values were taken from the γ-ray transmission method. The value 2.21+0.38 mg/cm^2 is estimated for the effective range of scattered electrons of ^{119}Sn. Auger electrons are also emitted as a result of the deexcitation of ^{119}Sn atoms, and these electrons will enhance the intensity of the conversion electron Mössbauer spectrum. Moreover, Tricker *et al.* pointed out that non-Mössbauer atoms (chromium or aluminium) enhanced the intensity of a Mössbauer spectrum when these atoms were evaporated on iron foil.[13] They concluded that electrons were emitted from the chromium or aluminium atoms by the X-rays which accompany the Mossbauer effect. Although the effects on the line width of the spectrum remain unsolved, the contribution may be assumed to be small.

Table 1. The effective ranges determined for the resonantly scattered electrons in tin compounds

Compound	^{119}Sn(mg/cm^2)	$\frac{100}{A}\cdot\frac{M}{m}$(mg/cm^2)
SnO_2	0.72±0.06	10.65±0.89
$CaSnO_3$	0.63±0.12	12.79±2.44
$BaSnO_3$	0.36±0.07	10.45±2.09
	Mean value :	11.30±1.81

X-Ray Diffraction Analysis. X-Ray diffractometry is a useful method for assignment of chemical species of a solid sample. In order to compare the characteristics of the X-ray diffractometry with the conversion electron Mössbauer spectroscopy for the corrosion sample, we examined the results obtained by using both these detection methods. For the purpose of the identification of corrosion products, we synthesized the chemically pure tin compounds which can be attributed to the corroded products based on the conversion electron Mössbauer spectroscopy, and measured their X-ray diffraction and transmission Mössbauer spectrum.

The Mössbauer data of the corrosion species produced by nitric acid indicate the presence of tin(IV) species similar to SnO_2. It is also known that a metallic tin plate reacts with diluted nitric acid to form metastannic acid, $SnO_2\cdot nH_2O$. The compound was prepared by according to the procedure of Weiser and Milligan,[14] and was checked by the X-ray diffractometry (see Fig. 7). We found good agreement between the pattern of the prepared sample and that of the tin plate corroded by 6.7M-nitric acid for 5.0 min, although those

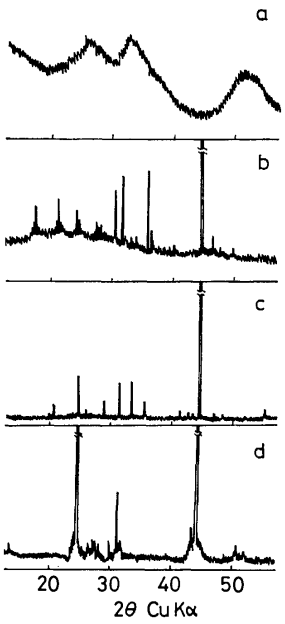

Fig. 6. X-Ray diffraction patterns. a) A tin plate corroded by 6.7 M-HNO_3 for 5 min, b) a tin plate corroded by 5.7 M-HCl for 6.5 h, c) a tin plate corroded by 9.0 M-H_2SO_4 for 3.8 d, d) a tin plate corroded by 27.0 M-HF for 6.2 d.

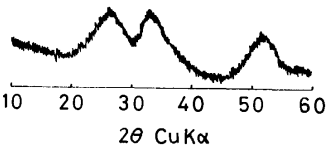

Fig. 7. X-Ray diffraction pattern of metastannic acid.

patterns are very broad, indicating an amorphous state. Transmission Mössbauer spectrum gives the I. S. value of 0.00 mm/s at room temperature for both samples. These results indicate the formation of metastannic acid, $SnO_2 \cdot nH_2O$, on the tin plate treated by 6.7M-nitric acid.

Mössbauer data of the tin plate corroded by 5.7M-hydrochloric acid for 6.5 h indicate a presence of Sn(II) and Sn(IV) corroded species. The X-ray diffraction pattern consists of many sharp lines and a broad line ranging from 20 to 35 deg. In order to identify the corroded products, the X-ray diffraction data were compared with those of Sn(II) compounds such as $SnCl_2$, $SnCl_2 \cdot 2H_2O$, and $Sn_4(OH)_6Cl_2$, and with $SnCl_4 \cdot 5H_2O$. X-Ray diffraction data of $Sn_4(OH)_6Cl_2$ agree the best with those of the corroded sample, as shown in Table 2. Since the Mössbauer parameters have not been reported for the compound, we prepared it by the procedure of Donaldson *et al.*[15] and accumulated the transmission spectrum at room temperature. The I. S. value and the quadrupole splitting (Q. S.) value are found to be 3.76 mm/s and 0.76 mm/s, respectively. The values are in good agreement with those of the corroded product found in a conversion electron spectrum. The conversion electron Mössbauer spectrum shows the presence of Sn(IV)

TABLE 2. X-RAY DIFFRACTION ANALYSIS OF A TIN PLATE CORRODED BY 5.7 M-HCl FOR 6.5 h

Sample 2		β-Sn[a]		$Sn_4(OH)_6Cl_2$[a]		Sample 2		β-Sn[a]		$Sn_4(OH)_6Cl_2$[a]	
d(Å)	I/I_0	d(Å)	I/I_0	d(Å)	I/I_0	d(Å)	I/I_0	d(Å)	I/I_0	d(Å)	I/I_0
1.67	37	1.659	17	1.675	30	2.71	30			2.70	20
1.83	22			1.828	50	2.82	72	2.793	90	2.82	80
1.91	20			1.893	30					2.85	80
1.90						2.93	63	2.92	100	2.90	40
				1.923	30					3.09	60
				1.937	40	3.18	36			3.18	20
1.96	30			1.969	20	3.27	40				
2.03	100	2.017	74	2.02	20	3.24				3.24	30
				2.14	40	3.45	35				
2.22	19			2.20	20	3.49				3.50	30
2.25	23			2.24	30	3.65	46				
2.29	23			2.28	30	3.71				3.64	30
				2.30	30					4.04	40
2.39	22			2.40	20	4.21	56			4.18	80
2.50	30			2.50	100					4.75	30
2.55	75			2.55	90					4.89	20
2.65	30			2.63	50	5.07	50			5.09	30
				2.64							

a) JCPDS data.

TABLE 3. X-RAY DIFFRACTION ANALYSIS OF A TIN PLATE CORRODED BY 9.0 M-H_2SO_4 FOR 3.8 d

Sample 3		β-Sn[a]		$SnSO_4$[a]		Sample 3		β-Sn[a]		$SnSO_4$[a]	
d(Å)	I/I_0	d(Å)	I/I_0	d(Å)	I/I_0	d(Å)	I/I_0	d(Å)	I/I_0	d(Å)	I/I_0
1.45	39	1.458	13			2.46	7			2.454	18
1.49	21	1.484	23			2.68	8			2.660	25
1.66	8					2.82	28	2.79	90		
1.67	10	1.659	17			2.93	15	2.92	100		
1.76	52			1.743	12	3.09	16			3.06	100
				1.735		3.34	8				
1.94	8					3.43	10				
2.04	100	2.017	74			3.57	33			3.55	50
2.08	7			2.089	50	4.28	14			4.25	30
2.10	7			2.101	50	4.42	9			4.39	25
2.14	6			2.130	12						
2.17	9			2.168	25						
2.18											

a) JCPDS data.

species with weak intensity in addition to the main peak of $Sn_4(OH)_6Cl_2$; the X-ray diffraction pattern also indicates the presence of amorphous species which may be ascribed to tin(IV) species produced on the tin plate. These observations lead us to the conclusion that $Sn_4(OH)_6Cl_2$ is the main product and some tin-(IV) species are produced on a tin plate treated by 5.7M-HCl.

Mössbauer spectra of the tin plate corroded by 9.0M-sulfuric acid for 3.8 d indicate the presence of Sn(II) compound. The X-ray diffraction data were compared with those of Sn(II) compound, as mentioned for the sample corroded by hydrochloric acid. The data of $SnSO_4$ are in good agreement with those of the tin plate corroded by 9.0M-sulfuric acid for 3.8 d (Table 3). The values of I. S. and Q. S. of $SnSO_4$ at room temperature are 3.98 mm/s and 0.95 mm/s, respectively. These values are in good agreement with those of the corroded species. The results indicate the formation of $SnSO_4$ of the tin plate corroded by 9.0M-sulfuric acid.

In the case of the sample corroded by 27.0M-hydrofluoric acid for 6.2 d, the conversion electron Mössbauer spectrum gives no definite peaks, the transmission spectrum gives only the β-Sn peak, and the X-ray diffraction pattern of the sample does not agree with any of the JCPDS data available for tin fluoride compounds.

The present results indicate the following conclusion: In order to determine the thin corrosion products formed on a metal surface, the observed peaks of X-ray diffraction pattern are so weak, as shown in Fig. 6, that the identification of the products is tedious and difficult. The transmission Mössbauer technique gives only the spectrum of the major substrate in a limited time of accumulation of the spectrum. The conversion electron Mössbauer technique, on the other hand, provides information concerning the chemical state of the products through the isomer shift and quadrupole splitting. Although the complete chemical form of the corroded products may not be determined, the conversion electron Mössbauer technique makes it very easy to cross-assign the weak peaks of the X-ray diffractometry to the possible chemical species.

References

1) K. R. Swanson and J. J. Spijkerman, *J. Appl. Phys.*, **41**, 3155 (1970).
2) G. W. Simmons, E. Kellerman, and H. Leidheiser, Jr., *Corrosion*, **29**, 227 (1973).
3) J. M. Thomas, M. J. Tricker, and A. P. Winterbottom, *J. Chem. Soc., Faraday Trans. 2*, **1975**, 1708.
4) M. J. Tricker, A. P. Winterbottom, and A. G. Freeman, *J. Chem. Soc., Dalton Trans.*, **1976**, 1289.
5) J. R. Gancedo, M. L. Martinez, and J. M. Oton, *J. Phys. (Paris), Colloq.*, **C6**, 297 (1976).
6) J. Stanek, J. Sawicki, and B. Sawicka, *Nucl. Instrum. Methods*, **130**, 613 (1975).
7) B. D. Sawicka, J. Sawicki, and J. Stanek, *J. Phys. (Paris), Colloq.*, **C6**, 879 (1976).
8) B. D. Sawicka, J. Sawicki, and J. Stanek, *Phys. Lett. A*, **59**, 1 (1976).
9) R. Oswald and M. Ohring, *J. Vac. Sci. Technol.*, **13**, 40 (1976).
10) C. L. Herzenberg and D. L. Riley, *Science*, **167**, 683 (1970).
11) W. Meisel, *Werkst. Korros.*, **21**, 249 (1970).
12) K. Endo, M. Shibuya, and H. Sano, *Radiochem. Radioanal. Lett.*, **28**, 363 (1977).
13) M. J. Tricker, L. A. Ash, and T. E. Cranshaw, *Nucl. Instrum. Methods*, **143**, 307 (1977).
14) H. W. Weiser and W. O. Milligan, *J. Phys. Chem.*, **36**, 3030 (1932).
15) J. D. Donaldson, W. Moser, and W. B. Simpson. *J. Chem. Soc. London*, **1963**, 1723.

Equilibrium Study of the Fe–V–S System by Thermogravimetry

Hiroaki WADA

National Institute for Researches in Inorganic Materials, Kurakake, Sakura-Mura, Niihari-Gun, Ibaraki 300-31

(Received September 7, 1977)

An equilibrium study of the Fe–V–S system was carried out in the range of $\log(P_{S_2}/\text{atm}) = -4$ to -0.8 at temperatures between 723 and 1093 K. The gravimetric method was employed by making use of a quartz spring balance. The partial pressure of sulfur was controlled in an N_2–sulfur vapor system by temperature regulation. The partial pressure of S_2 was calculated from the thermodynamic data, taking account of the existence of different molecular species: S_2 through S_8. Three kinds of ternary sulfides with different Fe/V ratios were used as starting material. The P_{S_2}-T-X relation was established through *in situ* measurements at high temperatures. It was found that the Fe–V–S system has an extensive ternary solid solution with the NiAs type of fundamental structure.

The compounds in the Fe–V–S system have not received much attention in the past, because they seem to occur in nature rather infrequently. Only the synthetic FeV_2S_4 compound, which is related to the ternary transition metal chalcogenides MM'_2S_4(M=Fe, Co,Ni; M′=Ti,V; X=S,Se), has recently been studied by solid state physicists, who reported its structural, magnetic and electrical properties.[1-4] However, very few studies have been published on the thermochemical aspects needed to determine the ternary phase relations in the Fe–V–S system.

Much information has now been obtained on the phase relations and crystal structures in the binary systems Fe–S[5] and V–S.[6] Vanadium sulfides, where the sulfur atoms are in hexagonal close packing, form the B8 (NiAs-type) structure at the composition VS, and the C6 ($Cd(OH)_2$-type) structure at VS_2. Within the composition limits VS–VS_2, structures intermediate between the B8 and C6 types are formed due to the removal of metal atoms from every second metal layer in the B8 structure. At lower temperatures, the vanadium vacancies are ordered within alternate metal layers, giving rise to ordered superstructures such as monoclinic V_3S_4(nonreduced space group I2/m referred to the fundamental NiAs-type cell) and monoclinic V_5S_8 (nonreduced space group F2/m).[7] With increasing temperature, the homogeneity ranges within those structures tend to be broadened. On the other hand, iron sulfides do not show the complete transition between the B8 and C6 structure types. The composition Fe_7S_8 is the stable limit of the B8 structure in the Fe–S system. When the number of metal vacancies increases beyond that in Fe_7S_8, a different structure type, such as cubic FeS_2(space group Pa3), becomes stable.

Accordingly, it is expected that the Fe–V–S system contains complicated ternary solid solutions based on the NiAs-type fundamental structure. In the solid solution, one end member is iron sulfide, FeS_x (NiAs-type) in the compositional range FeS–Fe_7S_8, while the other is one of the vanadium sulfides, such as VS_x (NiAs-type) in the compositional range VS–V_7S_8, V_3S_4 (distorted NiAs-type), or V_5S_8 (distorted NiAs-type). In order to clarify the behavior of ternary sulfides of the Fe–V–S system, it is important to determine in detail at high temperatures the phase relations and the compositional stability of the ternary solid solutions included in the system. Thus, the purpose of the present investigation was to establish the equilibrium diagrams of the sulfur-rich portion of the Fe–V–S system from the thermochemical viewpoint.

The equilibrium study was carried out mainly with a gravimetric method by making use of a quartz spring balance at 773—1093 K. The partial pressure of sulfur was controlled in an N_2–sulfur vapor system only by temperature regulation. The present paper is concerned with the calculation of the partial pressure of S_2 at specimen temperature in the employed experimental system and the P_{S_2} (equilibrium sulfur pressure)-T (temperature)-X (composition) relations of the Fe–V–S system at high temperatures.

Experimental

Materials. Reagent grade $VOSO_4 \cdot 3H_2O$ was mixed in ethanol with a reagent grade $FeSO_4 \cdot (NH_4)_2SO_4 \cdot 6H_2O$ in an agate mortar in desired quantitites. The mixture was dried, put in a quartz boat, and heated in an H_2S atmosphere at 1323 K for 4 h. The sulfide powder thus synthesized was quenched to room temperature and was used as the starting material. Prior to the experiments, the composition of the powder samples was determined by colorimetric methods for vanadium and ion and by weight-loss on oxidation to $xFe_2O_3 \cdot yV_2O_5$ at 873 K for sulfur. Fe/(Fe+V) ratios of the synthesized sulfides were in good agreement with those of mechanical mixtures of source materials within the accuracy of $\pm 0.5\%$. The over-all errors involved in the chemical analysis were $\pm 0.2\%$ by weight.

Sulfur Pressure Control. A direct sulfur pressure control method was employed in the equilibrium studies. The principal procedure is similar to that described by Wakihara *et al.*[8] The apparatus used for the equilibrium runs is shown schematically in Fig. 1. All this apparatus was constructed of quartz glass. The heating system was divided into five parts in order to keep each portion of the apparatus at the desired temperature. Nichrome wire (0.8 and 0.45 mm) and Pt–40%Rh wire (0.8 mm) were wound directly outside the quartz assembly as shown in Fig. 1 and fixed with an alumina cement. The temperatures of five portions of the system were controlled by chromel-alumel thermocouples.

Five hundred grams of guaranteed reagent grade sulfur was kept in the round-bottom reservoir A (2 dm^3). After passing nitrogen gas through the apparatus for 12 h, the sulfur was heated at 673 K and changed to the molten state by means of the heating mantle. Prior to use, the nitrogen gas was purifired by means of an MCN-005 type gas purifier

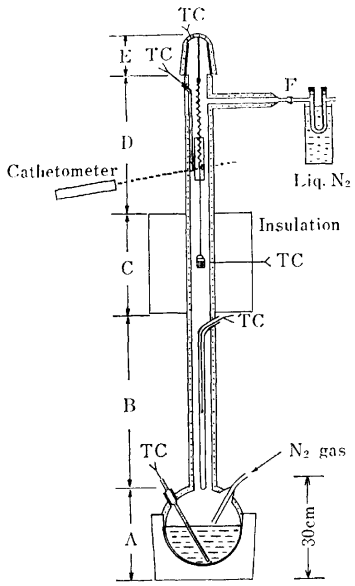

Fig. 1. Schematic diagram of apparatus.
Heating systems. A: The round-bottom reservoir is heated by means of heating mantle. B: Nichrome wire (0.8 mm) is used for a winding to maintain the minimum temperature zone over the central portion of B. C: The reaction chamber is wound with Pt-40%Rh wire coil (0.8 mm). The uncertainty in temperature is within ±3 K. D: The spring chamber is wound with Nichrome wire coil (0.45 mm). E: The cap is wound with Nichrome wire coil (0.8 mm). TC: Chromel-alumel thermocouples.

(Japan Pure Hydrogen Co.) in order to remove oxygen and water impurities. The saturated sulfur vapor over the molten sulfur was transported to the upper part of the apparatus by nitrogen gas at a constant rate (2 cm^3 of N_2/s). The central zone (width: 10 cm) of part B was held at the minimum temperature in all this apparatus so that the transported sulfur vapor from the reservoir became supersaturated and excess sulfur was condensed at this zone. Only the sulfur vapor which equilibriated at the minimum temperature zone was carried to the reaction chamber C. Thus, a desired partial pressure of sulfur was obtained by controlling the temperature within ±0.5 K at the minimum temperature zone. The upper portions, D and E, were also heated at higher temperatures than that of the minimum temperature zone so as to avoid any condensation of sulfur in the course of passing the atmosphere. At the outlet, F, sulfur was collected into a U-tube cooled by liquid nitrogen, and the weight of sulfur was measured for the calculation of partial pressure of S_2.

Thermogravimetry. For study of equilibrium experiments, a gravimetric method was employed, in which the elongation of a McBain balance could be followed by means of a cathetometer. The spring balance manufactured from a quartz glass fiber has the sensitivity of 67 mm per g weight at room temperature. The balance was suspended from a solid hook of a quartz rod in the center of the cap E. About 1 g of sulfide powder sample was placed in a quartz crucible (diameter: 16 mm, length: 16 mm, and weight: 280 mg) suspended from the top of the spring by strands of thin gold wire (0.2 mm). The length of the wire was adjusted in order that the crucible might be situated in the middle of the reaction chamber C. In order to observe the target visually, the spring chamber D was equipped with a transparent window (12×2.5 cm), which was not covered by the cement. A fluorescent lamp gave illumination from the rear side of the window. By making use of a quartz reference rod, the elongation of the spring was measured with the aid of a travelling microscope. The error in composition of sulfide specimens was estimated to be ±0.002 or sulfur to metal ratios, because the weighing could be read accurately to 0.2 mg, which corresponded to 0.001 cm of the smallest scale division.

Equilibrium was judged to be attained when the sample weight was constant. For log P_{S_2} of −2 and above, three hours were sufficient to attain equilibrium. For log P_{S_2} less than −3, twelve hours were found to be sufficient. The composition of the sulfide was calculated from the weight loss of the sample, assuming iron and vanadium to be involatile.

Besides the measurements described above, some supplemental experiments were carried out in order to examine the X-ray powder diffraction patterns of sulfides. A sample was placed in the crucible suspended from the cap E with a long platinum wire (0.2 mm) into the apparatus. After equilibrium was attained, the crucible was lifted up to the upper portion of the apparatus, taken out, and quenched in liquid nitrogen. Sulfides thus obtained were identified by using an X-ray diffractometer set up for Ni-filtered CuK_α radiation. The measurement was carried out at a goniometer scanning speed of 0.5° min^{-1}.

Results and Discussion

Calculation of Partial Pressure of S_2. The experimental results of the sulfur pressure measurements, in terms of the weight of collected sulfur at F, are presented in Table 1. The relationship between the weight of sulfur transported by unit volume of nitrogen and the temperature of the minimum temperature zone is given very well by the following formula (least squares treatment): $\log (w/mg\,dm^{-3}) = -3787\frac{1}{T/K} + 9.281$. This linear relationship indicates that the sulfur pressure was controlled precisely by the temperature regulation at the minimum temperature zone in the selected experimental system.

According to Rau *et al.*,[9] sulfur vapor contains molecular species from S_2 to S_8 at high temperatures below 1173 K. Therefore, it is necessary to calculate the partial pressure S_2 while considering the equilibrium between the different molecular species from S_2 to S_8.

Table 1. Relationships between the mass flow rate of sulfur and the temperature of the minimum temperature zone

Temperature (K)	Mass flow rate of sulfur (mg/dm^3 of N_2)
403	0.763
424	2.164
426	2.653
471	16.907
505	61.753
536	164.360
567	398.730

The partial pressure of S_2 at the specimen temperature was computed in the following way from the thermodynamic data of Rau *et al.* Assumptions were made that the sulfur vapor behaved ideally as a perfect gas and that a steady state of mass flow was set up in the experimental system. Then, P_{S_2} is given by the following equation:

$$P_{S_2} = \frac{m_2}{n + \sum_{i=2}^{8} m_i}, \quad (1)$$

where m_i and n are the number of moles of the sulfur vapor species S_i and of nitrogen, respectively, in the mass flow of gas for a given time interval t. A perfect gas obeys the following relations:

$$PV = (n + m_2 + m_3 + \cdots + m_8)RT, \quad (2)$$

and

$$P_{S_i} = m_i RT. \quad (3)$$

Substituting for m_i from Eq. 3 into Eq. 1, and rearranging, we obtain the following equation:

$$1 - \sum_{i=2}^{8} P_{S_i} = \frac{32.064\,n}{W} \sum_{i=2}^{8} iP_{S_i}, \quad (4)$$

where W represents the total amount of sulfur collected at the outlet within a time interval t. The equilibria connecting the various molecular species with S_2

$$S_i = (i/2)S_2 \quad (5)$$

are given by the equilibrium constant K_i

$$K_i = P_{S_2}^{i/2}/P_{S_i}. \quad (6)$$

Therefore, substitution of values of the equilibrium constant K_i into Eq. 4 through Eq. 6 yields the following expression as a function of P_{S_2}:

$$(2A+1)X^2 + \sum_{i=3}^{8} \frac{iA+1}{K_{S_i}} X^i - 1 = 0, \quad (7)$$

where $A = \frac{32.064n}{W}$ and $X = P_{S_2}^{1/2}$. Prior to the calculation of P_{S_2}, the equilibrium constant K_i was computed from the thermodynamic data of Rau *et al.* According to Eq. 7, the partial pressures of S_2, which were in equilibrium with the specimens, were calculated in the iterative Newton method from the data in Table 1. The physically meaningful value for P_{S_2} was selected. Values of log P_{S_2} are drawn in Fig. 2 as a function of the temperature at the minimum temperature zone with the specimen temperature as a parameter. The results for each given series are tied together by a smooth curve, which shows that the logarithmic values of P_{S_2} ranged from -4 to -0.8, corresponding to the change of temperature from 373 to 573 K. The uncertainty of log P_{S_2} was estimated to be ± 0.02 or less throughout the experimental range. From those smooth curves, the correction of P_{S_2} for specimen temperature could be made with sufficient accuracy. It will be seen that for specimen temperatures below 1000 K and also for values of log P_{S_2} higher than -2, the correction is not negligible.

Composition vs. P_{S_2} *Diagrams in the Fe–V–S System.* Representative selections of ternary sulfides in the Fe–V–S system (Fe/(Fe+V) mole ratios=0.05, 0.26, 0.35,

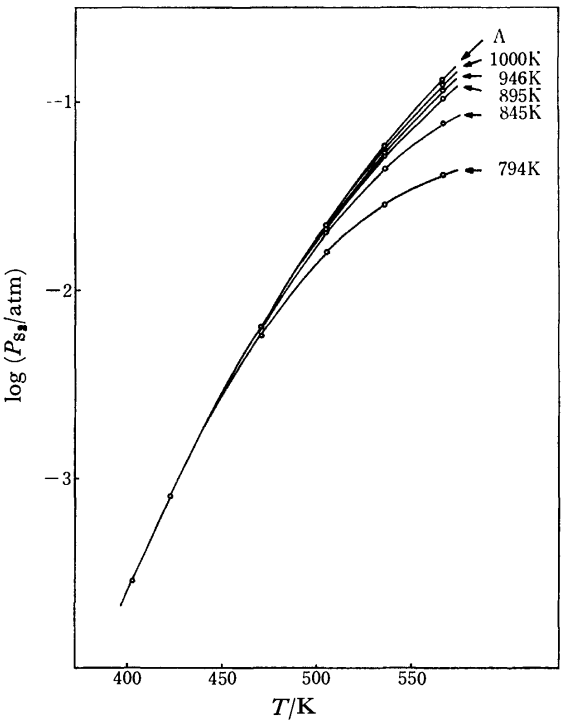

Fig. 2. Log P_{S_2} curve as a function of the temperature at the minimum temperature zone with the specimen temperature as a parameter.
A: Theoretical value, which is deduced from calculation of P_{S_2} on the basis of the assumption that sulfur vapor consists of only S_2 species.

respectively) have been subjected to an equilibrium study by the thermogravimetry. The experimental results of the investigation are shown graphically in Figs. 3—5. The isotherms drawn in Figs. 3—5 give the variation of equilibrium sulfur pressure P_{S_2} in relation to the composition of sulfides. The abscissa and ordinate are sulfur to metal ratio (S/(Fe+V)=X) and log P_{S_2}, respectively. Also, the phases as revealed by X-ray diffraction of the quenched specimens are given in the figures together with those judged from results of *in situ* measurements.

Figure 3 shows isotherms of the ternary sulfide with composition $Fe_{0.05}V_{0.95}S_x$. The composition covered between $Fe_{0.05}V_{0.95}S_{1.33}$ and $Fe_{0.05}V_{0.95}S_{1.60}$. Two discontinuities are found in the composition-P_{S_2} diagrams for 895 K in this region. One is in the range d—e ($1.45 \leqq X \leqq 1.46$), and the other in the range f—g ($1.55 \leqq X \leqq 1.56$). The horizontal isotherm described above represents a two-phase equilibrium. It becomes narrower and eventually vanishes with increasing temperature.

From Fig. 3, it is evident that the specimens at 895 K contain three phases: A, B, C. The tangent to the isothermal curves approaches gradually to a vertical line at the specific compositions of a ($X=1.33$) and c ($X=1.60$) in the phase A and C regions, respectively. At the same time, the sulfur pressure changes rapidly. Judging from this feature of the isotherms, it can be suggested that the A and C phases correspond to (Fe+V) : S=3 : 4 and (Fe+V) : S=5 : 8 phases, respectively. The sulfur-rich limit of the former extends to the com-

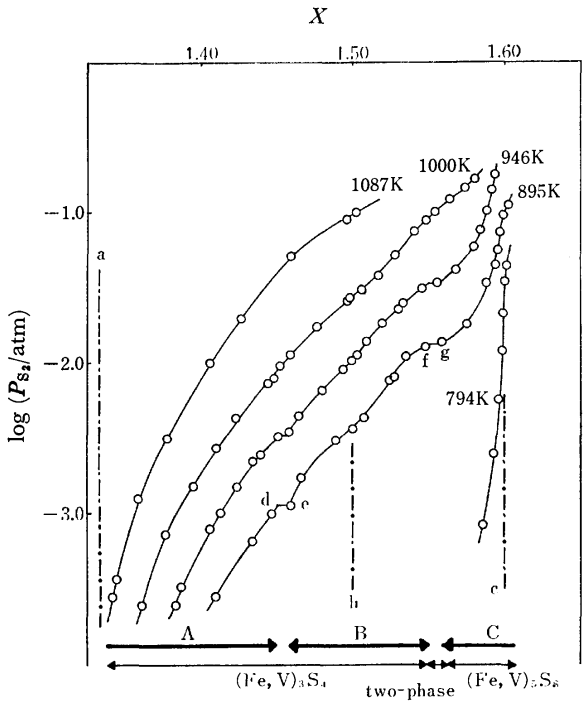

Fig. 3. P_{S_2}-composition (S/(Fe+V)=X) isotherms of $Fe_{0.05}V_{0.95}S_x$. Results of powder phase identifications are shown in lower part of figure together with results of phase identifications by thermogravimetry.
a: $(Fe_{0.05}V_{0.95})_3S_4$, b: $(Fe_{0.05}V_{0.95})_2S_3$,
c: $(Fe_{0.05}V_{0.95})_5S_8$.

position of X=1.45 and the metal-rich limit of the latter to X=1.56, where the isotherm becomes horizontal at 895 K. Within the phase B region ($1.46<X<1.55$), however, rapid change in the pressure at a specific composition is not observed. Instead, at the composition X=1.50 the curvature changes. A relatively small change in the pressure causes an appreciable variation of the composition, suggesting the flatness of the free energy surface. As evident in the curves for 1000 and 1087 K, the phases exhibit large mutual solubilities with increasing temperature.

A few remarks should be made here regarding the powder X-ray diffraction patterns of the quenched specimens. In contrast to the *in situ* observations described above, only two phases were detected in the range $1.33\leqq X\leqq 1.60$. Their X-ray powder patterns were similar to those of V_3S_4 and V_5S_8, respectively, in the V–S system. This suggests that Fe can substitute for V in both V_3S_4 and V_5S_8 phases due to the formation of ternary solid solutions. In the range, $1.55\leqq X\leqq 1.56$, a mixture of (Fe, V)$_3$S$_4$ and (Fe,V)$_5$S$_8$ patterns was obtained.

In the range, $1.45<X<1.55$, however, no mixture was obtained in the X-ray powder diffraction pattern; this result is inconsistent with the observation in Fig. 3. This is considered to originate from the difficulties that the phase in the range $1.46<X<1.55$ can hardly be distingushed from the (Fe,V)$_3$S$_4$ phase by X-ray powder analysis, due to the similarity of crystal structure. In fact, both phases show a large mutual solubility with increasing temperature (above 1000 K in Fig. 3). The unknown phase, B, may be inferred to be (Fe,V)$_2$S$_3$ phase, on the analogy of sesquisulfide V_2S_3, from a study of the V–S system.[10,11] In the present study, therefore, the phase described above is designated as the (Fe,V)$_2$S$_3$ phase for convenience throughout the paper.

Figure 4 shows isotherms with the composition $Fe_{0.264}V_{0.736}S_x$, richer in Fe than that in Fig. 3. The region covered experimentally lies between the composition $Fe_{0.264}V_{0.736}S_{1.333}$ and $Fe_{0.264}V_{0.736}S_{1.520}$. Two phases, A and B, exist in this range. Rapid increase of the pressure is observed near the stoichiometric compositions, $(Fe_{0.264}V_{0.736})_3S_4$ and $(Fe_{0.264}V_{0.736})_2S_3$. This indicates the existence of extensive ternary solid solutions such as (Fe,V)$_3$S$_4$ and (Fe,V)$_2$S$_3$, one end member of which is one of vanadium sulfides such as V_3S_4 and V_2S_3.

Again, the X-ray powder diffraction of the quenched specimen exhibits no difference between the two phases.

Figure 5 shows isotherms with the composition $Fe_{0.349}V_{0.651}S_x$. Within the present experimental pressure range, a large change in the pressure is observed only near the composition, X=1.33, in the phase A region. Therefore, it is considered that this phase is included in the region of the solid solution of the (Fe,V)$_3$S$_4$ phase.

As shown in Figs. 3—5, within the present experimental temperatures and Fe/V ratios, the features of isotherms depend upon compositions and temperature. With respect to isotherms, it is found that the sulfur content in the ternary sulfide which is equilibriated at the respective P_{S_2} values decreases with increasing Fe/V ratio.

This indicates that the equilibrium sulfur pressure of sulfides in the Fe–V–S system increases with decreasing vanadium content, when the S/(Fe+V) ratio is held

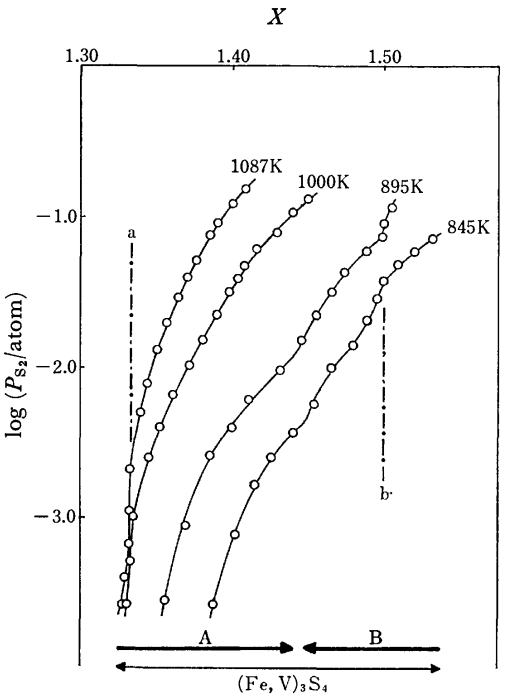

Fig. 4. P_{S_2}-composition isotherms of $Fe_{0.264}V_{0.736}S_x$.
a: $(Fe_{0.264}V_{0.736})_3S_4$, b: $(Fe_{0.264}V_{0.736})_2S_3$.

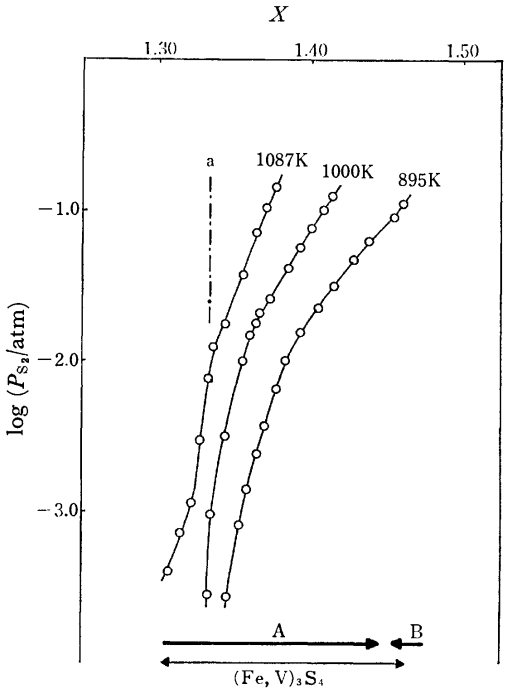

Fig. 5. P_{S_2}-composition isotherms of $Fe_{0.349}V_{0.651}S_x$.
a: $(Fe_{0.349}V_{0.651})_3S_4$.

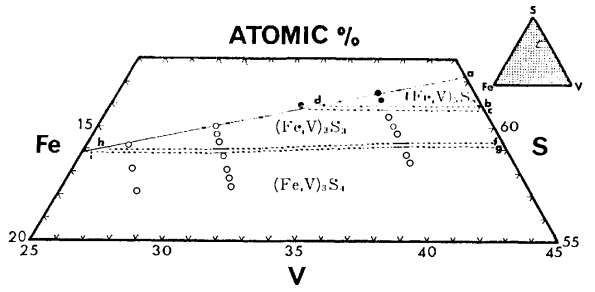

Fig. 6. Tentative phase diagram of the sulfur-rich portion of the Fe–V–S system for 895 K.
Two-phase fields are represented as follows
Area b-c-d-e: $(Fe,V)_5S_8+(Fe,V)_2S_3$, and Area f-g-h-i: $(Fe,V)_2S_3+(Fe,V)_3S_4$.
Phase identifications of quenched specimens by X-ray powder diffraction method are shown as follows
○: monoclinic V_3S_4-type structure,
●: monoclinic V_5S_8-type structure.

constant. From the experimental results described before, it is concluded that within the range Fe/(Fe+V) =0.05, 0.26, and 0.35, solid solution phases of $(Fe,V)_3S_4$, $(Fe,V)_2S_3$, and $(Fe,V)_5S_8$ are found and that the mutual solubility increases with increasing temperature (Figs. 3—5).

The tentative isothermal phase diagram in the sulfur-rich portion of the Fe–V–S system for 895 K was constructed on the basis of the results of thermogravimetry. The phase relations and their compositional limits are summarized in Fig. 6.

The iron-rich limits of solid solution phases such as $(Fe,V)_5S_8$ and $(Fe,V)_2S_3$ are determined by a smooth fitting of data points which are obtained under the highest sulfur pressure condition ($\log(P_{S_2}/\text{atm})=-0.95$) in this study. This boundary is drawn approximately as a straight line. The extension of this line intersects the boundary line, V–S, at the point a, whose composition is given as about 62.2 atomic % of sulfur. This value is in good agreement with that of the sulfur-rich limit of V_5S_8 phase ($VS_{1.64}$) which was reported by Saeki *et al.*[12] However, phase relations outside the line showing the iron-rich limits of solid solutions could not be determined owing to the limitation of the direct sulfur pressure control method and are omitted in Fig. 6.

With experimental data obtained in this study and with the homogeneity range of the compounds from the V–S system, as previously determined by De Vries and Jellinek[6] for V_5S_8 phase and by Nakahira *et al.*[11] for V_2S_3 and V_3S_4 phases, it was possible to draw two-phase fields. The boundaries of two-phase fields which show discontinuity of isotherms are represented as dotted lines nearly in parallel with the FeS–VS join. As shown in Fig. 6, two-phase mixtures of $(Fe,V)_5S_8+(Fe,V)_2S_3$ and $(Fe,V)_2S_3+(Fe,V)_3S_4$ are found in the range of S/(Fe+V) atomic ratios, 1.55—1.56 and 1.44—1.45 or 1.45—1.46, respectively.

Judging from the behavior of the iron-rich limits of solid solution fields, it was expected that the monoclinic $(Fe,V)_3S_4$ phase was stable over a wide compositional range. With the aid of a supplemental experiment using iron-rich ternary sulfides, the phase boundary of $(Fe,V)_3S_4$ was confirmed to be reached to the position of about 0.30 Fe/(Fe+V) ratio. Some representative unit-cell dimensions of quenched specimens in the $(Fe,V)_3S_4$ phase field are listed in Table 2. It is indicated that the axial dimensions, especially of the a- and c-axis, change smoothly with corresponding variations in Fe composition. From the results mentioned above, it is concluded that stoichiometric FeV_2S_4, as reported by many investigators, is not a specific ternary phase, but is included in the $(Fe,V)_3S_4$ solid solution fields.

The author is at present extending the present work to the iron-rich portion of the composition triangle of FeS–VS–S.

The author wishes to express his hearty thanks to Professor Mitsuoki Nakahira of Okayama College of Science for his encouragement and helpful discussions throughout this study.

TABLE 2. UNIT-CELL DIMENTIONS OF $(Fe,V)_3S_4$ SOLID SOLUTION

Composition	a(Å)	b(Å)	c(Å)	β(°)	Volume (Å^3)
$Fe_{0.05}V_{0.95}S_{1.39}$	5.860±3	3.285±2	11.355±1	91.97	218.5
$Fe_{0.26}V_{0.74}S_{1.38}$	5.855±2	3.291±1	11.297±5	91.94	217.5
$Fe_{0.35}V_{0.65}S_{1.39}$	5.848±2	3.291±1	11.237±5	91.95	216.2

References

1) B. L. Morris, R. H. Plovnick, and A. Wold, *Solid State. Commun.*, **7**, 291 (1969).
2) S. Muranaka and T. Takada, *Bull. Inst. Chem. Res., Kyoto Univ.*, **51**, 287 (1973).
3) S. Muranaka and T. Takada, *J. Solid State Chem.*, **14**, 291 (1975).
4) M. Cheverton and A. Sapet, *C. R. Acad. Sci., Paris*, **261**, 298 (1965).
5) G. Kullerud and H. S. Yoder, *Econ. Geol.*, **54**, 533 (1959).
6) A. B. De Vries and F. Jellinek, *Rev. Chim. Miner.*, **11**, 624 (1974).
7) I. Kawada, M. Nakano-Onoda, M. Ishii, M. Saeki, and M. Nakahira, *J. Solid State Chem.*, **15**, 246 (1975).
8) M. Wakihara, T. Uchida, and M. Taniguchi, *Mater. Res. Bull.*, **11**, 973 (1976).
9) H. Rau, T. R. N. Kutty, and J. R. F. Guedes de Carvalho, *J. Chem. Thermodyn.*, **5**, 833 (1973).
10) J. Tudo, *Rev. Chim. Miner.*, **2**, 53 (1965).
11) M. Nakahira, K. Hayashi, M. Nakano-Onoda, and K. Shibata, "Proc. 8th Int. Symp. on the Reactivity of Solids," ed by J. Wood *et al.*, Plenum Press, New York (1977), pp. 397—401.
12) M. Saeki, M. Nakano, and M. Nakahira, *J. Cryst. Growth*, **24/25**, 154 (1974).

Raman and Infrared Spectra of μ-O_2 Dicobalt(III) Complexes*

Takashi SHIBAHARA and Masayasu MORI

Department of Chemistry, Faculty of Science, Osaka City University, Sugimoto-cho, Sumiyoshi-ku, Osaka 558

(Received October 8, 1977)

Raman and infrared spectra of μ-hyperoxo and μ-peroxo ammine and cyano dicobalt(III) complexes have been studied and isotopic shifts of ν(OO) and ν(CoO) examined using ^{18}O. A μ-hyperoxo complex, $[(NH_3)_5Co(O_2)Co(NH_3)_5]X_5$ shows peaks around 1110, 620, and 440 cm^{-1} assignable to ν(OO), sν(CoO), and asν(CoO), respectively, whereas a μ-peroxo complex, $[(NH_3)_5Co(O_2)Co(NH_3)_5]X_4$ shows peaks around 805, 645, and 545 cm^{-1} assignable to ν(OO), sν(CoO), asν(CoO), respectively. These observed values are best reproduced, when the following force constants are assumed in the UBFF calculation: K(OO)=5.6, K(CoO)=1.40 mdyn/Å for μ-hyperoxo complexes and K(OO)=2.7, K(CoO)=2.15 mdyn/Å for μ-peroxo complexes. The calculated isotopic shifts are in good agreement with the observed ones. Raman and infrared spectra of dibridged μ-amido-μ-O_2 (both peroxo and hyperoxo) dicobalt(III) complex have also been characterized. A linear relationship has been found between ν(OO) and the bond order of the O_2 moiety in O_2-complexes in different oxidation states including alkali hyperoxide, alkali peroxide, hydrogen peroxide, oxygen, and O_2^+ species.

Although much work has been done on the preparation, reaction mechanisms and X-ray crystallography of O_2-bridged binuclear cobalt(III) complexes,[1] the information about the vibration of oxygen–oxygen and cobalt–oxygen bonding in the complexes has been relatively poor.[2-7]

The variation of O–O and Co–O stretching frequencies with the change in the oxidation state (*i.e.* peroxo to hyperoxo species) will give important information on the nature of the O–O and Co–O bonding.

As has been pointed out in the earlier communication,[7] the use of Raman spectroscopy is indispensable to obtaining the O–O stretching frequencies of substances having center of symmetry, since infrared spectroscopy does not give information in these cases. The recent development of the laser light source is beginning to afford Raman spectroscopy of colored substances such as many metal complexes, and is becoming to be a useful weapon in attacking these problems.

This paper will describe the O–O and Co–O stretching vibrations of μ-hyperoxo and μ-peroxo binuclear cobalt(III) complexes with and without additional NH_2-bridge as examined by using laser-Raman and infrared spectroscopy.

Experimental

Preparation. $[(NH_3)_5Co(O_2)Co(NH_3)_5]Cl_5\cdot 3H_2O$,[8] $[(NH_3)_5Co(O_2)Co(NH_3)_5](NO_3)_5$,[9] $[(NH_3)_5Co(O_2)Co(NH_3)_5](SO_4)_2HSO_4\cdot 3H_2O$,[10] $K_5[(CN)_5Co(O_2)Co(CN)_5]\cdot H_2O$,[11] $[(NH_3)_5Co(O_2)Co(NH_3)_5]Cl_4\cdot H_2O$,[12] $[(NH_3)_5Co(O_2)Co(NH_3)_5](NO_3)_4\cdot 2H_2O$,[12] $[(NH_3)_5Co(O_2)Co(NH_3)_5](SO_4)_2\cdot 3H_2O$,[12] $K_6[(CN)_5Co(O_2)Co(CN)_5]\cdot H_2O$,[13] $[(NH_3)_4Co(NH_2)(O_2)Co(NH_3)_4]Na(ClO_4)_4$,[3] and $[(NH_3)_4Co(NH_2)(O_2)Co(NH_3)_4]Cl_4\cdot 2H_2O$[3] were prepared as described in the references. In addition to the dihydrate of $[(NH_3)_4Co(NH_2)(O_2)Co(NH_3)_4]Cl_4$ cited above, the trihydrate $[(NH_3)_4Co(NH_2)(O_2)Co(NH_3)_4]Cl_4\cdot 3H_2O$ was also prepared. Although the factors which decide the number of water of crystallization have not yet been clarified, these two types are easily distinguished by infrared spectra, which will be discussed later.

Found: Co, 24.57; H, 6.17; N, 26.02%. Calcd for $[(NH_3)_4Co(NH_2)(O_2)Co(NH_3)_4]Cl_4\cdot 2H_2O$: Co, 24.56; H, 6.30; N, 26.26%.

Found: Co, 23.98; H, 6.32; N, 25.40%. Calcd for $[(NH_3)_4Co(NH_2)(O_2)Co(NH_3)_4]Cl_4\cdot 3H_2O$: Co, 23.67; H, 6.48; N, 25.31%.

$[(NH_3)_4Co(NH_2)(O_2)Co(NH_3)_4](NO_3)_4$ was prepared as described in Ref. 3. Two types (which we shall name α and β) of crystals were obtained by different ways of cooling. Rapid cooling with ice at the final stage of preparation tended to give crystals of the α-type, whereas slow cooling at room temperature gave crystals of the β-type. These two types are easily distinguished by infrared spectra (see below). From the X-ray powder pattern, it was made clear that the structure previously determined by X-ray single crystal analysis[14] was that of our β-type.

Found: α-type, Co, 21.37; N, 32.40%, β-type, Co, 21.26; N, 32.68%. Calcd for $[(NH_3)_4Co(NH_2)(O_2)Co(NH_3)_4](NO_3)_4$: Co, 21.42; N, 33.10%.

The following ^{18}O-labeled substances were prepared using $^{18}O_2$ gas (90%) obtained from International Chemical Nuclear Nuclear Corp.: $[(NH_3)_5Co(^{18}O_2)Co(NH_3)_5](NO_3)_5$, $[(NH_3)_5Co(^{18}O_2)Co(NH_3)_5]Cl_5\cdot 3H_2O$, $[(NH_3)_4Co(NH_2)(^{18}O_2)Co(NH_3)_4](NO_3)_4$, $[(NH_3)_4Co(NH_2)(^{18}O_2)Co(NH_3)_4]Cl_4\cdot 2H_2O$.

Spectroscopic Measurements. Raman spectra of the complexes in the solid state and in aqueous solutions were recorded on a JEOL JRS-Sl laser Raman spectrophotometer equipped with a rotating cell to avoid decomposition of samples. Krypton ion laser (5682 Å) was used as a light source. Infrared spectra were recorded as KBr disks and in Nujol mulls on a JASCO IR-S spectrophotometer (4000—400 cm^{-1}) and a DS-402G spectrophotometer (700—400 cm^{-1}). Samples dispersed homogeneously in polyethylene or Nujol mulls were used for the measurements in the far infrared region (400—30 cm^{-1}) with a Hitachi FIS-3 spectrophotometer.

Results and Discussion

Single-bridged μ-Hyperoxo Dicobalt(III) Complexes. Raman (solid samples) and infrared spectra of several single-bridged μ-hyperoxo dicobalt(III) complexes ((**1**), $[(NH_3)_5Co(O_2)Co(NH_3)_5]Cl_5\cdot 3H_2O$; (**2**), $[(NH_3)_5Co(O_2)Co(NH_3)_5](NO_3)_5$; (**3**), $[(NH_3)_5Co(O_2)Co(NH_3)_5](SO_4)_2\,HSO_4\cdot 3H_2O$; (**4**), $K_5[(CN)_5Co(O_2)Co(CN)_5]\cdot H_2O$) are shown in Fig. 1. Raman spectra of **1**, **2**, **3**, and **4** show strong peaks at about 1100 cm^{-1}, whereas no peak appears in the 900—1300 cm^{-1} region of the infrared spectra except in the case of **3**, which exhibits absorptions due to sulfate and hydrogensulfate

* Some parts of this paper have already been reported at XVIth International Conference on Coordination Chemistry, Dublin, 1974.

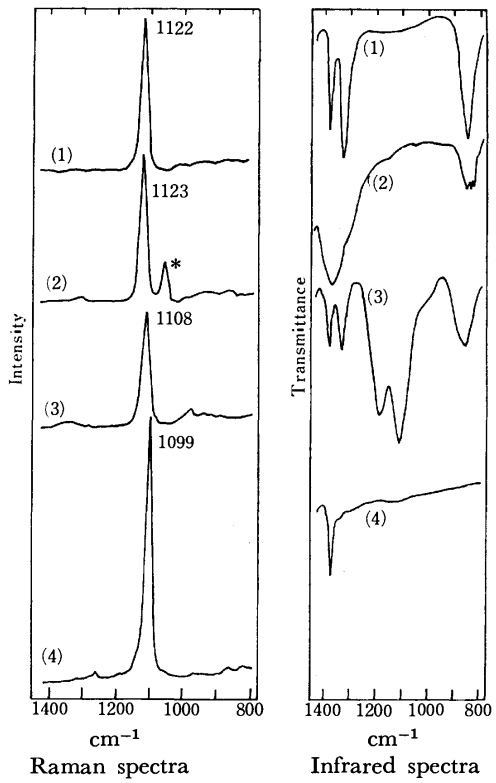

Fig. 1. Raman and infrared spectra of single-bridged μ-hyperoxo dicobalt(III) complexes in the rigion 1400—800 cm^{-1}.
(1): $[(NH_3)_5Co(O_2)Co(NH_3)_5]Cl_5 \cdot 3H_2O$,
(2): $[(NH_3)_5Co(O_2)Co(NH_3)_5](NO_3)_5$,
(3): $[(NH_3)_5Co(O_2)Co(NH_3)_5](SO_4)_2HSO_4 \cdot 3H_2O$,
(4): $K_5[CN)_5Co(O_2)Co(CN)_5] \cdot H_2O$.
*: $\nu_1(A_1')$ of NO_3^-.

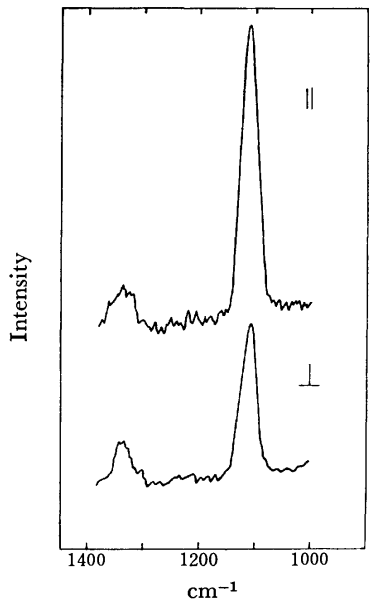

Fig. 2. Polarized Raman spectra of $[(NH_3)_5Co(O_2)$-$Co(NH_3)_5]Cl_5 \cdot 3H_2O$.

ions. X-Ray analyses by several authors[15–17] all revealed the Co–O–O–Co moieties of these complexes to be trans-planar (C_{2h} symmetry) or close to so. The in-plane vibrational modes can therefore be classified to A_g (Raman active and infrared inactive) and B_u (Raman inactive and infrared active) species. The Raman active band (A_g) at *ca.* 1100 cm^{-1} can be assigned to ν(OO); other vibrations belonging to A_g species (sν(CoO) and sδ(CoOO)) have too high frequencies to be assigned to these bands. As shown in Fig. 2, the degree of depolarization of Raman band at *ca.* 1100 cm^{-1} of a solution sample of the chloride is about one-half indicating that this vibration is totally symmetric. The Raman spectrum of $[CoCl(NH_3)_5]Cl_2$, having the same local symmetry (C_{4v}) as that around each cobalt atom in the μ-hyperoxo-bis[pentaamminecobalt(III)] complex has no peak in the 900—1250 cm^{-1} region. These facts also support the above assignment.

Infrared and Raman spectra of single-bridged μ-hyperoxo dicobalt(III) complexes in the KBr region are shown in Fig. 3, together with the infrared spectra of the chloride and nitrate of ^{18}O-substituted complexes. As shown in Fig. 3, the peaks at *ca.* 440 cm^{-1} in the infrared spectra are lowered by *ca.* 19 cm^{-1} by the substitution with ^{18}O. This confirms the conclusion by Ikawa *et al.*[4] who assigned the band to asν(CoO) from comparison of the infrared spectra of μ-hyperoxo complexes with those of μ-peroxo complexes and hexaammine cobalt(III) complex. The peaks in the range 505—470 cm^{-1} of the infrared spectra hardly shift indicating that the peaks are due to ν(CoN). Absence of any remarkable difference between ordinary and ^{18}O-substituted complexes in the far infrared region makes it difficult to assign δ(CoOO)(Fig. 4).[4] As regards to decaammine dicobalt(III) complexes, **1**, **2**, and **3**, the peaks at *ca.* 620 cm^{-1} in the Raman spectra (Fig. 3) are assigned to sν(CoO) by comparison with the infrared spectra (no peak around 620 cm^{-1}), although Strekas and Spiro[15] assigned the Raman band at 500 cm^{-1} to ν(CoO). The strong peaks at about 500 cm^{-1} in the Raman spectra can rather be assigned to ν(CoN), since $[CoCl(NH_3)_5]Cl_2$ also shows a strong peak at 494 cm^{-1} in the Raman spectrum. The Raman spectrum of the cyano complex **4** shows peaks at 610, 542, and 528 cm^{-1} and the peak at 610 cm^{-1} is assigned to sν(CoO) and the other two peaks are assigned to ν(CoC). A weak band assignable to sν(CoO) was observed at 618 cm^{-1} in the infrared spectrum, too. Appearance of this band can be attributed to the nonplanarity of the Co–O–O–Co moiety of the cyano complex; the following values were obtained from X-ray crystallography for the torsional angles: nitrate of the ammine complex,[16] 180°; sulfate tris-hydrogensulfate of the ammine complex,[17] 175°; potassium salt of the cyano complex,[18] 180 and 166° (two independent binuclear anions in the unit cell). The peaks at 551 and 543 cm^{-1} are assigned to ν(CoC) in the infrared spectrum of the cyano complex, since a peak assignable to ν(CoC) was observed at 565 cm^{-1} in the infrared spectrum of $K_3[Co(CN)_6]$.[19]

μ-Amido-μ-hyperoxo Dicobalt(III) Complexes. The Raman and infrared spectra of μ-amido-μ-hyperoxo bis[tetraamminecobalt(III)] chloride trihydrate (**5**) have peaks at 1075 and 1068 cm^{-1}, respectively, as shown in Fig. 5. These bands are assigned to ν(OO)

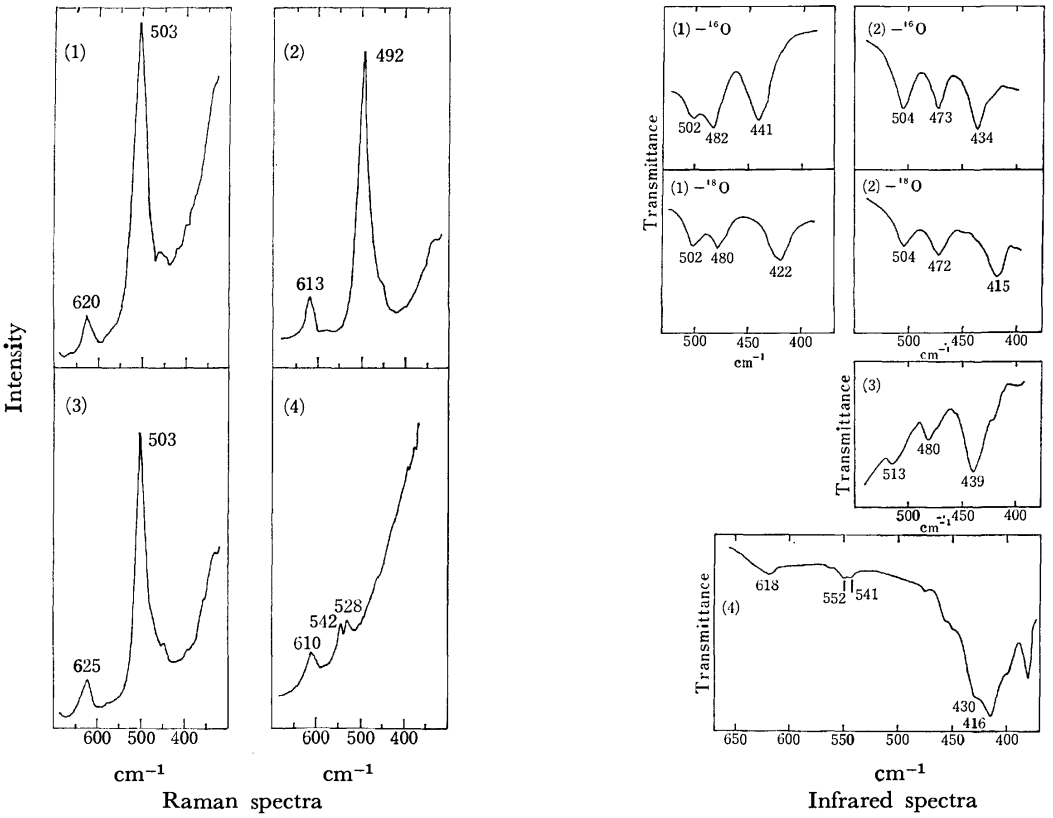

Fig. 3. Raman and infrared spectra of single-bridged μ-hyperoxodicobalt(III) complexes in the region 700—400 cm^{-1}. Each number represents the same compound as in Fig. 1.

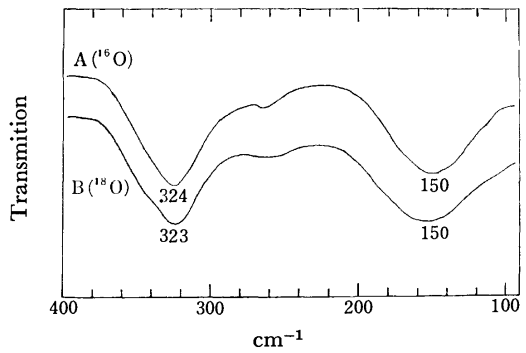

Fig. 4. Far infrared spectra of single-bridged μ-hyperoxo decaamine dicobalt(III) complexes.
(A): ^{16}O-$[(NH_3)_5Co(O_2)Co(NH_3)_5]Cl_5 \cdot 3H_2O$,
(B): ^{18}O-$[(NH_3)_5Co(O_2)Co(NH_3)_5]Cl_5 \cdot 3H_2O$.

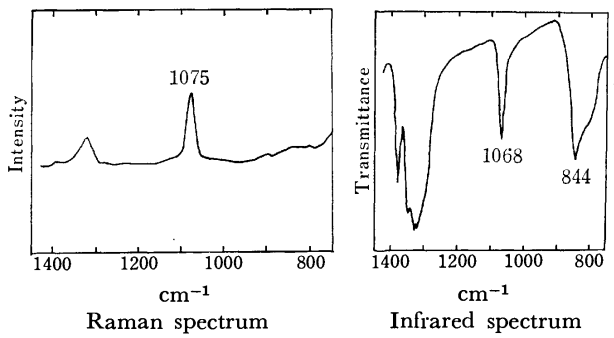

Fig. 5. Raman and infrared spectra of μ-amido-μ-hyperoxo bis[tetraamminecobalt(III)] chloride trihydrate, $[(NH_3)_4Co(NH_2)(O_2)Co(NH_3)_4]Cl_4 \cdot 3H_2O$.

by comparison with the peak positions in the Raman spectra of single-bridged μ-hyperoxo complexes and also by consideration of the degree of depolarization (*ca.* one-half) of the Raman band at *ca.* 1100 cm^{-1} of a solution samples of **5**, as shown in Fig. 6. Since the dibridged complex ion has no center of symmetry, any vibration should be both infrared and Raman active.

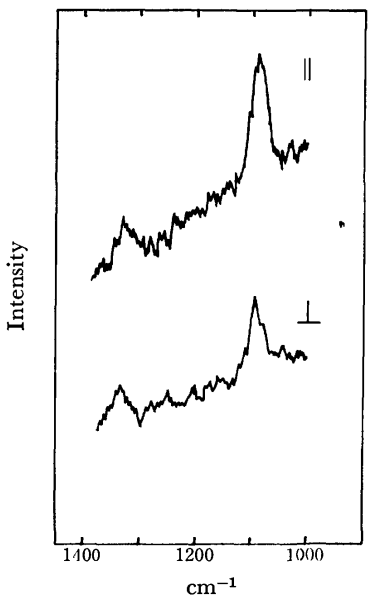

Fig. 6. Polarized Raman spectra of $[(NH_3)_4Co(NH_2)-(O_2)Co(NH_3)_4]Cl_4 \cdot 3H_2O$.

This is in accordance with the above observation. The chloride crystallizes in two forms, one with two moles of water and the other with three. They can easily be distinguished by the infrared spectra. The peak positions due to ν(OO) differ slightly (dihydrate, 1078 cm^{-1}; trihydrate, 1068 cm^{-1}) from each other and the band assigned to $\rho_r(NH_3)$ shows splitting in the dihydrate (dihydrate, 844 and 815 cm^{-1}; trihydrate, 844 cm^{-1}). The nitrate also has two crystal forms (cf. Experimental, Preparation.). Both are anhydrous and can be distinguished easily by infrared spectra. In addition to the difference in the peak position of ν(OO) (α-type, 1063 cm^{-1}; β-type, 1088 cm^{-1}), the spectrum of α-type shows a splitting of the band due to $\rho_r(NH_3)$ (α-type, 840 and 827 cm^{-1}; β-type, 830 cm^{-1}). As shown in Fig. 7, the O-O streching frequencies in the infrared spectra of ^{18}O-substituted complexes of the chloride ((A), $2H_2O$-type) and the nitrate ((B), α-type) are lower than those of the corresponding ^{16}O-complexes by 60 cm^{-1}. Since the difference in ν(OO) frequency between two crystal forms (in both chloride and

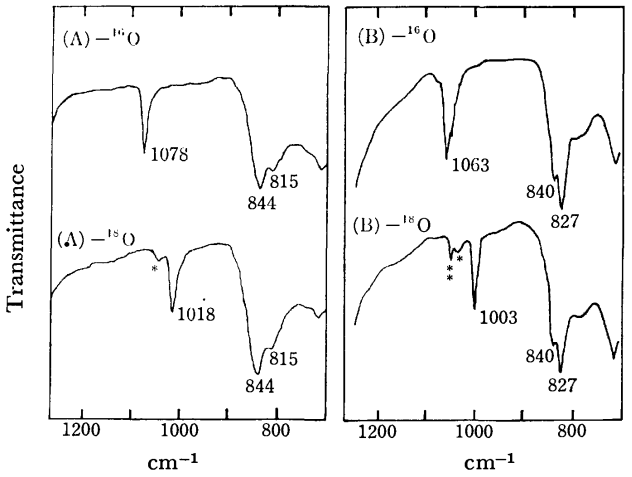

Fig. 7. Infrared spectra of chloride and nitrate of μ-amido-μ-hyperoxo bis[tetraamminecobalt(III)] in the region 1200—700 cm^{-1}.
(A): $[(NH_3)_4Co(NH_2)(O_2)Co(NH_3)_4]Cl_4 \cdot 2H_2O$,
(B): $[(NH_3)_4Co(NH_2)(O_2)Co(NH_3)_4](NO_3)_4$ (α-type),
*: $\nu(^{16}O^{18}O)$, **: $\nu_1(A_1')$ of NO_3^-.

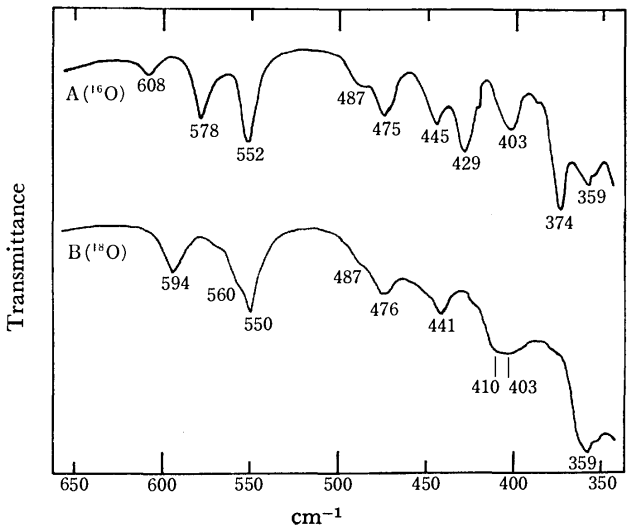

Fig. 8. Infrared spectrum of $[(NH_3)_4Co(NH_2)(O_2)$-$Co(NH_3)_4](NO_3)_4$ (α-type) in the region 650—350 cm^{-1}.

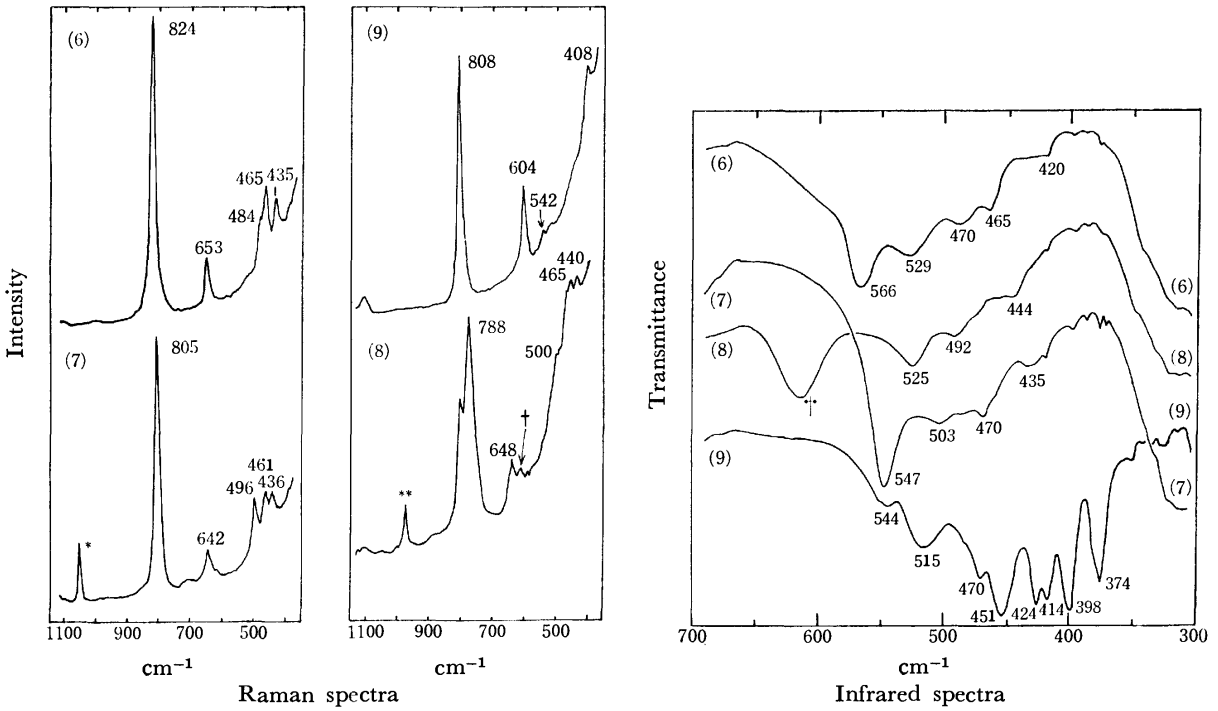

Fig. 9. Raman and infrared spectra of single-bridged μ-peroxo dicobalt(III) complexes.
(6): $[(NH_3)_5Co(O_2)Co(NH_3)_5]Cl_4 \cdot H_2O$, (7): $[(NH_3)_5Co(O_2)Co(NH_3)_5](NO_3)_4 \cdot 2H_2O$, (8): $[(NH_3)_5$-$Co(O_2)Co(NH_3)_5](SO_4)_2 \cdot 3H_2O$, (9): $K_6[(CN)_5Co(O_2)Co(CN)_5] \cdot H_2O$,
*: $\nu_1(A_1')$ of NO_3^-, **: $\nu_1(A_1)$ of SO_4^{2-}, †: $\nu_4(F_2)$ of SO_4^{2-}.

nitrate) is not negligible, it is important to compare the ν(OO) frequency of ^{16}O- and ^{18}O-compounds of the same crystal form.

Infrared spectra of ordinary and ^{18}O-substituted samples, of the nitrate (α-type) in the 650—350 cm^{-1} region are shown in Fig. 8, A and B, respectively. The peak at 429 cm^{-1} in A shifts to 410 cm^{-1} in B, whereas that at 374 cm^{-1} in A probably to *ca.* 360 cm^{-1} in B (overlapping with a peak at 359 cm^{-1} which does not shift). The peak at a higher frequency is assigned to sν(CoO) and that at a lower frequency to asν(CoO). Shifts of some other bands can also be observed; the peaks at 608 and 578 cm^{-1} in A disappeared and a new peak appeared at 594 cm^{-1} and a shoulder at 560 cm^{-1} in B. These two peaks are tentatively assigned to the combination bands of ν(CoO), ν(CoN), and ring deformation; if they were genuine ν(CoO)'s, the magnitude of the shifts would be expected to be *ca.* 25 cm^{-1}.

Single-bridged μ-Peroxo Dicobalt(III) Complexes. The Raman (1100—450 cm^{-1}) and infrared spectra (700—300 cm^{-1}) of single-bridged μ-peroxo dicobalt(III) complexes ((**6**), $[(NH_3)_5Co(O_2)Co(NH_3)_5]Cl_4\cdot H_2O$; (**7**), $[(NH_3)_5Co(O_2)Co(NH_3)_5](NO_3)_4\cdot 2H_2O$; (**8**), $[(NH_3)_5Co(O_2)Co(NH_3)_5](SO_4)_2\cdot 3H_2O$; (**9**), $K_6[(CN)_5Co(O_2)Co(CN)_5]\cdot H_2O$) are shown in Fig. 9. Strong bands assignable to ν(OO) are found around 800 cm^{-1} in the Raman spectra.[5-7] The degree of depolarization of these bands is *ca.* 0.3 indicating that the vibration is totally symmetric. The band at 600—660 cm^{-1} ((**6**), 653; (**7**), 642; (**8**), 648; (**9**), 604 cm^{-1}) in the Raman spectra are assigned to sν(CoO). Other bands in the Raman spectra are assigned to ν(CoN) for the compounds **6**(484, 465, and 435 cm^{-1}), **7**(496, 461, and 436 cm^{-1}), and **8**(500, 465, and 440 cm^{-1}). The bands with the highest wave number and at the same time the highest intensity in the KBr region of the infrared spectra of decaammine μ-peroxo compounds (**6**, 566 cm^{-1} and possibly 529 also; **7**, 547; **8**, 525 cm^{-1}) are assigned to asν(CoO). The bands in the region from 503 to 400 cm^{-1} are assigned to ν(CoN). As for the cyano compound **9**, the band at 515 cm^{-1} in the infrared spectrum is assigned to the asν(CoO), and the band at 544 cm^{-1} and the bands from 470 to 374 cm^{-1} are assigned to ν(CoC)+δ(CoCN), by the comparison with the infrared spectra of $K_3[Co(CN)_6]$.[19] The bands at 542 and 408 cm^{-1} in the Raman spectrum of **9** are also assigned to ν(CoC)+δ(CoCN).

μ-Amido-μ-peroxo Dicobalt(III) Complexes. The Raman and infrared spectra of $[(NH_3)_4Co(NH_2)(O_2)Co(NH_3)_4]Na(ClO_4)_4$ are shown in Fig. 10A and 10B, respectively. The ν(OO) in the infrared spectrum has been reported by Mori *et al.*[3] to be at 828 cm^{-1}. The Raman spectrum of this sample shows a distinct peak at 832 cm^{-1} which confirms the previous assignment. The band at 533 cm^{-1} in the infrared spectrum and

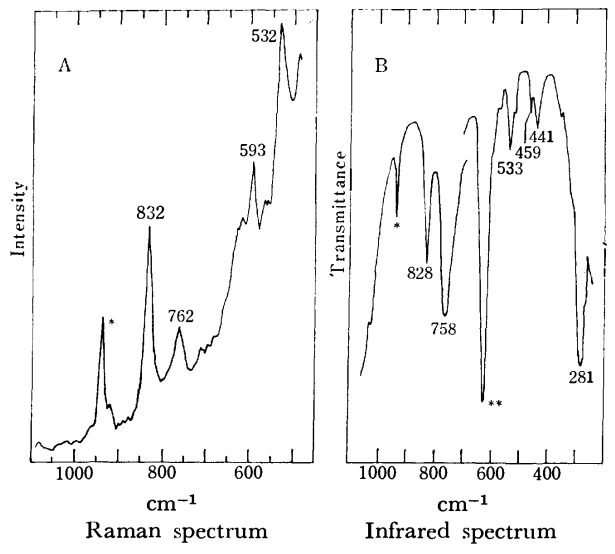

Fig. 10. Raman and infrared spectra of μ-amido-μ-peroxobis[tetraamminecobalt(III)] complex, $[(NH_3)_5Co(NH_2)(O_2)Co(NH_3)_4]Na(ClO_4)_4$.
*: $\nu_1(A_1)$ of ClO_4^-, **: $\nu_4(F_2)$ of ClO_4^-.

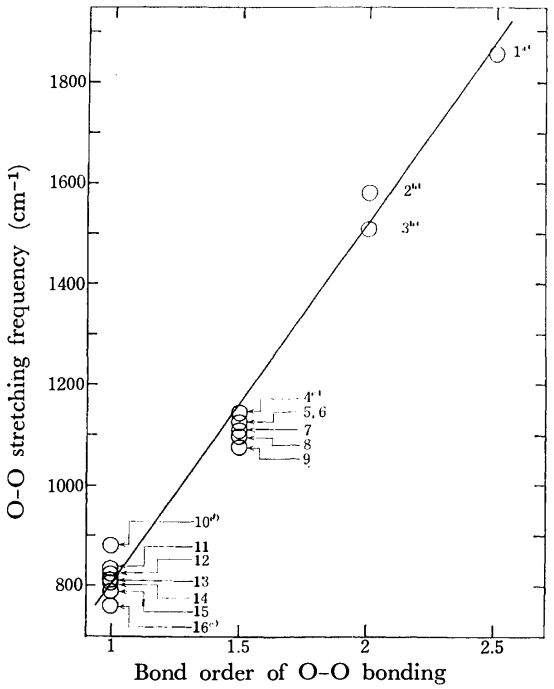

Fig. 11. Relationship between the bond order of oxygen-oxygen bonding and ν(OO) frequency.
(1): O_2AsF_6,[a] (2): $O_2(^3\Sigma_g^-)$,[b] (3): $O_2(^1\Delta_g)$, (4): KO_2,[c] (5): $[(NH_3)_5Co(O_2)Co(NH_3)_5](NO_3)_5$, (6): $[(NH_3)_5Co(O_2)Co(NH_3)_5]Cl_5\cdot 3H_2O$, (7): $[(NH_3)_5Co(O_2)Co(NH_3)_5](SO_4)_2\cdot HSO_4\cdot 3H_2O$, (8): $K_5[(CN)_5Co(O_2)Co(CN)_5]\cdot H_2O$, (9): $[(NH_3)_4Co(NH_2)(O_2)Co(NH_3)_4]Cl_4\cdot 3H_2O$, (10): H_2O_2,[d] (11): $[(NH_3)_4Co(NH_2)(O_2)Co(NH_3)_4]Na(ClO_4)_4$, (12): $[(NH_3)_5Co(O_2)Co(NH_3)_5]Cl_4\cdot H_2O$, (13): $K_6[(CN)_5Co(O_2)Co(CN)_5]\cdot H_2O$, (14): $[(NH_3)_5Co(O_2)Co(NH_3)_5](NO_3)_4\cdot 2H_2O$, (15): $[(NH_3)_5Co(O_2)Co(NH_3)_5](SO_4)_2\cdot 3H_2O$, (16): Na_2O_2.[e]

(a) J. Shamir, J. Binenboym, and H. H. Claassen, *J. Am. Chem. Soc.*, **90**, 6223 (1968). (b) G. Herzberg, "Spectra of Diatomic Molecules," van Nostrand (1950). (c) J. B. Bates, M. H. Brooker, and G. H. Boyd, *Chem. Phys. Lett.*, **16**, 391 (1972). (d) F. J. Blunt, P. J. Hendra, and J. R. Mackenzie, *Chem. Commun.*, **1969**, 278. (e) J. C. Evans, *Chem. Commun.*, **1969**, 682.

the bands at 593 and 532 cm^{-1} in the Raman spectrum are assigned tentatively to ν(CoO). Peaks at 762 cm^{-1} (Raman) and 758 cm^{-1} (infrared) are assigned to $\rho_r(NH_3)$.

Relationship between the Bond Order and the Oxygen–Oxygen Stretching Frequencies of O_2-compounds. An approximately linear relationship exists between the bond order of oxygen–oxygen bonding and ν(OO) as shown in Fig. 11. The relationship can be expressed by the following equation

$$\nu(OO) = 710 \times BO + 70,$$

where ν(OO) is the wave number of the O–O stretching vibration in cm^{-1} and BO is the bond order. The large differences of ν(OO) between μ-hyperoxo and μ-peroxo complexes clearly support the idea that these two kinds of complex have different oxidation states of bridging O_2-moieties, and that the cobalt atoms in both types of complex are of oxidation state three.[20] The substitution of ammonia with cyanide ions gives little influence on ν(OO) in both μ-hyperoxo and μ-peroxo complexes.

Calculations of Force Constants. The force constants of the single-bridged μ-hyperoxo and μ-peroxo complexes were calculated using UBFF and a four-body model (μ-hyperoxo, trans planar; μ-peroxo, torsional angle of 146°). The change of the torsional angle gave only a small influence on the calculated values. Bond lengths and angles used for the calculation were those of the nitrate[16] in the case of the μ-hyperoxo complex and those of the sulfate[22] in the case of the μ-peroxo complex. The calculated and observed values are summarized in Table 1, together with the force constants employed. The calculated isotopic shift of asν(CoO) for μ-hyperoxo complex is in good agreement with the observed ones.

Table 1. Observed and calculated frequencies of μ-hyperoxo and μ-peroxo dicobalt(III) complexes in cm^{-1}

	(A) $[(NH_3)_5Co(O_2)Co(NH_3)_5]X_5$				
			ν(OO)	sν(CoO)	asν(CoO)
Obsd	nitrate	^{16}O	1123	613	434
		^{18}O	—	—	415
	chloride	^{16}O	1122	620	441
		^{18}O	—	—	422
	sulfate	^{16}O	1108	625	439
Calcd		^{16}O	1114	621	439
		^{18}O	1050	587	420
(K(OO)=5.6, K(CoO)=1.40, H(CoOO)=0.30, F(CoO)=0.05 mdyn/Å)					
	(B) $[(NH_3)_5Co(O_2)Co(NH_3)_5]X_4$				
			ν(OO)	sν(CoO)	asν(CoO)
Obsd	nitrate	^{16}O	805	642	547
	chloride	^{16}O	824	653	566, 529
	sulfate	^{16}O	788	648	525
Calcd		^{16}O	799	649	543
(K(OO)=2.7, K(CoO)=2.15, H(CoOO)=0.30, F(CoO)=0.05 mdyn/Å)					

The O–O stretching frequencies in the Raman as well as the infrared spectra of the ^{18}O-substituted μ-amido-μ-hyperoxo complexes are lower by 60 cm^{-1} than those for the corresponding ^{16}O-complexes. The isotopic shift calculated from a simple valence force field and a five membered ring model Co–N–Co–O–O is 61 cm^{-1} with a force constant K(OO) of 5.1 mdyn/Å.

The authors are grateful to Professor T. Miyazawa of the University of Tokyo for valuable suggestions and to Drs. S. Hirai and T. Hinomoto of JEOL Ltd. for the measurement of Raman spectra.

References

1) A. G. Sykes and J. A. Weil, *Progr. Inorg. Chem.*, **13**, 1 (1970), and references cited therein.
2) N. Vannerberg, *Arkiv Kemi*, **20**, 245 (1963).
3) M. Mori, J. A. Weil, and M. Ishiguro, *J. Am. Chem. Soc.*, **90**, 615 (1968).
4) S. Ikawa, H. Hasebe, and M. Kimura, *Spectrochim. Acta*, **30A**, 151 (1974).
5) T. B. Freedman, C. M. Yoshida, and T. M. Loehr, *J. Chem. Soc., Chem. Commun.*, **1974**, 1016.
6) H. Siebert and S. Thym, *Z. Anorg. Allg. Chem.*, **399**, 107 (1973).
7) (A) T. Shibahara, *J. Chem. Soc., Chem. Commun.*, **1973**, 864. (B) T. Shibahara and M. Mori, XVIth International Conference on Coordination Chemistry, Proceedings R51 (1974).
8) V. M. Linhard and M. Weigel, *Z, Anorg. Allg. Chem.*, **308**, 254 (1961).
9) S. M. Jörgensen, *Z. Anorg. Chem.*, **5**, 185 (1894).
10) K. Gleu and K. Rehn, *Z. Anorg. Allg. Chem.*, **237**, 79 (1938).
11) M. Mori, J. A. Weil, and J. K. Kinnaird, *J. Phys. Chem.*, **71**, 103 (1969).
12) A. Werner and A. Mylius, *Z. Anorg. Chem.*, **16**, 262 (1898).
13) A. Haim and W. K. Wilmarth, *J. Am. Chem. Soc.*, **83**, 509 (1961).
14) C. G. Cristoph, R. E. Marsh, and W. P. Schaefer, *Inorg. Chem.*, **8**, 291 (1969).
15) T. C. Strekas and T. G. Spiro, *Inorg. Chem.*, **14**, 1421 (1975).
16) R. E. Marsh and W. P. Schaefer, *Acta Crystallogr., Sect. B*, **24**, 246 (1968).
17) W. P. Schaefer and R. E. Marsh, *Acta Crystallogr.*, **21**, 735 (1966).
18) F. Fronczek, W. P. Schaefer, and R. E. Marsh, *Inorg. Chem.*, **14**, 611 (1975).
19) I. Nakagawa, *Bull. Chem. Soc. Jpn.*, **46**, 3690 (1973).
20) J. A. Weil and J. K. Kinnaird, *J. Phys. Chem.*, **71**, 3341 (1967).

Kinetics and Mechanisms of the Reduction of Cobalt(III) Complexes by the Chromium(II) Complex Ligating *N*-(2-Hydroxyethyl)-ethylenediamine-*N*,*N*′,*N*′-triacetate

Hiroshi Ogino, Makoto Shimura, and Nobuyuki Tanaka
Department of Chemistry, Faculty of Science, Tohoku University, Sendai 980

(Received October 17, 1977)

The reduction of the cobalt(III) complexes, $CoX(NH_3)_5^{(3-m)+}$ (X^{m-}=Cl^-, Br^-, NCS^-, and H_2O) and $Co(en)_3^{3+}$, by Cr(II)-HEDTRA was studied by the stopped-flow method, where en and HEDTRA denote ethylenediamine and *N*-(2-hydroxyethyl)ethylenediamine-*N*,*N*′,*N*′-triacetatic acid respectively. From the kinetic behavior and the spectral properties of the immediate chromium(III) products, it is concluded that the Cr(II)-HEDTRA reductions of $CoX(NH_3)_5^{2+}$ (X^-=Cl^-, Br^-, and NCS^-) are of an inner-sphere type. The effect of the HEDTRA coordinated to chromium(II) on the rates of the electron-transfer reactions is discussed.

There has been much interest in the mechanisms of the electron-transfer reactions of $MX(NH_3)_5^{(3-m)+}$ (M= Co^{III} or Cr^{III}) with $Cr^{II}L(H_2O)^{(n-2)-}$, where X^{m-} denotes a potential bridging ligand.[1-7] The present authors proposed an inner-sphere mechanism for the reactions of $CrX(NH_3)_5^{2+}$ ($X=F^-$, Cl^-, Br^-, NCS^-, and OH^-) with $Cr^{II}(edta)(H_2O)^{2-}$ on the basis of the reactivity pattern.[2,3] A similar proposal has been made by Earley and Davies for the reactions of $CrX(NH_3)_5^{2+}$ ($X=Cl^-$ and OH^-) with several chromium(II)–amino polycarboxylates by considering the linear free energy relationship.[4,5] Diebler *et al.* reported that, from the findings on the isotopic fractionation effects, the reaction of $Co(OH)(NH_3)_5^{2+}$ with $Cr^{II}(edta)(H_2O)^{2-}$ is of an inner-sphere type.[6] Thorneley *et al.* investigated the reactions of several oxidants containing potential halide bridges with $Cr^{II}(edta)(H_2O)^{2-}$ and found that the final spectra recorded within 3 min of mixing always agreed with that of $Cr^{III}(edta)(H_2O)^-$.[7] Therefore, they proposed an outer-sphere mechanism for these reactions, because it was difficult to accept the idea the aquation of $Cr^{III}X(edta)^{2-}$ is rapid and complete within 3 min in view of the substitution inertness of chromium(III) complexes.

Quite recently, the present authors presented evidence that the reaction of $Co(OAc)(NH_3)_5^{2+}$ with $Cr^{II}L(H_2O)^{(n-2)-}$ is of an inner-sphere type, because the immediate chromium(III) product was $Cr^{III}(OAc)L^{(n-2)-}$ and aquated rapidly.[8] Therefore, the over-all reaction can be expressed in the following two stages:

$$Co(OAc)(NH_3)_5^{2+} + Cr^{II}L(H_2O)^{(n-2)-} \xrightarrow{k_{et}} Co^{2+} + 5NH_3 + Cr^{III}(OAc)L^{(n-2)-} + H_2O, \quad (1)$$

$$Cr^{III}(OAc)L^{(n-2)-} + H_2O \rightleftharpoons Cr^{III}L(H_2O)^{(n-3)-} + OAc^-. \quad (2)$$

It is also known that Reaction 3, involving OAc^-,[9] N_3^-,[10,11] or some other anions[12] as X^-, is reversible and extremely rapid:

$$Cr^{III}L(H_2O)^{(n-3)-} + X^- \underset{k_b}{\overset{k_f}{\rightleftharpoons}} Cr^{III}XL^{(n-2)-} + H_2O. \quad (3)$$

These observations indicate that the detection of the immediate chromium(III) product after the electron-transfer is the key to distinguishing the mechanisms. In order to ascertain the role of the coordinated amino polycarboxylates in the electron-transfer reactions and to elucidate the mechanism of the reactions, the previous work[8] has now been extended to the electron-transfer reactions of $CoCl(NH_3)_5^{2+}$, $CoBr(NH_3)_5^{2+}$, $Co(NCS)(NH_3)_5^{2+}$, $Co(NH_3)_5(H_2O)^{3+}$, and $Co(en)_3^{3+}$ ions with $Cr^{II}(hedtra)(H_2O)^-$. The findings on the reaction of $Co(en)_3^{3+}$ with $Cr^{II}(edta)(H_2O)^{2-}$ will also be given in this paper.

Experimental

Materials. The cobalt(III) complexes, $[CoCl(NH_3)_5](ClO_4)_2$,[13] $[CoBr(NH_3)_5](ClO_4)_2$,[14] $[Co(NCS)(NH_3)_5](ClO_4)_2$,[15] $[Co(NH_3)_5(H_2O)](ClO_4)_3$,[14] and $[Co(en)_3](ClO_4)_3$,[16] were prepared according to the literature. The solutions of $[Cr(H_2O)_6](ClO_4)_3$ and $[Cr(H_2O)_6](ClO_4)_2$ were prepared as has been described previously.[2] The $Cr^{II}(hedtra)(H_2O)^-$ and $Cr^{II}(edta)(H_2O)^{2-}$ were generated *in situ* by the injection of $Cr(H_2O)_6^{2+}$ solutions into excess HEDTRA and EDTA solutions respectively. All the solutions were prepared with redistilled water.

Kinetic Procedure. Many of the kinetic measurements were made with a Union-Giken RA 401 stopped-flow spectrophotometer and a Hitachi RSP-2 rapid scanning spectrophotometer. The dead time of mixing was approximately 0.5 ms for the former instrument and 20 ms for the latter instrument. Slow kinetic measurements were made with a Union-Giken SM 401 and a Hitachi EPS-3 recording spectrophotometer. All the kinetic measurements were made at I=1.0 ($NaClO_4$) under an atmosphere of nitrogen. The temperature was kept at 25.0 °C, unless otherwise stated. The hydrogen-ion concentrations of the solutions were adjusted with HEDTRA solutions as buffers, except for the reactions of $Co(en)_3^{3+}$ with $Cr^{II}(hedtra)(H_2O)^-$ and $Cr^{II}(edta)(H_2O)^{2-}$, which were performed in acetate buffer solutions. A Hitachi F-5 pH meter was used for the determination of the hydrogen-ion concentrations; the meter readings were calibrated against standard perchloric acid solutions.

The kinetics of the electron-transfer reactions was studied under the condition of $[Co(III)]_0 > [Cr(II)]_0$, where $[\ ]_0$ represents the initial concentration of the given species. The reactions were usually monitored by the appearance of the Cr(III)-HEDTRA or -EDTA complex at 545—550 nm. On the assumption that the electron-transfer reaction:

$$Co(III) + Cr(II)\text{-}L \xrightarrow{k_{et}} Co(II) + Cr(III)\text{-}L \quad (4)$$

proceeds by means of the second order rate law;

$$\frac{d[Cr(III)\text{-}Y]}{dt} = k_{et}[Co(III)][Cr(II)\text{-}L], \quad (5)$$

the following equation was derived:

$$\ln\left\{1+\frac{\varepsilon_{Co(III)}+\varepsilon_{Cr(II)}-\varepsilon_{Co(II)}-\varepsilon_{Cr(III)}}{A_t-A_\infty}[Co(III)]_\infty\right\} = [Co(III)]_\infty k_{et}t + \ln\frac{[Co(III)]_0}{[Cr(II)]_0}, \quad (6)$$

where A_t and A_∞ denote the absorbancies at time t and infinity respectively; $\varepsilon_{Co(III)}$, $\varepsilon_{Cr(II)}$, $\varepsilon_{Co(II)}$, and $\varepsilon_{Cr(III)}$, the molar absorption coefficients of the given species, and $[Co(III)]_\infty$, the concentration of Co(III) after the completion of the reaction. The value of the $\varepsilon_{Cr(II)}$ is so small that it can be neglected. The $[Co(III)]_\infty$ quantity was determined as follows. A known volume of the product solution was poured into an SP-Sephadex C-25 cation exchanger column in the Na^+ form. When the column was washed with water, only the unreacted cobalt(III) ions remained in the column, and they were eluted with 0.5—1.0 M NaCl solutions. The eluate was then acidified with hydrochloric acid. After the cobalt(III) ions in the solution has been reduced to cobalt(II) ions with amalgamated zinc, the cobalt(II) content was determined by Kitson's method.[17] The subtraction of $[Co(III)]_\infty$ from $[Co(III)]_0$ left $[Cr(II)]_0$. The plots of the left-hand side of Eq. 6 *vs.* the time gave straight lines for all the electron-transfer reactions within three half-lives.

The dependence of the observed rate constants on the hydrogen-ion concentrations was examined for all the electron-transfer reactions studied. Except for the reaction of $Co(NH_3)_5(H_2O)^{3+}$ with $Cr^{II}(hedtra)(H_2O)^-$, the observed rate constants were found to be independent of the hydrogen-ion concentrations under the present experimental conditions.

Results

Reaction of $Co(NH_3)_5(H_2O)^{3+}$ with $Cr^{II}(hedtra)(H_2O)^-$. The observed rate constants(k_{obsd}) of the electron-transfer reaction were dependent on the hydrogen-ion concentrations, as is shown in Table 1. The plots of k_{obsd} *vs.* $[H^+]^{-1}$ give a good linear relation. Therefore, the reaction obeys the rate law given in Eqs. 7 and 8:

$$\frac{d[Cr(III)\text{-}HEDTRA]}{dt} = k_{obsd}[Co(III)][Cr(II)], \quad (7)$$

$$k_{obsd} = \frac{a}{[H^+]} + b. \quad (8)$$

The values of a and b were determined to be 12.5± 0.5 s^{-1} and $(1.30\pm0.10)\times10^5$ M^{-1} s^{-1} respectively. No absorbance change subsequent to the electron-transfer reaction was observed.

Table 1. The acid dependence of the observed second-order rate constant for the reaction of $Co(NH_3)_5(H_2O)^{3+}$ with $Cr^{II}(hedtra)(H_2O)^-$

$[Co(III)]_0$ / 10^{-3} M	$[Cr(II)]_0$ / 10^{-3} M	$[H^+]$ / 10^{-5} M	k_{obsd} / 10^5 M^{-1} s^{-1}
2.36	1.52	1.99	7.51±0.17
2.37	1.76	3.15	5.40±0.25
2.32	1.53	5.73	3.98±0.18
2.34	1.60	6.14	3.43±0.10
2.30	1.25	7.21	3.01±0.09
4.73	4.02	7.21	2.60±0.11
2.37	1.23	37.8	1.60±0.04
2.29	1.39	47.6	1.51±0.10

Reactions of $Co(en)_3^{3+}$ with $Cr^{II}(hedtra)(H_2O)^-$ and $Cr^{II}(edta)(H_2O)^{2-}$. The rate constants of the electron-transfer reactions(k_{et}) are given in Table 2.

Reaction of $Co(NCS)(NH_3)_5^{2+}$ with $Cr^{II}(hedtra)(H_2O)^-$. The rate constant of the electron-transfer reaction of $Co(NCS)(NH_3)_5^{2+}$ with $Cr^{II}(hedtra)(H_2O)^-$ was determined and is given in Table 2. The electron-transfer reaction was found to be practically completed within 50 ms under the present experimental conditions. After this rapid reaction had been completed, the spectrum changed slowly, as is shown in Fig. 1. The absorption maxima of the immediate chromium(III) species produced by the electron-transfer reaction initially shifted to shorter wavelengths and then to longer wavelengths. These spectral changes indicate that the immediate chromium(III) species is converted to some other species in a complicated manner.

Reaction of $CoBr(NH_3)_5^{2+}$ with $Cr^{II}(hedtra)(H_2O)^-$. The electron-transfer reaction of this system was found to be completed within the time of mixing (<0.5 ms), so the k_{et} value was estimated to be more than 1×10^6 M^{-1} s^{-1}. The spectrum obtained immediately after the electron-transfer reaction (Curve A in Fig. 2) changed to that of $Cr^{III}(hedtra)(H_2O)$ (Curve B in Fig. 2) with the time scale of s, and the reaction was practically completed within 4 s. This spectral change obeyed the first-order kinetics; hence, the conventional plots, $\ln|A_t-A_\infty|$ *vs.* t at 430 nm, gave a linear relation

Table 2. The second-order rate constants (k_{et}/M^{-1} s^{-1}) for the electron-transfer reactions of cobalt(III) complexes with chromium(II) complexes

Oxidant	Reductant			Rate ratio	
	$Cr^{II}(hedtra)(H_2O)^-$	$Cr^{II}(edta)(H_2O)^{2-}$	$Cr(H_2O)_6^{2+}$	k(Cr-hedtra)/k(Cr)	k(Cr-edta)/k(Cr)
$Co(en)_3^{3+}$	$(3.14\pm0.16)\times10^3$ [a]	$(4.24\pm0.22)\times10^3$ [a]	3.4×10^{-4} [b]	9×10^6	1×10^7
$Co(OAc)(NH_3)_5^{2+}$	$(3.06\pm0.18)\times10^4$ [c]	1.0×10^4 [c]	0.35 [d]	9×10^4	3×10^4
$Co(NCS)(NH_3)_5^{2+}$	$(1.19\pm0.08)\times10^5$ [a]	——	19 [e]	6×10^3	—
$Co(NH_3)_5(H_2O)^{3+}$	$(1.3\pm0.1)\times10^5$ [a]	——	<0.1 [f]	$>1\times10^6$	—
$Co(OH)(NH_3)_5^{2+}$	$(2.06\pm0.13)\times10^7$ [a]	——	5.2×10^6 [f]	4	—
$CoCl(NH_3)_5^{2+}$	$>1\times10^6$ [a]	——	$(2.6\pm0.5)\times10^6$ [g]	>0.4	—
$CoBr(NH_3)_5^{2+}$	$>1\times10^6$ [a]	——	$(1.4\pm0.4)\times10^6$ [g,h]	>0.7	—

a) This work. b) Ref. 18. c) Ref. 8. d) Ref. 19. e) Ref. 20. f) Ref. 21. g) Ref. 22. h) at I=0.1 ($NaClO_4$).

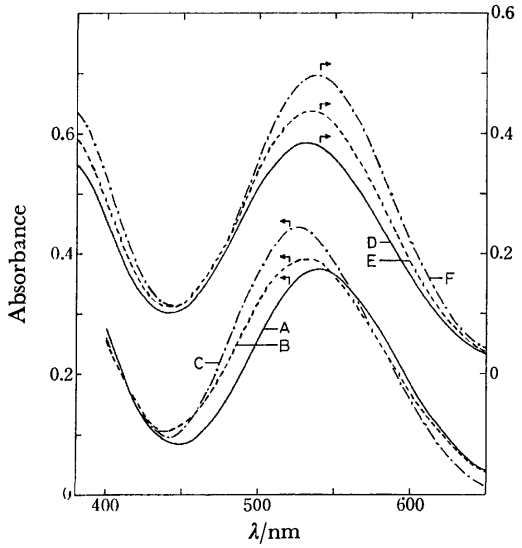

Fig. 1. Spectral changes after the electron-transfer reaction of $Co(NCS)(NH_3)_5^{2+}$ with $Cr^{II}(hedtra)(H_2O)^-$ at $[H^+]=1.99\times10^{-4}$ M, $[Co(NCS)(NH_3)_5^{2+}]_0=2.25\times10^{-3}$ M, $[Cr^{II}(hedtra)(H_2O)^-]_0=1.76\times10^{-3}$ M, and cell length=1 cm. Curves A, B, C, D, E, and F show the spectra obtained at $t=0.25$ s, 60 s, 120 s, 5 h, 49 h, and 147 h after the mixing respectively. The absorptions due to $Co(NCS)(NH_3)_5^{2+}$ unreacted and $Co^{II}(hedtra)(H_2O)^-$ produced are subtracted.

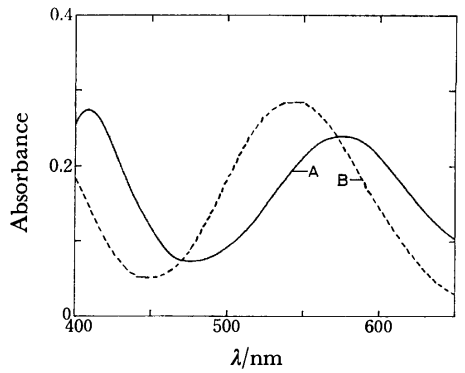

Fig. 2. Spectra obtained after the electron-transfer reaction of $CoBr(NH_3)_5^{2+}$ with $Cr^{II}(hedtra)(H_2O)^-$ at $[H^+]=1.73\times10^{-5}$ M, $[CoBr(NH_3)_5^{2+}]_0=4.00\times10^{-3}$ M, $[Cr^{II}(hedtra)(H_2O)^-]_0=1.89\times10^{-3}$ M, and cell length=1 cm. Curves A and B show the spectrum extraporated to $t=0$ and that obtained at $t=$ 25 s after the mixing respectively. The absorptions due to $CoBr(NH_3)_5^{2+}$ unreacted and $Co^{II}(hedtra)(H_2O)^-$ produced are subtracted.

within two half-lives. The observed rate constant was 2.0 s^{-1}. Therefore, the over-all reactions can be expressed in two stages given in Eqs. 9 and 10:

$$CoBr(NH_3)_5^{2+} + Cr^{II}(hedtra)(H_2O)^- \xrightarrow[\text{immeasurably fast}]{k_{et}} Co(II) + \text{Intermediate of Cr(III)}, \quad (9)$$

$$\text{Intermediate of Cr(III)} \xrightarrow[2.0\,s^{-1}]{} Cr^{III}(hedtra)(H_2O). \quad (10)$$

Reaction of $CoCl(NH_3)_5^{2+}$ with $Cr^{II}(hedtra)(H_2O)^-$. The electron-transfer reaction of this system was found to be completed within the time of mixing. The spectrum obtained immediately after the electron-transfer reaction did not change to that of $Cr^{III}(hedtra)(H_2O)$ directly. Figure 3 shows the spectral changes subsequent to the electron-transfer reaction of $CoCl(NH_3)_5^{2+}$ with $Cr^{II}(hedtra)(H_2O)^-$. The final spectrum, obtained 10 s after the electron-transfer reaction, was found to correspond to the absorption of $Cr^{III}(hedtra)(H_2O)$. The spectral changes shown in Fig. 3 can be reasonably explained by the occurrence of the following reactions:

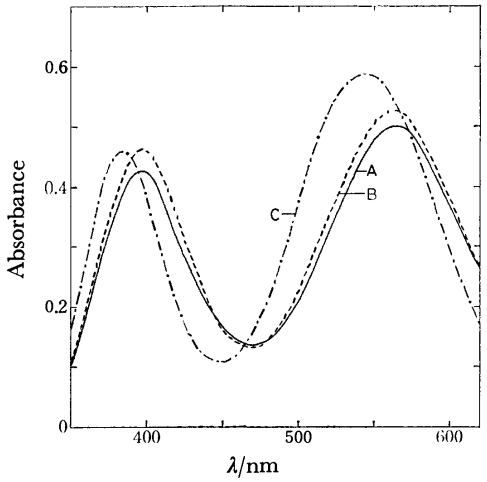

Fig. 3. Spectra obtained after the electron-transfer reaction of $CoCl(NH_3)_5^{2+}$ with $Cr^{II}(hedtra)(H_2O)^-$ at $[H^+]=1.14\times10^{-5}$ M, $[CoCl(NH_3)_5^{2+}]_0=4.83\times10^{-3}$ M, $[Cr^{II}(hedtra)(H_2O)^-]_0=3.91\times10^{-3}$ M, and cell length=1 cm. Curves A, B, and C show the spectra obtained at $t=0$, 0.12, and 10 s after the mixing. The absorptions due to $CoCl(NH_3)_5^{2+}$ unreacted and $Co^{II}(hedtra)(H_2O)^-$ produced are subtracted.

$$CoCl(NH_3)_5^{2+} + Cr^{II}(hedtra)(H_2O)^- \xrightarrow[\text{immeasurably fast}]{k_{et}} + \text{Intermediate (A) of Cr(III)} \ (Int_A), \quad (11)$$

$$Int_A \xrightarrow{k_A} \text{Intermediate (B) of Cr(III)} \ (Int_B), \quad (12)$$

$$Int_B \xrightarrow{k_B} Cr^{III}(hedtra)(H_2O). \quad (13)$$

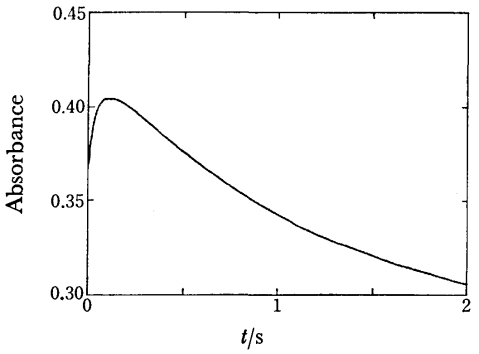

Fig. 4. The change of absorbance with time for the reactions subsequent to the electron-transfer reaction of $CoCl(NH_3)_5^{2+}$ with $Cr^{II}(hedtra)(H_2O)^-$ at 420 nm, $[H^+]=1.14\times10^{-5}$ M, $[CoCl(NH_3)_5^{2+}]_0=4.83\times10^{-3}$ M, $[Cr^{II}(hedtra)(H_2O)^-]_0=3.91\times10^{-3}$ M, and cell length=1 cm.

Table 3. The rate constants of Reaction 12 (k_A) and Reaction 13 (k_B)

$[Cr]_T$ / 10^{-3} M	$[H^+]$ / 10^{-5} M	T / °C	k_A / s^{-1}	k_B / s^{-1}
1.32	2.23	20.7	14.0±1.3	0.469±0.016
1.77	0.635	25.0	—	0.741±0.012
2.01	2.81	25.0	13.0±1.0	0.670±0.036
2.18	7.91	25.0	—	0.681±0.015
1.89	3.15	34.8	29.7±4.3	1.44 ±0.03
2.24	3.15	47.1	65±16	3.14 ±0.11

The change in the absorbance against time at 420 nm is exemplified in Fig. 4. The initial increase in the absorbance was assigned to the occurrence of Reaction 12, and the subsequent decrease in the absorbance, to that of Reaction 13. In accordance with these assignments, both the absorbance changes fit the first-order kinetics. The rate constant of Reaction 12 (k_A) was determined at 390 and 567 nm, while that of Reaction 13 (k_B) was determined at 420 and 510 nm. The values thus obtained are given in Table 3.

Discussion

Mechanism of the Reaction of $Co(NH_3)_5(H_2O)^{3+}$ with $Cr^{II}(hedtra)(H_2O)^-$. The observed second-order rate constants were considerably dependent on $[H^+]$, as is expressed in Eq. 8. If the acid-base equilibria for $Cr^{II}(hedtra)(H_2O)^-$ and $Co(NH_3)_5(H_2O)^{3+}$ are taken into consideration, the reaction in question can be expressed as the following four parallel reactions:

$$Co(OH)(NH_3)_5^{2+} + Cr^{II}(hedtra)(H_2O)^- \xrightarrow{k_1} \text{products}, \quad (14)$$

$$Co(NH_3)_5(H_2O)^{3+} + Cr^{II}(hedtra)(H_2O)^- \xrightarrow{k_2} \text{products}, \quad (15)$$

$$Co(OH)(NH_3)_5^{2+} + Cr^{II}(Hhedtra)(H_2O)_2 \xrightarrow{k_3} \text{products} \quad (16)$$

$$Co(NH_3)_5(H_2O)^{3+} + Cr^{II}(Hhedtra)(H_2O)_2 \xrightarrow{k_4} \text{products}. \quad (17)$$

Then, the following equation can be derived for the observed rate constant:

$$k_{obs} = \frac{\frac{k_1K_{Co}^H}{[H^+]} + k_2 + \frac{k_3K_{Co}^H}{K_{Cr}^H} + \frac{k_4[H^+]}{K_{Cr}^H}}{\left(1+\frac{K_{Co}^H}{[H^+]}\right)\left(1+\frac{[H^+]}{K_{Cr}^H}\right)}, \quad (18)$$

where k_1—k_4 denote the rate constants of Reactions 14—17 and where K_{Co}^H and K_{Cr}^H are defined as the equiliblium constants given by Eqs. 19 and 20 respectively:

$$K_{Co}^H = \frac{[H^+][Co(OH)(NH_3)_5^{2+}]}{[Co(NH_3)_5(H_2O)^{3+}]}, \quad (19)$$

$$K_{Cr}^H = \frac{[H^+][Cr^{II}(hedtra)(H_2O)^-]}{[Cr^{II}(Hhedtra)(H_2O)_2]}. \quad (20)$$

Although the value of K_{Cr}^H has not been reported, it may be estimated to be approximately $10^{-2.5}$ M from the corresponding values of the related complexes.[23] The value of K_{Co}^H has been reported to be $10^{-6.22}$ M at $I=0.3$ and 25 °C.[24] If the range of $[H^+]$ values employed in this work (2×10^{-5} M$<[H^+]<5\times10^{-4}$ M) and the magnitudes of K_{Cr}^H and K_{Co}^H values are taken into consideration, Eq. 18 can be simplified to

$$k_{obs} = \frac{k_1K_{Co}^H}{[H^+]} + k_2 + \frac{k_3K_{Co}^H}{K_{Cr}^H} + \frac{k_4[H^+]}{K_{Cr}^H}. \quad (21)$$

When Eq. 21 is compared with Eq. 8, it is evident that the last term on the right-hand side of Eq. 21 is negligibly small. The value of k_1 is calculated to be $(2.06\pm0.13)\times10^7$ M^{-1} s^{-1}. The value of b in Eq. 8 corresponds to the relation

$$b = k_2 + \frac{k_3K_{Co}^H}{K_{Cr}^H}. \quad (22)$$

This provides an example of a so-called proton ambiguity.[25,26] It would be reasonable to assume that the rate constant of the reaction of $Co(OH)(NH_3)_5^{2+}$ with $Cr^{II}(hedtra)(H_2O)^-$ (k_1) is larger than that with $Cr^{II}(Hhedtra)(H_2O)_2$ (k_3), because, in a closely related system, it has been shown that $Cr^{II}Y(H_2O)^{(n-2)-}$ is more reactive than its protonated form, $Cr^{II}(HY)(H_2O)^{(n-3)-}$; that is, the reaction of $Cr(OH)(NH_3)_5^{2+}$ with $Cr^{II}(edta)(H_2O)^{2-}$ has been found to proceed much faster than that with $Cr^{II}(Hedta)(H_2O)^-$.[3] Even if k_3 is equal to k_1, the value of $k_3K_{Co}^H/K_{Cr}^H$ amounts to 4×10^3 M^{-1} s^{-1}, whose contribution to the b value of Eq. 22 is only a small percentage. Hence the b value is considered to represent k_2 value itself.

Mechanisms of the Electron-transfer Reactions. The rate constants of the electron-transfer reactions of Co(III) complexes with $Cr^{II}Y(H_2O)^{(n-2)-}$ are summarized in Table 2, together with those with $Cr(H_2O)_6^{2+}$. Among them, the reactions of $Co(en)_3^{3+}$ with Cr(II) complexes are considered to proceed through an outer-sphere mechanism, because $Co(en)_3^{3+}$ has no bridging ligand.

On the bases of the extremely low basicity of a coordinated water molecule and a consideration of Marcus' cross reaction equation,[27] it has been proposed that water coordinated to a metal ion does not act as a bridging ligand in reduction by $Cr(H_2O)_6^{2+}$.[21] This proposal can be tested by a similar consideration of whether or not the electron-transfer reaction of $Co(NH_3)_5(H_2O)^{3+}$ with $Cr^{II}(hedtra)(H_2O)^-$ is of an outer-sphere type. According to Marcus' theory, the rate constant (k_{12}) of a cross reaction

$$Oxidant_1 + Reductant_2 \xrightarrow{k_{12}} Reductant_1 + Oxidant_2 \quad (23)$$

can be given as

$$k_{12} = \sqrt{k_{11}k_{22}K_{12}f}, \quad (24)$$

where k_{11} and k_{22} denote the rate constants of the exchange reactions; K_{12}, the equilibrium constant of Reaction 23; $\ln f=(\ln K_{12})^2/\{4\ln(k_{11}k_{22}/Z^2)\}$, and Z, the collision frequency. If Eq. 24 is compared for the two oxidants 1 and 1', say $Co(NH_3)_5(H_2O)^{3+}$ and $Co(en)_3^{3+}$, and a common reductant 2, the ratio of the rate constants can be expressed as

$$\frac{k_{12}}{k_{1'2}} = \sqrt{\frac{k_{11}}{k_{1'1'}}K_{11'}}, \quad (25)$$

Table 4. Comparison of the rate constants of the electron-transfer reactions of $Co(NH_3)_5(H_2O)^{3+}$ and $Co(en)_3^{3+}$ with various reductants

Reductant	$k_{et}/M^{-1}s^{-1}$		Rate ratio
	$Co(NH_3)_5(H_2O)^{3+}$	$Co(en)_3^{3+}$	$k(Co(NH_3)_5(H_2O)^{3+})/k(Co(en)_3^{3+})$
$Cr^{II}(hedtra)(H_2O)^-$	1.3×10^5 a)	3.14×10^3 a)	41
$Cr(bpy)_3^{2+}$	5×10^1 b,c)	1.8×10^2 b,c)	2.8×10^2
$Eu(H_2O)_6^{2+}$	1.5×10^{-1} b)	$\approx5\times10^{-3}$ b)	≈30
$V(H_2O)_6^{2+}$	5.3×10^{-1} d)	7.2×10^{-4} e)	7.4×10^2

a) This work. b) Ref. 20. c) at $I=0.1$ ($NaClO_4$). d) Ref. 28. e) Ref. 18.

where the f terms are ignored or considered to be cancelled. Equation 25 indicates that the rate ratio of $k_{12}/k_{1'2}$ is dependent only on the properties of the two oxidants 1 and 1'. The values of the rate ratios for the reductions of $Co(NH_3)_5(H_2O)^{3+}$ and $Co(en)_3^{3+}$ with various reductants are summarized in Table 4; they are quite similar to one another. This may support the thought that the $Cr^{II}(hedtra)(H_2O)^-$ reduction of $Co(NH_3)_5(H_2O)^{3+}$ is of an outer-sphere type.

It has been reported previously that the immediate chromium(III) product of the electron-transfer reaction of $Co(OAc)(NH_3)_5^{2+}$ with $Cr^{II}(hedtra)(H_2O)^-$ is $Cr^{III}(OAc)(hedtra)^-$ and that the inner-sphere electron-transfer is the dominant path of this reaction.[8] It would be reasonable to consider that the intermediate given in Eq. 9 is $Cr^{III}Br(hedtra)^-$. When it is assumed that the reaction proceeds exclusively through an inner-sphere mechanism, the absorption spectrum of $Cr^{III}Br(hedtra)^-$ can be estimated from the spectrum measured immediately after the electron-transfer reaction (see Fig. 2). The spectral data thus obtained and those of the related chromium(III) and cobalt(III) complexes are listed in Table 5. It is well known that the spectral shapes and absorption positions of the d-d bands of chromium(III) complexes are quite similar to those of the corresponding cobalt(III) complexes. The d-d absorption bands of the intermediate in question shift to longer wavelengths than those of $Cr^{III}(hedtra)(H_2O)$. A comparison of the data given in Table 5 will indicate that the assignment of the intermediate to $Cr^{III}Br(hedtra)^-$ is reasonable.

The intermediate formed by the reaction of $CoCl(NH_3)_5^{2+}$ with $Cr^{II}(hedtra)(H_2O)^-$ (Int_A) was found to be converted into another intermediate, Int_B, and finally into $Cr^{III}(hedtra)(H_2O)$ (see Eqs. 11—13). The spectral data of Int_A and Int_B, both given in Table 5, are very similar to each other, and so it is not unreasonable to conclude that both of the intermediates are $Cr^{III}Cl(hedtra)^-$. However, data sufficient to characterize the structural difference between these two intermediates are not available at present.

If the electron-transfer reaction of $Co(NCS)(NH_3)_5^{2+}$ with $Cr^{II}(hedtra)(H_2O)^-$ is of an outer-sphere type, the immediate product should be $Cr^{III}(hedtra)(H_2O)$. However, the spectrum of the immediate chromium(III) product in the electron-transfer reaction does not agree with that of $Cr^{III}(hedtra)(H_2O)$. This suggests that the possibility of an outer-sphere mechanism can be ruled out. The reactions of $Co(NCS)(NH_3)_5^{2+}$ and $Co(SCN)(NH_3)_5^{2+}$ with $Cr(H_2O)_6^{2+}$ have been observed to give $Cr(SCN)(H_2O)_5^{2+}$ and a mixture of $Cr(SCN)(H_2O)_5^{2+}$ and $Cr(NCS)(H_2O)_5^{2+}$ respectively.[31] Therefore, if the electron-transfer reaction of the present system proceeds through only an inner-sphere mechanism, it would be possible to assume the formation of $Cr^{III}(SCN)(hedtra)^-$ and/or $Cr^{III}(NCS)(hedtra)^-$. From independent experiments,[12] the reaction of $Cr^{III}(hedtra)(H_2O)$ with NCS^- was found to occur quite rapidly and reversibly as

$$Cr^{III}(hedtra)(H_2O) + NCS^- \rightleftharpoons Cr^{III}(NCS)(hedtra)^- + H_2O. \quad (26)$$

The absorption positions and intensities of the $Cr^{III}(NCS)(hedtra)^-$, which were determined from the equilibrium study of Reaction 26, are also given in Table 5. The spectrum of the immediate chromium(III) product in the present system does not agree with that of $Cr^{III}(NCS)(hedtra)^-$. The spectral changes after the electron-transfer reaction shown in Fig. 1 are very slow. This also indicates that the immediate product is not $Cr^{III}(NCS)(hedtra)^-$. Although the complicated spectral changes after the electron-transfer reaction cannot be explained thoroughly, the over-all features of the reaction of $Co(NCS)(NH_3)_5^{2+}$ with $Cr^{II}(hedtra)(H_2O)^-$ suggest that the reaction proceeds through an inner-sphere mechanism to give $Cr^{III}X(hedtra)^{n-}$, where X is an unidentified ligand.

Table 5. Absorption maxima (λ) and molar absorption coefficients (ε) of chromium(III) and cobalt(III) complexes of the $M^{III}X(hedtra)^{n-}$ type

Complex	λ/nm (ε/$M^{-1}cm^{-1}$)		Ref.
	First band	Second band	
$Cr(hedtra)(H_2O)$	545 (151)	385 (117)	9
$Co(hedtra)(H_2O)$	544 (245)	383 (197)	29
$Cr(NCS)(hedtra)^-$	535 (187)	392 (110)	12
$Cr(N_3)(hedtra)^-$	552 (207)	407 (130)	10
$Cr(OAc)(hedtra)^-$	556 (162)	394 (113)	9
$CrCl(hedtra)^-$ (Int_A) a)	565 (128)	397 (109)	This work
$CrCl(hedtra)^-$ (Int_B) a)	563 (136)	398 (121)	This work
$CoCl(hedtra)^-$	585 (278)	403 (251)	30
$CrBr(hedtra)^-$ a)	575 (127)	408 (145)	This work
$CoBr(hedtra)^-$	588 (241)	400 (243)	30

a) The spectral data were estimated on the assumption that the electron-transfer reaction of $CoCl(NH_3)_5^{2+}$ or $CoBr(NH_3)_5^{2+}$ with $Cr^{II}(hedtra)(H_2O)^-$ proceeds exclusively through the inner-sphere mechanism.

Rate Constants of the Electron-transfer Reactions. In the previous papers,[2,3] it was reported that Cr^{II}-

(edta) $(H_2O)^{2-}$ reacts with $CrX(NH_3)_5^{2+}$ ($X=F^-$, Cl^-, Br^-, NCS^-, and OH^-) much faster than $Cr(H_2O)_6^{2+}$ does, and this was explained by considering the change in the standard oxidation-reduction potentials of the Cr(II)–Cr(III) couples. Recently, Davies and Earley reported that the electron-transfer reactions of $CrCl(NH_3)_5^{2+}$ with some Cr(II)–amino polycarboxylate complexes followed the linear free-energy relationship with the slope ($\Delta\Delta G^*/\Delta\Delta G^\circ$) of 0.48, where $\Delta\Delta G^*$ and $\Delta\Delta G^\circ$ denote the change in the free energy of activation of the electron-transfer reactions and the free-energy difference between the chromium(II) and chromium(III) species respectively.[5] The data given in Table 2 show that the rate constants of the electron-transfer reactions of the cobalt(III) complexes with $Cr^{II}(hedtra)(H_2O)^-$ and $Cr^{II}(edta)(H_2O)^{2-}$ are larger than those of the corresponding reactions with $Cr(H_2O)_6^{2+}$. This rate enhancement may also be understood qualitatively by considering the free-energy change in the reactions. If the electron-transfer reactions of a common cobalt(III) complex with $Cr^{III}(H_2O)^{(n-2)-}$ and $Cr(H_2O)_6^{2+}$ follow the linear free-energy relationship with the slope of 0.5, 6×10^4 and 7×10^4 may be expected for the values of k(Cr-hedtra)/k(Cr) and k(Cr-edta)/k(Cr) respectively. Among the data shown in Table 2, the observed values of $Co(en)_3^{3+}$, $Co(NH_3)_5(H_2O)^{3+}$, and $Co(OH)(NH_3)_5^{2+}$ deviate considerably from the expected values. This may suggest that the assumption mentioned above is not satisfied for, at least, these systems, and that the other factors controlling the rates should be considered. The observed value for $Co(OH)(NH_3)_5^{2+}$ may be nearly a rate limit in the inner-sphere electron-transfer reactions containing Cr(II) ions as reductants.[32] This leads to the understanding that the free-energy change in the reaction by the coordination of HEDTRA to Cr(II) affects only slightly the rate of electron-transfer for, at least, the $Co(OH)(NH_3)_5^{2+}$ system.

Aquation Reactions of $Cr^{III}Cl(hedtra)^-$ and $Cr^{III}Br(hedtra)^-$ Subsequent to the Electron-transfer Reactions. It has been shown previously that the water position in the $Cr^{III}(hedtra)(H_2O)$ is a substitution-labile site.[9,10] This has been so postulated that the free $-CH_2CH_2OH$ existing in the complex ion acts as a nucleophile and catalyzes the substitution. It was found in this work that $Cr^{III}Cl(hedtra)^-$ and $Cr^{III}Br(hedtra)^-$ also aquate rapidly to give $Cr^{III}(hedtra)(H_2O)$. However, no formation of $Cr^{III}Cl(hedtra)^-$ or $Cr^{III}Br(hedtra)^-$ was observed upon the addition of an NaCl or NaBr solution up to a 1 M to $Cr^{III}(hedtra)(H_2O)$ solution. This may allow one to estimate that the formation constants of these mixed ligand complexes are less than 0.1 M^{-1}. The Eyring plot for the rate constants of the aquation reaction of $Cr^{III}Cl(hedtra)^-$ (the k_2 values are given in Table 3) gives activation parameters of $\Delta H^*=53.9\pm3.3$ kJ mol^{-1} and $\Delta S^*=-68\pm11$ J K^{-1} mol^{-1}. The large negative entropy of activation suggests an associative nature in the mechanism of this aquation reaction.

The authors wish to thank the Ministry of Education for Scientific Research Grant-in-Aid No. 147043. They also wish to thank Professor Kahei Takase of this department for allowing us to use a rapid-scanning spectrophotometer.

References

1) The following abbreviations are used throughout the paper: HEDTRA=*N*-(2-hydroxyethyl)ethylenediamine-*N*,*N*′,*N*′-triacetic acid, EDTA=ethylenediamine-*N*,*N*,*N*′,*N*′-tetraacetic acid, L=hedtra^{3-} or edta^{4-}, OAc^-=acetate, and en=ethylenediamine.
2) H. Ogino and N. Tanaka, *Bull. Chem. Soc. Jpn.*, **41**, 1622 (1968).
3) H. Ogino and N. Tanaka, *Bull. Chem. Soc. Jpn.*, **41**, 2411 (1968).
4) J. E. Earley, *Prog. Inorg. Chem.*, **13**, 243 (1970).
5) K. M. Davies and J. E. Earley, *Inorg. Chem.*, **15**, 1074 (1976).
6) H. Diebler, P. H. Dodel, and H. Taube, *Inorg. Chem.*, **5**, 1688 (1966).
7) R. N. F. Thorneley, B. Kipling, and A. G. Sykes, *J. Chem. Soc., A*, **1968**, 2847.
8) H. Ogino, M. Shimura, T. Watanabe, and N. Tanaka, *Inorg. Nucl. Chem. Lett.*, **12**, 911 (1976).
9) H. Ogino, T. Watanabe, and N. Tanaka, *Inorg. Chem.*, **14**, 2093 (1975).
10) H. Ogino, M. Shimura, and N. Tanaka, *Chem. Lett.*, **1976**, 127.
11) Y. Sulfab, R. S. Taylor, and A. G. Sykes, *Inorg. Chem.*, **15**, 2388 (1976).
12) H. Ogino, M. Shimura, and N. Tanaka, unpublished results.
13) W. A. Hynes, L. K. Yanowsky, and M. Shiller, *J. Am. Chem. Soc.*, **60**, 3053 (1938).
14) H. Diehl, H. Clark, and H. H. Willard, *Inorg. Synth.*, **1**, 186 (1939).
15) A. Werner, H. Müller, R. Klein, and F. Bräunlich, *Z. Anorg. Chem.*, **22**, 91 (1900).
16) J. B. Work, *Inorg. Synth.*, **2**, 221 (1946).
17) R. E. Kitson, *Anal. Chem.*, **22**, 664 (1950).
18) T. J. Przystas and N. Sutin, *J. Am. Chem. Soc.*, **95**, 5545 (1973).
19) M. B. Barrett, J. H. Swinehart, and H. Taube, *Inorg. Chem.*, **10**, 1983 (1971).
20) J. P. Candlin, J. Halpern, and D. L. Trimm, *J. Am. Chem. Soc.*, **86**, 1019 (1964).
21) D. L. Toppen and R. G. Linck, *Inorg. Chem.*, **10**, 2635 (1971).
22) J. P. Candlin and J. Halpern, *Inorg. Chem.*, **4**, 766 (1965).
23) L. G. Sillén and A. E. Martell, "Stability Constants of Metal-Ion Complexes," Spec. Publ. No. 25, Chem. Soc., London (1971).
24) R. C. Splinter, S. J. Harris, and R. S. Tobias, *Inorg. Chem.*, **7**, 897 (1968).
25) J. H. Espenson, *Inorg. Chem.*, **8**, 1554 (1969).
26) A. Haim, *Acc. Chem. Res.*, **8**, 264 (1975).
27) R. A. Marcus, *Ann. Rev. Phys. Chem.*, **15**, 155 (1964), and the references cited therein.
28) P. H. Dodel and H. Taube, *Z. Phys. Chem. (Frankfurt am Main)*, **44**, 92 (1965).
29) P. B. Wood and W. C. E. Higginson, *J. Chem. Soc.*, **1964**, 1484.
30) C. W. Van Saun and B. E. Douglas, *Inorg. Chem.*, **7**, 1393, (1968).
31) C. Shea and A. Haim, *J. Am. Chem. Soc.*, **93**, 3055 (1971).
32) R. C. Patel, R. E. Ball, J. F. Endicott, and R. G. Hughes, *Inorg. Chem.*, **9**, 23 (1970), and the references cited therein.

The Crystal Structure of Monoaquabis(1,10-phenanthroline)copper(II) Tetrafluoroborate $[Cu(H_2O)(phen)_2](BF_4)_2$

Hisayoshi NAKAI and Yukinao NODA

Department of Chemistry, Hyogo College of Medicine, Mukogawa-cho, Nishinomiya, Hyogo 663

(Received November 14, 1977)

The crystal of the title compound is monoclinic, with $a=19.099(6)$, $b=8.100(3)$, $c=16.177(5)$ Å, $\beta=100.54(5)°$, the space group of C2/c, and $Z=4$. The structure was determined from the counter data and was refined to $R=0.083$ for 1736 non-zero reflections. The coordination geometry of the copper atom is best described as a distorted trigonal bipyramid, in which the equatorial plane is composed of Cu, two N, and water O atoms, and the axial positions are occupied by two N atoms. The complex has a crystallographically imposed twofold axis which passes through the copper and the water oxygen atoms at the equatorial plane. The two phenanthroline ligands are related with each other by this axis.

In bis(bipyridine) and bis(phenanthroline)copper(II) complexes, the $Cu(chelate)_2^{2+}$ (chelate=bpy or phen) group is unable to assume a coplanar disposition about the copper atom because of the steric repulsions between the hydrogen atoms of these two chelates(I). Therefore, it has been shown that the bis(bipyridine)copper(II) complexes take a variety of stereochemistries, a distorted trigonal bipyramid[1-5] and *cis*-[6] and *trans*-distorted octahedra,[7,8] while the structure of the bis(phenanthroline)copper(II) complexes has not yet been investigated in detail.[9,10] As a part of our structural studies of such complexes, a single-crystal X-ray analysis has been carried out on $[Cu(H_2O)(phen)_2](BF_4)_2$.

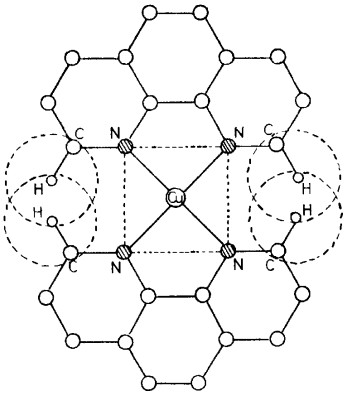

I

Experimental

The green crystals of $[Cu(H_2O)(phen)_2](BF_4)_2$ were prepared by a method similar to that used for the preparation of the corresponding nitrate;[9] they were then recrystallized from a water-methanol mixture. Found: C, 46.93; H, 2.96; N, 9.31%. Calcd for $Cu(phen)_2(BF_4)_2\cdot H_2O$: C, 46.83; H, 2.95; N, 9.10%.

Preliminary X-ray photographs taken with Cu$K\alpha$ radiation showed a Laue symmetry of 2/m, with systematic absences of hkl for $h+k=2n+1$ and $h0l$ for $l=2n+1$. The space group is either C2/c or Cc; the former was confirmed by a successful refinement of the structure.

A crystal with dimensions of $0.35\times0.36\times0.38$ mm was mounted on a glass fiber for data collection. The unit-cell dimensions were determined by a least-squares fit using 21 θ-values measured accurately on a diffractometer. Crystal data: $[Cu(H_2O)(phen)_2](BF_4)_2$, $M.W.=615.6$, monoclinic, $a=19.099(6)$, $b=8.100(3)$, $c=16.177(5)$ Å, $\beta=100.54(5)°$, $U=2460.5$ Å^3, $Z=4$, $D_c=1.66$, $D_m=1.64$ g cm^{-3}, Mo$K\alpha$ radiation($\lambda=0.71069$ Å), μ(Mo$K\alpha$)$=10.1$ cm^{-1}, space group C2/c.

The intensity data with $6°\leqq2\theta\leqq60°$ were collected at room temperature by the ω-2θ scan technique on a Philips PW1100 four-circle diffractometer using graphite-monochromated Mo$K\alpha$ radiation, a scan speed of 0.03° s^{-1}, a scan width of $(1.0+0.2\tan\theta)°$, and two 10-s background counts. Three standard reflections ($\bar{2}04$, $0\bar{2}0$, and 604), monitored every 4 h throughout the data collection, showed no significant variation in intensity. A total of 1736 intensities with $I_{top}-2\sqrt{I_{top}}\geqq I_{back}$ were classified as observed; I_{top} is the intensity(counts/s) measured at the top of the peak, and I_{back} is the mean background intensity(counts/s) obtained from the preliminary background measurement for 5 s on each side of the peak. The intensity data were processed with the computer program of Hornstra and Stubbe.[11] No absorption correction was made.

Structure Determination

The positions of the copper atoms were determined from a three-dimensional Patterson map, the space group being assumed to be C2/c. The structure was solved by the heavy-atom technique, and the positional and thermal parameters were refined by the block-diagonal least-squares method. The minimized function was $\Sigma w(F_o-|F_c|)^2$. A weighting scheme of the type suggested by Hughes[14] was applied using $w=1.0$ for $F_o\leqq F_{max}$ and $w=(F_{max}/F_o)^2$ for $F_o>F_{max}$; $F_{max}=31.0$ was found to be optimum. The atomic scattering curves were taken from Ref. 15. The initial refinement was carried out with isotropic thermal parameters. The thermal parameters of all the atoms except those of the BF_4^- ion converged at 3—5 Å^2, while those of the B and F atoms were found to be unusually large. In the subsequent refinement, the anisotropic thermal parameters were used for the Cu, C, N, and O atoms, but not for the B and F atoms. The R value was reduced to 0.116. Although introduction of anisotropic temperature factors for the B and F atoms as well as the other atoms reduced the R value further to 0.087, some of the F–B–F bond angles were found to be far from the tetrahedral angle (109°28′). In order to investigate carefully the electron-density distribution for the BF_4^- anion, we calculated a difference Fourier map in which the electron

TABLE 1. ATOMIC PARAMETERS AND THEIR STANDARD DEVIATIONS
OC indicates the occupancy factor of the atom in a distorted arrangement.

Atom	*x*	*y*	*z*	*B*/Å²	*OC*
Cu	0.0	0.0703(2)	0.25	a)	
O	0.0	−0.2060(10)	0.25	a)	
N(1)	0.0953(3)	0.0549(8)	0.3232(3)	a)	
N(2)	−0.0279(3)	0.1633(8)	0.3567(4)	a)	
C(1)	0.1555(4)	−0.0034(11)	0.3038(5)	a)	
C(2)	0.2180(4)	−0.0128(12)	0.3641(5)	a)	
C(3)	0.2184(4)	0.0399(10)	0.4438(5)	a)	
C(4)	0.1565(4)	0.1010(10)	0.4655(4)	a)	
C(5)	0.1514(5)	0.1628(12)	0.5477(5)	a)	
C(6)	0.0904(5)	0.2253(12)	0.5641(5)	a)	
C(7)	0.0271(4)	0.2296(10)	0.5007(4)	a)	
C(8)	−0.0402(5)	0.2894(12)	0.5140(5)	a)	
C(9)	−0.0962(5)	0.2875(12)	0.4497(6)	a)	
C(10)	−0.0893(4)	0.2231(12)	0.3704(5)	a)	
C(11)	0.0954(3)	0.1077(8)	0.4026(4)	a)	
C(12)	0.0302(4)	0.1675(9)	0.4204(4)	a)	
B(1a)	0.1727(6)	−0.4639(15)	0.3195(7)	2.9(0.2)	0.6
B(1b)	0.1468(11)	−0.4875(28)	0.3158(13)	3.5(0.3)	0.4
F(1a)	0.1237(7)	−0.3850(16)	0.2622(8)	8.3(0.3)	0.6
F(1b)	0.1538(12)	−0.3702(30)	0.2501(14)	10.2(0.5)	0.4
F(2a)	0.2338(8)	−0.3906(19)	0.3440(10)	10.2(0.4)	0.6
F(2b)	0.1712(19)	−0.3950(21)	0.3898(11)	7.5(0.4)	0.4
F(3a)	0.1423(9)	−0.4932(20)	0.3914(10)	10.5(0.4)	0.6
F(3b)	0.0810(17)	−0.5450(36)	0.3040(20)	13.4(0.8)	0.4
F(4a)	0.1875(6)	−0.6125(14)	0.2911(7)	7.1(0.2)	0.6
F(4b)	0.1877(10)	−0.6186(26)	0.3142(12)	9.1(0.5)	0.4
H(C1)	0.160(2)	−0.047(6)	0.243(3)	4.0	
H(C2)	0.260(3)	−0.058(7)	0.348(3)	4.0	
H(C3)	0.260(3)	0.025(7)	0.485(3)	4.0	
H(C5)	0.195(3)	0.187(7)	0.596(4)	4.0	
H(C8)	−0.041(3)	0.330(7)	0.566(3)	4.0	
H(C10)	−0.133(3)	0.225(7)	0.318(4)	4.0	
H(O)	0.030(3)	−0.281(7)	0.257(4)	4.0	

a) Anisotropic thermal factors are listed in Table 2.

TABLE 2. ANISOTROPIC THERMAL FACTORS[a] ($\times 10^4$) FOR THE NON-HYDROGEN ATOMS IN THE COMPLEX CATION

Atom	B_{11}	B_{22}	B_{33}	B_{12}	B_{13}	B_{23}
Cu	18.0(0.3)	171(2)	27.8(0.4)	0	−1.3(0.5)	0
O	28(2)	141(14)	67(4)	0	−3(5)	0
N(1)	21(1)	135(10)	33(2)	−8(7)	2(3)	−13(8)
N(2)	22(2)	153(11)	35(2)	15(7)	5(3)	10(8)
C(1)	20(2)	185(14)	48(4)	1(9)	0(4)	−28(12)
C(2)	22(2)	201(15)	49(4)	17(9)	1(4)	10(13)
C(3)	22(2)	179(17)	51(4)	0(9)	−13(4)	42(12)
C(4)	28(2)	155(15)	33(3)	−21(8)	−7(4)	19(9)
C(5)	37(3)	210(17)	30(3)	−36(11)	−6(4)	9(11)
C(6)	37(3)	203(17)	35(3)	−33(11)	−1(5)	19(12)
C(7)	32(2)	171(14)	30(3)	−17(9)	14(4)	16(10)
C(8)	46(3)	227(18)	33(3)	17(13)	26(5)	5(12)
C(9)	43(3)	214(18)	45(4)	50(13)	30(6)	7(13)
C(10)	29(2)	230(18)	39(3)	45(11)	11(4)	39(12)
C(11)	21(2)	105(11)	34(3)	−11(7)	−1(3)	22(8)
C(12)	27(2)	116(12)	31(3)	−13(8)	4(4)	6(9)

a) The anisotropic thermal factors are of the form: $\exp\{-(h^2B_{11}+k^2B_{22}+l^2B_{33}+hkB_{12}+hlB_{13}+klB_{23})\}$.

density due to the complex cation was eliminated. Figure 3 shows the resulting electron-density distribution, which can virtually account for the two azimuthally different BF_4^- ions in a statistical distribution. The weights of 0.6 and 0.4 for the BF_4^- ion with the subscript a and that with b(Fig. 3) were found to be optimum in view of the R value. Seven of the nine crystallographically independent hydrogen atoms could be located on the difference Fourier map calculated at this point. These seven hydrogen atoms were included in the final refinement, with an isotropic thermal parameter of 4.0 Å^2. The final R value was 0.083 for 1736 observed reflections. All the parameter shifts were less than 0.1σ in the final cycle of the refinement. The atomic coordinates and thermal parameters are listed in Tables 1 and 2. The observed and calculated structure factors are preserved at the Chemical Society of Japan(Document Number 7812). The computer programs used in the calculations were as follows: RSSFR-5[12] (Fourier synthesis), HBLS-V[13] (least-squares calculation), and DAPH[13] (interatomic distances and angles, least-squares plane, and coordinates of the H atoms). All the computations were carried out on a NEAC2200—700 computer at Osaka University.

Results and Discussion

The crystal is composed of the $[Cu(H_2O)(phen)_2]^{2+}$ cations and the tetrafluoroborate anions. The bond lengths and angles, with their estimated standard deviations, are given in Table 3.

Figure 1 shows a schematic drawing of the complex cation. There is a twofold axis which passes through the copper and the water-oxygen atoms and which relates the two phenanthroline ligands with each other. The central copper atom is surrounded by the four nitrogen atoms of the two phenanthroline ligands and one water-oxygen atom. The two Cu–N distances of 1.985(6) and 2.041(7) Å in the chelate ring are appreciably different. The Cu–O bond is 2.238(8) Å long.

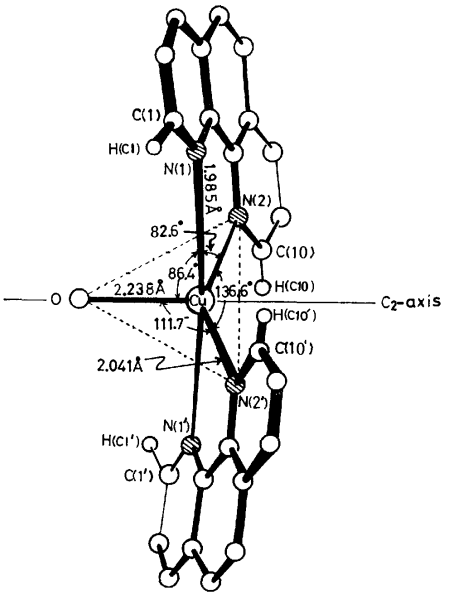

Fig. 1. A schematic drawing of the complex cation $[Cu(H_2O)(phen)_2]^{2+}$.

Among possible configurations for the five-coordinate complex, a trigonal-bipyramidal arrangement, II, and a square-pyramidal one, III, may be considered to be common in the $[Cu(chelate)_2X]^{n+}$ cations(chelate= phen or bpy).

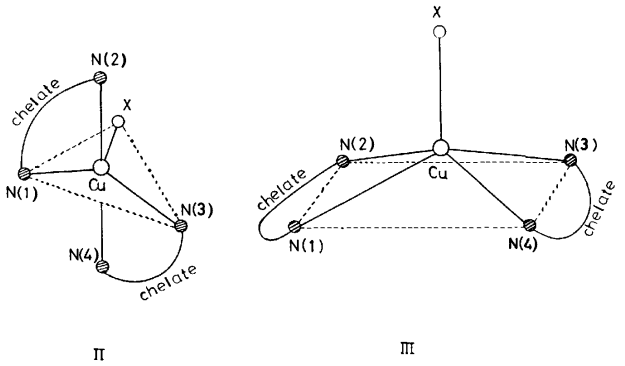

Several complexes with a II trigonal-bipyramidal stereochemistry have been found in $[Cu(bpy)_2X]^{n+}$-type complexes (X=I, NH_3, Cl, $CS(NH_2)_2$, and Cu^ICl_2).[1-5] As has been suggested by Stephens *et al.*, it is characteristic that the four Cu–N(bpy) distances in all those complexes except $[Cu(bpy)_2I]^+$ fall into two sets: the axial Cu–N(bpy) distances range from 1.96 to 2.00 Å and are significantly shorter (0.06—0.12 Å) than the equatorial ones. The N(1)–Cu–N(3) angle in the equatorial plane has been shown to be in the range of 109—123° in those complexes.[1-5]

On the other hand, a complex with a square-pyramidal stereochemistry, III, has not yet been found in the bis(phenanthroline)- and bis(bipyridine)copper(II) complexes. However, it has been recently shown that, when the two bipyridine ligands are coordinated to a copper atom in a square-planar arrangement, they must be twisted out of the central copper atom, in opposite directions about their individual C_2-axis by 15—20° towards a tetrahedral stereochemistry, because of the steric repulsions between the hydrogen atoms of the bipyridine ligands in the square-coplanar $Cu(bpy)_2^{2+}$ moiety(I).[7,8] Therefore, if a $[Cu(phen)_2X]^{n+}$ cation takes a square-pyramidal stereochemistry(III), the four nitrogen atoms of the $Cu(phen)_2^{2+}$ moiety in the basal plane should have a flattened tetrahedral disposition. Therefore, the N(1)–Cu–N(3) or N(2)–Cu–N(4) angle in III is presumably in the range of 150—160°. However, there must be no significant difference between the four Cu–N(phen) distances.

Judging from the details described above, the coordination geometry about the copper atom should be described as a distorted trigonal-bipyramid, because the two Cu–N distances for a given phenanthroline ligand are significantly different(Cu–N(1)=1.985(6) and Cu–N(2)=2.041(7) Å); the axial positions are occupied by N(1) and N(1'), while the Cu, N(2), N(2'), and O atoms lie on the trigonal plane. The angle of N(2)–Cu–N(2') in the trigonal plane is 137°; this value is, however, considerably larger than those (108—123°) found in the trigonal-bipyramidal complexes.[1-5] The

TABLE 3. BOND DISTANCES (l/Å) AND ANGLES (φ/°), WITH THEIR ESTIMATED STANDARD DEVIATIONS IN PARENTHESES[a)]

Cu-N(1) = 1.985(6)	B(1a)-F(1a) = 1.35(2)
Cu-N(2) = 2.041(7)	B(1a)-F(2a) = 1.31(2)
Cu-O = 2.238(8)	B(1a)-F(3a) = 1.41(2)
N(1)-C(1) = 1.33(1)	B(1a)-F(4a) = 1.34(2)
N(1)-C(11) = 1.35(1)	B(1b)-F(1b) = 1.45(3)
N(2)-C(10) = 1.32(1)	B(1b)-F(2b) = 1.42(3)
N(2)-C(12) = 1.37(1)	B(1b)-F(3b) = 1.32(4)
C(1)-C(2) = 1.40(1)	B(1b)-F(4b) = 1.32(3)
C(2)-C(3) = 1.36(1)	C(1)-H(C1) = 1.05(5)
C(3)-C(4) = 1.39(1)	C(2)-H(C2) = 0.97(6)
C(4)-C(5) = 1.44(1)	C(3)-H(C3) = 0.95(6)
C(4)-C(11) = 1.40(1)	C(5)-H(C5) = 1.06(6)
C(5)-C(6) = 1.34(1)	C(8)-H(C8) = 0.91(6)
C(6)-C(7) = 1.44(1)	C(10)-H(C10) = 1.07(6)
C(7)-C(8) = 1.43(1)	O-H(O) = 0.83(6)
C(7)-C(12) = 1.41(1)	
C(8)-C(9) = 1.35(1)	O···F(1a) = 2.75(2)
C(9)-C(10) = 1.41(1)	O···F(1b) = 3.22(3)
C(11)-C(12) = 1.41(1)	
N(1)-Cu-N(2) = 82.6(3)	C(4)-C(5)-C(6) = 121.4(9)
N(1)-Cu-N(2′) = 100.1(3)	C(4)-C(11)-C(12) = 120.8(6)
N(1)-Cu-O = 86.4(3)	C(5)-C(6)-C(7) = 121.1(9)
N(2)-Cu-O = 111.7(3)	C(6)-C(7)-C(8) = 124.4(8)
Cu-N(1)-C(11) = 112.9(5)	C(6)-C(7)-C(12) = 118.7(8)
Cu-N(1)-C(1) = 128.1(6)	C(7)-C(12)-C(11) = 119.9(7)
Cu-N(2)-C(10) = 130.9(6)	C(7)-C(8)-C(9) = 119.3(9)
Cu-N(2)-C(12) = 110.1(5)	C(8)-C(7)-C(12) = 116.9(8)
C(1)-N(1)-C(11) = 118.9(7)	C(8)-C(9)-C(10) = 120.8(9)
C(10)-N(2)-C(12) = 119.0(7)	F(1a)-B(1a)-F(2a) = 117(1)
N(1)-C(1)-C(2) = 121.2(8)	F(1a)-B(1a)-F(3a) = 108(1)
N(1)-C(11)-C(4) = 122.3(6)	F(1a)-B(1a)-F(4a) = 111(1)
N(1)-C(11)-C(12) = 116.9(6)	F(2a)-B(1a)-F(3a) = 108(1)
N(2)-C(10)-C(9) = 121.4(9)	F(2a)-B(1a)-F(4a) = 106(1)
N(2)-C(12)-C(7) = 122.6(7)	F(3a)-B(1a)-F(4a) = 106(1)
N(2)-C(12)-C(11) = 117.5(6)	F(1b)-B(1b)-F(2b) = 102(2)
C(1)-C(2)-C(3) = 120.1(9)	F(1b)-B(1b)-F(3b) = 100(2)
C(2)-C(3)-C(4) = 119.8(8)	F(1b)-B(1b)-F(4b) = 112(2)
C(3)-C(4)-C(5) = 124.3(8)	F(2b)-B(1b)-F(3b) = 104(2)
C(3)-C(4)-C(11) = 117.7(7)	F(2b)-B(1b)-F(4b) = 110(2)
C(5)-C(4)-C(11) = 118.0(7)	F(3b)-B(1b)-F(4b) = 99(2)

a) Estimated standard deviations are right-adjusted to the last digit of the preceding number. The atom with the prime is related by a twofold symmetry to the corresponding unprimed atom.

TABLE 4. LEAST-SQUARES PLANES AND DEVIATIONS OF ATOMS FROM THE PLANE (l/Å)

The equation of the plane is of the form $AX+BY+CZ+D=0$, where X, Y, Z, and D are measured in Å units. (The atoms marked by * are not included in the least-squares calculation.)

a) Phenanthroline ligand

$0.2954X+0.9161Y-0.2711Z+0.7571=0$

N(1)	0.026	N(2)	−0.038	C(1)	0.034	C(2)	0.004
C(3)	−0.016	C(4)	−0.025	C(5)	−0.021	C(6)	0.014
C(7)	0.018	C(8)	0.012	C(9)	0.016	C(10)	−0.012
C(11)	0.006	C(12)	−0.010	Cu*	−0.018	H(C1)*	0.050
H(C10)*	0.024						

b) Plane formed by Cu, N(2), and O atoms: $-0.8942X+0.0000Y-0.4477Z+1.1184=0$

c) Plane formed by Cu, N(1), and N(2) atoms: $0.2710X+0.9227Y-0.2743Z+0.7658=0$

d) Plane formed by Cu, N(1), and O atoms: $0.5880X-0.0000Y-0.8089Z+3.6511=0$

N(1)–Cu–O angle is 86.4°, and the N–Cu–N angle in the chelate ring is 82.8°.

On the basis of our previous X-ray examination of $[Cu(H_2O)(phen)_2](NO_3)_2$,[9] which was performed by the use of photographic data, the $[Cu(H_2O)(phen)_2]^{2+}$ cation was assigned a trigonal-bipyramidal structure, in which the axial and equatorial Cu–N distances were 1.99(1) and 2.03(1) Å respectively. Although the unit-cell dimensions of the $[Cu(H_2O)(phen)_2](BF_4)_2$ are different from those of the nitrate salt, the disposition of anions around the cation in the former resembles that in the latter; that is, these two crystal structures are roughly in agreement with each other. In the complex cation, there is no significant difference in the Cu–N distances, while the Cu–O distances are 2.18(1) Å in the NO_3^- salt and 2.238(8) Å in the BF_4^- salt, a difference of about 0.06 Å. However, the e.s.d. in the NO_3^- salt might be underestimated because it is based on photographic data. Therefore, we may regard the coordination geometries of these two complexes as essentially identical.

The phenanthroline ligands are planar within a maximum deviation of 0.04 Å(Table 4). The angle between the best planes of these two phenanthroline ligands is 47°. The H(C1)···H(C10′) distance is 2.43 Å; this value is equal to the sum of the van der Waals radii of the hydrogen atoms (Fig. 2). The bond lengths and angles agree with the values usually found in Cu(II)–phen complexes.[9,10,16,17] However, it is noted that the distances of C(2)–C(3), C(5)–C(6), and C(8)–C(9) are shorter than the others by 0.03—0.10 Å; such a trend has also been observed in the Cu(II)–phen complexes.

The arrangement of tetrafluoroborate ions is linked to the coordinated water molecules through O–H···F hydrogen bonding (O···F(1a)=2.75 Å) (Fig. 3). The B–F bond distances range from 1.32 to 1.45 Å, and the F–B–F angles, from 99 to 117°.

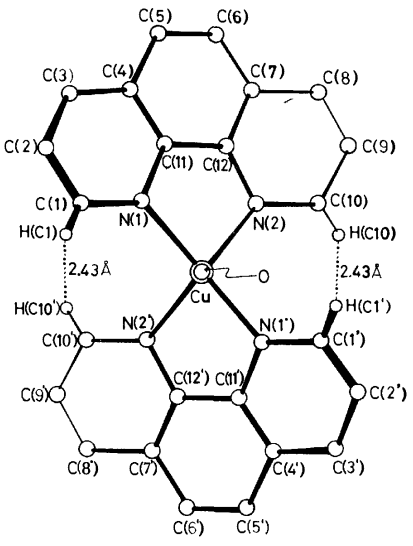

Fig. 2. The b axis projection of the complex cation $[Cu(H_2O)(phen)_2]^{2+}$.

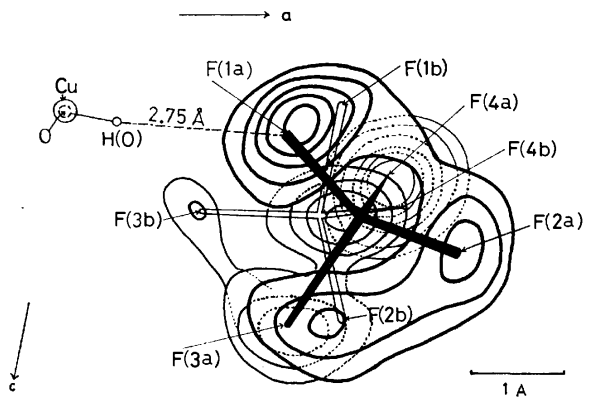

Fig. 3. The electron-density distribution of the disordered BF_4^- ion(O–H···F(BF_4^-) hydrogen bond, ——). The contours are at an arbitrary interval.

This work was supported in part by a Grant-in-Aid for Scientific Research from the Ministry of Education (No. 164174), for which the authors are grateful. The authors also wish to express their deep thanks to Professor Hisao Kuroya, Dr. Shun'ichiro Ooi, and Dr. Keiji Matsumoto of Osaka City University for allowing them to use a Philips PW1100 diffractometer.

References

1) G. A. Barclay, B. F. Hoskins, and C. H. L. Kennard, *J. Chem. Soc.*, **1963**, 5691.
2) F. S. Stephens, *J. Chem. Soc., Dalton Trans.*, **1972**, 1350.
3) F. S. Stephens and P. A. Tucker, *J. Chem. Soc., Dalton Trans.*, **1973**, 2293.
4) M. B. Ferrari, A. B. Corradi, G. G. Fava, C. G. Palmieri, M. Nardelli, and C. Pelizzi, *Acta Crystallogr., Sect. B*, **29**, 1808 (1973).
5) J. Kaiser, G. Brauer, and F. A. Schröder, *J. Chem. Soc., Dalton Trans.*, **1974**, 1490.
6) I. M. Procter and F. S. Stephens, *J. Chem. Soc. A*, **1969**, 1248.
7) H. Nakai, *Bull. Chem. Soc. Jpn.*, **44**, 2412 (1971).
8) M. B. Ferrari, G. G. Fava, and C. Pelizzi, *J. Chem. Soc., Chem. Commun.*, **1977**, 8.
9) H. Nakai and Y. Deguchi, *Bull. Chem. Soc. Jpn.*, **48**, 2557 (1975).
10) O. P. Anderson, *Inorg. Chem.*, **14**, 730 (1975).
11) J. Hornstra and B. Stubbe, PW1100 Data Processing Program, Philips Research Laboratories, Eindhoven, Holland.
12) T. Sakurai, The Universal Crystallographic Computing System(I), The Crystallographic Society of Japan(1967), p. 19.
13) T. Ashida, The Universal Crystallographic Computing System-Osaka, The Computation Center, Osaka University (1973), pp. 55, 63.
14) E. W. Hughes, *J. Am. Chem. Soc.*, **63**, 1737 (1941).
15) "International Tables for X-Ray Crystallography," Vol. 3, Kynoch Press, Birmingham (1962), p. 202.
16) D. L. McFadden and A. T. McPhail, *J. Chem. Soc., Dalton Trans.*, **1975**, 1993.
17) O. P. Anderson, *J. Chem. Soc., Dalton Trans.*, **1973**, 1237.

Relative Intensities of the Ligand-field Transition Bands in Tetragonal Chromium(III) and Cobalt(III) Complexes

Shuhei FUJINAMI, Muraji SHIBATA, and Hideo YAMATERA*

Department of Chemistry, Faculty of Science, Kanazawa University, Kanazawa 920

**Department of Chemistry, Faculty of Science, Nagoya University, Chikusa, Nagoya 464*

(Received November 16, 1977)

On the basis of a tetragonal (D_{4h}) model, the procedures for calculating the vibronically induced transition moment have been described, and a correlation in the band intensity between two nondegenerate transition components (A_2 and B_2) has been shown. The correlation has then been applied to understanding the characteristic absorption spectra of the *trans*-$[CrClF(NH_3)_4]^+$ and *trans*-$[CrF_2(NH_3)_4]^+$ complexes. Furthermore, an effect upon the band intensity caused by the configuration interactions among the E states has been proposed in order to explain the characteristic spectra of the *trans*-$[Co(C_2O_4)_2(py)_2]^-$ and *trans*-$[Co(CO_3)_2(py)_2]^-$ complexes. This treatment has been applied also to the spectra of cobalt(III) complexes with C_{4v} symmetry.

It is well known that the absorption spectra of *trans* complexes of the $[MX_2(NH_3)_4]^+$ type (M=Co and Cr; X=Cl and Br) exhibit marked splittings in the first absorption bands, this fact being well understood on the basis of the ligand-field theory.[1] Recently, it has been reported that the absorption spectra of a few chromium(III) complexes, such as *trans*-$[Cr(OH)_2(NH_3)_4]^+$, *trans*-$[CrF(OH)(NH_3)_4]^+$ and *trans*-$[CrF_2(NH_3)_4]^+$, show marked splittings in the second absorption bands, while the first bands are at the same time poorly or clearly split, the assignments of the bands being made on the basis of the angular overlap model.[2] Similar splittings in the second absorption bands have been reported with the *trans* complexes of the $[Co(OO)_2(py)_2]^-$ type (OO represents CO_3^{2-} or $C_2O_4^{2-}$), and the assignment of the split bands has been attempted by means of the angular overlap model.[3] These interesting aspects of the behavior of the splittings suggest that there is a certain correlation among the intensities of the split bands.

Early works on the band intensities of the ligand-field transitions were carried out by several workers[4–8] with respect to cubic complexes. Griffith[9] first applied the so-called tensor method to the calculation of the intensity, and then several workers[10–12] used the method for the parameterization of the band intensity with respect to complexes of rare earth elements.

There have also been a few investigations of the band intensity with respect to complexes with symmetry lower than the cubic. Dubicki and Day[13] measured the temperature dependence of the intensity of the ^4E_g ($^4T_{2g}$ parentage) band for *trans*-$[CrX_2(en)_2]ClO_4$ (X= Br or Cl) and found that the ^4E_g band borrows its intensity from the charge-transfer (CT) bands by means of the vibronic mechanism. In their treatment, however, only the admixtures of the excited ligand-field states with the ligand-to-metal CT states were taken into consideration.

The purpose of the present work was to find the correlation of the band intensities in a tetragonal cobalt(III) or a chromium(III) complex by applying the treatment of Dubicki and Day, with some modifications. That is, all kinds of admixtures of the ligand-field states with the CT states were considered in our treatment. In the first part of this paper, the mathematic formulation of the relative intensities of the ligand-field transitions will be described according to a model distorted weakly from a regular octahedron, and then the resultant formula will be proved by means of the spectral data of a few chromium(III) complexes. In the later part, the effect due to configuration interactions among the E states upon the band intensity will be discussed in connection with the spectral data for several cobalt(III) complexes.

Experimental

The *trans*-$[CoCl_2(NH_3)_4]Cl$, $[CoCl(NH_3)_5]Cl_2$, $[CoBr(NH_3)_5]Br_2$ and $[Cr(NH_3)_6](ClO_4)_3$ complexes were synthesized by the usual methods, while the *trans*-$[Co(CN)_2(NH_3)_4]Cl$ complex was prepared according to the literature.[14] The measurements of the absorption spectra in an aqueous solution were carried out with a Hitachi 323 recording spectrophotometer at room temperature. However, the spectrum of *trans*-$[CoCl_2(NH_3)_4]Cl$ was measured in a DMF solution. The absorption spectral data of the *trans*-$[CrF_2(NH_3)_4]^+$, *trans*-$[CrClF(NH_3)_4]^+$ and $[CoCl(CN)_5]^{3-}$ complexes were cited from the literature.[2,15] The curve analysis[3] of the absorption spectra was carried out at the Data Processing Center, Kanazawa University.

Methods of Calculation

Matrix Elements. The ligand-field transition between even-parity states is induced through odd-parity vibrations. The dipole-moment matrix element for the A′→B′ transition is given by[6]

$$\langle A'|\mathbf{P}|B'\rangle = \sum_D \frac{\langle A|\mathbf{P}|D\rangle\langle D|\mathbf{H}_v|B\rangle}{E_B - E_D} + \sum_C \frac{\langle B|\mathbf{P}|C\rangle\langle C|\mathbf{H}_v|A\rangle}{E_A - E_C}, \quad (1)$$

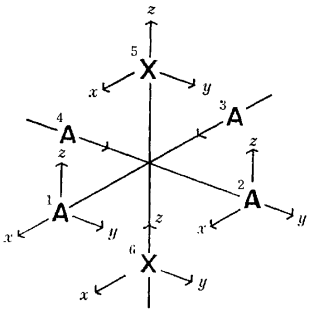

Fig. 1. Coordinate system in a D_{4h} model.

where the first term expresses the part caused by the admixtures of the D odd-parity states with the B excited-ligand-field states, and the second term, the part caused by the admixtures of the C odd-parity states with the A ground state. The $\mathbf{H}_v$ symbol denotes the vibrational Hamiltonian in a tetragonal complex. By adopting the coordinate system as in Fig. 1, $\mathbf{H}_v$ is written as follows:[16]

$$\begin{aligned}
\mathbf{H}_v(E_u^x(a)) &= (x_5+x_6-2x_0)(\partial/\partial x)(V_5+V_6)/2,\\
\mathbf{H}_v(E_u^x(b)) &= (x_2+x_4-2x_0)(\partial/\partial x)(V_2+V_4)/2,\\
\mathbf{H}_v(E_u^x(c)) &= (x_1+x_3-2x_0)(\partial/\partial x)(V_1+V_3)/2,\\
\mathbf{H}_v(A_{2u}(a)) &= (z_1+z_2+z_3+z_4-4z_0),\\
&\quad\times(\partial/\partial z)(V_1+V_2+V_3+V_4)/4,\\
\mathbf{H}_v(A_{2u}(b)) &= (z_5+z_6-2z_0)(\partial/\partial z)(V_5+V_6)/2,\\
\mathbf{H}_v(B_{2u}) &= (z_1+z_3-z_2-z_4)(\partial/\partial z)(V_1+V_3-V_2-V_4)/4,
\end{aligned} \tag{2}$$

where $V_j(j=1\text{—}6)$ represents the ligand-field potential at the jth position, and where x_j and z_j denote the nuclear displacements.

In a model of octahedron with weak tetragonal distortion, the excited-ligand-field states in a Co(III) complex are usually approximated by[8]

$$\begin{aligned}
|E_g^x(a)\rangle &= \{(yz)(y^2-z^2)\},\\
|E_g^x(b)\rangle &= \{(yz)(x^2)\},\\
|A_{2g}\rangle &= \{(xy)(x^2-y^2)\},\\
|B_{2g}\rangle &= \{(xy)(z^2)\}.
\end{aligned} \tag{3}$$

In the above determinants, each state is represented by a d-orbital component of the t_{2g} "hole" (yz or xy) and a d-orbital component of the occupied e_g orbital (y^2-z^2, x^2, x^2-y^2 or z^2). Thus, the wave function for $E_g^x(a)$ is:

$$\{(yz)(y^2-z^2)\} = \{|\cdots(\overset{+}{yz})(\overset{-}{y^2-z^2})(\overset{+}{zx})(\overset{-}{zx})(\overset{+}{xy})(\overset{-}{xy})| + |\cdots(\overset{+}{y^2-z^2})(\overset{-}{yz})\cdots|\}/\sqrt{2}.$$

On the other hand, there are two CT states which can be used as the odd-parity states; one is that of the ligand-to-metal charge transfer (LMCT), and the other, the metal-to-ligand charge transfer (MLCT). The CT states obtained by the use of the symmetry ligand orbitals listed in Table 1 are given in Table 2.

Our attention was given to the matrix elements in (1) in order to determine the CT states which contribute greatly to the intensities of the ligand-field transition bands; the Wigner-Eckart theorem[17] was useful in finding the non-vanishing matrix elements (the vibronic selection rule used in the calculation is given in Table 3). Among the non-vanishing matrix elements thus found, the elements such as $\langle y^2-z^2|\Gamma|\pi_\eta\rangle$, $\langle y^2-z^2|\Gamma|\sigma_\alpha\rangle$ and $\langle xy|\Gamma|\pi_\alpha\rangle$ (Γ represents $\mathbf{H}_v$ and $\mathbf{P}$) were considered to have small values because of the poor overlap integrals of the metal orbitals with the ligand orbitals. Furthermore, when the ligand-field potentials in a $\mathbf{H}_v$ lay outside the positions of the ligand orbitals used, the matrix elements associated with the $\mathbf{H}_v$ were considered to be quite small because of the three-centered integral. Since the numerators in (1) were expressed by products of the matrix elements of the $\mathbf{P}$ and those of the $\mathbf{H}_v$, the contribution from a product to the induced dipole moment was regarded to be negligible, at least when either of the two matrix elements was extraordinarily small.

Using the curled determinants, the states in a Cr(III) complex were easily correlated with the corresponding states in a Co(III) complex. The correlation table thus obtained is listed in Table 4. The states belonging to the A and B representations in the Co(III) complex correspond in turn to the states belonging to the B and A representations in the Cr(III) complex, while

Table 1. Symmetry ligand orbitals in the D_{4h} point group

Symmetry	Orbitals
E_u	$\sigma_\alpha=(\sigma_1+\sigma_3)/\sqrt{2}$
	$\sigma_\beta=(\sigma_2+\sigma_4)/\sqrt{2}$
E_u	$\pi_\alpha=(x_5+x_6)/\sqrt{2}$
	$\pi_\beta=(y_5+y_6)/\sqrt{2}$
E_u	$\pi_\xi=(x_2+x_4)/\sqrt{2}$
	$\pi_\eta=(y_1+y_3)/\sqrt{2}$
A_{2u}	$\sigma_\Gamma=(\sigma_5+\sigma_6)/\sqrt{2}$
A_{2u}	$\pi_\Gamma=(z_1+z_2+z_3+z_4)/2$
B_{2u}	$\pi_\zeta=(z_1-z_2+z_3-z_4)/2$

Table 2. Odd-parity charge-transfer states in the tetragonal Co(III) complex

Representation	LMCT	MLCT
$\|E_u^x\rangle$	$\{(\sigma_\alpha)(y^2-z^2)\}$	$\{(zx)(\sigma_\Gamma)\}$
	$\{(\sigma_\alpha)(x^2)\}$	$\{(xy)(\sigma_\beta)\}$
	$\{(\pi_\xi)(y^2-z^2)\}$	$\{(xy)(\pi_\eta)\}$
	$\{(\pi_\xi)(x^2)\}$	$\{(zx)(\pi_\Gamma)\}$
	$\{(\pi_\alpha)(y^2-z^2)\}$	$\{(zx)(\pi_\zeta)\}$
	$\{(\pi_\alpha)(x^2)\}$	$\{(xy)(\pi_\beta)\}$
$\|A_{2u}\rangle$	$\{(\sigma_\Gamma)(z^2)\}$	$[\{(yz)(\sigma_\beta)\}+\{(zx)(\sigma_\alpha)\}]/2$
	$\{(\pi_\Gamma)(z^2)\}$	$[\{(yz)(\pi_\eta)\}+\{(zx)(\pi_\xi)\}]/2$
	$\{(\pi_\zeta)(x^2-y^2)\}$	$[\{(yz)(\pi_\beta)\}+\{(zx)(\pi_\alpha)\}]/2$
$\|B_{2u}\rangle$	$\{(\sigma_\Gamma)(x^2-y^2)\}$	$[\{(yz)(\sigma_\beta)\}-\{(zx)(\sigma_\alpha)\}]/2$
	$\{(\pi_\Gamma)(x^2-y^2)\}$	$[\{(yz)(\pi_\eta)\}-\{(zx)(\pi_\xi)\}]/2$
	$\{(\pi_\zeta)(z^2)\}$	$[\{(yz)(\pi_\beta)\}-\{(zx)(\pi_\alpha)\}]/2$

Table 3. Vibronic selection rules in tetragonal Co(III) and Cr(III) complexes

	Transition	P	Admixture with excited state		Admixture with ground state	
			$\mathbf{H}_v$	D	$\mathbf{H}_v$	C
Co	$^1A_{1g}\rightarrow{}^1A_{2g}$	E_u	E_u	E_u	E_u	E_u
	$^1A_{1g}\rightarrow{}^1B_{2g}$	E_u	E_u	E_u	E_u	E_u
	$^1A_{1g}\rightarrow{}^1E_g$	A_{2u}	E_u	A_{2u}	E_u	E_u
		E_u	A_{2u}, B_{2u}	E_u	A_{2u}	A_{2u}
				E_u	B_{2u}	B_{2u}
Cr	$^4B_{1g}\rightarrow{}^4A_{2g}$	E_u	E_u	E_u	E_u	E_u
	$^4B_{1g}\rightarrow{}^4B_{2g}$	E_u	E_u	E_u	E_u	E_u
	$^4B_{1g}\rightarrow{}^4E_g$	A_{2u}	E_u	B_{2u}	E_u	E_u
		E_u	A_{2u}, B_{2u}	E_u	B_{2u}	A_{2u}
					A_{2u}	B_{2u}

Table 4. Correlation table of representations in tetragonal Co(III) and Cr(III) complexes

O_h Co(III) Complex	D_{4h} Co(III) Complex	D_{4h} Cr(III) Complex
$T_{1g}(t_{2g}^5e_g)$	E_g	$E_g(t_{2g}^2e_g)$
	A_{2g}	$B_{2g}(t_{2g}^2e_g)$
$T_{2g}(t_{2g}^5c_g)$	E_g	$E_g(t_{2g}^2e_g)$
	B_{2g}	$A_{2g}(t_{2g}^2e_g)$
$A_{1g}(t_{2g}^6)$	A_{1g}	$B_{1g}(t_{2g}^3)$
$T_{1u}(CT)$	E_u	$E_u(CT)$
	A_{2u}	$B_{2u}(CT)$
$T_{2u}(CT)$	E_u	$E_u(CT)$
	B_{2u}	$A_{2u}(CT)$

the states belonging to the E representation are common to both metal complexes.

Fenske[8] has stated that the $LM(t_{2g})CT$ transitions make no contribution to the intensities of the ligand-field transition bands. On this basis, the CT states listed in Table 2 were used for a Cr(III) complex only by exchanging A for B (or B for A). The intensity calculation for Cr(III) complexes was performed in the same way as that for Co(III) complexes.

Relative Intensities. Admixture with LMCT: In the case of Co(III) complexes, the matrix elements of the $^1A_{1g}\rightarrow{}^1A_{2g}$ transition were found to be the same as those of the $^1A_{1g}\rightarrow{}^1B_{2g}$ transition, although the coefficients differed from one another (see Table 5). On the basis of this result, in the case of a complex with only a σ-donating ligand such as NH_3 in the xy plane, the ratio of the oscillator strengths[18] of the $^1A_{2g}$ transition, $f(A_2)$, to that of the $^1B_{2g}$ transition, $f(B_2)$, was expressed by

$$\frac{f(A_2)}{f(B_2)} = k\frac{E(A_2)}{E(B_2)} \times \left(\frac{E(CT)-E(B_2)}{E(CT)-E(A_2)}\right)^2. \quad (4)$$

In this equation, $E(A_2)$, $E(B_2)$, and $E(CT)$ denote energy corresponding to each transition, and k is a coefficient, found to be 3 in this case. Hereinafter, the mechanism associated with $L(\sigma)MCT$ (or $ML(\sigma)$ CT) will be called the $L(\sigma)$-vibronic mechanism.

As is shown in Table 5, two $L(\pi)MCT$ participated in each transition through the vibronic mechanism (hereinafter called the $L(\pi)$-vibronic mechanism); for instance, with regard to the $^1A_{2g}$ transition, the $\langle x^2|\mathbf{P}|\pi_\xi\rangle$ and $\langle y^2-z^2|\mathbf{P}|\pi_\xi\rangle$ dipole moments appeared in the summation of the first term in (1). From the differences in the normalization constants of the (y^2-z^2) and (x^2) orbitals, it can easily be shown that

$$\langle y^2-z^2|\mathbf{P}|\pi_\xi\rangle = \sqrt{3}\langle x^2|\mathbf{P}|\pi_\xi\rangle. \quad (5)$$

On this basis, if the denominators in (1) were replaced by a mean value of the $L(\pi)MCT$ transition energies, the oscillator strengths in this $L(\pi)$-vibronic mechanism were evaluated by adding the two products of the matrix elements; consequently, the same equation as (4) was obtained, with the coefficient of 3/5. Similar equations were also derived between the $f(E_g(a))$ of the $^1E_g(a)$ and the $f(E_g(b))$ of the $^1E_g(b)$ transitions in both the $L(\sigma)$- and $L(\pi)$-vibronic mechanisms.

Admixture with MLCT: As is shown in Table 5, the matrix elements of the $^1T_{1g}$ parentage bands dif-

Table 5. Non-vanishing matrix elements

$\langle B|\mathbf{H}_v(E_u^y)|D(E_u^x)\rangle\langle D(E_u^x)|\mathbf{P}(E_u^x)|A\rangle$

	$A_{1g}\rightarrow A_{2g}$	$A_{1g}\rightarrow B_{2g}$
D : LMCT	$(-\sqrt{6}/2)\langle xy\|\mathbf{H}_v\|\sigma_\alpha\rangle\langle x^2\|\mathbf{P}\|\sigma_\alpha\rangle$	$(\sqrt{2}/2)\langle xy\|\mathbf{H}_v\|\sigma_\alpha\rangle\langle x^2\|\mathbf{P}\|\sigma_\alpha\rangle$
	$(-\sqrt{6}/2)\langle xy\|\mathbf{H}_v\|\pi_\xi\rangle\langle x^2\|\mathbf{P}\|\pi_\xi\rangle$	$(\sqrt{2}/2)\langle xy\|\mathbf{H}_v\|\pi_\xi\rangle\langle x^2\|\mathbf{P}\|\pi_\xi\rangle$
	$(\sqrt{2}/2)\langle xy\|\mathbf{H}_v\|\pi_\xi\rangle\langle y^2-z^2\|\mathbf{P}\|\pi_\xi\rangle$	$(\sqrt{6}/2)\langle xy\|\mathbf{H}_v\|\pi_\xi\rangle\langle y^2-z^2\|\mathbf{P}\|\pi_\xi\rangle$
D : MLCT	$\sqrt{2}\langle x^2-y^2\|\mathbf{H}_v\|\sigma_\beta\rangle\langle\sigma_\beta\|\mathbf{P}\|xy\rangle$	$\sqrt{2}\langle z^2\|\mathbf{H}_v\|\sigma_\beta\rangle\langle\sigma_\beta\|\mathbf{P}\|xy\rangle$
	$\sqrt{2}\langle x^2-y^2\|\mathbf{H}_v\|\pi_\eta\rangle\langle\pi_\eta\|\mathbf{P}\|xy\rangle$	$\sqrt{2}\langle z^2\|\mathbf{H}_v\|\pi_\eta\rangle\langle\pi_\eta\|\mathbf{P}\|xy\rangle$

$\langle B(E_g^x)|\mathbf{H}_v(E_u^y)|D(A_{2u})\rangle\langle D(A_{2u})|\mathbf{P}(A_{2u})|A\rangle$[a]

	$A_{1g}\rightarrow E_g(a)$	$A_{1g}\rightarrow E_g(b)$
D : LMCT	$(\sqrt{6}/2)\langle yz\|\mathbf{H}_v\|\sigma_\tau\rangle\langle z^2\|\mathbf{P}\|\sigma_\tau\rangle$	$(\sqrt{2}/2)\langle yz\|\mathbf{H}_v\|\sigma_\tau\rangle\langle z^2\|\mathbf{P}\|\sigma_\tau\rangle$
	$(\sqrt{6}/2)\langle yz\|\mathbf{H}_v\|\pi_\tau\rangle\langle z^2\|\mathbf{P}\|\pi_\tau\rangle$	$(\sqrt{2}/2)\langle yz\|\mathbf{H}_v\|\pi_\tau\rangle\langle z^2\|\mathbf{P}\|\pi_\tau\rangle$
	$(\sqrt{2}/2)\langle yz\|\mathbf{H}_v\|\pi_\zeta\rangle\langle x^2-y^2\|\mathbf{P}\|\pi_\zeta\rangle$	$-(\sqrt{6}/2)\langle yz\|\mathbf{H}_v\|\pi_\zeta\rangle\langle x^2-y^2\|\mathbf{P}\|\pi_\zeta\rangle$
D : MLCT	$1/\sqrt{2}\langle y^2-z^2\|\mathbf{H}_v\|\sigma_\beta\rangle\{\langle\sigma_\beta\|\mathbf{P}\|yz\rangle+\langle\sigma_\alpha\|\mathbf{P}\|zx\rangle\}$	$(1/\sqrt{2})\langle x^2\|\mathbf{H}_v\|\sigma_\beta\rangle\{\langle\sigma_\beta\|\mathbf{P}\|yz\rangle+\langle\sigma_\alpha\|\mathbf{P}\|zx\rangle\}$
	$1/\sqrt{2}\langle y^2-z^2\|\mathbf{H}_v\|\pi_\beta\rangle\{\langle\pi_\beta\|\mathbf{P}\|yz\rangle+\langle\pi_\alpha\|\mathbf{P}\|zx\rangle\}$	$(1/\sqrt{2})\langle x^2\|\mathbf{H}_v\|\pi_\beta\rangle\{\langle\pi_\beta\|\mathbf{P}\|yz\rangle+\langle\pi_\alpha\|\mathbf{P}\|zx\rangle\}$

$\langle B(E_g^x)|\mathbf{H}_v(A_{2u},B_{2u})|D(E_u^y)\rangle\langle D(E_u^y)|\mathbf{P}(E_u^y)|A\rangle$

	$A_{1g}\rightarrow E_g(a)$	$A_{1g}\rightarrow E_g(b)$
D : LMCT	$(\sqrt{6}/2)\langle yz\|\mathbf{H}_v\|\sigma_\beta\rangle\langle y^2\|\mathbf{P}\|\sigma_\beta\rangle$	$(\sqrt{2}/2)\langle yz\|\mathbf{H}_v\|\sigma_\beta\rangle\langle y^2\|\mathbf{P}\|\sigma_\beta\rangle$
	$(\sqrt{6}/2)\langle yz\|\mathbf{H}_v\|\pi_\beta\rangle\langle y^2\|\mathbf{P}\|\pi_\beta\rangle$	$(\sqrt{2}/2)\langle yz\|\mathbf{H}_v\|\pi_\beta\rangle\langle y^2\|\mathbf{P}\|\pi_\beta\rangle$
	$(\sqrt{2}/2)\langle yz\|\mathbf{H}_v\|\pi_\beta\rangle\langle z^2-x^2\|\mathbf{P}\|\pi_\beta\rangle$	$-(\sqrt{6}/2)\langle yz\|\mathbf{H}_v\|\pi_\beta\rangle\langle z^2-x^2\|\mathbf{P}\|\pi_\beta\rangle$
D : MLCT	$\sqrt{2}\langle y^2-z^2\|\mathbf{H}_v\|\sigma_\tau\rangle\langle\sigma_\tau\|\mathbf{P}\|yz\rangle$	$\sqrt{2}\langle x^2\|\mathbf{H}_v\|\sigma_\tau\rangle\langle\sigma_\tau\|\mathbf{P}\|yz\rangle$
	$\sqrt{2}\langle y^2-z^2\|\mathbf{H}_v\|\pi_\tau\rangle\langle\pi_\tau\|\mathbf{P}\|yz\rangle$	$\sqrt{2}\langle x^2\|\mathbf{H}_v\|\pi_\tau\rangle\langle\pi_\tau\|\mathbf{P}\|yz\rangle$
	$\sqrt{2}\langle y^2-z^2\|\mathbf{H}_v\|\pi_\zeta\rangle\langle\pi_\zeta\|\mathbf{P}\|yz\rangle$	$\sqrt{2}\langle x^2\|\mathbf{H}_v\|\pi_\zeta\rangle\langle\pi_\zeta\|\mathbf{P}\|yz\rangle$

a) $\langle B(E_g^x)|\mathbf{P}(E_u^y)|C(B_{2u})\rangle\langle C(B_{2u})|\mathbf{H}_v(B_{2u})|A\rangle$ is included in this case.

fered from those of the $^1T_{2g}$ parentage bands, though every coefficient was equal to $\sqrt{2}$ in both parentages. However, we could also show similar relations to (5) between the matrix elements in the transitions to the nondegenerate states (and between those in the transitions to the degenerate states). The same equations as (4) could be derived in both the L(σ)- and L(π)-vibronic mechanisms, where the k values were equal to 3.

In the case of the Cr(III) complexes, the resultant equations were also expressed by (4); however, the A_2 subscript (or B_2) had to be exchanged with B_2 (or A_2).

Results and Discussion

Nature of the A_2 and B_2 Transitions. Only a half of the calculated matrix elements of the first term in (1) are listed in Table 5, because the other half can easily be obtained by considering the symmetry. The matrix elements concerning the second term in (1) were obtained by exchanging the **P** in the first term with the $\mathbf{H}_v$.

From the present model of weak tetragonal distortion, it can be predicted that the intensities of the transitions to the nondegenerate excited states are independent of the ligand on the z axis (X in Fig. 1), since they are only related with the ligand orbitals on the xy plane (π_ξ, π_η, σ_α, and σ_β) through the E odd-vibrations occurring on the plane. This prediction is confirmed by the fact that the intensities of the $^4A_{2g}$ band in *trans*-$[CrX_2(NH_3)_4]^+$ (X=F^- and OH^-), whose tetragonal distortions seem to be small, are almost invariable, in comparison with the considerable variations in the intensities of the ^4E_g(b) bands. Moreover, the fact that the intensities of the $^4A_{2g}$ (or $^4B_{2g}$) bands are nearly equal to one-third of the intensity of the $^4T_{1g}$ (or $^4T_{2g}$) band in $[Cr(NH_3)_6]^{3+}$ supports the prediction from the present model.

The present model is applicable to the problem of A_2 and B_2 transitions in a C_{4v} complex for the following reason: The wave functions associated with the ligand orbitals on the xy plane are the same as those in the D_{4h} complexes. According to the ligand-field theory,[19] the ligand-field potential in a C_{4v} complex can be divided into two potentials in D_{4h} symmetry:

$$U_{C_{4v}} = U_{D_{4h}(A_{2u})} + U_{D_{4h}(A_{1g})}.$$

The first term can mix the states coming from even-parity states in D_{4h} with the states coming from odd-parity states under static conditions, and contributes only to the intensities of the E bands. On the other hand, the second term can mix the states coming from the odd-parity states in D_{4h} symmetry under vibronic conditions. In fact, in *trans*-$[CrF(OH)(NH_3)_4]^+$ the above-mentioned prediction holds.

Application to Tetragonal Complexes. As for Co(III) complexes, no absorption spectrum has been reported to exhibit distinct splittings in both the first and second absorption band regions. However, as for Cr(III) complexes, it has been reported that the absorption spectra in *trans*-$[CrF_2(NH_3)_4]^+$ and *trans*-$[CrClF(NH_3)_4]^+$ [2] show such splittings. Now, let us apply (4) to these complexes. Note that, in this application, the A_2 and B_2 subscripts in (4) must be exchanged with B_2 and A_2 respectively. The E(CT) values in these complexes are assumed to be *ca.* 55000 cm^{-1}, while the E(CT) value in $[Cr(NH_3)_6](ClO_4)_3$ lies above 52000 cm^{-1}. The $f(B_2)/f(A_2)$ value in (4) was calculated from the numerical data listed in Table 6, and found to be 1.36. On the other hand, the ratio calculated from the observed $f(B_2)$ and $f(A_2)$ values was 1.24 for the difluoro complex. As for *trans*-$[CrClF(NH_3)_4]^+$, the value calculated from the data of Table 6 was 1.52, and the value calculated from the observed data was 1.34, the two being roughly equal.

The angular overlap model[20] suggested that the extent of the tetragonal distortion due to M-L σ-bonding is expressed by the difference between two antibonding energies, $\sqrt{3}/4\{\langle z^2|\mathbf{A}|z^2\rangle - \langle x^2-y^2|\mathbf{A}|x^2-y^2\rangle\}$. In the case of the *trans*-$[M(X)_2(A)_4]$-type complex, the difference is rewritten as $\sqrt{3}(e_\sigma(X) - e_\sigma(A))/2$, where e_σ denotes the σ-antibonding parameter. It is known[2] that the σ-parameter related with the Cr–F bonding, e_σ(F), is slightly larger than that of the Cr–NH_3 bonding, e_σ(N). When these findings are taken into consideration, the tetragonal distortions in the Cr(III) complexes concerned are regarded as very small, and the excited states are sufficiently approximated by Eq. 3. Thus, it seems reasonable to use our model for the Cr(III) complexes with small distortions.

The Effect of Configuration Interactions. In a previous paper,[3] the band intensity in *trans*-$[Co(C_2O_4)_2$-

Table 6. Absorption spectral data[a] of Cr(III) complexes ($\bar{\nu}$ in 10^3 cm^{-1})

	$\bar{\nu}_{max}$	ε_{max}	$f\times10^7$	Assignment
trans-$[CrF_2(NH_3)_4]^+$ [b]	18.6(17.8)	13.8(8.8)	(0.98)	E_g(a)
	20.3(20.5)	14.9(14.7)	(2.62)	B_{2g}
	25.0(24.4)	10.9(8.5)	(1.12)	E_g(b)
	27.9(27.9)	11.1(10.8)	(2.10)	A_{2g}
trans-$[CrClF(NH_3)_4]^+$ [b]	17.8(17.7)	21.3(20.9)	(2.19)	E(a)
	20.2(20.7)	16.7(14.6)	(2.69)	B_2
	24.3(24.3)	16.8(15.4)	(1.96)	E(b)
	26.5(27.1)	17.2(12.8)	(2.01)	A_2
$[Cr(NH_3)_6]^{3+}$	21.0	47.9		T_{2g}
	29.4	39.8		T_{1g}

a) Analyzed values in parentheses. b) Ref. 2.

Table 7. Absorption spectral data of Co(III) complexes ($\bar{\nu}$ in 10^3 cm^{-1})

	$\bar{\nu}_{max}$	ε_{max}	$f\times10^7$	Assignment
trans-$[Co(CN)_2(NH_3)_4]^+$	20.3	15.4	1.81	A_{2g}
	24.0	66.3	12.2	E_g(a)
	31.4	67.6	14.9	(B_{2g}, E_g(b))
trans-$[Co(Cl)_2(NH_3)_4]^+$	15.9	42.7	5.11	E_g(a)
	20.7	21.8	3.96	A_{2g}
	26.3	44.6	11.8	(B_{2g}, E_g(b))
$[CoCl(NH_3)_5]^{2+}$	18.5	34.9	4.21	E(a)
	20.6	32.2	6.09	A_2
	27.7	49.1	9.34	(B_2, E(b))
$[CoBr(NH_3)_5]^{2+}$	18.0	44.4	5.64	E(a)
	20.5	35.4	6.50	A_2
trans-$[Co(CO_3)_2(py)_2]^-$ [a]	18.3	89.1	12.0	E_g(a), (A_{2g})
	23.4	35.5	5.58	B_{2g}
	26.5	57.5	6.51	E_g(b)
trans-$[Co(C_2O_4)_2(py)_2]^-$ [a]	18.4	57.5	8.25	E_g(a), (A_{2g})
	24.1	17.8	2.11	B_{2g}
	26.7	61.7	10.0	E_g(b)
$[CoCl(CN)_5]^{3-}$ [b]	25.5	200		E(a)
	32.2	97		A_2
$[Co(NH_3)_6]^{3+}$	21.0	47.9		T_{1g}
	29.4	39.8		T_{2g}
$[Co(CN)_6]^{3-}$	32.1	240		T_{1g}
	38.5	178		T_{2g}
$[Co(C_2O_4)_3]^{3-}$	16.6	148		T_{1g}
	23.6	200		T_{2g}

a) Ref. 3. b) Ref. 15.

$(py_2)]^-$ was treated by considering only the L(σ)-vibronic mechanism under a weak tetragonal distortion, and the intensity of the $^1A_{2g}$ band, which was not observed in the absorption spectrum, was estimated. The value reported there, $\varepsilon_{max}=19$, now seems to somewhat large in the light of the maximum ($\varepsilon_{max}=57.5$) of the observed band (the spectral data are summarized in Table 7). If the L(π)MCT contributes to the $^1A_{2g}$ band intensity, the ε_{max} value may be evaluated as a smaller one. However, in the case of *trans*-$[Co(C_2O_4)_2(py)_2]^-$, such a contribution seems to be negligible because the π-ligand orbitals of the O donors on the xy plane are utilized for σ-hybridizations. Thus, we re-evaluated that value by considering the configuration interactions among the E states.

When the distortion becomes large, the one-electron wave functions, y^2-z^2, x^2, z^2-x^2, and y^2, which have been used in the E states must be altered by the following respective functions:[20]

$$\begin{aligned}
\phi_a(x) &= a\phi(y^2-z^2) - b\phi(x^2),\\
\phi_b(x) &= b\phi(y^2-z^2) + a\phi(x^2),\\
\phi_a(y) &= -a\phi(z^2-x^2) - b\phi(y^2),\\
\phi_b(y) &= -b\phi(z^2-x^2) + a\phi(y^2),\\
&\text{where } a^2+b^2=1.
\end{aligned} \qquad (6)$$

When an expression for the $f(A_2)/f(B_2)$ ratio in a Co(III) complex was derived from these new wave functions of the E states, the expression was found to be the same as (4), although the k value varied as a function of the a coefficient. The change is illustrated in Fig. 2. When the L(σ)-vibronic mechanism participates and the e_σ(X) is larger than the e_σ(A), the k value decreases rapidly from 3 to 1.5 in the initial section of the a^2 value. On the other hand, in the case of $e_\sigma(X)<e_\sigma(A)$, the change of k with a^2 is quite different.

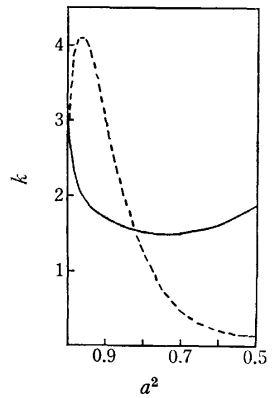

Fig. 2. Relationships between the coefficients k and a^2; —— $e_\sigma(X) > e_\sigma(A)$, ---- $e_\sigma(X)<e_\sigma(A)$.

It is reasonable to consider that e_σ(py) is larger than e_σ(O) in *trans*-$[Co(C_2O_4)_2(py)_2]^-$; if a sufficiently strong distortion is considered, the ε_{max} value of the $^1A_{2g}$ band is evaluated to be 10 for the bis(oxalato) complex. When the same calculations are carried out with a related dicarbonato complex, the results give $\varepsilon_{max}=16$. These values are much smaller than the observed ε_{max} values in the first absorption-band region ($\varepsilon_{max}=57.5$ for the bis(oxalato) complex and $\varepsilon_{max}=89.1$ for the dicarbonato complex). It is also possible to find an effect of the same kind in the polarized crystal spectra of *trans*-$K_2[Co(CN)(mal)_2(OH_2)]\cdot H_2O$;[21] two split bands have been observed in the second absorption-band region, while only one band assignable to E(a) has been observed in the first absorption-band region. This phenomenon can now be understood by considering the intensity of the A_2 band, which is too weak, compared with that of the B_2 band.

Whether or not a band splitting can be observed depends upon both the magnitude of the intensities and the extent of the energy separation of the split bands, but the latter is not discussed in this paper. The formula (4) derived in this paper is useful in evaluating the intensity of an unobservable band from the observed intensity of the other band. Thus, let us discuss the behavior of band intensities in cobalt(III) complexes in terms of the tetragonal distortion. Three cases—Case a, $e_\sigma(X)>e_\sigma(A)$; Case b, $e_\sigma(X)\simeq e_\sigma(A)$, and Case c, $e_\sigma(X)<e_\sigma(A)$—will be considered. In Case a, the intensity of the $^1A_{2g}$ band observed at the longest wavelength is quite small in comparison with that of the $^1B_{2g}$ band, because the calculated value of the energy part in (4) becomes small as a result of the large separation between the $^1A_{2g}$ and $^1B_{2g}$ bands, and because k also has a small value. This kind of complex will often exhibit marked

splittings in the $^1T_{2g}$ bands. In Case b, the $^1A_{2g}$-band intensity is anticipated to be comparable to the $^1B_{2g}$-band intensity because of the large k value ($k \simeq 3$). In this case, band splittings will be observed only in a complex with ligands showing a strong π-bonding or π-antibonding contribution. No typical example of this is found in Co(III) complexes, but the spectrum of *trans*-$[Co(CN)_2(NH_3)_4]^+$ probably is such a case, for the intensity of the $^1A_{2g}$ band is almost one-third of the intensity of the $^1T_{1g}$ band in $[Co(NH_3)_6]^{3+}$. This probability is supported by the fact that the π-bonding contribution of the CN^- ligand has been found through the infrared spectral[22] and the absorption spectral studies.[23] In Case c, the $f(A_2)/f(B_2)$ ratio becomes larger than unity, except for an extremely distorted complex, because the energy part in (4) takes a large value as a result of the small separation of the $^1A_{2g}$ and $^1B_{2g}$ bands, and because k also takes a large value. In this case, it will be easier to observe band splitting in the $^1T_{1g}$-band region rather than in the $^1T_{2g}$-band region. This seems to correspond to the large intensities of the $^1A_2$ bands in $[CoX(NH_3)_5]^{2+}$ ($X=Cl^-$ and Br^-) and $[CoCl(CN)_5]^{3-}$. When the distortion becomes extremely large, the $f(A_2)/f(B_2)$ ratio takes a value of roughly unity on account of the small value of k. An example is seen in the spectrum of *trans*-$[CoCl_2(NH_3)_4]^+$; the broad band in the $^1T_{2g}$-band region suggests that the $^1B_{2g}$-band intensity is comparable to the $^1A_{2g}$-band intensity.

References

1) H. Yamatera, *Bull. Chem. Soc. Jpn.*, **31**, 95 (1958).
2) J. Glerup, O. Mønsted, and C. E. Schäffer, *Inorg. Chem.*, **15**, 1399 (1976); J. Glerup and C. E. Schäffer, *Inorg. Chem.*, **15**, 1408 (1976).
3) Y. Ida, S. Fujinami, and M. Shibata, *Bull. Chem. Soc. Jpn.*, **50**, 2665 (1977).
4) S. Koide and M. H. L. Pryce, *Phil. Mag.*, **3**, 607 (1959).
5) C. J. Ballhausen and A. D. Liehr, *J. Mol. Spectrosc.*, **2**, 342 (1959).
6) R. Englman, *Mol. Phys.*, **3**, 48 (1960).
7) N. K. Harmer, *Mol. Phys.*, **5**, 455 (1962).
8) R. F. Fenske, *J. Am. Chem. Soc.*, **89**, 252 (1967).
9) J. S. Griffith, *Mol. Phys.*, **3**, 477 (1960).
10) B. R. Judd, *Phys. Rev.*, **127**, 205 (1962).
11) G. S. Ofelt, *J. Chem. Phys.*, **37**, 511 (1962).
12) W. T. Carnall, P. R. Fields, and B. G. Wybourne, *J. Chem. Phys.*, **42**, 3797 (1965).
13) L. Dubicki and P. Day, *Inorg. Chem.*, **10**, 2043 (1971).
14) K. Konya, H. Nishikawa, and M. Shibata, *Inorg. Chem.*, **7**, 1165 (1968).
15) V. M. Miskowski and H. B. Gray, *Inorg. Chem.*, **14**, 401 (1975).
16) I. Nakagawa and T. Shimanouchi, *Spectrochim. Acta*, **22**, 759 (1966).
17) J. S. Griffith, "The Irreducible Tensor Method for Molecular Symmetry Groups," Prentice-Hall, Englewood Cliffs, N. J., U. S. A. (1962).
18) C. J. Ballhausen, "Introduction to Ligand Field Theory," McGraw-Hill, New York, N. Y., Chap. 7.
19) S. Sugano, Y. Tanabe, and H. Kamimura, "Multiplets of Transition-Metal Ions in Crystals," Academic Press, New York and London (1970).
20) C. E. Schäffer, *Structure Bonding*, **5**, 68 (1968); C. E. Schäffer, *Pure Appl. Chem.*, **24**, 361 (1970).
21) S. Fujinami and M. Shibata, *Bull. Chem. Soc. Jpn.*, **46**, 3443 (1973).
22) L. H. Jones, *Inorg. Chem.*, **2**, 777 (1963).
23) H. B. Gray and N. A. Beach, *J. Am. Chem. Soc.*, **85**, 2922 (1963).

Synthesis and Unusual Properties of Trimethylsilylmethyl, Neopentyl, and Related Alkylthallium Compounds

Hideo KUROSAWA,* Shigeaki NUMATA, Toshifumi KONISHI, and Rokuro OKAWARA

Department of Petroleum Chemistry, Osaka University, Yamadakami, Suita, Osaka 565

(Received November 25, 1977)

Synthesis of some new trimethylsilylmethyl, neopentyl, and isobutylthallium compounds is described. Dialkylthallium halides containing these bulky alkyl substituents were found to be dimeric, in marked contrast to the polymeric dimethylthallium halide analogs. Trimethylsilylmethylthallium diisobutyrate possesses much higher stability than the methyl and ethylthallium analogs. These facts were discussed in terms of the steric bulk of the alkyl groups attached to thallium.

Organometallic compounds containing the trimethylsilylmethyl or neopentyl groups are of current interest because of abilities of these groups to apparently stabilize metal–carbon bonds.[1] Of particular importance in considering factors which affect kinetic stabilities and structural aspects of such a class of organometallic compounds is clearly bulkiness of the alkyl groups. We wish to describe synthesis of some new organothallium compounds containing bulky alkyl substituents whose unique properties may be contrasted with those of common, less bulky alkyl derivatives of thallium.[2]

Experimental

The infrared spectra were run on a Hitachi 225 or EPI-2G grating spectrophotometer. The ^{1}H NMR spectra were measured on a Japan Electron Optics JNM-PS-100 spectrometer. Molecular weights were determined in $CHCl_3$ at 25 °C using a Mechlorab vapor pressure osmometer Model 302. Tetrahydrofuran for the preparation of the Grignard and lithium reagents was dried with $LiAlH_4$.

Preparation of New Compounds. *Dialkylthallium Chlorides*: R_2TlCl ($R=Me_3CCH_2$, Me_2CHCH_2) were prepared in a manner similar to that[3] for obtaining $Pr^n{}_2TlCl$ from $TlCl_3$ and the appropriate Grignard reagents in tetrahydrofuran. Recrystallization from CH_2Cl_2 or $CHCl_3$ gave colorless needle-like crystals. *$(Me_3SiCH_2)_2TlCl$*: To a tetrahydrofuran solution (20 ml) of $TlCl_3$ (0.75 g; 2.4 mmol) was added lithiomethyltrimethylsilane,[4] which was prepared from Me_4Si (2.0 g; 24 mmol), *N,N,N′,N′*-tetramethylethylenediammine (2.8 g; 24 mmol) and 15 ml of 1.5 M Bu^nLi in hexane. Immediately metallic thallium formed and the solution became black. After stirring for 2 h, the reaction mixture was hydrolyzed with saturated aqueous ammonium chloride. The tetrahydrofuran extract was concentrated to give an oily product which was washed with water several times. Recrystallization from $CHCl_3$ gave white needles of $(Me_3SiCH_2)_2TlCl$ (0.34 g; 0.82 mmol). $(Me_3SiCH_2)_2TlBr$ was prepared from TlBr and Me_3SiCH_2Li in a similar manner. *$Me_3SiCH_2Tl(OOCPr^i)_2$*: Mercuric isobutyrate (0.30 g; 0.81 mmol) and $(Me_3SiCH_2)_2TlOOCPr^i$ (0.38 g; 0.81 mmol), which was prepared from $(Me_3SiCH_2)_2TlCl$ and $TlOOCPr^i$ in $CHCl_3$, were mixed in $CHCl_3$ (10 ml) at room temperature. The solid products obtained by vacuum evaporation of the solvent after 1 day were recrystallized from hexane to give 0.10 g (0.22 mmol) of $Me_3SiCH_2Tl(OOCPr^i)_2$. *$Me(Me_3SiCH_2)TlBr$*: Pyridinium perbromide (0.05 g; 0.19 mmol) and $(Me_3SiCH_2)_2TlCl$ (0.08 g; 0.19 mmol) were dissolved in 10 ml of $CHCl_3$. After 30 min tetramethyltin (0.04 g; 0.24 mmol) was added to the solution in order to methylate[5] a monoalkylthallium species produced *in situ*. After 1 h the solution was filtered. The solid products obtained by vacuum evaporation of the filtrate were recrystallized from $CHCl_3$ to give 0.06 g (0.16 mmol) of $Me(Me_3SiCH_2)TlBr$. $Me(Me_3SiCH_2)TlOOCPr^i$ was prepared from $Me(Me_3SiCH_2)TlBr$ and $TlOOCPr^i$ in $CHCl_3$. Recrystallization from hexane gave fine needles of the compound.

Analytical data of the new compounds thus obtained are summarized in Table 1. Infrared and ^{1}H NMR spectral data of the representative trimethylsilylmethyl compounds are shown in Table 2.

Pyrolysis of $(Me_2CHCH_2)_2TlCl$. 100 mg (0.28 mmol) of a solid sample of $(Me_2CHCH_2)_2TlCl$ in a sealed tube under reduced pressure (10^{-1} mmHg) was heated at 170 °C for 3 h. Sixty-five mg (0.27 mmol) of white powdery TlCl remained in the tube, and GLC analysis of gaseous products indicated

TABLE 1. PROPERTIES AND ANALYTICAL DATA OF ORGANOTHALLIUM COMPOUNDS

	Compound[a]	Mp (°C)	Found (Calcd) %C	Found (Calcd) %H	Mol wt Found (Calcd[b])	Concn[c]
1a	$R^1{}_2TlCl$	238	23.26 (23.20)	5.51 (5.35)	824 (828)	0.125
1b	$R^1{}_2TlBr$	234	21.53 (20.95)	5.24 (4.83)	920 (918)	0.152
2	$R^2{}_2TlCl$	>340	31.18 (31.43)	5.95 (5.80)	776 (762)	0.098
3	$R^3{}_2TlCl$[d]	e)	26.68 (27.14)	5.16 (5.12)	718 (708)	0.196
4	MeR^1TlBr	231	15.38 (15.53)	3.76 (3.65)	751 (772)	0.073
5	$R^1{}_2TlOOCPr^i$	72	31.04 (30.94)	6.32 (6.27)		
6	$R^1Tl(OOCPr^i)_2$	144	30.94 (30.60)	5.63 (5.41)		
7	$MeR^1TlOOCPr^i$	176	27.37 (27.46)	5.36 (5.38)		

a) $R^1=Me_3SiCH_2$, $R^2=Me_3CCH_2$, $R^3=Me_2CHCH_2$. b) As dimer. c) Mol%. d) % Tl, Found, 57.40: Calcd, 57.72. e) No definite melting point.

* To whom correspondence should be addressed.

TABLE 2. RELEVANT INFRARED[a] AND ^{1}H NMR[b] SPECTRAL DATA OF TRIMETHYLSILYLMETHYLTHALLIUM COMPOUNDS

Compound[c]		ν(Tl-C)		$^2J_{Tl-CH_2}$	$^2J_{Tl-CH_3}$
1a	R_2TlCl	520	491	537	
1b	R_2TlBr	520	489	536	
4	MeRTlBr	528	464	539	342
5	$R_2TlOOCPr^i$	514	478	566	
7	$MeRTlOOCPr^i$	d)	488	562	376
6	$RTl(OOCPr^i)_2$	d)		1121	

a) In Nujol mulls. ν in cm^{-1}. b) In $CDCl_3$. J in Hz. c) R=Me_3SiCH_2. d) Obscured by the ligand absorptions.

the presence of only isobutane and isobutene in almost 1 : 1 mole ratio. Also, 0.4 ml of $CDCl_3$ was added to a residual mixture, while kept at −78 °C, after a separate pyrolysis run carried out under the identical condition. The ^{1}H NMR spectrum of this $CDCl_3$ solution again confirmed the formation of only isobutane and isobutene (1 : 1) as chloroform-soluble products. No indication of the presence of 2,5-dimethylhexane could be obtained through GLC and ^{1}H NMR analyses.

Results and Discussion

Synthetic Route. Dialkylthallium halides, $(Me_3SiCH_2)_2TlX$ (**1a** X=Cl; **1b** X=Br) and $(Me_2RCCH_2)_2TlCl$ (**2** R=Me; **3** R=H) were prepared using the appropriate lithium or the Grignard reagents. **1a** was further derivatized to other trimethylsilylmethyl compounds of thallium as outlined in Scheme 1.

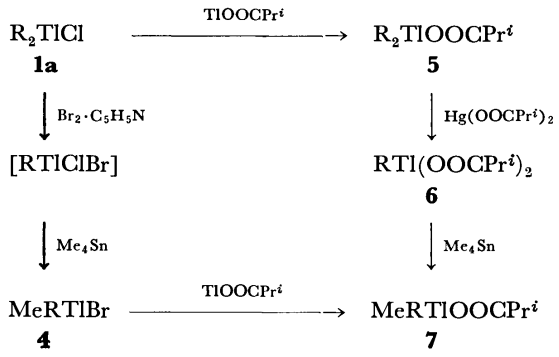

Scheme 1. R=Me_3SiCH_2.

Dialkylthallium Compounds. The trimethylsilylmethyl and neopentylthallium halides, **1a**, **1b**, **2**, and **4** possess good thermal stabilities comparable to those of dimethyl, diethyl or dipropyl analogs. However, interestingly, the diisobutylthallium derivative, **3** was found to be much less stable than not only **2** but Pr^n_2TlCl. Thus, even standing a crystalline sample of **3** at room temperature gradually caused decomposition to result in contamination of the sample with TlCl. Approximately 1 : 1 molar mixture of isobutane and isobutene was detected in the gaseous products from pyrolysis of the solid sample of **3** at 170 °C under reduced pressure for 3 h. 2,5-Dimethylhexane was not formed.

$$\underset{\mathbf{3}}{(Me_2CHCH_2)_2TlCl} \xrightarrow{\Delta} Me_3CH + Me_2C{=}CH_2 + TlCl$$

On the contrary, **2** and Pr^n_2TlCl were found to be totally stable under the same conditions. In view of this fact, it seems unlikely that the Tl–C bond strength in **3** is exceptionally weak. Although the precise mechanism of the decomposition of **3** yet remains to be elucidated, the presence of the labile β-methine hydrogen in the isobutyl group apparently is essential to the unique instability of this compound. In this regard, it should be mentioned that the removal of the β-methine hydrogen of the isobutyl group in $R(Me_2CHCH_2)Hg$ by a radical species promoted the liberation of isobutene and the homolytic fission of the Hg–R bond.[6]

Dimethylthallium halides are insoluble in non-coordinating solvents possibly due to the occurrence of the polymeric structure with a linear C–Tl–C unit lying perpendicular to the $(Tl–X)_n$ network as shown in **A** below.[7] It is well recognized[8] that the linear C–Tl–C configuration is energetically most favored in dialkylthallium compounds. On the contrary, **1**—**4** are all fairly soluble in $CHCl_3$ and benzene, and were found to be dimeric in $CHCl_3$ (Table 1) with a bent C–Tl–C configuration as suggested for **1a** and **1b** by the appearance of two TlC_2 stretching modes (Table 2).

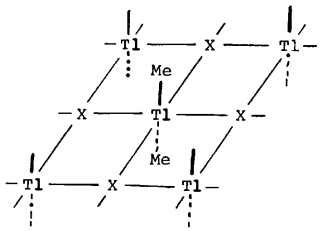

A (X=Cl, Br, I)

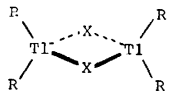

B (R=Me_3SiCH_2, Me_3CCH_2, Me_2CHCH_2; X=Cl, Br)

However, Pr^n_2TlCl was too insoluble to determine its molecular weight. We assume that a part of the reasons for the increased solubilities of **1**—**4**, compared to those of Me_2TlX and Pr^n_2TlCl, is steric; the steric bulk of the alkyl groups in **1**—**4** may have precluded the formation of the polymeric network with the Tl-X interaction as strong as that in $(Me_2TlX)_n$, as will be explained below. Thus, in molecular models for **1**, **2**, and **4** having a hypothetical structure similar to **A**, it is almost impossible to attach the Me_3SiCH_2 or Me_3CCH_2 groups, totally free of steric constraint, to each thallium atom in the $(Tl–X)_n$ layer which was constructed assuming the Tl–X bond length equal to that[7] in $(Me_2TlX)_n$. The most dominant repulsions observed in such models are those between the β-methyl substituents of one alkyl group and the CH_2 protons of the nearest alkyl or those between the former and the halogen atoms There exist similar kinds of, though to a lesser extent, steric repulsions in the similar model structure for **3**, while such model for Pr^n_2TlCl can now be readily constructed free of constraints without elongating the Tl–Cl distance found in $(Me_2TlCl)_n$.

A brief comparison of the electronic effects of the Me_3SiCH_2 and Me groups can be made on the basis of ^{1}H NMR spectral data. As shown in Table 2, J_{Tl-CH_2} and J_{Tl-CH_3} values of **7** are almost the same as those of **5** and $Me_2TlOOCPr^i$(377 Hz)[9], respectively.

Similarly, J_{Tl-CH_2} value of **1b** is very close to that of **4**. In view of the proposition[10] that thallium-proton spin-spin coupling constant is dominated by Fermi contact term, the results shown above suggest a similarity in the ability of the Me_3SiCH_2 and Me groups to affect the s-character in the bonds between thallium and these groups. A similar trend was also reported[11] that trans influences of the two groups are comparable in square planar Pt^{II} complexes.

Monoalkylthallium Compounds. It should be noted that **6** is much more stable than its methyl or ethyl analogs. Thus, for example, **6** can be recovered unchanged from hot methanol or dimethyl sulfoxide, while the latter two readily decomposed under the similar conditions to give thallium isobutyrate and $ROOCPr^i$ (R=Me, Et).[9] Kinetic studies on the similar decomposition of $MeTl(OAc)_2$ indicated the reaction to proceed through the nucleophilic attack of the acetate anion at the methyl carbon.[12] Therefore, the bulkiness of the Me_3SiCH_2 group almost certainly depresses the approach of a nucleophile at the α-carbon in **6**. A much higher stability of $PhCH(OMe)CH_2TlCl_2$[13] or a mononeopentylthallium halide species[14] than $MeTlX_2$ (X=Cl, Br) was also interpreted on similar grounds, although no detailed description on the isolation of the neopentyl derivative has yet appeared since its preliminary publication.

References

1) M. F. Lappert, Abstacts of 8th International Conf. Organometallic Chem., 1A21, Kyoto (1977).
2) A part of the present work has been communicated, S. Numata, H. Kurosawa, and R. Okawara, *J. Organomet. Chem.*, **70**, C21 (1974).
3) R. J. Meer and A. Bertheim, *Chem. Ber.*, **37**, 2051 (1904).
4) D. J. Peterson, *J. Organomet. Chem.*, **9**, 373 (1967).
5) M. Tanaka, H. Kurosawa, and R. Okawara, *J. Organomet. Chem.*, **18**, 49 (1969).
6) W. A. Nugent and J. K. Kochi, *J. Am. Chem. Soc.*, **98**, 5405 (1976).
7) H. D. Hausen, E. Veigel, and H. J. Guder, *Z. Naturforsch.*, **29b**, 269 (1974); H. M. Powell and D. M. Crowfoot, *Z. Kristallogr.*, **87**, 370 (1934).
8) P. J. Burke, L. A. Gray, P. J. C. Hayward, R. W. Matthews, M. McPatlin, and D. G. Gillies, *J. Organomet. Chem.*, **136**, C7 (1977).
9) H. Kurosawa and R. Okawara, *J. Organomet. Chem.*, **10**, 211 (1967).
10) J. V. Hatton, *J. Chem. Phys.*, **40**, 933 (1964).
11) M. R. Collier, C. Eaborn, B. Jovanovic, M. F. Lappert, L. M. Muir, and M. M. Truelock, *J. Chem. Soc., Chem. Commun.*, **1972**, 613.
12) U. Pohl and F. Huber, *J. Organomet. Chem.*, **116**, 141 (1976).
13) S. Uemura, A. Toshimitsu, and M. Okano, *Bull. Chem. Soc. Jpn.*, **49**, 2762 (1976).
14) M. D. Johnson, *Chem. Commun.*, **1970**, 1037.

ESR Studies of an Oxo-Bridged Manganese(III, IV) Complex of 2,2′-Bipyridine

Motomichi INOUE

Department of Chemistry, Nagoya University, Chikusa, Nagoya 464

(Received October 13, 1977)

ESR spectra were recorded on the single crystal of di-μ-oxo-tetrakis(2,2′-bipyridine)dimanganese(III,IV) perchlorate trihydrate. ESR signals attributable to the excited quartet state were observed in addition to an ESR signal due to the ground doublet state. From the temperature dependence of the signal intensities, the exchange integral was determined as $J/k=-207$ K. The spectrum of the quartet state exhibits a fine structure: $|D|$ and $|E|$ were estimated to be equal to 0.39 and 0.12 cm^{-1}, respectively. The constants are interpreted in terms of the dipole-dipole interaction and the crystal-field effect; the anisotropic part of the exchange interaction is negligibly small. The hyperfine structure in the spectrum of the doublet state indicates that odd electrons are distributed unequally on two manganese atoms in the dimer. This is due to an odd e electron (in the t_2^3-$t_2^3e^1$ system) localized mostly on one of the paired manganese atoms.

X-Ray crystal analysis and magnetic susceptibility measurement[1] showed that di-μ-oxo-tetrakis(2,2′-bipyridine)dimanganese(III,IV) perchlorate trihydrate, $[(bipy)_2Mn^{III}O_2Mn^{IV}(bipy)_2](ClO_4)_3\cdot 3H_2O$, is a good model compound for studying magnetic interaction between metal atoms in different oxidation states. As shown in Fig. 1, two manganese atoms bridged by two oxygen atoms are in different coordination fields. From the fact, it was suggested that Mn1 is a high spin d^4 ion, Mn^{3+}, and Mn2 a d^3 ion, Mn^{4+}. For a 2-3/2 spin system, four spin levels are derived with the energies $E_{1/2}=0$, $E_{3/2}=-3$, $E_{5/2}=-8$, and $E_{7/2}=-15J$ on the basis of the Hamiltonian,

$$\mathscr{H} = -2J\mathbf{S}_1\cdot\mathbf{S}_2. \quad (1)$$

The magnetic susceptibility[1] indicates that an antiferromagnetic interaction ($J/k=-147$ K) operates between the dissimilar ions. In the ESR spectrum,[2] a weak signal attributable to the excited states was observed in a region corresponding to $g=4$, in addition to a strong signal due to the ground state at a field of $g=2$. An ESR study of the excited states is expected to provide valuable information on the magnetic interaction. However, no detailed investigation has been undertaken. In the present investigation, ESR experiments have been carried out on the single crystal of the novel compound.

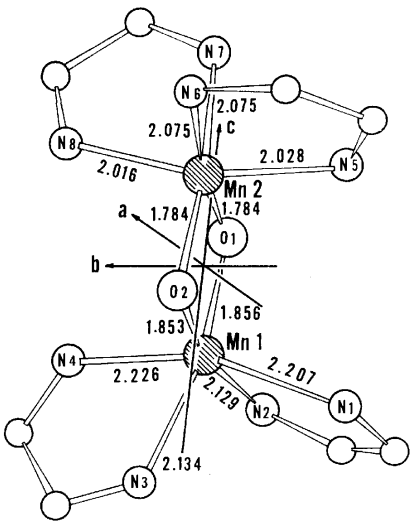

Fig. 1. Dimer structure of $[(bipy)_2MnO_2Mn(bipy)_2]^{3+}$.

Experimental

Single crystals of the complex were prepared by the method reported by Plaksin.[2] Deep green crystals were grown in the form of plates with well developed ab faces.

The ESR spectra were recorded by means of a JEOL ES-SCXA X-band ESR spectrometer equipped with a JEOL JM 350-MR electromagnet. Crystalline powders of MgO doped with Mn(II) ions were employed as a standard.

The crystal has a monoclinic space group $P2_1/c$ with four molecules per unit cell.[1,2] The Mn–Mn axis lies almost parallel to the bc plane and makes an angle of about 20° with the c axis. In a magnetic field applied along the ac plane, all molecules are magnetically equivalent. The ESR spectra were first recorded by rotating the crystal about its b axis, which coincides with one of the principal magnetic axes. An ESR signal exhibiting a hyperfine structure was observed at a field of $g=2$ (Fig. 2). Although the exact g factor was difficult to determine owing to the composite and asymmetric ESR curve, the anisotropy of the g factor was estimated to be 0.01 at most. The hyperfine structure showed no appreciable angular dependence. In addition to the main signal, weak signals were observed in regions of 1—2 and 5—11 kG (the unit G corresponds to 10^{-4} T in the SI unit system). Figure 2 shows an ESR spectrum for crystal orientation with the a axis perpendicular to magnetic field H_0. The positions of the weak signals exhibited marked angular dependence (Fig. 3). The maximum separation between the two signals was observed for $H_0\perp$a. The axis

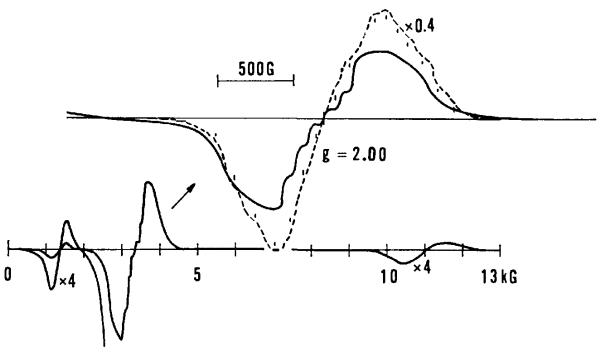

Fig. 2. ESR spectrum observed for H_0 applied along the K_m axis at 300 K. The broken curve displays the main signal ($g=2$) recorded at 183 K.

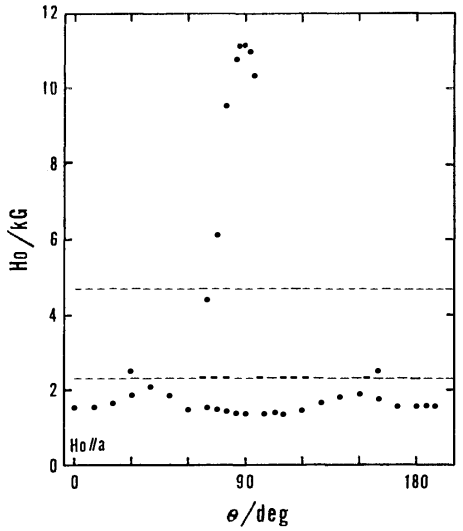

Fig. 3. Angular dependence of the positions of weak signals attributed to the quartet state for H_0 perpendicular to the b axis. The main signal ($g=2$) masks weak signals at fields between the broken lines.

K_m related to the maximum separation can be defined as one of the principal magnetic axes. Hence, the third axis coincides with the a axis. The ESR spectra were recorded by rotating the crystal about the K_m and a axes.

The temperature dependence of signal intensity was determined for the crystal orientations $K_m//H_0$ and b$//H_0$ (H_0 was applied along the bK_m plane) in a temperature range of 100—300 K.

Results

Temperature Dependence of Signal Intensity. The relative reciprocal intensity $I(293)/I(T)$ of the main signal observed at the field of $g=2$ is plotted against the temperature in Fig. 4. The intensity increases with decreasing temperature. On the other hand, the intensities of the weak signals decrease with decreasing temperature. The relative intensity $I(T)/I(293)$ of the signal at the lower field is shown in Fig. 4.

In a spin system having an exchange integral much larger than energies due to the zero-field splitting and the Zeeman term, the intensity $I_s(T)$ of an ESR signal attributed to the level S is proportional to $1/T$ and the unpaired-electron population $P_s(T)$ in the level:

$$I_S(T)\propto\frac{P_S(T)}{T}=\frac{(2S+1)\exp(-E_S/kT)}{T\sum_S(2S+1)\exp(-E_S/kT)}. \quad (2)$$

The population in each level is estimated as $P_{1/2}=0.66$, $P_{3/2}=0.30$, $P_{5/2}=0.04$, and $P_{7/2}=0.002$ at 300 K with the exchange integral determined from the magnetic susceptibility. The main signal is attributable to the ground doublet state, while the weak signals are attributable to the quartet state because contributions from the sextet and octet states are negligibly small. The intensity ratio of the weak signal to the main signal is expected to be proportional to $\exp(-3J/kT)$. The semilogarithmic plot of the ratio against $1/T$ yields a straight line over the temperature range investigated. From the slope, the exchange integral is determined

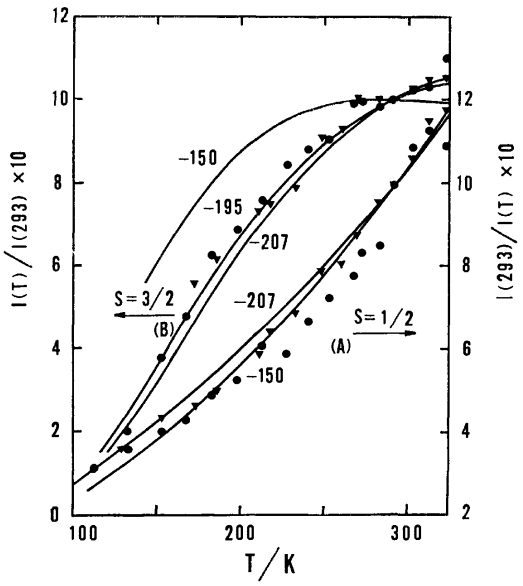

Fig. 4. Temperature dependence of signal intensities observed for $H_0//K_m$ (●) and $H_0\perp K_m$ (▼). The main signal (A) at $g=2$ and the weak signal (B) at the lower field are attributable to $S=1/2$ and $S=3/2$, respectively. The curves display relative intensities calculated with various J/k values.

to be −204 K (−142 cm^{-1}) for H_0//b and −210 K (−146 cm^{-1}) for $H_0//K_m$. The difference between the values cannot directly lead to the conclusion that the exchange interaction has an anisotropy, because the error of the integrated intensity amounts to about ±10 % and the uncertainty of temperature is estimated to be about 4°. Relative intensities calculated with the averaged value −207 K reproduce well the corresponding data (Fig. 4). Usually, magnetic susceptibility experiments give more accurate exchange integrals than ESR experiments. For the complex, however, the signal intensities can be determined separately for the two spin levels, and so the exchange integral determined by the present experiment seems to be highly reliable.

Spectrum of the Doublet State. The main signal attributed to the doublet state exhibits a hyperfine structure due to manganese nucleus-electron coupling. At low temperatures, the structure appears clearly on either side of the derivative curve as seen in Fig. 2. At least 16 lines can be found with spacings equal to 70—100 G: the structure consists of more than 11 lines expected for a pair of equivalent manganese atoms. This suggests that two manganese atoms in the dimer are not equivalent with each other, in line with the X-ray result showing that the two manganese atoms are in different oxidation states.

For H_0 along the aK_m plane, the g factor is approximately estimated to be equal to 2.00, the anisotropy being 0.01 at most. For crystal orientation in the ab plane, the g anisotropy is estimated to be less than 0.01.

Spectrum of the Quartet State. The shape and the resonance field of the signals depend markedly on the crystal orientation, but show no appreciable temperature dependence. The angular dependence of the position is shown in Fig. 3 for the crystal orientation in

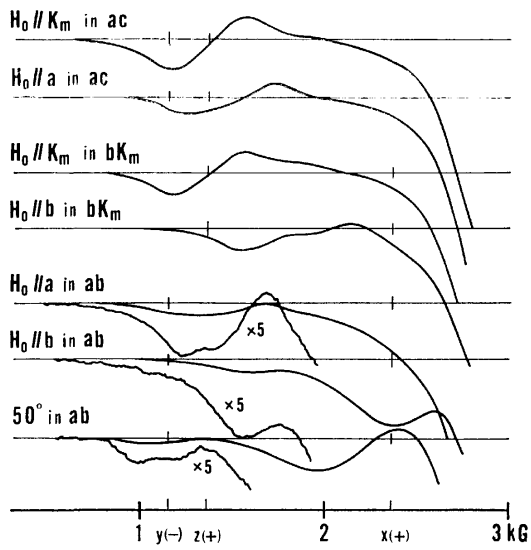

Fig. 5. Some spectra of the weak signal in the lower-field region.

H_0 along the ac plane. The intensity of the signals also depends on the crystal orientation. Especially, the signal in the higher field region is markedly angular dependent: no resonance line is observed above 100° of angle. An ESR pattern for H_0 along the bK_m plane resembles that for H_0 along the ac plane. When H_0 is applied along the ab plane, the crystal shows no ESR signal in the high field region. Figure 5 shows some spectra at the lower fields. The crystal oriented with its b axis parallel to H_0 shows different signals according to the direction of the microwave field H_1.

Because the exchange interaction energy is much larger than the Zeeman energy, the rate of mutual spin flipping is so high that only an average of two dissimilar spins is significant. In this case, the spin Hamiltonian for a pair of similar ions is applicable to the quartet state:

$$\mathscr{H} = g\mu_B \mathbf{S}\cdot\mathbf{H}_0 + D[S_z^2 - S(S+1)/3] + E(S_x^2 - S_y^2), \quad (3)$$

where x, y, and z axes are defined as local or molecular magnetic axes. The zero-field splitting constants D and E arise from the dipole-dipole interaction between two manganese atoms in the dimer, the anisotropic part of the exchange interaction, and the crystal field effect. When magnetic field is applied along the z axis, the following states and energy levels are derived.[3]

$$\theta_{\pm 3/2} = \cos\alpha_\pm |\pm\frac{3}{2}> + \sin\alpha_\pm |\mp\frac{1}{2}>, \quad (4)$$

$$\theta_{\mp 1/2} = -\sin\alpha_\pm |\pm\frac{3}{2}> + \cos\alpha_\pm |\mp\frac{1}{2}>, \quad (5)$$

$$W_{\pm 3/2} = \pm g_z\mu_B H_0/2 + [(D \pm g_z\mu_B H_0)^2 + 3E^2]^{1/2}, \quad (6)$$

$$W_{\mp 1/2} = \pm g_z\mu_B H_0/2 - [(D \pm g_z\mu_B H_0)^2 + 3E^2]^{1/2}. \quad (7)$$

In these expressions, $\tan 2\alpha_\pm = \sqrt{2}E/(g_z\mu_B H_0 \pm D)$. The energy levels for $H_0//x$ are derived as

$$W_{\pm 3/2} = \pm g_x\mu_B H_0/2 \pm [(g_x\mu_B H_0)^2 \mp (D-3E) g_x\mu_B H_0 + D^2 + 3E^2]^{1/2}, \quad (8)$$

$$W_{\pm 1/2} = \mp g_x\mu_B H_0/2 \pm [(g_x\mu_B H_0)^2 \pm (D-3E) g_x\mu_B H_0 + D^2 + 3E^2]^{1/2}. \quad (9)$$

The energy levels for $H_0//y$ are obtained by replacing $(D-3E)$ by $(D+3E)$. The transitions $\theta_{+3/2} \leftrightarrow \theta_{+1/2}$, $\theta_{+1/2} \leftrightarrow \theta_{-1/2}$, and $\theta_{-1/2} \leftrightarrow \theta_{-3/2}$ in H_0 directed to the i (x, y, or z) axis are abbreviated as i(+), i(0), and i(−), respectively. The transition probability depends on the $\alpha_\pm$ values and the direction of H_1 as well as H_0,[3] giving rise to the angular dependence of the signal intensity.

Four molecules in the unit cell are divided into two magnetically different groups: the Mn–Mn axes, which lie almost parallel to the ac plane, are inclined at +20 and −20°, respectively, with respect to the c axis, and the O–O axes are inclined at +40 and −40°, respectively, with the a axis. Thus, the principal zero-field splitting constants of the molecule cannot be determined definitely from the principal values of the crystal, since D and E in Eq. 3 are difficult to express as functions of angle. The following tentative analysis has been carried out. The Mn–Mn axis can be defined as one of the local principal axes, showing small deviation from the c axis approximately parallel to the K_m axis. Thus, the magnetic fields of z(+) and z(−) can be assumed to be equal to a set of the resonance fields observed for H_0 along K_m. The g values of the quartet state are presumed to be equal to those of the doublet state. On the basis of the assumptions, $|D|$ and $|E|$ are evaluated as 0.39 and 0.21 cm^{-1}, respectively. By use of the values, the transitions for H_0 directed to other principal axes are expected to take place at the fields $H_{y(+)}$=14.2, $H_{y(-)}$=1.15, $H_{x(+)}$=2.38, and $H_{x(-)}$=5.09 kG. The $|D|$ and $|E|$ values are so large that no i(0) transitions are allowed. The positions of the transitions in a magnetic field applied along the ab plane vary with crystal orientation in regions of $H_{x(+)}$–$H_{y(+)}$ and $H_{x(-)}$–$H_{y(-)}$. When H_0 makes 40 or 50° with the a axis, the spectrum shows resonance peaks at 1.36 and 2.27 kG (Fig. 5). A clear hump is observed at the high field side of the main signal, showing the presence of a signal at about 4 kG. The three transitions can be explained by $H_{y(-)}$, $H_{x(+)}$, and $H_{x(-)}$ fairly well, indicating that the tentative $|D|$ and $|E|$ values do not differ much from the inherent values. One of the principal axes is normal to the Mn–O_2–Mn plane, and the third axis is parallel to the O–O axis. It is noteworthy that $|E/D|$ of the complex is very large compared with the ratio ($\lesssim 1/3$) normally observed for metal complexes.

Discussion

The zero-field splitting constant arising from the dipole-dipole interaction between manganese atoms is evaluated as $D_{dip} \approx -3g^2\mu_B{}^2 r^{-3} = -0.26$ cm^{-1}, with the Mn–Mn distance 2.716 Å. The anisotropy of the exchange interaction is of the order of the magnitude $|D_{ex}| \approx |J(2-g)^2|$. Because the g factor is very close to 2.00, $|D_{ex}|$ is estimated to be less than 0.01 cm^{-1}. The value is negligibly small compared with $|D_{dip}|$. An additional contribution comes from the crystal field effect. Usually, the zero-field splitting constants of d^4 ions are much larger than those of d^3 ions.[4] Hence, Mnl makes a dominant contribution. The

constants of d^4 complexes are given by[3]

$$D_{cf} = -3\left(\rho+\frac{\lambda^2}{\Delta}\right)\left[\frac{2\Delta}{8\lambda}(2-g_{z'})-1\right], \quad (10)$$

$$E_{cf} = -\frac{1}{4}\left(\rho+\frac{\lambda^2}{\Delta}\right)\left(\frac{\Delta}{\lambda}\right)(g_{x'}-g_{y'}), \quad (11)$$

where x', y', and z' are defined as the local axes of the crystal field, λ is the spin-orbit coupling constant, Δ is the energy separation between Γ_3 and Γ_5 levels, and ρ is the constant of the spin-spin interaction. The values of λ and ρ are estimated to be equal to 88 and 0.18 cm^{-1}, respectively.[3] Usual manganese(III) complexes have Δ equal to 20 000 cm^{-1}. When $|g_{z'}-2| \approx 0.01$ and $|g_{x'}-g_{y'}|<0.01$, $|D_{cf}|$ is approximated to be equal to 0.7 cm^{-1}, and $|E_{cf}|$ is less than 0.3 cm^{-1}. The $|D_{cf}|$ and $|E_{cf}|$ values of Mn^{3+} in TiO_2 amount to 3.4 and 1.2 cm^{-1}, respectively.[3] This is the only example reported for Mn^{3+}, indicating that the aforementioned values of the complex are not overestimated. This suggests that the contribution from the crystal-field effect may be comparable to that from the dipole-dipole interaction. The octahedron of MnI is elongated along N1 and N4 directions, which are practically normal to the Mn–O_2–Mn plane. Because the z' axis is defined as a direction perpendicular to the plane, it is normal to the principal z axis of D_{dip}. Hence, D arises from D_{dip} and E_{cf}, and E is due to D_{cf}. This explains the large $|E/D|$ value. Although the uncertainty of the crystal orientation amounts to $\pm 5°$, the K_m axis deviates from the axis of D_{dip} directed to the Mn–Mn axis. This is probably due to a slight discordance between the crystal-field axis and dipolar-interaction axis systems. The zero-field splitting constants can be interpreted in terms of the dipole-dipole interaction and the crystal-field effect. The anisotropy of the exchange interaction is so small that the Hamiltonian (Eq. 1) of ideally isotropic interaction is valid for the complex.

The hyperfine structure in the ESR spectrum of the doublet state suggests that the odd electrons are unequally distributed on the two manganese atoms in the dimer. This situation is different from that in cobalt(III,IV) complexes, $[(NH_3)_5CoO_2Co(NH_3)_5]X_5$, in which an odd electron is distributed over the Co–O–O–Co system and the two cobalt atoms are equivalent with each other.[5] In the manganese(III,IV) complex, the spin delocalization takes place through the p orbitals of bridging oxygen atoms, giving rise to the antiferromagnetic interaction between the t_2^3 and $t_2^3e^1$ systems. The t_2 electrons forming $d\pi$–$p\pi$ bonds can be delocalized through the π systems, while the e electron occupying mostly the d_{z^2} orbital makes little contribution to the formation of Mn–O π bonding for symmetric and steric reasons, so that the e electron is stably localized on one of the paired manganese atoms or on MnI having the more distorted coordination field. For this reason, the two manganese atoms in the dimer differ from each other despite the strong exchange interaction operating between them.

This work was carried out preliminarily by use of a Varian E-3 ESR spectrometer at the Department of Chemistry, University of Florida. The author is much indebted to Dr. W. S. Brey, Jr. and Dr. R. C. Stoufer for their suggestions and support. The JEOL ESR spectrometer was purchased with a Grant-in-Aid for Scientific Research from the Ministry of Education.

References

1) P. M. Plaksin, R. C. Stoufer, M. Mathew, and G. J. Palenik, *J. Am. Chem. Soc.*, **94**, 2121 (1972).

2) P. M. Plaksin, Ph. D. Thesis, University of Florida, 1971.

3) A. Abragam and B. Bleaney, "Electron Paramagnetic Resonance of Transition Ions," Clarendon Press, Oxford, 1970.

4) H. A. Kuska and M. T. Rogers, "Radical Ions," ed. by E. T. Kaiser and L. Kevan, John Wiley & Sons, New York, N. Y. 1968, p. 579; B. A. Goodman and J. R. Rayner *Adv. Inorg. Nucl. Chem.*, **13**, 135 (1970).

5) M. Mori, J. A. Well, and J. K. Kinnaird, *J. Phys. Chem.*, **71**, 103 (1971); J. A. Well and J. K. Kinnaird, *J. Phys. Chem.*, **71**, 3341 (1971).

Liquid-phase Oxidation of Hydrocarbons with Molecular Oxygen. I. The Effects of Metal Ions and Their Ligands on Product Distribution in the Oxidation of Tetralin in Acetic Acid

Fujio MIZUKAMI and Juichi IMAMURA

National Chemical Laboratory for Industry, Honmachi, Shibuya-ku, Tokyo 151

(Received June 30, 1977)

Metal-ion catalyzed oxidation of tetralin and metal-ion catalyzed decomposition of α-tetralin hydroperoxide (THP) were carried out in acetic acid in both the presence and absence of an additive. It was found that the rate-determining step in the oxidation of tetralin is the decomposition of THP. The results also suggest that the decomposition of THP with cobalt catalysts proceeds by the inner-sphere mechanism. In the oxidation of tetralin catalyzed by first-transition-metal ions, excepting vanadium, cobalt showed the highest activity and the lowest selectivity of hydroperoxide, and chromium showed the highest ratio of α-tetralone to α-tetralol (On/Ol). The order of the activities of metal acetates in producing oxidation is in agreement with that of the activities of metal acetates in producing decomposition. Such agreement was also found for $Co(acac)_3$, $Cr(acac)_3$, $Mn(acac)_2$, and $Fe(acac)_3$ catalysts. For oxidation with $Co(OAc)_2 \cdot 4H_2O$ and $Cr(OAc)_3$, the product distributions were examined for various conversions of tetralin. In the both cases, the On/Ol ratios increase with increasing tetralin conversion. However, the mechanisms responsible for the increase in the On/Ol ratio appear to be different.

Liquid-phase oxidation of tetralin has been widely studied in both the presence and absence of a catalyst. The main products are known to be α-tetralin hydroperoxide (THP), α-tetralone and α-tetralol. According to previous studies,[1–10] the formation mechanism is understood as follows:

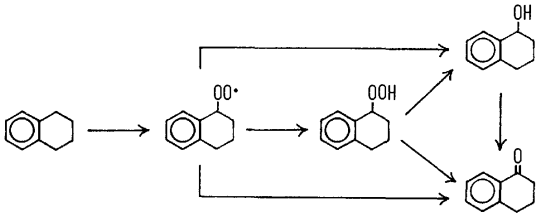

However, previous reports dealt mainly with kinetics and thus with reactions at low conversion in order to avoid complications. There are few data in the literature on the distribution of the products at high conversion.[6]

It is well known that transition-metal ions catalyze the oxidation of hydrocarbons and their catalytic activities are frequently related to their redox potentials.[11,12] It is also clear that metal ions in solution form complexes with solvent molecules, counter anions, *etc.*, and that the redox potentials of these ions are affected by ligands in the complex. However, there are not many reports dealing with the influence of ligands on the distribution of the products for metal-ion catalyzed autoxidation of aromatic hydrocarbons.

The aim of the present study is to elucidate the effects of various metal ions and their ligands on the oxidation of tetralin, in addition to the dependence of the product distribution on the catalyst and the substrate concentration at various reaction temperatures.

Experimental

Materials. The tetralin and metal salts employed were of reagent grade and were used without further purification. THP was synthesized according to the procedure of Knight and Swern.[13] This hydroperoxide was 99.8% pure as confirmed by iodometric titration.

Oxidation of Tetralin. A mixture (150 cm^3) of tetralin and acetic acid containing a catalyst was placed into an autoclave (sus-316) equipped with a magnetic stirrer and a thermocouple, and was warmed to the desired temperature. Oxygen was introduced into the autoclave through a pressure controller (the oxygen pressure was 20 kg/cm^2). The reaction temperature was controlled to within ±1.0 °C of the desired temperature by occasional cooling with water.

The reaction was terminated by stopping the oxygen feed and by quickly cooling the vessel in an ice-cold bath.

Decomposition of THP. A four-necked flask (200 cm^3, round-bottomed) equipped with a thermometer, a reflux condenser, a dropping funnel and a nitrogen inlet was filled with nitrogen gas. Into the flask, were placed a teflon stirring bar and a 50-cm^3 solution of acetic acid containing a catalyst. A stream of nitrogen was gently bubbled through the solution. The solution was then stirred and warmed to the desired temperature. To the vigorously stirred solution, was added a 25-cm^3 solution of acetic acid containing 2.50 g of THP and then the nitrogen stream was stopped. At hourly intervals, 1.5-cm^3 portions of the reaction mixture were withdrawn in a nitrogen atmosphere and were analyzed.

Analysis. The hydroperoxide concentration was determined by the usual method.[14]

α-Tetralone, α-tetralol and tetralin in the reaction mixture were identified and their amounts were determined using gas chromatography with a Shimadzu GC-4CPT chromatograph (2 m × 3 mm column packed with 10% Carbowax 4000 on Chromosorb AW, programming 5 °C/min from 120 to 170°, He 40 cm^3/min). *o*-Bromoanisole was used as an internal standard. Before GLC analysis, the remaining peroxide was reduced with an excess of triphenylphosphine.[15] The "net α-tetralol" is the difference between the total amount of α-tetralol after reduction and the amount of hydroperoxide before reduction.

Results and Discussion

The dissolving rate for molecular oxygen in a solution is frequently the rate-determining step in the liqid-phase autoxidation of hydrocarbons at atmospheric pressure. In the present study, the oxidation rate of tetralin in acetic acid was actually faster at higher pressure than at atmospheric pressure, and was nearly constant at oxygen pressures greater than 4 kg/cm^2. All runs in

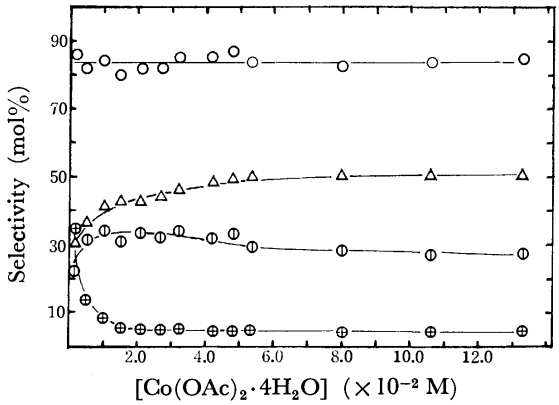

Fig. 1. The effect of cobalt acetate concentration on the oxidation of tetralin in acetic acid at 72.5±1.0 °C.
Reaction conditions: $[\text{tetralin}]_{\text{initial}}=3.85$ M; O_2 pressure, 20 kg/cm²; tetralin conversion, 20.0±1.5%.
△: Tetralone, ⓘ: tetralol, ⊕: peroxide, ○: total.

the present study were, therefore, carried out at an oxygen pressure of 20 kg/cm².

The Effects of the Cobalt and Tetralin Concentrations and the Reaction Temperature. The effect of the Co(OAc)₂·4H₂O concentration on the formation of products in the oxidation of tetralin in acetic acid at 72.5 °C is shown in Fig. 1. The dependence of the product distribution on the initial concentration of tetralin is shown in Fig. 2. Figure 3 shows the selectivities* of products at various reaction temperatures in the range from 50 to 110 °C. At reaction temperatures greater than 130 °C, hydroperoxide, α-tetralol and α-tetralone were obtained with lower selectivities than at reaction temperatures below 110 °C. At reaction temperatures

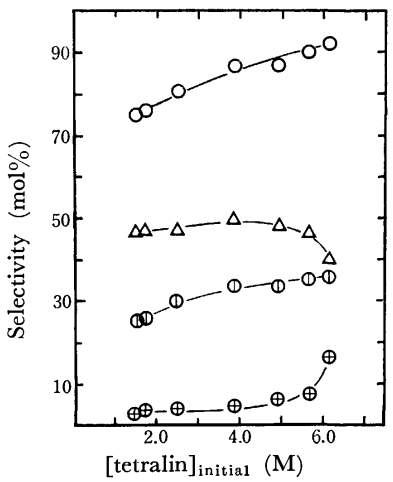

Fig. 2. The cobalt acetate catalyzed oxidation of tetralin in acetic acid at 72.5±1.0 °C.
Reaction conditions: $[\text{Co(OAc)}_2\cdot 4\text{H}_2\text{O}]=4.77\times10^{-2}$ M; O_2 pressure, 20 kg/cm²; tetralin conversion, 20.0±2.0%.
△: Tetralone, ⓘ: tetralol, ⊕: peroxide, ○: total.

* In this paper, the term "selectivity" means the molar percentage of the product to the amount of the converted tetralin.

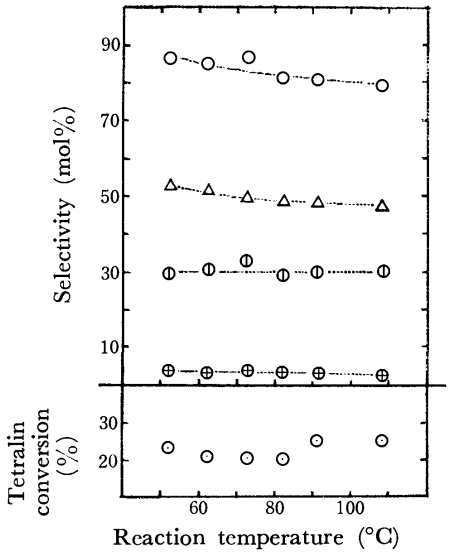

Fig. 3. The effect of reaction temperature on the oxidation of tetralin in acetic acid.
Reaction conditions: $[\text{Co(OAc)}_2\cdot 4\text{H}_2\text{O}]=4.77\times10^{-2}$ M; $[\text{tetralin}]_{\text{initial}}=3.85$ M; O_2 pressure, 20 kg/cm².
△: Tetralone, ⓘ: tetralol, ⊕: peroxide, ○: total.

above 120 °C, it was also difficult to carry out the oxidation of tetralin at an approximately constant temperature.

The selectivity of hydroperoxide formation decreases rapidly with increasing $\text{Co(OAc)}_2\cdot 4\text{H}_2\text{O}$ concentration (Fig. 1) and upon decreasing the initial tetralin concentration (Fig. 2). This result can be explained by the following reaction scheme which has been proposed

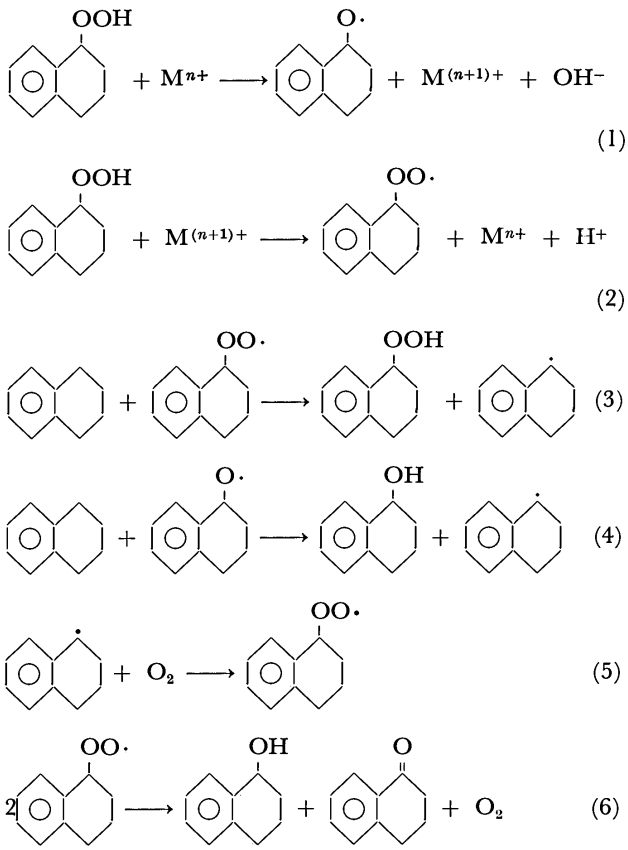

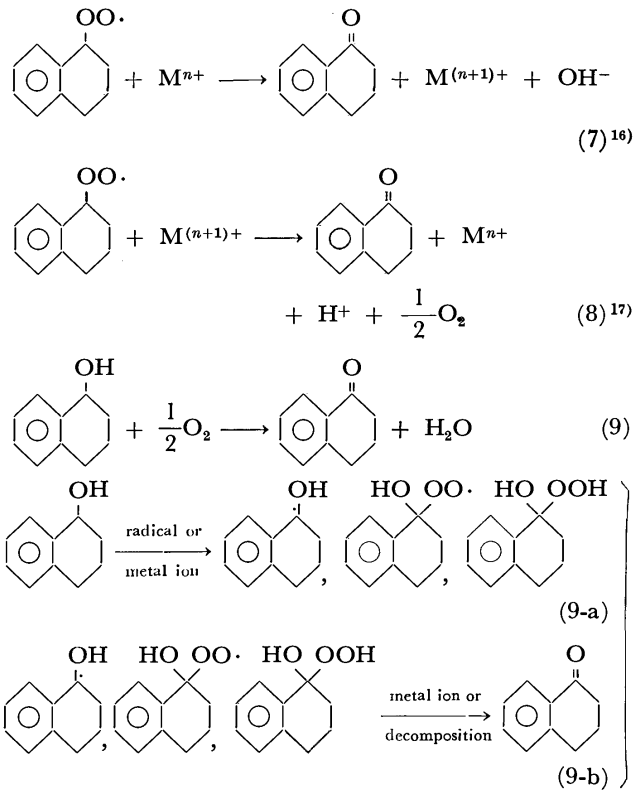

by other workers.[1-10,16,17] Transition-metal ions generally promote the decomposition of hydroperoxide following Reactions 1 and 2. Accordingly, the selectivity of hydroperoxide decreases with increasing $Co(OAc)_2 \cdot 4H_2O$ concentration.

Figures 4 and 5 show the product formation for various tetralin conversions. The product distributions shown in Fig. 4 are similar in tendency to those shown in Fig. 5, although the catalyst concentration depicted in Fig. 4 is different from that in Fig. 5. The α-tetralone selectivity increases with increasing tetralin conversion. For tetralin conversions above 20%, the percentage of the decrease in α-tetralol selectivity is

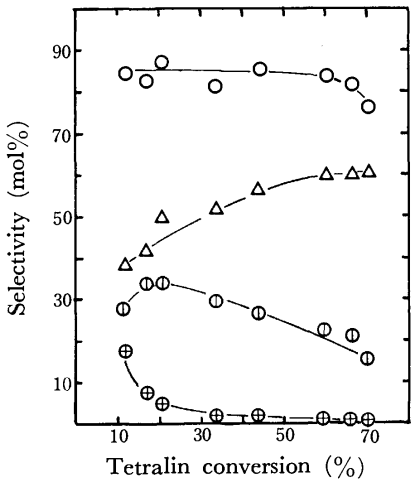

Fig. 4. The cobalt acetate catalyzed oxidation of tetralin in acetic acid at 72.5±1.0 °C.
Reaction conditions: $[Co(OAc)_2 \cdot 4H_2O] = 4.77 \times 10^{-2}$ M; $[tetralin]_{initial} = 3.85$ M; O_2 pressure, 20 kg/cm².
△: Tetralone, ⊖: tetralol, ⊕: peroxide, ○: total.

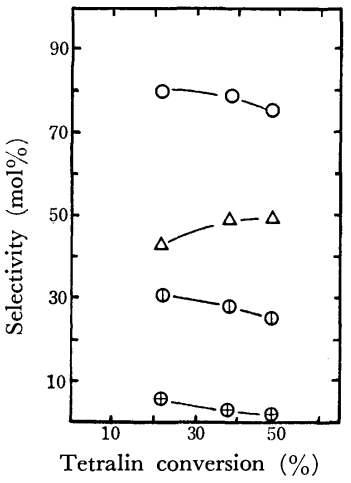

Fig. 5. The cobalt acetate catalyzed oxidation of tetralin in acetic acid at 72.0±2.0 °C.
Reaction conditions: $[Co(OAc)_2 \cdot 4H_2O] = 1.46 \times 10^{-2}$ M; $[tetralin]_{initial} = 3.50$ M; O_2 pressure, 20 kg/cm².
△: Tetralone, ⊖: tetralol, ⊕: peroxide, ○: total.

nearly equal to that of the increase in α-tetralone selectivity (Fig. 4). Martan *et al.*[6] have stated that, in the $Co(OAc)_2$-catalyzed co-oxidation of tetralin and α-tetralol in acetic acid at 80 °C, α-tetralol is oxidized at a rate 1.5 times faster than tetralin and gives α-tetralone in a 75% yield. Accordingly, the increase in α-tetralone selectivity for tetralin conversions above 20% appears to be mainly due to Reaction 9.

From Figs. 1—5, when cobalt(II) acetate is used as a catalyst and acetic acid as a solvent, the optimum conditions for obtaining α-tetralone are concluded to be as follows: a reaction temperature below 80 °C, an initial concentration of tetralin from 2.5 to 5 M, a catalyst concentration above 4.5×10^{-2} M and a tetralin conversion above 50%.

The Effect of Ligands. The effects of various counter anions and additives on the oxidation of tetralin catalyzed by cobalt ions are shown in Tables 1—4 and Fig. 6. It is clear that the additives used coordinate to the cobalt ion in a solution of acetic acid because the color of the solution containing cobalt acetate changes upon introduction of the additive.

As shown in Tables 1 and 3 and in Fig. 6, it is clear that cobalt(II) dibromide has a low catalytic activity although the rate of cobalt-catalyzed oxidation of tetralin is accelerated by adding potassium bromide to cobalt(II) acetate solutions (Co : KBr=1 : 1, molar ratio). This has already been observed and demonstrated kinetically.[7,10]

The tris(acetylacetonate)cobalt(III) complex ($Co(acac)_3$) showed a higher selectivity for hydroperoxide formation and a slower rate of oxidation than catalysts such as cobalt(II) carboxylates, cobalt(II) nitrate and bis(acetylacetonato)cobalt(II) complexes ($Co(acac)_2$ and $Co(acac)_2 \cdot 2H_2O$) (Tables 1 and 2, and Fig. 6). The addition of KF, pyridine (py) and 2,2'-bipyridine (bipy) to the $Co(OAc)_2 \cdot 4H_2O$ solution (Co-F, Co-py and Co-bipy) decreased the tetralin oxidation rate and increased the hydroperoxide selectivity (Tables 3 and 4, and Fig. 6). Thus, when hydroperoxide was ob-

Table 1. Product distribution for the cobalt salt catalyzed oxidation of tetralin

Catalyst	Tetralin conversion (%)	Selectivity (mol%)				Reaction temperature (°C)
		Tetralone	Tetralol	Peroxide	Total	
$Co^{II}(OAc)_2 \cdot 4H_2O$	20.9	49.1	32.3	4.8	86.2	72.5±0.5
$Co^{II}(C_6H_5CO_2)_2$	18.7	49.0	34.5	3.7	87.2	72.5±1.0
$Co^{II}(C_{18}H_{35}O_2)_2$	20.4	53.1	33.1	3.9	90.1	72.5±1.0
$Co^{II}(NO_3)_2 \cdot 6H_2O$	19.2	44.7	31.7	7.8	84.2	71.5±1.0
$Co^{III}(acac)_3$	19.9	41.9	29.0	18.4	89.3	72.5±1.0
$Co^{II}Br_2 \cdot 6H_2O$[a]	38.6	27.3	19.1	2.5	48.9	130—170

Reaction conditions : $[catalyst] = 4.77 \times 10^{-2}$ M, $[tetralin]_{initial} = 3.85$ M, the O_2 pressure was 20 kg/cm².
a) No oxygen absorption was observed for a period of 2 h at 72.5 °C.

Table 2. Product distribution for the acetylacetonato cobalt complex catalyzed oxidation of tetralin

Catalyst	Tetralin conversion (%)	Selectivity (mol%)				Reaction time (min)
		Tetralone	Tetralol	Peroxide	Total	
$Co^{II}(OAc)_2 \cdot 4H_2O$	22.3	53.2	30.3	4.3	87.8	40
$Co^{III}(acac)_3$	20.2	39.7	25.1	26.6	91.4	66
$Co^{II}(acac)_2$	19.0	46.9	30.9	6.0	83.8	37
$Co^{II}(acac)_2 \cdot 2H_2O$	17.6	48.9	32.1	5.3	86.3	35

Reaction conditions : $[catalyst] = 4.77 \times 10^{-2}$ M, $[tetralin]_{initial} = 3.85$ M, the reaction temperature was 50.0±1.0 °C, the O_2 pressure was 20 kg/cm².

Table 3. Product distribution for the cobalt acetate catalyzed oxidation of tetralin in the presence of additive

Additive	Tetralin conversion (%)	Selectivity (mol%)				Reaction time (min)
		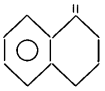	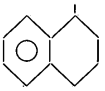	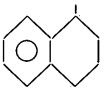	Total	
—	22.3	53.2	30.3	4.3	87.8	40
KCl	22.5	48.7	33.9	4.1	86.7	50
KBr	21.3	52.7	31.1	5.5	89.3	24
KSCN[a]	21.7	47.3	28.5	6.8	82.6	39
Pyridine	21.1	47.2	30.3	11.4	88.9	50
KF	23.3	43.8	28.8	15.2	87.8	64

Reaction conditions : $[Co(OAc)_2 \cdot 4H_2O] = [additive] = 4.77 \times 10^{-2}$ M, $[tetralin]_{initial} = 3.85$ M, the reaction temperature was 50.0±1.0 °C, the O_2 pressure was 20 kg/cm².
a) A brown material was deposited during the oxidation reaction.

Table 4. Product distribution for the cobalt acetate catalyzed oxidation of tetralin in the presence of bipyridine

Catalyst (M)		Tetralin conversion (%)	Selectivity (mol%)				Reaction temperature (°C)	Reaction time (min)
$Co(OAc)_2 \cdot 4H_2O$	Bipyridine		Tetralone	Tetralol	Peroxide	Total		
0.0052	0.0052	19.4	28.8	27.1	31.0	86.9	72.5±1.0	12
0.0105	0.0105	21.4	36.1	32.1	24.4	92.6	72.5±1.0	10
0.0159	0.0159	19.2	35.7	33.0	17.7	86.4	72.5±1.0	9
0.0213	0.0213	19.6	35.5	33.2	14.8	83.5	74.0±1.5	8
0.0266	0.0266	20.2	38.2	31.4	13.8	83.4	72.5±1.0	9
0.0051	0.0103	16.4	11.3	1.5	63.9	76.7	72.0±0.5	55
0.0104	0.0207	18.4	10.3	1.5	52.1	63.9	72.0±0.5	50
0.0107	—	20.9	40.6	34.7	8.0	83.3	64—70	12

Reaction conditions : $[tetralin]_{initial} = 3.85$ M, the O_2 pressure was 20 kg/cm².

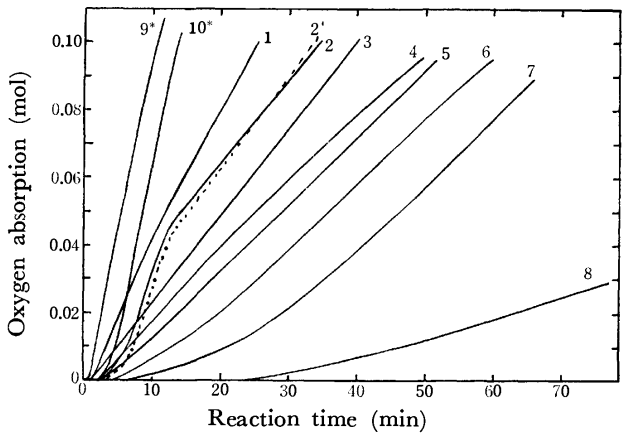

Fig. 6. The oxidation of tetralin in acetic acid at 50.0±1.0 °C.
Reaction conditions: [metal ion or complex]=[additive]=4.77×10^{-2} M; [tetralin]$_{initial}$=3.85 M; O_2 pressure, 20 kg/cm^2.
1: $Co^{II}(OAc)_2\cdot 4H_2O$+KBr (Co-Br), 2: $Co^{II}(acac)_2\cdot 2H_2O$, 2': $Co^{II}(acac)_2$, 3: $Co^{II}(OAc)_2\cdot 4H_2O$, 4: $Co^{II}(OAc)_2\cdot 4H_2O$+KCl (Co-Cl), 5: $Co^{II}(OAc)_2\cdot 4H_2O$+pyridine (Co-py), 6: $Co^{II}(OAc)_2\cdot 4H_2O$+KF (Co-F), 7: $Co^{III}(acac)_3$, 8: $Mn^{II}(OAc)_2\cdot 4H_2O$, 9*: $Co^{II}(OAc)_2\cdot 4H_2O$, 10*: $Co^{III}(acac)_3$.
*) The reaction temperature is 72.5±1.0 °C.

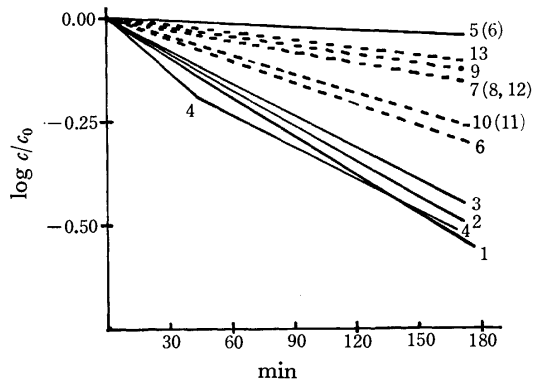

Fig. 7. The decomposition of THP in acetic acid.
——: Reaction temperature, 51.0±1.0 °C; [THP]$_{initial}$=2.00×10^{-1} M; [metal ion or complex]=[additive]=2.0×10^{-3} M.
----: Reaction temperature, 72.0±1.0 °C; [THP]$_{initial}$=2.00×10^{-1} M; [metal ion or complex]=6.0×10^{-3} M.
1: $Co^{II}(OAc)_2\cdot 4H_2O$, 2: $Co^{II}(OAc)_2\cdot 4H_2O$+pyridine (Co-py), 3: $Co^{II}(OAc)_2\cdot 4H_2O$+KF (Co-F), 4: $Co^{II}(acac)_2$, 5: $Co^{III}(acac)_3$, 6: $Mn^{II}(OAc)_2\cdot 4H_2O$, 7: $Cr^{III}(OAc)_3$, 8: $Ni^{II}(OAc)_2\cdot 4H_2O$, 9:$Cu^{II}(OAc)_2\cdot H_2O$, 10: $Cr^{III}(acac)_3$, 11: $Mn^{II}(acac)_2$, 12: $Ti^{IV}O(acac)_2$, 13: $Fe^{III}(acac)_3$.

tained in high selectivities, the oxidation rate of tetralin was low.

The decomposition of THP with five kinds of cobalt catalysts was also carried out in acetic acid at 51 °C in a nitrogen atmosphere. This was carried out at lower catalyst concentrations than those for the oxidation of tetralin, because the decomposition was too fast at high catalyst ([$Co(OAc)_2\cdot 4H_2O$]>6.0×10^{-3} M) concentrations. The decomposition rates were first order with respect to the hydroperoxide concentration. The decomposition order is $Co(acac)_2\simeq Co(OAc)_2\cdot 4H_2O$>Co-py>Co-F≫$Co(acac)_3$, as shown in Table 5 and Fig. 7. This order is consistent with that of the oxidation rates of tetralin at 50°, that is, $Co(acac)_2\simeq Co(OAc)_2\cdot 4H_2O$>Co-py>Co-F≫$Co(acac)_3$ (Tables 2 and 3, and Fig. 6) and also corresponds to the order of increasing hydroperoxide selectivities for oxidation ($Co(OAc)_2\cdot 4H_2O\simeq Co(acac)_2$ < Co-py < Co-F ≪ $Co(acac)_3$) (Tables 2 and 3, and Fig. 6). Yamada and Kamiya[18] have reported that the rate of $Co(OAc)_2$-catalyzed decomposition of THP in acetic acid at 50 °C lowers as the molar ratio of the bipy added to the cobalt(II) acetate is increased from zero to two. For the $Co(OAc)_2\cdot 4H_2O$-catalyzed oxidation of tetralin in acetic acid at

Table 5. Rate constants for the decomposition of THP in acetic acid

Catalyst: Metal salt or metal complex	Catalyst: Concentration (M)	Reaction temperature (°C)	Rate constant ($\times 10^{-3}$ min^{-1})
$Co^{II}(OAc)_2\cdot 4H_2O$	2.0×10^{-3}	51.0±1.0	7.5
Co-py[a]	2.0×10^{-3}	51.0±1.0	6.6
Co-F[b]	2.0×10^{-3}	51.0±1.0	5.8
$Co^{II}(acac)_2$	2.0×10^{-3}	51.0±1.0	10.0 6.2
$Co^{III}(acac)_3$	2.0×10^{-3}	51.0±1.0	0.7
$Mn^{II}(OAc)_2\cdot 4H_2O$	2.0×10^{-3}	51.0±1.0	0.6
	6.0×10^{-3}	72.0±1.0	3.9
$Cr^{III}(OAc)_3$	6.0×10^{-3}	72.0±1.0	2.0
$Ni^{II}(OAc)_2\cdot 4H_2O$	6.0×10^{-3}	72.0±1.0	1.9
$Cu^{II}(OAc)_2\cdot H_2O$	6.0×10^{-3}	72.0±1.0	1.7
$Cr^{III}(acac)_3$	6.0×10^{-3}	72.0±1.0	3.4
$Mn^{II}(acac)_2$	6.0×10^{-3}	72.0±1.0	3.3
$Ti^{IV}O(acac)_2$	6.0×10^{-3}	72.0±1.0	2.0
$Fe^{III}(acac)_3$	6.0×10^{-3}	72.0±1.0	1.5

a) $Co^{II}(OAc)_2\cdot 4H_2O$: pyridine=1 : 1 (molar ratio). b) $Co^{II}(OAc)_2\cdot 4H_2O$: KF=1 : 1 (molar ratio). [THP]$_{initial}$=2.00×10^{-1} M.

72.5 °C, the hydroperoxide selectivity increases as the ratio of the bipy to the cobalt(II) acetate is increased from zero to two (Table 4). Accordingly, the tetralin oxidation rate and the selectivity for the formation of hydroperoxide, for such cobalt catalysts, depend on the hydroperoxide decomposition rate.

From the above results, the decomposition mechanism of hydroperoxide can also be considered to be as follows. The catalytic decomposition of hydroperoxide by metal ions is thought to proceed *via* the formation of inner-sphere and/or outer-sphere complexes of metal ions with hydroperoxide[19] (inner-sphere[20-23] and/or outer-sphere mechanisms[20-23]). For the inner-sphere mechanism, the ligand attached to the metal ion must be replaced by the hydroperoxide, *i.e.*, $[ML_5Y]+ROOH \rightarrow [ML_5(ROOH)]+Y$. Such replacement is not required for the formation of the outer-sphere complex. Accordingly, decomposition by the outer-sphere mechanism will depend mainly on the redox potential of the complex. On the other hand, decomposition by the inner-sphere mechanism appears to depend on the mobility of the ligands attached to the metal ion, as well as on the redox potential of the metal ion.

The following facts are well known in coordination chemistry. Ligands such as py and F^- form strong coordination bonds with cobalt ions in comparison with ligands such as NO_3^-, Br^-, Cl^-, H_2O, and RCO_2^-.[20-24] For hydrolysis of the type, $[ML_5Y]+H_2O \rightarrow [ML_5(H_2O)]+Y$ ($M=Co^{III}$ or Cr^{III}, $L=NH_3$ or H_2O), the order of reactivities as far as the leaving group (Y) is concerned is $NO_3^- > Br^- > H_2O > AcO^- > F^- > NH_3$.[20,23,25] This is in good agreement with the order of stability constants of $[ML_5Y]$.[20,23] The cobalt complex having the $(t_{2g})^5(e_g)^2$ electron configuration ($Co^{II}(acac)_2L_2$, $L=H_2O$ or AcOH) has a faster rate for the ligand-replacement reaction than the corresponding cobalt complex having the $(t_{2g})^6(e_g)^0$ electron configuration ($Co^{III}(acac)_2L_2$, $L=H_2O$ or AcOH, L_2= acac).[20,23,25] In solution, $Co^{II}(acac)_2$ forms $Co^{II}(acac)_2L_2$ with solvent molecules such as AcOH and H_2O, although $Co^{II}(acac)_2$ has a tetrameric structure in the solid state.[22] 2,2'-Bipyridine coordinated to transition-metal ions generally can be replaced by other ligands only with difficulty.[20-24] Therefore, the fact that catalysts such as $Co(acac)_3$, Co-F, Co-py, and Co-bipy have high hydroperoxide selectivities for the oxidation of tetralin and low rates for the decomposition of THP is mainly correlated with the stability of the ligands attached to the cobalt ion if Reaction 1 and/or Reaction 2 proceed by the inner-sphere mechanism as follows:

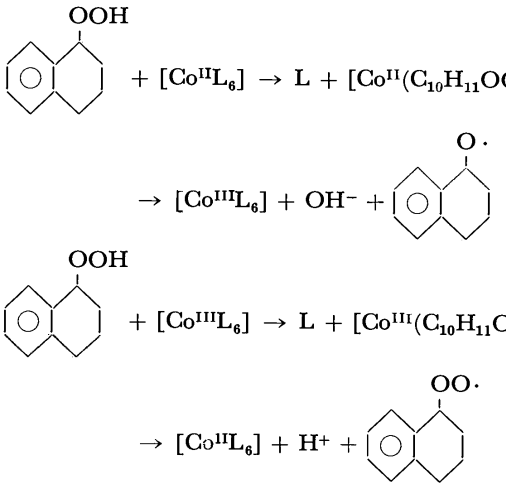

L : RCO_2^-, Br^-, Cl^-, F^-, OH^-, AcOH, H_2O, py,
L_2 : $acac^-$, bipy.

However, the possibility cannot be completely excluded that the high hydroperoxide selectivity and the low tetralin oxidation rate in the case of Co-py and Co-bipy are attributable to retarding effects of py and bipy on the autoxidation of hydrocarbons.[26,27]

When the bis(acetylacetonato)cobalt(II) complex is used as a catalyst, the oxygen absorption curve for the oxidation of tetralin has an irregular bending point (Fig. 6) and the decomposition of THP has two rate constants (Fig. 7 and Table 5). On the other hand, $Co(acac)_3$ shows neither such a bending point in the oxidation curve nor two decomposition rate constants. These results are interpreted as follows. Acetylacetonate in $Co(acac)_2L_2$ appears to be easily oxidized compared with that in $Co(acac)_3$ because $Co(acac)_2L_2$ is relatively labile. On the contrary, acetylacetonate in $Co(acac)_3$ is relatively difficult to oxidize because of the stability of $Co(acac)_3$. The redox potential and the rate of ligand replacement are also different from those for $Co(acac)_2L_2$ and the complex containing the new ligands which result from the oxidation of acetylacetonate. Therefore, the bis(acetylacetonato)-cobalt(II) complex is thought to show an irregular bending point in the oxidation and two decomposition rate constants.

The Effect of Metal Ions. The effects of various

Table 6. Product distribution for the metal acetate catalyzed oxidation of tetralin

Catalyst	Tetralin conversion (%)	Selectivity (mol%)				Molar ratio tetralone/tetralol	Reaction time (min)
		Tetralone	Tetralol	Peroxide	Total		
$Cr^{III}(OAc)_3$[a]	18.9	32.6	2.7	55.0	90.3	12.10	59
$Mn^{II}(OAc)_2 \cdot 4H_2O$	22.2	21.2	10.8	54.3	86.3	1.97	49
$Co^{II}(OAc)_2 \cdot 4H_2O$	20.9	49.1	32.3	4.8	86.2	1.52	7
$Ni^{II}(OAc)_2 \cdot 4H_2O$	20.5	18.0	8.4	68.0	94.4	2.15	53
$Cu^{II}(OAc)_2 \cdot H_2O$	18.8	16.3	8.9	59.9	85.1	1.83	285

Reaction conditions : [metal acetate] $=4.77 \times 10^{-2}$ M, $[\text{tetralin}]_{\text{initial}}=3.85$ M, the reaction temperature was 72.5± 1.0 °C, the O_2 pressure was 20 kg/cm^2.

a) A small part of the amount added remained undissolved.

Table 7. Product distribution for the acetylacetonato complex catalyzed oxidation of tetralin

Catalyst	Tetralin conversion (%)	Selectivity (mol%)				Molar ratio tetralone/tetralol	Reaction time (min)
		Tetralone	Tetralol	Peroxide	Total		
$Ti^{IV}O(acac)_2$[a]	17.6	17.5	15.1	33.4	66.0	1.16	300
$Cr^{III}(acac)_3$	20.3	30.9	9.4	50.1	90.4	3.30	64
$Mn^{II}(acac)_2$	20.6	21.3	11.9	52.3	85.5	1.79	70
$Fe^{III}(acac)_3$[a]	19.6	12.8	4.2	72.6	89.6	3.08	150
$Co^{III}(acac)_3$	19.9	41.9	29.0	18.4	89.3	1.44	12

Reaction conditions : [acetylacetonato complex] $=4.77\times10^{-2}$ M, $[\text{tetralin}]_{\text{initial}}=3.85$ M, the reaction temperature was 72.5±1.0 °C, the O_2 pressure was 20 kg/cm².
a) A small part of the amount added remained undissolved.

metal acetates and acetylacetonato complexes on the oxidation of tetralin in acetic acid at 72.5 °C are shown in Figs. 8—10 and Tables 6 and 7. The decomposition of THP with various metal acetates and acetylacetonato complexes was also carried out in acetic acid at 72.0 °C in a nitrogen atmosphere (Fig. 7 and Table 5).

In the oxidation of tetralin catalyzed by five kinds of metal acetates, the hydroperoxide selectivities increase in the order Co≪Mn≃Cr<Cu<Ni and the activity order of these catalysts is Co≫Mn≃Cr≃Ni>Cu (Table 6 and Fig. 8). This is in agreement with the order of activities for the decomposition of THP by these catalysts (Fig. 7 and Table 5). Therefore, the orders of the hydroperoxide selectivities and the oxidations rate are thought to arise from the differences in the decomposition rates of hydroperoxide produced in the oxidation of tetralin. The differences between the decomposition rates also appear to be mainly attributable to differences between the redox potentials of the five metal acetates in acetic acid because the activity order of these five metal acetates for the decomposition of THP is not consistent with the reactivity sequence predicted on the basis of crystal field theory[20,23] for the ligand-replacement reactions of the five

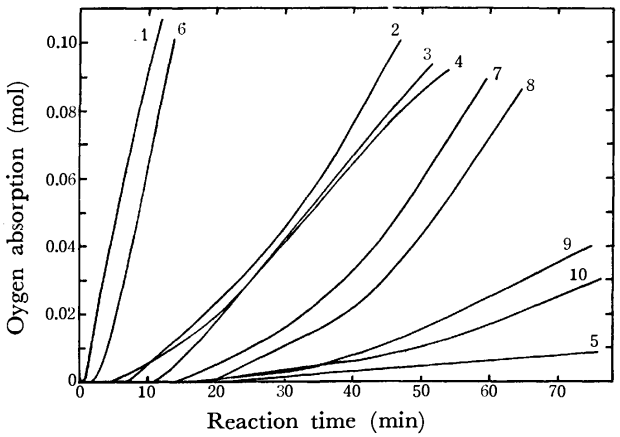

Fig. 8. The oxidation of tetralin in acetic acid at 72.5±1.0 °C.
Reaction conditions: [metal ion or complex] $=4.77\times10^{-2}$ M; $[\text{tetralin}]_{\text{initial}}=3.85$ M; O_2 pressure, 20 kg/cm².
1: $Co^{II}(OAc)_2\cdot4H_2O$, 2: $Mn^{II}(OAc)_2\cdot4H_2O$, 3: $Ni^{II}(OAc)_2\cdot4H_2O$, 4: $Cr^{III}(OAc)_3$, 5: $Cu^{II}(OAc)_2\cdot H_2O$, 6: $Co^{III}(acac)_3$, 7: $Cr^{III}(acac)_3$, 8: $Mn^{II}(acac)_2$, 9: $Ti^{IV}O(acac)_2$, 10: $Fe^{III}(acac)_3$.

metal acetato complexes. The fact that $Cu(OAc)_2\cdot H_2O$ exhibits a lower hydroperoxide selectivity than $Ni(OAc)_2\cdot4H_2O$ appears to involve the prolonged oxidation time of $Cu(OAc)_2\cdot H_2O$. The extent of thermal decomposition appears to become gradually greater with increasing reaction time. As a second reason, it is thought that the concentration of monomeric $Cu(OAc)_2\cdot H_2O$ increases during the prolonged reaction time. It has been reported that $Cu(OAc)_2\cdot H_2O$ is dimeric in many nonaqueous solvents[28,29] and partially dissociates into its monomeric form in acetic acid.[30] Imamura *et al.*[31] have also found that in the $Cu(OAc)_2\cdot H_2O$-catalyzed decomposition of THP in acetic acid at 80 °C, the addition of LiCl to the solution increases the concentration of monomeric copper(II) acetate and accelerates the decomposition of THP.

Agreement between the oxidation of tetralin and the decomposition of THP is also found for four acetylacetonato complexes, excepting $TiO(acac)_2$, as well as, for the five kinds of metal acetate catalysts. Specifically, the catalyst which exhibits a high hydroperoxide selectivity and a slow oxidation rate has a relatively low decomposition rate, *i.e.*, the orders of activities for oxidation, as well as for decomposition, are Co≫Cr≃Mn>Fe (Tables 5 and 7, and Fig. 7). This order appears to arise mainly from the differences in the redox potentials of the four acetylacetonato complexes in acetic acid because this order is inconsistent with the reactivity sequence expected on the basis of the stability constants[23,32,33] of acetylacetonato complexes for the ligand-replacement reaction. $TiO(acac)_2$, which has a d^0 system, is abnormal with respect to the acetylacetonato complexes used in the present work. This result cannot be interpreted explicitly at present.

As shown in Tables 6 and 7, the ratio of α-tetralone to α-tetralol (On/Ol) obtained for oxidation with a chromium catalyst is relatively high. The product distributions for oxidation with $Cr(OAc)_3$ were examined at various tetralin conversion. The selectivity of α-tetralone rises and that of hydroperoxide decreases as the conversion of tetralin increases for oxidation (Figs. 9 and 10). The degree of the increase in the α-tetralone selectivity is nearly equal to that of the decrease in the hydroperoxide selectivity. For $Cr(OAc)_3$-catalyzed decomposition of THP in acetic acid at 72.0 °C in a nitrogen atmosphere, α-tetralone and α-acetoxytetralin were obtained in about 70 and 10% selectivities, respectively, at 10—25% THP conversions.

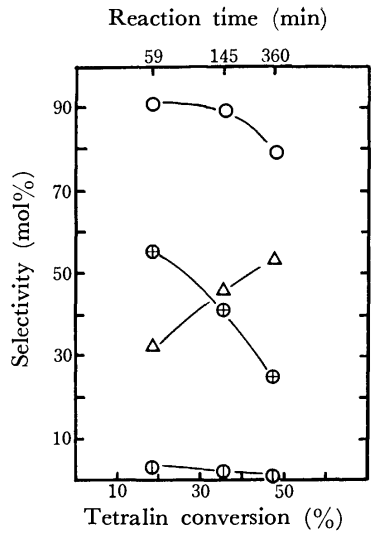

Fig. 9. The chromium(III) acetate catalyzed oxidation of tetralin in acetic acid at 72.5±1.0 °C.
Reaction conditions: $[Cr(OAc)_3]=4.77\times10^{-2}$ M; $[tetralin]_{initial}=3.85$ M; O_2 pressure, 20 kg/cm².
△: Tetralone, ⊕: tetralol, ⊕: peroxide, ○: total.

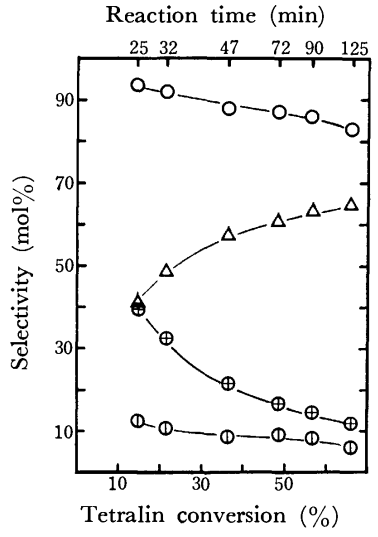

Fig. 10. The Cr-Co catalyzed oxidation of tetralin in acetic acid at 72.5±1.0 °C.
Reaction conditions: $[Cr(OAc)_3]=4.77\times10^{-2}$ M; $[Co(OAc)_2\cdot4H_2O=0.13\times10^{-2}$ M; $[tetralin]_{initial}=3.85$ M; O_2 pressure, 20 kg/cm².
△: Tetralone, ⊕: tetralol, ⊕: peroxide, ○: total.

α-Tetralol was produced only in small amounts. Therefore, it is thought that for $Cr(OAc)_3$-catalyzed oxidation, the main pathway which contributes to the increase of α-tetralone is not Reaction 9 but the THP dehydration reaction:

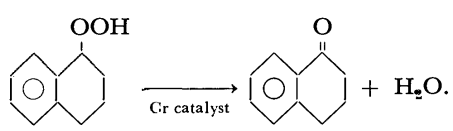

This dehydration reaction can be resolved into Reactions 2 (Cr^{3+} consumption) and 7 (Cr^{3+} regeneration) as far as the variable valence of the chromium ion is concerned. If hydroperoxide is dehydrated by a process in which the chromium valence remains unchanged, the formation of α-tetralone will be related to the hydration energy of the chromium ion. However, this is not the usual process for the decomposition of hydroperoxide catalyzed by a transition-metal ion. In addition, the increasing order of the On/Ol ratios for the metal-catalyzed oxidation of tetralin (Tables 6 and 7) is inconsistent with the order of hydration heats[20,23] of the first-transition-metal ions.

For the purposes of obtaining α-tetralone in higher yields, binary metal ions (Cr and Co) were used as a catalyst for the oxidation of tetralin (Fig. 10). However, the binary catalyst showed only a slight increase in the α-tetralone selectivity compared with the $Co(OAc)_2\cdot4H_2O$ catalyst (Figs. 4 and 10).

References

1) A. Robertson and W. A. Waters, *J. Chem. Soc.*, **1948**, 1574.
2) A. E. Woodward and R. B. Mesrobian, *J. Am. Chem. Soc.*, **75**, 6189 (1953).
3) Y. Kamiya, S. Beaton, A. Lafortune, and K. U. Ingold, *Can. J. Chem.*, **41**, 2020 (1963).
4) Y. Kamiya and K. U. Ingold, *Can. J. Chem.*, **42**, 2424 (1964).
5) A. Mukherjee and W. F. Graydon, *J. Phys. Chem.*, **71**, 4232 (1967).
6) M. Martan, J. Manassen, and D. Vofsi, *Tetrahedron*, **26**, 3815 (1970).
7) A. S. Hay and H. S. Blanchard, *Can. J. Chem.*, **43**, 1306 (1965).
8) A. I. Kamneva, V. I. Zakharova, L. N. Piterskii, V. A. Selenznev, and A. V. Artemov, *Neftekhimiya*, **15**, 403 (1975).
9) Y. Kamiya and K. U. Ingold, *Can. J. Chem.*, **42**, 1027 (1964).
10) Y. Kamiya, *Tetrahedron*, **22**, 2029 (1966).
11) T. Matsuzaki, J. Imamura, and N. Ohta, *Kogyo Kagaku Zasshi*, **71**, 700 (1968).
12) J. Manassen, *Catal. Rev.-Sci. Eng.*, **9**, 223 (1974).
13) H. B. Knight and D. Swern, *Org. Synth.*, **34**, 90 (1954).
14) W. O. Lundberg, "Autoxidation and Antioxidants," Vol. 1, Interscience Publication, New York (1961), p. 375.
15) L. Horner and W. Jurgeleit, *Justus Liebigs Ann. Chem.*, **591**, 138 (1955).
16) D. A. S. Ravens, *Trans. Faraday Soc.*, **55**, 1768 (1959).
17) Y. Kamiya, "Yuki-Sanka-Hanno," Gihodo, Tokyo (1973), p. 244.
18) T. Yamada and Y. Kamiya, presented at the 9th Symposium on Oxidation, Tokyo, Japan, November 25, 26 (1975).
19) G. C. Allen and A. Aguilo, "Oxidation of Organic Compounds," Vol. 2, Am. Chem. Soc. (1968), p. 63.
20) F. Basolo and R. G. Pearson, "Mechanism of Inorganic Reactions," John Wiley & Sons, New York (1967), pp. 80—88, 124—246, 454—525.
21) J. P. Candlin, K. A. Taylor, and D. T. Thompson, "Reaction of Transition-Metal Complexes," Elsevier Publishing Company, Amsterdam, London and New York (1968).
22) F. A. Cotton and G. Wilkinson, "Advanced Inorganic Chemistry," A Comprehensive Text, Interscience Publication, New York (1966).
23) K. Yamazaki, N. Tanaka, J. Matsuura, and R. Tamamushi, "Muki-Yoeki-Kagaku," Nankodo, Tokyo and Kyoto (1968), pp. 14—26, 69—97, 268—271.
24) L. E. Orgel, "An Introduction to Transition-Metal

Chemistry," John Wiley & Sons, New York (1966).
25) H. Taube, *Chem. Revs.*, **50**, 69 (1952).
26) A. H. Turner and W. A. Waters, *J. Chem. Soc.*, **1954**, 580; **1956**, 879.
27) C. F. Cullis and A. J. Waddington, *Trans. Faraday Soc.*, **53**, 1317 (1957).
28) R. Tsuchida, S. Yamada, and H. Nakamura, *Nature*, **178**, 1192 (1956).
29) R. L. Martin and A. Whitley, *J. Chem. Soc.*, **1958**, 1394.
30) J. K. Kochi and R. U. Subramanian, *Inorg. Chem.*, **4**, 1527 (1965).
31) S. Imamura, M. Teramoto, T. Sumi, and Y. Takegami, presented at the 8th Symposium on Oxidation, Osaka, Japan, November 21, 22 (1965).
32) L. G. Van Uitert, W. C. Fernelius, and B. E. Douglas, *J. Am. Chem. Soc.*, **75**, 457, 2736 (1953).
33) R. M. Izatt, W. C. Fernelius, C. G. Haas, Jr., and B. P. Block, *J. Phys. Chem.*, **59**, 170, 235 (1955).

A Synthetic Route to 3,3-Diphenyl-2-indolinone Derivatives

Manabu SENŌ, Shinsaku SHIRAISHI, Yukio SUZUKI, and Teruzō ASAHARA

Institute of Industrial Science, The University of Tokyo, Roppongi, Minato-ku, Tokyo 106

(Received July 4, 1977)

N-Aryl-α-chloro-α,α-diphenylacetimidoyl chlorides were prepared from Schiff bases and dichlorocarbene generated by use of the phase transfer catalyst. Treatment in sulfuric acid gave 3,3-diphenyl-2-indolinone derivatives. The synthetic route to 2-indolinone was found to give a higher overall yield than that by other methods. 2,2-Dichloro-1,3-diphenylaziridine gives α-chloro, α-acetoxy or α-hydroxy-α,α-diphenylacetanilide on treatment with sulfuric acid. Comparison of 2,2-dichloro-1,3-diphenylaziridine, 2,2-dichloro-1,3,3-triphenylaziridine and *N*-aryl-α-chloro-α,α-diphenylacetimidoyl chloride in their reactivities with sulfuric acid shows that the pathway of the reaction is governed by the character and number of substituents at the reaction center where carbonium ions are developed.

3,3-Diaryl-2-indolinone derivatives have pharmaceutical properties such as mothproofing,[1] laxative,[2] antibacterial and antiprotozoal[3] activities. Isacene (3,3-bis(*p*-acetoxy-phenyl)-2-indolinone) is used as a purgative. Copolymer of 3,3-bis(*p*-aminophenyl)-2-indolinone and benzophenone-tetracarboxylic dianhydride is useful as adhesive laminating resin for instrument boards, fiber and coating.[4] 3,3-Diaryl-2-indolinone derivatives were synthesized in various ways: from 2,3-indolinedione by the Grignard reaction,[5,6] from 2,3-indolinedione and diphenylurea with aluminium chloride,[8] form 3,3-dihalo-2-indolinone[5,7] or trichloroacetanilide[5] by the Friedel-Crafts reaction with benzene, by the reaction of *N'*-phenyldiphenylacetohydrazide with sodium,[9] α-acetoxy-α,α-diphenylacetyl chloride with aniline,[5] α-chloro-α,α-diphenylacetanilide with sodium hydride[10] or boron trifluoride etherate,[3] and by the treatment of α-hydroxy-α,α-diphenylacetanilide with sulfuric acid.[5,11-14] In a previous paper, we reported a synthetic route to various lactams from *gem*-dichloroaziridines or α-chloro-α,α-diphenylacetimidoyl chloride.[15] *gem*-Dichloroaziridines were prepared by the reaction of Schiff bases with dichlorocarbene. Makosza showed that the phase-transfer catalyst provides an excellent method for generation of dichlorocarbene.[16] Applying this method to the synthesis of 1-aryl-2,2-dichloro-3,3-diphenylaziridines, we obtained not 1-aryl-2,2-dichloro-3,3-diphenylaziridines but their isomerization products, *N*-aryl-α-chloro-α,α-diphenylacetimidoyl chlorides, in good yields. From these various 2-indolinone derivatives were obtained in good yields.

Results and Discussion

N-Benzhydrylideneanilines were prepared from benzhydrylidene dichloride and the corresponding aromatic amines in 40—60% yields(Table 1). The method[17] seems to give higher yields under moderate reaction conditions as compared with the other methods.[18,19] The *N*-benzhydrylideneanilines(**1a**—**e**) were allowed to react with dichlorocarbene generated by the method using phase-transfer catalyst. A chloroform solution of **1a**—**e** and an aqueous solution of 33.3 wt% NaOH

Table 1. *N*-Benzhydrylideneanilines

Compd No.	Ar	Yield, %	Mp, °C (lit)	IR, $\nu_{C=N}$, cm^{-1} (KBr disk)
1a	C_6H_5	60	112(113)[19]	1614
1b	*o*-CH_3-C_6H_4	63	50—51(51—52)[20]	1622
1c	*p*-CH_3-C_6H_4	53	48—49(48)[29]	1615
1d	*p*-Cl-C_6H_4	41	94—94.5(92—93)[21]	1612
1e	α-naphtyl	49	139—140(137.5)[29]	1601

Table 2. *N*-Aryl-α-chloro-α,α-diphenylacetimidoyl chlorides

Compd No.	Yield %	Mp, °C (lit)	IR, $\nu_{C=N}$, cm^{-1} (KBr disk)	NMR, ppm in $CDCl_3$	Formula	Found (Calcd), % C	H	N
2a	78	68.0—69.0 (70—71)[22]	1680	7.30(m)	$C_{20}H_{15}NCl_2$	70.54 (70.60)	4.40 (4.44)	3.94 (4.12)
2b	81	114.5—111.5	1672	7.30(m, 14) 2.10(s, 3)	$C_{21}H_{17}NCl_2$	71.45 (71.20)	4.87 (4.84)	4.03 (3.95)
2c	83	97.5—98.0 (92.5—94.0)[22]	1680	7.30(m, 14) 2.32(s, 3)	$C_{21}H_{17}NCl_2$	71.42 (71.20)	4.86 (4.84)	4.08 (3.95)
2d	75	109.0—110.0 (106.0—107.0)[22]	1655	7.30(m)	$C_{20}H_{14}NCl_3$	64.82 (64.11)	3.77 (3.77)	3.66 (3.74)
2e	71	106.0—107.0	1682	7.50(m)	$C_{24}H_{17}NCl_2$	74.21 (73.85)	4.48 (4.39)	3.64 (3.59)

and triethylbenzylammonium chloride(TEBA) were mixed and strirred at room temperature for 2 h to give the corresponding *N*-aryl-α-chloro-α,α-diphenylacetimidoyl chloride(**2a**—**e**) in quantitative yield. IR spectra of these compounds showed the characteristic strong absorption in the region 1650—1690cm^{-1}. The results are shown in Table 2.

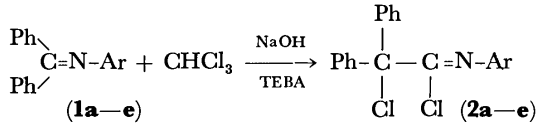

(**1a**—**e**) (**2a**—**e**)

In this formula, Ar stands for phenyl(**a**), *o*-tolyl(**b**), *p*-tolyl(**c**), *p*-chlorophenyl(**d**) and α-naphtyl(**e**).

The reaction would proceed *via* the formation of 1-aryl-2,2-dichloro-3,3-diphenylaziridines(**5a**—**e**) followed by its isomerization.

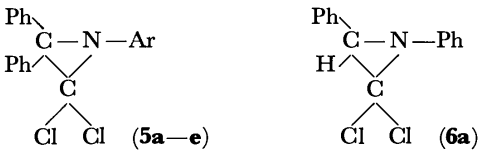

(**5a**—**e**) (**6a**)

Under the present reaction conditions, however, the aziridines(**5a**—**e**) were not isolated. Dichlorocarbenes generated in the phase-transfer catalytic system are known to be rich in reactivity.[23] The reactions take place at 5 °C or higher, since the reaction mixture becomes semi-solid at lower temperatures. Thus, the aziridines are not stabilized and isomerize into the corresponding *N*-aryl-α-chloro-α,α-diphenylacetimidoyl chloride.

On the other hand, the reaction of *N*-benzylideneaniline with chloroform in the presence of phase-transfer catalyst affords 2,2-dichloro-1,3-diphenylaziridine (**6a**) in a good yield, which dose not isomerize in this reaction system.[24] The difference in reactivity of aziridines 5 and 6 was revealed by DSC analyses. The DSC measurement of 2,2-dichloro-1-(*p*-chlorophenyl)-3,3-diphenylaziridine(**5d**), prepared by the reaction of **1d** with dichlorocarbene generated from *t*-BuOK–$CHCl_3$ in hexane at −5 °C, shows an exothermic peak at 362 K. It was confirmed from IR spectra before and after this peak that this transition is due to isomerization. Isomerization is accompanied by melting of the isomerized product **2d**, as revealed by observation under a microscope. The heat of transition combined with the heat of melting was determined to be −38.1 kJ mol^{-1}.

On the other hand, a separate run of **2d** showed an exothermic peak due to melting at 380 K, the heat of melting being 30.5 kJ mol^{-1}. Because of the melting point depression of the mixture, melting would be observed at the temperature of isomerization. By subtracting the heat of melting the heat of isomerization of **5d** into **2d** was determined to be −68.6 kJ mol^{-1}. On the other hand, aziridine **6a** was stable up to 404 K, where it was decomposed into several fragments. The difference in thermal behavior between **5d** and **6a** should be ascribed to the existence of two phenyl substituents at 3-position of **5d**. The substituents greatly affect the reactivity of aziridines.

N-aryl-α-chloro-α,α-diphenylacetimidoyl chlorides (**2a**—**e**) derived from **1a**—**e** were treated with sulfuric acid in acetic acid at room temperature for 2 h to give 3,3-diphenyl-2-indolinone derivatives(**4a**—**e**) in good yields. The formation of 3,3-diphenyl-2-indolinones proceeded also *via* *N*-aryl-α-hydroxy-α,α-diphenylacetamide(**3a**—**e**) obtained from hydrolysis of the corresponding *N*-aryl-α-chloro-α,α-diphenylacetimidoyl chlorides. The results are given in Tables 3 and 4.

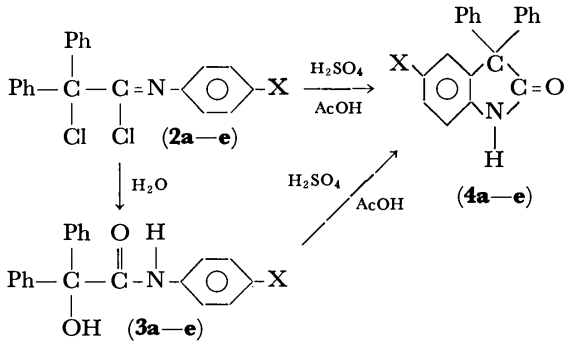

In the above formula, X denotes H(**a**), *o*-CH_3(**b**), *p*-CH_3(**c**), *p*-Cl(**d**) and 5,6-benzo(**e**).

Table 3. α-Hydroxy-α,α-diphenylacetanilides

Compd No.	Yield %	Mp, °C (lit)	IR, cm^{-1} (KBr disk)	NMR, ppm in $CDCl_3$	Formula	Found (Calcd), % C	H	N
3a	98	173.0—174.0 (174—175)[14]	3400 (ν_{OH}) 3330 (ν_{NH}) 1672 (ν_{CO})	7.40 (m, aromatic, 15) 3.57 (s, OH, 1)	$C_{20}H_{17}NO_2$	83.67 (84.19)	6.22 (6.01)	4.83 (4.91)
3b	98.4	149.0—149.8	3400 (ν_{OH}) 3355 (ν_{NH}) 1672 (ν_{CO})	7.30 (m, aromatic, 14) 3.98 (s, OH, 1) 2.00 (s, methyl, 3)	$C_{21}H_{19}NO_2$	78.69 (79.47)	6.10 (6.03)	4.38 (4·41)
3c	99.2	189.0—189.8 (190)[11]	3400 (ν_{OH}) 3300 (ν_{NH}) 1655 (ν_{CO})	7.30 (m, aromatic, 14) 3.65 (s, OH, 1) 2.35 (s, methyl, 3)	$C_{21}H_{19}NO_2$	78.81 (79.47)	6.16 (6.03)	4.36 (4.41)
3d	94.9	213.0—214.0 (210—212)[12]	3400 (ν_{OH}) 3340 (ν_{NH}) 1660 (ν_{CO})	7.25 (m, aromatic, 14) 3.30 (s, OH, 1)	$C_{20}H_{16}NO_2Cl$	70.04 (71.11)	4.82 (4.77)	4.11 (4.15)
3e	98.2	194.7—195.0 (195)[13]	3340 (ν_{NH}) 1668 (ν_{CO})	7.45 (m, aromatic, 17) 3.75 (s, OH, 1)	$C_{24}H_{19}NO_2$	81.23 (81.56)	5.51 (5.42)	3.90 (3.96)

Table 4. 3,3-Diphenyl-2-indolinones

Compd No.	Yield, % (a)	Yield, % (b)	Mp, °C (lit)	IR, cm^{-1} (KBr disk)	NMR, ppm in $CDCl_3$	Mass, *m/e*	Found (Calcd), % C	H	N
4a	96.0	79.7	222—225 (225—226)[14]	3300 (ν_{NH}) 1670 (ν_{CO})	7.30 (m)	285 (M^+), 257, 256 254, 208, 180	84.10 (84.19)	5.18 (5.30)	4.99 (4.91)
4b	86.0	87.8	256.5—257.5 (254—255)[12]	3160 (ν_{NH}) 1705 (ν_{CO})	7.30 (m)[c] 2.29 (s)	299 (M^+), 271, 270, 254, 222, 194	83.85 (84.25)	5.68 (5.72)	4.99 (4.68)
4c	70.0	57.2	284—285 (283—283.5)[25]	3260 (ν_{NH}) 1715 (ν_{CO}) 1672 (ν_{CO})	7.30 (m) 2.28 (s)	299 (M^+), 271, 270, 254, 222, 194	83.66 (84.25)	5.70 (5.72)	4.71 (4.68)
4d	65.5	56.5	266.0—266.5 (263—265)[12]	3250 (ν_{NH}) 1728 (ν_{CO}) 1681 (ν_{CO})	7.30 (m)	319 (M^+), 291, 290, 284, 254, 242, 214	75.01 (75.12)	4.52 (4.41)	4.31 (4.38)
4e	73.1	69.6	253.0—254.0 (254)[12]	3160 (ν_{NH}) 1702 (ν_{CO})	7.40 (m)	335 (M^+), 307, 306, 258, 230	84.60 (85.95)	5.07 (5.11)	4.11 (4.18)

a) Produced from the corresponding *N*-aryl-α,α-diphenylacetimidoyl chloride. b) Produced from the corresponding α-hydroxy-α,α-diphenylacetanilides. c) In DMSO-d_6.

Table 5. α,α-Diphenylacetanilide derivatives

Compd No.	Ar_1	Ar_2	Yield %	Mp, °C (lit)	IR, cm^{-1} (KBr disk)	NMR ppm in $CDCl_3$	Mass, *m/e*	Found (Calcd), % C	H	N
10a	C_6H_5	C_6H_5	48	179—180 (180)[26]	3310 (ν_{NH}) 1655 (ν_{CO})	7.3 (m) 5.1 (s)	287 (M^+), 194, 169 168, 167, 166, 165 153, 152, 120, 115	82.68 (83.68)	5.87 (5.96)	4.89 (4.87)
10b	C_6H_5	*p*-ClC_6H_4	25	205—206	3300 (ν_{NH}) 1655 (ν_{CO})	7.21 (m) 4.97 (s)	323, 321 (M^+), 169, 168, 167, 165, 152	73.95 (74.65)	5.03 (5.01)	4.42 (4.35)
10c	*p*-ClC_6H_4	C_6H_5	47	185—186 (182)[27]	3300 (ν_{NH}) 1660 (ν_{CO})	7.25 (m) 4.97 (s)	323, 321 (M^+), 204, 203, 202, 201, 169 166, 165, 120	75.59 (74.65)	5.08 (5.01)	4.32 (4.35)

IR spectra of these 2-indolinones show strong bands at 3160—3250cm^{-1} and 1670—1720cm^{-1}, assigned to cis bonded NH stretching and amide I, respectively. Compounds **4c** and **4d** show two bands ascribed to amide I, which seem to be due to free amide and dimer, since dilute solutions of **4c** and **4d** in chloroform show only a single band at 1721cm^{-1} and 1726cm^{-1}, respectively.

The reaction of **6a** with sulfuric acid gave α-chloro-α-phenylacetanilide(**7**) in 60% yield[15] Reexamination of this reaction confirmed that no intramolecular condensation of **6a** into 3-phenyl-2-indolinone occurs in H_2SO_4–AcOH mixture. The crude reaction product was carefully examined by silicagel column chromatography and α-hydroxy-α-phenylacetanilide(8) and α-acetoxy-α-phenylacetanilide(**9**) were isolated together with **7**. When **7** separated from the other products was treated with H_2SO_4–AcOH under similar conditions to those above, it remained unchanged. A similar treatment of **8** or **9** showed that they could be converted into each other.

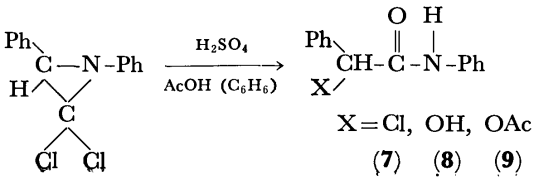

The results show that ring-opening of **6a** proceeds *via* an ion pair which can exchange its counter ions to some extent. However, **7** dose not undergo nucleophilic substitution. This would reflect lack in its ability of carbonium ion formation in H_2SO_4–AcOH.

To compare the catalytic ability of sulfuric acid with that of Lewis acid, some *gem*-dichloroaziridines were treated with aluminium chloride in benzene.* The reaction gave tarry products, from which Friedel-Crafts reaction products were isolated. From spectroscopic and elemental analyses these compounds were identified to be α,α-diphenylacetanilide derivatives(**10a—c**). The results are given in Table 5.

When **6a** was treated with sulfuric acid in the presence of benzene, the resulting products were **7**, **8** and **9**, **10a** not being obtained.

Treatment of **7a** with aluminium chloride in benzene afforded **10a**. This suggests that, if the reactions were carried out without addition of benzene, 3-phenyl-2-indolinone would be formed by intramolecular condensation. The reaction of *gem*-dichloroaziridines(**6a**,**6e**) with aluminium chloride was conducted in nitromethane, which dissolves aluminium chloride to form complexes. Compound **6d** stands for 2,2-dich-

* *gem*-Dichloroaziridines used were **6a**, 2,2-dichloro-1-(*p*-chlorophenyl)-3-phenylaziridine(**6b**), and 2,2-dichloro-3-(*p*-chlorophenyl)-1-phenylaziridine(**6c**).

loro-3-phenyl-1-(*m*-tolyl)aziridine. The reaction was carried out at various ratios of aluminium chloride to substrate, but the isolated products were acetanilide derivatives(**7a**,**7e**) in 30-60% yields.

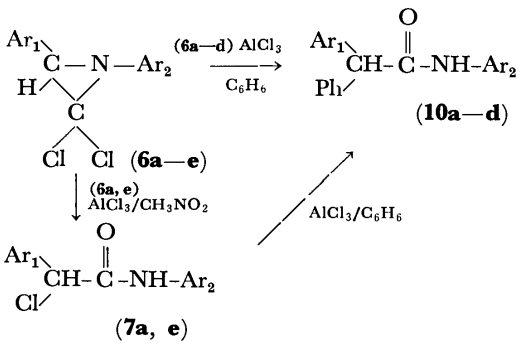

Treatment of 3-methyl-3-phenyl-1-(*m*-tolyl)-2,2-dichloro-aziridine(**11**) with H_2SO_4–AcOH gave *N*-(*m*-tolyl)-2-phenylpropene-amide(12). On the other hand, treatment of compound(**11**) with aluminium chloride in benzene gave *N*-(*m*-tolyl)-α-methyl-α,α-diphenylacetamide(**13**) and **12** in 41% and 6.3% yields, respectively. Treatment of **12** with aluminium chloride in benzene also gave **13**, probably owing to the presence of a small amount of water;2-indolinone derivative could not be obtained from 1-aryl-2,2-dichloro-3-methyl-3-phenylaziridine.

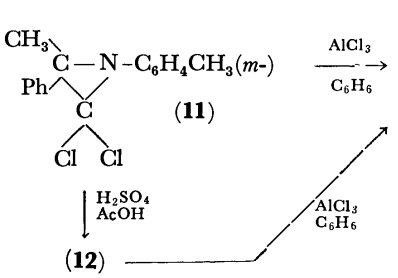

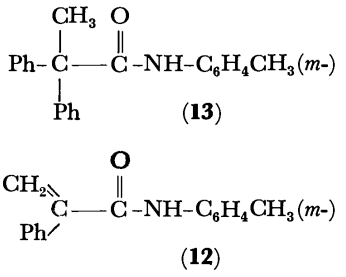

From a comparison of reactivities of these compounds, we see that intramolecular condensation into 2-indolinone occurs effectively only when stable carbonium ions are formed and the reaction pathway of dichloroaziridines is strongly governed by the character and number of substituents at the reaction center where carbonium ion is generated.

Experimental

*Preparation of Schiff Bases(**1a—e**).* A mixture of 0.3 mol of aromatic amine and 0.1 mol benzhydrylidene dichloride in 200 ml of benzene was heated to reflux with stirring for 2 h. The mixture was cooled and shaken with water to remove the amine hydrochloride. The organic layer was dried over anhydrous sodium sulfate and evaporated. Recrystalization of the residue from ethanol gave the corresponding Schiff base. The results are summarized in Table 1.

*Syntheses of N-Aryl-α-chloro-α,α-diphenylacetimidoyl Chlorides (**2a—e**) by Using Phase Transfer Catalyst.* A solution of 0.03 mol of *N*-benzhydrylideneaniline and 1 mmol of triethylbenzylammonium chloride in 50 ml of chloroform, and 75 g of an aqueous solution of 33.3 wt % sodium hydroxide were mixed and stirred at 5 °C for 30 min and then at room temperature for 2 h. The chloroform layer was separated and washed with dil. hydrochloric acid and then water. It was dried over sodium sulfate and evaporated. Recrystalization of the residue from hexane gave the corresponding *N*-aryl-α-chloro-α,α-diphenylacetimidoyl chloride. The results are summarized in Table 2.

*Syntheses of 2-Indolinones(**4a—e**).* 20 ml of concd H_2SO_4 was slowly added dropwise to a solution of *N*-aryl-α-chloro-α,α-diphenylacetimidoyl chloride(6 mmol) in 20 ml of glacial acetic acid. The mixture was then poured into 80 ml of water to form precipitates, which were collected by filtration. The crystals were dissolved in chloroform and washed with 0.5 M sodium hydrogencarbonate solution and then water. The chloroform solution was dried over anhydrous sodium sulfate. Evaporation of the solvent and recrystalization of the residue from an appropriate solvent gave a pure product. The results are summarized in Table 4.

*Hydrolysis of N-Aryl-α-chloro-α,α-diphenylacetimidoyl Chloride (**2a—e**).* A solution of 0.01 mol of *N*-aryl-α-chloro-α,α-diphenylacetimidoyl chloride in 50 ml of 33.3% aqueous dioxane was heated to reflux for 2 h. Evaporation of the solvent and recrystalization of the residue from ethanol gave *N*-aryl-α-hydroxy-α,α-diphenylacetamide(**3a—e**) quantitatively. The results are summarized in Table 3.

*Reaction of 2,2-Dichloro-1,3-diphenylaziridine(**6a**) in the Presence of Sulfuric Acid.* 50 ml of concd H_2SO_4 was slowly added dropwise to a solution of 15 mmol of 2,2-dichloro-1,3-diphenylaziridine in 50 ml of acetic acid. The mixture was heated at 60 °C for 30 min and then poured into 400 ml of water to form precipitates which were collected by filtration. The precipitates were dissolved in chloroform and the solution was washed with 0.5 M sodium hydrogencarbonate solution and then water. The combined aqueous layer was saturated with sodium chloride and shaken with chloroform. The combined chloroform solution was dried over anhydrous sodium sulfate and evaporated in vacuo. The residue was subjected to silicagel column chromatography: 9.6 mmol(64%) of α-chloro-α-phenylacetanilide(**7**) was eluted with chloroform and then 1.9 mmol(13%) of α-acetoxy-α-phenylacetanilide(**9**) and 1.5 mmol (10%) of α-hydroxy-α-phenylacetanilide(**8**) were separated with chloroform-ethyl acetate eluent in the order described. α-Chloro-α-phenylacetanilide(**7**); mp 149—150 °C (lit, 147—148 °C).[28] α-Hydroxy-α-phenylacetanilide(**8**); mp 150—151 °C (lit, 151—152 °C).[29] α-Acetoxy-α-phenylacetanilide(**9**); mp 118—119 °C(lit, 117.5 °C);[30] IR(KBr) 1738 cm^{-1}(CH_3COO, CO stretching), 1675 cm^{-1} (CONH, CO stretching); NMR($CDCl_3$), δ(ppm), 6.8—7.7 (m, aromatic, 10), 6.17(s, methyn, 1), 2.17(s, methyl, 3).

Reaction of gem*-Dichloroaziridines(**6a—c**) with Aluminium Chloride in Benzene.* A solution of 0.02 mol of *gem*-dichloroaziridine in 30 ml of benzene was slowly added dropwise to a solution of aluminium chloride(0.02 mol) in 10 ml of benzene. The mixture was stirred for 2 h and then poured into a hydrochloric acid solution. The organic layer separated

was washed with 0.5 M sodium hydrogencarbonate and then with water. It was dried over anhydrous sodium sulfate. After evaporation of benzene *in vacuo*, the residue was subjected to silicagel column chromatography using benzene as an eluent. The results are summarized in Table 5.

Reaction of gem-*Dichloroaziridines(**6a,d**) with Aluminium Chloride.* 0.02 mol of *gem*-dichloroaziridine in 30 ml of nitromethane was slowly added dropwise to a solution of aluminium chloride(0.02 mol) in 30 ml of nitromethane. The mixture was stirred for 2 h at room temperature. The resulting solution was treated as described in the preceding section. α-Chloro-α-phenylacetanilide(**7a**); mp 149—150 °C(lit, 147—148 °C).[28] α-Chloro-*N*-(*m*-tolyl)-α-phenylacetanilide(**7d**); mp 123.6—124.3 °C; IR(KBr) 3280 cm^{-1} (NH), 1670 cm^{-1} (CO); NMR($CDCl_3$) δ(ppm) 8.4(broad, 1, NH), 7.3(m, aromatic, 9), 5.44(s, methyn, 1), 2.29(s, methyl, 3); Found: C, 69.29; H, 5.49; N, 5.56%. Calcd for $C_{15}H_{14}NOCl$: C, 69.37; H, 5.43; N, 5.39%.

DSC Analyses. DSC analyses were performed on a Perkin-Elmer DSC-2 under the following conditions: heating rate 1.25 K/min, range 5 mcal/s, chart speed 10 mm/min. The DSC measurement of **5d** shows an exothermic peak of isomerization at 362 K, the heat of which was evaluated by comparison with a heat of fusion of indium. The heat of fusion of α-chloro-α,α-diphenylacetimidoyl chloride was determined in a similar way. DSC analysis of 2,2-dichloro-1,3-diphenylaziridine shows that it decomposes at 404 K.

References

1) J. R. Geigy, Swiss Patent 214900 (1941); *Chem. Abstr.*, **42**, 3579 (1941); K. Matsui and T. Kimijima, *Yuki Gosei Kagaku Kyokai Shi*, **9**, 92 (1951).

2) S. Loewe, *J. Phamacol. Exp. Ther.*, **94**, 288 (1948); M. H. Hubacher, S. Doernberg, and A. Horner, *J. Am. Pharm. Assoc.*, **42**, 23 (1953); R. G. Sanders, H. M. Baum, and G. J. Straub, *ibid.*, **40**, 340 (1951); G. Giuseppe, Ger. Patent 2129422 (1972); *Chem. Abstr.*, **76**, 140538 (1972).

3) C. E. William, U. S. Patent 3558653 (1971).

4) D. P. Franklin, U. S. Patent 3705869; *Chem. Abstr.*, **78**, 59024 (1973); D. P. Franklin, Ger. Patent 2257996 (1973); *Chem. Abstr.*, **79**, 67293 (1973); R. J. Kray, *Proc. Ann. Conf. Inst. Soc. Plast. Ind.*, **29**, 11C (1974).

5) R. F. Reeves and H. G. Lindwall, *J. Am. Chem. Soc.*, **64**, 1086 (1942).

6) W. C. Sumpter, *J. Am. Chem. Soc.*, **64**, 1736 (1942); W. C. Sumpter, M. Miller, and L. N. Hendric, *J. Am. Chem. Soc.*, **67**, 1656 (1945); J. Wegmann and H. Dahn, *Helv. Chem. Acta*, **29**, 415 (1946); B. Witkop and E. K. Arvid, *J. Am. Chem. Soc.*, **73**, 5664 (1951); S. Sarel and J. T. Klug, *Israel J. Chem.*, **2**, 143 (1964).

7) H. Wexler and Caraculacu, Isasi Sect. IC, 13 (1), 71 (1967); *Chem. Abstr.*, **69**, 106525 (1968).

8) D. P. Franklin, Ger. Patent 2258505 (1973); *Chem. Abstr.*, **79**, 105727 (1973).

9) J. Stanek, *Chem. Listy*, **37**, 161 (1943).

10) J. C. Sheehan and J. W. Frankenfeld, *J. Am. Chem. Soc.*, **83**, 4792 (1961); S. Sarel, J. T. Klug, E. Breaer, and F. D. Angel, *Tetrahedron Lett.*, **1964**, 1553.

11) P. A. Petyunin and I. S. Berdinskii, *Zh. Obshch. Khim.*, **21**, 1703 (1951).

12) P. A. Petyunin, I. S. Berdinskii, and N. G. Panferova, *Zh. Obshch. Khim.*, **27**, 1901 (1957).

13) P. A. Petyunin and N. G. Panferova, *Zh. Obshch. Khim.*, **21**, 1528 (1951).

14) P. A. Petyunin and N. G. Panferova, *J. Gen. Chem. (U.S.S.R)*, **17**, 502 (1947).

15) M. Senō, S. Shiraishi, Y. Suzuki, and T. Asahara, *Bull. Chem. Soc. Jpn.*, **49**, 1893 (1976).

16) M. Makosza, *Pure Appl. Chem.*, **43**, 439 (1975).

17) M. Pauly, *Ann. Chem.*, **187**, 214 (1877).

18) Dow Chem. Co., U. S. Patent 1938890 (1932).

19) G. Reddelien, *Ber.*, **46**, 2718 (1913).

20) G. Reddelien, *Ber.*, **48**, 1462 (1915).

21) E. Bergmann, L. Engel, and H. Mever, *Ber.*, **65**, 446 (1932).

22) K. Ichimura and M. Ohta, *Bull. Chem. Soc. Jpn.*, **40**, 1933 (1967).

23) C. M. Starks, *J. Am. Chem. Soc.*, **93**, 195 (1971).

24) We have synthesized various 1-aryl-2,2-dichloro-3-phenyl-aziridines in good yields under the same catalytic conditions.

25) J. C. Sheehan and J. H. Beeson, *J. Org. Chem.*, **31**, 1637 (1966).

26) H. Staudinger, *Ber.*, **38**, 1735 (1905).

27) W. Jungelt, D. Schmidt, R. Berhardt, and B. Stolze, *Z. Chem.*, **11**, 146 (1971).

28) R. E. Brooks, J. O. Edwards, G. Levey, and F. Smyth, *Tetrahedron*, **1966**, 1279.

29) Biscoff and Walden, *Ann. Chem.*, **279**, 123.

30) Anschutz and Bocker, *Ann. Chem.* **368**, 61.

Application of Electrochemical Recycle of Ti^{4+}-Ti^{3+} to Additive Dimerization of Butadiene with Hydroxylamine

Toshiro CHIBA and Yoshiyuki TAKATA*

Department of Applied Chemistry, Kitami Institute of Technology, Koen-chyo 165, Kitami 090

**Faculty of Engineering, Hokkaido University, Sapporo 060*

(Received July 9, 1977)

The electrolytic recycle of Ti^{4+}-Ti^{3+} has been employed for a redox-system consisting of hydroxylamine and Ti^{3+} which can produce amino radicals. From electroanalytical measurements, it was found that titanium(IV) chloride in hydrochloric methanol was reducible to Ti^{3+} with a sufficient current efficiency at the platinum electrode and the reduction was speeded up by an addition of hydroxylamine. On macro-scale electrolysis using a small amount of titanium(IV) chloride in the presence of 1,3-butadiene and hydroxylamine, the generated amino radical undergoes additive dimerization with butadiene and gives diaminooctadienes in reasonable yields.

The action of titanium(III) chloride on hydroxylamine in acid solution brings about the formation of an amino radical.[1] Previously, Coffman and his co-workers[2] showed that the amino radical generated in this way gave rise to additive dimerization with olefins to form the corresponding diamines. In these processes, one mole of titanium(III) chloride is consumed per mole of hydroxylamine, because Ti^{4+} produced in the redox-system cannot be rereduced by hydroxylamine. On the other hand, the electrocatalytic mechanism for the regeneration of Ti^{3+} from Ti^{4+} in the presence of hydroxylamine has been studied by different electroanalytical techniques,[3] but in most cases, oxalic acid was used as radical scavenger. Here we have examined the applicability of the Ti^{4+}-Ti^{3+} recycle by means of electrochemical reduction to Coffman's method, as depicted in Scheme 1.

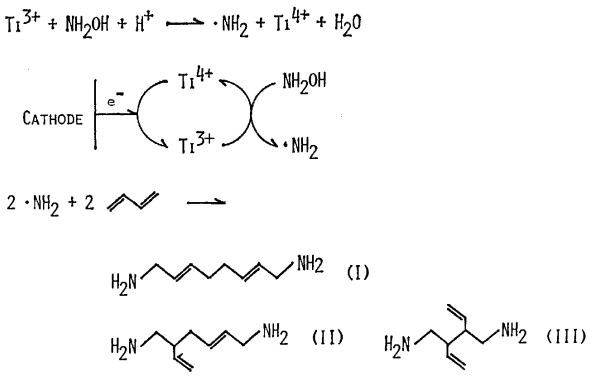

Scheme 1.

Ti^{3+} produced by the cathodic reduction of titanium(IV) chloride reduces hydroxylamine to amino radical along with the oxidation of itself to Ti^{4+}. The generated amino radical attacks 1,3-butadiene followed by additive dimerization to give diaminooctadienes, whereas the resulting Ti^{4+} undergoes rereduction at the cathode. According to the above recycle, this reaction is expected to occur sufficiently even when a small amount of titanium(IV) chloride is used.

Analogous processes, indirect electrochemical reductions which employ low-valent transition metal ions as a mediator, have been reviewed by Dietz and Lund.[4]

Results and Discussion

In the preliminary experiments, current-potential measurements were carried out on 2 M hydrochloric methanol, in both the presence and absence of titanium(IV) chloride.

As can be seen in Fig. 1, when a mercury pool was used as the cathode, the hydrochloric methanol without titanium(IV) chloride was not reduced below the potential of −1.1 V (SCE). An addition of hydroxylamine to the catholyte showed a similar current-potential curve; therefore, its reduction potential should be approximately −1.1 V or more cathodic. Hydrochloric methanol containing titanium(IV) chloride showed two reduction waves: the first wave was at −0.15 V and the

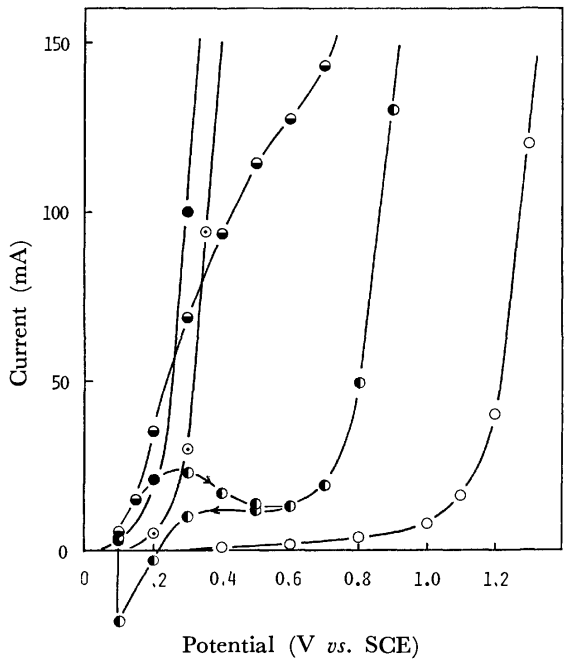

Fig. 1. Plots of current *vs.* cathode potential:
The relationships between current and potential were recorded automatically (sweep rate of 50 mV/s was used) but to economize on space tracings were prepared for reproduction herein. The measurements were carried out in 2 M HCl-MeOH at 25 °C.
a) On mercury; -○- in the absence and presence of $NH_2OH \cdot HCl$ (0.06 M), -◐- stationary curve in the presence of $TiCl_4$ (0.05 M), -◒- initial curve recorded immediately after adding $NH_2OH \cdot HCl$ (0.06 M). b) On platinum; -⊙- in the absence and presence of $NH_2OH \cdot HCl$ (0.06 M), -●- in the presence of $TiCl_4$ (0.05 M).

Table 1. Analytical results of Ti^{3+} generated on Pt cathode[a)]

No.	Catholyte		Constant current (A)	Consumed current (mF)	Cathode potential (V *vs.* SCE)	Conversion Found/Theoretical (%)
	$TiCl_4$ (mmol)	HCl-MeOH 80 ml				
1	9.3	2 M	1.0	3.1	0.21—0.26	80
2	9.3	2 M	1.0	6.2	0.20—0.30	64
3	9.3	2 M	1.0	9.3	0.21—0.35	56
4	9.3	2 M	0.5	3.1	0.19—0.23	84
5	9.3	2 M	0.5	6.2	0.19—0.31	73
6	9.3	2 M	0.5	9.3	0.18—0.35	67
7	9.3	2 M	0.2	9.3	0.13—0.33	74
8	9.3	0.5 M	1.0	9.3	0.21—0.36	49
9	18.6	2 M	1.0	9.3	0.19—0.26	71
10	18.6	5 M	1.0	9.3	0.20—0.28	71

a) Electrolyses were carried out in an ice bath. For volumetric determination of Ti^{3+}, the electrolysis solution was directly titrated with standard $FeCl_3$ solution in nitrogen atmosphere.

second was at −0.80 V. Further, an oxidation wave was observed on the anodic sweep in the vicinity of −0.15 V, which corresponded to the oxidation of the first reduction peak. It would arise from a reversible charge transfer of titanium ions. In polarographic studies,[5)] it has been confirmed that a mixture of titanium(IV)–titanium(III) chlorides in dilute hydrochloric acid showed a cathodic half-wave potential of −0.80 V where the Ti^{4+}-Ti^{3+} couple did not behave reversibly; however, in relatively concentrated solutions of hydrochloric acid, the wave was markedly shifted to a more positive position and was close to −0.15 V. Accordingly, the second wave may be attributed to the irreversible reduction of Ti^{4+}.

Under conditions of controlled potential electrolysis of titanium(IV) chloride in hydrochloric methanol at −0.3 V, the catholyte soon changed to a blue color, which suggests the occurrence of Ti^{3+}, and hence the first wave described above was undoubtedly exhibited by the reduction of Ti^{4+} to Ti^{3+}. Later, on addition of hydroxylamine to the catholyte, the electrolytic current suddenly increased, accompanied by a color change from blue to yellow. These observations indicate that Ti^{3+} is consumed for the reduction of hydroxylamine as soon as it is formed, and that the presence of hydroxylamine results in an acceleration of the cathodic reduction of Ti^{4+} by an electrocatalytic mechanism.

On the other hand, when platinum was used as the cathode, titanium(IV) chloride in hydrochloric methanol was reduced at a potential of −0.15 V, whereas the hydrochloric methanol alone initiated the reduction at −0.25V. Owing to the insignificant difference between the two potentials, platinum seemed entirely unsatisfactory as the generator cathode of Ti^{3+}. However, as shown in Table 1, titanium(IV) chloride was effectively reduced to Ti^{3+} even at the low concentration at the platinum cathode, although hydrogen evolution was observed at the end of the electrolysis. In fact, Malmstadt and Roberts[6)] reduced titanium(IV) chloride at a platinum cathode with 100% current efficiency in hydrochloric acid greater than 7 M. Since platinum was found to be available as the cathode, the mercury cathode was not used for macro-scale electrolysis, in spite of its much greater hydrogen overvoltage, because it is troublesome to handle.

On the basis of the electroanalytical results, preparative electrolyses were conducted under several conditions at the platinum cathode.

Figure 2 shows the results of constant current electrolyses of hydrochloric methanol containing hydroxylamine, 1,3-butadiene, and various amounts of titanium(IV) chloride. When the mol ratio of titanium(IV) chloride to hydroxylamine was more than 0.2, diaminooctadienes were obtained in yields of *ca.* 60% based on hydroxylamine. Immediately before the end of the electrolyses, namely, when the current

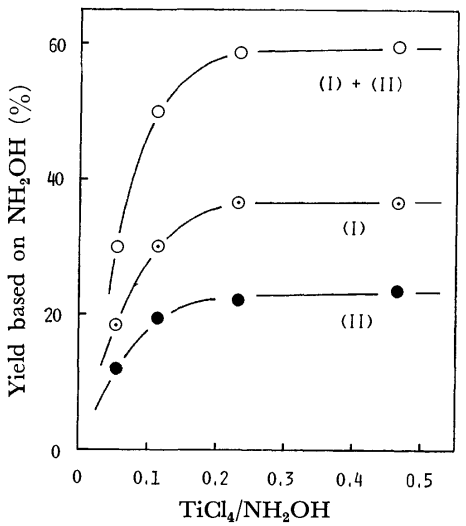

Fig. 2. Electrolyses of hydrochloric methanol containing hydroxylamine, butadiene, and various amounts of titanium (IV) chloride:
Catholyte: $NH_2OH \cdot HCl$, 36 mmol; C_4H_6, 180 mmol; 2 M HCl-MeOH, 80 ml. Constant current, 1.0 A. Consumed current, 37.3 mF.
(I) H_2N-CH_2CH=$CHCH_2CH_2CH$=$CHCH_2$-NH_2
(II) H_2N-$CH_2CH(-CH$=$CH_2)CH_2CH$=$CHCH_2$-NH_2

was consumed in slight excess of the quantity of electricity required to convert hydroxylamine, the catholyte assumed a blue color. This indicates that the reduction of Ti^{4+} and the subsequent reaction of Ti^{3+} with hydroxylamine proceed almost quantitatively. Consequently, under these conditions, the material yield would be governed by the reactivity of the amino radical with butadiene rather than the current efficiency for the generation of Ti^{3+}, although a certain amount of titanuim ions would be inactivated.

In the present reaction, three kinds of isomers of diaminooctadiene were considered, but (III) could not be detected in our experiments. The relative amounts of (I) and (II) were invariably 62:38. This is in agreement with the results in free radical polymerizations of 1,3-butadiene, in which the 1,4-addition reaction is more favorable than the 1,2-addition.[7]

Figure 3 shows the relationships among the consumed current, the current efficiency, and the product yield. The current efficiency for the formation of diamines linearly decreased with the increase of the consumed current, whereas the material yield based on hydroxylamine increased below the consumed current of 50 m farady (the theoretical extent of conversion of hydroxylamine is 67%), but above this value diamines were no longer produced.

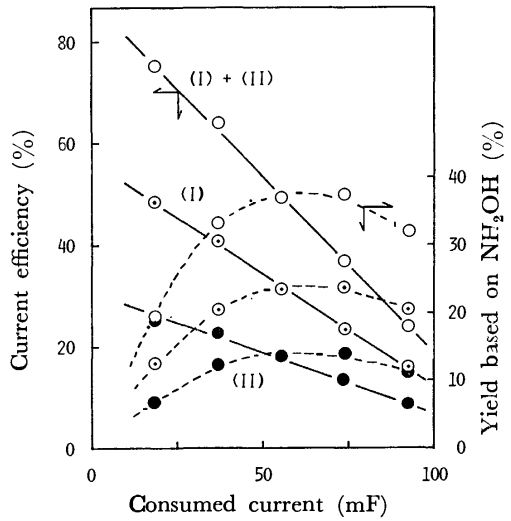

Fig. 3. The relationships among the current efficiency, consumed current, and the product yield:
Catholyte: $TiCl_4$, 9.3 mmol; C_4H_6, 72 mmol; $NH_2OH \cdot HCl$, 72 mmol; 2 M HCl-MeOH, 80 ml. Constant current, 1.0 A.

From the results in Figs. 2 and 3, Ti^{4+} is presumed to be rereduced 4—5 times on the electrode. Moreover, it is probable that water produced as the reaction proceeds renders Ti^{4+} inactive and gives rise to the side reaction. In fact, an addition of water to the catholyte greatly inhibited the electrolysis for the formation of diamines and caused the precipitation of titanium salt, gas evolution, and adhesion of tarry materials on the cathode.

Figure 4 shows the dependence of the amount of butadiene on the product yield. The use of a large excess of butadiene showed a tendency to increase the

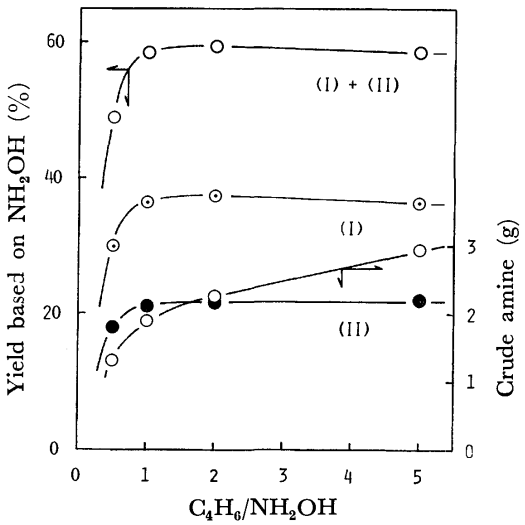

Fig. 4. The dependence of the amount of butadiene on the product yield:
Catholyte: $TiCl_4$, 9.3 mmol; $NH_2OH \cdot HCl$, 36 mmol; 2M HCl-MeOH, 80 ml. Constant current, 1.0 A. Consumed current, 37.3 mF.

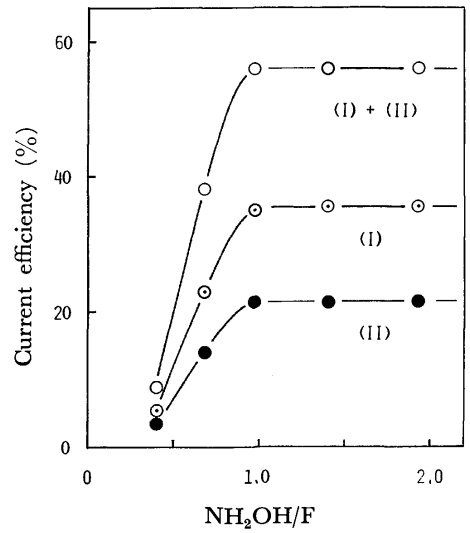

Fig. 5. The dependence of the amount of hydroxylamine:
Catholyte: $TiCl_4$, 9.3 mmol; C_4H_6, 180 mmol; 2 M HCl-MeOH, 80 ml. Constant current, 1.0A. Consumed current, 37.3 mF.

formation of materials with a high boiling point which were soluble in acidic solution. Thus it is probable that polymerization would occur. On the contrary, by the use of less than the theoretical amounts, for example, when the mol ratio of butadiene to hydroxylamine was 0.5, the yield of diaminooctadienes based on butadiene increased to over 90%.

Furthermore, as shown in Fig. 5, the product yield was hardly affected by even significant amounts of hydroxylamine, but was dependent on the consumed current. In order to run the electrolysis effectively, therefore, equimolar amounts of butadiene and hydroxylamine should be used.

Experimental

Reagents. Titanium(IV) chloride was purified by distillation after heating over mercury. Reagent grade hydroxylamine hydrochloride and 1,3-butadiene were used without purifications. Hydrochloride methanol was prepared by passage of dry hydrochloride through distilled methanol.

Apparatus. The instrument used to control potential and current for electroanalytical studies was a Nichia HP-E500H type potentiostat and a constant current unit. The electrode potential was scanned by means of a Nichia S-5A type potential programer. The relationship between current and potential was recorded on a Yokogawa 3077 X-Y recorder. Large scale electrolyses were performed with a Yanagimoto VE-8 potentiostat.

Current-potential measurements were made at 20 °C in a two-compartment H-type cell with a glass frit separating the compartments. The main compartment (25 ml) was provided with a working electrode (a smooth platinum plate or mercury pool, each area is 4 cm^2), a nitrogen gas bubbler, gas outlet, and a sce reference electrode. The other compartment (15 ml) contained a platinum wire as a counter electrode. All potentials were referred to the saturated calomel electrode.

Constant current electrolyses for preparative studies were carried out in a 100 ml-separable flask shielded from the anode compartment by a porous cup, and a reflux condenser (−10 °C) was connected to the cathode compartment. A cylindrical platinum net (4.5 cm in height, 11.0 cm in circumference, 55 mesh) was used at the cathode and the anode was a coil of platinum wire (0.8 mmϕ, 20 cm). The reference electrode was situated adjacent to the working electrode when necessary. The cell was cooled with ice water and nitrogen was bubbled through the cell during electrolysis.

Analytical. The amines were identified titrimetrically and spectroscopically. The amino nitrogen was analyzed by titration with perchloric acid in acetic acid in the usual manner. IR and mass spectra were recorded on a Hitachi 295 spectrophotometer and a Hitachi M-52 mass spectrometer, respectively. ^{1}H-NMR spectra were measured with a Hitachi 20A spectrometer using $CDCl_3$ as the solvent. Chemical shifts are given in ppm from TMS as the internal standard. Gas chromatographic analyses were conducted with a Hitachi 163 gas chromatograph using a 2-m glass column packed with 20% Apieson grease and 10% potassium hydroxyde on a 60—80 mesh Chromosorb W AW, a column temperature of 170 °C (preheater 200 °C), and a flow rate of 40 ml/min (nitrogen gas). Retention times for (I) and (II) isomers were 13.5 and 10.0 min, respectively.

For volumetric determination of Ti^{3+} generated cathodically, the electrolysis solution was directly titrated with 1.0 M ferric chloride in nitrogen atmosphere.

Electrolyses for Preparative Studies. A typical experimental procedure is as follows. The catholyte contained 36 mmol of $NH_2OH \cdot HCl$, 37 mmol of butadiene, and 9.3 mmol of $TiCl_4$ dissolved in 80 ml of 2 M HCl–MeOH. The electrolysis was carried out under a constant current at 1.0 A for 1 h. After the electrolysis, the blue catholyte was evaporated under reduced pressure. Then the residue was poured into a strong alkaline solution, and was extracted twice with a 20 ml portion of ether. The combined extracts were analyzed by GLPC. Analytical samples were obtained by fractional distillation. (I): Bp 91—94 °C/3 mmHg; IR (neat) ν 3370, 3280, 1600 (NH_2), 970 cm^{-1} (*trans* C=C); NMR ($CDCl_3$) δ 1.2 (4H, $-CH_2-\underline{NH_2}$), 2.1 (4H, $-\underline{CH_2}-CH=$), 3.2 (4H, $=CH-\underline{CH_2}-NH_2$), 5.5 ppm (4H, $-CH_2-\underline{CH}=\underline{CH}-CH_2-$); *MW* 140 (mass); Found: neut. equiv., 69.5. Calcd for $C_8H_{16}N_2$: neut. equiv., 70.1. (II): Bp 74—75 °C/3 mmHg; IR (neat) ν 3370, 3280, 1640, 1600 (NH_2), 970 (*trans* C=C), 910 cm^{-1} (term. vinyl); NMR ($CDCl_3$) δ 1.1 (4H, $-CH_2-\underline{NH_2}$), 2.1 (3H, $=CH-\underline{CH_2}-\underline{CH}-CH=$), 2.6 (2H, $-CH-\underline{CH_2}-NH_2$), 3.2 (2H, $=CH-\underline{CH_2}-NH_2$), *ca.* 5 (2H, $-CH=\underline{CH_2}$), 5.5 ppm (3H, $-CH_2-\underline{CH}=\underline{CH}-CH_2-$, $-\underline{CH}=CH_2$); *MW* 140 (mass); Found: neut. equiv., 69.8. Calcd for $C_8H_{16}N_2$: neut. equiv., 70.1.

References

1) a) P. Davis, M. G. Evans, and W. C. E. Higginson, *J. Chem. Soc.*, **1951**, 2563; b) H. Seaman, P. J. Taylor, and W. A. Waters, *ibid.*, **1954**, 4690; see also, Z. Yoshida, T. Matsumoto, and R. Oda, *Kogyo Kagaku Zasshi*, **65**, 46 (1962); Z. Yoshida, T. Matsumoto, and R. Oda, *ibid.*, **67**, 64, 67, 70, 72, 76 (1964); S. Maiti and M. K. Saha, *J. Polym. Sci. A-1*, **5**, 151 (1967); T. Kakurai, T. Sugata, and T. Noguchi, *Kobunshi Kagaku*, **25**, 120 (1968).

2) C. J. Albisetti, D. D. Coffman, F. W. Hoover, E. L. Jenner, and W. E. Mochel, *J. Am. Chem. Soc.*, **81**, 1489 (1959).

3) a) A. Blažek and J. Koryta, *Collect. Czech. Chem. Commun.*, **18**, 326 (1953); b) P. Delahay, C. C. Mattax, and T. Berzins, *J. Am. Chem. Soc.*, **76**, 5319 (1954); c) O. Fischer, O. Dracka, and E. Fischerova, *Collect. Czech. Chem. Commun.*, **26**, 1505 (1961); d) J. H. Christie and G. Lauer, *Anal. Chem.*, **36**, 2037 (1964); e) H. B. Herman and A. J. Bard, *ibid.*, **36**, 510 (1964); f) P. J. Lingane and J. H. Christie, *J. Electroanal. Chem.*, **13**, 227 (1967). *Cf.* T. H. Ridgway, R. P. Van Duyne, and C. N. Reilley, *ibid.*, **34**, 267 (1972).

4) R. Dietz and H. Lund, "Organic Electrochemistry," ed by M. M. Baizer, Marcel Dekker, Inc., New York (1973), Chap. 24. For the industrial importance, *cf.* R. Clarke, A. Kuhn, and E. Okoh, *Chem. Britain*, **11**, 59 (1975); and B. Kastening, International Symposium on Industrial Electrochemistry, Indian Institute of Technology, Madras, India, Dec., 1976, Abstruacts, p. 95.

5) J. J. Lingane and J. H. Kennedy, *Anal. Chim. Acta*, **15**, 294 (1956); see also, R. Strubl, *Collect. Czech. Chem. Commun.*, **10**, 475 (1938); M. Kolousek, *ibid.*, **11**, 592 (1939); R. Tamamushi, *Bull. Chem. Soc. Jpn.*, **23**, 220 (1950).

6) a) P. Arthur and J. F. Donahue, *Anal. Chem.*, **24**, 1612 (1952); b) H. V. Malmstadt and C. B. Roberts, *ibid.*, **27**, 741 (1955).

7) F. E. Condon, *J. Polym. Sci.*, **11**, 139 (1953).

Catalytic Hydrogenolysis of Phenothiazine, Thianthrene, and Phenoxathiin

Masatoshi NAGAI* and Noriyuki SAKIKAWA

Department of Industrial Chemistry, Faculty of Science and Engineering, Nihon University, Chiyoda-ku, Tokyo 101

(Received August 2, 1977)

Catalytic hydrogenolysis of phenothiazine, thianthrene, and phenoxathiin as appropriate model reactants in the competing reactions of sulfur, nitrogen, and oxygen removal over NH_4Y zeolite, pre-sulfided Co–Mo–Al_2O_3, and Ni–W–$SiO_2Al_2O_3$ catalysts has been carried out using the batch method. The cleavage patterns and the schemes in the hydrogenolysis of the three compounds and the active sites of an NH_4Y zeolite for the hydrogenolysis are discussed. The C–S bond in phenoxathiin was more prone to cleavage than the C–O bond, and the C–N bond in phenothiazine was not broken in our experiments. Sulfur removal from the three compounds took place more than the removal of nitrogen or oxygen. The reactivity over the zeolite Y, pre-sulfided Co–Mo–Al_2O_3, and Ni–W–$SiO_2Al_2O_3$ catalysts decreased in the order of phenothiazine > phenoxathiin > thianthrene, but in the absence of the catalyst the thermal stability was phenoxathiin > thianthrene > phenothiazine. In the hydrogenolysis of the three compounds over the NH_4Y catalyst the desulfurization activity of the zeolite Y catalyst was maximized when calcined at 500 °C. The reaction of phenoxathiin was found to be accelerated by Brönsted acid, but this did not hold true in the case of phenothiazine and thianthrene.

In previous papers,[1,2] catalytic hydrodesulfurization of dibenzothiophene, one of the condensed thiophene compounds in residual oils, over an NH_4Y or CoY zeolite catalyst has been studied in order to elucidate the behavior of high-molecular-weight aromatic sulfur compounds.

Catalitic hydrodesulfurization of petroleum fractions or coal oils occurs concurrently with the removal of nitrogen and oxygen. Consequently, we carried out a model experiment on the competitive reactions of S, N, and O removal during the hydrogenolysis of fuel oils. Thianthrene, phenothiazine, and phenoxathiin containing two atoms of sulfur and nitrogen or oxygen atoms in the compounds are regarded as appropriate model reactants.

There have been many studies of the hydrogenolysis of sulfur, nitrogen or oxygen compounds alone.[3-6] However, the only studies of hydrogenolysis of thianthrene on a silica–alumina catalyst were reported by Tits-Skvortsova *et al.*[7] Badger *et al.*[8] studied the mechanism of the desulfurization reaction using Raney nickel. Aiken *et al.*[9] studied the behavior of cyclic sulfur compounds such as dibenzothiophene and thianthrene. There have been no studies of the reaction of phenoxathiin or phenothiazine.

In the present paper, the hydrogenolysis of thianthrene, phenothiazine, and phenoxathiin as the model compounds over NH_4Y zeolite, pre-sulfided Co–Mo–Al_2O_3, and Ni–W–$SiO_2Al_2O_3$ catalysts has been carried out in order to study the competitive reactions of desulfurization, denitrogenation, and deoxygenation. The mechanism of hydrogenolysis of the three compounds and the active sites of the NH_4Y zeolite are discussed.

Experimental

Reactants and Catalysts. Thianthrene was prepared by our modification of the procedure given by Shirley.[10] Phenothiazine and phenoxathiin were prepared by methods previously described;[11,12] thianthrene: mp 157—158.5 °C (lit,[10] 149—154 °C); phenothiazine: 186.5—187.5 °C (lit,[13a] 187 °C); phenoxathiin: 57—58.5 °C (lit,[12] 57.5—58 °C).

NH_4(61%)NaY zeolite was prepared from NaY by a conventional ion exchange procedure using a solution of NH_4Cl–NH_4OH. The exchanged zeolite was then washed thoroughly with decationized water and dried at 100 °C in air. The pretreatment of zeolite was as follows. Glass ampoules containing 0.65 g of zeolite were placed in a furnance. The temperature was slowly raised to the desired calcination temperature and maintained for 4 h, at which time equilibrium had been established, and then the ampoules were sealed. Co–Mo–Al_2O_3 and Ni–W–$SiO_2Al_2O_3$ catalysts obtained commercially were pre-sulfided with a H_2S/H_2 volume ratio of 1/5 at 350 °C for a period of 3 h in the autoclave.

Apparatus and Procedure. Hydrogenolysis of the three compounds was carried out in a 100 ml autoclave with a stirrer driven magnetically. The catalyst and the substrate (0.017 mol) were put into the autoclave, which was then charged with hydrogen to the required pressure. The autoclave was placed in an electric furnance and the temperature was slowly raised to 350 °C and was kept constant, hydrogenolysis being allowed to start after 2 h. After the reaction was completed the autoclave was cooled to room temperature and the liquid reaction mixture and hydrogen sulfide in the autoclave were collected for analysis.

Analytical. Analysis of the liquid reaction mixture was made by gas chromatography using a 3 m column filled with a 5% Silicone OV-17 supported on Chromosorb W. The column was maintained at 70 °C (in the case of the analysis of benzene, benzenethiol, and phenol), 80 °C (for aniline), or 200 °C (for other high boiling compounds). A helium carrier gas was used at the flow rate of 40 ml/min. Ethylbenzene (70, 80 °C) and acenaphthene (200 °C) were used as internal standards for the measurement of the weight of compounds. Hydrogen sulfide in the gaseous products was trapped by lead acetate solution, resulting in the formation of lead sulfide, which was determined by gravimetric analysis. Most of the components were identified through their characteristic retention times in the columns. However, diphenyl disulfide produced during thianthrene hydrogenolysis was isolated by gas chromatography, and was identified by comparing the retention time on gas chromatography, mp 58—60 °C (lit,[13b] 61 °C), IR spectrum, and the fragmentation of the mass spectrum with those of the authentic sample. The stability of the zeolite structure was checked by an X-ray

* Present address: Department of Chemical Engineering, Faculty of Engineering, Tokyo University of Agriculture and Technology, Koganei-shi, Tokyo 184.

diffraction study. The degree of ion exchange was calculated from the sodium content of NH_4Y zeolite after ion exchange. Sodium was determined by chelate titration, using both uranyl acetate and nickel nitrate with a MX indicator.

Results and Discussion

The Cleavage Patterns. *Phenothiazine*: Phenothiazine was desulfided in the highest compounds of thianthrene, phenoxathiin, and phenothiazine; the results for the hydrogenolysis of phenothiazine are given in Table 1. The data where the zeloite Y and no catalyst were used indicated that diphenylamine and a small amount of carbazole and aniline were observed in the products. Hence, the cleavage pattern and the pathways in phenothiazine hydrogenolysis over the NH_4Y catalyst were considered with Scheme 1. As diphenylamine was usualy produced in the presence of the pre-sulfided Co–Mo–Al_2O_3 and Ni–W–$SiO_2Al_2O_3$ catalysts, only pathway (1) appeared to be followed. Degradation reactions of diphenylamine and carbazole occur hardly at all, because benzene was not observed and very little aniline was produced. Because no dibenzothiophene was produced while carbazole was produced in the phenothiazine reaction, we concluded that the C–N bond in the molecule is not broken, while the C–S bond is easily broken.

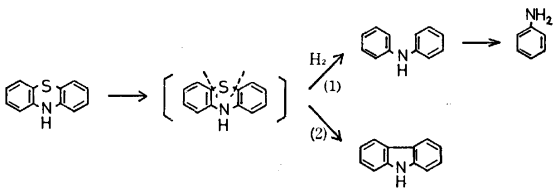

Scheme 1.

Thianthrene: The results for the hydrogenolysis of thianthrene over the pre-sulfided Co–Mo–Al_2O_3, Ni–W–$SiO_2Al_2O_3$, and zeolite Y catalysts, and for the hydrogenolysis without catalysts are given in Table 2. Obolentsev and Mashkina[14] identified *o*-(phenylthio)-benzenethiol in thianthrene hydrogenolysis over a sulfided Co–Mo–Al_2O_3 catalyst and proposed Reaction Scheme 2. In our experiment, however, the products of thianthrene hydrogenolysis over the catalysts used were primarily benzene, diphenyl sulfide and diphenyl disulfide, and *o*-(phenylthio)benzenethiol could not be confirmed. Hence, Scheme 2 is doubtful.

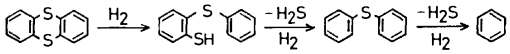

Scheme 2.

It seems likely that the thianthrene molecule is distorted on the S–S line,[15] and that the molecule is adsorbed to the catalyst at one or usually at two sulfur atoms, while 2 or more of the 4 C–S bonds in the molecule

Table 1. Catalytic hydrogenolysis of phenothiazine*)

Catalyst	NH_4Y[a)] 350 °C	NH_4Y[a)] 500 °C	NH_4Y[a)] 600 °C	None[b)]	Ni–W–$SiO_2Al_2O_3$[c)]	Co–Mo–Al_2O_3[d)]
Sulfur removed[e)] (mol%)	15.8	23.4	22.6	6.2	44.7	33.0
Percentage of products[f)] (%)						
Benzene	0	0	0	0	0	0
Aniline	+	0.2	0.3	0	+	0
Diphenylamine	13.2	20.1	19.7	3.1	38.6	33.9
Carbazole	0.2	0.8	0.3	0.7	0	0
Phenothiazine	86.6	79.0	79.7	96.2	61.4	66.1

*) Hydrogenolysis conditions—catalyst, 0.65 g; initial hydrogen pressure, 50 kg/cm² (at 70 °C); reaction temp (a,b): 350 °C, (c,d): 250 °C. a) Zeolites prepared by calcination of NH_4Y at various temperatures. c,d) Presulfiding condition—catalyst, 5 g; initial hydrogen pressure, 50 kg/cm² (room temp); time, 3 h. e) The yields were calculated from lead sulfide after the hydrogen sulfide in gaseous effluents was trapped in lead acetate solution. f) Products except gaseous effluents.

Table 2. Catalytic hydrogenolysis of thianthrene[a)]

Catalyst	NH_4Y 350 °C	NH_4Y 500 °C	NH_4Y 600 °C	None	Ni–W–$SiO_2Al_2O_3$	Co–Mo–Al_2O_3
Sulfur removed (mol%)	9.1	13.4	12.5	1.3	7.2	15.0
Percentage of products (%)						
Benzene	3.5	19.7	23.7	0	0.8	11.8
Benzenethiol	1.2	2.1	0.8	0	0	0
I[b)]	+	0.4	0.4	0	0	+
Diphenyl sulfide	1.7	3.5	4.0	0	3.4	5.9
Dibenzothiophene	1.0	3.3	2.8	2.2	0	0
Diphenyl disulfide	0.4	0.7	1.2	0	9.7	11.7
Thianthrene	92.0	70.4	67.1	97.8	86.2	70.6

a) The conditions in this table are similar to those in Table 1. b) Unidentified product.

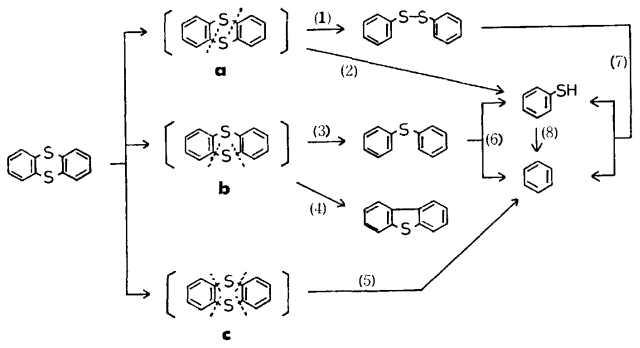

Scheme 3.

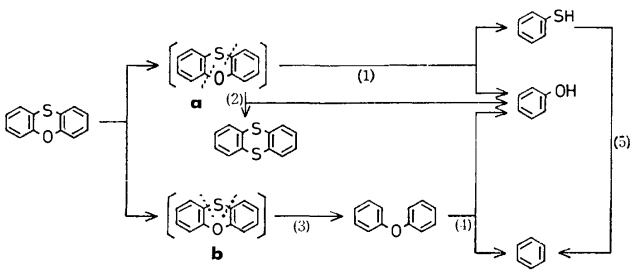

Scheme 4.

are broken. We propose Scheme 3, which occurs with the three ways of cleavage (**a**, **b**, **c**), as a modification of Scheme 2 for thianthrene hydrogenolysis. When only an atom of sulfur is adsorbed and two C–S bonds are broken, and cleavage pattern (**b**) is expected to occur, pathways (3) and (4) are thought to take place. If it is assumed that thianthrene is adsorbed at both sulfur atoms, the hydrogenolysis of thianthrene proceeds according to cleavage patterns (**a**) and (**c**). In pattern (**a**), the two diagonal C–S bonds in thianthrene are simultaneously broken to give benzenethiol (2), or the S–S bonds form to give diphenyl disulfide, which is desorbed (1). On the other hand, in pattern (**c**) the simultaneous loss of two sulfur atoms from thianthrene results in the formation of benzene in pathway (5).

The amounts of the products given in Table 2 suggest that cleavage patterns (**a**) and (**c**) predominate in thianthrene hydrogenolysis over the pre-sulfided Co–Mo–Al_2O_3 and Ni–W–$SiO_2Al_2O_3$ catalysts. During pyrolysis, only pattern (**b**) occurred and the loss of an atom of sulfur allowed thianthrene to pass to the more stable planar form of dibenzothiophene (4).[16] In the presence of the zeolite Y catalyst, pattern (**b**) appeared to predominate over pattern (**a**).

Phenoxathiin: The data for phenoxathiin hydrogenolysis over various catalysts are given in Table 3. The table shows that thianthrene and benzenethiol were produced in phenoxathiin hydrogenolysis over the NH_4Y zeolite catalyst, but were not observed over the pre-sulfided Co–Mo–Al_2O_3 and Ni–W–$SiO_2Al_2O_3$ catalysts and without catalysts. Grib *et al.*[17] reported that thianthrene and phenoxathiin were obtained by the reaction of diphenyl sulfide and diphenyl ether over an $AlCl_3$ catalyst, and that the formation of phenoxathiin was apparent, while that of thianthrene was not. We will now consider the hydrogenolysis mechanism (Scheme 4) which includes two kinds of cleavage patterns in order to explain the formation of thianthrene and benzenethiol and the absence of diphenyl sulfide in the products. For cleavage pattern (**a**) in Scheme 4 we assumed that the desorption of phenol is faster than that of benzenethiol, and that two molecules of benzenethiol combine on the surface of the catalyst to form thianthrene, which is then desorbed. Only in the case of the pre-sulfided Co–Mo–Al_2O_3 and Ni–W–$SiO_2Al_2O_3$ catalysts does cleavage pattern (**b**) take place. 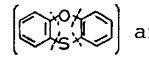 and 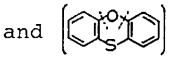 are not thought to take place because diphenyl sulfide and dibenzothiophene were not observed in the products and because a little benzene was produced. The distribution of the products in Table 3 shows that the primary product was diphenyl ether produced by the fission of the C–S bond in phenoxathiin. The fact that cleavage of the C–S bond in one-point adsorption is easier than the simultaneous cleavage of the C–O and C–S bonds in two-point adsorption of the sulfur and oxygen atoms can be explained by the greater electron density of sulfur atoms compared with oxygen atoms.[18] When comparing the reactivity of the three compounds where no catalyst was used in Tables 1, 2 and 3, phenoxathiin is the most stable of the three compounds, and the thermal stability order is pheno-

Table 3. Catalytic hydrogenolysis of phenoxathiin[a]

Catalyst	NH_4Y			None	Ni-W-$SiO_2Al_2O_3$	Co-Mo-Al_2O_3
	350 °C	500 °C	600 °C			
Sulfur removed (mol%)	8.9	13.4	6.6	1.0	34.1	26.8
Percentage of products (%)						
Benzene	2.5	5.1	3.5	0.3	0.6	0.7
Benzenethiol	1.2	0.4	+	0	0	0
Phenol	7.8	8.5	8.0	0	1.8	1.5
Diphenyl ether	5.7	15.1	11.6	0	31.6	19.0
Diphenyl sulfide	0.2	0	0	0	0	0
Phenoxathiin	81.7	67.6	75.4	99.7	65.9	78.9
Thianthrene	0.8	1.5	1.2	0	0	0
II[b]	0	1.7	0.3	0	0	0

a) The conditions in this table are similar to those in Table 1. b) Unidentified product.

xathiin > thianthrene > phenothiazine. The reactivity of the compounds over the zeolite Y, pre-sulfided Co–Mo–Al_2O_3, and Ni–W–$SiO_2Al_2O_3$ catalysts, however, decreased in the order phenothiazine>phenoxathiin> thianthrene, which is different from the order in the absence of catalysts. The product percentages in Tables 1 and 2 show that diphenyl ether is less readily decomposed than diphenyl sulfide.

The Active Sites of NH_4Y Zeolite in the Hydrogenolysis. The percentage of sulfur removed (H_2S produced) in the hydrogenolysis of phenothiazine, thianthrene, and phenoxathiin over the NH_4Y zeolite catalyst as a function of the calcination temperature is shown in Fig. 1. The percentage of sulfur removed from all three substrates was greatest at a calcination temperature of *ca.* 500 °C, just as in the case of dibenzothiophene over the NH_4Y catalyst. The percentage of sulfur removed decreased in the order of phenothiazine>phenoxathiin>thianthrene. This order was the same when the Co–Mo–Al_2O_3 and Ni–W–$SiO_2Al_2O_3$ catalysts were used, as can be seen in Tables 1, 2, and 3. The activity

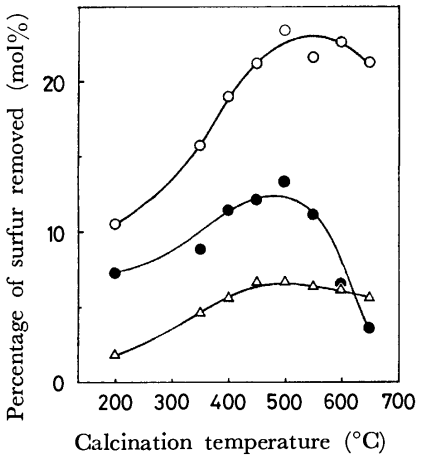

Fig. 1. The relations between the percentage of sulfur removed and calcination temperatures of the NH_4Y zeolite in the hydrogenolysis of phenothiazine (○), thianthrene (△), and phenoxathiin (●).

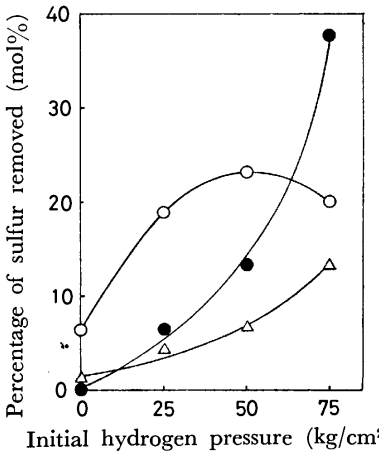

Fig. 2. The effect of the initial hydrogen pressure on the percentage of sulfur removed in the hydrogenolysis of phenothiazine (○), thianthrene (△), and phenoxathiin (●) over the NH_4Y catalyst calcined 500 °C.

of the zeolite catalyst during thianthrene reaction did not appreciably vary for calcination temperatures of the catalyst above 500 °C. The percentage of sulfur removed from phenoxathiin was greatly affected by the pretreatment temperature, reaching a maximum at 500 °C. The percentage of sulfur removed decreased sharply at temperatures above 500 °C. It has been proposed that the Brönsted acid sites on the NH_4Y zeolite are converted to Lewis acid sites when pretreatment is carried out at temperatures higher than 500 °C, as a result of the elimination of water.[19,20] Hence, the percentage of sulfur removed from phenoxathiin would be expected to decrease rapidly with decreasing Brönsted acid sites. The effect of the initial hydrogen pressure on the percentage of sulfur removed is given in Fig. 2. Sulfur removed during phenoxathiin hydrogenolysis increased considerably with increasing pressure of initial hydrogen. Therefore, the hydrogenolysis of phenoxathiin over the NH_4Y catalyst is accelerated by the Brönsted acid sites produced during calcination.

More phenol than phenyl ether was formed in phenoxathiin hydrogenolysis over the NH_4Y catalyst calcined at 350 °C, but less phenol than phenyl ether was produced over the NH_4Y catalyst at calcination temperatures above 500 °C. This is thought to be due to the fact that the reaction:

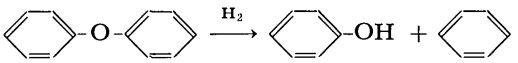

is accelerated by the Brönsted acid sites produced at the lower calcination temperatures.

In the hydrogenolysis of phenothiazine and thianthrene it is not yet understood what acid sites promote the reaction. As in the hydrodesulfurization of dibenzothiopene, however, sulfur removal was greatest when zeolite prepared by calcination of NH_4Y at temperatures of *ca.* 500 °C was used. There can therefore be no doubt that the acid sites play a role in the hydrogenolysis reaction.

We are grateful to Professor Kunio Itabashi and Dr. Hideo Urimoto, of Nihon University, and Associate Professor Toshiaki Kabe, the Tokyo University of Agriculture and Technology, for valuable discussions. We are also indebted to Mr. Hiroshi Tokita for assistance during the course of the experiments.

References

1) M. Nagai, H. Urimoto, and N. Sakikawa, *Nippon Kagaku Kaishi*, **1975**, 356.

2) M. Nagai, S. Obata, M. Yamada, and N. Sakikawa, *Nippon Kagaku Kaishi*, **1976**, 956.

3) O. Weisser and S. Landa, "Sulphide Catalysts, Their Properties and Application," Pergamon-Vieweg, New York (1973), Chap. 6.

4) S. A. Qader, W. H. Wiser, and G. R. Hill, *Ind. Eng. Chem., Process Dev.*, **7**, 390 (1968).

5) P. H. Emmett, Ed., "Catalysis," Reinhold Publishing Corp., Vol. 5, New York (1955), Chap. 6.

6) K. Itabashi, Ph. D. Thesis, University of Nihon, Tokyo, Japan, 1966.

7) I. N. Tits-Skvortsova, A. I. Leonora, S. Y. Levina,

and E. A. Karaseva, *Zh. Obshch. Khim.*, **23**, 303 (1953).
8) G. M. Badger, P. Cheuychit, and W. H. Sasse, *Aust. J. Chem.*, **17**, 366 (1964).
9) J. Aitken, T. Heeps, and W. Steedman, *Fuel*, **47**, 353 (1968).
10) D. A. Shirley, "Preparation of Organic Intermediates," John Wiley & Sons, New York (1951), p. 276.
11) Yuki Gosei Kyokai, Ed., "Yuki Kagobutsu Gosei Ho," Vol. 1, Gihodo, Tokyo (1949), p. 106.
12) C. M. Suter and C. E. Maxwell, *Org. Synth.*, Coll. Vol. II, 485 (1943).
13) Infrared Data Committee of Japan, Ed., "IRDC Cards, (a): No. 1915; (b): No. 6572," Nankodo, Japan (1966).
14) Ref. 3, p. 106.
15) S. Hosoya, *Acta Crystallogr.*, **16**, 310 (1963).
16) G. Saint-Ruf, J. Servoin-Sidoline, and J. P. Coic, *J. Org. Chem.*, **11**, 287 (1974).
17) A. V. Grib, T. P. Tolstaya, and A. V. Petrakov, *Izv. Akad. Nauk SSSR, Ser. Khim.*, **1970**, 2752.
18) M. Kamiya, *Bull. Chem. Soc. Jpn.*, **43**, 3929 (1970).
19) D. N. Stamires and J. Turkevich, *J. Am. Chem. Soc.*, **86**, 749 (1964).
20) J. B. Uytterhoeven, L. G. Christner, and W. K. Hall, *J. Phys. Chem.*, **69**, 2117 (1965).

Heterofulvalenes. I. 5-Aza- and 6-Aza-1,4-dithiafulvalenes

Jyuzo NAKAYAMA, Yukie WATABE, and Masamatsu HOSHINO

Department of Chemistry, Faculty of Science, Saitama University, Urawa, Saitama 338

(Received August 16, 1977)

5-Aza, 2,3-benzo-5-aza-, 6-aza-, and 2,3-benzo-6-aza-1,4-dithiafulvalenes were synthesized and their spectroscopic properties are described. For example, the reaction of 2-methylthio-1,3-dithiolylium iodide with pyrrole gave 2-(2-pyrrolyl)-1,3-dithiolylium iodide in a 92% yield, which was treated with DBU, giving rise to 5-aza-1,4-dithiafulvalene as thermally-stable orange crystals in an 82% yield. Several reactions found during the course of these synthetic studies are also reported.

Recent findings concerning the highly-conductive charge-transfer salt (**1**) of tetrathiafulvalene and tetracyanoquinodimethane have created a wide and expanding interest in convenient methods of synthesizing a variety of tetrathiafulvalene derivatives and their tetraselenafulvalene analogs.[1] The synthesis of azadithiafulvalenes, **2b** and **c**, and **3c** and **d**, has been reported by Gompper and Weiss.[2] However, no report of the synthesis of the parent compounds, **2a** and **3a**, has appeared, although 1,4-dithiafulvalene (**4**) has already been synthesized.[3] Compounds **2** and **3** are iso-π-electronic with **4** and sesquifulvalene (**5**)[4] and may be aromatic if dipolar structures such as **2'** or **3'** contribute to the ground state of these molecules. Here, the synthesis of **2a**, **3b**, their benzo-derivatives, and their spectroscopic properties are reported. At the beginning of these studies, parent

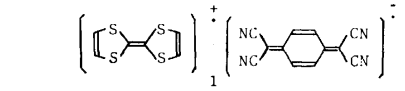

1

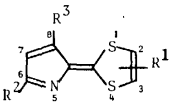

2a; $R^1 = R^2 = R^3 = H$
b; $R^1 = Ph$, $R^2 = R^3 = Me$
c; $R^1 = R^2 = R^3 = Ph$

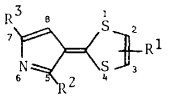

3a; $R^1 = R^2 = R^3 = H$
b; $R^1 = H$, $R^2 = R^3 = Me$
c; $R^1 = Ph$, $R^2 = R^3 = Me$
d; $R^1 = R^2 = R^3 = Ph$

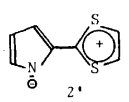

2'

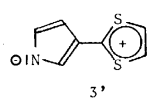

3'

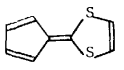

4

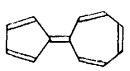

5

compounds **2a** and **3a** were considered too thermally unstable to be isolated because Gompper and Weiss were not able to isolate **2b** and **3c** (they can be maintained in acetonitrile at room temperature for several hours).[2] The synthesis of benzo-derivatives of **2** and **3** were then undertaken in the expectation that they would be more stable than the parent compounds. The starting materials, **7**, **8**, and **9**, were easily obtained by reactions of benzodithiole **6** with pyrroles in acetic acid.[5]

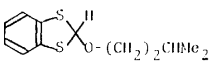

6

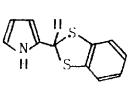

7

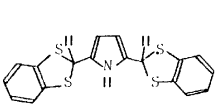

8

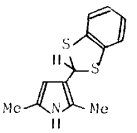

9

Tritly tetrafluoroborate (**10**) can abstract a hydride from 1,3-benzodithiole to give 1,3-benzodithiolylium tetrafluoroborate (**14**) in a good yield.[6] Thus, the reaction of **7** with an equimolar amount of **10** was carried out in acetonitrile at room temperature with the expectation of obtaining the dithiolylium salt, **15a**. However, the reaction gave 2,5-tritylpyrrole (**13**) in a 54% yield (based on **10**). The use of 2 molar amounts of **10** gave **13** in a 62% yield. The structure of **13** was confirmed by comparison with an authentic sample prepared in a 71% yield by the reaction of 2 equivalents of **10** with pyrrole. The formation of **13** from **7** and **10** may proceed *via* the formation of **11** as a transient intermediate. This would not be unexpected in view of the facile formation of **13** by the action of 2 equivalents of **10** with pyrrole. Ipso-substitution to form a sterically-unfavorable intermediate, **12**, and subsequent elimination of the dithiolylium salt (**14**) produced **13** The formation of the heteroaromatic salt, **14**, serves as a driving force for the latter reaction. Actually, evidence of the formation of **14** is found in the fact that treatment of the reaction mixture with triethylamine gave dibenzotetrathiafulvalene (**16**) in a low yield (2%). The formation of **16** from **14** by treatment

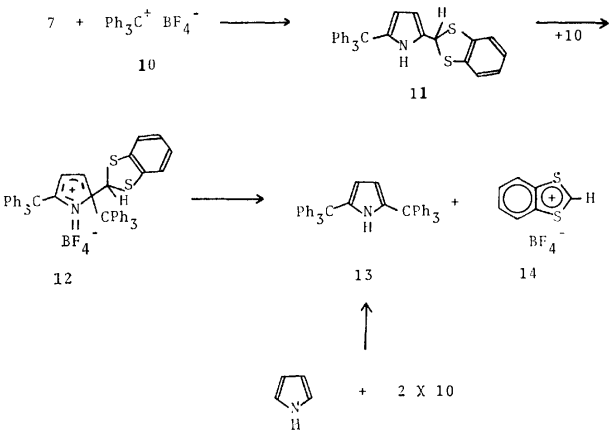

10 11 12 13 14

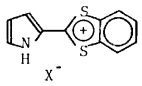

15a; X = BF_4
b; X = ClO_4

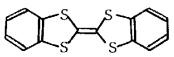

16

with a base is well documented.[6]

Although the reaction of **7** with **10** failed to give the expected product, treatment of **8** with **10** gave salt **17** as unstable yellowish-brown crystals in a 51% yield. Treatment of **17** with triethylamine in acetonitrile at room temperature quantitatively gave the azadithiafulvalene, **18**. Compound **18**, on being treated with tetrafluoroboric acid, gave salt **17**, but neither methyl iodide nor benzoyl chloride reacted with **18** in boiling acetonitrile or in acetonitrile at room temperature, respectively.

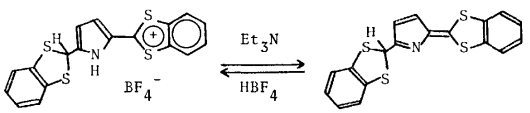

17 18

The reaction of **9** with **10** gave compound **19** (17%) and triphenylmethane (56%). Although the formation of triphenylmethane is indicative of the formation of the expected salt, **20a**, it was not isolated in pure form. Salt **14** also serves as hydride acceptor and is a milder reagent than **10**.[6,7] Therefore, **9** was allowed to react with **14**. The reaction carried out in acetonitrile at room temperature gave **20a** (20%), **21** (36%), and **22** (15%). Compound **14** in the reaction with **9** undergoes both hydride abstraction to form **20a** and electrophilic substitution to form **21**. The formation of compound **22** is the result of hydride abstraction from **21** by **14**. Salts **20a** and **22** could not be separated from each other, but the ratio of **20a** to **22** formed was easily determined by NMR analysis since both salts could be prepared by other methods described below. Compound **21** was prepared in a 93% yield from 2,5-dimethylpyrrole and 2 equivalents of **6** in acetic acid. Treatment of **21** with an equimolar amount of **14** gave salt **22** in a 76% yield. The reaction of **21** with **10** gave impure **22** in a diminished

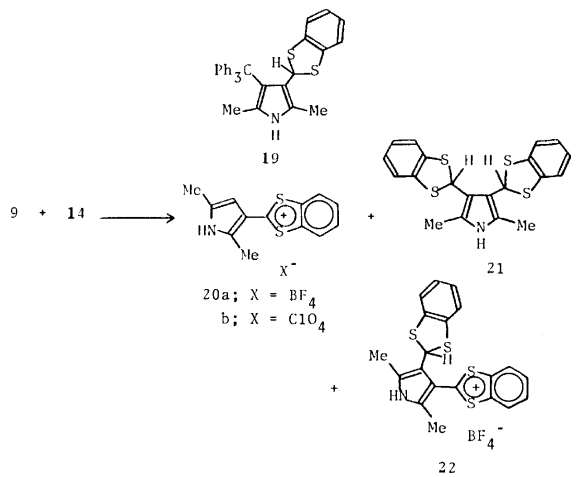

19

20a; X = BF_4
b; X = ClO_4

21

22

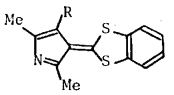

23; R = 1,3-Benzodithiol-2-yl
27; R = H

yield. Treating **22** with diazabicyclo[5.4.0]-undec-7-ene(DBU) gave the azathiafulvalene, **23**, in a 92% yield.

Since the reactions described above failed to produce clean samples of salts **15a** and **20a**, synthesis of these salts from salt **24**[8] was attempted. Pyrrole reacted smoothly with **24** in acetonitrile at room temperature and the expected perchlorate, **15b**, was obtained in an 84% yield. Similarly, salt **20b** was prepared from **24** and 2,5-dimethylpyrrole in a 67% yield. Treatment of an acetonitrile solution of **15b** with DBU gave the azadithiafulvalene, **25**, as an orange crystalline precipitate in a 31% yield. The addition of 2,3-dichloro-5,6-dicyano-*p*-benzo-quinone (DDQ) to the filtrate gave 1 : 1 charge transfer salt **26** of DDQ and **25** in a 37% yield. Salt **26** may consist of the radical anion of DDQ and the radical cation of **25** (the structure of **25** under active investigation in this laboratory). In a similar manner, salt **20b** was converted to **27** in a 68% yield.

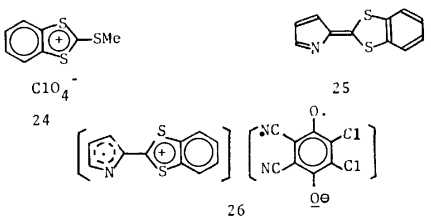

24 25

26

The finding that **25** and **27** thus obtained are thermally more stable than expected was encouragement to prepare parent compound **2a**. Thus, pyrrole was allowed to react with an equimolar amount of iodide **28**[9] in acetonitrile at room temperature for 2 days to gave the dithiolylium iodide, **29**, in a 92% yield. Treatment of **29** with DBU gave 5-aza-1,4-dithiafulvalene (**2a**) as orange crystals in an 82% yield. **2a** is thermally stable and can be stored in a refrigerator indefinitely. Similarly, salt **30** was prepared in an 83% yield from 2,5-dimethylpyrrole and **28**. Salt **30** was also converted to the thermally-stable azadithiafulvalene, **3b**, by treatment with DBU in

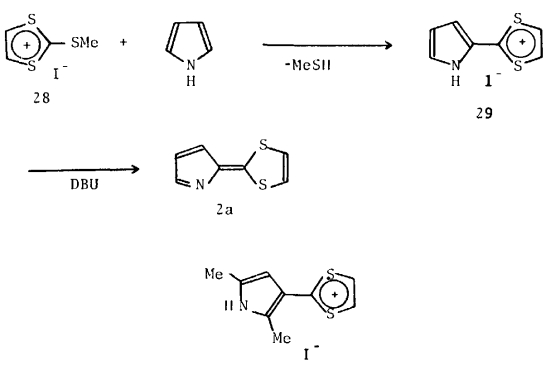

28 29

2a

30

a 70% yield. **3b** is less stable than **2a** and decomposed to tarry materials in solution.

NMR data for 1,3-dithiolylium salts and azadithiafulvalenes are summarized in Table 1. For comparison with these compounds, data for **7**, **8**, and **9** were also included. In the NMR spectrum of **8**, the pyrrole-ring proton signal appears at δ 6.07 as a doublet (due to long-range coupling with the N–H proton[10]).

On the other hand, the pyrrole-ring proton signal of the dithiolylium salt, **17**, occurs as two doublets at δ 6.78 and 7.52. A large low-field shift observed in going from **8** to **17** is attributed to the inductive effect of the positively-charged 1,3-benzodithiolylium nuclei. The high-field doublet of **17** can be assigned to the C-4 H of the pyrrole ring because the influence of the dithiolylium nuclei is less at this position. For the same reason, the pair of doublets of **29** at δ 6.66(J=5 and 3 Hz) can be assigned to the C-4 H of the pyrrole rings. The coupling constant between the C-3 H and C-4 H is 5 Hz for **17**. Therefore, the pair of doublets of **29** at δ 7.69 (J=5 and 1 Hz) and δ 7.88(J=3 and 1 Hz) can be assigned to C-3 H and C-5 H, respectively. The appearance of the benzene-ring proton signal of the 1,3-dithiolylium nuclei of **17** an **15b** as a typical AA'XX' pattern symmetrical about its center indicates that the conjugation between the two rings is not strong enough to hinder free rotation about the pinch bond. The same holds true for **29** since the dithiolylium-ring proton signal appears as a sharp singlet at δ 8.56. However, the chemical-shift value of δ 8.56, when compared to the value of δ 8.66 observed for the ring protons of **28** in deuteriofluoroacetic acid, suggests a significant contribution of structure **29'** to the ground state of

Table 1. NMR data

Compound	Solvent	δ (ppm) with TMS as internal reference
8	$CDCl_3$	6.07 (2H, d, J=2.6 Hz, pyrrole ring), 6.26 (2H, s, methine), 6.9—7.2 (8H, 2AA'BB' m, benzene ring), 8.8 (1H, very broad m, NH)
17	CF_3CO_2D	6.02 (1H, s, methine), 6.78 (1H, d, J=5 Hz, 4-C H of pyrrole ring), 7.52 (1H, d, J=5 Hz, 3-C H of pyrrole ring), 7.0—7.4 (4H, AA'BB' m, benzene ring protons of benzodithiol-2-yl group), 7.7—8.3 (4H, AA'XX' m, benzodithiolylium nucleus)
18	$CDCl_3$	6.06 (1H, s, methine), 6.65 (1H, d, J=4 Hz, 7-C H), 6.9—7.7 (9H, m, 8-C H + benzene ring protons)
7	$CDCl_3$	6.0—6.2 (2H, complex m, 3- and 4-C H's of pyrrole ring), 6.32 (1H, s, methine) 6.58 (1H, m, 5-C H of pyrrole ring), 6.9—7.3 (4H, AA'BB' m, benzene ring), 8.5 (1H, broad m, NH)
15b	DMSO-d_6	6.80 (1H, dd, J=5 and 3 Hz, 4-C H of pyrrole ring), 7.7—8.0 (3H, 3-C H + half of AA'XX' m of benzene ring protons), 8.10 (1H, dd, J=3 and 1 Hz, 5-C H), 8.3—8.6 2H, m, half of AA'XX' m)
25	$CDCl_3$	6.55 (1H, d, J=5 Hz, 7-C H), 7.05—7.65 (5H, m, 8-C H + benzene ring protons), 7.71 (1H, s, 6-C H)
29	DMSO-d_6	6.66 (1H, dd, J=5 and 3 Hz, 4-C H), 7.69 (1H, dd, J=5 and 1 Hz, 3-C H), 7.88 (1H, dd, J=3 and 1 Hz, 5-C H), 8.56 (2H, s, dithiolylium nucleus)
2a	CCl_4	6.40 (1H, d, J=4 Hz, 7-C H), 6.78 (2H, s, dithiole ring), 6.94 (1H, d, J=4 Hz, 8-C H), 7.52 (1H, s, 6-C H)
	CH_3CN	6.54 (1H, d, J=4 Hz, 7-C H), 7.23 (2H, s, dithiole ring), 7.16 (1H, d, J=4 Hz, 8-C H), 7.58 (1H, s, 6-C H)
9	$CDCl_3$	2.16 (3H, s, 5-C methyl), 2.18 (3H, s, C-2 methyl), 6.08 (1H, d, J=2.5 Hz, C-4 H of pyrrole ring), 6.40 (1H, s, methine), 6.9—7.3 (4H, AA'BB' m, benzene ring), 7.45 (1H, broad m, NH)
20b	DMSO-d_6	2.22 (3H, s, 5-C methyl), 2.62 (3H, s, 2-C methyl), 6.55 (1H, broad s, 4-C H), 7.7—8.5 (4H, AA'XX' m, benzodithiolylium nucleus)
27	$CDCl_3$	2.17 (3H, broad s, 7-C methyl), 2.40 (3H, s, 5-C methyl), 5.95 (1H, broad s, 8-C H), 7.1—7.6 (4H, complex m, benzene ring)
22	DMSO-d_6	2.45 (3H, s, 5-C methyl), 2.72 (3H, s, 2-C methyl), 7.42 (1H, s, methine), 7.0—7.6 (4H, AA'BB' m, benzene ring protons of benzodithiol-2-yl group), 7.7—8.7 (4H, AA'XX' m, benzodithiolylium nucleus)
23	$CDCl_3$	2.47 (3H, s, methyl), 2.52 (3H, s, methyl), 6.8—7.7 (9H, m, benzene ring protons+methine proton)
30	DMSO-d_6	2.23 (3H, broad s, 5-C methyl), 2.55 (3H, s, 2-C methyl), 6.48 (1H, broad s, 4-C H), 8.49 (2H, s, dithiolylium ring)
3b	$CDCl_3$	2.15 (3H, broad s, 7-C methyl), 2.32 (3H, s, 5-C methyl), 5.86 (1H, broad s, 8-C H), 6.73 (2H, s, dithiole ring)
	CH_3CN	6.05 (1H, broad s, 8-C H), 7.10 (2H, s, dithiole ring)
	$(CH_3)_2CO$	5.95 (1H, broad s, 8-C H), 7.23 (2H, s, dithiole ring)

29, since **28'** is known to contribute significantly to the ground state of **28**.[11]

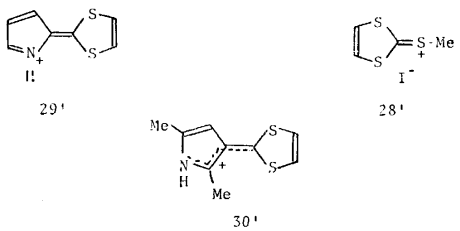

The formation of dithiolylium salt **20b** from **9** was also accompanied by a large low-field shift of the pyrrole-ring protons. The singlet due to the C-2 methyl of the pyrrole ring of **20b** is shifted to lower field by 0.44 ppm compared the that of **9**, whereas the singlet due to the C-5 methyl, which is broadened by long-range coupling with the C-4 H, is shifted to lower field by only 0.06 ppm and the broad singlet due to the C-4 H to lower field by only 0.47 ppm. This indicates that structure **30'** contributes significantly to the ground state of **30**. The chemical shift value of δ 8.49 of the dithiolyium-ring proton signal of **30** is also indicative of the contribution of **30'** as described for **29**. Free rotation about the pinch bond also occurs in this case.

In azadithiafulvalene **18**, the doublet at δ 6.65 can be assigned to the C-7 H (the C-8 H signal was obscured by signals due to the benzene-ring protons), which is less influenced than is the C-8 H by the electronegative nitogen atom and hence is expected to resonate at a higher value of the field than the C-8 H. The coupling constant between the C-7 H and C-8 H is 4 Hz in **18**. Accordingly, the doublet of **25** at δ 6.55 (J=4 Hz) and that of **2a** at δ 6.40 (J=4 Hz) can be assigned to the C-7 H, the doublet of **2a** at δ 6.94 (J=4 Hz) to the C-8H, and the singlet of **25** at δ 7.71 and that of **2a** at δ 7.52 to the C-6 H. The dithiole-ring proton signals of **2a** and **3b** appear as a singlet at δ 6.78 in carbon tetrachloride and at δ 6.73 in deuteriochloroform. This may be due to accidental equivalence of the two protons rather than rotation about the pinch bond. Evidence for this description comes from the fact that the benzene-ring proton signals of **25** and **27** appear as a complex multiplet, but not as a symmetrical AA'BB' pattern. The chemical-shift values of δ 6.78 and 6.73 of the dithiole-ring proton signals of **2a** and **3b** are slightly lower than the reported value (δ 6.60) of the dithiole-ring protons of 1,4-dithiafulvalene (**4**),[3] thus suggesting that the contribution of a dipolar structure is somewhat larger in **2a** and **3b** than in **4** due to the influence of the electronegative nitrogen atom. Here, of particular interest, is the large solvent effect observed with **2a** and **3b**. The dithiole-ring proton signals of **2a** were shifted to lower field by 0.45 ppm upon changing the solvent from carbon tetrachloride to acetonitrile, the other protons also being shifted to lower field (0.06 ppm for C-6 H, 0.22 ppm for C-7 H, and 0.14 ppm for C-8 H). The dithiole-ring protons of **3b** were also shifted to lower field by 0.37 and 0.50 ppm upon changing the solvent from deuteriochloroform to acetonitrile and acetone, respectively. This may be ascribed to the increased contribution of dipolar structures, such as **2'** and **3'**, in the polar solvents. A contribution from a dipolar structure increases the dithiolylium character of the dithiole ring of **2** and **3**, and the ring-current effect induced by the aromatic sextet formed in both rings may result in a shift to lower field. However, the possibility cannot be excluded that this low-field shift is the result of charge-transfer interactions of **2a** and **3b** with the solvent molecules, in which **2a** and **3b** serve as electron donors and acetonitrile or acetone as electron acceptors. UV data for dithiolylium salts, **29** and **30**, and azadithiafulvalenes, **2a** and **3b**, are listed in Table 2. The resemblance of the spectral features of **29** and **2a** probably reflects the similarity between the electronic structures of both compounds. On the other hand, conversion of **30** to **3b** resulted in a considerable change in spectral features. Changing the solvent from carbon tetrachloride to acetonitrile causes a slight bathochromic shift of the longest absorptions of **2a** and **3b**, probably because these strong absorptions are π-π^* transitions and, therefore, the more polar excited states are more stabilized in the polar solvent than are the ground states.

TABLE 2. UV DATA

Compound	Solvent	λ_{max} (nm) (log ε)
29	CH_3CN	440 (4.46), 424 (4.50), 247 (4.27)
2a	CCl_4	441 (4.19), 421 (4.19), 400sh (3.93), 320sh (2.74)
	CH_3CN	443 (4.47), 423 (4.40), 404sh (4.13), 312 (2.57)
30	CH_3CN	418(4.29), 350(3.85), 246(4.26)
3b	CCl_4	393 (*ca.* 3.7), 380 (*ca.* 3.6)[a]
	CH_3CN	396 (*ca.* 4.0)[a]

a) Accurate log ε values could not be obtained because of the instability of the sample in solutions.

Experimental

2-Isopentoyloxy-1,3-benzodithiole (**6**),[12] 2-(1,3-benzodithiol-2-yl)-, 2,5-bis(1,3-benzodithiol-2-yl)-, and 2,5-dimethyl-3-(1,3-benzodithol-2-yl)pyrroles (**7**, **8**, and **9**),[5] trityl tetrafluoroborate (**10**),[13] 1,3-benzodithiolylium tetrafluoroborate (**14**),[6] 2-methylthio-1,3-benzodithiolylium perchlorate (**24**),[8] and 2-methylthio-1,3-dithiolylium iodide (**28**)[9] were prepared by methods in the literature. Acetonitrile was refluxed and distilled from calcium hydride, and stored over molecular sieves. Ether was distilled and dried over molecular sieves.

Reaction of 7 with 10. To a stirred and ice-cooled solution of **7** (1.10 g; 5 mmol) in dry acetonitrile (15 ml) was added dropwise a solution of **10** (1.65 g; 5 mmol) in dry acetonitrile (10 ml) over a period of 20 min. Stirring was continued for 0.5 h while the mixture was brought to room temperature. The resulting precipitate was collected by filtration, washed with acetonitrile (10 ml), and dried to give 0.61 g (44%) of 2,5-ditritylpyrrole (**13**). The combined filtrate and washings were evaporated and the residue was subjected to silica gel column chromatography. Elution with carbon tetrachloride gave additional **13** (0.14 g; 10%). **13**; mp 229–230 °C (from benzene), colorless granules, IR (Nujol) 3400 cm^{-1} (NH), NMR ($CDCl_3$) δ 5.87 (2H, d, J=*ca.* 2.6 Hz)

and 7.0—7.3 (30 H, m). Found: C, 91.42; H, 5.97; N, 2.31%. Calcd for $C_{42}H_{33}N$: C, 91.43; H, 6.03; N, 2.54%.

To a stirred and ice-cooled solution of **7** (1.10 g; 5 mmol) in acetonitrile (15 ml) was added dropwise an acetonitrile solution (10 ml) of **10** (3.30 g; 10 mmol) over a period of 25 min. The ice bath was removed and the mixture was stirred for 1 h. The precipitate was filtered, washed with acetonitrile, and dried to give 1.32 g (48%) of **13**. Triethylamine (2 ml) was added to the dark reddish-brown filtrate and the mixture was evaporated. The residue was subjected to chromatography on silica gel. Elution with carbon tetrachloride gave triphenylmethane (0.32 g), dibenzotetrathiafulvalene (**16**) (0.02 g; 2%), mp and mixed mp with an authentic specimen[6] 236—237 °C, **13** (0.39 g; 14%), and trityl alcohol (0.43 g).

*2,5-Ditritylpyrrole (**13**) from **10** and Pyrrole.* To a stirred and ice-cooled solution of pyrrole (0.34 g; 5 mmol) in 15 ml of acetonitrile was added dropwise a solution of **10** (3.30 g; 10 mmol) in 20 ml of acetonitrile over a period of 0.5 h. A white solid began to precipitate during the addition. The mixture was stirred for 1.5 h at room temperature and then 2 ml of triethylamine was added. The precipitate was collected, washed with acetonitrile, and dried, yielding 1.95 g (71%) of **13**, mp 229—230 °C, undepressed on admixture with the products from **7** and **10**.

*2-[5-(1,3-Benzodithiol-2-yl)-2-pyrrolyl]-1,3-benzodithiolylium Tetrafluoroborate (**17**).* A solution of **10** (3.9 g; 12 mmol) in 25 ml of acetonitrile was added dropwise to a stirred and ice-cooled suspension of **8** (3.72 g; 10 mmol) in acetonitrile (80 ml) over a period of 20 min. The mixture was warmed to room temperature for 20 min and stirred for an additional 45 min. Ether (150 ml) was added to the mixture to precipitate the product. The precipitate was collected and washed with ether to give 2.32 g (51%) of **17** as yellowish-brown crystals. This was purified by dissolution in acetonitrile and reprecipitation with ether (attempted recrystallization from several solvents produced tarry materials). **17**; mp 179—180 °C (dec.), IR (Nujol) 3405 (NH) and 1000—1100 cm^{-1} (BF_4^-). Found: C, 46.50; H, 2.63; N, 2.87%. Calcd for $C_{18}H_{12}NS_4BF_4$: C, 47.27; H, 2.64; N, 3.06%.

*6-(1,3-Benzodithiol-2-yl)-2,3-benzo-5-aza-1,4-dithiafulvalene (**18**).* Triethylamine (1.5 ml) was added with stirring to an ice-cooled solution of **17** (1.08 g; 2.4 mmol) in acetonitrile (30 ml). Immediately, a yellow precipitate of **18** was separated out, which was then collected and washed with acetonitrile to give 0.85 g (98%) of **18**, which melted at 147—151 °C (decomp.). The crude material gave satisfactory results upon elemental analysis. Found: C, 58.50; H, 3.06; N, 3.79; S, 34.39%. Calcd for $C_{18}H_{11}NS_4$: C, 58.54; H, 3.00; N, 3.79; S, 34.66%.

***17** from **18** by Treatment with Tetrafluoroboric Acid.* **18** (185 mg; 0.5 mmol) was added with stirring to 4 ml of ice-cooled tetrafluoroboric acid. The mixture was stirred for 0.5 h at 0 °C. The yellowish-brown precipitate of **17** was filtered, washed with ether, and dried. It weighed 222 mg (97%).

*Reaction of **9** and **10**.* To a stirred and ice-cooled solution of **9** (1.24 g; 5 mmol) in 15 ml of acetonitrile was added dropwise a solution of **10** (1.65 g; 5 mmol) in 15 ml of acetonitrile over a period of 25 min. Stirring was continued for 2.5 h while the mixture was brought to room temperature. The precipitate was collected by filtration to give 0.5 g of a brown solid. The filtrate was diluted with 200 ml of ether and filtration of the resulting precipitate gave an additional 0.7 g of the brown solid; the IR spectrum of the solid had characteristic absorptions due to NH and BF_4^- groupings (3200 and 1000—1100 cm^{-1}), but did not result in a pure material upon repeated recrystallization. The filtrate was evaporated. The residue along with the brown solid from the reaction mixture were subjected to chromatography on silica gel. Elution with carbon tetrachloride gave 0.68 g of triphenylmethane, 0.50 g (17%) of 2,5-dimethyl-3-(1,3-benzodithiol-2-yl)-4-tritylpyrrole (**19**), and small amounts of a few unidentified products. **19**; mp 258—261 °C (dec.) (from benzene), colorless granules, IR (Nujol) 3360 cm^{-1} (NH). Found: C, 78.52; H, 5.55; N, 2.72%. Calcd for $C_{32}H_{27}NS_2$: C, 78.51; H, 5.56; N, 2.86%.

*Reaction of **9** with **14**.* 1.44 g (6 mmol) of **14** dissolved in 15 ml of acetonitrile was added dropwise to a stirred and ice-cooled suspension of 1.23 g (5 mmol) of **9** in 15 ml of acetonitrile over a period of 15 min. Stirring was continued for 2 h while the mixture was brought to room temperature. Filtration of the resulting precipitate and washing with acetonitrile gave 0.71 g (36%) of **21**. Ether (250 ml) was added to the brown filtrate and the precipitate was filtered to give 0.68 g of orange crystals which melted at 186—192 °C (dec). NMR analysis showed that the precipitate consisted of **20a** and **22** in a ratio of *ca.* 4:3 (in 20 and 15% yield, respectively). 2,5-Dimethyl-3,4-bis(1,3-benzodithiol-2-yl)pyrrole (**21**); mp 242—245 °C (dec) (from benzene), faint pale yellow granules, IR (Nujol) 3350 cm^{-1} (NH). Found: C, 60.45; H, 4.34; N, 3.15%. Calcd for $C_{20}H_{17}NS_4$: C, 60.11; H, 4.29; N, 3.51%.

***21** from **6** and 2,5-Dimethylpyrrole.* 2,5-Dimethylpyrrole (0.48 g; 5 mmol) and **6** (2.40 g; 10 mmol) were dissolved in 10 ml of acetic acid. The mixture was allowed to stand at room temperature overnight. The resulting crystalline precipitate was filtered and washed with methanol. The near-white solid weighed 1.86 g (93%), mp 242—245 °C (dec), undepressed upon admixture with a specimen from **9** and **14**.

*2-[2,5-Dimethyl-4-(1,3-benzodithiol-2-yl)-3-pyrrolyl]-1,3-benzodithiolylium Tetrafluoroborate (**22**).* To a suspension of **21** (1.67 g; 4.2 mmol) in acetonitrile (25 ml) was added dropwise a solution of **14** (1.44 g; 6 mmol) in 15 ml of acetonitrile over a period 20 min. The mixture was stirred overnight and the resulting precipitate was filtered and washed with ether to give 1.06 g (52%) of **22**. Dilution of the filtrate with ether (150 ml) gave additional **22** (0.48 g; 24%). **22**: mp 223—226 °C (dec) (from acetonitrile), orange needles, IR (Nujol) 3250 (NH) and 1000—1100 cm^{-1} (BF_4^-). Found: C, 49.52; H, 3.35; N, 2.80; S, 26.79%. Calcd for $C_{20}H_{16}NS_4BF_4$: C, 49.48; H, 3.32; N, 2.89; S, 26.42%.

*5,7-Dimethyl-8-(1,3-benzodithiol-2-yl)-2,3-benzo-6-aza-1,4-dithiafulvalene (**23**).* 1,8-Diazabicyclo[5.4.0]undec-7-ene (DBU) (0.5 ml) was added with stirring to an ice-cooled suspension of formation of **22** (0.20 g; 0.41 mmol) in 10 ml of acetonitrile. Immediately, a bright orange precipitate of **23** appeared with the disappearance of **22**. Filtration of the precipitate and washing with acetonitrile (5 ml) gave 0.15 g (92%) of **23**, mp 204—209 °C (dec), which gave satisfactory results upon elemental analysis without further purification. Found: C, 60.55; H, 3.99; N, 3.51%. Calcd for $C_{20}H_{15}NS_4$: C, 60.45; H, 3.81; N, 3.53%.

*2-(2-Pyrrolyl)-1,3-benzodithiolylium Perchlorate (**15b**).* Salt **24** (0.60 g; 2 mmol) was added in small portions to a stirred solution of pyrrole (134 mg; 2 mmol) in acetonitrile (20 ml). The mixture was stirred for 3 days. The precipitate was filtered, washed with ether, and dried to give 0.53 g (84%) of **15b**, mp>230 °C (dec) (from acetonitrile-ether), yellowish-brown needles. Found: C, 41.61; H, 2.54; N, 4.47; S, 20.28%. Calcd for $C_{11}H_8NS_2ClO_4$: C, 41.57;

H, 2.54; N, 4.41; S, 20.18%.

*2-(2,5-Dimethyl-3-pyrrolyl)-1,3-benzodithiolylium Perchlorate (**20b**).* A mixture of **24** (0.60 g; 2 mmol) and 2,5-dimethylpyrrole (0.19 g; 2 mmol) was stirred overnight at room temperature. The precipitate was filtered, washed with ether, and dried to give 0.35 g (51%) of **20b**. Dilution of the filtrate and collection of the resulting precipitate gave another crop of **20b** (0.12 g; 16%). **20b**; mp 225—227 °C (from acetonitrile), yellow needles, IR (Nujol) 3200 cm^{-1} (NH). Found: C, 45.14; H, 3.50; N, 4.07; S, 18.77%. Calcd for $C_{13}H_{12}NS_2ClO_4$: C, 45.15; H, 3.50; N, 4.05; S, 18.54%.

*2-(2-Pyrrolyl)-1,3-dithiolylium Iodide (**29**).* A mixture of pyrrole (0.27 g; 4 mmol) and **28** (1.10 g; 4 mmol) in acetonitrile (40 ml) was stirred for 2 days at room temperature. The precipitate was collected, washed with ether, and dried to give 1.08 g (92%) of **29**, mp 190—191 °C (dec) (from acetonitrile) yellowish-brown scales, IR (KBr), 3050, 1550, 1425, 1400, 1140, 1050, and 862 cm^{-1}. Found: C, 28.54; H, 2.05; N, 4.35; S, 21.71%. Calcd for $C_7H_6INS_2$: C, 28.48; H, 2.05; N, 4.75; S, 21.73%.

*2-(2,5-Dimethyl-3-pyrrolyl)-1,3-dithiolylium Iodide (**30**).* 2,5-Dimethylpyrrole (0.57 g; 6 mmol) and **28** (1.66 g; 6 mmol) was stirred in 40 ml of acetonitrile at room temperature for 2 days. The precipitate was filtered, washed with acetonitrile, and dried to give 1.60 g (83%) of **30**, mp 214—219 °C (dec) (from acetonitrile), yellowish-brown needles, IR (KBr) 3050, 2980, 1605, 1430, 1350, 1260, 1020, 920, 780, 725, and 710 cm^{-1}. Found: C, 33.46; H, 3.09; N, 4.48; S, 19.80%. Calcd for $C_9H_{10}INS_2$: C, 33.44; H, 3.12; N, 4.33; S, 19.84%.

*2,3-Benzo-5-aza-1,4-dithiafulvalene (**25**) and Its Charge-transfer Salt, **26**, with DDQ.* DBU (0.2 ml) was added to a stirred and ice-cooled suspensin of **15b** (0.20 g; 0.6 mmol) in acetonitrile (10 ml). Immediately, the formation of a yellow precipitate of **25** occurred with the disappearance of **15b**. After 5 min, the precipitate was filtered quickly, washed with acetonitrile, and dried to give 40 mg (31%) of **25**, mp>130 °C (dec) Found: C, 60.81; H, 3.25; N, 6.15; S, 29.54%. Calcd for $C_{11}H_7NS_2$: C, 60.83; H, 3.25; N, 6.45, S, 29.47%. DDQ (*ca.* 0.2 g) was added to the combined filtrate and washings. The resulting dark violet precipitate was filtered, washed with methanol, and dried to give 163 mg (37%) of **26**, which melted at 225—226 °C (dec). IR (Nujol) 2200 (CN), 1570, and 1550 cm^{-1}. Found: C, 50.80; H, 1.87; N, 9.11%. Calcd for $C_{19}H_7O_2Cl_2N_3S_2$: C, 51.35; H, 1.59; N, 9.46%.

*5,7-Dimethyl-2,3-benzo-6-aza-1,4-dithiafulvalene (**27**).* DBU (0.2 ml) was added to a stirred and ice-cooled suspension of **20b** (173 mg; 0.5 mmol) in 6 ml of acetonitrile. The precipitate was filtered after 5 min, washed with acetonitrile, and dried to give 83 mg (68%) of **27** as orange crystals, which melted at 182—185 °C (dec). Found: C, 63.50; H, 4.54; N, 5.70; S, 25.64%. Calcd for $C_{13}H_{11}NS_2$: C, 63.67; H, 4.52; N, 5.71; S, 26.10%.

*5-Aza-1,4-dithiafulvalene (**2a**).* DBU (0.5 ml) was added with stirring to an ice-cooled suspension of **29** (0.40 g; 1.36 mmol) in 7 ml of acetonitrile. Immediately, the mixture turned dark red with the disappearance of **29**. After 10 min, the mixture was diluted with 100 ml of ether, washed with saturated an aqueous sodium chloride solution (50 ml × 5), and dried. Evaporation of the ether left a red oily residue, to which hexane (10 ml) was added. It was allowed to stand in a refrigerator for 2 days. The oil crystallized, and was filtered and washed with hexane to give 0.18 g (82%) of **2a** as orange needles, which melted at 85—87 °C. IR (KBr) 1538, 1500, 1355, 1012, 842, and 740 cm^{-1}. Found: C, 50.21; H, 3.05; N, 8.26; S, 38.15%. Calcd for $C_7H_5NS_2$: C, 50.31; H, 3.02; N, 8.38; S, 38.30%.

*5,7-Dimethyl-6-aza-1,4-dithiafulvalene (**3b**).* To a stirred and ice-cooled suspension of **30** (323 mg; 1 mmol) was added DBU (0.2 ml). Immediately, the mixture turned red with the disappearance of **30** and the separation of an orange precipitate. After 10 min, the precipitate was filtered, washed with acetonitrile, and dried to give 117 mg (70%) of **3b** as orange crystals, which melted at 105—109 °C (dec). IR (KBr) 2920, 1535, 1475, 1315, 1270, 1000, 980, and 700 cm^{-1}. Found: C, 55.17; H, 4.64; N, 6.88; S, 32.71%. Calcd for $C_9H_9NS_2$: C, 55.38; H, 4.65; N, 7.18; S, 32.79%. The addition of tetracyanoquinodimethane (TCNQ) (*ca.* 0.1 g) to the filtrate gave a small amount of a greenish-black precipitate, which was assumed to be a charge-transfer salt of **3b** and TCNQ.

References

1) M. Narita and C. U. Pittman, Jr., *Synthesis*, **1976**, 489.
2) R. Gompper and R. Weiss, *Angew. Chem., Int. Ed. Engl.*, **7**, 296 (1968); R. Weiss and Gompper, *Tetrahedron Lett.*, **1970**, 481.
3) R. Gompper and E. Kutter, *Chem. Ber.*, **98**, 2825 (1965).
4) M. Neuenschwander and W. K. Schenk, *Chimia*, **26**, 194 (1972).
5) J. Nakayama, M. Imura, and M. Hoshino, *Chem. Lett.*, **1975**, 1319.
6) J. Nakayama, K. Fujiwara, and M. Hoshino, *Chem. Lett.*, **1975**, 1099 and *Bull. Chem. Soc. Jpn.*, **49**, 3567 (1976).
7) J. Nakayama, K. Yamashita, M. Hoshino, and T. Takemasa, *Chem. Lett.*, **1977**, 789.
8) R. Gompper and E. Kutter, *Chem. Ber.*, **98**, 1365 (1965).
9) E. Klingsberg, *J. Am. Chem. Soc.*, **86**, 5290 (1964).
10) N. F. Chamberlain, "The Practice of NMR Spectroscopy," Plenum Press, New York and London (1974), p. 311.
11) K. Sakamoto, N. Nakamura, M. Ōki, J. Nakayama, and M. Hoshino, *Chem. Lett.*, **1977**, 1133.
12) J. Nakayama, *Synthesis*, **1975**, 38.
13) H. J. Dauben, Jr., L. R. Honnen, and K. M. Harmon, *J. Org. Chem.*, **25**, 1442 (1960).

Structure-taste Relationship of Novel α-L-Aspartyl Dipeptide Sweetners*

Muneji Miyoshi, Ken-ichi Nunami, Hiroshi Sugano, and Toshiyuki Fujii

Research Laboratory of Applied Biochemistry, Tanabe Seiyaku Co. Ltd., Kashima-3-chome, Yodogawa-ku, Osaka 532

(Received August 18, 1977)

A sweetness potency was found in novel α-L-aspartyl dipeptide analogs which were quite stable on heating in an aqueous solution. The insertion of a methylene group into the peptide chain of α-L-aspartyl dipeptide esters mostly decreased the potency of the sweetness. However, the further exchange of the carbonyl and oxygen functions with each other on the ester group of a *C*-terminal β-alkyl-β-aminopropionic acid was found to increase the sweetness. Thus, *N*-(α-L-aspartyl)-*O*-pivaroyl-D-alaninol, *N*-(α-L-aspartyl)-*O*-cyclobutylcarbonyl-D-alaninol and *N*-(α-L-aspartyl)-*O*-cyclopropylcarbonyl-D-alaninol were all more than 200 times as sucrose.

Since the discovery[1] of the potent sweet taste of the α-L-aspartyl-L-phenylalanine methyl ester (APM), the special interest in dipeptide sweetners has increased and a large number of analogs related to APM have been synthesized. In the light of the data on the structure-taste relationship so far accumulated,[2-6] L-aspartic acid with unsubstituted α-amino and β-carboxyl groups is rather essential for sweetness. However, a considerable modification of a *C*-terminal amino acid may increase the sweetness when both the steric and hydrophobic properties fall into the requirements of a receptor site. In fact, Fujino[7] replaced the phenylalanine moiety with aminomalonates and found that α-L-aspartylaminomalonic acid with methyl fenchyl diester groups has, surprisingly, a potency 22000—33000 times as sweet as sucrose.

Some of the α-L-aspartyl-D-alanyl and α-L-aspartyl-D-seryl dipeptides which have relatively larger ester groups on the *C*-terminal D-amino acid have also been found to show considerable sweetness. It has been elucidated that both of the substituents on the α-carbon of a *C*-terminal amino acid should be strictly restricted as to sterical requirements; one is "a smaller part", while the other is "a larger part" with a hydrophobic group. When both of the parts involve a carboxyl group such as the aminomalonates, the potency of the sweetness of the dipeptide is greater than any other analogs so far reported. We are interested in such a role of the carboxyl group as the third hydrophobic group.

On the other hand, the dipeptide ester has a serious disadvantage in its practical use as a low-calory sweetner. On heating the aqueous solution of a dipeptide ester, the presence of the ester group readily causes the formation of a piperazinedione, which in turn leads to a loss of sweetness. In order to exclude the cyclization of the dipeptide esters to piperazinedione, it would be of interest to synthesize a series of dipeptide analogs whose backbones are elongated by one more methylene group.

For inserting a methylene group, two potential positions are conceivable with respect to the α-L-aspartyl dipeptide ester, *i.e.*, two types of dipeptide esters with the following structures, (**Ia** and **Ib**), respectively:

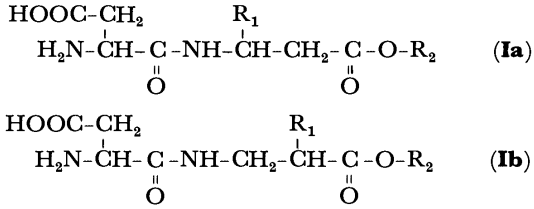

(**Ia**)

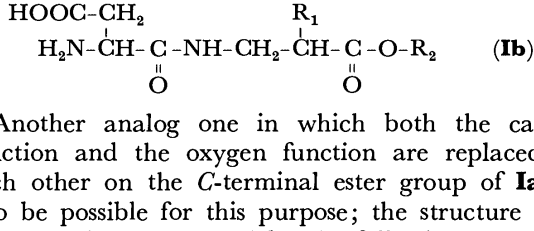

(**Ib**)

Another analog one in which both the carbonyl function and the oxygen function are replaced with each other on the *C*-terminal ester group of **Ia** may also be possible for this purpose; the structure of this type may be represented by the following general formula (**II**):

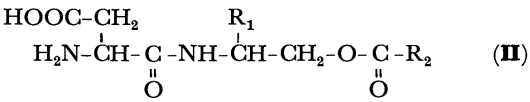

(**II**)

In the present paper, we wish to report on the structure–taste relationship of α-L-aspartyl dipeptide analogs of the above three types; all of them have both an elongated peptide chain and a carboxyl group in the molecule.

Results and Discussion

Synthesis of α-L-Aspartyl Dipeptide Analogs. The types of **Ia** and **Ib** correspond to the dipeptide esters in which a *C*-terminal amino acid is replaced by either β-alkyl-β-amino-propionic acid or α-alkyl-β-aminopropionic acid respectively. Several β-alkyl-β-aminopropionic acids were synthesized from the corresponding diazoketones according to the method reported by Shiba.[8] α-Alkyl-β-aminopropionic acids were obtained by the condensation of *N*-(chloromethyl)phthalimide with the diethyl alkylmalonates according to the method reported by Buco[9] and Böhme.[10] Some α-aminomethylmalonic acid esters were synthesized *via* a new method[11] recently developed in our laboratory; the condensation of alkylmalonate with *N*-(benzyloxycarbonyl)-acetoxymethylamine, which had been prepared from benzyloxycarbonylglycine by an electrochemical oxidation. The synthesis of the desired dipeptide esters of **Ia** and **Ib** was carried out by the DCC coupling of O^4-benzyl *N*-benzyloxycarbonyl-α-L-aspartate with β-alkyl-β-aminopropionic acid or α-alkyl-β-aminopropionic acid respectively as an amino component, followed by catalytic hydrogenolysis. 2-Amino-D-alkanols were derived from the corresponding *N*-benzyloxycarbonyl

* A part of this work was presented at the 34th National Meeting of the Chemical Society of Japan, Hiratsuka, April 4, 1976.

D-amino acid esters by $NaBH_4$ reduction,[12] followed by catalytic hydrogenolysis After coupling with O^1-*p*-nitrophenyl O^4-benzyl *N*-benzyloxycarbonyl-α-L-aspartate, *O*-acylation was carried out with various acyl halides in pyridine to give protected *O*-acyl-2-(α-L-aspartylamino)-alkanols. Subsequent hydrogenolysis afforded the desired dipeptide esters of the **II** type, as is shown in Scheme 1.

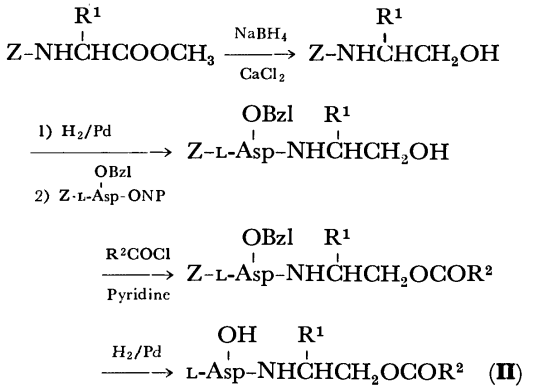

Scheme 1.

Stability in an Aqueous Solution. All of the α-L-aspartyl dipeptide analogs synthesized in the present study were found to be quite stable on heating in an aqueous solution. Table 1 presents the results of the stability test between APM and *N*-(α-L-aspartyl)-*O*-cyclobutylcarbonyl-D-alaninol (**46**), which is 220 times as sucrose. Aqueous solutions and the buffer solutions (pH 4 and pH 7), each containing 0.2% of one of the above compounds, were heated in a sealed tube at 100 °C for 1 h. The unchanged amounts of the compounds in each solution were determined by means of an amino-acid analyzer. All of the taste panelers felt that the solution of **46** was substantially unchanged in taste after heating as compared with the corresponding unheated solutions.

Table 1. Unchanged amounts after heating each solution at 100 °C for 1 h

Solution	APM (%)	**46** (%)
Water	94.5	96.6
pH 4 soln.	91.1	97.0
pH 7 soln.	9.2	85.8

Structure-taste Relationship. It has widely been accepted that in the structure of α-L-aspartyl dipeptide esters a side chain (R_1) of a *C*-terminal amino acid must be a larger hydrophobic group when the configuration is L-form, while the D-form is required when R_1 is a smaller one. In a series of APM, the ester group corresponds to the "smaller part" and the sweetness decreases as an alkyl chain (R_2) of the ester group becomes larger. In a series of α-L-aspartyl-D-alanine esters, the ester group comes to serve as the "larger part", thus, there would be room to elongate the ester group by the insertion of a methylene group within the allowable steric requirements mentioned above.

However, the elongation of a peptide chain would cause its bond angle to be more or less distorted and make it difficult to maintain the same conformation, even when both the configuration and the bulkiness of R_1 and R_2 are equal to those of the parent α-L-aspartyl dipeptide esters. As a typical example of how to estimate briefly such a steric effect of distortion, Table 2 shows a comparison of the sweetness among the analogs of L-Asp–D-Ala–OPr, all of which have, as a whole, the same chain length. Compound **Ib** scarcely showed any sweetness, probably because the insertion of a methylene into this position would effect a conformational change at both the side chain and the ester group of the *C*-terminal amino acid. On the contrary, in the cases of **Ia** and **II**, such a distortion can occur only at the position of the ester group; thus, a less conformational change would result in the exhibition of a considerable sweetness. It is of interest that **II** shows a greater sweetness than **Ia**. A CPK model of L-Asp–D-Ala–OPr is found to resemble the former rather than the latter because of the exchange of the carbonyl function and the oxygen atom.

Table 2. Analogs of L-Asp-D-Ala-OPr

Type	L-Asp-X	Sweetness
D-Ala-OPr	-NH-CH(CH₃)-C(=O)-O-CH₂-CH₂-CH₃	170[3]
Ia (**1**)	-NH-CH(CH₃)-CH₂-C(=O)-O-CH₂-CH₃	20
Ib (**18**)	-NH-CH₂-CH(CH₃)-C(=O)-O-CH(CH₃)₂	2
II (**34**)	-NH-CH(CH₃)-CH₂-O-C(=O)-CH₂-CH₂-CH₃	100

None of the analogs in the types of **Ia** and **Ib** synthesized in the present study showed a potency than 20 times as sucrose. Further, α-L-aspartyl-aminomethylmalonates, which involve one more methylene group in the skeleton of α-L-aspartyl-amino-malonates reported by Fujino, had no sweetness at all. The results are summarized in Tables 3 and 4. Mazur[3] synthesized various L-aspartic acid amides and found that most of them showed less sweetness. The **Ib** type should, rather, be regarded as a kind of L-aspartic acid amide, one which has a branched primary amine with one or two carbonyl groups among its substituents. Taking the above observations into account, we mainly focused on the type of **II** and synthesized the analogs with various chain lengths at the ester group.

The potencies of the sweetness of *O*-acyl-2-(α-L-aspartylamino)alkanols (Type **II**) are listed in Table 5. The side chain (R_1) of 2-amino-D-alkanols corresponds to the "smaller part," and when R_1 is methyl, that is, D-alaninol, most of the analogs showed a considerable sweetness with a good aftertaste, like sucrose. In this case, the potency of the sweetness tends to in-

Table 3. Sweetness of L-aspartyl dipeptide(**Ia**)

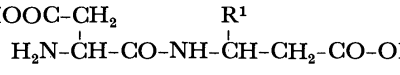

(L)

Compd No.	R^1	R^2	Configuration	Mp (°C)	Sweetness
1	CH_3	CH_2CH_3	D	150—154	20
2	CH_3	$CH(CH_3)_2$	D	152.5—154.5	9
3	CH_3	$CH(CH_3)CH_2CH_3$	D	139.5—142	5
4	CH_3	$C(CH_3)_3$	D	109 (dec.)	6
5	CH_3	*cyclo*-C_5H_9	D	144.5—147	5
6	CH_2CH_3	CH_2CH_3	DL	136.5—138	5
7	CH_2CH_3	$CH(CH_3)_2$	DL	129—132	0
8	CH_2CH_3	*cyclo*-C_5H_9	DL	119—121	0
9	CH_2Ph	CH_2CH_3	L	124—127	0

Table 4. Sweetness of L-aspartyl dipeptide(**Ib**)

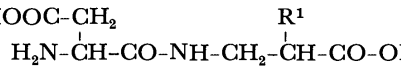

(L) (DL)

Compd No.	R^1	R^2	Mp (°C)	Sweetneess
10	H	$CH_2CH_2CH_2CH_3$	163.5—165.5	0
11	H	$CH(CH_3)CH_2CH_3$	160.5—162.5	7
12	H	$C(CH_3)_3$	175.5—177.5	3
13	H	$CH(CH_2CH_3)_2$	150—152.5	5
14	H	$CH(CH_3)CH_2CH_2CH_3$	150—152.5	6
15	H	*cyclo*-C_5H_9	152.5—154	18
16	H	*cyclo*-C_6H_{11}	156.5—158	20
17	H	*cyclo*-$C_6H_{10}CH_3$[2-]	132—135	0
18	CH_3	$CH(CH_3)_2$	154—160	2
19	CH_3	$C(CH_3)_3$	136—138	4
20	CH_3	*cyclo*-C_5H_9	148—149	9
21	CH_3	*cyclo*-C_6H_{11}	150—152	10
22	CH_2Ph	CH_3	170—175	0
23	CO_2CH_3	CH_3	62— 66	0
24	CO_2CH_3	*cyclo*-C_5H_9	80— 84	0
25	CO_2CH_3	*cyclo*-C_6H_{11}	79— 84	0

crease as an alkyl group (R_2) of the *O*-acyl residue—"a larger part"—becomes bulky with a branched short chain: *iso*-propyl and *t*-butyl isomers (**38**, **44**) are sweeter than those with less branched chains (**37**, **41**, **42**, **43**). Cycloalkyl isomers are also sweet. Thus, among the series of D-alaninol synthesized, *O*-pivaroyl (**44**) and *O*-cyclobutylcarbonyl (**46**) analogs become 240 and 220 times as sweet as sucrose respectively. When R_2 is a linear alkyl group, the potency of the sweetness decreases as the carbon number of an alkyl chain becomes greater, showing that the chain length of the dipeptide molecule must be strictly restricted; the order of sweetness is ethyl (**34**)> methyl (**33**)>butyl (**41**). A similar result was observed in the cycloalkyl groups: cyclobutyl (**46**)> cyclopropyl (**40**)>cyclopentyl (**49**), and the analogs with 3,3-dimethylcyclobutyl (**50**), cyclohexyl (**51**), or phenyl (**52**) were not sweet any more.

In a series of D-serinol, in which R_1 is the hydroxymethyl group, R_2 must be rather small to exhibit a considerable sweetness: the potency becomes 135 times as sucrose when R_2 is ethyl (**54**) or cyclopropyl (**55**), while it decreases as R_2 becomes bulky (**60** and **61**). Ariyoshi[5] reported on the dipeptide esters of β-hydroxy α-(α-L-aspartylamino)acids and found that L-Asp–D-Ser–OPr was the sweetest (320 times as sucrose). It is noted that this compound has the same chain length on the *C*-terminal amino acid as our *N*-(α-L-aspartyl)-*O*-propionyl-D-serinol (**54**).

In the cases of 2-amino-1-butanol (R_1; ethyl, **62**-**68**), *O*-methylserinol (R_1; methoxymethyl, **69**, **70**), and valinol (R_1; *iso*-propyl, **71**—**77**). the potency of the sweetness tends to decrease as compared with those of D-alaninol and D-serinol, though a tendency similar to that described above was observed concerning the requirement of the size of R_2. It was found that leucinol (**80**), isoleucinol (**81**), and phenylalaninol (**82**), which have such bulky groups on the side chain, showed no sweetness, not even when R_2 was the methyl group.

On the contrary, 2-aminoethanol (R_1; H), which has no side chain and which is the smallest analog

Table 5. Sweetness of L-aspartyl dipeptide(**II**)

$$HOOC\text{-}CH_2 \qquad R^1$$
$$H_2N\text{-}\overset{|}{C}H\text{-}CO\text{-}NH\text{-}\overset{|}{C}H\text{-}CH_2\text{-}O\text{-}CO\text{-}R^2$$
(L)

Compd No.	R^1	R^2	Configuration	Mp (°C dec)	Sweetness
26	H	CH_3	—	163—165	3
27	H	CH_2CH_3	—	171—172	6
28	H	$CH_2CH_2CH_3$	—	172—174	5
29	H	$CH(CH_3)_2$	—	175—177	20
30	H	*cyclo*-C_3H_5	—	155—159	15
31	H	*cyclo*-C_4H_7	—	166.5—170	13
32	H	$C(CH_3)_3$	—	140—143	30
33	CH_3	CH_3	D	146—149	60
34	CH_3	CH_2CH_3	D	155—156	100
35	CH_3	$CH=CH_2$	D	226	100
36	CH_3	$CH_2CH_2CH_3$	DL	164—166	25
37	CH_3	$CH_2CH_2CH_3$	D	151—152	50
38	CH_3	$CH(CH_3)_2$	D	154—155	120
39	CH_3	$C(CH_3)=CH_2$	D	230	130
40	CH_3	*cyclo*-C_3H_5	D	146.5—149	200
41	CH_3	$CH_2CH_2CH_2CH_3$	D	157—159	5
42	CH_3	$CH(CH_3)CH_2CH_3$	D	126	150
43	CH_3	$CH_2CH(CH_3)_2$	D	163—166.5	50
44	CH_3	$C(CH_3)_3$	D	145—147	240
45	CH_3	*cyclo*-$C_3H_4CH_3$[2-]	D	151—153	60
46	CH_3	*cyclo*-C_4H_7	D	168.5—170	220
47	CH_3	$CH(CH_2CH_3)_2$	D	126.5—127.5	40
48	CH_3	*cyclo*-$C_4H_6CH_3$[2-]	D	134—135	160
49	CH_3	*cyclo*-C_5H_9	D	162—165	60
50	CH_3	*cyclo*-$C_4H_6(CH_3)_2$[3,3-]	D	148—150.5	0
51	CH_3	*cyclo*-C_6H_{11}	D	186—188	0
52	CH_3	C_6H_5	D	179—182	0
53	CH_2OH	CH_3	D	206.5—207	25
54	CH_2OH	CH_2CH_3	D	203—204	135
55	CH_2OH	*cyclo*-C_3H_5	D	172.5—175	120
56	CH_2OH	$CH(CH_3)_2$	D	209—211	40
57	CH_2OH	$CH_2CH_2CH_3$	D	197—199	5
58	CH_2OH	*cyclo*-C_4H_7	D	185—190	65
59	CH_2OH	$C(CH_3)_3$	D	203—204	25
60	CH_2OH	$CH(CH_3)CH_2CH_3$	D	195—196	20
61	CH_2OH	*cyclo*-C_5H_9	D	191.5—192.5	10
62	CH_2CH_3	CH_3	DL	112—117	10
63	CH_2CH_3	CH_2CH_3	DL	128—130	20
64	CH_2CH_3	$CH(CH_3)_2$	DL	134—138	15
65	CH_2CH_3	*cyclo*-C_3H_5	DL	90—92	15
66	CH_2CH_3	*cyclo*-C_4H_7	DL	94.5—101	15
67	CH_2CH_3	$CH_2CH_2CH_2CH_3$	DL	131—135	0
68	CH_2CH_3	*cyclo*-C_5H_{11}	DL	135—138	0
69	CH_2OCH_3	CH_3	DL	50	2
70	CH_2OCH_3	CH_2CH_3	DL	77—79	10
71	$CH(CH_3)_2$	CH_3	DL	130—137	25
72	$CH(CH_3)_2$	CH_3	D	174—175	50
73	$CH(CH_3)_2$	CH_2CH_3	D	138—141	50
74	$CH(CH_3)_2$	$CH(CH_3)_2$	D	148—151	15
75	$CH(CH_3)_2$	*cyclo*-C_3H_5	D	129—133	20
76	$CH(CH_3)_2$	*cyclo*-C_4H_7	D	94.5—97	13
77	$CH(CH_3)_2$	$CH_2CH_2CH_3$	D	136—138	3
78	$CH_2CH_2CH_3$	CH_3	DL	175—177	3
79	$CH_2CH_2CH_3$	CH_2CH_3	DL	145—147	0
80	$CH_2CH(CH_3)_2$	CH_3	DL	112—117	0
81	$CH(CH_3)CH_2CH_3$	CH_3	DL	129—133	0
82	CH_2Ph	CH_3	L	89—92	0

of this series, was found to show some sweetness (**26**—**32**). It is noted that none of the *O*-acyl-2-(α-L-aspartylamino)-L-alkanol synthesized was sweet, showing that the configuration of the *C*-terminal amino acid must be D-form to exhibit the taste.

Summarizing the above observations, we may derive the following conclusions concerning the structure-taste relationship of our L-aspartyl dipeptide sweetners: (1) the insertion of a methylene group into the peptide chain generally causes a significant disadvantage; (2) the further exchange of the carbonyl and oxygen functions on the ester group of a *C*-terminal α-alkyl-β-aminopropionic acid has rather a good effect on exhibiting sweetness; (3) in the series of *O*-acyl-2-(α-L-aspartylamino)alkanols, the structural requirements for the mutual sizes between the side chain (R_1) and the alkyl group (R_2) of the *O*-acyl residue are nearly equal to those previously proposed for the structure-taste relationship of α-L-aspartyl dipeptide esters, and (4) the configuration of the 2-aminoalkanol esters should be D-form, the same as the corresponding α-L-aspartyl-D-alanine esters.

Experimental

The melting points were determined using a Yamato melting-point apparatus and were uncorrected. The IR spectra were measured with a Shimadzu IR-27G infrared spectrometer; the H^1 NMR spectra, with a Hitachi Perkin-Elmer R-20A high-resolution NMR spectrometer, using tetramethylsilane as the internal standard, and the optical rotations, with a Perkin-Elmer 141 polarimeter. The quantitative determination on peptides was performed by the use of a Hitachi KLA-3B automatic amino-acid analyzer.

*Typical Procedure for the Preparation of β-Alkyl-β-amino-propionic Acid and α-Alkyl-β-aminopropionic Acid Derivatives (**Ia** and **Ib**).* *D-3-(Benzyloxycarbonylamino)butyric Acid*: Methyl D-3-(benzyloxycarbonylamino)butyrate was obtained as a colorless oil from *N*-benzyloxycarbonyl-D-alanine (8.92 g) by means of the previously reported method.[8] This methyl ester was saponified with methanolic sodium hydroxide in the usual manner to give the title compound as colorless needles, which were then recrystallized from ethyl acetate-petroleum ether; yield, 4.0 g (42.2%); mp 104—104.5 °C; $[\alpha]_D^{22}$ −5.5° (*c* 1, acetone); IR (Nujol) 3300, 1685, 1550 cm^{-1}; NMR ($CDCl_3$) δ 1.24 (d, 3H, *J*=6 Hz), 2.54 (d, 2H, *J*=6 Hz), 3.8—4.4 (m, 1H), 5.10 (s, 2H), 5.0—5.8 (broad, 1H), 7.32 (s, 5H), 7.2—7.5 (broad, 1H); Found: C, 60.81; H, 6.42; N, 5.81%. Calcd for $C_{12}H_{15}NO_4$: C, 60.75; H, 6.37; N, 5.90%.

DL-2-Methyl-3-(benzyloxycarbonylamino)propionic Acid: Diethyl phthalimidomethyl-methylmalonate was prepared from diethyl methylmalonate (21 g in THF 50 ml) with 65% sodium hydride (4.1 g) and *N*-(chloromethyl)phthalimide (19.5 g in THF 150 ml) by means of the previously reported method.[10] These crystals obtained were recrystallized from ethyl acetate-hexane; yield, 28.6 g (85.5%); mp 98—99 °C. The hydrolysis of the compound obtained above was followed by column chromatography (Dianion SK 1b, H^+ form). The eluate with 5% aqueous ammonia was concentrated to dryness *in vacuo* to afford DL-2-methyl-3-aminopropionic acid as colorless crystals, which were used without further purification. The benzyloxycarbonylation of this compound was carried out by Schotten-Baumann's method to afford the title compound as colorless needles, which were then recrystallized from ethyl acetate-hexane; yield, 7.0 g (73.8%); mp 65—66.5 °C; IR (Nujol) 3340, 1715, 1685 cm^{-1}; NMR ($CDCl_3$) δ 1.23 (d, 3H, *J*=7 Hz), 2.4—3.1 (m, 1H), 3.40 (t, 2H, *J*=7 Hz), 5.10 (s, 2H), 5.1—5.6 (broad, 1H), 7.33 (s, 5H), 10.70 (s, 1H); Found: C, 60.68; H, 6.45; N, 5.79%. Calcd for $C_{12}H_{15}NO_4$: C, 60.72; H, 6.37; N, 5.90%.

Ethyl D-3-[(N-Benzyloxycarbonyl-O⁴-benzyl-α-L-aspartyl)-amino]butyrate: Ethyl D-3-(benzyloxycarbonylamino)butyrate was obtained as a colorless oil by treating D-3-(benzyloxycarbonylamino)butyric acid (2.73 g) with thionyl chloride (2 ml) in ethanol (10 ml). The oil was then dissolved in a mixture of *N*,*N*-dimethylformamide (5 ml) and tetrahydrofuran (20 ml), and the solution was cooled to 0 °C. To this were added O^4-benzyl *N*-benzyloxycarbonyl-α-L-aspartate (3.57 g), 1-hydroxybenzotriazole (1.35 g), and dicyclohexylcarbodiimide (2.1 g). The reaction mixture was stirred for 1 h at 0 °C and for 5 h at room temperature, and then the insoluble materials were filtered off. The filtrate was concentrated to dryness *in vacuo*, and the residue was dissolved in ethyl acetate (50 ml). The solution was washed with aqueous saturated sodium hydrogencarbonate (10 ml), 1% hydrochloric acid (10 ml), and water (10 ml), and then dried over magnesium sulfate. The solution was concentrated to dryness *in vacuo*, and the oily residue thus obtained was purified by chromatography on silica gel (80 g, Kiesel gel 60) with benzene-ethyl acetate (9:1) to afford the title compound as colorless needles, which were subsequently recrystallized from ethyl acetate-petroleum ether; yield, 2.7 g (57.4%); mp 91—92 °C; $[\alpha]_D^{22}$ −7.0° (*c* 0.5, MeOH), IR (Nujol) 3310, 1730, 1695, 1650 cm^{-1}; NMR ($CDCl_3$) δ 1.16 (d, 3H, *J*=7 Hz), 1.22 (t, 3H, *J*=7 Hz), 2.45 (d, 2H, *J*=6 Hz), 2.5—3.27 (m, 2H), 4.11 (quartet, 2H, *J*=7 Hz), 4.1—4.8 (m, 2H), 5.12 (s, 4H), 5.92 (broad d, 1H, *J*=9 Hz), 6.89 (broad d, 1H, *J*=9 Hz), 7.33 (s, 10H); Found: C, 63.77; H, 6.53; N, 5.86%. Calcd for $C_{25}H_{30}N_2O_7$: C, 63.82; H, 6.43; N, 5.95%.

*Ethyl D-3-(α-L-Aspartylamino)butyrate (**1**)*: Ethyl D-3-[(*N*-benzyloxycarbonyl-O^4-benzyl-α-L-aspartyl)amino]butyrate (1.2 g) was dissolved in methanol (20 ml). The hydrogenolysis of this compound was then carried out over palladium black (0.1 g) for 2 h at room temperature under an atmospheric pressure of hydrogen. After the catalyst had been filtered off, the filtrate was concentrated to dryness *in vacuo* to give **1** as crystals, which were then triturated with ether and filtered; yield 0.54 g (85.6%); mp 150—154 °C; $[\alpha]_D^{22}$ −9.7° (*c* 0.5, DMF); IR (Nujol) 3300, 1730, 1660 cm^{-1}; NMR (DMSO-d_6) δ 1.15 (d, 3H, *J*=7 Hz), 1.21 (t, 3H, *J*=7 Hz), 2.2—2.7 (m, 4H), 3.6—4.4 (m, 2H), 4.10 (quartet, 2H, *J*=7 Hz), 5.49 (s, 3H), 8.2—8.7 (broad, 1H); Found: C, 48.59; H, 7.51; N, 11.20%. Calcd for $C_{10}H_{18}N_2O_5$: C, 48.77; H, 7.36; N, 11.37%.

*Typical Procedure for the Preparation of (Aminomethyl)-Malonic Acid Derivatives (**Ib**).* *N-(Benzyloxycarbonyl)acetoxymethylamine*: Benzyloxycarbonylglycine (14.6 g) was dissolved in acetic acid (80 ml), to which we then added solium acetate (2.05 g). The solution was electrolyzed at 15—20 °C using 3×4 cm^2 of the carbon anode which was placed 0.5 cm apart from the carbon cathode. An electrolysis current was maintained at 1A during the electrolysis. After 6 h, the electrolyzed solution was evaporated to dryness *in vacuo*. The oily residue was dissolved in ethyl acetate, and the solution was washed with aqueous saturated sodium hydrogencarbonate and water, and then dried over magnesium sulfate. This solution was concentrated to dryness *in vacuo* to give the title compound as a colorless oil; yield, 12.7 g (79.4%); IR (film) 3340, 1730, 1520 cm^{-1}; NMR ($CDCl_3$), δ 2.0 (s, 3H), 5.13 (s, 2H), 5.16 (d, 2H), 5.9—6.5 (broad s, 1H), 7.35 (s, 5H).

Dicyclohexylammonium Cyclopentyl Malonate: The condensation of malonic acid (20.8 g) was carried out under reflux in benzene (150 ml) containing *p*-toluenesulfonic acid monohydrate (3.8 g), using a Dean-Stark's apparatus, to give dicyclopentyl malonate as a colorless oil. This compound was subsequently saponified with 2.5 M methanolic potassium hydroxide (80 ml) at room temperature for 2 h. After acidification with 6 M hydrochloric acid, the solution was extracted with ether (300 ml). The organic layer was washed with water (30 ml) and then dried over magnesium sulfate. To the solution we added dicyclohexylamine (36.2 g) to afford the title compound as colorless needles; yield, 32.6 g (46.2%); mp 113—115 °C; IR (Nujol) 1735, 1635, 1570 cm^{-1}; NMR (DMSO-d_6), δ 0.7—2.3 (m, 28H), 2.65—3.20 (broad, 2H), 2.94 (s, 2H), 4.85—5.20 (broad, 1H), 6.8—7.4 (broad, 2H); Found: C, 67.59; H, 9.98; N, 3.96%, Calcd for $C_{20}H_{35}NO_4$: C, 67.30; H, 10.11; N, 4.03%.

Cyclopentyl Methyl Malonate: Dicyclohexylammonium cyclopentyl malonate (10.6 g) was suspended in ether (200 ml), and 1 M sulfuric acid (20 ml) was added to the mixture under stirring. The organic layer was washed with water (20 ml) and dried over magnesium sulfate. The solution was concentrated to dryness *in vacuo*, the oily residue was dissolved in ether (50 ml), and then diazomethane in ether was added to this solution. The reaction mixture was concentrated to dryness *in vacuo* to afford the title compound as a colorless oil, which was distilled at 93 °C at 3 mmHg; yield, 4.6 g (82.4%); IR (film) 1730 cm^{-1}; NMR ($CDCl_3$), δ 1.5—2.1 (m, 8H), 3.32 (s, 2H), 3.72 (s, 3H), 5.05—5.4 (broad, 1H).

Cyclopentyl Methyl (Benzyloxycarbonylaminomethyl)malonate: *N*-(Benzyloxycarbonyl)acetoxymethylamine (2.23 g) was dissolved in *N,N*-dimethylformamide (10 ml), after which the mixture was cooled to 0 °C. To this we added cyclopentyl methyl malonate (1.86 g) and 65% sodium hydride (0.4 g) in *N,N*-dimethylformamide under vigorous stirring. The reaction mixture was stirred at room temperature for 15 h and then concentrated to dryness *in vacuo*. The oily residue thus obtained was dissolved in ethyl acetate, and the solution was washed with water saturated with sodium hydrogencarbonate, 1% hydrochloric acid, and water, and then dried over magnesium sulfate. The dried solution was concentrated to dryness *in vacuo*, and the residue was purified on a silica gel column (80 g, Kiesel gel 60), using benzene–ethyl acetate (95:5) as the eluate, to give the title compound as a colorless oil; yield, 2.84 g (79.3%); IR (film) 3370, 1730, 1520 cm^{-1}; NMR ($CDCl_3$), δ 1.4—1.9 (m, 8H), 3.65 (2H), 3.72 (s, 3H), 5.1 (s, 2H), 5.1—5.7 (m, 3H), 7.36 (s, 5H).

Cyclopentyl Methyl (N-Benzyloxycarbonyl-O⁴-benzyl-α-L-aspartylamino)malonate: Cyclopentyl methyl (benzyloxycarbonylaminomethyl)malonate (1.1 g) and oxalic acid dihydrate (0.2 g) were dissolved in methanol (20 ml). To this solution we added palladium black (0.1 g), and the hydrogenolysis was carried out under an atmospheric pressure of hydrogen. After the catalyst had been filtered off, the filtrate was concentrated to dryness *in vacuo* to give cyclopentyl methyl (aminomethyl)malonate as crystalline hemioxalic acid salt.

These crystals, O^1-*p*-nitrophenyl O^4-benzyl *N*-benzylocycarbonyl-α-L-aspartate (1.43 g), and 1-hydroxybenzotriazole (0.44 g), were dissolved in *N,N*-dimethylformamide (20 ml), after which the solution was cooled to 0 °C. Into this triethylamine (0.42 ml) was stirred. The reaction mixture was stirred at the same temperature for 30 min, and then diluted with ethyl acetate (100 ml). The solution was washed with aqueous saturated sodium hydrogencarbonate, 1% hydrochloric acid, and water, and then dried over magnesium sulfate. The dried solution was concentrated to dryness *in vacuo*, and the oily residue thus obtained was purified on a silica gel column (45 g, Kiesel gel 60), using benzene–ethyl acetate (83:17) as the eluate, to afford the title compound as a colorless oil; yield, 0.44 g (26.0%); IR (film) 3340, 1730, 1670, 1530 cm^{-1}; NMR ($CDCl_3$), δ 1.5—1.9 (m, 8H), 2.45—3.2 (m, 2H), 3.65 (2H), 3.72 (s, 3H), 3.7—3.85 (m, 1H), 4.45—4.7 (m, 1H), 5.12 (s, 4H), 5.1—5.3 (m, 1H), 5.82 (d, 1H, J=9 Hz), 6.7—7.1 (m, 1H), 7.32 (s, 10H).

Cyclopentyl Methyl (α-L-Aspartylaminomethyl)malonate (24): The hydrogenolysis of cyclopentyl methyl (*N*-benzyloxycarbonyl-O^4-benzyl-α-L-aspartylamino)malonate (0.4 g) was carried out in methanol using palladium black (0.1 g) under an atmospheric pressure of hydrogen. After the catalyst had been filtered off, the filtrate was concentrated to dryness *in vacuo*. The residue was dissolved in a small amount of water and then lyophylized; yield, 0.17 g (71.0%); mp 80—84 °C (dec); IR (Nujol) 1730, 1675 cm^{-1}; NMR (DMSO-d_6) δ 1.65 (broad s, 8H), 2.2—2.6 (2H), 3.65 (d, 2H, J=8 Hz), 3.68 (s, 3H), 3.7—3.9 (broad, 2H), 5.0—5.3 (broad s, 1H), 5.9—6.5 (broad s, 3H), 8.2—9.0 (broad s, 1H); Found: C, 48.16; H, 7.09; N, 7.89%. Calcd for $C_{14}H_{22}N_2O_7 \cdot H_2O$: C, 48.27; H, 6.74; N, 8.04%.

Typical Procedure for the Preparation of 2-Amino-D-alkanol Derivatives (II). *Methyl* N-*Acetyl*-O-*benzyl*-D-*serinate*: Thionyl chloride (16 g) was vigorously stirred, drop by drop, into methanol (80 ml) at −10 °C. To this solution we then added *N*-acetyl-*O*-benzyl-D-serine (19 g) at the same temperature. The reaction mixture was stirred at room temperature for 2 h and then concentrated to dryness *in vacuo* below 30 °C. The residue was disolved in ethyl acetate (100 ml), and the solution was washed with aqueous saturated sodium hydrogencarbonate (10 ml), 1% hydrochloric acid (10 ml), and water, and then dried over magnesium sulfate. The solution was concentrated to dryness *in vacuo* to give the title compound as colorless needles, which were subsequently recrystallized from ethyl acetate–petroleum ether; yield, 19.3 g (96.1%); mp 66—67 °C; $[\alpha]_D^{25}$ −11.8° (*c* 1.02, MeOH); IR (Nujol) 3290, 1750, 1635 cm^{-1}; NMR ($CDCl_3$) δ 2.01 (s, 3H), 3.55—4.00 (m, 2H), 3.72 (s, 3H), 4.50 (s, 2H), 4.65—4.88 (m, 1H), 6.50 (broad d, 1H, J=10 Hz), 7.30 (s, 5H); Found: C, 62.30; H, 6.86; N, 5.60%. Calcd for $C_{13}H_{17}NO_4$: C, 62.14; H, 6.82; N, 5.57%.

Methyl N-*Benzyloxycarbonyl*-D-*alaninate*: Thionyl chloride (6 ml) was vigorously stirred, drop by drop, into methanol (30 ml) at −10 °C. To this solution we then added *N*-benzyloxycarbonyl-D-alanine (6.7 g) at the same temperature. The reaction mixture was treated in the manner described above to give the title compound as colorless needles, which were subsequently recrystallized from ethyl acetate–hexane; yield, 6.40 g (90.0%); mp 48—49 °C; $[\alpha]_D^{25}$ +34.7° (*c* 1, MeOH); IR (Nujol) 3350, 1750, 1680 cm^{-1}; NMR ($CDCl_3$) δ 1.41 (d, 3H, J=7 Hz), 3.73 (s, 3H), 4.39 (quartet, 1H, J=7 Hz), 5.12 (s, 2H), 5.1—5.65 (broad, 1H), 7.35 (s, 5H); Found: C, 60.39; H, 6.44; N, 6.20%. Calcd for $C_{12}H_{15}NO_4$: C, 60.75; H, 6.37; N, 5.90%.

" N-*Acetyl*-O-*benzyl*-D-*serinol*: To a suspension of sodium borohydride (3.42 g) and calcium chloride (10 g) in tetrahydrofuran (75 ml), we added methyl *N*-acetyl-*O*-benzyl-D-serinate (7.5 g) in tetrahydrofuran (75 ml) at room temperature. After the reaction mixture had then been stirred for 2 h at the same temperature, the insoluble materials were removed by filtration and the filtrate was concentrated to dryness *in vacuo*. The oily residue was dissolved in ethyl acetate (100 ml). The solution was washed with water (20 ml) and dried over magnesium sulfate. The dried solution was concentrat-

ed to dryness *in vacuo* to give the title compound as a colorless oil; yield, 6.2 g (93.0%); $[\alpha]_D^{22}$ −28.6° (*c* 0.71, MeOH); IR (film) 3300, 1650, 1550 cm^{-1}; NMR ($CDCl_3$) δ 2.00 (s, 3H), 3.19 (broad s, 1H), 3.55—4.34 (m, 5H), 4.52 (s, 2H), 6.36 (broad d, 1H, J=8 Hz), 7.33 (s, 5H).

N-*Benzyloxycarbonyl*-D-*alaninol*: To a suspension of sodium borohydride (3.4 g) and calcium chloride (10 g) in tetrahydrofuran (75 ml), we added methyl *N*-benzyloxycarbonyl-D-alaninate (7.11 g) in tetrahydrofuran (75 ml) at room temperature. The reaction mixture was then treated in the manner described above to give the title compound as colorless needles, which were subsequently recrystallized from ethyl acetate–hexane; yield, 4.7 g (75.0%); mp 81—82 °C; $[\alpha]_D^{25}$ +4.9° (*c* 0.87, MeOH); IR (Nujol) 3460, 1695, 1660 cm^{-1}; NMR ($CDCl_3$) δ 1.12 (d, 3H, J=7 Hz), 2.93 (broad s, 1H), 3.41—4.15 (m, 3H), 5.09 (s, 2H), 5.10—5.40 (broad, 1H), 7.32 (s, 5H); Found: C, 62.78; H, 7.25; N, 6.74%. Calcd for $C_{11}H_{15}NO_3$: C, 63.14; H, 7.23; N, 6.69%.

O^3-*Benzyl*-D-*serinol Hydrochloride*: A solution of *N*-acetyl-O^3-benzyl-D-serinol (6.2 g) in 4 M hydrochloric acid (15 ml) was heated at 70 °C for 100 min under vigorous stirring. The reaction mixture was concentrated to dryness *in vacuo* to give the title compound as colorless needles, which were then recrystallized from methanol–ether; yield, 5.25 g (86.8%); mp 133.5—134.5 °C; $[\alpha]_D^{25}$ +4.6° (*c* 1.01, MeOH); IR (Nujol) 3360, 1590, 1380 cm^{-1}; NMR (DMSO-d_6) δ 3.00—3.90 (m, 5H), 4.56 (s, 2H), 4.20—5.00 (broad, 1H), 7.39 (s, 5H), 8.36 (broad s, 3H); Found: C, 55.00; H, 7.41; N, 6.43; Cl, 16.41%. Calcd for $C_{10}H_{16}NO_2Cl$: C, 55.17; H, 7.41; N, 6.44; Cl, 16.29%.

N-*(*N-*Benzyloxycarbonyl*-O^4-*benzyl*-α-L-*aspartyl)*-O^3-*benzyl*-D-*serinol*: To a solution of O^3-benzyl-D-serinol hydrochloride (2.2 g), triethylamine (1.4 ml), and 1-hydroxybenzotriazole (1.4 g) in *N,N*-dimethylformamide (30 ml), we added O^1-*p*-nitrophenyl O^4-benzyl *N*-benzyloxycarbonyl-α-L-aspartate (4.8 g). The reaction mixture was stirred for 30 min at 0 °C and then diluted with ethyl acetate (100 ml). The solution was washed with 3% aqueous ammonia, 1% hydrochloric acid, and water, and then dried over magnesium sulfate. The dried solution was concentrated to dryness *in vacuo* to give the title compound as colorless needles, which were subsequently recrystallized from ethyl acetate–petroleum ether; yield, 3.25 g (62.5%); mp 102—104 °C; $[\alpha]_D^{22}$ −22.3° (*c* 0.65, MeOH); IR (Nujol) 3450, 3300, 1730, 1680, 1650 cm^{-1}; NMR ($CDCl_3$) δ 2.50—3.30 (m, 3H), 3.50—4.35 (m, 5H), 4.47 (s, 2H), 4.40—4.90 (m, 1H), 5.10 (s, 4H), 6.00 (d, 1H, J=10 Hz), 6.80—7.15 (m, 1H), 7.32 (s, 15H); Found: C, 66.87; H, 6.25; N, 5.20%. Calcd for $C_{29}H_{32}N_2O_7$: C, 66.91; H, 6.20; N, 5.38%.

N-*(*N-*Benzyloxycarbonyl*-O^4-*benzyl*-α-L-*aspartyl)*-D-*alaninol*: The hydrogenolysis of *N*-benzyloxycarbonyl-D-alaninol (1 g) in methanol over palladium black (0.1 g) was carried out for 1.5 h under an atmospheric pressure of hydrogen. After the catalyst had been filtered off, the filtrate was concentrated to dryness *in vacuo* to give D-alaninol as a colorless oil. The D-alaninol thus obtained and 1-hydroxybenzotriazole (0.7 g) were dissolved in *N,N*-dimethylformamide (15 ml) and the solution was cooled to 0 °C. To this solution we then added O^1-*p*-nitrophenyl O^4-benzyl *N*-benzyloxycarbonyl-α-L-aspartate (2.3 g). The reaction mixture was stirred for 30 min at 0 °C, and then diluted with ethyl acetate (10 ml). The solution was washed with 3% aqueous ammonia, 1% hydrochloric acid, and water, and then dried over magnesium sulfate. The dried solution was concentrated to dryness *in vacuo* to give the title compound as colorless needles, which were subsequently recrystallized from ethyl acetate-hexane; yield, 1.3 g (65.9%); mp 111—113 °C; $[\alpha]_D^{25}$ −0.7° (*c* 0.76, MeOH); IR (Nujol) 3460, 3300, 1740, 1690, 1640 cm^{-1}; NMR ($CDCl_3$) δ 1.07 (d, 3H, J=7 Hz), 2.60—3.20 (m, 3H), 3.30—4.25 (m, 3H), 4.30—4.85 (m, 1H), 5.09 (s, 4H), 6.08 (broad d, 1H, J=10 Hz), 6.47—6.85 (broad, 1H), 7.32 (s, 10H); Found: C, 63.72; H, 6.49; N, 6.93%. Calcd for $C_{22}H_{26}N_2O_6$: C, 63.75; H, 6.32; N, 6.76%.

N-*(*N-*Benzyloxycarbonyl*-O^4-*benzyl*-α-L-*aspartyl*-O^1-*isobutyryl*-O^3-*benzyl*-D-*serinol*: *N*-(*N*-Benzyloxycarbonyl-O^4-benzyl-α-L-aspartyl)-O^3-benzyl-D-serinol (1.6 g) was dissolved in pyridine (20 ml), and the solution was cooled to 0 °C. To the solution we then added, drop by drop, isobutyryl chloride (0.96 g), after which the reaction mixture was stirred at room temperature for 1.5 h. The solution was concentrated to dryness *in vacuo*, and the resulting residue was dissolved in ethyl acetate (100 ml). The solution was washed with 1% hydrochloric acid, aqueous saturated sodium hydrogencarborate, and water, and then dried over magnesium sulfate. The dried solution was concentrated to dryness *in vacuo*, and the oily residue thus obtained was subjected to column chromatography on silica gel (50 g, Kiesel gel 60), using benzene–ethyl acetate (4:1). The eluate was concentrated to dryness *in vacuo* to give the title compound as colorless needles, which were subsequently recrystallized from ethyl acetate–petroleum ether; yield, 1.66 g (91.2%); mp 103—103.2 °C; $[\alpha]_D^{22}$ −6.6° (*c* 1, MeOH); IR (Nujol) 3300, 3270, 1725, 1685, 1665 cm^{-1}; NMR ($CDCl_3$) δ 1.11 (d, 6H, J=7 Hz), 2.26—3.26 (m, 3H), 3.27—3.67 (m, 2H), 4.04—4.80 (m, 4H), 4.47 (s, 2H), 5.10 (s, 4H), 5.90 (broad d, 1H, J=10 Hz), 6.85 (broad d, 1H, J=8 Hz), 7.32 (s, 15H); Found: C, 67.11; H, 6.60; N, 4.90%. Calcd for $C_{33}H_{28}N_2O_8$: C, 67.10; H, 6.49; N, 4.74%.

N-*(*N-*Benzyloxycarbonyl*-O^4-*benzyl*-α-L-*aspartyl)*-O-*propionyl*-D-*alaninol*: *N*-(*N*-Benzyloxycarbonyl-O^4-benzyl-α-L-aspartyl)-D-alaninol (0.88 g) was dissolved in pyridine (15 ml), and the solution was cooled to 0 °C. To the solution propionyl chloride (0.6 g) was added, drop by drop, after which the reaction mixture was stirred at room temperature for 1.5 h. The solution was treated in the manner described above to give the title compound as colorless needles, which were subsequently recrystallized from ethyl acetate-hexane; yield, 0.88 g (88.0%); mp 90—91 °C; $[\alpha]_D^{25}$ −4.0° (*c* 1, MeOH); IR (Nujol) 3310, 1740, 1700, 1660 cm^{-1}; NMR ($CDCl_3$) δ 1.10 (d, 3H, J=6 Hz), 1.12 (t, 3H, J=7 Hz), 2.33 (quartet, 2H, J=7 Hz), 2.50—3.25 (m, 2H), 3.80—4.85 (m, 4H), 5.12 (s, 4H), 5.92 (broad d, 1H, J=9 Hz), 6.30—6.80 (broad, 1H), 7.33 (s, 10H); Found: C, 63.91; H, 6.55; N, 5.92%. Calcd for $C_{25}H_{30}N_2O_7$: C, 63.81; H, 6.43; N, 5.95%.

N-(α-L-*Aspartyl*)-O^1-*isobutyryl*-D-*serinol* ***(56)***: *N*-(*N*-Benzyloxycarbonyl-O^4-benzyl-α-L-aspartyl)-O^1-isobutyryl-O^3-benzyl-D-serinol (1.4 g) was dissolved in a mixture of methanol (100 ml) and water (5 ml). The hydrogenolysis of this compound was carried out over palladium black (0.2 g) for 20 h at room temperature at 3 kg/cm^2 of hydrogen. After the catalyst had then been filtered off, the filtrate was concentrated to dryness *in vacuo* to give **56** as crystals, which were subsequently triturated by methanol and filtered; yield, 0.63 g (96.3%); mp 209—211 °C (dec); $[\alpha]_D^{20}$ +12.7° (*c* 0.5, AcOH); IR (Nujol) 3270, 1730, 1680 cm^{-1}; NMR (D_2O+TFA) δ 1.14 (d, 6H, J=7 Hz), 2.41—3.0 (m, 1H), 3.09 (d, 2H, J=7 Hz), 3.50—3.90 (m, 2H), 3.95—4.50 (m, 4H); Found: C, 47.91; H, 7.28; N, 10.14%. Calcd for $C_{11}H_{20}N_2O_6$ C, 47.82; H, 7.30; N, 10.14%.

N-*(*α-L-*Aspartyl)*-O-*propionyl*-D-*alaninol* ***(34)***: *N*-(*N*-Benzyloxycarbonyl-O^4-benzyl-α-L-aspartyl)-*O*-propionyl-D-alaninol (0.5 g) was dissolved in methanol (20 ml). The

hydrogenolysis of this compound was carried out over palladium black (0.1 g) for 2 h at room temperature under an atmospheric pressure of hydrogen. After the catalyst had been filtered off, the filtrate was concentrated to dryness *in vacuo* to give **34** as crystals, which were subsequently triturated by ether and filtered; yield, 0.25 g (95.4%); mp 155—156 °C (dec.); $[\alpha]_D^{22}$ +29.6° (*c*, 0.7, H_2O); IR (Nujol) 3310, 1740, 1660 cm^{-1}; NMR (DMSO-d_6) δ 1.03 (t, 3H, J=7 Hz), 1.10 (d, 3H, J=8 Hz), 2.34 (quartet, 2H, J=7 Hz), 2.30—2.65 (m, 2H), 3.40—4.45 (m, 4H), 5.28 (broad s, 3H), 8.1—8.65 (broad, 1H); Found: C, 45.59; H, 7.53; N, 10.74%. Calcd for $C_{10}H_{18}N_2O_5 \cdot H_2O$: C, 45.44; H, 7.63; N, 10.60%.

N-(α-L-*Aspartyl*)-O-*cyclopropylcarbonyl*-D-*alaninol* (**40**): *N*-(*N*-Benzyloxycarbonyl-O^4-benzyl-α-L-aspartyl)-*O*-cyclopropylcarbonyl-D-alaninol (0.96 g) was dissolved in methanol (20 ml). The hydrogenolysis of this compound was carried out in the manner described above. After the catalyst had been filtered off, the filtrate was concentrated to dryness *in vacuo* to give **40** as crystals, which were subsequently triturated by ether and filtered; yield, 0.5 g (96.9%); mp 146.5—149 °C (dec); $[\alpha]_D^{25}$ +27.4° (*c* 0.52, H_2O); IR (Nujol) 3320, 1730, 1660 cm^{-1}; NMR (DMSO-d_6) δ 0.87 (d, 3H, J=7 Hz), 0.92—1.3 (m, 4H), 1.45—1.9 (m, 1H), 2.23—2.6 (m, 2H), 3.52—4.2 (m, 4H), 5.40 (broad s, 3H), 8.2—8.7 (broad, 1H); Found: C, 51.00; H, 7.12; N, 10.67%. Calcd for $C_{11}H_{18}N_2O_5$: C, 51.15; H, 7.02; N, 10.85%.

N-(α-L-*Aspartyl*)-O-*cyclobutylcarbonyl*-D-*alaninol* (**46**): *N*-(*N*-Benzyloxycarbonyl-O^4-benzyl-α-L-aspartyl)-*O*-cyclobutylcarbonyl-D-alaninol (0.99 g) was subjected to hydrogenolysis to afford **46** by the procedure described above; yield, 0.52 g (95.6%); mp 168—170 °C (dec); $[\alpha]_D^{25}$ +29.8° (*c* 0.51, H_2O); IR (Nujol) 3330, 1730, 1660 cm^{-1}; NMR (DMSO-d_6) δ 1.06 (d, 3H, J=7 Hz), 1.8—2.6 (m, 8H), 2.9—3.3 (m, 1H), 3.6—4.2 (m, 4H), 5.40 (broad s, 3H), 8.1—8.7 (broad, 1H); Found: C, 52.69; H, 7.51; N, 10.15%. Calcd for $C_{12}H_{20}N_2O_5$: C, 52.93; H, 7.40; N, 10.29%.

Measurement of the Potency of Sweetness. The relative potencies of sweetness were determined based on a panel evaluation by six persons. A 100 mg portion of *O*-acyl-2-(α-L-aspartylamino)alkanol was dissolved in 5 ml of water. Various concentrations of aqueous solutions of sucrose (2, 4, 6, 8, 10, and 12%) were prepared as standard solutions. Every paneler kept 5 ml of the samples in his mouth for 5 s and compared the relative potencies of sweetness with that of the standard solution. When the potency of sweetness of a sample was higher than that of the standard solution, the solution of the sample was diluted more than twice in order to obtain the potency of sweetness more exactly.

The authors are indebted to Dr. Ichiro Chibata for his kind guidance throughout this study. Their thanks are also due to Drs. Hiroshi Itoh and Keisuke Kawashima for their valuable discussions and participation in the panel evaluation of the relative potencies of sweetness.

References

1) R. H. Mazur, J. M. Schlatter, and A. H. Goldkamp, *J. Am. Chem. Soc.*, **91**, 2684 (1969).
2) R. H. Mazur, A. H. Goldkamp, P. A. James, and J. M. Schlatter, *J. Med. Chem.*, **13**, 1217 (1970).
3) R. H. Mazur, J. A. Reuter, K. A. Swiatek, and J. M. Schlatter, *J. Med. Chem.*, **16**, 1284 (1973).
4) a) J. M. Schlatter, Ger. Offen. 1936159 (1970); b) T. Sheehan, *ibid.*, 2054545 (1971); c) N. Nakajima, H. Aoki, M. Fujino, O. Nishimura, and M. Wakimasu, *ibid.*, 2141771 (1972); d) N. Nakajima, H. Aoki, M. Fujino, O. Nishimura, M. Wakimasu, and M. Mano, *ibid.*, 2160042 (1972); e) J. J. Dhlmans, and W. H. J. Boesten, Neth. Appl. 7012897, 7012898, and 7012899; f) R. H. Mazur, A. H. Goldkamp, and J. M. Schlatter, Japan Pat. 7339 (1972); g) R. H. Mazur, J. M. Schlatter, and J. Myron, Fr. Addn. 2114657 (1973); h) Y. Fujimoto, Japan Pat. 8829 (1973).
5) Y. Ariyoshi, N. Yasuda, and T. Yamatani, *Bull. Chem. Soc. Jpn.*, **47**, 326 (1974).
6) M. Goodman and C. Gilon, "Peptides 1974," ed by Y. Wolman, John Wiley & Sons, New York, and Israel Universities Press, Jerusalem (1975), p. 271.
7) M. Fujino, M. Wakimasu, K. Tanaka, H. Aoki, and N. Nakajima, *Naturwissenschaften*, **60**, 351 (1973).
8) T. Wakamiya, H. Uratani, and T. Shiba, *Bull. Chem. Soc. Jpn.*, **48**, 2401 (1975).
9) S. R. Buco, *J. Am. Chem. Soc.*, **69**, 254 (1947).
10) H. Böhme, R. Broese, and F. Eiden, *Chem. Ber.* **92**, 1258 (1959).
11) H. Horikawa, T. Iwasaki, K. Matsumoto, and M. Miyoshi, *Tetrahedron Lett.*, **1976**, 191.
12) J. Kollonitsch, O. Fuchs, and V. Gabor, *Nature*, **175**, 346 (1955).

Boron Trifluoride Hydrate-catalyzed Ethylation of Benzene with Ethyl-1-^{13}C Fluoride and Ethyl-1,1-d_2 Fluoride

Toshiyuki OYAMA, Toshio HAMANO,* Katsuyuki NAGUMO,* and Ryohei NAKANE

The Institute of Physical and Chemical Research, Wako, Saitama 351

**Department of Applied Chemistry, Waseda University, Shinjuku-ku, Tokyo 160*

(Received August 22, 1977)

In the ethylation of benzene with ethyl-1-^{13}C fluoride and ethyl-1,1-d_2 fluoride in boron trifluoride hydrate, almost a 50% isotope position rearrangement in the ethyl group of ethylbenzene was found, whereas in the boron trifluoride-catalyzed ethylation in excess benzene no rearrangement was observed. Based on these results, it was suggested that an electrophile is an ethyl cation in the ethylation of benzene in excess boron trifluoride hydrate and a nonionized polar complex in the boron trifluoride-catalyzed ethylation in excess benzene.

The ethylation of benzene with ethyl fluoride in donor solvents using boron trifluoride as the catalyst proceeds through the formation of a nonionized polar complex, $C_2\overset{\delta+}{H}_5F\cdot\overset{\delta+}{B}F_3$, and the relative rates of toluene to benzene, k_T/k_B, were found to be 2.7 in nitromethane and 2.3 in excess aromatics.[1] On the other hand, in the boron trifluoride-catalyzed ethylation carried out in a nonpolar solvent such as hexane or cyclohexane, the electrophile is an ethyl carbocation, since the ethylation with ethyl fluoride-2-^{14}C indicated the migration of radioactivity from the β- to the α-carbon atom of the ethyl group.[2] In ethylation and isopropylation in hexane, an anomalous substrate selectivity was found (k_T/k_B=0.61 and 0.70 respectively).[3] The nonpolar solvents in which the alkylations are carried out contain a trace of water. Therefore, an alkylation catalyst in nonpolar solvents would be a hydrate of boron trifluoride, which is a strong proton-acid catalyst.[3]

In the present investigation, the ethylation of benzene with ethyl-1-^{13}C fluoride and ethyl-1,1-d_2 fluoride in boron trifluoride monohydrate has been carried out to obtain evidence of the incipient ethyl carbocation as an ethylation agent.

Experimental

Materials. The benzene was dried over calcium hydride. The boron trifluoride was obtained from the Hashimoto Kasei Co., Ltd. The ethyl-1-^{13}C fluoride was prepared from ethyl-1-^{13}C iodide (*ca.* 20 ^{13}C atom%. Prochem, The British oxygen Co., Ltd.) by reaction with mercuric fluoride[4], which had itself been prepared from mercuric chloride with elemental fluorine (Daikin Kogyo Co.) and purified by distillation at low temperatures. The ethyl-1,1-d_2 fluoride was prepared from ethyl-1,1-d_2 alcohol,[5] which had itself been obtained by the reduction of phenyl acetate with lithium aluminium deuteride[6] (99 D atom%. Merck Sharp and Dohme Co., Ltd.); yield: 80.6%, IR(gas): ν_{max} 2240, 2140 (C-D) 1180, 1170, 1155, 970, 960, and 955 (C-F) cm^{-1}; NMR (−40 °C): δ 1.05 (m of d, J_{CH-CF}=25.8 Hz, J_{CH-CD}= 1.02 Hz). The ethylbenzene-2,2-d_2 was prepared by the hydrolysis of 2-phenylethyl-1,1-d_2 magnesium bromide prepared from the bromide and magnesium turnings in dry ether at the reflux temperature for 1.5 hours. IR(neat): ν_{max} 2955, 2880, 2220, and 2130 cm^{-1}; MS:*m/e* 108 (M^+), 91 (base peak). The 2-phenylethyl-1,1-d_2 bromide was prepared from 2-phenylethyl-1,1-d_2 alcohol and a 47% solution of hydrogen bromide by the method in the literature.[7] IR: ν_{max} 2280, 2240, and 2160 cm^{-1}. The alcohol was obtained by the reduction of ethyl phenylacetate with lithium aluminium deuteride in an ether solution.

Procedure. The boron trifluoride monohydrate was prepared by passing anhydrous boron trifluoride gas into distilled water cooled in an ice bath. The resultant hydrate was a heavy, fuming liquid with a specific gravity of 1.77 at 25 °C; it made a clean homogeneous solution with a small amount of benzene (0.5 g benzene/1000 g BF_3-hydrate). Ethylation was carried out by bubbling ethyl fluoride gas into the solution (424 g) for 30 min at room temperature. After the introduction of ethyl fluoride (2.4 mmol), the solution was quenched in ice water. A small amount of unreacted benzene and the products were extracted with dichloromethane. The organic layer was washed with a 5% $NaHCO_3$ aq solution and then with water. The organic solution was dried over calcium chloride, and the solvent was removed by fractional distillation. The products were subjected to GLC, NMR, and GC-MS measurements. Boron trifluoride catalyzed ethylation with ethyl fluoride in excess benzene as a donor solvent was carried out according to the previously described method.[2] GLC analysis was carried out on a Hitachi Perkin Elmer gas chromatograph F6-D. The ^{1}H-NMR spectra were determined on a JEOL C-60HL. apparatus. The ^{13}C-NMR spectra were measured on a JEOL JNM-FX100 Fourier-transform NMR spectrometer. Tetramethylsilane was used as an internal reference. The mass spectra were obtained on a Hitachi RMU-6M mass spectrometer. The IR spectra were taken on a Shimadzu grating Infrared Spectrophotometer IR-27G.

Results and Discussion

In the ^{13}C-NMR spectrum (shown in Fig. 1) of the products of the ethylation of benzene with ethyl-1-^{13}C fluoride in boron trifluoride hydrate, both methyl and methylene carbon signals (15.63 and 28.89 ppm respectively) appeared strongly in a ratio of 40:60 (corrected by relative sensitivity) as compared with those of the aromatic ring (para:125.55 ppm, ortho:127.81 ppm, meta:128.29 ppm). This indicates that almost equal amounts of ethyl-1-^{13}C-benzene and ethyl-2-^{13}C-benzene were produced in this reaction. In the boron trifluoride-catalyzed ethylation with ethyl-1-^{13}C fluoride in excess benzene, it was estimated from the ^{13}C-NMR spectrum (shown in Fig. 2) that about 95% of the products consisted of ethyl-1-^{13}C-benzene. The ^{1}H-NMR spectrum of the product of the same reaction with ethyl-1,1-d_2 fluoride consists only of a methyl-group proton peak at δ=1.23 ppm, with a multiplicity due to H–D coupling (J_{H-D}=1.4 Hz), as is shown in

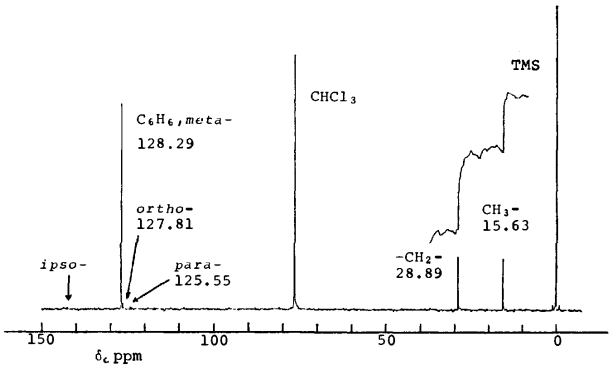

Fig. 1. ^{13}C-NMR spectrum (25 MHz FT) of ethylbenzene (in $CHCl_3$ and C_6H_6) obtained from the ethylation of benzene in boron trifluoride hydrate.

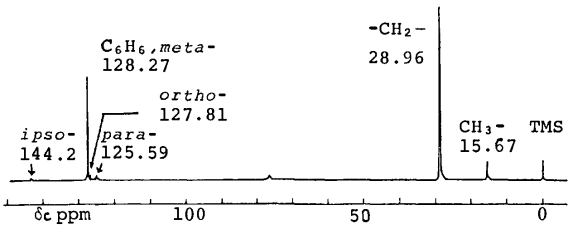

Fig. 2. ^{13}C-NMR spectrum (25 MHz FT) of ethylbenzene (in benzene) obtained from the boron trifluoride catalyzed ethylation in excess benzene.

Fig. 3; no resonance peak due to the methylene proton was observed. Therefore, it is evident that the only ethylated product was ethyl-1,1-d_2-benzene. On the other hand, the ^{1}H-NMR spectrum of the ethylbenzene (shown in Fig. 4) produced in boron trifluoride hydrate displays a multiplet peak of a methylene proton besides a multiplet peak of a methyl group. This product was also analyzed by GC-MS. It was determined from the peak-heights ratio of the $C_6H_5CH_2^+$, $C_6H_5CDH^+$, and $C_6H_5CD_2^+$ ions that the ethylbenzene produced was a mixture of $C_6H_5CH_2CD_2H$, $C_6H_5CDHCDH_2$, and $C_6H_5CD_2CH_3$ in a ratio of 68:95:42. Therefore, the obtained ^{1}H-NMR spectrum is a superposition of the resonance peaks of the isotopic ethyl group with a multiplet due to H–H and H–D coupling.

In order to confirm that the rearranged ethylbenzene

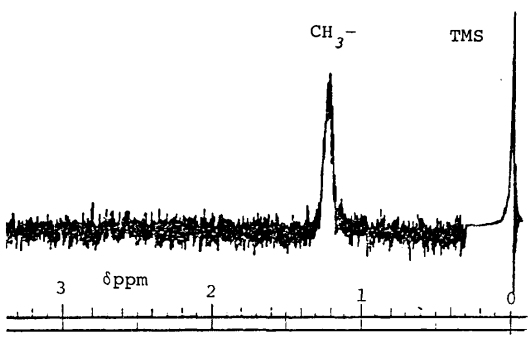

Fig. 3. ^{1}H-NMR spectrum (60 MHz methyl and methylene region) of ethylbenzene (in CCl_4) obtained from the boron trifluoride catalyzed ethylation in excess benzene.

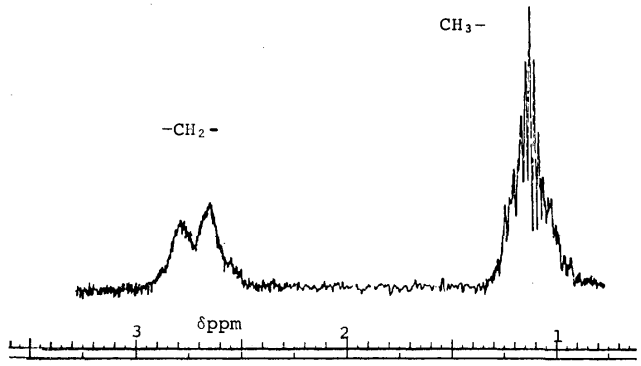

Fig. 4. ^{1}H-NMR spectrum (60 MHz methyl and methylene region) of ethylbenezene (in CCl_4) obtained from the ethylation of benzene in boron trifluoride hydrate.

was obtained by the ethylation reaction in the first step, and not by the secondary isotope-position scrambling of the ethylbenzene which is formed in the first step, ethyl-1-^{13}C-benzene and ethyl-2,2-d_2-benzene were placed in contact with boron trifluoride hydrate under the same conditions as in the ethylation reaction. No isotope-position rearrangement in the ethyl group was observed.

It is well known that, in the consideration of primary alkyl halides with aromatics under the Friedel-Crafts condition, a rearrangement of the alkyl group usually results; this has been interpreted in terms of carbocation formation and rearrangement. All such mechanisms, however, involve primary-to-secondary carbocation conversions. Therefore, it seemed of interest to investigate the primary-to-primary rearrangement of the ethyl group. Roberts *et al.*[8] and Lee *et al.*[9] have reported that the ethylation with ethyl-2-^{14}C halide gave unrearranged products. One of the present authors[2] previously found that, in the boron trifluoride-catalyzed ethyaltion of benzene with ethyl-2-^{14}C fluoride in nitromethane, only a little isotope position rearrangement in the ethyl group took place.

Now, in the ethylation with ethyl-1-^{13}C fluoride and ethyl-1,1-d_2 fluoride in excess benzene, no isotope-position-rearranged product was obtained. These facts show that the boron trifluoride catalyst forms, with ethyl fluoride, the nonionized complex in the Friedel-Crafts ethylation in the donor solvent and that the complex attacks the aromatic ring carbon without rearrangement. The ethylation proceeds *via* an S_N2 displacement reaction on the complex.

Boron trifluoride monohydrate,[10] which is formed by introducing an equal amount of boron trifluoride into

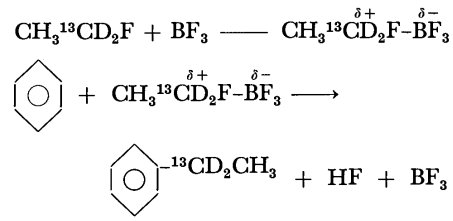

Scheme 1.

water, is a heavy, fuming liquid and is a strong proton acid of the hydroxyfluoroboric-acid type. This hydrate is used as a catalyst for polymerizations and alkylations.[11] When the hydrate of boron trifluoride reacts with ethyl fluoride, an ethyl cation or its ion pair is produced, and internal 1,2-hydride and deuteride shifts occur almost completely in the ethyl group before the ethyl cation combines with the benzene ring. Thus,

$$CH_3{}^{13}CH_2F + HBF_3OH \rightleftharpoons CH_3{}^{13}CH_2{}^+\text{-}HOBF_3{}^- + HF$$

$$\begin{array}{ccc} CH_3{}^{13}CH_2{}^+ & \overset{\sim H^-}{\rightleftharpoons} & {}^{13}CH_3CH_2{}^+ \\ \downarrow \text{PhH} & & \downarrow \text{PhH} \\ Ph{}^{13}CH_2CH_3 & & PhCH_2{}^{13}CH_3 \end{array}$$

$$\begin{array}{ccccc} CH_3CD_2{}^+ & \overset{\sim H^-}{\rightleftharpoons} & CD_2HCH_2{}^+ & \overset{\sim D^-}{\rightleftharpoons} & CDH_2CDH^+ \\ \downarrow \text{PhH} & & \downarrow \text{PhH} & & \downarrow \text{PhH} \\ PhCD_2CH_3 & & PhCH_2CD_2H & & PhCDHCDH_2 \end{array}$$

Scheme 2.

the ethylation with the isotope-position-rearranged ethyl cation or its ion pair gave a mixture of isotopic ethylbenzene. These facts suggest that the ethyl cation of its ion pair is the electrophile in boron trifluoride hydrate-catalyzed ethylation. In a competitive ethylation an anomalous relative rate ($k_T/k_B=0.8$), as in a nonpolar solvent, was obtained in boron trifluoride hydrate.[12] The ethylation of benzene with boron trifluoride and ethyl-2-^{14}C fluoride, carried out in a nonpolar solvent such as hexane and cyclohexane, gave isotope-position-rearranged ethylbenzene, indicating the ethyl-cation formation in the course of the reaction.[2] Therefore, it may be concluded that the ethylation catalyst in a nonpolar solvent is a boron trifluoride hydrate.

The authors wish to thank Mr. Jun Uzawa for measuring the NMR spectra.

References

1) R. Nakane, O. Kurihara, and A. Natsubori, *J. Am. Chem. Soc.*, **91**, 4528 (1969).
2) A. Natsubori and R. Nakane, *J. Org. Chem.*, **35**, 3372 (1970).
3) R. Nakane, O. Kurihara, and A. Takematsu, *J. Org. Chem.*, **36**, 2753 (1971).
4) A. L. Henne and T. Midhley, *J. Am. Chem. Soc.*, **58**, 884 (1936).
5) R. S. Tipson, *J. Org. Chem.*, **9**, 239 (1944); W. F. Edgell and L. Parts, *J. Am. Chem. Soc.*, **77**, 4902 (1955).
6) A. Murray and D. L. Williams, "Organic Syntheses with Isotopes," Part 2, Interscience, New York (1958), p.1341.
7) G. Schroeter, L. Lichtenstadt, and O. Irineu, *Ber.*, **51**, 1599 (1918).
8) R. M. Roberts, G. A. Ropp, and O. K. Neville, *J. Am. Chem. Soc.*, **77**, 1764 (1955).
9) C. C. Lee, M. C. Hamblin, and N. James, *Can. J. Chem.*, **36**, 1597 (1958).
10) a) C. A. Wamser, *J. Am. Chem. Soc.*, **73**, 409 (1951); b) N. N. Greenwood and R. L. Martin, *J. Chem. Soc.*, **1951**, 1915; c) N. N. Greenwood and R. L. Martin, *J. Chem. Soc.*, **1953**, 1427; d) P. Diel, *Helv. Phys. Acta*, **31**, 685 (1958); e) S. Pawlenko, *Z. Anorg. Allg. Chem.*, 300, 152 (1959).
11) a) A. V. Topchiev *et al.*, "Boron Fluoride and its Compounds as Catalysts in Organic Chemistry," Pergamon Press, New York (1959); b) J. T. Kelly and R. J. Lee, *Ind. Eng. Chem.*, **47**, 757 (1955); c) R. J. Lee, H. M. Knight, and J. T. Kelly, *Ind. Eng. Chem.*, **50**, 1001 (1958); d) N. Yoneda and H. Ohtsuka, *Kogyo Kagaku Zasshi*, **72**, 1743 (1969).
12) R. Nakane and A. Takematsu, unpublished results.

Metalloporphyrins. III.[1] Photoinduced Acylamination of Zinc Porphyrins by Use of Acyl Azides

Kunihiro ICHIMURA

Research Institute for Polymers and Textiles, Sawatari 4, Kanagawa-ku, Yokohama 221

(Received August 31, 1977)

Visible light irradiation of a solution of zinc octaethylporphin (ZnOEP) in the presence of acyl azide gives zinc complex of 5-acylamino-2,3,7,8,12,13,17,18-octaethylporphin together with a small amount of zinc complex of 21-acylamino-2,3,7,8,12,13,17,18-octaethylporphin. Zinc 5,10,15,20-tetraphenylporphin (ZnTPP) is coverted into zinc complex of 21-acylamino-5,10,15,20-tetraphenylporphin in a similar way. The pyrolysis of the *N*-acylaminated ZnOEP affords the rearrangement product in addition to ZnOEP, while *N*-acylaminated ZnTPP is converted into ZnTPP on heating. The spectroscopic properties of these photoproducts are given.

Photochemical studies on metalloporphyrins have hitherto been focused on their photoreduction and photooxidation in particular in relation to the function of photosynthetic pigments and the degradation of biological macrocycles. Little work has been done regarding other photochemical reactions of the macrocyclic ligands.[2] During the course of an investigation on the fluorescence quenching of metalloporphyrins, acyl azide was found to effectively quench the emission of zinc octaethylporphin (ZnOEP) (**1**), the fluorescence intensity decreasing gradually during the course of measurement. These observations prompted us to study the photolysis of ZnOEP–acyl azide system.[3] This paper describes the photoinduced acylamination at the *meso*-position and at the pyrrolic nitrogen of the macrocycle resulting from the sensitized decomposition of acyl azide. This type of photochemical conversion was extended to zinc tetraphenylporphin (ZnTPP) (**2**), yielding *N*-acylaminated ZnTPP. This seems to be a first example of the photoinduced substitution on metalloporphyrins.

Results and Discussion

When a dichloromethane solution of ZnOEP was irradiated with light of wavelength>450 nm in the presence of a slight excess of aromatic acyl azide under argon stream, the color of the solution immediately darkend. The irradiation period was dependent upon the nature of acyl azide; an electron-withdrawing group except nitro group on benzoyl residue accelerates the photolysis (Table 1). The reaction was followed by TLC, and two photolytic products were isolated by preparative TLC. The red major product showing larger R_f-value has typical visible bands of metal complexes and the CO stretching vibration owing to amide

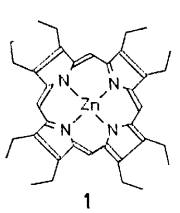
1

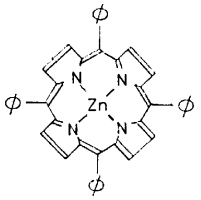
2

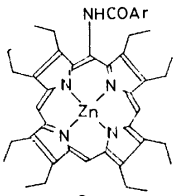

3

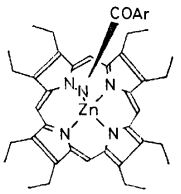

4

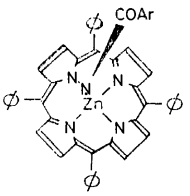

8

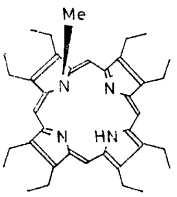

9

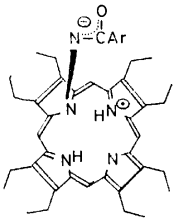
10

Table 1. *meso*-Acylaminooctaethylporphinatozinc (**3**)

	Ar	Mp (dec)	Irradiation time (h)	Yield[a]	Elementary analyses (%) Found C	Found H	Found N	Calcd C	Calcd H	Calcd N
3a	C_6H_5	307—309 °C	4	58%	71.65	6.80	9.54	71.99	6.89	9.97
3b	*p*-$MeOC_6H_4$	295—301	6	50	69.91	6.98	9.14	70.70	6.88	9.38
3c	*p*-ClC_6H_4	324—325	2	61	63.57	6.40	9.16	68.79	6.44	9.32
3d	*p*-CNC_6H_4	305—307	0.2	59	70.76	6.40	10.86	71.18	6.52	11.33
3e	*p*-$NO_2C_6H_4$	298—299	14	55	67.60	6.20	10.56	67.73	6.53	11.03
3f	*m*-$NO_2C_6H_4$	277—279	15	65	67.31	6.14	10.42	67.73	6.53	11.03
3g	α-Naphthyl	283—286	2	47	72.92	6.89	9.18	73.55	6.70	9.14
3h	Cinnamoyl	296—306	1	43	72.64	6.88	9.27	72.69	6.92	9.43

a) A small amount of ZnOEP recovered unchanged on photolysis is not taken into consideration.

group (Table 2). From the NMR spectra the amide group can be ascribed to the *meso*-substituent of the macrocyclic ligand, since the ethyl protons are no longer equivalent and three *meso*-protons are observed in the intensity ratio 1:2.[4,5] Appearance of new NMR proton signals due to aryl ring derived from acyl azide as well as the elementary analyses suggest that ZnOEP is substituted by ArCONH– or ArNHCO– group at the *meso*-position (Table 1 and 3). The structure having the former group for the major product (**3**; Ar=Ph) was unequivocally elucidated by identification of the photoproduct from ZnOEP–benzoyl azide system with the authentic sample prepared by the benzoylation of *meso*-aminooctaethylporphin,[5] followed by metallization.

The NMR spectra of the minor photoproducts chelated by zinc (Table 4) show the presence of four *meso*-protons in the intensity ratio 2:2 and the remarkable high field shift of the aryl protons derived from acyl azide, indicating that acylimino (ArCON) or its isomer (ArNCO) is bound to the pyrrolic nitrogen of ZnOEP (Table 5). Determination of the structure having the former group (**4**) was made by IR spectral analysis of the photoproduct starting from ZnOEP-*p*-cyanobenzoyl azide; $\bar{\nu}_{CN}$ at 2232 cm^{-1} is in line with that of *p*-cyanobenzoyl-*p*-toluide (**5**) and *N'*,*N'*-dimethylhydrazide (**6**) at 2233 cm^{-1} rather than that of *N*,*N*-dimethyl-*N'*-(*p*-cyanophenyl)urea (**7**) at 2223 cm^{-1}. The shift of the amide carbonyl frequency to lower wavelength at *ca.* 1610 cm^{-1} of this type of compound can be interpreted in terms of the bond formation between zinc and the acylamino nitrogen[6] (Table 6). The metal complexes exist as neutral species, in contrast to *N*-alkylporphins which require counter anion like halogenide

Table 2. Visible and infrared spectra of zinc *meso*-acylaminooctaethylporphins (**3**)

	λ_{max} nm ($\varepsilon \times 10^{-4}$) in CH_2Cl_2	$\bar{\nu}_{max}$ cm^{-1} in KBr
3a	412(42.0), 504(0.26), 540(1.95), 578(1.60)	3400, 1655, 1503
3b	412(46.0), 504(0.24), 540(1.71), 578(1.33)	3300, 1645, 1520
3c	412(40.6), 504(0.27), 540(1.90), 578(1.58)	3300, 1643, 1520
3d	412(43.5), 504(0.22), 540(1.93), 578(1.62)	3400, 2233, 1660, 1510
3e	411(40.0), 503(0.34), 541(1.86), 579(1.53)	3400, 1660, 1528, 1343
3f	412(38.5), 505(0.25), 541(1.88), 579(1.61)	3400, 1640, 1532, 1350
3g	414(40.5), 504(0.29), 542(2.02), 580(1.60)	3400, 1660
3h	412(43.5), 504(0.27), 541(2.07), 578(1.70)	3280, 1665, 1625

Table 3. NMR spectra of *meso*-acylaminooctaethylporphinatozinc (**3**)

	Solvent[a]	*meso*-H	Aryl-H	Ring-H
3a	DC	10.02 (s, 3H),	7.7—8.0 (m, 3H)	
3b	TFA	10.91, 11.02	7.67 (d, 2H, 9 Hz) 8.73 (d, 2H, 9 Hz)	−3.01 (2H), −4.13 (2H)
3c	TFA	10.88, 10.98	8.05 (d, 2H, 10.5 Hz)	−2.90 (2H), −4.00 (2H)
3d	DC	10.11 (s, 2H), 10.20 (s, 2H)	7.79 (d, 2H, 5.5 Hz), 8.57 (d, 2H, 5.5 Hz)	
3e	DC	9.97 (s, 2H), 10.10 (s, 2H)	8.55 (s, 4H)	
3f	TFA	10.90, 11.00	8.23 (m, 1H) 9.00—9.46 (m, 2H) 9.60—9.90 (m, 1H)	−2.86 (2H), −3.95 (2H)
3g	TFA	10.73, 10.91	7.79—9.05 (m, 7H)	−2.70 (2H), −3.98 (2H)
2h	TFA	10.56, 10.70	7.2—8.2 (m, 6H) 8.62 (d, 1H, 15 Hz)	−2.90 (2H), −4.08 (2H)

a) DC; chloroform-*d*. TFA; trifluoroacetic acid.

Table 4. *N*-Acylaminooctaethylporphins (**10**) and their zinc complexes (**4**)

	Ar		Elementary analyses (%) Found C	H	N	Calcd C	H	N
10a	C_6H_5	Free base	79.40	7.85	10.31	78.96	7.87	10.72
4c	*p*-ClC_6H_4	Zn salt	68.49	6.82	9.03	68.79	6.44	9.32
4d	*p*-CNC_6H_4	Zn salt	70.79	6.81	10.89	71.18	6.52	11.33
10d	*p*-CNC_6H_4	Free base	77.53	7.52	11.98	77.82	7.43	12.39
10h	Cinnamoyl	Free base	79.09	7.90	10.21	79.47	7.86	10.31

to form the metal complexes.[7-12] Another metal complex of this type of anomalous coordination has been reported.[13]

The photochemical acylamination on porphyrin ring has been extended to ZnTPP (**2**) (Table 7). The structure of the zinc complex of the photoproduct has been clarified by NMR spectra (Table 8). Protons attributable to acyl group derived from acyl azide undergo considerable high field shift as in the case of **4**. The number of β-pyrrolic protons remains eight; two singlets for four protons and an AB quartet for four protons. The zinc macrocycles show similar polarization of the amide CO and the cyano group like **4**, supporting the structure (**8**) (Table 9).

The structure of the photoproducts in the present work demonstrates the resemblance of the photolysis to the nitrene reaction. The reactions of nitrene or carbene with metalloporphyrins investigated so far fall into four categories, although no photochemically induced reaction has been reported; *a*) insertion at the *meso*-position,[14,15] *b*) addition on the pyrrolic nitrogen atom,[7-9,16] *c*) addition to the β,β-double bond of pyrrolic ring to give cyclopropane derivatives,[7,15,17] and *d*) formation of a metal-carbon bond.[18] The *meso*-acylaminated photoproducts (**3**) seem to be formed by reaction *a*), and the *N*-acylaminated macrocycles (**4**) and (**8**) by reaction *b*). The azacyclopropane derivative according to reaction *c*) has not yet been isolated in the photolysis of ZnOEP–acyl azide.

The photolysis of zinc porphyrin–acyl azide system is of synthetic value for the introduction of a functional group at the *meso*-position of the symmetrical macrocycles and particularly for the preparation of *N*-substituted macrocycles which are attracting attention as regards structural problems and chemical reactivity. Since the *N*-acylaminated porphins are the first example of the macrocycle bearing *N*-substituent other than alkyl, the NMR spectra and chemical reactivity of **4** and **8** have

TABLE 5. NMR SPECTRA OF *N*-ACYLAMINOOCTAETHYLPORPHINS (**10**) AND THEIR ZINC COMPLEXES (**4**) IN $CDCl_3$

	CH_3CH_2	CH_3CH_2	*meso*-H	Acyl-H	Ring-H
10a	1.51 (t, 6H) 1.91 (t, 6H) 2.00 (t, 12H)	*ca.* 4.18	10.66 (s, 2H) 10.71 (s, 2H)	3.16—3.39 (m, 2H) 5.40—5.75 (m, 2H) 6.06—6.37 (m, 1H)	−0.98 (2H)
4c	1.43 (t, 6H) 1.95 (t, 18H)	*ca.* 4.16	10.39 (s, 2H) 10.52 (s, 2H)	*ca.* 3.90 (2H) 5.79 (d, 2H, 8 Hz)	
10c	1.50 (t, 6H) 1.88 (t, 6H) 1.93 (t, 6H) 1.96 (t, 6H)	*ca.* 4.18	10.52 (s, 2H) 10.55 (s, 2H)	3.11 (d, 2H, 8 Hz) 5.42 (d, 2H, 8 Hz)	
4d	1.46 (t, 6H) 1.98 (t, 18H)	*ca.* 4.18	10.42 (s, 2H) 10.56 (s, 2H)	*ca.* 4.03 (2H) 6.12 (d, 2H, 8 Hz)	
10d	1.52 (t, 6H) 1.88 (t, 6H) 1.93 (t, 6H) 1.98 (t, 6H)	*ca.* 4.18	10.57 (s, 2H) 10.61 (s, 2H)	3.28 (d, 2H, 8 Hz) 5.78 (d, 2H, 8 Hz)	−1.36 (2H)
10h	1.54 (t, 6H) 1.90 (t, 6H) 1.96 (t, 6H) 2.00 (t, 6H)	*ca.* 4.18	10.54 (s, 4H)	5.35 (m, 2H) 6.6—6.9 (m, 3H) 3.01 (d, 1H, 15 Hz)	

TABLE 6. VISIBLE AND INFRARED SPECTRA OF *N*-ACYLAMINOOCTAETHYLPORPHINS (**10**) AND THEIR ZINC COMPLEXES (**4**) IN DICHLOROMETHANE

	λ_{max} ($\varepsilon \times 10^{-4}$) in nm	$\bar{\nu}_{max}$ in cm^{-1}
10a	401(10.8), 530(0.74), 566(1.28), 612(0.26)	1610, 1560
4c	410(19.0), 530(0.94), 563(1.57), 606(1.02)	1610, 1560
4d	410(17.1), 530(0.83), 563(1.18), 606(0.84)	2232, 1615, 1550
10d	402(11.5), 529(0.77), 565(1.27), 610(0.30)	2229, 1608
10h	404, 526, 562, 605	1645, 1590, 1560

TABLE 7. 21-ACYLAMINO-5,10,15,20-TETRAPHENYLPORPHINATOZINC (**8**)

	Ar	Irradiation time (h)	Yield (%)	Elementary analyses (%) Found C	Found H	Found N	Calcd C	Calcd H	Calcd N
8c	*p*-ClC_6H_4	15	69	73.19	4.23	7.98	73.63	3.88	8.43
8d	*p*-CNC_6H_4	15	62	75.51	4.08	9.87	75.94	3.93	10.23
8h	Cinnamoyl	12	67	77.07	4.35	8.32	77.31	4.29	8.51

a) Based on the consumed ZnTPP.

Table 8. NMR spectra of zinc complexes of 21-acylamino-5,10,15,20-tetraphenylporphin (**8**) in $CDCl_3$

	Acyl-H	β-Pyrrole-H
8c	3.93 (d, 2H, 8 Hz), 5.87 (d, 2H, 8 Hz)	7.88 (s, 2H), 9.05 (d, 2H, 4.5 Hz), 9.27 (d, 2H, 4.5 Hz), 9.03 (s, 2H)
8d	4.05 (d, 2H, 8 Hz), 6.15 (d, 2H, 8 Hz)	7.85 (s, 2H), 9.45 (d, 2H, 4.5 Hz), 9.65 (d, 2H, 4.5 Hz), 9.43 (s, 2H)
8h	2.51 (d, 1H, 15.8 Hz), 4.68 (d, 1H, 15.8 Hz), 5.9—6.2 (m, 2H) 6.6—6.9 (m, 2H)	— , 9.02 (d, 2H, 4.5 Hz), 9.23 (d, 2H, 4.5 Hz), 9.00 (s, 2H)

Table 9. Visible and infrared spectra of zinc complexes of 21-acylamino-5,10,15,20-tetraphenylporphin (**8**)

	λ_{max} ($\varepsilon \times 10^{-4}$) nm in CH_2Cl_2	$\bar{\nu}_{max}$ cm^{-1} (KBr)
8c	438(28.5), 559(0.79), 587(1.17), 609(1.41)	1616
8d	437.5(28.9), 555(0.76), 587(1.18), 608(1.29)	2234, 1614
8h	438.5(26.2), 558(0.80), 587(1.10), 610(1.33)	1638, 1598

been studied in detail. First the magnetic shielding effect of the macrocycles on the protons of *N*-acylamino group should be mentioned. Storm and Corwin showed that a plot of the incremental shift of *N*-alkyl substitutent (Δ in ppm) *vs.* the square of the reciprocal of the distance (r in Å) of the alkyl group from the current loop gives a straight line.[19] *N*-Acylamino group of **4** and **8** is approximately perpendicular to the plane of the macrocycles, as in the case of metal-free and metal containing *N*-alkylporphyrins (Fig. 1).[13,20-22] When the distance of protons on acyl including cinnamoyl group from the plane is estimated in the same way as in the work of Storm and Corwin, a plot of Δ between *N*-acylaminoporphin and the corresponding acyl amide as the reference compound against r^{-2} is found to give a straight line coinciding with the line for *N*-alkyl porphin (Fig. 2).

It was found that **4** and **8** are readily demetallized even when a solution of the complexes in dichloromethane was passed through a silica gel column. The anomalous instability of the zinc chelation reflects the

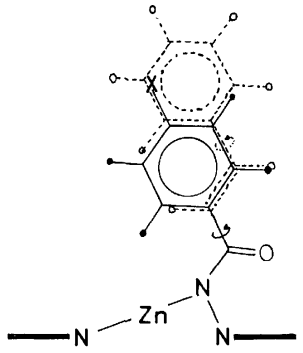

Fig. 1. The presumable stereochemistry of the zinc complexes of *N*-(*p*-substituted benzoylamino)porphin (full line) and *N*-(cinnamoylamino)porphin (broken line).

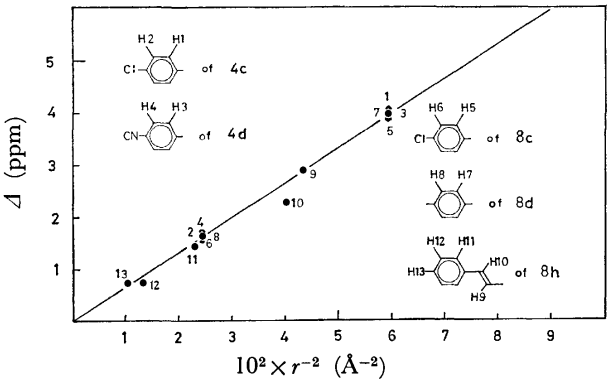

Fig. 2. A plot of the difference in chemical shift (Δ) between zinc complexes of *N*-acylaminoporphin and the corresponding acyl amide against the square of the reciprocal of the distance of the acyl protons from the current loop (r). This line is obtained by Storm and Corwin for *N*-alkyletioporphyrin-II.[19] The number of the plot refers to the acyl proton sketched in the Figure.

sp^3 character of the pyrrolic nitrogen bounded by the acylamino group. The stronger basicity of this nitrogen may accelerate the removal of zinc. The metal-free *N*-acylaminooctaethylporphins give characteristic spectroscopic data. The CO frequency of the acylamino group shows a considerable shift to lower wavenumber at *ca.* 1610 cm^{-1} (Table 6), indicating a strong polarization of the CO bond. The visible spectra are no longer similar to those of *N*-methyloctaethylporphin (**9**) having four visible bands but resemble that of monocation of **9** (Fig. 3). This suggests that the metal-free *N*-acylaminoporphin possesses the betaine structure (**10**) which has a strong polarized acylamino residue and monocationic macrocyclic system. Furthermore, two magnetically equivalent protons attributable to the ring protons support the structure. The unusually good solubility of this compound in methanol is also consistent with the polar structure.

The thermal decomposition of *N*-alkylated porphyrins leads to *a*) elimination of the alkyl,[7,23] *b*) isomerization to *meso*-alkylporphin,[16] *c*) migration of the alkyl to the β-pyrrolic position,[7,20] and *d*) formation of a novel macrocyclic system, homoporphyrin.[16] It was found that *N*-acylaminoporphyrins and their zinc complexes show similar pyrolytic behavior. When the crystals of **4d** were heated above 200 °C, ZnOEP and 3d were isolated in the ratio 1:2.1. The thermal conversion was also carried out in boiling *o*-dichloroben-

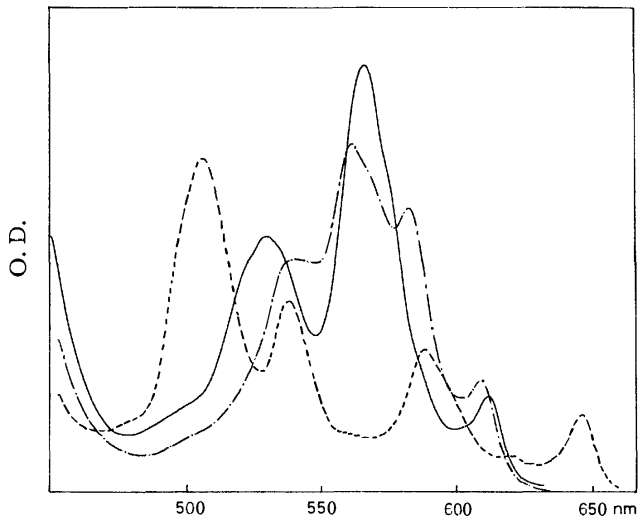

Fig. 3. The visible electronic absorption spectsa of *N*-benzoylaminooctaethylporphin (**10a**) in CH_2Cl_2 (——), *N*-methyloctaethylporphin (**9**) in CH_2Cl_2 (----), and **9** in CH_2Cl_2 containing acetic acid (—·—·—·—).

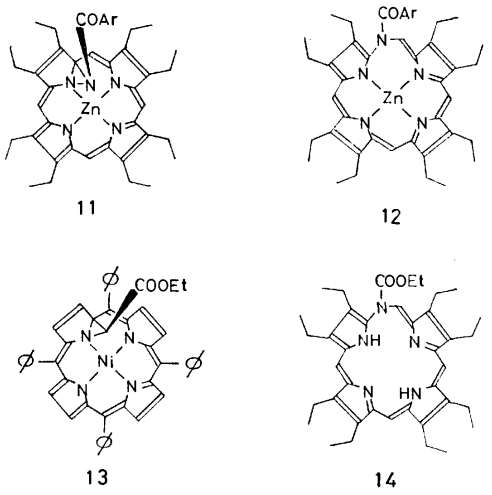

zene whithin a few minutes. The thermolysis of **10d** required more drastic conditions, giving OEP and the free base of **3d** in the product ratio 1:0.1. **8d** decomposed smoothly on heating in boiling *o*-dichlorobenzene.

The rearrangement of **4** to **3** occurs presumably through the diaziridine (**11**) and the azahomoporphyrin (**12**) as in the case of *N*-alkylporphyrins.[16] Although the aziridine intermediate (**13**) corresponding to **11** has been isolated in the thermal conversion of *N*-ethoxycarbonylethyltetraphenylporphinatonickel,[16] rapid ring contraction of **12** to the *meso*-substituted porphyrin takes place either upon heating or chelation.[14] Observation of the isosbestic points in the spectral change of **4d** and **8d** in boiling toluene suggests that both **11** and **12** are extremely short-lived.

Experimental

All melting points are not corrected. Visible, IR, and NMR spectra were recorded on a Hitachi type 323 spectrophotometer, and Hitachi EPI-3G spectrophotometer, and a JEOL C-60 HL type nuclear magnetic spectrometer, respectively. The preparative TLC was carried out with use of silica gel plates activated at 130 °C for 3 h.

Materials. Zinc octaethylporphin was recrystallized from toluene, and determination of its purity was made by means of visible spectrum and TLC on silica gel using benzene–hexane as an eluent. Commercial tetraphenylporphinatozinc (Strem Chemicals Inc.) was used without purification. Acyl azides were purified by passing a dichloromethane solution through a short column of silica gel, followed by recrystallization.

5-Benzoylamino-2,3,7,8,12,13,17,18-octaethylporphin. 5-Amino-2,3,7,8,12,13,17,18-octaethylporphin[5] (12.1 mg) was dissolved in 1 ml dry pyridine, and 50.0 mg of benzoyl chloride was added to the solution under stirring. A color change, violet→blue→olive green→violet, was observed. After 40 min stirring, the solution was poured into chloroform–water and the chloroform layer was separated, washed with dil acetic acid (×1), water (×3) and dried over anhydrous magnesium sulfate. After the solvent has been evaporated, the residue was chromatographed on silica gel plates with use of dichloromethane as an eluent. A red band was collected, and the product was extracted with dichloromethane containing methanol and recrystallized from dichloromethane–hexane. Red violet needles (6 mg) of mp 312—313 °C with decomposition was obtained. Found: C, 79.21; H, 8.10; N, 10.25%. Calcd for $C_{43}H_{49}N_5$: C, 78.96; H, 7.87; N, 10.72%. $\bar{\nu}_{max}$ (KBr): 3280 and 1643 cm^{-1}. λ_{max} in CH_2Cl_2: 405, 502, 536, 570, and 623 nm. Treatment with zinc acetate in chloroform–methanol gave the zinc complex.

Photolysis of Octaethylporphinatozinc in the Presence of Acyl Azide. To a solution of ZnOEP (120 mg) in 200 ml dichloromethane was added 1.5 molar amount of acyl azide, and the solution was irradiated with a 450 W high pressure mercury arc filtered with a Corning filter C. S. No.3—69 under argon bubbling and efficient stirring. The photolysis was followed by TLC and visible spectra. The irradiated solution was evaporated under reduced pressure, and the residue was chromatographed on silica gel plates with use of chloroform or dichloromethane–acetone as an eluent. The chromatogram was complex, two red bands being collected. The main red band having larger R_f-value gave red violet crystals of 5-acylamino-2,3,7,8,12,13-17,18-octaethylporphinatozinc (**3**) which were recrystallized from dichloromethane–methylcyclohexane. Identification of the benzoylamino derivative (**3a**) as well as its metal-free macrocycle with the authentic samples prepared as above was performed by TLC, IR, and visible spectra. The results are summarized in Table 1. The visible and IR spectra are given in Table 2. Methyl protons of ethyl group at the β-pyrrole positions undergo deshielding in the NMR spectra. The *meso*-protons are also influenced by the introduction of the *meso*-substitutent, being split into two signals in the intensity ratio 1:2. When the spectra are measured in trifluoroacetic acid, **3** is demetallized to form the dication and exhibits four ring NH protons in the intensity ratio 2:2. All the NMR signals are characteristic to *meso*-substituted octaethylporphin.[24] The protons of aroyl group show down field shift (Δ=*ca.* 0.8 ppm for protons at the *ortho*-position of phenyl) as a result of magnetic anisotropy of the porphyrin ring system. The acylamino group is thus positioned within the loop of the macrocycles. It is noteworthy that cinnamoylamino group in **3h** is in the *trans*-configuration (J=15 Hz); no sensitized isomerization of the cinnamoyl group exists during the course of photolysis.

The second product with smaller R_f-value was in some cases isolated in a demetallized state and recrystallzied from

dichloromethane–methylcyclohexane. Treatment of the metal-free products with zinc acetate gave zinc complexes which were found to be demetallized during the chromatographic work-up. This anomalous instability of the zinc complex indicates that the demetallization takes place not during the course of photolysis but on the chromatographic separation. When purified dichloromethane was used as an eluent, the zinc complexes were isolated from the photoproducts by TLC on silica gel. The demetallization must be caused by trace amount of acidic impurity in the eluent. The second TLC fraction was treated with zinc acetate, washed with water, and evaporated to dryness to give 20-acylamino-2,3,7,8,12,13,17,18-octaethylporphinatozinc (**4**) which was recrystallized from chloroform–methylcyclohexane. The results are given in Table 4. NMR, and visible and IR spectra are given in Tables 5 and 6, respectively.

Photolysis of 5,10,15,20-Tetraphenylporphinatozinc–Acyl Azide. A solution of ZnTPP (200 mg) and 5 molar amount of acyl azide in 100 ml of dichloromethane was irradiated in the same way as in the case of ZnOEP. The resulting dark brown solution was evaporated to dryness, and the residue was chromatographed on a silica gel column with use of dichloromethane as an eluent. After eluting recovered ZnTPP, the eluent turned into a dichloromethane–acetone mixture (100:1 v/v). An emerald-green fraction was obtained and evaporated to dryness. TLC of the residue on silica gel revealed that the fraction is composed of two products. The one with larger R_f-value having λ_{max} at 438, 554, 586, 609, and 636 nm was converted, on treatment with hydrochloric acid, into the other with smaller R_f-value having λ_{max} at 433, 460, 550, 590, and 649 nm. The latter was reversely converted into the former on treatment with zinc acetate. Accordingly, the residue of the mixture was treated with zinc acetate in chloroform–methanol, followed by washing with water and drying with anhydrous sodium sulfate. 21-Acylamino-5,10,15,20-tetraphenylporphinatozinc (**8**) was recrystallized from dichloromethane–hexane as dark blue crystals. The results are given in Table 7. NMR, and visible and IR spectra are given in Tables 8 and 9, respectively.

Pyrolysis of N-Acylaminoporphyrins and the Zinc Complexes. The crystals of 21-(*p*-cyanobenzoylamino)-2,3,7,8,12,13,17,18-octaethylporphinatozinc (**8d**) were heated at *ca.* 200 °C for a short time and chromatographed on a silica gel column with use of dichloromethane as an eluent. The first red fraction was identified with ZnOEP by TLC and visible spectrum. The second red fraction was identified with 5-(*p*-cyanobenzoylamino)-2,3,7,8,12,13,17,18-octaethylporphinatozinc (**3d**) (TLC and visible spectrum). The product ratio of ZnOEP to **3d** was determined spectrophotometrically to be 1 : 2.1. The crystals of the metal-free 21-(*p*-cyanobenzoylamino)-2,3,7,8,12,13,17,18-octaethylporphin (**10d**) were heated at *ca.* 270 °C, and the products were separated and identified to be OEP and 5-(*p*-cyanobenzoylamino)-2,3,7,8,12,13,17,18-octaethylporphin (TLC and visible spectrum). The product ratio of OEP to the rearranged product was 1 : 0.1. The pyrolytic product of 21-(*p*-cyanobenzoylamino)-5,10,15,20-tetraphenylporphinatozinc (**8d**) in the crystalline state was identified with ZnTPP.

Heating of the zinc complexes (**4d** and **8d**) in boiling *o*-dichlorobenzene resulted in the same products as those obtained by pyrolysis in the crystalline state, while the metal-free *N*-(*p*-cyanobenzoylamino)octaethylporphin was recovered unchanged under the same pyrolytic conditions. A solution of the *N*-acylaminated zinc complexes was heated in benzene or toluene. Samples were taken at intervals, and the reaction was followed spectrophotometrically. The spectral changes demonstrated isosbestic points for both zinc complexes.

References

1) Part II: K. Ichimura, *Chem. Lett.*, **1977**, 641.
2) a) F. R. Hopf and D. G. Whitten, in "Porphyrins and Metalloporphyrins," ed by K. M. Smith, Elsevier, Amsterdam (1975), p. 667; b) D. Mauzerall and F. T. Hong, in Ref. 2a, p. 701; c) J.-H. Fuhrhop, *Angew. Chem.*, **86**, 363 (1974).
3) As a preliminary report: K. Ichimura, *Chem. Lett.*, **1976**, 641.
4) H.-H. Inhoffen, J.-H. Fuhrhop, H. Voigt, and H. Brockmann Jr., *Liebigs Ann. Chem.*, **695**, 133 (1966).
5) R. Bonnett and G. F. Stephenson, *J. Org. Chem.*, **30**, 279 (1965).
6) K. Nakamoto, "Infrared Spectra of Inorganic and Coordination Compounds," Wiley-Interscience, New York (1970), p.332.
7) B. Shears, B. Shah, and P. Hambright, *J. Am. Chem. Soc.*, **93**, 776 (1971).
8) B. Shah, B. Shears, and P. Hambright, *Inorg. Chem.*, **10**, 1825 (1971).
9) R. Grigg, G. Shelton, and A. Sweeney, *J. Chem. Soc., Perkin Trans. 1*, **1972**, 1789.
10) H. J. Callot, *Bull. Soc. Chim. Fr.*, **1972**, 4387.
11) H. J. Callot and Th. Tschamber, *Bull. Soc. Chim. Fr.*, **1973**, 3192.
12) P. Batten, A. Hamilton, A. W. Johnson, G. Shelton, and D. Ward, *J. Chem. Soc., Chem. Commun.*, **1974**, 550.
13) H. J. Callot, Th. Tschamber, B. Chevier, and R. Weiss, *Angew. Chem.*, **87**, 545 (1975).
14) R. Grigg, *J. Chem. Soc., C*, **1971**, 3664.
15) H. J. Callot and A. W. Johnson, *J. Chem. Soc., Perkin Trans. 1*, **1973**, 1424.
16) H. J. Callot and Th. Tschamber, *J. Am. Chem. Soc.*, **97**, 6175 (1975).
17) H. J. Callot, *Tetrahedron Lett.*, **1972**, 1011.
18) H. J. Callot and E. Scheaffer, *Tetrahedron Lett.*, **1977**, 239.
19) C. B. Storm and A. H. Corwin, *J. Org. Chem.*, **29**, 3700 (1964).
20) G. M. McLauphlin, *J. Chem. Soc., Perkin Trans. 2*, **1974**, 136.
21) D. E. Goldberg and K. M. Thomas, *J. Am. Chem. Soc.*, **98**, 913 (1976).
22) O. D. Anderson and D. K. Lavalle, *J. Am. Chem. Soc.*, **98**, 4670 (1976).
23) H. J. Callot and Th. Tschamber, *Bull. Soc. Chim. Fr.*, **1973**, 112.
24) H. Sheer and J. J. Katz, in Ref. 2a, p. 399.

A Comparative Study of the Photo-induced Berson-Willcott Rearrangement of Methyl 3-Isopropyl-1a,7b-dihydro-1*H*-cyclopropa[*a*]naphthalene-1-*exo*- and 1-*endo*-acetate

Masahiko KATO, Masakazu TSUJI, and Toshio MIWA

Faculty of Science, Osaka City University, Sugimoto-cho, Sumiyoshi-ku, Osaka 558

(Received September 6, 1977)

The effect of 1-*exo*- and 1-*endo*-methoxycarbonylmethyl groups on the course of the photo-induced Berson-Willcott rearrangement of methyl 1a,7b-dihydro-1*H*-cyclopropa[*a*]naphthalene-1-acetate have been studied. Different reaction rates with the same final products have been observed and are discussed from the view of the stereochemical course of the reaction, which strongly supports the 60°-mechanism, *i.e.*, a slither motion of C-1 with inversion of configuration.

The photo-induced rearrangements of some benzonorcaradiene derivatives have been studied extensively.[1-5]

Swenton *et al.* demonstrated that the direct irradiation of 7b-cyano-1a,7b-dihydrocyclopropa[*a*]naphthalene (**1**) lead smoothly to products, **2** and **4**, through intermediate **3**. They discussed a decrease in the quantum yield of disappearance of 7b-methoxycarbonyl-1a,7b-dihydrocyclopropa[*a*]naphthalene (**5**) compared with that of **1** and the rearrangement towards **6**, in addition to **7**, on irradiation of **5** in terms of increased peri-interaction, which retarded the formation of **7**, in the intermediate **8**.

Such interaction was not observed in the intermediates, **3** and **9**, leading to **2** and **6** respectively; thus the formation of the latters becomes favorable.[3]

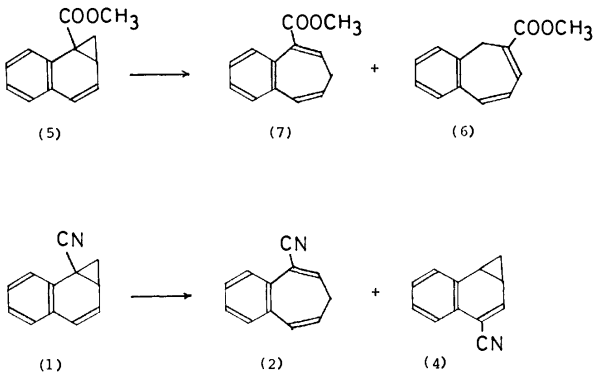

Scheme 1.

The photo-induced rearrangement of an *exo-endo* mixture of methyl 1a,7b-dihydro-1*H*-cyclopropa[*a*]-naphthalene-1-acetates, (**10**) and (**11**), has been investigated and gives, in addition to naphthalene, **12**, **13**—**16**.[4] The stereochemical course of the rearrangement of **10** and/or **11** to methyl 2a,7a-dihydro-7*H*-cyclobut[*a*]indene-7-*anti*-acetate (**15**) has been reported.[5] However, since compounds **10** and **11**

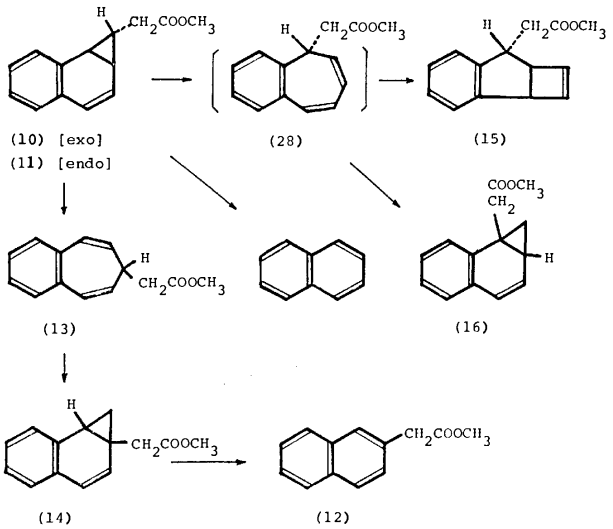

Scheme 2.

interconvert with each other under thermal (90 °C, 5 min) and photolytic conditions,[4] it was uncertain as to whether either one or both of the isomeric esters had actually rearranged to **15**.

The *exo-endo* interconversion between **10** and **11** occurs apparently through **17** by the fission of the C_{1a}–C_{7b} bond.[4] Since substitution on the C_3 with a bulky group (R) would retard the interconversion by way of peri-interaction, this would be expected to effect the photochemical reaction pathways as reported by Swenton *et al.* Therefore isopropyl derivatives, **18** and **19**, were selected as candidates for the present study.

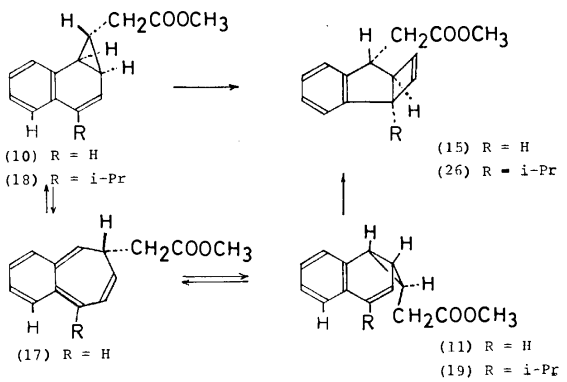

Scheme 3.

These compounds were thought to be suitable in order to gain more profound insight into the stereochemical course of the benzonorcaradiene system. Up to date, there have been no reports about the comparative study on the photochemical behavior of *exo* and *endo* isomers of 1-substituted 1a,7b-dihydro-1*H*-cyclopropa[*a*]naphthalene derivatives. The *endo* isomer was of special interest since it should exibit a repulsive interaction between the pi-electron(s) on the six-membered ring and the substituent on C-1. The presence of such an interaction may possibly cause an alteration of the reaction rates or pathway.

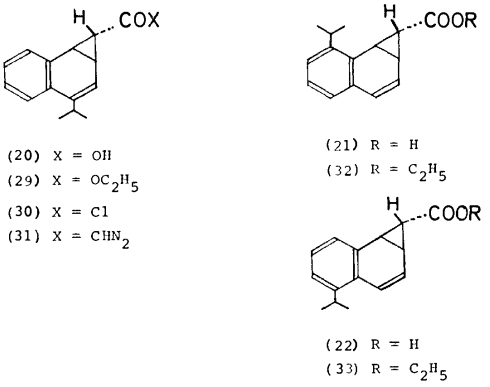

Scheme 4.

Results and Discussion

3-Isopropyl-1a,7b-dihydro-1*H*-cyclopropa[*a*]naphthalene-1-*exo*-carboxylic acid (**20**) was formed as the main product, along with **21** and **22**, from the reaction of 1-isopropylnaphthalene (**23**) with ethyl diazoacetate and subsequent hydrolysis. Arndt-Eistert reaction of **20** gave the desired compound **18**, the 3-isopropyl derivative of **10**, as a crystalline product, mp 84.5—85.5 °C. Compound **18** exhibited a well defined NMR spectrum (100 MHz); an olefinic proton doublet at δ=6.01 and isopropyl signals at 1.12(d) and 1.13(d) (6H) and 2.90 (1H, septet). Signals attributable to three protons on the cyclopropane ring were similar in their chemical shifts and coupling constants to those of **10**,[4] which indicated that the configuration of the methoxycarbonylmethyl group was *exo*. The UV spectrum was also similar in shape to that of **10**[4] but the maximum (278 nm) showed a small bathochromic shift effected by the substitution with the isopropyl group.

Heating **18** to 130 °C for 30 min, gave an equilibrium mixture composed of **18** and **19** in the ratio of 3 : 2. Isolation of **19** from the mixture was achieved using column chromatography on Silicic Acid with hexane–ether (95:5 v/v) eluant. The structure of **19** was assigned on the basis of the spectral data. The UV spectrum was superimposable with that of **18**. The NMR spectrum of **19** showed signals attributable to the three protons on the cyclopropane ring at δ=1.6—1.9 (H_1), 2.24 (H_{1a}), and 2.57 (H_{7b}, t). Double resonance spectrum obtained by irradiation at H_2 gave the coupling constants ($J_{H_1-H_{1a}}=J_{H_1-H_{7b}}=7.5$; $J_{H_{7b}-H_{1a}}=9$), which defined a *cis* relation to each other. The *endo* configuration of the methoxycarbonylmethyl group was further supported by the higher field resonance of the methylene proton signals compared with those of the *exo*-isomer **18**. When heated above 130 °C, **19** gave the same mixture of **18** and **19** as that obtained from **18** by the same treatment.

Both **18** and **19** were found to be thermally stable below 100 °C, and did not interconvert under the influence of UV irradiation, as expected from the above data.

Direct irradiation of **18** in methanol through a Pyrex filter with use of a HPL for 20 min gave **23**, methyl 9-isopropyl-5*H*-benzocycloheptene-5-acetate (**24**), methyl 5-isopropyl-7*H*-benzocycloheptene-7-acetate (**25**), *exo*-and *endo*-isomers of methyl 2a-isopropyl-2a,7a-dihydro-7*H*-cyclobut[*a*]indene-7-acetate (**26**, **27**), in 10, 35, 15, 12, and 6% yields, respectively, estimated by GLC (15% polydiethylene glycol adipate

Table 1. Estimated yields of products in the course of irradiation of **18** and **19** (8×10^{-4} mol/l MeOH)

Irradiation time (h)	Starting material	Eicosane (%)	% Yields of products[a]					
			18 or **19**	**23**	**25**	**24**	**26**	**27**
0	**18**	15.4	100					
	19	12.7	100					
1	**18**	15.4	42.8	5.1	11.1	24.6	1.0	0.8
	19	12.7	24.0	6.2	7.2	42.3	3.5	1.9
2	**18**	15.4	14.1	8.4	14.8	35.2	5.8	3.2
	19	12.7	3.6	9.3	9.8	47.0	13.9	6.9
3	**18**	15.4	4.5	10.2	14.8	35.4	11.8	6.0
	19	12.7	—	9.6	8.1	37.2	19.8	9.6
4	**18**	15.3	—	11.2	15.3	29.9	17.0	8.7
	19	12.7	—	9.4	6.4	17.1	32.4	16.1
5	**18**	15.3	—	11.0	11.7	26.0	22.1	10.4
	19	12.7	—	10.6	6.0	21.0	31.3	15.1
6	**18**	15.4	—	14.1	3.3	17.4	26.6	13.0
	19	12.7	—	11.0	5.2	15.5	34.5	17.9

a) The amount of each compound was estimated by their peak areas relative to that of eicosane.

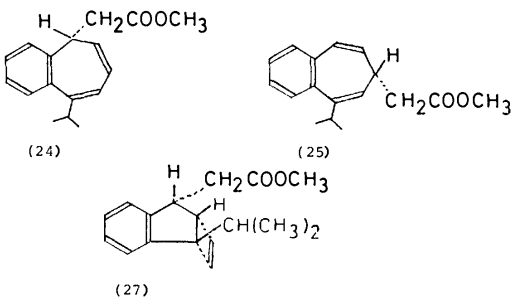

Scheme 5.

on Chromosorb WAW). Photolysis of the *endo* isomer (**19**) gave essentially the same products, except in their yields (Table 1).

The structures of these compounds were determined on the basis of their spectral data. The UV spectrum of **24** showed a maximum at 271 nm which suggested the presence of 5*H*-benzocycloheptene moiety (λ_{max} 275 nm).[7] Although the NMR spectrum taken at room temperature was too broad to investigate spin-spin coupling, those obtained at +2——45 °C clearly demonstrated fine splitting. The presence of three vicinal olefinic protons was observed from the NMR spectra (δ=5.45, 5.91, 6.45; $J_{H_4-H_5}$=5.5; $J_{H_5-H_6}$=9.5; $J_{H_6-H_7}$=5 Hz). The coupling pattenrs of the benzylic methine proton and the acetate-methylene protons defined the position of the substituents.

The UV spectrum of **25** was similar to that of 7*H*-benzocycloheptene (λ_{max} 228 (ε 44000); 256 ^{sh} nm (ε 5200).[7] The presence of 1H signal (δ=6.47), corresponding to the proton alpha to phenyl group, determined the position of the isopropyl group to be C-2. The proton-proton coupling pattern of >CH–CH_2–COO [ABX type: J_{AB}=15.5; J_{AX}=10; J_{BX}= 5.5 Hz] supported that of methyl 7*H*-benzocycloheptene-7-acetate. Direct irradiation of **24** gave mainly a mixture of **26** and **27** in a ratio of 2 : 1. The UV spectra, together with the coupling pattern of the olefinic proton signals in the NMR spectra suggested the presence of the 2a,7a-dihydro-7*H*-cyclobut[*a*]-indene structure. The absence of a lower field signal characteristic of the benzylic methine proton on the cyclobutene ring for both compounds, **26** and **27**, assigned the position of the isopropyl group on C-1. The *endo* structure for **27** was assigned from a larger separation of the two olefinic proton signals, caused by the proximity effect of the methoxycarbonyl group, and the larger splitting signal of the proton on C-5, coupled with the proton on C-4, compared with those of **26**.

It was observed in the photochemical reactions of **18** and **19** that the primary rearrangement products, **24** and **25**, were formed as the major products. Benzonorcaradiene derivatives were not detected in the products. In the photolysis of **10**, **28** was not detected and **13** was obtained in a small amount in the photolysate; further rearranged products were formed, even if the reaction was interupted at the initial stage.[4,7] Cycloheptatrienes are not planar molecules but have the boat conformations,[8] therefore

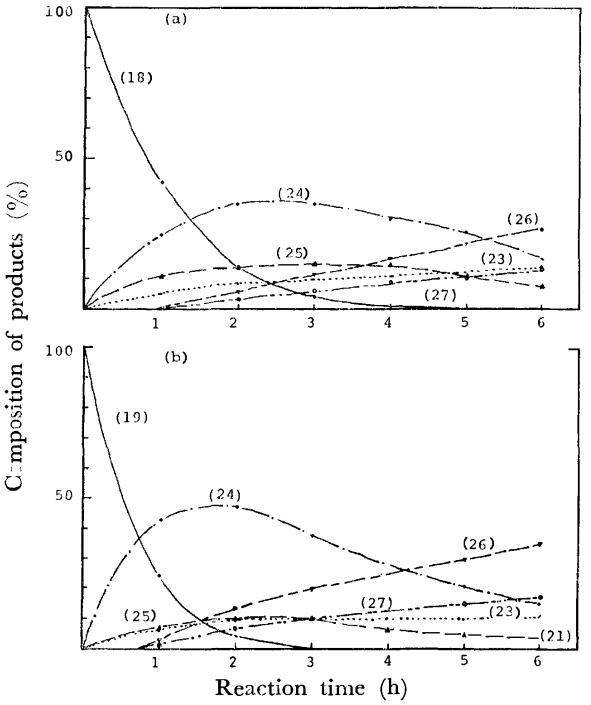

Fig. 1. Plots of the products composition *versus* irradiation time. Starting materials; (a) **18** and (b) **19**.
·····: (**23**), —·—·—: (**24**), ———: (**25**), – – – –: (**26**), ————————: (**27**).

the isopropyl group in **24** and **25** appears to be fixed in a non-coplanar position with respect to the peri C–H bond thereby minimising the mutual steric interaction. The isopropyl group on C-3 in **14** or **16** appears to be fixed near the coplanar position to the peri C–H bond, causing a large repulsive interaction. These steric repulsions give rise to interupt further rearrangement of the primary photo-products, **24** and **25**, to benzonorcaradienes.

To determine the relative reactivities of the isomeric esters, **18** and **19**, they were photolyzed independently in methanol at the same concentrations (8×10^{-4} mol/l). Eicosane was added as an internal standard and the merry-go-round apparatus was used. The products were analysed for by GLC at regular time intervals and the results are given in Fig. 1.

At the initial stage of the reaction, it may be seen that the rate of formation of **24** from **19** was twice as effective as that of **24** from **18**, in conjugation with the disappearance of **19** which disappeared twice as fast as that of **18**. Initially the rate of formation of **25** from **19** looks slower than that from **18**. However, as the decrease in concentration of **19** is much faster than that of **18**, the ratio of concentrations of **25**/**19** and that of **25**/**18** at low conversion (after one hour irradiation) are important and are almost similar (0.30 and 0.26, respectively).

Since the UV spectra of the isomeric esters, **18** and **19**, are superimposable, the methoxycarbonylmethyl group on C-1 appears to have little influence on the electronic state of the cyclopropane ring. Assuming that the electronic structures of the esters

are quite similar to each other except for steric requirements, the differences in reactivities between **18** and **19** will be determined by the degree of steric freedom in the intermediates from **18** and **19**. Berson,[9] Woodward and Hoffman[10] have suggested that the Berson-Willcott rearrangement of simple norcaradienes must follow after either one of the two possible modes of mechanisms, *i.e.*, the 60°- and the 120°-mechanism. When these mechanisms are applied to the present photo-induced rearrangement of **18** and **19**, the change in steric interference will govern the reaction pathway as shown in Schemes 6 and 7.

Path a

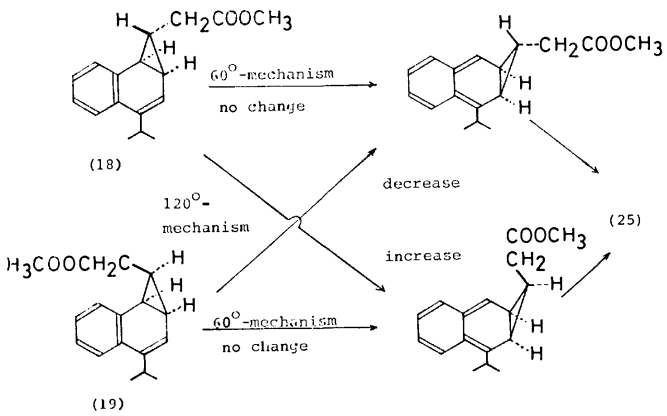

Scheme 6.

As observed from previous experiments on optically active **10**,[10] high stereospecificity of these reactions suggests that the reaction may follow either of the two mechanisms.

If the reactions toward Path a follow 60°-mechanism, formation of **25** from both **18** and **19** will proceed at similar rates. If it follows 120°-mechanism, formation of **25** from **18** will become less than that from **19**. The results on the ratios of concentrations (**25**/**19** and **25**/**18**) at low conversion discussed above support the 60°-mechanism.

Similarly, since formation of **24** from **18** is apparently retarded compared with that from **19** (Fig. 1), another Path b clearly follows the 60°-mechanism, that is, slither motion of C-1 with inversion of the

Path b

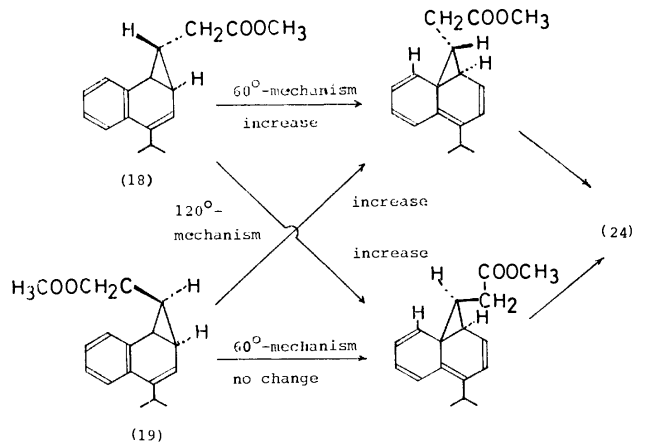

Scheme 7.

configuration. This latter claim is in line with the results obtained from the study on an photo-induced rearrangement of optically active substance **10**.[5]

The data supports the 60°-mechanism for the photo-induced rearrangement of methyl 3-isopropyl-1a,7b-dihydro-1*H*-cyclopropa[*a*]naphthalene-1-acetate in both directions. The precise stereochemistry for Path a has recently been established with use of the optically active 3-*t*-butyl derivative of **10** and the results will be reported elswhere.

Experimental

The NMR spectra were obtained on a JEOL Model PS-100 spectrometer with carbon tetrachloride as the solvent and TMS as the internal standard, unless otherwise specified. The chemical shifts are expressed in ppm from TMS. The IR spectra were recorded on a JASCO spectrometer Model IRE and the UV on a Hitachi Recording Spectrometer Model 323. GLC analysis was carried out on a Varian Aerograph Model 90P gas chromatograph under quoted conditions. The light source for photolysis, used throughout this experiments, was a Ushio high pressure mercury lamp, UM-452, with Pyrex filter.

*Synthesis of 3-Isopropyl-1a,7b-dihydro-1*H*-cyclopropa*[a]*naphthalene-1-*exo*-carboxylic Acid (**20**). Reaction of Isopropylnaphthalene (**23**) with Ethyl Diazoacetate*: To 24.6 g (0.144 mol) of **23**, containing 195 mg of copper powder heated at 145—150 °C, was added drop by drop 2.88 g (25.2 mmol) of ethyl diazoacetate over a period of 1 h with vigorous stirring. The mixture was further stirred for 2 h at 145 °C (gas evolution; 610 ml at 25 °C, 95% of theoretical), and then 21.5 g of **23** was recovered by distillation (97—100 °C/7 mmHg). The experiment was repeated three times and the collected residue taken in CH_2Cl_2 was filtered from copper powder and subsequently distilled to give 7.34 g of yellow liquid, bp 136—140.5 °C (1 mmHg). Repeated column chromatography of the distillate on Silicic Acid[11] (hexane-ether 19 : 1 v/v) gave three fractions: Fr. 1; 2.32 g [**29**+**32**]; Fr. 2; 1.73 g [**29**+**32**+**33**]; Fr. 3; 2.08 g [**29**+**33**].

Alkaline Hydrolysis of Fraction 3. The above Fr. 3 (2.08 g), dissolved in 0.5 M 85% aq ethanolic KOH (32 ml) was refluxed for 3 h. The resulting solution was then diluted with water (32 ml) and reduced to half volume under reduced pressure. After being washed with ether, the ice-cooled aq solution was acidified carefully with cold 2 M HCl in the presence of 30 ml of ether. The separated aq solution was extracted three times with ether, and the combined ether extracts were washed with saturated aq NaCl and dried (anhyd Na_2SO_4). After subsequent evaporation of ether, the remaining crystalline acid mixture was recrystallized from aq methanol to give **20** (647 mg) and a 1 : 1 mixture of **20** and **22** (390 mg). **20** mp 200—201.5 °C. IR ν_{max}^{Nujol}: 2650, 2560, 1680, 955 cm^{-1}. NMR ($CDCl_3$) δ=0.78 (1H, t, J=3.5 Hz), 1.14 (3H, d, J=6.5 Hz), 1.17 (3H, d, J=6.5 Hz), 2.75 (1H, d,d,d, J=8, 5.5, 3.5 Hz), 3.01 (1H, septet, J=6.5 Hz), 3.16 (1H, d,d, J=8, 3.5 Hz), 6.16 (1H, d, J=5.5 Hz), 7—7.6 (4H, m), 7.9 (1H, b). Found: C, 78.66; H, 7.10%. Calcd for $C_{15}H_{16}O_2$: C, 78.92; H, 7.06%.

*Preparation of Methyl 3-Isopropyl-1a,7b-dihydro-1*H*-cyclopropa*[a]*naphthalene-1-*exo*-acetate (**18**).* To a cold solution of **20** (3.03 g, 13.3 mmol) dissolved in benzene (66 ml), was added oxalyl chloride (10 g, 80 mmol). After stirring for 4 h at room temperature, the solution was evaporated below 20 °C and the residue was evaporated with benzene (three times, each 10 ml) under reduced pressure to give an acid

chloride (**30**) as an orange liquid. **30** IR $\nu_{max}^{liq.film}$: 1758 cm^{-1}.

To the dried ether solution of diazomethane, prepared from *N*-nitroso-*N*-methylurea (24 g), 50% aq KOH (75 ml) and ether (240 ml), was added drop by drop **30**, dissolved in benzene (15 ml), over a period of 2 h with cooling (ice-water). After further stirring for 1.5 h at that temperature, the mixture was evaporated and taken in dichloromethane. After drying, the solution was evaporated below 20 °C under reduced pressure to give an orange solid (**31**) (4.06 g). IR ν_{max}^{Nujol}: 2055, 1610 cm^{-1}.

The diazomethyl ketone (**31**), dissolved in 1240 ml of methanol was divided into three portions. Each portion was independently irradiated under nitrogen with an HPL for 40 min with external cooling (ice-water) and collected. Subsequent evaporation of solvent left an orange liquid (3.74 g), which was chromatographed on Silicic Acid (120 g) using hexane-ether (9:1 v/v) as the solvent to give **18** as light yellow crystals (1.86 g; 54.4%). Recrystallization from hexane gave colorless crystals, **18**, 1.26 g; mp 84.5—85.5 °C. **18** IR ν_{max}^{Nujol}: 1730, 1460, 1380, 1207, 1192, 1168, 995, 762, 740 cm^{-1}. UV λ_{max}^{EtOH} (log ε): 224.5 (4.29), 231 (4.28), 237.5 $^{infl.}$(4.13), 278 (3.77), 307$^{infl.}$nm(3.35). NMR δ=0.26 (1H, t,t, J=7, 4.3 Hz), 1.12 (3H, d, J=6.5 Hz), 1.13 (3H, d, J=6.5 Hz), 1.76 (1H, d,d,d, J=4.3, 5.5, 8.2 Hz), 2.18 (1H, d,d, J=4.3, 8.2 Hz), 2.31 and 2.34 (-CH_2-CH<, J_{AB}=15.8 Hz, J_{AX}=J_{BX}=7 Hz), 2.90 (1H, septet, J=6.5 Hz), 3.56 (3H, s), 6.01 (1H, J=5.5 Hz), 6.95—7.6 (4H, m). Found: C, 79.60; H, 7.86%. Calcd for $C_{17}H_{20}O_2$: C, 79.65; H, 7.86%.

*Methyl 3-Isopropyl-1a,7b-dihydro-1*H*-cyclopropa*[a]*naphthalene-1*-endo-*acetate (19)*. Compound **18** (20 mg), dissolved in DMSO-d_6 (0.5 ml) in a sealed NMR tube, was kept at 130 °C to give a mixture of **18** and **19**. The product ratios were estimated every 10 min by means of the NMR spectra. Ratio (**18**:**19**): After 10 min (2:1) 20 min (3:2); 30 min (3:2).

To obtain **19** in quantity, **18** (250 mg) was heated at 140 °C for 30 min and the product was chromatographed on 60 g of Silicic Acid (hexane-ether 95 : 5 v/v). Following to **18**, a mixture of **18** and **19** (rich in **19**) was obtained. Further chromatography gave a sample of **19** (50 mg) as a colorless liquid. This was further purified by distillation at 60 °C (1 mmHg) with the aid of a sublimation apparatus. **19** NMR δ=1.20 (3H, d, J=7 Hz), 1.25 (3H, d, J=7 Hz), 1.6—1.9 (-CH_2-CH<), 2.24 (H_{1a}, m), 2.57 (H_{7b}, t, J=7.5 Hz), 3.06 (1H, septet, J=7 Hz), 3.53 (3H, s), 5.89 (1H, d, J=5.5 Hz), 7.08—7.5 (4H, m). UV λ_{max}^{EtOH} (log ε): 224.5 (4.22), 231(4.21), 237.5$^{infl.}$(4.08), 278(3.70), 307$^{infl.}$nm(3.21). Mass spectrum (JMS-D300); M^+ (*m/e*): 256.145; Calcd for $C_{17}H_{20}O_2$; 256.146.

Irradiation of 18 in Methanol: Identification of Products. Compound **18** (300 mg), dissolved in methanol (320 ml), was irradiated using an HPL under nitrogen for 15 min with external cooling (ice-water). After evaporation of the solvent, the residue (303 mg), taken in hexane-ether (90 : 10 v/v), was developed on 30 g of Silicic Acid and elution was continued with the same solvent (95:5 v/v). Each 15 ml-fraction was collected separately and the solvent evaporated to give fractions as follows: Fr. 1—3, 15 mg (**23**); Fr. 6—7, 5 mg (**26**, **27**, and **25**); Fr. 8—9, 76 mg (**25** (main) and **24** (minor)); Fr. 10, 31 mg (**24**); Fr. 11—15, 100 mg (**18**).

Fraction 8 and 9 were rechromatographed on 20 g of Silicic Acid (hexane-ether 95 : 5 v/v) to give a pale yellow liquid (14 mg; **25**), which was purified by means of GLC [5% Silicone OV-17 on Chromosorb WAW, 1/4″×3 m; column temperature, 173 °C; He flow rate, 40 ml/min; retention time, **25** 12.6 min]. **25** NMR δ=0.735 (3H, d, J=7 Hz), 1.20 (3H, d, J=7 Hz), 2.2—2.45 (1H) and 2.48—2.65 (2H) [AB_2 type], 2.93 (1H, septet, J=7 Hz), 3.60 (3H, s), 5.44 (1H, d, J=5 Hz), 5.80 (1H, d,d, J=5, 10 Hz), 6.47 (1H, d, J=10 Hz), 7.05—7.2 (3H, m), 7.24—7.65 (1H, m). UV λ_{max}^{EtOH} (log ε): 227 (4.55), 255$^{infl.}$nm(3.85). Found: C, 79.66; H, 7.90%. Calcd for $C_{17}H_{20}O_2$: C, 79.65; H, 7.86%.

Fraction 10 (31 mg) was rechromatographed on 8 g of Silicic Acid (hexane-ether 95 : 5 v/v) to give a sample of **24** (10 mg). This compound could not be purified by GLC owing to a very slow isomerization to isomer(s) with the same retention time under these conditions. For CH analysis, GLC separation was carried out [5% Silicone OV-17, 170 °C; He, 40 ml/min]. **24** NMR δ=0.9—1.5 (6H, bm), 2.2—3.1 (3H, bm), 3.22 (1H, septet, J=7 Hz), 3.65 (3H, bs), 5.35—5.6 (1H, bm), 5.8—6.1 (1H, bm), 6.25—6.5 (1H, bm), 7.0—7.7 (4H, m); (CD_3OD) at +1 °C δ=0.96 (3H, d, J=7 Hz), 1.35 (3H, d, J=7 Hz), 2.77—2.99 (1H) and 3.07 (2H) [AB_2 type], 3.51 (weak s, axial-$COOCH_3$?)[12], 3.65 (3H, s, $COOCH_3$), 5.45 (1H, d,d, J=9.5, 5.5 Hz), 5.97 (1H, bd, d, J=9.5, 5 Hz), 6.45 (1H, d, J=5.5 Hz), 7.11—7.75 (4H, m). UV λ_{max}^{EtOH} (log ε): 271 (3.82); λ_{min} 246 nm (3.61). Found: C, 79.68; H, 7.91%. Calcd for $C_{17}H_{20}O_2$: C, 79.65; H, 7.86%.

To obtain **26** and **27** in quantity, photolysis of **18** was performed for 30 min. Fractions corresponding to Fr. 6—7 of the above mentioned chromatography were separated and purified by means of GLC [15% polydiethylene glycol adipate, 184 °C; He, 40 ml/min; retention times; **26**, 10 min; **27**, 12 min]. **26** (solidified) IR $\nu_{max}^{liq.film}$: 1730, 1480, 1460, 1440, 1365, 1250, 1165, 1040, 1000, 770, 759, 742 cm^{-1}. NMR δ=0.82(3H, d, J=6.5 Hz), 0.99(3H, d, J=6.5 Hz), 2.22 (1H, septet, J=6.5Hz), 2.21 and 2.51(CH_2, AB part of ABX type, J_{AB}=15.5 Hz, J_{AX}=10 Hz, J_{BX}=5.5 Hz), 2.84 (1H, bs, $\Delta\tau_{1/2}$=3.5 Hz), 3.31 (1H, d,d,d, J=10, 5.5, 1.5Hz), 3.62(3H,s), 6.04(1H, d, J=2.7Hz), 6.25 (1H, d, J=2.7Hz), 6.98—7.18 (4H, m). UV λ_{max}^{EtOH} (log ε): 262 (2.89), 268.5 (3.07), 275.5 nm (3.10). Found: C, 79.69; H, 7.91%. Calcd for $C_{17}H_{20}O_2$: C, 79.65; H, 7.86%. **27** IR $\nu_{max}^{liq.film}$: 1730, 1480, 1460, 1440, 1390, 1366, 1165, 995, 880 ,855, 812, 778, 760, 725 cm^{-1}. NMR δ=0.84 (3H, d, J=6.5Hz), 1.01 (3H, d, J=6.5Hz), 2.23 (1H, septet, J=6.5 Hz), 2.32—3.1(2H, m), 3.48(2H, bs, $\Delta\tau_{1/2}$=8 Hz), 3.64 (3H, s), 5.95(1H, d, J=2.7 Hz), 6.37 (1H, d, J=2.7Hz), 6.9—7.3 (4H, m). UV λ_{max}^{EtOH}: 262, 268.5, 275.5 nm.

Short Period Irradiation of 18 and 19 in Methanol. Compound **19** (40 mg), dissolved in methanol (105 ml), was irradiated for 5 min using an HPL with external cooling (ice-water) under nitrogen. After the solvent had been carefully evaporated below 20 °C, the products were analyzed by NMR and GLC. The NMR spectrum revealed that the mixture did not contain any of the *exo*-isomer, **18**. The GLC analysis [15% polydiethylene glycol adipate on Chromosorb WAW, 187 °C; He, 40 ml/min] showed it contained six species, estimated as follows: Retention time (product ratio) : 4.9 min (**23**, 7.5%), 12.8 min (**26**, 5.2%), 14.4 min (**27**, 3.4%), 18.2 min (**25**, 9.0%), 21 min (**24**, 44%), 28.4 min (**19**, 30%).

An identical experiment using the same concentration of **18**, instead of **19**, in methanol was carried out. The products did not contain any of **19** and the ratio of products were obtained as follows: **23**, 9.7%; **26**, 3.2%; **27**, 1.5%, **25**, 14.5% **24**, 33%; **18**, 38.3%.

Irradiation of 24. Compound **24** (60 mg), dissolved in methanol (130 ml), was irradiated with an HPL under nitrogen with external cooling. The occurrence of **26** and

27, in compensation for **24**, was observed by monitoring the reaction using GLC [10% Apiezone L on Chromosorb WAW, 190 °C; He, 40 ml/min: Compound (retention time); **26** (8.8 min), **27** (10 min), **24** (13.2 min)] and NMR [**26** δ=6.04 (d), 6.25 (d): **27** δ=5.95 (d), 6.37 (d): **24** δ=5.35—5.6 (bm)] measurements.

*Competitive Photo-induced Reaction of **18** and **19**.* Each 15 ml of a solution of **18** or **19**, (each 50 mg) dissolved in methanol (244ml) separately, was charged in Pyrex test tubes (ϕ1.5×13 cm), which were stoppered after flushing with nitrogen. Seven tubes each were arranged in a merry-go-round apparatus, cooled with ice-water, and irradiated concurrently with an HPL settled in the center of the apparatus. The reaction products from **18** and **19** were monitored every hour using GLC [15% polydiethylene glycol adipate on Chromosorb WAW, 175 °C; He, 40 ml/min]. The results are given in Table 1.

The authors are grateful to Mr. Jun-ichi Goda for the analytical data and to Mr. Kozo Shibata for measurement of the high resolution mass spectrum.

References

1) G. W. Gruber and M. Pomerantz, *J. Am. Chem. Soc.*, **91**, 4004 (1969).

2) M. D. Madigan and J. S. Swenton, *J. Am. Chem. Soc.*, **93**, 6316 (1971).

3) J. S. Swenton, K. A. Burdett, D. M. Madigan, T. Johnson, and P. D. Rosso, *J. Am. Chem. Soc.*, **97**, 3428 (1975).

4) M. Kato, M. Kawamura, Y. Okamoto, and T. Miwa, *Tetrahedron Lett.*, **1972**, 1171.

5) M. Kato, M. Funakura, M. Tsuji, and T. Miwa, *J. Chem. Soc., Chem. Commun.*, **1976**, 63.

6) In the case of **10**, the equilibrium (**10**⇌**13**=2 : 1) is established after 5 min at 90 °C.

7) M. Pomerantz, G. W. Gruber, *J. Am. Chem. Soc.*, **93**, 6615 (1971).

8) M. Traetteberg, *J. Am. Chem. Soc.*, **86**, 4265 (1964).

9) J. A. Berson, *Acc. Chem. Res.*, **1**, 152 (1968).

10) R. B. Woodward and R. Hoffmann, "The Conservation of Orbital Symmetry" Verlag Chemie, Bergstrsse, Germany (1970), pp. 132—140.

11) Mallinckrodt Chemical Works Silicic Acid (100 mesh) analytical grade was used throughout this experiment.

12) It has been found that methyl 5*H*-benzocycloheptene-5-carboxylate exists in an equilibrated mixture of the two conformers with pseudo-equatorial and a pseudo-axial methoxycarbonyl groups, which were detected by a low temperature NMR spectroscopy (below −90 °C)[M. Kato, K. Takatoku, S. Ito, and T. Miwa, unpublished work]. Likewise, **24** seems to exist in such mixture and the presence of 9-isopropyl group in **24** would make the interconversion much more difficult.

Vinyl Polymerization. 368.[1] Polymerization of Methyl Methacrylate with the System of RNA, Water and Cu(II) Ion

Minoru IMOTO, Yoshiyuki NISHIDA, Toshiyuki YOSHIKAWA, and Tatsuro OUCHI

Department of Applied Chemistry, Faculty of Engineering, Kansai University, Suita, Osaka 564

(Received September 14, 1977)

The radical polymerization of methyl methacrylate (MMA) was carried out with the system of ribonucleic acid (RNA), Cu(II) ion and water. The generation of free radical was found to take place in the water layer where RNA and Cu(II) ion exist. Urea shows a promoting activity. The effects of pH of water medium and temperature on the conversion of MMA were investigated. A reaction mechanism was proposed.

The so-called uncatalyzed polymerization is a novel reaction, in which macromolecule (or oligomer) in water phase incorporates vinyl monomer from monomer phase, forms a complex with water, monomer and Cu(II) ion, and generates free radicals. The radical polymerization proceeds in the water phase, *i.e.*, predominantly in the hydrophobic area formed by macromolecules. The present paper deals with radical polymerization of methyl methacrylate (MMA) initiated with a system of aqueous copper(II) chloride solution and RNA which was used as macromolecule. Sugiyama and Lee independently reported the polymerization of MMA with the system of RNA, water and Cu(II) ion in the presence or absence of carbon tetrachloride.[2] They investigated in detail only the case in which carbon tetrachloride is present. The present paper is concerned with the case in which it is absent and might be of value for reference.

Experimental

Materials. Commercial RNA from yeast (Sigma Chemical Co. 6750, Lot. 124C-8150) was used. Water was ion-exchanged and redistilled. Copper(II) chloride of special commercial grade was used without further purification. MMA, styrene, and acrylonitrile were purified by the usual method and redistilled before use.

Preparation of Buffer Solutions. These were prepared by use of following systems: pH 3.0—6.0: M/10 citric acid-M/5 Na_2HPO_4; pH 7: M/15 Na_2HPO_4-M/15 KH_2PO_4; pH 8—9: M/10 HCl-M/20 $Na_2B_4O_7$; pH 10: M/20 $Na_2B_4O_7$-M/10 NaOH; pH 11—12 M/10 NaOH-M/10 Na_2HPO_4.

Procedure. Monomer, the aqueous solution of RNA and $CuCl_2 \cdot 2H_2O$ were placed in an ampoule. The ampoule was flushed with nitrogen, frozen, evacuated at 0.1 mmHg, and scaled. The ampoule was shaken in a thermostat. After the reaction, the contents of the ampoule were poured into a large amount of methanol in order to precipitate the polymer. The polymer was collected on a glass filter, thoroughly washed with methanol and water and dried. The number-average degree of polymerization (P_n) of poly-MMA was estimated by gel permeation chromagraphy, using tetrahydrofuran as an eluent.

Results and Discussion

Selectivity of Vinyl Monomer. Polymerization of vinyl monomers was carried out in the presence of RNA, water and Cu(II) ion. The results are given in Table 1. The polymerization of acrylonitrile took place easily in the absence of RNA, by the charge transfer polymerization with Cu(II) ion.[3] The conversion of styrene was due to thermal polymerization.

Table 1. Selectivity of vinyl monomer
(Monomer 3 cm³, H_2O 10 cm³, $CuCl_2 \cdot 2H_2O$ 5×10^{-4} g; 85 °C, 5 h)

RNA/g	Conversion/%		
	MMA	AN	St
0	1.2	8.7	4.2
0.02	6.2	1.3	3.8

Table 2. Activity of metallic salts
(Metallic salts 2.9×10^{-6} mol. MMA 3 cm³, H_2O 10 cm³; 85 °C, 5 h)

RNA/g	Conversion/%				
	$MgCl_2 \cdot 6H_2O$	$FeCl_3 \cdot 6H_2O$	$FeCl_2 \cdot (4H_2O)$	$MnCl_2 \cdot 4H_2O$	$CuCl_2 \cdot 2H_2O$
0.02	1.7	2.6	2.5	2.6	6.2
0	1.2	1.7	1.8	1.8	1.2

It is evident that only MMA was polymerized by RNA.

Effect of Metallic Ion on Polymerization. In order to investigate the effect of metallic ion on polymerization, five kinds of metallic chlorides were added to the reaction system. The results are given in Table 2. Copper(II) chloride was the most active promotor for polymerization, and was thus used in subsequent polymerizations.

Figure 1 shows the effect of the amount of Cu(II) ion on the conversion of MMA. A maximum conver-

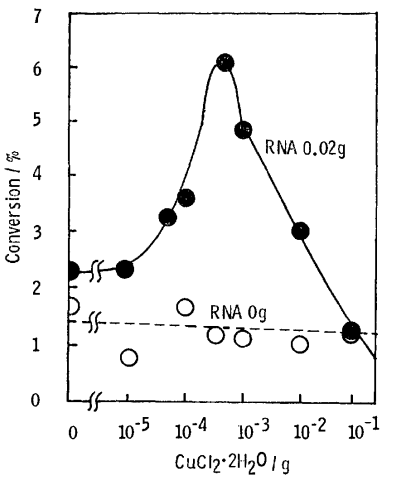

Fig. 1. Conversion of MMA *vs.* amount of Cu(II) ion. MMA 3 cm³, H_2O 10 cm³; 85 °C, 5 h.

sion of MMA was obtained at 5×10^{-4} g of copper(II) chloride. On the other hand, in the absence of Cu(II) ion, the polymerizations was hardly accelerated at all. The open circles indicate the conversion of MMA by thermal polymerization (1.2% in average). Cu(II) ion was found to be very effective.

Proof of Radical Mechanism. In order to confirm the view that polymerization proceeds through a radical mechanism, the copolymerization of MMA with styrene was carried out. The results are shown in Fig. 2. A radical mechanism was verified from the curve.

Locale of the Reaction. In order to find the locale of the generation of the initiating radical, polymerization of MMA was carried out without shaking. The ampoule containing 3 cm^3 of MMA, 0.02 g of RNA, 5×10^{-4} g of $CuCl_2\cdot2H_2O$ and 10 cm^3 of water was allowed to stand at 85 °C. The contents consist of two layers (Fig. 3(a)). As the polymerization proceeded, the water layer became turbid by the polymerized MMA (Fig. 3(b)). After 7 h, the MMA-layer was pipetted out and poured into methanol (conversion: 1.4%, $\bar{P}_n$ of poly-MMA: 1.3×10^4). The water layer was also poured into methanol (conversion: 9.8%, $\bar{P}_n$ of poly-MMA: 1.4×10^{-4}). From the results, it was concluded that the polymerization initiated with RNA takes place in the water layer. The conversion of 1.4% in MMA phase was the result of thermal polymerization.

Effects of the pH of Water Layer on the Conversion of MMA. The results obtained are shown in Fig. 4. The conversion of MMA shows a maximum at pH 8, it being

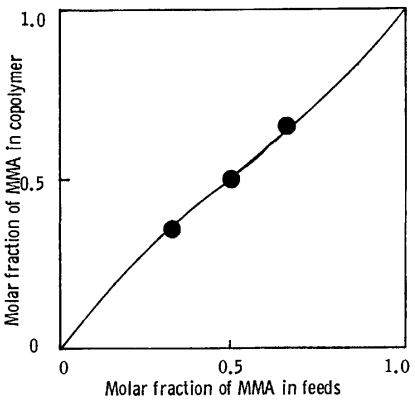

Fig. 2. Copolymerization of MMA and styrene. RNA 0.02 g, $CuCl_2\cdot2H_2O$ 5×10^{-4} g, H_2O 10 cm^3; 85 °C, 5 h.

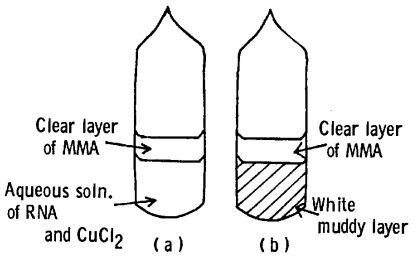

Fig. 3. Appearance of the ampoule on standing polymerization.

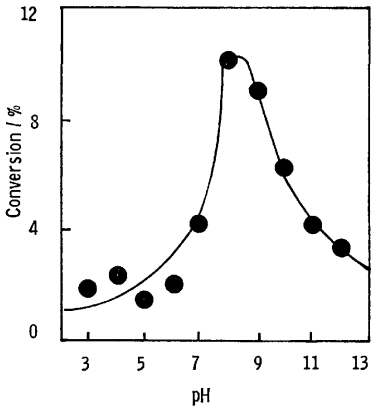

Fig. 4. Conversion of MMA *vs.* pH of aqueous phase. RNA 0.02 g, MMA 3 cm^3, $CuCl_2\cdot2H_2O$ 5×10^{-4} g, H_2O 10 cm^3; 85 °C, 5 h.

assumed that in the acidic medium, the phosphonate group has the undissociated form I. The decrease in the conversion in acidic medium can be explained by the loss of ionized form II. In the basic medium, the conversion decreased. It seems that NH_2 or NH group of nucleic acid bases becomes free from protonated structure and can easily form a complex with copper(II) ion. Thus when too much NH_2 or NH group exists, the effective activity of Cu(II) ion is lost and the

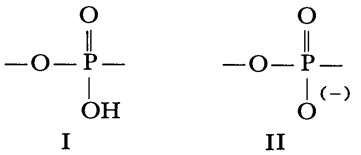

conversion decreases. Such a retarding effect of free NH_2 group was discussed in the polymerization of MMA initiated with Nylon-3[4].

Effect of Urea on Conversion of MMA. Recently, it was found by Imoto *et al.* that urea can promote the conversion of MMA remarkably in radical polymerization initiated by the system of Cu(II) ion, water and Nylon-3[5] or α-amylase.[6] Urea is known as a denaturing agent of proteins. The tertiary structure of a protein molecule can be unfolded to form new hydrogen bonds between urea and peptide chain. Urea reveals its activity as shown in Table 3, even though the promoting effect is not so large.

Table 3. Effect of urea on the polymerization (RNA 0.02 g, MMA 3 cm^3, $CuCl_2\cdot2H_2O$ 5×10^{-4} g, H_2O 10 cm^3; 85 °C, 5 h)

Urea/g	Conversion/g	$\bar{P}_n$ of Poly-MMA
0	6.2	—
0.05	10.5	3.5×10^4
0.10	11.2	3.4×10^4

Effect of Temperature on the Conversion of MMA. The results are shown in Fig. 5.

Mechanism of Initiation. Polymerization is considered to start by the incorporation of MMA into a

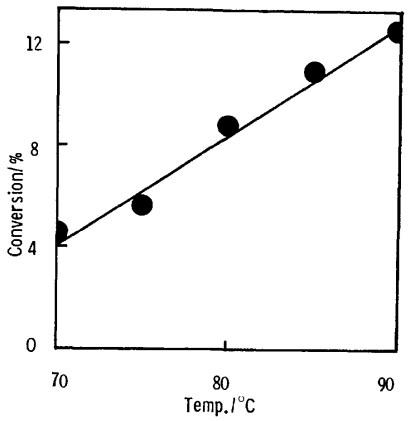

Fig. 5. Conversion of MMA *vs.* polymerization temperature. RNA 0.02 g, MMA 3 cm³, $CuCl_2 \cdot 2H_2O$ 5×10^{-4} g, pH 8, Buffer solution 10 cm³; 85 °C, 5 h.

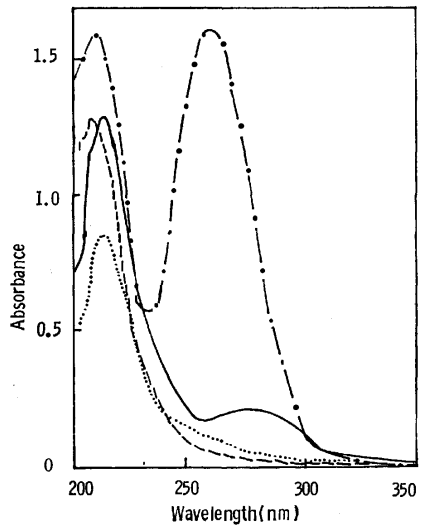

Fig. 6. UV-spectra measured in aqueous solution at 4.7—5.7 of pH.

Reference	Sample
—— ——	$CuCl_2 \cdot 2H_2O$
-·-· ——	RNA
—— RNA	$CuCl_2 \cdot 2H_2O$ + RNA
····· RNA + $CuCl_2 \cdot 2H_2O$	RNA + $CuCl_2 \cdot 2H_2O$ + MMA

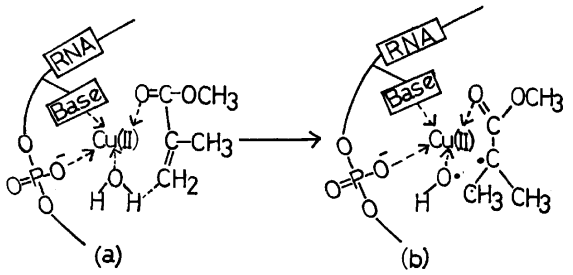

Fig. 7. Assumed initiation mechanism.

hydrophobic area formed by RNA molecules. RNA then forms a complex with Cu(II) ion, MMA and water. This is verified partially by the spectral study (Fig. 6). $CuCl_2$ solution in water showed a peak at 208 nm which corresponds to the complex $[Cu(II)\text{-}(OH^-)_x(H_2O)_{4-x}]$. The λ_{max} of water (vapor) is 167 nm[7]. By complexing with Cu(II) ion, this absorption maximum is consisdered to shift to 208 nm, *i.e.*, the λ_{max} of 208 nm corresponds to $Cu(II)(OH^-)_x(H_2O)_{4-x}$. The value of x may be small in the present measurement. RNA solution in water showed a peak at 260 nm which is due to RNA. The peak shifted to 275 nm in the RNA–$CuCl_2$–H_2O solution. This is considered to be an evidence of complex formation of Cu(II) ion with RNA. However, further addition of MMA to the solution of RNA and $CuCl_2$ showed no peak of complexed MMA in this region of wavelength. The ionized phosphonate group was assumed to be necessary, too much free NH_2 or NH group retarding the polymerization. The complex is indicated in Fig. 7(a). As regards the generation of the free radical, we have repeatedly proposed the hydrogen atom transfer from water molecule to MMA as shown in Fig. 7(b).

References

1) M.Imoto, T. Ouchi, M. Sakae, and H. Yamamoto, *Makromol. Chem.*, in press.
2) K. Sugiyama and S. W. Lee, *J. Polym. Sci., Polym. Lett. Ed.*, **15**, 17 (1977).
3) J. Furukawa, "Senikinzokushokubaijugo," Kagakudojin, 1st ed, 1972, p. 155.
4) T. Ouchi, T. Nishimura, and M. Imoto, *J. Polym. Sci., Polym. Chem. Ed.*, **14**, 2695(1976).
5) T.Nishimura, T. Ouchi, and M. Imoto, *Makromol. Chem.*, **177**, 1895(1976).
6) M. Imoto, N. Sakade, and T. Ouchi, *J. Polym. Sci., Polym. Chem. Ed.*, **15**, 499(1977).
7) H. Tsubomura, K. Kimura, K. Kaya, J. Tanaka, and S. Nagakura, *Bull. Chem. Soc. Jpn.*, **37**, 417(1964).

The Reactions of a Variety of Diazo Compounds with Sulfur Dioxide in Ethanol

Toyoshige TANABE and Toshikazu NAGAI

Institute of Chemistry, College of General Education, Osaka University, Toyonaka, Osaka 560

(Received September 16, 1977)

The reactions of several diazomethanes bearing a variety of substituents with sulfur dioxide were carried out in ethanol. The reaction of a diazomethane possessing an electron-releasing group gave the olefin as the major product. On the contrary, the ethyl ethers were predominantly afforded from the reactions of the diazomethanes containing an electron-withdrawing group. Moreover, the ethyl alkanesulfonates were obtained in the cases bearing the substituent of an intermediate electronic character. The observed product distribution is interpreted in terms of the nucleophilicity of the α-carbon atom of the diazomethane: the preference of the formation of sulfene by the electrophilic attack of SO_2 on the diazomethane to the acid-catalyzed decomposition by ethyl hydrogen sulfite reflects the nucleophilicity of the α-carbon atom in the diazomethane.

The reactions of diazoalkanes with sulfur dioxide in aprotic solvents are well known to lead to a sulfene intermediate *in situ* followed by the formation of episulfone, olefin, and the carbonyl compounds.[1] In a previous paper,[2] we demonstrated that this reaction certainly proceeds *via* sulfene by the use of enamine as a trapping reagent. Ethanol, one of the typical protic solvents, is also known to act as a trapping agent of the sulfene derived from alkanesulfonyl chloride and triethylamine.[3] However, in the system of diazoalkane and sulfur dioxide, contrary to the amine–chloride system, diazoalkane is liable to undergo decomposition by ethyl hydrogen sulfite, which is at equilibrium with ethanol and sulfur dioxide(Scheme 1, Route B). For example, Hesse and Majmudar[4] reported that ethyl ethoxyacetate was afforded from ethyl diazoacetate and that benzhydryl ethyl sulfite, whose structure had not yet been entirely established, was obtained from diphenyldiazomethane; therefore, the reaction proceeds not by a sulfene mechanism, but by a mechanism involving a protic acid.

In the present paper, we will describe how the possibility of an electrophilic attack of sulfur dioxide on the diazo compound to form sulfene(Scheme 1, Route A) can not be precluded as the initial stage of the reaction even in the system of ethanol and sulfur dioxide, depending on the substituents of diazomethane. Furthermore, as for the follow-up reaction of sulfene (formed *via* Route A), the reaction of sulfene with a new molecule of a diazo compound to give olefin (Route A_1) was found possibly to take place in competition with the trapping of sulfene by ethanol to yield the sulfonate(Route A_2).

Results and Discussion

NMR Study of the Interaction between Ethanol and SO_2. In order to obtain information on the interaction of ethanol and SO_2, the NMR spectra of these solvent mixtures at various ratios were measured, adding CCl_4 to keep the concentration of ethanol constant. The results are listed in the table. Upon an increase in the relative amount of SO_2, the signal of the hydroxylic hydrogen atom gradually shifts to a higher magnetic field, as may be seen in the table. This observation may be attributed to the cleavage of the hydrogen-bonding self association of ethanol by a weak interaction between the oxygen atom of ethanol and the sulfur atom of SO_2, like I as well as the methanol–SO_2 system which was previously reported.[5] If ethyl hydrogen sulfite(II), the OH-proton signal of

$$(C_2H_5OH)_4 \overset{SO_2}{\rightleftharpoons} 4\ \underset{\mathbf{I}}{\begin{matrix} C_2H_5 \\ H \end{matrix}\!\!>\!O\cdots S<\!\!\begin{matrix} O \\ O \end{matrix}} \rightleftarrows 4\ \underset{\mathbf{II}}{C_2H_5O\text{-}S\text{-}OH \\ \quad\quad\ \ \| \\ \quad\quad\ \ O}$$

which would appear in a very low field, were formed in an appreciable amount, the observed chemical shift (δOH) should go to a lower field because δOH must be the average chemical shift of two exchangeable hydroxylic protons of ethanol and II. Therefore, an

Table. The chemical shifts of protons of EtOH under the influence of SO_2

[EtOH] mol%	Molar ratio SO_2 : CCl_4	δOH ppm	δCH_2 ppm	δCH_3 ppm
83.1	0 : 100	5.01	3.38	0.93
84.0	25 : 75	5.00	3.38	0.93
82.8	39 : 61	4.95	3.33	0.88
82.3	58 : 42	4.95	3.36	0.92
84.2	82 : 18	4.89	3.31	0.88
82.6	100 : 0	4.84	3.32	0.88

Measured at 26° C; external standard, TMS.

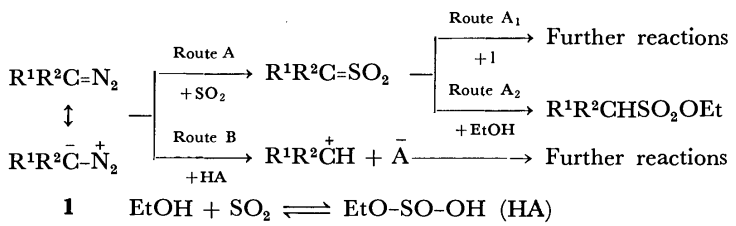

1 $EtOH + SO_2 \rightleftharpoons EtO\text{-}SO\text{-}OH$ (HA)

Scheme 1.

$R^1R^2CN_2 + SO_2 + EtOH \longrightarrow R^1R^2C{=}CR^1R^2 + R^1R^2CHSO_2\text{-}OEt$

1a R^1=*p*-tolyl, R^2=H — *cis*-**2a** 21%[a] **3a** 23%; *trans*-**2a** 38%

$+ R^1R^2C{=}N\text{-}N{=}CR^1R^2 + R^1\text{-}CO\text{-}R^2$

4a 9% **5a** 4%

$R^1R^2CN_2 + SO_2 + EtOH \longrightarrow R^1R^2CHSO_2\text{-}OEt$

1b R^1=R^2=phenyl — **3b** 87%

1c R^1,R^2=fluorenylidene — **3c** 89%

$R^1R^2CN_2 + SO_2 + EtOH \longrightarrow R^1R^2CHO\text{-}SO\text{-}OEt + R^1R^2CH\text{-}OEt$

1d R^1=*p*-nitrophenyl, R^2=H — **6d** 4% **7d** 79%

1e R^1=ethoxycarbonyl, R^2=H — **7e** 81%

Scheme 2. The reactions of diazo compounds(**1**) with SO_2 in ethanol.

a) The yields are in mol% based on the **1** used for **3**, **5**, **6**, and **7**, and based on a half mole of the **1** used for **2** and **4**.

ethanol solution of SO_2 consists largely, if not entirely, of ethanol and SO_2 rather than of ethyl hydrogen sulfite.

Reactions of Diazo Compounds in Ethanol–SO_2 System. The reactions of diazoalkanes(**1**) bearing a variety of substituting groups were carried out by passing gaseous SO_2 through an ethanol solution of **1** for a period of 1 h at 20 °C. The results are summarized in Scheme 2.

In the reaction of **1a**, *cis*- and *trans*-di-*p*-tolylethylene (**2a**) were afforded as the major products in yields of 21 and 38% respectively, together with ethyl *p*-tolylmethanesulfonate(**3a**) (23%), *p*-tolualdehyde azine(**4a**) (9%), and *p*-tolualdehyde(**5a**) (4%). Moreover, there was no proton signal at around δ=5 ppm[6] which could be assigned to the methylidyne proton of the corresponding *cis*- and *trans*-episulfone, 2,3-di-*p*-tolylthiirane 1,1-dioxide. This result may be ascribed to the low stability of episulfone under these reaction conditions; they might undergo decomposition to yield stilbene derivatives.[1b,7]

When **1b** or **1c** was used, the corresponding sulfonate, ethyl diphenylmethanesulfonate(**3b**) or ethyl 9-fluorenesulfonate(**3c**), was predominantly afforded. As for the structure of the reaction product of **1b**, benzhydryl ethyl sulfite(**6b**) was proposed, though not fully established, by Hesse and Majmudar.[4] This product was identified as **3b** and not the isomeric **6b** from the evidence of the mass fragmentation and the IR spectrum, in which two characteristic absorption bands of $-SO_2-$ were observed at 1168 and 1345 cm^{-1}. These observations were also made in **3c**.

On the other hand, ethyl ether, **7d** or **7e**, was exclusively afforded from the reaction of **1d** or **1e** respectively, in which an electron-withdrawing substituent is attached. This type of product is commonly obtained from the acid-catalyzed decomposition of diazo compounds in ethanol and from the thermolysis and the photolysis of diazo compounds in ethanol. In the reaction of **1d**, *p*-nitrobenzyl ethyl sulfite(**6d**) was also obtained in a very low yield(4%). Further, in the case of **1e**, the reaction did not practically proceed under the condition described above; the reaction was, instead, carried out at 40 °C for 2 h.

From the results presented above, it is clear that the product distribution was drastically varried with the electronic character of the substituent in **1**, that is, according to the nucleophilicity of the α-carbon atom in **1**.

Reaction Mechanism. Two different explanations are apparently possible to account for the decomposition of the diazo compounds(**1**) in the ethanol–SO_2 system and the formation of the various compounds, **2**—**7**: a reaction *via* sulfene[1] and an acid-catalyzed reaction.[8]

In the reaction of **1b**, the exclusive formation of **3b** is best explained by the process *via* the sulfene intermediate. If the decomposition proceeded by II, the reaction would result in the formation of benzhydryl ethyl ether, tetraphenylethylene, or benzhydryl ethyl sulfite as likely in a protic-acid decomposition. Hence, the possibility of acid catalysis can be ruled out. In this system, a sulfene intermediate was formed *in situ* by the electrophilic attack of SO_2 on **1b**, followed by the addition to ethanol, thus affording **3b**. This is also the case with the reaction of **1c**. As in these two cases, in the reaction of **1a**, which has a more electron-releasing substituent, sulfonate(**3a**) was also given in a 23% yield. In this instance, however, the major product was olefin, *cis*- and *trans*-**2a**(21 and 38% respectively). For the formation of this type of compound, both the sulfene process[1] and acid decomposition[8] are possible. If the latter process is involved in the present reaction, ethyl ether may be formed. Ethyl ether was not, however, obtained here. Furthermore, azine(**4a**) and aldehyde(**5a**) can not be afforded by acid decomposition.

As an alternative, the route involving a sulfene intermediate seems rather attractive as an explanation of the formation of **2a**, together with **4a** and **5a**. According to this process, sulfene was first generated *in situ* by the electrophilic attack of SO_2 on **1a**, with the loss of N_2. The further electrophilic attack of this sulfene intermediate on another, **1a**, rather than ethanol provides the transient 1,3,4-thiadiazoline 1,1-dioxide derivative(**9**), without the loss of N_2, or provides the thiirane 1,1-dioxide derivative(**10**), with the loss of N_2, which then lead to **2a** or **4a** (Scheme 3).[9] Furthermore, **5a** was afforded by the reaction of sulfene and SO_2.[1]

On the contrary, ethers are the major products in the cases bearing electron-withdrawing substituents like **1d** and **1e**. A sulfene mechanism can not give a satis-

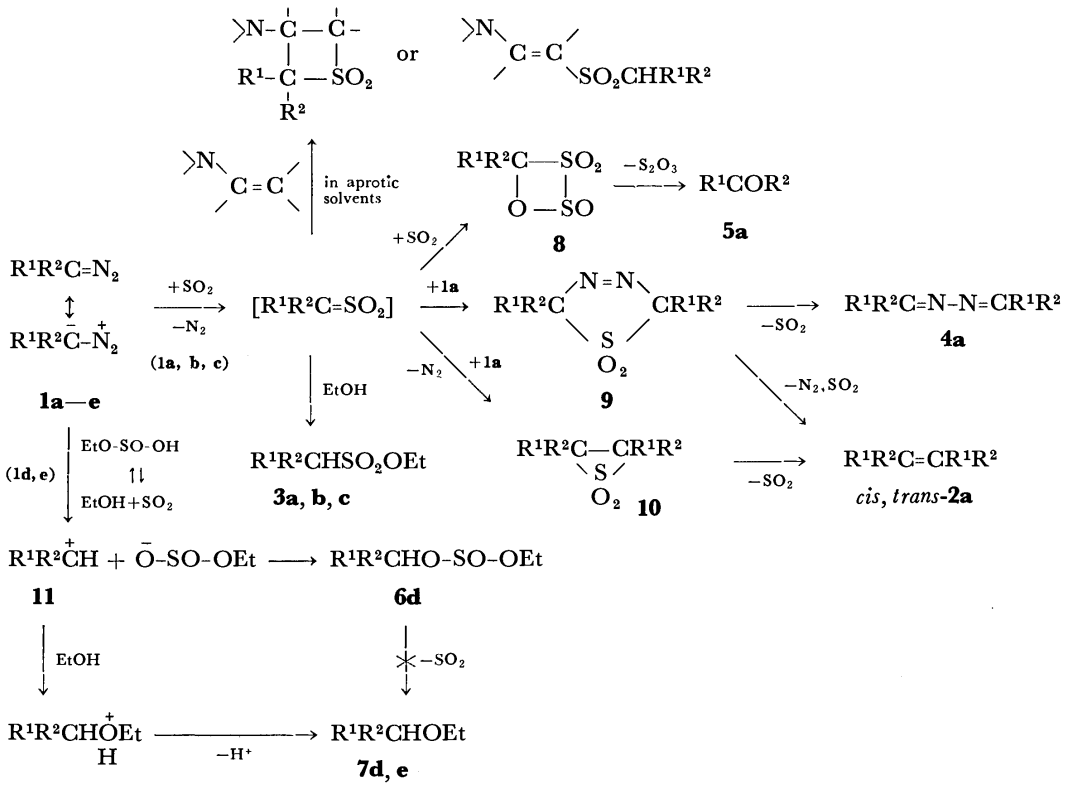

Scheme 3.

factory explanation of the formation of **7d** and **7e**. If a sulfene intermediate is involved, the expected product is a sulfonate like **3**. Rather, **7d** or **7e** is the typical product of an acid-catalyzed decomposition of diazo compounds, as has already been mentioned. **1d** and **1e** did not show sufficient reactivity against SO_2 because of the low electron density on the α-carbon atom. Actually, **1d** showed a slower decolorization than the other diazomethanes(**1a**, **b**, and **c**). Especially, **1e** did not react against SO_2 positively under ordinary reaction conditions. Furthermore, **1e** was recovered in the reaction of **1e** with SO_2 at 20 °C in benzene in the presence of 1-morpholino-2-methylpropene, which traps the sulfene intermediate to afford the additive product.[2] Therefore, the most reasonable and acceptable mechanistic route for the formation of ether, **7d** or **7e**, is that the carbonium ion(**11**) is first formed by protonation to diazomethane with a small amount of ethyl hydrogen sulfite, which is at equilibrium with ethanol and SO_2; this is followed by the addition to ethanol, giving **7d** or **7e** in a catalytic manner. As for the formation of **7e**, Hesse and Majmudar[4] proposed a route involving the decomposition of sulfite(**6**), which is yielded by the collapse of **11** with the conuter-ion. In the current observation, **6d** was isolated in a very low yield(4%); this compound is too stable to undergo decomposition to afford **7d**.

According to the observed results and the discussions presented above, the mechanism of the decomposition of the diazomethanes and the follow-up reaction, in the ethanol–SO_2 system depend on the structures of the diazomethanes. An acid-catalyzed decomposition may be limited to the diazo compounds with a relatively strong electron-withdrawing group, while a sulfene formation is regarded as much more likely for the more nucleophilic diazomethanes: olefin or sulfonate was afforded *via* the sulfene from the diazomethane, in which the α-carbon atom has a comparatively high electron density, or from that of an intermediate electronic character, respectively. To clarify the scope and limitations of this reaction, further investigation will be necessary; however, it should be noted here that not all kinds of the diazomethanes are decomposed by a protic acid.

Experimental

The NMR spectra were recorded on a Varian EM-360 (60MHz) instrument in $CDCl_3$, with TMS as the internal standard. The IR spectra were measured with a Hitachi 215 spectrophotometer. The mass spectra were run on a VD-10001-A Hitachi spectrometer.

Materials. All the diazo compounds were prepared by known procedures: *p*-tolyldiazomethane(**1a**),[10] diphenyl diazomethane(**1b**),[11] 9-diazofluorene(**1c**),[12] *p*-nitrophenyldiazomethane(**1d**),[13] and ethyl diazoacetate(**1e**).[14] The sulfur dioxide was dried by passing it through $CaCl_2$ and P_2O_5 tubes. The ethanol was purified[15] and dried by refluxing it over magnesium metal. The carbon tetrachloride was purified by the ordinary method[15] and was dried over activated molecular sieves, MS-4A.

Procedure. *NMR Study*: The solutions to be studied were prepared by passing SO_2 slowly through ethanol until saturation. After determining the amount of SO_2, definite amounts of CCl_4 and ethanol were added to this solution. These operation were carried out under a good dry condition. The solution was then transferred into

an NMR tube, and the tightly cap-sealed tube was submitted to NMR analysis at 26 °C.

General Method for the Reaction of ***1*** *with SO_2 in Ethanol.* In a 100-ml, three-necked flask equipped with a magnetic stirrer, a gas inlet tube, a thermometer, and a calcium chloride drying tube we placed 5 mmol of **1** and 100 ml of anhydrous ethanol. Gaseous SO_2 was then introduced into this solution at 20 °C for a period of 1 h. After the decolorization of the solution and the evolution of N_2 was complete, the solvent and the excess SO_2 were removed *in vacuo* at room temperature. An aliquot of the residue was dissolved in $CDCl_3$ and analyzed by NMR; then the NMR solvent was removed, and the combined residue was separated by preparative silica gel column chromatography, if necessary. An analytically pure sample was obtained by recrystallization from suitable solvents.

The Reaction of ***1a.*** The reaction was carried out using twice the amount of **1a**. According to the NMR spectrum, five kinds of products were contained in the crude reaction mixture. These products were submitted to the preparative silica gel column chromatograph. *cis-* and *trans-***2a** were eluted first by benzene; these two geometric isomers were isolated by fractional recrystallization from ethanol. The isolated yields of *cis-* and *trans-***2a** were 21 and 38% respectively. *cis*-Di-*p*-tolylethylene (*cis-***2a**) was crystallized from ethanol; colorless prisms; mp 31—32 °C (lit, 32.3 °C).[16] NMR: δ 2.30(6H, s, methyl), 6.50(2H, s, vinyl), and 7.00 and 7.15(each 4H, d, J=8 Hz, phenyl). MS: m/e=208(M^+). *trans*-Di-*p*-tolylethylene(*trans-***2a**) was recrystallized from ethanol; colorless leaflets; mp 183—184 °C (lit, 179—180 °C).[17] NMR: δ 2.30(6H, s, methyl), 6.98 (2H, s, vinyl), and 7.10 and 7.37(each 4H, d, J=8Hz, phenyl). Found: C, 91.75; H, 7.74%. Calcd for $C_{16}H_{16}$: C, 92.26; H, 7.74%. *p*-Tolualdehyde azine(**4a**) was obtained as the second eluate by the use of benzene; its yield was estimated to be 9% from the intensity of the NMR spectrum of a reaction mixture. The recrystallization from acetone gave pale yellow prisms; mp 159—160 °C(lit, 157 °C).[18] IR(KBr): 1615 cm^{-1}(C=N). NMR: δ 2.40(6H, s, methyl), 7.26 and 7.77 (each 4H, d, J=8.5Hz, phenyl), and 8.65 (2H, s, methylidyne). Found: C, 81.32; H, 6.83; N, 11.66%. Calcd for $C_{16}H_{16}N_2$: C, 80.99; H, 6.85; N, 11.65%. *p*-Tolualdehyde(**5a**) and ethyl *p*-tolylmethanesulfonate(**3a**) were eluted by ether as the final fraction in yields of 4 and 23% respectively. The **5a** was identified by the comparison of its IR and NMR spectra with those of an authentic specimen. The **3a** was purified by further silica gel column chromatography and was recrystallized from ethanol; colorless plates; mp 40—41 °C. IR(KBr): 1170, 1175, 1350, and 1355 cm^{-1} (SO_2). NMR: δ 1.30(3H, t, J=7 Hz, $CH_2\underline{CH_3}$), 2.37 (3H, s, CH_3), 4.12 (2H, q, J=7 Hz, $\underline{CH_2}CH_3$), 4.30 (2H, s, benzylic), and 7.25 (4H, broad s, phenyl). MS: m/e=214(M^+),105 (p-CH_3-C_6H_4-CH_2^+).

Reaction of ***1b.*** The white crystalline was obtained in a 87% yield by removing the solvent; subsequent recrystallization from ethanol gave colorless needles of ethyl diphenylmethanesulfonate (**3b**); mp 70—71 °C. IR (KBr): 1168 and 1345 cm^{-1}(SO_2). NMR: δ 1.15(3H, t, J=6Hz, CH_3), 4.00(2H, q, J=6Hz, CH_2), 5.50(1H, s, methylidyne), and 7.23—7.73(10H, m, phenyl). MS: m/e=276(M^+), 167(Ph_2CH^+). Found: C, 65.12; H, 5.77%. Calcd for $C_{15}H_{16}O_3S$: C, 65.21; H, 5.84%.

Reaction of ***1c.*** In the same manner as has been described above, a white powder, ethyl 9-fluorenesulfonate (**3c**), was obtained in a 89% yield; it was subsequently recrystallized from ethanol; colorless needles; mp 94.5—95.5 °C. IR(KBr): 1175 and 1355 cm^{-1}(SO_2). NMR: δ 0.93(3H, t, J=7Hz, CH_3),3.87(2H, q, J=7Hz, CH_2), 5.37(1H, s, methylidyne), and 7.2—8.1(8H, m, aromatic). MS: m/e=274(M^+), 165($M^+-C_2H_5SO_3$). Found: C, 65.96; H, 5.24%. Calcd for $C_{15}H_{14}O_3S$: C, 65.96; H, 5.15%.

Reaction of ***1d.*** The reaction was carried out using 10 mmol of **1d**. The crude reaction mixture was chromatographed over silica gel. *p*-Nitrobenzyl ethyl ether(**7d**), fractionated as the first eluate, was purified by further column chromatography; a pale yellow oil. IR: 1515 and 1345 cm^{-1}(NO_2), 1105 cm^{-1}(C-O-C). NMR: δ1.27(3H, t, J=7 Hz, CH_3), 3.60(2H, q, J=7 Hz, OCH_2CH_3), 4.59 (2H, s, benzylic), and 7.50 and 8.18(each 2H, d, J=8.5Hz, phenyl). MS: m/e=181(M^+), 152(p-NO_2-C_6H_4-CH_2O^+), 136(p-NO_2-C_6H_4-CH_2^+), 106(p-O-C_6H_4-CH_2^+). *p*-Nitrobenzyl ethyl sulfite(**6d**) was also separated in a 4% yield by further elution with benzene; it was recrystallized from ethanol as colorless needles; mp 87—88 °C. IR(KBr): 1175 cm^{-1}(O-SO-O), 1345, 1355, 1515, and 1525 cm^{-1}(NO_2). NMR: δ 1.33(3H, t, J=7Hz, CH_3), 4.23(2H, q, J=7Hz, OCH_2CH_3), 4.41(2H, s, benzylic), and 7.60 and 8.26(each 2H, d, J=8Hz, phenyl). MS: m/e=245(M^+), 152(p-NO_2-C_6H_4-CH_2O^+), 136(p-NO_2-C_6H_4-CH_2^+), 106(p-O-C_6H_4-CH_2^+).

Reaction of ***1e.*** Although the reaction did not practically proceed under ordinary conditions, it was accomplished at 40 °C for 2 h using 15 mmol of **1e** and 60 ml of ethanol. The oily crude product, obtained in an 81% yield by fractional distillation under reduced pressure, was identified as ethyl ethoxyacetate(**7e**); a colorless oil. IR: 1753 cm^{-1} (C=O), 1138 and 1205 cm^{-1}(C-O-C). NMR: δ 1.23(3H, t, J=6.5Hz, $OCH_2\underline{CH_3}$), 1.27(3H, t, J=7Hz, $CO_2CH_2\underline{CH_3}$),3.60(2H, q, J=6.5Hz, OCH_2CH_3), 4.03(2H, s, OCH_2CO), and 4.21(2H, q, J=7Hz, $CO_2\underline{CH_2}CH_3$). MS: m/e=103($M^+-C_2H_5$), 88($M^+-C_2H_4O$).

Reaction of ***1e*** *with SO_2 in the Presence of Enamine.* The reaction was tried using 10 mmol of **1e**, 10 mmol of 1-morpholino-2-methylpropene, and 50 mmol of SO_2 in 100 ml of benzene in the manner described in the previous paper,[2] but **1e** was recovered from the reaction mixture by distillation under reduced pressure.

References

1) For a review, see: a) G. Opitz, *Angew. Chem. Int. Ed. Engl.*, **6**, 107 (1967); b) N. H. Fischer, *Synthesis*, **1970**, 393; c) T. Nagai and N. Tokura, *Int. J. Sulfur Chem.*, **7B**, 207 (1972).

2) T. Tanabe and T. Nagai, *Bull Chem. Soc. Jpn.*, **50,** 1179 (1977).

3) a) W. E. Truce, R. W. Campbell, and J. R. Norell, *J. Am. Chem. Soc.*, **86**, 288 (1964); b) W. E. Truce and R. W. Campbell, *ibid.*, **88**, 3599 (1966); c) J. F. King and T. Durst, *ibid.*, **86,** 287 (1964); **87**, 5684 (1965).

4) G. Hesse and S. Majmudar, *Chem. Ber.*, **93**, 1129 (1960).
Staudinger and Pfenninger reported that ethyl diphenylmethanesulfonate was obtained from diphenyldiazomethane under similar conditions: H. Staudinger and F. Pfenninger, *Ber.*, **49**, 1941 (1916).

5) T. Nagai, H. Abe, and N. Tokura, *Bull. Chem. Soc. Jpn.*, **42,** 1705 (1969).

6) For instance, the methylidyne proton signals of *cis*-2,3-diphenylthiirane 1,1-dioxide are at 5.21 ppm: N. Tokura, T. Nagai, and S. Matsumura, *J. Org. Chem.*, **31**, 349 (1966).

7) F. G. Bordwell, J. M. Williams, Jr., E. B. Hoyt, Jr., and B. B. Jarvis, *J. Am. Chem. Soc.*, **90**, 429 (1968).

8) For a review, see: R. A. More O'Ferrall, "Advances in Physical Organic Chemistry," Vol. 5, Academic Press, New York (1967), p. 331.
9) The SO_2-elimination of the azosulfone **9** providing the azine **4a** can be interpreted as a thermally allowed, linear cheletropic reaction: R. B. Woodward and R. Hoffmann, *Angew. Chem. Int. Ed. Engl.*, **8**, 781 (1969).
10) W. R. Bamford and T. S. Stevens, *J. Chem. Soc.*, **1952**, 4775.
11) L. I. Smith and K. L. Howard, *Org. Synth.*, Coll. Vol. III, 351 (1955).
12) H. Staudinger and O. Kupfer, *Ber.*, **44**, 2207 (1911).
13) H. W. Davies and M. Schwarz, *J. Org. Chem.*, **30**, 1242 (1965).
14) L. F. Fieser and M. Fieser, "Reagents for Organic Synthesis," I, John Wiley and Sons, New York (1967), p. 367.
15) J. A. Riddick and W. B. Bunger, "Organic Solvents," 3rd ed, Wiley-Interscience, New York (1970).
16) J. Coops, G. J. Hoijtink, Th. J. E. Kramer, and A. C. Faber, *Recl. Trav. Chim. Pays-Bas*, **72**, 765 (1953).
17) G. Bulmer and F. G. Mann, *J. Chem. Soc.*, **1945**, 666.
18) M. P. Grammaticakis, *Bull. Soc. Chim. Fr.*, **1948**, 973.

The Intrachain Aminolysis of a Terminal *p*-Nitrophenyl Ester Group by a Terminal 4-Pyridyl Group Attached to Both Ends of a Poly(oxyethylene) Chain*

Masahiko SISIDO, Eiichi YOSHIKAWA, Yukio IMANISHI, and Toshinobu HIGASHIMURA

Department of Polymer Chemistry, Kyoto University, Kyoto 606

(Received September 24, 1977)

The intrachain aminolysis by a terminal 4-pyridyl group of a *p*-nitrophenyl ester group at the other terminal of a poly(oxyethylene) chain was investigated. The rate constants of the intrachain reaction were determined as a function of the degree of polymerization, *n*, of the poly(oxyethylene) chain over the range of 5—33 at 15, 25, and 35 °C. The rate constant was at its maximum at $n=7$ and decreased with an increase in the chain length. A comparison of the data with those obtained with polysarcosine chain showed that the intrachain reaction proceeded more effectively in the latter chain. Some thermodynamic considerations were made as to the cyclization process of a poly(oxyethylene) chain.

Many types of intramolecular reactions in which a polymeric molecule participates have been investigated. For a quantitative understanding of these reactions, including enzymic reactions, the investigation of the intramolecular reaction between two functional groups connected by a polymeric chain with a definite chain length is very useful.[1] The polymer molecules of this type can be shown schematically as an X–Y-type polymer, where X and Y denote the reactive groups. The intramolecular reaction of X and Y is different from the intermolecular one to an extent which is determined by the constraint imposed by the conformation of the polymer chain.

In a previous paper of this series,[2] an intrachain aminolysis on a polysarcosine chain with a terminal *p*-nitrophenoxycarbonyl group and a terminal 4-pyridyl group was investigated. The rate constant of the intrachain reaction decreased monotonously with an increase in the chain length. This observation is not in accordance with the chain length-ring-closure probability relationship predicted by the Monte Carlo calculation of the polysarcosine chain.[3] The calculation predicted a maximum intrachain rate constant at $n=7$ (*n* is the number of sarcosine units). In this study, the same sort of reaction was examined with poly(oxyethylene) chains with the degrees of polymerization, *n*, from 5 to 33. The results were compared with those obtained with the polysarcosine chain. The poly(oxyethylene) chain was employed to connect the functional groups because; (1) it readily dissolves in water; (2) it can be synthesized by anionic polymerization and the degree of polymerization is controlled by the monomer/initiator ratio;[4] and (3) its physical properties, such as the average dimensions in solution have been widely investigated.

Experimental

Preparation and Characterization of Polymer Samples. Poly(oxyethylene) with a terminal *p*-nitrophenoxycarbonyl group and a terminal 4-pyridyl group (I) was synthesized as is shown in Scheme 1.[2]

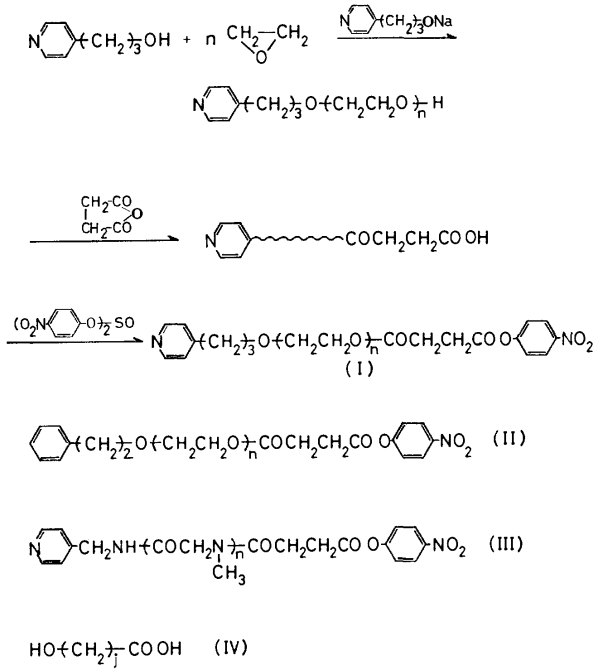

Scheme 1.

Ethylene oxide was polymerized in dioxane by using a mixture of 3-(4-pyridyl)-1-propanol (3 part) and its sodium salt (1 part).[4] All the polymerization procedures, including the preparation of the catalyst solution, were carried out in a vacuum line. After the reaction mixture had been allowed to stand for a week at 60 °C, the reaction tube was opened and an excess amount of succinic anhydride was added immediately. After a few hours, a three-fold excess of bis(*p*-nitrophenyl)sulfite was added and the mixture was left overnight at 25 °C. The polymer sample was then separated from the low-molecular-weight compounds by preparative gel-chromatography using a Sephadex LH-20 column equilibrated with dioxane. The fractions containing polymer samples were freeze-dried from dioxane. A polymer sample with a terminal phenyl group instead of a pyridyl group (II) was synthesized by using phenethyl alcohol as the initiator.

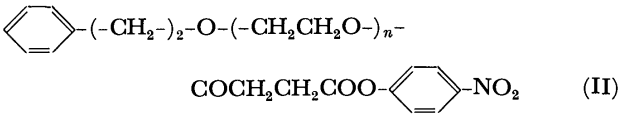

Polymers with degrees of polymerization higher than 40 were precipitated from the polymer mixture with ether.

* Intrachain Reaction of a Pair of Reactive Groups Attached to Polymer Ends. Part VI.

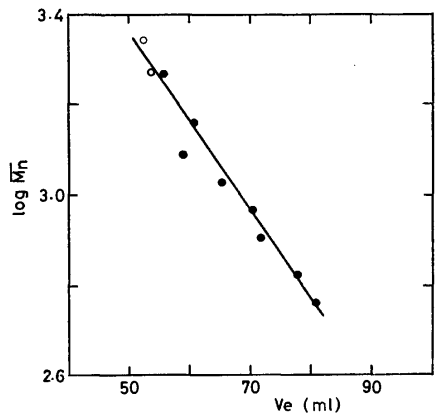

Fig. 1. Relation between the number-average molecular weight of poly(oxyethylene) and the elution volume at the peak position. The number-average molecular weight was calculated according to Eq. 1 (●) or determined by vapor-pressure osmometry (○).

The number-average molecular weight of the ether-precipitated polymers was measured by means of vapor-pressure osmometry. The low-molecular-weight samples, which were freeze-dried from the dioxane solution, usually contained trace amounts of a residual solvent and so were not suitable for the molecular-weight determination by the above method. Therefore, their molecular weight was determined on the basis of the elution volume in the gel chromatogram. Plots of the elution volume against the number-average molecular weight calculated by Eq. 1[4] are shown in Fig. 1. The

$$\bar{n} = [\text{Monomer}]/[\text{Initiator}]. \quad (1)$$

molecular weights measured by vapor-pressure osmometry are also plotted against the elution volume (open circles). Since the experimental points of different kinds (open and closed circles) lie on the same line, the following relation should hold between the elution volume, V_e, and the number-average degree of polymerization, $\bar{n}$:

$$V_e = 104 - 31 \log \bar{n}. \quad (2)$$

In the following part, the discussion will be based on the degree of polymerization calculated by Eq. 2. The number-average degrees of polymerization for polymers carrying a terminal phenyl group were determined in a similar way. The results of the polymer characterization are summarized in Table 1.

Table 1. Characterization of polymer samples

Initiator	$\bar{n}$ Calcd by Eq. 1	$\bar{n}$ Determined by VPO	$\bar{n}$ Determined by GPC
3-(4-Pyridyl)-1-propanol	5.2		4.8
	7.0		6.9
	9.7		11
	12.7		12
	15.6		17
	20.0		27
	25.7		24
	36.3		33
	31.7	35	40
	35.0	38	43
β-Phenetyl alcohol	4.6		2.4
	9.2		14
	13.4		13
	18.5		18
	18.1	28	27

The agreement of the molecular weights calculated from Eq. 1 with the observed values suggests a Poisson-type molecular-weight distribution for the polymer samples.[4] The narrow molecular-weight distribution was actually indicated by the elution diagram.

The amount of pyridyl group incorporated into a polymer end was estimated by means of the absorbance of the pyridyl group (260 nm, $\varepsilon = 2.01 \times 10^3$) for the ether-precipitated high-molecular-weight polymers. The ratios of the observed amount to the calculated amount for the complete incorporation were 0.88 ($\bar{n}=42$) and 0.95 ($\bar{n}=80$). These data show that the incorporation is nearly quantitative.

Measurements. The aminolysis reactions were carried out at pH 6.1 (phosphate buffer, $\mu=0.067$).[2] The reaction was followed by recording the absorbance (320 nm) of the *p*-nitrophenol liberated. The concentration of the terminal ester group was adjusted to about 5×10^{-5} M. At this dilute concentration the contribution from the intermolecular reactions can be ignored (see below). The iodometry[5] showed no evidence of the formation of poly(oxyethylene) micelles at this concentration. The fraction of free pyridyl groups at pH 6.1 has been estimated to be about 0.93,[2] irrespective of the reaction temperature.

Results and Discussion

Evaluation of Rate Constants of the Intrachain Reaction. The intrachain aminolysis was carried out at 15, 25, and 35 °C. Figure 2 shows a typical first-order plot for the reaction at 25 °C. The rate of the reaction depends unambiguously upon the chain length. The slope affords an apparent rate constant, k_{obsd}, which should consist of these three terms:

$$k_{obsd} = k_1 + k_s + k_2[\text{Pyr}], \quad (3)$$

where k_1, k_s, and k_2 denote the rate constants for the intrachain aminolysis, spontaneous hydrolysis, and

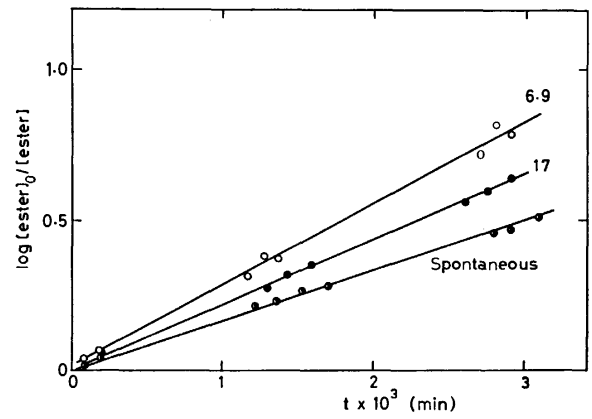

Fig. 2. Typical first-order plot for the reaction of polymer (I) having different chain lengths; 25 °C, pH=6.1. Numbers in the Figure indicate the number-average degrees of polymerization of poly(oxyethylene) chain. The bottom line represents the spontaneous hydrolysis of the polymer (II) (n=18).

Table 2. Rate constants for spontaneous hydrolysis (k_s) and intermolecular reaction by pyridine (k_2)

	$\bar{n}$	Temp (°C) 15	25	35
k_s	2.4	0.9×10^{-4}	2.9×10^{-4}	5.9×10^{-4}
(min^{-1})	7.4	0.9		
	12.5	1.0	3.5	5.4
	17.5	1.4	3.6	4.6
	27.4	1.2	3.5	4.7
	average	1.1×10^{-4}	3.3×10^{-4}	5.1×10^{-4}
k_2	2.4	2.0×10^{-2}	4.3×10^{-2}	1.3×10^{-1}
(M^{-1} min^{-1})	7.4	2.1		
	12.5	1.8	7.5	1.2
	17.5		4.4	1.5
	27.4	2.1	4.8	1.2
	average	2.0×10^{-2}	5.3×10^{-2}	1.3×10^{-1}

intermolecular aminolysis respectively. The concentration of the terminal pyridyl group is denoted as [Pyr]. The k_s value was determined from the spontaneous hydrolysis of the phenyl-terminated polymer (II) under the same conditions. The k_2 value was estimated from the pyridine-catalyzed aminolysis of the polymer (II). The results are collected in Table 2. The k_s and k_2 values were not affected by the chain length, indicating the same inherent reactivity of the terminal ester groups attached to poly(oxyethylene) with different chain lengths. The value of k_2 is so small that the contribution from the intermolecular reaction can be ignored when the polymer concentration is as low as 5×10^{-5} M.

The rate constant of the intrachain aminolysis, k_1, was calculated according to Eq. 3; it is plotted in Fig. 3 as a function of the degree of polymerization of the poly(oxyethylene) chain. It is interesting to note that the intrachain reaction is most efficient at $\bar{n}=7$. Undoubtedly the conformational constraints imposed by the poly(oxyethylene) chain caused this marked dependence on the chain length. The presence of the optimum chain length has been expected as a result of some conformational calculations and has actually been observed in some intrachain reactions.[3,6,7] The chain-length dependence of k_1 was more marked at higher temperatures. This trend indicates that the cyclic conformations, which are necessarily taken up to substantiate the intrachain reaction, have a large entropy at the optimum chain length resulting in the high intrachain reactivity. This view is consistent with the thermodynamic consideration (see below).

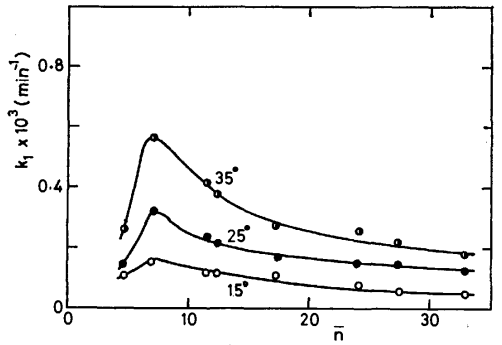

Fig. 3. Dependence of the rate constant of intrachain aminolysis k_1 on the degree of polymerization of poly(oxyethylene) at three different temperatures, pH=6.1.

Comparison with the Intrachain Reaction on a Polysarcosine Chain. To compare the present data with those obtained with other polymer chains, the chain-length dependence of k_1/k_2, the intrachain rate constant relative to the intermolecular one, was examined. The rate-constant ratio eliminates the ambiguity arising from the different inherent reactivities of the terminal groups. The rate-constant ratios are shown in Fig. 4, together with the data obtained with the polysarcosine chain (III)[2] and the polymethylene chain (IV).[6] The data for the polymethylene chain have been obtained by the intramolecular esterification

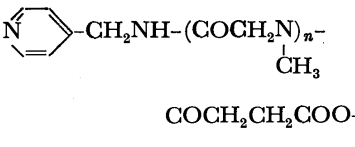

(III)

$$HO\text{-}(\text{-}CH_2\text{-})_j\text{-}COOH \qquad \text{(IV)}$$

(lactone formation) of ω-hydroxycarboxylic acid in a benzene solution at 80 °C.[7] For the other two poly-

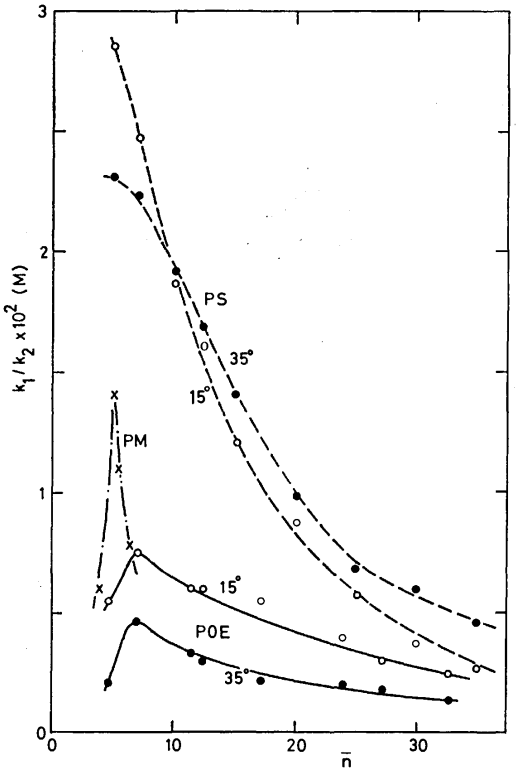

Fig. 4. Comparison of the rate-constant ratio of intrachain and intermolecular aminolyses k_1/k_2 among three polymers, *i.e.*, poly(oxyethylene) (POE), polysarcosine (PS), and polymethylene (PM). For polymethylene chains, $\bar{n}$ was calculated as $\bar{n}=(j/3)-2$.

mers, the reaction was an intrachain aminolysis. Obviously the polysarcosine and polymethylene chains are more efficient in the intrachain reaction; in other words, they take cyclic conformations more easily than poly(oxyethylene) chain. This finding is somewhat unexpected, since the latter chain appears to be more flexible due to the presence of oxygen atoms in the main chain, which are sterically less hindered than others. A Monte Carlo calculation may provide information concerning the ease of cyclization of these chains.[8] It is interesting that the population of the cyclic conformations of the poly(oxyethylene) chain increases with decreasing the temperature, whereas it increases with polysarcosines having larger chain lengths than $\bar{n}=10$ with a rise in temperature. This difference indicates the difference in the thermodynamic properties of the two chains.

Activation Parameters. The Arrehenius plots of the rate constants of the intrachain aminolysis are shown in Fig. 5. The activation parameters (ΔH_1^*, ΔS_1^*) were derived from the slope and the intercept of each straight line in Fig. 5. These parameters contain contributions from the conformational change requied for the cyclization (ΔH_c^*, ΔS_c^*) and those from the electronic change accompanying the reaction (ΔH_e^*, ΔS_e^*) as

$$\Delta H_1^* = \Delta H_c^* + \Delta H_e^*,$$
$$\Delta S_1^* = \Delta S_c^* + \Delta S_e^*. \quad (4)$$

ΔH_e^* and ΔS_e^* should be independent of the chain length. The electronic contributions can be evaluated from the activation parameters for the intermolecular reactions, ($\Delta H_2^*=14.4$ kcal/mol, $\Delta S_2^*=-15.3$ eu). Following the discussion reported previously,[2] the enthalpy for the electronic change of the intrachain reaction is equal to that of the intermolecular reaction, and the electronic entropy of the intrachain reaction is smaller by the bimolecular encounter term ($\Delta S_b^*=-3.6$ eu) than that of the intermolecular reaction. Thus, the following relations hold:

$$\Delta H_e^* = \Delta H_2^*,$$
$$\Delta S_e^* = \Delta S_2^* - \Delta S_b^*. \quad (5)$$

Using these relations, the activation parameters for the conformational change were calculated and plotted as a function of the degree of polymerization of the poly(oxyethylene) chain (Fig. 6). The activation enthalpy for conformational change is negative, irrespective of the chain length, indicating that cyclic conformations are of a lower conformational energy than linear ones. The chain-length dependence of the conformational enthalpy shows a tendency opposite to that observed in the rates of intrachain reactions; *e. g.*, at the optimum chain length ($\bar{n}=7$), the activation enthalpy is at maximum. It is, therefore, feasible to say that the chain-length dependence of the intrachain reaction of poly(oxyethylene) is governed mainly by the conformational entropy. This finding contrasts with that obtained for polysarcosine, where the conformational enthalpy was a dominant factor in the intrachain reaction.[2] As may be seen from Fig. 7, the compensation plot for ΔH_c^* and ΔS_c^* falls on a straight line, giving an isokinetic tempera-

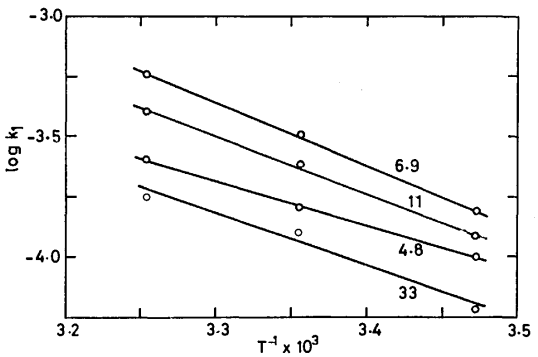

Fig. 5. Typical Arrhenius plot of the rate constants of intrachain aminolysis of poly(oxyethylene). Numbers in the Figure are the degree of polymerization of poly(oxyethylene).

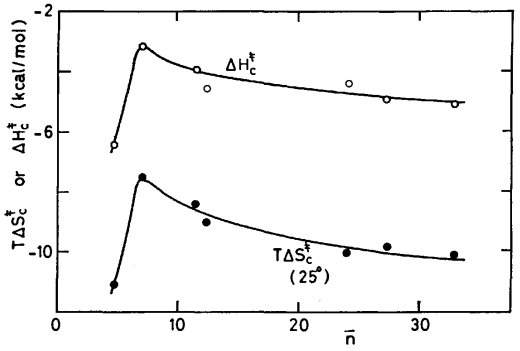

Fig. 6. Activation parameters for the conformational change accompanied with the intrachain reaction of poly(oxyethylene), plotted against the degree of polymerization.

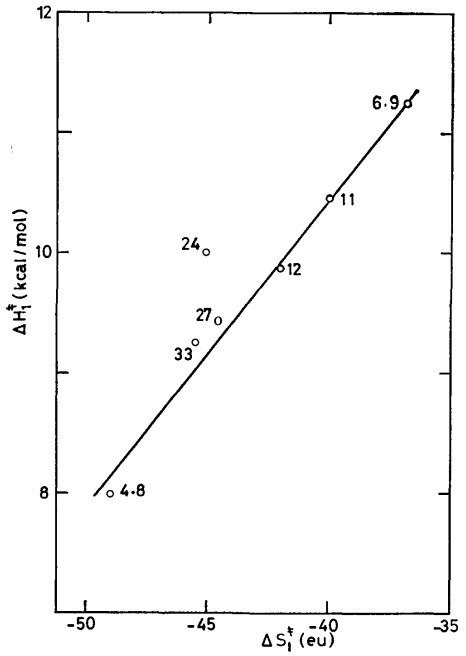

Fig. 7. Compensation plot of the activation parameters. Numbers in the Figure show the degree of polymerization of poly(oxyethylene).

ture of 2 °C. A similar relation has also been observed in the intrachain aminolysis of polysarcosine[2] and in the intrachain charge-transfer complex of polysarcosine.[9,10] Therefore, it is likely that some conformational mechanism operates to compensate for the entropy loss accompanying the cyclization, hence stabilizes the cyclized conformation. The solvation of the polymer chain has been suggested to play an important role in the compensation mechanism.[10] However, the details of the solvent effect still remain unclear in the present case.

To conclude, an optimum chain length was observed in the intrachain reaction between two terminal groups of the poly(oxyethylene) chain. Intrachain reactions on the poly(oxyethylene) chain took place less efficiently than those on polysarcosine and polymethylene chains.

References

1) M. Sisido, *Polym. J.*, **3**, 84 (1972); **4**, 534 (1973).
2) M. Sisido, T. Mitamura, Y. Imanishi, and T. Higashimura, *Macromolecules*, **9**, 316 (1976).
3) M. Sisido, Y. Imanishi, and T. Higashimura, *Macromolecules*, **9**, 320 (1976).
4) B. Wojtech, *Makromol. Chem.*, **66**, 180 (1963).
5) M. J. Schick, ed, "Nonionic Surfactants," Marcel Dekker, New York (1967).
6) M. Sisido, *Macromolecules*, **4**, 737 (1971).
7) M. Stoll and A. Rouvé, *Helv. Chim. Acta*, **18**, 1087 (1935).
8) M. Sisido, Y. Imanishi, and T. Higashimura, *Bull. Chem. Soc. Jpn.*, **51**, 1469 (1978).
9) M. Sisido, H. Takagi, Y. Imanishi, and T. Higashimura, *Macromolecules*, **10**, 125 (1977).
10) H. Takagi, M. Sisido, Y. Imanishi, and T. Higashimura, *Bull. Chem. Soc. Jpn.*, **50**, 1807 (1977).

A Monte Carlo Study of the Intrachain Reaction on a Poly(oxyethylene) Chain*

Masahiko Sisido, Yukio Imanishi, and Toshinobu Higashimura
Department of Polymer Chemistry, Kyoto University, Kyoto 606
(Received September 24, 1977)

Monte Carlo calculation was performed to estimate the ring-closure probability of a poly(oxyethylene) chain. The calculation was made for various chain lengths on the basis of a rotational isomeric state model in which the intrachain atomic overlaps were excluded in terms of the hard-sphere model. The chain-length dependence of the ring-closure probability thus obtained was compared with that of the rate-constant ratio of the intrachain reaction *vs.* the intermolecular reaction previously reported. For longer chains, the calculation agreed well with the experimental data. For shorter chains, the agreement was less satisfactory; this discrepancy was attributed to the effect of the bulky terminal groups of the poly(oxyethylene) chain. The thermodynamic parameters for the cyclization were determined, and it was found that the chain-length dependence of the ring-closure probability is mainly governed by the conformational enthalpy.

Intrachain reactions of X–Y-type polymers may provide information concerning the flexibility of a polymer chain, which is hard to determine quantitatively by other means. Provided that the reaction requires a moderately high activation energy, the rate of intrachain reaction on a polymer chain should be proportional to the ring-closure probability of the polymer chain.[1] The ring-closure probability of a polymer chain has been reported to be sensitive to the conformational property of the polymer chain.[2] In other words, the intrachain reaction on a polymer chain is strongly affected by the nature of the polymer chain. In this respect, a comparison of the experimental results of the intrachain reaction with the conformational calculation would seem to be interesting. This sort of comparison has been made for intrachain reactions on polymethylene chains,[1,3,4] polysarcosine chains,[5,6] and RNA chains.[7,8] The ring-closure probabilities of various condensation polymers have also been calculated in connection with the ring-chain equilibria in solution and in bulk.[9]

In our previous investigations,[7,8] a polysarcosine chain was used as a "spacer" for an intrachain aminolysis of a *p*-nitrophenyl ester group by a 4-pyridyl group in an aqueous solution. When the rate constants of the intrachain reaction were compared with those calculated by the Monte Carlo method, a fairly good agreement was found between them. This prompted us to carry out the Monte Carlo calculation for the poly(oxyethylene) chain, which has been used as a "spacer" for the same intrachain reaction.[10] Since the poly(oxyethylene) chain is different from other chains in its preference for the *gauche* conformational state for each bond, characteristic behavior in the ring-closure probability is expected. The ring-closure probability was calculated as a function of the chain length and was compared with experimental data on the rate-constant ratio of intrachain to intermolecular reactions. The agreement between them was compared with that previously obtained with polysarcosine.

Conformational calculations of poly(oxyethylene) chains have been conducted by Mark and Flory[11] and recently by Abe and Mark[12] on the basis of the *t-g* rotational isomer model. The most characteristic feature of the chain is the preference for the *gauche* rotational state, for reasons not yet completely clear. In the present calculation, therefore, the "*gauche* effect" was taken into consideration by adding a corrective energy for the *gauche* state, as was recently suggested by Abe and Mark.[12] By using these effective parameters, the conformational properties, such as the average dimensions and the dipole moment of poly(oxyethylene) chains, have been successfully reproduced.[12] Hence, the same parameters were used in the present Monte Carlo calculation.

Procedures for the Monte Carlo Calculation

Structure and Energy Parameters. As has been stated above, some ambiguity remains as to the conformational parameters for poly(oxyethylene) chains. In this study, the most recent values proposed by Abe and Mark[12] were used (Table 1). It should be noted that the rotational angles for the *gauche* states, $\phi_g\pm$, are taken as $\pm 110°$ instead of the usual value of $\pm 120°$. However, such small changes in the parameters did not cause any significant change in the ring-closure probability calculated. The bulkiness of the two terminal groups, a 4-pyridyl group and a *p*-nitrophenoxycarbonyl group, was not taken into considereation, and the computation was carried out for the skeletal structure I. It has been shown that the excluded volume effect is

$$\text{C-O-(-C-C-O-)}_m\text{-C},\ m=3\text{—}20 \qquad \text{(I)}$$

essential in the calculation of the ring-closure probability.[3] In this calculation, the skeletal overlaps were excluded in such a way that the conformations in which any pair of skeletal atoms fall within the sum of their atomic radii (Table 1) are rejected.

Table 1. Structure and energy parameters of poly(oxyethylene)

l(C-O)=1.43 Å, l(C-C)=1.53 Å,
$\angle$COC=$\angle$CCO=111.5°
ϕ_g(C-O)=ϕ_g(C-C)=$\pm$110°,
$E_{\sigma 2}$=−0.5 kcal/mol, $E_{\sigma 2'}$=0.9 kcal/mol,
$E_{\omega 2}$=0.4 kcal/mol.

For notations, see Ref. 12.

* Intrachain Reaction of a Pair of Reactive Groups Attached to Polymer Ends. Part VII.

Evaluation of the Ring-Closure Probability. The ring-closure probability is expressed as the ratio of the (conformational) partition function for ring conformations to that of the total ones. If a chain is regarded as cyclic when it takes an end-to-end distance, r, shorter than the critical distance, r_0, then the ring-closure probability is expressed as

$$W(r<r_0) = Z(r<r_0)/Z_t. \quad (1)$$

If the excluded volume effect is taken into account in the Monte Carlo calculation, the two partition functions should be estimated by generating the non-self-intersecting chains randomly. However, since the exclusion of the overlapping conformations requires a very long computation time, the exclusion process was performed after cyclic conformations were generated. For this purpose, Eq. 1 was rewritten as[6]

$$W(r<r_0) = \frac{Z(r<r_0)/Z_0}{Z_t/Z_0}, \quad (2)$$

where Z_0 is the total partition function for the conformations including any atomic overlaps. To calculate the numerator, a number of conformations were first generated without excluding the atomic overlaps, and then the check for the skeletal overlap was made only for the cyclic ($r<r_0$) conformations. The denominator represents the fraction of the non-self-intersecting conformations. This quantity can be calculated accurately from a relatively small number of Monte Carlo samples. The average value of the numerator was determined from 80000 Monte Carlo chains including skeletal overlaps. This procedure was repeated five times to obtain a total average of 400000 chains. The denominator was determined from $10000\times5=50000$ chains. In this case, the scattering among the five averages was not significant.

Results and Discussion

The ring-closure probabilities for poly(oxyethylene) chains whose chain lengths, m, range from 3 to 20 are shown in Fig. 1 for $r_0=6$ Å and in Fig. 2 for $r_0=4$ Å. The small open circles indicate the average value for 80000 chains, and the large open circles, the total average for 400000 chains. The probability shows a peak at $m=4$ or 5, indicating the presence of the optimum chain length for the intrachain reaction. In the two figures, the Monte Carlo data for polysarcosine chains[6] are also shown; they have been obtained by means of a hard-sphere model, without taking the conformational energy into account. The ring-closure probability for polysarcosine chains also shows a maximum, but the optimum chain length is considerably longer than that of poly(oxyethylene) chains. The ring-closure probability has been calculated for polymethylene chains[1] and found to reach a maximum at $j=20$, where j is the number of methylene units and corresponds approximately to 3 m. Therefore, the optimum chain length for the cyclization of poly(oxyethylene) chains is much shorter than for the other two chains. The conclusion from the calculation is undoubtedly related to the preference of a poly(oxyethylene) chain

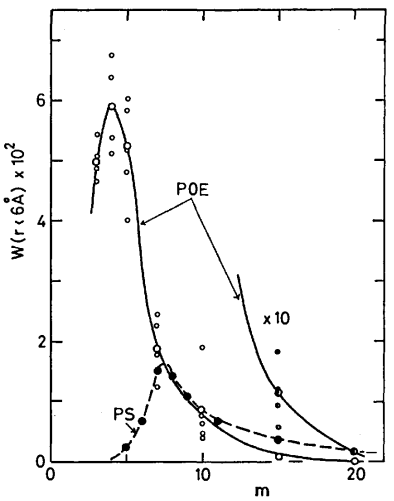

Fig. 1. Ring-closure probabilities for poly(oxyethylene) chain calculated for $r_0=6$Å. Small circles (○, ◐) indicate the local averages for 80000 chains and large circles (○, ◐) the total average for 400000 chains. (◐) and (◐) represent $W(r<6\text{Å})\times10^3$ for clarity for longer chains. Data for polysarcosine chain[6] are also shown with (●).

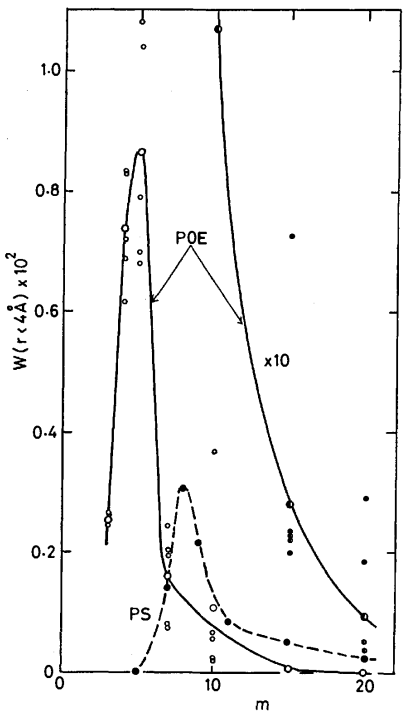

Fig. 2. Ring-closure probabilities for poly(oxyethylene) chain calculated for $r_0=4$Å. For the notations, see Fig. 1.

for *gauche* rotational states. Apart from the extraordinary high tendency to cyclize into a six-membered ring, which has been commonly found for various chains and is not included in the figures, the ring-closure probability at the optimum chain length is very large for poly(oxyethylene) chains. However, the probability decreases drastically with an increase in the chain length. For longer chains than $m=10$, the probability becomes smaller than that of polysarcosine chains, and

at $m=20$ it virtually vanishes.

The ratio of the rate constants for intra- and intermolecular reactions is related to the ring-closure probability, thus[1,3]

$$\frac{k_1}{k_2}=\frac{3000W(r<r_0)}{4\pi r_0^3 N_a}\ \text{mol/dm}^3, \tag{3}$$

where r_0 is the critical distance for the reaction and N_a is the Avogadro number. The ratios calculated for poly(oxyethylene) and polysarcosine chains by using the ring-closure probability for $r_0=4$ Å are shown in Fig. 3 (top), and there compared with the experimental results (bottom). The abscissa of Fig. 3 is taken as $n=m-2$ to match the actual structure (II) with the structure (I) of the poly(oxyethylene) model:

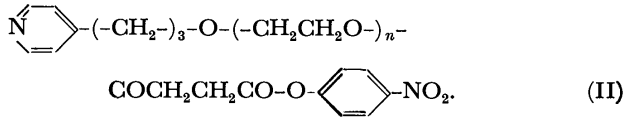

The agreement between the calculation and the experiment is fairly good for polysarcosine chain, except that the optimum chain length is not seen in the experimental data.[5] In contrast, with poly(oxyethylene) chains the optimum point is actually observed. However, the experimental rate-constant ratio at the optimum point is 10 times as small as the calculated one. For chains longer than $m=10$, the experimental rate-constant ratios for the poly(oxyethylene) chains are smaller than for the polysarcosine chains, as is to be expected from the calculation. The small ring-closure probabilities for long poly(oxyethylene) chains may be attributed to the high tendency to form small rings. In Fig. 3 the yield of cyclic n-mer in the oligomerization of ethylene oxide in dioxane initiated by BF_3 is also shown.[13] Because of the lack of detailed experimental data, however, the rate constant ratio cannot be obtained. In this case no bulky terminal group is present; hence, the yield can be compared with the k_1/k_2 calculated without considering the bulkiness of the two terminal groups. This permits a more direct comparison between the experimental and the calculated values than in the case of the intrachain reaction. In fact, a sharp maximum is seen in the yield of cyclic oligomers; this maximum is shorter by one oxyethylene unit than the calculated one. In summary, the results of the calculation on poly(oxyethylene) chains agreed with the observations of the intrachain reactions for longer chains. The deviation for shorter chains may be attributed to the steric repulsion between two terminal groups, which has not been taken into account in the calculation.

The ring-closure probabilities calculated at 15, 25, and 35 °C were used to determine thermodynamic parameters, ΔH_c and ΔS_c, for the conformational change accompanying the cyclization. The enthalpy change, ΔH_c, was determined from the temperature dependence of the ring-closure probabilities calculated for the same 80000 Monte Carlo samples. The total average for 400000 chains was calculated by using these locally averaged values. The entropy change, ΔS_c, was determined by using the total averages of the enthalpy and the ring-closure probability. The

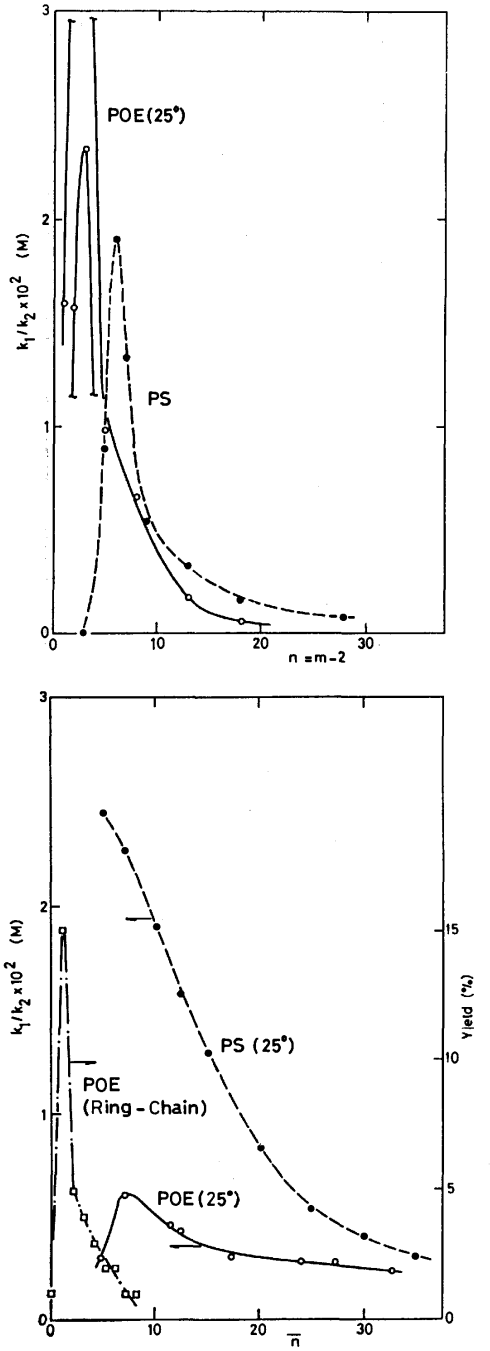

Fig. 3. Comparison of the observed (bottom) and the calculated (top) rate-constant ratio for intra- and intermolecular reactions. In the bottom, POE(Ring-Chain) represents the yield of cyclic oligomer in the ring-chain equilibrium attained in the oligomerization of ethylene oxide.[13] In the top, the data for poly(oxyethylene) chain having $n=4$ and 5 are subtracted by 3×10^{-2} for clarity. The abscissa is taken as $n=m-2$ to match the actual structure (II) with the model structure (I).

results are shown in Fig. 4, where the local average values of ΔH_c are indicated by small circles, and the total average, by a large circle. It is clear that the chain-length dependence of ΔH_c virtually determines the chain-length dependence of the ring-closure pro-

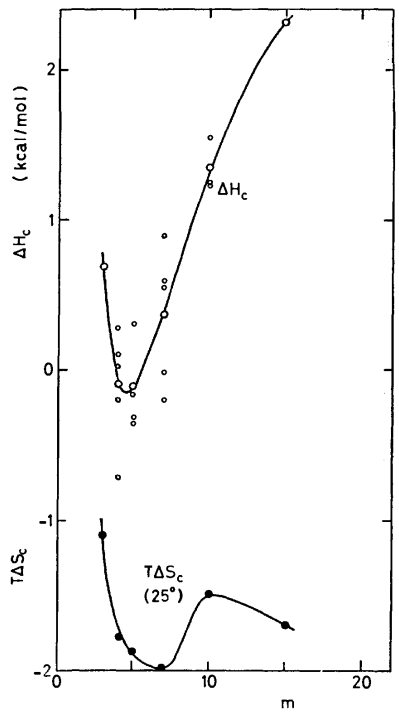

Fig. 4. Thermodynamic parameters for the cyclization and the chain length of poly(oxyethylene). Small and large open circles (○, ◯) indicate the local and the total averages of ΔH_c, respectively.

bability and, hence, the ease of the intrachain reaction. At the optimum chain length in the calculated k_1/k_2, ΔH_c is nearly zero, indicating that no excess energy is required for the optimum cyclization. The predominance of the enthalpy factor is somewhat unexpected, since it is natural to consider that the ease of the intrachain reaction is determined by the fraction of cyclic conformations and, hence, by the entropy factor. The predominance of the enthalpy factor has been found in the calculation for the ring-closure probability of polymethylene chains[3] and actually observed in some intrachain reactions on polysarcosine.[5] However, the entropy factor has been found experimentally to be important in the intrachain reaction on poly(oxyethylene) chains.[10] Since the chain-length dependence of the thermodynamic parameters has been reported to change drastically in different solvents,[14,15] the solvation of polymer chains may be another important factor in determining the thermodynamic parameters. The plot of the calculated values of ΔH_c against the calculated values of ΔS_c did not result in a straight line. This is in marked contrast with the same sort of plot between the experimental values of ΔH_c and ΔS_c, which gave a straight line.[10] This difference may also be attributed to the effect of solvation which operates in the real reaction, but which was ignored in the calculation. The solvation must compensate for the disadvantage due to the loss of entropy in a cyclic conformation and stabilize the latter, but the mechanism of solvation is not yet clear.

The authors wish to thank Mr. Eiichi Yoshikawa for his preliminary calculation of the chain conformations of poly(oxyethylene).

References

1) H. Morawetz and N. Goodman, *Macromolecules*, **3**, 699 (1970).
2) For example, see H. Yamakawa, "Modern Theory of Polymer Solutions," Harper and Row, New York (1971).
3) M. Sisido, *Macromolecules*, **4**, 737 (1971).
4) M. A. Winnik, R. E. Truman, G. Jackowski, D. S. Saunders, and S. G. Whittington, *J. Am. Chem. Soc.*, **96**, 4843 (1974).
5) M. Sisido, T. Mitamura, Y. Imanishi, and T. Higashimura, *Macromolecules*, **9**, 316 (1976).
6) M. Sisido, Y. Imanishi, and T. Higashimura, *Macromolecules*, **9**, 320 (1976).
7) C. DeLisi, *Biopolymers*, **11**, 2251 (1972).
8) H. Rubin and H. R. Kallenbach, *J. Chem. Phys.*, **62**, 2766 (1975).
9) J. A. Semlyen, *Adv. Polym. Sci.*, **21**, 41 (1976).
10) M. Sisido, E. Yoshikawa, Y. Imanishi, and T. Higashimura, *Bull. Chem. Soc. Jpn.*, **51**, 1464 (1978).
11) J. E. Mark and P. J. Flory, *J. Am. Chem. Soc.*, **88**, 3702 (1966).
12) A. Abe and J. E. Mark, *J. Am. Chem. Soc.*, **98**, 6468 (1976).
13) J. Dale, G. Borgen and K. Daasvatn, *Acta Chem. Scand.*, **B28**, 378 (1974).
14) M. Sisido, H. Takagi, Y. Imanishi, and T. Higashimura, *Macromolecules*, **10**, 125 (1977).
15) H. Takagi, M. Sisido, Y. Imanishi, and T. Higashimura, *Bull. Chem. Soc. Jpn.*, **50**, 1807 (1977).

Syntheses and Reactions of 10-(2,2'-Biphenylylene)-9-phenanthrone Derivatives and Some Consideration of Ethyl Isomers in Their Analogous Series

Takao Ooya,* Masahiro Minabe, and Kazuo Suzuki

Department of Industrial Chemistry, Faculty of Engineering, Utsunomiya University, Ishiicho, Utsunomiya 321-31

(Received October 3, 1977)

The Wagner-Meerwein rearrangement of 9'-methyl-9,9'-bifluoren-9-ol yielded 10-(2,2'-biphenylylene)-9-methylenephenanthrene. Ozonolysis of the phenanthrene afforded 10-(2,2'-biphenylylene)-9-phenanthrone. This pinacolone was converted into 2'-(9-fluorenyl)biphenyl-2-carboxylic acid. Oxidation of 4,9'-bifluoren-9-one, which was obtained by ring closure of the acid, gave 9'-hydroxy-, 9'-benzyl-, and 9'-benzyloxy-4,9'-bifluoren-9-one. Isomers of 2,2'-diethyl-9,9'-bifluorene-9,9'-diol were obtained by reduction of 2-ethyl-9-fluorenone. The pinacols were rearranged to the corresponding pinacolones, which were cleaved into carboxylic acids. The structural assignment of these isomers was made by spectral analyses.

It has been reported that pinacol-pinacolone rearrangement of 9,9'-bifluorene-9,9'-diol (**1a**) yields 10-(2,2'-biphenylylene)-9-phenanthrone (**2a**),[1] which does not give the corresponding oxime.[2] Spiran **2a** is cleaved into 2'-(9-fluorenyl)biphenyl-2-carboxylic acid (**3a**) by the action of potassium hydroxide in ethanol.[3]

The present paper deals, firstly, with other synthetic procedures of **2a** through 9,9'-bifluoren-9-ol derivatives, and also with the conversion of **2a** to 4,9'-bifluorene (**4**),[4] which has previously been obtained *via* ring closure of (2-biphenylyl)-(4-fluorenyl)methanol.

Ashby *et al.*[5] reported that reduction of phenyl 2-methylphenyl ketone afforded *meso*- and *dl*-1,2-diphenyl-1,2-di(2-methylphenyl)ethane-1,2-diol. Some bromo-derivatives of **1a** and **2a** have been obtained by the Clemmensen reduction of the corresponding ketones, but their isomers have not been isolated.[6] Pinacolic rearrangement of 2,3-di(2-fluorenyl)-butane-1,2-diol gave exclusively 3,3-di(2-fluorenyl)-butan-2-one.[7]

This paper is concerned, secondly, with the formation and rearrangement of *meso*-(**1b**) and *dl*-2,2'-diethyl-9,9'-bifluorene-9,9'-diol (**1c**). Finally, transformations of 2-ethyl-(**2b**) and 7-ethyl-10-(4-ethyl-2,2'-biphenylylene)-9-phenanthrone (**2c**) to 2,2-diethyl-(**5b**) and 7,2'-diethyl-4,9'-bifluoren-9-one (**5c**) are dealt with briefly here.

Results and Discussion

Synthesis and Transformations of 10-(2,2'-Biphenylylene)-9-phenanthrone (2a). A new spiran, 10-(2,2'-biphenylylene)-9-methylenephenanthrene (**6a**), was obtained by the Wagner-Meerwein rearrangement of 9'-methyl-9,9'-bifluoren-9-ol and also by dehydration of 10-(2,2'-biphenylylene)-9-methyl-9-phenanthrol (**6b**). The NMR of one of the fixed methylene protons on **6a**, H_a, appears at higher field (4.73 ppm) than that of H_b (5.20 ppm), owing to the ring current of the spiro fluorenylidene plane which lies close to the methylene group (Scheme 1).

Ozonolysis of **6a** gave the known ketone **2a**, which was also obtained by the reaction between 9'-bromo-9,9'-bifluoren-9-ol and silver oxide. The reaction of **2a** with 9-lithiofluorene gave 2-[2'-(9-fluorenyl)]-biphenylyl 9-fluorenyl ketone (**7**), as in the case[3] of **3a**. The fission between the highly-polarized carbonyl carbon and the spiro carbon atoms would be due to the stabilization of carbanion (A) resulting from an attack of the nucleophilic species, as occurs with the Haller-Bauer reaction.[8]

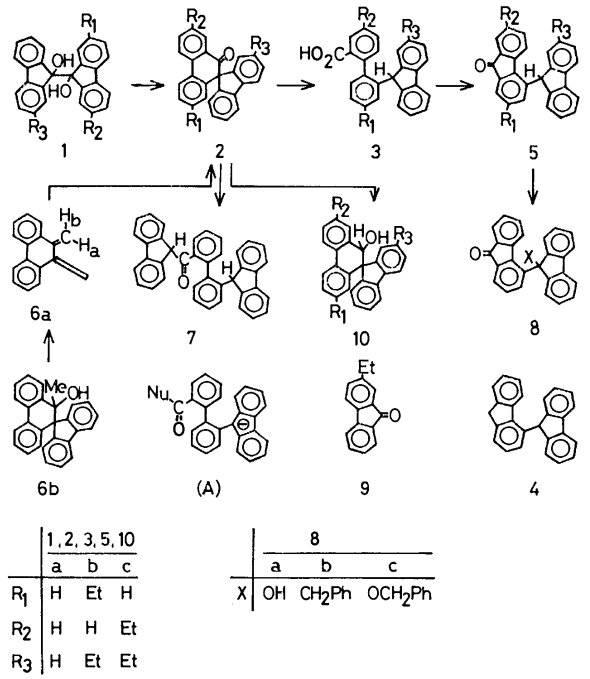

1,2,3,5,10	a	b	c
R_1	H	Et	H
R_2	H	H	Et
R_3	H	Et	Et

8	a	b	c
X	OH	CH_2Ph	OCH_2Ph

Scheme 1.

Dehydration of acid **3a** gave 4,9'-bifluoren-9-one (**5a**), which was reduced to authentic **4**. Oxidation of **5a** with Triton B-oxygen gave the expected 9'-hydroxy-4,9'-bifluoren-9-one (**8a**) in a good yield under mild conditions. If the oxidation was carried out in boiling pyridine, 9'-benzyl-(**8b**) and 9'-benzyloxy-4,9'-bifluoren-9-one (**8c**) were also obtained. Radical halogenation of **5a** with *N*-bromosuccinimide, on the other hand, did not yield 9'-bromo-4,9'-bifluoren-9-one.

These findings can be accounted for by the constrained state around the 9'-position of **5a**; the 9'-radical of **5a** may be coupled with the smaller benzyl radical,

* Present address: Institute of Pharmacology, Banyu Pharmaceutical Co., Ltd., Meguro, Tokyo 153.

but not with the larger bromine atom.

*Syntheses of 2,2'-Diethyl-9,9'-bifluorene-9,9'-diols(**1b**,**1c**).* The reduction of 2-ethyl-9-fluorenone (**9**)[9] gave the corresponding pinacol, which has a broad melting point. The NMR spectrum of the pinacol shows the existence of *meso*-(**1b**) and *dl*-isomers (**1c**) in the ratio of 1:1. A small amount of **1b** was separated by recrystallization of the mixture. Pure **1b** was isomerized to a mixture of **1b** and **1c** by UV irradiation.

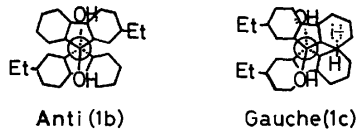

Scheme 2.

The conformation of **1b** would be represented as *anti* form because of the repulsion between the two bulky fluorene rings. Isomeric **1c** may be in *gauche* form, which twists to avoid the repulsion between two ethyl groups, as shown in Scheme 2. The assignment may be supported from the finding that the ethyl protons of **1b** are shifted to lower fields than those of **1c** due to the magnetic anisotropy effect of the aromatic rings.[10] Additionally, two protons of 8,8'-positions on **1c** locate on the shielding zone of the fluorene rings and are shifted to a higher field (6.58 ppm).[11]

*Transformations of Ethyl-substituted 10-(2,2'-Biphenylylene)-9-phenanthrones(**2b**,**2c**).* The pinacol-pinacolone rearrangement of **1b** and **1c** gave non-stereoselectively pinacolones **2b** and **2c** in the ratio of 1:1. The NMR spectra show that one ethyl group of **2b** is shifted to higher fields than the other in **2b**, higher also than those of **2c**.

The ethyl protons on the phenanthrone ring of **2b** would be more shielded than those of **2c**, because the ethyl group in the former is located in the shielding zone of the fluorenylidene ring, whereas in the latter, it undergoes a deshielding effect because of the 9-carbonyl group (Scheme 3).

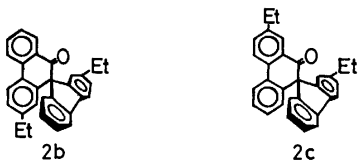

Scheme 3.

Compounds **2b** and **2c** were reduced to 2-ethyl-(**10b**) and 7-ethyl-10-(4-ethyl-2,2'-biphenylylene)-9-phenanthrol (**10c**), respectively. Also, **2b** and **2c** were converted into ethyl-substituted 4,9'-bifluoren-9-ones, **5b** and **5c**, through the corresponding carboxylic acids, **3b** and **3c**. The reactions of **3b** and **3c** with copper powder gave the original **2b** and **2c**.

Experimental

All the mps are uncorrected. The IR spectra were obtained as KBr pellets using an IR-G spectrophotometer (JASCO). The MS spectra were measured with a RMU-6E apparatus (Hitachi, Ltd.) by means of a direct inlet system. The NMR spectra were obtained with a JNM-C60-HL spectrometer (JEOL), using TMS as an internal reference.

9'-Methyl-9,9'-bifluoren-9-ol. A lithium derivative of 9-methylfluorene[12] (5.4 g) was prepared in the usual manner[13] and allowed to react with fluorenone (4.3 g) in benzene (40 ml) at 5—10 °C. Upon stirring at 50 °C for 2 h, the resulting mixture was treated with aqueous NH_4Cl (5%) solution. The organic layer was dried (Na_2SO_4) and chromatographed on an alumina column to give a crystalline product, which was recrystallized from cyclohexane-benzene (1:1) to give 7.2 g (84%) of the alcohol: Mp 174—176 °C; IR: 3540 cm^{-1} (-OH); ^1H NMR (C_6D_6): δ 1.65 (1H, s), 1.95 (3H, s), 6.82—8.48 (16H, m); MS, *m/e*, 360 (M^+), 343, 181, 179, 165. Found: C, 90.31; H, 5.80%. Calcd for $C_{27}H_{20}O$: C, 89.97; H, 5.59%.

The alcohol was treated with HBr in AcOH at 20 °C to yield 9-methyl-9'-bromo-9,9'-bifluorene (90%): Mp 175 °C (dec); MS, *m/e*, 424, 422 (M^+), 343. Found: C, 76.25; H, 4.89%. Calcd for $C_{27}H_{19}Br$: C, 76.60; H, 4.52%.

This bromide (1.0 g) was refluxed for 8 h with KOH (0.264 g) in EtOH (250 ml) to give 9-methyl-9'-ethoxy-9,9'-bifluorene (0.70 g, 76%): Mp 208—210 °C; ^1H NMR (C_6D_6): δ 1.01 (3H, t, J=7.1 Hz), 2.00 (3H, s), 2.89 (2H, q), 6.70—7.42 (16H, m); MS, *m/e*, 388 (M^+), 343. Found: C, 89.75; H, 6.44%. Calcd for $C_{29}H_{24}O$: C, 89.65; H, 6.23%.

Wagner-Meerwein Rearrangement of 9'-Methyl-9,9'-bifluoren-9-ol. A mixed powder of the alcohol (0.2 g) and P_2O_5 (0.2 g) was heated at 200 °C under 2 Torr for 15 min to yield 0.15 g (79%) of **6a** as sublimate: Mp 238.5—239.5 °C; IR: 905 cm^{-1} (>C=CH_2); ^1H NMR (CCl_4): δ 4.73 (1H, s), 5.20 (1H, s), 6.38—8.02 (16H, m). Found: C, 94.87; H, 5.14%. Calcd for $C_{27}H_{18}$: C, 94.70; H, 5.30%.

*Synthesis and Dehydration of 10-(2,2'-Biphenylylene)-9-methyl-9-phenanthrol (**6b**).* A 0.34-g portion of **2a** in 70 ml of benzene was added to a MeMgI solution and the mixture was refluxed for 1 h to yield 0.28 g (78%) of **6b**: Mp 185—187 °C; IR: 3570 cm^{-1} (-OH); ^1H NMR (CCl_4): δ 1.29 (3H, s), 1.48 (1H, s), 6.54—7.95 (16H, m); MS, *m/e*, 360 (M^+), 342. Found: C, 90.12; H, 5.57%. Calcd for $C_{27}H_{20}O$ C, 89.97; H, 5.59%.

A mixed powder of **6b** (0.05 g) and P_2O_5 was heated at 200 °C under reduced pressure for 10 min to afford 0.036 g (76%) of **6a**, identical in all respects with the specimen obtained above.

*Synthesis of Pinacolone **2a**. a)*: A solution of 0.34 g of **6a** in 30 ml of $CHCl_3$ was treated with ozone at −15 °C for 1 h. Upon evaporation of the solvent, the resulting ozonide was treated with Zn-dust (0.1 g) in AcOH (10 ml) to afford 0.21 g (61%) of **2a**, identical in all respects with the sample obtained by the authentic method: Mp 256—258 °C (lit,[3] mp 256 °C, dec); IR: 1676 cm^{-1} (>C=O).

b) From 9'-Bromo-9,9'-bifluoren-9-ol: A solution of 1.73 g of 9,9'-bifluoren-9-ol[14] and 1.08 g of NBS in 100 ml of benzene was refluxed for 7 h to afford 1.82 g (86%) of 9'-bromo-9,9'-bifluoren-9-ol (mp 150.0—150.5 °C) and 0.05 g of **2a**. Found for the bromide: C, 73.18; H, 3.96%. Calcd for $C_{26}H_{17}OBr$: C, 73.42; H, 4.03%.

A solution of 0.2 g of the bromohydrin in 20 ml of dioxane was refluxed with 0.13 g of Ag_2O for 4 h; 0.09 g (56%) of **2a** was obtained.

*Ring Cleavage of **2a**. a)*: A solution of **2a** (1.4 g) in EtOH (100 ml) containing EtONa (1.36 g) was refluxed for 11 h. The reaction mixture was poured into water and neutralized with hydrochloric acid. The precipitate was collected, dried, and recrystallized from EtOH to give 1.1 g (75%) of **3a**:

Mp 244—245 °C (lit,[3] mp 243—244 °C); IR: 3370 (-OH), 1696 cm^{-1} (>C=O); MS, *m/e*, 362 (M^+), 345, 344, 317, 316, 197, 165.

A solution of **3a** (1.5 g) in MeOH (80 ml) was refluxed with concd H_2SO_4 (2 ml) for 13 h. Upon the usual treatment, 1.30 g (83%) of the methyl ester was obtained: Mp 155—157 °C; IR: 1714 cm^{-1} (>C=O); ^1H NMR (C_6D_6): δ 3.35 (3H, s), 5.07 (1H, s), 6.33—8.02 (16H, m); MS, *m/e*, 376 (M^+), 344, 316, 211, 165. Found: C, 86.24; H, 5.39%. Calcd for $C_{27}H_{20}O_2$: C, 86.14; H, 5.36%.

b): A solution of 2.1 g of **2a** in 20 ml of xylene was added to a refluxing xylene solution of 9-lithiofluorene for 20 min and the mixture was refluxed for 4 h to yield 0.08 g (3%) of **7**: Mp 286—288 °C; IR: 1653 cm^{-1} (>C=O); MS, *m/e*, 510 (M^+), 317, 316, 193, 165. Found: C, 91.96; H, 4.83%. Calcd for $C_{39}H_{26}O$: C, 91.74; H, 5.13%.

Reaction of Carboxylic Acid 3a. a): A suspension of **3a** (1.6 g) and polyphosphoric acid (PPA, 15 ml) was stirred at 130 °C for 13 h. The reaction mixture was poured into cold water and the dried precipitate was chromatographed in benzene on an alumina column to yield 1.2 g (78%) of **5a**: Mp 216.5—218 °C; IR: 1697 cm^{-1} (>C=O); ^1H NMR (CCl_4): δ 5.89 (1H, s), 6.56—8.29 (15H, m); MS, *m/e*, 344 (M^+), 316, 315, 165. Found: C, 90.49; H, 4.48%. Calcd for $C_{26}H_{16}O$: C, 90.67; H, 4.68%.

The corresponding oxime was prepared by refluxing a solution of **5a** (0.26 g), $HONH_2 \cdot HCl$ (0.06 g), NaOH (0.04 g), H_2O (5 ml) in EtOH (30 ml) for 1 h: yield 0.12 g (44%); mp 219—221 °C; IR: 3510 cm^{-1} (-OH). Found: C, 86.59; H, 4.91; N, 4.03%. Calcd for $C_{26}H_{17}NO$: C, 86.88; H, 4.77; N, 3.90%.

b): A powdered mixture of 0.40 g of sodium salt of **3a** and 2.0 g of soda lime was allowed to stand at 270 °C for 10 min. The reaction mixture was extracted with benzene to give 0.064 g (19%) of 9,9'-spirobifluorene, which was identical with that obtained by the method described in the literature:[15] Mp 199—200 °C (lit,[15] mp 198—199 °C); MS, *m/e*, 316 (M^+).

Acids **3b** and **3c** were treated in a similar way, but the corresponding spirans were not isolated.

Reduction of 5a. Ketone **5a** (3.0 g) was refluxed with HI (48 ml, 57%) and P (red, 4.8 g) in AcOH (200 ml) for 15 h. The reaction mixture was poured into water and the precipitate was washed with aqueous $Na_2S_2O_3$ (5%) solution, dried, and recrystallized from AcOH to give **4** (2.13 g, 74%), identical in all respects with an authentic sample:[4] Mp 166—168 °C; ^1H NMR (CCl_4): δ 3.95 (2H, s), 6.09 (1H, s), 6.36—8.35 (15H, m).

Oxidation of 5a with Triton B-Oxygen. a): To a solution of **5a** (1.5 g) and Triton B (40%, 1.5 ml) in pyridine (30 ml), oxygen was introduced gently at 32—38 °C with stirring for 3 h. The resulting mixture was poured into water and extracted with benzene. The organic layer was washed with water, dried (Na_2SO_4), and chromatographed on a silica gel column to yield 1.2 g (73%) of **8a**: Mp 207.5—209 °C; IR: 3465 (-OH), 1686 cm^{-1} (>C=O); ^1H NMR ($CDCl_3$): δ 2.87 (1H, s), 6.58—7.85 (15H, m). MS, *m/e*, 360 (M^+), 344. Found: C, 86.74; H, 4.18%. Calcd for $C_{26}H_{16}O_2$: C, 86.65; H, 4.48%.

b): The same reaction was carried out under boiling conditions; 0.11 g (7%) of **8a**, 0.60 g (31%) of **8b** (mp 243.5—244.5 °C), and 0.35 g (17%) of **8c** (mp 190—192 °C) were isolated by means of a method similar to the above. IR of **8b**: 1705 cm^{-1} (>C=O); ^1H NMR ($CDCl_3$): δ 3.79 (2H, s), 5.80—8.59 (20H, m); MS, *m/e*, 434 (M^+), 343, 342, 91. Found: C, 91.16; H, 4.93%. Calcd for $C_{33}H_{22}O$: C, 91.21; H, 5.10%. IR of **8c**: 1704 cm^{-1} (>C=O); ^1H NMR ($CDCl_3$): δ 4.22 (2H, s), 6.77—7.87 (20H, m): MS, *m/e*, 450 (M^+), 359, 343, 342, 91. Found: C, 88.32; H, 4.83%. Calcd for $C_{33}H_{22}O_2$: C, 87.97; H, 4.92%.

Synthesis and Photo-isomerization of 2,2'-Diethyl-9,9'-bifluorene-9,9'-diol (1b, 1c). a): Ketone **9** (11.5 g) was treated with $TiCl_4$ (15.8 g)-Zn (10.8 g) in THF (130 ml) by the procedure described elsewhere.[16] After treatment in the usual manner,[7] 9.4 g (81%) of crude pinacol was obtained, which was confirmed to be a mixture of **1b** and **1c** (1:1) by NMR: Mp 156—164 °C; IR: 3385 cm^{-1} (-OH, broad); ^1H NMR (C_6D_6): δ 1.04 (3H, t, J=7.5 Hz), 1.12 (3H, t, J=7.5 Hz), 2.44 (2H, q), 2.57 (2H, q), 3.09 (2H, s, -OH), 6.58 (1H, s), 6.80—7.48 (13H, m); MS, *m/e*, 418 (M^+), 400, 209, 193, 181, 165. Found: C, 85.97; H, 6.49%. Calcd for $C_{30}H_{26}O_2$: C, 86.09; H, 6.26%.

The crude pinacol was purified by repeated recrystallization from cyclohexane and benzene (1:1) to yield 0.9 g of **1b**: Mp 180—182 °C; IR: 3470, 3370 cm^{-1} (-OH); ^1H NMR (C_6D_6): δ 1.12 (6H, t), 2.57 (4H, q), 3.12 (2H, s), 6.80—7.48 (14H, m). Found: C, 85.99; H, 6.25%.

b): A solution of 4.2 g of **9** in 40 ml of THF was allowed to react with MeMgI (40 mmol) in the presence of $FeCl_3$ (0.1 g) by the procedure described elsewhere.[5] The resulting mixture was treated with aqueous NH_4Cl (5%) solution and extracted with benzene. The organic layer was dried (Na_2SO_4) and chromatographed on a silica gel column to afford 2.84 g (67%) of a mixture of **1b** and **1c** (1:1).

c): Pinacol **1b** (0.100 g) in ether (10 ml) was irradiated with a high pressure mercury lamp (100 W) for 8 h to give a mixture of **1b** (61%) and **1c** (39%), which were determined by means of NMR analysis.

Rearrangement of 1b and 1c. An isomeric mixture of **1b** and **1c** (0.75 g) was refluxed with concd H_2SO_4 (0.5 ml) in AcOH (15 ml) for 1 h. The mixture was poured into water to give precipitates which were submitted to NMR analysis; **2b** (49.5%) and **2c** (50.5%) were confirmed.

Fractional crystallization of the reaction mixture from EtOH gave 0.10 g (14%) of **2b**, mp 112—114.5 °C, and 0.22 g (31%) of **2c**, mp 192.5—193.5 °C. IR of **2b**: 1686 cm^{-1} (>C=O); ^1H NMR (C_6D_6) : δ 0.75 (3H, t, J=7.5 Hz), 0.93 (3H, t, J=7.5Hz), 2.03 (2H, q), 2.30 (2H, q), 6.68—8.35 (14H, m); MS, *m/e*, 400 (M^+), 372, 371, 343, 327,197, 165. Found: C, 90.12; H, 5.80%. Calcd for $C_{30}H_{24}O$: C, 89.96; H, 6.04%. IR of **2c**: 1673 cm^{-1} (>C=O); ^1H NMR (C_6D_6): δ 0.90 (3H, t, J=7.5 Hz), 0.94 (3H, t, J=7.5Hz), 2.30 (2H, q), 2.34 (2H, q), 6.73—8.20 (14H, m); MS, *m/e*, 400 (M^+), 372, 371, 343, 327, 194, 179. Found: C, 89.65; H, 6.01%.

Reduction of 2b and 2c. A mixture of **2b** (0.258 g) and $LiAlH_4$ (0.06 g) in THF (25 ml) was refluxed for 3 h. After decomposition with AcOEt (5 ml) and with hydrochloric acid (5%), the reaction mixture was extracted with benzene to yield 0.155 g (60%) of **10b**: Mp 140.5—142.5 °C; IR: 3530, 3400 cm^{-1} (-OH); ^1H NMR (C_6D_6): δ 0.80 (3H, t, J=7.8 Hz), 0.88 (3H, t, J=6.9 Hz), 1.43 (1H, d, J=6.6 Hz, -OH), 2.10 (2H, q, J=7.8 Hz), 2.26 (2H, q, J=6.9Hz), 5.15 (1H, d, J=6.6 Hz), 6.59—7.93 (14H, m) ; MS, *m/e*, 402 (M^+), 373, 345, 326. Found: C, 89.33; H, 6.74%. Calcd for $C_{30}H_{26}O$: C, 89.51; H, 6.51%.

Alcohol **10c** (0.36 g, 72%) was obtained from **2c** (0.50 g) by the method similar to that of **10b**: Mp 167—169 °C; IR: 3540 cm^{-1} (-OH); ^1H NMR (C_6D_6): δ 0.88 (3H, t, J=7.8 Hz), 1.10 (3H, t, J=7.5 Hz), 1.43 (1H, d, J=6.3 Hz, -OH), 2.26 (2H, q, J=7.8 Hz), 2.49 (2H, q, J=7.5 Hz), 5.19 (1H, d, J=6.3Hz), 6.65—7.95 (14H, m); MS, *m/e*,

402 (M^+), 373, 209. Found: C, 89.48; H, 6.54%. Calcd for $C_{30}H_{26}O$: C, 89.51; H, 6.51%.

Ring Cleavage of **2b** *and* **2c**. *a)*: A solution of **2b** (0.50 g) in EtOH (25 ml) was mixed with NaOH (0.26 g) dissolved in water (5 ml) and the mixture was refluxed for 2 h. Upon treatment in a manner similar to that employed in the cleavage of **2a**, 0.40 g (77%) of **3b** was isolated: Mp 203—204 °C; IR: 3420 (-OH), 1690 cm^{-1} (>C=O); MS, *m/e*, 418 (M^+), 400, 372, 343. Found: C, 85.73; H, 6.38%. Calcd for $C_{30}H_{26}O_2$: C, 86.09; H, 6.26%.

A mixture of **3b** (0.30 g) in MeOH (20 ml) containing concd H_2SO_4 (0.5 ml) was refluxed for 8 h. The methyl ester of **3b** (0.24 g, 77%) was obtained by recrystallization from MeOH: mp 144—146 °C; IR: 1721 cm^{-1} (>C=O); ^1H NMR (CCl_4): δ 1.11 (3H, t, J=8.1 Hz), 1.21 (3H, t, J=7.8 Hz), 2.49 (2H, q, J=8.1 Hz), 2.64(2H, q, J=7.8 Hz), 3.76 (3H, s), 4.90 (1H, s,) 6.06—8.23 (14H, m). MS, *m/e*, 432 (M^+), 400, 193, 165. Found: C, 85.98; H, 6.77%. Calcd for $C_{31}H_{28}O_2$: C, 86.08; H, 6.53%.

b): Isomeric **3c** (0.91 g, 87%) was obtained from **2c** (1.0 g) in a manner similar to that given above: Mp 195.5—197 °C; IR: 3420 (-OH), 1696 cm^{-1} (>C=O); MS, *m/e*, 418 (M^+), 400, 372, 343, 209, 193, 165. Found: C, 85.94; H, 6.22%. Calcd for $C_{30}H_{26}O_2$: C, 86.09; H, 6.26%.

Methyl ester (0.22 g, 71%) of **3c** was obtained from **3c** (0.30 g) by the same procedure as was employed above: Mp 110—112 °C; IR: 1721 cm^{-1} (>C=O); ^1H NMR (CCl_4): δ 1.22 (3H, t, J=7.5Hz), 1.32 (3H, t, J=7.2 Hz), 2.63(2H, q, J=7.5 Hz), 2.75 (2H, q, J=7.2 Hz), 3.76 (3H, s), 4.94 (1H, s), 6.32—8.02 (14H, m); MS, *m/e*, 432 (M^+), 400, 193. Found: C, 85.98; H, 6.70%. Calcd for $C_{31}H_{28}O_2$: C, 86.08; H, 6.53%.

Ring Closure of **3b** *and* **3c**. *a)*: Compound **3b** (0.45 g) was treated with PPA (10 ml), as in the case of **3a**, to afford **5b** (0.10 g, 23%): Mp 182—183.5 °C; IR: 1706 cm^{-1} (>C=O); ^1H NMR (CCl_4): δ 1.09 (3H, t, J=7.5 Hz), 1.23 (3H, t, J=8.1 Hz), 2.48 (2H, q, J=7.5 Hz), 2.71 (2H, q, J=8.1 Hz), 5.87 (1H, s, >CH-), 6.50 (1H, s), 7.09—8.26 (12H, m); MS, *m/e*, 400 (M^+), 371, 343, 327, 313. Found: C, 89.75; H, 6.26%. Calcd for $C_{30}H_{24}O$: C, 89.96; H, 6.04%.

b): Isomeric **5c** (0.03 g, 14%) was obtained from **3c** (0.25 g) by the same procedure as that described above: Mp 194.5—196 °C; IR: 1700 cm^{-1} (>C=O); ^1H NMR ($CDCl_3$): δ 1.18 (3H, t, J=7.8 Hz), 1.29 (3H, t, J=8.4 Hz), 2.58 (2H, q, J=7.8 Hz), 2.60 (2H, q, J=8.4 Hz), 5.81 (1H, s), 6.46—8.07 (13H, m); MS, *m/e*, 400 (M^+), 371, 343. Found: C, 90.09; H, 5.82%. Calcd for $C_{30}H_{24}O$: C, 89.96; H, 6.04%.

c): A mixture of **3b** (0.40 g) and copper powder (0.90 g) in quinoline (20 ml) was refluxed for 3 h. After cooling, hydrochloric acid (10%, 50 ml) was added to the solution and the resulting mixture was extracted with benzene (20 ml). The organic layer was chromatographed on a silica gel column to yield 0.25 g (65%) of **2b**.

Isomeric **3c** (0.40 g) was converted into **2c** (0.17 g, 44%) by the same procedure.

References

1) J. Suszko and R. Schillak, *Rocz. Chem.*, **14**, 1216 (1934).
2) A. Werner and A. Brob, *Ber.*, **37**, 2887 (1904).
3) H. Klinger and C. Lonnes, *Ber.*, **29**, 2152 (1896).
4) K. Suzuki, *Technol. Rept. Tohoku Univ.*, **19**, 63 (1954).
5) E. C. Ashby, J. D. Buhler, I. G. Lopp, T. L. Wiesemann, J. S. Bower, Jr., and J. T. Laemmle, *J. Am. Chem. Soc.*, **98**, 6561 (1976).
6) K. Suzuki, T. Maeda, N. Nawa, and Y. Sōda, *Bull. Chem. Soc. Jpn.*, **35**, 1299 (1962); K. Suzuki, M. Fujimoto, M. Murakami, and M. Minabe, *ibid.*, **40**, 1259 (1967).
7) M. Minabe, M. Yoshida, M. Fujimoto, and K. Suzuki, *J. Org. Chem.*, **41**, 1935 (1976).
8) K. Hamlin and A. Weston, *Org. React.*, **9**, 2 (1957).
9) S. Kajigaeshi, M. Fujimoto, S. Fujisaki, T. Kunishige, and M. Mashihara, *Nippon Kagaku Zasshi*, **89**, 416 (1968).
10) A. Rieker and H. Kessler, *Tetrahedron Lett.*, **1969**, 1227; M. Nakamura and M. Ōki, *Chem. Lett.*, **1975**, 671; M. Nakamura, N. Nakamura, and M. Ōki, *Bull. Chem. Soc. Jpn.*, **50**, 2986 (1977).
11) M. Minabe and K. Suzuki, *J. Org. Chem.*, **40**, 1298 (1975).
12) K. L. Schoen and E. I. Becker, *Org. Synth.*, Coll. Vol. IV, 623 (1963).
13) M. Minabe and K. Suzuki, *Bull. Chem. Soc. Jpn.*, **48**, 1301 (1975).
14) S. Kajigaeshi, *Nippon Kagaku Zasshi*, **82**, 1712 (1961).
15) R. Clarkson and M. Gomberg, *J. Am. Chem. Soc.*, **52**, 2884 (1930).
16) T. Mukaiyama, T. Sato, and J. Hanna, *Chem. Lett.*, **1973**, 1041.

Liquid Phase Peptide Synthesis by the Fragment Condensation on Soluble Polymer Support. I. Efficient Coupling and Relative Reactivity of a Peptide Fragment with Various Coupling Reagents

Mitsuaki NARITA

Department of Industrial Chemistry, Tokyo University of Agriculture and Technology, Nakamachi, Koganei, Tokyo 184

(Received October 3, 1977)

The fragment condensation on the soluble polymer support using dicyclohexylcarbodiimide (DCCI) plus 1-hydroxy-1*H*-benzotriazole (HOBt), diethoxyphosphoryl cyanide (DEPC), and triphenylphosphine (Ph_3P) plus di-2-pyridyl disulfide ($(PyS)_2$) as coupling reagents gave rise to efficient coupling (86—99% yield) of the peptide fragment, *t*-butyloxycarbonyl-L-*O*-benzyl-tyrosylglycylglycyl-L-phenylalanine [Boc-L-Tyr(Bzl)-Gly-Gly-L-Phe-OH], to the amino free terminal of Leu anchored to the soluble polymer support, H-L-Leu-OCH_2-resin. Relative reactivity ratios of Boc-amino acids and Boc-L-Tyr(Bzl)-Gly-Gly-L-Phe-OH with H-L-Leu-OCH_2-resin in the coupling reaction using the three coupling reagent systems could be easily determined by use of amino acid ratios in the acid hydrolysates of the resulting peptide resins in which they were taken. The peptide chain length of Boc-L-Tyr(Bzl)-Gly-Gly-L-Phe-OH has no influence on the reactivity of *C*-terminal amino acid in the coupling reaction using DCCI plus HOBt or DEPC as a coupling reagent when Boc-L-Phe-OH was replaced with Boc-L-Tyr(Bzl)-Gly-Gly-L-Phe-OH. The coupling reagent, Ph_3P plus $(PyS)_2$, brought about a marked decrease in the reactivity of the fragment peptide acid.

Through progress in peptide chemistry the synthesis of several large proteins has been achieved by means of solid phase[1] and classical solution methods.[2] However, difficulties arise when these methods are applied to large molecule peptides and proteins. Heterogeneous reaction conditions in solid phase peptide synthesis cause the formation of deletion and truncated sequences,[3] diffusion, slow reaction rates[4] of coupling and removal of protecting groups, solvation problems,[5] and formidable separation of the desired peptide from a large number of similar products. There is a drastic decrease in the overall yield of synthesis, and further progress in peptide synthesis along classical lines is hindered mainly because of the low solubility of polypeptides in organic solvents and the difficulty of removing the side products in the process of synthesis.[2]

In these embarrassing situations, it is evident that a considerable modification of present techniques is necessary for the synthesis of homogeneous proteins of a defined structure. Solid phase peptide synthesis using the fragment condensation procedure is expected to be of value for the synthesis of large molecule peptides and proteins.[6] This strategy will alleviate sequence-dependent problems in coupling and deprotecting steps, formation of failure sequences, and the difficulty in purification of the desired peptide. The serious problem in this method is, however, of low yield in the coupling steps due mainly to restriction of permeability of the peptide fragment into the random closs-linked polymer support anchored amino free terminal of peptide. It can be expected that use of a soluble polymer support in the fragment condensation procedure eliminates it to attain efficient coupling.

Soluble polymer supports were used in the stepwise elongation of peptide chains.[4,7] Kinetic studies of the coupling reaction using the soluble polymer support indicate that the rate is of the same order of magnitude as that of classical liquid phase peptide synthesis,[4a] approximately 100 times faster than that of solid phase peptide synthesis.[4b]

In this paper, we wish to report that the new technique described here can achieve the efficient coupling of the fragment peptide acid using dicyclohexylcarbodiimide (DCCI) plus 1-hydroxy-1*H*-benzotriazole (HOBt),[8] triphenylphosphine (Ph_3P) plus di-2-pyridyl disulfide ($(PyS)_2$),[9] and diethoxyphosphoryl cyanide (DEPC)[10] as coupling reagents. The relative reactivity of a tetrapeptide fragment is practically the same as that of carboxylic acid of the amino acid corresponding to the carboxyl terminal of the fragment.

Results and Discussion

Fragment Condensation of Boc-L-Tyr(Bzl)-Gly-Gly-L-Phe-OH on the Soluble Polymer Support Using DCCI plus HOBt, DEPC, and Ph_3P plus $(PyS)_2$ as Coupling Reagents. Three systems of coupling reagents, DCCI plus HOBt, DEPC, and Ph_3P plus $(PyS)_2$, were investigated for the fragment condensation of Boc-L-Tyr(Bzl)-Gly-Gly-L-Phe-OH with the amino free terminal of Leu anchored to the soluble polymer support, H-L-Leu-OCH_2-resin. Soluble chloromethylated polystyrene (Cl content: 0.91 mmol/g) was prepared by the copolymerization of (chloromethyl) styrene (a mixture of *m*- and *p*-isomers 7 : 3) with styrene (molar ratios 1 : 9) using azobisisobutyronitrile as an initiator. H-L-Leu-OCH_2-resin (Leu content: 0.62 mmol/g) and Boc-L-Tyr(Bzl)-Gly-Gly-L-Phe-OH were prepared in the usual way.[7b,11]

On the basis of the amino component attached to the polymer, three equivalent each of the fragment peptide carboxylic acid and a coupling reagent are employed in order to pursue an efficient coupling. The reaction was performed in *N,N*-dimethylformamide (DMF) at 0—5 °C for 2 h and then at room temperature for 3 h. In the case of Ph_3P plus $(PyS)_2$, the coupling reaction was carried out with a threefold excess of the carboxyl component and a 30-fold excess each of Ph_3P and $(PyS)_2$. The reaction mixture was poured into methanol followed by the addition

Boc-L-Tyr(Bzl)-Gly-Gly-L-Phe-OH

$$+ \text{H-L-Leu-OCH}_2\text{-resin} \xrightarrow[\text{in DMF, 0—5 °C, 2 h and then r. t., 3 h}]{\text{coupling reagent}}$$

Boc-L-Tyr(Bzl)-Gly-Gly-L-Phe-L-Leu-OCH_2-resin

of a small amount of saturated aqueous sodium chloride. The precipitated peptide resin was filtered off and washed successively with water and methanol in order to remove the soluble reactant. In each case, recovery of the resulting peptide polymer by precipitation from the solution in DMF with methanol was more than 93% on the basis of yields. Amino acid analyses of the resulting peptide resins and coupling yields with various coupling reagents are summarized in Table 1. The average yield of the coupling reaction was calculated from the recovery of Phe and Gly in the acid hydrolysate taking the recovery of Leu as the standard. The fragment condensation on the soluble polymer support, especially when DCCI plus HOBt and DEPC were used as coupling reagents, could achieve efficient coupling (96—99% yield) of the tetrapeptide acid to the amino free terminal of Leu on the soluble polymer support.

Relative Reactivities of Boc-Amino Acids and Boc-L-Tyr(Bzl)-Gly-Gly-L-Phe-OH with H-L-Leu-OCH_2-resin in the Coupling Reaction. In order to find out to what extent the peptide chain length influences the reactivity of the *C*-terminal amino acid in the fragment condensation reaction, and the effect of the coupling reagent on the reactivity of the tetrapeptide acid when Boc-L-Phe-OH is replaced by Boc-L-Tyr(Bzl)-Gly-Gly-L-Phe-OH, the technique as given in the following was used. Relative reactivities of Boc-amino acids with H-L-Leu-OCH_2-resin were first determined with use of various coupling reagents. The results are summarized in Table 2. As a typical example (run 1), starting with 200 mg of H-L-Leu-OCH_2-resin containing 0.124 mmol of Leu, the coupling reaction was carried out with a three-fold excess each of Boc-Gly-OH, Boc-L-Val-OH, and Boc-L-Phe-OH and a nine-fold excess (an equimolar amount with the total of the

TABLE 1. AMINO ACID ANALYSES OF Boc-L-Tyr(Bzl)-Gly-Gly-L-Phe-L-Leu-OCH_2-resins AND COUPLING YIELDS WITH VARIOUS COUPLING REAGENTS

Coupling reagent	Amino acid content (mmol/g)				Average yield of coupling[a] (%)
	Tyr[b]	Gly	Phe	Leu	
DCCI + HOBt[c]	0.38	0.85	0.42	0.44	96
DCCI + HOBt[d]	0.39	0.89	0.45	0.46	97
DEPC[c]	0.42	0.88	0.45	0.45	99
$Ph_3P + (PyS)_2$[c]	0.31	0.71	0.35	0.41	86

a) Calculated from the recovery of Phe and Gly in the acid hydrolysate taking the recovery of Leu as a standard. b) Acid hydrolysis of tyrosyl peptides usually gave low recovery of Tyr (K. Watanabe and K. Inouye, *Bull. Chem. Soc. Jpn.*, **50**, 201 (1977)). c) Reaction carried out with stirring at 0—5 °C for 2 h and then at room temperature for 3 h. d) Reaction carried out with stirring at 0—5 °C for 2 h and then at room temperature for 20 h.

TABLE 2. AMINO ACID ANALYSES OF PEPTIDE RESINS AND RELATIVE REACTIVITIES OF BOC-AMINO ACIDS AND Boc-L-Tyr(Bzl)-Gly-Gly-L-Phe-OH IN THE COUPLING REACTION WITH H-L-Leu-OCH_2-resin USING VARIOUS COUPLING REAGENTS

Run No.	Coupling reagent	Acid components[b]	Amino acid content (mmol/g)				Relative reactivities[a] (Amino acid ratios)		
			Gly	Val	Leu	Phe	Gly	Val	Phe
1	DCCI+HOBt[c]	A	0.209	0.054	0.552	0.281	3.9	1.0	5.2
2	DEPC[c]	A	0.263	0.063	0.545	0.203	4.2	1.0	3.2
3	$Ph_3P+(PyS)_2$[d]	A	0.308	0.012	0.561	0.199	25.7	1.0	16.6
4	DCCI+HOBt[c]	B	—	0.131	0.544	0.401	—	1.0	3.1
5	DEPC[c]	B	—	0.136	0.572	0.397	—	1.0	2.9
6	$Ph_3P+(PyS)_2$[d]	B	—	0.019	0.531	0.467	—	1.0	24.6
7	DCCI+HOBt[c]	C	0.722	0.118	0.467	0.346	(3.1)	1.0	2.9
8	DEPC[c]	C	0.711	0.118	0.484	0.353	(3.0)	1.0	3.0
9	$Ph_3P+(PyS)_2$[d]	C	0.224	0.246	0.470	0.112	(0.46)	1.0	0.46

a) Determined with use of the amino acid ratios of resulting peptide resins taking the recovery of Val as a standard. b) Abbreviations; A: mixture of an equivalent each of Boc-Gly-OH, Boc-L-Val-OH, and Boc-L-Phe-OH, B: mixture of an equivalent each of Boc-L-Val-OH and Boc-L-Phe-OH, C: mixture of an equivalent each of Boc-L-Val-OH and Boc-L-Tyr(Bzl)-Gly-Gly-L-Phe-OH. c) A three-fold excess each of carboxyl components and an equimolar amount of the total of the carboxyl components of a coupling reagent were used. d) The coupling reaction was carried out with a three-fold excess each of carboxyl components and a two-fold excess of the total of the carboxyl components each of Ph_3P and $(PyS)_2$.

carboxyl components) of DCCI and HOBt each in 20 ml of DMF at 0—5 °C for 2 h and at room temperature for 13 h. The resulting peptide resin by precipitation from the solution in DMF with methanol was subjected to acid hydrolysis with propionic acid–12 M HCl (2: 1 v/v) at 115 °C for 35 h followed by the amino acid analysis. Relative reactivities of Boc–amino acids were determined using the amino acid ratios of the resulting peptide resin taking the recovery of Val as a standard. Relative reactivity of Boc–L-Tyr-(Bzl)–Gly–Gly–L-Phe–OH was also determined by a similar procedure using a combination of carboxyl components.

It seems that in each coupling reagent (except DCCI plus HOBt), peptide bonds involving Boc–L-Phe–OH and Boc–L-Val–OH which have bulky side chains are not formed as readily as Boc–Gly–OH forms peptide bond. A marked influence of bulky side chains on a decrease in the rate of the reaction was observed when Ph_3P plus $(PyS)_2$ was used as a coupling reagent (run Nos. 1—3, Table 2).

Relative reactivities using DCCI plus HOBt as a coupling reagent:

Boc-L-Phe-OH > Boc-Gly-OH > Boc-L-Val-OH

Relative reactivities using DEPC as a coupling reagent:

Boc-Gly-OH > Boc-L-Phe-OH > Boc-L-Val-OH

Relative reactivities using Ph_3P plus $(PyS)_2$ as a coupling reagent:

Boc-Gly-OH > Boc-L-Phe-OH $\gg$ Boc-L-Val-OH

The values reflect the reactivities of the intermediates formed by the reactions of coupling reagents with Boc–amino acids (Fig. 1).

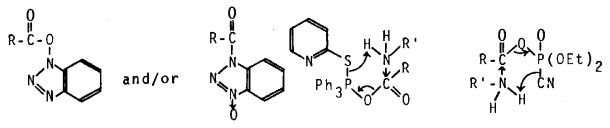

I II III

Fig. 1. Intermediates for the corresponding coupling reagents (DCCI+HOBt,[12] $Ph_3P+(PyS)_2$,[9] and DEPC[10]).

The data runs 4—9, Table 2 show that the relative reactivities of Boc–L-Val–OH, Boc–L-Phe–OH, and Boc–L-Tyr(Bzl)–Gly–Gly–L-Phe–OH are as follows:

Coupling reagents: DCCI + HOBt and DEPC

Boc-L-Tyr(Bzl)-Gly-Gly-L-Phe-OH

= Boc-L-Phe-OH > Boc-L-Val-OH

Coupling reagent: $Ph_3P + (PyS)_2$

Boc-L-Phe-OH $\gg$ Boc-L-Val-OH >

Boc-L-Tyr(Bzl)-Gly-Gly-L-Phe-OH

The results indicate that the peptide chain length of Boc–L-Tyr(Bzl)–Gly–Gly–L-Phe–OH has no influence on the reactivity of the *C*-terminal amino acid in the coupling reaction using DCCI plus HOBt and DEPC as coupling reagents. A marked decrease in the reactivity of the *C*-terminal amino acid of the tetrapeptide acid was observed when Ph_3P plus $(PyS)_2$ was used as a coupling reagent. The differences due to coupling reagents can be attributed to the steric hindrance effect of the peptide chain on the intermediates I, II, and III.

Fragment condensation on the soluble polymer support could achieve efficient coupling of the tetrapeptide acid to the amino free terminal anchored to the soluble polymer support. Relative reactivities of Boc–amino acids and the peptide fragment could be easily determined by use of amino acid ratios in the acid hydrolysates of the resulting peptide resins in which they were taken. Thus it was found that the peptide chain length of Boc–tetrapeptide acid has no influence on the reactivity of the *C*-terminal amino acid in the coupling reaction using DCCI plus HOBt and DEPC as coupling reagents. However, a marked decrease in the reactivity of the *C*-terminal amino acid of the tetrapeptide was observed when Ph_3P plus $(PyS)_2$ was used as a coupling reagent.

The versatility of this new approach eliminates shortcomings of the solid phase and the classical liquid phase peptide syntheses, their merits, namely the inherent simplicity of synthesis using polymer supports and the advantage of carrying out the peptide synthesis under homogeneous conditions, being preserved. It promises the possibility of unequivocal chemical synthesis of homogeneous proteins of defined structures.

Experimental

Boc–amino acids were prepared according to Nagasawa *et al.*[13] HOBt, DEPC, and $(PyS)_2$ were prepared by the methods given by Konig and Geiger,[8] Takamizawa *et al.*[14] and Matsueda *et al.*,[18] respectively. All other reagents were commercial products. DMF was purified as follows. To benzene-dried DMF was added phenyl isothiocyanate (1% by volume) followed by distillation under reduced pressure. It was then redistilled under reduced pressure. Optical rotations were taken in a 1-dm cell on a Jasco Model ORD/UV-5 optical rotatory dispersion recorder. Amino acid analyses were performed on a Hitachi Liquid Chromatograph, Model 034. Hydrolyses of peptide resins were carried out on 20—40 mg samples of resins with propionic acid–12 M HCl (2 : 1 v/v) at 115 °C for 35 h.

Soluble Chloromethylated Polystyrene. Styrene, 28.12 g (0.27 mol), 4.58 g (0.03 mol) of (chloromethyl)styrene (Tokyo Kasei Co., a mixture of *m*- amd *p*-isomers (7 : 3)), and 0.25 g (1.5 mmol) of azobisisobutyronitrile were dissolved in 100 ml of benzene. The solution in a polymerization tube was sealed off *in vacuo* and heated in a bath maintained at 70±0.5 °C for 38 h. The solution was poured into methanol to obtain a soluble chloromethylated polystyrene. The product was dried *in vacuo* at 75—80 °C for 20 h. The yield was 20.3 g. The chlorine content of the polymer was determined by the Volhard method to get a value of 0.91 mmol per 1 g of resin.

H–L-Leu–OCH₂–resin. Esterification of the chloromethylated polystyrene with Boc–L-Leu–OH was carried out at room temperature for 7 days.[7b] Boc–L-Leu–OCH_2–resin: Leu content, 0.61 mmol/g (amino acid analysis); Cl content, 0.20 mmol/g (titrated by Volhard method). After attachment of Leu to the polymer support, residual benzylic chlorides were removed by the reaction with sodium

acetate in DMF at 105 °C for 24 h. The final chlorine content was less than 0.02 mmol/g. H-L-Leu-OCH_2-resin was prepared by a similar procedure.[7b] H-L-Leu-OCH_2-resin: Leu content, 0.62 mmol/g (amino acid analysis).

Boc-L-Tyr(Bzl)-Gly-Gly-L-Phe-OCH_3. Boc-L-Tyr(Bzl)-Gly-Gly-L-Phe-OCH_3 was prepared with use of DCCI plus HOBt as a coupling reagent,[11] mp 114—116 °C, $[\alpha]_D^{21}=+13.1°$ ($c=2.0$, CH_3OH) (lit,[11] mp 108—110 °C, $[\alpha]_D=+26.3°$ ($c=1.0$, CH_3OH)). It was also prepared by the following procedure. To a mixture of 3.73 g (0.01 mol) of Boc-L-Tyr(Bzl)-OH and 3.63 g (0.011 mol) of H-Gly-Gly-L-Phe-OCH_3·HCl in 30 ml of DMF was added 1.80 g (0.011 mol) of DEPC in 10 ml of DMF at 0 °C, followed by the addition of 2.1 g (0.021 mol) of triethylamine in 10 ml of DMF during 5 min. The mixture was strired at 0 °C for 1 h and then at room temperature overnight. The reaction mixture was diluted with 300 ml of ethyl acetate, successively washed three times with 5% hydrochloric acid, twice with 10% aqueous sodium chloride, three times with saturated aqueous sodium hydrogencarbonate, and twice with 10% aqueous sodium chloride, and dried over sodium sulfate. Removal of solvent *in vacuo* afforded the crude peptide (6.10 g). Recrystallization from ethyl acetate gave a substance, mp 114—116 °C, $[\alpha]_D^{21}=+12.9°$ ($c=1.0$, CH_3OH). Amino acid ratios in acid hydrolysate: Tyr 0.93, Gly 2.00, Phe 1.01 (Found: C, 64.27; H, 6.42; N, 8.87%).

Boc-L-Tyr(Bzl)-Gly-Gly-L-Phe-OH. To the tetrapeptide methyl ester, 3.5 g(5.0 mmol) in 60 ml of methanol, was added 12 ml of 0.5 M aqueous sodium hydroxide and stirred overnight at room temperature. Removal of solvent *in vacuo* afforded the crude peptide sodium salt, which was treated with 10% citric acid to give the tetrapeptide acid, 2.85 g. Recrystallization from water-methanol (3 : 1) gave a pure material, mp 104—107 °C, $[\alpha]_D^{21}=+21.0°$ ($c=1.0$, CH_3OH) (lit,[11] mp 95—96 °C, $[\alpha]_D=+34.3°$ ($c=0.95$, CH_3OH)). Amino acid ratios in acid hydrolysate: Tyr 0.91, Gly 2.00, Phe 1.00 (Found: C, 63.33; H, 6.15; N, 9.02%).

Boc-L-Tyr(Bzl)-Gly-Gly-L-Phe-L-Leu-OCH_2-resin. H-L-Leu-OCH_2-resin, 200 mg(Leu content: 0.124 mmol), was dissolved in 10 ml of DMF. To the solution was added 224 mg (0.37 mmol) of Boc-L-Tyr(Bzl)-Gly-Gly-L-Phe-OH, followed by the addition of 0.37 mmol of a coupling reagent at 0—5 °C. The reaction mixture was stirred at 0—5 °C for 2 h and then at room temperature for 3 h. To DCCI and DEPC, used as coupling reagents, were added 0.37 mmol of HOBt and 0.37 mmol of triethylamine, respectively. In the case of Ph_3P plus $(PyS)_2$, the coupling reaction was carried out with a three-fold excess of the carboxyl component and a 30-fold excess each of Ph_3P and $(PyS)_2$. The solution was poured into 200 ml of methanol followed by 30 ml of saturated aqueous sodium chloride. The precipitated peptide resin was filtered off, and washed successively with water and methanol to remove the soluble reactant. The yields were 253 mg (DCCI plus HOBt), 277 mg (DEPC), and 243 mg (Ph_3P plus $(PyS)_2$) (dried *in vacuo* for 2 days).

Relative Reactivities of Boc-Amino Acids and Boc-L-Tyr(Bzl)-Gly-Gly-L-Phe-OH in the Coupling Reaction. H-L-Leu-OCH_2-resin, 200 mg (Leu content: 0.124 mmol), and a three equivalent each of carboxyl components were dissolved in 20 ml of DMF. To the solution was added a coupling reagent, an equivalent mole with the total of the carboxyl components, under cooling with ice-cold water. When DCCI and DEPC were used as coupling reagent, an equivalent each of HOBt and triethylamine was added, respectively, after addition of the coupling reagent. In the case of Ph_3P plus $(PyS)_2$, the coupling reaction was carried out with a three-fold excess each of carboxyl components and a two-fold excess of the total of the carboxyl components each of Ph_3P and $(PyS)_2$. The reaction mixture was stirred for 2 h in an ice bath and 13 h at room temperature. The work-up was essentially the same as described above. The peptide resins were subjected to acid hydrolyses.

The work was carried out with a Grant-in-aid for Scientific Research from the Ministry of Education. Thanks are due to Prof. M. Akiyama for his support and Mrs. M. Asuke of this department for elemental analyses.

References

1) (a) R. B. Merrifield, *J. Am. Chem. Soc.*, **85**, 2149 (1963); (b) B. Gutte and R. B. Merrifield, *J. Biol. Chem.*, **246**, 1922 (1971); (c) C. H. Li and D. Yamashiro, *J. Am. Chem. Soc.*, **92**, 7608 (1970); (d) B. Gutte, *J. Biol. Chem.*, **250**, 889 (1975); (e) N. H. Tan and E. T. Kaiser, *J. Org. Chem.* **41**, 2787 (1976).

2) S. R. Jenkins, R. F. Nutt, R. S. Dewey, D. F. Veber, F. W. Holly, W. J. Paleveda, Jr., T. Lanza, Jr., R. G. Strachan, E. F. Schoenewaldt, H. Barkemeyer, M. J. Dickinson, J. Sondey, R. Hirschmann, and E. Walton, *J. Am. Chem. Soc.*, **91**, 505 (1969).

3) E. Bayer, H. Eckstein, K. Hagele, W. A. König, W. Brünig, H. Hagenmaier, and W. Parr, *J. Am. Chem. Soc.*, **92**, 1735 (1970).

4) (a) E. Bayer, M. Mutter, R. Uhmann, J. Polster, and H. Mauser, *J. Am. Chem. Soc.*, **96**, 7333 (1974); (b) J. J. Maher, M. E. Furey, and L. J. Greenberg, *Tetrahedron Lett.*, **1971**, 27.

5) D. Yamashiro, J. Blake, and C. H. Li, *Tetrahedron Lett.*, **1976**, 1469.

6) (a) H. Yajima and H. Kawatani, *Chem. Pharm. Bull.*, **19**, 1905 (1971); (b) H. Yajima and Y. Kiso, *ibid.*, **22**, 1087 (1974); (c) R. Matsueda, H. Maruyama, E. Kitazawa, H. Takahagi, and T. Mukaiyama, *J. Am. Chem. Soc.*, **97**, 2573 (1975); (d) K. Neubert and H. D. Yakubuke, *J. Prakt. Chem.*, **317**, 448 (1975); (e) C. Di Bello, A. Marigo, O. Buso, and A. Lucchiari, *Tetrahedron Lett.*, **1977**, 1135.

7) (a) M. M. Shemyakin, Yu. A. Ovchinnikov, A. A. Kinyushkin, and I. V. Kozhevnikova, *Tetrahedron Lett.*, **1965**, 2323; (b) B. Green and L. R. Garson, *J. Chem. Soc., C*, **1969**, 401; (c) E. Bayer and M. Mutter, *Nature*, **237**, 512 (1972); (d) H. Hagenmaier, *Z. Physiol. Chem.*, **356**, 777 (1975).

8) W. König and R. Geiger, *Chem. Ber.*, **103**, 788 (1970).

9) T. Mukaiyama, R. Matsueda, and M. Suzuki, *Tetrahedron Lett.*, **1970**, 1901.

10) (a) S. Yamada, Y. Kasai, and T. Shioiri, *Tetrahedron Lett.*, **1973**, 1595; (b) T. Shioiri, K. Ninomiya, and S. Yamada, *J. Am. Chem. Soc.*, **94**, 6203 (1972).

11) W. Voelter, E. Pietrzik, and H. Kalbacher, *Tetrahedron Lett.*, **1976**, 2119.

12) (a) K. Horiki, *Tetrahedron Lett.*, **1977**, 1897; (b) K. Horiki, *ibid.*, **1977**, 1902.

13) T. Nagasawa, K. Kuroiwa, K. Narita, and Y. Isowa, *Bull. Chem. Soc. Jpn.*, **46**, 1296 (1973).

14) A. Takamizawa, Y. Sato, and S. Tanaka, *Yakugaku Zasshi*, **85**, 298 (1965).

15) R. Matsueda, H. Maruyama, M. Ueki, and T. Mukaiyama, *Bull. Chem. Soc. Jpn.*, **44**, 1373 (1971).

The Reactions of Group V Metal Amide with Sulfur Dioxide

Fumio Ando, Jugo Koketsu, and Yoshio Ishii
Department of Industrial Chemistry, Chubu Institute of Technology, Matsumoto, Kasugai, Aichi 487

(Received October 14, 1977)

Tris(dialkylamino)-arsines (I), -stibines (II), and -bismuthines (III) react with sulfur dioxide to give the corresponding tetraalkylsulfurous diamides and the corresponding metal oxides or polymers containing the metals. The reactivity of these metal amides in view of the fastness of the initial reactions follows the order III>II>I, however, the yields decrease in the order I>II>III. Tris(dialkylamino)phosphines, on the other hand, give hexaalkylphosphoric triamides and hexaalkylphosphorothioic triamides in a ratio of 2 : 1. The reactivity of the various phosphorus compounds toward sulfur dioxide increases with increasing nucleophilicity of the phosphorus atom; $P(NEt_2)_3 > Ph_2PNEt_2 > Ph_2POEt > PhP(OEt)_2 > P(OEt)_3$. The reaction mechanism of compounds (I), (II), and (III) with sulfur dioxide is different from that of the phosphorus amides.

Sulfur dioxide is unique in the point that it exhibits both nucleophilic and electrophilic behavior.[1] Many studies of the reaction of sulfur dioxide with organometallic compounds have been reported.[2,3] Lappert *et al.* have found that the reaction of sulfur dioxide with (dimethylamino)trimethyltin affords the insertion product,[4]

$$Me_3SnNMe_2 + SO_2 \rightarrow Me_3SnOSNMe_2 \quad (1)$$
$$\qquad\qquad\qquad\qquad\qquad\qquad\quad \| \; O$$

The reaction of tris(dialkylamino)boron with sulfur dioxide yields tetraalkylsulfurous diamides and tris-(dimethylamino)boroxin,[5]

$$3B(NR_2)_3 + 3SO_2 \rightarrow 3(R_2N)_2SO + (R_2NBO)_3. \quad (2)$$

The group V metal amides; $P(NR_2)_3$, $As(NR_2)_3$, $Sb(NR_2)_3$, and $Bi(NR_2)_3$ are very reactive compounds and thus are valuable as synthetic intermediates. They are known to react with ketones,[6-8] acetic anhydride,[7,9] and heterocumulenes,[7,9] but there is no report concerning their chemistry with sulfur dioxide. This paper describes the reactions of the group V metal amides with sulfur dioxide, and a reaction mechanism is proposed based on relative reactivities.

Results and Discussion

Tris(dimethylamino)-, tris(diethylamino)-, and tris-(dipropylamino)-arsine reacted with sulfur dioxide at −30 °C to give the corresponding tetraalkylsulfurous diamides and As_2O_3 which was identified by X-ray powder diffraction.

$$2As(NR_2)_3 + 3SO_2 \rightarrow 3(R_2N)_2SO + As_2O_3. \quad (3)$$

The sulfurous diamides were identified by comparison of their IR and NMR spectra with those of authentic samples obtained by the reaction of thionyl chloride with the corresponding secondary amines.[10,11] The identity of the sulfurous diamides was confirmed by the fact that their reaction with acetic anhydride gave the appropriate *N,N*-dialkylacetamides accompanied by the evolution of sulfur dioxide.[12]

The reaction of tris(dialkylamino)-stibines and -bismuthines with sulfur dioxide proceeded more vigorously, but the yield of sulfurous diamides was lower than the case of tris(dialkylamino)arsine. In addition to sulfurous diamides, in both cases polymeric residues, which were formulated on the basis of elemental analyses as $(R_2NSbO)_n$ or $(R_2NBiO)_n$, are formed. IR spectra of the residues showed a stretching mode for Sb–O–Sb at 750—715 cm^{-1} and for Bi–O–Bi at 630—620 cm^{-1}.[13]

$$M(NR_2)_3 + SO_2 \rightarrow (R_2N)_2SO + \frac{1}{n}(R_2NMO)_n. \quad (4)$$

M = Sb and Bi

These residues are hydrolyzed in the presence of hot water to afford Sb_2O_3 or Bi_2O_3 which was identified by X-ray powder diffraction.

There is a similarity between the reactions described here and the amination reactions of carbonyl compounds with group V metal amides.[8] Bismuth amides react with sulfur dioxide most vigorously. The reactivity order in view of the fastness of the initial reaction is Bi>Sb>As, whereas, the yields of sulfurous diamides decrease as follows As>Sb>Bi (Table 1). A mechanism for the reaction can be discussed in terms of the nucleophilicity of nitrogen atom and the affinity of the metal atom for oxygen. The first step involves the nucleophilic attack by the nitrogen atom of the metal amide on the sulfur atom of sulfur dioxide thus forming an insertion product.

$$(R_2N)_3M \rightarrow R_2N \quad O \| S=O \rightarrow \left[(R_2N)_2M\text{-}O \; | \; R_2N\text{-}S=O \right]$$
$$\rightarrow \left[R_2N\text{-}M\text{-}O \; | \; R_2N \;\; S(O)NR_2 \right] \rightarrow (R_2N)_2SO + \frac{1}{n}[R_2NMO]_n \quad (5)$$

The degree of ionic character of metal–nitrogen bonds increases with decreasing electronegativity of the central metal. The rates of the initial addition step are found to be parallel with the ionic degree of the metal–nitrogen bonds. On the other hand, the affinity of metal atoms

Table 1. Yields(%) of tetraalkylsulfurous diamide in the reaction of $M(NR_2)_3$ with SO_2

M	R		
	Me	Et	Pr
As	76	75	88
Sb	62	48	49
Bi	46	45	46

for oxygen decreases in the order; As>Sb>Bi.[8,14] Therefore, bismuth amides are the most reactive in the initial step, but their poor affinities for oxygen result in decreased yields of the sulfurous diamides as the result of the formation of the polymeric residues which contain the dialkylamino moieties instead of the metal oxides.

When tris(dialkylamino)phosphines were treated with sulfur dioxide, hexaalkylphosphoric triamides and hexaalkylphosphorothioic triamides were obtained in the ratio of 2:1.

$$3(R_2N)_3P + SO_2 \rightarrow 2(R_2N)_3P{=}O + (R_2N)_3P{=}S \quad (6)$$

Similarly, (diethylamino)diphenylphosphine, ethyl diphenylphosphinite and ethyl diphenylphosphinothioite gave the corresponding P=O and P=S compounds in the ratio of 2:1. The reactivity of the various trivalent phosphorus compounds toward sulfur dioxide was compared by means of GLC analysis. The order of the reactivity, $P(NEt_2)_3 > Ph_2PNEt_2 > Ph_2POEt > PhP(OEt)_2 > P(OEt)_3$, is parallel with the order of electron density on the phosphorus atom.[15,16] Tris(diethylamino)phosphine has the highest electron density on the phosphorus atom because of the (p-d)π interaction between the nitrogen atom and the phosphorus atom. In the case of phosphites, although there may be some degree of oxygen to phosphorus (p-d)π bonding, the inductive effect of oxygen atoms provide a greater influence on the reactivity. Thus it would appear most reasonable to expect that the reactive site on the aminophosphine is the phosphorus atom instead of the nitrogen atom. On this basis a tentative mechanism for the reaction is as follows.

$$(R_2N)_3P + S{=}O \rightarrow (R_2N)_3\overset{+}{P}{-}S{=}O \rightarrow (R_2N)_3P{<}\begin{matrix}S{=}O\\ O\end{matrix}$$

$$\rightarrow (R_2N)_3PO + [SO]$$

$$[SO] \rightarrow \frac{1}{2}(S) + \frac{1}{2}SO_2$$

Nucleophilic attack by the phosphorus atom on the sulfur atom of sulfur dioxide occurs as the first step of the reaction, and follows the formation of the P–O bond, generating the products. This mechanism is principally the same as that proposed by Smith *et al.* for the reaction of phosphines with sulfur dioxide.[17,18] Aminophosphines exhibit an ambident nature in their reactions with various kinds of electrophilic reagents, such as phenyl cyanate, and β-propiolactone.[19,20] In the reaction with cyclic carbonates, the nitrogen atom of the aminophosphine acts as the nucleophilic site whereas in the reaction with alkyl benzenesulfonate, the phosphorus atom attacks the electrophilic reagent forming the phosphonium salt.[21,22] Although it is very difficult to predict which atom of the aminophosphines acts as a nucleophilic site, the HSAB concept may prove helpful. Since the phosphorus atom of the aminophosphine is softer than the nitrogen atom, a soft electrophile would be expected to prefer to interact with the phosphorus atom. The striking difference in mechanism of the reaction of sulfur dioxide with aminophosphines and with aminoarsines, aminostibines and aminobismuthines is not explainable on the basis of HSAB theory. The fact that the metal sulfides of the type, $(R_2N)_3M{=}S$ where M=As, Sb, and Bi were not formed suggests that the poorer stability of the M=S bond relative to P=S may be a factor of significant importance.

Experimental

All the reactions were carried out under an argon atmosphere. The IR, NMR, and mass spectra were recorded on a Shimadzu IR-430 spectrometer, a JEOL-C60 HL spectrometer, and a JMS-D300 spectrometer, respectively. GLC analyses were carried out on a Simadzu GC 6A apparatus, using PEG 6000 (10%)-Shimalite W 301 (1 m) column with helium as the carrier gas.

Materials. Tris(dialkylamino)arsines, -stibines, and -bismuthines were prepared by the methods priviously reported[9,23]: $As(NMe_2)_3$; bp 68—72 °C/18 mmHg, $As(NEt_2)_3$; bp 62—65 °C/0.3 mmHg, $As(NPr_2)_3$; bp 82—86 °C/0.08 mmHg, $Sb(NMe_2)_3$; bp 55—61 °C/5 mmHg, $Sb(NEt_2)_3$; bp 59—62 °C/0.02 mmHg, $Sb(NPr_2)_3$; bp 107—111 °C/0.1 mmHg, $Bi(NMe_2)_3$; bp 34—36 °C/0.2 mmHg, $Bi(NEt_2)_3$; bp 75—77 °C/0.12 mmHg, $Bi(NPr_2)_3$; bp 73—77 °C/0.05 mmHg. All the phosphorus compounds used in this experiment are synthesized according to the methods described in the literature.[24] Sulfur dioxide, obtained from a commercial source, was dried by passage through concentrated sulfuric acid. Organic solvents were dried by conventional methods.[25]

Reaction of Tris(dialkylamino)arsines with Sulfur Dioxide. Dry sulfur dioxide was bubbled through tris(dimethylamino)-arsine (2.67 g, 12.9 mmol) in diethyl ether (5 ml) at −30 °C. An exothermic reaction took place to give a white precipitate. After removal of the precipitate, the solvent and excess SO_2, tetramethylsulfurous diamide (2.00 g, 76%) was obtained by distillation under reduced pressure; bp 70—73 °C/16 mmHg, mp 30—30.5 °C, IR (neat) ν(S=O) 1150, $\nu(NC_2)$ 930, 908, ν(S–N) 670, 656, 646 cm^{-1}, NMR ($CHCl_3$) δ 2.62, MS *m/e* 136 (M^+).

Similar treatment of tris(diethylamino)arsine (5.09 g, 17.5 mmol) with sulfur dioxide resulted in the formation of tetraethylsulfurous diamide (3.77 g, 75%); bp 82—84 °C/3 mmHg, n_D^{20} 1.4635, IR(neat), ν(S=O) 1110 cm^{-1}, $\nu(NC_2)$ 924, 894, 876 cm^{-1}, ν(S–N) 652 cm^{-1}, NMR ($CHCl_3$) δ 1.10 (3H, t), 3.06 (2H, q), MS *m/e* 192 (M^+). Reaction of tris-(dipropylamino)arsine (4.16 g, 11.1 mmol) with sulfur dioxide gave tetrapropylsulfurous diamide (3.63 g, 88%); bp 66—68 °C/0.03 mmHg, n_D^{20} 1.4667, IR (neat) ν(S=O) 1110 cm^{-1}, $\nu(CN_2)$ 692 cm^{-1}, NMR ($CHCl_3$); δ 0.89 (3H, t), 1.53 (2H, m), 2.94 (2H, t), MS *m/e* 248 (M^+).

Reaction of Tris(diethylamino)stibine with Sulfur Dioxide. When sulfur dioxide was passed through an ethereal solution of tris(diethylamino)stibine (1.93 g, 5.71 mmol) at −30 °C, a violent reaction took place to give a yellowish white precipitate, which was filtered and washed twice with ether. The filtrate was distilled to give tetraethylsulfurous diamide (0.79 g, 48%), bp 44—46 °C/0.02 mmHg. The polymeric residue exhibited Sb–O–Sb bands at 750, 616 cm^{-1} and several absorptions ascribed to the diethylamino moiety. (Found: C, 23.6%, H, 4.98%. Calcd for $C_4H_{10}NOSb$; C, 22.90%, H, 4.80%.)

Reaction of Tris(diethylamino)bismuthine with Sulfur Dioxide. Tris(diethylamino)bismuthine (2.85 g, 6.70 mmol) reacted readily with sulfur dioxide to give hexaethylsulfurous diamide (0.88 g, 45%) and a yellowish white precipitate; IR (KBr) 618 cm^{-1} (Bi–O–Bi). (Found: C, 16.4%, H, 3.66%, Calcd for $C_4H_{10}NOBi$; C, 16.17%, H, 3.39%)

Table 2. Spectroscopic data of the products of the reaction between several phosphorus compounds and SO_2

Compound	NMR δ (TMS)	IR ν(P=O or P=S) cm^{-1}
$Ph_2P(O)NEt_2$	1.07(6H, t), 3.07(4H, m, $J_{PNCH}=11.4$ Hz), 7.51, 7.90(10H, m)	1180
$Ph_2P(S)NEt_2$	1.07(6H, t), 3.07(4H, m, $J_{PNCH}=11.2$ Hz), 7.50, 7.90(10H, m)	753, 578
$Ph_2P(O)OEt$	1.35(3H, t), 4.30(2H, m, $J_{POCH}=7.1$ Hz)	1225
$Ph_2P(S)OEt$	1.31(3H, t), 4.10(2H, m, $J_{POCH}=8.8$ Hz)	782, 610
$Ph_2P(O)SEt$	1.29(3H, t), 2.84(2H, m, $J_{PSCH}=11.6$ Hz), 7.51, 7.87(10H, m)	1200
$Ph_2P(S)SEt$	1.25(3H, m, $J_{PSCH}=2.1$ Hz),	785
	2.84(2H, m, $J_{PSCH}=7.3$ Hz), 7.46, 7.85(10H, m)	630

Reaction of Tris(dialkylamino)phosphines with Sulfur Dioxide. Sulfur dioxide was bubbled through tris(dimethylamino)phosphine (1.65 g, 10.1 mmol) in diethyl ether (5 ml) at −30 °C. After removal of the volatile materials, the reaction mixture was distilled to give a fraction having a boiling point of 53—72 °C/0.6 mmHg. The distillate showed two spots on thin layer chromatograph at $R_f=0.87$ and 0.19. Separation of the distillate by a column chromatograph (silica gel-chloroform) gave hexamethylphosphorothioic triamide (0.53 g, 27%) as a first eluate and hexamethylphosphoric triamide (0.87 g, 48%) as a second eluate, as identified by the comparison of their IR and NMR spectra with those of authentic materials.[24] Similarly, sulfur dioxide was passed through an ethereal solution of tris(diethylamino)phosphine (1.83 g, 7.40 mmol) at −30 °C, and the reaction mixture was distilled. The fraction of the bp range 36—86 °C/0.1 mmHg was collected, and column chromatograph of this fraction gave hexaethylphosphorothioic triamide (0.56 g, 27%) $R_f=0.70$, NMR ($CHCl_3$) δ 1.11 (3H, t), 3.14 (2H, m, $J_{PNCH}=11.6$ Hz). IR ν(P=S) 798, 696 cm^{-1}, and hexaethylphosphoric triamide (0.98 g, 50%), NMR ($CHCl_3$) δ 1.22 (3H, t), 3.31 (2H, m, $J_{PNCH}=16.5$ Hz), IR ν(P=O) 1205 cm^{-1}. Reaction of tris(dipropylamino)phosphine with sulfur dioxide gave hexapropylphosphorothioic triamide (0.37 g, 20%), NMR ($CHCl_3$) δ 0.86 (3H, t), 1.56 (2H, m), 2.96 (2H, m), IR ν(P=S) 796, 736 cm^{-1}, and hexapropylphosphoric triamide (0.82 g, 45%), NMR ($CHCl_3$) δ 0.91 (3H, t), 1.63 (2H, m), 3.01 (2H, m), IR ν(P=O) 1242 cm^{-1}.

The similar treatment of (diethylamino)diphenylphosphine, ethyl diphenylphosphinite and ethyl diphenylphosphinothioite with sulfur dioxide gave the corresponding P=O and P=S compounds in the ratio of 2:1. And the spectral data of these products are shown in Table 2.

Effect of Substituent on the Reactivity. A reaction of a phosphorus (III) compound (0.1 mol/l) with a large excess sulfur dioxide was initiated at −55 °C by mixing THF solutions of each reagent containing an internal standard. Aliquots of the reaction mixture were withdrawn at appropriate times, and the remaining amount of the phosphorus (III) compound was determined by GLC analysis (Table 3).

Reaction of Tetraalkylsulfurous Diamide with Acetic Anhydride. Acetic anhydride (1.3 g, 11.1 mmol) was added to an ice-cooled ethereal solution of tetramethylsulfurous diamide (1.51 g, 11.1 mmol) with stirring. An exothermic reaction took place accompanied by the evolution of a gas. After removal of the solvent, *N,N*-dimethylacetamide (17.4 g, 90%) was obtained by distillation, bp 67—70 °C/20 mmHg. Similarly an equimolar reaction of tetraethylsulfurous diamide (1.56 g, 8.13 mmol) with acetic anhydride gave *N,N*-diethylacetamide (1.63 g, 87%), bp 101—104 °C/55 mmHg.

Table 3. Remaining amount of trivalent phosphorus compounds after 40 min

Compound	Concentration (mmol/l)
$P(NEt_2)_3$	0
Ph_2PNEt_2	14.2
Ph_2POEt	21.8
$PhP(OEt)_2$	51.6
$P(OEt)_3$	98.6

The authors wish to thank Professor D. Hendricker of Ohio University for valuable discussions and correcting English.

References

1) A. Wojcicki, "Adavances in Organometallic Chemistry," Academic Press, Vol. 12, (1974), p. 13—81.
2) C. W. Fong and W. Kitching, *J. Organomet. Chem.*, **22**, 95 (1970).
3) U. Kunze and J. D. Koola, *J. Organomet. Chem.*, **80**, 281 (1974).
4) T. A. George, K. Tones, and M. F. Lappert, *J. Chem. Soc.*, **1965**, 2157.
5) H. Noth and P. Schweizer, *Chem. Ber.*, **97**, 1464 (1964).
6) H. Weingarten and W. A. White, *J. Org. Chem.*, **31**, 4041 (1966).
7) J. Koketsu and Y. Ishii, *J. Chem. Soc., C*, **1971**, 511.
8) F. Ando, K. Ohashi, and J. Koketsu, *Bull. Chem. Soc. Jpn.*, **49** 727 (1976).
9) F. Ando, T. Hayashi, K. Ohashi, and J. Koketsu, *J. Inorg. Nucl. Chem.*, **37**, 2011 (1975).
10) R. Patetzald and E. Ronsch, *Spectrochim. Acta*, **26A**, 569 (1970).
11) T. Keat, D. S. Ross, and D. W. A. Sharp, *Spectrochim. Acta.*, **27A**, 2219 (1971).
12) T. Mukaiyama, H. Takei, and H. Shimizu, *Bull. Chem. Soc. Jpn.*, **40**, 939 (1967).
13) E. Maslowsky, Jr., *J. Organomet. Chem.*, **70**, 153 (1974).
14) D. Brandes and A. Blaschette, *J. Organomet. Chem.*, **73**, 217 (1974).
15) G. Aksnes and D. Aksnes, *Acta Chem. Scand.*, **18**, 38 (1964).
16) J. Schemidt, *Z. Naturforsch.*, **27b**, 600 (1972).
17) B. C. Smith and G. H. Smith, *J. Chem. Soc.*, **1965**, 5516.
18) E. Fluck and H. Binden, *Z. Anorg. Allg. Chem.*, **354**, 139 (1967).
19) J. Koketsu, S. Sakai, and Y. Ishii, *Kogyo Kagaku Zasshi*, **72**, 2503 (1969).
20) J. Koketsu, S. Kojima, and Y. Ishii, *Bull. Chem. Soc. Jpn.*, **43**, 3232 (1970).
21) J. Koketsu, S. Sakai, and Y. Ishii, *Kogyo Kagaku Zasshi*, **73**, 201 (1970).
22) J. Koketsu and Y. Ishii, *Bull. Chem. Soc. Jpn.*, **43**, 2527 (1970).
23) K. Moedritzer, *Inorg. Chem.*, **3**, 609 (1964).
24) G. M. Kosolapoff and L. Maier, "Organic Phosphorus Compounds," Wiley-Interscience, Vol. 4, 5 (1972—1973).
25) J. A. Riddick and W. B. Binger, "Organic Solvents," 3rd ed, Wiley-Interscience, New York (1970),

The Reaction of 1,3,5-Triazine with Aromatic Nitrile Oxides. A New Synthesis of 3-Substituted 1,2,4-Oxadiazoles

Masahiro KURABAYASHI and Christoph GRUNDMANN

National Chemical Laboratory for Industry, Mita, Meguro-ku, Tokyo 153

Department of Chemistry, Carnegie-Mellon University, 4400 Fifth Avenue, Pittsuburgh, Pennsylvania 15213

(Received October 17, 1977)

The cycloaddition of aromatic nitrile oxides(**2a**=benzo-; **2b**=*p*-tolu-; **2c**=mesitylenecarbo-) with 1,3,5-triazine(**1**) is reported. The corresponding 3-substituted 1,2,4-oxadiazoles(**3a,b,c**) are obtained in fair yields only when BF_3 is added. It was stoichiometrically confirmed that one mol of **1** behaves so as to supply three mols of azomethine radicals. A reaction scheme initiated from a two-step cycloaddition of **2** to **1** activated by BF_3 is suggested. The mixture, **1** : **2c** : BF_3=1 : 3 : 1, afforded a better yield of **3c**(69%) than an equimolar mixture of **2c** with ethyl formimidate or formamidine.

Grundmann and Kreutzberger[1-5] have investigated a variety of reactions of 1,3,5-triazine(**1**) with many kinds of nucleopiles. This paper is concerned with an unpublished reaction of **1** with nitrile oxides(**2**) which are well-known 1,3-dipoles for cycloaddition.[6a] Several aromatic **2** were treated with **1**, but 3-substituted 1,2,4-oxadiazoles(**3**), potential intermediates for organic synthesis, were obtained in fair yields only when boron trifluoride diethyl etharate(BF_3) was added to the mixtures.

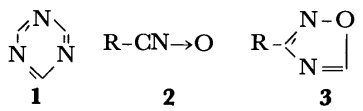

1 **2** **3**

2a, **3a**: R=C_6H_5
2b, **3b**: R=*p*-$CH_3C_6H_4$
2c, **3c**: R=2,4,6-$(CH_3)_3C_6H_2$

Experimental

Materials. **1** was prepared by Schaefer's method,[3] mp 81.6 °C(85—86),[3] N, 51.83% (52.13). Benzohydroximoyl chloride, mp 51.7 °C(49—50),[7] and *p*-toluhydroximoyl chloride, mp 67.2 °C, Cl, 20.90%(20.90) were obtained from the corresponding aldoximes by the usual manner.[7] **2c** was obtained by the previously reported method[8] from 2,4,6-trimethylbenzaldehyde oxime, mp 112.5—113.5 °C (114).[6] Hydrogen cyanide was generated from potassium cyanide and sulfuric acid and distilled over posphorus pentaoxide, bp 26 °C.

Typical Procedure for the Reaction of 1 with 2. An equivalent amount of triethylamine is added to a tetrahydrofuran (THF) solution of a few grams of benzohydroximoyl chloride and *p*-toluhydroximoyl chloride, respectively, to generate **2a** and **2b**, and thus precipitated triethylamine hydrochloride is removed by filtration. These procedures and the handling of the resulting solutions of **2a** and **2b** are carried out under cooling with salt and ice mixture. **2c** is stable for a long time in both solid and solution at room temperature.[6]

In the case of *Method A*, BF_3 is added dropwise to a mixture of **1** and the smallest amount of solvent under stirring. To the resulting slurry a solution of **2** is added within half an hour. In the case of *Method B*, BF_3 is added to a solution of **1** and **2**. After the stirring has been continued according to the time and temperature schedule given in Figs. 1 and 2 and Table 2, the reaction mixture is neutralized with an aqueous potassium carbonate solution, separated from the solvent by means of mild evacuation, and then shaken with heptane. The extract is analyzed by the use of gas-liquid phase chromatography(GLC) to determine the yield of **3**, and then distilled *in vacuo*. A fraction of **3** underwent further

TABLE 1. ANALYTICAL DATA OF 3-SUBSTITUTED 1,2,4-OXADIAZOLES(**3**) (1 Torr=133.322 Pa)

3	Bp, *t*/°C (Torr)	Mp, *t*/°C	M_W[a]	C %	H %	N[b] %
3a	70 (71—2)[11]	19.2 (15.5)[11]	146 (146.2)	65.77 (65.74)	4.13 (4.14)	19.07 (19.17)
3b	81	34.0	160 (160.2)	67.38 (67.48)	5.05 (5.03)	17.53 (17.49)
3c	91.5	62.4	188 (188.2)	70.07 (70.18)	6.45 (6.43)	14.92 (14.88)

	IR, cm^{-1}[c]					NMR ($CDCl_3$), ppm[d]			
3a	3125	1520—1320	1100	880	788	7.5 (t, 3) Ph-3,4,5	8.1 (d, 2) Ph-2,6	8.8 (s, 1) C_2ON_2-5	
3b	3115	1530—1320	1100	880	745	2.4 (s, 3) 4-Me	7.3 (d, 2) Ph-3,5	8.0 (d, 2) Ph-2,6	8.7 (s, 1) C_2ON_2-5
3c	3115	1530—1315	1108	852	722	2.2 (s, 6) 2,6-Me	2.3 (s, 3) 4-Me	7.0 (s, 2) Ph-3,5	8.9 (s, 1) C_2ON_2-5

a) From the parent peak of MS. Theoretical values are given in parentheses. b) From elemental analysis. Calculated values are given in the parentheses. c) Be common in 3-substituted oxadiazole group. d) Assignments are shown under each peak.

Table 2. Reaction of aromatic nitrile oxides(**2**) with 1,3,5-triazine(**1**)[a]

2	Solvent (cm³/mol of **1**)		Reaction[b] method	Temp Initial	Temp End	Yield[c]
				t/°C		%
2a	THF	(1650)	*A*	−20	60	26.6
2b	THF	(1350)	*A*	−20	60	11.9
2c	THF	(3000)	*A*	40	60	51.8
2c	Benzene	(3000)	*B*	40	80	35.2
2c	Benzene	(900)	*B*	40	80	69.0

a) All the reactions were carried out with the molar ratio, **1** : **2** : BF_3 = 1 : 3 : 1. b) See Experimental. c) Theoretical yield of **3** based on **2**.

purification on preparative GLC for supplying the analytical data given in Table 1.

Results and Discussion

The following was confirmed by a preliminary test: **1** is stable to BF_3 in inert solvents at temperatures up to 60 °C and produces an adduct of fine needles with BF_3. **2c** is unstable under the same conditions and rapidly converted into mesitylenecarbonitrile and a caramel-like polymer. When **1**, **2c**, and BF_3 are put together, the self-conversion of **2c** competes with the cycloaddition leading to **3c**.

The yield of **3c** is its maximum when the molar ratio of BF_3 to **1** is 0.3—0.5, as shown in Fig. 1; when the ratio is increased beyond this range, the yield is decreased, probably because of the extensive advance of the self-conversion of **2c**. Increase in the concentrations of the reactants and a molar ratio of **1** to **2** are effective for suppressing the self-conversion of **2**, and as a result, an increase in the yield of **3**, and also the dropwise addition of **2** to a mixture of **1** and BF_3 is similarly effective (Table 2). Use of BF_3 is also effective in the case of **2a** and **2b** in spite of their smaller steric hindrances than **2c**. The yields of **3a** and **3b** were both poor presumably because of the poor stability of **2a** and **2b**.[6b]

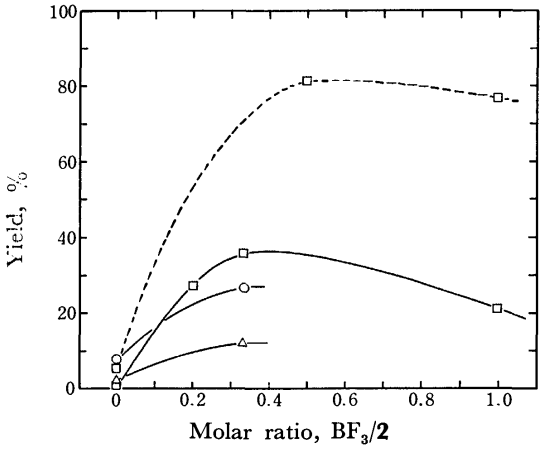

Fig. 1. Plots of yield of **3** based on **2** *vs.* molar ratio of BF_3 to **2**. —○—: **1** : **2a** : THF = 1 mol : 3 mol 1500 cm³ by reaction *Method A*, —△—: **1** : **2b** : THF = 1 mol : 3 mol : 1500 cm³ by reaction *Method A*, —□—: **1** : **2c** : benzene = 1 mol : 3 mol : 3000 cm³ by reaction *Method B*, --□--: **1** : **2c** : benzene = 1 mol : 1 mol : 1000 cm³ by reaction *Method B*.

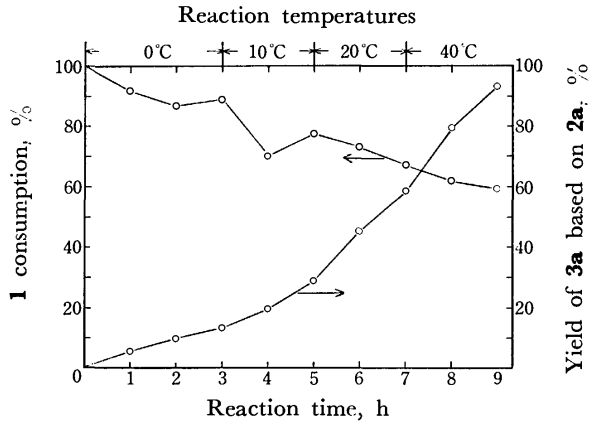

Fig. 2. Time dependence of the composition of the reaction mixture started with the ratio, **1** : **2c** : BF_3 : benzene = 1 mol : 1 mol : 0.5 mol : 1000 cm³.

Equation 1 satisfies the experimental fact that the yield of **3c** amounted to 69% when the reaction was started with the molar ratio of **1** to **2c** as one-third (see Table 2).

$$\mathbf{1} + 3\,\mathbf{2} \longrightarrow 3\,\mathbf{3} \qquad (1)$$

It is noticeable that several dipolarophiles such as aliphatic carbonyls and nitriles without electron attractive moieties can be activated by an addition of BF_3 to undergo cycloaddition with **2**.[9] The role of BF_3 in the cycloaddition in this study is thought to activate the dipolarophile, **1**, too. The reaction scheme is inferred as Eq. 2.

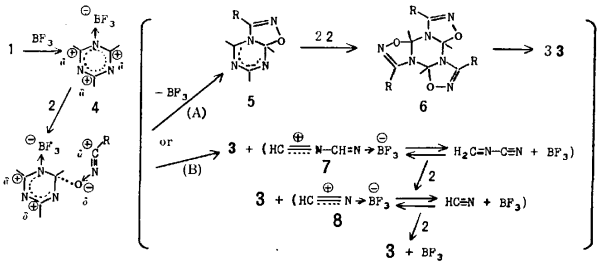

(2)

4 presumed to be an activated form of **1** by BF_3 is attacked on the carbon atom by the oxygen atom of **2** and then derived to the 1:1 adduct, **5**, or split to **3** and **7** by way of a two-step cycloaddition. Additional two moles of **2** may attack the intermediates, **5** or **7** and **8**, resulting in three molecules of **3** by the route A or B. When the initial molarities of **1** and **2c** have been made equal, merely one-third mole of **1** is consumed for the formation of every one mole of **3c** during the reaction (Fig. 2). This shows that the intermediate systems containing **5** or **7** and **8** are more susceptible to the attack of **2** than **4**. Whether route A or B prevails could not be verified,[10] since these intermediates have never been isolated.

The formation of maximal 3 mol of **3** from 1 mol of **1** demonstrates the usefulness of **1** as a starting material

TABLE 3. REACTION OF **2c** WITH HYDROGEN CYANIDE AND ITS DERIVATIVES TO FORM **3c**[a]

Dipolarophile (mol/mol-**2c**)	Catalyst (mol/mol-**2c**)	Solvent	Reaction temp t/°C	Yield[b] %
HCN (3)[c]	BF_3 (0.5)	Benzene	0—60	0
$HC(NH)OC_2H_5$ (1)[d]	—	EtOH	17—40	33.4
$HC(NH)NH_2$ (1)[e]	—	EtOH	11—60	59.0

a) 2000 cm^3 of solvent was used for one mol of **2c**. b) Theoretical yield of **3c** based on **2c**. c) Hydrogen cyanide was mostly recovered unreacted. d) An equiv. amount of 1,8-diazabicyclo[5,4,0]undec-7-ene was added to the mixture of ethyl formimidate hydrochloride and **2c**. e) An equiv. amound of triethylamine was added to the mixture of formamidine hydrochloride and **2c**.

for **3**. As a comparison, hydrogen cyanide and its two derivatives were subjected to cycloaddition with **2c**.

$$\left.\begin{array}{l}\mathrm{HCN}\\ \mathrm{HC(NH)OC_2H_5}\\ \mathrm{HC(NH)NH_2}\end{array}\right\} \xrightarrow{\mathbf{2c}} \mathbf{3c} \qquad (3)$$

The results are given in Table 3. It is seen that formamidine is comparative to **1** with respect to the yield of **3c**. However, formamidine is usually prepared from hydrogen cyanide *via* formimidate. Thus it is less accessible than **1** which is prepared directry from hydrogen cyanide.[3] As regards synthesis of **3** without use of **2**, the reactions of amidoxime with acetic formic unhydride,[11] formamide,[12] trialkyl orthoformates,[14,15] and *N*,*N*-dimethyl-α,α-dimethoxymethylamine[15] have been reported to give sometimes good yields.

The authors wish to express their thanks to Mr. Jyunichi Fujishima, Tokai University, for his assistance.

References

1) C. Grundmann and A. Kreutzberger, *J. Am. Chem. Soc.*, **77**, 6559 (1955).
2) A. Kreutzberger and C. Grundmann, *J. Org. Chem.*, **26**, 1121 (1961).
3) C. Grundmann, *Angew. Chem.*, **75**, 393 (1963).
4) A. Kreutzberger and G. Stevens, *J. Chem. Soc., C*, **1969**, 1282.
5) A. Kreutzberger, *Tetrahedron*, **28**, 4877 (1972); *ibid.*, **32**, 1073 (1976).
6) a) C. Grundmann and P. Grünauger, "The Nitrile Oxides," Springer-Verlag, Berlin-Heiderberg-New York (1971); b) *ibid.*, p. 18.
7) Houben-Weyl, "Methoden der Org. Chem.," 4th ed, G. Thieme, Stuttgart (1965), Vol. 10/4, p. 100.
8) C. Grundmann and T. Dean, *J. Org. Chem.*, **30**, 2809 (1965).
9) S. Morrocchi, A. Ricca, and L. Vero, *Tetrahedron Lett.*, **1967**, 331.
10) There is some evidence to substantiate route A:—1 : 3 adducts similar to **6** have been proposed as intermediates in the reaction of **1** with primary amines[1,3-5] or active methylenes;[2] The mixture of hydrogen cyanide, **2c**, and BF_3 in benzene yielded no **3c**, suggesting inertness of **8** toward **2** (Table 3).
11) R. Lenaers, C. Moussebois, and F. Floy, *Helv. Chim. Acta*, **45**, 441 (1962).
12) C. Moussebois, *Bull. Soc. Chim. Belges*, **76**, 92 (1967); *Chem. Abstr.*, **67**, 64304t (1967).
13) Toyama Chem. Ind., Jpn, Patent 6802354 (1968); *Chem. Abstr.*, **69**, 66771h (1968).
14) J. Claisse, M. Foxton, G. Gregory, A. Sheppard, E. Tiley, W. Warburton, and M. Wilson, *J. Chem. Soc., Perkin Trans. 1*, **1973**, 2241.
15) J. Maddison, P. Seale, E. Tiley, and W. Warburton, *J. Chem. Soc., Perkin Trans. 1*, **1974**, 81.

The Role of the Charge-transfer Complex in the Photocopolymerization of Oxygen with Styrene and α-Methylstyrene

Toshiyuki KODAIRA, Kohzoh HASHIMOTO, Yoshihiko SAKANAKA, Sumio TANIHATA, and Katsuki IKEDA

Department of Industrial Chemistry, Faculty of Engineering, Fukui University, Fukui 910

(Received October 25, 1977)

The effect of the wavelength of irradiated light on the photocopolymerizations of oxygen with styrene (**1**) and α-methylstyrene (**2**) was investigated in connection with the charge-transfer bands observed between these monomers and oxygen, with the latter as an electron acceptor. It appeared that the excitation of the charge-transfer bands is responsible for the copolymerizations and that the photoabsorptions due to **1** and **2** do not contribute to the reactions, although the excited singlet states of these compounds were quenched by oxygen according to a Stern-Volmer plot.

The bathochromic shifts of the electronic absorption bands of several monomers including styrene (**1**) and α-methylstyrene (**2**) were observed while the electronic spectra were measured for these compounds saturated with oxygen.[1] The extra absorption bands were attributed to contact charge-transfer (CT) complexes between them and oxygen, with the latter as an electron acceptor, by taking into consideration the similar absorptions observed for various organic substances.[2] The photopolymerization of **1** in the presence of oxygen revealed that the CT-band plays an important role as a light-absorbing species in the formation of the alternating copolymer of **1** with oxygen.[1] Some contribution from the exciplex between oxygen and the excited singlet **1** to the formation of the alternating copolymer was also suggested based upon the measurements of the fluorescence spectra of **1** in the presence of oxygen under various pressures, but no detailed polymerization data were reported in connection with the excitation of **1**.[1] For this reason, the effect of the wavelength of irradiated light on the photocopolymerization of **1** with oxygen has been investigated to get further information on the contribution from the excited singlet **1** to the copolymerization. During the course of this study, it appeared that **2** also yields an alternating copolymer, with oxygen as a comonomer, on the excitation of **2** in the region of the CT-band. Therefore, similar experiments have also been carried out for **2**. Photo- and thermal-copolymerizations of these compounds by using azobisisobutyronitrile have already been reported,[3-6] but their direct photocopolymerizations have not yet been studied except for the work[1] in this laboratory.

This subject is interesting in connection with the direct photooxygenation reaction, which has been studied in only a few works,[7-9] in contrast to the extensive studies of the photosensitized oxygenation.[10]

Experimental

Materials. The monomers and oxygen were purified as has been described previously.[1]

Polymerization. The apparatus used for the copolymerization of **1** with oxygen[1] was adopted, but a polymerization tube made of quartz was used for all the copolymerizations unless otherwise noted in the text. A trap protected from atmospheric moisture by calcium chloride and immersed in a dry ice–methanol bath was added at the outlet of a refluxing condenser to collect the volatile products. After a given time, the unreacted monomers were distilled off through a vacuum line without heating. The residues were weighed in order to determine the yield of polyperoxide. The distillate was treated with an aqueous semicarbazide hydrochloride solution containing potassium acetate.

Photoirradiation. Photoirradiations were carried out using one of the following three lamps; a Riko 30-watt low-pressure mercury lamp (Model UVL-30A), a Toshiba 100-watt high-pressure mercury lamp (Model SHL-100UV2), and an Ushio 2000-watt xenon lamp (Model UXL-2003D). The wavelength was controlled by means of a Toshiba colored glass filter or a monochrometer (Ritsu Applied Optics Co., Ltd., Model MC-30). In the latter case, the distances from the lamp to the entrance slit of the monochrometer and from the exit slit to the polymerization tube were 21 and 27 cm, respectively. The width of both the slits was 8 mm.

Measurements of Light Intensities. The light intensities of the Xe-lamp at arbitrarily chosen wavelengths were determined by means of a potassium tris(oxalato)ferrate(III) actinometer,[11] using the apparatus for the copolymerization. The results are illustrated in Fig. 1. The light intensities of the low-pressure mercury lamp with and without the application of an UV-29 filter are also given in Fig. 1. The quantum efficiency at 253.7 nm of the actinometer was used for the calculation of the photointensities of the lamp, though it irradiates light of various wavelengths.

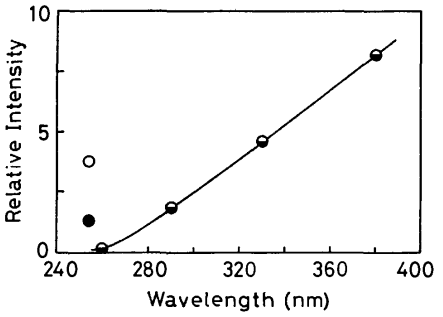

Fig. 1. Photointensities of a xenon lamp (◒) and a low pressure mercury lamp with an UV-29 filter (●) and without it (○). Light detected for the low pressure mercury lamp under the application of the filter consists of higher wavelength bands than the emission band at 253.7 nm because of the almost complete shielding of it by the filter, but the photointensity was depicted at the wavelength for convenience. Distance between light and polymerization tube was 10 cm for the mercury lamp and see experimental section for the xenon lamp.

Measurements of Spectra and Viscosity. Measured as has been described previously.[1)]

Results and Discussion

The amount of residue after the evaporation of the unreacted **1** from the reaction mixture is plotted *versus* the wavelength of the light irradiated in Fig. 2. The absorptions of **1** saturated with nitrogen and oxygen are also illustrated in Fig. 2. The yield of the copolymer increases with an increase in the wavelength of the irradiated light and then decreases after attaining a maximum at about 335 nm, though the intensity of the light increases as the wavelength becomes longer, as is shown in Fig. 1. The photointensity in the shorter-wavelength region is too weak to deduce a conclusion in connection with the intensity of light and the polymer yield. Therefore, the copolymerization was undertaken under the irradiation by the low-pressure mercury lamp. Its most prominent emission band, at 253.7 nm, is in the region where **1** has a strong absorption. The results are shown in Table 1. The emission intensity of the mercury lamp is comparable with that of the Xe-lamp at 320 nm (Fig. 1), but the polymer yield is only one-third of the yield by the Xe-lamp at that wavelength. The application of the UV-29 filter which cuts off emission at 253.7 nm did not reduce the polymer yield, as was expected from the decrease in the photointensity. Further, it must be noticed that the filter also lowers the light intensity at longer wavelengths to some extent. These results suggest that the polymer obtained by using the low-pressure mercury lamp is mainly due to the absorption of light at the longer wavelengths irradiated from the lamp. The alternating copolymer of **1** with oxygen decomposes to produce benzaldehyde and formaldehyde when exposed to ultraviolet light.[12)] The yields of benzaldehyde, determined as its semicarbazone, are also plotted *versus* the wavelength of the light irradiated in Fig. 2. The formaldehyde was qualitatively identified as paraformaldehyde when the white powder detected in the cold trap of the outlet was analyzed by comparing its IR spectrum with that of an authentic sample. It has already been confirmed that these decomposition products do not contribute to the initiation reaction of the copolymerization.[1)]

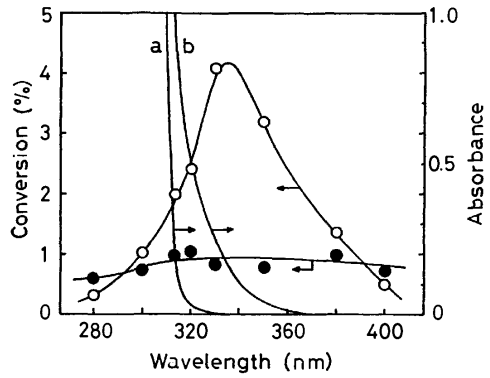

Fig. 2. Electronic spectra of **1** saturated with nitrogen (a) and oxygen (b), and the dependence of the reaction products on the wavelength of the light irradiated. ○: Copolymer, ●: benzaldehyde. Conversions for these compounds were determined based upon **1**. Time 9 h, temp 30 °C, and oxygen 18.5 ml/min.

TABLE 1. PHOTOCOPOLYMERIZATION OF OXYGEN WITH **1** AND **2** BY MEANS OF A LOW-PRESSURE MERCURY LAMP[a)]

Monomer	Filter	Conv. %	BA[b)] %	APH[c)] %
1	—	0.8	0.6	—
1	UV-29	0.5	0.7	—
2	—	1.3	—	0.9
2	UV-29	0.8	—	0.7

a) Temp, 30°C; time, 9 h; oxygen, 18.5 ml/min; distance between light and polymerization tube, 10 cm. Conversion and yield of BA and APH were determined based upon monomers. b) Benzaldehyde. c) Acetophenone.

A similar investigation was carried out for **2**. The dependence of the yield of the residue on the wavelength of the light irradiated is shown in Fig. 3, together with the absorption spectra of **2** saturated with nitrogen and oxygen. The residue was confirmed to be an alternat-

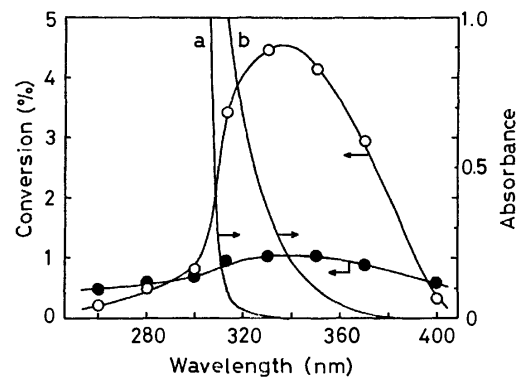

Fig. 3. Electronic spectra of **2** saturated with nitrogen (a) and oxygen (b), and the dependence of the reaction products on the wavelength of the light irradiated. ○: Copolymer, ●: acetophenone. Conversions for these compounds were determined based upon **2**. Conditions are the same as described in Fig. 2.

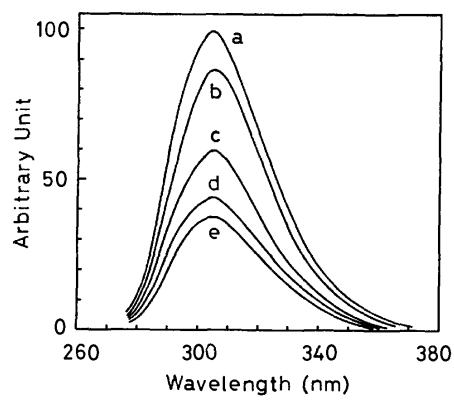

Fig. 4. Fluorescence of **2**. Solvent *n*-hexane, concentration 2×10^{-4} mol/l, excitation 265 nm. Partial pressure of oxygen in the mixture of nitrogen and oxygen: a 0, b 0.2, c 0.5, d 0.8, and e 1.0.

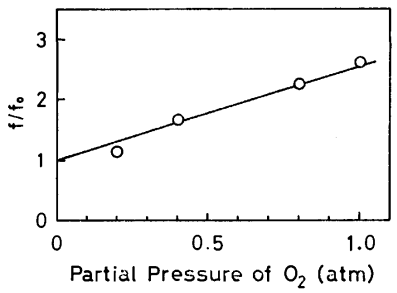

Fig. 5. Stern-Volmer plot of fluorescence at 305 nm for **2**-oxygen system. Conditions are the same as described in Fig. 4.

ing copolymer of **2** with oxygen, based upon its IR spectrum and that of an authentic sample.[5] The results obtained by using the low-pressure mercury lamp as a light source are given in Table 1. These results indicate that the photoabsorption of the CT-band between **2** and oxygen is responsible for the formation of the alternating copolymer, while that of **2** does not contribute to the copolymerization.

Based upon the quenching process of the fluorescence of **1** by oxygen, it has been considered that the exciplex of the excited singlet **1** with oxygen also contributes to the photoinduced alternating copolymerization of **1** with oxygen.[1] However, the results obtained in this work are in contrast to this suggestion. For this reason, the interaction of oxygen with the singlet excited state of **2** has been investigated by measuring the fluorescence spectra of **2** in the presence of oxygen under various pressures. As is shown in Figs. 4 and 5, the fluorescence of **2** is quenched by oxygen according to a Stern-Volmer plot, though it is not quenched so effectively as in the case of **1** under the conditions described. Accordingly, it appeared that the interaction between the singlet excited state and oxygen does not contribute to the initiation reaction of the copolymerization in the case of **2**, either.

The alternating copolymer of **2** with oxygen decomposes to yield acetophenone and formaldehyde on photoirradiation.[5] The former was, in fact, detected in the distillate of the unreacted monomer as its semicarbazone. The white solid precipitated in the cold trap was identified as paraformaldehyde by measuring the IR spectra. The yield of acetophenone was determined quantitatively; it is plotted against the wavelength in Fig. 3. The addition of one-fourth of the maximum yield of acetophenone to the polymerization system did not cause any change in the yield of polyperoxide as compared with the polymerization under normal conditions, *i.e.*, the copolymerization without acetophenone. The polyperoxide thus formed acts as an initiator for the photocopolymerization, as is shown in Table 2, but the results indicate that the initiation of the copolymerization proceeds more effectively through the excitation of the CT-band than the initiation through peroxide.

Thus, the photoabsorption of the CT-bands plays a fundamental role in the copolymerization of oxygen with **1** and **2**, and the excited singlet states of both the monomers do not contribute to the copolymerizations.

Table 2. Photocopolymerization of **2** with oxygen by means of a high-pressure mercury lamp in a hard glass ampoule[a]

Polyperoxide[b] %	Conv. %	APH[c] %
0	8.8	4.0
3.0	13.9[d]	7.4

a) See footnote of Table 1. b) Alternating copolymer of **2** with oxygen. c) Acetophenone. d) Polyperoxide added was not subtracted.

However, the maximum polymer yield is slightly shifted to a longer wavelength region than the wavelength expected from the CT-bands. One reason for this is the fact that the intensity of the irradiated light decreases with the decrease in the wavelength. The other is the absorption of light by **1** and **2**, which does not contribute to the reactions, because the sharp decrease in the polymer yield begins at the wavelength where the absorption bands of **1** and **2** appear.

The contribution to the copolymerizations by the triplet states excited directly by the singlet states of **1** and **2** is excluded on the basis of the following considerations. The singlet-triplet transition of **1** has been observed around 463 nm,[13] while that of **2** is expected to be detected at a longer wavelength region judging from the effect of the substituents on the transition of aromatic and olefinic compounds,[14] though the datum for the singlet-triplet transition for **2** is not available.

The reduced viscosities measured for the copolymers of oxygen with **1** and **2** were found to be in the region from 0.06 to 0.08 dl/g. The values were scattered, without any significant trend with respect to the polymerization conditions.

Financial support (Grant-in-Aid No. 975439) by the Ministry of Education, Japanese Government, is acknowledged.

References

1) T. Kodaira, K. Hayashi, and T. Ohnishi, *Polym. J.*, **4**, 1 (1973).
2) For instance, H. Tsubomura and R. S. Mulliken, *J. Am. Chem. Soc.*, **82**, 5966 (1960).
3) A. A. Miller and F. R. Mayo, *J. Am. Chem. Soc.*, **78**, 1017 (1956).
4) J. A. Haward and K. U. Ingold, *Can. J. Chem.*, **43**, 2729 (1965).
5) F. R. Mayo and A. A. Miller, *J. Am. Chem. Soc.*, **80**, 2480 (1958).
6) H. Hock and M. Siebert, *Chem. Ber.*, **87**, 546 (1954).
7) J. C. Chien, *J. Phys. Chem.*, **69**, 4317 (1965).
8) V. I. Stenberg, R. D. Olson, C. T. Wang, and N. Kulevsky, *J. Org. Chem.*, **32**, 3227 (1967).
9) H. Tsubomura, T. Yagishita, and H. Toi, *Bull. Chem. Soc. Jpn.*, **46**, 3051 (1973).
10) T. Tachibana, Ed., "Shin Jikken Kagaku Kohza," Maruzen, Vol. 15, Sanka to Kangen I-1, Tokyo (1976), pp. 515—561.
11) C. G. Hatchard and C. A. Parker, *Proc. R. Soc. London, Ser. A*, **235**, 518 (1956).
12) F. R. Mayo and A. A. Miller, *J. Am. Chem. Soc.*, **78**, 1023 (1956).
13) D. F. Evans, *J. Chem. Soc.*, **1957**, 1351.
14) D. F. Evans, *J. Chem. Soc.*, **1959**, 2753.

Studies on the Liquid Phase Oxidation of Nitroalkylbenzenes Catalyzed by Transition Metal and Bromide Ions

Ryoichi HASEGAWA[1] and Yoshio KAMIYA

Department of Reaction Chemistry, Faculty of Engineering, The University of Tokyo, Hongo, Tokyo 113

(Received October 15, 1976)

The liquid phase autoxidation of nitroalkylbenzenes catalyzed by transition metal and bromide ions in acetic acid was investigated at 55—85 °C. A remarkable synergistic effect was found on the mixtures of metal catalysts composed of cobalt and other transition metals, the maximum reaction rate being observed at the molar ratio of Co : Mn : Br = 1 : 0.005—0.01 : 1—2. The rate of oxygen absorption of *p*- or *m*-nitroalkylbenzenes was affected by the partial pressure of oxygen, showing deviation from the first order dependency on the substrate concentration in contrast to the case of ordinary alkylbenzenes. The results can be explained by the retardation effect due to nitro compounds which might result from the reaction with alkyl radicals and the deactivation of metal catalysts. *o*-Nitroalkylbenzenes except nitroethylbenzene show a great resistivity against the oxidation. The retardation effect can be ascribed to the inhibiting effect due to inactive free radicals and also to the various reduced products resulting from the intramolecular reaction of nitro groups and active radicals. It was found that the autoxidation of *p*-nitrotoluene catalyzed by Co–Mn–Br catalyst proceeds very rapidly at temperatures as low as 85 °C, yeilding mostly *p*-nitrobenzoic acid along with a small amount of *p*-nitrobenzaldehyde.

The autoxidation of alkylbenzenes catalyzed by transition metal and bromide ions in acetic acid has been studied by many workers.[2-6] The liquid phase oxidation of nitroalkylbenzenes is important from the viewpoint of chemical industry, it is also interesting theoretically because of the difficulty of the reaction due to electron-withdrawing tendency of the nitro group, though this has not been clarified. Chervinskii and Kovalev reported the oxidation of *p*-nitrotoluene catalyzed by transition metal stearates and tetrabromoethane in propionic or butyric acids at 140—160 °C,[7,8] but we have confirmed that the selectivity of the reaction is low because of complicated side reactions. They reported the oxidation of nitrosubstituted *o*-xylenes,[9] but did not clarify the effect of the nitro group. Several patents which have been published for the oxidation of *p*- or *m*-nitrotoluenes[10-15] with severe conditions attached, do not furnish satisfactory data for a theoretical approach on the effect of the nitro group.

We have thoroughly studied the effect of the nitro group in the autoxidation of nitroalkylbenzenes catalyzed by transition metal and bromide ions in acetic acid and found that the oxidation proceeds easily at temperatures as low as 85 °C under restricted reaction conditions.

Experimental

Materials. Acetic acid, various metal acetates and alkali bromides of reagent grade were used. Nitrotoluenes, 2,4-dimethylnitrobenzene, *p*-nitroethylbenzene and nitrobenzene were purified by the usual method: distillation or recrystallization after washing with dilute sulfulic acid, aqueous alkali, water and drying. Chlorobenzene and *o*-dichlorobenzene were distilled after being dried over calcium chloride. *p*-Chlorotoluene, *o*-nitroethylbenzene, *o*-nitroacetophenone, *o*-nitrobenzaldehyde, *p*-nitrobenzaldehyde and other organic compounds of reagent grade were used after treatment with active alumina, when necessary.

Procedure. The rate of oxygen absorption was measured under atmospheric oxygen according to the method of Kamiya,[16,17] but in the case of the experiment under positive pressure, it was determined by measuring the very small pressure variation in a constant volume reactor.

Analysis. A gas chromatograph (Shimadzu GC-4BP-TF) was mainly used for analysis of the reaction products. The conditions were as follows, Column: 3% Silicone OV-17, on Chromosorb WHP, 1.5 m, 145 °C, Detector: FID, 250 °C, N_2-Flow rate: 40 ml/min, Injection temperature: 260 °C.

Results and Discussion

Feature of the Metal Catalyst. Oxidation of *p*-nitrotoluene and *p*-chlorotoluene was carried out in acetic acid in the presence of various catalysts. The steady state rate of oxidation is shown in Fig. 1. The general feature of the oxygen absorption curves was not affected by the concentration of catalyst or

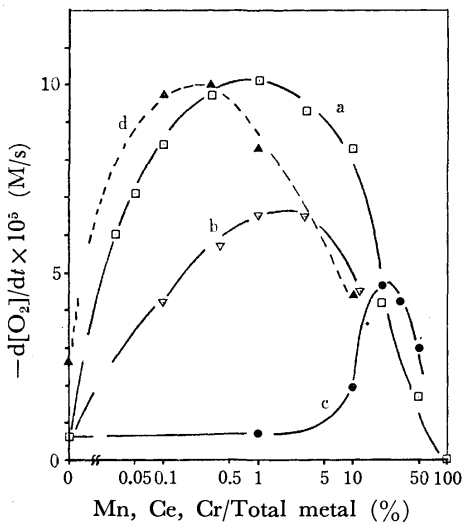

Fig. 1. Relation between catalyst composition and the rate of oxidation in acetic acid.
Total metal 3.6×10^{-2} M, NaBr 6.1×10^{-2} M, 85 °C.
a: *p*-Nitrotoluene 1.69 M, $Co(OAc)_2 \cdot 4H_2O$, $Mn(OAc)_2 \cdot 4H_2O$, b: *p*-nitrotoluene 1.69M, $Co(OAc)_2 \cdot 4H_2O$, $Ce(OAc)_3 \cdot H_2O$, c: *p*-nitrotoluene 1.69M, $Co(OAc)_2 \cdot 4H_2O$, $Cr(OAc)_3 \cdot H_2O$, d: *p*-chlorotoluene 1.69M, $Co(OAc)_2 \cdot 4H_2O$, $Mn(OAc)_2 \cdot 4H_2O$.

substrate, a straight line being obtained until a considerable amount of substrate was consumed. The activity of catalysts decreased in the order, Co–Mn–Br> Co–Ce–Br> Co–Cr–Br, no appreciable catalysis being observed in other combinations of metal ions. Maximum reaction rates were obtained in metal mixtures of Co–Mn, Co–Ce, and Co–Cr at molar ratios of 99 to 1, 98 to 2 and 75 to 25, respectively. However, the Co–Mn ratio reported in the oxidation of *p*-xylene and ethylbenzene catalyzed by Co–Mn–Br is 80 to 20.[5] In the following experiments, Co–Mn–Br catalyst was mainly used at the molar ratio of Co : Mn : Br=99 : 1 : 170 because of its high activity. With regard to the molar ratio of bromide ion to total metal ions, no significant difference was observed between the ratios from 1 : 1 to 2 : 1. The effect of counter cation on bromide ion was striking. In the case of alkali earth metal ions (*e. g.* Mg^{2+}, Ca^{2+}, and Ba^{2+}), the initial reaction rate was considerably high but decreased very soon, in similar way to that in the oxidation of ordinary alkylbenzenes.[18]

Effect of Catalyst Concentration. The oxygen absorption rate is nearly of second order in catalyst at lower concentrations, but independent of the catalyst concentration above 3.6×10^{-2} M. This effect is not so significant in the oxidation of ordinary alkylbenzenes catalyzed by Co–Br catalyst.[19,20] The difference is related to the substrates, but not to catalysts, because this effect was not so remarkable in the oxidation of ethylbenzene catalyzed by Co–Mn–Br catalyst. Since odd electron density at the benzylperoxyl radical center should decrease by electron-withdrawing substituents, the reaction of *p*-nitrobenzylperoxyl radical with metal ion at low oxidation state ($Me^{2+}+RO_2\rightarrow Me^{3+}\cdot RO_2$) leading to chain termination should be accelerated. Thus no increase of oxidation rate was observed with increasing catalyst concentration.

Effect of the Partial Pressure of Oxygen. The effect of oxygen partial pressure is shown in Fig. 2,

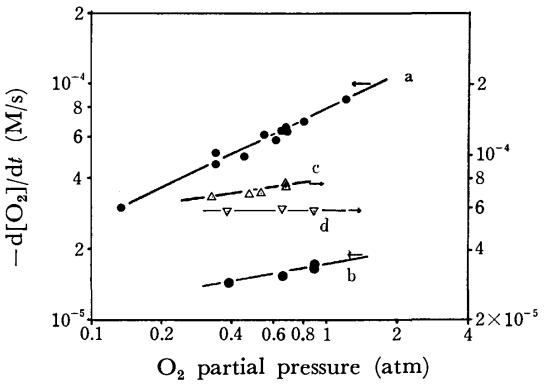

Fig. 2. The rate of oxidation of *p*-nitrotoluene, *m*-nitrotoluene, and *p*-chlorotoluene catalyzed by Co–Mn–Br catalyst in acetic acid as a function of oxygen partial pressure.
$Co(OAc)_2\cdot4H_2O$: $Mn(OAc)_2\cdot4H_2O$: NaBr=99 : 1 : 170, total metal 1.2×10^{-2} M.
a: *p*-Nitrotoluene 1.69 M, 85 °C, b: *p*-nitrotoluene 1.69 M, 65 °C, c: *m*-nitrotoluene 1.69 M, 85 °C, d: *p*-chlorotoluene 1.69 M, 65 °C.

indicating a slight positive effect on the rate of oxidation of nitrotoluenes. However, in the case of ordinary alkylbenzenes below 100 °C, this effect is negligible at pressures above 0.5 atm.[5,22] Since the reaction of substituted benzyl radical with molecular oxygen has been concluded to have no significant effect due to substituents,[23,24] the effect of partial pressure of oxygen is attributable to the following inhibiting effect due to the nitro group.

According to Jackson and Waters,[25] *O,N*-dibenzyl-*N*-phenylhydroxylamines, *N*-benzylanilines, anilines and resinous materials were obtained, after toluene, aromatic nitro compounds and *t*-butyl peroxide had been allowed to react at the reflux point for 80 h. They postulated the following mechanism for the reaction.

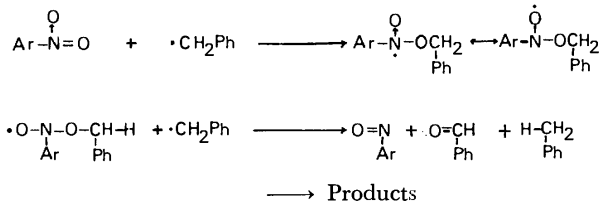

Scheme 1.

Aromatic nitro compounds are known to be oxidizing agents which become reduced in the course of reaction, the reduced products acting as inhibitor or retarder in radical polymerization.[26–28]

Since there exist more than 1000-fold excess of nitro groups as compared with oxygen in *p*-nitrotoluene oxidation, a small portion of active radicals may react with nitro groups, even if the reaction betwen *p*-nitrobenzyl or *p*-nitrobenzoyl radicals and oxygen proceeds rapidly. Accordingly, various inhibitors could be formed in the solution, and the reaction rate would decrease by reduction in oxygen partial pressure.

Substrate Concentration. Although the rate of oxidation of *p*-nitrotoluene is of first order with respect to substrate at concentrations below 0.3 M, the order decreases with increase in concentration. However, the first order dependency is observed at high concentration region in the oxidation of ethylbenzene, *p*-xylene and toluene.[5] The inhibition effect due to nitrobenzene in the oxidation of *p*-nitrotoluene was examined, acetic acid being replaced partly by nitrobenzene. The decrease in oxidation rate of *p*-nitrotoluene by nitrobenzene addition corresponds to the negative deviation from linearity at high concentration of *p*-nitrotoluene (Fig. 3). Although chlorobenzene or *o*-dichlorobenzene was similarly treated in place of nitrobenzene, they exhibited positive effect for the *p*-nitrotoluene oxidation. When the same amount of nitrobenzene as substrate was added in the oxidation of *p*-chlorotoluene, correlation between the rate of oxidation and concentration of substrate were similar to those of *p*-nitroethylbenzene and *p*-nitrotoluene. The anomality in the oxidation of nitroalkylbenzenes compared with the case of hydrocarbons having no nitro substituent can be explained in terms of the effect of the aromatic nitro group.

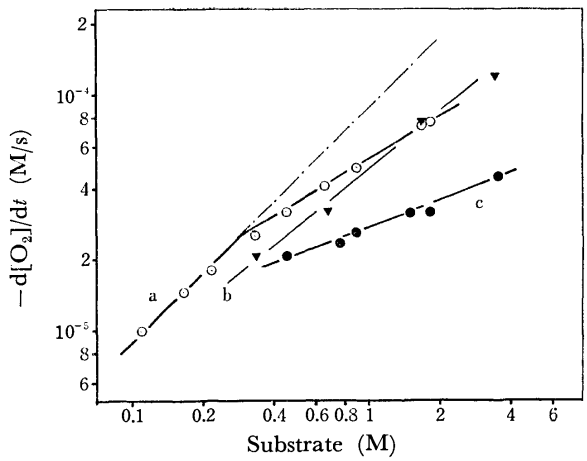

Fig. 3. The rate of oxidation of *p*-nitrotoluene *m*-nitrotoluene, and *p*-nitroethylbenzene catalyzed by Co-Mn-Br catalyst in acetic acid as a function of substrate concentration.
$Co(OAc)_2 \cdot 4H_2O$: $Mn(OAc)_2 \cdot 4H_2O$: NaBr=99 : 1 : 170, total metal 1.2×10^{-2} M.
a: *p*-Nitrotoluene 85 °C, b: *m*-nitrotoluene 85 °C, c: *p*-niroethylbenzene 55 °C.

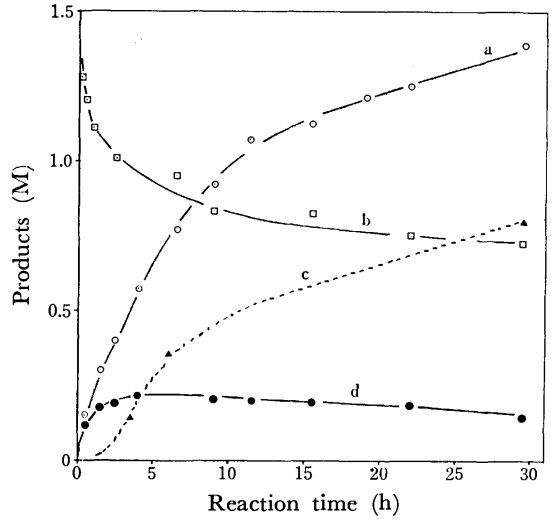

Fig. 4. Products distribution in the oxidation of *p*-nitrotoluene at 85 °C in acetic acid.
$Co(OAc)_2 \cdot 4H_2O$: $Mn(OAc)_2 \cdot 4H_2O$: NaBr = 99 : 1 : 170, total metal 1.2×10^{-2} M, *p*-nitrotoluene 1.69 M.
a: Absorbed O_2, b: *p*-nitrotoluene, c: *p*-nitrobenzoic acid, d: *p*-nitrobenzaldehyde.

Two possibilities have been suggested for the negative effect of the nitro group in *p*-nitrotoluene oxidation;[7,8] interruption of the chains, and complex formation with catalyst, which has low activity in chain initiation.

Although the reaction conditions or catalyst composition differ from those of Chervinskii and Kovalev, our results support their view.

While there is no evidence for complex formation between catalyst and nitro compounds as well as its inactivity, the aromatic nitro compounds having high dielectric constants may coordinate to metal ion and deactivate the catalyst as in the action of water. The effect of substrate concentration in the oxidation of nitroalkylbenzenes should be due to the catalyst deactivating tendency by the complex formation and the chain terminating inclination by the reaction with active radical.

Reaction Products. Main products were *p*-nitrobenzaldehyde, *p*-nitrobenzoic acid and water in the oxidation of *p*-nitrotoluene in acetic acid. Small amounts (1—2% selectivity) of *p*-nitrobenzyl bromide and *p*-nitrobenzyl acetate were formed simultaneously. The total yield of these products per reacted nitrotoluene was 101%, and 69.5% of inorganic bromide ion initially added was found to be converted into organic bromide (*p*-nitrobenzyl bromide) at 48% conversion of *p*-nitrotoluene. The relation between oxidation products of *p*-nitrotoluene and the reaction time is shown in Fig. 4. Main products in the oxidation of *p*- or *o*-nitroethylbenzene in propionic acid were nitroacetophenones, 1-(nitrophenyl)ethanols, and water. As in the case of *p*-nitrotoluene, 1-(nitrophenyl)ethyl bromides and 1-(nitrophenyl)ethyl propionates were formed. The relation between the oxidation products and the reaction time is shown in Fig. 5. In all cases, the esters are considered to be formed through the following pathways.

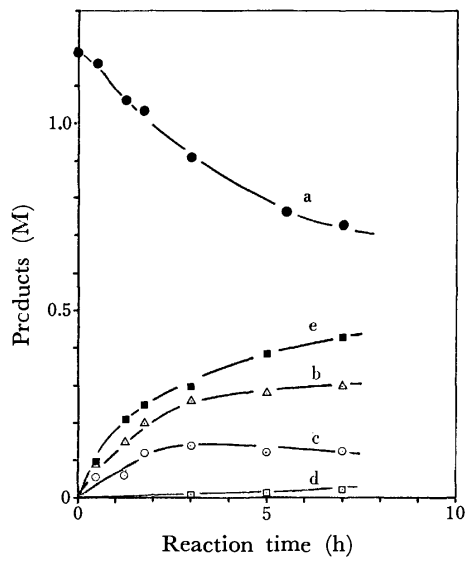

Fig. 5. Products distribution in the oxidation of *p*-nitroethylbenzene at 90 °C in propionic acid.
$Co(OAc)_2 \cdot 4H_2O$: $Mn(OAc)_2 \cdot 4H_2O$: NaBr = 99 : 1 : 170, total metal 1.2×10^{-2} M, *p*-nitroethylbene 1.19 M.
a: *p*-Nitroethylbenzene, b: *p*-nitroacetophenone, c: 1-(*p*-nitrophenyl)ethanol, d: 1-(*p*-nitrophenyl)ethyl propionate, e: absorbed O_2.

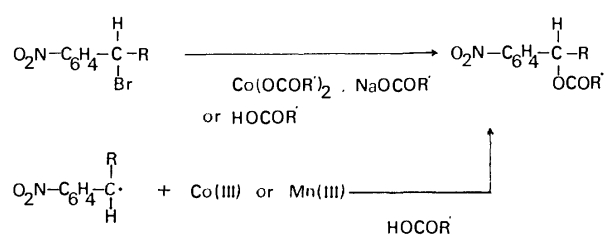

Scheme 2.

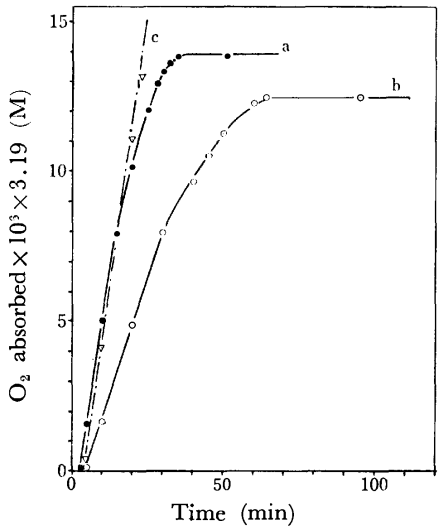

Fig. 6. Oxygen absorption curves of the *p*-nitrotoluene oxidation in the presence of *o*-nitrotoluene or *o*-nitroacetophenone at 85 °C in acetic acid.
$Co(OAc)_2 \cdot 4H_2O$: $Mn(OAc)_2 \cdot 4H_2O$: NaBr = 99 : 1 : 170, total metal 1.2×10^{-2} M.
a: *o*-Nitrotoluene addition, b: *o*-nitroacetophenone addition, c: *p*-nitrotoluene only, 1.69 M.

Oxidation of o-*Nitroalkylbenzenes.* When *o*-nitrotoluene was allowed to the oxidation catalyzed by Co–Mn–Br catalyst, the reaction did not proceed. As shown in Fig. 6, the oxidation of *p*-nitrotoluene in the presence of equal amounts of *o*-nitrotoluene or *o*-nitroacetophenone stops at low conversion (a few persent), as does the oxidation of 2,4-dimethylnitrobenzene. This suggests that *o*-nitrosubstituted toluene and acetophenone produce inhibitors during oxidation.

Intramolecular reaction should take place in the case of *o*-nitroalkylbenzenes. Intramolecular reaction proceeds advantageously as compared to intermolecular reaction. The reaction intermediates are supposed to form five or six membered rings.

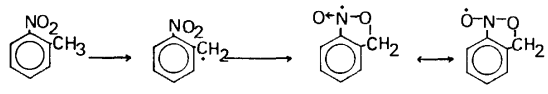

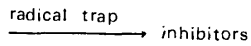

Scheme 3.

o-Nitrobenzaldehyde or *o*-nitroacetophenone formed as primary oxidation products are subjected to similar reactions. Inhibiting effect due to *o*-nitrotoluene or *o*-nitroacetophenone can be explained in terms of the intramolecular reaction between active radical and nitro group.

The oxidation of 2,4-dimethylnitrobenzene was carried out in acetic acid under the following conditions. Substrate concentration=1.51 M, molar ratio of $Co(OAc)_2 \cdot 4H_2O$, $Mn(OAc)_2 \cdot 4H_2O$ and NaBr=99 : 1 : 170, and 65 °C. When the catalyst concentration (total metal) decreased in the order 2.4×10^{-2} M, 1.2×10^{-2} M and 8×10^{-3} M, the oxidation stopped at 10 min, 70 min and did not stop over 150 min, respectively. The oxidation of 2,4-dimethylnitrobenzene stops at lower conversion as concentration of the catalyst increases. Reasons for this might be as follows. I) The metal catalyst itself stops the autoxidation chain by the reaction with peroxyl radical. II) The metal catalyst produces inhibitors in the course of the reaction.

The following reaction has been reported in studies of photochemical reaction[29] and mass spectrometry of the *o*- or *peri*-nitro substituted aromatics.[30]

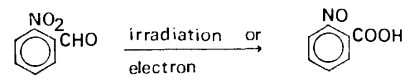

Scheme 4.

The electron of the metal may enhance the rate of reaction, and a direct reaction between the catalyst and the nitro group can not be discarded.

However, when *o*-nitrobenzaldehyde or nitrobenzene was treated with equal amount of Co–Mn–Br catalyst at 80 °C in acetic acid in the absence of oxygen, no change took place. The effect of phenols which can be produced by the acid catalyzed decomposition of hydroperoxides should be negligible in acetic acid, where strong acid is absent. Thus, the inhibition effect at high concentration of catalyst on the oxidation of 2,4-dimethylnitrobenzene can be ascribed mainly to the chain termination due to metal ions. This can be correlated to the discussion on the effect of catalyst concentration.

The oxidation of *o*-nitroethylbenzene proceeded until 45% conversion. The rate of *o*-nitrocumene was extremely low as compared with that of *p*-isomer. Thus, of the *o*-nitro-substituted toluene, ethylbenzene and cumene, the oxidation of only *o*-nitroethylbenzene proceeded fairly rapidly. This can be attributed to:

I) The reactivity of *o*-nitroethylbenzene is expected to be higher than that of *o*-nitrotoluene or *o*-nitrocumene, since one of the secondary benzylic hydrogen atoms should be free from hydrogen bonding with the oxygen atom of nitro group. This would overcome the negative effect due to the nitro group.

II) The primary oxidation products, *o*-nitroacetophenone and 1-(*o*-nitrophenyl)ethanol, are relatively stable against autoxidation.

One of the authors (R.H) wishes to thank Dr. E. Niki, Mr. H. Tsutsumi, and Mr. S. Komoto for their advice and encouragement, and also to the staff of Nippon Kayaku Co., Ltd. for permission to publish this work.

References

1) Present address: Dyestuff Research Laboratory, Nippon Kayaku Co., Ltd., Shimo 3-26-8, Kita-ku, Tokyo 115.
2) D. A. S. Ravens, *Trans. Faraday Soc.*, **55**, 1768 (1959).
3) A. S. Hay and H. S. Blanchard, *Can. J. Chem.*, **43**, 1306 (1965).
4) Y. Kamiya, *Tetrahedron*, **22**, 2029 (1966).
5) Y. Kamiya, "Oxidation of Organic Compounds," **2**, Am. Chem. Soc. (1968), p. 193.
6) C. E. H. Bawn and T. K. Wright, *Discuss. Faraday Soc.*, **46**, 164 (1969).

7) K. A. Chervinskii and V. I. Kovalev, *Khim. Tekhnol.* **12**, 83 (1969).
8) K. A. Chervinskii, *Khim. Tekhnol.*, **11**, 60 (1968).
9) K. A. Chervinskii and V. I. Kovalev, *Zh. Fiz. Khim.*, **43** 2062 (1969).
10) U. S. Patent 2833816.
11) U. S. Patent 3030414.
12) U. S. Patent 3030415.
13) Brit. Patent 814487.
14) Japan Patent Kokai 75 96539.
15) U. S. S. R. Patent 224510.
16) Y. Kamiya and M. Kashima, *J. Cataly.*, **25**, 326 (1972).
17) Y. Kamiya, *Kogyo Kagaku Zasshi*, **68**, 1877 (1965).
18) Y. Kamiya, "Yuki Sanka Hanno," Gihodo, Tokyo (1973), p. 147.
19) Y. Kamiya, *Kogyo Kagaku Zasshi*, **69**, 897 (1966).
20) Y. Kamiya, *Bull. Chem. Soc. Jpn.*, **39**, 2211 (1966).
21) Y. Kamiya, *J. Catal.*, **33**, 480 (1974).
22) H. Takeyama, *Shokubai*, **7**, 352 (1965).
23) G. A. Russell *et al.*, *J. Org. Chem.*, **32**, 137 (1967).
24) A. A. Miller and F. R. Mayo, *J. Am. Chem. Soc.*, **78**, 1017 (1956).
25) R. A. Jackson and W. A. Waters, *J. Chem. Soc.*, **1960**, 1653.
26) C. C. Price and D. A. Durham, *J. Am. Chem. Soc.*, **65**, 757 (1943).
27) P. D. Bartlett and H. Kwart, *J. Am. Chem. Soc.*, **74**, 3969 (1952).
28) Gingras and W. A. Waters, *J. Chem. Soc.*, **1954**, 1920.
29) Giacomo Giamician, *Ber.*, **1901**, 2040.
30) J. Harley-Mason, *J. Chem. Soc.*, *B*, **1966**, 396.

1,3-Dipolar Cycloadditions to Bicyclic Olefins. IV. The Influence of Non-neighboring Double Bonds on the Stereoselectivity in 1,3-Dipolar Cycloadditions to Bicyclo[*n*.2.2]alkadienes[1]

Hisaji TANIGUCHI, Toshikazu IKEDA, and Eiji IMOTO

Department of Applied Chemistry, College of Engineering, University of Osaka Prefecture, Mozu-Umemachi, Sakai, Osaka 591

(Received November 17, 1977)

1,3-Dipoles, such as phenylglyoxylonitrile oxide (**1**), benzonitrile oxide, and phenyl azide, undergo cycloadditions to the more electron-rich double bond of 2,3-bis(methoxycarbonyl)bicyclo[2.2.2]octa-2,5-diene (**5**) to afford only *endo* adducts. The cycloadditions of these 1,3-dipoles to the more electron-rich double bond of 6,7-bis(methoxycarbonyl)bicyclo[3.2.2]nona-6,8-diene (**6**) give only *exo* adducts. Benzonitrile-*N*-phenylimine (**4**) undergoes cycloadditions to both the more electron-rich and the more electron-poor double bonds of **5** or **6**. The reaction of **4** with **5** yields two *endo* adducts, and the reaction of **4** with **6** gives two *exo* adducts. However, the cycloaddition of **1** to 5,6-*endo*,*endo*-bis(methoxycarbonyl)bicyclo[2.2.2]oct-2-ene affords both the *exo*- and *endo* adducts. The reason for the predominant *endo* cycloadditions toward **5** and *exo* cycloadditions toward **6** is discussed.

In a previous paper, it was reported that 1,3-dipolar cycloadditions to norbornenes follow the "*exo* rule" of Alder and Stein, but that those to norbornadienes do not follow this rule.[2] This difference in reactivity has been ascribed to the fact that, in norbornadienes, the homoconjugations are present on their *endo* sides, while in norbornenes such interactions can not be present.[2] This assumption prompted us to examine the stereochemistry of the 1,3-dipolar cycloadditions to other bicyclic olefins with two carbon-carbon double bonds within each molecule, such as bicyclo[*n*.2.2]alkadienes($n \geqq 2$). Therefore, the 1,3-dipolar cycloadditions of phenylglyoxylonitrile oxide(**1**), benzonitrile oxide(**2**), phenyl azide(**3**), and benzonitrile-*N*-phenylimine(**4**) to 2,3-bis(methoxycarbonyl)bicyclo[2.2.2]octa-2,5-diene(**5**), or 6,7-bis(methoxycarbonyl)bicyclo[3.2.2]nona-6,8-diene (**6**) were carried out. Moreover, for comparison, the 1,3-dipolar cycloaddition of **1** to 5,6-*endo*,*endo*-bis(methoxycarbonyl)bicyclo[2.2.2]oct-2-ene(**7**), which is a corresponding monoene of **5**, was also carried out. In this paper, it will be emphasized that the interaction between the two carbon-carbon double bonds in **5** or **6** is an important factor controlling the stereochemistry of the additions of 1,3-dipoles to these double bonds.

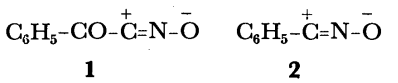

1 **2** **3**

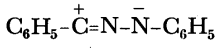

4

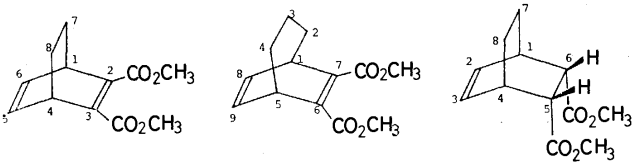

5 **6** **7**

Results

1,3-Dipolar Cycloadditions. The nitrile oxide, **1**, was easily prepared by the treatment of α-chloro-α-hydroxyiminoacetophenone(**8**) with triethylamine (TEA).[3] In order to avoid the dimerization of the nitrile oxide, **1**, to 3,4-dibenzoyl-1,2,5-oxadiazole 2-oxide(**9**), the reaction was carried out with low stationary concentrations of **1**. A dilute THF solution of TEA was slowly stirred into a solution of a mixture of **5** and **8** in THF cooled in an ice-bath.[4] This cycloaddition afforded only one *endo* adduct, 5-benzoyl-8,9-bis(methoxycarbonyl)-2,6-*endo*-3-oxa-4-azatricyclo-[5.2.2.$0^{2,6}$]undeca-4,8-diene(**10**). The cycloaddition of **1** to **6** was carried out by a similar method. In this case, the reaction gave only one *exo* adduct, 5-benzoyl-11,12-bis(methoxycarbonyl)-2,6-*exo*-3-oxa-4-azatricyclo-[5.3.2.$0^{2,6}$]dodeca-4,11-diene(**11**). The monoadducts which were produced by the addition of **1** to the more electron-poor double bonds of **5** and **6** and the bisadducts were not detected at all. These findings show that the nitrile oxide, **1**, acts as an electron-accepting 1,3-dipole toward **5** and **6**.[5]

The cycloadditions of **2** to **5** and **2** to **6** were carried out by a procedure similar to that described above. In these reactions also, the nitrile oxide, **2**, attacked the more electron-rich double bonds of **5** and **6** to give 8,9-bis(methoxycarbonyl)-5-phenyl-2,6-*endo*-3-oxa-4-azatricyclo[5.2.2.$0^{2,6}$]undeca-4,9-diene(**12**) and 11,12-bis(methoxycarbonyl)-5-phenyl-2,6-*exo*-3-oxa-4-azatricyclo[5.3.2.$0^{2,6}$]dodeca-4,11-diene(**13**) respectively. These findings show that **2** also acts as an electron-accepting 1,3-dipole toward **5** and **6**.[5]

The cycloaddition of the azide, **3**, to **5** was carried out as follows. The benzene solution of a mixture of **3** and **5** was allowed to stand in the dark for two weeks at room temperature. The subsequent usual work-up of the reaction mixture gave only one *endo* adduct, 8,9-bis(methoxycarbonyl)-5-phenyl-2,6-*endo*-3,4,5-triazatricyclo[5.2.2.$0^{2,6}$]undeca-3,8-diene(**14**). A similar treatment of **3** with **6** afforded one *exo* adduct, 11,12-bis(methoxycarbonyl)-5-phenyl-2,6-*exo*-3,4,5-triazatricyclo[5.3.2.$0^{2,6}$]dodeca-3,11-diene(**15**). These findings show that the dipole, **3**, acts as an electron-accepting 1,3-dipole toward **5** and **6**.[5] This is consistent with the fact that the dipole, **3**, acts as an electron-accepting 1,3-dipole toward norbornene and cyclopentene.[5,6]

The nitrilimine, **4**, which was prepared from *N*-phenylbenzenecarbohydrazonoyl chloride(**16**)[7] and TEA in benzene, underwent 1,3-dipolar cycloaddition

to **5** to afford a mixture of two monoadducts, 8,9-bis(methoxycarbonyl)-3,5-diphenyl-2,6-*endo*-3,4-diazatricyclo[5.2.2.$0^{2,6}$]undeca-4,8-diene(**17**) and 2-*exo*,6-*exo*-bis(methoxycarbonyl)-3,5-diphenyl-2,6-*endo*-3,4-diazatricyclo[5.2.2.$0^{2,6}$]undeca-4,8-diene(**18**). A similar treatment of **4** with **6** gave two *exo* adducts, 11,12-bis(methoxycarbonyl)-3,5-diphenyl-2,6-*exo*-3,4-diazatricyclo[5.3.2.$0^{2,6}$]dodeca-4,11-diene(**19**) and 2-*endo*,6-*endo*-bis(methoxycarbonyl)-3,5-diphenyl-2,6-*exo*-3,4-diazatricyclo[5.3.2.$0^{2,6}$]dodeca-4,11-diene(**20**). The cycloadducts, **17** and **19**, are those which were produced by the addition of **4** to the more electron-rich double bonds of **5** and **6**, while the **18** and **20** adducts are those which were produced by the addition of **4** to the more electron-poor double bonds of **5** and **6**. These results indicate that the dipole, **4**, acts both as an electron-accepting 1,3-dipole and as an electron-donating one toward **5** and **6**.[5]

The cycloaddition of **1** to **7** was carried out by the method described above. This reaction gave a mixture of the *exo*- and *endo* adducts, 5-benzoyl-8-*endo*, 9-*endo*-bis(methoxycarbonyl)-2,6-*exo*-3-oxa-4-azatricyclo[5.2.2.$0^{2,6}$]undec-4-ene(**21**) and 5-benzoyl-8-*endo*, 9-*endo*-bis(methoxycarbonyl)-2,6-*endo*-3-oxa-4-azatricyclo[5.2.2.$0^{2,6}$]undec-4-ene(**22**) in yields of 29% and 6% respectively, with a recovery of 63% of **7**.

TABLE 1. YIELDS AND PRODUCT COMPOSITIONS

Olefin	1,3-Dipole	Adduct	Yield[a] (%)	Composition *exo* (%)	Composition *endo* (%)	Recovery of olefin (%)
5	**1**	**10**	98	0	100	0
6	**1**	**11**	76	100	0	14
5	**2**	**12**	79	0	100	9
6	**2**	**13**	77	100	0	11
5	**3**	**14**	70	0	100	23
6	**3**	**15**	67	100	0	21
5	**4**	**17**	53	0	68	35
		and				
		18		0	32	
6	**4**	**19**	75	81	0	17
		and				
		20		19	0	
7	**1**	**21**	35	83	17	63
		and				
		22				

a) The yields are based on the starting olefins.

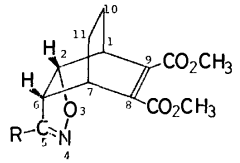

10, R = C_6H_5CO
12, R = C_6H_5

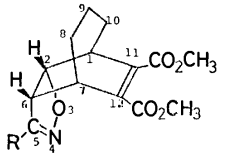

11, R = C_6H_5CO
13, R = C_6H_5

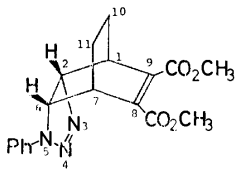

14

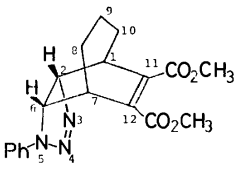

15

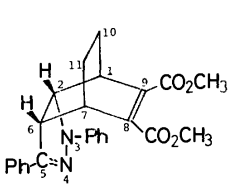

17

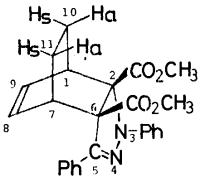

18

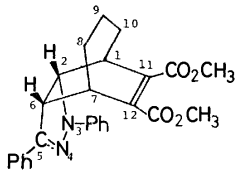

19

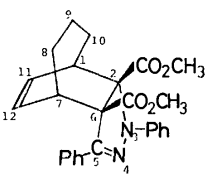

20

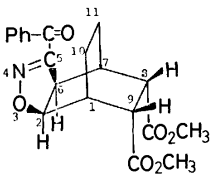

21

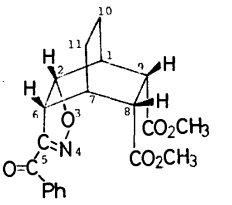

22

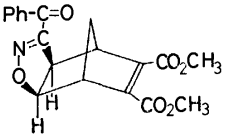

24

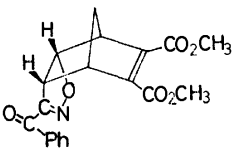

25

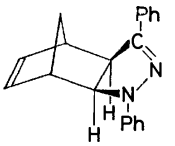

27

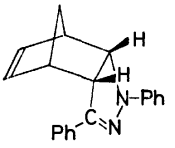

28

Analyses of NMR Spectra of Adducts. The *exo*- or *endo* assignment of each adduct was based on the NMR data(Table 2). The configurations of all the adducts except for **18** and **20** could be determined from the chemical shifts of their methoxycarbonyl groups. As is shown in Table 2, for the **10**—**15** and **22** adducts, one of the two methoxycarbonyl groups of each adduct appeared in a field higher by 0.21—0.48 ppm than the other. Moreover, the low-field methoxycarbonyl groups have chemical shifts of about δ 3.7—3.8 ppm which resemble the chemical shifts of mehtoxycarbonyl goups of the referential compounds (**5**, **6**, and dimethyl maleate (**23**)). For the **17** and **19** adducts the two methoxycarbonyl groups of each adduct appeared in fields higher by about 0.3—0.4 ppm than those of

Table 2. Chemical shifts of methoxycarbonyl groups and vinyl protons in adducts and referential compounds[a,b]

Compound	CO_2CH_3		$\Delta\delta$[c]	Vinyl protons
10	3.44	3.78	0.34	
12	3.38	3.74	0.36	
14	3.38	3.75	0.37	
17	3.33	3.45	0.42[d]	
11	3.50	3.75	0.25	
13	3.49	3.74	0.25	
15	3.50	3.71	0.21	
19	3.44	3.54	0.32[e]	
21	3.63	3.67	0.04	
22	3.16	3.62	0.48	
23	3.81	3.81	0.00	
24	3.78[f]	3.81[f]	0.03	
25	3.33[f]	3.78[f]	0.45	
5	3.73	3.73	0.00	6.34
6	3.75	3.75	0.00	6.27
7	3.58[g]	3.58[g]	0.00	6.33[g]
18	3.58	3.68	0.10	5.93[h]
20	3.62	3.69	0.07	5.80[h]
26				6.25[i]
27				6.25[f]
28				5.89[f]

a) The spectra were recorded at 60 MHz. b) Expressed in δ ppm units, with TMS as the internal standard, in $CDCl_3$ solutions. c) The difference in chemical shift between the high-field methoxycarbonyl and the low-field methoxycarbonyl protons. d) The difference between the chemical-shift value (3.81) of the methoxycarbonyl of dimethyl maleate and the average of the values, 3.33 and 3.45. e) The difference between the chemical-shift value (3.81) of the methoxycarbonyl of dimethyl maleate and the average of the values, 3.44 and 3.54. f) Ref. 2. g) K. Tori, Y. Takano, and K. Kitakonoki, *Chem. Ber.*, **97**, 2798 (1964). h) The value at the center of the ABq. i) K. Tori, Y. Hata, R. Muneyuki, Y. Takano, T. Tsuji, and H. Tanida, *Can. J. Chem.*, **42**, 926 (1964).

the referential compound, **23**. The molecular models of the adducts reveal that the high field methoxycarbonyl groups lie in the shielding cones of benzene rings attached on the heterocyclic moieties of the adducts. On the other hand, the **21** adduct exhibited the chemical shifts of the two methoxycarbonyl groups at δ 3.63 and 3.67 ppm, whose values were normal. This indicated that the adduct has the *exo* configuration. Such an assignment has also been carried out for the *exo*- and *endo* adducts, **24** and **25**, formed by the cycloaddition of **1** to 2,3-bis(methoxycarbonyl)-norbornadiene.[2] The configurations of the **18** and **20** adducts were determined as follows. The vinyl protons of these adducts appeared as AB quartets of doublets in fields higher by about 0.3—0.4 ppm than those of the referential compounds, **5**, **6**, **7**, and bicyclo[2.2.2]-oct-2-ene(**26**). These up-field shifts are probably due to the diamagnetic anisotoropy effects of the carbon-nitogen double bonds.[8] This finding indicates that the vinyl protons of these adducts are placed above the carbon-nitrogen double bonds of the heterocyclic moieties. The structures of **18** and **20** are consistent with this finding. Such an assignment has also been carried out for the *exo*- and *endo* adducts, **27** and **28**, formed by the cycloaddition of **4** to norbornadiene.[2]

Discussion

This kind of 1,3-dipolar cycloaddition has been shown to be a kinetically controlled reaction.[1,2,9] Hence, all the adducts obtained here are kinetically controlled products.

About Steric Hindrance. Two 7,8-*syn*-hydrogen atoms are present on the *exo* side of **5**, but such hydrogen atoms are absent on the *endo* side. A similar difference in steric hindrance is present between the *exo*- and *endo* sides of **6**. For this reason, it might appear that the steric hindrance is a factor which brings about the highly stereoselective cycloadditions of 1,3-dipoles toward the dienes, **5** and **6**.

From the fact that the cycloaddition of **1** to **7** gave both the *exo*- and *endo* adducts, however, we doubt the above explanation based on the steric hindrance theory. The molecular models of **5** and **7** show that the difference in steric crowding between the *exo*- and *endo* sides of **5** is smaller than that in steric crowding between the *exo* and *endo* sides of **7**. This implies that the *endo*/*exo* product ratio for the cycloaddition of **1** to **5** must become closer to unity than that for the cycloaddition of **1** to **7**, provided that the preferred direction of reaction is controlled only by the steric hindrance. As Table 1 shows, however, the *endo*/*exo* product ratio for the cycloaddition of **1** to **5** is infinity, while that for the cycloaddition of **1** to **7** is 0.21. This finding shows that the direction of the attack of the 1,3-dipole, **1**, on the double bond of **5** can not be determined only by the steric hindrance. For the same reason, the predominant *exo* cycloaddition of **1** to **6** can not be explained by the steric hindrance alone. For all the other cycloadditions carried out here as well, these findings suggest that the steric hindrance is not a main factor controlling the stereochemistry of these reactions.

The Interaction of the Two Carbon-Carbon Double Bonds.

a) For bicyclo[2.2.2]octa-2,5-diene and bicyclo-[3.2.2]nona-6,8-diene, the presence of a homoconjugation between the two non-neighboring carbon-carbon double bonds has been found by investigating the photoelectron spectroscopy of these dienes.[10]

b) The relative rate ratios of the cycloadditions of **4** to cyclohexene, cyclopentene, 1-heptene, dimethyl maleate, and dimethyl fumarate can be derived from the data of Eckell *et al.*[5c] (Table 3). Table 3 suggests that the dipole, **4**, undergoes cycloadditions to the more electron-poor double bonds of the dienes, **5** and **6**, rather than to the more electron-rich double bonds. In practice, however, the 1,3-dipolar cycloadditions occured preferentially on the more electron-rich double bonds of **5** and **6** (Table 4). This attack on the reverse site must be ascribed to the interaction between the two non-neighboring carbon-carbon

TABLE 3. RELATIVE RATES OF THE ADDITION OF 4[a)]

Compound	Relative rates
Cyclohexene	1
Cyclopentene	8.7
1-Heptene	9.1
Dimethy maleate	530
Dimethy fumalate	19, 100

a) Derived from Ref. 5c.

TABLE 4. THE ATTACKING SITE OF 4 ON 5 AND 6

Diene	Electron-rich double bond (%)	Electron-poor double bond (%)
5	68	32
6	81	19

double bonds of **5** or **6**, as will be described below.

A Tentative Explanation of the Highly Stereoselective Cycloadditions. a) The LU-Controlled Reactions of 1,3-Dipoles with the Dienes, 5 and 6: As has described above, the 1,3-dipoles **1**—**4**, act as electron-accepting dipoles toward the more electron-rich double bonds of **5** and **6**. In Houk's terminology, these cycloadditions are called LU-controlled reactions.[5b)] In these cases, the interaction of the dipole LUMO(lowest unoccupied molecular orbital) with the dipolarophile HOMO (highest occupied molecular orbital) is greatest.[5b)] The predominant *endo* cycloadditions toward **5** and *exo* cycloadditions toward **6** can be reasonably explained by the orbital mixing rule.[11)] This rule treats the extension of an orbital at an interacting center in a certain direction. Now, we shall consider the orbital extension of the HOMO of the more electron-rich double bond (C_5–C_6) of **5** to the *exo*- and *endo* sides. The rehybridization originates from the mixing of the C_5–C_6 σ orbital in the C_5–C_6 π orbital(HOMO) under the influence of the C_2–C_3 π orbital(HOMO). The C_5–C_6 double bond interacts with the C_2–C_3 double bond on the *endo* side, as has been described above. The three orbitals and their energy relation are shown in Fig. 1.[12)] From the orbital mixing rule, it can be predicted that the HOMO of the C_5–C_6 double bond extends more to the *endo* side than to the *exo* side (Fig. 1.). Consequently, the 1,3-dipoles, **1**—**4**, attack predominantly from the *endo* side. In the same treatment, the HOMO of the C_8–C_9 double bond of **6** can be predicted to extend more greatly to the *exo* side than to the *endo* side. This explains the predominant *exo* cycloaddition to the C_8–C_9 double bond of **6**. Such a treatment has also been carried out for the HOMO of norbornene.[11a)]

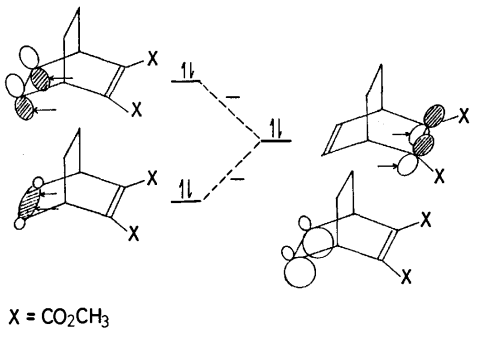

Fig. 1. Origin and direction of nonequivalent HOMO extension of **5**.

b) *The HO-Controlled Reaction of the Nitrilimine, 4, with 5 and 6*: The 1,3-dipole, **4**, acts as an electron-donating dipole toward the more electron-poor double bonds of **5** and **6**, as has been described above. In Houk's terminology, these cycloadditions are called HO-controlled reactions.[5b)] In these cases, the interaction of the dipole HOMO with the dipolarophile LUMO is greatest.[5b)] Hence, we shall consider the orbital extension of the LUMO of the more electron-poor double bond(C_2–C_3) of **5** using the orbital mixing rule in order to explain the predominant endo cycloaddition of **4** to this double bond. In this case, the interaction among the three orbitals, the C_2–C_3 σ^* orbital, the C_2–C_3 π^* orbital(LUMO), and the C_5–$C_6\pi^*$ orbital(LUMO), is taken account of on the *endo* side. The three orbitals and their energy relation are shown in Fig. 2.[14)] The orbital mixing rule predicts that the LUMO of the C_2–C_3 double bond will extend more to the *endo* side than to the *exo* side (Fig. 2.). Consequently, the dipole, **4** attacks predominantly from the *endo* side. In the same treatment, the LUMO of the C_6–C_7 double bond of **6** is predicted to extend more to the *exo* side than to the *endo* side. This reasonably explains the predominant *exo* cycloaddition of **4** to the C_6–C_7 double bond of **6**.

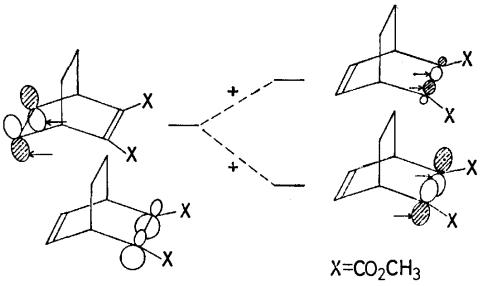

Fig. 2. Origin and direction of nonequivalent LUMO extension of **5**.

Experimental

Materials. The precursors of 1,3-dipoles (**8**,[3)] **16**,[15)] and *N*-hydroxybenzenecarboximidoyl chloride (**29**)[16)]) and the azide, **3**,[17)] were prepared by methods described in the literature. The dienes, **5**[18)] and **6**,[19)] and the monoene, **7**,[20)] were also prepared by the methods described in the literature.

Cycloaddition of 1 to 5. Into a stirred solution of **5** (1.10 g, 5.0 mmol) and **8**(0.92 g, 5.0 mmol) in dry THF (15 cm^3) cooled in an ice bath, a solution of triethylamine (TEA) (0.65 g, 6.5 mmol) in dry THF (10 cm^3) was added, drop by drop, over a period of 1 h. After an additional stirring for 1 h at the same temperature, the resulting triethylammonium chloride was removed by filtration. The TLC of the filtrate showed only one spot (elution with benzene–ether(9:1)). After the evaporation of the solvent, the yellowish residue was washed with several drops of 95%

EtOH. The solid was separated by filtration and dried under reduced pressure to give 1.79 g(98%) of the adduct, **10**. It was recrystallized from 95% EtOH to afford colorless needles: Mp 97—98 °C; IR(KBr) 1733(ester C=O), 1710(ester C=O), 1650(C=O), 1440 and 1280 cm^{-1}; NMR ($CDCl_3$) δ=1.56(4H, m, CH_2CH_2), 3.44(3H, s, 8-CO_2CH_3), 3.58(1H, m), 3.76(1H, m), 3.78(3H, s, 9-CO_2CH_3), 3.95 (1H, dd, J=10 and 4 Hz, 6-H), 4.98(1H, dd J=10 and 4 Hz, 2-H), and 7.3—8.3 ppm (5H, m).

Found: C, 65.03; H, 5.10; N, 3.56%. Calcd for $C_{20}H_{19}N_1O_6$: C, 65.03; H, 5.19; N, 3.79%.

*Cycloaddition of **1** to **6**.* A solution of **6**(710 mg, 3.0 mmol) and **8**(551 mg, 3.0 mmol) in dry THF(15cm^3) was treated with TEA(370 mg, 3.7 mmol) in dry THF(10 cm^3) as has been described above. A similar work-up of the reaction mixture and evaporation of the solvent produced a yellowish viscous oil. This oil showed, on TLC with benzene–ether(95 : 5), two marked spots, at R_f 0.45(**6**) and at R_f 0.32(**11**). The oil was chromatographed on silica gel (200—300 mesh). Elution with benzene–ether(95 : 5) gave **6**(96 mg, recovery 14%) and a white solid of **11**(877 mg, 76%). The solid was recrystallized from MeOH to afford colorless leaves: Mp 98—99 °C; IR(KBr) 1735(ester C=O), 1715(ester C=O), 1660(C=O), 1440, 1275, and 1260 cm^{-1}; NMR($CDCl_3$) δ=1.74(6H, s, $(CH_2)_3$), 3.27(1H, m), *ca.* 3.5(1H, m), 3.50(3H, s, 12-CO_2CH_3), 3.75(3H, s, 11-CO_2CH_3), 4.18(1H, dd, J=10.5 and 1.5 Hz, 6-H), 5.18(1H, dd, J=10.5 and 2.5 Hz, 2-H), and 7.1—8.2 ppm(5H, m).

Found: C, 65.75; H, 5.51; N, 3.55%. Calcd for $C_{21}H_{21}N_1O_6$: C, 65.78; H, 5.52; N, 3.65%.

*Cycloaddition of **2** to **5**.* A solution of **5**(1110 mg, 5.0 mmol) and **29**(778 mg, 5.0mmol) in dry THF(15 cm^3) was treated with TEA(610 mg, 6.0 mmol) in dry THF(10 cm^3) by a procedure like that described above. A similar work-up of the reaction mixture and evaporation of the solvent gave a yellowish viscous oil. On TLC with benzene–ether (95:5), the oil showed three spots, at R_f 0.75(3,4-diphenyl-1,2,5-oxadiazole 2-oxide (**30**)), R_f 0.40(**5**), and R_f 0.13(**12**). The oil was column chromatographed on silica gel with benzene–ether (95:5) to give a white solid of **30**(37 mg, mp 115—116 °C (lit,[21] mp 112 °C)), **5**(116 mg, recovery 10%), and a solid of **12**(1331 mg, 78%).

Adduct **12** : Mp 148—149 °C(colorless cubic crystals from MeOH); IR(KBr) 1705(ester C=O), 1433, and 1290 cm^{-1} ; NMR($CDCl_3$) δ=1.46 and 1.62(4H, ABq, J=12 Hz, CH_2CH_2), 3.38(3H, s, 8-CO_2CH_3), *ca.* 3.5(1H, m), 3.65(1H, m), 3.74(3H, s, 9-CO_2CH_3), 3.88(1H, dd, J=10 and 3 Hz, 6-H), 4.93(1H, dd, J=10 and 4.0 Hz, 2-H), and 7.2—7.8 ppm(5H, m).

Found: C, 66.91; H, 5.50; N, 4.15% Calcd for $C_{19}H_{19}N_1O_5$: C, 66.85; H, 5.61; N, 4.10%.

*Cycloaddition of **2** to **6**.* A solution of **6**(710 mg, 3.0 mmol) and **29**(476 mg, 3.0 mmol) in dry THF(15 cm^3) was treated with TEA(370 mg, 3.7 mmol) in dry THF(10 cm^3) as has been described above. A similar work-up of the reaction mixture and evaporation of the solvent afforded a yellowish viscous oil, which showed three spots on TLC with benzene–ehyl acetate(95:5). It was column chromatographed on silica gel. Elution with benzene–ethyl acetate (95:5) gave **30**(24 mg), **6**(78 mg, recovery 11%),and a solid of **13**(819 mg, 77%).

Adduct **13** : Mp 129—130 °C(colorless cubic crystals from MeOH–H_2O); IR(KBr) 1720(ester C=O), 1440, and 1295 cm^{-1}; NMR($CDCl_3$) δ=1.71(6H, s, $CH_2CH_2CH_2$), 3.11(1H, m), 3.38(1H, m), 3.49(3H, s, 12-CO_2CH_3), 3.74 (3H, s, 11-CO_2CH_3), 4.12(1H, dd, J=10.5 and 1.5 Hz, 6-H), 5.26(1H, dd, J=10.5 and 2.5 Hz, 2-H), and 7.2—7.8 ppm (5H, m).

Found: C, 67.37; H, 5.89; N, 3.98%. Calcd for $C_{20}H_{21}N_1O_5$: C, 67.59; H, 5.96; N, 3.94%.

*Cycloaddition of **3** to **5**.* A mixture of **5**(560 mg, 2.5 mmol) and **3**(298 mg, 2.5 mmol) was dissolved in dry benzene (5 cm^3). After the solution had then been allowed to stand in the dark for two weeks at room temperature, it showed two spots(**5** and **14**) on TLC with benzene–ethyl acetate(8:2). After the removal of the solvent, the residue was column chromatographed on alumina. Elution with benzene–ehtyl acetate(8:2) gave **5**(129 mg, recovery 23%). Further elution with the same solvent afforded **14** (600 mg, 70%), which was subsequently recrystallized from MeOH to give colorless prisms: Mp 151—152 °C; IR(KBr) 1715(ester C=O), 1605, 1493, 1440, and 1300 cm^{-1}; NMR($CDCl_3$) δ= 1.47 and 1.68(4H, ABq, J=11 Hz, CH_2CH_2), 3.38(3H, s, 8-CO_2CH_3), 3.75(3H, s, 9-CO_2 CH_3), 3.6—3.9(2H, m), 4.10(1H, dd, J=11.5 and 3.5 Hz, 6-H), 4.86(1H, dd, J= 11.5 and 3.5 Hz, 2-H), and 6.7—7.6 ppm(5H, m).

Found: C, 63.49; H, 5.50; N, 12.30%. $C_{18}H_{19}N_3O_4$: C, 63.33; H, 5.61; N, 12.31%.

*Cycloaddition of **3** to **6**.* A solution of **6**(708 mg, 3.0 mmol) and **3**(357 mg, 3.0 mmol) in dry benzene(3 cm^3) was allowed to stand in the dark for one week at room temperature. Then, the solution showed three spots (**3**, **6**, and **15**) on TLC with benzene–ethyl acetate(9:1). The solvent was evaporated under reduced pressure to give a residue, which was column chromatographed on alumina with benzene–ethyl acetate(9:1) to afford a trace amount of **3**, **6**(148 mg, recovery 21%), and **15**(713 mg, 67%).

Adduct **15**: Mp 137—139 °C(colorless leaves from MeOH); IR(KBr) 1710(ester C=O), 1600, 1490, 1433, and 1287 cm^{-1}; NMR($CDCl_3$) δ=1.73(6H, s, $CH_2CH_2CH_2$), 3.38 (1H, m), 3.50(3H, s, 12-CO_2CH_3), *ca.* 3.7(1H, m), 3.71(3H, s, 11-CO_2CH_3), 4.37(1H, dd, J=12 and 1.5 Hz, 6-H), 5.01(1H, dd, J=12 and 2 Hz, 2-H), and 6.8—7.6 ppm (5H, m).

Found: C, 64.26; H, 6.06; N, 11.81%. Calcd for $C_{19}H_{21}N_3O_4$: C, 64.21; H, 5.96; N, 11.83%.

*Cycloaddition of **4** to **5**.* A mixture of **5**(558 mg, 2.5 mmol) and **16**(576 mg, 2.5mmol) was dissolved in dry benzene(10 cm^3). Into the solution, TEA(940 mg, 9.3 mmol) was then added all at once, after which the solution was allowed to stand in the dark for two weeks at room temperature. The resulting ammonium chloride was removed by filtration. The filtrate showed, on TLC with benzene, four spots, at R_f 0.65(**16**), R_f 0.25(**18**), R_f 0.16(**5**), and R_f 0.09(**17**). A large amount of the solvent was removed under reduced pressure. Then, the concentrated solution was chromatographed on silica gel. Subsequent elution with benzene afforded a solid of **16**(229 mg, recovery 40%), a solid of **18**(174 mg, 17%), **5**(193 mg, recovery 35%), and a yellow solid of **17**(379 mg, 36%) in that order.

Adduct **17**: Mp 169—170 °C(yellow sticks from EtOH); IR(KBr) 1717(ester C=O), 1600, 1500, and 1300 cm^{-1}; NMR($CDCl_3$) δ=1.49 and 1.69(4H, ABq, J=10 Hz, CH_2-CH_2), 3.33(3H, s, CO_2CH_3), 3.45(3H, s, CO_2CH_3), 3.55 (1H, m), 3.89(1H, dd, J=12 and 2.5 Hz, 6-H), 3.90(1H, m), 4.45(1H, dd, J=12 and 2.5 Hz, 2-H), and 6.6—7.8 ppm(10H, m).

Found: C, 72.22; H, 5.97; N, 6.97%. Calcd for $C_{25}H_{24}N_2O_4$: C, 72.10; H, 5.81; N, 6.73%.

Adduct **18**: Mp 217—219 °C(colorless cubic crystals from hexane–benzene); IR(KBr) 1742(ester C=O), 1737(ester C=O), 1600, 1593, 1500, 1262 cm^{-1}; NMR($CDCl_3$) δ=

1.12(2H, d, J=8 Hz, 10-*syn* H and 11-*syn* H), 2.35(2H, d, J=8H, 10-*anti* H and 11-*anti* H), 3.58(3H, s, CO_2CH_3), 3.68(3H, s, CO_2CH_3), 3.5—3.7(2H, m), 5.86 and 6.01(2H, ABq of d, $J_{8,9}$=8 Hz and $J_{7,8}=J_{1,9}$=6.5 Hz, 8-H and 9-H), and 6.8—7.9 ppm(10, m).

Found: C, 71.94; H, 5.65; N, 6.68%. Calcd for $C_{25}H_{24}N_2O_4$: C, 72.10; H, 5.81; N, 6.73%.

Cycloaddition of ***4*** *to* ***6***. A mixture of **5**(710 mg, 3.0 mmol), **16**(692 mg, 3.0 mmol), and TEA(1130 mg, 11.2 mmol) was dissolved in dry benzene(10 cm³). The solution was then allowed to stand for 24 h, and the resulting triethylammonium chloride was removed by filtration. On TLC with benzene, the filtrate showed four spots, at R_f 0.79(**16**), R_f 0.36(**20**), R_f 0.25(**6**), and R_f 0.20(**19**). After the removal of the solvent, the residue was chromatographed on silica gel. Elution with benzene gave a trace of **16**, a solid of **20**(176 mg, 14%), **6**(123 mg, recovery 17%), and a yellow solid of **19** (792 mg, 61%), in that order.

Adduct **19**: Mp 181—183 °C(yellow sticks from ethyl acetate–EtOH); IR(KBr) 1713(ester C=O), 1593, 1492, and 1285 cm⁻¹; NMR($CDCl_3$) δ=1.78(6H, s, $CH_2CH_2CH_2$), 3.30 (1H, m), 3.44(3H, s, CO_2CH_3), 3.54(3H, s, CO_2CH_3), *ca.* 3.6(1H, m), 4.18(1H, dd, J=12 and 1.5 Hz, 6-H), 4.68(1H, dd, J=12 and 2 Hz, 2-H), and 6.7—8.0 ppm(10H, m).

Found: C, 72.60; H, 6.06; N, 6.44%. Calcd for $C_{26}H_{26}N_2O_4$: C, 72.54; H, 6.09; N, 6.51%.

Adduct **20**: Mp 198—200 °C(colorless needles from EtOH); IR(KBr) 1740(ester C=O), 1720(ester C=O), 1595, 1587, 1500, 1492, and 1255 cm⁻¹; NMR($CDCl_3$) δ=1.1—2.5(6H, m, $CH_2CH_2CH_2$), 3.0—4.0(2H, m), 3.62(3H, s, CO_2CH_3), 3.69(3H, s, CO_2CH_3), 5.71 and 5.90(2H, ABq of d, $J_{11,12}$= 8 Hz and $J_{1,11}=J_{7,12}$=6.5 Hz, 11-H and 12-H), and 6.7—8.0 ppm(10H, m).

Found: C, 72.35; H, 6.03; N, 6.39%. Calcd for $C_{26}H_{26}N_2O_4$: C, 72.54; H, 6.09; N, 6.51%.

Cycloaddition of ***1*** *to* ***7***. Into a solution of **7**(1120 mg, 5.0 mmol) and **8**(920 mg, 5.0 mmol) in dry THF(15 cm³) cooled in an ice bath, a solution of TEA(620 mg, 6.1 mmol) in dry THF (10 cm³) was stirred, drop by drop, over a period of 1 h. After an additional 1 h's stirring at the same temperature, the resulting ammonium chloride was removed by filtration. The filtrate showed, on TLC with hexane–acetone (7 : 3), four spots, at R_f 0.47(**7**), R_f 0.41(**9**), R_f 0.35(**21**), and R_f 0.32(**22**). The solvents was evaporated under reduced pressure to give a residue. It was column-chromatographed on silica gel. Elution with hexane–acetone(31:12) gave **7** (705 mg, recovery 63%), 405 mg of **9**(mp, 76—78 °C(lit[3] 78—80 °C), a white solid of **21**(540 mg, 29%), and a white solid of **22**(110 mg, 6%) in that order.

Adduct **21**: Mp 113—114 °C(colorless plates from EtOH); IR(KBr) 1750(ester C=O) and 1660 cm⁻¹(C=O); NMR($CDCl_3$) δ=1.4—1.6(4H, m, CH_2CH_2), 2.50(1H, m), 2.77(1H, m), 3.00—3.15(2H, m, 8-H and 9-H), 3.63(3H, s, CO_2CH_3), 3.67(3H, s, CO_2CH_3), 3.88(1H, dd, J=12 and 3.5 Hz, 6-H), 5.27(1H, dd, J=12 and 3.5 Hz, 2-H), and 7.3—8.2 ppm(5H, m).

Found: C, 64.57; H, 5.76; N, 3.58%. Calcd for $C_{20}H_{21}N_1O_6$: C, 64.68; H, 5.70; N, 3.77%.

Adduct **22**: Mp 104—108 °C(dec); IR(KBr) 1750(ester C=O), 1725(ester C=O), and 1660 cm⁻¹(C=O); NMR($CDCl_3$) δ=1.3—2.0(4H, m, CH_2CH_2), 2.35—2.55(2H, m), 3.03(2H, broad, 8-H and 9-H), 3.16(3H, s, 8-CO_2CH_3), 3.62(3H, s, 9-CO_2CH_3), 4.30(1H, dd, J=12 and 4.0 Hz, 6-H), 5.28(1H, dd, J=12 and 4.0 Hz, 2-H), and 7.4—8.2 ppm(5H, m).

Found: C, 64.94; H, 5.85; N, 3.82%. Calcd for $C_{20}H_{21}N_1O_6$: 64.68; H, 5.70; N, 3.77%.

References

1) Preceding paper: H. Taniguchi and E. Imoto, *Bull. Chem. Soc. Jpn.*, submitted for publication.

2) H. Taniguchi, T. Ikeda, Y. Yoshida, and E. Imoto, *Bull. Chem. Soc. Jpn.*, **50**, 2694 (1977).

3) Y. Otsuji, Y. Tsujii, A. Yoshida, and E. Imoto, *Bull. Chem. Soc. Jpn.*, **44**, 223 (1971).

4) Since Compound **8** is very soluble in THF(solubility, 1250 mg/cm³ at 25 °C), the hydrogen-bonded complex between **8** and **5** (or **6**) can not be formed in THF.[1]

5) According to the calculations of Houk *et al.* for various 1,3-dipoles, the nitrile oxides, **1** and **2**, acts as electron-accepting 1,3-dipoles toward a variety of dipolarophiles. Phenyl azide also acts as an electron-accepting 1,3-dipole toward the electron-rich double bonds. The nitrilimine, **4**, varies its electron-accepting or donating character according to the kind of dipolarophile. a) K. N. Houk, J. Sims, R. E. Duke, Jr., R. W. Strozier, and J. K. George, *J. Am. Chem. Soc.*, **95**, 7287 (1973); b) K. N. Houk, J. Sims, C. R. Watts, and L. J. Luskus, *ibid.*, **95**, 7301 (1973); c) A. Eckell, R. Huisgen, R. Sustmann, G. Wallbillich, D. Grashey, and E. Spindler, *Chem. Ber.*, **100**, 2192 (1967).

6) R. Huisgen, G. Szeimies, and L. Möbius, *Chem. Ber.*, **100**, 2494 (1967).

7) Since Compound **16** is sufficiently soluble in benzene (solubility, 91 mg/cm³), the compound may not associate with **5** (or **6**) in benzene.[1]

8) L. M. Jackman and S. Sternhell, "Application of Nuclear Magnetic Resonance Spectroscopy in Organic Chemistry," 2nd ed, Pergamon Press, London (1969), Chap. 2-2.

9) H. Taniguchi, Y. Yoshida, and E. Imoto, *Bull. Chem. Soc. Jpn.*, **50**, 3335 (1977).

10) a) H. Bock and B. G. Ramsey, *Angew. Chem. Int. Ed. Engl.*, **12**, 734 (1973); b) P. Bischof, J. H. Hashmall, E. Heilbronner, and V. Hornung, *Helv. Chim. Acta*, **52**, 1745 (1969); c) M. J. Coldstein, S. Natowsky, E. Heilbronner, and V. Hornung, *Helv. Chim. Acta*, **56**, 294 (1973).

11) a) S. Inagaki, H. Fujimoto, and K. Fukui, *J. Am. Chem. Soc.*, **98**, 4054 (1976); b) K. Fukui, "Kagaku Hanno To Denshi No Kido," Maruzen, Tokyo (1976), Chaps. 3 and 4; c) K. Fukui, *Kagaku To Kogyo*, **29**, 666 (1976).

12) The energy relation of these three orbitals comes from the energy levels of the C–C σ and C–C π orbitals of ethylene[13] and the energy level of the C–C π orbital of dimethyl maleate.[5a,13]

13) a) W. L. Jorgensen and L. Salem, "The Organic Chemist's Book of Orbitals," Academic Press, New York, New York(1973), p. 81; b) R. Sustmann and H. Trill, *Tetrahedron Lett.*, **1972**, 4271; c) D. W. Turner, C. Baker, A. D. Baker, and C. R. Brundle, "Molecular Photoelectron Spectroscopy," Wiley, London, Interscience(1970), p. 61.

14) The energy relation of these three orbitals comes from the energy levels of the C–C σ^* and C–C π^* orbitals of dimethyl maleate[5a,13] and the energy level of the π^* orbital of ethylene.[5a,13]

15) R. Huisgen, M. Seidel, G. Wallbillich, and H. Knupfer, *Tetrahedron*, **17**, 3 (1962).

16) P. Pajahopalan, B. G. Advani, and C. N. Talaty, *Org. Synth.*, Coll. Vol. V, 505 (1973).

17) R. O. Lindsay and C. F. H. Allen, *Org. Synth.*, Coll. Vol. III, 710 (1955).

18) O. Diels and K. Alder, *Justus Liebigs Ann. Chem.*, **490**, 236 (1931).

19) H. Prinzbach and H-G. Schmidt, *Chem. Ber.*, **107**, 1988 (1974).

20) O. Diels and K. Alder, *Justus Liebigs Ann. Chem.*, **460**, 98 (1928).

21) A. Werner and H. Buss, *Ber.*, **27**, 2197 (1894).

Synthetic Studies on Quinoxaline Antibiotics. Synthesis of Quinoxaline-2-carbonyl Tetradepsipeptide Derivatives Related to Triostin A*

Masaru SHIN, Ken INOUYE, and Hideo OTSUKA

Shionogi Research Laboratory, Shionogi & Co., Ltd., Fukushima-ku, Osaka 553

(Received November 26, 1977)

The synthesis is described of four quinoxaline-2-carbonyl (Qxc) tetradepsipeptide derivatives, Qxc-D-Ser[Z-MeCys(Bzl)-MeVal]-Ala-OH, Qxc-D-Ser[Bpoc-MeCys(Bzl)-MeVal]-Ala-OBu^t (**2**), Qxc-D-Ser(Z-MeVal)-Ala-MeCys(Bzl)-OH, and Qxc-D-Ser(Bpoc-MeVal)-Ala-MeCys(Bzl)-OBu^t, corresponding to the partial structure of a quinoxaline antibiotic, triostin A. The Qxc group was introduced at the dipeptide or tripeptide stage with Qxc-ONp as acylating agent. Qxc-D-Ser-Ala-OBu^t and Qxc-D-Ser-Ala-MeCys(Bzl)-OBu^t were acylated with Z-MeVal-OH by using *p*-toluenesulfonyl chloride as activating agent to give the desired depsipeptides in excellent yields, whereas the acylation with Bpoc-MeVal-OH by the same procedure was unsuccessful. The latter could be achieved by the *N,N'*-carbonyldiimidazole method, though the yields were relatively low. The treatment of compound **2** with an aqueous acetic acid-formic acid mixture for removal of the Bpoc group brought about concomitant formation of *cyclo*[-MeCys(Bzl)-MeVal-].

The quinoxaline antibiotics[1] are produced by various species of streptomycetes including *S. aureus* and reported active against gram-positive bacteria, certain tumors and to inhibit DNA-dependent RNA synthesis. The triostins, a family of the quinoxaline antibiotics, were isolated by Shoji *et al.*[2] and their structure was determined by Otsuka and Shoji[3] to be a quinoxaline-2-carbonyl(Qxc)-peptide lactone with a bridged disulfide linkage (Fig. 1). As a result of the recent NMR and MS studies, the structure of echinomycin[4] (quinomycin A[5]), which is also a member of the quinoxaline antibiotics, has been revised,[6] while that of triostin A has rather been confirmed.[7] Some synthetic studies on these antibiotics have appeared, in which the Qxc derivatives of some amino acids,[8] peptides,[9] and related compounds[10] were prepared. Very recently Ciardelli and Olsen[11]

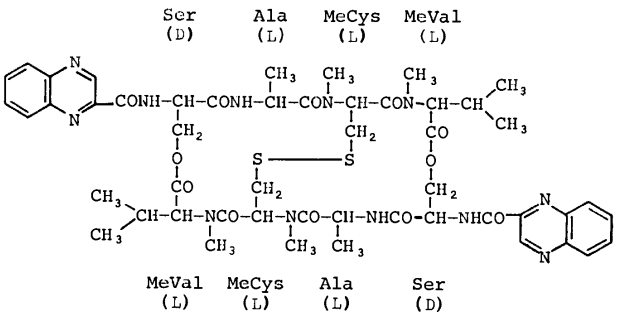

Fig. 1. Structure of triostin A.[3]

have reported the synthesis of des-*N*-tetramethyltriostin A, an analogue differing from the natural compound by lack of the *N*-methyl groups on the cysteine and valine residues. This desmethyl analogue had no activity toward *Staphylococcus aureus*, however.[11] We wish now to report the synthesis of tetradepsipeptide derivatives, Qxc-D-Ser[Z-MeCys(Bzl)-MeVal]-Ala-OH (**1**), Qxc-D-Ser[Bpoc-MeCys(Bzl)-MeVal]-Ala-OBu^t (**2**), Qxc-D-Ser(Z-MeVal)-Ala-MeCys(Bzl)-OH (**3**), and Qxc-D-Ser(Bpoc-MeVal)-Ala-MeCys-(Bzl)-OBu^t (**4**), which has been performed as a step toward the total synthesis of triostin A.

As is seen in Fig. 1, the structure of triostin A has the point of symmetry and can be split into two equal portions, each containing one Qxc group and four different amino acid residues, D-Ser, Ala, MeCys, and MeVal. Thus, the formation of the desired octadepsipeptide ring may be accomplished by combining a selected pair of the two halves, and a key to the total synthesis may be the choice of the position at which the ring is closed. The ring-closure by the lactonization between the MeVal and the D-Ser residues seems to be inadequate, because the low reactivity of the hydroxyl group of serine would require the carboxyl component highly activated,[12] and this could be a cause for some side reactions and racemization. The cyclization should, therefore, be carried out at a peptide bond. The synthesis of compounds **1**, **2**, **3**, and **4** was performed along this line.

Quinoxaline-2-carboxylic acid (Qxc-OH) as a starting material was synthesized by the method of Keller-Schierlein and Prelog[1b] from 2-methylquinoxaline *via* 2-styrylquinoxaline as intermediate. *N*-Methyl-L-valine was prepared according to the procedure of Quitt *et al.*[13] and *N*-methyl-*S*-benzyl-L-cysteine was derived from L-thiazolidine-4-carboxylic acid as described by Yamashiro *et al.*[14] As a reagent for introducing the Qxc group quinoxaline-2-carboxylic acid *p*-nitrophenyl ester (Qxc-ONp) was prepared by the treatment of Qxc-OH with *p*-nitrophenyl trifluoroacetate[15] in pyridine. Qxc-ONp was also prepared from Qxc-OH and *p*-nitrophenol by the mixed acid anhydride method using benzenesulfonyl chloride. This crystalline compound is stable, but readily reacts

---

* Abbreviations used in this communication are those recommended by the IUPAC-IUB Commission on Biochemical Nomenclature [*Biochemistry*, **5**, 2585 (1966); *ibid.*, **6**, 362 (1967); *ibid.*, **11**, 1726 (1972)] and include MeCys: *N*-methyl-L-cysteine, MeVal: *N*-methyl-L-valine, Qxc: quinoxaline-2-carbonyl, Z: benzyloxycarbonyl, Boc: *t*-butoxycarbonyl, Bpoc: 2-(4-biphenylyl)-2-propoxycarbonyl, Bzl: benzyl, OBu^t: *t*-butoxy, ONp: *p*-nitrophenoxy, DCC: dicyclohexylcarbodiimide, CDI: *N,N'*-carbonyldiimidazole, CDMI: 2,2'-dimethyl-1,1'-carbonyldiimidazole, Tos-Cl: *p*-toluenesulfonyl chloride, TFA: trifluoroacetic acid, TEA: triethylamine, DCHA: dicyclohexylamine, DMF: *N,N*-dimethylformamide, and THF: tetrahydrofuran.

with amines to give their Qxc derivatives. In view of the general trend that a *p*-nitrophenyl ester is less reactive toward alcohols than the corresponding acid chloride, Qxc–ONp may be more suitable than Qxc–Cl[10] for the preferential *N*-acylation in the presence of the hydroxyl group of serine residue.

Synthesis of compounds **1** and **2** was performed as illustrated in Fig. 2. Compound **5** was hydrogenolyzed to remove the Z group and the product was acylated with an equimolar amount of Qxc–ONp to give a crystalline Qxc-dipeptide (**6**) in a moderate yield. Compound **6** was also synthesized by Gerchakov and Schultz[9] from Qxc–D-Ser–OH and H–Ala–OBu^t, but the mp and $[\alpha]_D$ values reported are significantly lower than those of our product. This might be an indication of some racemization which could occur in the coupling reaction with a Qxc–amino acid as carboxyl component. The subsequent acylation of **6** with Bpoc–MeVal–OH at the hydroxyl group of serine residue could be achieved by the CDI[16] or CDMI[17] method to give compound **7**, though the yield was relatively low. This contrasts with the finding by Chen *et al.*[18] that the CDI (and the mixed anhydride) methods are unsuccessful in such depsipeptide bond formation. When the MeVal was introduced by using Z–MeVal–OH[19] and Tos–Cl in some excess, the desired depsipeptide,Qxc–D-Ser(Z–MeVal)–Ala–OBu^t, was obtained in an excellent yield. However, the same method failed to give componud **7**, probably because the symmetrical anhydride, which could be formed from Bpoc–MeVal–OH by means of Tos–Cl,[20] was sterically hindered by the bulky Bpoc

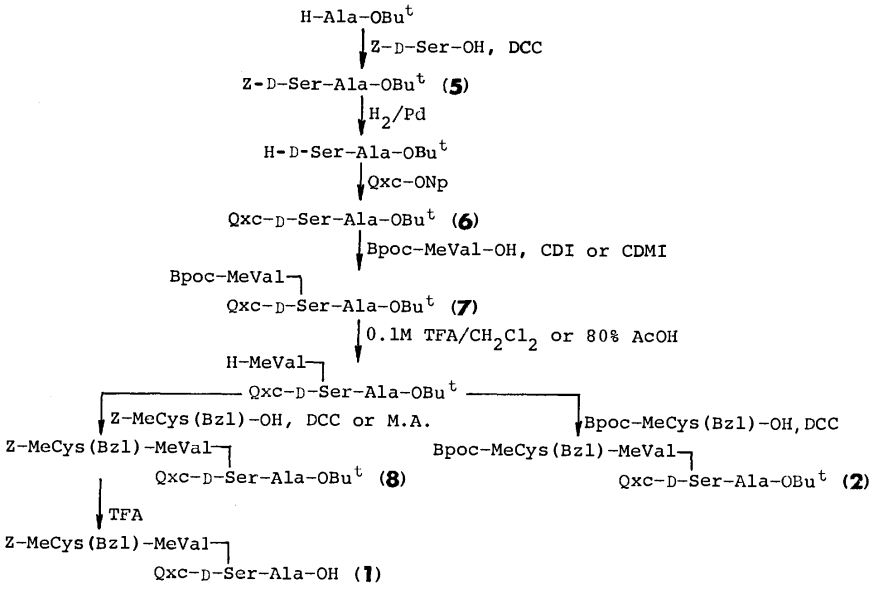

Fig. 2. Synthesis of tetradepsipeptide derivatives related to triostin A (part 1).

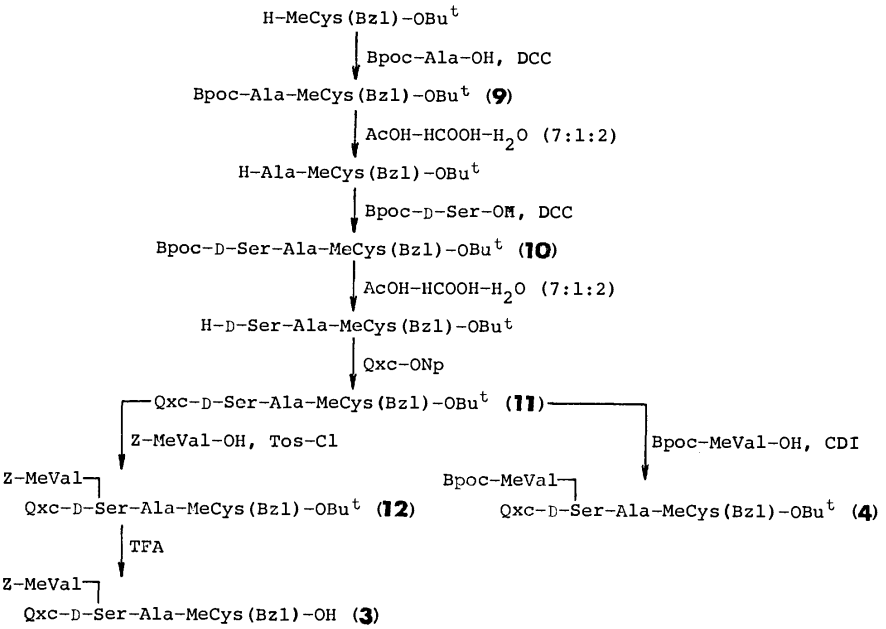

Fig. 3. Synthesis of tetradepsipeptide derivatives related to triostin A (part 2).

groups. Compound **7** was then treated with 0.1 M TFA in dichloromethane at room temperature or with 80% acetic acid at 70 °C to remove the Bpoc group. The resulting compound was coupled with Z–MeCys(Bzl)–OH[14] by the DCC or mixed anhydride method and with Bpoc–MeCys(Bzl)–OH by the DCC method to give **8** and **2**, respectively, in moderate yields. The treatment of **8** with TFA yielded **1** as desired, but the treatment of **2** with an aqueous acetic acid–formic acid mixture[21] yielded not the desired Qxc–D-Ser[H–MeCys(Bzl)–MeVal]–Ala–OBu^t but two major products, which were isolated and identified as *cyclo*[–MeCys(Bzl)–MeVal–] and **6**, respectively. The data of MS supported the structure of the cyclic compound. In view of this easy formation of the cyclic dipeptide by intramolecular aminolysis, compound **2** does not seem to be useful as intermediate for the total synthesis of triostin A. We next tried, therefore, to synthesize **3** and **4** according to the procedure illustrated in Fig. 3.

Bpoc–Ala–OH[22] and H–MeCys(Bzl)–OBu^t prepared according to Roeske[23] were coupled with DCC to give a dipeptide (**9**). The treatment of **9** with an acetic acid–formic acid–water mixture[21] yielded the N^{α}-free compound, which was coupled with Bpoc–D-Ser–OH by the DCC method. The crystalline tripeptide derivative (**10**) thus obtained was treated with acid as above, followed by acylation with Qxc–ONp to produce compound **11**. In the subsequent step Z–MeVal–OH was introduced by the use of Tos–Cl and Bpoc–MeVal–OH by the CDI method to the hydroxyl group of D-Ser residue of **11** to give **12** and **4**, respectively. As in the synthesis of **7**, Bpoc–MeVal–OH could not be introduced by the Tos–Cl method. The treatment of **12** with TFA gave **3** in a moderate yield. In the synthesis of **1**, **2**, **3**, and **4**, most of the intermediates as well as the final products resisted at crystallization, probably because of the presence of *N*-methylamino acid(s) in their molecules. These amorphous products were purified extensively by means of silica gel column chromatography. The tetradepsipeptide derivatives thus obtained, **3** and **4** in particular, would serve as intermediates for the production of triostin A. The final steps toward this goal are now in progress.

Experimental

Thin-layer chromatography (TLC) was performed on silica gel plates (Kieselgel GF_{254} or precoated Kieselgel $60F_{254}$, Merck) with the following solvent systems (ratios by volume): A, ethyl acetate; B, benzene–ethyl acetate (1 : 1); C, benzene–ethyl acetate (7 : 3); D, benzene–ethyl acetate–acetic acid (70 : 30 : 3); E, dichloromethane–ethyl acetate (9 : 1); F, dichloromethane–ethyl acetate (8 : 2); G, cyclohexane–ethyl acetate (2 : 8); H, chloroform–methanol (95 : 5); I, chloroform–methanol (8 : 2); J, chloroform–methanol–acetic acid (95 : 5 : 3); K, chloroform–methanol–acetic acid (90 : 10 : 3); L, 1-butanol–acetic acid–water (4 : 1 : 2). For column chromatography Kieselgel 60 (Merck) was used throughout unless otherwise specified.

D-Serine was purchased from Fluka AG, Buchs, Switzerland and 2-methylquinoxaline from Aldrich Chemical Co., Inc., Milwaukee, Wisconsin, U. S. A. *N*-Methyl-L-valine ($[\alpha]_D^{23}$ +32.5 ±0.8° (*c* 1.0, 6M HCl); lit,[13] $[\alpha]_D^{23}$ +33.1° (*c* 1, 6M HCl)), *N*-methyl-*S*-benzyl-L-cysteine (mp 202—203 °C dec, $[\alpha]_D^{23.5}$ +67.2 ±1.2° (*c* 1.0, 1M HCl); lit.[14] mp 205—206 °C dec, $[\alpha]_D^{20}$ +67.5° (*c* 1, 1M HCl)), and quinoxaline-2-carboxylic acid (mp 228—229 °C; lit,[4b] mp 211—212 °C) were synthesized according to the literature.

p-Nitrophenyl Quinoxaline-2-carboxylate (Qxc–ONp). *a) With p-Nitrophenyl Trifluoroacetate*: To a solution of quinoxaline-2-carboxylic acid (13.93 g, 80 mmol)[4b] in anhydrous pyridine (80 ml) was added *p*-nitrophenyl trifluoroacetate (20.69 g, 88 mmol)[15] and the mixture was stirred at 25 °C for 3.5 h. The desired product was precipitated by the addition of cold water (400 ml). Recrystallization from ethyl acetate gave needles; yield 21.57 g (91%), mp 198—199 °C. Found: C, 61.14; H, 3.13; N, 14.32%. Calcd for $C_{15}H_9N_3O_4$: C, 61.02; H, 3.07; N, 14.23%.

b) With Benzenesulfonyl Chloride and p-Nitrophenol: Quinoxaline-2-carboxylic acid (0.52 g, 3 mmol) in anhydrous pyridine (20 ml) was allowed to react with benzenesulfonyl chloride (0.77 ml, 6 mmol) at 0 °C for 5 min and to this was added *p*-nitrophenol (0.42 g, 3 mmol). The mixture was stirred at 0 °C for 60 min and then ice-cold water (100 ml) was introduced. The precipitate collected was recrystallized from ethyl acetate; yield 0.42 g (47%), mp 197—198 °C. Found: C, 60.80; H, 3.14; N, 14.35%.

Bpoc–MeVal–OH. *N*-Methyl-L-valine (3.94 g, 30 mmol)[13] was dissolved in 40% benzyltrimethylammonium hydroxide in methanol (Triton B, 13.7 ml) and the solution was evaporated *in vacuo*. The residue was, after evaporation from DMF, dissolved in DMF (15 ml) together with Bpoc–N_3 (11.25 g, 40 mmol)[21] and TEA (11.2 ml), and the mixture was stirred at 40 °C for 60 min. Some water (60 ml) was added and the mixture was washed with ether. The aqueous solution was then acidified with ice-cold M citric acid at 0 °C. The oily precipitate which separated was extracted with ether. The organic extracts were combined, dried (Na_2SO_4) and evaporated to give the desired product, which was crystallized from ethyl acetate–petroleum ether; yield 4.33 g (34%), mp 138.5—139 °C, $[\alpha]_D^{20.5}$ −60.1± 1.0° (*c* 1.0, methanol). TLC: homogeneous (H_2SO_4) in system D. Found: C, 71.66; H, 7.40; N, 4.20%. Calcd for $C_{22}H_{27}NO_4$: C, 71.52; H, 7.37; N, 3.79%.

Bpoc–MeCys(Bzl)–OH·DCHA. *N*-Methyl-*S*-benzyl-L-cysteine (9.01 g, 40 mmol)[14] was acylated with Bpoc–N_3 (13.99 g, 50 mmol) in the same manner as described above for Bpoc–MeVal–OH. The oily product was dissolved in ether (20 ml) and DCHA (4.53 g, 25 mmol) was added. The crystalline precipitate which formed was filtered off and recrystallized from methanol–ether; yield 13.55 g (53%), mp 146—148 °C, $[\alpha]_D^{20}$ −53.9 ±1.0° (*c* 1.0, methanol). TLC: homogeneous (H_2SO_4) in systems D and J. Found: C, 72.72; H, 8.20; N, 4.51; S, 4.94%. Calcd for $C_{39}H_{52}N_2O_4S$: C, 72.63; H, 8.13; N, 4.34; S, 4.97%.

Bpoc–D-Ser–OH·H$_2$O. This compound was prepared in the same manner as for Bpoc–MeVal–OH. Crystallization from chloroform–petroleum ether gave the desired product in a 73.5% yield; mp 76—77 °C, $[\alpha]_D^{23}$ +7.6 ±0.5° (*c* 1.0, methanol). TLC: homogeneous (H_2SO_4) in system M. Found: C, 63.25; H, 6.91; N, 4.12%. Calcd for $C_{19}H_{21}NO_5\cdot H_2O$: C, 63.15; H, 6.42; N, 3.88%.

The DCHA salt prepared in the usual manner showed mp 152—154 °C, $[\alpha]_D^{23}$ −4.3 ±0.5° (*c* 1.0, methanol).

H–MeCys(Bzl)–OBu^t·HCl. *N*-Methyl-*S*-benzyl-L-cysteine (2.25 g, 10 mmol)[14] was treated with 2-methylpropene in dioxane (15 ml) in the presence of sulfuric acid

(1.5 ml) according to Roeske[23] to give the corresponding *t*-butyl ester, which was isolated as the hydrochloride and recrystallized from dichloromethane-ethyl acetate; yield 1.81 g (57%), mp 153—153.5 °C, $[\alpha]_D^{23.5}$ −11.9 ±0.6° (*c* 1.0, methanol). TLC: homogeneous (H_2SO_4) in system L. Found: C, 56.53; H, 7.62; N, 4.38; S, 10.03; Cl, 11.25%. Calcd for $C_{15}H_{23}NO_2S$: C, 56.68; H, 7.61; N, 4.41; S, 10.09; Cl, 11.15%.

Z-D-Ser-Ala-OBu^t (5). Z-D-Ser-OH (4.78 g, 20 mmol)[24] and H-Ala-OBu^t (2.90 g, 20 mmol) were coupled with DCC (4.13 g, 20 mmol) in ethyl acetate-dichloromethane (2 : 5, 70 ml) at 5 °C for 20 h. After the dicyclohexylurea which had separated was filtered off, the filtrate was evaporated *in vacuo*. The residue was dissolved in ethyl acetate and the solution was washed with ice-cold M hydrochloric acid and M sodium hydrogencarbonate, dried (Na_2SO_4), and evaporated *in vacuo* to give the desired product, which was recrystallized from ethyl acetate-petroleum ether; yield 5.12 g (70%), mp 89—90 °C, $[\alpha]_D^{28}$ −14.4 ±0.5° (*c* 1.1, methanol). TLC: homogeneous (ninhydrin, after pretreatment with HBr) in systems A and I. Found: C, 59.32; H, 7.08; N, 7.68%. Calcd for $C_{18}H_{26}N_2O_6$: C, 59.00; H, 7.15; N, 7.64%.

Qxc-D-Ser-Ala-OBu^t (6). Compound **5** (7.33 g, 20 mmol) was hydrogenolyzed over palladium in methanol for 2 h to give H-D-Ser-Ala-OBu^t as an oil. This was then allowed to react with Qxc-ONp (5.91 g, 20 mmol) in ethyl acetate (100 ml) at 25 °C for 20 h. The product was purified on a silica gel column with chloroform-methanol (9:1) as solvent. The fractions containing the desired material as a single component, as examined by TLC, were combined and evaporated *in vacuo* to give a crystalline residue. This was recrystallized from benzene-hexane; yield 5.90 g (76%), mp 99—100 °C, $[\alpha]_D^{27}$ −114.2 ±2.9° (*c* 0.5, methanol), −100.4 ±1.7° (*c* 0.9, DMF). λ_{max}^{MeOH} 243 nm (ε 43 700), 320 nm (ε 7 450), 325 nm (ε 7 440). TLC: homogeneous (H_2SO_4) in system A. Lit: mp 94—96 °C, $[\alpha]_D^{27}$ −79.2° (*c* 5, DMF).[9] Found: C, 58.94; H, 6.18; N, 14.47%. Calcd for $C_{19}H_{24}N_4O_5$: C, 58.75; H, 6.23; N, 14.42%.

Qxc-D-Ser(Z-MeVal)-Ala-OBu^t. *a) Carbonyldiimidazole Method*: To a solution of Z-MeVal-OH (0.29 g, 1.1 mmol)[19] in anhydrous THF (4 ml) was added CDMI (0.21 g, 1.1 mmol) and the mixture was stirred at 25 °C for 25 min. To this was added compound **6** (0.43 g, 1 mmol) with some THF as solvent. After the reaction mixture had been kept at 25 °C for 2 days, the product was precipitated by the addition of water and extracted with ethyl acetate. The organic solution was dried (Na_2SO_4) and evaporated *in vacuo* to give a residue, which was purified on a silica gel column with benzene-ethyl acetate (1:1) as solvent; yield 0.19 g (30%), $[\alpha]_D^{25}$ −93.7 ±2.9° (*c* 0.5, methanol). TLC: homogeneous (H_2SO_4) in systems A and B. Found: 62.36; H, 6.45; N, 10.87%. Calcd for $C_{33}H_{41}N_5O_8$: C, 62.35; H, 6.50; N, 11.02%.

b) p-Toluenesulfonyl Chloride Method: Z-MeVal-OH (2.65 g, 10 mmol) was allowed to react with Tos-Cl (1.43 g, 7.5 mmol) in dry pyridine (10 ml) at 0 °C for 15 min. To this was added **6** (2.01 g, 5 mmol) and the mixture was stirred at 0 °C for 3 h. The product was precipitated by the addition of water and purified as described above in a); yield 2.88 g (91%), $[\alpha]_D^{25}$ −91.5 ±2.6° (*c* 0.5 methanol). TLC: homogeneous (H_2SO_4) in systems A and B. Found: C, 62.38; H, 6.21; N, 10.89%.

Qxc-D-Ser(Bpoc-MeVal)-Ala-OBu^t (7). Bpoc-MeVal-OH (3.70 g, 10 mmol) was allowed to react with CDI (1.78 g, 11 mmol) in anhydrous THF at 0 °C. When effervescence ceased compound **6** (3.88 g, 10 mmol) was added. The mixture was stirred at 25 °C for 5 h, after which the product was precipitated with water. Purification on a silica gel column with dichloromethane-ethyl acetate (8 : 2) as solvent afforded **7** as glassy material; yield 2.93 g (40%), $[\alpha]_D^{24.5}$ −62.2 ±2.1° (*c* 0.5, methanol). TLC: homogeneous (H_2SO_4) in systems D and F. Found: C, 66.34; H, 6.80; N, 9.85%. Calcd for $C_{41}H_{49}N_5O_8$: C, 66.55; H, 6.75; N, 9.61%.

Compound **7** was also synthesized under the same conditions except for the use of CDMI in place of CDI; yield 28%, $[\alpha]_D^{27}$ −60.9 ±2.1° (*c* 0.5, methanol).

Qxc-D-Ser[Z-MeCys(Bzl)-MeVal]-Ala-OBu^t (8). *a) Mixed Anhydride Method*: Compound **7** (0.44 g, 0.6 mmol) was treated with 0.1M TFA in dichloromethane (60 ml) at 25 °C for 60 min to give Qxc-D-Ser(H-MeVal)-Ala-OBu^t. The mixture was neutralized with TEA (0.75 ml, 5.4 mmol) and concentrated to *ca.* 5 ml. Z-MeCys(Bzl)-OH, derived from the DCHA salt (0.49 g, 0.9 mmol)[14] by the treatment with Dowex 50W × 8 (H^+ form) in 50% ethanol, and TEA (0.13 ml, 0.9 mmol) were dissolved in dichloromethane (5 ml) and ethyl chloroformate (0.09 ml, 0.9 mmol) was added at −10 °C. The resulting solution of the anhydride was mixed with a solution of the N^α-free tridepsipeptide obtained above and TEA (0.83 ml) was added. The reaction mixture was kept at 5 °C for 16 h. The product precipitated by the addition of water was chromatographed repeatedly on silica gel columns with chloroform-methanol (99 : 1) as solvent; yield 0.26 g (51%), $[\alpha]_D^{25}$ −146.5 ±3.7° (*c* 0.4, methanol). TLC: homogeneous (H_2SO_4) in system K. Found: C, 62.58; H, 6.34; N, 9.98; S, 4.09%. Calcd for $C_{44}H_{54}N_6O_9S$: C, 62.69; H, 6.46; N, 9.97; S, 3.80%.

b) DCC Method: Compound **7** (1.48 g, 2 mmol) was deblocked with 80% acetic acid (50 ml) at 70 °C for 60 min. The solvent was evaporated *in vacuo* and the residue was precipitated from ether-petroleum ether. The oily precipitate separated by decantation was lyophilized from 0.05M hydrochloric acid to give the N^α-free depsitripeptide hydrochloride. This was then coupled with Z-MeCys(Bzl)-OH, derived from the DCHA salt (1.08 g, 2 mmol), by means of DCC (0.41 g, 2 mmol) in dichloromethane in the presence of TEA (0.28 ml, 2 mmol) at 5 °C overnight. The reaction mixture was worked up in the usual manner and the resulting product was purified on a silica gel column with benzene and benzene-ethyl acetate systems (7:3 and 1:1) as solvent. The fractions of the last solvent system were combined and evaporated *in vacuo* to give **8** in pure form; yield 1.19 g (71%), $[\alpha]_D^{22}$ −137.7 ±3.6° (*c* 0.5, methanol). TLC: homogeneous (H_2SO_4) in systems B and C. Found: C, 62.56; H, 6.28; N, 9.74; S, 4.02%.

Qxc-D-Ser[Z-MeCys(Bzl)-MeVal]-Ala-OH (1). Compound **8** (0.84 g) was treated with anhydrous TFA (10 ml) at 25 °C for 60 min. After removal of TFA by evaporation *in vacuo* the residue was dissolved in ethyl acetate and the solution was washed with water, dried (Na_2SO_4) and evaporated *in vacuo* to give glassy material; yield 0.77 g (97%), $[\alpha]_D^{23.5}$ −142.7 ±3.6° (*c* 0.5, methanol). TLC: homogeneous (H_2SO_4) in systems B and J. Found: C, 60.81; H, 5.94; N, 10.41; S, 4.52%. Calcd for $C_{40}H_{46}N_6O_9S$: C, 61.05; H, 5.89; N, 10.68; S, 4.07%.

Qxc-D-Ser[Bpoc-MeCys(Bzl)-MeVal]-Ala-OBu^t (2). Compound **7** (0.74 g, 1 mmol) was deblocked with 80% acetic acid to give the N^α-free tridepsipeptide, which was converted into the hydrochloride as in the synthesis of **8**. This was then coupled with Bpoc-MeCys(Bzl)-OH, derived from the DCHA salt (0.65 g, 1 mmol) by shaking with M

citric acid in the presence of dichloromethane, by the DCC method as described above for compound **8**. The product was chromatographed on a silica gel column with benzene-ethyl acetate (7:3) as solvent; yield 0.57 g (60%), $[\alpha]_D^{22}$ −121.5 ±3.6° (*c* 0.5, methanol). TLC: homogeneous (H_2SO_4) in systems B and D. Found: C, 65.72; H, 6.61; N, 8.78; S, 3.76%. Calcd for $C_{52}H_{62}N_6O_9S$: C, 65.94; H, 6.60; N, 8.87; S, 3.38%.

Treatment of **2** *with Aqueous Acetic Acid-Formic Acid Mixture. Formation of* Cyclo[-*MeCys(Bzl)-MeVal*-]. Compound **2** (0.38 g, 0.4 mmol) was treated with acetic acid-formic acid-water (7:1:2, 4 ml)[21] at 25 °C for 2 h. The solvent was evaporated *in vacuo* and the oily residue was precipitated from ethyl acetate-petroleum ether. The resulting material was subjected to a column of silica gel (26 g) and eluted with benzene-ethyl acetate (7:3, 200 ml) and then with ethyl acetate (150 ml). The ethyl acetate fractions were combined and evaporated *in vacuo*. The residue (0.22 g) was rechromatographed on a silica gel column (25 g, Kieselgel H, Merck) with chloroform-methanol (95:5) as solvent. Tubes 15—17 (5 g/tube) were combined and evaporated *in vacuo* to give an oil (72 mg, 56% as *cyclo*[-MeCys(Bzl)-MeVal-]); $[\alpha]_D^{26}$ −43.5 ±1.7° (*c* 0.5, methanol). Found: C, 63.00; H, 7.59; N, 8.42; S, 9.61%. Calcd for $C_{17}H_{24}N_2O_2S$: C, 63.72; H, 7.55; N, 8.74; S, 10.00%. MS, *m/e* 320 (M), 229, 197, 183, 155, and 91.[25]

From tubes 19—24 (5 g/tube) was obtained a crystalline material, which was recrystallized from benzene-hexane (118 mg, 76% as compound **6**); mp 96—98 °C, $[\alpha]_D^{22}$ −109.0 ±0.7° (*c* 0.5, methanol). IR, identical with that of an authentic sample of **6**.

Bpoc-Ala-MeCys(Bzl)-OBu^t ***(9)***. H-MeCys(Bzl)-OBu^t·HCl (6.36 g, 20 mmol) was treated with 50% potassium carbonate at 0 °C in the presence of ether and the organic phase was dried (Na_2SO_4) and evaporated *in vacuo* to give the corresponding free base. This was then coupled with Bpoc-Ala-OH (6.55 g, 20 mmol)[22] by means of DCC (4.13 g, 20 mmol) in ethyl acetate (10 ml). The reaction mixture was worked up in the usual manner to give an oily product, which was chromatographed on a silica gel column with benzene-ethyl acetate (8:2) as solvent to give **9** in pure form; yield 11.19 g (95%), $[\alpha]_D^{22}$ −106.9 ±1.5° (*c* 1.0, methanol). TLC: homogeneous (H_2SO_4) in systems C and E. Found: C, 69.25; H, 7.24; N, 4.59; S, 5.36%. Calcd for $C_{34}H_{42}N_2O_5S$: C, 69.12; H, 7.17; N, 4.74; S, 5.43%.

Bpoc-D-Ser-Ala-MeCys(Bzl)-OBu^t ***(10)***. Compound **9** (10.63 g, 18 mmol) was treated with a mixture of acetic acid-formic acid-water (7:1:2; 100 ml) at 25 °C for 2 h. The solvent was evaporated *in vacuo* and the residue was treated with saturated potassium carbonate in the presence of ethyl acetate. The organic solution was washed with saturated sodium chloride, dried (Na_2SO_4) and evaporated *in vacuo* to give H-Ala-MeCys(Bzl)-OBu^t as an oil. This was then coupled with Bpoc-D-Ser-OH (6.18 g, 18 mmol) by the DCC method in dichloromethane in the usual manner. The product was chromatographed on a silica gel column (Kieselgel H, Merck) with ethyl acetate-cyclohexane (8:2) as solvent and crystallized from ethyl acetate-petroleum ether to give fine needles; yield 8.80 g (76%), mp 128—129 °C, $[\alpha]_D^{23}$ −42.6±1.6° (*c* 0.5, methanol). TLC: homogeneous (ninhydrin, after pretreatment with HCl) in system D. Found: C, 65.39; H, 6.95; N, 6.47; S, 4.74%. Calcd for $C_{37}H_{47}N_3O_7S$: C, 65.66; H, 6.99; N, 6.20; S, 4.73%.

Qxc-D-Ser-Ala-MeCys(Bzl)-OBu^t ***(11)***. Compound **10** (6.78 g, 10 mmol) was treated with acetic acid-formic acid-water (7:1:2) at 25 °C for 2 h to give the N^{α}-free tripeptide and this was allowed to react with Qxc-ONp (3.25 g, 11 mmol) in ethyl acetate in the presence of TEA (1.54 ml) for 20 h. The product was purified on a silica gel column with chloroform-methanol (9:1) as solvent; yield 3.90 g (65%), mp 60—70 °C, $[\alpha]_D^{22}$ −153.6±3.8° (*c* 0.5, methanol). TLC: homogeneous (H_2SO_4) in systems A and H. Found: C, 59.99; H, 6.32; N, 11.86; S, 5.29%. Calcd for $C_{30}H_{37}N_5O_6S$: C, 60.49; H, 6.26; N, 11.76; S, 5.38%.

Qxc-D-Ser(Z-MeVal)-Ala-MeCys(Bzl)-OBu^t ***(12)***. Z-MeVal-OH (0.42 g, 1.6 mmol)[19] was coupled with **11** (0.48 g, 0.8 mmol) by means of Tos-Cl (0.23 g, 1.2 mmol) in pyridine, as in the synthesis of Qxc-D-Ser(Z-MeVal)-Ala-OBu^t. The crude product was purified by repeated chromatography on silica gel columns with chloroform-methanol (95:5) and ethyl acetate-cyclohexane (8:2) as solvent; yield 0.48 g (72%), $[\alpha]_D^{22}$ −129.8±3.4° (*c* 0.5, methanol). TLC: homogeneous (H_2SO_4) in systems G and H. Found: C, 62.47; H, 6.28; N, 9.77; S, 4.03%. Calcd for $C_{44}H_{54}N_6O_9S$: C, 62.69; H, 6.46; N, 9.97; S, 3.80%.

Qxc-D-Ser(Z-MeVal)-Ala-MeCys(Bzl)-OH ***(3)***. Compound **12** (0.42 g, 0.5 mmol) was treated with TFA (5 ml) at 25 °C for 30 min. After removal of TFA by evaporation *in vacuo* the residue was dissolved in ethyl acetate and the solution was washed with water, dried (Na_2SO_4) and evaporated *in vacuo* to give a glassy material, which was purified by chromatography on a silica gel column (Kieselgel H, Merck) with chloroform-methanol-acetic acid (90:10:3) as solvent; yield 0.37 g (94%), $[\alpha]_D^{25.5}$ −126.1±3.3° (*c* 0.5, methanol). TLC: homogeneous (H_2SO_4) in system K. Found: C, 60.35; H, 5.81; N, 10.42; S, 4.34%. Calcd for $C_{40}H_{46}N_6O_9S$: C, 61.05; H, 5.89; N, 10.68; S, 4.07%.

Qxc-D-Ser(Bpoc-MeVal)-Ala-MeCys(Bzl)-OBu^t ***(4)***. Bpoc-MeVal-OH (0.55 g, 1.5 mmol) was allowed to react with CDI (0.29 g, 1.8 mmol) in anhydrous THF at 25 °C for 30 min. To this was added a solution of **11** (0.60 g, 1.0 mmol) in THF. The mixture was stirred at 25 °C for 22 h and evaporated *in vacuo*. The residue was, after being washed with water, purified on a silica gel column (Kieselgel H, Merck) with chloroform-methanol (98:2) as solvent; yield 0.20 g (21%), $[\alpha]_D^{26.5}$ −99.6±2.6° (*c* 0.5, methanol). TLC: homogeneous (H_2SO_4) in systems C, G, and J. Found: C, 65.62; H, 6.58; N, 8.63; S, 3.62%. Calcd for $C_{52}H_{62}N_6O_9S$: C, 65.94; H, 6.60; N, 8.87; S, 3.38%.

References

1) K. Katagiri, T. Yoshida, and K. Sato, "Antibiotics," Vol. 3, ed by J. W. Corcoran and F. E. Hahn, Springer Verlag (1975), p. 234 and references cited therein.

2) J. Shoji and K. Katagiri, *J. Antibiot.*, **A14**, 335 (1961); H. Otsuka and J. Shoji, *ibid.*, **A19**, 128 (1966).

3) H. Otsuka and J. Shoji, *J. Antibiot.*, **A16**, 52 (1963); J. Shoji, K. Tori, and H. Otsuka, *J. Org. Chem.*, **30**, 2772 (1965); H. Otsuka and J. Shoji, *J. Antibiot.*, **A18**, 134 (1965); H. Otsuka and J. Shoji, *Tetrahedron*, **21**, 2931 (1965); *ibid.*, **23**, 1535 (1967).

4) a) R. Corbaz, L. Ettlinger, E. Gäumann, W. Keller-Schierlein, F. Kradolfer, L. Neipp, V. Prelog, P. Reusser, and H. Zähner, *Helv. Chim. Acta*, **40**, 199 (1957); b) W. Keller-Schierlein and V. Prelog, *ibid.*, **40**, 205 (1957); c) W. Keller-Schierlein, M. Lj. Mihailović, and V. Prelog, *ibid.*, **42**, 305 (1959).

5) T. Yoshida and K. Katagiri, *J. Antibiot.*, **A14**, 330 (1961).

6) D. G. Martin, S. A. Mizsak, C. Biles, J. C. Stewart, L. Baczynskyj, and P. A. Meulman, *J. Antibiot.*, **28**, 332 (1975); A. Dell, D. H. Williams, H. R. Morris, G. A. Smith,

J. Feeney, and G. C. K. Roberts, *J. Am. Chem. Soc.*, **97**, 2497 (1975).
7) H. Otsuka, J. Shoji, K. Kawano, and Y. Kyogoku, *J. Antibiot.*, **29**, 107 (1976).
8) S. Gerchakov, P. J. Whitman, and H. P. Schultz, *J. Med. Chem.*, **9**, 266 (1966).
9) S. Gerchakov and H. P. Schultz, *J. Med. Chem.*, **12**, 141 (1969).
10) H. C. Koppel, I. L. Honigberg, R. H. Springer, and C. C. Cheng, *J. Org. Chem.*, **28**, 1119 (1963).
11) T. L. Ciardelli and R. K. Olsen, *J. Am. Chem. Soc.*, **99**, 2806 (1977).
12) J. Meienhofer, *J. Am. Chem. Soc.*, **92**, 3771 (1970).
13) P. Quitt, J. Hellerbach, and K. Vogler, *Helv. Chim. Acta*, **46**, 327 (1963).
14) D. Yamashiro, H. L. Aanning, L. A. Branda, W. D. Cash, V. V. S. Murti, and V. du Vigneaud, *J. Am. Chem. Soc.*, **90**, 4141 (1968).
15) S. Sakakibara and N. Inukai, *Bull. Chem. Soc. Jpn.*, **37**, 1231 (1964); *ibid.*, **38**, 1979 (1965).
16) H. A. Staab, *Justus Liebigs Ann. Chem.*, **609**, 75 (1957); *Angew. Chem.*, **68**, 754 (1956).
17) S. Akabori, S. Sakakibara, and M. Shin, Proceedings of the 2nd Symposium on Peptide Chemistry, Osaka, 1963, Institute for Protein Research, Osaka University (1963), p. 39.
18) W.-Y. Chen, M.-L. Hsu, and R. K. Olsen, *J. Org. Chem.*, **40**, 3110 (1975).
19) Pl. A. Plattner, K. Vogler, R. O. Studer, P. Quitt, and W. Keller-Schierlein, *Helv. Chim. Acta*, **46**, 927 (1963); J. R. McDermott and N. L. Benoiton, *Can. J. Chem.*, **51**, 1915 (1973).
20) J. H. Brewster and C. J. Ciotti, Jr., *J. Am. Chem. Soc.*, **77**, 6214 (1955).
21) P. Sieber and B. Iselin, *Helv. Chim. Acta*, **51**, 622 (1968).
22) S. S. Wang and R. B. Merrifield, *Int. J. Pept. Protein Res.*, **1**, 235 (1969); E. Schnabel, G. Schmidt, and E. Klauke, *Justus Liebigs Ann. Chem.*, **743**, 69 (1971).
23) R. Roeske, *J. Org. Chem.*, **28**, 1251 (1963).
24) E. Baer and J. Maurukas, *J. Biol. Chem.*, **212**, 25 (1955); H. Adkins, R. M. Ross, D. C. Schroeder, C. L. Mahoney, and W. W. Gilbert, *J. Am. Chem. Soc.*, **76**, 147 (1954).
25) MS was measured by Dr. Yuzo Nakagawa of this laboratory on a Hitachi mass spectrometer.

Reactions of Aromatic Compounds in Molten Salts. II. The Rearrangement of Phenylhydrazine to Give *o*-Phenylenediamine in a Molten Mixture of $AlCl_3$–NaCl–KCl

Hisao IMAIZUMI, Yoji HASHIDA, and Kohji MATSUI

Faculty of Engineering, Gunma University, Kiryu, Gunma 376

(Received December 26, 1977)

Phenylhydrazine gave *o*-phenylenediamines as the major product upon heating in a molten mixture of $AlCl_3$–NaCl–KCl. In the molten mixture, some aromatic compounds gave the corresponding aromatic amines in good yields in the presence of phenylhydrazine, suggesting that the method provides a novel direct process for the preparation of aromatic amines.

Many derivatives of *N*-substituted aniline have been known to rearrange to give *C*-substituted anilines; as examples, Bamberger's phenylhydroxylamine[2] and phenylnitroamine rearrangement,[3] Chattaway's *N,N*-diacylaniline rearrangement,[4] Fischer-Hepp's rearrangement,[5] Hofmann-Martin's alkylaniline rearrangement,[6] and Reilly-Hickinbottom's *N*-alkylaniline rearrangement[7] can be cited.

On the other hand, phenylhydrazine is known to give *p*-phenylenediamine upon heating in the presence of hydrochloric acid; in this case, however, no detectable formation of *o*-phenylenediamine was observed.[8] Phenylhydrazine has also been known to decompose to give aniline, benzene, ammonia, and other products upon heating in the presence of Lewis acid,[9] metals[10] or phenylhydrazine hydrochloride.[11] However, the reaction to give *o*-phenylenediamine has not been reported. We have now found that, in a molten mixture of $AlCl_3$–NaCl–KCl, phenylhydrazine gives *o*-phenylendiamine and that several aromatic compounds yield the corresponding amines in the presence of phenylhydrazine in the molten mixture.

Experimental

All the melting points are uncorrected. The structural assignment of the reaction products was done by means of their NMR, MS, IR, UV spectra, and elemental analyses and by a mixed-melting-point-test with an authentic sample.

Materials. The $AlCl_3$, NaCl, KCl, and other inorganic materials used were of a reagent grade. The organic materials used were purified by distillation or recrystallization, and their purities were checked by TLC or GLC before use.

A typical example of the reaction will now be described; 5 ml of phenylhydrazine (0.051 mol) was stirred, drop by drop, into a molten mixture of $AlCl_3$–NaCl–KCl in an atmosphere of prepurified nitrogen. After stirring at a given temperature for a given time, the reaction mixture was poured into a mixture of 500 ml of 0.1 M HCl and 100 g of ice. After a small amount of the insoluble matter had then been filtered off, the filtrate was made alkaline and the reaction products were extracted with diethyl ether. The solvent was removed by distillation; then the reaction products were separated and purified by column chromatography. The quantitative determinations of the reaction products were carried out by GLC (Column:Lubrol MO 15%/Cromsorb WAW, 4 mm × 1 m).

Results and Discussion

Formation of o-*Phenylenediamine.* When phenylhydrazine (0.05 mol) was heated at 100 °C in a mixture of $AlCl_3$–NaCl–KCl (0.60:0.23:0.17 mol), aniline and *o*-phenylenediamine were both obtained in about a 30% yield; however, no *p*-phenylenediamine was detected in the reaction mixture. The yield of *o*-phenylenediamine was affected very much by the Lewis acids used. When $ZnCl_2$ was used instead of $AlCl_3$, the yield of *o*-phenylenediamine decreased considerably. However, in the reaction of phenylhydrazine in a molten mixture of CuCl–NaCl–KCl (0.60 : 0.20 : 0.20 mol) at 200 °C, aniline was the sole major product; *o*-phenylenediamine was not detected at all in the reaction mixture. Similar results were also obtained in the reactions of

TABLE 1. EFFECTS OF MOLTEN SALT COMPOSITION ON PRODUCT YIELDS IN THE REACTIONS OF PHENYLHYDRAZINE

Composition (mol)	Condition		Conv. (%)	Products (%)			
	Temp (°C)	Time (h)		Aniline	*o*-Phenylene diamine	Chloro-aniline	Benzidine
$AlCl_3$: NaCl : KCl (0.60 : 0.23 : 0.17)	100	1	100	30	30	—	—
$ZnCl_2$: NaCl : KCl (0.60 : 0.20 : 0.20)	200	5	81	27	12	—	—
CuCl : NaCl : KCl (0.60 : 0.20 : 0.20)	200	0.5	100	45	—	—	—
$SnCl_4$[a] (0.5)	100	1	80	33	—	—	—
$TiCl_4$[a] (0.5)	120	2	91	52	—	—	—
PH·HCl[b1]	100	2	100	15	3	10	32
PH·HCl[b2]	100	2	100	14	2	8	33

5.0 ml (0.0508 mol) of $C_6H_5NHNH_2$ was used.

a) Phenylhydrazinium salt was insoluble in $SnCl_4$ or $TiCl_4$. b) A $AlCl_3$: NaCl : KCl mixture(=0.60 : 0.23 : 0.17) and 7.4 g (0.06 mol) of phenylhydrazine hydrochloride were used. b_1) Phenylhydrazine hydrochloride was added to a molten mixture of 100 °C. b_2) The temperature of a mixture of $AlCl_3$, NaCl, KCl, and phenylhydrazine hydrochloride was gradually raised to 100 °C.

phenylhydrazine in $SnCl_4$ and $TiCl_4$.

When phenylhydrazine hydrochloride was heated in a molten mixture of $AlCl_3$: NaCl : KCl (0.60 : 0.23 : 0.17 mol) at 100 °C, *o*-phenylenediamine was obtained only in low yields; on the contrary, benzidine became the major product in this case. These results are summarized in Table 1.

From the reaction products and their yields, *o*-phenylenediamine is assumed to be produced from the phenylhydrazine–$AlCl_3$ complex formed by the HCl–$AlCl_3$ exchange from phenylhydrazine hydrochloride. On the other hand, chloroanilines would result from the chlorination of aniline with the chlorine formed by the oxidation of hydrochloric acid by the air included in the voluminous phenylhydrazine hydrochloride powder; benzidine would be formed from the aniline produced by the decomposition of phenylhydrazine hydrochloride, as has been reported in the previous paper.[1)]

When phenylhydrazine was heated in a molten mixture of $AlCl_3$–NaCl–KCl (0.60 : 0.23 : 0.17 mol) at 120 °C, the yield of *o*-phenylenediamine varied depending upon the amount of the molten mixture employed, as is shown in Fig. 1. The results show that an excess of $AlCl_3$ is necessary for the formation of *o*-phenylenediamine in good yields.

Decomposition of Phenylhydrazine–$AlCl_3$ Complex. Phenylhydrazine is known to form a complex with $AlCl_3$ of a molar ratio of 2 : 1.[12)] Therefore, the thermal behavior of the complexes of phenylhydrazine with $AlCl_3$ were investigated in order to make clear the reaction of phenylhydrazine in the molten salt. The complexes were prepared by mixing phenylhydrazine with powdered $AlCl_3$ in benzene. When the ratio of $AlCl_3/PhNHNH_2$ is less than unity, the complex was obtained as a crystalline solid. In the range of ratios above unity, however, the complex obtained was a viscous molten mass from which the complete removal of benzene was very difficult. In some cases, the yield of aniline (based on the phenylhydrazine) was found to exceed 100% (the best yield was about 150%, in the case of a $AlCl_3/PhNHNH_2$ molar ratio of 3), suggesting that the residual benzene in the complex was aminated to give aniline. In these cases, the yields of *o*-phenylenediamine remained low.

On the other hand, in the reactions using the complexes prepared in petroleum ether the yield of *o*-phenylenediamine increased with an increase in the $AlCl_3/PhNHNH_2$ ratio until about 2 (the best yield was 30%); however, aniline was obtained only in low yields, as may be anticipated in the absence of benzene. From these results, it is obvious that the formation of *o*-phenylenediamine and the amination of benzene take place competitively.

When phenylhydrazine was heated with powdered $AlCl_3$ in benzene under reflux, the solubility of the resulting complex was found to vary depending upon the $AlCl_3/PhNHNH_2$ ratio. In the range of the ratios below 0.6, the complex was isolated as a white solid which was insoluble in the solvent. However, in the range of the ratios above 0.8, the resulting complex was soluble in the solvent to give a clear orange solution. These observations indicate that the composition of the complex varied with the change in the $AlCl_3/PhNHNH_2$.

Fig. 2 shows the results of the reactions of the phenylhydrazine–$AlCl_3$ complex in benzene. From Fig. 2, it is clear that the decomposition of phenylhydrazine takes place in the range of $AlCl_3/PhNHNH_2$ ratios above unity and that the yield of *o*-phenylenediamine increases with an increase in the ratio until 2, showing that stoichiometrically at least 1 mol of $AlCl_3$ to 1 mol of phenylhydrazine is necessary for the formation of *o*-phenylenediamine. In this case, the formation of aniline from benzene was also observed.

Decomposition of Phenylhydrazine–$AlCl_3$ Complex in Monosubstituted Benzene Derivatives. When phenylhydrazine was heated in a molten mixture of $AlCl_3$: NaCl : KCl in the presence of *p*-chloroaniline at 100 °C, no 4-chloro-*o*-phenylenediamine was detected (Table 2), indicating that the amination of aromatic amine did not take place under these reaction conditions. To get more insight into the amination in the molten mixture, the amination of several monosubstituted benzene derivatives was investigated. The results are shown in Table 3. Two noticeable points in

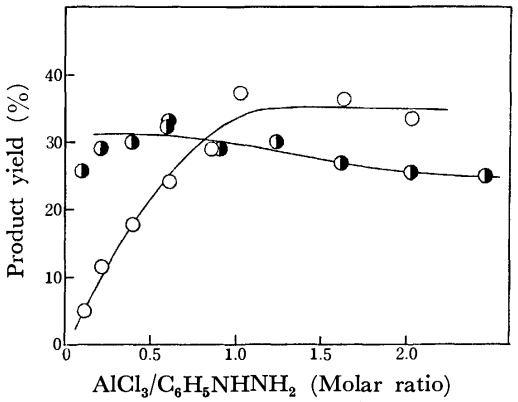

Fig. 1. Effect of amount of molten salt on product yield.
Molar ratio: $AlCl_3$: NaCl : KCl = 0.60 : 0.23 : 0.17.
Temperature: 120 °C, Time: 1 h.
◑: Aniline, ○: *o*-phenylenediamine.

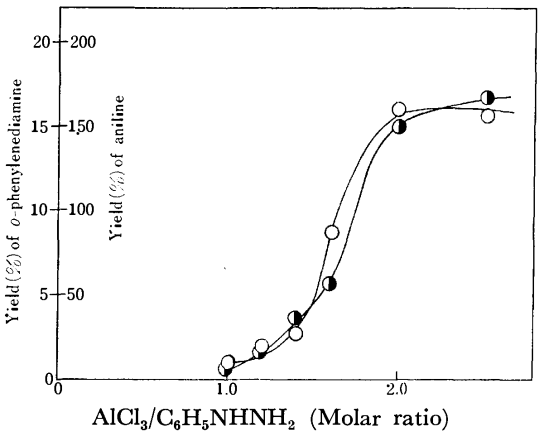

Fig. 2. Product yields in the decomposition of phenylhydrazine–$AlCl_3$ complex in refluxing benzene.
◑: Aniline, ○: *o*-phenylenediamine.

Table 2. Reaction of phenylhydrazine in molten salt in the presence of *p*-chloroaniline at 100 °C

Condition		Conv. (%)	Products (%)		
Temp (°C)	Time (h)		Aniline	*o*-Phenylene-diamine	Chloro-*o*-phenylene-diamine
100	1	100	24	37	—
100	1	100	21	46	—

$AlCl_3$: NaCl : KCl = 0.60 : 0.23 : 0.17 mol.
0.051 mol of $C_6H_5NHNH_2$ and 0.051 mol of *p*-chloroaniline were used.

Table 3. Yields of monosubstituted anilines

X-Substituted benzene derivative	Conv. (%)	Aniline (%)	*o*-Phenylene-diamine (%)	X-substituted aniline derivative (%)		
				o-	*m*-	*p*-
X = $-CH_3$	100	77	11		45	
-H	100	150	16	—	—	—
-Cl	100	34	16	6	20	
-F	100	44	19	4	1	10

$AlCl_3$ = 0.105 mol; $C_6H_5NHNH_2$ = 0.0518 mol.
Benzene derivative, 30 ml; heated for 1 h under reflux.

Table 3 are that, even though all of these aromatic compounds were aminated, the total yield of toluidines was higher than those of chloro- and fluoroaniline, and that the amination took place at the ortho and para positions to the fluoro substituents. These results suggest that the reaction takes place by means of a mechanism of electrophilic substitution; the fact that the amination of chloroaniline did not take place may be understood to indicate that chloroaniline combines at first with $AlCl_3$ to form a inert complex towards an electrophile. Accordingly, the formation of *o*-phenylenediamine is not considered to result from the amination of aniline, but may be assumed to result from the rearrangement of the phenylhydrazine–$AlCl_3$ complex. This is because, if *o*-phenylenediamine were produced by the intermolecular amination of aniline by an electrophile such as NH_2^+, *p*-phenylenediamine should be produced at the same time.

When $AlCl_3$ was added to a solution of phenylhydrazine in dioxane, the UV spectrum of phenylhydrazine (λ_{max} 293 nm) showed a blue shift, and at the point of a $AlCl_3/PhNHNH_2$ ratio of 1/2,[12] the spectrum coincided in position with that of phenylhydrazine hydrochloride ($PhNHNH_2$: HCl = 1 : 1, λ_{max} 272 nm). In phenylhydrazine, the β-amino group is more basic than the α-amino group; therefore, a 2:1 complex between phenylhydrazine and $AlCl_3$ may be expected to possess the skeleton described below:

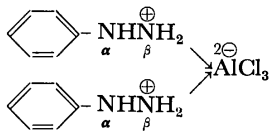

The fact that 1 mol of $AlCl_3$ is necessary for each mole of phenylhydrazine for the formation of *o*-phenylenediamine, as is shown in Fig. 2, suggests that an additional attack by $AlCl_3$ upon the 2 : 1 complex is essential. Thus, the reaction of the phenylhydrazine–$AlCl_3$ com-

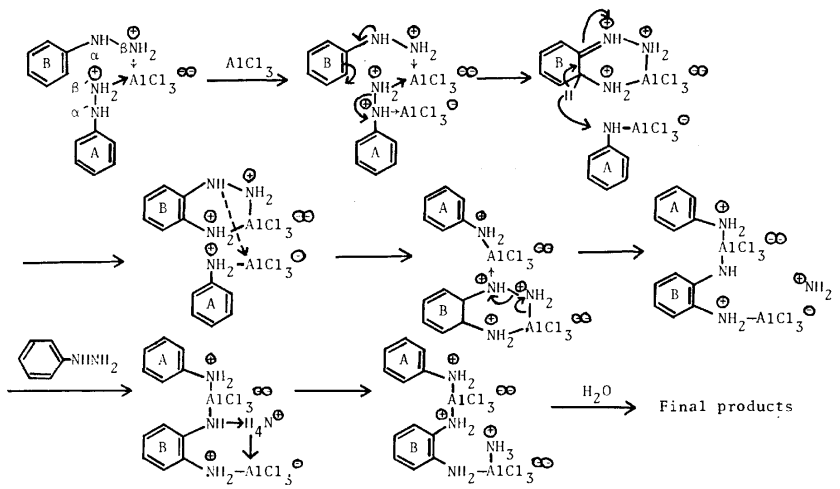

Scheme 1.

plex to give *o*-phenylenediamine in the molten salt may be reasonably explained by a process shown in Scheme 1.

1) The formation of a 2:1 complex from phenylhydrazine and $AlCl_3$.

2) An additional attack by $AlCl_3$ upon one of the N_α atoms (N_α'), resulting in a new complex which has a N atom of a high electrophilicity as a result of the electrostatic repulsion between N_α' and N_β' atoms.

3) In the new complex, even though the electron-donating ability of the N_β atom is low, the electron density of the B phenyl group will be high at the ortho and para positions. Therefore, the electrophilic attack by N_β' upon the ortho carbon atom would take place without difficulty through the 6-membered transition state.

Step 3 would be the key step for the reaction; the following sequences of the reaction would proceed according to the process shown in Scheme 1, in which only the skeletons of the complexes are shown because the exact compositions of the complexes including the ligands are still uncertain. During the reaction, the nitrenium cation is assumed to be produced, even though its formation has not been confirmed; the nitrenium cation may react with phenylhydrazine to give the ammonium cation in a manner similar to that of the phenylnitrenium cation.[13] In fact, ammonia was detected during the course of the reaction.

The amination of aromatic compounds by the phenylhydrazine–$AlCl_3$ complex to give the corresponding derivatives of aniline would take place in a manner similar to that described above, as is shown in Scheme 2.

Several methods have been reported for the direct amination of aromatic compounds in the presence of Lewis acid: the aminations by hydroxylamine,[14] by hydrazoic acid,[15] and by *N*-chlorodialkylamine[16] may be cited. As to the amination by means of hydrazine, however, only the photochemical amination of cyclohexane has been reported.[17] Thus, the amination of aromatic compounds described above may provide a novel direct method for the preparation of aromatic amines; in addition, this method may be expected to develop into a general method of the amination of aromatic compounds using hydrazine and its derivatives in the presence of Lewis acid.

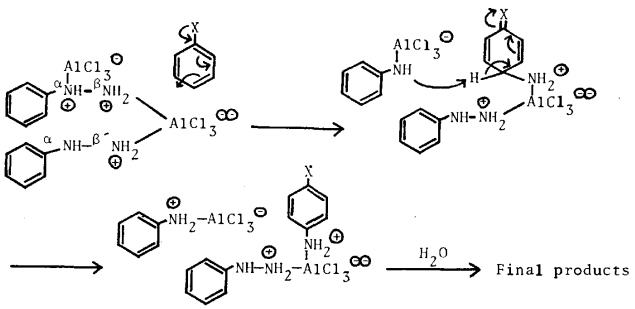

Scheme 2. Probable process for the amination benzene derivatives.

References

1) Part I of this series: H. Imaizumi, S. Sekiguchi, and K. Matsui, *Bull. Chem. Soc. Jpn.*, **50**, 948 (1977).

2) E. Bamberger, *Ber.*, **27**, 1347 (1894); *Ann.*, **424**, 233, 297 (1921).

3) E. Bamberger and K. Landsteiner, *Ber.*, **27**, 359 (1894); *ibid.*, **28**, 399 (1895); *ibid.*, **30**, 1248 (1897).

4) F. D. Chattaway, *J. Chem. Soc.*, **85**, 386 (1904); J. F. J. Dippy and V. Moss, *ibid.*, **1952**, 2205.

5) O. Fischer and E. Hepp, *Ber.*, **19**, 2991 (1886).

6) A. W. Hofmann and C. M. Martius, *Ber.*, **4**, 742 (1871); A. W. Hofmann, *ibid.*, **5**, 720 (1872).

7) J. Reilly and W. J. Hickinbottom, *J. Chem. Soc.*, **117**, 103 (1920); H. Hart and J. R. Kosak, *J. Org. Chem.*, **27**, 116 (1962).

8) J. Thiele and L. H. Wheeler, *Ber.*, **28**, 1538 (1895).

9) A. E. Abuzov and V. M. Tikhvinskii, *J. Russ. Phys. Chem. Soc.*, **45**, 69 (1913); *Chem. Abstr.*, **7**, 2225 (1913); A. E. Abuzov and V. M. Tinkhvinskii, *Ber.*, **43**, 2295 (1910); K. Clusius and M. Hoch, *Helv. Chim. Acta*, **33**, 2122 (1950); R. C. Aggarwal and R. C. Makhja, *Z. Anorg. Allg. Chem.*, **336** 81 (1965), *Chem. Abstr.*, **64**, 7662 g (1966).

10) A. Koraczynski and L. Kierzek, *Gazz. Chim. Ital.*, **55**, 361 (1925); *Chem. Abstr.*, **20**, 598 (1926).

11) M. Busch and R. Knoll, *J. Prakt. Chem.*, **116**, 39 (1927); J. Kenner and E. C. Knight, *Ber.*, **69**, 341 (1936).

12) S. Prasad and L. Prasad, *J. Proc. Inst. Chemists (India)*, **36**, 293 (1964); *Chem. Abstr.*, **63**, 5545f (1965).

13) R. A. Abramovitch and B. A. Davis, *Chem. Rev.*, **64**, 174 (1964).

14) P. Kovacic and R. P. Bennett, *J. Am. Chem. Soc.*, **83**, 221 (1961); P. Kovacic and J. L. Foote, *ibid.*, **83**, 743 (1961); R. N. Keller and D. A. S. Smith, *ibid.*, **68**, 899 (1946).

15) G. M. Hoop and J. M. Tedder, *J. Chem. Soc.*, **1961**, 4685; K. Schmidt, *Ber.*, **57**, 704 (1924).

16) H. Bock and K. L. Kompa, *Chem. Ber.*, **99**, 1347 (1966).

17) Y. Ogata, Y. Izawa, H. Tomioka, and T. Nishizawa, *Tetrahedron*, **22**, 1557 (1966).

Polymeric Alkoxyalkylaluminum Compounds by Novel Reductive Cleavage of Saturated Cyclic Ethers. A New Organometallic Reagent in Organic Synthesis

Mitsuhiro SUMITANI, Kazuhiko KANEMITSUYA, Hajime YASUDA, and Hisaya TANI

Department of Polymer Science, Faculty of Science, Osaka University, Toyonaka, Osaka 560

(Received November 10, 1977)

Insertion of aluminum to the C–O–C bond of saturated cyclic ethers by the $HgCl_2$–$ZnCl_2$–MeI catalyst system led to the reductive cleavage of 5, 6, and 7 membered ring ethers to give polymeric alkoxyalkylaluminum compounds. The relative rate of the reaction was increased in the order of tetrahydrofuran, 3-methyltetrahydrofuran, 2-methyltetrahydrofuran, 2,5-dimethyltetrahydrofuran, tetrahydropyran, oxepane, 7-oxabicyclo[2.2.1]-heptane, and 2-methyltetrahydropyran. The cleaved cyclic ethers are bonded with aluminum atoms bifunctionally and the resulting polymeric aluminum compound gave dideuterio alcohols upon deuterolysis. Addition reaction of allyl halides and reduction of chloral with the aluminum compound provided a novel route for the preparation of unsaturated alcohols.

A number of methods for the cleavage of saturated cyclic ethers have been reported and summarized in several reviews.[1–4] Both acid[5–8] and base[9–11] catalyzed cleavages are known and the ring opening mechanism,[12,13] ring size effects[14] and influences of the group substituted on the ring[15,16] have been extensively studied. Most of the studies reported so far are concerned with the stoichiometric reactions between cyclic ethers and ring cleaving agent. We present here a novel direct reaction of saturated cyclic ethers with aluminum which led to the reductive cleavage of 5, 6, and 7 membered cyclic ethers. Remarkable points of this reaction lie in the following points; 1) metallic aluminum, a neutral reactant, can undergo the stoichiometric reaction with cyclic ethers to give a new type of aluminum compounds, 2) the order in reactivity of the cyclic ethers follows that of the steric effects of the alkyl group on the ring and of the carbon chain consisting the ring, and 3) this method has the advantages of experimental simplicity and broad applicability for the preparation of unsaturated alcohols with elongated carbon chain from allyl halides.

Results and Discussion

Reductive Cleavage of Cyclic Ethers by Aluminum. In our search for the new method for activating main group metals, we found an unusual reductive cleavage of tetrahydrofuran(THF) with aluminum to give polymeric alkoxyalkylaluminum compounds. The reaction proceeded by employing the aluminum turnings activated not only with mercury(II) halides, in accordance with the general procedure,[17] but also with a minute quantity of organic halides. All of the mercury(II) or mercury(I) halides, $HgBr_2$, Hg_2Br_2, $HgCl_2$, Hg_2Cl_2, HgI_2, and Hg_2I_2, were effective as catalysts in various concentrations from 0.1 to 0.4 mol% when it was used simultaneously with an organic halide in concentrations of 4.0—8.0 mol% to aluminum turnings. Iodine, alkyl iodides and bromides were preferred over chloro compounds. The addition of zinc chloride to the HgX_2–RX catalyst system brought about a remarkable acceleration of the reaction. The use of the catalyst system composed of $HgCl_2$(2 mol%)–MeI(4.0 mol%)–$ZnCl_2$(4.0 mol%) resulted in the formation of the tetrahydrofuran-aluminum compound **1** in 93% yield as listed in Table 1. When an excess of THF(10 equivalent mole) reacted at 80 °C for 70 h, aluminum was consumed completely and a liquid amalgam was precipitated. The hydrolysis of the amalgam with 10 M HCl and the chemical analysis of the hydrolyzate by the 8-quinolinol method showed that 99% of mercury and 68% of zinc added to the system were reduced to metals as amalgam. As the promotors, $FeCl_3$ and $TiCl_4$ were also effective, but the use of zinc chloride was more favorable with respect to the reproducibility of the reaction. No reaction occurred when boron, magnesium, calcium or alkali metals were used in place of aluminum. It

TABLE 1. YIELDS OF THE ALUMINUM-THF COMPOUND **1** WITH VARIOUS CATALYST SYSTEMS[a]

Catalyst component			Reaction conditions		Yields (%)
HgX_2 (mol%)	RX (mol%)	Promotor (mol%)	Time (h)	Temp (°C)	
8.0($HgCl_2$)	0.0	0.0	240	80	0
2.0($HgCl_2$)	4.0(MeI)	0.0	170	80	22
2.0($HgCl_2$)	4.0(MeI)	4.0($ZnCl_2$)	70	80	93
2.0($HgCl_2$)	4.0(MeI)	4.0($ZnCl_2$)	240	40	0
0.0	4.0(MeI)	4.0($ZnCl_2$)	240	80	0
2.0(HgI_2)	4.0(MeI)	4.0($ZnCl_2$)	70	80	95
2.0(HgI_2)	4.0(BuCl)	4.0($ZnCl_2$)	70	80	15
2.0(HgI_2)	4.0(MeI)	4.0($FeCl_3$)	70	80	85

a) The g-atom/mol ratio of aluminum to THF was 1 ; 4.

may be noted that the present reaction is characteristic to cyclic ethers and, hence, acyclic ethers such as diethyl or dipropyl ether can be used as a solvent.

Characterization of the Aluminum Compoumds. The aluminum compound **1** thus obtained was soluble in benzene or ether. It gave terminally dideuterated 1-butanol C_4H_8DOD quantitatively upon deuterolysis and produced no detectable amount of by-product as evidenced by GC and TLC. The molecular weight of **1** determined cryoscopically in benzene corresponded to that of $(Al_2C_{12}H_{24}O_3)_n$ where $n=2$. The ratio of aluminum to 1-butanol analyzed with the 8-quinolinol method and GC was 2:3. PMR spectral data taken in benzene also agreed with the following structure. Proton signals assigned to CH_2 adjacent

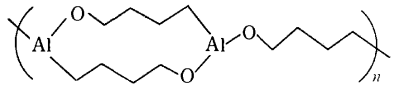

1

to Al, internal CH_2, and CH_2 bonded with oxygen atoms appeared at δ 0.54, 1.84, and 3.92 ppm in 1:2:1 peak area ratio. When 4 mol% of $FeCl_3$ or $TiCl_4$ was used as a promotor instead of zinc chloride, the molecular weight of the aluminum compound increased to 1050—1105 which corresponds to $(Al_2C_{12}H_{24}O_3)_4$, but the NMR data coincided in chemical shift and peak area ratio with that of **1**. In the similar manner, 3-methyltetrahydrofuran-aluminum **2**, 2-methyltetrahydrofuran-aluminum **3**, 2,5-dimethyltetrahydrofuran-aluminum **4**, tetrahydropyran-aluminum **5**, oxepane-aluminum **6** and 7-oxabicyclo[2.2.1]-heptane-aluminum **7** compounds could be prepared individually by using the $HgCl_2$–$ZnCl_2$–MeI catalyst system. All of these aluminum compounds gave the corresponding dideuterio alcohols upon deuterolysis and have oligomeric structures similar to **1** where $n=2$ (Table 2). PMR spectral data of **5** and **6** were in accord in chemical shift with that of **1** within 10 Hz.

Steric and Ring Size Effect of the Cyclic Ethers. The reactions mentioned above were of the second order and the relative rate of reactions is listed in Table 3. A higher homologue, 2-methyltetrahydropyran, had no reactivity and was recovered quantitatively. The order in reactivity of cyclic ethers which form **1**, **2**, **3** and **4** is consistent with the half-lives for the nucleophilic cleavage of those ethers with organolithium compounds[18,19] but not consistent with the order in reactivity of cyclic ethers toward electrophiles[20] or their basicities against various acids,[21,22] nevertheless this reaction was initiated with a Lewis acid catalyst system. The substitution of THF with methyl group in α position caused to the remarkable decrease in reactivity. In case of 7-oxabicyclo[2.2.1]heptane, which may be considered as *cis*-2,5-dimethyltetrahydrofuran with methyl group bound together in a bridge, the reactivity was significantly small compared to 2,5-dimethyltetrahydrofuran. This should be ascribed to the cage effect derived from the bulky bicyclic ring.[21] In the reaction of 2-methyltetrahydrofuran, the substituted carbon atom is known to be attacked preferentially by both nucleophilic[18,19] and electrophilic[23] reagents. However, the ring cleavage of 2-methyltetrahydrofuran by the present method afforded **3a** stereoselectively (99%). The yield of **3b** was only 1%. The compound **2** also gave the abnormal product predomonantly; *i.e.*, the ratio of 2-methyl- to 3-methylbutanol was 74 : 26. These results are concordant with the reductive cleavage of 2-methyltetrahydrofuran by a bulky nucleophile, $LiAlH(OtBu)_3$-BH_3,[24] which gave only 2-methylbutanol. Thus the ring opening of cyclic ethers with aluminum was oriented mainly by the steric effect of subsituents rather than the ionic or inductive effects. The ratio of **3a** to **3b**(99 : 1) was proportional to that of relative rates of reaction between THF and 2,5-dimethyltetrahydrofuran, 92 : 8. The orientation of the ring opening of 2-methyltetrahydrofuran was, therfore, interpreted in terms of the steric effect of substituents.

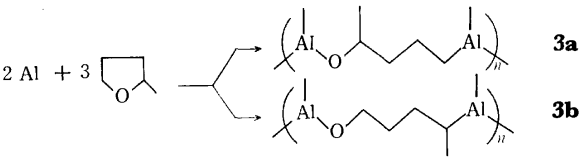

3a

3b

To elucidate the ring size effect, the reaction of 3, 4, 5, 6, and 7 membered ring ethers bearing no methyl substituents was examined. Comparison of these ethers showed that the rate of reaction increased in the order of 5>6>7 membered ring. Three and four membered ring ethers are unfortunately too sensitive to the catalyst to permit the comparative studies(polymerization occurred preferentially). This order varies inversely as the order of inductive effect, 7>6>5, and is not consistent with that of pK_a values[21] of cyclic ethers or the strain energies, ΔG,[25] which

TABLE 2. CHARACTERIZATION OF ALUMINUM-CYCLIC ETHER COMPOUNDS

Compound	Mol wt Found(Calcd)	Al (%) Found(Calcd)	Hydrolysis product
1	520 (270)	19.8 (20.0)	1-butanol
2	605 (312)	17.3 (17.3)	2-methyl-1-butanol 3-methyl-1-butanol
3	620 (312)	17.1 (17.3)	2-pentanol
4	690 (354)	15.2 (15.2)	2-hexanol
5	590 (312)	16.8 (17.3)	1-pentanol
6	701 (354)	15.3 (15.2)	1-hexanol
7	705 (348)	15.7 (15.5)	cyclohexanol

TABLE 3. COMPARATIVE RATES OF REACTION OF CYCLIC ETHERS

Cyclic ethers	Initial rate const $10^4 k$ (l/mol h)
Tetrahydrofuran	378.4
3-Methyltetrahydrofuran	154.5
2-Methyltetrahydrofuran	67.4
2,5-Dimethyltetrahydrofuran	15.4
Tetrahydropyran	9.1
Oxepane	8.1
7-Oxabicyclo[2.2.1]heptane	2.2

increased in order of 7>6>5. Although systematic data about the steric effect of cyclic ethers are lacking, those of linear ethers[26] clearly showed that the steric effect was reversed by the inductive effect. The order in reactivity of 5, 6, and 7 membered ring ethers should be, therfore, ascribed to the steric effect of the methylene chain on the ring.

The steric effect observed in the present system is unusually large. This unique behavior may be interpreted with the concept that the real catalyst is formed on the aluminum surface to proceed a kind of template reaction. The following examination supports this assumption; *i.e.*, aluminum turnings activated with the above mentioned catalyst at 40 °C in THF was washed thoroughly with excess of anhydrous ether to remove unreacted catalyst components. Although no ring opening had occurred at this temperature, the aluminum turnings thus treated were already activated and they maintained the activity to give **1** by the reaction with freshly introduced THF at 80 °C. In addition, aluminum chloride, methylalminum dichloride, and dimethylaluminum chloride, candidates of the real catalyst which could be formed[27,28] from the mixture of aluminum, mercury(II) chloride, zinc chloride, and methyl iodide, had no catalytic activity. The stoichiometric reaction of the catalyst, $HgCl_2$–$ZnCl_2$–MeI, with THF gave no ring opening products, unless aluminum was present in the system. On the bases of these results, we can reasonably conclude that the ring cleavage occrured certainly on the aluminum surface and the large steric effect observed in this system was caused by the metal surface reaction.

This method was less applicable to the cleavage of aromatic cyclic ethers whose ring were stabilized by the conjugation effect.[29] The reaction of 2,3-dihydrobenzofuran and 1,3-benzodioxole with aluminum resulted in the formation of 2-ethylphenol and catechol, respectively, in 10—20% yield. Desired *o*-methoxyphenol was not obtained from 1,3-benzodioxole.

Preparation of Unsaturated Alcohols from Cyclic Ethers. The cleaved cyclic ether is bonded with aluminum atoms bifunctionally, differing from the alkoxy group of the aluminum alkoxide. By taking advantage of the bifunctional nature of the cleaved cyclic ether, the addition of allyl group to the terminal methylene of the cleaved tetrahydrofuran was attempted. The addition of 2 mol. of 3-bromopropene to **1** at 80 °C resulted in the formation of 6-hepten-1-ol in only 5% yield upon hydrolysis, but the addition of cupric or cuprous compounds($CuBr_2$ or CuBr, 1 mol% to the aluminum compound) as catalyst brought about the increase of the yield to 70%. They were more effective as catalyst than Cd, Zn, Ni(II), Co(II), Pd(II), or Fe(III) compound as the latter was reduced immediately to the metal. In a similar manner, the reaction of **2** with 3-bromopropene gave 2-methyl-6-hepten-1-ol(75%) and 3-methyl-6-hepten-1-ol(25%) in 62% yield and **3** gave 7-octen-2-ol in 65% yield. The reaction of **1** with *trans*-1-chloro-2-butene in the presence of $CuBr_2$(1.0 mol%) gave 5-methyl-6-hepten-1-ol and 6-octen-1-ol with 1 : 1 ratio in 60% yield. The isomer, 3-chloro-1-butene also gave the same alcohols with 1 : 1 ratio in 63% yield under the same

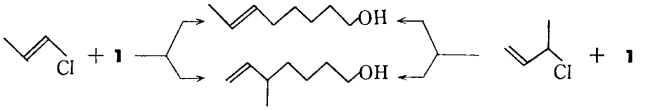

reaction conditions(80 °C for 10 h). This suggests that the ratio of two isomeric butenyl cations formed in both reactions are identical with each other. Thus the polymeric alkoxyalkylaluminum reagents are preferred for the preparation of unsaturated alcohols with elongated carbon chain from allyl halides. Elongation of the carbon chain with diiodomethane was also possible. For example, the reaction of **1** with diiodomethane at 80 °C for 20 h gave 5-iodopentanol in 49% yield upon hydrolysis.

In order to explore the reducing ability of **1**—**3**, reduction of chloral was examined. Two moles of **1** reduced three moles of chloral resulting in the formation of 2,2,2-trichloroethanol and 3-buten-1-ol in 77% yield. The following intermediate can be considered for this reaction. The reducing ability of **1** is similar

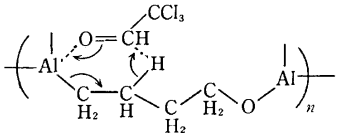

to that of triethylaluminum.[30] Acetaldehyde and acetone were not reduced with **1**. Similarly, **2** gave 2-methyl-3-buten-1-ol and 3-methyl-3-buten-1-ol in 7 : 3 ratio and **3** gave 4-penten-2-ol by the reaction with chloral.

Thus, a series of polymeric alkoxyalkylalumunum compounds obtained here has a large utility in the novel synthesis of unsaturated alcohols with or without elongated carbon chain.

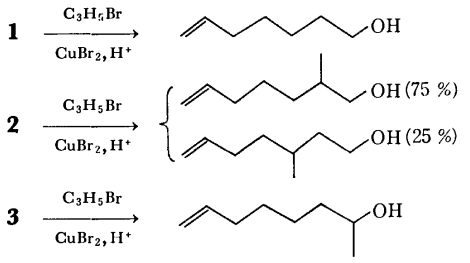

Experimental

All the cyclic ethers obtained commercially were dried over sodium/potassium alloy and distilled. Aluminum foil (99.99% in purity, thickness 0.025 mm, 2.0×2.0 mm width, Nakarai Chem.), aluminum powder(99% purity, Alfa Chem.) and aluminum foil for kitchen use (97% purity, Toyo Aluminum Tech.) were used as the Aluminum turnings. Anhydrous metal halides were prepared by heating the hydrates in vacuum at the prescribed temperature. Reactions were carried out under nitrogen using the two-necked glass tube(30×150 mm, thickness 2.0 mm). GC analysis and the separation of the reaction products were made with Yanagimoto Model G-80 and Varian-Aerograph

Model 700 gas chromatographs. PMR spectra were taken with a Varian Model A-60 instrument and MS with a Hitachi RMU-7HR spectrometer. IR spectra were recorded on a Hitachi Model EPI-2 spectrometer.

*Preparation of **1** from THF.* To the aluminum turnings (2.7 g, 0.1 g-atom) in THF(40 ml, 0.4 mol), a mixture of mercury(II) chloride(0.54 g, 2.0 mol% to aluminum), zinc chloride(0.54 g, 4.0 mol%), and methyl iodide(0.25 ml, 4.0 mol%) was added as catalyst. After the tube was sealed and shaken for 70 h at 80 °C in a temperature controlled water bath equipped with a vibrator, benzene(120 ml) was added to the product. The colorless benzene solution was transferred with a hypodermic syringe to remove the residual aluminum amalgam and was evaporated to dryness to give **1** as a semi-solid substance. Any differences in reactivity were not observed among the three brands of aluminum turnings used in this experiment.

*Preparation of Aluminum Compounds **2**—**6**.* In essentially the same way as described above, the reaction of 2-methyltetrahydrofuran, 3-methyltetrahydrofuran, 2,5-dimethyltetrahydrofuran, tetrahydropyran, and oxepane(0.4 mol) with aluminum turnings(2.7 g, 0.1 g-atom) were carried out at 80 °C for 150 h. The resulting products were dissolved in benzene (120 ml) and poured into hexane(300 ml) to precipitate the compound. After decantation, the precipitates **2**—**6** were dried *in vacuo* to give semi-solid materials.

*Deuterolysis of the Compound **1**—**7**.* The aluminum compounds **1**—**7**(50 mmol) were deuterolyzed at 0 °C with deuterium oxide(5 ml) in ether(50 ml). Isomeric alcohols were separated with a preparative GC using a column(4 m) packed with 15% Silicone DC-500 on 40/60 mesh Celite 545. The position of deuteriums in the resulting alcohols was determined with IR, PMR, and MS, by reference to alcohols obtained by hydrolysis.

*Butan-4-*d-*1-ol-*d *from **1***: IR(neat) 2490(ν OD), 2180 cm^{-1} (ν CD). PMR($CDCl_3$) δ 3.68(2H, q, CH_2O), 1.52(4H, m, CH_2), 0.99(2H, m, CH_2D). MS *m/e* 76(M^+), 74, 57, 32.

*2-Methylbutan-4-*d-*1-ol-*d *from **2***: IR(neat) 2483(ν OD), 2182 cm^{-1}(ν CD). PMR($CDCl_3$) δ 3.62(2H, t, CH_2O), 1.50 (3H, m, CH_2CH), 0.93(5H, m, CH_3 and CH_2D). MS *m/e* 90(M^+), 88, 71, 32.

*3-Methylbutan-4-*d-*1-ol-*d *from **2***: IR(neat) 2485(ν OD), 2180 cm^{-1}(ν CD). PMR($CDCl_3$) δ 3.68(2H, t, CH_2O), 1.51 (3H, m, CH_2CH), 0.93(5H, d, CH_3 and CH_2D). MS *m/e* 90(M^+), 88.

*Pentan-5-*d-*2-ol-*d *from **3***: IR(neat) 2489(ν OD), 2179 cm^{-1} (ν CD). PMR($CDCl_3$) δ 3.80(1H, m, CH), 1.48(4H, m, CH_2), 1.18(3H, d, CH_3), 0.93(2H, m, CH_2D). MS *m/e* 90(M^+), 88, 75, 71, 32.

*Hexan-6-*d-*2-ol-*d *from **4***: IR(neat) 2490(ν OD), 2175 cm^{-1} (ν CD). PMR($CDCl_3$) δ 3.80(1H, m, CH), 1.31(6H, m, CH_2), 1.18(3H, d, CH_3), 0.92(2H, q, CH_2D). MS *m/e* 104 (M^+), 85, 57, 32.

*Pentan-5-*d-*1-ol-*d *from **5***: IR(neat) 2490(ν OD), 2182 cm^{-1} (ν CD). PMR($CDCl_3$) δ 3.62(2H, t, CH_2O), 1.40(6H, m, CH_2), 0.90(2H, m, CH_2D). MS *m/e* 88(M^+-2), 71, 55, 32.

*Hexan-6-*d-*1-ol-*d *from **6***: IR(neat) 2485(ν OD), 2170 cm^{-1} (ν CD). PMR($CDCl_3$) δ 3.67(2H, m, CH_2O), 1.38(8H, m, CH_2), 0.90(2H, m, CH_2D). MS *m/e* 102(M^+-2), 85, 67, 32.

*Cyclohexan-4-*d-*ol-*d *from **7***: IR(neat) 2489(ν OD), 2208, 2109 cm^{-1}(ν CD). PMR($CDCl_3$) δ 3.63(1H, m, CH), 1.78—1.32(9H, m, CH_2 and CHD). MS *m/e* 102(M^+), 83, 32.

Reaction of Aromatic Cyclic Ethers with Aluminum. To a mixture of 2,3-dihydrobenzofuran(5.7 ml, 50 mmol) and aluminum(1.4 g, 50 mg-atom) in benzene(15 ml) was added the catalyst, $HgCl_2$-$ZnCl_2$-MeI(4, 8, and 8 mol%, respectively). The mixture was heated at 80 °C for 100 h, hydrolyzed at 0 °C and then distilled. Deuterolysis of the product gave 2-ethyl-phenol-d_2 in 15% yield. IR(neat) 2558(ν OD), 2447 cm^{-1}(ν CD). PMR($CDCl_3$) δ 6.82(4H, m, CH), 2.59 (2H, q, CH_2), 1.20(2H, t, CH_2D). MS *m/e* 124(M^+). Phthalan had no reactivity toward aluminum even carrying out the reaction at 120 °C for 150 h. The reaction of 1,3-benzodioxole(6.1 g, 50 mmol) with aluminum(1.4 g) at 100 °C for 150 h resulted in the formation of catechol in 20% yield.

*Allylation of **1**—**3** with 3-Bromopropene.* To a stirred mixture of anhydrous 3-bromopropene(10.4 ml, 120 mmol) and $CuBr_2$(0.18 g, 0.8 mmol) was added compounds **1**—**3** (40 mmol) in benzene(30 ml). After the reaction was allowed to proceed at 80 °C for 20 h, products were hydrolyzed, filtered and distilled. Yields, 65—75%.

*6-Hepten-1-ol from **1***: IR(neat) 3340, 915 cm^{-1}. PMR ($CDCl_3$) δ 5.71, 4.90(3H, m, CH_2=CH), 3.65(2H, t, CH_2), 2.01(2H, m, CH_2), 1.87(1H, s, OH), 1.38(6H, m, CH_2). MS *m/e* 114(M^+).

*3-Methyl-6-hepten-1-ol from **2***. IR(neat) 3340, 915 cm^{-1}. PMR($CDCl_3$) δ 5.69, 4.95(3H, m, CH_2=CH), 3.63 (2H, t, CH_2), 2.02(2H, m, CH_2), 1.83(1H, s, OH), 1.63(1H, m, CH), 1.38(4H, m, CH_2), 0.94(3H, d, CH_3). MS *m/e* 127(M^+-1).

*2-Methyl-6-hepten-1-ol from **2***. IR(neat) 3350, 915 cm^{-1}. PMR($CDCl_3$) δ 5.68, 4.89(3H, m, CH_2=CH), 3.44(2H, d, CH_2), 2.05(2H, m, CH_2), 1.80(1H, s, OH), 1.65(1H, m, CH), 1.33(4H, m, CH_2), 0.98(3H, d, CH_3). MS *m/e* 127(M^+-1).

*7-Octen-2-ol from **3***. IR(neat) 3380, 915 cm^{-1}. PMR ($CDCl_3$) δ 5.78, 4.79(3H, m, CH_2=CH), 3.76(1H, m, CH), 1.99(2H, t, CH_2), 1.91(1H, s, OH), 1.38(6H, m, CH_2), 1.18 (3H, d, CH_3). MS *m/e* 127(M^+-1).

*Reaction of **1** with 1-Chloro-2-butene and 3-Chloro-1-butene.* A solution of **1**(5.4 g, 40 mmol) in benzene(30 ml) was added to a stirred mixture of anhydrous *trans*-1-chloro-2-butene (11.8 ml, 120 mmol) and $CuBr_2$(0.18 g, 0.8 mmol). The mixture was heated to 80 °C for 20 h and then hydrolyzed. Resulting two alcohols(with 1:1 ratio) were separated with GC. Typical yield, 63% based on **3**.

a) trans-*6-Octen-1-ol*: IR(neat) 3340(ν OH), 967(ν *trans* C=C). PMR($CDCl_3$) δ 5.42(2H, m, CH), 3.60(2H, t, CH_2O), 1.96(2H, m, CH_2), 1.82(1H, s, OH), 1.61(3H, m, CH_3), 1.38(6H, m, CH_2). MS *m/e* 128(M^+).

b) 5-Methyl-6-hepten-1-ol: IR(neat) 3370(ν OH), 920 cm^{-1}(ν C=C). PMR($CDCl_3$) δ 5.60, 4.95(3H, m, CH_2=CH), 3.63(2H, t, CH_2O), 2.05(1H, m, CH), 1.39(6H, m, CH_2), 0.99(3H, d, CH_3). MS *m/e* 128(M^+).

The same alcohols were obtained also from the reaction of 3-chloro-1-butene(12.7 ml, 120 mmol) with **1**(5.4 g) in 63% yield with 1:1 ratio.

*Addition of Methylene Iodide to **1**.* To a solution of **1** prepared from aluminum(1.4 g) and excess of tetrahydrofuran(40 ml) was added directly methylene iodide(16.1 ml, 0.2 mol) and the mixture was heated to 80° for 20 h. Distillation of the hydrolyzate gave 5-iodo-1-pentanol in 49% yield based on **1**. IR(neat) 3390(ν OH), 722 cm^{-1}(ν CI). PMR($CDCl_3$) δ 3.61(2H, t, CH_2O), 3.18(2H, t, CH_2I), 1.89 (1H, s, OH), 1.56(6H, m, CH_2). MS *m/e* 213(M^+-1).

*Reduction of Chloral with **1**—**3**.* To a solution of **1** (5.4 g, 40 mmol) in benzene(30 ml) was added dropwisely anhydrous chloral(11.8 g, 80 mmol) dried over calcium hydride with vigourous stirring at 20 °C. The mixture was heated at 60° for 3 h and then hydrolyzed. The resulting 2,2,2-trichloroethanol and 3-buten-1-ol obtained from the benzene fraction were identified with authentic samples. The yield of 3-buten-1-ol was 77% based on **1**. In the similar

manner, reduction of chloral with **2** gave 3-methyl-3-buten-1-ol(30%). Which was identified with the commercial sample, and also 2-methyl-3-buten-1-ol(70%). IR(neat) 3330 (ν OH), 905 cm^{-1}(ν CH_2=CH). PMR($CDCl_3$) δ 5.8—5.1 (3H, m, CH_2=CH), 3.68(2H, d, CH_2O), 2.01(1H, m, CH), 1.95(1H, s, OH), 1.33(3H, d, CH_3). MS *m/e* 86(M^+), 85. Typical yield was 70%. Reduction of chloral with **3** under the same reaction condition gave 4-penten-2-ol in 70% yield and it was identified with the authentic sample.

References

1) A. Lüttringhaus and G. vonSääf, *Angew. Chem.*, **51**, 915 (1938).
2) R. L. Burwell, Jr., *Chem. Rev.*, **54**, 615 (1954).
3) R. E. Parker and N. S. Isaacs, *Chem. Rev.*, **59**, 737 (1959).
4) S. Patai, "The Chemistry of the Ether Linkage," Interscience Publishers (1967).
5) D. Jaques and J. A. Leistein, *J. Chem. Soc.*, **1961**, 4963.
6) R. C. Larock, *J. Org. Chem.*, **39**, 3721 (1974).
7) S. Sakai, H. Tanaka, and Y. Ishii, *Kogyo Kagaku Zasshi*, **69**, 1388 (1966).
8) E. Mincione, *Ric. Sci.*, **39**, 424 (1969).
9) R. E. Goldsberry, D. E. Lewis, and K. Cohn, *J. Organomet. Chem.*, **15**, 491 (1968).
10) F. Patat, *Chimia(Aarau)*, **18**, 233 (1964).
11) A. G. Evans, M. LI. Jones, and N. H. Rees, *J. Chem. Soc., B*, **1969**, 894.
12) H. H. Wassermann and N. E. Aubrey, *J. Am. Chem. Soc.*, **78**, 1726 (1956).
13) J. K. Addy and R. E. Parker, *J. Chem. Soc.*, **1965**, 644.
14) H. C. Brown, R. S. Fletcher, and R. B. Johannesen, *J. Am. Chem. Soc.*, **73**, 212 (1951); H. C. Brown, *J. Chem. Soc.*, **1956**, 1248.
15) D. E. McLaghlin, M. Tamres, S. Searles, Jr., and S. Nukina, *J. Inorg. Nucl. Chem.*, **17**, 112 (1961).
16) H. H. Sisler and P. E. Perkins, *J. Am. Chem. Soc.*, **78**, 1135 (1956).
17) W. G. Dauben, D. F. Dickel, O. Jeger, and V. Prelog, *Helv. Chim. Acta*, **36**, 325 (1953).
18) R. B. Bates, L. M. Kroposki, and D. E. Potter, *J. Org. Chem.*, **37**, 560 (1972).
19) S. C. Honeycutt, *J. Organomet. Chem.*, **29**, 1 (1971).
20) S. Sakai, S. Sakano, and Y. Ishii, *Kogyo Kagaku Zasshi*, **69**, 1211 (1966).
21) E. M. Arnett and C. Y. Wu, *J. Am. Chem. Soc.*, **84**, 1684 (1962).
22) W. Strohmeier and A. Echte, *Z. Elektrochem.*, **61**, 549 (1957).
23) H. Alper and C.-C. Huang, *J. Org. Chem.*, **38**, 64 (1973).
24) H. C. Brown, S. Krishnamurthy, and R. A. Coleman, *J. Am. Chem. Soc.*, **94**, 1750 (1972).
25) A. S. Pell and G. Pilcher, *Trans. Faraday Soc.*, **60**, 71 (1959).
26) B. Rubin, H. H. Sisler, and H. Schechter, *J. Am. Chem. Soc.*, **74**, 877 (1952).
27) A. vonGosse and J. M. Mavity, *J. Org. Chem.*, **5**, 106 (1940).
28) A. G. Pozamantir and M. L. Genusov, *J. Gen. Chem. USSR*, **32**, 1149 (1962).
29) Yu. Maksyutin, Yu. L. Frolov, A. V. Kalabina, and V. A. Sheveleva, *Zh. Fiz. Khim.*, **38**, 2604 (1964).
30) H. Meerwein, G. Hinz, H. Majert, and H. Sonke, *J. Prakt. Chem.*, **147**, 226 (1936).

Photoreaction of 1-(1-Cycloalkenyl)-4-phenyl-1-butanone under Neutral and Acidic Conditions

Masaru TADA, Tetsuro MAEDA, and Hiroshi SAIKI

Department of Chemistry, School of Science and Engineering, Waseda University, Shinjuku, Tokyo 160

(Received October 29, 1977)

UV irradiation of 1-(1-cycloalkenyl)-4-phenyl-1-butanones gives differing products depending on the reaction conditions, neutral or acidic. In benzene 1-(1-cyclopentenyl)-4-phenyl-1-butanone gives 4-phenylspiro[4,4]-nonan-1-one, formed by the intramolecular abstraction of hydrogen, and 4-cyclopentylidene-4-phenylbutanal, formed by Norrish type I fission of the spiro ketone. 1-(1-Cyclohexenyl)-4-phenyl-1-butanone does not exibit this behavior. Both ketones give the reduction products, 1-cyclopentyl-4-phenyl-1-butanone and 1-cyclohexyl-4-phenyl-1-butanone, under the action of trifluoroacetic acid, and cyclized products, 7-phenylperhydro-4-indenone and 4-phenylperhydro-1-naphthelenone, under the action of boron trifluoride etherate. The reaction processes under acidic conditions have both an ionic and a free radical nature. The results have lead to the proposition of the mechanism involving electron transfer, proton transfer, and hydrogen abstraction.

Much attention has been paid to the intramolecular exciplex between two aromatic groups or between an aromatic moiety and a non-aromatic functional group.[1,2] It appears that the formation of the exciplex is dependent upon the length of the bridge connecting the two chromophores. Excited complexes have been postulated as the intermediates of intramolecular photochemical reactions.[3-5] Following the study on the photochemistry of 1-(1-cycloalkenyl)-2-phenyl-1-ethanones (Ia, Ib, and Ic)[6] and 1-(1-cycloalkenyl-3-phenyl-1-propanones (IIa and IIb),[7] the photoreactions of 1-(1-cycloalkenyl)-4-phenyl-1-butanones (IIIa and IIIb) having the trimethylene bridge between the enone and phenyl groups have been investigated. The UV irradiation of Ia, Ib, and Ic under acidic conditions or in protic media induces photo-coupling between the β-position of the enones and the ortho-position of the phenyl group.[6] Similarly the irradiation of IIb under acidic conditions gives the same type of photoproduct. Irradiation of IIa under neutral conditions, on the other hand, gives a product derived from the intramolecular abstraction of hydrogen by the β-carbon of the enone moiety.[7]

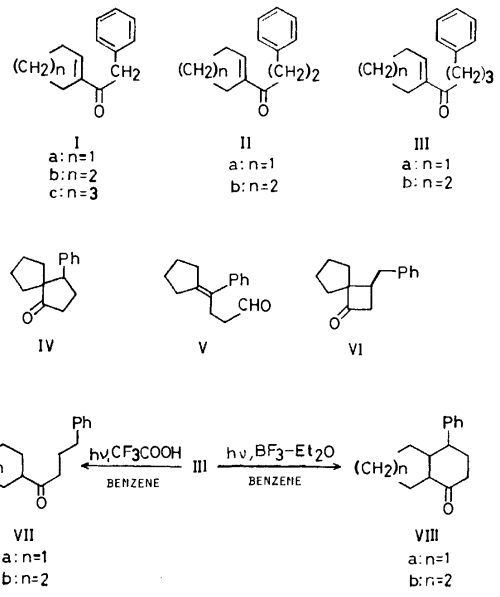

The 1-(1-cycloalkenyl)-4-phenyl-1-butanones (IIIa and IIIb) have a trimethylene bridge by which the two chromophores may be expected to interact more effectively than I or II.[3-5] The present study demonstrates that the photochemical behavior of III is completely different from that of I and II.

Results and Discussion

Photoreaction under Neutral Conditions. Irradiation (10 h) of a solution of 1-(1-cyclopentenyl)-4-phenyl-1-butanone (IIIa) in benzene gave a spiro ketone IV and an aldehyde V in 24 and 17% yields, respectively. The structures of IV and V were deduced from spectral data. The IR absorptions of IV at 1735, 765, and 700 cm^{-1} show the presence of a five membered ketone and a monosubstituted benzene ring. The IR absorption at 2710 cm^{-1} and NMR signal at δ 9.85 (t, J=2 Hz) of V are due to an aldehyde group, and the IR absorptions at 775 and 700 cm^{-1} show the presence of a monosubstituted benzene ring. The IR absorption of the crude product from the irradiation of IIIa showed an absorption at 1774 cm^{-1} and this indicated the product VI having a cyclobutanone structure. This minor product, which was not isolated, appears to be formed by the intramolecular abstraction of the hydrogen at C_3-methylene by the β-carbon of the enone moiety of IIIa.[7] The product IV appears to be formed by the intramolecular abstraction of the benzylic hydrogen by the β-carbon of the enone moiety of IIIa. The formation of aldehyde V showed an induction period and hence V appears to be a secondary product from IIIa through the spiro ketone IV. This was ascertained by the direct irradiation of IV. Norrish type I fission of IV and hydrogen transfer account for the transformation of IV to V.

1-(1-Cyclohexenyl)-4-phenyl-1-butanone (IIIb) in benzene, in contrast, did not react even after prolonged irradiation (24 h). This may be explained in terms of the preferential dissipation of the excited energy due to the cis-trans isomerization of the cyclohexene moiety.[8]

Photoreaction under Acidic Conditions. A solution of 1-(1-cyclopentenyl)-4-phenyl-1-butanone (IIIa) or 1-(1-cyclohexenyl)-4-phenyl-1-butanone (IIIb) in benzene

Table 1. Yield of VIIa from IIIa (0.1 M in toluene) depending upon the amount of CF_3COOH

CF_3COOH (M)	Yield of VIIa (%)
0.03	trace
0.06	44
0.12	76
0.23	84

was irradiated for 32 or 70 h in the presence of 0.05 M trifluoroacetic acid, giving the dihydro derivatives VIIa and VIIb in yields of 63 and 40%, respectively. GLC analysis of the product mixture showed the formation of 1,2-diphenylethane and carbon dioxide when the reaction of IIIa was carried out in degassed toluene. The yield of VIIa was dependent on the amount of trifluoroacetic acid used and was improved up to 84% by using two equivalents of the acid in toluene (Table 1). These results demonstrate the involvement of free radical hydrogen abstraction and the degradation of trifluoroacetic acid. The photoreaction of IIIa in 2-propanol, however, did not give the reduction product, and this suggests that the reaction takes a mechanism other than a simple hydrogen abstraction from the solvent. Under the conditions in which essentially entire incident light was absorbed in the $n\pi^*$ region of IIIa, the relative rates of the photoreduction (relative quantum yield in the approximation) were dependent on the molar polarization of the solvent used as seen in Fig. 1. The figures in parentheses in Fig. 1 are the relative rates of hydrogen abstraction by an excited benzophenone.[9] The retardation of the photo-reduction in benzene, an extremely poor hydrogen donor, explain this behavior. This suggests the polar nature of the photo-reduction and some dependence on the hydrogen donating ability of the solvent. The photo-reduction takes place only in the presence of a strong Brønsted acids such as trifluoroacetic acid (pK_a: 0.2). The weaker acids like benzoic acid (pK_a: 4.20), acetic acid (pK_a: 4.75), or phenol (pK_a: 10.00) can not induce the reaction.

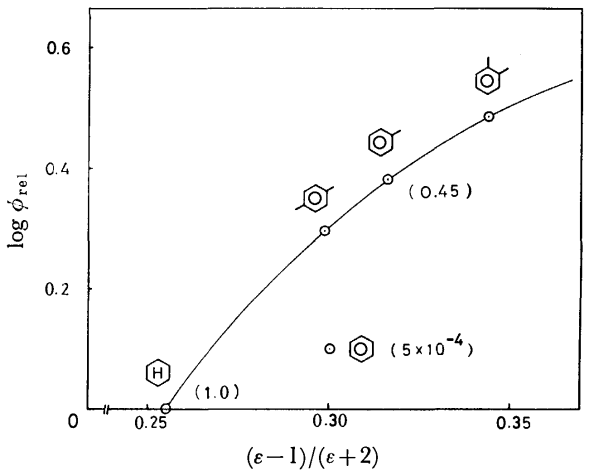

Fig. 1. Relation between the relative quantum yield of VIIa and the polarization of solvents. (The figures in parentheses are the relative rates of H-abstraction by an excited benzophenone.[9])

A solution of 1-(1-cycloalkenyl)-4-phenyl-1-butanone (IIIa and IIIb) in benzene containing 0.05 M boron trifluoride etherate was irradiated for 20 h, the cyclized products VIIIa and VIIIb were obtained in 25 and 30% yields, respectively. The structures of products VIIIa and VIIIb were deduced from permanganate oxidation which gave banzoic acid and spectroscopic data (VIIIa, 1705, 760, and 700 cm^{-1}; VIIIb, 1710, 760, and 700 cm^{-1}). These data indicate the presence of a six-membered ketone and a monosubstituted benzene ring. Though the stereochemistry of the products VIIIa and VIIIb was not defined, only one of the possible stereoisomers was detected by GLC analysis. This type of ortho-cyclization also took place under catalysis of other Lewis acids such as tin(IV) chloride and titanium(IV) chloride (0.05 M). The reaction in hydrogen donating solvents such as toluene and xylene in the presence of boron trifluoride etherate did not give the products VIIIa and VIIIb in reasonable yields but gave the reduction products VIIa and VIIb predominantly (see next section).

Reaction Mechanism. The two types of reaction do not take place in the absence of trifluoroacetic acid or a Lewis acid and do not occur intermolecularly between 1-acetylcyclopentene (0.1 M) and tuluene under the same reaction conditions as for IIIa. This result indicates that an intramolecular interaction between the phenyl group and the enone moiety, at least in the excited state, is necessary for the photoreaction of IIIa and IIIb under acidic conditions, and that the existence of an acid must enhance the interaction. The UV-spectra of IIIa and IIIb are essentially the same as the spectrum of the 1:1 mixture of 1-acetylcyclopentene or 1-acetylcyclohexene and toluene, and therefore there is no evidence for the interaction between the two chromophores in the ground state. The enone moieties of IIIa and IIIb are nonemissive and only a weak fluorescence from the aromatic moieties may be observed. The intensity is much weaker than that of toluene and this is thought due to the efficient quenching of the excited state of the aromatic moiety by the intramolecular enone group. An α,β-unsaturated ketone has the intrinsic ability to quench the excited singlet state of an aromatic molecule. Thus 1-acetylcyclopentene quenched the fluorescence of toluene, 1-methylnaphthalene, and anthracene by diffusion controlled-rates (10^9—10^{10} M^{-1} s^{-1}). The quenching rates were obtained from the slopes of Stern-Volmer plots ($k_q\tau_0$) and the reported lifetimes (τ_0) of the aromatic compounds.[10] The weak fluorescence of IIIa and IIIb is suggested due to the strong intramolecular interaction between the two chromophores in the singlet excited state. For the acid-coordinated species of IIIa and IIIb, the interaction between the two chromophores would be expected to be CT-type and the excitation of either a donor (aromatic moiety) or an acceptor (enone moiety) promotes the interaction. Though the excited state responsible for the photoreactions cannot be specified, the excitation of either chromophore must form an essentially similar CT-state. In addition it is highly possible that the photoreaction of IIIa and IIIb occurs from the new CT-excitation

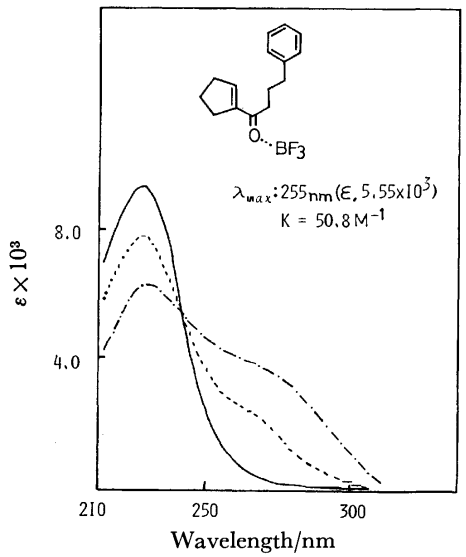

Fig. 2. UV absorption of IIIa (1.26×10^{-4} M in hexane) in the presence of BF_3-Et_2O: ——, 0 M; ----, 1.06×10^{-2} M; —·—·, 2.65×10^{-2} M.

indicated by the UV spectra of IIIa and IIIb in the presence of an acid.

In the presence of boron trifluoride etherate, the UV spectrum of IIIa in hexane (2.52×10^{-4} M) shows a broad band at around 260 nm with concomitant decrease in $\pi\pi^*$ absorption at 232 nm as shown in Fig. 2. The analysis of the spectrum having an isosbestic point at 242 nm by the Rose-Drago's method,[11] monitoring at 250, 260, 270, and 280 nm, gave λ_{max}^{hexane} 255 nm (ε 5550) and the stability constant $K=50.8\ M^{-1}$ for the complex X between IIIa and boron trifluoride. The complexing of boron trifluoride to α,β-unsaturated ketones has been reported by UV,[12] IR,[13] and NMR[14] spectra. A similar behavior was observed with trifluorocetic acid (10^{-3}—10^{-2} M) in the $n\pi^*$ region of IIIa in higher concentration (1.26×10^{-2} M), though the dilute solution of IIIa (1.26×10^{-4} M) showed only a slight bathochromic shift in $\pi\pi^*$ region. These results indicate that the enone IIIa is coordinated

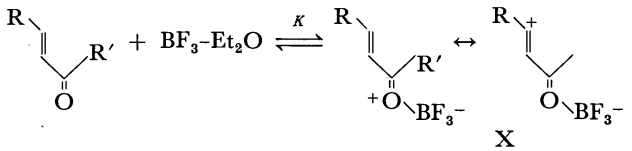

effectively with a Lewis acid or a strong Brønsted acid under the reaction conditions—enone III 0.1 M and acid 0.05—0.06 M. The necessity for acid in the two types of photoreactions, suggests the direct involvement of the acid-coordinated form (X) of the starting ketone. The quenching of the photo-products VIIa and VIIIa by 1,3-pentadiene gave linear Stern-Volmer plots with $k_q\tau$ value of 88 M^{-1} for VIIa and 158 M^{-1} for VIIIa. If this quenching is due to the energy transfer from the triplet enone to the diene, the quenching rates would be expected to be diffusion-controlled ($k_p=ca.\ 10^{10}\ M^{-1}\ s^{-1}$), and the lifetime ($\tau$) of the triplet enone would fall into 10^{-9}—10^{-8} s. These values are too small for the normal triplet species and hence the quenchable intermediate appears to be a singlet or triplet species with an unusually short lifetime.

TABLE 2. SOLVENT EFFECT ON THE YIELD OF VIIa AND VIIIa FROM IIIa (0.1 M)

BF_3-Et_2O (0.05 M) solvent	Yield of VIIa (%)	Yield of VIIIa (%)	CF_3COOH (0.05 M) solvent	Yield of VIIa (%)	Yield of VIIIa (%)
Benzene	1.5	25	Benzene	43	7
Toluene	18	1.0	Toluene	80	2
o-Xylene	26	0	*o*-Xylene	80	0
Cyclohexane	8	1.3	Cyclohexane	29	4
			Hexane	16	3

The photoreactions in benzene were selective with the acid used. The reaction under boron trifluoride etherate gave the cyclized product VIII whereas the reaction under trifluoroacetic acid gave largly the reduction product VII. The variation in the yields are listed in the Table 2. The reaction in the hydrogen donating solvents such as toluene and *o*-xylene gave largly the reduction product found under both trifluoroacetic acid and boron trifluoride etherate. Thus the hydrogen donating ability of the solvent appears to be an important factor in the discrimination of the two types of photoreactions.

For the photoreaction of ketone IIIa and IIIb the mechanism shown in Fig. 3 is proposed on the basis of the experimental results; (a) the radical and ionic nature of the photochemical process, (b) the degradation of trifluoroacetic acid to carbon dioxide, (c) the necessity and reality of the intramolecular interaction in the excited state, (d) the existence of acid coordination to the enone and its enhancement of the intramolecular interaction between the two chromophores, (e) quenching, and (f) the solvent effect on the yield and distribution of products.

Excitation of the acid-coordinated enone—$n\pi^*$ excitation or direct CT-excitation of the complex X—forms an intramolecular singlet excited complex (X*) having CT-character, in which the phenyl group works as as an electron donor and the enone group works as an electron accepter. An electron transfer in this excited complex gives a radical ion pair XI. When the acid A is BF_3, the loss of BF_3 and the simultaneous proton transfer from the benzylic position to oxygen gives a

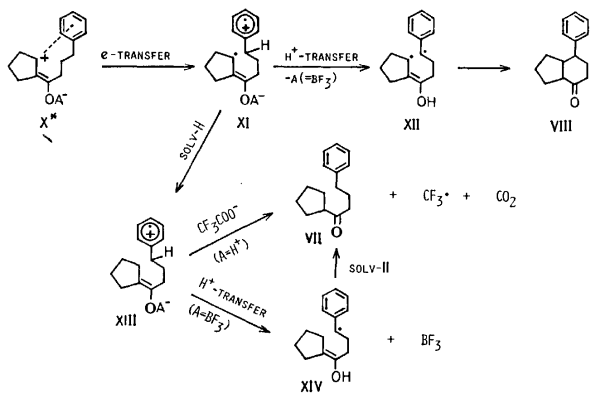

Fig. 3. Reaction scheme.

diradical XII, and the coupling of the diradical forms the photo-cyclization product VIII. In hydrogen donating solvents, the hydrogen abstraction by XI from the solvent gives a radical ion XIII. When the acid is CF_3COOH, another electron transfer from CF_3COO^- to XIII forms the reduction product VII and carbon dioxide. When the acid A in XIII is BF_3, the proton transfer from benzylic position to oxygen with simultaneous loss of BF_3 gives the benzyl radical XIV which forms the reduction product VII by another hydrogen abstraction from the solvent. This reaction mechanism accounts for solvent-polarity, the hydrogen donating ability of the solvent, and the acid—Brønsted or Lewis acid—on the product formation. The photoreactions observed for III were not observed in the case of I and II. The variation in the reactivity upon reaction conditions was again not observed with I and II. The interaction between the two chromophores in the excited state of III appeares to be stronger than that in I and II.[15] Evidently the trimethylene bridge combining the phenyl and the enone groups in III appeares to be an important factor for the different reactivity of III from those of I and II.

Experimental

Preparation of 1-(1-Cyclopentenyl)-4-phenyl-1-butanone (IIIa) and 1-(1-Cyclohexenyl)-4-phenyl-1-butanone (IIIb). Ketones IIIa and IIIb were synthesized from 4-phenylbutanoyl chloride and cycloalkene by the modified method of Cook and Hawett[16] for the synthesis of 1-(1-cyclohexenyl)-2-phenyl-1-ethanone (Ib). Dichloromethane was the solvent instead of carbon disulfide and $SnCl_4$ the acid catalyst. The reaction was carried out at a lower temperature (−80—−100 °C) under an atmosphere of nitrogen. Under these conditions clean 1-(2-chlorocycloalkyl)-4-phenyl-1-butanone was the product. 1-(2-Chlorocyclopentyl)-4-phenyl-1-butanone was dehydrochlorinated by refluxing the benzene solution in the presence of triethylamine. 1-(2-Chlorocyclohexyl)-4-phenyl-1-butanone was dehydrochlorinated in *N,N*-dimethylaniline at 180 °C. IIIa; bp 152 °C/0.3 mmHg. MS *m/e* 214 (M^+). IR(neat): 1655, 1613, 745, and 690 cm^{-1}. NMR(CCl_4): δ 7.20 (5H, m) and 6.80 (1H, br s). Semicarbazone; mp 123.5—125.0 °C. Found: C, 70.99; H, 7.85; N, 15.48%. Calcd for $C_{16}H_{21}N_3O$: C, 70.82; H, 7.80; N, 15.48%. IIIb; bp 115—120 °C/0.1 mmHg. MS *m/e* 228 (M^+). IR(neat): 1655, 1610, 750, and 700 cm^{-1}. NMR(CCl_4): δ 7.20 (5H, m), and 6.80 (1H, br s). Semicarbazone; mp 145 °C. Found: C, 71.73; H, 8.28; N, 14.96%. Calcd for $C_{17}H_{23}N_3O$: C, 71.54; H, 8.12; N, 14.73%.

Absorption and Emission Spectra of IIIa and IIIb. Hexane and cyclohexane were purified by passing over a long column of activated silica gel. The effect of BF_3-Et_2O on the absorption spectrum of IIIa was studied in hexane (IIIa, 2.52×10^{-4}M) containing 1.06—2.65×10^{-2} M BF_3-Et_2O in both sample and reference cells, and the results are shown in Fig. 2. The effect of CF_3COOH was studied in the same manner by using 1.26×10^{-4}M solution of IIIa and 1.44×10^{-3}—4.40×10^{-2}M CF_3COOH in hexane, and the $\pi\pi^*$ absorption shifted from 232 to 242 nm. The effect of CF_3COOH on $n\pi^*$ band was studied by using 1.26×10^{-2}M solution of IIIa and 2.63×10^{-3}—2.30×10^{-2}M CF_3COOH in hexane, and an isosbestic point was observed at 333 nm. Fluorescence spectra were measured by a Hitachi MPF-4 spectrophotometer using cyclohexane purged by argon as solvent. IIIa fluoresces weakly at 300—350 nm and it appeares in the same region to the $n\pi^*$ absorption of IIIa. The weakness of the fluorescence is not thought entirely due to the absorption by the enone at the concentrations for the measurement of fluorescence($<10^{-3}$ M). The concentrations of toluene and IIIa in hexane were adjusted to absorb the same quanta of light at 270nm for the measurement of the relative intensity of fluorescence. The intensity of fluorescence from IIIa under these conditions was much weaker than that of toluene, Φ(toluene)/Φ(IIIa)$>$200.

Fluorescence Quenching of Aromatic Compounds by 1-Acetylcyclopentene. The hexane solutions of (a) toluene (1.90×10^{-3} M), (b) 1-methylnaphthalene (1.45×10^{-3} M), and (c) anthracene (1.40×10^{-3}M), were used for the quenching experiments and were excited at 260nm (a), and 300 nm (b, c). The intensities of fluorescence were monitored at the emission maxima at 283 (a), 325 (b), and 400 nm (c). The concentration limits of the quencher, 1-acetylcyclopentene, were 3.64×10^{-4} to 5.82×10^{-3}M. The slopes of the Stern-Volmer plots ($k_q\tau_0$) were 427 (a), 265 (b), and 84 M^{-1} (c).

Irradiation of IIIa and IIIb under Neutral Conditions. The solution of IIIa (700 mg) in 150 ml of thiophene-free benzene was internally irradiated by a 450W high pressure mercury lamp mounted in a Pyrex cooling jacket. During the reaction the solution was stirred magnetically and kept in an atmosphere of argon. Reaction products were obtained by distillation, 100—120 °C/0.1mmHg, after evaporation of the solvent *in vacuo*. GLC analysis (5% PEG-20M on Chromosorb W, 200 °C) of the crude product showed two main peaks attributed to spiro ketone IV and aldehyde V beside small peaks attributed to the starting material IIIa and a minor product. The aldehyde V was collected by preparative GLC (120 mg, 17%). Since the spiro ketone IV was difficult to purify by preparative GLC, the aldehyde was destroyed by AgO treatment[17] of the crude product before GLC, IV (170 mg, 24%).

Irradiation of IIIb in the same manner did not give the product but recovered the starting material. IV, an oil. *MW* Found: *m/e* 214.1342. Calcd for $C_{15}H_{18}O$: *m/e* 214.1357. IR(neat): 1735, 765, and 700 cm^{-1}. NMR(CCl_4): 7.30 (5H, m). V, an oil, *MW* Found: *m/e* 214.1342. Calcd for $C_{15}H_{18}O$: *m/e* 214.1357. IR(neat): 2710, 1728, 775, and 700 cm^{-1}. NMR(CCl_4): δ 9.85 (1H, t, J=2 Hz), 7.20 (5H, m), and 2.68 (2H, t, J=7 Hz).

Photoreaction of IIIa and IIIb in the Presence of CF_3COOH.

a) Preparative Experiment: The solution of IIIa or IIIb (500 mg) in 140 ml of thiophene-free benzene was purged by argon and CF_3COOH added to make 0.05M CF_3COOH. Irradiation was carried out (32 h for IIIa and 70 h for IIIb) in the same manner as described for the photoreaction of IIIa in benzene. The reaction solution was passed through an alumina column to remove the acid and concentrated *in vacuo*. Distillation of the residue by a Kugelrohr apparatus gave product VIIa (*ca.* 110 °C/0.1 mmHg) in 63% yield and VIIb (*ca.* 120 °C/0.1 mmHg) in 40% yield. The products VIIa and VIIb were identified by IR, NMR, and GLC analyses with the authentic samples prepared by hydrogenation of IIIa and IIIb over Pd-C catalyst.

b) Detection of Carbon Dioxide: The solution of IIIa (50 mg) in toluene (4 ml) containing 0.05 M CF_3COOH was degassed by the freeze-thaw method and kept under an atomosphere of argon. After irradiation for 9 h, 3 ml of the gaseous layer was introduced into GLC (3 mm $\phi\times$

2.25 m silica gel 60/80 mesh, room temperature). The relative peak intensity of carbon dioxide from the irradiated sample and the sample kept in the dark was 16:1.

c) Solvent Effect: Enone IIIa was dissolved in cyclohexane, benzene, toluene, *p*-xylene and *o*-xylene to make the concentration of each solution to be 0.21M. This concentration was enough to absorb more than 99% of the incident light from the lamp in the $n\pi^*$ region of the enone. To each solution was added 50 μl of CF_3COOH (0.32M) and the solution in the Pyrex tube was irradiated under argon using a Rikosha merry-go-round type irradiation apparatus equiped with a 450W high pressure mercury lamp. The relative rates—the relative quantum yield—of the product were determined by GLC analysis of the product using 3-phenyl-1,3-dihydroisobenzofuran-1-one as an internal reference. The results are shown in Fig. 1.

Photoreaction of IIIa and IIIb in the Presence of Lewis Acid. a) Preparative Experiments: The solution of IIIa or IIIb (800 mg) in 150 ml of thiophene-free benzene containing a Lewis acid (0.05M) was irradiated for 20 h in the same manner as described for the reaction in benzene. The Lewis acid was removed by passing an alumina column by benzene. Alumina chromatography eluted by hexane-dichloromethane and recrystallization from hexane gave the cyclized product VIIIa (25%/BF_3–Et_2O, 63%/$SnCl_4$) or VIIIb (30%/BF_3–Et_2O). The reactions on other solvents are summarized in Table 2. VIIIa; mp 78 °C. Found: C, 84.00; H, 8.54%. Calcd for $C_{15}H_{18}O$: C, 84.07; H, 8.47%. MS *m/e* 214(M^+). IR(neat): 1705, 760, and 700 cm^{-1}. NMR(CCl_4): δ 7.26 (5H, m) and 3.30—3.60 (1H, m). VIIIb; mp 82 °C. Found: C, 84.11; H, 8.85%. Calcd for $C_{16}H_{20}O$: C, 84.16; H, 8.83%. MS *m/e* 228 (M^+). IR(neat): 1710, 760, and 700 cm^{-1}. NMR(CCl_4): δ 7.00 (5H, m) and 3.00—3.40 (1H, m).

b) Solvent Effect: The 0.1 M solution of IIIa in 8 ml of cyclohexane, benzene, toluen, or *o*-xylene containing 0.05 M BF_3–Et_2O was irradiated for 20 h in the same manner as the irradiation of IIIa in the presence of CF_3COOH. The products VIIa and VIIIa were analyzed by GLC (3% OV-17 on Chromosorb W, 190 °C) using an internal reference and the results are summarized in Table 2.

Permanganate Oxidation of the Product VIIIa and VIIIb. The mixture of the one of the products (10 mg) and $KMnO_4$ (36 mg) in 1 ml of water was stirred for 15 h at room temperature. The reaction mixture was extracted with benzene after addition of concd-HCl and the extract treated with an ethereal solution of diazomethane. The methyl ester was identified as methyl benzoate by GLC analysis (3% OV-17 on Chromosorb W). No trace of methyl phthalate was detected.

Quenching Experiments. a): Six Pyrex tubes containing enone IIIa (25 mg), CF_3COOH (15 μl), and dried toluene (3 ml) had 0, 3, 6, 10, 12, and 15μl of 1,3-pentadiene added. The solutions were irradiated using a merry-go-round apparatus for 2 h. After passing the solution through alumina, each sample was analyzed by GLC using an internal reference. Stern-Volmer plots of the product formation gave a linear plot with $k_q\tau$ value of 88 M^{-1}.

b): The mixture of IIIa (21.8 mg), BF_3–Et_2O (20 μl), and benzene (3 ml) containing varing amounts of 1,3-pentadiene was irradiated for 35 h in the same manner as the experiment (*a*) in this section. The product was identified by GLC using ethyl oleate as an internal reference. The Stern-Volmer plots of the product formation were found to be linear having a $k_q\tau$ value of 158 M^{-1}.

References

1) (a) A. Lablache-Combier, *Bull. Soc. Chim. Fr.*, **1972**, 4791; (b) J. N. Pitts, Jr., G. S. Hammond, and K. Gallnick ed, "Advances in Photochemistry," Vol. 10, John-Wiley & Sons, New York, (1977) p. 359—465.

2) R. Ide, Y. Sakata, S.Misumi, T. Okada, and N. Mataga, *J. Chem. Soc., Chem. Commun.*, **1972**, 1009.

3) Y. Sato, H. Nakai, T. Mizuguchi, Y. Hatanaka, and Y. Kanaoka, *J. Am. Chem. Soc.*, **98**, 2349 (1976).

4) D. Brice-Smith, A. Gilbert, and G. Klunklin, *J. Chem. Soc., Chem. Commun.*, **1973**, 330.

5) S. Naruto and O. Yonemitsu, *Tetrahedron Lett.*, **1975**, 3399.

6) M. Tada, H. Saiki, K. Miura, and H. Shinozaki, *J. Chem. Soc., Chem. Commun.*, **1975**, 55; *Bull. Chem. Soc. Jpn.*, **49**, 1666 (1976).

7) M. Tada, H. Saiki, H. Mizutani, and K. Miura, *Bull. Chem. Soc. Jpn.*, **51**, 343 (1978).

8) P. E. Eaton, *Acc. Chem. Res.*, **1**, 50 (1968).

9) S. Murov, "Handbook of Photochemistry," Marcel Dekker, Inc., New York (1973). p. 67.

10) Ref. 9, p. 1.

11) N. J. Rose and R. S. Drago, *J. Am. Chem. Soc.*, **81**, 6138 (1959).

12) G. Gallardo-Herrero, G. Torri, J. F. Gal and M. Azzaro, *Tetrahedron Lett.*, **1972**, 4553.

13) A. Pagliardivi, G. Turro, L. Elegart, and M. Azzaro, *Tetrahedron Lett.*, **1972**, 4241.

14) J. S. Hartman and P. Stilbs, *Tetrahedron Lett.*, **1975**, 3497.

15) E. A. Chandrass and C. J. Dempster, *J. Am. Chem. Soc.*, **92**, 3586 (1970). See also Refs. 1 and 2.

16) J. W. Cook and C. L. Hawett, *J. Chem. Soc.*, **1933**, 1098.

17) M. Fieser and L. Fieser, "Reagents for Organic Synthesus," Vol. 2, Wiley-Interscience, New York (1969), p. 369.

Magnitude of Mercury Levels in Fish Muscle Tissue from South Carolina Waters

Andrew K. Koli and Edward McClary

South Carolina State College, Orangeburg, South Carolina 29117 U. S. A.

(Received November 13, 1976)

Many of the world's great gastronomic materpieces are based on fish from both freshwater and saltwater. The danger for human health, due to fish consumption, has been very well recognized. A survey of mercury residues in freshwater fish was undertaken to see if the problem of the magnitude of mercury contamination was evident in the South Carolina Fishery. These investigations were initiated to determine mercury levels in fish from a variety of South Carolina Waters. Samples of fish from freshwater sources all over the state of South Carolina were collected during 1974 and 1975. The species composition of the collections generally reflects the fish populations of the water sampled. Mercury determinations were made on 100 samples of fish taken from 22 locations covering 46 South Carolina counties. Triplicate samples of fish tissues were analyzed using flameless atomic absorption procedures. Findings of this report are that magnitude of mercury levels of fish from Lake Jocassee and Edisto River have been found to be higher than other waterways surveyed. Mercury levels exceeding the U. S. Food and Drug Administration guideline of 0.5 ppm have been found in Brown Trout, Pike and Mudfish. Different patterns of mercury concentration occurred between different tissues. Larger fish contain higher concentration of mercury than do smaller fish of the same species.

A survey of mercury residues in freshwater fish was undertaken in July 1974. These investigations were initiated to determine mercury levels in fish from a variety of South Carolina waters. The survey was undertaken to see if the problem of the magnitude of mercury contamination was evident in the South Carolina Fishery. The danger for human health, due to fish consumption, has been very well recognized. The first known cases of human poisoning from fish contaminated with methylmercury were reported in Japan, on Minamata.[1,2] Samples of fish from freshwater sources all over the state of South Carolina were collected during the summers of 1974 and 1975. Mercury determinations were made on 100 samples of fish taken from 22 locations covering 46 South Carolina counties. The species composition of the collections generally reflects the fish populations of the waters sampled. Triplicate samples of fish tissue were analyzed using flameless atomic absorption procedures out-lined by Hatch and Ott.[3] The significant findings of this report are that magnitude of mercury levels of fish from Lake Jocassee and Edisto River have been found to be higher than other waterways surveyed. Mercury levels exceeding the U.S. Food and Drug Administration guideline of 0.5 ppm for muscle tissue have been found in Brown Trout, Pike and Mudfish. Different patterns of mercury concentration occurred between different tissues. Larger fish contain higher concentration of mercury than do smaller fish of the same speices as reported by Scott and Armstrong.[4]

Experimental

Sample Collection. Samples of fish from freshwater sources of lakes, rivers, streams and ponds all over the state of South Carolina were collected during the summers of 1974 and 1975. Lakes include Marion, Moultrie, Murray, Clark Hill, Keowee, Wateree, Jocassee, Greenwood, Hartwell, Wylie, Robinson, Secession, and Cherokee Falls and rivers include Edisto River and Savannah River.

The fish collected were Bluegill (*Lepomis macrochirus*), White Bass (*Roccus crysops*), Largemouth Bass (*Micropeterus salmoides*), Brown Trout (*Salmo trutta*), Channel Catfish (*Ictalurus Punctatus*), Pike (*Esox lucius*), Black Crappie (*Pomoxis nigromaculatus*), Redbreast (*Lepomis auritus*), Shad (*Alosa sapidissima*), Warmouth (*Lepomis gulosus*), Striped Bass (*Roccus saxatilis*), Mudfish (*Amia calva*), Jackfish (*Caranx hippos*), Shiner (*Notropis spp*), and Carp.

Wet Digestion. Fish tissue, 0.2 to 0.3g were weighed accurately and placed in the bottom of a clean dry Erlenmeyer flask which is closed with a polyethylene stopper. Samples were digested with 5 ml of 9M sulfuric acid and 1 ml of 5.6M nitric acid mixture. The sample flasks were incubated in a shaking water bath at 58°C until the tissue was completely dissolved giving a clear solution (50—60 min). Sample flasks were removed from the bath and allowed to cool in ice. Chemical oxidation of the samples were carried out by addition of 5 ml of 5% potassium permanganate slowly with swirling in each flask. Samples were kept overnight before analysis without apparent loss of mercury. Enough water was added to make the total volume approximately 125 ml. 1.5% Hydroxylamine hydrochloride solution, 5 ml, was added to reduce the excess permanganate. After 30 s, 5 ml of 10% Tin(II) chloride solution was added and immediately attached the flask to the aeration system.[5]

Mercury Determination by Atomic Absorption. Digests were analyzed using flameless atomic absorption spectrophotometry procedures outlined by Hatch and Ott[3] and Uthe *et al.*[5] as modified for use with a Perkin Elmer, Coleman MAS-50 mercury analyzer. Determination of mercury in fish tissue was measured in parts per million (ppm). The analytical error was $\pm 10\%$ at 0.1 ppm mercury level.

Results and Discussion

Mercury determinations were made on 100 samples taken from 22 locations covering 46 South Carolina counties. The species composition of the collections generally reflects the fish populations of the waters sampled. All South Carolina fish analyzed countained mercury. Mercury levels in fish averaged 0.13 ppm and ranged between 0.02 and 0.64 ppm.

Different species vary in mercury content and larger fish contain higher concentrations of mercury than do small fish of the same species taken from the same water. Pike, Mudfish, Brown Trout and Largemouth Bass showed higher mercury concentrations, while the pan-

Table 1. Magnitude of mercury levels in fish muscle tissue from various South Carolina waters

Station	Date	Species	Weight (g)	Mercury in wet weight (ppm)
Lake Secession	2/3/75	Striped bass	679	0.03
	2/3/75	Striped bass	657	0.03
	2/5/75	White bass	627	0.05
	2/5/75	White bass	463	0.12
	2/5/75	White bass	495	0.13
	2/17/75	White bass	873	0.11
	2/17/75	White bass	705	0.09
	2/17/75	Black crappie	703	0.09
	3/3/75	Shad	164	0.21
	3/3/75	Shad	179	0.19
	3/3/75	Shad	194	0.16
	3/5/75	White bass	536	0.11
	3/5/75	Black crappie	400	0.08
	3/5/75	Shad	219	0.10
	3/5/75	White catfish	258	0.07
	3/19/75	White bass	502	0.10
Lake Wylie	5/26/75	Bluegill	73	0.02
(4-Season fishing)	5/26/75	Bluegill	78	0.03
	5/26/75	Bluegill	61	0.03
	5/29/75	Redbreast	66	0.04
	5/29/75	Redbreast	49	0.04
	5/29/75	Redbreast	45	0.03
Lake Wateree	6/4/75	Channel catfish	161	0.06
(Great Falls)	6/4/75	Channel catfish	131	0.03
	6/4/75	Channel catfish	95	0.02
Lake Robinson	5/19/75	Redbreast	253	0.05
(Near dam)	5/19/75	Bluegill	51	0.04
	5/19/75	Bluegill	40	0.04
	5/20/75	Bluegill	49	0.03
	5/20/75	Bluegill	42	0.04
	5/20/75	Bluegill	41	0.04
Lake Jocassee	5/21/75	Bluegill	17	0.02
(Boat dock)	10/13/75	Bluegill	117	0.31
	10/13/75	Bluegill	86	0.29
	10/13/75	Bluegill	86	0.18
	10/13/75	Bluegill	59	0.20
(Devil's fork)	2/9/76	Brown trout	1927	0.53
	2/19/76	Brown trout	1542	0.58
	2/19/75	Brown trout	2041	0.51
Lake Moultrile	7/18/74	Redbreast	25	0.16
(Monck's corner)	7/18/74	Bluegill	51	0.10
(Harry's fish camp)	9/30/75	Redbreast	106	0.14
	9/30/75	Redbreast	99	0.06
	9/30/75	Redbreast	76	0.08
	10/2/75	Bluegill	113	0.05
	10/2/75	Bluegill	93	0.04
	10/2/75	Bluegill	71	0.03
	10/6/75	Bass	54	0.08
	10/6/75	Bass	46	0.06
(Bonneau Dykes)	10/8/75	Channel catfish	172	0.06
	10/8/75	Channel catfish	113	0.04
Edisto River	7/18/74	Bluegill	29	0.48
(Orangeburg)	7/18/74	Warmouth	76	0.49
	1/22/75	Mudfish	2000	0.63
	1/22/75	Bass	53	0.45
	1/22/75	Warmouth	143	0.38
	7/15/75	Bluegill	29	0.36
	1/27/75	Largemouth bass	483	0.59
Lake Murray	7/25/74	Catfish	50	0.06
(Below dam)	7/25/74	Catfish	37	0.08
(Hendrix landing)	7/9/75	Pike	741	0.64
Lake Hartwell	9/16/74	Catfish	41	0.14
(Gulley)				
(Stone creek clove)	7/29/74	Bluegill	59	0.06
	7/29/74	Bass	52	0.07
	7/29/74	Bluegill	49	0.03
(Jewel Bridge)	10/16/75	Bluegill	112	0.14
	10/16/75	Bluegill	107	0.09
	10/16/75	Bluegill	102	0.09
	10/16/75	Bluegill	80	0.07
	10/22/75	Bluegill	79	0.08
	10/22/75	Bluegill	73	0.08
	10/22/75	Bluegill	70	0.06
	10/22/75	Bluegill	60	0.09
Lake Keowee	10/1/74	Bluegill	102	0.12
	10/1/74	Bluegill	86	0.08
	10/1/74	Bluegill	45	0.04
	9/24/74	Bluegill	41	0.08
Lake Marion	1/16/75	Bluegill	15	0.06
(Santee refuge)	1/16/75	Redbreast	33	0.06
	1/16/75	Jackfish	206	0.18
	1/20/75	Bass	352	0.09
	1/20/75	Shiner	39	0.03
Clark Hill reservoir	3/10/75	Redbreast	63	0.07
	3/10/75	Redbreast	42	0.04
	3/10/75	Redbreast	28	0.02
	3/10/75	Redbreast	23	0.02
Lake Greenwood	6/16/75	Bluegill	57	0.08
(Floyd's landing)	6/16/75	Bluegill	83	0.02
	6/16/75	Bluegill	58	0.02
Savannah River	2/19/75	Mudfish	972	0.17
	2/19/75	Catfish	188	0.09
	2/19/75	Catfish	140	0.06
(Cohan's bluff)	9/17/75	Redbreast	329	0.14
	9/17/75	Bluegill	82	0.06
	9/17/75	Redbreast	266	0.04
Cherokee Falls	10/27/75	Catfish	95	0.06
(Below dam)	10/27/75	Catfish	81	0.05
	10/27/75	Catfish	77	0.06
	10/27/75	Catfish	62	0.04
	10/29/75	Catfish	674	0.19

fishes, including Bluegill, Redbreast, Shad, Warmouth, Catfish, Carp, Shiner often showed low concentrations.

Mercury levels exceeding the U.S. Food and Drug Administration guideline of 0.5 ppm for flesh have been found in Pike, Trout and Mudfish. No fish weighing less than a thousand grams had mercury levels above the currently accepted guideline of 0.5 ppm. Of the three fish weighing more than a thousand grams whole body weight, a Pike (1.0 kg) had muscle mercury levels of 0.64 ppm; Mudfish (2.0 kg) had muscle mercury levels of 0.63 ppm and Brown Trout (1.9 kg) had muscle mercury levels of 0.53 ppm.

Concentrations increased with increased body weight and biological amplification or magnification of mercury occurred through the food chain. Mudfish feeds on the bottom sediments and that might be the reason for higher mercury content. Pike and Trout seem to have higher mercury levels because of their predatory (carnivorous) eating habits.

Mercury levels in fish samples taken from Lake Secession ranged from 0.03 to 0.21 ppm; Lake Wylie ranged form 0.02 to 0.04 ppm; Lake Wateree ranged from 0.02 to 0.06 ppm; Lake Robinson ranged from 0.03 to 0.05 ppm; Lake Jocassee ranged from 0.02 to 0.58 ppm; Lake Moultrie ranged from 0.03 to 0.16 ppm; Edisto River ranged from 0.36 to 0.63 ppm; Lake Murray ranged from 0.06 to 0.64 ppm; Lake Hartwell ranged from 0.03 to 0.14 ppm; Lake Keowee ranged from 0.04 to 0.12 ppm; Lake Marion ranged from 0.03 to 0.18 ppm; Lake Clark Hill ranged from 0.02 to 0.07 ppm; Lake Greenwood ranged from 0.02 to 0.08 ppm; Savannah River ranged from 0.06 to 0.17 ppm and Lake Cherokee Falls ranged from 0.04 to 0.19 ppm (Table 1).

Mercury levels in Bluegill taken from Lake Jocassee and Edisto River were about one order higher than all other lakes and rivers surveyed. Matsunaga[6] has reported that mercury levels in fish taken from rivers containing mercury of 0.02 μg/l were about one order higher than natural rivers containing mercury of 0.002 μg/l. Thus, the higher levels of mercury found in both Edisto River and Lake Jocassee Fish can be related to pollution due to exposure to waters from sewege, agricultural drainage, industry waste water, and surface pollutants.

In this study, mercury in waters and in sediments was also determined (Tables 2 and 3). The mercury levels of water from Lake Jocassee and Edisto River were higher than all other Lakes and Rivers.

Relative Mercury Content of Fish Tissues. The mercury levels in different tissues, liver, kidney, muscle, skin, bone, gills, scales, fin, gonads, brain, stomach, spleen and heart of Brown Trout were determined. It seems different patterns of mercury concentration occur between tissues (Fig. 1). This was concluded from the analysis of Brown Trout from Lake Jocassee. We selected this species as an ideal to find out patterns of mercury levels in different tissues, since it had more than 0.5 ppm mercury content which is the upper limit according to Food and Drug Administration guideline.

The mercury content of fin, eye, scales, skin, bone,

Table 2. Water qtality data

Sample station	pH	Mercury level (μg/l)
Lake Jocassee	6.3	0.025
Edisto River	6.5	0.026
Lake Wylie	6.8	<0.01
Lake Wateree	6.6	<0.01
Lake Robinson	6.5	<0.01
Lake Moultrie	6.9	<0.01
Lake Murray	6.7	<0.01
Lake Hartwell	6.5	<0.01
Lake Keowee	6.4	<0.01
Lake Marion	6.7	<0.01
Lake Clark Hill	6.6	<0.01
Lake Greenwood	6.7	<0.01
Savannah River	6.5	<0.01
Cherokee Falls	6.6	<0.01

Table 3. Sediment quality data

Sample station	Sediment type	Mercury level in dry weight (ppm)
Lake Jocassee	Coarse sand	0.07
Edisto River	Coarse sand	0.06
Lake Wylie	Fine sand	0.02
Lake Wateree	Fine sand	0.02
Lake Robinson	Fine sand	0.02
Lake Moultrie	Fine sand	0.01
Lake Murray	Fine sand	0.01
Lake Hartwell	Fine sand	0.03
Lake Keowee	Fine sand	0.03
Lake Marion	Fine sand	0.02
Lake Clark Hill	Fine sand	0.01
Lake Greenwood	Fine sand	0.02
Savannah River	Fine sand	0.03
Cherokee Falls	Fine sand	0.01

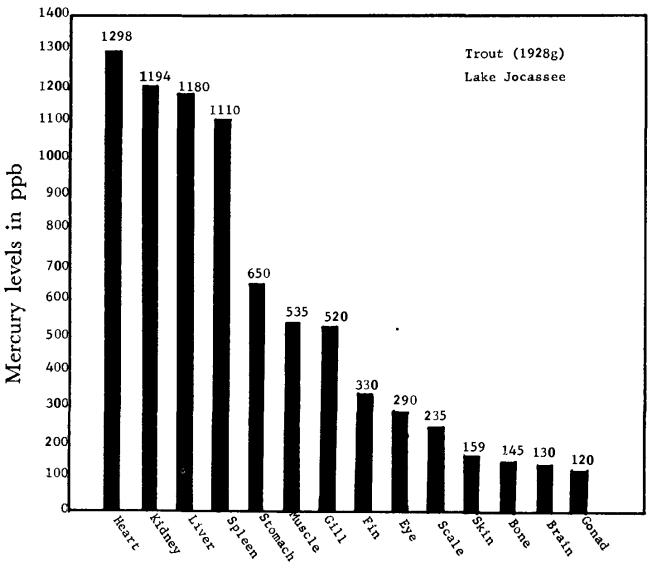

Fig. 1. Relative mercury content of fish tissues of Brown Trout.

brain and gonads was relatively low. Stomach, muscle and gills were intermediate in mercury content. Higher levels of mercury occurred in liver, kidney, spleen and heart (Fig. 1). It seems highly vascularized blood tissues had the highest mercury content than other tissues analyzed. The patterns of concentration occurred between tissues seemed characteristics of species, and suggests that patterns of uptake, accumulation and elimination differ between species.

Conclusions

The significant findings of this report are that magnitude of mercury levels of fish from Lake Jocassee and Edisto River have been found to be higher than other waterways surveyed. Carnivorous and bottom-feeding fishes are the most reliable indicators of mercury pollution. Mercury levels exceeding the U.S. Food and Drug Administration guideline of 0.5 ppm for muscle tissue have been found in Brown Trout, Pike and Mudfish. Different patterns of mercury concentration occurred between different tissues Larger fish contain higher concentration of mercury than do smaller fish of the same species.

This work is a result of research grant supported by CSRS Grant No. 416-05-01, U.S. Department of Agriculture, in cooperation with Cooperative State Research Service, USDA. The authors thank Dr. R.L. Hurst, Vice-President of Research, Planning and Extension and Dr. S. S. Sandhu, Head of water Pollution Laboratory for their help in this research.

References

1) L. T. Kurland, S. M. Faro, and H. Seidler, *World Neurol*, **1**, 370 (1960).

2) M. Kutsuma, "Study group of Minamata Disease," Kumamoto University, Kumamoto, Japan (1968).

3) W. R. Hatch and W. L. Ott, (Determination of submicrogram quantities of mercury by atomic absorption spectrophotometry), *Anal. Chem.*, **40**, 2085 (1968).

4) Scott and Armstrong, *J. Fish. Res. Board of Canada*, **79**, 1685 (1972).

5) J. M. Uthe, F. A. J. Armstrong, and M. P. Stainton, (Mercury determinations in fish samples by wet digestion and flameless atomic absorption spectrophotometry), *J. Fish. Res. Board of Canada*, **27**, 805 (1970).

6) K. Matsunaga, *Nature*, **257**, 49 (1975).

Investigation on the Lanthanoid Chelates of 1-Phenyl-3-methyl-4-benzoyl-5-pyrazolone. An Examination of the Phenomenon of Hypersensitivity

Ajoy Roy and K. Nag*

Department of Inorganic Chemistry, Indian Association for the Cultivation of Science, Calcutta 700032, India

(Received February 25, 1977)

1-Phenyl-3-methyl-4-benzoyl-5-pyrazolone (Hpmbp) form complexes with lanthanoids of the type $Ln(pmbp)_3 \cdot nH_2O$ ($n=4$ for La—Sm, and $n=1$ for Eu—Yb and Y), $Ln(pmbp)_3 \cdot 2pyridine \cdot 2H_2O$, $Ln(pmbp)_3 \cdot (2,2'\text{-bipyridine/}1,10\text{-phenanthroline}) \cdot C_2H_5OH$, $NH_4[Ln(pmbp)_4] \cdot C_2H_5OH$ and $Q^+[Ln(pmbp)_4] \cdot C_2H_5OH$, where Q^+ is the quaternary ammonium cation of piperidine, pyrrolidine or morpholine. These compounds have been characterized from physicochemical studies. The electronic spectra of the Nd(III) complexes have been studied in detail to investigate the phenomenon of hypersensitivity with respect to the coordination environment and solvent medium. In these compounds solvent does not play a significant role to cause variation in hypersensitivity. The oscillator strengths of the hypersensitive transition in these compounds show the following trend: $Q^+[Nd(pmbp)_4] > Nd(pmbp)_3 \cdot phen > Nd(pmbp)_3 \cdot bpy > Nd(pmbp)_3 \cdot 2py \cdot 2H_2O > Nd(pmbp)_3 \cdot 2H_2O$. In the Pr(III) complexes the band due to $^3H_4 \rightarrow {}^1D_2$ transition has been found to be hypersensitive, and the gradation of intensity due to this band follows almost the same trend as in the corresponding Nd(III) complexes.

Since the introduction of 1-phenyl-3-methyl-4-benzoyl-5-pyrazolone (Hpmbp) as a chelate-forming extractant by Jensen[1] extensive studies have been made on the use of this reagent for solvent extraction and separation of various metal ions[2,3]. The versatility of Hpmbp is comparable to the more popular extractant thenoyltrifluoroacetone (Htta).[4] In previous publications[5,6] we have reported solvent extraction behavior of the entire lanthanoid series using Hpmbp as the extractant and have noted the "tetrad effect" in the series.

Although composition and stability constants of extracted binary or ternary complexes (formed in the presence of Lewis bases during synergistic extraction) of Hpmbp with various metal ions have been determined, characterization of these compounds in the solid state have been scarcely made. To our knowledge only Cu(II) and VO^{2+} chelates have been investigated so far.[7] We wish to report here synthesis and characteristics of several types of lanthanoid chelates with Hpmbp. Our interest in these compounds stems from a desire to investigate the phenomenon of hypersensitivity which is a subject of considerable interest.

Experimental

Materials. Lanthanoids oxides (99.9% pure) were obtained from Johnson Matthey (U.K.) and A.D. Mackay (U.S.A.). Hpmbp was prepared by a modified procedure[8] of Jensen.[1] The compound in its keto form was obtained by recrystallization from (1 : 4) ethanol-water mixture (mp 120 °C, lit, 122 °C) and in the enol form from heptane (mp 91 °C, lit, 92 °C).

Preparation of the Chelates. The method adopted for the preparation of a particular type of lanthanoid chelate is the same for all the metal ions. Here preparations are described with respect to neodymium.

$Nd(pmbp)_3 \cdot 4H_2O$: Hydrated neodymium nitrate (1 mmol) and Hpmbp (3 mmol) were dissolved separately in ethanol (10 ml), then mixed together and stirred for a few minutes. Water was slowly added to the solution until precipitation of the compound occurred. After stirring the mixture for 30 min, the compound was filtered and washed thoroughly with water and petroleum ether. The compound was recrystallized from ethanol-water mixture (1 : 1).

$Nd(pmbp)_3 \cdot 2py \cdot 2H_2O$: One g (*ca.* 1 mmol) of $Nd(pmbp)_3 \cdot 4H_2O$ was dissolved in 30 ml ethanol. To it 1 g (12 mmol) of pyridine was added and the solution was refluxed on a water bath for 4 h. After filtration, the filtrate was concentrated to a small volume. The compound separated was filtered, and was washed with cold ethanol and petroleum ether.

$Nd(pmbp)_3(bpy/phen) \cdot C_2H_5OH$: To an ethanolic solution (10 ml) of hydrated neodymium nitrate (1 mmol) an ethanol solution (15 ml) containing 3 mmol of Hpmbp, 1 mmol of 2,2'-bipyridine (or 1,10-phenanthroline) and 3 mmol of sodium hydroxide was added in a dropwise manner with stirring. The mixture was stirred for 30 min and the volume was then reduced to about 5 ml, cooled and filtered. The product was washed with water, a small amount of cold ethanol and finally with benzene. The compound was recrystallized from (1 : 1) ethanol-water mixture.

*$Q^+[Nd(pmbp)_4] \cdot C_2H_5OH$***: To a stirred ethanol solution (25 ml) containing 1 mmol of hydrated neodymium nitrate and 4 mmol of Hpmbp was slowly added 4 mmol of the heterocyclic base (diluted in 5 ml of ethanol). The mixture was stirred for 30 min, evaporated to $\approx$10 ml, filtered, and the product was washed with petroleum ether and water. It was recrystallized from (2 : 1) ethanol-water mixture.

$NH_4[Nd(pmbp)_4] \cdot C_2H_5OH$: In the above preparation instead of adding a heterocyclic base ammonia gas was passed through the solution for 30 min. The mixture was filtered and the filtrate was evaporated almost to dryness. The compound separated was collected and recrystallized from (1:1) ethanol-water mixture.

All these compounds were obtained in high yield, 70—90%.

Analyses. Carbon, hydrogen and nitrogen were analysed in the microanalytical laboratory of this Institute. Lanthanoids were estimated after decomposing the compounds with acid mixtures (HNO_3-$HClO_4$) and titrating with Na_2H_2-edta using Xylenol Orange as the indicator.[9]

Physical Measurements. Conductivity measurements were carried out using a Philips PR 9500 conductivity bridge. Infrared spectra were recorded on Perkin-Elmer 225/621 spectrometers in KBr pellets (in the range 4000—400 cm^{-1}). and in nujol or hexachlorobutadiene mulls (between 700—200 cm^{-1}). Electronic spectral measurements were carried

* For correspondence.

** Q^+ is the quaternary ammonium cation of morpholine, piperidine or pyrrolidine.

Table 1. Analytical data

Compound	C%		H%		N%		M%	
	Calcd	Found	Calcd	Found	Calcd	Found	Calcd	Found
Hpmbp	73.38	73.27	5.40	5.18	10.07	10.01	—	—
$Nd(pmbp)_3 \cdot 4H_2O$	58.45	58.63	4.49	4.72	8.02	7.95	15.75	15.40
$Nd(pmbp)_3 \cdot 2H_2O$	60.53	59.96	4.25	4.41	8.31	8.25	14.24	14.10
$Nd(pmbp)_3 \cdot py_2 \cdot 2H_2O$	62.62	62.08	4.53	4.82	9.58	9.45	12.32	12.18
$Nd(pmbp)_3 \cdot bpy \cdot C_2H_5OH$	64.24	63.92	4.54	4.42	9.51	9.37	12.24	12.37
$Nd(pmbp)_3 \cdot phen \cdot C_2H_5OH$	64.86	64.70	4.41	4.29	9.93	9.21	11.99	11.80
$Hpiper[Nd(pmbp)_4] \cdot C_2H_5OH$	65.01	64.86	5.06	4.95	9.10	9.20	10.40	11.25
$Hpyrrol[Nd(pmbp)_4] \cdot C_2H_5OH$	64.82	64.70	4.96	4.81	9.20	9.35	10.52	10.65
$Hmorph[Nd(pmbp)_4] \cdot C_2H_5OH$	64.00	63.87	4.51	4.40	9.09	9.00	10.39	10.52
$NH_4[Nd(pmbp)_4] \cdot C_2H_5OH$	63.84	63.80	4.71	4.78	9.58	9.53	10.94	10.86
$Eu(pmbp)_3 \cdot H_2O$	61.12	61.16	4.10	4.26	8.39	8.27	15.18	15.11
$Y(pmbp)_3 \cdot H_2O$	64.71	64.50	4.33	4.45	8.88	8.65	10.47	10.42
$Sm(pmbp)_2 \cdot bpy \cdot C_2H_5OH$	63.90	63.81	4.48	4.37	9.47	9.41	12.68	12.75
$Su(pmbp)_3 \cdot bpy$	63.81	63.70	4.10	4.15	9.76	9.65	13.08	13.01
$Gd(pmbp)_3 \cdot phen \cdot C_2H_5OH$	64.25	64.42	4.37	4.28	9.23	9.15	12.93	12.82
$Hpiper[Pr(pmbp)_4] \cdot C_2H_5OH$	64.16	65.08	5.07	5.00	9.12	9.12	10.21	10.30
$Hpiper[Pr(pmbp)_4]$	65.61	65.60	4.79	4.71	9.44	9.52	10.32	10.24
$Hpyrrol[Er(pmbp)_4] \cdot C_2H_5OH$	63.74	63.31	4.88	4.74	9.04	9.08	11.99	11.87
$Hmorph[Yb(pmbp)_4] \cdot C_2H_5OH$	62.76	62.25	4.80	4.74	8.91	8.85	12.23	12.30

py, pyridine; bpy, 2,2′-bipyridine; phen, 1,10-phenanthroline; piper, piperidine; pyrrol, pyrrolidine; morph, morpholine.

out either on a Spectro MOM 201 or a Hilger UV-spek spectrophotometer. For measurements in the visible range, the solutions used mostly had a concentration $\approx 1 \times 10^{-2}$ M. The oscillator strength (P) was determined from the relation[10]

$$P = 4.31 \times 10^{-9}\left[\frac{9n}{(\eta+2)^2}\right]\varepsilon_1(\nu_1)\mathrm{d},$$

where n is the refractive index of the medium, ε_1 is the molar extinction coefficient and ν_1 is the energy of transition in cm^{-1}. The band areas were measured by a planimeter.

Results and Discussion

The analytical data of the lanthanoid complexes are summarized in Table 1. In general, the compounds are freely soluble in acetone, ethanol and chloroform, less soluble in benzene, and insoluble in hydrocarbon solvents. These compounds are generally light yellow in color, but the neodymium compounds show dichroic behavior; violet in the day light and greenish-yellow under a fluorescent lamp. The compounds of the type, $Q^+[Ln(pmbp)_4]$ and $[Ln(pmbp)_3L]$ (where L is 2,2′-bipyridine or 1,10-phenanthroline) contain one molecule of ethanol as the solvent of crystallization which can be removed by heating at *ca.* 60 °C for an hour. The tris-chelates of the lower lanthanoids (La—Sm) having the composition $Ln(pmbp)_3.4H_2O$ contain two coordinated water molecules. The two solvated water molecules may be removed by heating at 100 °C for 2 h. Thermal analysis shows that $Ln(pmbp)_3.2H_2O$ is stable up to 200°C, and beyond this temperature further loss of water molecules cause decomposition of the compound. On the other hand, the tris-chelates of the higher lanthanoids (Eu onward), $Ln(pmbp)_3 \cdot H_2O$ do not contain any water of crystallization. Conductivity measurements of the tetrakis-chelates in nitrobenzene show that Λ_M values are in the range 20—25 $ohm^{-1}\,cm^2\,mol^{-1}$ which are consistent with the 1:1 electrolytic behavior of the compounds.[11]

Hpmbp can be isolated both in keto and enol forms (Ia, Ib). The reagent is comparatively a strong acid, ($pK_a = 4.10^5$) and although its distribution constrants in various solvents have been determined[2], no information regarding the keto-enol equilibrium in organic solvents is known. Unfortunately, the reagent does not have enough solubility in major organic solvents suitable for studying NMR spectra. In an attempt to study this equilibrium the electronic spectra of Hpmbp in several organic solvents have been recorded. The pertinent data summarized in Table 2 show that the reagent has two absorption bands, but neither of these can be related to a particular tautomer. On the contrary, both the bands are composite type, having significant contribution of the either forms. It may be mentioned that the enol form is obtained by recrystallization from heptane.[1-4] On this basis one may expect that in heptane the reagent remains at least 98% in the enol form, if not exclusively. It follows from Table 2 that the decreased order of molar absorptivity of the lower wavelength band with respect to solvent is, heptane>methanol>ethanol>chloroform; whereas the corresponding order for the higher wavelength band is, chloroform>heptane>carbon tetrachloride>methanol>ethanol. It is well-known that an enol content increases with the decrease in dielectric constant of a solvent. On this basis the higher wavelength band gives an indication of the decreased order of the enol content, although the position of chloroform is confusing. Attempt was also made to determine keto-enol ratio by Meyer's bromine absorption method.[12] However, this approach was unsuccessful because bromine nonselectively gets absorbed both by

Table 2. Electronic spectral data of Hpmbp

Solvent	λ_{max} (nm)	ε
Methanol	236	16840
	273	17300
Ethanol	238	16190
	278	15080
Heptane	242	19200
	289	17570
Chloroform	246	15350
	287	17950
Carbon tetrachloride	—	—
	291	17490

the double bond and the phenyl rings.

The IR spectrum of the enolic form of the ligand shows a broad band at 2540 cm^{-1} which is evidently due to hydrogen bonded OH. Hpmbp contains a large number of bands in the region 1700—200 cm^{-1} which rendered frequency assignments somewhat difficult. It is possible, however, to obtain some useful information regarding the metal–ligand bonding. For example, the ligand bands at 1662 and 1638 cm^{-1} are considerably shifted to lower frequency $\approx$1610 cm^{-1} in the metal chelates and thus can be related to the C=O stretching. On the other hand, a band at 1590 cm^{-1} in the ligand remains unaltered in the chelates and is therefore due to phenyl ring stretching. Similarly, another unaffected band at 1575 cm^{-1} appears to be due to C=C/C=N stretchings. The ligand band at 1545 cm^{-1} which gets displaced to 1525—1500 cm^{-1} in the complexes has major contribution due to C=O stretching. The remaining large number of bands which are mostly composite type do not undergo major shift in frequency in the complexes. A broad band in the complexes observed at 3400—3300 cm^{-1} is either due to the water molecules (in the tris-chelates) or the ethanol molecule (in the tetrakis- or the adduct type chelates). It has been observed that although the ligand has a weak band at 410 cm^{-1}, in the tris- or the adduct type chelates another new band appears at 400 cm^{-1}. In the tetrakis-chelates this band is observed at 435—440 cm^{-1}. We infer this band as due to Ln–O stretching. Indeed Liang *et al.*[13] also observed that Ln–O stretching vibration appears at 400—420 cm^{-1} in a large number of lanthanoid β-diketonates of both tris- and tetrakis-type.

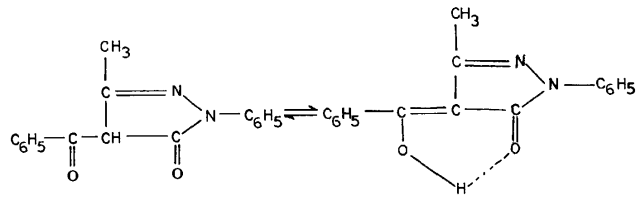

Ia Ib

The electronic spectral characteristics of the compounds under discussion have been studied in detail with respect to those derived from Nd(III) and to a limited extent for the Pr(III) complexes. Admittedly useful information could have been obtained for the Ho(III) and Er(III) complexes but their hypersensitive bands appear in the region where there is considerable absorbance due to ligand/or charge-transfer tail.

Table 3 lists the oscillator strengths for several non-hypersensitive transitions in the neodymium complexes in several solvents. It may be noted from a comparison of these values with those of neodymium perchlorate[14] that the coordination environment or the solvent medium have little effect on the variation of band intensities. This is in accordance with the model proposed by Judd[15] and Oflet[16] for the intensities of f-f transitions.

In Table 4 the oscillator strengths (P) for the hypersensitive transition in the Nd(III) complexes have been summarized. It may be noted that in the $Q^+[Nd(pmbp)_4]$ type complexes P values are independent of the Q^+ cations and there is a marginal variation in hypersensitivity with respect to the solvent medium. Interestingly, in $Q^+[Nd(sdbm)_4]$ chelates (Hsdbm=1,3-diphenyl-3-thioxo-1-propanone) we noted[17] that while Q^+ ions had no effect, however, the oscillator strengths in acetone were significantly higher than in chloroform and benzene. We rationalized this variation by invoking a difference in symmetry of the dissociated (in acetone) and undissociated (in chloroform or benzene) form of the complexes. The fact that the $Q^+[Nd(pmbp)_4]$ complexes do not show such a behavior implies that dissociation of these complexes do not profoundly affect their symmetries. According to Henrie *et al.*[18] symmetry does have implication on the overall intensity but hypersensitivity *per se* can not be classified as being due to a symmetry phenomenon.

Table 4 reveals that the gradation of hypersensitivity in the compounds is $Q^+[Nd(pmbp)_4]>Nd(pmbp)_3\cdot phen > Nd(pmbp)_3\cdot bpy > Nd(pmbp)_3\cdot 2py\cdot 2H_2O > Nd(pmbp)_3\cdot 2H_2O$. The greater hypersensitivity of the tetrakis complexes over the tris species can be rationalized by invoking an important observation made by Barnes and Pincott[19] that not only are the energies of the lanthanoid charge-transfer transitions dependent on the ligand but also they increase in a stepwise manner with the stepwise addition of ligands. Similar observation as the present one was made by us[17,20] previously for β-thioxo ketonates and also by Poluektov *et al.*[21] for a number of phenolic ligands.

Table 4 shows that the addition of heterocyclic donors to the tris-chelate do as not profoundly increase hypersensitivity in the adducts. Sinha *et al.*[22] observed that hypersensitivity in neodymium complexes shows the trend phen>bpy>H_2O, but the differences are not much. Our results also show a similar trend. Sinha *et al.*[22] related the above trend to the poor donor capacity of nitrogen atom toward lanthanoid ions which indeed is an estabilshed fact.[23] Sinha and Green reported[24] that the formation constants of lanthanoid-phen or bpy complexes are extremely low, log $K_1\approx 1$.

Literature shows[25–27] that the increased order of hypersensitivity in tris-β-diketonates is hexafluoroacetylacetone < trifluoroacetylacetone < acetylacetone <benzoylacetone< thenoyltrifluoroacetone < dibenzoylmethane. In the corresponding β-thioxo ketonates also the following trend was observed by us[17,20] 4-phenyl-4-thioxo-2-butanone<4-thenoyl-4-thioxo-1,1,1-trifluoro-2-butanone < 1,3-diphenyl-3-thioxo-1-propanone. These results combined together imply that hypersensitivity

Table 3. Oscillator strength (P) of some non-hypersensitive transition in neodymium complexes

Compound	Solvent	$P \times 10^6$		
		$^4I_{9/2}$ $^4F_{3/2}$ (10800—11800 cm^{-1})	$^4I_{9/2} \rightarrow {}^4F_{5/2}$, $^2H_{9/2}$ (11800—13000 cm^{-1})	$^4I_{9/2} \rightarrow {}^4F_{7/2}$, $^4S_{3/2}$ (13000—14100 cm^{-1})
$Nd(ClO_4)_3$	$DClO_4$-HClO	2.57[a]	8.54[a]	8.78[a]
$Nd(pmbp)_2 \cdot 2H_2O$	Chloroform	2.84	11.51	9.89
	Acetone	2.30	10.44	10.86
	Benzene	2.92	10.17	10.70
	Methanol	2.77	11.44	11.12
$Nd(pmbp)_3 \cdot py_2 \cdot 2H_2O$	Chloroform	2.75	10.77	8.92
$Nd(pmbp)_3 \cdot bpy \cdot C_2H_5OH$	Chloroform	3.16	11.20	11.22
	Methanol	3.28	11.11	11.45
	Acetone	3.22	11.35	11.17
	Benzene	2.67	11.05	10.37
$Nd(pmbp)_3 \cdot phen \cdot C_2H_5OH$	Chloroform	2.86	11.13	10.86
$NH_4[Nd(pmbp)_4] \cdot C_2H_5OH$	Chloroform	2.75	11.13	9.89
$Hpiper[Nd(pmbp)_4] \cdot C_2H_5OH$	Chloroform	2.48	11.47	11.47
$Hpyrrol[Nd(pmbp)_4] \cdot C_2H_5OH$	Chloroform	2.88	11.39	10.70
$Hmorph[Nd(pmb)_4] \cdot C_2H_5OH$	Chloroform	2.85	11.47	11.08
	Methanol	3.38	11.12	11.05
	Acetone	3.46	8.87	9.85
	Benzene	2.68	11.05	10.73

a) Data taken from Ref. 14.

Table 4. Oscillator strength of hypersensitive transition in neodymium complexes

Compound	$P \times 10^6$ ($^4I_{9/2} \rightarrow {}^4G_{5/2}$, $^2G_{7/2}$) 16250—18250 cm^{-1}				
	Acetone	Benzene	Chloroform	Dioxane	Methanol
$Nd(pmbp)_3 \cdot 2H_2O$	57.4	59.2	56.8	57.7	51.1
$Nd(pmbp)_3 \cdot py_2 \cdot 2H_2O$	—	—	62.1	—	—
$Nd(pmbp)_3 \cdot bpy \cdot C_2H_5OH$	62.1	65.9	66.7	63.8	57.2
$Nd(pmbp)_3 \cdot phen \cdot C_2H_5OH$	—	—	71.3	—	—
$NH_4[Nd(pmbp)_4] \cdot C_2H_5OH$	—	—	74.9	—	—
$Hpiper[Nd(pmbp)_4] \cdot C_2H_5OH$	—	—	78.2	—	—
$Hpyrrol[Nd(pmbp)_4] \cdot C_2H_5OH$	—	—	75.6	—	—
$Hmorph[Nd(pmbp)_4] \cdot C_2H_5OH$	77.2	76.3	74.9	73.1	71.7

of lanthanoid complexes generally increases with the increases in pK_a value of the ligand. However, there are exceptions to this generality. For example, pK_a of Hdbm is greater than Hsdbm, but the neodymium complex of Hsdbm shows greater band intensification.[17] This is due to more covalent interaction in the thio compound as sulfur acts as a softer base. A comparison of the oscillator strengths of Hpmbp complexes (Table 4) with the β-diketonates reported in literature[25-27] reveals that in spite of weaker basicity, the oscillator strengths of Hpmbp complexes are rather high. Moreover, lanthanoid–pmbp complexes have relatively high formation constants ($\log \beta_3 \approx 12$—13)[28] which indicate that probably the complexes are stabilized to a great extent through covalent interaction. Menzel *et al.*[7] also indicated higher covalency in Cu(pmbp)$_2$ compared to Cu(II) acetylacetonate.

Henrie *et al.*[18] have recently proposed a mechanism to explain the phenomenon of hypersensitivity which suggests that hypersensitive transitions aries from metal-ligand covalency *via* charge-transfer levels. The greater the covalent interaction greater will be the hypersensitivity. On this premise Henrie *et al.*[18] further proposed a correlation between P and pK_a. From the present study we conclude that hypersensitivity indeed increases with greater covalent interaction, but a linear correlation between hypersensitive band intensity and ligand basicity appears to be an overemphasized one.

The electronic spectral characteristics of the Pr(III) complexes in chloroform have been investigated. The hypersensitive transition, $^3H_4 \rightarrow {}^3F_2$ (*ca.* 5.2×10^3 cm^{-1}) was beyond the range of measurement. Although $^3H_4 \rightarrow {}^3P_2$ and $^3H_4 \rightarrow {}^1D_2$ transitions have been reported[29] to exhibit hypersensitivity, they do not obey quadrupole selection rules. In the Pr(III)–pmbp complexes, $^3H_4 \rightarrow {}^3D_2$ transition is completely swamped by the ligand/or charge-transfer tail, which also considerably modified the bands due to $^3H_4 \rightarrow {}^3P_1$, $^1I_6$ ($\approx 21.2 \times 10^3$ cm^{-1}) transitions. The molar extinction coefficients of $^3H_4 \rightarrow {}^1D_2$ transition ($\approx 17.6 \times 10^3$ cm^{-1}) in the complexes on comparison with the corresponding value for the aquated Pr^{3+} ion reveal that there is significant increase in intensity in the complexes. In fact, the gradation in intensity is almost similar to the one observed in the Nd(III) complexes. In view of the exceptional behavior of Pr(III) in its hypersensitivity which still remains as

one of the major problems in lanthanoid intensity theory,[30] no attempt has been made to evaluate the oscillator strengths for $^3H_4 \rightarrow {}^1D_2$ transition.

The authors express their sincere thanks to Prof. B. J. Hathaway of the University College, Cork, Ireland, and Dr. P. L. Goggin of the University of Bristol for recording infrared spectra of the compounds.

References

1) B. S. Jensen, *Acta Chem. Scand.*, **13**, 1668 (1959).
2) O. Navratil, *Chem. Listy*, **68**, 470 (1974). A review.
3) G. N. Rao and J. S. Thakur, *J. Sci. Indust. Res. (India)*, **34**, 110 (1975). A review.
4) Yu. A. Zolotov, "Extraction of Chelate Compounds" (Engl. Translation), Ann Arbor-Humphrey Science Publishers (1970), p. 227.
5) A. Roy and K. Nag, *Indian J. Chem.*, **15A**, 474 (1977).
6) A. Roy and K. Nag, *J. Inorg. Nucl. Chem.*, **40**, 331 (1978).
7) E. R. Menzel, D. R. Lorenz, J. R. Wasson, K. R. Radigan, and B. J. McCormick, *J. Inorg. Nucl. Chem.*, **38**, 993 (1976).
8) Yu. A. Zolotov, V. G. Lambrev, and M. K. Chamutova, *Dokl. Akad. Nauk SSSR*, **165**, 117 (1965).
9) S. J. Lyle and M. Rehman, *Talanta*, **10**, 1177 (1963).
10) D. M. Gruen, C. W. Dekock, and R. L. McBeth, *Adv. Chem. Ser.*, **71**, 102 (1967).
11) W. J. Geary, *Coord. Chem. Rev.*, **7**, 1177 (1971).
12) K. Meyer, *Chem. Ber.*, **45**, 2843 (1912).
13) C. Y. Liang, E. J. Schmitschek, and T. A. Trias, *J. Inorg. Nucl. Chem.*, **32**, 811 (1970).
14) W. R. Carnall, P. R. Fields, and B. G. Wybourne, *J. Chem. Phys.*, **42**, 3797 (1965).
15) B. R. Judd, *Phys. Rev.*, **127**, 750 (1962).
16) G. S. Oflet, *J. Chem. Phys.*, **37**, 511 (1962).
17) K. Nag and M. Chaudhury, *Inorg. Chem.*, **15**, 2291 (1976).
18) D. E. Henrie, R. L. Fellows, and G. R. Choppin, *Coord. Chem. Rev.*, **18**, 199 (1976).
19) J. C. Barnes and H. Pincott, *J. Chem. Soc. A*, **1966**, 842.
20) K. Nag and M. Chaudhury, *Inorg. Nucl. Chem. Lett.*, **12**, 307 (1976).
21) N. S. Poluektov, M. A. Tishchenko, and G. E. Gerasimenko, *Dokl. Akad. Nauk SSSR*, **213**, 1334 (1973).
22) S. P. Sinha, P. C. Mehta, and S. S. L. Surana, *Mol. Phys.*, **23**, 807 (1972).
23) J. H. Forsberg, *Coord. Chem. Rev.*, **10**, 195 (1973).
24) S. P. Sinha and R. D. Green, *Spectrosc. Lett.*, **4**, 399 (1971).
25) D. G. Karraker, *Inorg. Chem.*, **6**, 1863 (1967).
26) P. C. Mehta and S. P. Tandon, *J. Chem. Phys.*, **53**, 414 (1970).
27) L. I. Kononenko, M. A. Tishchenko, and U. N. Drobyazko, *Zh. Anal. Khim.*, **26**, 729 (1971).
28) A. Roy and K. Nag, unpublished result.
29) R. D. Peacock, *Chem. Phys. Lett.*, **7**, 187 (1970).
30) R. D. Peacock, *Struct. Bonding*, **22**, 83 (1975).

Conductance Behavior of Manganese Soap Solutions in 1-Butanol and 3-Methyl-1-butanol

R. P. VARMA, K. SINGH,* and H. SINGH*

Department of Chemistry, D.A.V. College, Muzaffarnagar 251001, India

** Department of Chemistry, J.V. College, Baraut, 250611, Meerut, India*

(Received August 12, 1977)

The specific conductance of manganese soap solutions in 1-butanol and 3-methyl-1-butanol has been measured at temperatures in the range 35—50 °C. Manganese soaps form micellar aggregates and the CMC, which decreases with increase in chain length of the soaps of saturated fatty acids, was found to be independent of the nature of the solvent. Conductance behavior of soaps is given by the equation $\log \lambda_M = A + B \log C$ where A and B are constants and C is the concentration in mol/dm^3. Constant A increases with increase in temperature and chain length of the soap. Constant B is independent of temperature but varies with soap chain. Molecular conductance at infinite dilution, λ_∞, dissociation constant, K, activation energy of conductance, ΔE_λ, and heat of dissociation, $\Delta H°$, have been evaluated.

Measurement of the conductance of metal soaps involves no special problem except the application of external electrical forces. Since the mobility of the ion present as simple species resembles that of dissociated salts and differs markedly from that of aggregated ions, there is an abrupt change in specific conductance at CMC. Electrical conductance of various ionic agents has been reported.[1-4] The conductance of sodium and potassium soaps in ethanol, toluene, and pyridine was determined[5] and sodium oleate in ethanol was reported[6] to behave as simple electrolyte. Several workers[7-9] have studied the CMC of magnesium, calcium, barium, and strontium soap solutions and determined parameters such as K, λ_∞, and $\Delta H°$. From the conductance behavior[10] of magnesium soaps in lower aliphatic alcohols, it was confirmed that CMC is uneffected by change in temperature. An investigation of CMC of nickel, cobalt, and iron soaps has been made[11] by conductance measurement at different temperatures.

We have studied the conductance of manganese soaps (oleate, laurate, decanoate and octanoate) in 1-butanol and 3-methyl-1-butanol at different temperatures in order to a) determine the CMC of the soap solutions, b) confirm the effect of temperature, if any, on CMC, and c) determine dissociation constant, K, molecular conductance at infinite dilution, λ_∞ and heat of dissociation, $\Delta H°$.

Experimental

Materials. 1-Butanol, 3-methyl-1-butanol, manganese chloride, oleic acid, and octanoic, decanoic and lauric acids (Merck or B.D.H. reagent grade) were used. The fatty acids were purified by distillation under reduced pressure, the purity being confirmed by bp measurements.

Preparation of Soaps. Manganese soaps were prepared by the interaction of manganese chloride solution in a small quantity of distilled water with a hot solution of sodium soap, the latter being added drop-wise while the whole mass was continuously stirred at 50—55 °C. The precipitate was filtered and washed with hot water until the filtrate gave no reaction to manganese chloride. After initial drying in an air oven (100—105 °C) final drying was carried out under reduced pressure.

Apparatus and Procedure. All the measurements were carried out in a thermostat at constant temperature (±0.05 °C). A conductivity bridge (Phillips, PR 9500, India) and a dipping type conductivity cell were used for measuring the conductance of soap solutions. All data were obtained by concentration runs, solutions were diluted by adding the solvent in a desired proportion and the conductance was measured. The reproducibility of the results was verified by repeating the measurements.

Results and Discussion

Specific conductance, κ, of manganese soap solutions increases with increasing concentrations of soap solutions at different temperatures. The κ-C plots (Fig. 1) are characterised by an intersection of two straight lines at a definite concentration called CMC (Table 1). The values of CMC of soaps are unaffected by change in temperature but decrease with increasing chain length of the soap.

Molecular conductance, λ_M, obtained from the measured specific conductance of solutions decreases with increase in the concentration of the soap solutions. The plots (Fig. 2) of λ_M *vs.* $C^{1/2}$ are concave upward.

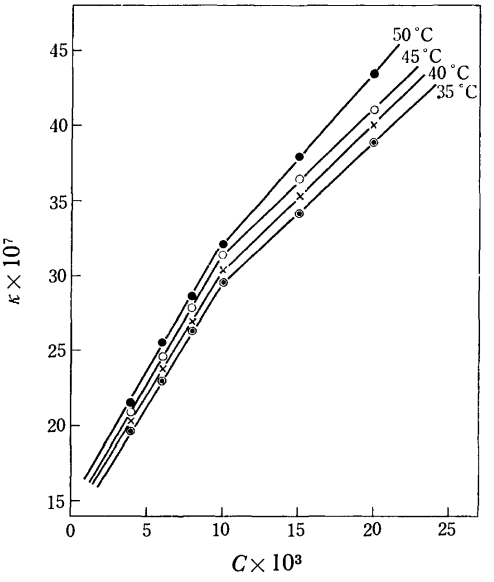

Fig. 1. Plot of specific conductivity, κ *vs.* concentration, C, of manganese oleate in 1-butanol at temperatures, 35—50 °C.

Table 1. Values of CMC and heat of dissociation, ΔH° in kcal of manganese soaps at all temperatures (35—50 °C)

Soap	1-Butanol		3-Methyl-butanol	
	CMC	ΔH°	CMC	ΔH°
Oleate	0.010 M	25.51	0.008 M	10.08
Laurate	0.007 M	27.51	0.007 M	13.29
Decanoate	0.008 M	30.25	0.008 M	39.42
Octanoate	0.009 M	33.04	0.009 M	43.54

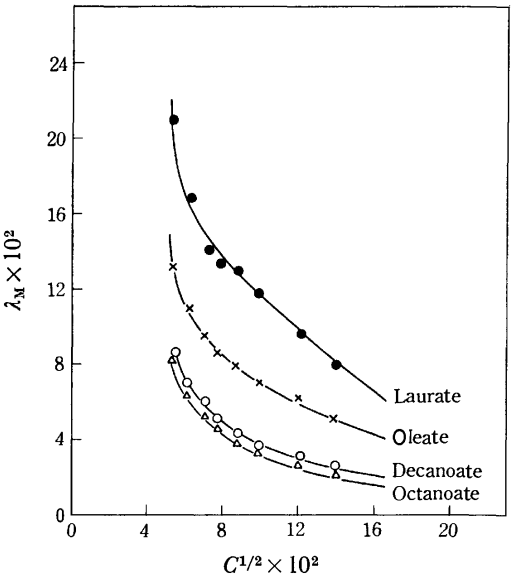

Fig. 2. Plot of molecular conductivity, λ_M, *vs.* square root of concentration, $C^{1/2}$, of manganese soaps in 3-methyl-1-butanol at 35 °C.

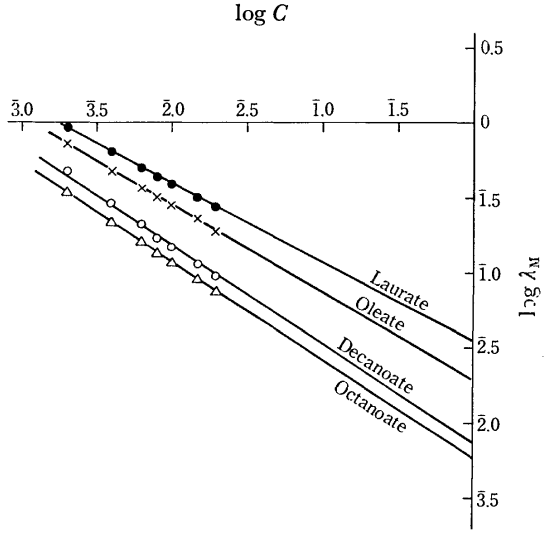

Fig. 3. Plot of $\log \lambda_M$ *vs.* $\log C$ of manganese soaps at 35 °C in 1-butanol.

This is due to the weak electrolyte behavior of the soaps.

The conductance behavior of manganese soap solutions at various temperatures (Fig. 3) is represented by

$$\log \lambda_M = A + B \log C, \quad (1)$$

where A and B are constants and C is the concentration in mol/dm^3

The values of constants A and B have been found from the slopes and intercepts of the linear plots of $\log \lambda_M$ *vs.* $\log C$ (Table 2). It is seen that constant A in 1-butanol is higher than 3-methyl-1-butanol varying with soap at different temperatures in the order

laurate>oleate>decanoate>octanoate

Constant B (Table 3) is independent of temperature which supports the idea that CMC remains unaffected by temperature.

The molecular conductance temperature variation can be expressed by

$$\lambda_M = Ae^{-\Delta E_\lambda / RT}, \quad (2)$$

where A and ΔE_λ are constants.

Constant ΔE_λ is of importance, since information can be obtained on the aggregation by measuring the activation energy of conductance. The plots of $\log \lambda_M$ *vs.* $1/T$ are straight lines in alcohols. The activation energy of conductance, ΔE_λ has been calculated from the slopes of linear plots. Table 4 indicates and appreciable difference in the values of ΔE_λ below an above CMC which supports the micellar behavior of manganese soaps in alcohols.

Dissociation Constant, Heat of Dissociation, and Molecular Conductance at Infinite Dilution. Manganese soap has been reported to behave as a weak electrolyte in dilute solutions,[13] the dissociation of soap can thus be derived as follows:

$$\underset{C(1-\alpha)}{(COOR)_2Mn} \rightleftharpoons \underset{C\alpha}{Mn^{2+}} + \underset{2C\alpha}{2RCOO^-}, \quad (3)$$

$$K = \frac{[Mn^{2+}][RCOO^-]^2}{[(COOR)_2Mn]} \quad (4)$$

$$= \frac{4C^2\alpha^3}{1-\alpha} . \quad (5)$$

The degree of dissociation, α, of soaps in solution is very small. Ionic concentration would be low and interionic effects can be neglected. On replacing $\alpha = \lambda_M/\lambda_\infty$ and rearranging, we obtain

$$C^2\lambda_M^2 = \frac{K\lambda_\infty^3}{4\lambda_M} - \frac{\lambda_\infty^2 K}{4} . \quad (6)$$

The plots of $C^2\lambda_M^2$ *vs.* $1/\lambda_M$ are linear below CMC and the equation fails above this concentration. The values of K and λ_∞ obtained from Eq. 6 at different temperatures are given in Tables 5 and 6.

The dissociation constant decreases with increase in temperature and decrease in dielectric constant of the solvent. In a medium of low dielectric constant, the electrostatic attractive forces between positive and negative ions are large, giving rise to diminished small dissociation.

The heat of dissociation, ΔH° has been calculated from the slopes of the plots of $\log K$ *vs.* $1/T$ and is given in Table 1. We see that the values of ΔH° decrease with increase in the chain length of soap.

Molecular conductance at infinite dilution, λ_∞ increases with increase in temperature which is due to the decrease in the viscosity of solvent. The rise in temperature causes increase in ionic mobility despite the fact that the addition of the soap increases the viscosity of the solvent.

TABLE 2. VALUES OF A OF MANGANESE SOAPS AT TEMPERATURES IN THE RANGE 35—50 °C

Solvent	Temp °C	Constant A			
		Oleate	Laurate	Decanoate	Octanoate
1-Butanol	35	$\bar{2}.32$	$\bar{2}.58$	$\bar{3}.86$	$\bar{3}.80$
	40	$\bar{2}.34$	$\bar{2}.62$	$\bar{3}.88$	$\bar{3}.82$
	45	$\bar{2}.36$	$\bar{2}.66$	$\bar{3}.90$	$\bar{3}.86$
	50	$\bar{2}.38$	$\bar{2}.72$	$\bar{3}.90$	$\bar{3}.88$
3-Methyl-1-butanol	35	$\bar{3}.86$	$\bar{2}.00$	$\bar{3}.30$	$\bar{3}.24$
	40	$\bar{3}.90$	$\bar{2}.06$	$\bar{3}.36$	$\bar{3}.28$
	45	$\bar{3}.92$	$\bar{2}.08$	$\bar{3}.38$	$\bar{3}.30$
	50	$\bar{3}.98$	$\bar{2}.10$	$\bar{3}.40$	$\bar{3}.36$

TABLE 3. VALUES OF B OF MANGANESE SOAPS AT TEMPERATURES IN THE RANGE 35—50 °C

Solvent	Temp °C	Constant B			
		Oleate	Laurate	Decanoate	Octanoate
1-Butanol	35	0.56	0.52	0.66	0.64
	40	0.56	0.52	0.66	0.64
	45	0.56	0.50	0.66	0.62
	50	0.56	0.50	0.66	0.62
3-Methyl-1-butanol	35	0.48	0.52	0.64	0.66
	40	0.48	0.50	0.62	0.64
	45	0.48	0.50	0.62	0.66
	50	0.50	0.50	0.62	0.62

TABLE 4. RANGE OF ACTIVATION ENERGY OF CONDUCTANCE, ΔE_λ FOR MANGANESE SOAPS BELOW AND ABOVE CMC

Soap	ΔE_λ in kcal			
	1-Butanol		3-Methyl-1-butanol	
	below CMC	above CMC	below CMC	above CMC
Oleate	1.37—1.38	1.83—1.84	1.37—1.60	1.60—1.80
Laurate	1.37—1.84	2.30—3.21	0.60—1.37	1.37—2.06
Decanoate	0.92—1.37	1.83—1.84	0.91—0.92	1.37—2.06
Octanoate	0.91—0.92	1.83—2.29	1.14—1.60	1.83—2.00

TABLE 5. VALUES OF DISSOCIATION CONSTANTS, K, FOR MANGANESE AT TEMPERATURES IN THE RANGE 35—50 °C

Solvent	Temp °C	$K \times 10^5$			
		Oleate	Laurate	Decanoate	Octanoate
1-Butanol	35	6.874	0.494	22.000	33.300
	40	3.852	0.326	7.960	13.140
	45	1.920	0.153	5.810	8.000
	50	0.968	0.074	1.280	2.489
3-Methyl-1-butanol	35	2.500	3.692	0.078	0.347
	40	3.212	3.241	0.032	0.154
	45	1.703	2.110	0.012	0.073
	50	1.279	1.341	0.004	0.016

Table 6. Values of molecular conductivity at infinite dilution, λ_∞, at temperatures in the range 35—50 °C

Solvent	Temp °C	λ_∞			
		Oleate	Laurate	Decanoate	Octanoate
1-Butanol	35	1.230	1.800	0.962	0.600
	40	1.477	2.158	1.487	0.818
	45	1.882	2.800	1.530	1.000
	50	2.932	3.454	2.500	1.501
3-Methyl-1-butanol	35	0.200	0.319	0.336	0.173
	40	0.208	0.330	0.444	0.233
	45	0.227	0.385	0.600	0.306
	50	0.250	0.457	0.925	0.500

We appreciate the laboratory facilities provided by college authorities and the advice given by Dr. K. N. Mehrotra.

References

1) M. E. L. McBain, W. B. Dye, and S. A. Johnston, *J. Am. Chem. Soc.*, **61**, 3210 (1939).
2) A. Lottermoser, and F. Puschel, *Kolloid-Z.*, **63**, 175 (1933).
3) A. W. Ralston and C. W. Hoerr, *J. Am. Chem. Soc.*, **64**, 772 (1942).
4) H. F. Walton, E. N. Hiebert, and E. H. Sholtes, *J. Colloid Sci.*, **1**, 385 (1946).
5) S. S. Bhatnagar, and M. Prasad, *Kolloid-Z.*, **34**, 193 (1924).
6) W. A. Patrick, W. L. Hyden, and E. F. Milan, *J. Phys. Chem.*, **29**, 1004 (1925).
7) R. P. Varma, and K. Kumar, *Cellul. Chem. Technol.*, **9**, 23 (1975).
8) R. P. Varma, and P. Bahadur, *Cellul. Chem. Technol.*, **9**, 393 (1975).
9) R. P. Varma, and R. Dayal, *J. Am. Oil Chem. Soc.*, **53**, 39 (1976).
10) R. P. Varma, and K. Kumar, *Kolloid-Z. Z. Polym.*, in press.
11) R. P. Varma, H. K. Bhargava, and R. Dayal, *Roczniki Chemii. ann. Soc. Chim. Polonorum*, **50**, 307 (1976).
12) K. N. Mehrotra, and R. P. Varma, *J. Am. Oil Chem. Soc.*, **45**, 673
13) R. P. Varma, and P. Bahadur, *Cellul. Chem. Technol.*, **8**, 27 (1974).

Effect of Monohydroxy Alcohols and Urea on the CMC of Surfactants

H. N. SINGH and Shanti SWARUP,
Department of Chemistry, Aligarh Muslim University, Aligarh 202001, India
(Received September 26, 1977)

The effect of monohydroxy alcohols on the critical micelle concentration (CMC) of anionic and cationic surfactants have been studied by a conductometric method. The CMC was found to decrease by adding small quantities of alcohol and raised again at higher alcohol concentrations. The CMC decreasing effect has been discussed on the basis of more ordered water cavity formed around the added alcohol molecules and their increasing effect by the partition of alcohol between the micellar and the bulk phase leading to the break-down of the micelles. The effect of urea on CMC in alcohol–water mixtures has been studied and its CMC increasing effect explained.

The properties of aqueous solutions of aliphatic monohydric alcohols are of interest in the field of surface chemistry; especially their effect on the phenomenon of micellization of surfactants. Since water–alcohol-surfactant systems are so frequently used as media in the studies of chemical equilibria and reaction rates,[1] it is very essential to investigate the nature of the alkyl groups in the alcohol on the CMC of surfactants.

The driving force for the formation of nonionic micelles in water being the hydrophobic interactions between the hydrocarbon portion of the surfactant has been treated quantitatively,[2] but this treatment in case of ionic micelles was less satisfactory.[3] The most satisfactory way of investigating the effect of hydrophobic interaction on ionic micelle formation would be to study the micellar properties of ionic surfactants in altered water structure by adding small quantities of alcohols of varying chain length. But one could not rule out the possibility of incorporation of alcohol molecules into the micelles.

The CMC decreasing effect due to incorporation of alcohol molecules between the soap micelles has been advocated by many workers.[4–6] Branched chain alcohols at low concentrations were found ineffective while the higher homologous alcohols caused depression of the CMC. Addition of various amphiphiles to micellar soap solutions caused the electrical conductivity to increase.[8] The effect of C_2—C_{10} alcohols on the CMC of soap solutions was investigated by electrical conductivity and distribution methods.[9–10] The CMC raising effect of ethanol and methanol at higher concentration is well studied.[12–19]

Virtually all substances containing hydrophobic moities decrease the concentration of an amphiphile in equilibrium with its micelles.[20] This decrease can be explained only by the incorporation of the added substances into the micelle, since simple addition of the alcohol and similar substances to the solvent must diminish the hydrophobic effect, that is, it would decrease the standard chemical potential of monomer for the micelle forming amphiphile without any effect on the standard chemical potential of micelle and would therefore increase the CMC. In related work, the effect of urea on micelle formation has been found to increase the CMC, though, it could not be incorporated into the micelle.[21–23]

From the detailed literature survey on the effect of additives, particularly alcohols and other related substances, which markedly influence the hydrophobic effect and the micelle formation,[24] it seems that there exist two different views regarding the effect of additives on micelle formation. The first deals with the solubilization of alcohols in micelle[11,21,25] and the second view is that additives have direct effect on the water structure.[26–28]

Recent investigations[29,30] further indicate that the role of alcohols in micelle formation could be explained on the basis of several factors. It may be possible that the alcohol molecules may modify water structure if present in very small concentration. At higher concentrations some other effects like the alteration in the dielectric constant of the solvent or the partition of alcohol molecules between bulk and the micellar phase[31–33] or the diminishing of the hydrophobic effect[20] may be more important. At very high alcohol concentration a shift in equilibrium between surfactant monomers and micelles towards monomer may be possible due to high solvent power of alcohol for the hydrophobic part of the surfactant ion.

The main objects of the present investigation were (a) to extend information on the influence of the solvent on the micelle formation due to alteration in water structure by gradual addition of alcohols in very small amounts and (b) to study the effect of urea on micelle formation in the altered water structure.

Experimental

Sodium dodecylsulfate (SDS) was purchased from BDH (England). It was first recrystallized from ethanol–acetone mixture. Traces of unreacted alcohol were removed by extracting it with petroleum ether (60 h) and chloroform (100 h). The surfactant was dried after filtration in a hot air oven to a constant weight. The absence of any unreacted alcohol was ascertained from the absence of OH peak in the IR spectrum. The microanalysis of the compound showed: C=49.73, H=9.02, S=11.00%; calculated values C=49.8, H=8.9, S=11.06%. The purity was also confirmed from the absence of minimum in the surface tension *vs.* log concentration plots. Cetyltrimethylammonium bromide (CTMAB) was BDH reagent grade quality. It was recrystallized from acetone, repeated thrice. Demineralized double distilled water was used throughout this work. The specific conductivity of water was 20.0×10^{-6} to 21.7×10^{-6} $ohm^{-1}\,cm^{-1}$. CMC values of SDS and CTMAB, determined by conductivity method in water at 30 °C were 8.6 and 0.97 $mmol/dm^3$ respectively, are in good agreement with literature values[12] at 25 °C. 1-Propanol, 1-butanol, 1-hexanol, and cyclohexanol were all BDH laboratory reagents while 1-pentanol and cyclopentanol were E. Merk products. These

alcohols were distilled under reduced pressure and the middle fractions of the distillate were used.

Water-alcohol mixtures of several compositions were prepared by mixing requisite quantity of alcohol in water. Stock solutions of surfactants were prepared by weighing. The conductometric measurements of surfactant solutions were made by a Philips conductivity meter model PR 9500 at a frequency of 1000 Hz using platinized electrodes of known cell constant. After measuring the conductivity of the solvent, small volumes of the stock solution (50 mmol/dm^3 surfactant solution) were added and the conductivity noted after each addition and thorough mixing to a constant reading. The specific conductivity was calculated after applying the solvent correction. The CMC values were determined at the break points of nearly two straight line portion of the specific conductivity *versus* concentration plots.

Results

The specific conductivity, K, *vs.* concentration, C, plots for SDS and CTMAB in different compositions of 1-propanol-water mixtures are shown in Fig. 1. The plots for other alcohol-water mixtures were similar. The variation of CMC with the mole fraction of alcohol, χ, are shown in Fig. 2 and the effect of urea on the CMC in alcohol-water mixtures resulting in minima in CMC, where the water is supposed to be in most ordered form, are given in Table 1. The slopes of K *vs.* C plots for SDS below and above CMC in different alcohols are given in Table 2.

Discussion

The highly structured tetrahedral arrangement of water molecules in the liquid state would have to be disrupted by the addition of any solute.[20] When alcohols are added into water, some hydrogen bonds must be broken, and new hydrogen bonds between water and alcohol would be formed. But the hydrogen bond formation between alcohol and water does not seem very tangible because in liquid alcohol the tendency for O–H···O bond formation is likely to be as strong as in water, though such hydrogen bonds cannot comprise an isotropic net work filling the entire solvent space due to the presence of alkyl side chains. However, the addition of alcohols to water, if results in the rapture of hydrogen bonds of the latter, the major contribution to the free energy of transfer of alcohol to water would be a positive enthalpy term. Instead, as reported[34] earlier, the transfer to water is actually slightly favored energetically. The positive value of change in standard chemical potential for the transfer of aliphatic alcohols from pure liquid to water resulting from a negative entropy change has been explained by the fact that the water molecules at the surface of the cavity created by a nonpolar part must be capable of rearranging themselves in order to regenerate the broken hydrogen bonds, create a higher degree of local ordering than exists in pure liquid water.[20] Hence it is reasonable to expect that the addition of higher alcohols to water may result in the ordering of water structure at concentrations lower than their lower counterparts.

In fact, the CMC lowering of surfactants by the small addition of alcohols may be due to their direct action on water structure and the subsequent addition

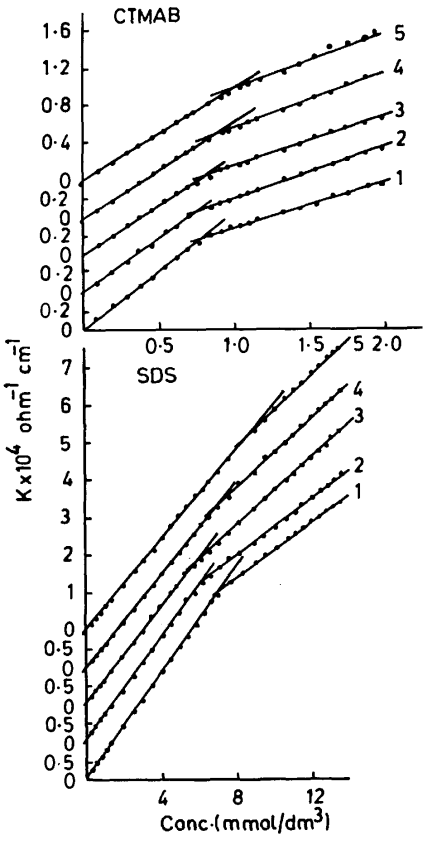

Fig. 1. Specific conductivity *vs.* concentration plots for surfactants in 1-propanol-water mixture at 30 °C.
1: $\chi=23\times10^{-4}$, 2: $\chi=72\times10^{-4}$, 3: $\chi=124\times10^{-4}$, 4: $\chi=177\times10^{-4}$, 5: $\chi=251\times10^{-4}$.

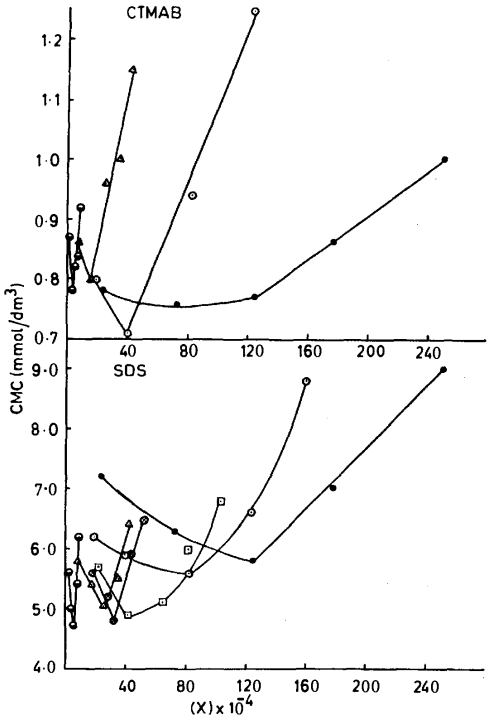

Fig. 2. The variation of CMC with χ.
—●—: 1-Propanol, —⊙—: 1-butanol, —△—: 1-pentanol, —◒—: 1-hexanol, —⊡—: cyclopentanol, —○—: cyclohexanol.

Table 1. CMC (mmol/dm³) values of SDS and CTMAB in presence of various concentrations of urea at 30 °C

The mole fraction (χ) of alcohol in water is taken at minimum in CMC.

SDS

Urea	1-Propanol ($\chi=124\times10^{-4}$)		1-Butanol ($\chi=82\times10^{-4}$)		1-Pentanol ($\chi=25\times10^{-4}$)		1-Hexanol ($\chi=5.7\times10^{-4}$)		Cyclopentanol ($\chi=40\times10^{-4}$)		Cyclohexanol ($\chi=32\times10^{-4}$)	
	CMC	%CMC increase	CMC	%CMC increase	CMC	%CMC increase	CMC	%CMC increase	CMC	%CMC increase	CMC	%CMC increase
0M[a]	5.8	—	5.6	—	5.0	—	4.7	—	4.9	—	4.8	—
1M	6.5	12	6.2	11	5.8	16	5.6	19	6.0	22	5.7	18
3M	8.0	38	7.5	34	7.2	44	6.9	47	7.4	51	7.0	25
6M	No micelles		No micelles		No micelles		10.0	112.76	No micelles		No micelles	

CTMAB

Urea	1-Propanol ($\chi=72\times10^{-4}$)		1-Butanol ($\chi=40\times10^{-4}$)		1-Hexanol ($\chi=28\times10^{-4}$)	
	CMC	%CMC increase	CMC	%CMC increase	CMC	%CMC increase
0M	0.76	—	0.72	—	0.78	—
1M	0.82	7.9	0.79	9.7	0.80	2.6
3M	1.33	75	1.08	50	0.92	18
6M	1.55	10	1.21	68	—	—

a) 1M=mol/dm³.

Table 2. Slopes (ohm^{-1} cm^{-1}/mol dm^{-3}) above and below the CMC of alcohol-water mixtures at 30 °C

1-Propanol (χ)		0	23×10^{-4}	72×10^{-4}	124×10^{-4}	177×10^{-4}	251×10^{-4}
Slope	above CMC	0.030	0.030	0.035	0.040	0.045	0.047
	below CMC	0.065	0.070	0.069	0.070	0.068	0.069
1-Butanol (χ)		0	19×10^{-4}	40×10^{-4}	82×10^{-4}	123×10^{-4}	159×10^{-4}
Slope	above CMC	0.030	0.040	0.050	0.052	0.055	0.057
	below CMC	0.065	0.069	0.070	0.071	0.070	0.070
1-Pentanol (χ)		0	8×10^{-4}	17×10^{-4}	25×10^{-5}	34×10^{-4}	42×10^{-4}
Slope	above CMC	0.030	0.040	0.043	0.050	0.052	0.055
	below CMC	0.065	0.070	0.069	0.069	0.070	0.070
1-Hexanol (χ)		0	2.8×10^{-4}	4.3×10^{-4}	5.7×10^{-4}	7.6×10^{-4}	8.4×10^{-4}
Slope	above CMC	0.030	0.040	0.042	0.044	0.046	0.049
	below CMC	0.065	0.072	0.070	0.070	0.070	0.069
Cyclopentanol (χ)		0	21×10^{-4}	40×10^{-4}	63×10^{-4}	81×10^{-4}	102×10^{-4}
Slope	above CMC	0.030	0.040	0.045	0.050	0.055	0.057
	below CMC	0.065	0.070	0.069	0.070	0.070	0.069
Cyclohexanol (χ)		0	17×10^{-4}	28×10^{-4}	32×10^{-3}	43×10^{-4}	52×10^{-4}
Slope	above CMC	0.030	0.042	0.050	0.055	0.058	0.055
	below CMC	0.065	0.070	0.070	0.071	0.070	0.069

may cause secondary effects such as their solubilization in micelle and decrease of hydrophobic effect. A perusal of Fig. 2 shows that the CMC values of SDS decrease by the gradual increase in the mole fraction of alcohol in water and increase further after attaining a minimum value. The mole fraction of alcohols where the CMC minima occur also depend upon the length of the hydrocarbon chain. It may, therefore, be concluded from these observations and the above mentioned facts that the initial addition of alcohol to water causes the ordering of water which in turn reduces the CMC to a minimum value. From Fig. 2 it is also noted that the CMC values at the minimum decrease gradually with increase of the length of the hydrocarbon chain in the alcohol. This further supports the view[20] that the formation of the cavity of more ordered water molecules is favored by the long hydrocarbon chain of the alcohols. In presence of such a cavity a decrease in CMC is not unexpected.

In case of cyclic alcohols, *viz.*, cyclopentanol and cyclohexanol, the CMC minimum occurs at higher mole fraction of alcohols as compared with their linear-chain counterparts. This indicates that these alcohols possess less proton accepting capacity in solvent water to result in the well organized alcohol-water hydrogen bond formation or to create a cavity of more ordered water molecules. Apart from these mixtures having a more organised solvent structure, the higher CMC values at the minimum further suggest that the degree of association of the surfactant is slightly restricted due to steric reasons.

Studies have also been made with a cationic surfactant, CTMAB. The CMC values of CTMAB in different compositions of alcohols are given in Fig. 2.

In all the alcohol–water mixtures, the CMC values initially decrease, pass through a minimum and increase further, with the increase in the mole fraction of alcohols. Unlike anionic surfactant (SDS) no systemetic trend in the CMC values at the minimum is observed with the increase in the length of the hydrocarbon chain in alcohols. At this stage it is difficult to comment on the behavior of a cationic surfactant in alcohol–water mixtures.

The role of the water cavity in micelle formation has been further verified by studying the effect of urea on CMC. Urea is a strong water structure breaker, in presence of alcohols it may destroy the cavity of ordered water structure. It is, therefore, expected that the CMC should increase with the increase in the concentration of urea. Table 1 shows the effect of urea on the CMC of SDS and CTMAB in presence of constant concentration of alcohols. The percent increase in the CMC values are also included in Table 1. These results indicate that the addition of urea results in the breaking of water structure even at the concentration of alcohols where it is expected to be more ordered. This effect is so pronounced in lower alcohols that no micelle formation takes place when the concentration of urea exceeds 3 mol/dm^3. It is intresting to note that the CMC increasing effect of 1 mol/dm^3 urea is much smaller for cyclopentanol and cyclohexanol which further supports the conclusion that the water cavity formed in presence of cyclic alcohols is less ordered. However, an irregular change in the CMC values of CTMAB (Fig. 2) with the hydrophobicity of the alcohol indicates that the water molecules do not have a unique way of arranging themselves, but that different arrangements are possible depending upon the precise spatial requirements.[20] A comparison of percent increase in CMC in 3 mol/dm^3 urea (Table 1) may lead to the conclusion that the higher alcohols may be readily partitioned in cationic micelle than in an anionic micelle.

In case of anionic surfactants a further increase in CMC in higher concentration of alcohols suggests that some other factor, influencing the micelle formation, must be taken into account. A micelle formed in presence of an alcohol is likely to contain alcohol molecules in its oriented structure.[4,5] These alcohol molecules, introduced between the soap ions and the micelle, will produce a further charge separation. Owing to the lowered charge density the conditions are thus more favorable to abnormally small atmosphere and inclusion effects. This partition of additive between the solution and the micelles may be sensitive to the structure of the polar third component and the temperature. It is probably due to the above fact that no micelle formation is observed in all the alcohol–water mixtures in presence of 6 mol/dm^3 urea except in 1-hexanol which is less polar.

The inclusion and the micelle breakdown effect of alcohols[11,25,30] may further be reflected from the slopes of *K vs. C* plots below and above the CMC in different compositions of alcohols. The slopes for SDS in alcohol–water mixtures are given in Table 2.

A perusal of Table 2 shows that the slopes below the CMC remain nearly constant irrespective of the composition and the chain length of the added alcohol which indicate that alcohol molecule is not incorporated at all with the surfactant monomers. Approximately 8% higher values of slopes than in pure water may be due to modification of water structure by the added alcohols. The inclusion of alcohol molecules into the surfactant micelle is clearly reflected from the decrease in slopes above the CMC. It is also clear that the inclusion effect is stronger for alcohols with larger alkyl chains which brings about the reduction of the surface-charge density on the micelle. Similar conclusions have been given by Shirahama and Kashiwabara.[24] Larger values of slopes in higher alcohols (C_4—C_6) and their gradual increase with alcohol content indicates that the partition of alcohol into the micelle results in a slight increase in the conductivity due to release of few surfactant anions from the micellar to the bulk phase. The high solvent power of alkyl chains of the alcohol for surfactant tails may shift the equilibrium from aqueous micellar to the alcoholic environment (hydrocarbon like) in higher alcohols which could create a separate phase of reversed micelles.[35,36]

The authors are thankful to Prof. W. Rahman, Head, Department of Chemistry, for his keen interest in the work.

References

1) J. H. Fendler and E. J. Fendler, "Catalyses in Micellar and Macromolecular Systems," Academic Press, New York (1975).
2) D. C. Poland and H. A. Scheraga, *J. Phys. Chem.*, **69**, 2431 (1965).
3) D. C. Poland and H. A. Scheraga, *J. Colloid Interface Sci.*, **21**, 273 (1966).
4) J. H. Schulman and A. H. Hughes, *Biochem. J.*, **29**, 1242 (1935).
5) W. D. Harkins, R. W. Mattoon, and R. Mittelmann, *J. Chem. Phys.*, **15**, 763 (1947).
6) B. D. Flockhart and A. R. Ubbelhode, *J. Colloid Sci.*, **8**, 428 (1953).
7) S. H. Herzefeld, M. L. Corrin, and W. D. Harkins, *J. Phys. Colloid Chem.*, **54**, 271 (1950).
8) A. J. Hyde and A. S. C. Lawrence, *Proc. 3rd Int. Congr. Surface Activity.* (Univ. Press, Mainz, Germany,) **1**, 21 (1960).
9) K. Shinoda, *Bull. Chem. Soc. Jpn.*, **26**, 101 (1953).
10) K. Shinoda, *J. Phys. Chem.*, **58**, 1136 (1954).
11) A. S. C. Lawrence and J. T. Pearson, *Trans. Faraday Soc.*, **63**, 495 (1967).
12) P. Mukherjee and K. J. Mysels, Criti. Micelle Conc. of Aq. Surfactant System. Nath. Bu. Standards Pub., NSRDS. NBS-36, U. S. Govt. Printing Office, (1971).
13) B. D. Flockhart, *J. Colloid Sci.*, **12**, 557 (1957).
14) M. L. Corrin and W. D. Harkins, *J. Chem. Phys.*, **14**, 640 (1946).
15) A. F. H. Ward, *J. Chem. Soc.*, **1**, 522 (1939).
16) A. F. H. Ward, *Proc. R. Soc. London, Ser. A*, **176**, 412 (1940).
17) K. Shirahama and R. Matuura, *Bull. Chem. Soc., Jpn.*, **38**, 373 (1965).
18) W. U. Malik, Surendra P. Verma, and P. Chand, *Indian J. Chem.*, **8**, 826 (1970).

19) F. Franks and D. J. G. Ives, *Quart. Rev.*, **20**, 1 (1966).
20) C. Tanford, "The Hydrophobic Effect, Formation of Micelles and Biological Membranes," John Wiley, New York (1973), p. 84.
21) M. F. Emerson and A. Holtzer, *J. Phys. Chem.*, **71**, 3320 (1967).
22) L. Benjamin, *J. Colloid Interface Sci.*, **22**, 386 (1966).
23) J. M. Corkill, J. F. Goodman, and J. R. Tate, in "Hydrogen-bonded Solvent Systems," ed by A. K. Covington and P. Jones, Taylor and Francis, Ltd. London (1968).
24) K. Shirahama and T. Kashiwabara, *J. Colloid Interface Sci.*, **36**, 65 (1971).
25) W. Kauzman, *Adv. Protein Chem.*, **14**, 1 (1959).
26) P. Mukherjee and A. Ray, *J. Phys. Chem.*, **67**, 190 (1963).
27) H. S. Frank, *Fed. Proc. Suppl.*, **15**, 51 (1965).
28) H. A. Scheraga, *Ann. N. Y. Acad. Sci.*, **125**, 253 (1965).
29) J. W. Larsen and L. B. Tepley, *J. Colloid Interface Sci.*, **49**, 113 (1974).
30) H. N. Singh, S. Singh, and D. S. Mahalwar, *J. Colloid Interface Sci.*, **59**, 386 (1977).
31) N. Nishikido, Y. Moroi, H. Uehara, and R. Matuura, *Bull. Chem. Soc. Jpn.*, **47**, 2634 (1974).
32) M. Manabe, K. Shirahama, and M. Koda, *Bull. Chem. Soc. Jpn.*, **49**, 2904 (1976).
33) K. Hayase and S. Hayano, *Bull. Chem. Soc., Jpn.*, **50**, 83 (1977).
34) H. S. Frank and M. W. Evans, *J. Chem. Phys.*, **13**, 507 (1945).
35) S. Friberg and S. I. Ahmad, *J. Phys. Chem.*, **75**, 2001 (1971).
36) S. I. Ahmad and S. Friberg, *J. Am. Chem. Soc.*, **95**, 5196 (1972).

NOTES

BULLETIN OF THE CHEMICAL SOCIETY OF JAPAN, VOL. 51 (5), 1539—1540 (1978)

CNDO/2 Calculations of MeSEt, MeS-*n*-Pr, MeS-*n*-Bu, $(Et)_2S$, EtS-*n*-Pr, EtS-*n*-Bu, and $(n\text{-Pr})_2S$[1]

Masaru OHSAKU,* Norihisa BINGO, Hiroshi FUJIWARA, and Hiromu MURATA

Department of Chemistry, Faculty of Science, Hiroshima University, Higashisenda-machi, Hiroshima 730

(Received March 25, 1977)

Synopsis. CNDO/2 sp calculations were carried out for MeSEt, MeS-*n*-Pr, MeS-*n*-Bu, $(Et)_2S$, EtS-*n*-Pr, EtS-*n*-Bu, and $(n\text{-Pr})_2S$. The stable conformations of these molecules were discussed.

Conformational analyses of MeSEt have been performed extensively on the basis of the vibrational spectra and a normal coordinate treatment[2-4] and on the basis of vapor-phase electron diffraction.[5] With the MeS-*n*-Pr,[6-8] MeS-*n*-Bu,[6,7,9] $(Et)_2S$,[2,9] EtS-*n*-Pr,[6,7,9] EtS-*n*-Bu,[6,7] and $(n\text{-Pr})_2S$[6,7] molecules the conformations have also been analysed by means of IR and Raman spectroscopy. However, the interpretations of the observed results were not always consistent with each other. In particular, the conformation about the C–S bond remains vague. In the present study, in order to obtain useful information on the skeletal conformation, especially about the C–S bond, we have investigated the conformational analyses of these molecules by the aid of the CNDO/2 method.[10]

The molecular geometry used is as follows: for MeSEt–referred to the data of elctron diffraction,[5] r(C–H)=1.117, r(C–S)=1.818, r(C–C)=1.526 Å, and ϕ(CSC)=103.9°; for the other molecules, r(C–H)=1.09, r(C–S)=1.81, r(C–C)=1.54 Å, and ϕ(CSC)=105°; while the other angles were assumed to be tetrahedral. The dihedral angles of these sulfides were taken to be 180 and 60° for the T and G conformations respectively, according to the energy minima of MeSEt, to be shown later. The observed data are summarized in Table 1.

Figure 1 shows that the T form is more stable than the G form in MeSEt. The results of the present calculations, therefore, are in good agreement with our observed results,[2] but they do not agree with the

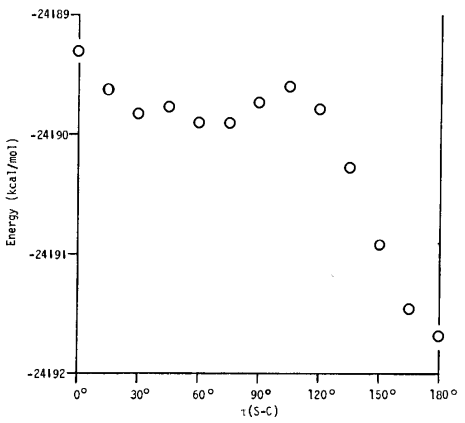

Fig. 1. Total energy as a function of the internal rotation angle in CS-CC.

TABLE 1. OBSERVED STABILITY/CONFORMATION AND ENTHALPY DIFFERENCES (cal/mol) OF DIALKYL SULFIDES

Molecule	Stability/Conformation[a]	Enthalpy differences	Ref
CS-CC	T*>G		2
	G*>T	30±50(gas), 140±50(liq)	4, 3
CS-C-CC (1)	around 1, T*		7
	GT*		8
CS-C-C-CC (1)	around 1, T*		7
	TTT*		9
CC-S-CC	TT*		2
	TT*>GG>TG	$\Delta H_{TT-TG}=460\pm100$(liq) $\Delta H_{GG-TG}=40\pm50$(liq)	9
CC-S-C-CC (1)	around 1, T*		7
	TTT*		9
CC-S-C-C-CC (1)	around 1, T*		7
CC-C-S-C-CC (1 1)	around 1, T*		7

a) With asterisk — the most stable form (conformation) in the crystalline solid state.

* To whom all correspondence should be addressed.

CS-C-CC	$TG_{0.\gtrsim 29}TT_{\underline{1.\gtrsim 85}}GG_{0.\gtrsim 05}GT_{\underline{62\gtrsim}}$ GG' = G'G
CS-C-C-CC	$TGT_{0.\gtrsim 15}TGG_{0.\gtrsim 07}TTT_{0.\gtrsim 25}TTG_{\underline{1.\gtrsim 66}}GGT_{0.\gtrsim 02}GTT_{0.\gtrsim 14}GGG_{0.\gtrsim 07}GTG$
CC-S-CC	$TT_{\underline{1.\gtrsim 71}}TG_{\underline{1.\gtrsim 70}}GG_{\underline{37\gtrsim}}$ GG'
CC-S-C-CC	$TTG_{0.\gtrsim 31}TTT_{\underline{1.\gtrsim 39}}GTG_{0.\gtrsim 29}GTT_{0.\gtrsim 13}TGG_{0.\gtrsim 06}TGT_{\underline{1.\gtrsim 65}}GGG_{0.\gtrsim 04}GGT$
CC-S-C-C-CC	$TTGG_{0.\gtrsim 11}TTTT_{\underline{1.\gtrsim 59}}GTGG_{0.\gtrsim 08}GTTT_{0.\gtrsim 18}TGGT_{0.\gtrsim 04}TGTT_{0.\gtrsim 03}GTTG_{0.\gtrsim 18}TGTG_{\underline{1.\gtrsim 62}}GGGG$
CC-C-S-C-CC	$GTTG_{0.\gtrsim 32}TTTG_{0.\gtrsim 32}TTTT_{\underline{1.\gtrsim 48}}GTGG_{0.\gtrsim 06}TGTG_{0.\gtrsim 23}TTGG_{0.\gtrsim 06}TTGT_{\underline{1.\gtrsim 79}}GGGG_{0.\gtrsim 08}TGGT$

Fig. 2. Stability as a function of the internal rotation angle. Small figures indicate the energy difference, in kcal/mol, while those with underlines indicate fairly large differences.

latest observations[3,4] that the G form is more stable than the T form, although the energy difference observed between the two forms is very small.

Also, for the other longer methyl substituents, the sp calculations indicate that the forms which have the T conformation around the CS–R bond are more stable than those of the G conformation, as is summarized in Fig. 2. For example, for CS–C–C–CC, the TGT and TTT forms, for example, were estimated to be more stable than the other forms, *e.g.*, GGT and GGG. The calculations, therefore, explain reasonably well the experimental results.[6,7,9] With the ethyl substituents, the calculations indicate that the forms which have the TT conformation about the CC–S–R bonds are the most stable ones. For example, for CC–S–C–CC, the TTG and TTT forms can be expected from the calculations to be more stable than the other forms. The present results agree well with the observed ones.[6,7,9] Moreover, the calculations show that the TT form about the CCC–S–CCC bonds is the most stable of all. This agrees well with our previous inference, in which the molecule may all have the *trans* form in the crystalline solid state, judging from the IR spectra of the molecule.[6,7] As has been noted previously,[7] the stable conformation around the C–C bond adjacent to the C–S bond was the T form in the crystalline state, while the conformation around the C–S bond was fairly difficult to determine from only the vibrational spectra and the normal coordinate treatment. In the present case, therefore, the sp calculations and the treatment of the molecular vibrations play complementary roles.

Generally, the present method reproduces the energy-minimum conformations of the simple normal dialkyl sulfides fairly well. Therefore, this method is a helpful method of analysing the vibrational data of these molecules.

The authors wish to thank Professor Akira Imamura of the Shiga University of Medical Science for his helpful advice. Thanks are also due to Dr. Hiroatsu Matsuura of the University of Tokyo for sending us preprints of Refs. 4 and 9.

References

1) Presented in part at the 34th National Meeting of the Chemical Society of Japan, Hiratsuka, April, 1976.
2) M. Ohsaku, Y. Shiro, and H. Murata, *Bull. Chem. Soc. Jpn.*, **45**, 954 (1972); **45**, 956 (1972); **46**, 1399 (1973).
3) N. Nogami, H. Sugeta, and T. Miyazawa, *Bull. Chem. Soc. Jpn.*, **48**, 3573 (1975).
4) M. Sakakibara, H. Matsuura, I. Harada, and T. Shimanouchi, *Bull. Chem. Soc. Jpn.*, **50**, 111 (1977).
5) K. Oyanagi, T. Fukuyama, and K. Kuchitsu, Preprints of the 32nd National Meeting of the Chemical Society of Japan, Vol. 1, p. 112 (1975).
6) M. Ohsaku, *J. Sci. Hiroshima Univ.*, **A38**, 51 (1974).
7) M. Ohsaku, *Bull. Chem. Soc. Jpn.*, **48**, 1037 (1975).
8) N. Nogami, H. Sugeta, and T. Miyazawa, *Chem. Lett.*, **1975**, 147.
9) M. Ohta, Y. Ogawa, H. Matsuura, I. Harada, and T. Shimanouchi, *Bull. Chem. Soc. Jpn.*, **50**, 380 (1977).
10) D. P. Santry and G. A. Segal, *J. Chem. Phys.*, **47**, 158 (1967).

BULLETIN OF THE CHEMICAL SOCIETY OF JAPAN, VOL. 51 (5), 1541—1542 (1978)

The Verification of Three-Dimensional Aromaticity: Tricarbonyliron Complexes of Olefins

Jun-ichi AIHARA

Department of Chemistry, Faculty of Science, Hokkaido University, Sapporo 060

(Received June 30, 1977)

Synopsis. Using Mingos's Hückel molecular-orbital model, polyolefins were found to be markedly aromatized by the coordination of tricarbonyliron. The Dewar-type resonance energies calculated for the title compounds are consistent with their chemistry.

In 1956, Longuet-Higgins and Orgel pointed out the possibility that quite an unstable cyclobutadiene molecule can be stabilized by combination with a suitable transition-metal compound.[1] In 1965, Pettit *et al.* first achieved such a stabilization of cyclobutadiene by adding tricarbonyliron to it.[2] The chemistry of transition-metal complexes of olefins has since been rapidly developed.[3,4] In parallel with this, two important concepts have been employed to elucidate the stability of these complexes; one is a symmetry-based molecular-orbital approach derived from perturbation-theory arguments,[5,6] and the other is the eighteen-electron (or inert-gas) rule.[4,7]

On the other hand, the present author has been developing a graph-theoretical theory of aromaticity within the framework of the Hückel molecular-orbital (HMO) theory.[8–10] The aromaticity theory is characterized by its ability to determine the Dewar-type resonance energy[11] of any conjugated compound without parametrization. Recently, Mingos reported his attempt to frame tricarbonyliron complexes of typical olefins by means of the HMO theory.[7] Accordingly, it can now be shown that the theory of aromaticity can be extended to verify the aromaticities of three-dimensional conjugated systems in these complexes.

In applying the graph-theoretical theory of aromaticity[8–10] to the tricarbonyliron complexes, Mingos's HMO model[7] was adopted in its original form. The signs of the iron-carbon resonance integrals were chosen in a way which reflects the phase changes in the set of basis orbitals. The absolute values of all the resonance integrals were taken to be equal to that of the carbon-carbon resonance integral (β_{C-C}). The Coulomb integral of iron was taken to be equal to $\alpha_C - \beta_{C-C}$, where α_C signifies the Coulomb integral of carbon. The resonance energies of typical tricarbonyliron complexes were calculated according to a procedure previously described;[8] they are presented in Table 1.

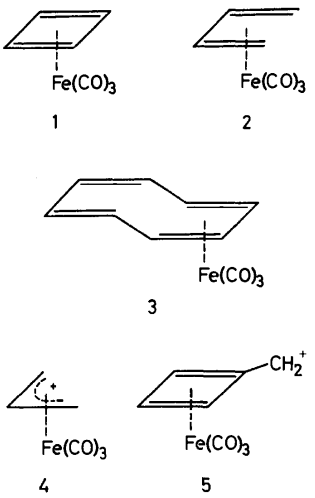

Table 1. Resonance energies of tricarbonyliron complexes of typical olefins

Complex	Resonance energy (β)
1[2,13]	0.894
2[15]	0.646
3[16]	0.671
4[17]	0.373
5[18]	0.593

Alone, the olefins investigated here are not aromatic, because they do not have positive resonance energies. The resonance energies are −1.226 for cyclobutadiene, 0.000 for butadienene, −0.594 for cyclooctatetraene, 0.000 for an allyl cation, and −0.401 for a methylenecyclobutadiene cation, all in units of β. Accordingly, it should be noted that the resonance energies of these olefins dramatically increase when they form complexes with tricarbonyliron.[12]

Since it has been fully proved that the resonance energy of this type excellently correlates with the experimental stability for a wide variety of conjugated compounds,[8,9,11] we might safely say that these olefins are markedly aromatized by the coordination of tricarbonyliron. The positive resonance energy is a distinct indication of aromaticity. This fact clearly supports the view of Pettit *et al.*,[13] who first insisted that the tricarbonyliron complex of cyclobutadiene is aromatic because of its tendency toward electrophilic substitution reactions.[14] An analogous trend in the reactivity is also found among the other tricarbonyliron complexes listed in Table 1.[15–18] The results of the present approach are, of course, consistent with Mingos's conclusion, based on the eighteen-electron rule, leading to the stabilization of these complexes.[7] The decrease in the degree of bond alternation gives further support to the aromaticities of the complexes.[7,19]

In contrast to the aromatic compounds so far identified, each of the tricarbonyliron complexes has a three-dimensional conjugated system. They can, hence, be considered to be the first examples of three-dimensional aromatic compounds ascertained in terms of

the Dewar concept of aromaticity.[8,9,11] The application of the HMO theory to the other organometallic compounds[3,4] and also to such hydrocarbons as a square-pyramidal $C_5H_5^+$ species[20] would help to extend the concept of three-dimensional aromaticity.

This work was motivated by Dr. Shigeo Yoneda's article on three-dimensional aromaticity [Kagaku Sôsetsu, **15**, 36 (1977)]. The use of the facilities of the Hokkaido University Computing Center is gratefully acknowledged.

References

1) H. C. Longuet-Higgins and L. E. Orgel, *J. Chem. Soc.*, **1956**, 1969.
2) G. F. Emerson, L. Watts, and R. Pettit, *J. Am. Chem. Soc.*, **87**, 132 (1965).
3) H. W. Quinn and J. H. Tsai, *Adv. Inorg. Chem. Radiochem.*, **12**, 217 (1969); E. W. Abel and F. G. A. Stone, *Quart. Rev.*, **23**, 325 (1969).
4) C. A. Tolman, *Chem. Soc. Rev.*, **1**, 337 (1972).
5) M. J. S. Dewar, *Bull. Soc. Chim. Fr.*, **18**, C71 (1951); J. Chatt and L. A. Duncanson, *J. Chem. Soc.*, **1953**, 2939.
6) M. Elian and R. Hoffmann, *Inorg. Chem.*, **14**, 1058 (1975).
7) D. M. P. Mingos, *J. Chem. Soc. Dalton*, **1977**, 20, 26, 31.
8) J. Aihara, *J. Am. Chem. Soc.*, **98**, 2750 (1976); *ibid.*, **99**, 2048 (1977); *Kagaku No Ryoiki*, **30**, 379 (1976).
9) J. Aihara, *J. Am. Chem. Soc.*, **98**, 6840 (1976); *J. Org. Chem.*, **41**, 2488 (1976); *Kagaku No Ryoiki*, **30**, 812 (1976).
10) A definition of resonance energy presented in a recent paper [J. Aihara, *Bull. Chem. Soc. Jpn.*, **50**, 2010 (1977)] is not used here because the original definition proposed in Ref. 8 appears most suitable for describing the stability of any conjugated system. Note that the reference energy in Ref. 8 defines the lowest energy of the reference structure relative to which aromatic stabilization is considered. For all the conjugated systems investigated here, however, both definitions of resonance energy give the same results.
11) M. J. S. Dewar and G. J. Gleicher, *J. Am. Chem. Soc.*, **87**, 685, 692 (1965); M. J. S. Dewar and C. de Llano, *ibid.*, **91**, 789 (1969); J. Aihara, *Kagaku No Ryoiki*, **30**, 269 (1976).
12) Note that, in each of these tricarbonyliron complexes, one of the iron d orbitals and any three carbon p_π orbitals which are arranged in sequence and coordinated to the iron atom form a singly twisted conjugated ring (*i.e.*, a Möbius ring) because of the nodal characteristics of d orbitals. Such four-membered Möbius rings make a significant contribution to the aromaticity of the entire conjugated system.[9] In this context, the hypothetical Möbius cyclobutadiene can be considered to be highly aromatic. See, *e.g.*, J. Aihara, *Bull. Chem. Soc. Jpn.*, **48**, 517 (1975).
As a general rule, polyolefins do not tend to form very stable compounds in which only one double bond is coordinated to a transition metal atom. See, *e.g.*, F. A. Cotton and G. Wilkinson, "Advanced Inorganic Chemistry," 3rd ed, Wiley-Interscience, New York, N. Y. (1972), Chap. 23. This fact is consistent with the above structural consideration of conjugated systems.
13) J. D. Fitzpatrick, L. Watts, G. F. Emerson, and R. Pettit, *J. Am. Chem. Soc.*, **87**, 3254 (1965).
14) There has been a qualitative idea that aromatic compounds should be unusually stable, and that, typically, they should undergo substitution rather than addition reactions. See, *e.g.*, B. A. Hess, Jr., and L. J. Schaad, *J. Org. Chem.*, **36**, 3418 (1971).
15) B. F. Hallam and P. L. Pauson, *J. Chem. Soc.*, **1958**, 642; O. S. Mills and G. Robinson, *Proc. Chem. Soc.*, **1960**, 421.
16) T. A. Manuel and F. G. A. Stone, *Proc. Chem. Soc.*, **1959**, 90; *J. Am. Chem. Soc.*, **82**, 366 (1960); A. Nakamura and N. Hagihara, *Bull. Chem. Soc. Jpn.*, **32**, 880 (1959); M. D. Rausch and G. N. Schrauzer, *Chem. Ind.*, **1959**, 957.
17) G. F. Emerson, J. E. Mahler, and R. Pettit, *Chem. Ind.*, **1964**, 836.
18) J. D. Fitzpatrick, L. Watts, and R. Pettit, *Tetrahedron Lett.*, **1966**, 1299; R. E. Davis, H. D. Simpson, and R. Pettit, *J. Am. Chem. Soc.*, **93**, 6688 (1971).
19) T. Nakajima, *Top. Curr. Chem.*, **32**, 1 (1972); H. Kuroda, T. Ohta, and T. L. Kunii, "Aromaticity, Pseudo-Aromaticity, Anti-Aromaticity," ed by E. D. Bergman and B. Pullman, Israel Academy of Sciences and Humanities, Jerusalem (1971), pp. 236—255.
20) W. D. Stohrer and R. Hoffmann, *J. Am. Chem. Soc.*, **94**, 1661 (1972); S. Masamune, M. Sakai, and H. Ona, *ibid.*, **94**, 8955 (1972); S. Masamune, M. Sakai, H. Ona, and A. J. Jones, *ibid.*, **94**, 8956 (1972).

BULLETIN OF THE CHEMICAL SOCIETY OF JAPAN, VOL. 51 (5), 1543—1544 (1978)

Studies on Spontaneous Emulsification. III. Molecular Interaction at the Oil–Water Interface

Keizo OGINO and Hidetoshi UMETSU

Faculty of Science and Technology, Science University of Tokyo, Noda, Chiba 278

(Received August 19, 1977)

Synopsis. At the oil-water interface, measurements of the interfacial tension were performed simultaneously with the observation of spontaneous emulsification. The effects of an oil-soluble alcohol (1-dodecanol) and a water-soluble surfactant (SDS) on the interfacial tension and on the spontaneous emulsification were studied.

In previous papers,[1,2] the molecular interactions at the Nujol–water interface were studied in relation to the kinds of additives and the tendency of spontaneous emulsification.

In this study, sodium dodecyl sulfate (SDS) was used as a water-soluble surfactant and dodecane containing 1-dodecanol as an oil phase. All have 12 carbon atoms in the hydrocarbon chains, and consequently this system is advantageous for studying the details of the interactions between the molecules causing the spontaneous emulsification.

The interfacial tension showed a minimum value when the 1-dodecanol molar fraction in the oil phase was approximately from 0.05 to 0.10 for all SDS concentrations in the water phase.

Spontaneous emulsification was not observed at the minimum interfacial tension, while it was observed when the molar fraction of 1-dodecanol in dodecane exceeded 0.10 and the concentration of SDS was 6×10^{-3} M*. Spontaneous emulsification with 1-dodecanol was also observed only above an SDS concentration of 4×10^{-3} M.

Experimental

Materials. SDS obtained from the Wako Pure Chemical Industries, Ltd., was purified by recrystallization from ethanol, and extracted with petroleum ehter. Dodecane was supplied from the Nikko Petrochemical Co., Ltd., and 1-dodecanol from the Wako Pure Chemical Industries, Ltd.

Apparatus. The interfacial tension was measured using a Shimadzu Seisakusho, Ltd., Wilhelmy-type Surface Tensiometer.

Procedure. Dodecane and 1-dodecanol were mixed in various proportions to prepare the oil phase, and SDS was dissolved in distilled water. The measurement of the interfacial tension was started 10 min after the beginning of the contact between oil and water phases. Spontaneous emulsification was observed with the unaided eye and was photographed. All measurements carried out at 25 °C.

Results and Discussion

Decrease in Interfacial Tension. The interfacial tension was measured for various compositions of the oil phase consisting of dodecane and 1-dodecanol, as well as for various concentrations of SDS in the water phase. From this the effects of these variations on the interfacial tension were derived.

Figure 1 shows the effect of the variation of the SDS concentration on the interfacial tension for each composition of the oil phase. It is apparent from Fig.1 that the interfacial tension is lowered by the addition of 1-dodecanol in dodecane, and that the extent of the lowering is larger for smaller 1-dodecanol fractions in the oil phase. In this connection, the tension at the interface between the oil phase with a small molar fraction of 1-dodecanol and the water phase, including SDS, was measured. From Fig. 2, it is clear that the interfacial tension decreases greatly when the fraction of 1-dodecanol in the oil phase is in the range from 0.03 to 0.10. The interfacial tension was reduced to about 0.5 dyn**/cm for SDS concentrations

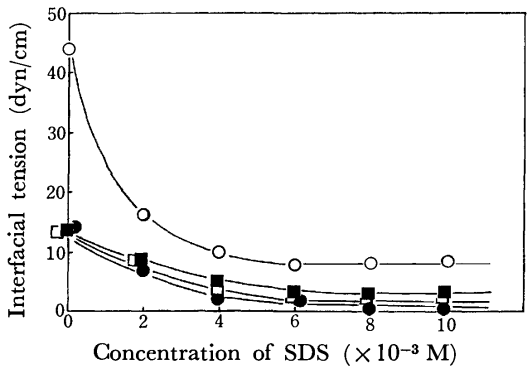

Fig. 1. The effect of concentration of SDS on the interfacial tension at the oil/SDS solution interface. Mole fraction of oil phase (dodecane : 1-dodecanol ○: (1.00 : 0.00), ●: (0.80 : 0.20), □: (0.60 : 0.40) ■: (0.00 : 1.00)

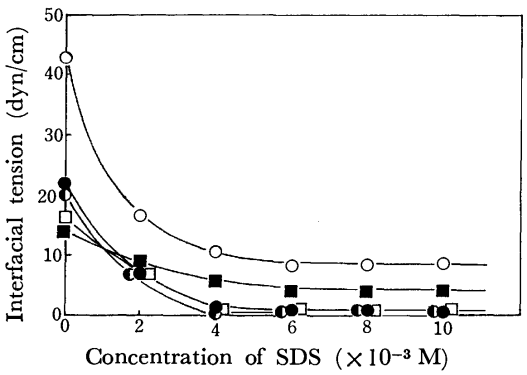

Fig. 2. The effect of concentration of SDS on the interfacial tension at the oil/SDS solution interface. Mole fraction of oil phase (dodecane : 1-dodecanol) ○: (1.00 : 0.00), ●: (0.97 : 0.03), ◐: (0.95 : 0.05) □: (0.90 : 0.10), ■: (0.00 : 1.00).

* Throughout this paper 1 M=1 mol dm^{-3}.

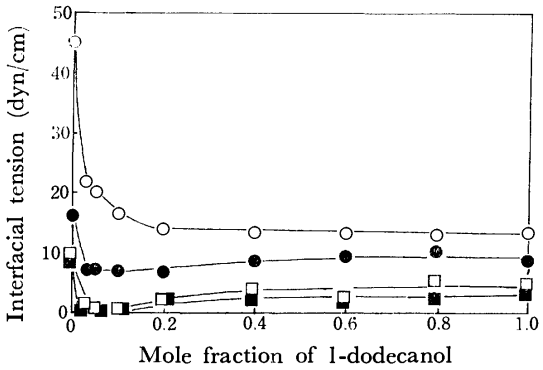

Fig. 3. The effect of composition of oil phase on the interfacial tension at the oil/SDS solution interface. Water phase ○: Water, ●: 2×10^{-3} M, □: 4×10^{-3} M, ■: 6×10^{-3} M.

above 6×10^{-3} M.

The relation between the composition of the oil phase and the interfacial tension is shown in Fig. 3. As is seen in the figure, the minimum value of the interfacial tension appears in the 1-dodecanol molar fraction range of 0.05 to 0.10 for concentrations of the SDS solution above 2×10^{-3} M. The minimum value of such a relation would be the result of molecular interaction between SDS and 1-dodecanol at the interface. When the concentration of 1-dodecanol in the oil phase is so low that no monolayer is formed, for example less than 0.05, and a solution including the other molecular species is injected, a variety of phenomena may occur.[3] If very small quantities of molecular species are present at the oil–water interface, they will eventually, by the processes of diffusion and convection, cause fluctuation, resulting in a large change in the interfacial tension.

Spontaneous Emulsification. The entire contour of the relation of the interfacial tension with the phase composition appearing separately in Figs. 1, 2, and 3 are shown together in Fig. 4. In this figure, the dotted line shows the critical SDS concentration at which spontaneous emulsification begins to occur, with the phases showing milky turbidity.

Figure 5 shows that spontaneous emulsification does not occur even for a SDS concentration in the water phase of 10×10^{-3} M, when the 1-dodecanol molar

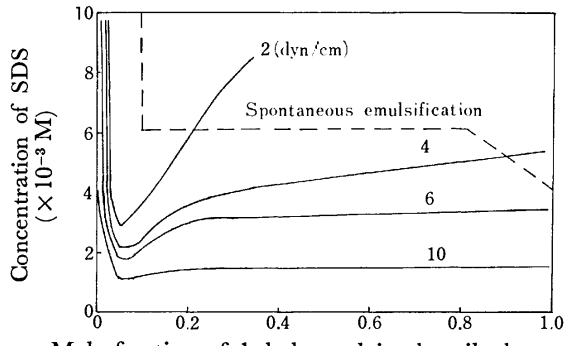

Fig. 4. The contour line of the infacial tension at the Dodecane & 1-dodecanol/SDS solution interface.

** Throughout this paper 1 dyn = 10^{-5} N.

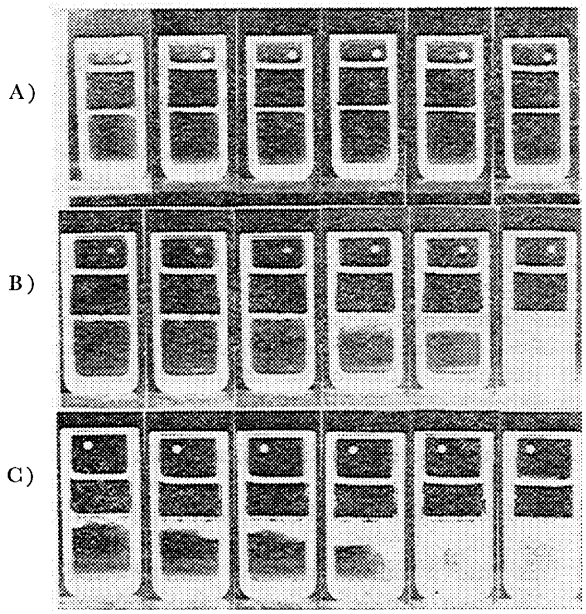

Fig. 5. Observation for spontaneous emulsification.
A) Oil phase dodecane: 1-dodecanol = 0.95 : 0.05. Water phase 10×10^{-3} M SDS solution.
B) Oil phase dodecane: 1-dodecanol = 0.90 : 0.10 Water phase 6×10^{-3} M SDS solution.
C) Oil phase dodecane: 1-dodecanol = 0.80 : 0.20 Water phase 6×10^{-3} M SDS solution.

fraction in the oil phase is 0.05. However, this occurs for SDS concentrations above 6×10^{-3} M, when the 1-dodecanol molar fraction is 0.10 and 0.20. It is apparent that the limit of the appearance of spontaneous emulsification depends on the SDS concentration and the composition of the oil phase rather than on the value of the minimum interfacial tension.

Schulman and Cockbain[4] have shown that spontaneous emulsification occurs when a complex is formed between an oil-soluble substance and a water-soluble surfactant at the oil–water interface. Mori *et al.*[5] have reported the existence of a complex between SDS and 1-dodecanol, and have shown the ratio of alcohol to sulfate to be 0.53—0.63.

In this work, no spontaneous emulsification was observed when the 1-dodecanol molar fraction was less than 0.05, although the interfacial tension showed a minimum. The amount of the complexes formed between the two components must be too small to be detectable with the unaided eye and, consequently, the visual change must be the change introduced by the complex formation.

References

1) K. Ogino and M. Ota, *Yukagaku*, **23**, 28 (1974).
2) K. Ogino and M. Ota, *Bull. Chem. Soc. Jpn.*, **49**, 1187 (1976).
3) J. H. Schulman and E. K. Rideal, *Proc. R. Soc. London, Ser. B*, **122**, 29, 46 (1937).
4) J. H. Schulman and E. G. Cockbain, *Trans. Faraday Soc.*, **36**, 651 (1940).
5) Y. Mori, K. Motomura, and R. Matsuura, *Bull. Chem. Soc. Jpn.*, **44**, 2078 (1971).

BULLETIN OF THE CHEMICAL SOCIETY OF JAPAN, VOL. 51 (5), 1545—1546 (1978)

Proton Magnetic Relaxation Time T_1 of Water in Acrylamide Gel

Seiji KATAYAMA, Yoji ARATA,* and Shizuo FUJIWARA*
Shizuoka College of Pharmacy, 2-2-1, Ojika, Shizuoka 422
**Department of Chemistry, Faculty of Science, The University of Tokyo, Hongo, Tokyo 113*
(Received August 30, 1977)

Synopsis. Proton magnetic relaxation time T_1 of water in polyacrylamide gel was measured. The results have been interpreted in terms of the contribution from dissolved oxygen and the intrinsic nature of gel. A minimum of $1/T_1$ appears in a system with a *ca.* 2.8% concentration of acrylamide, corresponding to the lowest concentration for gel formation.

The proton spin lattice relaxation time, T_1, of water which is held in a polyacrylamide gel was measured in order to compare the motion of water molecules in the gel with that of bulk water. The gel was prepared by the copolymerization of acrylamide and *N,N'*-methylenebisacrylamide in heavy water, the mole ratio of acrylamide and *N,N'*-methylenebisacrylamide being approximately 80 to 1. The T_1 values of water were measured by the adiabatic rapid passage method using a JNM-C-60H high resolution NMR spectrometer at 60 MHz.

Samples were used under four different conditions: 1) undegassed, 2) degassed at about 10^{-5} mmHg, 3) degassed and polymerized by addition of a small amount of ammonium persulfate to accelerate polymerization, and 4) polymerized without degassing. For samples 3) and 4), no appreciable difference was observed between the values of $1/T_1$ before and immediately after the addition of ammonium persulfate. T_1 measurements were carried out in each case after sufficient elapse of time. The dissolved oxygen in each sample was thus sufficiently in equilibrium with the air pressure contacted (degassed and undegassed conditions).

Plots of $1/T_1$ against the concentration of acrylamide are shown in Figs. 1, 2, and 3. Linearity holds between the acrylamide content and $1/T_1$ of water in acrylamide solutions under atomospheric pressure (Fig. 1). We see that the $1/T_1$ values are considerably shortened by degassing. The paramagnetic effect of dissolved oxygen plays an important role in determining the relaxation.[1,2]

Polymerization causes a remarkable change in the $1/T_1$ values (Fig. 2). The $1/T_1$ values are reduced in a drastic way by polymerization of the solutions at lower concentrations of acrylamide, $1/T_1$ becoming minimum and then increasing.

In marked contrast, no such minimum can be observed in the case of degassed polymer samples (Fig. 3 A). The values of $1/T_1$ observed when the degassed samples are polymerized deviate from a straight line before polymerization (Fig. 3 B). At lower concentrations,

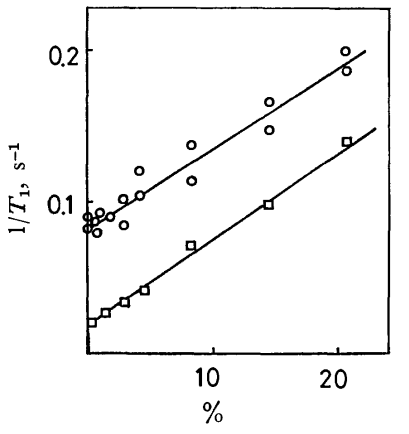

Fig. 1. Plots of $1/T_1$'s of water in acrylamide aqueous solutions *vs.* acrylamide content. —○—: Undegassed samples, —□—: degassed samples.

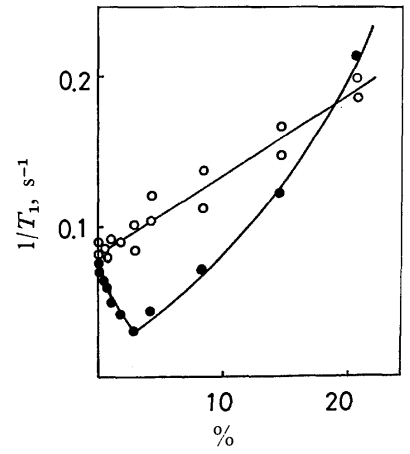

Fig. 2. Plots of $1/T_1$'s of water *vs.* acrylamide content. —○—: Undegassed samples, —●—: Undegassed polymer samples.

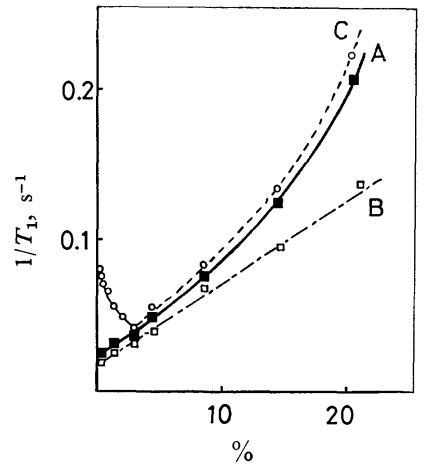

Fig. 3. Plots of $1/T_1$'s of *vs.* water acrylamide content. A —■—: Degassed polymer samples, B —□—: degassed samples, C —○—: undegassed polymer samples.

the line of $1/T_1$ for the polymerized samples (Fig. 3A) nearly coincides with that of samples before polymerization (Fig. 3B), whereas at higher concentrations, the $1/T_1$ values for the polymerized samples (Fig. 3A) increase drastically and are in accord with that for the undegassed polymer samples (Fig. 3C). The fact that very little difference can be observed in the $1/T_1$ values between both polymer samples produced from the degassed and undegassed solutions might indicate that both polymerized samples are essentially the same as regards relaxation of water.

The proton relaxation of water in the polyacrylamide gel is written as

$$(1/T_1)_{obsd} = (1/T_1)_{O_2} + (1/T_1)_{gel},$$

where $(1/T_1)_{obsd}$ is the observed value, $(1/T_1)_{O_2}$ the contribution from the oxygen molecule and $(1/T_1)_{gel}$ the term arising from the intrinsic nature of the gel. It may be concluded that in the sol phase at concentrations lower than 2.8%, the term $(1/T_1)_{O_2}$ dominantly determines T_1, with a negligible contribution from $(1/T_1)_{gel}$. The decrease of $1/T_1$ value with increase in the concentration of acrylamide in this range may be interpreted by the fact that the solubility of oxygen in the polymer solution is reduced with the increase in the concentration of acrylamide.

The above interpretation was deduced from the T_1 data and is not the final conclusion. In the gel phase, $(1/T_1)_{gel}$ becomes dominant, suggesting that the relaxation time T_1 of the water proton in a confined space of the polyacrylamide gel is considerably shortened in comparison with that in bulk water. Two types of water, "bound" and "free" have been assumed to exist in explaining a similar relaxation behavior in biological systems.[3-7] The presence of a small proportion of water having an increased relaxation rate in the bound state can produce a marked reduction in the observed relaxation times.[8-11]

It can be concluded that the minimum point of $1/T_1$ corresponds to the critical concentration at which the gel can be formed.

References

1) F. Bloch, W. W. Hansen, and M. Packard, *Phys. Rev.*, **70**, 474 (1946).
2) R. Hausser and F. Noack, *Z. Naturforsch.*, **20**, 1688 (1965).
3) O. Hechter, T. Wittstruck, N. McNiven, and G. Lester, *Proc. Natl. Sci. U.S.*, **46**, 783 (1970).
4) C. Sterling and M. Masuzawa, *Macromol. Chem.*, **116**, 140 (1968).
5) D. E. Woessner, B. S. Snowden, Jr. and Y. C. Chiu, *J. Colloid Interface Sci.*, **34**, 283 (1970).
6) D. E. Woessner and B. S. Snowden, Jr., *J. Colloid Interface Sci.*, **34**, 290 (1970).
7) D. E. Woessner and B. S. Snowden, Jr., *Ann. N.Y. Acad. Sci.*, **204**, 113 (1973).
8) J. R. Zimmerman and W. E. Brittin, *J. Phys. Chem.*, **61**, 1328 (1957).
9) E. D. Finch, J. F. Harmon, and B. H. Muller, *Arch. Biochem. Biophys.*, **147**, 299 (1971).
10) R. Cooke and R. Wein, *Biophys. J.*, **11**, 1002 (1971).
11) R. Cooke and R. Wein, *Ann. N.Y. Acad. Sci.*, **204**, 197 (1973).

BULLETIN OF THE CHEMICAL SOCIETY OF JAPAN, VOL. 51 (5), 1547—1548 (1978)

Complex Anion Radical Salts Derived from Dicyanomethylenetrinitrofluorene

Yoshio MATSUNAGA and Yuji YOSHIDA

Department of Chemistry, Faculty of Science, Hokkaido University, Sapporo 060

(Received October 25, 1977)

Synopsis. Four anion radical salts of the 2 : 3 type were derived from 9-dicyanomethylene-2,4,7-trinitrofluorene. Their electronic spectra, the ESR spectra characteristic of triplet excitons, and the electrical properties were measured.

9-Dicyanomethylene-2,4,7-trinitrofluorene (DTF) has been known to form anion radical salts with a number of onium cations.[1,2] All the cations so far examined have given salts of the 1:1 type. However, Dupuis and Néel have reported the isolation of 1,2,3-trimethylbenzimidazolium salts not only of the 1:1 type, but also of the 1:2 type.[2] In addition, they have noted that the salts prepared by the reduction of DTF with onium iodides tend to include an excess of DTF, which could be eliminated by repeated recrystallizations from acetonitrile. Consequently, it seemed highly likely that some complex anion radical salts could be obtained if the preparation conditions and the cations were appropriately selected.

As has been described by Mukherjee and Levasseur,[1] DTF was prepared by a condensation reaction between 2,4,7-trinitrofluorenone, Eastman reagent-grade, and malononitrile in methanol, and was then recrystallized from acetonitrile. The anion radical salts were obtained by mixing DTF and the onium iodide, separately dissolved in hot acetonitrile, in a mole ratio of 3:2 under a nitrogen atmosphere. The mole ratio employed by Dupuis and Néel was reversed here in order to attempt the isolation of possible complex salts. The greenish-black products were recrystallized two or three times from acetonitrile. Although we examined a number of cations, only the following four complex salts could be isolated (two independent preparations were analysed for each salt). With tetrapropylammonium, Found: C, 59.19, 58.93; H, 4.90, 4.91; N, 16.18, 15.85%. Calcd for $[(C_3H_7)_4N]_2(DTF)_3$: C, 59.13; H, 4.89; N, 16.28%. With tetrabutylammonium, Found: C, 60.81, 60.68; H, 5.89, 5.77; N, 14.28, 13.63%. Calcd for $[(C_4H_9)_4N]_2(DTF)_3$: C, 61.02; H, 5.57; N, 15.12%. With propyltriphenylphosphonium, Found: C, 62.28, 63.68; H, 3.51, 3.45; N, 11.83, 12.19%. With isopropyltriphenylphosphonium, Found: C, 63.07, 63.26; H, 3.56, 3.48; N, 11.89, 12.03%. Calcd for $[C_3H_7(C_6H_5)_3P]_2(DTF)_3$: C, 63.57; H, 3.50; N, 12.36%. The composition was checked by measuring the ratio of optical density at 515 nm to that at 380 nm, following Dupuis and Néel. The optical density at the former wavelength arises solely from the anion, but that at the latter, from both the anionic and neutral species. Dupuis and Néel have found that the ratio is about 0.64 in the 1 : 1 salt and 0.34 in the 1 : 2 salt. The values observed with our salts were in the range from 0.42 to 0.48, and so seemed to be consistent with the proposed composition.

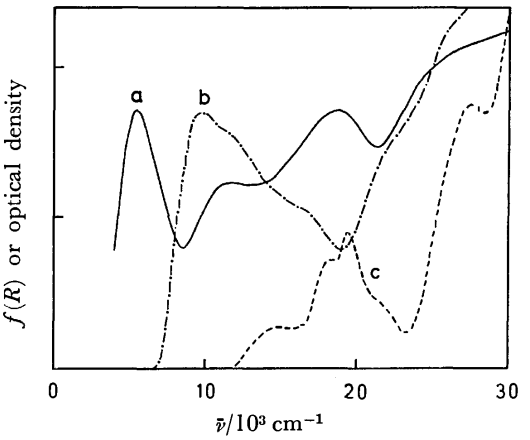

Fig. 1. Diffuse reflection spectra of (a) isopropyltriphenylphosphonium-DTF(2 : 3), (b) lithium-DTF (1 : 1), and (c) absorption spectrum of the DTF^- ion in acetone.

The solid-state spectra of the four salts, as recorded on a Beckman DK-2A spectroreflectometer, are similar to each other. In Fig. 1, the spectra of the isopropyltriphenylphosphonium salt and the simple lithium salt, plotted using the Kubelka-Munk function, are compared with the absorption spectrum of the latter dissolved in acetone. The band around 5.5×10^3 cm^{-1} appears in all the solid complex salts and may be assigned to the charge-transfer transition from the highest occupied level of the DTF anion to the lowest vacant level of the DTF molecule. The second band, located near 11×10^3 cm^{-1}, observable also with the simple salt, may arise from the charge-transfer interaction between the anions.

In the ESR spectra of the present salts taken at the X-band, the appearance of three pairs of resonance lines characteristic of triplet-spin excitons was noted in the temperature range from 30 to 120 °C. No change in the separation of the pair was detected in the measured range; however, the collapse of the inner two pairs by broadening was observed at the highest temperature employed. For the sake of simplicity, an isotropic g value was assumed to be equal to the free electron value; then, the principal axis splittings are related to the zero-field splitting parameters, D and E, by the following equations:

$$d_1 = 2|D/g\beta|,$$
$$d_2 = |D/g\beta| + 3|E/g\beta|,$$
$$d_3 = |D/g\beta| - 3|E/g\beta|,$$

where d_i is the measured separation and β is the Bohr magneton. The numbering, i, is given starting from

Table 1. Zero-field splitting parameters and singlet-triplet separation energies of the complex anion radical salts derived from dicyanomethylenetrinitofluorene

Cation	$\lvert D/g\beta \rvert$ /G	$\lvert E/g\beta \rvert$ /G	J/eV
Tetrapropylammonium	99.5	2.2	0.31
Tetrabutylammonium	97.8	3.9	0.42
Propyltriphenylphosphonium	98.3	3.7	0.28
Isopropyltriphenylphosphonium	95.2	3.4	0.32

the outermost pair of resonance lines. The estimated parameters are summarized in Table 1. The magnitude depends on the average spatial distribution of the correlated spins of the exciton. When the spins interact strongly, the parameters may be expected to increase. The values of $|D/g\beta|$ in our salts, 95—99 G, are close to those in the complex TCNQ salts of the 2:3 type, 100 G, while the simple TCNQ salts are known to give values of 140—170 G, and the complex salts of the 1:2 type, about 70 G.[3] Thus, one may be led to the conclusion that the spins in the DTF salts are as delocalized as those in the TCNQ salts and are more delocalized than those in the anion radical salts derived from 2,3-dicyano-1,4-naphthoquinone studied earlier.[4] Taking the peak height or the peak-to-peak intensity on the first derivative curve as a measure of the relative intensity of the ESR absorption for a triplet state, I, the following approximation was found to be well-obeyed;

$$I \times T \propto \exp(-J/kT),$$

where J is the energy for the singlet-triplet separation. The energies listed in Table 1 are comparable with the values for the dicyanonaphthoquinone salts. The absence of any appreciable exciton-exciton exchange in the DTF salts is consistent with such large separation energies.

The electrical resistivities, ρ, observed with polycrystalline compactions were in the order of 10^4 or 10^5 ohm cm at room temperature. These values are close to those reported by Dupuis and Néel for their simple DTF salts containing aromatic counter ions with large polarizabilities.[5] The temperature-dependence recorded employing the potential-probe method described before[6] does not fit in with the usual exponential law, $\rho=\rho_0 \exp(E/kT)$. The increase at high temperatures was found for the tetrabutylammonium and propyltriphenylphosphonium salts. Such behavior is not unexpected when the conduction is extrinsic in the measured range, but the impurity concentration is low. The intrinsic resistivities of the present complex anion radical salts at room temperature may be higher by a factor of tens or hundreds than the observed values.

The present work was partially supported by a Grant-in-Aid for Scientific Research from the Ministry of Education (No. 234028).

References

1) T. K. Mukherjee and L. A. Levasseur, *J. Org. Chem.*, **30**, 644 (1965).
2) P. Dupuis and J. Néel, *C. R. Acad. Sci., Ser. C*, **268**, 557 (1969).
3) T. Hibma, P. Dupuis, and J. Kommandeur, *Chem. Phys. Lett.*, **15**, 17 (1972).
4) I. Maki, Y. Matsunaga, M. Nakakura, and A. Nonaka, *Bull. Chem. Soc. Jpn.*, **48**, 1368 (1975).
5) P. Dupuis and J. Néel, *C. R. Acad. Sci., Ser. C*, **268**, 653 (1969).
6) K. Kan and Y. Matsunaga, *Bull. Chem. Soc. Jpn.*, **45**, 2096 (1972).

BULLETIN OF THE CHEMICAL SOCIETY OF JAPAN, VOL. 51 (5), 1549—1550 (1978)

Spectroscopic Similarity of Charge-Transfer Absorptions in Crystalline Complex Ion Radical Salts

Yôichi IIDA

Department of Chemistry, Faculty of Science, Hokkaido University, Sapporo 060

(Received October 29, 1977)

Synopsis. Charge-transfer transition between ion radical molecules takes place in crystalline ion radical salts. Spectroscopic similarity of the charge-transfer absorptions between certain systems of complex ion radical salts has been studied with use of a one-dimensional Hubbard model.

In most solid ion radical salts, the planar ion radical molecules are known to form, in themselves, a face-to-face stacking into infinite one-dimensional columns so as to make a large overlap between their half-occupied molecular orbitals.[1-5] In this case, since any individual radical molecule interacts through charge-transfer most strongly with two other neighboring radicals, the electronic spectrum of the solid salt differs distinctly from the monomer spectrum of the radical ion in solution, showing a charge-transfer transition between ion radicals in the low-energy region.[6,7]

Two kinds of solid ion radical salts are known:[1-7] (a) simple ion radical salts in which each ion radical molecule has one unpaired electron, considered to be a one-dimensional system of sites with half-occupied orbital; (b) complex ion radical salts, which include not only ion radicals but also formally neutral parent molecules, belonging to a one-dimensional system of sites with less than half-occupied orbital. In the present paper, it is shown that the charge-transfer absorption of the system with less than half-occupied orbital has spectroscopic properties similar to those for the system with more than half-occupied orbital.

In order to describe a narrow energy band with strong electron correlation in the crystalline ion radical salts, we consider a system of electrons expressed by the Hubbard Hamiltonian,[8]

$$\mathscr{H} = \sum_{i,j,\sigma} t_{ij} C_{i\sigma}{}^{+} C_{j\sigma} + I \sum_{i} n_{i\downarrow} n_{i\uparrow}, \tag{1}$$

where $n_{i\sigma}=C_{i\sigma}{}^{+}C_{i\sigma}$, and $C_{i\sigma}{}^{+}$ and $C_{i\sigma}$ are the creation and annihilation operators of an electron with σ-spin at the i-th site, respectively, t_{ij} is the transfer matrix element between the i-th and j-th sites, the intra-site Coulomb repulsive potential, I, appearing only when two electrons with up and down spins are at the same site. We consider one-dimensional stack of planar molecules including unpaired electrons in the solid state, and apply the one-particle Green's function given by Hubbard (often referred to as Hubbard I).[8] For the sake of simplicity, we assume non-alternant linear chain of equivalent sites for which the transfer matrix element, denoted by $T<0$, is taken only between the nearest neighbor sites. Discussion is restricted to the spectroscopic feature of the charge-transfer absorption. The charge-transfer absorption due to the transition of electrons with up spin in such one-dimensional column is given by[9]

$$\mathrm{Re}\sigma_{xx}(\omega) \propto A_{+}(\omega)\theta_{+}(\omega) + A_{-}(\omega)\theta_{-}(\omega), \tag{2}$$

$$A_{\pm}(\omega) = \frac{e^2}{2}\frac{I^2 n_{\downarrow}(1-n_{\downarrow})}{\omega^2\sqrt{\omega^2-4I^2n_{\downarrow}(1-n_{\downarrow})}}\sqrt{4T^2-\varepsilon_{\pm}(\omega)^2}, \tag{3}$$

$$\varepsilon_{\pm}(\omega) = -I(2n_{\downarrow}-1) \pm \sqrt{\omega^2-4I^2n_{\downarrow}(1-n_{\downarrow})}, \tag{4}$$

where ω is the frequency of electromagnetic wave absorbed by electrons with up spin, $n_{\downarrow}=<n_{i\downarrow}>$ being the mean number of electrons with down spin per site in the Hartree-Fock scheme.[8] $\theta_{\pm}(\omega)$ is the term related to Fermi distribution function, $f(E)$, and is given by $f(E_{\pm}{}^{L})-f(E_{\pm}{}^{U})$, where

$$E_{\pm}^{L} = \frac{1}{2}\left\{\varepsilon_{\pm}(\omega)+I-\sqrt{(\varepsilon_{\pm}(\omega)+I)^2-4I(1-n_{\downarrow})\varepsilon_{\pm}(\omega)}\right\}, \tag{5}$$

$$E_{\pm}^{U} = \frac{1}{2}\left\{\varepsilon_{\pm}(\omega)+I+\sqrt{(\varepsilon_{\pm}(\omega)+I)^2-4I(1-n_{\downarrow})\varepsilon_{\pm}(\omega)}\right\}. \tag{6}$$

If we assume a paramagnetic state (*i.e.*, $n_{\downarrow}=n_{\uparrow}$), an expression of the charge-transfer absorption similar to Eqs. 3 and 4 is obtained for electrons with down spin. Hereafter, we take only the absorption due to electrons with up spin. The character of the charge-transfer absorption of a complex ion radical salt with mean number of electrons, $n_{\downarrow}$, then depends strongly on $n_{\downarrow}$, $(0\leq n_{\downarrow}\leq 1)$.

We next consider complex ion radical salts in which the mean number of electrons with down spin is given by $1-n_{\downarrow}$. We also assume a paramagnetic state and magnitudes of I and T common to those of the $n_{\downarrow}$ system, respectively. The charge-transfer absorption of the $(1-n_{\downarrow})$ system is given by

$$\mathrm{Re}\sigma'_{xx}(\omega) \propto A_{+}'(\omega)\theta_{+}'(\omega) + A_{-}'(\omega)\theta_{-}'(\omega), \tag{7}$$

where $A_{\pm}'(\omega)$ and $\theta_{\pm}'(\omega)$ are derived from $A_{\pm}(\omega)$ and $\theta_{\pm}(\omega)$ by replacing $n_{\downarrow}$ by $1-n_{\downarrow}$, respectively. However, if we pay attention to the forms of Eqs. 3 and 4, we note that

$$A_{\pm}'(\omega) = \frac{e^2}{2}\frac{I^2 n_{\downarrow}(1-n_{\downarrow})}{\omega^2\sqrt{\omega^2-4I^2n_{\downarrow}(1-n_{\downarrow})}}\sqrt{4T^2-\varepsilon_{\pm}'(\omega)^2}, \tag{8}$$

$$\varepsilon_{\pm}'(\omega) = -\varepsilon_{\mp}(\omega). \tag{9}$$

Thus, we obtain

$$A_{\pm}'(\omega) = A_{\mp}(\omega). \tag{10}$$

The charge-transfer absorption of the $(1-n_{\downarrow})$ system is then given by

$$\mathrm{Re}\sigma_{xx}'(\omega) \propto A_{-}(\omega)\theta_{+}'(\omega) + A_{+}(\omega)\theta_{-}'(\omega). \tag{11}$$

As for the term related to the Fermi distribution function, the Fermi energy for the $(1-n_{\downarrow})$ system differs from that for the $n_{\downarrow}$ system. However, if the intra-site Coulomb repulsion energy is much greater

than the energy due to the observed temperature, we can put $\theta_{\pm}(\omega)\approx 1$ and $\theta'_{\pm}(\omega)\approx 1$. The magnitudes of I for a number of organic ion radical salts have been reported to be of the order of 1 eV.[9] This is found to be much larger than the room-temperature energy of ≈ 0.026 eV. Under these conditions, the charge-transfer absorption of $\mathrm{Re}\sigma'_{xx}(\omega)$ for the $(1-n_{\downarrow})$ system has spectroscopic properties identical with those of $\mathrm{Re}\sigma_{xx}(\omega)$ for the $n_{\downarrow}$ system, except for a difference between $\theta_{\pm}(\omega)$ and $\theta'_{\mp}(\omega)$. The symmetrical point with respect to the number of electrons with down spin is then at $n_{\downarrow}=1/2$. The system $n_{\downarrow}=1/2$ corresponds to the half-occupied orbital system of simple ion radical salt where each site has one unpaired electron. If we consider a system of complex ion radical salt with $n_{\downarrow}<1/2$, we can expect another kind of complex ion radical salt of $1-n_{\downarrow}>1/2$ with the common I and T values. Thus the spectroscopic features of the charge-transfer absorptions of both less than half-occupied orbital system (the $n_{\downarrow}$ system) and more than half-occupied orbital system (the $1-n_{\downarrow}$ system) are similar.

With respect to negatively charged ion radical salts, 7,7,8,8-tetracyanoquinodimethane (TCNQ) has been known to form a number of complex anion radical salts, as well as simple anion radical salts, with various counter cations.[1-6] Different stoichiometries of the type $(M^+)_m(TCNQ)_n^{m-}$ are obtainable even for a single cation, M^+. For example, morpholinium–TCNQ forms $(m:n)=(1:1)$, $(2:3)$, and $(3:4)$ crystalline anion radical salts,[5,10] while methyltriphenylphosphonium–TCNQ gives $(1:1)$ and $(1:2)$ salts.[1,6] The salts with $(1:1)$ composition correspond to simple anion radical salts of half-occupied orbital system, while those with other compositions are complex anion radical salts. Not only simple TCNQ anion radical salts but also complex ones show strong charge-transfer absorptions due to the transitions between unpaired electrons in the low-energy regions.[6,9] So far, only the complex salts with less than half-occupied orbital system (*i.e.*, $m<n$) are known. No experimental data have been given on the formation and thus the spectroscopic properties of the complex salts with more than half-occupied orbital system (*i.e.*, $m>n$). However, the above theoretical prediction strongly suggests that the spectroscopic features of the charge-transfer absorption of $(M^+)_m(TCNQ)_n^{m-}$, $(m<n)$, salt are very similar to those of $(M^+)_{2n-m}(TCNQ)_n^{(2n-m)-}$ salt of more than half-occupied orbital system, as long as the assumptions for deriving Eqs. 2—11 hold for these two compounds.

As for positively charged ion radical salts, few compounds are known to form crystalline complex cation radical salts with diamagnetic counter anions. For example, tetrathiafulvalene (TTF) forms such cation radical salts as $(TTF)_n^{m+}(I^-)_m$, $(m:n=0.7:1)$.[11] There should be spectroscopic similarity of the charge-transfer absorptions between complex cation radical salts of less than half-occupied and more than half-occupied orbital systems. The situation would be analogous to that of complex anion radical salts.

The author wishes to thank Dr. Kenn Kubo for his useful suggestions.

References

1) L. R. Melby, R. J. Harder, W. R. Hertler, W. Mahler, R. E. Benson, and W. E. Mochel, *J. Am. Chem. Soc.*, **84**, 3374 (1962).
2) W. J. Siemons, P. E. Bierstedt, and R. G. Kepler, *J. Chem. Phys.*, **39**, 3523 (1963); R. G. Kepler, *J. Chem. Phys.*, **39**, 3528 (1963).
3) G. R. Anderson and C. J. Fritchie, Jr., Second National Meeting, Society for Applied Spectroscopy, San Diego, Paper 111 (1963).
4) H. Kobayashi, Y. Ohashi, F. Marumo, and Y. Saito, *Acta Crystallogr., Sect. B*, **26**, 459 (1970), and the references cited therein.
5) T. Sundaresan and S. C. Wallwork, *Acta Crystallogr., Sect. B*, **28**, 491, 3507 (1972).
6) Y. Iida, *Bull. Chem. Soc. Jpn.*, **42**, 71, 637 (1969).
7) Y. Iida, *Bull. Chem. Soc. Jpn.*, **43**, 2772 (1970); **44**, 663, 1777 (1971); **45**, 105, 624 (1972).
8) J. Hubbard, *Proc. R. Soc. London, Ser. A*, **276**, 238 (1963).
9) Y. Iida, *Bull. Chem. Soc. Jpn.*, **50**, 1445 (1977); Y. Iida, *Bull. Chem. Soc. Jpn.*, **51**, 434 (1978).
10) J. C. Bailey and D. B. Chesnut, *J. Chem. Phys.*, **51**, 5118 (1969).
11) J. J. Daly and F. Sanz, *Acta Crystallogr., Sect. B*, **31**, 620 (1975); C. K. Johnson and C. R. Watson, Jr., *J. Chem. Phys.*, **64**, 2271 (1976).

BULLETIN OF THE CHEMICAL SOCIETY OF JAPAN, VOL. 51 (5), 1551—1552 (1978)

Surface Tensions of Several Rare-earth Chlorides and Binary NaCl–YCl_3 System in Molten State

Kazuo IGARASHI, Junichi MOCHINAGA, and Shiro UEDA

Department of Synthetic Chemistry, Faculty of Engineering, Chiba University, Yayoi-cho, Chiba 280

(Received November 2, 1977)

Synopsis. The surface tensions of YCl_3, $LaCl_3$, $PrCl_3$, $NdCl_3$, $GdCl_3$, and $DyCl_3$, and binary NaCl–YCl_3 system in molten state were measured by a maximum bubble pressure method, and the results were represented by empirical formulas as functions of temperature. Surface enthalpies of rare-earth chlorides were calculated from the formulas.

Surface tension is important for thermodynamic considerations, since it is related to the interaction between the species in the melts and is necessary for calculating surface properties such as surface enthalpy and surface entropy. The surface tensions of binary $LaCl_3$–alkali chloride and –alkaline earth chloride systems in molten state have been reported by Smirnov and Stepanov[1] and those of binary $NdCl_3$–alkali chloride systems in molten state by Kurmaev *et al.*[2] In the present experiment, the surface tensions of YCl_3, $LaCl_3$, $PrCl_3$, $NdCl_3$, $GdCl_3$, and $DyCl_3$, and binary NaCl–YCl_3 system were measured, and represented by empirical formulas as functions of temperature. Negative deviation from the surface tension calculated by use of Guggenheim's equation[3] for ideal solution takes place in the isotherm of surface tension for binary NaCl–YCl_3 system.

Experimental

Materials. Rare-earth chlorides were prepared by the similar procedure to that given in the previous paper.[4] NaCl of analytical grade was dried by heating *in vacuo* at temperature 50 °C below the melting point for several hours. Argon gas was purified by passing through P_2O_5 and heated Ti sponges at 1000 °C.

Measurement. Maximum bubble pressure method was used. Two types of capillaries were used, one made of transparent quartz and the other of Pt-Rh(10% Rh) alloy. The surface tensions of binary NaCl–YCl_3 mixture melts were measured with the quartz capillary. The pressure of argon bubbles in the melts was measured with a manometer containing dibutyl phthalate, which was kept at 30.4±0.1 °C in a water bath. The surface tensions were calculated by means of Schrödinger's[5] equation giving the relation between bubble pressure and surface tension. The surface tension of NaCl and $CaCl_2$ in molten state were measured to check the apparatus, the observed values being in good agreement with the data given by Bloom *et al.*[6] and Grjotheim *et al.*[7]

Results and Discussion

Surface Tensions of Rare-earth Chlorides. The temperature dependence of the surface tensions for YCl_3, $LaCl_3$, $PrCl_3$, $NdCl_3$, $GdCl_3$, and $DyCl_3$ in molten state are shown in Fig. 1. The surface tension decreases linearly with increasing temperatrue within the range of measurement. The values

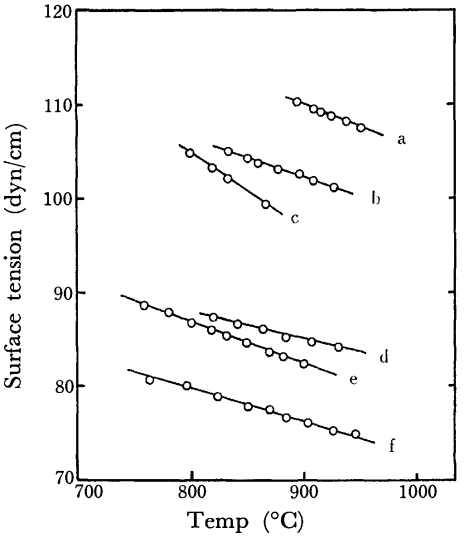

Fig. 1. Surface tensions of rare-earth chloride melts. a: $LaCl_3$, b: $PrCl_3$, c: $NdCl_3$, d: $GdCl_3$, e: $DyCl_3$, f: YCl_3.

TABLE 1. SURFACE TENSION EQUATIONS OF PURE MOLTEN SALTS

Salt	$\gamma=a+bt$ γ : (dyn/cm), t(°C)	σ (dyn/cm)	Temp range (°C)
YCl_3	$\gamma=106.3-0.0334t$	0.158	768—946
$LaCl_3$	$\gamma=147.9-0.0423t$	0.121	892—950
$PrCl_3$	$\gamma=135.9-0.0372t$	0.034	830—926
$NdCl_3$	$\gamma=173.4-0.0855t$	0.166	800—865
$GdCl_3$	$\gamma=110.1-0.0278t$	0.139	820—930
$DyCl_3$	$\gamma=124.4-0.0465t$	0.069	760—901

are represented by linear empirical formulas as functions of temperature. The formulas are given in Table 1, together with standard error, σ.

The values obtained for $LaCl_3$ melts were slightly lower than that reported by Smirnov *et al.*[8]

Surface Enthalpies of Rare-earth Chlorides. The surface enthalpies of rare-earth chlorides in molten state were calculated by the equation

$$H^s = \gamma - T\left(\frac{d\gamma}{dT}\right),$$

where H^s is the surface enthalpy in erg/cm^2, γ the surface tension of molten salt in dyn/cm, and T the absolute temperature. The results are given in Table 2. Comparing the surface enthalpies of the molten chlorides with those of other molten salts, we see that the molten chlorides have similar surface enthalpies except for YCl_3, $NdCl_3$, and $GdCl_3$ melts. The values of

Table 2. Surface enthalpies of pure molten salts

Salt	H^s (erg/cm^2)
YCl_3	115.4
$LaCl_3$	159.5
$PrCl_3$	146.1
$NdCl_3$	196.8
$GdCl_3$	117.7
$DyCl_3$	137.1

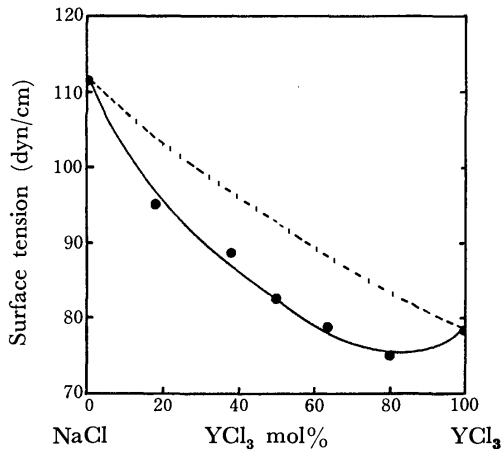

Fig. 2. Isotherm of surface tension of molten binary NaCl-YCl_3 mixture at 825 °C.
—●—: Observed surface tensions, ----: calculated surface tensions by use of the Guggenheim's equation for ideal solution.

Table 3. Surface tension equations of molten binary NaCl-YCl_3 system

YCl_3 (mol%)	$\gamma=a+bt$ γ : (dyn/cm), t(°C)	σ (dyn/cm)	Temp range (°C)
0.0	$\gamma=173.1-0.0747t$	0.180	830—950
17.7	$\gamma=165.2-0.0853t$	0.332	819—910
38.1	$\gamma=140.2-0.0628t$	0.420	747—901
50.0	$\gamma=111.8-0.0346t$	0.113	787—857
63.8	$\gamma=108.0-0.0350t$	0.136	795—938
80.0	$\gamma=94.9-0.0239t$	0.166	806—876
100.0	$\gamma=106.3-0.0334t$	0.158	768—946

the molten YCl_3 and $GdCl_3$ were intermediate between those of the molten chlorides and covalent liquids such as benzene and methanol, the value of $NdCl_3$ being larger than that of the others.

Binary NaCl-YCl_3 Mixture. The isotherm of surface tension of molten binary NaCl-YCl_3 mixture at 825 °C is shown in Fig. 2. The surface tensions are represented by empirical formulas as functions of temperature. The results are given in Table 3. In binary molten salt mixtrures with a common anion, the surface tensions show a negative deviation from

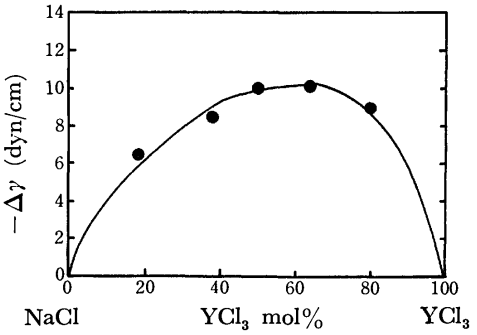

Fig. 3. Negative deviation of molten binary NaCl-YCl_3 mixture at 825 °C.

surface tension isotherms of ideal solution calculated by use of Guggenheim's equation. In this binary NaCl-YCl_3 mixture, a large negative deviation was observed. The negative deviation at 825 °C is shown in Fig. 3.

The maximum value of the deviation was observed at about 65 mol% in YCl_3. For the calculations of surface tensions, the densities of these melts were used with the data given in previous papers.[9-11]

The calculations were carried out with the computer at Chiba University.

The authors wish to thank Mr. T. Matsumaru for his kind assistance.

References

1) a) M. V. Smirnov and V. P. Stepanov, *Tr. Inst. Elektrokhim., Akad. Nauk SSSR, Ural Filial*, **12**, 3 (1969); b) M. V. Smirnov and V. P. Stepanov, *ibid.*, **12**, 9 (1969); c) M. V. Smirnov and V. P. Stepanov, *ibid.*, **14**, 58 (1970); d) V. P. Stepanov and M. V. Smirnov, *ibid.*, **14**, 62 (1970).

2) R. Kh. Kurmaev, L. A. Kupriyanova, N. A. Maltsev, and V. A. Krokhim, *Izv. Vyssh. Ucheb. Zaved., Tsvet. Met.*, **17**, 28 (1974).

3) E. A. Guggenheim, "Mixtures," Oxford University Press, London (1952), p. 176.

4) J. Mochinaga and K. Irisawa, *Bull. Chem. Soc. Jpn.*, **47**, 364 (1974).

5) E. Schrödinger, *Ann. Phys.*, **46**, 413 (1917).

6) H. Bloom, F. G. Davis, and D. W. James, *Trans. Faraday Soc.*, **56**, 1179 (1960).

7) K. Grjotheim, J. L. Holm, B. Lillebuen, and H. A. Oye, *Acta Chem. Scand.*, **26**, 2050 (1972).

8) M. V. Smirnov, V. A. Khokhlov, and V. P. Stepanov, "Electrochemistry of Molten and Solid Electrolytes," Vol. 7, (1969) p. 31.

9) K. Cho, K. Irisawa, J. Mochinaga, and T. Kuroda, *Electrochim. Acta*, **17**, 1821 (1972).

10) J. Mochinaga and K. Igarashi, *Bull. Chem. Soc. Jpn.*, **48**, 713 (1975).

11) J. Mochinaga, K. Igarashi, H. Kuroda, and H. Iwasaki, *Bull. Chem. Soc. Jpn.*, **49**, 2625 (1976).

BULLETIN OF THE CHEMICAL SOCIETY OF JAPAN, VOL. 51 (5), 1553—1554 (1978)

Characteristic Behavior of Damping Coefficient of Capillary Wave on Surfactant Solution

Minoru SASAKI, Tatsuya YASUNAGA, Minoru ASHIDA, and Haruki KAN

Department of Chemistry, Faculty of Science, Hiroshima University, Higashisenda-machi, Horishima 730

(Received November 15, 1977)

Synopsis. The damping coefficient of a capillary wave on decylamine hydrochloride and octylamine hydrochloride solutions decreased abruptly in the vicinity of a critical micelle concentration. The phenomenon observed was well interpreted by an equation derived on the basis of a surface mechanical impedance.

The dynamic properties of surfactants existing on a surface have been studied by means of capillary wave technique.[1-4] Most of the experimental studies have been carried out on the surfactant solutions below a critical micelle concentration (CMC) and the phenomena observed have been attributed to the diffusion and adsorption-desorption of surfactants between the surface and the bulk phase.

Preliminary measurements on decylamine hydrochloride (DeAC) solution above the CMC revealed that the damping coefficient of the wave decreases abruptly in the vicinity of the CMC. The purpose of this paper is to study the above phenomenon on the DeAC and octylamine hydrochloride (OAC) solutions above the CMC.

Experimental

The apparatus employed was the same as that reported previously.[1] The frequency range of measurement was 45 to 600 Hz at 25±0.4 °C.

The DeAC and OAC were prepared from decylamine (purity, 99.8%) and octylamine (purity, 99.9%) according to the previous procedure,[4] respectively. The CMC values of the DeAC and OAC solutions were determined to be 62 and 180 mM*, respectively.

Results and Discussion

The frequency dependence of the damping coefficient, α, was measured in the DeAC and OAC solutions above the CMC. The results are shown in Figs. 1 and 2, together with the data on the solutions below the CMC.[4] As can be seen from these figures, the α/f values on the solutions above the CMC are considerably smaller than those below the CMC, where f is the frequency. If the phenomenon is related to some chemical relaxation, the α/f value should be greater than that based on only the diffusion of surfactants between surface and bulk phase. This prediction, however, contradicts the present result.

One next considers the effect of a bending viscosity which has been observed on a highly condensed insoluble monolayer.[5] The theoretical curve of α/f based on the bending viscosity is shown by the curve

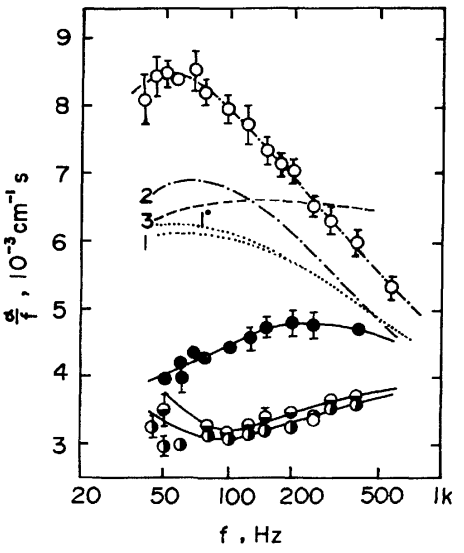

Fig. 1. Frequency dependence of α/f on the DeAC solutions. curves 1(C>CMC) and 1'(C<CMC): theoretical curves based on only the diffusion, curve 2: theoretical curve based on the relaxation, curve 3: theoretical curve based on the bending viscosity.[5] The solid lines shown the theoretical curves calculated by Eq. 3.
○: 50 mM (below the CMC), ●: 62.5 mM (G^σ = 1.8 dyn cm^{-1}, $\eta^\sigma = 3.9\times10^{-3}$ dyn cm^{-1} s), ◒: 70 mM ($G^\sigma = 3.1$ dyn cm^{-1}, $\eta^\sigma = 3.5\times10^{-3}$ dyn cm^{-1} s), ◑: 80 mM ($G^\sigma = 3.0$ dyn cm^{-1}, $\eta^\sigma = 4.3\times10^{-3}$ dyn cm^{-1} s).

3 in Fig. 1. As can be seen from this figure, the tendency of this curve differs from that of the experimental curve.

Let us introduce a surface mechanical impedance, Z, concerned with the normal stress which is proportional to the rate of change in the curvature of the surface, ζ. The boundary condition for the balance of the normal stress at the gas-liquid interface is represented by the following relation:[6]

$$\gamma\zeta + p - 2\eta\frac{\partial v}{\partial y} - Z\frac{\partial\zeta}{\partial t} = 0, \qquad (1)$$

where y is a rectangular coordinate tangent to the surface at rest, v the component in the y direction, γ the surface tension, p the hydrostatic pressure, η the viscosity, and t the time. Furthermore, one assumes that Z is given by the linear combination of the elasticity, G^σ, and the viscosity, η^σ, as follows:

$$(2i\pi fZ)^{-1} = \{G^{\sigma-1} + (2i\pi\eta^\sigma f)^{-1}\}^{-1}. \qquad (2)$$

According to the previous treatment,[6] a combination of Eqs. 1 and 2 gives the following equation for α:

* Throughout this paper, 1 mM = 10^{-3} mol dm^{-3}.

$$\frac{\alpha}{f} = \frac{4\pi}{3c}(\varepsilon_{ela}+\varepsilon_r)_{im} - \frac{4\pi^2 k G^{\sigma 2}\eta^\sigma f}{3\rho c^3\{G^{\sigma 2}+(2\pi\eta^\sigma f)^2\}}, \quad (3)$$

where ε_{ela} and ε_r are the parameters concerned with the surface viscoelaticity and the relaxation,[6] respectively; ρ is the density, k the wave number, c the propagation velocity, and the subscript im indicates the imaginary part. In the present case, ε_r was ignored because of the absence of the relaxation. The theoretical curves calculated by Eq. 3 are shown by the solid lines in Figs. 1 and 2. Here, the values of the parameters G^σ and η^σ in Eq. 3 were determined so as to reduce the residual variance about the regression line. As can be seen from these figures, the experimental values fall on the theoretical curves. This fact suggests the validity of the present theory.

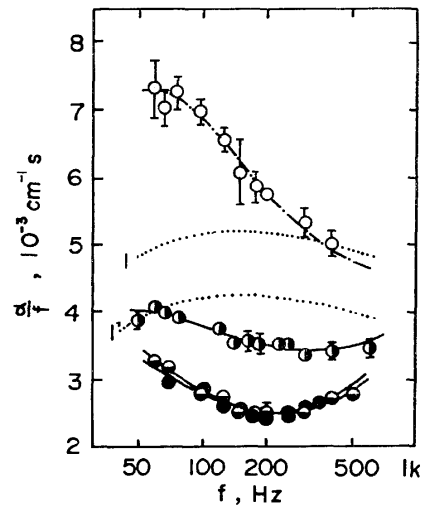

Fig. 2. Frequency dependence of α/f on the OAC solutions. curves 1(C>CMC) and 1'(C<CMC): theoretical curves based on only the diffusion. The solid lines show the theoretical curves calculated by Eq. 3.
○: 114 mM (below the CMC), ◑: 250 mM (G^σ = 2.4 dyn cm^{-1}, $\eta^\sigma = 1.0\times10^{-3}$ dyn cm^{-1} s), ◒: 280 mM (G^σ = 3.7 dyn cm^{-1}, $\eta^\sigma = 1.4\times10^{-3}$ dyn cm^{-1} s), ●: 351 mM (G^σ = 3.8 dyn cm^{-1}, $\eta^\sigma = 2.0\times10^{-3}$ dyn cm^{-1} s).

Since we have no direct measure of G^σ and η^σ, we infer their validity from the following consideration. According to the present idea, the dynamic surface tension in the case of $f \gg \eta^\sigma/G^\sigma$ is expressed by a sum of γ and G^σ. From the data of the dynamic surface tension in sodium dodecyl sulfate solution above the CMC,[7] the G^σ value was obtained to be *ca.* 3 dyn cm^{-1} (1 dyn = 10^{-5} N). This value is of the same order as that obtained in the present work (3.8 dyn cm^{-1} in the 351 mM OAC solution). This agreement in the order of magnitude gives further evidence of the validity of the present theory. No consideration for η' was made.

Further clarification for G^σ and η^σ will be reported in a subsequent paper.

References

1) M. Sasaki, T. Yasunaga, and N. Tatsumoto, *Bull. Chem. Soc. Jpn.*, **50**, 858 (1977).
2) J. Lucassen and H. S. Hansen, *J. Colloid Interface Sci.*, **22**, 32 (1966).
3) J. Lucassen and H. S. Hansen, *J. Colloid Interface Sci.*, **23**, 319 (1967).
4) M. Sasaki, T. Yasunaga, S. Satake, and M. Ashida, *Bull. Chem. Soc. Jpn.*, **50**, 3144 (1977).
5) E. Mayer and J. D. Eliassen, *J. Colloid Interface Sci.*, **37**, 228 (1971).
6) M. Sasaki, T. Yasunaga, and N. Tatsumoto, *Bull. Chem. Soc. Jpn.*, **50**, 852 (1977).
7) D. K. Owens, *J. Colloid Interface Sci.*, **29**, 496 (1969).

BULLETIN OF THE CHEMICAL SOCIETY OF JAPAN, VOL. 51 (5), 1555—1556 (1978)

Temperature Effect on the Molecular Weight and the Optical Purity of Anhydropolyaspartic Acid Prepared by Thermal Polycondensation

Etsuo KOKUFUTA, Shinnichiro SUZUKI, and Kaoru HARADA

Department of Chemistry, The University of Tsukuba, Sakura-mura, Niihari-gun, Ibaraki, 300-31

(Received November 16, 1977)

Synopsis. Anhydroyplyaspartic acid (APAA) was prepared by the thermal polycondensation of L-aspartic acid in the solid state at 160—220 °C for 5 h. The effect of temperature on molecular weight and optical purity of APAA was investigated. The molecular weight increases rapidly in the temperature range 180—200 °C, the yield of APAA also increasing rapidly. The optical purity decreases rapidly with rise in temperature from 160—180 °C.

In recent years, the thermal polycondensation of α-amino acids has drawn attention in view of the prebiotic formation of polypeptides. Aspartic acid yields anhydropolyaspartic acid (APAA) by thermal polycondensation in the solid state at around 200 °C.[1] APAA was converted into polyaspartic acid (PAA) having α- and β-aspartyl residues by alkaline hydrolysis.[2] Studies on the chemical structure[2–5] and potentiometric titration behavior[6] for APAA and PAA have been reported. However, little attention has been paid to the temperature effect on the physical properties of these polyamino acids prepared by thermal polycondensation.

In the present study, the effect of reaction temperature on the molecular weight, yield and optical purity of APAA was examined.

Experimental

Materials. L-Aspartic acid (10.0 g, 0.0752 mol) was packed tightly on the bottom of a 0.5 litre Erlenmeyer flask and was heated at various temperatures (160—220 °C) for 5 h under nitrogen atmosphere. The reaction time (5 h) was chosen since the yields of APAA become almost constant by heating at 180 and 200 °C for 5 h.[7] The slightly colored product was suspended in water and then dialyzed against distilled water for 5—6 days.[3] The weight losses of the products obtained at 160 and 220 °C during the dialysis are 97 and 29%, respectively. The insoluble material was collected by filtration and washed with distilled water and ethanol. APAA obtained was dried at 120 °C over phosphorus pentaoxide under reduced pressure for 4 days. PAA was prepared from APAA in the same way as described earlier.[6,7] APAA and PAA were characterized by infrared spectra and potentiometric titrations. PAA was titrated with 0.1 M NaOH, whereas APAA previously treated with 0.1 M NaOH was back-titrated with 0.1 M HCl.

Viscometric Measurement. Viscometric measurements were carried out to investigate the change of molecular weight of APAA by reaction temperature. APAA was dissolved in 0.5 M NaOH and allowed to stand at 25 °C for 24 h. Measurements were carried out at 25±0.01 °C with a Ubbelohde capillary viscometer with 388.5 s flowing time for water at 25 °C. The reduced viscosity (η_{sp}/C) was determined at a constant concentration (C=0.179 g/dl).

Titration of N-Terminal Amino Groups with Perchloric Acid. The molecular weight of PAA derived from APAA prepared at various temperatures was determined by means of N-terminal amino group titration. PAA (20 mg) was dissolved in 5 ml of purified *N,N*-dimethylformamide. The sample solutions were titrated with 0.02 M perchloric acid with a microburet. The crystal violet was used as an indicator.

Determination of Optical Purity. APAA (20 mg) was hydrolyzed with 6 M HCl (5 ml) in a sealed tube at 110 °C for 24 h under reduced pressure. The hydrolyzate was evaporated to dryness, and the residue was dissolved in 6 M HCl. The molar ellipticity [θ] was measured with a JASCO model J-20C recording spectropolarimeter at wavelength 236 nm. On the other hand, the [θ] value at 236 nm for a standard solution of L-aspartic acid in 6 M HCl was also obtained. The concentrations of aspartic acid in the hydrolyzed samples and the standard solution (0.05—0.1 mol/l) were measured with a Yanagimoto model LC-5S amino acid analyzer. The optical purity of anhydroaspartyl residue in APAA was estimated by the ratio of the [θ] value of the sample solution to that of the standard solution.

Results and Discussion

APAA prepared by thermal polycondensation is mainly composed of the imide structure and is quantitatively hydrolyzed to aspartic acid.[2,3,7] The

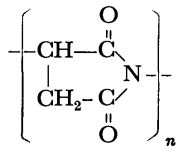

structure is also supported by the results of potentiometric titration and infrared spectra. The molecular weight of repeating unit was estimated to be 99±2 for APAA and 115±1 for PAA by means of potentiometric titration. The infrared spectrum of APAA shows moderate absorption at 1780 cm^{-1}

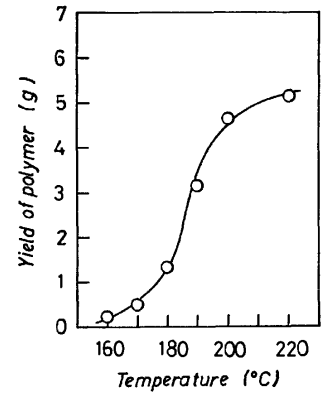

Fig. 1. Temperature effect on the yield of APAA. The yield is represented by the weight of APAA obtained from 10.0 g of L-aspartic acid.

and strong absorption at 1715 cm^{-1}, indicating the presence of 5-membered cyclic imide,[3,8] and moderate absorption at 1530 cm^{-1}(amide II). The infrared spectrum of PAA shows strong absorption at 1720 cm^{-1} (COOH), 1650 cm^{-1} (amide I), and 1530 cm^{-1} (amide II).

The relationship between the yield of APAA and the reaction temperature is shown in Fig. 1. It is seen that the yield of APAA rapidly increases with rise in reaction temperature from 180—200 °C. On the other hand, aspartic acid hardly undergoes polycondensation at all by heating below 160 °C.

The effect of reaction temperature on the molecular weight of APAA was investigated by means of viscometric measurement for APAA in 0.5M NaOH, and N-terminal amino group titration for PAA prepared from APAA. The results are shown in Fig. 2. Assuming that degradation of the polypeptide chain does not occur during the course of partial alkaline hydrolysis of the imide structure of APAA, we can estimate the molecular weight of APAA by means of the N-terminal amino group titration of PAA. The result obtained indicates that the molecular weight of APAA increases rapidly in the temperature range 180—200 °C. This is also supported by the result obtained by the viscometric measurement of APAA. It is evident that the molecular weight of APAA increases rapidly in the temperature range at which the yield of APAA increases rapidly.

The effect of reaction temperature on the optical

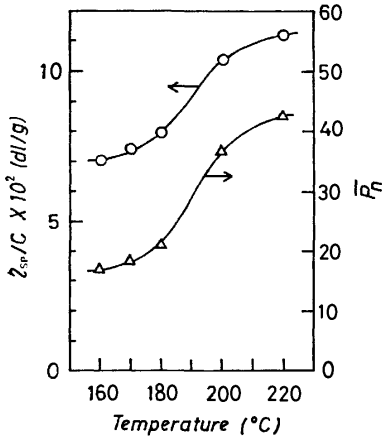

Fig. 2. Temperature effect on the molecular weight of APAA.
The reduced viscosity (η_{sp}/C) of APAA was determined in 0.5 M NaOH at C=0.175 g/dl.
The $\overline{P}_n$ represents the number-average degree of polymerization of PAA.

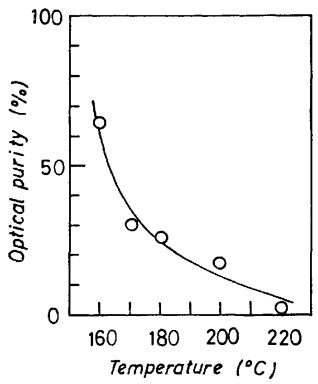

Fig. 3. Temperature effect on the optical purity of APAA.

purity of APAA is shown in Fig. 3. The optical purity decreases rapidly with rise in temperature from 160—180 °C, approaching almost zero percent in the region above 220 °C at which higher yield and higher molecular weight of APAA are obtained. The optical purity of aspartyl residue in the copolymer of aspartic acid and glutamic acid, prepared by thermal polycondensation in the molten state at 170 °C for 3 h, was also almost zero percent.[9] It seems that the racemization of L-aspartic acid by the thermal polycondensation in the molten state takes place faster than that in the solid state.

This work was partially supported by a Scientific Research Grant from the Ministry of Education.

References

1) J. Kovacs, I. Könyves, and A. Pusztai, *Experientia*, **9**, 459 (1953).
2) J. Kovacs, H. N. Kovacs, I. Könyves, J. Csaszar, T. Vajda, and H. Mix, *J. Org. Chem.*, **26**, 1084 (1961).
3) A. Vegotsky, K. Harada, and S. W. Fox, *J. Am. Chem. Soc.*, **80**, 3361 (1958).
4) K. Harada and S. W. Fox, *Biosystems*, **7**, 213 (1975).
5) S. Andini, E. Benedetti, L. Ferrara, L. Paolillo, and P. A. Temussi, *Origins of Life*, **6**, 147 (1975).
6) E. Kokufuta, S. Suzuki, and K. Harada, *Biosystems*, **9**, 211 (1977).
7) S. W. Fox and K. Harada, "A Laboratory Manual of Analytical Methods of Protein Chemistry," Vol. 4, ed by P. Alexander and H. P. Lundgren, Pergamon Press (1966), pp. 129—132.
8) L. J. Bellamy, "The Infrared Spectra of Complex Molecules," John Wiley & Sons, Inc., New York (1954), pp. 175—179.
9) E. Kokufuta, S. Suzuki, and K. Harada, Abstr. II, p. 1225, 36th National Meeting of the Chemical Society of Japan, Osaka, April 1977.

BULLETIN OF THE CHEMICAL SOCIETY OF JAPAN, VOL. 51 (5), 1557—1558 (1978)

Distribution of Trace Rare Earth Element Ions in the Crystallization Process of Alums

Hitoshi KANNO,* Hiroshi WAKITA, and Hiroshi HAMAGUCHI**

Department of Chemistry, The University of Tokyo, Hongo, Bunkyo-ku, Tokyo 113

(Received August 16, 1977)

Synopsis. The distribution coefficients of rare earth element ions between alums and aqueous solution were determined.

We have studied the effects of ionic size on the distribution of trace ions between crystal and aqueous solution. Rare earth element ions are suitable for this purpose, since they are all similar in chemical properties, differing only in ionic size.[1] In addition, the large variety of alums and the existence of more than 200 different compounds with the structure $M(I)M(III)(RO_4)_2 \cdot 12H_2O$, ($M(I)=Na^+$, K^+, NH_4^+, Rb^+, Cs^+, Tl^+ ···; $M(III)=Al^{3+}$, Ga^{3+}, In^{3+}, Cr^{3+}, ···; R=S, Se, ···)[2] provide us a good chance to clarify the effects of ion size and chemical nature on trace ion distribution.

As a first step we took up $KAl(SO_4)_2 \cdot 12H_2O$, $NH_4Al(SO_4)_2 \cdot 12H_2O$, and $NH_4Fe(SO_4)_2 \cdot 12H_2O$ as host crystals. The crystals were grown at room temperature by evaporating aqueous alum solutions containing rare earth element (REE) ions and alkali ions, the concentration of each element (other than potassium) being *ca.* 40 ppm. The contents of REE in both crystal and solution were determined by non-destructive neutron activation analysis.[3] Alkali ion contents were qualitatively measured by both atomic absorption spectroscopy[4] and neutron activation analysis (for Rb and Cs).

The distribution coefficient of REE is tentatively expressed by

$$D = \frac{X_i^s(1\text{ g of crystal})}{X_i^l(1\text{ ml of residual solution})},$$

where X_i is the content of rare earth element i in either crystal or solution, and subscripts s and l denote crystal and residual solution, respectively. The results are plotted against the ionic radius of REE. We see distinct dependence of the distribution coefficient on ionic size for potassium alum but not for ammonium alums, indicating that M(I) ion in the alum greatly affects the distribution pattern of trace ions (Fig. 1).

There are three possible mechanisms in the incorporation of trace ions in the crystallization process, *i. e.*, surface adsorption, occlusion and solid solution formation.[5] Solid solution formation is considered to be the main mechanism because the distribution coefficient is dependent on the ionic size of REE for potassium alum. In contrast to silicate minerals in which the smaller the difference in ionic size between host and guest

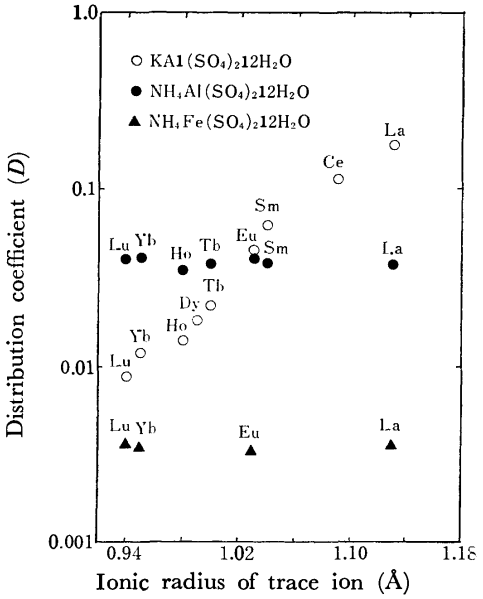

Fig. 1. Distribution coefficient of REE ion between alum and aqueous solution.

ions is the more easily the guest ions replace the host ions in the crystal,[6,7] La^{3+} ion which has the largest difference in ionic size with the host Al^{3+} ion gives the highest *D* value in potassium alum. This seems to be associated with hydration of ions and with the coordination number change of REE ions from aqueous solutions to alum crystals. In alum crystals each M(III) ion is surrounded by six water molecules, whereas in aqueous solution the lighter REE members (La^{3+}—Nd^{3+}) tend to have 9-coordination and the heavier members (Ga^{3+}—Lu^{3+}) are generally 8-coordinate.[1b] Furthermore the experimental evidence that while a smaller ion has a small number of near neighbor water molecules the larger polarizing power of the smaller ion will lead to a larger solvated radius may account for the higher *D* values for the lighter REE members than the heavier ones.

Another interesting feature is the difference in *D* values between the two ammonium alums. This apparent difference is largely due to their solubility difference, Fe-alum being soluble in cold water about 8 times larger than Al-alum.[8] In fact, the ratio (number of REE)/(number of host element) is almost the same for both Al- and Fe-crystals. This is an additional evidence for solid solution formation in the trace REE ions in the alum crystals.

As for alkali ions, the members larger in ionic radius than the host ions are found to have almost completely moved into crystal from the solution.

* Present address: Department of Chemistry, Meisei University, Hino, Tokyo 191.

** Present address: Japan Analytical Center, Funado, Itabashi, Tokyo 174.

The authors wish to thank Professor Kenji Tomura and Dr. Hideo Higuchi for their help in activation analysis.

References

1) (a) G. T. Seaborg and J. J. Katz, "The Actinide Elements," McGraw-Hill, New York (1954); (b) F. A. Cotton and G. Wilkinson, "Advanced Inorganic Chemistry," 3rd ed, Wiley-Interscience, New York (1972), p. 1059.

2) (a) H. Lipson and C. A. Beevers, *Proc. R. Soc. London, Ser. A*, **148**, 664 (1935); (b) S. Haussühl, *Z. Kristallogr.*, **116**, 371 (1961).

3) T. Bereznai, *J. Radioanal. Chem.*, **9**, 81 (1971).

4) W. Slavin, "Atomic Absorption Spectroscopy," Wiley & Sons, New York (1968).

5) W. L. McIntire, *Geochim. Cosmochim. Acta*, **27**, 1209 (1963).

6) A. E. Ringwood, *Geochim. Cosmochim. Acta*, **7**, 189, 242 (1955).

7) N. Onuma, H. Higuchi, H. Wakita, and H. Nagasawa, *Earth Planet. Sci. Lett.*, **5**, 47 (1968).

8) R. C. Weast, Ed, "Handbook of Chemistry and Physics," 57th ed, CRC Press, Ohio (1976), pp. B87, B88.

BULLETIN OF THE CHEMICAL SOCIETY OF JAPAN, VOL. 51 (5), 1559—1560 (1978)

The Separation of Iron(III), Cobalt(II), Nickel(II), Copper(II), Zinc(II), Mercury(II), Lead(II), Cadmium(II), and Palladium(II) as Their SDBM (3-Mercapto-1,3-diphenyl-2-propen-1-one) Complexes by Thin Layer Chromatography on Silica Gel

Takaharu HONJO, Hiromi HONNAMI, and Toshiyasu KIBA

Department of Chemistry, Faculty of Science, Kanazawa University, Marunouchi, Kanazawa, 920

(Received September 26, 1977)

Synopsis. The separation of iron(III), cobalt(II), nickel(II), copper(II), zinc(II), mercury(II), lead(II), cadmium(II), and palladium(II) as their SDBM chelates has been achieved successfully on the thin layer of silica gel with such developing solvents as carbon tetrachloride, 1,1,1-trichloroethane, trichloroethylene, tetrachloroethylene, and carbon disulfide.

A new chelating reagent, 3-mercapto-1,3-diphenyl-2-propen-1-one(abbreviated as SDBM), has been found to form stable and extractable chelates of a specific color,[1,2] and it has been used for the determination of mercury(II) by means of the radioisotope dilution method[3] and for the spectrophotometric determination of iron(II, III), nickel(II), and copper(II).[4,5] In an attempt to widen the analytical application of this reagent, the metal ions have now been extracted in cyclohexane containg SDBM, and the metal chelates thus extracted have been chromatographed on the thin layer of silica gel with various organic solvents.

Experimental

The SDBM was synthesized by a modification of the method of Chaston *et al.*[6] A 5.0-g portion of dibenzoylmethane and 200 ml of absolute ethanol were put into a 500-ml flask, and then the vessel was cooled to 0—10 °C in an ice bath containing only ice or a freezing mixture with potassium chloride. The dried hydrogen chloride gas was passed through the solution for 10—30 min, after which the dried hydrogen sulfide gas was passed through for 1—2 h. There was no problem in the preparation of SDBM even if the hydrogen sulfide gas was passed into the solution first. The dehydration of ethanol, hydrogen sulfide, and hydrogen chloride might lead a worker to a successful synthesis of SDBM as in the synthesis of STTA.[7] The dark red solution was allowed to stand in an ice bath for 30—60 min and was then poured into ice water. The red crystalline product was filtered off, washed with water, and recrystallized from absolute ethanol or petroleum ether to give red crystals of the compound; yield, 60—70%; mp 76.5—78.0 °C. The developing solvents were all reagent-grade materials and were purified by the ordinary method, if necessary. The sample solutions for the thin layer chromatography were metal-SDBM chelates in cyclohexane, which were prepared as follows: a 10^{-2}—10^{-1} M salt solution was adjusted to pH 1—10, and then this solution was shaken with 10^{-3} M SDBM in cyclohexane for from 30 min to 2 h. The SDBM was found to remain mostly in the cyclohexane phase when the pH of the aqueous solution was below pH 10. Cadmium(II) and iron(III) gave large amounts of insoluble chelates in cyclohexane. Mercury(II), lead(II) and palladium(II) gave some insoluble chelates in cyclohexane. The experimental procedures and conditions for the thin layer chromatography of these metal chelates were almost the same as have previously been described.[8]

Results and Discussion

Each SDBM chelate extracted in cyclohexane showed its own specific color of the respective absorption maximum (Table 1), and was stable for at least several days. The results after the development of these SDBM metal chelates, including SDBM itself, with individual solvents on a thin layer of silica gel are given in Table 2. The compounds could be identified only by observing each specific color on the chromatoplate. The chelates may be classified into four groups in terms of their chromatographic behavior: 1) Chelates which do not migrate from the sample spot (with cyclohexane). 2) Chelates which can be developed to a moderate distance over a comparatively wide range (with carbon tetrachloride, 1,1,1-trichloroethane, trichloroethylene, tetrachloroethylene, carbon disulfide, chloroform, benzene, chlorobenzene, and *o*-dichlorobenzene). By using these solvents, the mutual separation of various metal chelates was achieved successfully. 3) Chelates which move up to the solvent front (with acetone, ethyl acetate, and diethyl ether). 4) Chelates which cause a remarkable tailing during development (with methanol and ethanol). By using a binary mixture of solvents in a 1:1 volume ratio, SDBM and its metal chelates were developed to a moderate distance (Table 3). It was observed that the Co-SDBM chelate was trans-

TABLE 1. COLOR, ABSORPTION MAXIMA, AND EXTRACTION pH OF SDBM AND ITS METAL CHELATES IN CYCLOHEXANE

Compound	Color	Absorption maxima (nm)	Extraction pH
SDBM	Reddish orange	328, 410	—
$Fe(SDBM)_3$	Greenish brown	260, 324, 409	2—8
$Co(SDBM)_3$	Brown	305	6—8
$Ni(SDBM)_2$	Reddish brown	307, 400, 436	6—8
$Cu(SDBM)_2$	Olive brown	290, 345, 418	3—6
$Zn(SDBM)_2$	Yellow	310, 410	6—8
$Hg(SDBM)_2$	Pale yellow	276, 350	1—6
$Pb(SDBM)_2$	Orange yellow	318, 411	4—8
$Cd(SDBM)_2$	Yellow	275, 388	6—8
$Pd(SDBM)_2$	Orange	285, 460	1—8

TABLE 2. R_f VALUES OF SDBM AND ITS METAL CHELATES WITH VARIOUS PURE DEVELOPING SOLVENTS ON SILICA GEL AT ROOM TEMPERATURE (22—25 °C)

Developing solvent	Dielectric constant	Developing time (min)*	Metal									
			Fe	Co	Ni	Cu	Zn	Hg	Pb	Cd	Pd	SDBM
Methanol	32.6	70	0.94	0.40—0.95	0—0.88	0—0.92	0.85—0.99	a)	0.94	0—0.92	0—0.92	0.71—0.92
Ethanol	24.3	80	0.86—1.00	0.73—0.99	0.38—0.99	0.76—0.96	0.86—0.99	0.92	0.86—0.99	0.86—0.99	0.62—0.98	0.97
Acetone	20.7	17	0.99	0.98	0.99	0.98	0.99	0.99	0.99	0.99	0.98	0.99
Ethyl acetate	6.0	30	1.00	0.99	0.91	0.99	0.99	0.94	0.99	0.99	0.99	0.99
Diethyl ether	4.3	18	a)	0.94	0.95	0.93	0.97	a)	a)	a)	a)	0.96
Carbon tetrachloride	2.2	70	0.14	0.05	0.23	0.15	0	0	0.39	0	0.19	0.43
Chloroform	4.8	50	0.43	0.83	0.91	0.90	0	0.48	0.77	0	0.92	0.86
1,1,1-Trichloroethane	7.5	43	0.41	0.53	0.66	0.62	0	0.49	0.69	0	0.64	0.69
Trichloroethylene	3.4	36	0.16	0.29	0.57	0.54	0.06	0.09	0.66	0.01	0.63	0.64
Tetrachloroethylene	2.3	38	0.18	0.04	0.17	0.12	0.03	0	0.41	0	0.16	0.43
Carbon disulfide	2.6	15	0.11	0.05	0.15	0.12	0.03	0.02	0.42	0	0.16	0.43
Cyclohexane	2.0	60	0	0	0	0	0	0	0.08	0	0	0.09
Benzene	2.3	36	0.93	0.91	0.93	0.88	0	a)	0.90	0	0.94	0.90
Chlorobenzene	5.6	28	a)	0.68	0.90	0.84	0.01	0.09	0.80	0	0.96	0.84
o-Dichlorobenzene	9.9	70	a)	0.96	0.97	0.95	0	0.10	0.87	0	0.87	0.92

* The developing time for a distance of 10 cm. The average deviation of the R_f values was 0.01. a) The spots disappeared during the development.

TABLE 3. R_f VALUES OF SDBM AND ITS METAL CHELATES WITH VARIOUS MIXED DEVELOPING SOLVENTS ON SILICA GEL AT ROOM TEMPERATURE (22—25 °C)

Developing solvent (1 : 1, v/v)	Developing time (min)*	Metal					
		Co	Ni	Cu	Zn	Cd	SDBM
Cyclohexane-Chloroform	40	0.26	0.49	0.46	0.08	0	0.63
Cyclohexane-*o*-Dichlorobenzene	50	0.05	0.15	0.13	0.03	0	0.29
Carbon tetrachloride-Chloroform	45	0.50	0.76	0.74	0	0	0.75
Carbon tetrachloride-Carbon disulfide	20	0.06	0.20	0.17	0.07	0	0.49
Chloroform-Carbon disulfide	22	0.43	0.70	0.64	0.01	0.06	0.72

* The developing time for a distance of 10 cm. The average deviation of the R_f values was 0.01.

formed into $Co(SDBM)_3$ chelates.[8] Some representative chromatograms of SDBM and its metal chelates with pure solvents and their mixture are shown in Fig. 1. In general, the greater the polarity of the solvent, the greater the distance of the development of metal chelates on the chromatographic plate. The R_f values of the SDBM chelates with various solvents generally increased in the following order: Cd(II), Zn(II)<Hg(II)<Fe(III), Co(III)<Cu(II)<Ni(II), Pd(II)<Pb(II), (SDBM). The R_f values of the SDBM chelates of Co(II), Ni(II), Cu(II), Zn(II), and Cd(II) with the binary solvent mixture have the same tendency in their change as those of the single solvents. The R_f values of the SDBM chelates are smaller than those of the STTA chelates, while the R_f sequence of the SDBM chelates is almost the same as that of the STTA chelate series except for the Pb(II) complex, the R_f of which behaves much like the ligand; the latter sequence is: Cd(II)< Zn(II) < Pb(II), (STTA) < Hg(II) < Co(II, III) < Cu(II)<Ni(II).[9] In general, the discrepancy in the R_f values of the ligands and their metal chelates

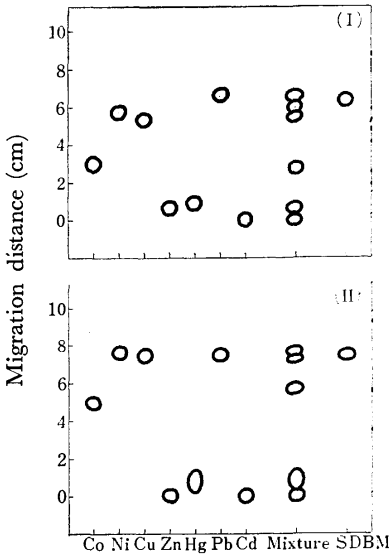

Fig. 1. Chromatogram of SDBM, its metal chelates, and the chelate mixtures with single component solvent and binary solvent mixture.
SDBM, Chelate: *ca.* 5×10^{-4} M (3—6 μl).
Developing solvent: (I) Trichloroethylene, (II) carbon tetrachloride-chloroform.

may be caused by the differences in hydrogen bonding or dipole-dipole interaction among the ligands, each chelate, and silanol or siloxane on the surface of silica gel involving the competition adsorption of the developing solvents and metal chelates with or without the ligands. In conclusion, carbon tetrachloride, 1,1,1-trichloroethane, trichloroethylene, tetrachloroethylene, and carbon disulfide were found to be suitable developing solvents for the mutual separation of metals as their SDBM chelates by means of thin layer chromatography on silica gel.

References

1) T. Honjo and T. Kiba, *Bunseki Kagaku*, **21**, 676 (1972).
2) T. Honjo and H. Freiser, Abstracts I, p. 538. 36th National Meeting of Chemical Society of Japan, East Osaka, April, 1977.
3) H. Tanaka, N. Nakanishi, Y. Sugiura, and A. Yokoyama, *Bunseki Kagaku*, **17**, 1428 (1968).
4) E. Uhlemann and H. Müller, *Anal. Chim Acta*, **41**, 311 (1968).
5) M. Chikuma, A. Yokoyama, Y. Ooi, and H. Tanaka, *Chem. Pharm. Bull.*, **23**, 507 (1975).
6) S. H. H. Chaston, S. E. Livingstone, T. N. Lockyer, V. A. Pickeles, and J. S. Shannon, *Aust. J. Chem.*, **18**, 673 (1965).
7) T. Honjo and T. Kiba, *Bull. Chem. Soc. Jpn.*, **45**, 185 (1972).
8) A. Yokoyama, S. Kawanishi, M. Chikuma, and H. Tanaka, *Chem. Pharm. Bull.*, **15**, 540 (1967).
9) T. Honjo and T. Kiba, *Bull. Chem. Soc. Jpn.*, **46**, 3768 (1973).

BULLETIN OF THE CHEMICAL SOCIETY OF JAPAN, VOL. 51 (5), 1561—1562 (1978)

An X-Ray Photoelectron Spectroscopic Study of Biuret Metal Complexes

Tooru YOSHIDA, Kiyoshi YAMASAKI, and Shigemasa SAWADA

Osaka Prefectural Industrial Research Institute, Enokojima, Nishi-ku, Osaka 550

(Received October 21, 1977)

Synopsis. The mode of the co-ordination of biuret in biuret metal complexes has been examined by means of X-ray photoelectron spectroscopy. It has been found that the C(1s), O(1s), and N(1s) binding energies were clearly different among the bidentated, O-, and N-co-ordinated structures, and the monodentated O-co-ordinated one.

Biuret ($NH_2CONHCONH_2$) is known to form the following three types of complexes:

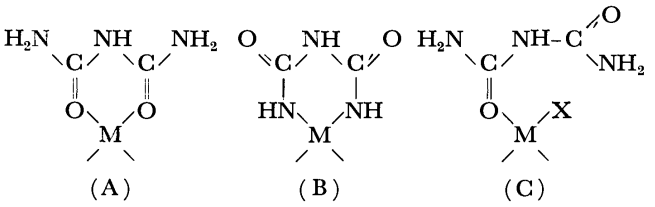

(A) (B) (C)

The structure (A) was found by the X-ray analysis for bis(biuret)copper(II) chloride[1] and bis(biuret)-zinc(II) chloride.[2] The structure (B) was found for dipotassium bis(biureto)cuprate(II) tetrahydrate.[1] The structure (C) was found for bis(biuret)cadmium(II) chloride.[3] The structures of the other metal complexes have been studied in the solid state by various kinds of physicochemical techniques.[4]

The purpose of this study is to examine the mode of the co-ordination of biuret in the metal complexes by means of X-ray photoelectron spectroscopy(XPS).

The X-ray photoelectron spectra were measured on an AEI ES200 spectrometer. AlK_α(1486.6 eV) X-ray radiation was used as the excitation source. The samples were ground to powder and then dusted onto double-backed adhesive tape. The measurements were run at room temperature under a vacuum of about 10^{-7} Torr. The binding energies were corrected by using the value of 285.0 eV for the C(1s) level resulting from the contaminated carbon. The reproducibilities of the values thus obtained were within ±0.1 eV. All the compounds used and their binding energies measured are given in Table 1. Biuret of an analytical grade was used after recrystallization from ethanol. All the complexes were prepared based upon the literature methods.[4c]

The C(1s), O(1s), and N(1s) electron spectra of biuret and all the biuret complexes except for K_2[M(biureto)$_2$] (M : Cu, Ni) showed approximately symmetrical single peaks, whose full-widths at the half-maximum heights were 1.8—2.0 eV in the C(1s) and O(1s) spectra, and 2.1—2.2 eV in the N(1s). These results suggest the presence of only one kind of carbon, oxygen, and nitrogen atoms. The N(1s) spectrum of dipotassium bis(biureto)niccolate(II) showed an unsymmetrical peak, as is shown in Fig. 1. This suggests the presence of two kinds of nitrogen atoms as well as dipotassium bis(biureto)cuprate(II). The two peaks, a and b, shown by the broken lines in the figure were obtained by a graphical resolution.

TABLE 1. MEASURED BINDING ENERGIES

Compond	Binding energy (eV)				
	C(1s)	N(1s)	O(1s)	Cl($2p_{3/2}$)	Metal($2p_{3/2}$)
$Cu(LH_2)_2Cl_2$	290.1	400.6	533.0	198.5	936.0
$Ni(LH_2)_2Cl_2$	289.9	400.4	532.6	198.5	856.9
$Co(LH_2)_2Cl_2$	289.9	400.5	532.7	198.6	782.1
$Mn(LH_2)_2Cl_2$	289.9	400.4	532.6	198.5	642.3
$Cd(LH_2)_2Cl_2$	289.6	400.3	532.2	199.0	406.0[a]
$Hg(LH_2)_2Cl_2$	289.5	400.2	532.1	199.4	101.5[b]
K_2NiL_2	287.9	399.7; 398.2	530.8		855.0
$K_2CuL_2 \cdot 2H_2O$	288.1	399.7; 398.0	531.0		934.7
LH_2	289.5	400.2	532.2		
$NiCl_2$				199.4	856.9
$CuCl_2$				199.4	935.8
KCl				198.2	

LH_2 indicates $H_2NCONHCONH_2$. a) Cd($3d_{5/2}$). b) Hg($4f_{7/2}$).

Co-ordination through the two oxygen atoms of biuret can be expected to increase contributions from the structures of the following types:

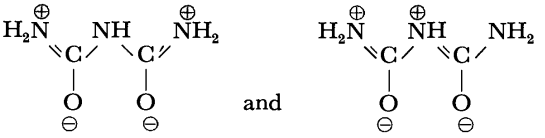

This should result in an increase in the N(1s) binding energy of the complexes.

In fact, the N(1s) binding energies of [M(biuret)$_2$]-Cl_2 (M: Cu, Ni, Co, Mn) were 0.2—0.4 eV higher than that of biuret. The presence of only one symmetrical peak in the N(1s) spectra suggests that the differences among the charges on the three nitrogen atoms in the molecule are not large enough to be detected by XPS. The increase in the C(1s) and O(1s) binding energies of the four complexes above, 0.2—0.4 and 0.4—0.6 eV respectively, compared with those of biuret may be explained by the displacement of

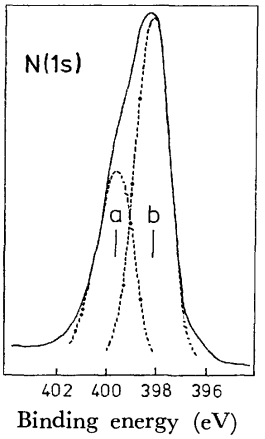

Fig. 1. N(1s) electron spectrum of dipotassium bis-(biureto)niccolate(II).

the charge through the oxygen atom to the metal ion upon the complex formation. The Cl($2p_{3/2}$) binding energies of these complexes were 0.3—0.4 eV higher than that of KCl, and 0.8—0.9 eV lower than those of $NiCl_2$ and $CuCl_2$. This indicates that the bond character between the Cl^- ion and the metal ion in these complexes is more ionic than that in $NiCl_2$ and $CuCl_2$, but not so ionic as in KCl. This does not contradict the finding[1] derived from the X-ray analysis for bis(biuret)copper(II) chloride.

The XPS results presented above lead to the conclusion that the co-ordination modes of biuret are the same in the four metal complexes above.

The C(1s), O(1s), and N(1s) binding energies and the shape of each peak of $M(biuret)_2Cl_2$ (M: Cd, Hg) were almost the same as those of the biuret, and the Cl($2p_{3/2}$) binding energies were similar to those of $NiCl_2$ and $CuCl_2$. These suggest that, in the two complexes, the charge displacement on the complex formation occurs mainly between the metal and the Cl^- ions, and that the co-ordination mode in the Hg complex is the same as that[3] in the Cd.

In the case of dipotassium bis(biureto)niccolate(II), it can be considered that two biuret molecules are co-ordinated to the metal atom, each through two nitrogen atoms of the amide groups, just as in the case of dipotassium bis(biureto)cuprate(II).[1] This co-ordination mode can be expected to increase contributions from structures of the following types:

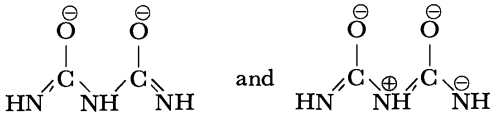

This should result in a decrease in the O(1s) binding energy of the complex and an appreciable separation of the N(1s) binding energies for the two kinds of nitrogen atoms, central and terminal.

In fact, the C(1s) and O(1s) binding energies of the complexes were 1.6 and 1.4 eV lower in the nickel complex, and 1.4 and 1.2 eV lower in the copper complex, than those of the biuret. Furthermore, the separation energies of the two kinds of peaks with the intensity ratio of about 1 : 2 observed in the N(1s) spectra of the nickel and the copper complexes were 1.5 and 1.7 eV respectively. The two peaks in both complexes could be assigned to the central and terminal nitrogen atoms respectively.

The difference (1.9 eV) between the Ni($2p_{3/2}$) binding energies of dipotassium bis(biureto)niccolate(II) and bis(biuret)nickel(II) chloride may be mainly due to the following differecnes in the bonding types. Firstly, the former complex contains biuret in an anionic species, while the latter contains biuret in a cationic species. That is, the possibility of increasing the electron density on the metal atom is larger in the former case than in the latter. Secondly, the coordination atoms in the two complexes are different, being nitrogen atoms and oxygen atoms respectively. That is, the covalent character of the coordination bond of dipotassium bis(biureto)niccolate(II) is larger than that in bis(biuret)nickel(II) chloride; the electron density on the metal atom is larger in the former complex than in the latter. The difference (1.3 eV) between the Cu($2p_{3/2}$) binding energies of the two analogous copper complexes may be explained in the same way.

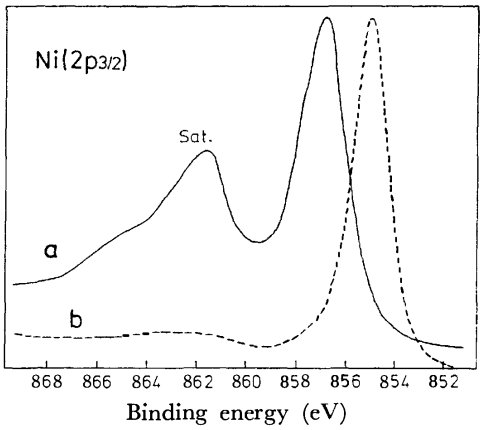

Fig. 2. Ni($2p_{3/2}$) electron region spectra.
a: Bis(biuret)nickel(II) chloride, b: dipotassium bis(biureto)niccolate(II)

XPS can differentiate specifically between the paramagnetic and diamagnetic characters of nickel(II) compounds.[5] That is, the intense shake-up satellites due to the 3d→4s, 4p transition are found on the high-energy side of the primary peak in the former in the 2p electron region, but they are absent in the latter.

Figure 2 shows the spectra of bis(biuret)nickel(II) chloride and dipotassium bis(biureto)niccolate(II) in the $2p_{3/2}$ electron region. The former complex exhibited a strong satellite peak, but the latter did not. This satellite peak was similar to those of other paramagnetic nickel compounds[6] in its intensity and its separation energy from the main peak. This suggests that the latter complex is of the low-spin type, and the former, the high-spin type. This agrees with the reported results[4c] on their magnetic properties.

References

1) H. C. Freeman, J. E. W. L. Smith, and J. C. Taylor, *Nature (London)*, **184**, 707 (1959).

2) M. Nardelli, G. Fava, and G. Giraldi, *Acta Crystallogr.*, **16**, 343 (1963).

3) L. Cavalca, M. Nardelli, and G. Fava, *Acta Crystallogr.*, **13**, 594 (1960).

4) a) B. B. Kedzia, P. X. Armendarez, and K. Nakamoto, *J. Inorg. Nucl. Chem.*, **30**, 849 (1968); b) K. Aida, Y. Musya, and S. Kinumaki, *Inorg. Chem.*, **2**, 1268 (1963); c) A. W. Mclellan and G. A. Melson, *J. Chem. Soc., A*, **1967**, 137; d) G. A. Melson, *J. Chem. Soc., A*, **1967**, 669.

5) a) L. J. Matienzo, W. E. Swartz, Jr., and S. O. Grim, *Inorg. Nucl. Chem. Lett.*, **8**, 1085 (1972); b) L. J. Matienzo and S. O. Grim, *ibid.*, **9**, 731 (1973); c) L. Yin, I. Adler, T. Tsang, L. J. Matienzo, and S. O. Grim, *Chem. Phys. Lett.*, **24**, 81 (1974).

6) L. J. Matienzo, L. Yin, S. O. Grim, and W. E. Swartz, Jr., *Inorg. Chem.*, **12**, 2762 (1973).

BULLETIN OF THE CHEMICAL SOCIETY OF JAPAN, VOL. 51 (5), 1563—1564 (1978)

Preparation of *trans*-Dichlorocobalt(III) Complexes of *N*-Alkylethylenediamines

Taku KITAMURA, Masahiko SABURI, and Sadao YOSHIKAWA

Department of Synthetic Chemistry, Faculty of Engineering, The University of Tokyo, Hongo, Bunkyo-ku, Tokyo 113

(Received October 25, 1977)

Synopsis. *N*-Alkylethylenediamine ($RNHCH_2CH_2NH_2$; R=butyl, hexyl, isobutyl, and isopropyl) complexes of the type $[CoCl_2(diamine)_2]X$ prepared by usual air-oxidation method except the case of R=isopropyl. The *N*-ipren (R=isopropyl) complex was obtained by employing methanol as the solvent. A brief consideration of the steric effect of *N*-isopropyl group was given.

In the past ten years cobalt(III) complexes of *N*-methylethylenediamine(*N*-meen) and other *N*-methyl-1,2-diamines were studied extensively. The presence of secondary N atom, which provides a new asymmetric center upon coordination, opened a variety of problems in the stereochemistry of metal complexes.[1-4] However, the cobalt(III) complexes of other *N*-alkyl-1,2-diamines such as *N*-eten,* *N*-npren,* *N*-nbuen,* *etc.* were attracted little attention.[5-7]

Basolo obtained the *trans*-dichlorobis(diamine)-cobalt(III) complexes (diamine = *N*-eten, and *N*-npren) as the crystalline products.[5] However, the *N*-nbuen complex of the same type was not isolated in the pure crystalline form, though its formation could be acknowledged from the green color of a reaction mixture.[5] In this note we report the prerartion of *trans*-dichlorocobalt(III) complexes of various *N*-alkylethylenediamines including *N*-nbuen by an air-oxidation method.

Experimental

Ligands. To a solution of 2-bromoethylamine hydrobromide (52g; 0.25 mol) in ethanol (150 cm^3) was added *N*-monoalkylamine (1.3—1.5 mol) and the solution was heated under reflux for 7 h. Ethanol and excess amine were distilled off under reduced pressure and the oily residue was dissolved in a small volume of water (*ca.* 50—100 cm^3). An excess amount of sodium hydroxide (*ca.* 40 g) was added to the solution in small portions, with occasional removing of white precipitate (NaBr) by filtration through a glass filter. When the diamine separated from aqueous alkali, it was extracted with ether (total 300 cm^3). The ether extracts were combined and dried over potassium hydroxide pellets overnight. Ether was removed by distillation, and the diamine which remained was distilled at atmospheric or under reduced pressure. Yield; 45—60%. Bp: *N*-nbuen, 160 °C (atmospheric); *N*-ipren, 140 °C (atmospheric); *N*-ibuen, 160 °C (atmospheric); *N*-nhxen, 105—108 °C/17 mmHg; *N*-chxen, 115—116 °C/29 mmHg.

trans-$[CoCl_2(N\text{-}nbuen)_2]ClO_4$. To a solution of $CoCl_2 \cdot 6H_2O$ (2.38 g; 0.01 mol) in water (30 cm^3) was added *N*-nbuen (2.4 g; 0.02 mol), and the solution was aerated for 6 h at room temperature. After 15 cm^3 of concd hydrochloric acid had been added, the solution was evaporated on a water bath at 75—80 °C. When the volume was reduced to ca. 20 cm^3, 60% perchloric acid (3 cm^3) was added and the mixture was cooled in a refrigerator. Dull yellow-green crystals which deposited were collected, washed successively with cold water, ethanol, and ether, and air-dried. Yield, 1.50 g. The product was recrystallized from methanol. Found: C, 31.39; H, 7.15; N, 12.00%. Calcd for $C_{12}H_{32}N_4O_4Cl_3Co$: C, 31.22; H, 6.99; N, 12.14%.

trans-$[CoCl_2(N\text{-}ibuen)_2]ClO_4$ was obtained by the same procedure as that for the above *N*-nbuen complex, using *N*-ibuen in place of *N*-nbuen. Found: C, 30.19; H, 6.93; N, 11.96%. Calcd for $C_{12}H_{32}N_4O_4Cl_3Co$; C, 31.22; H, 6.99; N, 12.14%.

trans-$[CoCl_2(N\text{-}nhxen)_2]ClO_4$. To a solution of $CoCl_2 \cdot 6H_2O$ (1.19 g; 0.005 mol) in water (15 cm^3) was added a solution of *N*-nhxen (1.97 g; 0.012 mol) in ehtanol (15 cm^3), and the solution was aerated for 5 h, adding occationaly a few cm^3 of ethanol to dissolve deep brown oily materials. After 15 cm^3 of concd hydrochloric acid was added, the resultant solution was evaporated on a water bath at 75—80 °C. When a small amount of green crystals appeared, the mixture was cooled to room temperature, and then 60% perchloric acid (5 cm^3) was added. The oily product which deposited was separated by decantation, and crystallized from ethanol solution. Found: C, 37.11; H, 7.89; N, 10.69%. Calcd for $C_{16}H_{40}N_4O_4Cl_3Co$; C, 37.11; H, 7.79; N, 10.82%.

trans-$[CoCl_2(N\text{-}ipren)_2]_2(ZnCl_4)$. Cobalt(II) chloride hexahydrate (1.19 g; 5 mmol) dissolved in methanol (20 cm^3) was added dropwise to a solution of *N*-ipren (1.02 g; 10 mmol) in methanol (30 cm^3) with continuous bubbling of air. After the addition had been completed, air was passed through the solution for further 3 h, adding occasionally a few cm^3 of methanol to maintain the volume of reaction mixture at 40—50 cm^3. Then, methanol was rotary-evaporated and the residue was dissolved in concd hydrochloric acid (15 cm^3). The solution was heated on a boiling water bath for 30 min, and then evaporated on a rotary evaporator to a volume of 20 cm^3. After solid $ZnCl_2$ (5 g) had been added, the blue-green solution was cooled in a refrigerator overnight. Green crystals which appeared were filtered off, washed with cold hydrochloric acid, ethanol, and then ether, and dried under reduced pressure. Found: C, 27.49; H, 6.73; N, 13.08. Calcd for $C_{20}H_{56}N_8Cl_8Co_2Zn$: C, 27.44; H, 6.45; N, 12.80%.

Measurements. Absorption spectra were obtained on a Shimadzu UV-210 spectrometer.

Results and Discussion

Basolo observed that addition of *N*-ipren to an aqueous solution of coblat(II) chloride resulted in the

* Abbreviations of *N*-alkylethylenediamine ($RNHCH_2CH_2NH_2$) are as follows: *N*-eten (R=ethyl)=*N*-ethylethylenediamine, *N*-npren (R=propyl)=*N*-propylethylenediamine, *N*-nbuen (R=butyl)=*N*-butylethylenediamine, *N*-nhxen (R=hexyl)=*N*-hexylethylenediamine, *N*-ipren (R=cyclohexyl)=*N*-isopropylethylenediamine, *N*-ibuen (R=isobutyl)=*N*-isobutylethylenediamine, *N*-chxen (R=cyclohexyl)=*N*-cyclohexylethylenediamine.

separation of cobalt(II) hydroxide.[5] This implies that the introduction of the bulky isopropyl group disturbs the coordination of *N*-ipren to the Co^{2+} ion due to steric hindrances and that the Co^{2+} ion interacts with hydroxide ions to deposite as cobalt(II) hydroxide. We supposed that the coordination of *N*-ipren to the Co^{2+} ion might be permitted to give rise to *trans*-$[CoCl_2(N\text{-ipren})_2]^+$, if the coexistence of hydroxide could be prevented by using an organic solvent. It was actually observed that the air-oxidation of a mixture of Co^{2+} and *N*-ipren in methanol resulted in the formation of *trans*-$[CoCl_2(N\text{-ipren})_2]^+$ after the treatment with HCl. The addition of $ZnCl_2$ to the reaction mixture gave crystals of the *N*-ipren complex of tetrachlorozincate(II) ($ZnCl_4^{2-}$) salt, though the yield was relatively low (*ca.* 20%). A similar effect of organic solvent which improves the formation of complex ions has been noted for the *trans*-dichlorocobalt(III) complex of 1,3-diaminopropane.[8]

On the other hand, *trans*-dichlorocobalt(III) complexes of *N*-nbuen, *N*-nhxen, and *N*-ibuen were readily obtained as perchlorate salts with considerable yields according to the usual air-oxidation method in aqueous media. It was noted that *N*-ibuen behaved in the same manner as *N*-nbuen, though the isobutyl group, as well as the isopropyl group, had a branch at the alkyl substituent. This indicates that primary *N*-alkyl groups permit the coordination of *N*-substituted en to the Co^{2+} ion even in aqueous solution.

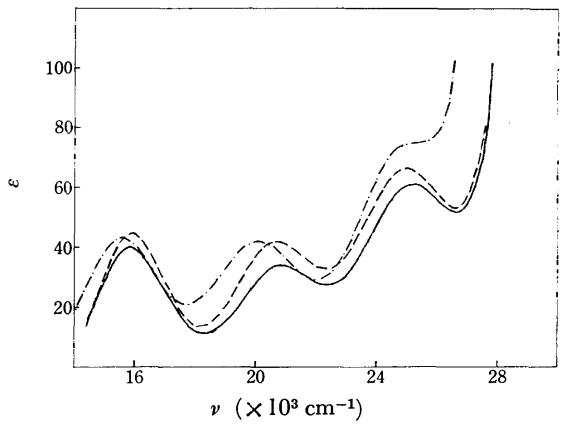

Fig. 1. Absorption spectra of *trans*-$[CoCl_2(diamine_2]^+$: *N*-nbuen (——), *N*-nhxen (— — —), and *N*-ipren (—·—·—).

The difference between isopropyl and other primary alkyl groups was also observed in the absorption spectra of *trans*-$[CoCl_2(diamine)_2]^+$ complexes. As Fig. 1 shows, the absorption maxima(15600, 20100, and 25000(sh) cm^{-1}) of the *N*-ipren compex shift to the lower energy side by 300—600 cm^{-1} than those of the other complexes (*N*-nbuen; 15900, 20800, and 25300 cm^{-1}. *N*-nhxen; 15900, 20700, and 25000 cm^{-1}. *N*-ibuen; 15900, 20700, and 25100 cm^{-1}). The red shift should be ascribed to the steric effects caused by the bulkiness of isopropyl group.

It is very suggestive that *N*-chxen no longer forms the *trans*-dichlorocobalt(III) complex according to the same method as for the *N*-ipren complex. The cyclohexyl group is also a secondary alkyl group but its bulkiness should have more significant effects than that of isopropyl. Thus, it seems likely that the isopropyl group has the critical size not to prevent the formation of Co(III) species by air-oxidation.

References.

1) D. A. Buckingham, L. G. Marzilli, and A. M. Sargeson, *J. Am. Chem. Soc.*, **89**, 825 (1967).
2) D. A. Buckingham, L. G. Marzilli, and A. M. Sargeson, *Inorg. Chem.*, **5**, 915 (1968).
3) M. Saburi, Y. Tsujito, and S. Yoshikawa, *Inorg. Chem.*, **9**, 1476 (1970).
4) J. A. Tiethof and D. W. Cooke, *Inorg. Chem.*, **11**, 315 (1973) and references therein.
5) F. Basolo, *J. Am. Chem. Soc.*, **75**, 227 (1953).
6) R. N. Keller and L. J. Edwards, *J. Am. Chem. Soc.*, **74**, 215 (1952).
7) T. Kitamura, M. Saburi and S. Yoshikawa, *Inorg. Chem.*, **16**, 585 (1977).
8) J. C. Bailar, Jr. and J. B. Work, *J. Am. Chem. Soc.*, **68**, 232 (1946).

BULLETIN OF THE CHEMICAL SOCIETY OF JAPAN, VOL. 51 (5), 1565—1566 (1978)

Solvolysis in Carboxamides. III.[1] Solvolysis Rates of 1-Adamantyl Bromide and Tosylate, 2-Adamantyl Tosylate, and *t*-Butyl Chloride in Carboxamides

Seiki SAITO, Kenji DOIHARA, Toshio MORIWAKE, and Kunio OKAMOTO*

Department of Synthetics Chemistry, School of Engineering, Okayama University, Tsushima, Okayama 700

**Department of Hydrocarbon Chemistry, Faculty of Engineering Kyoto University, Sakyo-ku, Kyoto 606*

(Received June 24, 1977)

Synopsis. Rate constants for the solvolysis of 1-adamantyl bromide and tosylate, 2-adamantyl tosylate, and *t*-butyl chloride in the four carboxamide solvents, *i. e.*, *N,N*-dimethylacetamide, *N,N*-dimethylformamide, *N*-methylacetamide, and *N*-methylformamide, have been determined. The role of the carboxamides as solvolytic solvents has been discussed on the basis of linear free-energy relationship.

Although carboxamides, such as *N,N*-dimethylacetamide (DMA), *N,N*-dimethylformamide (DMF), *N*-methylacetamide (NMA), and *N*-methylformamide (NMF), are expected to be particularly effective solvents for S_N1 solvolyses because of their highly polar characteristics,[2] little has been studied on the solvolytic feature of these solvents.[1,3]

It has been commonly accepted that the rate of solvolysis of the adamantyl system reflects the rate of the ionization process, because, for this system, neither rate-determining elimination nor solvation at the rear side of a leaving group is possible. Thus, in the assessment of the ionizing power of solvolytic solvents, the adamantyl system, including 1-adamantyl bromide[4] (**1**) and tosylate[4b,5] (**2**), and 2-adamantyl tosylate[6] (**3**) has been used as the reference compound. In the present paper we wish to report on the ionizing powers of the carboxamides, *i.e.*, DMA, DMF, NMA, and NMF, by the use of above mentioned tertiary systems **1** and **2**, **3**, and *t*-butyl chloride (**4**).

Results and Discussion

The first-order rate constants for the solvolysis of **1**, **2**, **3**, and **4** in the carboxamide solvents are shown in Table 1 along with the *Y* and *m* values.[7] A linear relation between log k_1 and *Y* has been observed for the carboxamide solvolysis of **1**, **2**, and **3**, and another linear relation has also been observed for many other solvents, including carboxamides, with a range of solvolytic reactivities varying over 8 (for **1**), 5 (for **2**), and 6 (for **3**) powers of ten, excluding the points for carboxylic acids[5,6c,6d] for **2** and **3**, aqueous trifluoroethanols[4a,6e] for **1** and **3**, and phenolic solvents[4b] for **1** and **2**. The correlation coefficients for the latter *m*-*Y* relation are 0.996, 0.990, and 0.998, respectively for **1**, **2**, and **3**. On the basis of these linear free-energy relationships, it is expected that the four carboxamide solvents would cause the solvolytic ionization even in the solvolyses of a secondary system,[8] though their ionizing powers are comparatively low (−1.51—−4.28 as measured by *Y*-values).

The importance of the nature of a leaving group is demonstrated when the correaltion between the rates for **1** and **2** in several groups of solvents is examined (Fig. 1). The data for the different solvent systems are clearly represented by five lines in Fig. 1. A similar type of dispersion has been found by Harris *et al.*[4c] in the plots of the log k_1 for **4** against log k_1 for **1** in aqueous ethanols and aqueous trifluoroethanols, and they have suggested that this dispersion is a diagnostic for nucleophilic solvent assistance.[6c] Our findings for the adamantyl systems, in which nucleophilic solvent assistance[6c] is prohibited, suggest that, besides the factor pointed out by Harris *et al.*,[4c] the non-electrostatic contribution (*i. e.*, hydrogen-bonding to the leaving group)[4c] to the ionization is important and different from a group of solvents to

TABLE 1. FIRST-ORDER RATE CONSTANTS (k_1)[a] FOR THE SOLVOLYSIS OF ADAMANTYL COMPOUNDS AND *t*-BUTYL CHLORIDE AT 25 °C AND THE CORRELATION BETWEEN log k_1 (ADAMANTYL) AND *Y*[b]

Amide	$k_1/(10^{-5}\ s^{-1})$				*Y*
	t-BuCl	1-AdBr	1-AdOTs	2-AdOTs	
DMA	4.87×10^{-5}	3.81×10^{-8} [c]	4.15×10^{-3}	2.91×10^{-7}	−4.28
DMF	2.40×10^{-4}	4.23×10^{-7}	2.89×10^{-2}	1.54×10^{-6}	−3.59[d]
NMA	4.73×10^{-3}	3.03×10^{-5}	8.25×10^{-1}	2.67×10^{-5}	−2.29
NMF	2.87×10^{-2}	5.23×10^{-4}	8.03	1.78×10^{-4}	−1.51
m (Amides)[e]	1.00	1.48	1.18	0.997	
m (Solvents)[f]	1.00	1.27	1.15	0.874	

a) Extrapolated from data at other temperatures (33—145 °C), except for the run, 1-AdOTs in NMF. b) P. R. Wells, *Chem. Rev.*, **63**, 171 (1963). c) Calculated from the plot of log k_1 *vs.* *Y*. d) The reported values:[3b] −3.47. e) The *m* values of the substrates calculated merely for the carboxamides. f) The *m* values for k_1's respectively in 22, 17, and 12 solvents, including the carboxamides; for k_1's in hydroxylic solvents, see Refs. 4a, 5, 6c—e, and J. M. Harris, A. A. Becker, J. F. Fagan, and F. A. Walden, *J. Am. Chem. Soc.*, **94**, 4484 (1974).

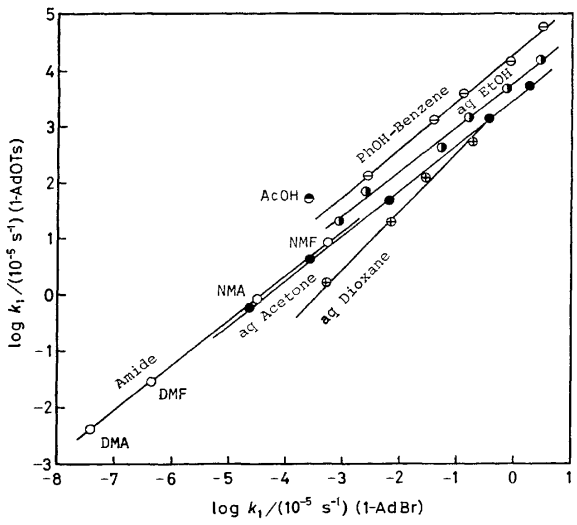

Fig. 1. Correlation of the rates of 1-AdOTs with that of 1-AdBr at 25 °C in different groups of solvents; from Table 1 and Refs. 4a, 4b, and 5.

another, though the definite conclusion is to be expected in a future work.

Experimental

Substrates and Solvents. 1-Adamantyl bromide, mp 119—120 °C (lit[9] mp 119—120 °C), 1-adamantyl tosylate, mp 79—83 °C (lit[10] mp 78—83 °C), and 2-adamantyl tosylate, mp 82.3—83 °C (lit,[6e] mp 82.1—83.4 °C) were prepared following the published methods.[5,11] *t*-Butyl chloride (commercial) was dried ($CaCl_2$) and distilled immediately before use. The four carboxamides were purified by the method described in a previous paper.[1]

Kinetic Measurements. Rates of solvolysis of the tosylates **2** and **3**, and the halides **1** and **4** were respectively determined by an acid-base titration (KOH in EtOH, Thymol Blue–phenolphthalein mixed indicator) and by haldie ion titration (the Volhard method[12]), employing the usual sealed-ampoule technique. As to the run for the tosylates, an acid-catalyzed hydrolysis of the carboxamides due to water contained in the solvent even after rigorous purification, has made an experimental infinity titer greater than the theoretical one. After appropriate correction for the above difference, a good first-order behavior was observed for all kinetic runs over two to three half-lives both in the absence and presence of added pyridine, except for the solvolysis of **2** in DMA at higher temperatures in which the first-order plot showed a downward drift after 25% completion. Linearity of the Arrhenius plot held also for all cases. In the case of **4**, the rate constant was calculated using a theoretical infinity titer.

Solvolysis Products. On the basis of GLC and NMR spectroscopy, the solvolysis products of **1**, **2**, and **3** in the carboxamides were identified to be mixtures of adamantanol and adamantyl esters which were furnished by the hydrolysis of initial ion-pair intermediate and of cationic imidate,[1] respectively.

References

1) Part II. S. Saito, T. Yabuki, T. Moriwake, and K. Okamoto, *Bull. Chem. Soc. Jpn.*, **51**, 529 (1978).

2) G. R. Reader and J. F. Gormlye, *J. Am. Chem. Soc.*, **73**, 5731 (1951).

3) a) N. Kornblum and R. K. Blackwood, *J. Am. Chem. Soc.*, **78**, 4037 (1956); b) S. D. Ross and M. M. Labes, *ibid.*, **79**, 4155 (1957); c) S. G. Smith, A. H. Fainberg, and S. Winstein, *ibid.*, **83**, 618 (1961); d) J. W. Wilt, R. G. Stein, and W. J. Wagner, *J. Org. Chem.*, **32**, 2097 (1967); e) S. Saito, T. Yabuki, T. Moriwake, and K. Okamoto, *Bull. Chem. Soc. Jpn.*, **46**, 1795 (1973); f) M. Anteunis and H. L. Peeters, *J. Org. Chem.*, **40**, 307 (1975); g) H. L. Peeters and M. Anteunis, *ibid.*, **40**, 312 (1975).

4) a) D. J. Raber, R. C. Bingham, J. M. Harris, J. L. Fry, and P. v. R. Schleyer, *J. Am. Chem. Soc.*, **92**, 5977 (1970); b) K. Okamoto, M. Matsubara, and T. Kinoshita, *Bull. Chem. Soc. Jpn.*, **45**, 1191 (1972); c) J. M. Harris, D. J. Raber, W. G. Neal, Jr., and M. D. Dukes, *Tetrahedron Lett.*, **1974**, 2331; d) J. M. Harris, D. L. Mount, M. R. Smith, and S. P. McManus, *J. Am. Chem. Soc.*, **99**, 1283 (1977).

5) D. N. Kevill, K. C. Kolwyck, and F. L. Weitl, *J. Am. Chem. Soc.*, **92**, 7300 (1970).

6) a) J. L. Fry, C. J. Lancelot, L. K. M. Lam, J. M. Harris, R. C. Bingham, D. J. Raber, R. E. Hall, and P. v. R. Schleyer, *J. Am. Chem. Soc.*, **92**, 2538 (1970); b) J. L. Fry, J. M. Harris, R. C. Bingham, and P. v. R. Schleyer, *ibid.*, **92**, 2540 (1970), c) P. v. R. Schleyer, J. L. Fry, L. K. M. Lam, and C. J. Lancelot, *ibid.*, **92**, 2542 (1970); d) T. W. Bentley and P. v. R. Schleyer, *ibid.*, **98**, 7658 (1976); e) F. L. Schadt, T. W. Bentley, and P. v. R. Schleyer, *ibid.*, **98**, 7667 (1976).

7) E. Grunwald and S. Winstein, *J. Am. Chem. Soc.*, **70**, 846 (1948).

8) It has been found that *exo*-2-norbornyl-3-*endo*-*d* tosylate rearranges to 7-*anti*-*d* tosylate in a significant extent in the course of solvolysis in DMA (S. Saito, T. Moriwake, K. Takeuchi, and K. Okamoto, submitted for publication in *Bull. Chem. Soc. Jpn.*)

9) St. Landa, S. Kriebel, and E. Knobloch, *Chem. Listy*, **48**, 61 (1954).

10) M. L. Sinnott, H. L. Storesund, and M. C. Whiting, *Chem. Commun.*, **1969**, 1000.

11) a) H. Stetter and C. Wulff, *Chem. Ber.*, **93**, 1366 (1960). b) P. v. R. Schleyer and R. D. Nicholas, *J. Am. Chem. Soc.*, **83**, 182 (1961).

12) A. H. Fainberg and S. Winstein, *J. Am. Chem. Soc.*, **78**, 2770 (1954).

BULLETIN OF THE CHEMICAL SOCIETY OF JAPAN, VOL. 51 (5), 1567—1568 (1978)

Effect of Hydration on the Thermal Denaturation of Lysozyme as Measured by Differential Scanning Calorimetry

Yukihisa FUJITA and Yukinao NODA

Department of Chemistry, Hyogo College of Medicine, Mukogawa, Nishinomiya, Hyogo 663

(Received August 31, 1977)

Synopsis. The thermal properties of the lysozyme-water system were investigated by differential scanning calorimetry under varied water contents, ranging from 0.05 to 1.6 g per g of protein. The temperature, T_d, and the enthalpy change, ΔH_d, of denaturation at water contents below 0.75 g/g showed strong dependencies on the hydration. At higher water contents, however, T_d and ΔH_d were almost independent of the degree of hydration, showing values almost identical to those in solution.

Recent studies have revealed that water plays a prominent role in the structure and biological function of proteins, but there are many problems remaining unsolved. The hydration process of proteins have been extensively studied by various techniques, such as gravimetric measurements (sorption isotherms),[1,2] IR[3] and NMR spectroscopy.[4] Calorimetric measurements of the hydrated proteins can also provide instructive information on the interaction between protein and water.

This paper will describe the effect of hydration on the thermal denaturation of lysozyme as measured by differential scanning calorimetry.

Experimental

Materials. The hen egg-white lysozyme used in the present study was a three-times-recrystallized sample(lot 74C—8040) from Sigma Chemicals Co. All the chemicals employed for the control of the relative humidities were of a reagent grade and were used without further purification.

Methods. The thermal denaturation of lysozyme was measured with a Rigaku Denki standard-type differential scanning calorimeter. The samples(5—10 mg) were packed in sealable pans and kept in humidostates at appropriate relative humidities in order to adjust the water contents by conditioning for 5 days, then the pans were sealed. The relative humidity was varied by placing saturated aqueous solutions in contact with an excess of various solutes at 293 K.[5] The samples with water contents higher than 1 g/g were prepared by adding twice-distilled water.

For calorimetric measurements, the heating rate was 2.5 K/min. This heating rate was found to be preferable in terms of the sharpness of the resulting thermograms and their reproducibility.

The water content and the dry mass of the sample were gravimetrically determined by drying the punctured sample pan at 378 K *in vacuo* for 24 h. The molecular weight of lysozyme was taken as 14300.[6]

Results and Discussion

Figure 1 shows typical thermograms measured at three different water contents. The thermal denaturation was accompanied by an endothermal heat effect. The temperature, T_d, and the enthalpy change, ΔH_d, of the denaturation were estimated

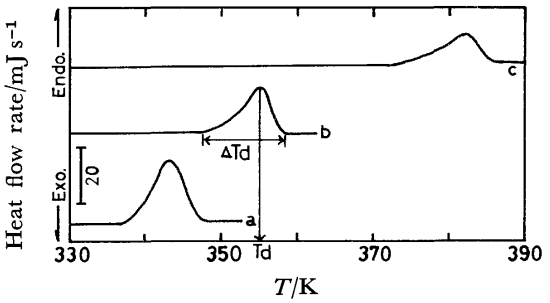

Fig. 1. DSC thermograms of lysozyme.
Water contents and sample weights are (a) 1.13, 6.2; (b) 0.27, 4.8; (c) 0.10 g/g, 4.2 mg.

from the temperature of the peak and the peak-area respectively in the thermogram obtained. The temperature width of the denaturation peak, ΔT_d, was also estimated as the temperature difference between the onset and the outset of the endothermal peak in the thermogram. Unfortunately, these values could not estimated at water contents lower than about 0.05 g/g, because these thermal decomposition occurred instead of thermal denaturation.

The T_d, ΔT_d and ΔH_d are plotted as a function of the water content in Figs. 2 and 3 respectively. These values similarly showed marked dependencies on the water content. At water contents above 0.75 g/g, both T_d and ΔH_d were slightly dependent on the water content. The mean values in this region were 341.7 K and 313 kJ/mol, almost identical to those measured for lysozyme in solution.[7,8] It seems reasonable to assume that a similar conformational change which takes place in solution occurs in a solid state containing much water; the interaction between protein

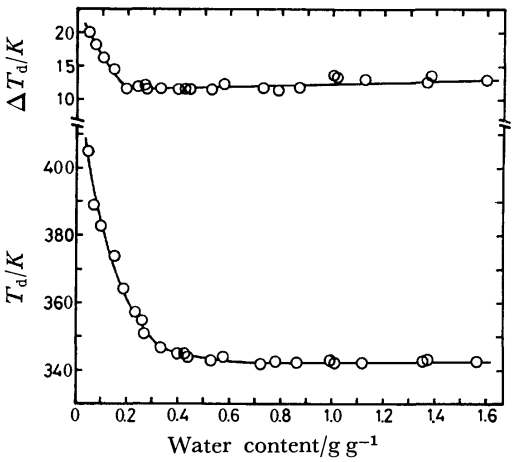

Fig. 2. Temperature of denaturation, T_d, and temperature width of denaturation peak, ΔT_d, of lysozyme as a function of water content.

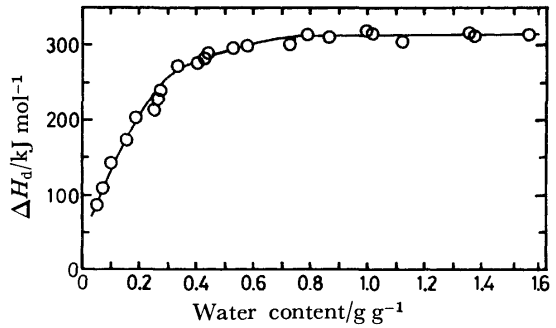

Fig. 3. Enthalpy change of denaturation, ΔH_d, of lysozyme as a function of water content.

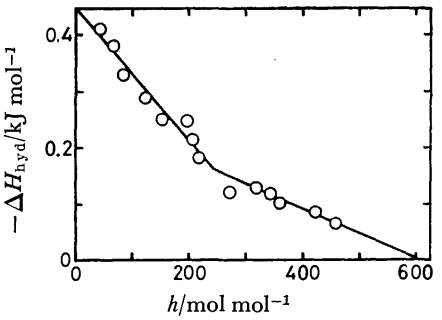

Fig. 4. The plot of the contribution by removal of the water from the hydrated protein, ΔH_{hyd}, to the enthalpy change of denaturation *vs.* the degree of hydration, h.

molecules does not influence the unfolding of the molecule. In addition, this indicates that the hydration of lysozyme, an essential process for stabilizing its spatial structure in water, is completed at about 0.75 g of water per g of protein, equivalent to about 600 moles of water per mol of protein.

Below the water content of 0.75 g/g, the T_d increased gradually with a decrease in the water content, until the increase became much more marked at water contents lower than about 0.3 g/g. The ΔH_d, on the other hand, decreased with a decrease in the water content in the same region of water content. The ΔT_d showed an almost constant value at water contents higher than about 0.15 g/g, but increased markedly at water contents lower than this value.

To analyze the experimental data we assumed that the observed enthalpy change of the thermal denaturation of lysozyme, ΔH_d, was expressed as follows:

$$\Delta H_d = \Delta H_{comp} + (600-h)\Delta H_{hyd}$$

where ΔH_{comp} is the enthalpy change of the denaturation of the completely hydrated protein, h is the degree of hydration, as expressed by the number of moles of water adsorbed per mole of protein, and ΔH_{hyd} is the contribution made by the removal of the water from the hydrated protein, as expressed on the basis of one mole of water per mol of protein. As is shown in Fig. 3, the hydration of lysozyme was completed at about 600 moles of water per mol of protein, and ΔH_d showed an almost constant value at water contents higher than 600 mol/mol, therefore, ΔH_{comp} was regarded as identical to ΔH_d, 313 kJ/mol, in this region. The plot of ΔH_{hyd} against the degree of hydration is shown in Fig. 4. The ΔH_{hyd} decreased with an increase in the h, this relationship could be represented by two segments of the straight line. This indicates that the effect of hydration on the stabilization of protein decreases with an increase in the degree of hydration; the interaction between protein and water decreases with an increase in the degree of hydration, and the dependence of protein–water interaction on the degree of hydration changes at about 240 mol/mol, equivalent to a water content of 0.3 g/g.

It is interesting to note that a break in the dependence of the protein–water interaction on the water content is seen near 0.3 g of water per g of protein. Harvey and Hoekstra[9] have reported that the dielectric properties of the adsorbed water on lysozyme changed at the same water content. A recent calorimetric study of frozen protein solutions[10] has revealed that the threshold water contents for the unfreezable and freezable water fractions with heats of fusion different from that of the bulk water are about 0.3 and 0.7 g/g respectively. The water content of 0.3 g/g corresponds to about 3.5 molecules of water per ploar amino acid residue in the lysozyme molecule. Below the water content of 0.3 g/g, the water molecules are probably bound by hydrogen bonds to the polar amino acid residues on the surface of protein. It seems likely that the exhaustive removal of these associated water molecules brings about changes in the structure of protein[11] and in the mechanism of denaturation, as suggested by the curve for ΔT_d in Fig. 2.

At water contents above 0.3 g/g, the protein–water interaction was weaker than that at lower water contents. In the range of water content between 0.3 and 0.75 g/g, some water molecules may ambivalently interact not only with the water strongly bound to hydrogen-bonding sites of the protein, but also with the normal bulk water, which probably paly an essential role in stabilizing the native conformation of the protein.

It will be interesting to study the contribution of hydration to the stabilization of protein in further detail.

References

1) H. B. Bull, *J. Am. Chem. Soc.*, **66**, 1499 (1944).
2) L. H. Reyerson and W. S. Hnojewyi, *J. Phys. Chem.*, **64**, 811 (1960).
3) M. Ruegg and H. Hani, *Biochim. Biophys. Acta*, **400**, 17 (1975).
4) W. S. Jr. Brey, T. E. Evans, and L. H. Hitzrot, *J. Colloid Interface Sci.*, **26**, 306 (1968).
5) Chem. Soc. Jpn., Ed., "Kagaku Benran," Maruzen, Tokyo (1966), p. 67.
6) R. E. Canfield, *J. Biol. Chem.*, **238**, 2698 (1963).
7) F. Delben and V. Creascenji, *Biochim. Biophys. Acta*, **194**, 615 (1969).
8) J. M. O'Reilly and F. E. Karasz, *Biopolymers*, **9**, 1429 (1970).
9) S. C. Harvey and P. Hekstra, *J. Phys. Chem.*, **76**, 2987 (1972).
10) M. Ruegg, V. Moor, and B. Blanc, *Biochim. Biophys. Acta*, **400**, 334 (1975).
11) N. Hanafusa, *Teion Kagaku*, **B**, **27**, 11 (1969).

BULLETIN OF THE CHEMICAL SOCIETY OF JAPAN, VOL. 51 (5), 1569—1570 (1978)

The Reaction of O(^{3}P) Atoms with Indene and Phenanthrene Induced by the γ-Radiolysis of Liquid Carbon Dioxide

Seizi GOTO, Akira HORI, Setsuo TAKAMUKU,* and Hiroshi SAKURAI

The Institute of Scientific and Industrial Research, Osaka University, Yamadakami, Suita, Osaka 565

(Received October 17, 1977)

Synopsis. The γ-radiolysis of liquid CO_2 with indene and phenanthrene gives the corresponding oxirane and carbonyl compounds, together with some products which are unexpected on the basis of the reaction of (^{3}P) with aliphatic olefins: (i) the corresponding cyclic carbonate; (ii) 1*H*-2-benzopyran and a dimer for indene, and (iii) dibenz[*b*,*d*]oxepin and 2,2′-biphenyldicarbaldehyde for phenanthrene. The mechanisms of the formation of these products are discussed.

It has been shown that the γ-radiolysis of CO_2 in the liquid phase produces oxygen atoms.[1] We have recently studied the radiolysis of liquid CO_2 with various organic compounds, such as olefins,[2] saturated hydrocarbons,[3] and phenylacetylenes,[4] and have observed the formation of the corresponding oxidation products. On the basis of the reaction mechanism, it has been concluded that the most reasonable oxidizing species must be a ground-state oxygen atom. Recently, Wojnarovits *et al.*[5] also indicated the formation of O(^{3}P) atoms in the γ-radiolysis of a cyclohexene-liquid CO_2 mixture. Therefore, one may expect the radiolysis of liquid CO_2 to be useful for the generation of O(^{3}P) atoms in the liquid phase. The purpose of this work is to clarify the reactivity of O(^{3}P) atoms with condensed-ring compounds, such as indene and phenanthrene, the reactions of which with oxygen atoms are not known, and to explore the possibility of capturing CO_2 by intermediates of the reactions of O(^{3}P) atoms with the above compounds.

The irradiation of an indene-liquid CO_2 mixture was carried out using a ^{60}Co source at 0 °C; the results are summarized in Table 1. The following features were observed; (i) the products were 1H-2-benzopyran (**1**), 1,2-epoxyindan (**2**), 2-indanone (**3**), 1-indanone (**4**), 1,2-indandiyl carbonate (**5**), and an indene dimer (**6**),[6] among which **2** and **3** were the main products; (ii) the total *G* values of the oxygen-containing products were *ca.* 5.3 and 3.8 for 2 and 17 hrs irradiation respectively, which are consistent with the $G(CO)=3.5$—5.0 obtained by the γ-radiolysis of liquid CO_2 at −48 °C,[1] and hence the *G* values suggested that the oxygen atoms generated on the radiolysis of liquid CO_2 are trapped effectively by indene; (iii) on the basis of the γ-irradiation to **2** or **3** in liquid CO_2,[7] it was found that the further reactions of the main products to form their isomers and **5** are negligibly small, except for a slight isomerization of **2** to **3**, and (iv) 1*H*-2-benzopyran (**1**) was formed by the pyrolysis of **2** at 300 °C.

Table 1. Radiolysis of the indene-liquid CO_2 system

Irrad. time (h)	Conv. (%)	Product yield (%)[a] (*G* value)					
		1	**2**	**3**	**4**	**5**	**6**
2	4.2	2.8 (0.17)	29 (1.7)	51 (3.1)	3.3 (0.19)	1.7 (0.10)	7.8 (0.47)
17	42	1.5 (0.11)	24 (1.7)	23 (1.7)	2.7 (0.20)	1.4 (0.10)	1.0 (0.07)

a) All the products were analyzed with a 3-m PEG 20 M column at 150 °C. The product yields are based on the amount of indene consumed.

* To whom correspondence should be addressed.

On the basis of these observations, we propose the following scheme for the formation of the oxygen-containing products of indene:

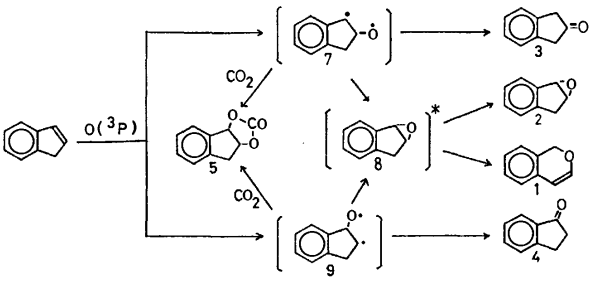

In the first step, the oxygen atom adds to the double bond of indene, preferentially at the C-2 carbon atom. The biradical (**7** or **9**) thus formed undergoes ring closure to an epoxide or undergoes a rearrangement to the carbonyl compounds (**3** or **4**); 2-indanone(**3**) is also produced, partly by the further isomerization of the **2** primarily produced. The epoxide (**8**) initially formed may possess a vibrationally excess energy and may be rearranged partly to **1**. Furthermore,

Table 2. Radiolysis of the phenanthrene-liquid CO_2 system

Irrad. time (h)	Conv. (%)	Product yield (%)[a] (*G* value)				
		10	**11**	**12**[b]	**13**	**14**
3	5	1.3 (0.04)	35 (1.1)	46 (1.4)	2.9 (0.09)	0.9 (0.03)
17	15	1.2 (0.02)	6.1 (0.10)	15 (0.24)	2.6 (0.04)	4.4[c] (0.07)

a) All the products were analyzed with a 1-m Silicone OV-17 column at 180 °C. b) This product was determined to be 9-methoxyphenanthrene. c) The addition of isopropyl alcohol (13 mmol) decreased the yield of **14** to trace amounts.

the biradical (**7** or **9**) captures CO_2 to form **5**, probably because of its dipolar character.

In the case of phenanthrene (Table 2), the products were dibenz[*b*,*d*]oxepin (**10**), 9,10-dihydro-9,10-epoxyphenanthrene (**11**), 9-phenanthrol (**12**), 9,10-dihydro-9,10-phenanthrylene carbonate (**13**), and 2,2'-biphenyldicarbaldehyde (**14**). The main products were **11** and **12**. The further reactions of the main products to form their isomers, **13** and **14**, are negligibly small, because the γ-radiolysis of liquid CO_2 in the presence of **11** or **12** gave such products in very low yields (the *G* values were all less than 0.03). Consequently, the initial reaction of the oxygen atom is the addition to the 9,10-bond of phenanthrene, the so-called K-region, to form a biradical:

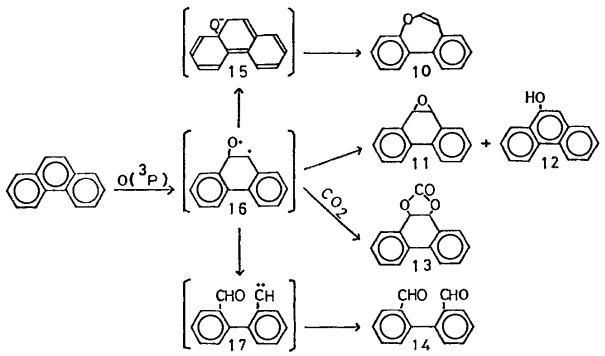

The biradical (**16**) may be transformed into the products by the following possible modes: (i) the ring closure or rearrangement of **16** to give **11** or **12** respectively; (ii) the ring closure to **15**, which then undergoes thermal valence isomerization to **10**; (iii) capturing CO_2 to form **13**, or (iv) the fission of a carbon-carbon bond of **16** to form a carbene (**17**), which is then oxidized to **14**. The (ii) mode is also observed in the photorearrangement of **11** to **10**.[8] Although there is no direct evidence for the (iv) mode, it may be supported by the following facts: (a) the addition of isopropyl alcohol, which is known to react with a carbene,[9] to this reaction system resulted in a pronounced decrease in the **14**, despite the fact that the yields of the other products remained unaltered, and (b) the radiolysis of the *trans*-stilbene-benzene-liquid CO_2 system gave benzaldehyde, diphenylmethane, and 7-phenylcycloheptatriene, besides oxirane and carbonyl compounds, whose formation can be explained by the following scheme:[10]

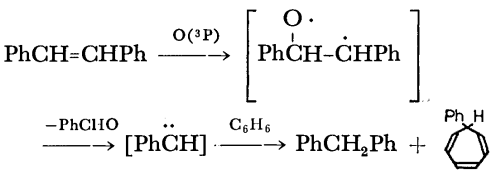

Experimental

Procedure. The experimental procedures were essentially the same as those reported previously in the reaction of atomic oxygen with alkanes.[3] A mixture of liquid CO_2 (1.4 mol) and indene (4.3 mmol) or phenanthrene (2.8 mmol) in a stainless-steel autoclave was irradiated by means of a ^{60}Co source at 0 °C. The dose rate, as measured by ferrous sulfate dosimetry, was 1.7×10^{19} eV/g h. The products were identified by a comparison of the retention times of the GLPC and the mass spectra with those of authentic samples.

Materials. Commercial indene and phenanthrene were purified by distillation and by recrystallization from methanol respectively before use. The carbon dioxide (99.99%, Fuji Koatsu Gas Co., Ltd.) was used without further purification. Authentic samples of the products, **1**,[11] **2**,[12] **3**,[13] **4**,[14] **10**,[8] **11**,[15] **12**,[16] and **14**,[17] were prepared by the literature procedures. 1,2-Indandiyl carbonate (**5**) and **13** were prepared by reactions of *cis*-1,2-indandiol and *cis*-9,10-dihydroxy-9,10-dihydrophenanthrene with diethyl carbonate respectively, according to the method of Overberger and Drucker.[18] All the products synthesized were identified by means of their melting points and NMR spectra or by means of their mass spectra.

References

1) D. L. Baulch, F. S. Dainton, and R. L. S. Willix, *Trans. Faraday Soc.*, **61**, 1146 (1965); A. R. Anderson and D. A. Dominey, *Radiat. Res. Rev.*, **1**, 269 (1968); M. Yoshimura M. Chosa, Y. Soma, and M. Nishikawa, *J. Chem. Phys.*, **57**, 1626 (1972).

2) H. Sakurai, K. Akimoto, S. Toki, and S. Takamuku, *Chem. Lett.*, **1975**, 469.

3) A. Hori, S. Takamuku, and H. Sakurai, *J. Org. Chem.*, **42**, 2318 (1977).

4) A. Hori, S. Takamuku, and H. Sakurai, *J. Chem. Soc., Chem. Commun.*, **1976**, 686.

5) L. Wojnarovits, S. Hirokami, and S. Sato, *Bull. Chem. Soc. Jpn.*, **49**, 2956 (1976).

6) The mechanism of the formation of **6** will be reported and discussed elsewhere.

7) The γ-radiolysis of liquid CO_2 in the presence of **2** (2.3 mmol) or **3**(2.3 mmol) was carried out under conditions similar to those used for indene-liquid CO_2 system. Only small amounts of the products, **1**, **3**, **4**, and **5**, were formed for **2**, and the *G* values were as follows: **1** ($G=0.02$); **3** (0.79); **4** (0.01); **5** (0.02). In the case of **3**, no such products could be detected.

8) D. M. Jerina, B. Witop, C. L. Meintosch, and O. L. Chapmann, *J. Am. Chem. Soc.*, **96**, 5578 (1974); N. E. Brightwell and G. W. Griffin, *J. Chem. Soc., Chem. Commun.* **1973**, 37.

9) P. Scheiner, *J. Org. Chem.*, **34**, 199 (1969).

10) K. Akimoto, S. Takamuku, and H. Sakurai, unpublished results.

11) H. Kristinson, R. A. Matter, and G. W. Griffin, *Chem. Commun.*, **1966**, 415.

12) C. J. W. Brooks and L. Young, *J. Biochem.*, **63**, 264 (1956).

13) J. E. Horan and R. W. Schiesser, *Org. Synth.*, Coll. Vol. V, 647 (1973).

14) R. A. Pacaud and C. F. H. Allen, *Org. Synth.*, Coll. Vol. II, 336 (1950).

15) M. S. Newman and S. Blum, *J. Am. Chem. Soc.*, **86**, 5599 (1964).

16) L. F. Fieser, R. P. Jacovsen, and C. C. Price, *J. Am. Chem. Soc.*, **58**, 2163 (1936).

17) P. S. Bailey and R. E. Erickson, *Org. Synth.*, Coll. Vol. IV, 489 (1973).

18) C. G. Overberger and A. Drucker, *J. Org. Chem.*, **29**, 365 (1964).

BULLETIN OF THE CHEMICAL SOCIETY OF JAPAN, VOL. 51 (5), 1571—1572 (1978)

Syntheses of Aromatic Mannich Bases Involving Nitrogen Heterocycles by Means of Amine-exchange Reaction

Hiroyoshi KAMOGAWA, Kuniaki KUBOTA, and Masato NANASAWA

Department of Applied Chemistry, Yamanashi University, Takeda 4, Kofu, Yamanashi 400

(Received November 1, 1977)

Synopsis. Amine-exchange reactions of aliphatic Mannich bases involving nitrogen heterocycles, such as 2-(2-dimethylaminoethyl)-substituted pyridine, quinoline, benzothiazole, and 3,3-dimethyl-3*H*-indole, with arylamines readily provided the corresponding aromatic Mannich bases which are otherwise hardly accessible.

A few amine-exchange reactions involving aliphatic Mannich bases and arylamines have been reported.[1,2] In spite of their expected usefulness in organic synthesis, however, the results so far reported have been limited only to those for Mannich bases containing ketone carbonyls.

In the course of the synthetic studies of the polymerizable Mannich bases containing aromatic functional groups,[3] we have successfully attempted the amine-exchange reactions of aliphatic Mannich bases involving nitrogen heterocycles with arylamines; thereby we have isolated, in reasonable yields, the aromatic Mannich bases, which could not be synthesized directly from the corresponding 2-methyl-substituted nitrogen heterocycles, formalin, and arylamines.

Amine-exchange reactions take place as follows.

$$RCH_2CH_2NMe_2 + ArNH_2 + HCl$$

1—4

1: R =

3: R = 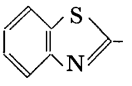

2: R = 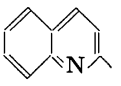

4: R = 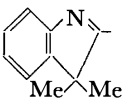

$$\longrightarrow RCH_2CH_2NHAr + Me_2NH\cdot HCl$$

5a—d: R =

6a—d: R = 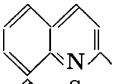

7a—g: R = 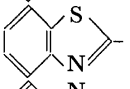

8a—e: R = 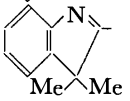

It has been found that, by refluxing the ingredients in ethanol–water for 4—25 h, exchange reactions take place readily to afford the corresponding products (**5**—**8**). Table 1 gives the results obtained.

It may be seen that from this table that good nucleophiles, such as *p*-anisidine and *p*-toluidine generally provided better yields of the exchange products than poor nucleophiles such as *p*-nitroaniline and *p*-aminobenzoic acid. *p*-Nitroaniline, a poor nucleophile, failed even to react with 2-(2-dimethylaminoethyl)-substituted pyridine (**1**), and quinoline (**2**). Moreover, the reactivity of the Mannich base in the exchange reaction is considerably affected by the cyclic portion of the molecule, providing this decreasing order of reactivity: **3**, **4**, **2**, and **1**. The most reactive Mannich base, **3**, reacted successfully with all the arylamines employed.

Table 1. AMINE-EXCHANGE REACTIONS OF MANNICH BASES

No.		Ar	Yield, %	Mp, °C
1→	**5a**	*p*-$OCH_3\cdot C_6H_4$-	37.2[a]	Oily product
	5b	*p*-$CH_3\cdot C_6H_4$-	34.0[a]	
	5c	C_6H_5-	30.3[a]	
	5d	*p*-$NO_2\cdot C_6H_4$-	0[a]	
2→	**6a**	*p*-$OCH_3\cdot C_6H_4$-	39.1[b]	Oily product
	6b	*p*-$CH_3\cdot C_6H_4$-	35.9[b]	
	6c	C_6H_5-	31.0[b]	
	6d	*p*-$NO_2\cdot C_6H_4$-	0[b]	
3→	**7a**	*p*-$OCH_3\cdot C_6H_4$-	58.0[b]	80—82
	7b	*p*-$CH_3\cdot C_6H_4$-	60.6[b]	85—88
	7c	C_6H_5-	32.4[c]	Viscous mass
	7d	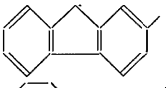	48.2[b]	151—154
	7e	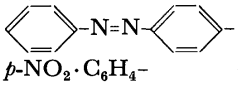	57.5[b]	89—92
	7f	*p*-$NO_2\cdot C_6H_4$-	41.3[b]	85—90
	7g	*p*-$COOH\cdot C_6H_4$-	27.7[b]	70—73
4→	**8a**	*p*-$OCH_3\cdot C_6H_4$-	44.1[b]	91—93
	8b	*p*-$CH_3\cdot C_6H_4$-	62.2[b]	103—105
	8c	C_6H_5-	40.9[b]	128—131
	8d	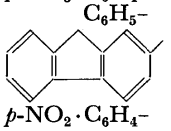	73.7[b]	119—122
	8e	*p*-$NO_2\cdot C_6H_4$-	Trace[b]	—

a) 25 h refluxing in $EtOH/H_2O$ (1/1). b) 4 h refluxing in $EtOH/H_2O$ (1/1). c) With tar.

Although the mechanism of the reaction is not exactly known, the fact that amine-exchange reactions also took place readily between aliphatic Mannich bases containing a β-dimethylaminoethyl group attached to a nitrogen heterocycle and arylamines indicates that the synthetic procedure for aromatic Mannich bases by amine-exchange reaction is generally applicable to Mannich bases containing a β-alkylaminoethyl group.

Experimental

The infrared, ^{1}H-NMR, and mass spectra were recorded on a Hitachi 215 spectrophotometer, a JNM-PMX 60 spectrometer, and a Hitachi RMU-6 MG spectrometer, respectively, all under standard measurement conditions. The elemental analyses were carried out using a Perkin-Elmer

250 instrument.

Syntheses of Starting Mannich Bases. A conventional procedure[4] was employed. Thus, in a typical example, for obtaining 2-(β-dimethylaminoethyl)-3,3-dimethyl-3*H*-indole (**4**), 9.5 g (60 mmol) of 2,3,3-trimethyl-3*H*-indole, 4.9 g (60 mmol) of dimethylamine hydrochloride, and 6 ml (60 mmol) of 37% formalin in 30 ml of ethanol were refluxed for 4 h. The resulting dark red solution was diluted with water and extracted with ether three times. The dark aqueous layer was then basified with aqueous sodium hydroxide, and the resulting orange oil was extracted with ether, followed by washing with water, drying over anhydrous sodium sulfate, and evaporation *in vacuo* to leave a red viscous mass, which was subsequently recrystallized from ethanol–water to afford light orange crystals (mp 58—60 °C) in a 33% yield. Found: C, 77.59; H, 9.42; N, 12.99%. Calcd for $C_{14}H_{20}N_2$: C, 77.78; H, 9.26; N, 12.96%. IR(CCl_4): 2970—2860 (CH_2, CH_3), 2820, 2760 (NMe_2), 1600 (aryl), 1450 cm^{-1}. NMR(CCl_4): δ 1.3 (m, 6H, 2Me), 2.2 (s, 6H, NMe_2), 2.4—4.0 (m, 4H, $2CH_2$), 6.8—7.8 (m, 4H, ArH) ppm. Mass (*m/e*) 216(M^+).

2-(β-Dimethylaminoethyl)-pyridine (**1**), -quinoline (**2**), and -benzothiazole (**3**) were obtained in similar manners in 44% (oil), 42% (oil), and 40% (oil) yields, respectively, their analytical and spectral data also being satisfactory.

Amine-exchange Reactions. In a typical example, 0.52 g (2.5 mmol) of **3**, 0.36 g (2.5 mmol) of *p*-toluidine hydrochloride, and 10 ml of ethanol–water (1/1 v/v) were refluxed for 4 h. The resulting yellow solution, with the red oil separated, was extracted with ether and water; the yellow organic layer was then dried over anhydrous sodium sulfate and evaporated *in vacuo* at 50 °C to leave a red viscous mass, which was subjected to silica gel-column chromatography to collect benzene–ether elutes. Recrystallizations from benzene provided orange-yellow crystals (**7b**) (mp 85—88 °C) in a 60.6% yield. Found: C, 71.51; H, 6.00; N, 10.37%. Calcd for $C_{16}H_{16}N_2S$: C, 71.64; H, 5.97; N, 10.45%. IR(CCl_4): 3390 (NH), 3000—2860 (CH_3, CH_2), 1600 (aryl), 1430 cm^{-1}. NMR (CCl_4): δ 2.2 (s, 3H, CH_3), 3.0—5.0 (m, 5H, NH+$2CH_2$), 6.3—8.3(m, 8H, ArH) ppm. Mass(*m/e*): 268(M^+, 20), 120 (100).

The reactions for the other combinations in Table 1 were carried out in similar manners, the identifications of the products by CHN analyses and the infrared, NMR, and mass spectra being satisfactory.

References

1) J. C. Craig and M. Moyle, *J. Org. Chem.*, **29**, 410 (1964); *ibid.*, **23** 2779 (1963).

2) J. V. Greenhild and M. Ramli, *Tetrahyd. Let.*, **1973**, 4059.

3) H. Kamogawa, K. Kubota, and M. Nanasawa, *Bull. Chem. Soc. Jpn.*, **51**, 561, (1978).

4) R. Adams, *Org. React.*, **1**, 336 (1942).

BULLETIN OF THE CHEMICAL SOCIETY OF JAPAN, VOL. 51 (5), 1573—1574 (1978)

Studies on Heterocyclic Analogs of Azulenes. IV.[1] Behavior of 2-Chlorocyclohepta[*b*]pyrrole Derivatives toward Phosphorus Ylide

Tarozaemon NISHIWAKI, Noritaka ABE, Kozue ISHIDA, and Kaoru MIURA

Department of Chemistry, Yamaguchi University, Yamaguchi 753

(Received November 4, 1977)

Synopsis. The transylidation reaction of methyl (triphenylphosphoranylidene)acetate with 2-chlorocyclohepta[*b*]pyrrole derivatives has been studied. 3,8-Disubstituted derivatives gave a transylidation product only, whereas 3-substituted derivatives afforded not only a transylidation products but also the compounds formed by the addition of ylide at C-8. ^{13}C NMR spectra of the transylidation products are recorded in part.

The transylidation reaction[2] has been utilized for the preparation of heterocyclic ylides[3] and alkyl- and alkenyl-substituted hetreocycles.[4] The present study was undertaken from our interest[1,5] in the reactivities of 2-chlorocyclohepta[*b*]pyrrole derivatives toward nucleophiles.

The reaction of methyl (triphenylphosphoranylidene)acetate (**5**) with 2-chloro-3-ethoxycarbonyl-8-phenyl- (**1**) and 2-chloro-3-cyano-8-*p*-methoxyphenylcyclohepta[*b*]pyrrole (**2**), respectively, proceeded to give the corresponding phosphoranes (**6**) and (**7**). However, 2-chloro-3-cyanocyclohepta[*b*]-pyrrole (**3**), when treated with **5**, gave a complex mixture of products, among which a transylidation product (**8**), 2-chloro-3-cyano-8-methylcyclohepta[*b*]-pyrrole (**10**), and 2-chloro-1-cyano-4-(methoxycarbonyl)cyclohepta[1,2,3-*hi*]indolizine (**11**) were characterized. The reaction of 2-chloro-3-(ethoxycarbonyl)-cyclohepta[*b*]pyrrole (**4**) with **5** proceeded in a similar way to give a number of compounds besides (**9**). Most of them were obtained in small quantities, too unstable to be identified.

Phosphoranes (**6**—**9**) were characterized by spectral methods. IR spectra of the products show a ν(C=O) absorption at 1650—1615 cm^{-1}, characteristic of the phosphoranes possessing an α-carboxylic ester group,[6] whereas their mass spectra contain abundant ions at *m/e* 108, 152, 183, 185, and 262 which are diagnostic of (triphenylphosphoranylidene)acetates.[7] ^{13}C NMR spectra provide a conclusive evidence in favor of the structures (**6**—**9**). The ^{13}C chemical shifts and ^{13}C- ^{31}P couplings for these products (Table 1) were easily assigned by reference to the spectra of the related azaazulenes and data on phosphoranes.[8] We see that there are long-range couplings (J=6—12 Hz) involving ^{31}P nucleus and each of the ring carbons-2 and -3; the structure in which the ylide moiety is attached to C-8 is not compatible with the observations. The phosphoranes are protonated by acid. As an example, UV spectrum of **9**, when determined for a neutral solution, displays absorptions at 272, 309, 354, and 448 nm. However, the spectrum taken in the presence of trifluoroacetic acid (265, 286^{sh}, 345, and 482 nm) resembles that of 1,2-dihydro-3-ethoxycarbonyl-2-[cyano(ethoxycarbonyl)methylene]-cyclohepta[*b*]pyrrole.[1] This fact indicates that protonation occurred at the ring nitrogen atom. The spectrum of the neutral solution was also obtained on basification of the acidified solution.

Table 1. Partial ^{13}C chemical shifts and $J_{^{31}P-^{13}C}$ values of **6**, **8**, **9**

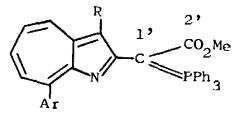

Carbon	**6**	**8**	**9**
1′	129.4(112.3)	131.0(112.3)	131.0(129.4)
2′	168.0(13.4)	166.6(14.6)	168.6(14.6)
2	168.5(6.1)	168.8(7.0)	169.1(12.2)
3	114.7(8.5)	92.2(9.8)	115.2(8.5)
3a	147.5	150.5	146.7
4	129.1	128.8	130.4
5	126.6	126.7	129.5
6	129.8	129.4	130.7
7	129.1	127.6	130.3
8	130.3	132.9	132.6
8a	154.6	157.1	158.1

Compound **10** was identified by a comparison of its melting point with that reported.[9] The NMR spectrum of **11** indicates the presence of a 2,3,8-trisubstituted cyclohepta[*b*]pyrrole ring, whereas its UV spectrum suggests the presence of a chromophore more extended than that of **3**. From these results, together with the presence of additional two sets of one-proton doublets at δ 6.58 and 6.74 (J=8 Hz) in its NMR spectrum, we assigned the structure.

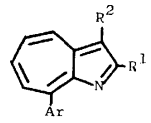

1 R^1=Cl, R^2=CO_2Et, Ar=Ph
2 R^1=Cl, R^2=CN, Ar=*p*-$MeOC_6H_4$
3 R^1=Cl, R^2=CN, Ar=H
4 R^1=Cl, R^2=CO_2Et, Ar=H
6 R^1=C(CO_2Me)=PPh_3, R^2=CO_2Et, Ar=Ph
7 R^1=C(CO_2Me)=PPh_3, R^2=CN, Ar=*p*-$MeOC_6H_4$
8 R^1=C(CO_2Me)=PPh_3, R^2=CN, Ar=H
9 R^1=C(CO_2Me)=PPh_3, R^2=CO_2Et, Ar=H

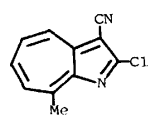

10

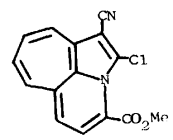

11

It is concluded that the C-6 and C-8 positions of 2-chlorocyclohepta[*b*]pyrroles are reactive toward nucleophiles despite the presence of a good leaving group at the most electron deficient C-2 and reactivities of these three positions depend on the reaction conditions[1] and the nature of nucleophiles.

Experimental

Melting points were uncorrected. IR spectra were recorded for nujol mulls. ^{1}H NMR spectra were obtained with a Varian HA-100 spectrometer at 100 MHz (solvent $CDCl_3$; Me_4Si as internal standard), and ^{13}C NMR spectra with a JEOL FX-100 spectrometer (solvent $CDCl_3$). UV spectra were measured for chloroform solutions. Molecular weights were determined by mass spectrometry with a Hitachi RMU 7 spectrometer. Chromatography was performed on Kiesel gel 60. Yields are based on unrecovered starting material.

*Reaction of **1** with **5**.* A mixture of **1** (1.00 g, 3.21 mmol) and **5** (2.08 g, 6.2 mmol) in xylene (100 ml) was heated under reflux for 5.5 h, and then heated with 10% aqueous sodium carbonate solution (20 ml) for 30 min. Water was added and the mixture was extracted with chloroform, the extracts being dried and evaporated. Chromatography of the residue with chloroform afforded triphenylphosphine oxide (1.12 g). Further elution with chloroform and benzene-ethyl acetate (4:1) gave **6** (0.25 g, 66%), orange prisms (from cyclohexane), mp 183—184 °C, NMR δ=1.52 (3H, t, J=7 Hz), 3.43 (3H, s), 4.47 (2H, q, J=7 Hz), 6.82 (2H, d, J=8 Hz), 6.96—7.48 (15H, m), 7.52—7.80 (6H, m), 8.72—8.90 (1H, dm, J=8 Hz); UV_{max} 264 nm (log ε 4.35), 305 (4.30), 365 (3.84), 458 (4.18); IR 1685 (C=O), 1640 cm^{-1} (C=O). Found C, 76.57; H, 5.39; N, 2.05; P, 4.78%. Calcd for $C_{39}H_{32}NO_4P$: C, 76.84; H, 5.29; N, 2.30; P, 5.08%.

*Reaction of **2** with **5**.* A mixture of **2** (0.77 g, 2.61 mmol) and **5** (2.18 g, 6.53 mmol) in xylene (100 ml) was heated under reflux for 8.5 h and the solvent was then evaporated. Chromatography of the residue with benzene-chloroform (2:1) gave **2** (0.195 g). An oil eluted with chloroform was re-chromatographed with benzene-chloroform (1 : 2) to give **7** (0.24 g, 21%) as a red oil, which on trituration in petroleum ether-dichloromethane partly solidified, mp 115—116 °C, NMR δ=3.63 (3H, s), 3.82 (3H, s), 6.48 (2H, d, J=8 Hz), 6.83 (2H, d, J=8 Hz), 6.9—8.4 (19H, m); UV_{max} 266 nm (log ε 4.16), 312 (4.18), 360^{sh} (3.75), 383^{sh} (3.70), 464 (3.98); IR 2200 (C≡N), 1650 cm^{-1} (C=O). Found: C, 76.42; H, 5.16; N, 4.07; P, 5.74%. Calcd for $C_{38}H_{29}N_2O_3P$: C, 77.02; H, 4.93; N, 4.73; P, 5.23%.[10] Elution with chloroform-ethyl acetate gave an inseparable mixture of **5** and **7**.

*Reaction of **3** with **5**.* A mixture of **3** (2.00 g, 10.6 mmol) and **5** (7.60 g, 22.8 mmol) in xylene (150 ml) was heated under reflux for 8.5 h, hydrolyzed with 10% aqueous sodium carbonate solution (*vide supra*), and worked up as above. Chromatography with benzene gave **11** (0.084 g, 7%), brownish violet prisms (from benzene), mp 219 °C, NMR δ=3.74 (3H, s), 5.45 (1H, dd, J=11 and 8 Hz), 5.73 (1H, dd, J=12 and 8 Hz), 6.20 (1H, d, J=11 Hz), 6.58 (1H, d, J=8 Hz), 6.74 (1H, d, J=8 Hz), 7.27 (1H, d, J=12 Hz); UV_{max} 265 nm (log ε 4.43), 273 (4.45), 369 (4.03), 393 (4.08), 417 (4.09), 463 (2.96), 499 (3.03), 540 (3.04), 591 (2.94), 650 (2.65); IR 2200 (C≡N), 1690 cm^{-1} (C=O). Found: C, 63.43; H, 3.27; Cl, 12.54; N, 9.71%. Calcd for $C_{15}H_9ClN_2O_2$: C, 63.28; H, 3.19; Cl, 12.45; N, 9.84%. Elution with benzene-chloroform (3:1) gave **10** (0.083 g, 9%), mp 201 °C (lit,[9] mp 202 °C), Found: C, 65.16; H, 3.32; N, 13.92%. Further elution with benzene-chloroform (3:1) afforded **3** (1.19 g) and elution with benzene-chloroform (1:4) gave triphenylphosphine oxide (5.54 g). Elution with chloroform gave **8** (0.79 g, 38%), orange prisms (from cyclohexane-dichloromethane), mp 210 °C, NMR δ=3.65 (3H, s), 7.3—7.9 (19H, m), 8.24 (1H, d, J=9 Hz); UV_{max} 269 nm (log ε 4.34), 307 (4.31), 318^{sh} (4.23), 354 (3.76), 450 (4.22); IR 2200 (C≡N), 1650 cm^{-1} (C=O). Found: C, 76.20; H, 4.52; N, 5.72; P, 6.64%. Calcd for $C_{31}H_{23}N_2O_2P$: C, 76.53; H, 4.77; N, 5.76; P, 6.37%.

*Reaction of **4** with **5**.* A mixture of **4** (2.00 g, 8.49 mmol) and **5** (6.60 g, 20.4 mmol) in xylene (150 ml) was heated under reflux for 18.5 h, hydrolyzed (*vide supra*), and worked up as above. Elution with chloroform-ethyl acetate (1:1) gave **4** (0.296 g) and triphenylphosphine oxide (3.07 g) and elution with ethyl acetate afforded **9** (0.53 g, 14%), orange needles (from cyclohexane), mp 198 °C, NMR δ=1.46 (3H, t, J=7 Hz), 3.43 (3H, s), 4.43 (2H, q, J=7 Hz), 7.25—7.95 (19H, m), 8.75 (1H, dm, J=10 Hz); UV_{max} 272 nm (log ε 4.47), 309 (4.25), 354 (3.81), 448 (4.19); IR 1675 (C=O), 1615 cm^{-1} (C=O). Found: C, 74.16; H, 5.15; N, 2.51; P, 5.77%. Calcd for $C_{33}H_{28}NO_4P$: C, 74.28; H, 5.29; N, 2.63; P, 5.81%.

We thank Dr. A. Mori, Kyushu University, and Dr. T. Morita, Tohoku University, for NMR spectral determinations.

References

1) Part III, N. Abe and T. Nishiwaki, *Bull. Chem. Soc. Jpn.*, **51**, 667 (1978).
2) For a review see H. J. Bestmann, *Angew. Chem.*, **77**, 651 (1965).
3) J. J. Pappas and E. Gancher, *J. Heterocycl. Chem.*, **5**, 123 (1968).
4) E. C. Taylor and S. F. Martin, *J. Am. Chem. Soc.*, **96**, 8095 (1974).
5) N. Abe, *Heterocycles*, **4**, 221 (1976).
6) M. A. Shaw, J. C. Tebby, R. S. Ward, and D. H. Williams, *J. Chem. Soc., C*, **1967**, 2442; J. J. Pappas and E. Gancher, *J. Org. Chem.*, **31**, 1287 (1966).
7) R. G. Cooks, R. S. Ward, D. H. Williams, M. A. Shaw, and J. C. Tebby, *Tetrahedron*, **24**, 3289 (1968).
8) G. A. Gray, *J. Am. Chem. Soc.*, **95**, 7736 (1973).
9) S. Seto and T. Nozoe, *Proc. Jpn. Acad.*, **32**, 765 (1956).
10) Compound **7** was not obtained in an analytically pure state as shown by microanalytical data and the presence of an additional small peak at δ 3.93 in its ^{1}H NMR spectrum. It was difficult to crystallize and to separate completely from **5**, which resulted in unsatisfactory analytical data.

BULLETIN OF THE CHEMICAL SOCIETY OF JAPAN, VOL. 51 (5), 1575—1576 (1978)

Electrosynthesis of Hetero-Hetero Atom Bonds. I. A Direct Preparation of Bis(dialkylthiocarbamoyl) Disulfides from Dialkylamines and Carbon Disulfide

Sigeru TORII, Hideo TANAKA, and Kiyosi MISIMA

Department of Industrial Chemistry, School of Engineering, Okayama University, Okayama 700

(Received December 3, 1977)

Synopsis. Bis(dialkylthiocarbamoyl) disulfides were synthesized directly from dialkylamines and carbon disulfide by electrolysis under constant voltage using an undivided cell. The electrochemical reaction was carried out effectively in a two-layer system of electrolysis solvents, *e. g.*, water-chloroform, water-dichloromethane, water-1,2-dichloroethane, and water-carbon disulfide. Likewise, the electrolysis could be performed in a homogeneous solution using dimethylformamide and/or acetonitrile.

Bis(dialkylthiocarbamoyl) disulfides **1** are industrial chemicals of importance for use as vulcanization accelerators[1] and fungicides.[2] Two methods of preparation have been widely used, one involving

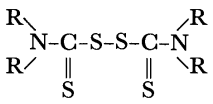

1: R=C_1-C_4

the oxidation of ammonium dialkyldithiocarbamates[3] and the other that of alkali dialkyldithiocarbamates.[4] Both methods require stoichiometric amounts of oxidizing agents which give rise to environmental problems. A clean process using few chemical reagents is desirable. We wish to report the direct electrosynthesis of **1** form dialkylamines and CS_2 by two methods, one involving a two-layer system for the continuous extraction of **1** and the other a homogeneous solvent system.[5]

For the two-layer system the following solvent combinations are used; water–chloroform, water–dichloromethane, water–1,2-dichloroethane, and water–CS_2. A schematic sketch of the apparatus for laboratory scale electrolysis is given in Fig. 1. Electrolysis was carried out in an aqueous solution (upper layer) containing the dithiocarbamates **2**,[3] prepared *in situ*

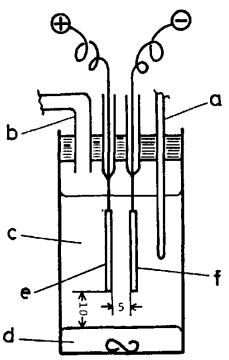

Fig. 1. Electrolysis cell.
a: Thermometer; b: gas lead pipe; c: aqueous layer; d: extraction layer; e: anode; f: cathode.

by stirring a mixture of dialkylamines and CS_2, using an undivided cell fitted with platinum and/or carbon electrodes under a constant terminal voltage of 2.0 V (0.75—1.15 V *vs.* SCE).[6] The results are given in Table 1. Over 1.0—1.1 F/mol of electricity, the current becomes almost zero. During the course of the reaction,

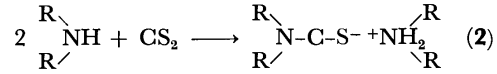

(**2**)

electrolysis efficient extraction of **1** with dichloromethane (lower layer) proceeds spontaneously. Removal of the extracting solvent afforded the solid material **1**(R=Me, Et, and Pr) in 76—99% yields (1, 2, 5, and 7). When electrolysis of **2**(R=Et) in an aqueous solution was carried out at 2 V without using the extracting solvents, the initial current was 27 mA/cm². Soon the platinum anode became covered with **1** as a pale yellow film and about 1 h later the passage of current stopped. Work-up of the electrolytic solution afforded **1** in 5—20% yields, indicating that the presence of extracting solvents in the lower layer contributes a great deal to the continuous electrolysis of **2**.

The electrolysis of a more bulky amine such as dibutylamine with CS_2 in a water dichloromethane system gave **1** in poor yield (9), because of the low solubility of **2** (R=Bu) in water, resulting in by-products.[7] However, electrolysis in a water–CS_2 system for 60 h afforded **1** (R=Bu) in 86% yield without pro-

TABLE 1. ELECTROLYSIS OF AMMONIUM DIALKYLDITHIOCARBAMATES[a]

Entry	Amine[b] R	Amine[b] mmol	CS_2 mmol	Solvent[c] (ml)	Current mA/cm²	Temp °C	Time[d] h	Yield[e] %
1	Me	6.0	3.0	CH_2Cl_2-H_2O (3/20)	27—0.1	3— 5	26	99
2	Me	6.0	3.0	CH_2Cl_2-H_2O (3/20)	13—0.7	14—16	20	76[f]
3	Me	6.0	3.0	CH_2ClCH_2Cl-H_2O (5/20)	17—0.7	24—26	22	97
4	Me	6.0	3.0	$CHCl_3$-H_2O (3/20)	20—0.7	23—25	22	87
5	Et	5.3	2.6	CH_2Cl_2-H_2O (3/20)	23—0.1	19—21	8	99
6	Et	3.0	excess	CS_2-H_2O (3/20)	15—0.2	17—20	9	99
7	Pr	4.0	2.0	CH_2Cl_2-H_2O (3/20)	9—0.1	15—18	23	80
8	Pr	3.0	excess	CS_2-H_2O (3/20)	7—0.03	18—20	48	96
9	Bu	3.0	1.5	CH_2Cl_2-H_2O (3/20)	1—0.03	16—17	17	28
10	Bu	2.0	excess	CS_2-H_2O (3/20)	1—0.07	17—18	60	86
11	Me	9.0	3.0	MeCN (20)	19—13	12—14	3	79
12	Et	6.0	3.0	MeCN (20)	22—6	10—12	1.7	99
13	Et	6.0	3.0	DMF (20)	13—3	10—11	3.5	99
14	Pr	6.0	3.0	DMF (20)	8—0.4	10—13	6	99
15	Bu	6.0	3.0	DMF (20)	9—0.2	9—12	5	100

a) Carried out under voltage of 2 V using Pt foil electrodes (3 cm²). b) Aqueous 50% Me_2NH used. c) Containing 160 mg of NH_4Cl (1—10) or 100 mg of Et_4NClO_4 (11—15). d) 1.01—1.05 F/mol passed. e) Isolated yields based on CS_2 (1—5, 7, 9, and 11—15) or amines (6, 8, and 10). f) Carbon electrodes (3 cm²) used.

ducing by-products (10).

Choice of CS_2 for diethylamine, dipropylamine, and dibutylamine as an extracting solvent was found suitable, since electrolysis could be carried out without preparing **2** by adding appropriate amines to the aqueous solution, product **1** moving smoothly into the lower layer. Upon concentration of the CS_2 fraction, disulfides **1** were obtained in 86—99% yields as fine crystals (6, 8, and 10). It is well known that dithiocarbamate ion, upon one electron oxidation on the anode followed by the coupling of the thio radical, gives **1**.[8] In the course of electrolysis of **2**, dialkylammonium ions, upon discharge on the cathode, liberate dialkylamines, which can react with CS_2 to regenerate **2**. Consequently, most of the dialkylamines used (6, 8, and 10) could be converted into **1**.

$$R_2\overset{+}{N}H_2 \xrightarrow[-\frac{1}{2}H_2]{+e} R_2NH \xrightarrow{CS_2} \mathbf{2}$$

We further investigated the direct synthesis of **1** from dialkylamines and CS_2 in a homogeneous solvent using MeCN and/or DMF. Electrolysis of a solution of two parts of diethylamine and one part of CS_2 in MeCN was carried out by using platinum electrodes at 2 V in the presence of tetraethylammonium perchlorate as a supporting electrolyte (12). After 1.05 F/mol of electricity had been passed, work-up of the solution afforded **1** in 99% yield.

Experimental

All melting points are uncorrected. Carbon-13 NMR spectra (CMR) were taken at 25.05 MHz in the Fourier mode using a JEOL FX-100 spectrometer. Samples were dissolved in $CDCl_3$ containing Me_4Si as an internal standard.

*Preparation of **1** from Dialkylamines and Carbon Disulfide in a Two-layer Solution.* A typical procedure is as follows: A mixture of aqueous 50% Me_2NH (0.80 ml, 6.0 mmol) and CS_2 (0.18 ml, 3.0 mmol) in water (20 ml) was stirred for *ca.* 1 h at room temperature. To this solution were added NH_4Cl (160 mg) and CH_2Cl_2 (3 ml), Pt electrodes (3 cm^2) being immersed in the aqueous layer. The mixture was electrolysed at 2 V (0.79—0.90 V *vs.* SCE) at 3—5 °C for 26 h. The current densities varied from 27 to 0.1 mA/cm^2 during the course of electrolysis. The CH_2Cl_2 layer (lower layer) was separated, washed with brine, and dried (Na_2SO_4.) Removal of the solvent afforded **1** (R=Me, 357 mg, 99%): mp 143—145 °C from EtOH (lit,[4e] mp 145—146 °C); CMR ($CDCl_3$) δ 193.3 (s, C=S), 47.4, 42.2 (q, CH_3).

The reaction conditions and results are given in Table 1, 1—10. Physical and spectral data of **1** (R=Et, Pr, and Bu) are as follows.

Compound **1** (R=Et): Mp 69—70.5 °C from EtOH (lit,[4e] mp 69.5—70.5 °C); CMR ($CDCl_3$) δ 192.4 (s, C=S), 52.0, 47.6 (t, CH_2), 13.4, 11.4 (q, CH_3).

Compound **1** (R=Pr): Mp 48.5—49.5 °C from EtOH (lit,[4e] mp 49—50.5 °C); CMR ($CDCl_3$) δ 193.2 (s, C=S), 59.2, 55.1 (t, CH_2N), 21.7, 19.6 (t, CH_2), 11.3 (q, CH_3).

Compound **1** (R=Bu):[4e] CMR ($CDCl_3$) δ 192.9 (s, C=S), 57.4, 53.2 (t, CH_2N), 30.2, 28.1 (t, C_β), 20.1 (t, C_γ), 13.8 (q, CH_3).

*Preparation of **1** from Dialkylamines and Carbon Disulfide in Acetonitrile.* A mixture of Et_2NH (0.62 ml, 6.0 mmol), CS_2 (0.18 ml, 3.0 mmol), and Et_4NClO_4 (100 mg) in MeCN (20 ml) was electrolyzed at 2 V (0.75—1.10 V *vs.* SCE) at 10—12 °C using Pt electrodes (3 cm^2). After a current of 3.15×10^{-3} F had been passed for 1.7 h, the mixture was concentrated *in vacuo*. The residue was worked up to give **1** (R=Et, 99%): Mp 69—70.5 °C from EtOH (lit,[4e] mp 69.5—70.5 °C). Similarly, DMF was used for the preparation of **1** (R=Et, Pr, and Bu). The conditions and results are given in Table 1, 11—15.

*Electrolysis of Diethylammonium Diethyldithiocarbamate **2** (R=Et) in Water.* A mixture of Et_2NH (0.62 ml, 6.0 mmol), CS_2 (0.18 ml, 3.0 mmol), and NH_4Cl (160 mg) in water (20 ml) was stirred at 14 °C for 1 h to give a homogeneous solution of **2** (R=Et).[3c] The aqueous solution was electrolyzed at 2 V (0.75—0.85 V *vs.* SCE) at 13—15 °C with Pt electrodes (3 cm^2). At the beginning of the reaction the current density was 27 mA/cm^2. After 10 min, pale yellow precipitates were deposited on the anode. After 1 h the anode was covered with the precipitates as a film and the current was reduced to almost zero. Electrolysis was continued for further 2.5 h (total 0.3×10^{-3} F). After the usual work-up 35 mg (8%) of **1** (R=Et) was obtained.

References

1) (a) D. Jaroszuska, *Polimery*, **10**, 403 (1965); (b) T. Azami and I. Yamatsu, *Nippon Gomu Kyokaishi*, **37**, 413 (1964); (c) C. M. Hayes and A. Gaydash, Fr. Pat. 1322580 (1963).

2) (a) F. Mailath, F. Medve, and M. Jozsef, *Acta Pharm. Hung.*, **44**, 71 (1974); (b) M. Murata and F. Sakabe, *Nippon Nogei Kagaku Kaishi*, **35**, 1158 (1961); (c) W. M. Linfield and R. E. Casely, *Am. Perfumer Cosmet.*, **77**, 103 (1962).

3) (a) J. J. Tazuma and A. Bergomi, Ger. Pat. 2349313 (1974); (b) H. S. Adamus and L. Meuser, U.S. Pat. 1782111 (1930); (c) J. V. Braum, *Ber.*, **35**, 817 (1902).

4) (a) E. Chrabknowski, Z. Michalski, and J. Sroczinski, Fr. Pat. 1552795 (1969); (b) W. Budd and E. M. Katt, U. S. Pat. 3255250 (1966); (c) J. M. Aulbaugh and W. R. Trutna, U. S. Pat. 3147308 (1964); (d) M. E. Miville, Ger. Pat. 1023030 (1958); (e) S. Akerström, *Arkiv. Kemi.*, **14**, 384 (1959).

5) A similar attempt involving electrolysis of an aqueous solution of sodium dithiocarbamates using an alternating current has been reported. However, the low solubility of **1** for water along with the low current efficiency (12.5%) gives rise to difficulties: J. A. Gardner, U. S. Pat., 2385410 (1945).

6) Change in the cell voltage did not affect product selectivity and yields.

7) In the course of electrolysis of **2** in water-CH_2Cl_2, methylene bis(dialkyldithiocarbamate) was obtained as a by-product (R=Me, Et, <1%; R=Pr, 5—10%; R=Bu, 65—70%). Formation of the by-product could be surpressed by use of carbon disulfide as an extracting solvent. Methylene bis(dimethyldithiocarbamate) has been prepared from CH_2Cl_2 and sodium dimethyldithiocarbamate: T. Nakai and M. Okawara, *Chem. Lett.*, **1974**, 731.

8) G. Cauguis and D. Lachenal, *J. Electroanal. Chem. Interfacial Electrochem.*, **43**, 205 (1973).

BULLETIN OF THE CHEMICAL SOCIETY OF JAPAN, VOL. 51 (5), 1577—1578 (1978)

Studies on Aziridine-2-carboxylic Acid. I. Synthesis of the Optically Active L-Aziridine-2-carboxylic Acid and Its Derivatives

Kiichiro NAKAJIMA, Fumiko TAKAI, Takumi TANAKA, and Kenji OKAWA

Department of Chemistry, Faculty of Science, Kwansei Gakuin University, Nishinomiya 662

(Received December 9, 1977)

Synopsis. Lithium L-aziridine-2-carboxylate was synthesized from *N*-trityl-L-aziridine-carboxylic acid benzyl ester by the treatment with trifluoroacetic acid followed by the saponification with lithium hydroxide. Several *N*-acylaziridine-2-carboxylic acid esters were synthesized in good yield.

Due to acid labile properties of the aziridine ring, no optically active aziridine-2-carboxylic acid has been synthesized. Only racemic aziridine-2-carboxylic acid has been isolated as a lithium salt in poor yield from methyl 2,3-dibromopropionate by the treatment of liquefied ammonia.[1]

The peptide derivatives of aziridine-2-carboxylic-acid(Azy),[2] however, were prepared *via* *N*-trityl-*O*-tosyl(or *O*-mesyl)β-hydroxy amino acid peptides.[3]

We have undertaken to synthesize L-isomer of Azy since it is of great use in the synthesis of Azy containing peptides.

Lithium L-aziridine-2-carboxylate has been prepared from the corresponding *N*-trityl-*O*-tosyl-L-serine benzyl ester as shown in following Scheme 1. The key step of the detritylation procedure was accomplished by the action of trifluoroacetic acid solution at low temperature, several *N*-acyl-L-Azy–OBzl derivatives being synthesized in good yield as shown in Scheme 2.

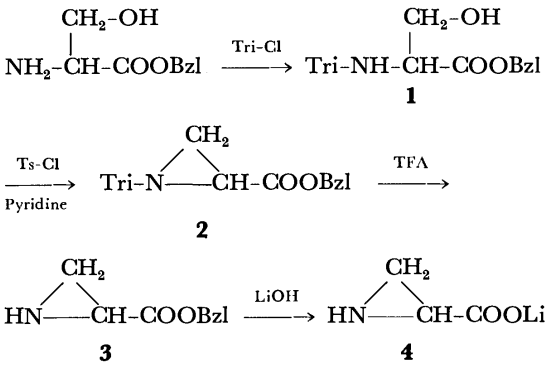

Scheme 1.

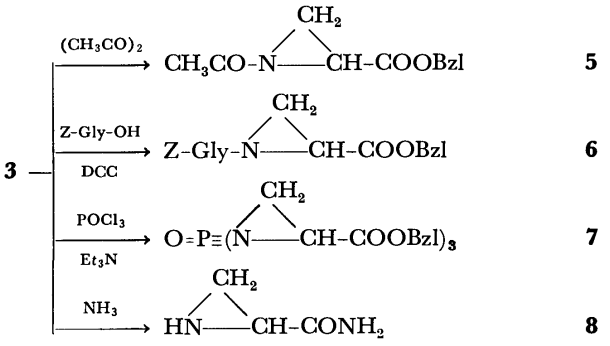

Scheme 2.

Experimental

All the melting points are uncorrected. The IR and NMR spectra were recorded on Hitachi EPI-G3 and Hitachi R-20B spectrometers, respectively. The purity of the synthetic compounds was confirmed by thin layer chromatography on silica gel G.

Tri-L-Ser-OBzl (1): To a solution of L-Ser–OBzl benzenesulfonate (56 g, 0.15 mol) and Et_3N (42 ml, 0.3 mol) in $CHCl_3$ (100 ml) was added a solution of Tri-Cl (41.8 g, 0.15 mol) in $CHCl_3$ (80 ml) with stirring at 0 °C. After the reaction mixture had been stirred for 24 h at 0 °C, the solution was washed with 10% citric acid and water, and dried over Na_2SO_4. After removal of the solvent, **1** was obtained in theoretical yield as an oily product; $[\alpha]_D^{25}$ +64.8° (*c* 1.0, MeOH). Found: C, 79.43; H, 6.32; N, 3.42%. Calcd for $C_{29}H_{27}O_3N$: C, 79.61; H, 6.22; N, 3.20%.

Tri-L-Azy–OBzl (2): To a solution of **1** (65.6 g, 0.15 mol) in dry pyridine (200 ml) was added a solution of Ts-Cl (85.8 g, 0.45 mol) in dry pyridine (50 ml) at −10 °C for 1 h. After the reaction mixture had been stirred for 24 h at 0 °C, the solvent was removed *in vacuo* and the residual oil was partitioned between ethyl acetate and water. The organic layer was washed with 10% citric acid and water, and dried over Na_2SO_4. The ethyl acetate was removed *in vacuo* to give an oily product (84.3 g, 95% yield as a *O*-tosylate). The oil was dissolved in dry THF (100 ml), and Et_3N (39.2 ml, 0.28 mol) was added. After the THF solution had been refluxed at 75 °C for 24 h, the reaction mixture was concentrated *in vacuo* and the residue was dissolved in ethyl acetate. The organic layer was washed with 10% citric acid, 1M sodium hydrogencarbonate and water, and dried over Na_2SO_4. The solvent was removed *in vacuo*, and the product was crystallized from ethyl acetate–ether–hexane; yield, 31.4 g (57.8%); mp 114—116 °C; $[\alpha]_D^{20}$ −95.5° (*c* 1.0, THF). IR: 1722, 1590, 1095 cm^{-1}; NMR (CCl_4): δ 2.10, 1.32 (2H 2q, J_{trans}=3.1 Hz, J_{cis}=6.3 Hz, J_{gem}=1.8 Hz, β-proton); 1.87 (1H q, J_{trans}=3.1 Hz, J_{cis}=6.3 Hz, α-proton). Found: C, 82.90; H, 5.84; N, 3.25%. Calcd for $C_{29}H_{25}O_2N$: C, 83.03; H, 6.01; N, 3.34%.

L-*Azy–OBzl (3)*: To a solution of **2** (5.04 g, 12 mmol) in $CHCl_3$ (10 ml) and absolute MeOH (10 ml, used as a scavenger of trityl group), was added TFA (20 ml) with stirring at −5 °C, and the solution was stirred for 2 h. The solvent was removed *in vacuo* and the residual oil was partitioned between ether and water. Sodium hydrogencarbonate was added to the aqueous layer producing alkaline solution, and the isolated oil was extracted with ether. After being dried over Na_2SO_4, the solvent was removed *in vacuo* to give an oily product; yield, 1.92 g (90.2%); $[\alpha]_D^{23}$ −56.8° (*c* 1.0, THF). IR: 3320, 1730, 1090 cm^{-1}; NMR ($CDCl_3$): δ 2.03, 1.88 (2H 2q, J_{trans}=3.0 Hz, J_{cis}=6.0 Hz, J_{gem}=1.5 Hz, β-proton); 2.58 (1H q, J_{trans}=3.0 Hz, J_{cis}=6.0 Hz, α-proton); 1.43 (1H bs, H–N<); 5.19 (2H s, C_6H_5–

CH_2–O–); 7.36 (5H s, C_6H_5–CH_2–O–). Found: C, 67.52; H, 6.31; N, 7.76%. Calcd for $C_{10}H_{11}O_2N$: C, 67.78; H, 6.26; N, 7.91%.

L-*Azy-OLi* (**4**): To a solution of **3** (540 mg, 3.05 mmol) in absolute MeOH (3 ml) was added a solution of LiOH (115.2 mg, 2.74 mmol) in water (1 ml) with stirring at −10 °C. After the reaction mixture had been stirred for 6 h at −5 °C, the solvent was removed *in vacuo*. EtOH was added to a residual oily product and the crystals obtained were collected by filtration. The crystals (**6**) were obtained in theoretical yield; mp 260 °C dec; $[\alpha]_D^{23}$ −39.5° (*c* 1.0, H_2O). IR: 3440, 3275, 1590, 1095 cm^{-1}; NMR (D_2O): δ 1.80, 1.75 (2H 2q, J_{trans}=3.6 Hz, J_{cis}=5.8 Hz, J_{gem}=1.5 Hz, β-proton); 2.36 (1H q, J_{trans}=3.6 Hz, J_{cis}=5.8 Hz, α-proton). Found: C, 38.68; H, 4.18; N, 15.21%. Calcd for $C_3H_4O_2NLi$: C. 38.73; H, 4.34; N, 15.05%.

Ac-L-*Azy-OBzl* (**5**): To a solution of **3** (2.2 g, 12.4 mmol) and Et_3N (3.5 ml, 24.8 mmol) in $CHCl_3$ (20 ml) was added acetic anhydride (1.1 ml, 12.4 mmol) with stirring at −5 °C, followed by stirring at 0 °C for 4 h. The reaction mixture was washed with 10% citric acid and water, and dried over Na_2SO_4. The solvent was removed *in vacuo* to give an oily product; yield, 2.28 g (84.4%); $[\alpha]_D^{23}$ −39.6° (*c* 1.0, MeOH). IR: 1740, 1708, 1081 cm^{-1}; NMR ($CDCl_3$): δ 2.59, 2.48 (2H 2q, J_{trans}=2.9 Hz, J_{cis}=5.9 Hz, J_{gem}=1.5 Hz, β-proton); 3.18 (1H q, J_{trans}=2.9 Hz, J_{cis}=5.9 Hz, α-proton); 2.21 (3H s, CH_3–CO–); 5.20 (2H s, C_6H_5–CH_2–O–); 7.37 (5H s, C_6H_5–CH_2–O–). Found: C, 65.58; H, 5.86; N, 6.20%. Calcd for $C_{12}H_{13}O_3N$: C, 65.74; H, 5.98; N, 6.39%.

Z-Gly-L-*Azy-OBzl* (**6**): To a solution of Z-Gly-OH (540 mg, 2.6 mmol) and **3** (460 mg, 2.6 mmol) in $CHCl_3$ (20 ml) was added a solution of DCC (540 mg, 2.6 mmol) in $CHCl_3$ (5 ml) with stirring at −5 °C. After the reaction mixture had been stirred for 6 h, the produced *N,N'*-dicyclohexylurea was filtered off. The filtrate was washed with 1M sodium hydrogencarbonate, 10% citric acid and water, and dried over Na_2SO_4. The solvent was removed *in vacuo* to give the desired product, which was crystallized from ethyl acetate–ether– hexane; yield, 870 mg (90.8%); mp 42—43 °C; $[\alpha]_D^{23}$ −44.5° (*c* 1.0, $CHCl_3$). NMR ($CDCl_3$): δ 2.51, 2.07 (2H m, β-proton); 3.22 (1H q, J=4.8, 3.5 Hz, α-proton); 4.00 (2H d, J=5.5 Hz, –NH–CH_2–CO–); 5.09, 5.18 (4H 2s, $2C_6H_5$–CH_2–O–); 5.37 (1H bs, –NH–CO–); 7.33 (10H s, $2C_6H_5$–CH_2–O–). Found: C, 65.29; H, 5.36; N, 7.48%. Calcd for $C_{20}H_{20}O_5N_2$: C, 65.21; H, 5.47; N, 7.61%.

O=*P*≡(L-*Azy-OBzl*)$_3$ (**7**): To a solution of **3** (1.8 g, 10.1 mmol) and $POCl_3$ (0.23 ml, 2.5 mmol) in $CHCl_3$ (5 ml) at 0 °C was added a solution of Et_3N (1.06 ml, 7.63 mmol) in $CHCl_3$ (1ml) with stirring. After the reaction mixture had been stirred at 0 °C for 3 h, the solution was washed with 1M sodium hydrogencarbonate, 10% citric acid and water, and then dried over Na_2SO_4. The solvent was removed *in vacuo*, and the residual oil was subjected to column chromatography on silica gel using ethyl acetate–$CHCl_3$–benzene (5:1:1 v/v) to give a pure product; yield, 1.09 g (76.0%); $[\alpha]_D^{23}$ −94.7° (*c* 1.0, MeOH). IR: 1745, 1082, 1175—1180, 1250—1290 cm^{-1}; NMR ($CDCl_3$): δ 2.59, 2.72, 3.34 (3H 3q, J=1.6, 3.0 Hz, J=1.6, 6.0 Hz, J=3.0, 6.0Hz, aziridine ring); 2.59, 2.52, 3.09 (3H 3q, J=1.6, 3.0 Hz, J=1.6, 6.0 Hz, J=3.0, 6.0 Hz, aziridine ring); 2.36, 2.36, 2.60 (3H 3q, J=1.6, 3.0 Hz, J=1.6, 6.0 Hz, J=3.0, 6.0 Hz, aziridine ring). Found: C, 62.65; H, 5.16; N, 7.04%. Calcd for $C_{30}H_{30}O_7N_3P$: C, 62.60; H, 5.26; N, 7.29%.

L-*Azy-NH*$_2$ (**8**): Dry ammonia gas was bubbled into a solution of **3** (306.7 mg, 1.73 mmol) in absolute MeOH (10 ml) at 0 °C for 20 min. The reaction mixture was allowed to stand overnight at room temperature.. After the solvent had been removed *in vacuo*, ether was added to a residual oily product and the resulting crystals were collected; yield, 133.7 mg (89.7%); mp 141—142 °C; $[\alpha]_D^{23}$ −44.8° (*c* 1.07, DMF). NMR ($CDCl_3$): δ 1.78, 1.70 (2H 2q, J_{trans}=3.6 Hz, J_{cis}=5.7 Hz, J_{gem}=1.5 Hz, β-proton); 2.38 (1H q, J_{trans}=3.6 Hz, J_{cis}=5.7 Hz, α-proton); 1.78 (1H s, H–N<); 7.50 (2H br, –$CONH_2$). Found: C, 41.78; H, 7.16; N, 32.43%. Calcd for $C_3H_6ON_2$: C, 41.85; H, 7.02; N, 32.54%.

References

1) R. A. Clark, Ph. D. Thesis, University of Maryland, Maryland, U. S. A., 1966.

2) Abbreviations according to IUPAC-IUB commisison, *J. Biol. Chem.*, **247**, 977 (1972), are used. Z: benzyloxycarbonyl, Tri: trityl, DCC: dicyclohexylcarbodiimide, Bzl: benzyl. "Azyline" is used as the name of an aziridine-2-carboxylic acid, "Azy" being its abbreviation.

3) K. Okawa, K. Nakajima, T. Tanaka, and Y. Kawana, *Chem. Lett.*, **1975**, 591; K. Nakajima, O. Kanda, and K. Okawa, proceedings of the 14th Symposium on Peptide Chemistry, p. 17, Hiroshima, 1976.

BULLETIN OF THE CHEMICAL SOCIETY OF JAPAN, VOL. 51 (5), 1579—1580 (1978)

Rotational Isomerism and Vibrational Assignments of Monobromothioacetic Acid

H. S. RANDHAWA* and W. WALTER

Institut für Organische Chemie und Biochemie der Universität Hamburg, Federal Republic of Germany

(Received May 2, 1977)

Synopsis. The infrared and Raman spectra of monobromothioacetic acid have been recorded and vibrational assignments proposed for the two symmetrical rotational isomers present in the acid.

In our earlier paper[1] we have investigated the vibrational and NMR spectra of mono- and dichlorothioacetic acids in relation to the rotational isomerism and hydrogen bonding. As a part of the aforesaid studies we had the occasion to synthesize mono- and dibromothioacetic acids. In the present article we have characterized monobromothioacetic acid and made vibrational assignments corresponding to the two symmetrical rotational isomers present in this acid.

Experimental

Monobromothioacetic acid was prepared by the following reaction:

$$BrCH_2COCl + H_2S \xrightarrow[-15\,^\circ C]{AlCl_3} BrCH_2C\begin{Bmatrix}O\\S\end{Bmatrix}H + HCl$$

The diethyl ether extract of the reaction mixture was distilled thrice under vacuum. The deep yellow colored liquid with bp 27—28 °C/0.2 mmHg; $n_D^{20}=1.5643$ collected under dry nitrogen was used in the spectral measurements and for characterization. The yield was 35%. Elemental analysis: $BrCH_2C\begin{Bmatrix}O\\S\end{Bmatrix}H$(27—28 °C/0.2 mmHg): Found: C, 15.35; H, 2.11; Br, 51.73; S, 20.43%. Calcd: C, 15.48; H, 1.93; Br, 51.61; S, 20.64%.

The spectra were recorded by the same apparatus as described in a previous paper.[1] The infrared and Raman band frequencies (in cm^{-1}) along with the relative intensities are given in Table 1. The NMR signals (in 3% $CDCl_3$/TMS) for SH and CH_2 protons were found to be at δ values of 4.8 and 4.00 ppm respectively.

Results and Discussion

Table 1 reveals that the number of normal motions observed in the Raman (liquid) and infrared (liquid film and vapors) spectra are more than the expected number of vibrations *i.e.* $3N-6=12A'+6A''$. In transition from liquid to gaseous phase, a change in relative intensity of some of the infrared bands (Table 1) is observed. Moreover three and two bands were observed in the C–Br and C–S stretching regions respectively, while two bands were observed for each of the C=O stretching and CSH in-plane deformation regions. All these experimental observations show that there are two symmetrical rotational isomers present in the liquid and gaseous states of this acid like its chloro analogue *i. e.* $ClCH_2CO\begin{Bmatrix}O\\S\end{Bmatrix}H$.[1]

TABLE 1. INFRARED AND RAMAN BAND FREQUENCIES (in cm^{-1}) OF MONOBROMOTHIOACETIC ACID

Raman Liquid	Infrared		Assignment, species
	Liquid film	Vapor	
3010 m, dp	3000 m	—	CH_2 asymstr, A″
2948 vst	2943 m	2955 w, 2920 w	CH_2 symstr, A′
2560 vst	2544 vst	2582 vw	SH str, A′
1699 m, 1685 m	1715 vst, 1680 vst	1720 vst, —	C=O str, A′
1415 w, 1390 mw	1410 st, 1385 vst	1410 w, —	CH_2 scissor, A′
1250 m, 1215 mw	1245 sh, 1210 st	—, 1210 w	CH_2 wag, A′
1160 vw, 1140 vw	1150 st, —	1155 sh, 1125 st	CH_2 twist, A″
1050 vw, 1090 vw	1035 vst, 1087 sh	1025 st, 1070 mw	C-C str, A′
910 w, 865 m	905 m, 840 m	900 m, 840 m	CSH bend, A′
750 st, 725 m, 710 m	735 m, 705 w	—	C-Br str, A′
655 m, 565 m	—	—	C-S str, A′
450 m, 525 st	—	—	OCS bend, A′
430 m	—	—	CSH bend, A″
410 vw, 398 vw, dp	—	—	C=O wag, A″
255 m, 330 m	—	—	CCBr bend, A′
180 mw, 153 mw, dp	—	—	C-C torsion, A″

dp, depolarized; st, strong; vst, very strong; m, medium; mw, medium weak; sh, shoulder; w, weak; vw, very weak; sym, symmetric; asym, asymmetric; str, stretch; the rotational isomers are assumed to be symmetrical.

* To whom all queries should be made: H. S. Randhawa, Department of Chemistry, Punjab Agricultural University, Ludhiana, India.

There is strong resemblance between the spectra of thioacids and their corresponding acyl halides.[1] Thus from the well known spectra of $BrCH_2COCl$[2] and $ClCH_2C\{^{O}_{S}\}H$[1] the assignments of the vibrational motions for the $BrCH_2$–C– and COSH structural parts of $BrCH_2C\{^{O}_{S}\}H$ are made and given in Table 1. The difference between the IR and Raman band frequencies (Table 1) *e. g.* for SH and C=O stretching modes may be due to the cyclic H-bonded dimers as in the carboxylic acids. The position of SH stretching motion at higher wave number in the vapor phase than in the liquid phase infrared spectrum is the normal behavior of an SH group.[3,4]

Our assignments for the normal motions of this acid are in good agreement (except for the C–C torsional frequency) with those of Nakagawa *et al.* on $BrCH_2COCl$.[2] The bands positioned at 181 cm^{-1} and 157 cm^{-1} in $BrCH_2COCl$[2] have been assigned to the in-plane bending vibration. Since the C–C torsional frequency must be influenced by the mass of the halogenated and thiocarboxyl groups, we prefer to assign the depolarized Raman bands at 180 and 153 cm^{-1} in $BrCH_2C\{^{O}_{S}\}H$ to the A'' C–C torsional vibration for each of the two rotational isomers. These bands are positioned at 205 and 180 cm^{-1} in $ClCH_2C\{^{O}_{S}\}H$.[1]

One of the authors (H. S. R) is grateful to the Alexander Von Humboldt Stiftung for financial support of this work.

References

1) H. S. Randhawa and W. Walter, *J. Mol. Struct.*, **38**, 89 (1977) and the references cited therein.

2) I. Nakagawa, I. Ichishima, K. Kuratani, T. Miyazawa, T. Shimanouchi, and S. I. Mizushima, *J. Chem. Phys.*, **20**, 1720 (1952).

3) H. S. Randhawa, C. O. Meese, and W. Walter, *J. Mol. Struct.*, **36**, 25 (1977).

4) H. S. Randhawa, W. Walter, and C. O. Meese, *J. Mol. Struct.*, **37**, 187 (1977).

An Infrared Study of Acid Sites on Silica-Alumina Catalysts Poisoned with Sodium Hydroxide[1)]

Jun-ichiro TAKE, Toshiaki UEDA, and Yukio YONEDA

Department of Synthetic Chemistry, Faculty of Engineering, The University of Tokyo, Hongo, Bunkyo-ku, Tokyo, 113

(Received July 29, 1977)

We investigated the effect of NaOH impregnation on the acidic properties (the type, strength, and amount of acid sites) of silica–alumina by means of IR spectroscopy of chemisorbed pyridine. Most acid sites on the unpoisoned catalyst were of the Lewis type. Some Lewis-bound pyridine was retained on the surface even at 400 °C, but the pyridinium ion was eliminated at 300 °C, indicating that the strong acid sites were also of the Lewis type. Impregnated NaOH affected both Lewis and Brønsted sites. An increase in the amount of NaOH resulted in the elimination of the Brønsted acid sites of medium strength, and also in a significant reduction in the number of Lewis acid sites over the whole range of acid strength. Weak Brønsted acid sites showed no marked change in number. When the NaOH-impregnated catalysts were exposed to pyridine, a new IR band appeared at about 1445 cm^{-1}; this band is attributable to pyridine associated with the Na ions on the surface.

The infrared spectroscopy of pyridine chemisorbed on solid acids permits the differentiation of Lewis acid sites from Brønsted ones.[2,3)] Since the strength of acid sites should be related to the upper limit of the temperature at which the sites are capable of holding pyridine molecules, a measure of the acid strength may be given in terms of the evacuation temperature of chemisorbed pyridine. Thus, the acid-strength distributions of Brønsted and Lewis acid sites will be determined by means of the IR spectroscopy of chemisorbed pyridine combined with its evacuation temperature, which is successively elevated. Recently, a similar IR technique has been applied to silica–alumina[4)] and Y zeolite[5)] catalysts for the purpose of investigating the influence of aluminium extraction on the surface acid properties.

Previous studies have shown that Na-poisoned silica–alumina catalysts decrease in catalytic activity for cumene cracking,[6)] the isomerization of dialkylbenzenes,[6)] and propene origomerization.[7)] A few brief studies have been reported on the effect of alkali-poisoning on the acidic properties of silica–alumina. Parry[2)] has reported that Na-poisoning (0.8 mg-ion/g) markedly reduced the number of Brønsted acid sites on silica–alumina, and also weakened the Lewis acid sites. The IR spectral data obtained by Bourne, Cannings, and Pitkethly[8)] show a partial and nonselective poisoning of the Brønsted and Lewis acid sites on "aluminium-on-silica" with sodium (0.71 wt%). Basila, Kantner, and Rhee[3)] have reported that the K-poisoning (*ca.* 1 mg-ion/g) of silica–alumina resulted in the elimination of the Brønsted sites and a severe weakening of the Lewis acid sites. The present study was undertaken in order to see, in detail, the effect of NaOH poisoning on the acidic properties of silica–alumina by means of the IR spectroscopy of pyridine, which was retained on the surface after evacuation at successively elevated temperatures.

Experimental

Materials. The Na-poisoned silica–alumina catalysts (SA-1-Na-1, -2, -3, and -4) were prepared by soaking the cracking catalyst (SA-1, 13% Al_2O_3) in an aqueous solution of sodium hydroxide and by then evaporating it to dryness.

TABLE 1. CATALYSTS

Symbol	Surface area m^2/g	Na^+ content mg-ion/g
SA-1	540	0.003
SA-1-Na-1	450	0.048
SA-1-Na-2	480	0.087
SA-1-Na-3	480	0.168
SA-1-Na-4	452	0.807

Some physical properties of these catalysts shown in Table 1 are taken from previous papers.[6,9)] The silica gel (S-3, 600 m^2/g) and γ-alumina (A-1, 170 m^2/g) were prepared by the neutral hydrolysis of ethyl orthosilicate and aluminium isopropoxide, respectively, and by calcination at 550 °C in air for 7 h. The two starting materials were distilled two or three times before use. The pyridine was distilled from a reagent of a GR grade, dried over KOH under a vacuum, and finally vacuum-distilled into a vessel containing a molecular sieve 5A, which had been evacuated *in situ* at 350 °C for 2 h before use.

Sample Preparation and IR Cell. Self-supporting 20-mm diameter wafers of the catalysts were formed by pressing about 50 mg of the samples at 3200 kg/cm^2 in a conventional KBr die. The cell was described in detail in a previous paper.[10)]

Procedures. The wafer mounted in a sample holder was pretreated first in a dry oxygen stream at 550 °C for 2 h and then in a wet oxygen stream at 150 °C for 0.5 h. Afterwards, it was activated in the cell by evacuation at 10^{-4}—10^{-5} mmHg and at 450 °C for 2 h, and then cooled to room temperature. Pyridine vapor (about 16 mmHg) was allowed to equilibrate with the wafer at 150 °C for 1 h after the background spectrum had been recorded. The wafer was evacuated at 150 °C for 1 h and then successively at the desired temperatures for 1 h. After each evacuation, the spectra were recorded on a model DS-401G grating spectrometer (Nihon Bunko) at room temperature. The spectra were scanned at a rate of 1/6 cm^{-1}/s on an expanded wave-number scale (*ca.* 3.3 mm/cm^{-1}). The spectral slit width was approximately 3 cm^{-1} in the 1300—1600 cm^{-1} region.

The band area (or integrated absorbance) was used for the quantitative measurements. The backgrounds for the integration of the bands of adsorbed pyridine were constructed in the same manner as that used by Hughes and White.[11)] The integrated absorbances were normalized so as to indicate

the absorbance per unit of "optical thickness" of the wafer. This normalized absorbance, AS/W (cm/g), corresponds to the $\varepsilon M/W$ quantity, where A and ε are, respectively, the integrated absorbance and the apparent integrated molar absorption coefficient of a band, where M is the amount (mmol) of the responsible species, and where S and W are the cross section (cm^2) and weight (g) of the wafer, respectively.

Results and Discussion

Spectra of Adsorbed Pyridine. The absorption spectrum of pyridine adsorbed on S-3 showed that the adsorbate was hydrogen-bonded (HPY) after evacuation for 1 h at room temperature. The characteristic bands appeared at around 1440 and 1600 cm^{-1}, in accordance with Parry's results.[2] The bands disappeared completely upon evacuation at 120 °C for 1 h.

The A-1 catalyst produced Lewis-bound pyridine (LPY) which gave rise to characteristic bands at 1450 and 1492 cm^{-1} when the adsorbed pyridine was evacuated at 150 °C for 1 h. The peak of the 19*b* mode of LPY was slightly shifted from 1450 to 1458 cm^{-1} as the evacuation temperature was raised from 150 to 300 °C. After evacuation at 300 °C, a weak shoulder remained at around 1452 cm^{-1}; the 19*a* mode (1492 cm^{-1}) also split into two bands at 1500 and 1492 cm^{-1}. A similar shift of the 19*b* mode has been reported for η-alumina.[2] No conversion occurred from LPY into the pyridinium ion (BPY) exhibiting characteristic bands at around 1540 and 1490 cm^{-1}, on dosing water vapor, as has been reported in the literature.[2,3,11]

The spectra of pyridine adsorbed on SA-1 and Na-poisoned SA-1 are illustrated in Fig. 1. After evacuation at 150 °C for 1 h, the pyridine adsorbed on SA-1 displayed three bands, at 1455, 1493, and 1540 cm^{-1}, indicating the coexistence of Lewis and Brønsted acid sites on the surface. The 19*b* mode (1540 cm^{-1}) of BPY disappeared upon evacuation at 300 °C for 1 h (Spectrum b). It has already been shown that this disappearance is accompanied by a partial loss of the Brønsted acid sites.[10]

The splitting of the bands at 1455 and 1493 cm^{-1} took place after evacuation at 300 °C, as was also observed for A-1. The original bands remained with reduced intensities, and additional bands appeared at 1462 and 1497 cm^{-1} (Spectrum b). The 1462 cm^{-1} band, as well as the 1458 cm^{-1} band for A-1, is probably due to another kind of pyridine bound to a Lewis acid site stronger than that characterized by the 1455 cm^{-1} band. Other researchers have reached the same conclusion.[2,4,8] The appearance of the 1497 cm^{-1} band is probably related to the same Lewis acid site as that for the band at 1462 cm^{-1}. The 19*b* mode (1455 and 1462 cm^{-1}) of LPY still remained even after evacuation at 400 °C (Spectrum c), in contrast with that of BPY. This fact implies that the strong acid sites on SA-1 are of the Lewis type. The addition of water vapor converted LPY into BPY, as is well known.

When the Na-poisoned catalysts were exposed to pyridine vapor and then evacuated at 150 °C for 1 h, the adsorbed pyridine produced the same spectra as those obtained for SA-1, except for the appearance of a new band. The new absorption occurred at 1445 cm^{-1} without the appearance of the 1600 cm^{-1} band characteristic of HPY; it was especially pronounced for SA-1-Na-4 (Fig. 1B). This band disappeared upon evacuation at 200 °C for SA-1-Na-1 or -2, but it remained even after evacuation at 300 °C for SA-1-Na-4. Additionally, the band is very similar in frequency to a band at 1438—1445 cm^{-1} due to pyridine adsorbed on the Na ion in Na-exchanged X or Y zeolites.[12] Therefore, the new band is attributable to pyridine associated with the Na ion on the surface, rather than to hydrogen-bonded pyridine. A similar band has also been found on Na-exchanged "aluminium-on-silica."[8] The three

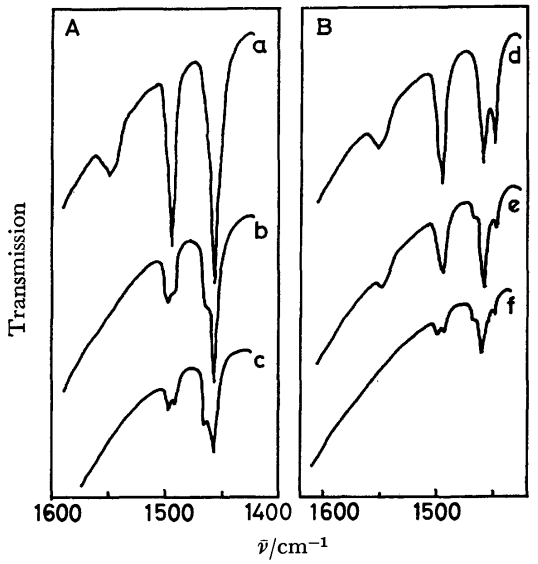

Fig. 1. Infrared spectra of pyridine chemisorbed on silica–alumina catalysts. Spectra A with SA-1 were recorded after evacuation at 150 (a), 300 (b), and 400 °C (c); spectra B with SA-1-Na-4 were obtained after evacuation at 150 (d), 200 (e), and 300 °C (f).

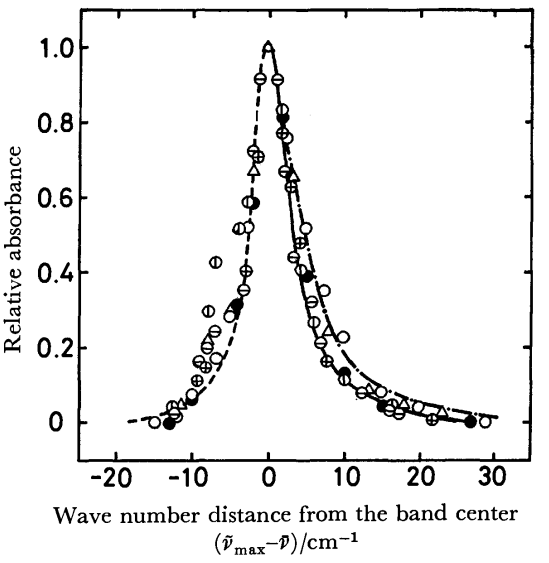

Fig. 2. Band shapes of the 19*b* mode (1455 cm^{-1}) due to Lewis-bound pyridine on various catalysts.
△, ○: SA-1 (150 °C evac.); ●: SA-1 (200 °C evac.); ◑: SA-1 (300 °C evac.); ⊖: SA-1-Na-1 (200 °C evac.); ⊕: SA-1-Na-2 (200 °C evac.).

other bands at 1455, 1490, and 1540 cm^{-1} behaved in essentially the same way as SA-1 when the evacuation temperature was raised or when water vapor was dosed. Since the 1455 cm^{-1} band overlapped to a considerable extent with the 1445 cm^{-1} band (Fig. 1B), the deconvolution of the observed band into these two components was necessary for quantitative measurements of the Lewis acid sites on the Na-poisoned catalysts. The deconvolution was carried out in the manner described below.

Deconvolution of the Overlapped Bands Near 1450 cm^{-1}. In Fig. 2, representative absorption bands at 1455 cm^{-1} are plotted in a normalized form for the catalysts which exhibit no absorption band at 1445 cm^{-1}. The solid and chain lines in Fig. 2 represent two types of Lorentz curves, whose respective half-widths are 7 and 10 cm^{-1}. Apparently, the right half of an absorption curve is fitted approximately by a Lorentz curve with a half-width of 10 cm^{-1} for the bands recorded after evacuation at 150 °C, or by one with a half-width of 7 cm^{-1} for the bands obtained after evacuation at 200 or 300 °C. A Lorentz curve (broken line) with a half-width of 5 cm^{-1} fits the left half of an absorption curve for all the bands, except for a shoulder at around 1460 cm^{-1}.

The procedure for resolving the 1455 cm^{-1} band from the 1445 cm^{-1} band is based on these findings, as illustrated in Fig. 3. First, the shape of the right half of the 1455 cm^{-1} band was determined by drawing a Lorentz curve (broken line) with a half-width of 7 or 10 cm^{-1} from the peak onto the lower-frequency side. Secondly, the absorption curve (dotted line) of the 1445 cm^{-1} band was determined by subtracting the absorption curve of the 1455 cm^{-1} band from the observed curve (solid line).

Changes in Acidic Properties. The two bands at 1455 and 1540 cm^{-1} were chosen to measure the numbers of the Lewis and Brønsted acid sites, respectively. Figure 4 shows the integrated absorbances of the two bands recorded after evacuation at the indicated temperatures for all the catalysts. These absorbances are related quantitatively to the numbers of acid sites capable of retaining the pyridine at the respective temperatures. Since the apparent integrated molar absorption coefficient is approximately the same for the two bands.[11,13] The results shown in Fig. 4 also permit a direct comparison between the Lewis and Brønsted acidities. The acid-strength distributions of the Lewis and Bronsted acids are given in Table 2, in which the number of acid sites is represented as the ratio relative to the total amount of the corresponding type of acid for each catalyst. In Table 3, the integrated absorb-

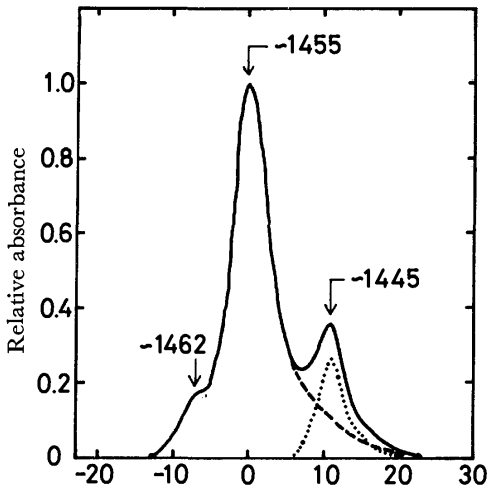

Fig. 3. Illustration of deconvolution of the observed band into the 1455 and 1445 cm^{-1} bands. Original spectrum was recorded after evacuation of pyridine chemisorbed on SA-1-Na-2 at 200 °C.

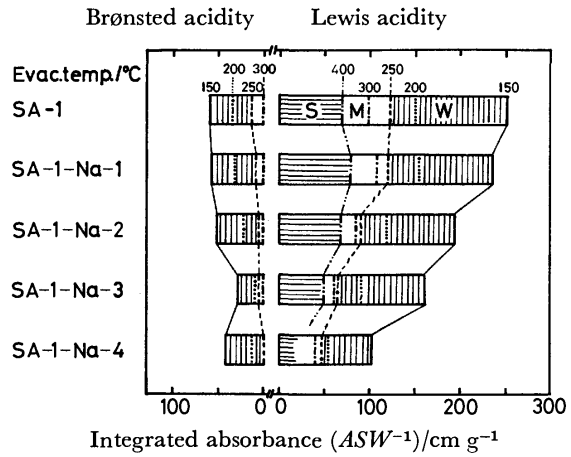

Fig. 4. Acidic properties of catalysts.
S: Strong, M: medium, W: weak.

Table 2. Acid-strength distribution

	Lewis acid			Brønsted acid		
	Weak[a)]	Medium[a)]	Strong[a)]	Weak	Medium	Strong
SA-1	0.51	0.14	0.35	0.77	0.23	0
SA-1-Na-1	0.48	0.19	0.33	0.87	0.13	0
SA-1-Na-2	0.53	0.11	0.35	0.91	0.09	0
SA-1-Na-3	0.60	0.10	0.30	0.88	0.12	0
SA-1-Na-4	0.54	0.46		1.0	0	0

a) Weak and medium sites are incapable of retaining the pyridine in the evacuation temperature (T_e) ranges of $150 < T_e/°C \leqq 250$ and $250 < T_e/°C \leqq 400$, respectively; strong sites are capable of retaining the pyridine at $T_e/°C = 400$; their amounts are given as ratios relative to the total amount of the corresponding type of acid for each catalyst.

TABLE 3. INTEGRATED ABSORBANCES[a] OF THE 1445 cm^{-1} BAND ON Na-POISONED CATALYSTS

Catalyst	Evacuation temperature/°C		
	150	200	300
SA-1-Na-1	17	0	0
SA-1-Na-2	27	0	0
SA-1-Na-3	35	7	0
SA-1-Na-4	38	13	3

a) ASW^{-1}/cm g^{-1}.

ances of the 1445 cm^{-1} band are listed for the Na-poisoned catalysts.

Figure 4 indicates that most (*ca.* 80%) of the acid sites on unpoisoned SA-1 are of the Lewis type. Of the Lewis acid sites, about 35% are so strong as to be capable of holding the pyridine even at 400 °C; about a half are weak, so the pyridine is evolved at 250 °C; the remainder are medium in acid strength. The Brønsted acid sites are not so strong as the Lewis acid sites, since they are incapable of retaining the pyridine even at 300 °C. A similar trend is also found in the results of Ballivet, Barthomeuf, and Pichat.[4] Therefore, such a trend seems general in the acidic properties of dehydroxylated silica–alumina.

The poisoning effect of the impregnated NaOH is apparent on both Lewis and Brønsted acidities, as may be seen in Fig. 4. The Lewis acid sites are markedly decreased in number as the Na^+ content is increased. However, the acid-strength distribution of Lewis acid sites shows no significant change, as is shown in Table 2. This implies that the poisoning action is exerted to an almost equal extent on the sites over the whole range of acid strength; hence, it does not mean that the impregnated NaOH weakens the Lewis acid sites, in contrast with the results of the previous researchers.[3] Of the Brønsted acid, a considerable change in the acid-strength distribution is noticed (Table 2). The Brønsted acid sites of medium strength are decreased in number with an increase in the Na^+ contents, and finally are eliminated (Fig. 4 and Table 2). The weak Bronsted acid sites show no significant change in number. Consequently, the Brønsted acid sites on the poisoned catalysts are weakened and also reduced in number with the impregnated NaOH.

Therefore, the present data confirm the general agreement in the literature[2,3,8] that alkali ions affect both Lewis and Brønsted acid sites over silica–alumina. Such behavior of alkali ions cannot be expected only as a result of their exchange with the protons of Brønsted acid sites. Many other complex chemical processes are probably involved in alkali poisoning. For example, our poisoned catalysts are probably partially hydrolyzed during the course of preparation. There are some differences in the poisoning effect between the present results and those in the literature,[2,3] as has been mentioned above. This strongly suggests that the poisoning effect of alkali ions also considerably varies depending on the preparation of poisoned catalysts. Thus, one must be careful about interpreting the results of alkali ion poisoning unless the effect of poisoning has been well characterized.

Table 3 indicates that, in the range of low Na^+ content (SA-1-Na-1 and -2), the absorbance of the 1445 cm^{-1} band after evacuation at 150 °C increases almost proportionally to the increase of Na^+ content, but its increase becomes slight more and more as the Na^+ content is additionally increased (SA-1-Na-3 and -4). This finding implies that, in the range of high Na^+ content, the number of pyridine molecules interacting with the Na ions is limited. However, the interaction is strengthened more and more with an increase in the Na^+ contents. Therefore, these findings suggest that, when the Na ions are increased in amount, they may be distributed in groups over the surface. This type of distribution may restrict sterically the number of pyridine molecules interacting with the Na ions, but may enhance electrostatically the interacting power of the Na ions.

References

1) Presented at the 28th National Meeting of the Chemical Society of Japan, Tokyo, April 1973.
2) E. P. Parry, *J. Catal.*, **2**, 371 (1963).
3) M. R. Basila, T. R. Kantner, and K. H. Rhee, *J. Phys. Chem.*, **68**, 3197 (1964).
4) D. Ballivet, D. Barthomeuf, and P. Pichat, *J. Chem. Soc., Faraday Trans. 1*, **68**, 1712 (1972).
5) R. Beaumont, P. Pichat, D. Barthomeuf, and Y. Trambouze, *Proc. 5th Intern. Congr. Catalysis*, (Miami Beach, 1972), **1**, 9-343, North-Holland Publishing Co., Amsterdam (1973).
6) H. Matsumoto, J. Take, and Y. Yoneda, *J. Catal.*, **11**, 211 (1968).
7) M. Misono and Y. Yoneda, *Bull. Chem. Soc. Jpn.*, **40**, 42 (1967).
8) K. H. Bourne, F. R. Cannings, and R. C. Pitkethly, *J. Phys. Chem.*, **74**, 2197 (1970).
9) J. Take, H. Kawai, and Y. Yoneda, *Bull. Chem. Soc. Jpn.*, **50**, 2428 (1977).
10) K. Mizuno, M. Ikeda, T. Imokawa, J. Take, and Y. Yoneda, *Bull. Chem. Soc. Jpn.*, **49**, 1788 (1976).
11) T. R. Hughes and H. M. White, *J. Phys. Chem.*, **71**, 2192 (1967).
12) J. Ward, *J. Catal.*, **10**, 34 (1968); *ibid.*, **14**, 365 (1969); B. V. Liegme and W. K. Hall, *Trans. Faraday Soc.*, **62**, 3219 (1966); Y. Watanabe and H. W. Habgood, *J. Phys. Chem.*, **72**, 3066 (1968).
13) J. Take, M. Ikeda, and Y. Yoneda, *Bull. Chem. Soc. Jpn.*, **50**, 49 (1977).

Defect Chemistry of Barium Monoferrite, $BaFe_2O_{4-\delta}$

Akio NAKAMURA,* Shigeru YAMAUCHI, Kazuo FUEKI, and Takashi MUKAIBO

Department of Industrial Chemistry, Faculty of Engineering, The University of Tokyo, Hongo, Bunkyo-ku, Tokyo 113

(Received August 16, 1977)

In order to obtain information on the defects in ternary oxide systems, the nonstoichiometry and electrical conductivity of $BaFe_2O_4$ were determined at temperatures between 1050 and 1125 °C. The electrical conductivity was found to be proportional to $P_{O_2}^{-1/6}$. This relationship suggests that $BaFe_2O_4$ is an oxygen deficient n-type semiconductor at high temperatures. The nonstoichiometry was proportional to $P_{O_2}^{-1/2.88}$. In order to interpret the dependence of electrical conductivity and nonstoichiometry on the oxygen partial pressure, various defect models were examined. As a result the following equilibria were selected from among the oxygen vacancies $V_O^{\cdot\cdot}$ and V_O^{x}, and oxygen gas.

$$\text{null} = (1/2)O_2 + V_O^{x}$$
$$V_O^{x} = V_O^{\cdot\cdot} + 2e'$$

An analysis based on the above defect model explains the data well.

The defect chemistry of oxides is important for the elucidation of transport-phenomena mechanisms, such as electrical conduction, diffusion, metal oxidation, sintering and the other processes for fabricating ceramic materials and heterogeneous catalysts. Although extensive research has been carried out on point defects in simple oxides,[1-3] few studies on defects in complex oxides have been published. Most of the ternary oxide systems studied so far are spinels and perovskite-structure oxides.[4-6] In order to obtain more information about defects in ternary oxide systems of other types of crystal structure, an investigation of the nonstoichiometry δ and the electrical conductivity σ of $BaFe_2O_{4-\delta}$ of stuffed tridymite structure was carried out.

Experimental

Materials. Reagent-grade barium carbonate and hematite of 99.99% purity were mixed in a ratio of Ba/Fe= 1/2. The mixture was cold-pressed into pellets and fired in air at 1100 °C for 12 h to form barium ferrite. One of the sintered pellets was ground and the powder was cold pressed. Then, it was heated again to 1300 °C for 6 h and examined using the X-ray powder diffraction method. The powder was found to consist of β'-$BaFe_2O_4$, a low-temperature modification of barium monoferrite.[7]

The sintered pellets were crushed to grains of 1—2 mm in diameter and used as the sample for the nonstoichiometric measurements. The sintered rectangular specimen, 2× 1.5× 15 mm, was used for the mesurement of the electrical conductivity. The relative density was 88%.

Measurements. The nonstoichiometry of $BaFe_2O_{4-\delta}$ was determined gravimetrically by means of a Shimadzu RMB-50 micro balance at temperatures between 1050 and 1125 °C. The sensitivity of the balance was 1 μg. Details of the equipment have been described elesewhere.[8]

About one gram of the sample was placed in a platinum basket, which was then suspended from the balance by fine alumina fibers. The nonstoichiometry δ was assumed to be zero in 1 atm of oxygen since almost no weight change was observed even when the oxygen pressure was changed from 1 to 0.01 atm at constant temperature. The nonstoichiometry was calculated from the difference in the sample weight in CO_2–CO gas mixtures and in 1 atm of oxygen.

The electrical conductivity was measured using the d.c. four-probe method. Four platinum wires were connected to the sample using platinum paste. Details of the equipment and experimental procedure have been described elsewhere.[9]

Results and Discussion

Nonstoichiometry. A plot of $\log \delta$ against $\log P_{O_2}$ is presented in Fig. 1. The linear relationship between $\log \delta$ and $\log P_{O_2}$ indicate that δ is proportional to $P_{O_2}^{-1/m}$. The values of m calculated from the slope are

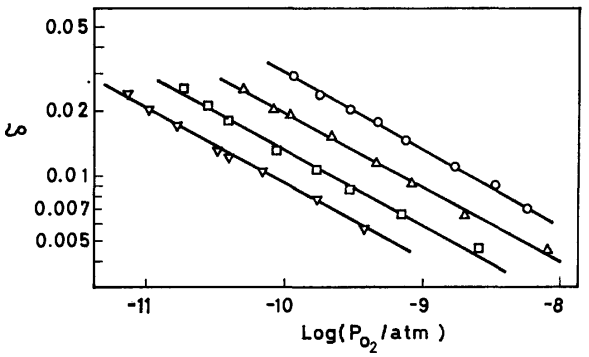

Fig. 1. Dependence of nonstoichiometry δ in $BaFe_2O_{4-\delta}$ on oxygen partial pressure.
▽: 1050 °C, □: 1075 °C, △: 1100 °C, ○: 1125 °C.
The symbols for identification of the temperature is the same through Figs. 1 to 4.

Table 1. Summary of the powers of P_{O_2} from the nonstoichiometric and electric conductivity data

$\frac{t}{°C}$	m[a]	m'[b]
1050	2.88±0.02[c]	6.6±0.1
1075	2.85±0.03	6.2±0.1
1100	2.85±0.01	6.0±0.05
1125	2.95±0.01	5.5±0.1

a) m is from $\delta \propto P_{O_2}^{-1/m}$. b) m' is from $\sigma \propto P_{O_2}^{-1/m'}$. c) The errors indicated are for one standard deviation.

*Present address: Research and Development Laboratory TDK Electronics Corporation, 15-7, Higashi Owada 2-Chome, Ichikawa, Chiba 272-01.

given in the second column of Table 1. The mean value of m is 2.88. If the chemical potential of the oxygen atom in the oxide is expressed as

$$\mu_O = \mu_O^\circ + \frac{1}{2}RT \ln P_{O_2}, \quad (1)$$

the relative partial molar enthalpy of the oxygen atom at a constant composition is given by

$$\Delta H_O^\circ = \partial\left(\frac{1}{2}RT \ln P_{O_2}\right)\Big/\partial(1/T).$$

The ΔH_O° values for $BaFe_2O_{4-\delta}$ are listed in the second column of Table 2. ΔH_O° increases slightly with increasing δ.

TABLE 2. PARTIAL MOLAR ENTHALPY OF THE OXYGEN ATOM AND THE ACTIVATION ENERGY FOR ELECTRICAL CONDUCTIVITY

δ	ΔH_O° / kcal mol^{-1}	ΔH_A / kcal mol^{-1}
0.006	77.1±4.6	12.04±2.66
0.010	77.9±3.0	13.12±1.68
0.012	79.0±3.0	11.88±1.37
0.015	80.5±2.5	12.95±0.85
0.020	86.1±3.0	13.49±1.0

Electrical Conductivity. Figure 2 shows the results of the electrical conductivity measurements. The conductivity decreases with increasing oxygen partial pressure. This result indicates that $BaFe_2O_4$ is an oxygen deficient, n-type oxide and that the dependence of conductivity on the oxygen pressure is given by $\sigma = P_{O_2}^{-1/m'}$. The values of m' are given in the third column of Table 1. The values are scattered with the mean value being 6.1.

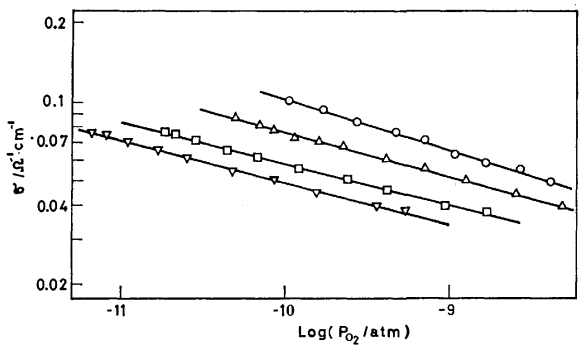

Fig. 2. Dependence of conductivity on oxygen partial pressure.

From the temperature dependence of the conductivity, the apparent activation energy for electronic conduction was calculated for a fixed composition. The results are given in the third column of Table 2. Although the standard deviations are relatively large, it appears that the apparent activation energy is independent of composition. The mean value is 12.7 kcal/mol.

Defect Models and the Expected Pressure Dependence of δ and σ. Measurements on nonstoichiometry and electrical conductivity have revealed that the dependence of the nonstoichiometry on oxygen partial pressure is different from that of the electrical conductivity, that is, the oxygen-pressure dependence is $P_{O_2}^{-1/2.88}$ for nonstoichiometry and $P_{O_2}^{-1/6.1}$ for conductivity. In order to interpret the difference in oxygen-pressure dependence consistently, a thermodynamic calculation was carried out on the defect concentration of oxygen deficit, n-type oxides on the basis of several defect models and the calculated results were compared with the data.

Interstitial cation models cannot be used to interpret the oxygen-pressure dependence, so oxygen vacancy models were examined. If V_O^x, $V_O^{\cdot}$, and $V_O^{\cdot\cdot}$ represent the neutral oxygen vacancy, the oxygen vacancy associated with one electron, and an oxygen vacancy free of electrons, respectively, the chemical equilibria relevant to these vacancies can be written as follows:

$$\text{null} = (1/2)O_2(g) + V_O^x, \quad K_1 = [V_O^x]P_{O_2}^{1/2}, \quad (2)$$

$$V_O^x = V_O^{\cdot\cdot} + 2e', \quad K_2 = n^2[V_O^{\cdot\cdot}]/[V_O^x], \quad (3)$$

$$V_O^x = V_O^{\cdot} + e', \text{ and } K_3 = n[V_O^{\cdot}]/[V_O^x], \quad (4)$$

where K_1, K_2, and K_3 are equilibrium constants, the brackets express the concentration of the respective oxygen vacancies in units of moles per mole of $BaFe_2O_{4-\delta}$ and n is the concentration of electrons in the same units. The electrical neutrality condition is

$$n = 2[V_O^{\cdot\cdot}] + [V_O^{\cdot}]. \quad (5)$$

The nonstoichiometry, δ, and electrical conductivity, σ, are related to the oxygen-vacancy concentrations by

$$\delta = [V_O^x] + [V_O^{\cdot}] + [V_O^{\cdot\cdot}] \quad (6)$$

and

$$\sigma = (N_A/V_m)ne\mu = kn, \quad (7)$$

where V_m is the molar volume of $BaFe_2O_{4-\delta}$, N_A the Avogadro number, e the electronic charge, and μ the electron mobility. k is substituted for $(N_A/V_m)eu$ for the sake of simplification.

In the following, several defect models and the results of thermodynamic calculations on the basis of these models are described.

For the "A" models, one of the three kinds of oxygen vacancies are assumed to be predominant. If $V_O^{\cdot}$ is predominant, the elimination of V_O^x and $V_O^{\cdot\cdot}$ in Eqs. 5 and 6 and combining Eqs. 2, 4, 5, and 6 result in a relation whereby both δ and σ depend on $P_{O_2}^{-1/4}$. Let us call this the "A-2" model. Two other models, "A-1" and "A-3", are also proposed. The oxygen-pressure dependence of δ and σ for the "A" models is summarized in the first three lines of Table 3.

For the "B" models, two of the three kinds of oxygen vacancies are assumed to be predominant. Three models, "B-1", "B-2", and "B-3", and the oxygen-pressure dependence of δ and σ are as shown in the fourth to sixth lines of Table 3.

All three kinds of oxygen vacancies are assumed to prevail for the "C" model. The oxygen-pressure dependence of δ and σ is given in the last line of Table 3.

The observed pressure dependence is $P_{O_2}^{-1/2.88}$ for δ and $P_{O_2}^{-1/6}$ for σ. Therefore, two kinds of models, "B-3" and "C", appear to be appropriate for interpreting the observed results.

Thermodynamic Calculations on the Basis of the "C" Model. Equation 2 gives the concentration of V_O^x as

Table 3. Models and oxygen-pressure dependence

	Model	Condition	Oxygen-pressure dependence m[a)]	m'[b)]
A	A-1	$[V_O^x] \gg [V_O^{\cdot}], [V_O^{\cdot\cdot}]$	2	
A	A-2	$[V_O^{\cdot}] \gg [V_O^x], [V_O^{\cdot\cdot}]$	4	4
A	A-3	$[V_O^{\cdot\cdot}] \gg [V_O^x], [V_O^{\cdot}]$	6	6
B	B-1	$[V_O^x], [V_O^{\cdot}] \gg [V_O^{\cdot\cdot}]$	2—4	4
B	B-2	$[V_O^{\cdot}], [V_O^{\cdot\cdot}] \gg [V_O^{\cdot}]$	4—6	4—6
B	B-3	$[V_O^x], [V_O^{\cdot\cdot}] \gg [V_O^{\cdot}]$	2—6	6
	C	$[V_O^x] \approx [V_O^{\cdot}] \approx [V_O^{\cdot\cdot}]$	2—6	4—6

a) m is from $\delta \propto P_{O_2}^{-1/m}$. b) m' is from $\sigma \propto P_{O_2}^{-1/m'}$.

$$[V_O^x] = K_1 P_{O_2}^{-1/2}. \quad (8)$$

From Eqs. 3, 4, and 7,

$$[V_O^{\cdot}] = K_3[V_O^x]/n = K_1K_2kP_{O_2}^{-1/2}\sigma^{-1}, \quad (9)$$

$$[V_O^{\cdot\cdot}] = K_2[V_O^x]/n^2 = K_1K_3k^2P_{O_2}^{-1/2}\sigma^{-2}, \quad (10)$$

and, therefore,

$$P_{O_2}^{1/2} = K_1 + K_1K_3k\sigma^{-1} + K_1K_2k^2\sigma^{-2}. \quad (11)$$

Employing the observed values of δ, σ, and P_{O_2}, a least-squares calculation was carried out for Eq. 11, but no equilibrium constants simultaneously satisfying Eq. 11 could be found. Thus, "C" model was excluded from consideration and a detailed examination of the "B-3" model was carried out.

Thermodynamic Calculations on the Basis of the "B-3" Model. Omitting $[V_O^{\cdot}]$ in the right-hand side of Eq. 5, we obtain the neutrality condition,

$$n = 2[V_O^{\cdot\cdot}]. \quad (12)$$

Combination of Eqs. 2, 3, 7, and 12 yields

$$\sigma = (2K_1K_2k^3)^{1/3}P_{O_2}^{-1/6}. \quad (13)$$

Figure 3 shows a σ-$P_{O_2}^{-1/6}$ plot for the observed data. It is seen that Eq. 13 holds for the oxygen-pressure dependence of the conductivity. The concentrations of $V_O^{\cdot\cdot}$ and V_O^x can be expressed in terms of σ using Eqs. 2, 3, 7, and 12 as follows:

$$[V_O^{\cdot\cdot}] = n/2 = \sigma/2k \quad (14)$$

and

$$[V_O^x] = n^2[V_O^{\cdot\cdot}]/K_2 = \sigma^3/2K_2k^3. \quad (15)$$

Inserting Eqs. 14 and 15 into Eq. 6, and omitting $[V_O^{\cdot}]$, we obtain

$$2\delta/\sigma = 1/k + \sigma^2/K_2k^3. \quad (16)$$

This equation implies that a plot of $2\delta/\sigma$ against σ^2 would give a straight line and the value of k and the equilibrium constant K_2 could then be determined from the intercept and the slope of the line. Figure 4 shows a plot of $2\delta/\sigma$ *vs.* σ^2. Evidently, the data at constant temperature fall along a straight line. This result supports the "B-3" model.

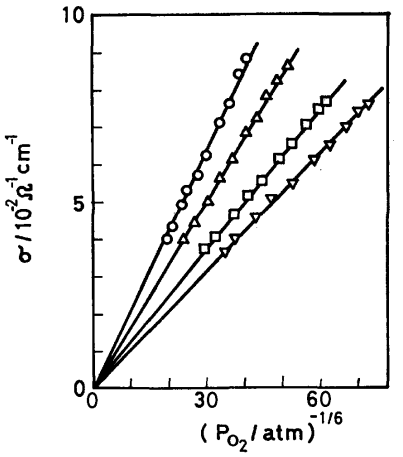

Fig. 3. The plot of σ against $P_{O_2}^{-1/6}$.

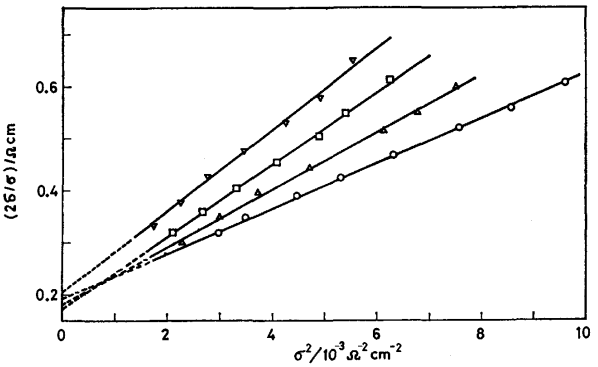

Fig. 4. The plot of $2\delta/\sigma$ against σ^2.

The k value calculated from the intercept is given in the second column of Table 4. The value of k appears to be independent of temperature in the temperature range between 1052 and 1125 °C. The average of k in this temperature range was 5.3 ± 0.4 cm^{-1} Ω^{-1}. From this value, the electron mobility was evaluated to be $(3.9\pm0.3)\times10^{-3}$ cm^2 V^{-1}.

The slope is listed in the third column of Table 4. The equilibrium constants, K_2, calculated from the slope and k are given in the fourth column of Table 4. Equa-

Table 4. Calculation of equilibrium constants, K_1 and K_2

t / °C	k / cm^{-1} Ω^{-1}	$1/(K_2k^3)$ / cm^3 Ω^3	K_2 / 10^{-5}	$2K_1K_2k^3$ / 10^{-10} atm$^{1/2}$ cm^{-3} Ω^{-3}	K_1 / 10^{-8} atm$^{1/2}$
1050	4.8±0.2	78±2	8.6±1.4	8.9±0.7	3.5±0.4
1075	5.8±0.2	69±1	9.7±1.0	19.1±0.6	6.6±0.3
1100	5.5±0.2	55±2	12.3±1.9	46.3±0.8	12.6±0.6
1125	5.1±0.1	43.0±0.3	15.6±0.2	95.1±0.7	20.5±1.6
	average: 5.3±0.4				
$\Delta S°$/cal mol^{-1}			3.8±2.4		32.1±2.2
$\Delta H°$/kcal mol^{-1}			29.7±3.3		87.5±2.2

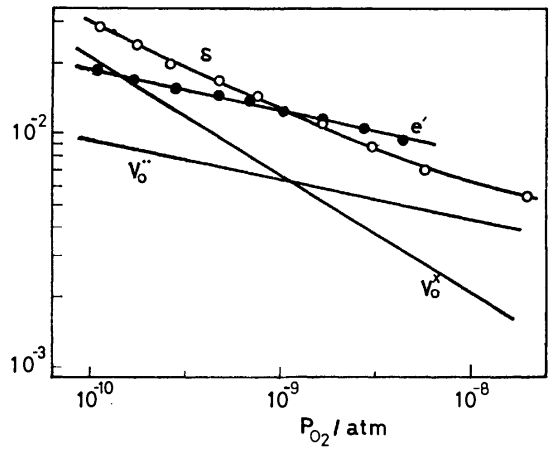

Fig. 5. Concentration of point defects in $BaFe_2O_{4-\delta}$ at 1125 °C.
○: δ, ●: concentration of conduction electron.

tion 13 indicates that the slope of the σ-$P_{O_2}^{-1/6}$ plot gives the value of $2K_1K_2k^3$, which is presented in the fifth column of Table 4. From this value and the slope obtained from Fig. 4, the equilibrium constant K_1 was calculated. The results are given in the last column of Table 4.

The concentrations of the lattice defects, V_0^x, $V_0^{\cdot\cdot}$ and electrons, and the nonstoichiometry, δ, were calculated from the values of K_1 and K_2 in Table 4. They are plotted together with δ in Fig. 5. The open circles designate the observed nonstoichiometric data and the solid circles designate the electron concentration calculated from the observed concentration data and the value of the electron mobility (3.9×10^{-3} cm^2 V^{-1}). It is seen that the oxygen vacancies V_0^x tend to dissociate into $V_0^{\cdot\cdot}$ and electrons as the oxygen partial pressure increases. The agreement is very good for both the electron concentration and the nonstoichiometry. Thus, the "B-3" model explains well the observed results.

The temperature dependence of the equilibrium constants, K_1 and K_2, can be represented by

$$K = \exp(\Delta S^\circ/R)\exp(-\Delta H^\circ/RT). \quad (17)$$

The values of ΔH° and ΔS° with one standard deviation are indicated in Table 4. The enthalpy change for Eq. 2 is 87.5 kcal/mol and that for Eq. 3 is 29.7 kcal/mol.

From these results it is concluded that the "B-3" model is best of those listed in Table 3 for interpreting the observed data for δ and σ.

References

1) F. A. Kroeger, "The Chemistry of Imperfect Crystals," North Holland Publ. Co., Amsterdam (1974).
2) P. Kofstad, "Nonstoichiometry, Diffusion, and Electrical Conductivity in Binary Metal Oxides," John Wiley, New York (1972).
3) L. Eyring and M. O'Keefe, eds., "The Chemistry of Extended Defects in Non-Metallic Solids," North Holland Publ. Co., Amsterdam (1970).
4) H. Schmalzried and C. Wagner, *Z. Phys. Chem. (Frankfurt am Main)*, **B31**, 198 (1962).
5) A. M. J. H. Seuter, *Philips Res. Rept.*, Suppl. No. 3 (1974).
6) S. A. Long and R. N. Blumenthal, *J. Am. Ceram. Soc.*, **54**, 610 (1971).
7) S. Meriani, *Acta Crystallogr., Sect. B*, **28**, 1241 (1972).
8) A. Nakamura, S. Yamauchi, K. Fueki, and T. Mukaibo, submitted to the *J. Phys. Chem. Solids.*
9) K. Endo, S. Yamauchi, K. Fueki, and T. Mukaibo, *J. Solid State Chem.*, **19**, 13 (1976).

Molecular Structure of 2,2-Dichloropropane as Determined by a Combined Use of the Electron-diffraction Data and the Spectroscopic Moments of Inertia

Masashi HIROTA, Takao IIJIMA,* and Masao KIMURA**

Department of Chemistry, Faculty of Science, Hokkaido University, Sapporo 060

(Received August 31, 1977)

The molecular structure of 2,2-dichloropropane has been determined by the joint analysis of the electron-diffraction data and the moments of inertia obtained by Matsumura and Takeo by means of microwave spectroscopy. Under the assumptions that r_g(C–H) is in the range of 1.100—1.110 Å and that φ_α(HCH) is larger than 107.0°, the structure parameter values have been determined (with the limits of error in parentheses) to be as follows: r_g(C–Cl), 1.799(3) Å; r_g(C–C), 1.523(4) Å; r_g(Cl···Cl), 2.910(1) Å; r_g(C···Cl), 2.702(1) Å; φ_{av}(ClCCl), 108.3(3)°, and φ_{av}(CCC), 113.0(4)°. The r_g-structure determined in the present study is in perfect conformity with the r_0-structure determined by Matsumura and Takeo. The C–Cl and C–C distances are shorter than the corresponding distances in 2-chloropropane.

Since Lide and Jen first pointed out the systematic elongation of C–Cl bonds in a series of molecules (methyl, ethyl, isopropyl, and *t*-butyl chlorides),[1] the environment effect on bond lengths in the halogen derivatives of alkanes has been the subject of many studies. A similar systematic elongation of the C–F bonds observed for the fluorine derivatives of alkanes may be involved in studies of the environment effect.[2] Recently, Matsumura and his collaborators have carried out extensive microwave studies of the chlorine and fluorine derivatives of methane.[3] From their results and those for halogenated ethanes and propanes quoted in the literature, they have systematized changes in the carbon-halogen bond lengths with the number of halogen atoms and methyl groups attached to the carbon atom in question. However, the comparisons of the bond lengths so far reported are, in most cases, based upon the r_s distances determined by microwave spectroscopy.[4]

In the present authors' opinion, the r_g distances are preferable to the r_s distances for comparing bond lengths, as was mentioned in the preceding paper on 2-chloropropane.[5] However, high-precision data on the r_g-structures of halogenated alkanes are rather few. The present paper will report the structure of 2,2-dichloropropane as determined by a combined use of the electron-diffraction data obtained by the present study and the moments of inertia obtained by Matsumura and Takeo by microwave spectroscopy,[6] as part of a series of studies of the molecular structures of chlorinated alkanes.

Experimental

A guaranteed reagent purchased from Nakarai Chemicals, Ltd., was used without further purification. Diffraction photographs were taken at room temperature, 20 °C, on the unit eqipped with an r^3-sector[7] under the following experimental conditions: camera lengths, 244.3 and 109.3 mm; accelerating voltage, 42 kV; beam current, 0.15 μA; exposure times, about 70 s for the short camera length and about 50 s for the long camera length; sample pressure, 50 Torr.[8] The wavelength, or the scale factor, was determined by reference to the pattern of carbon disulfide taken under the same experimental conditions. The covered s ranges were 3—19 Å^{-1} and 6—40 Å^{-1} for the long and short camera distances respectively. Two plates from the long camera distance and five plates from the short camera distance were selected for analysis.

Analysis of the Diffraction Data

The reduction of the observed total intensities to the molecular intensities[9] and the determination of the parameter values by the least-squares method were carried out following our usual procedure.[10] The following assumptions were set up with respect to the molecular geometry: (1) C_{2v} symmetry for the molecule as a whole, (2) local C_{3v} symmetry for the methyl tops, (3) zero tilt angles for the methyl tops, *i.e.*, the C_3 axes of the methyl tops coincident with the C–C bond axes, (4) staggered conformation about the C–C bonds with HCCCH in plane, as was assumed for 2-chloropropane. The mean amplitudes were fixed at values calculated using the Urey-Bradley force field proposed by Green and Harrison.[11] The calculated mean amplitudes for the main distances are shown in Table 1.

TABLE 1. CALCULATED MEAN AMPLITUDES AT 20 °C (in Å units)

Distance	Calculated mean amplitude	
C–Cl	0.0631	
C–C	0.0519	
C–H	0.0784	
Cl···Cl	0.0851	
C···Cl	0.0769	
Cl:::H_{gauche}	0.1833	H in CCC plane
	0.2113	H out of CCC plane
Cl:::H_{trans}	0.1061	
C···C	0.0788	

Starting with the r_0-structure reported by Matsumura and Takeo,[6] four distances, Cl···Cl, C–Cl, C···Cl, and C–C, were adjusted by fixing the r_a(C–H) and φ_α(HCH) at plausible values.[4,12] Since the contributions to the molecular intensities are small from the distances

* Present address: Gakushuin University, Mejiro, Tokyo 171.

** To whom correspondence should be addressed.

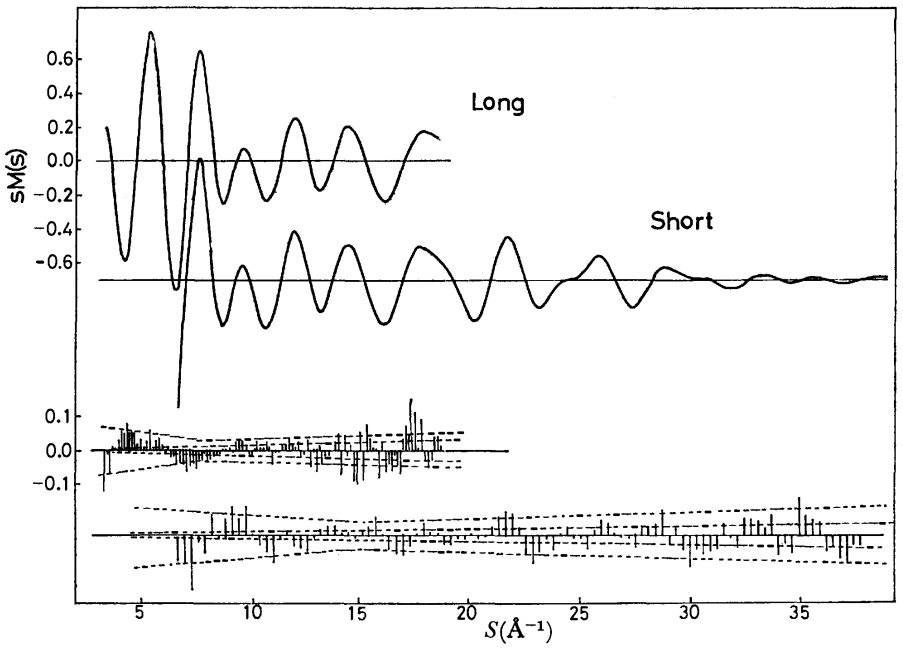

Fig. 1. The best fit theoretical molecular intensity curves, $sM(s)$, and the differences, $sM(s)^{obsd}-sM(s)^{calcd}$, for typical data from the long and the short camera distances. In the afferences, the inner broken lines indicate the limit of detection in photometry and the outer broken lines the estimated limit of errors in the observed intensities; see Ref. 5. The ordinate for the differences is taken twice as large as that for the intensity curves.

TABLE 2. RESULTS OF ELECTRON DIFFRACTION (distance in Å; angle in degree units)[a]

Distance	r_g	r_α^0 [b]
Cl···Cl	2.903(7)	2.902
C–Cl	1.797(4)	1.792
C···Cl	2.702(4)	2.700
C–C	1.519(6)	1.515
Index of resolution	0.98—1.04	

a) The values in parentheses indicate the limits of error, which were estimated from the random errors and the error in the scale factor. The uncertainty included in the scale factor is ±0.10% in the distances. The r_a(C–H) and the φ_α(HCH) were assumed to be 1.110 Å and 108.5° respectively. b) As to the conversion of r_g to r_α^0, see text. The uncertainties in the r_α^0 values are equivalent to those in the r_g values.

involving H atoms, the influence of the assumed distances on the results is insignificant; the converged values vary only by one-thousandth angstrom or less as long as the φ_α(HCH) and the r_a(C–H) values are limited within reasonable ranges (see Ref. 12 and also the next section). The final results are listed in Table 2, while the best-fit theoretical intensity curves and the residuals for the observed intensities for typical plates are shown in Fig. 1. The residuals are depicted on a double scale. The inner broken lines on the residuals indicate the limit of detection in photometry, while the outer ones indicate the boundary of the distribution of the residuals in the molecular intensities observed by a normal technique.[13]

Joint Analysis

The moments of inertia of $(CH_3)_2C^{35}Cl_2$ and $(CH_3)_2C^{35}Cl^{37}Cl$ in the ground state have been reported by Matsumura and Takeo.[6] Since the $^{35}Cl^{37}Cl$ species does not provide additional information,[5] only the moments of inertia of $(CH_3)_2C^{35}Cl_2$ were used for the joint analysis in the present study. These effective moments of inertia, $I^{(eff)}$, were corrected for the vibrational effect and converted into the moments of inertia, $I^{(z)}$, for the zero-point average structure.[14] The corrections, ΔI, were calculated by using the force constants given by Green and Harrison.[11] The barrier to the hindered rotation about the C–C axis was estimated to be about 3.4 kcal/mol.[11] In general, somewhat different ΔI values are obtained by using either one of two alternatives, the small-amplitude[14] or the large-amplitude treatment[15] for the methyl torsion. The

TABLE 3. EFFECTIVE MOMENTS OF INERTIA, THE VIBRATIONAL CORRECTION, AND THE MOMENTS OF INERTIA FOR THE ZERO-POINT AVERAGE STRUCTURE OF $(CH_3)_2C^{35}Cl_2$ (in amu Å² units)[a]

	$I^{(eff)}$ [b]	ΔI	$I^{(z)}$ [c]
a	138.056	0.108	138.164
b	205.617	0.112	205.729
c	234.154	0.044	234.198

a) The corrections were calculated by the small-amplitude treatment. See text. b) Calculated from the observed rotational constants by using, as the conversion factor, 505376 MHz amu Å². c) $I^{(z)}=I^{(eff)}+\Delta I$.

barrier to the hindered rotation of this molecule is almost the same as that of 2-chloropropane.[5] Therefore, the differencc in the r_z(C–H) value or in the φ_z(HCH) value of the 2,2-dichloropropane obtained by the two treatments is practically the same as that in the case of 2-chloropropane.[5] In the present analysis, the small-amplitude treatment was adopted; the ΔI and $I^{(z)}$ values thus obtained are listed in Table 3, together with $I^{(eff)}$. The ΔI and the $I^{(z)}$ values to be obtained by the large-amplitude treatment can be estimated by referring to the results of 2-chloropropane.[5] In either treatment, the same r_g values are finally yielded. The r_g distances determined by the electron diffraction were converted into the r_α^0 distances by correcting them for the anharmonic term, the centrifugal stretching, and the perpendicular vibration. The r_α^0 values thus obtained are also entered in Table 2. The Morse asymmetry constants, a_3, were assumed to be 2.0, 2.1, and 2.0 Å^{-1} for the C–Cl, C–C, and C–H distances respectively, and zero for all the non-bonded atom pairs.

The structure of 2,2-dichloropropane is defined by the six parameters, r(C–C), r(Cl···Cl), r(C···Cl), r(C–H), and ∠HCH, under the same assumptions with respect to the geometry as those employed in the analysis of the electron-diffraction data. In determining these six parameter values, the three moments of inertia can be used in addition to the two r_α^0 values for the bonded distances determined by the electron diffraction. Obviously these five experimental values are not sufficient for determining the six parameters of this molecule. Thus, a reasonable assumption as to the ranges of r(C–H) and ∠HCH was used and the skeletal parameters were determined with smaller uncertainties than those of the electron-diffraction results.

The analysis was done through the following steps. For the bonded distances, r(C–C) and r(C–Cl), the results obtained by the electron diffraction are illustrated in a two-dimensional space, as is shown in Fig. 2, where the axes are scaled in r_α^0 derived from r_g. In Fig. 2, the O point indicates the best-fit values determined by the electron diffraction, while the ellipse shows the boundary of the total limits of error, which were estimated from the random errors obtained by the least-squares refinement and the error included in the scale factor. The straight line S shows the direction of change in r(C–C) and r(C–Cl) with a change in the scale factor. For any pair of the C–C and C–Cl distances, the three moments of inertia give the relation among the other four parameters. When the A, B, C, and D points are chosen on the S line in Fig. 2, the relations can be represented by the corresponding parallel straight lines in the r(C–H)–∠HCH space, as is shown in Fig. 3. The relations may be described numerically as follows; (1) for any pair of r(C–C) and r(C–Cl), a variation of ±0.005 Å in r(C–H) is equivalent to variations of ±0.22° in ∠HCH, ∓0.0004 Å in r(Cl···Cl) (or ∓0.02° in ∠ClCCl), without any change in the C···Cl distance, and (2) an increase of 0.01% in both r(C–C) and

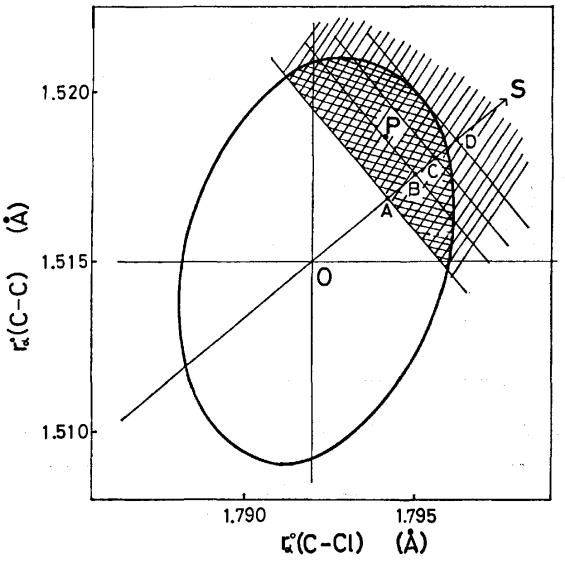

Fig. 2. The allowed range of the r_α^0(C–Cl) and r_α^0(C–C) distances. The shading indicates the range allowed by the spectroscopic moments of inertia under the conditions that the r_α^0(C–H) is in the range of 1.075—1.085 Å and the φ_α(HCH) is larger than 107.0°. The cross-shaded area is the range allowed by both electron diffraction results and the spectroscopic moments of inertia under the same conditions. The O point shows the best fit values which were obtained by converting the r_g values determined by electron diffraction into the r_α^0 values and the P point is the center of the cross-shaded area. The limits of error in the r_α^0 values are taken to be identical to those in the experimental r_g values. See text about other details.

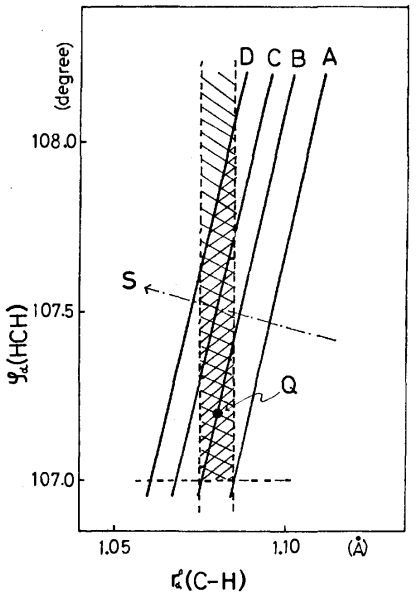

Fig. 3. The correlation diagram of the r_α^0(C–H) and the φ_α(HCH) which satisfy the three observed $I^{(z)}$. The region assumed for the r_α^0(C–H) and the φ_α(HCH) is indicated by shading. The pararell lines, A, B, C, and D, corresponds to the A, B, C, and D points in Fig. 2 respectively. The S line with an arrow indicates the direction of an increase in the scale factor. The upper boundary limited by the D line is determined by the electron diffraction results. The cross-shaded area then corresponds to that in Fig. 2. The Q point indicates the final representative values which are compatible with the P point in Fig. 2.

r(C–Cl) is equivalent to either changes of +0.11° in ∠HCH and +0.0003 Å in r(C···Cl), or changes of −0.0025 Å in r(C–H), +0.0004 Å in r(C···Cl), and +0.0002 Å in r(Cl···Cl).

Here, we put restrictions on the allowed ranges of the r(C–H) and ∠HCH. In various molecules which are about the size of the present one, the r_g(C–H) have been found in the ranges of 1.100—1.110 Å, which corresponds to the range of 1.075—1.085 Å in r_α^0(C–H), and the φ_α(HCH) have been found to be larger than 107.0°. Thus, the r_α^0(C–H) and φ_α^0(HCH) values of the present molecule were assumed to be in the ranges of values mentioned above. This region is indicated by shading in Fig. 3. It may be seen that line A in Fig. 3 is a limiting case in which the line is scarcely in contact with the region allowed by the restrictions for r(C–H) and ∠HCH. Accordingly, the A point in Fig. 2 represents the lower limit of the allowed region with respect to the scale factor. When the r(C–C) and the r(C–Cl) change along a line perpendicular to the S line, changes in the moments of inertia due to a change in the r(C–C) are almost cancelled by those due to a change in the r(C–Cl); consequently, the calculated values of the moments of inertia do not change practically. Thus, the relation between r(C–H) and ∠HCH shown by the A, B, C, and D lines in Fig. 3 holds well for any pair of the C–C and C–Cl distances on the lines perpendicular to the S line through the A, B, C, and D points in Fig. 2 respectively. In Fig. 2, the line through the A point, which corresponds to the A line in Fig. 3, is, then, the lower boundary in the r(C–C)–r(C–Cl) space. The shaded area in Fig. 2 is the region thus limited.

The upper boundary in the r(C–C)–r(C–Cl) space is formed by the error-ellipse of the electron-diffraction results. The line tangent to the ellipse and perpendicular to the S line in Fig. 2 passes through the D point. Then, the D line in Fig. 3 becomes the corresponding upper boundary in the r(C–H)–∠HCH space. The allowed regions thus determined are shown as the cross-shaded area in Figs. 2 and 3. In this procedure, the allowed ranges of the r(Cl···Cl) and the r(C···Cl) are concurrently determined, since the areas in Figs. 2 and 3 also define the ranges of these parameters, though implicitly.

The values of r(C–Cl) and r(C–C) at the approximate center, P, of the cross-shaded area in Fig. 2 were taken as the final ones. The final values for the other four parameters were chosen at the middle point of the ranges of the parameters which are compatible with the values of r(C–C) and r(C–Cl) given by the P point. The final values for r(C–H) and ∠HCH thus determined are represented by the Q point in Fig. 3. The results are summarized in Table 4. In the table, the allowed ranges for the parameters are given by the farthest separations from the respective final value in the allowed region, such as the cross-shaded area in Fig. 2. The allowed ranges for the skeletal parameters are narrower than those for the r_α^0 values determined by the electron diffraction alone. (*cf.* Table 2). This is because we assumed the C–H distance and the HCH angle to be within the limited ranges of values. The uncertainties included in the $I^{(z)}$ values are estimated to be 0.01 amu Å^2.[16] The corresponding variations in the parameter-values are only ±0.0007 Å for the C–H distance and ±0.03° for the HCH angle, and negligible for the other distances. Therefore, the uncertainties in the $I^{(z)}$ values do not affect the final allowed ranges.

TABLE 4. RESULTS OF THE COMBINED ANALYSIS[a]

	r_{av} or φ_{av}	Allowed range	r_g[c]
C–Cl	1.794	±0.003	1.799
C–C	1.519	±0.004	1.523
Cl···Cl	2.908	±0.001	2.910
C···Cl	2.700	±0.001	2.702
C–H	[1.080[b]	±0.005	1.101]
ClCCl[d]	108.3	±0.3	
CCC[d]	113.0	±0.4	
HCH	[107.2[b]	+0.9 −0.2]	
CCCl[d]	108.9	±0.4	

a) Distances in Å units, and angles in degree units. The r_{av}(C–H) and the φ_{av}(HCH) were assumed to be in the range of 1.075—1.085 Å and larger than 107.0° respectively; they are indicated by brackets. See text. b) The values obtained by the large-amplitude treatment would be 1.090 Å for the r_{av}(C–H) and 107.4° for the φ_{av}(HCH). c) The limits of error in the r_g values are equivalent to the allowed ranges of the r_{av}. d) Calculated from the distance-parameters.

Discussion

The r_0-structure determined by Matsumura and Takeo[6] is reproduced in the third column of Table 5 and compared with the result obtained by the present study in the second column of the table. The r_g(C–C) and r_g(C–Cl) values differ slightly from the r_0 values. However, if the difference in their physical meanings is taken into account,[17] such differences between r_g and r_0 as are shown in the table may be said to be reasonable. Thus, except for the structure of the methyl top, the two results are in good agreement with each other.

A comparison with the structure of 2-chloropropane

TABLE 5. COMPARISON OF THE STRUCTURES OF 2,2-DICHLOROPROPANE DETERMINED BY THE PRESENT AND THE MICROWAVE STUDIES, AND THE STRUCTURE OF 2-CHLOROPROPANE (in Å and degree units)

	2,2-Dichloropropane		2-Chloropropane
	r_g or φ_{av} (Present study)	r_0 (Matsumura *et al.*)[a]	r_g or φ_{av} (Iijima *et al.*)[b]
C–Cl	1.799 (3)	1.793 (5)	1.812 (1)
C–C	1.523 (4)	1.522 (assumed)	1.527 (1)
ClCCl	108.3 (0.3)	108.2 (0.5)	
CCC	113.0 (0.4)	113.0 (0.5)	112.7 (0.4)
CCCl[c]	108.9 (0.4)	108.9	109.0 (0.2)

a) Ref. 6. b) Ref. 5. c) Calculated from the other parameter values.

reported previously, which is also shown in Table 5, shows that the C–C and C–Cl distances are shorter in 2,2-dichloropropane than those in 2-chloropropane. An increase in the number of Cl atoms results in the shortenings of the C–C and C–Cl bonds. In spite of the contraction of the C_2CCl_2 frame of 2,2-dichloropropane, the valence angles, CCC and CCCl, are the same as those in 2-chloropropane, while the ClCCl angle is much smaller than the tetrahedral angle. Probably, the repulsive interactions between the two methyl tops and between the methyl top and the chlorine atom overcome the interaction between the two chlorine atoms.

The numerical computations were performed on a FACOM 230-75 of the Hokkaido University Computing Center and on a FACOM 270-20 in the laboratory of Professor Kimio Ohno, to whom the authors' thanks are due. The authors also wish to thank Dr. Chi Matsumura of the National Chemical Laboratory for Industry for permitting them to use his results prior to publication.

References

1) D. R. Lide, Jr., and M. Jen, *J. Chem. Phys.*, **38**, 1504 (1963).

2) See, *e.g.*, L. Nygaard, *Spectrochim. Acta*, **22**, 1261 (1966); H. Kakubari, T. Iijima, and M. Kimura, *Bull. Chem. Soc. Jpn.*, **48**, 1984 (1975).

3) Y. Fujimori, M. Ayabe, K. Endo, Y. Kamura, H. Takeo, and C. Matsumura, the 32nd National Meeting of the Chemical Society of Japan, Tokyo, April, 1975. A part of the results is published in; H. Takeo and C. Matsumura, *Bull. Chem. Soc. Jpn.*, **50**, 636 (1977).

4) As for the definitions of various distances, see, *e.g.*, K. Kuchitsu and S. J. Cyvin, "Molecular Structures and Vibrations," ed by S. J. Cyvin, Elsevier, Amsterdam (1972), Chap. 12; see also L. S. Bartell, K. Kuchitsu, and H. M. Seip. *Acta Crystallogr., Sect. A*, **32**, 1013 (1976). φ_a-denotes valence angles in the r_a-structure, while r_{av} and φ_{av} are used for values determined by a joint analysis.

5) T. Iijima, S. Seki, and M. Kimura, *Bull. Chem. Soc. Jpn.*, **50**, 2568 (1977).

6) C. Matsumura and H. Takeo, Symposium on Molecular Structure, Nagoya, Oct. 1973.

7) Y. Murata, K. Kuchitsu, and M. Kimura, *Jpn. J. Appl. Phys.*, **9**, 591 (1970).

8) 1 Torr = 101325/760 Nm^{-2}, 1 Å = 10^{-10}m.

9) The numerical data of the total intensity and the background for typical plates are deposited with the Chemical Society of Japan (Document No. 7814).

10) S. Konaka and M. Kimura, *Bull. Chem. Soc. Jpn.*, **43**, 1693 (1970).

11) J. H. S. Green and D. J. Harrison, *Spectrochim. Acta, Part A*, **27**, 1217 (1971).

12) In practice, the ranges of the r_a(C-H) and the φ_a(HCH) adopted were 1.08—1.10 Å and 108—110° respectively. See the section on joint analysis in the text.

13) A few points fall outside the expected limits of error. In the present analyses, all the observed values were employed. However, they do not affect the results. See Ref. 5.

14) K. Kuchitsu, "MTP International Review of Science, Physical Chemistry, Series One," Vol. 2, ed by G. Allen, Medical and Technical Publishing Co., Oxford (1972), Chap. 6.

15) T. Iijima and S. Tsuchiya, *J. Mol. Spectrosc.*, **44**, 88 (1972).

16) See footnote 22 in Ref. 5.

17) See, *e.g.*, Y. Morino, K. Kuchitsu, and T. Oka, *J. Chem. Phys.*, **36**, 1108 (1962).

The Molecular Structure of Ethyl Chloride as Determined by a Combined Use of the Electron-diffraction Data and the Spectroscopic Moments of Inertia

Masashi HIROTA, Takao IIJIMA,* and Masao KIMURA**

Department of Chemistry, Faculty of Science, Hokkaido University, Sapporo 060

(Received August 31, 1977)

The molecular structure of ethyl chloride has been determined by a joint analysis of the electron-diffraction data and the moments of inertia obtained by Schwendeman and Jacobs by means of microwave spectroscopy. In the analysis, a staggered conformation with C_s symmetry for the molecule and a local C_{3v} symmetry about the C–C axis for the methyl group were assumed. Under the further assumptions that $\varphi_{av}(HCH)_{CH_3}$ is $109.2\pm2°$ and $\varphi_{av}(CCH)_{CH_3}$ is in the range of 113.6—109.6°, the following parameter values were determined: r_g(C–C), 1.528(4) Å; r_g(C–Cl), 1.802(3) Å; r_g(C···Cl), 2.746(5) Å; $r_g(C–H)_{CH_3}$, 1.103(4) Å; $\varphi_{av}(HCH)_{CH_3}$, 110.0(1.6)°; and φ_{av}(CCCl), 110.7(0.3)°. The r_g and r_s distances for the C–Cl and C–C bonds of various chlorinated alkanes were plotted against the difference between the numbers of methyl groups and chlorine atoms, $\Delta n=n(CH_3)-n(Cl)$. In general, as the number of chlorine atoms increases, both distances become shorter, though the r_g distances are longer than the r_s distances by 0.01—0.03 Å.

In order to examine the environment effect on the bond lengths in the halogen derivatives of alkanes, precise structural determinations of chlorinated alkanes have been initiated[1] and in the preceding paper the structure of 2,2-dichloropropane has been reported.[2] As one of this series of studies, the results for ethyl chloride will be reported in the present paper.

Several microwave studies of this molecule can be found in the literature.[3–6] Among them, Schwendeman and Jacobs studied the widest variety of isotopic species and determined the r_s-structure.[6] Their data on the moments of inertia contain information necessary for our purpose, and the r_s-structure will serve for comparison with the r_g-structure determined by the present study.

According to them and also to Lide,[5] the barrier to the hindered rotation is about 3.6 kcal/mol, a value which is very close to those for propane,[7] 2-chloropropane,[8] and 2,2-dichloropropane.[9] This means that the torsional motion may be regarded as a small amplitude vibration in evaluating the vibrational correction of the present molecule as of the other molecules mentioned above; this correction is necessary to convert the r_g values determined by the electron diffraction and the observed moments of inertia, $I^{(eff)}$, into the values in the zero-point average structure, r_α^0 or $I^{(z)}$.[10] In this study, therefore, the vibrational correction has been carried out by the small-amplitude treatment[11] after the manner adopted in previous papers.[1,2]

Experimental

The sample of ethyl chloride was a guaranteed reagent purchased from Nakarai Chemicals, Ltd., and was used without further purification. Diffraction photographs were taken with a unit in our laboratory at room temperature, 20 °C. The other experimental conditions were as follows: camera length, 109 mm; accelerating voltage, 42 kV; beam current, 0.1 μA; sample pressure, 50 Torr,[12] and exposure time, 110 s. The covered s range was 6—40 $Å^{-1}$.[12] The wavelength, or the scale factor, was determined by reference to the diffraction pattern of carbon disulfide taken under the same experimental conditions. Three plates were selected for analysis.

Analysis of Electron-diffraction Data

The observed total intensities[13] were reduced to the molecular intensities, $sM(s)$, following our usual procedure.[14] The molecular intensities thus obtained were used for the refinement of the molecular parameter values by means of the least-squares method.[14] In the refinement, the following assumptions were made as to the molecular geometry: (1) a staggered conformation with C_s symmetry for the molecule as a whole; (2) a local C_{3v} symmetry for the methyl group; (3) a zero tilt angle for the methyl group, and (4) r_a(C–H) distances equal to 1.105 Å, $\varphi_\alpha(CCH)_{CH_3}=111.6°$, $\varphi_\alpha(HCH)_{CH_3}=109.2°$, and $\varphi_\alpha(HCH)_{CH_3}=108.5°$. These assumed values were taken from the r_s-structure determined by Schwendeman and Jacobs.[6] The values left to be determined are, then, the bonded C–Cl and C–C distances and the non-bonded C···Cl distance. All the mean amplitudes were fixed at values calculated using the force field proposed by Dempster and Zerbi.[15] The calculated mean amplitudes for the main distances are listed in Table 1. The Morse asymmetry constants, a_3, were assumed to be 2.0, 2.1, and 2.0 $Å^{-1}$ for the C–Cl, C–C, and C–H distances respectively, and zero for all non-bonded atom pairs, in the estimation of the asymmetry parameters, κ. As long as the distances and

Table 1. Calculated mean amplitudes at 20 °C (in Å units)

Distance	Calculated mean amplitude
C–Cl	0.0533
C–C	0.0510
C–H	0.0784
C···Cl	0.0799
Cl···H	0.1068
Cl:::H_{trans}	0.1062
Cl:::H_{gauche}	0.1813

* Present address: Gakushuin University, Mejiro, Tokyo 171.

** To whom correspondence should be addressed.

Table 2. Results of electron diffraction (in Å units)[a]

	r_g[b]	r_α^0[c]
C···Cl	2.739(11)	2.733
C–Cl	1.798(5)	1.795
C–C	1.523(8)	1.520
Index of resolution	0.93—1.04	

a) The geometry of the methyl group was assumed at the values determined by microwave spectroscopy. See text. b) The values in parentheses indicate the limits of error, which were estimated from the random errors obtained in the least-squares adjustment and the systematic errors included in the scale factor, which was ±0.06 % in distances. c) r_α^0 were derived from r_g; see text. The errors are regarded to be the same as those for r_g.

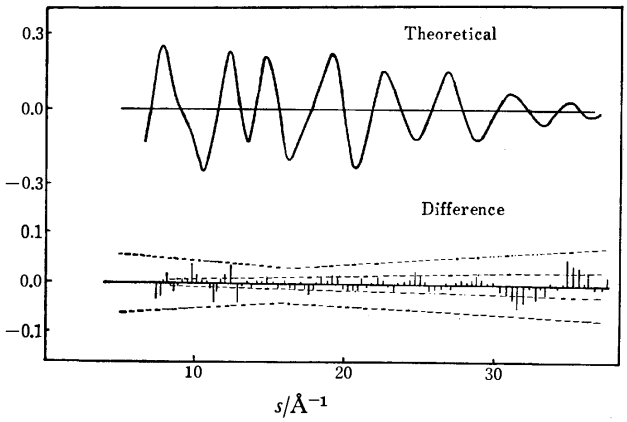

Fig. 1. The theoretical molecular intensity curve, $sM(s)$, for the best fit parameters, and the difference, $sM(s)^{obsd}-sM(s)^{calcd}$. In the difference, the inner broken lines indicate the limit of detection in photometry, and the outer broken lines the estimated limit of errors in the observed intensities; see Ref. 1. The ordinate for the difference curve is enlarged twice as large as that of the intensity curve.

angles in the methyl group are assumed to be within the ranges of plausible values (see the next section), the converged C–Cl, C–C, and C···Cl values change by only one or two thousandths Å, a value which is much smaller than the limits of error.

The results of the least-squares analyses are listed in Table 2. Figure 1 shows the theoretical molecular intensity curve for the best-fit parameters and the difference between the theoretical and observed intensities.

Joint Analysis

The r_g values obtained by the electron-diffraction were converted into the r_α^0 values using the parallel and perpendicular mean amplitudes calculated at 293 and 0 K, the centrifugal stretching, and the assumed Morse asymmetry constants. The r_α^0 values thus obtained are also entered in Table 1.

The moments of inertia have been determined by Schwendeman and Jacobs for seven isotopic species, including the parent $CH_3CH_2{}^{35}Cl$ species.[6] Among them, the ^{37}Cl-species and ^{13}C-species do not provide additional information useful for our purpose,[1] and the species containing a partially deuterated methyl group would not be helpful for the determination of the molecular structure because they have no local C_{3v} symmetry in the r_z-structure and so only increase the number of parameters to be determined. Thus, we made use of the moments of inertia of only two species, $CH_3CH_2{}^{35}Cl$ and $CH_3CD_2{}^{35}Cl$. The observed moments of inertia, $I^{(eff)}$, were corrected for the harmonic vibrations by means of the small-amplitude treatment and were converted into the zero-point moments of inertia, $I^{(z)}$. The results are listed in Table 3.[16]

Table 3. Observed and corrected moments of inertia and the vibrational corrections (in amu Å² units)[a]

		$I^{(eff)}$	ΔI	$I^{(z)}$
$CH_3CH_2{}^{35}Cl$	a	16.121	0.020	16.141
	b	91.992	0.139	92.131
	c	101.843	0.084	101.927
$CH_3CD_2{}^{35}Cl$	a	20.935	0.021	20.956
	b	94.414	0.124	94.538
	c	105.902	0.083	105.985

a) The conversion factor: 505376 MHz amu Å². b) $I^{(z)}=I^{(eff)}+\Delta I$. c) The uncertainties included in ΔI, and accordingly in $I^{(z)}$ also, are estimated to be about 10% of the corrections themselves; see Ref. 1. The joint analysis was, therefore, carried out by assuming the uncertainties in $I^{(z)}$ to be ±0.01 amu Å².

The isotope effect for the C–H distance, $\delta(C-D)=r_z(C-D)-r_z(C-H)$, was estimated and assumed to be -0.0007 ± 0.0014 Å.[17] However, the $\varphi_z(DCD)$ and the $\varphi_z(CCD)$ values were added in parameters because no appropriate method of estimation has been found. Taking all the $r_g(C-H)$ distances to be equivalent, the difference between the $r_z(C-H)_{CH_3}$ and $r_z(C-H)_{CH_2}$ distances was estimated to be 0.007 Å by converting the r_g values into the corresponding r_z values. Thus the number of parameters to be adjusted becomes nine (see Table 5 below), while the available data are two bonded distances determined by the electron diffraction and the six moments of inertia. The C···Cl distance obtained by the electron diffraction was not used, for the r_α^0 value derived from the r_g value might not be accurate enough; anharmonicity for a non-bonded atom-pair is still ambiguous. Therefore, the value of $\varphi_z(HCH)_{CH_3}$ was assumed to be $109.2\pm2°$ by referring to the reported r_s-structure[6] (see also Table 5).[18] The eight parameters to be determined are r(C–C), r(C–Cl), r(C···Cl), $r(C-H)_{CH_2}$, $\angle HCH_{CH_2}$, δ(DCD) ($=\angle DCD_{CD_2}-\angle HCH_{CH_2}$), $\angle CCH_{CH_2}$, and δ(CCD) ($=\angle CCD_{CD_2}-\angle CCH_{CH_2}$).

However, in fitting the eight parameters to the eight observed quantities, the allowed ranges for r(C–C) and r(C–Cl) could never be smaller than the limits of error of the electron-diffraction results, and the values of the other parameters may include both unreasonably large and small values. Therefore, the reported r_s-structure[6] was again used in order to restrict the $\varphi_z(CCH)_{CH_3}$ so that it was in the range of $111.6\pm2.0°$.[18]

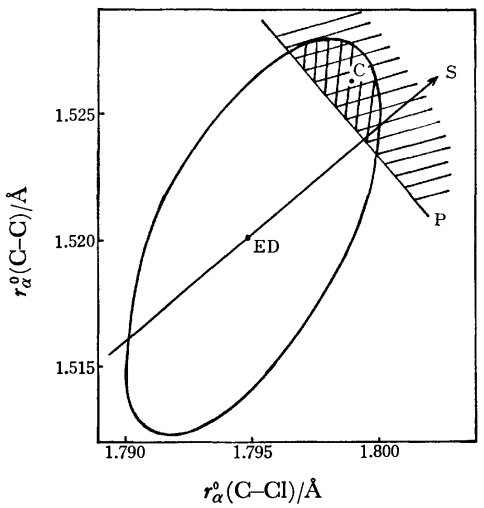

Fig. 2. The diagram of the allowable range of the C–Cl and C–C distances. The ED point indicates the best values determined by electron diffraction. The shaded area is allowed by the moments of inertia when the isotope effect, δ(C–D), is taken as −0.0007 Å and the C point indicates the final values. See text for the details. The cross-shaded area is allowed by both the electron diffraction data and the moments of inertia.

Figure 2 shows the r(C–C) and r(C–Cl) values allowed by the electron-diffraction data and the six moments of inertia under the assumptions and the restriction mentioned above. In this figure, the ED point represents the best values determined by electron diffraction, while the ellipse shows the total limits of error estimated from both the random error obtained by the least-squares adjustment and the systematic error included in the scale factor. The straight line, S, indicates the direction of change in the distances with the change in the scale factor. On the other hand, the shading in Fig. 2 indicates the area obtained by projecting the region allowed by the six moments of inertia onto the r(C–C)-r(C–Cl) plane. The P line perpendicular to the S line represents a lower bondary of the allowed region on the r(C–C)-r(C–Cl) plane, when δ(C–D) is taken to be −0.0007 Å. Thus, the cross-shaded area is the region of the r(C–C) and r(C–Cl) values allowed by both the electron-diffraction data and the moments of inertia. The final r_{av}(C–C) and r_{av}(C–Cl) values, represented by the point C in Fig. 2, were taken at the center of a rectangle which contained the allowable region and had its sides parallel to S and P. With these r_{av}(C–C) and r_{av}(C–Cl) values, and on the assumptions that $\varphi_{av}(HCH)_{CH_3}$= 109.2°, that δ(C–D) = −0.0007 Å, and that $\varphi_{av}(CCH)_{CH_3}$ was in the range of 113.6—109.6°, the final values for the other parameters were determined; with these values the six moments of inertia were satisfied best. The results are listed in the 2nd column of Table 4.

The errors listed in Table 4 were estimated as follows: ε_1 are the limits of the allowable parameter values explored with the C–C and the C–Cl values in the allowed region shown in Fig. 2; ε_2 are the limits of error due to the uncertainty included in ΔI, ±0.01 amu Å^2;[19] ε_3 were estimated by considering that the assumed $\varphi_z(HCH)_{CH_3}$ included an uncertainty of ±2°; ε_4 and ε_4' were estimated from the uncertainty included in the isotope effect for the C–H distance. As was mentioned before, the uncertainty in the δ(C–D) was estimated to be ±0.0014 Å. A change in the δ(C–D) causes the P line to shift parallel to itself in Fig. 2 and, consequently, influences the limits of error in two manners. The first influence appears as the shift of the C point, while the second one brings about a change in the width of the allowed region on the C–Cl *vs.* C–C map. A decrease in the δ(C–D) makes the P line shift in the direction of the scale factor decrease. Therefore, in order to estimate errors, it is necessary to estimate only the

Table 4. Results of the joint analysis (in Å and degree units)

	r_{av} or φ_{av}	ε_1	ε_2	ε_3	ε_4	ε_4'	ε_0
C–C	1.5262	$^{+0.0018}_{-0.0022}$	—	—	−0.002	±0.002	±0.004
C–Cl	1.7990	$^{+0.0010}_{-0.0025}$	—	—	−0.001	±0.001	±0.003
C···Cl	2.7399	$^{+0.0028}_{-0.0011}$	±0.0002	±0.0025	−0.002	±0.002	±0.005
$C–H_{CH_3}$[a]	1.082	$^{+0.001}_{-0.001}$	±0.001	±0.003	+0.001	±0.001	±0.004
HCH_{CH_3}	109.8	$^{+0.35}_{-0.35}$	±0.2	±1.5	−0.4	±0.4	±1.6
CCH_{CH_3}	110.6	$^{+3.0}_{-0.0}$	±0.2	±1.0	+2.0	—	±3.0
HCH_{CH_3}	[109.2][c]						
δ(C–D)[b]	[−0.0007][c]						
δ(DCD)[b]	0.2	$^{+0.05}_{-0.05}$	±0.1	±0.8	+0.1	—	±0.9
δ(CCD)[b]	0.8	$^{+0.2}_{-1.0}$	±0.1	±0.3	+0.4	—	±1.1

a) $r_z(C–H)_{CH_3} - r_z(C–H)_{CH_3} = -0.007$ Å. b) $\delta(C–D) = r_z(C–D) - r_z(C–H)$; $\delta(DCD) = \varphi_z(DCD) - \varphi_z(HCH)$; $\delta(CCD) = \varphi_z(CCD) - \varphi_z(CCH)$. c) These values were assumed. The errors associated with the assumptions are estimated as ε_3, ε_4, and ε_4'. See text.

Table 5. Final parameter values
(in Å and degree units)

	r_{av} or φ_{av}	r_g	r_s[a]
C–C	1.526(4)	1.528(4)	1.520(3)
C–Cl	1.799(3)	1.802(3)	1.788(2)
C···Cl	2.740(5)	2.746(5)[d]	(2.730)[f]
$C-H_{CH_3}$	1.091(4)[b,c]	1.103(4)	1.091(10)
HCH_{CH_3}	110.0(1.6)[c]		108.5(0.5)
CCH_{CH_3}	110.6(3.0)		111.6(0.5)
δ(DCD)[e]	0.2(0.9)		
δ(CCD)[e]	0.8(1.0)		
CCCl	110.7(0.3)[f]		111.0(0.1)
HCH_{CH_3}	[109.2][g]		109.2(0.5)
δ(C–D)	[−0.0007][g,h]		

a) Ref. 6. b) $r_z(C-H)_{CH_3}-r_z(C-H)_{CH_3}=-0.007$ Å. c) 0.009 Å and 0.2° were added to the values in Table 3 in order to convert them into the values for the torsionless molecule. d) Converted from r_{av} assuming the asymmetry constant to be zero. e) $\delta(DCD)=\varphi_z(DCD)_{CD_3}-\varphi_z(HCH)_{CH_3}$; $\delta(CCD)=\varphi_z(CCD)_{CD_3}-\varphi_z(CCH)_{CH_3}$. f) Calculated from the other parameter values. g) These values were assumed in the joint analysis. See text. h) $\delta(C-D)=r_z(C-D)_{CD_3}-r_z(C-H)_{CH_3}=-0.0007\pm0.0014$ Å.

influence of the decrease in the δ(C–D). ε_4 and ε_4' are uncertainties related to the shift of the C point and the increase in the allowed region respectively, when $\delta(C-D)=-0.0007-0.0014$ Å. A similar effect of the uncertainty of $\angle HCH_{CH_3}$ to the allowed region on the C–C *vs.* C–Cl was negligibly small. In order to assign the total errors, it seems safe to adopt as great error as possible in the present case. Therefore, as for ε_1 we adopted a greater value, irrespective of its sign, while for ε_4 we ignored the fact that it is applicable only in the specified direction. Then the total errors, ε_0, were estimated by considering all these errors to be independent of one another: they are listed in the last column of Table 4. Table 5 shows the final values for r_{av} and φ_{av}, their limits of error, and the r_g values derived from the r_{av}. In order to compare the C–H distances and HCH angles in various molecules, it is desirable to list these parameters in the state in which the torsional motions are eliminated.[20] Therefore, Table 5 gives the r_{av}(C–H) and the φ_{av}(HCH) for the torsionless state. They were obtained by adding 0.009 Å and 0.2° respectively to the r_{av} and φ_{av} obtained by the small-amplitude treatment.[1]

Discussion

We adopted the value of 2.746 Å as the final r_g(C···Cl) distance, the value of 2.739 Å obtained by the electron-diffraction being consistent with it within the limits of error. In deriving the r_g value from the r_{av} value, the Morse asymmetry constant a_3 for this non-bonded distance was assumed to be zero. However, the possibility of a_3 having a negative value has been pointed out in the study of 2-chloropropane[1] and also in the recent studies of $CHBr_3$, CH_2Br_2[21] and $CHCl_3$.[22] In the present case, a negative a_3 brings the r_g(C···Cl) obtained by the joint analysis closer to the diffraction value, although the large uncertainty of the latter makes it difficult to place any significance on the closeness of the two values. A similar situation was also found in the Cl···Cl distance of 2,2-dichloropropane.[2]

In the present analysis, we had to assume the symmetry of the methyl group. As a result, only the average values of the C–H distances and the HCH angles were determined for the structure of the methyl group. According to the microwave study by Zeil *et al.*, the r_s-structure of the methyl top does not have C_{3v} local symmetry.[23] However, since the method of using these r_s data in the determination of the r_g or r_{av} structure has not been established, the precise structure of the methyl group of this molecule in terms of r_g or r_{av} is left unsolved. Similar situations are probably more or less present for other molecules as well. This seems to pose a problem for the future.

The last column of Table 5 shows the r_s values reported by Schwendeman and Jacobs.[6] It should be

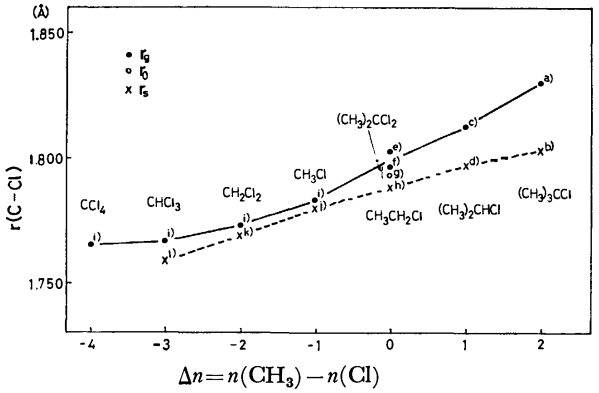

Fig. 3. The r_g(C–Cl) and r_s(C–Cl) distances of chlorinated alkanes plotted against $\Delta n=n(CH_3)-n(Cl)$: a) Ref. 25; b) Ref. 26; c) Ref. 1; d) Ref. 8; e) the present study; f) Ref. 2; g) r_0 value, Ref. 24; h) Ref. 6; i) preliminary results in our laboratory, which are almost the same as those reported so far; j) Ref. 12; k) Ref. 28; l) Ref. 29.

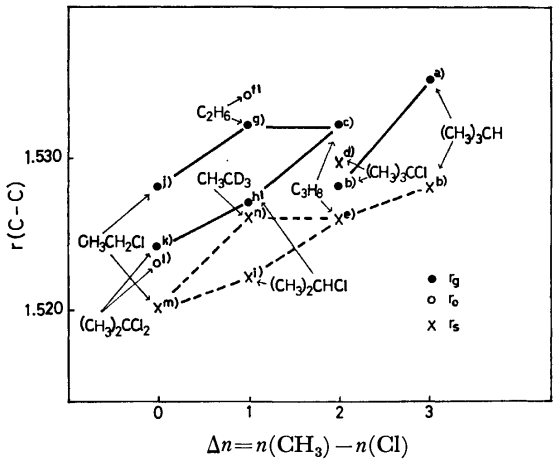

Fig. 4. The r_g(C–C) and r_s(C–C) distances of chlorinated alkanes plotted against $\Delta n=n(CH_3)-n(Cl)$; a) Ref. 30; b) Ref. 25; c) Ref. 31; d) Ref. 26; e) Ref. 32; f) Ref. 33; g) Ref. 34; h) Ref. 1; i) Ref. 8; j) the present study; k) Ref. 2; l) Ref. 24; m) Ref. 23; n) Ref. 35.

noted that the r_s distances are all shorter than the corresponding r_g distances.

Matsumura and his co-workers showed that the C–Cl and C–C r_s distances for various chlorinated alkanes exhibit systematic changes against the difference between the numbers of methyl groups and chlorine atoms attached to the carbon atom, $\Delta n = n(CH_3) - n(Cl)$.[24] Their results are reproduced in Figs. 3 and 4, together with the plotting of the r_g values. As may be seen in Fig. 3, the C–Cl distances become shorter as Δn decreases; if Δn is the same, the C–Cl distances are also the same. For the C–C distances in Fig. 4, the situation is a little more complicated. For compounds consisting of the same number of carbon atoms, the one with more chlorine atoms has a shorter C–C distance, while compounds with the same number of chlorine atoms have nearly the same C–C distance. The r_g distances show a similar tendency, but generally they are longer than the corresponding r_s distances. An exception is found in the C–C distance of *t*-butyl chloride, in which the r_s value could be unusual, for the central carbon is very close to the center of gravity of the molecule.

The numerical computations were performed on a FACOM 230-75 of the Hokkaido University Computing Center and also on a FACOM 270-20 in the laboratory of Professor Kimio Ohno, to whom the authors' thanks are due.

References

1) T. Iijima, S. Seki, and M. Kimura, *Bull. Chem. Soc., Jpn.*, **50**, 2568 (1977).
2) M. Hirota, T. Iijima, and M. Kimura, *Bull. Chem. Soc. Jpn.*, **51**, 1589 (1978).
3) R. S. Wagner and B. P. Dailey, *J. Chem. Phys.*, **26**, 1588 (1957).
4) A. I. Barchuker, T. M. Murina, and A. M. Prokhorov, *Opt. Spektrosk.*, **4**, 521 (1958).
5) D. R. Lide, Jr., *J. Chem. Phys.*, **30**, 37 (1959).
6) R. H. Schwendeman and G. D. Jacobs, *J. Chem. Phys.*, **36**, 1245 (1962).
7) 3.40 kcal/mol; D. M. Grant, R. J. Pugmire, R. C. Livingston, K. A. Strong, H. L. McMurry, and R. M. Brugger, *J. Chem. Phys.*, **52**, 4424 (1970).
8) 3.45 kcal/mol; F. L. Tobiason and R. H. Schwendeman, *J. Chem. Phys.*, **40**, 1014 (1964).
9) 3.40 kcal/mol; J. H. S. Green and D. J. Harrison, *Spectrochim. Acta*, **27A**, 1217 (1971).
10) As for the definitions of various distances, see, *e.g.*, K. Kuchitsu and S. J. Cyvin, "Molecular Structures and Vibrations," ed by S. J. Cyvin, Elsevier, Amsterdam (1972), Chap. 12; see also L. S. Bartell, K. Kuchitsu, and H. M. Seip, *Acta Crystallogr., Sect. A*, **32**, 1013 (1976). φ_α denotes valence angles in the r_α-structure, while r_{av} and φ_{av} are used for the values determined by a joint analysis; see T. Fukuyama and K. Kuchitsu, *J. Mol. Struct.*, **5**, 131 (1970).
11) K. Kuchitsu, "MTP International Review of Science, Physical Chemistry Series One," Vol. 2, ed by G. Allen, Medical and Technical Publishing Co., Oxford (1972), Chap. 6.
12) 1 Torr = 101325/760 Nm^{-2}, 1 Å = 10^{-10} m.
13) The observed intensities and the background for typical plates have been deposited with the Chemical Society of Japan (Document No. 7813).
14) S. Konaka and M. Kimura, *Bull. Chem. Soc. Jpn.*, **43**, 1693 (1970).
15) A. B. Dempster and G. Zerbi, *J. Mol. Spectrosc.*, **39**, 1 (1971).
16) The $I^{(eff)}$ values in Table 2 are slightly different from those quoted in Schwendeman and Jacobs. This is a result of the difference in the conversion factor used.
17) This uncertainty in the δ(C–D) was estimated from an uncertainty of ± 0.5 $Å^{-1}$ in the Morse asymmetry constant.
18) The uncertainty of $\pm 2°$ is probably a good estimate for an angle of the r_s-structure to be used in zero-point average structure. See Ref. 1.
19) See Table 3, footnote c, and also Ref. 1.
20) T. Iijima and S. Tsuchiya, *J. Mol. Spectrosc.*, **44**, 88 (1972).
21) K. Tamagawa and M. Kimura, unpublished data.
22) H. Kunimi and M. Kimura, unpublished data.
23) Private communication.
24) Y. Fujimori, M. Ayabe, K. Endo, Y. Kamura, H. Takeo, and C. Matsumura, 32nd National Meeting of the Chemical Society of Japan, Tokyo, April, 1975. A part of the results have been published in H. Takeo and C. Matsumura, *Bull. Chem. Soc. Jpn.*, **50**, 636 (1977), and K. Endo, H. Takeo, and C. Matsumura, *ibid.*, **50**, 626 (1977).
25) R. L. Hilderbrandt and J. D. Wieser, *J. Chem. Phys.*, **55**, 4648 (1971); *ibid.*, **56**, 1143 (1972).
26) D. R. Lide, Jr., and M. Jen, *J. Chem. Phys.*, **38**, 1504 (1963).
27) C. C. Costain, *J. Chem. Phys.*, **29**, 864 (1958).
28) $r_s = 1.769$; C. Matsumura, private communication. $r_0 = 1.772$; R. J. Myers and W. D. Gwinn, *J. Chem. Phys.*, **20**, 1420 (1952).
29) M. Jen and D. R. Lide, Jr., *J. Chem. Phys.*, **36**, 2525 (1962).
30) R. L. Hilderbrandt and J. D. Wieser, *J. Mol. Struct.*, **15**, 27 (1973).
31) T. Iijima, *Bull. Chem. Soc. Jpn.*, **45**, 1291 (1972).
32) D. R. Lide, Jr., *J. Chem. Phys.*, **33**, 1514 (1960).
33) $r_0 = 1.534$; D. E. Shaw and W. L. Welsh, *Can. J. Phys.*, **44**. 3823 (1967).
34) T. Iijima, *Bull. Chem. Soc. Jpn.*, **46**, 2311 (1973).
35) E. Hirota, K. Matsumura, M. Imachi, M. Fujio, Y. Tsuno, and C. Matsumura, *J. Chem. Phys.*, **66**, 2660 (1977).

The Effect of Poly(oxyethylene) Alkyl Ethers, Alkanediols, and Alkanols on the Critical Micelle Concentration of Sodium Dodecyl Sulfate

Masahiro MANABE and Masaharu KODA

Department of Industrial Chemistry, Niihama Technical College, Niihama, Ehime 792

(Received September 5, 1977)

The effect of the addition of the homologues of poly(oxyethylene) alkyl ethers ($C_mH_{2m+1}(OCH_2CH_2)_nOH$: $m=3$—6, $n=1$—4), α,ω-alkanediols ($m=4$—6, 8), and 1-alkanols ($m=2$—7) on the critical micelle concentration (CMC) of sodium dodecyl sulfate (SDS) was examined. The homologous additives are appropriate for studying the effect of polar groups as well as an alkyl group. The CMC decreases with an increase in the concentration of additive. The rate of CMC-decrease estimated at the infinite dilution of the additive increases with the length of alkyl chain in each homologue. The dependence of the rate on the alkyl chain length is the same for all the homologues with longer chain ($m \geqq 4$ for ethers and alkanols, and $m > 6$ for alkanediols). This is ascribed to the complete transfer of the long alkyl chain into the interior of micelles. The dependence of rate on the number of polar groups (OH, OCH_2CH_2) is as follows. The rate for alkanediol is lower than that for alkanol with a given alkyl chain. The rate for ethers increases asymptotically with the length of oxyethylene chain. The result for alkanediol is ascribed to the pronounced hydrophilic nature, and that for ethers to the reduction of electrostatic repulsive force between ionic head groups of the surfactant in micelles.

Successive addition of a small amount of normal 1-alkanols and their isomers to a surfactant solution depresses critical micelle concentration (CMC) of several, ionic[1-3] and nonionic[4] surfactants. The rate of CMC-decrease, defined as the decrement of CMC caused by unit increase of additive concentration, increases with an increase in the number of carbon atoms of the alkyl chain. Systematic studies on the effect of additives have so far been restricted to alkanols, because of the authors' interest[1-4] in the hydrophobic behavior of the alkyl chain in the additives dissolved in the surfactant solutions. No systematic study seems to have been made on the effect of additives having various hydrophilic polar groups on the CMC of surfactant solutions. The study is necessary for finding the factor governing the micelle formation and solubilization of surfactants.

This paper deals with the effect of homologous additives, poly(oxyethylene) alkyl ethers, α,ω-alkanediols, and 1-alkanols, on the CMC of sodium dodecyl sulfate. The homologues are appropriate for studying the effect of their polar groups as well as a methylene group in their alkyl chain, since the hydrophilic property of the additives can be altered successively by the number of oxyethylene and hydroxyl groups. The present study gives information on the mixed micelle, consisting of an ionic surfactant and a poly(oxyethylene)-type nonionic one.[5-10]

Experimental

Materials. Sodium dodecyl sulfate (SDS), water, normal 1-alkanols (C_2—C_7), and poly(oxyethylene) alkyl ethers ($C_mH_{2m+1}(OCH_2CH_2)_nOH$: $m=3$, $n=1$; $m=4$, 5, $n=1$—4) were the same as given in the previous studies.[11,12] The ethers ($m=6$, $n=1$, 2, Tokyo Kasei Kogyo Co., Ltd. G. R. grade) were used without further purification. α,ω-Alkanediols (C_4—C_6, C_8) were used after distillation through a 1 m column under reduced pressure.

Determination of CMC. The conductivity of aqueous SDS solution prepared with a solvent containing a small amount of the additives was measured on a Yanagimoto Model MY-7 conductivity meter. Measurements were carried out in a water-thermostat controlled within 25± 0.01 °C. The critical micelle concentration (CMC) of SDS in an aqueous additive solution was taken as the SDS concentration at the break point in the plot of specific conductance *vs.* SDS concentration.[13] The CMC of SDS in water was determined to be 8.30 mmol/kg.

Results and Discussion

For all the additives, the CMC of SDS decreases linearly with an increase in the concentration of the additives within their low concentration regions, deviating gradually upwards from linearity at higher concentrations as shown in Fig. 1 for 1-pentanol and its derivatives. This is in line with the systems of alkanols and surfactants.[1-4] The rate of CMC-decrease, k, is determined by the limiting slope of the straight line where at least four points fall on each straight line. The values of k are given in Table 1.

The logarithm of $-k$ is plotted in Fig. 2 against the number of carbon atoms, m, in alkyl chain in each homologue. The lines are of similar form, a monotonic

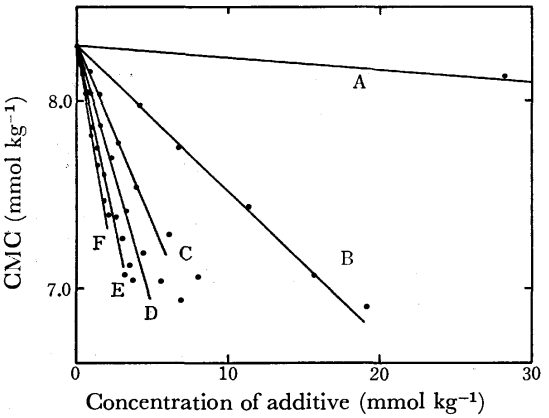

Fig. 1. The relation between CMC of SDS and concentration of additives (1-pentanol derivatives). A: Alkanediol, B: alkanol, C: ether, $n=1$, D; $n=2$, E: $n=3$, F; $n=4$.

TABLE 1. THE VALUE OF k FOR HOMOLOGOUS ADDITIVES

m	$-k$ (mol kg^{-1}/mol kg^{-1})					
	n of ether[a]				Alkanol	Alkane-diol
	1	2	3	4		
2					0.0013	
3	0.021				0.0087	
4	0.072	0.11	0.14	0.18	0.028	0.0012
5	0.19	0.28	0.38	0.47	0.078	0.0066
6	0.48	0.78			0.21	0.022
7					0.53	
8						0.18

a) Poly(oxyethylene) alkyl ether.

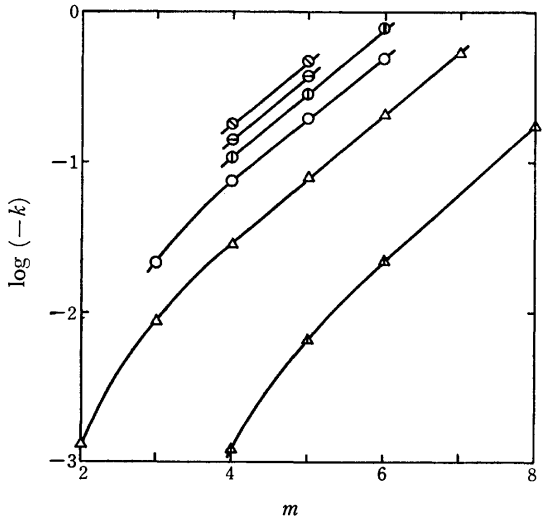

Fig. 2. The relation between log(−k) and alkyl chain length (m). Homologue of alkanediol (△), alkanol (△), ethers of n=1 (○), n=2 (◐), n=3 (⊖), n=4 (⊘).

increase in log (−k) as a function of m being found to be linear above a certain number of m. For each homologous series, a standard free energy change of transfer per methylene group, $\Delta G°(CH_2)$, from aqueous environment to micelles can be calculated by [2,3]

$$\Delta G°(CH_2) = -RT\,\mathrm{d}\ln(-k)/\mathrm{d}m \qquad (1)$$

or by its approximation

$$\Delta G°(CH_2) = -RT\{\ln(-k_{m+1}) - \ln(-k_m)\} \qquad (2)$$

as a function of m. The $\Delta G°(CH_2)$ value, calculated from each pair of neighboring k values taken from the appropriate column in Table 1, is plotted against m in Fig. 3. The plots of alkanol and its poly(oxyethylene) ethers can be regarded as giving a single curve. For all the homologues, the absolute value of $\Delta G°(CH_2)$ decreases initially with the increasing m, and then takes a constant value (−590 cal/mol CH_2)* from about m=4 for alkanols and ethers, and from about 6 for alkanediols. The value is comparable with the corresponding free energy value in the process of hydrophobic bond formation (*ca.* −600 cal/mol CH_2).[14,15] Thus, for each series of homologues including alkanediols which bears polar

* 1 cal=4.18$_4$ J.

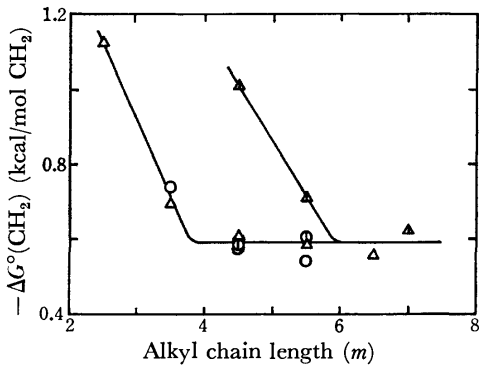

Fig. 3 The relation between $\Delta G°(CH_2)$ and alkyl chain length (m). The mark of each homologue is the same as that in the legend in Fig. 2.

groups at both end positions of the alkyl chain, the methylene groups remote from the polar group by more than about three carbon atoms can be transferred from aqueous environment to the non-polar interior of micelles. This is in line with the view that, in the process of micelle formation of surfactant alone, the hydration of the four methylene groups adjacent to its head group is retained.[16] In other words, the shorter alkyl-chain compounds are probably transferred incompletely (at most, up to the surface region of micelles) or not at all (changing only the property of aqueous medium) owing to their remarkable miscibility with water. The results are supported by the previous findings[11] that the partial molar volumes of 1-butanol and longer-chain 1-alkanols are higher in the micellar solution of SDS than in water, no difference being observed for 1-propanol and lower ones; the lower alkanols are not solubilized to a great extent.

The relation between log (−k) and the number of hydroxyl groups and oxyethylene groups (n) is shown in

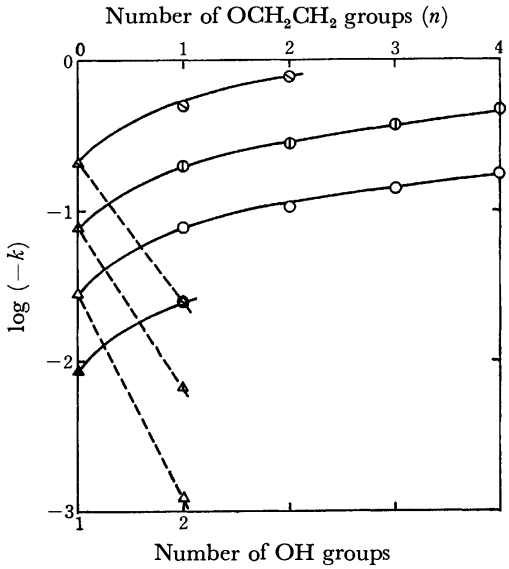

Fig. 4. The relation between log(−k) and the number of oxyethylene (n) and of hydroxyl groups. Solid line refers to ether: m=3 (●), m=4 (○), m=5 (◐), m=6 (⊘), and broken line to hydroxyl derivatives: m=3 (▲), m=4 (△), m=5 (◭), m=6 (◬).

Fig. 4. With alkanediols, log $(-k)$ is lower than that for alkanol with the same alkyl chain. However, for ethers, log $(-k)$ increases asymptotically with an increase in n, where alkanol is regarded as an ether with $n=0$. The tendencies are also seen in Fig. 1.

When a small amount of a nonionic amphiphilic substance is added to an ionic surfactant solution to form mixed micelles, the following main factors controlling the CMC-decrease can be considered: (i) thermodynamic factor by which the free energy of mixing decreases, and (ii) electrostatic factor by which the repulsive force decreases among ionic head groups in the surface region of micelles. Both hydroxyl and oxyethylene groups are hydrophilic.[12,13] From the view that an additive dissolves undergoing partition between a polar aqueous phase and a non-polar micellar one, the decreasing tendency of log $(-k)$ with the number of hydroxyl groups (Fig. 4) might be caused for the reason that alkanediol is more difficult to be transferred to the micellar phase than alkanol because of the higher hydrophilicity of the former. Thus, (i) would be the predominant factor.

The tendency of ethers to increase (Fig. 4) is explained as follows. The oxyethylene chain, which wedges off among the ionic head groups, occupies a large space in the ionic surface region of micelles to reduce ionic repulsive force. In addition, the hydrophilic nature of an oxyethylene group is less remarkable than that of a hydroxyl group.[18] The increase in the number of oxyethylene groups may not prevent effectively the solubilization of an additive in contrast with that in the number of hydroxyl groups. Thus, factor (ii) is likely to be more effective than factor (i). The present results are reasonably compared with those of the mixed micelles consisting of an ionic surfactant and a poly(oxyethylene)-type nonionic one, since the present ethers are similar to the nonionic surfactant in molecular structure. This explanation is in line with the results of potentiometric study on a mixed surfactant system: the degree of dissociation of the mixed micelles increases with an increase in the proportion of nonionic component.[8,10] It is also supported by the results obtained in the determination of CMC, in which the break in the curve of specific conductance *vs.* concentration of SDS in water becomes less sharp[5,10] with increase in the content of additive. The tendency becomes remarkable as the oxyethylene chain in ethers is lengthened. The asymptotical curve for ethers (Fig. 4) suggests that an oxyethylene group more remote from the alkyl chain has fewer occasions to approach the surface of micelle near enough to interact appreciably with ionic head groups scattering on it. Another suggestion is as follows. The longer the oxyethylene chain, the more powerful the hydrophilic nature of the ether molecule, and the more difficult the transfer of the ether molecule into micelles, as in the case of alkanediol. As a result, factor (i), the decrease of ether-concentration in micelles, may be added gradually to factor (ii).

We thank Prof. Ryohei Matuura, Kyusyu University, and Prof. Mituru Tanaka, Fukuoka University, for their encouragement.

References

1) S. H. Herzfeld, M. L. Corrin, and W. D. Harkins, *J. Phys. Colloid Chem.*, **54**, 271 (1950).
2) K. Shinoda, *J. Phys. Chem.*, **58**, 1136 (1954).
3) K. Shirahama and T. Kashiwabara, *J. Colloid Interface Sci.*, **36**, 65 (1971).
4) N. Nishikido, Y. Moroi, H. Uehara, and R. Matuura, *Bull. Chem. Soc. Jpn.*, **47**, 2634 (1974).
5) O. Yoda, K. Meguro, T. Kondo, and T. Ino, *Nippon Kagaku Zasshi*, **77**, 905 (1955).
6) T. Nakagawa and H. Inoue, *Nippon Kagaku Zasshi*, **78**, 636 (1957).
7) A. M. Mankowich, *J. Am. Oil Chem. Soc.*, **41**, 449 (1964).
8) J. M. Corkill, J. F. Goodman, and J. R. Tate, *Trans. Faraday Soc.*, **60**, 986 (1964).
9) M. J. Schick and D. J. Manning, *J. Am. Oil Chem. Soc.*, **43**, 133 (1966).
10) F. Tokiwa and N. Moriyama, *J. Colloid Interface Sci.*, **30**, 338 (1969).
11) M. Manabe, K. Shirahama, and M. Koda, *Bull. Chem. Soc. Jpn.*, **49**, 2904 (1976).
12) M. Manabe, M. Koda, and K. Shirahama, *Bull. Chem. Soc. Jpn.*, **48**, 3553 (1975).
13) The CMC values of SDS for 1-alkanols were shown in detail elsewhere: M. Manabe and M. Koda, *Memoirs of the Niihama Technical College*, **13**, 57 (1977).
14) I. J. Lin and P. Somasundaran, *J. Colloid Interface Sci.*, **37**, 731 (1971).
15) P. Molyneux, C. T. Rhode, and J. Swarbrick, *Trans. Faraday Soc.*, **60**, 1043 (1964).
16) J. M. Corkill, J. F. Goodman, and T. Walker, *Trans. Faraday Soc.*, **63**, 768 (1976).
17) M. J. Schick, Ed., "Nonionic Surfactants," Marcel Dekker, Inc., New York (1967), p. 478.
18) J. T. Davies and E. K. Rideal, "Interfacial Phenomena," Academic Press, New York (1963), p. 374.

Vibrational Spectra and Normal Coordinate Calculations for Trimethylaluminium-Ammonia

Fumio WATARI, Shigenori SHIMIZU,* Koyo AIDA, and Eiji TAKAYAMA**
Department of Applied Science, Faculty of Engineering, Tohoku University, Sendai 980
(Received September 9, 1977)

Studies were carried out on the infrared spectra (33—4000 cm^{-1}) of four isotopic trimethylaluminium-ammonia complexes, $(CH_3)_3AlNH_3$, $(CD_3)_3AlNH_3$, $(CH_3)_3AlND_3$, and $(CD_3)_3AlND_3$, in the solid state at low temperature, and on the Raman spectra (0—4000 cm^{-1}) in the solid state and in solution of dichloromethane and of benzene at ambient temperature. Assignments for all fundamentals except internal torsion were made on the basis of C_{3v} molecular symmetry. For the sake of confirmation normal coordinate calculations were carried out utilizing a symmetry force field. The Al–N stretching force constant was found to be 1.544 mdyn/Å.

Numerous vibrational studies have been made on the coordination complexes of boron compounds with derivatives of the Group Vb elements. However, few studies are known for the addition complexes of aluminium compounds,[1-5] belonging to the same group as that of boron.

The present study was undertaken to observe the vibrational spectra of trimethylaluminium–ammonia complexes, to assign vibrational fundamentals and to calculate force constants, especially that of the Al–N bond. Complete vibrational analyses for these complexes might provide interesting information on the electron donor-acceptor bond, which in turn can be compared with other physical and chemical properties.

Experimental

All manipulation of chemical substances was done in the conventional vacuum line, because of inflammability of trimethylaluminium and sensitivity of the addition complexes to moisture.

Trimethylaluminium was prepared by the reaction of dimethylmercury(II) with aluminium powder in slight excess in a sealed tube with a break-seal, following the procedure of Wartik and Schlesinger.[6] Dimethyl-d_6-mercury-(II) was used for the preparation of trimethylaluminium-d_9. Ammonia generated by dropping commercial aqueous ammonia over solid potassium hydroxide was collected in a U-type trap immersed in liquid nitrogen. Ammonia-d_3 was prepared by the reaction of deuterium oxide with magnesium nitride[7] in the vacuum line. These substances were purified by fractional distillation in the vacuum line.

Trimethylaluminium–ammonia complex for infrared work was prepared by condensing trimethylaluminium and ammonia in a 1 : 2 mole ratio into a small reaction tube with a stopcock and a ground-joint at liquid nitrogen temperature. After closing the stopcock the tube was left to reach room temperature. It was then opened to the vacuum line for a while in order to remove volatile substances.

The aluminium content was determined by the EDTA method.[8] Calcd for $(CH_3)_3AlNH_3$: Al, 30.3%. Found: Al, 29.3%.

Infrared spectra were recorded on a Perkin-Elmer Model 337 spectrophotometer in the region 4000—400 cm^{-1}. Frequencies were read on a Hitachi QPD-33 recorder by abscissa expansion with use of a Perkin-Elmer Expanded Scale Readout Kit. The instrument was calibrated in the usual manner.[9] The spectra were obtained for the samples deposited onto a CsI plate cooled with liquid nitrogen. Before recording the spectra, the samples were annealed until the spectra showed no change.

Far infrared spectra were obtained between 400 and 33 cm^{-1} with a Hitachi FIS-III spectrophotometer which was evacuated in order to remove atmospheric water vapor. The instrument was calibrated by means of water vapor frequencies. The sample was sublimed onto a polyethylene window cooled with liquid nitrogen, and annealed in a similar manner to that for the midinfrared study. The double chopping method was used for recording the spectra to avoid the radiation effect resulting from the temperature difference between the sample and the reference beam path.

Raman spectra were recorded in the range 0—4000 cm^{-1} on a JEOL JRS-S1 laser Raman spectrophotometer equipped with an NEC GLG-108 50 mW He–Ne laser. The spectrophotometer was calibrated with the emmission lines of neon. The spectra were obtained at ambient temperature in the solid state and in the saturated solution of dichloromethane and of benzene, sealed in a capillary of about 1.5 mm o.d.

Results and Vibrational Assignments

The infrared and Raman spectra of four isotopic trimethylaluminium–ammonia complexes are shown in Figs. 1—3. The vibrational frequencies are given in Tables 1—4. A molecular symmetry of C_{3v}, with the C_3 axis coinciding with the Al–N bond, is assumed for trimethylaluminium–ammonia. From group theory, the molecule is expected to have $10A_1$, $5A_2$, and 15E modes, in which the A_2 mode is inactive in both the infrared and Raman spectra, and the A_1 and E modes are active in both.

CH_3 and CD_3 Modes. The CH_3 stretches are observed around 2900 cm^{-1} in the infrared spectra. The three asymmetric stretches are contained within a single intense absorption at 2910 cm^{-1} for $(CH_3)_3AlNH_3$ and at 2915 cm^{-1} for $(CH_3)_3AlND_3$. On deuteration of the methyl groups these stretches shift and split into two at 2184 and 2179 cm^{-1} for the NH_3 adduct, and at 2184 and 2177 cm^{-1} for the ND_3 adduct. The two symmetric methyl stretches are observed to be accidentally degenerate at 2874 cm^{-1} for $(CH_3)_3AlNH_3$ and at 2872 cm^{-1} for $(CH_3)_3AlND_3$, the modes shifting to 2089 cm^{-1} and to 2090 cm^{-1} on deuteration of the

* Present address: Nagano Research Institute for Health and Pollution, Komemura, Amori, Nagano 380.
** Present address: National Institute for Researches in Inorganic Materials, Sakura-Mura, Niihari-Gun, Ibaraki 300-31.

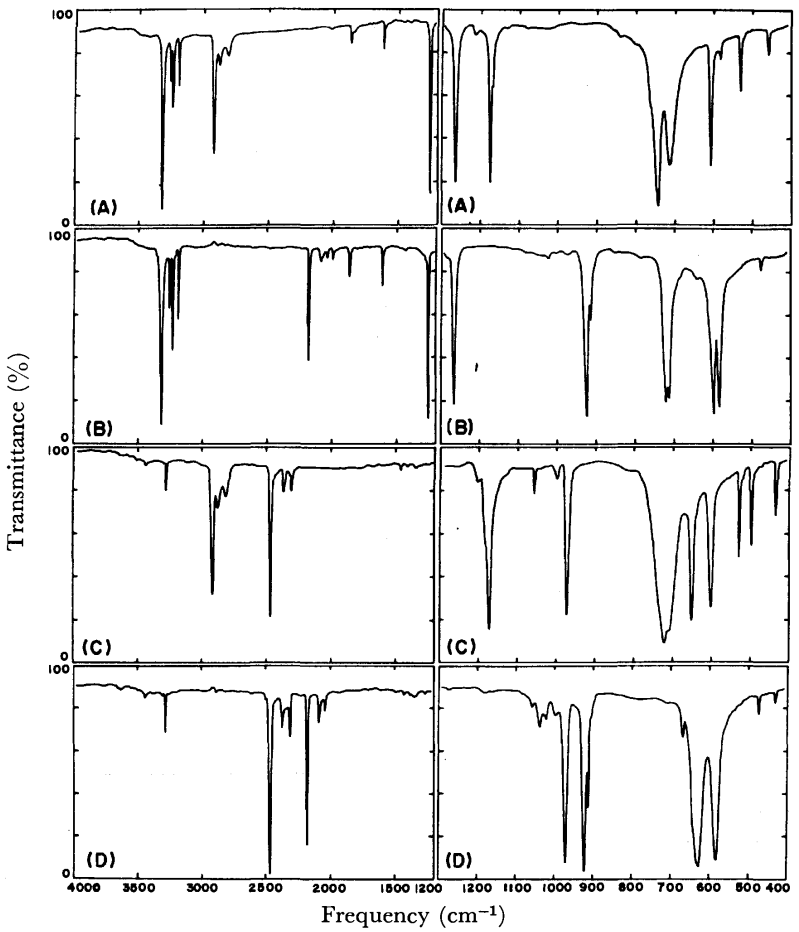

Fig. 1. Infrared spectra of (A) $(CH_3)_3AlNH_3$, (B) $(CD_3)_3AlNH_3$, (C) $(CH_3)_3AlND_3$, and (D) $(CD_3)_3$ $AlND_3$ recorded at −196 °C.

methyl groups. The Raman bands corresponding to the lower frequency infrared absorptions are polarized.

Degenerate methyl deformation is observed very weakly and broadly around 1470 and 1410 cm^{-1} in the infrared spectra. The frequencies are not definite, whereas the modes of $(CD_3)_3AlND_3$ are observed at 1038 cm^{-1} (ν_{21}) and 1021 cm^{-1} (ν_4 and ν_{22}). The deformation of $(CD_3)_3AlNH_3$ is too weak for the frequency to be defined.

Symmetric methyl deformation is observed as a singlet at 1172 cm^{-1} for $(CH_3)_3AlNH_3$ and at 1173 cm^{-1} for $(CH_3)_3AlND_3$. In the Raman spectra, the modes are observed at 1163 cm^{-1} and at 1165 cm^{-1} with a shoulder on the high-frequency side, the higher frequency bands being polarized. Consequently the 1172 and 1173 cm^{-1} infrared absorptions are assigned to the symmetric methyl deformation of A_1 symmetry, and the 1163 and 1165 cm^{-1} Raman bands, of E symmetry. The CD_3 modes are observed in the infrared spectra at 914 and 923 cm^{-1} for $(CD_3)_3AlNH_3$, and at 913 and 921 cm^{-1} for $(CD_3)_3AlND_3$, the lower frequency absorptions of which are weak. The Raman bands corresponding to the lower frequency infrared absorptions are strong and polarized.

The CH_3 rocks are assigned to absorptions at 743 cm^{-1} (ν_{25} and ν_{26}) and 712 cm^{-1} (ν_7) for $(CH_3)_3AlNH_3$, and at 720 cm^{-1} (ν_{25}) and 710 cm^{-1} (ν_7 and ν_{26}) for $(CH_3)_3AlND_3$. The CD_3 rocks are observed at 586 and 584 cm^{-1} in the infrared spectra for $(CD_3)_3AlNH_3$ and $(CD_3)_3AlND_3$, respectively, without splitting.

NH_3 and ND_3 Modes. The symmetric NH_3 stretch is assigned to an infrared absorption observed at 3254 cm^{-1} for the $(CH_3)_3Al$ and at 3252 cm^{-1} for the $(CD_3)_3Al$ adduct. On deuteration, the mode shifts from 3254 to 2369 cm^{-1} and from 3252 to 2373 cm^{-1}. The corresponding Raman bands are clearly polarized, though observed only weakly because of insufficient sensitivity of a photomultiplier in this region. The degenerate stretches are assigned to the most intense absorptions of these regions observed at 3313, 3312, 2463, and 2468 cm^{-1} for trimethylaluminium–ammonia-d_0, -d_9, -d_3, and -d_{12}, respectively.

The degenerate NH_3 deformation is observed at 1615 and 1618 cm^{-1} in the infrared spectrum for $(CH_3)_3$-$AlNH_3$ and $(CD_3)_3AlNH_3$, respectively. The ND_3 deformation shows no clear band in the infrared and Raman spectra, being observed at 1180 cm^{-1} as a shoulder on the high-frequency side of the symmetric CH_3 deformation or an extremely weak band in the infrared spectrum.

The symmetric NH_3 deformation is assigned to a band at 1263 and 1265 cm^{-1} in the infrared spectrum for $(CH_3)_3AlNH_3$ and $(CD_3)_3AlNH_3$, respectively. It shifts to 974 and 971 cm^{-1} on deuteration of the ammonia

TABLE 1. OBSERVED AND CALCULATED FREQUENCIES (cm^{-1}) FOR $(CH_3)_3AlNH_3$[a]

No.[b]	Infrared Solid	Raman[c] Solid	Raman[c] Solution	Calcd	PED
1	3254 m	3261	3274 p	3253	$98F_1$
2	2915 m	2919	2922	2918	$100F_2$
3	2874 w	2882	2889 p	2874	$97F_3$
4	1410 vw			1414	$97F_4$
5	1263 s			1265	$71F_5$, $28F_1$
6	1173 s	1173 sh	1185 p	1175	$92F_6$
7	712 s	706	705	715	$89F_7$
8	533 m	525	524 p	539	$70F_8$, $20F_9$
9	461 w	457	451 p	470	$68F_9$, $22F_8$
10	188 w	184		184	$93F_{10}$
16	3312 s	3320		3317	$100F_{16}$
17	2915 m	2919	2922	2920	$99F_{17}$
18	2915 m	2919	2922	2919	$99F_{18}$
19	2874 w	2882	2889	2875	$98F_{19}$
20	1615 w			1617	$100F_{20}$
21	1470 vw	1436	1436	1445	$96F_{21}$
22	1410 vw			1414	$96F_{22}$
23		1163		1170	$92F_{23}$
24	712 s	706	705	716	$68F_{24}$, $14F_{27}$, $10F_{26}$
25	743 s	737	734	750	$73F_{25}$, $14F_{26}$
26	743 s	737	734	743	$70F_{26}$, $24F_{25}$
27	608 s	605	597	619	$62F_{27}$, $23F_{24}$
28	214 m	215		213	$87F_{28}$
29	171 m	167		168	$94F_{29}$

a) Abbreviations: v, very; w, weak; m, medium; s, strong; sh, shoulder; p, polarized. b) Vibrational modes referring to the numbers are given in Table 5. c) Raman intensities are not given since photomultiplier sensitivity varies in a wide range within the spectral region.

TABLE 2. OBSERVED AND CALCULATED FREQUENCIES (cm^{-1}) FOR $(CD_3)_3AlNH_3$[a]

No.[b]	Infrared Solid	Raman[c] Solid	Raman[c] Solution	Calcd	PED
1	3252 m	3260	3276 p	3253	$98F_1$
2	2179 m	2182	2184	2171	$99F_2$
3	2089 w	2096	2100 p	2088	$94F_3$
4	(1021)[d]		1033 p?	1021	$98F_4$
5	1265 s	1269	1265	1265	$71F_5$, $28F_1$
6	914 w	916	921 p	910	$81F_6$, $12F_8$
7	586 s	594	580 p	588	$51F_7$, $28F_9$
8	482 w	474	469 p	475	$40F_8$, $36F_7$, $21F_9$
9		440	423 p	441	$46F_9$, $39F_8$
10	165 w	155		167	$91F_{10}$
16	3312 s	3331		3317	$100F_{16}$
17	2184 m	2182	2184	2173	$91F_{17}$
18	2179 m	2182	2184	2171	$91F_{18}$
19	2089 w	2096	2100	2086	$98F_{19}$
20	1618 w			1617	$100F_{20}$
21	(1038)[d]	1039	1042	1042	$97F_{21}$
22	(1021)[d]			1021	$97F_{22}$
23	923 s	924 sh	931 sh	915	$78F_{23}$, $17F_{27}$
24	716[e] s	703	696	710	$86F_{24}$
25	586 s			556	$42F_{25}$, $40F_{26}$, $11F_{27}$
26	586 s			561	$44F_{26}$, $51F_{25}$
27	600 s	594		592	$65F_{27}$, $14F_{24}$, $11F_{23}$
28	187 m	185		188	$74F_{28}$, $12F_{29}$
29	154 m	143		156	$85F_{29}$, $13F_{28}$

a) For abbreviations, see Table 1. b, c) See the corresponding footnotes to Table 1. d) Frequencies in parentheses were not observed for this compound, but taken as the same values as those of the corresponding modes of $(CD_3)_3AlND_3$ for the normal coordinate calculations. e) This frequency is the average of 721 and 712 cm^{-1} observed as a doublet.

Table 3. Observed and calculated frequencies (cm^{-1}) for $(CH_3)_3AlND_3$[a]

No.[b]	Infrared Solid	Raman[c] Solid	Raman[c] Solution	Calcd	PED
1	2369 w	2373	2384 p	2370	$95F_1$
2	2910 s	2924	2920	2918	$100F_2$
3	2872 w	2883	2886 p	2874	$97F_3$
4	1410 vw		1407 p	1414	$97F_4$
5	974 s	987		971	$65F_5$, $30F_1$
6	1172 s	1177 sh	1179 p	1175	$94F_6$
7	710 s	716	711	713	$90F_7$
8	532 m	525	521 p	535	$81F_8$, $10F_9$
9	439 w	434	398 p	442	$75F_9$, $11F_8$
10	180 w	183	184	180	$91F_{10}$
16	2463 s	2484	2500	2459	$99F_{16}$
17	2910 s	2924	2920	2920	$99F_{17}$
18	2910 s	2924	2920	2918	$99F_{18}$
19	2872 w	2883	2886	2875	$98F_{19}$
20	1180 sh			1180	$99F_{20}$
21	1470 vw	1436	1436	1445	$96F_{21}$
22	1410 vw		1407	1414	$96F_{22}$
23		1165		1170	$92F_{23}$
24	501 m	497		495	$86F_{24}$
25	720 s	716	716	749	$80F_{25}$, $11F_{26}$
26	710 s	716	711	744	$76F_{26}$, $17F_{25}$
27	654 s	650	636	656	$72F_{27}$, $13F_{26}$
28	211 m	203		212	$89F_{28}$
29	160 m	165	156	160	$93F_{29}$

a) For abbreviations, see Table 1. b, c) See the corresponding footnotes to Table 1.

Table 4. Observed and calculated frequencies (cm^{-1}) for $(CD_3)_3AlND_3$[a]

No.[b]	Infrared Solid	Raman[c] Solid	Raman[c] Solution	Calcd	PED
1	2373 w	2377	2385 p	2370	$95F_1$
2	2177 s	2187	2182	2171	$99F_2$
3	2090 w	2093	2097 p	2088	$94F_3$
4	1021 w			1021	$98F_4$
5	971 s	974		971	$65F_5$, $30F_1$
6	913 m	912	919 p	910	$81F_6$, $12F_8$
7	584 s	585	580 p	579	$59F_7$, $17F_9$
8	478 w	473	469 p	471	$60F_8$, $24F_7$
9	435 w	415	392	419	$59F_9$, $17F_8$, $11F_5$
10	162 w	150	165	163	$90F_{10}$
16	2468 s	2485	2500	2459	$99F_{16}$
17	2184 s	2187	2182	2173	$91F_{17}$
18	2177 s	2187	2182	2171	$91F_{18}$
19	2090 w	2093	2097	2086	$95F_{19}$
20	1180 vw			1180	$99F_{20}$
21	1038 w	1037	1035	1042	$97F_{21}$
22	1021 w			1021	$97F_{22}$
23	921 s	924 sh	928 sh	914	$77F_{23}$, $17F_{27}$
24		490 sh		490	$80F_{24}$, $13F_{27}$
25	584 s			559	$83F_{25}$
26	584 s			562	$83F_{26}$
27	628 s	629	637	622	$63F_{27}$, $12F_{24}$, $11F_{23}$
28	184 m	180		187	$80F_{28}$
29	146 m	150	141	149	$89F_{29}$

a) For abbreviations, see Table 1. b, c) See the corresponding footnotes to Table 1.

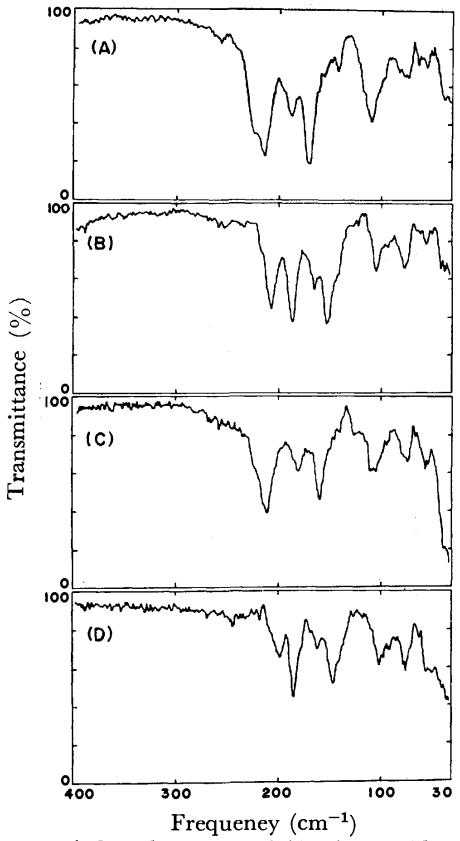

Fig. 2. Far infrared spectra of (A) $(CH_3)_3AlNH_3$, (B) $(CD_3)_3AlNH_3$, (C) $(CH_3)_3AlND_3$, and (D) $(CD_3)_3AlND_3$ recorded at −196°.

group.

The NH_3 rock is observed at 712 cm^{-1} coinciding with the CH_3 (A_1) rocking frequency for $(CH_3)_3AlNH_3$, and at 721 and 712 cm^{-1} as a doublet for $(CD_3)_3AlNH_3$. The mode shifts to 501 cm^{-1} for $(CH_3)_3AlND_3$. For $(CD_3)_3AlND_3$, no absorption is found around 500 cm^{-1}, but a shoulder is observed at 490 cm^{-1} in the Raman spectrum and assigned to the ND_3 rock.

Skeletal Modes. The symmetric AlC_3 stretches are observed at almost definite frequency of 530 cm^{-1} for the $(CH_3)_3Al$ and of 480 cm^{-1} for the $(CD_3)_3Al$ adducts. The mode gives the strongest polarized Raman line. The degenerate AlC_3 stretch, coupling with deformation of the methyl and ammonia groups, is observed in the 650—600 cm^{-1} region.

The AlC_3 deformation is observed in the 210—150 cm^{-1} region (Tables 1—4).

The Al–N stretch is observed in the 460—435 cm^{-1} region in the infrared spectrum. The absorption is weak, and not observed for $(CD_3)_3AlNH_3$. The corresponding Raman band is weak, but polarized. In a solution Raman spectrum, this mode is observed to shift toward the lower frequency than that in the solid state.

Normal Coordinate Calculations

The normal coordinate analysis was undertaken to confirm the assignments. The calculation was made by Wilson's *GF* matrix method on an ACOS 77/700 computer at the Computer Center, Tohoku University,

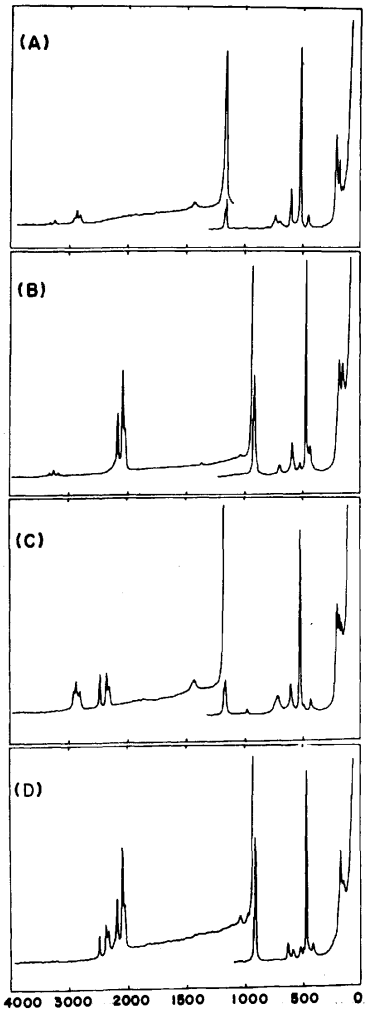

Fig. 3. Raman spectra of (A) $(CH_3)_3AlNH_3$, (B) $(CD_3)_3AlNH_3$, (C) $(CH_3)_3AlND_3$, and (D) $(CD_3)_3AlND_3$ recorded in the solid state at ambient temperature.

by means of the usual iterative least-squares procedure.

The *G* matrix was calculated using structural parameters of Cl_3AlNH_3[10] and $(CH_3)_3AlN(CH_3)_3$[11] determined by electron-diffraction studies; r(N–H)=1.03 Å (assumed), r(C–H)=1.09 Å, r(Al–C)=1.987 Å, r(Al–N)=2.099 Å (taken from $(CH_3)_3AlN(CH_3)_3$), $\angle$(H–N–H)=112.79°, $\angle$(Al–C–H)=111.8°, and $\angle$(C–Al–N)=102.3°. Symmetry coordinates similar to those for trimethylarsine-borane[12] were used.

Infrared frequencies were used for the calculations. The Raman frequencies observed in the solid state were used for vibrations which frequencies were not accurate from the infrared spectra but accurate enough from the Raman effect. The torsional mode was neglected in the E class. The frequencies were weighted by $(1/\lambda)$ in the least-squares routine, but the CH_3 degenerate deformation frequencies were weighted by 0.1 because of inaccuracy. The least-squares refinement was carried out in terms of symmetry force constants, fitted to the observed frequencies for the four isotopic species simultaneously. The calculated frequencies are given for the four isotopic species in Tables 1—4, together with the potential energy distributions, the average

Table 5. Symmetry force constants and their uncertainties for trimethylaluminium–ammonia[a)]

			σ				σ
$\nu(NH_3)$	F_1	5.593	0.087	$\nu(NH_3)$	E_{16}	5.919	0.027
$\nu(CH_3)$	F_2	4.543	0.009	$\nu(CH_3)$	F_{17}	4.551	0.023
$\nu(CH_3)$	F_3	4.642	0.042	$\nu(CH_3)$	F_{18}	4.542	0.023
$\delta(CH_3)$	F_4	0.548	0.003	$\nu(CH_3)$	F_{19}	4.667	0.092
$\delta(NH_3)$	F_5	0.689	0.033	$\delta(NH_3)$	F_{20}	0.595	0.013
$\delta(CH_3)$	F_6	0.400	0.009	$\delta(CH_3)$	F_{21}	0.571	0.009
$\rho(CH_3)$	F_7	0.332	0.004	$\delta(CH_3)$	F_{22}	0.547	0.009
$\nu(AlC_3)$	F_8	2.312	0.063	$\delta(CH_3)$	F_{23}	0.391	0.018
$\nu(AlN)$	F_9	1.544	0.059	$\rho(NH_3)$	F_{24}	0.300	0.030
$\delta(AlC_3)$	F_{10}	0.508	0.017	$\rho(CH_3)$	F_{25}	0.400	0.009
				$\rho(CH_3)$	F_{26}	0.381	0.009
	$F_{1,5}$	−0.992	0.069	$\nu(AlC_3)$	F_{27}	2.087	0.098
	$F_{3,6}$	−0.214	0.065	$\delta(AlC_3)$	F_{28}	0.482	0.036
	$F_{6,8}$	−0.103	0.028	$\rho(AlC_3)$	F_{29}	0.409	0.037
	$F_{5,9}$	0.073	0.033				
	$F_{8,9}$	0.082	0.040		$F_{19,23}$	−0.175	0.157
					$F_{20,24}$	−0.089	0.115
					$F_{23,27}$	−0.090	0.045
					$F_{24,27}$	0.032	0.017
					$F_{26,27}$	0.198	0.076

a) Stretching force constants in mdyn/Å, bending constants in mdyn Å/(radian)^2, stretching-bending interactions in mdyn/radian. ν, stretching; δ, deformation; ρ, rocking; σ, dispersion.

errors being 0.51 and 0.97% for the A_1 and E vibrations, respectively. The sum of the weighted squares of errors, $\Sigma(\lambda_{obsd}-\lambda_{calcd})^2/\lambda_{obsd}$, was 1.83×10^{-3} for the A_1 species vibrations and 1.45×10^{-2} for the E species. The symmetry force constants and their uncertainties from the last cycle of the least-squares refinement are given in Table 5.

Discussion

In the far infrared spectra, another absorption in the skeletal deformation region was observed at around 220 cm^{-1} as a shoulder for the $(CH_3)_3Al$ adduct and at about 200 cm^{-1} for the $(CD_3)_3Al$, which remained unassigned. This may be due to the torsional mode of the methyl groups active in both the infrared and the Raman spectrum. They seem to be rather intense as being due to torsions, the deuteration shift (20 cm^{-1}) appearing to be too small.[13)] An infrared strong absorption at 604 cm^{-1} of $(CH_3)_3AlND_3$ also remained unassigned. Attempts to assign the vibrational mode was unsuccessful.

The symmetric AlC_3 stretch is mixed with the Al–N stretch, also with the CD_3 rock for the $(CD_3)_3Al$ adduct. The frequencies are in almost fixed region at 530 cm^{-1} for the $(CH_3)_3Al$ adducts and at 480 cm^{-1} for the $(CD_3)_3Al$, not being influenced on deuteration of the ammonia group, whereas the degenerate AlC_3 stretch is mixed with the NH_3 or ND_3 rock and the frequencies are higher for the ND_3 adducts than those of the NH_3.

Studies on boron adducts have shown the Raman technique to be more sensitive to the donor-acceptor bond stretching mode than the infrared technique.[14–17)] The Al–N stretch of the $(CH_3)_3AlNH_3$ molecule is weak in intensity in the infrared spectrum and also unexpectedly weak in the Raman effect.

Agreement between the observed and calculated frequencies is satisfactory. The vibrational assignments are supported by the product rule ratios given in Table 6, where the theoretical ratios were calculated from the determinant of the G matrices.

The Al–N force constant is compared with that of

Table 6. Comparison of product rule ratios for the various isotopic combinations of the $(CH_3)_3AlNH_3$ molecule[a)]

	A_1		E	
	Calcd	Theoret.	Calcd	Theoret.
$(CH_3)_3AlNH_3/(CD_3)_3AlND_3$	9.79	9.68	34.4	32.6
$(CD_3)_3AlNH_3/(CD_3)_3AlND_3$	1.91	1.90	2.78	2.66
$(CH_3)_3AlND_3/(CD_3)_3AlND_3$	4.96	4.93	12.1	11.9
$(CH_3)_3AlNH_3/(CH_3)_3AlND_3$	1.97	1.96	2.85	2.74
$(CD_3)_3AlNH_3/(CH_3)_3AlND_3$	0.385	0.386	0.230	0.223
$(CH_3)_3AlNH_3/(CD_3)_3AlNH_3$	5.12	5.07	12.4	12.2

a) The theoretical values were calculated from the determinants of the G matrix, as $|G|/|G'|$.

Table 7. Comparison of bond distances, stretching force constants and stretching frequencies of Al–N bond, and heats of formation

	r(Al–N) Å	f(Al–N) mdyn/Å	ν(Al–N) cm^{-1}	$-\Delta H$ kJ/mol
$Cl_3AlN(CH_3)_3$	1.96[18]	2.251[4]	565[4]	198.7[11]
	1.945[19]			
Cl_3AlNH_3	1.996[10]	1.912[4]	579[4]	
		1.875[21]		
$H_3AlN(CH_3)_3$	2.063[20]	2.321[4]	525[4]	
			533[22]	
$(CH_3)_3AlN(CH_3)_3$	2.099[11]			125.3[23]
				128.4[11]
$(CH_3)_3AlNH_3$		1.544[a]	461[a]	115.2[23]

a) This work.

other addition compounds containing an Al–N bond in Table 7, where their Al–N bond distances, Al–N stretching frequencies and heats of formation are also given. We can not find any trend from the frequencies of the Al–N stretching mode, probably because of its mixing with other vibrational modes. However, we find correlations between the bond distances, the Al–N force constants (except that of $H_3AlN(CH_3)_3$) and the heats of formation. Considering that ammonia is a weaker base than trimethylamine and the heat of formation of $(CH_3)_3AlNH_3$ is less than that of $(CH_3)_3AlN(CH_3)_3$, the Al–N bond distance of $(CH_3)_3AlNH_3$ would be greater than that of $(CH_3)_3AlN(CH_3)_3$. The force constant 2.321 mdyn/Å for $H_3AlN(CH_3)_3$ seems quite large as compared with the Al–N bond distances. Though we have only a limited number of data and detailed vibrational analysis would be necessary for other compounds, it appears that the Al–N force constant of 1.544 mdyn/Å is reasonable for trimethylaluminium-ammonia.

References

1) J. Goubeau and H. Siebert, *Z. Anorg. Allg. Chem.*, **254**, 126 (1947).

2) W. Zeil, R. Dautel, and W. Honsberg, *Ber. Bunsenges. Phys. Chem.*, **60**, 1131 (1956); R. Dautel and W. Zeil, *ibid.*, **64**, 1234 (1960); H. Roszinski, R. Dautel, and W. Zeil, *Z. Phys. Chem. N. F.*, **36**, 26 (1963).

3) G. Schomburg and E. G. Hoffmann, *Ber. Bunsenges., Phys. Chem.*, **61**, 1110 (1957).

4) W. Sawodny and J. Goubeau, *Z. Phys. Chem. N. F.*, **44**, 227 (1965).

5) I. R. Anderson, F. R. Forgaard, and A. Haaland, *Acta Chem. Scand.*, **26**, 1947 (1972).

6) T. Wartik and H. I. Schlesinger, *J. Am. Chem. Soc.*, **75**, 835 (1953).

7) L. Duparc, P. Wenger, and Ch. Urfer, *Helv. Chim. Acta*, **13**, 650 (1930).

8) G. E. Coates and J. Graham, *J. Chem. Soc.*, **1963**, 233.

9) R. N. Jones and A. Nadeau, *Spectrochim. Acta*, **20**, 1175 (1964).

10) M. Hargittai, I. Hargittai, V. P. Spiridonov, M. Pelissier, and J. -F. Labbare, *J. Mol. Struct.*, **24**, 27 (1975).

11) G. A. Anderson, F. R. Forgaard, and A. Haaland, *Acta Chem. Scand.*, **26**, 1947 (1972).

12) F. Watari, *Bull. Chem. Soc. Jpn.*, **50**, 1287 (1977).

13) J. R. Durig, S. M. Craven, K. K. Lau, and J. Bragin, *J. Chem. Phys.*, **54**, 479 (1971); J. R. Durig, S. M. Craven, and J. Bragin, *ibid.*, **52**, 2046, 5663 (1970).

14) R. C. Taylor and T. C. Bissot, *J. Chem. Phys.*, **25**, 780 (1956).

15) J. D. Odom, B. A. Hudgens, and J. R. Durig, *J. Phys. Chem.*, **77**, 1972 (1973).

16) J. D. Odom, S. Reithmiller, J. D. Witt, and J. R. Durig, *Inorg. Chem.*, **12**, 1123 (1973).

17) J. D. Odom, J. A. Barnes, B. A. Hudgens, and J. R. Durig, *J. Phys. Chem.*, **78**, 1503 (1974).

18) D. F. Grant, R. C. G. Killean, and J. L. Lawrence, *Acta Crystallogr., Sect. B*, **25**, 377 (1969).

19) A. Almenningen, A. Haaland, T. Haugen, and D. P. Novak, *Acta Chem. Scand.*, **27**, 1821 (1973).

20) A. Almenningen, G. Gunderson, T. Haugen, and A. Haaland, *Acta Chem. Scand.*, **26**, 3928 (1972).

21) S. J. Cyvin, B. N. Cyvin, and I. Hargittai, *J. Mol. Struct.*, **23**, 385 (1974).

22) G. W. Fraser, N. N. Greenwood, and B. P. Straughen, *J. Chem. Soc.*, **1963**, 3742.

23) C. H. Henrickson, D. Duffy, and D. D. Eyman, *Inorg. Chem.*, **7**, 1047 (1968).

Beam Studies of the Ion-Molecule Reaction $CO_2^+ + D_2 \rightarrow DCO_2^+ + D$

Hiroshi TOCHIHARA* and Yoshitada MURATA*

Department of Chemistry, Faculty of Science, Gakushuin University, Mejiro, Toshima-ku, Tokyo 171

(Received September 19, 1977)

Reaction cross sections of the reaction $CO_2^+ + D_2 \rightarrow DCO_2^+ + D$ have been measured over the range of the collision energies $E=0.4$ to 4 eV in the center of mass system. The cross section was obtained from relative values of the reaction $Ar^+ + D_2 \rightarrow DAr^+ + D$ by using the mixed ion beam method. The observed cross sections are about half of the Langevin-Gioumousis-Stevenson cross sections and show approximately $E^{-1/2}$ dependence.

Since the molecular beam technique has been used with great success, the ion beam technique has also been employed for ion-molecule reactions. This method has enabled the study of collision energy dependence of the reaction cross section. The following reactions have been studied extensively:[1-5]

$$Ar^+ + D_2 \longrightarrow DAr^+ + D, \quad \Delta E = -1.2\ \text{eV}, \quad (1)$$

$$CO^+ + D_2 \longrightarrow DCO^+ + D, \quad \Delta E = -2.0\ \text{eV}, \quad (2)$$

and

$$N_2^+ + D_2 \longrightarrow DN_2^+ + D, \quad \Delta E = -2.5\ \text{eV}, \quad (3)$$

where ΔE denotes the heat of reaction. These reactions are exothermic. The cross sections in these reactions are in proportional to $E^{-1/2}$ at low energies (below 1 eV in the center of mass system**) and decrease more steeply with increasing collision energy. The cross section, σ, of Reactions 1 and 2 is in good agreement with the Langevin-Gioumousis-Stevenson (LGS) cross section[6] below 1 eV.[2-4] For Reaction 3 σ is about twice as large as the LGS cross section.[1,4,5]

In this paper, the reaction

$$CO_2^+ + D_2 \longrightarrow DCO_2^+ + D, \quad \Delta E = -1.1\ \text{eV}, \quad (4)$$

was investigated. Since the incident ion of this reaction is more complex than those of Reactions 1—3, a different energy dependence of σ can be expected. This reaction has been studied by several methods such as flowing afterglow,[7] mass-spectrometry,[8,9] ion cyclotron resonance mass-spectrometry,[10,11] and energy analysis of product ions.[12] In these studies except for the last method, reaction rate constants were observed only at thermal or a little higher energies. Recently, Mahan and Schubart investigated the velocity vector distribution of DCO_2^+ in detail.[13]

Experimental

An apparatus for the study of the ion-molecule reaction was constructed chiefly to determine the collision energy dependence of σ. The beam-collison chamber method was employed and a schematic diagram of the apparatus is shown in Fig. 1. The main chamber was evacuated to a pressure around 10^{-4} Pa and operated at around 10^{-3} Pa during the experiment.

The ion source used was a Bayard-Alpert gauge type. The impact energy of the electrons was about 33 eV. The electron current was 1×10^{-5} A and the pressure of the gas

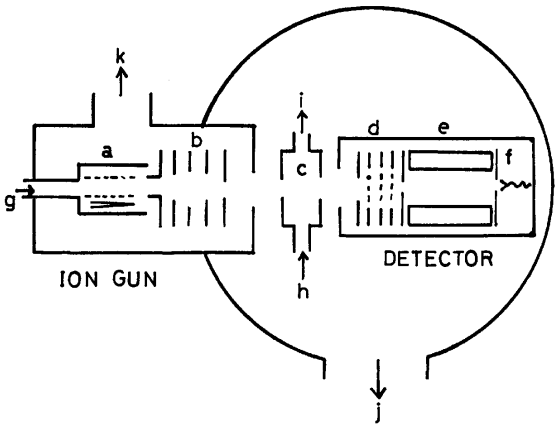

Fig. 1. Schematic diagram of the apparatus. a: Ion source, b: extracting electrode, einzel lens, and aperture, c: collision chamber, d: detection aperture and three-fold plane grids, e: quadrupole mass filter, f: channel electron multiplier, g: gas inlet to ion source, h: gas inlet to collision chamber, i: to ionization gauge, j: to 10 in. oil diffusion pump, k: to 2 in. oil diffusion pump.

introduced into the ion source was about 5×10^{-3} Pa. An attenuation experiment[14] ensured that the CO_2^+ ion beam produced by 33 eV electron impact in the present experiment did not contain any appreciable amount of metastable ions.

The collision chamber was 15 mm thick and the entrance and exit apertures were 2 and 3 mm in diameter, respectively. The distance between the center of the collision chamber and the detection aperture, 4 mm in diameter, was 20.5 mm. Hence, the detection angle was $\pm 5.6°$ at the center of the collision chamber. A quadrupole mass filter was used. In the present experiment, the transmittance of the incident and the product ions in the mass filter is almost the same, since the difference between their masses is small ($\Delta M=2$). Mass-analyzed ions were detected by a channel electron multiplier. A pulse counting system was used for detection, and the pulse height was such that the counting efficiency for all ionic species was about unity.

The pressure of the target gas in the collision chamber was measured with an ionization gauge which was mounted on the collision chamber. Since it was not suitable to keep the ionization gauge on during the collision experiment, the relationship between the reading of the ionization gauge and the revolution number of a variable leak valve was measured. During the experiment, the pressure of the target gas in the collison chamber was determined only by the revolution number of the variable leak valve. To realize the single collision condition and to obtain as many product ions as possible the pressure of D_2 was around 0.2 Pa throughout the present experiment. Under the single collision condition, σ was obtained by using the thin target formula, $\sigma = i/(INL)$

* Present address: The Institute for Solid State Physics, The University of Tokyo, Roppongi, Minato-ku, Tokyo 106.

** Hereafter, the collision energy is in the center of mass system.

where N is the number density of the target molecules, L is the collision path length, and I and i are the intensities of the incident and the product ions respectively.

It is difficult to obtain the absolute value of N. Hence, we obtained experimentally the relative cross section of Reaction 4 with respect to Reaction 1, *i.e.*, the cross section was obtained from the equation $\sigma_4=\sigma_1 i_4 I_1/i_1 I_4$, where the subscripts 1 and 4 denote Reactions 1 and 4 respectively. The mixed ion beam of Ar^+ and CO_2^+ was employed, which was made by introducing the mixed gases of Ar and CO_2 into the ion source. The intensities, i_1/I_1 and i_4/I_4, were observed under the same scattering condition, *i.e.*, the same number density of D_2 and the same geometry.

Results and Discussion

The cross section σ_1 has been obtained in good agreement by three different groups over a wide range of collision energies.[3] Therefore, Reaction 1 was thought suitable as a reference reaction. The average value $\hat{\sigma}_1$ of σ_1's reported is shown by a solid line in Fig. 2 as a function of the collision energy. The cross section, σ_4, was obtained from the equation $\sigma_4=\hat{\sigma}_1(i_4/I_4)/(i_1/I_1)$ and was plotted as a function of the collision energy (Fig. 2). Differences, between the incident and product ions, in the transmittance of the mass filter and in the counting efficiency of the multiplier have been ignored in this experiment, as mentioned in the Experimental.

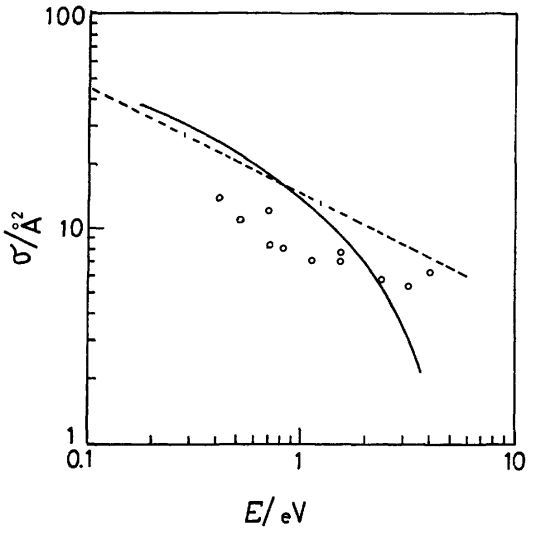

Fig. 2. Reaction cross section σ *vs.* collision energy E for Reaction 4. Open circles, observed cross sections; broken line, LGS cross section.[6] Solid line: average cross section for Reaction 1, $\hat{\sigma}_1$.[3]

In order to obtain an accurate value of σ_4, all of the product ions, DAr^+ or DCO_2^+, had to be collected in both reactions. The collection efficiency of DAr^+ for Reaction 1 in the present experiment was estimated by using data of the angular distribution observed by Herman *et al.*[15] The estimated values were about 70 and 90% at the collision energies 0.4 and 0.7 eV, respectively, and over 95% above 0.7 eV. In the estimation, the geometry mentioned above was used, and the collimated incident beam and the perfect alignment of the detection system were assumed.

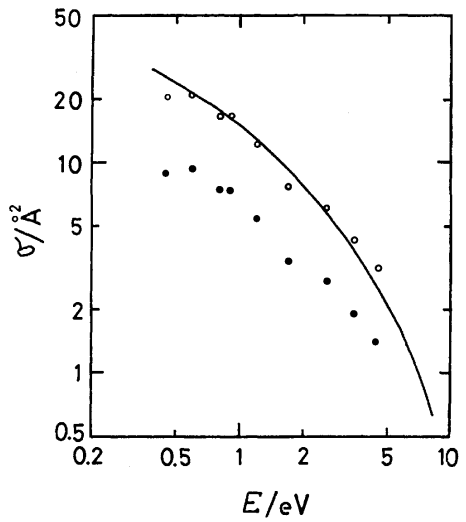

Fig. 3. Reaction cross section σ *vs.* collision energy E for Reaction 1. Solid line, average cross section, $\hat{\sigma}_1$[3]; closed circles, observed cross sections derived from the thin target formula; open circles, observed cross sections normalized to $\hat{\sigma}_1$ at 0.8 eV.

Further data on the collection efficiency in Reaction 1 has been obtained by comparing the energy dependence of the observed cross sections, the closed circles in Fig. 3, with that of $\hat{\sigma}_1$, the solid line in Fig. 3. The observed cross sections were matched to $\hat{\sigma}_1$ at 0.8 eV by multiplying by a constant. The fitted values, the open circles in Fig. 3, are in good agreement with $\hat{\sigma}_1$. This agreement may indicate that the collection efficiency of DAr^+ in the present experiment was almost the same as that of other experiments,[2-4] and that the discrepancy between the observed cross section and $\hat{\sigma}_1$ was caused by an incorrect value of the observed pressure of D_2 in the collision chamber.

The angular distribution of DCO_2^+ reported by Mahan and Schubart[13] was similar to that of DAr^+ in the laboratory system at 2 and 5 eV. Hence, the cross sections, σ_4, obtained in the present experiment give accurate values.

The magnitude of the cross section σ_4 was about 50% of $\hat{\sigma}_1$ in the low energy region and almost the same or larger at energies higher than 2.5 eV. The cross section σ_4 was approximately proportional to $E^{-1/2}$ over the energy range studied in the present experiment, and the magnitude of σ_4 was about 50% of the LGS cross section.

Mahan and Schubart detected the DCO^+ ion in the collision of CO_2^+ with D_2 above the collision energy 1 eV.[13] The peak height corresponding to DCO^+ on the contour map at 4.36 eV, at which the scattering intensity of DCO^+ was strongest, was only 5% of that corresponding to DCO_2^+. Thus, the small cross section was not caused by other reactive collisions.

The magnitude of σ_4 was observed to be about 50% of the LGS cross section which is in good agreement with that obtained by other techniques. Harrison and Myher studied Reaction 4 by mass-spectrometry and observed the reaction rate constant to be 0.6×10^{-9} $cm^3\ s^{-1}$ at a collision energy 0.3 eV.[8] McAllister and

Pitman measured the rate constant by ion cyclotron resonance mass-spectrometry and reported it to be 0.5×10^{-9} cm^3 s^{-1} at thermal energy.[11] These values are about 50% of the rate constant value predicted by the polarization theory,[6] 1.1×10^{-9} cm^3 s^{-1}. That the small rate constant is not due to charge transfer or other reactive collision has been reported.[10]

The small value of σ for Reaction 4 will be discussed by the modified polarization theory, by which the magnitude of the cross section for Reaction 3 can be explained. This will be described and presented in detail in a later paper.[16] Under this theory the incident ion is regarded as a two- or three-centered charged particle.

In Reactions 1—3, σ decreases more steeply than $E^{-1/2}$ with increasing collision energy above 1 eV,[1-5] as is illustrated by the solid line in Fig. 2 for Reaction 1. σ_4 does not illustrate this behaviour. It appears that this steep decrease of σ at the high collision energy is due to the dissociation of the product ion. In Reaction 4, the collision energy may be transferred efficiently into the internal energy of DCO_2^+ and distributed to all vibrational modes. Moreover, the minimum collision energy, above which DCO_2^+ dissociates into $CO_2 + D^+$ or $CO_2^+ + D$, is about 8 eV, if the spectator-stripping reaction occurs. The experiments of Mahan and Schubart indicate that the spectator-stripping reaction is the dominant process of Reaction 4.[13]

Hiroshi Tochihara acknowledges thanks to the Itoh Science Foundation and Matsunaga Science Foundation for partial financial support.

References

1) R. B. Turner, M. A. Fineman, and R. F. Stebbings, *J. Chem. Phys.*, **42**, 4088 (1965).
2) J. B. Homer, R. S. Lehrle, J. C. Robb, and D. W. Thomas, *Nature*, **202**, 795 (1964).
3) M. Henchman, "Ion-Molecule Reactions," Vol. 1. ed by J. L. Franklin, Plenum Press, New York (1972), pp. 101, 259.
4) D. Hyatt and K. Lacmann, *Z. Naturforsch., Teil A*, **23**, 2080 (1968).
5) P. M. Hierl, L. W. Strattan, and J. R. Wyatt, *Int. J. Mass Spectrom. Ion Phys.*, **10**, 385 (1972/1973).
6) G. Gioumousis and D. P. Stevenson, *J. Chem. Phys.*, **29**, 294 (1958).
7) F. C. Fehsenfeld, A. L. Schmeltekopf, and E. E. Ferguson, *J. Chem. Phys.*, **46**, 2802 (1967).
8) A. G. Harrison and J. J. Myher, *J. Chem. Phys.*, **46**, 3276 (1967).
9) K. R. Ryan, *J. Chem. Phys.*, **61**, 1559 (1974).
10) D. L. Smith and J. T. Futrell, *Int. J. Mass Spectrom. Ion Phys.*, **10**, 405 (1972/1973).
11) T. McAllister and P. Pitman, *Int. J. Mass Spectrom. Ion Phys.*, **19**, 423 (1976).
12) A. Ding, *Z. Naturforsch., Teil A*, **24**, 856 (1969).
13) B. H. Mahan and P. J. Schubart, *J. Chem. Phys.*, **66**, 3155 (1977).
14) B. R. Turner, J. A. Rutherford, and D. M. J. Compton, *J. Chem. Phys.*, **48**, 1602 (1968).
15) Z. Herman, J. Kerstetter, T. Rose, and R. Wolfgang, *Discuss. Faraday Soc.*, **44**, 123 (1967).
16) H. Tochihara and Y. Murata, to be published.

Linear Free Energy Relationships in Heterogeneous Catalysis. XIII. The Dehydration of Aliphatic Alcohols over Silica-Alumina

Jun-ichiro TAKE, Tadayuki MATSUMOTO, and Yukio YONEDA

Department of Synthetic Chemistry, Faculty of Engineering, The University of Tokyo, Hongo, Bunkyo-ku, Tokyo 113

(Received October 5, 1977)

In order to survey the applicability of linear free-energy relationships to the catalytic dehydration of aliphatic alcohols, isopropyl alcohol and *n*-, *s*-, and *t*-butyl alcohols were dehydrated over silica-alumina at 54—166 °C. The dehydration was zero order in alcohol over the pressure range of 0.01 to 0.1 atm. The true activation energies were 32.0, 35.3, 31.7, and 29.9 kcal/mol for isopropyl alcohol and *n*-, *s*-, and *t*-butyl alcohols, respectively. The zero-order rate constants were exclusively affected by the activation energy. A linear relationship was found between the true activation energy, as well as the logarithm of the zero-order rate constant, and the heterolytic bond dissociation energy for the C–O bond in alcohols, $D(R^+OH^-)$. The activation energy increased and the rate constant decreased with an increase in the $D(R^+OH^-)$. These correlations were explained in terms of the heterolytic fission of the C–O bond in the rate-determining step.

The catalytic dehydration of alcohols on oxides has been extensively studied and reviews have appeared by Winfield,[1] Pines and Manassen,[2] Knözinger,[3] and Notari.[4] However, there have been few studies of linear free-energy relationships (LFER) and, furthermore, such studies as have been made have been restricted mainly to alumina. In previous LFER studies of the dealkylation[5] and isomerization[6] of alkylbenzenes over silica–alumina, we found that the apparent activation energies, as well as the logarithms of the first-order rate constants, have linear correlations with $\Delta H_C^+(R)$, the enthalpy change for hydride abstraction from the corresponding paraffin.

The present study was devoted to a surve of the applicability of the LFER to the catalytic dehydration of aliphatic alcohols over silica–alumina.

Experimental

Materials. The silica–alumina (SA-1, 13% Al_2O_3) in powder form was taken from the same batch as that used earlier.[6] The catalyst was calcined at 550 °C for 8 h in the atmosphere. The alcohols used were GR-grade reagents: the isopropyl alcohol and *n*- and *s*-butyl alcohols were dried over CaO and distilled; the *t*-butyl alcohol was shaken with $CaCl_2$ for 20 min and then distilled. The alcohols were finally stored over a molecular sieve 4A.

Apparatus. A continuous-flow mode was used for the reaction, as is shown in Fig. 1. Hydrogen as a carrier gas was deoxygenated with a Deoxo column (B), divided into three streams, and then dried by means of dry ice–ethanol traps (D_1—D_3). Each alcohol was introduced into the first hydrogen stream with a flow rate of about 40 STP ml/min from a microfeeder (F), vaporized, and then diluted with the second hydrogen stream, whose flow rate was usually above 600 STP ml/min. A vessel (H, with an effective volume of about 90 ml) filled with glass beads reduced a small but unnegligible cyclic fluctuation (*ca.* ±15%) in the feed rate of the reactant to a satisfactory extent (below ±5%). A conventional TCD cell (G) in the vaporizer (I) monitored the reactant pressure. The stream through a glass reactor (J) was led to a gas-sampling valve (K) of a GLC apparatus (M). A wet gas meter (N) determined the total flow rate of the carrier gas after the removal of the condensable materials with a dry ice–ethanol or an ice–NaCl trap (D_4). A column of PEG 400 (2m) or of PEG 6000 (0.7 m) was used for analysis. In some experiments, a DMS column (6 m) was also used for the analysis of olefins.

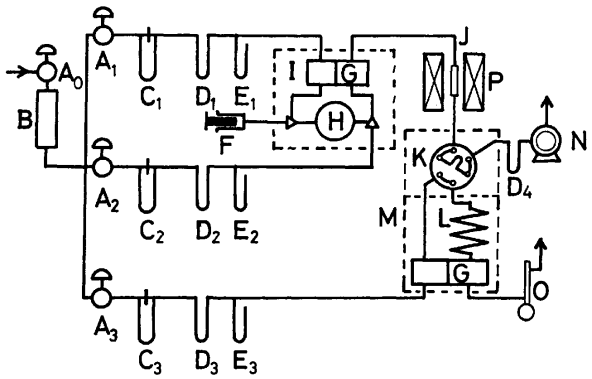

Fig. 1. Schematic diagram of the apparatus.
(A) Pressure regulator, (B) Deoxo column, (C) orifice meter, (D) cold trap, (E) mercury manometer, (F) microfeeder, (G) TCD cell, (H) vessel (*ca.* 90 ml), (I) vaporizer, (J) reactor, (K) six-way gas-sampling valve, (L) analytical column, (M) GLC apparatus, (N) wet gas meter, (O) soap-film meter, (P) furnace.

Procedures. The catalyst was held in the reactor with quartz wool plugs and activated at 450 °C for 1—2 h in a hydrogen stream with a flow rate of about 50 ml/min. The alcohol pressure was modified over the range of 0.01 to 0.1 atm by changing the feed rate of the alcohol. The alcohol were dehydrated at 120—166 °C for a primary alcohol, at 100—145 °C for a secondary one, and at 54—80 °C for a tertiary one. A proper amount of the catalyst (0.01—5.4 g) was used depending upon the reaction temperature and the reactivity of the alcohols. In all the runs, the fractional conversion was less than 0.1 (in most runs, less than 0.05), so that the reactor was regarded as differential. Under the above reaction conditions, only a dehydration reaction occurred to yield olefin, which resulted from β-elimination, and water. No other products were dected by GLC. The activity of the catalyst was almost constant during the course of the reaction.

Results

External Diffusion Effects. These experiments were performed with the most reactive *t*-butyl alcohol and moderately reactive *s*-butyl alcohol by changing the total flow rate of the carrier gas. The results are shown

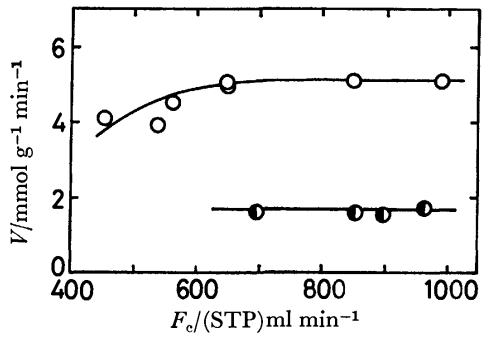

Fig. 2. Influence of flow rate of carrier on dehydration rate.
○: *t*-Butyl alcohol at 80 °C and 0.025 atm;
◐: *s*-butyl alcohol at 135 °C and 0.01 atm.

in Fig. 2. The dehydration rates of *t*-butyl alcohol at 80 °C, the highest in the present study, show no change in magnitude when the flow rate of the carrier is kept higher than about 650 STP ml/min, indicating that no external diffusion affects the reaction rate under such conditions. The carrier was, therefore, passed through at a flow rate higher than 650 STP ml/min in all subsequent runs.

Effects of Alcohol Pressure. The effect of the alcohol pressure on the dehydration rate was investigated at the high-temperature extreme for each alcohol. As is shown in Fig. 3, the dehydration rates are zero order in alcohol over the entire pressure range employed,

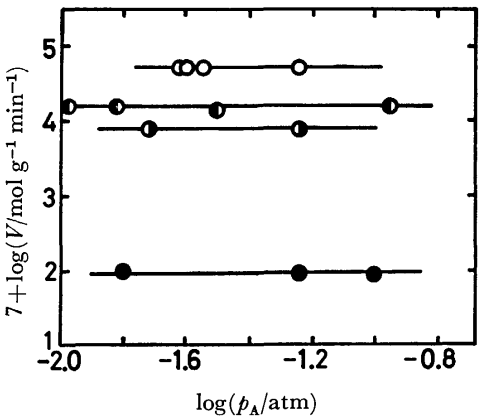

Fig. 3. Influence of alcohol pressure on dehydration rate.
○: *t*-Butyl alcohol (80 °C); ◐: *s*-butyl alcohol (136 °C); ●: butyl alcohol (149 °C); ◑: isopropyl alcohol (145 °C).

implying that the rate-determining step is one which involves the reactions of adsorbed species. The zero-order kinetics should hold over the entire temperature range applied to each alcohol since the heat of adsorption is generally exothermic. With *t*- and *s*-butyl alcohols this was ascertained to be the case. The dehydration rates, therefore, give the rate constants of the dehydration of the adsorbed species.

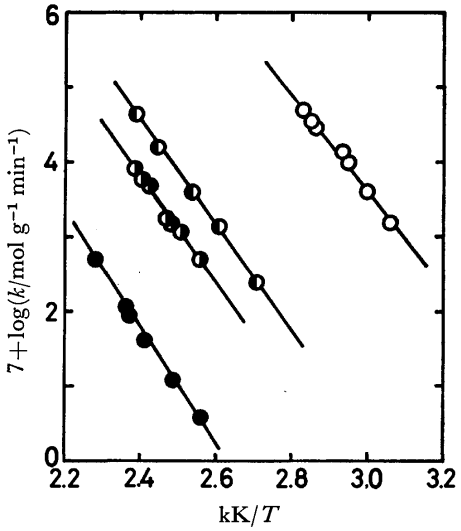

Fig. 4. Influence of temperature on dehydration rate constant.
○: *t*-Butyl alcohol; ◐: *s*-butyl alcohol; ●: butyl alcohol; ◑: isopropyl alcohol.

Effects of Reaction Temperature. The experiments were carried out at a constant alcohol pressure of about 0.02 atm. The zero-order rate constants are plotted in Arrhenius diagrams (Fig. 4). The Arrhenius parameters were determined by means of a least-squares method. The results are given in Table 1. This table also shows, as $\log(k/k_0)$, the rate constants relative to those for butyl alcohol at the low- and high-temperature extremes used. The rate constants for temperatures not covered by the experimental data were determined by extrapolation.

Internal Diffusion Effects. The effects were examined using the formula given by Weisz:[7]

$$\phi = \frac{dN}{dt}\frac{1}{C_0}\frac{R^2}{D_{eff}},$$

where dN/dt is the reaction rate in mol s^{-1} cm^{-3}; C_0,

Table 1. Rate constants and Arrhenius parameters for the dehydration of alcohols over silica–alumina

Alcohol	$\log(k/k_0)$[a] at t/°C=166	$\log(k/k_0)$[a] at t/°C=54	E_A[b] / kcal mol⁻¹	$\log\left(\frac{A}{\text{mol g}^{-1}\text{ min}^{-1}}\right)$[b]
Butyl	0	0	35.3±0.6	13.5±0.3
Isopropyl	1.85	2.41	32.0±1.3	13.7±0.7
s-Butyl	2.49	3.11	31.7±0.7	14.2±0.4
t-Butyl	5.39	6.32	29.9±0.2	16.2±0.2

a) The rate constant, k_0, is for butyl alcohol dehydration; k_0/mol g^{-1} $min^{-1}=7.8\times10^{-5}$ and 7.3×10^{-11} at t/°C=166 and 54, respectively. b) E_A is the zero-order activation energy; A, the preexponential factor.

the reactant concentration in mol cm^{-3}; R, the catalyst particle radius in cm, and D_{eff}, the effective diffusion constant in $cm^2\ s^{-1}$. In the present study, the extreme values for these coefficients are as follows: $dN/dt=10^{-4}$ mol s^{-1} cm^{-3}; $C_0=10^{-6}$ mol cm^{-3}; $R=10^{-3}$ cm. According to Weisz, the approximate value of D_{eff} is 10^{-3} for the system of a gel such as silica–alumina with a high surface area and a reactant whose molecular weight is about 150. From these data we obtain $\Phi=10^{-1}$. Weisz has shown that the diffusion effect can be excluded when $\Phi\leqslant 6$ for zero-order reactions.

Discussion

Table 1 shows that α-methylation (isopropyl to *t*-butyl) has a marked effect on the rate of dehydration, whereas the effect of β-methylation (isopropyl to *s*-butyl) is small. Thus, the reactivity of alcohols falls in the following order: butyl≪isopropyl<*s*-butyl≪*t*-butyl for dehydration. This trend is quite similar to that of the increasing stability of alkyl cations (see $\Delta H^\circ_f(R^+)$ in Table 2). Analogous rate relationships are found in the literature concerning a variety of heterogeneously or homogeneously catalyzed elimination reactions in the gas phase: the dealkylation of monoalkylbenzenes over silica–alumina;[5a] the dehydration of aliphatic alcohols over alumina[8] and hydroxyapatite,[9] or with gaseous hydrogen halide molecules;[10] the dehydrohalogenation of monohaloalkanes over salt catalysts,[11] and the dehydrosulfurization of alkyl mercaptans over silica–alumina.[12] The rate-constant data in Fig. 4 and Table 1 are for zero-order kinetics; therefore, the activation energies should not include heats of adsorprion. The major factor affecting the dehydration rates is clearly the activation energy, since the preexponential factor, A, does not vary except in the case of *t*-butyl alcohol. The activation energy decreases in the following order:

butyl > isopropyl > *s*-butyl > *t*-butyl

A similar sequence is also found in the literature.

Mochida and Yoneda[5b] obtained a linear relationship between the apparent activation energy, or the logarithm of the first-order rate constants, for the dealkylation of monoalkylbenzenes over silica–alumina and $\Delta H_C{}^+(R)$, the enthalpy change for the hydride abstraction from the corresponding paraffins. They explained this relationship in terms of the heterolytic fission of the C_{alkyl}–C_{phenyl} bond in the rate-determining step. For the gas-phase dehydrohalogenation of monohaloalkanes, Maccoll and his co-workers[10] found a linear relationship between the activation energy and the heterolytic bond dissociation energy of the C–X bond, $D(R^+\ X^-)$ (in this case, X=Cl, Br, and I). This correlation led them to the conclusion that the rate of elimination was determined by the heterolysis of the C–X bond.

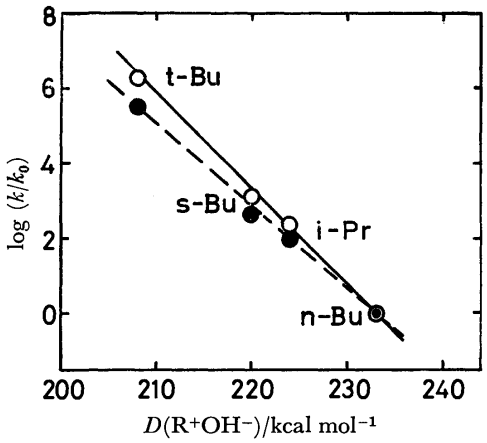

Fig. 5. Correlations of dehydration rate constant on silica–alumina with heterolytic bond dissociation energy, $D(R^+OH^-)$, of the C–O bond.
○: At t/°C=54; ●: at t/°C=166.

Table 2. Heterolytic bond dissociation energy and related thermodynamical quantities[a,b,c]

R and X	ΔH°_f(R or X)[d] kcal mol^{-1}	IP(R)[e] or EA(X) kcal mol^{-1}	$\Delta H^\circ_f(R^+$ or $X^-)$ kcal mol^{-1}	ΔH°_f(ROH)[f] kcal mol^{-1}	ΔH°_f(RH)[f] kcal mol^{-1}	$D(R^+OH^-)$ kcal mol^{-1}	$D(R^+H^-)$ kcal mol^{-1}
R=							
Et	25.7	193.3	219.0	−56.12	−20.24	242	273
n-Pr	21.0	186.8	207.8	−61.55	−24.82	236	267
i-Pr	17.6	174.1	191.7	−65.15	−24.82	224	251
n-Bu	16.0	184.7	200.7	−65.15	−30.15	233	265
i-Bu	14.0	184.7	198.7	−67.9[g]	−32.15	234	265
s-Bu	12.4	170.9	183.3	−69.86	−30.15	220	248
t-Bu	6.8	159.8	166.6	−74.7[h]	−32.15	208	233
X=							
OH	9.3	42.2[i]	−32.9				
H	52.1	17.9[j]	34.2				

a) ΔH°_f is the standard heat of formation; IP, the ionization potential; EA, the electron affinity; $D(R^+X^-)$, the heterolytic bond dissociation energy for the R–X bond. b) $\Delta H^\circ_f(R^+)=\Delta H^\circ_f(R)+IP(R)$, $\Delta H^\circ_f(X^-)=\Delta H^\circ_f(X)-EA(X)$, $D(R^+X^-)=\Delta H^\circ_f(R^+)+\Delta H^\circ_f(X^-)-\Delta H^\circ_f(RX)$. c) Et=ethyl, Pr=propyl, Bu=butyl. d) J. A. Kerr, *Chem. Rev.*, **66**, 465 (1966). e) F. P. Lossing and G. P. Semeluk, *Can. J. Chem.*, **48**, 955 (1970). f) D. S. Stull, E. F. Westrum, Jr., and G. C. Sinke, "The Chemical Thermodynamics of Organic Compounds," John Wiley & Sons, New York (1969). g) H. A. Skinner and A. Snelson, *Trans. Faraday Soc.*, **56**, 758 (1960). h) E. T. Beynon and J. J. McKetta, *J. Phys. Chem.*, **67**, 2761 (1963). i) L. M. Branscom, *Phys. Rev.*. **148**, 11 (1966). j) D. Feldmann, *Z. Naturforsch.*, **25a**, 621 (1970).

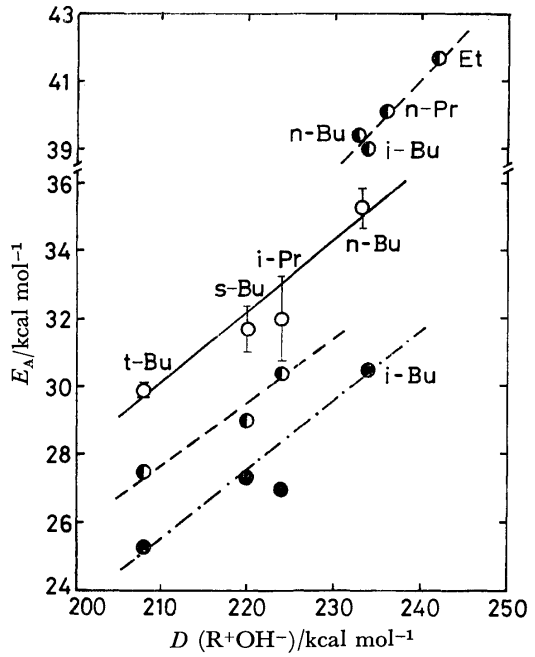

Fig. 6. Correlations of zero-order activation energy for alcohol dehydration on various catalysts with heterolytic bond dissociation energy, D(R$^+$OH$^-$), of the C–O bond.
○: The present study (on silica–alumina); ●: Knözinger and Scheglila[8] (on γ-alumina); ◐: Kibby and Hall[9] (on Ca-deficient hydroxyapatite).

Figure 5 shows the correlation between the relative rate constant of dehydration and the heterolytic bond dissociation energy, D(R$^+$OH$^-$), for alcohols. The relationship of the activation energy with D(R$^+$OH$^-$) is also shown in Fig. 6. From the definition, D(R$^+$X$^-$) is the enthalpy change of the RX→R$^+$+X$^-$ process, where R is the alkyl group, and X, the substituent, such as OH, halogen or H, so that the previous parameter, ΔH_{C^+}(R), is D(R$^+$H$^-$). The bond energy, D(R$^+$X$^-$), was calculated for X=OH and H from recent thermodynamical data, as is shown in Table 2. Although D(R$^+$X$^-$) has a linear correlation with ΔH_{C^+}(R) for each X$^-$, the former seems more attractive than the latter in that it may function as a simple parameter describing the effects of both R and X on the reactivity.

The logarithms of the rate constants relative to that for butyl alcohol have a linear relationship with D(R$^+$OH$^-$) over the range of about six orders of magnitude in the rate constants (Fig. 5), indicating that the lower the heterolytic bond dissociation energy, the higher the rate constant. The activation energies also show a linear relationship with D(R$^+$OH$^-$) (Fig. 6); that is, the activation energy increases with an increase in D(R$^+$OH$^-$). Both linear correlations can readily be explained in terms of the heterolytic rupture of the C–O bond in the rate-determining step. Yamaguchi and Tanabe[13] found no primary isotope effect of C_β–D in the zero-order dehydration of 2-propanol-d_8 on silica–alumina at 160 °C; they proposed an E1-like mechanism. Thus, the presently obtained LFER, in cooperation with the isotope-effect data, strongly supports the E1-like character of the alcohol dehydration over silica–alumina.

Knözinger and Scheglila[8] found high primary isotope effects in the zero-order dehydration of C_β-deuterated butyl alcohols, $(CH_3)_2CDCH_2OH$, $C_2D_5CH(OH)CH_3$, and $(CD_3)_3COH$, on alumina at 120—200 °C. They deduced an E2-like mechanism which contains a certain degree of ionic contributions. Their activation-energy data on undeuterated alcohols[8,14] are also plotted in Fig. 6. These activation energies also fall on a straight line, which is separate from, but nearly the same in slope as the line for silica–alumina. Comparisons of the two linear correlations provide information concerning the rate-determining participation of the heterolytic C–O bond fission during the E2-like dehydration couse. The equality in the slope indicates that the heterolytic bond strength of the C–O bond plays as important a role in determining the activation energy for the E2-like dehydration as it does for the E1-like dehydration. The heterolytic loosening of the C–O bond in the transition state may not differ much in the two modes of dehydration.

Furthermore, the activation energy on silica–alumina is approximately 5 kcal/mol higher than that on alumina for each alcohol, as is shown in Fig. 6. Knözinger and Scheglila[8] also found that the deuterium effect on the preexponential factor, A_H/A_D, was approximately 0.01 for each alcohol. More recently, this abnormally low A_H/A_D ratio was taken as evidence by the same group of researchers[14] to demonstrate a certain tunnel contribution to the β-proton abstraction. The tunnel effect is also supported, though they did not claim so, by their own experimental results that the deuterium effect on the activation energy, E_D-E_H, was about 5 kcal/mol for each alcohol.[8] This effect greatly exceeds in magnitude the zero-point energy difference between the C_β–H and C_β–D stretching vibrations in the initial state, ΔE_0, which is about 1.1 kcal/mol for the substrates in question. The $E_D-E_H<\Delta E_0$ relation also provides strong evidence for proton tunneling.[15] The difference of about 5 kcal/mol for E_D-E_H is comparable to the activation-energy difference between silica–alumina and alumina for the undeuterated alcohol dehydration. The activation energies for deuterated alcohol dehydration on alumina and those for undeuterated alcohol dehydration on silica–alumina will, therefore, fall on a single straight line if they are plotted in Fig. 6. Since tunneling should be much less in the β-deuteron abstraction than in the β-proton abstraction, the observed tunneling contribution to the β-proton abstraction presumably explains most of the slight lowering of the activation energy in the dehydration of undeuterated alcohols over alumina. In addition, the stabilization of the transition state through the interaction of β-deuterium, probably, with a basic site does not seem very large. Therefore, it is highly probable that the activation energy for the E2-like dehydration is determined primarily by the heterolytic bond strength of the C–O bond, much as with that for the E1-like dehydration.

Figure 6 also shows a plot of the activation-energy data reported by Kibby and Hall,[9] who obtained them from the zero-order reaction rates on calcium-deficient hydroxyapatite at 150—400 °C; they presumed an E1-like mechanism for tertiary alcohol and an E2-like one

with an ionic character for primary and secondary alcohols. The sequence of increasing activation energy is the same as that of increasing $D(R^+OH^-)$. Isopropyl alcohol and *s*- and *t*-butyl alcohols fall on a single straight line, which is quite similar in both slope and the magnitude of activation energy to those for silica–alumina and alumina, although primary alcohols appear to follow a separate straight line. It is clear that, on this catalyst, the activation energy is also determined by the heterolytic bond strength of the C–O bond.

In spite of the fact that these three catalysts are quite different materials, the alcohol dehydrations catalyzed by them are very similar in the magnitude of the activation energy and its dependence upon $D(R^+OH^-)$. This may be a reflection of a similarity in the nature of the active centers which first attack the oxygen atom of the C–O bond. As such active centers, Knözinger and his co-workers,[3] and Kibby and Hall[9] proposed acidic surface hydroxyls on their catalysts. With silica–alumina, Brønsted acid sites are most likely to be active centers in view of the experimental finding[16] that the response of the ethanol dehydration rates to the Na^+-poisoning of silica–alumina is very similar to that of the cumene dealkylation rates, which have been believed to be determined by the Brønsted acidity. For alumina[17,18] and even silica–alumina,[19] on the other hand, another active-center model has been proposed in which incompletely coordinated aluminium ions in the surface are responsible for attacking the oxygen atom of the C–O bond. This problem, then, requires further investigations to be solved.

References

1) M. E. Winfield, "Catalysis," Vol. 7, ed by P. H. Emmett, Reinhold, New York (1960), p. 93.
2) H. Pines and J. Manassen, *Adv. Catal.*, **16**, 49 (1966).
3) H. Knözinger, *Angew. Chem. Int. Ed. Engl.*, **7**, 791 (1968).
4) B. Notari, *Chim. Ind. (Milan)*, **51**, 1200 (1969).
5) (a) I. Mochida and Y. Yoneda, *J. Catal.*, **7**, 386 (1967); (b) *ibid.*, **8**, 223 (1967).
6) (a) H. Matsumoto, J. Take, and Y. Yoneda, *J. Catal.*, **11**, 211 (1968); (b) *ibid.*, **19**, 113 (1970).
7) P. B. Weisz, *Z. Phys. Chem. (N. F.)*, **11**, 1 (1957).
8) H. Knözinger and A. Scheglila, *J. Catal.*, **17**, 252 (1970).
9) C. L. Kibby and W. K. Hall, *J. Catal.*, **29**, 144 (1973).
10) A. Maccoll, "Advances in Physical Organic Chemistry," Vol. 3, ed by V. Gold, Academic Press, London and New York (1965), p. 91.
11) H. Noller, P. Andréu, and M. Hunger, *Angew. Chem. Int. Ed. Engl*, **10**, 172 (1971).
12) M. Sugioka, T. Yotsuyanagi, and K. Aomura, *Kogyo-Kagaku Zasshi*, **73**, 2172 (1970).
13) T. Yamaguchi and K. Tanabe, *Nippon Kagaku Kaishi*, **1973**, 240.
14) H. Knözinger, H. Buhl, and K. Kochloefl, *J. Catal.*, **24**, 57 (1972).
15) (a) L. Fandersburk and E. S. Lewis, *J. Am. Chem, Soc.*, **86**, 2531 (1964). (b) V. J. Shiner and B. Martin, *Pure Appl. Chem.*, **8**, 371 (1964).
16) J. Take and Y. Yoneda, unpublished data.
17) H. Arai, J. Take, Y. Saito, and Y. Yoneda, *J. Catal.*, **9**, 146 (1967).
18) Y. Soma, T. Onishi, and K. Tamaru, *Trans. Faraday Soc.*, **65**, 2215 (1969).
19) K. V. Topchieva, K. Yun Pin, and I. V. Smirnova *Adv. Catal.*, **9**, 799 (1957).

Minima in the Solubilities of Normal Alkane Derivatives with a Polar Group in Water

Nobuo NISHINO and Masao NAKAMURA

Department of Chemistry, Faculty of Science, Tokai University, Kitakaname, Hiratsuka 259-12

(Received October 6, 1977)

The change in the solubility in water with the temperature was measured for alkanols, alkylamines, and alkanoic acids. It has been found that a minimum exists commonly on the solubility-temperature curve. This minimum dissolution point, P_m, may be regarded as a characteristic point with respect to the solute. The change in the solubility with the temperature has been explained in terms of the increase in the partial molar enthalpy of the solute in solution with an increase in the temperature, which results from the breakdown of the ice-like structure of water formed around the nonpolar alkyl group. Both the concentration, x_m, and temperature, T_m, at point P_m decrease with an increase in the number of carbon atoms in the alkyl group, m. The decrease in $\ln x_m$ by the addition of one methylene group is steeper in the order of alkanoic acids, alkylamines, and alkanols, while the corresponding decrease in T_m shows the reverse order. In addition, T_m is related to the cohesive energy of the solute in the pure state.

Aqueous nonionic surfactant solutions suddenly become turbid above a certain temperature, which is called the cloud point,[1] while nicotine and like-compounds have both upper and lower critical consolution temperatures in water,[2,3] although a substance is usually more soluble at a higher temperature in an ordinary or regular solution.[4,5] Several concepts have been presented in attempts to interpret these anomalous solubility phenomena in water. One is that the hydrogen bonding between a water molecule and a polar group of the organic solute decreases as the temperature rises,[6] and another is that a nonpolar hydrocarbon or rare gas molecule in water promotes the formation of the structure of water around it, while the structure gradually breaks down with a rise in the temperature.[7–9] The above concepts, however, cannot explain the solubility phenomena quantitatively, and the states in water of organic compounds have not yet been understood sufficiently. In the present paper, in order to study the states of organic compounds in water, the change in the solubility with the temperature was measured for several normal alkane derivatives, which have a polar group in the molecule to increase the solubilities. A minimum was commonly observed on the solubility-temperature curve.

Experimental

Normal alkane derivatives as the solutes were selected from the 1-, 2-, and 3-alkanol, alkylamine, and alkanoic acid series, each of which is liquid over the temperature range under investigation. The samples are commercially available as G. R. -grade materials from Wako Pure Chemical Industries, Ltd.; the Kanto Chemical Co., Inc.; Nakarai Chemicals, Ltd.; the Sumida Chemical Co., Ltd., and the Tokyo Kasei Kogyo Co., Ltd. They were used without further treatment except for those of 1-alkanol series, which were dried over calcium oxide and kept in ampoules in contact with magnesium powder before use. The solvent was obtained by distilling ion-exchanged water from an alkaline potassium permanganate solution after refluxing for 15 h.

Twenty to thirty glass ampoules containing aqueous solutions of *ca.* 5 cm^3 of various concentrations near the solubility at room temperature for each compound were immersed in a water thermostat. The distinction between clean and turbid ampoules was made after a time long enough for equilibrium to be established, say *ca.* 2 h, at each temperature. Observations were made at 2- to 5-K intervals from 275 to 360 K. The smooth curve drawn to separate the clean and turbid regions in the concentration-temperature diagram was regarded as the solubility curve.

The heat of evaporation was estimated according to the vapor-pressure method described in a previous paper,[10] except for using a spinning-band type of precision distillation apparatus (Tokyo Kagaku Seiki Co.).

Results and Discussion

The solubilities in the mole fraction, x_2, measured are plotted against the temperature, T, in Figs. 1 and 2. Alkanols, alkylamines, and alkanoic acids commonly show decreasing and increasing solubilities with temperature in lower- and higher-temperature regions respectively. Each curve, then, has a minimum point

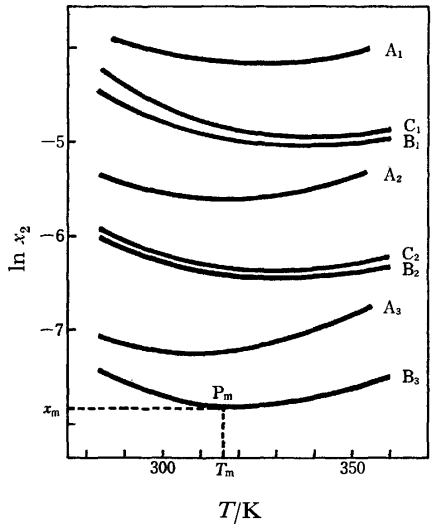

Fig. 1. Solubility of alkanol series in water as a function of temp.
A_1: 1-Butanol, A_2: 1-pentanol, A_3: 1-hexanol, B_1: 2-pentanol, B_2: 2-hexanol, B_3: 2-heptanol, C_1: 3-pentanol, C_2: 3-hexanol, P_m: minimum dissolution point, x_m: minimum dissolution concn, T_m: minimum dissolution temp.

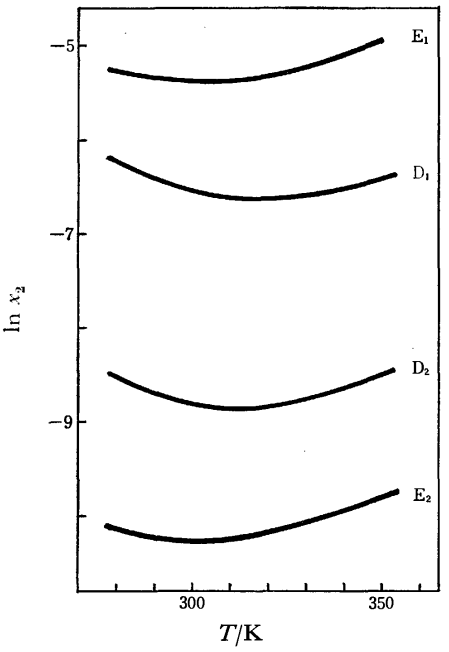

Fig. 2. Solubility of alkylamine and alkanoic acid series in water as a function of temp.
D_1: Hexylamine, D_2: heptylamine, E_1: pentanoic acid, E_2: hexanoic acid.

in solubility, which is referred to as the minimum dissolution point, P_m, as is indicated in Fig. 1. This minimum point may be regarded as a characteristic point with respect to the solute in water as a solvent. The concentration and temperature at that point are termed the minimum dissolution concentration, x_m, and the minimum dissolution temperature, T_m, respectively. The appearance of these minima resembles the dependence of the critical micelle concentration, CMC, on the temperature, T, for aqueous surfactant solutions measured by Shinoda.[9] He has described how the iceberg formation of water molecules around the monodisperse solute rather enhances the CMC, the logarithm of which would be decreased linearly with T^{-1} if the solution behaved regularly, and the iceberg formation increases with the temperature depression.

Bohon and Claussen[11] have estimated the heat of solution from such solubility curves for aromatic compounds by assuming that the heat of solution is proportional to the tangent of the curve of $\ln x_2$ *vs.* T^{-1}. This assumption, however, is valid only when the organic phase in equilibrium with the aqueous solution contains no water or a constant amount of it, regardless of the temperature. It may be reasonable, nevertheless, to consider that the change in the solubility with the temperature shown in Figs. 1 and 2 is predominantly due to the increase in the heat of solution at an infinite dilution with the temperature, because the solubility of water in an organic phase is expected to vary less with the temperature. The heat of solution at an infinite dilution is the difference between the partial molar enthalpy of the solute in an infinitely dilute solution and the molar enthalpy in the pure state of the solute; in addition, the heat of solution is equal to the sum of the heat of evaporation of the pure solute and the heat of condensation of the solute from the vapor phase to the solution, according to Hess' law. The heat of evaporation may be assumed to be constant in the measured temperature range for each solute, because the logarithm of the vapor pressure decreases linearly with T^{-1}, as is shown in Figs. 5 and 6. The increase in the heat of solution, therefore, may be attributed mainly to the increase in the partial molar enthalpy of the solute in the solution through the heat of condensation, which shows that some endothermic changes proceed on and/or around the solute molecules with the temperature rise. Since all the solubility curves in Figs. 1 and 2 are similar in shape, regardless of the nature of the polar group, such endothermic changes may be attributed commonly to the nonpolar alkyl group. Frank and Evans[7] have described how the rare gases and hydrocarbon gases form icebergs when they dissolve in cold water; how, as the temperature is raised, these icebergs melt, giving rise to the enormous partial molar heat capacity of these gases in water, and how, at still higher temperatures, the heat of evaporation from the aqueous solution becomes negative. The solubility of most gases in water shows a minimum when plotted against the temperature. Following the above description, the solubility curves in Figs. 1 and 2 can be explained by considering that the ice-like structure of water is also formed around the nonpolar alkyl group of alkanol, alkylamine, or alkanoic acid in water, which structure breaks down as the temperature is raised.

The relations between $\ln x_m$ and the number of carbon atoms in an alkyl chain, m, for the respective series are shown in Fig. 3. The value of $\ln x_m$ decreases linearly with m for the 1- and 2-alkanol series, and these two lines are nearly parallel to each other. The decrease in $\ln x_m$ from 3-pentanol to 3-hexanol is nearly equal

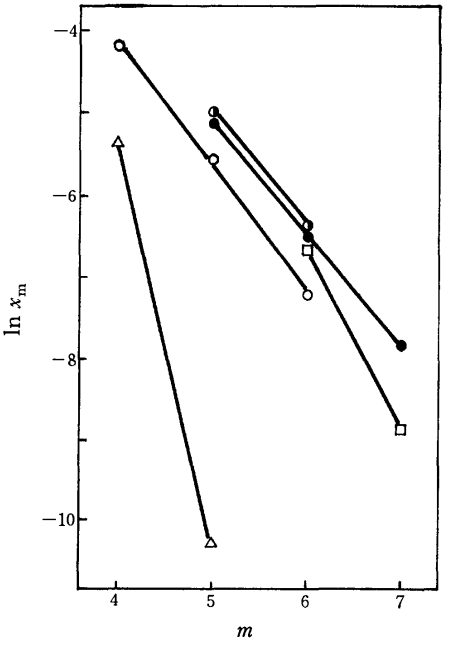

Fig. 3. Minimum dissolution concn as a function of number of carbon atom in alkyl group.
○: 1-Alkanol, ●: 2-alkanol, ◑: 3-alkanol, □: alkylamine, △: alkanoic acid.

to the slopes of the straight lines for the 1- and 2-alkanol series. The decrease of $\ln x_m$ by the addition of one methylene group is different according to the kind of polar group attached to the molecule; the order is as follows:

$$-COOH > -NH_2 > -OH.$$

It has previously been determined[12] that the slopes of the logarithm of solubility *vs.* m values of more than 9 both for the alkanoic acid series at 298 K and for the alkylamine series at 295 K are very close to the slope for the alkanol series in Fig. 3. The larger decrease for the alkylamine or alkanoic acid series in Fig. 3 can then be expected to be reduced gradually to that for the alkanol series, when m increases up to the range out of the influence of the polar group. These phenomena may be interpreted in terms of a higher free energy of a methylene group under the influence of the attached polar group than that out of the influence of the polar group.[13] The farther the methylene group is apart from the polar group, the easier is the structure of water to be formed around it, since the effect of the polar group decreases with the distance. The steeper decrease in $\ln x_m$ for the alkanoic acid series than for the alkylamine series in Fig. 3 can be explained by the smaller carbon number, m, in the former series, although the former series have slightly weaker polarities or dissociation constants.[14] In addition, in the alkanol series, the closer the OH groups are to the center, the more soluble they are when they have the same m, as is shown in Fig. 3. This may be explained in terms of the increasing number of methylene groups within the influence of an OH group as the OH group is closer to the center of the molecule, but the difference between the 2- and 3-alkanol series is not appreciable.

The minimum dissolution temperature, T_m, also decreases with an increase in the number of carbon atoms, m, for those series, as is shown in Fig. 4. The decrease in T_m upon the addition of one methylene group is steeper in the reverse order of that of $\ln x_m$ in Fig. 3. The T_m values show the following order:

3-alkanol > 2-alkanol > alkylamine > 1-alkanol > alkanoic acid,

if m is constant in the range of 5 and 6.

The characteristic point, P_m, of a solute in an aqueous solution is expected to be related to the characteristics of the solute itself, especially, for example, the cohesion between molecules. The heat of evaporation, $\Delta_e h_2^\circ$, can be considered a measure of the cohesive energy.[10] The vapor pressures, p, of the solutes in their pure states

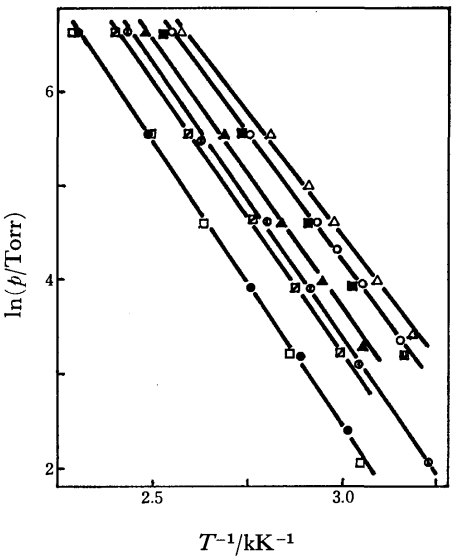

Fig. 5. Vapor pressure of alkanol series as a function of temp.
○: 1-Butanol, ◑: 1-pentanol, ●: 1-hexanol, ■: 2-pentanol, ⊠: 2-hexanol, □: 2-heptanol, △: 3-pentanol, ▲: 3-hexanol.

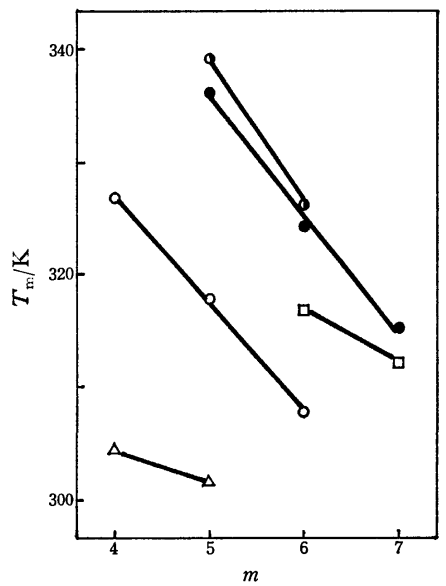

Fig. 4. Plots of minimum dissolution temp *vs.* number of carbon atom in alkyl group.
○: 1-Alkanol, ●: 2-alkanol, ◑: 3-alkanol, □: alkylamine, △: alkanoic acid.

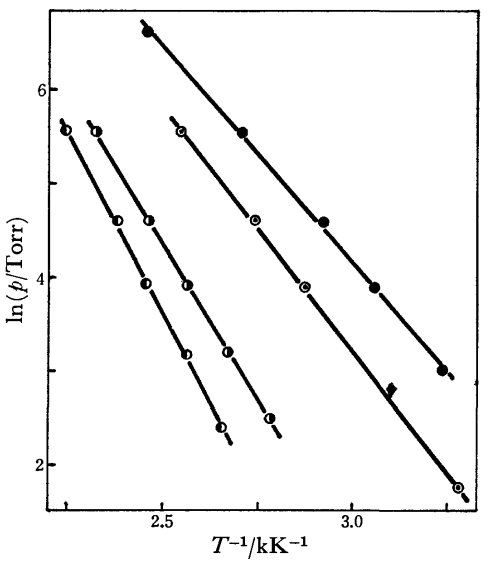

Fig. 6. Vapor pressure of alkylamine and alkanoic acid series as a function of temp.
●: Hexylamine, ⊙: heptylamine, ◑: pentanoic acid, ◐: hexanoic acid.

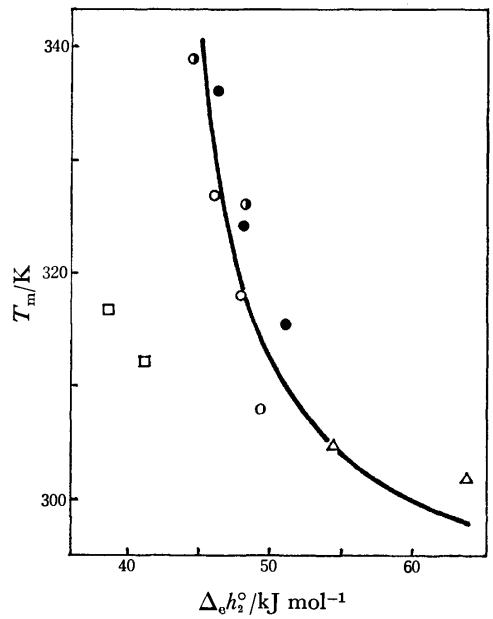

Fig. 7. Plots of minimum dissolution temp *vs.* heat of evaporation.
○: 1-Alkanol, ●: 2-alkanol, ◑: 3-alkanol, □: alkylamine, △: alkanoic acid.

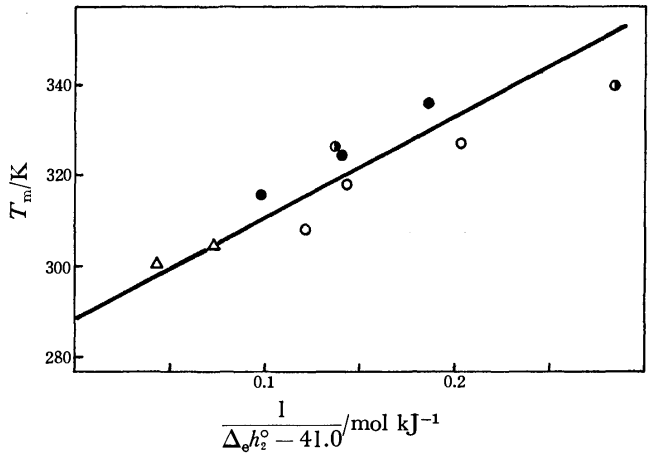

Fig. 8. T_m *vs.* $\frac{1}{\Delta_e h_2^\circ - 41.0}$ plots.
Marks are the same as in Fig. 7.

were measured in the temperature range between 305 and 445 K. As has been mentioned above, $\ln p$ decreases linearly with T^{-1} for each solute, as is shown in Figs. 5 and 6. The heat of evaporation, $\Delta_e h_2^\circ$, was estimated from the slope according to the Clausius-Clapeyron equation. It has been found that $\Delta_e h_2^\circ$ has a certain relation to T_m except for the alkylamine series, as is shown in Fig. 7. The relation may be expressed by

$$T_m = \frac{223}{\Delta_e h_2^\circ - 41.0} + 288, \qquad (1)$$

as is shown as the straight line in Fig. 8 and as the curve in Fig. 7. It should be noted that Eq. 1 should be applied to the compounds having $\Delta_e h_2^\circ$ values higher than 41.0 kJ mol^{-1} and T_m values larger than 288 K.

References

1) K. Shinoda, "Solvent Properties of Surfactant Solutions," ed by K. Shinoda, Marcel Dekker, New York (1967), p. 27.
2) C. S. Hudson, *Z. Phys. Chem.*, **47**, 113 (1903).
3) H. L. Cox and L. H. Cretcher, *J. Am. Chem. Soc.*, **48**, 451 (1926).
4) J. H. Hildebrand and R. L. Scott, "Regular Solutions," Prentice-Hall, Englewood Cliffs, New Jersey (1962).
5) E. A. Guggenheim, "Mixtures," Oxford University Press, Oxford (1952).
6) K. Shinoda, T. Nakagawa, B. Tamamushi, and T. Isemura, "Colloidal Surfactants," Academic Press, New York and London (1963), p. 129.
7) H. S. Frank and M. W. Evans, *J. Chem. Phys.*, **13**, 507 (1945).
8) K. Shinoda and M. Fujihira, *Bull. Chem. Soc. Jpn.*, **41**, 2612 (1968).
9) K. Shinoda, *Proc. 6th Intern. Congr. Surface Active Substance*, **2**, 891 (1972).
10) M. Nakamura, K. Eda, and K. Kosiyama, *Bull. Chem. Soc. Jpn.*, **47**, 2877 (1974).
11) R. L. Bohon and W. F. Claussen, *J. Am. Chem. Soc.*, **73**, 1571 (1951).
12) I. J. Lin and P. Somasundaran, *J. Colloid Interface Sci.*, **37**, 731 (1971).
13) D. B. Dahlberg, *J. Phys. Chem.*, **76**, 2045 (1972).
14) "Landolt-Börnstein Tabellen," 6 Aufl., II Band, 7 Teil, Springer-Verlag (1960), p. 847.

A Localized Molecular Orbital Calculation of Chemically Interacting Systems. Interaction between Amines and Carbonyls

Tsutomu MINATO, Hiroshi FUJIMOTO, and Kenichi FUKUI

Faculty of Engineering, Kyoto University, Sakyo-ku, Kyoto 606

(Received October 11, 1977)

The bond interchange in the course of the addition of amine to carbonyl has been studied by means of a localized molecular orbital method with a clear chemical-bond concept, and the mechanism of the addition has been elucidated theoretically. It is ascertained by the present calculation that the charge transfer interaction from the highest occupied molecular orbital of amine to the lowest unoccupied molecular orbital of carbonyl is of importance to form a new nitrogen-carbon bond. Furthermore, the stereospecificity of the nucleophilic addition to a double or triple bond has been studied. When an intermediate is created by the addition of a nucleophile to the unsaturated bond, it is suggested that the intermediate is reactive for the electrophilic attack on the side *trans* to the new bond formed by the first attack. This is reasoned in terms of the mode of orbital interaction.

Addition of amine to carbonyl is one of the simplest nucleophilic reactions.[1] Recently, the course of the addition was studied experimentally by analyzing the molecular structure of adducts of amine to ketone with presumably different strength of the interaction.[2] The path of the approach of amine to carbonyl revealed in the work is expected to provide us with valuable information for a theoretical study of chemical reactions. In general, the path of the chemical reaction is governed by various energy factors in a molecular orbital (MO) viewpoint.[3] A partitioning analysis of the interaction energy suggested that the exchange and charge transfer (CT) interactions are generally of importance in the interaction between two reagents, while the Coulomb interaction plays a dominant role in an early stage of ionic reactions.[4] Even in ionic cases, however, the CT interaction is the origin of the formation of new chemical bonds.[5]

In discussing the orientation and stereoselection in chemical reactions, the CT interaction from the highest occupied (HO) MO of electron donors to the lowest unoccupied (LU) MO of electron acceptors is usually of a particular importance.[5] The HOMO and LUMO of many molecules, however, are delocalized over p atomic orbitals (AO's) of component heavy atoms and hydrogen 1s AO's. The s AO's of first and second row atoms are found for the most part in low-lying MO's. When a configuration interaction expansion of the wavefunction of the interacting system is carried out in terms of various kinds of the electron configurations, there is non-negligible contribution of the charge transferred and locally excited configurations from low-lying MO's, in addition to the major charge transferred configurations from the HOMO to the LUMO. Therefore, the formation of new bonds and the loosening of old bonds, together with the rehybridization at the reaction centers, may be interpreted by means of orbital interactions between the isolated molecules including the HOMO-LUMO interactions.

In general, the MO's of a sizable molecule are delocalized over the constituent AO's and the bonding property of a given atom pair is discussed by means of the electron density contour,[6] the overlap population[7] and the bond energy.[8] On the other hand, the method of the Edmiston-Ruedenberg localized MO (LMO)[9] presents us an alternative way of visualizing the chemical bonds in a chemically graspable manner. It may be worthwhile to show that the application of the LMO method to chemically interacting systems is really helpful in disclosing the mechanism of bond interchange and rehybridization in the course of the reaction. These are interesting problems in organic chemistry.

In the present paper, we first apply the LMO method to the chemically interacting system composed of amine and carbonyl in order to obtain a theoretical way of representing the bond interchange and rehybridization in the course of the addition reaction. Next, the mechanism of the addition is clarified by the mode of the orbital interaction mentioned above. Furthermore, the general aspect of the nucleophilic addition to unsaturated bonds is explained schematically in terms of the shape of MO's of the isolated reactants.

Calculation of Assumed Reaction Models

Method of Calculation. In this study, a system composed of an ammonia and a formaldehyde is selected as a reaction model in the calculation of the LMO's. The canonical MO's (CMO's) of the isolated molecules and the reacting system which are transformed into the LMO's[9] are obtained by the INDO MO method.[8]

Figure 1 illustrates the geometry of assumed reaction models. In the present calculation, three variables (R, r, and θ) are changed. The geometry of ammonia[10] is kept frozen throughout the calculation, whereas that of formaldehyde[11] is deformed. The parameter, R, means the intermolecular distance between the nitrogen atom (N) of ammonia and the carbon atom (C) of formaldehyde. "r" is the distance of the C=oxygen (O) bond of formaldehyde, and "θ" is defined as the angle between the C=O bond and the methylene plane of formaldehyde. A preliminary calculation on this system gives a result which is in a fairly good agreement with the experimental reaction path.[2] In consideration of the preliminary result and the experimental reaction path, the angle between the N···C line and the C=O is fixed to be 107° in the present calculation. The N···C distance, R, is restricted to the range, 3.0—2.0 Å. At R=3.0 and 2.5 Å, the geometry of formaldehyde is not deformed (r=1.21 Å and θ=0°),[11] whereas at R=2.2

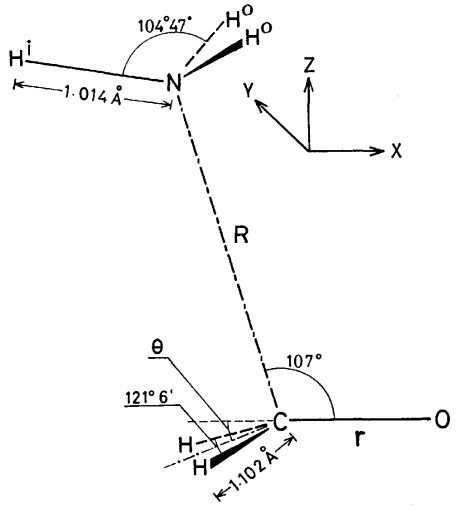

Fig. 1. The assumed reaction model employed for the calculation of the LMO.

and 2.0 Å it is deformed to give the minimum total energy of the interacting system at each value of R (r=1.25 Å, θ=10° at R=2.2 Å and r=1.27 Å, θ=15° at R=2.0Å). On these models, the LMO's of the reacting system are calculated.

The energy of each LMO (B_i) is calculated to study the formation and disappearance of the bond.[12] The energy, B_i, is represented by the sum of the electron energy (E_i^{el}) of the LMO and the nuclear repulsion energy.

$$B_i = E_i^{el} + E_i^{n}. \quad (1)$$

The nuclear repulsion energy is partitioned and assigned to the bonds according to the procedure introduced by Parks and Parr.[13] E_i^n in Eq. 1 is the partitioned nuclear repulsion energy assigned to the bond i.

Furthermore, the LMO is expanded in terms of the CMO's of ammonia and formaldehyde in order to see the origin of the bond formation, the bond cleavage and the rehybridization in the course of the reaction.[5b]

$$\phi_{LMO} = \sum_{i=1}^{7} C_i a_i + \sum_{j=1}^{10} D_j b_j. \quad (2)$$

ϕ_{LMO} is one of the LMO's of the reacting system. The CMO of ammonia is defined a_i, while that of formaldehyde is named b_j. The suffix attached to the right bottom of "a" and "b" stands for the numbering order counted from the lowest occupied MO.

Results. In Fig. 2, the CMO's of ammonia and formaldehyde are schematically depicted. In Fig. 3, the shapes of the LMO's of these are also schematically pictured. They are three N–H (hydrogen) bond orbitals and an N lone pair orbital in ammonia, and two C–H bond orbitals, two O lone pair orbitals and two C–O bent bond orbitals in formaldehyde. The upper C–O bent bond orbital is hereafter called the CO bond 1, and the lower one is called the CO bond 2. For each value of R, the energies of LMO's are calculated. The result is given in Table 1. In Table 1, it is shown that the N lone pair orbital is stabilized. This corresponds to the formation of the N···C bond. On the other hand, the two C–O bent bond orbitals are

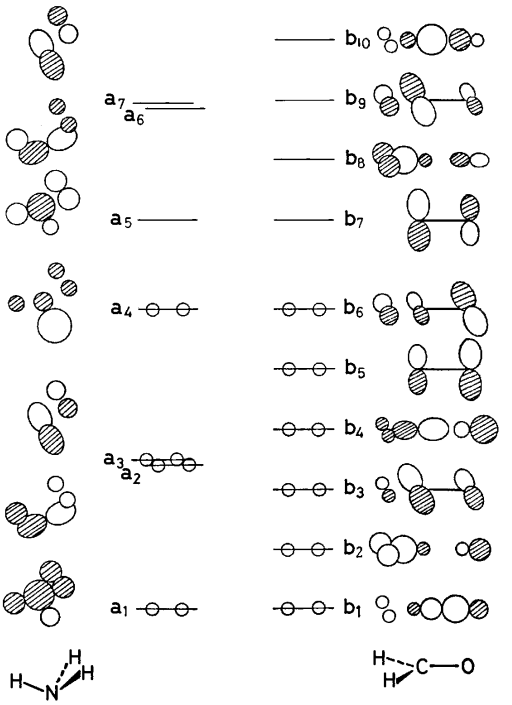

Fig. 2. The shape of the CMO's of the isolated ammonia and formaldehyde.

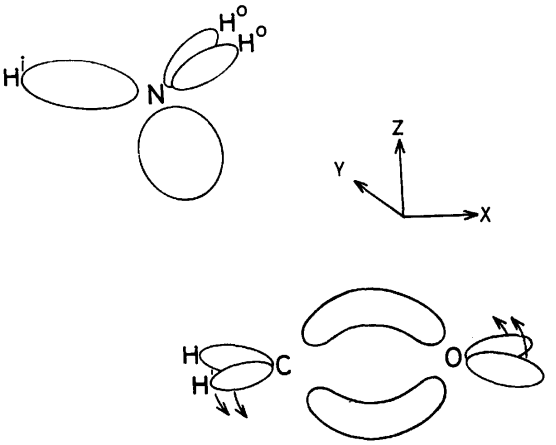

Fig. 3. The shape of the LMO's of the isolated ammonia and formaldehyde.

destabilized, indicating the weakening of the bonds. Interestingly, the CO bond 2 is loosened more easily than the CO bond 1, and the latter is even stabilized at R=2.0 Å. A more detailed discussion on this point will be given later. It is found from Table 1 that the remaining bond orbitals do not change much in comparison with the three bond orbitals mentioned above.

Let us examine the change in the LMO's for the N lone pair and the two C–O bonds. These bonds are considered to participate significantly in the addition reaction. In Fig. 4, the LMO corresponding to the N lone pair is pictured. It is shown that the N lone pair orbital begins to deform so that it would include the component of the carbon AO's. The s-nature of the N lone pair orbital of the isolated ammonia is calculated to be 35.5%, and that at R=2.0 Å is found

TABLE 1. THE CALCULATED ENERGY OF THE BOND ORBITALS IN THE ADDITION OF AMMONIA TO FORMALDEHYDE
The NH bond is the N–H^{i} bond of ammonia which is in the N–C–O plane.
The NH^{o} bonds are not in the N–C–O plane.

R/Å		CO bond 1	CO bond 2	CH bond	CH bond	O lone pair	O lone pair	N lone pair	NH^{o} bond	NH^{o} bond	NH^{i} bond
	E_i^{el}	−212.25	−212.25	−168.27	−168.27	−211.73	−211.73	−148.85	−151.44	−151.44	−151.44
8	E_i^{n}	79.78	79.78	100.28	100.28	62.02	62.02	42.60	65.65	65.65	65.65
	B_i	−132.47	−132.47	−67.99	−67.99	−149.71	−149.71	−106.25	−85.79	−85.79	−85.79
	E_i^{el}	−245.42	−245.30	−204.20	−204.20	−242.73	−242.73	−202.13	−201.79	−201.79	−201.01
3.0	E_i^{n}	113.47	113.47	136.41	136.41	93.09	93.09	95.62	115.51	115.51	114.70
	B_i	−131.95	−131.83	−67.79	−67.79	−149.64	−149.64	−106.51	−86.28	−86.28	−86.31
	E_i^{el}	−250.71	−250.65	−210.32	−210.32	−246.89	−246.89	−212.15	−210.30	−210.30	−209.21
2.5	E_i^{n}	119.09	119.09	142.82	142.82	97.59	97.59	104.85	123.57	123.57	122.42
	B_i	−131.62	−131.56	−67.50	−67.50	−149.30	−149.30	−107.30	−86.73	−86.73	−86.79
	E_i^{el}	−252.53	−250.22	−213.19	−213.19	−247.70	−247.70	−220.47	−216.73	−216.73	−215.34
2.2	E_i^{n}	121.28	121.28	145.56	145.56	98.85	98.85	111.31	129.12	129.12	127.65
	B_i	−131.25	−128.94	−67.63	−67.63	−148.85	−148.85	−109.16	−87.61	−87.61	−87.69
	E_i^{el}	−260.68	−244.38	−215.66	−215.66	−248.37	−248.37	−228.26	−222.22	−222.22	−220.57
2.0	E_i^{n}	123.69	123.69	148.37	148.37	100.34	100.34	116.53	133.54	133.54	131.81
	B_i	−136.99	−120.69	−67.29	−67.29	−148.03	−148.03	−111.73	−88.68	−88.68	−88.76

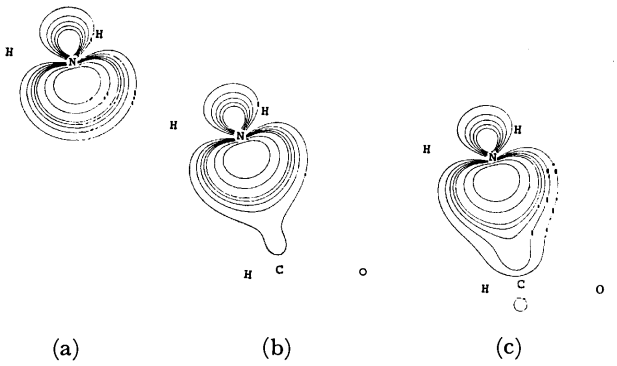

(a) (b) (c)

Fig. 4. The lone pair orbital of ammonia (N lone pair). The contour lines show the electron density. Each line indicates 0.1, 0.2, 0.3, 0.5, 0.7, 1.0 and 1.5 e/Å^3 from out side.
(a); The lone pair orbital of the isolated ammonia. (b); The lone pair orbital at R=2.2 Å. (c); The lone pair orbital at R=2.0 Å.

to be 35.3%. It is suggested, therefore, that ammonia gets into the interaction with formaldehyde, without changing its hybridized state significantly. The N lone pair orbital at R=2.5 Å corresponding to the N···C bond in the reacting system is expanded in terms of the CMO's of the two reactants.

$$\psi_{\text{N lone pair}} = 0.933a_4 - 0.343a_1 + 0.110b_7 + 0.020b_8 + \cdots \quad (3)$$

In Eq. 3, the coefficients larger than 0.02 (absolute value) are displayed. From Eq. 3, it is found that in addition to the dominant interaction between the HOMO (a_4) of ammonia and the LUMO (b_7) of formaldehyde, there are certain contributions of the low-lying and high-lying sigma MO's (a_1 and b_8). The former sigma MO, a_1, contributes to build up a hybridized orbital of ammonia (sp^3), and the latter, b_8, contributes to the change of the hybridization of the carbon of formaldehyde ($sp^2 \rightarrow sp^3$). The CT interaction from the HOMO (a_4) to the LUMO (b_7) is primarily important in the formation of the new N···C bond, and then the low-lying and high-lying MO's contribute to the rehybridization of the reacting centers.

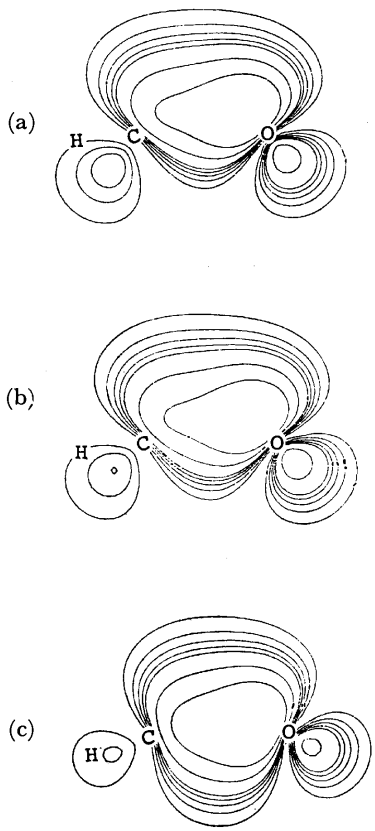

(a) (b) (c)

Fig. 5. One of the bent bond orbitals of formaldehyde (CO bond 1). The contour line means the same as is used for the lone pair orbital.
(a); One of the bent bond orbitals of the isolated formaldehyde. (b); The bent bond orbital at R=2.2 Å. (c); The bent bond orbital at R=2.0 Å.

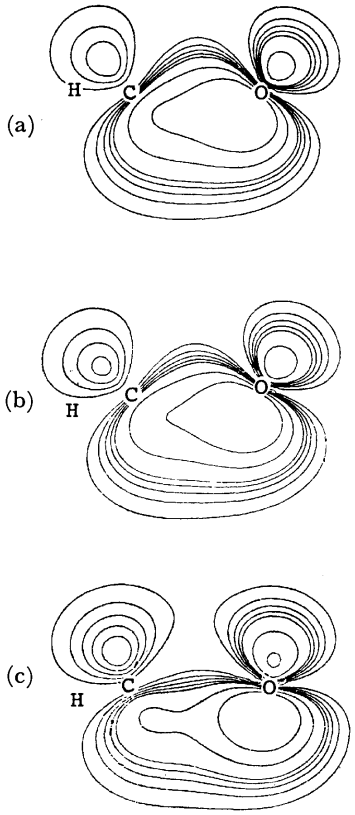

Fig. 6. The other bent bond orbital of formaldehyde (CO bond 2). The contour line means the same as is used for the lone pair orbital.
(a); The other bent bond orbital of the isolated formaldehyde. (b); The bent bond orbital at R=2.2 Å. (c); The bent bond orbital at R=2.0 Å.

In Figs. 5 and 6, the two bent bond orbitals of the C=O double bond are drawn. Let us compare Fig. 5 with Fig. 6. This comparison, together with the energy change of the bond orbitals in Table 1, shows that the CO bond 1 is converted into the CO sigma bond, whereas the CO bond 2 is transformed into the O lone pair. This result seems to be interesting in regard to the stereospecific phenomena observed in the nucleophilic additions as will be shown in the next section.

The result obtained here is explicable in terms of the orbital interaction in the following manner. In Fig. 7, the mode of the orbital interaction of the HOMO of ammonia with the π (b_5) and π^* (b_7) orbitals of formaldehyde is schematically illustrated. The interaction of the a_4 with the π and π^* leads to two occupied MO's (ψ_1 and ψ_2) and one unoccupied MO (ψ_3) of the composite system. Among the three MO's, ψ_1, ψ_2 and ψ_3, the mixing of the π and π^* through the a_4 is the largest in the ψ_2.[14] If our attention is focused on the sign of the component MO's the ψ_2 is represented[15] as

$$\psi_2 = a_4 - \pi + \pi^*.$$

The mixing of the π and π^* through the a_4 contributes to the polarization of the electrons in the direction from the carbon atom to the oxygen atom, although this mixing does not give the difference of the polarization between the upper and lower sides of the molecular

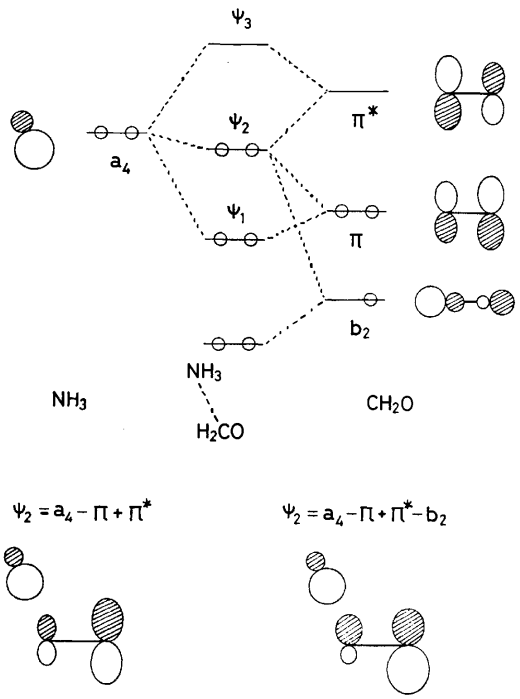

Fig. 7. The schematic representation of the electron polarization by the orbital mixing of the b_2, π, and π^* through the a_4.

plane of formaldehyde. However, the b_2 mixes into the ψ_2 through the interaction with the a_4, and then the ψ_2 is rewriten[15] as

$$\psi_2 = a_4 - \pi + \pi^* - b_2.$$

Consequently, the polarization of the C=O bond is more effective in the lower side of the molecular plane of formaldehyde than the upper side. From the above result, it is considered that in the addition of ammonia to formaldehyde one of the C=O bent bond orbitals (CO bond 1) is converted into the C–O sigma bond and the other (CO bond 2) is transformed into the O lone pair. That is, the O lone pair stays as far away from the N···C bond as possible.

In the present calculation, the LMO's representing the C–H bonds of formaldehyde are shown to be pushed down by the approach of ammonia as is indicated by the arrow in Fig. 3, whereas the O lone pair orbitals are lifted, when the nuclear framework is kept unchanged. Such rehybridizations on the carbon atom and oxygen atom are obviously in favor of the change of the CO bond 2 to the O lone pair spreading over the region opposite to the initial attack at the carbon atom. The rehybridization of the carbon is explicable in terms of the orbital mixing of the b_2, b_5, and b_7 through the interaction with the a_4. This orbital mixing is shown in Eq. 4.

$$\psi_{\text{CH bond}} = 0.238b_1 + 0.624b_2 + 0.586b_3 - 0.226b_4 + 0.018b_5 - 0.395b_6 - 0.039b_7 + \cdots. \quad (4)$$

In Eq. 4, the expansion coefficients are obtained at R=2.0 Å and the values larger than 0.015 (absolute value) are displayed. The rehybridization on the oxygen is also explicable in the way similar to that on the carbon. In Eq. 5, the expansion coefficients which

are obtained at R=2.0 Å are shown and those smaller than 0.015 (absolute value) are neglected.

$$\psi_{\text{O lone pair}} = 0.345b_1 - 0.316b_2 + 0.395b_3 - 0.491b_4 + 0.198b_5 + 0.586b_6 - 0.016b_7 + \cdots. \quad (5)$$

In Eqs. 4 and 5, the coefficient of the a_4 is very small, but when the CMO's of the interacting system are expanded by the use of those of the isolated molecules, the mixing of the b_2, b_5, and b_7 is shown to be due to the interaction with the a_4. It should be noted that the LMO's representing the N–H bonds are not changed markedly in the present calculation.

Let us summarize the results obtained so far. When the C=O double bond of the formaldehyde is represented by two bent bond orbitals, the attack of ammonia to the C=O bond is shown to bring about the breaking of the bent bond orbital on the side opposite to the attack. The bond orbital is shown to be converted into the O lone pair orbital having large amplitudes on the side opposite to the initial attack at the carbon atom. Furthermore, the C–H bonds and the O lone pairs are shown to rotate to assist the transformation of the bent bond orbital into the O lone pair. In the present calculation, the system composed of ammonia and formaldehyde is selected as a reaction model. It is reasonable to consider that a compound with a double bond or triple bond (A=B or A≡B) has π, π^*, and σ MO's which are delocalized over A and B. Consequently, the result obtained by the present calculation on such a simple system seems to be generalized for the nucleophilic additions to the unsaturated compounds. The electron pair dislodged from the double bond or triple bond will stay as far away from the electron pair of the nucleophile as possible. Then, the addition to an unsaturated bond initiated by a nucleophile is expected to be trans if the intermediate reacts with an electrophile without the change of its conformation. In the next section, this expectation will be compared with the experimental data reported so far.

Comparison with Experimental Results

In the previous section, the change of the chemical bonds in the course of the addition of ammonia to formaldehyde was investigated by the use of the LMO method. The intermediate produced by the initial attack of the nucleophile to a double bond or triple bond is predicted to be more reactive for the *trans*-approach of the electrophile than the *cis*-approach. In this section, the validity of the prediction is checked by investigating the stereochemistry of the products of the nucleophilic additions reported so far.

First, let us investigate the nucleophilic additions to double bonds. The additions are known to be stereospecific.[16,17] In the reaction of 1-cyanocyclohexene with malonic ester, 72% of product is the *cis* and only 28% the *trans* isomer, and probably no equilibration of the products takes place.[16] Evidently, this result is attributable to the preference of *trans* addition.

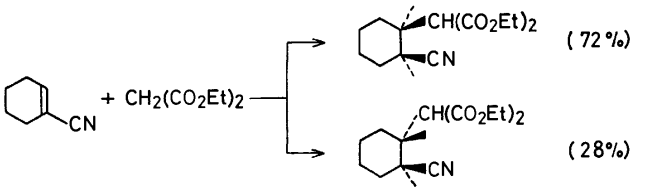

Similarly, the addition of *p*-toluenethiol to 1-(*p*-tolylsulfonyl) cyclohexene gives a *cis* product.[17]

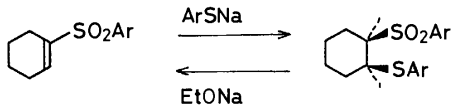

(Ar = p-$CH_3C_6H_4$-)

The stereochemistry of the nucleophilic addition to acetylene is known as *trans*.[18,19] The addition of sodium methoxide in methanol to phenylacetylene gives *cis*-*β*-methoxystyrene,[18] and a similar addition of sodium methanethiolate gives *cis*-*β*-(methylthio)stylene.[19]

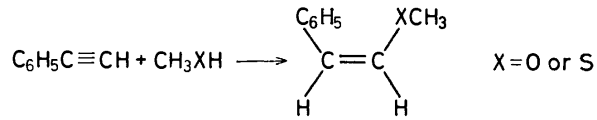

The product obtained from sodium *p*-toluenethiolate and 2-butyne, 2-(*p*-tolylthio)-2-butene, is also assigned the *trans* structure on the basis of infrared evidence[19] and this reaction appears to involve the *trans* addition.

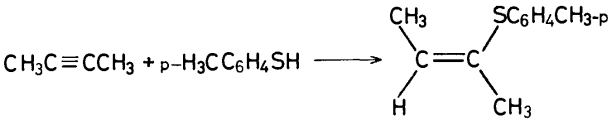

Hegarty and McCormack have suggested from the experimental result that the nucleophilic attack on alkylidyneammonium ion by acetate ion is stereospecific, giving rise to just a single imine isomer.[20]

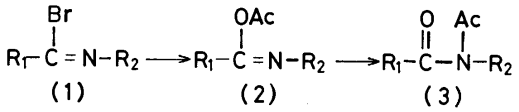

The treatment of *N*-(α-bromoalkylidene) amine (**1**) in 1 : 1 acetone–water in the presence of sodium acetate gives the *O*-acyl compound (**2**), which is uncontaminated by the isomer (**3**). The isoimide structure is rare in organic chemistry and is generally limited to cyclic materials in which the rearrangement to the imide is inhibited.[21] They attributed the stability of the *O*-acyl structure to its existence in the configuration (**5**) in which the nucleophilic lone pair electrons on the neighboring nitrogen and the acyl group would be *trans*. It has been demonstrated that the starting bromide (**1**) reacts *via* rate-determining alkylideneammonium ion (**4**) formation in aqueous acetone.[22] They

have concluded that the nucleophilic attack by acetate ion on (**4**) must, therefore, be stereospecific as is shown in the following scheme.[20]

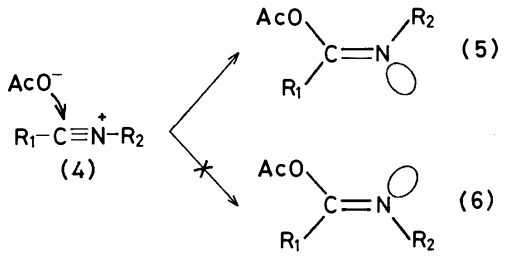

Their suggestion is in agreement with the prediction in the present work.

Conclusion

In this work, the LMO method is applied to the addition of ammonia to formaldehyde. The bond interchange in the course of the reaction is investigated and some comparative studies between the present results and the experimental data reported so far are made. Then, the conclusion obtained here is as follows.

In the addition of ammonia to formaldehyde, the LMO method is convenient to represent the bond interchange in the course of the reaction. In this addition reaction, the electron pair contributed by ammonia and that dislodged from the double bond of formaldehyde tend to stay as far away from each other as possible. It is suggested that this trend is general in nucleophilic additions to an unsaturated bond. Therefore, the intermediate created by the attack of a nucleophile to the unsaturated bond is more reactive at the *trans* position to the new bond than at the *cis* position.

The authors would like to express their gratitude to the Data Processing Center, Kyoto University, for its generous permission to use the FACOM 230-75 computer. The MO calculation was carried out under financial support of the Ministry of Education of Japan (Grant-in-Aid 139012).

References

1) (a) R. L. Reeves, "The Chemistry of the Carbonyl Group," Vol. 1, ed by S. Patai, John Wiley & Sons, London (1966); (b) Y. Ogata and A. Kawasaki, "The Chemistry of the Carbonyl Group," Vol. 2, ed by S. Patai, John Wiley & Sons, London (1970).

2) H. B. Bürgi, J. D. Dunitz, and E. Shefter, *J. Am. Chem. Soc.*, **95**, 5065 (1973).

3) (a) G. Klopman, *J. Am. Chem. Soc.*, **90**, 223 (1968); (b) L. Salem, *ibid.*, **90**, 543, 553 (1968); (c) K. Fukui and H. Fujimoto, *Bull. Chem. Soc. Jpn.*, **41**, 1989 (1968).

4) (a) K. Fukui, H. Fujimoto, and S. Yamabe, *J. Phys. Chem.*, **76**, 232 (1972); (b) H. Fujimoto, M. Katata, S. Yamabe, and K. Fukui, *Bull. Chem. Soc. Jpn.*, **45**, 1320 (1972).

5) (a) H. Fujimoto, S. Yamabe, and K. Fukui, *Bull. Chem. Soc. Jpn.*, **44**, 2936 (1971); (b) H. Fujimoto, S. Kato, S. Yamabe, and K. Fukui, *J. Chem. Phys.*, **60**, 502 (1974).

6) E. A. Laws, R. M. Stevens, and W. N. Lipscomb, *J. Am. Chem. Soc.*, **94**, 4461 (1972).

7) R. S. Mulliken, *J. Chem. Phys.*, **23**, 1833, 1841, 2338, 2343 (1955).

8) J. A. Pople and D. L. Beveridge, "Approximate Molecular Orbital Theory," McGraw-hill, New York (1970).

9) C. Edmiston and K. Ruedenberg, *Rev. Mod. Phys.*, **35**, 457 (1963).

10) D. M. Dennison, *Rev. Mod. Phys.*, **12**, 175 (1940).

11) G. Herzberg, "Molecular Spectra and Structure," D. Van Nostrand Co., New York (1966).

12) G. Frenking, H. Kato, K. Hirao, and K. Fukui, *Bull. Chem. Soc. Jpn.*, **48**, 2769 (1975).

13) J. M. Parks and R. G. Parr, *J. Chem. Phys.*, **28**, 335 (1958).

14) S. Inagaki, H. Fujimoto, and K. Fukui, *J. Am. Chem. Soc.*, **98**, 4054 (1976).

15) When the CMO's of the interacting system at $R=$ 2.5 Å are expanded in terms of the CMO's of ammonia and formaldehyde, the expansion coefficients of the ϕ_2 are obtained as follows.

$$\phi_2 = 0.922a_4 - 0.343b_5 - 0.108b_2 + 0.106b_7 + \cdots$$

The coefficients larger than 0.10 (absolute value) are displayed in the above equation.

16) R. A. Abramovitch and J. M. Muchowski, *Can. J. Chem.*, **38**, 557 (1960).

17) W. E. Truce and A. J. Levy, *J. Am. Chem. Soc.*, **83** 4641 (1961).

18) S. I. Miller, *J. Am. Chem. Soc.*, **78**, 6091 (1956).

19) W. E. Truce and J. A. Simms, *J. Am. Chem. Soc.*, **78**, 2756 (1956).

20) A. F. Hegarty and M. T. McCormack, *J. Chem. Soc., Chem. Commum.*, **1975**, 168.

21) C. G. McCarthy, "The Chemistry of the Carbon-Nitrogen Double Bond," ed by S. Patai, Wiley, New York (1970).

22) A. F. Hegarty, M. P. Cashman, and F. L. Scott, *J. Chem. Soc., Perkin Trans. 2*, **1972**, 44.

The Structure of the Cyclodextrin Complex. VI. The Crystal Structure of α-Cyclodextrin-*m*-Nitrophenol (1: 2) Complex

Kazuaki HARATA, Hisashi UEDAIRA, and Jiro TANAKA*

Research Institute for Polymers and Textiles, Sawatari-4, Kanagawa-ku, Yokohama 221
**Department of Chemistry, Faculty of Science, Nagoya University, Chikusa-ku, Nagoya 464*

(Received October 13, 1977)

α-Cyclodextrin (α-CDx) forms a 1: 2 crystalline complex with *m*-nitrophenol (*m*-NP). The crystal structure was determined by the X-ray method. The crystal is orthorhombic, and the space group is $P2_12_12$ with $Z=2$. The cell dimensions are $a=22.231(7)$, $b=16.865(6)$, and $c=8.152(1)$ Å. The structure was solved on the basis of the nearly isomorphous structure of the α-CDx–sodium benzenesulfonate complex by using 2246 reflections, and refined by the block-diagonal least-squares method to the final *R*-value of 0.10. The framework of the crystal is built up of a stack of α-CDx molecules with a head-to-tail arrangement along the two-fold axis, showing a channel-type structure. Two *m*-NP molecules are statistically disordered on the two-fold axis. One is located in the channel, while the other is sandwiched between the α-CDx molecules. In the channel, the nitro group of *m*-NP is inserted into the α-CDx ring from the secondary hydroxyl side, and the phenolic hydroxyl group is hydrogen-bonded to the primary hydroxyl group of the next α-CDx molecule. The enthalpy change was calculated for the complex formation in an aqueous solution. The calculated results are in qualitatively agreement with the observed values. The catalytic ability of α-CDx in the hydrolysis of substituted phenyl acetates was discussed on the basis of the structural data.

α-Cyclodextrin (α-CDx), which is a doughnut-shaped oligosaccharide consisting of α-1,4-linked six D-glucose residues, forms a number of inclusion complexes with a variety of guest molecules in aqueous solutions and in the crystalline state.[1,2] In solution, α-CDx catalyzes several chemical reactions,[3] so it has been referred to as enzyme model. The stereospecific catalysis has been observed in the hydrolysis of substituted phenyl acetates;[4] *m*-nitrophenyl acetate decomposes about fifty times faster than *p*-nitrophenyl acetate. In the previous paper,[5] it was shown that the low catalytic ability of α-CDx in the hydrolysis of *para*-substituted phenyl acetates can be ascribed to the structure of the α-CDx–ester inclusion complex. The X-ray analysis of the α-CDx–*m*-nitrophenol (1: 2) complex was carried out to investigate the geometry of inclusion in relation to the stereospecificity of the α-CDx-catalyzed reactions as well as the α-CDx–substrate interaction. The energy of the complex is calculated by using the structural data to investigate the intermolecular force for complex formation.

Table 1. Crystal data

$C_{36}H_{60}O_{30}\cdot 2C_6H_5NO_3\cdot 6H_2O$		
Formula weight		1359.2
Crystal system		Orthorhombic
Space group		$P2_12_12$
	Z	2
Cell dimensions	a	22.231(7) Å
	b	16.865(6)
	c	8.152(1)
Cell volume	V	3056.5 Å^3
Density	D_m	1.47 g·cm^{-3}
	D_x	1.48

Experimental

A yellowish and needle-like crystal of the α-CDx–*m*-NP (1:2) complex was obtained by allowing an aqueous solution containing α-CDx and *m*-NP with a 1: 1 molar ratio to stand. The determination of lattice parameters and the intensity measurement were carried out on a Rigaku automatic four-circle diffractometer with graphite-monochromated Cu $K\alpha$ radiation. The crystal was enclosed in a quartz capillary with a small amount of water, since the crystal breaks up in the air. 2246 independent reflections with $|F_o|\geqq 3\sigma(F)$ were collected up to 120° in 2θ by using the 2θ-ω scan technique. No correction was made for absorption and extinction. The crystal data are given in Table 1.

Determination and Refinement of the Structure

The crystal of the α-CDx–*m*-NP complex is nearly isomorphous with the crystals which have the channel-type structure. A set of coordinates of α-CDx found in the α-CDx–sodium benzenesulfonate complex[6] was used to calculate the initial phases, which were refined by the block-diagonal least-squares method. The *m*-NP and water molecules were found on an electron-density map. The primary hydroxyl groups of α-CDx were found to be statistically disordered. Each occupancy factor of 0.5 was estimated from the electron-density map, but the values were not refined. The determination of the atomic parameters of the *m*-NP molecule (*m*-NP-2) located on the c axis failed, owing to the disordered structure. The position and orientation of *m*-NP-2 were then determined by the rigid-body least-squares method; the structure of *m*-NP-2 was built up by using the bond distances and angles of *p*-NP in the α-CDx–*p*-NP complex.[5] The atomic parameters of the other molecules were refined by the block-diagonal least-squares method. The quantity minimized was $\Sigma w(|F_o|-|F_c|)^2$, with $w=1.0$ for all reflections. The final *R*-value was 0.10. The atomic scattering factors were taken from "International Tables for X-Ray Crystallography."[7] The atomic parameters are listed in Table 2. The observed and calculated structure factors are given in Table 3.**

** Tables 3 and 4 are kept as a Document at the office of The Chemical Society of Japan (Document No. 7815).

TABLE 2. FINAL ATOMIC PARAMETERS ($\times 10^4$)
The anisotropic thermal factors are of the form: $\exp[-(B_{11}h^2+B_{22}k^2+B_{33}l^2+B_{12}hk+B_{23}kl+B_{31}lh)]$.

	x	y	z	B_{11}	B_{22}	B_{33}	B_{12}	B_{23}	B_{31}
C(1,G1)	1445(5)	2422(7)	3587(15)	24(3)	40(5)	146(21)	-5(7)	57(20)	-22(14)
C(2,G1)	1172(5)	2880(7)	5017(16)	16(2)	47(5)	168(21)	-2(6)	-19(20)	-30(13)
C(3,G1)	492(5)	2612(7)	5228(14)	16(2)	40(5)	136(20)	3(6)	-14(17)	-19(12)
C(4,G1)	167(4)	2799(6)	3622(13)	14(2)	43(5)	121(17)	-4(5)	57(18)	-15(11)
C(5,G1)	479(5)	2331(8)	2207(14)	12(2)	73(7)	126(20)	5(7)	15(21)	2(12)
C(6,G1)	208(6)	2625(12)	521(15)	22(3)	137(13)	110(21)	21(11)	11(31)	0(13)
O(2,G1)	1514(4)	2656(5)	6449(12)	27(2)	52(4)	232(19)	8(5)	-43(17)	-69(12)
O(3,G1)	241(3)	3110(5)	6499(10)	26(2)	51(4)	125(13)	7(5)	-28(14)	-13(9)
O(4,G1)	-414(3)	2447(4)	3846(9)	16(2)	33(3)	131(13)	0(4)	12(12)	-12(8)
O(5,G1)	1098(3)	2639(5)	2158(10)	21(2)	56(4)	153(15)	1(5)	79(14)	-2(9)
O(6A,G1)	474(8)	2301(13)	-643(21)	26(4)	91(12)	160(33)	26(13)	-12(36)	8(21)
O(6B,G1)	221(9)	3309(11)	102(24)	39(6)	48(8)	220(36)	10(12)	56(33)	-27(26)
C(1,G2)	2394(5)	-447(7)	3649(18)	16(3)	49(6)	238(27)	-2(6)	63(24)	9(16)
C(2,G2)	2528(6)	82(7)	5123(18)	22(3)	29(4)	271(26)	0(6)	33(22)	-67(16)
C(3,G2)	2014(5)	694(7)	5296(15)	24(3)	39(5)	139(21)	-8(6)	25(18)	-30(14)
C(4,G2)	1952(5)	1152(7)	3659(15)	18(2)	38(5)	162(21)	4(6)	26(19)	-22(14)
C(5,G2)	1846(6)	592(7)	2257(14)	35(4)	42(5)	119(20)	39(8)	25(18)	18(16)
C(6,G2)	1824(8)	990(10)	571(18)	57(6)	74(9)	174(27)	72(12)	70(26)	84(22)
O(2,G2)	2541(5)	-431(5)	6495(12)	54(4)	43(4)	228(19)	11(6)	19(17)	-143(16)
O(3,G2)	2186(4)	1265(5)	6553(11)	35(2)	42(4)	158(16)	1(5)	1(14)	-57(11)
O(4,G2)	1417(3)	1618(4)	3878(10)	18(2)	27(3)	154(14)	-5(4)	22(11)	-6(9)
O(5,G2)	2348(4)	30(5)	2217(10)	25(2)	45(4)	209(16)	9(5)	62(16)	54(11)
O(6A,G2)	1924(11)	562(12)	-609(22)	60(8)	59(9)	135(31)	57(15)	-23(31)	-6(29)
O(6B,G2)	2222(9)	1314(12)	109(25)	38(6)	62(10)	210(38)	-7(13)	24(36)	-27(28)
C(1,G3)	923(5)	-2945(7)	3520(18)	20(3)	42(5)	217(26)	8(6)	10(22)	-6(15)
C(2,G3)	1358(6)	-2886(7)	5022(17)	30(3)	40(5)	167(22)	-9(7)	32(20)	-19(16)
C(3,G3)	1549(5)	-2001(7)	5242(13)	22(3)	41(5)	91(18)	6(6)	-2(16)	1(12)
C(4,G3)	1822(5)	-1684(6)	3651(13)	18(2)	33(4)	100(17)	-2(6)	-2(16)	-5(12)
C(5,G3)	1392(5)	-1794(7)	2177(14)	26(3)	40(5)	127(20)	-22(7)	-15(18)	7(14)
C(6,G3)	1718(7)	-1622(11)	558(16)	42(5)	107(11)	99(21)	-52(13)	-10(26)	23(17)
O(2,G3)	1024(4)	-3169(6)	6372(12)	32(2)	62(5)	212(19)	-13(6)	112(18)	-45(13)
O(3,G3)	2008(3)	-1968(5)	6469(10)	22(2)	57(4)	127(14)	-1(5)	36(14)	-15(9)
O(4,G3)	1858(3)	-852(4)	3934(10)	15(2)	34(3)	153(14)	-6(4)	-13(12)	-2(9)
O(5,G3)	1239(3)	-2652(5)	2129(10)	19(2)	45(4)	152(14)	-7(4)	-31(13)	39(9)
O(6A,G3)	1385(11)	-1815(11)	-658(23)	53(8)	142(18)	94(30)	-68(21)	4(42)	10(26)
O(6B,G1)	2131(9)	-2026(11)	84(26)	48(7)	49(8)	221(38)	-20(13)	-67(33)	107(29)
O(W1)	1409(7)	6339(7)	-689(14)	96(6)	55(5)	231(24)	33(10)	-7(20)	-70(21)
O(W2)	1674(4)	3399(6)	-602(12)	37(3)	56(5)	219(20)	-19(6)	-24(17)	27(13)
O(W3)	1778(4)	4890(7)	709(11)	34(3)	72(5)	179(16)	-8(7)	17(18)	-3(12)
C(1,N1)	316(5)	4971(7)	5231(13)	24(3)	27(4)	151(19)	3(6)	-14(18)	-4(13)
C(2,N1)	612(6)	4936(7)	3741(17)	35(4)	32(5)	227(26)	3(7)	-29(24)	40(19)
C(3,N1)	320(7)	4956(10)	2291(17)	62(6)	36(5)	209(25)	-24(13)	-34(27)	55(21)
O(1,N1)	1160(7)	4928(12)	3670(24)	21(4)	70(9)	241(36)	15(11)	-40(41)	-11(24)
O(2,N1)	1155(9)	4784(13)	6963(24)	33(5)	82(12)	211(38)	3(14)	34(38)	4(26)
O(3,N1)	303(9)	4939(19)	8086(21)	41(7)	138(17)	134(29)	59(21)	53(49)	25(24)
N(1,N1)	601(9)	4879(15)	6868(28)	20(5)	64(12)	236(46)	3(13)	13(45)	21(26)

	x	y	z		x	y	z
C(1,N2)	-24	-23	6035	C(6,N2)	-524	396	6590
C(2,N2)	330	-468	7068	O(1,N2)	517	-877	9854
C(3,N2)	184	-495	8731	O(2,N2)	-176	415	3362
C(4,N2)	-311	-70	9290	O(3,N2)	606	-322	3850
C(5,N2)	-662	382	8225	N(1,N2)	142	22	4295

Description and Discussion of the Structure

The structure and numbering scheme of the complex are shown in Figs. 1 and 2. The schematic drawing of the crystal structure is given in Fig. 3. The α-CDx molecules are stacked along the two-fold axis to form an endless cylinder, showing a channel-type structure. One *m*-NP molecule (*m*-NP-2) is included in the cylinder, while the other (*m*-NP-1) is located outside the α-CDx ring.

Structure of α-CDx. Bond distances, angles, and conformation angles are given in Tables 4—6. The geometrical data for α-CDx are shown in Table 7. The bond distances and angles are in good agreement with those found in the other α-CDx complexes with the channel-type structure.[6,8-10] The primary hydroxyl groups are statistically disordered, showing *gauche-trans* and *gauche-gauche* conformations. The C–O bonds of these groups are abnormally short, but a similar shortening of the disordered C–O bond has been observed in α-L-sorbose[11] and the α-CDx complexes with Methyl Orange.[9] The α-CDx ring is distorted from the regular hexagonal symmetry owing to the inclusion of the planar molecule. The diagonal O(4, G3)···O(4, G3*) distance is longer by 0.4 Å than the O(4, G2)··· O(4, G2*) distance. The distortion of the α-CDx ring

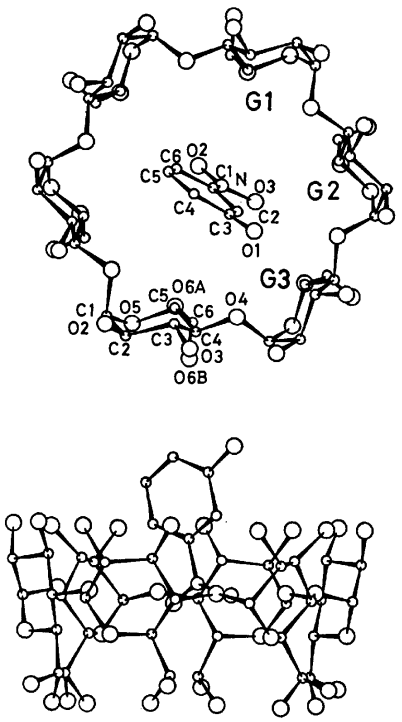

Fig. 1. The structure and numbering scheme of the α-cyclodextrin–*m*-nitorophenol complex.

Table 5. Average bond distances and angles for the glucose residue

Standard deviations given in parentheses were estimated according to $\sigma=[\sum_{i=1}^{3}(x_i-\bar{x})^2/2]^{1/2}$, where x_i is the bond distance or angle in the i-th glucose residue and $\bar{x}$ is the average value. A prime (′) indicates an atom in the adjacent glucose residue.

I. Bond distances (l/Å)			
C(1)–C(2)	1.538(23)	C(4)–C(5)	1.536(31)
C(1)–O(5)	1.429(12)	C(4)–O(4)	1.431(7)
C(1)–O(4′)	1.402(29)	C(5)–C(6)	1.548(28)
C(2)–C(3)	1.565(20)	C(6)–O(6A)	1.249(29)
C(2)–O(2)	1.422(18)	C(6)–O(6B)	1.171(57)
C(3)–C(4)	1.535(11)	C(5)–O(5)	1.474(12)
C(3)–O(3)	1.444(13)		
II. Bond angles (ϕ/°)			
C(2)–C(1)–O(5)	107.5(16)	C(3)–C(4)–O(4)	103.5(3)
C(2)–C(1)–O(4′)	109.1(12)	C(5)–C(4)–O(4)	106.9(9)
O(5)–C(1)–O(4′)	110.5(10)	C(4)–C(5)–C(6)	111.2(31)
C(1)–C(2)–C(3)	108.5(1)	C(4)–C(5)–O(5)	106.3(14)
C(1)–C(2)–O(2)	105.7(4)	C(6)–C(5)–O(5)	105.1(21)
C(3)–C(2)–O(2)	110.9(11)	C(5)–C(6)–O(6A)	112.2(35)
C(2)–C(3)–C(4)	108.8(14)	C(5)–C(6)–O(6B)	121.5(15)
C(2)–C(3)–O(3)	107.5(11)	C(4)–O(4)–C(1′)	118.7(15)
C(4)–C(3)–O(3)	107.9(9)	C(5)–O(5)–C(1)	114.0(14)
C(3)–C(4)–C(5)	110.4(17)		

is small compared with the α-CDx–*p*-NP complex; the maximum difference in the O(4)···O(4) distances is 0.9 Å in the *p*-NP complex. The O(4)···O(4) distances between the adjacent glucose residues indicate that the deformation of the pyranose ring is also small in the *m*-NP complex.

Table 6. Conformation angles (ϕ/°) in α-cyclodextrin

A prime (′) indicates an atom in the adjacent glucose residue.

	G1	G2	G3	Average
C(1)–C(2)–C(3)–C(4)	−59.4	−55.5	−55.2	−56.7
C(2)–C(3)–C(4)–C(5)	59.6	56.6	55.7	57.3
C(3)–C(4)–C(5)–O(5)	−61.5	−57.5	−55.4	−58.1
C(4)–C(5)–O(5)–C(1)	67.6	62.9	62.9	64.5
C(5)–O(5)–C(1)–C(2)	−68.5	−64.2	−65.9	−66.2
O(5)–C(1)–C(2)–C(3)	61.4	59.0	58.8	59.7
O(4′)–C(1)–C(2)–O(2)	57.8	56.5	60.6	58.3
O(2)–C(2)–C(3)–O(3)	69.1	72.3	71.7	71.0
O(3)–C(3)–C(4)–O(4)	−72.7	−70.6	−73.7	−72.3
O(4)–C(4)–C(5)–C(6)	78.0	71.9	79.4	76.4
O(5)–C(5)–C(6)–O(6A)	−64.1	−40.2	−57.8	−54.0
O(5)–C(5)–C(6)–O(6B)	53.9	57.4	49.2	53.5
C(4)–C(5)–C(6)–O(6A)	−175.0	−158.4	−171.7	−168.4
C(4)–C(5)–C(6)–O(6B)	57.1	60.8	64.7	60.9
C(2)–C(1)–O(4′)–C(4′)	−130.3	−132.4	−129.3	−130.7
O(5)–C(1)–O(4′)–C(4′)	111.5	107.2	113.1	110.6
C(1)–O(4′)–C(4′)–C(3′)	127.8	129.9	129.1	128.9
C(1)–O(4′)–C(4′)–C(5′)	−114.7	−112.7	−116.4	−114.6

Table 7. Geometrical data for α-cyclodextrin

An asterisk (*) indicates an atom related by the two-fold symmetry.

I. Selected interatomic distances between glucose residues (l/Å)			
O(4, G1)–O(4, G2)	4.303		
O(4, G2)–O(4, G3)	4.279		
O(4, G3)–O(4, G1*)	4.186		
O(2, G1)–O(3, G2)	2.788		
O(3, G1)–O(2, G3*)	2.821		
O(2, G2)–O(3, G3)	2.858		
O(4, G1)–O(4, G1*)	8.444		
O(4, G2)–O(4, G2*)	8.346		
O(4, G3)–O(4, G3*)	8.745		
II. Least-squares planes and deviations of atoms (l/Å)			
i) $-0.3217X+0.9334Y-0.1590Z=3.0664$			
C(1, G1)[a]	−0.747	C(4, G1)[a]	0.751
C(2, G1)	−0.020	C(5, G1)	−0.020
C(3, G1)	0.018	O(5, G1)	0.021
ii) $0.6457X+0.7498Y-0.1445Z=3.1405$			
C(1, G2)[a]	−0.695	C(4, G2)[a]	0.693
C(2, G2)	−0.010	C(5, G2)	−0.010
C(3, G2)	0.010	O(5, G2)	0.011
iii) $0.9585X-0.2357Y-0.1603Z=3.3949$			
C(1, G3)[a]	−0.711	C(4, G3)[a]	0.679
C(2, G3)	−0.012	C(5, G3)	−0.012
C(3, G3)	0.011	O(5, G3)	0.013
iv) $0.0000X+0.0000Y+1.0000Z=3.1679$			
O(4, G1)	−0.034	O(4, G1*)	−0.034
O(4, G2)	−0.004	O(4, G2*)	−0.004
O(4, G3)	0.038	O(4, G3*)	0.038

a) The atom not included in the plane.

Structure of m-*Nitrophenol.* Both *m*-NP molecules (*m*-NP-1 and *m*-NP-2) are statistically disordered on the two-fold axis, as shown in Fig. 2. The benzene ring of

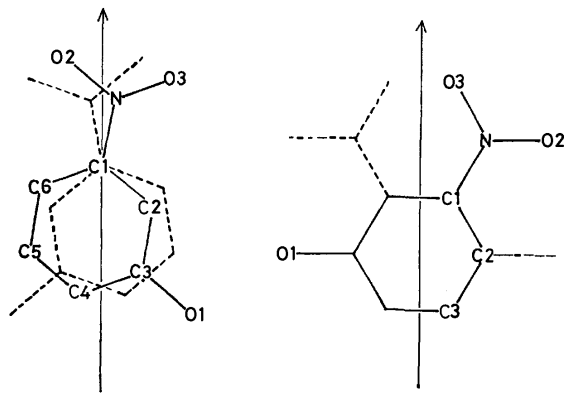

Fig. 2. Schematic drawings of the disordered structures of *m*-NP-1 (right) and *m*-NP-2 (left). The transposed structure by the two-fold axis is shown by broken lines.

TABLE 8. BOND DISTANCES AND ANGLES IN *m*-NITROPHENOL WITH ESTIMATED STANDARD DEVIATIONS

An asterisk (*) indicates an atom related by the two-fold symmetry.

I. Bond distances (l/Å)	
C(1, N1)–C(2, N1)	1.382(17)
C(1, N1)–C(1*, N1)	1.410(16)
C(2, N1)–C(3, N1)	1.349(20)
C(3, N1)–C(3*, N1)	1.431(21)
C(2*, N1)–O(1, N1)	1.218(23)
C(1, N1)–N(1, N1)	1.485(25)
N(1, N1)–O(2, N1)	1.246(30)
N(1, N1)–O(3, N1)	1.198(33)
II. Bond angles (ϕ/°)	
C(1, N1)–C(2, N1)–C(3,N1)	122.7(13)
C(2, N1)–C(3, N1)–C(3*, N1)	118.8(13)
C(2, N1)–C(1, N1)–C(1*, N1)	118.5(11)
C(1*, N1)–C(2*, N1)–O(1, N1)	121.2(14)
C(3*, N1)–C(2*, N1)–O(1, N1)	116.1(15)
C(2, N1)–C(1, N1)–N(1, N1)	125.6(13)
C(1*, N1)–C(1, N1)–N(1, N1)	115.6(12)
C(1, N1)–N(1, N1)–O(2, N1)	119.4(19)
C(1, N1)–N(1, N1)–O(3, N1)	120.1(21)
O(2, N1)–N(1, N1)–O(3, N1)	120.4(24)

m-NP-1 shows the two-fold symmetry. The bond distances and angles (Table 8) are normal. The nitrophenyl group of *m*-NP-2 is not parallel to the two-fold axis, but makes an angle of 14.2°. The *m*-NP-2 molecule seems to be loosely bound, since the average thermal factor of the molecule is relatively large (22.7 Å^2).

Geometry of Inclusion. Intermolecular distances between α-CDx and *m*-NP-2 are given in Table 9. In the channel, the *m*-NP-2 molecules are located at a position similar to that of the *N,N*-dimethylaminophenyl group found in the Methyl Orange complexes.[9] The nitro group is inserted into the α-CDx cavity from the secondary hydroxyl side. The phenolic hydroxyl group is hydrogen-bonded to O(6A, G3) of the next α-CDx molecule. The benzene ring is surrounded by O(3)···O(6) hydrogen bonds. Thus, the adjacent α-CDx molecules are connected not only by the O(3)···O(6) hydrogen bonds, but also by the guest molecule. The nitro group is in close contact with the glycosidic oxygen atom.

TABLE 9. SELECTED INTERMOLECULAR DISTANCES

I. O(3)···O(6) distances along the channel (l/Å)		
O(3, G1)–O(6A, G1)	(a)	2.749
O(3, G2)–O(6A, G2)	(a)	2.664
O(3, G3)–O(6A, G3)	(a)	2.733
O(3, G1)–O(6B, G1)	(a)	2.957
O(3, G2)–O(6B, G2)	(a)	2.901
O(3, G3)–O(6B, G3)	(a)	2.961
II. Intermolecular distances involving *m*-nitrophenol (l/Å)		
C(1, N1)–O(3, G1)		3.310
C(3, N1)–O(6B,G1)		3.309
N(1, N1)–O(3, G1)		3.103
O(1, N1)–O(W3)		2.779
O(1, N1)–C(2, G2)	(g)	3.090
O(1, N1)–O(2, G2)	(g)	2.953
O(3, N2)–O(4, G3)		2.922
O(3, N2)–C(5, G3)		3.328
O(1, N2)–C(5, G3)	(c)	3.124
O(1, N2)–C(6, G3)	(c)	3.007
O(1, N2)–O(6A, G3)	(c)	2.529
C(5, N2)–O(6A, G3)	(e)	3.042
III. Intermolecular distances involving water (l/Å)		
O(W1)–O(W3)		2.818
O(W2)–O(W3)		2.741
O(W2)–O(5, G1)		2.889
O(W2)–O(2, G1)	(a)	2.735
O(W1)–O(5, G3)	(b)	2.884
O(W1)–O(2, G3)	(d)	2.676
O(W2)–O(6B, G3)	(f)	2.783
O(W3)–O(2, G2)	(g)	2.790

Code	Symmetry operator		
None	x,	y,	z
a	x,	y,	$1+z$
b	x,	$-1+y$,	z
c	x,	y,	$-1+z$
d	x,	$-1+y$,	$1+z$
e	$-x$,	$-y$,	$-1+z$
f	$1/2-x$,	$-1/2+y$,	$-z$
g	$1/2-x$,	$-1/2+y$,	$1-z$

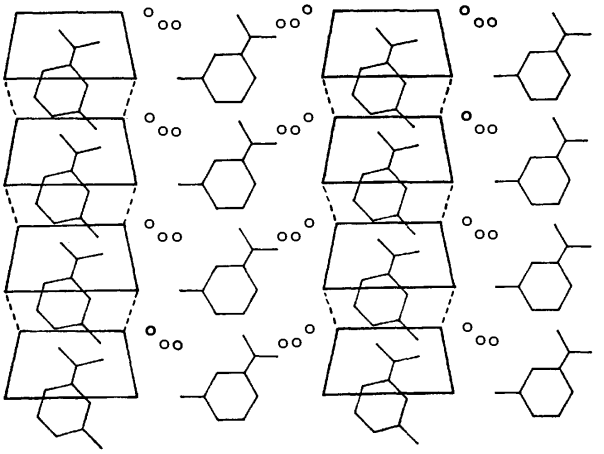

Fig. 3. A schematic drawing of the crystal structure. Circles indicate water molecules. Broken lines denote hydrogen bonds linking α-cyclodextrin molecules along the channel.

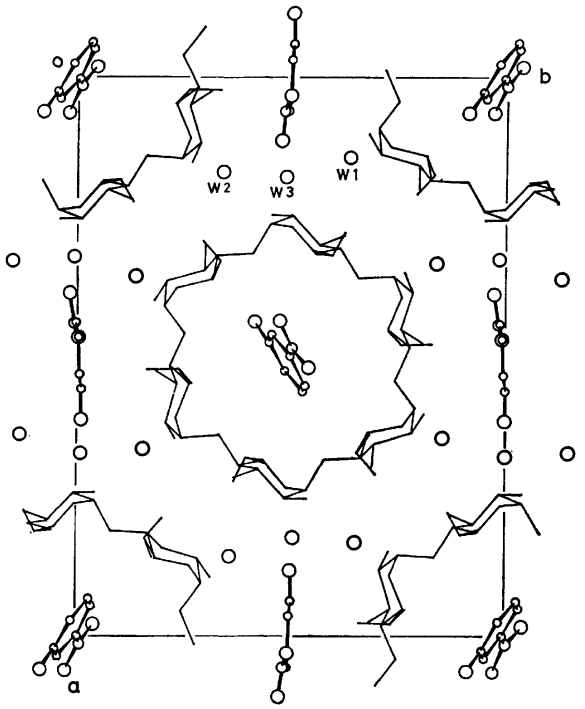

Fig. 4. The crystal structure projected to the ab plane. Circles indicate atoms in water and *m*-nitrophenol molecules.

The shortest distance is 2.922 Å, which is slightly shorter than the normal van der Waals contact of 3.04 Å.[12]

Crystal Structure. The crystal structures are shown in Figs. 4 and 5. The framework of the crystal is built up of a stack of α-CDx molecules with the head-to-tail arrangement along the two-fold axis. The *m*-NP-1 molecule is located nearly parallel to the ac plane in the space between the α-CDx molecules. The phenolic hydroxyl group forms two hydrogen bonds with O(W3) and O(2, G2) (Table 9). The benzene ring is sandwiched by the two α-CDx molecules. Water molecules are distributed in the space outside the channel, and they are linked each other by hydrogen bonds. W1 and W2 are also found in the other channel-type crystals,[6,8–10] but W3 is replaced by the sodium or potassium ion. W1 and W2 form O(2)···water···O(5) hydrogen bonds connecting the adjacent two α-CDx molecules along the channel. The space where *m*-NP-1 is located is filled with water molecules in the other channel-type crystals.

The channel-type structure with the head-to-tail arrangement of α-CDx molecules has been observed in the complexes with ionic guests. In these complexes, the primary hydroxyl groups of α-CDx form hydrogen bonds with the ionized group of the guest molecule. In the *m*-NP complex, however, the guest molecule has no ionized group. The phenolic hydroxyl group is hydrogen-bonded to the primary hydroxyl group of α-CDx. Therefore, the ionic guest is not necessarily required to form the channel-type structure, but the hydrogen bond with the primary hydroxyl group seems to be important.

Calculation of the Heat of the Complex Formation in Aqueous Solution

Method of Calculation. In the crystalline state, the uncomplexed α-CDx molecule contains two water molecules in its cavity.[13] If we assume the same structure in aqueous solution, the two water molecules will be released by the complex formation. The heat of the complex formation of α-CDx with *m*-NP and *p*-NP in aqueous solution was calculated for the following equilibrium at 25 °C:

$$\alpha\text{-CDx}\cdot 2H_2O + \text{guest} \rightleftarrows \alpha\text{-CDx–guest} + 2H_2O. \quad (1)$$

The enthalpy change is expressed as

$$\Delta H = H(\alpha\text{-CDx–guest}) + H(2H_2O) - H(\alpha\text{-CDx}\cdot 2H_2O) - H(\text{guest}), \quad (2)$$

$$= \Delta H^s + \Delta H^c + \Delta H^i, \quad (3)$$

where ΔH^s, ΔH^c, and ΔH^i are the enthalpy changes for the solvation, the conformation, and the interaction of α-CDx with the included molecules, respectively. The interaction energy and conformational energy were calculated on the basis of the non-bonded interatomic interaction.[6] The procedure of evaluating the solvation energy is generally the same as used in the earlier work,[6] but the following modifications were made: (1) the cavity term was calculated according to Pierotti[14] and (2) the dipole-dipole interaction was taken into account in the calculation of the electrostatic term (see Appendix).

Parameters. The van der Waals volumes of the

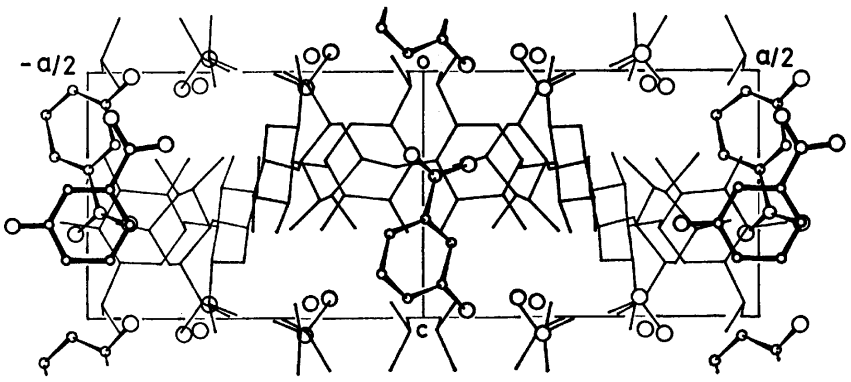

Fig. 5. The crystal structure projected to the ac plane. Circles indicate atoms in water and *m*-nitrophenol molecules.

TABLE 10. VAN DER WAALS VOLUMES

H_2O	20.58 Å^3
m-NP	113.1
p-NP	113.1
α-CDx–$2H_2O$	1120.0
α-CDx–*m*-NP	1232.3
α-CDx–*p*-NP	1186.5

complexes were estimated from the X-ray data, and those of the other molecules were calculated by using the van der Waals volumes of atoms and groups.[12] The group dipole moments were taken from the literature[15] and the average polarizabilities were estimated from the atomic polarizabilities.[16] The coefficients of the Lennard-Jones potential function were calculated according to Goebel *et al.*[17,18] The atomic charges of the glucose residue were taken from Rao,[19] and those of *m*-NP and *p*-NP were calculated by the CNDO/2 MO method.[20]

TABLE 11. ATOMIC CHARGES

I. *m*-Nitrophenol			
C(1)	0.06	O(1)H	−0.12
C(2)	−0.04	O(2)	−0.33
C(3)	0.19	O(3)	−0.34
C(4)	−0.02	H(C2)	0.04
C(5)	0.02	H(C4)	0.02
C(6)	0.00	H(C5)	0.02
N	0.47	H(C6)	0.03
II. *p*-Nitrophenol			
C(1)	0.01	O(1)H	−0.09
C(2)	0.05	O(2)	−0.34
C(3)	−0.06	O(3)	−0.34
C(4)	0.21	H(C2)	0.03
C(5)	−0.05	H(C3)	0.02
C(6)	0.04	H(C5)	0.02
N	0.47	H(C6)	0.03

Results of the Calculation and Discussion

The calculated enthalpy changes are given in Table 12. These values are in qualitatively agreement with the observed ones.[21] The enthalpy change of the *p*-NP complex is three times greater than that of the *m*-NP complex. In both complexes, the effect of the solvation energy is small and negative for the complex formation. The hydrogen-bond energy was not included in the calculation, but a part of it was taken into account in terms of the electrostatic energy and the van der Waals energy. The contribution of the hydrogen-bond energy to the complex formation has been considered to be small in aqueous solution.[3]

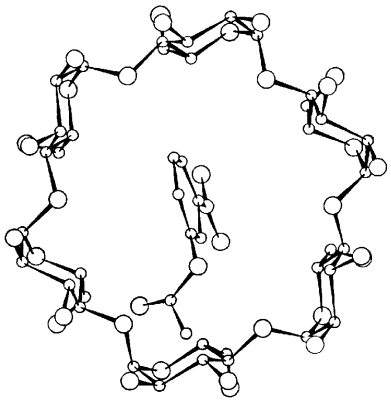

Fig. 6. An expected structure of the α-cyclodextrin–*m*-nitrophenyl acetate complex.

In the crystalline complexes, a remarkable change of the α-CDx conformation is observed between the complexed state and the uncomplexed state.[22] The calculated conformational energy of the *m*-NP complex is lower than that of the uncomplexed state, suggesting that the α-CDx conformation is stabilized by the complex formation. On the other hand, the *p*-NP complex gives a higher conformational energy than the uncomplexed α-CDx. This high energy may be due to the deformation of the α-CDx ring caused by the deep penetration of the bulky and planar molecule. Thus, the inclusion of *p*-NP makes the α-CDx conformation unstable, but the strong interaction of *p*-NP with α-CDx gives the large interaction energy. In the case of the *m*-NP complex, only the partial penetration of the guest molecule is possible because of the steric hindrance. The relatively weak interaction between α-CDx and *m*-NP gives a small deformation of the α-CDx ring. The calculated results indicate the importance of the interaction energy, and suggest that the conformational energy and the solvation energy are not the major components of the binding force in the *m*-NP and *p*-NP complexes. This has also been pointed out by Bergeron *et al.* on the basis of the spectroscopic investigations of α-CDx complexes with substituted *p*-nitrophenols.[23]

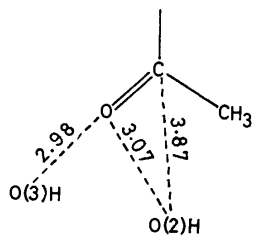

Fig. 7. A schematic drawing of the contact between the acetyl group of *m*-nitrophenyl acetate and the secondary hydroxyl groups of α-cyclodextrin.

TABLE 12. CALCULATED ENTHALPY CHANGE FOR THE COMPLEX FORMATION

	ΔH^s mol^{-1} kcal	ΔH^c mol^{-1} kcal	ΔH^i mol^{-1} kcal	ΔH mol^{-1} kcal	ΔH(obsd)[a] mol^{-1} kcal
α-CDx–*m*-NP	1.64	−0.69	−4.61	−3.66	−7.8
α-CDx–*p*-NP	1.42	0.92	−13.68	−11.34	−7.3

a) See Ref. 22.

Catalytic Property of α-Cyclodextrin

In the α-CDx catalyzed hydrolysis of substituted phenyl acetates, the reaction mechanism has been interpreted in terms of the nucleophilic attack of the secondary hydroxyl group of α-CDx on the carbonyl carbon atom of the ester.[4] The low reactivity of α-CDx in the hydrolysis of *para*-substituted phenyl esters has been discussed on the basis of the geometry of the α-CDx–*p*-NP complex.[5] The nitrophenyl group is so rigidly fixed in the α-CDx ring that the carbonyl carbon atom of the ester could hardly have close contacts with the secondary hydroxyl groups without the large deformation of the α-CDx ring.

In the α-CDx–*m*-NP complex, the guest molecule was found to be partially inserted into the α-CDx ring from the secondary hydroxyl side. The phenolic hydroxyl group is separated by more than 4.7 Å from the secondary hydroxyl groups. When *m*-nitrophenyl acetate forms a complex in the same manner, the acetyl group may have close contacts with the secondary hydroxyl groups. The expected structure of the *m*-nitrophenyl acetate complex is shown in Fig. 6, where the conformation of the acetyl group was assumed to be the same as that found in *p*-nitrophenyl acetate.[24] The distances between the carbonyl oxygen atom and the vicinal secondary hydroxyl groups are 2.98 and 3.07 Å (Fig. 7), suggesting that the structure of the complex is stabilized by hydrogen bonds. The carbonyl carbon atom is located at the distance of 3.87 Å from the secondary hydroxyl group. Unlike *p*-NP, *m*-NP is loosely bound to the α-CDx cavity. The carbonyl carbon atom can easily approach closer to the secondary hydroxyl group by the small displacement of the guest molecule and the deformation of the α-CDx ring. The hydrolysis of the ester bond is interpreted in terms of the tetrahedral intermediate.[25,26] When the carbonyl carbon atom is attacked by the O(2) hydroxyl group (Fig. 7), which is possibly ionized in a relatively high pH condition,[4] the hydrogen bond involving the O(3) hydroxyl group may stabilize the tetrahedral intermediate and lower the activation energy. Acetyl α-CDx, which is formed by the release of *m*-NP, may be decomposed by water. Although simplified, this proposed reaction mechanism is similar to that of the chymotrypsin-catalysis,[27] indicating that α-CDx is a good enzyme model.

Appendix

The pair potential of the dipole-dipole interaction between μ_1 of the solvent molecule and μ_{2i} of the i-th group of the solute molecule is given by $-2\mu_1^2\mu_{2i}^2/(3kTr^6)$,[28] where k is the Boltzmann constant. The distance between these dipoles is

$$r = (R^2+l^2-2Rl\cos\theta)^{1/2}, \quad \text{(A1)}$$

where l and R are the distances from the center of the solute molecule to the i-th group of the solute molecule and to the solvent molecule respectively, and where θ is the angle made by the corresponding two vectors. Then, by averaging over l and θ, we obtain

$$U_{ei}(R) = \frac{-\mu_1^2\mu_{2i}^2}{kT\varepsilon(R_2-l_{2i}^\circ)^3}\int_0^{R_2-l_{2i}^\circ}\int_0^\pi \frac{l^2\sin\theta \mathrm{d}\theta\mathrm{d}l}{r^6}, \quad \text{(A2)}$$

where l_{2i}° is the radius of the i-th group. The effective dielectric constant was assumed to be

$$\varepsilon = 1 + (\varepsilon_0-1)(1-\exp[(R_1+R_2-R)/2R_1]), \quad \text{(A3)}$$

where R_1 and R_2 are the van der Waals radii of the solvent and solute molecules respectively, and where ε_0 is the dielectric constant of the solvent. Thus, the electrostatic energy is

$$H_e^s = \frac{-D}{2R_2^3}\sum_i \frac{\mu_{2i}^2}{\left(1-\frac{D\alpha_{2i}}{R_2^3}\right)} + 4\pi\rho\int_{R_0}^\infty \sum_i U_{ei}(R)R^2\mathrm{d}R, \quad \text{(A4}$$

with $D=2(\varepsilon_0-1)/(2\varepsilon_0+1)$ and $R_0=R_1+R_2$, where ρ is the number density of the solvent.

The van der Waals interaction energy is given by[29]

$$H_v^s = 4\pi\rho\left[1-\frac{3(n^2-1)}{4(n^2+2)}\right]\int_{R_0}^\infty \sum_i U_{vi}(R)R^2\mathrm{d}R. \quad \text{(A5)}$$

The pair potential of the i-th atom in the solute molecule and the solvent molecule is

$$U_{vi}(R) = \frac{3}{2(R_2-l_{2i}^\circ)^3}\int_0^{R_2-l_{2i}^\circ}\int_0^\pi\left(\frac{a_i}{r^{12}}-\frac{c_i}{r^6}\right)l^2\sin\theta\mathrm{d}\theta\mathrm{d}l, \quad \text{(A6)}$$

where a_i and c_i are the coefficients of the potential function, and where l_{2i}° is the radius of the i-th atom.

References

1) J. A. Thoma and L. Stewart, "Starch: Chemistry and Technology," Vol. I, ed by R. L. Whistler and E. F. Pashall, Academic Press, New York (1965), pp. 209—249.
2) F. R. Senti and S. R. Erlander, "Non-stoichiometric Compounds," ed by L. Mandelcorn, Academic Press, New York (1964), pp. 568—605.
3) D. W. Griffiths and M. L. Bender, *Adv. Catal.*, **23**, 209 (1973).
4) R. L. VanEtten, J. F. Sebastian, C. A. Clows, and M. L. Bender, *J. Am. Chem. Soc.*, **89**, 3242 (1967).
5) K. Harata, *Bull. Chem. Soc. Jpn.*, **50**, 1416 (1977).
6) K. Harata, *Bull. Chem. Soc. Jpn.*, **49**, 2066 (1976).
7) "International Tables for X-Ray Crystallography," Vol. IV, Kynoch Press, Birmingham (1974), pp. 72—75.
8) A. Hybl, R. E. Rundle, and D. E. Williams, *J. Am. Chem. Soc.*, **87**, 2779 (1965).
9) K. Harata, *Bull. Chem. Soc. Jpn.*, **49**, 1493 (1976).
10) K. Harata, *Bull. Chem. Soc. Jpn.*, **50**, 1259 (1977).
11) H. Kim and R. D. Rosenstein, *Acta Crystallogr.*, **22**, 648 (1967).
12) A. Bondi, *J. Phys. Chem.*, **68**, 441 (1964).
13) P. C. Manor and W. Saenger, *J. Am. Chem. Soc.*, **96**, 3630 (1974).
14) R. A. Pierotti, *J. Phys. Chem.*, **69**, 281 (1965).
15) "Lange's Handbook of Chemistry," ed by J. A. Dean, McGraw-Hill, New York (1973).
16) J. Ketelaar, "Chemical Constitution," Elsevier Publishing Co., New York (1958), p. 91.
17) C. V. Goebel, W. L. Dimpfl, and D. A. Brant, *Macromolecules*, **3**, 644 (1970).
18) D. A. Brant and P. J. Flory, *J. Am. Chem. Soc.*, **87**, 2791 (1965).

19) V. S. R. Rao, "Handbook of Biochemistry and Molecular Biology: Lipids, Carbohydrates, Steroids," ed by G. D. Fasmann, CRC Press, Cleveland (1975), pp. 474—481.
20) J. A. Pople and D. L. Beveridge, "Approximate Molecular Orbital Theory," McGraw-Hill, New York (1970).
21) E. A. Lewis and L. D. Hansen, *J. Chem. Soc., Perkin Trans.* 2, **1973**, 2081.
22) W. Saenger, M. Noltemeyer, P. C. Manor, B. Hingerty, and B. Klar, *Bioorg. Chem.*, **5**, 187 (1976).
23) R. J. Bergeron, M. A. Channing, G. J. Gibeily, and D. M. Pillor, *J. Am. Chem. Soc.*, **99**, 5146 (1977).
24) R. Guttormson and B. E. Robertson, *Acta Crystallogr., Sect. B*, **28**, 2702 (1972).
25) M.L. Bender, *J. Am. Chem. Soc.*, **73**, 1626 (1951).
26) H. B. Buergi, *Angew. Chem.*, **87**, 461 (1975).
27) D. M. Blow, *Acc. Chem. Res.*, **9**, 145 (1976).
28) J. O. Hirshfelder, C. F. Curtis, and R. B. Bird, "Molecular Theory of Gases and Liquids," John Wiley & Sons, New York (1954).
29) O. Sinanoglu, "Molecular Associations in Biology," ed by B. Pullman, Academic Press, New York (1968), pp. 427—445.

Application of Microwave Spectroscopy to Kinetic Study of the Reaction of Carbonyl Sulfide with Atomic Oxygen

Noritetsu YOSHIDA* and Shuji SAITO**

Sagami Chemical Research Center, Nishi-Ohnuma, Sagamihara 229

(Received October 21, 1977)

Microwave spectroscopy has been applied to the determination of the rate constant for OCS+O→SO+CO. A short cell of a parallel-plate type was devised for the detection of the SO radicals produced in a fast flow reactor. Production of the SO radical was traced by measuring its spectral line intensity under the condition of [OCS]≫[O]. The rate constant for the reaction was determined to be $(7.1\pm0.7)\times10^9$ cm³/mol·s at room temperature (24—25) °C, in good agreement with the values obtained by other methods.

Microwave spectroscopy has been so far mainly concerned with molecular structural studies. Recently some of its applications to the studies of reaction mechanisms have been reported, examples of which are the detection of transient species and the quantitative analysis of final products. In the former studies, about forty species of free radicals, unstable molecules and molecular ions have been detected, though major interest has been focused on their structures. The latter kind of studies have been encouraged by the establishment of an improved technique[1] for measuring the relative intensities of microwave absorption lines. The catalytic hydrogen-exchange reaction of propene with deuterium or deuterium oxide has been thoroughly investigated by analyzing the geometric isomers of deuterated propenes produced. Thus the adsorbed species of propene on various catalysts have been clarified more precisely than before.[2] Other catalytic reactions have been also investigated with remarkable success.[3]

The success of these applications is entirely due to the high specificity of microwave spectroscopy with respect to the detection of molecular species and its high sensitivity. These distinctive features led to the application of microwave spectroscopy to the kinetic studies of gas-phase fast reactions reported here. The reaction investigated was

$$OCS + O \xrightarrow{k} SO + CO. \quad (1)$$

The initial step of the reaction of carbonyl sulfide with atomic oxygen has been investigated kinetically by means of ESR and MS spectroscopies.[4] Reliable values of the rate constant k reported in five seperate studies[5-9] enable the applicability of the microwave spectroscopic technique to be tested.

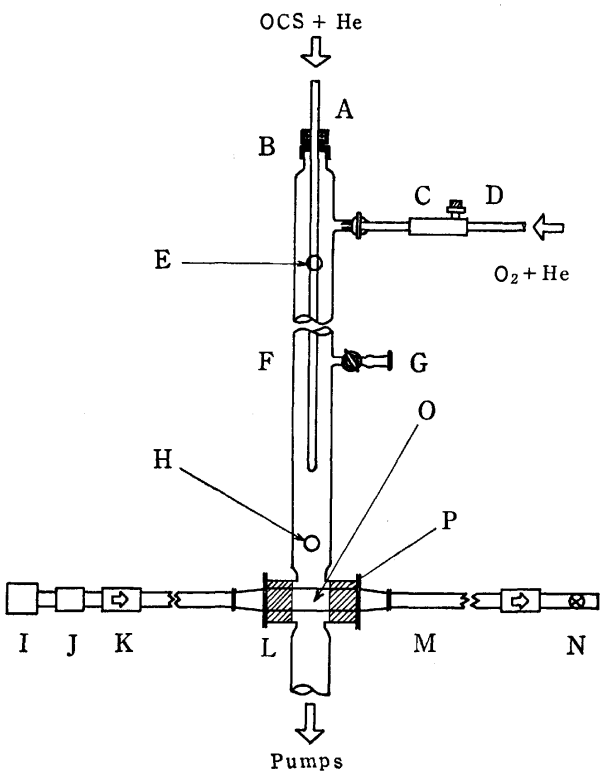

Fig. 1. Schematic diagram of experimental apparatus. A: Injector tube, B: O-ring sliding seal, C: microwave discharge cavity, D: quartz tube, E: McLeod gauge, F: flow tube, G: additional tap for thermal decomposition of CH_2CH_2SO, H: capacitance manometer, I: klystron, J: power attenuator, K: ferrite isolator, L: absorption cell, M: X-band waveguide, N, crystal detector, O: Stark electrode, P: Teflon block.

Experimental

The reaction of carbonyl sulfide with atomic oxygen was studied at about 0.13 Torr at room temperature (24—25) °C, by the use of a fast flow reactor with a microwave spectroscopic detection system. The apparatus used is shown schematically in Fig. 1. The reactor consisted of a flow tube (36 mm inner diameter Pyrex) coated with H_3PO_4 for reducing atom recombination, a movable injector tube (10 mm outer diameter Pyrex) with nine evenly spaced small holes on its head, and a microwave discharge tube (9 mm inner diameter quartz) equipped with an Evenson-Broida type 2a cavity operating at 2450 MHz. A Baratron capacitance manometer (MKS Instruments, Inc.) and a McLeod gauge were placed at about 10 and 94 cm upstream from the microwave absorption cell, respectively.

The atomic oxygen was produced by passing a mixture of O_2 and He through a microwave discharge tube. About 2.5% of the O_2 molecules dissociated into O atoms. Carbonyl sulfide gas, diluted with He was fed into the partially dissociated O_2 flow via the injector. The duration of the reaction was controlled by the distance between the injector head and the cell. The injector was moved less than 50 cm in each run, which covered

* Present address: Department of Chemistry, Faculty of Science, Kobe University, Rokkodai, Nada, Kobe 657.

** Present address: Institute for Molecular Science, Myodaiji, Okazaki 444.

the reaction range of about 50 ms. Flow rates of the gases were controlled by means of stainless steel needle valves, monitored roughly with glass flow meters, and determined accurately by measuring the pressure rise in a bulb known volume after each run. The initial concentration of oxygen atoms, $[O]_0$, was titrated with NO_2[10] in the absence of OCS, by visual observation of the greenish yellow afterglow emitted by the recombination reaction of O with NO in the presence of an excess of O atoms over NO_2 molecules.

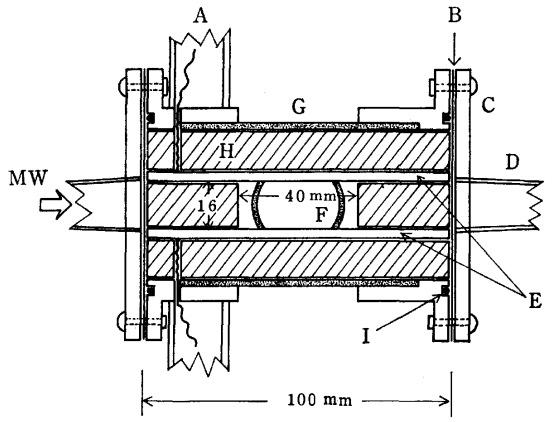

Fig. 2. Cross-sectional view of microwave absorption cell.
A: Stark input, B: mica window, C: blass flange, D: tapered transition unit, E: Stark electrodes, F: flow tube, G: Pyrex tube (55 mmϕ), H: Teflon block, I: O-ring.

The cross-sectional view of the microwave absorption cell is shown in Fig. 2, where the direction of the gas flow is perpendicular to the plane of the paper. A pair of gold-plated brass plates ($3\times30\times100$ mm), which served as Stark electrodes, were fixed 16 mm apart from each other in a Pyrex tube (55 mm outer diameter). Unessential spaces in the cell were filled up with Teflon blocks in order to obtain a smooth gas flow. The effective absorption length of the cell was 40 mm. The cell was completely vacuum-tight with O-rings and mica windows for microwave. A pair of ferrite isolators were incorporated to prevent multiple reflection of the microwave in the cell.[1] They were placed 80 cm apart from the cell (see Fig. 1) to avoid the influence of their magnetic field leakage upon the paramagnetic species SO. The microwave spectrometer used was a conventional one with 110 kHz sinusoidal Stark modulation.[11]

The SO appearance was monitored by observing a microwave absorption line at 13044 MHz, the transition $J,K=1,2\leftarrow1,1$.[12] The signal was recorded very slowly (1 MHz/min) with a time constant of 3 s in order to obtain almost true line shape. Three or four sweep runs were averaged for each signal. As the sinusoidal Stark modulation was used, the observed signal was the first derivative of the Lorenzian absorption line. The absolute intensity is proportional to $H\cdot(\Delta\nu)^2$, where H and $\Delta\nu$ denote the peak-to-peak amplitude and the width of the derivative,[13] respectively. In the determination of the rate constant k for Reaction 1, however, only the relative amplitude of the signal was sufficient to obtain relative concentration of SO, since the widths were practically constant over the reaction range. The signal intensity, H, was calibrated into the absolute concentration only to examine the stoichiometry of Reaction 1. The calibration was performed by using another source of SO, that is, the thermal decomposition of ethylene episulfoxide (CH_2CH_2SO) in He at 600 °C,[14] and by titrating with NO_2:[15] $SO+NO_2\rightarrow SO_2+NO$.

The sample gases, helium (airco, 99.9995%), oxygen (Toyo Sanso, 99.99%) and carbonyl sulfide (Matheson, 97.5%), were taken directly from their respective cylinders. Matheson NO_2 was purified by mixing it with O_2 and passing it over evaporated P_2O_5 films. This was followed by vigorous pumping of the white frozen solid at 77 K, in order to remove the impurities of H_2O and NO. Ethylene episulfoxide was prepared by the reaction of ethylen episulfide with *m*-chloroperbenzoic-acid in CH_2Cl_2[16] at −10 °C, and was purified by distillation under reduced pressure.

Results and Discussion

Performance of the Spectrometer. The quantitative steady-state experiment, such as the present one, indispensably requires a detection system which is stabilized over a long period of time and whose response is proportional to the concentration of species to be detected. This aspect was examined using a flow of OCS highly diluted with He at about 0.05 Torr. The signal amplitude of the OCS ($J=1\leftarrow0$, 12163 MHz), having a signal-to-noise ratio of about 50, was monitored over 4 h. Maximum fluctuation of the amplitude was about 3%, while that of the total pressure was only 0.5%. Figure 3

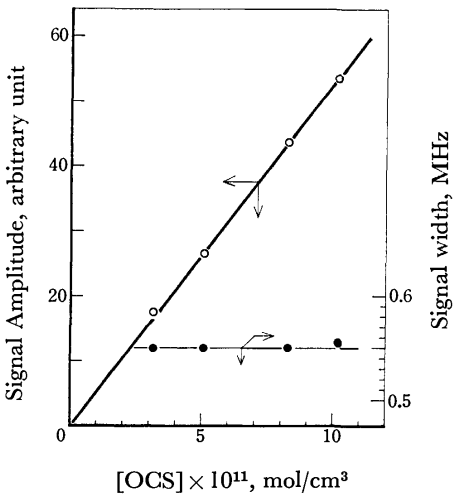

Fig. 3. Peak-to-peak amplitude and width of OCS first-derivative signal (12163 MHz) *vs.* OCS concentration. T: 27.5 °C, P: 0.0572−0.0591 Torr, He flow: 9.86 μmol/s, Noise level: 0.3 unit.

shows plots of the signal amplitudes and widths as a function of OCS concentration. The linearity of the spectrometer is clearly shown in the figure, where the signal amplitude is directly proportional to the concentration while the signal width remains constant. Figure 3 also indicates the sensitivity of the spectrometer. On the basis of the noise intensity of 0.3 unit in the above results, the OCS signal with the signal-to-noise ratio of 2 corresponds to 2×10^{-12} mol/cm³. The minimum detectable concentration of SO was proved to be 1×10^{-12} mol/cm³.

Determination of the Rate Constant k. In order to perform an exact analysis of a flow system, it would be necessary to employ a laborious treatment. In the present study it was assumed that the radial concentration gradients and axial diffusion rates were negligible

and that the parabolic velocity distribution could be replaced by an average velocity (v). Furthermore it was assumed that Reaction 1 operated simply and other side reactions were ignored. Then the solution of the rate equation becomes

$$k \cdot t = -\frac{1}{[OCS]_0 - [O]_0} \cdot \ln \frac{[O] \cdot [OCS]_0}{[O]_0 \cdot [OCS]}. \quad (2)$$

The present experiments were performed under a condition of a large excess of carbonyl sulfide, $[OCS]_0 \gg [O]_0$, so that [OCS] is essentially constant throughout the reaction. Equation 2 can be reduced under this condition, and replacement of $[O]_0$ by $[SO]_\infty$ yields

$$k \cdot [OCS]_0 \cdot t = \ln (1 - [SO]/[SO]_\infty)^{-1}, \quad (3)$$

where $[OCS]_0$ is the initial concentration of carbonyl sulfide and $[SO]_\infty$ the concentration of the SO radicals after infinite time. In Fig. 4, typical plots of $\ln(1-[SO]/[SO]_\infty)^{-1}$ *vs.* t are shown for various empirically adjusted values of $[SO]_\infty$. It may be seen that initial time, $t=0$, can be arbitrarily chosen without loss of generality. As shown in Fig. 4, plots for $[SO]_\infty=22$ (arbitrary units)

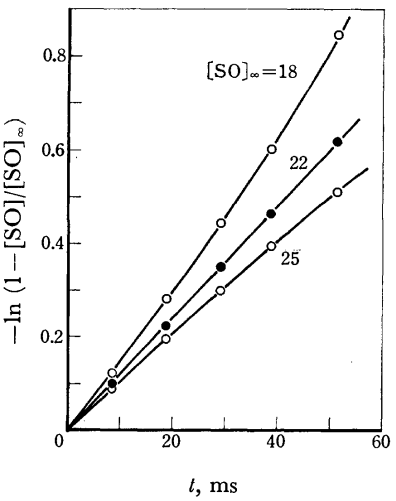

Fig. 4. Typical logarithmic plots of the SO appearance in the reaction of OCS+O→SO+CO for various empirically adjusted values of $[SO]_\infty$.
T: 24.0 °C, P: 0.1304 Torr, v: 9.6 m/s, $[OCS]_0$: 1.64×10^{-9} mol/cm³.

produced a linear curve, while the others did not. The values of k obtained from the slopes of several such linear plots are given in Table 1, and the values of k determined by other workers using MS and ESR spectrometers are also listed for comparison. The values of v and $[OCS]_0$ given in the table were determined at the pressure calculated for the center of the range of the OCS-injection point. The average k thus obtained was 7.1×10^9 cm³/mol·s, which agrees well with the values reported by other workers.

Reliability of the Observed Values. An important point in the kinetic studies by the measurement of a product species is how much the product may be lost by side reactions. The O/SO stoichiometry in Reaction 1 was thus examined by comparing $[O]_0$ and $[SO]_\infty$,

Table 1. The rate constant k for OCS+O → SO+CO

Expt No.	T (°C)	P (Torr)	v (m/s)	$[OCS]_0$ (mol/cm³)	k (cm³/mol·s)
1	25.0	0.1298	9.4	1.57×10^{-9}	7.3×10^9
2	24.3	0.1304	9.6	1.64×10^{-9}	7.0×10^9
3[a]	24.0	0.1372	8.8	1.57×10^{-9}	7.1×10^9
					(av.$=7.1 \times 10^9$)
Ref. 5	25.0[b]			Detector: MS	6.7×10^9
6	25.0[b]			MS	6.0×10^9
7	room temperature			MS	5.5×10^9
8	24.0			ESR	8.5×10^9
9	24.0			ESR	7.2×10^9

a) Effect of metal surface was examined. b) The value calculated from the Arrhenius expression

because if the loss of SO by side reactions was significant, $[SO]_\infty$ should be smaller than $[O]_0$. In the case of Expt 1 in Table 1, $[O]_0$ was found to be 2.1×10^{-11} mol/cm³ by the NO_2-titration, while the adjusted $[SO]_\infty$ value was 2.0×10^{-11} mol/cm³. This good agreement confirms the stoichiometry, and hence supports the assumption of the negligible side reactions. This result is concordant with that reported by Westenberg and deHaas,[8] who confirmed this stoichiometry under highly diluted conditions by monitoring both O and SO with an ESR spectrometer.

The most serious difficulty of the microwave technique may arise from the possible effect of the metal surface of the Stark electrodes on the kinetic measurement, particularly in the case of transient species. In order to assess the error, k was determined when a gold-plated brass plate having almost the same surface area as the electrodes was inserted into the flow tube. The result is listed in Table 1 as Expt 3. Comparison of the results demonstrates that there was little difference in the values of k determined with and without the extra metal surface in the flow tube. Therefore, the surface of the Stark electrodes was considered to have little effect on the kinetic measurement.

The microwave absorption cell has a detection zone of about 3 cm. It takes about 2 ms for the flowing gas molecules to pass through the absorption cell. It is not always negiligibly small in comparison with the time range within which the reaction was monitored, but it may be reasonable to consider that the response of the spectrometer corresponds to the concentration at a fixed point in the cell.

The radial concentration gradients and the axial diffusion rate may be evaluated by the diffusion aspect of reactants, and the values of r^2/D and the ratio $k \cdot [OCS]_0 \cdot D/v^2$ are measures of them, where D denotes the diffusion coefficient of the O atoms in He and r the radius of the flow tube. Recently Goldberg and Crowe reported the value of D as 1300 cm²/s at 0.6 Torr and at 280 K.[17] The value corrected to 0.13 Torr is 6000 cm²/s, according to the relation $D=D_0(P_0/P)$ where D_0 is the diffusion coefficient at an arbitrary value of P_0,[18] the small contribution due to temperature dependence being ignored. Thus the value of r^2/D is 0.7 ms in He and $k \cdot [OCS]_0 \cdot D/v^2 \ll 1$. Therefore, the corrections for both effects may

be negligible. In the case of the viscous pressure drop, it was about 7—9% within the range where the OCS-injection point was shifted. Westenberg and deHaas reported,[19] "Simply using the pressure at the center of the measurement section to compute flow velocity and reactant concentration yielded essentially the same rate constant as was obtained with more sophisticated corrections for the pressure drop." The effect was assumed to be of the same magnitude in our experiments, since the present conditions were almost the same as theirs.

On these basis the assumptions used in determining k were considered to be reasonable. Stability of the flow system as well as of the detection system was satisfactory, as was described in the previous section. Thus the origin of the errors in the measurement may be ascribed mainly to the relative readings of the signal amplitudes and to the determination of the slopes of the pseudo-first order plots. These measurement errors were roughly estimated to be about $\pm 10\%$.

The results obtained above demonstrate that the microwave spectroscopic technique offers a reliable and powerful means for gas kinetic studies, in spite of some limitations to its applications, *e.g.*, non-polar substances cannot be detected, and the applicable pressure-range is limited normally to 10^{-1}—10^{-2} Torr. Nevertheless, high specificity of the microwave spectrum makes this technique most suitable among the available techniques (ESR, MS, *etc.*) for reactions concerned with isotopic and geometric isomers. In addition to the determination of reaction rate constants, it may be possible by this technique to determine the life-time of transient species and the diffusion coefficients of gaseous substances regardless of their stabilities.

The authors wish to express their gratitude to Professor Yonezo Morino for continuing encouragement and helpful advice, and to Mr. Fumio Makino for construction of the microwave spectrometer with great competence.

References

1) A. S. Esbitt and E. B. Wilson, Jr., *Rev. Sci. Instrum.*, **34**, 901 (1963).
2) Y. Morino and E. Hirota, *Nippon Kagaku Zasshi*, **85**, 535 (1964); K. Hirota, Y. Hironaka, and E. Hirota, *Tetrahedron Lett.*, **1964**, 1645; T. Ueda, J. Hara, K. Hirota, S. Teratani, and N. Yoshida, *Z. Phys. Chem. (Frankfurt am Main)*, **64**, 64 (1969); T. Kondo, S. Saito, and K. Tamaru, *J. Am. Chem. Soc.*, **96**, 6857 (1974).
3) K. Hirota, *Proc. Intern. Congr. Catalysis, 5-th, Miami*, **1**, c-37 (1972).
4) F. Kaufman, *Ann. Rev. Phys. Chem.*, **20**, 45 (1969).
5) K. Hoyermann, H. G. Wagner, and J. Wolfrum, *Ber. Bunsenges. Phys. Chem.*, **71**, 603 (1967).
6) K. H. Homann, Gg. Krome, and H. G. Wagner, *Ber. Bunsenges. Phys. Chem.*, **72**, 998 (1968).
7) J. O. Sullivan and P. Warneck, *Ber. Bunsenges. Phys. Chem.*, **69**, 7 (1965).
8) A. A. Westenberg and N. deHaas, *J. Chem. Phys.*, **50**, 707 (1969).
9) W. H. Breckenridge and T. A. Miller, *J. Chem. Phys.*, **56**, 465 (1972).
10) F. Kaufmann, *Proc. R. Soc. London, Ser, A*, **247**, 123 (1958).
11) S. Saito, *J. Mol. Spectrosc.*, **30**, 1 (1969).
12) F. X. Powell and D. R. Lide, Jr., *J. Chem. Phys.*, **41**, 1413 (1964).
13) C. P. Poole, Jr., "Electron Spin Resonance," John Wiley & Sons, New York (1967), Chap. 20.
14) S. Saito, *Bull. Chem. Soc. Jpn.*, **42**, 667 (1969).
15) M. A. A. Clyne, C. J. Halstead, and B. A. Thrush, *Proc. R. Soc. London, Ser. A*, **295**, 355 (1966).
16) A. Negishi, K. Saito, S. Saito, and M. Fukuyama, Preprints for the 21-st Annual Meeting of the Chemical Society of Japan, Suita (April 1, 1968).
17) I. B. Goldberg and H. R. Crowe, *J. Phys. Chem.*, **80**, 2407 (1976).
18) J. P. Appleton, "Diffusion and Heat Transfer in Chemical Kinetics," ed by D. A. Frank-Kamenetskii, Plenum Press, New York (1969), p. 207.
19) A. A. Westenberg and N. deHaas, *J. Chem. Phys.*, **46**, 490 (1967).

Diffusion Coefficients of Argon in Aqueous Ethanol and 1,4-Dioxane Solutions and of Methane in Aqueous Ethanol Solutions*

Yūkō Taira, Kunio Matsuda, and Koichiro Nakanishi**

Department of Industrial Chemistry, Faculty of Engineering, Kyoto University, Kyoto 606

(Received October 24, 1977)

The diffusion coefficients of argon in water-rich regions of aqueous solutions of ethanol and of 1,4-dioxane and those of methane in aqueous solutions of ethanol have been measured by using a diaphragm cell apparatus, designed after Hildebrand *et al.*, for dissolved gases in liquid. The diffusivity of gases was found to show much anomaly which might be ascribed to the structural change of water due to the addition of another solvent. The viscosity reduced diffusion coefficient $D\eta$ (D: diffusion coefficient, η: viscosity coefficient) has a maximum value in dilute aqueous solution of both ethanol and 1,4-dioxane.

Studies have been made recently on the diffusivity of dilute solute in a variety of mixed solvents.[1-4] Iodine was used as a solute and the influence of its specific interaction with the solvents upon diffusivity was examined. Among the mixed solvents examined so far, aqueous alcohol solutions exhibit anomaly in diffusivity which is reverse in direction to that in other solvent systems.[1] It was pointed out that this anomaly may have close connection with the destruction or stabilization of water structure as revealed by solubility and other thermodynamic data.[5]

The purpose of the present study is to elucidate this phenomenon through the determination of diffusion coefficient of inert solute in aqueous solutions. Nakanishi *et al.* measured the diffusion coefficient of various gases dissolved in liquid by diaphragm cell method.[6] A diffusion apparatus has been constructed by utilizing the same diaphragm as employed previously. The diffusion coefficients of argon in water-rich regions of aqueous solution of ethanol and of 1,4-dioxane and those of methane in water-rich region of aqueous solutions of ethanol have been measured. In this paper are given the results of these measurements and a discussion based on the effect of structural change in water on gas diffusivity.

Experimental

Gases and Other Materials. Argon and methane of 99.998 and 99.95% purity were used. The gases were introduced into the apparatus after passing through a column of dehydrating agent $CaCl_2$. Guaranteed ethanol and 1,4-dioxane were used as solvent. Water was deionized and distilled three times.

Apparatus. The fundamental design of the diffusion apparatus shown in Fig. 1 is similar to that used by Hildebrand and co-workers.[6,7] The apparatus consists of three main parts, diffusion cell, gas buret and degassing device. Each of the valves used to separate the parts of the apparatus is a high vacuum glass stopcock, except for the Teflon greaseless needle valve (valve 9) used to avoid the contact of grease with solvent. The diffusion cell consists of two glass bulbs between which the diaphragm is placed. The diaphragm was cut from that prepared by Hildebrand and co-workers,[6,7b] the cross section being the same 5.65 cm^2 and the length 1.00 cm.

During the course of measurements the diffusion cell was immersed in a water thermostat kept at 25.00±0.05 °C. The gas buret was covered with a jacket in which thermostatted water (25.0±0.1 °C) was circulated.

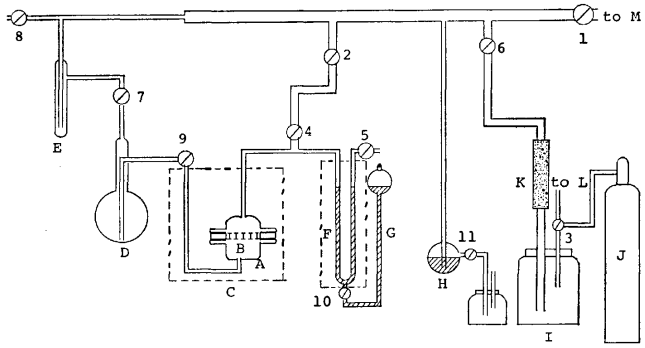

Fig. 1. Schematic diagram of diffusion apparatus.
A: Diffusion cell, B: diaphragm, C: water thermostat, D: degassing flask, E: trap, F: gas buret, G: mercury reservoir, H: open manometer, I: gas reservoir, J: cylinder, K: column of dehydrating reagent, L: gas bag, M: rotary pump, 1—11: valve or stopcock.

Operation. Before the diffusion run, *ca.* 380 ml of solvent was placed in a degassing flask (Fig. 1, D). The flask was then immersed in a Dewar vessel and the liquid was degassed thoroughly by the freeze-and-thaw method *in vacuo*. The number of the times the freeze-and-thaw procedure had to be repeated depended on the sample liquid, but usually five to seven times appeared necessary for complete degassing, which was judged from the disappearance of bubble on thawing. Valve 9 was then closed, and the diffusion cell evacuated.

After degassing was completed, a small amount of sample gas (=1/5 atm) was admitted into the diffusion cell from the gas reservoir. Valves 7 and 8 were then opened to increase the pressure in the degassing flask to ordinary pressure, and the degassed liquid was rapidly transferred to the diffusion cell by opening valve 9. When the surface of liquid layer reached about 1.0 mm above the upper end of the diaphragm, valve 9 was closed in order to complete the introduction of solvent to the diffusion cell. Next, mercury was introduced into the gas buret and the gas was admitted into the vapor space of the diffusion cell. Valve 5 was kept open and the gas pressure in the cell was made to be equal to the atmospheric pressure. The water thermostat placed on a laboratory jack was raised to immerse the diffusion cell in it, and kept at 298.15±0.05 K.

The gas above the liquid surface dissolved in the liquid layer to form a saturated solution and then diffused *via* diaphragm into the liquid phase underneath. After the concentration gradient is established in the diaphragm, diffusion takes place in a steady state and can be followed by the decrease in the

* Diffusion in Mixed Solvents. Part V.

** To whom correspondence should be addressed.

amount of gas as measured by the rise of the mercury column in the gas buret F.[8] The pressure of gas was equalized to atmospheric pressure by adjusting the amount of mercury in the gas buret. The rise Δh in mercury level was measured with a cathetometer. Thus Δh can be determined as a function of times Δt and the diffusion coefficient can be calculated from the slope of Δh *vs.* Δt plot.

Calculation of Diffusion Coefficient. For the diaphragm method, Fick's first law of diffusion can be written as

$$dn/dt = DA\Delta c/L, \quad (1)$$

where dn/dt (mol s^{-1}) is the number of mole of the diffusant which passes through the diaphragm in unit time, A (cm^2) the cross section of diaphragm, L (cm) the length of diaphragm, Δc (mol cm^{-3}) the concentration difference, and D (cm^2 s^{-1}) the diffusion coefficient.[9] If the gas can be assumed to be ideal, then the amount of gas dissolved as a result of steady progress of diffusion is given by

$$dn/dt = d(PV/RT)/dt = (P/RT)\Delta V/\Delta t, \quad (2)$$

where P is the partial pressure of gas, ΔV the volume decrease of gas due to dissolution, R the gas constant, T the temperature and Δt the time increment. Substitution of Eq. 2 into Eq. 1 gives

$$D = (LP/ART\Delta c)(\Delta V/\Delta t). \quad (3)$$

ΔV can be measured by the change in mercury level Δh in the gas buret as

$$\Delta V = A_m \Delta h, \quad (4)$$

where A_m is the cross section of gas buret. The concentration difference $\Delta c(t)$ can be expressed by

$$\Delta c(t) = (c_0 P/P_0)\Delta c^*(t), \quad (5)$$

where $c_0 = X/V_1^0$ is the concentration of the saturated solution of gas at $P = P_0$ and $\Delta c^*(t)$ a correction term due to the change in concentration difference with the advancement of diffusion of gas into lower vessel of the diffusion cell. Here X is the solubility of gas given in terms of the mole fraction in the liquid phase and V_1^0 is the molar volume of solvent. P_0 is taken to be the atmospheric pressure so that X is the solubility at 1 atmosphere.

The diffusion coefficient D can be calculated by the following equation, obtained from Eqs. 3, 4, and 5:

$$D = (LA_m P_0/ART c_0)(\Delta h/\Delta c^*\Delta t), \quad (6)$$

$$= K(\Delta h/\Delta c^*\Delta t c_0), \quad (7)$$

where K is the apparatus constant and K/c_0 is also a constant for the combination of gas and solvent. Thus we can calculate D from the slope of linear relation between $\Delta h/\Delta c^*$ and Δt.

In order to use Eq. 7 for the calculation of D, it is necessary to apply some corrections to Δh and Δc^*. Since Δh is influenced by the change in atmospheric pressure, a correction should be made by means of the equation

$$\Delta h = \Delta h_0 - (V_g/A_m)(\Delta P/P), \quad (8)$$

where V_g is the volume of vapor phase, ΔP the fluctuation of atmospheric pressre and Δh_0 the manometer (gas buret) reading. On the other hand, the correction for the concentration change can be estimated by

$$\Delta c^* = 1 - (P/RT)(A_m/V_1)(\Delta h^*(\Delta t)/c_0), \quad (9)$$

where V_1 is the volume of degassed solvent and $\Delta h^*(\Delta t)$ is the change in mercury level after the steady state was attained. The relation is somewhat ambiguous as the amount of gas dissolved before the establishment of steady state of diffusion is unknown. When V_1 is sufficiently large, the correction is negligible.

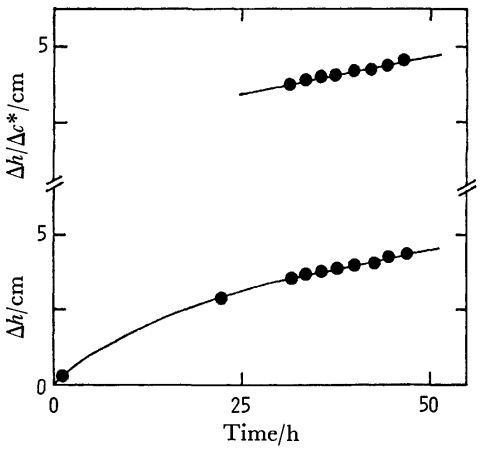

Fig. 2. Plot of height change in buret against time.

The present technique is an absolute method for the measurement of D without use of any apparatus constant determined by calibration with a gas of known D. It is in contrast to the conventional diaphragm cell technique for which the determination of cell constant is indispensable.

An example of $\Delta h/\Delta c^*$ *vs.* Δt plot is given in Fig. 2. The plot shows a downward curvature in the initial stage indicating gradual attainment of the steady concentration gradient and linearity. It requires about one day to establish a stationary state of diffusion in aqueous solutions.[10] The diffusion coefficient can be calculated from the slope of the straight line.

Apparatus Constants and Physical Constants Used. Instead of carrying out calibration measurement with a gas of known D, several apparatus constants should be determined in advance. The values of each constant used in most measurements with gases of unknown D are as follows.

$$A = 5.65\ cm^2,\ L = 1.00\ cm,\ A_m = 0.326\ cm^2,$$

$$V_1 = 257\ cm^3,\ \text{and}\ V_g = 144\ cm^3.$$

Somewhat different values of V_1 and V_g were used in part of the measurements since it was necessary to overhaul and reconstruct the apparatus during the course of the present study.

In order to calculate the diffusion coefficient, it is necessary to use physical constants such as gas solubility, vapor pressure, and density of solvent. Gas solubility data given by Ben-Naim and Baer[11] and Cargill and Morrison[12] (argon in ethanol+water solutions), Ben-Naim and Moran[13] (argon in 1,4-dioxane+water solutions) and Ben-Naim[14] (methane in ethanol +water solutions) were used. The density and vapor pressure of all the solvents have been taken from the compilation of Timmermans.[15]

Results and Discussion

Diffusion Coefficient of Argon and Methane in Water. In order to confirm the reliability of the apparatus, comparison has been made between the present data for pure solvents and those in literature. The diffusion coefficients of argon and methane have been studied extensively. Figures 3 and 4 show both data as a function of temperature. We have found that the diffusion coefficient of argon in water is 2.22×10^{-5} cm^2 s^{-1}. Literature values scatter a great deal. However, the reliable data by Duda[16] and Baird and Davidson[17] seem to converge to about 2.0×10^{-5} cm^2 s^{-1} at 25 °C. The agreement between both data is reasonable, though the present value is about 10% higher. The results for

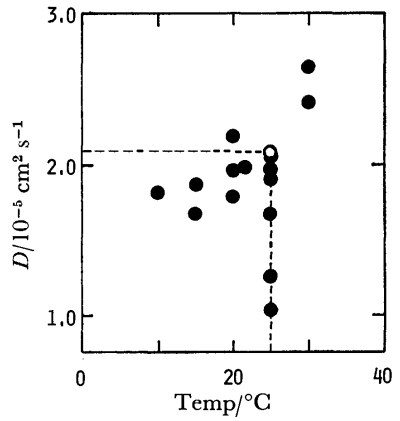

Fig. 3. Diffusion coefficient of argon in water as a function of temperature. ○: This work, ●: literature value.

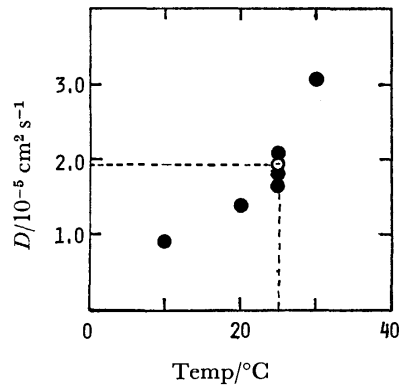

Fig. 4. Diffusion coefficient of methane in water as a function of temperature. ○: This work, ●: literature value.

methane do not scatter much, the representative datum due to Witherspoon and Saraf[18] being 1.88×10^{-5} cm^2 s^{-1} at 25 °C, in perfect agreement with the present data. It is thus concluded that the present data can be regarded as reliable.

Diffusion Coefficients in Aqueous Solutions. The diffusion coefficients of argon in aqueous solution of ethanol and in aqueous solution of 1,4-dioxane and of methane in aqueous solution of ethanol have been measured at 298.15 K. The measurements are restricted to water-rich regions. The results are given in Table 1, the values being an average of the results of two or three runs. Reproducibility is satisfactory, deviation being less than

Table 1. Diffusion coefficients of argon and methane in aqueous solutions at 298.15 K

Ar−H_2O+EtOH		Ar−H_2O+$C_4H_8O_2$		CH_4−H_2O+EtOH	
x_{EtOH}	D[a]	$x_{dioxane}$	D	x_{EtOH}	D
0	2.22	0	2.22	0	1.88
0.045	1.87	0.015	2.19	0.045	1.61
0.090	1.53	0.060	2.09	0.090	1.04
0.150	1.02	0.150	1.35	0.150	0.43
0.250	1.12	0.200	1.54	0.200	0.52
		0.250	1.85	0.250	0.54

a) 10^5 cm^2 s^{-1}.

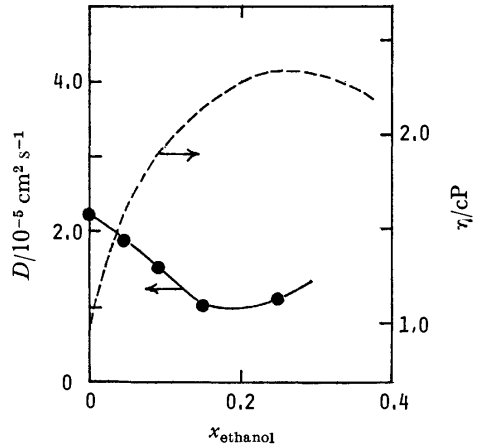

Fig. 5. Diffusion coefficients of argon in aqueous solutions of ethanol at 298.15 K.

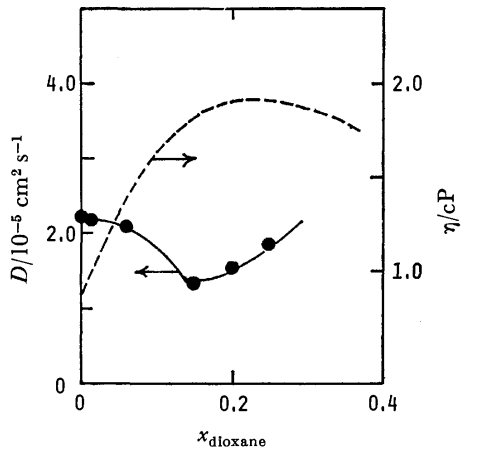

Fig. 6. Diffusion coefficients of argon in aqueous solutions of 1,4-dioxane at 298.15 K.

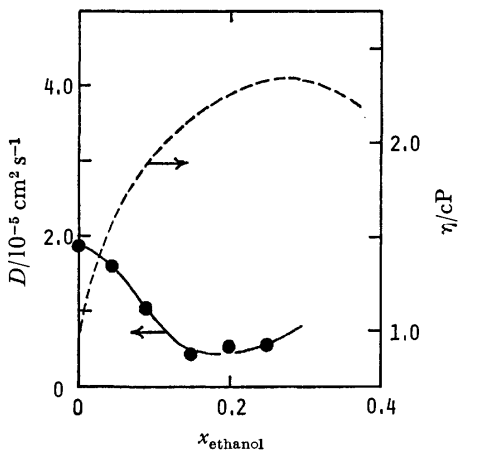

Fig. 7. Diffusion coefficients of methane in aqueous solution of ethanol at 298.15 K.

±4%. The diffusion coefficients and the viscosity coefficient η of the mixed solvents are plotted against the mole fraction of ethanol or 1,4-dioxane in Figs. 5—7.

The viscosity of solvent increases with the addition of ethanol until the mole fraction of ethanol x_{EtOH} exceeds 0.25, at which the viscosity becomes maximum. A

similar tendency can be seen for 1,4-dioxane solutions. On the other hand, the diffusion coefficient decreases rapidly with the addition of ethanol or 1,4-dioxane, becoming minimum near $x=0.2$, and then increasing. Thus D and η are inversely proportional with each other.

Anomaly in $D\eta$ vs. x Plot. It is common practice to reduce the D value with η to examine the behavior of the product $D\eta$ as a function of the composition of mixed solvents. We have recently studied the diffusion in mixed solvents using iodine as a solute and found that $D\eta$ value of iodine becomes maximum in aqueous alcohol (ethanol and *t*-butyl alcohol) solutions near $x_{alcohol}=0.1$ to 0.2.[1] A similar anomaly has been reported by Perkins and Geankoplis[19] for acetic acid in aqueous ethanol solutions. The minimum diffusion coefficient does not necessarily correspond to maximum viscosity. It is thus of interest to examine the relation $D\eta$ *vs.* x. Figure 8 shows the plot of $D\eta$ against x for argon and methane in aqueous ethanol solutions. It should be noted that a small peak appears in the region $x_{EtOH}<0.1$. This may be characteristic of aqueous alcohol solutions and aqueous solutions of all the compounds acting as a structural maker. Although 1,4-dioxane has been regarded often as a structural breaker, it may act as a structural maker as far as diffusivity concerned.

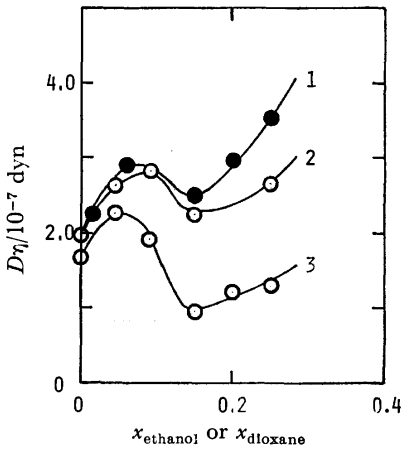

Fig. 8. Isoviscous diffusion coefficients as a function of mole fraction of ethanol or 1,4-dioxane in aqueous solutions. 1: Argon in 1,4-dioxane solutions, 2: argon in ethanol solutions, 3: methane in ethanol solutions.

Comparison between Ar and CH_4 and between Ethanol and 1,4-Dioxane Solutions. The diffusivity of gases in aqueous ethanol solution has been studied extensively.[20,21] The dependence of diffusion coefficient on the molar composition is complicated, varying with gas. In view of the complicatedness of the problem, we confine our attention to a comparison only between the three data obtained in the present study.

First we deal with the difference in the diffusivity of argon in aqueous ethanol solution and in aqueous 1,4-dioxane solution. When ethanol or 1,4-dioxane is added to water, viscosity increases a great deal to the same extent. However, the decrease in diffusivity is fairly large in ethanol solution, while that in 1,4-dioxane solution is small. This may be interpreted as follows. There should be various kinds of cavities in three dimensional hydrogen bonding structure in water. The size of these cavities is thought to be *ca.* 5.8—6.6 Å.[22] Since 1,4-dioxane shows no self-association, the cavity can be occupied by 1,4-dioxane molecule dissolved in water. In fact, the self-diffusion of 1,4-dioxane decreases distinctly with the increase in $x_{dioxane}$ in aqueous solution.[23] When argon diffuses in aqueous 1,4-dioxane solution, capture of argon molecule in the water cavity is reduced. Rapid diffusion may be energetically favorable. In spite of a large viscosity increase, the diffusion of argon would not decrease much. On the other hand, the addition of ethanol to water may enlarge and stabilize the cavity in water. Therefore, in aqueous ethanol solution, argon can be easily trapped in the cavity and its diffusion coefficient will decrease a great deal with the addition of ethanol into water.

The diffusion coefficient of methane in aqueous ethanol solutions is always smaller than that of argon in the same solutions. This reflects the difference in the size of diffusant. For the size effect on diffusivity, Ross and Hildebrand[7] have proposed an empirical relation, $D\sigma^2=$constant, where σ is the diameter of diffusant. Witherspoon and Saraf[18] showed that a relation, $D\sigma=$constant, seems to be also valid for the diffusion of gaseous hydrocarbons in water. In the present case, it can be shown that the latter gives a better fit. Thus

$$D_{Ar}\sigma_{Ar} = D_{CH_4}\sigma_{CH_4}, \qquad (10)$$

seems to be valid in water. It is of interest to examine whether D_{Ar}/D_{CH_4} is a constant in aqueous ethanol solutions. Figure 9 shows D_{Ar}/D_{CH_4} *vs.* x_{EtOH} plot. The ratio becomes maximum near $x_{EtOH}=0.1$—0.15. This indicates that the capture of solute in the cavity of water enlarged by the introduction of ethanol depends appreciably on the kind of solute and the effect can be clearly seen in the composition range where the anomaly of aqueous ethanol solution is often observed.[5] The characteristics of the diffusivity of solutes in dilute aqueous solutions is too complicated to deduce a clear-cut interpretation. It seems necessary to accumulate experimental data for various solutes in aqueous mixed solvents at different temperatures.

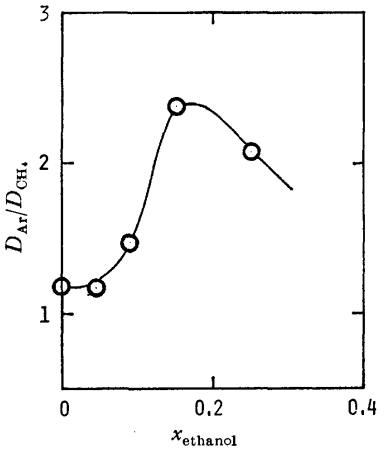

Fig. 9. Ratio of diffusion coefficient between argon and methane as a function of mole fraction of ethanol in aqueous solution.

The authors thank Mr. Soto Asakura for his cooperation in the earlier stage of the work. They are grateful to Prof. Nobuatsu Watanabe for his interest and discussion.

References

1) K. Nakanishi and T. Ozasa, *J. Phys. Chem.*, **74**, 2956, (1970).
2) K. Nakanishi, T. Ozasa, and K. Ashitani, *J. Phys. Chem.*, **75**, 963 (1971).
3) K. Nakanishi and S. Kitajima, *J. Phys. Chem.*, **76**, 2470 (1972).
4) K. Nakanishi and Y. Furusawa, *J. Chem. Eng. Data*, **23**, 101 (1978).
5) F. Franks and D. S. Reid, in F. Franks ed, "Water," Vol. 2, Plenum Press, New York (1973), Chapt. 5.
6) K. Nakanishi, E. M. Voigt, and J. H. Hildebrand, *J. Chem. Phys.*, **42**, 1860 (1965).
7) (a) M. Ross and J. H. Hildebrand, *J. Chem. Phys.*, **40**, 2397 (1964); (b) R. J. Powell and J. H. Hildebrand, *J. Chem. Phys.*, **55**, 4715 (1971).
8) It is possible that a stagnant layer is formed just below the diaphragm if no stirring is applied in the degassed liquid phase. However, no retardation of diffusion was observed in the experiment carried out with the same diaphragm as that used here.[6] No stirrer was attached to the diffusion cell in the present experiment.
9) The method of calculation of diffusion coefficient described here is based on the one established by Hildebrand and co-workers.[6,7] No detailed description of this method has been given.
10) The time required for the establishment of steady state diffusion seems to be longer than expected.
11) A. Ben-Naim and G. Baer, *Trans. Faraday Soc.*, **60**, 1736 (1964).
12) R. W. Cargill and T. J. Morrison, *J. Chem. Soc. Faraday Trans. 1*, **71**, 618 (1975).
13) A. Ben-Naim and G. Moran, *Trans. Faraday Soc.*, **61**, 821 (1965).
14) A. Ben-Naim, *J. Solution Chem.*, **2**, 425 (1973).
15) J. Timmermans, "Physico-Chemical Constants of Binary Systems in Concentrated Solutions," Vol. 4, Interscience (1960).
16) J. L. Duda, *AIChE J.*, **14**, 286 (1968).
17) M. H. I. Baird and J. F. Davidson, *Chem. Eng. Sci.*, **17**, 473 (1962).
18) P. A. Witherspoon and D. N. Saraf, *J. Phys. Chem.*, **69**, 3752 (1965).
19) L. R. Perkins and C. J. Geankoplis, *Chem. Eng. Sci.*, **24**, 1035 (1969).
20) Y. D. Tang and D. M. Himmelblau, *AIChE J.*, **11**, 54 (1965).
21) E. Sada, S. Kito, T. Oda, and Y. Ito, *Chem. Eng. J.*, **10**, 155 (1975).
22) F. Franks, in F. Franks ed, "Water," Vol. 2, Plenum Press, New York (1973), Chapt. 4.
23) T. Erdey-Gruz and B. Levay, *Acta Chim. (Budapest)*, **69**, 215 (1971).

The Structure of the Cyclodextrin Complex. VII. The Crystal Structure of the α-Cyclodextrin-DMSO-Methanol (1: 1: 2) Dihydrate Complex A Simultaneous Inclusion of DMSO and Methanol

Kazuaki HARATA

Research Institute for Polymers and Textiles, Sawatari-4, Kanagawa-ku, Yokohama 221

(Received October 25, 1977)

The crystal structure of the α-cyclodextrin(α-CDx)–DMSO–methanol (1: 1: 2) dihydrate complex was determined by the X-ray method. The crystal is monoclinic, and the space group is $P2_1$ with $Z=2$. The cell dimensions are $a=9.505(1)$, $b=14.150(1)$, $c=19.738(2)$ Å, and $\beta=102.88(1)°$. The structure was solved by an inspection of a Patterson map and by a trial-and-error method, and was refined by the block-diagonal least-squares method to the final R-value of 0.083 for 3732 reflections. The α-CDx ring is nearly hexagonal, with diagonal distances of 8.40—8.53 Å between the glycosidic oxygen atoms. The α-CDx molecules are arranged to form molecular layers perpendicular to the ac plane. The DMSO molecule is located on the secondary hydroxyl side in the α-CDx cavity, forming two hydrogen bonds with the adjacent α-CDx molecules. One methanol molecule is found on the primary hydroxyl side in the cavity, while the other is located outside the cavity. Two water molecules are distributed in the space between α-CDx molecules.

Extensive studies of inclusion and catalysis by cyclodextrins have been described.[1–3] The structure and binding force of α-cyclodextrin (α-CDx) complexes have been discussed on the basis of the structure of crystalline adducts obtained from aqueous solutions.[3–5] Recently, α-CDx was found to form complexes in a DMSO solution, and lyophobic binding has been proposed.[6] From the NMR study,[7] it seems that cyclodextrins form intramolecular O(3)–H···O(2) hydrogen bonds between the adjacent glucose residues in a DMSO solution, although the α-CDx complexes crystallized from aqueous solutions show both O(2)–H···O(3) and O(3)–H···O(2) hydrogen bonds.[4,8,9] α-CDx crystallizes from a DMSO–methanol solution. The crystal structure was determined in order to investigate the conformation of α-CDx and the α-CDx-solvent interaction in non-aqueous solutions.

Experimental

A needle-like crystal of the α-CDx–DMSO–methanol (1: 1: 2) dihydrate complex was obtained from a DMSO–methanol (1: 2) solution containing α-CDx hexahydrate (*ca.* 5%). The diffraction experiments were carried out with the crystal enclosed in a quartz capillary including a drop of mother liquor, since the crystal breaks up in air. The determination of the lattice parameters and the intensity measurement were performed on a Rigaku automatic four-circle diffractometer with graphite-monochromated Cu $K\alpha$ radiation. 3732 independent reflections with $|F_o| \geqq 3\sigma(F)$ were obtained up to 150° in 2θ by using the 2θ-ω scan technique. No corrections were made for absorption or extinction.

Crystal Data: $C_{36}H_{60}O_{30}\cdot C_2H_6OS\cdot 2CH_4O\cdot 2H_2O$, *FW* 1151.1, monoclinic, space group $P2_1$, $Z=2$, $a=9.505(1)$, $b=14.150(1)$, $c=19.738(2)$ Å, $\beta=102.88(1)°$, $V=2587.0$ Å^3, $D_m=1.46$, $D_x=1.478$ g·cm^{-3}.

Determination and Refinement of the Structure

The orientation of the α-CDx molecule in the unit cell was deduced from an inspection of a Patterson map. The position of the molecule was determined by the trial-and-error method. Then, the rigid-body least-squares technique was adopted in order to refine the position and orientation of each glucose residue. DMSO, methanol, and water molecules were found on Fourier and difference-Fourier maps. The primary hydroxyl groups of the G5 residue was found to be statistically disordered. The occupancy factors were estimated from an electron-density map, but they were not refined. Fifty-four hydrogen atoms were found on a difference-Fourier map. The refinement of atomic parameters was carried out by the block-diagonal least-squares method. The thermal factors of the hydrogen atoms were fixed as isotropic ones of the carbon or oxygen atoms to which they are bonded. The quantity minimized was $\Sigma w(|F_o|-|F_c|)^2$, with $w=1.0$ for all the reflections used. The final R-value was 0.083. The atomic scattering factors were taken from "International Tables for X-Ray

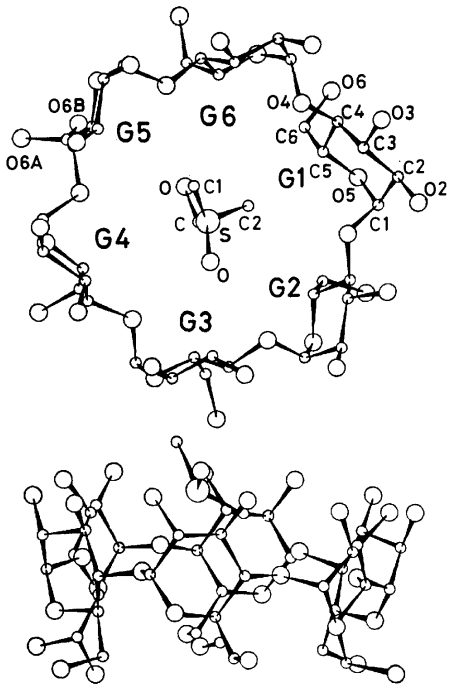

Fig. 1. Structure and numbering scheme of the α-cyclodextrin–DMSO–methanol complex.

TABLE 1. FINAL ATOMIC PARAMETERS FOR NON-HYDROGEN ATOMS ($\times 10^4$)

The anisotropic thermal factors are of the form: $\exp[-(B_{11}h^2+B_{22}k^2+B_{33}l^2+B_{12}hk+B_{23}kl+B_{31}lh)]$.

	x	y	z	B_{11}	B_{22}	B_{33}	B_{12}	B_{23}	B_{31}
C(1,G1)	466(11)	7045(8)	342(5)	93(14)	32(6)	18(3)	52(15)	6(7)	-5(10)
C(2,G1)	-601(11)	6475(7)	650(5)	76(13)	26(5)	17(3)	-3(13)	-12(6)	-6(9)
C(3,G1)	176(12)	5938(7)	1293(5)	101(14)	24(5)	17(3)	-21(14)	6(6)	0(10)
C(4,G1)	1422(12)	5346(7)	1124(5)	133(15)	21(5)	10(2)	-4(15)	7(6)	18(10)
C(5,G1)	2400(12)	5940(8)	758(5)	122(15)	37(6)	13(3)	6(16)	1(7)	21(10)
C(6,G1)	3493(12)	5350(8)	480(6)	103(15)	36(6)	23(3)	27(16)	-3(8)	17(11)
O(2,G1)	-1651(8)	7088(6)	835(4)	91(10)	37(4)	23(2)	19(11)	-2(5)	10(8)
O(3,G1)	-790(9)	5342(6)	1533(4)	156(13)	37(4)	28(3)	-34(13)	3(6)	60(9)
O(4,G1)	2267(7)	5018(5)	1773(3)	95(9)	25(4)	15(2)	-14(10)	-1(4)	3(7)
O(5,G1)	1514(7)	6421(5)	164(3)	88(9)	30(4)	13(2)	13(10)	-1(4)	26(6)
O(6,G1)	2902(10)	4547(6)	103(4)	174(14)	37(5)	24(2)	23(14)	-8(6)	26(9)
C(1,G2)	2282(12)	10468(7)	1141(5)	125(15)	22(5)	19(3)	-16(15)	-1(7)	1(11)
C(2,G2)	778(11)	10275(8)	1172(5)	98(14)	29(5)	19(3)	-16(15)	7(7)	-2(10)
C(3,G2)	555(11)	9213(7)	1220(4)	121(15)	21(5)	9(2)	7(14)	-5(5)	9(9)
C(4,G2)	1114(11)	8698(7)	669(5)	87(13)	19(5)	13(2)	16(13)	1(6)	2(9)
C(5,G2)	2624(11)	9004(7)	608(6)	91(14)	24(5)	25(3)	-11(15)	-2(7)	-6(11)
C(6,G2)	3031(13)	8632(9)	-46(6)	128(17)	45(7)	28(4)	-15(19)	-22(9)	68(13)
O(2,G2)	372(8)	10761(6)	1741(4)	116(11)	35(4)	25(2)	26(12)	-21(5)	-3(8)
O(3,G2)	-945(8)	9019(5)	1176(4)	99(10)	35(4)	21(2)	-21(11)	-7(5)	12(7)
O(4,G2)	1147(7)	7711(5)	844(3)	103(10)	22(3)	8(2)	-19(10)	-5(4)	-3(6)
O(5,G2)	2664(7)	10020(5)	567(3)	97(9)	27(4)	17(2)	-15(10)	4(4)	12(7)
O(6,G2)	1974(11)	8807(7)	-654(4)	245(17)	55(6)	17(2)	1(17)	-3(6)	43(10)
C(1,G3)	6761(11)	10819(7)	3328(5)	75(12)	24(5)	18(3)	1(13)	9(6)	10(9)
C(2,G3)	5247(12)	11151(8)	3418(5)	120(16)	38(6)	12(3)	32(16)	12(7)	-4(10)
C(3,G3)	4081(11)	10655(8)	2939(5)	75(13)	37(6)	18(3)	15(15)	7(7)	2(9)
C(4,G3)	4235(12)	10783(7)	2178(5)	127(16)	27(5)	11(2)	-7(15)	-8(6)	2(10)
C(5,G3)	5782(12)	10545(7)	2099(5)	97(14)	27(5)	20(3)	4(15)	11(6)	-20(10)
C(6,G3)	6079(14)	10839(10)	1421(5)	156(19)	64(8)	13(3)	20(21)	-12(8)	-2(11)
O(2,G3)	5246(9)	10989(6)	4139(3)	154(13)	56(5)	10(2)	34(13)	2(5)	15(7)
O(3,G3)	2727(8)	11034(6)	2988(4)	100(11)	57(5)	26(2)	36(13)	24(6)	29(8)
O(4,G3)	3224(7)	10154(5)	1773(3)	97(10)	27(4)	17(2)	-16(10)	7(4)	-24(7)
O(5,G3)	6807(7)	11008(5)	2624(3)	77(9)	45(4)	14(2)	-17(11)	9(5)	5(6)
O(6,G3)	5719(9)	11790(6)	1246(4)	171(14)	48(5)	13(2)	-64(14)	7(5)	-9(8)
C(1,G4)	9463(11)	7811(8)	4581(5)	88(14)	44(6)	11(2)	2(15)	1(7)	10(9)
C(2,G4)	8881(10)	8577(7)	5011(5)	71(12)	33(5)	12(2)	5(13)	-1(6)	3(9)
C(3,G4)	7692(10)	9138(8)	4561(5)	63(12)	46(6)	13(2)	38(14)	13(7)	23(9)
C(4,G4)	8210(9)	9525(7)	3920(4)	46(11)	31(5)	13(2)	-17(13)	9(6)	-5(8)
C(5,G4)	8852(11)	8748(8)	3540(5)	86(13)	40(6)	16(3)	-5(15)	5(7)	28(10)
C(6,G4)	9637(12)	9132(10)	2994(6)	120(17)	64(8)	21(3)	22(20)	22(9)	57(12)
O(2,G4)	8424(8)	8094(6)	5565(3)	124(11)	48(5)	14(2)	45(12)	8(5)	26(7)
O(3,G4)	7400(9)	9901(6)	4976(4)	162(13)	43(5)	14(2)	59(13)	-9(5)	17(8)
O(4,G4)	6905(7)	9846(5)	3448(3)	69(8)	32(4)	14(2)	-24(9)	4(4)	-4(6)
O(5,G4)	9953(7)	8249(5)	4035(4)	60(8)	35(4)	20(2)	5(10)	8(5)	16(6)
O(6,G4)	10889(10)	9648(8)	3322(6)	160(15)	73(7)	54(4)	-56(18)	20(9)	101(13)
C(1,G5)	7112(12)	4430(7)	3973(5)	108(15)	27(5)	18(3)	-5(15)	-10(6)	-5(10)
C(2,G5)	7098(11)	4788(8)	4704(5)	93(14)	38(6)	16(3)	24(15)	10(7)	-10(10)
C(3,G5)	7197(11)	5883(8)	4693(5)	86(13)	43(6)	14(3)	-36(15)	-1(7)	19(9)
C(4,G5)	8474(10)	6194(7)	4415(5)	66(12)	28(5)	17(3)	-18(13)	-5(6)	0(9)
C(5,G5)	8480(11)	5731(8)	3712(5)	81(13)	44(6)	15(3)	-29(15)	-7(7)	0(9)
C(6,G5)	9957(15)	5927(10)	3517(7)	165(21)	64(9)	38(5)	-102(23)	-57(11)	106(16)
O(2,G5)	5766(8)	4501(6)	4864(4)	125(11)	54(5)	20(2)	-37(13)	8(6)	37(8)
O(3,G5)	7268(8)	6214(6)	5381(3)	132(11)	48(5)	15(2)	-47(12)	-19(5)	45(8)
O(4,G5)	8269(7)	7209(5)	4321(3)	47(8)	32(4)	18(2)	3(9)	3(4)	12(6)
O(5,G5)	8403(7)	4710(5)	3790(3)	75(9)	41(4)	17(2)	1(10)	-10(5)	21(7)
O(6A,G5)	11182(23)	5955(19)	3897(13)	44(27)	56(17)	26(8)	-28(36)	26(19)	-5(23)
O(6B,G5)	10030(15)	5524(10)	2906(7)	167(20)	65(9)	37(5)	-17(23)	7(11)	97(16)
C(1,G6)	2651(10)	4046(7)	1836(5)	72(12)	23(5)	16(3)	-10(13)	1(6)	2(9)
C(2,G6)	2443(11)	3711(8)	2553(5)	90(13)	37(6)	11(2)	-18(15)	-5(6)	8(9)
C(3,G6)	3499(13)	4247(8)	3112(5)	142(17)	38(6)	10(2)	-13(16)	1(6)	37(10)
C(4,G6)	5043(11)	4151(7)	3018(5)	96(14)	25(5)	12(2)	0(14)	9(6)	7(9)
C(5,G6)	5129(11)	4405(8)	2281(4)	99(14)	48(6)	6(2)	-32(16)	5(6)	23(9)
C(6,G6)	6631(12)	4133(10)	2128(6)	83(14)	67(8)	22(3)	17(18)	-8(9)	39(11)
O(2,G6)	1030(8)	3839(6)	2636(4)	89(10)	52(5)	27(2)	-46(12)	-9(6)	-25(8)
O(3,G6)	3436(9)	3870(7)	3784(3)	177(13)	67(6)	10(2)	-98(16)	-7(6)	28(8)
O(4,G6)	5895(7)	4775(5)	3502(3)	82(9)	20(3)	15(2)	-9(9)	0(4)	-6(6)
O(5,G6)	4074(7)	3903(5)	1782(3)	100(9)	34(4)	12(2)	2(10)	-14(4)	15(6)
O(6,G6)	6864(10)	3124(7)	2233(5)	161(14)	57(6)	35(3)	53(16)	-26(7)	2(11)
S(1,DS)	3821(12)	7756(-)	3670(3)	875(31)	62(3)	54(2)	-14(17)	-4(5)	89(14)
C(1,DS)	3519(25)	7052(18)	4425(13)	295(41)	126(19)	100(12)	95(47)	139(26)	127(37)
C(2,DS)	3029(34)	7317(26)	2896(13)	511(72)	227(35)	54(9)	-80(86)	-34(31)	-38(41)
O(1,DS)	3359(11)	8678(8)	8350(5)	204(17)	76(7)	43(4)	-48(20)	-42(9)	34(13)
C(1,M1)	126(16)	6895(12)	6767(9)	140(22)	72(11)	57(7)	0(25)	5(14)	89(20)
O(1,M1)	1022(11)	7647(8)	6632(5)	144(15)	86(8)	40(3)	37(18)	24(9)	18(11)
C(1,M2)	6107(25)	7534(20)	1769(15)	271(42)	132(21)	120(15)	94(51)	21(31)	168(42)
O(1,M2)	6726(23)	6739(15)	1921(11)	561(48)	194(20)	131(11)	255(54)	173(26)	402(41)
O(W1)	6671(11)	7601(7)	9644(5)	199(17)	55(6)	42(4)	13(17)	-3(8)	-59(13)
O(W2)	333(13)	7634(8)	8436(6)	265(22)	49(6)	58(5)	-40(20)	20(9)	-46(16)

Crystallography."[10] The atomic parameters are listed in Tables 1 and 2,* while the observed and calculated structure factors are given in Table 3.*

Description and Discussion of the Structure

Structure of α-CDx. The structure and numbering scheme of α-CDx are shown in Fig. 1. The bond distances, angles, and conformation angles are given in Tables 4—6.* The geometrical data for the α-CDx ring are shown in Tables 7 and 8. The average bond distances and angles are in good agreement with those found in other α-CDx complexes.[5,8,9,11-21] The primary hydroxyl group of the G5 residue is statistically disordered. The occupancy factors are 0.3 for O(6A, G5) and 0.7 for O(6B, G5). The C(6)–O(6A) and C(6)–O(6B) bonds show *gauche-gauche* and *gauche-trans* conformations respectively. The other primary hydroxyl groups are in the *gauche-gauche* conformation. The C(6)–O(6A) and C(6)–O(6B) bonds are significantly short, but a similar shortening of the disordered C–O bond has been observed in α-L-sorbose[22] and α-CDx complexes with Methyl Orange[12] and *m*-nitrophenol.[15]

The six glycosidic oxygen atoms form a nearly regular hexagon. The diagonal O(4)···O(4) distances of the α-CDx ring deviate 0.08 Å at most from their average value of 8.47 Å. These six O(4) atoms are coplanar within 0.14 Å. The average O(4)···O(4) distance between the adjacent glucose residues is 4.24 Å, with a maximum deviation of 0.05 Å. The symmetrical α-CDx ring has been also found in the sodium 1-propanesulfonate complex,[14] but the torsion-angle index[23] indicates that the conformation of pyranose rings changes slightly. The torsion-angle indices (128—136°) are significantly larger than those found in the sodium 1-propanesulfonate complex (126.6—128.5°).

Intramolecular O(2)···O(3) hydrogen bonds are observed between the adjacent glucose residues (Table 7). From the NMR spectra of cyclodextrins in a DMSO solution, only the O(3)–H···O(2) hydrogen bond has been suggested.[7] In the DMSO–methanol complex there are four O(3)–H···O(2) hydrogen bonds, but a O(2)–H···O(3) hydrogen bond is also observed between the G1 and G2 residues. The O(2)···O(3) distance between the G1 and G6 residues (3.25 Å) is too large for the hydrogen bond.

TABLE 5. AVERAGE BOND DISTANCES AND ANGLES FOR THE GLUCOSE RESIDUE

The standard deviations were estimated according to $\sigma=[\sum_{i=1}^{6}(x_i-\bar{x})^2/5]^{1/2}$, where x_i referes to the bond distances or angles in the i-th residue and $\bar{x}$ is the average value. A prime indicates the atom in the adjacent glucose residue.

I. Bond distances (l/Å)			
C(1)–C(2)	1.53(3)	C(3)–O(3)	1.42(1)
C(1)–O(5)	1.41(1)	C(4)–C(5)	1.54(1)
C(1)–O(4′)	1.42(1)	C(4)–O(4)	1.43(2)
C(2)–C(3)	1.51(3)	C(5)–C(6)	1.53(3)
C(2)–O(3)	1.43(2)	C(5)–O(5)	1.44(2)
C(3)–C(4)	1.53(2)	C(6)–O(6)	1.40(5)
II. Bond angles (ϕ/°)			
C(2)–C(1)–O(5)	110(2)	C(3)–C(4)–C(5)	112(1)
C(2)–C(1)–O(4′)	108(2)	C(3)–C(4)–O(4)	106(1)
O(5)–C(1)–O(4′)	111(1)	C(5)–C(4)–O(4)	109(1)
C(1)–C(2)–C(3)	110(2)	C(4)–C(5)–C(6)	113(2)
C(1)–C(2)–O(2)	109(3)	C(4)–C(5)–O(5)	110(1)
C(3)–C(2)–O(2)	111(2)	C(6)–C(5)–O(5)	106(1)
C(2)–C(3)–C(4)	111(1)	C(5)–C(6)–O(6)	113(3)
C(2)–C(3)–O(3)	109(2)	C(4)–O(4)–C(1′)	119(1)
C(4)–C(3)–O(3)	110(2)	C(1)–O(5)–C(5)	114(2)

TABLE 7. GEOMETRICAL DATA FOR THE α-CYCLODEXTRIN RING[a]

I. O(4)···O(4) distances (l/Å)			
O(4, G1)···O(4, G2)	4.26(1)		
O(4, G1)···O(4, G6)	4.29(1)		
O(4, G2)···O(4, G3)	4.19(1)		
O(4, G3)···O(4, G4)	4.27(1)		
O(4, G4)···O(4, G5)	4.19(1)		
O(4, G5)···O(4, G6)	4.24(1)		
O(4, G1)···O(4, G4)	8.40(1)		
O(4, G2)···O(4, G5)	8.53(1)		
O(4, G3)···O(4, G6)	8.49(1)		
II. Torsion-angle index (ϕ/°)			
G1 residue	133	G4 residue	130
G2 residue	133	G5 residue	136
G3 residue	134	G6 residue	128
III. Intramolecular hydrogen bonds (l/Å)			
		H···O	O···O
O(2, G1)–H···O(3, G2)		2.27(13)	2.86(1)
O(3, G3)–H···O(2, G2)		2.34(13)	2.96(1)
O(3, G4)–H···O(2, G3)		1.97(13)	2.79(1)
O(3, G5)–H···O(2, G4)		1.88(13)	2.87(1)
O(3, G6)–H···O(2, G5)		1.93(13)	2.85(1)

a) Estimated standard deviations are shown in parentheses.

TABLE 8. LEAST-SQUARES PLANES AND DEVIATIONS OF ATOMS (l/Å)

The plane equation is of the $AX+BY+CZ=D$ form, where X, Y, and Z are the coordinates in Å along the a, b, and c* axes respectively.

I. The plane through six O(4) atoms.

$0.772X-0.105Y-0.627Z=-1.756$

O(4, G1)	−0.06	O(4, G4)	0.03
O(4, G2)	0.14	O(4, G5)	0.07
O(4, G3)	−0.13	O(4, G6)	−0.04

II. Deviations of atoms from the plane through C(2), C(3), C(5), and O(5).

Residue	C(1)	C(2)	C(3)	C(4)	C(5)	O(5)
G1	0.69	0.01	−0.01	−0.63	0.01	−0.01
G2	0.66	0.02	−0.02	−0.58	0.02	−0.02
G3	0.70	0.01	−0.01	−0.62	0.01	−0.01
G4	0.68	0.01	−0.01	−0.65	0.01	−0.01
G5	0.71	0.02	−0.02	−0.65	0.02	−0.02
G6	0.68	0.00	−0.00	−0.64	0.00	−0.00

* Tables 2—4 and 6 are kept at the office of the Chemical Society of Japan (Document No. 7818).

Table 9. Bond distances and angles in DMSO and methanol[a)]

I.	Bond distances (l/Å)	
	S(1, DS)–C(1, DS)	1.87(3)
	S(1, DS)–C(2, DS)	1.67(3)
	S(1, DS)–O(1, DS)	1.45(1)
	C(1, M1)–O(1, M1)	1.43(2)
	C(1, M2)–O(1, M2)	1.27(3)
II.	Bond angles (ϕ/°)	
	C(1, DS)–S(1, DS)–C(2, DS)	115(1)
	C(1, DS)–S(1, DS)–O(1, DS)	100(1)
	C(2, DS)–S(1, DS)–O(1, DS)	118(1)

a) Estimated standard deviations are shown in parentheses.

Table 10. Intermolecular distances between α-cyclodextrin and included molecules[a)]

I.	α-Cyclodextrin···DMSO (l/Å)	
	O(2, G3)–O(1, DS)	3.71(1)
	O(3, G3)–O(1, DS)	3.73(1)
	C(3, G3)–O(1, DS)	3.47(2)
	O(4, G4)–O(1, DS)	3.99(1)
	O(3, G5)–C(1, DS)	3.83(3)
	C(3, G5)–C(1, DS)	3.80(3)
	O(4, G1)–C(2, DS)	3.19(3)
II.	α-Cyclodextrin···methanol (l/Å)	
	C(5, G5)–O(1, M2)	3.83(2)
	C(6, G6)–O(1, M2)	3.71(2)
	O(6B, G5)–O(1, M2)	3.73(3)
	C(5, G6)–O(1, M2)	3.77(2)

a) Estimated standard deviations are shown in parentheses.

α-CDx-Guest Interaction. The bond distances and angles in DMSO and methanol are given in Table 9. The S(1, DS)–C(1, DS) bond is longer by 0.2 Å than the S(1, DS)–C(2, DS) bond. A similar inequality of the S–C bonds has been observed in the crystal structure of DMSO.[24)] The S–O bond is shorter by 0.09 Å than that found in the crystalline DMSO. The C–O bond of M2 is shorter by 0.16 Å than that of M1. This may be due to the large thermal motion as has been found in the α-CDx–methanol complex.[8)]

The intermolecular distances between α-CDx and included guests are shown in Table 10. The sulfur atom is located at the center of the circle composed of the twelve secondary hydroxyl groups. The C(2, DS) methyl group is inserted into the α-CDx cavity, while the C(1, DS) methyl group protrudes from the cavity. The shortest contact of DMSO with α-CDx is that of 3.47 Å found between O(1, DS) and C(3, G3), suggesting van der Waals contact. The M2 methanol is located nearly parallel to the O(4) plane on the primary hydroxyl side of the cavity. In the α-CDx–methanol complex,[8)] the methanol molecule is found in a similar position, being hydrogen-bonded to the primary hydroxyl group with the *gauche-trans* conformation. In the DMSO–methanol complex, C(6, G5)–O(6B, G5) bond is in the *gauche-trans* conformation, but the O(6B, G5)···O(1, M2) distance of 3.73 Å is too large for the hydrogen bond.

Table 11. Intermolecular distances less than 3.0 Å (l/Å)[a)]

O(6, G4)–O(1, DS)	(a)	2.72
O(6B, G5)–O(2, G6)	(a)	2.66
O(2, G4)–O(1, M1)	(a)	2.93
O(6, G3)–O(6, G6)	(b)	2.76
O(2, G1)–O(1, M2)	(c)	2.95
O(3, G3)–O(6, G4)	(c)	2.80
O(3, G1)–O(6B, G5)	(c)	2.66
O(6, G2)–O(W2)	(d)	2.68
O(2, G1)–O(W1)	(e)	2.63
O(2, G2)–O(W2)	(f)	2.74
O(3, G1)–O(6, G2)	(g)	2.85
O(6, G1)–O(3, G2)	(g)	2.88
O(6, G3)–O(W1)	(h)	2.79
O(2, G3)–O(3, G5)	(h)	2.78
O(2, G4)–O(3, G6)	(h)	2.64
O(2, G6)–O(W2)	(i)	2.80
O(6, G6)–O(1, M1)	(j)	2.74
O(2, G5)–O(1, DS)	(j)	2.75
O(6, G1)–O(W1)	(j)	2.81
O(3, G4)–O(6A, G5)	(k)	2.80

Code	Symmetry code		
a	$1+x$,	y,	z
b	x,	$1+y$,	z
c	$-1+x$,	y,	z
d	x,	y,	$-1+z$
e	$-1+x$,	y,	$-1+z$
f	$-x$,	$1/2+y$,	$1-z$
g	$-x$,	$-1/2+y$,	$-z$
h	$1-x$,	$1/2+y$,	$1-z$
i	$-x$,	$-1/2+y$,	$1-z$
j	$1-x$,	$-1/2+y$,	$1-z$
k	$2-x$,	$1/2+y$,	$1-z$

a) Estimated standard deviations are in the range from 0.01 to 0.03 Å.

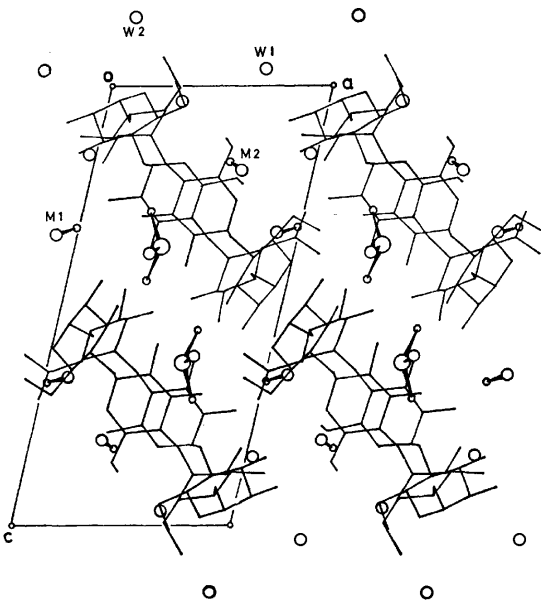

Fig. 2. The crystal structure projected on the ac plane. Circles indicate atoms in DMSO, methanol, and water molecules.

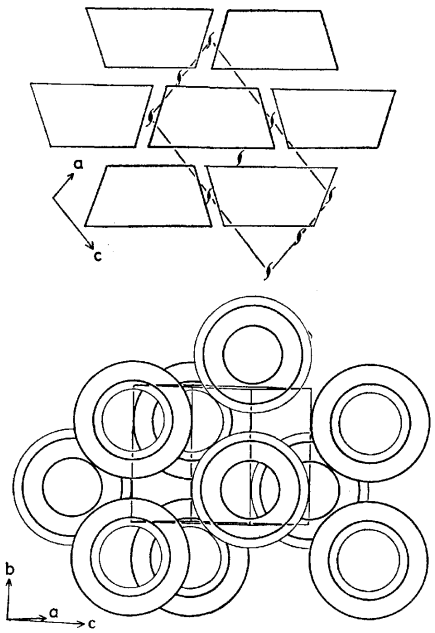

Fig. 3. A schematic drawing of the packing of α-cyclodextrin molecules.

Crystal Structure and Hydrogen Bonds. The crystal structure is shown in Fig. 2. The packing scheme of α-CDx molecules is illustrated in Fig. 3. The α-CDx molecules are arranged to form molecular layers parallel to the $(10\bar{2})$ plane. The α-CDx cavity is not connected to that of the next layer, but both ends of the cavity are open to the space between the α-CDx rings in the next layer. A similar packing of α-CDx molecules has been observed in the α-CDx complexes with *para*-disubstituted benzenes. Adjacent α-CDx molecules are linked by hydrogen bonds. In a layer, O(6, G3)–O(6, G6) (b), O(3, G1)–O(6, G2) (g), O(6, G1)–O(3, G2) (g), and O(3, G4)–O(6A, G5) (k) hydrogen bonds are observed. The adjacent layers are connected by O(6B, G5)–O(2, G6) (a), O(3, G3)–O(6, G4) (c), O(3, G1)–O(6B, G5) (c), O(2, G3)–O(3, G5) (h), and O(2, G4)–O(3, G6) (h) hydrogen bonds.

The DMSO molecule forms two hydrogen bonds with O(6, G4) (a) and O(2, G5) (j) in the next layer. The O(2)–H···DMSO hydrogen bond has also been proposed from the NMR study.[7] The methanol molecule (M2) in the α-CDx cavity is hydrogen-bonded to O(2, G1) (c), while the other methanol molecule (M1) forms two hydrogen bonds with O(2, G4) (a) and O(6, G6) (j). Thus, the DMSO and M2 methanol molecules are strongly bound to the α-CDx molecules in the next layer, although the interaction with the host α-CDx molecule seems to be weak. Each water molecule forms three hydrogen bonds with hydroxyl groups of α-CDx; O(W1) is linked to O(2, G1) (e), O(6, G3) (h) and O(6, G1) (j), while O(W2) is linked to O(6, G2) (d), O(2, G2) (f), and O(2, G6) (i).

From the DMSO methanol solution, a different crystal, which is more unstable, was obtained. The cell dimensions are $a=14.298$, $b=12.305$, $c=15.828$ Å, and $\beta=113.59°$, and the space group is $P2_1$. β-CDx crystallizes in an orthorhombic form; $a=11.428$, $b=15.549$, $c=40.025$ Å, and the space group is $P2_12_12_1$. We are attempting to elucidate these structures in order to investigate the conformation of cyclodextrins in non-aqueous solutions.

The author wishes to thank Dr. Hisashi Uedaira for supporting this study and for his helpful discussions. The computation was carried out on a HITAC 8450 computer in our laboratory.

References

1) J. A. Thoma and L. Stewart, "Starch: Chemistry and Technology," Vol. I, ed by R. L. Whistler and E. F. Pashall, Academic Press, New York (1965), pp. 209—249.
2) F. R. Senti and S. R. Erlander, "Non-stoichiometric Compounds," ed by L. Mandelcorn, Academic Press, New York (1964), pp. 568—605.
3) D. W. Griffiths and M. L. Bender, *Adv. Catal.*, **23**, 209 (1973).
4) W. Saenger, M. Noltemeyer, P. C. Manor, B. Hingerty, and B. Klar, *Bioorg. Chem.*, **5**, 187 (1976).
5) K. Harata, *Bull. Chem. Soc. Jpn.*, **49**, 2066 (1976).
6) B. Siegel and R. Breslow, *J. Am. Chem. Soc.*, **97**, 6869 (1975).
7) M. St-Jacques, P. R. Sundararajan, K. J. Taylor, and R. H. Marchessault, *J. Am. Chem. Soc.*, **98**, 4386 (1976).
8) B. Hingerty and W. Saenger, *J. Am. Chem. Soc.*, **98**, 3357 (1976).
9) K. Harata, *Bull. Chem. Soc. Jpn.*, **50**, 1416 (1977).
10) "International Tables for X-Ray Crystallography," Vol. IV, Kynoch Press, Birmingham (1974), pp. 72—75.
11) K. Harata, *Bull. Chem. Soc. Jpn.*, **48**, 2409 (1975).
12) K. Harata, *Bull. Chem. Soc. Jpn.*, **49**, 1493 (1976).
13) K. Harata, *Carbohydr. Res.*, **48**, 265 (1976).
14) K. Harata, *Bull. Chem. Soc. Jpn.*, **50**, 1259 (1977).
15) K. Harata, H. Uedaira, and J. Tanaka, *Bull. Chem. Soc. Jpn.*, **51**, 1627 (1978).
16) A. Hybl, R. E. Rundle, and D. E. Whilliams, *J. Am. Chem. Soc.*, **87**, 2779 (1965).
17) R. K. McMullan, W. Saenger, J. Fayos, and D. Mootz, *Carbohydr. Res.*, **31**, 211 (1973).
18) P. C. Manor and W. Saenger, *J. Am. Chem. Soc.*, **96**, 3630 (1974).
19) W. Saenger, R. K. McMullan, J. Fayos, and D. Mootz, *Acta Crystallogr. Sect. B*, **30**, 2019 (1974).
20) W. Saenger, K. Beyer, and P. C. Manor, *Acta Crystallogr. Sect. B*, **32**, 120 (1976).
21) W. Saenger and M. Noltemeyer, *Chem. Ber.*, **109**, 503 (1976).
22) K. Kim and R. D. Rosenstein, *Acta Crystallogr.*, **22**, 648 (1967).
23) A. D. French and V. G. Murphy, *Carbohydr. Res.*, **27**, 391 (1973).
24) R. Thomas, C. B. Shoemaker, and K. Eriks, *Acta Crystallogr.*, **21**, 12 (1966).

Neutron Diffraction Study of the Structure of Liquid Water

Norio OHTOMO* and Kiyoshi ARAKAWA

Research Institute of Applied Electricity, Hokkaido University, Sapporo 060

**Faculty of Engineering, Hokkaido University, Sapporo 060*

(Received October 28, 1977)

The structure factor for heavy water at 17 °C up to the Q value of 18 Å^{-1} has been determined by means of the time-of-flight (TOF) diffraction method using pulsed neutrons produced by LINAC. The result has been compared with structure factors calculated on the basis of the various structure models of liquid water; the "uncorrelated orientation model" and the "watery model" (Page and Powles), the "near-neighbor model" (Narten) and the "revised watery model" (authors). None of these models has been found to fit the neutron diffraction data satisfactorily over the entire range of Q, though our curve is somewhat improved in comparison with the curves for earlier models. Some discussions about the various structure models of liquid water have been made.

The neutron diffraction method has proved to be a powerful means for the determination of the structure of liquids for these two decades, and its applications into the studies of the structure of liquid water have been carried out since those by Brockhouse[1] and by Springer *et al.*[2] Recently, two remarkable studies of the liquid structure of water using the method have appeared, which have been given by Page and Powles[3] and by Narten,[4] and further, the structure factors at higher Q values have been reported.[5,6] However, the experimental data are still limited at present.

Among these studies the results[3] obtained by Page and Powles and those[4] by Narten are the most important and interesting from the view-point of the liquid structure of water. The observed structure factors obtained by both of them are found to be not so different from each other, but their conclusions on the structure models of water are largely inconsistent. It has been reported by Narten that the calculated structure factor curve based on his "near neighbor model" is in very good agreement with his observed one. However, because several arbitrarily adjustable parameters are used in his analysis, the physical reality of the model is obscured. On the other hand, any of the structure models treated in Page and Powles' paper has not fitted the diffraction data over the whole range of Q (up to the Q value of 10 Å^{-1}) and has been disproved by them.

Thus, in order to elucidate the structure of liquid water, the authors have carried out a study by the TOF diffraction technique using the electron linear accelerator as a neutron source, which has been developed recently and has turned out to be more favorable for diffraction studies of liquids than that using a reactor as the source.[7]

Experimental

i) Apparatus and Procedures. In the TOF diffraction method the analyzing actions are performed by the TOF technique, where the time-of-flight, t[μs] is measured for neutrons of various magnitudes of wavelength λ [Å] at a fixed angle 2θ [degree].[8] The momentum transfer is $\hbar Q$ and the magnitude of Q becomes

$$Q = \frac{4\pi}{\lambda}\sin\theta = 3177\frac{L_0+L}{t}\sin\theta, \qquad (1)$$

where L_0 [m] and L [m] is the flight path of the incident and scattered neutron beam, respectively. $\hbar$ is $h/2\pi$ and h is Planck constant. The schematic diagram of the apparatus is shown in Fig. 1.

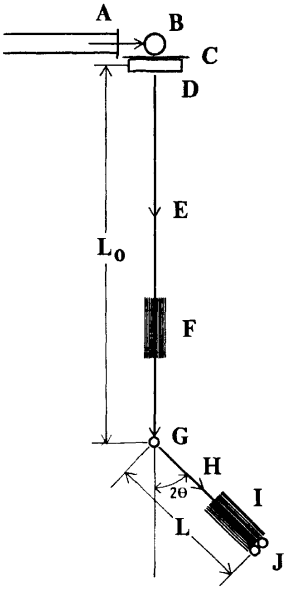

Fig. 1. Schematic diagram of the apparatus.
A: Pulsed electron beam, B: Pb target, C: Cd sheet, D: H_2O moderator assembly, E: incident neutron beam, F: Soller collimator, G: sample, H: scattered neutron beam, I: Soller collimator, and J: ^{3}He couter.

The measurement has been carried out using a pulsed neutron source which is connected to the electron linear accelerator (LINAC) at the Department of Atomic Engineering, Faculty of Engineering, Hokkaido University. In the LINAC a burst of 45 MeV (the pulse width, 3 μs and the repetition frequency of pulse, 100 pps) impinges on a water-cooled heavy metal target (lead) and pulsed photo-neutrons are produced through the (γ, n) reaction in the target. The neutrons are moderated by a water slab ($250\times250\times25$ mm^2) and become low energy neutrons in the Maxwell-Boltzmann distribution.[9] For the purpose of reducing the widening of pulse width caused by reflected neutrons a Cd sheet is inserted between the target and the water slab. The intensity and pulse width of these low energy neutrons are dependent on the shape, dimmension and arrangement of the target and the water slab, and then the neutron source system is optimized for raising up the resolution and accuracy in the present experiment.[10]

The pulsed beam of heterochromatic neutrons is scattered isotropically by the sample after passing through a flight tube set in a shielding wall and the neutrons scattered to the direction of the angle 2θ are detected by a counter. The neutron beam is collimated by two Soller collimators composed of

parallel Cd-plated sheets before and behind the sample. The slit width of the Soller collimator governs primarily the resolving power as a spectrometer, and, when the measurement is carried out at a small angle, it should be designed to be narrow enough.

The neutrons scattered by the sample are detected by a ^{3}He counter and are analyzed by a multi-channel time analyzer. Time analysis is carried out with a channel width of 20 μs and a channel number 512. The lower limit of Q in the present experiment becomes about 1 Å^{-1} at the scattered angle $2\theta=50°$ with the flight path of 7 m.

ii) Resolution. The fractional resolution $\Delta Q/Q$ is expressed as

$$\frac{\Delta Q}{Q}=\left[(\Delta\theta\cot\theta)^2+\left(\frac{\Delta t}{t}\right)^2+\left(\frac{\Delta L}{L_0+L}\right)^2\right]^{1/2}, \quad (2)$$

where $\Delta\theta$, Δt, and ΔL represent the uncertainties in θ, t, and L_0+L, respectively. $\Delta\theta$ is attributed to the widening of the beam $\Delta\theta_1$, which is determined by the slit width of the Soller collimator, as well as to the widening of the beam along the length of the detector and the sample. $\Delta\theta_1$ in the present Soller collimator becomes about 1.72° and this governs $\Delta\theta/\theta$. Δt is determined from the pulse width of the electron beam τ_p in LINAC, the mean-emission-time at the moderator τ_m and the channel width τ_c in the multi-channel time analyzer. The magnitude of τ_m is determined from theoretical and experimental considerations,[10] which becomes about 1 μs at $\lambda=0.3$ Å and increases about 25 μs at $\lambda=1.8$ Å. In the present experiment $\tau_p=3$ μs and $\tau_c=20$ μs. At small wavelength of neutrons τ_c becomes dominant in Δt. The magnitude of ΔL is calculated from the effective radius of the radiation surface of the neutron source (=15 cm) and the diameter of the detector (=2.5 cm).

Table 1. The resolving power $\Delta Q/Q$

λ[Å]	$\Delta\theta\cot\theta$	$\Delta L/(L_0+L)$	$\Delta t/t$	$\Delta Q/Q$
1.8	0.066	0.021	0.017	0.070
0.3	0.066	0.021	0.044	0.082

The resolving power $\Delta Q/Q$ is given in Table 1 for two magnitudes of wavelength. In addition to the estimation of $\Delta Q/Q$ described above the experimental determination of $\Delta Q/Q$ is also carried out, together with the calibration of Q, through the scattering experiment for polycrystalline samples such as Fe, Zr, Cu, *etc.* which have clear and known Bragg reflection peaks.

Experimental Results

Scattering measurements have been carried out at 17 °C for the sample (99.75% D_2O) which was contained in a vessel of Al foil (100 mm long, 9.0 mm in diameter; 0.017 mm wall thickness) and for a vanadium rod of the same shape and dimmension as the sample which was used as a standard and further carried out for the estimation of the contribution of background scattering. In Fig. 2 the count rate time-spectrum (the raw data of the scattering) is given, normalized in burst number of LINAC, where the spectrum for vanadium and that for background are smoothed. The magnitudes of resolution ΔQ are given as triangles along the abscissa axis. The statistical error is smaller than 1.7% in the range of $Q>2$ Å^{-1}, and becomes about 7% for $Q\approx1$ Å^{-1}. The effective range of Q in the present experiment is up to 18 Å^{-1}.

In order to determine the structure factors relevant to the molecular model of liquid, the following contributions to observed values as well as the absolute calibration should be subtracted: the multiple scattering, the absorption, the background counting and the inelastic scattering (the Placzek correction). In the present study, firstly, all data are smoothed according to the least square fitting procedure and, thereafter, the

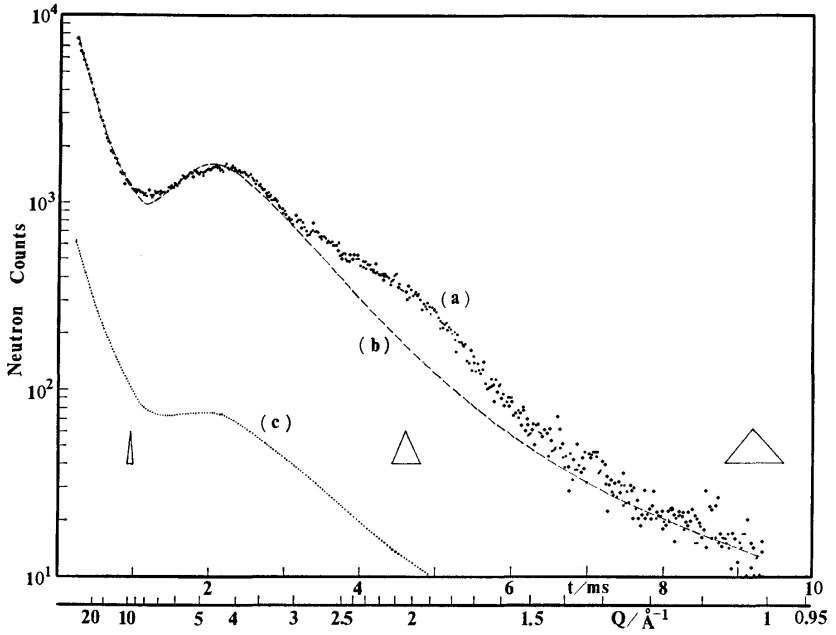

Fig. 2. Time-of-flight spectra.
(a) • : D_2O (17 °C)+background, (b) ——: vanadium rod+background, (c) ·····: background.
The magnitudes of the instrumental resolution are indicated by triangles at three points.

following corrections and reduction are made for the smoothed spectrum.

a) The multiple scattering correction: Blech and Averbach's method[11] has been used for the correction to multiple scattering. The effect of double scattering only is taken into consideration and three or more-fold scattering is ignored. We applied this correction to the scattering data of D_2O and those of vanadium rod.

b) The absorption correction: Paalman and Pings' method[12] has been applied to the absorption correction, which is used as the absorption correction in X-ray analysis for samples and vessels of cylindrical or ring shape.

c) The background correction: The background data shown in Fig. 2 has been subtracted from the scattering data for the sample and the vanadium rod after the application of the multiple scattering and absorption corrections.

d) The Placzek correction: Powles[6] proposed the method of the Placzek correction for the TOF diffraction method using the LINAC pulsed neutron source. There exist some semiempirical schemes for applying the correction, but any more rigorous numerical procedure applicable over a wide range of Q has not been discovered.[13] Then, we have applied this method in the present analysis. Page and Powles used 6.7 A.U. as the value of the effective mass M_{eff},[3] which is the mean mass of the component nuclei of a heavy water molecule. In the present analysis we have used the linearly interpolated values of M_{eff} between 2 A.U. at 20 Å^{-1} and 20 A.U. at 2 Å^{-1}. The Placzek correction rises steadily from about 2% at 2 Å^{-1} to about 8% at 10 Å^{-1}, and amounts to 16% at 18 Å^{-1}.

After the application of all corrections the calibration to the absolute cross-section scale has been carried out by comparison of the count rate time-spectrum from the sample D_2O with that from a polycrystalline vanadium rod which is usually regarded as an isotropic and incoherent scatterer. The effect of the corrections described above is seen in Fig. 3 by comparing two

Table 2. The observed absolute neutron scattering factor $S_m(Q)$ as a function of scattering vector Q [Å^{-1}] for heavy water at 17 °C

Q	$S_m(Q)$	Q	$S_m(Q)$	Q	$S_m(Q)$
1.0	0.207	4.8	0.287	11.6	0.323
1.1	0.237	5.0	0.284	11.8	0.324
1.2	0.253	5.2	0.279	12.0	0.327
1.3	0.282	5.4	0.277	12.2	0.330
1.4	0.325	5.6	0.291	12.4	0.333
1.5	0.395	5.8	0.300	12.6	0.335
1.6	0.465	6.0	0.309	12.8	0.336
1.7	0.549	6.2	0.316	13.0	0.337
1.8	0.565	6.4	0.317	13.2	0.339
1.9	0.656	6.6	0.324	13.4	0.342
2.0	0.698	6.8	0.331	13.6	0.343
2.1	0.628	7.0	0.339	13.8	0.344
2.2	0.553	7.2	0.349	14.0	0.345
2.3	0.496	7.4	0.355	14.2	0.345
2.4	0.475	7.6	0.360	14.4	0.344
2.5	0.454	7.8	0.366	14.6	0.342
2.6	0.435	8.0	0.375	14.8	0.339
2.7	0.398	8.2	0.380	15.0	0.335
2.8	0.374	8.4	0.382	15.2	0.332
2.9	0.348	8.6	0.381	15.4	0.330
3.0	0.337	8.8	0.375	15.6	0.327
3.1	0.328	9.0	0.374	15.8	0.323
3.2	0.311	9.2	0.370	16.0	0.318
3.3	0.306	9.4	0.368	16.2	0.315
3.4	0.313	9.6	0.367	16.4	0.310
3.5	0.319	9.8	0.362	16.6	0.307
3.6	0.320	10.0	0.350	16.8	0.307
3.7	0.321	10.2	0.342	17.0	0.306
3.8	0.319	10.4	0.338	17.2	0.307
3.9	0.318	10.6	0.333	17.4	0.312
4.0	0.317	10.8	0.327	17.6	0.313
4.2	0.315	11.0	0.323	17.8	0.318
4.4	0.306	11.2	0.320	18.0	0.318
4.6	0.300	11.4	0.320	18.2	0.318

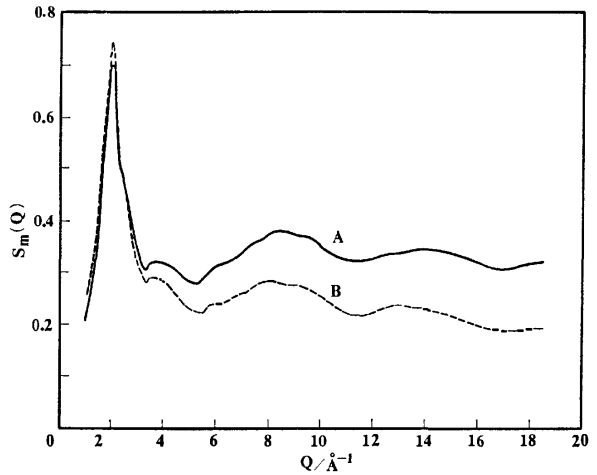

Fig. 3. The effect of the corrections for the observed structure factor $S_m(Q)$.
A: Fully corrected structure factor, B: the background correction only.

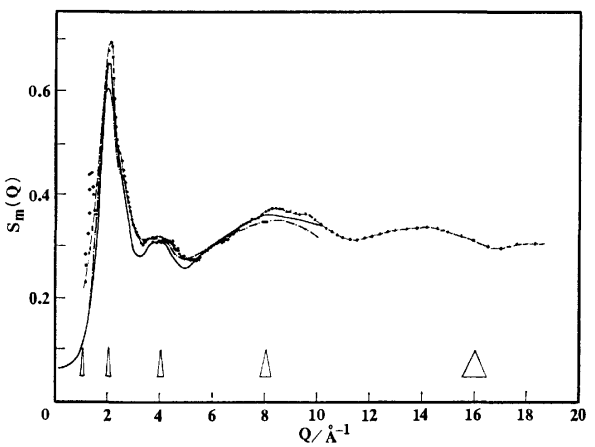

Fig. 4. The observed structure factors.
-●-: $S_m(Q)$ by the authors, (17 °C), ——: $S_m(Q)$ by Narten, (25 °C), ·····: $S_m(Q)$ by Page and Powles, (22 °C).

curves: the curve A (fully corrected structure factor) and the curve B (the background correction only). The difference between two curves shows the effect of the multiple scattering, the absorption and the Placzek correction. The absolute structure factor, $S_m(Q)$ for liquid D_2O thus determined after all corrections and calibration is tabulated in Table 2, and shown again in Fig. 4, together with the factors given by Page and Powles and by Narten for comparison.

Analysis of Neutron Diffraction Data

i) The Method of Analysis. It is well known that strong orientational correlations are present between adjacent water molecules in liquid water. Then, we will analyze the present data using a model in line with the correlated orientation model[3] with respect to the nearest neighbor configuration of molecules.

Firstly, under the assumption that the relative orientation of pairs of molecules is correlated in a way which is independent of molecular separarion,[14] the structure factor $S_m(Q)$ becomes[3]

$$S_m(Q) = f_1(Q) + f_{2C}(Q)[S_C(Q) - 1], \quad (3)$$

where $f_1(Q)$ and $S_C(Q)$ are the intramolecular contribution and the molecular-centre structure factor, respectively. $f_{2C}(Q)$ is a factor resulting from the orientational configuration between neighboring molecules.

Here we consider what we call the "revised watery model," that is, a revised model originating from the "watery model" proposed first by Page and Powles.[3] In the model the relative orientation of adjacent molecules is shown in Fig. 5. The water molecules constituting the tetrahedral pentamer (Fig. 5) are classified into three groups according to the manner of hydrogen-bonding: 1) a central molecule in which two OD bonds are hydrogen-bonded (Fig. 5(c)), 2) two molecules in which one OD bond is hydrogen-bonded (Fig. 5(a)), and 3) two molecules in which two OD bonds are free (Fig. 5(b)). The non-hydrogen-bonded bond length r_{OD} is 0.96 Å (the length of the bond in the vapor molecule) and the hydrogen-bonded bond length r_{OD} 1.01 Å (the length of the bond in heavy ice I). The separation r_{OO} for hydrogen bond O-D···O is taken to be 2.82 Å.[15]

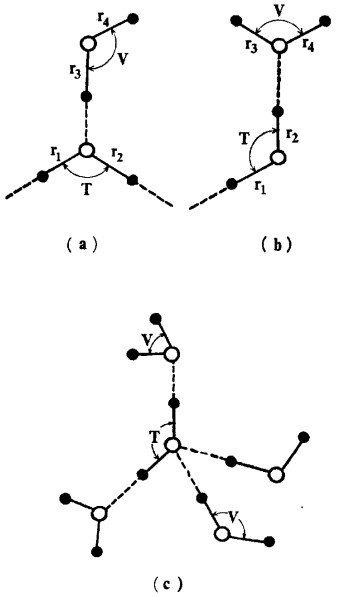

Fig. 5. The structure of the "revised watery model."
●: Deuteron nucleus, ○: oxygen nucleus.
Two types of hydrogen-bonded pairs between the central molecule and the peripheral one in the tetrahetral star-pentamer, (a): r_1, r_2, and r_3=1.01 Å, r_4=0.96 Å, (b): r_1 and r_2=1.01 Å, r_3 and r_4=0.96 Å. (c): the configuration of the tetrahedral coordination.
The four hydrogen-bonded molecules are rotating freely about each O-D···O axis. V=104.5°, T=109.5°.

The structure factor for heavy water is calculated by means of Eq. 3. The intramolecular contribution, $f_1(Q)$, consists of three varieties of factors (Fig. 5) for 1)—3) described above, and the intermolecular contribution is $f_{2C}(Q)[S_C(Q)-1]$, where the factor, $f_{2C}(Q)$, is the sum of two terms as the following equation:

$$f_{2C}(Q) = \frac{1}{2}[f^{a}_{2CW}(Q) + f^{b}_{2CW}(Q)]. \quad (4)$$

$f^{a}_{2CW}(Q)$ and $f^{b}_{2CW}(Q)$ are the structure factor for the configurations (a) and (b) in Fig. 5, respectively. These two are expressed as

$$f^{a}_{2CW}(Q) = [b_O^2 + b_O b_D\{3j_0(Qr^{i}_{OD}) \exp(-\gamma^{i}_{OD}Q^2) + j_0(Qr^{v}_{OD}) \exp(-\gamma^{v}_{OD}Q^2)\} + 2b_D^2\{j_0(Qr_s) \exp(-\gamma_s Q^2) + L(Q)\}]/(b_O + 2b_D)^2, \quad (5)$$

and

$$f^{b}_{2CW}(Q) = [b_O^2 + 2b_O b_D\{j_0(Qr^{i}_{OD}) \exp(-\gamma^{i}_{OD}Q^2) + j_0(Qr^{v}_{OD}) \exp(-\gamma^{v}_{OD}Q^2)\} + 2b_D^2\{j_0(Qr_p) \exp(-\gamma_{r,p}Q^2) + M(Q)\}]/(b_0 + 2b_D)^2, \quad (6)$$

where

$$j_0(Qr) = \frac{\sin Qr}{Qr}, \quad (7)$$

$$L(Q) = \frac{1}{\pi}\int_0^{\pi} j_0[Qh_L(\xi)] \exp(-\gamma_{h,L}Q^2)d\xi, \quad (8)$$

$$M(Q) = \frac{1}{\pi}\int_0^{\pi} j_0[Qh_M(\xi)] \exp(-\gamma_{h,M}Q^2)d\xi, \quad (9)$$

$$h_L(\xi) = \left[r^{i}_{OD}{}^2 + r^{v}_{OD}{}^2 + \frac{2}{3}r^{i}_{OD}r^{v}_{OD}\{\cos(\pi - V) - 2\sqrt{2}\cos\xi \sin(\pi - V)\}\right]^{1/2}, \quad (10)$$

$$h_M(\xi) = \left[r^{i}_{OD}{}^2 + r^{v}_{OD}{}^2 + \frac{2}{3}r^{i}_{OD}r^{v}_{OD}\left\{\cos\left(\frac{V}{2}\right) - 2\sqrt{2}\cos\xi \sin\left(\frac{V}{2}\right)\right\}\right]^{1/2}, \quad (11)$$

$$r_p = 2\left[r^{v}_{OD}{}^2 + \left(\frac{p}{2}\right)^2 - r^{v}_{OD}p\cos\delta\right]^{1/2}, \quad (12)$$

$$\delta = \cos^{-1}[(r^{v}_{OD}{}^2 + p^2 - r^{i}_{OD}{}^2)/2r^{v}_{OD}p], \quad (13)$$

$$p = [r^{i}_{OD}{}^2 + r^{v}_{OD}{}^2 - 2r^{i}_{OD}r^{v}_{OD}\cos T]^{1/2}, \quad (14)$$

and

$$r_s = 2r^{i}_{OD}\cos\left(\frac{T}{2}\right). \quad (15)$$

$b_0=0.577\times10^{-12}$ cm and $b_D=0.67\times10^{-12}$ cm are the coherent scattering length for oxygen and deuteron, respectively. The intramolecular oxygen-to-deuteron distance r_{OD}^{l} is the length of the O—D bond in heavy ice I and r_{OD}^{v} that in the vapor. $2\gamma_{OD}^{l}$, $2\gamma_{OD}^{v}$, $2\gamma_{h,L}$, $2\gamma_{h,M}$, $2\gamma_S$, and $2\gamma_{r,P}$ are the mean-square variation to the distance r_{OD}^{l}, r_{OD}^{v}, $h_L(\xi)$, $h_M(\xi)$, r_S, and r_P, respectively, and their magnitudes are known from various sources.[16,17] The variation is assumed to be proportional to the corresponding bond length,[18] being taken to be 0.06 Å per 1 Å for bond length. $V=104.5°$ is the DOD angle for the molecule in the vapor and T the tetrahedral angle. ξ is the average rotational angle in relation to the average of the intermolecular distance r_{DD}.[19] The molecular-centre structure factor, $S_C(Q)$, is obtained from X-ray scattering data.[16]

ii) Results and Comparison with Previous Works. The structure factor $S_m(Q)$ for the "revised watery model," which has been calculated using Eqs. 3—15 is given in Fig. 6 and compared with the experimental $S_m(Q)$ (Table 2, Fig. 4). The comparison with the calculated $S_m(Q)$ for other models is shown in Fig. 7; the "uncorrelated orientation model" and the "watery model" (Page and Powles).[3] The agreement between calculated and experimental $S_m(Q)$ is not satisfactory as seen in Fig. 6 but slightly improved in comparison with other models as seen in Fig. 7.

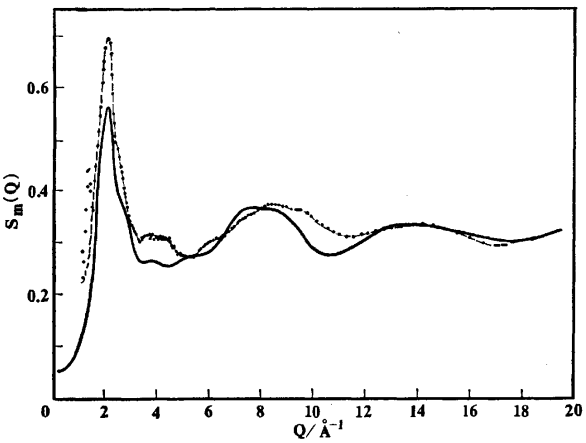

Fig. 6. The comparison between the calculated $S_m(Q)$ values for the "revised watery model" and the observed ones.
——: The calculated $S_m(Q)$ for the "revised watery model," -●-: the observed $S_m(Q)$.

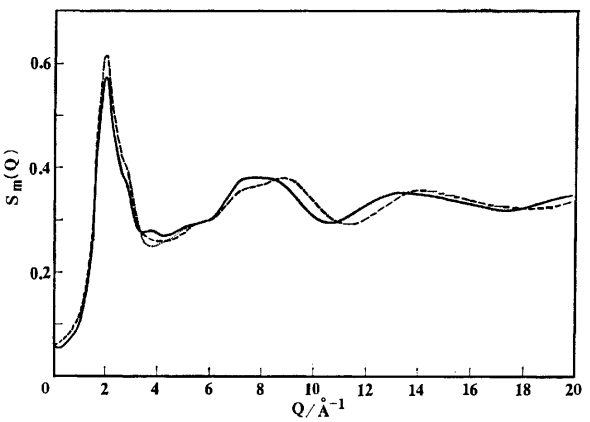

Fig. 7. The comparison between the calculated curve of $S_m(Q)$ for the "revised watery model" and the curves for other models.
——: $S_m(Q)$ for the "revised watery model," ——: $S_m(Q)$ for the "watery model," ……: $S_m(Q)$ for the "uncorrelated orientation model."

Three experimental curves, which have been given by Page and Powles, by Narten and by the authors, are compared in Fig. 4. The main features of the curves consist of the largest peak at 2 Å^{-1}, a bump about 4 Å^{-1} and a broad peak ranging over 7—10 Å^{-1}, including a rather smaller but clear shoulder at 2.8 Å^{-1}. The absolute magnitude of these peaks may be regarded as being possessed of some uncertainties, taking into consideration the fact that a certain arbitrariness is present in the application of various kinds of corrections, for example, the assignment of M_{eff} in the Placzek correction *etc.* However, the position of the peaks and shoulder is unchanged at all before and after applying the corrections, as clearly seen in Fig. 3. In analyzing the data we must take into consideration these facts. From Figs. 3, 4, 6, and 7, it can be said that the behavior of curves near 4 Å^{-1} is important in judging the adequacy of the model proposed, which has been noted by Page and Powles.[3] Our model as well as others given in Fig. 7 is not successful in this respect, though our curve is somewhat improved.

The disagreement of the first peak which is seen in Fig. 6 is attributed to the ignorance of some long range order with the period of about 3 Å, probably. This may be ascribed to the presence of unbonded water molecules which is practically ignored in the present model as well as in Page and Powles' models (except the "uncorrelated orientation model") and Narten's model, considering the fact that the first peak is the highest in the "uncorrelated orientation model" (Page and Powles). In order to improve that we must use a mixture model,[20] which is impossible without introducing some adjustable parameters in the analysis.

Narten calculated $S_m(Q)$ according to his near-neighbor model,[4,21] where one oxygen atom as an

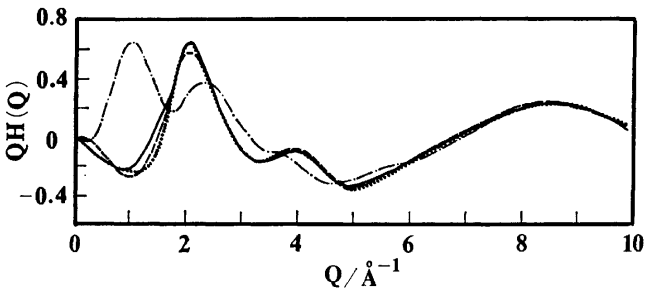

Fig. 8. The weighted structure function $QH(Q)$ calculated for Narten's model.
……: The observed curve by Narten, ——: the calculated curve by Narten, ——: the calculated curve by the authors for all $r_{o\alpha\beta}=3$ Å, -·-·-: the calculated curve by the authors for all $r_{o\alpha\beta}=5$ Å.
$H(Q)=S_m(Q)-\sum_{n=1}^{3}b_n^2/(\sum_{n=1}^{3}b_n)^2$, ($H(Q)$ is Eq. 10 in Ref. 4).

origin is surrounded by four other oxygens at the corners of a regular tetrahedron like Fig. 5 (c) and the region beyond the discrete structure is regarded as a uniform distribution of atoms, and obtained a very good fit with his experimental curve as shown in Fig. 8 which has been reprinted from his paper.[4] In order to investigate the nature of Narten's model, we have attempted to reproduce the calculation of $S_m(Q)$ according to the same procedures as described in that text, using quite identical values for molecular parameters except those for $r_{c\alpha\beta}$.[22] We have obtained the best curve for the assignment that all $r_{c\alpha\beta} \equiv 3$ Å $= r_c$, which are the separation between the nucleus α in the central molecule and the nucleus β in the continuum region. The magnitude of $r_{c\alpha\beta} \approx 3$ Å is clearly too small. It should be larger than 4.5 Å, considering the size of the discrete structure. When the larger values than 3 Å are assigned to any of $r_{c\alpha\beta}$, the shape and features of the $QH(Q)$ *vs.* Q curve are found to vary and the good fit is quite missed. Then, it is concluded for Narten's model that the assignment of implausibly small values to the parameter $r_{c\alpha\beta}$ is needed for obtaining the fit to the experimental data, and, otherwise it is not attained. Thus, the success reported in his paper[4] has turned out to be only apparent.

The authors are grateful to Associate Professor Takaaki Matsumoto and Mr. Masanobu Senda of Faculty of Engineering, Hokkaido University for their kindful cooperation in carrying out the experiment.

References

1) B. N. Brockhouse, *Nuovo Cimento Suppl.*, **9**, 45 (1958).
2) T. Springer, C. Hofmeyer, S. Kornblicher, and H. D. Lemmel, *Proc. Intern. Conf. on Peaceful Uses of Atomic Energy*, 3rd, Geneva (1964), Vol. 2, p. 351.
3) D. I. Page and J. G. Powles, *Mol. Phys.*, **21**, 901 (1971).
4) A. H. Narten, *J. Chem. Phys.*, **56**, 5681 (1972).
5) G. Walford, J. H. Clarke and J. C. Dore, *Mol. Phys.*, **33**, 25 (1977).
6) J. G. Powles, *Mol. Phys.*, **26**, 1325 (1973).
7) Y. Ishikawa and N. Watanabe, *Butsuri*, **28**, 461 (1973).
8) R. N. Sinclair, D. A. G. Johnson, J. C. Dore, J. H. Clarke and A. C. Wright, *Nucl. Instr. and Meth.*, **117**, 445 (1974).
9) K. Inoue, N. Ohtomo, H. Iwasa, and Y. Kiyanagi, *J. Nucl. Sci. Technol.*, **11**, 228 (1974).
10) N. Ohtomo and K. Inoue, *Bull. Fac. Eng. Hokkaido Univ.*, **73**, 105 (1974); *J. Nucl. Sci. Technol.*, **12**, 384 (1975); K. Inoue and N. Ohtomo, *J. Nucl. Sci. Technol.*, **13**, 389 (1976).
11) I. A. Blech and B. L. Averbach, *Phys. Rev.*, **137**, A1113 (1965).
12) H. H. Paalman and C. J. Pings, *J. Appl. Phys.*, **33**, 2635 (1962).
13) A. K. Soper, G. W. Neilson, J. E. Enderby, and R. A. Howe, *J. Phys. C: Solid State Phys.*, **10**, 1793 (1977).
14) J. G. Powles, *Adv. in Phys.*, **22**, 1 (1973).
15) K. Arakawa, K. Tokiwano, and K. Kojima, *Bull. Chem. Soc. Jpn.*, **50**, 65 (1977).
16) A. H. Narten and H. A. Levy, *J. Chem. Phys.*, **55**, 2263 (1971).
17) W. S. Benedict, N. Gailar and E. K. Plyler, *J. Chem. Phys.*, **24**, 1139 (1956); S. Shibata and L. S. Bartell, *J. Chem. Phys.*, **42**, 1147 (1965); W. C. Ermler and C. W. Kern, *J. Chem. Phys.*, **55**, 4851 (1971).
18) A. H. Narten, M. D. Danford, and H. A. Levy, *Discuss. Faraday Soc.*, **43**, 97 (1967).
19) In the paper of Page and Powles, this average angle ξ is represented by the notation ν defined in Eqs. 12 and 13 in Ref. 3.
20) K. Arakawa, *Kagaku Sosetsu*, No. 11, 35 (1976).
21) A. H. Narten, M. D. Danford, and H. A. Levy, *J. Chem. Phys.*, **46**, 4875 (1967); A. H. Narten and H. A. Levy, *Science*, **165**, 447 (1969).
22) The OD and DD distances and their rms variations $(2\gamma)^{1/2}$ are taken to be
$r_{OD} = 0.934$ Å, $(2\gamma_{OD})^{1/2} = 0.138$ Å,
$r_{DD} = 1.53$ Å, $(2\gamma_{DD})^{1/2} = 0.24$ Å,
according to Ref. 4.

Light Scattering Study of Local Structures in Solutions. Structure-Forming Effect of Non-Associative Solvent on Ethanol Aggregate

Tsunetake FUJIYAMA and Masami TANAKA

Department of Chemistry, Faculty of Science, Tokyo Metropolitan University, Setagaya-ku, Tokyo 158

(Received, October 31, 1977)

Light scattering spectra were observed for binary mixtures of ethanol and carbon tetrachloride, and of ethanol and cyclohexane at various concentrations. The Rayleigh intensities were reduced to concentration fluctuation values. From the observed concentration fluctuation values, the mean association numbers of ethanol at each concentration were calculated. The results were compared with that observed in ethanol–chloroform system, where associative interaction between ethanol and chloroform molecules is expected. The concentration dependencies of the mean association numbers suggested that these non-associative solvent molecules (carbon tetrachloride and cyclohexane) promote the formation of large local structure in ethanol solution.

Local fluctuation of concentration is considered to afford information which is useful to understand the mixing of liquid from a molecular viewpoint. Based upon this belief, we have planned a series of studies on analysis of temperature and concentration dependencies of concentration fluctuation through observation of light scattering spectra.[1]

First the relationship between concentration fluctuation and Rayleigh intensities has been theoretically established.[2] Then, a theory has been proposed for determining local structures existing in associated solutions from the observed concentration fluctuation in various concentrations and at various temperatures,[3,4] and the method has been applied successfully for the studies of local structures in a few kinds of binary solutions.[3–6]

In the study of the local structures which are formed in ethanol–chloroform solution, it has been emphasized that the associative interaction between chloroform and ethanol molecules arrests the growth of the local structure of ethanol and keeps the mean association number of ethanol molecules constant for all the ethanol concentrations. It is of much interest, therefore, to see the effect of non-associative solvents like cyclohexane, in place of associative solvents like chloroform, on the local structure formation of ethanol. In the present report, we will discuss the formation of local structures in ethanol–cyclohexane and ethanol–carbon tetrachloride solutions on the basis of the quantitative analysis of the concentration fluctuation measured by the light scattering spectra.

Experimental

The samples used in the present study were commercially available reagents. Ethanol was purified by distillation after elimination of water by zeolite A-3. Carbon tetrachloride and cyclohexane were purified by distillation. The binary solutions of ethanol–carbon tetrachloride and ethanol–cyclohexane were made dust-free by the use of a millipore filter FG of 0.2 μm pore size. Mole fraction of sample solutions was determined from the weight and density of each component. The refractive indices of the samples were measured by means of a Shimadzu-Bausch Lomb Abbe refractometer 3L. Density data were found in the literature.[7] The composition derivative of the refractive index at the mole fraction, x, was estimated from the refractive indices measured at $x\pm0.05$. The temperature derivative of the refractive index at the temperature, T, was estimated from the refractive indices measured at $T\pm10$ °C.

Light scattering spectra were recorded by using a spectrometer which is composed of a He–Ne gas laser source (NEC, GLG 108, 60 mW) and a pressure scanning Fabry-Perot interferometer. The spacer between the interferometer ethalon has a thickness of 6 mm, giving a free spectral range of 0.82 cm^{-1} and over-all instrumental half-width of about 0.042 cm^{-1}. Details of the spectrometer and the sampling technique have been reported elsewhere along with the reliability of the observed spectral parameters.[1,2]

The temperature of the sample solutions was controlled by a high temperature cell which was made by the authors. A temperature constancy of ±1 °C was obtained with the use of the apparatus.

Results and Discussion

Light Scattering Spectra and Concentration Fluctuation. Figure 1 shows the light scattering spectra for the ethanol–carbon tetrachloride and ethanol–cyclohexane systems. It is seen from these figures that the Rayleigh intensity increases in magnitude on passing from pure liquids to binary solutions. After separating the Rayleigh part from the observed spectra, a Rayleigh intensity was expressed relative to a Rayleigh intensity of pure ethanol. Then the concentration fluctuation,

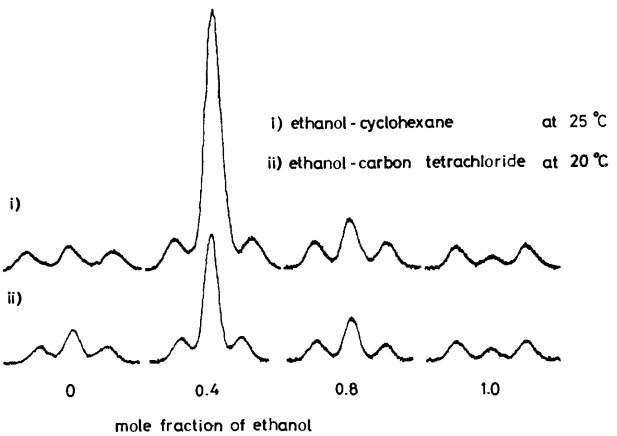

Fig. 1. Observed light scattering spectra for i) ethanol–carbon tetrachloride and ii) ethanol–cyclohexane systems. The concentration is expressed in terms of the mole fraction of ethanol.

$N\langle(\Delta x)^2\rangle$, was calculated from the relation,[2]

$$N\langle(\Delta x)^2\rangle = \frac{N_A\rho}{M}\left(\frac{\lambda_i^4}{\pi^2}\right)\frac{1}{4n^2\left(\frac{\partial n}{\partial x}\right)^2_{T,P}}\{(R_{90})_R-(R_{90})_S\}, \quad (1)$$

where N is the total number of molecules included in the field within which the concentration fluctuation is considered, N_A the Avogadro number, M the mean molecular weight, n the refractive index, ρ the density, λ_i the wavelength of the incident light, x the mole fraction of ethanol, and $(R_{90})_R$ the Rayleigh ratio for a Rayleigh line. $(R_{90})_S$ is the Rayleigh ratio for entropy fluctuation and is expressed by the relation

$$(R_{90})_S = (\pi^2/\lambda_i^4)\frac{4kn^2T^2}{C_{pg}\rho}\left(\frac{\partial n}{\partial T}\right)^2_{P,x}, \quad (2)$$

where k is the Boltzmann constant, T the absolute temperature, and C_{pg} the isobar heat capacity per gram. The C_{pg} values were found in the literature[8] only for the pure liquids studied in this work. The C_{pg} values for the binary solutions were estimated from the C_{pg} values of the pure component liquids by assuming the relation

$$C_{pg} = x_1C^1_{pg} + x_2C^2_{pg}, \quad (3)$$

where C_{pg} and x_i are the isobar heat capacity and the mole fraction of the i-th component, respectively. The error expected to the C_{pg} values thus obtained was estimated to be about a few percent by considering the C_{pg} values observed for the binary solution of ethanol and methylcyclohexane.[9] As $(R_{90})_R$ is much larger than $(R_{90})_S$ in the present binary mixture, the over-all errors which should be attached to the concentration fluctuation values are mainly determined by the uncertainties expected for the observed composition derivatives fo refractive indices (see Eq. 1).

In Figs. 2 and 3, the concentration fluctuations thus obtained are plotted against the mole fraction, x, of ethanol for ethanol–carbon tetrachloride and for ethanol–cyclohexane systems, respectively. The dashed lines in these figures correspond to the concentration fluctuation expected for an ideal binary solution. The over-all errors which should be attached to the concentration fluctuations are indicated by the vertical lines. It is seen from these figures that the observed concentration fluctuations are generally larger than that of an ideal binary solution. The concentration fluctuation takes a maximum value at $x=0.5$ for an ideal binary solution, while the observed concentration fluctuation takes maximum values at the mole fraction smaller than 0.5 for both carbon tetrachloride and cyclohexane solutions. In ethanol–carbon tetrachloride solution, the concentration fluctuation assumes much larger value for all x than that of an ideal binary solution, and takes maximum value at $x=0.3$ at 20 °C.

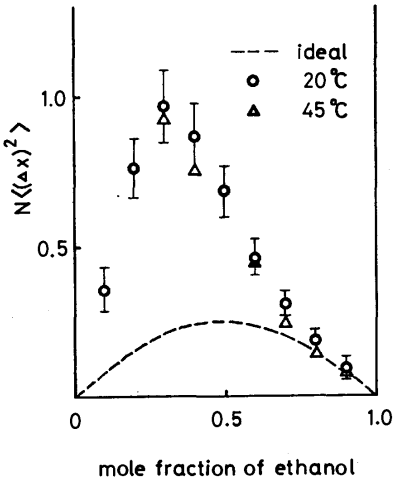

Fig. 2. Observed concentration fluctuation for ethanol–carbon tetrachloride system at the temperatures of 20 and 45 °C. Errors are indicated by the horizontal lines.

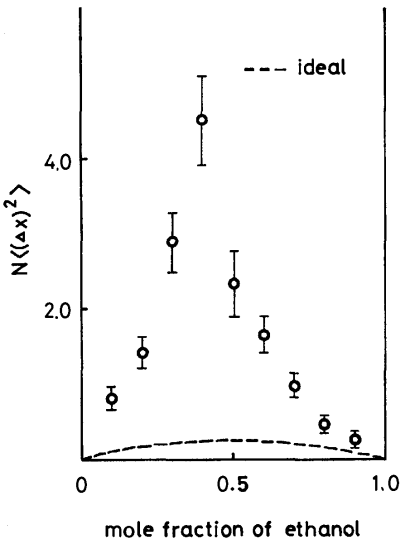

Fig. 3. Observed concentration fluctuation for ethanol–cyclohexane system at the temperature of 25 °C. Errors are indicated by the horizontal lines.

These specific concentration dependencis of the concentration fluctuation may arise from intermolecular interactions between component molecules. Taking into account the possible intermolecular interactions such as hydrogen bonding formation, we tried to estimate possible local structures expected in these ethanol solutions through theoretical consideration of the observed concentration dependencies of the concentration fluctuation.

Determination of Mean Association Number of Ethanol. In our previous reports[4,5] we have presented the associated complex model which can explain the relation between the associated complex formation and the concentration fluctuation in solutions. The associated complex formation in binary solutions would be classified into three cases: 1) the case where association between the same species occurs, 2) the case where association between different species occurs, and 3) the case where association between the same species and between different species occur simultaneously.

It has been shown that, the case 1), the concentration fluctuation takes a larger values than that of an ideal binary solution thoughout the whole concentration (see the systems "A and B_l" and "A_l and B_l" of the previous, report[4]). In the case 2), the concentration fluctuation

takes a smaller value than that of an ideal binary solution throughout the whole concentration (see the system "A and AB" or "B and AB" of the previous report[4]). In the case 3), on the other hand, the concentration fluctuation takes both larger and smaller values than that of an ideal binary solution (see the results for ethanol–chloroform system of the previous report[5]).

As the observed concentration fluctuations of Figs. 2 and 3 are always much larger than that of an ideal binary solution, the states of mixing of the solutions in question must belong to the case 1). In ethanol–carbon tetrachloride and ethanol–cyclohexane systems, it is hardly possible to imagine the associated complex formation between carbon tetrachloride molecules or between cyclohexane molecules. Therefore, we assume that l numbers of ethanol molecules associate with each other, and the resultant associated complex behaves as an independent molecule in these solutions. Then, the relation between the concentration fluctuation, $\langle(\Delta x)^2\rangle$, and the mean association number, l, of ethanol molecule is formulated to be[3,4]

$$N\langle(\Delta x)^2\rangle = x(1-x)\{x+l(1-x)\},$$

or

$$l = \frac{N\langle(\Delta x)^2\rangle - x^2(1-x)}{x(1-x)^2}, \qquad (4)$$

where x is the mole fraction of ethanol. Thus, the mean association number of ethanol can be obtained from Eq. 4 and the observed concentration fluctuation value at each concentration. The mean association numbers thus obtained for ethanol–carbon tetrachloride and ethanol–cyclohexane systems are plotted against the mole fraction of ethanol, respectively, in Figs. 4 and 5.

Local Structures in Ethanol Solutions. It is seen from Figs. 4 and 5 that the mean association number of ethanol molecules changes its magnitude with the change of the concentration. In the case of ethanol–carbon tetrachloride solution at 20 °C, the observed mean association number increases up to about 7 with the increase of ethanol mole fraction up to 0.3 and, then, gradually decreases with the successive increase in ethanol concentration. Almost the same concentration dependence can be seen in Fig. 5 for ethanol–cyclohexane solution. In this case, the maximum mean

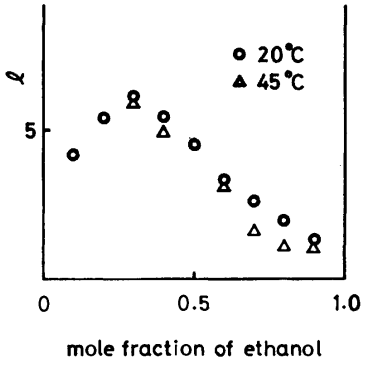

Fig. 4. Concentration dependence of mean association numbers of ethanol molecules observed in ethanol–carbon tetrachloride system.

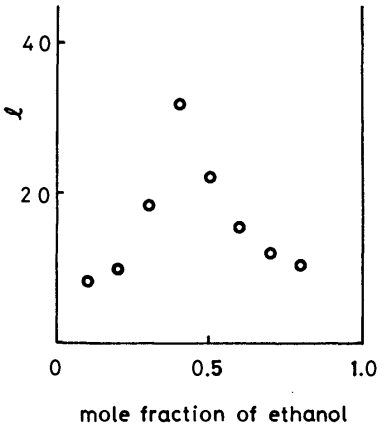

Fig. 5. Concentration dependence of mean association numbers of ethanol molecules observed in ethanol–cyclohexane system.

association number of ethanol is about 32 at 25 °C and is much larger than that observed in carbon tetrachloride solution. These results are in good contrast with the results obtained for ethanol–chloroform solution, namely, the mean association number of ethanol is about 3 for all the ethanol concentrations.[5]

It has been emphasized in the previous reports on the ethanol–chloroform system that the associative interaction between chloroform and ethanol molecules arrests the growth of the local structure of ethanol by truncating the successive growth of hydrogen bonding between ethanol molecules. The remarkable increase of the mean association number observed in the present systems is apparently consistent with this viewpoint, because the interaction between ethanol and cyclohexane or between ethanol and carbon tetrachloride is very weak in comparison with that between ethanol and chloroform molecules. However, the mean association number takes a maximum value in both cyclohexane and carbon tetrachloride solutions. At ceartain ethanol concentration the mean association number began to increase with the increase of ethanol concentration. It may be considered, therefore, that these non-associative solvent molecules promote the formation of larger local structure of ethanol molecules by surrounding and isolating the individual aggregate of ethanol molecules. Then, the decrease of the mean association number of ethanol molecules in the high ethanol concentration range can be understood reasonably, if we remind the fact that the mean association number in pure liquid ethanol is about 3—4.[10,11] As the mole fraction of ethanol increases, the number of carbon tetrachloride or cyclohexane molecules surrounding the ethanol aggregate becomes too small, and consequently neighbouring aggregates merge into more extensive aggregates, which assumes the character of pure liquid ethanol. As the mean association number of ethanol in pure liquid is about 3—4, the above situation is reflected upon the gradual decrease of the mean association number of ethanol from the maximum value down to 3—4, or the gradual breakdown of the local structure of ethanol in these solutions.

The difference between the maximum mean associa-

tion numbers observed in the ethanol–carbon tetrachloride and ethanol–cyclohexane solutions suggests the existence of very weak, but considerable degree of associative interaction between ethanol and carbon tetrachloride molecules in the binary solution of ethanol and carbon tetrachloride.

Concluding Discussion. From the discussion of the preceding paragraphs, the effects of the solvent molecules on a mean association number of ethanol may be summarized as the followings.

1) In the mixture of ethanol and the solvent which is associative with ethanol, the mean association number of ethanol does not exceed 3—4. The associative solvent molecule arrests the formation of large local structure of ethanol by truncating the seccessive hydrogen bond formation. In this sense, the associative solvent like chloroform has structure-breaking property.

2) The mean association number of ethanol increases remarkably in the mixture of ethanol and the solvent which is non-associative with ethanol. In this sense, the non-associative solvents like cyclohexane and carbon tetrachloride have structure-forming property.

The decrease of the mean association number with the increase of ethanol concentration in the ethanol-rich solution can be explained by the decrease of the structure-forming property of the non-associative solvent molecules with the decrease of the concentration of the non-associative solvent.

References

1) K. Iwasaki, M. Tanaka, and T. Fujiyama, *Bunko Kenkyu*, **25**, 134 (1976).
2) K. Iwasaki, M. Tanaka, and T. Fujiyama, *Bull. Chem. Soc. Jpn.*, **49**, 2719 (1976).
3) T. Kato and T. Fujiyama, *J. Phys. Chem.*, **80**, 2771 (1976).
4) K. Iwasaki, Y. Katayanagi, and T. Fujiyama, *Bull. Chem. Soc. Jpn.*, **49**, 2988 (1976).
5) T. Kato and T. Fujiyama, *J. Phys. Chem.*, **81**, 1560 (1977).
6) K. Iwasaki and T. Fujiyama, *J. Phys. Chem.*, **81**, 1908 (1977).
7) J. A. Barker, I. Brown, and F. Smith, *Discuss. Faraday Soc.*, **15**, 142 (1953); G. Scatchard and F. G. Satkiewicz, *J. Am. Chem. Soc.*, **86**, 130 (1964).
8) "International Critical Tables," McGraw-Hill, New York (1926). T. Nakamura, Y. Murakami, and R. Fujishiro, *Nippon Kagaku Kaishi*, **1976**, 1034.
9) S. C. P. Hwa and W. T. Ziegler, *J. Phys. Chem.*, **70**, 2572 (1966).
10) A. N. Fletcher, *J. Phys. Chem.*, **76**, 2562 (1972).
11) E. E. Tucker, S. B. Farnham, and S. D. Christian, *J. Phys. Chem.*, **73**, 3820 (1969).

The Application of a Quadrupole Mass Spectrometer to a Study of Methane Oxidation in Shock Waves

Yoshiaki HIDAKA, Midori NAGAYAMA, and Masao SUGA

Department of Chemistry, Faculty of Science, Ehime University, Bunkyo-cho, Matsuyama 790

(Received November 4, 1977)

A part of the mass-spectrometer shock-tube apparatus was improved, and its working characteristics were examined. The oxidation of methane was studied with this apparatus over the temperature range of 1800—2500 K and the total pressure range of 360—560 Torr at O_2/CH_4 ratios of 1—3. The induction period was measured by monitoring the oxygen concentration, and the following equation was found to hold:

$$\tau = 4.54 \times 10^{-10}[CH_4]^{0.37}[O_2]^{-0.64} \exp(35600/RT)\ \text{s}$$

in which the concentrations were expressed in mol per cubic centimeter.

We have previously tried to apply a quadrupole mass spectrometer to fast reactions in shock waves, and have reported the devices and characteristics of the ion source.[1] This mass-spectrometer shock-tube apparatus has since been used for the study of the decomposition of N_2O and C_2H_4.[2] However, this apparatus still has two problems. One was that the rise time of the signal on the oscillogram is suddenly prolonged by the contamination of the ion-repeller electrode. The other is the overlapping of an abnormal signal with the monitored signal of the reactant or product; this abnormal signal does not come from any of the reactants or products.[2]

The methane oxidation in a shock wave has been studied in detail by many investigators.[3-16] There is a tendency for the measured apparent activation energies to depend on the total experimental pressures, as has been mentioned by Cooke *et al.*[15] Therefore, it can be seen that the apparent activation energies previously reported may be classified roughly into two groups: about 33 kcal mol^{-1} (below 1 atm) and 50 kcal mol^{-1} (above 2 atm). The studies under low-pressure conditions (below 1 atm) are few in number than those at high pressures. It also has not become sufficiently apparent whether or not the apparent activation energy at low pressures is lower than that at high pressures.

In the present paper, we wish to report on the improvement of the apparatus and its working characteristics. Another purpose of this paper is to confirm the apparent activation energy in the oxidation of methane at relatively low pressures (below 560 Torr).

Experimental

Apparatus. The scheme of the shock tube which connects with the quadrupole mass spectrometer is given in Fig. 1. The details of the shock tube have already been described.[1,2] In the present experiment, barium titanate gauges of G_2 and G_3 were used instead of platinum resistance gauges. The barium titanate gauge G_3 was mounted flush with the inside surface of the end wall of the shock tube. A pinhole leak 20 μm in diameter was at the center of a small disk 10 mm in diameter and 1 mm thick, which was mounted flush with the inside surface of the end plate of the shock tube.

In the previous experiments, the quadrupole mass spectrometer and the shock tube were placed at right angles to one another so that the beam of gas molecules emerging from the pinhole leak entered into the ion source at right angles with the quadrupole Rod (L-type).[1] In the present experiment, though, the quadrupole mass spectrometer and shock tube

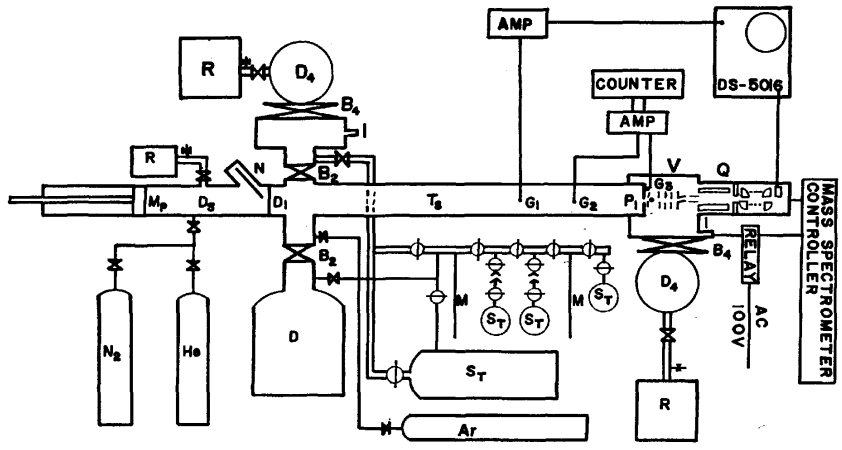

Fig. 1. Schematic diagram of the apparatus.
M_p: Movable piston, D_s: driver section, N: needle, D_i: diaphragm, D: dumping tank, B_2: 2-inch butterfly valve, I: ionization gauge, B_4: 4-inch butterfly valve, D_4: 4-inch diffusion pump, R: rotaty pump, S_T: storage tank, M: manometer, T_s: test section, G_1, G_2, G_3: barium titanate pressure gauge, P_1: pinhole leak of 20 μm in diameter, V: vacuum chamber, Q: quadrupole mass spectrometer,

were placed at an angle of 180° to one another so that the beam of gas molecules might enter straightforwardly into the ion source from the opposite direction of the quadrupole Rod (I-type). A 4-inch oil diffusion pump with a liquid nitrogen trap was connected to the vacuum chamber, and the diffusion pump and the vacuum chamber were separated by a 4-inch butterfly valve.

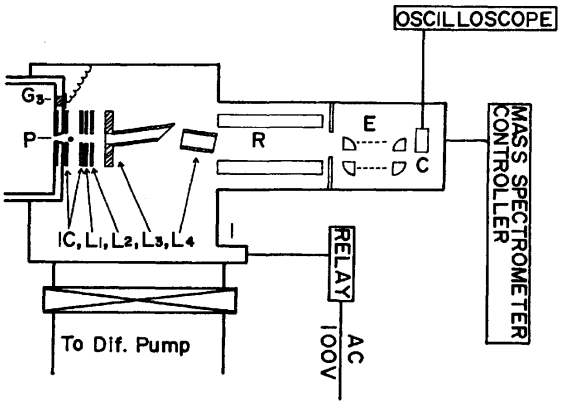

Fig. 2. Schematic diagram of the ion source, the vacuum chamber and the end section of the shock tube.
G_3: Barium titanate pressure gauge, P: pinhole leak of 20 μm, IC: ionization chamber, L_1, L_2, L_3, and L_4: ion lens electrodes, R: Rod, E: secondary electron multiplier, C: ion collector, I: ionization gauge.

A scheme of the ion source and the end section of the shock tube is shown in Fig. 2. The ion source consisted of the following parts: an ionization chamber (IC), an electron repeller (ER), a filament (F), an electron target (T), and focusing lenses (L_1, L_2, L_3, and L_4). Most of the metal parts were made of stainless steel. The tungsten filament, which was 0.2 mm in diameter, was wound in a six-turn helix. The L_1 and L_2 lens electrodes were 4 mm in inner diameter and 0.5 mm long. The ion-lens electrodes of L_3 and L_4 were constructed of pipes 4 mm and 6 mm in inner diameter, and 40 mm and 30 mm in length, respectively. They were placed at an angle of 10° to the axis of the shock tube, and also the exit of the L_3 lens was cut at an angle of 30°, as is shown in Fig. 2. The electron inlet slit (1.5 mm in diameter) was devised so as to set the edge of the leak side of the ionization chamber as near as possible. Consequently, the distance between the pinhole and the electron-inlet slit was shortened to about 4 mm. The voltage supplied to each electrode of the ion source could be changed as follows:

V_{ER}: +30—−150 V, V_{IC}: +150—+20 V,

V_T: +150—+30 V, V_{L_1}, V_{L_2}, V_{L_3}: +150—−110 V,

V_{L_4}: +150—0 V.

Sample gases behind reflected shock waves were directly introduced into the ionization chamber through the pinhole leak 20 μm in diameter and were ionized in the ionization chamber. Then, the formed ions were extracted from the ionization chamber into the ion lenses and transported into the analyzer tube (the quadrupole Rod). The ions filtered by the Rod were led to the secondary electron multiplier, and the ion-current generated from the electron multiplier was measured by means of an oscilloscope (Iwatsu DS-5158).

Materials. The compositions of the reaction mixtures used were

(A) 1% CH_4, 2% O_2, 97% Ar,

(B) 1% CH_4, 3% O_2, 96% Ar,

(C) 2% CH_4, 2% O_2, 96% Ar.

The methane, oxygen, and argon were obtained from commercial cylinders; their purities were 99.9, 99.9, and 99.99% respectively. The initial pressures of the reaction mixtures were always about 10 Torr.

Procedure. The test section of the shock tube and the vacuum chamber in which the ion source had been installed were evacuated to 2×10^{-6} Torr and 3×10^{-7} Torr respectively by two pumping systems, both of which had 4-inch oil diffusion pumps with liquid nitrogen traps. When the sample gas of about 10 Torr was admitted into the test section of the shock tube, the pressure in the vacuum chamber normally indicated a value of 4×10^{-6} Torr. The driver section was evacuated by means of a rotary pump, prior to admitting the driver gas He, until the residual gas pressure was about 1×10^{-3} Torr. Shock waves were fired within two minutes after the isolation of the pumpimg system, because the leaking and outgassing rate of the test section was about 1.57×10^{-3} Torr l/min. The operations of the pinhole leak were always checked by monitoring the inside pressure of the vacuum chamber using the ionization gauge (I). That is, before each run, the pressure in the vacuum chamber must indicate the value of 4×10^{-4} Torr when dried nitrogen gas of about 1 atm is admitted into the test section; also, the pressure must indicate the value of 4×10^{-6} Torr when a sample gas of about 10 Torr is admitted into the test section.

On the other hand, the quadrupole mass spectrometer was always adjusted and checked thus:

(1) Each electrode voltage (V_{ER}, V_{IC}, V_T, V_{L_1}, V_{L_2}, V_{L_3}, and V_{L_4}) was tentatively set up so that the detecting sensitivity of the quadrupole mass spectrometer might become a maximum.

(2) Then, a standard gas whose composition was 2% N_2 +98% Ar was heated by reflected shock waves, and the oscillogram of N_2 was observed by using the ion signal of the mass position, $m/e=28$. If necessary, the voltage, V_{L_3}, of the lens electrode (L_3) was readjusted so that the time-history curve of of N_2 could level off to a constant value during about 1000 μs.

(3) This adjustment in (2) was made for each series of experimental runs. When the detecting sensitivity of the mass spectrometer became so low that the variation in the ion-current could not be observed, the ion source had to be cleaned. The adjustment as described above was then done again.

After a series of adjustments, the reaction mixtures were heated by reflected shock waves, and the oscillogram of O_2^+ ($m/e=32$) was monitored and analyzed. With a universal counter (Iwatsu US-6141) with a precision of ±0.1 μs, the velocity of the shock waves was determined by detecting their passage between two gauges, G_2 and G_3. By assuming the gas to be ideal, the thermodynamic properties of the gas behind the reflected shock waves were calculated from the three conservation equations and from the measured incident-shock velocity.

Characteristics of Improved Ion Source. When we try to design an ion source for the study of fast reactions, the following requirements are essential, as was mentioned in a previous paper:[1]

(1) The molecules emerging from the pinhole at the end plate of the shock tube should be ionized fast.

(2) The ions thus formed should be extracted fast from

the ionization chamber.

(3) Unionized molecules should be withdrawn fast from the ionization chamber.

(4) Collisions of ions with neutral molecules emerging from the pinhole should be limited.

In the case of using the L type reported previously, ions formed by the electron bombardment needed to be forcibly extracted from the ionization chamber at right angles with the beam of the gas molecules emerging from the pinhole leak. An ion-repeller electrode had to be provided in the ion source so that the ion formed might be expelled effectively and quickly from the ionization chamber; consequently, at about 700 Torr (the pressure behind reflected shock wave) the rise time obtained was less than 10 μs. When the ion-repeller electrode was omitted from this ion source, the rise time was above 150 μs. The contamination on the ion-repeller electrode tended to increase in every experimental run and resulted in prolonging the rise time of an ion signal. This trouble happened irregularly and abruptly when the experimental runs were repeated more than 50 times. The complete adjustment of the rise time was not easy; indeed, it was the most difficult technique among the experimental procedures.

In the case of the I type, a fairly short rise time (20—50 μs) could be obtained over the pressure range of 360—560 Torr in spite of omitting the ion-repeller electrode. Since the rise time is inversely proportional to the pressure of the reflected shock wave, it can be deduced that this value is close to that in the L type. We infer that the fairly short rise time was obtained in spite of omitting the ion-repeller electrode, because the molecules emerging from the pinhole leak enter the ionization chamber, and the ions formed by an electron bombardment are expelled from that chamber. The direction of these molecules and ions is the same as in the I type; moreover, these molecules flow with a large translation energy in the direction of the ion lenses.[1)]

In the I type, the troubles in the rise time were eliminated. This may be because the ion-repeller electrode was omitted from the ionization source. The rise time did not vary even if the experimental runs were repeated more than 200 times.

There is another problem, "the abnormal signal." Since, in this kind of study, the reaction gas is generally diluted with large quantities of Ar, the high range of the detecting sensitivity of the multiplier and the amplifier needs to be employed for observing the time history of reactants or products on the oscillogram. When a high detecting sensitivity was used, an abnormal signal was observed; it always had to be subtracted in the data analysis as if it were a background signal.[2)] It was considered that this abnormal signal was not attributable to ions but to neutral species possessing a high translational energy.[2)] In order to separate the ions and neutral species, the lenses of L_3 and L_4 were designed as is shown in Fig. 2. The abnormal signal could be almost eliminated by this device. By this improvement of the ion source, the sensitivity was lowered slightly, but both the resolution of the mass spectrometer and the rise time of the ion signal did not vary at all.

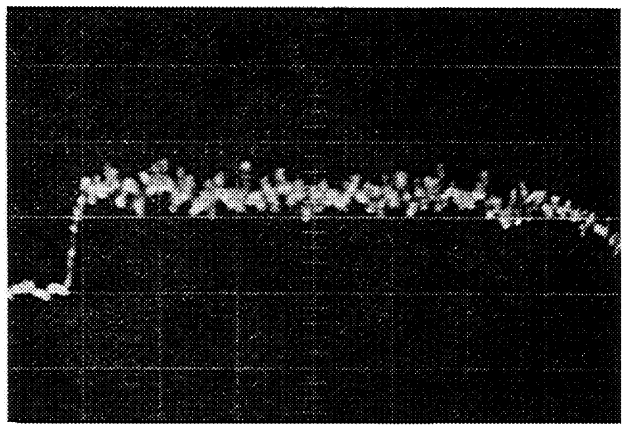

Fig. 3. Typical oscillogram of N_2^+ ($m/e=28$).
Sweep=200 μs/div., $T_5=1908$ K, $P_5=430$ Torr. Supplied voltages: $V_{ER}=+22$ V, $V_{IC}=+130$ V, $V_T=+130$ V, $V_{L_1}=+70$ V, $V_{L_3}=-116$ V, $V_{L_4}=+92$ V, $V_{L_4}=+110$ V, $V_{Rod}=+110$ V.

This apparatus had been previously checked with the time history of Ar^+ ($m/e=40$).[2)] In the present experiment, it was checked with the time history of N_2^+ ($m/e=28$) using a gas mixture (2% N_2+98% Ar). A typical time history of N_2^+ is shown in Fig. 3. In this cheking, it is necessary that the time history of N_2^+ measured on the oscillogram rise rapidly and remain constant for more than 1000 μs.

Results and Discussion

Some typical oscillograms of reactants (CH_4 and O_2) and the main products (H_2O, CO, and CO_2) near 1940 K are shown in Fig. 4. All of these are measured with a same ionizing energy of 24 eV. The time history of a product (H_2O, CO, or CO_2) keeps a base level for a certain time after shock heating, and then begins to rise gradually. On the contrary, the time history of a reactant (CH_4 or O_2) rises rapidly, keeps a nearly constant value for a while, and then falls exponentially until an equilibrium is reached. There is a lag time in the apparatus which has been defined as the time elapsing from the beginning of the reflected shock-wave signal to the beginning of the ion-current signal.[1)] If the induction period is calibrated by monitoring the time history of one of the products, the lag time needs to be measured in preliminary experiments beforehand.

In the present study, the induction period is defined as the time elapsing between the reflected shock arrival and the onset of the rapid decrease in the oxygen concentration; it is measured by monitoring the O_2^+ ($m/e=32$) signals at an ionizing energy of 110 eV, as is shown in Fig. 5. The induction period is calibrated as is shown in Fig. 6, which is obtained by averaging the noise of an observed signal (Fig. 5). Since "the lag time" of the apparatus is cancelled in the calibration in Fig. 6, it is not necessary to take account of this. This is a reason for monitoring the concentration of the O_2 reactant in a series of experimental runs.

In order to monitor the time hisroty of O_2^+, a high detecting sensitivity was required. A high ionizing energy 110 eV, was adopted in order to achieve a higher detecting sensitivity. When this high ionizing energy was adopted, many fragments appeared. When the ion signals at $m/e=16$ were monitored at the ionizing energy of 110 eV, it was the signal of CH_4^+ plus O^+ which was considered to consist of fragment ions of H_2O, CO, and CO_2. When we monitored the concentration of CH_4, the ionizing energy had to be kept lower at the expense of the detecting sensitivity. This was another reason to monitor the concentration of O_2.

Table 1 summarizes the results of the induction periods, τ, together with the conditions of the experimental runs.

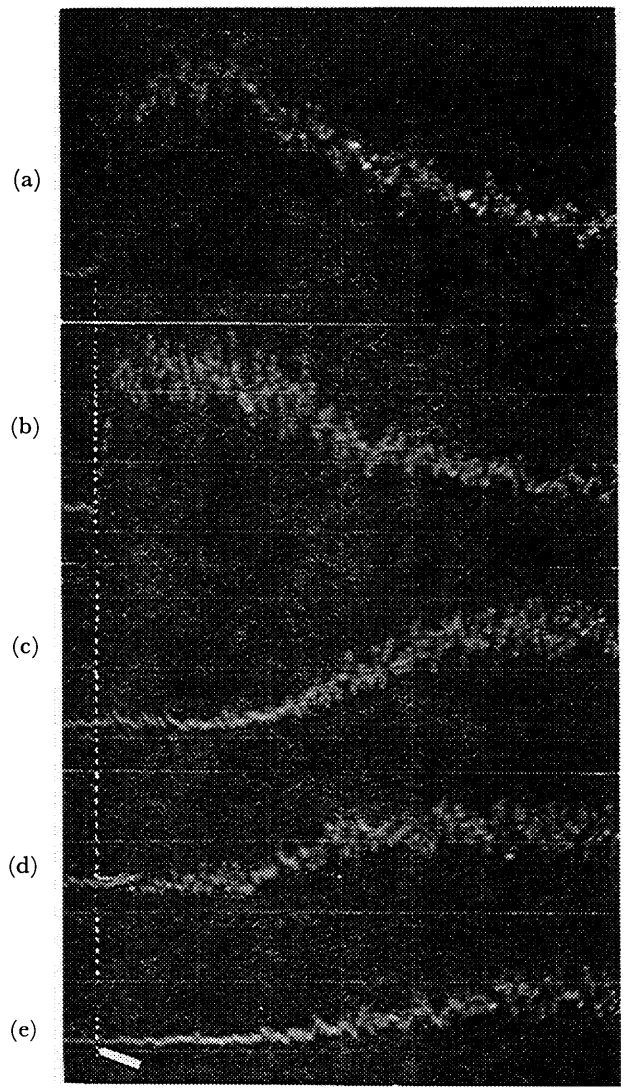

Fig. 4. Some typical oscillograms of species on the methane oxidation near 1940 K.
Sweep=200 μs/div. (a) Time history curve of O_2^+ (m/e=32), T_5=1956 K, P_5=416 Torr. (b) Time history curve of CH_4^+ (M/e=16), T_5=1944 K, P_5=413 Torr. (c) Time history curve of H_2O^+ (m/e=18), T_5=1936 K, P_5=412 Torr. (d) Time history curve of CO^+ (m/e=28), T_5=1938 K, P_5=412 Torr. (e) Time history curve of CO_2^+ (m/e=44), T_5=1947 K, P_5=414 Torr. Supplied voltages: V_{ER}=+18 V, V_{Ic}=+44 V, V_T=+45 V, V_{L_1}=+42 V, V_{L_2}=−90 V, V_{L_3}=+13 V, V_{L_4}=0 V, V_{Rod}=+23 V,

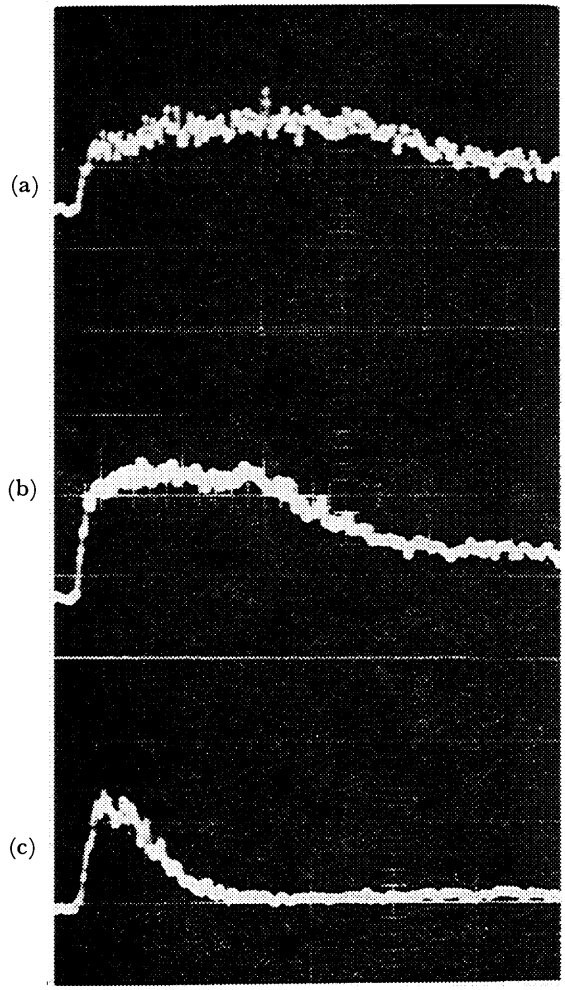

Fig. 5. Typical time history curves of O_2^+ (m/e=32), on oscillograms.
Sweep=200 μs/div. Supplied voltages: V_{ER}=+22 V, V_{IC}=+130 V, V_T=+130 V, V_{L_1}=+70 V, V_{L_2}=−116 V, V_{L_3}=+92 V, V_{L_4}=+110 V, V_{Rod}=+110 V.
(a) Shock No. 110, (b) Shock No. 201, (c) Shock No. 310.

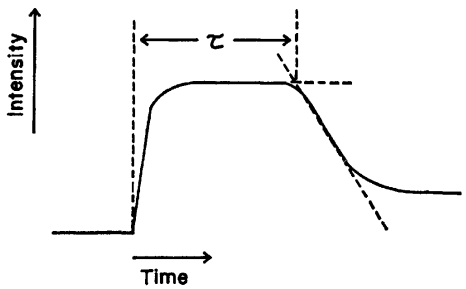

Fig. 6. Definition of the induction period.

Figure 7 shows the plot of log τ *versus* $1/T$ for three composition groups, A, B, and C. It can readily be seen that the values of log τ in each group fall on a single line and that all the lines are parallel. Figure 8 shows the plotting of log τ $[CH_4]^{-0.37}$ $[O_2]^{0.64}$ *versus* $1/T$ for the three groups of A, B, and C. All the points fit a single straight line. The temperature coefficient of the induction periods can be obtained from the slope of the line drawn in Fig. 8. Over the temperature range covered by the present experiment, the induction periods can be represented as

$$\tau = 4.54 \times 10^{-10}[CH_4]^{0.37}[O_2]^{-0.64} \exp(35600/RT)\ \text{s},$$

in which concentrations are expressed in mol per cubic centimeter.

In the study of oxidation reactions in shock waves, induction periods have been considered to be a useful parameter in elucidating a reaction mechanism. The terms "induction period of ignition" and "induction period" have been used in studies of methane oxidation

Table 1. Experimental conditions and induction periods

Series	Shock No.	T_5/K	P_5/Torr	τ/μs
A	101	1860	389	741
	102	2060	447	339
	103	1875	393	551
	104	2390	553	81
	105	2220	499	167
	106	2328	535	82
	107	2068	453	345
	108	1965	437	470
	110	1877	394	680
	113	2080	457	281
	115	2253	511	172
	117	2465	578	79
	119	2060	450	266
	120	1915	409	580
B	201	1925	417	431
	203	2045	448	270
	204	2230	514	110
	207	2145	492	186
	208	2280	519	87
	211	1813	487	648
	213	2285	524	125
	214	1950	425	330
C	301	1907	406	815
	302	1945	417	560
	303	2087	462	300
	305	2355	549	125
	306	2130	576	255
	307	1862	392	890
	308	2005	435	415
	309	2187	494	235
	310	2458	579	125

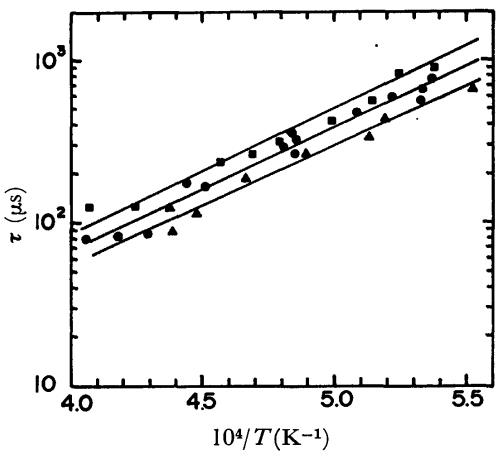

Fig. 7. A plot of log τ *versus* $1/T$ for three composition groups.
■: 2% CH_4+2% O_2, ●: 1% CH_4+2% O_2, ▲: 1% CH_4+3% O_2.

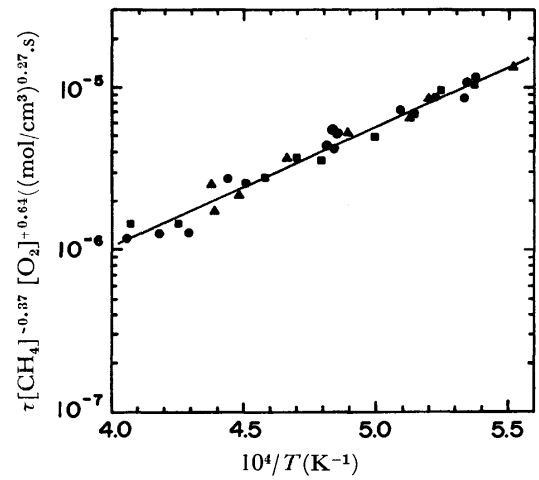

Fig. 8. A plot of log τ $[CH_4]^{-0.37}$ $[O_2]^{0.64}$ *versus* $1/T$ for three composition groups.
■: 2% CH_4+2% O_2, ●: 1% CH_4+2% O_2, ▲: 1% CH_4+3% O_2.

using the shock waves although there is same uncertainty in their definitions. The first study of the induction period of methane oxidation in shock waves was carried out by Skinner and Ruehrwein in 1959.[3] Afterwards, a considerable number of data have been reported by many investigators.[4-16] Most of the reported activation energies center around 50 kcal/mol (at high pressures (above 2 atm)) or 33 kcal/mol (at low pressures (below 1 atm)).

Our experimental results indicate that the reaction of methane oxidation passes through two steps: the first step (during the induction period) is characterized by a very slow decrease in the oxygen concentration, while the second step (after the induction period) is followed by a rapid decrease. The induction periods are measured by monitoring the oxygen concentration; thereby, an apparent activation energy of 35.6 kcal/mol is obtained over the pressure range of 360—560 Torr and the temperature range of 1800—2500 K. The value of the apparent activation energy obtained is in good agreement with the values obtained by Cooke *et al.*,[15] Higgin *et al.*,[10] and Kistiakowsky *et al.*[4] in spite of the differences in the method of measurement. On the other hand, although we have tried analysing the time history of the O_2 concentration after the induction period, we have not yet obtained any useful information on the methane oxidation.

References

1) M. Suga and Y. Hidaka, *Mass Spectroscopy*, **23**, 23 (1975).
2) Y. Hidaka, *J. Sci. Hiroshima Univ., Ser. A*, **38**, 301 (1974).
3) G. B. Skinner and R. A. Ruehrwein, *J. Phys. Chem.*, **63**, 1736 (1959).
4) G. B. Kistiakowsky and L. W. Richards, *J. Chem. Phys.*, **36**, 1707 (1962).
5) H. Miyama and T. Takeyama, *J. Chem. Phys.*, **40**, 2049 (1963).
6) T. Asaba, K. Yoneda, N. Kakihara, and T. Hikita, "Symp. Combust. 9th," Academic Press (1963), p. 193.
7) H. Miyama and T. Takeyama, *Bull. Chem. Soc. Jpn.*,

38, 37 (1965).
8) G. P. Glass, G. B. Kistiakowsky, J. V. Michael, and H. Niki, "Symp. Combust. 10th," Combustion Institute (1965), p. 513.
9) R. I. Soloukhin, "Symp. Combust. 11th," Combustion Institute (1967), p. 671.
10) R. M. R. Higgin and A. Williams, "Symp. Combust. 12th," Combustion Institute (1969), p. 579.
11) D. J. Seery and C. T. Bowman, *Combust. Flame*, **14**, 37 (1970).
12) D. F. Cooke and A. Williams, "Symp. Combust. 13th," Combustion Institute (1971), p. 757.
13) A. Lifshitz, K. Scheller, A. Burcat, and G. B. Skinner, *Combust. Flame*, **16**, 311 (1971).
14) T. Tsuboi and H. G. Wagner, "Symp. Combust. 15th," Combustion Institute (1974), p. 883.
15) D. F. Cooke and A. Williams, *Combust. Flame*, **24**, 245 (1975).
16) A. Grillo and M. W. Slack, *Combust. Flame*, **27**, 377 (1976).

Molecular Dissociation of 3-Cyclopenten-1-one Photosensitized by Excited Mercury ($^3P_1$)

Kazumoto NAKAMURA, Seiichro KODA, and Kazuo AKITA

Department of Reaction Chemistry, Faculty of Engineering, The University of Tokyo, Bunkyo-ku, Hongo, Tokyo 113

(Received November 11, 1977)

The mercury photosensitized decomposition of 3-cyclopenten-1-one produced carbon monoxide and 1,3-butadiene in equal quantum yields as the exclusive products, independent on the absence or presence of nitrogen oxide. Thus the process was a molecular dissociation. The quantum yield was dependent on the pressure of argon added as a third body and revealed a maximum at the pressure of about 100 mmHg. A possible reaction scheme was proposed to explain the above kinetic behavior. It was suggested that the vibrationally excited state of 3-cyclopenten-1-one was a main precursor to decompose to carbon monoxide and 1,3-butadiene. An energy about 20 kcal·mol^{-1} was estimated to be lost before its production from the original triplet state 3-cyclopenten-1-one according to the proposed reaction scheme. This result is compared with the behaviors of excited 3-cyclopenten-1-ones produced by different excitation procedures.

Mechanisms of pyrolyses, photolyses and photosensitized reactions of saturated cyclic ketones and cyclic unsaturated hydrocarbons have been well elucidated in recent years.[1] But those of unsaturated cyclic ketones are rarely investigated. Among them is 3-cyclopenten-1-one (abbreviated as CP). Dolbier and Frey[2] studied the thermal decomposition of this ketone. Hess and Pitts[3] reported the direct photolysis at 313 nm briefly. In both cases, carbon monoxide (CO) and 1,3-butadiene (BD) were exclusive products. To our knowledge, however, there is no report on the mercury photosensitization of this ketone.

During our study of the atomic oxygen reaction with 1,3-cyclopentadiene,[4] CP was proposed as an important intermediate to decompose to CO and BD. The spin state of the intermediate cyclopentenone could be either singlet or triplet. Apart from the oxygen atom reaction, a triplet state CP is expected to be prepared through mercury photosensitization of the ketone itself. Moreover, the energy which is transferred from the excited mercury atom to the ketone should be 113 kcal·mol^{-1} or less, which is relatively close to the possible excess energy possessed by the intermediate CP of the atomic oxygen reaction with cyclopentadiene; that is about 105 kcal·mol^{-1}.[5]

Thus we are interested in the possible difference in the mechanism of decomposition of CP excited by mercury photosensitization from those of cyclopentenones excited thermally or by direct photon absorption, or prepared through the reaction of oxygen atoms with 1,3-cyclopentadiene. This matter will be discussed after the photosensitized decomposition of CP is described.

Experimental

Materials. The preparative method of 3- and 2-cyclopenten-1-one were described by Hess and Brown.[6] The crude pentenones were purified by repeated distillations. Gas-chromatographic analyses showed that the CP and the 2-cyclopenten-1-one were more than 99 and 97% pure, respectively.

Commercially obtained argon (pure grade; the purity is more than 99.99%; from Takachiho Shoji Co., Ltd.), nitrogen, CO, BD, and 1-butyne (the four gases are of research grade from Takachiho Shoji Co., Ltd.) were used without further purification. Commercially obtained dinitrogen oxide, nitrogen oxide and ethane (all, research grade; from Takachiho Shoji Co., Ltd.) were distilled several times *in vacuo* before use.

Cyclobutene (CB) was synthesized through the photoisomerization of BD according to the method described by Srinivasan[7] and purified gas-chromatographically.

Apparatus. The cyclindrical quartz photochemical cell was 5 cm in diameter and 10 cm long, equipped with a gas circulation line with a glass-made circulation pump having Teflon bearings, mercury store, a U-type trap, and a reservoir. The total volume of the reaction system mentioned above was 650 ml. A conventional vacuum system was used for gas handling.

The 253.7 nm light source was a flat-spiral low pressure mercury resonance lamp (Ushio Electric Inc., type UTL-7SQ). The light from the lamp passed through a glass filter (Toshiba Kasei Co., Ltd., UV-D25) to get rid of the radiation below 200 nm, an iris (diameter 10 mm), a quartz lens (f=10 cm) and a quartz beam splitter. The transmitted light reached the cell. The reflected light at right angles from the beam splitter reached a phototube (Hamamatsu TV Co., Ltd., R765). Thus the relative intensity of this radiation could be monitored to be corrected for any fluctuation of the radiation all through the experimental runs.

Experimental Procedure. A measured amount of CP (and nitrogen oxide, if necessary) was introduced into the reaction system. Then argon, if necessary, was added through a slightly opened stopcock until the desired total pressure was reached. The gas mixture was circulated all through the total reaction system by means of the circulation pump for at least an hour before photolysis. Within an hour, mercury vapor evaporated from the mercury store into the gas mixture until the equilibrium pressure at the temperature was reached. Irradiation was carried out for a desired period, while the gas mixture was being circulated.

After the irradiation, the gas mixture was treated as follows. In the experiments without argon, the mixture was divided to three portions. The first portion, non-condensable at liquid nitrogen temperature, was collected by a Toepler pump. The other two portions, one of which was not condensable at Dry Ice–methanol temperature (−78 °C) and the other of which, condensable at that temperature, were sampled in gas samplers cooled at the adequate temperatures, respectively. In the experiments with argon, a part of the mixture was expanded into a gas sampler. The remaining part was pumped out very slowly through several spiral traps immersed in a Dry

TABLE 1. ESTIMATION OF THE PERCENTAGE ABSORPTION OF LIGHT IN VARIOUS GAS MIXTURES

Run	$P_{C_2H_6}$ (mmHg)	P_{N_2O} (mmHg)	$P_{C_5H_6O}$ (mmHg)	P_{NO} (mmHg)	P_{Ar} (mmHg)	a ($\times 10^{-8}$ A)	b ($\times 10^{-10}$ A)	c ($\times 10^{-2}$)	d (%)
1[a]	0.0	0.0				5.40	299.6	55.5	0.0
2	99.8	104.2				5.49	14.7	2.68	95.2
3	99.3	101.4				5.16	14.0	2.71	95.1
4	103.6	107.8				5.26	15.9	3.02	94.6
5			10.3	0.0	0.0	5.39	17.3	3.14	94.3
6			10.9	0.0	0.0	4.63	15.5	3.38	93.9
7			9.2	10.9	456.9	5.14	11.1	2.16	96.1
8			10.1	4.3	469.2	5.14	12.1	2.36	95.8
9			10.2	21.7	461.6	6.00	14.1	2.43	95.6
10			10.1	26.7	444.7	5.29	12.2	2.30	96.8

Reaction temperature; 25±3 °C. a) Without any mercury. *a*: The reflected light (phototube current) from the beam splitter. *b*: The leaking light (phototube current). *c*: *b*/*a*. *d*: The percentage of absorption $((1-(c_1/c_1))\times 100)$.

Iice–methanol bath. The collection efficiency of the traps was checked for BD and was found to be at least 95%.

Analyses of Products. The products were identified and analysed quantitatively by means of gas-chromatography (Yanagimoto Seisakusho Co., Ltd., G80-PT(TCD), G80-FTP (FID)) with several appropriate columns. The columns used were 3,4-dimethylsulfolane (4.5 m, 0 °C) and Squalane (3 m, 30 or 90 °C) for BD and also for lower hydrocarbons, Molecular Sieve 5A (2.25 m, 60 °C) for nitrogen and CO, bis(2-ethylhexyl)phthalate (2.25 m, 70 °C) and Polyethylene Glycol 20M (2.25 m, 100 °C) for searching for other possible products of a larger molecular weight. Usually a thermal conductivity detector was used for nitrogen and CO and a flame ionization detector for hydrocarbons.

In the experiments with argon, the product CO could not be separated from the large amount of argon by a conventional method. Thus the part which represented the total photolysed mixture correctly, and had been expanded into a gas sampler, was introduced into the gas-chromatograph after being got rid of the condensable products at Dry Ice–methanol temperature. The product CO was then separated from argon through the Molecular Sieve 5A column in the gas-chromatograph, converted to methane by the reduction with the carrier gas hydrogen at 320 °C through the nickel catalyst column (from Gasukuro Kogyo Co., Ltd.) connected to the Molecular Sieve 5A column directly, and then detected with a flame ionization detector. Carbon monoxide of more than 30 ppm in argon could be analysed quantitatively by the above procedure, provided that the total mixture of 3000 mmHg·cm^3 was introduced to the gas-chromatograph.

Measurements of the Intensity of Light Which Leaks out from the Cell. The intensity of the light coming out from the inside of the cell (transmitted light and re-emitted light from the excited mercury) was measured with a phototube at various positions around the cell. The total amount of the leaking light could be then estimated by summing the measured intensity values with taking into account the geometry of the cell.

Estimation of the Amount of Absorbed Light in the Cell. The amount of the light which leaked out from the cell was measured by the above procedure under several different experimental conditions as shown in Table 1. Thus the percentage of the absorption was always about 95%, in various experimental runs including the case of the photolysis of the mixture of dinitrogen oxide and ethane. Then the amount of absorbed light in the cell could be calculated based on the experimental nitrogen yield from the photolysis of dinitrogen oxide–ethane; the quantum yield of the nitrogen production is unity according to Ref. 8.

Results

The main products were CO and BD. Trace amounts of C_2 and C_3 hydrocarbons, 1,2-butadiene and 1-butyne were detected in some experiments, especially when the conversion was high. But they were always produced in negligibly small quantum yields. No other C_4H_6 isomers such as CB and 3-methylcyclopropene could be detected. Their quantum yields should be less than 0.002, considering from the detection limit of our analysis. Small amount of 2-cyclopenten-1-one, one of the isomers of cyclopentenones, were detected in some experiments. But quantitative analyses gave relatively poor reproducibility for this product, possibly because of its easiness to adsorb on the wall of the reaction and/or analysis systems. Thus quantitative analyses were confined to CO and BD.

The quantum yield of carbon monoxide was independent on the irradiation time as shown in Fig. 1, which guaranteed that no secondary photolysis of the products proceeded to appreciable extents under the

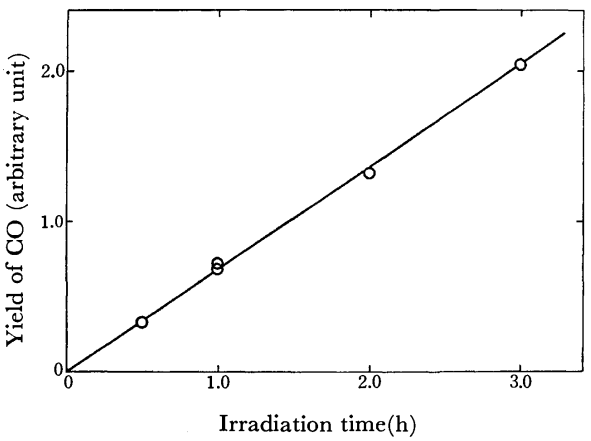

Fig. 1. Yield of carbon monoxide *versus* irradiation time
Pure CP (10.0—12.4 mmHg) was photosensitized, at 20—25 °C. The yield of CO is corrected for the variation of the light intensity.

Table 2. The quantum yields of carbon monoxide and 1,3-butadiene

Run	$P_{C_5H_6O}$ (mmHg)	P_{Ar} (mmHg)	P_{NO} (mmHg)	ϕ_{CO}	ϕ_{BD}	ϕ_{BD}/ϕ_{CO}
5	10.3	0.0		0.874	n.d.	n.d.
6	10.9	0.0		0.849	0.876	1.03
7	9.2	456.9	10.9	0.568	0.590	1.04
8	10.1	469.2	4.3	0.685	0.701	1.04
9	10.2	461.6	21.7	0.399	0.410	1.03
10	10.1	444.7	26.7	0.427	0.412	0.97
11	10.1	316.3		0.814	0.847	1.04
12	10.8	88.1		0.954	0.901	0.94
13	11.3	0.0		0.854	0.828	0.97
14	10.5	0.0		0.855	0.876	1.02
15	10.3	492.3		0.678	0.740	1.09
16	10.5	275.8		0.877	0.860	0.98
17	10.5	45.5		0.914	0.947	1.04
18	10.5	647.2		0.606	0.618	1.02
19	9.8	137.7		0.913	0.904	0.99
				average		1.01 ± 0.04

n.d.=not determined. Reaction conditions; irradiation time, 1.0 or 2.0 h, reaction temperature, 25 ± 3 °C.

present conditions.

Table 2 shows the quantum yields of CO and BD. In some experiments, argon was added in order to know its effect as a third body. Argon is known not to quench excited mercuries in any appreciable extent. In several experiments, nitrogen oxide as a radical scavenger[9] was added. The ratio of the quantum yield of CO versus that of BD was found to be always very close to unity under various conditions, as shown in the last column of the table.

We carried out one special experimental run where the mixture of methane (656 mmHg) and CP (10 mmHg) was photolysed. No C_4H_6 isomers other than BD could be detected. The yield of CB, if it were produced, should be less than 0.03% of that of BD produced, judging from the gas-chromatographic sensitivity.

Discussion

Molecular Dissociation. As shown in Table 2, the ratio of the quantum yield of CO to that of BD was about unity in any experiment under various conditions. Even in the experiments where nitrogen oxide was added, the ratio did not change. The decrease of the yield of CO and BD with the addition of NO should be attributed to the quenching effect of NO for the excited mercuries. These observations show that CO and BD are produced *via* a common intermediate, and no radical species seems to contribute to the production of CO and BD. Therefore, the main reaction is considered to be a molecular dissociation of a certain excited CP to produce CO and BD, under the present conditions.

Absence of Excited Cyclobutene as an Intermediate. BD is considered to be produced through a molecular dissociation as stated in the previous section. One possibility is that BD is, in fact, produced as a secondary product through isomerization from some other vibrationally excited C_4H_6 isomers which might be produced primarily. Among C_4H_6 isomers other than BD, CB seems to be the most plausible primary species, because CB could be produced as a molecular dissociation product from excited CP without any serious rearrangements of molecular structures and also because it is known to isomerize thermally to BD exclusively.[10] Thus we must determine whether BD is produced *via* the excited CB intermediate, CB*, or is produced directly. Because some part of CB* should be collisionally stabilized and analysed as CB, we can estimate the fraction of the process *via* CB*, X, based on the fraction of CB among product C_4H_6 isomers (CB+BD), β, which is experimentally obtainable. Here, the following scheme is assumed.

$$\text{Intermediate}\,(C_5H_6O) \longrightarrow CO + CB^* \quad k_a \quad (1)$$

$$\longrightarrow CO + BD \quad k_b \quad (2)$$

$$CB^* \longrightarrow BD \quad k_{iso} \quad (3)$$

$$CB^* + M \longrightarrow CB + M \quad \alpha k_\omega \quad (4)$$

(α=collisional deactivation efficiency, k_ω=kinetic collision frequency at the pressure)

X and β are equated to the rate constants, as follows.

$$X = \frac{k_a}{k_a+k_b} \quad (5)$$

$$\beta = \frac{k_a}{k_a+k_b} \times Y \quad (6)$$

Here, $Y=\alpha k_\omega/(\alpha k_\omega+k_{iso})$. Therefore, X can be calculated from β and Y.

$$X = \beta Y^{-1} \quad (7)$$

The value β is determined experimentally. The value Y can not be obtained experimentally, but may be approximately estimated by simple statistical considerations as described below. At first, the rate constant k_{iso} is calculated by the following equation when the excess energy of CB* is E.

$$k_{iso} = A(1-E_a/E)^{s-1} \quad (8)$$

By use of $s=10$, $E_a=32.9$ kcal·mol^{-1}, $A=10^{13.3}$ s^{-1} and $E=66$ kcal·mol,$^{-1}$ k_{iso} is calculated to be 1×10^{10} s^{-1}. Here, the value $s=10$ is claimed to be optimum to explain the experimental results of the thermal isomerization of CB,[10,11] and then rate parameters E_a and A are taken from the data of the thermal isomerization.[10] The excess energy E is estimated as follows. It is likely that about 105 kcal·mol^{-1} energy is transferred to CP from the $^3P_1$ mercury, referred to the experimental results of Montague and Rowland.[12] According to the simple statistical consideration, CB* possesses the excess energy which is equivalent to the available energy multiplied by the ratio of the number of internal degrees of freedom of CB(24) to that of CP(30). The available energy is equal to the transferred energy (105 kcal·mol^{-1})+ the heat of reaction of the dissociation of CP to CO and CB (-23 kcal·mol^{-1}). Its twenty four-thirtieth is 66 kcal·mol^{-1}. Secondly, the term αk_ω is estimated by adopting 1×10^7 s^{-1} as the kinetic

collision frequency at 1 mmHg and by use of appropriate α values. α is 0.24 for methane[13] and unity deactivation efficiency is assumed for CP.

Thus, the value of Y is estimated to be 0.14 in the experiment with 656 mmHg of methane (CP, 10 mmHg) and to be 0.0099 in the experiments without additive gases (CP, 10 mmHg). As described in the result section, CB could not be found both in the experiment with 656 mmHg of methane and in the experiments without additive gases. Correspondingly, the possible maximum of β is 3×10^{-4} in both cases. According to Eq. 7, the possible maximum of X should be then 2×10^{-3} in the experiment with 656 mmHg of methane and 3×10^{-2} in the experiments without additive gases.

The above discussions show that the process *via* the excited CB contributes to a very small extent, if at any. BD must be produced as the primary dissociation product from the molecular dissociation.

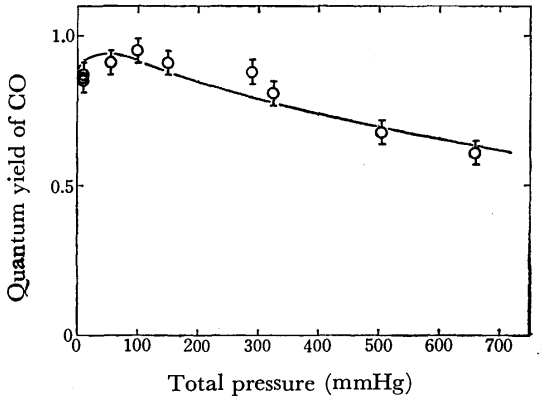

Fig. 2. Quantum yield of carbon monoxide versus total pressure.
Data are from Table 2. total pressure=Ar pressure+ CP pressure (9.8—11.3 mmHg)

Reaction Scheme. Figure 2 shows the relationship between the quantum yield of CO, ϕ_{CO}, and the total pressure. Here, the total pressure is the sum of the pressure of CP which was about 10 mmHg all through the experimental runs and the pressure of argon which was varied.

The fact that the extrapolation value of the plots to zero pressure is not unity suggests the existence of a channel through which products other than CO and BD are produced. Those products could not be clearly identified, but the isomer 2-cyclopenten-1-one is one possibility. The complex dependence of ϕ_{CO} on the pressure indicates the existence of several consecutive competitions between stabilization and dissociation to produce CO and BD. At least two independent processes which are affected by collisions are required in order to explain the positive and then negative pressure dependence of ϕ_{CO}. It is very plausible that the vibrationally excited state of CP is the immediate precursor to decompose to CO and BD, taking into account the facts that the products of pyrolysis of CP is exclusively CO and BD,[2] and that the Woodward-Hoffmann rule indicates the possibility of the production of CB from electronically excited CP's, against our observation.

As a simple model which satisfy the above considerations, we propose the following reaction scheme.

$$C_5H_6O(S_0) + Hg(^3P_1) \longrightarrow C_5H_6O(T) + Hg(^1S_0) \quad (9)$$

$$C_5H_6O(T) \longrightarrow CO + BD \quad (10)$$

$$C_5H_6O(T) \longrightarrow \text{other products except CO and BD} \quad (11)$$

$$C_5H_6O(T) + M \longrightarrow C_5H_6O(T') + M \quad (12)$$

$$C_5H_6O(T') \longrightarrow C_5H_6O(S_0^*) \quad (13)$$

$$C_5H_6O(S_0^*) \longrightarrow CO + BD \quad (14)$$

$$C_5H_6O(S_0^*) + M \longrightarrow C_5H_6O(S_0) + M \quad (15)$$

Here, M means a third body. Argon and CP are not differentiated from each other, though they may have different quenching ability. We did not vary the pressure of CP to reveal its different quenching ability from argon, because of its low vapor pressure at room temperature, which is 13 mmHg.

The reaction 10 may be a single process as described above or more plausibly a consecutive process (Eqs. 10a and 10b),

$$C_5H_6O(T) \longrightarrow C_5H_6O(S_0^\dagger), \quad (10a)$$

$$C_5H_6O(S_0^\dagger) \longrightarrow CO + BD, \quad (10b)$$

where $S_0^\dagger$ means a vibrationally excited ground state of CP with a larger excess energy than S_0^*. The process (Eq. 10a) is a collision free intersystem crossing. Because of the very large amount of excess energy of $S_0^\dagger$, its subsequent process is almost confined to the dissociation (Eq. 10b) under the present pressures. The T' state is either the vibrationally relaxed T state or any other different triplet state with a lower triplet energy. S_0^* means a vibrationally excited S_0 state, and is assumed to possess less energy than is originally transferred from the excited mercury because of the collisional deactivation (Eq. 12).

According to the above scheme, we can derive.

$$\phi_{CO} = \frac{1}{1+(k_{11}/k_{10})+(k_{12}M/k_{10})} + \frac{k_{12}M/k_{10}}{1+(k_{11}/k_{10})+(k_{12}M/k_{10})}\cdot\frac{1}{1+k_{15}M/k_{14}}. \quad (16)$$

Adoptation of appropriate values for the ratios of the rate constants is found to result in coincidence between the experimentall values and calculated values according to Eq. 16 within experimental errors. When the optimum values, $k_{11}/k_{10}=0.15$, $k_{12}/k_{10}=5\times10^{-2}$ mmHg^{-1}, $k_{15}/k_{14}=9\times10^{-4}$ mmHg^{-1} are adopted, the calculated values of ϕ_{CO} are shown as a bold line in Fig. 2. Though these rate ratios could not be determined unequivocally, the allowable range of k_{15}/k_{14} to satisfy the experimental results was found to be between 1×10^{-3} and 7×10^{-4} mmHg^{-1}. This range could be rather unequivocally determined, because the relationship between ϕ_{CO} and the pressure is determined by this ratio almost exclusively, when the pressure is above 150 mmHg.

Adoptation of a multi-step deactivation process in place of Eqs. 14 and 15 was found to result in a little better coincidence, but the improvement was minor. Thus we consider that the scheme (Eqs. 9—15) is enough to explain the experimental results. This scheme is also

compatible with the considerations of the excess energy of the intermediate S_0^* state, as will be described in the next section.

Excess Energy of the Excited Ground State 3-Cyclopenten-1-one. The experimental value of k_{15}/k_{14} gives the value of k_{14} as 1.1×10^9 s^{-1} on the basis of the assumption, $k_{15}=1\times10^6$ mmHg^{-1}·s^{-1}. Here, the k_{15} value of one-tenth (which is the collisional deactivation efficiency) of the gas kinetic collision frequency is used.[13] The excess energy of S_0^* can be estimated by use of

$$k(E) = A(1-E_a/E)^{s-1}. \quad (17)$$

Here, $k(E)$ is a rate constant of decomposition when an excess energy is E. We get $E=86.6$ kcal·mol^{-1} by using the values of A ($10^{14.5}$ s^{-1}) and E_a (51.3 kcal·mol^{-1}) taken from the experiment of Dolbier and Frey,[2] and assuming $s=15$. The possible range of the ratio k_{15}/k_{14} between 1×10^{-3} and 7×10^{-4} mmHg^{-1} corresponds to the range of the excess energy E between 86.2 and 87.1 kcal·mol^{-1}. The estimation of the excess energy is also dependent on the assumed value of the collisional deactivation efficiency. For example, unit efficiency, which is an unlikely large efficiency, result in the increase of the excess energy about 10 kcal·mol^{-1}. But even in this case, the excess energy is still smaller by about 10 kcal·mol^{-1} than the energy, about 105 kcal·mol^{-1}, which is originally transferred to CP from the excited mercury. Thus the dissociating intermediate S_0^*, and also T′ seem to be deactivated by 20 kcal·mol^{-1} or so before the dissociation. The energy loss should be due to the vibrational deactivation process (Eq. 12) in the triplet state.

Triplet State of 3-Cyclopenten-1-one. CP possesses two active chromophores which are relatively independent on each other; they are C=O and C=C double bond. Then two kinds of triplet states of low energy are expected to exist; one is $^3(n-\pi^*)$ mainly excited in the C=O chromophore (T_a) and the other is $^3(\pi-\pi^*)$ mainly excited in the C=C chromophore (T_b).

The absorption spectrum of CP measured by Hess and Pitts[3] clearly shows two different absorption systems, one of which is relatively weak ($\varepsilon\approx10$ l·mol^{-1}·cm^{-1}) and in the region from 250 to 320 nm, and the other is strong ($\varepsilon\approx10^3$ l·mol^{-1}·cm^{-1}) and in the region from 180 to 230 nm. The upper state of the first system is safely assigned to $^1(n-\pi^*)$ of the C=O chromophore. The upper state of the second system is not clear enough, but might be $^1(\pi-\pi^*)$ of the C=C chromophore. The 0–0 energies of the two systems are apparently 86 kcal·mol^{-1} and 114 kcal·mol^{-1}, respectively, judging from their absorption spectra. Considering that the difference between a $^1(n-\pi^*)$ state and the corresponding $^3(n-\pi^*)$ is usually about 5 kcal·mol^{-1} or so,[14] the T_a state may be above the ground state by about 80 kcal·mol^{-1}. The difference between a $^1(\pi-\pi^*)$ and the corresponding $^3(\pi-\pi^*)$ is usually large and also varies very much from molecule to molecule. The fact that the rotation around the C–C axis is restricted due to the ring structure in the case of CP, makes it more difficult to presume the energy of T_b.[15] It is thus difficult to decide which is the lowest triplet state. Anyhow, at least one triplet state whose triplet energy is around the same as the excess energy of the assumed T′ state seems to exist. Thus our assumption of the two-step consecutive deactivation process ((Eqs. 12, 15); the first step in the triplet vibrational manifold and the second step in the ground state vibrational maifold) is self-consistent.

Comparison among the Excited 3-Cyclopenten-1-ones from Different Excitation Methods. Hess and Pitts[3] obtained CO and BD with the quantum yield of 0.87 in the direct photolysis of CP by using 313 nm light (91.3 kcal·mol^{-1}) at 35 mmHg of total pressure. A singlet ($^1(n-\pi^*)$) CP is considered to be produced as a primary product through the direct photon absorption. Provided that the dissociation is from the vibrationally excited ground state molecule which has been prepared from the singlet excited state through internal conversion, the excess energy of the decomposing molecule is calculated to be about 90 kcal·mol^{-1} by the similar procedure as described in the fourth section, based on the above quantum yield (0.87 at 35 mmHg). The excess energy is then very near the initial excitation energy. Thus it is plausible that the singlet $^1(n-\pi^*)$ state CP changes before any appreciable collisions to a vibrationally excited ground state molecule, which then decomposes unimolecularly.

In the reaction of atomic oxygen with 1,3-cyclopentadiene, we assumed the existence of an excited CP as the intermediate to decompose to CO and BD (the corresponding process is expressed by Eq. IV in the previous paper[4]). Provided that the intermediate is a vibrationally excited ground state CP, its excess energy is estimated to be 104 kcal·mol^{-1}, by the similar calculation procedure based on the data presented in Fig. 7 of the paper. On the other hand, the heat of reaction of the process, $O(^3P)+1,3$-cyclopentadiene→ 3-cyclopenten-1-one, is 102 kcal·mol^{-1}, which is near the above estimated excess energy.

Thus in the above two excitation procedures, the collisional events do not seem to affect the processes preceding the decomposition, which should be attributed to the rapid conversion of the primary products to the corresponding vibrationally excited ground state CP's. We found a moderate pressure effect of the quantum yield of the products in the case of the mercury photosensitization, and attributed it to the collisional deactivation in the triplet state, as described before. A relatively long triplet lifetime is expected because of the possibly slow intersystem crossing.

Our reaction scheme is based on a very simple kinetic treatment of the CO quantum yield, and might be modified with future additional informations. We wish to stress, however, that the pressure dependence of ϕ_{CO} in the mercury photosensitization is somewhat different from those in the other two excitation systems even though the products are CO and BD in every case. The existence of this difference is independent on the assumption of reaction schemes.

The authors are grateful to Associate Professor S. Tsuchiya of the University of Tokyo for his encouragement.

References

1) J. G. Calvert and J. N. Pitts, Jr., "Photochemistry," John Wiley, New York (1966); C. H. Bamford and C. F. H. Tipper, "Comprehesive Chemical Kinetics," Vol. 5, Elsevier Publishing Company, New York (1972).
2) W. R. Dolbier, Jr. and H. M. Frey, *J. Chem. Soc., Perkin Trans. 2*, **1967**, 1674.
3) L. D. Hess and J. N. Pitts, Jr., *J. Am. Chem. Soc.*, **89**, 1973 (1967).
4) K. Nakamura and S. Koda, *Int. J. Chem. Kinet.*, **9**, 67 (1977).
5) In the estimation, we used -11.8 kcal·mol^{-1} for the standard heat of formation of 3-cyclopenten-1-one. The value was estimated from the group added theory. P. I. Gold, *Chem. Eng.*, 112 (1969).
6) H. M. Hess and H. C. Brown, *J. Org. Chem.*, **32**, 4138 (1967).
7) R. Srinivasan, *J. Am. Chem. Soc.*, **85**, 4045 (1963).
8) R. J. Cvetanovic, W. E. Falconer, and K. R. Jennings, *J. Chem. Phys.*, **35**, 1225 (1961); M. G. Bellas, V. Rousseau, O. P. Strauz and H. E. Gunning, *J. Chem. Phys.*, **47**, 768 (1964).
9) J. Heicklen and N. Cohen, *Adv. Photochem.*, **5**, 157 (1967).
10) W. P. Hauser and W. D. Walters, *J. Phys. Chem.*, **67**, 1328 (1963).
11) R. J. Robinson and K. A. Holbrook, "Unimolecular Reactions," Wiley-Interscience, New York (1972), p. 249.
12) D. C. Montague and F. S. Rowland, *J. Am. Chem. Soc.*, **91**, 7230 (1969).
13) D. L. Bunker, "Theory of Elementary Gas Reaction Rates," Pergamon Press, London (1967); Japanese Translation by H. Miyama and T. Fueno, Tokyo Kagaku Dojin, Tokyo (1970), p. 86.
14) J. A. Barltrop and J. D. Coyle, "Excited States in Organic Chemistry, John Wiley, New York (1975), p. 53.
15) I. Sauers, L. A. Grezzo, S. W. Staley, and J. H. Moore, Jr., *J. Am. Chem. Soc.*, **98**, 4218 (1976).

Luminescence Properties and the Primary Process of Photochromism of 2-(2-Hydroxyphenyl)benzothiazole

Ryoichi NAKAGAKI,* Takayoshi KOBAYASHI,** and Saburo NAGAKURA*,**

**The Institute for Solid State Physics, The University of Tokyo, Minato-ku, Tokyo 106*

***The Institute of Physical and Chemical Research, Wako, Saitama 351*

(Received November 12, 1977)

The luminescence behavior of 2-(2-hydroxyphenyl)benzothiazole at 77 K was studied in detail, special attention being paid to dual fluorescence at ≈500 and ≈370 nm and also to phosphorescence at ≈500 nm. From the dependence of these emission bands upon the hydrogen-bonding ability of solvents and the excitation spectra, it is concluded that the short- and long-wavelength fluorescence bands are due to the intermolecularly hydrogen-bonded enol imine and the keto amine produced from the intramolecularly hydrogen-bonded enol, respectively, and that the phosphorescence is due to the intermolecularly hydrogen-bonded enol imine. The estimated quantum yield of the enol fluorescence gives further support to the formation scheme of the photochromic colored species previously presented. The rate constants of the intramolecular hydrogen transfer at 77 and 293 K are evaluated to be larger than 4×10^{10} s^{-1} and 3×10^{12} s^{-1}, respectively.

Photochromism of *N*-salicylideneanilines has been interpreted to be an enol-keto phototautomerization, which involves not only hydrogen transfer but a geometrical change in the molecular framework.[1-4]

In a previous paper, the photochromism of *N*-salicylideneanilines, including 2-(2-hydrophenyl)benzothiazole (HBT), was studied at room temperature.[4] From the FT infrared absorption measurement, we presented the direct evidence of the keto amine form for the colored species of *N*-salicylideneanilines. Furthermore, with the aid of picosecond time-resolved spectroscopy, we found the transient precursor from which the colored species and the *cis*-keto amine were produced.

Cohen and Flavian observed anomalously red-shifted fluorescence for *N*-salicylideneanilines and suggested from the comparison with absorption spectra that it was attributed to the keto tautomer formed during the lifetime of the enol excited state. But they could not observe separately a long-lived component (phosphorescence) appearing in the same wavelength region.[5]

In the present work, we have studied in detail the fluorescence and phosphorescence spectra, lifetimes, and fluorescence quantum yields of HBT and related heterocyclic compounds in various solvents. The main aim of the present study is to investigate the effect of hydrogen bonding upon the luminescence properties in order to obtain further support for the mechanism of photochromism, and to estimate the rate constant of intramolecular hydrogen transfer.

Experimental

The compounds employed in the present work are 2-(2-hydroxyphenyl)bonzothiazole (HBT), 2-(2-methoxyphenyl)benzothiazole (MBT), and 2-(2-hydroxyphenyl)benzoxazole (HBO). Commercially available HBT and HBO were chromatographed from benzene on activated alumina. MBT was obtained by two methods; treatment of HBT with dimethyl sulfate and synthesis according to the method in literature.[6] Solvents used in the present study are: PM (1: 1 by volume of spectro-grade isopentane and spectro-grade methylcyclohexane), DCM (dichloromethane), AN (spectro-grade acetonitrile), AA (acetic acid), EPA (5: 5: 1 by volume of spectro-grade diethyl ether, isopentane, and ethanol), EM (1: 1 by volume of spectro-grade ethanol and methanol), and DMF (*N*,*N*-dimethylformamide).

Ultraviolet absorption spectra were measured with a Cary 14 RI recording spectrophotometer. Phosphorescence spectra and their decay times were measured with a conventional phosphoroscope by employing a 1 kW Hg arc as an exciting light source. Emission spectra were measured with a Spex 1700-II grating monochromator equipped with an EMI 6256S photomultiplier and a PAR 128 lock-in amplifier. Fluorescence and phosphorescence excitation spectra were measured by exciting samples with monochromatic light at various wavelengths obtained with a 1 kW Xe lamp and the Spex monochromator, and by detecting emission intensities by the combination of a Bausch and Lomb 0.5 m monochromator with the photomultiplier and the lock-in amplifier. The quantum yield ratio between the short- and long-wavelength fluorescences was obtained by comparing the integratedintensities of the corresponding bands in the corrected emission spectra.

The fluorescence quantum yield of HBT excited at 354 nm was determined with use of a Shimadzu RF-502 spectrofluorometer. The standard material was 9,10-diphenylanthracene, the quantum yield of which was determined to be 0.93 in 3-methylpentane.[7] A flash-photolysis apparatus at room temperature and method for the determination of fluorescence lifetimes were described previously.[4] The flash photolysis experiments were carried out at 77 K with an apparatus at Institute of Applied Electricity, Hokkaido University.[8]

Results and Discussion

Fluorescence and Absorption Spectra of HBT, MBT, and HBO. The absorption and emission spectra of HBT, MBT, and HBO are given in Figs. 1, 2, and 3, respectively. HBT and MBT belong to 2-phenyl derivatives of benzothiazole and have similar molecular structures. Their emission properties, however, are quite different. In EPA at 77 K HBT shows dual fluorescence with peaks at 500 and 370 nm, while MBT exhibits single fluorescence as a mirror image of the absorption band.

The short-wavelength fluorescence of HBT shows vibrational structure pertinent to the 2-phenyl derivatives of benzothiazole like MBT,[9] and therefore is attributed to the lowest excited singlet state of the enol tautomer.

The Stokes shift amounts to 8500 cm^{-1} for the long-

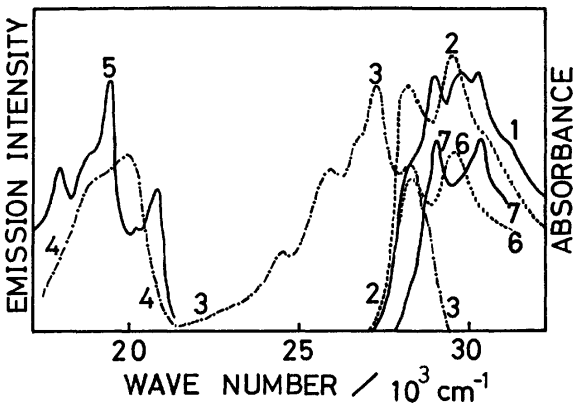

Fig. 1. The absorption, emission, and excitation spectra of HBT at 77 K: curve 1, absorption in EPA; curve 2, absorption in PM; curve 3, fluorescence of the enol imine in EPA; curve 6, fluorescence excitation spectrum of the keto amine in EPA; curve 7, fluorescence and phosphorescence excitation spectrum of the enol imine in EPA. Curves 3, 4, and 5 were measured under the excitation at 313 nm.

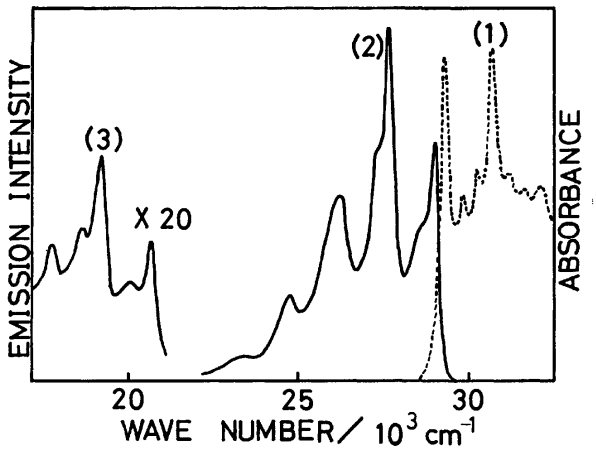

Fig. 2. The absorption (curve 1), fluorescence (curve 2), and phosphorescence (curve 3) spectra of MBT in EPA at 77 K. Curves 2 and 3 were measured under the excitation at 313 nm.

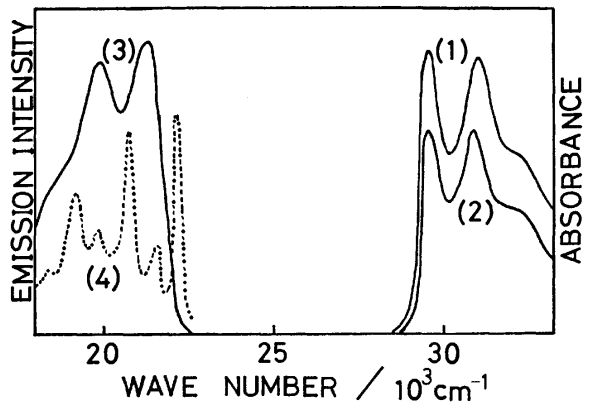

Fig. 3. The absorption and emission spectra of HBO at 77 K: curve 1, absorption in EPA; curve 2, absorption in PM curve 3, fluorescence of the keto amine in PM; curve 4, phosphorescence of the enol imine in PM. Curves 3 and 4 were measured under the excitation at 313 nm.

wavelength fluorescence of HBT. This suggests that the molecular framework changes in the excited state of the long-wavelength fluorescence. HBT can tautomerize from the enol imine to the keto amine, whereas MBT cannot. The excitation spectrum of the long-wavelength fluorescence of HBT in EPA at 77 K agrees well with the absorption spectrum of the HBT enol imine with the intramolecular hydrogen bond in PM at 77 K. This indicates that the long-wavelength fluorescence of HBT is due to the keto amine tautomer produced through hydrogen transfer in the excited state of the enol imine with the intermolecular hydrogen bond.

The relative intensities of the two fluorescence bands of HBT in solution are dependent on the solvent. The intensity of the short-wavelength fluorescence increases on going from the non-hydrogen-bonding or weakly hydrogen-bonding solvents (PM, DCM, and AN) to the strongly hydrogen-bonding solvents (AA, EPA, EM, and DMF). The fluorescence quantum yield ratios $\phi_f(E)/\phi_f(K)$ in various solvents are given in Table 1,

Table 1. $\phi_f(E)/\phi_f(K)$ in various solvents at 77K

	$\phi_f(E)/\phi_f(K)$
PM	$\leqslant 0.015$
DCM	$\leqslant 0.015$
AN	0.036 ± 0.002
AA	0.092 ± 0.005
EPA	1.6 ± 0.1
EM	3.0 ± 0.1
DMF	12 ± 1

where $\phi_f(E)$ and $\phi_f(K)$ are the fluorescence quantum yields for short- and long-wavelengths, respectively. When the short-wavelength fluorescence was too weak to be measured, an upper limit of $\phi_f(E)/\phi_f(K)$ was estimated from the limitation of detection. From these results and the discussion given above, it is concluded that the short-wavelength fluorescence of the dual emission is due to the enol imine with the intermolecular hydrogen bond, and the long-wavelength fluorescence to the keto amine produced by the hydrogen transfer in the excited state of the intramolecularly hydrogen-bonded enol imine. The absorption spectrum of HBT in EPA at 77 K is in good agreement with the superposition of the short- and long-wavelength fluorescence excitation spectra. In other words, the spectrum is interpreted as the superposition of the absorption spectra of the intramolecularly and intermolecularly hydrogen-bonded enol species of HBT.

Phosphorescence Spectra of HBT and MBT. HBT and MBT exhibit phosphorescence similar to that of 2-phenylbenzothiazole with respect to transition energy and vibrational structure.[9] The phosphorescence of HBT was observed only in the hydrogen-bonding solvents (AA, EPA, EM, and DMF). The $T_n \rightarrow T_1$ transition band of HBT was observed around 425 nm in EPA at 77 K, but not in the non-hydrogen-bonding solvent, PM at 77 K. In the HBT with the intramolecular hydrogen bond, hydrogen transfer through the bond occurs so fast that no triplet enol imine can be

formed. The excitation spectrum of HBT phosphorescence in EPA at 77 K is identical with that of the short-wavelength enol imine fluorescence. Thus the phosphorescence of HBT is assigned to the enol imine tautomer with the intermolecular hydrogen bond. The phosphorescence of the keto amine tautomer of HBT might appear above 600 nm from the position of the fluorescence band of the keto tautomer and the ordinary energy separation between π-π^* excited singlet and triplet states.

Relaxation Processes of Excited HBT in Hydrogen-bonding and Non-hydrogen-bonding Solvents. The relaxation processes after photoexciation of the HBT enol imine for HBT in non-hydrogen-bonding or weakly hydrogen-bonding solvents and in strongly hydrogen-bonding solvents are summarized in Figs. 4(a) and 4(b), respectively. In the former case in which HBT with the intramolecular hydrogen bond exists, the hydrogen transfer through the bond proceeds very fast in the excited state and the intermediate, X, is detected by picosecond time-resolved spectroscopy.[4] The photochromic state P and the *cis*-keto amine were formed from X competitively. In the latter case in which both intramolecular and intermolecular hydrogen bonded species coexist in equilibrium in the ground state, besides the processes mentioned above, the formation and decay processes of the triplet enol imine occur. "Sol" in Fig. 4(b) refers to a solvent molecule.

Electronic Spectra of HBO and HBT. The absorption spectrum of HBO in EPA at 77 K is essentially the same as that in PM (Fig. 3), showing that the dominant species in EPA at 77 K is the enol imine with the intramolecular hydrogen bond. The intramolecular hydrogen bond of HBO is more stable than that of HBT,[10] as Durmis *et al.* showed in their study of the dissociation constants.[11]

The emission spectra of HBO in PM are shown in Fig. 3. The emission properties of HBO in EPA at 77 K are very similar to those in PM at 77 K. The intensity of the keto amine fluorescence is much larger than that of the enol imine fluorescence or phosphorescence. The ratio $\phi_f(E)/\phi_f(K)$ was estimated to be less than 0.01 both in EPA and in PM at 77 K. The excitation spectra of the keto amine fluorescence and the enol imine phosphorescence agree with the absorption spectrum in PM at 77 K.

A difference between HBT and HBO is seen with respect to the yield of enol triplet formation. In PM at room temperature, the $T_n \leftarrow T_1$ transition was observed with HBO but not with HBT, while the photochromic transient absorption was observed with HBT but not with HBO. The phosphorescence of the enol imine with the internal hydrogen bond was observed with HBO but not with HBT at 77 K. These facts indicate that the intersystem crossing yield of the enol tautomer is larger for HBO than for HBT. The relaxation processes after photoexcitation of the HBO enol tautomer in EPA and in PM at 77 K are summarized in Fig. 5.

Primary Process of Photochromism. The yield $\phi_f(K)$

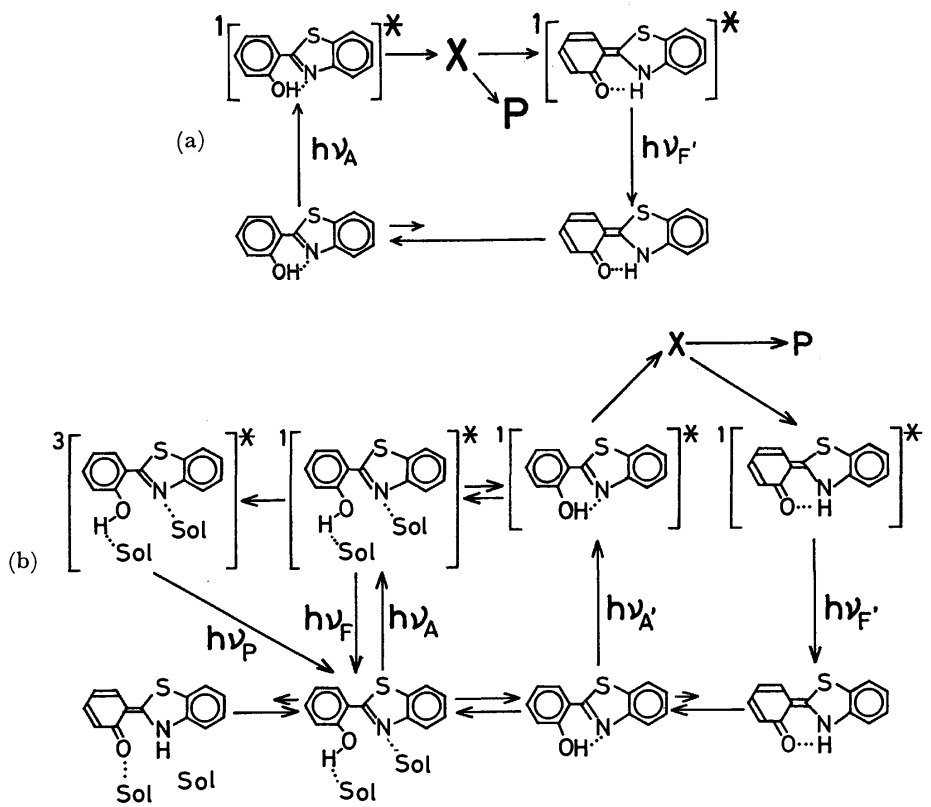

Fig. 4. Schematic diagrams representing the ground state equilibrium and relaxation processes in the excited state of HBT.
(a) In the weakly hydrogen-bonding or non-hydrogen bonding solvents.
(b) In the strongly hydrogen-bonding solvents.

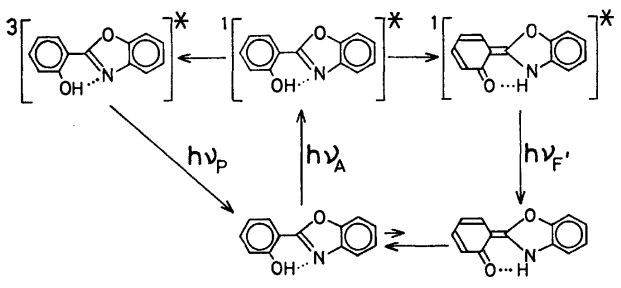

Fig. 5. Schematic diagram representing the ground state equilibrium and relaxation processes in the excited state of HBO.

of HBT in PM at 77 K was determined to be 0.36, and the ratio $\phi_f(E)/\phi_f(K)$ was estimated to be less than 0.015 (Table 1). From these values $\phi_f(E)$ at 77 K was evaluated to be less than 5.4×10^{-3}. For HBT in PM at 293 K, the yield $\phi_f(K)$ was determined to be 0.006, and the ratio $\phi_f(E)/\phi_f(K)$ was estimated to be less than 0.012. Thus the yield $\phi_f(E)$ at 293 K was evaluated to be less than 7.2×10^{-5}.

The enol fluorescence radiative rate constant k_f^e was estimated to be $2.3\times10^8\ s^{-1}$.[12] From this value and the yield $\phi_f(E)$, the lifetime of the enol imine fluorescent state was estimated to be shorter than 3.1×10^{-13} s. This is much shorter than the lifetime of the precursor, X, of the photochromic species (53 ps) determined in previous study.[4] This means that the enol imine fluorescent state is not the precursor. Thus we obtain an additional support for the scheme in which P is not formed directly from the enol excited state.

Estimation of the Rate Constant of the Intramolecular Hydrogen Transfer. The rate constants of the intramolecular hydrogen transfer at 77 and 293 K were estimated from the enol imine fluorescence quantum yield, which is given by

$$\phi_f(E) = \frac{k_f^e}{k_f^e + k_{fq}^e + k_{HT}}, \qquad (1)$$

where k_{fq}^e and k_{HT} represent the rate constants of the radiationless transition other than hydrogen transfer and of the intramolecular hydrogen transfer in the excited singlet state of the enol imine, respectively. From the decay times of the enol imine fluorescent state in the hydrogen bonding media, $(k_f^e + k_{fq}^e)$ in PM was estimated to be about $1\times10^9\ s^{-1}$ at 77 K. By putting the numerical values into Eq. 1, k_{HT} was evaluated to be larger than $4\times10^{10}\ s^{-1}$ at 77 K. At room temperature, $(k_f^e + k_{fq}^e)$ is at most of the order of $10^{11}\ s^{-1}$; k_{HT} was estimated from the values mentioned above to be larger than $3\times10^{12}\ s^{-1}$ in PM at 293 K.[13] By assuming an Arrhenius equation with a frequency factor of $10^{13}\ s^{-1}$ for k_{HT}, an upper limit of 0.9 kcal/mol was estimated for the barrier to the hydrogen transfer.[14] The value of k_{HT} at 77 K is greater than that for the 1,7-diazaindene hydrogen bonded dimer in 3-methylpentane at 77 K ($5\times10^8\ s^{-1}$) by a factor of at least 80,[15] and at 293 K it is greater than the value for 2,4-bis(dimethylamino)-6-(2-hydroxy-5-methylphenyl)-1,3,5-triazine in cyclohexane at 298 K ($1.1\times10^{10}\ s^{-1}$) by a factor of at least 270.[16] These large k_{HT} values can be explained as follows.

(1) A strong intramolecular hydrogen bond is formed in the HBT ground state, as shown by the pK_a value, NMR and IR spectroscopy and X-ray crystal analysis.[11,5,17] The O–N distances in the six-membered chelate ring are 2.605 Å for HBT, 2.584 Å for *N*-(5-chlorosalicylidene)aniline, and 2.609 Å for 2-chloro-*N*-salicylideneaniline.[18] These are examples of the shortest O–N distance in the OH···N hydrogen bond systems, the average O–N distance of which is 2.80 Å.[19] This strong intramolecular hydrogen bond favors the rapid hydrogen transfer in the excited state.

(2) Upon photoexcitation the phenolic hydroxyl group becomes more acidic and the imino nitrogen more basic than in the ground state. A similar situation has been reported for intramolecularly hydrogen-bonded salicylic acid derivatives.[20]

We are greatly indebted to Prof. Katsumi Kimura and Dr. Yohji Achiba, Hokkaido University, for their kindness in performing flash photolysis experiments at 77 K. We wish to thank Dr. Kazuo Shibata and Dr. Yorinao Inoue, the Institute of Physical and Chemical Research, for their kindness in putting the spectrofluorometer (Shimadzu RF-502) at our disposal.

References

1) (a) R. S. Becker and W. F. Richey, *J. Am. Chem. Soc.*, **89**, 1298 (1967): (b) W. F. Richey and R. S. Becker, *J. Chem. Phys.*, **49**, 2092 (1968).

2) (a) M. Ottolenghi and D. S. McClure, *J. Chem. Phys.*, **46**, 4613, 4620 (1967): (b) R. Potashnik and M. Ottolenghi, *ibid.*, **51**, 3671 (1969): (c) T. Rosenfeld, M. Ottolenghi, and A. Y. Meyer, *Mol. Photochem.*, **5**, 39 (1973).

3) (a) M. D. Cohen and G. M. J. Schmidt, *J. Phys. Chem.*, **66**, 2442 (1962): (b) M. D. Cohen, Y. Hirshberg, and G. M. J. Schmidt, *J. Chem. Soc.*, **1964**, 2051.

4) R. Nakagaki, T. Kobayashi, J. Nakamura, and S. Nagakura, *Bull. Chem. Soc. Jpn.*, **50**, 1909 (1977).

5) M. D. Cohen and S. Flavian, *J. Chem. Soc., B*, **1967**, 317, 321.

6) H. P. Lankelma and P. X. Sharnoff, *J. Am. Chem. Soc.*, **53**, 2654 (1931).

7) J. V. Morris, M. A. Mahaney, and J. R. Huber, *J. Phys. Chem.*, **80**, 969 (1976).

8) Y. Achiba and K. Kimura, *Chem. Phys. Lett.*, **48**, 107 (1977).

9) A. Olszowski, H. Romanowski, and Z. Ruziewicz, *Bull. Acad. Pol. Sci., Ser. Sci. Math. Astr. Phys.*, **21**, 381 (1973).

10) On treatment with dimethyl sulfate under the usual conditions, HBT is easily methylated but HBO is hardly converted into the corresponding methoxy derivative. This reflects the difference in stability of the intramolecular hydrogen bond between HBT and HBO.

11) J. Durmis, M. Karvaš, and Z. Maŭásek, *Collect. Czech. Chem. Commun.*, **38**, 215, 224, 243 (1973).

12) The fluorescence radiative rate constant k_f^e was calculated by Förster's formula:

$$k_f^e = 2.88\times10^{-9}n^2\int\frac{(2\nu_0-\nu)^3}{\nu}\varepsilon(\nu)d\nu.$$

13) This value of k_{HT} is of the same order or a little larger than the usual values of the rate constants of vibrational relaxation in condensed media. This suggests that the intramolecular hydrogen transfer occurs from not only the thermalized

state in the lowest excited singlet state (S_1) but levels of S_1, and gives a plausible explanation for dependence on the excitation wavelength of the quantum yield of the photochromic colored species reported by Rosenfeld *et al.*[2c]

14) The hydrogen transfer in the enol excited state is a cooperative phenomenon, in which such particular vibrations as the stretching vibrations of the phenolic hydroxyl group and the aromatic nucleus of the salicylaldehyde moiety, participate. Consequently, it is reasonable to assume that the rate constant of phototautomerization follows the Arrhenius equation with a frequency factor of 10^{13} s^{-1}, which is commonly observed for the order of the stretching vibration frequency in the excited state.

15) M. A. El-Bayoumi, P. Avouris, and W. R. Ware, *J. Chem. Phys.*, **62**, 2499 (1975).

16) H. Shizuka, K. Matsui, Y. Hirata, and I. Tanaka, *J. Phys. Chem.*, **80**, 2070 (1976).

17) P. Stenson, *Acta Chem. Scand.*, **24**, 3729 (1970).

18) (a) J. Bregman, L. Leiserowitz, and G. M. J. Schmidt, *J. Chem. Soc.*, **1964**, 2068; (b) J. Bregman, L. Leiserowitz, and K. Osaki, *ibid.*, **1964**, 2086.

19) G. C. Pimentel and A. L. McClellan, "The Hydrogen Bond," W. H. Freeman and Co., San Francisco (1960), p. 289.

20) A. Weller, "Progress in Reaction Kinetics," Vol. 1, ed by G. Porter, Pergamon Press Ltd., London (1961), pp. 188—214.

Selective Hydrogen Atom Abstraction by H Atoms in Radiolysis and Photolysis at 77 K: Decane-d_{22}, Tetramethylsilane, and Xenon Matrices

Tetsuo MIYAZAKI,* Joji KASUGAI, Manabu WADA, and Kazuhisa KINUGAWA

Department of Synthetic Chemistry, Faculty of Engineering, Nagoya University, Chikusa-ku, Nagoya 464

(Received November 19, 1977)

The selective formation of HD and solute radicals in the radiolysis of n-$C_{10}D_{22}$ doped with n-$C_{10}H_{22}$ at 77 K is explained quantitatively by the mechanism of a selective hydrogen-atom-abstraction reaction by D atoms. The selective hydrogen-atom abstraction by H atoms is found also in tetramethylsilane and xenon matrices as well as in the alkane matrix. The rate constants of the abstraction reaction by H atoms are compared with the bond energies of the solvent and solute molecules. The bond energy of the solvent molecule is always higher than that of the solute molecule. Even if the difference in the bond energy between the solvent and the solute is very small, the k(solute)/k(solvent) ratio is quite large. The k(solute)/k(*neo*-C_5H_{12}) ratios for different solutes in a neopentane matrix are not influenced by the differences in the bond energy among the solutes. Since an isotope effect on the selective hydrogen-atom abstraction reaction is small, the effect may diminish the possibility of the quantum mechanical tunneling abstraction by thermal H atoms. The energy loss of hot H atoms in a Xe matrix is discussed.

Since hydrogen and alkyl radicals are the predominant products in the radiolysis of alkanes in the solid phases, C–H bond rupture, with the resultant formation of the H atom, is one of the most important processes in the radiolysis of solid hydrocarbons. H atoms may play also an important role in the radiation effect of polymers[1] and biological solid substances.[2]

Recently Miyazaki *et al.* have found a quite interesting phenomenon concerning a hydrogen-atom abstraction reaction by H atoms in solid alkane mixtures at 77 K.[3] When H atoms are produced at 77 K by the UV-photolysis of hydrogen halide or by the radiolysis of solvent neopentane, the H atoms react selectively with the solute alkane, resulting in the formation of solute radicals. The experimental basis for the reaction of the H atoms has been described fully in previous papers.[3a,b,e] This phenomenon has also been found in several alkane matrices, such as neopentane,[3a,b] isobutane,[3a,c] 2,2,3,3-tetramethylbutane,[3c] cyclopropane,[3c] cyclohexane,[3d] pentane,[3d] and 3-methylpentane-d_{14}.[4]

Though a number of studies of the reaction of H atoms have been undertaken previously in gas and liquid phases at temperatures higher than room temperature, the studies in the solid phase at low temperatures have been limited to a few examples. The selective hydrogen-atom-abstraction reaction by H atoms in the solid phase at 77 K has raised new problems concerning its reaction kinetics. If hot H atoms are involved in the reaction, they must migrate a long distance through the alkane matrix 77 K without losing their kinetic energies. If thermal H atoms are involved, the activation energy for hydrogen-atom abstraction must be nearly zero in the alkane matrix at 77 K, though the value amounts to 7—10 kcal/mol in the gas phase.[5] Therefore, the study of the behavior of H atoms in the solid phase is important in solid-reaction kinetics as well as in solid-radiation chemistry.

The research described herein was undertaken in order to obtain further information about the reaction of the H atoms at 77 K. Answers to the following three questions have been sought: (1) Lund *et al.*[6] have reported that when n-$C_{10}D_{22}$ doped with a small amount of n-$C_{10}H_{22}$ is γ-irradiated at 77 K, solute $C_{10}H_{21}$ radicals are formed in a much higher yield than would be expected from the concentration. They ascribed this result to the excitation transfer from deuterated to protiated molecules. The results, however, can be explained also by a selective hydrogen-atom-abstraction reaction by D atoms. Recently it has been reported independently by two groups[7,8] that HD is formed selectively in the radiolysis of n-$C_{10}D_{22}$–n-$C_{10}H_{22}$ mixtures at 77 K. The results were interpreted qualitatively by quite different mechanisms: a mechanism of excitation transfer[7] and one of selective hydrogen-atom abstraction by the D atom.[8] In order to discriminate the two mechanisms, the estimation of the yield of hydrogen *via* the molecular detachment process in the radiolysis of pure n-$C_{10}D_{22}$ and n-$C_{10}H_{22}$ at 77 K is important. In this study, the yield of hydrogen *via* the molecular detachment will be reported first. Then, we will give an answer to a question of which of the two mechanisms can best explain the absolute yields of the isotopic composition of the hydrogen gas. (2) The selective hydrogen-atom abstraction by H atoms has been found previously in alkane matrices at 77 K. Does the selective reaction take place also in matrices other than alkanes? Here we have examined tetramethylsilane (TMS) and xenon matrices at 77 K. (3) Selective hydrogen-atom abstraction reactions by H atoms have been found in several alkane matrices at 77 K. What are the rate constants of these reactions? Is there any relationship between the rate constants and the C–H bond energies?

Experimental

The D content of decane-d_{22}, supplied by Merck Sharp and Dohm, Canada, Ltd., is 99%. Tetramethylsilane (TMS), supplied by the Merck Co., is more than 99.7 mol%. Xenon, supplied by the Takachiho Shoji Co., is more than 99.9 mol%. The other reagents used in this study are the same as those used before.[3c]

UV illumination was provided by Toshiba medium-pressure

* All correspondence should be addressed.

mercury lamps. γ-Irradiation was done by Co-60 at a dose rate of 2.3×10^{19} eV/g h.

The hydrogen was analyzed by means of a gas buret connected to a Toepler pump and mass spectrometer (RMS-4 Hitachi mass spectrometer). The yields are the averages of two runs. The free radicals were measured at 77 K with a JES-3BX ESR spectrometer. The microwave power levels used did not result in the saturation of the signal of the alkyl radicals.

Results and Discussion

Selective Hydrogen-atom-abstraction Reaction in Decane-d_{22}. In order to discuss the mechanisms for the formation of hydrogen in the radiolysis of n-$C_{10}D_{22}$–n-$C_{10}H_{22}$ mixtures, the yields of the hydrogen gas formed in an unimolecular reaction must first be estimated, though this process has been tentatively neglected in a recent paper.[7] The formation of H_2 from decane at 77 K can be represented as follows:

$$RH \begin{cases} \rightsquigarrow R\cdot + H & (1) \\ \rightsquigarrow \text{Olefin} + H_2 & (2) \end{cases}$$

$$2H \longrightarrow H_2 \quad (3)$$

$$H + RH \longrightarrow R\cdot + H_2 \quad (4)$$

Here, RH and R· represent the decane and the alkyl radicals respectively. Since the alkyl radicals produced by the radiolysis of decane at 77 K are isolated radicals,[6b,9] it is assumed here that all of the alkyl radicals are trapped at 77 K. The formation of one hydrogen molecule by an H atom produces two alkyl radicals. Therefore, a half of $G(R\cdot)$ corresponds to the amount of H_2 formation by an H-atom process. The G-value for the formation of a $C_{10}H_{21}$ radical in the radiolysis of pure n-$C_{10}H_{22}$ at 77 K has been reported as 5.4,[6b] 3.1,[9] and 6.0,[10] the mean value being 4.8. Therefore, $G(H_2)$ from the H-atom process is $4.8/2=2.4$. $G(C_{10}D_{21})$ in the radiolysis of n-$C_{10}D_{22}$ at 77 K has been reported as 4.1[6b] and 3.1,[9] the mean value being 3.6. $G(H_2)$ and $G(D_2)$ in the radiolysis of pure n-$C_{10}H_{22}$ and n-$C_{10}D_{22}$ at 77 K were measured here as 4.3 and 2.9 respectively at a dose of 3.4×10^{19} eV/g. Therefore, the molecular yields are (4.3—2.4) for n-$C_{10}H_{22}$ and (2.9—1.8) for n-$C_{10}D_{22}$. The ratios of G(hydrogen) by the molecular process to G(hydrogen) by the atomic process are 0.79 for n-$C_{10}H_{22}$ and 0.61 for n-$C_{10}D_{22}$. A similar high molecular yield was reported previously in the radiolysis of solid n-C_6H_{14} at 77 K.[11] The G-values of hydrogen in the radiolysis of n-$C_{10}D_{22}$–n-$C_{10}H_{22}$ mixtures at 77 K are shown in Fig. 3. The results obtained by Lund *et al.*[7] are approximately the same as those obtained by present authors. There is a possibility that hydrogen might react with alkyl radicals during the melting of the irradiated sample, as was observed in irradiated polyethylene.[12] Since the activation energy for this reaction is 13 kcal/mol, however, it takes several hours for the reaction to occur at room temperature.[12] Therefore, we can neglect the possibility that the hydrogen produced by the radiolysis of decane might react with the alkyl radicals while the irradiated decane is warmed up.

Three mechanisms explaining the hydrogen yields will be compared: energy transfer with the resultant formation of a thermal H atom, energy transfer with the resultant formation of a hot H atom, and selective hydrogen-atom abstraction by a D atom. The hydrogen yields are calculated from the yields of the alkyl radicals, which were measured by ESR spectroscopy,[6] and are compared with the hydrogen yields obtained here experimentally.

A) Energy transfer with the resultant formation of a thermal H atom.

$$C_{10}D_{22} \rightsquigarrow C_{10}D_{22}^* \quad (1)$$

$$C_{10}D_{22}^* \longrightarrow C_{10}D_{21} + D \quad a \quad (2)$$

$$\searrow\ C_{10}D_{20} + D_2 \quad 0.305a \quad (3)$$

$$C_{10}D_{22}^* + C_{10}H_{22} \longrightarrow C_{10}D_{22} + C_{10}H_{22}^* \quad (4)$$

$$C_{10}H_{22} \rightsquigarrow C_{10}H_{22}^* \quad (5)$$

$$C_{10}H_{22}^* \longrightarrow C_{10}H_{21} + H \quad b \quad (6)$$

$$\searrow\ C_{10}H_{20} + H_2 \quad 0.395b \quad (7)$$

$$2D \longrightarrow D_2 \quad a^2/[2(a+b)] \quad (8)$$

$$2H \longrightarrow H_2 \quad b^2/[2(a+b)] \quad (9)$$

$$D + H \longrightarrow HD \quad 2ab/[2(a+b)] \quad (10)$$

Here, a and b are the yields of the $C_{10}D_{21}$ and $C_{10}H_{21}$ radicals respectively, which were obtained by ESR spectroscopy.[6] The G-value of the alkyl radicals is taken as 3.6. The excited $C_{10}D_{22}$ molecule, produced by γ-irradiation, transfers its energy to the solute $C_{10}H_{22}$ (Reactions 1 and 4). It is assumed here that the decomposition of excited decane produces thermal atoms and hydrogen molecules (Reactions 2, 3, 6, and 7). The thermal atoms recombine with each other at 77 K (Reactions 8, 9, and 10). The calculated G-values of hydrogen are shown in Fig. 1. $G(H_2)$ increases remarkably with an increase in the concentration of $C_{10}H_{22}$. G(HD) increases sharply at a low concentration of $C_{10}H_{22}$ and then reaches a plateau at a higher concentration.

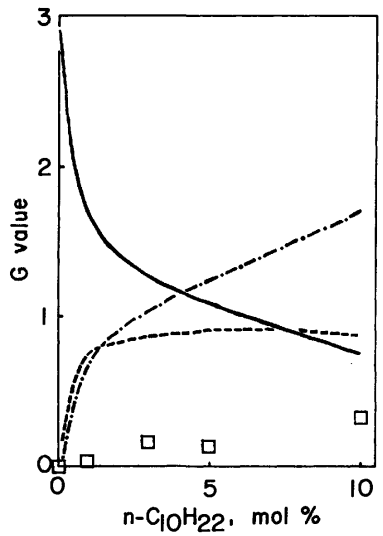

Fig. 1. Yields of hydrogen calculated by the model of energy transfer, with the resultant formation of the thermal H atom.
——, D_2; ——, HD; -·-·-, H_2; □, H_2 obtained experimentally.

The calculated G-values do not coincide at all with the experimental $G(H_2)$.

B) Energy transfer with the resultant formation of a hot H atom.

$$C_{10}D_{22} \rightsquigarrow C_{10}D_{22}^* \quad (1)$$

$$C_{10}D_{22}^* \longrightarrow C_{10}D_{21} + D \qquad c \quad (2)$$

$$\searrow\ C_{10}D_{20} + D_2 \qquad 0.61c \quad (3)$$

$$C_{10}D_{22}^* + C_{10}H_{22} \longrightarrow C_{10}D_{22} + C_{10}H_{22}^* \quad (4)$$

$$C_{10}H_{22} \rightsquigarrow C_{10}H_{22}^* \quad (5)$$

$$C_{10}H_{22}^* \longrightarrow C_{10}H_{21} + H \qquad d \quad (6)$$

$$\searrow\ C_{10}H_{20} + H_2 \qquad 0.79d \quad (7)$$

$$D + C_{10}D_{22} \longrightarrow C_{10}D_{21} + D_2 \qquad c(1-x) \quad (11)$$

$$D + C_{10}H_{22} \longrightarrow C_{10}H_{21} + HD \qquad cx \quad (12)$$

$$H + C_{10}D_{22} \longrightarrow C_{10}D_{21} + HD \qquad d(1-x) \quad (13)$$

$$H + C_{10}H_{22} \longrightarrow C_{10}H_{21} + H_2 \qquad dx \quad (14)$$

Here, c and d are the yields of hot D atoms and hot H atoms respectively, which are calculated from the yields of $C_{10}D_{21}$ and $C_{10}H_{21}$ radicals.[6] x represents the mole fraction of the solute $C_{10}H_{22}$. The excited $C_{10}D_{22}$ molecule transfers its energy to the solute $C_{10}H_{22}$ (Reaction 4). It is assumed that the decomposition of excited decane produces hot H(or D) atoms and hydrogen molecules (Reactions 2, 3, 6, and 7). The hot atoms abstract H or D atoms from decane molecules (Reactions 11, 12, 13, and 14). It is assumed here that $k_{11}=k_{12}$ and $k_{13}=k_{14}$. The G-value of the alkyl radical is taken as 3.6. Though the total alkyl-radical yields in the A and B mechanisms are the same, c(or d) is different from a(or b) because of the different mechanisms of the radical formations in the two mechanisms. The calculated G-values of hydrogen are shown in in Fig. 2. $G(D_2)$ approaches zero at 10 mol% of $C_{10}H_{22}$, while $G(HD)$ and $G(H_2)$ increase remarkably with an increase in the concentration of $C_{10}H_{22}$. The calculated

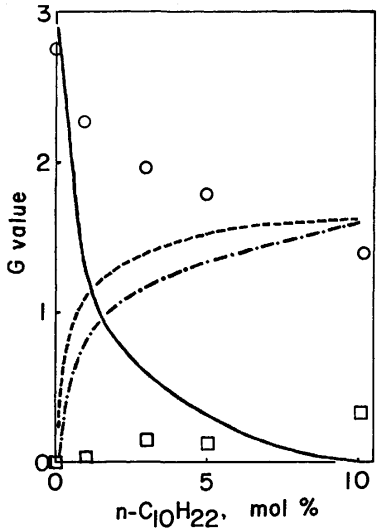

Fig. 2. Yields of hydrogen calculated by the model of energy transfer, with the resultant formation of the hot H atom.
——, D_2; ——, HD; -·-·-, H_2; ○, D_2 obtained experimentally; □, H_2 obtained experimentally.

G-values do not coincide at all with the experimental $G(D_2)$ and $G(H_2)$.

C) Selective hydrogen atom abstraction by a D atom.

Recently it has been found that H atoms, produced by the radiolysis of solvent alkane at 77 K, react selectively with solute alkane to produce solute alkyl radicals.[3] Though it has been suggested that this mechanism may play only a minor role,[6] we will discuss here the possibility.

$$C_{10}D_{22} \rightsquigarrow C_{10}D_{22}^* \quad (1)$$

$$C_{10}D_{22}^* \longrightarrow C_{10}D_{21} + D \qquad e(1-x) \quad (2)$$

$$\searrow\ C_{10}D_{20} + D_2 \qquad 0.61e(1-x) \quad (3)$$

$$C_{10}H_{22} \rightsquigarrow C_{10}H_{22}^* \quad (5)$$

$$C_{10}H_{22}^* \longrightarrow C_{10}H_{21} + H \qquad 1.33ex \quad (6)$$

$$\searrow\ C_{10}H_{20} + H_2 \qquad 1.05ex \quad (7)$$

$$D + C_{10}D_{22} \longrightarrow C_{10}D_{21} + D_2 \qquad e(1-x)^2/[Kx+1-x] \quad (11)$$

$$D + C_{10}H_{22} \longrightarrow C_{10}H_{21} + HD \qquad ex(1-x)K/[Kx+1-x] \quad (12)$$

$$H + C_{10}D_{22} \longrightarrow C_{10}D_{21} + HD \qquad 1.33ex(1-x)/[Kx+1-x] \quad (13)$$

$$H + C_{10}H_{22} \longrightarrow C_{10}H_{21} + H_2 \qquad 1.33ex^2K/[Kx+1-x] \quad (14)$$

Here, e is a half of the yield of $C_{10}D_{21}$ radicals in the radiolysis of pure n-$C_{10}D_{22}$ and is taken as 1.8 G-unit. [The amounts of Reactions 2 and 3 at $x=0$]/[the amounts of Reactions 6 and 7 at $x=1$] is equal to $[G(D_2)$ in pure n-$C_{10}D_{22}]/[G(H_2)$ in pure n-$C_{10}H_{22}]$, that is, 0.67. The D atoms produced by the radiolysis of n-$C_{10}D_{22}$ react selectively with the solute $C_{10}H_{22}$ to form $C_{10}H_{21}$ radicals. It is assumed that $k_{12}/k_{11}=k_{14}/k_{13}$, which is denoted by K. K is estimated to be 61 by using the yields[6] of the $C_{10}H_{21}$ and $C_{10}D_{21}$ radicals. The calculated yields for D_2, HD, and H_2 are shown in Fig. 3. The coincidence of the calculated curves with the experimental yields may be good, if we take into consideration of the fact that the calculation for the final products has been based upon independent results, that is to say, the yields of free radicals as measured by ESR spectroscopy. If K is taken tentatively as 27, the coincidence becomes much better, as is shown in Fig. 3.

Therefore, we can conclude that the selective formation of the solute $C_{10}H_{21}$ radical and HD in the radiolysis of the n-$C_{10}D_{22}$–n-$C_{10}H_{22}$ mixture at 77 K is not due to the energy transfer from the solvent to the solute, but to the selective hydrogen-atom abstraction from the solute by the D atom. The reaction-rate constant (k_{12}) of the D atom with n-$C_{10}H_{22}$ is 27 times greater than that (k_{11}) with n-$C_{10}D_{22}$.

Though the experimental results obtained here are approximately the same as those reported by Lund *et al.*,[7] the conclusion of this work is quite different from that of Ref. 7. This difference is caused by the following two factors. First, Lund *et al.* neglected tentatively the formation of hydrogen by a molecular detachment process. On the contrary, the yield of the molecular detachment process is estimated experimental-

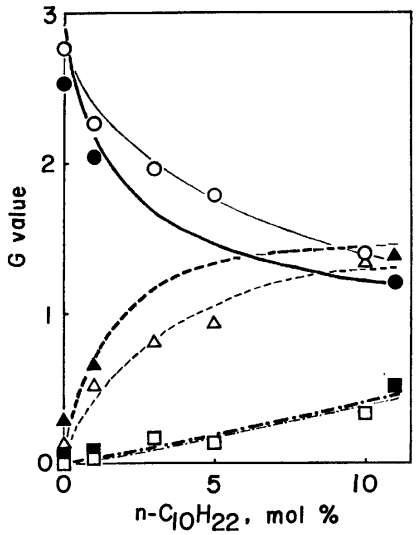

Fig. 3. Comparison of experimental hydrogen yields with the yields calculated by the model of selective hydrogen-atom abstraction by the D atom. Since the results by Lund *et al.* are relative yields, the *G*-values by Lund *et al.* are calculated by using the total *G*-value of hydrogen in this work.
○: D_2 obtained experimentally in this work, ●: D_2 obtained experimentally by Lund *et al.*, △: HD obtained experimentally in this work, ▲: HD obtained experimentally by Lund *et al.*, □: H_2 obtained experimentally in this work, ■: H_2 obtained experimentally by Lund *et al.*, ——: D_2 calculated by taking K as 61, ------: HD calculated by taking K as 61, - - - -: H_2 calculated by taking K as 61, ——: D_2 calculated by taking K as 27, ------: HD calculated by taking K as 27, - · - · -: H_2 calculated by taking K as 27.

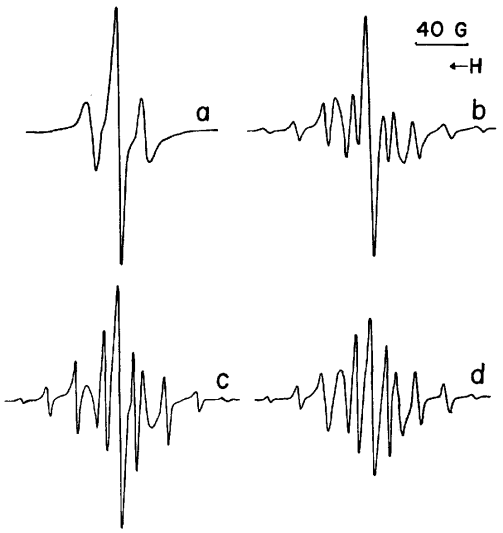

Fig. 4. ESR spectra of irradiated tetramethylsilane(TMS) at 77 K. The unit of the solute concentration is mol/100 mol of TMS.
a: γ-Irradiated TMS, b: γ-irradiated TMS-i-C_4H_{10}-(0.46), c: γ-irradiated TMS-i-C_4H_8(0.1), d: UV-irradiated TMS-i-C_4H_{10}(0.75)-HI(0.2).

ly in this paper and the process is taken into consideration in the discussion. Second, since it has been found that H atoms react quite selectively with the solute alkane in alkane mixtures at 77 K,[3] the possibility of a high selectivity for the H atom abstraction reaction by D atoms has been considered in this paper. Lund *et al.*, however, neglected the possibility of the high selective reaction of D atoms at 77 K.

Selective Hydrogen-atom-abstraction Reaction in Tetramethylsilane (TMS). Figure 4a shows the ESR spectra of γ-irradiated pure TMS at 77 K. The spectrum of the three broad lines with a separation of 20.8 G is attributable to the $(CH_3)_3\dot{S}iCH_2$ (TMS·) radical. Figures 4a and c show the ESR spectra of γ-irradiated TMS containing i-C_4H_{10} and i-C_4H_8 respectively. The spectra consist of three broad lines, which are attributable to the TMS· radical, and eight narrow lines with a separation of 22.8 G, which are attributable to the t-C_4H_9 radical. Figure 4d shows the ESR spectra of UV-illuminated TMS containing i-C_4H_{10} and HI. The spectra consist of three broad lines, ascribed to the TMS· radicals, and eight narrow lines, ascribed to the t-C_4H_9 radical.

The yields of the radicals in Fig. 4b can be estimated by the integration of the spectrum. From the decomposition of the integrated spectrum into t-C_4H_9 and TMS· radicals, the amount of the t-C_4H_9 radical is estimated to be 13% of the total radical yield. Since an electron fraction of i-C_4H_{10} in the TMS-i-C_4H_{10} (0.46 mol/100 mol of TMS) mixture is 0.0031, the formation of the t-C_4H_9 radical is sensitized 42-fold. Therefore, some activation, produced by the γ-irradiation of TMS, is transfrred to the i-C_4H_{10} solute.

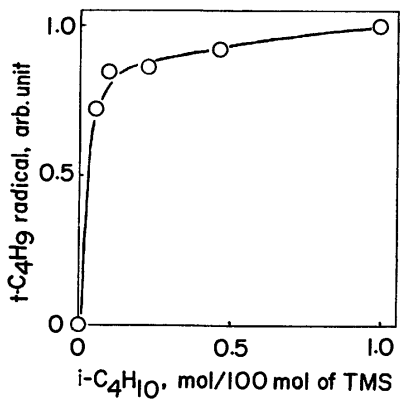

Fig. 5. Yields of the t-C_4H_9 radical against the concentration of i-C_4H_{10} in the radiolysis of TMS-i-C_4H_{10} mixtures at 77 K.

The yields of the t-C_4H_9 radicals are shown in Fig. 5 as a function of the i-C_4H_{10} concentration. The yields do not increase linearly with an increase in the i-C_4H_{10} concentration; at low concentrations they rise steeply, and then approach a plateau value at higher concentrations. This nonlinear increase in the yields indicates also that the formation of the t-C_4H_9 radical does not result from the direct absorption of the ionizing radiation by i-C_4H_{10}, but from the activation transfer from TMS to i-C_4H_{10}.

It is suggested by the following two reasons that the mechanism of the activation transfer may be due to a selective hydrogen-atom-abstraction reaction from i-

C_4H_{10} by H atoms, as is observed in the radiolysis of alkane mixtures:[3] (1) When isobutane is added to TMS, the t-C_4H_9 radical is formed by the addition of the H atom to the olefin (Fig. 4c). (2) When H atoms are produced by the photolysis of hydrogen iodide in TMS containing a small amount of i-C_4H_{10}, the H atoms react selectively with the i-C_4H_{10} solute to form t-C_4H_9 radicals (Fig. 4d).

A maximum yield of t-C_4H_9 radicals in the radiolysis of TMS–i-C_4H_{10} mixture amounts to 15% of the total radical yield. 50% of the total radical yields corresponds to the yields of TMS· radicals which are produced by the decomposition of TMS molecules (*cf.* Reactions 15 and 16). Therefore, 30% of the H atoms produced by the radiolysis of TMS migrate to the i-C_4H_{10} solute. The rest react promptly with TMS molecules (Reaction 17).

$$\text{TMS} \longrightarrow \text{TMS}\cdot + H_{ab} \quad (15)$$

$$\text{TMS} \longrightarrow \text{TMS}\cdot + H_{mig} \quad (16)$$

$$H_{ab} + \text{TMS} \longrightarrow \text{TMS}\cdot + H_2 \quad (17)$$

$$H_{mig} + i\text{-}C_4H_{10} \longrightarrow t\text{-}C_4H_9 + H_2 \quad (18)$$

$$H_{mig} + \text{TMS} \longrightarrow \text{TMS}\cdot + H_2 \quad (19)$$

H_{ab} represents an H atom which reacts promptly with TMS and does not migrate through the matrix. H_{mig} represents an H atom which can migrate through the matrix and reacts with i-C_4H_{10} or TMS during its excursion. It is uncertain at present whether the difference between H_{ab} and H_{mig} atoms is due to the difference in their kinetic energies or to that in the initial direction of their translational motions, the possibility of which was suggested in a recent paper.[13]

TABLE 1. H ATOMS PRODUCED IN THE RADIOLYSIS AND PHOTOLYSIS IN THE ALKANE MATRIX AT 77 K[a]

Matrix	Method of production of H atom	Fractions of two kinds of H atoms	
		H_{ab}, %	H_{mig}, %
neo-C_5H_{12}	radiolysis of *neo*-C_5H_{12}	54[b]—36[c]	46[b]—64[c]
neo-C_5H_{12}	photolysis of HI[d]	<10	>90
TMB[e]	radiolysis of TMB[f]	60	40
TMB[e]	photolysis of HI[g]	60	40
TMS[h]	radiolysis of TMS[i]	70	30
TMS[h]	photolysis of TMS[j]	70	30

a) The unit of the solute concentration in the footnotes is mol/100 mol of the solvent molecule. The concentrations of solute alkanes in this work are sufficient to capture almost all the H_{mig} atoms. b) The value is obtained in the radiolysis of *neo*-C_5H_{12}–i-C_4H_{10}(2). c) The value is quoted from the results by Iwasaki *et al.* in the radiolysis of *neo*-C_5H_{12}–c-C_6H_{12}(2) (*cf.* M. Iwasaki, K. Toriyama, K. Nunome, M. Fukaya, and H. Muto, *J. Phys. Chem.*, **81**, 1410 (1977)). d) The value is obtained in the photolysis of *neo*-C_5H_{12}–i-C_4H_{10}(2)–HI(0.5). e) TMB is 2,2,3,3-tetramethylbutane. f) The value is obtained in the radiolysis of TMB–C_3H_8 (4.9). g) The value is obtained in the photolysis of TMB–C_3H_8 (3.6)–HI(0.5). h) TMS is tetramethylsilane. i) The value is obtained in the radiolysis of TMS–i-C_4H_{10}(1.0). j) The value is obtained in the photolysis of TMS–i-C_4H_{10}(0.8)–HI(0.2).

Therefore, the notation of H_{ab} and H_{mig} is a phenomenological discrimination of the two kinds of hydrogen atoms; one reacts promptly with the solvent, while the other migrates through the solvent to react with a solute alkane. The presence of two kinds of H atoms is observed also in other alkane matrices. The results are summarized in Table 1. The relative yields of H_{mig} decrease in the following order: neopentane, 2,2,3,3-tetramethylbutane, and tetramethylsilane. The yields might be influenced by a crystalline structure, the rigidness of the solid, and so on.

Selective Hydrogen-atom-abstraction Reaction in Xenon.

When xenon containing a small amount of i-C_4H_{10} and HI is illuminated at 77 K by ultraviolet light, t-C_4H_9 radicals are clearly observed by ESR spectroscopy. The ESM spectra were reported in a previous paper.[14] The efficiency of the formation of butyl radicals is approximately the same as that in the photolysis of the *neo*-C_5H_{12}–i-C_4H_{10}–HI system at 77 K. H atoms, produced by the photolysis of HI, migrate through a xenon matrix and react with the i-C_4H_{10} solute (Reactions 20 and 21):

$$\text{HI} \xrightarrow{h\nu} \text{H} + \text{I} \quad (20)$$

$$\text{H} + i\text{-}C_4H_{10} \longrightarrow H_2 + t\text{-}C_4H_9 \quad (21)$$

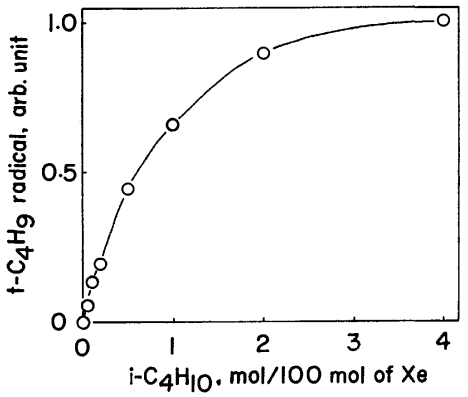

Fig. 6. Yields of the t-C_4H_9 radical against the concentration of i-C_4H_{10} in the UV-photolysis of Xe–i-C_4H_{10}–HI(0.15 mol/100 mol of Xe) at 77 K.

The yields of the t-C_4H_9 radicals are shown in Fig. 6 as a function of the i-C_4H_{10} concentration. A crude estimation of the average distance that the H atoms must be able to travel is available from the yields in Fig. 6. The simplest approach is to use a "target" model in which an H atom travels through a certain volume of the matrix where n atoms of xenon exit. When one molecule of i-C_4H_{10} exists in this volume, the H atom reacts with the i-C_4H_{10} solute. The ratio of the yield (I) of a t-C_4H_9 radical at the i-C_4H_{10} concentration (c mol/mol of Xe) to that (I_∞) at an infinite i-C_4H_{10} concentration is expected to be of the form

$$I/I_\infty = 1 - \exp(-nc). \quad (a)$$

It is assumed that I_∞ is approximately the same as the yield of a t-C_4H_9 radical at 4 mol/100 mol of Xe. Equation a can be expressed as

$$-\log\{1-(I/I_\infty)\} = nc \log e. \quad (b)$$

A good linear relationship between $-\log\{1-(I/I_\infty)\}$ and i-C_4H_{10} concentration is obtained. The actual value found for n is 114. It is concluded that the H atoms produced by the photolysis of HI migrate through 114 atoms of xenon at 77 K.

Correlation between the Rate Constant for H-atom Abstraction and the C–H Bond Energy. A selective hydrogen-atom-abstraction reaction by H atoms has been found previously in several matrices, such as n-$C_{10}D_{22}$, TMS, and Xe matrices. It is interesting to summarize the selectivities of the reactions in these matrices. H atoms which can migrate through the matrix are formed by

$$RH \rightsquigarrow H_{mig} + R\cdot \quad (22)$$

$$(HI \xrightarrow{h\nu} H_{mig} + I) \quad (23)$$

$$H_{mig} + SH \xrightarrow{k(\text{solute})} H_2 + S\cdot \quad (24)$$

$$H_{mig} + RH \xrightarrow{k(\text{solvent})} H_2 + R\cdot \quad (25)$$

the radiolysis of solvent molecules (RH) or by the photolysis of hydrogen iodide (Reactions 22 or 23). They react selectively with solute molecules (SH). It is assumed here that the H atoms may react also with solvent molecules, competing with Reaction 24. If the rate of the formation of H_{mig} is expressed as I, the following relationship is obtained by a steady-state treatment:

$$\frac{1}{r(S\cdot)} = \frac{1}{I} + \frac{k(\text{solvent})[RH]}{Ik(\text{solute})[SH]}, \quad (c)$$

where $r(S\cdot)$ is the rate of the formation of the solute radical and where k is the rate constant. The yields of the solute radical per unit of time ($r(S\cdot)$) have been measured here and in previous studies[3e] as a function of the solute concentration ([SH]). Linear relationships between $1/r(S\cdot)$ and [RH]/[SH] are obtained in many systems. The slope-to-intercept ratios give k(solvent)/k(solute), shown in Table 2.

The values of k(solute)/k(solvent) ranged from 5200 in TMS to 27 in n-$C_{10}D_{22}$. The bond-dissociation energy for the C–H bond and the difference in the bond energy between a solvent and a solute are shown in the fifth and sixth columns in Table 2 respectively. Two conclusions can be drawn from these results. First, the bond energy of the solvent molecule is always higher than that of the solute molecule. Even if the difference in the bond energy between the solvent molecule and the solute molecule is very small, the k(solute)/k(solvent) ratio is quite large. Second, the k(solute)/k(*neo*-C_5H_{12}) ratios for different solutes in a neopentane matrix are of the same order of magnitude, though the difference in the C–H bond energy between the solutes amounts to 7 kcal/mol.

The first conclusion may suggest that the selective abstraction reaction is not caused by hot H atoms with extremely high energies. In order to verify the second conclusion, the competitive reaction of H atoms with C_2H_6 and c-C_6H_{12} has been studied in the neopentane matrix at 77 K.[15] The experimental value for $k(c$-$C_6H_{12})/k(C_2H_6)$ is 3.7, though the difference in bond energy between C_2H_6 and c-C_6H_{12} is 4 kcal/mol. If the selective hydrogen-atom-abstraction reaction is caused by a thermal H atom, a small difference in a bond energy causes a large k(solute)/k(solvent) because of a reaction at a very low temperature, such as 77 K. For example, $k(C_2H_6)/k($*neo*-$C_5H_{12})$ amounts to 400—500, though the difference in the bond energy between C_2H_6 and *neo*-C_5H_{12} is only 1.3 kcal/mol. The hypothesis of the thermal H atom expects that $k(c$-$C_6H_{12})/k(C_2H_6)$ will also be very large because of the large difference of bond energies (4 kcal/mol) betweeen c-C_6H_{12} and C_2H_6. Therefore, the experimental value of $k(c$-$C_6H_{12})$/

Table 2. Rate constant for H-atom-abstraction reaction by H(or D) atom at 77 K

Solvent	Solute	Source of H (or D) atom[a]	$\frac{k(\text{solute})}{k(\text{solvent})}$	C–H bond energy[b] kcal/mol		Difference[c] kcal/mol
				Solv.	Solu.	
TMS[d]	i-C_4H_{10}	rad of TMS	5200	99.3[e]	91.0	8.3
neo-C_5H_{12}	c-C_6H_{12}	rad of C_5H_{12}	810[f]	99.3	94.0	5.3
	i-C_4H_{10}	photo of DBr	780[f]		91.0	8.3
	i-C_4H_{10}	photo of HI	700[f]		91.0	8.3
	C_2H_6	photo of HI	490[g]		98.0	1.3
	C_2H_6	rad of C_5H_{12}	380[h]		98.0	1.3
c-C_3H_6	C_2H_6	rad of C_3H_6	630[f]	101.0	98.0	3.0
TMB[i]	C_3H_8	rad of TMB	100[f]	99.3[e]	94.5	4.8
	C_3H_8	photo of HI	50[f]		94.5	4.8
i-C_4H_{10}	C_3H_8	photo of HI	39[f]	98[j]	94.5	3.5
	C_3H_8	rad of C_4H_{10}	11[f]		94.5	3.5
n-$C_{10}D_{22}$	n-$C_{10}H_{22}$	rad of $C_{10}D_{22}$	27			1.2[k]

a) Rad and photo represent radiolysis and photolysis respectively. b) The value is quoted from the paper by J. A. Kerr, *Chem. Rev.*, **66**, 465 (1966). Solv. and solu. represent solvent and solute molecules respectively. c) Difference in C–H bond energy between solvent and solute. d) TMS is tetramethylsilane. e) It is assumed that the C–H bond energies of TMS and TMB are approximately the same as that of *neo*-C_5H_{12}. f) The value is calculated from the results in Ref. 3e. g) The value is calculated from the results by T. Wakayama, T. Miyazaki, and Z. Kuri. h) The value is calculated from the results by T. Miyazaki. i) TMB is 2,2,3,3-tetramethylbutane. j) The value is the energy of the primary C–H bond. k) The value is the difference in zero-point energy between C–H and C–D bonds.

Table 3. Isotope effect on selective hydrogen-atom-abstraction reaction by H(or D) atoms at 77 K

Method of production of H(or D) atoms	Reaction	$k(H)/k(D)$
Selective H-atom-abstraction reaction by H atom at 77 K		
Radiolysis of solvent *neo*-C_5H_{12} at 77 K[a]	$H+i\text{-}C_4H_{10} \longrightarrow H_2+t\text{-}C_4H_9$ ($i\text{-}C_4H_9D$) (HD)	1.1
Photolysis of HI in *neo*-C_5H_{12} at 77 K[a,b]	$H+i\text{-}C_4H_{10} \longrightarrow H_2+t\text{-}C_4H_9$ ($i\text{-}C_4H_9D$) (HD)	1.7—2.5
Photolysis of HI in Xe at 77 K[c]	$H+i\text{-}C_4H_{10} \longrightarrow H_2+t\text{-}C_4H_9$ ($i\text{-}C_4H_9D$) (HD)	4—5
Radiolysis of solvent *n*-$C_{10}D_{22}$ at 77K[c]	$D+C_{10}H_{22} \longrightarrow HD+C_{10}H_{21}$ ($C_{10}D_{22}$) (D_2) ($C_{10}D_{21}$)	27
Hot-atom reaction		
Photolysis of HBr in gas phase at about 300 K[d]	$H+CH_3CD_3 \longrightarrow H_2$ or HD	2.4—3.1
Photolysis of HI in gas phase at 313 K[e]	$H+C_2H_5D \longrightarrow H_2$ or HD (CH_3CD_3)	4.8—8.5
Recoil T atom in gas phase[f]	$T+C_2H_4 \longrightarrow HT$ (C_2D_4) (DT)	1.27
Thermal abstraction reaction at 77 K		
Electron attachment to CH_3Cl at 77 K[g]	$CH_3+CH_3OD \longrightarrow CH_4+CH_2OD$ (CD_3OD)	>1000
Radiolysis of CH_3CN at 77 K[h]	$CH_3+CH_3CN \longrightarrow CH_4+CH_2CN$ (CD_3CN)	>28000

a) Ref. 3b. b) Ref. 3a. c) This work. d) Hot H atoms have energies of 1.1—2.9 eV; G. D. Beverly and R. M. Martin, *J. Phys. Chem.*, **81**, 2063 (1976). e) Hot H atoms have an energy of 1.8 eV; K. Hong and G.J. Mains, *J. Phys. Chem.*, **76**, 3337 (1972). f) J. W. Root, W. Breckenridge, and F.S. Rowland, *J. Chem. Phys.*, **43**, 3694 (1965). g) Ref. 19b. h) Ref. 19c.

$k(C_2H_6)=3.7$ cannot be explained by the hypothesis of a thermal H atom. It is interesting to note that $k(c\text{-}C_6H_{12})/k(C_2H_6)$ is 3.5 for a hot tritium atom reaction[16] and about 6 for a hot CH_3 radical reaction in the photolysis of CH_3I.[17] The experimental value obtained in the neopentane matrix is approximately of the same order of magnitude as that in the hot-atom reaction.

Isotope Effects on the H-atom Abstraction Reaction at 77 K. The isotope effects on the hydrogen-atom-abstraction reaction are summarized in Table 3. $k(H)$ and $k(D)$ represent the rate constants of the H-abstraction and D-abstraction reactions respectively. The values in the *neo*-C_5H_{12} and Xe matrices were estimated from the yields of $t\text{-}C_4H_9$ radicals produced by the radiolysis or photolysis in *neo*-C_5H_{12} (or Xe) containing 2 mol% of $i\text{-}C_4H_{10}$ or $i\text{-}C_4H_9D$ at 77 K. The isotope effects in the neopentane matrix ranged from 1.1 to 2.5.[18] In order to confirm the isotope effect in the *neo*-C_5H_{12} matrix, a competitive reaction of H atoms with C_2H_6 and $c\text{-}C_6H_{12}$ (or $c\text{-}C_6D_{12}$) has been studied at 77 K. The experimental value for $k(H)/k(D)$ of cyclohexane in the neopentane matrix is 7.3.[15] Recently it has been reported that a thermal CH_3 radical abstracts a hydrogen atom at 77 K by mean of quantum mechanical tunneling.[19] The most important characteristic of this mechanism is a quite large isotope effect (*cf.* Table 3). The value for $k(H)/k(D)$ in the neopentane matrix is quite different from the value for quantum mechanical tunneling. On the contrary, the value in the neopentane matrix is approximately the same as the value for hot-atom reactions in the gas phase.

Energy Loss of Reactive H Atoms in the Solid Phase. Since the energy of the first excited state of alkane (7—8 eV)[20] is much larger than the bond energy of the C–H bond (4 eV),[21] and since the energy of ultraviolet light (4.9 eV) is much larger than the bond energy of HI (3.1 eV),[21] the H atom produced by the radiolysis of alkane or by the photolysis of HI must have, initially, an excess energy of 2—3 eV. Recently it has been reported that the H atoms produced in the gas phase by electron impact on hydrocarbons have kinetic energies of 1.8—3.8 eV.[22] Now, we will discuss the problem of whether or not the H atoms with the excess energy lose their energy completely during their excursion in the crystal at 77 K.

The photolysis of the Xe–$i\text{-}C_4H_{10}$–HI mixture is the simplest way to discuss the energy loss of hot H atoms. When the photolysis of HI is caused by a 2537 Å light, the initial kinetic energy of an H atom is 20 kcal/mol if the iodine atom is produced in the $^2P_{1/2}$ excited state and 41 kcal/mol if it is produced in the $^2P_{3/2}$ ground state.[23] The experimental results in Fig. 6 indicate that the H atoms produced in the photolysis of HI migrate through 114 atoms of Xe at 77 K. In order to estimate the number of H atoms colliding with Xe atoms during the excursion, three cases are considered here. First, if the collision efficiency of an H atom with solute $i\text{-}C_4H_{10}$ is the same as that of Xe, the number of collisions of the H atom with Xe is 114 until the H atom reacts with $i\text{-}C_4H_{10}$. Second, since the crystalline structure of Xe is face-centered cubic,[24] a channeling wall[25] consists of four Xe atoms. If the $i\text{-}C_4H_{10}$ solute

exists as a defect in the channeling zone, it may be assumed that the collision efficiency of an H atom with i-C_4H_{10} is four times as large as that with Xe. In this case, the collision number of the H atom with Xe is 114/4(=28.5). Third, an i-C_4H_{10} molecule may exist in a lattice of crystalline Xe. It may be assumed that H atoms react with i-C_4H_{10} whenever they approach nearest neighboring Xe atoms around i-C_4H_{10}. The collision efficiency of H atoms with i-C_4H_{10} is 12 times as large as that with Xe. In this case, the collision number of an H atom with Xe is 114/12(=9.5).

The reactive H atom loses its energy by elastic collisions with Xe molecules. The energy loss by a single collision is expressed as

$$\frac{E_0-E'}{E_0} = \frac{2M_1M_2}{(M_1+M_2)^2}(1-\cos\theta), \qquad \text{(d)}$$

where E_0 and E' are the kinetic energies before and after a collision respectively.[26] M_1 and M_2 are the masses of the H atom and the Xe atom respectively. θ is the diffraction angle of the H atom caused by the collision. The mean value of the energy loss ($\langle E'/E_0 \rangle$) is obtained by means of the following equation:

$$\left\langle \frac{E'}{E_0} \right\rangle = 1 - \int_0^{\pi/2} \frac{2M_1M_2}{(M_1+M_2)^2}(1-\cos\theta)\mathrm{d}\theta. \qquad \text{(e)}$$

When an H atom has, initially, a kinetic energy of 41 or 20 kcal/mol, the final energy of the H atom after the excursion in a xenon matrix is calculated by means of Eq. e for all three cases of the collision number. As is shown in Table 4, the final energy ranges from 11 to 39 kcal/mol, depending on the models for collisions and the initial energies of the H atoms. Since the activation energy for the hydrogen-atom-abstraction reaction of an H atom with i-C_4H_{10} is 7.4 kcal/mol,[5] the H atom has enough energy for a chemical reaction with i-C_4H_{10} after the excursion in the Xe matrix.

Table 4. Final energy of reactive H atom in Xe matrix at 77 K

	Collision efficiency with solute		
	1	4	12
Collision number	114	28.5	9.5
Final energy of H atom with 41 kcal/mol,[a] kcal/mol	23	36	39
Final energy of H atom with 20 kcal/mol,[b] kcal/mol	11	18	19

a) The H atom has initially a kinetic energy of 41 kcal/mol. b) The H atom has initially a kinetic energy of 20 kcal/mol.

The theoretically estimated energies of 11—39 kcal/mol are high in comparison with the activation energy of 7.4 kcal/mol. Therefore, there remains the important question of why the H atoms with the energies of 11—39 kcal/mol abstract selectively the tertiary H atom of i-C_4H_{10}. We cannot give a good explanation of this problem as yet. Two possibilities are plausible. One is that the real energy of the reactive H atoms is near the threshold of the hydrogen abstraction reaction. The other is that the reaction in the solid state at low temperature shows the selectivity under the influence of the crystalline fields. For example, when isobutane is exposed to γ-irradiation[27] or hot-atom attack[14] at 77 K in a polycrystalline medium, the isobutyl radical is formed, while in a glassy state the tertiary butyl radical is formed. In the radiolysis of 2,3-dimethylbutane at 77 K, the $\cdot CH_2CH(CH_3)CH(CH_3)_2$ radical is formed in crystal-I, while the $CH_3\dot{C}(CH_3)CH(CH_3)_2$ radical is formed in crystal-II.[28] When glassy 3-methyl alkane are exposed to γ-irradiation, hot-atom attack, hot-radical attack, or photosensitization by aromatic solutes, radicals are formed predominantly by the rupture of secondary C–H bonds rather than by that of the weak tertiary or of the more abundant primary bonds.[29]

In conclusion, we cannot give a decisive answer to the question of whether the reactive H atoms in the radiolysis and the photolysis of solid mixtures at 77 K are thermal or hot. We will try, however, to give a probable hypothesis for further investigation. The remarkable selectivity for the reaction may diminish the possibility of hot H atoms with extremely high energies. The small isotope effect on the reaction may diminish the possibility of a quantum mechanical tunneling abstraction[19] by thermal H atoms, Since the rate constants and isotope effects for solute molecules in *neo*-C_5H_{12}-alkane mixtures are approximately the same as those for hot-atom reactions, H atoms with epithermal energy may be responsible for the reaction. When the H atoms produced by the radiolysis of the solvent alkane or by the photolysis of hydrogen halide are incident upon the channeling zone[25,3c] of the matrix, the H atoms may travel a long distance by a succession of glancing collisions with the channel walls of the solvent molecules and may then react with a solute alkane which may exist as a defect in the matrix.

The D atoms produced by the photolysis of DI react selectively with 3-methylpentane-h_{14} in 3-methylpentane-d_{14} glass at 77 K.[4] There is, however, no experimental information on the kinetic energy of the D atoms. The problem of whether the D atoms in 3-methylpentane-d_{14} glass are thermal or hot atoms requires further study in the future.

The authors wish to express their appreciation to Professor Kenji Fueki of Nagoya University for his fruitful discussions. The authors wish also to thank Dr. Kozo Matsumoto of Nagoya University for his mass spectroscopic analysis.

References

1) A. Charlesby, Proceedings of the 1962 Tihany Symposium on Radiation Chemistry, Akademiai Kiado, Budapest, 1964, p. 175.

2) W. Flossman, E. Westhof, and A. Muller, *Int. J. Radiat. Biol.*, **28**, 105 (1975). Previous papers concerning the role of the H atom in biological substances are cited therein.

3) a) T. Wakayama, T. Miyazaki, K. Fueki, and Z. Kuri, *J. Phys. Chem.*, **77**, 2365 (1973); b) T. Miyazaki and T. Hirayama, *J. Phys. Chem.*, **79**, 566 (1975); c) T. Miyazaki, K. Kinugawa, M. Eguchi, and S. M. L. Guedes, *Bull. Chem. Soc. Jpn.*, **49**, 2970 (1976); d) T. Miyazaki, S. M. L. Guedes, L. G. A. Silva, and L. Fernandes, *Bull. Chem. Soc. Jpn.*, **50**, 301

(1977); e) T. Miyazaki, K. Kinugawa, and J. Kasugai, *Radiat. Phys. Chem.*, **10**, 155 (1977).
4) D. D. Wilkey and J. E. Willard, *J. Chem. Phys.*, **64**, 3976 (1976).
5) B. A. Thrush, *Prog. React. Kinet.*, **3**, 89 (1965).
6) a) T. Gillbro and A. Lund, *Chem. Phys. Lett.*, **27**, 300 (1974); b) T. Gillbro and A. Lund, *Int. J. Radiat. Phys. Chem.*, **8**, 625 (1976).
7) O. Claesson and A. Lund, *Chem. Phys. Lett.*, **47**, 155 (1977).
8) T. Miyazaki, *Radiat. Phys. Chem.*, **10**, 219 (1977).
9) M. Iwasaki, K. Toriyama, H. Muto, and K. Nunome, *J. Chem. Phys.*, **65**, 596 (1976).
10) D. D. Wilkey, H. W. Fenrick, and J. E. Willard, *J. Phys. Chem.*, **81**, 220 (1977).
11) L. Kevan and W. F. Libby, *J. Chem. Phys.*, **39**, 1288 (1963).
12) D. C. Waterman and M. Dole, *J. Phys. Chem.*, **74**, 1913 (1970).
13) K. Kinugawa, T. Miyazaki, and H. Hase, *Radiat. Phys. Chem.*, **10**, 341 (1977).
14) T. Wakayama, T. Miyazaki, K. Fueki, and Z. Kuri, *Bull. Chem. Soc. Jpn.*, **44**, 2619 (1971).
15) Although the details will be given elsewhere, some of the results were presented by T. Miyazaki *et al.* at the 20th Japanese Conference of Radiation Chemistry, Sapporo, Japan, October, 1977.
16) E. Tachikawa and F. S. Rowland, *J. Am. Chem. Soc.*, **90**, 4767 (1968).
17) R. E. Rebbert and P. Ausloos, *J. Chem. Phys.*, **48**, 306 (1968).
18) Recent results obtained by T. Miyazaki *et al.* by the method of a competitive reaction also support this value.
19) a) R. J. LeRoy, E. D. Sprague, and F. Williams, *J. Phys. Chem.*, **76**, 546 (1972); b) A. Campion and F. Williams, *J. Am. Chem. Soc.*, **94**, 7633 (1972); c) E. D. Sprague, *J. Phys. Chem.*, **81**, 516 (1977).
20) J. W. Raymonda and W. T. Simpson, *J. Chem. Phys.*, **47**, 430 (1967).
21) V. I. Vedeneyev, L. V. Gurvich, V. N. Kondratyev, V. A. Medvedev, and Ye. L. Frankevich, "Bond Energies, Ionization Potentials, and Electron Affinities," translated to English by W. C. Price, London, Edward Arnold (1966).
22) K. Ito, N. Oda, Y. Hatano, and T. Tsuboi, *Chem. Phys.*, **21**, 203 (1977).
23) S. Adita and J. E. Willard, *J. Am. Chem. Soc.*, **88**, 229 (1966).
24) R. W. G. Wyckoff, "Crystal Structures," John Wiley & Sons (1965), p. 10.
25) T. Miyazaki, *Bull. Chem. Soc. Jpn.*, **50**, 1625 (1977).
26) A. Kanpanetz, "Theoretical Physics," translated to Japanese by T. Yamanouchi and H. Takami, Iwanami Shoten (1964), p. 48.
27) a) T. Miyazaki, T. Wakayama, K. Fueki, and Z. Kuri, *Bull. Chem. Soc. Jpn.*, **42**, 2086 (1969); b) T. Wakayama, T. Miyazaki, K. Fueki, and Z. Kuri, *J. Phys. Chem.*, **74**, 3584 (1970); c) Y. Saitake, T. Wakayama, T. Kimura. T, Miyazaki, K. Fueki, and Z. Kuri, *Bull. Chem. Soc. Jpn.*, **44**, 301 (1971).
28) M. Fukaya, T. Wakayama, T. Miyazaki, Y. Saitake, and Z. Kuri, *Bull. Chem. Soc. Jpn.*, **46**, 1036 (1973).
29) a) D. J. Henderson and J. E. Willard, *J. Am. Chem. Soc.*, **91**, 3014 (1969); b) T. Ichikawa and N. Ohta, *J. Phys. Chem.*, **81**, 560 (1977).

Heterogeneous Catalysis in Liquid-Phase Oxidation of Olefin. II. Dependence of the Structure of Vanadium-Chromium Binary Oxide Catalyst for Oxidation of Cyclohexene on the Method of Preparation

Katsuomi TAKEHIRA, Takashi HAYAKAWA, Toshio ISHIKAWA

Catalysis Division, National Chemical Laboratory for Industry, Mita, Meguro-ku, Tokyo 153

(Received December 1, 1977)

The influence of preparative conditions on the structure and catalytic activity of V–Cr oxide catalyst for the liquid-phase oxidation of cyclohexene has been investigated. Three series of binary oxide, V–Cr-D, V–Cr-E, and V–Cr-F, were prepared from acidic, neutral, and alkaline media, respectively. The specific activity of the catalyst was found to be in the order: V–Cr-D>V–Cr-E>V–Cr-F, the catalyst prepared from acidic medium showing the highest activity. The results of structure analysis showed the formation of several chromium isopolyvanadates, *i.e.*, chromium pyrovanadate, chromium metavanadate, and unknown phase (probably chromium polyvanadates), together with V_2O_5, Cr_2O_3, and solid solution of Cr^{6+} in V_2O_5 lattice. The formation of chromium isopolyvanadate having a higher degree of condensation of the vanadate anion was promoted by use of a more acidic medium in the catalyst preparation. The higher activity for autoxidation was obtained with the catalyst containing the more condensed isopolyvanadate. Epoxidation seems to proceed by the hydroperoxide intermediate mechanism on the active site differing from that for autoxidation.

Properties of heterogeneous catalysts in liquid-phase oxidation of cyclohexene were studied using several binary oxides containing vanadium.[1] Vanadium–chromium system (V–Cr) was found to be relatively active for the oxidation, in which epoxidation of cyclohexene also proceeded. The insoluble catalyst system seems to contain two types of active site, one effective for autoxidation of cyclohexene, *i.e.*, for radical chain reaction, and the other for selective epoxidation of cyclohexene with 1-cyclohexenyl hydroperoxide (HPO) formed by autoxidation. The activity of the V–Cr catalyst for oxidation of acrylaldehyde is considerably affected by its preparative conditions.[2] It seems that the active species is a chromium isopolyvanadate and its formation is promoted by use of an acidic medium. We have studied the effects of the methods of preparation of the V–Cr catalyst on its property. Three series of vanadium–chromium oxide were prepared from acidic, neutral, and alkaline media, and their structures and catalytic activity for oxidation of cyclohexene have been investigated in detail.

Experimental

Catalysts. Three series of binary oxide catalyst were prepared in the following way. A combination of three raw materials such as V_2O_5 hydrate+$Cr(NO_3)_3 \cdot 9H_2O$, V_2O_5 hydrate+$Cr(OH)_3$ hydrate, or NH_4VO_3+$Cr(OH)_3$ hydrate was employed in the preparation of the catalysts from acidic, neutral, or alkaline media, respectively.

The raw materials were mixed and kneaded with a small amount of water at 80 °C for 6 h, dried at 100 °C for one day, and calcined at 450 °C* for 5 h in air. The resulting three series of binary oxide, each consisting of catalysts of different compositions, are denoted by V–Cr-D (from acidic), V–Cr-E (from neutral), V–Cr-F (from alkaline medium). V_2O_5 hydrate was prepared as previously reported,[1] and $Cr(OH)_3$ hydrate was obtained as precipitate by addition of dilute ammonia to an aqueous solution of $Cr(NO_3)_3 \cdot 9H_2O$. The catalyst was pulverised and used as powder of particle size smaller than 100 mesh. The composition (in terms of atomic % of Cr/(V+Cr)), symbol, and specific surface area (S_s) are given in Table 1.

Apparatus and Procedure of Catalytic Reaction. The oxidation reaction was carried out at 60 °C for 5 h under 1 atm of O_2 pressure using a batch system.[1] 20.0 ml of cyclohexene, 50.0 ml of benzene as solvent, and 50.0 mg of the binary oxide catalyst were used in each reaction.

Analyses of Reaction Products and Catalysts. The reaction products, HPO and cyclohexene oxide (OXIDE), were determined by the iodometric method and gas-chromatography.[1]

The structure of the catalyst was studied by means of X-ray diffraction and infrared absorption, the surface area being obtained by the BET method.[1] Differential thermal analysis and thermo gravimetric analysis of the samples before calcination were carried out with a Thermoflex YGHD type thermal analyser (Rigaku Denki Co.). Electron spin resonance absorption spectra were recorded with a JES-3BX type ESR spectrometer (X-band). For removal of V_2O_5, the catalyst was immersed in 6 M ammonia for two days, separated by filtration, washed with water, and dried at 150 °C for one day.

Results

Surface Area of Catalyst. The surface area of catalyst varies a great deal with the preparative conditions and composition of catalyst (Table 1), the value being in the order: V–Cr-F>V–Cr-E>V–Cr-D. The catalyst prepared from the more alkaline medium shows a higher value.

X-Ray Diffraction of Catalyst. Typical diffraction patterns of the binary system catalysts are shown in Fig. 1. The formation of two phases, X and Y, besides V_2O_5 and Cr_2O_3 in the V–Cr catalyst used for acrylaldehyde oxidation has been recognized by X-ray diffraction analysis.[2] In the present work, these four phases were also observed. The diffraction lines are

* Formation of several chromium isopolyvanadates is expected in this binary system.[2] 450 °C was shosen as temperature of calcination so that these isopolyvanadates, *i.e.*, $Cr(VO_3)_3$,[3] $(Cr_2O)(VO_3)_4$,[4] and $Cr_4(V_2O_7)_3$,[5] might be obtained in stable form.

TABLE 1. COMPOSITION, SYMBOL, AND SPECIFIC SURFACE AREA OF CATALYST

Composition Cr/(V+Cr) (atomic %)	D-Series Symbol	S_s (m^2/g)	E-Series Symbol	S_s (m^2/g)	F-Series Symbol	S_s (m^2/g)
0	D-0	4.1	E-0	5.2	F-0	7.1
10	D-1	11.3	E-1	9.1	F-1	10.1
20	D-2	10.1	E-2	13.6	F-2	23.6
30	D-3	7.9	E-3	12.4	F-3	37.7
40	D-4	8.7	E-4	15.7	F-4	57.1
50	D-5	8.3	E-5	13.9	F-5	73.3
60	D-6	8.2	E-6	18.6	F-6	73.6
70	D-7	7.7	E-7	17.0	F-7	82.5
80	D-8	8.0	E-8	10.7	F-8	65.8
90	D-9	7.3	E-9	10.7	F-9	43.4
100	D-10	8.7	E-10	36.3	F-10	47.2

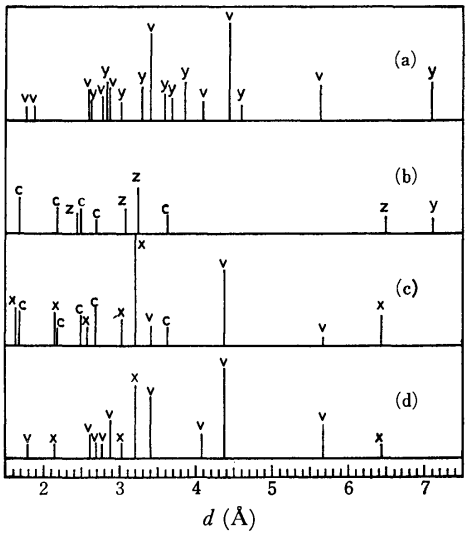

Fig. 1. X-Ray diffraction patterns of V–Cr catalysts.
v: V_2O_5, y: phase Y, x: phase X, z: phase Z, c: Cr_2O_3.
(a) D-3, (b) D-7, (c) E-5, (d) F-3.

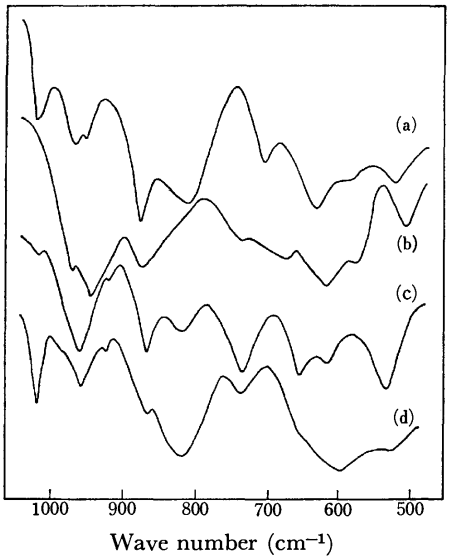

Fig. 2. Infrared spectra of V–Cr catalysts.
(a) D-3, (b) D-7, (c) E-5, (d) F-3.

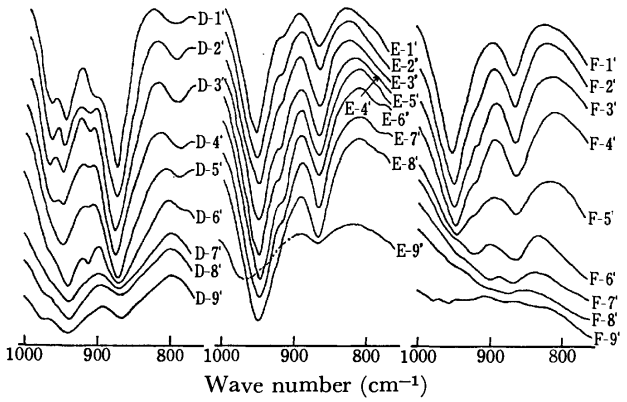

Fig. 3. Infrared spectra of V–Cr catalysts treated with NH_3.

classified into four groups; v, c, x, and y (belong to V_2O_5, Cr_2O_3, X, and Y, respectively). Several unknown lines (z) appeared in V–Cr-D catalysts of higher Cr content. The lines y were found only in V–Cr-D catalysts, while the lines *x* were observed in the other binary system, V–Cr-E and V–Cr-F. Furthermore, the *d*-spacing value of the strongest line of V_2O_5: d=4.38 Å (001 plane) increased in proportion to the Cr content, reaching 4.47 Å in D-4, only in the patterns of V–Cr-D catalysts.

Infrared Spectra. Infrared spectra of the catalysts before and after treatment with ammonia are shown in Figs. 2 and 3, respectively. Mark (') shows the catalyst treated with ammonia. The spectrum changes considerably with composition and the preparing conditions. An absorption band at about 1020 cm^{-1} (Fig. 2) is assigned to the stretching vibration of V=O bond in V_2O_5.[6] The band in D-1 and D-2 broadens toward frequency slightly lower than 1020 cm^{-1}. D-1'–D-4' show the spectra which coincide fairly well with those of chromium metavanadate ($Cr(VO_3)_3$).[7] The spectra of E-1'—E-8' and F-1'—F-5' might be due to chromium pyrovanadate ($Cr_4(V_2O_7)_3$).[7] The band observed at about 800 cm^{-1} in D-1'—D-5' is also recognized, though weak, in E-6'—E-8'.

DTA and TGA of Catalyst. In order to clarify the solid-phase reaction during the preparation of the catalysts, thermoanalyses of the samples after being dried at 100 °C (before calcination) were carried out in the range 100—750 °C. The results are shown in Fig. 4. The sharp endothermic peak at 680 °C is due to the melting of V_2O_5, and the sharp exothermic one observed with the decrease of weight at 410 °C might be due to the dehydration of $Cr(OH)_3$.[8] Several endo- and exothermic peaks observed between 100 and 200 °C with the samples of D-series are mainly due to the decomposition of chromium nitrate. An exothermic peak observed with D-0 at 320 °C seems to be due to dehydration of V_2O_5 hydrate. The peak shifted toward high temperature by addition of $Cr(NO_3)_3$. An exothermic peak at *ca.* 410 °C in D-series of high Cr content (Fig. 4, D-5) recognized with weight loss proportional to the Cr content, might be due to the dehydration of

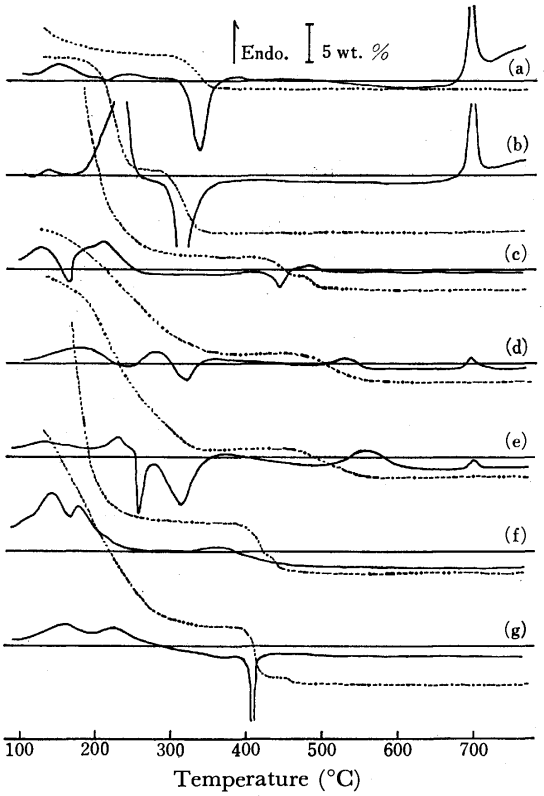

Fig. 4. DTA and TGA curbes of V–Cr binary oxides.
(a) D-0, (b) F-0, (c) D-5, (d) E-5, (e) F-5, (f) D-10, (g) E-10.
—— DTA, ------ TGA.

$Cr(OH)_3$ formed by the partial hydrolysis of $Cr(NO_3)_3$ during the course of mixing of the raw materials. The samples of E-series show several obscure peaks with weight loss below 300 °C, and an exothermic peak in the vicinity of 500 °C (Fig. 4, E-5). The weight loss at about 320 °C decreases with increase in Cr content, that at about 500 °C being roughly proportional to the Cr content. The temperature of the latter peak was lowered with increase in Cr content. Series-F show an exothermic peak at about 210°C, two exothermic peaks at about 220 and 300 °C, and a weak endothermic peak near 500 °C (Fig. 4, F-5). The peaks at 210 and 300 °C are due to the decomposition of ammonium metavanadate. The weak endothermic peak at 500 °C is accompanied by weight loss proportional to the Cr content as in the case of V–Cr-E.

ESR Spectra of Catalyst. The form of spectra varies remarkably, depending on the preparing conditions of catalyst. Typical spectra are shown in Fig. 5. D-1—D-3 show spectra consisting of a strong narrow signal superposed on a broad one (Fig. 5, a and b), the narrow signal having a peak-to-peak line width (ΔH_{msl}) of 60—110 G and g value of 1.96. The intensity of the narrow signal is higher in the catalysts having lower Cr content, the strongest one being observed with D-1. The catalyst of low Cr content in E and F-series also show similar types of spectrum, but the intensity of the narrow signal is very weak. Furthermore, ΔH_{msl} of the broad signal varies a great deal; 300—500 G in V–Cr-D, and

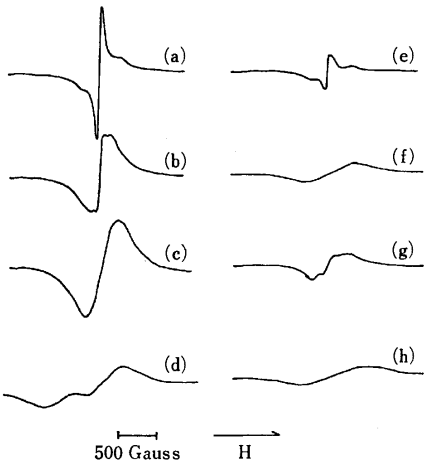

Fig. 5. ESR spectra of V–Cr catalysts.
(a) D-1, (b) D-2, (c) D-5, (d) D-7, (e) E-1, (f) E-7, (g) F-1, (h) F-7.

400—1200 G, being very broad, in both V–Cr-E and V–Cr-F. Thus, the broad signals in V–Cr-D series are clearly distinguishable from those of V–Cr-E and V–Cr-F series. In the case of D-4 and D-5, the narrow signal is probably hindered by the broad signal which is observed strongly. D-6—D-9 show spectra having additional maximum in weak fields (Fig. 5, d).

Results obtained for the single component catalysts are as follows. D-0, E-0, and F-0 show a very weak signal having ΔH_{msl} of about 80 G and g value of 1.96, while the spectra of Cr_2O_3 vary depending on the preparing conditions. D-10 shows a spectrum similar to D-7, however, the spectra of both E-10 and F-10 consist of a single broad signal.

Oxidation Reaction. The reaction results obtained for the three series of V–Cr catalysts are shown in Figs. 6 and 7. The order of specific activity shown in terms of the maximum rate of oxygen absorption per unit

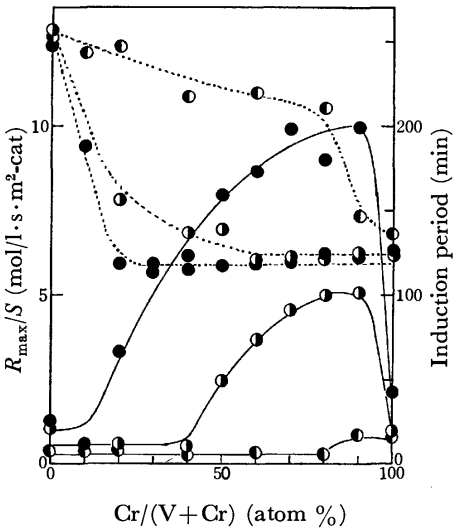

Fig. 6. Specific activities of V–Cr catalysts and induction periods of oxygen uptakes.
● V–Cr-D, ◑ V–Cr-E, ◐ V–Cr-F,
—— specific activity, ------ induction period.

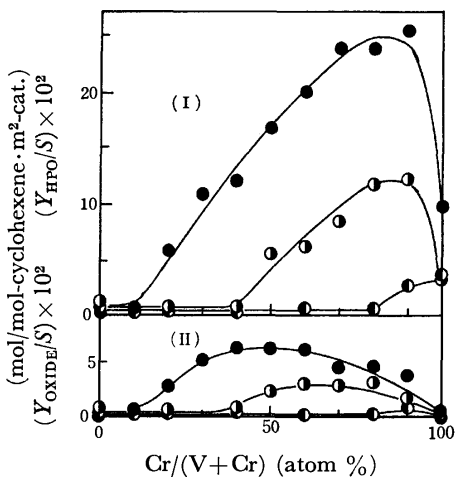

Fig. 7. Formations of HPO (I) and OXIDE (II) in the oxidations with V–Cr catalysts.
● V–Cr-D, ◑ V–Cr-E, ◐ V–Cr-F.

surface area of the catalyst (R_{max}/S) is: V–Cr-D>V–Cr-E>V–Cr-F (Fig. 6). The activity of each binary system is high when Cr content is high, the highest value being obtained at 90 atom % of Cr in all the three series. An induction period for oxygen uptake was 120—130 min with the relatively active catalysts, *i.e.*, D-2—D-9 and E-5—E-9, and the higher content of Cr caused decrease in its value (Fig. 6). Fig. 7 shows the yield of HPO or OXIDE per unit surface area of each catalyst (Y_{HPO}/S or Y_{OXIDE}/S). The values of Y_{HPO}/S show a very similar tendency to the oxygen uptake in Fig. 6. OXIDE was obtained only with the catalyst active for HPO formation. However, dependency of epoxidation on the catalyst composition differs clearly from that of HPO formation, the maximum value of Y_{OXIDE}/S being obtained with the catalyst with much less Cr content.

Discussion

Structure of Catalyst. Solid solution is formed in the binary oxide containing V, such as V–Mo and V–W.[6] For V–Cr system, Kurina *et al.*[9] reported that the solid solution is formed in the binary oxide prepared from NH_4VO_3 and $Cr(NO_3)_3\cdot9H_2O$.

By means of X-ray analysis, a diffraction pattern of V_2O_5, and an increase in *d*-spacing of 001 plane proportional to the Cr content, following Vegard's law were observed in D-1—D-4 catalysts. An interfacial solid solution seems to be formed in the catalysts. These catalysts show a narrow signal in their ESR spectra, the values of *g* and ΔH_{msl} being very similar to the values of the weak signal of the V_2O_5 spectra. The weak signal of V_2O_5 is thought to be due to quadrivalent vanadium ions, V^{4+}, resulting from lattice defects.[6] The narrow signal might be due to V^{4+} ions. The reduction of vanadium species is considered to occur as a result of the charge compensation of the chromium atoms (probably, Cr^{6+}) introduced into the lattice of V_2O_5 by the formation of the solid solution. This is supported by the fact, in D-1 and D-2, the infrared absorption band at 1020 cm^{-1} broadens toward lower frequency. The broadening may be due to the formation of V^{4+}=O bond, resulting from solid solution. In both series of V–Cr-E and V–Cr-F, the catalysts containing a small amount of Cr show a very weak narrow signal in their ESR spectra, its highest intensity being observed with E-1 and F-1.** However, no clear change in the *d*-spacing was observed. This suggests that the amount of solid solution is considerably smaller in both V–Cr-E and V–Cr-F than in V–Cr-D. The intensity of the narrow signal can be put in the order: V–Cr-D>V–Cr-E>V–Cr-F. It is suggested that more acidic preparative conditions are favorable for the formation of solid solution.

By means of X-ray diffraction, three phases, X, Y, and Z were observed in the catalysts. The patterns of X and Y coincide with those of $Cr_4(V_2O_7)_3$[5] and $Cr(VO_3)_3$,[3] respectively. Phases X and Y might be chromium pyrovanadate and chromium metavanadate, respectively. The *d*-spacing values of lines classified into z in V–Cr-D (Fig. 1, b) vary somewhat depending on the composition of catalyst, the lines z being hardly attributed to single component. Phase Z might be a mixture of several compounds. In order to clarify the influence of preparing conditions on the formation of these phases, the intensities of two characteristic peaks selected for two phases, $Cr_4(V_2O_7)_3$ (d=3.19 Å) and $Cr(VO_3)_3$ (d=3.87 Å), in Fig. 1, are plotted as a function of the composition of each catalyst series, together with that of both phases of V_2O_5 (d=4.37 Å) and Cr_2O_3

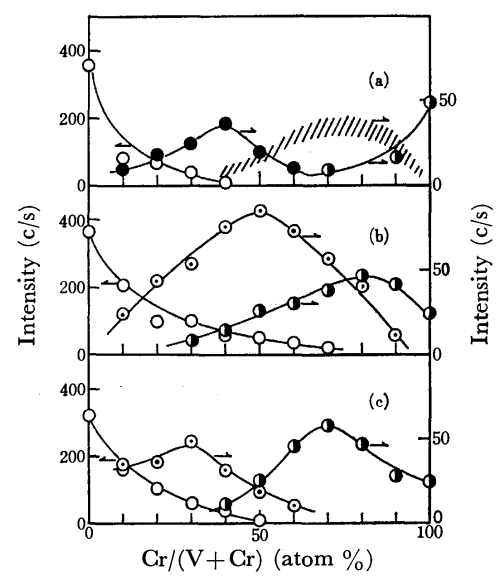

Fig. 8. Intensities of X-ray diffraction lines.
(a) V–Cr-D (b) V–Cr-E (c) V–Cr-F
○ d=4.38 Å (V_2O_5), ⊙ d=3.19 Å ($Cr_4(V_2O_7)_3$), ● d=3.87 Å ($Cr(VO_3)_3$), /// $d\simeq$3.2 Å (phase z), ◑ d=2.67 Å (Cr_2O_3).

** No narrow signal was observed in the catalyst prepared from NH_4VO_3 and $Cr(NO_3)_3\cdot9H_2O$.[2] However, Kurina *et al.*[9] reported that the binary oxide similarly prepared shows the narrow signal of V^{4+} in the solid solution, its intensity reaching maximum at 5 mol% of Cr. Disappearance of the narrrow signal seems to be due to the fact that the signal was hindered by the strong broad one, since the catalysts contain more than 17% of Cr.

(d=2.67 Å) (Fig. 8). In order to show the existence of phase Z, the line near d=3.2 Å was selected for the sake of convenience. Its intensity is indicated by shading. The intensity of the peak of $Cr(VO_3)_3$, recognized only in D-1—D-6 catalysts, was observed to reach a maximum at 40 atom % of Cr. The values of Cr content at the maximum intensity of the $Cr_4(V_2O_7)_3$ peak are *ca.* 50 and 30 atom % in V–Cr-E and V–Cr-F, respectively.

The infrared spectra suggest the formation of $Cr(VO_3)_3$ in the catalysts of D-1—D-4 and $Cr_4(V_2O_7)_3$ in E-1—E-8 and F-1—F-5. The compositions of these catalysts coincide with those classified by X-ray analysis, with respect to the formation of $Cr(VO_3)_3$ and $Cr_4(V_2O_7)_3$. However, a very weak absorption band was observed at about 800 cm^{-1} in E-6′—E-8′, in spite of the absence of $Cr(VO_3)_3$ The results suggest the formation of amorphous $Cr(VO_3)_3$. According to the report given by Olivier,[7] the absorption bands between 750 and 1050 cm^{-1} are assigned to the stretching vibrations of V–O bonds, varying markedly with the type of isopolyvanadate anion. $Cr(VO_3)_3$ has a chain structure of VO_6 octahedra connected with each other by sharing an edge,[10] the bands in its spectrum being assigned as: 970 and 945 cm^{-1} to $\nu_s VO_2$ and 915 and 800 cm^{-1}*** to VO_6. On the other hand, $Cr_4(V_2O_7)_3$ contains V_2O_7 group which consists of two VO_3 pyramids linked by a V–O–V bridge.[11] The following assignments might be made: 950 cm^{-1} to $\nu_s VO_3$ and 870 cm^{-1} to $\nu_{as} VO_3$. Catalysts D-6—D-9 containing phase Z as classified by X-ray analysis show very broad bands centered at *ca.* 940 and 870 cm^{-1} in the range of V–O stretching vibrations. No such spectra seem to have been reported. They suggest some chromium polyvanadates containing anions of higher degrees of condensation. The nature of the anionic vanadate species in alkaline, neutral, and acidic solutions has been the subject of numerous investigations. A typical example of the types of vanadate anions is as follows.[12]

pH	6.7	9.6	12.6
anion	poly→←meta→←pyro→←ortho		

It is reasonably considered that chromium polyvanadates are formed in D-6—D-9 whose preparing conditions are more acidic than those of D-1—D-5. The fact that D-6—D-9 show some randomness in the d-spacing values and the frequencies of infrared absorption might be due to the diversity of the type of polyvanadate.

Samples of the binary system show thermal changes not observed in each of the one component systems (Fig. 4). In each of the three series, the endothermic peak due to the melting of V_2O_5 was rapidly weakened with the increase in Cr content, not being observed in the sample containing less amount of V than 40 atom %. This suggests that some solid-phase reactions took place during the course of calcination. It is considered that the weight loss observed at *ca.* 500 °C especially in E and F-series is mainly due to the dehydration of $Cr_4(V_2O_7)_3 \cdot nH_2O$.[5] The dehydration is more difficult than that of $Cr(VO_3)_3 \cdot mH_2O$, requiring a long period or a higher temperature. There is a possibility that undesirable water remains in the binary catalysts. However, the infrared spectra of the catalysts show no absorption band of H–O–H bending vibration at *ca.* 1600 cm^{-1}, indicating that the dehydration is nearly completed by at 450 °C for 5 h.

The electron spin resonance spectra show broad signals whose value of ΔH_{msl} vary considerably. ΔH_{msl} of these signals were relatively small in V–Cr-D, but fairly large in both V–Cr-E and V–Cr-F. The peak-to-peak height was especially great in V–Cr-D. It is difficult to assign these broad signals. However, the relatively strong signal observed in D-2—D-6 might be assigned to a paramagnetic species included in $Cr(VO_3)_3$, since its intensity correlates fairly well with the amount of $Cr(VO_3)_3$ estimated from the results of X-ray diffraction and infrared analysis. In a similar manner, the very broad signals observed with some V–Cr-E and V–Cr-F catalysts may be assigned to a paramagnetic species in $Cr_3(V_2O_7)_4$. The broadening of these signals might be due to the dislocalization of the unpaired electron owing to the ordering of the structure containing the paramagnetic species. In the infrared spectra of E-6—E-8, a weak absorption band was observed which may be assigned to the stretching vibration of VO_6 in $Cr(VO_3)_3$. However, the electron spin resonance spectra of these catalysts show no broad signal of $Cr(VO_3)_3$, contrary to our expectation. Spectra having an additional maximum in weak fields were observed in D-7–D-10, the intensity increasing with the amount of Cr_2O_3 estimated by X-ray diffraction. This type of signal seems to be due to Cr_2O_3. However, E-10 and F-10 show only a broad signal, suggesting a difference between Cr_2O_3 prepared from $Cr(NO_3)_3$ and that from $Cr(OH)_3$.

Relationship between Structure and Catalytic Activity. The correlation of the catalyst composition to R_{max}/S differs clearly from that to Y_{OXIDE}/S, in each series of binary system (Figs. 6 and 7). The oxygen uptake is rationally assumed to be mainly due to the radical chain reaction. It is considered that the active species for autoxidation differs from that for epoxidation. Since epoxidation was observed only with the catalysts which gave HPO (Fig. 7), epoxidation is thought to proceed selectively with HPO. Thus, the results we obtained support the suggestion that epoxidation proceeds by a hydroperoxide intermediate mechanism catalyzed by the vanadium–chromium oxide having two types of active site, one effective for the autoxidation and the other for the selective epoxidation.[1]

The activity for autoxidation shown by R_{max}/S might be explained as follows. Chromium polyvanadates and $Cr(VO_3)_3$ were observed in the catalysts of D-series; $Cr(VO_3)_3$ (suggested only by the infrared absorption) and $Cr_4(V_2O_7)_3$ in those of E-series; and $Cr_4(V_2O_7)_3$ in those of F-series. From a comparison of the distribution of these isopolyvanadates in the three series with specific activities (Fig. 6), it seems that the activity for autoxidation is largely affected by the type of chromium isopolyvanadate in the catalyst, its activity being in the order: chromium polyvanadates $> Cr(VO_3)_3 > Cr_4(V_2O_7)_3$.

*** The band at about 800 cm^{-1} was assigned to the stretching of V–O–V bond.[2] However, the assignment to VO_6 octahedron may be more reasonable because of the absence of the band in the spectrum of $Cr_4(V_2O_7)_3$.

Chromium isopolyvanadate with a higher degree of condensation shows a higher activity. The long induction periods observed in all the reactions may be due to the accumulation of HPO. Thus, autoxidation is considered to be initiated by the radical decomposition of HPO with the binary catalyst. According to the results of Meyer *et al*,;[13] chromium oxide decomposes hydroperoxide, it is thought that the active species for autoxidation contains chromium.**** The correlation of catalyst composition to Y_{HPO}/S is similar to that to R_{max}/S. This is explained by the fact that HPO is the main product of the autoxidation of cyclohexene by radical chain mechanism.

Concerning epoxidation, exact discussions are difficult since it may have first-order dependence on HPO concentration. All we can say is that the active species for the epoxidation differs from that for the autoxidation. It might consist of vanadium.

Studies on the vapor-phase oxidation with V system catalysts[6] show that the formation of solid solution causes the increase of catalytic activity. However, no such phenomenon has been observed. This might result from the difference in the catalytic mechanism between liquid-phase and vapor-phase oxidation.

Higher activity of the V–Cr catalyst was obtained by use of the more acidic medium. This might result from the variety of vanadate anions formed on mixing of the raw materials. It is suggested that various isopolyvanadate anions form depending on the acidity of medium.[12] Their existence may largely influence the structure and activity of the binary oxide catalyst.

**** In order to study the surface state of the catalysts, X-ray photoelectron spectroscopy was carried out. No shift was observed in the V $2p_{3/2}$ line between $V_2O_5(V^{5+})$ and V_2O_4 (V^{4+}),[14] but some shift was recognized in the Cr $2p_{3/2}$ line between $Cr_2O_3(Cr^{3+})$ and $K_2Cr_2O_7(Cr^{6+})$.[15] The binding energies of Cr in the binary catalysts remain approximately constant, 587 eV (Cr $2p_{1/2}$) and 557 eV (Cr $2p_{3/2}$), suggesting that chromium species on the surface of the catalysts have the same charge (probably of Cr^{3+}).

References

1) K. Takehira and T. Ishikawa, *Bull. Chem. Soc. Jpn.*, **49**, 2351 (1976).
2) K. Takehira, T. Nishimura, M. Araki, T. Hayakawa, and T. Ishikawa, *Nippon Kagaku Kaishi*, **1974**, 652.
3) J. Amiel, D. Olivier, and M. Dessolin, *C. R. Acad. Sci., Ser. C*, **264**, 1045 (1967).
4) D. Olivier, *C. R. Acad. Sci., Ser. C.* **264**, 1176 (1976).
5) D. Olivier and P. Rabette, *C. R. Acad. Sci., Ser. C*, **265**, 1451 (1967).
6) S. Yoshida, *Shokubai*, **10**, 90 (1968) and references cited therein.
7) D. Olivier, *C. R. Acad. Sci., Ser. C*, **272**, 1225 (1971).
8) T. Nishimura, T. Hayakawa, M. Araki, K. Takehira, and T. Ishikawa, *J. Nat. Chem. Labr. Ind.*, **68**, 249 (1973).
9) L. N. Kurina, O. N. Ediseeva, V. F. Anufrienko, S. T. Chistanova, N. M. Simkin, and V. A. Zozulya, *Kinet. Katal.* **11**, 614 (1970); V. A. Anufrienko, S. T. Chistanova, and L. N. Kurina, *ibid.*, **11**, 1079 (1970).
10) J. C. Bouloux and J. Galy, *Bull. Soc. Chim. Fr.*, **1969**, 736.
11) D. Olivier, *Rev. Chim. Miner.*, **6**, 1033 (1969).
12) G. A. Tsigdinos and C. J. Hallada, "Isopoly Compounds of Molybdenum, Tungsten, and Vanadium," *Molybdenum Chemicals Bulletin Cdb-14* (February 1969), p. 20.
13) C. Meyer, G. Clement, and J. C. Balaceanu, *Proc. Int. Congr. Catal., 3rd 1964*, **1**, 184 (1965).
14) J. C. Helmer, *J. Electron Spectrosc.*, **1**, 259 (1972/73).
15) M. Valdeievre, H. Baussart, R. Delobel, and J. M. Leroy, *Bull. Soc. Chim. Fr.*, **1975**, 2467.

Calorimetric Study of the Glassy State. XIV. Calorimetric Study on Unusual Glass Transition Phenomena in $CFCl_2$-$CFCl_2$

Kōji Kishimoto,* Hiroshi Suga, and Syûzô Seki

Department of Chemistry, Faculty of Science, Osaka University, Toyonaka, Osaka 560

(Received December 1, 1977)

The heat capacities of the glassy crystalline, plastic crystalline, and liquid phases of $CFCl_2$–$CFCl_2$ were measured by an adiabatic calorimeter over a temperature range from 13 to 310 K, with a sample of 99.93% purity. The triple point was determined to be 297.91 K, the enthalpy and entropy of fusion being 3.666 kJ mol^{-1} and 12.30 J K^{-1} mol^{-1}, respectively. Three kinds of relaxation phenomena were found during the heat capacity measurement centered at around 60, 90, and 130 K, respectively. The first was attributable to the β relaxation. The second was for primary glass transition, where overall rotation or reorientation of the molecules might be frozen. The third was analyzed by ascribing it to the freezing of conversion between the trans and the gauche conformers of the molecule. Activation enthalpy for the internal rotation and energy difference between the two conformers were determined to be 41 kJ mol^{-1} and (790 ± 60) J mol^{-1}, respectively. This experiment provides the first example in which three different freedoms of molecular motion are frozen successively at different temperatures as the crystal is cooled down. An effort to get a possible low-temperature ordered crystalline phase was partially successful by long annealing of the crystal. The extremely sluggish nature of the phase transition into the ordered phase will be related with the slow rate of the internal rotation of the molecule below the transition temperature.

In order to clarify the nature of vitrification process from molecular viewpoint, it is indispensable, at the present stage, to choose as simple a system as possible where degrees of freedom to be taken into account are so restricted in its number that rigorous treatment will be approached. Glassy crystal meets this requirement since it has three-dimensional long-range periodicity which eliminates the complication in considering positional disorder. In hopes of the elucidation of freedoms frozen below a glass transition temperature, T_g, the present material was chosen from the viewpoint of simple molecular structure with internal degrees of definite nature. Kolesov *et al.*[1] already measured the heat capacity of this material and found a type-G transition at around 90 K, according to the phenomenological classification advanced by Guthrie and McCullough.[2] They also reported that this compound has a plastic crystalline phase below its melting point. However, the detailed trend of the heat capacity in the transition region was not delineated in their calorimetric study and they did not mention any relaxational nature of the anomaly. To clarify the nature of the anomaly is the first motivation for the present study. As judged by intuitive plausibility, the transition which they called type-G transition is likely to be a glass transition from the plastic crystal to a glassy crystal. If so, a low-temperature ordered phase must be found by careful thermal treatment. This is another principal object of the study.

Experimental

Material. About 200 g of the compound purchased from E. Merck AG. was first purified by distillation at atmospherric pressure. The middle fraction was subjected to fractional melting in a thermostated bath controllable within $\pm$ 1 mK and then purified by molecular sieve (Linde 3A) to remove low molecular weight compounds as impurities, and finally fractionally distilled *in vacuo*. The calorimeter cell had been attached in advance to the purification system. The purified sample was transferred into the calorimeter cell and then an inlet capillary tubing was pinched off. The analysis of the fractional melting process of the sample, as will be described later, indicated the impurity content of 0.07%.

Heat Capacity Measurement. The heat capacity was measured by the adiabatic calorimeter reported previously.[3] The calorimeter cell was a gold-plated copper can of internal volume 30 cm^3. A sample of 48.121 g (*in vacuo*) was loaded into the cell. No exchange gas was admitted inside the cell. The density of the crystal used in buoyancy correction was calculated from an X-ray diffraction data. A working platium thermometer was calibrated against the International Practical Temperature Scale of 1968 after the completion of the measurement.

X-Ray Diffraction. Preliminary X-ray investigation of the crystal at room temperature was done by the rotating-crystal method. Single crystal was grown from the liquid within a pyrex capillary tubing. X-ray diffraction phtograph was taken at 15 °C by a cylindrical camera of diameter 5.712 cm with Cu K_α radiation

Results and Discussion

X-Ray Diffraction. The observed X-ray diffraction patterns are well indexed as those of the bcc lattice with the cell constant of (0.718 ± 0.004) nm at 15 °C. The rotation photograph has only four reflections, corresponding to (110), (200), (211), and (220) planes, even for prolonged irradiation. This arises from the rapid falling-off in intensity with increasing reflection angle and reflects the fact that the crystal is highly disordered. This behavior is one of the characteristic natures of the plastic crystal.

Determination of Purity. A fractional melting experiment was carried out to determine the melting point and the purity of the sample. In Fig. 1 the reciprocal of the fraction of the sample melted, $1/f$, is plotted against the equilibrium final temperature, T_f, for each energy input. As extremely long time was required for the establishment of thermal equilibrium during the

* Present address: Industrial Research Lab., Kao Soap Co., Ltd., Wakayama.

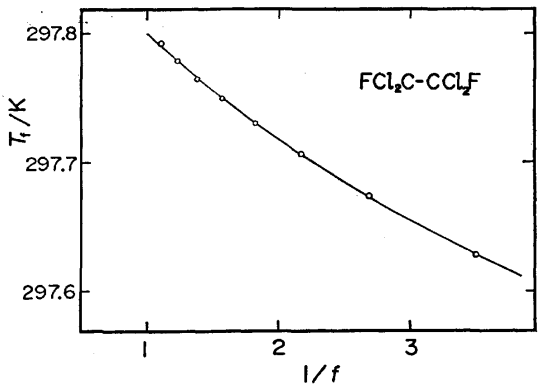

Fig. 1. The equilibrium melting temperature of CCl_2F–CCl_2F plotted against the reciprocal of fraction melted.

TABLE 1. THE EQUILIBRIUM TEMPERATURES DURING FUSION PROCESS OF CCl_2F–CCl_2F

f	$1/f$	T_f/K
0.2856	3.501	297.6273
0.3726	2.684	297.6737
0.4605	2.171	297.7063
0.5491	1.821	297.7305
0.6381	1.567	297.7498
0.7273	1.375	297.7650
0.8167	1.225	297.7789
0.9060	1.104	297.7924

T_{tp}=297.91 K
Purity=99.93%

melting process, the extrapolated value of the temperature to the time being infinite at each energy input was taken as T_f. These values are given in Table 1. Since T_f versus $1/f$ does not yield a straight line, we employed Mastrangelo-Dornte's method[4] in which they derived a solid solution treatment for calorimetric melting point data. By use of this treatment the purity and the triple point of the sample were determined to be 99.93% and 297.91 K, respectively. The enthalpy of fusion was measured twice. These cryoscopic data are given in Table 2. The small entropy of fusion as well as its high crystallographic symmetry indicate that the crystal belongs to the category of plastic crystal originally defined by Timmermans.[5]

TABLE 2. CRYOSCOPIC DATA OF CCl_2F–CCl_2F

T_{tp}/K	ΔH_m/J mol^{-1}	ΔS_m/J K^{-1} mol^{-1}
297.91	3666	12.30

Heat Capacity. The experimental values of the molar heat capacities are listed in Table 3 and presented graphically in Fig. 2. These series of measurements are numbered in chronological order so that their thermal history of the sample may be followed. Also, the approximate temperature increments employed in the measurements may be deduced from the differences in the adjacent average temperatures. Curvature correction was made along the same line as in Ref. 6, whereas the vaporization correction was not made because of

TABLE 3. MOLAR HEAT CAPACITIES OF CCl_2F–CCl_2F

T_{av}/K	C_p/J K^{-1} mol^{-1}	T_{av}/K	C_p/J K^{-1} mol^{-1}
Series 1		229.23	156.05
		232.05	156.68
106.09	132.62	235.02	157.30
108.30	133.05	238.13	158.05
110.64	133.55	241.23	158.95
112.97	133.83	244.31	159.54
115.28	134.36	247.39	160.38
117.55	134.50	250.44	161.14
119.92	135.11	253.35	161.80
122.37	135.62	256.39	162.58
Series 2		Series 6	
127.24	137.13	259.89	163.53
130.09	138.27	263.14	164.33
132.90	139.03	266.37	165.25
135.71	139.05	269.59	166.25
138.50	139.54	272.80	167.13
141.30	139.98	275.99	168.09
144.09	140.49	279.16	169.19
146.84	140.88	282.32	170.20
149.57	141.43	285.46	171.04
152.30	141.83	288.58	172.48
		291.68	173.61
Series 3		294.92	174.74
150.73	141.62	Series 7	
153.56	142.06		
156.41	142.55	279.77	169.28
159.37	143.04	282.97	170.26
162.40	143.52	286.17	171.34
165.42	144.09	289.36	172.67
168.99	144.57	292.54	173.85
Series 4		Series 8	
171.90	145.28	298.96	178.45
174.81	145.52	301.23	178.77
177.69	145.90	304.26	179.20
180.57	146.50	307.29	179.73
183.43	147.05	310.33	180.13
186.27	147.60		
189.10	148.04	Series 9	
191.92	148.68		
194.73	149.06	94.17	130.81
197.51	149.50	96.86	131.29
200.37	150.07	99.53	131.77
203.31	150.67	102.26	132.31
206.24	151.17	105.06	132.65
209.16	152.03		
212.07	152.41	Series 10	
214.96	153.04		
217.84	153.67	115.30	134.24
220.71	154.32	117.63	134.64
223.56	154.85	119.96	135.07
		122.29	135.47
Series 5		124.66	135.94
		127.08	136.39
226.40	155.41	129.53	136.99

TABLE 3. (Continued)

T_{av}/K	C_p/J K^{-1} mol^{-1}	T_{av}/K	C_p/J K^{-1} mol^{-1}
132.04	138.23	66.40	68.15
134.63	139.29	68.65	69.88
137.34	139.27	70.88	71.63
		73.14	73.49
Series 11		75.42	75.44
		77.78	77.54
158.65	142.81	80.29	80.14
161.32	143.13	82.85	83.41
163.98	145.29	85.31	88.25
166.57	150.60	87.63	99.79
169.18	145.66	89.82	127.66
171.86	145.11	91.96	130.78
174.52	145.55		
		Series 13	
Series 12			
		99.99	129.16
13.93	16.57	103.33	129.82
15.10	18.68	106.63	130.52
16.46	21.18	109.90	131.19
18.20	24.22	113.14	131.93
20.09	27.21	116.35	132.61
21.87	29.84	119.54	133.21
23.60	32.25	121.83	133.61
25.38	34.57	124.99	134.51
27.24	36.83	128.11	135.78
29.00	38.75	131.27	136.94
30.88	40.52	134.50	137.53
32.83	42.37	137.70	137.85
34.69	44.01	140.88	138.51
36.66	45.56	144.05	139.10
38.66	47.23	147.74	139.80
40.59	48.60	150.88	140.53
42.53	50.01	153.99	141.34
44.49	51.40		
46.38	52.69	Series 14	
48.26	53.99		
50.21	55.35	157.36	142.11
52.32	56.79	160.41	143.60
54.48	58.36	163.65	151.37
56.70	59.99	166.68	210.52
59.13	61.84	169.32	213.47
61.65	63.90	172.33	149.40
64.07	66.06	175.51	146.21

lack of the vapor pressure data. As is seen in Fig. 2, the plastic crystal is easily brought into a glassy crystalline state through a glass transition region centered around 90 K. This is really a glass transition phenomenon since the characteristic enthalpy relaxation was observed at this temperature region, as will be shown later. The heat capacities of the glassy crystal plotted in Fig. 2 are for the sample cooled at the rate of 0.2 K min^{-1} from 210 K to temperatures below T_g.

Usually plastic crystal undergoes a transformation on cooling to different phase with ordered molecular orientation in accord with the third law of thermodynamics. The expected ordered phase, however, can not be realized in this crystal by a simple cooling. Therefore,

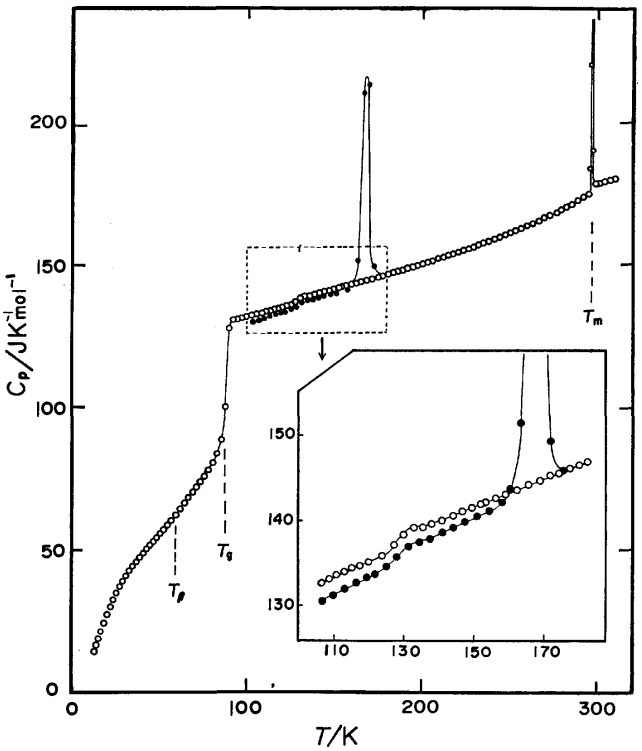

Fig. 2. The heat capacities of CCl_2F–CCl_2F.
○; Rapidly cooled specimen,
●; annealed specimen for 50 days below 120 K.

the sample was first cooled down to 13 K and then annealed in the temperature range between 77 and 160 K for 50 days. This thermal treatment proves to be partially successful for inducing a low-temperature phase. The major feature of the heat capacity for this sample (solid circle in Fig. 2) is a sharp peak at 170 K which is undoubtedly the transition point T_t, separating an ordered and the plastic phases. Extremely long equilibration time was required during the phase transition, and this indicates the first order nature of the transition. The heat capacities below T_t are 0.9% smaller than those for the supercooled plastic crystalline phase, while above T_t both of the values agree within the experimental precision.

The heat capacities of the glassy crystal and its simple extrapolation to higher temperatures serve as an approximation to those for the ordered crystal. Comparing the heat capacity lowering of 0.9% with the heat capacity jump at T_g, it is estimated that 2—3% of the plastic crystalline phase was transformed into the ordered phase by the above thermal treatment. On the other hand, fewer ($\approx$0.16%) ordered phase was obtained by the same procedure except that the sample had not been cooled down to 13 K. Being cooled down to the liquid hydrogen temperature seems to be indispensable for some other kinds of materials to produce their ordered phases as suggested by Finke and Messerly.[7] The fact that the rate of nucleation is accelerated by cooling the crystal to 13 K supports the prevailing idea that some kinds of molecular rearrangement still occur even below T_g. This suggests a potential existence of another relaxation phenomenon below the primary glass transition.

Thermodynamic Functions. Thermodynamic func-

TABLE 4. THERMODYNAMIC FUNCTIONS OF CCl_2F–CCl_2F

T / K	C_p / J K^{-1} mol^{-1}	$S°-S°_0$ / J K^{-1} mol^{-1}	$(H°-H°_0)/T$ / J K^{-1} mol^{-1}	$-(G°-H°_0)/T$ / J K^{-1} mol^{-1}
		Glassy crystalline and Plastic crystalline phases		
10	(8.866)	(3.466)	(2.543)	(0.923)
20	27.11	15.43	10.43	5.00
30	39.69	28.99	18.24	10.75
40	48.19	41.64	24.72	16.91
50	55.19	53.15	30.12	23.03
60	62.53	63.84	34.90	28.94
70	70.96	74.13	39.46	34.67
80	79.83	84.15	43.92	40.23
90	128.13	95.07	49.38	45.69
100	131.79	108.85	57.53	51.32
110	133.42	121.49	64.35	57.14
120	135.05	133.17	70.18	62.99
130	138.26	144.08	75.27	68.81
140	139.80	154.38	79.82	74.56
150	141.45	164.08	83.88	80.21
160	143.09	173.26	87.53	85.74
170	144.77	181.99	90.84	91.15
180	146.47	190.31	93.89	96.43
190	148.19	198.28	96.70	101.58
200	150.05	205.93	99.32	106.61
210	152.03	213.29	101.78	111.51
220	154.09	220.41	104.11	116.30
230	156.23	227.31	106.33	120.98
240	158.50	234.01	108.46	125.55
250	160.96	240.53	110.51	130.02
260	163.61	246.89	112.50	134.39
270	166.40	253.12	114.44	138.67
273.15	167.31	255.05	115.05	140.00
280	169.33	259.22	116.35	142.87
290	172.37	265.22	118.23	146.99
		Liquid phase		
300	178.59	283.43	132.33	151.11
310	180.09	289.32	133.85	155.47

tions at regular temperature intervals were obtained by numerical integration of the smoothed values of the experimental heat capacities. They are all tabulated in Table 4. In the derivation of these apparent thermodynamic functions, the glassy crystalline phase at 0 K was taken as a reference state instead of a crystalline phase which obeys the third law of thermodynamics, because of the failure in preparing pure low-temperature ordered phase. Below 13 K, the values of heat capacity contributing to the thermodynamic functions were calculated on the basis of the effective frequency distribution[8,9] given in the inset in Fig. 3.

Primary and β Relaxation. β relaxation was first observed calorimetrically in the glassy state of isopropylbenzene.[8] An analogous thermal anomaly was observed in the glassy crystalline state of the present material. Figure 4 represents the thermal drifts encountered during the course of heat capacity measurement. These drifts of the calorimeter temperature are the sum of the quasi-adiabatic drifts due to small heat leakage in the calorimetric system and the drifts due to enthalpy relaxations which are responsible for configurational or other changes possibly occurring in the sample. The values shown in this figure are corresponding to the initial drifts taken just after a uniform distribution of the calorimetric temperature which is realized about 5 min after an energy input. Changes in signs of the temperature drifts on heating from exothermic to endothermic ones characteristic of enthalpy relaxation phenomena were observed centering at around 60, 90, and 130 K. The change found around 60 K is attributed to the β relaxation. Associated with this relaxation, the heat capacity increases stepwise by amount of ≈2 J K^{-1} mol^{-1} around 60 K. Figure 3 indicates the excess heat capacity responsible for the β relaxation over those extrapolated from below T_β (see Fig. 2). This extrapolation was carried out by employing the method of effective frequency distribution[8,9] with 22 values for C_p between 14 and 52 K. The inset in this figure is the effective frequency distribution which reproduces best the heat capacity data below 52 K. The nature and the possible origins of β relaxations in glassy liquid and glassy crystal were discussed by Johari[10] based on the dielectric observation. The second found around 90 K in Fig. 4 is attributed to the primary glass transition, where overall rotation or reorientation of molecules might be frozen.

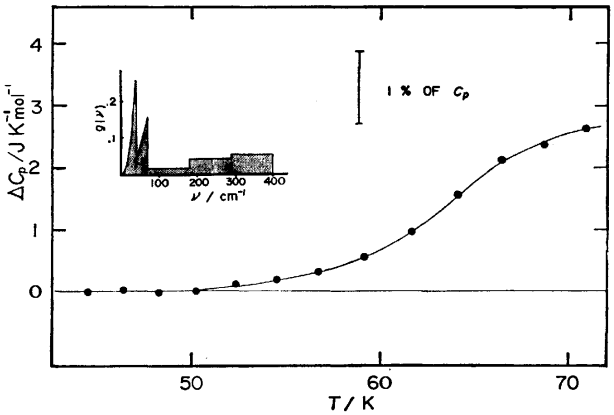

Fig. 3. Excess heat capacities responsible for β relaxation over those extrapolated from T_β.

Anomalous Heat Capacity around 130 K. The heat capacity data above 100 K are reproduced in Fig. 5 on an enlarged scale. The anomalous heat capacities observed around 130 K are accompanied by temperature drifts characteristic of those observed around glass

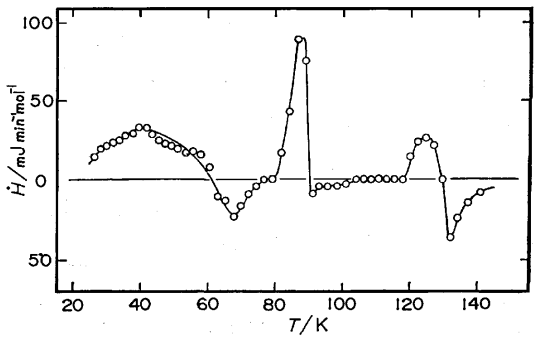

Fig. 4. Spontaneous temperature drifts of calorimeter plotted as a function of temperature.

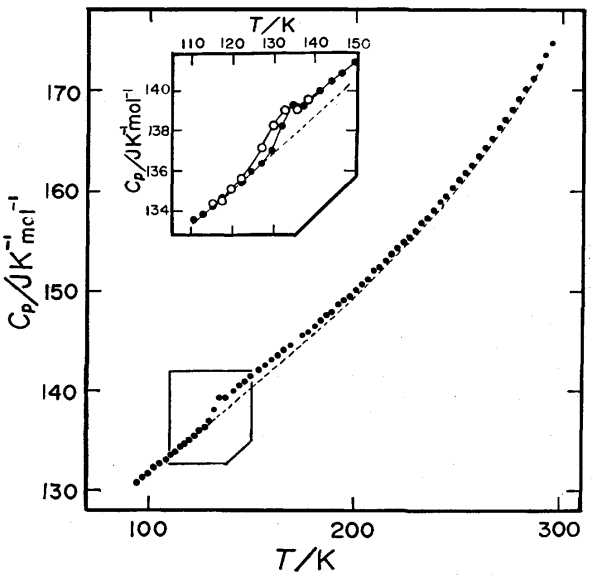

Fig. 5. The heat capacities of CCl_2F–CCl_2F above 100 K on an enlarged scale.
●; Rapidly cooled specimen,
○; annealed specimen at 125 K for about 40 h.

transition region. Taking into account the step-like increase in heat capacity and the nature of temperature drifts, we can conclude that the anomaly arises from relaxational effect of some degrees of freedom. One possible candidate is freezing-in of the conversion between trans and gauche conformers of the molecule. Based on the assumptions that the frequencies of C–C torsional modes are the same for both conformers and that the conversion has little effect on the lattice vibration, the excess heat capacity due to the conversion is approximately described by the Schottky heat capacity.

Newmark and Graves[11] found that the energy of the gauche conformer was 690 J mol^{-1} above the trans conformer in a mixed solvent $CFCl_3$–CF_2Cl_2. Newmark and Sederholm[12] obtained the value 510 J mol^{-1} for the energy difference in $CFCl_3$ solution. Therefore the trans conformer was assumed to be more stable one in the plastic crystalline phase. Then, the molar Schottky heat capacity C_{sch} is given by the following equation:

$$C_{sch} = \frac{\Delta H^2 \exp(\Delta H/RT)}{2RT^2\left[1+\frac{1}{2}\exp(\Delta H/RT)\right]^2}\cdot\theta(T-T_g), \quad (1)$$

where ΔH is the enthalpy difference between the trans and the gauche conformers, R the gas constant, and θ the step function. Below T_g, there exists no contribution to the Schottky heat capacity because of the freezing-in of the conversion. Then, ΔH in this equation can be obtained from C_{sch} at T_g which is corresponding to the heat capacity jump at T_g in Fig. 5. By taking into account of the irreversible enthalpy relaxation effect, the heat capacity jump is assessed to be (1.1±0.2) J K^{-1} mol^{-1} at 130 K, which gives the value (790±60) J mol^{-1} for ΔH. The broken curve in Fig. 5 represents the heat capacities obtained by subtracting C_{sch} from the measured molar heat capacities. This broken curve gives a reasonable extrapolation of the heat capacity below 130 K up to the triple point. Comparison of our value (790±60) J mol^{-1} with the following three values, that is, (i) ΔH=800 J mol^{-1} obtained by Pethrick *et al.*[13] based on the IR and Raman data of Kagarise *et al.*,[14] (ii) ΔH=690 J mol^{-1} obtained by Newmark and Graves and (iii) ΔH=510 J mol^{-1} by Newmark and Sederholm described above, supports the validity of the proposed model for the explanation of the heat capacity anomaly appeared around 130 K.

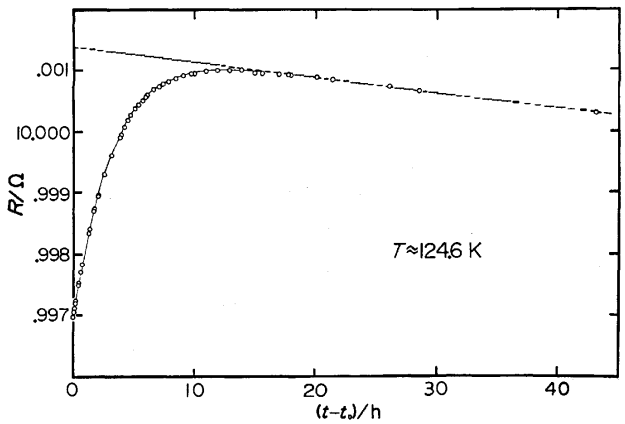

Fig. 6. The temperature drifts due to the enthalpy relaxation phenomenon are plotted as a function of time. The ordinate represents the readings of the platinum resistance thermometer.

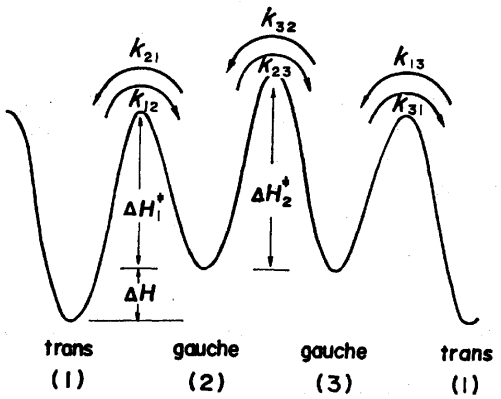

Fig. 7. The enthalpy curve as a function of the coordinate of internal rotation around the C–C bond of CCl_2F–CCl_2F.

The exothermic drifts measured at 124.6 K are plotted in Fig. 6 as a function of time. The broken line indicates the heat leakage caused by the imperfection of adiabatic control. It was assessed to be 28 μW. The difference between the solid and the broken lines is attributed to the enthalpy relaxation inside the specimen, which can be fitted considerably well to an exponential function. The relaxation time at 124.6 K turned out to be 10.4 ks. The process of trans-gauche conversion is very similar to that of unimolecular reactions. In Fig. 7, the states labeled 1, 2, and 3 correspond to trans, gauche, and gauche conformers, respectively. Dynamical equilibrium among them is established above the frozen-in temperature. The transition from state i to state j is assumed to take place with a transition probability k_{ij}.

From the symmetry of the potential function, the following relations can be obtained,

$$k_{32} = k_{23},\ k_{13} = k_{12},\ \text{and}\ k_{31} = k_{21}. \quad (2)$$

Between 1 and 2, and 2 and 3, there exist activated states whose potential barriers have heights of ΔH_1^* and ΔH_2^*, respectively. The rate equation for the occupational probablities of the states may be expressed in a matrix form,

$$\dot{P}(t) = D \cdot P(t), \quad (3)$$

where

$$P(t) = \begin{pmatrix} P_1(t) \\ P_2(t) \\ P_3(t) \end{pmatrix}$$

$$D = \begin{bmatrix} -2k_{12} & k_{21} & k_{21} \\ k_{12} & -(k_{21}+k_{23}) & k_{23} \\ k_{12} & k_{23} & -(k_{21}+k_{23}) \end{bmatrix}. \quad (4)$$

The rate equation has the solution

$$P(t) = (\exp Dt) \cdot P(0) = Te^{\Lambda t}T^{-1}P(0). \quad (5)$$

T is the matrix that diagonalizes D, and Λ is the diagonal matrix:

$$\Lambda = T^{-1}DT = \begin{bmatrix} 0 & 0 & 0 \\ 0 & -(k_{21}+2k_{12}) & 0 \\ 0 & 0 & -(k_{21}+2k_{23}) \end{bmatrix}. \quad (6)$$

Hence $P(t)$ is readily obtained as

$$P(t) = \begin{bmatrix} P_1^\circ & 2m & 0 \\ P_2^\circ & -m & n \\ P_3^\circ & -m & -n \end{bmatrix} \cdot \begin{pmatrix} 1 \\ \exp(-t/\tau_1) \\ \exp(-t/\tau_2) \end{pmatrix}, \quad (7)$$

where $\tau_1^{-1}=k_{21}+2k_{12}$, $\tau_2^{-1}=k_{21}+2k_{23}$, the coefficients m and n are evaluated from the initial conditions, and P_i° the equilibrium occupational probability of state i.

The internal energy arising from the freedom of internal rotation, H_{int}, is given as follows by taking the trans conformer as the reference state of energy,

$$H_{\text{int}} = \Delta H(P_2+P_3) = \Delta H[2P_2^\circ - 2m\exp(t/\tau_1)]. \quad (8)$$

It is noticeable that the enthalpy relaxation is dominated by a single relaxation time, whereas the dielectric relaxation time for this system is dependent on both τ_1 and τ_2.[15] On the other hand, according to the theory of absolute reaction rate[16] k_{12} can be written in the following form by assuming a transmission coefficient of nearly unity,

$$k_{12} = \frac{kT}{h}\frac{F^*}{F_1}\exp[-(\Delta H_1^* + \Delta H)/RT] \simeq \frac{kT}{h}\left[1-\exp\left(-\frac{h\nu}{kT}\right)\right]\exp[-(\Delta H_1^* + \Delta H)/RT], \quad (9)$$

where F_1 and F^* are the partition functions of the trans conformer for the ground and the activated states, respectively. ν is the C–C torsional frequency, and the other symbols obey the conventional terminology. Similarly, k_{21} and k_{23} are of the form

$$k_{21} \simeq \frac{kT}{h}\left[1-\exp\left(-\frac{h\nu}{kT}\right)\right]\exp\left(-\frac{\Delta H_1^*}{RT}\right),$$

and

$$k_{23} \simeq \frac{kT}{h}\left[1-\exp\left(-\frac{h\nu}{kT}\right)\right]\exp\left(-\frac{\Delta H_2^*}{RT}\right). \quad (10)$$

Assuming $\Delta H \ll \Delta H_1^*$ gives $k_{12}=k_{21}$, and as a result, $\tau_1^{-1} = 3k_{21}$. Equation (8) yields the relation that the enthalpy relaxation time τ is equal to $1/3\,k_{21}$.

ΔH^* can be calculated to be 39.8 kJ mol^{-1} by use of the value 82 cm^{-1} [13] for ν together with the value for τ at 124.6 K. This result agrees well with the value of (38 ± 1) kJ mol^{-1} obtained by Newmark and Graves[11] and of (40 ± 0.4) kJ mol^{-1} obtained by Newmark and Sederholm.[12] The relaxation time at infinite temperature, τ_0, is of the order of 10^{-13} s. The large activation enthalpy in this highly halogenated ethane seems to arise from steric hindrance of the bulky halogen atoms in the eclipsed state. Since all molecules in the low-temperature ordered phase should be in only one and the same conformer, either trans or gauche form, the molecules must rearrange themselves to go to the most stable conformer by exceeding the activated state in the course of the phase transition of the plastic crystalline phase into the ordered phase. Thus one of the reasons for the extremely sluggish nature of the phase transition of the present material seems to be the slow rate of the trans-gauche conversion below T_t (170 K).

The authors express their sincere thanks to Associate Professor Yōzō Chatani for taking the X-ray diffraction photographs

References

1) V. P. Kolesov. V. N. Vorob'ev, and E. A. Sarzhina, *Preprint of Third Intern'l Conf. on Chem. Thermodyn.*, **2**, 33 (1973).
2) G. B. Guthrie and J. P. McCullough, *J. Phys. Chem. Solids*, **18**, 53 (1965).
3) H. Suga and S. Seki, *Bull. Chem. Soc. Jpn.*, **38**, 1000 (1965).
4) S. V. R. Mastrangelo and R. W. Dornte, *J. Am. Chem. Soc.*, **77**, 6200 (1955).
5) J. Timmermans, *J. Phys. Chem. Solids*, **18**, 1 (1961).
6) E. F. Westrum, Jr., G. T. Furukawa, J. P. McCullough, Adiabatic low-temperature calorimetry. In "Experimental Thermodyamics," Vol. 1, ed by J. P. McCullough, D. W. Scott, Butterworths, London (1968).
7) H. L. Finke and J. F. Messerly, *J. Chem. Thermodyn.*, **5**, 247 (1973).
8) K. Kishimoto, H. Suga, and S. Seki, *Bull. Chem. Soc. Jpn.*, **46**, 3020 (1973).
9) M. Sorai and S. Seki, *J. Phys. Soc. Jpn.*, **32**, 382 (1972).
10) G. P. Johari, *Ann. New York Acad. Sci.*, **279**, 117 (1976).
11) R. A. Newmark and E. R. Graves, *J. Phys. Chem.*, **72**, 4299 (1968).
12) R. A. Newmark and C. H. Sederholm, *J. Chem. Phys.*, **43**, 602 (1965).
13) R. A. Pethrick and E. Wyn-Jones, *J. Chem. Soc., Ser. A*, **1971**, 54.
14) R. E. Kagarise and W. Daasch, *J. Chem. Phys.*, **23**, 113 (1955).
15) K. Kishimoto, Doctoral Thesis, Osaka University, 1976. The dipole moment correlation function $\Gamma(t)$ for this system is given by the following equation,

$$\Gamma(t) = \frac{3}{2}P_2^\circ + \frac{3}{4}P_1^\circ \exp(-t/\tau_1) + \frac{1}{4}\exp(-t/\tau_2).$$

16) S. Glasstone, K. S. Laidler, and H. Eyring, "Theory of Rate Process" McGraw-Hill Book Co., Inc., New York (1941).

Interactions of Calcium Ions with Carbohydrates: Crystal Structure of Calcium DL-Glycerate Dihydrate

Tooru TAGA, Makoto OHASHI, and Kenji OSAKI

Faculty of Pharmaceutical Sciences, Kyoto University, Sakyo-ku, Kyoto 606

(Received December 8, 1977)

The crystal structure of calcium DL-glycerate dihydrate has been determined by the heavy atom method. The crystal is monoclinic, space group $P2_1/c$, with unit cell dimensions: $a=14.40$, $b=7.63$, $c=10.40$ Å, and $\beta=98.8°$. Two independent glycerate anions have different conformations. β-Hydroxy oxygen in one conformer is trans-gauche to α-carboxy carbon and α-hydroxy oxygen, while that in the other conformer is gauche-gauche. Ca–O interactions and hydrogen bonds stabilize the crystal structure. The calcium ion is bound to three glycerate anions and two water molecules, the two glycerate anions chelating the calcium ion with the α-carboxy oxygen and α-hydroxy oxygen, and third glycerate anion bonding to the calcium ion with β-hydroxy oxygen. Seven oxygens surround a calcium ion in a distorted pentagonal biprism arrangement with Ca–O distances ranging from 2.32 to 2.47 Å.

A ^{1}H NMR study on lanthanoid complexes of polyhydroxy α-carboxylic acids in an aqueous solution indicates that the ligand anion has a conformation suitable for the complex formation with the cation and usually chelates the cation with α-carboxy oxygen, α-hydroxy oxygen, and β-hydroxy oxygen.[1,9] The same type of 'three O atoms' chelation to a calcium ion has been observed in the crystal structures of Ca-arabonate·$5H_2O$[11] and CaBr-lactobionate·$4H_2O$.[12] However, such a chelate form may not be always necessary for a stable calcium binding to β-hydroxy carboxylic acid in the crystal state, since the calcium binding features in Ca-tartrate·$3H_2O$[20] and Ca-glucarate·$4H_2O$[10] differ from that mentioned above. The calcium ion is generally coodinated with seven to nine oxygens in a crystalline state, and the oxygen polyhedra observed in a number of calcium carbohydrate crystals[8-32] are largely distorted from the idealized form. In the present investigation we were, therefore, interested in the conformation of the glycerate anion and in the chelating feature of the anion with the calcium ion; the steric arrangement of the ligand oxygens around the calcium ion in the crystal structure received special attention.

Experimental

Colorless monoclinic crystals of calcium glycerate dihydrate $Ca(C_3H_5O_4)_2\cdot 2H_2O$ were obtained by slow evaporation of the saturated aqueous solution. Prelimilary experiments indicated that the space group is $P2_1/c$, from the systematic absences of $h0l$ and $0k0$ for l and k odd, and that the unit cell dimensitions are $a=14.40(7)$, $b=7.63(4)$, $c=10.40(4)$ Å, and $\beta=98.8(3)°$, from Weissenberg photographs calibrated by NaCl standard powder lines. $V=1129$ Å^3, $Z=4$, and $D_x=1.68$ g/cm^3. Equi-inclination Weissenberg photographs were taken by rotating the crystal about the b- and c-axes, using nickel-filtered Cu $K\alpha$ radiation. Intensity data were collected on a SYNTEX AD-1 densitometer controlled by a NOVA 1200 computer acting in cooperation with a DIABLO-31 disk drive. Structure factors of 1150 independent reflections were obtained through the usual data reduction procedure.

Positional parameters of the calcium ion were determined from sharpened Patterson maps and those of carbon and oxygen atoms were determined from the Fourier maps synthesized with phases of the calcium ion. Six cycles of block-diagonal least-squares refinement with the anisotropic thermal parameters gave an R-value of 0.14.

TABLE 1. ATOMIC PARAMETERS AND THEIR ESTIMATED STANDARD DEVIATIONS

The values have been multiplied by 10^4. Temperature factors are in the form $T^{-1}=\exp(\beta_{11}h^2+\beta_{22}k^2+\beta_{33}l^2+2\beta_{12}hk+2\beta_{13}hl+2\beta_{23}kl)$.

	x	y	z	β_{11}	β_{22}	β_{33}	β_{12}	β_{13}	β_{23}
Ca	2712(2)	498(4)	1357(3)	22(1)	85(5)	49(2)	5(3)	12(1)	−2(4)
C(1)	1694(10)	4143(18)	585(14)	36(7)	79(28)	79(16)	−17(12)	20(9)	−14(17)
C(2)	1534(10)	4109(18)	2040(14)	39(7)	83(29)	63(15)	5(12)	20(8)	16(16)
C(3)	491(10)	4456(24)	2091(15)	38(8)	168(35)	86(17)	13(16)	18(9)	42(23)
O(1a)	2000(7)	2811(13)	132(9)	62(7)	113(22)	54(10)	27(10)	26(7)	−12(12)
O(1b)	1547(77)	5607(14)	25(9)	55(6)	105(20)	61(10)	−3(11)	22(6)	7(13)
O(2)	1773(7)	2382(14)	2495(9)	52(6)	107(20)	68(11)	27(10)	35(7)	12(13)
O(3)	339(7)	4443(20)	3432(11)	36(6)	360(37)	85(12)	−5(13)	27(7)	−24(20)
C(4)	3897(9)	−830(19)	−886(12)	36(7)	98(29)	36(11)	−16(11)	12(7)	−6(15)
C(5)	4066(9)	−2417(20)	−10(13)	26(6)	103(27)	52(14)	16(12)	10(8)	−14(17)
C(6)	3804(9)	−4104(20)	−742(14)	26(6)	140(33)	64(15)	−3(12)	12(8)	−15(18)
O(4a)	3371(7)	342(13)	−603(9)	48(6)	93(19)	70(10)	19(9)	28(6)	7(13)
O(4b)	4317(7)	−839(14)	−1895(9)	44(6)	154(24)	59(10)	−20(10)	25(6)	−3(13)
O(5)	3549(6)	−2161(13)	1067(8)	36(5)	143(22)	37(9)	23(9)	15(5)	−3(12)
O(6)	2909(6)	−4006(13)	−1510(9)	28(5)	104(20)	70(10)	−12(8)	15(6)	2(11)
O(7)	1322(6)	−1110(13)	655(11)	29(5)	122(21)	111(13)	−12(8)	19(7)	−9(14)
O(8)	3987(7)	2286(14)	2103(11)	34(5)	99(21)	121(14)	5(9)	17(7)	−23(14)

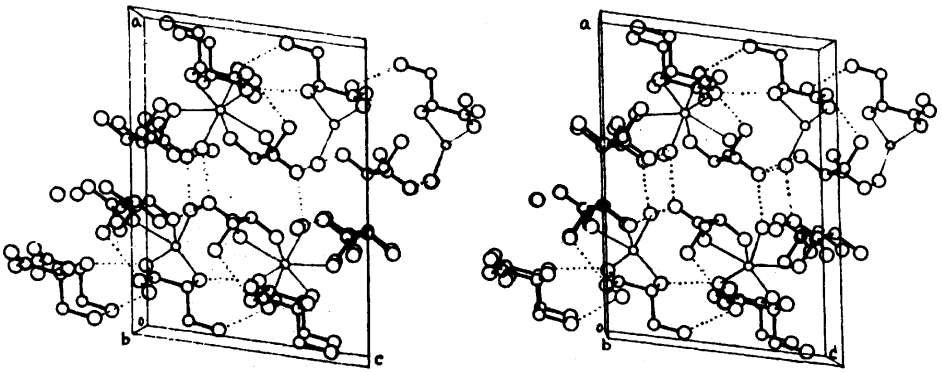

Fig. 1. Stereo-representation of the crystal structure of calcium DL-glycerate dihydrate. Ca, C, and O atoms are represented by the small, middle, and large circles, respectively. The hydrogen bonds and the Ca–O contacts are indicated by the dotted and full lines.

The hydrogen atom positions were assumed from the difference Fourier maps synthesized at this stage. After the Zachariazen extinction correction was applied for the reflection data, three more cycles of full-matrix least-squares refinement including the hydrogen atoms in the structure factor calculations reduced the R-value to 0.095. Atomic scattering factors were obtained from the International Tables for X-Ray Crystallography IV.[6] All computations for the structure analysis were undertaken by using a KPAX program system which included the UNICS programs on a FACOM M-190 in the Data Processing Center of Kyoto University.

The final atomic parameters and their estimated standard deviations are given in Table 1, and the observed and calculated structure factors at the final stage are listed in Table 2.[7]

Results and Discussion

Crystal Packing. Calcium-oxygen interactions and hydrogen bonds stabilize the crystal structure. Figure 1 shows the crystal packing and Table 3 lists the hydrogen-bond distances. All hydrogen atoms of hydroxyl groups and water molecules participate in the hydrogen bonds. The O atoms related to O(4b) and O(8) by 2_1 symmetry through 1/2, 0, 1/4, and 1/2, 0, 3/4 form an infinite hydrogen-bond chain along the b-axis. O(3), O(7), and their centrosymmetrically related O atoms form a square linkage of hydrogen-bonds about the $\bar{1}$ site, 0, 0, 0, and 0, 1/2, 1/2. Three glycerate anions and two water molecules are bound to a calcium ion, the two glycerate anions chelating the calcium ion with α-carboxy and α-hydroxy oxygens, and the one glycerate anion bonding to the calcium ion through the β-hydroxy oxygen. Figure 2 shows the environment of the calcium ion, which is surrounded by seven oxygens in a distorted pentagonal biprism arrangement, five glycerate oxygens being approximately coplanar (Table 4). The Ca–O distances range from 2.32 to 2.47 Å. The O–Ca–O angles within the pentagonal plane range from 65 to

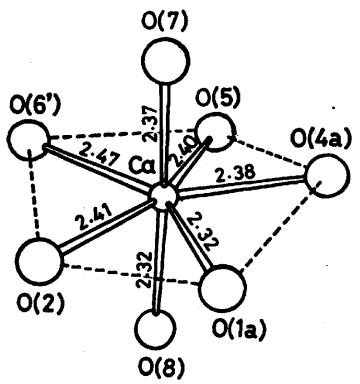

Fig. 2. The calcium ion coordination shell. Atom O(6′) is generated from O(6) by the symmetry operation $x, -1/2-y, 1/2+z$. The estimated standard deviation of a Ca–O distance is 0.02 Å.

TABLE 3. HYDROGEN-BOND DISTANCES

Donor Acceptor	Distance	Symmetry operation for acceptor O
O(2)···O(1a)	2.72 Å	$x, 1/2-y, 1/2+z$
O(3)···O(7)	2.74	$-x, 1/2+y, 1/2-z$
O(5)···O(4b)	2.71	$x, -1/2-y, 1/2+z$
O(6)···O(1b)	2.73	$x, -1+y, z$
O(7)···O(3)	2.82	$x, 1/2-y, -1/2+z$
O(7)···O(1b)	2.62	$x, -1+y, z$
O(8)···O(4b)	2.72	$1-x, -y, -z$
O(8)···O(4b)	2.92	$x, 1/2-y, 1/2+z$

TABLE 4. LEAST-SQUARES PLANE OF FIVE OXYGENS AROUND CALCIUM ION AND ATOMIC DEVIATIONS

The plane is defined by $Ax+By+Cz=D$ where x, y, and z are in Å along the axes a and b and the normal to the ab plane. An asterisk indicates an atom not used in the plane calculation.

$A=0.7703$, $B=0.5345$, $C=0.3471$, and $D=3.521$.

Atom	Deviation (Å)
Ca	−0.007
O(1a)	0.124
O(2)	−0.002
O(4a)	−0.217
O(5)	0.218
O(6′)	−0.117
O(7)*	2.355
O(8)*	−2.326

80°, while the O–Ca–O angles out of the plane range from 85 to 99°. The O(7)–Ca–O(8) angle is 175°. The estimated standard deviations of the O–Ca–O angles are less than 1°.

Geometry of the Glycerate Anions. The conformations of the two crystallographically independent glycerate anions differ from each other (Fig. 3). The bond lengths and angles, and the torsion angles about the C–C bond for each conformer are given in Tables 5 and 6. The C(3)–O(3) bond is trans to C(1)–C(2) about the C(2)–C(3) bond in one conformer, while C(6)–O(6) is gauche to C(4)–C(5) about C(5)–C(6) in the second conformer. Similar conformational dimorphism has been observed in the crystals of potassium salts of gluconic acid[8] and of calcium and potassium salts of glucaric acid.[9,10] Although in these crystals each conformer is crystallized in different crystal forms, the two conformers in the present case are crystallized together into one crystal structure. The ^{1}H NMR studies of glyceric acid in an aqueous solution[1,2] showed that the two β-protons are asymmetric in an unprotonated carboxyl state and the glycerate anion has two or more different conformations in the solution. The two conformers observed here may be therefore energetically very close to each other. For both conformers, α-hydroxy oxygen lies approximately on the same plane of the carboxyl group; the atomic deviations from the least-squares plane of the carboxyl group are given in Table 7. The nonbonding distances between α-hydroxy oxygen and one of the carboxy oxygen are 2.55 Å for O(1a)···O(2) and 2.57 Å for O(4a)···O(5). The stability of such a planar α-hydroxy carboxyl arrangement was discussed by Newton and Jeffrey.[3]

The Polyhedron of Oxygen Atoms about a Calcium Ion. Oxygen-polyhedra about a cation in inorganic crystals can be generally classified into a limited number of typically regular forms, depending on a coordination number; for instance, cube, square antiprism, and dodecahedron are usual forms for eight-coordination, and pentagonal biprism, monocapped octahedron, and monocapped trigonal biprism for seven-coordination.[4] The square antiprism for eight-coordination is the most usual form observed to data in the calcium carbohydrate crystals.[10–32] The pentagonal biprism, as observed in

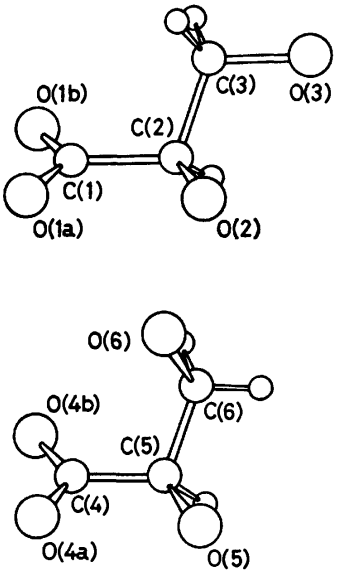

Fig. 3. Two conformations of glyceric anions. Both conformers are shown in the D-isomers.

Table 5. Bond lengths and angles, and their estimated standard deviations

Bond length		Bond angle	
C(1)–C(2)	1.57(2) Å	C(1)–C(2)–C(3)	109(1)°
C(2)–C(3)	1.54(2)	O(1a)–C(1)–O(1b)	127(1)
C(1)–O(1a)	1.24(2)	O(1a)–C(1)–C(2)	118(1)
C(1)–O(1b)	1.27(2)	O(1b)–C(1)–C(2)	114(1)
C(2)–O(2)	1.43(2)	C(1)–C(2)–O(2)	106(1)
C(3)–O(3)	1.46(2)	C(3)–C(2)–O(2)	110(1)
		C(2)–C(3)–O(3)	109(1)
C(4)–C(5)	1.52(2)	C(4)–C(5)–C(6)	112(1)
C(5)–C(6)	1.52(2)	O(4a)–C(4)–O(4b)	125(1)
C(4)–O(4a)	1.25(2)	O(4a)–C(4)–C(5)	119(1)
C(4)–O(4b)	1.30(2)	O(4b)–C(4)–C(5)	109(1)
C(5)–O(5)	1.46(2)	C(4)–C(5)–O(5)	108(1)
C(6)–O(6)	1.41(2)	C(6)–C(5)–O(5)	113(1)
		C(5)–C(6)–O(6)	112(1)

Table 6. Torsion angles about the C–C bonds

Bond	Angle
O(1a)–C(1)–C(2)–C(3)	−119.8°
O(1b)–C(1)–C(2)–C(3)	64.7
O(1a)–C(1)–C(2)–O(2)	−2.2
O(1b)–C(1)–C(2)–O(2)	−177.6
C(1)–C(2)–C(3)–O(3)	−179.5
O(2)–C(2)–C(3)–O(3)	65.4
O(4a)–C(4)–C(5)–C(6)	−122.8
O(4b)–C(4)–C(5)–C(6)	56.3
O(4a)–C(4)–C(5)–O(5)	1.4
O(4b)–C(4)–C(5)–O(5)	−179.4
C(4)–C(5)–C(6)–O(6)	48.2
O(5)–C(5)–C(6)–O(6)	−73.2

Table 7. Least-squares plane of five atoms of carboxyl and α-hydroxyl groups, and atomic deviations

The plane is defined by $Ax+By+Cz=D$ where x, y, and z are in Å along the axes a and b and the normal to the ab plane. An asterisk indicates an atom not used in the plane calculation.

$A=0.908$	$A=0.715$
$B=0.289$	$B=-0.462$
$C=0.302$	$C=0.525$
$D=1.045$	$D=7.229$

Atom	Deviation (Å)	Atom	Deviation (Å)
C(1)	0.026	C(4)	−0.003
C(2)	0.001	C(5)	0.009
C(3)*	1.280	C(6)*	1.185
O(1a)	−0.007	O(4a)	0.004
O(1b)	−0.014	O(4b)	−0.004
O(2)	−0.006	O(5)	−0.006
O(3)*	1.260	O(6)*	2.399
Ca*	−0.630	Ca*	0.511

the present crystal, has been found in the crystal structures of α-D-xylose $CaCl_2 \cdot 3H_2O$,[13] β-D-fructose $CaBr_2 \cdot 2H_2O$,[14] and α,α'-D-trehalose $CaBr_2 \cdot H_2O$;[15] all seven-coordinations about a calcium ion in the carbohydrate crystals are in this form. The pentagonal biprism may be therefore the most favored arrangement of oxygens about a calcium ion for the seven-coordination. This fact is evidenced by the Doyl-Britten calculations of repulsive potential energy between ligand atoms of simple seven-coordination models.[5] The Ca–O distance, averaged for those in 22 structures observed hitherto,[10–32] is 2.445 Å for Ca–O (carboxy oxygen), 2.488 Å for Ca–O (hydroxy oxygen), and 2.442 Å for Ca–O (water oxygen), the Ca–O (hydroxy oxygen) being slightly larger than the others. Thus, the partial charge and the dipole moment on the ligand oxygen apparently influence the Ca–O distance. The large distortion of the actual oxygen-polyhedron about a calcium ion may be due to such different Ca–O interactions which depend on the ligand oxygens, in addition to a steric restriction by covalent bonds bridged between two or more ligand oxygens and to the effect of crystal field, especially of the hydrogen-bonds which formed around the oxygen-polyhedron.

We wish to thank Miss Shizuko Matsumoto for her experimental assistance.

References

1) T. Taga, Y. Kuroda, and M. Ohashi, *Bull. Chem. Soc. Jpn.*, in press.
2) D. T. Sawyer and J. R. Brannan, *Anal. Chem.*, **38**, 192 (1966).
3) M. D. Newton and G. A. Jeffery, *J. Am. Chem. Soc.*, **99**, 2413 (1977).
4) A. F. Wells, "Structural Inorganic Chemistry," Clarendon Press, Oxford (1975), pp. 60—70.
5) D. Britton, *Can. J. Chem.*, **41**, 1632 (1963).
6) "International Table for X-Ray Crystallography IV," Kynoch Press, Birmingham (1974), p. 71.
7) Table 2 is kept in the office of the Chemical Soiety of Japan, 1-5 Kanda-Surugadai, Chiyoda-ku, Tokyo 101, (Document No. 7817).
8) N. C. Panagiotopolous, G. A. Jeffrey, S. J. La Palaca, and W. C. Hamilton, *Acta Crystallogr., Sect. B*, **30**, 1421 (1974).
9) T. Taga, Y. Kuroda, and K. Osaki, *Bull. Chem. Soc. Jpn.*, **50**, 3083 (1977).
10) T. Taga and K. Osaki, *Bull. Chem. Soc. Jpn.*, **49**, 1517 (1976).
11) S. Furberg and S. Helland, *Acta Chem. Scand.*, **16**, 2373 (1962).
12) W. J. Cook and C. E. Bugg, *Acta Crystallogr., Sect. B*, **29**, 215 (1973).
13) G. F. Richards, *Carbohydr. Res.*, **26**, 448 (1073).
14) W. J. Cook and C. E. Bugg, *Acta Crystallogr., Sect. B*, **32**, 656 (1976).
15) W. J. Cook and C. E. Bugg, *Carbohydr. Res.*, **31**, 265 (1973).
16) I. Nitta and K. Osaki, *X-Ray*, **5**, 37 (1948).
17) C. Sterling, *Acta Crystallogr.*, **18**, 917 (1965).
18) M. P. Gupta, S. M. Prasad, R. G. Sahu, and B. N. Sahu, *Acta Crystallogr., Sect. B*, **28**, 135 (1972).
19) C. I. Branden and B. O. Soderberg, *Acta Chem. Scand.*, **20**, 730 (1966).
20) G. K. Ambady, *Acta Crystallogr., Sect. B*, **24**, 1548 (1968).
21) V. A. Uchtman and R. P. Oerter, *J. Am. Chem. Soc.*, **95**, 1802 (1973).
22) B. Sheldrick, *Acta Crystallogr., Sect. B*, **30**, 2056 (1974).
23) R. Norrestam, P. E. Werner, and M. V. Glehn, *Acta Chem. Scand.*, **22**, 1395 (1968).
24) A. A. Balchin and C. E. Carlisle, *Acta Crystallogr.*, **19**, 103 (1965).
25) J. P. Glusker, J. A. Minkin, and C. A. Casciato, *Acta Crydtallogr., Sect. B*, **27**, 1284 (1971).
26) S. E. B. Gould, R. O. Gould, C. A. Rees, and W. E. Scott, *J. Chem. Soc., Perkin Trans. 2*, 237 (1975).
27) S. Thanomkul, J. A. Hjortas, and H. Sorum, *Acta Crystallogr., Sect. B*, **32**, 920 (1976).
28) W. J. Cook and C. E. Bugg, *Acta Crystallogr., Sect. B*, **29**, 2404 (1973).
29) D. C. Craig, N. C. Stephenson, and J. D. Stevens, *Carbohydr. Res.*, **22**, 494 (1972).
30) C. E. Bugg, *J. Am. Chem. Soc.*, **95**, 908 (1973).
31) W. J. Cook and C. E. Bugg, *Acta Crystallogr., Sect. B*, **32**, 656 (1976).
32) D. C. Craig, N. C. Stephenson, and J. D. Stevens, *Cryst. Struct. Commun.*, **3**, 195 (1974).

Kinetic Studies of the Dimerization Reaction of Thionine by the Laser Raman Temperature-jump Method

Wataru INAOKA, Shoji HARADA, and Tatsuya YASUNAGA

Department of Chemistry, Faculty of Science, Hiroshima University, Higashisenda-machi, Hiroshima 730

(Received December 23, 1977)

Kinetic studies of the dimerization reaction of thionine in an aqueous solution have been performed by the laser temperature-jump method with the use of the stimulated Raman effect in high-pressure H_2 gas. From the concentration dependence of the relaxation time, the formation and dissociation rate constants of the thionine dimer have been obtained. The data have been confirmed by the equilibrium constant, independently obtained spectrophotometrically. The formation rate constant of the dimer was very large, and the process was revealed to be a diffusion-controlled reaction, similar to those with other dyes.

The aggregation of a dye in solution is interesting not only in itself but also as a model system of molecular aggregation in the biochemical field. Many spectrophotometric[1-5] and polarographic[6] investigations have been performed. The kinetic investigations have, however, been limited in number because of their rapid aggregation rates and other experimental restrictions. The laser-heating temperature-jump method has a decisive advantage over the usual Joule-heating one for kinetic studies of the dye aggregation; it enables the measurement of a very rapid reaction with a time constant in even the nsec region and needs no addition of salts, which is undesirable for studies of the dye aggregation in solution. The recently developed method of the laser-heating T-jump with the use of a stimulated Raman effect in liquid N_2[7] or high-pressure H_2 gas[8] has much improved the applicability. In the present study, the laser T-jump method with a stimulated Raman effect in H_2 gas was applied to kinetic studies of the aggregation reaction of thionine in an aqueous solution.

Experimental

Materials. Thionine hydrochloride was purchased from Wako Pure Chemical Industries, Ltd. It was recrystallized from water and then dried at 105 °C for 12 h. The purity of the dye was confirmed by means of CHN gravimetric analysis. Distilled and deionized water was used throughout. The pH of the solution was controlled to 3.5 by the addition of nitric acid to prevent the dye decomposition.

Spectrophotometric Measurement. The equilibrium constant of the monomer-dimer reaction of thionine was determined spectrophotometrically with a Union Giken SM-401 spectrophotometer. The measurement was performed at 25 °C.

Laser Raman Temperature-jump Apparatus. The apparatus used in this study was a modification of that described by Ameen.[8] A schematic diagram of our apparatus is shown in Fig. 1. The giant pulse laser (Japan Electron Optics Laboratory Co., Ltd. Type JLS-G-3) operates in the Q-switched mode with a rotating prism. The neodymium-doped glass rod (100 mm long, 12.5 mm diam.) delivers a maximum energy of 3 J in 25 ns at a wavelength of 1060 nm. The laser beam was focused into the Raman cell by means of a $f=50$ cm quartz lens. The Raman cell consists of a stainless steel tube (100 cm long, 20 mm i.d.) with 15 mm quartz windows at the ends and filled with H_2 gas of about 80 atm. Several kinds of lights with different wavelengths are emitted. To select only the 1890 nm light, a Si-coated filter (transmittance of 1060 nm, 8.5%; 1890 nm, 93%) was used, and then the light was again focused into the sample cell by means of a $f=20$ cm quartz lens. The sample cell is made of two glass plates, with a spacer between them. Several spacers 0.1—0.5 mm thick were used. In order to prevent cavitation, a pressure of a few atm was exerted on the sample solution. The Raman cell, filter, and lens were completely covered to prevent the visible light produced by the Raman scattering from entering the photomultiplier. The laser axis was aligned by means of a conventional laser beam. The relaxation effect was monitored photometrically. The light from a 500-W xenon lamp was monochronized and focused into the sample cell. A shutter was used to prevent the decoloration of the sample. The detection axis was aligned so as to have an angle of about 30 degrees to the laser axis, –thus having a long path length in the solution. As a photomultiplier tube, 931A (Hamamatsu TV Co., Ltd.) was employed. The output signal was amplified and led to the emitter follower, the filter, and the oscilloscope. The apparatus was calibrated by means of the phenolred (1 mM)–ammonia (2.3 M) system at pH 7.9. This system is known to have a large enthalpy change and a very short relaxation

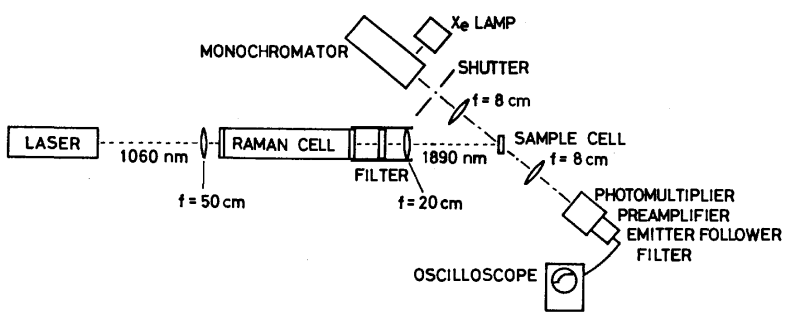

Fig. 1. Schematic diagram of the laser temperature-jump apparatus with use of the stimulated Raman effect in H_2 gas.

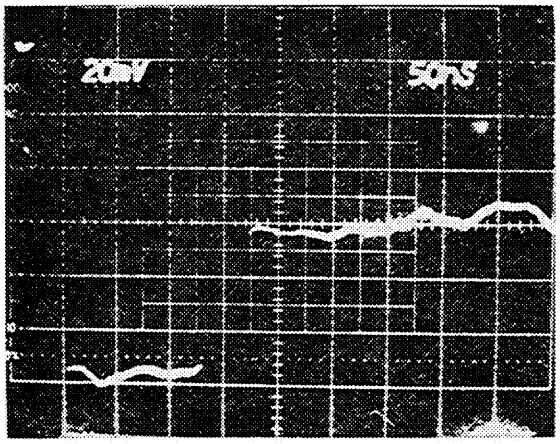

Fig. 2. Spectrum in the phenolred (1 mM)–ammonia (2.3 M) system at pH 7.9, 25 °C; sweep 50 ns/div.

time of about 10 ns.[9] The spectrum is shown in Fig. 2. In the case of a heating volume of 5 μl, the magnitudes of the temperature-jump and the heating-time constant were determined to be 3 °C and 50 ns respectively.

Results and Discussion

Thionine is known to aggregate in an aqueous solution and a monomer-dimer equilibrium is established:

$$2T \underset{k_{-1}}{\overset{k_1}{\rightleftarrows}} T_2, \qquad (1)$$

where k_1 and k_{-1} are the formation and dissociation rate constants respectively. The equilibrium constant, K, of this system is expressed by $K=[T_2]/[T]^2=k_1/k_{-1}$, where $[T]$ and $[T_2]$ denote the monomer and dimer concentrations respectively. In order to obtain the K value, spectrophotometric studies were performed with the following equation:[10]

$$\left(\frac{\varepsilon_M-\varepsilon}{C_0}\right)^{1/2} = \left(\frac{2K}{\Delta\varepsilon}\right)^{1/2}\{\Delta\varepsilon-(\varepsilon_M-\varepsilon)\}, \qquad (2)$$

where ε_M: the molar extinction coefficient of the monomer.
ε: the apparent molar extinction coefficient.
$\Delta\varepsilon$: the difference between the molar extinction coefficient of the monomer and that of the dimer.
C_0: the initial concentration of the dye.

According to Eq. 2, a plot of $\{(\varepsilon_M-\varepsilon)/C_0\}^{1/2}$ *vs.* $(\varepsilon_M-\varepsilon)$ will give a straight line with the intercept $(2K\Delta\varepsilon)^{1/2}$ on the ordinate and $\Delta\varepsilon$ on the abscissa. On this basis, we evaluated ε_M as the best choice to obtain a straight line with the measured values of ε and C_0. The value of K was obtained as 750 M^{-1} at 25 °C. In comparison with the previously reported values of this dye,[2,11,12] the present result seems to be satisfactory.

The kinetic measurements were carried out at 25 °C. The concentration of the dye was ranged from 0.2 to 2.4 mM. The concentration change was monitored at the monomer band (λ=597 nm). The relaxation phenomenon was observed over all the concentration range and was characterized by a single relaxation time. The concentration dependence of the relaxation time, τ, is expressed as follows:

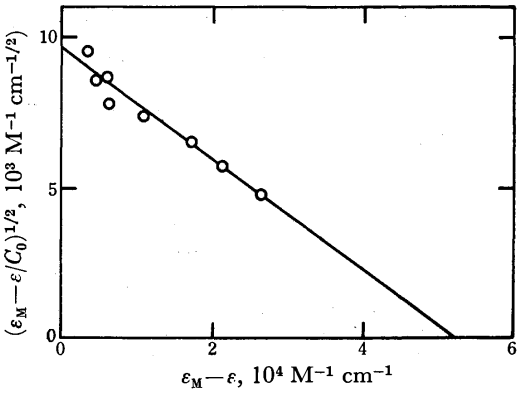

Fig. 3. Plots to determine the equilibrium constant K of dimerization at pH 3.5, 25 °C.

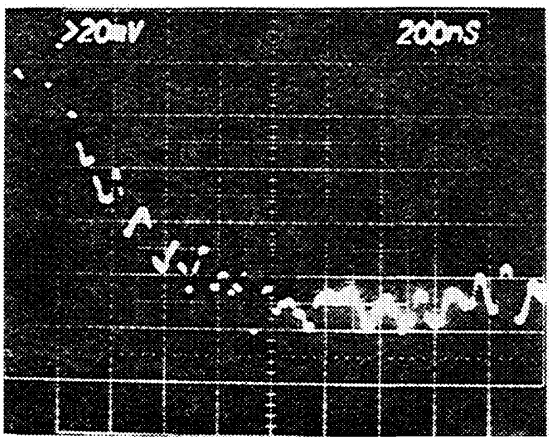

Fig. 4. Typical relaxation spectrum in 2 mM thionine at pH 3.5, 25 °C, wavelength 597 nm; sweep 200 ns/div.

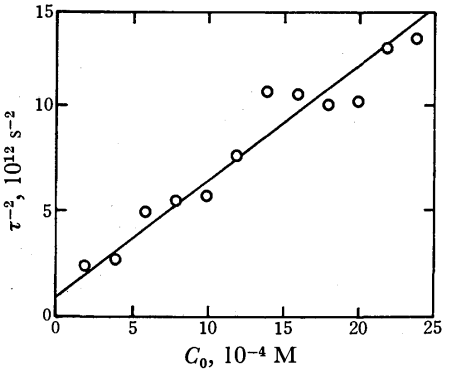

Fig. 5. Plots of τ^{-2} *vs.* C_0 at pH 3.5, 25 °C.

$$\tau^{-1} = 4k_1[T] + k_{-1}. \qquad (3)$$

This equation can be arranged more conveniently with the initial concentration of the dye:

$$\tau^{-2} = k_{-1}^2 + 8k_1k_{-1}C_0. \qquad (4)$$

The experimentally obtained values of τ^{-2} are plotted against C_0 in Fig. 5. Each value is the average of at least ten runs. The linearity of these plots indicates that the observed relaxation effect is based on the monomer-dimer reaction of the dye. The rate constants were evaluated to be $k_1=7.1\times10^8$ M^{-1} s^{-1} and $k_{-1}=9.4\times10^5$

Table 1. Summary of the rate and equilibrium constants for dimerization reactions at 25 °C

Dye	k_1 (10^8, $M^{-1}s^{-1}$)	k_{-1} (10^6, s^{-1})	K (M^{-1})	Ref.
Ethidium bromide	4.6	6.7	69	13
Proflavine	7.9	2.0	395	14
Acridine orange	2.7	0.018	15000	15
N^6,N^9-Dimethyl-adenine	9.3	50	19	16
Thionine	7.1	0.94	750	This work

s^{-1} from the slope and the intercept respectively of this straight line. The resultant equilibrium constant given by the ratio of these values is in good agreement with that derived spectrophotometrically. The rate constants were then compared with those obtained for other dyes; they are listed in Table 1. The rate and equilibrium constants of thionine are very analogous to those of proflavine. This fact is confirmed by their similar structures. As can be said for other dyes, the value of k_1 of thionine is very large and close to that of the diffusion-controlled association reaction.[17] If the dimerization process of the dye is a diffusion-controlled reaction, the value of k_1 will decrease in the case of a bulky dye molecule since the diffusion coefficient depends on the volume of the molecule. These tendencies in Table 1 show that the dye aggregation process is a diffusion-controlled reaction. In contrast to the small difference between the k_1 values, the values of k_{-1} differ remarkably; *i.e.*, the difference in the equilibrium constants is directly reflected in the values of k_{-1}. The good linear relationship between log k_{-1} and log K pointed out by Turner *et al.*[13] is here supported.

The authors gratefully acknowledge the support of the Toray Science Foundation.

References

1) L. V. Levshin and V. K. Gorshkov, *Opt. Spectrosc.*, **10**, 401 (1961).
2) E. Rabinowitch and L. F. Epstein, *J. Am. Chem. Soc.*, **63**, 69 (1941).
3) V. Zanker, *Z. Phys. Chem.*, **199**, 225 (1952).
4) M. Hida, A. Yabe, H. Murayama, and M. Hayashi, *Bull. Chem. Soc. Jpn.*, **41**, 1776 (1968).
5) K. K. Rohatgi and G. S. Singhal, *J. Phys. Chem.*, **70**, 1695 (1966).
6) P. J. Hillson and R. B. Makay, *Trans. Faraday Soc.*, **61**, 374 (1965).
7) D. H. Turner, G. W. Flynn, N. Sutin, and J. V. Beitz, *J. Am. Chem. Soc.*, **94**, 1554 (1972).
8) S. Ameen, *Rev. Sci. Instrum.*, **46**, 1209 (1975).
9) G. W. Hoffman, Ph, D. Dissertation (University of Braunschweig, Braunschweig, 1972).
10) G. Schwarz, S. Klose, and W. Balthasar, *Eur. J. Biochem.*, **12**, 454 (1970).
11) M. Hida and T. Sanuki, *Bull. Chem. Soc. Jpn.*, **43**, 2291 (1970).
12) R. E. Ballard and C. H. Park, *J. Chem. Soc., Ser. A*, **8**, 1340 (1970).
13) D. H. Turner, R. Yuan, G. W. Flynn, and N. Sutin, *Biophys. Chem.*, **2**, 385 (1974).
14) D. H. Turner, G. W. Flynn, S. K. Lunberg, L. D. Faller, and N. Sutin, *Nature*, **239**, 215 (1972).
15) G. G. Hammes and C. D. Hubbard, *J. Phys. Chem.*, **70**, 1615 (1966).
16) D. Porschke and F. Eggers, *Eur. J. Biochem.*, **26**, 490 (1972).
17) I. Amdur and G. G. Hammes, "Chemical Kinetics," McGraw-Hill, New York (1966).

Acidic Property and Catalytic Activity of Tungsten Oxide

Hideshi HATTORI, Noriyoshi ASADA, and Kozo TANABE
Department of Chemistry, Faculty of Science, Hokkaido University, Sapporo 060
(Received January 5, 1978)

A maximum activity of tungsten oxide for the isomerization of 1-butene was observed when the catalyst was evacuated at 600 °C, the ratio of *cis*-2-butene to *trans*-2-butene being 1.4. The activity was lost by the addition of NH_3, but not affected by the addition of CO_2 or H_2O. The oxidation states of tungsten oxide treated with hydrogen at 550 and 650 °C were $WO_{2.89}$ and WO_2, respectively. The activity of $WO_{2.89}$ for the double bond isomerization of 1-butene was almost the same as that of WO_3, but the activity of WO_2 for the double bond and skeletal isomerization of 1-butene and the dehydration of isopropanol was higher than that of WO_3 or $WO_{2.89}$. The coisomerization of *cis*-2-butene-d_0/d_8 revealed that the double bond isomerization of butenes proceeds by an intermolecular hydrogen transfer mechanism. When *cis*-2-butene-d_8 was introduced to the catalyst on which *cis*-2-butene-d_0 had been preadsorbed, the reactant and the product containing much of H were obtained, no d_0-species being observed. It was concluded that the active sites for the isomerization of butenes are protons of polymerized butene formed by the adsorption on Lewis acid sites of tungsten oxide surface and the isomerization takes place *via* carbenium ion intermediates.

Tungsten oxide mixed with SiO_2 or Al_2O_3 is a well-known catalyst for the hydration[1] and disproportionation[2] of olefins. Combined with MoO_3, NiO, V_2O_5, or CeO_2, tungsten oxide becomes catalytically active for the hydrocracking,[3] hydrotreating[4] and reforming[5] of hydrocarbons, the isomerization of paraffins,[6] and the oxidative dehydrogenation of butene.[7] Thus, tungsten oxide is one component of industrially important catalysts. Tungsten oxide itself is known to catalyze the oxidation of 1-butene to carbon dioxide[8] and tungsten oxide reduced with hydrogen was reported recently to catalyze the isomerization and hydrocracking of heptane, the dealkylation of isopropyl benzene and the dehydration of isopropyl alcohol, where the change in catalytic action with the change of oxidation state and acidic property of tungsten oxide was studied.[9] The present work was initiated to learn more about the role of acid-base property of tungsten oxide for the isomerization of butenes and to elucidate the nature of active sites and the reaction mechanism.

Experimental Methods

Tungsten trioxide was prepared by calcination of ammonium paratungstate $[(NH_4)_{10}W_{12}O_{41}\cdot 5H_2O]$ at 550 °C for 10 h in air. This was used for the reaction after evacuation at different temperatures for 3 h. X-Ray diffraction patterns were recorded on a Toshiba ADG-301 with a powdered sample over the range of $2\theta = 10$—60°. Cu K_α was used as the radiation source.

1-Butene was purified by passage through 4A molecular sieves kept at −78 °C. Perdeuterated *cis*-2-butene was prepared by exchange of butenes with D_2 over MgO.[10] Isopropanol was purified by passage through 4A molecular sieves at 0 °C.

Two different types of reactors were employed. A recirculation reactor which had a volume of 270 cm^3 was used for kinetic measurements of the double bond and skeletal isomerization of 1-butene and the dehydration of isopropanol. Reaction products were periodically withdrawn from the system and analyzed by gas chromatography. For the isomerizations, a 4-m gas chromatographic column containing propylene carbonate on Celite 545 was operated at 0 °C. For the dehydration, a 1-m column packed with TPC on Celite 545 was operated at 100 °C.

In poisoning experiments, NH_3, H_2O, CO_2, and a mixture of H_2O and CO_2 were used as poisons. The catalyst that had been evacuated at 500 °C was exposed to a poison at 100 °C for 30 min (NH_3, H_2O+CO_2) or 60 min (H_2O, CO_2) and then evacuated at 100 °C for 1 or 3 h.

Oxygen and H_2 treatments were carried out as follows. To the catalyst that had been evacuated at 500 °C, 15 Torr of O_2 was admitted at 500 °C and recirculated at this temperature for 1 h, the trap attached to the recirculating loop being cooled by liquid N_2. After the treatment, the catalyst was evacuated at 500 for 30 min. Hydrogen treatment was performed at 500 and 650 °C. In the treatment at 500 °C, 50 Torr of H_2 was admitted to the catalyst that had been evacuated at 500 °C and recirculated for 1 h with a liquid N_2 trap. The catalyst was evacuated at 500 °C for 1 h. In the treatment at 650 °C, the catalyst that had been evacuated at 650 °C was exposed to 400 Torr of H_2. After H_2 was recirculated for 5 h with a liquid N_2 trap, the catalyst was evacuated with a gradual rise of temperature and finally evacuated at 700 °C for 1 h.

For the deuterium tracer experiments, a microcatalytic pulse reactor was employed. About 29 μmol of *cis*-2-butene was introduced into the He stream (flow rate, 35 ml/min) ahead of the catalyst. The produced butenes were gas chromatographically separated. The separated isomers were trapped at −196 °C and subjected to a mass spectrographic analysis. Mass spectra were recorded on Hitachi mass spectrometer RMU-2 at low ionization voltage. A deuterated catalyst was prepared by exposure of D_2O vapor at 400 °C to the catalyst that had been evacuated at 500 °C and then evacuated at 500 °C for 3 h. Another deuterated catalyst was obtained by exposure of D_2O vapor at 100 °C to the 500 °C evacuated catalyst, followed by evacuation at this temperature for several hours.

Results

Activity was expressed by percent conversion of 1-butene per unit time, min, per unit weight of catalyst, g, at the initial stage of the reaction. The variations of the activity for the isomerization of 1-butene at 100 °C and the ratio of *cis*-2-butene to *trans*-2-butene are shown in Fig. 1 as a function of evacuation temperature of the catalyst. The activity reaches a maximum value on evacuation at 600 °C. The ratio of *cis*-2-butene to *trans*-2-butene gradually decreases from 1.7 to 1.2 with

Table 1. Effect of poisoning on activity and *cis*-/*trans*-2-butene

Evac. temp, °C	Poison	Poisoning temp, °C	Evac. after temp, °C	Poisoning time, min	Activity %min^{-1} g^{-1}	Relative activity	*cis*-/*trans*-2-Butene
500	—	—	—	—	5.87	1.00	1.41
500	NH_3	100	100	30	0.00	0.00	
500	CO_2	100	100	60	4.73	0.81	1.66
500	H_2O	100	100	60	5.05	0.86	1.75
500	H_2O	100	100	1	5.02	0.85	2.70
500	H_2O+CO_2	100	100	30	7.35	1.25	2.15

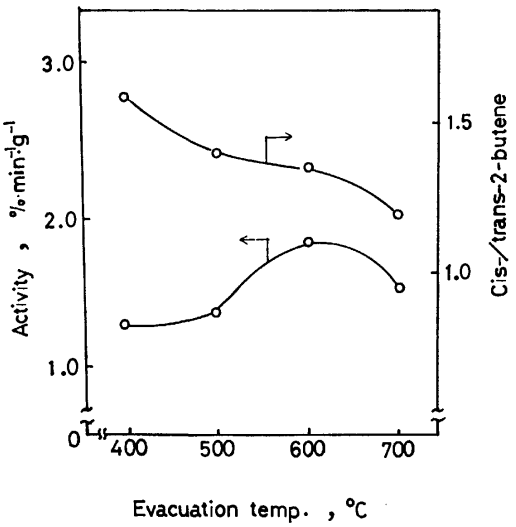

Fig. 1. Effect of evacuation temperature of WO_3 on activity and selectivity for isomerization of 1-butene.

a rise of evacuation temperature.

Poisoning effects of NH_3, CO_2, H_2O, and a mixture of CO_2 and H_2O on the activity and the ratio of *cis*-2-butene to *trans*-2-butene are included in Table 1. Ammonia completely poisoned the active sites, while CO_2, H_2O, and a mixture of CO_2 and H_2O scarcely showed poisoning effect. A mixture of CO_2 and H_2O even increased a little the activity.

The catalysts evacuated at various temperatures showed yellow color and the X-ray diffraction pattern of WO_3. During the treatment with H_2 at 500 °C, 0.00048 mol/g of H_2 was consumed, which corresponds to the number of H_2 required for the change of WO_3 to $WO_{2.89}$. The catalyst became dark blue on the treatment and showed the X-ray diffraction pattern of mixture of WO_3 and $WO_{2.87}$. The treatment with H_2 at 650 °C resulted in a consumption of 0.0046 mol/g of H_2, which corresponds to the number of H_2 required for the change of WO_3 to WO_2. The resulting catalyst was brown and showed the X-ray diffraction pattern of WO_2. The effects of the treatments are given in Table 2. The treatment with H_2 or O_2 at 500 °C did not result in an appreciable effect on the activity for the double bond isomerization of 1-butene. However, the treatment with H_2 at 650 °C greatly increased the activities for the double bond and skeletal isomerizations and the dehydration of isopropanol.

Results of microcatalytic tracer experiments are given in Table 3. In the coisomerization of *cis*-2-butene-d_0/d_8 over WO_3 that had been evacuated at 500 °C, a large number of exchanged isotopic species were produced in 1-butene and *trans*-2-butene. The number of H(or D) atoms exchanged per molecule (AEM value) was calculated from the equation,[11]

$$\mathrm{AEM} = \sum_{i=0}^{4} i \cdot N_i + \sum_{i=5}^{8} (8-i) \cdot N_i,$$

where N_i is the fraction of isotopic species containing i D atoms. The AEM values of the products were close to 0.5 (see Table 3). This indicates that the double bond isomerization involves intermolecular hydrogen transfer.[11]

In the isomerization of *cis*-2-butene over the deuterated catalyst that was evacuated at 500 °C after exposed to D_2O, negligible amounts of D atoms were incorpo-

Table 2. Effect of pretreatments of tungsten oxide on double bond isomerization of 1-butene, dehydration of 2-propanol, and skeletal isomerization of 1-butene

Evac. temp, °C	Treatment reagent	Treated temp, °C	Evac. after treatment temp, °C	Evac. after treatment time, min	Activity %min^{-1} g^{-1}	Relative activity	*cis*-/*trans*-2-Butene
500	—	—	—	—	1.17[a]	1.00	1.41
500	H_2	500	500	60	1.04[a]	0.89	1.40
500	O_2	500	500	60	1.34[a]	1.14	1.76
700	—	—	—	—	0.92[a]	1.00	1.20
650	H_2	650	700	180	2.09[a]	2.21	1.40
700	—	—	—	—	109.4[b]	1.00	—
650	H_2	650	700	180	316.6[b]	2.89	—
700	—	—	—	—	0.10[c]	1.00	—
650	H_2	650	700	180	0.92[c]	8.88	—

a) Double bond isomerization at 100 °C over 0.5 g of WO_x. b) Dehydration of 2-propanol at 100 °C over 50 mg of WO_x. c) Skeletal isomerization at 400 °C over 0.5 g of WO_x.

TABLE 3. RESULTS OF MICROCATALYTIC TRACER EXPERIMENTS AT 100 °C

Reactions and Catalysts	Pulse number	Products kinds	Products %	Isotopic distributions, % d_0	d_1	d_2	d_3	d_4	d_5	d_6	d_7	d_8	AEM[e]	ϕ[f]
a	1	1	6.02	46.36	18.9	3.1	0.7	0.5	0.9	5.5	18.2	5.9	0.609	
		t	19.65	35.8	13.7	2.6	0.7	0.9	2.3	7.5	20.3	16.3	0.667	
		c	74.33	41.5	6.0	0.8	0.3	0.3	0.6	2.7	12.5	35.2	0.297	
b	1	1	7.07	97.90	2.0	0.10	0	0	0	0	0	0		2.20
		t	29.72	98.14	1.74	0.12	0	0	0	0	0	0		1.98
		c	63.21	98.92	1.08	0	0	0	0	0	0	0		1.08
c	1	1	5.04	0.34	0.26	0.20	0.20	0.54	1.56	6.12	28.04	62.74		7.46
		t	16.09	0.46	0.27	0.10	0.11	0.50	1.69	7.36	27.22	62.28		7.44
		c	78.87	0.57	0.38	0	0	0.24	0.48	21.8	13.03	83.11		7.73
c	2	1	4.76	1.23	1.10	0.17	0.14	0.28	0.56	2.86	17.55	76.10		7.546
		t	13.71	0.29	0.06	0	0	0.36	0.77	3.12	17.73	77.66		7.695
		c	81.53	0.16	0	0	0	0.16	0.15	1.33	8.97	89.24		7.860
d	1	1	7.01	78.23	18.05	2.90	0.82	0	0	0	0	0		0.263
		t	29.13	79.58	17.29	2.50	0.63	0	0	0	0	0		0.241
		c	63.86	92.00	7.03	0.84	0.13	0	0	0	0	0		0.091
d	2	1	7.46	95.88	3.86	0.27	0	0	0	0	0	0		0.0440
		t	23.28	95.29	4.16	0.55	0	0	0	0	0	0		0.0526
		c	69.26	98.07	1.74	0.19	0	0	0	0	0	0		0.0212

a) Coisomerization of *cis*-2-butene-d_0/d_8 over WO_3. b) Isomerization of *cis*-2-butene-d_0 over WO_3 treated with D_2O at 400 °C. c) Isomerization of *cis*-2-butene-d_8 over WO_3 treated with *cis*-2-butene-d_0 at 100 °C. d) Isomerization of *cis*-2-butene-d_0 over WO_3 treated with D_2O at 100 °C. e) $\mathrm{AEM}=\sum_{i=0}^{4} iN_i+\sum_{i=5}^{8} iN_i$. f) $\phi=\sum_{i=0}^{8} iN_i$.

rated into butenes. However, over the deuterated catalyst that was evacuated at 100 °C after being deuterated, a considerable number of D atoms were incorporated into the products. The cumulative number of D atoms picked up by butenes till the 3rd slug was 29.2×10^{17} atoms/g.

Over the catalyst that had been evacuated at 500 °C, a slug of *cis*-2-butene-d_8 was introduced after 4 slugs of *cis*-2-butene-d_0. The products as well as the reactant contain a large number of H exchanged isotopic species. The average number of D atoms per molecule, ϕ value, was calculated from the equation,

$$\phi = \sum_{i=0}^{8} i \cdot N_i.$$

The ϕ values of 1-butene, *trans*-2-butene, and *cis*-2-butene were 0.54, 0.56 and 0.27, respectively (Table 3). There was a very small amount of d_0 species which would be detected if adsorbed butene-d_0 were replaced by butene-d_8.

Discussion

All results obtained can be explained in terms of acidic property of the catalyst.

Strong poisoning effect with NH_3 suggests that the acid sites are acting as active sites for the double bond isomerization of butene. In the acid-catalyzed isomerization of 1-butene, the ratio of *cis*-2-butene to *trans*-2-butene is usually close to unity.[12] The ratios obtained over tungusten oxide treated under different conditions were close to unity, which also supports that the acid sites are active. No poisoning effect with CO_2 indicates that the basic sites, even if present, do not participate in the reaction.

Since the reaction involves intermolecular hydrogen transfers and the active sites are acidic, it is quite plausible that the reaction intermediate is a carbenium ion. In the reaction over the deuterated catalyst that was evacuated at 500 °C after D_2O treatment, the numbers of D atoms incorporated into the products were small. On the other hand, considerable numbers of D atoms were incorporated into the products when *cis*-2-butene was reacted over the deuterated catalyst evacuated at 100 °C after D_2O treatment. Therefore, the surface OH groups on the catalyst evacuated at 100 °C participate in the reaction as a source of H^+, but the OH groups on the catalyst evacuated at 500 °C, even if they present, do not participate. Instead of surface OH groups, H^+ is provided by preadsorbed butene over the catalyst evacuated at 500 °C, since much of H^+ was contained in the reaction products of *cis*-2-butene-d_8 over the catalyst on which *cis*-2-butene-d_0 had been preadsorbed. The butene which serves as the source of H^+ may not retain the form of C_4H_8 and may be polymerized on the acid sites of Lewis type, because the preadsorbed butene-d_0 was not replaced by the introduction of butene-d_8. This type of active sites were proposed by Kimura and Ozaki for the isomerization of butenes over SiO_2–Al_2O_3.[13]

The addition of water retarded the reaction of heptane,[9] but it did not appreciably retard the isomerization of 1-butene. This is considered due to that the protons formed by the adsorption of water on Lewis acid sites act as active sites for the isomerization of 1-butene, but not for the reaction of heptane.

The treatment with H_2 at 500 °C did not result in the reduction of WO_3 to WO_2, but only to $WO_{2.87}$, while

the treatment with H_2 at 650 °C resulted in the formation of WO_2. The increase in the activity for the isomerization of butene by the treatment with H_2 at 650 °C indicates that the acidity and acid strength of WO_2 are higher than those of WO_3 or $WO_{2.87}$. The enhancement of acidic property by the treatment at 650 °C also interprets the increases of the activities for the dehydration of isopropanol and the skeletal isomerization of 1-butene, which are known as acid-catalyzed reaction.

References

1) C. H. Kline and V. Kollonitsh, *Ind. Eng. Chem.*, **57**, 53 (1965).
2) R. L. Banks and G. C. Bailey, *Ind. Eng. Chem.*, **3**, 170 (1964).
3) U. S. Pat. (M. W. Kellogs) 3043769 (1962).
4) U. S. Pat. (Pure oil) 2964463 (1960).
5) German Pat. (BASF) 864721 (1953).
6) A. V. Aganov, V. A. Khavkin, L. N. Osipov, and S. P. Rogov, *Novosti Neft. Gaz. Tekhn. Neft. i Neftekhim*, **9**, 3 (1962): *Chem. Abstr.*, **60**, 10444*e* (1964).
7) T. G. Alkhazov, M. S. Belenky, and R. I. Alekseyeva, Proc. 4th Intern. Congr. Catalysis, **I**, 243, Akademiai Kiado, Budapest, 1971.
8) R. I. Alekseyeva, T. G. Alkazov, P. M. Bidzinova, and M. S. Belenky, *Azerb, Khim. Zh.*, **6**, 45 (1968); *Chem. Abstr.*, **71**, 64601*v* (1969).
9) Y. Kamiya and E. Ogata, Proc. 5th Intern. Congr. Catalysis, **II**, **93**-1291, North Holland Publishing Co., 1973.
10) H. Hattori and A. Satoh, *J. Catal.*, **45**, 32 (1976).
11) J. W. Hightower and W. K. Hall, *J. Am. Chem. Soc.*, **89**, 778 (1967).
12) J. W. Hightower and W. K. Hall, *Chem. Eng. Prog.*, **63**, 122 (1967).
13) A. Ozaki and K. Kimura, *J. Catal.*, **3**, 395 (1964).

Abnormal Hyperchromism of the n→π* Absorption Band of Acetone in Protic Solvents

Masako YUDASAKA and Haruo HOSOYA

Department of Chemistry, Faculty of Science, Ochanomizu University, Bunkyo-ku, Tokyo 112

(Received January 11, 1978)

Concentration dependence (1—10^{-4} molar fraction) of the UV absorption spectra of the binary mixtures of (i) acetone–water, (ii) acetone–ethanol, and (iii) diisobutyl ketone–ethanol systems was studied. In (i) and (ii) distinct spectral changes of three steps were observed in succession, while in (iii) gradual changes in two steps were observed. The intensities of the n→π* band of very dilute solutions for these systems are enhanced, respectively, by 40, 20, and 15 per cent. The results were interpreted as the following stepwise equilibria

$$A + B \rightleftarrows AB, \quad AB + B \rightleftarrows AB_2, \quad AB_2 + B \rightleftarrows AB_3$$

for (i) and (ii), while in (iii) the last step is obscured, where A and B denote, respectively, ketone and water or ethanol molecules. The structure of AB_3 is discussed.

The n→π* absorption bands of ketones have been extensively studied and known to show blue shift in protic solvents.[1,2] However, most of the studies on the solvent effect of the electronic absorption spectra have been performed using dilute solutions. Above all Bayliss and Wills-Johnson extensively measured the n→π* bands of various ketones and nitro-compounds in a number of solvents and claimed that the intensity change can be explained mainly by the dispersion force, even for the cases where hydrogen bonding exists.[3] They found that, among the various solvents studied, water has by far the most peculiar effect to increase the oscillator strength as large as 40 per cent in dilute solution, but they failed to observe the concentration dependence. Gorubunov and Naberukhin measured the concentration dependence of IR and UV spectra of acetone–water mixtures in a wide range and attributed them to the two step hydrogen bonding forming acetone–water and acetone–$(water)_2$ complexes.[4] However, their conclusions are not decisive yet, since they did not analyze the intensity change. Further, Lavrik and Naberukhin proposed that cooperative effects of the hydrogen bonding of water molecules are operative in dilute aqueous non-electrolyte solutions.[5] On the other hand, Reuben explained the concentration dependence of the NMR spectra of acetone-water mixture by the existence of two different hydrogen bonding species, *i.e.*, acetone–water and $(acetone)_2$–water.[6]

Summarizing these studies, it is plausible to assume at least the following three different hydrogen bonding species for explaining the spectral change of the acetone–water mixture.

$$R_2CO + HOH \rightleftarrows R_2CO \cdots HOH \quad (AB) \quad (1)$$

$$R_2CO \cdots HOH + R_2CO \rightleftarrows R_2CO \cdots HOH \cdots OCR_2 \quad (A_2B) \quad (2)$$

$$R_2CO \cdots HOH + HOH \rightleftarrows R_2CO \cdots (HOH)_2 \quad (AB_2) \quad (3)$$

For acetone–alcohol mixtures similar arguments may apply but without assuming the A_2B type species.

As argued from the above discussion the concentration dependence of the n→π* absorption bands of ketone in protic solvents needs to be remeasured carefully, and also the effects of the proton donating and accepting powers of the solvent and solute should be studied in order to settle the discussions above.

In this study we have performed accurate measurements of the n→π* absorption bands of the binary mixture of acetone–water, acetone–ethanol, and diisobutyl ketone–ethanol systems over the full concentration range, *i.e.*, from pure acetone liquid down to very dilute solutions as low as $\approx 10^{-4}$ molar fraction.[7] The conclusions obtained in this study are as follows.

i) The intensity of the n→π* absorption bands of ketones in protic solvents such as water and alcohols increases steadily but not monotonously as the concentration of the ketone decreases, and as yet no lower limit of the concentration is obtained below which the spectrum is stable.

ii) This concentration dependence of the n→π* absorption bands of acetone in water can be interpreted as the stepwise equilibria involving successive coordination of the protic solvent molecules through hydrogen bonding as

$$A \longrightarrow AB(A_2B) \longrightarrow AB_2 \longrightarrow AB_3.$$

Especially in the very low concentration of acetone (below 10^{-2} molar fraction), it is essential to assume the third water molecule which causes extraordinary enhancement of the n→π* absorption band by forming AB_3 species as

$$R_2CO \cdots (HOH)_2 + HOH \rightleftarrows R_2CO \cdots (HOH)_3 \quad (AB_3). \quad (4)$$

iii) Almost the same but a little different mechanism can be applied to other combinations of ketones and protic solvents, the difference being attributed to the strength of the hydrogen bonding.

iv) It became clear that any discussion on the solvent effect is liable to be in serious error unless concentration dependence in a wide range down to lower molar fraction is studied.

Experimental

Acetone and ethanol of G. R. grade were dried over molecular sieve 3A and distilled several times until the refractive indices got close to the literature values. Water for spectral measurements was passed through the ion exchange resin and distilled. Crude diisobutyl ketone was purified by the courtesy of Shimadzu Seisakusho using a preparative

gas chromatograph. It is reported that the gas chromatogram analysis assures 100% purity. The refractive index also agreed with the literature value, 1.4122. The molar fraction of the solutions was determined by weight using measuring flasks.

The UV spectra of ketones in water and ethanol of wide range of concentrations were measured with a Shimadzu D-40R recording spectrophotometer at room temperature. In order to check the linearity in the high optical density region, the influenece of the stray light of the recorded intensity was checked by using the calibrated potassium chromate in aqueous 0.05 M KOH solutions. Various fused quartz cells of the lengths, 5, 1, 0.5, and 0.1 cm, with stoppers and quartz assembling cells of 0.01 cm were used depending on the concentration of ketones. The length of the 0.01 cm cells was calibrated using a micrometer, while other cells were calibrated by measuring the standard spectra. In the case where the absorbance gets larger than 2, the reference light was diminished by using a wire net whose absorbance is nearly equal to unity in the wavelength region between 350 and 230 nm. Reproducibility of the spectra was strictly checked.

The temperature dependence of the n→π^* band of acetone in water was checked in the range 20—50 °C by using a cell jacket through which water from a constant temperature bath is circulated.

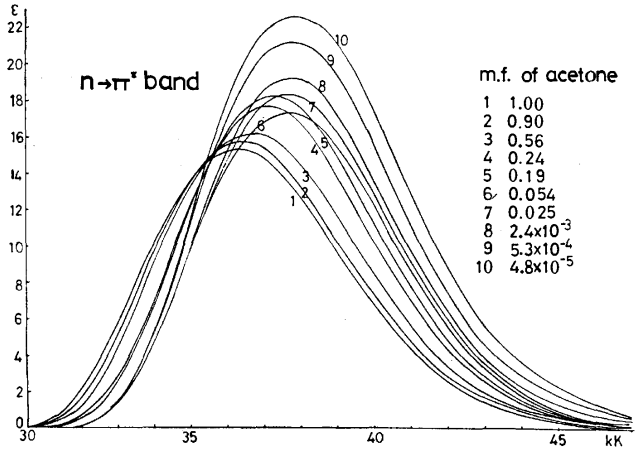

Fig. 1. The concentration dependence of the n→π^* absorption band of acetone in the binary mixtures with water.

Results

Acetone–Water System. As shown in Fig. 1, the n→π^* absorption band of the acetone-water system changes so slightly in the concentration range (Region I) between 1.0 and 0.15 molar fraction (x_A) that only a vague isosbestic point can be observed. Below 0.15 down to 0.05 of x_A (Region II) the intensity of the band slowly diminishes. Further, as the concentration gets lower (Region III) the intensity (ε_{max}) of the band monotonously increases and we could not observe the convergence limit at the infinite dilution.

In order to see the spectral change in more detail in the low concentration range, λ_{max} and ε_{max} are plotted against the logarithm of x_A as in Fig. 2.[8] It should be noted that both the curves have similar concentration dependence and their inflexion points are found nearly in the same concentration region. To see this more

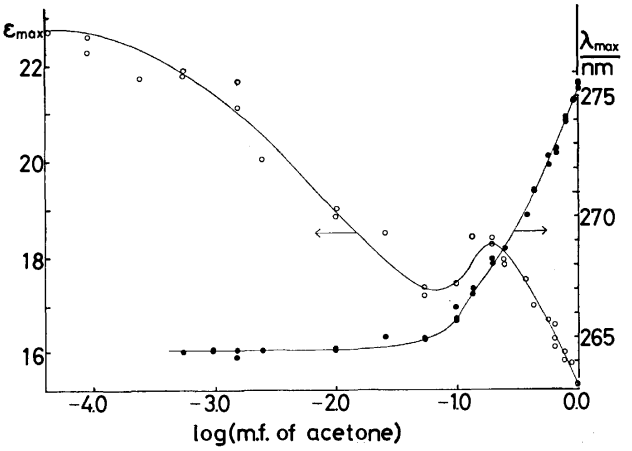

Fig. 2. The λ_{max}—log x_A and ε_{max}—log x_A plots of the acetone–water system, x_A being the molar fraction of acetone.

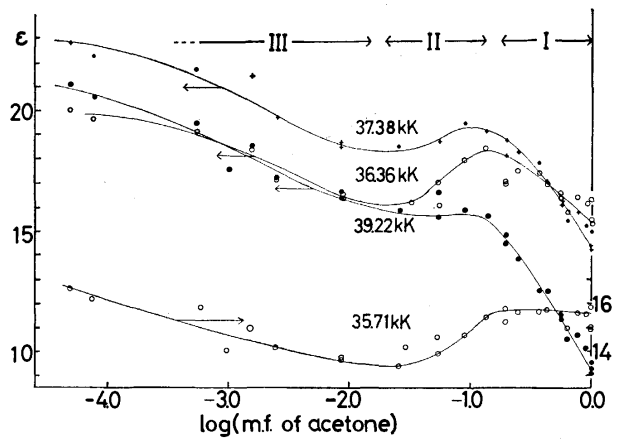

Fig. 3. The plots of ε—log x_A for the acetone–water system indicating three stepwise equilibria, Regions I—III.

quantitatively, the plots of ε—log x_A at various wavelengths are given in Fig. 3. For a single equilibrium as A+B⇌AB, the plotted curve should be something like a sigmoid one unless the wavelength is chosen at the isosbestic point.[9] For stepwise equilibria the plotted curve is expected not exactly but approximately to be a composite of the curves of the component equilibria. If a few wavelengths are carefully chosen for this plot one can easily decompose the whole change into the component equilibria.[10] This is the case with Fig. 3, where the wavelengths 35710 and 39220 cm^{-1} are so chosen from the isosbestic points for the first and second steps, respectively, that the spectral changes in the other steps clearly come out. The wavelengths 36360 and 37380 cm^{-1} are chosen so as to get zig-zag plots and are advantageous over the region above 40000 or below 34000 cm^{-1} giving monotonously increasing or decreasing curve. Now it is unambiguous that we are really observing three distinct equilibria as in Regions I—III mentioned above.

Acetone–Ethanol System. As seen in Fig. 4 the n→π^* band of acetone in ethanol does not effectively show wavelength shift (4 nm to blue) but gains only small fraction (about 20 per cent) of intensity as the concen-

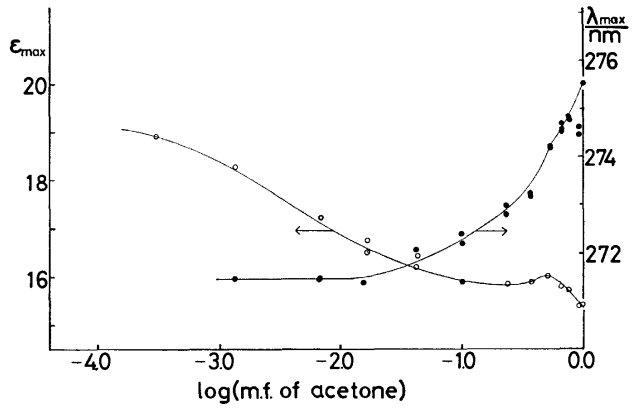

Fig. 4. The λ_{max}—log x_A and ε_{max}—log x_A plots of the acetone–ethanol system.

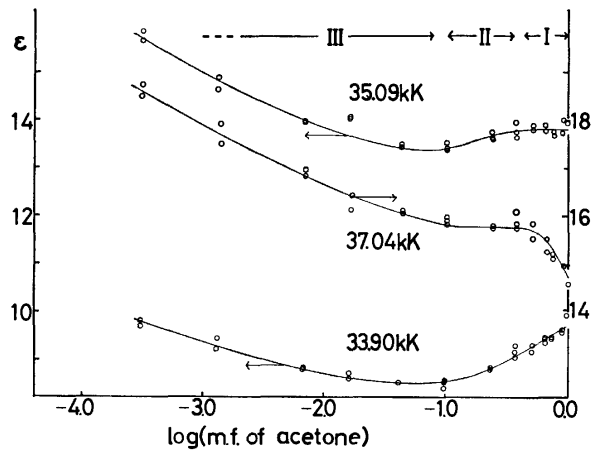

Fig. 5. The plots of ε—log x_A for the acetone–ethanol system indicating three stepwise equilibria, Regions I—III.

tration gets lower than 10^{-2} molar fraction or 0.2 M. However, if the ε—log x_A plot is taken as in Fig. 5, this spectral change also reveals three successive equilibria as in the acetone-water system. The only differences are: (i) the x_A regions in which the first and second steps occur are shifted to higher x_A values, and (ii) the degree of hyperchromism and blue shift are small. Acetone–methanol mixtures show almost the same but a little

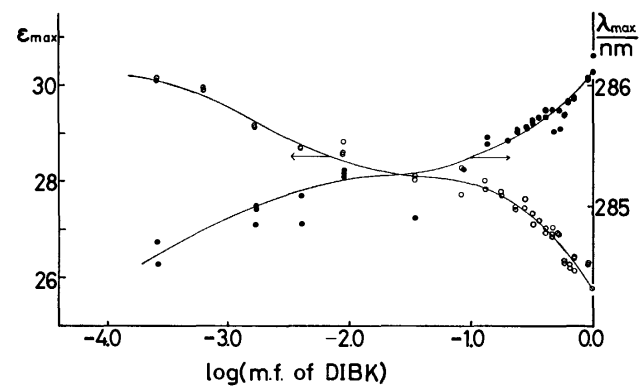

Fig. 6. The λ_{max}—log x_A and ε_{max}—log x_A plots of the diisobutyl ketone–ethanol system.

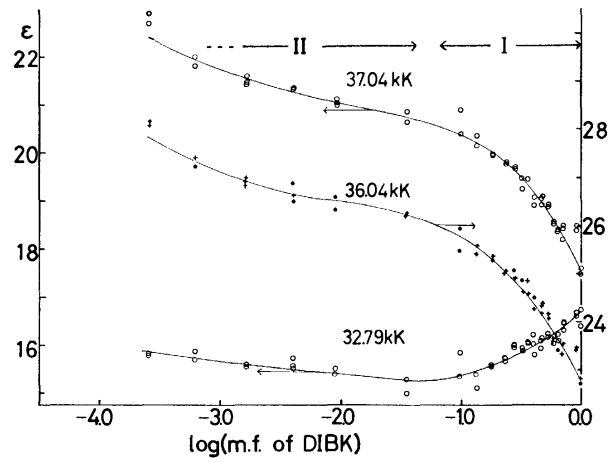

Fig. 7. The plots of ε—log x_A for the diisobutyl ketone–ethanol system.

pronounced spectral changes as the acetone–ethanol system. On the other hand, the binary mixture of acetone–dioxane does not show appreciable spectral change comparable at least with that of acetone–ethanol.[11]

Diisobutyl Ketone–Ethanol System. As shown in Figs. 6 and 7, the n→π^* band and its concentration dependence of this binary mixture is different from the case of the acetone–ethanol mixture in three points: (i) the intensity is considerably larger, (ii) in the low concentration range the intensity is monotonously growing up with small (1.5 nm) blue shift, and (iii) only two successive equilibria can be seen below and above 0.03 molar fraction indicating the low ability of diisobutyl ketone toward hydrogen bonding.

Discussion

Expected Spectral Changes of Various Hydrogen-Bonded Species. By taking account of the several mechanisms proposed by many authors, the spectral changes obtained above can be interpreted in terms of the successive change of the equilibria (1)—(4). In the following discussion the hydrogen-bonded species composed of the m ketone and n water molecules will be denoted as A_mB_n (see Chart 1). Before going into the details in the stepwise equilibria, let us try to estimate the possible change in the intensity and the wavelength at the absorption maximum.

The blue shift of AB or A_2B relative to A is known to be due to the net stabilization of the ground state by the hydrogen bonding with protic solvent molecules. Since

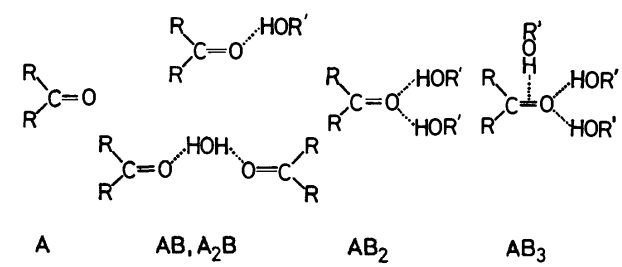

Chart 1.

we are observing the signal from the acetone molecule, it is very difficult to distinguish between AB and A_2B, if any, from the change of the n→π* absorption band. Thus in the following discussion no attempt is tried to elucidate the relative ratio of AB to A_2B. However, this ambiguity has little effect on the discussion of the succeeding changes, *i.e.*, equilibria (3) and (4).

If the second solvent molecule is to attack the second lobe of the lone pairs of the carbonyl oxygen atom, further blue shift is expected for AB_2 relative to AB. According to the *ab initio* molecular orbital calculation by Iwata and Morokuma on the A, AB, and AB_2 species of formaldehyde, the same magnitude of blue shift is predicted both in the two equilibria (1) and (3).[12] It is reasonable to expect that nearly the same argument is applied to the case of acetone in water. For the case of acetone and alcohol, the magnitudes of these shifts may be smaller, reflecting the weaker hydrogen bond.

On the other hand, the intensity of the n→π* band of AB is supposed to be larger than that of AB_2 since the potential of the electrons of the carbonyl group of AB has at most the C_s symmetry rather than the C_{2v} symmetry of AB_2 and releases the n→π* transition from having the forbidden character. The intensity of the band of AB_2 may be a little larger than that of A due to the labile and fluctuating hydrogen bonds which distort the C_{2v} symmetry.

As to the position of the attack by the third solvent molecule, two possible structures, I and II, are proposed for AB_3, where the carbon and oxygen atoms are attacked, respectively.

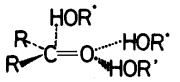

I

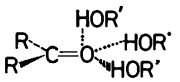

II

Since we cannot predict *a priori* which structure is more plausible for AB_3 species, let us look into the results of the *ab initio* calculation of the hydrogen bonding effect on the n→π* transition of acetone. According to Iwata and Morokuma[12] the energy of the n→π* transition is unchanged both for structures I′ and II′, in which a water molecule attacks from above the molecular plane of free formaldehyde.

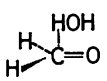

I′

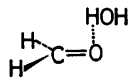

II′

However, there is no guaranty that this is also true for the attack of the third water molecule as in I and II. Del Bene has performed the population analysis for the species A and AB, where water molecules are situated in the formaldehyde plane, and found that the π-electron density of the oxygen atom is increased every time the first and second water molecules pulls the lone pair electrons through the σ-type hydrogen bonding.[13] This result is in favor of structure II but not decisive yet.

Anyway we can expect strong hyperchromism by the third water molecule to break the C_{2v} symmetry.

On the other hand, large blue shift is not expected for AB_3 species as the π-electron but not the lone pair electron is purturbed in either of the proposed structures.

Interpretation of the Spectral Changes in Terms of the Stepwise Equilibria. Now turn to the spectral change of the acetone–water system. In going from $x_A=1$ to 0.12, the n→π* band is shifted to blue by 0.15 eV with a moderate intensification. This change is in consistent with the expectation that the first water molecule attacks the carbonyl oxygen lone pair as in equilibrium (1) in agreement with the results of *ab initio* calculations.[12,13] The second change from $x_A=0.12$ to 0.03 is a hypochromism with a further but small blue shift (0.03 eV). The symmetrical coordination of the water molecules (equilibrium (3)) may lower the intensity of the n→π* band. Although two independent *ab initio* calculations[12,13] give much larger blue shift for AB_2 species there is no other candidate for explaining this spectral change in Region II.

For the concentration region below $x_A=0.03$ (Region III) the intensity of the n→π* band is monotonously growing up to the extraordinary large ε_{max} value without blue shift. That this sharp increase in the intensity is an abnormal phenomenon can be realized by replotting the curve in Fig. 2 against x_A, instead of log x_A. Further, as shown in Figs. 4 and 5, a similar spectral change as Regions I, II, and III is observed also for the acetone–ethanol and the acetone–methanol (not shown) system, the same mechanism should be applied to these systems. As far as we know, only water, methanol, and ethanol are the strongly perturbing solvents for the intensity of the n→π* band toward the infinite dilution without blue shift.[11]

Thus we can safely conclude that in the binary mixtures of acetone–water and acetone–alcohol the three successive hydrogen bonding equilibria (1), (3), and (4) take place. It should be noted here that although in the latter system A_2B species or equilibrium (2) is absent, the overall spectral change is essentially the same as that of the former system. This justifies the above statement that ambiguity in the ratio of AB to A_2B in the acetone–water system has little effect on the succeeding equilibria (3) and (4).

The different feature (ii) of ethanol from water stated in Results can be explained by assuming a smaller perturbation of ethanol molecule to the carbonyl group relative to that of water molecule. Whereas the main cause of the difference (i) can be attributed to the fact that, in spite of the weaker hydrogen bonding ability, ethanol molecules are more ready to associate with ketone molecules than water molecules owing to the strong tendency toward the self-association of water molecules as discussed by Gorubunov and Naberukhin.[4]

The bulky alkyl groups of a diisobutyl ketone molecule are likely to break the C_{2v} symmetry of the electronic structure of the carbonyl group reducing the forbidden character of the n→π* band more than that of acetone. These bulky alkyl groups are considered to hinder ethanol molecules from associating with the carbonyl group, so that AB_2 species is difficult to be formed and a considerable amount of AB species is seen until fairly lower concentration range. The bulky alkyl groups of the diisobutyl ketone are thus responsible for the

TABLE 1. ABSORPTION CHARACTERISTICS OF THE TYPICAL HYDROGEN-BONDED SPECIES OF KETONES AND WATER OR ETHANOL

Item		a	b	c	d
Region			I	II	III
Acetone–Water	x_A	1.0	0.133	0.054	4.82×10^{-5}
	λ_{max}/nm	275.2	267.0	264.9	264.5
	ε_{max}	15.4	18.5	17.4	22.8
	$\Delta\nu_{1/2}$/kK	6.10	6.12	6.11	6.43
Acetone–Ethanol	x_A	1.0	0.515	0.099	3.02×10^{-4}
	λ_{max}/nm	275.2	274.2	272.4	271.5
	ε_{max}	15.4	16.0	15.9	18.9
	$\Delta\nu_{1/2}$/kK	6.10	6.25	6.51	6.35
Diisobutyl Kteone–Ethanol	x_A	1.0	0.0348	6.16×10^{-4}	
	λ_{max}/nm	286.1	285.3	284.6	
	ε_{max}	25.8	28.1	31.0	
	$\Delta\nu_{1/2}$/kK	5.40	5.48	5.53	

a) Spectrum of A. b) Spectrum of $AB(A_2B)$ mixed with those of A and AB_2. c) Spectrum of AB_2 mixed with those of AB and AB_3. d) Spectrum of AB_3 mixed with that of AB_2. See text for further explanation.

differences (i) and (iii) stated above. The difference (ii) is also attributed to the bulky alkyl groups. Although in the previous section, the geometry of AB_2 species does not break the C_{2v} symmetry of the carbonyl group, it is reasonable to consider that this is not the case for bulky alkyl groups which may be twisted by the two ethanol molecules to make the intensity of the n→π^* band increase accompanying blue shift. As the result the intensity of the n→π^* band increases with blue shift.

Summarizing the above discussion absorption characteristics of the typical hydrogen-bonded species of ketones and water or ethanol are given in Table 1. Note, however, that this table was prepared so as to demonstrate how the spectrum of ketones changes with the decrease of the concentration in water and alcohols. The spectra of the pure liquid acetone and diisobutyl ketone are given under item a. The values under item b do not represent the spectrum of pure AB or A_2B species but that of the liquid mixtures at the border of Regions I and II, where AB or A_2B is thought to be predominant. The value under item c corresponds to the mixture at the border of Regions II and III, where AB_2 species predominates. Since the spectra of acetone under item d are the observed limits, the intensity of the band of pure AB_3 species is expected to be larger.

Although the change in the oscillator strength is not given in Table 1, it can be estimated to be roughly proportional to the change of ε_{max} as the half-band width is kept constant in a wide range for each system.

Other Theories. Bayliss and Wills-Johnson[3] calculated the change in the oscillator strength of the n→π^* bands of ketones and nitroalkanes based on their quantum mechanical model in which the total fluctuating field

$$\boldsymbol{R}^* = \alpha_s(\nu)\boldsymbol{m}\sum_k \boldsymbol{r}_k^{-6}[\boldsymbol{m} - 3(\boldsymbol{m}\cdot\boldsymbol{r}_k)\boldsymbol{r}_k]$$

caused by the solvent molecules surrounding the cavity acts on the solute chromophore, where $\alpha_s(\nu)$ is the solvent polarizability, $\boldsymbol{m}$ is the dipole moment of the solute, and $\boldsymbol{r}_k$ is the distance vector pointing to the k-th solvent molecule from the solute molecule. Although these authors could explain the "solvent dependence" of the relative intensity of the n→π^* band even for the aqueous solution, this model cannot explain the "concentration dependence," *i.e.*, the sudden rise in the intensity in the low concentration range below 10^{-2} molar fraction in water and even in ethanol, because it is impossible for any of the quantity, $\alpha_s(\nu)$, $\boldsymbol{m}$, or $\boldsymbol{r}_k$ to change sharply in this region.[14]

According to Lavrik and Naberukhin,[5] in the binary mixtures of water and non-electrolyte the cooperative effect of the hydrogen-bonded network of the liquid water predominates below 0.05 molar fraction of the non-electrolyte and this effect is greatly diminished either in ethanol or at high temperature around 60 °C. However, we have found that the behavior of the n→π^* band observed in the acetone-ethanol system as shown in Figs. 4 and 5 is essentially the same as that for the acetone–water system and that the intensity of the n→π^* band of acetone in water is even five per cent larger than the value at 20 °C. Thus we can conclude that contrary to the case of the Raman band intensity the cooperative effect of water is not responsible for the enhancement of the n→π^* band of ketones in dilute aqueous solutions.

It is generally accepted that the "solvent effect" of the electronic absorption spectra of most organic compounds can well be understood in terms of the polarizability, dielectric constant, dipole moment of the solvent, and the relevant interactions between the solute and solvent. However, the experimental data to be considered are usually taken from the measurements on "dilute solutions," and no systematic analysis has been done on the concentration dependence rather than the solvent dependence of the solvent effect, since it has not been realized that the former effect happens to compete with the latter as in this study. Thus one of the most important consequences of the present investigation is to give a warning that any discussion on the solvent effect of the electronic spectra is liable to be in serious error unless concentration dependence in a wide range

down to lower concentrations is studied.

A preliminary work of this study was initiated by Miss Akiko Motoyama now in Japan Association for International Chemical Information, to whom the authors' hearty thanks are due. The authors also thank Dr. Koichi Ohno of the University of Tokyo, Professor Tsunetake Fujiyama of Tokyo Metropolitan University, and Professor Yusei Maruyama of Ochanomizu University for their continuous interest, criticism, and helpful suggestions. For the troublesome purification of diisobutyl ketone the authors are greatly indebted to Dr. Yoshihiko Moriyama of the University of Tokyo and Research Laboratory staffs of Shimadzu Seisakusho. The present work was partially supported by a Grant-in-Aid for Scientific Research from the Ministry of Education.

References

1) H. H. Jaffé and M. Orchin, "Theory and Application of Ultraviolet Spectroscopy," John Wiley, New York (1962).
2) J. N. Murrell, "The Theory of the Electronic Spectra of Organic Molecules," Methuen, London (1963).
3) N. S. Bayliss and G. Wills-Johnson, *Spectrochim. Acta, Part A*, **24**, 551, 563 (1968).
4) B. Z. Gorubunov and Yu. I. Naberukhin, *Zh. Strukt. Khim.*, **15**, 8 (1974).
5) N. L. Lavrik and Yu. I. Naberukin, *ibid.*, **17**, 466 (1976).
6) J. Reuben, *J. Am. Chem. Soc.*, **91**, 5725 (1969).
7) Sterically crowded diisobutyl ketone is hardly soluble in water.
8) To the authors' awareness the concentration dependence of the $n\rightarrow\pi^*$ band of acetone in water has never been reported in the full concentration range except by Gorubunov and Naberukhin,[4] who, however, observed only the λ_{max} change as in Fig. 2.
9) H. Hosoya and S. Nagakura, *Spectrochim. Acta*, **17**, 324 (1961); H. Hosoya, J. Takaka, and S. Nagakura, *J. Mol. Spectrosc.*, **8**, 257 (1962).
10) H. Hosoya, S. Hosoya, and S. Nagakura, *Nippon Kagaku Zasshi*, **88**, 797 (1967).
11) A. Motoyama and H. Hosoya, unpublished.
12) S. Iwata and K. Morokuma, *J. Am. Chem. Soc.*, **95**, 7563 (1973).
13) J. E. Del Bene, *J. Am. Chem. Soc.*, **95**, 6517 (1973); **96**, 5643 (1974).
14) According to the observed concentration dependence of the refractive index (present study) and dielectric constant[15] of the binary mixtures of acetone and water, there is no sharp change in the low acetone concentration region.
15) Drude, *Z. Phys. Chem.*, **23**, 267 (1897).

Electrical and Spectroscopic Investigations of Molecular Layers of Fatty Acids Including Carotene

Toshihiro OHNISHI, Masahiro HATAKEYAMA, Naoto YAMAMOTO, and Hiroshi TSUBOMURA

Department of Chemistry, Faculty of Engineering Science, Osaka University, Toyonaka, Osaka 560

(Received January 17, 1978)

Spectroscopic and electrical studies have been made for the mono- and multi-molecular layers of barium stearate mixed with carotene. The results of the electronic spectra have indicated that the carotene molecules lie parallel to the monolayer plane and are aggregated. The capacitances measured are expressed well as those of parallel plate capacitors. From these results, the structure of the layers containing carotene has been deduced.

Kuhn and his colaborators have extensively investigated the physicochemical phenomena occurring at interfaces of Langmuir films made of some organic molecules such as fatty acid salts and organic dyes.[1,2]

We have investigated the electrical and spectroscopic properties of sandwitch-type assemblies of fatty acid salt layers mixed with *all-trans*-β-carotene in order to clarify the structure of these layers and its relation with the electrical properties.

Experimental

Aluminum/Langmuir film/aluminum junctions were prepared as follows. Aluminum film was evaporated on a slide glass using 99.999% aluminum at a pressure of 10^{-5} Torr. Monolayers or multilayers were deposited on such films by means of the Langmuir-Blodgett technique.[3] Finally, aluminum was evaporated in an array of stripes on the layers as shown in Fig. 1. The effective electrode area of each

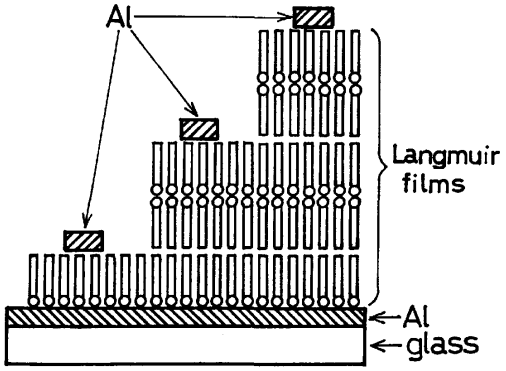

Fig. 1. The structure of Al/monolayers/Al assemblies.

of the junctions formed was about 0.1 cm^2. The monolayers were spread on an aqueous subphase containing 3×10^{-5} M barium chloride and 4×10^{-4} M potassium bicarbonate by introducing a small amount of a benzene solution of a fatty acid or a mixture of fatty acid and β-carotene. The water used as the subphase was prepared by distilling deionized water twice. Oleic acid was used as a piston oil having a surface pressure of 29.5 dyn/cm. Stearic acid from Sigma Chemical Co., 99% pure arachidic acid and 99% pure behenic acid both from Nakarai Chem. Co. were purified by recrystallization twice from distilled ethanol solutions. *All-trans*-β-carotene, 97% pure, from Merk & Co. was used without further purification. Capacitance measurements were made with a Yokogawa-Hewlett-Packard 4265B bridge at 1 kHz, 20 mV peak-to-peak. Absorption spectra were measured by use of a Cary 15 spectrophotometer.

Results and Discussion

Electronic Absorption Spectra. Figure 2 shows the electronic absorption spectra, measured at normal incidence, of various molecular layers of barium stearate mixed with β-carotene. The benzene solution of carotene is well known to have a strong absorption due to the $^1B\leftarrow{}^1A$ transition with fine structures in the region from 500 to 350 nm. The absorption spectra of the layers are somewhat different from that in solution. The peak positions of the layers, 513, 474, and 447 nm are essentially the same as those of a β-carotene film formed on glass by solvent evaporation from a benzene solution containing carotene and stearic acid at the same molar ratio, and are at slightly shorter wavelengths than those reported for a solid state carotene film by Rosenberg *et al.*[4] When the number of the superposed monolayers increased, the absorption intensity increased proportionally, but no change in the spectral shape was found.

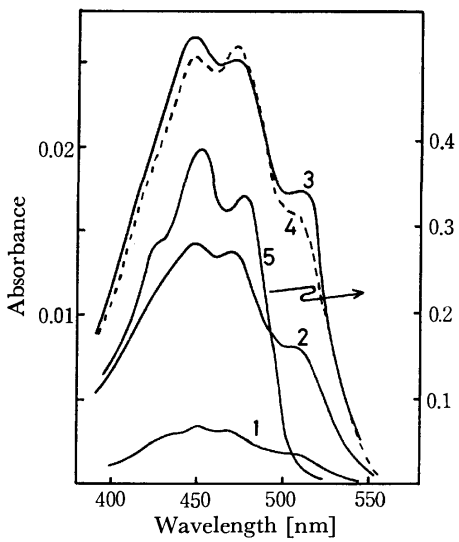

Fig. 2. Absorption spectra of Langumuir films containing *all-trans*-β-carotene taken at normal incidence: (1) monomolecular layer. (2) 3 molecular layers. (3) 5 molecular layers. (4) 5 molecular layers at an angle of incidence of 45°. (5) The hexane solution of β-carotene. All films are made of a mixture of β-carotene and barium stearate in a molar ratio of 1 : 12.3.

The $^1B\leftarrow{}^1A$ transition moment of carotene lies in the molecular plane and directs along the polyene chain. Therefore, if the carotene molecules are assumed to lie

perpendicularly on the glass plane, no absorption should be observed with light of normal incidence. On the other hand, if the carotene molecules are assumed to be randomly oriented, the absorption intensity should change with the angle of incidence, θ, being proportional to $1/\cos\theta$. Finally, if the molecules are assumed to lie parallel to the glass, the absorption intensity is expected to be proportional to $(1+\cos^2\theta)/(2\cos\theta)$, so that the ratio of the absorption intensity measured at $\theta=45°$ to that at $\theta=0°$ is calculated to be 1.06. In the present work, the absorption spectrum obtained at an angle of incidence of 45° showed no significant difference in shape and intensity from that obtained at normal incidence (Fig. 2). This result suggests that the carotene molecules lie parallel to the glass plate. The large difference between the absorption spectrum of carotene in the layers and that in solution can be explained by taking account of the aggregation of the molecules in the former. Based on these results, a plausible model for the structure of the mixed monolayers is shown schematically in Fig. 3.[5] It is reasonable to assume that the carotene molecules are stacked face to face on the glass plane in view of the π-π type molecular interaction giving a large amount of stabilization.

Capacitance Measurements. Figure 4 shows the reciprocal of capacitance per unit area measured for barium stearate layers with and without β-carotene versus the number of superposed monolayers between aluminum electrodes. The capacitance, C, of these layers, being regarded as parallel type capacitors, is expressed as a function of the number of the monolayers, n, as follows:

$$1/C = 1/C_{ox} + (d/\varepsilon_0\varepsilon)n, \quad (1)$$

where C_{ox} is the capacitance due to the oxide layer presumably formed on the aluminum electrode surface, ε_0 is the dielectric constant of vacuum, ε is the relative permittivity of the organic layers, and d is the thickness of the monolayer. As is seen from Fig. 4, a good linear relationship is obtained between $1/C$ and n for all cases.

By taking the relative permittivity of aluminum oxide to be 8,[6] the oxide thickness is calculated to be 35 Å for the stearate layer assemblies and 42 Å for the mixed layer assemblies from the $1/C$ values extrapolated to $n=0$. Similar plots were made for other fatty acid salts and the d/ε values derived from the slopes are listed in Table 1. Using the d values obtained by Kuhn *et al.*,[7] the ε values were derived for the fatty acid salts as seen in Table 1, being in good agreement with those obtained by Kuhn *et al.*[8] and Reynolds *et al.*[9]

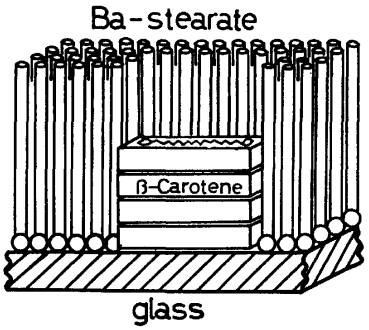

Fig. 3. Schematic representation of the mixed layer of *all-trans*-β-carotene and a fatty acid salt.

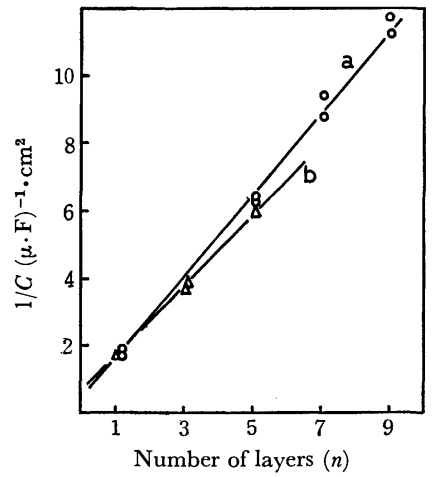

Fig. 4. Reciprocal of capacitance, $1/C$, *vs.* predicted number of layers, n; (a) for the monolayers of barium stearate and (b) for those mixed with β-carotene in a mole ratio of 1: 12.3.

Table 1. The d/ε and ε of fatty acid salts obtained from the capacitance measurements

Material	d/ε (Å)	d[a] (Å)	ε
Barium stearate	10.5	25.8	2.46
Barium arachidate	11.6	28.0	2.41
Barium behenate	13.0	30.2	2.32
Barium stearate–β-carotene	9.7		

a) Taken from Ref. 8.

Somewhat smaller d/ε values were obtained for the mixed layers than those for the pure barium stearate layers. Assuming that the electric polarization of the mixed layer is a simple sum of those by the fatty acid salt array and the carotene array indicated in Fig. 3, the capacitance of the layer can be calculated only if the stacking number of β-carotene molecules in each of the monolayer is assumed. Using the d/ε values obtained both for the fatty acid salt layers and for the mixed layers, the molecular cross-section of barium stearate of 20 Å^2, the molecular plane area of carotene of 230 Å^2, the thickness of the carotene plane of 4 Å, and ε of carotene assumed to be 2.5 or 3.0,[10] the number derived is 3.58 or 4.09, respectively. The relative actual thickness of the carotene layers is such as illustrated in Fig. 3. In the above discussion, it was assumed that there are no interstices between the molecular layers.

Surface pressure-area (π-A) curve measured for β-carotene at the air–water interface has been measured. It is in good agreement with that obtained by Leblanc and Orger.[11] The limiting area of 18.0 Å^2 per molecule was derived by extrapolating the steep part of the π-A curve. This corresponds to the cross sectional area of β-carotene calculated from the molecular structural model, indicating that the β-carotene molecules are standing perpendicularly on the surface. The π-A curves

for samples containing both carotene and fatty acid in various molar ratios have also indicated the perpendicular standing of β-carotene. Therefore, the structure proposed in Fig. 3 for the mixed Langumuir film of β-carotene with the fatty acid salt seems to be formed when the layer was transferred from the air–water interface onto the glass surface.

References

1) H. Kuhn, D. Möbius, and H. Bücher, "Techniques of Chemistry," Vol. 1, Part 3B, ed by A. Weissberger and B. W. Rossiter, Wiley, New York (1972), p. 577.

2) H. Bücher, K. H. Drexhage, M. Fleck, H. Kuhn, D. Möbius, F. P. Schäfer, J. Sondermann, W. Sperling, P. Tillmann, and J. Wiegand, *Molecular Crystals*, **2**, 199 (1967).

3) K. B. Blodgett, *J. Am. Chem. Soc.*, **56**, 495 (1934); *ibid.*, **57**, 1007 (1935). I. Langmuir, *Trans. Faraday Soc.*, **15**, 62 (1920).

4) T. N. Misra and B. Rosenberg, *J. Chem. Phys.*, **48**, 5734 (1968).

5) In this figure, β-carotene molecules are shown to exist as a single molecular column surrounded by the fatty acid. Naturally, it is possible that they form larger islands consisting of two or more columns in the fatty acid.

6) J. C. Fisher and I. Giaever, *J. Appl. Phys.*, **32**, 172 (1961).

7) B. Mann, H. Kuhn, and L. v. Szentpláy, *Chem. Phys. Lett.*, **8**, 82 (1971).

8) B. Mann and H. Kuhn, *J. Appl. Phys.*, **42**, 4398 (1971).

9) H. H. Race and S. I. Reynolds, *J. Am. Chem. Soc.*, **61**, 1425 (1936).

10) The values of the permittivity are 2.44 for benzene and 2.85 for napthalene in solid state, respectively. It is presumed that β-carotene has a value in permittivity near those of unsaturated hydrocarbons such as benzene and naphthalene.

11) R. M. Leblanc and B. H. Orger, *Biochim. Biophys. Acta*, **275**, 102 (1972).

The Crystal and Molecular Structures of Pyrrolidinium *p*-Chlorobenzoate and Pyrrolidinium *p*-Toluate

Setsuo KASHINO, Shin-ichi KATAOKA, and Masao HAISA

Department of Chemistry, Faculty of Science, Okayama University, Tsushima, Okayama 700

(Received January 27, 1978)

The crystal structures of pyrrolidinium *p*-chlorobenzoate (PYC) and pyrrolidinium *p*-toluate (PYT) have been determined from visually estimated Cu $K\alpha$ data. The crystals of PYC are orthorhombic, space group Pbca, $a=9.53(1)$, $b=27.28(3)$, $c=9.39(2)$ Å, and $Z=8$. Those of PYT are monoclinic, space group $P2_1/c$, $a=14.66(3)$, $b=9.00(2)$, $c=9.44(1)$ Å, $\beta=101.3(4)°$, and $Z=4$. The structures of PYC and PYT were refined by the block-diagonal least-squares method to R values of 0.073 and 0.089 for 855 and 1277 non-zero reflections, respectively. In both PYC and PYT, the pyrrolidinium and benzoate ions are linked together by two kinds of N–H···O hydrogen bonds to form a ribbon along the twofold screw axis. The shorter hydrogen bond [N···O 2.697(7) Å for PYC, 2.674(5) Å for PYT] lies nearly perpendicular to the twofold screw axis, and the longer bond [N···O 2.730(7) Å for PYC, 2.738(5) Å for PYT] makes an angle of about 20° with the axis. The O···N···O angle is near to the regular tetrahedral angle [105.4(2)° for PYC, 107.1(2)° for PYT]. The crystals of PYC are isomorphous with those of piperidinium *p*-chlorobenzoate, piperidinium *p*-bromobenzoate, piperidinium *p*-toluate and pyrrolidinium *p*-bromobenzoate, but PYT crystallizes in a subgroup of the space group of the others because of the cooperative effects of the bulkiness of the methyl group and the ring size of the base moiety. The pyrrolidine rings in PYC and PYT take an approximate C_S symmetry.

Previously, we have shown that the crystals of piperidinium *p*-chlorobenzoate (PIC), piperidinium *p*-bromobenzoate (PIB) and piperidinium *p*-toluate (PIT) are isomorphous.[1,2] The present investigation was undertaken in order to elucidate the effect of the ring size of the base moiety and the effect of the *para* substituent of the acid moiety on the crystal structure and on the geometry of hydrogen bond in the crystals. The conformation of the pyrrolidine ring in the solid state is of additional interest.

Experimental

The compounds were prepared by dissolving equimolar quantities of the acid and the base in dry benzene, in a similar manner described for piperidinium benzoates.[3] Crystallographic data for PYC, PYT and pyrrolidinium *p*-bromobenzoate (PYB) are listed in Table 1, and experimental details are in Table 2.

As the crystals of these compounds decomposed gradually, the specimens were sealed in glass capillaries. The intensity data were collected on the equi-inclination Weissenberg photographs using Cu $K\alpha$ radiation. Intensities were esti-

Table 1. Crystallographic data

	Pyrrolidinium *p*-chlorobenzoate (PYC) $(C_4H_8NH_2)^+(ClC_6H_4CO_2)^-$	Pyrrolidinium *p*-bromobenzoate (PYB) $(C_4H_8NH_2)^+(BrC_6H_4CO_2)^-$	Pyrrolidinium *p*-toluate (PYT) $(C_4H_8NH_2)^+(CH_3C_6H_4CO_2)^-$
F.W.	227.7	272.2	207.3
Mp (°C)	127—129	123—124	133—134
Morphology	plates developed {010}	plates developed {010}	plates developed {100}
Crystal system	orthorhombic	orthorhombic	monoclinic
Space group	Pbca	Pbca	$P2_1/c$
a (Å)	9.53(1)	9.44(1)	14.66(3)
b	27.28(3)	27.49(3)	9.00(2)
c	9.39(2)	9.41(1)	9.44(1)
β (°)			101.3(4)
D_m (g cm^{-3})	1.24	1.48	1.12
		(Weld pycnometer and liquid paraffin)	
D_x	1.240	1.480	1.128
Z	8	8	4
$F(000)$	960	1104	448

Table 2. Experimental details

	PYC	PYT
μ (cm^{-1}) for Cu $K\alpha$	32.2	6.5
Dimensions of crystals used (mm)	0.60×0.16×0.22 0.20×0.20×0.95	0.18×1.1×0.22 0.30×0.30×1.1
Layers photographed	$0kl$ to $5kl$ $hk0$ to $hk5$	$h0l$ to $h6l$ $hk0$ to $hk6$
No. of observed reflections	855	1277
Percent to accessible	31	45
B (Å^2) from Wilson's plot	6.8	6.6

TABLE 3. ATOMIC PARAMETERS

(a) Final atomic parameters for the non-hydrogen atoms ($\times 10^4$) with their e.s.d.'s in parentheses. The β_{ij}'s are defined by $\exp(-\beta_{11}h^2-\beta_{22}k^2-\beta_{33}l^2-\beta_{12}hk-\beta_{13}hl-\beta_{23}kl)$.

	x	y	z	β_{11}	β_{22}	β_{33}	β_{12}	β_{13}	β_{23}
Pyrrolidinium *p*-chlorobenzoate (PYC)									
C(1)	3810(7)	1285(2)	8577(6)	145(9)	16.9(1.0)	148(9)	5(5)	−16(17)	−5(5)
C(2)	3367(7)	1639(2)	9552(7)	200(11)	18.1(1.0)	155(9)	11(6)	40(19)	4(5)
C(3)	3886(8)	2120(3)	9468(8)	208(13)	23.0(1.3)	173(11)	16(7)	−24(21)	−4(6)
C(4)	4797(8)	2237(3)	8367(8)	162(11)	21.3(1.2)	197(11)	−13(6)	−80(20)	8(6)
C(5)	5201(9)	1892(3)	7395(9)	198(12)	25.2(1.3)	170(10)	−3(7)	71(20)	17(7)
C(6)	4738(8)	1416(2)	7489(8)	168(10)	18.7(1.0)	160(8)	−1(6)	10(18)	4(6)
C(7)	3247(7)	766(2)	8660(6)	157(10)	18.5(1.0)	129(8)	12(5)	−48(17)	2(5)
O(8)	2460(5)	669(2)	9718(6)	201(8)	23.3(0.9)	228(8)	−11(4)	131(15)	−4(4)
O(9)	3635(6)	456(2)	7758(5)	259(9)	20.0(0.7)	134(7)	−0(4)	3(13)	−10(4)
Cl(10)	5420(3)	2839(1)	8233(5)	363(5)	21.4(0.3)	268(4)	−56(2)	−119(8)	16(2)
N(11)	2945(5)	306(2)	4970(5)	139(7)	17.8(0.8)	130(7)	4(4)	28(12)	1(4)
C(12)	1631(7)	588(3)	4800(9)	144(10)	25.1(1.3)	241(13)	34(6)	27(22)	−14(7)
C(13)	2037(10)	1034(4)	4037(14)	221(16)	33.4(2.2)	614(35)	53(9)	17(39)	104(14)
C(14)	3347(11)	964(4)	3369(10)	339(20)	32.5(2.0)	286(18)	−17(10)	17(32)	97(9)
C(15)	3992(8)	489(3)	3883(8)	177(12)	24.5(1.3)	180(11)	−10(6)	34(20)	11(6)
Pyrrolidinium *p*-toluate (PYT)									
C(1)	7555(3)	8818(4)	7260(4)	56(2)	119(5)	164(6)	16(5)	39(6)	58(10)
C(2)	8174(3)	9775(5)	8148(5)	61(2)	161(7)	205(7)	−8(7)	17(7)	−21(11)
C(3)	9103(3)	9821(5)	8021(6)	60(3)	175(7)	310(10)	−5(7)	−4(8)	−22(15)
C(4)	9447(3)	8960(6)	7025(7)	52(2)	199(8)	357(11)	22(7)	73(8)	45(16)
C(5)	8819(3)	8018(6)	6159(6)	67(3)	196(8)	296(10)	30(8)	89(8)	−49(15)
C(6)	7896(3)	7929(5)	6282(5)	60(2)	152(6)	211(7)	26(6)	43(7)	−20(12)
C(7)	6539(3)	8799(5)	7361(4)	64(2)	146(6)	165(6)	6(6)	52(6)	56(10)
O(8)	6264(2)	9800(4)	8106(4)	68(2)	291(7)	268(6)	−18(6)	107(6)	−187(11)
O(9)	6015(2)	7833(3)	6659(3)	63(2)	155(4)	246(5)	−34(5)	39(5)	16(8)
C(10)	10475(4)	9034(8)	6916(10)	60(3)	301(13)	650(23)	−3(11)	160(14)	−39(29)
N(11)	5587(2)	4964(4)	7214(4)	57(2)	139(5)	167(5)	0(5)	49(5)	5(8)
C(12)	6087(3)	4712(6)	8762(5)	78(3)	259(9)	137(6)	−22(9)	32(6)	−31(13)
C(13)	7006(4)	4020(8)	8616(6)	83(4)	440(16)	196(8)	126(13)	−18(8)	−91(20)
C(14)	6948(4)	3553(7)	7130(6)	78(3)	299(11)	225(9)	115(10)	34(8)	−19(17)
C(15)	5970(3)	3852(6)	6334(5)	74(3)	224(8)	147(6)	21(8)	55(6)	−39(12)

(b) Positional($\times 10^3$) and isotropic thermal parameters for the hydrogen atoms.

	x	y	z	B/Å^2	x	y	z	B/Å^2	Bonded to
	PYC				PYT				
H(16)	269(7)	157(2)	1047(7)	5.1(1.6)	791(4)	1036(7)	888(6)	7.9(1.6)	C(2)
H(17)	346(7)	237(3)	1008(10)	8.2(2.3)	948(4)	1052(6)	869(5)	6.6(1.3)	C(3)
H(18)	567(7)	199(3)	672(8)	6.1(1.9)	896(4)	749(6)	536(6)	7.9(1.5)	C(5)
H(19)	503(7)	114(2)	690(7)	4.8(1.6)	749(3)	735(5)	561(5)	5.8(1.2)	C(6)
H(20)	309(6)	32(2)	588(6)	3.1(1.4)	569(3)	590(5)	706(5)	4.7(1.1)	N(11)
H(21)	272(7)	−8(2)	486(7)	4.7(1.6)	486(3)	488(5)	722(4)	4.1(1.0)	N(11)
H(22)	116	66	584	6.8	618(4)	559(6)	925(6)	6.8(1.4)	C(12)
H(23)	89	39	412	6.8	574(3)	403(5)	915(5)	5.8(1.2)	C(12)
H(24)	218	134	490	6.8	761(6)	484(11)	896(9)	16.6(3.3)	C(13)
H(25)	122	117	335	6.8	723(6)	346(10)	927(8)	14.2(2.5)	C(13)
H(26)	403	128	353	6.8	755(6)	389(10)	670(8)	14.4(2.7)	C(14)
H(27)	315	94	221	6.8	716(4)	253(7)	694(6)	8.6(1.6)	C(14)
H(28)	499	57	442	6.8	594(3)	416(6)	534(5)	5.7(1.2)	C(15)
H(29)	409	23	302	6.8	550(4)	291(7)	628(6)	8.2(1.5)	C(15)
H(30)					1095(6)	834(12)	779(9)	17.6(3.1)	C(10)
H(31)					1066(5)	1006(8)	695(7)	10.7(2.1)	C(10)
H(32)					1057(6)	850(10)	601(8)	14.2(2.6)	C(10)

mated visually and corrected for Lorentz and polarization factors and spot shape.

Structure Determination and Refinement

The structures were solved from sharpened Patterson maps, and refined by block-diagonal least-squares calculations. For PYC an extinction correction was applied at the stage of $R=0.089$, for the four strongest reflections according to the formula $I_{corr}=I_{obsd}/(1-1.3\times 10^{-4} I_{obsd})$. In the subsequent refinements, the parameters of the H atoms attached to the C atoms of pyrrolidine ring were fixed. The weighting scheme used was $w=1.0$ for $0<|F_o|\leq F_{max}$, and $w=(F_{max}/|F_o|)^2$ for $|F_o|>F_{max}$, where F_{max} was 18.0. The final R value was 0.073 for 855 non-zero reflections.

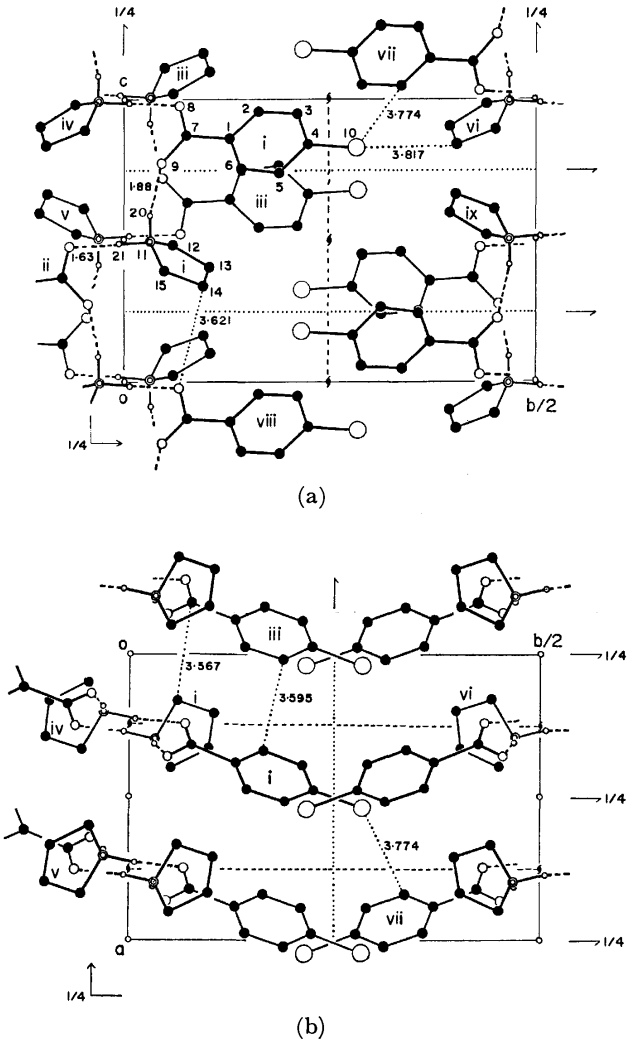

Fig. 1. Projections of the crystal structure of PYC along the a axis (a), and the c axis (b).
Broken lines show hydrogen bonds, and dotted lines intermolecular contacts.
Symmetry code: i x, y, z; ii $1/2-x, -y, -1/2+z$; iii $-1/2+x, y, 3/2-z$; iv $1/2-x, -y, 1/2+z$; v $1-x, -y, 1-z$; vi $x, 1/2-y, 1/2+z$; vii $1/2+x, 1/2-y, 2-z$; viii $x, y, -1+z$; ix $1/2+x, 1/2-y, 1-z$.

For PYT a difference Fourier map revealed all the H atoms at the stage of $R=0.104$. Further refinements gave a final R value of 0.089 for 1277 non-zero reflections. The same weighting scheme as that for PYC was used with $F_{max}=10.0$.

The final atomic parameters are listed in Table 3.[4]

The atomic scattering factors were taken from International Tables for X-Ray Crystallography.[5] The computations were carried out on a NEAC 2200-500 computer at the Okayama University Computer Center. The programs used were HBLS-5 and DAPH.[6]

Results and Discussion

The projections of the crystal structure of PYC viewed along a and c axes are shown in Fig. 1, and those of PYT along c and b axes in Fig. 2. Some intermolecular distances are summarized in Table 4. Bond lengths and angles are listed in Table 5.

Crystal Structures. The crystals of PYC are isostructural with those of piperidinium compounds *i.e.* PIC, PIB, and PIT, and also with PYB, judging from the space group, the cell dimensions, and the intensity distribution.

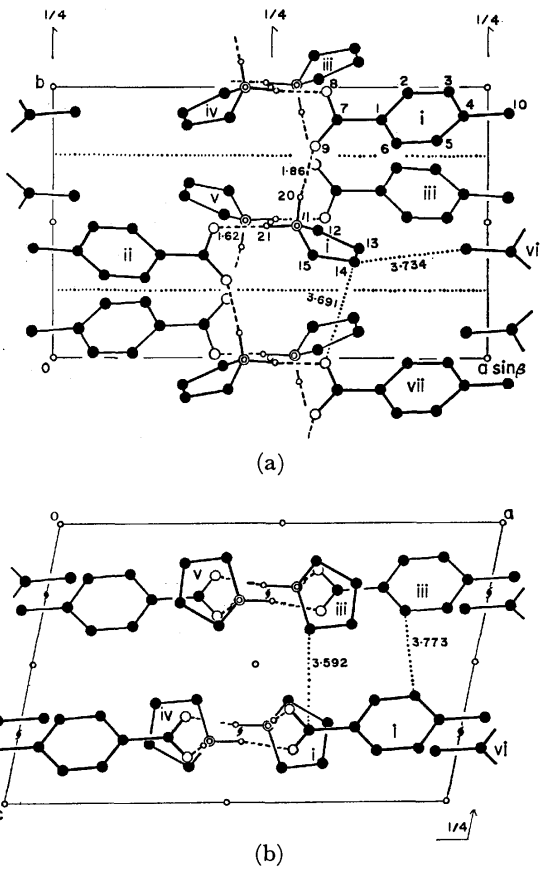

Fig. 2. Projections of the crystal structure of PYT along the c axis (a), and the b axis (b).
Broken lines show hydrogen bonds, and dotted lines intermolecular contacts.
Symmetry code: i x, y, z; ii $1-x, -1/2+y, 3/2-z$; iii $x, 3/2-y, -1/2+z$; iv $1-x, 1/2+y, 3/2-z$; v $1-x, 1-y, 1-z$; vi $2-x, -1/2+y, 3/2-z$; vii $x, -1+y, z$; viii $x, 3/2-y, 1/2+z$.

TABLE 4. INTERMOLECULAR DISTANCES (Å) FROM THE MOLECULE (i) WITH THEIR e.s.d.'s IN PARENTHESES
Symmetry code is given in the legend of Figs. 1 and 2.

PYC					
C(7)	H(20^{i})	2.89(6)	H(21)	H(28^{v})	2.65
C(2)	C(5^{iii})	3.595(11)	Cl(10)	H(26^{vi})	2.77
C(12)	C(7^{iii})	3.567(11)	Cl(10)	C(14^{vi})	3.817(11)
H(22)	C(1^{iii})	2.86	Cl(10)	H(16^{vii})	2.97
H(22)	C(6^{iii})	2.92	Cl(10)	C(2^{vii})	3.774(8)
H(22)	C(7^{iii})	2.83	H(27)	O(8^{viii})	2.54
C(7)	H(21^{iv})	2.38(7)	H(27)	H(16^{viii})	2.41
O(9)	H(21^{iv})	2.57(7)	C(14)	O(8^{viii})	3.621(12)
O(9)	H(23^{iv})	2.67	Cl(10)	H(25^{ix})	3.18
O(9)	H(29^{v})	2.95			
PYT					
C(7)	H(20^{i})	2.88(5)	C(7)	H(21^{iv})	2.37(4)
C(5)	C(2^{iii})	3.773(8)	O(9)	H(21^{iv})	2.59(4)
H(18)	C(2^{iii})	2.98(6)	H(21)	H(28^{v})	2.61(7)
H(28)	O(8^{iii})	2.44(5)	C(14)	C(10^{vi})	3.734(12)
C(7)	C(12^{iii})	3.592(7)	H(26)	C(10^{vi})	2.94(9)
C(7)	H(22^{iii})	2.93(6)	H(26)	H(30^{vi})	2.22(14)
O(9)	H(22^{iii})	2.73(6)	H(27)	C(2^{vii})	3.00(6)
C(6)	H(24^{iii})	2.94(10)	C(14)	O(8^{vii})	3.691(7)

The pyrrolidinium and *p*-chlorobenzoate ions are linked together by two kinds of hydrogen bonds [N(11)–H(21)···O(8^{ii}) and N(11)–H(20)···O(9)] to form a ribbon along the twofold screw axis parallel to ***c***. The ribbons related by an a-glide plane are held together side by side by van der Waals interactions to form a sheet parallel to (010). The sheets related by a c-glide plane are stacked along ***b*** to complete a whole crystal.

In the crystals of PYT, similar hydrogen bonds to those in PYC effect a ribbon around the twofold screw axis at $x=1/2$. The ribbons related by a c-glide plane are held together to form a sheet parallel to (100). The sheets are stacked along ***a***. The axes ***a*** sin β, ***b***, and ***c*** of PYT correspond to the axes ***b***/2, ***c***, and ***a*** of PYC, respectively.

In both PYC and PYT six close contacts between the

TABLE 5. BOND LENGTHS (Å) AND ANGLES (°) WITH THEIR e.s.d.'s IN PARENTHESES

	PYC (X=Cl)	PYT (X=C)
C(1)–C(2)	1.395(10)	1.404(6)
C(2)–C(3)	1.405(11)	1.391(8)
C(3)–C(4)	1.388(11)	1.387(9)
C(4)–C(5)	1.364(11)	1.393(9)
C(5)–C(6)	1.376(11)	1.383(8)
C(6)–C(1)	1.397(10)	1.387(6)
C(1)–C(7)	1.516(9)	1.511(6)
C(7)–O(8)	1.272(8)	1.257(6)
C(7)–O(9)	1.254(8)	1.259(5)
C(4)–X(10)	1.753(8)	1.533(12)
N(11)–C(12)	1.479(10)	1.495(6)
N(11)–C(15)	1.512(9)	1.496(6)
C(12)–C(13)	1.464(16)	1.515(9)
C(13)–C(14)	1.410(17)	1.451(10)
C(14)–C(15)	1.514(13)	1.507(8)
N(11)–H(20)	0.86(6)	0.88(5)
N(11)–H(21)	1.08(7)	1.06(4)
C(1)–C(2)–C(3)	120.2(7)	119.8(5)
C(2)–C(3)–C(4)	118.4(7)	122.3(5)
C(3)–C(4)–C(5)	121.1(7)	116.9(6)
C(4)–C(5)–C(6)	121.1(7)	122.1(5)
C(5)–C(6)–C(1)	119.4(7)	120.6(5)
C(6)–C(1)–C(2)	119.6(6)	118.5(4)
C(3)–C(4)–X(10)	118.7(6)	121.0(6)
C(5)–C(4)–X(10)	120.1(6)	122.2(6)
C(2)–C(1)–C(7)	120.3(6)	120.0(4)
C(6)–C(1)–C(7)	120.0(6)	121.6(4)
C(1)–C(7)–O(8)	116.3(6)	117.1(4)
C(1)–C(7)–O(9)	119.5(6)	118.8(4)
N(11)–C(12)–C(13)	105.1(8)	104.6(5)
C(12)–C(13)–C(14)	109.9(10)	108.8(6)
C(13)–C(14)–C(15)	109.4(9)	107.5(5)
C(14)–C(15)–N(11)	103.3(6)	105.1(4)
C(15)–N(11)–C(12)	108.3(5)	106.3(4)
H(20)–N(11)–C(12)	103(4)	105(3)
H(21)–N(11)–C(12)	109(4)	108(2)
H(20)–N(11)–C(15)	123(4)	115(3)
H(21)–N(11)–C(15)	113(4)	115(2)

TABLE 6. GEOMETRY OF HYDROGEN BONDS
Lengths in Å and angles in degree.

	PYC	PYT	PIC	PIB	PIT
N(11)···O(8^{ii})	2.697(7)	2.674(5)	2.674(10)	2.687(8)	2.698(5)
N(11)–H(21)···O(8^{ii})	174(6)	170(4)			175(4)
C(12)–N(11)···O(8^{ii})	112.5(4)	113.8(3)	108	109	108.7(4)
C(15)–N(11)···O(8^{ii})	111.2(4)	112.2(3)	106	108	108.1(4)
C(7^{ii})–O(8^{ii})···N(11)	111.0(4)	113.6(3)	112	111	110.2(3)
N(11)···O(9)	2.730(7)	2.738(5)	2.722(11)	2.762(9)	2.766(6)
N(11)–H(20)···O(9)	168(5)	175(4)			161(4)
C(12)–N(11)···O(9)	103.2(4)	104.3(3)	102	101	101.0(4)
C(15)–N(11)···O(9)	116.0(4)	112.9(3)	124	123	122.2(4)
O(8^{ii})···N(11)···O(9)	105.4(2)	107.1(2)	107	105	105.2(3)
Angle between N(11)···O(9) bond and the 2_1 axis along which the bond extends	16	19	22	21	21
Angles between the plane perpendicular to the 2_1 axis and					
N(11)···O(8^{ii}) bond, δ_1	5	−3	3	2	2
C(7)···X(10) axis, δ_2	4	−2	3	4	4
carboxylate group plane, δ_3	56	53	56	55	55
benzene ring plane, δ_4	54	44	48	48	47

ribbons are concerned with the atoms in the pyrrolidine ring as seen from Table 4. However, the contacts around C(13) in the ring are rather loose; the closest being C(13)···C(1^{iii}) 3.866(15) Å in PYC, and C(13)···C(6^{viii}) 3.780(9) Å in PYT.

Geometry of the Hydrogen Bonds. The geometry in PYC and PYT is summarized in Table 6, along with that in the piperidinium compounds. In all these crystals the hydrogen bond N(11)···O(8^{ii}) lies nearly perpendicular to the twofold screw axis along which the ribbon extends, as seen in δ_1, and the bond N(11)···O(9) makes a constant angle of about 20° with the twofold screw axis. Thus the angle O(8^{ii})···N(11)···O(9) is near to the regular tetrahedral angle. The N(11)···O(8^{ii}) bond is shorter and hence stronger than the N(11)···O(9) bond. The former associates with the nearly tetrahedral C–N···O and C–O···N angles, and with linear N–H···O angle. Dihedral angle, δ_3, between the carboxylate group and the plane perpendicular to the twofold screw axis remains almost constant throughout the compounds, and the long axis of the acid anion lies nearly on the plane as seen from δ_2 in Table 6.

Morphotropism. In the structures of PYC, PYT and the piperidinium compounds many contacts between the ribbons are concerned with the atoms of the base moiety. Thus the effect of ring size of the bases is reflected in the thickness of the ribbons, hence in the cell dimension along ***a*** for PYC and ***c*** for PYT. The values for the pyrrolidinium compounds are smaller than those for the piperidinium compounds. Furthermore, the angle of the long axis of the acid anion with (010) in PYC, 70°, is widened from 64—61° in the piperidinium compounds. This is also the case for the corresponding angle with (100) in PYT, the angle here being 75°.

It has been shown[2] that in the piperidinium compounds the contacts around the *p*-substituents are rather loose and hence the crystal structures are little affected by the bulkiness of the substituents. On the other hand, in PYC the contacts become close as an effect of the ring size mentioned above: Cl···H(26^{vi}) 2.77 Å, Cl···H(16^{vii}) 2.97 Å. Therefore, a mode of stacking of the sheets seems to be more largely affected by the bulkiness of the substituents in the pyrrolidinium compounds than in the piperidinium compounds. The reason why PYT crystallizes in a subgroup of the space group Pbca is the disappearance of the c-glide plane by the cooperative effects of the bulkiness of the methyl group and the thickness of the ribbon.

Molecular Structures. (*a*) *Benzoate Ions*: The benzene rings are planar within 0.015 Å, as shown in Table 7. The dihedral angle between the ring and the carboxylate group is 1.9° for PYC, while is 9.7° for PYT. This difference is mainly due to the difference in δ_4 in Table 6. The inner angle at C(4) for PYT is smaller than the sp^2 angle as found in PIT and in many methyl substituted benzene derivatives.[7,8]

(*b*) *Pyrrolidinium Ions*: The torsion angles, χ_i (mod. 5), of the five bonds of the pyrrolidine rings are listed in Table 8. The χ_i in PYC corresponds to χ_{i-1} in PYT, being close to 0° for $i=3$. Hence, in PYC C(12) deviates from the plane through the other non-hydrogen atoms in the ring, while N(11) deviates in PYT, as seen from Table 7. Thus, the pyrrolidine ring in PYC and PYT take an approximate C_s (envelope) symmetry, the mirror plane passing through C(12) in PYC and N(11) in PYT.

In both PYC and PYT the C–C–C angles in the rings are slightly larger than the C–C–N angles. The C–N–C angles are close to the sp^3 angle. The C(13)–C(14) bonds are shortened by the unusually large vibrational motions of C(13) in the direction perpendicular to the ring planes, as found in prolyl residues of some oligopeptides.[9]

Table 7. The least-squares planes and displacements (Å) of the atoms from the planes $X=ax+cz\cos\beta$, $Y=by$, $Z=cz\sin\beta$.

(I) Benzene ring

PYC: $-0.7747X+0.2375Y-0.5860Z+6.6943=0$

PYT: $0.0851X-0.7246Y+0.6839Z+0.3216=0$

	PYC	PYT
C(1)[a]	−0.0054	−0.0047
C(2)[a]	0.0147	−0.0027
C(3)[a]	−0.0112	0.0047
C(4)[a]	−0.0019	−0.0058
C(5)[a]	0.0112	−0.0047
C(6)[a]	−0.0073	0.0146
C(7)	0.0278	−0.0558
O(8)	−0.0358	−0.2831
O(9)	0.0378	0.0749
X(10)	0.0020	0.0068

(II) Carboxylate group

PYC: $-0.7904X+0.2492Y-0.5596Z+6.4968=0$

PYT: $-0.0449X+0.6035Y-0.7961Z+1.0003=0$

C(1)[a]	−0.0060		0.0032
C(7)[a]	0.0221		−0.0146
O(8)[a]	−0.0076		0.0046
O(9)[a]	−0.0075		0.0072

(III) Pyrrolidine ring

PYC: $-0.4617X-0.5114Y-0.7247Z+5.0955=0$

PYT: $-0.3593X-0.8980Y+0.2539Z+4.3613=0$

PYC			PYT
N(11)[a]	−0.0088	N(11)	−0.4110
C(12)	0.2914	C(12)[a]	−0.0119
C(13)[a]	0.0098	C(13)[a]	0.0191
C(14)[a]	−0.0148	C(14)[a]	−0.0202
C(15)[a]	0.0138	C(15)[a]	0.0132

a) Atoms used for the calculation of the planes.

Table 8. The torsion angles (°) in the pyrrolidine rings

	PYC	PYT
χ_0: C(15)–N(11)–C(12)–C(13)	−19.9	26.0
χ_1: N(11)–C(12)–C(13)–C(14)	18.5	−13.7
χ_2: C(12)–C(13)–C(14)–C(15)	−9.9	−3.6
χ_3: C(13)–C(14)–C(15)–N(11)	−2.6	19.5
χ_4: C(14)–C(15)–N(11)–C(12)	14.0	−28.5

References

1) S. Kashio, Y. Sumida, and M. Haisa, *Acta Crystallogr., Sect. B*, **28**, 1374 (1972).

2) S. Kashino, *Acta Crystallogr., Sect. B*, **29**, 1836 (1973)
3) S. Kashino, K. Kanei, and S. Hasegawa, *Bull. Chem. Soc. Jpn.*, **45**, 1247 (1972).
4) A list of structure factors has been deposited at the Chemical Society of Japan (Document No. 7819).
5) "International Tables for X-Ray Crystallography," Vol. III, Kynoch Press, Birmingham (1962), p. 202.
6) "The Universal Crystallographic Computing System-Osaka," The Computation Center, Osaka University. (1973).
7) A. Domenicano, A. Vaciago, and C. A. Coulson, *Acta Crystallogr., Sect. B*, **31**, 221 (1975).
8) M. Haisa, S. Kashino, Y. Matsuzaki, R. Kawai, and K. Kunitomi. *Acta Crystallogr., Sect. B*, **33**, 2449 (1977).
9) T. Ashida and M. Kakudo, *Bull. Chem. Soc. Jpn.*, **47**, 1129 (1974).

Charge-Transfer Character in the Intramolecular Hydrogen Bond: Vacuum Ultraviolet Spectra of Acetylacetone and Its Fluoro Derivatives

Hiroshi NAKANISHI, Hiroshi MORITA, and Saburo NAGAKURA

The Institute for Solid State Physics, The University of Tokyo, Roppongi, Minato-ku, Tokyo 106

(Received January 28, 1978)

Near and vacuum UV absorption spectra of trifluoroacetylacetone (TFAC) and hexafluoroacetylacetone (HFAC) were measured at room temperature in the vapor phase and in perfluorohexane in the 30000—80000 cm^{-1} region, together with a vacuum UV absorption spectrum of acetylacetone in the 60000—80000 cm^{-1} region. By the aid of the modified CNDO-CI calculation, each of the observed valence-shell transition bands was assigned to the π–π^*, π–σ^*, or σ–σ^* transition. The third σ–σ^* bands observed at 65200 cm^{-1} for acetylacetone, at 78000 cm^{-1} for TFAC, and at 70400 cm^{-1} for HFAC were concluded to be rich in the CT character pertinent to hydrogen bond. In particular, the third σ–σ^* band of HFAC was found to be the CT band pertinent to hydrogen bonding in the sense that the contribution of the CT configuration to the excited state amounts to 67.4%.

Importance of the charge-transfer (CT) mechanism in hydrogen bond has been recognized by many authors from theoretical[1-7] and experimental[8-10] points of view. The CT mechanism can strongly be supported by the observation of the CT band pertinent to hydrogen bond.[11] The CT character of intramolecular hydrogen bond in the ground and excited electronic states was investigated for the hydrogen maleate anion;[12,13] the theoretical and experimental results indicated that the first π-π^* band which is rich in the CT character pertinent to the hydrogen bond is covered by the strong second π-π^* band at 210 nm.[13]

The enol forms of acetylacetone, trifluoroacetylacetone (TFAC), and hexafluoroacetylacetone (HFAC) have a strong intramolecular hydrogen bond with the O···O distance of 2.38—2.55 Å as revealed from X-ray diffraction[14] and gas-phase electron diffraction studies.[15,16] In a previous paper,[17] we reported the electronic structures and spectra of the keto and enol forms of acetylacetone in the 30000—61000 cm^{-1} region, and discussed the CT character of the intramolecular hydrogen bond of the enol form. Concerning the electronic structures and spectra of the fluoroacetylacetones, only a few studies have been made.[18-20]

Our previous study[17] of the electronic structure and spectrum of acetylacetone led us to the expectation that a band rich in the CT character might appear in a higher energy region than 61000 cm^{-1}. In the present paper, we extend the spectral region to 80000 cm^{-1} in the vacuum ultraviolet (VUV) region and measure the absorption spectra of acetylacetone in the vapor phase and of TFAC and HFAC in the vapor phase and in perfluorohexane. From analysis of the experimental results by the modified CNDO-CI method[21] and the configuration analysis method,[22] the nature of the valence-shell transition and Rydberg excitation bands is discussed, special attention being paid to the identification of the CT band pertinent to the intramolecular hydrogen bond.

Experimental

Materials. TFAC (Dotait G.R. Grade) and HFAC (Dotait G. R. Grade) were purified by repeating vacuum distillation three times immediately before use. Acetylacetone and perfluorohexane were purified in the same way as reported previously.[17]

Measurement. Near UV (30000—50000 cm^{-1}) absorption spectra were measured with a Cary recording spectrophotometer Model 14. VUV (50000—80000 cm^{-1}) absorption spectra were measured with a Johnson-Onaka type VUV spectrophotometer,[23] the sample chamber and detector system of which were modified as shown in Fig. 1. A hot cathode deuterium discharge lamp and Tanaka type xenon and krypton continuum lamps driven with microwave excitation (2450 MHz) were used as VUV light sources. Cells with MgF_2 or LiF windows of 5—10 cm light path lengths and a 0.01 cm quartz cell were used for the measurement in the vapor phase and in the solution, respectively. The vapor pressure of the sample was regulated with a cryogenic bath at various temperatures.

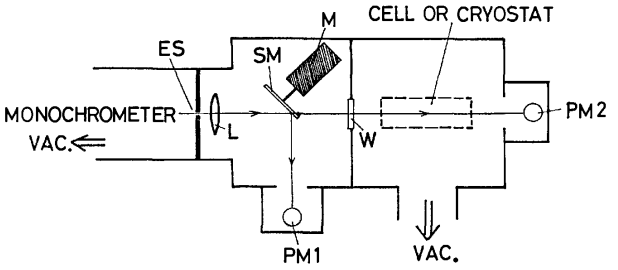

Fig. 1. Schematic diagram of the sample chamber and detector system of the VUV spectrophotometer. ES; Exit slit, L; MgF_2 lens (f=60 mm), SM; rotating sector mirror, M; oilless motor, W; MgF_2 window, PM 1 and 2; photomultipliers (HTV R106) coated with sodium salicylate.

Theoretical

The modified CNDO-CI method[21] was applied to the enol forms of acetylacetone, TFAC, and HFAC to investigate the valence-shell transitions. The semiempirical parameters of H, C, and O atoms were the same as reported previously.[17,21] The parameters of F atom were adopted as follows; the one-center Coulomb repulsion integral, γ_F=19.36 eV, the bonding parameter, β_F^0=−40.0 eV, and the $(I+A)/2$ values, 32.772 eV for the 2s AO, and 11.580 eV for the 2p AO. Preliminary calculations for such fluorinated molecules as carbon

tetrafluoride, carbonyl fluoride, trifluoroacetoaldehyde, and trifluoroacetic acid with the use of these parameters showed that the calculated transition energies and oscillator strengths agree well with the observed values. In the configuration interaction (CI) treatment of TFAC and HFAC, 40 singly excited π-π^* and σ-σ^* configurations and 40 singly excited π-σ^* and σ-π^* configurations were taken into account.

The actual calculations were made for two different geometrical structures, symmetrical and asymmetrical ones. Symmetrical molecular structures of TFAC and HFAC were taken from the results of gas-phase electron diffraction studies,[15] the linear symmetrical intramolecular hydrogen bond, O···H···O being assumed, and asymmetrical molecular structures were taken from the results by nonempirical calculations,[24,25] a non-linear asymmetrical intramolecular hydrogen bond being taken from the X-ray diffraction study.[26]

The configuration analysis was applied to the third σ-σ^* excited state (calculated at 9.02 eV)[17] of the enol form of acetylacetone. The procedure for the analysis was described in detail in the previous paper.[17]

Results and Discussion

The VUV Absorption Spectrum of Acetylacetone. Figure 2 shows the VUV spectrum in the 50000—80000 cm^{-1} region measured with acetylacetone in the vapor phase at room temperature. Since acetylacetone predominantly exists as the enol form in the vapor phase (96.2% at 20 °C),[17] the spectrum in Fig. 2 is ascribed to the enol form. We can see from Fig. 2 that strong bands appear at 65200 cm^{-1} (8.08 eV) and $\approx$79000 cm^{-1} ($\approx$9.8 eV) and shoulders at $\approx$60000 cm^{-1} ($\approx$7.4 eV) and $\approx$71000 cm^{-1} ($\approx$8.8 eV). Table 1 shows theoretical values of the transition energies and oscillator strengths of the valence-shell transition bands, together with the observed values (for the theoretical and observed results below 8 eV, see Table 1 in Ref. 17). From the comparison between the observed and calculated results, the strong 8.08 eV band (oscillator strength, $f\approx0.5$) can safely be assigned to the third σ-σ^* transition (calculated at 9.02 eV) because of its large oscillator strength among the bands calculated in 7.5—10.0 eV region. The other three observed bands at $\approx$7.4 eV, $\approx$8.8 eV, and $\approx$9.8 eV can be assigned to the third π-π^* transition (calculated at 8.46 eV), the fourth σ-σ^* transition (calculated at 9.94 eV), and the fourth π-π^* transition (calculated at 10.15 eV), respectively.

Table 1. Transition energies ($^1\Delta E$(eV)) and oscillator strengths (f) observed and calculated for some higher excited states of the enol form of acetylacetone[a]

Assignment	Obsd[b]		Calcd		Main config.[c]
	$^1\Delta E$	f	$^1\Delta E$	f[d]	
σ(n)-σ^*			8.38	0.002(x)	20—23
π-π^*	$\approx$7.4	$\approx$0.1	8.46	0.120(y)	17—21
σ-π^*			8.58	0.004(z)	(16,13)—21
π-σ^*			8.60	0.009(z)	19—26
σ(n)-σ^*			8.93	0.022(y)	20—(27, 24)
π-σ^*			9.00	0	19—(27, 24)
σ(n)-σ^*	8.08	$\approx$0.5	9.02	0.685(x)	{20—26 {14—21
σ-π^*			9.06	0	15—21
π-σ^*			9.78	0.019(z)	19—(28, 23, 25)
σ(n)-σ^*	$\approx$8.8		9.94	0.045(x)	20—(25, 23)
σ(n)-σ^*			10.04	0.006(y)	20—(27, 24)
π-π^*	$\approx$9.8		10.15	0.050(x)	{14—21 {20—26
σ-π^*			10.57	0	16—22
σ-π^*			10.69	0.001(z)	(18, 15)—22

a) For lower excited states ($\leq$8 eV), see Table 1 in Ref. 17. b) Observed value in the vapor phase. c) Main electron configurations of the respective excited states are shown. (i,j)-k denotes the singly excited configurations, i-k and j-k, and i-(k,l), the singly excited configurations, i-k and i-l. The shapes of MO's are shown in Fig. 5 in Ref. 17. d) The direction of the transition moment is shown in the parentheses, the x-axis being taken to be parallel to the O···H···O bond within the molecular (x-y) plane.

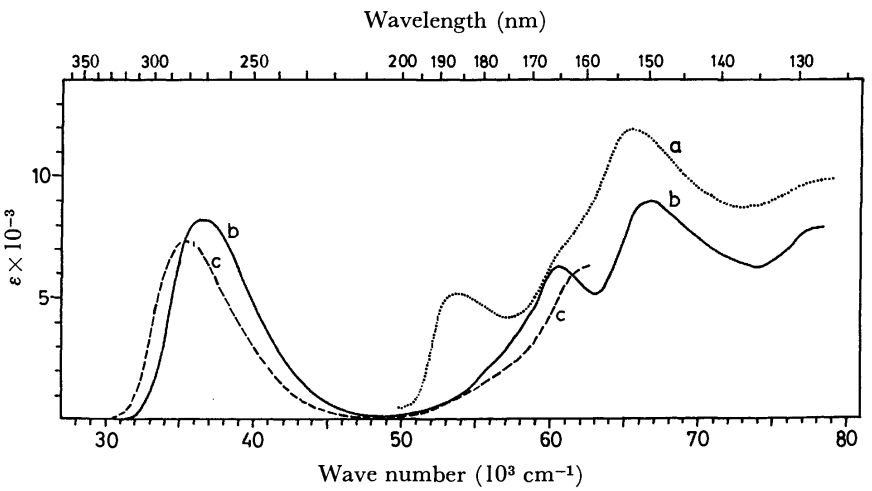

Fig. 2. Near and vacuum UV absorption spectra measured with (a) acetylacetone in the vapor phase, (b) TFAC in the vapor phase, and (c) TFAC in perfluorohexane at room temperature.

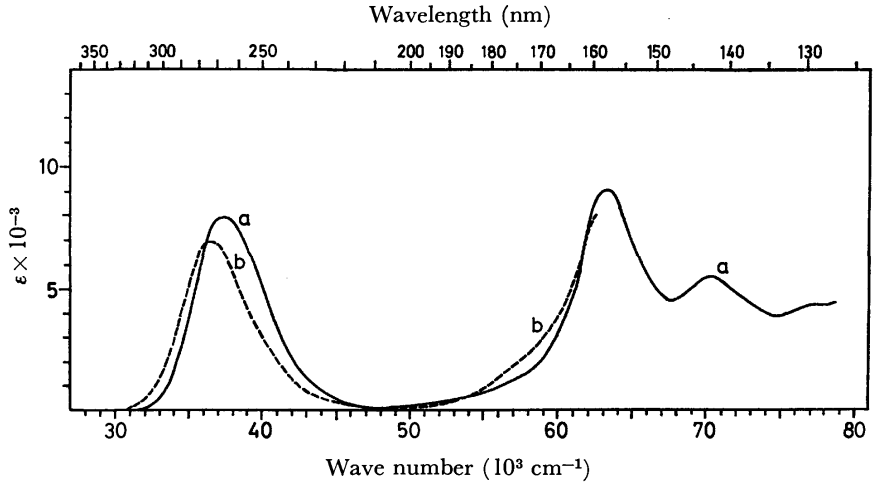

Fig. 3. Near and vacuum UV absorption spectra of HFAC measured (a) in the vapor phase and (b) in perfluorohexane at room temperature.

Electronic Absorption Spectra of TFAC and HFAC. Near and vacuum UV absorption spectra in the 30000—80000 cm^{-1} region measured with TFAC and HFAC at room temperature are shown in Figs. 2 and 3, respectively. As pointed out by the NMR studies,[27,28] substitution of the methyl group(s) in acetylacetone by the more electronegative trifluoromethyl group(s) preponderates the enol tautomer in the keto-enol equilibrium; TFAC and HFAC exist almost completely (95—100%) as the enol form in the vapor phase and in nonpolar solvents at room temperature. Therefore, the observed spectra shown in Figs. 2 and 3 are ascribed to the enol form.

The TFAC vapor spectrum in Fig. 2 has absorption peaks at 36670 cm^{-1} (4.55 eV), 60600 cm^{-1} (7.51 eV), 66700 cm^{-1} (8.27 eV), and 78000 cm^{-1} (9.7 eV), and shoulders at ≈56000 cm^{-1} (≈6.9 eV) and ≈71000 cm^{-1} (≈8.8 eV). The HFAC vapor spectrum in Fig. 3 has absorption peaks at 37450 cm^{-1} (4.64 eV), ≈57000 cm^{-1} (≈7.1 eV) (as a weak shoulder), 63700 cm^{-1} (7.90 eV), 70400 cm^{-1} (8.73 eV), and ≈77000 cm^{-1} (≈9.5 eV).

Comparison between the spectra in the vapor phase and in the solution in Fig. 2 shows that the 60600 cm^{-1} band of TFAC in the vapor phase disappears in the solution. This means that the band is assigned to the Rydberg excitation band.[29] The Rydberg excitation energy satisfies the following formula;[29]

$$h\nu = I_p - 109737/(n-\delta)^2, \quad (1)$$

where $h\nu$ is the excitation energy (cm^{-1}), I_p is the ionization potential (cm^{-1}), n is the principal quantum number, and δ is the quantum defect. By the use of the first I_p value (9.93 eV) determined by photoelectron spectroscopy,[30] the δ value of the 60600 cm^{-1} band was determined to be 0.63, corresponding to $n=3$. This strongly suggests that the band is due to the transition to the 3p Rydberg orbital from the highest occupied π orbital. The band intensity is of the same order of magnitude as the π-3p Rydberg band of acetylacetone[17] observed at 53300 cm^{-1}. The corresponding Rydberg transition band is expected to appear at ≈67000 cm^{-1} for HFAC from the first ionization potential of 10.72 eV.[30] But it is covered by strong valence-shell transition bands and cannot be observed.

Theoretical transition energies and oscillator strengths of the valence-shell transitions of the enol forms of TFAC and HFAC were calculated on the basis of two kinds of (*i.e.*, symmetrical and asymmetrical) molecular structures. The results for lower excited states of both the TFAC and HFAC molecules are rather insensitive to

Table 2. Transition energies ($^1\Delta E$(eV)) and oscillator strengths (f) observed and calculated for the enol form of trifluoroacetylacetone

Assignment	Obsd[a]		Calcd[b]		Main config.[c]
	$^1\Delta E$	f	$^1\Delta E$	f[d]	
σ(n)–π*			2.90	0.000$_6$(z)	29—30
π–π*	4.55	0.18	4.75	0.162 (x$_y$)[e]	28—30
σ(n)–π*			5.17	0.000(z)	29—31
σ–π*			7.35	0.000$_5$(z)	26—30
π–σ*	≈6.9	≈0.03	7.58	0.014(z)	28—32
π–π*	8.27	≈0.25	7.35	0.225(y$_x$)[f]	28—31
σ(n)–σ*			7.99	0.102(x$_y$)[e]	29—32
σ–π*			8.14	0.001(z)	28—30, 26—31
σ–π*			8.57	0.016(z)	27—30
π–σ*			8.67	0.004(z)	28—34
π–σ*			8.78	0.017(z)	28—33
σ(n)–σ*	≈8.8		8.97	0.259(x$_y$)[e]	29—34, 29—33
σ–π*			9.21	0.009(z)	24—30, 23—30
σ(n)–σ*	9.7		9.34	0.372(x)	29—33, 29—34
π–σ*			9.57	0.014(z)	28—36
π–π*			9.75	0.310(y)	25—30

a) Observed value in the vapor phase. b) Calculated value for the symmetrical molecular structure of the enol form. c) Main electron configurations of the respective excited states are shown. d) The direction of the transition moment is shown in the parentheses, the x-axis being taken to be parallel to the O···H···O bond within the molecular (x-y) plane as is shown in Fig. 8(a). e) y-Component of the transition moment contributes appreciably to x-component. f) x-Component of the transition moment contributes appreciably to y-component.

the molecular structures, and from semiquantitative view-points, the same conclusions are derived concerning the assignments and characterizations of the observed bands.

Table 2 shows the theoretical results calculated for the symmetrical molecular structure of the enol form of TFAC compared with the observed values. The 4.55 eV band can safely be assigned to the first π-π^* transition (calculated at 4.75 eV) and corresponds to the 4.72 eV band of acetylacetone. The strong 61700 cm^{-1} (7.65 eV) band in the solution is assigned to the second π-π^* transition (calculated at 7.35 eV). In the vapor phase, the second π-π^* band shifts to the shorter wavelengths. The theoretical result predicts that the weak band at $\approx$6.9 eV can be assigned to the first π-σ^* transition (calculated at 7.58 eV), and that the strong 8.27 eV band in the vapor phase is composed of the second π-π^* transition and the first σ-σ^* transition (calculated at 7.99 eV). Moreover, from the comparison between the observed and calculated results, the $\approx$8.8 eV band and the 9.7 eV band are assigned to the second (calculated at 8.97 eV) and third (calculated at 9.34 eV) σ-σ^* transitions, respectively.

Table 3 shows the theoretical results of the valence-shell transitions calculated for the symmetrical molecular structure of the enol form of HFAC, together with the observed values. The 4.64 eV band can be assigned to the first π-π^* transition (calculated at 4.48 eV). The weak band at $\approx$7.1 eV in the vapor phase is also observed in perfluorohexane, and is assigned to the first π-σ^* transition (calculated at 7.59 eV). The strong 7.90 eV band is ascribed to the superposition of the second π-π^* (calculated at 7.29 eV) and first σ-σ^* (calculated

TABLE 3. TRANSITION ENERGIES ($^1\Delta E$(eV)) AND OSCILLATOR STRENGTHS (f) OBSERVED AND CALCULATED FOR THE ENOL FORM OF HEXAFLUOROACETYLACETONE

Assignment	Obsd[a]		Calcd[b]		Main config.[c]
	$^1\Delta E$	f	$^1\Delta E$	f[d]	
$\sigma(n)$-π^*			2.65	0.000_8(z)	38—39
π-π^*	4.64	0.20	4.48	0.124(x)	37—39
$\sigma(n)$-π^*			4.85	0	38—40
σ-π^*			7.31	0	35—39
π-σ^*	$\approx$7.1	$\approx$0.02	7.59	0.011(z)	37—41
π-π^*	7.90	$\approx$0.3	7.29	0.207(y)	37—40
$\sigma(n)$-σ^*			7.54	0.146(x)	38—41
σ-π^*			7.91	0.003(z)	34—39
σ-π^*			8.09	0	36—39 38—40
$\sigma(n)$-σ^*			8.17	0.004(y)	38—42
π-σ^*			8.44	0	37—42
π-σ^*			8.55	0.007(z)	37—43
$\sigma(n)$-σ^*	8.73	$\approx$0.15	8.87	0.347(x)	38—43
σ-π^*			8.97	0.027(z)	28—39 35—40 34—39
π-σ^*			9.29	0.032(z)	37—44
$\sigma(n)$-σ^*			9.44	0.014(y)	38—45
$\sigma(n)$-σ^*	$\approx$9.5		9.52	0.087(x)	38—44
π-π^*			9.83	0.235(y)	33—39

a) Observed value in the vapor phase. b) Calculated value for the symmetrical molecular structure of the enol form. c) Main electron configurations of the respective excited states are shown. d) The direction of the transition moment is shown in the parentheses, the x-axis being taken to be parallel to the O···H···O bond within the molecular (x-y) plane as is shown in Fig. 8(b).

TABLE 4. RESULTS OF THE CONFIGURATION ANALYSIS (WEIGHTS) FOR THE GROUND AND THE THIRD σ–σ^* EXCITED STATES OF THE ENOL FORM OF ACETYLACETONE[a]

	Structure	Reference Configuration[b,c]	State	
			Ground	Third σ–σ^*[d]
I	(OH-O$^+$)+(O$^+$H-O)[e]	i,j-36, 36	0.1101	—
II	(OH-O$^+$)−(O$^+$H-O)	i,j-36, 36	—	0.0999
III	(O–H···O)+(O···H–O)	i-36	0.4166	—
		i-36+π–π^*[f]	0.0194	0.1588
		i-36+σ–σ^*[f]	0.0153	0.1065
		(Total for sym. covalent structure)	(0.4513)	(0.2653)
IV	(O–H···O)−(O···H–O)	i-36	—	0.1892
		i-36+π–π^*[f]	—	0.0088
		i-36+σ–σ^*[f]	—	0.0061
		(Total for antisym. covalent structure)	—	(0.2041)
V	$O^{-1/2}H^+O^{-1/2}$	G^0[g]	0.3942	—
		π–π^*[h]	0.0184	0.1503
		σ–σ^*[h]	0.0153	0.1098
		i,j-k,l	0.0013	0.0190
		(Total for $O^{-1/2}H^+O^{-1/2}$ structure)	(0.4292)	(0.2791)
		Total	0.9906	0.8484
II+IV	Total for CT structure		—	0.3040

a) The results for the first π–π^* and the first σ–σ^* excited states are shown in Table 3 of Ref. 17. b) i and j denote the 20 occupied MO's of the anion, and k and l, the 15 vacant MO's of the anion. The 1s orbital of the hydrogen-bonded hydrogen is numbered as the 36th vacant orbital. c) i–k and i, j–k,l denote the singly and doubly excited reference configurations, respectively. d) The strong band observed at 8.08 eV in Fig. 2. e) The ionic structure, $((\underline{O^+H^-O})+(\underline{OH^-O^+}))$, is also involved. f) Doubly excited configurations, i, j–k, 36.

g) The ground reference configuration coincides with the ground state of the anion. h) Singly excited configurations, i–k.

at 7.54 eV) transitions. The shift to the longer wavelengths of the second π-π^* and first σ-σ^* bands of HFAC compared to the corresponding bands of TFAC is consistent with the theoretical predictions in Tables 2 and 3. The 8.73 eV band is safely assigned to the third σ-σ^* transition (calculated at 8.87 eV). The $\approx$9.5 eV band may tentatively be assigned to the fifth σ-σ^* transition (calculated at 9.52 eV).

Electronic Structures of the Intramolecular Hydrogen Bonds of Acetylacetone, TFAC, and HFAC. The previous paper[17] shows that the CT configuration characteristic of the intramolecular hydrogen bond corresponds to the one electron excitation from the nonbonding orbital to the antibonding orbital in the hydrogen bond. In the case of acetylacetone, the 20—26 configuration is the CT configuration (see Fig. 5 in Ref. 17.), and contributes mainly to the first π-π^* band (observed at 4.72 eV) (9.8%), the third σ-σ^* band (observed at 8.08 eV) (40.3%), and the fourth π-π^* band (observed at $\approx$9.8 eV) (16.3%). In acetylacetone, the third σ-σ^* band is richest in the CT character.

The CT character in the intramolecular hydrogen bond of acetylacetone was investigated quantitatively by the configuration analysis method; the result for the third σ-σ^* band is tabulated in Table 4, together with the result for the ground state (for the purpose of comparison, also see Table 3 in Ref. 17). In this table, the CT structure corresponds to the antisymmetric covalent structure IV and antisymmetric ionic structure II. Both structures contribute considerably (30.4%) to the third σ-σ^* excited state, revealing us that the band is rich in the CT character pertinent to the hydrogen bond.

Figures 4 and 5 show the energy levels of TFAC and HFAC, respectively, calculated by the modified CNDO-CI method for some low-lying π-π^* and σ-σ^* excited states of the enol form with the symmetrical molecular structures. In the figures, i–j represents a singly excited configuration caused by the one-electron excitation from

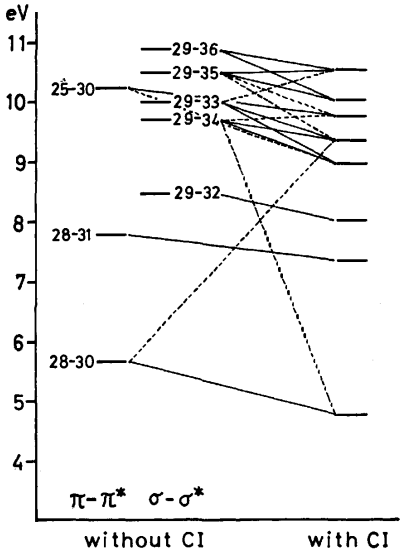

Fig. 4. Energy levels calculated with and without CI treatment for some lower π–π^* and σ–σ^* excited states of the enol form of TFAC.

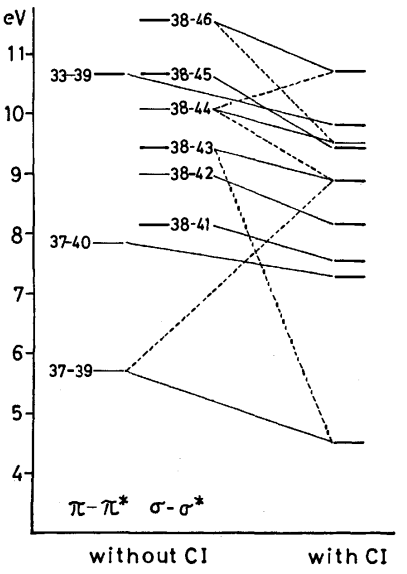

Fig. 5. Energy levels calculated with and without CI treatment for some lower π–π^* and σ–σ^* excited states of the enol form of HFAC.

the i-th occupied MO to the j-th vacant MO. From the shapes of the MO's of TFAC and HFAC (see Figs. 6 and 7), the CT configuration characteristic of the intramolecular hydrogen bond is the 29-34 configuration for TFAC and the 38-43 configuration for HFAC. As for TFAC, the 29-34 CT configuration interacts significantly with the 29-33 σ-σ^*, 25-30 π-π^*, and 28-30 π-π^* configurations, and contributes significantly to the first π-π^* (calculated at 4.75 eV), the second σ-σ^*

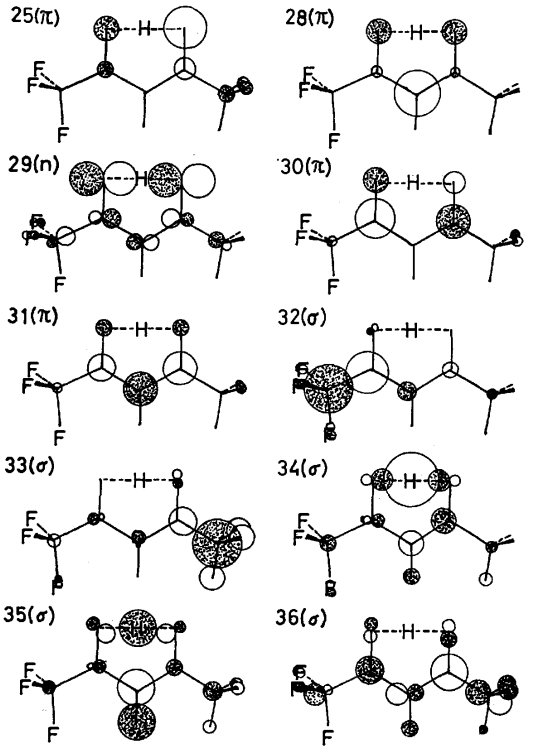

Fig. 6. Schematic shapes of some occupied and vacant MO's of the enol form of TFAC. The 29th MO is the highest occupied one.

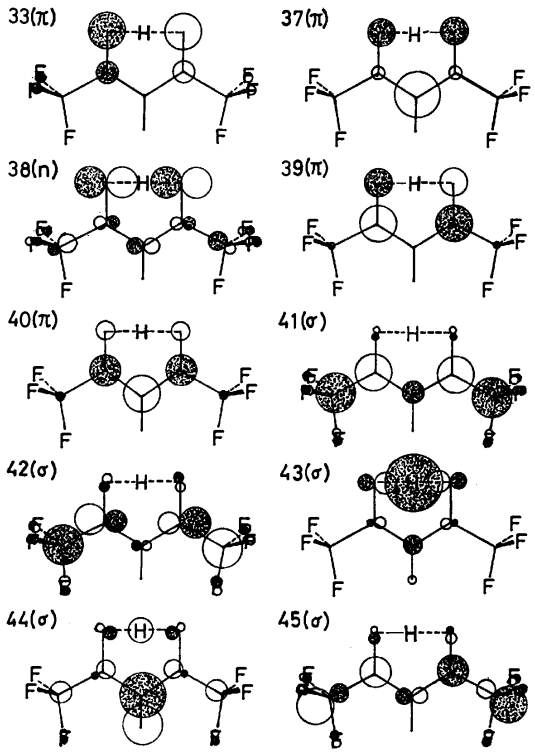

Fig. 7. Schematic shapes of some occupied and vacant MO's of the enol form of HFAC. The 38th MO is the highest occupied one.

(calculated at 8.97 eV), the third σ-σ* (calculated at 9.34 eV), and the third π-π* (calculated at 9.75 eV) excited states. The first π-π* band (observed at 4.55 eV) is mainly composed of the 28-30 π-π* (85.1%) and 29-34 CT (5.9%) configurations; the second σ-σ* band (observed at ≈8.8 eV), of the 29-34 CT (33.7%), 29-33 σ-σ* (31.8%), and 25-30 π-π* (11.4%) configurations; and the third σ-σ* band (observed at ≈9.7 eV), of the 29-33 σ-σ* (35.2%), 29-34 CT (22.0%), 29-35 σ-σ* (10.2%), and 28-30 π-π* (4.8%) configurations. The theoretical results calculated by the modified CNDO-CI method predict that the second and third σ-σ* bands are rich in the CT character pertinent to the hydrogen bond in TFAC.

In the case of HFAC, the 38-43 CT configuration interacts significantly with the 37-39 π-π* and 38-44 σ-σ* configurations, and contributes to the first π-π* (calculated at 4.48 eV) and the third σ-σ* (calculated at 8.87 eV) excited states. The first π-π* band (observed at 4.64 eV) is composed of the 37-39 π-π* (83.6%) and 38-43 CT (7.2%) configurations, and the third σ-σ* band (observed at 8.73 eV), of the 38-43 CT (67.4%), 38-44 σ-σ* (5.9%), and 37-39 π-π* (5.5%) configurations. The theoretical calculation predicts that the third σ-σ* band is the CT band characteristic of the intramolecular hydrogen bond of HFAC. It is noteworthy that the first π-π* bands of acetylacetone, TFAC, and HFAC observed at 4.5—4.7 eV have the CT character pertinent to the hydrogen bond by 5—10%.

Electron Densities of TFAC and HFAC. Figure 8 shows electron densities in the ground state calculated for the symmetrical molecular structures of the enol forms of TFAC and HFAC. By substituting the methyl

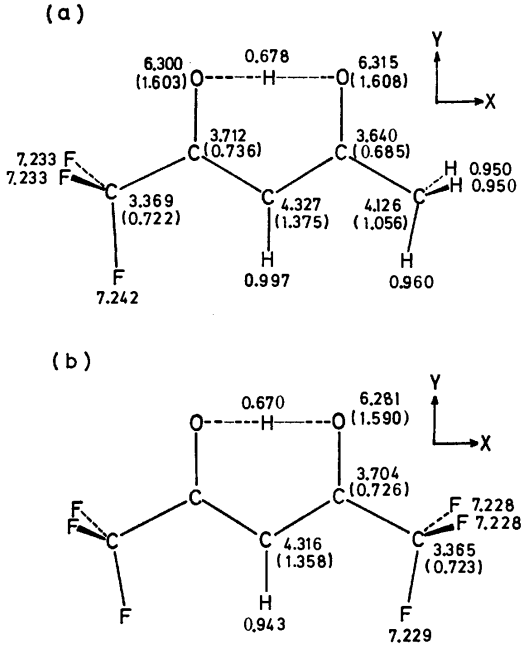

Fig. 8. Total and π-(in parentheses) electron densities calculated for the ground states of (a) TFAC and (b) HFAC.

group(s) by the trifluoromethyl group(s), the σ-electron density on the hydrogen-bonded hydrogen atom slightly decreases, and the π-electron densities increase on carbonyl carbon atoms with the decrease on oxygen atoms. The dipole moments of TFAC and HFAC were calculated to be 3.42 and 0.69 D, respectively. The cancellation between the dipole moments in the carbonyl groups and in the trifluoromethyl groups is responsible for the small dipole moment of HFAC.

The authors are indebted to Dr. J. Nakamura, the Institute of Physical and Chemical Research, for her helpful advice in modifying the VUV instrument. This work was partially supported by a Grant-in-Aid for Scientific Research from the Ministry of Education.

References

1) K. Nukasawa, J. Tanaka, and S. Nagakura, *J. Phys. Soc. Jpn.*, **8**, 792 (1953).
2) H. Tsubomura, *Bull. Chem. Soc. Jpn.*, **27**, 445 (1954).
3) C. A. Coulson, *Research*, **10**, 149 (1957).
4) F. B. van Duijneveldt and J. N. Murrell, *J. Chem. Phys.*, **46**, 1759 (1967).
5) S. Bratož, "Advances in Quantum Chemistry," Vol. 3, ed by P. O. Löwdin, Academic Press, New York (1967), p. 209.
6) P. A. Kollman and L. C. Allen, *Chem. Rev.*, **92**, 283 (1972).
7) K. Morokuma, S. Iwata, and W. A. Lathan, "The World of Quantum Chemistry," ed by R. Daudel and B. Pullman, D. Reidel, Dordrecht, Holland (1974); H. Umeyama and K. Morokuma, *J. Am. Chem. Soc.*, **99**, 1316 (1977), and references cited therein.
8) H. Tsubomura, *J. Chem. Phys.*, **23**, 2130 (1955); *ibid.*, **24**, 927 (1956).
9) S. Nagakura and M. Gouterman, *J. Chem. Phys.*, **26**, 811 (1957).

10) H. Ratajczak, *J. Phys. Chem.*, **76**, 3000, 3999 (1972); H. Ratajczak and W. J. Orville-Thomas, *J. Chem. Phys.*, **58**, 911 (1973); H. Ratajczak, W. J. Orville-Thomas, and C. N. R. Rao, *Chem. Phys.*, **17**, 197 (1976), and references cited therein.
11) R. S. Mulliken and W. B. Person, "Molecular Complexes," Wiley-Interscience, New York (1969).
12) S. Nagakura, *J. Chim. Phys.*, **61**, 217 (1964).
13) H. Morita, K. Fuke, and S. Nagakura, *Bull. Chem. Soc. Jpn.*, **50**, 645 (1977).
14) J. P. Schaefer and P. J. Wheatley, *J. Chem. Soc., A*, **1966**, 528.
15) A. L. Andreassen, D. Zebelman, and S. H. Bauer, *J. Am. Chem. Soc.*, **93**, 1148 (1971); A. L. Andreassen and S. H. Bauer, *J. Mol. Struct.*, **12**, 381 (1972).
16) A. H. Lowrey, C. George, P. D'Antonio, and J. Karle, *J. Am. Chem. Soc.*, **93**, 6399 (1971).
17) H. Nakanishi, H. Morita, and S. Nagakura, *Bull. Chem. Soc. Jpn.*, **50**, 2255 (1977).
18) R. N. Haszeldine, W. K. R. Musgrave, F. Smith, and L. M. Turton, *J. Chem. Soc.*, **1951**, 609.
19) E. M. Larsen, G. Terry, and J. Leddy, *J. Am. Chem. Soc.*, **75**, 5107 (1953).
20) R. L. Belford, A. E. Martell, and M. Calvin, *J. Inorg. Nucl. Chem.*, **2**, 11 (1956).
21) H. Morita, K. Fuke, and S. Nagakura, *Bull. Chem. Soc. Jpn.*, **49**, 922 (1976).
22) H. Baba, S. Suzuki, and T. Takemura, *J. Chem. Phys.*, **50**, 2078 (1968).
23) K. Kaya and S. Nagakura, *J. Mol. Spectrosc.*, **44**, 279 (1972).
24) J. E. Del Bene and W. L. Kochenour, *J. Am. Chem. Soc.*, **98**, 2041 (1976).
25) G. Karlström, B. Jönsson, B. Roos, and H. Wennerström, *J. Am. Chem. Soc.*, **98**, 6851 (1976).
26) D. E. Williams, *Acta Crystallogr.*, **21**, 340 (1966).
27) J. L. Burdett and M. T. Rogers, *J. Am. Chem. Soc.*, **86**, 2105 (1964).
28) R. L. Lintvedt and H. F. Holtzclaw, Jr., *J. Am. Chem. Soc.*, **88**, 2713 (1966).
29) M. B. Robin, "Higher Excited States of Polyatomic Molecules," Vol. 1, Academic Press, New York (1974).
30) C. Nishijima, H. Nakayama, T. Kobayashi, and K. Yokota, *Chem. Lett.*, **1975**, 5.

The Crystal and Molecular Structure of Oxydi(carboxymethyl)bis-(triphenylphosphine)palladium(II), [Pd($C_4H_4O_3$)(PPh_3)$_2$]

Yukio ZENITANI, Haruo TOKUNAN, Yasushi KAI, Noritake YASUOKA, and Nobutami KASAI*

Department of Applied Chemistry, Faculty of Engineering, Osaka University, Yamadakami, Suita, Osaka 565

(Received February 7, 1978)

The molecular structure of oxydi(carboxymethyl)bis(triphenylphosphine)palladium(II), [Pd($C_4H_4O_3$)(PPh_3)$_2$] has been determined by means of X-ray diffraction. The crystal belongs to the orthorhombic system, space group $P2_12_12_1$, with four formula units in a cell with dimensions of $a=16.320(2)$, $b=20.104(2)$, and $c=10.271(2)$ Å. $R=0.058$ for 4732 non-zero relfections. The feature of the structure is that the palladium atom is chelated by an acetic anhydride to form a six-membered ring [Pd–C=2.141(13) and 2.124(11) Å], and the palladium atom has a square-planar geometry.

Interesting studies on the synthesis and reactivity of a series of organopalladium complexes with the palladium–carbon σ-bond have been reported.[1-4] Stimulated by the stereochemical interests, X-ray molecular structures of [Pd($C_4H_4O_3$)(PPh_3)$_2$], [Pd($C_2H_2O_2$)(PPh_3)(py)],[2] [Pd(acac)$_2$(PPh_3)$_2$],[5] [Pd($C_6H_9O_3$)$_2$(MePy)$_2$][4], [PdCl($CH_2COCH_2COOCH_2Ph$)(Py)$_2$],[6] and [Pd(CH_2COOH)(acac)(PPh_3)][7] have been determined. This paper deals with the structure of [Pd($C_4H_4O_3$)(PPh_3)$_2$], of which preriminary result has been reported briefly.[2]

Experimental

Pale yellow, polyhedral crystal of [Pd($C_4H_4O_3$)(PPh_3)$_2$] were kindly supplied by Professor S. Kawaguchi and his co-workers of the Osaka City University. Preliminary X-ray work showed that the crystals belong to the orthorhombic system and that the space group is $P2_12_12_1$ (No. 16, absent reflections, $h00$; $h=2n+1$, $0k0$; $k=2n+1$, and $00l$; $l=2n+1$). Accurate unit-cell dimensions were determined by a least-squares fit using 2θ values of 20 strong reflections measured on a Rigaku automated, four-circle, single crystal diffractometer.

Crystal Data: $C_{40}H_{34}O_3P_2Pd$, *F. W.*=731.1, orthorhombic, space group, $P2_12_12_1$, $a=16.320(2)$, $b=20.104(2)$, $c=10.271(2)$ Å. $U=3369.8(8)$ Å^3, $D_m=1.41$ g·cm^{-3} (by flotation in aqueous solution of zinc iodide), $Z=4$, $D_c=1.44$ g·cm^{-3}, Mo $K\alpha_1$ ($\lambda=0.70926$ Å).

For the intensity measurement, a crystal with approximate dimensions of $0.18\times0.25\times0.30$ mm was used. Data were collected on the Rigaku diffractometer using graphite monochromatized Mo $K\alpha$ radiation. All data within a 2θ sphere of 60° ($\sin\theta/\lambda=0.70$) were measured using the θ-2θ scan technique. The integrated intensity was determined by scanning over the peak at a rate of 2°min^{-1} and subtracting the background obtained by averaging the two values measured for 10 s at both ends of a scan; the scan width of each reflection was $\Delta(2\theta)=(1.6+0.7\tan\theta_c)°$, where θ_c is the calcualated Bragg angle for Mo $K\alpha_1$ ($\lambda=0.70926$ Å). A total of 5482 independent reflections was collected, of which the number of non-zero reflections was 4732. The intensities of three standard reflections (060, 004, and 3,18,2) were measured periodically; no intensity decrease in these reflections was observed during the experiment. Usual Lorentz and polarization corrections were made, but the absorption correction was ignored ($\mu=6.73$ cm^{-1} for Mo $K\alpha$).

* To whom the correspondence should be addressed.

TABLE 1. FRACTIONAL ATOMIC COORDINATES (estimated standard deviations in parentheses)

	x	y	z
Pd	0.09161(3)	0.02528(3)	0.08560(6)
P(1)	0.0590(1)	−0.0859(1)	0.0541(2)
P(2)	−0.0334(1)	0.0597(1)	0.1767(2)
O(1)	0.2499(4)	0.1201(4)	−0.0230(10)
O(2)	0.3246(4)	0.0560(4)	0.1071(12)
O(3)	0.1476(5)	0.1845(3)	−0.0905(10)
C(1)	0.2087(5)	0.0054(5)	−0.0002(13)
C(2)	0.2664(5)	0.0583(5)	0.0371(12)
C(3)	0.1718(6)	0.1461(4)	−0.0095(13)
C(4)	0.1307(6)	0.1251(4)	0.1122(11)
C(11)	−0.0070(4)	−0.0959(4)	−0.0873(8)
C(12)	−0.0280(6)	−0.0391(5)	−0.1571(8)
C(13)	−0.0803(7)	−0.0434(6)	−0.2667(10)
C(14)	−0.1110(6)	−0.1075(7)	−0.3024(10)
C(15)	−0.0865(7)	−0.1646(6)	−0.2343(10)
C(16)	−0.0365(5)	−0.1594(5)	−0.1277(8)
C(21)	0.1424(4)	−0.1453(4)	0.0208(8)
C(22)	0.1677(5)	−0.1567(5)	−0.1078(9)
C(23)	0.2321(7)	−0.2006(5)	−0.1293(11)
C(24)	0.2686(7)	−0.2344(6)	−0.0270(13)
C(25)	0.2453(8)	−0.2206(7)	0.0971(14)
C(26)	0.1805(6)	−0.1774(6)	0.1223(10)
C(31)	0.0117(5)	−0.1241(4)	0.1970(7)
C(32)	−0.0557(5)	−0.1679(4)	0.1883(9)
C(33)	−0.0833(6)	−0.1996(4)	0.3011(9)
C(34)	−0.0460(6)	−0.1886(4)	0.4201(10)
C(35)	0.0198(5)	−0.1436(5)	0.4275(8)
C(36)	0.0475(5)	−0.1110(4)	0.3171(8)
C(41)	−0.1198(5)	0.0028(4)	0.2028(8)
C(42)	−0.1659(5)	−0.0182(4)	0.0939(10)
C(43)	−0.2320(5)	−0.0611(5)	0.1077(11)
C(44)	−0.2523(5)	−0.0839(5)	0.2326(12)
C(45)	−0.2080(6)	−0.0645(5)	0.3386(11)
C(46)	−0.1404(5)	−0.0206(5)	0.3277(8)
C(51)	−0.0135(5)	0.0945(4)	0.3383(8)
C(52)	0.0507(6)	0.0667(5)	0.4079(11)
C(53)	0.0658(7)	0.0884(6)	0.5372(11)
C(54)	0.0208(7)	0.1383(5)	0.5928(12)
C(55)	−0.0426(8)	0.1664(6)	0.5221(11)
C(56)	−0.0599(6)	0.1453(5)	0.3933(11)
C(61)	−0.0856(5)	0.1256(3)	0.0855(8)
C(62)	−0.1625(5)	0.1492(5)	0.1224(9)
C(63)	−0.1980(6)	0.2026(5)	0.0582(10)
C(64)	−0.1596(7)	0.2299(5)	−0.0502(11)
C(65)	−0.0858(7)	0.2036(4)	−0.0946(10)
C(66)	−0.0490(6)	0.1519(4)	−0.0263(9)

Solution and Refinement of the Structure

The structure was solved by the heavy atom method. The palladium and two phosphorus atoms were located from a three-dimensional Patterson function. All the remaining non-hydrogen atoms were located by successive Fourier syntheses. The structure was refined by the block-diagonal least-squares procedure. The HBLS V program[8] was used, the function minimized being $(|F_o|-k|F_c|)^2$, where k is a single scale factor. Several cycles of isotropic refinement reduced the R_1 factor ($R_1=\sum||F_o|-|F_c||/\sum|F_o|$) to 0.092 for non-zero reflections, and no abnormal thermal parameter was observed. Anisotropic thermal parameters were introduced for palladium and phosphorus atoms for several cycles of refinement, and then for all the non-hydrogen atoms. The difference synthesis, based on the final atomic parameters, did not reveal any hydrogen atoms. Finally,

Table 2. Anisotropic thermal parameters ($\times 10^4$) expressed in the form: $\exp\{-(\beta_{11}h^2+\beta_{22}k^2+\beta_{33}l^2+\beta_{12}hk+\beta_{13}hl+\beta_{23}kl)\}$ (estimated standard deviations in parentheses)

	β_{11}	β_{22}	β_{33}	β_{12}	β_{13}	β_{23}
Pd	21.6(1)	12.8(1)	84.5(5)	−2.8(3)	11.1(6)	−8.0(5)
P(1)	21.0(5)	11.6(4)	61(2)	−2.1(8)	2(2)	−2(1)
P(2)	22.3(6)	14.2(4)	65(2)	3.5(9)	5(2)	−3(2)
O(1)	36(3)	25(2)	284(16)	−13(4)	82(12)	2(9)
O(2)	31(3)	44(3)	304(18)	−4(5)	−32(13)	−59(13)
O(3)	63(4)	25(2)	204(12)	−4(4)	63(14)	46(9)
C(1)	27(3)	22(2)	231(18)	−20(4)	83(13)	−66(11)
C(2)	26(3)	23(2)	202(18)	−3(5)	64(13)	−5(11)
C(3)	33(4)	16(2)	201(17)	−18(4)	54(13)	−12(10)
C(4)	37(3)	14(2)	154(14)	−11(4)	22(12)	−29(8)
C(11)	23(2)	19(2)	59(6)	0(3)	−1(8)	−1(7)
C(12)	44(4)	30(3)	65(8)	17(6)	−5(9)	7(8)
C(13)	47(5)	45(4)	90(10)	30(7)	−13(12)	7(10)
C(14)	37(4)	56(5)	92(10)	−5(7)	−34(11)	−37(12)
C(15)	42(4)	41(3)	88(9)	−35(7)	6(12)	−21(10)
C(16)	31(3)	26(2)	76(8)	−14(5)	4(9)	−13(7)
C(21)	21(2)	14(2)	82(8)	4(3)	10(7)	−2(6)
C(22)	31(3)	28(2)	81(9)	1(5)	16(9)	−12(8)
C(23)	41(4)	32(3)	125(13)	5(6)	23(12)	−34(10)
C(24)	54(5)	39(4)	162(17)	55(8)	24(16)	−8(14)
C(25)	61(6)	57(5)	142(14)	86(9)	41(18)	59(16)
C(26)	42(4)	38(3)	102(11)	41(6)	−3(11)	4(10)
C(31)	27(3)	14(2)	61(7)	2(3)	0(7)	1(5)
C(32)	31(3)	17(2)	94(9)	−8(4)	−3(9)	−2(7)
C(33)	38(4)	18(2)	110(10)	−13(5)	5(11)	15(7)
C(34)	43(4)	21(2)	95(9)	4(5)	19(12)	18(9)
C(35)	36(3)	28(2)	62(7)	5(5)	−3(9)	15(8)
C(36)	29(3)	20(2)	76(8)	5(4)	−4(8)	−36(7)
C(41)	25(3)	14(2)	85(8)	11(3)	2(8)	−3(6)
C(42)	25(2)	23(2)	109(9)	−0(4)	−3(9)	11(9)
C(43)	31(3)	23(2)	142(13)	−2(5)	−13(11)	13(10)
C(44)	29(3)	22(2)	173(15)	−1(5)	20(12)	21(10)
C(45)	37(4)	25(3)	122(12)	2(5)	36(11)	30(9)
C(46)	31(3)	20(2)	93(8)	8(5)	28(9)	28(8)
C(51)	27(3)	18(2)	83(8)	−0(4)	−2(8)	−13(7)
C(52)	48(4)	33(3)	96(10)	26(6)	−20(13)	−50(10)
C(53)	60(6)	39(4)	108(11)	20(8)	−61(14)	−32(11)
C(54)	51(5)	32(3)	107(11)	1(6)	−1(14)	−30(11)
C(55)	62(6)	33(3)	112(12)	2(7)	6(15)	−59(11)
C(56)	37(4)	27(3)	127(12)	11(5)	4(12)	−51(10)
C(61)	30(3)	15(1)	72(6)	−2(4)	16(10)	5(6)
C(62)	32(3)	23(2)	99(10)	12(5)	−0(10)	10(8)
C(63)	45(4)	23(2)	105(11)	24(5)	−35(11)	−3(8)
C(64)	57(5)	21(2)	128(13)	9(6)	−36(14)	−4(9)
C(65)	57(4)	21(2)	85(8)	1(6)	−7(14)	7(8)
C(66)	37(4)	17(2)	87(9)	−0(4)	2(10)	1(7)

Table 3. Bond lengths and bond angles (estimated standard deviations in parentheses)

Bond lengths [l/Å]			
Pd–P(1)	2.320(2)	Pd–P(2)	2.349(2)
P(1)–C(11)	1.818(8)	P(1)–C(21)	1.844(8)
P(1)–C(31)	1.828(8)	P(2)–C(41)	1.836(8)
P(2)–C(51)	1.830(9)	P(2)–C(61)	1.832(9)
Pd–C(1)	2.141(13)	Pd–C(4)	2.124(11)
C(1)–C(2)	1.473(18)	C(3)–C(4)	1.479(17)
C(2)–O(2)	1.192(18)	C(3)–O(3)	1.202(17)
C(2)–O(1)	1.412(16)	C(3)–O(1)	1.386(17)
C(11)–C(12)	1.390(13)	C(12)–C(13)	1.415(16)
C(13)–C(14)	1.432(18)	C(14)–C(15)	1.403(18)
C(15)–C(16)	1.369(14)	C(16)–C(11)	1.426(12)
C(21)–C(22)	1.404(12)	C(22)–C(23)	1.390(15)
C(23)–C(24)	1.387(18)	C(24)–C(25)	1.359(20)
C(25)–C(26)	1.394(18)	C(26)–C(21)	1.375(14)
C(31)–C(32)	1.412(12)	C(32)–C(33)	1.397(13)
C(33)–C(34)	1.382(14)	C(34)–C(35)	1.406(14)
C(35)–C(36)	1.387(12)	C(36)–C(31)	1.390(11)
C(41)–C(42)	1.413(13)	C(42)–C(43)	1.387(15)
C(43)–C(44)	1.402(17)	C(44)–C(45)	1.365(16)
C(45)–C(46)	1.416(14)	C(46)–C(41)	1.408(12)
C(51)–C(52)	1.386(14)	C(52)–C(53)	1.421(16)
C(53)–C(54)	1.367(17)	C(54)–C(55)	1.385(17)
C(55)–C(56)	1.418(17)	C(56)–C(51)	1.392(14)
C(61)–C(62)	1.394(13)	C(62)–C(63)	1.388(14)
C(63)–C(64)	1.390(15)	C(64)–C(65)	1.392(16)
C(65)–C(66)	1.390(14)	C(66)–C(61)	1.399(12)
Bond angles [ϕ/°]			
P(1)–Pd–P(2)	98.05(7)	P(1)–Pd–C(1)	88.1(4)
P(2)–Pd–C(4)	86.0(3)	C(1)–Pd–C(4)	87.8(5)
C(2)–O(1)–C(3)	117.6(11)	Pd–C(1)–C(2)	109.2(9)
C(1)–C(2)–O(1)	113.6(11)	C(1)–C(2)–O(2)	129.6(13)
O(1)–C(2)–O(2)	116.8(12)	C(4)–C(3)–O(1)	113.2(11)
C(4)–C(3)–O(3)	128.3(12)	O(1)–C(3)–O(3)	118.3(12)
Pd–C(4)–C(3)	107.3(8)		
Pd–P(1)–C(11)	110.8(3)	Pd–P(1)–C(21)	118.7(3)
Pd–P(1)–C(31)	113.0(3)	C(11)–P(1)–C(21)	102.5(4)
C(11)–P(1)–C(31)	110.2(4)	C(21)–P(1)–C(31)	100.8(4)
Pd–P(2)–C(41)	122.8(3)	Pd–P(2)–C(51)	108.6(3)
Pd–P(2)–C(61)	114.4(3)	C(41)–P(2)–C(51)	104.0(4)
C(41)–P(2)–C(61)	99.6(4)	C(51)–P(2)–C(61)	105.6(4)
P(1)–C(11)–C(12)	117.8(7)	P(1)–C(11)–C(16)	122.1(6)
C(12)–C(11)–C(16)	120.1(8)	C(11)–C(12)–C(13)	120.7(9)
C(12)–C(13)–C(14)	117.9(11)	C(13)–C(14)–C(15)	120.6(12)
C(14)–C(15)–C(16)	120.5(11)	C(11)–C(16)–C(15)	120.1(9)
P(1)–C(21)–C(22)	119.8(6)	P(1)–C(21)–C(26)	119.8(7)
C(22)–C(21)–C(26)	120.3(8)	C(21)–C(22)–C(23)	118.3(9)
C(22)–C(23)–C(24)	121.2(11)	C(23)–C(24)–C(25)	119.3(12)
C(24)–C(25)–C(26)	120.9(13)	C(21)–C(26)–C(25)	119.7(11)
P(1)–C(31)–C(32)	122.7(6)	P(1)–C(31)–C(36)	117.1(6)
C(32)–C(31)–C(36)	120.2(7)	C(31)–C(32)–C(33)	118.9(8)
C(32)–C(33)–C(34)	121.2(9)	C(33)–C(34)–C(35)	119.2(9)
C(34)–C(35)–C(36)	120.6(8)	C(31)–C(36)–C(35)	119.9(8)
P(2)–C(41)–C(42)	118.7(7)	P(2)–C(41)–C(46)	121.7(6)
C(42)–C(41)–C(46)	119.7(8)	C(41)–C(42)–C(43)	121.2(9)
C(42)–C(43)–C(44)	118.8(11)	C(43)–C(44)–C(45)	120.7(11)
C(44)–C(45)–C(46)	121.9(10)	C(41)–C(46)–C(45)	117.8(8)
P(2)–C(51)–C(52)	116.6(7)	P(2)–C(51)–C(56)	123.5(7)
C(52)–C(51)–C(56)	119.8(9)	C(51)–C(52)–C(53)	119.4(10)
C(52)–C(53)–C(54)	121.4(11)	C(53)–C(54)–C(55)	118.9(11)
C(54)–C(55)–C(56)	121.0(11)	C(51)–C(56)–C(55)	119.4(10)
P(2)–C(61)–C(62)	121.7(7)	P(2)–C(61)–C(66)	119.6(6)
C(62)–C(61)–C(66)	118.6(8)	C(61)–C(62)–C(63)	120.7(9)
C(62)–C(63)–C(64)	119.8(10)	C(63)–C(64)–C(65)	120.2(10)
C(64)–C(65)–C(66)	119.6(10)	C(61)–C(66)–C(65)	120.8(9)

TABLE 4. LEAST-SQUARES PLANES THROUGH VARIOUS GROUPS OF ATOMS AND THE DEVIATIONS (l/Å) OF THE ATOMS FROM THE PLANE

Equation of the plane is of the form $AX+BY+CZ+D=0$, where X, Y, Z, and D are measured in Å unit; $X=ax$, $Y=by$, and $Z=cz$.
(Atoms marked by * are not included in the least-squares calulation.)

(a)	Coordination plane						
	$-0.3546X+0.2240Y-0.9078Z+1.2106=0$						
	Pd	−0.004	P(1)	−0.021	P(2)	0.026	C(1)	0.029
	C(4)	−0.027	C(2)*	−0.414	C(3)*	0.963	O(1)*	0.520
(b)	Plane defined by C(1), C(2), O(1), and O(2)						
	$-0.5838X+0.2492Y+0.7727Z+1.9597=0$						
	C(1)	−0.003	C(2)	0.009	O(1)	−0.003	O(2)	−0.004
(c)	Plane defined by C(3), C(4), O(1), and O(3)						
	$-0.3942X-0.7739Y-0.4956Z+3.3519=0$						
	C(3)	0.022	C(4)	−0.007	O(1)	−0.007	O(3)	−0.009
(d)	Phenyl ring 1 (C(11)—C(16))						
	$-0.4947X+0.1173Y+0.5956Z+0.6837=0$						
	C(11)	0.013	C(12)	−0.006	C(13)	−0.009	C(14)	0.020
	C(15)	−0.016	C(16)	−0.001	P(1)*	0.048		
(e)	Phenyl ring 2 (C(21)—C(26))						
	$0.6570X+0.7505Y+0.0714Z+0.6470=0$						
	C(21)	−0.004	C(22)	0.003	C(23)	0.015	C(24)	−0.030
	C(25)	0.021	C(26)	−0.004	P(1)*	0.023		
(f)	Phenyl ring 3 (C(31)—C(36))						
	$-0.6369X+0.7527Y+0.1666Z+1.6461=0$						
	C(31)	−0.017	C(32)	0.007	C(33)	0.007	C(34)	−0.010
	C(35)	−0.001	C(36)	0.015	P(1)*	−0.173		
(g)	Phenyl ring 4 (C(41)—C(46))						
	$0.6120X-0.7812Y-0.1232Z+1.4936=0$						
	C(41)	−0.004	C(42)	0.017	C(43)	−0.012	C(44)	0.001
	C(45)	0.003	C(46)	0.001	P(2)*	−0.001		
(h)	Phenyl ring 5 (C(51)—C(56))						
	$0.6336X+0.6829Y-0.3636Z+0.1006=0$						
	C(51)	−0.004	C(52)	0.017	C(53)	−0.012	C(54)	0.001
	C(55)	−0.005	C(56)	0.007	P(2)*	−0.084		
(i)	Phenyl ring 6 (C(61)—C(66))						
	$-0.4768X-0.6575Y-0.5834Z+1.4762=0$						
	C(61)	−0.030	C(62)	0.035	C(63)	−0.010	C(64)	−0.020
	C(65)	0.020	C(66)	0.007	P(2)*	−0.112		

four cycles of refinement converged to $R_1=0.058$ ($R_2=0.070$) for 4732 non-zero reflections. The largest shifts in positional and thermal parameters were about 0.02σ and 0.3σ, respectively. The atomic scattering factors used in the calculations were those of Hanson and co-workers.[9] The final positional and thermal parameters are listed in Tables 1 and 2.**

Description of the Structure

Molecular Structure. The perspective view of the $[(Pd(C_3H_4O_3)(PPh_3)]$ molecule is given in Fig. 1, with numbering scheme of atoms. A stereoscopic drawing of the molecule and the coordination geometry around the palladium atom are given in Figs. 2 and 3, respectively. Bond lengths and bond angles are given in Table 3. Least-squares planes of various groups of atoms and

** The Table of observed and calculated structure factors are kept as Document No. 7820 at the Chemical Society of Japan.

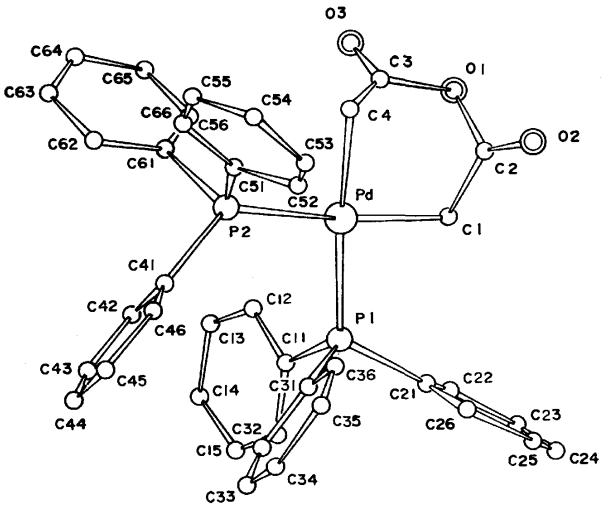

Fig. 1. Perspective view of the molecule with the numbering scheme of atoms.

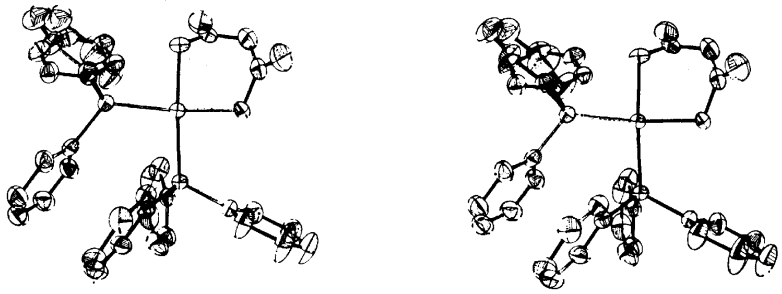

Fig. 2. A stereoscopic view of the molecule. Non-hydrogen atoms are represented by the thermal ellipsoids at 50% probability level.

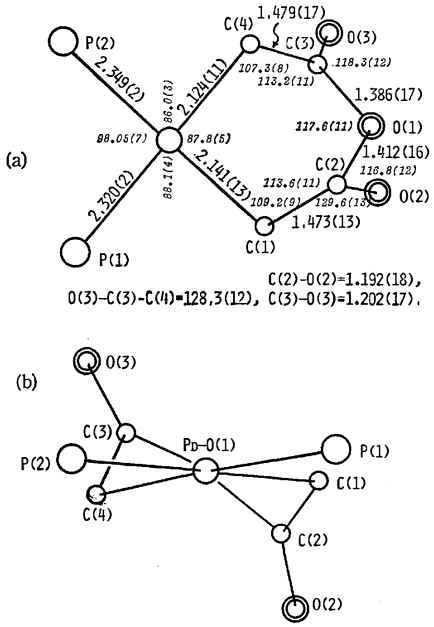

Fig. 3. The coordination geometry around the palladium atom. (a) Selected bond lengths [l/Å] and bond angles [ϕ/°]. (b) Viewed down along the Pd···O(1).

deviations of atoms from these planes are listed in Table 4.

The remarkable feature of the molecular structure is that this complex contains a carbon-bonded chelated ring of acetic anhydride (Fig. 1). The palladium atom has a square-planar geometry coordinated by two sp^3 carbon atoms (C(1) and C(4)) of the chelate ring and two phosphorus atoms: the mean and maximum deviations of atoms from the best plane being 0.023 and 0.029 Å.

The bond lengths between the palladium and two carbon atoms (C(1) and C(4)) are equal: 2.141(13) and 2.124(11) Å, which are longer ones of the Pd(II)–C-(sp^3) bonds.[6] The C(1)–Pd–C(4) angle [87.8(5)°] is slightly smaller than 90°.

The Pd–P bond lenghts [2.320(2) and 2.349(2) Å] are not equal, and these values are slightly longer than those of 2.232(3) Å in $[Pd(C_2H_2O_2)(PPh_3)(py)]$,[2] 2.235(1) Å in $[Pd(CH_2COOH)(acac)(PPh_3)]$,[7] and 2.258(4) Å in $[Pd(acac)_2(PPh_3)]$.[5] The P(1)–Pd–P(2) angle of 98.05(7)° is larger than 90° because of steric interaction between two triphenylphosphine ligands.

In the chelate ring of acetic anhydride, the C(1)–C(2) and C(3)–C(4) bond lenghts of 1.473(18) and 1.479(19) Å are compared with those ovserved in C–C=O moieties in many organic compounds [av 1.506(5) Å].[10] The C(2)=O(2) and C(3)=O(3) bond lengths are 1.192(18) and 1.202(17) Å, respectively, which are equal to those in aldehydes and ketones [av 1.215(5) Å],[10] and that in α-oxalic acid [1.207(1) Å].[11] The C(2)–O(1) and C(3)–O(1) bond lengths [1.412(16) and 1.386(17) Å] have intermediate values between those observed in saturated [av 1.426(5) Å] and conjugated heterocyclic C–O bonds [1.371(16) Å (in furan)].[12] The C(1)–C-(2)–O(1) and C(4)–C(3)–O(1) angles [113.6(11) and 113.2(11)°] are much smaller, whereas the C(1)–C(2)–O(2) and C(4)–C(3)–O(3) angles [129.6(13) and 128.3-(12)°] are much larger than 120°. However, the C(1), C(2), O(1), and O(2) atoms and C(3), C(4), O(1), and O(3) atoms respectively lie on a plane: the dihedral angles between these planes being 69.8°. The dihedral angles between these planes and the coordination plane are 64.0 and 65.4°, respectively: the O(2) and O(3) atoms being above and below the coordination plane

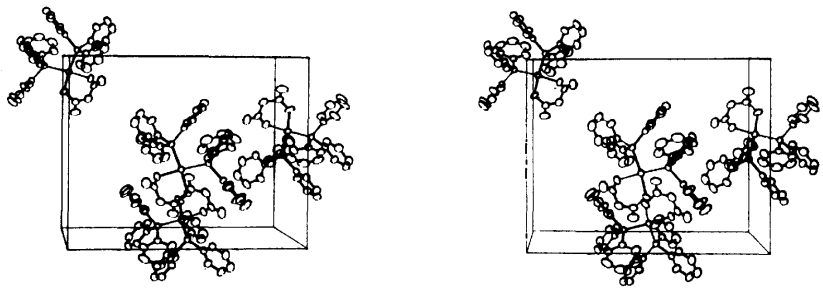

Fig. 4. A stereoscopic drawing of the molecular packing in the unit cell.

TABLE 5. INTERMOLECULAR ATOMIC CONSTANTS WITHIN 3.5 Å

O(2)–C(53)[a]	3.48(2) Å	Code for superscript
O(1)–C(64)[b]	3.44(2)	a) $0.5-x, \quad -y, -0.5+z$
O(3)–C(63)[b]	3.41(2)	b) $0.5+x, 0.5-y, \quad -z$

(Fig. 3(b)). The Pd–C(1)–C(2) and Pd–C(4)–C(3) angles [109.2(9) and 107.3(8)°] have normal tetrahedral values.

Both phosphorus atoms show deviations from the tetrahedral geometry: the C(11)–P(1)–C(21) and C(21)–P(1)–C(31) [102.5(4), and 100.8(4)°] and C(41)–P(2)–C(51), C(41)–P(2)–C(61), and C(51)–P(2)–C(61) angles [104.0(4), 99.6(4), and 105.6(4)°] being much smaller, whereas Pd–P(1)–C(21) and Pd–P(1)–C(31) [118.7(3) and 113.0(3)°] and Pd–P(2)–C(41) angle [122.8(3) Å] being larger than the tetrahedral angle. Six phenyl rings attached to the phosphorus atoms heve normal structure [C–C (av)=1.395 Å and C–C–C (av)=120.0°].

Crystal Structure. Figure 4 shows a stereoscopic view of the molecular packing in the unit-cell along the c axis. The intermolecular atomic contacts less than 3.5 Å are listed in Table 5: no short interatomic distance being found.

Computations throughout the present study were carried out on a NEAC 2200-700 computer at the Osaka University. Figures 2 and 4 were drawn on the NUMERICON 7000 system at Osaka University with a local version of ORTEP.[13]

The authors wish to express their deep thanks to Professor Shinichi Kawaguchi and co-workers of the Osaka City University for supplying crystals and helpful discussions.

References

1) S. Baba, T. Ogura, and S. Kawaguchi, *Inorg. Nucl. Chem. Lett.*, **7**, 1195 (1971); *Bull. Chem. Soc. Jpn.*, **47**, 665 (1974).

2) S. Baba, T. Ogura, S. Kawaguchi, H. Tokunan, Y. Kai, N. Yasuoka, and N. Kasai, *J. Chem., Soc., Chem. Commum.*, **1972**, 910.

3) S. Baba, T. Sobata, T. Ogura, and S. Kawaguchi, *Bull. Chem. Soc. Jpn.*, **47**, 2792 (1974).

4) S. Okeya, S. Kawaguchi, N. Yasuoka, Y. Kai, and N. Kasai, *Chem. Lett.*, **1976**, 53.

5) M. Horike, Y. Kai, N. Yasuoka, and N. Kasai, *J. Organomet. Chem.*, **72**, 441 (1974).

6) M. Horike, Y. Kai, N. Yasuoka, and N. Kasai, *J. Organomet. Chem.*, **86**, 269 (1975).

7) Y. Zenitani, K. Inoue, Y. Kai, N. Yasuoka, and N. Kasai, *Bull. Chem. Soc. Jpn.*, **49**, 1531 (1976).

8) T. Ashida, "The Universal Crystallographic Computing System-Osaka," The Computation Center, Osaka University, (1973), p. 55.

9) H. P. Hanson, P. Herman, J. D. Lea, and S. S. Skillman, *Acta Crystallogr.*, **17**, 1040 (1964).

10) L. E. Sutton, ed, "Tables of Interatomic Distances and Configuration in Molecules and Ions, Supplement," 1956—1959, The Chem. Soc. (1965), pp. S15s, and S22s.

11) J. L. Derissen and P. H. Smit, *Acta Crystallogr., Sect. B*, **30**, 2240 (1974).

12) B Bak, L. Hansen, and J. Rasrtup-Andersen, *Discuss. Faraday Soc.*, **19**, 30 (1955).

13) C. K. Johnson, *ORTEP*, Report ORNL-3794, Oak Ridge National Laboratory, Tenn., (1965).

Fluorescence Lifetime Measurements of Morin-Metal Ion Complexes

Tsuguo SAWADA, Takeshi SHIBAMOTO, and Hitoshi KAMADA
Faculty of Engineering, The University of Tokyo, Hongo, Bunkyo-ku, Tokyo 113
(Received June 8, 1977)

Fluorescence lifetimes of morin complexes of Be(II), Zn(II), Al(III), Ga(III), In(III), Th(IV), Zr(IV), and Sn(IV) extracted into isopentyl alcohol from the acid solution at various pH values were investigated. The result indicates that the Al(III), Ga(III), and In(III) complexes change their compositions according to the change of pH. More detailed investigations by the use of mole ratio method suggest that Al(III), Ga(III), and In(III) form complexes having two different mole ratios of 1 to 1 and 1 to 2 (metal ion: morin). Fluorescence lifetimes were changed according to the changes of the composition of the complex and the differences of the metal ion.

Morin (3,5,7,2′,4′-pentahydroxyflavone) has been widely used as an analytical reagent for fluorometric determinations.

It reacts with Be(II), Zn(II), Al(III), Ga(III), In(III), Sn(IV), Th(IV), Zr(IV), and so on to form fluorescent complexes. The Al(III),[1] Zr(IV),[2] and Be(II)[3] complexes exhibit especially intense green fluorescence, and morin has been utilized very often for the determination of trace amounts of these metal ions. The fluorescence system resulting from the reaction between Al(III) and morin has been applied also to the determination of inorganic ions such as F^- by the use of its quenching ability.[4]

Katyal[5] discussed summarily the analytical utilities of flavonoid compounds including morin. The compositions of complexes formed between morin and metal ions have been investigated by several workers. Biryuk and Rabitskaya[6] reported that In(III)-morin complex with the mole ratio of 1 : 1 is formed at pH 3.6. Recently Katyal and Prakash[7] reported that Al(III) and Ga(III) give the morin complexes with the same composition as the In(III) complex at pH 3.6. In the case of Th(IV) complex, two different results were obtained by Fletcher *et al.*[8] and by Blank *et al.*[9]: that is, 1 : 2 and 1 : 3 complexes, respectively.

In the present paper, we report the new results that complexes with two different mole ratios are formed in Al(III)-, Ga(III)-, In(III)-, and Be(II)-morin systems, while Zn(II), Th(IV), Zr(IV), and Sn(IV) react with morin to give the complexes with a single mole ratio by the measurement of the fluorescence lifetime of these complexes. Although these complexes showed very similar fluorescence spectra, explicitly different fluorescence lifetimes were determined.

Experimental

Reagents and Procedure. Aluminium(III) and gallium(III) stock solutions were obtained by dissolving each metal in concentrated hydrochloric acid. An indium(III) solution was prepared by dissolving indium(III) hydroxide in boiling hydrochloric acid. Other metal ion solutions were prepared by dissolving each salt in hydrochloric acid. Working solutions of each metal ion were prepared by diluting the stock solutions with distilled water to about 10 mM.

Morin of high purity was purchased from Merck. Solutions of morin were prepared by dissolving the solid material in methanol. Spectral grade methanol and high purity isopentyl alcohol were purchased from Wako Junyaku, Co., Ltd. All the reactions of complexation were done in hydrochloric acid solutions at various pH values, and the complexes obtained were almost extracted into isopentyl alcohol, as described elsewhere.[10] After the extraction solutions were degassed by bubbling with high purity nitrogen for 5 min, fluorescence and excitation spectra and fluorescence lifetimes were measured.

Apparatus. Fluorescene and excitation spectra were measured with a Hitachi MPF-4 fluorometer. Fluorescence lifetimes were measured by the use of a home-made time-correlated single photon counting apparatus.[11] Although the time-resolution is 0.1 ns, the exciting light pulse has a time-duration of 1.6 ns. Therefore, the values of fluorescence lifetimes shorter than 2.0 ns were corrected by the deconvolution method.

Results and Discussion

Aluminium(III)-Morin Complex. Figure 1 shows fluorescence and excitation spectra of the aluminium-morin complex in isopentyl alcohol. The complex was formed in hydrochloric acid solutions at pH 1.0 and 3.0. Morin itself does not fluoresce in acid solutions. As is seen in this figure, the maximum fluorescence wavelengths are 495 nm at pH 1.0 and 503 nm at pH 3.0.

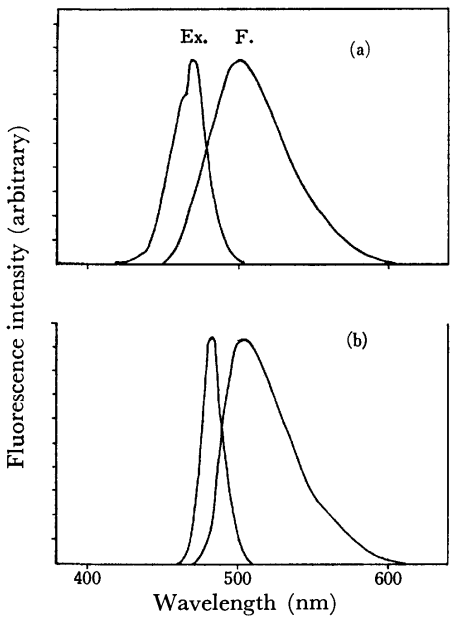

Fig. 1. Fluorescence and excitation spectra of Al(III)-morin complex in isopentyl alcohol; (a) pH 1.0 and (b) pH 3.0.

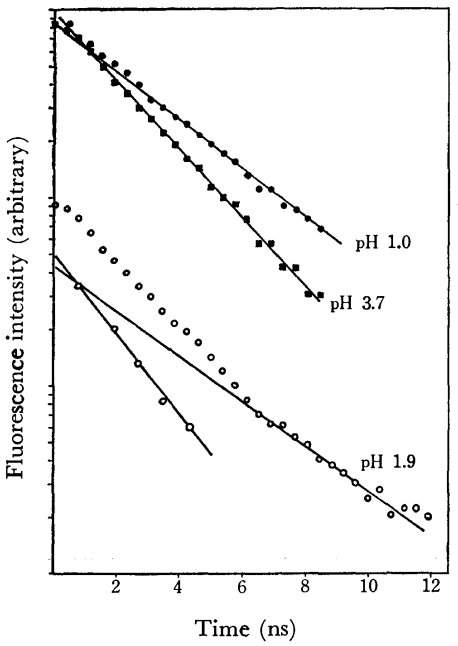

Fig. 2. Semilogarithmic plots of the decay time of the fluorescence of Al(III)–morin complex.

There is little difference between the fluorescence spectra at pH 1.0 and 3.0, while the excitation spectra are very different.

Figure 2 shows a semilogarithmic plot of the fluorescence intensity *vs.* time in order to obtain the fluorescence lifetime of the aluminium complex. As shown in Fig. 2, the decay time of fluorescence of the complex extracted at pH 1.9 has two different exponential features. On the contrary, the plots for those extracted both at pH 1.0 and 3.7 give single exponential decay times. Moreover, the component with the longer lifetime in the two fluorescence decays at pH 1.9 agrees with that at pH 1.0, and the component with the shorter lifetime with that at pH 3.7, within experimental errors. The value of the longer lifetime component is (3.3 ± 0.1) ns and that of the shorter lifetime component is (2.0 ± 0.3) ns. These results suggest that the composition of aluminium-morin complex changes near pH 2. The composition of aluminium to morin was estimated by the mole ratio method. The result is shown in Fig. 3,

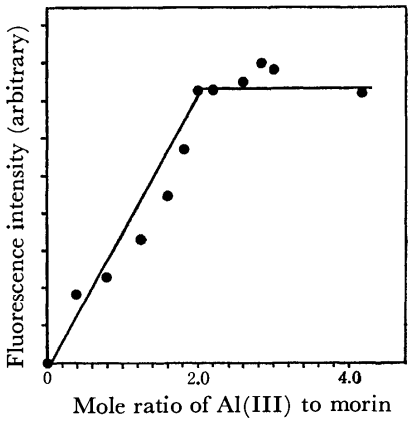

Fig. 3. The mole ratio method for Al(III)–morin complex formed at pH 1.3.

which confirms the aluminium-morin ratio of 1 : 2 for the complex formed at pH 1.0. The composition of complex at pH 3.0 was also investigated and the result obtained was in good agreement with that in the literature.[7] The structure of the complex has not been established yet, but the metal ion is assumed to be substituted for the hydrogen of the hydroxyl group at the 3- or 5-position.[10]

Gallium(III)- and Indium(III)–Morin Complexes. Figures 4 and 5 show fluorescence spectra of gallium-

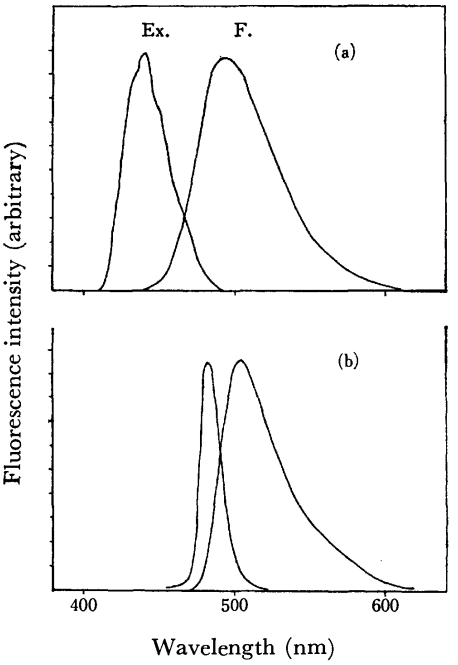

Fig. 4. Fluorescence and excitation spectra of Ga(III)–morin complex in isopentyl alcohol; (a) pH 1.0 and (b) pH 3.0.

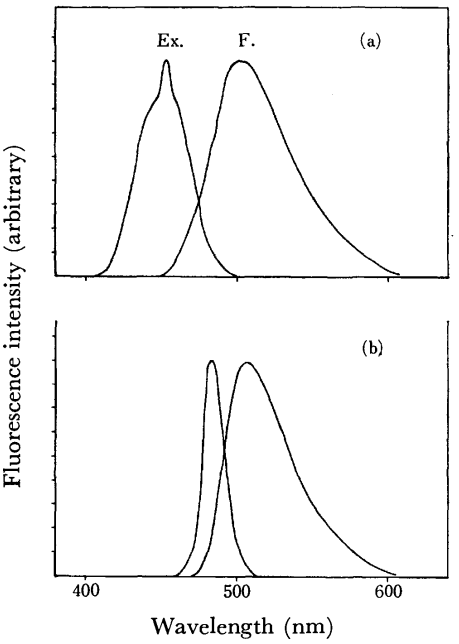

Fig. 5. Fluorescence and excitation spectra of In(III)–morin complex in isopentyl alcohol; (a) pH 1.3 and (b) pH 3.6.

and indium–morin complexes and their excitation spectra at two different pH values. The decay curve of the fluorescence showed a single exponent at each pH value. The results of the fluorescence lifetime measurement were that the longer lifetime component of the gallium complex is (2.7±0.1) ns and the shorter one is (1.6±0.4) ns. As for the indium complex, the longer lifetime component is (4.6±0.1) ns and the shorter one is (3.5±0.1) ns. Dependencies of the shape and wavelength of fluorescence and excitation spectra on pH were in good agreement with those in the case of the aluminium complex. However, the fluorescences of the gallium and indium complexes were unstable in comparison with that of the aluminium complex. Therefore, no reliable composition of these complexes has been determined by the mole ratio method. However, the same conclusion about the composition as that obtained in the aluminium complex is predictable, because aluminium, gallium, and indium belong to the same group IIIb.

Beryllium(II)-Morin Complex. Beryllium ion reacted with morin to form a stable complex in both acid and basic solutions. If forms a complex with the mole ratio of 1 : 2 (beryllium: morin) in hydrochloric acid at pH 2.0 and its fluorescence lifetime was estimated to be (2.1±0.1) ns. Some differences in fluorescence and excitation spectra can be seen between the complexes obtained at pH>3.4 and at pH 2.0. The fluorescence lifetime obtained at pH 4.3 is (4.8±0.3) ns, although the mole ratio has not been determined because of the poorness of experimental reproducibility.

Thorium(IV)–, Zirconium(IV)–, Tin(IV)–, and Zinc-(IV)-Morin Complexes. These complexes obtained in acid media are considered to have a single mole ratio, since the fluorescence lifetime values showed no change in the pH range of 1–5. As for the thorium and zirconium complexes, the mole ratio of metal ions to morin was estimated to be 1 : 2. However, the mole ratio of tin– and zinc–morin complexes has not been determined, because the complexes were unstable.

The fluorescence lifetime values obtained in this work are summarized in Table 1.

TABLE 1. FLUORESCENCE PROPERTIES OF METAL ION–MORIN COMPLEXES IN ISOPENTYL ALCOHOL

Metal ion	Mole ratio (metal ion: morin)	F_{max} (nm)	E_x (nm)	Fluoresence lifetime (ns)
Al(III)	1 : 2	495	438	3.3±0.1
	1 : 1	503	483	2.0±0.3
Ga(III)	1 : 2	500	468	2.7±0.1
	1 : 1	503	483	1.6±0.4
In(III)	1 : 2	500	452	4.6±0.1
	1 : 1	506	483	3.5±0.1
Be(II)	1 : 2	500	438	2.1±0.1
	1 : 1 (?)	508	451	4.8±0.3
Zn(II)	—	502	468	2.1±0.3
Th(IV)	1 : 2	513	483	2.6±0.3
Zr(IV)	1 : 2	508	440	4.6±0.3
Sn(IV)	—	—	—	2.3±0.4

References

1) C. E. White and C. S. Lowe, *Ind. Eng. Chem., Anal. Ed.*, **12**, 229 (1940).
2) R. A. Geiger and E. B. Sandell, *Anal. Chim. Acta*, **16**, 346 (1957).
3) E. B. Sandell, *Ind. Eng. Chem., Anal. Ed.*, **12**, 674 (1940).
4) H. H. Willard and C. A. Horton, *Anal. Chem.*, **24**, 862 (1952).
5) M. Katyal, *Talanta*, **15**, 95 (1968).
6) E. A. Biryuk and R. V. Ravitsukaya, *Ukr. Khim. Zh.*, **36**, 121 (1970).
7) M. Katyal and S. Prakash, *Talanta*, **24**, 367 (1977).
8) M. H. Fletcher and R. G. Milky, *Anal. Chem.*, **28**, 1402 (1956).
9) A. B. Blank, I. I. Mirenskaya, and L. M. Satanovsii, *Zh. Analit. Khim.*, **30**, 1116 (1975).
10) E. B. Sandell, "Colorimetric Determination of Traces of Metals," 3rd ed, Interscience Publisher's, New York (1959).
11) T. Sawada and H. Kamada, *Bunseki Kagaku*, **22**, 881 (1973).

Reactions between PbO and TiO_2 under Hydrothermal Conditions

Shoji KANEKO and Fumio IMOTO

Department of Industrial Chemistry, Faculty of Engineering, Shizuoka University, Johoku, Hamamatsu 432

(Received July 29, 1977)

The phase relation of products obtained by the reaction between PbO and TiO_2 under hydrothermal conditions up to 500 °C and 500 kg/cm² for 5h has been investigated. The yield and crystallographic properties of purified $PbTiO_3$ depend upon the PbO/TiO_2 mole ratio (Pb/Ti ratio) in raw mixtures as well as the reaction temperature. Both $PbTiO_3$ and $PbTi_3O_7$ are synthesized at a remarkably low temperature under hydrothermal conditions, as compared with the ignition process in air. Pure and well-crystallized $PbTiO_3$ is obtained by heat-treating above 400 °C at Pb/Ti ratios greater than 1.0 and by dissolving excess PbO with acetic acid. $PbTi_3O_7$ coexists occasionally with $PbTiO_3$ to some extent at Pb/Ti ratios less than 1.0, but appears as a single phase in the temperature range 100—450 °C at the Pb/Ti ratio 0.33. The unit cell volume of $PbTiO_3$ prepared at lower temperature is considerably large, suggesting a loosely-packed structure. The compound is always of tetragonal form containing no metastable cubic form.

Three compounds, Pb_2TiO_4,[1] $PbTiO_3$,[2] and $PbTi_3O_7$[3] have been reported in the system PbO–TiO_2, although the phase diagram has not been completed so far. The existence of Pb_2TiO_4 was denied by Matsuo and Sasaki.[4] Aykan[3] found a novel compound $PbTi_3O_7$ by the reaction between PbO and TiO_2 in the TiO_2-rich region. Kato *et al.*[5] analyzed the structure in detail using a single crystal prepared by a flux method. Lobachev[6] also found a new phase in the system PbO–TiO_2–KF–H_2O under hydrothermal conditions and determined the composition as $PbTi_3O_7$ by chemical analysis. His X-ray data, however, were insufficient, differing from those of other investigators.[3,5]

$PbTiO_3$ has a tetragonal form at room temperature, the axial ratio (c/a=1.065) being the largest of perovskite-type compounds. It is transformed reversibly from tetragonal to cubic around 490 °C (Curie point),[7] and is important as a component of complex perovskite-type compounds, especially piezoelectrics such as PZT ceramics.[8]

In previous papers[9,10] dealing with the reaction of oxides under hydrothermal conditions, it was shown that the crystallization and anatase-rutile transformation of TiO_2 was markedly accelerated, and fine-grained (below 200 Å) $BaTiO_3$ of tetragonal form easily synthesized. A hydrothermal reaction seems to be suitable for the preparation of inorganic powders containing a volatile component such as PbO.

We have investigated the phase relation of the products by the reaction between PbO and TiO_2 in order to find the optimum conditions for the preparation of pure $PbTiO_3$ under hydrothermal conditions.

Experimental

Starting Materials and Procedures. Hydrous titanium dioxide (TiO_2: 83.6 wt%, H_2O: 10.8 wt%, SO_3: 5.6 wt%) was prepared by the neutralization of titanium sulfate with aqueous ammonia (sulfate-process). This compound (TiO_2: 91.9 wt%, H_2O: 8.1 wt%) was also prepared by the hydrolysis of titanium tetrachloride with heating at about 100 °C (chloride-process). Both of them were considered to be the most reactive source of TiO_2.

Hydrous titanium dioxide and guaranteed reagent lead monoxide (purity 99.0 wt%, Koso Chemical Co., Ltd.) were weighed to prepare a mixture of a certain PbO/TiO_2 mole ratio (Pb/Ti ratio). A gold vessel containing raw materials and water was placed in a cylindrical autoclave of 100 cm³ volume, and subjected to various conditions up to 500 °C and 500 kg/cm² for 5 h. Products were washed several times with 5% acetic acid and distilled water by decantation in order to remove excess PbO, then dried at 80 °C in an oven.

Chemical Analysis. Dried products were analyzed by the following method. About 0.6 g of a sample is accurately weighed and dissolved in 20 ml of hot sulfuric acid with 6 g of ammonium sulfate. After cooling, lead sulfate is precipitated by addition water and filtered off for weighing. Hydrous titanium dioxide is precipitated from the filtrate by addition of aqueous ammonia. After filtration and ignition, the precipitate is weighed as total TiO_2, *i.e.*, unreacted TiO_2 and TiO_2 in $PbTiO_3$. The yield of $PbTiO_3$ is calculated by

$$\text{Yield (\%)} = \frac{\text{Weight of } TiO_2 \text{ in } PbTiO_3 \text{ equimolar to } PbSO_4}{\text{Weight of total } TiO_2} \times 100. \quad (1)$$

X-Ray Diffraction. The products were identified by means of X-ray diffraction using Geigerflex, Type D-2* with nickel-filtered Cu $K\alpha$ radiation. The crystallite size was calculated from Scherrer's equation[11] with Warren's correction, employing half value widths of $PbTiO_3$ (110) and Si (111) reflections. Lattice constants of tetragonal $PbTiO_3$ were determined by (110) and (200) reflections using Si as an internal standard.

Results and Discussion

Reaction Products under Various Conditions. Poorly-crystallized $PbTiO_3$ was formed at Pb/Ti ratio 1.0 and 200 °C, with an unknown phase X and a small amount of lead sulfate attributed to the sulfate ion contained in hydrous titanium dioxide[9] (Fig. 1). Above 300 °C, the unknown phase disappeared with increase of $PbTiO_3$. $PbTiO_3$ appeared as a single phase in a considerably wide temperature range. Under hydrothermal conditions, the synthesis of $PbTiO_3$ was initiated at a temperature as low as 170 °C, which was much lower than 550 °C in the ignition process reported by Okazaki *et al.*[12] and somewhat higher than 60 °C in the wet synthesis of $BaTiO_3$.[13] Figure 2 shows a similar

* Rigaku Denki Co., Ltd. Tokyo, Japan.

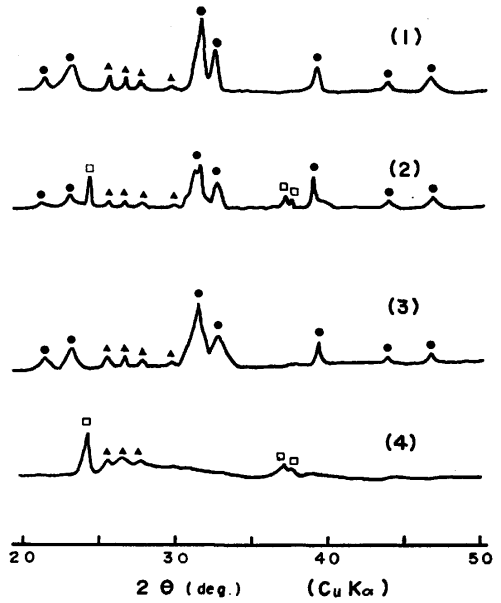

Fig. 1. X-Ray diffraction patterns of the products. (1) Pb/Ti ratio=1.0, 300 °C, (2) Pb/Ti ratio=1.0, 200 °C, (3) Pb/Ti ratio=0.8, 300 °C, (4) Pb/Ti ratio=0.8, 200 °C. ●: $PbTiO_3$, ○: $PbTi_3O_7$, ▲: $PbSO_4$, □: unknown phase.

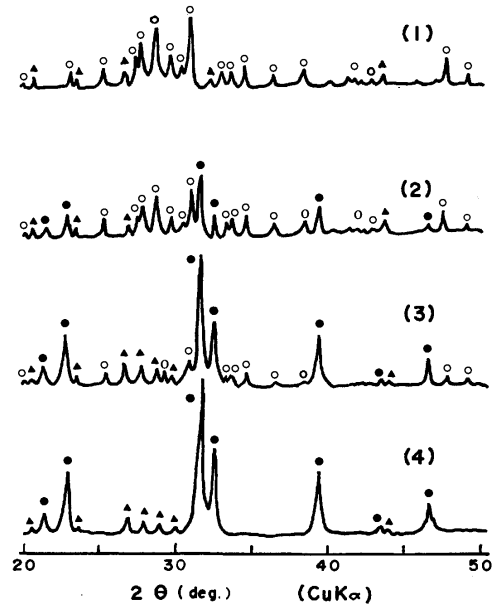

Fig. 2. X-Ray diffraction patterns of the products at various Pb/Ti ratios and 400 °C. (1) Pb/Ti ratio=0.33, (2) Pb/Ti ratio=0.5, (3) Pb/Ti ratio=0.7, (4) Pb/Ti ratio=1.0. ●: $PbTiO_3$, ○: $PbTi_3O_7$, ▲: $PbSO_4$.

phase relation at 400 °C. $PbTi_3O_7$ was observed as a single phase at Pb/Ti ratio 0.33. $PbTi_3O_7$ and $PbTiO_3$ coexisting at Pb/Ti ratios 0.45—0.7, the latter predominated high Pb/Ti ratio.

The relationship between Pb/Ti ratio, temperature and phase is shown in Fig. 3. The diagram is divided into four zones: (1) coexistence of amorphous and unknown phases, (2) $PbTiO_3$, (3) $PbTi_3O_7$, and (4)

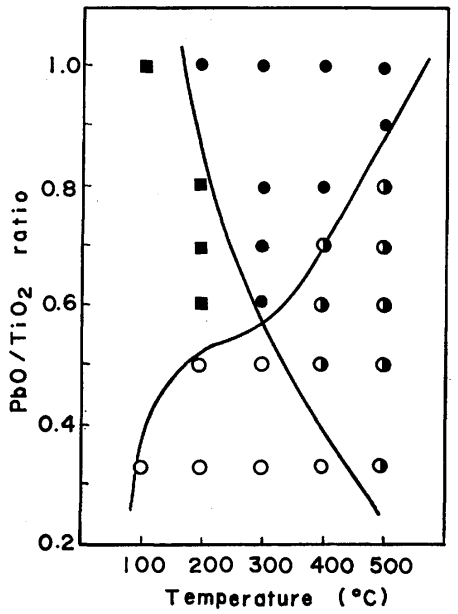

Fig. 3. Phase relation in the reaction between PbO and TiO_2 under hydrothermal conditions. ■: Amorphous and unknown phase, ●: $PbTiO_3$, ○: $PbTi_3O_7$, ◑: $PbTiO_3+PbTi_3O_7$.

coexistence of $PbTiO_3$ and $PbTi_3O_7$. It is remarkable that $PbTi_3O_7$ was solely obtained in a wide and low temperature range 100—450 °C under hydrothermal conditions, as compared with the narrow temperature range 800—850 °C in the ignition process in the air.[3]

Crystallographic Properties of $PbTiO_3$. In the lattice constants of $PbTiO_3$, *a* for the specimens treated at lower temperatures is slightly smaller than the value

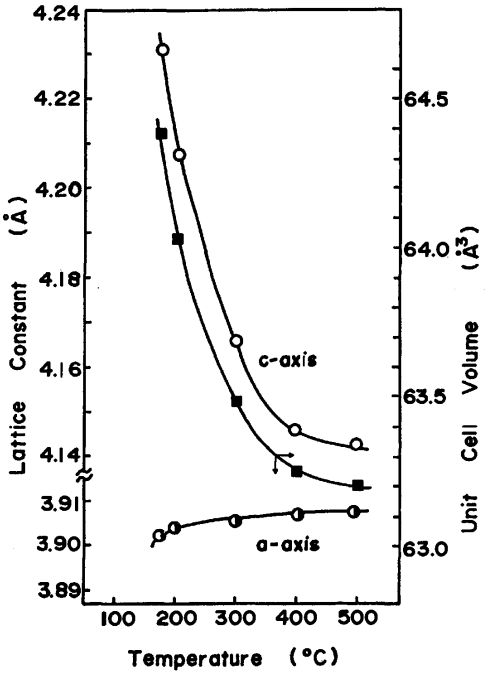

Fig. 4. Variations of lattice constants and unit cell volume of hydrothermal $PbTiO_3$ with reaction temperature.

reported** whereas c is relatively larger (Fig. 4), indicating that the unit cell expands to the direction of c-axis by loose packing of each ion. With increase in temperature, c decreases markedly and the axial ratio (c/a) gradually approaches the value 1.065,** the unit cell volume (a^2c) changing in a similar way to c. In contrast, hydrothermal $BaTiO_3$, as well as wet-synthesized $BaTiO_3$,[13,14] are of cubic form presumed to be a metastable state, being transformed into tetragonal form with increase in temperature.[11] The difference between $PbTiO_3$ and $BaTiO_3$ seems to arise primarily from the difference in ionic properties of lead and barium. The tolerance factor, or the fraction of ion packing, in $PbTiO_3$ is smaller than that in $BaTiO_3$; each ion in the former moves more easily around than that in the latter in the crystal lattice. In addition, lead ion is more readily polarized than barium ion. The anisotropy of the crystal structure is more enhanced in $PbTiO_3$.

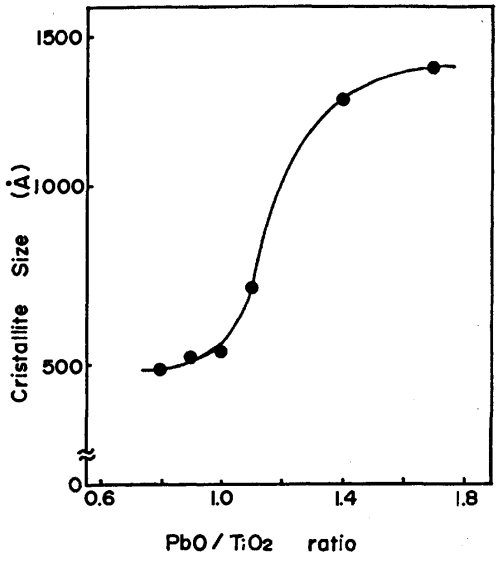

Fig. 5. Crystallite size of hydrothermal $PbTiO_3$ at 500 °C as a function of Pb/Ti ratio.

The crystallite size of $PbTiO_3$ increases from 500 to 1400 Å with increase in the Pb/Ti ratio (Fig. 5). The size of starting hydrous titanium dioxide is about 80 Å, the reaction temperature being too low to expect crystal growth by the solid state reaction. Thus the crystal growth suggests that the hydrothermal reaction proceeds through the solution-precipitation mechanism based on the large dissolving power of hydrothermal media.

TiO_2 obtained by the chloride-process was also examined as a starting material to avoid the formation of the by-products resulting from impurities. As shown in Fig. 6, the specimens prepared from TiO_2 by the chloride-process generally give sharper X-ray profiles than those for the specimens prepared from TiO_2 by the sulfate-process. No preheating TiO_2 by the sulfate-process contains both H_2O and SO_3. It loses almost H_2O at about 570 °C, then releasing SO_3 and crystallizes completely. On the other hand, no preheating TiO_2 by the chloride-process contains H_2O alone and loses it at 300 °C.[9] When used no preheating TiO_2 or TiO_2 preheated at 600 °C, the X-ray profiles of $PbTiO_3$ were sharp [Fig. 6(1)], but when used TiO_2 preheated at 400 °C, the profile was broad. When used no preheating TiO_2, the profile was very sharp, but when used TiO_2 preheated over 400 °C, the profiles were rather broad [Fig. 6(2)]. If we assume that the sharper X-ray profile

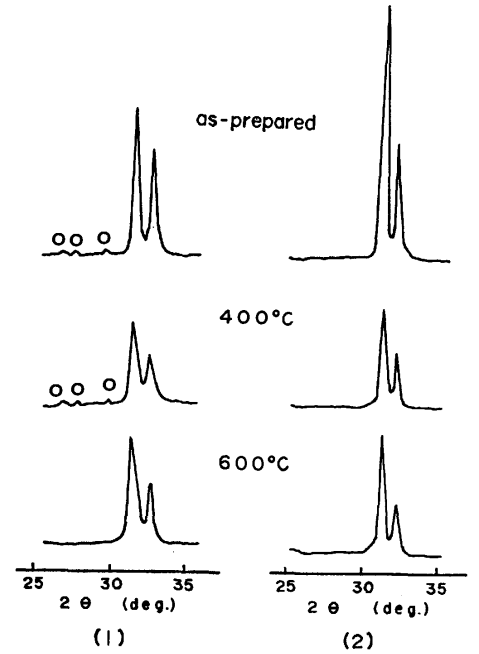

Fig. 6. X-Ray profiles of hydrothermal $PbTiO_3$ prepared from two kinds of TiO_2 pre-heated at various temperatures. (1) TiO_2 prepared by the sulfate-process, (2) TiO_2 prepared by the chloride-process. ○: $PbSO_4$.

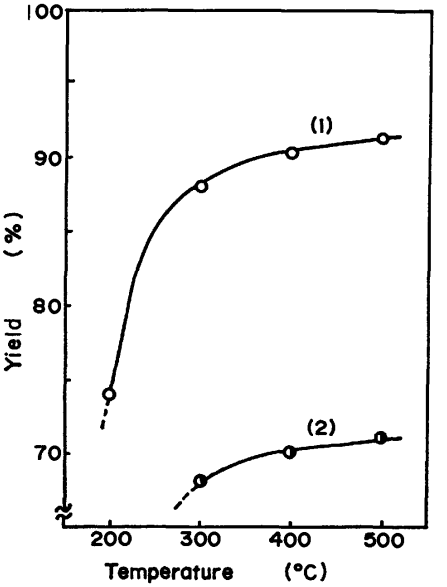

Fig. 7. Relationship between yield of hydrothermal $PbTiO_3$ and reaction temperature. (1) Pb/Ti ratio= 1.0, (2) Pb/Ti ratio=0.8.

** From "Powder Diffraction File, Card No. 4-0477," lattice constants a and c of $PbTiO_3$ are 3.899 Å and 4.153 Å, respectively. Unit cell volume, a^2c=63.138 Å^3 and axial ratio, c/a=1.065 are calculated from these values.

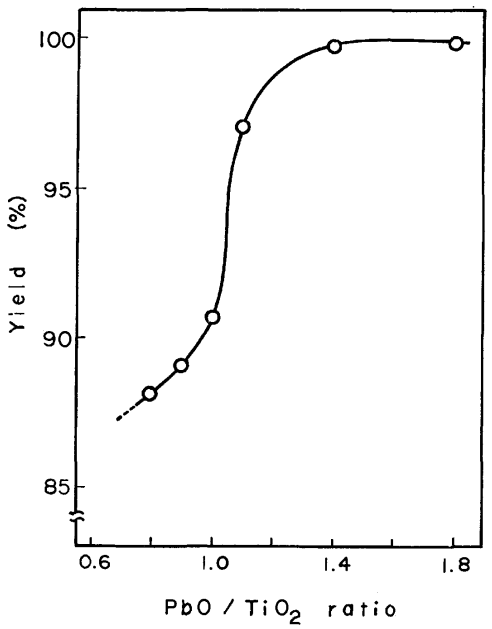

Fig. 8. Relationship between yield of hydrothermal $PbTiO_3$ and Pb/Ti ratio at 500 °C.

is related to better crystallinity, OH or H_2O on the surface of TiO_2 promotes crystallization, while the sulfate ion retards it. For the preparation of pure and well-crystallized $PbTiO_3$ it is advantageous to use no preheating TiO_2 by the chloride-process containing much H_2O and no sulfate ion.

Yield of $PbTiO_3$. At the Pb/Ti ratios 0.8—1.0, the yield increases with in temperature, the reaction proceeding almost completely up to 400 °C (Fig. 7). The yield was 90.7% at the Pb/Ti ratio 1.0 and 400 °C. However it is estimated to be over 95% after the correction for the consumption of PbO by the preferential reaction with sulfate ion contained in hydrous titanium dioxide converting to lead sulfate. Figure 8 shows the relation between yield and the Pb/Ti ratio at 500 °C. When the Pb/Ti ratio exceeds 1.0, the yield reaches 100% after the correction described above. The yield changes considerably with the Pb/Ti ratio and reaction temperature.

The authors wish to thank Mr. Kenji Kamo and Mr. Tohru Yamamoto for technical assistence throughout the course of this work.

References

1) I. N. Belyaev and A. K. Nesterova, *J. Gen. Chem. USSR* (English Transl.), **22**, 469 (1952).
2) D. G. Nickolson, *Ind. Eng. Chem.*, **29**, 716 (1937).
3) K. Aykan, *J. Am. Ceram. Soc.*, **51**, 577 (1968).
4) Y. Matsuo and H. Sasaki, *J. Am. Ceram. Soc.*, **46**, 409 (1963).
5) K. Kato, I. Kawada, and K. Muramatsu, *Acta Crystallogr., Sect. B*, **30**, 1634 (1974).
6) A. N. Lobachev, Ed, "Crystallization Processes under Hydrothermal Conditions," (English Transl.), Consultants Bureau, New York (1973), p. 81.
7) G. Shirane and S. Hoshino, *J. Phys. Soc. Jpn.*, **6**, 265 (1951).
8) B. Jaffe, R. S. Roth, and S. Marzullo, *J. Appl. Phys.*, **25**, 809 (1954).
9) F. Imoto and S. Kaneko, *Kogyo Kagaku Zasshi*, **74**, 591 (1971).
10) S. Kaneko and F. Imoto, *Nippon Kagaku Kaishi*, **1975**, 985.
11) H. P. Klug and L. E. Alexander, "X-Ray Diffraction Procedures for Polycrystalline and Amorphous Materials," 2nd ed, John Wiley and Sons, New York (1974), p. 687.
12) K. Okazaki, T. Yoshioka, and K. Takahashi, *Yogyo Kyokai Shi*, **73**, 17 (1965).
13) T. Kubo, M. Kato, and T. Fujita, *Kogyo Kagaku Zasshi*, **71**, 114 (1968).
14) S. Naka, F. Nakakita, Y. Suwa, and M. Inagaki, *Bull. Chem. Soc. Jpn.*, **47**, 1168 (1974).

Bivalent and Tervalent Cobalt Complexes of 4-(2-Pyridylazo)resorcinol, 1-(2-Pyridylazo)-2-naphthol, and their Thiazolyl Analogs in Aqueous and Aqueous Dioxane Media. Rapid-scan Spectral and Kinetic Studies*

Katsura MOCHIZUKI, Taira IMAMURA, Tasuku ITO, and Masatoshi FUJIMOTO
Department of Chemistry, Faculty of Science, Hokkaido University, Sapporo 060
(Received August 29, 1977)

The reactions of Co^{2+} with 4-(2-pyridylazo)resorcinol (PAR), 1-(2-pyridylazo)-2-naphthol (PAN), and their thiazolyl analogs TAR and TAN in aqueous or aqueous dioxane media are followed by a rapid-scan spectroscopic method combined with stopped-flow technique. The step of the fast formation of cobalt(II) complexes is clearly discriminated from the subsequent slower step of oxidation to the cobalt(III) state. Formation and redissolution of transient insoluble intermediates are observed in the stopped-flow signals for the light scattered by the reaction mixture. The metal-to-ligand ratio in the short-lived intermediate cobalt(II) complex of PAR and PAN is determined to be 1 : 2 by applying the method of continuous variation to the fast change in stopped-flow signals. The rate constants k_1 and k_2 for the step of formation of 1 : 1 cobalt(II) complex with the species LHH* and LH^- of PAR in aqueous solution and with the species LH_2^+ and LH of PAN in 5%(v/v) dioxane–water are determined to be $k_1 = 4.8 \times 10^4$ and $k_2 = 9.8 \times 10^4$ dm^3 mol^{-1} s^{-1}, and $k_1 < 10^3$ and $k_2 = 4.6 \times 10^3$ dm^3 mol^{-1} s^{-1}, respectively.

Some *ortho*-hydroxy azo compounds shown in Fig. 1 are reported to behave as terdentate ligands[1,2] forming colored chelates with many metal ions.[3] PAN and PAR have been used as sensitive analytical reagents for the spectrophotometric determination of cobalt.[4,5]

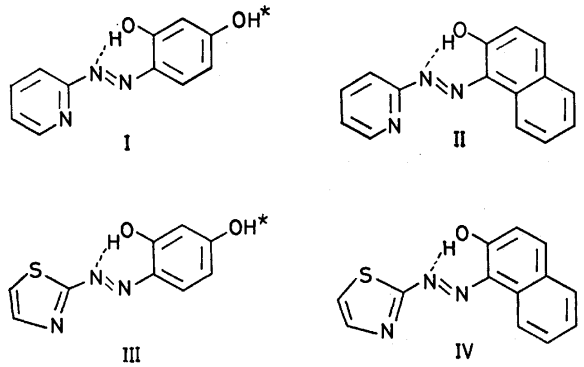

Fig. 1. Structural formulae of the ligands. I: 4-(2-pyridylazo)resorcinol (PAR), II: 1-(2-pyridylazo)-2-naphthol (PAN), III: 4-(2-thiazolylazo)resorcinol (TAR), IV: 1-(2-thiazolylazo)-2-naphthol (TAN).

As regards the cobalt chelates of PAN and PAR, a number of data have been reported on the composition and the stability constants.[3,6,7] On the basis of the measurements of magnetic susceptibility, Iwamoto and Fujimoto provided an evidence for the formation of cobalt(III) complexes in a solution prepared from Co^{2+} and PAR or PAN.[8] This result has been supported by the studies on the substitution reaction with EDTA[5,9] and also by the proton magnetic resonance studies of the isolated complex.[10,11] Although the cobalt(III) complexes of these heterocyclic *ortho*-hydroxy azo compounds have been well characterized, no studies on cobalt(II) chelates have been reported so far.

In the present study, we have confirmed the formation of transient intermediate cobalt(II) complexes in the course of the reaction between Co^{2+} and the ligands I—IV using a rapid-scan spectrophotometer equipped with a stopped-flow cell. The formation and redissolution of hardly visible fine precipitates in the course of the reaction between Co^{2+} and PAN or TAN were also revealed by applying the stopped-flow technique to the measurements of the change in intensity of the scattered light.[12] The metal-to-ligand ratio in the transient cobalt(II) complexes, the mechanisms and the kinetic data for the step of formation of 1 : 1 cobalt(II) complexes, and some results on the cobalt(III) complexes are discussed.

Experimental

Materials. Deionized water was distilled. Reagent grade materials were used unless otherwise specified.

The cobalt(II) perchlorate solution was prepared by heating cobalt(II) chloride with a small excess of perchloric acid until no trace of chloride ion was detected. The solution was standardized titrimetrically with EDTA using Xylenol Orange as an indicator.

PAR was synthesized by the usual method,[13] and recrystallized several times from 1 : 1(v/v) ethanol–water to yield reddish yellow needles of the monohydrate of the monosodium salt. Found: C, 51.34; H, 3.97; N, 16.26%. Calcd for $C_{11}H_8N_3O_2Na \cdot H_2O$: C, 51.77; H, 3.95; N, 16.47%. The concentration of PAR in the aqueous stock solution (*ca.* 10^{-4} mol dm^{-3}) was calculated from its weight.

Commercial PAN, TAR, and TAN (Dojindo, Kumamoto) were used without further purification. The purity was confirmed by elemental analyses. Stock solutions of these compounds (1×10^{-4} mol dm^{-3}) were prepared by dissolving the reagent in 50%(v/v) dioxane–water. The concentrations were calculated from the weighed amount.

A neutral 1 : 2 cobalt(III) complex of PAR, [$Co^{III}L(LH^*)$] was prepared as follows, where LH* stands for the ligand with an undissociated *para*-hydroxyl group.† The stoichio-

* Prensented in part at the 1977 Winter Meeting in Hokkaido of the Chemical Society of Japan and the Japan Society for Analytical Chemistry, Sapporo, February 2, 1977, Abstracts, p. 11, and at the 36th National Meeting of the Chemical Society of Japan, Osaka, April 1, 1977, Abstracts Vol. 1, p. 18.

† Hereafter "PAR" stands for L^{2-}, LH^-, LH^{*-}, and/or LHH*, where H* denotes the proton of the *para*-hydroxyl group (Fig. 1).

metric amounts of cobalt(II) perchlorate and PAR were slowly mixed with vigorous stirring at pH 6.0—6.5. Precipitates formed gradually. Then the pH of the solution was lowered to 4.0 by adding dropwise dilute perchloric acid in order to complete the precipitation. The solution was allowed to stand for 24 h. Precipitates were filtered off, washed thoroughly with water and ethanol, and dried at 80 °C. The content of cobalt was determined titrimetrically with EDTA using Cu–PAN as an indicator after decomposition of the complex by heating with hydrogen peroxide and sulfuric acid. Found: C, 52.87; H, 3.66; N, 16.58; Co, 11.38%. Calcd for $C_{22}H_{15}N_6O_4Co \cdot H_2O$: C, 52.39; H, 3.20; N, 16.66; Co, 11.69%.

A pale-colored anion-exchange resin QAE-Sephadex A-25 in the Cl-form and a pale-colored cation exchanger SP-Sephadex C-25 in the Na-form were used in order to discern the sign of the net charge on the final cobalt(III)–PAR species formed in the reaction at various pH by the sensitive coloration on the resin grains.

Measurements. The absorption spectra were measured with a Hitachi recording spectrophotometer model EPS-3T.

Fast changes in the absorption spectra and the rate of complex formation were measured with a Union Giken rapid-scan spectrophotometer model RA-1300 equipped with a stopped-flow cell.

The stopped-flow signal for the scattered light[12] was also observed with this apparatus.

All measurements were carried out at 25.0±0.2 °C. The ionic strength was maintained at 0.1 mol dm^{-3} with sodium perchlorate. The pH of the solution was adjusted with acetate or hexamine buffers and measured with a Radiometer pH-meter 4d (Copenhagen) equipped with a glass electrode type G 202B and a reference calomel electrode type 401. The pH-meter readings for the 5 or 10% (v/v) dioxane–water solutions were used without correction.[14]

Results and Discussion

I. Rapid-scan Spectral Studies. Cobalt–PAR. Rapid-scan Spectra: Figure 2(a) shows a typical example of the spectral change for the reaction of Co^{2+} and PAR in aqueous solution at pH 5.46. Each spectrum was rapidly scanned at appropriate time intervals after the solution containing cobalt(II) perchlorate in excess was rapidly mixed with a PAR solution by the stopped-flow technique. The figure clearly indicates that two steps are involved in the reaction.

At the initial stage, the spectrum of the reaction mixture changed rapidly with an isosbestic point at 450 nm. The absorption around 400 nm due to the free ligand PAR decreased with the increase of a new absorption around 500 nm due to the complex. The rapid spectral change ceased in *ca.* 40—50 ms after mixing. Then a relatively slow spectral change occurred with other isosbestic points at 330 and 435 nm. The final equilibrium was attained in *ca.* 3 min under the given conditions.

The change in the rapid-scan spectra for the reaction of Co^{2+} and PAR at pH 2.72 (Fig. 2(b)) differs from that at pH 5.46 (Fig. 2(a)), but it is still evident that two steps with two sets of isosbestic points are involved in the reaction.

In each case, the final spectrum coincides with the spectrum of $[Co^{III}(par)_2]$, which was obtained under the same conditions either with an equilibrated solution

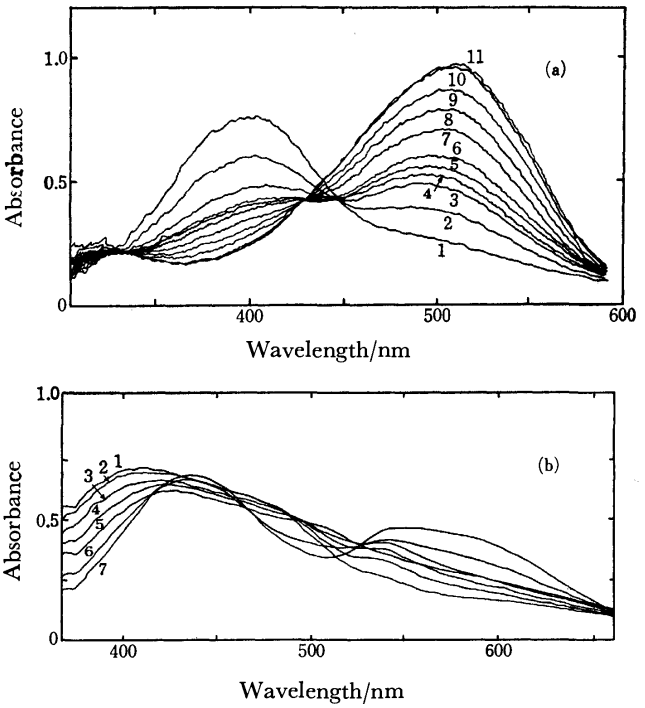

Fig. 2. (a) Rapid-scan spectra for the reaction of 7.64 × 10^{-4} mol dm^{-3} cobalt(II) perchlorate and 3.31 × 10^{-5} mol dm^{-3} PAR at pH 5.46, I=0.1 ($NaClO_4$), and 23 °C, measured at 0 (1), 10 (2), 25 (3), 50 (4), 100 ms (5), 0.5 (6), 5 (7), 20 s (8), 1 (9), 2 (10), and 3 min (11) after mixing. Scan rate: 300 nm/5 ms.

(b) Rapid-scan spectra for the reaction of 1.53 × 10^{-3} mol dm^{-3} cobalt(II) perchlorate and 3.57 × 10^{-5} mol dm^{-3} PAR at pH 2.72, I=0.1 ($NaClO_4$), and 25 °C, measured at 0 (1), 10 (2), 25 (3), 50 (4), 100 ms (5), 1 s (6), and 3 min (7) after mixing. Scan rate: 300 nm/5 ms.

prepared by mixing Co^{2+} and PAR in the molar ratio of 1 : 2 or with an aqueous solution of the isolated 1 : 2 cobalt(III) complex $[Co^{III}L(LH^*)]$ (Fig. 7).

Stopped-flow Signal: Figure 3 shows the change in absorbance with time at 510 nm in the course of the reaction under the same conditions as in Fig. 2(a). The stopped-flow signal also discriminates the fast reaction from the slower one. The rate of the first step

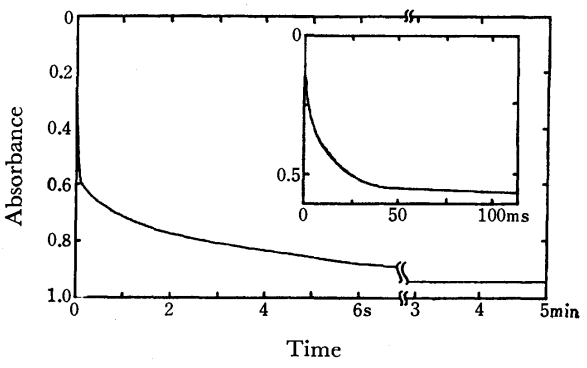

Fig. 3. Stopped-flow signal at 510 nm for the reaction of Co^{2+} and PAR. The experimental conditions are the same as those for Fig. 2(a). Inset shows an expanded signal for the initial stage of the reaction.

was found to be enhanced under the same conditions with the increase in the initial concentration of Co^{2+} ion (*vide infra*). This result indicates that the first step is the complex formation process. On the other hand, the effects of hydrogen peroxide on the reaction between Co^{2+} and PAR reveal that the second step involves the oxidation of cobalt(II)–PAR complex. When the solution of PAR containing 6% H_2O_2 was mixed with a Co^{2+} solution under the same conditions as in Fig. 3, only the second step was accelerated several-fold, leaving the first step essentially unaffected.

Substitution Reaction with EDTA: The results on the substitution reaction of cobalt–PAR complexes with EDTA also provide a further evidence for the presence of the Co(II) state in the initial stage of the present reaction and of the Co(III) state in the final stage. The solution containing Co^{2+} ion in excess was rapidly mixed with a yellow PAR solution at pH 5 with a microsyringe. The red color of the solution thus formed turned orange by the subsequent rapid addition of EDTA. The color change indicates the liberation of yellow ligand PAR, suggesting the presence of labile Co(II) state immediately after the rapid mixing of Co^{2+} and PAR.[15]

However, when once the final equilibrium is attained, the red color of the solution never changes on addition of even a large excess of EDTA. This fact suggests the formation of inert cobalt(III)–PAR complexes and the absence of labile cobalt(II)–PAR complexes in this stage of the reaction. The observed color changes are summarized in Scheme 1 together with those for the cobalt–PAN system.

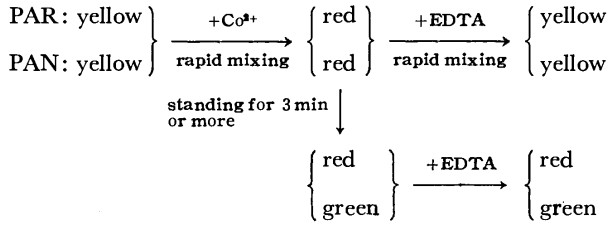

Scheme 1. Color change at pH *ca.* 5.

Ion-exchange Behavior of the Final Products: The nature of the final products was also proved by their ion-exchange behavior. The final product obtained at pH 2.72 was strongly adsorbed on the cation-exchange resin but not on the anion-exchange resin. On the other hand, the final product at pH 5.46 was strongly adsorbed on the anion-exchange resin but not on the cation-exchange resin. These facts lead to the conclusion that the final product is a tervalent cobalt complex with two ligand molecules having dissociated or undissociated *para*-hydroxyl groups with respect to the azo group; the final products at pH 2.72 and 5.46 are a cationic species $[Co^{III}(LH^*)_2]^+$ and an anionic species $[Co^{III}L_2]^-$, respectively. The net charge on the final product is supported by the pK_a value of the *para*-hydroxyl group of the ligand in $[Co(par)_2]$ (*vide infra*). It should be noted that 1:2 complexes are finally formed even though a large excess of Co^{2+} reacts with the ligand PAR.

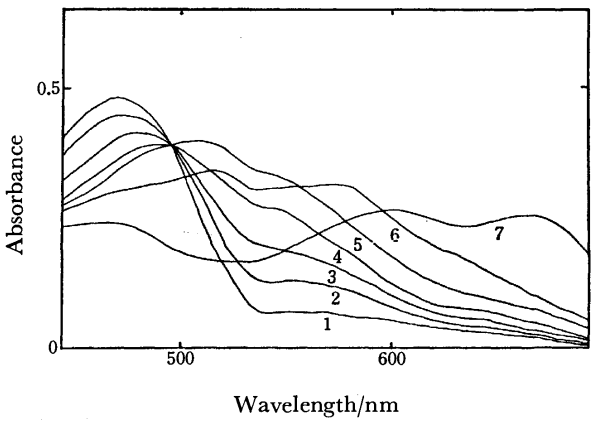

Fig. 4. Rapid-scan spectra for the reaction of 7.65×10^{-4} mol dm^{-3} cobalt(II) perchlorate and 2.99×10^{-5} mol dm^{-3} PAN in 5%(v/v) dioxane–water mixture at pH 4.72, I=0.1 ($NaClO_4$), and 25 °C, measured at 0 (1), 0.04 (2), 0.1 (3), 0.2 (4), 0.4 (5), 4 s (6), and 4 min (7) after mixing. Scan rate: 300 nm/20 ms.

Cobalt–PAN. Rapid-scan Spectra: Figure 4 shows the change of rapid-scan spectra for the reaction of Co^{2+} ion and PAN at pH 4.72. The experiments were carried out in 5%(v/v) dioxane–water solutions because of the very low water-solubility of PAN. At the initial stage, the spectrum of the reaction mixture changes rapidly with an isosbestic point at 490 nm. The absorption around 470 nm due to the free ligand PAN decreases in 400 ms with the increase of a new absorption around 540 nm due to a red-colored complex. This absorption in turn decreases in a few minutes with the increase of an absorption around 650 nm due to the formation of a green-colored complex.

The lability of the cobalt in the red and the green complex was confirmed by means of the substitution reaction with EDTA. The results shown in Scheme 1 indicate the formation of a red-colored labile cobalt(II) complex immediately after the rapid mixing of Co^{2+} and PAN and the subsequent slow formation of a green-colored inert cobalt(III) complex. These observations, together with the results of the kinetic study, indicate that the two-step reaction in Fig. 4 corresponds to the fast formation of cobalt(II)–PAN complex and the subsequent slow oxidation to a cobalt(III)–PAN complex $[Co^{III}(pan)_2]$.

However, no isosbestic point was observed for the oxidation step in contrast to the observation for the corresponding step of the cobalt–PAR system. For the reaction of Co^{2+} with PAN the formation of a neutral insoluble intermediate $[Co^{II}(pan)_2]^0$ was expected, as observed for the Ni^{2+}–PAN system.[12] In order to confirm this expectation, the stopped-flow signal of the scattered light was measured for the reaction of the Co^{2+}–PAN system.

Stopped-flow Signals for Scattered Light: Figure 5 shows the change in intensity of scattered light in the course of the reaction. The intensity increases after a short induction period and then decreases gradually. The feature is essentially independent of the wavelength of the incident monochromatic light in the range 400—600 nm. The induction period appearing at the initial

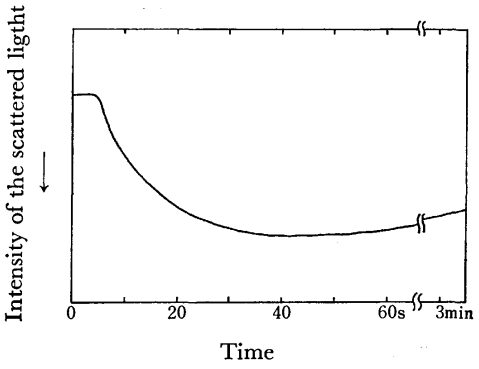

Fig. 5. Stopped-flow signal of the scattered light for the reaction of 1.91×10^{-5} mol dm^{-3} cobalt(II) perchlorate and 2.99×10^{-5} mol dm^{-3} PAN in 5%(v/v) dioxane–water mixture at pH 4.72, I=0.1 ($NaClO_4$) and 25 °C.

stage of the reaction corresponds to the formation of the cobalt(II)–PAN complex prior to the crystal growth. The subsequent increase in the intensity of the scattered light is due to the formation and the growth of the insoluble crystals of $[Co^{II}(pan)_2]^0$. The final decreasing portion of the signal indicates the process of redissolution of the insoluble intermediate. This corresponds to the step of oxidation of $[Co^{II}(pan)_2]^0$ forming a more soluble $[Co^{III}(pan)_2]^+$ complex. The lack of an isosbestic point in the spectra for the second step of the present reaction shown in Fig. 4 is due to the formation of an insoluble intermediate $[Co^{II}(pan)_2]^0$.

Cobalt–TAR and Cobalt–TAN. Similar spectral changes were observed for the reactions of Co^{2+}–TAR and –TAN. The ligands TAR and TAN, which have a thiazolyl group instead of pyridyl group in PAR and PAN, are insoluble in water. The experiments were, therefore, carried out in a 5 or 10%(v/v) dioxane–water solution. The spectral change for these systems also consists of a fast and a subsequent slower step. Two sets of distinct isosbestic points were observed in the spectra for the reaction of Co^{2+} and TAR, while no isosbestic point was observed for the second step of the Co^{2+}–TAN system.

Experiments on the substitution reactions of the intermediates and the final products with EDTA were carried out for both the cobalt-TAR and the cobalt–TAN system in the same way as described for the PAR and the PAN system. Stopped-flow signals for the scattered light similar to the signal shown in Fig. 5 were observed for the Co^{2+}–TAN reaction.

It is concluded that the reactions of Co^{2+}–TAR and –TAN proceed by the same mechanism as for the Co^{2+}–PAR and –PAN systems, respectively. In each system, the first and the second step correspond to the formation of cobalt(II) complex and subsequent oxidation, respectively. The reaction of cobalt(II) with TAN involves the formation of insoluble intermediate, $[Co^{II}(tan)_2]^0$.

Effect of Oxygen on the Oxidation of Cobalt(II) Complexes. In order to ascertain if the cobalt(II) complexes are stable in deoxygenated media, we carried out spectrophotometric measurements for the cobalt(II)–PAN and the cobalt(II)–PAR system with a device connected to a vacuum system (Fig. 6). In this device the solutions of Co^{2+} and the ligand were separately degassed beforehand by freezing several times. Then the solutions were mixed and introduced into the optical cell *in vacuo*. This approach succeeded in detection of the cobalt(II)–PAN and the cobalt(II)–PAR complex even with an ordinary spectrophotometer, since in the measurements with this device the rate of oxidation was lowered by 50—60 times for both systems as compared with that in undegassed solutions. Spectra thus obtained were identical with those of the cobalt(II) complexes observed transiently by the rapid-scan spectrophotometer. It is concluded that $[Co^{II}(pan)_2]$ and $[Co^{II}(par)_2]$ complexes are oxidized by oxygen in the solution and that even a trace amount of oxygen takes part in the oxidation to cobalt(III) complexes.

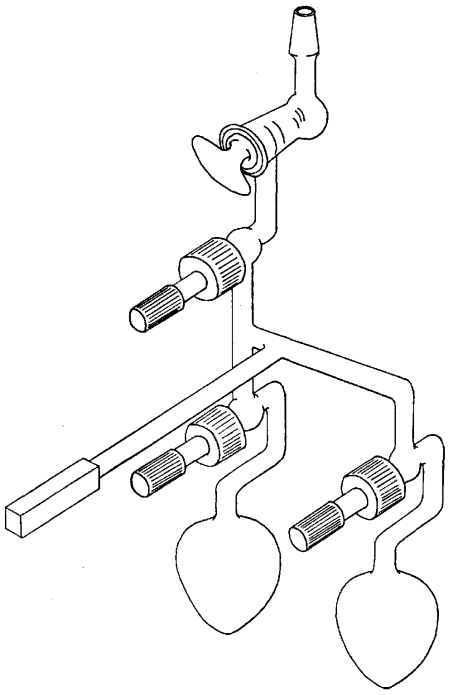

Fig. 6. Evacuable mixing device for measurements of absorption spectra in deoxygenated systems.

II. Equilibrium and Kinetic Studies. Composition of the Cobalt–PAR and –PAN Complexes. The Composition of the short-lived intermediate cobalt(II) complexes was determined to be 1 : 2 by applying the method of continuous variation to the first rapid change of the stopped-flow signals as shown in the inset of Fig. 3. The composition of the cobalt(III) complexes of PAR and PAN in the aqueous and the 50%(v/v) dioxane–water solutions, respectively, was determined also to be 1 : 2 by the usual continuous variation method.

Protonation-Deprotonation of $[Co^{III}(par)_2]$. Figure 7 shows the pH-dependence of the spectrum of an aqueous solution of the isolated cobalt(III)–PAR complex $[Co^{III}L(LH^*)]$. The same pH-dependence of the spectrum was also observed with an equilibrated solution prepared from Co^{2+} and PAR in a molar ratio of 1 : 2. It is attributed to the protonation-deprotonation of the *para*-hydroxyl group of the coordinated

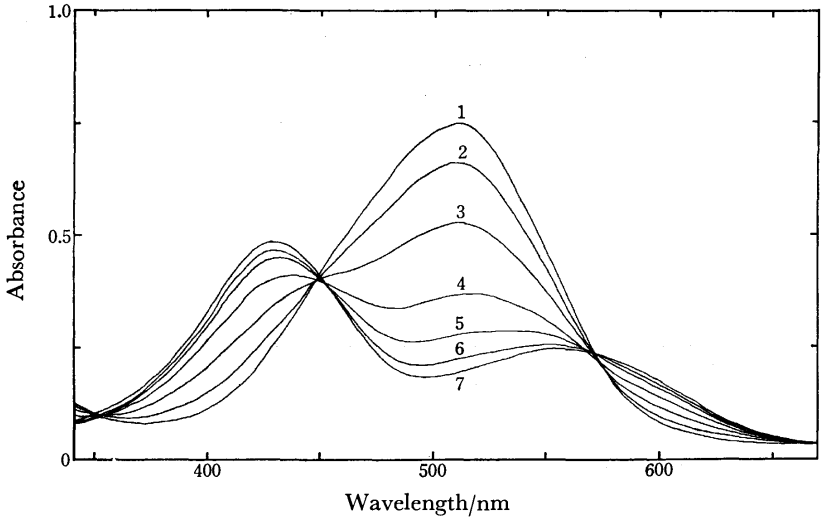

Fig. 7. Absorption spectra of the aqueous solution of $[Co^{III}(par)_2]$ as a function of pH at 25 °C and I=0.1 ($NaClO_4$). $[Co^{III}(par)_2]$= 1.26×10^{-5} mol dm^{-3}. pH=9.29 (1), 5.05 (2), 4.39 (3), 3.73 (4), 3.26 (5), 2.77 (6), and 1.88 (7).

PAR in the inert cobalt(III) complex.

Acid-dissociation constants for

$$[Co^{III}(LH^*)_2]^+ \overset{K_{a1}}{\rightleftharpoons} [Co^{III}L(LH^*)] + H^+$$

and

$$[Co^{III}L(LH^*)] \overset{K_{a2}}{\rightleftharpoons} [Co^{III}L_2]^- + H^+$$

were determined from the result shown in Fig. 7. The plots of absorbance *vs.* pH at 420, 510, and 600 nm indicate that the values of pK_{a1} and pK_{a2} are not quite different from each other, the average value being 4.1.[16]

From these results and the ion-exchange behavior the cobalt(III)–PAR complexes are found to be in the form of an anionic $[Co^{III}L_2]^-$ (λ_{max}=510 nm, ε_{max}=57000) at pH 6 or higher, and a cationic $[Co^{III}(LH^*)_2]^+$ (λ_{max}=430 nm, ε_{max}=37500; λ_{max}=558 nm, ε_{max}= 18300) at pH 2 or lower. Features of the spectral change depicted in Fig. 7 suggest the formation of a neutral species $[Co^{III}L(LH^*)]^0$, since two sets of isosbestic points are observed at 452 and 568, and 448 and 574 nm.[17]

Overall Reaction Mechanisms for the Formation of Cobalt(III) Complexes. On the basis of the results given above the overall reaction mechanisms for the formation of 1:2 cobalt(III) complexes with the ligands PAR and PAN are summarized in Schemes 2 and 3, respectively. It should be noted that cobalt(II) complexes are oxidized only *via* formation of 1:2 complexes, $[Co^{II}(par)_2]$ or $[Co^{II}(pan)_2]$.

Kinetics on the Formation of Cobalt(II) Complexes. Kinetic measurements were carried out under the conditions of Co^{2+} ion in large excess over the ligand. For the calculation of rate constants, the first rapid change in the stopped-flow signal was analyzed after subtracting the part of slower oxidation step involved in the signal. The stopped-flow signals were followed at the absorption maxima for the 1:2 cobalt(II) complexes and for the free ligands PAR or PAN as well. Both signals for the fast complex formation gave a single exponential curve characterized by the same pseudo-first-order rate constant, k_{obsd}. The result and the values of k_{obsd} suggest that the coordination of the first ligand is the rate-determining step, the coordination of the second ligand molecule proceeding very fast.

Cobalt(II)–PAR: The rate of formation of cobalt(II)–PAR complex was determined in aqueous solution at pH 3—6 with 10—100 fold excess of Co^{2+} ion over the ligand. The absorbance change at 510 nm was used for the calculation of rate constants. The pseudo-first-order rate constant k_{obsd} showed first-order dependence on the total concentration of Co^{2+}, [Co], at constant pH as shown by

$$k_{obsd} = k_f[Co] + k_d. \quad (1)$$

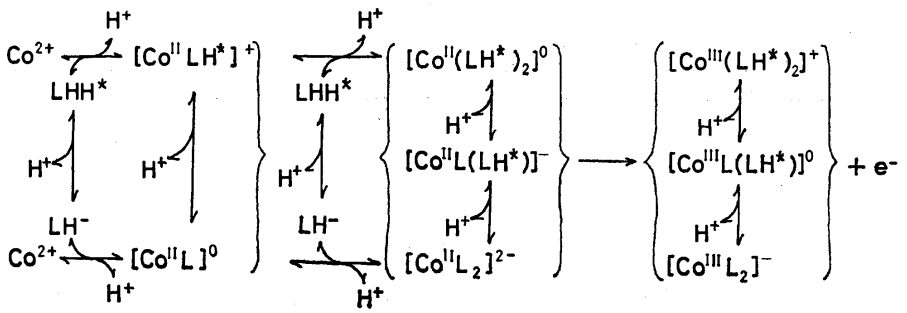

Scheme 2. Overall reaction mechanism for the formation of $[Co^{III}(par)_2]$.[1]

Table 1. Kinetic data[a] for the formation of cobalt(II) complexes at 25 °C and I=0.1 ($NaClO_4$)

Ligand	[Co] 10^{-3} mol dm^{-3}	at pH	Rate constant k_{obsd}/s^{-1} 3.03	4.10	4.62	4.95	5.60
PAR[b]	0.38		7.0	28	37	38	39
	0.77		23	44	59	60	72
	1.53		45	83	110	120	130
	2.30		67	120	140	160	200
	3.06		83	—	180	210	240
	k_f/10^4 dm^3 mol^{-1} s^{-1}		2.8	4.7	5.4	6.1	7.7
	k_d/s^{-1} [e]		3.0	15	19	22	23
		at pH	3.83	4.45	4.72	5.03	
PAN[c]	0.38		1.7	1.7	2.3	2.2	
	0.77		3.4	3.7	4.5	4.3	
	1.53		6.8	6.6	8.3	9.9	
	2.30		9.9	9.8	11	12	
	3.06		12	14	14	15	
	k_f/10^3 dm^3 mol^{-1} s^{-1}		4.1	4.4	4.5	4.8	
	k_d/s^{-1} [e]		0.3	0.2	0.5	0.5	

Ligand	[Co] 10^{-3} mol dm^{-3}	Rate constant k_{obsd}/s^{-1} at pH 4.7
TAR[c]	0.38	44
	0.77	68
	1.53	110
	2.30	150
	3.06	210
	k_f/10^4 dm^3 mol^{-1} s^{-1}	6.1
	k_d/s^{-1} [e]	20
		at pH 4.7
TAN[d]	0.38	4.0
	0.77	6.4
	1.53	12
	2.30	14
	3.06	19
	k_f/10^3 dm^3 mol^{-1} s^{-1}	5.6
	k_d/s^{-1} [e]	2

a) Experimental error ± 15%. Value of pH kept within ±0.05. Concentration of the ligands in the range (2—4)×10^{-5} mol dm^{-3}. b) Measured in water. c) Measured in 5%(v/v) dioxane–water. d) Measured in 10%(v/v) dioxane–water. e) Ref. 20.

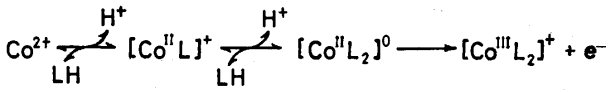

Scheme 3. Overall reaction mechanism for the formation of $[Co^{III}(pan)_2]$.

Forward and backward rate constants, k_f and k_d, were evaluated from the slope and the intercept of the linear plot of k_{obsd} against [Co] (Table 1). Under the experimental conditions the mechanism for the step of formation of 1 : 1 cobalt(II)–PAR complex was postulated as follows, the hydrolysis of Co^{2+} being neglected.[18]

$$\begin{array}{ccc} Co^{2+} + LHH^* & \underset{k_{-1}}{\overset{k_1}{\rightleftharpoons}} & CoLH^{*+} + H^+ \\ K_a \uparrow\downarrow & & K_G \uparrow\downarrow \\ Co^{2+} + LH^- + H^+ & \underset{k_{-2}}{\overset{k_2}{\rightleftharpoons}} & CoL + 2H^+ \end{array}$$

According to this mechanism, the overall formation rate constant k_f is expressed by

$$k_f = \frac{k_1[H] + k_2K_a}{[H] + K_a} \quad (2)$$

or

$$k_f(1 + K_a[H]^{-1}) = k_1 + k_2K_a[H]^{-1}, \quad (3)$$

where K_a denotes the acid-dissociation constant of *para*-hydroxyl proton of PAR. The plot of $k_f(1+K_a[H]^{-1})$ against $[H]^{-1}$ gives a straight line. The rate constants k_1 and k_2 were determined from the intercept and the slope to be 4.8×10^4 and 9.8×10^4 dm^3 mol^{-1} s^{-1}, respectively, using the value pK_a=5.6.[7]

Cobalt(II)–PAN: The rate of formation of the cobalt(II)–PAN complex was measured with 5%(v/v) dioxane–water solutions at pH 3—5 with 10—100 fold excess of Co^{2+} ion over the ligand. For the calculation of rate constants, the stopped-flow signal at 540 nm, the absorption maximum of the 1 : 2 complex, was used. The pseudo-first-order rate constant, k_{obsd}, at constant pH showed first-order dependence on [Co], as shown by Eq. 1 (see Table 1). The k_f values obtained from the linear plot show a slight dependence of [H]. The pH-dependence of k_{obsd} is interpreted by the following reaction scheme.

$$\begin{array}{ccc} Co^{2+} + LH_2^+ & \underset{k_{-1}}{\overset{k_1}{\rightleftharpoons}} & Co^{II}L^+ + 2H^+, \\ K_a' \uparrow\downarrow & & k_2 \nearrow\swarrow k_{-2} \\ Co^{2+} + LH + H^+ & & \end{array}$$

where LH_2^+ denotes a unipositive species of PAN protonated on the pyridyl nitrogen having $K_a'=10^{-2.9}$.[19] According to this mechanism the overall formation rate constant k_f is expressed by

$$k_f = \frac{k_1[H] + k_2K_a'}{[H] + K_a'} \quad (4)$$

or

$$k_f(1 + K_a'[H]^{-1}) = k_1 + k_2K_a'[H]^{-1}. \quad (5)$$

The plot of $k_f(1+K_a'[H]^{-1})$ against $[H]^{-1}$ gives a straight line. The rate constants k_1 and k_2 were determined from the intercept and the slope to be $<10^3$ and 4.6×10^3 dm^3 mol^{-1} s^{-1}, respectively.

The rate constants k_f and k_d were also evaluated for the TAR and the TAN complex. The data obtained for the cobalt(II)–TAR and –TAN systems would be explained by the mechanisms for the PAR and the PAN complex, respectively.

The rate constants are summarized in Tables 1 and 2. It is noticeable in Table 2 that the protonated cationic species of PAN is inert for the complex formation of Co^{2+} as was found in the reaction of Ni^{2+} and PAR,[21] suggesting that the first coordinating group in PAR and PAN is the pyridyl group in the ligands.

Wilkins reported the kinetic data on the reactions of a neutral ligand 4-(2-pyridylazo)-*N*,*N*-dimethylaniline

Table 2. Rate constants for the formation of cobalt(II) complexes at 25 °C and I=0.1 ($NaClO_4$)

Ligand		Rate constant	
PAR	LH_2	k_1/dm^3 mol^{-1} s^{-1}	4.8×10^4
	LH^-	k_2/dm^3 mol^{-1} s^{-1}	9.8×10^4
PAN	LH_2^+	k_1/dm^3 mol^{-1} s^{-1}	$<10^3$
	LH	k_2/dm^3 mol^{-1} s^{-1}	4.6×10^3
PAD[a]		k_f/dm^3 mol^{-1} s^{-1}	4.0×10^4
H_2O[b]		k_{H_2O}/s^{-1}	1.1×10^6

a) Ref. 22. b) Ref. 27.

(PAD) with Co^{2+} or Ni^{2+} ion.[22] PAD is a bidentate ligand having a structure similar to that of PAR except for the absence of intramolecular hydrogen-bond. In his paper, the values of the formation constant of the outer-sphere complex for the neutral ligand species, K_{os},[23] and the distance of closest approach of the reactant molecules, a, are estimated to be 0.1 dm^3 mol^{-1} and 5 Å, respectively. Since the rate constants reported for the reactions of Co^{2+} and PAD are in the same order of magnitude as the rate constants for the reactions of Co^{2+} and the neutral species of PAR, LH_2 (see Table 2), it would be reasonable to assume that the reaction of PAR and Co^{2+} also proceeds by the same mechanism as in the case of PAD and that the internal rotation of the resorcinol moiety around the C–N axis in PAR preceded by the rupture of the stable intramolecular hydrogen-bond does not eventually lower the overall rate of complex formation.

However, in the reaction of Co^{2+} and PAN the formation rate constant is smaller by one order of magnitude than that of the corresponding reaction of PAR. This difference observed in similar ligands might be explained by the following: (a) the difference in values of K_{os}[23] for the two systems, (b) the effect of small amounts of dioxane added in the case of PAN on the rate constants, (c) retardation of complex formation by the relative slowness of the internal rotation of the bulky naphthol moiety in PAN for the formation of the terdentate complex,[1] and (d) steric hindrance caused by the shape of a bulky ligand PAN on the first coordination site in the ligand.

As regards (a), if the relatively small rate constants for the Co^{2+}–PAN system as compared with the case of Co^{2+}–PAR were attributed to the lower values of K_{os}, the reaction distance a for the complex formation of PAN would be evaluated to be 2—3 Å.[25] This is about a half of the value of a estimated by Funahashi and Tanaka for the Ni^{2+}–PAR system,[25] and would be too small as the reaction distance for the Co^{2+}–PAN system. The second possibility (b) is also not essential, since the rate constant of complex formation of a similar ligand TAR is in the same order of magnitude even in dioxane–water media as that of PAR observed in aqueous media. Therefore, it would be reasonable to infer that the intervening step of internal rotation of the bulky naphthol moiety around the C–N axis (c) and a steric hindrance caused by the particular shape of the bulky PAN molecule on the site of the first coordination at the pyridyl nitrogen atom (d) would essentially be responsible for the retardation of the overall reaction in PAN. The smaller rate constants observed for the reaction of Ni^{2+} and PAN as compared with those of Ni^{2+} and PAR would also be attributed to the difference in character of these ligands.[26]

References

1) S. Ooi, D. Carter, and Q. Fernando, *Chem. Commun.*, **1967**, 1301.

2) M. Kurahashi, *Chem. Lett.*, **1974**, 1271; *Bull. Chem. Soc. Jpn.*, **49**, 127, 872, 1419, 2927, 3053 (1976).

3) S. Shibata, "2-Pyridylazo Compounds in Analytical Chemistry," in "Chelates in Analytical Chemistry," ed by H. A. Flaschka and A. J. Barnard, Jr., Vol. 4, Marcel Dekker, Inc., New York, N. Y. (1972), p. 1; R. G. Anderson and G. Nickless, *Analyst*, **92**, 207 (1967); **93**, 13, 20 (1968); S. Shibata, *Bunseki Kagaku*, **21**, 551 (1972); H. Wada, *ibid.*, **21**, 543 (1972); H. R. Hovind, *Analyst*, **100**, 769 (1975).

4) K. L. Cheng and R. H. Bray, *Anal. Chem.*, **27**, 782 (1955); G. Goldstein, D. L. Manning, and O. Menis, *ibid.*, **31**, 192 (1959); T. Yotsuyanagi, R. Yamashita, and K. Aomura, *ibid.*, **44**, 1091 (1972).

5) R. Yamashita, T. Yotsuyanagi, and K. Aomura, *Bunseki Kagaku*, **20**, 1282 (1971) and the literatures cited therein.

6) T. Iwamoto, *Bull. Chem. Soc. Jpn.*, **34**, 605 (1961); *cf.*, "Stability Constants," Special Publication No. 17, The Chemical Society (London) (1964), p. 657 and 701; "Stability Constants, Supplement No. 1," Special Publication No. 25, The Chemical Society (London) (1971), p. 661, 738, 590, and 714.

7) M. Hniličková and L. Sommer, *Collect. Czech. Chem. Commun.*, **26**, 2189 (1961).

8) T. Iwamoto and M. Fujimoto, *Anal. Chim. Acta*, **29**, 282 (1963).

9) K. Mochizuki, T. Imamura, T. Ito, and M. Fujimoto, *Chem. Lett.*, **1976**, 1207.

10) M. Široki, L. Marić, Z. Štefanac, and M. J. Herak, *Anal. Chim. Acta*, **75**, 101 (1975).

11) T. Ito, K. Mochizuki, T. Komazawa, and M. Fujimoto, presented at the 1976 Summer Meeting in Hokkaido of the Chemical Society of Japan and the Japan Society for Analytical Chemistry, Kitami, July 19, 1976, Abstracts, p. 12.

12) K. Mochizuki, T. Imamura, T. Ito, and M. Fujimoto, *Chem. Lett.*, **1977**, 1239.

13) F. H. Pollard, P. Hanson, and W. J. Geary, *Anal. Chim. Acta*, **20**, 26 (1959).

14) N. Yoshida and M. Fujimoto, *Bull. Chem. Soc. Jpn.*, **50**, 1328 (1977).

15) On standing for a long time at room temperature this solution turned again reddish orange. The final product was $[Co^{III}(par)_2]$ (See Ref. 9).

16) It is difficult to determine spectrophotometrically the values of pK_{a1} and pK_{a2} separately, because $[Co^{III}L(LH^*)]$ shows approximately an average spectrum of $[Co^{III}(LH^*)_2]^+$ and $[Co^{III}L_2]^-$. From the results of the solvent extraction Yotsuyanagi and Hoshino reported the values $pK_{a1}=3.64$ and $pK_{a2}=4.41$. See T. Yotsuyanagi and H. Hoshino, *Bunseki*, **1976**, 743. Corsini *et al.* have determined pK_{a1} and pK_{a2} in 50%(v/v) dioxane–water by potentiometric titration to be 4.8 and 6.0, respectively. See A. Corsini, Q. Ferdinando, and H. Freiser, *Anal. Chem.*, **34**, 1090 (1962).

17) On standing overnight around pH 4 the solution of the cobalt(III)–PAR complex gave even in 10^{-5} mol dm^{-3} a reddish orange flocculent precipitate of $[Co^{III}L(LH^*)]^0$.

18) "Stability Constants," Special Publication No. 17, The Chemical Society (London) (1964), p. 54.
19) G. Nakagawa and H. Wada, *Nippon Kagaku Zasshi*, **84**, 639 (1963).
20) The intercepts of the linear plot of k_{obsd} *vs.* [Co] would give the values of backward rate constant k_d. However, the value of k_d can not immediately be assigned to the rate-determining step responsible for the reverse reaction. The value of k_d thus derived might include the rate constants for the dissociation of the second and/or the first coordinated ligand molecule in the complex.
21) M. Fujimoto, presented at the 21st Meeting on the Coordination Chemistry, Nagoya, October 17, 1971, Abstracts, p. 87.
22) R. G. Wilkins, *Inorg. Chem.*, **3**, 520 (1964).
23) According to Fuoss[24] the association constant of outer-sphere complex K_{os} is expressed as $K_{os}=(4\pi Na^3/3000)\cdot \exp[-U(a)/kT]$, where $U(a)=z_1z_2e^2/aD-z_1z_2e^2k/D(1+\kappa a)$ and $\kappa=(8\pi Ne^2I/1000DkT)^{1/2}$, N is Avogadro's number, a the reaction distance, *i.e.*, the distance of closest approach for the reactant molecules to form the outer-sphere complex, z the net charge of the reactants, D the bulk dielectric constant, e the elementary charge, k the Boltzmann's constant, and I the ionic strength.
24) R. M. Fuoss, *J. Am. Chem. Soc.*, **80**, 5059 (1958).
25) For the reactions involving a neutral reactant species K_{os} is reduced to $K_{os}=4\pi Na^3/3000$. Funahashi and Tanaka suggested that the value of K_{os} for the reaction of Ni^{2+} and LH^-, a uninegative species of PAR, is comparable to the values of K_{os} for the reactions of neutral ligand species of similar size. Namely, they assumed that the uninegative ligand PAR behaves like an uncharged ligand irrespective of the presence of a remote charge on the bulky ligand molecule. S. Funahashi and M. Tanaka, *Inorg. Chem.*, **8**, 2159 (1969).
26) C. D. Hubbard and D. Pacheco A, *J. Inorg. Nucl. Chem.*, **39**, 1373 (1977).
27) T. J. Swift and R. E. Connick, *J. Chem. Phys.*, **37**, 307 (1962).

Copper(II)-2,2′-Bipyridine-Eriochrome Cyanine R Ternary Complex and Its Application to the Spectrophotometric Determination of Copper(II)

Ryoei Ishida, Hifumi Narita, and Koichi Tonosaki

Department of Chemistry, Faculty of Science, Hirosaki University, Hirosaki, Aomori 036

(Received September 26, 1977)

Copper(II) ion reacted with 2,2′-bipyridine (bpy) and Eriochrome Cyanine R (ECR) to give one of two kinds of ternary complexes according to the amount of reagents in a weakly basic medium. The combining ratios of three components in the complexes were estimated to be Cu(II): bpy: ECR=1: 1: 2 and 1: 1: 1, respectively, the former having an absorption maximum at 515 nm and the latter at 550 nm. The color development of the 1: 1: 2 complex was utilized in the spectrophotometric determination of copper(II) at microgram level. The ternary complex gave a maximum absorbance at 515 nm in the pH range 10.2—10.6. Under optimum pH, 2,2′-bipyridine and Eriochrome Cyanine R concentrations, a linear relationship holds between the absorbance of the complex and copper(II) concentration up to 6×10^{-5} mol dm^{-3}. The apparent molar absorption coefficient at 515 nm is about 20400 dm^3 mol^{-1} cm^{-1}, corresponding to Sandell's sensitivity index of 0.003_1 μg cm^{-2}.

Eriochrome Cyanine R (ECR), sodium 2″-sulfo-5,5′-dimethyl-4-hydroxyfuchsone-3,3′-dicarboxylate, a dyestuff of the triphenylmethane series like Chromazurol S, has been used for the spectrophotometric determination of aluminium(III),[1-3] beryllium(II)[4,5] and scandium(III),[6] and others. While 2,2′-bipyridine (bpy) is a sensitive and selective reagent for iron(II),[7,8] it has been reported to form a 1: 2 complex with copper(I), and a 1: 3 complex with copper(II).[9]

In a previous paper, the formation reaction of Cu(II)–bpy–Chromazurol S mixed ligand complex and its application to the spectrophotometric determination of copper(II) was reported.[10]

The present paper deals with studies on the color reaction forming the ternary complex composed of copper(II), 2,2′-bipyridine and Eriochrome Cyanine R, which has a structure similar to that of Chromazurol S, and on the spectrophotometric determination of copper(II) by means of this ternary complex. The composition of the ternary complex as well as the fundamental conditions for the determination of copper(II) are discussed.

Experimental

Reagents. Copper(II) Standard Stock Solution (1.00×10^{-2} mol dm^{-3}): Copper metal (Purity: 99.99%) was dissolved in a small amount of dilute nitric acid, with heating, and the solution was evaporated nearly to dryness on a water bath. The residual contents were dissolved in water containing nitric acid, and the solution was diluted with water in a volumetric flask (nitric acid was added to make the final acidity 0.01 mol dm^{-3}).

Standard Solution: The stock solution was diluted as required.

2,2′-Bipyridine Solution (1.00×10^{-3} mol dm^{-3}): 2,2′-Bipyridine (Wako Pure Chemical Industries, Ltd.) was dissolved in water containing hydrochloric acid (final concentration of hydrochloric acid: 0.002 mol dm^{-3}).

Eriochrome Cyanine R Solution (2.00×10^{-3} mol dm^{-3}): Eriochrome Cyanine R (Merck & Co., Inc.) was dissolved in water containing hydrochloric acid (final concentration of hydrochloric acid: 0.008 mol dm^{-3}). The acidified Eriochrome Cyanine R solution was stable for at least 1 year.

Buffer Solution: A borate buffer solution was prepared by mixing 0.1 mol dm^{-3} solution of borax and 0.2 mol dm^{-3} solution of hydrochloric acid or sodium hydroxide.

Triton X-100 Solution (1%, v/v): This was prepared by diluting polyethylene glycol mono[*o*-(1,1,3,3-tetramethylbutyl)phenyl]ether (BDH Chemicals Ltd.) with water.

All the other reagents were of analytical reagent grade. Doubly distilled water was used.

Apparatus. A Hitachi model 124 double-beam recording spectrophotometer and a Hitachi 139 spectrophotometer were used for measuring absorbance in glass cells of 10-mm pathlength. Measurements were carried out at 25±0.1 °C.

A Hitachi-Horiba model F-7 glass electrode pH meter was used for pH measurements.

Standard Procedure. An aliquot of a standard copper(II) solution was transferred to a 25-cm^3 volumetric flask, and then 2,2′-bipyridine and Eriochrome Cyanine R solutions were added. The flask was filled up to about 10 cm^3 by adding water. The pH value was adjusted with a buffer solution, the ionic strength of the solution being controlled to 0.1 with the amount of buffer solution. The total volume of the solution was made up to the mark with water. After gentle mixing, the absorbance of the resulting solution was measured against the reagent blank obtained in the same way.

Results and Discussion

Absorption Spectra. Suk and Mikeťuková[11] reported that Eriochrome Cyanine R dissociates in aqueous solution as follows:

$$H_5ECR^+ \rightleftarrows H_4ECR^0 \rightleftarrows H_3ECR^- \rightleftarrows H_2ECR^{2-} \rightleftarrows HECR^{3-} \rightleftarrows ECR^{4-}$$

The absorption spectra of each species caused by the acid dissociation of Eriochrome Cyanine R in aqueous medium are shown in Fig. 1. No spectrum of the neutral species H_4ECR^0 is shown, since it is almost insoluble in water. In the reaction, mainly the $HECR^{3-}$ species takes part in the color development.

The absorption spectra of the reagent blank (bpy and ECR) and the ternary complex with copper(II) at pH 10.4 are shown in Fig. 2. For the sake of comparison the spectrum of Cu(II)–ECR binary complex at the same pH value is also given. The absorption spectrum of the reagent blank (Curve 1) coincides with that of Eriochrome Cyanine R itself. Thus it seems that there is no interaction between Eriochrome Cyanine R and 2,2′-bipyridine. The maximum absorption wavelengths of both the binary and the ternary complexes are found

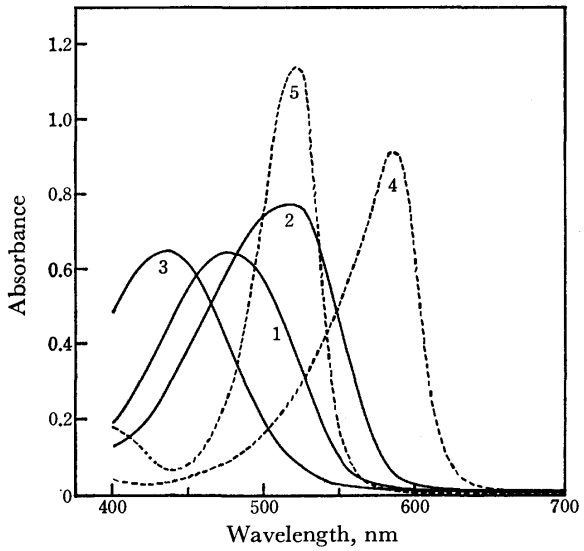

Fig. 1. Absorption spectra of Erichrome Cyanine R at various acidities.
Concn of ECR—1, 2 and 3: 6.0×10^{-5} mol dm^{-3}, 4 and 5: 3.0×10^{-5} mol dm^{-3}; acidity—1: pH 1.35 (H_3ECR^-), 2: pH 3.50 (H_2ECR^{2-}), 3: pH 9.00 ($HECR^{3-}$), 4: pH 13.5 (ECR^{4-}), 5: 9 mol dm^{-3} H_2SO_4 (H_5ECR^+).

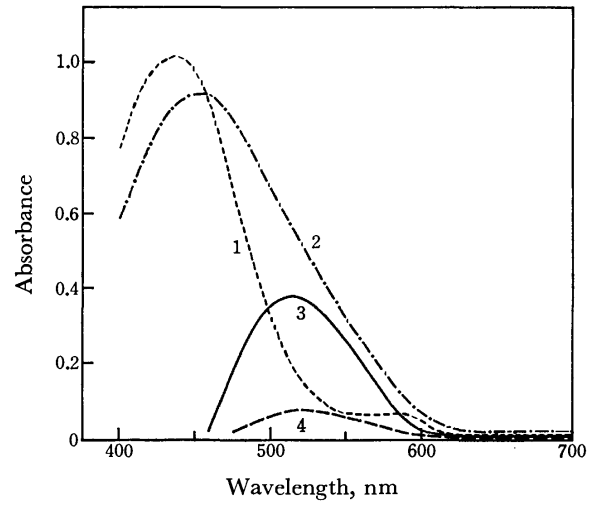

Fig. 2. Absorption spectra of Cu(II)-bpy-ECR complex and binary Cu(II)-ECR complex.
Concn of Cu(II), bpy and ECR: 2.0×10^{-5} mol dm^{-3}, 4.0×10^{-5} mol dm^{-3} and 1.0×10^{-4} mol dm^{-3}, respectively; pH: 10.4, ionic strength: 0.1; 1: reagent blank *vs.* water, 2: Cu(II)-bpy-ECR *vs.* water, 3: Cu(II)-bpy-ECR *vs.* reagent blank, 4: Cu(II)-ECR *vs.* ECR.

at about 515 nm. The addition of 2,2′-bipyridine to the Cu(II)-ECR complex gives rise to a large hyperchromic shift at the maximum absorption wavelength. The hyperchromic effect is probably due to the increment of molecular cross section caused by the combination with 2,2′-bipyridine. It follows that the sensitivity of the color development increases remarkably (about 5-fold).

The absorption spectra of colored solutions at different pH values were measured against the reagent blanks

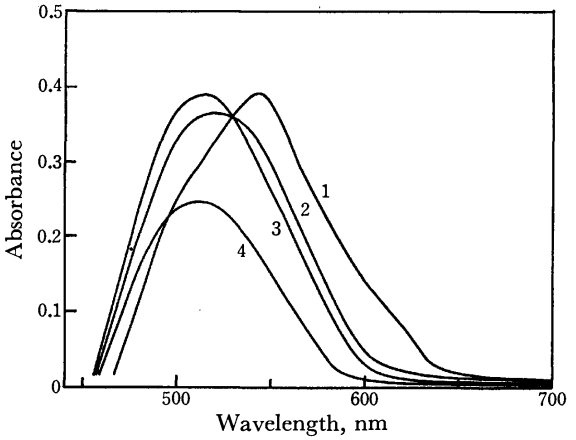

Fig. 3. Absorption spectra of Cu(II)-bpy-ECR complex at various pH values.
Concn of Cu(II), bpy and ECR: 2.0×10^{-5} mol dm^{-3}, 4.0×10^{-5} mol dm^{-3} and 1.0×10^{-4} mol dm^{-3}, respectively; Triton X-100: 0.04%, ionic strength: 0.05; 1: pH 9.60, 2: pH 10.00, 3: pH 10.31, 4: pH 11.15.

(Fig. 3). At pH above 10, the maximum absorption wavelength is found at 515 nm, the spectra showing similar shapes. At pH below 10, each peak is shifted toward a longer wavelength, and at pH below 9.5, a part of the formed complex precipitates, even in the presence of Triton X-100 (0.04%).

The concentration of Eriochrome Cyanine R was kept constant and varying amounts of an equimolar mixed solution of copper(II) and 2,2′-bipyridine were added. The absorption spectra were measured against the water blank. The results for pH 10.4 are shown in Fig. 4.

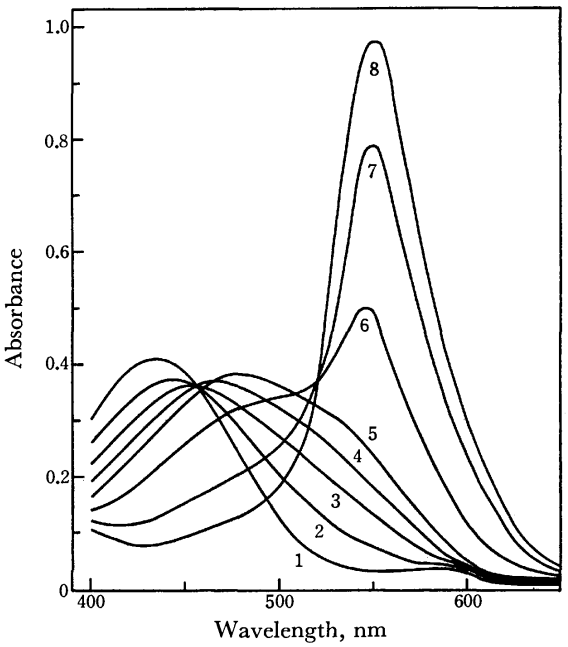

Fig. 4. Absorption spectra of Cu(II)-bpy-ECR system.
Concn of ECR: 4.0×10^{-5} mol dm^{-3}; pH: 10.4, Triton X-100: 0.04%, ionic strength: 0.05; each concn of Cu(II) and bpy (mol dm^{-3})—1: 0, 2: 5.0×10^{-6}, 3: 1.0×10^{-5}, 4: 1.5×10^{-5}, 5: 2.0×10^{-5}, 6: 3.0×10^{-5}, 7: 4.0×10^{-5}, 8: 5.0×10^{-5}.

Under the conditions of excess copper(II), a part of the complex formed precipitate. However, by addition of Triton X-100 the complex existed in a homogeneous dispersed state without formation of any precipitate. An absorption band appears with a maximum at 550 nm in accordance with the increasing amounts of the mixed solution of copper(II) and 2,2′-bipyridine, indicating that there are two absorbing species under these conditions (Fig. 4).

Composition of the Ternary Complexes. From the results given in Figs. 2 and 4, it seems that two kinds of complexes can be formed in a weakly basic pH medium (pH 10.4), according to the concentration ratio of the reagents.

A triangular coordinate method extended to three-component system of the continuous variation plot was applied to the determination of the composition of ternary complexes. The sum of the initial concentrations of copper(II), 2,2′-bipyridine and Eriochrome Cyanine R in the solution was kept constant, and preparation of the colored solution was carried out with 45 different compositions. The absorbance of the solution was measured against the reagent blank at 515 and 550 nm. The results are shown in Figs. 5 and 6, respectively. The contour lines in both figures show various compositions of equal absorbance. At 515 nm, maximum absorbance is obtained at the mole ratio of Cu(II) : bpy : ECR=0.25 : 0.25 : 0.5, namely 1 : 1 : 2 (Fig. 5). Similarly, at 550 nm, maximum absorbance is obtained at the mole ratio of Cu(II) : bpy : ECR= 1 : 1 : 1 (Fig. 6).

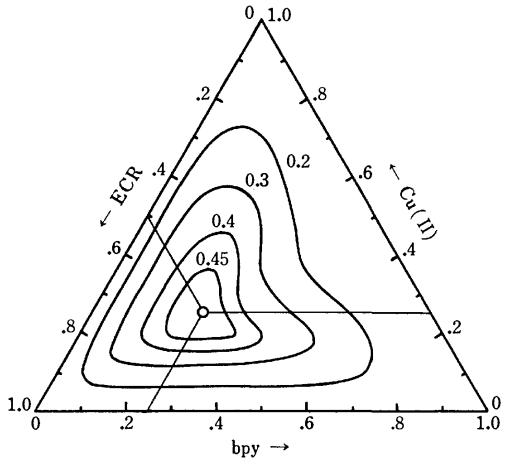

Fig. 5. Continuous variation method applied to three-component system of Cu(II)-bpy-ECR complex.
Total concn of Cu(II), bpy and ECR: 1.5×10^{-4} mol dm^{-3}; pH: 10.4, Triton X-100: 0.04%, ionic strength: 0.05, wavelength: 515 nm.

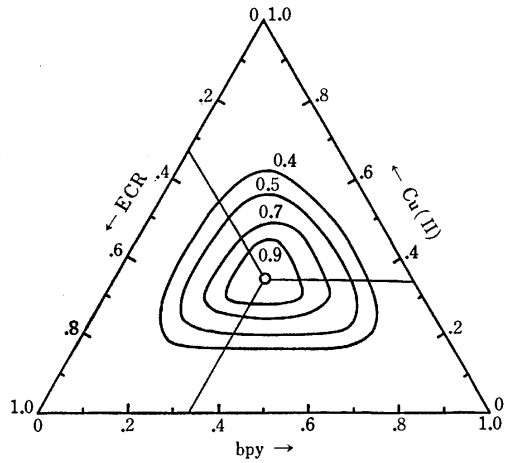

Fig. 6. Continuous variation method applied to three-component system of Cu(II)-bpy-ECR complex.
Wavelength: 550 nm; the other conditions except wavelength are the same as those in Fig. 5.

In the above experiments (Figs. 3, 4, 5, and 6) nonionic surfactant Triton X-100 was used as a solubilizing agent of the ternary complex. Addition of Triton X-100, however, had no effect on the light absorption of solutions.

From the results (Figs. 4, 5, and 6) it is evident that two types of ternary complex are formed successively, according to the amount of reagent, at pH 10.4, the combining ratio of Cu(II): bpy: ECR being confirmed to be 1 : 1 : 2 in one and 1 : 1 : 1 in the other. The maximum absorption wavelengths of the 1 : 1 : 2 and 1 : 1 : 1 complexes were 515 and 550 nm, respectively. In Cu(II)–bpy–Chromazurol S ternary complex[10] only the 1 : 1 : 2 species is formed.

The color development of the 1 : 1 : 2 complex with absorption maximum at 515 nm in a weakly basic pH medium was utilized in the spectrophotometric determination of copper(II). Conditions for the color development were investigated.

Effect of pH. The effect of pH on the color development of the ternary complex was studied with solutions adjusted to various pH values. The results are shown in Fig. 7. The maximum and nearly constant absorbance is obtained over the pH range 10.2—10.6.

Effect of 2,2′-Bipyridine and Eriochrome Cyanine R Concentrations. With the concentration of copper(II) kept constant, varying amounts of reagent were added, and the absorbances of the resulting solutions were measured against the reagent blanks. The results are shown in Fig. 8. When the concentration of 2,2′-bipyridine was varied and the concentrations of copper(II) and Erio-

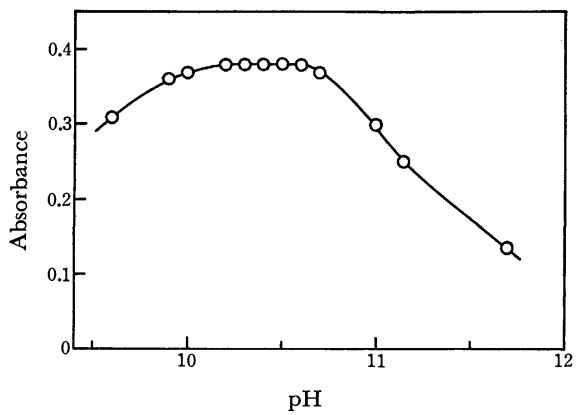

Fig. 7. Effect of pH on the absorbance of Cu(II)-bpy-ECR complex.
Concn of Cu(II), bpy and ECR: 2.0×10^{-5} mol dm^{-3}, 4.0×10^{-5} mol dm^{-3} and 1.0×10^{-4} mol dm^{-3}, respectively; ionic strength: 0.1, wavelength: 515 nm.

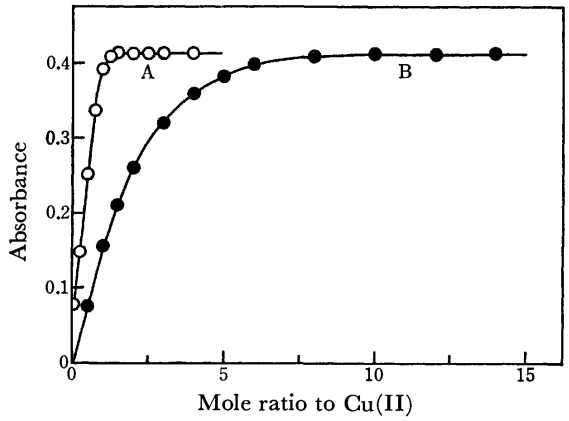

Fig. 8. Effect of 2,2′-bipyridine and Eriochrome Cyanine R concentrations on the absorbance of Cu(II)-bpy-ECR complex.
Concn of Cu(II): 2.0×10^{-5} mol dm^{-3}, pH: 10.4, ionic strength: 0.1, wavelength: 515 nm; A: [bpy]/[Cu(II)], ECR: 2.0×10^{-4} mol dm^{-3}, bpy varying; B: [ECR]/[Cu(II)], bpy: 4.0×10^{-5} mol dm^{-3}, ECR varying.

chrome Cyanine R were kept constant, the constant and maximum absorbance was obtained with a concentration ratio higher than 1.5-fold of 2,2′-bipyridine to copper(II) (Curve A). The absorbance at mole ratio of zero in curve A corresponds to that of the binary Cu(II)–ECR complex. In the same way, the effect of various Eriochrome Cyanine R concentrations is shown by curve B. More than 10-fold excess of Eriochrome Cyanine R over the copper(II) concentration is necessary in order to obtain the maximum color intensity.

Effect of Time. Color development of the ternary complex was almost instantaneous, the absorbance remaining unchanged for several hours.

Calibration Curve. A calibration curve was made under optimum conditions. A linear concentration-absorbance relationship is obtained in the copper(II) concentration up to 6×10^{-5} mol dm^{-3}. The regression equation of the calibration curve obtained by a least squares method is as follows:

$$\log (I_0/I) = 20433[\mathrm{Cu(II)}] + 0.005_5 \qquad (1)$$

Experimental conditions:
- bpy: 2.0×10^{-4} mol dm^{-3}
- ECR: 5.0×10^{-4} mol dm^{-3}
- pH: 10.4
- Ionic strength: 0.1
- Wavelength: 515 nm

Here, $\log(I_0/I)$ and [Cu(II)] are the absorbance of ternary complex against the reagent blank as reference and the concentration (mol dm^{-3}) of copper(II) in the solution, respectively. As is evident from Eq. 1, the apparent molar absorption coefficient of the complex is about 20400 dm^3 mol^{-1} cm^{-1}, corresponding to Sandell's sensitivity index of 0.003_1 μg cm^{-2}. When this is compared with indices of other similar ternary systems, its sensitivity is lower than that of the method using Neocuproine and Chromazurol S (0.002_2 μg cm^{-2}),[12] but comparable to that of the method using 2,2′-bipyridine and Chromazurol S (0.003_1 μg cm^{-2}).[10]

Effect of Diverse Ions. The influence of several cations which might introduce a large error in the determination of copper(II), and that of a few anions as masking agents were examined. The results are given in Table 1. All the cations interfere with the copper(II) determination. Beryllium(II), cobalt(II), nickel(II), and manganese(II) give high positive error, and iron(III) gives negative error. Tartrate, citrate and cyanide ions inhibit color formation of the ternary complex. Fluoride and phosphate ions, however, have almost no influence on the ternary complex formation, even in large amounts. Sodium fluoride and sodium phosphate can, therefore, serve as excellent masking agents. Among the coexisting cations in Table 1, metal cations except beryllium(II) and cobalt(II) can be effectively masked by using appropriate amounts of either fluoride or phosphate.[12,13]

Table 1. Influence of several foreign ions

Foreign ion	Ion added (μmol)	Absorbance[a] (515 nm)	Relative error (%)
	Nil	0.414	
Beryllium(II)	0.5	1.022	146.9
Cobalt(II)	0.5	0.542	30.9
Nickel(II)	0.5	0.484	16.9
Manganese(II)	0.5	0.457	10.4
Thorium(IV)	0.5	0.444	7.2
Aluminium(III)	0.5	0.417	0.7
Iron(III)	0.5	0.392	−5.3
Fluoride	50	0.416	0.5
	150	0.412	−0.5
	200	0.401	−3.1
Phosphate	5	0.409	−1.2
	25	0.397	−4.1
	50	0.393	−5.1
Tartrate	12.5	0.349	−15.7
	50	0.247	−40.3
Citrate	12.5	0.334	−19.3
	50	0.238	−42.5
Cyanide	2.5	0.030	−92.8
	5	0.011	−97.3

Copper(II) taken: 31.8 μg; a) Each result is the average of three separate analyses.

References

1) T. Millner, *Z. Anal. Chem.*, **113**, 83 (1938).
2) F. Richter, *Z. Anal. Chem.*, **126**, 426 (1943).
3) Y. Shijo and T. Takeuchi, *Bunseki Kagaku*, **17**, 323 (1968).
4) U. T. Hill, *Anal. Chem.*, **30**, 521 (1958).
5) H. Kohara, N. Ishibashi, and K. Fukamachi, *Bunseki Kagaku*, **17**, 1400 (1968).
6) T. Fujinaga, T. Kuwamoto, S. Tsurubo, and K. Kuwabara, *Bunseki Kagaku*, **13**, 127 (1964).
7) F. Blau, *Ber.*, **21**, 1077 (1888).
8) M. L. Moss and M. G. Mellon, *Ind. Eng. Chem., Anal. Ed.*, **14**, 826 (1942).
9) E. I. Onstott and H. A. Laitinen, *J. Am. Chem. Soc.*, **72**, 4724 (1950).
10) R. Ishida and K. Tonosaki, *Nippon Kagaku Kaishi*, **1975**, 1496.
11) V. Suk and V. Miketuková, *Collect. Czech. Chem. Commun.*, **24**, 3629 (1959).
12) R. Ishida and K. Tonosaki, *Bunseki Kagaku*, **25**, 625 (1976).
13) R. Ishida, *Bull. Chem. Soc. Jpn.*, **42**, 1011 (1969).

Conditions for the Precipitation of Heavy Metals from Wastewater by the Lime Sulfurated Solution (Calcium Polysulfide) Process

Toshiro ARATANI, Kiyochika YAHIKOZAWA,* Hitoshi MATOBA,**
Shigeki YASUHARA, and Takeo YANO

Department of Chemical Engineering, College of Engineering, University of Osaka Prefecture, Mozu-Ume, Sakai, Osaka 591

**Department of Chemical Engineering, College of Textile Science and Technology, Shinshu University, Tokida, Ueda, Nagano 386*

(Received September 28, 1977)

A new chemical precipitation process utilizing CaS_x solution as a single coagulant was tested for the removal of heavy metals from a batch stirred vessel. The precipitation of heavy metals from the simulated wastewater was investigated under varing conditions of pH, temperature, and heavy metal concentrations. Several agitating speeds were studied for the gases (atmospheric air and CO_2 gas) blown into the water to decompose the coagulant (CaS_x). The findings are as follows: Heavy metal removal in keeping with the water quality standards in Japan was achieved for the simulated wastewater having pH's between 3 and 11, and the temperatures from 10 to 85 °C. The agitating speed for optimum removal was found to be 10 Hz. More than 250 ppm of the initial heavy metal concentration gives sufficient removal at stoichiometric quantities of coagulant, while less than 50 ppm of the initial concentration results in rather poor removal owing to the colloidal properties of the metal sulfide or hydroxide. For low concentrations of heavy metals, several units of the coagulant over stoichiometric amount are necessary for sufficient precipitation to achieve the water quality standards.

The effluent from the industry and the cities known as wastewater has various pH's, temperatures and concentrations of contaminants. Therefore, in designing and operating wastewater treatment plants, information about the properties of the wastewater to be treated and the precipitating conditions are of great importance. For the removal of heavy metals, there have been many processes with high efficiency.[1] Among these, the chemical precipitation processes are most widely put into practice.[2,3] The temperature and pH of the wastewater, the initial concentration of heavy metals, the amount of coagulant to be injected, and the agitating speed of the stirrer are known to adversely affect the heavy metal removal by chemical precipitation.[1]

In the previous work,[4] a new chemical precipitation process has been developed to cope with the severe water quality standards in Japan for Hg^{2+}, Cd^{2+}, and Cr(VI). This process utilizes "Lime Sulfurated Solution" as a single coagulant to precipitate the heavy metals from wastewater as metal sulfides or hydroxides. Kinetic studies on this process have already been done for the removal of heavy metals: Hg^{2+}, Cd^{2+}, Cu^{2+}, Zn^{2+}, Pb^{2+}, Cr^{3+}, and Cr(VI).[4,5]

In the present study, optimum precipitating conditions have been discussed. The conditions for effective coagulation were investigated experimentally in a batch stirred vessel for the removal of Cd^{2+} and Cr(VI) from simulated wastewater at various pH's, temperatures, and initial concentrations of the heavy metals.

Lime Sulfurated Solution (Calcium Polysulfide) Process

According to previous studies on the apparent kinetics,[4,5] the principal reactions for the precipitation of heavy metals by this process may be summarized as follows.

$$CaS_x + \frac{3}{2}O_2 \longrightarrow CaS_2O_3 + (x-2)S, \quad (1)$$

$$CaS_x + CO_2 + H_2O \longrightarrow CaCO_3 + H_2S + (x-1)S. \quad (2)$$

CaS_x which is the main component of the lime sulfurated solution reacts with O_2 or CO_2 which is blown into the wastewater, and this liberates CaS_2O_3, H_2S, and S (solid sulfur particles), as shown in Eqs. 1 and 2. Bivalent heavy metals denoted by M^{2+} are precipitated as metal sulfides by CaS_2O_3 and H_2S according to Eqs. 3 and 4.

$$M^{2+} + CaS_2O_3 + H_2O \longrightarrow MS + CaSO_4 + 2H^+, \quad (3)$$

$$M^{2+} + H_2S \longrightarrow MS + 2H^+. \quad (4)$$

Trivalent heavy metals, the sulfides of which are usually unstable in water as is the case of Cr^{3+}, may be precipitated as metal hydroxides by the alkaline base of the lime sulfurated solution. Sexi-chromium Cr(VI) (dichromate) is reduced to Cr^{3+} by H_2S or CaS_2O_3 and precipitated as $Cr(OH)_3$.

$$Cr(VI) + \frac{3}{2}H_2S \longrightarrow Cr^{3+} + \frac{3}{2}S + 3H^+, \quad (5)$$

$$Cr(VI) + \frac{3}{2}CaS_2O_3 + \frac{3}{2}H_2O \longrightarrow Cr^{3+} + \frac{3}{2}CaSO_4 + \frac{3}{2}S + 3H^+. \quad (6)$$

The experimental findings of previous studies[4,5] may be summarized as follows;

(1) Heavy metals, especially Hg^{2+}, Cd^{2+}, and Cr(VI) may be treated below the water quality standards in Japan within 60 min of processing time (fixed temperature of 25 °C, initial pH of 5.0, initial heavy metal concentration of 25 ppm with the amount of the coagulant: $R_m=25$). R_m is defined as the mole ratio of sulfur in CaS_x per M^{2+}.

2) The processing time is dependent on the kinds of

** Present address: Ataka Kogyo Co. Ltd., Sueyoshibashi, Minamiku, Osaka 542.

heavy metals and gases (air and CO_2) used for the decomposition of CaS_x, and varies from 5 to 60 min. The rate of precipitation for the bivalent heavy metals is determined by that of the CaS_x decomposition, which is accelerated by CO_2 blowing. The rate of $Cr(OH)_3$ floc formation can be favored by aeration. The pH values of the water treated with aeration or CO_2 blowing were found to change to 7 and 6, respectively.

Experimental

The precipitation of heavy metals at various conditions by CaS_x solution was carried out in a batch stirred vessel with gas (air or CO_2) blowing. The vessel was made of glass and cylindrical in shape and had a flat bottom. The diameter and height of the vessel were, respectively, 15 and 22 cm. Four baffles were positioned symmetrically on the inside wall of the vessel. The vessel contents were agitated by a six-bladed turbine driven by a variable speed electric motor. The vessel was immersed in a constant temperature bath, maintained between 10 and 85 °C by set of control systems consisting of a contact thermometer and a heater or cooler. The gas (air or CO_2) for the decomposition of CaS_x was blown through a pipe of 1 mm inner diameter attached just below the center of the turbine. Simulated wastewater containing heavy metals as soluble salts (nitrates were used for bivalent metals and potassium dichromate was used for sexi-chromium) was poured into the vessel. After ensuring steady state conditions in the vessel, removal of the heavy metals was started by injecting the coagulant (CaS_x solution). The sample liquor taken from the vessel at predetermined time intervals was filtered on a No. 5C filter paper and, if necessary, by a membrane filter and analyzed by an atomic absorption spectrophotometer according to JIS-K0102.

Results and Discussion

Effect of the Injected Amount of the Coagulant. Removal experiments were undertaken for Cd^{2+} as the representative of the bivalent heavy metals which were precipitated as metal sulfides, and for Cr(VI) as one of the multivalent heavy metals precipitated as metal hydroxides after reduction to the trivalent state.

Figure 1 shows the concentration of Cd^{2+} in the filtrate plotted against the processing time for the various mole ratios (R_m) of sulfur in CaS_x solution per metal (at 25 °C, agitating speed of 10 Hz, and initial heavy metal concentration (C_0) of 25 ppm). The CO_2 gas was blown in at the rate of 0.5 dm^3/min. The steady state concentration is likely to be realized after 80 to 120 min of the processing time and enough removal was found to be attained for R_m over 25. The steady state concentrations of Cd^{2+} after 120 min were measured for various values of C_0 and R_m (the same operating conditions as the data in Fig. 1). The result is shown in Fig. 2. For the highest value of C_0=1000 ppm, R_m=5.9 was found sufficient to achieve the water quality standard (criterion). Since x atoms of sulfur in the polysulfide are necessary to precipitate an ion of Cd^{2+} if the reactions proceed as described by Eqs. 1 to 4, then $R_m=x$ is the theoretical stoichiometric amount of the coagulant. x in CaS_x is reported as x=4.7 to 5.4.[6] The higher R_m value observed here, *i.e.*, R_m=5.9 is a little more than the stoichiometric amount for C_0=1000 ppm. One explanation for this may be that the sulfur from the CaS_x partly leaks as H_2S from the liquid phase to the exhaust gas phase, though the H_2S generated is in relatively smaller quantities under aeration than CO_2 blowing. Figure 3 illustrates the precipitation of Cd^{2+}, when CO_2 gas is used as the blowing gas instead of air. For the same values of C_0, R_m values increased a little with CO_2 blowing, in comparison with aeration. This increase may be due to the fact that CO_2 blowing generates H_2S which tends to leak from the liquid phase to the exhaust gas phase without any precipitating reaction with Cd^{2+}. Aeration generates mainly CaS_2O_3 which does not leak from the liquid phase. This leakage may explain the higher R_m values in Fig. 3 (CO_3 blowing) than that in Fig. 2 (aeration). CO_2 blowing had the advantage over aeration in that it shortened the processing time.[4] Aeration was found to utilize the sulfur from CaS_x more effectively than CO_2 blowing in the batch process. With decrease in C_0 from 1000 ppm, values of R_m (to achieve the same standard) increased gradually as shown in Figs. 2 and 3 for both cases of aeration and CO_2 blowing. A reason for this increase may be the generation of finer particles of metal sulfide for the lower values of C_0. These finer particles may pass the No. 5C filter paper and may be detected as apparent liquid phase concentration by atomic absorption to give high concentration of Cd^{2+} in the filtrate.

The behavior of these suspended fine particles was investigated by the following experiments. The sample liquors were filtered by membrane filters of various pore sizes. The filtrates were acidified with HCl to dissolve the metal sulfides and the atomic absorption was measured. Figures 4 and 5 show the apparent particle size distributions of the suspended colloidal CdS. These distributions are calculated from the filtrate concentrations based on the assumption that the membrane filter works like a standard mesh. As may be seen from

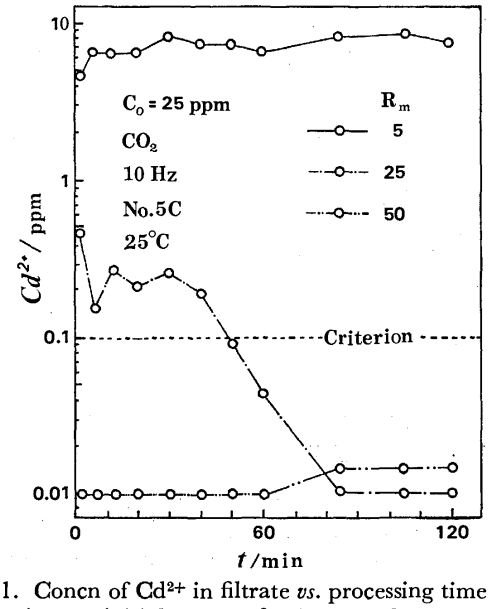

Fig. 1. Concn of Cd^{2+} in filtrate *vs.* processing time (CO_2 blowing, at initial concn of Cd^{2+}; C_0=25 ppm, agitating speed of 10 Hz, filtered on No. 5C, for mole ratio of coagulant to heavy metal; R_m=5, 25, and 50).

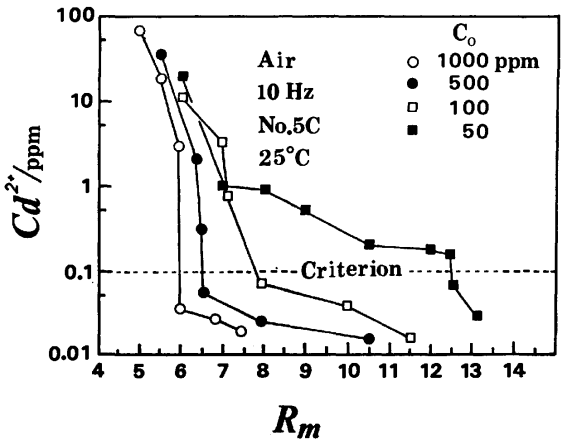

Fig. 2. Concn of Cd^{2+} in filtrate after 120 min of aeration *vs.* R_m (at 25 °C, 10 Hz, by No. 5C, for C_0=1000, 500, 100 and 50 ppm).

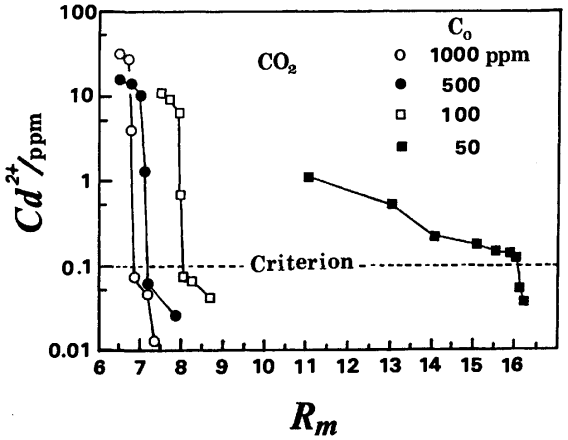

Fig. 3. Concn of Cd^{2+} after 120 min of CO_2 blowing *vs.* R_m.

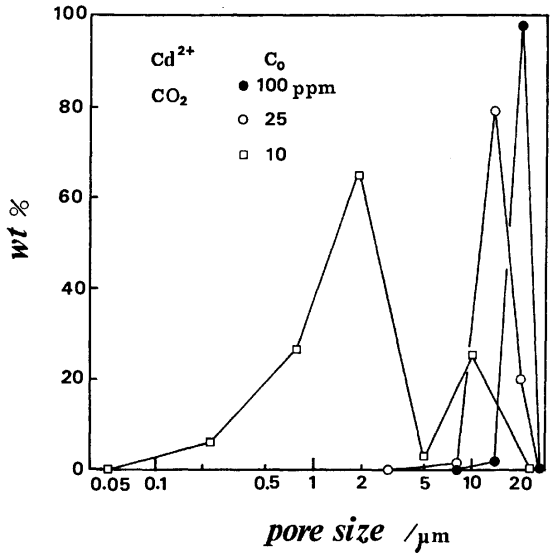

Fig. 4. Apparent particle size distribution of CdS, at 25 °C, R_m=25, with CO_2 blowing, for C_0=100, 25, and 10 ppm.

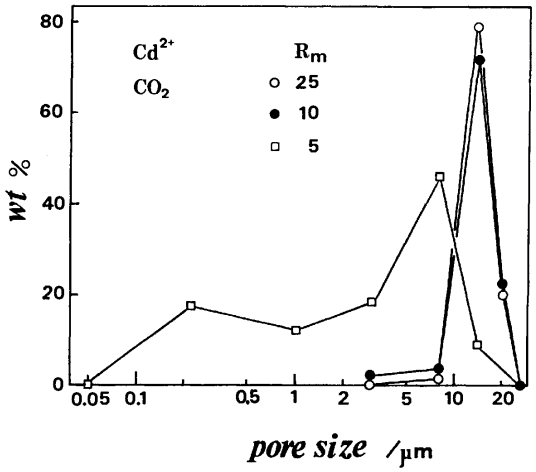

Fig. 5. Apparent particle size distribution of CdS, at 25 °C, C_0=25 ppm, with CO_2 blowing, for R_m=25, 10, and 5.

Fig. 4, decreases in C_0 gives rise to the generation of fine particles for R_m=25. Increase in R_m results in the generation of the big particles, as shown in Fig. 5. To separate the precipitated CdS completely for R_m=25 and C_0=25 ppm, a filter having a maximum pore size of 3 μm was suitable as may be seen from Figs. 4 and 5. The mean particle size of this process was found to be over 8 μm from Figs. 4 and 5, for R_m greater than 10 and C_0 greater than 25 ppm.

Processing results of Cr(VI) by CaS_x are shown in Fig. 6 with aeration and in Fig. 7 with CO_2 blowing. The residual concentration of total chromium in the filtrate after 180 min of the processing time is shown as the ordinate. As observed with Cd^{2+}, the concentration decreases critically near the theoretical stoichiometric injection of CaS_x only for aeration. If the reducing reactions follows Eqs. 1 to 5 or 6 and x is taken as 4.7 to 5.4,[6] the theoretical stoichiometric amount of CaS_x needed to treat Cr(VI) is $R_m=(3/2)x$, that is, R_m=7.1 to 9.1. Figure 8 shows the apparent particle size distribution of $Cr(OH)_3$ flocs. CO_2 blowing was found to give a finer particle size than aeration. On comparing Figs. 6 and 7, values of R_m (to achieve the standard) are observed to differ more evidently with aeration and CO_2 blowing than those with Cd^{2+} (see Figs. 2 and 3). CdS flocs have almost the same particle size distribution both for CO_2 blowing and aeration. On the other side, $Cr(OH)_3$ flocs formed by the CaS_x process with CO_2 blowing are relatively fine and need more processing time to flocculate than with aeration. This slow flocculation was observed as a gradual decrease in the amount of the light green particles ($Cr(OH)_3$) (the suspension was held in the filtrate for about 60 min with the CO_2 blowing).

Effect of Temperature. Figure 9 shows the concentration of Cd^{2+} in the filtrate (No. 5C) after 120 min of the processing time plotted against the temperature of the simulated wastewater (CO_2 blowing for C_0=25 ppm). For large values of R_m and C_0, the removal of Cd^{2+} is almost independent of the temperature. The temperature may not have such an effect on the precipitation of Cd^{2+} with large values of R_m and C_0 when

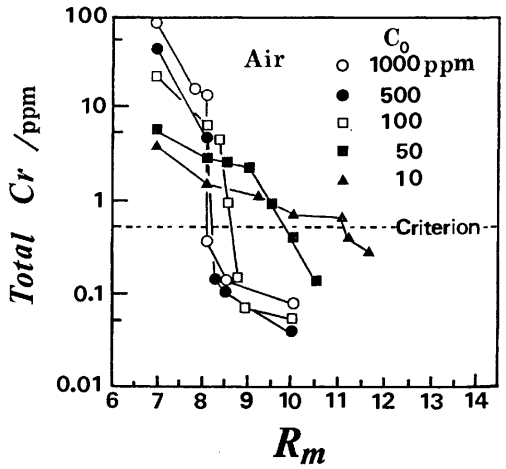

Fig. 6. Concn of total Cr after 180 min of aeration *vs.* R_m, at 25 °C, 10 Hz, by No. 5C, for C_0=1000, 500, 100, 50, and 10 ppm.

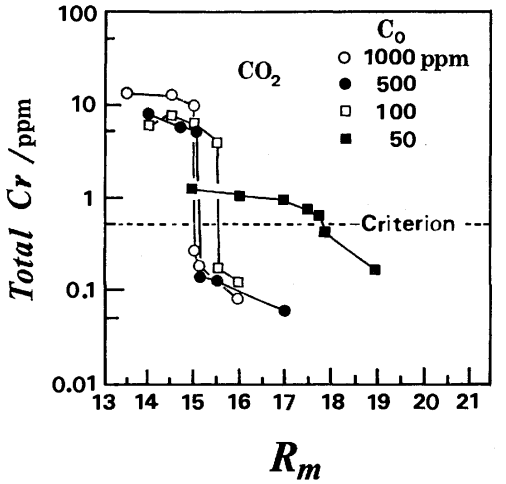

Fig. 7. Concn of total Cr after 180 min of CO_2 blowing *vs.* R_m.

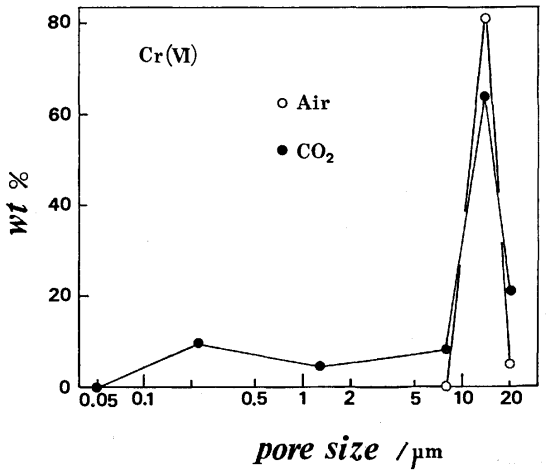

Fig. 8. Apparent particle size distribution of $Cr(OH)_3$, at 25 °C, C_0=25 ppm, after 15 min from the start of run with aeration or CO_2 blowing.

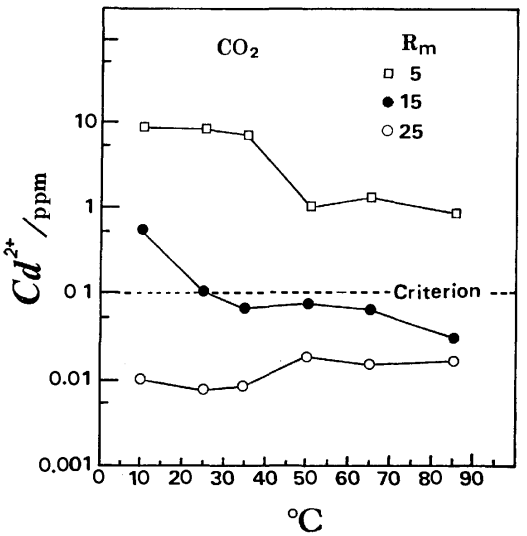

Fig. 9. Effect of temperature: Concn of Cd^{2+} *vs.* processing temperature, with CO_2 blowing, at 25 ppm, by No. 5C, for R_m=5, 15, and 25.

the particle size is large. The precipitation seems to be related to the temperature of the wastewater for R_m=5 which gives fine particles as shown in Fig. 5. Removal meets the criterion conditions for wastewater between 10 and 85 °C. Thus the CaS_x process is able to cope with variations in the temperature of the wastewater to be treated.

Effect of Agitating Speed. The removal of Cd^{2+} is shown plotted against the agitating speed of the impeller for C_0=1000 ppm and 50 ppm in Figs. 10 and 11, respectively. For C_0=1000 ppm which produces a precipitate of large particle size, the removal is almost independent of change in the agitating speed. For C_0= 50 ppm which generates the fine suspended particles, the agitation affects the removal. The removal is thought to be promoted by the agitation which accelerates the flocculation. However, removal at an agitation higher than 10 Hz results in adverse removal, and this may be due to the fragmentation of the flocs, once

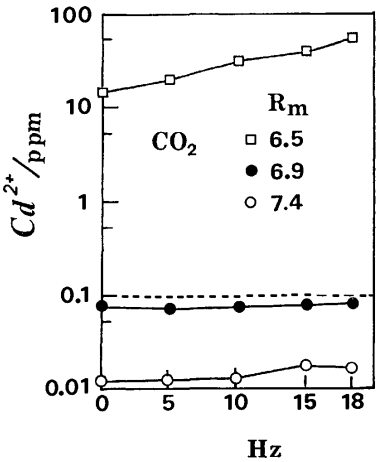

Fig. 10. Effect of agitating speed: Concn of Cd^{2+} after 120 min of CO_2 blowing *vs.* Hz, at C_0=1000 ppm, 25 °C, by No. 5C.

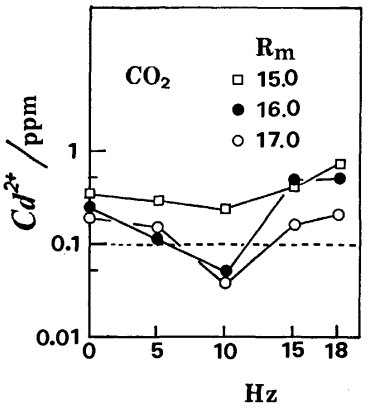

Fig. 11. Concn of Cd^{2+} with CO_2 blowing *vs.* Hz, at $C_0=50$ ppm.

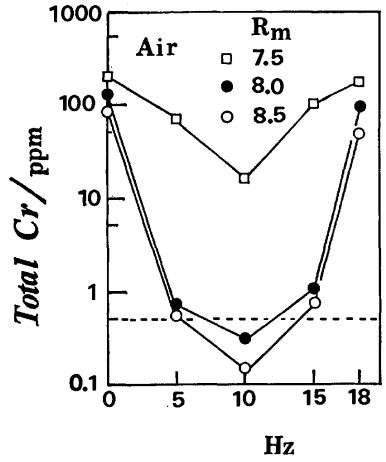

Fig. 12. Effect of agitating speed: Concn of total Cr after 180 min of aeration *vs.* Hz, at $C_0=1{,}000$ ppm, 25 °C, by No. 5C.

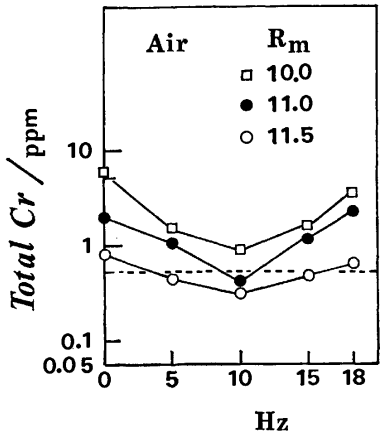

Fig. 13. Concn of total Cr with aeration *vs.* Hz, at $C_0=50$ ppm.

coagulated, by the vigorous mechanical agitation. The fragmentation may produce fine particles that pass through the No. 5C filter paper and detected as apparent Cd^{2+} concentration by atomic absorption measurements.

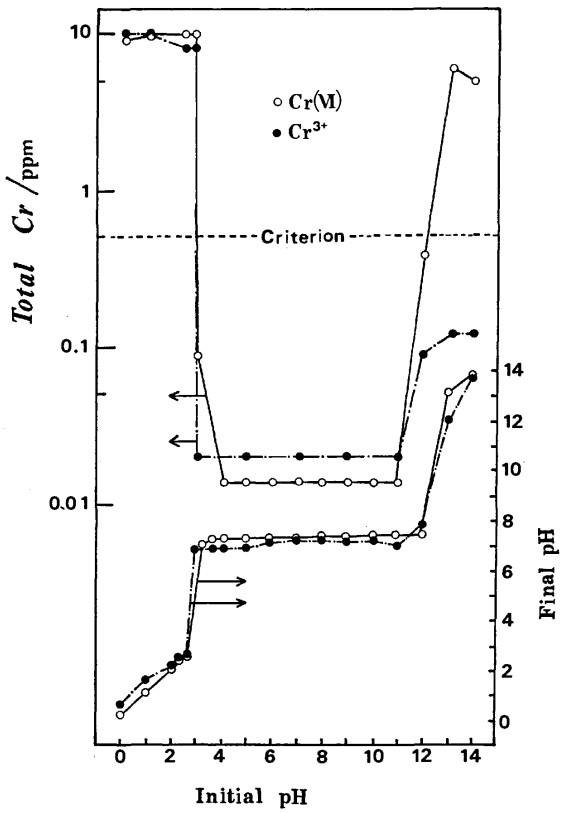

Fig. 14. Effect of pH: Concn of total Cr after 180 min of aeration *vs.* initial pH, at $C_0=25$ ppm, $R_m=25$, 25 °C, by No. 5C: Final pH *vs.* initial pH.

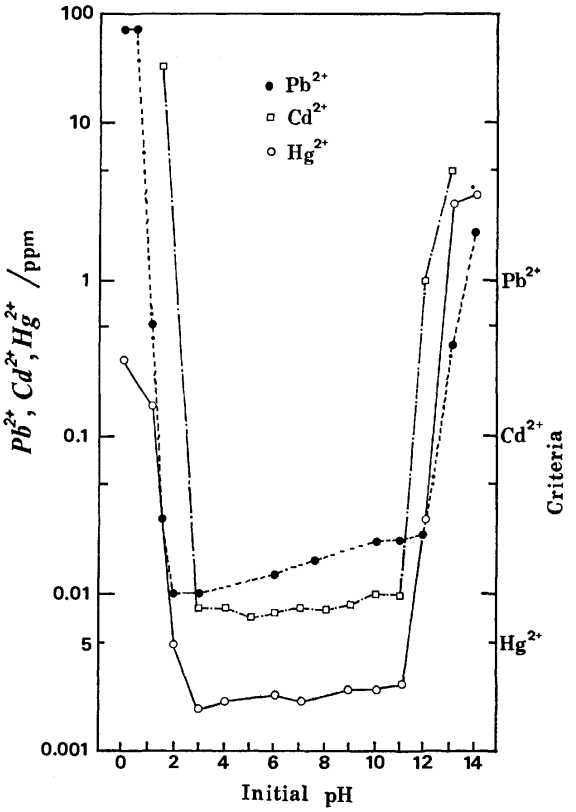

Fig. 15. Effect of pH: Concn of Pb^{2+}, Cd^{2+}, Hg^{2+} *vs.* initial pH at $C_0=25$ ppm, $R_m=25$, 25 °C, by No. 5C.

For the removal of Cr(VI), the effect of the agitating speed is shown in Fig. 12 with $C_0=1000$ ppm and Fig. 13 with $C_0=50$ ppm. In contrast to the Cd^{2+} removal, at $C_0=1000$ ppm the Cr(VI) removal was more affected by the aeration than at $C_0=50$ ppm. In the present, the reason for this is not so evident. Possibly, this may be due to the differences between metal sulfides and hydroxides in their mechanisms of flocculation.

Effect of pH. The results of removal with the wastewater having the initial pH from 0 to 14 are shown in Figs. 14 and 15. With a slightly acidic wastewater, the acid in the water may be neutralized by the strong alkaline base of the coagulant, *i.e.*, lime sulfurated solution. With alkaline water, it is neutralized by the acid of the blown gas (CO_2 in air or CO_2 gas) and by the protons liberated as stated in Eqs. 1 to 5. Figure 14 shows the removal of Cr^{3+} and Cr(VI) from simulated wastewater having pH's between 0 to 14. The final pH's are almost constant around pH=7.0, and the removal is satisfactory for the initial pH's between 3 and 11. Figure 15 shows the results of Pb^{2+}, Cd^{2+}, and Hg^{2+} removal from the wastewater of various initial pH's. The same pH range of removal is observed for these bivalent metals as that for Cr^{3+} and Cr(VI). For the other heavy metals Ni^{2+}, Zn^{2+}, and Cu^{2+}, approximately the same removal range of pH has been reported.[5]

Conclusion

The above experiments help to clarify the conditions of the CaS_x process for the removal of heavy metals from wastewater. The experimental findings are summarized as follows.

1) Almost stoichiometric amount of the coagulant is enough for the precipitation of heavy metals when their concentrations are more than about 100 ppm. When the concentrations are less than 100 ppm, several portions of coagulant are needed because of the colloidal properties of the precipitates.

2) The wastewater at wide temperature and pH range is expected to be treated far below the water quality standards for heavy metals in Japan.

The authors wish to thank Prof. Dr. Ryozo Ito of Osaka University, Profs. Drs. Takataro Suda and Yoshiki Sanoh of Shinshu University, and Assoc. Prof. Dr. Kei Miyanami of University of Osaka Prefecture for their useful discussions.

The authors wish to express their thanks to Messrs. Teruhisa Nakashiba, Kiyoshi Inoue, and Jun Akai for assistance in the experimental work.

The present work was partially supported by Grant-in-Aid for Developmental Scientific Research from the Ministry of Education.

References

1) E. F. Gloyna and W. W. Eckenfeder, Jr. Ed, "Water Quality Improvement by Physical and Chemical Process," Vol. III, The University of Texas Press (1970), p. 219.

2) M. Munemori, T. Aoki, Y. Inoue, and T. Hata, the 26th IUPAC Congress, 7A-501, Tokyo, Sept. 1977.

3) N. R. Iammartino, *Chem. Eng. (N. Y.)*, Feb. 13th, 36 (1975).

4) K. Yahikozawa, T. Aratani, R. Ito, T. Suda, and T. Yano, *Bull Chem. Soc. Jpn.*, **51**, 613 (1978).

5) T. Aratani *et al.*, Presentation No. A303/304, the 40th Annual Meeting of the Soc. of Chem. Engr. of Japan, Nagoya, April 1975.

6) W. F. Giggenbach, *Inorg. Chem.*, **13**, 1724 (1974).

Synthesis of Oxide-Chalcogenides. I. Hydrothermal Synthesis of Sarabauite $CaSb_{10}O_{10}S_6$ and Related Compounds*

Kozo Nagashima, Masataka Ogino, and Izumi Nakai
Department of Chemistry, The University of Tsukuba, Sakura-mura, Ibaraki 300-31
(Received October 8, 1977)

Single crystals of a recently described metal oxide sulfide mineral sarabauite and three related oxide-sulfides of alkaline earths and antimony were hydrothermally synthesized. (1) $CaSb_{10}O_{10}S_6$: color, carmine red; crystal system, monoclinic; space group, C2/c. (2) Compound in Sr–Sb–O–S system (O<S), blackish silver, monoclinic, $P2_1/a$. (3) Compound in Ba–Sb–O–S system (O>S), reddish orange, triclinic P1 or $P\bar{1}$. (4) Compound in Ba–Sb–S–O system (O<S), blackish brown, monoclinic, $P2_1/a$.

A new oxide-sulfide of calcium and antimony with the formula $CaSb_{10}O_{10}S_6$ was first found as a beautiful scarlet colored mineral from the Sarabau mine, Malaysia, and reported as a mineral sarabauite.[1] The mineral and three compositionally related compounds in the M^{II}–Sb–O–S system (where M^{II} represents an alkaline earth metal), have been hydrothermally synthesized. This paper reports the preparation and chemical and physical properties of sarabauite and the three related oxide sulfide compounds. The three compounds have not been found in nature. Their preparation has not been reported.

Experimental

The following CP-grade reagents were used for the syntheses: CaO, $SrCO_3$, $BaCO_3$, Sb_2S_3, and Sb_2O_3. They were taken in the required ratios and mixed in an agate motor. Seventy milligrams of the mixture and 0.07 ml of water were sealed in either a gold or platinum tube: length 35 mm, inner diam. 2.7 mm. The conventional hydrothermal method, using stellite bombs of the test-tube type, was employed throughout the investigation. Syntheses were conducted under hydrothermal conditions in the temperature range 100—650 °C under 500—2000 kg/cm² pressure for 1—360 h.

The products were examined by means of the Weissenberg and precession methods, X-ray powder diffraction method, DTA, TGA, and microscope. Some were subjected to electron microprobe analysis.

Results and Discussion

Sarabauite. Single crystals up to 3 mm long have been synthesized by subjecting a mixture of the composition CaO: Sb_2S_3: Sb_2O_3 in the ratio 1:2:3 for three days at 400 °C and 1000 kg/cm² pressure. The crystals are transparent with a carmine red color similar to that of natural sarabauite. The twelve strongest X-ray powder reflections obtained by the diffractometer method are given in Table 1, together with the reflections for natural sarabauite for the sake of comparison. They are in good agreement. The unit cell dimensions for the synthesized $CaSb_{10}O_{10}S_6$ calculated from the powder data are a=25.39(4), b=5.655(5), c=16.92(3) Å and β=117.5(2)°. The values are very close to those for natural sarabauite: a=25.37(2), b=5.654(1), c=16.87(1) Å and β=117.58(4). The Weissenberg and precession photographs of the product reveal that it belongs to the same space group as sarabauite *i.e.* C2/c.[2] Thermal analyses (DTA and TGA) were performed at a heating rate of 2.5 °C/min. The DTA curve (Fig. 1) shows two exothermic peaks starting at 410 and 490 °C. The former is accompanied by weight loss. The corresponding peaks for natural sarabauite are found to start at 420 and 490 °C. The decomposition products at 490 °C

Table 1. X-Ray powder reflections of synthesized $CaSb_{10}O_{10}S_6$ and natural sarabauite (Cu/Ni, diffractometer method)

$CaSb_{10}O_{10}S_6$		Sarabauite		
d/Å	I/I_0	d/Å	I/I_0	hkl
11.25	20	11.33	20	200
4.469	20	4.462	36	$\bar{3}12$
4.227	40	4.227	42	$\bar{6}02$
3.931	20	3.924	30	$\bar{1}13$
3.470	50	3.466	78	312
3.218	100	3.215	100	$\bar{5}14$
3.184	40	3.182	60	511
3.162	50	3.164	50	$\bar{8}02$
2.820	70	2.817	88	020
2.720	40	2.718	28	$\bar{2}06$
2.587	20	2.583	40	$\bar{4}21$
2.058	20	2.058	29	025

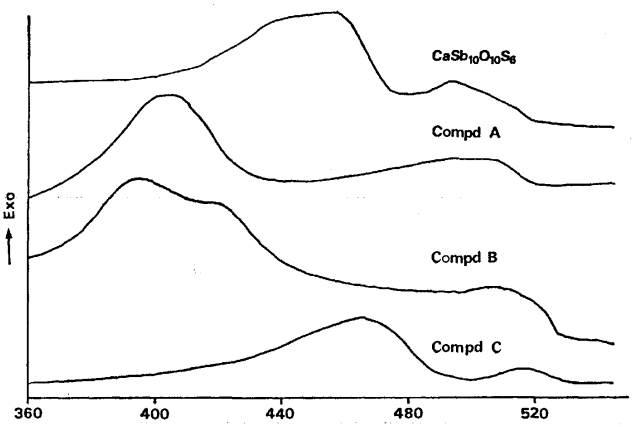

Fig. 1. DTA curves of $CaSb_{10}O_{10}S_6$, Compd A, Compd B, and Compd C.

* Presented at the 36th National Meeting of the Chemical Society of Japan, April 1977, and partly at the 1976 National Meeting of the Mineralogical Society of Japan, June 1976.

were found by X-ray analysis to be Sb_2O_3, Sb_2O_4, and $CaSb_2O_6$.

The density 4.9 g/cm³ determined by a Berman balance agrees with the calculated density 4.96 g/cm³ for $CaSb_{10}O_{10}S_6$ if we adopt the measured unit cell data and $Z=4$. The synthesized crystals have been identified as sarabauite $CaSb_{10}O_{10}S_6$.

Crystal habits of the synthesized sarabauite are tabular or columnar parallel to the b-axis. The former is characterized by the well developed {100} face.

The sarabauite phase was found to be formed in the temperature range 230—560 °C at a 1000 kg/cm² pressure. The product often included recrystallized acicular Sb_2S_3 and polygonal Sb_2O_3. The rate of sarabauite formation is scarcely influenced by variations in pressure up to 2000 kg/cm². One experiment carried out in a silica tube at 500 °C resulted in sarabauite formation at a 20 kg/cm² pressure. Formation of sarabauite proceeded so rapidly that the sarabauite phase appeared within 1 h at 500 °C and 1000 kg/cm². The presence of water is essential for the formation of sarabauite. Attempts at synthesis in a dry atmosphere at temperatures below 500 °C were unsuccessful.

Three compounds related to the above were prepared as follows: compound A, Sr–Sb–O–S system; compound B and compound C, Ba–Sb–O–S system. Their chemical compositions are given in Table 2. The analysis was carried out with an electron microprobe analyzer, measurements being made at 15 kV using Sb_2S_3, Sb_2S_2O, Sb_2O_3, $BaSO_4$, and $SrCO_3$ as standards. Since the correction procedures for the oxide–sulfide system are not well established in electron microprobe analysis, the values given should be considered approximate. The crystallographic data are summarized in Table 3. The crystal system and possible space group were determined by means of Weissenberg and precession photographs. The unit cell dimensions were obtained on an automated four-circle diffractometer using Mo $K_{\alpha 1}$ radiation for A and B and Cu $K_{\alpha 1}$ radiation for C. The 12 strongest X-ray powder lines are given in Table 4. Indexing is in line with the space groups, unit cell constants and X-ray intensity data of the single crystals.

Table 2. Electron microprobe chemical analysis of compounds A, B, and C

	Compd A		Compd B		Compd C	
	wt%	r[a)]	wt%	r[a)]	wt%	r[a)]
Sr	4.7	0.9				
Ba			10.9	1.4	7.6	1.0
Sb	72.1	10	68.9	10	69.4	10
O	6.5	6.9	9.3	10	6.2	6.8
S	18.6	9.8	11.6	6.4	16.1	8.8
Total	101.9		100.7		99.3	

a) Atomic ratio, basis Sb=10.

Sr–Sb–O–S System: Compound A. A mixture of $SrCO_3$: Sb_2S_3: Sb_2O_3 in the ratio 1: 2: 3 was maintained for 214 h at 450 °C and 1030 kg/cm². The color of the crystal is blackish silver and by transmitted light red, giving a metallic luster and columnar shape elongated along the b-axis, and often showing parallel growth. The determined density is 4.6 g/cm³ which is slightly less than the 4.9 g/cm³ for sarabauite. The DTA and TGA curves are characterized by an exothermic peak starting at 380 °C, accompanied by weight loss, and one starting at 460 °C (Fig. 1). An X-ray powder study for the product at 460 °C showed that it consists of a mixture of Sb_2O_4 and $SrSb_2O_6$. Compound A is formed in the temperature range 460—540 °C under 1000 kg/cm².

Ba–Sb–O–S System: 1) Compound B. A mixture of $BaCO_3$: Sb_2S_3: Sb_2O_3 in the ratio 1: 2: 3 was maintained at 520 °C and 500 kg/cm² for 219 h. The crystals obtained are reddish orange and transparent, possessing resinous luster similar to that of sarabauite.

The habit is tabular or columnar parallel to the b-axis. The measured density is 5.4 g/cm³. Figure 1 shows the result of DTA. The curve consists of two exothermic peaks starting at 370 and 500 °C, the former being accompanied by weight loss resulting from thermal decomposition. The temperature range for the formation of compound B is similar to that for sarabauite: 290—550 °C under 1000 kg/cm².

2) Compound C. Crystals up to 1 mm in length have been prepared by heating the mixture for B at 500 °C and 1000 kg/cm² for 110 h. The color is blackish brown and by transmitted light, red, respectively. C is a sulfur rich oxide–sulfide as compared to B (Table 2). It is characterized by its extremely large unit cell (Table 3). It appears columnar in shape, showing parallel growth along the b-axis in many cases. The product usually contains some of compound B. The result of DTA, given in Fig. 1, shows two exothermic peaks, one starting at 420 °C with weight loss and the other at 500 °C. The optimum temperature range

Table 3. Crystallographic data

		$CaSb_{10}O_{10}S_6$	Compd A	Compd B	Compd C
Crystal system		monoclinic	monoclinic	triclinic	monoclinic
Space group		C2/c	$P2_1/a$	P1 or $P\bar{1}$	$P2_1/a$[a)]
Cell parameters	a/Å	25.39(4)	27.217(4)	13.949(3)[b)]	38.286(3)
	b/Å	5.655(5)	5.7759(5)	5.5511(9)	5.7156(4)
	c/Å	16.92(3)	16.657(2)	11.083(3)	22.343(2)
	α/°			100.15(2)	
	β/°	117.5(2)	91.09(1)	67.53(2)	
	γ/°			97.07(2)	99.266(8)

a) 1st setting. b) The corresponding reduced cell[3)] (a', b', c', α', β', and γ') is given as follows: $a'=c$, $b'=a$, $c'=b$, $\alpha'=\gamma$, $\beta'=\alpha$, and $\gamma'=\beta$.

Table 4. Twelve strongest X-ray powder reflections of compounds A, B, and C (Cu/Ni, diffractometer method)

Compd A			Compd B			Compd C		
d/Å	I/I_0	hkl	d/Å	I/I_0	hkl	d/Å	I/I_0	hkl
4.298	40	$\bar{4}11$	10.10	40	101	3.936	30	$\bar{3}14$
		403	4.124	60	302			610
3.583	80	610	3.470	50	401	3.678	60	314
3.393	100	014			012	3.393	50	$\bar{7}14$
3.108	60	$\bar{6}04$			$11\bar{2}$	3.294	60	11.0.2
3.054	80	604	3.388	50	212	3.127	40	$\bar{2}16$
2.899	70	020	3.289	40	$\bar{1}1\bar{3}$			11.0.3
2.839	30	$\bar{1}21$	3.111	50	$\bar{3}1\bar{3}$			$\bar{1}16$
		121	2.945	100	$31\bar{1}$	2.935	50	10.1.0
2.758	30	320			$\bar{3}11$	2.906	40	12.0.3
		812			403			10.1.1
2.677	30	$\bar{4}15$	2.788	80	411	2.834	50	$\bar{4}20$
2.467	20	10.1.0			$\bar{4}01$	2.797	100	008
		$\bar{1}0.0.3$	2.690	60	104	2.767	50	$\bar{5}21$
2.092	50	624	2.661	80	304			$\bar{3}17$
		008	2.558	40	503	2.712	60	$\bar{5}22$
1.888	30	14.0.2	1.994	40	$\bar{4}03$	2.526	50	11.0.6
					505			
					023			

for the synthesis of compound C is 450—500 °C under a pressure of 1000 kg/cm².

The authors wish to express their thanks to Mr. Ko Hirata and Mr. Toyohiko Okumura, Electron Optics Division, JEOL. Ltd. for their help in the electron microprobe analysis. Thanks are also due to Prof. Nobuo Morimoto and Dr. Kichiro Koto of I.S.I.R., Osaka University for their help in the X-ray diffraction studies.

References

1) I. Nakai, H. Adachi, S. Matsubara, A. Kato, K. Masutomi, T. Fujiwara, and K. Nagashima, *Am. Mineral.*, **63** (1978), in press.

2) I. Nakai. K. Koto, K. Nagashima, and N. Morimoto, *Chem. Lett.*, **1977**, 275.

3) J. D. H. Donnay, Ed, "Crystal Data," American Crystallographic Association (1963), p. 2.

Note added in proof

A new oxide-selenide of barium and antimony, Compound D, has been synthesized by heating a mixture of $BaO:Sb_2Se_3:Sb_2O_3$ in the ratio 1:2:3 with 5% NaOH solution for 110 h under hydrothermal conditions.

The crystals are red, and transparent having resinous luster and columnar shape. X-Ray data show them to be hexagonal, space group $P6_3$ or $P6_3/m$, with $a=14.41(1)$, and $c=5.552(3)$ Å. The strongest X-ray powder lines are: 12.62(30)(100), 4.168(40)(300), 3.601(30)(220), 3.333(50)(301), 3.124(40)(040), 3.027(90)(221), 2.943(60)(311), 2.727(100)(140). The DTA curve shows an exothermic peak starting at 495 °C, accompanied by weight loss. Compound D is formed in the temperature range 300—650 °C under 1000 kg/cm².

Synthesis and Spectroscopy of Acetato and Dithiocarbamate Complexes of Bis(cyclopentadienyl)zirconium(IV)

Hideo SUZUKI, Toshio TAKIGUCHI, and Yoshikane KAWASAKI*

Department of Synthetic Chemistry, Faculty of Technology, Gunma University, Kiryu, Gunma 376
**Department of Petroleum Chemistry, Faculty of Engineering, Osaka University, Yamada-Kami, Suita, Osaka 565*

(Received October 14, 1977)

Several acetato and dithiocarbamate complexes of bis(cyclopentadienyl)zirconium(IV), $Cp_2Zr(X)OAc$ (X= Me, Cl, OAc), $Cp_2Zr(X)dmtc$ (X=Me, Cl; dmtc=S_2CNMe_2), and $Cp_2Zr(X)detc$ (X=Me, Cl; detc=S_2CNEt_2) have been prepared. Infrared, ^1H NMR and mass spectra of these complexes suggest the chelation of acetato (except for one acetato group in $Cp_2Zr(OAc)_2$) and dithiocarbamate groups, affording 18-electron configuration of the zirconium atom. The infrared spectrum of diacetate bis(cyclopentadienyl)zirconium(IV) shows that one acetato group acts as bidentate ligand and the other as unidentate. Remarkable benzene- and hexafluorobenzene-induced shifts were observed in the ^1H NMR signal of methyl group attached to the zirconium atom and the dithiocarbamate group.

The structure and reactivity of bis(cyclopentadienyl)-zirconium(IV) complexes are of considerable interest in comparison with those of titanium analogs in view of the fact that the zirconium atom has larger ionic radius and smaller ionization potentials than the titanium atom.

Very few[1-3] 18-electron bis(cyclopentadienyl)zirconium complexes $Cp_2Zr\begin{matrix}X\\ \leftarrow L\\ Y\end{matrix}$, which are thought to be a reaction intermediate, have been reported. In these complexes the X, Y, and L groups take coplanar three coordinated configuration. Brainina *et al.*[4] reported the preparation of acetate chlorobis(cyclopentadienyl)zirconium(IV) but gave no spectral data. Wailes *et al.*[5] reported only ^1H NMR data of diacetate bis(cyclopentadienyl)zirconium(IV) in $CDCl_3$. Neither groups, however, made any suggestions for the structures.

This paper reports the preparation of several dithiocarbamate bis(cyclopentadienyl)zirconium(IV), with some spectroscopic discussion on their structures. No dithiocarbamate derivatives of bis(cyclopentadienyl)zirconium(IV) have been reported, except for monocyclopentadienylzirconium(IV) complex $CpZr(S_2CNMe_2)_3$.[6] The preparation of some acetate bis(cyclopentadienyl)-zirconium(IV) is also reported.

Experimental

General. Preparation and recrystallization were carried out under argon or nitrogen atmosphere. Solvents were dried in the usual manner and distilled. Chlorobis-(cyclopentadienyl)(methyl)zirconium(IV) and thallium(I) dimethyl and diethyldithiocarbamate were prepared by the procedures reported.[7,8] Thallium(I) acetate and thallium(I) dithiocarbamates were used as a fine powder stored over P_2O_5. Infrared and mass spectra were recorded on a Hitachi 225 spectrophotometer and a JEOL model JMS-07 spectrometer, respectively. ^1H NMR spectra were recorded on a JEOL model JNM-PS-100 spectrometer operating at 100 MHz and a Varian A60-D spectrometer operating at 60 MHz. Chemical shifts were measured relative to tetramethylsilane as an internal standard. Melting points were measured in sealed capillary tubes and are uncorrected.

Preparation. Acetato Bis(cyclopentadienyl)(methyl)zirconium(IV) **1**: Thallium(I) acetate (0.58 g, 2.2 mmol) was gradually added to a solution of chlorobis(cyclopentadienyl)(methyl)zirconium(IV) (0.54 g, 2 mmol) in 50 ml of dichloromethane and the mixture was stirred at room temperature for 4 h. The filtrate was evaporated *in vacuo*, and the yellow residue was recrystallized twice from benzene–hexane to give white crystals **1** (0.21 g, 35% yield). Am attempt to prepare **1** by the reaction of $(Cp_2ZrMe)_2O$[9] with Ac_2O was unsuccessful, although $Cp_2Zr(Cl)OAc$ was prepared[4] by the treatment of $(Cp_2ZrCl)_2O$ with Ac_2O.

Acetato Chlorobis(cyclopentadienyl)zirconium(IV) **2**: Dichlorobis(cyclopentadienyl)zirconium(IV) (0.58 g, 2 mmol) was treated with thallium(I) acetate (0.58 g, 2.2 mmol) to give **2** (0.40 g, 64% yield) after recrystallization twice from dichloromethane–hexane.

Diacetate Bis(cyclopentadienyl)zirconium(IV) **3**: Sodium acetate (0.36 g, 4.4 mmol) was added to a solution of dichloro bis(cyclopentadienyl)zirconium(IV) (0.58 g, 2 mmol) in 40 ml of benzene and the mixture was refluxed for 6 h with stirring. The yellow filtrate was evaporated *in vacuo*. The orange residue was recrystallized three times from benzene–hexane to give white crystals **3** (0.30 g, 45% yield).

Dimethyldithiocarbamate Bis(cyclopentadienyl)(methyl)zirconium(IV) **4**, *Dimethyldithiocarbamate Chlorobis(cyclopentadienyl)-zirconium(IV)* **5**, *Diethyldithiocarbamate Bis(cyclopentadienyl)-(methyl)zirconium(IV)* **6**, *and Diethyldithiocarbamate Chlorobis-(cyclopentadienyl)zirconium(IV)* **7**: Complexes **4**—**7** were obtained as white crystals in 45(for **4**)—85%(for **7**) yield by the reaction of $Cp_2ZrMeCl$ or Cp_2ZrCl_2 with thallium(I)-dimethyl- or diethyldithiocarbamate in a similar way to

Table 1. Analytical data and melting points of $Cp_2Zr(X)Y$

	Complexes	Mp(°C)	Found (Calcd) % C	H	N
1	$Cp_2Zr(Me)OAc$	92—94	52.29 (52.84)	5.45 (5.35)	—
2	$Cp_2Zr(Cl)OAc$	137—138	45.06 (45.62)	4.04 (4.15)	—
3	$Cp_2Zr(OAc)_2$	100—101	49.65 (49.53)	4.62 (4.75)	—
4	$Cp_2Zr(Me)dmtc$[a]	156—158	46.93 (47.15)	5.35 (5.37)	4.01 (3.93)
5	$Cp_2Zr(Cl)dmtc$[a]	208 dec	41.22 (41.41)	4.22 (4.28)	3.65 (3.71)
6	$Cp_2Zr(Me)detc$[b]	131—132	50.80 (51.01)	5.96 (6.15)	3.23 (3.72)
7	$Cp_2Zr(Cl)detc$[b]	186 dec	44.05 (44.47)	4.95 (4.98)	3.43 (3.46)

a) dmtc=S_2CNMe_2. b) detc=S_2CNEt_2.

that for **1** and **2**.

Results and Discussion

Acetato Derivatives (1—3). In the monoacetato complexes **1** and **2**, ν_{as}(OCO) and $\Delta(\nu_{as}-\nu_s)$ values (Table 2) suggest that the acetato group belongs to the category of the chelating structure[10] in the solid state. On the other hand, in the diacetate derivative **3** one acetato group acts as the bidentate ligand and the other as unidentate in the solid state. Bridging and ionic structures of the acetate groups are excluded on the basis of molecular weight measurements and negligible molar conductivities (Table 3). In mass spectra of these complexes no ion heavier than the parent ion or the $(M-Me)^+$ ion was detected (Table 4). The results suggest the following structures I and II for complexes **1**—**3** in the solid state. The IR spectra of **1** and **2** in

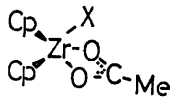

1 (X=Me)
2 (X=Cl)
(I)

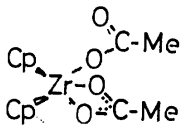

3
(II)

CH_2Cl_2, however, give additional weak bands at *ca.* 1640 and 1300 cm^{-1}. The results indicate that there is some portion of III in equilibrium with I in CH_2Cl_2.

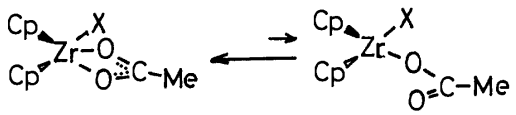

(I) (III)

The structure of **3** is of interest as compared with that of analogous titanium(IV) complex $Cp_2Ti(OAc)_2$.[11] In the latter both acetate groups are unidentate, although the bidentate acetate group was reported for Cp_2Ti^{III}-OAc.[12] The difference in structure of these diacetate complexes might be mainly due to the difference in their ionic radii (Ti(IV) 0.62—0.65 Å, Zr(IV) 0.79—0.87 Å). In the ^1H NMR spectrum of **3** methyl signals of the two acetate groups were observed as a singlet resonance even at −91 °C in CH_2Cl_2. The IR spectrum of **3** in CH_2Cl_2 shows little difference from that in the solid state. The IR and ^1H NMR data suggest that there is a rapid interconversion process IIa—IIb between two acetate groups in CH_2Cl_2.

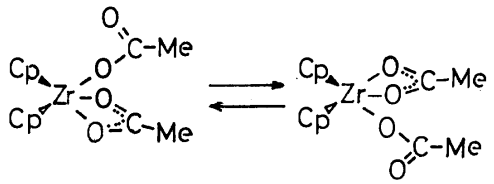

(IIa) (IIb)

Dithiocarbamate Derivatives (4—7). IR spectra: The νC=N frequency of complexes **4**—**7** together with that of methyl dialkyldithiocarbamate, tetraalkylthiuram disulfide, and sodium dialkyldithiocarbamate is summarized in Table 2. The IR spectra of complexes **4**—**7** in CH_2Cl_2 show little difference from those in the solid state. Complexes **4**—**7** exhibited the νC=N band at higher frequency than the corresponding unidentate dithiocarbamate compounds containing the same *N,N*-dialkyl group. The frequency of this band of **4**—**7** is nearly the same as that of $CpZr(S_2CNR_2)_3$,[6,17] in which chelation of the dithiocarbamate groups has been demonstrated by X-ray crystal analysis.[6] Thus the higher νC=N values suggest the chelation of dithiocarbamate groups in the complexes.

^1H NMR Spectra and the Structures: One sharp N–Me proton signal was observed at 23 °C in CH_2Cl_2 in complexes **4** and **5**, the latter showing two N–Me proton signals under 0 °C. One kind of sharp N–CH_2 and two

Table 2. IR data[a] for the complexes (in cm^{-1})

Complexes	ν_{as}(OCO)	ν_s(OCO)[b]	Δ[c]	ν Zr–Me
1	1533	1467	66	440
2	1535	1465	70	—
3	1642 1540	1305 1480	337 60	—

Complexes	νC=N[d]	νZr–S	νZr–Me
4	1512	358 355	425
5	1523	367	—
6	1495	360	423
7	1500	366	—

a) Nujol mulls. b) Hexachlorobutadiene mulls. c) $\Delta=\nu_{as}(OCO)-\nu_s(OCO)$. d) Reported νC=N values in unidentate dithiocarbamate compounds. Me_2NCS_2Me[13] 1498; $(Me_2NCS_2)_2$[14] 1505; $Me_2NCS_2Na\cdot H_2O$[15] 1480; Et_2NCS_2Me[13] 1489; $(Et_2NCS_2)_2$[16] 1487; $Et_2NCS_2Na\cdot xH_2O$ 1475.

Table 3. Mol wt and molar conductivities of $Cp_2Zr(X)OAc$

Complexes	Mol wt[a]	(Calcd)	Molar conductivity[b] ($\times 10^{-3}$ M concn)	
1	330	(295)	0.032	(1.03)
2	325	(316)	0.020	(1.02)
3	360	(340)	0.074	(0.59)

a) Determined cryoscopically in C_6H_6.
b) Ω^{-1} cm^2 mol^{-1} in CH_2Cl_2 at 25 °C.

Table 4. Mass spectral data[a] for $Cp_2Zr(X)Y$

Complexes	Temp °C	*m/e* (intensity) assignment
1	100	279(100) $[M-Me]^+$, 43(10)$MeC^+=O$
2	150	314(13)M^+, 279(15) $[M-Cl]^+$, 249 (100) $[M-Cp]^+$, 43(19)$MeC^+=O$
3	100	273(100) $[M-Cp]^+$, 43(33)$MeC^+=O$
4	150	340(100) $[M-Me]^+$, 88(7)$Me_2NC^+=S$
5	200	375(6)M^+, 340(22) $[M-Cl]^+$, 310 (100) $[M-Cp]^+$, 88(15)$Me_2NC^+=S$
6	130	368(100) $[M-Me]^+$, 116(17)$Et_2NC^+=S$
7	150	403(5)M^+, 368(2) $[M-Cl]^+$, 338(100) $[M-Cp]^+$, 116(2)$Et_2NC^+=S$

a) Ionizing voltage: 30 eV.

Table 5. ^{1}H NMR data[a] for complexes in CH_2Cl_2, C_6D_6, and C_6F_6 (Zr)=Cp_2Zr

Complexes		Assignment	CH_2Cl_2[b]	C_6D_6[b]	C_6F_6[c]	Δ[d]	Δ^*[e]
1	(Zr)OAc Me	Cp	5.92	5.73	5.85	+0.19	−0.07
		C–Me	1.80	1.61	1.80	+0.19	+0.00
		Zr–Me	0.00	0.43	−0.35	−0.43	+0.35
2	(Zr)OAc Cl	Cp	6.20	5.86		+0.34	
		C–Me	1.96	1.61		+0.35	
3	(Zr)OAc OAc	Cp	6.23	5.98		+0.25	
		C–Me	2.00	1.82		+0.18	
4	(Zr)dmtc Me	Cp	5.79	5.73	5.65	+0.06	+0.14
		N–Me	3.25[f]	2.69	3.40	+0.53	−0.15
		Zr–Me	−0.06	0.47	−0.43	−0.53	+0.37
5	(Zr)dmtc Cl	Cp	6.09	5.96		+0.13	
		N–Me	3.30[g]	2.58		+0.72	
6	(Zr)detc Me	Cp	5.88	5.72	5.70	+0.16	+0.18
		N–CH_2	3.72(q)	3.38(q) 3.36(q)	3.92(q)	+0.35	−0.20
		C–Me	1.19(t)[h] 1.21(t)[h]	0.89(t) 0.86(t)	1.40(t)	+0.33	−0.20
		Zr–Me	−0.06	0.47	−0.43	−0.53	+0.37
7	(Zr)detc Cl	Cp	6.07	6.00		+0.07	
		N–CH_2	3.75(q)	3.37(q)		+0.38	
		C–Me	1.26(t)[h] 1.24(t)[h]	0.86(t)		−0.39	
	(Zr)Me_2[i]	Cp	6.08	5.80	6.05	+0.28	+0.03
		Zr–Me	−0.40	−0.14	−0.57	−0.26	−0.17
	(Zr)MeCl	Cp	6.22	5.73		+0.49	
		Zr–Me	0.28	0.32		−0.04	
	(Zr)Cl_2	Cp	6.68	5.83		+0.85	

a) δ value (ppm); (q) quartet; (t) triplet; other, sharp singlet except as noted. b) Recorded on a JEOL model JNM-PS-100 spectrometer at 23 °C operating at 100 MHz. c) Recorded on a Varian A-60-D spectrometer at 40 °C operating at 60 MHz. d) $\Delta=\delta(CH_2Cl_2)-\delta(C_6D_6)$. e) $\Delta^*=\delta(CH_2Cl_2)-\delta(C_6F_6)$. f) Singlet even at −97 °C. g) Coalesces to doublet at 0 °C. h) Coalesces to triplet at about 34 °C. i) Ref. 7.

sorts of sharp C–Me proton signals were observed at 23 °C in complexes **6** and **7**. The C–Me proton signals coalesced at 34 °C. On the other hand, very broad N–Me and N–CH_2 proton signals were observed in Me_2NCS_2Me and Et_2NCS_2Me at 23 °C in CH_2Cl_2, due to the high rotational barrier around the S_2C=N bond.[13] The chemical shifts of *N*-alkyl protons of complexes **4**—**7** are nearly the same as those of $CpZr(S_2CNR_2)_3$. The IR and ^{1}H NMR data suggest that these dithiocarbamate groups complexes **4**—**7** are chelating in the solid state and in CH_2Cl_2. The two *N*-alkyl protons might be magnetically equivalent by the following equilibration IVa—IVc over −97 °C in **4**, 0 °C in **5**, and 34 °C in **6** and **7**.

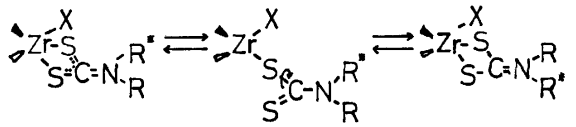

(IVa) (IVb) (IVc)

Chemical Shifts of Cp Proton, and Solvent-induced Shifts. Table 5 shows ^{1}H NMR data for complexes **1**—**7** in CH_2Cl_2, C_6D_6, and C_6F_6 together with those for Cp_2Zr-Me_2, $Cp_2Zr(Me)Cl$, Cp_2ZrCl_2. In a series of $Cp_2Zr(X)$-OAc the order of high field shifts of Cp proton in CH_2Cl_2 is X=Me>Cl≥OAc (unidentate). Similarly in Cp_2Zr-(X)Me the order is X=dmtc>detc>OAc(chelating)>Me>Cl, and in $Cp_2Zr(X)Cl$ it is X=detc≥dmtc>OAc-(chelating)≥Me>Cl. Thus the overall order of high field shifts of the Cp proton in CH_2Cl_2 is as follows: dmtc≥detc>OAc(chelating)≥Me>Cl≥OAc(unidentate). The signals of Cp proton in bis(cyclopentadienyl)-zirconium(IV) complexes in $CDCl_3$ shift in general to high field in line with electron donating effect of ligands on the zirconium atom.[18] The order is in line with that of electron donating ability of ligands. Remarkably low field shifts for (Zr)–CH_3 proton signals and high field shifts for N–CH_3 proton signals in dithiocarbamate groups were observed in benzene (Tables 5). The specific benzene-induced solvent shifts are interpreted by the following benzene-solute stereospecific interaction. Benzene–dithiocarbamate interaction has been

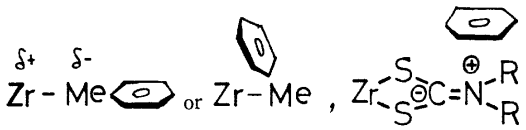

reported by Hatton and Richards[19-20] and Honda *et al.*[21-22] Hexafluorobenzene[23-24] induces low field shifts of protons at the electron-deficient site in a solute molecule and high field shifts of protons at the electron-rich site, the direction of these shifts being reversed in ben-

zene. In our zirconium complexes appreciable hexafluorobenzene induced shifts were also observed in (Zr)–CH_3, N–CH_3, and N-CH_2CH_3 proton signals.

One of us (H. S) is grateful to Prof. Rokuro Okawara, Dr. Masanori Wada and Dr. Hideo Kurosawa, Osaka University, for their encouragement and valuable discussions.

References

1) G. Fachinetti, C. Floriani, F. Marchetti, and S. Merlino, *J. Chem. Soc., Chem. Commum.*, **1976**, 522.

2) E. M. Brainina, E. V. Bryukhova, B. V. Lokshin, and N. S. Alimov, *Izv. Akad. Nauk SSSR, Ser. Khim*, **1973**, 891.

3) H. A. Martin, P. J. Lemaire, and F. Jellinek, *J. Organomet. Chem.*, **14**, 149 (1968).

4) E. M. Brainina, M. Kh, Minacheva, B. V. Lokhin, E. I. Fedin, and P. V. Petrovskii, *Izv. Akad. Nauk SSSR, Ser. Khim*, **1969**, 2492.

5) P. C. Wailes, H. Weigold, and A. P. Bell, *J. Organomet. Chem.*, **33**, 181 (1971).

6) A. H. Bruder, R. C. Fay, D. F. Lewis, and A. A. Sayler, *J. Am. Chem. Soc.*, **98**, 6932 (1976). IR(Nujol) 1510 (ν C=N), and 350 cm^{-1} (ν Zr–S); NMR ($CDCl_3$) δ=6.13(Cp), 3.36, 3.35, 3.30, and 3.29 (N–Me).

7) P. C. Wailes, H. Weigold, and A. P. Bell, *J. Organomet. Chem.*, **34**, 155 (1972).

8) S. Akerstorm, *Arkiv. Kemi.*, **24**, 495 (1965).

9) This compound was obtained in 65% yield as shiny white crystals by the reaction of Cp_2ZrMe_2 with MeOH in CH_2Cl_2, and recrystallization from CH_2Cl_2–hexane. (Cp_2·$ZrMe)_2O$: mp 160 °C (dec); IR(Nujol) 745 (ν Zr–O–Zr) and 450 cm^{-1} (νZr–Me); NMR(C_6D_6) δ=5.93 (10H, s, Cp) and 0.24 (3H, s, Me); MS(150 °C, 75 eV), *m/e* (rel intensity), 486 (100, M−Me); Found: C, 53.75; H, 5.51%. Calcd for $C_{22}H_{26}OZr_2$: C, 54.05; H, 5.36%.

10) N. W. Alcock, V. M. Tracy, and T. C. Waddington, *J. Chem. Soc., Dalton Trans.*, **1976**, 2243.

11) G. G. Dvoryantseva, Yu. N. Sheinker, A. N. Nesmeyanov, D. V. Nogina, N. A. Lazareva, and V. A. Dubovitskii, *Dokl. Akad. Nauk SSSR.*, **161**, 603 (1965).

12) R. S. P. Coutts and P. C. Wailes, *Aust. J. Chem.*, **20**, 1579 (1967).

13) C. E. Holloway and M. H. Gitlitz, *Can. J. Chem.*, **45**, 2659 (1967).

14) F. A. Cotton and J. A. McCleverty, *Inorg. Chem.*, **3**, 1398 (1964).

15) C. ÓConnor, J. D. Gilbert, and G. Wilkinson, *J. Chem. Soc., A*, **1969**, 84.

16) N. K. Wilson, *J. Phys. Chem.*, **75**, 1067 (1971).

17) This compound was obtained as white crystals by the treatment of Cp_2ZrCl_2 with NaS_2CNEt_2 in CH_2Cl_2 at r. t. $CpZr(S_2CNEt_2)_3$: mp 185—186 °C; IR (Nujol) 1493 (ν C=N), 371 and 362 cm^{-1} (ν Zr–S); NMR ($CDCl_3$) δ=6.08 (5H, s, Cp), 3.76 (12H, m, 10 lines, N–CH_2) and 1.24 (18H, m, 6 lines, C–Me); Found: C, 39.80; H, 5.86; N, 6.99%. Calcd for $C_{20}H_{35}N_3S_6Zr$: C, 39.96; H, 5.87; N, 6.99%.

18) P. C. Wailes, "Organometallic Chemistry of Titanium, Zirconium and Hafnium," Academic Press (1974), p. 115.

19) J. V. Hatton and R. E. Richards, *Mol. Phys.*, **3**, 253 (1960).

20) J. V. Hatton and R. E. Richards, *Mol. Phys.*, **5**, 139 (1962).

21) M. Honda, M. Komura, Y. Kawasaki, T. Tanaka, and R. Okawara, *J. Inorg. Nucl. Chem.*, **30**, 323 (1968).

22) M. Honda, Y. Kawasaki, and T. Tanaka, *Tetrahedron Lett.*, **1967**, 3313.

23) R. D. Bertrand, R. D. Compton, and J. G. Verkade, *J. Am. Chem. Soc.*, **92**, 2702 (1970).

24) R. S. Armstrong, M. J. Aroney, R. K. Duffin, H. J. Stootman, and R. J. W. Le Fevre, *J. Chem. Soc., Perkin Trans. 2*, **1973**, 1362.

Five-coordinate Bis(8-aminoquinoline) Nitrosylcobalt Complexes

Eiichi MIKI, Hiromichi OKAMURA,* Kunihiko MIZUMACHI, and Tatsujiro ISHIMORI

Department of Chemistry, College of Science, Rikkyo University, 3-Chome, Nishi-Ikebukuro, Toshima-Ku, Tokyo 171

(Received December 6, 1977)

$[Co(C_9H_8N_2)_2NO]X_2 \cdot nH_2O$ ($C_9H_8N_2$=8-aminoquinoline; X=Cl, Br, I, NO_3, ClO_4, and $SO_4/2$; n=0, 1, 1.5, and 2) was isolated by the reaction of nitrogen oxide with a mixture of the corresponding cobalt(II) salt and 8-aminoquinoline in methanol. The IR, UV, and molar conductivity measurements suggest that the geometry of the cation is a tetragonal pyramid with an apical NO^-.

Nast *et al.* reported that paramagnetic deep blue compounds formulated as $[Co(C_9H_8N_2)_2NO]X_2$ ($C_9H_8N_2$=8-aminoquinoline; X=Cl and NO_3) had been isolated by the reaction of nitrogen oxide with $CoX_2(C_9H_8N_2)_2$ in methanol, and that the geometry of the complex cation was a tetragonal pyramid with an apical NO^-, its N–O stretching vibration being assigned to a *ca.* 1170 cm^{-1} band.[1] Subsequently, it was established that N–O stretching vibrations for nitrosylcobalt complexes with this geometry can be observed in the region 1620—1710 cm^{-1} and most of the compounds are diamagnetic.[2,3] N–O stretching vibrations for compounds bridged by a NO group and those for compounds containing an anion of dimer of nitrosyl group such as a hyponitrite ion were observed in the region 1300—1550 and 920—1270 cm^{-1}, respectively.[4,5]

The authors reinvestigated the reaction of nitrogen oxide with $CoX_2(C_9H_8N_2)_2$ to make clear the detals. In this paper, they report the syntheses and characterization of some new five-coordinate mononitrosyl complexes which are different from the compounds isolated by Nast *et al.*[1]

Experimental

Preparations. The compounds were prepared by the use of a Schlenk apparatus under nitrogen atmosphere. Four mmol of 8-aminoquinoline was added to *ca.* 50 cm^3 of deoxygenated methanol solution containing 2 mmol of cobalt(II) salt to give a deep orange solution. Nitrogen oxide (of purity more than 99.0%) purchased from Seitetsu Kagaku Co., Ltd., after being further purified by passing it through a trap at −80 °C, was then passed into this solution at room temperature causing the solution to darken gradually with the formation of a precipitate. This precipitation was not reported by Nast *et al.*[1] After the nitrogen oxide had been replaced with nitrogen, the precipitate was collected by filtration, washed with methanol and diethyl ether, successively in air, and dried over anhydrous calcium chloride under vacuum. Yield, 500—700 mg. The elementary analyses are given in Table 1. The filtrate was wine red. The same compounds could also be prepared by the reaction of $CoX_2(C_9H_8N_2)_2$ with the nitrogen oxide in methanol, but could not be prepared by exposure of $CoX_2(C_9H_8N_2)_2$ in the solid state to the nitrogen oxide under *ca.* 1 atmosphere at room temperature. The ^{15}NO(^{15}N atom%=95.5) analogues were prepared in a vacuum system on a scale half of the ordinary one by the use of *ca.* 3 mmol of ^{15}NO derived from $K^{15}NO_3$.

The wine red filtrate was dropped into a large volume of petroleum ether or diethyl ether (*ca.* 500 cm^3), while being stirred, to give the paramagnetic deep blue precipitate reported by Nast *et al.*[1]

$[CoNO(diars)_2](ClO_4)_2$ (diars=1,2-bis(dimethylarsino)benzene), $[CoINO(diars)_2]ClO_4$, and their ^{15}NO-substituted compounds were synthesized by the use of a vacuum system in accordance with Ref. 6.

Measurements. The magnetic susceptibility was measured by the Gouy method. The IR spectra were measured as Nujol and hexachlorobutadiene mulls in the region 200—4000 cm^{-1} on JASCO 402G and JASCO IR-F spectrometers. The wave numbers of the observed bands were calibrated with polystyrene film and water vapor. The UV spectra in *N,N*-dimethylformamide were measured with a Hitachi 124 spectrometer and the diffuse reflection spectra with a Hitachi EPS-3T spectrometer. The molar conductivities in *N,N*-dimethylformamide were measured in the range $(2.5—10)\times10^{-3}$ M at 25 °C (±0.1 °C) with a universal bridge (Model 4225A of Yokogawa-Hewlett-Packard Ltd.). The *N,N*-dimethylformamide was purified by the standard method, its electrolytic conductivity being $(1.1—2.3)\times10^{-5}$ S m^{-1}.

Results and Discussion

Properties of the Compounds. All the compounds obtained were stable in air, and were soluble in water, methanol, and ethanol to give wine red solutions from which the deep blue compounds reported by Nast *et al.*

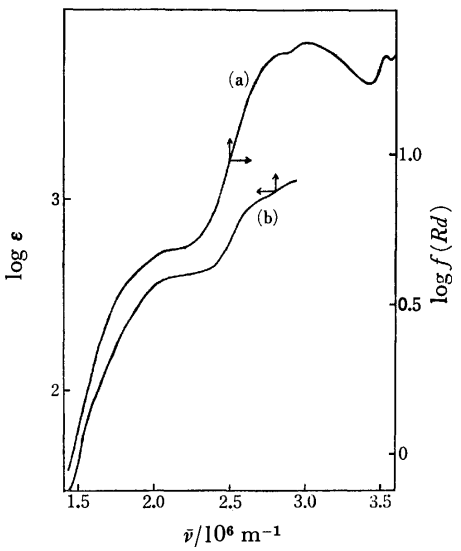

Fig. 1. UV spectra of $[Co(C_9H_8N_2)_2NO](NO_3)_2$; a: in *N,N*-dimethylformamide(1.266×10^{-4} M), b: in the solid state.

* Present address: Synthetic Chemistry Laboratory, Nisso Chemicals Co., Ltd., 12-8, Goi-Minamikaigan, Ichihara, Chiba 290.

Table 1. Elementary analyses of the compounds

Compound		Co	C	H	N	Halogen	H_2O	S/%
$[Co(C_9H_8N_2)_2NO]Cl_2\cdot 2H_2O$ (khaki)	Calcd	12.17	44.65	4.16	14.46	14.65		
	Found	12.2	47.29	4.23	14.43	14.49		
$[Co(C_9H_8N_2)_2NO]Br_2\cdot 2H_2O$ (brown)	Calcd	10.28	37.72	3.52	12.23	27.88		
	Found	10.5	40.18	3.60	12.05	27.65		
$[Co(C_9H_8N_2)_2NO]I_2\cdot H_2O$ (chocolate)	Calcd	9.08	33.31	2.79	10.78	39.10	2.78	
	Found	9.06	33.28	2.76	10.39	38.35	3.08	
$[Co(C_9H_8N_2)_2NO](ClO_4)_2$ (russet)	Calcd	10.23	37.52	2.80	12.15	12.31		
	Found	10.4	37.48	2.81	12.27	12.28		
$[Co(C_9H_8N_2)_2NO](NO_3)_2$ (dark brown)	Calcd	11.75	43.13	3.22	19.56			
	Found	11.9	43.41	3.32	19.22			
$[Co(C_9H_8N_2)_2NO]SO_4\cdot 1.5H_2O$ (khaki)	Calcd	11.78	43.21	3.83	14.00		5.40	6.41
	Found	11.8	42.77	3.71	13.93		5.34	6.17
$[Co(C_9H_8N_2)_2NO]SO_4\cdot H_2O$[a] (khaki)	Calcd	11.99	44.00	3.69	14.25		3.67	6.52
	Found	12.0	43.11	3.58	14.03		3.64	6.12

a) This compound could be obtained from $[Co(C_9H_8N_2)_2NO]SO_4\cdot 1.5H_2O$ by drying it over P_4O_{10} in vacuum.

Table 2. IR data and molar conductivities of the compounds

Compound	νNO / cm^{-1}	δCoNO / cm^{-1}	νCoN / cm^{-1}	Λ[a] / 10^{-4} S m^2 mol^{-1}	Slope[b]	Electrolyte type
$[CoCl(en)_2NO]ClO_4$				153	560	1:1
$[Ru(phen)_3]I_2\cdot H_2O$				244	1200	2:1
$[Co(phen)_3]Br_3$				356	3120	3:1
$[Co(C_9H_8N_2)_2NO[Cl_2\cdot 2H_2O$	1651 vs (26)[c]	520 w(8)	308 sh?	e)		
$[Co(C_9H_8N_2)_2NO]Br_2\cdot 2H_2O$	1662 vs (28)	520 w(8)	305 w(4)	171	1180	2:1
$[Co(C_9H_8N_2)_2NO]I_2\cdot H_2O$	1670 vs	517 sh?	d)	230	950	2:1
$[Co(C_9H_8N_2)_2NO](ClO_4)_2$	1715 vs (29)	501 w(4)?	d)	275	1230	2:1
$[Co(C_9H_8N_2)_2NO](NO_3)_2$	1683 vs (29)	520 w(6)	d)	253	1470	2:1
$[Co(C_9H_8N_2)_2NO]SO_4\cdot 1.5H_2O$	1635 vs, br	d)	d)	e)		
$[Co(C_9H_8N_2)_2NO]SO_4\cdot H_2O$	1632 vs, br	d)	d)	e)		

a) Molar conductivities at 2.5×10^{-3} M. b) $(\Lambda_0-\Lambda)/\sqrt{C}$ where Λ_0 is molar conductivity at infinite dilution, Λ being that at C mol/dm^3. c) The value in parentheses indicates observed ^{15}N-isotopic shift. d) Not observed. e) Unstable in *N,N*-dimethylformamide. νNO, N–O stretching vibration. δCoNO, Co–N–O bending vibration. νCoN, Co–N stretching vibration. vs, very strong; w, weak; sh, shoulder; br, broad.

precipitate by addition of petroleum ether or diethyl ether. UV spectra of the wine red solutions were consistent with those of the deep blue compounds. All of the compounds except the chloride and sulfate were stable in *N,N*-dimethylformamide for a few hours. Although they could not be purified by recrystallization from *N,N*-dimethylformamide, they gave excellent results for the elementary analyses.

Magnetic susceptibilities, χ_g, for the chloride, bromide, iodide, perchlorate, and nitrate are -0.38, $+1.33$, -0.06, $+0.01$, and -0.14×10^{-6} cm^3 g^{-1}, respectively. Thus, all the compounds are essentially diamagnetic. The slight paramagnetism is probably due to contamination by a small amount of the deep blue compound (μ_B=3.45 and 2.95 B. M. for the chloride and nitrate, respectively) reported by Nast *et al.* considering the synthetic conditions.

UV Spectra and Molar Conductivities. The spectral figures in *N,N*-dimethylformamide are similar to those of the diffuse reflection as shown in Fig. 1. Hence, the structures of the cation in the solid state of the bromide, iodide, perchlorate, and nitrate may be the same as those in *N,N*-dimethylformamide. The UV spectra in *N,N*-dimethylformamide show a peak or shoulder at $(1.9—2.1)\times 10^6$ m^{-1} with log ε=2.7—2.8, which is a characteristic band of a tetragonal pyramid-type nitrosyl complex with an apical NO^- group.[2]

The measurement of the molar conductivity was carried out within *ca.* one hour after the compounds had been dissolved. The molar conductivities were compared with those of 3:1-, 2:1-, and 1:1-type electrolytes by the method of Feltham and Hayter.[7] The results in Table 2 show that the compounds are 2:1-type electrolytes.

IR Spectra. The wave numbers and their assignments due to the CoNO group are summarized in Table 2.

No isotopic shift upon ^{15}NO-substitution was observed in the bands at *ca.* 1100 cm^{-1}, while the bands at 1630—1720 cm^{-1} shifted downwards by 26—29 cm^{-1}. Hence, the latter can be assigned to the N–O stretching vibrations.

The isotopic shift in the region 200—700 cm^{-1} was carefully measured because a number of bands due to 8-aminoquinoline disturbed the assignments of skeletal vibrations due to the CoNO group. The 500—520 cm^{-1} bands showed the isotopic shift, its value being 4—8 cm^{-1}. The 305 cm^{-1} band for the bromide shifted to 301 cm^{-1}; however, no band in the region of 300 cm^{-1} was observed for the other compounds. This can be

explained from the fact that a very strong band at 290—300 cm^{-1} due to the coordinated 8-aminoquinolines overlapped the bands due to the CoNO group.

For nitrosylcobalt complexes, the N–O stretching vibration of the NO^- complex is observed in the region 1570—1710 cm^{-1}, while that of the NO^+ complex such as $[CoNO(diars)_2](ClO_4)_2$ at 1846 cm^{-1}.[2,3,6,8] The ^{15}N-isotopic shift of the N–O stretching vibration for $[CoNO(diars)_2](ClO_4)_2$ was 36 cm^{-1}, this value being quite similar to the isotopic shift, 35 cm^{-1}, calculated by a linear Co–N–O arrangement. On the other hand, the isotopic shift of the N–O stretching vibrations for the NO^- complexes such as $[Co(NH_3)_5NO]Cl_2$ (νNO, 1614 cm^{-1}), $[Co(OClO_3)(en)_2NO]ClO_4$ (νNO, 1661 cm^{-1}), $Co\{S_2CN(CH_3)_2\}_2NO$ (νNO, 1624 cm^{-1}), and $[CoINO(diars)_2]ClO_4$ (νNO, 1575 cm^{-1}) was in the range 25—29 cm^{-1}.[9] Thus, the value of the ^{15}N-isotopic shift for the N–O stretching vibration is sensitive to the metal–N–O bond angle.

Skeletal vibrations of the metal–N–O group are observed in the wide region 280—600 cm^{-1}, which have been established from the ^{15}NO-substitution.[9] For NO^+ complexes, the skeletal vibrations are observed in the limited region *ca.* 450—650 cm^{-1}. For example, those for $[CoNO(diars)_2](ClO_4)_2$ in the present work were observed at 477 and 501 cm^{-1}, the ^{15}N-isotopic shifts being 10 and 11 cm^{-1}, respectively. For NO^- complexes, the metal–N stretching and the metal–N–O bending vibrations are observed in the regions, 280—340 and 500—620 cm^{-1}, respectively, and the ^{15}N-isotopic shift for the former vibration is generally smaller than that for the latter one. Thus, the 500—520 cm^{-1} bands for the present compounds can be assigned to the Co–N–O bending and the *ca.* 300 cm^{-1} bands to the Co–N stretching vibrations. Similar vibrational frequencies are also observed in a strongly bent nitrosyl, XNO (X= F, Cl, and Br); the X–N–O bending vibrations appear in the region 550—780 cm^{-1}, the X–N stretching vibrations in the region 270—520 cm^{-1}. The ^{15}N-isotopic shift of the X–N–O bending vibration is 14—18 cm^{-1}, that of the X–N stretching one being 2.2—2.5 cm^{-1}.[10]

The position of the N–O stretching vibration, its ^{15}N-isotopic shift, and the far IR measurement suggest that the present compounds are formulated as NO^- complex.

IR bands due to the stretching vibration of Co–X (X=Cl, Br, and I) are usually observed in the region 170—350 cm^{-1}, and the bands due to the Co–O stretching vibration resulted from coordination of perchlorate, nitrate, and sulfate ions to the cobalt atom in the region 200—350 cm^{-1}.[11,12] Spectral figures in the region 200—350 cm^{-1} for the compounds were very similar to each other. This finding supports the contention that the anions are not in the coordination sphere, which is also suggested from the molar conductivity measurements.

It is well known that geometry of five-coordinate mononitrosyl complexes with a CoNO group, the formal oxidation state of which is II, is divided into two forms: a tetragonal pyramid with an apical NO^- and a trigonal bipyramid with an equatorial NO^+.[3] From the experimental results, the geometry of the cation of the present compounds is considered to be a tetragonal pyramid with an apical NO^-.

The compounds reported in this paper may be a precursor of the deep blue compounds isolated by Nast *et al.*[1] considering the synthetic conditions and the properties of the compounds.

The authous express their appreciation to Mr. Osamu Sakuma of Rikkyo University, for his technical assistance. The present work was supported in part by a Grant-in-Aid (No. 254208 in 1977) for Scientific Research from the Ministry of Education.

References

1) R. Nast, H. Bier, and J. Gremm, *Chem. Ber.*, **94**, 1185 (1961).
2) M. Tamaki, I. Masuda, and K. Shinha, *Bull. Chem. Soc. Jpn.*, **42**, 2858 (1969).
3) J. H. Enemark and R. D. Feltham, *Coord. Chem. Rev.*, **13**, 339 (1974).
4) J. C. Bailar Jr., H. J. Emeléus, Sir R. Nyholm, and A. F. Trotman-Dickenson, Ed, "Comprehensive Inorganic Chemistry," Vol. 5, Pergamon Press, Oxford (1973), p. 118.
5) H. Okamura, E. Miki, K. Mizumachi, and T. Ishimori, *Bull. Chem. Soc. Jpn.*, **49**, 666 (1976) and references cited therein; E. Miki and T. Ishimori, *ibid.*, **49**, 987 (1976).
6) R. D. Feltham and R. S. Nyholm, *Inorg. Chem.*, **4**, 1334 (1965).
7) R. D. Feltham and R. G. Hayter, *J. Chem. Soc.*, **1964**, 4587.
8) T. B. Jackson, M. J. Baker, J. O. Edwards, and D. Tutas, *Inorg. Chem.*, **5**, 2046 (1966).
9) E. Miki, K. Mizumachi, and T. Ishimori, *Bull. Chem. Soc. Jpn.*, **46**, 3779 (1973); *ibid.*, **47**, 656, 3068 (1974); *ibid.*, **48**, 2975 (1975).
10) L. H. Jones, "Inorganic Vibrational Spectroscopy," Vol. 1, Marcel Dekker, New York, N. Y. (1971), p. 79.
11) K. Nakamoto, "Infrared Spectra of Inorgamic and Coordination Compounds," 3rd ed, Wiley-Interscience, New York, N. Y. (1970).
12) J. R. Ferraro, "Low Frequency Vibration of Inorganic and Coordination Compounds," Plenum Press, New York, N. Y. (1971).

The Polymorphic Crystallization of Titanium(IV) Oxide under Hydrothermal Conditions. II.[1] The Roles of Inorganic Anions in the Nucleation of Rutile and Anatase from Acid Solutions

Fujio Izumi

National Institute for Research in Inorganic Materials, Sakura-mura, Niihari-gun, Ibaraki 300-31

(Received December 7, 1977)

Titanic acid was treated with hydrochloric, nitric, sulfuric, and hydrofluoric acids at 350 °C and 49 MPa to give titanium(IV) oxide. With increasing acid concentration, its polymorphic forms changed from anatase to rutile in hydrochloric and nitric acids, but from anatase to rutile, then back to anatase in sulfuric and hydrofluoric acids. Rutile and anatase crystals were grown from 1.7—9.5 mol dm^{-3} hydrofluoric acid at 360—560 °C by the temperature-drop method. Lower temperatures and higher concentrations of the acid favored anatase formation. The mechanisms for crystallization of the two forms are discussed by considering the chemical behavior of titanium(IV) complexes involved in their primary nucleation.

Titanium(IV) oxide occurs naturally in three minerals: rutile (tetragonal), brookite (orthorhombic), and anatase (tetragonal). Rutile and anatase can readily be prepared in a large variety of ways;[2] they are produced industrially for use as important white pigments. By contrast, brookite has rarely been synthesized by conventional methods.[3,4] On the basis of thermochemical data, Navrotsky and Kleppa[5] established that anatase is thermodynamically always unstable with respect to rutile. Anatase formation should, therefore, be regarded as metastable crystallization. Many reports have been published on the kinetics and mechanism of the irreversible anatase-rutile phase transition.[6]

There is some information in the literature regarding the crystallization and chemical reactivities of the two polymorphs under hydrothermal conditions. Osborn[7] was the first to find that, in pure water, anatase was converted into rutile above *ca.* 600 °C, which is a good deal lower than the temperatures of the anatase-rutile transformation in air. Hydrothermal treatment of hydrous titanium(IV) oxide (titanic acid) with pure water yielded rutile and/or anatase; lower temperatures, and to a lesser extent lower pressures, favored the unstable formation of anatase.[3,4,8,9] Single crystals of rutile have been grown from sulfuric acid[10] and from solutions of several fluorides.[11,12] The previous work in this series[1] has shown that anatase crystals can be successfully grown from potassium fluoride–dipotassium hydrogenphosphate solutions at less than 600 °C.

Few papers report the polymorphism of titanium(IV) oxide in acid solutions, apart from the formation of hydrated titanium(IV) oxide of poor crystallinity at temperatures below 100 °C and at atmospheric pressure.[2] The present investigation deals chiefly with the hydrothermal synthesis of rutile and anatase in four different mineral acids. Attention will be paid to the roles of dissolved anions in the nucleation of the oxide, as in the preceding paper.[1] Information of this type is indispensable for an understanding of the mechanisms by which rutile and anatase are crystallized under hydrothermal conditions.

Experimental

Materials. Titanium(IV) ethoxide obtained commercially was used without further purification. The single crystal of rutile-type titanium(IV) oxide produced by the Verneuil technique was a highly-purified product from Nakazumi Crystal, Ltd. Rutile powder of 99.99% purity was obtained from the Kojundo Kagaku Kenkyusho. All the other reagents used were of a GR grade.

Preparation of Amorphous Titanic Acid. Titanium(IV) ethoxide was poured into a large excess of pure water. The white precipitate which formed was washed several times with pure water by decantation, filtered off with suction, and then dried over phosphorus(V) oxide at ambient temperature under reduced pressure. Thermogravimetry showed that this sample contained *ca.* 23 wt% of water, which was released almost completely at 420 °C in static air.

Hydrothermal Treatment of Titanic Acid with Acid Solutions. Titanic acid (30 mg) and mineralizer solutions (0.1 cm^3) were sealed into welded gold capsules 4 mm in diameter and 30 mm in effective length. Four capsules were placed together in a cold-seal pressure vessel (Nikkiso NK-H25-III) with a capacity of 27 cm^3 and an i.d. of 12.7 mm. Most of the unoccupied space above the capsules was filled with a hastelloy rod to minimize the temperature differences both between the interior and exterior of the pressure vessel and between the capsule ends.[13] The vessel was then allowed to heat to 350 °C in a tubular furnace arranged vertically. The reaction temperature was measured with an external chromel-alumel thermocouple. The pressures generated within the capsules were balanced by water pumped into the pressure vessel and measured with a Bourdon gauge.

Recrystallization of Titanium(IV) Oxide in Fluoride Solutions by Means of a Double-capsule Technique. Small pieces (0.1—4 mm in size) of broken single crystals of rutile (Ru-I) and rutile powder (Ru-II) were used as starting materials. Either Ru-I (0.15 g) or Ru-II (0.1 g) was contained in a gold capsule 4 mm in diameter and 10 mm long, with a small hole. This nutrient capsule was fixed at one end of a larger gold capsule 5 mm in diameter and 60 mm in effective length. After 0.5 cm^3 of a mineralizer solution had been added, the larger capsule was sealed by crimping and welding the other end shut. This double capsule was placed in a conventional cold-seal pressure vessel (Nikkiso NK-H25-I: capacity, 5.5 cm^3; i.d., 6.4 mm), which was set horizontally in a tubular furnace. The temperature gradient between the capsule ends varied from 40 to 90 °C. The solid in the nutrient capsule was dissolved and then transported to the other end, where titanium(IV) oxide recrystallized spontaneously from supersaturated solutions.

The phases which formed were identified by X-ray powder diffraction using nickel-filtered Cu $K\alpha$ radiation. The relative amounts of rutile and anatase in their mixtures were

calculated from the X-ray intensities of the strongest reflections for rutile (d=0.3245 nm) and anatase (d=0.351 nm).[14] Acid solutions were standardized against a sodium hydroxide solution.

Chemical Analysis of Fluoride Ions Coprecipitated with Titanium(IV) Oxide. A sample ground into a powder was fused with about 2.5 g of potassium sodium carbonate in a platinum crucible at 900 °C. After the resulting cake had been transferred quantitatively to a distillation flask together with a small amount of water, 15 cm^3 of concentrated sulfuric acid was slowly added into the flask, which was cooled in an ice bath. The mixture was steam-distilled at 130—150 °C until *ca.* 80 cm^3 of distillate was collected. The total volume of the solution was then adjusted to 100 cm^3 with pure water. About 90% of fluorine could be recovered as hexafluorosilicic acid by following the above procedure. The fluoride ion concentration of the distillate was determined colorimetrically with Dotite Alfusone (lanthanum–alizarin complexone).[15]

Results

Titanic acid was treated isothermally with dilute acids of various concentrations as well as pure water for *ca.* 70 h at 350 °C and 49 MPa. Rutile and/or anatase were crystallized by the action of hydrochloric, nitric, sulfuric, and hydrofluoric acids on the amorphous reactant. Anatase was formed exclusively in pure water. These products were fully crystalline powders, white or yellow-tinged white except for those obtained by using 0.1—1.0 mol dm^{-3} hydrofluoric acid, in which bluish-gray powders formed. This exceptional coloration will later be discussed in some detail. An attempt to prepare titanium(IV) oxide in about 7.5 mol dm^{-3} phosphoric acid failed; only a highly insoluble, poorly crystallized phosphate of titanium(IV) was formed.

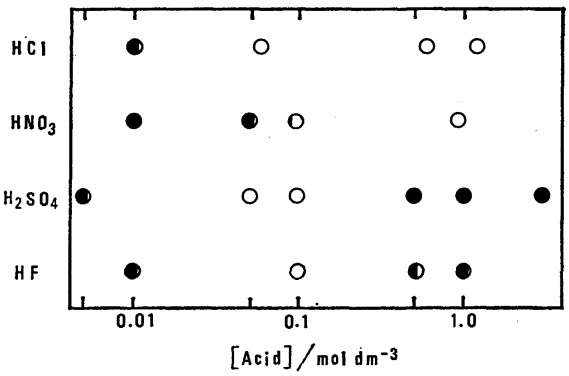

Fig. 1. Crystallization of rutile and anatase from titanic acid in four mineral acids at 350 °C and 49 MPa (t= 70 h). ○: Rutile, ●: anatase. Percentage of area of each circle shaded indicates percentage of anatase in the mixture.

Figure 1 shows the effects of the acid and its concentration on the relative amounts of rutile and anatase. With increasing acid concentration, the polymorphic forms of titanium(IV) oxide changed from anatase to rutile in hydrochloric acid and nitric acid, but from anatase to rutile, then to anatase again in sulfuric acid and hydrofluoric acid. The crystallization behavior of the oxide in the presence of hydrochloric acid is similar to that reported earlier by Matthews.[9] On the basis of experiments with only pure water, hydrochloric acid, and a sodium carbonate solution, he claimed that neutral, basic, and weakly acidic media were favorable for anatase formation, whereas more strongly acid environments resulted in the appearance of rutile. Judging from the conflicting results obtained by use of sulfuric acid and of hydrofluoric acid, his conclusion is highly questionable. The observations presented above support the idea that polymorphic crystallization of titanium(IV) oxide from aqueous solution is susceptible to the influence of not only the acid concentration but also the kind of acid.

Several representative specimens prepared hydrothermally were observed by scanning electron microscopy

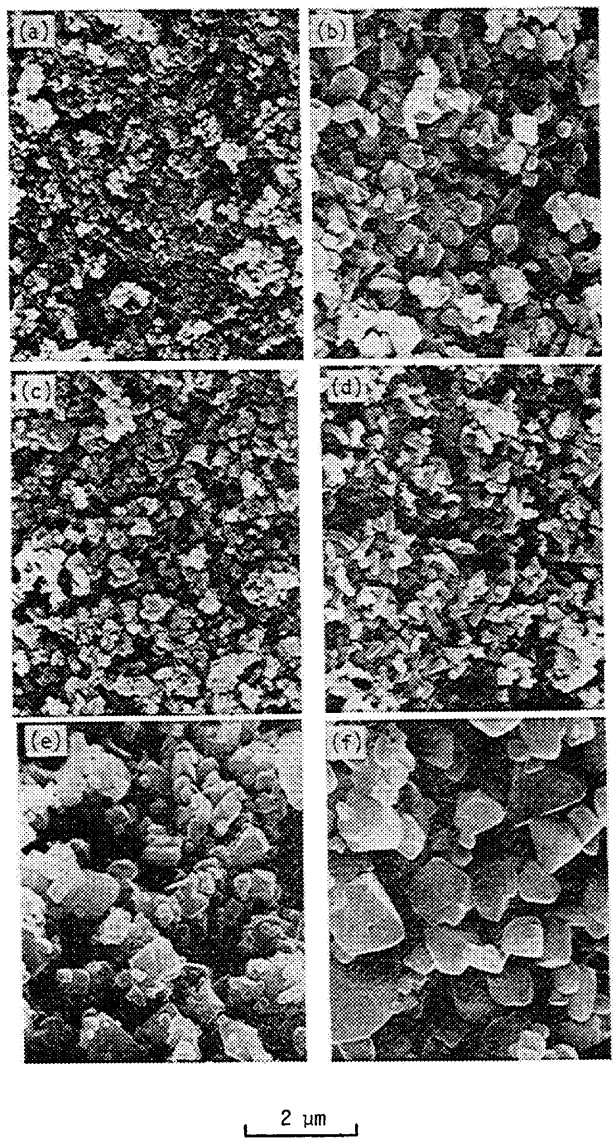

Fig. 2. Scanning electron micrographs of rutile and anatase prepared from titanic acid in dilute acids at 350 °C and 49 MPa.
(a) Anatase, pure water; (b) rutile, 0.058 mol dm^{-3} HCl; (c) rutile, 0.92 mol dm^{-3} HNO_3; (d) rutile, 0.049 mol dm^{-3} H_2SO_4; (e) anatase, 1.0 mol dm^{-3} H_2SO_4; (f) rutile, 0.10 mol dm^{-3} HF.

(Fig. 2). In pure water, anatase occurred as aggregates of reasonably equidimensional crystallites of the order of 0.1 μm in diameter [Fig. 2(a)]. The formation of the finely dispersed product is evidently due to the very low solubilities of titanic acid and the resulting anatase in pure water.

As pointed out by Matthews,[9] the anatase must be crystallized *via* the gradual structural rearrangement of the reactant with liberation of water. Dehydration probably precedes the structural rearrangement in the same way as in the crystallization of anatase by thermal dehydration of titanic acid in air. Titanic acid, which was amorphous to X rays, is assumed to have already a short-range order analogous in structure to anatase. Hence, anatase nucleation is readily induced in the reactive starting material and followed by a series of epitaxial growth processes. Practically the same reaction scheme as proposed above holds also for anatase formation in acids with concentrations lower than 50 mol m^{-3} (see Fig. 1).

By contrast, rutile and anatase grew into relatively large particles with characteristic crystal habits in acids of concentrations higher than 50 mol m^{-3} [Fig. 2 (b) to (f)]. The gross morphologies of their grains were quite different from those of the titanic acid grains from which they were obtained. Rutile crystallized in columns 0.07—0.2 μm in diameter from 49 mol m^{-3} sulfuric acid [Fig. 2(d)]. All the other products in acid solutions consisted of polygonal microcrystals with smooth faces. These observations are compatible with the dissolution and precipitation mechanism described below.

Amorphous titanic acid has much higher free energies of formation than has any polymorph of titanium(IV) oxide, with the result that mineralizer solutions equilibrated with titanic acid become supersaturated with respect to both rutile and anatase. Subsequently, rutile or anatase nucleates spontaneously and grows by transfer of material from titanic acid. Rutile growth at the expense of fully crystalline anatase seems to proceed to a very small extent, if at all, at a temperature as low as 350 °C.

Titanium(IV) oxide was more soluble in hydrofluoric acid than in any of the other mineral acids at relatively low temperatures, making it possible to grow crystals of rutile and anatase from the acid by the temperature-drop method.[16] It was transported from the cold to the hot zone (retrograde solubility) in 1.7—9.5 mol dm^{-3} hydrofluoric acid over the temperature range 320 to 600 °C under a constant pressure of 49 MPa. For this reason, its dissolution in hydrofluoric acid must be exothermic, at least under the above conditions.[17] Hydrofluoric acid enabled the oxide to be transported much more rapidly than did alkali fluoride solutions.[1,11,12] Unless otherwise stated, the reaction temperatures described below refer to those at the hot (crystallization) zone. Titanium(IV) compounds where fluorine is a dominant element were never formed, even in hydrofluoric acid at a concentration as high as 9.5 mol dm^{-3}, in disagreement with earlier work by Kuznetsov and Panteleev.[18]

Figure 3 gives the results of mole fraction of anatase in titanium(IV) oxide formed in the temperature range 360—560 °C *versus* concentration of hydrofluoric acid.

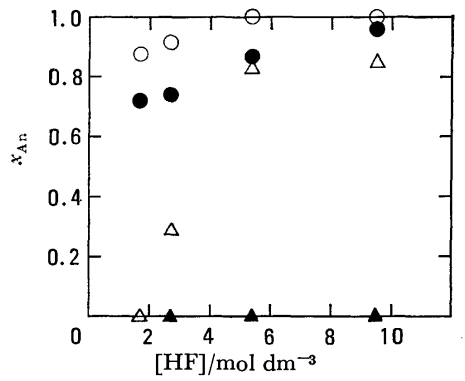

Fig. 3. Mole fraction of anatase in titanium(IV) oxide crystallized from hydrofluoric acid, x_{An}, *vs.* concentration of hydrofluoric acid. Nutrient, Ru-I; P=49 MPa; t=5—11 d. $x_{An}=w_{An}/(w_{Rn}+w_{An})$, where w_{Ru} and w_{An} are, respectively, the weights of rutile and anatase in the product. ○: 360 °C, ●: 400 °C, △: 480 °C, ▲: 560 °C.

As expected, higher concentrations of hydrofluoric acid and especially lower temperatures favored the precipitation of titanium(IV) oxide as anatase. Anatase was converted into rutile to a greater extent with rising reaction temperature; only rutile appeared at 560 °C or above. Anatase which was pure to X rays could be isolated at 360 °C from 5.4—9.5 mol dm^{-3} hydrofluoric acid.

Both rutile and anatase were obtained as almost opaque grains, blue or bluish black and less than 1 mm

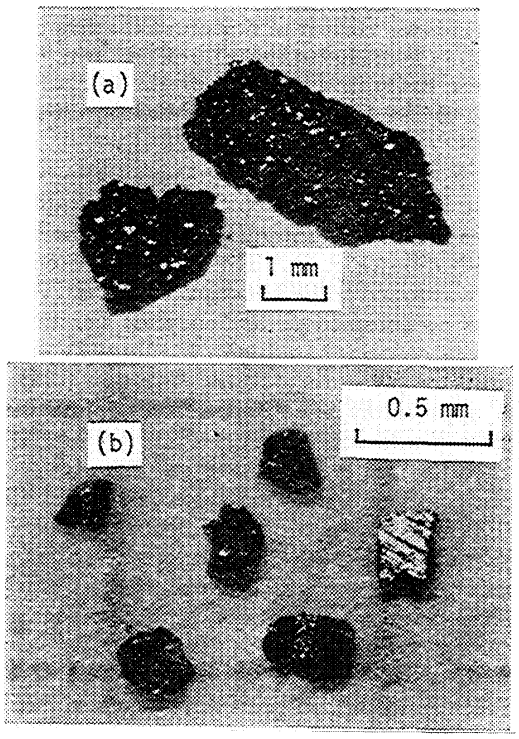

Fig. 4. Crystals of titanium(IV) oxide grown from hydrofluoric acid.
(a) Aggregates of rutile crystals. [HF]=1.7 mol dm^{-3}; θ=480 °C; t=258 h.
(b) Plate crystals of anatase. [HF]=9.5 mol dm^{-3}; θ=400 °C; t=139 h.

in size, or as their irregular aggregates (Fig. 4). Anatase was hardly distinguishable from rutile without the aid of X-ray analysis. Anatase grew at such high supersaturations that most crystals were anhedral and had rather rough surfaces. It was also found as subhedral plate crystals [Fig. 4(b)]. The Laue in conjunction with the oscillation methods showed these single-domain crystals to be tabular on {001}. The anatase which was prepared in 9.5 mol dm^{-3} hydrofluoric acid at 400 °C was submitted to high-temperature X-ray diffraction. When heated in air at a temperature-scan rate of 6.5 °C min^{-1}, it began to change into rutile at 970 °C and disappeared by 1210 °C.

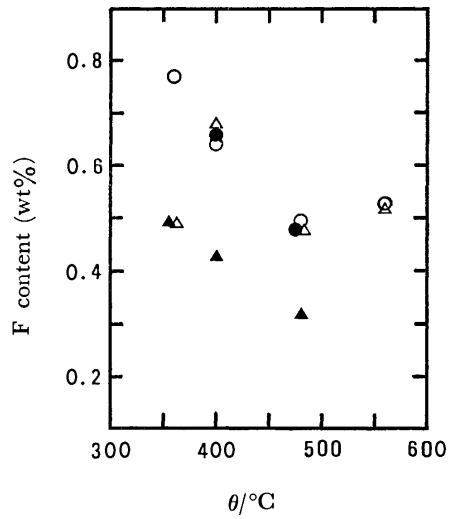

Fig. 5. Fluorine content of titanium(IV) oxide crystallized from hydrofluoric acid *vs.* reaction temperature. Nutrient, Ru-I; P=49 MPa; t=5—11 d. ○: 9.5 mol dm^{-3}, ●: 5.4 mol dm^{-3}, △: 2.7 mol dm^{-3}, ▲: 1.7 mol dm^{-3}.

Fluoride ions in parent solutions were readily taken up into the lattice of titanium(IV) oxide in the course of its crystallization (Fig. 5). The fluorine content of the products was found to lie between 3200 and 7700 ppm. There was no conspicuous tendency for the amount of fluoride ions coprecipitated with titanium(IV) oxide to vary with temperature. Rutile did not differ from anatase appreciably in the partition of fluoride ions between solid and aqueous phases.

Chamberland *et al.*[19,20] have successfully prepared the black compound titanium fluoride oxide, TiFO, in which titanium is formally in a valence state of +3. It is isostructural with rutile and characterized by its n-type semiconducting properties. Furthermore, they have established that, for the titanium fluoride oxides system, nonstoichiometry can easily be achieved to form a series of solid solutions with the general formula TiF_xO_{2-x} ($0<x<1$). As described previously, anatase and rutile were crystallized as bluish-gray powders only by the action of dilute hydrofluoric acid on titanic acid. The almost colorless, transparent crystals of rutile used as a starting material turned blue during hydrothermal reactions in hydrofluoric acid. These blue crystals of rutile contained about 330 ppm of fluorine and showed an ESR spectrum characteristic of the presence of titanium(III) ions at liquid helium temperature.

All these facts provide convincing evidence that titanium(IV) oxide prepared in hydrofluoric acid owes its intense color not to the nonstoichiometry, which is expressed as TiO_{2-x} ($x<8\times10^{-3}$),[11,21] but to point defects arising from the non-equilibrium incorporation of fluoride ions into the growing crystals of rutile and anatase. In fact, crystals of titanium(IV) oxide prepared in various solutions containing fluoride ions (see Table 1) became darker with increasing fluorine content. Fluoride ions presumably substitute oxide ions with similar size in a random way to form $[Ti(O,F)_6]$ octahedra; this substitution causes equal numbers of titanium(IV) ions to be replaced by titanium(III) ions to maintain electrical neutrality. Reduction of quadrivalent titanium to trivalent titanium in the absence of any powerful reducing agent is not surprising because reducing atmospheres usually predominate under hydrothermal conditions.

Discussion

The factors governing hydrothermal crystallization of rutile and anatase should be considered in the light of both the crystal structures of the two modifications and the chemical properties of titanium(IV) species in aqueous solution. Figure 6 illustrates the structures of rutile

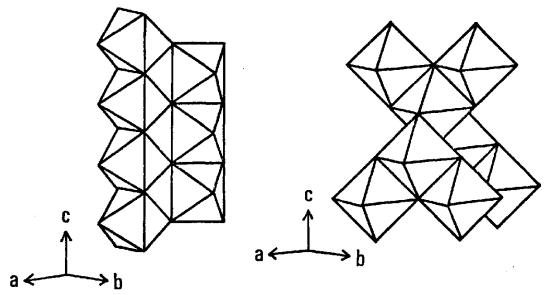

Fig. 6. Structures of rutile and anatase drawn as arrays of regular octahedra joined by common corners and edges.

and anatase. In both crystal lattices, every titanium(IV) ion is surrounded by six oxide ions arranged octahedrally (slightly distorted), and each oxide ion by three titanium(IV) ions. Rutile consists of $[TiO_6]$ octahedra linked by sharing two opposite edges to form chains parallel to the c-axis. In less dense anatase, each $[TiO_6]$ octahedron shares edges with four adjacent $[TiO_6]$ octahedra, which form spiral chains round each four-fold axis. It follows from the above structural consideration that the formation of linear polynuclear species containing bidentate oxo or hydroxo bridges between titanium(IV) ions will give rise to rutile nucleation, while nonlinear ones must pass into anatase nuclei.

We shall, for the moment, confine ourselves to speculating about the nucleation process in solutions containing fluoride ions. Table 1 summarizes the results of a series of experiments on crystallization of titanium(IV) oxide from fluoride solutions by the temperature-drop

TABLE 1. HYDROTHERMAL CRYSTALLIZATION OF TITANIUM(IV) OXIDE FROM VARIOUS SOLUTIONS CONTAINING FLUORIDE IONS

Run No.	Nutrient[a]	Mineralizer solution	θ_1[b] °C	θ_2[b] °C	P MPa	t h	w[c] mg	Products[d]	F content (wt%)
1[e]	Ru-II	1.42 mol/kg NH_4F	$\theta_1 \rightarrow$ 480		49	95		Ru	
2[e]	Ru-II	1.45 mol/kg NH_4F 0.16 mol/kg $(NH_4)_2HPO_4$	$\theta_1 \rightarrow$ 480		49	89		An>U.P.	
3	Ru-I	2.0 mol/dm³ NH_4F	430→480		49	162	136	Ru(52%) An(48%)	1.4
4	Ru-II	2.0 mol/dm³ NH_4F	400→480		49	190	89	Ru	
5	Ru-I	2.0 mol/dm³ KF	454←500		49	184	9	Ru	
6	Ru-I	2.0 mol/dm³ KF	530←600		78	163	59	Ru	0.21
7[e]	Ru-I	0.91 mol/kg KF	529←600		98	353	61	Ru	0.14
8[e]	Ru-I	0.93 mol/kg KF 0.155 mol/kg K_2HPO_4	546←600		98	329	52	An[f]	0.032

a) Ru-I, small pieces of broken single crystals of rutile; Ru-II, rutile powder. b) θ_1, temperature of the cold zone; θ_2, temperature of the hot zone. Arrows show the direction of transport of titanium(IV) oxide. c) Weight of transported titanium(IV) oxide. d) Ru, rutile; An, anatase; U.P., unknown phosphate. e) See Ref. 1. f) The phosphorus content of this product was determined to be 12 ppm.

method.[22] Strange to say, the polymorphic crystallization of the oxide from a 2 mol dm^{-3} solution of ammonium fluoride at 480 °C depended on the grain size of the original charge. A mixture of rutile and anatase separated out with Ru-I, whereas rutile alone was isolated by using Ru-II instead. The reasons for these reproducible phenomena have not been established. The crystallization behavior of titanium(IV) oxide in hydrofluoric acid was essentially uninfluenced by a change of the source material. Rutile was formed exclusively out of potassium fluoride solutions, regardless of the size of the starting rutile.[1]

The small, highly charged metals of Group IVA in the highest oxidation state of +4 are typical hard acids[23] and hence have strong affinities for hard bases such as fluoride,[24,25] sulfate (HSO_4^- and SO_4^{2-}),[26] and phosphate ($H_2PO_4^-$, HPO_4^{2-}, and PO_4^{3-}) ions. Since anatase was crystallizable from solutions containing fluoride ions with rutile as the nutrient in some instances, Ti–O–Ti and $Ti\langle^{O}_{O}\rangle Ti$ bonds in starting rutile are assumed to be thoroughly broken on dissolution in fluoride solutions. As a result, mononuclear titanium(IV) complexes are formed in which each titanium(IV) ion is octahedrally coordinated to hard bases including the fluoride ion, oxide ion, hydroxide ion, and water. The directions of transport of titanium(IV) oxide along temperature gradients show that it has negative partial molar enthalpies of solution in hydrofluoric acid and ammonium fluoride solutions, but positive ones in potassium fluoride solutions.[17] These experimental results indicate that the dissolved species in the above two types of fluoride solutions differ markedly from one another in composition and structure.

Mononuclear fluoro complexes of titanium(IV) are unstable toward hydrolysis at high supersaturations, where they are polymerized through fluctuation to afford polynuclear complexes (embryos) related structurally to either rutile or anatase. Further progress of polymerization leads to rutile or anatase nucleation, which is followed by the growth of the resulting crystal nuclei.

Phosphate ions dissolved in parent solutions were most effective in catalyzing anatase formation and/or retarding rutile formation (Runs No. 2 and No. 8).[1] On addition of an adequate amount of phosphate ions to fluoride solutions, titanium(IV) ions almost certainly form mixed-ligand complexes with fluoride and phosphate ions. In this case, phosphate ions bound coordinatively to titanium(IV) ions have a decisive influence on the selective nucleation of anatase. A crystalline phosphate of titanium(IV), together with anatase, precipitated from an ammonium fluoride–diammonium hydrogenphosphate solution (Run No. 2).[1] The concomitant formation of the phosphate undoubtedly reflects the strong complexation between titanium(IV) and phosphate ions. Duncan and Richards[27] have recently demonstrated that sulfate ions slow down the rate of hydrolysis of titanium(IV) ions by occupying a place in the first coordination sphere of each titanium(IV) ion.

Metal oxides in contact with air or water vapor are normally covered with a monomolecular hydroxide layer,[28,29] evidently because hydroxide ions can fit nearer to the centers of positive charge than half the quantity of oxide ions. Hydroxyl groups on the surface of titanium(IV) oxide are amphoteric; basic hydroxyl groups are readily exchangeable for foreign anions such as fluoride, sulfate, and phosphate ions in acidic or neutral media.[28,29] These facts suggest that the above anions are appreciably chemisorbed onto the surfaces of crystals (nuclei) of rutile and anatase under hydrothermal conditions as well.

The ease with which fluoride ions are incorporated into the lattice of titanium(IV) oxide is ascribable not only to the similarities in ionic radius and electronegativity between the fluoride and oxide ions, but also to the surface coverage by fluoride ions during crystal growth. As Table 1 and Fig. 5 show, the bulk uptakes of fluoride ions into titanium(IV) oxide crystallized from three different fluoride solutions (*ca.* 2 mol dm^{-3}) decreased in the order:

$$NH_4F > HF > KF$$

Anatase crystals grown from a potassium fluoride solution with addition of phosphate ions (Run No. 8) contained far fewer fluoride ions in solid solution than rutile crystals obtained in a potassium fluoride solution (Run No. 7). Very few phosphate ions were coprecipitated with anatase. These findings provide some indirect evidence for the adsorption (desorption) of phosphate ions on (from) the growing surface of anatase.

As the concentration of complexing anions is increased, their uptake at nucleus (crystal)/solution interfaces must also increase. When titanium(IV) oxide nucleates at high supersaturations through the hydrolytic polymerization of the dissolved species, anions initially bound to titanium(IV) ions are partly retained by the resulting polynuclear species on their surfaces and partly released into aqueous phases. Of course, the modes and extent of surface complexing by these ligands foreign to the titanium(IV) oxide lattice greatly affect the relative rates at which rutile and anatase nucleate, thus determining the structures of its crystal nuclei and macrocrystals.

In contrast with the three complexing anions already described, chloride and nitrate ions are known to be generally unattached to the surface of titanium(IV) oxide,[29] owing to their weak ability to complex the titanium(IV) ion. Those polymeric ions analogous in structure to rutile which contain as anions only oxide and hydroxide ions are formed selectively in hydrochloric and nitric acids.

The overall excess free energy, ΔG, between a crystal nucleus and the solute in solution is equal to the sum of the surface excess free energy, ΔG_s, and the volume excess free energy, ΔG_v:[30]

$$\Delta G = \Delta G_s + \Delta G_v$$

ΔG_s is the excess free energy between the surface of the nucleus and the bulk of the nucleus, and ΔG_v the excess free energy between a very large crystal and the solute in solution. Let us suppose that values of ΔG_s for anatase nuclei are smaller than those for rutile ones with comparable dimensions, as a result of the chemisorption of fluoride, sulfate, and phosphate ions. Then we find the possibility that the critical nucleus of anatase is more thermodynamically stable than that of rutile.[30,31] In other words, the relative stabilities for the two polymorphs of large particle size can be reversed in the nuclear state. The metastable formation of anatase in sulfuric and hydrofluoric acids with concentrations higher than 0.5 mol dm^{-3} (Fig. 1), as well as in fluoride solutions containing phosphate ions (Table 1), may be attributed to the pronounced stabilization of anatase nuclei by adsorption of sulfate, fluoride, or phosphate ions.

The details of the mechanisms whereby rutile and anatase are crystallized remain unknown, since we are technically incapable of observing the hydrothermal crystallization process *in situ*.

The author is much indebted to Michiko Kobayashi and Yoshiyuki Yajima for their experimental assistance in the chemical analyses and to Masayuki Tsutsumi for his cooperation in the scanning electron microscopy The author also benefited from stimulating discussions with the members of Seventh Research Group of this institute.

References

1) Part I: F. Izumi and Y. Fujiki, *Bull. Chem. Soc. Jpn.*, **49**, 709 (1976).
2) "Gmelins Handbuch der Anorganischen Chemie," Titan, Verlag Chemie, Weinheim (1951) pp. 226—231.
3) I. Keesmann, *Z. Anorg. Allg. Chem.*, **346**, 30 (1966).
4) E. Schwarzmann and K. -H. Ognibeni, *Z. Naturforsch., Teil B*, **29**, 435 (1974).
5) A. Navrotsky and O. J. Kleppa, *J. Am. Ceram. Soc.*, **50**, 626 (1967).
6) K. J. D. MacKenzie, *Trans. J. Br. Ceram. Soc.*, **74**, 77 (1975) and references cited therein.
7) E. F. Osborn, *J. Am. Ceram. Soc.*, **36**, 147 (1953).
8) F. Dachille, P. Y. Simons, and R. Roy, *Am. Mineral.*, **53**, 1929 (1968).
9) A. Matthews, *Am. Mineral.*, **61**, 419 (1976).
10) M. L. Harvill and R. Roy, "Crystal Growth," ed by H. S. Peiser, Pergamon Press, Oxford (1967), p. 563.
11) V. A. Kuznetzov, *J. Cryst. Growth*, **3,4**, 405 (1968).
12) M. Passaret, Y. Toudic, A. Regreny, R. Aumont, and J. F. Bayon, *J. Cryst. Growth*, **13, 14**, 524 (1972).
13) A. L. Boettcher and D. M. Kerrcik. "Research Techniques for High Pressure and High Temperature," ed by G. C. Ulmer, Springer-Verlag, New York (1971), p. 179.
14) R. A. Spurr and H. Myers, *Anal. Chem.*, **29**, 760 (1957).
15) H. Hashitani, H. Yoshida, and H. Muto, *Bunseki Kagaku*, **16**, 44 (1967).
16) A preliminary report on this subject has been published: F. Izumi, H. Kodama, and Y. Fujiki, *Inorg. Nucl. Chem. Lett.*, **13**, 157 (1977).
17) L. Pauling, "General Chemistry," 3rd ed, W. H. Freeman, San Francisco (1970), p. 450.
18) V. A. Kuznetsov and V. V. Panteleev, *Kristallografiya*, **10**, 445 (1965).
19) B. L. Chamberland and A. W. Sleight, *Solid State Commun.*, **5**, 765 (1967).
20) B. L. Chamberland, A. W. Sleight, and W. H. Cloud, *J. Solid State Chem.*, **2**, 49 (1970).
21) R. N. Blumenthal and D. H. Whitmore, *J. Electrochem. Soc.*, **110**, 92 (1963).
22) Some of these data have been reported in Ref. 1.
23) R. G. Pearson, *J. Chem. Educ.*, **45**, 581, 643 (1968).
24) V. Caglioti, L. Ciavatta, and A. Liberti, *J. Inorg. Nucl. Chem.*, **15**, 115 (1960).
25) Yu A. Buslaev, D. S. Dyer, and R. O. Ragsdale, *Inorg. Chem.*, **6**, 2208 (1967).
26) J. Beukenkamp and K. D. Herrington, *J. Am. Chem. Soc.*, **82**, 3025 (1960).
27) J. F. Duncan and R. G. Richards, *N. Z. J. Sci.*, **19**, 171, 179, and 185 (1976).
28) H. P. Boehm, *Angew. Chem.*, **78**, 617 (1966); *Angew. Chem., Int. Ed. Engl.*, **5**, 533 (1966).
29) H. P. Boehm, *Discuss. Faraday Soc.*, **52**, 264 (1971).
30) R. Kiriyama, Y. Bando, and T. Takada, *Kagaku Sosetsu*, **9**, 61 (1975).
31) A fuller discussion of this notion will be published in *Gendai Kagaku* (in press).

Nuclear Magnetic Resonance Study of Exchanging Systems. XI.[1] ^{13}C NMR Spectra of 9-Ethyltriptycene Derivatives and the Restricted Rotation of the Ethyl Group

Hiroshi NAKANISHI and Osamu YAMAMOTO

National Chemical Laboratory for Industry, Honmachi, Shibuya-ku, Tokyo 151

(Received August 16, 1977)

9-Ethyl-1,4-dimethoxytriptycene, 1,5-dichloro-9-ethyltriptycene, and 9-ethyl-1,4-dimethyltriptycene were prepared. The ^{13}C NMR spectra of these compounds were measured at low temperatures in order to obtain information about the restricted rotation of the ethyl group. It was found that the former two compounds have the *meso* isomer as well as the *dl* isomer. Different chemical shifts of the methylene carbons in the ethyl group, C(2) and C(3) of the benzene A ring, and some quaternary carbons in the two isomers of 9-ethyl-1,4-dimethoxytriptycene indicate that the 120° rotation around C_{sp_3}–C_{sp_2} single bond in the ethyl group deforms the benzene or bicyclo-[2.2.2]octatriene skeleton. The complete line-shape analyses of the temperature-dependent ^{13}C NMR spectra of this compound were performed, and the thermodynamic static parameters and activation parameters of the ethyl rotation were determined. The correlation between the rotational barriers of the alkyl groups and their bulkiness was briefly discussed.

One of the most interesting recent topics in internal rotation studies using dynamic NMR spectroscopic methods is the restricted rotation around C_{sp_2}–C_{sp_2} single bond in sterically overcrowded molecules.[2–5] A number of the rotations of sterically larger groups, for example, *t*-butyl, isopropyl, and ortho-substituted aryl groups, have been investigated, becuase the rotational barriers of these groups are quite high as a result of the severe steric repulsion. Recently, even the rotation of a methyl group, the smallest alkyl group, was found to be strongly restricted on the NMR time scale in several compounds.[6–11] The restricted rotation around the C_{sp^3}–C_{sp^3} single bond in 9-alkyltriptycene derivatives has intensively studied by Ōki[5] and his co-workers, while the rotations of the methyl (**1**)[8,9] benzyl,[12,13] isopropyl (**2**),[14] *t*-butyl (**3**),[10] 1,1-dimethyl-2-phenylethyl,[15] aryl,[16,17] and chloromethyl[18] groups were investigated by the ^1H NMR spectroscopic methods. From these studies, it has been made clear that the rotational barriers of 9-alkyl or aryl groups in triptycene derivatives are strongly influenced by the bulkiness of these groups as well as by the substituents at the peri positions of the benzene rings. However, the rotation of an ethyl group in triptycene derivatives has not yet been studied, and it is important to study systematically how the barriers of the rotations of the alkyl groups at the 9-position in the triptycene derivatives (**1**—**6**) change when the bulkiness of the alkyl group changes in such an order as; methyl, ethyl, isopropyl, and *t*-butyl groups,.

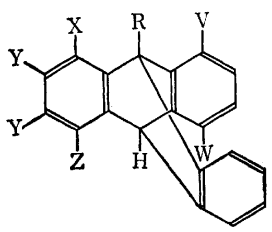

1: R=Me
2: R=^{i}Pr
3: R=^{t}Bu
4: R=Et, X=Z=OMe, Y=V=W=H
5: R=Et, X=W=Cl, Y=Z=V=H
6: R=Et, X=Z=Me, Y=V=W=H

When the three groups or atoms bonded to α-carbon in the 9-substituent alkyl group are not all the same, there is a possibility for two rotational isomers (*i.e.*, *dl* and *meso* forms) to exist (see the Newman projection). In the case of 9-isopropyltriptycene derivatives, however, it was reported in an ^1H NMR spectral study[14] that only the *dl* isomer exists. This may be ascribed to a great destabilization in the *meso* isomer by the severe steric repulsion between the peri-substituent and the two methyl groups. Therefore, from the point of view of the steric repulsion, there may be a possibility for the meso isomer as well as the *dl* one to exist in 9-ethyltriptycene derivatives, for the repulsion in question in the ethyl compound is considered to be much smaller than in the isopropyl analogue. Thus, if this is so, the rotation of the 9-ethyl group in the triptycene derivatives is an isomerization process between the *dl* and *meso* isomers. Therefore, it will be interesting to study the stability of these isomers.

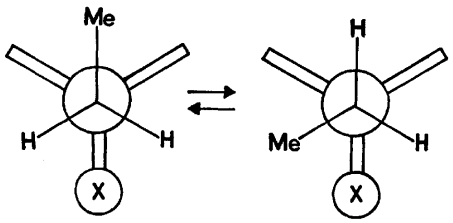

meso *dl*

It is well known that ^{13}C NMR chemical shifts are strongly influenced by the steric compression effect as well as by the electronic effects in sterically overcrowded molecules. Recently an interesting tendency in the ^{13}C NMR chemical shift was found in dibenzobicyclo[2.2.2]-octatriene derivatives.[19] Therefore, it may be worthwhile to study also the correlation between the ^{13}C chemical shifts and the steric repulsion in the sterically overcrowded 9-ethyltriptycene derivatives.

In this work, we chose to study 9-ethyl-1,4-dimethoxytriptycene (**4**), 1,5-dichloro-9-ethyltriptycene (**5**), and 9-ethyl-1,4-dimethyltriptycene (**6**), for the rotation of the ethyl group in these compounds was expected to be strongly restricted on the NMR time scale because of

the strong repulsion between the ethyl group and the peri-substitutents on the rigid triptycene skeleton. Moreover, since the rotational barriers of the methyl,[8,9] isopropyl,[14] and *t*-butyl[10] groups in triptycene derivatives with the same substituents (described above) have already been studied, it is convenient to know the barriers of the ethyl groups in **4**—**6** in order to discuss the correlation of the barriers with the bulkiness of the alkyl groups and the peri-substituents.

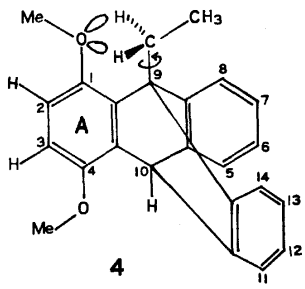

4

Experimental

Materials. **4** was prepared by means of a benzyne reaction between ethylanthracene[20] and 1,4-dimethoxybenzyne, which had been prepared from phenylsodium and 1-chloro-2,5-dimethoxybenzene under nitrogen according to a method similar to that in literature.[9] The purification was made three times by Al_2O_3 chromatography. Mp 179—181 °C, MS, Found: *m/e* 342.162. Calcd for $C_{24}H_{22}O_2$: M+, 342.162.

1,5-Dichloro-9-ethylanthracene (7). A solution of 28.0 g of 1,5-dichloroanthraquinone, 7.0 g of red phosphor, 57 ml of 57% aqueous hydroiodic acid, and 800 ml of acetic acid were heated and stirred at *ca.* 140 °C for 7 h. After cooling, the precipitant was filtered and dissolved in chloroform. After the chloroform solution had then been filtered again to exclude the red phosphor, the solution was dried with anhydrous potassium carbonate. Then, 18.3 g of 1,5-dichloroanthrone (**8**) was obtained by evaporating the solvent. 1,5-Dichloro-9-ethyl-9-hydroxy-10-dihydroanthracene (**9**) was prepared by the Grignard reaction of **8** and ethyl magnesium bromide in dry benzene. The yield was 65%. **7** was prepared by dehydration reaction of 15 g of **9** and 200 g of diphosphorus pentaoxide in 400 ml of benzene at room temperature for 10 h. The solution was decanted, washed with aqueous sodium hydrogencarbonate, and dried over potassium chloride. After the evaporation of the solvent, the residue was recrystallized three times from chloroform and methanol (1: 1) mixed solvent. The yield was 23%. Mp 100—102 °C.

1,5-Dichloro-9-ethyltriptycene (5). Into a refluxing solution of 1.3 g of butyl nitrite and 3.5 g of **7** in 150 ml of dry dichloromethane was added a solution of 1.8 g of anthranilic acid in 150 ml of dry ether over a period of 40 min with stirring. The solution was then refluxed for half an hour, washed with aqueous potassium carbonate, and dried over potassium chloride. The purification was made by Al_2O_3 chromatography and by three recrystallizations from a chloroform and methanol (1: 1) mixed solvent. The yield was *ca.* 30%. Mp 208—210 °C, MS, Found: *m/e* 350.072. Calcd for $C_{22}H_{16}Cl_2$: M+, 350.063.

9-Ethyl-1,4-dimethylanthracene (10). **10** was prepared from 1,4-dimethyl-anthraquinone of a commercial origin by a similar method. The yield was *ca.* 14% from the anthraquinone. Mp 63—64 °C.

9-Ethyl-1,4-dimethyltriptycene (6). **6** was prepared from **10** and anthranilic acid by a similar method. The purification was made by SiO_2 chromatography. The yield was *ca.* 20%. Mp 219—221 °C, MS, Found: *m/e* 310.176. Calcd for $C_{24}H_{22}$: M+, 310.172.

The purity of these compounds was checked by means of the ^{13}C-NMR spectra.

NMR Spectral Measurements. The ^{13}C-NMR spectra of these compounds were recorded by the pulsed FT method on NEVA NV-14 (15.087 MHz) and Varian XL-100-15 (25.162 MHz) spectrometers with Varian 620/L computers. The sample concentrations and solvents were as follows: 13 wt% in $CDCl_3+CS_2+CD_3COCD_3$ (5: 5:1) for **4**, 10 wt% in $CDCl_3+CS_2$ (1: 2) for **5**, and 21 wt% in $CDCl_3+CS_2$ (1: 2) for **6**. The temperature was read by means of a calibrated copper-constantan thermocouple.

Molecular-weight Determinations. High-resolution molecular-weight determinations were carried out on a CEC high-resolution mass spectrometer, Model 21-110 B, with a direct-inlet system and an ionization potential of 70 eV.

Spectral Calculations. The calculations of the theoretical spectra in the complete line-shape analyses were made using program EXNMR **1*** on a FACOM 270/30 computer.

Results and Discussion

The Temperature-dependence of the ^{13}C NMR Spectra and the Rotational Isomers of the Ethyl Groups in 4—6. The total spectrum of **4** at ambient temperature is shown in Fig. 1 (a). The spectrum shows that the signals of methyl and methylene carbons of the ethyl group are singlets and that the line broadening occurs in two signals at this temperature. An ^1H undecoupled ^{13}C spectrum

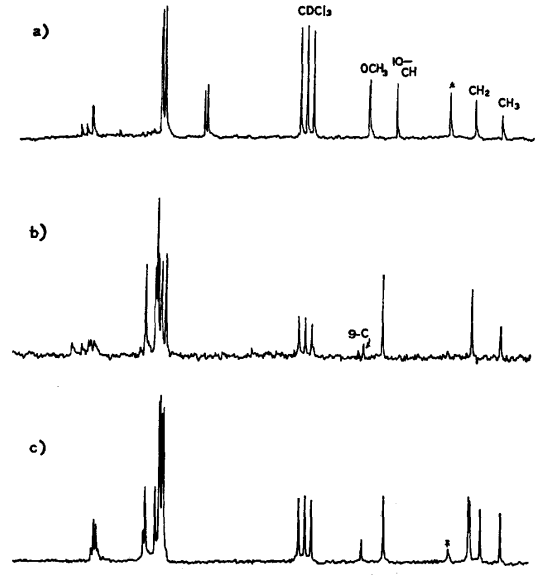

Fig. 1. ^{13}C NMR spectra of **4**—**6**.
a) The spectrum of **4**. Spectral width (SW): 2500 Hz, pulse width (PW): 45 μ, pulse delay (PD): 10, sensivity enhancement (SE): 0.2 s, the number of accumulation (NT): 3500. * impurity. b) The spectrum of **5**. SW: 2500 Hz, PW: 45 μ, PD: 15 s, SE: 0.2 s, NT: 4500. c) The spectrum of **6**. SW: 2500 Hz, PW: 45 μ, PD: 8 s, SE: 0.2 s, NT: 2000. * impurity.

* A modified version of EXNMR 0.[21]

of **4** shows that the higher-field peak of the ethyl group can be assigned to the methyl carbon, as expected. The degree of the line broadening in the methyl signal is larger than that in the methylene signal. The line broadening indicates that the rotation of the ethyl group is quite rapid at room temperature. This is reasonable,

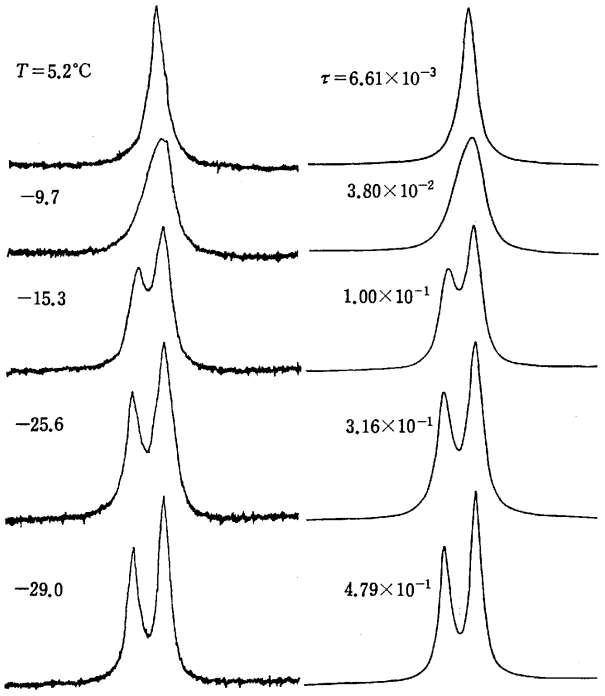

Fig. 2. The observed (left) and calculated (right) ^{13}C spectra of the methyl carbons of the ethyl groups in the *meso* and *dl* isomers of **4** at several temperatures. τ is a mean life time.

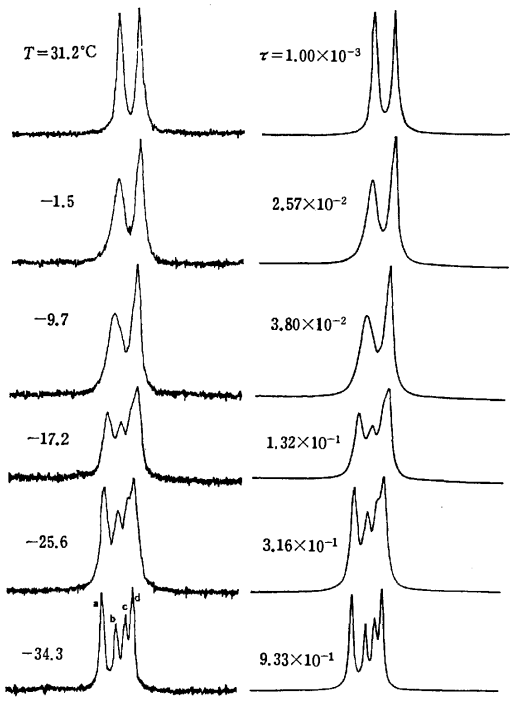

Fig. 3. The observed (left) and calculated (right) ^{13}C spectra of the aromatic CH carbons at 2 and 3 positions of **4** at several temperatures.

for it has been reported that , at room temperature, the rotation of the isopropyl group in 9-isopropyltriptycene derivatives is frozen,[14] while that of the methyl group in the methyl analogues is extremely rapid.[9] Then, in order to freeze the rotation, the ^{13}C spectra of **4** were measured at low temperatures (see Figs. 2 and 3). At −29.0 °C, the methyl signal of the ethyl group consists of two sharp peaks. This means a sufficiently slow rotation at this temperature. The intensity of the higher-field peak is stronger than that of the lower one: the intensity ratio of the former to the latter is 59/41 at −29.0 °C. Taking the steric repulsion between the ethyl and methoxyl groups into account (see the Newman projection), the *meso* isomer can be expected to be more stable than the *dl* isomer. Therefore, the strong peak at the higher filed is assigned to the *meso* isomer, and the weak peak at the lower field to the *dl* isomer.

The signal of the methylene carbon also shows line broadening when the temperature is lowered. At −28.1 °C, the signal consists of two sharp peaks. The intensity of the higher-field peak is stronger than that of the lower-field one, so the former peak is assigned to the *meso* isomer.

The signals of the methoxy carbons do not show any line broadening at low temperatures.

The signals of the aromatic CH carbons in **4** show unexpectedly simple spectral patterns (the higher- and lower-field parts) at ambient temperature (see Fig. 1 (a)). In the higher-field part, the two peaks at 109.6 and 110.5 ppm from TMS are assigned to C(2) and C(3) with reference to the CH signal of *p*-dimethoxybenzene (δ: 114.8). In the lower-field part, the signals of eight other CH carbons [C(5)–C(8), and C(11)–C(14)] apparently show a simple line shape (three peaks), as is shown in Fig. 1 (a), probably because of the signal overlapping and the signal averaging by a rapid rotation of the ethyl group at room temperature. As the temperature is lowered, the signals of these carbons become broader, until finally they consist of many sharp peaks at such conformationally frozen temperatures as −28.1 °C. This line-shape behavior is reasonable, because C(8) and C(14) are near the rotating ethyl group and the chemical shifts of these carbons in the *dl* isomer can be different from those in the *meso* isomer.

Surprisingly, it was found that the peaks of aromatic C(2) and C(3) also show line broadening at low temperatures, and the separate sharp peaks of the two isomers appear at −34.3 °C, as is shown in Fig. 3. The two stronger peaks are assigned to the *meso* isomer, and the intensity ratio of the *meso* isomer to the *dl* isomer is 60/40, which is the same as in the analysis of the methyl carbon signals.

The ^{13}C spectrum of **5** at room temperature is shown in Fig. 1 (b). The signals of the methyl and methylene carbons are singlets. Although the signal of the methylene carbon is a sharp singlet, the line-width of the methyl carbon signal is considerably large. The line broadening in the methyl signal is explained by the existence of both *meso* and *dl* isomers and the signal coalescence due to the rapid exchange between the two isomers. When the temperature is lowered, however, it was found that the methyl signal shows the following curious tempera-

ture-dependent behavior: as the temperature is lowered, the signal first shows little line broadening up to *ca.* −30 °C, but when the temperature is more deeply decreased, it becomes sharper instead of being separated into two peaks, until finally its peak height is almost the same as that of the bridge-head methine carbon at −62.5 °C. This interesting phenomenon can be accounted for as follows. When the temperature is lowered from 31.0 °C to *ca.* −30 °C, two contradictory phenomena, *i.e.*, the increased line broadening due to the slower exchange rate with the temperature decrease, and the decreased line broadening due to the smaller population of the less stabilized isomer (*dl* isomer) at the lower temperature, occur, causing the degree of the line broadening in the methyl signal to be almost unchanged. Then, at the lower temperatures, the population of the *dl* isomer becomes so small that the former effect becomes negligibly small, until at last the line broadening cannot be observed. These discussions lead to the conclusion that the population of the less stabilized *dl* isomer in **5** is much smaller than in **4**. This may be reasonable, because the steric repulsion between the ethyl group and the peri-substituted chlorine atom in **5** is larger than that between the ethyl group and the methoxy oxygen atom in **4**.

In extending the discussion, it may be expected that **6** with a methyl group at a peri position, has more of the *dl* isomer than **4** and **5**, because the bulkiness of a methyl group is smaller than those of the methoxyl group and the chlorine atom, so the steric repulsion in question in **6** is smaller than those in **4** and **5**. Contrary to expectations, the signals of the methyl and methylene carbons in the ethyl group of **6** show little line broadening in the temperature range from 31.0 °C to *ca.* −50 °C. This quite unexpected result may be explained by the absence for the *dl* isomer. However, there remains a possibility that the two rotational isomers do exist, but the chemical shift differences between the two isomers of the methyl and methylene carbons in the ethyl group are so small and/or the rotational barrier is so small that the line broadening does not occur at these temperatures. At present, we cannot conclude which is true in **6**. If the former case is true, we should consider, in addition to the steric factors, some unknown interaction in **4** which may stabilize the *dl* isomer for example, an interaction between the methylene group and the methoxy oxygen atom ($CH_2\cdots O$).

In this work, it has been made clear that the two rotational isomers around the C_{sp_3}–C_{sp_3} single bond at the 9-position of triptycene exist in **4** and **5**. The results make a clear constanst to the fact that, in 9-isopropyltriptycene derivatives (**2**), only the *dl* isomer exists; the *dl* isomer is the more stable isomer in this case.[14] This interesting contrast may be caused by the great unstability of the *meso* isomer in **2** due to the severe steric repulsion between the two methyl groups and the peri-substituent (see the Newman projections **11** and **12**).

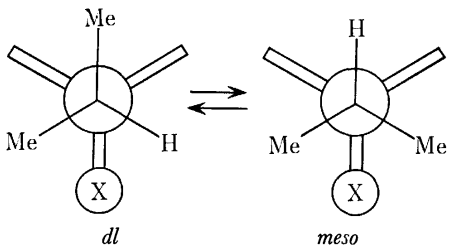

dl **11** *meso* **12**

TABLE 1. THE ^{13}C CHEMICAL SHIFTS OF **4**—**6** (ppm from TMS)

	4		**5**		**6**
	31.0 °C	−28.1 °C	31.0 °C		31.0 °C
CH_3(Et)	12.4	12.1 12.9	12.2		12.3
CH_2(Et)	21.4	20.8	21.9		22.6
OCH_3	56.3 56.5	55.9			
CH_3(arom)					18.9 22.8
C(9)		56.6	57.8		58.2
C(10)	47.3	46.8	51.4		51.0
C(2), C(3)	109.6 110.5	108.4 108.7 109.2 109.9			126.2 129.5
Other aromatic CH carbons	123.5 124.5 124.6	121.1 123.7 124.0 124.3 124.7	122.8 123.4 124.0 124.5 125.0	125.6 125.9 129.0	123.6 123.9 124.5 124.8
Quaternary carbons	147.0 148.8 150.6	145.6[a] 146.1 147.8 149.8	142.9 143.4 144.5 145.1 145.7	146.5 147.3 150.6	130.5 145.0 145.7 146.5 147.3

a) Two other shoulder peaks are present in this region.

The ^{13}C NMR Chemical Shifts and the Conformations of the Two Isomers in 4. The ^{13}C chemical shifts of **4**—**6** are listed in Table 1. As has been described previously, the higher-field peak of the methyl carbon in the ethyl group of **4** is assigned to the *meso* isomer on the basis of the peak intensities and the degree of the unstability caused by the steric repulsion. The validity of the assignment is strongly suppoted by the steric compression shift. Since the steric repulsion between the methyl and methoxyl groups in the *dl* isomer is larger than in the *meso* isomer as has been described above, the signal of the methyl carbon in the *dl* isomer should be at a lower field than that in the *meso* isomer because of the large lower-field shift due to the steric compression.[22]

The fact that there is a difference between the chemical shifts of the methylene carbons in the two isomers of **4** is quite unexpected if we consider only the simple Newman projection model described above, for it is assumed in the model that all of the distances between the methylene carbon and the other atoms or groups are equal in the two isomers. It has been considered thus far that such carbons as the methylene carbons in **4**, which are positioned on the rotational axis, are all

equivalent. This remarkable fact may be explained, however, by different geometries of the methylene groups in the two isomers in the severely compressed environment around the ethyl group in **4**, or by an unknown interaction between the methylene group and the oxygen lone pair, an interaction which may be caused by the extreme proximity of the two groups. Previously, in dimethyl 9-isopropyl-9,10-ethenoanthracene-11,12-dicarboxylate (**13**), we found a similar interesting unequality in chemical shifts between the signals of the methine carbons in the isopropyl groups in the *dl* and *meso* isomers, which are both positioned on the rotational axis.

It is very interesting to find the unequality between the chemical shifts of C(2) and C(3) in the *dl* isomer and those in the *meso* isomer. Since the distances between these two carbons and the rotating ethyl group are very great, the steric and anisotropic effects on the chemical shifts of these carbons can be considered to be negligibly small. Therefore, the fact indicates that the electronic states of these carbons of the *dl* isomer are different from those of the *meso* isomer.

The determination of the pairs of the C(2) and C(3) in the two isomers was made by a careful investigation of the temperature-dependent line shape in the computer simulation analyses (Peaks a—b and c—d; see Fig. 3), although it could not be determined which signal in C(2) and C(3) is at the higher field. The chemical shift differences ($\Delta\delta$=4.9 and 10.7 Hz) are almost comparable to those of the methylene and methyl signals ($\Delta\delta$=8.3 and 12.5 Hz respectively). The large differences between the chemical shifts in the two isomers may be caused by the following two possibilities. The steric repulsion between the ethyl and methoxyl groups in the *dl* isomer is so severe that the angle between the C–OCH_3 bond and the 1,4-dimethoxy substituted benzene ring (A ring) is a little deformed. In the *meso* isomer, the steric repulsion is not so severe, and so the deformation is considered to be negligibly small (see the Newman projection). The deformation influences the conformation of the A ring and so has an effect on the electronic state of the ring. This causes the chemical shifts of C(2) and C(3) in the *dl* isomer to be different from those in the *meso* isomer. The second possibility is the deformation of the bicyclo[2.2.2]octatriene skeleton by the strong repulsion in the *dl* isomer, such as was found in **13**. If this happens, the signals of C(9), C(10), and other quaternary carbons would be different from each other in the two isomers.

The signal of the quaternary carbon C(9) is masked by the strong methoxy carbon signals at room temperature, but it appears as a separate peak at −25.6 °C (δ: 56.6), because the peaks of the methoxy carbon signals shift to a little higher field as the temperature is lowered. However, it cannot be immediately concluded that C(9) gives only one peak, for there remains a possibility that the other peak is masked by the methoxy carbon signals if the chemical shifts of the two isomers are different from each other.

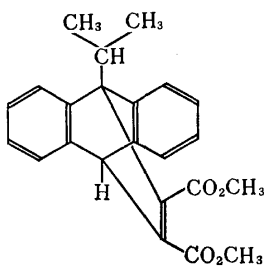

13

The signal of C(10) methine carbon does not show line-broadening at low temperatures. However, this does not directly mean that there is the same conformation in the two isomers, because even if they are different, the chemical shift difference between the C(10) signals in the two isomers is not always large because of the long distance between C(10) and the ethyl group. It is worthwhile to point out that the signal of C(10) in **4** (δ: 47.3) is at a much higher field than those in **5** and **6** (δ: 51.4 and 51.0 respectively). It may be that the anomalous high-field shift of the C(10) signal in **4** indicates a conformation of the bicyclo[2.2.2]octatriene skeleton in **4** different from those in **5** and **6**.

The signals in the lowest field region (145—150 ppm from TMS) consist of three peaks at room temperature (see Fig. 1(a)). When the temperature is lowered, line broadening occurs in these peaks. At −34.3 °C, the signals consist of six peaks. The temperature-dependent signals should be assigned to quaternary carbons at the ring junction or to C(1) and C(4) carbons, judging from their long relaxation times (T_1) and the comparison with the chemical shifts of **5**—**6**, *p*-dimethoxybenzene, and 9-methyltriptycene. Unfortunately, however, more exact assignments cannot be made because of the closeness of their signals. At any rate, it is certain from the line-shape changes that the signals of some quaternary carbons are different between the two isomers.

Therefore, from the results and the discussion presented above, we cannot determine which possibility (*i.e.*, the deformation of the A ring or that of bicyclo[2.2.2]octatriene skeleton) is true here. In any case, it is a very important fact, from the point of view of structural chemistry, that a simple 120° rotation of the small ethyl group around the C_{sp_3}–C_{sp_2} single bond of the 9-position in **4** deforms the benzene ring or bicyclo[2.2.2]octatriene skeleton, both which are known to have very solid structures.

The Static and Dynamic Parameters of the Rotation of the Ethyl Group in 4. The populations of the two isomers in **4** were determined using a computer simulation in the trial-and-error method in the conformationally frozen temperature range, independently in the two regions of the methyl signals in the ethyl group and of C(2) and C(3) signals. The values obtained in the two regions were in good agreement with each other at all temperatures. The static thermodynamic parameters ($\Delta G°$, $\Delta H°$, and $\Delta S°$) of the isomerization between

Table 2. The static thermodynamic parameters of the rotation of the ethyl group in **1** (at 25.0 °C)

$\Delta G°$ (kcal/mol)	$\Delta H°$ (kcal/mol)	$\Delta S°$ (e.u.)
0.12±0.13	0.80±0.13	2.3±0.4

TABLE 3. THE ACTIVATION PARAMETERS OF THE ROTATION AROUND THE C_{sp_2}–R BOND IN 9-ALKYLTRIPTYCENE DERIVATIVES (AT 25.0 °C)

		R	E_a (kcal/mol)	$\Delta G^{\neq}$ (kcal/mol)	$\Delta H^{\neq}$ (kcal/mol)	$\Delta S^{\neq}$ (e.u.)	Ref.
Compound	**1a**	Me	7.8±0.6	8.8±0.3	7.2±0.6	−5.4±2.0	9
	4	Et(1)[a]	14.9±0.6	13.8±0.3	14.3±0.6	1.7±0.7	This work
		Et(2)[b]	13.6±0.6	13.8±0.3	13.0±0.6	−2.7±0.7	
	2a	^{i}Pr[c]	25.4±1.1	23.6±0.3	24.8±1.1	3.9±2.7	14
	3a	^{t}Bu[d]	>30	—	—	—	

a) Values of the rotation from the *meso* isomer to the *dl* one. b) Values of the rotation from the *dl* isomer to the *meso* one. c) Values of the rotation from the *d*(*l*) isomer to the *l*(*d*) one. d) Assumed value (three methyl carbon peaks of the *t*-butyl group do not show line broadening at 180 °C).

the *meso* and *dl* isomers in **4** were determined from the Arrhenius plot of the populations of the two isomers. The result are shown in Table 2.

In order to obtain the activation parameters of the ethyl rotation in **4**, the computer similation of the temperature-dependent spectra was performed using the modified Bloch equation method, which has been described before.[21]

The complete line-shape analyses were carried out for the methyl and C(2) and C(3) signals independently, changing the rotational rate k and the population ratio between the two isomers at each temperature. Several calculated spectra thus obtained are shown in Figs. 2 and 3. The rotational rate obtained in the two regions were in excellent agreement with each other at all temperatures, within the experimental errors. The activation parameters were determined from the Arrhenius plots of k's and Eyrings's equations. The results are given in Table 3. In Table 3, the activation parameters of the R–C(9) rotations in 1,4-dimethoxy-9-methyltriptycene (**1a**),[9] 1,4-dimethoxy-9-isopropyltriptycene (**2a**),[14] and 1,4-dimethoxy-9-*t*-butyltriptycene (**3a**) are also listed in order to facilitate a comparison of rotational barriers.

The two activation energies E_a (Et1) and E_a (Et2) of **4**, which correspond to the two rotations from the conformation at the ground state to that at the transition state for the *meso* and *dl* isomers respectively, are larger than that of the methyl analogue (**1a**) and much smaller than that of the isopropyl one (**2a**). These data are reasonable considering the bulkiness of the alkyl group at the 9-position of the triptycene derivatives. It can be considered that the conformations of these compounds are *gauche* form at the ground states and *eclipsed* form at the transition states, as is shown in the Newman projections of Fig. 4. If we simply assume that the energies concerning the rotational barriers of the alkyl groups are mainly influenced by the steric repulsions between the three peri-substituents of the benzene rings and the methyl groups and/or hydrogen atoms in the 9-alkyl groups, and that the deformation of the geometries of the 9-alkyl groups in question is neglibibly small, and finally, that in the estimation of the steric repulsion energies between these groups and atoms in the ground and transition states, an additive nature is effective in **1a**, **2a**, and **4**, simple calculations of the activation energies in these compounds can be made. These calculation shows that the activation energy differences

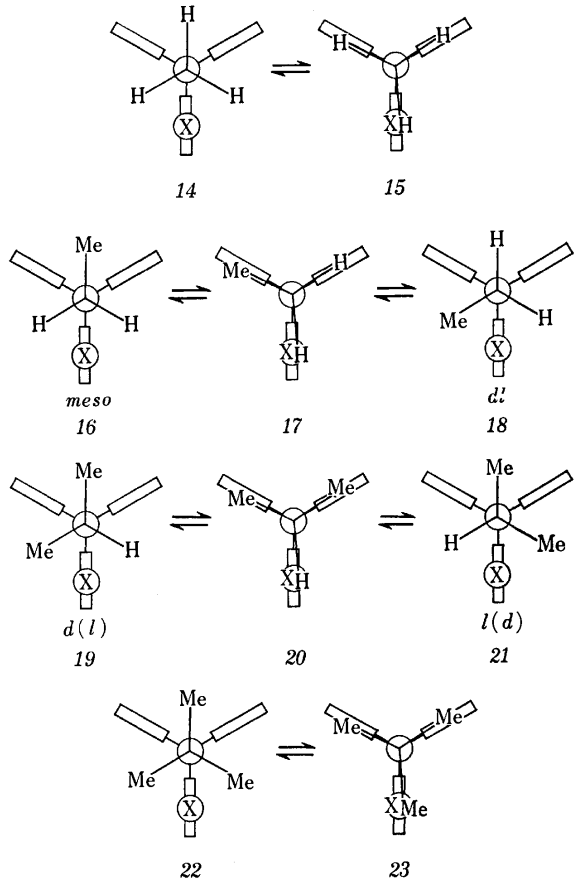

Fig. 4. The Newman projections of the conformations at the ground and transition states of the rotations of the 9-alkyl groups in 1,4-dimethyltriptycene derivatives (**1a**, **2a**, **3a**, and **4**). (X=OMe).

$\Delta E_a(1)$ and $\Delta E_a(2)$ [$\Delta E_a(1)=E_a(\text{Et1})-E_a(\text{Me})$, $\Delta E_a(2)=E_a(\text{Et2})-E_a(\text{Me})$] must be equal to $\Delta E_a(4)$, and $\Delta E_a(3)$ [$\Delta E_a(4)=E_a(^i\text{Pr})-E_a(\text{Et2})$, $\Delta E_a(3)=E_a(^i\text{Pr})-E_a(\text{Et1})$] respectively. In real, however, $\Delta E_a(3)$ and $\Delta E_a(4)$ (10.5 and 11.8 kcal/mol respectively) are much larger than $\Delta E_a(1)$ and $\Delta E_a(2)$ (7.1 and 5.8 kcal/mol respectively). This means that the steric repulsion energy between the two methyl groups in the isopropyl group and the benzene rings at the transition state of **2a** (*cf.* **20**) is not equal, but is much larger than twice the steric repulsion energy of one methyl group and the benzene ring in **4** (*cf.* **17**). The

results indicate much increased steric overcrowding of the isopropyl group against the three peri-substituents in **2a** in comparison with that in **4**. In this connection, it is reasonable that the rotational barrier of the *t*-butyl analogue (**3a**) is much larger than that in **2a**, for, at the transition state of **3a** (**23**), one methyl group must have an *eclipsed* conformation against the largest peri-subsituted methoxy oxygen atom, and the other two methyl groups, against the peri-hydrogen atoms, thus, the repulsion energy becomes extremely high, although, at the ground state, the steric repulsion in the *gauche* form (**22**) is considerably larger than that in **2a** (**19**).

The simple calculations beased on the above assumptions are not valid in the estimation of the steric repulsion energies of severely overcrowded molecules. In a sense, this is an expected result. It is very difficult to estimate quantitatively the correlation between the steric bulkiness of the alkyl groups and the rotational barriers of the alkyl groups in these overcrowded molecules.

The authors wish to express their hearty thanks to Professor Michinori Ōki and Dr. Fumio Suzuki of the University of Tokyo for their helpful discussions, and Mr. Nobuhide Wasada of our Laboratory for his kind measurements of the mass spectra of the compounds studied.

References

1) The preceding papre: H. Nakanishi, H. Fujita, and O. Yamamoto, *Bull. Chem. Soc. Jpn.*, **51**, 214 (1978).
2) H. Kessler, *Angew. Chem. Int. Ed. Engl.*, **9**, 219 (1970).
3) I. O. Sutherland, *Annu. Rep. NMR. Spectrosc.*, **4**, 71 (1971).
4) S. Sternhell, "Dynamic Nuclear Magnetic Resonance Spectroscopy," ed by L. M. Jackman and F. A. Cotton, Academic Press, New York (1975), Chap. 6.
5) M. Ōki, *Angew. Chem.*, **88**, 67 (1976).
6) H. Nakanishi, O. Yamamoto, M. Nakamura, and M. Ōki, *Tetrahedron Lett.*, **1973**, 727.
7) M. Nakamura, M. Ōki, and H. Nakanishi, *Tetrahedron*, **30**, 543 (1974).
8) M. Nakamura, M. Ōki, and H. Nakanishi, *J. Am. Chem. Soc.*, **95**, 7169 (1973).
9) M. Nakamura, M. Ōki, H. Nakanishi, and O. Yamamoto, *Bull. Chem. Soc. Jpn.*, **47**, 2415 (1974).
10) H. Nakanishi and O. Yamamoto, *Bull. Chem. Soc. Jpn.*, in press.
11) J. E. Anderson and D. I. Rawson, *J. Chem. Soc., Chem. Commum.*, **1973**, 830.
12) F. Suzuki and M. Ōki, *Tetrahedron Lett.*, **1974**, 2845.
13) F. Suzuki and M. Ōki, *Bull. Chem. Soc. Jpn.*, **48**, 596 (1975).
14) F. Suzuki, M. Ōki, and H. Nakanishi, *Bull. Chem. Soc. Jpn.*, **47**, 3114 (1974).
15) G. Yamamoto and M. Ōki, *J. Chem. Soc., Chem. Commum.*, **1974**, 713.
16) M. Nakamura and M. Ōki, *Bull. Chem. Soc. Jpn.*, **48**, 2106 (1975).
17) M. Nakamura, H. Kihara, and M. Ōki, *Tetrahedron Lett.*, **1976**, 1207.
18) N. M. Sergeyev, K. F. Abdulla, and V. R. Shvarchenko, *J. Chem. Soc., Chem. Commum.*, **1972**, 368.
19) H. Nakanishi, Y. Kitagawa, O. Yamamoto, and M. Ōki, *Org. Magn. Reson.*, **9** 118 (1977).
20) R. LaLonde and R. Calas, *Bull. Soc. Chim. Fr.*, **1959**, 766.
21) O. Yamamoto, K. Hayamizu, H. Nakanishi, and M. Yanagisawa, *J. Nat. Chem. Lab. Ind.* [*Tokyo*], **69**, 14 (1974).
22) G. J. Martin, M. L. Martin, and S. Odiot, *Org. Magn. Reson.*, **7**, 2 (1975).

The Synthesis of New Flavones with a 4*H*,10*H*-Benzo[1,2-*b*: 3,4-*b*']dipyran-4,10-dione Skeleton and the Light Resistannce of These Compounds

Makoto KANETA, Hiroshi HIKICHI, Seiichi ENDO, and Noboru SUGIYAMA*

Fukushima Technical College, Iwaki-shi, Fukushima 970

**Department of Chemistry, Tokyo Kyoiku University, Otsuka, Bunkyo-ku, Tokyo 112*

(Received August 16, 1977)

Six analogous new flavones with a skeleton similar to arthraxin, which is a light-stable, natural, new flavone, have been synthesized by the use of a modification of Allan-Robinson's flavone synthesis. The structures of these compounds were elucidated by means of the Gibbs reaction, NMR, and mass spectrometry. The light resistance of these flavones was then examined by means of UV spectrometry. The results indicate that these flavones, with a 4*H*,10*H*-benzo[1,2-*b*: 3,4-*b*'] dipyran-4,10-dione skeleton, in contrast with natural common flavonol and arthraxin, show a high resistance to light.

In a previous paper,[1] we reported the isolation and structure of a new flavone arthraxin (**1**) from the grass *Arthraxon hispidus*, which had been used as a source of natural dyestuff for the light-stable, yellow coloring "Kihachijo," produced on Hachijo Island, Japan. In our succesive studies,[2,3] arthraxin, in contrast with flavonol, was found to show a high resistance to light. This result suggests that the flavones which have a skeleton similar to arthraxin's 4*H*,10*H*-benzo[1,2-*b*: 3,4-*b*']dipyran-4,10-dione skeleton will be stable to light. To make clear this problem, we have synthesized a series of new flavones with skeletons similar to arthraxin and have examined the light resistance of these compounds by UV spectrometry.

Synthesis of Six Analogous New Flavones with a 4H,10H-Benzo[1,2-b: 3,4-b']dipyran-4,10-dione Skeleton. These compounds, **6**, **7**, **8**, **9**, **10**, and **11**, have been synthesized according to the annexed scheme.

2,4-Diacetylphloroglucinol (**2**) was prepared by saturating a glacial acetic acid solution of phloroglucinol with boron trifluoride gas.[4] The condensation of **2** with potassium benzoate and benzoic anhydride yielded 8-acetyl-5,7-dihydroxyflavone (**3**). By using

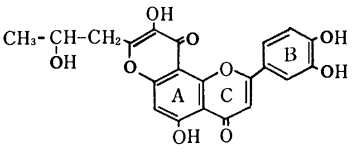

1 Arthraxine

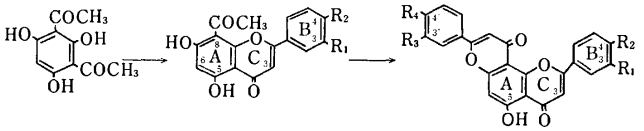

2 **3** $R_1=R_2=H$; **4** $R_1=H$, $R_2=OCH_3$; **5** $R_1=R_2=OCH_3$; **6** $R_1=R_2=R_3=R_4=H$; **7** $R_1=R_2=R_3=H$, $R_4=OCH_3$; **8** $R_1=R_2=H$, $R_3=R_4=OCH_3$; **9** $R_1=R_3=H$, $R_2=R_4=OCH_3$; **10** $R_1=H$, $R_2=R_3=R_4=OCH_3$; **11** $R_1=R_2=R_3=R_4=OCH_3$

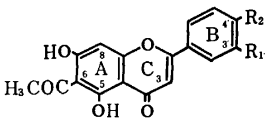

3b $R_1=R_2=H$
4b $R_1=H$, $R_2=OCH_3$
5b $R_1=R_2=OCH_3$

potassium *p*-anisate and *p*-anisic anhydride or potassium veratrate and veratric anhydride instead, 8-acetyl-5,7-dihydroxy-4'-methoxyflavone (**4**) or 8-acetyl-5,7-dihydroxy-3',4'-dimethoxyflavone (**5**) was obtained respectively. The alternative structures, 6-acetyl-5,7-dihydroxyflavone (**3b**), 6-acetyl-5,7-dihydroxy-4'-methoxyflavone (**4b**), and 6-acetyl-5,7-dihydroxy-3',4'-dimethoxyflavone (**5b**), were rejected after a study of the NMR spectra of Compounds **3**, **4**, and **5** indicated the presence of the C-6 proton and because the negative Gibbs reaction[5] indicated the presence of C substitution in the C-8 position. The signals at 6.40, 6.41, and 6.43 ppm of **3**, **4**, and **5** can be assigned to the C-6 proton in the A-ring, because the C-6 and C-8 protons of the 5,7-disubstituted flavones appear in the regions of 6.25—6.5 ppm for the C-6 proton and 6.5—6.9 ppm for the C-8 proton.[6,7] The Gibbs reaction with *N*-chloro-2,6-dichloro-*p*-benzoquinone 4-imine has been used for the

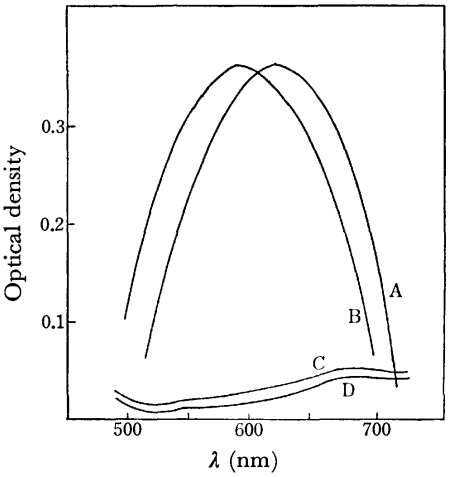

Fig. 1. UV spectra of the compounds treated with the Gibbs reagent.
A: Phenol, B: *o*-cresol, C: Compd **3**, D: Compd **4**.

detection of unsubstituted CH para to a phenolic hydroxyl group at the C-5 position. On treatment with the Gibbs reagent, a phenolic compound which is unsubstituted in the para position to the phenolic hydroxyl group gives the blue-green color of the indophenol derivative, with an absorption peak at 500—900 nm.[5] Compounds **3**, **4**, and **5** showed negative Gibbs reactions. This constitutes further evidence that **3**, **4**, and **5** do not have the C-8 proton which is in the para position to the C-5 hydroxyl group.

Heating **3** with potassium *p*-anisate and *p*-anisic anhydride yielded a new flavone, 2-phenyl,8-(4-methoxyphenyl)-4*H*,10*H*-benzo[1,2-*b*: 3,4-*b'*]dipyran-4,10-dione (**7**). By using potassium benzoate and benzoic anhydride or potassium veratrate and veratric anhydride instead, 2,8-diphenyl-4*H*,10*H*-benzo[1,2-*b*: 3,4-*b'*]dipyran-4,10-dione (**6**) or 2-phenyl,8-(3,4-dimethoxyphenyl)-4*H*,10*H*-benzo[1,2-*b*: 3,4-*b'*]dipyran-4,10-dione (**8**) was obtained. When **4** was used for the condensation with potassium veratrate and veratric anhydride, 2-(4-methoxyphenyl)-8-(3,4-dimethoxyphenyl)-4*H*,10*H*-benzo[1,2-*b*: 3,4-*b'*]dipyran-4,10-dione (**10**) was obtained.

According to the usual Allan-Robinson's flavone synthesis, Compound **6** is synthesized by heating a mixture of **3** which has been synthesized from **2**, potassium benzoate, and benzoic anhydride in a ratio of about 1: 2: 4 mol for several hours. However, we could synthesize **6** directly from **2** by heating a mixture of **2**, potassium benzoate, and benzoic anhydride in a ratio of about 1: 4: 8 mol for 10—12 h. In this way, Compounds (**9**) and (**11**) were also synthesized. The NMR and mass spectral data as well as the negative Gibbs reaction support the **6**, **7**, **8**, **9**, **10**, and **11** structures.

*Light Resistance of New Synthesized Flavones with a 4H,10H-Benzo[1,2-*b*: 3,4-*b'*]dipyran-4,10-dione Skeleton.* The light resistance of the following flavones, has been examined by means of the UV spectra; quercetin, morin, arthraxin (**1**), **7**, **9**, and **11**. The methanol solution of a sample prepared at a constant concentration was irradiated with a 200 W high-pressure mercury lamp

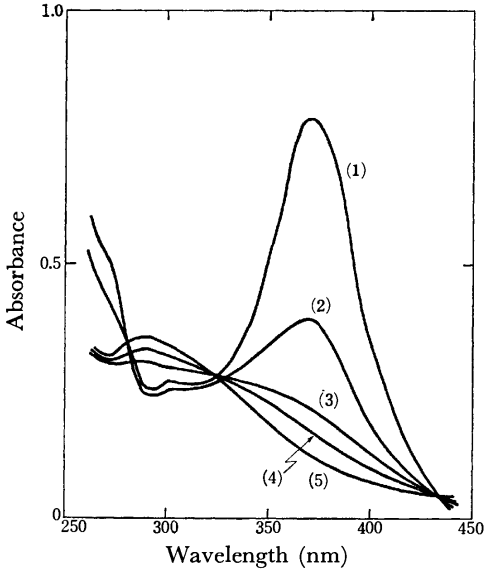

Fig. 2. Time change during irradiation of the spectrum of quercetin in methanol.
(1): 0 h irradiation, (2): 3 h, (3): 5 h, (4): 8 h, (5): 15 h.

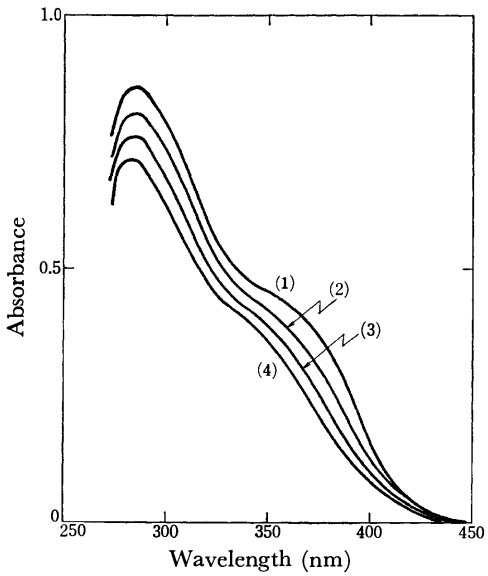

Fig. 3. Time change during irradiation of the spectrum of Compound **9** in methanol.
(1): 0 h irradiation, (2): 3 h, (3): 5 h, (4): 8 h, (5): 15 h.

Table 1. Decrease ratio of the concentration calculated from the intensity of Band I

	Flavonol		Flavone with a 4*H*,10*H*-benzo[1,2-*b*: 3,4-*b'*]-dipyran-4,10-dione skeleton			
			Natural	Synthesized		
	Quercetin[a] (370 nm)	Morin (370)	Arthraxin (340)	Compound **7** (358)	Compound **9** (355)	Compound **11** (356)
0 h						
3	50.2	69.2	8.8	8.4	8.0	2.8
5	71.7	80.8	13.3	13.2	11.9	3.7
8	78.8	86.5	18.0	15.7	15.9	4.5
15	83.5	92.0	23.5	18.1	21.1	6.4
22	84.5	94.2	27.6	20.5	24.1	8.8
50			36.4	24.7	27.9	16.1

a) λ_{max} of Band I of the samples are shown in the respective parentheses.

through a quartz glass tube, with a water-cooled jacket, under bubbling air. The UV spectrum of an aliquot portion was then recorded at intervals of 3, 5, 8, 15, 22, and 50 h. The resistance to light was measured in terms of the decrease ratio of the concentration calculated from the intensity of Band 1, defined as the peak absorption intensity in the 350—450 nm region.

The results tabulated in Table 1 indicate that the synthesized flavones with a 4*H*,10*H*-benzo[1,2-*b*: 3,4-*b*']dipyran-4,10-dione skeleton, in contrast with flavonol and arthraxin, show a high resistance to light when air is bubbled into the methanol solution.

Experimental

The melting points are uncorrected. The NMR spectra were taken at 60 MHz with a Hitachi high-resolution nuclear magnetic resonance spectrometer, R-24 A. All the samples were run as 5—10% solutions in deuteriochloroform. The mass spectra were determined by a direct sample introduction using a Hitachi mass spectrometer, model RMU-6MG, under the following conditions: ionizing voltage; 70 eV, Samples **3**, **4**, and **5**; 20 eV, Samples **6**, **7**, **8**, **9**, **10**, and **11**; accelerating voltage; 3 kV, Samples **3**, **4**, and **5**; 3.2 kV, Samples **6**, **7**, **8**, **9**, **10**, and **11**; ion-source temperature; 170 °C, Samples **6**, **8**, and **10**, 200 °C, Samples **3**, **4**, and **5**; 220 °C, Samples **7**, **9**, and **11**.

2,4-Diacetylphloroglucinol (2). A solution of phloroglucinol (25 g) in warm glacial acetic acid (150 ml) was saturated with boron trifluoride gas and was then set aside for 1 h. The reaction mixture was poured into water (1300 ml), and the orange solid which separated was collected and recrystallized from aqueous ethanol to give nearly colorless needles (17 g); mp 164 °C (lit,[4] mp 168 °C).

8-Acetyl-5,7-dihydroxyflavone (3). A mixture of **2** (20 g), benzoic anhydride (88 g), and potassium benzoate (32 g) was heated at 170—175 °C for 6 h. The product was boiled for a short time with a mixture of ethanol (750 ml), water (90 ml), and potassium hydroxide (60 g). After the subsequent evaporation of the solvent under reduced pressure, the residue was redissolved in water (1000 ml). The solution was saturated with carbon dioxide, and the brown precipitate which separated was collected, washed, and dried (14 g). The product was purified on a silica gel column by eluting it successively with benzene, benzene–ethyl acetate (1: 1), and ethyl acetate. The fraction which was eluted with benzene–ethyl acetate was evaporated to dryness, and the residue was recrystallized from ethanol to give **3** (4.15 g) as yellow needles; mp 210 °C; NMR ($CDCl_3$), 2.81 (s, 3H, $COCH_3$), 6.40 (s, 1H, H-6), 6.66 (s, 1H, H-3), 7.4—8.0 (m, 5H, H-2′, 3′, 4′ 5′, 6′); M(mass spectrum), 296. $C_{17}H_{12}O_5$ requires M, 296.

The Gibbs Reaction. A small quantity (about 1 mg) of Samples **3**, **4**, **5**, **6**, **7**, **8**, **9**, **10**, and **11** was placed in a measuring cylinder and dissolved in pyridine (1 ml). To the solution we then added 5 ml of a freshly prepared Gibbs reagent solution (*N*-chloro-2,6-dichloro-*p*-benzoquinone diimine (10 mg) in pyridine (5 ml)), after which the mixture was diluted to 20 ml with a sodium borate buffer (pH 9.2). The absorption spectrum was determined between 10 and 20 min. All the samples, **3**—**11**, showed negative Gibbs reactions.

8-Acetyl-5,7-dihydroxy-4′-methoxyflavone (4). Compound **4** (15 g) was synthesized from **2** (18.7 g), *p*-anisic anhydride (90 g), and potassium *p*-anisate (35 g) by a way similar to that used in synthesizing **3**. Compound **4** was obtained as yellow needles; mp 181 °C; NMR ($CDCl_3$), 2.75 (s, 3H, $COCH_3$), 3.82 (s, 3H, OCH_3), 6.41 (s, 1H, H-6), 6.73 (s, 1H, H-3), 6.93, 7.09 (d, 2H, 3′, 5′-H), 7.79, 7.94 (d, 2H, 2′, 6′-H); M(mass spectrum), 326. $C_{18}H_{14}O_6$ requires M, 326.

8-Acetyl-5,7-dihydroxy-3′,4′-dimethoxyflavone (5). Compound **5** (7.5 g) was synthesized from **2** (8 g), veratric anhydride (35 g), and potassium veratrate (13 g) by a way imilar to that used in synthesizing **3**. Compound **5** was obtained as yellow needles; mp 251 °C; NMR ($CDCl_3$), 2.75 (s, 3H, $COCH_3$). 3.70 (s, 3H, OCH_3), 3.90 (s, 3H, OCH_3), 6.43 (s, 1H, H-6), 6.66 (s, 1H, H-3), 6.73—6.88 (m, 1H, H-5′), 7.40—7.58 (m, 2H, H-2′, 6′); M (mass spectrum), 356. $C_{19}H_{16}O_7$ requires M, 356.

*2-Phenyl-8-(4-methoxylhenyl)-4*H,*10*H-*benzo*[*1,2*-b: *3,4*-b′]-*dipyran-4,10-dione (7).* A mixture of **3** (1 g), *p*-anisic anhydride (17 g), and potassium *p*-anisate (3 g) was heated at 170 °C for 8 h. The product was boiled for 30 min with a mixture of ethanol (125 ml), water (30 ml), and potassium hydroxide (10 g). After the evaporation of the solvent, the residue was redissolved in water. The solution was saturated with carbon dioxide, and the precipitate which was thus separated was collected, washed, and dried (450 mg). The product was purified on a silica gel column by eluting it successively with benzene, benzene–ehytl acetate (15: 1), benzene–ethyl acetate (1: 1), and benzene–ethyl acetate (1: 5). The fraction which was eluted with benzene–ethy acetate (15: 1) was evaporated to dryness, and, the residue was recrystallzed from ethanol to give **7** (*ca.* 40 mg) as yellow needles; mp 139 °C; NMR ($CDCl_3$), 3.87 (s, 3H, OCH_3), 6.45 (s, 1H, H-6), 6.72 (s, 1H, H-3), 7.3—7.8 (m, 10H); M (mass spcetrum), 412. $C_{25}H_{16}O_6$ requires M, 412.

*2-Phenyl-8-(3,4-dimethoxyphenyl)-4*H,*10*H-*benzo*[*1,2*-b:*3,4*-b′]-*dipyran-4,10-dione (8).* Compound **8** (850 mg) was synthesized from **3** (1 g), veratric anhydride (20 g), and potassium veratrate (4 g) by a way similar to that used in synthesizing **7**. Compound **8** was obtained as yellow needles, mp 151 °C; NMR ($CDCl_3$), 3.85 (s, 3H, OCH_3), 3.91 (s, 3H, OCH_3), 6.45 (s, 1H, H-6), 6.73 (s, 1H, H-3), 6.9—7.9 (m, 9H); M (mass spectrum), 442. $C_{26}H_{18}O_7$ requires M, 442.

*2-(4-Methoxyphenyl)-8-(3,4-dimethoxyphenyl)-4*H,*10*H-*benzo*[*1,2*-b: *3,4*-b′]*dipyran-4,10-doine (10).* Compound **10** (700 mg) was syntheized from **4** (1.3 g), veratric anhydride (23.5 g), and potassium veratrate (4.1 g) by a way similar to that used in synthesizing **7**. Compound **10** was obtained as yellow needles; mp 168 °C; NMR ($CDCl_3$), 3.82 (s, 3H, OCH_3), 3.87 (s, 3H, OCH_3), 3.90 (s, 3H, OCH_3), 6.42 (s, 1H, H-6), 6.70 (s, 1H, H-3), 6.9—8.0 (m, 8H); M (mass spectrum), 472. $C_{27}H_{20}O_8$ requires M, 472.

*2,8-Diphenyl-4*H,*10*H-*benzo*[*1,2-b*: *3,4-b*′]*dipyran-4,10-dione (6).* A mixture of **2** (3 g), benzoic anhydride (25 g), and potassium benzoate (9 g) in a ratio of about 1: 4: 8 mol was heated at 170 °C for 11 h. The product was boiled for 30 min with a mixture of ethanol (200 ml), water (70 ml), and potassium hydroxide (43 g). After the evaporation of the solvent under reduced pressure, the residue was redissolved in water. The solution was saturated with carbon dioxide, and the precipitate which was thus separated was collected, washed, and dried (2.9 g). The product was purified on a silica gel column by eluting it successively with benzene–ethyl acetate (1: 1), ethyl acetate, ethyl acetate–acetone (1: 1), acetone, acetone–methanol (1: 1), and methanol. The fraction which was eluted with acetone was evaporated to dryness, and the residue was recrystallized from ethanol to give (**6**) as pale yellow needles; mp 272 °C; NMR ($CDCl_3$), 6.76 (s, 1H), 6.94 (s, 1H), 7.30—7.62 (m, 7H), 7.81—8.05 (m, 4H); M (mass spectrum), 382. $C_{24}H_{14}O_5$ requires M, 382.

*2-(4-Methoxyphenyl)-8-(4-methoxyohenyl)-4*H,*10*H-*benzo*[*1,2*-b:

3,4-b']*dipyran-4,10-dione* (*9*). Compound **9** (1.2 g) was synthesized from **2** (1 g), *p*-anisic anhydride (11 g), and potassium *p*-anisate (3.7 g) by a way similar to that used in synthesizing **6**. Compound **9** was thus obtained as yellow needles; mp 286 °C; NMR ($CDCl_3$), 3.71 (s, 3H, OCH_3), 3.81 (s, 3H, OCH_3), 6.40 (s, 1H), 6.80 (s, 1H), 6.9—8.1 (m, 9H); M (mass spectrum), 442. $C_{26}H_{18}O_7$ requires M, 442.

*2-(3,4-Dimethoxyphenyl)-8-(3,4-dimethoxyphenyl)-4*H,*10*H-*benzo*[*1,2*-b: *3,4*-b']*dipyran-4,10-dione* (*11*). Compound **11** (600 mg) was synthesized from **2** (1 g), veratric anhydride (13.5 g), and potassium veratrate (4.3 g) in a way similar to that used in synthesizing **6**. Compound **11** was thus obtained as yellow needles; mp 225 °C; NMR ($CDCl_3$), 3.65, 3.73, 3.88, 3.95 (all s, 3H, OCH_3), 6.43 (s, 1H), 6.70 (s, 1H), 6.9—8.1 (m, 7H); M (mass spectrum), 502. $C_{28}H_{22}O_9$ requires M, 502.

References

1) M. Kaneta and N. Sugiyama, *J. Chem. Soc., C*, **1971**, 1982.
2) M. Kaneta and N. Sugiyama, *Bull. Chem. Soc. Jpn.*, **44**, 3211 (1971).
3) M. Kaneta and N. Sugiyama, *Bull. Chem. Soc. Jpn.*, **46**, 2265 (1973).
4) T. W. Campbell and G. M. Coppinger, *J. Am. Chem. Soc.*, **73**, 2708 (1951).
5) F. E. King and L. C. Manning, *J. Chem. Soc.*, **1957**, 563.
6) J. Massicot and J. P. Marthe, *Bull. Soc. Chim. Fr.*, **1962**, 1962.
7) J. Massicot, J. P. Marthe, and S. Heitz, *Bull. Soc. Chim. Fr.*, **1963**, 2712.

Aromaticity-Based Theory of Pericyclic Reactions

Jun-ichi AIHARA

Department of Chemistry, Faculty of Science, Hokkaido University, Sapporo 060

(Received August 26, 1977)

The resonance energies of conjugated compounds in the electronically excited state were calculated on the basis of the aromaticity theory previously reported by us. The allowednesses of pericyclic reactions were predicted by means of these resonance energies. The predictions based on the resonance energy difference (RED) between the pericyclic transition state and the reactant(s) are in general agreement with the experiment.

Dewar-type resonance energy is an excellent aromaticity index for a conjugated compound.[1] It is defined as the difference between the energy of a conjugated compound and the energy of a "localized structure." Here, a "localized structure" signifies an olefinic reference structure which is hypothetically free from aromaticity. During the last three years we have been developing an analytical theory of aromaticity by means of the HMO theory, and have succeeded in formulating a characteristic polynomial for a "localized structure" of a conjugated compound.[2-5] A characteristic polynomial for the localized structure has been termed a "reference polynomial."[2] The π energy calculated from a reference polynomial can be interpreted as the π energy which a compound would possess if it were absolutely olefinic in nature.[2,3] On this basis, we could satisfactorily evaluate the aromatic resonance energy for any kind of conjugated compound and its ions.[2-5]

In this paper, we will show that the same definition of resonance energy can be applied to conjugated compounds in the excited state, and that it can be used as a new reactivity index for judging the allowedness of related pericyclic (*i.e.*, concerted) reactions.

Aromaticity in an Excited-State Species

A criterion of aromaticity in an electronically excited species is a comparison of the π energies of the compound and its localized structure (*i.e.*, its reference structure),[2] but in this case both structures must be in an equivalent excited state. We will here restrict our consideration to the lowest excited state, because, in most cases, any higher excited state will rapidly relax to the lowest excited state.[6] This means that, in most photochemical reactions, only the lowest excited state is important.

Let a characteristic polynomial for a conjugated compound and a corresponding reference polynomial be written respectively as

$$P(X) = X^N + \sum_{k=1}^{N} a_k X^{N-k} \tag{1}$$

and

$$R(X) = X^N + \sum_{k=1}^{N} b_k X^{N-k}, \tag{2}$$

where N is the number of atoms in the conjugated system. The coefficients, a_k and b_k, can be enumerated graphically with little difficulty.[2,3,7]

The roots of a secular equation, $P(X)=0$, are arranged in decreasing order as

$$X = X_1, X_2, \cdots, X_{N-1}, X_N. \tag{3}$$

The roots of a corresponding reference equation, $R(X)=0$, are arranged analogously in decreasing order as

$$X = X_1^*, X_2^*, \cdots, X_{N-1}^*, X_N^*. \tag{4}$$

The resonance energy of a conjugated system, RE, is then defined as

$$RE = \sum_{m}^{\text{occ.}} g_m(X_m - X_m^*), \tag{5}$$

where m runs over all the occupied π-molecular orbitals and where g_m is the number of electrons which occupy the m-th orbital. The resonance energy of any conjugated compound in any excited state can be calculated from this expression simply by adjusting the g_m values to its electronic configuration.

Resonance Energies of Annulenes in the Lowest Excited State

The resonance energies of ordinary annulenes (*i.e.*, Hückel annulenes) can be calculated straightforwardly from Eq. 5. The resonance energies of unrealistic Möbius annulenes (*i.e.*, singly twisted annulenes)[8] can also be calculated in the same manner. A reference polynomial for a Möbius annulene is identical with that for an ordinary annulene of the same size because the coefficients of the reference polynomials for both annulenes depend solely upon the connectivity of carbon atoms.[9] More accurately, each coefficient of a reference polynomial is a function of the bond (or heterobond) parameters squared (k^2).[3] Therefore, the coefficients of a reference polynomial are independent of the sign of any bond parameter. The π-orbital energies for the Hückel and Möbius benzenes, together with those for their reference structure, are shown in Fig. 1. Table 1 contains the resonance energies obtained for the Hückel and Möbius annulenes.

It is noteworthy that the aromaticity of a Möbius annulene in the ground state is determined by the converse of the Hückel (4n+2) rule, in agreement with a conclusion by Heilbronner.[8] The sign and the magnitude of the resonance energy for any ground-state annulene are essentially the same as those previously reported by us.[10] On the other hand, either conformation of any annulene in the excited state can be predicted to have an aromatic character opposite to that in the ground state. For example, a Hückel benzene (*i.e.*, an ordinary benzene) is the most stable annulene in the ground state, but the resonance energy becomes greatly negative when it is electronically excited. Such a situation is best represented by a high reactivity of

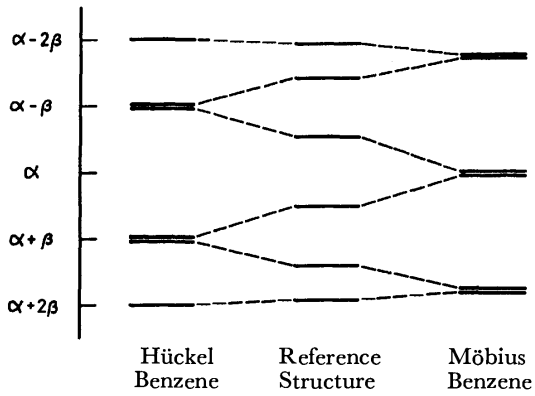

Fig. 1. Orbital correlations between benzenes and their reference structure.
Dashed lines indicate orbital correlations, which are drawn according to the principle described in J. Aihara, *Bull. Chem. Soc. Jpn.*, **50**, 2010 (1977). However, another definition of resonance energy given therein is not used in this paper, because the original definition (Ref. 2) is more practical and physically meaningful. Note that the reference energy in Ref. 2 defines the lowest energy of the reference structure.

Table 1. Resonance energies of annulenes

Species	Resonance energy (β)	
	Ground state	Excited state
Hückel cyclobutadiene	−1.226	0.305
Möbius cyclobutadiene	0.431	−0.867
Hückel benzene	0.273	−0.692
Möbius benzene	−0.799	0.236
Hückel cyclooctatetraene	−0.595	0.186
Möbius cyclooctatetraene	0.201	−0.550
Hückel[10]annulene	0.159	−0.451
Möbius[10]annulene	−0.474	0.152

this compound in the excited state. Benzene often forms benzvalene, Dewar benzene, and prismane when it is irradiated by ultraviolet light.[11]

Pericyclic Reactions with a Monocyclic Transition State

The above aspect of the aromaticity of annulene reminds us of the stereoselectivity of pericyclic reactions. Thus far, two principal approaches, the frontier orbital method[12] and the correlation diagram method,[13] have been widely employed to explain a number of pericyclic reactions. An alternative approach was made by Dewar[14] and Zimmerman,[15] who independently considered an aromatic property of a transition state as a determinant for the allowedness of pericyclic reactions.

Since, at any point along the reaction coordinate, a set of electrons are cyclically delocalized over the reacting centers, a transition state of the pericyclic reaction can be considered as a kind of cyclic conjugated system. For example, a transition state of a $[4_s+2_s]$ Diels-Alder reaction is isoconjugate with a Hückel benzene. According to an aromaticity-based theory of pericyclic reactions,[14,15] this reaction is thermally allowed because benzene is aromatic in the ground state. Dewar and Zimmerman thus showed that the problem of pericyclic reactions is identical in principle with that of aromaticity. The utility of this approach depends on the facility with which one can predict whether or not a given pericyclic transition state is aromatic. However, there has been no satisfactory theory of aromaticity for conjugated systems in the excited state. Their account of photochemical pericyclic reactions hence appeared less persuasive than that of thermal pericyclic reactions.

Now, we have an analytical theory of aromaticity[2-5] applicable to the excited-state species. By correlating the present resonance energies of annulenes (Table 1) with the pericyclic reactions whose transition states are monocyclic, we can safely predict that, if a pericyclic transition state is electronically equivalent to an annulene in an aromatic state, the reaction is allowed, while if it is not, the reaction is forbidden. Here, an aromatic state signifies a state in which the compound has a positive resonance energy, whether or not it is a ground-state species. On this basis, it can be predicted that a $[4_s+2_s]$ Diels-Alder reaction is photochemically forbidden, since a corresponding Hückel benzene has a negative resonance energy in the excited state. This is, of course, in harmony with the fact that such a reaction has not been reported.

Accordingly, an aromaticity-based theory of pericyclic reactions can be generalized into a single definitive rule: pericyclic reactions, both thermal and photochemical, take place *via* aromatic transition states. Since there are no exceptions to the Woodward-Hoffmann rules, there are no exceptions to this rule, either.

Pericyclic Reactions with a Polycyclic Transition State

Even though a pericyclic reaction has a polycyclic transition state, we can expect that an analogous consideration can be applied to it. In this case, the reactants are often cyclic conjugated compounds, and they may have an aromatic character. In order to take this new factor into account, we propose a new quantity, defined as the resonance energy difference (RED) between the pericyclic transition state and the reactants. This quantity reflects the relative aromatic stabilization of the transition state as compared with that of the reactants in an equivalent electronic state.

After extensive numerical analysis, the RED was found to give an excellent reactivity index for pericyclic reactions of any type. In Table 2 some typical pericyclic reactions with a polycyclic transition state are listed, together with their RED values. In calculating these RED values, some substituents, denoted therein as R_1 and R_2, were ignored for the sake of simplicity. As is shown in this table, the RED must be positive in order for the reaction to be allowed. The reaction is predicted to be allowed *via* a transition state with the largest RED value. When the RED is smaller than that, the reaction cannot be expected to occur, in accord with the experimental results.

Such a trend in reactivity strongly suggests that an

TABLE 2. RED VALUES FOR TYPICAL PERICYCLIC REACTIONS

Type of reaction	Stereochemistry	RED (β)	Allowedness
A	(4_s+2_a) or (4_a+2_s)	0.02	Yes[a]
	(4_s+2_s)[k] or (4_a+2_a)	−0.26	No
B	(4_a+2_a)	0.80	Yes[b]
	(4_s+2_a)[k] or (4_a+2_s)[k]	−0.28	No
C	Disrotatory	0.25	Yes[c]
	Conrotatory	−0.71	No
D	Disrotatory	0.23	Yes[d]
	Conrotatory	−0.52	No
E	Conrotatory	0.06	Yes[e]
	Disrotatory	−0.18	No
F	(6_s+4_s)	0.16	Yes[f]
	(6_s+4_a)[k] or (6_a+4_s)[k]	−0.29	No
G	(8_s+2_s)	0.19	Yes[g]
	(8_s+2_a) or (8_a+2_s)	−0.30	No
H	(14_a+2_s)	0.08	Yes[h]
	(14_a+2_a) or (14_s+2_s)	0.00	No
I	Disrotatory-disrotatory	0.25	Yes[i]
	Conrotatory-disrotatory[k]	0.28	No
J	Conrotatory-disrotatory	0.40	Yes[j]
	Disrotatory-disrotatory	−0.47	No

a) During the reaction two bonds are simultaneously formed, one bond between C_1 and C_3, and the other bond between C_2 and C_6: G. S. Hammond, N. J. Turro, and R. S. H. Liu, *J. Org. Chem.*, **28**, 3297 (1963); G. S. Hammond and R. S. H. Liu, *J. Am. Chem. Soc.*, **85**, 477 (1963). b) During the reaction two bonds are simultaneously formed, one bond between C_1 and C_5 and the other bond between C_2 and C_8: R. Criegee and R. Askani, *Angew. Chem., Int. Ed. Engl.*, **7**, 537 (1968). c) S. Masamune, S. Tanaka, and R. T. Seidner, *J. Am. Chem. Soc.*, **91**, 7769 (1969). d) S. Masamune and R. T. Seidner, *J. Chem. Soc., Chem. Commun.*, **1969**, 542. e) K. A. Muszkat and E. Fisher, *J. Chem. Soc. B*, **1967**, 662; F. B. Mallory, C. S. Wood, and J. T. Gordon, *J. Am. Chem. Soc.*, **86**, 3094 (1964). f) K. Houk, Dissertation, Harvard University (1968). See also Ref. 13. g) R_1 = —$COOCH_3$: A. Galbraith, T. Small, R. A. Barnes, and V. Boekelheide, *J. Am. Chem. Soc.*, **83**, 453 (1961). h) R_2 = —CN: W. von E. Doering, cited in Ref. 13. i) During the reaction two bonds, a and b, are simultaneously broken: T. J. Katz, E. J.Wang, and N. Acton, *J. Am. Chem. Soc.*, **93**, 3782 (1971); Ref. 16. j) During the reaction two bonds, a and b, are simultaneously broken: G. L. Closs and P. E. Pfeiffer, *J. Am. Chem. Soc.*, **90**, 2452 (1958); H. M. Frey and I. D. R. Stevens, *Trans. Faraday Soc.*, **61**, 90 (1969); R. Srinivasan, A. A. Levi, and I. Haller, *J. Phys Chem.*, **69**, 1775 (1965); Ref. 16. k) Heavy steric hindrance does not allow this reaction path, either.

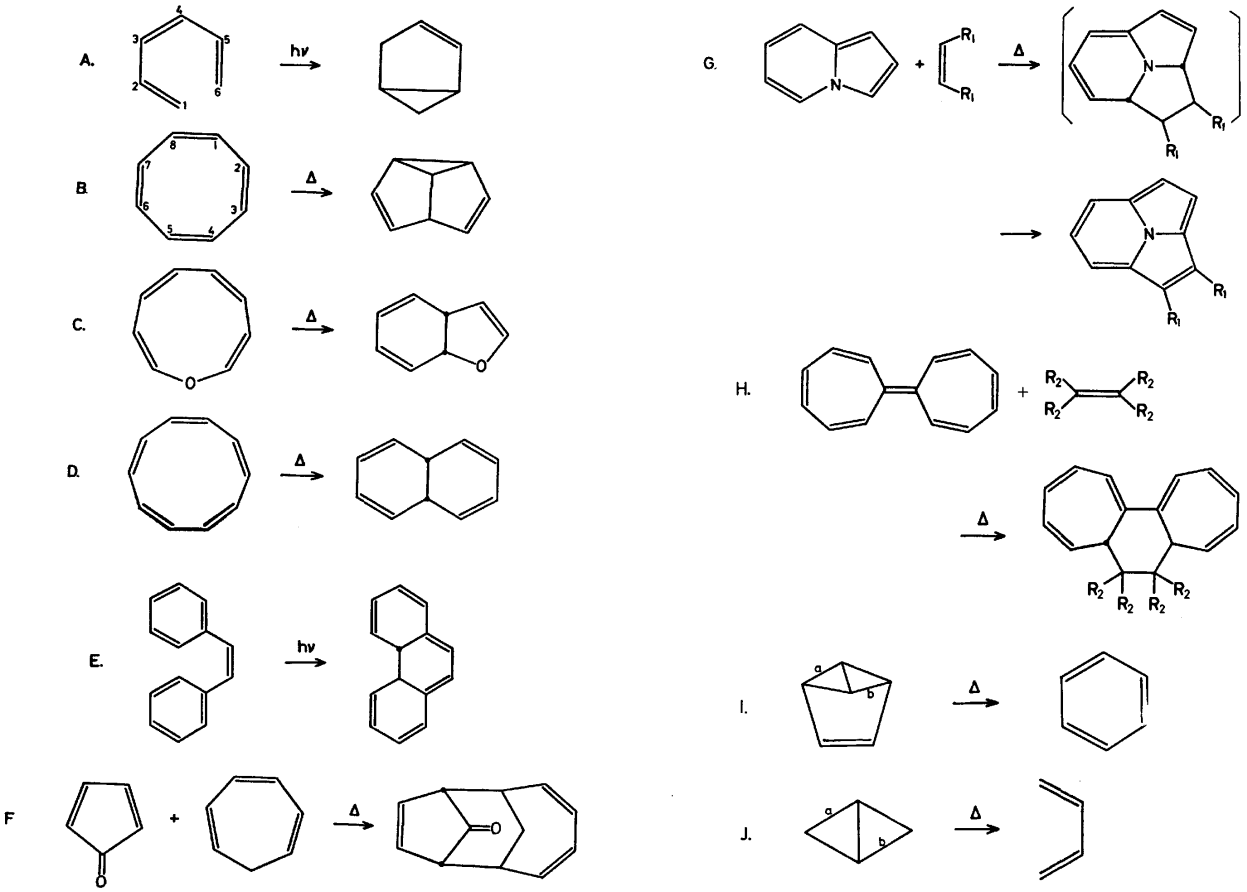

The conformation of the product shown in each of these chemical equations is the one obtained from the allowed reaction path.

actual transition state of a pericyclic reaction must be more aromatic, or less antiaromatic, than the reactants and any other transition state imaginable in an equivalent electronic state. This trend appears to be justified by the view that a more aromatic state might more easily be reached in the course of the reaction. All the pericyclic reactions investigated can be explained in this manner.

Therefore, the definitive rule found above for pericyclic reactions with a monocyclic transition state must neccessarily be modified to include all kinds of pericyclic reactions as follows: Pericyclic reactions, both thermal and photochemical, take place *via* more aromatic transition states than the reactants. In the case of pericyclic reactions with a monocyclic transition state, the RED agrees exactly with the resonance energy of the transition state.

Above all, it should be noted that, on the basis of the present approach, we can avoid a certain ambiguity encountered in applying the Woodward-Hoffmann rules to pericyclic reactions with a polycyclic transition state. For example, the fact that the conversion of benzvalene to benzene is thermally allowed in a disrotatory-disrotatory manner (Reaction I in Table 2), whereas the same stereochemical conversion of bicyclobutane to butadiene is thermally forbidden (Reaction J in Table 2), cannot be explained in terms of orbital correlations between reactants and products.[16]

This problem can, in principle, be solved by means of the present aromaticity-based theory. The reason for the occurrence of the former reaction is that the resonance energy of the transition state, which is something like tricyclo[3.1.0.$0^{4,6}$]hexatriene, is positive. On the contray, the resonance energy of a transition state for the latter reaction, which is something like propalene, is negative. They are 0.253 and -0.473 respectively in units of β. Since the reactants for both reactions are nonaromatic, the RED for only the former reaction is positive. In agreement with a suggestion of Dewar and Kirschner,[16] a double bond in benzvalene obviously plays a significant role in determining both the aromaticity of the transition state and the allowedness of this reaction.

In this context, one comment must be made here. A thermal conrotatory-disrotatory conversion of benzvalene to benzene (Ia) can also be predicted to have a positive RED value (see Table 2). Unfortunately, this value is considerably larger than that for a thermal disrotatory-disrotatory conversion of the same compound (Ib). However, heavy steric hindrance forbids the occurrence of the former reaction (*i.e.*, Ia). It goes without saying that the steric effect is one of the crucial factors in determining the allowedness of any pericyclic reaction.

Apart from the steric effect, the suspicion that an actual reaction may not follow a reaction path with the maximum RED value seems to be related to a fault in the HMO model, rather than to one in the present approach to pericyclic reactions. According to our simplest HMO model, the energy of the transition state for Ia is estimated to be larger than that for Ib. This difficulty can be overcome simply by improving the HMO model so as to reproduce the actual transition states for both reactions (*i.e.*, Ia and Ib). Because any actual reaction occurs along the lowest-energy path, an actual transition state for Ib should be energetically lower than that for Ia. Logically, the RED for Ib is larger than that for Ia. For such a reason, the slight inconsistency found in Table 2 should be ascribed to a rather incomplete HMO model, in which bond alternation and the like are not taken into consideration.

Concluding Remarks

We now feel confident that the degree of aromaticity in a conjugated transition state is an important factor in determining the allowedness of pericyclic reactions. We might safely conclude that pericyclic reactions with the largest RED occur only thermally or photochemically, depending upon the electronic state concerned. It goes without saying that a heavy steric hindrance may forbid an electronically-allowed reaction. It is clear that the present approach complements and completes the aromaticity-based theory of pericyclic reactions, originally proposed by Dewar[14] and Zimmerman.[15] From this standpoint, the new concept of the aromaticity of the excited-state species also seems to have been explained fairly well, although it is not easy to estimate this aromaticity experimentally. The introduction of actual bond alternation would obviously improve the value of the RED as a reactivity index.[3]

The author would like to thank Professor Takashi Tsuji for his help in preparing Table 2. The use of the facilities of the Hokkaido University Computing Center is acknowledged.

References

1) M. J. S. Dewar and G. J. Gleicher, *J. Am. Chem. Soc.*, **87**, 685, 692 (1965); M. J. S. Dewar and C. de Llano, *ibid.*, **91**, 789 (1969); J. Aihara, *Kagaku No Ryoiki*, **30**, 269 (1976).

2) J. Aihara, *J. Am. Chem. Soc.*, **98**, 2750 (1976); *Kagaku No Ryoiki*, **30**, 379 (1976).

3) J. Aihara, *J. Am. Chem. Soc.*, **98**, 6840 (1976).

4) J. Aihara, *J. Am. Chem. Soc.*, **99**, 2048 (1977).

5) J. Aihara, *J. Org. Chem.*, **41**, 2488 (1976).

6) See, *e.g.*, P. A. Leermarker, "Energy Transfer and Organic Photochemistry," ed by A. A. Lamora and N. J. Turro, Interscience, New York, N.Y. (1969), Chap. 1.

7) H. Hosoya, *Theor. Chim. Acta*, **25**, 215 (1972); A. Graovac, I. Gutman, N. Trinajstić, and T. Žikvović, *ibid.*, **26**, 67 (1972).

8) E. Heilbronner, *Tetrahedron Lett.*, **1964**, 1932.

9) A. Graovac and N. Trinajstić, *J. Mol. Struct.*, **30**, 416 (1976).

10) J. Aihara, *Bull. Chem. Soc. Jpn.*, **48**, 517 (1975).

11) See, *e.g.*, W. J. le Noble, "Highlights of Organic Chemistry," Marcell Dekker, New York, N.Y. (1974), Chap. 11.

12) K. Fukui, "Theory of Orientation and Stereoselection," Springer Verlag, Heidelberg, Germany (1970).

13) R. B. Woodward and R. Hoffman, "The Conservation of Orbital Symmetry," Verlag Chemie-Academic Press, Weinheim/Bergst., Germany (1970).

14) M. J. S. Dewar, *Tetrahedron Suppl.*, **8**, 75 (1966);

"The Molecular Orbital Theory of Organic Chemistry," McGraw-Hill, New York, N.Y. (1969), Chap. 8; *Angew. Chem., Int. Ed. Engl.*, **10**, 761 (1971).
15) H. E. Zimmerman, *J. Am. Chem. Soc.*, **88**, 1564, 1566 (1966); *Angew. Chem., Int. Ed. Engl.*, **8**, 1 (1969); *Acc. Chem. Res.*, **4**, 272 (1971).
16) M. J. S. Dewar and S. Kirschner, *J. Am. Chem. Soc.*, **97**, 2932 (1975).

Solvent Effects on the Photoamination of 1-Amino-2,4-dibromoanthraquinone. I. Photoamination in Benzene *via* Intramolecular Charge Transfer Excited Triplet State

Haruo INOUE and Mitsuhiko HIDA

Department of Industrial Chemistry, Faculty of Technology, Tokyo Metropolitan University, Fukazawa, Setagaya-ku, Tokyo 158

(Received September 19, 1977)

The bromine atom at the 4 position of 1-amino-2,4-dibromoanthraquinone (**1**) was substituted by butylamine and aniline by the irradiation of visible light. In ethanol the dissolved oxygen promoted the reaction and anthracene, a triplet quencher, had little effect. In benzene, the dissolved oxygen retarded the reaction and anthracene had a considerable quenching effect. Kinetic analysis indicated that in ethanol the photoamination of **1** proceeds mainly through the interaction of **1** in $S_1(^1CT)$ with the ground state oxygen, while in benzene it does through the $T_1(^3CT)$ of **1** without the aid of oxygen. The detailed reaction mechanism in benzene has been discussed and the rate constant of each process including the deactivation constant of the upper excited $T_2(^3n\pi^*)$ level evaluated.

The photochemical behavior of anthraquinone derivatives has attracted attention for a long time in relation to the photofading of vat dyes and the photosensitized oxidation. Many intensive studies have been made on the photoreduction, the photoannelation, and the photosubstitution.[1] Anthraquinone derivatives have four $\pi\pi^*$ absorption bands in the region of the wavelength between 220 nm and 350 nm, and $n\pi^*$ band at the longer wavelength near 400 nm. When electron donating substituents such as hydroxyl, amino, and methylamino groups are introduced in to the nucleus, a new $\pi\pi^*$ absorption band, an intramolecular charge transfer band, appears in the visible region. It has been emphasized that the triplet excited $n\pi^*$ state is reactive in almost all the photochemical reactions of anthraquinones, while the excited CT state has little reactivity and the introduction of an electron donating substituent renders the excited anthraquinone extremely unreactive.[1] However, recently a new photosubstitution reaction of aminohaloanthraquinone has been reported: the bromine atom of sodium 1-amino-4-bromoanthraquinone-2-sulfonate **3** has been substituted by ammonia and alkylamine by the irradiation of visible light.[2] The oxygen molecule is indispensable for the photoamination and the mechanism has been postulated that the photoamination proceeds through an exciplex or an encounter complex formation between **3** in its excited ^1CT state and the ground sate oxygen, followed by an attack of amine to produce the aminated product as shown below.[3]

$$AQ^*(^1CT) + {}^3O_2 \longrightarrow [AQ^{\delta+} \cdots O_2^{\delta-}]$$

$$[AQ^{\delta+} \cdots O_2^{\delta-}] \swarrow \quad \downarrow \text{Amine}$$

$$AQ + O_2 \qquad \text{Amination}$$

This photoamination appears to be the first example of a reaction which proceeds *via* the excited CT state of anthraquinone derivatives.

In this paper the photoamination of 1-amino-2,4-dibromoanthraquinone **1** by butylamine has been investigated. Very large solvent effects were observed between the photoamination of **1** in benzene and that in ethanol: both the reactive state of the excited **1** and the reaction mechanism changed with the nature of the solvents used.

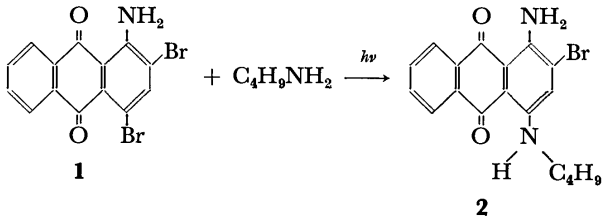

1 **2**

Experimental

1-Amino-2,4-dibromoanthraquinone **1** was prepared by the bromination of sodium 1-amino-4-bromoanthraquinone-2-sulfonate **3** with bromine and was purified by repeated recrystallizations from ethanol. Shimadzu UV-200 spectrophotometer was used for the measurement of the visible and UV spectra, and Hitachi MPF-4 spectroflurometer for the measurement of the fluorescence spectra. The quantum yield of the photoamination of **1** was determined by the potassium tris(oxalto)ferrate(III) chemical actinometer according to the method recommended by Hatchard and Parker.[4] The reaction mixture was irradiated by means of a 500 W xenon lamp (USHIO UXL-500 DXO) or a 100 W high-pressure mercury lamp (Eikosha) through the following filter system: soda glass for the irradiation of light of $\lambda > 300$ nm, a Toshiba interference filter KL-40 for monochromatic light of $\lambda = 400$ nm, and a Toshiba interference filter KL-47 and a glass filter VY-45 for monochromatic light of $\lambda = 470$ nm, respectively.

Results and Discussions

*The Photoamination of **1** in Benzene.* A solution of **1** (1.00×10^{-4} mol/dm^3) and butylamine (5.00×10^{-2} mol/dm^3) in benzene was irradiated by the light of $\lambda > 300$ nm, and a new absorption band appeared in the region between 500 and 700 nm which is characteristic of the aminated product **2**, having the isosbestic points at $\lambda = 390$ and 512 nm. TLC analysis (silica gel, eluent: 93: 7 benzene–acetone) of the irradiated mixture indicated that only **2** was produced in the reaction system. From these results it was concluded that the photoreaction of **1** with butylamine in benzene gave only the aminated product **2**. After evaporating the solvent from the irradiated mixture, the aminated product **2** was seperated by silica gel column chromatography and purified by repeated recrystallizations from

hexane. (Found: C, 58.02; H, 4.55; N, 7.56%).

Solvent Effects on the Photoamination of 1. The solvent effects on the photoamination of **1** with butylamine are shown in Table 1. Very large solvent effects were observed. In ethanol, 1) the dissolved oxygen promoted the photoamination of **1**, but **1** had a poor reactivity under a nitrogen atmosphere, 2) a little quenching effect was observed by the addition of anthracene, and 3) the yield (%) of **2** was not equivalent to the conversion (%) of **1** and the ratio (0.79) between them was unchanged during the photoreaction. The last result suggests that the simultaneous photodecomposition of **1** accompanied by the photoamination took place as observed in the photoamination of **3** in aqueous 2-propanol. In benzene, 1) the dissolved oxygen retarded the photoamination and **1** was rather reactive under a nitrogen atmosphere, 2) a considerable quenching effect was observed by the addition of anthracene, and 3) the yield of **2** was equal to the conversion of **1**, suggesting that the photoamination of **1** proceeded quantitatively.

TABLE 1. SOLVENT EFFECTS ON THE PHOTOAMINATION OF **1** BY BUTYLAMINE[a)]

Solvent	Φ_{N_2}[b)] / Φ_{Air}	Quenching effect by anthracene[c)]	Yield of **2** / conversion of **1**
Ethanol	0.13	△[d)]	0.79
Benzene	1.50	○[e)]	1.00

a) **1** (1.00×10^{-4} mol/dm^3); butylamine (5.00×10^{-2} mol/dm^3); in ethanol or benzene; light of $\lambda>420$ nm. b) Φ_{N_2} and Φ_{Air} are the quantum yield of the photoamination of **1** under nitrogen and air, respectively. c) [Anthracene] = 1.00×10^{-2} mol/dm^3. d) Little quenching. e) Considerable quenching.

Absorption and Fluorescence Emission Spectra of 1. The absorption and the fluorescence emission spectra of **1** shown in Fig. 1 have two distinct characteristics. 1) The λ_{max} of the first absorption band in ethanol exibits a red shift of 5 nm compared with that in benzene and the λ_{max} of the fluorescence spectrum exibits a red shift of 21 nm. This supports the theory that **1** in the excited state has an intramolecular CT nature. 2) Contrary to the usual solvent effect,[5)] the relative intensity of the fluorescence spectrum in benzene is weaker by a factor of ten than that in ethanol under the same conditions. This suggests that **1** in its ^{1}CT state in benzene is deactivated more than ten times as effectively as in ethanol, possibly by a process such as an enhanced intersystem crossing to the triplet state.

Energy Diagram of the Excited State of 1. An introduction of substituent to the anthraquinone nucleus is thought to have little effect on the position of the nπ^* level,[1b)] so that the ^{1}nπ^* and ^{3}nπ^* levels of **1** are supposed to lie in the neighborhood of those of anthraquinone, 280 kJ/mol and 259 kJ/mol respectively. As the absorption and the fluorescence spectra were still structureless even at 77 K, the 0-0 band in the first absorption band of **1** was estimated from the intersection of the absorption and the fluorescence spectra in a mirror image relation.[6)] The ^{1}CT level of **1** was supposed to be at 218 kJ/mol in ethanol and 228 kJ/mol in benzene, respectively.

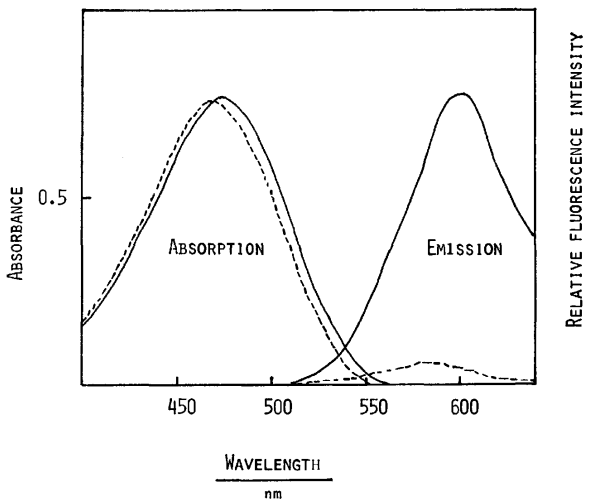

Fig. 1. Absorption and fluorescence spectra of **1**. [**1**] = 1.00×10^{-4} mol/dm^3, ——: in ethanol, ——: in benzene.

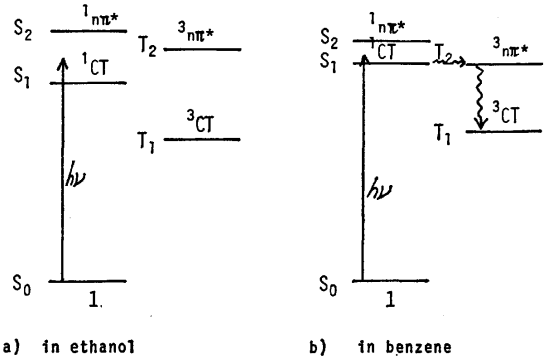

Fig. 2. Energy diagram of the excited state of **1**.

Thus, the ^{1}CT level of **1** in ethanol was considered to be a little lower than the ^{3}nπ^* level as illustrated in Fig. 2a. In benzene the absorption and the fluorescence spectra indicate the ^{1}CT level of **1** being situated at a higher position than that in ethanol. Moreover, the nπ^* level of **1** in a non-polar solvent such as benzene lies in a relatively lower position than that in a polar protic solvent such as ethanol, and it may be reasonably accepted that in benzene the ^{1}CT level lies in close contiguity to the ^{3}nπ^* level as shown in Fig. 2b. An inversion of the disposition between the ^{1}CT and the ^{3}nπ^* levels may take place by the variation of the solvent polarity. On the basis of the energy diagram of the excited states of **1** (Fig. 2a and b), the solvent effects on the photoamination can be discussed as follows. In ethanol **1** is excited to the ^{1}CT level by an irradiation of the first absorption band of **1** and the photoamination takes place in a similar manner to the case of **3** in aqueous 2-propanol. In benzene, because of a close contiguity or an inversion of the disposition between $S_1(^1CT)$ and the $T_2(^3n\pi^*)$ levels, both levels interact more strongly with each other than in ethanol, resulting in enhancement of the intersystem crossing process. Thus the relative fluorescence intensity of **1** in benzene becomes weaker by a factor of ten compared with that in ethanol. Consequently, the $T_1(^3CT)$ level

of **1** is supposed to be largely populated by the irradiation of the first absorption band of **1** in benzene by the dominant deactivation process of $S_1(^1CT) \rightsquigarrow T_2(^3n\pi^*) \rightsquigarrow T_1(^3CT)$. Then, the photoamination is supposed to proceed mainly from the $T_1(^3CT)$ without the aid of the dissolved oxygen.

Effect of Oxygen in Benzene. The quenching experiments by the dissolved oxygen in benzene gave a linear Stern-Volmer plot (Fig. 3), indicating that the dissolved oxygen acted as a quencher of the photoamination of **1** in benzene and the photoreaction proceeds through the one excited state of **1**. From the slope of the linear plot, $k_q \cdot \tau_1$ was found to be 513 dm³/mol, where k_q denotes the quenching rate constant by oxygen and τ_1 the lifetime of the excited state quenched by oxygen, respectively.

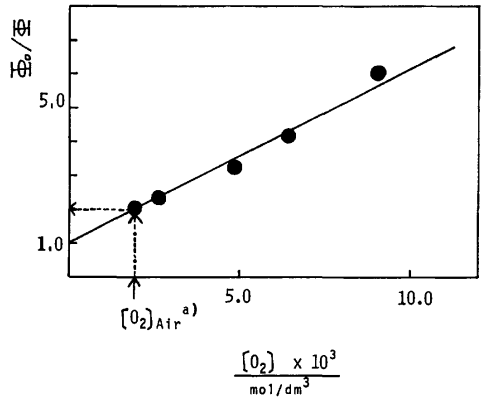

Fig. 3. Stern-Volmer plot for the quenching effect of oxygen on the photoamination of **1** (1.00×10^{-4} mol/dm³) by butylamine (5.00×10^{-2} mol/dm³) in benzene by the irradiation of the light of $\lambda = 470$ nm.
a) The concentration of the dissolved oxygen in the air saturated benzene.

Effect of the Triplet Sensitizer in Benzene. The benzene solution of **1** (1.00×10^{-4} mol/dm³) and butylamine (5.00×10^{-2} mol/dm³) with or without a triplet sensitizer (1.00×10^{-2} mol/dm³) was irradiated by monochromatic light of $\lambda = 400$ nm under nitrogen. In the presence of benzil ($E_T = 226$ kJ/mol) and fluorenone ($E_T = 226$ kJ/mol) as triplet sensitizers the reaction was promoted by a factor of 1.8 and 10, respectively. These results indicate that the photoamination proceeds through the triplet excited state of **1**. As the triplet levels of both benzil and fluorenone are lower than the $T_2(^3n\pi^*)$ of **1**, it is supposed that the photoreaction proceeds through the $T_1(^3CT)$ level.

Effect of the Triplet Quencher in Benzene. Cyclooctatetraene (COT) and anthracene did not affect the fluorescence intensity of **1**. Thus, they were expected to act as a triplet quencher but not as a singlet quencher. The Stern-Volmer plot was shown in Fig. 4 when COT ($E_T = 163$ kJ/mol) was used as a triplet quencher. A linear relationship between Φ_0/Φ and the concentration of COT was observed and its slope was 52 dm³/mol under nitrogen and 28 dm³/mol in aerated solution, respectively, that is, the lifetime of the excited state of **1**, quenched by COT, depended upon the presence of

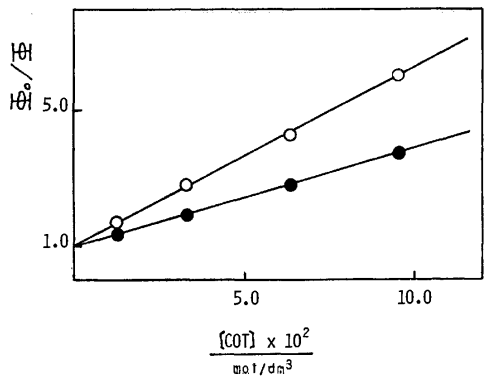

Fig. 4. Stern-Volmer plot for the quenching effect of cyclooctatetraene on the photoamination of **1** (1.00×10^{-4} mol/dm³) by butylamine (5.00×10^{-2} mol/dm³) in benzene by the irradiation of the light of $\lambda = 470$ nm.
○: Under nitrogen, ●: under air.

the dissolved oxygen, suggesting that the dissolved oxygen may interact with the same state as that quenched by COT. These results, in addition to the above sensitizing experiments, lead to the conclusion that the photoamination of **1** proceeded through the $T_1(^3CT)$ level of **1** which can be quenched by both the dissolved oxygen and COT.

In the presence of anthracene ($E_T = 176$ kJ/mol), the Stern-Volmer plot for the photoamination of **1** was also found to be linear (Fig. 5). A different result with COT was obtained. The slope of the Stern-Volmer plot was the same both under nitrogen and air, that is, the lifetime of the excited state of **1** quenched by anthracene was not affected by the presence of oxygen. This suggests that anthracene interacts in the quenching manner with the different excited state of **1** from the $T_1(^3CT)$ which is quenched by oxygen. It is been reported that the photoreduction of anthraquinone *via* the $^3n\pi^*$ level is efficiently quenched by anthracene.[7] Davies *et al.* reported the quenching of the $T_2(^3n\pi^*)$ level of 1-dimethylaminoanthraquinone by anthracene.[8] The quenching effect on the photoamination of **1** by anthracene in this study is understandable by

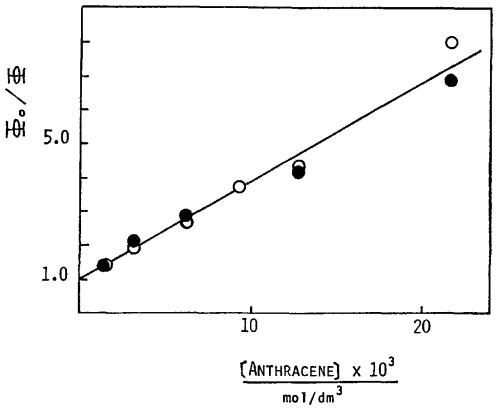

Fig. 5. Stern-Volmer plot for the quenching effect of anthracene on the photoamination of **1** (1.00×10^{-4} mol/dm³) by butylamine (5.00×10^{-2} mol/dm³) by the irradiation of the light of $\lambda = 470$ nm.
○: Under nitrogen, ●: under air.

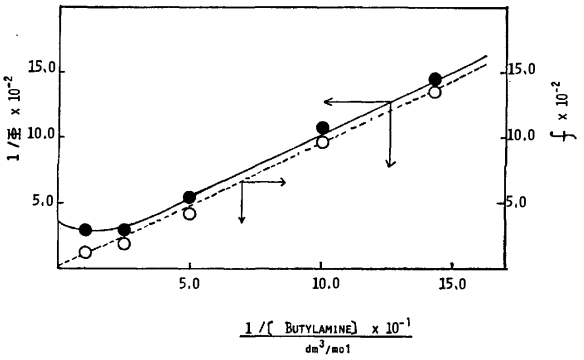

Fig. 6. Effect of the concentration of butylamine on the photoamination of **1** (1.00×10^{-4} mol/dm³) in benzene. -●-: $1/\Phi$ *vs.* 1/[Butylamine], -○-: f *vs.* 1/[Butylamine].

assuming that the $T_2(^3n\pi^*)$ level of **1** is quenched by anthracene. Thus, the $T_1(^3CT)$ level of **1** in benzene, which was quenched by COT (E_T=163 kJ/mol), but not by anthracene (E_T=176 kJ/mol), was supposed to lie in the range of 163—176 kJ/mol.

Effect of the Concentration of Butylamine in Benzene. The plot of the reciprocal of the quantum yield of the photoamination of **1** *versus* the reciprocal of the concentration of butylamine gave the curve as shown in Fig. 6. This curve may be explained by assuming that the amine molecule participates not only in the process leading to the aminated product **2**, but also in the quenching. Since anthraquinonesulfonic acids and aminoanthraquinones have been reported to be photoreduced *via* their $^3n\pi^*$ state by an electron transfer from amines or inorganic anions in polar solvents,[9,10] it may be possible that in non-polar benzene, butylamine as an electron donor interacts with **1** in the $T_2(^3n\pi^*)$ level in a quenching manner to the photoamination of **1** which proceeds through the $T_1(^3CT)$ level of **1**. If butylamine interacts with the $T_2(^3n\pi^*)$ level in a quenching manner to the photoamination, the lifetime of the $T_2(^3n\pi^*)$ level, τ_2, should be shortened by an increase in concentration of butylamine: the slope of the Stern-Volmer plot (Fig. 5) expressed as $k_q'\cdot\tau_2$, where k_q denotes the quenching rate constant of $T_2(^3n\pi^*)$ by anthracene and τ_2 the lifetime of $T_2(^3n\pi^*)$, should decrease with an increase in concentration of the amine. The slope of the Stern-Volmer plot in different concentration of the amine are listed in Table 2. It is seen that the slope of the Stern-Volmer plot,

TABLE 2. EFFECT OF THE CONCENTRATION OF BUTYLAMINE ON THE SLOPE OF THE STERN-VOLMER PLOT IN FIG. 5

$\frac{[\text{Butylamine}]\times10^2}{\text{mol/dm}^3}$	2.00	5.00	10.0
$\frac{\text{Slope } (k'_q\cdot\tau_2)}{\text{dm}^3/\text{mol}}$	380	290	210

$k_q'\cdot\tau_2$, decreased with an increase in concentration of the amine. Consequently, it may be concluded that butylamine interacts with **1** in the $T_2(^3n\pi^*)$ level in a quenching manner. The quenching effect by the amine may be explained by assuming an exciplex

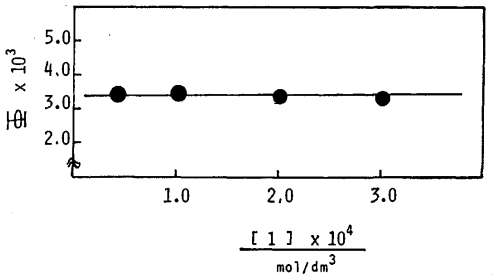

Fig. 7. Effect of the concentration of **1** on the photoamination of **1** by butylamine (5.00×10^{-2} mol/dm³) by the irradiation of the light of λ=470 nm.

formation such as $[AQ^{\delta-}\cdots Amine^{\delta+}]$ which whould not lead to the aminated product **2**, but be deactivated to the ground state of **1** and the amine in non-polar benzene.

Effect of the Concentration of 1 in Benzene. The quantum yield of the photoamination remained unchanged by the variation of the concentration of **1** (Fig. 7). This precludes the possibility that **1** participates in the photoamination as depicted below.

$$AQ^* + AQ \longrightarrow [AQ^{\oplus}\cdots AQ^{\ominus}]$$

$$[AQ^{\oplus}\cdots AQ^{\ominus}] \xrightarrow{\text{Amine}} \text{Amination}$$

$$[AQ^{\oplus}\cdots AQ^{\ominus}] \longrightarrow 2AQ$$

The Reaction Mechanism of the Photoamination of 1 in Benzene. On the basis of the above experimental results, the reaction scheme for the photoamination of **1** may be depicted as Fig. 8.

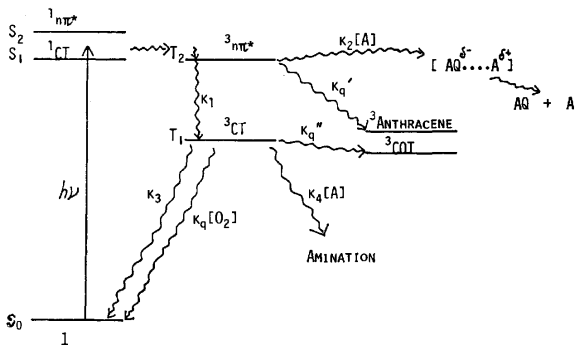

Fig. 8. Reaction scheme of the photoamination of **1** by butylamine in benzene.

The quantum yield for the production of **2** under nitrogen without a triplet quencher may be expressed by

$$\Phi = \Phi_{isc}\cdot\left(\frac{k_1}{k_1+k_2[A]}\right)\cdot\left(\frac{k_4[A]}{k_3+k_4[A]}\right)\cdot\alpha, \qquad (1)$$

where Φ_{isc} = the efficiency of the intersystem crossing of $S_1(^1CT) \rightsquigarrow T_2(^3n\pi^*)$,
k_i = the rate constant of each process indicated in Fig. 8,
A = butylamine,
and α = the yield of the aminated product **2** for every collision between the amine and **1** in its $T_1(^3CT)$ level.

The reciprocal of the quantum yield is thus expressed by

$$\frac{1}{\Phi} = \frac{1}{\Phi_{isc}\cdot\alpha}\cdot\left(1+\frac{k_2[A]}{k_1}\right)\cdot\left(1+\frac{k_3}{k_4[A]}\right). \quad (2)$$

Hence, a plot of the reciprocal of the quantum yield *versus* the reciprocal of the concentration of butylamine would be expected to show the result given in Fig. 6.

With dissolved oxygen present, the Stern-Volmer equation may be expressed by

$$\frac{\Phi_0}{\Phi} = 1 + \frac{k_q[O_2]}{k_3+k_4[A]}. \quad (3)$$

When COT was used as a triplet quencher,

$$\frac{\Phi_0}{\Phi} = 1 + \frac{k_q''[COT]}{k_3+k_4[A]+k_q[O_2]} \quad (4)$$

and in the case of anthracene,

$$\frac{\Phi_0}{\Phi} = 1 + \frac{k_q'[Anthracene]}{k_1+k_2[A]}. \quad (5)$$

A plot of Φ_0/Φ *versus* the concentration of each quencher used should give a linear relationship (Figs. 3, 4, and 5). Equation 4 indicates that the slope of the plot in Fig. 4 means to be $k_q''/(k_3+k_4[A]+k_q[O_2])$, which should be dependent upon the concentration of the dissolved oxygen as discussed before. The ratio between the slope of the plot (Fig. 4) for the results under nitrogen and air (52/28=1.9), corresponding to $1+k_q[O_2]_{air}/(k_3+k_4[A])$, agrees with the value of $\Phi_0/\Phi=1+k_q[O_2]_{air}/(k_3+k_4[A])=2.0$ obtained from Fig. 3 and Eq. 3 at the air saturated oxygen concentration. Equation 5 indicates that the slope of the plot, Φ_0/Φ *versus* [Anthracene] (Fig. 5), should be independent of the concentration of the dissolved oxygen.

By combining the values of the slopes of the lines represented by Figs. 3, 4, and 5 with Eqs. 3, 4, and 5, the following rate constants relationships were obtained;

$$\frac{k_q}{k_3+k_4[A]} = 513\ dm^3/mol, \quad (6)$$

where $[A]=5.00\times10^{-2}$ mol/dm^3,

$$\frac{k_q''}{k_3+k_4[A]} = 52\ dm^3/mol, \quad (7)$$

where $[A]=5.00\times10^{-2}$ mol/dm^3, and

$$\frac{k_q'}{k_1+k_2[A]} = 210, 290, \text{and } 380\ dm^3/mol, \quad (8)$$

where $[A]=1.00\times10^{-1}$, 5.00×10^{-2}, and 2.00×10^{-2} mol/dm^3, respectively.

Equation 8 gave the value of $k_1/k_q'=2.1\times10^{-3}$ mol/dm^3 and $k_2/k_q'=2.7\times10^{-2}$ mol/dm^3, respectively. Assuming that the quenching rate constant of $T_2(^3n\pi^*)$ by anthracene is $k_q'=1.6\times10^{10}$ dm^3/(mol·s) which is a diffusion controlled one, k_1 and k_2 may be calculated as $k_1=3.4\times10^7$ s^{-1} and $k_2=4.3\times10^8$ dm^3/(mol·s), respectively.

If Eq. 2 is rewritten using Eq. 9, the value of f calculated by using the k_1 and k_2 obtained above, with the reciprocal of the concentration of butylamine would be expected to exibit a linear relationship.

$$f = \frac{1}{\Phi}\left(\frac{k_1}{k_1+k_2[A]}\right) = \frac{1}{\Phi_{isc}\cdot\alpha}\cdot\left(1+\frac{k_3}{k_4[A]}\right) \quad (9)$$

A plot of f *versus* the reciprocal of the concentration of butylamine gave a linear relationship as indicated by the dotted line in Fig. 6. These results support the reaction scheme shown in Fig. 8. It may be seen from Eq. 9 that the ratio between the slope and the intercept in the plot of f *versus* the reciprocal of the concentration of the amine (Fig. 6) is equal to k_3/k_4. The value of k_3/k_4 was obtained as 0.50 mol/dm^3. Supposing the quenching rate constant of $T_1(^3CT)$ by oxygen k_q to be the diffusion controlled one (1.6×10^{10} dm^3/(mol·s)), k_3 and k_4 may be determined by substituting the value of k_3/k_4 into Eq. 6 as $k_3=2.8\times10^7$ s^{-1} and $k_4=5.7\times10^7$ dm^3/(mol·s), respectively. Moreover, the substitution of the value of k_3 and k_4 into Eq. 7 reveal the quenching rate constant of $T_1(^3CT)$ by COT, k_q'', to be 1.6×10^9 dm^3/(mol·s), which is one order of magunitude smaller than the diffusion controlled rate. It has been reported that the quenching rate by energy transfer drops very quickly from the diffusion controlled rate when the acceptor triplet level approaches that of the donor within 13—17 kJ/mol.[11] This may be valid in the case of $T_1(^3CT)$ (E_T=163—176 kJ/mol) of **1** as a donor level and COT (E_T=163 kJ/mol) as an acceptor. The rate constant in the reaction scheme of Fig. 8 determined by these kinetic analysis are tabulated in Table 3.

Table 3. Rate constants in the reaction scheme for the photoamination of **1** by butylamine in benzene[a]

k_1 / s^{-1}	k_2 / dm^3/(mol·s)	k_3 / s^{-1}	k_4 / dm^3/(mol·s)	k_q'' / dm^3/(mol·s)
3.4×10^7	4.3×10^8	2.8×10^7	5.7×10^7	1.6×10^9

a) They were determined on the assumption that k_q, $k_q'=1.6\times10^{10}$ dm^3/(mol·s) (diffusion controlled rate), respectively.

It is significant that these rate constants, especially the deactivation constant of the upper excited level $T_2(^3n\pi^*)$ can be determined kinetically, which is rarely possible in many cases because of the short lifetime of the upper excited level. The deactivation constant k_1 corresponding to the reciprocal of the lifetime of $T_2(^3n\pi^*)$ level was revealed to have a value of 3.4×10^7 s^{-1} comparable to that of the lowest excited triplet level $T_1(^3CT)$ ($k_3=2.8\times10^7$ s^{-1}). Davies *et al.* reported the photoreduction of 1-dimethylaminoanthraquinone by hydrogen abstraction *via* its upper excited level $T_2(^3n\pi^*)$ and pointed out that anthraquinone derivatives might have a lifetime long enough to photoreact in their upper excited $T_2(^3n\pi^*)$ level.[8] This has been demonstrated in this study. That the $T_2(^3n\pi^*)$ level of **1** has such a long lifetime of *ca.* 30 ns in contrast to those of T_2 of substituted anthracenes (*ca.* 0.3 ns) and naphthalene (*ca.* 10 ps) would be unusual. These values were kinetically determined by Liu *et al.*[12,13]

Previously it has been reported that in contrast to the aliphatic amines, aromatic amines appeared not to photoreact with sodium 1-amino-4-bromoanthraquinone-2-sulfonate **3** in polar medium. As stated above, in polar solvent the photoamination proceeds through the $S_1(^1CT)$ level interacting with the ground state oxygen along with the simultaneous production of the peroxide, probably derived from the superoxide ion O_2^-.[3] Consequently it was considered that the

aromatic amine was oxidized predominantly by the peroxide produced in the reaction system, resulting in the suppression of the photoamination in polar solvent. These considerations suggest that aromatic amines would be expected to photoreact with **1** in benzene, in which the photoamination proceeds without the aid of oxygen. In fact, in benzene under a nitrogen atmosphere effective photoamination of **1** with aromatic amine, aniline, was observed.

References

1) a) J. M. Bruce, *Quart. Rev.*, **21**, 405 (1967); b) D. Schulte-Frohlinde and C. V. Sonntag, *Zh. Phys. Chem.*, **44** 314 (1965); c) H. Inoue and M. Hida, *Yuki Gosei Kagaku Kyokai Shi*, **32**, 348 (1974).

2) a) H. Inoue, M. Hida, T. D. Tuong, and T. Murata, *J. Chem. Soc., Chem. Commum.*, **1971**, 1347.
b) H. Inoue, M. Hida T. D. Tuong, and T. Murata, *Bull. Chem. Soc. Jpn.*, **46**, 1759 (1973).

3) H. Inoue, K. Nakamura, S. Kato, and M. Hida, *Bull. Chem. Soc. Jpn.*, **48**, 2872 (1975).

4) C. G. Hatchard and C. A. Parker, *Proc. R. Soc. London, Ser. A*, **235**, 518 (1956).

5) Usually, it may be supposed that the fluorescence intensity of **1** should be weaker in ethanol than that in benzene because of a probable large deactivation through the hydrogen bond between **1** and ethanol as observed in the case of 2-piperidinoanthraquinone: A. K. Davies, G. A. Gee, J. F. Mckeller, and G. O. Phillips, *J. Chem. Soc., Perkin Trans. 2*, **1973**, 1742.

6) From the intersection of the absorption and the fluorescence spectra, the ^{1}CT level of 1-aminoanthraquinone in ethanol was also estimated to lie in 218 kJ/mol, which agreed very well with that (218 kJ/mol) determined in EPA matrix at 77 K: H. H. Dearman and A. Chan, *J. Chem. Phys.*, **44**, 416 (1966).

7) K. Tickle and F. Wilkinson, *Trans. Farady Soc.*, **61**, 1981 (1965).

8) A. K. Davies, R. Ford, J. F. McKeller, and G. O. Phillips, *J. Chem. Soc., Perkin Trans. 2*, **1972**, 923.

9) V. A. Kuzmin and A. K. Chibisov, *J. Chem. Soc., Chem. Commum.*, **1971**, 1559.

10) H. Inoue, K. Kawabe, N. Kitamura, and M. Hida, *Chem. Lett.*, **1977**, 987.

11) A. A. Lamola, "Energy Transfer and Organic Photochemistry," John Willey & Sons, Inc. (1969), p. 47.

12) R. S. H. Liu and J. R. Edman, *J. Am. Chem. Soc.*, **91**, 1492 (1969).

13) C. C. Ladwig and R. S. H. Liu, *J. Am. Chem. Soc.*, **98**, 8093 (1976).

The Effects of Solvents on the IR and PMR Spectra of Intramolecular OH···π and OH···O Hydrogen Bonded Systems[1)]

Shinichi UEJI

Institute of Chemistry, College of General Education, Kobe University, Tsurukabuto, Nada, Kobe 657

(Received October 7, 1977)

The effects of solvents on the intramolecular OH···π and OH···O hydrogen bonding in 2-arylphenols and 2,6-diarylphenols have been studied by examining the OH stretching IR absorption spectra in a range of solvents. The solvent shifts of the hydrogen bonded bands, νOH···π and νOH···O, followed the *G* correlation and the BHW plot. The success of both correlations suggests that the solvent shifts are primarily due to a specific solvent-solute association, even in relatively non-polar solvents. The solvent sensitivity of the OH···π and OH···O hydrogen bonded bands depended on the stereo-chemical environment around the hydrogen bonded system rather than on such electronic factors as the strength of the hydrogen bonding. On the basis of the relationship between the solvent sensitivity and the structural changes over a group of phenols, a simplified model for the solvent-solute association is put forward. Furthermore, this simplified model is also discussed in terms of the aromatic solvent-induced shifts in the PMR spectra.

Since the first observation of the solvent sensitivity of the hydrogen bonded OH frequency,[2)] considerable attention has been focused on the solvent effects on IR frequency shifts.[3–6)] However, the problem is not yet completely settled.

In the IR study of the solvent effects on the hydrogen bonded bands, Bellamy, Morgan, and Pace[3)] attributed the origin of solvent shifts to the specific association of solvents with the hydrogen bonded complex;

$$\text{S–H} \cdots \text{O–H} \cdots \text{B(Base)},$$

where S–H denotes the solvent molecule. Later, Yoshida and Ōsawa[4)] interpreted the solvent shifts in terms of the dipolar association model, in which the solvent is preferentially oriented with its bond dipole toward the lone pair dipole of the hydroxyl group in the hydrogen bonded system. Furthermore, they assumed that the dipolar association exists as the following geometry.[4a)]

$$\begin{array}{l} \overset{\delta-}{\text{O}}\text{H} \cdots \overset{\delta+}{\text{B}} \\ \vdots \\ \underset{\delta+}{\text{H}}\text{–}\underset{\delta-}{\text{S}} \end{array}$$

Most of the studies in this field have been concerned with the intermolecular hydrogen bonding. However, there has been little systematic study of the intramolecular hydrogen bonding, primarily because of the complexity of the factors affecting the solvent sensitivity. In case of the intramolecular hydrogen bonding, the solvent shifts can be expected to be affected by the geometric effects as well as the electronic effects if the specific solvent-solute association is an important factor in determining the solvent shifts.

In this paper, the effects of solvents on the intramolecular OH···π and OH···O hydrogen bonding in 2-arylphenols (**1**—**7**) and 2,6-diarylphenols (**8**—**13**) are investigated by means of IR spectroscopy, and the solvent-solute association model is discussed through the geometric effects on the solvent sensitivity.

^{1}H NMR spectroscopy is also a powerful method for the study of the geometry for the solvent-solute association model. The aromatic solvent-induced shifts in the PMR spectra of Compound (**8**) are nicely explained in terms of the model derived from the IR study.

2-arylphenols

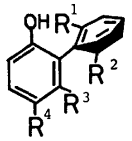

1 $R^1=R^2=R^3=R^4=H$
2 $R^1=R^2=R^4=H$, $R^3=CH_3$
3 $R^1=R^3=CH_3$, $R^2=R^4=H$
4 $R^1=OH$, $R^2=R^3=R^4=H$
5 $R^1=OH$, $R^2=R^3=CH_3$, $R^4=H$
6 $R^1=OCH_3$, $R^2=R^3=^4R=H$
7 $R^1=R^2=R^3=H$, $R^4=NO_2$

2,6-diarylphenol

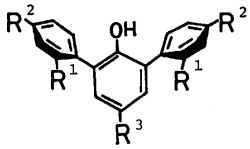

8 $R^1=R^2=R^3=H$
9 $R^1=CH_3$, $R^2=R^3=H$
10 $R^1=R^2=H$, $R^3=NO_2$
11 $R^1=CH_3$, $R^2=H$, $R^3=NO_2$
12 $R^1=H$, $R^2=CH_3$, $R^3=NO_2$
13 $R^1=H$, $R^2=C(CH_3)_3$, $R^3=NO_2$

Results and Discussion

IR Spectra. In nonpolar solvents such as CCl_4, 2-arylphenols (**1**, **2**, **3**, **5**, and **7**) show the doublet νOH absorptions, corresponding to the free and the intramolecularly OH···π hydrogen bonded hydroxyl groups, while 2,6-diarylphenols (**8**—**13**) have only a singlet νOH due to the intramolecular OH···π hydrogen bonding. In addition to the observed doublet, the other 2-arylphenols (**4** and **6**) exhibit a broad third band centered at about 3450 cm^{-1}, indicating the presence of intramolecular OH···O hydrogen bonding. These assignments are based on the reported IR spectra of similar compounds.[7,8)] Some typical νOH absorption spectra are reproduced in Fig. 1.

Table 1 summarizes the intramolecularly OH···π and OH···O hydrogen-bonded OH stretching frequencies in the same set of solvents, together with the solvent constants. The OH···π and OH···O frequencies in the

Table 1. Intramolecular OH···π and OH···O hydrogen bonded OH stretching frequencies (cm^{-1}) in the same set of solvents[a] and solvents constants

Solvent	Solvent constants G	$\Delta\nu/\nu$	1	2	3	4 OH···π	4 OH···O	5
(Vapor)	0	0	(3587)	(3580)	(3571)	(3569)	(3538)	(3553)
Hexane	44	7.0	3573.0	3566.6	3558.3	3558.4	—b)	3544.3
Cyclohexane	49	7.6	3570.2	3564.2	3557.5	3556.6	—b)	3543.9
Decalin	58	8.8	3566.6	3563.0	3555.7	3555.7	3483	3542.0
Tetrachloroethylene	64	9.4	3565.7	3560.2	3553.0	3554.8	3478	3541.1
Carbon tetrachloride	69	9.9	3564.8	3561.1	3553.9	3555.7	3474	3542.0
Benzene	80	11.1						
Dichloromethane	100	14.0	3554.8	3550.5	3542.7	3549.3	3440	3534.8
Bromoform	118	17.0	3547.5	3544.0	3539.4	3540.3	3429	3530.5

Solvent	6 OH···π	6 OH···O	7	8	9	10	11	12	13
(Vapor)	(3579)	(3499)	(3569)	(3573)	(3567)	(3554)	(3545)	(3547)	(3546)
Haxane	3566.6	3460	3551.1	3560.2	3554.8	3539.3	3532.0	3533.0	3533.0
Cyclohexane	3564.1	3456	3548.4	3558.5	3553.8	3536.6	3531.4	3531.4	3531.4
Decalin	3563.9	3450	3543.9	3555.5	3551.0	3533.9	3525.7	3527.5	3526.6
Tetrachloroethylene	3561.4	3442	3542.0	3555.7	3549.4	3531.1	3524.8	3525.0	3526.4
Carbon tetrachloride	3562.0	3441	3543.9	3555.7	3550.0	3532.0	3527.5	3527.5	3527.5
Benzene				3549.3	3544.1	3524.0	3518.6	3518.0	3516.7
Dichloromethane	3551.7	3409	3527.6	3543.8	3539.0	3519.7	3513.0	3512.8	3513.0
Bromoform	3545.5	3397	3520.9	3540.2	3535.7	3514.1	3511.0	3510.5	3511.0

a) The νOH frequencies differ slightly from the results for the same materials reported in a preliminary communication.[1] The data were obtained in separate experimental studies on different spectrometers. b) The apparent intensity was too weak to obtain a reliable value.

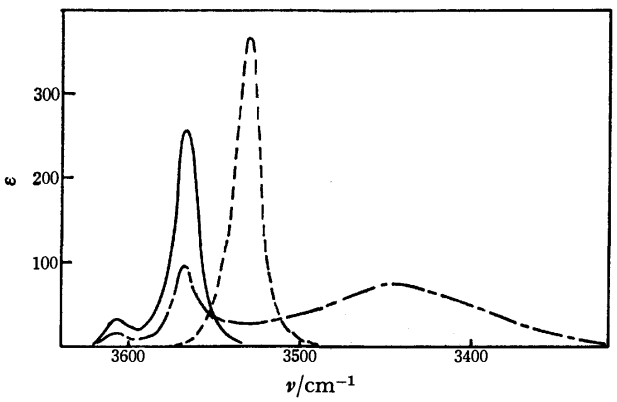

Fig. 1. νOH Absorptions of **1**, **6**, and **10** in CCl_4.
——(**1**), ——(**6**), ——(**10**).

vapor phase were estimated by interception at $G=0$ in the G correlations (see Fig. 2), according to the previously reported procedure.[2,4] The G value is the solvent constant empirically assigned to the solvent by Allerhand and Schleyer in order to explain the solvent sensitive IR bands.[2] The relative solvent shifts, $\Delta\nu/\nu$, of the νC=O of acetophenone are used as the reference value in the Bellamy-Hallam-Williams (BHW) plot.[9] The choice of solvents was limited to inert solvents which can not act as proton acceptors, because the proton acceptor solvents produce intermolecular hydrogen bonding.[10,11]

It is found from Table 1 that the frequencies of the hydrogen bonded bands, νOH···π and νOH···O, are fairly sensitive to the change of solvent. These solvent shifts correlate linearly with both the G and $\Delta\nu/\nu$ values. Figures 2 and 3 show the G correlation and the BHW plot respectively. The success of both correlations suggests that the operation of the solvation mechanism in the OH···π bonded system is similar to that in the

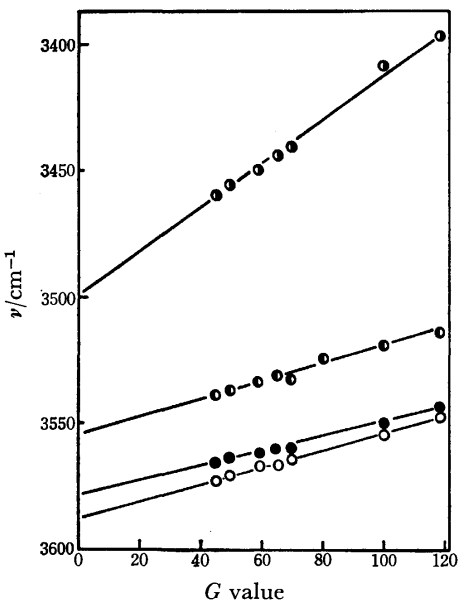

Fig. 2. Correlation of the OH stretching frequencies of OH···π and OH···O hydrogen bonds with the G values of the solvents.
1 (○), **6** (OH···π, ●; OH···O, ◑), **10** (◐).

TABLE 2. SOLVENT SENSITIVITY, IR SPECTRAL DATA, AND DIHEDRAL ANGLE OF THE OH···π AND OH···O HYDROGEN-BONDED SYSTEMS

		a	$1/S$	$\Delta\nu_{max}$/cm^{-1} [a]	A_i/A_f [b]	Dihedral angle (θ)/deg	K band λ_{max}/nm
2-Arylphenols							
1		0.33	0.69	42.2	6.7	50° [e]	245.5
2		0.30	0.64	47.5	11.2	60° [e]	245.5
3		0.27	0.56	54.5	16.4	70° [e]	240.0
4	OH···π	0.23	0.50	44.5	9.1		
	OH···O	0.94	2.00	126	—[c]		
5		0.19	0.40	62.7	42.0	70°—90°	Submerged
6	OH···π	0.28	0.60	42.8	7.8		
	OH···O	0.85	1.90	164	39.7		
7		0.40	0.87	47.3	9.6		
2,6-Diarylphenols				$\nu_{i\,max}$/cm^{-1} [d]	$A_i\times10^{-4}$ [f]		
8		0.28	0.61	3555.7	1.89	60°(52°) [g]	241.0
9		0.27	0.58	3550.0	2.01	70°	236.0
10		0.34	0.74	3532.0	2.60	(58°) [g]	
11		0.30	0.67	3527.5	2.85		
12		0.32	0.74	3527.5	2.73		
13		0.32	0.75	3527.5	3.04		

a) νOH(free)–νOH(OH···π or OH···O). b) Relative integrated intensities; A_i(OH···π or OH···O)/A_f(free). c) The A_i value could not be determined because of the very weak intensity. d) νOH···π. e) See Ref. 8. f) Integrated intensisies; A_i(OH···π)/mol^{-1} l cm^{-2}. g) Our X-ray results; see Ref. 20.

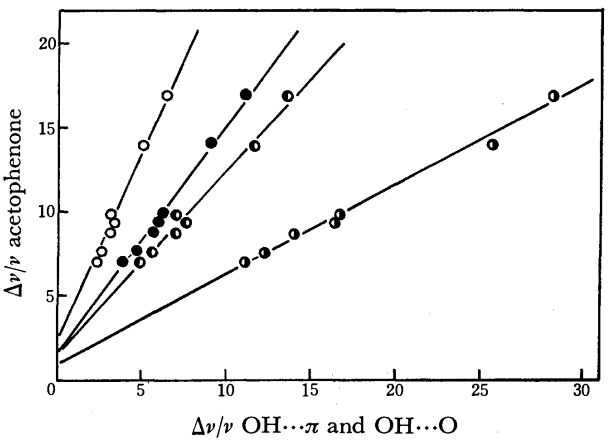

Fig. 3. BHW plots of νOH···π and νOH···O frequencies against the νC=O frequencies of acetophenone.
1 (●), **5** (○), **7** (◐), **6** (OH···O; ◑).

carbonyl group[12] and that the solvent shifts are mainly produced by a specific solvent-solute association rather than by general dielectric effects, because (1) Bellamy *et al.* showed that the solvent dependency of the νC=O frequency is primarily due to a specific solvent-solute association,[9] and (2) the G value does not fit the KBM, Pullin, and Buckingham equations based on the dielectric theory.[2]

As can be seen from Figs. 2 and 3, the slopes in both correlations vary widely from compound to compound. It is known that the slope of the G correlation (a)[2] and the reciprocal slope of the BHW plot ($1/S$)[13] become direct measures of the solvent sensitivity.

Table 2 lists the a and $1/S$ values, the IR spectral data, and the dihedral angle between the phenol ring and the proton acceptor ring. In the IR data, both A_i/A_f and $\Delta\nu_{max}$ can indicate the strength of the hydrogen bonding in 2-arylphenols.[14] With 2,6-diarylphenols without a free hydroxyl group, both A_i and $\nu_{i\,max}$ are adopted as a measure of the strength of the OH···π bonding.[15] The dihedral angle was roughly estimated from the K-band maxima of these compounds in heptane in the UV spectra, according to the established method.[8,16] From the data in Table 2, the strength of the OH···π hydrogen bonding is found to increase with the increase in the dihedral angle. This trend is consistent with those reported by Ōki and Iwamura,[8] who studied the steric effects on the OH···π hydrogen bonding in 2-arylphenols.

For the intermolecular hydrogen bonding, Yoshida *et al.*[4] reported the parallelism between the $1/S$ value and the strength of the hydrogen bonding. This fact is consistent with the dipolar association theory, in which the bond dipole of the solvent associates with the lone pair dipole of the hydrogen bonded system, because the lone pair dipole increases with the strength of the hydrogen bonding.

In case of the OH···π hydrogen bonding, the component of the dipole electric field is in the $\overset{\delta-}{\text{O}}\text{H}\overset{\delta+}{\leftarrow}\pi$ direction, because the charge-transfer plays an important role in this hydrogen bonded system.[17] Furthermore, the oxygen lone pair dipole on the OH group reinforces the component of the dipole due to the charge-transfer. Therefore, the dipolar association theory can also be applied to the intramolecular OH···π hydrogen bonding now being studied, as with the ordinary hydrogen bonding.

In contrast to Yoshida's result, it is clear from Table 2 that the proportional correlation between the solvent sensitivity and the strength of the OH···π bonding does not hold in this case; rather, both the a and $1/S$ values seem to be inversely proportional to the A_i, A_i/A_f, ν_i, and $\Delta\nu$ values. However, it seems that our

observation can be reconciled with Yoshida's dipolar association theory by considering the difference between inter- and intramolecular hydrogen bonded system.

For the intermolecular hydrogen bonding, such electronic effects as the strength of the hydrogen bonding are important factors in the dipolar association. On the other hand, for the intramolecular hydrogen bonding, the steric effects on the dipolar association seem to play a larger part than the electronic effects,[18] since the OH···π bonded system is fixed in the same molecule by the molecular geometry. Therefore, the lack of the correlation proposed by Yoshida *et al.* can be interpreted by assuming that the steric effects are so great that the electronic effects are masked.

By comparing the solvent sensitivity for the compound pairs of **1** and **7**, **8** and **10**, and **9** and **11**, it is noted that the nitrophenols (**7**, **10**, and **11**) show a and $1/S$ values larger than those for the corresponding phenols without the nitro group (**1**, **8**, and **9**) (see Table 2). The electron withdrawing nitro substituent produces a stronger OH···π hydrogen bonding, but does not greatly alter the stereochemical environment around the dipole of the OH···π bonded system. For these pairs of compounds, therefore, only the electronic effects can be operative in determining the solvent sensitivity. This result supports the dipolar association theory.

In order to investigate the steric effects on the dipolar association, both a and $1/S$ values are compared with the structural changes over a group of phenols. As can be seen from Table 2, both a and $1/S$ values appear to decrease with an increase in the dihedral angle; the observed order in the solvent sensitivity for the similar structural class is as follows; **7**>**1**>**2**>**3**, **4**>**5**, **8**>**9**, **10**>**11**, **10**≃**12**≃**13**. This suggests that the solvent sensi tivity is greatly affected by the steric factors, and supports the specific dipolar association mechanism in solvation to the OH···π bonded system.

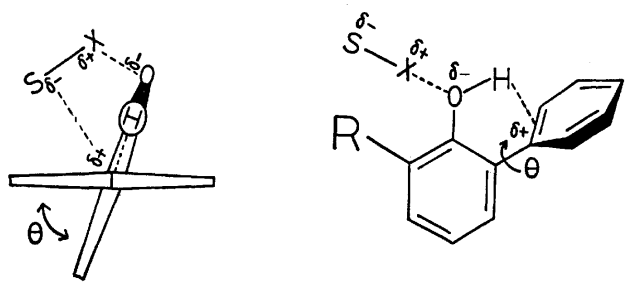

geometry (I) R=H or aryl. geometry (II)

Fig. 4. Schematic representation of the dipolar association between the bond dipole of the solvent and the dipole of the OH···π bonded system. S–X; solvent, θ; dihedral angle.

From the dihedral angular dependence of the solvent sensitivity, we propose a simplified model with the geometry (I) for the dipolar association between the dipole of the OH···π bonded system (involving the lone pair dipole) and the bond dipole of the solvent molecule, as is shown in Fig. 4. This model is based on a specific 1:1 solvent-solute interaction. The geometry (I) indicates that the approach of the bond dipole of the solvent to the dipole of the OH···π bonded system is made difficult by the larger dihedral angle, since the steric repulsion between the solvent molecule and the proton acceptor ring becomes more severe with an increase in the dihedral angle.

As another model, the geometry (II), in which the positive end of the dipole of the solvent associates with negative end of the dipole (the lone pair electrons) of the OH···π bonded system, is also shown in Fig. 4. In this model, however, there are no steric effects on the solvent-solute association, and so Yoshida's correlation should be held throughout all the phenols studied here. It seems that this model is significant only in a protic solvent[19] because of the formation of hydrogen bonding.

In the competitive intramolecular hydrogen bond formation between the OH···π and OH···O systems in **4** and **6**, the latter system shows a remarkably large solvent sensitivity. The OH···O hydrogen bonding in the biphenyl skeleton is possible only in either a planar or nearly planar conformation,[7b] while the OH···π hydrogen bonding is favored for the conformation in which the dihedral angle becomes larger.[8] For example, 2-arylphenol (**5**), with a nearly perpendicular conformation, shows no OH···O bonding, but a strong OH···π interaction (see Table 2). Furthermore, in general, the strength of the OH···O bonding is greater than that of the OH···π bonding (see Table 2). Therefore, the trend in the observed solvent sensitivity can be interpreted in terms of both electronic and dihedral angular effects, supporting the model with the geometry (I).

Another steric factor which can affect the solvent sensitivity is the presence of alkyl substituents in the proton acceptor ring. In addition to the dihedral angular effects, an *ortho* methyl group in the proton acceptor ring also hinders the bond dipole of the solvent from approaching the dipole of the OH···π bonded system, as is anticipated from the geometry (I). Furthermore, the introduction of the alkyl group to the *para* position of the proton acceptor ring (**12** and **13**) produces little variation in the solvent sensitivity (see Table 2). If the dipolar association exists in the geometry (II), the dipolar association will be made difficult by the presence of the *para* alkyl group, because the *para* alkyl group on the opposite side of the OH···π bond is expected to hinder the approach of the solvent molecule (the positive end of the dipole) to the lone pair electrons on the oxygen atom (the negative end of the dipole). Therefore, the absence of any effects of the *para* alkyl group on the solvent sensitivity agrees with the geometry (I), because the alkyl group at the *para* position is well removed from the site of the dipolar association.

PMR Spectra. The chemical shifts (δ) of the PMR spectra of 2,6-diphenylphenol (**8**) in CCl_4, in benzene-d_6, and hexafluorobenzene and the solvent shifts ($\Delta\delta=\delta_{CCl_4}-\delta_{C_6D_6 \text{ or } C_6F_6}$) are given in Table 3. For comparison, this Table also includes the IR frequency shifts in these solvents. Compound (**8**) with a single polar site was selected for this study, because the aromatic solvent-induced shifts (ASIS) become more complex for a compound with multiple polar sites.[21] The observed ASIS are due to the dipolar association of the aromatic solvent with the OH···π bonded system,

Table 3. Proton chemical shifts (δ) and OH stretching frequencies (νOH) in CCl_4, C_6D_6, and C_6F_6 and solvent shifts ($\Delta\delta$ and $\Delta\nu$OH) of 2,6-diphenylphenol

Proton chemical shifts (ppm)			
	OH proton		
	CCl_4	C_6D_6	C_6F_6
δ	5.12	5.15	5.36
$\Delta\delta$		−0.03	−0.24
	2,6-Ring protons[a]		
	CCl_4	C_6D_6	C_6F_6
δ	7.42	7.13	7.43
$\Delta\delta$		0.28	−0.01
OH stretching frequencies (cm^{-1})			
	CCl_4	C_6H_6	C_6F_6
νOH	3555.7	3549.3	3559.3
$\Delta\nu$OH		6.4	−3.6

a) Estimated from the δ value of the strongest peak.

not to the intermolecular OH···π bond formation,[22] since these IR shifts follow a common pattern obtained for other inert solvents studied here (see Figs. 2 and 3).

It is known[24] that the direction of the ASIS with C_6D_6 is opposed to that with C_6F_6. As may be seen in Table 3, however, both C_6D_6 and C_6F_6 produced more complex ASIS results. This seeming anomaly can be interpreted by assuming the asymmetric deformation of the geometry for the dipolar association caused by the steric requirement. In order to explain these ASIS results, the schematic representation of the dipolar association between the bond dipole of C_6D_6 and of C_6F_6 solvent molecules and the dipole of the OH···π bonded system is shown in Fig. 5; the direction of the bond dipole of the $\overset{\delta-}{C}\leftarrow\overset{\delta+}{D}$ bond in C_6D_6 shows a sign opposite to that of the $\overset{\delta+}{C}\rightarrow\overset{\delta-}{F}$ in C_6F_6.[24a]

In C_6D_6 solvent, a slight downfield shift for the OH proton and an upfield shift for the ring protons at the 2,6-positions of the phenol are observed. As is shown in model A, the π-electron cloud on the C_6D_6 molecule, which is attracted by the dipolar association, will be repelled by the π-electron cloud on the proton acceptor ring, thus increasing the angle, θ, between the dipole of the OH···π bonded system and the bond dipole of the overlying C_6D_6 solvent molecule. The large angle should cause a large remove of the OH proton from the center of the C_6D_6 molecule, so that the OH proton may be expected to lie near the edge of the aromatic shielding cone or the weak deshielding region of the C_6D_6 molecule. As another possible source of the ASIS effects, the charge polarization and variation in the bond order for the OH bond arising from a change in the solvent must be considered. On passing from CCl_4 to C_6H_6, the OH stretching frequency falls by 6.4 cm^{-1} (see Table 3). This electronic effect will cause the downfield ASIS of the OH proton. Thus, the slight deshielding of the OH proton in C_6D_6 can be explained in terms of the combination of the ring current and electronic effects. Furthermore, the upfield shifts for the ring protons must be considered in the same model. When the C_6D_6 solvent molecule approaches the proton acceptor ring (hereafter abbreviated as Ring I) with the positive end of the dipole, the other ring (hereafter Ring II) will be further removed from the same C_6D_6 solvent molecule. Therefore, the protons on Ring I will be strongly shielded, and those on Ring II, weakly deshielded. As the average ASIS effect, therefore, the upfield shift was observed in C_6D_6 solvent, supporting the model A.[25]

On the other hand, C_6F_6 gives a downfield shift in the OH proton and little variation in the ASIS of the ring protons. It is possible to expect the approach of the fluorine of the C_6F_6 periphery to the positive end of the dipole of the OH···π bonded system, since the van der Waals radius for fluorine (1.35 Å) is almost equal to that for hydrogen (1.2 Å). As is to be anticipated from the model B, the OH proton will be in the deshielding region of the C_6F_6 ring, in spite of the repulsion of the π-electron cloud on the C_6F_6 solvent molecule and the oxygen lone pair electrons. Accordingly, the OH proton should have a downfield shift, although the OH stretching frequency rises by 3.6 cm^{-1}. At the same time, this model shows that the protons on Ring I and II are in the deshielding and shielding region of the C_6F_6 solvent molecule respectively, since the C_6F_6 could be situated along the dipole of the OH···π bonded system. These ASIS, therefore, should cancel each other. In short, the direction of the ASIS can be nicely explained in terms of the model B.

Consequently, it is found that these ASIS results support the model derived from the IR study.

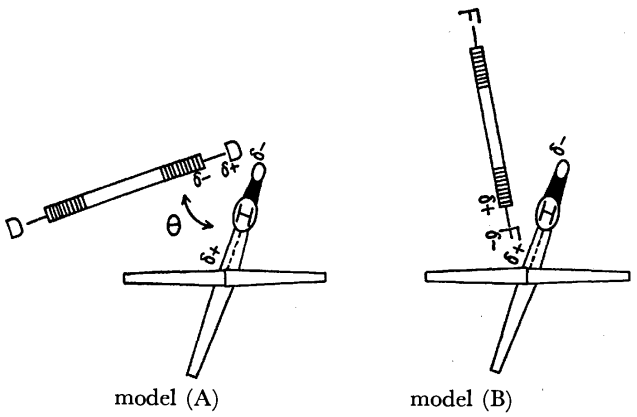

Fig. 5. Schematic representation of the dipolar association between the bond dipole of benzene and of hexafluorobenzene and the dipole of the OH···π bonded system.

Experimental

Measurement of the Spectra. The infrared spectra were recorded on a JASCO DS-701G grating spectrometer. The spectral slit width under high resolution conditions was 2 cm^{-1} in the region 3200—3700 cm^{-1}. Sodium chloride cells of 1 and 2 mm thicknesses were used. The concentration of phenols was about 5×10^{-3} M. The frequencies were calibrated by the standard absorption line of water vapor (3568.5 and 3447.2 cm^{-1}). The precision of the measure-

ments on νOH was about 2 cm^{-1} for the OH···π band and about 5 cm^{-1} for the broader OH···O band. All the measurements were carried out at 35 °C. Proton chemical shifts were measured on a JEOL PS-100 spectrometer operating at 100 MHz by using TMS as the internal standard at normal probe temperatures (*ca.* 35 °C). Frequency calibration was provided by the use of standard side-band techniques employing an audio-frequency counter. The measured relative chemical shifts are believed accurate to ±0.1 Hz. The ultraviolet absorption was obtained with a Hitachi 124 automatic recording spectrophtometer in 1.0 cm quartz cells at room temperature. The concentration of the samples in heptane was 10^{-5}—10^{-4} M.

Materials. Most of the solvents for spectra measurements were spectro-grade solvents and were used without further purification. Bromoform and decalin were purified by known methods.[27] Compound (**1**) was a commercial sample, recrystallized before use. Compounds (**2**),[8] (**3**),[8] (**4**),[28] (**5**),[29] (**6**),[28] (**7**),[7a] and (**12**)[30] were prepared according to the published procedures. Compounds (**8**)—(**11**) were prepared earlier.[10]

Preparation of ***13***. To a mixture of *t*-butyl chloride (4.3 g, 46.5 mmol) and **10** (2 g, 6.9 mmol) was added powered aluminium chloride (0.4 g, 3 mmol) at 40 °C. The mixture was then stirred for 5 h. A subsequent in the usual way gave a brown solid which was chromatographed on silica gel; elution with benzene–hexane (5: 1) afforded **13** (1.4 g, 52%). Recrystallization from benzene–hexane gave yellow plates; mp 162—164 °C. Found: C, 77.49; H, 7.29; N, 3.50%. Calcd for $C_{26}H_{29}O_3N$: C, 77.39; H, 7.24; N, 3.47%.

The author is indebted to Professor Emeritus Toshio Kinugasa of Kobe University for his valuable advice.

References

1) Part of this work was reported as a communication: S. Ueji and T. Kinugasa, *Tetrahedron Lett.*, **1976**, 2037.

2) A. Allerhand and P. von R. Schleyer, *J. Am. Chem. Soc.*, **85**, 371 (1963).

3) L. J. Bellamy, K. J. Morgan, and R. J. Pace, *Spectrochim. Acta, Part A*, **22**, 535 (1966).

4) a) Z. Yoshida and E. Ōsawa, *Nippon Koogyo Kagaku Zasshi*, **69**, 23 (1966); b) E. Ōsawa and Z. Yoshida, *Spectrochim. Acta, Part A*, **23**, 2029 (1967).

5) P. V. Huong and J. C. Lassegues, *Spectrochim. Acta, Part A*, **26**, 269 (1970).

6) L. J. Bellamy and R. J. Pace, *Spectrochim. Acta, Part A*, **27**, 705 (1971).

7) a) M. Ōki, H. Hosoya, and H. Iwamura, *Bull. Chem. Soc. Jpn.*, 34, 1391 (1961); M. Ōki and H. Iwamura, *ibid.*, **34**, 1395 (1961); b) W. F. Baitinger, Jr., P. von R. Schleyer, and K. Mislow, *J. Am. Chem. Soc.*, **87**, 3169 (1965); c) H. Musso and G. Sandrobk, *Ber.*, **97**, 2076 (1964).

8) M. Ōki and H. Iwamura, *J. Am. Chem. Soc.*, **89**, 576 (1967).

9) L. J. Bellamy and R. L. Williams, *Trans. Faraday Soc.*, **55**, 14 (1959). $\Delta\nu/\nu=[\nu(\text{vapor})-\nu(\text{solvent})]\times 10^3/\nu(\text{vapor})$.

10) S. Ueji, N. Ueda, and T. Kinugasa, *J. Chem. Soc., Perkin Trans. 2*, **1976**, 187.

11) T. Kinugasa, M. Nakamura, and S. Ueji, *J. Chem. Soc., Perkin Trans. 2*, **1976**, 1663.

12) The dipolar association mechanism in the carbonyl carbon system was found in the correlation between the *G* value and the ^{13}C chemical shift of the carbonyl carbon; S. Ueji and M. Nakamura, *Tetrahedron Lett.*, **1976**, 2549.

13) a) E. A. Cutmore and H. E. Hallam, *Trans. Faraday Soc.*, **58**, 40 (1962); b) H. E. Hallam and T. C. Tay, *ibid.*, **58**, 1299 (1962).

14) G. C. Pimental and A. L. McClellan, "The Hydrogen Bond," Freeman, San Francisco (1960), pp. 82—102.

15) For example, the $\nu_{1\,max}$ value was used as a measure of the strength of the OH···π bonding; H. Iwamura and K. Hanaya, *Bull. Chem. Soc. Jpn.*, **43**, 3901 (1970).

16) H. Suzuki, *Bull. Chem. Soc. Jpn.*, **32**, 1340, 1350, 1357 (1959); **33**, 109 (1960).

17) a) Z. Yoshida and N. Ishibe, *Bull. Chem. Soc. Jpn.*, **42**, 3254 (1969); b) M. Basila, R. L. Sailer, and L. R. Cousins, *J. Am. Chem. Soc.*, **87**, 1665 (1965).

18) According to the Keesom equation, the association energy, *E*, of a pair of dipoles in the vapor state is given by

$$E = -2/3\mu_1^2\cdot\mu_2^2/R^6\cdot k\cdot T$$

where μ_1 and μ_2 are the dipole moment of the dipole 1 and 2, *R* is the interdipolar distance, *k* is the Boltzman constant, and *T* is the absolute temperature; W. H. Keesom, *Z. Phys.*, **22**, 129 (1921). This equation means that the interdipolar distance greatly affects the dipolar association energy.

19) A similar model of the XH···O–H···OR_2 type was found in alcohol/ether complexes in proton donating solvents.[3,6]

20) a) K. Nakatsu, H. Yoshioka, K. Kunimoto, T. Kinugasa, and S. Ueji, *Acta Crystallogr., Sect. B*, in the press. b) K. Kinoshita, S. Nishigaki, H. Yoshioka, K. Nakatsu, T. Kinugasa, and S. Ueji, 36th National Meeting of the Chemical Society of Japan, Osaka, 1977.

21) The orientation of the aromatic solvent to alkyl and nitro groups attached to the aromatic ring was found in the literature; a) J. Ronayne and D. H. Williams, *J. Chem. Soc., B*, **1967**, 540; b) Y. Nomura and Y. Takeuchi, *Tetrahedron*, **25**, 3839 (1969).

22) Giles' refractive index measurement[23] for detecting intermolecular hydrogen-bonding pairs in solution shows no possibility of an intermolecular OH···π bond formation, presumably because the presence of the 2- and 6-phenyl groups of the phenol hinders the approach of the aromatic solvent to the OH group. The details of these refractometric results will be published elsewhere.

23) C. H. Giles and R. B. Mckay, *J. Biol. Chem.*, **237**, 3388 (1962). This method is a well-established, simple and sensitive one. (For example, see: Z. Yoshida, E. Ōsawa, and R. Oda, *J. Phys. Chem.*, **68**, 2895 (1964).)

24) a) R. D. Bertrand R. D. Compton, and J. G. Verkade, *J. Am. Chem. Soc.*, **92**, 2702 (1970); b) R. S. Amstrong, M. J. Aroney, R. K. Duffin, H. J. Srootman, and R. J. W. LeFevre, *J. Chem. Soc., Perkin Trans, 2*, **1973**, 1362; c) K. Nikki, N. Nakahata, and N. Nakagawa, *Tetrahedron Lett.*, **1975**, 3811.

25) This model seems to be consistent with the generally accepted model[21,26] in which the π-electron cloud on the C_6H_6 solvent molecule orients with the electron-deficient center on a solute molecule.

26) J. Ronaye and D. H. Williams, *Annu. Rev. NMR Spectrosc.*, **2**, 83 (1969).

27) A. Weissberger, ed, "Techniques of Chemistry," Vol 2; "Organic Solvents," 3rd ed, Wiley-Interscience, New York (1970).

28) H. Musso and H. G. Matthies, *Ber.*, **94**, 336 (1961).

29) H. Musso and W. Steckelberg, *Ann. Chem.*, **693**, 187 (1966).

30) H. B. Hill, *Am. Chem. J.*, **24**, 5 (1900).

The Reactions of 2-Arylacetylene-1-sulfonamides with Heterocumulenes

Kiyoshi HASEGAWA, Syuzi HIROOKA, Hiroshi KAWAHARA, Akihiko NAKAYAMA, Keiichi ISHIKAWA, Nobuyuki TAKEDA, and Hisakatsu MUKAI

Department of Industrial Chemistry, Faculty of Engineering, Toyama University, Takaoka-shi 933

(Received October 12, 1977)

The syntheses of new heterocyclic compounds by the reaction of 2-arylacetylene-1-sulfonamides **1**, (*Z*)-β-bromo- **12** or (*Z*)-α-chloro-β-styrenesulfonamides **13** with heterocumulenes are described. Weak base treatment of ureas $R^1C_6H_4C{\equiv}CSO_2NHC(=O)NHR^2$ prepared from **1** and isocyanates gave 2-amino-6-aryl-1,4,3-oxathiazine 4,4-dioxides, whereas strong base treatment of the ureas afforded 3-oxo-4,5-diphenyl-2,3-dihydro-1,2,4-thiadiazine 1,1-dioxides where R^2 is a phenyl group. The thiadiazines were also prepared by the strong base treatment of *N*-((*Z*)-α-bromo- or (*Z*)-β-chlorostyrylsulfonyl)-*N'*-phenylureas. The reaction of **1**, **12**, or **13** with isothiocyanates in the presence of weak base gave 3-amino-5-aryl-1,4,2-dithiazine 1,1-dioxides, but the major products produced were 3-amino-5-benzylidene-1,4,2-dithiazole 1,1-dioxides when **12a** was treated with isothiocyanates in the presence of strong base. The reaction of **1** with carbon disulfide and dimethyl sulfate in the presence of 5 M NaOH afforded 3-methylthio-5-benzylidene-1,4,2-dithiazole 1,1-dioxide with a small amount of 3-methylthio-5-aryl-1,4,2-dithiazine 1,1-dioxide. A mixture of both isomers was also prepared from **12a**. Possible mechanisms for the formation of the heterocycles from **1**, **12**, or **13** are suggested.

The syntheses of 5,6-dihydro-1,4,2-dithiazine 1,1-dioxide and 5,6-dihydro-1,2,4-thiadiazine 1,1-dioxide rings from β-styrenesulfonamides have been reported.[1-3] The synthesis of hitherto unknown 5,6-unsaturated heterocyclic systems is reported here. Since triple bonds are more susceptible to nucleophilic attack than double bonds,[4] reactions of 2-arylacetylene-1-sulfonamides **1**[5] with heterocumulenes such as isocyanate, isothiocyanate and carbon disulfide were investigated. This paper describes the syntheses of new 1,4,3-oxathiazine 4,4-dioxide, 2,3-dihydro-1,2,4-thiadiazine 1,1-dioxide, 1,4,2-dithiazine 1,1-dioxide and 1,4,2-dithiazole 1,1-dioxide derivatives. These heterocycles were also prepared from (*Z*)-β-bromo- **12**[5] and (*Z*)-α-chloro-β-styrenesulfonamides **13**.[5]

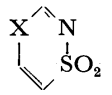

X=O, S

Results and Discussion

Reaction of the Sulfonamides with Isocyanates. A mixture of **1**, phenyl isocyanate **2** and K_2CO_3 in acetone was stirred for 30 min at 0—5 °C. Analytically pure potassium salts of *N*-(arylethynylsulfonyl)-*N'*-phenylureas **3** subsequently separated out. As the salts were immediately cyclized to 2-phenylamino-6-aryl-1,4,3-oxathiazine 4,4-dioxides **6** when dissolved in water,

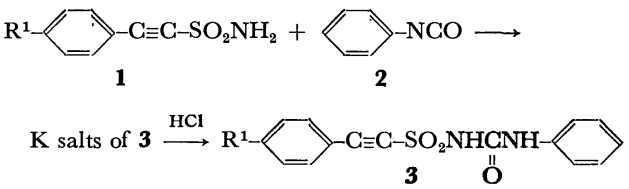

the sulfonylureas **3** were prepared by suspending the salts in aqueous 9 M HCl. All of the ureas **3** thus

TABLE 1. LIST OF THE UREAS **3**, **11**, **14**, AND **15**, AND THE THIOUREA **19**

Compd	R^1	R^2	Yield path(%)	Mp (°C)	Found %				Calcd %			
					C	H	N	S	C	H	N	S
3a	H		71	260—262	60.07	4.01	9.13		60.00	4.03	9.33	
3b	Cl		64	274—276	53.58	3.48	8.10	9.59	53.82	3.31	8.37	9.58
3c	Br		56	275—276	45.42	2.91	7.15	8.64	45.71	2.92	7.39	8.46
3d	CH_3		75	274—276	60.94	4.63	8.76		61.14	4.49	8.91	
11a	H	CH_3	D(85), E(84), F(80)	163—164	47.17	4.64	10.86	12.50	46.88	4.72	10.93	12.51
11b	H	C_2H_5	D(74), E(89)	154—156	49.13	5.26	10.16	11.61	48.89	5.22	10.37	11.86
11c	H	C_6H_{13}	E(51), F(80)	185—186	55.78	6.39	8.61		55.55	6.22	8.64	
11d	H	C_6H_5	D(43)	152—154	56.33	4.20	8.55		56.59	4.43	8.80	
14a	H	CH_3	87	206—207	37.86	3.55	8.75	10.12	37.63	3.45	8.78	10.05
14b	H	C_2H_5	90	216—217	39.90	3.71	8.26		39.65	3.93	8.41	
14c	H	C_6H_{13}	87	178—180	46.45	5.14	7.47	8.30	46.52	4.95	7.23	8.28
14d	H	C_6H_5	93	158—160	47.17	3.42	7.19	8.42	47.25	3.44	7.35	8.41
14e	Cl	C_6H_5	77	163—165	43.58	3.15	6.91		43.33	2.91	6.74	
15a	H	CH_3	86	208—209	43.76	4.00	10.14	11.65	43.72	4.04	10.20	11.67
15b	H	C_2H_5	59	176—178	45.60	4.69	9.56	11.18	45.75	4.54	9.70	11.10
15c	H	C_6H_{13}	89	189—190	52.81	5.30	8.11	9.07	52.55	5.59	8.17	9.35
15d	H	C_6H_5	94	166—168	53.76	3.98	8.28	9.51	53.49	3.89	8.32	9.52
19			72	108—113	41.58	4.05	9.90	21.93	41.30	3.82	9.64	22.05

obtained was analytically pure. Recrystallization was not attempted because of ready cyclization to **6**. The results are summarized in Table 1. The IR spectra of **3a**—**d** displayed absorption bands at 1670—1680 (C=O) and 2185—2195 (C≡C) cm^{-1}. The NMR and mass spectra were identical with those of **6a**—**d**.

1 reacted with alkyl isocyanates **4** to give only 2-alkylamino-6-aryl-1,4,3-oxathiazine 4,4-dioxides **7** as shown in Scheme 1.

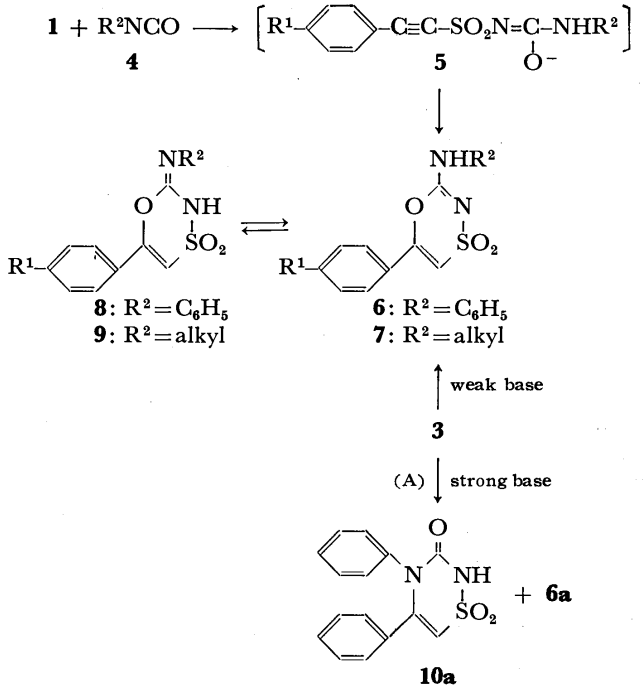

Scheme 1.

Treatment of **3a**—**d** with weak base (0.01—0.1 M K_2CO_3) gave a mixture of **6a**—**d** and their "imino" isomers **8a**—**c** (Table 2). Although "imino" isomers **9** were not isolated, the equilibrium between **7** and **9** (about 3: 1) in DMSO-d_6 was established by estimating the peak areas of the doublet due to NH**CH**$_3$ protons (δ=2.77, J=4.0 Hz) and the singlet due to NCH$_3$ protons (δ=2.76) in the NMR spectra of **7a**, **7d**, and **7e**.

Treatment of **3a** with strong base (1 M NaOH) at 45—50 °C for 4 h afforded a 96: 4 mixture of 3-oxo-4,5-diphenyl-2,3-dihydro-1,2,4-thiadiazine 1,1-dioxide **10a** and **6a**. **10a** was purified by fractional recrystallization (path A in Table 2). Aqueous 1 M NaOH has sufficient basicity to abstract a N'-proton from **3** and the resulting amide ion stabilized by a phenyl group seems to be responsible for the thiadiazine formation. The struc-

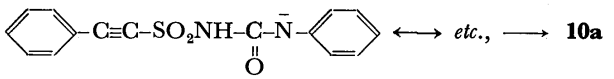

tures of **6**—**8** and **10a** were assigned on the basis of analytical and spectral data. The IR spectra of **6** and **7** showed C=N absorption bands adjacent to a SO_2 group at a lower frequency (1640 cm^{-1}) than those of **8** (1680 cm^{-1}). The IR spectrum of **10a** displayed absorption bands at 1680 (C=O) and 3080 (NH) cm^{-1}. These values are similar to the frequencies reported for 3-oxo-4-alkyl-5-aryl-2,3,5,6-tetrahydro-1,2,4-thiadiazine 1,1-dioxides.[3] The mass spectra of the oxathiazines **6**, **7** and **8** and **10a** showed fragment peaks assigned to $R^1C_6H_4CO^+$ and $C_6H_5CN^+C_6H_5$, respectively. The NMR spectra of **6**—**8** and **10a** displayed singlet CH signals in the region described in Table 2.

Strong base treatment of **6a** and **7a**—**b** gave N'-substituted N-(benzoylmethylsulfonyl)ureas **11** (path D in Table 1). A possible driving force for C–O fission is the abstraction of a vinyl proton on C_5 activated by an adjacent sulfonyl group.

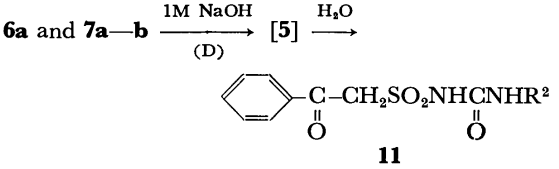

The thiadiazines **10** were also prepared from **14** (path B) or **15** (path C) under reaction conditions similar to those described in path A. **11** was prepared when R^2 groups in **14** and **15** are alkyls. The paths are illustrated in Scheme 2 and the results summarized in Tables 1 and

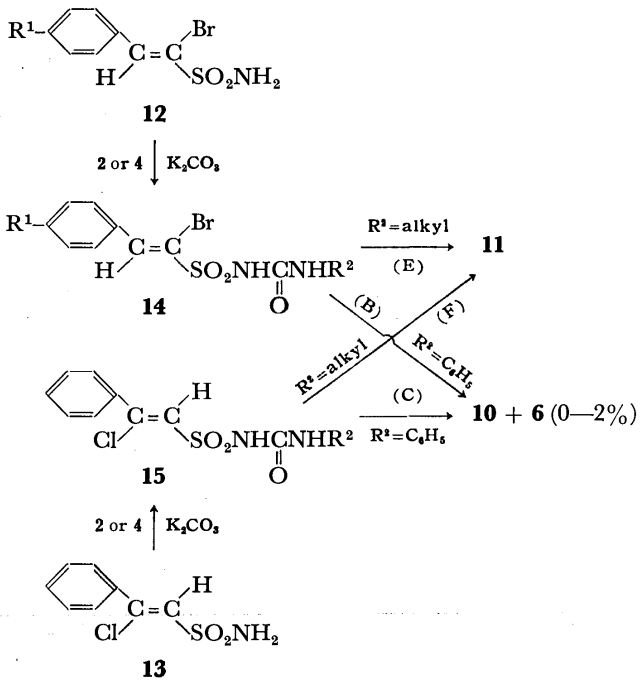

Scheme 2.

2. Two mechanisms for the formation of **10** are conceivable: (a) dehydrohalogenation followed by addition, or (b) addition followed by dehydrohalogenation. The mechanisms are similar to those suggested in the cyclization of N-(α-bromostyrylsulfonyl)amidines.[6] The reaction of **7a**, **14**, or **15** with 1 M NaOH proceeds slowly even at 10—20 °C, but attempts to detect and isolate the intermediates by IR and high-speed liquid chromatography were unsuccessful. At present it has not been established whether the reactions in paths B, C, E, and F involve the mechanism (a) or (b). N-(Styrylsulfonyl)-N'-alkyl(or phenyl)ureas[7] gave no cycloadducts as compared with ready cyclization of **3**, **14**, and **15**.

Table 2. List of heterocycles

Compd	R^1	R^2	Yield path (%)	Mp (°C)	δ_{CH} (ppm)	$\lambda_{max}^{C_2H_5OH}$ (ε_{max})	Found % (Calcd %) C	H	N	S
6a	H	C_6H_5	77	274—275	7.70	257 (18900)	60.14 (60.00	4.29 4.03	9.56 9.33	10.69 10.66)
6b	Cl	C_6H_5	73	279—280	a)	263 (17700)	53.57 (53.81	3.52 3.31	8.09 8.37	9.60 9.76)
6c	Br	C_6H_5	71	276—277	a)	258 (23800)	47.39 (47.50	2.90 2.92	7.26 7.39	8.68 8.46)
6d	CH_3	C_6H_5	90	277—278	7.62	262 (19700)	61.18 (61.14	4.60 4.49	8.66 8.91	10.17 10.18)
7a	H	CH_3	45[b]	230—231	7.56	260 (14800)	50.59 (50.42	4.07 4.23	11.61 11.76	13.28 13.46)
7b	H	C_2H_5	59[b]	203—204	7.60	260 (14000)	52.47 (52.38	4.52 4.80	11.19 11.11	12.68 12.71)
7c	H	C_6H_{13}	69[b]	211—213	7.60	266 (12600)	58.64 (58.81	6.05 5.92	8.88 9.15	9.65 10.47)
7d	Cl	CH_3	49[b]	238—239	7.64	266 (14800)	43.93 (44.13	3.36 3.33	10.14 10.30	11.32 11.76)
7e	Br	CH_3	55[b]	242—243	7.60	270 (16100)	38.03 (37.87	2.57 2.86	8.88 8.83	10.11 10.11)
8a	H	C_6H_5	9	169—170	c)	257 (19600)	59.80 (60.00	4.03 4.03	9.56 9.33)	
8b	Cl	C_6H_5	18	156—158	c)	262 (21500)	53.94 (53.81	3.37 3.31	8.17 8.37)	
8c	Br	C_6H_5	19	186—187	8.12	263 (22600)	47.33 (47.50	2.67 2.92	7.20 7.39)	
10a	H		A(40),[b] B(58)[b] C(55)[b]	188—190	6.85	247 (10900)	59.76 (60.00	4.19 4.03	9.14 9.33	10.67 10.66)
10b	Cl		B(56)[b]	198—200	6.82	247 (11700)	54.05 (53.81	3.28 3.31	8.15 8.36)	
10c	CH_3		B(53)[b]	202—204	c)	252 (11500)	61.18 (61.13	4.59 4.59	8.90 8.90)	
18a	H	CH_3	G(35)[b], H(34)[b], I(41)[b], M(66)[b]	188—190	7.55	244 (17500)	47.12 (47.25	3.71 3.97	11.18 11.02	25.08 25.20)
18b	H	C_2H_5	G(25)[b], I(40)[b], M(58)[b]	184—186	7.60	244 (18200)	49.51 (49.25	4.50 4.51	10.43 10.54	23.65 23.87)
18c	H	C_6H_5	G(35)[b], I(42)[b]	247—248	d)	274 (22300)	56.65 (56.94	3.74 3.82	8.64 8.86	20.03 20.23)
18d	Cl	CH_3	G(26)[b]	256—258	7.70	248 (18800)	41.81 (41.59	3.10 3.14	9.64 9.70	21.73 22.20)
18e	Br	CH_3	G(33)[b]	268—270	7.84	251 (18700)	36.19 (36.04	2.86 2.72	8.28 8.41	19.03 19.24)
18f	CH_3	CH_3	G(36)[b]	185—186	7.55	249 (16000)	49.38 (49.25	4.35 4.51	10.21 10.45	23.82 23.86)
21a	H	CH_3	J(58)[b]	210—212	7.62	296 (20900)	47.14 (47.25	4.15 3.97	10.82 11.02)	
21b	H	C_2H_5	J(63)[b]	174—175	7.63	296 (23200)	49.32 (49.25	4.52 4.51	10.15 10.54	23.58 23.87)
21c	H	C_6H_5	J(60)[b]	234—235	7.68	304 (32400)	56.73 (56.94	3.88 3.82	9.12 8.86	20.28 20.23)
24a[e]	H		42[b]	217—221	7.17		34.14 (34.27	3.22 3.20	4.20 4.44)	
25a	H		K(7[b], 9[f])	175—176	7.87	296 (22800)	44.04 (44.29	3.18 3.35	5.46 5.17	35.51 35.40)
25b	Cl		K(25[b], 31[f])	187—189	7.90	320 (21900)	39.00 (39.27	2.38 2.64	4.74 4.58	31.74 31.45)
25c	CH_3		K(13[b], 16[f])	149—151	7.80	322 (14800)	46.33 (46.29	3.91 3.89	4.94 4.91)	
26a	H		L(34)	162—163	7.83	252 (19000)	44.04 (44.29	3.18 3.35	5.46 5.17	35.51 35.40)
27	H		53	121—122	7.90	245 (9800)	41.74 (41.62	2.42 2.33	5.55 5.39)	

a) The NMR spectra could not be measured on account of the low solubility in usual solvent. b) Yield after recrystallization. c) The NMR spectra could not be measured on account of insufficient material. d) The CH proton is ambiguous because of overlapping with multiplet of phenyl protons. e) Dihydrate. f) Yield of a mixture of **25** and **26**, respectively.

Reaction of the Sulfonamides with Isothiocyanates. The reaction of **1**, isothiocyanates **16** and K_2CO_3 in acetone at 50—55 °C gave 3-alkylamino(or anilino)-5-aryl-1,4,2-dithiazine 1,1-dioxides **18**, which are the Michael cycloadducts of intermediate potassium salts of *N'*-substituted *N*-(arylethynylsulfonyl)thioureas **17** (path G). In contrast to the reaction of β-styrenesulfonamides

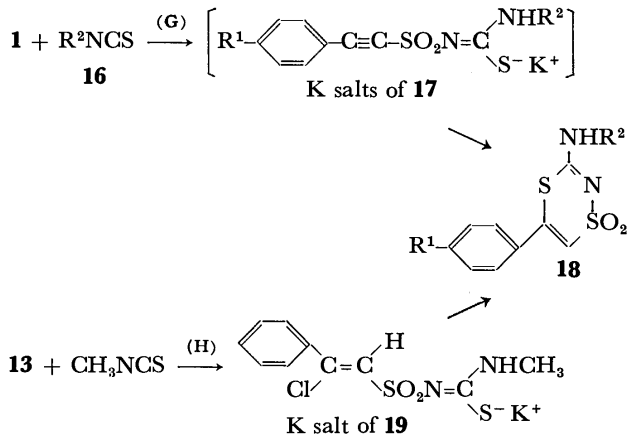

with **16**,[1] the potassium salts of **17** could not be isolated since they were soluble in warm acetone and their triple bonds were more susceptible to nucleophilic attack than their double bonds. Aqueous 5 M NaOH may be used in place of K_2CO_3.

The dithiazine **18a** ($R^2=CH_3$) was also prepared by the reaction of **13** with methyl isothiocyanate (path H) under conditions similar to those described for path G. The results are summarized in Table 2. The intermediate potassium salt of *N*-((*Z*)-β-chlorostyrylsulfonyl)-*N'*-methylthiourea **19** was isolated under ambient conditions (Table 1). The IR spectra of **18** showed typical C=N bands attached to a SO_2 group at 1570—1590 cm^{-1}. In the NMR spectra of **18**, a methine proton peak appeared as a singlet (Table 2). The mass spectra of **18** displayed fragment peaks assigned to $R^1C_6H_4CS^+$ and $R^1C_6H_4C(S)=CH^+$. The reaction of **12a** ($R^1=H$) with **16** in acetone in the presence of K_2CO_3 gave **18** along with small amounts of 3-alkylamino-5-benzylidene-1,4,2-dithiazole 1,1-dioxide **21** (path I in Table 2). The content ratios(%) of **18** were as follows: $R^2=CH_3$(96), C_2H_5(97), and C_6H_5(82).

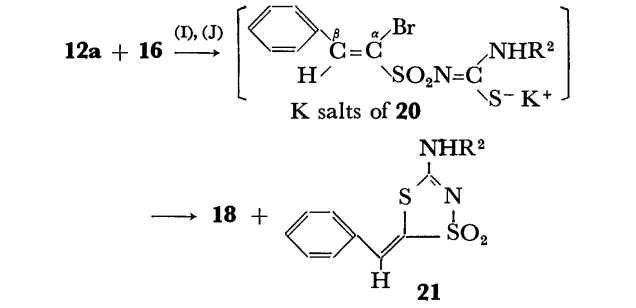

Potassium carbonate is not sufficiently basic to eliminate HX from **12**—**15**, thus the formation of **18** from **19** and **20** may proceed by the Michael addition followed by dehydrohalogenation. A similar reaction carried out in DMF in the presence of 10 M NaOH gave **21** along with small amount of **18** (path J). The content ratios(%) of **21** were as follows: $R^2=CH_3$(96), C_2H_5(97), and C_6H_5(96). The formation of **21** by path J may be explained in terms of S_N attack of a thiolate anion on the C_α atom, and this is favored under strongly basic conditions. **18** and **21** were purified by fractional recrystallization of the crude products of paths I and J, respectively. The structure of **21** was determined by means of the IR (1620 cm^{-1} for C=N), NMR (δ: *ca.* 7.65 for CH), UV and mass spectra, and also by elemental analysis (Table 2). All mass spectra of **21** displayed peaks due to $C_6H_5CH=CS^+$ but no peaks due to $C_6H_5CS^+$.

Reaction of the Sulfonamides with Carbon Disulfide. The reaction of **1** with CS_2 in the presence of 5 M NaOH at 0—3 °C and subsequent methylation yielded 3-methylthio-5-benzylidene-1,4,2-dithiazole 1,1-dioxide **25** in low yield together with a small amount of 3-methylthio-5-aryl-1,4,2-dithiazine 1,1-dioxide **26** (path K). Possible mechanisms for the formation of **25** and **26** are shown in Scheme 3. The content ratios of **25** and

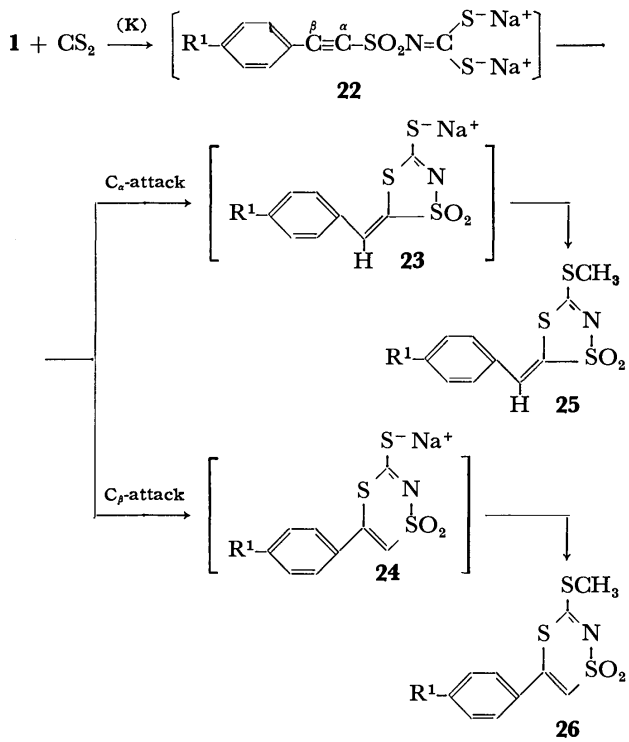

Scheme 3.

26 in the crude products were determined by evaluating the peak areas of the methyl protons and the results are as follows: R^1, yield % (ratio % of **25**)=H, 9(94), Cl, 31(92), and CH_3, 16(70). **25** was purified by fractional recrystallization of the crude products (Table 2), but **26** could not be purified.

The sulfonamide **12a** was reacted with CS_2 and dimethyl sulfate by a procedure similar to path K to give a 44: 56 mixture of **25a** and **26a** (91% yield). The mixture could not be separated into **25a** and **26a**, so intermediate **24a** was isolated and converted into **26a** by methylation (path L).

Chlorination of **26a** gave the 3-chloro derivative **27**

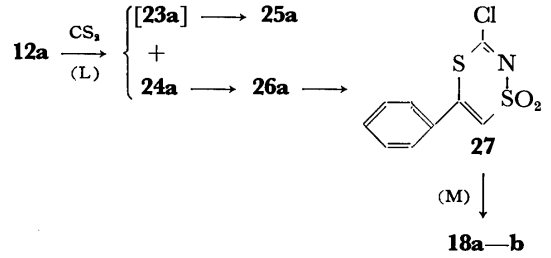

which was treated with amines to afford **18a** and **18b** (path M). The structure of **26a** was determined by the presence of $C_6H_5CS^+$ in the mass spectrum and also by the synthetic pathway **26a**→**18a**—**b**. The spectral data of **25a** differed from those of **26a** and **25a** displayed no peak due to $C_6H_5CS^+$.

3-Substituted 1,4,2-dithiazole 1,1-dioxide rings were previously prepared by the reaction of α-chloromethanesulfonamide with isothiocyanate or carbon disulfide.[9]

p-Substituent effect on the formation of **25** in path K was examined, but the results were not satisfactory as illustrated above (H≃Cl>CH_3). This may be due to low yield and formation of an unknown oily by-product. Further studies are required to clarify the mechanisms for paths K and L.

Experimental

The melting points were determined on a Yanagimoto micro melting-point measuring apparatus, MP-S2, and are uncorrected. The IR and UV spectra were recorded on a JASCO IRA-1 and Hitachi EPS-3T spectrometer, respectively. The NMR spectra were determined with a JEOL JNM-MH-100 spectrometer, with TMS as the internal standard and the mass spectra, with JEOL JNM-O1SG spectrometer. The high-speed liquid chromatographic (HLC) analysis was carried out using a JASCO FLC-150 apparatus equipped with a UV detector (254 nm) and a 0.5m×2.1 mm column packed with JASCO-DAC SV-02 (Solvent: methanol (20—50%)–water). Distribution of the isomers was determined by the results of NMR and HLC analyses. Spectral data are given only for a representative of each class.

N-(Arylethynylsulfonyl)-N'-phenylurea (3a). To a solution of **1a** (0.199 g, 0.0011 mol) in dry actone (3 ml) was added **2** (0.143 g, 0.0012 mol) and anhydrous K_2CO_3 (0.235 g, 0.0017 mol), and the mixture stirred for 30 min at 0—5° C. The resulting potassium salt of **3a** was filtered and suspended in aqueous 9 M HCl (5 ml). After standing for a night, the suspension was filtered to give 0.213 g (71%) of **3a** as analytically pure crystals: IR(KBr) 3340 (NH), 2180 (C≡C), 1620 (C=N), 1270 and 1140 (SO_2) cm^{-1}. *N,N'*-Diphenylurea (0.050 g) was obtained from the acetone filtrate, mp 238—239 °C (lit,[8] 235 °C).

2-Phenylamino-6-phenyl-1,4,3-oxathiazine 4,4-Dioxide (6a). When potassium salt of **3a** (0.102 g, 0.00030 mol) was dissolved in warm water (40—50 °C, 10 ml) or when **3a** (0.090 g, 0.00030 mol) was dissolved in warm aqueous 0.01—0.1 M K_2CO_3 (10 ml), **6a** began to separate out. After about 5 min, the reaction mixture was filtered to give 0.054 g (60%) of **6a**. The filtrate was acidified with conc HCl to afford 0.008 g (9%) of **8a**. Compound **6a** was recrystallized from CH_3OH and **8a** from CH_3OH–H_2O. When the reaction mixture was filtered after 12 h, 0.069 g (77%) of **6a** was obtained as shown in Table 2. **6a**: IR(KBr) 3260 (NH), 1640 (C=N), 1290 and 1160 (SO_2) cm^{-1}; NMR (DMSO-d_6) δ 7.20—7.70 (m, 10, $2C_6H_5$), 7.70 (s, 1, CH) and 7.96 ppm (broad, 1, NH); MS *m/e* 105 ($C_6H_5CO^+$), 118 (base peak, $C_6H_5C(O)=CH^+$), 236 (M^+-SO_2) and 300 (M^+). **8a**: IR (KBr) 3320 (NH), 1680 (C=N), 1330 and 1160 (SO_2) cm^{-1}. MS *m/e* 105 (base peak), 118, 236 and 300 (M^+). **8c** NMR (DMSO-d_6) δ 7.20—7.65 (m, 5, C_6H_5), 7.85—8.06 (dd, 4, C_6H_4), 8.10 (s, 1, CH) and 11.50 ppm (broad, 1, NH).

2-Methylamino-6-aryl-1,4,3-oxathiazine 4,4-Dioxides (7). To a solution of **1** (0.0010 mol) in acetone (4 ml) was added **4** (0.0011 mol) and anhydrous K_2CO_3 (0.0015 mol), and the solution stirred for 1 h at 20—25 °C. Oxathiazines **7a—c** were obtained by evaporation of the acetone filtrates, and **7d** and **7e**, which were almost insoluble in acetone, by filtration. **7e**: IR (KBr) 3300 (NH), 1650 (C=N), 1290 and 1130 (SO_2) cm^{-1}; NMR (DMSO-d_6) δ 2.76 (s, 0.7 H, $=NCH_3$), 2.77 (d, J_{NH-CH3}=4.0 Hz, 2.3H, CH_3), 7.60 (s, 1, CH), 7.72—7.78 (m, 4, C_6H_4), 8.40 (broad, 0.3H, SO_2NH) and 8.80 ppm (broad, 0.7H, NH); MS *m/e* 184±1 ($BrC_6H_4CO^+$), 197±1 (base peak, $BrC_6H_4C(O)=CH^+$), 253±1 (M^+-SO_2) and 317±1 (M^+).

3-Oxo-4,5-diphenyl-2,3-dihydro-1,2,4-thiadiazine 1,1-Dioxide (10a). *Path A*: A suspension of **3a** (0.060 g, 0.00020 mol) in aqueous 1M NaOH (2.0 ml, 0.0020 mol) was stirred at 45—50 °C for 4 h. The resulting clear solution was acidified with conc HCl to give 0.040 g of a 96: 4 mixture of **10a** and **6a**. Recrystallization of the crude mixture from benzene gave 0.024 g (40%) of **10a** and **6a** remained insoluble in warm benzene. **10a**: IR (KBr) 3080 (NH), 1680 (C=N), 1330 and 1160 (SO_2) cm^{-1}; NMR (DMSO-d_6) δ 6.85 (s, 1, CH), 7.12—7.30 (m, 10, $2C_6H_5$) and 8.60 ppm (broad, 1, NH), MS *m/e* 116, 145, 180 ($C_6H_5CN^+C_6H_5$), 193 (base peak, $C_6H_5C(NC_6H_5)=CH^+$), 236 (M^+-SO_2), 257 and 300 (M^+).

Path B: By using the way described in path A, 0.035 g (58%) of **10a** was obtained from **14d** (0.076 g, 0.00020 mol).

Path C: By using the way described in path A, 0.148 g (55%) of **10a** was obtained from **15d** (0.30 g, 0.00090 mol).

N-(Benzoylmethylsulfonyl)-N'-methylurea (11a). *Path D*: A solution of **7a** (0.238 g, 0.0010 mol) in aqueous 1M NaOH (10 ml, 0.0100 mol) was stirred at 50 °C for 4 h and acidified with conc HCl to give 0.217 g (85%) of **11a**. It was recrystallized from CH_3OH: IR (KBr) 3380 (NH), 1680 and 1660 (C=O), 1350 and 1160 (SO_2) cm^{-1}; NMR (DMSO-d_6)[10] δ 2.64 (d, J_{NH-CH3}=4.0 Hz, 3, CH_3), 5.20 (s, 2, CH_2), 6.35 (broad, 1, NH), 7.50—7.80 and 8.04—8.20 ppm (m, 5, C_6H_5), MS *m/e* 105 (base peak), 120, 131, 143, 174, 199, 225, and 238 (M^+-H_2O). The urea **11d** was obtained under the more drastic reaction conditions (20 equiv of 1M NaOH, 60—70 °C, 4h) because **6a** was almost insoluble in 10 equiv of 1M NaOH at 50 °C.

Path E: By using the way described in path D, 0.103 g (84%) of **11a** was obtained from **14a** (0.153 g, 0.00048 mol).

Path F: By using the way described in path D, 0.103 g (80%) of **11a** was obtained from **15a** (0.136 g, 0.00050 mol).

The ureas **11a** and **11d** were also prepared by stirring the acetone solution (3 ml) of benzoylmethanesulfonamide (0.0005 mol) with K_2CO_3 (0.00075 mol) and methyl and phenyl isocynate (0.00055 mol) for 2 h at 20—25 °C in 70 and 50% yields, respectively.

N-((Z)-α-Bromostyrylsulfonyl)-N'-methylurea (14a). To a solution of **12a** (0.40 g, 0.0015 mol) in dry acetone (4 ml) was added methyl isocynate (0.094 g, 0.00165 mol) and anhydrous K_2CO_3 (0.311 g, 0.00225 mol), and the mixture stirred for 2h at 55—60 °C. The resulting potassium salt was filtered and dissolved in water (20 ml). The solution was acidified with conc HCl to give 0.36 g (75%) of **14a**. An additional crop of **14a** (0.058 g, 12%) was obtained

from the acetone filtrate and recrystallized from CH_3OH: IR(KBr) 3360 (NH), 1660 (C=O), 1350 and 1160 (SO_2) cm^{-1}; NMR (DMSO-d_6)[10] δ 2.60 (d, J_{NH-CH3}=4.0Hz, 3, CH_3), 6.40 (broad, 1, NH), 7.48—7.60 and 7.80—7.96 (m, 5, C_6H_5) and 8.18 ppm (s, 1, CH); MS *m/e* 319±1 (M^+).

*N-((Z)-β-Chlorostyrylsulfonyl)-N'-methylurea (**15a**).* By using the way described in the synthesis of **14a**, 0.236 g (86%) of **15a** was obtained from the acetone filtrate of the reaction mixture of **13** (0.218 g, 0.0010 mol), methyl isocyanate (0.063 g, 0.0011 mol) and anhydrous K_2CO_3 (0.207 g, 0.0015 mol), and was recrystallized from CH_3OH–H_2O: IR (KBr) 3340 (NH), 1650 (C=O), 1340, 1175 and 1150 (SO_2) cm^{-1}; NMR (DMSO-d_6) δ 2.65 (d, J_{NH-CH3}=4.0 Hz, 3, CH_3), 3.90 (broad, 1, NH), 6.35 (broad, 1, SO_2NH), 7.30 (s, 1. CH) and 7.45—7.60 ppm (m, 5, C_6H_5); MS *m/e* 274±1 (M^+).

*3-Methylamino-5-phenyl-1,4,2-dithiazine 1,1-Dioxide (**18a**).* *path G*: To a solution of **1a** (3.0 g, 0.0165 mol) in acetone (23 ml) was added methyl isothiocyanate (1.33 g, 0.0182 mol) and anhydrous K_2CO_3 (3.42 g, 0.025 mol), and the mixture stirred for 3 h at 50—55 °C. The solution was filtered and the filtrate concentrated to dryness *in vacuo* to leave viscous oil. It was recrystallized three times from CH_3OH to give 1.47 g (35%) of **18a**: IR (KBr) 3240 (NH), 1590 and 1570 (C=N), 1280 and 1120 (SO_2) cm^{-1}; NMR (DMSO-d_6) δ 2.90 (s, 3, CH_3), 7.55 (s, 1, CH), 7.60 (s, 5, C_6H_5) and 9.50 ppm (broad, 1, NH): MS *m/e* 102, 121 ($C_6H_5CS^+$), 134 (base peak, $C_6H_5C(S)=CH^+$), 162, 190 (M^+–SO_2), and 254 (M^+).

Path H: By using the way described in path G, 0.085 g (34%) of **18a** was obtained from **13** (0.218 g, 0.0010 mol), methyl isothiocyanate (0.080 g, 0.0011 mol) and anhydrous K_2CO_3 (0.207 g, 0.0015 mol).

Path I: By using the way described in path G, 0.104 g (41%) of **18a** was obtained from **12a** (0.262 g, 0.0010 mol), methyl isothiocyanate (0.080 g, 0.0011 mol) and anhydrous K_2CO_3 (0.207 g, 0.0015 mol).

Path M: To a suspension of **27** (0.052 g, 0.00020 mol) in methanol (5 ml) was added 30% aqueous methylamine (0.21 g, 0.0020 mol), and the mixture stirred for 1 h at 50—55 °C. The clear solution was concentrated to dryness *in vacuo* to leave viscous oil. Water (2 ml) was added and the cooled precipitate was filtered to give 0.034 g (66%) of **18a**.

*3-Methylamino-5-benzylidene-1,4,2-dithiazole 1,1-Dioxide (**21a**).* *Path J*: To a solution of **12a** (0.262 g, 0.0010 mol) in DMF (2 ml) was added methyl isothiocyanate (0.080 g, 0.0011 mol) and aqueous 10 M NaOH (0.20 ml, 0.0020 mol), and the mixture stirred for 4h at 55—60 °C. Water (7 ml) was added to the solution and cooled precipitate filtered to afford 0.185 g of a 96: 4 mixture of **21a** and **18a**. It was recrystallized from CH_3OH to give 0.147 g (58%) of **21a**: IR (KBr) 3200 (NH), 1620 (C=N), 1290 and 1160 (SO_2) cm^{-1}; NMR (DMSO-d_6) δ 3.00 (s, 3, CH_3), 7.50 (s, 5, C_6H_5), 7.62 (s, 1, CH) and 9.50 ppm (broad, 1, NH); MS *m/e* 102, 108, 134 (base peak, $C_6H_5CH=CS^+$), 190 (M^+–SO_2) and 254 (M^+).

*3-Methylthio-5-benzylidene-1,4,2-dithiazole 1,1-Dioxide (**25a**).* *Path K*: To a solution of **1a** (0.72 g, 0.0040 mol) in DMF (4 ml) was added aqueous 5 M NaOH (1.60 ml, 0.0080 mol) and CS_2 (0.61 g, 0.0080 mol), and the mixture was stirred for 2 h at 0—3 °C. Dimethyl sulfate (0.55 g, 0.0044 mol) was then added to the red solution and the mixture stirred for 2 h at 0—3 °C. The resulting precipitate was filtered and washed with methanol to give 0.097 g (9%) of a 94: 6 mixture of **25a** and **26a**. It was recrystallized from CH_3OH to afford 0.078 g (7%) of **25a** as colorless columns: IR(KBr) 1510 (C=N), 1330 and 1160 (SO_2) 995, 960, 825 and 750 cm^{-1}; NMR (DMSO-d_6) δ 2.81 (s, 3, CH_3), 7.50—7.60 (m, 5, C_6H_5) and 7.87 ppm (s, 1, CH); MS *m/e* 102, 108, 134 (base peak, $C_6H_5CH=CS^+$), 207 (M^+–SO_2) and 271 (M^+).

*3-Methylthio-5-phenyl-1,4,2-dithiazine 1,1-Dioxide (**26a**).* *Path L*: To a solution of **12a** (1.00 g, 0.0038 mol) in DMF (8 ml) was added aqueous 10 M NaOH (0.76 ml, 0.0076 mol) and CS_2 (0.58 g, 0.0076 mol), and the mixture stirred for 2h at 15—20 °C. Evaporation of DMF *in vacuo* left a residue, which was recrystallized twice from aqueous 1M NaOH to give 0.50 g (42%) of **24a** as dihydrate: IR (KBr) 3550—3400 ($2H_2O$), 1350 and 1130 (SO_2) cm^{-1}; NMR (DMSO-d_6) δ 3.26 ($2H_2O$), 7.17 (s, 1, CH) and 7.54—7.58 ppm (m, 5, C_6H_5).

To a solution of **24a** (0.63 g, 0.0020 mol) in 2: 1 (v/v) CH_3OH–H_2O (10 ml) was added dimethyl sulfate (0.28 g, 0.0022 mol), and the mixture was stirred for 2h at 15—20 °C. The precipitate was filtered to give 0.43 g (80%) of **26a**. It was recrystallized from CH_3OH to give colorless needles: IR (KBr) 1510 (C=N), 1330 and 1150 (SO_2), 940 and 750 cm^{-1}; NMR (DMSO-d_6) δ 2.71 (s, 3, CH_3), 7.55–7.60 (m, 5, C_6H_5) and 7.83 (s, 1, CH); MS *m/e* 102 ,108, 121 ($C_6H_5CS^+$), 134 (base peak, $C_6H_5C(S)=CH^+$), 174, 198, 207 (M^+–SO_2) and 271 (M^+).

*3-Chloro-5-phenyl-1,4,2-dithiazine 1,1-Dioxide (**27**).* Excess chlorine was bubbled through a solution of **26a** (0.65 g, 0.0024 mol) in chloroform (10 ml) at 20—30 °C. The orange solution was concentrated to dryness *in vacuo* and the residue suspended in CCl_4 (5 ml). The mixture was filtered to give 0.33 g (53%) of **27** and recrystallized from CCl_4: IR (KBr) 1570 (C=N), 1330 and 1160 (SO_2) cm^{-1}; NMR (DMSO-d_6) δ 7.45—7.65 (m, 5, C_6H_5) and 7.90 ppm (s, 1, CH); MS *m/e* 102, 108, 121 ($C_6H_5CS^+$), 134 (base peak, $C_6H_5C(S)=CH^+$), 195 (M^+–SO_2) and 258 (M^+).

References

1) K. Hasegawa and S. Hirooka, *Bull. Chem. Soc. Jpn.*, **45**, 525 (1972).

2) K. Hasegawa and S. Hirooka, *Bull. Chem. Soc. Jpn.*, **45**, 1567 (1972).

3) K. Hasegawa and S. Hirooka, *Bull. Chem. Soc. Jpn.*, **45**, 1893 (1972).

4) J. March, "Advanced Organic Chemistry, Reactions, Mechanisms, and structure," McGraw-Hill, Tokyo (1968), p. 575.

5) K. Hasegawa, S. Hirooka, H. Kawahara, A. Tanaka, M. Nomura, and Y. Hori, *Bull. Chem. Soc. Jpn.*, **50**, 2346 (1977).

6) W. L. Matier, W. T. Comer, and A. W. Gomoll, *J. Med. Chem.*, **17**, 549 (1974).

7) K. Hasegawa and S. Hirooka, *Nippon Kagaku Kaishi*, **1972**, 1098.

8) T. L. Davis and K. C. Branchard, *Org. Synth.*, Coll. Vol. I, 453 (1956).

9) K. Dickore, R. Wegler, and K. Sasse, *Chem. Abstr.*, **68**, 105211b (1968). U. S. 3345374.

10) One of the two NH proton signals was not observed.

Photochemical Reactions of Aromatic Compunds. XXXI.[1] Exciplex Quenching by Pyridine, Methylated Pyridines, and Methylated Imidazoles and Termolecular Interaction in the Excited Singlet State

Tetsuro MAJIMA, Chyongjin PAC,* and Hiroshi SAKURAI

The Institute of Scientific and Industrial Research, Osaka University, Suita, Osaka 565

(Received October 24, 1977)

Pyridine, methylated pyridines, and methylated imidazoles quenched the exciplexes of aromatic nitrile–2,5-dimethylfuran or 2,5-dimethyl-2,4-hexadiene, and the rate constants for the exciplex quenching were obtained. The exciplex quenching by 2-methyl- and 2,6-dimethylpyridines was much less efficient than that by the other quenchers. The exciplex quenching was discussed in terms of the interaction of the n-orbital of the quenchers with the positive charge developed on the electron-donor side of the exciplexes. Curved Stern-Volmer plots were obtained in the quenching of aromatic nitrile fluorescence by 1-methylimidazole and/or 1,2-dimethylimidazole. On the basis of the kinetic results, the mechanism was discussed in terms of a termolecular interaction between excited singlet aromatic nitrile, the methylated imidazole as the π-donor, and the second one as the n-donor.

Exciplex formation has been recognized to be a general mechanistic pathway in fluorescence quenching[2,3] and has been suggested to precede photocycloadditions in a variety of reaction system.[4–6] We have also extensively investigated photocycloadditions of furan and olefinic compounds to aromatic nitriles, which have been suggested to occur *via* exciplexes.[7] In some exciplex-formation systems, the increase in the concentration of a precursor results in the formation of a termolecular excited complex (triplex), which arises from the interaction of a precursor with an exciplex.[8,9] This type of termolecular interaction can be considered to be rather general and has been suggested to be important in some photoreactions.[10] Caldwell and his co-workers reported a different type of termolecular interaction in the excited singlet state which occurs by means of the interaction of exciplexes with compounds which are not the precursors of the exciplexes and which possess either an electron-donor or an electron-acceptor nature.[11] In a previous paper,[12] we reported that pyridine quenches exciplexes which emit very weakly or which are not emissive at all. The exciplex quenching by pyridine provides a convenient method for establishing the existence of the exciplex intermediacy in our reaction systems. In the exciplex quenching, however, pyridine can act as either an n-donor or a π-acceptor, since it is weakly basic as well as π-deficient. In the present paper, we wish to report that pyridine, methylated pyridines, and methylated imidazoles quench the exciplexes of aromatic nitrile–2,5-dimethylfuran or 2,5-dimethyl-2,4-hexadiene by acting as n-donors, and that 1-methyl- and 1,2-dimethylimidazoles quench the fluorescence of aromatic nitriles by way of a termolecular process.

Results

Characteristics of Exciplexes. For exciplex-quenching experiments, we employed the exciplexes of 1- and 2-naphthonitriles (1- and 2-NN)–2,5-dimethylfuran (DF) and 9-cyanophenanthrene (9-CP)–2,5-dimethyl-2,4-hexadiene (DHD), since these exciplexes can be considered to be typical models of the supposed intermediates in our reaction systems and all are fairly emissive. Table 1 lists the lifetimes of the exciplexes in a benzene solution containing 0.3 mol dm^{-3} in DF or DHD, the exciplex emission maxima in benzene and ethyl acetate solutions containing 0.3 mol dm^{-3} in DF or DHD, the calculated dipole moments, and the apparent rate constants ($\gamma_0 k_e$) of the quenching of the aromatic nitrile fluorescence by DF or DHD.

Table 1. Characteristics of exciplexes

		Exciplex		
		1-NN–DF	2-NN–DF	9-CP–DHD
λ_{max}[a] (nm)	C_6H_6	435	413	440
	AcOEt	445	435	460
τ_{EX}[b] (ns)		32[c] (15)	28[c] (14)	21[d] (12)
Dipole moment[e] (D)		≈10	≈10	≈10
$\gamma_0 k_e$[f] (dm^3 mol^{-1} s^{-1}) $\times 10^{-9}$		8.1	2.6	8.1

a) Emission maxima of the exciplexes; 5×10^{-4} mol dm^{-3} in aromatic nitrile and 0.3 mol dm^{-3} in DF or DHD; ±2 nm. b) Lifetimes in degassed benzene; the numbers in parentheses are the lifetimes in air-saturated benzene; ±0.5 ns. c) Oxygen-quenching method. d) Determined by an N_2 laser-flash method. e) Calculated from the solvent shifts of the emission maxima. f) Apparent rate constants for the quenching of the aromatic nitrile fluorescence by DF or DHD.

The lifetime of the 9-CP–DHD exciplex was directly determined by monitoring the decay of the exciplex fluorescence at 440 nm using an N_2 laser. When the decay of the residual 9-CP fluorescence was monitored at 375 nm, two decays were observed; the lifetimes of the slow and rapid decay components were calculated to be 17 ns and less than 2 ns respectively. The slow-decay component apparently arises from the reversible dissociation of the exciplex into an excited singlet 9-CP and a ground-state DHD. However, the reversible dissociation can be considered to be not so significant, since the quenching of the 9-CP fluorescence by DHD occured at a diffusion-controlled rate. The lifetimes of

* To whom all correspondence should be addressed.

the 1-NN– and 2-NN–DF exciplexes were determined by the oxygen-quenching method proposed by Caldwell.[13]

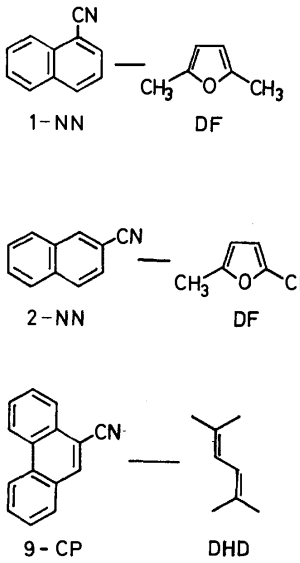

These exciplexes are charge-transfer complexes in nature, as is shown by the dipole moment, which was obtained by a usual method using plots of the wave numbers of the emission maxima in various solvents *vs.* $[(\varepsilon-1)/(2\varepsilon-1)-(n^2-1)/2(2n^2-1)]$,[14] where ε and n represent the dielectric constant and the refractive index of the solvent respectively. The slopes of the plots are commonly $(10\pm1)\times10^3$ cm^{-1}, which corresponds to *ca.* 10 Debey units of the dipole moment. The 9-CP–DHD exciplex crosses over a $2\pi+2\pi$ cycloadduct,[7f] while the 1- and 2-NN–DF exciplexes do not result in the formation of any stable products at room temperature. The UV spectra showed no indication of the formation of charge-transfer complexes in the ground state.

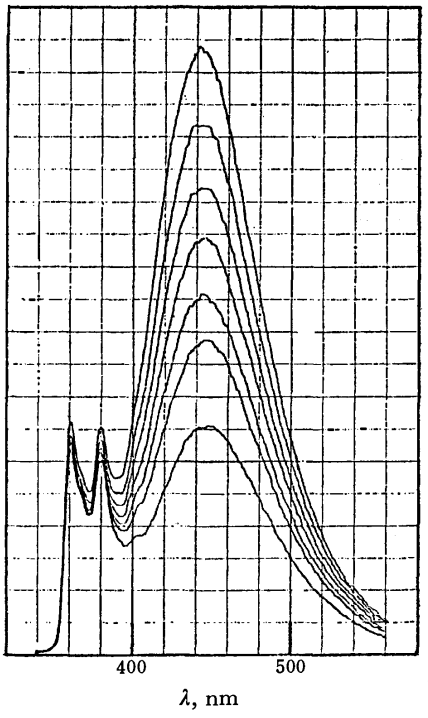

Fig. 1. Quenching of 9-CP–DHD exciplex by **1a** in deoxygenated benzene: $k_q\tau_{EX}=1.5$ dm^3 mol^{-1}.

Exciplex Quenching by Pyridine and Imidazole Compounds. For the exciplex quenching, we used pyridine (**1a**), 2-, 3-, and 4-methylpyridines (**1b**, **1c**, and **1d**), 2,6- and 3,5-dimethylpyridines (**1e** and **1f**), 1-methylimidazole (**2a**), and 1,2-dimethylimidazole (**2b**) as quenchers. The exciplex-quenching experiments were carried out as usual. Figure 1, for example, shows the spectral change in the fluorescence from a benzene solution containing 5×10^{-4} mol dm^{-3} in 9-CP and 0.3 mol dm^{-3} in DHD on the addition of **1a**. The exciplex emission with the maximum at 440 nm was significantly quenched. The plot of the relative intensities at 440 nm in the absence of and in the presence of **1a** (I^0_{EX}/I^Q_{EX}) *vs.* the concentrations of **1a** gave a linear line, the slope of which was 1.5 dm^3 mol^{-1} (Fig. 4); the rate constant (k_q) of the exciplex quenching was calculated to be 7.1×10^7 dm^3 mol^{-1} s^{-1} by applying the slope to Eq. a, where τ_{EX} and Q represent the lifetimes of an exciplex and an exciplex quencher respectively. Similarly, the rate

$$I^0_{EX}/I^Q_{EX} = 1 + k_q\tau_{EX}[Q] \qquad (a)$$

constants of the quenching of the 1- and 2-NN–DF exciplexes by pyridine were calculated to be 3.5×10^8 and 2.6×10^8 dm^3 mol^{-1} s^{-1} respectively.

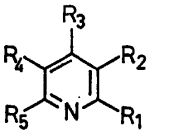

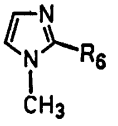

1a: $R_1=R_2=R_3=R_4=R_5=H$
1b: $R_1=CH_3$, $R_2=R_3=R_4=R_5=H$
1c: $R_2=CH_3$, $R_1=R_3=R_4=R_5=H$
1d: $R_3=CH_3$, $R_1=R_2=R_4=R_5=H$
1e: $R_1=R_5=CH_3$, $R_2=R_3=R_4=H$
1f: $R_2=R_4=CH_3$, $R_1=R_3=R_5=H$

2a: $R_6=H$
2b: $R_6=CH_3$

As is shown in Fig. 1, the residual 9-CP fluorescence at 360—380 nm was also slightly quenched by pyridine. Similarly, a slight quenching of the residual 1- and 2-NN fluorescence was also observed in the quenching of the 1- and 2-NN–DF exciplexes by pyridine. In contrast, the 2-NN or 9-CP fluorescence in the absence of DF or DHD was not quenched at all by pyridine, while the quenching of the 1-NN fluorescence by pyridine was relatively efficient, the rate constant being 3×10^8 dm^3 mol^{-1} s^{-1}. Therefore, the quenching of the residual 2-NN or 9-CP fluorescence can be ascribed to the decrease in the reversible dissociation of the exciplex because of the exciplex quenching. In the case of the 1-NN–DF exciplex, however, the slight quenching of the residual 1-NN fluorescence would be caused by either the exciplex quenching or the direct quenching of the excited singlet 1-NN by pyridine.

Table 2 lists the quenching constants ($k_q\tau^{air}_{EX}$) for each exciplex-quencher pair; they were obtained by the usual Stern-Volmer plots for air-saturated benzene and ethyl acetate solutions, using Eq. a but replacing τ_{EX} by τ^{air}_{EX}, the lifetime in air-saturated solutions. In order to avoid the quenching of excited-singlet aromatic

Table 2. Quenching of exciplex emission by exciplex quenchers[a)]

Quencher	$k_q\tau_{EX}^{air}$ (dm^3 mol^{-1})					
	1-NN–DF		2-NN–DF		9-CP–DHD	
	C_6H_6	AcOEt	C_6H_6	AcOEt	C_6H_6	AcOEt
1a	5.6(11.3)[b)]	9.6	3.6(7.2)[b)]	7.7	0.9(1.5)[b)]	2.6
1c	—	10.5	—	8.5	1.1	—
1d	8.0	11.0	—	9.3	1.4	3.3
1f	—	11.0	—	12.0	—	—
1b	0.8	≈1.0	—	≈0.5	<0.2	<0.2
1e	—	≈0.3	—	<0.1	<0.1	—
2a	37.5	—	20.5	—	4.9	9.0
2b	12.2	—	12.0	—	—	—

a) In air-saturated solutions; 5×10^{-4} mol dm^{-3} in aromatic nitriles and 0.3 mol dm^{-3} in DF or DHD. b) In degassed benzene.

nitrile, the concentrations of the quenchers were kept as low as the quenching of excited-singlet aromatic nitrile, which was negligible except for the exciplex quenching by **1b** and **1e**. There was no indication of the formation of any charge-transfer complexes between A or D and Q in the ground state.

*Quenching of Aromatic Nitrile Fluorescence by **2a** and **2b**.* The fluorescence of 1- and 2-NN was quenched by **2a**. Interestingly, the Stern-Volmer plots were not linear (Fig. 2). In the fluorescence quenching, very weak exciplex emissions appeared, but no isoemissive points could be observed. The 9-CP fluorescence was not quenched by **2a** at all. The quenching of the 2-NN and 9-CP fluorescence by **2b** gave, again, slightly curved Stern-Volmer plots, while that of the 1-NN fluorescence was efficient and gave a linear Stern-Volmer plot (Fig. 3). In the latter quenching, a fairly strong exciplex emission with the maximum at 408 nm appeared without an isoemissive point; it revealed its maximum intensity at the concentration of 1.8×10^{-2} mol dm^{-3} of added **2b**. A further increase in the **2b** concentration

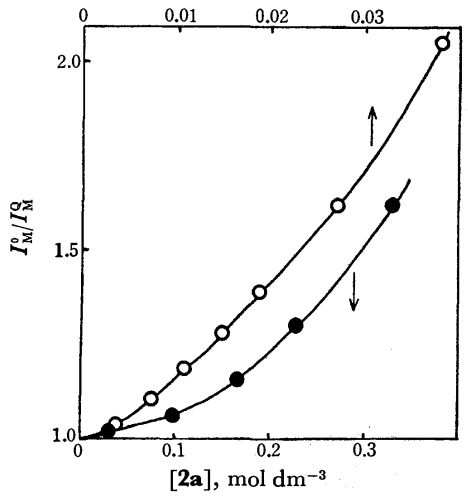

Fig. 2. Stern-Volmer plots for the quenching of 1-NN (-○-) and 2-NN (-●-) fluorescence by **2a** in air-saturated benzene, [1- and 2-NN]$=5\times10^{-4}$ mol dm^{-3}.

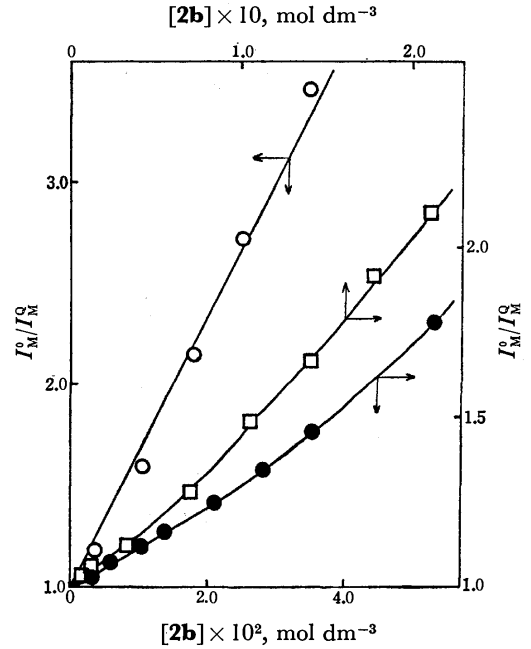

Fig. 3. Stern-Volmer plots for the quenching of 1-NN (-○-) 2-NN (-●-), and 9-CP (-□-) fluorescence by **2b** in air-saturated benzene, [Aromatic Nitrile]$=5\times10^{-4}$ mol dm^{-3}.

Table 3. Quenching of 1-NN fluorescence by **2b**[a)]

[**2b**]$\times10^2$ (mol dm^{-3})	0.36	1.1	1.8	2.5	3.6	5.4	7.2	10.8
I_M^0/I_M^Q [b)]	1.16	1.58	2.14	2.72	3.47	—	—	—
$\phi_{EX}/\phi_{EX}^{max}$ [c,d)]	0.47	0.92	1.00	0.99	0.93	0.80	0.69	0.54
L_{max}/L [d)]	0.77	0.90	1.00	1.11	1.32	1.48	1.79	2.28

a) In air-saturated benzene, 5×10^{-4} mol dm^{-3} in 1-NN. b) Relative intensities of the 1-NN fluorescence at 340 nm in the absence and in the presence of **2b**. c) Relative intensities of the exciplex emission at 408 nm. d) See the text.

resulted in a decrease in the exciplex emission. Table 3 summarizes the relative intensities of 1-NN fluorescence at 340 nm (I_M^0/I_M^Q) and those of the exciplex emission at 408 nm ($\phi_{EX}/\phi_{EX}^{max}$), the atterl of which are corrected by subtracting the intensity of the 1-NN fluorescence at 408 nm from the total intensity at this wavelength. The curved Stern-Volmer plots could be caused by the formation of charge-transfer complexes in the ground state. However, UV measurements eliminated this posibility.

Discussion

Mechanism of Exciplex Quenching. Scheme 1 shows the reaction processes involving the exciplex formation and the quenching of the exciplex, where A, D, $[A^-D^+]^*$, and Q represent the aromatic nitriles, DF or DHD, the exciplexes, and the exciplex quenchers respectively. Processes 1 and 4 involve all the unimolecular physical

$$A \xrightarrow{h\nu} {}^1A^*$$

$${}^1A^* \xrightarrow{1/\tau_M} A + h\nu' \text{ (or heat)} \quad (1)$$

$${}^1A^* + Q \xrightarrow{k_q'} A + Q \quad (2)$$

$${}^1A^* + D \underset{k_{-e}}{\overset{k_e}{\rightleftharpoons}} [A^-D^+]^* \quad (3)$$

$$[A^-D^+]^* \xrightarrow{k_d} A + D + h\nu'' \text{ (or heat)} \quad (4)$$

$$[A^-D^+]^* \xrightarrow{k_p} \text{Product(s)} \quad (5)$$

$$[A^-D^+]^* + Q \xrightarrow{k_q} A + D + Q \quad (6)$$

Scheme 1.

decays of A and $[A^-D^+]^*$ respectively. Equations b and c are the Stern-Volmer equations for the quenching of the Nonomer (A) fluorescence by D in the absence of Q and of exciplex emission at a constant concentration of D (0.3 mol dm^{-3}) by Q respectively.

$$I_M^0/I_M^Q = 1 + \gamma_0 k_e \tau_M [D] \quad (b)$$

$$\gamma_0 = (k_d + k_p)/(k_{-e} + k_d + k_p) \approx 1$$

$$I_{EX}^0/I_{EX}^Q = \left(1 + \frac{k_q' \tau_M [Q]}{1 + k_e \tau_M [D]}\right)(1 + k_q \tau_{EX} [Q]) \quad (c)$$

The value of γ_0 is nearly unity, since the fluorescence of A was quenched by D at a diffusion-controlled rate *i.e.*, $k_{-e} \ll k_d + k_p$; the exciplexes are almost irreversibly formed. In the presence of 0.3 mol dm^{-3} in D, therefore, Eq. c can be reduced to Eq. a, since $1 \gg k_q' \tau_M [Q]/(1 + k_e \tau_M [D])$. The calculated k_q values for the quenching of the exciplexes by pyridine are one or two orders lower than the diffusion-controlled rate, showing that pyridine is an inefficient quencher for the exciplexes. Significantly, however, pyridine does not quench the 2-NN and 9-CP fluorescence at all; thus, it can be used as a selective quencher for the exciplexes involving nitriles.[12] The photocycloaddition of DHD to 9-CP[7f] was also quenched by pyridine; the Stern-Volmer plot gave the $k_q \tau_{EX}$ value of 1.95 ± 0.5 dm^3 mol^{-1}, which is very similar to that obtained from exciplex-emission-quenching experiments (Fig. 4). The results clearly

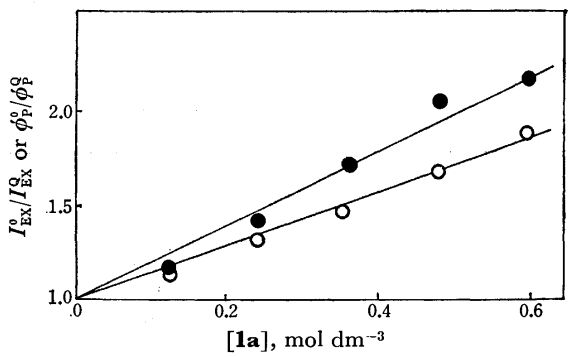

Fig. 4. Stern-Volmer plots for the quenching of 9-CP–DHD exciplex by **1a** in degassed benzene; fluorescence quenching (-○-) and product quenching (-●-) runs, [9-CP] = 5×10^{-4} mol dm^{-3} and [DHD] = 0.3 mol dm^{-3}.

demonstrate the intermediacy of the exciplex in the photocycloaddition.

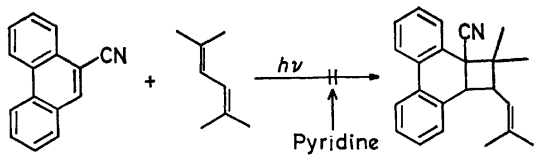

According to Caldwell's generalization of exciplex quenching,[11] an exciplex quencher possessing an electron-donor or electron-acceptor nature (Q_D or Q_A) interacts with an exciplex $[A^-D^+]^*$ on the D or A side *i.e.*, $A^{\delta-}\cdots D\cdots Q_D^{\delta+}$ or $Q_A^{\delta-}\cdots A\cdots D^{\delta+}$. This termolecular interaction results in exciplex quenching. Therefore, if pyridine acts as an n-donor in the exciplex quenching, the n-orbital of pyridine must perpendicularly approach to the molecular plane of the D side of exciplexes (I in Scheme 2). On the other hand, the pyridine which acts as a π-acceptor can interact with the A side of exciplexes with a sandwich type of configuration (II).

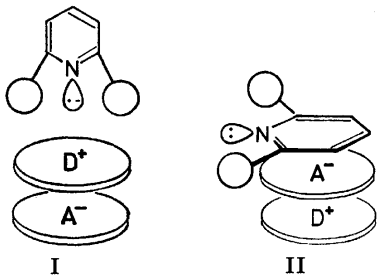

Scheme 2.

As is shown in Table 2, methyl substitution at the 2- and 2,6-positions of the pyridine ring commonly leads to a marked decrease in the quenching ability of the three exciplexes, while substitution at the other positions instead slightly enhances the quenching rate. The effect of the methyl groups at the 2- and 2,6-positions demonstrates the dominant n-donor character in the exciplex quenching. The methyl groups of **1b** and **1e** would sterically inhibit the approach of the n-orbital to the exciplexes within an effective distance for the

quenching. In the cases of the other methylated pyridines, such steric hindrance can not occur in the attack of the n-orbital on the exciplexes. Moreover, this mechanism is supported by the observation that the $k_q\tau_{EX}^{air}$ values increase with the increase in the base strength of the quenchers; methyl substitution in the pyridine ring enhances the base strength, and imidazole is much more strongly basic, but less π-defficient, than pyridine.[15] In line with this mechanism, **2a** is a much more efficient quencher than **1a**. Methyl substitution at the 2-position of the imidazole ring results, again, in a decrease in the quenching efficiency to some extent, though the steric effect is much smaller than that of the methyl group of **1b**; the difference in the steric effects can be easily predicted by molecular models. In conclusion, the exciplex quenching occurs by means of the attack of the n-orbital of the quenchers on the positive charge developed on the D side because of a high degree of charge-transfer contribution to the exciplexes. The ionic or charge-transfer nature of the exciplex quenching is supported by the observation that the $k_q\tau_{EX}^{air}$ values in ethyl acetate are greater than those in benzene.

Quenching of Aromatic Nitrile Fluorescence by 2a and 2b. The quenching of the 1- and 2-NN fluorescence by **2a** gave curved Stern-Volmer plots, which, it may be suggested, occur by way of a termolecular process involving the exciplexes of 1- and 2-NN–**2a**. The termolecular mechanism is further suggested by the observation that the emission of the 1-NN–**2b** exciplex increases up to the concentration of 1.8×10^{-2} mol dm^{-3} in **2b**, but decreases upon a further increase in the concentration of **2b**. In Scheme 3, therefore, the

$$A \xrightarrow{h\nu} {}^1A^* \tag{7}$$

$${}^1A^* \xrightarrow{1/\tau_M} A + h\nu' \text{ (or heat)} \tag{8}$$

$${}^1A^* + Q \underset{k_{-e}}{\overset{k_e}{\rightleftharpoons}} [AQ]^* \tag{9}$$

$$[AQ]^* \xrightarrow{k_f} A + Q + h\nu'' \tag{10}$$

$$[AQ]^* \xrightarrow{k_{it}} A + Q + \text{heat} \tag{11}$$

$$[AQ]^* + Q \xrightarrow{k_q} A + 2Q$$

Scheme 3.

reaction processes are shown, where A, Q, and [AQ]* denote the aromatic nitriles, **2a** or **2b**, and the exciplexes respectively. The process for the formation of stable products, [AQ]* and/or [AQ]*+Q→Products, can be discarded, since no products could be detected. Equation d represents the Stern-Volmer equation for the quenching of the aromatic nitrile fluorescence by Q, whereas Eq. e shows the quantum yield of the 1-NN–**2b** exciplex emission at a given concentration of Q.

$$I_M^0/I_M^Q = 1 + \left\{\frac{1+k_q\tau_{EX}^0[Q]}{1+(k_{-e}+k_q[Q])\tau_{EX}^0}\right\}k_e\tau_M[Q] \tag{d}$$

$$\tau_{EX}^0 = 1/(k_d+k_f)$$

$$\phi_{EX} = \left(\frac{I_M^Q}{I_M^0}\right)\left\{\frac{k_f\tau_{EX}^0}{1+(k_{-e}+k_q[Q])\tau_{EX}^0}\right\}k_e[Q] \tag{e}$$

If the reversible dissociation of the exciplex into $^1A^*$ and Q can be neglected (*i.e.*, $k_{-e}\ll k_d+k_f$), Eq. d can be reduced to a usual Stern-Volmer equation; thus, the fluorescence quenching would give a linear Stern-Volmer plot. The quenching of the 1-NN fluorescence by **2b** fits the case (Fig. 3); the k_e value was calculated to be $(9.3\pm1.0)\times10^9$ dm^3 mol^{-1} s^{-1} from the slope of the Stern-Volmer plot (71.0 dm^3 mol^{-1}) and the lifetime of the excited singlet 1-NN in air-saturated benzene (7.5 ± 0.5 ns). The occurrence of a diffusion-controlled fluorescence quenching demonstrates the negligible importance of the reversible dissociation.

If the reversible dissociation can not be neglected,

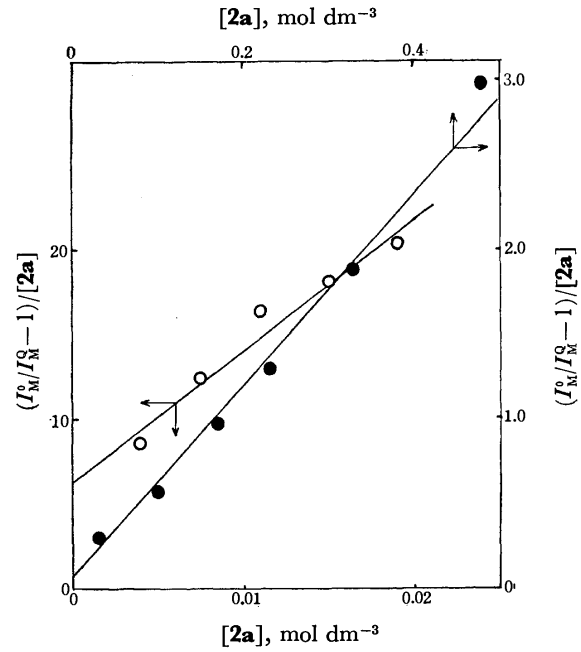

Fig. 5. Plots of $(I_M^0/I_M^Q-1)/[\mathbf{2a}]$ *vs.* [**2a**] for 1-NN (-○-) and 2-NN (-●-) using the data in Fig. 2.

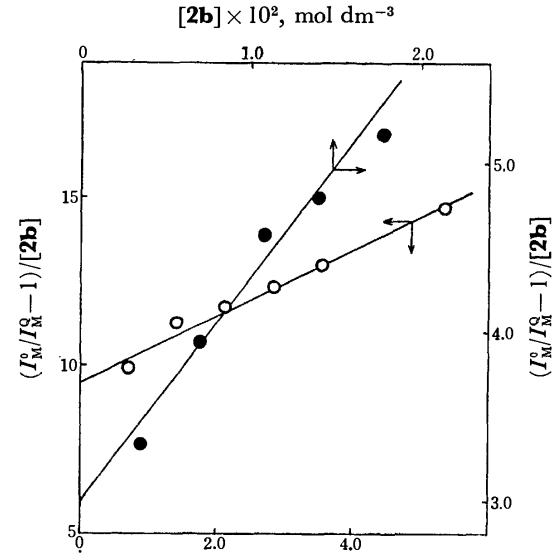

Fig. 6. Plots of $(I_M^0/I_M^Q-1)/[\mathbf{2b}]$ *vs.* [**2b**] for 2-NN (-○-) and 9-CP (-●-) using the data in Fig. 3.

TABLE 4. RATE CONSTANTS FOR QUENCHING OF AROMATIC NITRILE FLUORESCENCE BY **2a** AND **2b**[a)]

	2a		**2b**		
	1-NN	2-NN	1-NN	2-NN	9-CP
τ_M [b)] (ns)	7.5	10.0	7.5	10.0	10.0
$\{1/(1/\tau_{EX}^0+k_{-e})\tau_{EX}^0\}k_e\tau_M$ ($dm^3\ mol^{-1}$)	6.1	0.06	71.0	9.5	3.0
$k_e/(1/\tau_{EX}^0+k_{-e})\tau_{EX}^0$ ($dm^3\ mol^{-1}\ s^{-1}$)	8.1×10^8	6×10^6	9.3×10^9	9.5×10^8	3×10^8
$k_q\tau_{EX}^0$ ($dm^3\ mol^{-1}$)	179	93.3	22.0	10.0	4.4

a) In air-saturated benzene, 5×10^{-4} mol dm^{-3} in aromatic nitriles. b) Lifetimes of excited singlet aromatic nitriles in air-saturated benzene; ±0.5 ns.

Eq. d predicts non-linear Stern-Volmer plots (Figs. 2 and 3). Equation d can be transformed into Eq. f; thus, the plots of $(I_M^0/I_M^Q-1)/[Q]$ *vs.* [Q] are shown in Figs. 5 and 6, using the data in Figs. 2 and 3. Equation f predicts that the plots will be linear at lower concentrations of Q, provided $k_q[Q]\ll k_d+k_f+k_{-e}$, while a deviation from the linearity occurs at higher concentrations of Q. The results are in good accord with this prediction.

$$(I_M^0/I_M^Q-1)/[Q]=\frac{k_e\tau_M}{1+(k_{-e}+k_q[Q])\tau_{EX}^0}+\frac{k_e\tau_M k_q\tau_{EX}^0[Q]}{1+(k_{-e}+k_q[Q])\tau_{EX}^0} \quad (f)$$

When the slopes and intercepts in Figs. 5 and 6 applied to Eq. f, one can obtain the values of $\{1/(1/\tau_{EX}^0+k_{-e})\cdot\tau_{EX}^0\}k_e$ and $k_q\tau_{EX}^0$ listed in Table 4. The former is the apparent rate constant for the formation of the exciplex, in which the reversible dissociation of the exciplex is taken into account. In the case of the 2-NN–**2a** exciplex, the rate constant is three orders lower than the diffusion-controlled rate, suggesting the dominant dissociation; the exciplex formation must be isothermal or only slightly exothermic. In the cases of all the other exciplexes except the 1-NN–**2b** exciplex, the dissociation is also important. The curved Stern-Volmer plots arise from the quenching of the exciplexes by **2a** or **2b**. The $k_q\tau_{EX}^0$ values can be obtained by dividing the slopes by the intercepts in Figs. 5 and 6.

In the case of the 1-NN–**2b** exciplex, the $k_q\tau_{EX}^0$ value should be calculated by another method, since the Stern-Volmer plot for the quenching of the 1-NN fluorescence by **2b** gives a linear line. If Eq. g represents the maximum quantum yield of the 1-NN–**2b** exciplex emission observed in the presence of 1.8×10^{-2} mol dm^{-3} in **2b** ($[Q]_{max}$), Eq. h can be finally obtained by dividing Eq. g by Eq. e and by a subsequent transformation:

$$\phi_{EX}^{max}=\left(\frac{I_M^Q}{I_M^0}\right)_{max}\left(\frac{k_f\tau_{EX}^0}{1+k_q\tau_{EX}^0[Q]_{max}}\right)k_e[Q]_{max} \quad (g)$$

$$L_{max}/L=\left(\frac{\phi_{EX}^{max}}{\phi_{EX}}\right)\left(\frac{[Q]}{[Q]_{max}}\right)\left\{\frac{(I_M^Q/I_M^0)}{(I_M^Q/I_M^0)_{max}}\right\}=\left(\frac{1}{1+k_q\tau_{EX}^0[Q]_{max}}\right)(1+k_q\tau_{EX}^0[Q]) \quad (h)$$

Since the 1-NN–**2b** exciplex is almost irreversibly formed, k_{-e} was omitted in Eqs. e, g, and h. Thus, L_{max}/L was plotted *vs.* [Q] using the data in Table 3; a good linear line was thus obtained (Fig. 7). The $k_q\tau_{EX}^0$ value was calculated to be 22.0 $dm^3\ mol^{-1}$ by dividing the slope by the intercept, or 24.1 $dm^3\ mol^{-1}$ from the intercept. Although the latter must include a greater error than the former, the agreement between the calculated values is good within the limits of experimental error.

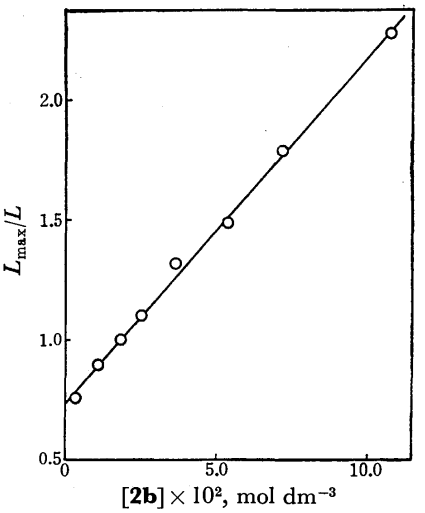

Fig. 7. Plots of L_{max}/L *vs.* [**2b**], using the data in Table 3.

The apparent rate constants for the formation of the 1- and 2-NN–**2a** exciplexes are much lower than those for the exciplexes of **2b**. This suggests that **2a** and **2b** act as π-donors in the exciplex formation, since **2b** is apparently a stronger π-donor than **2a**. In contrast, the $k_q\tau_{EX}^0$ values for 1- and 2-NN–**2a** system are about ten times greater than those for the 1- and 2-NN–**2b** system respectively. The difference between the $k_q\tau_{EX}^0$ values for **2a** and **2b** suggests that **2a** and **2b** act as n-donors in Process 11, as is illustrated as III; the methyl group at the 2-position of **2b** sterically inhibits the interaction of the n-orbital with the 1- and 2-NN–**2b** exciplexes, leading to lower k_q values than those for **2a**, as has been discussed in the foregoing section.

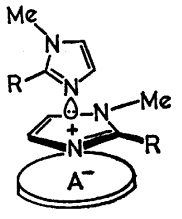

III

Unfortunately, the k_q values which are essential for the discussion can not be calculated, since the τ^0_{EX} values are not available. However, the participation of the n-orbital in Process 11 is further supported by the fact that DF and 1-methylpyrrole, which are strong π-donors but are very weakly basic, do not interact with the respective exciplexes of 1- or 2-NN up to 0.1 mol dm^{-3}, though they do quench the 1- and 2-NN fluorescence at a diffusion-controlled rate.[16] In summary, the termolecular interactions in the exciplex quenching and the quenching of aromatic nitrile fluorescence by **2a**, **b** occur upon the attack of **1** and **2** as n-donor, Q_n, on the exciplexes, $[A^-_\pi D^+_\pi]^*$ or $[A^-_\pi Q^+_\pi]^*$, giving rise to a purturbation of the exciplexes, by which non-radiative decays may be assisted. The interaction of triplexes, $[A_\pi D_\pi Q_n]^*$ or $[A_\pi Q_\pi Q_n]^*$, provokes an interesting speculation, though triplex emission could not be observed; the triplexes may rapidly collapse into the precursors in the ground state without emission and/or into triplet-state species. Alternatively, the interaction of Q_n with the exciplexes may cause a complete electron transfer from D_π or Q_π to A_π, leading to such ion-pairs as $[A^-_\pi \cdots (D_\pi Q_n)^+]_{solv}$ or $[A^-_\pi \cdots (Q_\pi Q_n)^+]_{solv}$; the electron reversal in the ion-pairs may exclusively occur to result in the collapse in to the precursors in the ground-state or triplet-state species because of the low polarity of the solvent. However, it should be pointed out that the decay channels are still open to question.

Experimental

The 1- and 2 naphthonitriles (Tokyo Kasei Co., Ltd.) were distilled under a high vacuum, chromatographed on silica gel, and recrystallized three times from hexane. The 9-cyanophenanthrene was prepared by a known method,[17] distilled under a high vacuum, and recrystallized three times from methanol. The 2,5-dimethyl-furan and 2,5-dimethyl-2,4-hexadine (Tokyo Kasei Co., Ltd.) were distilled from sodium under a pure nitrogen stream before use. The pyridine, methylated pyridines, 1-methylimidazole, and 1,2-dimethylimidazole (Tokyo Kasei Co., Ltd.) were all distilled from anhydrous potassium hydroxide under a pure nitrogen stream before use. The benzene and ethyl acetate (spectrograde, Nakarai Chemicals) were distilled before use.

The measurements of the fluorescence spectra and the fluorescence-quenching experiments were carried out with a Hitachi MPF-2A spectrofluorometer. The product analysis were carried out with a Shimadzu GC-2C gas chromatograph using a column of SE-30 (5% on Celite 545, 0.75 m) at 140—170 °C, a Hitachi R-24 (60 MHz) NMR spectrometer, and a Hitachi 124 UV spectrometer.

The authors wish to thank Professor Noboru Mataga and Dr. Tadashi Okada, Osaka University, for their help and guidance in the determination of the lifetime of the 9-CP–DHD exciplex. They are also indebted to Professor Haruo Shizuka, Gunma University, for the fluorescence lifetimes of 1- and 2-NN.

References

1) Part XXX: T. Majima, C. Pac, A. Nakasone, and H. Sakurai, *J. Chem. Soc., Chem. Commun.*, in press.

2) A. Weller, *Pure Appl. Chem.*, **16**, 115 (1968); J. B. Birks, "Photophysics of Aromatic Molecules," Wiley, New York, N. Y. (1970).

3) L. M. Stepenson and G. S. Hammond, *Pure Appl. Chem.*, **16**, 125 (1968); D. A. Labianca, G. N. Taylor, and G. S. Hammond, *J. Am. Chem. Soc.*, **94**, 3687 (1972); "The Exciplex," ed by M. Gordon and W. R. Ware, Academic Press, New York (1975); P. Froehlich and E. L. Wehry, in "Modern Fluorescence Spectroscopy," ed by E. L. Wehry, Plenum Press, Vol. 2, New York (1976), p. 319.

4) R. S. Davidson, "Molecular Association," ed by R. Foster, Academic Press, Vol. 1, New York (1975), p. 215; A. Lablache-Combier, *Bull. Chim. Soc. Fr.*, **1972**, 4792.

5) T. S. Cantrell, *J. Am. Chem. Soc.*, **94**, 5929 (1972); J. J. McCullough, R. C. Miller, D. Fung, and W. -S. Wu, *ibid.*, **97**, 5942 (1975); R. A. Caldwell and L. Smith, *ibid.*, **96**, 2994 (1974); N. C. Yang and K. Srinivasachar, *J. Chem. Soc., Chem. Commun.*, **1976**, 48; N. C. Yang, K. Srinivasachar, B. Kim, and J. Libman, *J. Am. Chem. Soc.*, **97**, 5006 (1975).

6) K. E. Wilzbach and L. Kaplan, *J. Am. Chem. Soc.*, **93**, 2073 (1971); J. Cornelisse, V. Y. Merritt, and R. Srinivasan, *ibid.*, **95**, 6197 (1973); R. M. Bowman, T. R. Chamberlain, C. -W. Huang, and J. J. McCullough, *ibid.*, **96**, 692 (1974); T. Sasaki, K. Kanematsu, and K. Hayakawa, *ibid.*, **95**, 5632 (1973); O. L. Chapman and R. D. Lura, *ibid.*, **92**, 6352 (1970); P. P. Wells and H. Morrison, *ibid.*, **97**, 154 (1975); F. D. Lewis and C. E. Hoyle, *ibid.*, **98**, 4338 (1976).

7) a) C. Pac, T. Sugioka, and H. Sakurai, *Chem. Lett.*, **1972**, 39; b) C. Pac, T. Sugioka, K. Mizuno, and H. Sakurai, *Bull. Chem. Soc. Jpn.*, **46**, 238 (1973); c) T. Sugioka, C. Pac, and H. Sakurai, *Chem. Lett.*, **1972**, 791 and 667; d) K. Mizuno, C. Pac, and H. Sakurai, *ibid.*, **1973**, 309; e) C. Pac, K. Mizuno, T. Sugioka, and H. Sakurai, *ibid.*, **1973**, 187; f) K. Mizuno, C. Pac, and H. Sakurai, *J. Am. Chem. Soc.*, **96**, 2993 (1974); g) K. Mizuno, C. Pac, and H. Sakurai, *J. Chem. Soc., Perkin Trans. 1*, **1974**, 2360; h) K. Mizuno, C. Pac, and H. Sakurai, *J. Chem. Soc., Chem. Commun.*, **1974**, 648; i) K. Mizuno, C. Pac, and H. Sakurai, *J. Chem. Soc., Perkin Trans. 1*, **1975**, 2221.

8) H. Beens and A. Weller, *Chem. Phys. Lett.*, **2**, 140 (1968).

9) J. Saltiel, D. E. Townsend, B. D. Watson, and P. Shannon, *J. Am. Chem. Soc.*, **97**, 5688 (1975).

10) a) J. Saltiel and D. E. Townsend, *J. Am. Chem. Soc.*, **95**, 6140 (1973); b) R. O. Campbell and R. S. H. Lin, *Mol. Photochem.*, **6**, 207 (1974); c) N. C. Yang, D. M. Shold, and B. Kim, *J. Am. Chem. Soc.*, **98**, 6587 (1976); d) J. Saltiel, D. E. Townsend, B. D. Watson, P. Shannon, and S. L. Finson, *ibid.*, **99**, 884 (1977).

11) a) R. A. Caldwell and L. Smith, *J. Am. Chem. Soc.*, **96**, 2994 (1974); b) D. Creed and R. A. Caldwell, *ibid.*, **96**, 7369 (1974); c) R. A. Caldwell, D. Creed, and H. Ohta, *ibid.*, **97**, 3246 (1975); d) D. Creed, R. A. Caldwell, H. Ohta, and D. C. DeMarco, *ibid.*, **99**, 277 (1977).

12) C. Pac and H. Sakurai, *Chem. Lett.*, **1976**, 1067.

13) The lifetimes were determined from the effect of aeration on the exciplex-emission intensity.[10c]

14) H. Beens, H. Knibbe, and A. Weller, *J. Chem. Phys.*, **47**, 1183 (1967).

15) L. A. Paquette, "Principles of Modern Heterocyclic Chemistry," W. A. Benjamin, New York (1968), pp. 183, 222.

16) Unpublished results.

17) J. E. Callen, C. A. Dornfeld, and G. H. Coleman, *Org. Shynth.*, Coll. Vol. III, 212 (1955).

The Reaction of Alkyl Halides with Mercury(II) and Potassium Thioacetates and Selenocyanates

Sakae UEMURA,* Nanao WATANABE,** Akio TOSHIMITSU, and Masaya OKANO
Institute for Chemical Research, Kyoto University, Uji, Kyoto 611
(Received October 28, 1977)

The reactions of alkyl halides with mercury(II) and potassium thioacetates afford alkyl thioacetates (RSCOMe), S_N1 and S_N2 type reactions taking place. In neither case is ROCSMe formed. Reactions with mercury(II) selenocyanate usually give only small amounts of alkyl selenocyanates and/or isoselenocyanates as isolated products except the case of benzyl bromide from which benzyl selenocyanate was obtained almost quantitatively. The ambident reactivity of this salt was revealed to be not so strong as that of mercury(II) thiocyanate. The reaction with potassium selenocyanate is also reported for comparison.

Mercury(II) thiocyanate reacts with alkyl halides in less-polar solvents to afford both alkyl isothiocyanates and thiocyanates, the former being predominant, in contrast to the reaction with the corresponding potassium salt in *N,N*-dimethylformamide (DMF), where alkyl thiocyanates are the main products.[1] We have carried out a similar reaction using mercury(II) thioacetate and selenocyanate to confirm the ambident reactivity of mercury(II) salt. The results are given herewith. For the sake of comparison reactions with the corresponding potassium salts were also carried out. It should be noted that the ambident character of potassium selenocyanate in the reaction with alkyl halide is known to some extent.[2]

Results and Discussion

Reaction with Mercury(II) or Potassium Thioacetate. The reaction was carried out by stirring equimolar amounts of alkyl halide and mercury(II) thioacetate in hexane at room or refluxing temperature as in the case of the reaction with mercury(II) thiocyanate.[1] It was found to be heterogeneous. The products were only alkyl thioacetates (**1**)[3] (Scheme 1), their formation being restricted to the cases of *t*-butyl and arylalkyl halides which can form the stable carbonium ions, all the starting alkyl halides being recovered unreacted in the other cases.

$$RX + Hg(SCOMe)_2 \xrightarrow{\text{hexane}} RSCOMe\ (\mathbf{1}) + Hg(X)SCOMe \quad (1)$$

The results show that the S_N1 type reaction might be involved, but when the homogeneous reactions of alkyl halides with potassium thioacetate were carried out in DMF, **1** was obtained in almost all cases except *t*-butyl halide (Scheme 2), suggesting the occurrence of S_N2

$$RX + KSCOMe \xrightarrow{\text{DMF}} (\mathbf{1}) + KX \quad (2)$$

type reaction. In all cases no ROCSMe were obtained. This indicates that mercury(II) thioacetate shows no ambident character, reflecting the significant difference in nucleophilic reactivity toward carbocation between sulfur and oxygen.[4] The attack by only S-site in the case of potassium thiocarboxylate is known in several cases such as the reaction of potassium thioacetate with alkyl tosylate[5] and that of potassium thiobenzoate with butyl halides.[6] Typical results are given in Table 1. An appreciable amount of thioacetic anhydride was also formed in the reaction of *t*-butyl bromide with the mercury(II) salts. Although the exact pathway for this anhydride is still ambiguous, it could not be formed by stirring mercury(II) thioacetate in hexane at room temperature for 24 h in the presence or absence of **1** (R=*t*-Bu).

Table 1. Reaction of alkyl halides with $Hg(SCOMe)_2$ or KSCOMe[a]

Alkyl Halide (RX)	Yield of **1**[b] From Hg salt (%)	From Hg salt (°C, h)	From K salt (%)	From K salt (°C, h)
n-BuBr	0	(65, 10)[c,d]	80	(25, 2)
i-PrBr	0	(65, 10)[c,d]	72	(25, 6)
t-BuBr	45	(25, 4)[e]	0	(75, 3)[d]
$PhCH_2Br$	53	(70, 8)	81	(75, 1)
PhCH(Me)Br	91	(25, 3)[f]	78	(75, 1)
Ph_2CHCl	99	(60, 1)	95	(70, 1)
c-$C_6H_{11}Br$	0	(68, 20)[d]	40	(75, 5)[g]

a) RX and metal thioacetate, each of 15 mmol. Solvent 20 ml; hexane in the case of Hg salt and DMF in the case of K salt. b) Isolated yield. c) Corresponding alkyl iodide was used. d) All alkyl halide was recovered unreacted. e) Other product; $(MeCO)_2S$ 42%. f) Other product; $(MeCO)_2S$ 7%. g) Other product; cyclohexane 28% (by GLC).

Reaction with Mercury(II) or Potassium Selenocyanate. When benzyl bromide was reacted with equimolar amount of mercury(II) selenocyanate in hexane or dibutyl ether at refluxing temperature for 0.5—1 h, benzyl selenocyanate [**2**(R=$PhCH_2$)] was obtained almost quantitatively. In the cases of almost all other alkyl or arylalkyl halides, however, the yields of the products, the corresponding selenocyanate (**2**) and isoselenocyanate (**3**) (Scheme 3), were quite low because of the rapid formation of lots of sticky solids containing mercury(II) salt, about 60—80% of the starting alkyl or arylalkyl halides being recovered unreacted. The situation was not improved by changing the

$$RX + Hg(SeCN)_2 \xrightarrow{\text{hexane}} RSeCN\ (\mathbf{2}) + RNCSe\ (\mathbf{3}) + Hg(X)SeCN \quad (3)$$

* To whom correspondence should be addressed.
** Koei Chemical Co., Ltd., Joto-ku, Osaka 536.

Table 2. Reaction of alkyl halides with $Hg(SeCN)_2$ or KSeCN

Alkyl halide (10 mmol)	Metal salt[a] (10 mmol)	Solvent (20 ml)	Temp (°C)	Time (h)	Products and yields (%)[b] 2	3
n-BuI	Hg	hexane	68	20	3[c]	0
n-BuBr	K	acetone	58	4	67	0
i-PrI	Hg	hexane	68	1	10[c]	8[c]
i-PrI	Hg	acetone	58	0.5	0	11[c]
i-PrI	K	acetone	58	4	74	0
t-BuBr	Hg	hexane	68	1	0	4[c]
t-BuBr	Hg	acetone	58	0.25	0	8[c]
t-BuBr	K	acetone	58	4	4[c]	7[c]
t-BuBr	K	EtOH	78	6	8[c]	11[c]
$PhCH_2Br$	Hg	$(n\text{-Bu})_2O$	70	0.5	99	0
$PhCH_2Br$	Hg	hexane	68	1	99	0
$PhCH_2Br$	K	acetone	58	3	97	0
PhCH(Me)Br	K	acetone	58	4	86	0
PhCH(Me)Br	K	DMF	80	1	64	0
Ph_2CHBr	K	acetone	58	4	80	0
Ph_3CCl	K	acetone	58	4	0	66

a) Hg and K designate $Hg(SeCN)_2$ and KSeCN, respectively. b) Isolated yield. c) By GLC. About 60—80% of alkyl halide was recovered unreacted.

solvent, reaction temperature, and molar ratio of the reactants. Although these solids were found to contain C and N, attempts to identify them were unsuccessful. The reason for the phenomena is not clear, but instability of the products, especially **3**, may be one cause.[7] In fact, when **3** (R=*t*-Bu), prepared separately,[7b] was heated in hexane for 1 h in the presence of an equimolar amount of mercury(II) selenocyanate and/or bromide, only half the amount of the starting material **3** was recovered. In the case of **2** (R=*i*-Pr), 75% of **2** was recovered by a similar treatment.

Formation of **3** from secondary and tertiary alkyl halides, although in low yield, suggests the ambident nature of mercury(II) selenocyanate. However, when the isomer ratio of **3**/**2** obtained from benzyl bromide[0 in hexane and $(n\text{-Bu})_2O$] is compared with that of $PhCH_2NCS/PhCH_2SCN$[0.56 in $(n\text{-Bu})_2O$][1] obtained in the reactions with mercury(II) thiocyanate, the ambident nature is clearly not so strong as in the case of mercury(II) thiocyanate. The exclusive formation of **2** ($R=PhCH_2$) indicates the predominant attack of the Se-site despite the fact that mercury is bonded with Se and not with N in mercury(II) selenocyanate.[8] This is probably due to the difference in nucleophilicity of Se and S. In this connection, the former is known to be a much stronger nucleophile than the latter in aliphatic nucleophilic substitution (S_N2).[9] Diphenylmethyl bromide reacts with potassium selenocyanate to give diphenylmethyl selenocyanate, while triphenylmethyl chloride gives only triphenylmethyl isoselenocyanate by a similar treatment.[2] In order to obtain authentic samples for alkyl selenocyanate and clarify the isomer distribution in the products, reactions with potassium selenocyanate were also carried out in acetone or DMF as solvent.[10] All alkyl halides except tertiary ones were found to give only the corresponding **2**, triphenylmethyl chloride affording only **3** and *t*-butyl bromide a small amount of a mixture of **2** and **3**.

Experimental

All the organic substrates except the solvents were used without further purification. Mercury(II) thioacetate[11] was prepared as follows. Thioacetic acid (10 g, 130 mmol) was slowly added to a chloroform (40 ml) suspension of mercury(II) oxide (yellow, 13 g, 6 mmol) at 5—10 °C with stirring for 1 h. The precipitated yellowish gray solid was collected and recrystallized from chloroform to give white leaflets; yield, 13.7 g (65%). Potassium thioacetate was prepared from thioacetic acid and $KHCO_3$.[12] Mercury(II) selenocyanate was prepared from mercury(II) nitrate and commercial potassium selenocyanate in water.[8] A sharp absorption at 2150 cm^{-1} ($\nu_{C\equiv N}$) in the IR spectrum (KBr disc) suggests the coordination of mercury with selenium.[8]

Gas chromatography (GLC) was used for detection of the isomer and determination of the isomer ratios, NMR analysis also being used in some cases. GLC analyses were carried out with a Shimadzu 5APTF apparatus using DEGS (1 m), Apiezon-L (1 m), and PEG-6000 (3 m) columns (carrier gas, N_2). The NMR and IR spectra were recorded on Varian EM-360 ($CDCl_3$, TMS, internal lock) and Hitachi EPI-S2 spectrometers, respectively.

All the products except **1** ($R=Ph_2CH$) and **2** (R=PhCHMe) are known compounds and were identified by NMR spectra and by comparison of their bp and mp with those in literature. The authentic samples of thioacetic anhydride,[13] **3** (R=*i*-Pr),[7a] and **3** (R=*t*-Bu)[7b] were prepared according to reported methods for identification of the products on GLC. **1** ($R=Ph_2CH$); bp 120—140 °C/5 mmHg, mp 39—40 °C (from EtOH); NMR δ 2.30 (s, 3H), 5.95 (s, 1H), 7.30 (s, 10H). **2** (R=PhCHMe); bp 120—125 °C/10 mmHg, NMR δ 2.30 (d, 3H), 4.90 (q, 1H), 7.39 (s, 5H).

Reaction of Benzyl Bromide with Mercury(II) Thioacetate in Hexane. Benzyl bromide (2.57 g, 15 mmol) was added to a stirred suspension of $Hg(SCOMe)_2$ (5.25 g, 15 mmol) in hexane (20 ml) at 30 °C, and the mixture was heated to 70 °C and kept for 8 h with stirring. The resulting red-brown suspension was cooled and filtered to remove

the red-brown precipitates which were found to contain C, H, and Br by analyses. The pale orange filtrate was washed with water and dried over Na_2SO_4. The GLC analysis of this filtrate showed the presence of one product and the absence of the starting benzyl bromide. Distillation afforded benzyl thioacetate [**1**(R=$PhCH_2$), 1.33 g, 53.4% yield, bp 100—102 °C/7 mmHg (lit,[5] bp 54 °C/0.05 mmHg)], leaving 0.14 g of residue. NMR δ 2.32 (s, 3H), 4.12 (s, 2H), 7.28 (s, 5H).

*Formation of Bis(diphenylmethyl) Sulfide (**4**).* Diphenylmethyl chloride (2.03 g, 10 mmol) was added to a stirred suspension of $Hg(SCOMe)_2$ (1.75 g, 5 mmol) in hexane (20 ml) at 40 °C and the resulting heterogeneous mixture was heated to 70 °C and kept for 2 h with stirring. After being cooled, the yellow orange precipitates were filtered and the filtrate was treated as above. GLC analysis of the filtrate showed the absence of diphenylmethyl chloride and the presence of **1** (R=Ph_2CH). Evaporation of the solvent left 2.10 g of an oil shown by NMR to consist of 1.20 g (5 mmol) of **1** (R=Ph_2CH) and 0.90 g (2.5 mmol) of **4**. The residue after distilling **1** (R=Ph_2CH) off was solidified and recrystallized from petroleum ether to afford 0.83 g of pure **4**; mp 63—65 °C (lit,[3] mp 66.5 °C), NMR δ 4.72 (s, 2H), 6.85—7.5 (m, 20H).

Reaction of Benzyl Bromide with Mercury(II) Selenocyanate in (n-Bu)$_2$O. Benzyl bromide (1.11 g, 6.5 mmol) was added to a stirred suspension of $Hg(SeCN)_2$ (2.68 g, 6.5 mmol) in (n-Bu)$_2$O (20 ml) at 85 °C, and the mixture was kept for 0.5 h with stirring. The reaction mixture was cooled and filtered in order to remove the orange sticky precipitates. Removal of (n-Bu)$_2$O from the filtrate gave white solids of crude benzyl selenocyanate [**2** (R=$PhCH_2$), 1.12 g, 94% yield] which were recrystallized from aqueous ethanol; mp 69—70 °C (lit,[10] mp 71.5 °C, 72 °C), NMR δ 4.25 (s, 2H), 7.33 (s, 5H).

This work was partly supported by a Grant-in-Aid from the Ministry of Education.

References

1) N. Watanabe, M. Okano, and S. Uemura, *Bull. Chem. Soc. Jpn.*, **47**, 2745 (1974).
2) C. Th. Pedersen, *Acta Chem. Scand.*, **17**, 1459 (1963).
3) Even when two equivalents of alkyl halide to one equivalent of the mercury(II) salt were used, only one equivalent of **1** was formed at most. In this case the dialkyl sulfide was also formed as a by-product probably through the reaction of product **1** or the corresponding thiol with excess alkyl halide (see Experimental). The formation of dialkyl sulfide from thiol and alkyl halide has long been known: A. Schönberg, O. Schütz, and S. Nickel, *Ber.*, **61**, 2175 (1928).
4) See for example, C. D. Ritchie, *Acc. Chem. Res.*, **5**, 348 (1972); C. D. Ritchie, *J. Am. Chem. Soc.*, **97**, 1170 (1975).
5) J. H. Chapman and L. N. Owen, *J. Chem. Soc.*, **1950**, 579.
6) J. W. Kimball and E. E. Reid, *J. Am. Chem. Soc.*, **38**, 2758 (1916).
7) On the preparation and instability of **3**, see for example Ref. 2 and also a) W. J. Franklin and R. L. Werner, *Tetrahedron Lett.*, **1965**, 3003; b) N. Sonoda, G. Yamamoto, and S. Tsutsumi, *Bull. Chem. Soc. Jpn.*, **45**, 2937 (1972).
8) E. E. Aynsley, N. N. Greenwood, and M. J. Sprague, *J. Chem. Soc.*, **1965**, 2395.
9) See for example, E. S. Gould, "Mechanism and Structure in Organic Chemistry," Holt, Rinehart and Winston, New York (1959), pp. 259—260.
10) The reaction of alkyl halide with potassium selenocyanate in ethanol is well-known for the preparation of **2**. See for example; H. Rheinboldt, Methoden der Organischen Chemie (Houben-Weyl), ed by E. Müller, Vol. 9, Georg Thieme Verlag, Stuttgart (1955), p. 939.
11) N. Tarugi, *Gazz. Chem. Ital.*, **25**, 341 (1895).
12) I. T. Barnish and M. S. Gibson, *J. Chem. Soc., C*, **1970**, 854.
13) W. A. Bonner, *J. Am. Chem. Soc.*, **72**, 4270 (1950).

The Reactions of Olefins with Chloromethoxymethane or Dimethoxymethane in Nitriles

Yasuo WADA,* Takeshi YAMAZAKI,* Kazuo NISHIURA,* Shigeo TANIMOTO, and Masaya OKANO**

Institute for Chemical Research, Kyoto University, Uji, Kyoto 611

(Received November 7, 1977)

The Lewis acid-catalyzed reactions of olefins with chloromethoxymethane (CM) or dimethoxymethane (DM) and aliphatic or aromatic nitriles afforded the 1 : 1 : 1 adducts and/or their hydrolysis products in various yields, together with the 1 : 1 olefin–CM (or DM) adducts. $AlCl_3$, $FeCl_3$, $ZnCl_2$, and $SnCl_4$ were effective catalysts for the reaction with CM, whereas BF_3 and $SnCl_4$ were effective for that with DM. In the case of cyclohexene, the addition proceeded in the *trans*-manner; *i.e.*, the methoxymethyl group and the nitrile molecule were added to the olefin from opposite sides.

Several modifications of the Ritter reaction with various positive halogen compounds (*e.g.*, Cl_2,[1] Br_2,[1] ClOH,[1] BrN_3,[2] $ClNHCONH_2$,[3] $Cl_2NCOOEt$,[4] and Cl_2NSO_2Ph[5]), a nitronium salt,[6] and a carbenium salt[7] have been reported. However, in the last case the reaction of styrene with a methoxycarbenium salt and acetonitrile to produce *N*-(2-methoxy-1-phenylpropyl) acetamide is the sole example thus far examined, and only a brief description on it has been given. In order to know the nature of such a reaction involving the attack of a carbenium ion and to save the trouble of pre-preparing a carbenium salt, we examined three-component reactions of olefins with readily available sources of a methoxymethyl cation, such as chloromethoxymethane (CM), dimethoxymethane (DM), or trimethoxymethane (TM), and nitriles in the presence of Lewis acid catalysts. Except for the case of TM, the reactions proceeded smoothly and afforded the desired adducts (**1**) and/or their hydrolysis products (**2**) in various yields (Eq. 1), together with other products, including the 1 : 1 olefin–CM(or DM) adducts. The present paper will be concerned with these results.

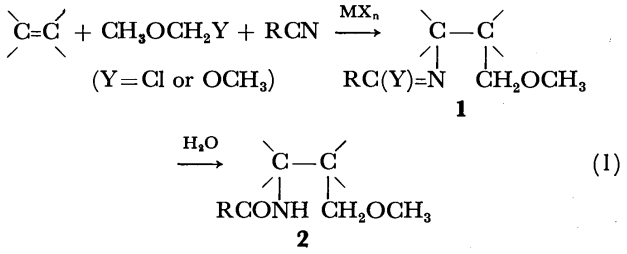

(1)

In this connection, the Lewis acid-catalyzed reactions of α-halo ethers,[8] 1,1-dialkoxymethanes,[9] or trialkoxymethanes[10] with olefins to yield the corresponding 1 : 1 adducts were known in the 1950's (Eqs. 2 and 3).

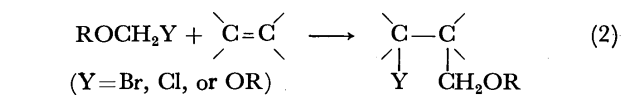

(2)

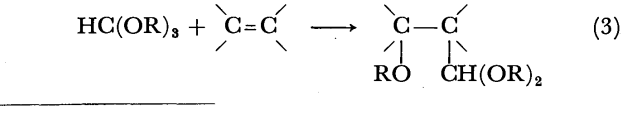

(3)

* Koei Chemical Co., Ltd., Joto-ku, Osaka 536.

** To whom correspondence should be addressed.

Results and Discussion

The treatment of cyclohexene with CM in acetonitrile in the presence of a Lewis acid catalyst at room temperature for 24 h, followed by a work-up procedure with aqueous Na_2CO_3, gave the following three compounds as the main products: a *N*-[2-(methoxymethyl)-cyclohexyl]acetamide (**2a**, R=CH_3), a 1-chloro-2-(methoxymethyl)cyclohexane (**3a**, Y=Cl), and probably 3-methoxymethyl-1-cyclohexene (**4'a**) (see Eq. 6). The first compound corresponds to the hydrolysis product of the 1 : 1 : 1 olefin–CM–nitrile adduct and the second one, to the 1 : 1 olefin–CM adduct, while the last one may come from the intermediate cation **5a** in the addition and/or from the 1 : 1 adduct, **3a**. However, a blank experiment revealed that the latter possibility (the dehydrochlorination of **3a**) can be excluded, at least during the work-up procedure. Further, it was confirmed by a separate experiment that **3a** (Y=Cl) does not react with acetonitrile to afford **2a** and either **4a** or **4'a**, even in the presence of equimolar amounts of $AlCl_3$ or $FeCl_3$, under the given reaction conditions. When propionitrile and some aromatic nitriles were used as solvents in place of acetonitrile, the corresponding 1 : 1 : 1 adducts were obtained similarly. Generally, the reactions were accompanied by a considerable formation of tarry materials (which were probably formed by further acid-catalyzed reactions of the products, **3a**, **4a** and/or **4'a**). Several results of the reaction of cyclohexene with CM are summarized in Table 1.

As can be seen from the table, $AlCl_3$, $FeCl_3$, $ZnCl_2$, and $SnCl_4$ were superior to $HgCl_2$ and BF_3 as catalysts. When equimolar amounts of these effective catalysts were used in acetonitrile, the combined yields of **2a**, **3a**, and **4'a** were nearly 55—60% (based on the consumed cyclohexene), and the proportions of **2a** (R=CH_3) changed appreciably with the nature of the catalysts. The best yield (41%) of **2a** was obtained by the use of one equivalent of $AlCl_3$. Though it is known that the basicity of benzonitrile is lower than that of acetonitrile, the former nitrile afforded the corresponding amide (**2a**, R=C_6H_5) in considerable yields with selectivities comparable to those of the case of acetonitrile (*e.g.*, $AlCl_3$-catalyzed, the **2a**/**2a**+**3a**+**4'a** ratio was 0.69/1 for CH_3CN and 0.71/1 for C_6H_5CN). Such a result may reflect a considerable stabilization through conjuga-

TABLE 1. REACTION OF CYCLOHEXENE WITH CM IN NITRILES

Ether (CM), 100 mmol; Cyclohexene, 100 mmol; Nitrile, 1000 mmol. Reaction conditions: 20—25 °C, 24 h.

Nitrile	MX_n (equiv)	Method[a]	Product and yield (%)[b,c]			Recovered olefin (mmol)[c]
			2a	**3a** (Y=Cl)	**4'a**	
CH_3CN	$ZnCl_2$(1/3)	A	22	10	17	11
CH_3CN	$ZnCl_2$(1)	B	31	9	16	5
CH_3CN	$FeCl_3$(1/3)	A	24	5	12	24
CH_3CN	$FeCl_3$(1)	A	34	13	8	0
CH_3CN	$FeCl_3$(1)	B	34	13	10	1
CH_3CN	$AlCl_3$(1/3)	A	21	3	15	17
CH_3CN	$AlCl_3$(1)	A	41	6	11	2
CH_3CN	$AlCl_3$(1)	B	41	10	8	4
CH_3CN	$SnCl_4$(1/3)	A	24	7	10	5
CH_3CN	$SnCl_4$(1)	B	33	13	9	0
CH_3CN	$HgCl_2$(1/3)	A	15	13	16	24
CH_3CN	$BF_3 \cdot Et_2O$(1/3)	A	9	19	7	41
C_2H_5CN[e]	$AlCl_3$(1)	B	34	7	15	6
C_6H_5CN[e]	$ZnCl_2$(1/3)	A	17[d]	18	7	13
C_6H_5CN[e]	$AlCl_3$(1)	B	44[d]	8	10	0
p-$CH_3C_6H_4CN$[e]	$AlCl_3$(1)	B	20[d]	6	6	1
p-ClC_6H_4CN[e,f]	$ZnCl_2$(1/3)	A	11[d]	12	7	31

a) Method A: The ether was added to a mixture of olefin, nitrile, and the catalyst. Method B: The catalyst was added to a mixture of olefin, the ether, and nitrile. b) Based on the olefin consumed. c) Determined by GLC, unless otherwise noted. d) Isolated yield after chromatography. e) Experiment on the scale of 1/2. f) The amount of nitrile was 250 mmol, and CCl_4 (60 ml) was added as the solvent.

TABLE 2. REACTION OF OLEFINS WITH CM IN ACETONITRILE

Ether (CM), 100 mmol; Olefin, 100 mmol; Nitrile, 1000 mmol. Reaction conditions: 20—25 °C, 24 h.

Olefin	MX_n (equiv)	Method[a]	Product and yield (%)[b,c]		
			2	**3** (Y=Cl)	**4** or **4'**
n-$C_4H_9CH=CH_2$	$AlCl_3$(1)	B	44	5	4
n-$C_4H_9CH=CH_2$	$ZnCl_2$(1/3)	A	24	20	7
$(CH_3)_2C=CH_2$	$FeCl_3$(1)	B	7	0	0
$C_6H_5CH=CH_2$	$ZnCl_2$(1)	B	9	6[d]	0

a), b), c) See footnotes in Table 1. d) The 2: 1 styrene–CM adduct was also formed (4%).

tion in the imidoyl cation, **6**, formed by the attack of benzonitrile on the cation **5** (see Eq. 6).

When the reaction was applied to three typical terminal olefins in acetonitrile, the yields of the 1: 1: 1 adducts varied significantly (Table 2). From 1-hexene, the expected adduct **2b** (R=CH_3), following Markovnikov's rule, was obtained in a yield similar to that in the case of cyclohexene. Although the successful addition of nitriles to 2-methylpropene has been known in the Ritter reaction (in H_2SO_4–HOAc),[1] our reaction gave a poor yield of the expected adduct **2c** (R=CH_3) and a large amount of a tarry product. In the case of styrene, the 1: 1 adduct **3d** (Y=Cl) became the principal product, and the yield of the desired adduct, **2d** (R=CH_3), was also quite poor.

Next, a similar treatment of cyclohexene with DM in place of CM in acetonitrile resulted in the formation of the following four products: a methyl *N*-[2-(methoxymethyl)cyclohexyl]ethanimidate (**1a**, Y=OCH_3, R=CH_3), the actamide **2a** (R=CH_3), a 1-methoxy-2-(methoxymethyl)cyclohexane (**3a**, Y=OCH_3), and the olefin **4'a** (see Eq. 6). The first and third compounds correspond to the 1: 1: 1 olefin–DM–nitrile adduct and the 1: 1 olefin–DM adduct respectively. For this reaction, the apparent effectiveness of catalysts decreased in this order: $BF_3 > SnCl_4 > AlCl_3 > FeCl_3 \gg ZnCl_2$ and $HgCl_2$ (both almost ineffective), in contrast to the case of CM. When two-thirds equivalents of $BF_3 \cdot Et_2O$ was used, the combined yield of **1a** and **2a** (R=CH_3 each) was found to be 39%; this value was comparable to the highest yield of **2a** (R=CH_3) in the reaction with CM. By a separate experiment, it was confirmed that **1a** (Y=OCH_3, R=CH_3) can be readily converted into **2a** (R=CH_3) by hydrolysis with 5% aqueous NaOH (under reflux, 2 h). Most of the **2a** product may arise from **1a** (Y=OCH_3) during the work-up procedure, but another route *via* **1a** (Y=Cl) can not be excluded when metal chlorides are used as catalysts. In addition, a controlled experiment revealed that **3a** (Y=OCH_3) does not react with acetonitrile in the presence of $BF_3 \cdot Et_2O$ to afford **1a** or **2a** under the given reaction conditions. Some typical data of the reaction with DM are given in Table 3.

1-Hexene and styrene can be used as the olefin component for this reaction, but 2-methylpropene failed to undergo the reaction (Table 4). Here, it would be worthwhile to note that the reaction with CM is somewhat preferable to that with DM for the one-step preparation of the 1: 1: 1 adducts, **2**, from cyclohexene or 1-hexene, but the latter reaction is prefered for the preparation of **2** (*via* **1**) from styrene.

The following pathway, which is analogous to that of the Ritter reaction, appears to be consistent with all

Table 3. Reaction of cyclohexene with DM in nitriles

Ether, (DM) 100 mmol; Cyclohexene, 100 mmol; Nitrile, 1000 mmol, Reaction conditions: 20—25 °C, 24 h.

Nitrile	MX_n (equiv)	Method[a]	Product and yield (%)[b,c]				Recovered olefin (mmol)[c]
			1a (Y=OCH_3)	**2a**	**3a** (Y=OCH_3)	**4'a**	
CH_3CN	$BF_3 \cdot Et_2O$(1/2)	B	21	13	1	7	16
CH_3CN	$BF_3 \cdot Et_2O$(2/3)	B	25	11	1	9	13
CH_3CN[e]	$BF_3 \cdot Et_2O$(2/3)	B	24	11	1	11	12
CH_3CN	$BF_3 \cdot Et_2O$(1)	B	1	5	1	7	9
CH_3CN	$SnCl_4$(1/2)	B	21	8	2	10	11
CH_3CN	$SnCl_4$(2/3)	B	16	9	1	9	8
CH_3CN	$AlCl_3$(1/2)	B	9	15	1	11	26
CH_3CN	$FeCl_3$(1/2)	B	3	15	1	6	49
C_6H_5CN[f]	$BF_3 \cdot Et_2O$(2/3)	B	36	2[d]	3	14	21
C_6H_5CN[f]	$SnCl_4$(1/2)	B	28	4[d]	2	12	13

a), b), c), d) See footnotes in Table 1. e) Reaction time: 48 h. f) Experiment on the scale of 1/2.

Table 4. Reaction of olefins with DM in acetonitrile

Ether (DM), 100 mmol; Olefin, 100 mmol; Nitrile, 1000 mmol. Reaction conditions: 20—25 °C, 24 h.

Olefin	MX_n (equiv)	Method[a]	Product and Yield (%)[b,c]			
			1 (Y=OCH_3)	**2**	**3** (Y=OCH_3)	**4** or **4'**
n-$C_4H_9CH=CH_2$	$BF_3 \cdot Et_2O$(2/3)	B	19	8	3	22
n-$C_4H_9CH=CH_2$	$SnCl_4$(1/2)	B	19	8	2[d]	12
$C_6H_5CH=CH_2$	$BF_3 \cdot Et_2O$(2/3)	B	28	4	19	0
$C_6H_5CH=CH_2$	$SnCl_4$(1/2)	B	18	6	19[d]	0

a), b), c) See footnotes in Table 1. d) No **3** (Y=Cl) was detected.

Table 5. Physical properties and analytical data of the **1** and **2** products

Product; Bp(°C/Torr)[Mp(°C)]	H NMR (δ) (in $CDCl_3$)	Found (Calcd) (%)		
		C	H	N
1a (Y=OCH_3, R=CH_3)[a]; 105—106/15	3.50 (s, 3H), 3.20 (s, 3H), 3.6—2.7 (m, 3H), 1.80 (s, 3H), 2.0—1.0 (m, 9H)	66.43 (66.29	10.16 10.62	6.82 7.03)
1a (Y=OCH_3, R=C_6H_5); 108—110/2—3	7.5—7.2 (m, 5H), 3.75 (s, 3H), 3.20 (s, 3H), 3.5—2.8 (m, 3H), 2.1—0.8 (m, 9H)	73.64 (73.53	8.87 8.87	5.10 5.36)
1b (Y=OCH_3, R=CH_3); 105—107/28	3.58 (s, 3H), 3.4—3.1 (m, 3H), 3.30 (s, 3H), 1.84 (s, 3H), 1.8—1.0 (m, 8H), 0.9 (t, 3H)	65.93 (65.63	11.74 11.52	6.67 6.96)
1d (Y=OCH_3, R=CH_3); 101—103/2—3	7.4—7.1 (m, 5H), 4.65—4.25 (m, 1H), 3.65 (s, 3H), 3.30 (s, 3H), 3.5—3.15 (m, 2H), 1.82 (s, 3H), 2.2—1.7 (m, 2H)	70.87 (70.56	8.97 8.65	6.26 6.33)
2a (R=CH_3)[a]; 120—122/2—3, [110]	5.8 (b, 1H), 3.25 (s, 3H), 3.7—2.9 (m, 3H), 1.90 (s, 3H), 2.2—0.7 (m, 9H)	64.40 (64.83	10.21 10.34	7.47 7.56)
2a (R=C_2H_5); [90—90.5]	6.4 (b, 1H), 3.23 (s, 3H), 3.7—2.9 (m, 3H), 2.10 (q, 2H), 1.10 (t, 3H), 2.2—0.7 (m, 9H)	66.06 (66.29	10.75 10.62	6.94 7.03)
2a (R=C_6H_5); [120—121]	7.8—7.2 (m, 5H), 7.0 (b, 1H), 3.20 (s, 3H), 3.8—3.1 (m, 3H), 2.2—0.8 (m, 9H)	72.56 (72.84	8.76 8.56	5.55 5.56)
2a (R=p-$CH_3C_6H_4$); [129—129.5]	7.8—7.1 (m, 4H), 6.7 (b, 1H), 3.25 (s, 3H), 3.8—3.1 (m, 3H), 2.40 (s, 3H), 2.2—0.8 (m, 9H)	73.52 (73.53	9.06 8.87	5.48 5.36)
2a (R=p-ClC_6H_4); [160—162]	7.8—7.3 (m, 4H), 6.8 (b, 1H), 3.25 (s, 3H), 3.8—3.1 (m, 3H), 2.2—0. 8 (m, 9H)	63.82 (63.94	7.29 7.15	5.12 4.97)
2b (R=CH_3); 128—130/3, [115—116]	7.5 (b, 1H), 4.1—3.6 (m, 1H), 3.35 (t, 2H), 3.25 (s, 3H), 1.90 (s, 3H), 1.9—1.1 (m, 8H), 0.9 (t, 3H)	63.97 (64.13	11.07 11.30	7.61 7.48)
2c (R=CH_3); 109—110/4	7.1 (b, 1H), 3.40 (t, 2H), 3.30 (s, 3H), 1.86 (s, 3H), 1.86 (t, 3H), 1.33 (s, 6H)	60.14 (60.34	10.66 10.76	8.82 8.80)
2d (R=CH_3); 138—140/3	8.2 (b, 1H), 7.4—7.0 (m, 5H), 5.3—4.9 (m, 1H), 3.25 (s, 3H), 3.5-3.1 (m, 2H), 1.90 (s, 3H), 2.2—1.7 (m, 2H)	70.12 (69.53	8.02 8.27	6.16 6.76)

a) *trans*-Isomer.

of the results:

$$CH_3OCH_2Y + MX_n \rightleftharpoons CH_3OCH_2^+ + MX_nY^- \quad (4)$$
(Y=Cl or OCH_3)

$$R'R''C{=}CHR''' + CH_3OCH_2^+ \longrightarrow \left[\begin{array}{l} R'R''\overset{+}{C}\text{–}CHR''' \\ \qquad\quad | \\ \qquad CH_2OCH_3 \end{array}\right] \quad (5)$$

5

$$\mathbf{5} \xrightarrow{-H^+} R'R''C{=}CR'''(CH_2OCH_3)$$

4

or $R'(\text{–}H){=}CR''\text{–}CHR'''(CH_2OCH_3)$ (6a)

4'

$$\mathbf{5} \xrightarrow{MX_nY^-} \begin{array}{l} R'R''C\text{—}CHR''' \\ \quad | \quad | \\ \quad Y \quad CH_2OCH_3 \end{array} \quad (6b)$$

3

$$\mathbf{5} \xrightarrow{RCN} \left[\begin{array}{l} R'R''C\text{—}CHR''' \\ \overset{+}{R}C{=}N \quad | \\ \qquad\quad CH_2OCH_3 \end{array}\right] \xrightarrow{MX_nY^-}$$

6

$$\begin{array}{l} R'R''C\text{—}CHR''' \\ \quad | \quad | \\ RC(Y){=}N \quad CH_2OCH_3 \end{array} \xrightarrow{H_2O} \begin{array}{l} R'R''C\text{—}CHR''' \\ \quad | \quad | \\ RCONH \quad CH_2OCH_3 \end{array} \quad (6c)$$

1 **2**

a: R', R'''=$(CH_2)_4$, R''=H
b: R'=*n*-C_4H_9, R''=R'''=H
c: R'=R'''=CH_3, R''=H
d: R'=C_6H_5, R''=R'''=H

The attemped reaction using TM as the source of the methoxymethyl moiety under similar reaction conditions was unsuccesful. For example, when an equimolar mixture of cyclohexene and TM was treated with excess acetonitrile in the presence of $BF_3 \cdot Et_2O$ (2/3 equiv.) at room temperature for 48 h, only a small amount of a tarry product was formed, and most of the olefin was recovered.

Lastly, we wish to add a short comment on the stereochemical results of the reactions of cyclohexene in acetonitrile. When crude **2a** (R=CH_3) (obtained by the reaction with CM) was hydrolyzed by refluxing in aqueous HCl, *trans*-2- and probably *cis*-3-(methoxymethyl)cyclohexylamines (*trans*-**7** and *cis*-**8** respectively) were formed in a ratio of 9: 1, and no other products, including the *cis*-isomer of **7**, were found.[11] The configuration and conformation of **7** were deduced from the splitting of the C<u>H</u>(NH_2) proton in its NMR (100 MHz) spectrum, which indicates that this proton is in an *axial* position, coupled strongly to two adjacent *axial* protons and weakly to one adjacent *equatorial* proton (δ=2.42, d of t, J=4 and 10 Hz). In addition, the C<u>H</u>Cl proton of **3a** (Y=Cl) showed a quite similar splitting pattern at δ=3.74, indicating that its structure is also *trans* (diequatorial). An almost exclusive formation of *trans*-**7** was also observed when crude **1a** (Y=OCH_3) and crude **2a** (R=CH_3) (both obtained by the reaction with DM) were each subjected to hydrolysis in 10% aqueous HCl.[13] These results imply that the methoxymethyl cation and the nitrile molecule or Cl^- are added to cyclohexene from opposite sides. Since the absence of γ-methoxyl group participation in solvolytic reactions has been established by Winstein *et al.*,[14] the *trans*-addition *via* a four-membered cyclic oxonium ion intermediate is unlikely. The high stereoselectivity might be explained by assuming that, on the attack by the nucleophile upon the **5a** cation, the course leading to a thermodynamically more stable isomer becomes quite favorable for some reason.

Experimental

All the organic and inorganic materials were commercial products. The NMR spectra (in $CDCl_3$) were recorded with a Varian A-60 apparatus and a JEOL MH-100 apparatus. The GLC analyses were carried out on a Shimadzu 5APTF apparatus, using EGSS-X (30%)-Chromosorb-W(1 m) and PEG 6000 (3 m) columns (with N_2 as the carrier gas).

Reactions of Cyclohexene with CM or DM in Nitriles. Some typical examples are given below.

Method A: To a stirred mixture of cyclohexene (8.2 g, 100 mmol) and $FeCl_3$ (16.2 g, 100 mmol) in acetonitrile (41 g, 1000 mmol), CM (8.0 g, 100 mmol) was added, drop by drop, the temperature being maintained at near 5 °C by cooling with ice water. The mixture was stirred for 24 h at room temperature (20—25 °C) and then poured into a cooled solution of aqueous Na_2CO_3. After the basic mixture had then been stirred for 2 h at room temperature, the precipitated inorganic substance was filtered off and the filtrate was extracted with ether. Then the organic layer separated from the aqueous one was washed with aqueous NaCl and dried over anhydrous $MgSO_4$, and most of the solvent was evaporated. GLC analysis of the residue indicated the presence of **4'a** (probably) (1.0 g, 8 mmol), **3a** (Y=Cl) (2.1 g, 13 mmol), and **2a** (R=CH_3) (6.3 g, 34 mmol). Distillation afforded the following fractions: bp 65—95 °C/25 Torr [a mixture of **4'a** and **3a** (Y=Cl), 3 g], bp 119—123 °C/2—3 Torr [crude **2a** (R=CH_3), 6.5 g], and a brown, tarry residue (3.6 g).

Method B: To a stirred solution of cyclohexene (8.2 g, 100 mmol) and DM (7.6 g, 100 mmol) in acetonitrile (41 g, 1000 mmol), $BF_3 \cdot Et_2O$ (9.5 g, 67 mmol) was added slowly at near 5 °C; the resulting mixture was stirred for 24 h at room temperature. The work-up procedure was the same as above. GLC analysis showed the presence of unreacted cyclohexene (1.1 g, 13 mmol), **4'a** (1.0 g, 8 mmol), **3a** (Y=OCH_3) (0.1 g, 1 mmol), **1a** (Y=OCH_3, R=CH_3) (4.4 g, 22 mmol), and **2a** (R=CH_3) (1.8 g, 10 mmol). Distillation gave the following fractions: bp 65—95 °C/25 Torr [a mixture of **4'a** and **3a** (Y=OCH_3), 1.0 g], bp 103—108 °C/15 Torr [crude **1a** (Y=OCH_3, R=CH_3), 4.0 g], bp 119—123 °C/2—3 Torr [crude **2a** (R=CH_3), 1.6 g], and a tarry resudue (2.8 g).

In the reaction with CM or DM in benzonitrile, the **1a** adduct (Y=OCH_3, R=C_6H_5) could be separated by distillation, whereas the **2a** adduct (R=C_6H_5) was purely isolated from the residual solid by column chromatography [Wakogel, hexane–ether (1: 2)].

In GLC analysis, ethyl acetate, *p*-chlorotoluene, *p*-nitrotoluene, and benzophenone were used as internal standards for the estimation of cyclohexene, **4'a** and **3a** (Y=Cl), **3a** (Y=OCH_3) and **1a** (Y=OCH_3, R=CH_3), and **1a** (Y=OCH_3, R=C_6H_5) and **2a** (R=CH_3) respectively.

The physical properties of the products collected by means of the GLC technique, careful distillation, or recrystallization are as follows: **4'a**[15]: bp 77—78 °C/50 Torr (lit,[9b] bp 158 °C); NMR, δ=5.9—5.4 (m, 2H), 3.20 (s, 3H), 3.10

(d, 2H), 2.5—1.0 (m, 7H). *trans*-**3a** (Y=Cl): bp 95—97 °C/25 Torr (lit,[17,18] bp 109—113 °C/49 Torr); NMR (100 MHz), δ=3.74 (d of t, J=4 and 10 Hz, 1H), 3.50 (d, J=4 Hz, 2H), 3.30 (s, 3H), 2.3—1.0 (m, 9H). **3a** (Y=OCH_3): bp 106—108 °C/50 Torr (lit,[9b,18] bp 192—192.5 °C); NMR (100 MHz), δ=3.6—3.0 (m, 3H), 3.30 (s, 6H), 2.2—0.8 (m, 9H). The data on *trans*-**1a** (Y=OCH_3, R=CH_3), **1a** (Y=OCH_3, R=C_6H_5), *trans*-**2a** (R=CH_3), **2a** (R=C_2H_5), **2a** (R=C_6H_5), **2a** (R=*p*-$CH_3C_6H_4$), and **2a** (R=*p*-ClC_6H_4) are given in Table 5.

Hydrolysis of ***1a*** and ***2a***. When **1a** (Y=OCH_3, R=CH_3) (*ca.* 10 mmol) was heated in 5% NaOH under reflux for 2 h, **2a** (R=CH_3) was obtained in a *ca.* 95% yield. On the other hand, the hydrolysis of **1a** (*ca.* 10 mmol) with 10% HCl under reflux for 6 h afforded almost pure *trans*-**7** in a *ca.* 90% yield. When crude **2a** (R=CH_3) (prepared by the reaction with CM) (*ca.* 10 mmol) was hydrolyzed with 10% HCl under reflux for 6 h, a mixture of *trans*-**7** and *cis*-**8** (9: 1) was obtained in a high yield, whereas the acid-catalyzed hydrolysis of crude **2a** (R=CH_3) (obtained by the reaction with DM) afforded *trans*-7 almost exclusively. *trans*-**7**: bp 87—88 °C/19 Torr; Found (Calcd): C, 66.87 (67.09), H, 11.66 (11.96), N. 9.60 (9.78)%; NMR (100 MHz), δ=3.30 (d, J=4.5 Hz, 1H), 3.28 (d, J=4.5 Hz, 1H), 3.20 (s, 2H), 2.42 (d of t, J=4 and 10 Hz, 1H), 1.36 (s, 2H), 2.0—0.8 (m, 9H). *cis*-**8**: NMR (100 MHz), δ=3.25 (s, 3H), 3.15 (d, J=4.5 Hz, 1H), 3.31 (d, J=4.5 Hz, 1H), 2.60 (t of t, J=4 and 10 Hz, 1H), 1.25 (s, 2H), 2.1—0.7 (m,9H).

Reactions of Other Olefins with CM or DM in Nitriles The reactions were performed analogously to the cyclohexene experiment. The physical properties of the products (other than **1** and **2**, shown in Table 5) from other olefins are given below. *trans*-**4'b** (probably *trans*-1-methoxy-3-heptene): bp 78—79 °C/100 Torr (lit,[18,19] bp 58—59 °C/30 Totr); IR, 965 cm^{-1} (*trans*-CH=CH); NMR, 5.7—5.3 (m, 2H), 3.35 (t, J=6 Hz, 2H), 3.30 (s, 3H), 2.5—1.8 (m, 4H), 1.6—1.2 (m, 2H), 0.9 (t, 3H). **3b** (Y=Cl): bp 90—92 °C/23—25 Torr; Found (Calcd): C, 58.99 (58.35), H, 10.95 (10.40)%; NMR, δ=4.1—3.8 (m, 1H), 3.30 (t, J=5.5 Hz, 2H), 3.20 (s, 3H), 1.8—1.1 (m, 8H), 0.9 (t, 3H). **3b** (Y=OCH_3): bp 104—105 °C/100 Torr; Found (Calcd): C, 67.12 (67.45), H, 12.77 (12.58)%; NMR, δ=3.6—3.1 (m, 3H), 3.30 (s, 6H), 1.9—1.1 (m, 8H), 0.9 (t, 3H). **3d** (Y=Cl): bp 83—84 °C/3 Torr (lit,[20] bp 100—101.5 °C/6 Torr); NMR, δ=7.4—7.1 (m, 5H), 5.2—4.8 (m, 1H), 3.25 (s, 3H), 3.7—3.2 (m, 2H), 2.4—2.0 (m, 2H). **3d** (Y=OCH_3): bp 105 °C/11 Torr (lit,[9a] bp 151 °C/74 Torr); NMR, δ=7.4—7.2 (m, 5H), 4.4—4.1 (m, 1H), 3.30 (s, 3H), 3.20 (s, 3H), 3.6—3.2 (m, 2H), 2.2—1.75 (m, 2H).

We wish to thank Dr. Sakae Uemura, Institute for Chemical Research, Kyoto University, for his helpful discussions of the NMR data.

References

1) L. I. Krimen and D. J. Cota, *Org. React.*, **17**, 246 (1969).
2) F. Boerwinkle and A. Hassner, *Tetrahedron Lett.*, **1968**, 3921.
3) Y. Wada and R. Oda, *Bull. Chem. Soc. Jpn.*, **43**, 2167 (1970).
4) B. Crookes, T. P. Seden, and R. W. Turner, *J. Chem. Soc. Chem. Commun.*, **1968**, 342.
5) W. Theilacker, *Angew. Chem. Int. Ed. Engl.*, **6**, 94 (1967).
6) M. L. Scheinbaum and M. Dines, *J. Org. Chem.*, **36**, 3641 (1971).
7) W. A. Smit, A. V. Semenovsky, V. F. Kucherov, T. N. Chernova, M. Z. Krimer, and O. V. Lubinskaya, *Tetrahedron Lett.*, **1971**, 3101.
8) H. Gross and E. Höft, *Angew. Chem. Int. Ed. Engl.*, **6**, 342 (1967).
9) (a) R. Paul and S. Tchelitcheff, *Bull. Soc. Chim. Fr.*, **1951**, 125; (b) D. C. Dermer and J. J. Hawknis, *J. Am. Chem. Soc.*, **74**, 4595 (1952).
10) J. W. Copenhaver, U. S. Patent, 2677708 (1954) [*Chem. Abster.*, **49**, 1812 (1955)].
11) The minor product, *cis*-**8**, which is believed to be thermodynamically more stable than the *trans*-isomer,[12] may come from the attack of the nitrile on the 3-(methoxymethyl)-cyclohexyl cation formed from isomeric **5a** by a 1,2-hydride shift.
12) *Cf.* E. L. Eliel, N. L. Allinger, S. J. Angyal, and G. A. Morrison, "Conformational Analysis," Interscience Publishers, New York (1965), p. 53.
13) An attempt to elucidate the configuration and conformation of **3a** (Y=OCH_3) by NMR (100 MHz) failed because of an overlapping of the absorptions of the C<u>H</u>(OCH_3) and $C\underline{H}_2OCH_3$ protons.
14) S. Winstein, E. Allred, R. Heck, and R. Glick, *Tetrahedron*, **3**, 1 (1958).
15) The structure of the 1: 1 adduct was tentatively assigned as 1-methoxymethyl-1-cyclohexene by Dermer *et al.*,[9b] but our reinvestigation revealed that its structure should be 3- or 4-methoxymethyl-1-cyclohexene, not that of the 1-methoxymethyl isomer (based on its NMR spectral data). Though no decisive data are available at present, the 3-methoxymethyl structure seems more likely, judging from its boiling point (*cf.* the bp of the 4-methoxymethyl isomer,[16] 86—88 °C/100 Torr).
16) L. N. Owen and P. A. Robins, *J. Chem. Soc.*, **1949**, 331
17) S. D. Mekhtiev, B. F. Pishnamazzade, Sh. D. Gasanova, and R. M. Mamedova, *Dokl. Akad. Nauk Az. SSR*, **15**, 1115 (1959) [*Chem. Abstr.*, **54**, 24450 (1960)].
18) No stereochemical assignment was given in the literature cited.
19) A. N. Pudovik and V. I. Nikitina, *Zh. Obshch. Khim.*, **22**, 1553 (1952) [*Chem. Abstr.*, **47**, 8632 (1952)].
20) S. Mamedov and D. N. Khydyrov, *Zh. Obshch. Khim.*, **31**, 3905 (1961) [*Chem. Abstr.*, **57**, 11073 (1962)].

Synthesis of Stachyose Tetradecaacetate and An Isomer

Tetsuo SUAMI,* Toshiki OTAKE, Shigeru NISHIYAMA, Ryoichi ADACHI, and Katsumi NAKAMURA

Department of Applied Chemistry, Faculty of Engineering, Keio University, Hiyoshi, Yokohama 233

(Received November 9, 1977)

Condensation of 1′,2,2″,3,3′,3″,4,4′,4″,6′-deca-*O*-acetylraffinose (**1**) with 2,3,4,6-tetra-*O*-benzyl-D-galactopyranosyl chloride in the presence of tetraethylammonium chloride, followed by deacetylation, debenzylation and subsequent acetylation afforded stachyose tetradecaacetate. An isomer in which a terminal D-galctopyranosyl group is attached to the 6″-*O* of raffinose in β-anomeric linkage, was prepared by condensing **1** with 2,3,4,6-tetra-*O*-acetyl-α-D-galactopyranosyl bromide in the presence of mercury(II) cyanide. ^{13}C NMR spectra of stachyose tetradecaacetate and the isomer were discussed.

Stachyose was first discovered from a root of *Stachys tuberifera* (*Chorogi* in Japanese) by von Planta and Schulze in 1890.[1] Later this tetrasaccharide was found in other plants such as *Labiate*, *Pinuceae*, and *Leguminosae*.[2] The structure of stachyose was established by Onuki,[3] Laidlaw and Wylam,[4] and Hérissey and Courtois[5] as *O*-α-D-galactopyranosyl-(1→6)-*O*-α-D-galactopyranosyl-(1→6)-*O*-α-D-glucopyranosyl β-D-fructofuranoside.

In continuation of a previous study on sucrochemistry,[6] attempts were made to synthesize stachyose tetradecaacetate by condensing 1′,2,2″,3,3′,3″,4,4′,4″,6′-deca-*O*-acetylraffinose[6] (**1**) with 2,3,4,6-tetra-*O*-benzyl-D-galactopyranosyl chloride[7] (**2**). We now wish to report a successful synthesis of stachyose tetradecaacetate (**5**) by the condensation in the presence of tetraethyl ammonium chloride,[8–12] followed by deacetylation, debenzylation and subsequent acetylation.

Results and Discussion

When **1** was condensed with **2** in dichloromethane in the presence of tetraethylammonium chloride, *N,N*-diisopropylethylamine and molecular sieves at ambient temperature for a prolonged period, *O*-(2,3,4,6-tetra-*O*-benzyl-α-D-galactopyranosyl)-(1→6)-*O*-(2,3,4-tri-*O*-acetyl-α-D-galactopyranosyl)-(1→6)-*O*-(2,3,4-tri-*O*-acetyl-α-D-glucopyranosyl) 1,3,4,6-tetra-*O*-acetyl-β-D-fructofuranoside (**3**) was obtained as crystals. Deacetylation of **3** in methanolic sodium methoxide gave 2‴,3‴,4‴,6‴-tetra-*O*-benzylstachyose (**4**). Debenzylation of **4** in aqueous methanol in the presence of palladium catalyst under hydrogen atmosphere, followed by acetylation gave **5**. Compound **5** was identical with authentic stachyose tetradecaacetate.[3] Deacetylation of **5** gave stachyose (**6**) which was identical with an authentic sample.[3] The present synthesis substantiates the effectiveness and the high stereoselectivity of the Lemieux's condensation system.[8–11]

In contrast, when **1** was condensed with **2** in the presence of mercury(II) cyanide in benzene, the product was contaminated with an isomer (isostachyose derivative)[22]: *O*-(2,3,4,6-tetra-*O*-benzyl-β-D-galactopyranosyl)-(1→6)-*O*-(2,3,4-tri-*O*-acetyl-α-D-galactopyranosyl)-(1→6)-*O*-(2,3,4-tri-*O*-acetyl-α-D-glucopyranosyl) 1,3,4,6-tetra-*O*-acetyl-β-D-fructofuranoside. In this case, isolation of stachyose tetradecaacetate in a pure state was unsuccessful, owing to a similar chromatographic behavior of a contaminant in each step of the reactions. The contamination with isostachyose tetradecaacetate[22] (**7**) was demonstrated by measurement of ^{13}C NMR spectra of **5** and **7**. An authentic sample of **7** was prepared by condensing **1** with 2,3,4,6-tetra-*O*-acetyl-α-D-galactopyranosyl bromide[15] in the presence of mercury(II) cyanide in nitromethane.

^{13}C NMR spectra of sucrose octaacetate,[16] raffinose undecaacetate,[13] isoraffinose undecaacetate,[14] **5** and **7** have been determined. Assignments of the signals, obtained in accordance with the data for sucrose,[17–19] raffinose[19] and stachyose,[19] are given in Table 1.

The signals of the anomeric carbon atoms are readily recognized in the lower field (90.0—101.0 ppm). The chemical shift values for the anomeric carbon atoms of the α-D-glucopyranosyl moieties are almost the same in these cases (90.0—90.3 ppm). The anomeric carbon atoms of the α-D-galactopyranosyl groups (C-1″ and 1‴) reveal their signals at 95.9—96.2 ppm.

The signal of the anomeric carbon atom of the terminal β-D-galactopyranosyl group (C-1‴) in **7** (101.0 ppm) shifts downfield markedly from that of the corresponding α-D-galactopyranosyl group in **5** (96.2 ppm). This is in line with the fact that the C-1 of methyl α-D-glucopyranoside gives its signal in a 4.1 ppm higher field than that of the β-D-glucopyranoside.[20] This is also the

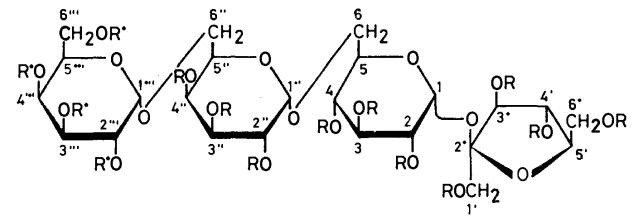

3 R=Ac, R′=$C_6H_5CH_2$
4 R=H, R′=$C_6H_5CH_2$
5 R=R′=Ac
6 R=R′=H

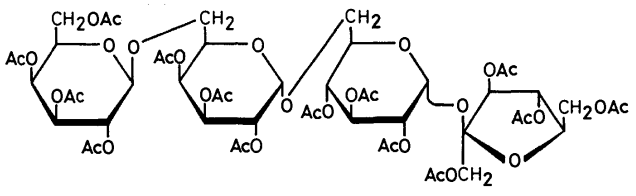

7

Scheme 1.

* To whom correspondence should be addressed.

TABLE 1. VALUES OF ^{13}C NMR CHEMICAL SHIFTS[a] OF SUCROSE OCTAACETATE, RAFFINOSE UNDECAACETATE, ISORAFFINOSE UNDECAACETATE, STACHYOSE TETRADECAACETATE (**5a**), AND ISOSTACHYOSE TETRADECAACETATE (**7**)

	Sucrose octaacetate[16]	Raffinose undecaacetate[13]	Isoraffinose undecaacetate[14]	Stachyose tetradecaacetate **5**	Isostachyose tetradecaacetate **7**
C-2′	104.1	104.9	104.4	104.8	104.6
C-1‴				96.2	101.0
C-1″		95.9	101.1	96.1	96.2
C-1	90.0	90.2	90.3	90.3	90.2
C-3′ (or 4′)	79.2	79.9	79.4	80.1	79.5
C-4′ (or 3′)	75.9	76.4	76.1	76.6	76.1
C-5′	75.2	75.9	75.4	76.1	75.4
Methine and methylene carbons of D-glucosyl and D-galactosyl moieties	70.4	70.5	71.2	70.4	70.9
	69.6	69.5	70.9	69.7 (2)	70.7
	68.6	69.4	70.5	68.7 (2)	70.5
	68.4	68.9	69.9	68.4	69.8
		68.3 (2)	69.2	68.3	69.6
		67.5	68.8	67.74	68.6 (4)
		66.4	68.6	67.70	67.7 (2)
		66.0	67.2	67.5	67.1 (2)
			67.0	67.1	65.8
				66.7	
				66.2	
				65.7	
C-1′, 6′, 6 (or 6″ or 6‴)	63.6	63.6	63.6	63.7	63.5
	62.9	61.9	62.9	62.1	62.5
	61.9	61.8	61.3	62.0	61.2

a) Chemical shifts are expressed in parts per million (ppm) downfield from the ^{13}C NMR resonance of tetramethylsilane.

case of the anomeric carbon atoms of the terminal D-galactopyranosyl groups in raffinose and isoraffinose undecaacetates (Table 1).

The presence of **7** as an impurity in stachyose tetradecaacetate was demonstrated by measuring its ^{13}C NMR spectrum and determining the optical rotation. The crude product of **5** showed a trace of the signal at 101.0 ppm and a slightly lower value of specific rotation as compared with that of an authentic sample.

Experimental

General Methods. Stachyose tetrahydrate (Aldrich Chemical Company, Inc., U. S. A.), mp 100—104 °C, $[\alpha]_D^{24}$ +133 °C (*c* 4, water), was used as an authentic sample. Melting points were determined in capillary tubes and are corrected. Solutions were concentrated under reduced pressure below 40 °C. Optical rotations were measured with a Japan Spectroscopic DIS-SL polarimeter. ^1H NMR spectra were recorded with a Varian XL-100 spectrometer at 100 MHz, peak positions being given in δ values. ^{13}C NMR spectra were determined with a Varian CFT-20 spectrometer at 20 MHz, the resonance signals being expressed in ppm downfield from the signal of tetramethylsilane. In both spectra, deuteriochloroform was used as a solvent and tetramethylsilane as an internal standard. IR spectra were recorded with a Hitachi 225 spectrophotometer in KBr disks. TLC was performed on Wakogel B-10 (Wako Pure Chemical Co. Ltd.) plates, silica gel (Wakogel C-300) being used for column chromatography. Acetylation was carried out with acetic anhydride in pyridine as usual.

*1′,2,2″,3,3′,3″,4,4′,4″,6′-Deca-O-acetylraffinose (**1**).* The compound was prepared by the method of Suami *et al.*[6] The product used in the present synthesis contained a trace amount of 1′,2,2″,3,3′,3″,4,4′,6′,6″-deca-*O*-acetylraffinose[6] which was detectable on TLC.

*O-(2,3,4,6-Tetra-O-benzyl-α-D-galactopyranosyl)-(1→6)-O-(2,3,4-tri-O-acetyl-α-D-galactopyranosyl)-(1→6)-O-(2,3,4-tri-O-acetyl-α-D-glucopyranosyl) 1,3,4,6-tetra-O-acetyl-β-D-fructofuranoside (**3**).* (a) Tetraethylammonium chloride (4.04 g), *N,N*-diisopropylethylamine (3.25 g) and molecular sieves 3A (5.2 g) were added to a solution of **1** (1.43 g) and 2,3,4,6-tetra-*O*-benzyl-D-galactopyranosyl chloride[7] (**2**, 12.1 g) in dichloromethane (40 ml). After 21 days at ambient temperature, the mixture was filtered and the filtrate was washed with cold water. The aqueous layer was extracted with chloroform, the chloroform layer being combined with the dichloromethane solution. After being dried over Na_2SO_4, the combined solution was concentrated. The residue was acetylated with acetic anhydride and pyridine in order to make the subsequent chromatographic separation easy. The acetylation product was purified on a silica gel column using 1:5 (v/v) 2-butanone–toluene. Fractions homogeneous on TLC (R_f 0.30) in the same solvent were combined and concentrated. The residue was recrystallized from 2-propanol to give 711 mg (32%) of **3**, mp 70—72 °C, $[\alpha]_D^{20}$ +91.9° (*c* 0.86, chloroform).

Found: C, 59.95; H, 5.98%. Calcd for $C_{72}H_{86}O_{31}$: C, 59.74; H, 5.99%.

Fractions homogeneous on TLC (R_f 0.17) in the same solvent were combined and concentrated. The residue was recrystallized from 3:2:5 (v/v) ethanol–methanol–water to give 349 mg (23%) of raffinose undecaacetate, mp 97—100 °C (Lit,[13] mp 99—101 °C).

(b) Mercury(II) cyanide (1.5 g) and drierite (3.0 g) were added to a solution of **1** (1.60 g) and **2** (3.51 g) in dry benzene (30 ml). The mixture was heated under reflux for 20 h with

mechanical agitation. The mixture was filtered and the filtrate was washed with sodium hydrogencarbonate solution and cold water. After being dried over Na_2SO_4, the solution was concentrated. The residue was purified on a silica gel column analogously as described in (a). Fractions practically homogeneous on TLC (R_f 0.30) in the same solvent as in (a) were combined and concentrated to dryness.
The residue was recrystallized from 2-propanol to give 1.12 g (45%) of crude **3**, mp 66—68 °C, $[\alpha]_D^{23}$ +88.2 ° (*c* 1.02, chloroform).

Found: C, 59.99; H, 5.87%. Calcd for $C_{72}H_{86}O_{31}$: C, 59.74; H, 5.99%.

Fractions homogeneous on TLC (R_f 0.54) in 20: 1 (v/v) chloroform-ethanol were combined and concentrated to give 205 mg (13%) of 1′,2,2″,3,3′,3″,4,4′,6′,6″-deca-*O*-acetylraffinose.[14]

Besides the products described above, 650 mg of a mixture of **3** and an isomer (isostachyose derivative)[22]: *O*-(2,3,4,6-tetra-*O*-benzyl-β-D-galactopyranosyl)-(1→6)-*O*-(2,3,4-tri-*O*-acetyl-α-D-galactopyranosyl)-(1→6)-*O*-(2,3,4-tri-*O*-acetyl-α-D-glucopyranosyl) 1,3,4,6-tetra-*O*-acetyl-β-D-fructofuranoside, was recovered from the column. The mixture showed two spots on TLC (R_f 0.30 and 0.29) in the same solvent system as described in (a) in an approximate ratio of 1: 1. An attempt to separate each component by repeated column chromatography was unsuccessful.

2‴,3‴,4‴,6‴-Tetra-O-benzylstachyose (4). (a) Compound **3** (669 mg) was deacetylated in 0.1 M methanolic sodium methoxide (10 ml) at ambient temperature overnight. After being neutralized with Amberlite IRA-120(H^+) resin, the solution was concentrated. The residue was purified on a silica gel column using 6: 18: 6: 1 (v/v) acetone–hlorocform–methanol–water. Fractions homogeneous on TLC (R_f 0.58) in 4: 9: 4: 1 (v/v) acetone–chloroform–methanol–water were combined and concentrated to give 471 mg (100%) of **4** as a glass, $[\alpha]_D^{20}$+81.7° (c 0.6, chloroform).

(b) Crude **3** (896 mg) was deaectylated analogously as described above to giv 596 mg (94%) of crude **4**, $[\alpha]_D^{20}$+96.2° (*c*, 1.04, chloroform).

1′,2,2‴,2‴,3,3′,3‴,3‴,4,4′,4‴,4‴,6′,6‴-Tetradeca-O-acetylstachyose (5). (a) Compound **4** (423 mg) was hydrogenated in 90% aqueous methanol (15 ml) in the presence of freshly prepared palladium black in hydrogen atmosphere (343 kPa) at 35 °C for a week in a Parr apparatus. During the course of hydrogenation, the pH of the solution was adjusted to 5 by adding a few drops of glacial acetic acid. The catalyst was filtered off and the filtrate was concentrated to dryness. The residue was acetylated, the product being purified on a silica-gel column using 1: 7 (v/v) acetone–benzene. Fractions homogeneous on TLC (R_f 0.62) in 1: 1 (v/v) 2-butanone–toluene were combined and concentrated. The residue was recrystallized from 2-propanol to give 248 mg (48%) of **5**, mp 93—95 °C, $[\alpha]_D^{21}$+123.0° (*c* 0.88, ethanol). The compound is identical with an authentic sample in ^1H NMR and IR spectra, showing no depression in mixed melting point determination with an authentic sample. Lit,[3] mp 95—96 °C, $[\alpha]_D^{22.5}$+120.2° (*c* 1.02, ethanol). ^1H NMR: δ 1.95 (s, 3, OAc), 2.02 (s, 3, OAc), 2.07 (s, 12, 4×OAc), 2.11 (s, 18, 6×OAc), 2.15 (s, 3, OAc), 2.19 (s, 3, OAc), 4.84 (dd, 1, $J_{1,2}$=4.2 Hz, $J_{2,3}$=10.0 Hz, H-2), 5.65 (d,1, H-1).

Found: C, 49.72; H, 5.62%. Calcd for $C_{52}H_{70}O_{35}$: C, 49.76; H, 5.62%.

(b) Crude **4** (600 mg) was worked up analogously as described above to give 236 mg (32%) of crude **5**, mp 93—95 °C, $[\alpha]_D^{22}$+117.9 ° (*c* 3.30, ethanol).

Found: C, 49.53; H, 5.47%. Calcd for $C_{52}H_{70}O_{35}$: C, 49.76; H, 5.62%.

Stachyose (6). Compound **5** (56 mg) was deacetylated in 0.1 M methanolic sodium methoxide (2 ml) at ambient temperature overnight. The solution was diluted with cold water and neutralized with Amberlite IR-120(H^+) resin. The solution was concentrated to dryness, and the residue was recrystallized from aqueous ethanol to give 14.2 mg (48%) of **6**. After 24 h in a vacuum desiccator with calcium chloride, the product melted at 122—123 °C, $[\alpha]_D^{20}$+140.2° (*c* 0.84, water). After being dried over phosphorus pentaoxide *in vacuo* at 45 °C for 72 h, the product gave correct analysis as a monohydrate, $[\alpha]_D^{20}$+147.3° (*c* 0.8, wster), its IR spectrum being superimposable on that of an authentic sample. Lit, $[\alpha]_D$+148.1° (*c* 9, water) (anhyd ous),[1] $[\alpha]_D^{20}$ +146° (*c* 2.05, water) (anhydrous),[3] $[\alpha]_D^{23}$+133° (*c* 4.5, water) (tetrahydrate).[21]

Found: C, 41.99; H, 6.70%. Calcd for $C_{24}H_{42}O_{21}\cdot H_2O$: C, 42.11; H, 6.48%.

O-(2,3,4,6-Tetra-O-acetyl-β-D-galactopyranosyl)-(1→6)-O-(2,3,4-tri-O-acetyl-α-D-galactopyranosyl)-(1→6)-O-(2,3,4-tri-O-acetyl-α-D-glucoyranosyl) 1,3,4,6-tetra-O-acetyl-β-D-fructofuranoside (7). Mercury(II) cyanide (2.0 g) and drierite (2.0 g) were added to a solution of **1** (0.81 g) and 2,3,4,6-tetra-*O*-acetyl-α-D-galactopyranosyl bromide[15] (1.03 g) in dry nitromethane (20 ml). After being left to stand for 4.5 h in the dark, the mixturr was filtered and the filtrate was concentrated. The residue was purified on a silica gel column using 2: 5 (v/v) 2-butanone–toluene. Fractions homogeneous on TLC (R_f 0.37) in 3: 5 (v/v) 2-butanone–toluene were combined and coccentrated. The residue was recrystallized from 2-propanol to give 588 mg (54%) of **7**, mp 89—91 °C, $[\alpha]_D^{21}$+69.4° (*c* 1.34, chloroform). ^1H NMR: δ 1.95 (s, 3, OAC), 1.97 (s, 3, OAc), 2.03 (s, 3, (OAc, 2.05 (s, 3, OAc), 2.06 (s, 3, OAc), 2.10 (s, 9, 3×OAc), 2.11 (s, 3, OAc), 2.12 (s, 3, OAc), 2.13 (s, 3, OAc), 2.15 (s, 3, OAc), 2.17 (s, 3, OAc), 2.20 (s, 3, OAc), 4.49 (d, 1, $J_{1''',2'''}$= 8.0 Hz, H-1‴), 4.85 (dd, 1, $J_{1,2}$=4.0 Hz, $J_{2,3}$=10.5 Hz, H-2), 5.73 (d, 1, H-1).

Found: C, 49.60; H. 5.58%. Calcd for $C_{52}H_{70}O_{35}$: C, 49.76; H, 5.62%.

We wish to express our thanks to Mr. Toshihide Ikeda for his technical assistance and to Mr. Saburo Nakada for the elemental analyses.

References

1) A. von Planta and E. Schulze, *Ber.*, **23**, 1692 (1890).
2) D. French, *Advances Carbohyd. Chem.*, **9**, 149 (1954).
3) M. Onuki, *J. Agr. Chem. Soc. Jpn.*, **8**, 445 (1932).
4) R. A. Laidlaw and C. B. Wylam, *J. Chem. Soc.*, **1953**, 567.
5) H. Hérissey, A. Wickstrom, and J. Courtois, *Bull. Soc. Chim. Biol.*, **33**, 642 (1951).
6) T. Suami, T. Otake, T. Ikeda, and R. Adachi, *Bull. Chem. Soc. Jpn.*, **50**, 1612 (1977).
7) P. W. Austin, F. E. Hardy, J. G. Buchanan, and J. Baddily, *J. Chem. Soc.*, **1964**, 2128; P. W. Austin, F. E. Hardy, J. G. Buchanan, and J. Baddily, *J. Chem. Soc.*, **1965**, 1419.
8) R. U. Lemieux, K. B. Hendriks, R. V. Stick, and K. James, *J. Am. Chem. Soc.*, **97**, 4056 (1975).
9) R. U. Lemieux and H. Driguez, *J. Am. Chem. Soc.*, **97**, 4063 (1975).
10) R. U. Lemieux and H. Driguez, *J. Am. Chem. Soc.*, **97**, 4069 (1975).
11) R. U. Lemieux, D. R. Bundle, and D. A. Barker, *J. Am.*

Chem. Soc., **97**, 4076 (1975).
12) D. D. Cox, E. K. Metzner, and E. J. Reist, Abstract of the 172nd ACS National Meeting San Fraccisco, Calif., U. S. A., Aug. 30, 1976.
13) C. Scheiber and H. Mittelmeier, *Ber.*, **23**, 1438 (1980); C. Tanret, *Bull. Soc. Chim. Fr.*, **13**, 261 (1895); R. L. Whistler and J. N. BeMiller, *Methods Carbohyd. Chem.*, **1**, 366 (1962).
14) T. Suami, T. Otake, T. Nishimura, and T. Ikeda, *Carbohydr. Res.*, **26**, 234 (1973); An isomeric raffinose where the terminal D-galactopyranosyl group attaches to the 6-*O* of sucrose in β anomeric linkage is tentatively referred to isoraffinose for the sake of convenience
15) H. Ohle, W. Marecek, and W. Bourjan, *Chem. Ber.*, **62**, 833 (1929).
16) C. S. Hudson and J. M. Johnson, *J. Am. Chem. Soc.*, **37**, 2748 (1915); T. Suami, T. Otake, S. Ogawa, T. Shoji, and N. Kato, *Bull. Chem. Soc. Jpn.*, **43**, 1219 (1970).
17) D. Doddrell and A. Allerhand, *J. Am. Chem. Soc.*, **93**, 2779 (1971).
18) R. Khan, *Adv. Carbohyd. Chem. Biochem.*, **33**, 278 (1976).
19) A. Allerhand and D. Doddrel, *J. Am. Chem. Soc.*, **93**, 2777 (1971).
20) D. E. Dorman and J. D. Roberts, *J. Am. Chem. Soc.*, **92**, 1355 (1970).
21) C. Tanret, *C. R. Acad. Sci.*, **134**, 1586 (1902); *Bull. Soc. Chim. Fr.*, **27**, 947 (1902); *Bull. Soc. Chim. Fr.*, **29**, 888 (1903).
22) An isomeric stachyose in which the terminal D-galactopyranosyl group attaches to the 6''-*O* of raffinose in β anomeric linkage is tentatively referred to isostachyose.

Studies of Peptide Antibiotics. XXXVIII.[1] Synthesis of *S,S'*-Bi([1-L-hemicystine]-gramicidin S), a Dimerized Analog of Gramicidin S

Kazuki SATO, Kazuo UEDA,* Michio KONDO,** Haruhiko AOYAGI, and Nobuo IZUMIYA

Laboratory of Biochemistry, Faculty of Science 33, Kyushu University, Higashi-ku, Fukuoka 812

(Received November 12, 1977)

To investigate the importance of the orientation of side chains of amino acid residues in gramicidin S (GS) for the antibacterial activity, a dimerized analog of GS, namely *S,S'*-bi([1-L-hemicystine]-GS) (**13**) was synthesized *via* removal of *p*-methoxybenzyl group of [1-*S*-*p*-methoxybenzyl-L-cysteine]-GS (**12**) and subsequent oxidation. Compound **12** showed the same antibacterial activity as GS, whereas **13** was inactive. The resemblance of ORD curves of the two analogs to that of GS suggested the similarity of peptide-backbone structure of these three compounds. Strong activity of **12** was explained by similar conformation of **12** to that of GS. To explain the inactivity of **13**, a molecular model was proposed; four hydrophilic side chains are located on surface of the molecule, whereas six hydrophobic are burried.

Gramicidin S (GS) is a cyclic decapeptide antibiotic possessing the amino acid sequence shown in Fig. 1. Several models have been proposed[2] for the conformation of GS in solid state and solution. The most favorable model is the intramolecular antiparallel β-form with four hydrogen bondings between the valyl and the leucyl residues.[3] A characteristic feature of this conformation is the orientation of side chains in which the charged Orn side chains were on one side and the hydrophobic Val and Leu side chains on the other side of the molecule.[4] Recently, Kato and Izumiya introduced the sidedness hypothesis which means that the sidedness in GS molecule is important for the antibacterial activity of GS.[5,6] The sidedness hypothesis are supported by the results from many investigations of synthetic amino acid-substituted analogs.[2]

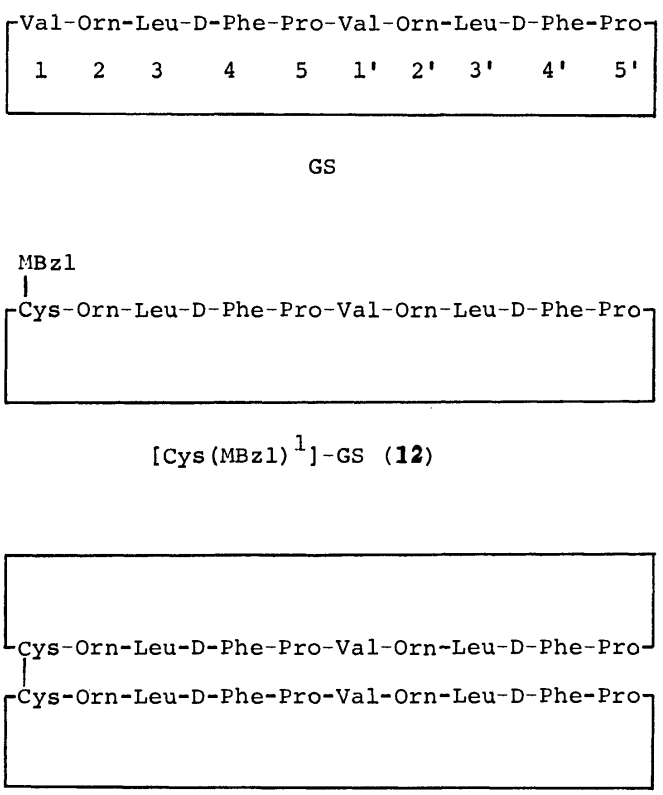

Fig. 1. Structure of GS and its analogs.

[3,3'-Di-*N*-methyl-L-leucine]-gramicidin S synthesized by Sugano *et al.*[7] showed the same antibacterial activity as GS. For the conformation of this analog, Kumar *et al.*[8] proposed a model, in which the side chains of Orn and Val were on the same side of the molecule, on the basis of NMR studies. On the other hand, Kato and Izumiya[5] showed the possibility of other two models which satisfy the sidedness hypothesis; the models were derived from the calculation of dihedral angles and other considerations. Therefore, it seemed interesting to synthesize an analog of GS which possesses a deviated conformation from the sidedness hypothesis. For this purpose, we selected a dimerized analog of GS containing a disulfide bridge. In this connection, it would be noteworthy that a synthetic digramicidin S, *cyclo*(–Val–Orn–Leu–D-Phe–Pro–)$_4$, possessed an appreciable antibacterial activity, and showed similar ORD curves as GS in ethanol, but quite different in aqueous urea.[9] These results suggested that digramicidin S also possesses somewhat GS-like orientation of side chains in spite of its soft and fairly different structures from that of GS.

The present paper deals with the synthesis, antibacterial properties, and ORD measurements of a dimerized analog of GS, *S,S'*-bi([1-L-hemicystine]-gramicidin S) (**13**), and a precursor of **13**, [1-*S*-*p*-methoxybenzyl-L-cysteine]-gramicidin S (**12**), the structure of them being shown in Fig. 1. The former compound, **13**, was a model in which the hydrophobic sides of two GS molecules were combined together by a disulfide bridge.

The synthesis of **12** was outlined in Fig. 2.[10] Cyclization reaction was achieved with leucyl residue at *C*-terminal.[11] Mercapto group of cysteine was protected with *p*-methoxybenzyl group which was removable smoothly with liquid hydrogen fluoride,[12] but stable for the treatment with hydrogen bromide in acetic acid. Mixed anhydride method was used for couplings between an amino acid and a peptide derivative, and azide method for fragment coupling and cyclization.

* Present address: Laboratory of Chemistry, College of General Education, Nagasaki University, Nagasaki 852.
** Present address: Department of Chemistry, Faculty of Science and Engineering, Saga University, Saga 840.

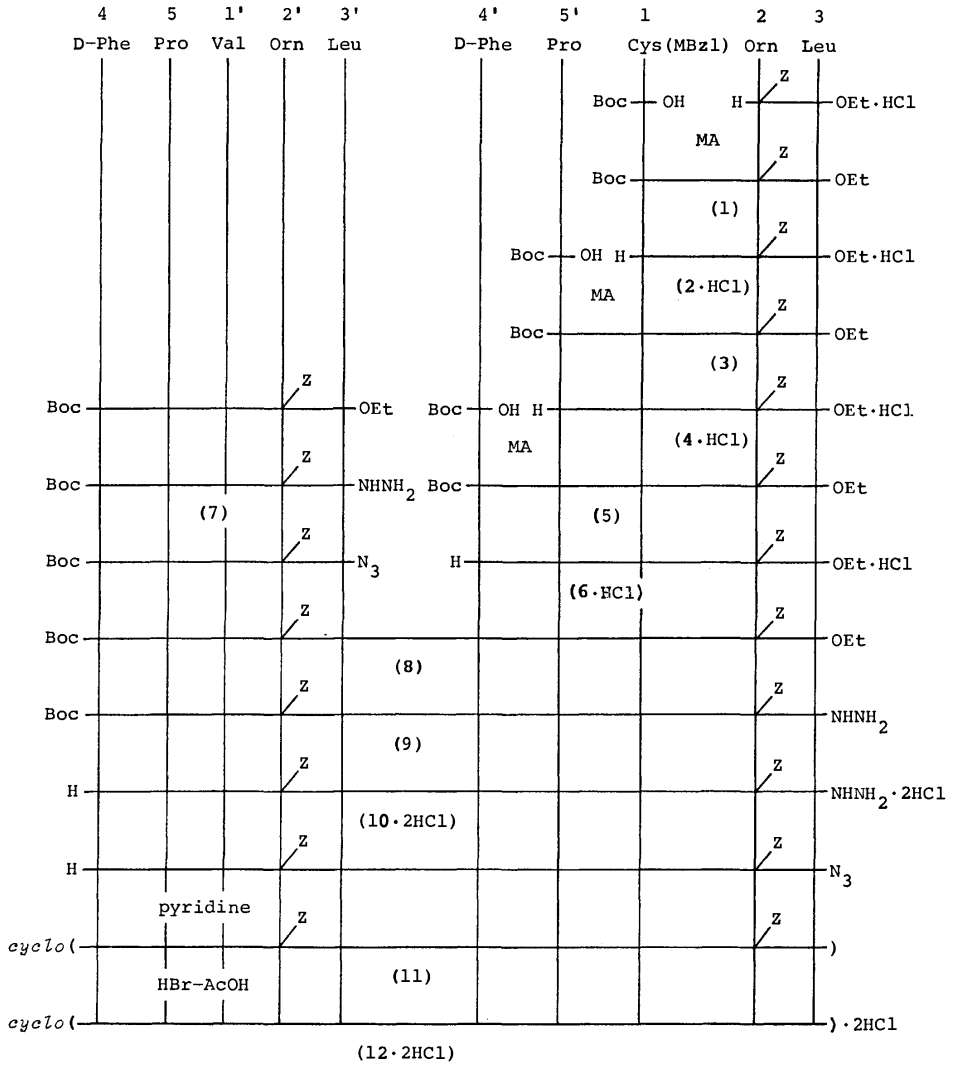

Fig. 2. Synthesis of [Cys(MBzl)[1]]-GS (**12**).

The pentapeptide ester (**6**) containing *S*-*p*-methoxybenzylcysteine residue was prepared by stepwise elongation from H–Orn(Z)–Leu–OEt·HCl[13] toward the amino end. Azide coupling of **6** and Boc-pentapeptide hydrazide (**7**) derived from Boc–D-Phe–Pro–Val–Orn(Z)–Leu–OEt[13] afforded a Boc-decapeptide ester (**8**), which was purified with silica gel column chromatography. Conversion of **8** to its hydrazide (**9**) and deblocking of Boc-group of **9** were performed without any difficulty. A key interemediate (**11**) was derived by the cyclization of **10** in a satisfactory yield of 64%. Z-groups of **11** were removed with hydrogen bromide in acetic acid and the dihydrobromide (**12**·2HBr) obtained was treated with Dowex 1 (OH^- form) to afford an acid-free **12**, which was converted to a dihydrochloride in a crystalline fine needle like GS dihydrochloride by the addition of ethanol and 1 M hydrochloric acid. The desired compound, **13**, was derived from **12** by the treatment with liquid hydrogen fluoride followed by oxidation with potassium hexacyanoferrate(III).[14] The molecular size of **13** shown in Fig. 1 was estimated by the fact that the elution volume of **13**·4HCl in the column chromatography of Sephadex G-25 coincided well with that of digramicidin S tetrahydrochloride.[9] The homogeneity of **12** and **13** was confirmed by paper and thin-layer chromatography, paper electrophoresis and elemental analysis.

Table 1. Antibacterial activity of GS and its analogs (Minimum inhibitory concentration, μg/ml)

Strain	GS	[Cys(MBzl)[1]]-GS (**12**)	*S,S'*-Bi([hemicystine[1]]-GS) (**13**)
Staphylococcus aureus	5	10	>100
Bacillus subtilis	2	5	>100
Escherichia coli	>100	>100	>100
Mycobacterium avium	100	>100	>100
Proteus vulgaris	>100	>100	>100

Antibacterial activities of **12** and **13** measured in nutrient agar are listed in Table 1. Compound **12** exhibited the same activity as GS against some organisms tested, whereas **13** was inactive. These data indicated that the Val[1] residue in GS was exchangeable to Cys(MBzl) residue without any significant effect on the antibacterial activity, and that the activity of **12**

was lost when the hydrophobic sides in position 1 were combined with a disulfide bridge.

The ORD curves of the two analogs as well as of GS are shown in Fig. 3. The fact that **12** exhibited closely similar curves to GS in EtOH (Fig. 3-a) and even in the strong denaturing agent such as 8 M urea (Fig. 3-b) suggested the rigid and stable conformation of **12** as well as natural GS. The dimerized analog, **13**, also exhibited the same pattern as GS though the negative trough was shallower than that of GS, the result suggesting that the structure of peptide-backbone was not changed significantly by the formation of a disulfide bridge.

The results of biological assay and ORD measurement

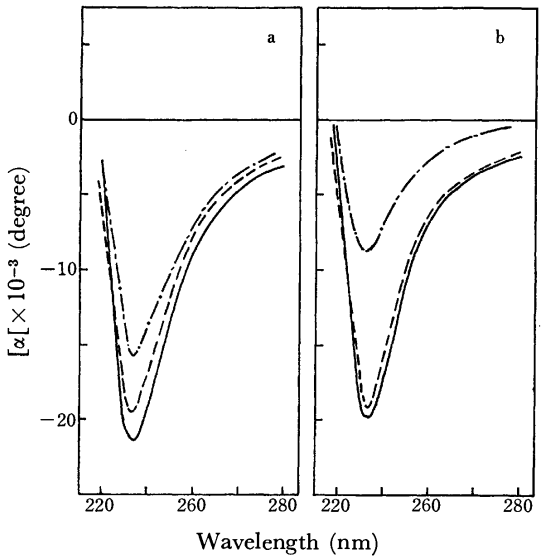

Fig. 3. ORD curves of GS and its analogs. Solvent: a, EtOH; b, 8 M urea. Curve: ——, GS; ----, **12**; -·-·-, **13**.

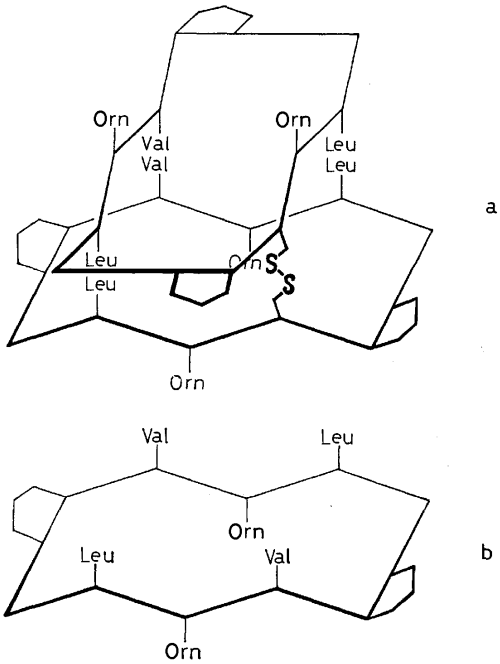

Fig. 4. A possible conformation (a) of a dimerized analog (**13**) and a conformation (b) of GS.

of **12** indicated the importance of definite orientation of side chains such that the hydrophilic side chains were on one side of a molecule and the hydrophobic were on the other side for the molecule such as GS and its active analogs. On the other hand, we propose a possible conformation (Fig. 4-a) of **13** suitable for the results of its biological assay and ORD measurement. In this model, (1) the H^{α}–C^{α} and C^{β}–S bonds are in antiperiplanar conformation regards to the C^{α}–C^{β} bond,[15] (2) the dihedral angle of C^{β}–S–S′–C^{β} is +90° (P-helical), and (3) charged side chains of four Orn residues are located on surface of the molecule, and bulky side chains of six Val and Leu residues make three pair of hydrophobic interactions in inside. In this connection, it would be noteworthy that NMR and CD studies on a bicyclic GS analog (cyclic decapeptide), [2,2′-cystine]-GS (**14**), revealed that its structure was identical with that of GS;[16] the fact indicated no distorting of the conformation of **14** by disulfide bridge which links the two β-antiparallel strands. The biological activity of **14**, however, has not been reported.

Experimental

All the melting points are uncorrected. The ratio in parentheses after a solvent system was indicated by vol. TLC was carried out on silica gel G (Merck) with the following solvent systems: R_f^1, CHCl–MeOH (5: 1); R_f^2, *n*-BuOH–AcOH–pyridine–H_2O (4: 1: 1: 2). Paper chromatography was carried out on Toyo Roshi No. 52 paper; R_f^3, same solvent as that used for R_f^2. Optical rotations were measured on a Union high sensitivity polarimeter PM-71. Amino acid analyses were performed with a Hitachi amino acid analyzer KLA-5. Molecular weight was determined with a Hitachi Osmometer, Model 115, MeOH being used as a solvent.

Boc-Cys(MBzl)-Orn(Z)-Leu-OEt (1). To a chilled solution of Boc-Cys(MBzl)-OH (5.12 g, 15 mmol) and TEA (2.1 ml, 15 mmol) in THF (30 ml) was added isobutyl chloroformate (1.97 ml, 15 mmol) at −10°C. After 10 min, a chilled solution of H-Orn(Z)-Leu-OEt·HCl[13] (6.65 g, 15 mmol) and TEA (2.1 ml, 15 mmol) in $CHCl_3$ (30 ml) was added. The mixture was left to stand at room temperature overnight, evaporated *in vacuo*, and the oily residue was dissolved in EtOAc. The solution was washed successively with 4% $NaHCO_3$, 10% citric acid and water, dried (Na_2SO_4), and evaporated under reduced pressure. The residual oil was solidified by the addition of ether and petroleum ether, and the product was recrystallized from EtOH–ether–petroleum ether; yield, 7.68 g (70%); mp 78—80 °C; $[\alpha]_D^{20}$—25.6 ° (*c* 1, EtOH); R_f^1 0.88.

Found: C, 60.90; H, 7.50; N, 7.77%. Calcd for $C_{37}H_{54}O^9N_4S$: C, 60.80; H, 7.45; N, 7.67%.

H-Cys(MBzl)-Orn(Z)-Leu-OEt·HCl (2·HCl). Compound **1** (6.58 g, 9 mmol) was dissolved in 2.8 M hydrogen chloride in EtOAc (64 ml). The solution was allowed to stand at room temperature for 1 h and then evaporated. Addition of ether to the oily residue gave hygroscopic crystals; yield, 5.47 g (91%); mp 170—171 °C; $[\alpha]_D^{20}$—10.6° (*c* 1, EtOH); R_f^1 0.80, R_f^2 0.84, R_f^3 0.93.

Found: C, 56.42; H, 7.08; N, 8.44%. Calcd for $C_{32}H_{46}O_7N_4S\cdot HCl\cdot H_2O$: C, 56.08; H, 7.21; N, 8.18%.

Boc-Pro-Cys(MBzl)-Orn(Z)-Leu-OEt(3). This was prepared from Boc-Pro-OH (1.64 g, 7.6 mmol) and **2**·HCl (5.09 g, 7.6 mmol) as described for the preparation of **1**.

The product was recrystallized from EtOH–ether; yield, 5.16 g (82%); mp 134—136 °C; $[\alpha]_D^{20}$—48.8° (*c* 1, EtOH); R_f^1 0.87.

Found: C, 60.44; H, 7.52; N, 8.39%. Calcd for $C_{42}H_{61}O_{10}N_5S$: C, 60.92; H, 7.43; N, 8.46%.

H–Pro–Cys(MBzl)–Orn(Z)–Leu–OEt·HCl (**4**·*HCl*). This was prepared from **3** (2.85 g, 3.5 mmol) as described for **2**·HCl; yield, 2.52 g (95%); mp 112—114 °C; $[\alpha]_D^{20}$—39.0° (*c* 1, EtOH); R_f^1 0.66, R_f^2 0.78.

Found: C, 57.37; H, 7.13; N, 8.87%. Calcd for $C_{37}H_{53}O_8N_4S$·HCl: C, 57.46; H, 7.17; N, 9.06%.

Boc–D-Phe–Pro–Cys(MBzl)–Orn(Z)–Leu–OEt (**5**). This was prepared from Boc–D-Phe–OH (0.85 g, 3.2 mmol) and **4**·HCl (2.47 g, 3.2 mmol) as described for **1**. The product was obtained as a foam; yield, 3.01 g (97%); $[\alpha]_D^{20}$—85.9° (*c* 2, EtOH); R_f^1 0.71.

Found: C, 62.66; H, 7.44; N, 8.50%. Calcd for $C_{51}H_{70}O_{11}N_6S$: C, 62.81; H, 7.24; N, 8.62%.

H–D-Phe–Pro–Cys(MBzl)–Orn(Z)–Leu–OEt·HCl (**6**·*HCl*). Compound **5** (1.95 g, 2 mmol) was treated with 2.8 M hydrogen chloride in EtOAc (14 ml) as described for **2**·HCl. The oily product was purified with a column (4.6×40 cm) of silica gel as follows. The crude **6**·HCl was applied on the column. The column was washed successively with EtOAc (1000 ml) and a mixture (300 ml) of EtOAc–EtOH (2:1), and eluted with EtOH (700 ml). Each fraction was assayed by TLC, and the fractions containing the desired product were evapotared to leave a foam; yfield, 1.29 g (70%); $[\alpha]_D^{20}$—119° (*c* 1, EtOH); R_f^1 0.62.

Found: C, 59.83; H, 7.00; N, 9.11%. Calcd for $C_{46}H_{62}O_9N_6S$·HCl·1/2H_2O: C, 60.01; H, 7.01; N, 9.13%.

Boc–D-Phe–Pro–Val–Orn(Z)–Leu–N_2H_3 (**7**). A solution of Boc–D-Phe–Pro–Val–Orn(Z)–Leu–OEt (0.86 g, 1 mmol)[13] and hydrazine hydrate (1.94 ml, 40 mmol) in DMF (6 ml) was allowed to stand at room temperature for 48 h. The solution was evaporated and the addition of water afforded a solid, which was recrystallized from MeOH–ether; yield, 0.77 g (92%); mp 178—182 °C; $[\alpha]_D^{20}$—62.8° (*c* 1, EtOH); R_f^1 0.72.

Found: C, 61.43; H, 7.95; N, 13.23%. Calcd for $C_{43}H_{64}O_9N_8$: C, 61.70; H, 7.71; N, 13.39%.

Boc–D-Phe–Pro–Val–Orn(Z)–Leu–D-Phe–Pro–Cys(MBzl)–Orn(Z)–Leu–OEt (**8**). To a solurion of **7** (313 mg, 0.37 mmol) in DMF (2 ml) were added 2.8 M hydrogen chloride in EtOAc (0.52 ml) and isopentyl nitrite (0.057 ml, 0.41 mmol) in DMF (0.57 ml) at −60 °C. After being left to stand at −20 °C for 10 min, the solution was cooled again to −60 °C and neurtalized with TEA (0.21 ml, 1.5 mmol). To this solution was added a chilled solution of **6**·HCl (337 mg, 0.37 mmol) and TEA (0.05 ml, 0.37 mmol) in DMF (1 ml). The reaction mixture was allowed to stir at 0 °C for 48 h and then evaporated. After the addition of 0.02 M citric acid (100 ml), the solid was collected and washed with water. The crude product was purified with a column (4.6×45 cm) of silica gel using $CHCl_3$–MeOH–AcOH (95:5:1) as a developing agent as described for **6**·HCl; yield, 370 mg (60%); mp 104—109 °C; $[\alpha]_D^{20}$—116° (*c* 0.5, EtOH); R_f^1 0.79.

Found: C, 63.32; H, 7.31; N, 9.96%. Calcd for $C_{89}H_{122}O_{18}N_{12}S·H_2O$: C, 63.32; H, 7.40; N, 9.95%.

Boc–D-Phe–Pro–Val–Orn(Z)–Leu–D-Phe–Pro–Cys(MBzl)–Orn(Z)–Leu–N_2H_3 (**9**). Compound **8** (336 mg, 0.2 mmol) was treated with hydrazine hydrate (0.39 ml, 8 mmol) as described for **7**; yield, 232 mg (70%); mp 208—209 °C $[\alpha]_D^{20}$—126° (*c* 0.5, EtOH); R_f^1 0.61.

Found: C, 61.12; H, 7.19; N, 11.55%. Calcd for $C_{87}H_{120}O_{17}N_{14}S·2H_2O$: C, 61.39; H, 7.34; N, 11.52%.

H–D-Phe–Pro–Val–Orn(Z)–Leu–D-Phe–Pro–Cys(MBzl)–Orn(Z)–Leu–N_2H_3·2HCl (**10**·2*HCl*). Compound **9** (216 mg, 0.13 mmol) was treated with 0.1 M hydrogen chloride in formic acid (3.3 ml) as described for **2**·HCl and the product was used for the next reaction without further treatment; yield, 196 mg (92%); R_f^1 0.58.

cyclo(*–D-Phe–Pro–Val–Orn(Z)–Leu–D-Phe–Pro–Cys(MBzl)–Orn(Z)–Leu–*) (**11**). To a solution of **10**·2HCl (178 mg, 0.11 mmol) in DMF (2 ml) were added 2.8 M hydrogen chloride in EtOAc (0.15 ml) and isopentyl nitrite (0.017 ml, 0.12 mmol) in DMF (0.17 ml) at −30 °C. After 30 min, the reaction mixture was added into pyridine (108 ml) at 0 °C. After being stirred at 5 °C for 4 days, the solution was evaporated and the residue was dissolved in a mixture (11 ml) of MeOH–H_2O (10:1). The solution was applied on columns (1.9×20 cm each) of Dowex 1 (OH^- form) and Dowex 50 (H^+ form). The columns were washed with the same solvent (200 ml); the combined effluent was evaporated to leave an oil which was solidified by the addition of water. The crude product dissolved in MeOH (2 ml) was applied on a column (1.8×110 cm)of Sephadex LH-20 which was developed with MeOH. The fractions with the desired product were evaporated and the oily residue was crystallized by the addition of ether and petroleum ether; yield, 106 mg (64%); mp 187—189 °C; $[\alpha]_D^{20}$—290° (*c* 0.5, MeOH); R_f^1 0.78.

Found: C, 63.54; H, 7.05; N, 10.71%; mol wt, 1541. Calcd for $C_{82}H_{103}O_{15}N_{12}S·H_2O$: C, 63.46; H, 7.15; N, 10.83%; mol wt, 1552.

cyclo(*–D-Phe–Pro–Val–Orn–Leu–D-Phe–Pro–Cys(MBzl)–Orn Leu–*)·2HCl ([*Cys(MBzl)*^{1}]–*GS*·2HCl) (**12**·2*HCl*). To a solution of **11** (96 mg, 0.06 mmol) in AcOH (1 ml) was added 25% hydrogen bromide in AcOH (0.2 ml). The rereaction mixture was allowed to stand at room temperature for 4 h, evaporated, and the yellowish residue was crystallized by the addition of ether. The crude dihydrobromide was dissolved in a mixture of MeOH–H_2O (4:1) and the solution was applied on a column (1.9×20 cm) of Dowex 1 (OH^- form). The peptide in the column was eluted with the same solvent and the combined effluent (200 ml) was evaporated to leave a solid. The product was recrystallized from EtOH–1 M HCl; yield, 62 mg (75%); mp 270—271 °C (dec); $[\alpha]_D^{20}$—297° (*c* 0.3, EtOH); R_f^2 0.84, R_f^3 0.80.

Found: C, 55.64; H, 7.59; N, 11.45%. Calcd for $C_{66}H_{96}O_{11}N_{12}S$·2HCl·5$H_2O$: C, 55.49; H, 7.61: N, 11.75%.

S,S'-Bicyclo(*–D-Phe–Pro–Val–Orn–Leu–D-Phe–Pro–hemicystyl–Orn–Leu–*)·4HCl (S,S'–*Bi*([*hemicystine*^{1}]–*GS*)·4HCl) (**13**·4*HCl*). To a mixture of **12**·2HCl (40 mg, 0.03 mmol) and anisole (0.16 ml) was added liquid hydrogen fluoride (5 ml) at 0 °C. The reaction mixture was stirred at 0 °C for 1 h and then evaporated *in vacuo*. The residue was dissolved in 1 M AcOH (50 ml) and the solution was washed with ether (20 ml×2) and then lyophilized. To a solution of the lyophilizate (30 mg) in 0.05 M ammonium acetate containing 30% MeOH (50 ml, pH 6.8) was added 0.01 M potassium hexacyanoferrate(III) (5.6 ml).[14] After being stirred for 10 min, Amberlite IR-45 (Cl^- form) resin was added into the solution, and the resin was filtered off and washed with 30% MeOH. The filtrate and washings were evaporated, the residue was dissolved in a mixture (3 ml) of AcOH–MeOH–H_2O (1:1:1), and the solution was applied on a column of Sephadex G-25 (2×80 cm) which was eluted with the same solvent. The fractions of the desired product were evaporated to leave a solid, which was recrystallized from EtOH–1 M HCl; yield, 15 mg (41%); mp 258—259 °C (dec); $[\alpha]_D^{20}$—287° (*c* 0.4, EtOH); R_f^2 0.75; R_f^3 0.80. Amino acid ratios in acid hydrolyzate; Phe

4.20, Pro 3.76, Val 1.92, cystine 0.90, Orn 4.12, Leu 4.00. Found: C, 53.43; H, 7.37; N, 12.07%. Calcd for $C_{116}H_{174}O_{20}N_{24}S_2 \cdot 4HCl \cdot 10H_2O$: C, 53.28; H, 7.63; N, 12.36%.

Paper Electrophoresis. This was carried out with Toyo Roshi No. 52 paper and a solvent system of HCOOH–AcOH–MeOH–H_2O (1: 3: 6: 10, pH 1.8) for 2.5 h at 500 V/30 cm. Figure 5 showed that each of the peptides (**12** and **13**) revealed a single spot.

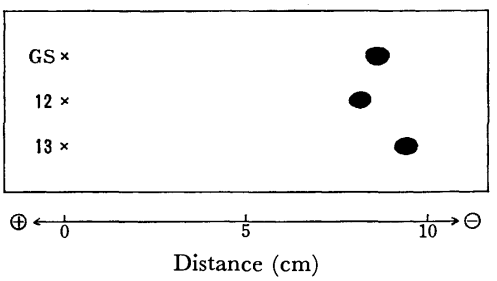

Fig. 5. Paper electrophoresis of GS and its analogs.

Microbiological Assays[17] *and ORD Measurements.* These were carried out as described in a previous paper,[13] the results being shown in Table I and Fig. 3.

The authors wish to express their thanks to Dr. T. Kato and Dr. M. Waki of this laboratory for their helpful discussions.

References

1) Part XXXVII of this series: H. Takiguchi, H. Nishikawa, S. Ando, and N. Izumiya, *Bull. Chem. Soc. Jpn.*, **51**, 297 (1978).

2) T. Kato and N. Izumiya, "Chemistry and Biochemistry of Amino Acids, Peptides, and Proteins", ed by B. Weinstein, Marcel Dekker, New York (1974), pp. 1—39.

3) D. C. Hodgkin and B. M. Oughton, *Biochem. J.*, **65**, 752 (1957), and the references cited in Ref. 2.

4) R. Schwyzer, "Amino Acids and Peptides with Antimetabolic Activity," Churchill, New York (1958), pp. 171—191.

5) T. Kato and N. Izumiya, *Biochim. Biophys. Acta*, **493**, 235 (1977).

6) In 1958, Schwyzer proposed the concept that GS shows the antibacterial activity because of a specific conformation of the molecule in which the charged side chains are on one side and the hydrophobic side chains on the other side.[4] For this concept, Kato and Izumiya introduced a term of sidedness hypothesis in 1977;[5] a term of sidedness itself appeared at first in 1975.[8]

7) H. Sugano, H. Abe, M. Miyoshi, T. Kato, and N. Izumiya, *Bull. Chem. Soc. Jpn.*, **47**, 698 (1974).

8) N. G. Kumar, N. Izumiya, M. Miyoshi, H. Sugano, and D. W. Urry, *J. Am. Chem. Soc.*, **97**, 4105 (1975).

9) S. Matsuura, M. Waki, T. Kato, and N. Izumiya, *Bull. Chem. Soc. Jpn.*, **46**, 977 (1973).

10) Abbreviations according to IUPAC-IUB Commission, *J. Biol. Chem.*, **247**, 977 (1972), are used throughout. Additional abbreviations: DMF, *N,N*-dimethylformamide; MA, mixed anhydride; MBzl, *p*-methoxybenzyl; TEA, triethylamine. Amino acid symbols except D-Phe denote the L-configuration.

11) M. Ohno, K. Kuromizu, H. Ogawa, and N. Izumiya, *J. Am. Chem. Soc.*, **93**, 5253 (1971).

12) S. Sakakibara, Y. Shimonishi, Y. Kishida, M. Okada, and H. Sugihara, *Bull. Chem. Soc. Jpn.*, **40**, 2164 (1967).

13) H. Abe, K. Sato, T. Kato, and N. Izumiya, *Bull. Chem. Soc. Jpn.*, **49**, 3113 (1976).

14) D. B. Hope, V. V. S. Marti, and V. du Vigneaud, *J. Biol Chem.*, **237**, 1563 (1962).

15) H. Sugeta, A. Go, and T. Miyazawa, *Chem. Lett.*, **1972**, 83.

16) U. Ludescher and R. Schwyzer, *Helv. Chim. Acta*, **54**, 1637 (1971); *ibid.*, **55**, 2052 (1972).

17) We are indebted to the staff of Takeda Chemical Industries, Ltd., for the assay.

Preparation of Organic Copper(I) Complexes by the Reactions of Methylbis(triphenylphosphine)copper(I) with Nitroalkanes, β-Diketones, and Cyanoalkanes[1)]

Takakazu YAMAMOTO, Minoru KUBOTA, Akira MIYASHITA, and Akio YAMAMOTO

Research Laboratory of Resources Utilization, Tokyo Institute of Technology, 4259 Nagatsuta-cho, Midori-ku, Yokohama 227

(Received November 16, 1977)

Reactions of a methylcopper complex $CH_3Cu(PPh_3)_2$(diethyl ether)$_{0.5}$ (PPh_3=triphenylphosphine) with three types of active hydrogen compounds HA give the corresponding copper derivatives of active hydrogen compounds formulated as $ACu(PPh_3)_2$. Nitroalkanes (nitromethane, nitroethane and 2-nitropropane) form copper complexes bonded through aci-nitro groups. β-Diketone and its analogs such as acetylacetone, diethyl malonate and ethyl acetoacetate react in their enol form to give six-membered *O,O'*-bonded chelates, whereas cyanoalkanes including acetonitrile, propionitrile, and malononitrile afford organocopper complexes having a direct Cu–C bond.

The non-transition metal derivatives of active hydrogen compounds such as diethyl malonate and malononitrile serve as convenient and versatile starting materials for the syntheses of various organic compounds. Extensive studies have been made on the preparation and properties of the non-transition metal derivatives of the active hydrogen compounds. However, only limited information is available on the transition metal derivatives of the active hydrogen compounds except for some β-diketones which form chelate complexes with the transition metals. In the course of studies on the chemical properties of alkylcopper complexes having tertiary phosphine ligands[2)] it was found that reactions proceed smoothly between the alkylcopper complexes and various active hydrogen compounds having nitro, β-dicarbonyl, or cyano group to afford various copper derivatives of the active hydrogen compounds in high yields.

In this paper we report the preparation of the copper derivatives of the active hydrogen compounds and discuss their structures. Marsich and Camus and co-workers recently reported the preparation of copper derivatives of active hydrogen compounds having β-dicarbonyl or nitro group by the reaction of arylcopper(I) with the active hydrogen compounds in the presence of phosphine ligands.[3)] Tsuda *et al.* reported the formation of (cyanomethyl)copper complexes by the decarbonylation of Cu(I) and Cu(II) cyanoacetates as well as by the reaction of t-$C_4H_9OCu(P(n\text{-}C_4H_9)_3)$ with CH_3CN.[4)] Utilization of (cyanomethyl)copper prepared *in situ* by the reaction of CuI with $LiCH_2CN$ for organic syntheses[5)] was also reported.

Results and Discussion

Reactions of Alkylcopper Complexes with Active Hydrogen Compounds. Alkylcopper complexes smoothly react with active hydrogen compounds having nitro, β-dicarbonyl, or cyano group. The methylcopper complex $CH_3Cu(PPh_3)_2(Et_2O)_{0.5}$ gives three types of complex in high yields (63—92%) depending on the nature of the active hydrogen compound.

An active hydrogen compound with more acidic hydrogen reacts more easily with the methylcopper complex. As an example, **1** reacts with malononitrile immediately at −30 °C, but the reaction of **1** with

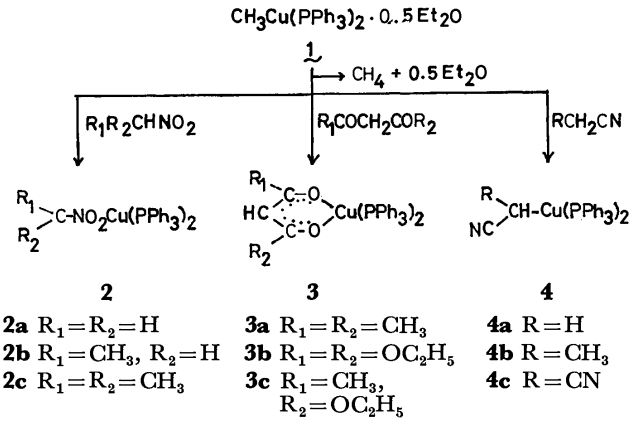

Fig. 1.

propionitrile at room temperature takes several hours to complete. All the complexes prepared are white indicating that the oxidation number of copper in the complexes is one. Type **2** and **3** complexes are soluble in organic solvents, but not the copper derivatives of cyanoalkanes, **4**. Most complexes are relatively insensitive to air, having very high thermal stability in the solid state. However, they are easily oxidized in solution, the thermal stability decreasing.

Of the products represented in Fig. 1, **2a**, **3a**, **3b**, **3c**, and **5** have been independently prepared by Marsich and Camus and co-workers through reactions of arylcopper(I) prepared *in situ* with the corresponding active hydrogen compounds in the presence of PPh_3.[3)] However, no NMR spectroscopic data have been given.[6)] Analytical and spectral data of the isolated complexes are summarized in Tables 1 and 2, respectively.

In addition to the nitromethanato complex **2a** they prepared a dinitrophenylmethane derivative of copper $(C_6H_5C(NO_2)_2)Cu(PPh_3)_2$, and confirmed by X-ray analysis that the copper atom in the complex is bonded to the dinitrophenylmethanato ligand through one of the two nitro groups in the solid state.[3d)] The IR and NMR spectroscopic data of complexes **2a**, **2b**, and **2c** support the view that the copper atom in these complexes is bonded to the nitroalkanato ligand through the same type of bonding (aci-nitro type bonding) as in the dinitrophenylmethane complex:

The ν(C=N) stretching frequencies of the nitroalkanes

TABLE 1. PREPARATION OF THE COPPER DERIVATIVES OF ACTIVE HYDROGEN COMPOUNDS ACCORDING TO Fig. 1.

Complex		Yield (%)	Mp (°C)	Found (Calcd), % C	H	N	M_w[a]
$Cu(CH_2NO_2)(PPh_3)_2$	**2a**[b]	89	177—182	68.7 (68.5	5.1 5.0	2.4 2.2)	
$Cu(CH(CH_3)NO_2)(PPh_3)_2$	**2b**	85	178—179	68.7 (68.9	5.0 5.2	2.2 2.1)	593 (676)
$Cu(C(CH_3)_2NO_2)(PPh_3)_2$	**2c**	63	172—173	69.5 (69.2	5.7 5.4	2.3 2.1)	
$Cu(CH(COCH_3)_2)(PPh_3)_2$	**3a**[b]	92	210—215	71.2 (71.6	5.3 5.4)		
$Cu(CH(COOC_2H_5)_2)(PPh_3)_2$	**3b**[b]	78	176—179	72.5 (72.2	5.9 5.8)		594 (747)
$Cu(CH(COCH_3)COOC_2H_5)(PPh_3)_2$	**3c**[b]	67	127—129	70.3 (70.3	5.7 5.4)		410 (717)
$Cu(CH_2CN)(PPh_3)_2$	**4a**	68	188	72.6 (72.7	5.2 5.1	2.1 2.2)	
$Cu(CH(CH_3)CN)(PPh_3)_2$	**4b**	72	179	72.7 (72.9	5.5 5.4	2.4 2.2)	
$Cu(CH(CN)_2)(PPh_3)_2$	**4c**	78	216	71.9 (71.7	4.6 4.8	4.2 4.3)	
$Cu(CH(CN)COOC_2H_5)(PPh_3)_2$	**5**[b]	84	166—167	70.2 (70.2	5.3 5.2	2.2 2.0)	601 (700)

a) Cryoscopic in benzene. b) Prepared independently by Marsich and Camus and co-workers.[3]

TABLE 2. IR AND NMR SPECTROSCOPIC DATA OF THE COPPER DERIVATIVES OF ACTIVE HYDROGEN COMPOUNDS

Complex	ν(CN) and ν(CO)[a] (cm^{-1})	$\Delta\nu$[b] (cm^{-1})	Relevant NMR signals and assignments[c] (δ, ppm from TMS)
2a	1582	24	5.76 (2H, s, CH_2) $\Delta\delta$=1.43[d]
2b	1580	25	1.95 (3H, d, 6 Hz, CH_3) $\Delta\delta$=0.40, 6.26 (1H, q, 6 Hz, CH) $\Delta\delta$=1.86
2c	1600 1580	55 30	2.16 (6H, s, CH_3) $\Delta\delta$=0.61
3a	1598 1510	*ca.*—110	2.04 (6H, s, CH_3), 5.56 (1H, s, CH)
3b	1643	—92	1.0 (6H, t, CH_3), 4.1 (4H, q, CH_2), 5.12 (1H, s, CH)
3c	1635	*ca.*—100	1.0 (3H, t, CH_3), 2.14 (3H, s, CH_3), 4.0 (2H, q, CH_2), 5.36 (1H, s, CH)
4a	2125	—120	
4b	2100	—140	
4c	2150 2095	—120 —175	
5	2180 1670	—70 —80	0.92 (3H, t, CH_3), 3.72 (1H, s, CH), 3.82 (2H, q, CH_2)

a) In KBr disk. ν(C=N) for **2a**, **2b**, and **2c**; ν(C=O) for **3a**, **3b**, and **3c**; (C≡N) for **4a**, **4b**, and **4c**; ν(C≡N) and (C=O) for **5**. b) $\Delta\nu=\nu(XY)_{complex}-\nu(XY)_{free}$ (X, Y=C, N, O). c) In $CDCl_3$ for **2a**; in C_6D_6 for the other complexes. d) $\Delta\delta=\delta_{complex}-\delta_{free}$. The triphenylphosphine signals are omitted from the table.

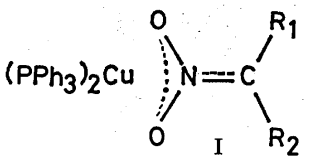

I

Fig. 2.

shift towards higher values on complex formation, the new bands appearing in the absorption regions characteristic of the aci-nitroalkanato anion.[7]

In the NMR spectra of the nitroalkanato complexes the α-proton signals of nitromethane and nitroethane are shifted to lower field by 1.44[6] and 1.86 ppm, respectively, and the α-methyl proton signals of nitroethane and 2-nitropropane to the same direction by 0.40 and 0.61 ppm, respectively. Since the protons attached to the carbon directly bonded to copper in alkylcopper complexes give rise to signals at relatively higher fields as compared with those in usual organic compounds,[2b] the low field shift of nitroalkane signals upon bonding to copper is not in line with the substitution of the nitroalkanes by copper at the α-position forming a nitroalkylcopper complexes.

The sp^2 character around the α-carbon in the aci-nitro type complex I accounts for the lowering of the

α-proton and α-methyl signals.

Since the nitroalkanato ligand $RCHNO_2$ is considered to be bonded to copper atom through the nitro group, the reaction of the complex with alkyl halide R'X is expected to give *O*-alkylated compound RCH=N(O)OR' as in the reactions of copper phenoxide with alkyl halides.[8] However, the reactions of complexes **2a**, **2b**, and **2c** with alkyl halides give α-*C* alkylated compounds $RCHR'NO_2$, *e.g.*,

$$\mathbf{2b} + CH_3I \xrightarrow[THF]{\text{r.t.}} \text{2-nitropropane (16\%)}$$

The α-alkylated compounds can be produced through a direct electrophilic attack of R'X at the α-carbon in the aci-nitromethanato ligand or through isomerization of the *O*-bonded species I to the *C*-bonded species.

On allowing complex **2a** to stand in chloroform at room temperature it is decomposed to release nitromethane.[6] Since employment of $CDCl_3$ does not cause the introduction of D into the nitromethane released, the possibility of the abstraction of hydrogen of chloroform by the nitromethanato ligand is excluded. The PPh_3 ligand coordinated with Cu may give its ortho hydrogen to the nitromethanato ligand with formation of ortho metalized PPh_3 ligand and nitromethane. This type of abstraction of ortho hydrogen of PPh_3 has been observed in the decomposition of $RhCH_3(PPh_3)_3$ in solutions.[9]

Cryoscopic determination of the molecular weight indicates that the nitroethanato complex has a monomeric structure in benzene with partial dissociation of the PPh_3 ligands.

The ν(C=O) bands assignable to free C=O groups of the β-dicarbonyl compounds (acetylacetone, diethyl malonate, ethyl acetoacetate) disappear on the complex formation with copper, new bands appearing in a lower frequency region which is shifted by *ca.* 100 cm^{-1} from the original ν(C=O). The IR data indicate the formation of an *O*,*O'*-bonded six-membered chelate β-dicarbonyl ligands, excluding the possible metalization of the β-dicarbonyl compounds through the α-carbon.[10] In the *C*-bonded complexes the ν(C=O) bonds are usually observed at much higher frequency, 1700—1800 cm^{-1}. The *O*,*O'*-bonded structure in $Cu(CF_3COCHCOCH_3)(PPh_3)_2$ has been established by X-ray crystallography.[11] The molecular weight determination of complexes **3b** and **3c** gave lower values than those calculated for each complex suggesting dissociation of one of PPh_3 ligands in benzene.

Some by-products such as the dimers of cyanoalkanes (*e.g.*, 2-aminocrotonitrile from acetonitrile) are formed in the metalization of cyanoalkanes by alkali metals, contamination of the alkali metal cyanoalkanate with the by-products being inevitable.[12] However, contamination of complexes **4a** and **4b** with the by-products is excluded since each IR spectrum of the complexes shows only a sharp ν(C≡N) band and acidolyses of the complexes with acetic acid give only the parent cyanoalkanes as confirmed by gas chromatography. Appearance of two ν(C≡N) bands in the IR spectrum of **4c** seems to be due to the separation of $\nu(CN)_{sym}$ and $\nu(CN)_{asym}$ vibrations in the dicyanomethanato ligand.

For the metal derivatives of cyanoalkanes the following forms (a)—(e) are conceivable ((c) is possible only when R=H):[12b]

MCHR–C≡N, MCR=C=NH, MC≡C–NHR,
(a) (b) (c)
RC≡C–NHM, HRC=C=NM
(d) (e)
M=metal

As for complexes **4a** and **4b**, however, the presence of the tautomeric species (b), (c), and (d) is not plausible since their IR spectra show no ν(N–H) band. Insolubility of complexes **4a**, **4b**, and **4c** prevents a detailed structural examination of the complexes by NMR spectroscopy, but form (a) is preferred to the other forms for the present copper derivatives of cyanoalkanes, since some sodium derivatives of cyanoalkanes are known to exist mainly in the *C*-bonded form and the ν(CN) bands of the present copper derivatives appear in the same range of the ν(CN) bands as in the sodium derivatives.[12a] The insolubility of the complexes in organic solvents (acetone, acetonitrile, tetrahydrofuran, benzene, chloroform *etc.*) suggests that the complexes are aggregated by intermolecular association between the CN group and copper.

In contrast to complexes **4a**, **4b**, and **4c** the copper derivative of the β-carbonyl cyanoalkane, ethyl cyanoacetate, is soluble in common organic solvents. The shift of the α-proton signal of ethyl cyanoacetate to lower magnetic field (NMR) by 0.27 ppm and a relatively large shift of ν(CO) band to lower frequency on the formation of the copper derivative suggest the formation of an *O*- and *NC*-bonded chelate:

The molecular weight determination of complex **5** also excludes the association of the complex through the CN group.

Experimental

General. Preparation and recrystallization of copper complexes were carried out under deoxygenated nitrogen or argon. IR spectra were recorded on a Hitachi Model 295 spectrometer in KBr discs, and ^{1}H-NMR spectra on a Japan Electron Optics Lab. JNM-PS-100 spectrometer (TMS as an internal standard). The amount of gas evolved was measured by volumetry and the composition of the gas was analyzed with a Hitachi RMU-5B mass-spectrometer and a Shimadzu GC-5B gas chromatograph. The microanalysis of carbon, hydrogen and nitrogen was performed by Mr. T. Saito with Yanagimoto CHN Autocorder Type MT-2. For analytical and spectral data see Tables 1 and 2.

Material. $CH_3Cu(PPh_3)_2$ $(Et_2O)_{0.5}$ **1** was prepared as reported previously.[2] Solvents were dried by the usual procedure, distilled, and stored under argon or nitrogen. Active hydrogen compounds were purified by distillation brfore use.

Preparations of Copper Derivatives of Nitroalkanes. *Complex 2a*: Nitromethane (3.00 g, 50 mmol) was introduced by a trap-to-trap distillation in a vacuum to complex **1** (100 g, 1.56 mmol) dissolved in tetrahydrofuran (THF, 10 ml). After the mixture had been stirred for 2 h at room temperature a colorless solution was obtained with evolution of methane (35.0 ml, S.T.P., 1.00 mol/Cu). Addition of diethyl ether (20 ml) to the solution and cooling gave white crystlas. They were washed with diethyl ether repeatedly

and dried in a vacuum to yield 899 mg of **2a** (1.39 mmol, 89%).

Complex 2b: Nitroethane (3.75 g, 50 mmol) was introduced to a THF (10 ml) solution of complex **1** (1.00 g, 1.56 mmol) in a vacuum. Stirring of the mixture for 2 h at 0 °C gave a colorless solution, releasing a quantitative amount of methane. Addition of diethyl ether (20 ml) to the solution and cooling afforded white crystals. They were recrystallized from THF and dried in a vacuum to give white crystals of **2b** (877 mg, 1.325 mmol. 85%).

Complex 2c: 2-Nitropropane (4.45 g, 50 mmol) was introduced by a trap-to-trap distillation in a vacuum to a THF (10 ml) solution of complex **1** (1.00 g, 1.56 mmol). Stirring the mixture at −20 °C for 2 h gave a light yellow solution with evolution of a quantitative amount of methane. A white solid was precipitated on condensation of the solution and was recrystallized from toluene-diethyl ether. The white crystals were dried in a vacuum to yield 644 mg (63%) of **2c**.

Preparation of Copper Derivatives of β-Dicarbonyl Compounds.

Complex 3a: Acetylacetone (90 mg, 1.00 mmol) was added to a THF (10 ml) solution of complex **1** (640 mg, 1.00 mmol) with a syringe at −78 °C. Stirring of the mixture at −30—0 °C for 2 h gave a colorless solution and methane. The solution was dried up and the residue was recrystallized from THF to give white crystals, which were dried in a vacuum to give 622 mg (92%) of **3a**.

Complex 3b and 3c: Complexes **3b** and **3c** were prepared in a similar way by the reactions of complex **1** 640 mg, 1.00 mmol) with diethyl malonate (160 mg, 1.00 mol) and ethyl acetoacetate (130 mg, 1.00 mmol), respectively (reaction conditions: −30—0 °C, 2 h).

Prepararions of Cyanoalkylcopper Complexes. *Complex 4a*: The reaction of complex **1** (640 mg, 1.00 mmol) with acetonitrils (2.0 g, 49 mmol) in THF (15 ml) at −10°C gradually produced a light yellow precipitate from a dark yellow solution with evolution of methane. After 5 h the precipitate was separated by filtration, washed with THF repeatedly, and dried in a vacuum to yield a pale yellow complex of **4a** (426 mg, 68%).

Complex 4b: Complex **4b** was prepared in the reaction of complex **1** (640 mg, 1.00 mmol) with propionitrile (2.9 g, 36 mmol) in 5 ml of THF solution at room temp. for 5 h. Work-up was carried out in the same way as in the preparation of **4a**. White yellow complex of **4b** (462 mg, yield 72%) was obtained.

Complex 4c: The reaction of complex **1** (1.10 g, 1.72 mmol) with malononitrile (113 mg, 1.72 mmol) in 10 ml of THF solution at −30 °C produced a white precipitate immediately with evolution of a quantitative amount of methane. The precipitate was washed with diethyl ether and THF and dried in a vacuum to yields a white complex of **4c** (870 mg, 78%).

Complex 5: The reaction of complex **1** (640 mg, 1 mmol) with ethyl cyanoacete (113 mg, 1 mmol) in THF solution at −30—0 °C for 2 h produced a colorless solution. The solution was dried up and the residue was recrystallized from diethyl ether and toluene and the crystals were dried in a vacuum to yield white crystals of **5** (582 mg, 78%).

References

1) A part of this paper was reported in "Symposium on the Utilization of Carbon Dioxide in Chemistry," No. 8, Tokyo, September (1975), cited in T. Osa "Chemistry o Carbon Dioxide-Basis for Utilization" Kyoritsu Chemistryf Library No. 11, Kyoritsu, Tokyo, p. 98 (1976). The reaction of organic copper derivatives with carbon dioxide will be published separately.

2) (a) A. Yamamoto, A. Miyashita, T. Yamamoto, and S. Ikeda, *Bull. Chem. Soc. Jpn.*, **45**, 1583 (1972); (b) A. Miyashita and A. Yamamoto, *Bull. Chem. Soc. Jpn.*, **50**, 1102 (1977); (c) A. Miyashita, T. Yamamoto, and A. Yamamoto, *Bull. Chem. Soc. Jpn.*, **50**, 1109 (1977); (d) T. Ikariya and A. Yamamoto, *J. Organomet. Chem.*, **72**, 145 (1975).

3) (a) N. Marsich and A. Camus, *J. Organomet. Chem.*, **81**, 87 (1974); (b) N. Marsich and A. Camus, *J. Inorg. Nucl. Chem.*, **39**, 275 (1977); (c) A. Camus, N. Marsich, and R. Mosca, *ibid.*, **38**, 1967 (1976); (d) A. Camus, N. Marsich, G. Nardin, and L. Randaccio, *J. Chem. Soc., Dalton. Trans.*, **1975**, 2560; (e) A. Camus, N. Marsich, G. Nardin, and L. Randaccio, *Inorg. Chim. Acta*, **17**, L33 (1976); (f) F. H. Jardin, *Adv. Inorg. Radiochem.*, **17**, 115 (1975).

4) (a) T. Tsuda, T. Nakatsuka, T. Hirayama, and A. Saegusa, *J. Chem. Soc., Chem. Commum.*, **1974**; 557; (b) T. Tsuda, T. Nakatsuka, and T. Sasegusa, Twenty Second Symposium on Organometallic Chemistry Japan, 211A, Tokyo (1974); (c) T. Saeguas, T. Tsuda, and T. Hashimoto, Annual Meeting of Chemical Society of Japan (autumn), 3122 (1972).

5) E. J. Corey and I. Kuwajima, *Tetrahedron Lett.*, **1972**, 487.

6) The methylene signal of the complex **2a** appears at 4.35 ppm in the NMR spectrum ($CDCl_3$).[3e] However, the signal appears to be due to the free CH_3NO_2 (4.35 ppm in $CDCl_3$) liberated from complex **2a**. When the NMR spectrum is taken immediately after the preparation of the sample or at low temperatures below −30 °C, the methylene signal of complex **2a** is observed at lower field (5.76 ppm), no peak being observed at 4.35 ppm (see the text and Table 2).

7) M. Brookes and N. Jonathan, *J. Chem. Soc., A.* **1968**, 1529.

8) T. Kawaki and H. Hashimoto, *Bull. Chem. Soc. Jpn.*, **45**, 1499 (1972).

9) W. Kein. *J. Organometl. Chem.*, **14**, 197 (1968).

10) (a) J. Lewis and C. Oldham, *J. Chem. Soc., A*, **1966**, 1456; (b) S. Baba, T. Ogura, and S. Kawaguchi, *Bull. Chem. Soc. Jpn.*, **47**, 665 (1974); (c) S. Okeya and S. Kawagucki, *Chem. Lett.*, **1976**; 53; (d) S' Okeya and S. Kawaguchi, *Inorg. Chem.*, **16**, 1730 (1977); (e) T. Ito, T. Kiriyama, and A. Yamamoto, *Bull. Chem. Soc. Jpn.*, **49**, 3250 (1976).

11) M. Bartlett and G. J. Palenik, *Acta Crystallogr., Sect. A*, **25**, S173 (1969).

12) (a) C. Krüger, *J. Orgamometal. Chem.*, **9**, 125 (1975); (b) W. H. Glaze and D. P. Duncha, *ibid.*, **99**, 11 (1975); (c) R. Das and C. A. Wilkie, *J. Am. Chem. Soc.*, **94**, 4555(1972).

1,3-Dipolar Cycloadditions of *N*-(*p*-Substituted benzylidene) *p*-Substituted Benzylamine *N*-Oxides with *trans*-Bis(*p*-substituted benzoyl)ethylenes and the Substituent Effects on the Reaction Rates

Keishi TADA, Tomoharu YAMADA, and Fujio TODA

Department of Synthetic Chemistry, Faculty of Engineering, The University of Tokyo, Hongo, Bunkyo-ku, Tokyo 113

(Received November 28, 1977)

1,3-Dipolar cycloadditions of *N*-(*p*-substituted benzylidene) *p*-substituted benzylamine *N*-oxides with *trans*-bis(*p*-substituted benzoyl)ethylenes gave the *trans*- and the *cis*-2,3-bis(*p*-substituted phenyl)-4,5-bis(*p*-substituted benzoyl)isoxazolidines. The configurations of the resulting isoxazolidines were determined by NMR spectra. The formation ratios of the *trans*- to *cis*-adducts were determined by liquid chromatography. The second-order rate constants in xylene at 60 °C were obtained by high speed liquid chromatographic analysis. The rates varied with the σ values of the substituents R_1 on the *N*-benzylidene benzylamine *N*-oxides and R_3 on the dibenzoylethylenes, and linear relationships between log *k* and σ have been established. These results indicate that the HOMO(*N*-oxide)–LUMO(dibenzoylethylene) interaction predominates. The ρ-values for R_1 and R_3 were respectively; $\rho=-0.41\pm0.01$, $\rho=+0.60\pm0.02$.

Several 1,3-dipolar cycloadditions of nitrones have been studied.[1-4] The reactions of *N*-benzylidene benzylamine-*N*-oxide with *trans*- or *cis*-dibenzoylethylene has been reported to give 2,3-diphenyl-4,5-dibenzoylisoxazolidine, quantitatively.[5] However the configurations of the resulting isoxazolidines have not been established.

In the reaction of a 1,3-dipole and a dipolarophile, the eight stereoisomers are affected by the following three factors: the orientation of the addition, the direction of the cycloaddition, that is, either *exo* or *endo* and the reaction mechanism, either one or two-step. However, there have been few reported cases in which stereoisomers were obtained by the two-step mechanism. In the system here, the C_{2h}-symmetry of the *trans*-dibenzoylethylene prevented the formation of the stereoisomers caused by the two orientations. If these reactions proceed by a concerted mechanism, only two stereoisomers caused by *exo*- and *endo*-additions, the *trans*- and *cis*-isoxazolidines are expected.

This paper will report the configurations of the resulting isoxazolidines and some reactions of *N*-(*p*-substituted benzylidene) *p*-substituted benzylamine *N*-oxides with *trans*-bis(*p*-substituted benzoyl)ethylenes. The formation ratios of *trans*- to *cis*-forms were investigated to determine the substituent effect or the steric effect.

There have been some quantitative reports in the literatures[6-8] on the effect of substituents on the reaction rates. This paper describes the substituent effects on the reaction rate, and a semiquantitative treatment of the correlation between log *k* and σ using the second-order perturbation theory.

Results and Discussion

1,3-Dipolar cycloadditions of *N*-(*p*-substituted benzylidene) *p*-substituted benzylamine *N*-oxides (**1a**—**f**) (DPN) with *trans*-bis(*p*-substituted benzoyl)ethylenes (**2a**—**c**) (DBE) were conducted in anhydrous benzene to give a mixture of two stereoisomeric isoxazolidines, quantitatively. The configurations of these were determined to be as expected the *trans*- and *cis*-2,3-bis-

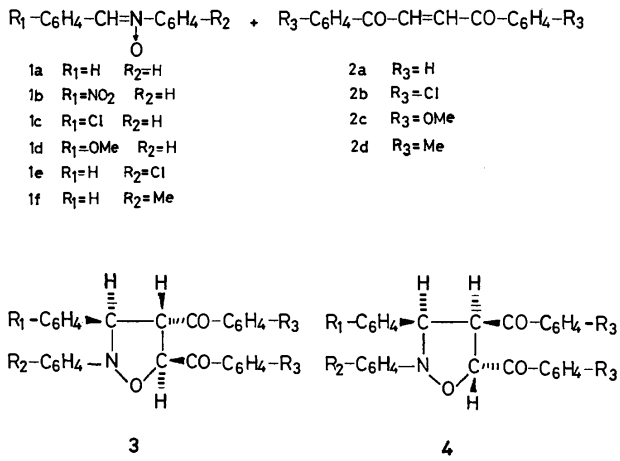

Scheme 1.

(*p*-substituted phenyl)-4,5-bis(*p*-substituted benzoyl)isoxazolidines, that is, **3** and **4** in Scheme 1. Thin-layer and high speed liquid chromatography have shown that the reaction mixture had no components other than the two stereoisomers. Column chromatography successfully isolated them from the reaction mixture.

The structures of **3** and **4** were determined by NMR spectra. For example, the NMR spectra of the *trans*- and *cis*-2,3-diphenyl-4,5-dibenzoylisoxazolidines which were produced by the reaction of *N*-benzylidene benzylamine *N*-oxide (**1a**) and dibenzoylethylene (**2a**) are shown in Fig. 1. In the spectrum of the *trans*-adduct (a), the peaks at $\delta=5.05$(d), 5.38(d-d) and 6.01(d) are C_3–H, C_4–H, and C_5–H, respectively. The decoupling signal of C_5–H turned the double-doublet peak of C_4–H to a doublet one. This result confirms these assignments. Coupling constants, C_3–H—C_4–H ($J_{3,4}$) and C_4–H—C_5–H($J_{4,5}$) were as follows; $J_{3,4}=6.0$ Hz, $J_{4,5}=3.4$ Hz. In the spectrum of the *cis*-adduct(b), the peaks C_3–H, C_4–H and C_5–H are situated at $\delta=5.44$(d), 5.82(d-d) and 6.32(d), respectively. The coupling constants are $J_{3,4}=7.5$ and $J_{4,5}=5.6$. In saturated or unsaturated rings, the *cis*-forms coupling constant is generally larger than that of the *trans*-form,[9,10] thus these stereoisomers were concluded to have the above configurations since

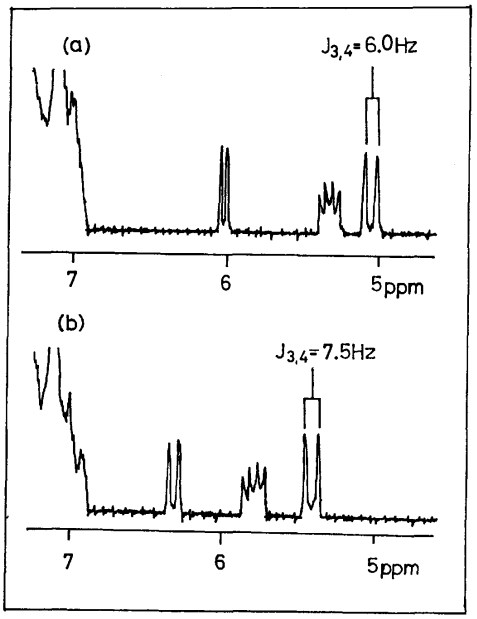

Fig. 1. NMR spectra of *trans*-(**3**) and *cis*-(**4**) isoxazolidine. (a); *trans* (b); *cis* (in DMSO-d_6, 60 MHz).

$7.5(J_{cis})>6.0(J_{trans})$. The observation that the *trans*-adduct, which is favored sterically, was the major product also supported these identifications. The NMR spectra of the other reaction products showed similar signal patterns.

DBE has C_{2h}-symmetry at the center of C=C double bond, so that two orientations of the addition give the same product. But there are two directions of the interaction between two components. *trans*-Isoxazolidine was formed through the *exo*-form transition state, and *cis*-isoxazolidine through the *endo*-form (Scheme 2).

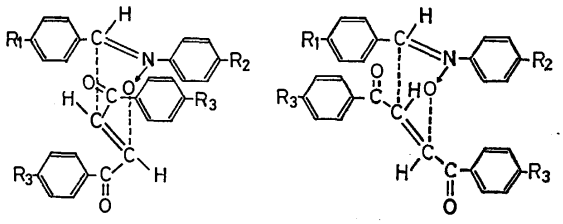

Scheme 2.

Melting points and the analytical data of the resulting isoxazolidines are summarized in Table 1. The formation ratios of the *trans*-forms to the *cis*-forms are also shown. They were determined by high speed liquid chromatography.

The reactions of nitrones with *N*-phenylmaleimides have been reported.[11,12] In this system the formation ratios varied in the range 1.5—3.9, depending on the electronic characters of the substituents on the nitrones and maleimides. This result suggests that the two reactant species orient in such a way that the interaction of the two dipole moments is favored (Scheme 3). Between log (I_t/I_c) and the Hammett σ values of the substituents on the nitrones and maleimides a linear

TABLE 1. THE MELTING POINTS AND THE ANALYTICAL DATA OF THE RESULTING ISOXAZOLIDINES AND THE FORMATION RATIOS

Run	Mp (°C)	Analytical data[a] (Calcd) C%	H%	N%	3/4
1a+**2a**	151.0—152.0	80.40	5.42	2.98	
	108.5—108.7	80.02	5.44	3.42	4.2
		(80.37	5.31	3.23)	
1b+**2a**	160.0—163.0	73.23	4.86	5.47	
	158.5—159.5	72.72	4.70	5.65	4.7
		(72.80	4.60	5.86)	
1c+**2a**	155.5—156.5	74.39	4.71	2.97	
	120.0—121.0	74.06	4.76	3.01	5.0
		(74.43	4.74	2.99)	
1f+**2a**	127 (dec)	80.06	5.82	2.95	
	117.3—117.5	80.30	5.76	3.03	3.0
		(80.51	5.63	3.14)	
1a+**2b**	141.0—143.5	69.28	4.21	2.81	
	127.0—127.5	69.47	4.21	2.83	4.0
		(69.33	4.21	2.79)	
1b+**2b**	—		—		4.5
1c+**2b**	213.0—214.5	65.14	4.02	2.42	
	156.5—158.0	64.80	3.80	2.60	4.7
		(64.88	3.76	2.61)	
1d+**2b**	145 (dec)	67.24	4.39	2.55	
	147.5—148.5	67.83	4.40	2.53	4.5
		(67.68	4.35	2.63)	
1e+**2b**	188.5—191.0	64.91	3.37	2.63	
	125.5—126.5	64.67	3.74	2.83	5.2
		(64.88	3.76	2.61	
1f+**2b**	121.5—123.0	70.12	4.74	2.55	
	129.5—130.0	69.85	4.49	2.71	3.9
		(69.77	4.49	2.71)	
1a+**2c**	—		—		4.4
1b+**2c**	143.5—145.0	68.68	4.91	5.03	
	139.0—141.5	68.90	4.91	5.12	6.3
		(69.14	5.20	5.20)	
1c+**2c**	122.0—124.0	70.38	5.00	2.61	
	125.0—126.0	70.32	4.95	2.66	4.5
		(70.52	4.96	2.65)	

a) The upper line is for the *cis*-form, and the lower line is for the *trans*-form.

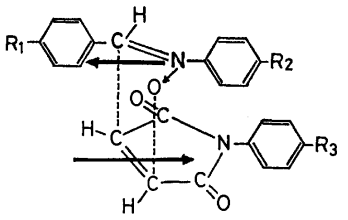

Scheme 3.

relationship has been established.

DBE has three planar configurations. Two of these have C_{2h}-symmetry, and the unsymmetric one is hindered sterically between a vinyl hydrogen and an *o*-hydrogen in the benzene ring. By this reasoning the dipole moment will have an insignificant influence on the formation ratios, and consequently the steric effect will be the predominant factor when the two components

are approaching and the π-orbitals begin to interact. The steric effect in the reaction of DPN with DBE would be expected to be greater than that in the reaction of DPN with *N*-phenylmaleimide. In this system the formation ratios are in the range 3.0—6.3, which are a little greater than the formation ratios of the maleimides. This result suggests that the *endo*-type addition is more hindered by the steric effect. In the reactions of DPNs with three DBEs, the values of the formation ratios are not so dissimilar, for example, the ratios of the reactions of **1a** with **2a**, **2b**, and **2c** are 4.2, 4.0, and 4.4, respectively, and the ratios of the reactions of **1c** with **2a**, **2b**, and **2c** are 5.0, 4.7, and 4.5, respectively.

The generation of C-T complexes between two benzene rings could be regarded as a factor governing the formation ratios. In *exo*- and *endo*-additions, the benzene ring of DPN makes about 90° with that of DBE when the two approach and interact in the most stable planar configurations, and about 30° in a less stable configuration. The generation of C-T complexes produces a fluorescence spectrum, but since this was not observed, this factor does not seem to have a predominating effect on the formation ratios.

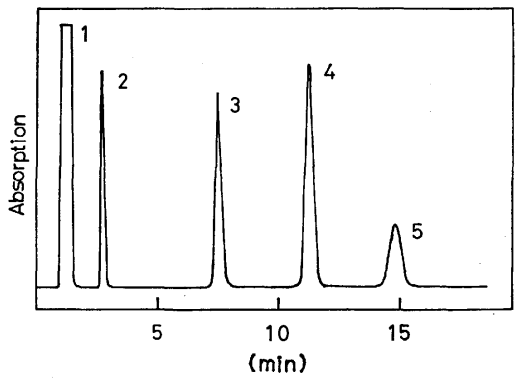

Fig. 2. The HLC chart of the reaction mixture of **1a** and **2a**.

In order to study the effects of substituents on the reaction rates, the rate constants of the reactions of **1a—d** with **2a—d** were determined by high speed liquid chromatography (HLC). Figure 2 shows an HLC chart of the reaction mixture of *N*-benzylidene benzylamine *N*-oxide (**1a**) and dibenzoylethylene (**2a**) at the middle stage of the reaction. The peaks 1, 2, and 4 are of xylene (solvent), nitrobenzene (standard) and DBE, respectively. Before reaction, there were only these three peaks, and as the reaction proceeded, peaks, 3 and 5 appeared and became larger. They are considered to be the *trans*- and *cis*-isoxazolidines. The R_f-values of *trans*-isoxazolidine is usually larger than that of *cis*-one, and the ratio of *trans*- to *cis*-isoxazolidine is greater than 1 due to the steric effect. From these facts, peak 3 is assigned as the *trans*-isomer, and peak 5 as the *cis*-isoxazolidine. The NMR spectra of the products further supported the assignments. In all cases, the peak of DPN was not found in the HLC chart because of a strong attachment to the packing material. In some cases the relative positions of the peaks of DBE and *cis*-isoxazolidine were reversed. In the plots of $1/C$ ("C" is the concentration of DPN or DBE, and the mol-concentrations of DPN and DBE were equal to each other throughout the reaction) *vs.* the reaction time, a linear relationship was established. Therefore, the cycloaddition proved to have a second-order rate constant, first-order with respect to each reactant species.

Table 2. The second-order rate constant k and $\log k$ of the reaction of **1** with **2** (in xylene, at 60 °C)

R_3		R_1: NO_2	Cl	H	MeO
Cl	$k\times10^3$	1.8	2.9	4.6	4.8
	$\log k$	−2.74	−2.54	−2.34	−2.32
H	$k\times10^3$	1.3	2.5	3.3	3.4
	$\log k$	−2.89	−2.60	−2.48	−2.47
Me	$k\times10^3$	1.1	2.2	2.6	2.5
	$\log k$	−2.96	−2.66	−2.59	−2.60
MeO	$k\times10^3$	1.0	1.8	2.1	3.2
	$\log k$	−3.00	−2.74	−2.68	−2.49

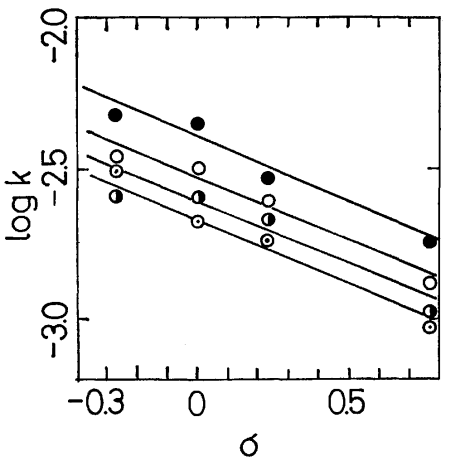

Fig. 3. The relation between the Hammett σ value of R_1 and $\log k$.
● Cl–DBE, ○ H–DBE, ◑ Me–DBE, ⊙ MeO–DBE.

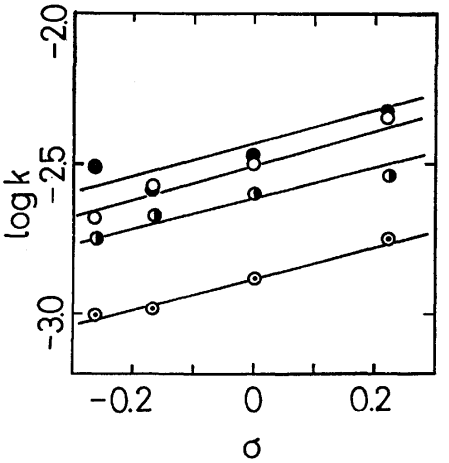

Fig. 4. The relation between the Hammett σ value of R_3 and $\log k$.
● MeO–DPN, ○ H–DPN, ◑ Cl–DPN, ⊙ NO_2–DPN.

The second-order rate constants k and log k are shown in Table 2. Figure 3 demonstrates the dependence of the σ value of R_1 on log k, and that the increasing negativity of R_1 brings about a decrease in rate. Plots of log k *vs.* the σ values of R_3 are shown in Fig. 4, which indicates the linear increase in rate when the negativity of R_3 is increased in every DPN. Thus the reaction rates are influenced by the energy difference, E_I(HOMO(1,3-dipole)–LUMO(dipolarophile)) more than E_{II}(HOMO(dipolarophile)–LUMO(1,3-dipole)). Therefore, these reactions belong to the Sustmann Type I.[8]

According to the perturbation theory, the interaction energy (ΔE) of the HOMO–LUMO combination is approximated as follows when a reaction belongs to the Sustmann Type I.[2,13,14]

$$\Delta E = \frac{(C_a C_d' \beta_{ad} + C_c C_e' \beta_{ce})^2}{E_I}, \quad (1)$$

where C and C' are the coefficients of the atomic orbitals of HOMO and LUMO, respectively, and β is the resonance integral. Assuming that the two resonance integrals are equal, $\beta_{ad}=\beta_{ce}=\beta$, and setting $(C_a C_d' + C_c C_e')^2=A$, Eq. 1 is turned into the following simple equation:

$$\Delta E = \frac{A\beta^2}{E_I}. \quad (2)$$

Since log k is proportional to ΔE, thus

$$\log k = m\frac{A\beta^2}{E_I} + q \quad (\text{"}m\text{" and "}q\text{" are constants}). \quad (3)$$

Here, E_I, the energy difference, is supposed to be a function of the electronic character of the substituents, R_1 and R_3. Assuming that E_I is the first-order function of σ, and setting E_0 the standard value of E_I when the σ value of the substituent is zero, we have, $E_I=E_0+n\sigma$. Thus, substituting we have

$$\log k = \frac{mA\beta^2}{E_0 + n\sigma} + q(\text{"}n\text{" is a constant}). \quad (4)$$

This equation shows that log k is the hyperbolic function of σ. When $n>0$, increasing σ decreases the value of log k since log $k<0$ and $mA\beta^2>0$. This relation is shown in Fig. 5-1. When $n<0$, the relation is as shown in Fig. 5-2. In each case, a linear relationship between log k and σ was observed. σ varied in the narrow range, $-0.3<\sigma<0.8$, and log k in the range $-3.00<\log k<-2.32$. These results are very sililar to the solid lines in Figs. 5-1 and 5-2, respectively.

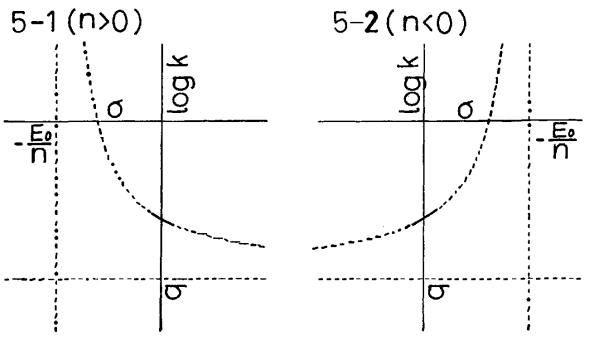

Fig. 5. The relation between log k and σ according to Eq. 4.

"n" is positive for the σ value of the substituent on a 1,3-dipole, and negative for that on a dipolarophile in Sustmann Type I reactions. In this way, log k is approximated to be the first-order function of σ in a very narrow range. Thus

$$\log k - q = \rho\sigma \quad (\text{"}\rho\text{" is a constant}). \quad (5)$$

From the experimental results, $\rho=-0.41\pm0.01$ for the σ value of the substituent R_1 and $\rho=+0.60\pm0.02$ for that of R_3 were obtained. Huisgen and coworkers have reported the linear correlation of log k ($\rho=0.77$) in the reaction of α-phenyl-*N*-methylnitrone with *p*-substituted styrene.[15] In the reaction of symmetrical bis(*p*-substituted benzoyl)-ethylenes with *N*-(*p*-substituted benzylidene) *p*-substituted benzylamine *N*-oxide, similar correlations of log k were observed.

Experimental

N-(p-Substituted benzylidene) p-Substituted Benzylamine N-Oxides(DPN). All DPNs were prepared in the usual manner.[16] Melting points and yields were as follows;

1a; mp; 111.0—112.0 °C yield; 40%
1b; mp; 182.0—183.0 °C yield; 34%
1c; mp; 149.0—150.0 °C yield; 45%
1d; mp; 134.5—136.0 °C yield; 27%
1e; mp; 169.0—171.0 °C yield; 63%
1f; mp; 122.0—123.5 °C yield; 24%

trans-Bis(p-substituted benzoyl)ethylenes (DBE). DBEs were prepared by the procedure of Conant and Lutz.[17–19] It has been established that the products by this method are only of the *trans*-form. Melting points and yields were as follows;

2a; mp; 106.5—108.0 °C (lit, 111 °C) yield; 30%
2b; mp; 170.5—171.5 °C (lit, 172 °C) yield; 13%
2c; mp; 166.0—166.5 °C (lit, 167.5—168.0 °C) yield; 16%
2d; mp; 147.0—148.0 °C (lit, 148 °C) yield; 18%

Reactions of DPNs with DBEs and Formation Ratios. All the reactions were carried out by the same method. For example, the reaction of *N*-benzylidene benzylamine *N*-oxide (**1a**) with *trans*-dibenzoylethylene (**2a**) was carried out as follows; **1a** (0.985 g(0.005 mol)) and **2a** (1.180 g(0.005 mol)) were dissolved in benzene (80 ml) and refluxed for about 3 h. The reaction was carried out in the dark, since **1a** is easily decomposed by sun-light. The reaction products, *trans*- and *cis*-isoxazolidines were isolated, respectively by column chromatography (200 mesh silica gel).

The formation ratios were determined by high speed liquid chromatography. The ε_{max} value of the *trans*-form was assumed to be equal to that of the *cis*-form. For example, the ε_{max} value of the *trans*-2,3-diphenyl-4,5-dibenzoylisoxazolidine and the *cis*-form were 32400 (247 nm) and 35300 (248 nm), respectively, consequently they can be assumed equal within an 8% difference. The HLC was performed using a stainless column (4 mmϕ × 50 cm) containing TSK-Gel LS310-P10 or Wakogel LC-ODS-10K. Chloroform and hexane were used as the eluent in various mixed ratios, depending on the samples and the gels. The flow rate was 2—4 ml/min. The eluate was analyzed by a UV detector in the range 254—270 nm region.

Kinetic Procedures. The rate constants were determined by HLC under the same conditions. A small amount of nitrobenzene (0.05 ml) was added to the reaction solvent

as a standard for analysis before reaction. Nitrobenzene has an ε_{max} at 252 nm, and the ε_{max} is 10000, so that only a small amount is sufficient for the standard. Moreovre, since the R_f-value was found to be near to 1 under the experimental conditions, there was no possibility for peak overlap.

The area ratio(r) of DBE peak relative to that of nitrobenzene at zero time (r_0) was obtained first. At time t, the residual concentration of DBE (C) was calculated by comparison of the area ratio (r_t) with r_0. Plots of $1/C$ *vs.* the reaction time (second) gave good linear relations, from which the second-order rate constants were obtained. The UV spectra of DBEs were as follows:

2a; $\lambda_{max}=262$ nm $\varepsilon_{max}=20000$
2b; $\lambda_{max}=272$ nm $\varepsilon_{max}=20800$
2c; $\lambda_{max}=241$ nm $\varepsilon_{max}=18300$
2d; $\lambda_{max}=275$ nm $\varepsilon_{max}=18000$

The spectra of all DBEs were satuarated at a concentration of about 10^{-4} mol/l. The concentration of samples in the detector were considered far below it, since the concentration of DBE in the reaction mixture was 1/30 mol/l in each case, a sample size was under 1 μl, and the flow rate of the eluent was about 4 ml/min. In point of fact none of the peaks of DBEs was saturated. For all DBEs, good linearity was found between the areas of the peak and the concentration under 10^{-4} mol/l.

For example, the reaction of *N*-benzylidene benzylamine *N*-oxide (**1a**) with dibenzoylethylene (**2a**) was carried out as the following; **2a** (0.236 g(0.001 mol)) was dissolved in anhydrous xylene (30 ml) containing nitrobenzene (0.05 ml). After the reaction temperature was controlled at 60 °C (±0.1), **1a** (0.197 g(0.001 mol)) was added and stirred well. At intervals of about twenty minutes, the reaction mixture was analyzed by HLC.

The authors are grateful to Dr. Yoshio Iwakura and the late Dr. Keikichi Uno for advice and helpful discussions.

The authors would like to thank Toyo Soda Manufacturing Co., Ltd. for a generous supply of TSK-Gel.

References

1) R. Huisgen, *Angew. Chem. Int. Ed. Engl.*, **2**, 565 (1963).
2) D. St. Black, R. F. Crozire, and V. C. Davis, *Synthesis*, **1975**, 205.
3) R. Huisgen, *J. Org. Chem.*, **41**, 403 (1975).
4) W. C. Herdson, *Chem. Rev.*, **72**, 157 (1972).
5) R. Huisgen, H. Hauck, R. Grashey, and H. Seidl, *Chem. Ber.*, **102**, 736 (1969).
6) K. N. Houk, J. Sims, R. E. Duke, Jr., R. W. Strozier, and J. K. George, *J. Am. Chem. Soc.*, **95**, 7287 (1973).
7) K. N. Houk, J. Sims, C. R. Watts, and L. J. Luskus, *J. Am. Chem. Soc.*, **95**, 7301 (1973).
8) R. Sustmann, *Pure Appl. Chem.*, **40**, 569 (1974); *Tetrahedron Lett.*, **1971**, 2717.
9) M. Joucla, J. Hamelin, and R. Carrie, *Bull. Soc. Chim. Fr.*, **11**, 3116 (1973).
10) R. Sustmann, R. Huisgen, and H. Huber, *Chem. Ber.*, **100**, 1802 (1967).
11) Y. Iwakura, K. Uno, and T. Hongu, *Bull. Chem. Soc. Jpn.*, **42**, 2882 (1969).
12) Y. Iwakura, K. Uno, Such-Ju Hong, and T. Hongu, *Bull. Chem. Soc. Jpn.*, **45**, 192 (1972).
13) R. Huisgen, *J. Org. Chem.*, **41**, 403 (1976).
14) R. F. Hudson, *Angew. Chem. Int. Ed. Engl.*, **12**, 36 (1973).
15) R. Huisgen, H. Seidl, and I. Bruning, *Chem. Ber.*, **102**, 1102 (1969).
16) *Org. Synth.*, Coll. Vol. V, 1124 (1973).
17) J. B. Conant and R. E. Lutz, *J. Am. Chem. Soc.*, **45**, 1303 (1923).
18) R. E. Lutz, *J. Am. Chem. Soc.*, **52**, 3423 (1930).
19) T. I. Crowell, G. C. Helsley, R. E. Lutz, and W. L. Scott, *J. Am. Chem. Soc.*, **85**, 443 (1963).

The Reaction of *N*-Alkylisoxazolium Salts with Hydroxylamine

Choji KASHIMA, Kimio ARAI, Satoshi IMADA, and Yoshihiko TSUDA

Department of Chemistry, University of Tsukuba, Sakura-mura, Niihari-gun, Ibaraki 300-31

(Received November 30, 1977)

The alternating transposition of C-3 and C-5 substituents on 3,5-disubstituted isoxazoles was found by refluxing a mixture of hydroxylamine hydrochloride, potassium carbonate, and 3,5-disubstituted 2-methylisoxazolium salts, derived from the corresponding isoxazoles. Under the same conditions, 3,5-disubstituted 2-*t*-butyl- or 2-benzhydrylisoxazolium salts gave the corresponding isoxazoles without alternation of the substituents.

The reactions of 3,5-dimethylisoxazole (**1**) with various electrophiles in the presence of sodium amide have been investigated.[1] The 5-methylisoxazoles have been prepared from β-amino enones on treatment with hydroxylamine.[2] However the sterically hindered 5-trichloroacetamido-2,2-dimethyl-4-hexen-3-one will not give the 5-methyl-3-*t*-butylisoxazole (**2**), so it was necessary to devise a general preparative method for the 5-methylisoxazoles.

On the basis of the reported reactions of *N*-alkylisoxazolium salts[3] with various nucleophiles such as potassium alkoxide,[4] Grignard reagents,[5] and sodium borohydride,[6] the 3,5-disubstituted 2-methylisoxazolium salts would be expected to react with hydroxylamine. Thus, treatment of a mixture of 2,3,5-trimethylisoxazolium iodide (**5**) and hydroxylamine hydrochloride with potassium methoxide in methanol gave **1** in good yield. In the same manner, treatment of a mixture of 2,3-dimethyl-5-phenylisoxazolium iodide (**6**) and hydroxylamine hydrochloride with potassium methoxide gave an isomeric mixture of 3-methyl-5-phenylisoxazole (**3**, 46%) and 5-methyl-3-phenylisoxazole (**4**, 54%). Treatment of the mixture with potassium carbonate as a base yielded the isomer **4** as the major product. Similarly the isoxazolium iodides **7** and **8**, and also the isoxazolium perchlorates **9** and **10** may be converted into the corresponding isoxazoles as shown in Table 1. These results reveal the alternating transposition of the substituent groups on isoxazoles proceeds smoothly on treatment of *N*-methylisoxazolium salts with hydroxylamine hydrochloride in the presence of potassium carbonate.

For the formation of the isoxazoles from *N*-methylisoxazolium salts, three possible reaction paths are shown in Fig. 1. The β-amino enone **11** may be prepared as the sole product by the reaction of **6** with potassium methoxide. The interconversion of **3** and **4** did not occur in the presence of hydroxylamine, so that path 1 may be omitted from the consideration of the formation of the alternating transposition product. A weak base, such as potassium carbonate is not able to abstract the proton on *N*-methyl group of **6**. Furthermore, the treatment of **11** with hydroxylamine hydrochloride in the presence of potassium methoxide or carbonate gave the isoxazole **3** as listed in Table 2. Thus the *N*-methylisoxazolium salts undergo the transposition reaction to give **4** in the manner shown in path 3, whereas the formation of **3** is considered to proceed *via* path 2.

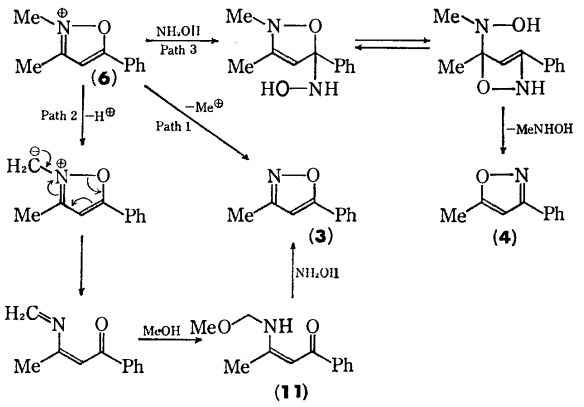

A mixture of 2-*t*-butyl-3-methyl-5-phenylisoxazolium perchlorate (**12**), hydroxylamine hydrochloride, and potassium carbonate was heated and gave **3** and **4** in 60 and 13% yields, respectively. Similarly, 2-benz-

Table 1. The reaction of *N*-alkylisoxazolium salts with hydroxylamine

Compd	R^2	R^3	R^5	Anion	Base	3,5-Disubstituted isoxazole		
						Total yield	Retention	Transposition
5	Me	Me	Me	I^-	KOMe	63	—	—
6	Me	Me	Ph	I^-	KOMe	72	46	54
5	Me	Me	Me	I^-	K_2CO_3	80	—	—
6	Me	Me	Ph	I^-	K_2CO_3	80	18	82
7	Me	Me	*t*-Bu	I^-	K_2CO_3	79	7	93
8	Me	Me	CH_2CH_2Ph	I^-	K_2CO_3	51	16	84
9	Me	Me	Ph	ClO_4^-	K_2CO_3	93	9	91
10	Me	Ph	Me	ClO_4^-	K_2CO_3	95	15	85
14	*t*-Bu	Me	Me	ClO_4^-	K_2CO_3	80	—	—
12	*t*-Bu	Me	Ph	ClO_4^-	K_2CO_3	73	82	18
15	Ph_2CH	Me	Me	ClO_4^-	K_2CO_3	86	—	—
13	Ph_2CH	Me	Ph	ClO_4^-	K_2CO_3	79	100	0

Table 2. The reaction of 1-substituted 3-(methoxymethylamino)-2-buten-1-ones with hydroxylamine

5-Subst.	Base	Isoxazole yield	Retention	Transposition
Me	MeOK	29	—	—
Ph	MeOK	36	100	0
t-Bu	MeOK	32	100	0
CH_2CH_2Ph	MeOK	36	100	0

hydryl-3-methyl-5-phenylisoxazolium perchlorate (**13**) gave **3** and methyl benzhydryl ether but no isomer **4**. The formation of compound **3** from **12** and **13** is assumed to proceed *via* path 1.

In conclusion, the treatment of *N*-methylisoxazolium salts with hydroxylamine hydrochloride in the presence of potassium carbonate gave alternation transposition compounds of oxygen and nitrogen atoms attached to the isoxazoles. In contrast, the same treatment of *N*-*t*-butyl- or *N*-benzhydrylisoxazolium salts afforded isoxazoles without alternating the hetero atoms.

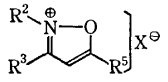

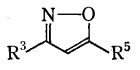

(**5**): R^2=R^3=R^5=Me X=I
(**6**): R^3=R^5=Me R^5=Ph X=I
(**7**): R^2=R^3=Me R^5=*t*-Bu X=I
(**8**): R^2=R^3=Me R^5=CH_2CH_2Ph X=I
(**9**): R^2=R^3=Me R^5=Ph X=ClO_4
(**10**): R^2=R^5=Me R^3=Ph X=ClO_4
(**12**): R^2=tBu R^3=Me R^5=Ph X=ClO_4
(**13**): R^2=Ph_2CH R^3=Me R^5=Ph X=ClO_4
(**14**): R^2=*t*-Bu R^3=R^5=Me X=ClO_4
(**15**): R^2=Ph_2CH R^3=R^5=Me X=ClO_4

(**1**): R^3=R^5=Me
(**2**): R^3=tBu R^5=Me
(**3**): R^3=Me R^5=Ph
(**4**): R^3=Ph R^5=Me
(**16**): R^3=CH_2CH_2Ph R^5=Me

Fig. 2.

Experimental

Materials. 2,3,5-Trimethyl- (**5**), 2,3-dimethyl-5-phenyl- (**6**), 2,3-dimethyl-5-*t*-butyl- (**7**), and 2,3-dimethyl-5-phenethylisoxazolium iodide (**8**) were prepared from the corresponding isoxazoles.[3] According to the method of Adachi,[5] 2,3-dimethyl-5-phenyl- (**9**) and 2,5-dimethyl-3-phenylisoxazolium perchlorate (**10**) were prepared. *N*-*t*-Butyl- and *N*-benzhydrylisoxazlium perchlorates were prepared by the method of Woodman.[7] The physical data of these isoxazolium salts are listed in Table 3.

General Procedure. To a mixture of MeOK (or K_2CO_3, 4.8 mmol) in methanol (30 ml) was added an isoxazolium salt (2.0 mmol) and hydroxylamine hydrochloride (2.4 mmol). The mixture was refluxed for 18 h, poured into ice-water, extracted with CH_2Cl_2, and dried over $MgSO_4$. The isoxazole yield was estimated by the peak area of gas chromatography and the product ratio calculated by the intensity of methyl proton signals in the NMR spectra.

3-t-Butyl-5-methylisoxazole (2).[8] The title compound was isolated by fractional distillation. Bp 110—114 °C/73 mmHg. NMR (δ): 1.32 (s, 9H), 2.37 (s, 3H) and 5.98 ppm (s, 1H). Found: C, 68.73; H, 9.42; N, 10.09%. Calcd for $C_8H_{13}NO$: C, 69.03; H, 9.41; N, 10.06%.

3-Phenethyl-5-methylisoxazole (16). The title compound was isolated by fractional distillation. Bp 121—127 °C/2 mmHg. NMR (δ): 2.35 (s, 3H), 2.94 (s, 4H), 5.74 (s, 1H) and 7.23 ppm (s, 5H). Found: C, 76.83; H, 6.78; N, 7.17%. Calcd for $C_{12}H_{13}NO$: C, 76.97; H, 7.00; N, 7.48%.

Isomerization of Isoxazole. The mixture of isoxazole (**3** or **4**, 2.0 mmol), hydroxylamine hydrochloride (2.6 mmol) and MeOK (or K_2CO_3, 2.8 mmol) in methanol (20 ml) was refluxed and the resulting mixture poured into water, and extracted with CH_2Cl_2. The product was analyzed by gas chromatography and NMR spectroscopy.

The Reaction of 3-(Methoxymethylamino)-2-buten-1-ones with Hydroxylamine. The mixture of 3-(methoxymethylamino)-2-buten-1-ones (2.0 mmol) and hydroxylamine hydrochloride (2.4 mmol) was treated with MeOK (or K_2CO_3, 2.4 mmol) by the procedure described in reference 2. The results are listed in Table 2.

References

1) C. Kashima, Y. Yamamoto, and Y. Tsuda, *Heterocycles*, **6**, 805 (1977).
2) C. Kashima, Y. Yamamoto, Y. Tsuda, and Y. Omote, *Bull. Chem. Soc. Jpn.*, **50**, 543 (1977).
3) W. Lampe and J. Smolinska, *Rocz. Chem.*, **28**, 163 (1954).
4) C. Kashima, N. Mukai, Y. Yamamoto, Y. Tsuda, and Y. Omote, *Heterocycles*, **7**, 241 (1977).
5) I. Adachi, K. Harada, M. Miyazaki, and H. Kano, *Chem. Pharm. Bull.*, **22**, 61 (1974).
6) I. Adachi, R. Miyazaki, and H. Kano, *Chem. Pharm. Bull.*, **22**, 70 (1974).
7) D. J. Woodman, *J. Org. Chem.*, **33**, 2397 (1968).
8) Coutrier reported[10] the preparation of isoxazole derivative from 5,5-dimethyl-2,4-hexanedione and hydroxylamine hydrochloride. The product was identified to be 3-methyl-5-*t*-butylisoxazole with the authentic sample.[11]
9) M. F. Coutrier, *C. R. Aced. Sci.*, **150**, 928 (1910).
10) C. Kashima, S. Tobe, N. Sugiyama, and M. Yamamoto, *Bull. Chem. Soc. Jpn.*, **46**, 310 (1973).

Table 3. Physical data and elemental analysis of *N*-alkylisoxazolium salts

Compd	R^2	R^3	R^5	Anion	Mp °C	Yield	Found C	Found H	Found N	Calcd C	Calcd H	Calcd N
5	Me	Me	Me	I^-	84	78	—	—	—	—	—	—
6	Me	Me	Ph	I^-	171	59	43.69	3.98	4.90	43.87	4.01	4.65
7	Me	Me	*t*-Bu	I^-	196	82	38.79	5.61	4.93	38.45	5.74	4.98
8	Me	Me	CH_2CH_2Ph	I^-	121	61	47.51	4.91	4.10	47.43	4.90	4.26
9	Me	Me	Ph	ClO_4^-	186	81	—	—	—	—	—	—
10	Me	Ph	Me	ClO_4^-	130	78	47.96	4.39	5.01	48.28	4.42	5.11
12	*t*-Bu	Me	Ph	ClO_4^-	146	75	53.07	5.75	4.62	53.26	5.74	4.44
14	*t*-Bu	Me	Me	ClO_4^-	120	34	—	—	—	—	—	—
13	Ph_2CH	Me	Ph	ClO_4^-	138	74	64.93	4.75	3.47	64.87	4.73	3.29
15	Ph_2CH	Me	Me	ClO_4^-	157	63	—	—	—	—	—	—

Cyclization of Isothiosemicarbazones. I. A New Route to 2-Mercaptoimidazole Derivatives and 4-Substituted Imidazoles[1)]

Chiji YAMAZAKI

Department of Chemistry, School of Hygienic Sciences, Kitasato University, Asamizodai, Sagamihara-shi 228

(Received November 30, 1977)

Some 1-arylmethyleneamino-2-mercapto-4-aryl-1*H*-imidazole derivatives were prepared by the condensation of isothiosemicarbazones of aromatic carbonyl compounds with phenacyl bromides. The 1,2,5-trisubstituted isomers were obtained by substitution of *dl*-α-bromophenylacetaldehyde for phenacyl bromide in this condensation. The reaction of isothiosemicarbazones of aliphatic carbonyl compounds with phenacyl bromides produced a dark, complex mixture from which the corresponding 1-alkylideneamino-2-mercapto-4-aryl-1*H*-imidazoles and 3,5-disubstituted 1,2,4-triazines were isolated in poor yields, with the latter being a main product or a sole heterocyclic product depending on the reaction conditions. Reductive cleavage of the cyclized products with zinc dust in acetic acid-acetic anhydride solution gave 1-acetyl-4-aryl-1*H*-imidazoles, which were readily hydrolyzed to 4-aryl-1*H*-imidazoles. The susceptibility to acid hydrolysis of the arylmethyleneamino group was dependent on the extent of conjugation between the azomethine double bond and the adjacent aromatic rings. Hydrazinolysis of the azomethine double bond yielded 1-amino-2-mercapto-4-aryl-1*H*-imidazoles in high yields. Their structures were established on the basis of NMR, IR, UV, and mass spectra as well as elemental analyses. Differentiation between 1,2,4- and 1,2,5-trisubstituted imidazoles was discussed.

Condensation of certain thiosemicarbazones of aromatic aldehyde with α-halo ketones leads to the formation of thiazole derivatives owing to the preferential attack of the most nucleophilic mercapto group on the halogen-bearing carbon of the halo ketone.[2)] If the potential mercapto group, however, is first blocked by alkylation, the reaction of *S*-alkylisothiosemicarbazone with an α-halo ketone should lead to the formation of an alkylthioimidazole. Very few examples have been known for cyclization of isothiosemicarbazone to a heterocyclic compound with retention of the alkylthio group.[3)] The present paper is concerned with an attempt to prepare imidazole derivatives by blocking the mercapto group of thiosemicarbazone with an alkyl, alkenyl, or arylalkyl group and condensing the isothiosemicarbazones with α-halo carbonyl compounds. The use of isothiosemicarbazone, especially of aromatic carbonyl compounds, allows to avoid extensive sulfide formation as encountered with the reaction between phenacyl bromide and *S*-benzylisothiourea[4)] which has a pronounced tendency to lose the thiol. This paper further describes reductive and hydrolytic cleavage of as well as hydrazinolysis of the cyclized products, as represented in Schemes 1 and 2.

In view of the fact that the condensation of isothiosemicarbazones (**1**) with *dl*-α-bromophenylacetaldehyde (**3**) gave sterically hindered 5-phenyl compounds (**5**), steric factor, as suggested in our preliminary report,[1)] should not be the directive force in the orientation of this ring closure. Differentiation between 4- and 5-phenyl-1*H*-imidazoles was made by observing the ortho deshielding phenomenon[5)] of the 4-phenyl protons and the C–H stretching absorption band at 5-position of the 1,2,4-trisubstituted imidazole series. Mass spectra showed no definitive difference between both isomers in

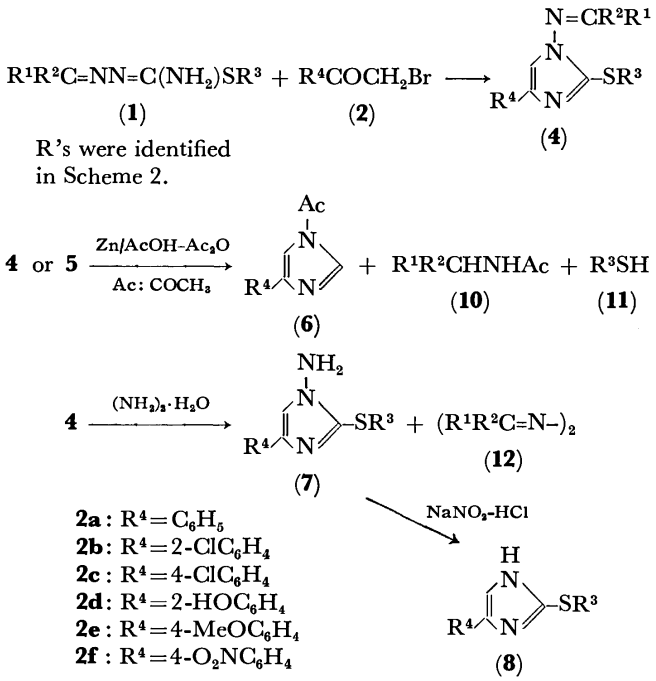

Scheme 1.

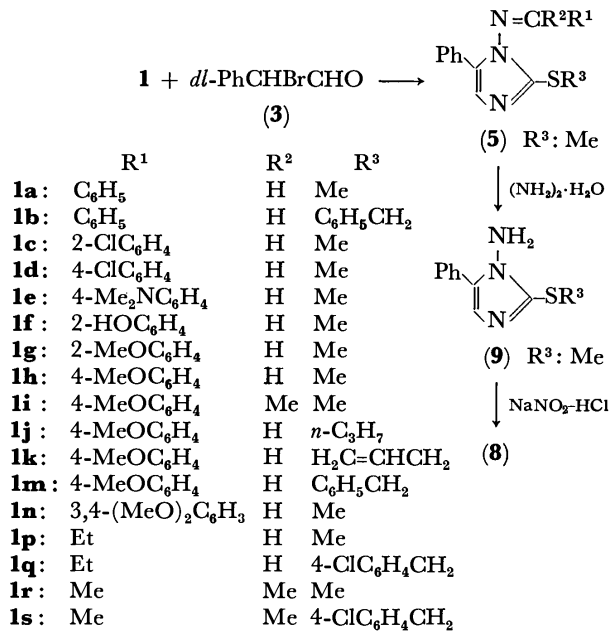

	R^1	R^2	R^3
1a:	C_6H_5	H	Me
1b:	C_6H_5	H	$C_6H_5CH_2$
1c:	2-ClC_6H_4	H	Me
1d:	4-ClC_6H_4	H	Me
1e:	4-$Me_2NC_6H_4$	H	Me
1f:	2-HOC_6H_4	H	Me
1g:	2-$MeOC_6H_4$	H	Me
1h:	4-$MeOC_6H_4$	H	Me
1i:	4-$MeOC_6H_4$	Me	Me
1j:	4-$MeOC_6H_4$	H	*n*-C_3H_7
1k:	4-$MeOC_6H_4$	H	H_2C=$CHCH_2$
1m:	4-$MeOC_6H_4$	H	$C_6H_5CH_2$
1n:	3,4-$(MeO)_2C_6H_3$	H	Me
1p:	Et	H	Me
1q:	Et	H	4-$ClC_6H_4CH_2$
1r:	Me	Me	Me
1s:	Me	Me	4-$ClC_6H_4CH_2$

Scheme 2.

determining the substitution pattern with the exception of compounds carrying an ortho-substituent on the arylmethyleneamino group.

Results and Discussion

The condensation of isothiosemicarbazones (**1**) with phenacyl bromides (**2**) was carried out by heating a mixture of **1** and **2** in acetonitrile in the presence of an excess of sodium hydrogencarbonate at 75 °C for 3 h under stirring. With a few exceptions, the imidazoles usually crystallized out of the reaction mixture upon cooling or even at still hot and could easily be isolated by filtration. Most of the products, after being washed with water to remove any inorganic salts, were sufficiently pure to use for further reactions indicated in Scheme 1. Isolation of **4h**, **4m**, and **4p** was accomplished by means of column chromatography. 2-Allylthio compound **4t** was isolated by crystallization from ethanol of an amorphous gum obtained after evaporation of the reaction mixture under reduced pressure. Alternative process in which a mixture of **1** and **2** (2: 1) in ethanol is heated at 75 °C (Method A) could be applied to the cyclization of **1e** to **4h** with rather better yields than in the standard procedure described above. In some cases, the use of excess **2** up to 50% was found to somewhat improve the yield of imidazoles. For example, the yield of **4j** increased to 66% when the ratio of **2a** to **1g** was raised to 1.5: 1 compared with the yield 40% in the ratio 1: 1. This modification, however, was not generally applicable because the excess **2** may prevent crystallization of a cyclized product from the reaction mixture. The use of a tertiary amine such as pyridine or triethylamine in place of sodium hydrogencarbonate resulted in the predominant formation of the corresponding quaternary ammonium bromide of these acid binders with **2** and gave no cyclized product. Attempts to cyclize **1s** and *p*-methoxyacetophenone *S*-benzylisothiosemicarbazone with **2a** were unsuccessful presumably due to their sterically unfavorable structure. Cyclization of *m*- and *p*-nitrobenzaldehyde *S*-methylisothiosemicarbazones was also failed because of the extremely poor solubility.

In sharp contrast to the behavior of the isothiosemicarbazones of aromatic carbonyl compounds, the reaction of those of aliphatic ones with **2** produced a dark resinous mass even at room temperature with a poor yield of imidazoles and therefore might be less valuable for preparative purpose. Isolation of the 1-alkylideneamino-1*H*-imidazoles (**4w**—**4z**) was accomplished by means of column chromatography on silica gel using a benzene–ethanol mixture as an eluent. Unfortunately, **4z** tends to lose the acetone during the working up to form **7a** and therefore the conversion of **1r** to imidazole was estimated on the basis of the yield of a relatively insoluble derivative such as **4o** which was obtained by reacting both **4z** and **7a** with anisaldehyde in an acidic medium. 4-Aryl-1*H*-imidazoles thus obtained were listed in Table 1.

The reaction of aliphatic isothiosemicarbazones with **2** was further complicated by the formation of 3,5-disubstituted 1,2,4-triazines (**15**) and sulfides (R^3SCH_2-COR^4) in addition to **4**, with the ratio of these products being dependent upon the particular isothiosemicarbazone and the reaction conditions. The standard procedure described in the beginning of this section generally gives **4** as a main product along with a minor product **15**, while the latter predominates under the conditions of Method A. For example, the reaction of **1p** with **2a** by that method produced 3-methylthio-5-phenyl-1,2,4-triazine (**15a**) in 8% yield with no imidazole formation, whereas the reaction of **1q** with **2a** in dimethyl sulfoxide (DMSO) in the presence of sodium hydrogencarbonate gave **4y** in 11% yield but no **15c** at all. Under the conditions of Method A, **15b** was obtained in less than 30% yields from the reaction of **1p** or **1r** with **2c**. Similarly, **1s** gave **15c** in 38% yield. The structure of **15a** was confirmed by the unambiguous synthesis reported by Paudler *et al.*[6] and **15b** was well consistent in the melting point with that of the literature.[7]

The triazine formation was attributed to the tendency of an aliphatic isothiosemicarbazone to split off the carbonyl component and can be explained as the result of oxidation at the α-carbon of **2** by isothiosemicarbazide (**13**) thus liberated by analogy with osazone or dioxime formation of α-halo carbonyl compounds.[8] Since the reaction mixture becomes acidic under the conditions of Method A, the rate of hydrolysis of isothiosemicarbazone should increase and the triazine formation will be accelerated. On the other hand, acidic media are generally unfavorable to the imidazole formation because protonation of **1** evidently inhibits the first step of this cyclization (Fig. 2). Furthermore, aldehyde isothiosemicarbazones, particularly those of aliphatic aldehyde, are likely susceptible to intramolecular cyclization under such conditions through the addition of the terminal amino group to the aldimine double bond to form a dihydro-1,2,4-triazole structure which is believed to be an intermediate in the formation of *N*-isopropenyl-1,2,4-triazoles in acetic acid.[9] Thus **1p** or **1q** cannot produce the corresponding 1-propylideneamino-1*H*-imidazole by the reaction with **2** or **3** unless a stronger base than the isothiosemicarbazone itself is present as acid binder. The fact that **1q** does not give **15c** in DMSO in the presence of sodium hydrogencarbonate can be rationalized in terms of the strong proton-accepting nature of this solvent. The reaction of **13** ($R^3=CH_3$) with **2** produced a highly darkened, complex mixture from which the corresponding **15** was isolated only in 4—8% yields. The alkylidene group of aliphatic isothiosemicarbazone may therefore serve as a protective group for controlled liberation of relatively unstable **13**, thereby leading to better yields of **15**. Taking into account of the facts that ammonium bromide and **14** ($R^3=CH_3$) were isolated in significant amounts from the reaction mixture of **1r** with **2a** and that the triazine formation occurred in the absence of oxygen, a mechanism for this reaction was suggested in Fig. 1.

The reaction conditions employed for the preparation of **4** were not very suitable for the reaction of **1** ($R^1=$ aryl) with **3** because of unstability of the halo aldehyde to sodium hydrogencarbonate. With the exception of **1p**, the condensation of **1** with **3** was thus carried out by

TABLE 1. 1-ALKYLIDENEAMINO- AND 1-ARYLMETHYLENEAMINO-2-MERCAPTO-4-ARYL-1*H*-IMIDAZOLES

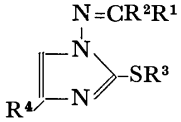

Compd No.	R^1	R^2	R^3	R^4	Yield (%)	Mp °C	Formula	Found (Calcd), % C	H	N	M+	IR[a] νC–H
4a	C_6H_5	H	Me	C_6H_5	70	144—145[b]	$C_{17}H_{15}N_3S$	69.33 (69.60	5.09 5.15	14.21 14.32	293 293)	3140
4b	C_6H_5	H	Me	*p*-ClC_6H_4	78	177—178[c]	$C_{17}H_{14}ClN_3S$	62.00 (62.29	4.34 4.30	12.50 12.82	327 327)	3140
4c	C_6H_5	H	Me	*p*-$MeOC_6H_4$	50	145—145.5[d]	$C_{18}H_{17}N_3OS$	66.80 (66.84	5.22 5.30	12.74 13.00	323 323)	3150
4d	C_6H_5	H	Me	*p*-$O_2NC_6H_4$	80	225—226[e]	$C_{17}H_{14}N_4O_2S$	60.18 (60.34	4.25 4.17	16.36 16.56	338 338)	3150
4e	C_6H_5	H	$C_6H_5CH_2$	C_6H_5	63	128—129[f]	$C_{23}H_{19}N_3S$	74.80 (74.78	5.16 5.18	11.18 11.38	369 369)	3150
4f	*o*-ClC_6H_4	H	Me	C_6H_5	77	149—150[c]	$C_{17}H_{14}ClN_3S$	62.23 (62.29	4.33 4.30	12.68 12.82	327 327)	3150
4g	*p*-ClC_6H_4	H	Me	C_6H_5	78	173.5—174[b]	$C_{17}H_{14}ClN_3S$	62.59 (62.29	4.37 4.30	12.70 12.82	327 327)	3150[j]
4h	*p*-$Me_2NC_6H_4$	H	Me	C_6H_5	49[g]	137—138[h]	$C_{19}H_{20}N_4S$	67.73 (67.84	6.01 5.99	16.82 16.66	336 336)	3150
4i	*o*-HOC_6H_4	H	Me	C_6H_5	73	176—178[b]	$C_{17}H_{15}N_3OS$	65.88 (66.01	4.92 4.89	13.59 13.58	309 309)	3145
4j	*o*-$MeOC_6H_4$	H	Me	C_6H_5	66	146—146.5[i]	$C_{18}H_{17}N_3OS$	67.05 (66.84	5.26 5.30	13.00 13.00	323 323)	3160[k]
4k	*p*-$MeOC_6H_4$	H	Me	C_6H_5	75	169—169.5[m]	$C_{18}H_{17}N_3OS$	66.82 (66.84	5.27 5.30	13.03 13.00	323 323)	3150[j]
4m	*p*-$MeOC_6H_4$	Me	Me	C_6H_5	38[g]	137—138[m]	$C_{19}H_{19}N_3OS$	67.68 (67.64	5.77 5.68	12.15 12.46	337 337)	3140
4n	*p*-$MeOC_6H_4$	H	Me	*o*-ClC_6H_4	58	142—142.5[n]	$C_{18}H_{16}ClN_3OS$	60.89 (60.41	4.39 4.51	11.74 11.74	357 357)	3160
4o	*p*-$MeOC_6H_4$	H	Me	*p*-ClC_6H_4	73	179—179.5[m]	$C_{18}H_{16}ClN_3OS$	60.48 (60.41	4.61 4.51	11.99 11.74	357 357)	3140
4p	*p*-$MeOC_6H_4$	H	Me	*o*-HOC_6H_4	8[g]	149—150[m]	$C_{18}H_{17}N_3O_2S$	64.16 (63.71	5.03 5.05	12.40 12.38	339 339)	3150
4q	*p*-$MeOC_6H_4$	H	Me	*p*-$MeOC_6H_4$	71	156.5—157[p]	$C_{19}H_{19}N_3O_2S$	64.37 (64.48	5.41 5.41	11.67 11.87	353 353)	3140
4r	*p*-$MeOC_6H_4$	H	Me	*p*-$O_2NC_6H_4$	77	215—216[q]	$C_{18}H_{16}N_4O_3S$	58.48 (58.69	4.39 4.38	14.99 15.21	368 368)	3140
4s	*p*-$MeOC_6H_4$	H	*n*-Pr	C_6H_5	67	143—143.5[b]	$C_{20}H_{21}N_3OS$	68.32 (68.36	6.13 6.02	11.73 11.96	351 351)	3120[v]
4t	*p*-$MeOC_6H_4$	H	$H_2C=CHCH_2$	C_6H_5	49	110—111[r]	$C_{20}H_{19}N_3OS$	68.75 (68.75	5.42 5.48	11.82 12.03	349 349)	3140
4u	*p*-$MeOC_6H_4$	H	$C_6H_5CH_2$	C_6H_5	38	136—137[d]	$C_{24}H_{21}N_3OS$	72.20 (72.16	5.32 5.30	10.33 10.52	399 399)	3150
4v	*p*-$MeOC_6H_4$	H	$C_6H_5CH_2$	*p*-ClC_6H_4	47	174—175[s]	$C_{24}H_{20}ClN_3OS$	66.52 (66.43	4.58 4.65	9.66 9.69	433 433)	3140
4w	Et	H	Me	C_6H_5	27[g]	179.5—180[i,u]	$C_{13}H_{16}ClN_3O_4S$	45.05 (45.15	4.60 4.66	12.09 12.15)		3150[t]
4x	Et	H	Me	*p*-ClC_6H_4	22[g]	104—104.5[r]	$C_{13}H_{14}ClN_3S$	55.90 (55.81	5.00 5.04	14.85 15.02)		3140
4y	Et	H	*p*-$ClC_6H_4CH_2$	C_6H_5	28[g]	107.5—108[i]	$C_{19}H_{18}ClN_3S$	63.77 (64.13	5.15 5.10	11.67 11.81)		3150
4z	Me	Me	Me	C_6H_5	8[g]	180—180.5[n,u]	$C_{13}H_{16}ClN_3O_4S$	45.23 (45.15	4.63 4.66	12.29 12.15)		3150[t]

a) The C–H stretching vibration of imidazole ring, cm^{-1} in KBr. b) Pale yellow needles from EtOH. c) Yellow needles from EtOH. d) Yellow plates from benzene–EtOH. e) Bright orange needles from pyridine. f) Light brown needles from MeCN. g) A homogeneous fraction from column chromatography. h) Pale yellow needles from MeOH. i) Yellow prisms from EtOH. j) 3155 cm^{-1} in $CHCl_3$. k) 3155 cm^{-1} in CCl_4. m) Pale yellow needles from benzene–EtOH. n) Colorless needles from EtOH. p) Pale yellow needles from pyridine–*i*-PrOH. q) Brown needles from pyridine. r) Pale yellow plates from EtOH. s) Yellow fine prisms from pyridine–EtOH. t) Free base in CCl_4. u) $HClO_4$ salt. v) Splitted into 3120 and 3090 cm^{-1} bands.

Table 2. 1-Alkylideneamino- and 1-arylmethyleneamino-2-methylthio-5-phenyl-1*H*-imidazoles

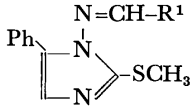

Compd No.	R^1	Yield[a] (%)	Mp °C	Formula	Found (Calcd), % C	H	N	M+	UV (MeOH) λ_{max} nm ($\varepsilon \times 10^{-4}$)		NMR[e] SCH_3	H-4
5a	C_6H_5	53	110—111[b]	$C_{17}H_{15}N_3S$	69.50 (69.60	5.21 5.15	14.48 14.32	293 293)	263 (2.82)	—	2.66	7.20
5b	*o*-ClC_6H_4	62	109—109.5[b]	$C_{17}H_{14}ClN_3S$	62.01 (62.29	4.37 4.30	12.76 12.82	327 327)	264 (2.28)	—	2.69	7.22
5c	*p*-ClC_6H_4	49	96.5—97[b]	$C_{17}H_{14}ClN_3S$	61.98 (62.29	4.22 4.30	12.88 12.82	327 327)	269 (2.65)	—	2.67	7.22
5d	*o*-HOC_6H_4	71	112—113[b]	$C_{17}H_{15}N_3OS$	65.79 (66.01	4.91 4.89	13.52 13.58	309 309)	267 (2.01)	335 (0.7)	2.68	7.21
5e	*o*-$MeOC_6H_4$	55	59.5—61[c]	$C_{18}H_{17}N_3OS$	66.59 (66.84	5.16 5.30	13.02 13.00	323 323)	267 (2.61)	332 (1.35)	2.67	7.29
5f	*p*-$MeOC_6H_4$	46	95—95.5[b]	$C_{18}H_{17}N_3OS$	67.00 (66.84	5.36 5.30	12.99 13.00	323 323)	281 (2.74)	306 (2.37)	2.67	7.24
5g	Et	15	38—39.5[d]	$C_{13}H_{15}N_3S$	63.80 (63.66	6.14 6.16	17.39 17.13)		276 (1.40)	—	2.61	7.06

a) For the product from a homogeneous fraction of column chromatogram. b) Yellow needles from *i*-PrOH. c) Yellow prisms from hexane–*i*-Pr_2O. d) Pale yellow crystals. e) δ, in $CDCl_3$.

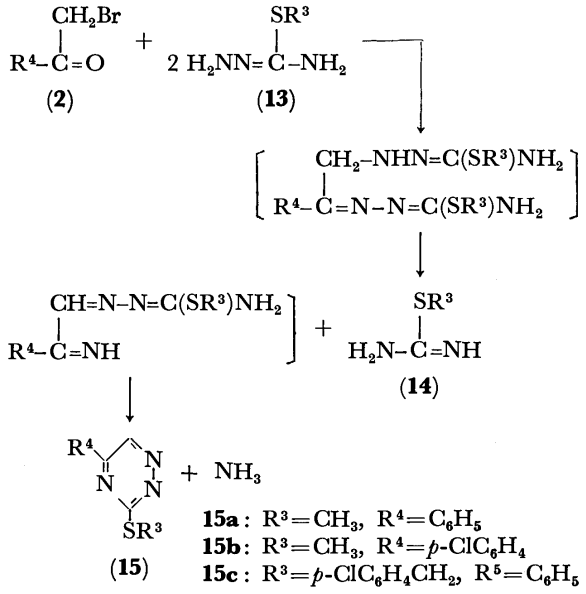

Fig. 1. A reaction mechanism for 1,2,4-triazine formation.

refluxing a mixture of **1** and **3** in a molar ratio of 2: 1 in acetonitrile without added sodium hydrogencarbonate and 5-phenyl-1*H*-imidazoles were isolated by means of column chromatography. As described above, **1p** did not produce the corresponding **5** under these reaction conditions but a complex mixture composed of many unidentifiable components. The standard procedure using sodium hydrogencarbonate was inevitably applied to the preparation of **5g** from **1p** in spite of the poor yield of this imidazole. 5-Phenyl-1*H*-imidazoles (**5**) thus obtained were listed in Table 2.

The structures of **4** and **5** were confirmed on the basis of analytical and spectral data (Tables 1—4) as well as their chemical transformation.

Table 3. Chemical shifts of phenyl protons on the imidazole ring (δ, in $CDCl_3$).

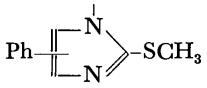

R^1	4-Phenyl H^o	$H^{m,p}$	Δ[a]	5-Phenyl $H^{o,m,p}$
C_6H_5	7.88	7.41	0.47	7.44
o-ClC_6H_4	7.92	7.39	0.53	7.42
p-ClC_6H_4	7.86	7.41	0.45	7.43
o-HOC_6H_4	7.87	7.38	0.49	7.41
o-$MeOC_6H_4$	7.92	7.42	0.50	7.42
p-$MeOC_6H_4$	7.88	7.39	0.49	7.40
Et	7.82	7.37	0.45	7.28

a) Differences (in ppm) between the chemical shifts of *ortho* (H^o) and *meta-para* ($H^{m,p}$) protons.

As has been observed by a number of investigators, the anisotropic deshielding of phenyl protons ortho to the heteroaromatic ring in phenylazoles disappeares or greatly diminishes when coplanarity between the two aromatic rings and the resulting resonance interaction is inhibited by the adjacent alkyl group on the azole ring.[5] The NMR spectral data (Table 3) showed that the ortho protons (H^o) in the compounds **4** obtained from the condensation with **2a** were deshielded by 0.45—0.53 ppm relative to the *meta*- and *para*-protons ($H^{m,p}$), whereas the phenyl protons in the compounds **5** gave a single signal only. Thus the phenyl group of **4** should lie at the position 4 and that of **5** is in the 5-position adjacent to the $R^1R^2C{=}N$ grouping.

Compounds which were derived from substituted phenacyl bromides (**2b**—**2f**) might also be expected to have the 4-aryl-1*H*-structure. The UV spectra of these compounds normally showed two maxima at near

TABLE 4. UV SPECTRA OF 1-ARYLMETHYLENEAMINO-2-METHYLTHIO-4-ARYL-1*H*-IMIDAZOLES

Compd No.	R^4	UV (MeOH) λ_{max} nm ($\varepsilon \times 10^{-4}$)		
4a	C_6H_5	279 (3.09)		344 (1.18)
4b	*p*-ClC_6H_4	283 (3.54)		345 (1.44)
4c	*p*-$MeOC_6H_4$	294 (3.66)		352 (1.27)
4f	C_6H_5	281 (3.37)		356 (1.04)
4g	C_6H_5	283 (3.72)		349 (1.33)
4i	C_6H_5	281 (3.17)		351 (1.84)
4j	C_6H_5	278 (2.74)		349 (1.73)
4k	C_6H_5	291 (2.90)		342 (2.20)
4m	C_6H_5	283 (3.41)		—
4n	*o*-ClC_6H_4	293 (2.46)		338 (2.20)
4o	*p*-ClC_6H_4	292 (3.06)		344 (2.29)
4p	*o*-HOC_6H_4	258 (1.55),	300 (2.70),	352 (2.18)
4q	*p*-$MeOC_6H_4$	290 (2.77)		348 (1.92)

280—290 and 340—350 nm with one or two inflections between these bands, with the former absorptions being more intense than the latter (Table 4). These characteristics in UV spectra are quite similar to those exhibited by 4-(unsubstituted phenyl) compounds (**4a**, **4f**—**g**, **4i**—**k**) and are essentially different from those of **5**, which had a main band within the limits λ_{max} 263—281 nm and $\varepsilon \times 10^{-4}$=2.01—2.82. The compound **4p**, which had an additional shorter band at 258 nm and a longer main band at 300 nm than the normal region, exhibited an intramolecularly hydrogen bonded O–H band (centered at 3050 cm^{-1}) at a concentration of 2.5×10^{-3} M in carbon tetrachloride. Such hydrogen bonding would be possible only in the 4-*o*-hydroxyphenyl structure because of lack of proton-accepting nature in N-1. Consequently the reaction between isothiosemicarbazones and phenacyl bromides should produce 4-aryl-1*H*-imidazoles independently of the nature of R's and the steric repulsion between R^4 and R^1R^2C=N groups in the transition state will have no effect upon the orientation of ring closure.

The 1,2,4- and 1,2,5-trisubstituted imidazoles could also be differentiated by their IR spectra. The differentiation of both series was based upon the appearance of a weak, but distinct absorption band at 3160—3140 cm^{-1} in the spectra of 1,2,4-trisubstituted isomers (Table 1). Such a difference consistently occurred between isomers both in crystalline materials in KBr disks and in carbon tetrachloride or chloroform solution and therefore does not reflect the difference between their crystal structures. This absorption band was absent in 5-deuterio compounds (**4g**-d_1 and **4k**-d_1) and thus assigned to a C–H stretching vibration at the 5-position of imidazole ring shifted to higher frequencies than usual aromatic region[10] presumably by steric compression.

o-Hydroxybenzylideneamino compounds **4i** and **5d** exhibited internally bonded O–H stretching bands (centered at 3220 and 3170 cm^{-1}) at 4×10^{-3} M in carbon tetrachloride. This observation suggests that the *o*-hydroxyphenyl group and the imidazole ring must be in *E* configuration about the azomethine double bond to which they attached. Other **4** and **5** may also be *E* form in view of the similarities of UV spectra observed between the members of each series. If they were in *Z* configuration, R^1 should be twisted out of the plane of the rest of molecule as evidenced by examination of a scale model. Thus the UV spectra of 4-aryl series would resemble that of **4m** which lacks the longer-wavelength band (Table 4) due to the steric inhibition of conjugation between R^1 and the heteroaromatic ring caused by the α-methyl group (R^2=CH_3); on the other hand, the UV spectra of 5-aryl series would become comparable with those of **5g**.

In mass spectrometry, molecular ions were obtained for all 1-arylmethyleneamino compounds studied (Tables 1 and 2) and always represented the base peak. Primary fragmentation occurred at the N–N bond, leading to an intermediate, M^+–R^1R^2C=N (≃100%), common to the 1,2,4- and 1,2,5-isomers. Another ionization occurred to produce R^1R^2C=N^+=CS (≈60%) which is also common to both isomers. Thus practically identical spectra resulted between the members of each pair of isomers except for **4f** and **4j** in which fragmentation M^+–Cl· and M^+–MeO· occurred only in 4-aryl compounds as shown by the appropriate metastable ions. The R^4CN^+ ion, one of the criteria on which the structural assignment had been made in Ref. 1, was invariably found in the spectra of both isomers in comparable abundance (9—38%) and therefore of no diagnostic value for differentiation.

Although no reaction intermediates have been isolated in this study, a probable reaction mechanism that accounts for the results obtained here was represented in Fig. 2.

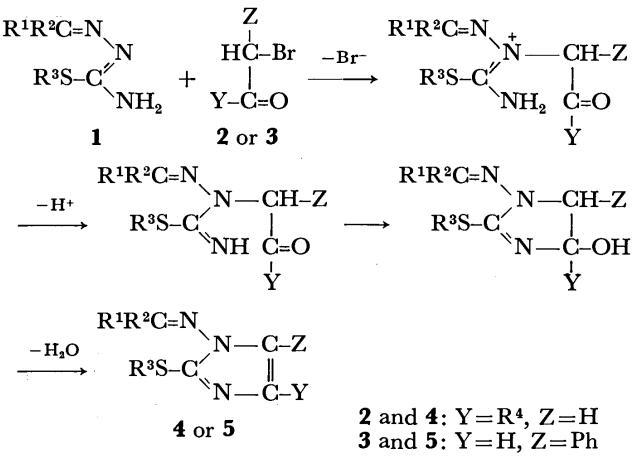

Fig. 2. A reaction mechanism for imidazole-ring formation.

The reaction should occur by the initial attack of N-2 which was believed to be the most nucleophilic center in **1**[11] on the α-carbon of **2** or **3**. An alternative path, in which the condensation of the terminal amino group of **1** with the carbonyl group of **2** or **3** is the first step, is unlikely to operate because the substitution of phenacyl chloride for **2a** resulted in substantial recovery of the starting materials under the same conditions. If the reaction proceeds through the latter path, there would accumulate an initial product, R^1R^2C=N–N=C(SR^3)–N=C(CH_2Cl)Ph, in the reaction mixture because of low reactivity of the halogen in phenacyl chloride.

Both 4- and 5-aryl-1*H*-imidazoles (**4** and **5**) were found to undergo reductive cleavage to 1-acetyl-4-aryl-1*H*-imidazoles (**6**), *N*-benzylacetamides (**10**), and thiols (**11**) upon stirring with acetic acid and zinc dust in the presence of acetic anhydride at room temperature. A possible product 1-acetyl-5-phenyl-1*H*-imidazole from **5a**, if any, may rapidly rearrange to a thermodynamically favorable 4-phenyl isomer through a reversible process of acetylation.[12] The benzylthio derivative (**4u**) was more resistant to the reduction than alkylthio compounds and prolonged reaction periods caused considerable formation of unidentifiable amorphous materials leading to a poor yield of **6**. The nitro group of **4d** was simultaneously reduced to give **6c**. The reduction of nitro group readily took place under the reaction conditions as evidenced by rapid disappearance of the red color due to this group prior to evolution of methanethiol and therefore a compound 1-acetyl-4-*p*-nitrophenyl-1*H*-imidazole could not be obtained by this process. The acetyl group at N-1 was susceptible to hydrolysis and partially splitted off in working up.

Two protons H-2 and H-5 on the imidazole ring of **6** appeared as two doublets with a coupling constant of 1.3 Hz at about δ 8.1 and 8.4 ppm in DMSO-d_6 due to cross-ring coupling. Peak assignment of these protons can unambiguously be made on the basis of the spectrum of 1-acetyl-4-phenyl-5-deuterio-1*H*-imidazole (**6a**-d_1) which lacks the upfield resonance. This is in accordance with the common practice of assigning H-2 to the most downfield resonance of 1-substituted imidazoles,[13] although H-2 is not always the most deshielded proton.[14]

Hydrolysis of the arylmethyleneamino to an amino group of **4g** or **4k** was unsuccessful either in aqueous ethanolic hydrogen chloride or sodium hydroxide solution at the reflux temperature over a period of 10 h with total recovery of the starting imidazoles (Table 5). The corresponding 5-phenyl isomers, however, underwent hydrolysis to an extent of 24 and 22%, respectively. Ortho substituents on the benzylideneamino group of **4** accelerated the rate of hydrolysis independently of whether it is electron-releasing or electron-withdrawing. No specific intramolecular catalysis[15] was observed. On the other hand, **4m** was hydrolyzed to 97% under the same conditions and the reaction was substantially completed within 30 minutes when the hydrolysis was carried out in concentrated hydrochloric acid at 130 °C. In view of these observations, the susceptibility to hydrolysis of arylmethyleneamino group directly reflects the diminished or inhibited conjugation between the azomethine double bond and the adjacent aromatic rings resulting from crowding around the double bond.

Hydrolytic products **7** and **9** could be obtained quantitatively by hydrazinolysis of **4** and **5**. When **4k** was heated with a large excess of hydrazine hydrate in

Table 5. Yield[a] of 1-aminoimidazoles from 1-arylmethyleneamino-2-methylthio-4- or 5-phenyl-1*H*-imidazoles

Substituents on the benzylideneamino group	4-Phenyl	5-Phenyl
o-Chloro	9	23
p-Chloro	0	24
o-Hydroxy	8	50
o-Methoxy	12	19
p-Methoxy	0	22
p-Methoxy-α-methyl	97	—

a) Estimated from NMR spectra after refluxing in aqueous ethanolic HCl for 10 h and evaporating under reduced pressure.

Table 6. 1-Amino-2-mercapto-4-aryl-1*H*-imidazoles

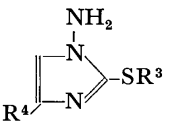

Compd No.	R^3	R^4	Yield (%)	Mp °C	Formula	Found (Calcd), % C	H	N	IR (KBr) νN–H[a]	NMR (CDCl$_3$), δ SCH_3	SCH_2	H-5
7a	Me	C_6H_5	98	122.5—123[b]	$C_{10}H_{11}N_3S$	58.55 (58.53	5.43 5.40	20.35 20.48)	3340—3100	2.59	—	7.20
7b	Me	*p*-$H_2NC_6H_4$	29	175—176[c]	$C_{10}H_{12}N_4S$	54.78 (54.54	5.53 5.49	25.68 25.44)	3350—3120	2.51	—	7.30[d]
7c	Me	*p*-ClC_6H_4	97[e]	138—139[f]	$C_{10}H_{10}ClN_3S$	50.08 (50.15	4.28 4.21	17.53 17.54)	3330—3140	2.64	—	7.30
7d	Me	*p*-$O_2NC_6H_4$	32	177.5—178[g]	$C_{10}H_{10}N_4O_2S$	48.18 (48.00	4.00 4.02	22.18 22.39)	3330—3130	2.62	—	7.96[d]
7e	*n*-Pr	C_6H_5	90[h]	79—80.5[i]	$C_{12}H_{15}N_3S$	61.91 (61.78	6.47 6.48	17.87 18.02)	3340—3140	—	3.04[j]	7.18
7f	H_2C=$CHCH_2$	C_6H_5	93	100—101[k]	$C_{12}H_{13}N_3S$	62.30 (62.32	5.71 5.67	18.16 18.17)	3350—3140	—	3.66[m]	7.19
7g	$C_6H_5CH_2$	C_6H_5	86	113—114[n]	$C_{17}H_{17}N_3S$	68.17 (68.31	5.37 5.38	14.88 14.94)	3320—3120	—	4.10	7.12

a) Composed of 4—5 bands, cm^{-1}. b) Lit,[18] mp 118 °C. c) Reddish beige plates from EtOH. d) In DMSO-d_6. e) Heated for 10 h. f) Colorless plates from EtOH. g) Yellowish orange needles from EtOH. h) Starting with **4s**. i) White needles from hexane. j) Triplet, J=6.8 Hz. k) Colorless needles from *i*-Pr_2O. *m*) Double triplet, J=6.5 and 0.8 Hz. n) Pale yellow prisms from EtOH.

2-methoxyethanol at 170 °C for 1.5 h, **7a** was obtained in 98% yield after isolation by means of column chromatography on silica gel. It was also possible to isolate and purify **7a** by extraction with methanol followed by recrystallization from benzene. In most cases, however, repeated recrystallizations were required to accomplish complete removal of azine **12** causing a considerable loss of the aminoimidazoles. The yields reported in Table 6 were those for a homogeneous fraction obtained by means of column chromatography except for **7b** and **7d**. 4-*p*-Nitrophenylimidazole **4d** gave **7b** in addition to the expected product **7d** as a result of simultaneous reduction of the nitro group. The treatment of **4t** with hydrazine hydrate was also complicated by concomitant reduction of the allyl to a propyl group, if the reaction mixture contained an acid or accidentally absorbed an acid vapor. The formation of **7e** reached the maximum 28.5% when 4 molar equivalents of acetic acid was present, while no reduction occurred in the absence of acid.[16] In contrast to certain methylthiotriazine derivatives,[6,17] nucleophilic attack by a hydrazine molecule on C-2 was not observed even after heating over a period of 10 h.

The aminoimidazoles **7** underwent deamination upon treatment with sodium nitrite in a hydrochloric acid–methanol mixture to give the corresponding 2,4-disubstituted imidazoles **8** in moderate yields. They were characterized by their IR spectra which exhibited a broad absorption band at 3060—2600 cm^{-1} due to the bonded N–H.

Pyl *et al.*[18] had reported a melting point of 118 °C for 1-amino-2-methylthio-4-phenyl-1*H*-imidazole. This value corresponds to that of **7a** but obviously not to 5-phenyl isomer **9**. The strength in support of the structure for **7a** may thus be obtained. However, there is no reason to believe it is the ring nitrogen which attacks the α-carbon of **2a** and not the amino nitrogen in the formation of the precursor 2-substituted 6-phenylimidazo[2,1-*b*][1,3,4]thiadiazole by the reaction between 2-amino-1,3,4-thiadiazole and **2a**.[18] Consequently the practical agreement in the melting point of **7a** with that of the literature may be insufficient as the basis for determination of the substitution pattern of all the present 1,2,4- and 1,2,5-trisubstituted imidazoles.

Experimental

Melting points were determined in an open glass capillary and are uncorrected. IR spectra were recorded on a Hitachi EPI-G2 grating spectrophotometer. Spectra of solutions were obtained in 0.1-mm KBr or 5-mm KRS-5 cells and those of solid samples taken in KBr disks. UV spectra were recorded on a Hitachi EPS-2 spectrophotometer and mass spectra (75 eV) on a Japan Electron Optics JMS-OlS or JMS-D100 mass spectrometer using a direct inlet procedure. ^1H NMR spectra were obtained on a Nichiden-Varian T-60 or a Hitachi R-24 spectrometer, both operating at 60 MHz. Chemical shifts were reported in δ ppm downfield from internal tetramethylsilane. Following abbreviations were used: s=singlet, d=doublet, t=triplet, m=multiplet, br=broad singlet, dt=double triplet, and vs=very strong.

α-Halo Carbonyl Compounds. Phenacyl bromides (**2a**—**2f**) were prepared from the corresponding acetophenones by the known methods[19] and **3** was obtained from phenylacetaldehyde according to the method described by Riehl.[20] NMR (CCl_4) 5.11 (d, 1, J=3.6 Hz, BrCH), 7.34 (s, 5, C_6H_5), 9.48 (d, 1, J=3.6 Hz, CHO). α-Ethoxyphenylacetaldehyde 2,4-dinitrophenylhydrazone,[21] mp 139 °C (lit,[22] mp 140 °C).

Isothiosemicarbazones. The compounds (**1a**—**1s**) were prepared by the procedure reported previously[11] with some appropriate modifications. New ones are: **1c**: white prisms (from hexane), mp 60—62 °C, yield 46%; NMR ($CDCl_3$) 2.51 (s, 3, SCH_3), 5.50 (br, 2, NH_2), 7.15—8.15 (m, 4, ring protons), 8.80 (s, 1, CH=N). Found: C, 47.37; H, 4.40; N, 18.42%. Calcd for $C_9H_{10}ClN_3S$: C, 47.47; H, 4.43; N, 18.45%. **1d**: pale yellow prisms (from *i*-PrOH), mp 98—100 °C, yield 49%; NMR ($CDCl_3$) 2.49 (s, 3, SCH_3), 5.50 (br, 2, NH_2), 7.33 (d, 2, J=8.5 Hz, ring protons), 7.66 (d, 2, J=8.5 Hz, ring protons), 8.33 (s, 1, CH=N). Found: C, 47.16; H, 4.38, N, 18.39%. Calcd for $C_9H_{10}ClN_3S$: C, 47.47; H, 4.43; N, 18.45%. **1e**[23]: yellow plates (from aq EtOH), mp 140—142 °C, yield 81%; NMR ($CDCl_3$) 2.48 (s, 3, SCH_3), 2.98 (s, 6, $N(CH_3)_2$), 5.40 (br, 2, NH_2), 6.68 (d, 2, J=9.6 Hz, ring protons), 7.62 (d, 2, J=9.6 Hz, ring protons), 8.32 (s, 1, CH=N). Found: C, 55.92; H, 6.70; N, 23.65%. Calcd for $C_{11}H_{16}N_4S$: C, 55.91; H, 6.83; N, 23.72%. **1f**: faintly yellow needles (from aq EtOH), mp 162.5—163 °C, yield 78%; NMR ($CDCl_3$–DMSO-d_6, 4: 1 by volume) 2.45 (s, 3, SCH_3), 6.25 (br, 2, NH_2), 6.70—7.50 (m, 4, ring protons), 8.22 and 8.37 (two s, 0.5, 0.5, CH=N), 11.15 and 11.46 (two br, 0.5, 0.5, OH).[24] Found: C, 51.72; H, 5.32; N, 19.95%. Calcd for $C_9H_{11}N_3OS$: C, 51.67; H, 5.30; N, 20.09%. **1g**: white needles (from hexane), mp 58.5—59 °C, yield 90%; NMR ($CDCl_3$) 2.49 (s, 3, SCH_3), 3.82 (s, 3, OCH_3), 5.50 (br, 2, NH_2), 6.80—8.10 (m, 4, ring protons), 8.78 (s, 1, CH=N). Found: C, 54.08; H, 5.99; N, 18.73%. Calcd for $C_{10}H_{13}N_3OS$: C, 53.80; H, 5.87; N, 18.83%. **1p**: white plates (from hexane), mp 67—68 °C, yield 65%; NMR ($CDCl_3$) 1.10 (t, 3, J=7.4 Hz, CCH_3), 2.36 (m, 2, CH_2), 2.42 (s, 3, SCH_3), 5.36 (br, 2, NH_2), 7.73 (t, 1, J=5.0 Hz, CH=N). Found: C, 41.62; H, 7.52; N, 28.95%. Calcd for $C_5H_{11}N_3S$: C, 41.37; H, 7.64; N, 28.95%. **1q**: white needles (from hexane), mp 82—83 °C, yield 83% NMR ($CDCl_3$) 1.13 (t, 3, J=7.4 Hz, CCH_3), 2.35 (m, 2, CCH_2), 4.22 (s, 2, SCH_2), 5.30 (br, 2, NH_2), 7.30 (s, 4, ring protons), 7.80 (t, 1, J=5.1 Hz, CH=N). Found: C, 51.93; H, 5.49; N, 16.38%. Calcd for $C_{11}H_{14}ClN_3S$: C, 51.66; H, 5.52; N, 16.43%. **1s**: pale yellow plates (from hexane), mp 77.5—78 °C, yield 63%; NMR ($CDCl_3$) 2.00 (s, 3, CCH_3), 2.01 (s, 3, CCH_3), 4.23 (s, 2, SCH_2), 5.14 (br, 2, NH_2), 7.25 (s, 4, ring protons). Found: C, 51.32; H, 5.50; N, 16.49%. Calcd for $C_{11}H_{14}ClN_3S$: C, 51.66; H, 5.52; N, 16.43%.

*Preparation of **4k** (a typical example).* A mixture of **1h** (0.56 g, 2.5 mmol), **2a** (0.60 g, 3.0 mmol), sodium hydrogencarbonate (0.63 g, 7.5 mmol), and MeCN (3 ml) was heated under stirring at 75 °C for 3 h. After cooling, the solids were filtered off, washed with cold MeCN, and then suspended in sufficient water to dissolve any inorganic salts. The insoluble crystals were collected on a filter, washed with water, and then dried to give **4k** (0.60 g, 75%), mp 169—169.5 °C. Recrystallization from benzene–EtOH did not raise the melting point, but resulted in improvement in the appearance of the crystal. When 0.75 g (3.75 mmol) of **2a** was used, the yield of **4k** increased to 0.65 g (80.3%). The 5-deuterio derivative (**4k**-d_1) was similarly prepared by substituting phenacyl-*methylene*-d_2 bromide ($C_6H_5COCD_2Br$), which in turn was obtained by brominating acetophenone-α,α,α-d_3 ($C_6H_5COCD_3$), for **2a** in 65% yield. Pale yellow needles (benzene–EtOH), mp 168—169 °C not depressed by **4k**. IR ($CHCl_3$) 2340 (C–D) cm^{-1}; NMR ($CDCl_3$) 2.70 (s, 3, SCH_3), 3.78 (s, 3, OCH_3), 6.87 (d,

2, J=8.7 Hz, *p*-methoxyphenyl protons), 7.21 (m, 3, $H^{m,p}$ of 4-phenyl), 7.63 (d, 2, J=8.7 Hz, *p*-methoxyphenyl protons), 7.69 (m, 2, H^{o} of 4-phenyl), 8.10 (s, 1, CH=N); M^+ 324 (M 324). Similarly, **4g**-d_1 was obtained in 64% yield as yellow needles, mp 173.5—174 °C. IR ($CHCl_3$) 2340 (C–D) cm^{-1}; NMR ($CDCl_3$) 2.67 (s, 3, SCH_3), 7.26 (m, 3, $H^{m,p}$ of 4-phenyl), 7.31 (d, 2, J=8.5 Hz, *p*-chlorophenyl protons), 7.65 (d, 2, J=8.5 Hz, *p*-chlorophenyl protons), 7.70 (m, 2, H^{o} of 4-phenyl), 8.08 (s, 1, CH=N); M^+ 328 (M 328).

Preparation of **5c** *(a typical example).* To a warm soln of **3** (0.5 g, 2.5 mmol) in MeCN (5 ml) was added **1d** (1.14 g, 5.0 mmol) and quickly dissolved with agitation. The reaction mixture solidified within a few min. After heating for 1 h at 83 °C, the solids were filtered off, washed with MeCN and then Et_2O. The filtrate and the washings were combined and evaporated. The residual liquid was dissolved in benzene (30 ml) and the soln was washed with 0.1 M hydrochloric acid and then with water. The organic layer was dried over anhyd. sodium sulfate and evaporated. The residue (0.73 g) was charged onto a silica gel column (40 g) and eluted by benzene–EtOH (98: 2 by volume). A homogeneous fraction (0.43 g, 52.4%) was crystallized from *i*-PrOH (0.5 ml) to give **5c** as bright yellow needles, mp 96—97 °C. Recrystallization from *i*-PrOH (1.0 ml) yielded yellow needles, mp 96.5—97 °C. NMR ($CDCl_3$) 7.45 (d, 2, J=8.0 Hz, *p*-chlorophenyl), 7.70 (d, 2, J=8.0 Hz, *p*-chlorophenyl), 8.22 (s, 1, CH=N).

Preparation of **5g**. A mixture of **1p** (0.73 g, 5.0 mmol), **3** (1.00 g, 5.0 mmol), sodium hydrogencarbonate (1.70 g, 20 mmol), and MeCN (10 ml) was stirred at 74 °C for 3 h and then filtered. After the inorganic salts were washed with MeCN, the filtrate and the washings were evaporated and the residue taken up in benzene (30 ml). When the soln was worked up in a similar manner to the preparation of **5c**, there was obtained **5g** as pale yellow prisms (0.19 g, 15%), mp 38—39.5 °C. NMR ($CDCl_3$) 1.11 (t, 3, J=7.0 Hz, CCH_3), 2.40 (m, 2, CH_2), 7.60 (t, 1, J=4.8 Hz, CH=N).

Reaction of **1p** *with* **2a**. A mixture of **1p** (0.73 g, 5 mmol), **2a** (1.0 g, 5 mmol), sodium hydrogencarbonate (1.7 g, 20 mmol), and MeCN (10 ml) was stirred at 75 °C for 3 h. The inorganic salts were filtered off and washed with benzene. The filtrate and the washings were combined and evaporated. The residue (1.41 g) was charged onto silica gel column (100 g) and eluted with benzene–EtOH (98: 2 by volume). Two fractions, an imidazole-rich fraction (0.53 g) containing a small amount of methyl phenyl sulfide and a triazine-rich fraction (0.17 g) were separated. The former was again subjected to column chromatography under the same conditions to give pure **4w** as a yellow oil (0.33 g, 27%). UV_{max} (MeOH) 254 (ε 20 100), 271 (ε 15 900), 311 (ε 8 300) nm; NMR ($CDCl_3$) 1.19 (t, 3, J=7.0 Hz, CCH_3), 2.52 (m, 2, CH_2), 2.70 (s, 3, SCH_3), 7.56 (s, 1, H-5), 7.79 (t, 1, J=4.8 Hz, CH=N). The perchlorate was prepared in a conventional manner; IR (KBr) 3170 (NH^+), 1100 *vs.* (ClO_4^-) cm^{-1}. The mixed melting point with a product prepared by reacting **7a** with propionaldehyde and salt-forming with perchloric acid did not show any depression (179.5 °C). The triazine-rich fraction was crystallized from *i*-PrOH (0.5 ml) to afford **15a** as pale yellow prisms (0.06 g), mp 99—99.5 °C (lit,[6] mp 99—100.5 °C); NMR ($CDCl_3$) 2.71 (s, 3, SCH_3), 7.52 (m, 3, $H^{m,p}$ of 5-phenyl), 8.10 (m, 2, H^{o} of 5-phenyl), 9.33 (s, 1, H-6). (Found: N, 20.97%). Methyl phenacyl sulfide separated from the imidazole-rich fraction exhibited the identical IR and NMR spectra with those of an authentic sample which was prepared by introducing methanethiol generated from a mixture of **14** (R^3=Me, as a sulfate) and aq sodium hydroxide into a soln of **2a** in Et_2O. 2,4-Dinitrophenylhydrazone: mp 164—165 °C (lit,[25] mp 164—165.5 °C).

Reaction of **1r** *with* **2a**. A solution of **1r** (10.0 g, 69 mmol) and **2a** (6.86 g, 34.5 mmol) in EtOH (100 ml) was heated at 70—75 °C for 3 h and then evaporated. The residue was taken up in chloroform and the soln was repeatedly washed with water acidified to pH 5 with hydrobromic acid. The organic layer was dried over anhyd. sodium sulfate and evaporated. The residue (6.69 g) was triturated with six 75 ml-portions of a hexane–diisopropyl ether mixture (2: 1 by volume) and the combined extracts were evaporated to give an oil (4.96 g). From a one-gram portion of this oil, there were separated **15a** (0.28 g, 20%), mp 95—98 °C; **4z** (0.13 g, 7.5%), NMR ($CDCl_3$) 1.90 (s, 3, CCH_3), 2.20 (s, 3, CCH_3), 2.61 (s, 3, SCH_3), 7.17 (s, 1, H-5), 7.35 (m, 3, $H^{m,p}$ of 4-phenyl), 7.80 (m, 2, H^{o} of 4-phenyl), perchlorate mp 180—180.5 °C, IR (KBr) 3180 (NH^+), 1120 (ClO_4^-) cm^{-1}; and impure **7a** (0.22 g). Ammonium bromise (0.38 g) and **14** (R^3=CH_3) as a picrate (1.0 g), mp 220 °C dec, not depressed on mixing with an authentic sample, were isolated from the aq washings. When **1s** was react d with **2a** by this method, **15c** was obtained in 38% yield and no imidazole was detected. Deep yellow powder (from EtOH), mp 115—116 °C; IR (KBr) 1540, 1500, 1250, 760 cm^{-1}; NMR ($CDCl_3$) 4.50 (s, 2, CH_2), 7.35 (m, 4, *p*-chlorophenyl protons), 7.55 (m, 3, $H^{m,p}$ of 5-phenyl), 8.10 (m, 2, H^{o} of 5-phenyl), 9.35 (s, 1, H-6). Found: C, 61.07; H, 3.92; N, 13.36%. Calcd for $C_{16}H_{12}ClN_3S$: C, 61,24; H, H, 3.80; N, 13.40%.

Reaction of **1r** *with* **2c**. A mixture of **1r** (1.45 g, 10 mmol), **2c** (3.50 g, 15 mmol), sodium hydrogencabronate (5.0 g, 60 mmol), and MeCN (20 ml) was heated at 80 °C under stirring for 5 h and the inorganic salts were filtered off. After the filtrate was evaporated, the residue was worked up by the same manner as that in the reaction with **2a** giving a hexane–diisopropyl ether extract (1.35 g) from which **15b** (0.18 g, 7.6%) was isolated by crystallization from *i*-PrOH. It was passed a silica gel column using chloroform as an eluent and the homogeneous fraction recrystallized from aq EtOH to afford yellow needles, mp 164—164.5 °C (lit,[7] mp 163 °C); NMR ($CDCl_3$) 2.71 (s, 3, SCH_3), 7.51 (d, 2, J=9.0 Hz, *p*-chlorophenyl protons), 8.12 (d, 2. J=9.0 Hz, *p*-chlorophenyl protons), 9.34 (s, 1, H-6). (Found: C, 50.46; H, 3.48; N, 17.80%). The mother liquor obtained after removal of **15b** was heated under reflux in EtOH (7 ml) containing concentrated hydrochloric acid (0.5 ml) and anisaldehyde (0.5 ml) for 30 min. When the reaction mixture was made basic (pH 9) with aq ammonia **4o** (0.57 g, 16%) precipitated. When **1r** (1.45 g, 10 mmol) was reacted with **2c** (1.17 g, 5 mmol) by heating in ethanolic soln at 65 °C for 4 h, there were obtained **15b** (0.33 g, 28%) and **4o** (0.30 g, 17%).

Reductive Cleavage of **4b** *(a typical example).* A mixture of **4b** (0.66 g), zinc dust (13.0 g), glacial acetic acid (42 ml), and acetic anhydride (21 ml) was stirred at room temperature for 3 h, filtered, and the filtrate was evaporated to give a residue which was then triturated with water (10 ml). The insoluble solid was collected by filtration, washed with water and then dried in vacuo giving **6b** (R^4=*p*-ClC_6H_4) (0.36 g, 82%), mp 180—183 °C. Recrystallization from EtOH yielded lustrous flat prisms. mp 186.5 °C. IR(KBr) 3140 (νC–H), 1720 *vs.* (C=O), 835 (δC–H) cm^{-1}. NMR (DMSO-d_6) 2.64 (s, 3, $COCH_3$), 7.39 (d, 2, J=8.2 Hz, *p*-chlorophenyl protons), 7.84 (d, 2, J=8.2 Hz, *p*-chlorophenyl protons), 8.17 (d, 1, J=1.3 Hz, H-5), 8.41 (d, 1, J=1.3 Hz, H-2). Found: C, 59.68; H, 4.00; N, 12.70%. Calcd for $C_{11}H_9ClN_2O$: C, 59.88; H, 4.11; N, 12.69%. The product (0.1 g) was hydrolyzed by refluxing in an EtOH–hydrochloric acid mixture to 4-*p*-chlorophenylimidazole hydro-

chloride which was then treated with aq sodium hydroxide soln and the free base (0.07 g, 87%) recrystallized from water affording 4-*p*-chlorophenylimidazole, mp 146—147 °C (lit,[26] mp 145—147 °C). IR(KBr) 3130—2600 *vs.* (N–H) cm^{-1}.

The following compounds were similarly obtained: **6a** ($R^4=C_6H_5$) from **4k** in 38% yield, mp 148—149 °C (lit,[27] mp 153 °C). IR (KBr) 1725 *vs.* (C=O) cm^{-1}; NMR (DMSO-d_6) 2.65 (s, 3, $COCH_3$), 7.32 (m, 3, $H^{m,p}$ of 4-phenyl), 7.81 (m, 2, H^o of 4-phenyl), 8.10 (d, 1, J=1.3 Hz, H-5), 8.38 (d, 1, J=1.3 Hz, H-2). (Found: N, 14.99%). 4-Phenylimidazole which was contained in the aq washings of **6a** was separated as picrate in 19% yield, mp 214—215 °C lit,[27] mp 215 °C). (Found: C, 48.17; H, 2.96; N, 18.77%). 1-Acetyl-4-phenyl-1*H*-imidazole was also obtained from **5a** in 55% yield, mp 149 °C not depressed by **6a** from **4k**. The 5-deuterio compound **4k**-d_1 gave **6a**-d_1 in 62% yield, mp 146—147 °C. IR(KBr) 1725 *vs.* (C=O) cm^{-1}; NMR (DMSO-d_6) 2.66 (s, 3, $COCH_3$), 7.30 (m, 3, $H^{m,p}$ of 4-phenyl), 7.82 (m, 2, H^o of 4-phenyl), 8.38 (s, 1, H-2). **6c** (R^4=*p*-AcNH-C_6H_4) from **4d** in 74% yield as colorless prisms, mp 258 °C (from AcOH–Ac_2O); IR(KBr) 1735 *vs.* (C=O), 1680 (C=O) cm^{-1}; NMR (CF_3CO_2D) 2.50 (s, 3, $COCH_3$), 2.91 (s, 3, $COCH_3$), 7.72 (s, 4, C_6H_4), 8.12 (d, 1, J=1.6 Hz, H-5), 9.29 (d, 1, J=1.6 Hz, H-2). Found: C, 64.30; H, 5.35; N, 17.13%. Calcd for $C_{13}H_{13}N_3O_2$: C, 64,18; H, 5.39; N, 17.27%. Selective hydrolysis at N-1 of **6c** was accomplished by agitating in water adjusted to pH 11 at room temperature and afforded 4-*p*-acetamidophenylimidazole, mp 250—250.5 °C (lit,[28] mp 250—251 °C); IR (KBr) 1685 cm^{-1} (C=O). (Found: C, 65.49; H, 5.50; N, 20.98%). **6d** (R^4=*p*-$MeOC_6H_4$) from **4c** in 78% yield as colorless needles, mp 184.5—185 °C (from EtOH); IR (KBr) 3140 (νC–H), 1730 *vs.* (C=O), 840 (δC–H) cm^{-1}; NMR (DMSO-d_6) 2.65 (s, 3, $COCH_3$). 3.78 (s, 3, OCH_3), 6.93 (d, 2, J=8.7 Hz, *p*-methoxyphenyl protons), 7.77 (d, 2, J=8.7 Hz, *p*-methoxyphenyl protons), 8.02 (d, 1, J=1.3 Hz, H-5), 8.37 (d, 1, J=1.3 Hz, H-2). Found: C, 66.45; H, 5.54; N, 12.98%. Calcd for $C_{12}H_{12}N_2O_2$: C, 66.65; H, 5.59; N, 12.96%. It was hydrolyzed to 4-*p*-methoxyphenylimidazole (75%), mp 137.5—138 °C (lit,[28] mp 136—137 °C); IR (KBr) 3100—2600 *vs.* (N–H) cm^{-1}. (Found: C, 68.92; H, 5.81; N, 16.25%).

*Reductive Cleavage of **4k** (another example for isolation of the cleaved products).* A mixture of **4k** (0.7 g), zinc dust (18 g), glacial acetic acid (70 ml), and acetic anhydride (28 ml) was stirred at room temperature for 2 h, filtered, and the filtrate was evaporated. The residue was heated with a mixture of water (10 ml) and MeOH (5 ml) and the aq extract was treated with a soln of picric acid (0.5 g) in water (30 ml) giving 4-phenylimidazole picrate (0.55 g, 69%). The mother liquor of picrate was evaporated and the residue was extracted with chloroform (50 ml). The extract was washed successsively with aq ammonia and water and then evaporated to afford **10** (R^1=*p*-$MeOC_6H_4$, R^2=H), mp 95—96 °C (0.35 g, 90%) (lit,[29] mp 95.5—97 °C). IR (KBr) 3250 (N–H), 1630 (C=O), 1255 (C–O–C) cm^{-1}; NMR ($CDCl_3$) 1.95 (s, 3, $COCH_3$), 3.74 (s, 3, OCH_3), 4.25 (d, 2, J=6.0 Hz, NCH_2), 6.30 (br, 1, NH), 6.77 (d, 2, J=8.3 Hz, ring protons), 7.12 (d, 2, J=8.3 Hz, ring protons). In the same manner, **4s**, **4t**, and **4u** gave 4-phenylimidazole picrate in 87, 73, and 17% yields, respectively.

*Hydrazinolysis of **4k** (a typical example).* A mixture of **4k** (0.24 g), 80% hydrazine hydrate (0.5 ml), and 2-methoxyethanol (2 ml) was heated to 165°C for 70 min and then evaporated. The residue was charged onto a silica gel column (30 g), eluted with chloroform, and the homogeneous fraction was evaporate giving practically pure **7a** (0.15 g, 98%), mp 119—120 °C. Recrystallization from benzene gave colorless needles, mp 122.5—123 °C. UV_{max} (MeOH) 271 nm (ε 16 900); NMR ($CDCl_3$) 4.70 (br, 2, NH_2), 7.30 (m, 3, $H^{m,p}$ of 4-phenyl), 7.71 (m, 2, H^o of 4-phenyl). From a fraction which preceded **7a**, there was obtained **12** (R^1=*p*-$MeOC_6H_4$, R^2=H), mp 167—169 °C (from benzene) (turned to a clear melt at 179—180 °C) (lit,[30] mp 167—163 °C). (Found: C, 71.78; H, 6.02; N, 10.31%). Alternatively, the residue obtained after evaporation of the reaction mixture was triturated with water and the insoluble solids were heated with MeOH at the reflux temperature for 30 min. Insoluble **12** was filtered off and the filtrate evaporated to give a residue which was then recrystallized from benzene affording **7a** (54%), mp 122—123 °C. According to the latter procedure, **5a** yielded **9** (74%) as colorless needles, mp 141—142 °C. UV_{max} (MeOH) 278 nm (ε 16 800); IR (KBr) 3340 and 3100 (NH) cm^{-1}; NMR ($CDCl_3$) 2.59 (s, 3, SCH_3), 4.55 (br, 2, NH_2), 7.00 (s, 1, H-4), 7.35 (s, 5, C_6H_5). Found: C, 58.75; H, 5.40; N, 20.66%; M^+, 205. Calcd for $C_{10}H_{11}N_3S$: C, 58.53; H, 5.40; N, 20.48%; M, 205.

*Hydrazinolysis of **4d**.* A mixture of **4d** (0.86 g), 80% hydrazine hydrate (7.5 ml), and 2-methoxyethanol (7.5 ml) was heated to 175 °C for 13 h[31] and then evaporated. The residual liquid was triturated with EtOH (6 ml) to crystallize **7d** (0.13 g, 20%), mp 177.5—178 °C (from EtOH). NMR (DMSO-d_6) 6.06 (br, 2, NH_2), 8.00 (d, 2, J=9.1 Hz, *p*-nitrophenyl protons), 8.23 (d, 2, J=9.1 Hz, *p*-nitrophenyl protons). The mother liquor after crystallization of **7d** was allowed to stand overnight and deposited **7b** (0.16 g, 29%) was collected by filtration, mp 175—176 °C (from EtOH). NMR (DMSO-d_6) 3.67 (br, NH_2), 5.88 (br, 2, NH_2), 6.54 (d, 2, J=8.6 Hz, *p*-aminophenyl protons), 7.38 (d, 2, J=8.6 Hz, *p*-aminophenyl protons). When the reaction was carried out by heating a mixture of **4d** (0.68 g), 80% hydrazine hydrate (6 ml), and 2-methoxyethanol (24 ml) for 2 h (**4d** had dissolved within 10 min) and concentrating the mixture to one half of the original volume, **7d** gradually crystallized (0.16 g, 32%), mp 177—178 °C.

*Hydrolysis of **4m**.* A soln of **4m** (0.92 g) in concentrated hydrochloric acid (20 ml) was heated to 130 °C for 30 min and the separated *p*-methoxyacetophenone (0.4 g, 98%) was removed by extraction with Et_2O. The aq layer was diluted with water (7 ml), made basic with aq ammonia, and extracted with chloroform (30 ml) giving **7a** (0.44 g, 79%), mp 120—122 °C.

*Deamination of **7**.* To a stirred mixture of **7a** (0.41 g), concentrated hydrochloric acid (4 ml), and MeOH (4 ml) was added a soln of sodium nitrite in water (0.1 g/ml) until an excess of nitrous acid remained after the last addition. Stirring was continued for 4 h at room temperature and the mixture was made alkaline (pH 10) with aq soln of sodium hydroxide. The solid was filtrered and washed with water giving **8a** (R^3=Me, $R^4=C_6H_5$) (0.26 g, 68%), mp 137—138 °C (lit,[32] mp 135.5—136.5 °C). IR (KBr) 3060—2600 (N–H) cm^{-1}. The following compounds were similarly obtained: **8b** (R^3=Me, R^4=*p*-ClC_6H_4): colorless plates (from *i*-PrOH), 84%, mp 181—182 °C; IR (KBr) 3050—2580 (N–H) cm^{-1}; NMR ($CDCl_3$) 2.64 (s, 3, SCH_3), 5.64 (br, 1, NH), 7.28 (d, 2, J=8.9 Hz, *p*-chlorophenyl protons), 7.36 (s, 1, H-4 or 5), 7.70 (d, 2, J=8.9 Hz, *p*-chlorophenyl protons). Found: C, 53.34; H, 4.08; N, 12.27%. Calcd for $C_{10}H_9ClN_2S$: C, 53.45; H, 4.04; N, 12.47%. **8c** (R^3=Me, R^4=*p*-$O_2NC_6H_4$): bright yellow needles (from benzene–MeOH), 47%, mp 211—212 °C; IR (KBr) 3140—2590 (N–H) cm^{-1}; NMR (CF_3CO_2D) 2.91 (s, 3, SCH_3), 7.88 (s,

1, H-4 or 5), 7.95 (d, 2, J=9.2 Hz, *p*-nitrophenyl protons), 8.48 (d, 2, J=9.2 Hz, *p*-nitrophenyl protons). Found: C, 51.24; H, 3.87; N, 18.03%. Calcd for $C_{10}H_9N_3O_2S$: C, 51.06; H, 3.86; N, 17.87%. **8d** (R^3=*n*-C_3H_7, R^4=C_6H_5): 48%, mp 79.5—80 °C (lit,[32] mp 78—79 °C), IR (KBr) 3050—2600 (N–H) cm^{-1}. (Found: C, 66.07; H, 6.53; N, 12.57%). **8e** (R^3=H_2C=$CHCH_2$, R^4=C_6H_5): colorless needles (from *i*-Pr_2O–hexane), 62%, mp 93—94 °C; IR (KBr) 3060—2550 (N–H) cm^{-1}; NMR ($CDCl_3$) 3.55 (dt, 2, J= 6.8 and 0.9 Hz, SCH_2), 5.00 (m, 2, =CH_2), 5.80 (m, 1, –CH=), 7.23 (m, 3, $H^{m,p}$ of phenyl), 7.32 (s, 1, H-4 or 5), 7.64 (m, 2, H^o of phenyl), 10.43 (s, 1, NH). Found: C, 66.56; H, 5.68; N, 12.73%. Calcd for $C_{12}H_{12}N_2S$: C, 66.65; H, 5.59; N, 12.96%. **8f** (R^3=$C_6H_5CH_2$, R^4=C_6H_5): 19%, mp 175—176 °C (lit,[4] mp 176.5—177.5 °C); IR (KBr) 3050—2580 (N–H) cm^{-1}. (Found: C, 72.00; H, 5.46; N, 10.30%).

The author wishes to thank Mr. Seizo Taira and Miss Tomoko Okawa for their assistance in the preparation of some compounds.

References

1) A part of this work was reported in a preliminary form: C. Yamazaki, S. Taira, and T. Okawa, *Chem. Lett.*, **1972**, 617.
2) (a) I. Simiti and M. M. Coman, *Ann. Chim. (Paris)*, **8**, 373 (1973); (b) I. Simiti and M. M. Coman, *Bull. Soc. Chim. Fr.*, **1969**, 3276; (c) I. Zugravescu and S. Avramovici. Analele Stiint. Univ. "*A. I. Cuza*" *Iasi, Sect. I.* **8**, 515 (1962); *Chem. Abstr.*, **59**, 10016h (1963); (d) A. A. Tsurkan, *Farm. Zh. (Kiev)*, **30**, 82 (1975).
3) (a) E. Hoggarth, *J. Chem. Soc.*, **1949**, 1160; (b) F. Kurzer and K. Douraghi Zadeh, *J. Chem. Soc.*, **1965**, 932.
4) R. M. Dodson, *J. Am. Chem. Soc.*, **70**, 2753 (1948).
5) (a) L. A. Lee and J. W. Wheeler, *J. Org. Chem.*, **37**, 348 (1972); (b) R. N. Butler, *Can. J. Chem.*, **51**, 2315 (1973); (c) L. G. Tensmeyer and C. Ainsworth, *J. Org. Chem.*, **31**, 1878 (1966).
6) W. W. Paudler and Teh-Kuei Chen, *J. Heterocycl. Chem.*, **7**, 767 (1970).
7) M. Tišler, *Croat. Chem. Acta*, **32**, 123 (1960).
8) (a) R. Belcher, W. Hoyle, and T. S. West, *J. Chem. Soc.*, **1958**, 2743; (b) F. Ramirez and A, F. Kirby, *J. Am. Chem. Soc.*, **74**, 4331 (1972).
9) C. Yamazaki, *Tetrahedron Lett.*, **1978**, 1295.
10) M. Cordes and J. L. Walter, *Spectrochim. Acta, Part A*, **24**, 237 (1968).
11) C. Yamazaki, *Can. J. Chem.*, **53**, 510 (1975).
12) (a) R. A. Olofson and R. V. Kendall, *J. Org. Chem.*, **35**, 2246 (1970); (b) E. F. Godefroi and J. H. F. M. Mentjens, *Recl. Trav. Chim. Pays-Bas*, **93**, 56 (1974).
13) G. S. Reddy, L. Mandell, and J. H. Goldstein, *J. Chem. Soc.*, **1963**, 1414.
14) H. R. Matthews and H. Rapoport, *J. Am. Chem. Soc.*, **95**, 2297 (1973).
15) R. L. Reeves, *J. Org. Chem.*, **30**, 3129 (1965).
16) This results are in accord with those reported by F. Aylward and M. Sawistowska, *Chem. Ind. (London)*, **1961**, 404.
17) J. Lee and W. W. Paudler, *J. Heterocycl. Chem.*, **9**, **995** (1972).
18) T. Pyl, F. Waschk, and H. Beyer, *Liebigs Ann. Chem.*, **663**, 113 (1963).
19) (a) L. C. King and G. K. Ostrum, *J. Org. Chem.*, **29**, 3459 (1964); (b) R. E. Lutz, R. K. Allison, G. Ashburn, P. S. Bailey, M. T. Clark, J. F. Codington, A. J. Deinet, J. A. Freek, R. H. Jordan, N. H. Leake, T. A. Martin, K. C. Nicodemus, R. J. Rowelett, Jr., N. H. Shearer, Jr., J. D. Smith, and J. W. Wilson, *J. Org. Chem.*, **12**, 617 (1947).
20) J. J. Riehl, *C. R. Acad. Sci., Rend.* **245**, 1321 (1957).
21) The halogen of **3** was labile and easily underwent solvolysis when the 2,4-dinitrophenylhydrazone was prepared in the presence of EtOH. See Ref. 8(b).
22) M. Kerfanto and F. Venien, *C. R. Acad. Sci.*, **261** (Groupe 8), 5535 (1965).
23) This compound had been described by the following authors without physical and preparative data: E. Hoggarth, A. R. Martin, N. E. Storey, and E. H. P. Young, *Brit. J. Pharmacol.*, **4**, 248 (1949).
24) This compound showed a set of signals for the azomethine and the hydroxyl protons. Presumably solvent-solute interaction is responsible for the phenomenone because its sharp melting point should preclude a possibility of isomeric mixture in the solid state.
25) H. Gilman and L. Fullhart, *J. Am. Chem. Soc.*, **71**, 1478 (1949).
26) T. O. Norris and R. L. McKee, *J. Am. Chem. Soc.*, **77**, 1056 (1955).
27) S. Cusmano and V. Sprio, *Gazz. Chim. Ital.*, **82**, 252 (1952); *Chem. Abstr.*, **47**, 7509 f (1953).
28) R. Weidenhagen and R. Herrmann, *Ber.*, **68**, 1953 (1935).
29) W. H. Carothers, C. F. Bickford, and G. J. Hurwitz *J. Am. Chem. Soc.*, **49**, 2908 (1927).
30) L. N. Ferguson and T. C. Goodwin, *J. Am. Chem. Soc.*, **71**, 633 (1949). Other mp's were reported, *e.g.*, (a) 179—179.5 °C (melted with cloud at 168 °C) by N. Schapiro, *Ber.*, **66**, 1103 (1933): (b) 169—170 °C by O. Tsuge and S. Kanemasa, *Bull. Chem. Soc. Jpn.*, **45**, 3591 (1972).
31) About 3 h were required for complete dissolution of **4d**.
32) P. M. Kochergin and M. N. Shchukina, *Zh. Obshch. Khim.*, **25**, 2182 (1955).

New β-Carbonylvinylpalladium(II) Complexes Derived from 2-Chlorovinyl Ketones and Tetrakis(triphenylphosphine)palladium(0)

Masayoshi ONISHI, Hideharu YAMAMOTO, and Katsuma HIRAKI

Department of Industrial Chemistry, Faculty of Engineering, Nagasaki University, Bunkyo-machi, Nagasaki 852

(Received December 3, 1977)

Chloro(*trans*-3-oxo-3-phenyl-1-propenyl)bis(triphenylphosphine)palladium(II), chloro(*trans*-3-oxo-3-*p*-tolyl-1-propenyl)bis(triphenylphosphine)palladium(II), chloro(3-oxo-1-cyclohexenyl)bis(triphenylphosphine)palladium(II), and chloro(5,5-dimethyl-3-oxo-1-cyclohexenyl)bis(triphenylphosphine)palladium(II) were prepared by reactions between $Pd(PPh_3)_4$ and linear or cyclic 2-chlorovinyl ketones. The halogen metathesis reactions with LiBr yielded the corresponding bromo complexes. Each of the β-carbonylvinyl groups in these eight complexes was found to be situated at the *trans* position to a palladium-halogen bond, on the basis of IR and ^{1}H-NMR studies. The complexes with the cyclic β-carbonylvinyl groups were rather stable. The oxidative addition of linear 2-chlorovinyl ketones proceeded with retention of configuration about the double bond.

Several investigations have been reported on the oxidative addition of vinyl halides, for example, polyhalogenated olefins,[1] fluorovinyl halides,[2] and some styryl halide derivatives[3] with a tris- or tetrakis(tertiary phosphine)platinum(0) complex. A few halogeno-substituted vinylpalladium(II) complexes have been obtained by the reactions of $[Pd(PPh_3)_4]$ with polyhalogenated olefins[4] or fluorovinyl halides.[5] Moreover, Murahashi *et al.*[6] reported cross-coupling reactions of vinyl halides with alkyl magnesium bromide catalysed by $[Pd(PPh_3)_4]$, *via* the oxidative addition.

Although 2-chlorovinyl ketones are very reactive and useful intermediates for the syntheses of some organic compounds,[7] only a few investigations have been reported concerning the reactions between linear 2-chlorovinyl ketones and iron,[8] tungsten,[9] or rhenium[10] carbonyl derivatives.

We have been interested in the ease of carbon-chlorine bond cleavage in the linear and cyclic chloro olefins activated by electron-withdrawing acyl groups. In the present research, 2-chlorovinyl ketones were found to react with $[Pd(PPh_3)_4]$ to yield several new β-carbonylvinylpalladium(II) complexes, and some properties of these complexes were studied.

Experimental

General Procedures. IR spectra were obtained using a Hitachi 285 grating spectrometer and a Shimadzu IR 450 spectrometer. ^{1}H-NMR spectra were run on a Japan Electron Optics Laboratory JNM-MH-100 spectrometer. Melting points were determined on a Yanagimoto MP-S3 microstage apparatus in capillary tubes in dinitrogen and are uncorrected.

Phenyl 2-chlorovinyl ketone,[7,11] *p*-tolyl 2-chlorovinyl ketone,[7,12] 3-chloro-2-cyclohexen-1-one,[13] and 3-chloro-5,5-dimethyl-2-cyclohexen-1-one[14] were prepared according to the methods described in the literature. Solvents were dried and distilled by the usual methods, and all operations were performed in an atmosphere of dry dinitrogen.

Reactions of the Linear 2-Chlorovinyl Ketones with $Pd(PPh_3)_4$.

Phenyl 2-chlorovinyl ketone (0.60 g) in 8 ml of benzene was added dropwise to a suspension of $Pd(PPh_3)_4$ (3.40 g) in 25 ml of benzene, and the mixture was stirred at room temperature for two days. Benzene was removed *in vacuo* from the suspension, and the residue was extracted with dichloromethane. The extract was evaporated to dryness and the resulting solid was washed with acetone, ethanol, and diethyl ether to yield chloro(*trans*-3-oxo-3-phenyl-1-propenyl)bis(triphenylphosphine)palladium(II) (**1**), 0.56 g.

Chloro(*trans*-3-oxo-3-*p*-tolyl-1-propenyl)bis(triphenylphosphine)palladium(II) (**2**) was obtained similarly.

Reactions of the Cyclic 2-Chlorovinyl Ketones with $Pd(PPh_3)_4$.

A mixture of $Pd(PPh_3)_4$ (3.10 g) and 3-chloro-2-cyclohexen-1-one (0.71 g) in 25 ml of benzene was warmed at *ca.* 60 °C for 3 h. The solvent was removed *in vacuo* and the resulting residue was recrystallized from benzene to give a pale yellow powder of chloro(3-oxo-1-cyclohexenyl)bis(triphenylphosphine)palladium(II) (**3**), 1.71 g.

Chloro(5,5-dimethyl-3-oxo-1-cyclohexenyl)bis(triphenylphosphine)palladium(II) (**4**) was prepared by a similar method.

*Halogen Metathesis Reactions of **1**, **2**, **3**, and **4**.* The complex **1** (0.25 g) and LiBr (0.05 g) were mixed in 12 ml of acetone and the suspension was stirred at room temperature for four days. The resulting precipitate was collected and washed with acetone, ethanol, and diethyl ether to yield a pale yellow powder of bromo(*trans*-3-oxo-3-phenyl-1-propenyl)bis(triphenylphosphine)palladium(II) (**5**), 0.07 g.

Bromo(*trans*-3-oxo-3-*p*-tolyl-1-propenyl)bis(triphenylphosphine)palladium(II) (**6**), bromo(3-oxo-1-cyclohexenyl)bis(triphenylphosphine)palladium(II) (**7**), and bromo(5,5-dimethyl-3-oxo-1-cyclohexenyl)bis(triphenylphosphine)palladium(II) (**8**) were prepared by a method similar to **5**.

Results and Discussion

Four new β-carbonylvinylpalladium(II) complexes: **1**, **2**, **3**, and **4**, were obtained from the oxidative addition reaction between $Pd(PPh_3)_4$ and 2-chlorovinyl ketones. The halogen metathesis reaction with lithium bromide yielded the corresponding bromo complexes: **5**, **6**, **7**, and **8**. The cyclic 2-chlorovinyl ketones, such as 3-chloro-2-cyclohexen-1-one, were more thermally unstable and sensitive to moisture than the linear ketones. However, the reaction of the cyclic ketones

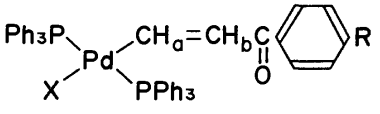

1 ; R = H , X = Cl
2 ; R = CH3 , X = Cl
5 ; R = H , X = Br
6 ; R = CH3 , X = Br

Table 1. Yields and properties of the palladium complexes

Complex	Yield (%)	Mp (°C)[a]	Color	C (%)		H (%)	
				Calcd	Found	Calcd	Found
1	24	>112	Pale yellow	67.77	67.73	4.68	4.66
2	31	>126	Pale yellow	68.07	67.91	4.84	4.79
3	84	>191	Pale yellow	66.24	66.61	4.90	4.95
4	28	>146	Off white	66.93	67.03	5.23	5.44
5	27	>116	Pale yellow	64.19	64.66	4.43	4.52
6	41	>127	Off white	64.54	64.23	4.59	4.56
7	66	>118	Pale yellow	62.59	62.91	4.63	4.66
8	81	>179	Pale yellow	63.36	63.37	4.96	5.06

a) With decomposition in dinitrogen.

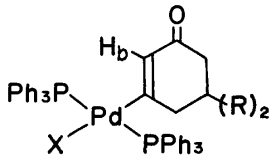

3 ; R = H , X = Cl
4 ; R = CH_3 , X = Cl
7 ; R = H , X = Br
8 ; R = CH_3 , X = Br

with $Pd(PPh_3)_4$ took place only at temperatures above 50 °C, while that of the linear ketones proceeded smoothly at room temperature. When the solvents were not sufficiently dried, the complexes with the linear β-carbonylvinyl groups decomposed partially and turned brown. Yields, analytical data, and the properties of the eight complexes prepared are summarized in Tables 1, 2, and 3. These complexes were readily soluble in dichloromethane and hot benzene, and the complexes with the linear β-carbonylvinyl groups were also moderately soluble in benzene at room temperature.

The complexes obtained in this study possess a palladium-vinyl σ bond, judging from the halogen metathesis reaction and the existence of ν(Pd–Cl) bands shown in Table 2.

The ν(C=C) stretching frequencies of all the complexes were lowered about 45—80 cm^{-1} relative to those of the starting 2-chlorovinyl ketones. These lowering shifts of the ν(C=C) frequencies were probably associated with some double-bonding character between the d orbitals of palladium and the sp^2 carbon atom. The ν(C=O) stretching frequencies of the complexes with the cyclic β-carbonylvinyl groups were shifted by 25—60 cm^{-1} towards lower wavenumbers, relative to those of the starting ketones. The lowering shifts of the ν(C=O) frequencies were possibly due to an extension of the π-conjugation through the β-carbonylvinylpalladium moiety. On the other hand, the complexes with the linear β-carbonylvinyl groups showed small lowering shifts (*ca.* 10 cm^{-1}) of the ν(C=O) frequencies, in comparison with the starting 2-chlorovinyl ketones. This fact might correspond to a small degree of additional

Table 2. Characteristic IR bands of the complexes[a]

Complex	ν(C=O)	ν(C=C)	ν(Pd–Cl)
1	1650	1533	290
2	1642	1517	280
3	1640	1540	280
4	1645	1560	285
5	1648	1530	—
6	1642	1517	—
7	1630	1540	—
8	1635	1555	—

a) Measured in KBr disc, values in cm^{-1}.

Table 3. ^{1}H-NMR data of the palladium complexes[a,b]

Complex	H_b			CH_3	$-CH_2-$
	δ, ppm	J_{PH}, Hz	J_{ab}, Hz	δ, ppm	δ, ppm
1	6.17(dt)	2.1	15.5	—	—
2	6.15(dt)	2.3	18.0	2.31(s)	—
3	6.18(t)	2.2	—	—	0.54(m), 1.28(t), 2.05(t)
4	6.10(t)	3.1	—	0.00(s)[c]	0.95(s), 2.17(s)
5	6.10(d)[d]	—	17.0	—	—
6	6.11(dt)	2.1	14.0	2.31(s)	—
7	6.18(t)	2.4	—	—	0.54(m), 1.26(t), 2.04(t)
8	6.17(t)	2.7	—	0.06(s)[c]	0.99(s), 2.27(s)

a) Measured in deoxygenated CD_2Cl_2 using tetramethylsilane as the internal standard.
b) Abbreviations used: s=singlet, d=doublet, t=triplet, dt=double triplet, m=multiplet.
c) Chemical shifts were referenced to dichloromethane, whose resonance was δ 5.31 ppm downfield from tetramethylsilane. d) The coupling with ^{31}P could not be detected. See the text.

extension of the π-conjugation, owing to the complex formation.

It has been well known that the aryl 2-chlorovinyl ketones used in this study have a *trans* configuration about the double bond.[7] The ^{1}H-NMR couplings J_{ab} of the vinyl protons, H_a and H_b in **1**, **2**, **5**, and **6**, were about 14.0—18.0 Hz, which were of the order expected for *trans*-AB coupling across a double bond, and indicated that the *trans* arrangement of these protons was retained in these four complexes. No signal for H_a protons could be distinguished owing to the overlapping with many aromatic protons.

H_b resonances of the complexes with the linear and cyclic β-carbonylvinyl groups showed a double triplet and a triplet, respectively. These triplet splittings for both kinds of complexes were ascribed to the coupling with two equivalent phosphorus-31 atoms and indicated a *trans* geometry of the two triphenylphosphine ligands. (In the complex **5**, the coupling with phosphorus-31 could not be detected, because of its fairly fast decomposition.) Table 2 also shows reasonable ν(Pd–Cl) frequencies for the *trans* position to the palladium-carbon σ bond.

In addition, the resonances of the methyl groups in **4** and **8** showed large high-field shifts. The reason for these shifts was probably explained by the ring current of phenyl groups of triphenylphosphine.

The palladium-carbon σ bonds in the eight complexes studied here were stabilized by β-carbonylvinyl groups to some degree, and these complexes were stable in the solid state under dinitrogen at room temperature for several weeks. In a deoxygenated dichloromethane solution, the complexes with the cyclic β-carbonylvinyl groups were stable for more than a week at room temperature, whereas the complexes with the linear ones began to decompose in 1 h. This high stability of the former complexes can be accounted for probably by the steric hindrance of the cyclic β-carbonylvinyl groups against the species which attack the palladium-carbon σ bond.

We are grateful to Professor Keinosuke Hamada and Mr. Hirofumi Morishita, Nagasaki University, for their help with the Far IR measurements.

References

1) W. J. Bland and R. D. W. Kemmitt, *J. Chem. Soc., A*, **1968**, 1278.
2) A. J. Mukhedkar, M. Green, and F. G. A. Stone, *J. Chem. Soc., A*, **1970**, 947.
3) B. E. Mann, B. L. Shaw, and N. I. Tucker, *J. Chem. Soc., A*, **1971**. 2667.
4) P. Fitton and J. E. McKeon, *Chem. Commun.*, **1968**, 4.
5) A. J. Mukhedkar, M. Green, and F. G. A. Stone, *J. Chem. Soc., A*, **1969**, 3023.
6) M. Yamamura, I. Moritani, and S. Murahashi, *J. Organomet. Chem.*, **91**, C39 (1975).
7) A. E. Pohland and W. R. Benson, *Chem. Rev.*, **66**, 161 (1966).
8) A. N. Nesmeyanov, L. V. Rybin, M. I. Rybinskaya, and Yu. A. Ustynyuk, *Zh. Obshch. Khim.*, **37**, 1587 (1967).
9) A. N. Nesmeyanov, L. V. Rybin, M. I. Rybinskaya, and V. S. Kaganovich, *Izv. Akad. Nauk SSSR, Ser. Khim.*, **1971**, 348.
10) A. N. Nesmeyanov, V. S. Kaganovich, L. V. Rybin, P. V. Petrovskii, and M. I. Rybinskaya, *Izv. Akad. Nauk SSSR, Ser. Khim.*, **1971**, 1576.
11) S. Wakayama, T. Itoh, and K. Suginome, *Nippon Kagaku Zasshi*, **76**, 94 (1955).
12) N. K. Kochetkov, A. Yu. Khorlin, and M. Yu. Karpeiskii, *Zh. Obshch. Khim.*, **26**, 595 (1956).
13) A. W. Crossley and P. Hass, *J. Chem. Soc.*, **83**, 494 (1903).
14) A. W. Crossley and H. Rondel, *J. Chem. Soc.*, **83**, 110 (1903).

1,3-Dipolar Cycloadditions to Bicyclic Olefins. V. The Stereo- and Regiochemistry of 1,3-Dipolar Cycloadditions to Several Unsymmetrical Bicyclic Olefins[1,2]

Hisaji TANIGUCHI, Toshikazu IKEDA, and Eiji IMOTO

Department of Applied Chemistry, College of Engineering, University of Osaka Prefecture, Mozu-Umemachi, Sakai, Osaka 591

(Received December 12, 1977)

Each of the 1,3-dipolar cycloadditions of phenylglyoxylonitrile oxide (**1**), methylglyoxylonitrile oxide (**2**), benzonitrile oxide (**3**), and phenyl azide to 2-phenylsulfonyl-2-azabicyclo[3.2.1]octa-3,6-diene (**6**) occurs only to the C_6–C_7 double bond, affording two exo regioisomers. Each of the cycloadditions of **1**, **2**, and **3** to 2-phenylsulfonyl-2-azabicyclo[3.2.1]oct-3-ene (**7**) gives only one exo adduct. The cycloaddition of *C,N*-diphenylnitrone to 2-methylenenorbornane (**8**) gives a mixture of two exo adducts. These results show that the "exo rule" can be extended to the 1,3-dipolar cycloadditions to the bicyclic olefins, **6**, **7**, and **8**. Tentative explanations are offered to account for the exo stereoselectivity and the regio-selectivity in these cycloadditions.

1,3-Dipolar cycloadditions to norbornenes follow the "exo rule."[3] However, a previous paper reported that those to norbornadienes do not follow this rule.[4] This reactivity difference has been ascribed to the presence of homoconjugation in norbornadiene.[4] These results and the assumption prompted us to ascertain to what cases the "exo rule" could be extended. We undertook to study it through 1,3-dipolar cycloadditions to the following three kinds of bicyclic olefins: (i) 2-phenylsulfonyl-2-azabicyclo[3.2.1]octa-3,6-diene (**6**), which has a formally different homoconjugation from norbornadiene;[5] (ii) 2-phenylsulfonyl-2-azabicyclo[3.2.1]oct-3-ene (**7**), which has an unsaturated bridge larger by one nitrogen atom than that of norbornene, and (iii) 2-methylenenorbornane (**8**), whose double bond is of the exo type. The 1,3-dipolar cycloadditions of phenylglyoxylonitrile oxide (**1**), methylglyoxylonitrile oxide (**2**), benzonitrile oxide (**3**), and phenyl azide (**4**) to **6** or **7** and the 1,3-dipolar cycloaddition of α,*N*-diphenylmethanimine *N*-oxide (**5**) to **8** were carried out. Since all the bicyclic olefins used here were unsymmetrical, the regiochemistry of these cycloadditions was also studied.

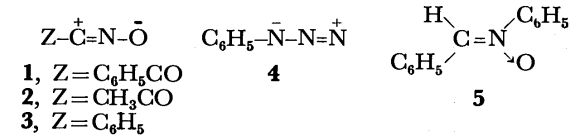

1, $Z=C_6H_5CO$
2, $Z=CH_3CO$
3, $Z=C_6H_5$

4

5

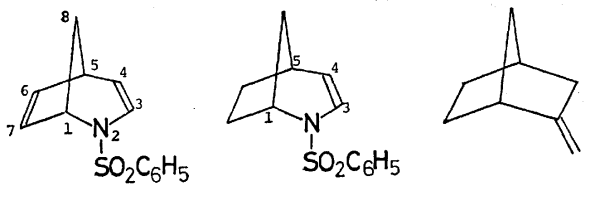

6 **7** **8**

Results

1,3-Dipolar Cycloadditions. The slow addition of a dilute THF solution of triethylamine (TEA) to a stirred solution of **6** and α-chloro-α-hydroxyiminoacetophenone (**9**), which is a precursor of **1**, in THF cooled in an ice bath gave two exo adducts, 8-phenylsulfonyl-5-benzoyl-2,6-*exo*-3-oxa-4,8-diazatricyclo[5.3.1.$0^{2,6}$]-undeca-4,9-diene (**10**) and 10-phenylsulfonyl-5-benzoyl-2,6-*exo*-3-oxa-4,10-diazatricyclo[5.3.1.$0^{2,6}$]undeca-4,8-diene (**11**). The cycloadditions of **2** to **6** and **3** to **6** were carried out by a method like that described above. The reaction of **2** to **6** afforded two exo adducts, 5-acetyl-8-phenylsulfonyl-2,6-*exo*-3-oxa-4,8-diazatricyclo-[5.3.1.$0^{2,6}$]undeca-4,9-diene (**12**) and 5-acetyl-10-phenylsulfonyl-2,6-*exo*-3-oxa-4,10-diazatricyclo[5.3.1.$0^{2,6}$]-undeca-4,8-diene (**13**). Moreover, the reaction of **3** with **6** also produced two exo adducts, 8-phenylsulfonyl-5-phenyl-2,6-*exo*-4,8-diazatricyclo[5.3.1.$0^{2,6}$]undeca-4,9-diene (**14**) and 10-phenylsulfonyl-5-phenyl-2,6-*exo*-4,10-diazatricyclo[5.3.1.$0^{2,6}$]undeca-4,8-diene (**15**). All the adducts obtained in the above reactions are produced by the addition of the nitrile oxides, **1**—**3**, to the C_6=C_7 double bond of **6**. The adducts which were to be produced by the addition of the nitrile oxides to the other carbon-carbon double bond (C_3=C_4 double bond) of **6**, the endo adducts, and the bisadducts were not detected at all.

The reaction of the azide, **4**, with an equiv of **6** in dry benzene at room temperature led to the formation of two exo monoadducts, 10-phenylsulfonyl-5-phenyl-2,6-*exo*-3,4,5,10-tetraazatricyclo[5.3.1.$0^{2,6}$]undeca-3,8-diene (**16**) and 8-phenylsulfonyl-5-phenyl-2,6-*exo*-3,4,5,8-tetraazatricyclo[5.3.1.$0^{2,6}$]undeca-3,9-diene (**17**). Similary, the adducts which were to be produced by the attack of **4** on the C_3=C_4 double bond of **6**, the endo adducts, and the bisadducts were not detected at all.

The yields of the adducts obtained in the reactions of **1**—**4** with **6** and the product compositions are summarized in Table 1.

The cycloadditions of the nitrile oxides, **1**—**3**, to **7** was carried out in a manner similar to that described above. Each of the three reactions gave only one exo adduct, 2-phenylsulfonyl-6-benzoyl-3,7-*exo*-4-oxa-2,5-diazatricyclo[6.2.1.$0^{3,7}$]undec-5-ene (**18**), 6-acetyl-2-phenylsulfonyl-3,7-*exo*-4-oxa-2,5-diazatricyclo[6.2.1.$0^{3,7}$]-undec-5-ene (**19**), or 2-phenylsulfonyl-6-phenyl-3,7-*exo*-4-oxa-2,5-diazatricyclo[6.2.1.$0^{3,7}$]undec-5-ene (**20**). When these reactions were carried out at 0 °C, the yields of the adducts were low. When the reaction temperature was raised to 66 °C, the yields of the adducts (**18**, **19**) increased, but no other product was

TABLE 1. THE YIELDS OF ADDUCTS AND PRODUCT COMPOSITIONS IN THE REACTIONS OF **1**—**4** WITH **6**

1,3-Dipole	Adduct	Yield (%)	Composition (%)	Recovery of **6** (%)
1	**10**	97[a]	67	0
	11		33	
2	**12**	94[a]	76	0
	13		24	
3	**14**	96[a]	71	0
	15		29	
4	**16**	78[b]	87	8
	17		13	

a) At 0 °C in THF. b) At r.t. for one week in C_6H_6.

TABLE 2. THE YIELDS OF ADDUCTS IN THE REACTIONS OF **1**—**3** WITH **7** IN THF

1,3-Dipole	Temp (°C)	Adduct	Yield (%)	Recovery of **7** (%)
1	0	**18**	12	73
	66	**18**	56	27
2	0	**19**	10	79
	66	**19**	45	39
3	0	**20**	33	50
	66	**20**	33	52

obtained (Table 2).

A solution of **4** and **7** in dry benzene was allowed to stand in the dark for one week at room temperature; however, this treatment gave no adduct.

When a solution of the nitrone, **5**, in toluene containing two equiv. of **8** was refluxed, a 1 : 1 mixture of two exo adducts, 1′-*exo*,3′-*endo*-2′,3′-diphenylspiro[norbornane-2,5′[1′]oxa[2′]azacyclopentane] (**21**) and 1′-*exo*,3′-*exo*-2′,3′-diphenylspiro[norbornane-2,5′[1′]oxa[2′]azacyclopentane] (**22**), was obtained in an 83% yield.

The above results show that the "exo rule" can be extended to the 1,3-dipolar cycloadditions to the bicyclic olefins, **6**, **7**, and **8**.

The separation or the isolation of the adducts from the reaction mixture was carried out using column chromatography on silica gel or alumina.

*Determination of Configurations of Adducts. a) Adducts (**10**—**17**) obtained in Cycloadditions to **6***: The structural assignments of the adducts were made on the basis of the NMR chemical shifts (Table 3), the coupling constants (Table 4), the spin-spin decouplings, and the nuclear Overhauser effects (NOE).[6]

In each adduct, the signal which appeared as a double doublet in the region of δ 6.50—6.66 was assigned to the vinyl proton, 9-H. This was confirmed by the spin-decoupling technique; the vinyl proton was coupled to the adjacent vinyl proton (J=8.0 or 7.5 Hz) and to the bridgehead proton which neighbors on the nitrogen atom (J=1.0 or 1.5 Hz). This finding indicates that all the adducts (**10**—**17**) are produced by the addition of 1,3-dipoles to the C_6=C_7 double bond of **6**.

The signals of the 2-H and the 6-H in each adduct appeared as simple doublets. The coupling constant between the 2-H (or 6-H) and the adjacent bridgehead proton was 0 Hz, as is shown in Table 4. This finding shows that all the adducts are produced by the attack of 1,3-dipoles on **6** from the exo side.

Each adduct pair, **10** and **11**, **12** and **13**, **14** and **15**, or **16** and **17**, consists of regioisomers to each other. The distinction between the **12** and **13** regioisomers was achieved by NOE experiments. Irradiation at the frequency of the 1-H of the adduct, **12**, caused a 24% increase in the integral of the multiplet (δ=5.00—5.12, 2-H and 6-H), but brought about no increase in the integral of the doublet (6-H). The saturation of the 7-H of the adduct, **13**, gave rise to a 20% enhancement of the integral of the 8-H and a 5% enhancement of that of the 6-H. These findings show that the oxygen atom of the isoxazoline moiety in the **12** adduct is on the opposite side of the molecule from the *N*-phenylsulfonyl group, while the corresponding oxygen atom of the adduct, **13**, is on the same side of the molecule as the *N*-phenylsulfonyl group. The difference in the chemical

TABLE 4. COUPLING CONSTANTS IN ADDUCTS (**10**—**17**)[a,b]

Adduct	$J_{1,2}$	$J_{2,6}$	$J_{6,7}$	$J_{7,8}$	$J_{8,9}$	$J_{9,10}$	$J_{10,1}$	$J_{7,9}$	$J_{1,9}$
10	0	8.5	0	—	—	8.0	8.0	1.0	0
11	0	8.5	0	8.0	8.0	—	—	0	1.0
12	0	8.5	0	—	—	8.0	8.0	1.5	0
13	0	8.5	0	8.0	8.0	—	—	0	1.0
14	0	8.5	0	—	—	8.0	8.0	1.0	0
15	0	8.5	0	8.0	8.0	—	—	0	1.0
16	0	9.5	0	7.5	7.5	—	—	0	1.0
17	0	9.5	0	—	—	7.5	7.5	1.0	0

a) The spectra were recorded at 60 MHz. b) J values in Hz.

TABLE 3. CHEMICAL SHIFTS OF ADDUCTS (**10**—**17**)[a,b]

Adduct	1-H	2-H	6-H	7-H	8-H	9-H	10-H	$\Delta\delta$[c]
10	2.70	5.00	3.77	4.88	—	6.60	5.14	1.23
11	4.54	4.92	4.20	2.73	5.38	6.50	—	0.72
12	2.69	5.00	3.49	4.68	—	6.60	5.12	1.51
13	4.53	4.93	3.96	2.63	5.34	6.52	—	0.97
14	2.70	5.12	4.10	4.50	—	6.64	5.22	1.02
15	4.52	4.91	4.21	2.55	5.37	6.57	—	0.70
16	*ca.* 4.7	4.82	4.25	2.60	5.28	6.64	—	0.57
17	2.88	5.12	4.28	*ca.* 4.4	—	6.66	5.49	0.84

a) The spectra were recorded at 60 MHz. b) Expressed in δ ppm units, with TMS as the internal standard, in $CDCl_3$ soln. c) The shift difference between the 2-H and the 6-H.

shift between the 2-H and the 6-H of the **12** adduct is greater by 0.54 ppm than the corresponding difference between the 2-H and the 6-H of the **13** adduct. Such a chemical-shift difference was applied to the distinction between the **10** and **11**, or **14** and **15** regioisomers (Table 3).

The distinction between the **16** and **17** regioisomers was also achieved by observing the NOE. Irradiation at the frequency of the bridgehead proton, 7-H, of the **16** adduct brought about an increase of 9% in the integral of the doublet (6-H) and an increase of 9% in the integral of the vinyl proton, 8-H, but caused no increase in the integral of the doublet (2-H). Also, the empirical data[7] suggest that the high-field doublet of the two doublet is due to the 6-H which is adjacent to the phenyl group. These findings show that the phenyl group is on the opposite side of the molecule from the *N*-phenylsulfonyl group, as is shown in the structure (**16**). In the case of the **17** adduct, it was confirmed by irradiation at the frequency of the bridgehead proton, 1-H, of this adduct that the phenyl group is on the same side of the molecule as the *N*-phenylsulfonyl group. An increment of 25% was observed in the integral of the multiplet, which consisted of a low-field doublet (2-H) and a triplet (10-H).

Table 5. The NMR data of adducts (**18**—**20**)[a,b]

Adduct	1-H	3-H	7-H	8-H	$J_{3,7}$	$J_{7,8}$
18	4.01	6.65	3.72	2.58	10	0
19	4.00	6.58	3.52	—	9.5	0
20	4.00	6.60	3.65	2.32	9.5	0

a) The spectra were recorded at 60 MHz. b) The chemical shifts are expressed in δ ppm units, with TMS as the internal standard, in $CDCl_3$ soln. J values in Hz.

b) Adducts (18—20) Obtained in Cycloadditions to 7: The structural assignments of the **18**—**20** adducts were carried out by means of their NMR data (Table 5). Each spectrum of these adducts showed two simple doublets at δ *ca.* 3.6 and *ca.* 6.6 (Table 5). The high-field doublet in each spectrum was assigned to the 7-endo H by making a comparison between its spectrum and the spectrum of the exo adduct (**25**)[4] formed in the cycloaddition of **1** to norbornadiene; in the spectrum of Compound **25**, the 6-endo H appears at δ 3.78 ppm as a simple doublet.[4] From the fact that the coupling constant between the 7-H and the adjacent bridgehead proton, 8-H, in each adduct is 0 Hz, it can be said that each adduct is an exo adduct; the dihedral angle between the 7-H and the 8-H is close to 90°.

c) The 21 and 22 Adducts: Since no hydrogen atom is attached to the 2-carbon atom of the **8** olefin, it is impossible to determine the structure of the 1 : 1 adducts obtained in the cycloaddition of **5** to **8** on the basis of the NMR spectrum alone. A solid obtained in this cycloaddition consisted of the two exo adducts **21** and **22**, not of the endo adducts, **23** and **24**. This was confirmed by the following observations. (i) The NMR spectrum of a mixture of **21** and **22** showed the signal of their 5′-methylene protons at δ 2.2—2.9 as a multiplet. This chemical-shift value indicated that these adducts are produced by the attack of the oxygen atom in the nitrone, **5**, on the 2-carbon atom in the olefin, **8**. (ii) It was revealed by the double-resonance technique that the solid obtained in this cycloaddition consisted of two adducts. Each 4′-H of the two adducts (**21** and **22**) has the same chemical shift (δ=4.61). When their 4′-H's were irradiated with an additional radio frequency at the resonance position, the multiplet which appeared at δ 2.2—2.9 was transformed into eight sharp peaks, which consisted of two sets of AB quartets (J_{AB}=11.0 and 14.0 Hz) assigned to 5′-methylene protons in **21** and to those in **22**. (iii) The hydrogenolysis of the solid which consisted of **21** and **22** gave only 2-phenethyl-2-*exo*-norbornanol (**26**) in a 79% yield. The structure of this alcohol was established by comparison with the corresponding endo alcohol (**27**), which had been prepared by a method like that described in the literature.[8]

These findings (i—iii) indicate that the solid obtained in this cycloaddition consists of the two exo adducts, **21** and **22**.

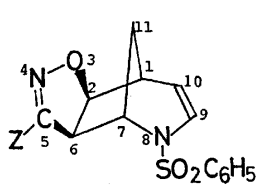

10, Z=C_6H_5CO
12, Z=CH_3CO
14, Z=C_6H_5

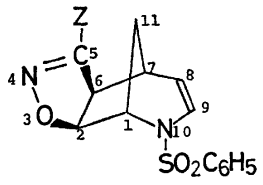

11, Z=C_6H_5CO
13, Z=CH_3CO
15, Z=C_6H_5

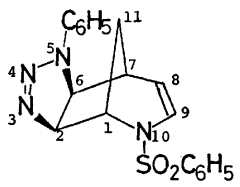

16

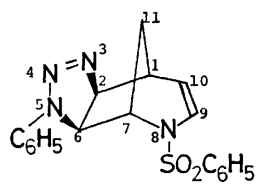

17

18, Z=C_6H_5CO
19, Z=CH_3CO
20, Z=C_6H_5

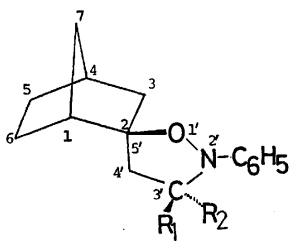

21
22

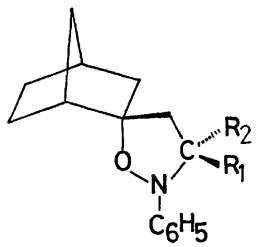

23
24

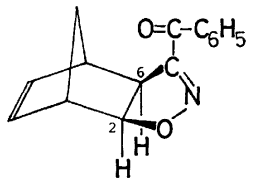

25

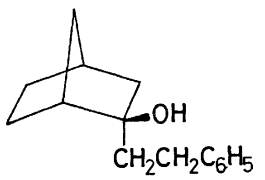

26

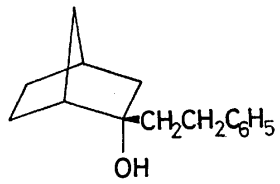

27

Discussion

This kind of 1,3-dipolar cycloaddition has been shown to be a kinetically controlled reaction.[4,9]

A Tentative Explanation of the exo Stereoselectivity. In view of the results obtained in previous work,[2,4] it may be suggested that the dipoles used here, **1**—**5**, act as electron-accepting 1,3-dipoles toward the olefins, **6**—**8**. This indicates that the present 1,3-dipolar cycloadditions may be classified as LU-controlled reactions.[10] On the other hand, it has been suggested by the orbital mixing rule that the highest occupied molecular orbital (HOMO) of norbornene extends more to the exo side than to the endo side because of the interaction beteen the HOMO of the carbon-carbon double bond and the strained methano-bridge orbital.[11] Each olefin used here has a strained methano-bridge such as norbornene. Similarly, it can be predicted by the orbital mixing rule that the HOMO of the carbon-carbon double bond in each olefin extends more to the exo side than to the endo side.[12] Consequently, the dipoles, **1**—**5**, attack the olefins, **6**—**8** from their exo sides.

Attacking Site of 1,3-Dipoles on 6. Although the **6** olefin has two double bonds which are to be attacked by 1,3-dipoles, cycloaddition occurs only to the C_6=C_7 double bond, not to the enamine-type double bond (C_3=C_4 double bond). This phenomenon may be ascribed to the following factors (i—iii): (i) In the 2-azabicyclo[3.2.1]octa-3,6-diene system (**28**,[5] **29**,[13] and **30**[5]), the signals of the 4-H and the 7-H shift to lower fields with an increase in the value of Hammett's σ_p[14] of the *N*-substituent, *R* (Fig. 1). Also, both the 4-H and the 7-H appear at higher fields than the 6-H. These findings indicate that not only the 4-carbon atom, but also the 7-carbon atom, is under the influence of the electron-donating character of the nitrogen atom. (ii) From the structural consideration of **6**, the interaction of the HOMO of the C_6=C_7 double bond with the methano-bridge orbital is assumed to be greater than that of the HOMO of the C_3=C_4 double bond with the methano-bridge orbital, so that the extension of the HOMO of the C_6=C_7 double bond into the exo side may be greater than that of the HOMO of the C_3=C_4 double bond.[15] (iii) The bulky *N*-substituent (phenylsulfonyl group) may hinder the approach of 1,3-dipoles to the C_3=C_4 double bond. From the fact that phenyl azide addition to bicyclo[3.2.1]octa-2,6-diene (**31**) occurs only to the C_6=C_7 double bond from the exo side,[16] however, this factor seems less probable.

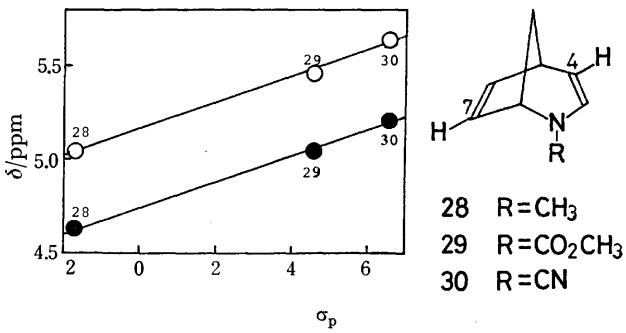

28 R=CH_3
29 R=CO_2CH_3
30 R=CN

Fig. 1. Chemical shifts (TMS as an internal standard, in CCl_4 solutions) of vinyl protons of 2-azabicyclo-[3.2.1]octa-3,6-diene system *vs.* Hammett's σ_p.
○: 7-H, : ●4-H.

TABLE 6. CHEMICAL SHIFTS OF VINYL PROTONS IN **6** AND **7**[a]

Olefin	3-H	4-H	6-H	7-H
6	6.30	5.1—5.5	6.14	5.1—5.5
7	6.37	5.19		

a) The spectra were recorded at 60 MHz. Expressed in δ ppm units, with TMS as the internal standard, in $CDCl_3$ soln.

Regioselectivity. In the **6** diene, the δ values of its vinyl protons (Table 6)[17] suggest the π electron-cloud on the C_6–C_7 double bond is polarized. This may be caused by the electron-donating character of the nitrogen atom, as has been described above, and by the structural characteristics of the bicyclic dienes with a bicyclo[3.2.1]octane skeleton.[19] In the **7** olefin, the π electron-cloud on the C_3=C_4 double bond may be polarized because of the electron-donating character of the nitrogen atom (see Table 6). In the **8** ofefin, the calculations of Houk *et al.* for the HOMO of ethylenes substituted by alkyl groups[21] suggest that the π electron-cloud of the double bond is polarized. As far as the present cycloadditions are concerned, it may be concluded from the product compositions (Table 1) and the structures of the adducts that the orientation in which the plus poles of 1,3-dipoles attack the minus poles of dipolarophiles is preferred.[22]

Conclusion

The "exo rule" can be applied to 1,3-dipolar cycloadditions to bicyclic olefins with a moiety of the bicyclo-[*n*.2.1]alkane(*n*=2 and 3) skeleton, except for norbornadienes, and can also be applied to such a cycloaddition to 2-methylenenorbornane.

Experimental

Materials. The precursors of the nitrile oxides (**9**),[23] α-chloro-α-hydroxyiminoacetone (**32**),[24] and *N*-hydroxybenzenecarboximidoyl chloride (**33**)[25] and the 1,3-dipoles

(**4**[26] and **5**[27]) were prepared by methods described in the literature. The olefines, **6**,[18] **7**,[18] and **8**,[28] were also prepared by methods described in the literature.

*Cycloaddition of **1** to **6**.* Into a stirred solution of 6 (494 mg, 2.0 mmol) and **9** (367 mg, 2.0 mmol) in dry THF (10 cm^3) cooled in an ice bath, a solution of triethylamine (TEA) (250 mg, 2.5 mmol) in dry THF (5 cm^3) was added, drop by drop, over a period of 1 h. After an additional 1 h's stirring at the same temperature, the resulting triethylammonium chloride was removed by filtration. The filtrate showed, on TLC with benzene–ether (97: 3), two spots at R_f 0.40 (**11**) and at R_f 0.33 (**10**). The evaporation of the solvent left a residue. The residue was chromatographed on silica gel (200—300 mesh). Elution with benzene–ether (97: 3) gave **11** (252 mg, 32%) and **10** (513 mg, 65%), in that order.

Adduct **10**: mp 119—121 °C (colorless cubic crystals from EtOH); IR(KBr) 1650 (C=O), 1642, 1570, 1453, 1362, 1340, 1255, and 1175 cm^{-1} (SO_2).

Found: C, 64.12; H, 4.64; N, 7.20%. Calcd for $C_{21}H_{18}N_2O_4S_1$: C, 63.94; H, 4.61; N, 7.10%.

Adduct **11**: mp 124—125 °C (colorless needles from 95% EtOH); IR (KBr) 1660 (C=O), 1640, 1575, 1450, 1360, 1340, and 1173 cm^{-1} (SO_2).

Found: C, 64.07; H, 4.57; N, 7.20%. Calcd for $C_{21}H_{18}O_4S_1$: C, 63.94; H, 4.61; N, 7.10%.

*Cycloaddition of **2** to **6**.* A solution of **6** (494 mg, 2.0 mmol) and **32** (250 mg, 2.0 mmol) in dry THF (10 cm^3) was treated with TEA (250 mg, 2.5 mmol) in dry THF (5 cm^3) as has been described above. A similar work-up of the reaction mixture and evaporation of the solvent produced a viscous oil, which was solidified by the addition of a few drops of CCl_4. The solid was separated by filtration and dried under a vacuum to give 621 mg (94%) of a mixture of **12** and **13**. The NMR spectrum of the mixture showed that the **12**/**13** product ratio was 76/24. The mixture was chromatographed on silica gel. Elution with benzene–ether (97: 3) gave **13** and **12**, in that order.

Adduct **12**: mp 148—149 °C (coloeless leaves from EtOH); IR (KBr) 1693 (C=O), 1639, 1575, 1457, 1362, 1340, and 1172 cm^{-1} (SO_2); MS (80 eV), *m/e* 332, 289, 221, and 80.

Found: C, 57.63; H, 4.65; N, 8.51%. Calcd for $C_{16}H_{14}N_2O_4S_1$: C, 57.81; H, 4.86; N, 8.43%.

Adduct **13**: mp 129—130 °C (colorless needles from EtOH): IR (KBr) 1700 (C=O), 1639, 1580, 1458, 1360, 1345, and 1180 cm^{-1} (SO_2); MS (80 eV), *m/e* 332, 289, 221, and 80.

Found: C, 58.02; H, 4.81; N, 8.63%. Calcd fro $C_{16}H_{16}N_2O_4S_1$: C, 57.81; H, 4.96; N, 8.43%.

*Cycloaddition of **3** to **6**.* A solution of **6** (494 mg, 2.0 mmol) and **33** (311 mg, 2.0 mmol) in dry THF (10 cm^3) was treated with TEA (250 mg, 2.5 mmol) in dry THF (10 cm^3) by a procedure like that described above. A similar work-up of the reaction mixture and evaporation of the solvent gave 703 mg (96%) of a mixture of **14** and **15**. The NMR spectrum of the mixture showed that the **14**/**15** product ratio was 71/29. The solid was recrystallized from benzene to give colorless, pure **14**. The evaporation of benzene from the mother liquor afforded a residue, which was chromatographed on silica gel with benzene–ether(95: 5) to give **15** and **14**, in that order.

Adduct **14**: mp 214—215 °C (colorless leaves from benzene); IR(KBr) 1635, 1450, 1360, 1335, and 1172 cm^{-1}.

Found: C, 65.68; H, 4.95; N, 7.88%. Calcd for $C_{20}H_{18}N_2O_3S_1$: C, 65.55; H, 4.96; N, 7.65%.

Adduct **15**: mp 151—153 °C (colorless cubic crystals from EtOH–$CHCl_3$); IR (KBr) 1640, 1452, 1360, 1340, and 1172 cm^{-1}.

Found: C, 65.34; H, 4.76; N, 7.64% Calcd for $C_{20}H_{18}N_2O_3S_1$: C, 65.55; H, 4.96; N, 7.65%.

*Cycloaddition of **4** to **6**.* A mixture of **6** (494 mg, 2.0 mmol) and **4** (238 mg, 2.0 mmol) was dissolved in dry benzene (5 cm^3). The solution was then allowed to stand in the dark for one week at room temperature. The resulting white solid was separated from the solution by filtration, washed with a small amount of cold benzene, and dried under a vacuum to give pure **16** (343 mg, 47%). The filtrate was evaporated to afford a residue, which was subsequently chromatographed on alumina. Elution with $CHCl_3$ gave **6** (38 mg, recovery 8%), **17** (76 mg, 10%), and an additional amount of **16** (156 mg, 21%), in that order.

Adduct **16**: mp 179—181 °C (from MeOH); IR (KBr) 1632, 1600, 1505, 1488, 1350, and 1177 cm^{-1}.

Found: C, 62.38; H, 4.88; N, 15.25%. Calcd for $C_{19}H_{18}N_4O_2S_1$: C, 62.28; H, 4.95; N, 15.29%.

Adduct **17**: mp 165—167 °C (from MeOH); IR (KBr) 1639, 1603, 1500, 1363, and 1180 cm^{-1}.

Found: C, 62.20; H, 5.01: N, 15.27%. Calcd for $C_{19}H_{18}N_4O_2S_1$: C, 62.28; H, 4.95; N, 15.29%.

*The Nuclear Overhauser Effects Experiments in the **12**, **13**, **16**, and **17** Adducts.* The NOE in the NMR of these adducts were measured in well-deoxygenated $CDCl_3$ solutions. Table 7 shows the results.

Table 7. NOE experiments in four adducts (**12**, **13**, **16**, and **17**)

Adduct	Signal-irradiated	Proton-affected	Enhancement (%)
12	1-H	10-H	24
		2-H	
		6-H	0
13	7-H	8-H	20
		6-H	5
		2-H	0
16	7-H	8-H	9
		6-H	9
		2-H	0
17	1-H	10-H	24
		2-H	
		6-H	0

*Cycloaddition of **1** to **7**.* *a) At 66 °C*: Into a refluxing solution of **7** (375 mg, 1.5 mmol) and **9** (275 mg, 1.5 mmol) in dry THF (5 cm^3) warmed in a water bath, we stirred, drop by drop over a 2-h period, a solution of TEA (200 mg, 2.0 mmol) in dry THF (5 cm^3). After an additional 1 h's stirring at the same temperature, the resulting ammonium chloride was removed by filtration. The filtrate showed, on TLC with benzene, their spots. After the removal of the solvent, the residue was chromatographed on silica gel. Elution with benzene gave a small amount of 3,4-dibenzoyl-1,2,5-oxadiazole 2-oxide (**34**) (mp 76—78 °C, (lit,[23] 78—80 °C)), **7** (103 mg, recovery 27%), and **18** (335 mg, 57%), in that order.

Adduct **18**: mp 188—190 °C (colorless cubic crystals from $CHCl_3$–EtOH); IR(KBr) 1648 (C=O), 1562, 1448, 1337, and 1167 cm^{-1}.

Found: C, 63.68; H, 4.98; N, 7.16%. Calcd for $C_{21}H_{20}N_2O_4S_1$: C, 63.61; H, 5.09; N, 7.07%.

b) At 0 °C: The same reaction was carried out under similar conditions, but the reaction temperature was maintained at 0 °C instead of at 66 °C. A similar work-up of

the reaction mixture gave **34**, **7** (272 mg, recovery 72%), and **18** (72 mg, 12%).

Cycloaddition of 2 to 7. *a) At 66* °C: A solution of **7** (375 mg, 1.5 mmol) and **32** (182 mg, 1.5 mmol) in dry THF (5 cm^3) was treated with TEA (200 mg, 2.0 mmol) in dry THF (5 cm^3) as described above. A similar work-up of the reaction mixture produced an oil after the evaporation of THF. The oil showed, on TLC with benzene, three spots—at R_f 0.34 (**7**), R_f 0.25 (3,4-diacetyl-1,2,5-oxadiazole 2-oxide (**35**)), and R_f 0.12 (**19**). The oil was chromatographed on silica gel with benzene to give **7** (145 mg, recovery 39%), an oil of **35** (20 mg), and **19** (218 mg, 45%). The structure of **35** was confirmed by the elemental analysis ($C_6H_6N_2O_4$) and by comparing its IR spectrum with that of the analogous furoxan, **34**.

Adduct **19**: mp 156—158 °C (colorless plates from EtOH); IR (KBr) 1692 (C=O), 1580, 1447, 1347, and 1173 cm^{-1}.

Found: C, 57.35; H, 5.48; N, 8.40%. Calcd for $C_{16}H_{18}N_2O_4S_1$: C, 57.46; H, 5.44; N, 8.38%.

b) At 0 °C: The same recation was carried out under similar conditions, but the reaction temperature was kept at 0 °C. A similar work-up of the reaction mixture gave **7** (295 mg, recoverry 79%), a small amount of **35**, and **19** (51 mg, 10%).

Cycloaddition of 3 to 7. *a) At 66* °C; A solution of **7** (375 mg, 1.5 mmol) and **33** (233 mg, 1.5 mmol) in dry THF (5 cm^3) was treated with TEA (200 mg, 2.0 mmol) in dry THF (5 cm^3) as has been described above. A similar work-up of the reaction mixture gave 3,4-diphenyl-1,2,5-oxadiazole 2-oxide (**36**) (mp 115—116 °C (lit,[29] mp 112 °C)), **7** (194 mg, recovery 52%), and **20** (184 mg, 33%).

Adduct **20**: mp 227—229 °C (colorless cubic crystals from EtOH–$CHCl_3$); IR(KBr) 1453, 1400, 1342, and 1178 cm^{-1}.

Found: C, 64.94; H, 5.41; N, 7.57%. Calcd for $C_{20}H_{20}N_2O_3S_1$: C, 65.19: H, 5.48; N, 7.60%.

b) At 0 °C: The same reaction was carried out under similar conditions, but the reaction temperature was kept at 0 °C. A similar work-up of the reaction mixture gave **36**, **7** (187 mg, recovery 50%), and **20** (185 mg, 33%).

Treatment of 4 with 7. A solution of **7** (375 mg, 1.5 mmol) and **4** (180 mg, 1.5 mmol) in dry benzene was allowed to stand in the dark for one week at room temperature. Then, the solution showed, on TLC with benzene, only two spots—at R_f 0.80 (**4**) and R_f 0.47 (**7**).

Cycloadditon of 5 to 8. A solution of **8** (2.22 g, 16.3 mmol) and **5** (1.60 g, 8.2 mmol) in dry toluene (4 cm^3) was heated under reflux for 24 h. The solvent was then removed under reduced pressure to give a solid which consisted of **5** and a mixture of **21** and **22**. It was column chromatographed on silica gel. Elition with benzene gave 2.25 g (83%) of a mixture of **21** and **22**. The NMR spectrum of the mixture showed that the **21**/**22** product ratio was *ca.* 1/1. The 1:1 mixture of **21** and **22**: mp 108—116 °C (from hexane); IR (KBr) 1600, 1500, and 1285 cm^{-1}; NMR ($CDCl_3$ δ=6.8—7.5 (20H, m), 4.61 (2H, t, J=8.0 Hz, 4′-H of **21** and 4′-H of **22**), 2.24 and 2.88 (2H, ABq of d, J=14.0 and 8.0 Hz, 5′-CH_2 of **21** or **22**), 2.20 and 2.86 (2H, ABq of d J=11.0 and 8.0 Hz, 5′-CH_2 of **21** and **22**), and 1.0—2.6 (20H, m).

Found: C, 82.69; H, 7.52; N, 4.81%. Calcd for $C_{21}H_{23}N_1O_1$: C, 82.58; H, 7.59; N, 4.59%.

Hydrogenolysis of a Mixture of 21 and 22. To a solution of a mixture of **21** and **22** (305 mg, 1.0 mmol) in ethyl acetate (10 cm^3), 5% paradium-on-carbon catalyst (300 mg) was added. The solution was then shaken with hydrogen for 3 days at room temperature in a low-pressure apparatus. After the removal of the catalyst by filtration, the solvent was evaporated under reduced pressure to afford an oil. The oil showed, on TLC with hexane–ether (6:4), two spots—at R_f 0.36 (**26**) and R_f 0.23 (aniline). The oil was chromatographed on silica gel. Elution with hexane–ether (6:4) gave pure **26** (171 mg, 79%).

Product **26**: oil; IR (naet) 3380 (OH), 1605, 1500, and 1475 cm^{-1}; NMR ($CDCl_3$) δ=7.21 (5H, m) and 1.1—2.9 (15H, m); 2-phenethyl-2-*exo*-norbornyl phenylcarbamate: mp 116—117 °C (from hexane).

Found: C, 78.99; H, 7.50; N, 4.23%. Calcd for $C_{22}H_{25}N_1O_2$: C, 78.77; H, 7.51; N, 4.18%.

*Preparation of 2-Phenethyl-2-*endo*-norbornanol (27).* This compound was prepared by a procedure similar to that described in the literature.[8] Phenethyl bromide (14.8 g, 0.08 mol) dissolved in dry ethyl ether (25 cm^3) was stirred, drop by drop, into a suspension of magnesium turnings (1.82 g, 0.075 mol) in dry ether (50 cm^3) containing a small amount of I_2. The resulting solution was treated dropwise with 2-norbornanone (5.50 g, 0.05 mol) in dry ether (25 cm^3). After this addition was complete (45 min), the reaction mixture was stirred for 1 h, after which it was hydrolyzed with a saturated aq solution of ammonium chloride and extracted with ether (3×50 cm^3). The ether layer was separated, dried over $MgSO_4$, and evaporated to yield a colorless oil (**27**): bp 132—134 °C/1.2 Torr; IR(neat) 3360 (OH), 1605, 1500, and 1455 cm^{-1}; NMR ($CDCl_3$) δ=7.21 (5H, s) and 1.0—2.9 (15H, m); 2-phenethyl-2-*endo*-norbornyl phenylcarbamate: mp 160—162 °C (from benzene–hexane).

Found: C, 78.92; H, 7.32; N, 4.23%. Calcd for $C_{22}H_{25}N_1O_2$: C, 78.77; H, 7.51; N, 4.18%.

References

1) Presented at the 36th National Meeting of the Chemical Society of Japan, Higashi-Osaka, Japan, April 1977, Abstracts II, 3S 11.

2) Preceding paper: H. Taniguchi, T. Ikeda, and E. Imoto, *Bull. Chem. Soc. Jpn.*, **51**, 1495 (1978).

3) a) K. Alder and G. Stein, *Justus Liebigs Ann. Chem.*, **485**, 211, 223 (1931); b) K. Alder and G. Stein, *ibid.*, **501**, 1 (1933); c) K. Alder and G. Stein, *ibid.*, **515**, 165, 185 (1935); d) K. Alder, H-J. Ache, and F. H. Flock, *Chem. Ber.*, **93**, 1888 (1960).

4) H. Taniguchi, T. Ikeda, Y. Yoshida, and E. Imoto, *Bull. Chem. Soc. Jpn.*, **50**, 2694 (1977), and the references cited therein.

5) A. G. Anastassiou and H. Kasmai, *J. Chem. Soc., Chem. Commum.*, **1975**, 201.

6) F. A. L. Anet, and A. J. R. Bourn, *J. Am. Chem. Soc.*, **87**, 5250 (1965).

7) a) P. Scheiner, *Tetrahedron*, **24**, 349 (1967); b) R. Huisgen, L. Moebius, G. Mueller, J. Stangle, G. Szeimes, and J. M. Vernon, *Chem. Ber.*, **98**, 3992 (1965); c) D. Barraclough, J. S. Oakland, and F. Scheinmann, *J. Chem. Soc., Perkin Trans. 1*, **1972**, 1500.

8) E. M. Burgess, H. R. Penton, Jr., and E. A. Taylor, *J. Org. Chem.*, **38**, 26 (1973).

9) a) H. Taniguchi, Y. Yoshida, and E. Imoto, *Bull. Chem. Soc. Jpn.*, **50**, 3335 (1977); b) H. Taniguchi and E. Imoto, *Bull. Chem. Soc. Jpn.*, in press.

10) In LU-controlled reactions, the interaction of the dipole LUMO (lowest unoccupied molecular oribital) with the dipolarphile HOMO (highest occupied molecular orbital is greatest: K. N. Houk, J. Sims, C. R. Watts, and L. J. Luskus, *J. Am. Chem. Soc.*, **95**, 7301 (1973).

11) a) S. Inagaki, H. Fujimoto, and K. Fukui, *J. Am. Chem. Soc.*, **98**, 4054 (1976); b) K. Fukui, "Kagaku Hanno To Denshi No Kido," Maruzen, Tokyo (1976), Chaps. 3 and 4; c) K. Fukui, *Kagaku To Kogyo*, **29**, 666 (1976).

12) As has been described above, in the 2-azabicyclo-[3.2.1]octa-3,6-diene system the exsistence of homoconjugation has been found by NMR and UV spectroscopy.[5] From the structure of **6**, however, it may be considered that this homoconjugation on the endo side is weaker than that of norbornadiene,[4] so the interaction between the HOMO of the carbon-carbon double bond on the exo side in this system would surpass the homoconjugation on the endo side.

13) H. Taniguchi, K. Umano, and E. Imoto, unpublished data.

14) D. H. McDaniel and H. C. Brown, *J. Org. Chem.*, **23**, 420 (1958).

15) This can be deduced from the orbital mixing rule.[11] According to this rule, the resonance integrals as well as the orbital energies are important factors in the second-order pertubed orbital (see Ref. 11).

16) R. S. McDaniel and A. C. Oehlschlager, *Can. J. Chem.*, **48**, 345 (1970).

17) It has been reported that the vinyl protons (6-H and 7-H) of the diene, **6**, appear at δ 5.15—5.5 and 6.15 respectively.[18] However, that these assignments are incorrect has been found by a re-examination of its NMR spectrum (a double-resonance technique was used).

18) A. C. Oehlschlarger and L. H. Zalkow, *J. Org. Chem.*, **30**, 4205 (1965).

19) In the NMR spectrum of **31** in THF, the 6-H which corresponds to the 7-H of the olefin, **6**, appears in a field higher by 0.53 ppm than the 7-H which corresponds to the 6-H of the olefin, **6**.[20]

20) S. Winstein, M. Ogliaruso, M. Sakai, and J. M. Nicholson, *J. Am. Chem. Soc.*, **89**, 3656 (1967).

21) K. N. Houk, J. Sims, R. E. Duke, Jr., R. W. Strozier, and J. K. George, *J. Am. Chem. Soc.*, **95**, 7287 (1973).

22) In the reactions of 1,3-dipoles with the **7** and **8** olefins the cycloaddition of the reverse orientation did not occur. This may result from both the polarized carbon-carbon double bonds in these olefins, described above, and the steric hindrance (in the cycloadditions to **7**, the steric hindrance between the *N*-phenylsulfonyl group in **7** and the substituents in 1,3-dipoles, and in the cycloaddition of **5** to **8**, the steric hindrance between the methano-bridge in **8** and the phenyl group attached to the carbon atom in **5**).

23) Y. Otsuji, Y. Tsujii, A. Yoshida, and E. Imoto, *Bull. Chem. Soc. Jpn.*, **44**, 223 (1971).

24) Y. Otsuji, H. Nishikawa, and E. Imoto, the 30th National Meeting of the Chemical Society of Japan, Higashi-Osaka, April 1974, Abstracts III, p. 1302.

25) P. Pajahopalan, B. G. Advani, and C. N. Talaty, *Org. Synth.*, Coll. Vol. V, 505 (1973).

26) R. O. Lindsay and C. F. H. Allen, *Org. Synth.*, Coll. Vol. III, 710 (1955).

27) S. R. Sandler and W. Karo, "Organic Functional Group Preparations III," Academic Press, New York (1972), p. 307.

28) H. C. Brown and K-T. Liu, *J. Am. Chem. Soc.*, **97**, 600 (1975).

29) A. Werner and H. Buss, *Chem. Ber.*, **27**, 2197 (1894).

The Reactions of 2-Fluoro-1,3,5-trinitrobenzene (FTNB) as a New Condensing Reagent

Katsuhiko INOMATA, Hideki KINOSHITA, Hirohiko FUKUDA, Kumiko TANABE, and Hiroshi KOTAKE

Department of Chemistry, Faculty of Science, Kanazawa University, Kanazawa 920

(Received December 13, 1977)

2-Fluoro-1,3,5-trinitrobenzene (FTNB) was found to be a useful new condensing reagent. Various amides, esters and thiocarboxylic *S*-esters were prepared in good yields from carboxylic acids with the reagent.

As has been reported in a preliminary communication,[1] we have examined the reaction of various polynitrohalobenzenes with carboxylic acids in the presence of a base and have found that the readily available 2-fluoro-1,3,5-trinitrobenzene (FTNB) is most reactive for the amide formation. In this paper we wish to report that FTNB is a useful new condensing reagent for the preparation of amides, esters, and thiocarboxylic *S*-esters from carboxylic acids.

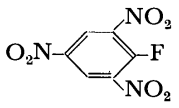

FTNB

Preparation of Amides. When triethylamine was added to a mixed solution of an equimolar amount of FTNB and carboxylic acid (**1a**—**h**) in acetonitrile at room temperature under a nitrogen atmosphere, a facile reaction began immediately; we checked the reaction by means of TLC. The spots of the starting materials, FTNB and carboxylic acid, disappeared, and a new spot of the intermediate appeared. After 1 h twice a molar quantity of aniline was added to the solution at room temperature, the reaction mixture was stirred for 1 h and then worked up to give the corresponding anilide (**2a**—**h**) in an excellent yield, as is listed in Table 1.

From these results, it will be noted that 2,2-dimethylpropanoic acid (**1e**) produces the initial active intermediate as fast as other carboxylic acids, but that the subsequent nucleophilic reaction of aniline with the intermediate is relatively slow. These differences in reactivity appear to be based on the differences in steric hindrance.

This versatile compound, FTNB, also proved to be an excellent condensing reagent for peptide synthesis, which will be described elsewhere.

Preparation of Esters and Thiocarboxylic S-*Esters.* In order to compare the results with those described above for amides, the same carboxylic acids (**1a**—**f**) except **1i** were used first and the corresponding benzyl ester derivatives (**3a**—**f, i**) were prepared. The benzyl group is a useful carboxyl-protecting group because it is easily cleaved by reductions.

The initial step in the formation of the active intermediate from carboxylic acid and FTNB was carried out in a similar manner; however, it was found that the subsequent nucleophilic reaction of benzyl alcohol to the intermediate in the presence of a base was very slow at room temperature. Consequently, the reaction with benzyl alcohol was run by refluxing to give the desired benzyl esters in good yields, as is shown in Table 2.

The low yields or the relatively slow reaction rates in the cases of 2,2-dimethylpropanoic acid (**1e**) and 2-methylpropanoic acid (**1f**) probably reflect the steric

Table 1. Preparation of anilides from carboxylic acids and aniline with FTNB

FTNB + RCO_2H + Et_3N —(r.t., 1 h, in CH_3CN)→ —(2 $PhNH_2$, r.t., (A))→ RCONHPh

1a—h **2a—h**

	RCO_2H	Time (A)	Isolated yield (%) **2a—h**	Mp (°C)[a]
1a	$PhCH{=}CHCO_2H$	1 h	quant.	151—152
1b	$PhCO_2H$	1 h	93	161—162
1c	$PhCH_2CO_2H$	1 h	88	116—117
1d	Z-Gly-OH	1 h	87	143—144
1e	$(CH_3)_3CCO_2H$	2 days	93	128—131
1f	$(CH_3)_2CHCO_2H$	2.5 h	96	103—105
1g	CH_3CO_2H	1.5 h	82	111—113
1h	$CH_3(CH_2)_{12}CO_2H$	2 h	89	83—84

a) They were in accordance with the values cited in the literatures (see Ref. 2 except for **2d**[3]).

Table 2. Preparation of benzyl esters from corboxylic acids and benzyl alcohol with FTNB

FTNB + RCO_2H + Et_3N

1a—f, i

—(r.t., 2 h, in CH_3CN)→ —($PhCH_2OH$, base, reflux, (B))→ RCO_2CH_2Ph

3a—f, i

	RCO_2H	Base	Time (B)	Isolated yield (%) **3a—f, i**	$\nu_{C=O}$ (cm^{-1})
1a	$PhCH{=}CHCO_2H$	Et_3N	3 h	89	1710
1b	$PhCO_2H$	Et_3N	3 h	80	1710
1c	$PhCH_2CO_2H$	Et_3N	2 h	91	1730
1d	Z-Gly-OH	Et_3N	2 h	81	1715
1e	$(CH_3)_3CCO_2H$	Et_3N	92 h	27	1725
	$(CH_3)_3CCO_2H$	Et_3N	92 h	42[a]	1725
	$(CH_3)_3CCO_2H$	DBU	92 h	41	1725
1f	$(CH_3)_2CHCO_2H$	Et_3N	20 h	50	1730
	$(CH_3)_2CHCO_2H$	Et_3N	20 h	72[a]	1730
	$(CH_3)_2CHCO_2H$	DBU	20 h	78	1730
1i	$CH_3(CH_2)_6CO_2H$	Et_3N	5 h	95	1735

a) A 1.5 equivalent of benzyl alcohol was used.

Table 3. Preparation of esters of benzoic acid and thiobenzoic *S*-acid

FTNB + $PhCO_2H$ + Et_3N —(r.t., 2 h, in CH_3CN)→ —(RYH (**4a—h**), Et_3N, (C))→ PhCOYR (Y=O, S) **5a—h**

	RYH	Conditions (C)	Isolated yield (%) **5a—h**	$\nu_{C=O}$ (cm^{-1})
4a	Cl_3CCH_2OH	r.t., 2 h	81	1735
4b	*t*-C_4H_9OH	reflux, 4 h	0	—
4c	*p*-$NO_2C_6H_4OH$	r.t., 5 h	94	1735
4d	C_6Cl_5OH	r.t., 22 h	71	1750
4e	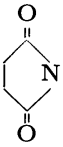	r.t., 30 min	83	1765, 1735
4f	*n*-C_4H_9SH	r.t., 3 h	96	1660
4g	*p*-$CH_3C_6H_4SH$	r.t., 1 h	87	1660
4h	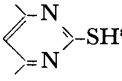 [a]	r.t., 6 h	64	1670
	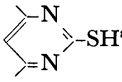 [a]	r.t., 6 h	76[b]	1670

a) A HCl salt was used and neutralized *in situ* with Et_3N.
b) A 1.5 equivalent of **4h** was used.

hindrance as well as the formation of 2,2-dimethylpropananilide (**2e**). The use of excess benzyl alcohol or 1,5-diazabicyclo[5.4.0]undec-5-ene (DBU) as a base was effective in such a case.

Various esters of benzoic acid (**5a—e**) and of thiobenzoic *S*-acid (**5f—h**) were prepared by this reaction; the results are shown in Table 3.

The failure to prepare *t*-butyl benzoate (**5b**) suggests that this reaction is also affected by the steric hindrance of alcohol; the fact that all the reactions (except that of *t*-butyl alcohol (**4b**)) proceeded at room temperature, unlike the case of benzyl alcohol, can be explained on the basis of the high nucleophilicity of the anions produced by the reaction of **4a**, **c—h** with triethylamine.

The extension of this reaction to macrolide synthesis is in progress.

Mechanism. The probable course of this reaction is illustrated in the following scheme. First, an anionic sigma complex (**6**) is formed *via* the aromatic nucleophilic addition of a carboxylate anion to FTNB, followed by the elimination of the picrate anion to produce an acyl fluoride (**7**), which then reacts with a nucleophile, R'YH, to give the corresponding product (**8**). Support for this scheme was found in the reaction of FTNB with cinnamic acid (**1a**) and triethylamine to isolate cinnamoyl fluoride by sublimation.

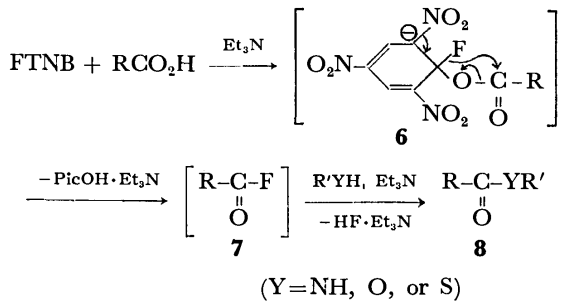

(Y=NH, O, or S)

Experimental

All the melting points are uncorrected. The proton NMR spectra were recorded on a JEOL JNM-MH 60 spectrometer. The chemical shifts are reported on the δ scale relative to TMS as the internal standard. The IR spectra were taken with a JASCO IRA-1 diffraction grating infrared spectrometer.

Materials. The acetonitrile used here was distilled according to the usual method and was stored over molecular sieves as a drying agent. 2-Fluoro-1,3,5-trinitrobenzene (FTNB, recrystallized from benzene; mp 127—128 °C [lit,[4] mp 122—123 °C or 130—131.5 °C]) was readily prepared using a modification of the procedure for the nitration of 1-fluoro-2,4-dinitrobenzene by 25% fuming sulfuric acid and fuming nitric acid (sp gr about 1.50). 2-Mercapto-4,6-dimethylpyrimidine hydrochloride was prepared by the reported procedure.[5] Thin-layer chromatography (TLC) and column chromatography were performed on Merck's Kieselgel 60 PF_{254} (Art. 7749) and on Alumina Woelm B (Akt. 1), respectively.

Cinnamanilide (2a). To a mixed solution of FTNB (116 mg, 0.5 mmol) and cinnamic acid (74 mg, 0.5 mmol) in acetonitrile (3 ml) was added an acetonitrile solution (1 ml) of triethylamine (55 mg, 0.55 mmol) at room temperature under a nitrogen atmosphere. After 1 h, a solution of aniline (93 mg, 1 mmol) in acetonitrile (1 ml) was added to the solution, after which the reaction mixture was stirred for an additional hour at room temperature. The solution was then evaporated under reduced pressure, and the residue was partitioned between ethyl acetate and a saturated solution of $NaHCO_3$. The organic layer was further washed with 1M HCl and a saturated solution of NaCl, dried over anhydrous Na_2SO_4, filtered, and evaporated to dryness under reduced pressure. The desired product, cinnamanilide, was separated from the residue by preparative TLC (development with 5:3 benzene: ethyl acetate) in a nearly quantitative yield (112 mg, mp 151—152 °C [lit,[2] mp 153 °C]).

In a similar manner, other anilides (**2b—h**) were prepared in excellent yields from the corresponding carboxylic acids and aniline with FTNB. The results are listed in Table 1.

Benzyl Cinnamate (3a). To an acetonitrile solution (3 ml) of FTNB (231 mg, 1 mmol) was added a mixed solution of cinnamic acid (148 mg, 1 mmol) and triethylamine (101 mg, 1 mmol) in acetonitrile (5 ml) at room temperature under a nitrogen atmosphere. After this mixture had been stirred for 2 h, a solution of benzyl alcohol (108 mg, 1 mmol) and triethylamine (101 mg, 1 mmol) in acetonitrile (4 ml) was added, and the reaction mixture was refluxed for 3 h. The solvent was removed under reduced pressure, and the residue was then dissolved in benzene, followed by injection into one end of a short column of basic alumina. The triethylammonium picrate was removed efficiently by elution with benzene. The eluate from the column was condensed, and pure benzyl cinnamate was separated from the residue by prepatative TLC (development with 5:1 benzene: hexane) in an 89% yield (212 mg).

The other examples reported in Tables 2 and 3 were carried out in a similar manner. The spectral data, physical proper-

ties, and analytical data of the products are listed below.

3a: oil, NMR (CCl_4) δ 5.09 (s, 2H), 6.29 (d, 1H, J=17 Hz), 7.22 (m, 10H), 7.56 (d, 1H. J=17 Hz). **3b**: oil, NMR (CCl_4) δ 5.20 (s, 2H), 7.0—7.5 (m, 8H), 7.8—8.1 (m, 2H). **3c**: oil, NMR (CCl_4) δ 3.48 (s, 2H), 4.94 (s, 2H), 7.11 (s, 5H), 7.13 (s, 5H). **3d**: mp 68—70 °C, NMR ($CDCl_3$) δ 3.86 (d, 2H, J=6 Hz), 4.98 (s, 2H), 5.03 (s, 2H), 5.1—5.6 (broad, 1H), 7.21 (s, 10H). **3e**: oil, NMR (CCl_4) δ 1.19 (s, 9H), 4.99 (s, 2H), 7.22 (s, 5H). **3f**: oil, NMR (CCl_4) δ 1.13 (d, 6H, J=7 Hz), 2.46 (h, 1H, J=7 Hz), 4.93 (s, 2H), 7.15 (s, 5H). **3i**: oil, NMR (CCl_4) δ 0.6—1.9 (m, 13H), 2.26 (t, 2H, J=7 Hz), 5.01 (s, 2H), 7.27 (s, 5H).

5a: oil, NMR (CCl_4) δ 4.82 (s, 2H), 7.1—7.6 (m, 3H), 7.8—8.2 (m, 2H). **5c**: mp 139—142 °C (lit,[2] mp 142.5 °C). **5d**: mp 159—160 °C (lit,[2] mp 159—160 °C). **5e**: mp 139—140 °C, NMR (CCl_4) δ 2.86 (s, 4H), 7.3—7.8 (m,3H), 8.0—8.3 (m, 2H).

*S-(4,6-Dimethyl-2-pyrimidyl) Thiobenzoate (**5h**).* To a mixed solution of FTNB (231 mg, 1 mmol) and benzoic acid (122 mg, 1 mmol) in acetonitrile (6 ml) was added an acetonitrile solution (2 ml) of triethylamine (101 mg, 1 mmol) at room temperature under a nitrogen atmosphere. After 2 h, a mixed solution of 2-mercapto-4,6-dimethylpyrimidine hydrochloride (265 mg, 1.5 mmol) and triethylamine (253 mg, 2.5 mmol) in acetonitrile (10 ml) was added to the solution, after which the reaction mixture was stirred for an additional 6 h at room temperature. The solvent was removed under reduced pressure; the residue was then dissolved in benzene, followed by injection into one end of a short column of basic alumina. After elution with benzene, the eluate was condensed, and pure **5h** was separated from the residue by preparative TLC (development with 5:1 benzene: ethyl acetate) in a 76% yield (278 mg): mp 74—77 °C (recrystallized from cyclohexane), NMR (CCl_4) δ 2.41 (s, 6H), 6.78 (s, 1H), 7.2—7.5 (m, 3H), 7.7—8.0 (m, 2H). Found: C, 63.90; H, 4.94; N, 11.94%. Calcd for $C_{13}H_{12}N_2OS$: C, 63.92; H, 4.95; N, 11.47%.

The other thiocarboxylic *S*-esters, **5f** and **5g**, were prepared in a similar manner. Their spectral data and physical properties are listed below.

5f: oil, NMR (CCl_4) δ 0.7—1.9 (m, 7H), 2.97 (t, 2H, J=7 Hz), 7.1—7.5 (m, 3H), 7.6—8.1 (m, 2H). **5g**: mp 74—75 °C (lit,[6] mp 75°C).

Cinnamoyl Fluoride. To an acetonitrile solution (3 ml) of FTNB (231 mg, 1 mmol) was added a mixed solution of cinnamic acid (148 mg, 1 mmol) and triethylamine (101 mg, 1 mmol) in acetonitrile (5 ml) at room temperature under a nitrogen atmosphere. After the mixture had been stirred for 2 h, the solvent was removed under reduced pressure; then we sublimed cinnamoyl fluoride (102 mg) from the residue *in vacuo* in a 68% yield: mp 30 °C (lit,[7] mp 31—31.5 °C), IR 1782, 1615, 1182, 1092 cm^{-1}; NMR ($CDCl_3$) δ 6.32 (d·d, 1H, J_{HH}=16.2 Hz, J_{HF}=7.2 Hz), 7.44 (m, 5H), 7.82 (d, 1H, J_{HH}=16.2 Hz).

References

1) H. Kotake, K. Inomata, H. Kinoshita, K. Tanabe, and O. Miyano, *Chem. Lett.*, **1977**, 647.

2) J. R. A. Pollock and R. Stevens, Ed, "Dictionary of Organic Compounds," Maruzen, Tokyo (1965).

3) J. P. Greenstein and M. Winitz, "Chemistry of the Amino Acids," Vol. 2, John Wiley & Sons, New York (1961), p. 973.

4) (a) G. C. Shaw III and D. L. Seaton *J. Org. Chem.*, **26**, 5227 (1961); (b) R. E. Parker and T. O. Read, *J. Chem. Soc.*, **1962**, 9.

5) R. R. Hunt, J. F. W. McOmie, and E. R. Sayer, *J. Chem. Soc.*, **1959**, 525.

6) Deutschen Chemischen Gesellschaft, "Beilsteins Handbuch der Organischen Chemie," Band IX, p. 421.

7) F. Seel and J. Langer, *Chem. Ber.*, **91**, 2553 (1958).

Asymmetric Reduction of Prochiral Ketones with Chiral Hydride Reagents Prepared from Lithium Aluminium Hydride and (*S*)-2-(*N*-Substituted aminomethyl)pyrrolidines

Masatoshi ASAMI, Hiroyasu OHNO, Susumu KOBAYASHI, and Teruaki MUKAIYAMA
The University of Tokyo, Hongo, Bunkyo-ku, Tokyo 113
(Received December 20, 1977)

Asymmetric reduction of prochiral ketones with various hydride reagents prepared from lithium aluminium hydride and (*S*)-2-(*N*-substituted aminomethyl)pyrrolidines, derived easily by four steps from commercially available (*S*)-proline, yields optically active alcohols with 13—92% optical purity having the *S*-configuration.

Asymmetric reduction of prochiral carbonyl compounds by chiral hydride reagents has been the object of extensive work and a number of methods have been reported.[1] Most of such works have been developed based on the use of chiral hydride reagents obtained by reaction of $LiAlH_4$ and chiral ligands such as alkaloids,[2] sugar derivatives,[3] amino alcohols,[4,5] chiral oxazolines,[6] tartaric acid derivatives,[7] chiral diols,[8] or chiral amines.[9] Relatively high optical yield (<83%) was achieved in the case of the reduction of acetophenone by using these ligands.

On the other hand, during the course of our synthetic investigation utilizing the onium salts of azaaromatics, we have reported the convenient and efficient methods for the optical interconversion of chiral secondary alcohols,[10a] and transformation of the alcohols to chiral halides,[10b] thiols,[10c] and primary amines.[10d] This prompted us to study on the exploration of a new and efficient chiral ligand, and (*S*)-2-(anilinomethyl)pyrrolidine (**5a**) is found to be efficient for the reduction of acetophenone to yield (*S*)-1-phenylethanol with 92% optical purity as briefly reported in the previous communication.[11] (Scheme 1).

(*S*)-2-(*N*-substituted aminomethyl)pyrrolidines (**5a**—**1**) were easily prepared from readily available (*S*)-proline as shown in the following scheme (Scheme 2): (*S*)-Proline (**1**) was converted to (*S*)-*N*-(benzyloxycarbonyl)-proline (**2**) by treatment with benzyloxycarbonyl chloride and sodium hydrogencarbonate. Then it was transformed into the corresponding amides (**3a**—**1**) by treatment with *N*-methylmorpholine, ethyl chloroformate and amines. *N*-Substituted (*S*)-prolinamides (**4a**—**1**) were obtained by the hydrogenolysis of the amides **3a**—**1** in the presence of 5% Pd–C catalyst under hydrogen atmosphere at ordinary pressure. The amides **4a**—**1** were further reduced to the required chiral diamines, (*S*)-2-(*N*-substituted aminomethyl)pyrrolidines **5a**—**1**, tabulated in Table 1.

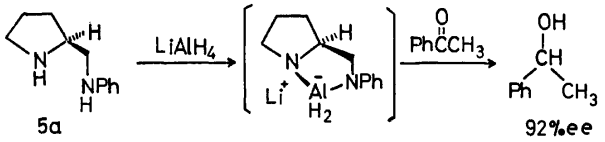

Scheme 1.

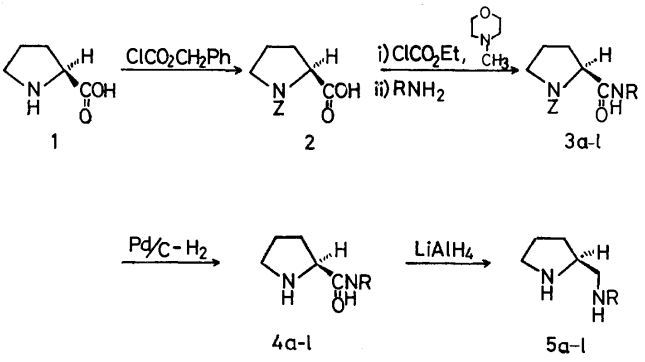

Scheme 2.

In the first place, we examined suitable reaction conditions using chiral diamine **5a** as ligand and acetophenone as model substrate. The reactions were carried out as follows: The diamine **5a** in ether, THF, or toluene was added to the standardized $LiAlH_4$

TABLE 1. PHYSICAL PROPERTY OF (*S*)-2-(*N*-SUBSTITUTED AMINOMETHYL)PYRROLIDINES **5a**—**1**

No.	Chiral diamines substituent	$[\alpha]_D$ (EtOH)	Bp
5a	Ph	$[\alpha]_D^{24}$+19.7° (*c* 1.04)	111—112 °C/0.55 mmHg
5b	Isopropyl	$[\alpha]_D^{26}$+16.5° (*c* 1.07)	59—62 °C/4 mmHg
5c	Hexyl	$[\alpha]_D^{24}$+13.9° (*c* 1.13)	66—70 °C/0.25 mmHg
5d	Cyclohexyl	$[\alpha]_D^{24}$+10.3° (*c* 1.01)	78—80 °C/0.4 mmHg
5e	(*R*)-1-Phenylethyl	$[\alpha]_D^{24}$+53.5° (*c* 1.02)	110—118 °C/1 mmHg
5f	(*S*)-1-Phenylethyl	$[\alpha]_D^{24}$−43.0° (*c* 1.10)	106—116 °C/0.7 mmHg
5g	1-Naphtyl	$[\alpha]_D^{24}$+29.5° (*c* 1.03)	159—161 °C/0.3 mmHg
5h	2-Methoxyphenyl	$[\alpha]_D^{24}$+25.2° (*c* 1.08)	150 °C/0.6 mmHg
5i	4-Methoxyphenyl	$[\alpha]_D^{24}$+14.4° (*c* 0.97)	130—132 °C/0.25 mmHg
5j	2-Pyridyl	$[\alpha]_D^{24}$+21.3° (*c* 1.16)	102—106 °C/0.025 mmHg
5k	4-Pyridyl	$[\alpha]_D^{24}$+1.90° (*c* 0.68)	130—140 °C/0.04 mmHg
5l	3,4-Dichlorophenyl	$[\alpha]_D^{24}$+9.46° (*c* 0.96)	150—153 °C/0.25 mmHg

Table 2. Asymmetric reduction of acetophenone with $LiAlH_4$-chiral diamine **5a** complex

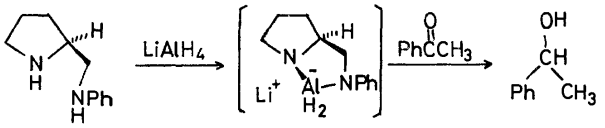

Exp	Solvent	Temp (°C)	Molar ratio[a)]	Additive	Yield (%)	$[\alpha]_D$ (*c*, cyclopentane)	Optical purity (%)[b)]
1	Ether	−40	B	—	68	$[\alpha]_D^{31}$ −35.5° (7.30)	82
2	Ether	−78	A	—	68	$[\alpha]_D^{22}$ −33.8° (7.27)	78
3	Ether	−78	B	—	84	$[\alpha]_D^{22}$ −36.1° (7.39)	84
4	Ether	−78	C	—	88	$[\alpha]_D^{22}$ −38.2° (7.17)	89
5	Ether	−100	B	—	81	$[\alpha]_D^{25}$ −37.5° (7.25)	87
6	Ether	−100	C	—	93	$[\alpha]_D^{26}$ −39.8° (7.28)	92
7	THF	−78	B	—	54	$[\alpha]_D^{24}$ + 8.3° (4.00)	19
8	Toluene	−78	B	—	—[c)]		
9	Ether	−78	B	TMEDA	67	$[\alpha]_D^{25}$ − 7.6° (6.88)	18
10	Ether	−78	B	DME	84	$[\alpha]_D^{24}$ −16.6° (7.39)	38
11	Ether	−78	B	$MgBr_2$	85	$[\alpha]_D^{24}$ −10.7° (7.17)	25

a) $LiAlH_4$: **5a**: Acetophenon A 1.3: 1.5: 1, B 1.75: 2.00: 1, C 2.36: 2.73: 1. b) Based on $[\alpha]_D^{21}$ −43.1° (*c* 7.19, C_5H_{10}) reported by S. Yamaguchi and H.S. Mosher, *J. Org. Chem.*, **38**, 1970 (1973). c) Only trace of alcohol was detected by TLC.

solution. On addition of the diamine **5a**, *ca.* 2 mol of hydrogen gas evolved and white precipitates, presumably, the diamine **5a**–$LiAlH_4$ complex appeared in ether or toluene. But, in the case of THF, almost homogeneous solution resulted. After the evolution of gas had been completed, the mixture was stirred at room temperature for 1 h. Then it was cooled and was add d acetophenone. Stirring was continued for additional 3 h at the temperature and it was hydrolyzed to yield 1-phenylethanol. In the cases when additives (*N*,*N*,*N*′,*N*′-tetramethylethylenediamine (TMEDA), 1,2-dimethoxyethane (DME), or $MgBr_2$) were used, they were added before lowering the temperature and the mixture was stirred at room temperature for about 1 h. Then it was cooled to −78 °C and added acetophenone and treated similarly. The results are summarized in Table 2.

These results indicate that ether is preferred as solvent and the optical purity increased by lowering the reaction temperature [Exp. 1, 3, 5, and 4, 6]. The molar ratio of each substances also affect both synthetic and optical yields. The presence of additives such as TMEDA, DME or $MgBr_2$ caused the decrease of optical purity, which indicates that lithium ion plays an important role in the present asymmetric reductions.

The effect of the *N*-substituents in the ligand diamines **5a**—**l** on the enantioselectivity in the present asymmetric reduction were examined with various *N*-substituted diamines **5a**—**l**–$LiAlH_4$ complexes under the same reaction conditions as Exp. 3 by employing the asymmetric reduction of acetophenone as a model. The results are summarized in Table 3. Relatively high optical purities were attained when *N*-aryl substituted diamines–$LiAlH_4$ complexes were employed as chiral hydride reagent. Electron-withdrawing group (3,4-dichloro) or electron-donating group (4-methoxyl) in *N*-aryl substituent did not cause the remarkable effect both on the synthetic and optical yields, but methoxyl group on the *o*-position (2-methoxyl) in *N*-aryl substituent which can coordinate to the metal atom, either lithium or aluminium of the bicyclic hydride reagents, deactivated the reagent.

Table 3. Asymmetric reduction of acetophenone with $LiAlH_4$-chiral diamines **5a**—**l** complex

Exp.	Diamines **5** R	Alcohol Yield (%)	Alcohol $[\alpha]_D$ (*c*, cyclopentane)	Alcohol Optical purity (%)
3	**a** Ph	84	$[\alpha]_D^{22}$ −36.1° (7.39)	84
12	**b** Isopropyl	65	$[\alpha]_D^{24}$ −20.1° (7.13)	47
13	**c** Hexyl	45	$[\alpha]_D^{25}$ −21.3° (2.11)	49
14	**d** Cyclohexyl	78	$[\alpha]_D^{26}$ −25.5° (6.74)	59
15	**e** (*R*)-1-Phenylethyl	69	$[\alpha]_D^{22}$ −22.2° (7.67)	52
16	**f** (*S*)-1-Phenylethyl	72	$[\alpha]_D^{23}$ −23.0° (7.53)	54
17	**g** 1-Naphtyl	67	$[\alpha]_D^{28}$ −33.3° (5.80)	77
18	**h** 2-Methoxyphenyl	18	$[\alpha]_D^{25}$ 0° (5.37)	0
19	**i** 4-Methoxyphenyl	63	$[\alpha]_D^{28}$ −32.5° (5.75)	76
20	**j** 2-Pyridyl	88	$[\alpha]_D^{24}$ − 1.0° (7.23)	2
21	**k** 4-Pyridyl[a)]	64	$[\alpha]_D^{28}$ + 3.0° (6.75)	7
22	**l** 3,4-Dichlorophenyl	66	$[\alpha]_D^{28}$ −33.3° (5.74)	77

a) Small amount of THF was used.

Further, the diamine–$LiAlH_4$ complex was applied to the asymmetric reduction of various ketones by choosing diamine **5a**–$LiAlH_4$ complex and diamine **5d**–$LiAlH_4$ complex as the chiral hydride reagents. In every case, the reactions were carried out according to a similar procedure as mentioned above and corresponding alcohols were obtained as summarized in Table 4.

As the result, in the case of the ketones having aromatic ring attached to the carbonyl group gave fairly good optical purities (50—85% with diamine **5a**–$LiAlH_4$ complex), but satisfactory results could not be obtained in the case of normal aliphatic ketones. We assume that enantioselectivities were induced by both electronic

Table 4. Asymmetric reduction of various ketones with $LiAlH_4$–chiral diamine **5a** complex and $LiAlH_4$–chiral diamine **5d** complex

Exp	Ketone	Diamine 5 R		Alcohol[a] Yield (%)	Alcohol[a] $[\alpha]_D$ (c. solv.)	Alcohol[a] Optical Purity (%)
23	PhCOEt	**a**	Ph	90	$[\alpha]_D^{25}$ −23.7° (neat)	85[b]
24	$PhCOCHMe_2$	**a**	Ph	80	$[\alpha]_D^{23}$ −27.0° (6.79, ether)	57[c]
25	α-Tetralone	**a**	Ph	94	$[\alpha]_D^{22}$ +16.3° (4.12, $CHCl_3$)	50[d]
26	$PhCH_2COMe$	**a**	Ph	85	$[\alpha]_D^{25}$ +12.9° (5.19, C_6H_6)	31[e]
27	n-$C_6H_{13}COMe$	**a**	Ph	77	$[\alpha]_D^{25}$ + 1.27° (neat)	13[f]
28	PhCOEt	**d**	Cyclohexyl	40	$[\alpha]_D^{28}$ −28.9° (5.40, $CHCl_3$)	63[b]
29	$PhCOCHMe_2$	**d**	Cyclohexyl	83	$[\alpha]_D^{28}$ −24.0° (7.20, ether)	51[c]
30	α-Tetralone	**d**	Cyclohexyl	80	$[\alpha]_D^{28}$ + 1.36 (4.42, $CHCl_3$)	4[d]

a) All these alcohols have *S*-configuration. b) Based on $[\alpha]_D^{25}$ 27.7° (neat), $[\alpha]_D$ 45.45° (*c* 5.15, $CHCl_3$) reported by R. H. Pickard and J. Kenyon, *J. Chem. Soc.*, **99**, 45 (1911); *ibid* **105**, 1115 (1914). c) Based on $[\alpha]_D^{20}$ 47.7° (*c* 7, ether) reported by R. MacLeod, F. J. Welch and H. S. Mosher, *J. Am. Chem. Soc.*, **82**, 876 (1960). d) Based on $[\alpha]_D^{17}$ 32.7° (*c* 4.1, $CHCl_3$) reported by A. G. Davies and A. M. White, *J. Chem. Soc.*, **1952**, 3300. e) Based on $[\alpha]_D^{20}$ 41.8° (*c* 5.26, C_6H_6) reported by R. H. Pickard and J. Kenyon *J. Chem. Soc.*, **105**, 1115 (1914), f) Based on $[\alpha]_D^{25}$ 9.57° (neat) reported by S. J. Cristol, B. Franzus, A. Shadan, *J. Am. Chem. Soc.*, **77**, 2512 (1955).

and steric effects of the aromatic ring in the ketones attached to the carbonyl group. That is, the conjugation effect puts the aromatic ring and carbonyl group on the same plane. This makes possible to distinguish a sharp steric difference of the two substituents and enantioface of unsymmetrical ketones during hydride transfer to attain relatively high optical yield.

Although the precise mechanism of this asymmetric reduction is not clear, we assume that high enantioselectivity, namely, all of the produced alcohols have *S*-configuration (except the case THF was used as solvent) with high optical purity, in the present asymmetric reduction of prochiral ketones is due to the following factors: 1) The diamines, a simple structure having only one asymmetric carbon, produce the effective chiral environment by the treatment with $LiAlH_4$. This may be due to the formation of sterically restricted *cis*-fused bicyclic hydride reagents, creating the additional chiral center on the nitrogen atom in the pyrrolidine ring. 2) The reactivity of the two hydrogen atoms contained in this chiral reagent is remarkably different. Actually only one hydrogen atom was consumed by the reaction with ketones, but the other remained unreacted because of large steric hinderance. 3) Lithium ion, presumably coordinating to the nitrogen atoms on the pyrrolidine ring and/or on the side chain in the diamine–$LiAlH_4$ complex, restrict the direction of approach of the ketones.

Table 5. Comparison of various chiral reducing reagents prepared from $LiAlH_4$ and chiral ligands (optical purity)

Ketone	Ligand: Sugar[3a] derivative	Ligand: Darbon[a] [4]	Ligand: Chiral oxazoline[6]	Ligand: Chiral amine[9]	**5a**
PhCOMe	71	75	65	43	84 (92)[b]
PhCOEt	46	—	62	52	85
$PhCOCHMe_2$	—	48	43	—	57
α-Tetralone	—	—	4	—	50
$PhCH_2COMe$	—	—	1	—	31
n-$C_6H_{13}COMe$	25	—	4 (6)	—	13

a) (+)-(2*S*,3*R*)-4-Dimethylamino-3-methyl-1,2-diphenyl-2-butanol. b) at −100 °C.

In conclusion, it is noteworthy that the diamine **5a** produces effective chiral hydride reagent with $LiAlH_4$ and reduces prochiral ketones, including acetophenone, propiophenone, phenyl isopropyl ketone, α-tetralone, benzyl methyl ketone and 2-octanone, to afford corresponding chiral alcohols with 13—92% optical purity having *S*-configuration.

Experimental

Spectra. NMR were obtained on a Hitachi R-24 spectrometer. Infrared spectra were taken using a Hitachi EPI-G2 spectrometer. Mass spectra were taken using a Hitachi RMU-6 spectrometer. Optical rotations were taken on a JASCO DIP-SL automatic polarimeter using 1-dm or 1-cm thermostated microcell. Products were identified by NMR and IR with authentic samples.

Materials. All solvents used were distilled according to the general methods and stored over sodium metal as a drying agent. Further ether and THF were distilled from $LiAlH_4$ prior to use. A supernatant of etheral $LiAlH_4$ solution was stored in a flask closed with a rubber septum.

(S)-N-(Benzyloxycarbonyl)prolinanilide ***3a.*** Commercial *(S)*-proline **1** (11.5 g, 0.1 mol), sodium hydrogencarbonate (20.16 g) and benzyloxycarbonyl chloride (32 g, 30—35% toluene solution) in 150 ml of water were stirred for 2 h at room temperature. Then sodium hydrogencarbonate (10.08 g) and benzyloxycarbonyl chloride (32 g, 30—35% toluene solution) were added and stirred for 3 h at room temperature. The reaction mixture was washed two times with 50 ml of ether and the aqueous layer was acidified (pH 3—4) by 6M HCl. The mixture was extracted four times with ethyl acetate (250 ml) and the extracts were dried over Na_2SO_4. The solvent was evaporated and *(S)-N-*(benzyl-

oxycarbonyl)proline **2** (24.1 g, 96.8%, $[\alpha]_D^{22}-40.4°$ (*c* 1.027, EtOH) was obtained. Under an argon atmosphere (*S*)-*N*-(benzyloxycarbonyl)proline **2** (18.7 g) in 250 ml of ethyl acetate was added *N*-methylmorpholine (7.6 g) in 10 ml of ethyl acetate at −15 °C. And ethyl chloroformate (8.1 g) in 10 ml of ethyl acetate was added slowly to the solution at −15 °C during 5 minutes then aniline (7.0 g) in 20 ml of ethyl acetate was added to the reaction mixture at −15 °C. The mixture was kept at −15 °C for 1 h and at 0 °C for 1 h then gradually up to room temperature and it was stirred overnight. To the mixture was added 150 ml of ethyl acetate, and 100 ml of water. Then organic layer was washed with aqueous 4% sodium hydrogencarbonate solution, saturated sodium chloride solution, 2% hydrochloric acid, and saturated sodium chloride solution (50 ml each) successively. Then organic layer was dried over Na_2SO_4 and concentrated to give crude (*S*)-*N*-(benzyloxycarbonyl)prolinanilide **3a** (22.8 g). Recrystallyzation from acetone afforded 18.7 g (77%, mp 141—141.5 °C, $[\alpha]_D^{23}-63.2°$ (*c* 0.997, EtOH). Found: C, 70.07; H, 6.18; N, 8.65%. Calcd for $C_{19}H_{20}O_3N_2$: C, 70.35; H, 6.22; N, 8.64%. By similar prodecure amides **3b**—**1** were obtained.

(S)-2-(Anilinomethyl)pyrrolidine **5a**. *(S)-N*-(Benzyloxycarbonyl)prolinanilide **3a** (21 g) and 5% Pd—C catalyst (1g) were stirred vigorously in methanol (120 ml) under hydrogen atmosphere for 3 h. Then reaction mixture was filtered through celite and the filtrate was concentrated to give crude (*S*)-prolinanilide **4a**, which was recrystallized from cyclohexane to afford pure **4a** (11.5 g, 94%, mp 76—77 °C, $[\alpha]_D^{27}-71.0°$ (c 1.025, EtOH)). Found: C, 69.53; H, 7.58; N, 14.84%. Calcd for $C_{11}H_{14}ON_2$: C, 69.44; H, 7.42; N, 14.73%. **4a** (10.5 g) in 35 ml of THF was added to the $LiAlH_4$ (4.2 g) in 40 ml of THF at 0 °C under an argon atmosphere. The reaction mixture was stirred overnight at 0 °C and hydrolyzed with saturated sodium sulfate solution. After removal of the inorganic material and concentration of organic layer, fractional distillation under reduced pressure afforded a colorless oil **5a** (7.2 g, 81%, bp 111—112 °C/0.55 mmHg, $[\alpha]_D^{24}+19.7°$ (*c* 1.087, EtOH); IR 3280 cm^{-1} (N-H); NMR ($CDCl_3$) δ=0.93−2.13 (m, 5H), 2.35—3.46 (m, 5H), 4.10 (br, 1H), 6.33—6.86 (m, 3H), 6.86—7.38 (m, 2H). MS (70 eV), *m/e*, 176 (M^+), 107, 77, 70, and 43. By similar procedure diamines **5b**—**1** were also prepared. **5b**; IR 3280 cm^{-1} (N-H); NMR ($CDCl_3$) δ=1.00 (d, 6H), 1.32 (s, 2H), 1.20—2.03 (m, 4H), 2.30—3.34 (m, 6H). Found: C, 67.84; H, 13.00; N, 19.64%. Calcd for $C_8H_{18}N_2$: C, 67.55; H, 12.75; N, 19.64%. **5c**; IR 3280 cm^{-1} (N-H); NMR ($CDCl_3$) δ=0.62—1.95 (m, 15H), 1.21 (s, 2H), 1.91—3.32 (m, 7H); MS (70 eV), *m/e*, 185 (M^++1), 114, 70, 43. Found: C,71.49; H, 13.42; N, 15.48%. Calcd for $C_{11}H_{24}N_2$: C, 71.68; H, 13.12; N, 15.20%. **5d**; IR 3270 cm^{-1} (N-H); NMR ($CDCl_3$) δ=0.59—2.06 (m, 14H), 1.40 (s, 2H), 2.06—3.29 (m, 6H); MS (70 eV), *m/e*, 183 (M^++1), 112, 70, 43. Found: C, 72.50; H, 12.42; N, 15.30%. Calcd for $C_{11}H_{22}N_2$: C, 72.47; H, 12.61; N, 15.37%. **5e**; IR 3280 cm^{-1} (N-H); NMR ($CDCl_3$) δ=0.76—1.91 (m, 4H), 1.27 (d, 3H), 1.64 (s, 2H), 2.20—3.06 (m, 5H), 3.65 (q, 1H), 6.99—7.39 (m, 5H). Found: C, 76.67; H, 10.04; N, 13.77%. Calcd for $C_{13}H_{20}N_2$: C, 76.42; H, 9.87; N, 13.71%. **5f**; IR 3280 cm^{-1} (N-H); NMR ($CDCl_3$) δ=0.69—2.05 (m, 4H), 1.29 (d, 3H), 1.83 (s, 2H), 2.29—3.13 (m, 5H), 3.70 (q, 1H), 6.88—7.43, (m 5H). Found: C, 76.36; H, 9.65; N, 13.79%. Calcd for $C_{13}H_{20}N_2$: C, 76.42, H, 9.87, N, 13.71%. **5g**; IR 3350 cm^{-1} (N-H); NMR ($CDCl_3$) δ=0.90—1.98 (m, 5H), 2.42—3.55 (m, 5H), 4.92 (br, 1H), 6.49 (dd, 1H), 6.99—7.97 (m, 6H); MS (70 eV), *m/e*, 226 (M^+), 157, 70, 43. **5h**; IR 3400 cm^{-1} (N-H); NMR ($CDCl_3$) δ=1.05—2.20 (m, 5H), 2.52—3.63 (m, 6H), 3.79 (s, 3H), 6.25—6.94 (m, 4H); MS (70 eV), *m/e*, 206 (M^+), 137, 70, 43. **5i**; IR 3330 cm^{-1} (N-H); NMR ($CDCl_3$) δ=1.03—2.10 (m, 4H), 2.50—3.50 (m, 7H), 3.63 (s, 3H), 6.20—6.77 (m, 4H); MS (70 eV), *m/e*, 206 (M^+), 137, 70, 43. **5j**; IR 3300 cm^{-1} (N-H); NMR ($CDCl_3$) δ= 1.00—2.50 (m, 5H), 2.55—3.85 (m, 5H), 4.25 (br, 1H), 6.27—6.75 (m, 2H), 7.33 (dt, 1H), 8'08 (d, 1H); MS (70 eV), *m/e*, 178 (M^++1), 108, 70, 43. Found: C, 68.01; H, 8.51; N, 24.01%. Calcd for $C_{10}H_{15}N_3$: C, 67.76; H, 8.53; N, 23.71%. **5k**; IR 3300 cm^{-1} (N-H); NMR ($CDCl_3$) δ= 0.50—2.23 (m, 4H), 2.44 (s, 1H), 2.59—3.78 (m, 5H), 5.04 (br, 1H), 6.41 (d, 2H), 8.14 (d, 2H); MS (70 eV), *m/e*, 178 (M^++1), 108, 70, 43. **5l**; IR 3350 cm^{-1} (N-H); NMR ($CDCl_3$) δ=0.97—2.13 (m, 5H), 2.35—3,50 (m, 5H), 4.41 (br, 1H), 6.29 (dd, 1H), 6.55 (dd, 1H), 7.03 (d, 1H); MS (70 eV), *m/e*, 244 (M^+), 175, 70, 43.

Asymmetric Reduction of Ketone with $LiAlH_4$–Diamine **5a** *Complex in Ether (Representative example).* The diamine **5a** (359.3 mg, 2.04 mmol) in 2 ml of ether was added to a standardized ethereal solution of $LiAlH_4$ (2.86 ml, 1.77 mmol) over ten minutes at room temperature under an argon atmosphere. On addition of **5a**, hydrogen gas evolved and white precipitates appeared. After stirring for 1 h at room temperature, propiophenone (134 mg, 1.00 mmol) in 2 ml of ether was added at −78 °C, and the reaction mixture was stirred for 3 h. The mixture was hydrolyzed with 0.4 ml of water and washed successively with 8 ml of 0.5 N hydrochloric acid and saturated sodium chloride solution. The ethereal layer was dried over Na_2SO_4 and the solvent was removed. The crude product was purified by preparative TLC to give 1-phenyl-1-propanol (120.0 mg, 90%). Further it was purified for the measurement of specific rotation by bulb to bulb distillation [175 °C (bath temperature/21 mmHg], and 104.3 mg of the alcohol was obtained, $[\alpha]_D^{25}$—23.65° (neat). Most of the chiral diamine was recovered from the aqueous layer by usual work up.

Asymmetric Reduction Acetophenone with $LiAlH_4$–Diamine **5a** *Complex in THF (or toluene).* Under an argon atmosphere, $LiAlH_4$ in ether (2.79 ml, 2.66 mmol) was transfered into the flask. The ether was removed under reduced pressure at room temperature for about 1 h, then 5.5 ml of THF was added. The diamine **5a** (540.2 mg, 3.07 mmol) in 4 ml of THF was added to the solution over ten minutes at room temperature. After stirring for 1 h at toom temperature, acetophenone (180.3 mg, 1.5 mmol) was added at —78 °C and the mixture was stirred for 3 h. The reaction mixture was treated similarly as mentioned above and 1-phenylethanol (97.3 mg, 54%) was obtained, which was further purified for the measurement of specific rotation by bulb to bulb distillation [150—160 °C (bath temperature)/21 mmHg], and 86 mg of alcohol was obtained, $[\alpha]_D^{24}+8.25°$ (*c* 4.00, cyclopentane).

Asymmetric Reduction of Acetophenone with $LiAlH_4$–Diamine **5a** *in the Presence of Additives.* The diamine **5a** (539 mg, 3.07 mmol)–$LiAlH_4$ complex (2.66 mmol) in 8 ml of ether was added TMEDA (307 mg, 2.66 mmol) in 2 ml of ether at room temperature. After stirring for 1 h, acetophenone (180.5 mg, 1.5 mmol) was added to the reaction mixture at −78 °C, which was stirred for 3 h. After the reaction mixture was treated similarly, 1-phenylethanol (122.5 mg, 67%) was obtained, which was further purified by bulb to bulb distillation [150—160 °C (bath temperature)/21 mmHg] and 115.9 mg of alcohol was obtained, $[\alpha]_D^{25}-7.6°$ (*c* 6.88, cyclopentane).

The present work was partially supported by a Grant-in-Aid for Scientific Research from the Ministry

of Education (203014).

References

1) J. D. Morrison and H. S. Mosher, "Asymmertric Organic Reactions," Prentice Hall Englewood Cliffs, N. J. (1971), pp. 203—218.

2) O. Cervinka and O. Bebousky, *Collect. Czech. Chem. Commum.*, **32**, 3897 (1967), and references cited therein.

3) a) S. R. Landor and A. R. Tachell, *J. Chem. Soc., C.*, **1966**, 2280; S. R. Landor, B. J. Miller, and A. R. Tachell, *ibid.*, **1967**, 197; b) N. Baggett and P. Stribblehill, *J. Chem. Soc., Perkin Trans. 1*, **1977**, 1123.

4) S. Yamaguchi and H. S. Mosher, *J. Org. Chem.*, **38**, 1970 (1973).

5) I. Jaquet and J. P. Vigneron, *Tetrahedron Lett.*, **1974**, 2065.

6) A. I. Meyers and P. M. Kendall, *Tetrahedron Lett.*, **1974**, 1337.

7) D. Seebach and D. Herman, *Chem. Ber.*, **107**, 1748 (1974).

8) R. Haller and H. J. Schneider, *Chem. Ber.*, **106**, 1312 (1973).

9) S. Yamaguchi, F. Yasuhara, and K. Kabuto, *J. Org, Chem.*, **42**, 1578 (1977).

10) a) T. Mukaiyama and K. Hojo, *Chem. Lett.*, **1976**, 893; b) K. Hojo and T. Mukaiyama, *ibid.*, **1976**, 619. T. Mukaiyama, S. Shoda, and Y. Watanabe, *ibid.*, **1977**, 383; c) K. Hojo, H. Yoshino, and T. Mukaiyama, *ibid.*, **1977**, 133, 437; d) K. Hojo, S. Kobayashi, K. Soai, S. Ikeda, and T. Mukaiyama, *ibid.*, **1977**, 635.

11) T. Mukaiyama, M. Asami, J. Hanna, and S. Kobayashi, *Chem. Lett.*, **1977**, 783.

Formaldehyde Polymers. 22.[1] Reaction Products of 6,8-Dimethyl-4-chromanone with Formaldehyde—On the Dimeric Products—

Akira NINAGAWA and Haruo MATSUDA

Department of Petroleum Chemistry, Faculty of Engineering, Osaka University, Yamadakami, Suita, Osaka 565

(Received December 21, 1977)

The reaction of 6,8-dimethyl-4-chromanone with formaldehyde has been carried out in 96% sulfuric acid. From the mother liquors after obtaining 5-hydroxymethyl-6,8-dimethyl-4-chromanone, the methylene and oxydimethylene dimers of 6,8-dimethyl-4-chromanone, 6,6′,8,8′-tetramethyl-5,7′-methylenedichroman-4,4′-dione and bis(6,8-dimethyl-4-oxochroman-5-ylmethyl) ether, respectively, were isolated by recrystallization. ^{1}H- and ^{13}C-NMR spectra of 5-hydroxymethyl-6,8-dimethyl-4-chromanone in 96% sulfuric acid show the existence of 6,8-dimethyl-4-oxochroman-5-ylmethyl cation. The intermediate ion is stable, not reacting in sulfuric acid.

In a previous paper,[1] a report was given on the reactions of 4-chromanones with formaldehyde carried out in the presence of sulfuric acid or polyphosphoric acid. The reaction products of 4-chromanone, 6- as well as 8-methyl- and 5,7-dimethyl-4-chromanone with formaldehyde were the polymers linked by methylene bridges, while 6,8-dimethyl-4-chromanone gave only 5-hydroxymethyl-6,8-dimethyl-4-chromanone.

In this paper, the isolation of dimeric products from the reaction products of 6,8-dimethyl-4-chromanone with formaldehyde in the presence of sulfuric acid and the spectral characteristic of 5-hydroxymethyl-6,8-dimethyl-4-chromanone in sulfuric acid are reported.

Results and Discussion

Isolation of the Dimeric Compounds. The reaction of 6,8-dimethyl-4-chromanone (**1**) with formaldehyde was carried out in different mol ratios of the reactants in the presence of 96% sulfuric acid. The products are given in Table 1.

Table 1. Reaction of 6,8-dimethyl-4-chromanone with formaldehyde at 60 °C

Exp. No.	Reactant (mol)		CH_2O/**1** (mol ratio)	H_2SO_4 (g)	Time (hr)	Products and Yield (%)		
	1	CH_2O				**2**	**3**	**4**
1	0.10	0.05	0.5	38	4	—	3.1	—
2	0.20	0.10	0.5	80	4	0.5	—	—
3	0.20	0.10	0.5	80	8	0.15	0.9	—
4	0.28	0.28	1.0	230	6	36.	1.2	—
5	0.50	0.60	1.2	1000	4	55.	—	—
6	0.80	1.17	1.5	3000	4	60.	—	0.3

The reaction products of **1** with formaldehyde in a 2: 1 molar ratio in sulfuric acid were 5-hydroxymethyl-6,8-dimethyl-4-chromanone (**2**) and 6,6′,8,8′-tetramethyl-5,7′-methylenedichroman-4,4′-dione (**3**). The low yield of **2** is due to a lower fractionation of **2** from a mixture of unreacted **1** and **2**, and the solubility of **2** in aqueous sulfuric acid solution. With increase of the mol ratio the yield of **2** increased, another dimeric compound, bis(6,8-dimethyl-4-oxochroman-5-ylmethyl) ether (**4**) being obtained with **2** from the reaction product (6, Table 1).

Structures of the Dimeric Compounds. The ^{1}H-NMR spectra of the methylene dimer **3** and the oxydimethylene dimer **4** are given in Table 2.

Table 2. ^{1}H-NMR spectra of methylene dimer **3** and oxydimethylene dimer **4**

	Methylene dimer **3** (CCl_4; 1.0%)	Oxydimethylene dimer **4** (CCl_4; 5.0%)
Aromatic	7.08(1H, s) 6.17(1H, s)	6.98(2H, s)
Methylene between two aromatic rings	4.20(2H, s)	4.85(4H, s)
Pyrone ring	4.45(2H, t[a]) 4.40(2H, t[a]) 2.69(2H, t[a]) 2.65(2H, t[a])	4.41(4H, t[b]) 2.67(4H, t[b])
Methyl	2.65(3H, s) 2.20(3H, s) 2.04(3H, s) 1.96(3H, s)	2.30(6H, s) 2.11(6H, s)

a) J=6.7 Hz. b) J=6.7 Hz.

The ^{1}H-NMR spectrum of **3** shows two sharp singlet of aromatic protons, four sharp singlet of methyl protons and four sets of triplet of pyrone ring protons, while that of **4** shows a sharp singlet of aromatic protons, two sharp singlet of methyl protons and two sets of triplet of pyrone ring protons. The ^{1}H-NMR spectrum of the oxydimethylene dimer **4** is very similar to that of the symmetrical methylene dimers of 6- and 8-methyl-4-chromanone.[2] It is thought that an oxydimethylene bridge of **4** is formed between 5- and 5′-positions of 6,8-dimethyl-4-chromanones and a methylene bridge of **3** between 5- and 7′-positions of 6,8-dimethyl-4-chromanones.

Reactivity of 5-Hydroxymethyl-6,8-dimethyl-4-chromanone. Reactions of **2** with **1** or *p*-cresol which is more active than **1**[3] were carried out in the presence of sulfuric acid.

Table 3. Reaction conditions for the reaction of 5-hydroxymethyl-6,8-dimethyl-4-chromanone with 6,8-dimethyl-4-chromanone or *p*-cresol

Reactant (mmol)			H_2SO_4 (g)	Temp (°C)	Time (h)
2	**1**	*p*-Cresol			
25.0	50.0	—	40.0	60	4
1.0	2.0	—	16.6	80	6
1.0	—	2.0	16.6	80	6

Table 4. ^{1}H-NMR spectra of 5-hydroxymethyl-6,8-dimethyl-4-chromanone in 96% sulfuric acid and carbon tetrachloride

Solvent	Conc. (wt %)	2-H	3-H	5-CH_2	6-CH_3	8-CH_3	7-H	OH
H_2SO_4	2.1	4.39(t)[a]	3.09(t)[a]	5.68(s)	1.86(s)	1.82(s)	7.30(s)	c)
CCl_4	5.7	4.45(t)[b]	2.78(t)[b]	4.46(s)	2.32(s)	2.14(s)	7.05(s)	3.38(s)

a) J=7.4 Hz. b) J=6.6 Hz. c) Not observable in 96% H_2SO_4.

Table 5. ^{13}C-NMR spectra of 6,8-dimethyl-4-chromanone and 5-hydroxymethyl-6,8-dimethyl-4-chromanone in 96% sulfuric acid and deuteriochloroform[a]

Chromanones	Solvent	Conc. (wt %)	C-2	C-3	C-4	C-5	C-6	C-7	C-8	C-9	C-10	6-CH_3	8-CH_3	CH_2OH
1	H_2SO_4	11.9	65.7	31.4	202.7	125.0	133.9	151.9	129.9	168.0	114.6	19.5	14.3	—
	$CDCl_3$	36.5	66.5	37.2	190.8	123.6	129.1	137.0	126.0	157.6	120.2	19.7	14.9	—
	Δ	—	−0.8	−5.8	11.9	1.4	4.8	14.9	3.9	10.4	−5.6	−0.2	−0.6	—
2	H_2SO_4	7.7	68.3	28.1	206.5	144.0	128.6	152.6	127.5	160.6	120.7	16.8	12.9	89.4
	$CDCl_3$	13.5	66.3	39.0	196.0	138.0	129.4	139.4	126.8	160.0	120.2	18.8	15.7	59.5
	Δ	—	2.0	−10.9	10.5	6.0	−0.8	13.2	0.7	0.6	0.5	−2.0	−2.8	29.9

a) Chemical shifts are reported in ppm relative to Me_4Si. Δ=(H_2SO_4−$CDCl_3$) is the chemical shift difference.

The reaction conditions are given in Table 3. **2** was recovered from the reaction mixtures under these reaction conditions.

NMR Spectra of 5-Hydroxymethyl-6,8-dimethyl-4-chromanone in Sulfuric Acid. ^{1}H-NMR spectra of **2** in carbon tetrachloride and 96% sulfuric acid as solvents are given in Table 4. The chemical shift of the methylene protons of 5-hydroxymethyl group in 96% sulfuric acid moves towards lower magnetic fields relative to carbon tetrachloride. The remarkable ^{1}H-NMR down field shift of the absorption of the methylene protons on the 5-position of **2** together with the data in carbon tetrachloride suggest that **5a** is a more suitable representation for the ion **5b**. This chemical shift difference resembles that reported for 2-methyl-1-oxonia-1-cyclopentene hexachloroantimonate[5] and for 5-hexen-2-one in sulfuric acid.[6]

The spectrum of **2** in sulfuric acid remained unchanged even after being heated at 80 °C for 3 h. This indicates that five-menbered oxonium ion **5a** is very stable in sulfuric acid.

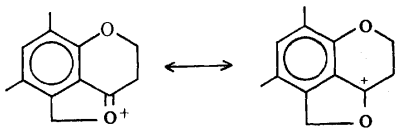

5a **5b**

The ^{13}C-chemical shifts for **1** and **2** obtained in 96% sufuric acid and deuteriochloroform, as well as the chemical shift difference, Δ, between these two solvents are given in Table 5. Chemical shifts were assigned by comparison with the spectra of 4-chromanone,[7] and by consideration of the known substituent effects of methyl,[8] and hydroxymethyl groups.[9] All the assignments are supported by off-resonance decoupling experiments. A positive Δ indicates that the resonance is deshielded in sulfuric acid relative to deuteriochloroform.

Larger deshielding patterns (+Δ) of **2** except the aromatic carbons are observed for C-4 and CH_2OH with the shift of CH_2OH larger than that of C-4. The observed chemical shift trends for **2** are interpreted to result predominantly from 5-methylene cation. Larger contribution from resonance form **5a**, which places positive charge on oxygen of ketone, can be used to rationalize the deshielding noted for this carbon.

The chemical shift change of C-4 for **2** is smaller than that observed for **1** which is protonated in 96% sulfuric acid.[10] Chemical shift changes associated with the aromatic ring seem to result from further inductive and positive charge delocalization effects on these carbons.

Reaction of 1 with Formaldehyde in Sulfuric Acid. The orientation of **1** of the cationic substants appears to be 5- and 7-positions on account of the inductive effects of two methyl groups.[1] In an acid catalyzed reaction of aromatic compounds with formaldehyde, it is probable that the hydroxymethyl cation (CH_2OH^+) is generated at first to react with **1**. Accordingly, 5- and 7-hydroxymethyl derivatives of **1** should be generated. 5-Hydroxymethyl derivative **2** was isolated from the reaction products. 5,7'-Methylene dimer **3** was obtained, but not 7-hydroxymethyl derivative.

The oxonium ion **5a** formed from 5-hydroxymethyl derivative is very stable, not reacting with **1** in 96% sulfuric acid. After being poured into water, **2** was regenerated.

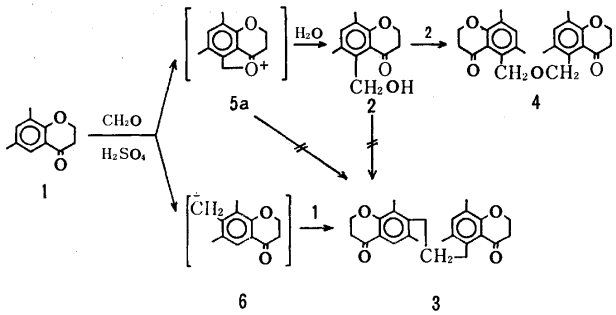

Scheme 1.

It seems that 5,7′-methylene dimer **3** arises from 7-hydroxymethyl derivative by a benzyl cation process. It is proposed that a hydroxide ion is first abstracted yielding the 7-methylene cation **6**, which then attacks on 5-position of **1** to give **3**.

4 might be formed from **2** during post-treatment of the reaction mixture.

A reasonable reaction mechanism might be as shown in Scheme 1.

Experimental

General. Melting points are uncorrected. IR spectra were obtained as KBr pellets on a Hitachi EPI-G2 spectrophotometer. Mass spectra were obtained on a Hitachi RMU-6 mass spcetrometer at 70 eV, and ^{1}H-NMR spectra on a JEOL Model PS-100 spectrometer with tetramethylsilane (Me_4Si) as an internal standard. Chemical shift values are given in terms of δ (ppm). ^{13}C-NMR spectra were obtained on a JNM-FX60 spectrometer. Chemical shifts in deuteriochloroform were measured using Me_4Si as an internal standard. Chemical shifts in 96% sulfuric acid were obtained relative to external deuteriochloroform and converted to the Me_4Si scale by the relationship $\delta Me_4Si = \delta CDCl_3 + 77.1$.

Materials. 6,8-Dimethyl-4-chromanone (**1**) was prepared by the previous method,[2] bp 108—110 °C/2 mmHg [lit,[2] bp 121.5—122 °C/7 mmHg]. Commercial 1,3,5-trioxane and 96% sulfuric acid were used.

*Reactions of **1** with Formaldehyde.* The general procedure is as follows. A mixture of **1** (0.10—0.80 mol) and 1,3,5-trioxane (0.05—1.17 mol) in 96% sulfuric acid (38—3000 g) was stirred at 60 °C.

After completion of the reaction, the reaction mixture was poured into ice water. Crystalline material was obtained by filtration. Benzene solution of the filtrate was washed successively with sodium hydroxide solution and water, dried over anhydrous sodium sulfate, and then condensed to a yellow paste. Both products were dissolved in hot ligroin and allowed to stand at room temperature. The first precipitate was **2**. Concentration and cooling of the mother liquor gave **3** or **4**. These products were purified as follows.

*5-Hydroxymethyl-6,8-dimethyl-4-chromanone (**2**)*: The first product separated from the hot ligroin solution of the reaction products was recrystallized from ligroin. Colorless needle crystals were obtained; mp 95—97 °C (lit,[2] mp 94—95 °C). The structure of this product was confirmed by IR, ^{1}H-NMR and MS spectra.

*6,6′,8,8′-Tetramethyl-5,7′-methylenedichroman-4,4′-dione (**3**)*: The compound soluble in the mother liquor after obtaining **2**, was fractionally recrystallized from hexane to give colorless needle crystals; mp 195—197 °C. IR; 1675 (ν C=O) and 885 (δ CH, aromatic, isolated H) cm^{-1}. MS; *m/e* 364 (M^+, 70.3%), 349 ($M^+ - CH_3$, 55.0%), 346 ($M^+ - H_2O$, 100%), and 189 ($M^+ - C_{11}H_{11}O_2$, 72.0%). Found: C, 75.64; H, 6.48%. Calcd for $C_{23}H_{24}O_4$: C. 75.80, H, 6.64%. ^{1}H-NMR spectrum of **3** is shown in Table 2.

Reduction of **3**; Reduction of **3** was carried out by the Clemmensen method.[11] To a mixture of 5.0 g of amalgamated zinc, 6.0 ml of water, 0.31 ml of concentrated hydrochloric acid and 20 ml of toluene was added 0.5 g of **3**. The mixture was refluxed briskly for 24 h, during which time a 3.0 ml portion of concentrated hydrochloric acid was added every 8 h. The solution was cooled to room temperature and the aqueous layer was separated and extracted with benzene. The combined benzene and toluene solutions were washed with water and dried over calcium chloride. After removal of the solvents, the residue was chromatographed on silica gel (Merk, silica gel 60 pre-paked column for LC size B) with benzene as an eluent to give 0.2 g of 6,6,′8,8′-tetramethyl-5,7′-methylenedichroman. Colorless oil. IR(neat); 1100 (ν C–O–C) and 875 (δ CH, aromatic, isolated H) cm^{-1}, the absorption at 1675 cm^{-1} disappearing. MS; *m/e* 336 (M^+, 19.5%) and 174 ($M^+ - C_{11}H_{13}O$, 100%). Found: C, 81.85; H, 8.08%. Calcd for $C_{23}H_{28}O_2$: C, 82.10; H, 8.39%. ^{1}H-NMR (CCl_4; 6.0%); 6.68 (1H, s, Ph), 5.95 (1H, s, Ph), 3.61 (2H, s, PhC$\underline{H}_2$Ph), 4.03 (4H, t, J=5.8 Hz, 2- and 2′-CH_2), 2.63 (2H, t, J=6.9 Hz, 4- or 4′-CH_2), 1.87 (2H, m, 3- or 3′-CH_2), 2.45 (2H, t, J=6.9 Hz, 4′- or 4-CH_2), 1.79 (2H, m, 3′- or 3-CH_2), 2.14 (3H, s, CH_3), 2.10 (3H, s, CH_3), 2.01 (3H, s, CH_3), and 1.91 (3H, s, CH_3).

*Bis(6,8-dimethyl-4-oxochroman-5-ylmethyl) Ether (**4**)*: The product separated from the ligroin solution (6, Table 1) was recrystallized repeatedly from ligroin to give **4**. mp 177—179 °C. IR; 1680 (ν C=O) and 1075 (ν C–O–C) cm^{-1}. MS; *m/e* 349 (M^+, trace), 205 ($M^+ - C_{12}H_{13}O_2$, 100%), and 190 (54.7%). Found: C, 73.08; H, 6.64%. Calcd for $C_{24}H_{26}O_5$: C, 73.08; H, 6.64%. ^{1}H-NMR spectrum of **4** is shown in Table 2.

*Reactions of **2** with **1** or p-Cresol.* A typical procedure is as follows. A mixture of **2** (0.21 g) and *p*-cresol (0.21 g) in sulfuric acid (16.6 g) was stirred at 80 °C for 6 h. The reaction mixture was then poured into ice water and extracted with chloroform. The chloroform layer was washed with aqueous sodium hydroxide solution and water, successively. After removal of the solvent, the residue was confirmed by IR and ^{1}H-NMR spectra.

References

1) Part 21: A. Ninagawa, Y. Oomi, and H. Matsuda, *Nippon Kagaku Kaishi*, **1976**, 1926.

2) A. Ninagawa, Y. Oomi, H. Matsuda, and S. Matsuda, *Nippon Kagaku Kaishi*, **1973**, 1621.

3) The reactivity of *p*-cresol towards electrophilic reagents appears to be higher than that of **1**. The reaction rate of **1** with formaldehyde in dioxane in the presence of perchloric acid at 60 °C was 1/2 of that of *m*-xylene with formaldehyde[1] and the reaction rate of *m*-xylene with formaldehyde catalyzed by perchloric acid in acetic acid at 60 °C was 1/1650 of that of *p*-cresol with formaldehyde.[4]

4) M. Imoto, C. Huang, S. Yoshioka, and T. Uehara, *Kogyo Kagaku Zasshi*, **65**, 613 (1962).

5) H. R. Ward and P. D. Sherman, Jr., *J. Am. Chem. Soc.*, **90**, 3813 (1968).

6) C. U. Pittman, Jr. and S. P. McManus, *Chem. Commun.*, **1968**, 1479.

7) M. S. Chauhan and I. W. J. Still, *Can. J. Chem.*, **53**, 2880 (1975).

8) G. C. Levy and G. L. Nelson, "Carbon-13 Nuclear Magnetic Resonance for Organic Chemists," Wiley Interscience, New York (1972), p. 81.

9) J. B. Stothers, "Carbon-13 NMR Spectroscopy," Academic Press, New York, N. Y. (1972), p. 197.

10) A. Ninagawa, R. Nomura, and H. Matsuda, The 20th Meeting of the Japan Petroleum Institute, 1977.

11) E. L. Martin, "Organic Reactions," Vol. 1, Chap. 7, p. 155.

Synthetic Bilayer Membranes with Anionic Head Groups*

Toyoki KUNITAKE and Yoshio OKAHATA

Department of Organic Synthesis, Faculty of Engineering, Kyushu University, Fukuoka 812

(Received January 6, 1978)

Anionic amphiphiles which possess two normal alkyl groups as the hydrophobic residue and sulfonate, phosphate or carboxylate groups as the hydrophilic residue were prepared. Most of these compounds aggregate extensively in water to form vesicles and lamellae which are probably formed by the molecular bilayer. These aggregates are quite similar to the lecithin liposome with respect to the restricted molecular motion and cholesterol binding.

The bilayer structure similar to that of biomembranes has been prepared mostly from biolipid molecules and related compounds (lecithins and modified lecithins). Although molecular bilayers can be prepared also from other simpler compounds, they are usually unstable and/or formed under rather exotic conditions.[1-3]

A series of dimethyldialkylammonium salts (C_nC_m-N^+2C_1) aggregate extensively in water to form stable structures similar to that of the biomembrane.[4,5] The aggregate structure (lamella or vesicle) depends on the length of the alkyl group, and no structure was found when one of the alkyl group was octyl or shorter. The results suggest that the formation of the stable molecular bilayer is a general physicochemical phenomenon and that particular molecular structure of biolipids is determined by biological necessity.

In order to establish the generality of bilayer formation, we prepared some amphiphilic compounds which possess anionic hydrophilic groups (phosphate, carboxylate and sulfonate) and two alkyl chains. The aggregation behavior of these compounds would be of interest since biolipid molecules contain phosphate, carboxylate and sulfonate groups in the hydrophilic head group. The chemical structures of the compounds used in this study are shown below.

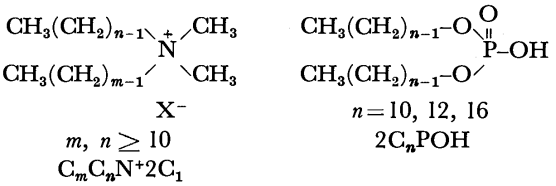

$m, n \geq 10$
$C_mC_nN^+2C_1$

$n = 10, 12, 16$
$2C_nPOH$

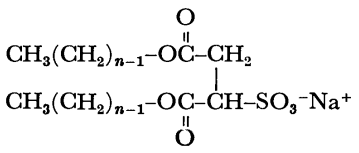

$n = 10, 12, 16$
$2C_nSO_3^-Na^+$

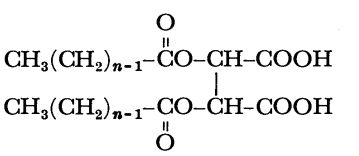

$n = 13$
$2C_n2COOH$

* Contribution No. 477 from this department.

Experimental

Preparation of $2C_nSO_3Na$. This type of compound is known as a lipophilic surfactant such as Aerosol OT. Maleic anhydride and twice molar alkyl bromides were heated in toluene in the presence of a few drops of concentrated sulfuric acid, and azeotropic water was removed for 3 h. The solvent was then removed and the residue was recrystallized twice: didecyl maleate, mp 40—42 °C (colorless flakes from hexane); didodecyl maleate, mp 53—55 °C (colorless flakes from hexane); dihexadecyl maleate, mp 64—65 °C (colorless flakes from toluene). These dialkyl maleates and equimolar amounts of $NaHSO_3$ were dissolved in a small amount of water, and allowed to react with stirring at 100 °C for 2—3 h[6] Water was removed *in vacuo* and the residue was dissolved in a large amount of hot methanol in order to separate inorganic materials. Colorless powder was recovered by removal of methanol and dried. NMR spectra are in line with the expected structures[7] The following characteristic bands were observed in the IR spectrum: 1725 cm^{-1} ($\nu_{c=o}$), 1250 cm^{-1} (ν_{so_3}, ν_{c-o-c}) and 1050 cm^{-1} (ν_{so_3}). The elemental analyses are summarized in Table 1.

Table 1. Elemental analysis

Compound		C	H
$2C_{10}SO_3Na$	Calcd for $C_{24}H_{45}SO_7Na \cdot 6H_2O$	47.35	9.10
	Found	46.68	9.06
$2C_{12}SO_3Na$	Calcd for $C_{28}H_{53}SO_7Na \cdot 4H_2O$	53.48	9.78
	Found	54.83	8.48
$2C_{16}SO_3Na$	Calcd for $C_{36}H_{69}SO_7Na \cdot 4H_2O$	58.35	10.47
	Found	58.48	9.29
$2C_{16}POH$	Calcd for $C_{32}H_{67}PO_4$	70.33	12.27
	Found	70.70	12.81
$2C_{12}POH$	Calcd for $C_{24}H_{51}PO_4$	66.32	11.83
	Found	66.43	12.01
$2C_{10}POH$	Calcd for $C_{20}H_{43}PO_4$	63.46	11.46
	Found	64.39	11.69
$2C_{13}COOH$	Calcd for $C_{32}H_{58}O_8$	73.03	12.19
	Found[a]	67.34	10.24

a) About 4 mol% of myristic acid is contained.

Preparation of $2C_nPOH$.[8] $POCl_3$ and three equivalents of the respective alcohols were refluxed in benzene for 18—20 h. The solvent was removed and the residue recrystallized twice or more: didecyl phosphate, mp 33—34 °C (colorless granules from hexane); didodecyl phosphate, mp 51—52 °C (colorless granules from hexane); dihexadecyl phosphate, mp 66—68 °C (colorless granules from benzene). The elemental analyses are given in Table 1. IR and NMR spectral data are in line with the expected structures: IR, $\nu_{p=o}$ 1230 cm^{-1}, ν_{p-o-c} 1060 cm^{-1}.

Preparation of $2C_{13}2COOH$.[9] Myristoyl chloride (24.7 g,

0.1 mol) in toluene was added to a pyridine solution of 7.5 g (0.05 mol) of *dl*-tartaric acid at 10 °C over a period of 30 min, the mixture being then stirred at room temperature for 1 h. Precipitates formed were separated and the solution was concentrated. The solid product was recrystallized twice from hexane, mp 49—50 °C. IR and NMR spectra are consistent with the expected structure but the elemental analysis shows some deviations from the calculated values. (Table 1, footnote).

Electron Microscopy. Weighed amounts of $2C_nSO_3Na$ were suspended in water (1—40 ml) and sonicated for 5—15 min using a Branson cell disruptor. $2C_nPOH$ and $2C_{13}$-2COOH were dissolved in water of pH 9 and sonicated. The final pH of the solutions was 8—9. All of these stock solutions were 10 mM. The stock solution (1 ml) was mixed with 1 ml of appropriate staining reagents (2% aqueous uranyl acetate, 2% aqueous phosphotungstic acid (pH 7), or 2% aqueous ammonium molybdate), sonicated for 15 s, kept for 30—60 min in an ice-water bath, and applied to carbon grids. A Hitachi electron microscope, model H-500 was used.

Results and Discussion

Electron Micrograph. All the dialkyl compounds were soluble under the conditions employed, giving clear to slightly turbid aqueous solutions. Multi-walled vesicles are observed in the electron micrograph of aqueous $2C_{12}SO_3Na$ (Fig. 1a). In contrast, no structure was detected for a 10 mM solution of Aerosol OT which posesses 2-ethylhexyl groups in place of dodecyl group.

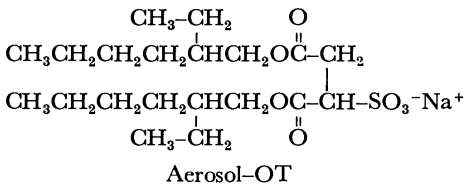

Aerosol-OT

Lamellar structures are observed in the electron micrograph of aqueous $2C_{16}SO_3Na$ (Fig. 1b). However, vesicle structure is observed for $2C_{12}POH$ and $2C_{10}POH$ (Fig. 1c).

The layer width of these aggregates is 3—5 nm. This suggests that the molecular bilayer as in biomembranes is formed as the basic structural unit. The electron microscopic observation is summarized in Table 2. The aggregate weight determined by means of the light scattering method is also given. They are in the range of 2—20 million daltons, and much larger than those observed for the conventional anionic micelles: 10^5 daltons for sodium dodecyl sulfate.[10]

Table 2. Electron microscopy

Compound[a]	Stock solution 10 mM	Electron micrograph	Aggregate weight[b] 10^{-6}·dalton
$2C_{16}SO_3Na$	slightly turbid	lamella	—
$2C_{12}SO_3Na$	clear to slightly turbid	large vesicle	22
$2C_{10}SO_3Na$	clear	large vesicle	1.9
$2C_{16}POH$	slightly turbid	lamella	12
$2C_{12}POH$	slightly turbid	vesicle	20
$2C_{10}POH$	clear	vesicle	4.4
$2C_{13}2COOH$	slightly turbid[c]	vesicle	—

a) All compounds are in anionic form in the stock solution. b) Light scattering instrument: Union Giken Co. (Japan) Model LS-600. Light source. He–Cd laser. c) Prone to precipitate upon cooling.

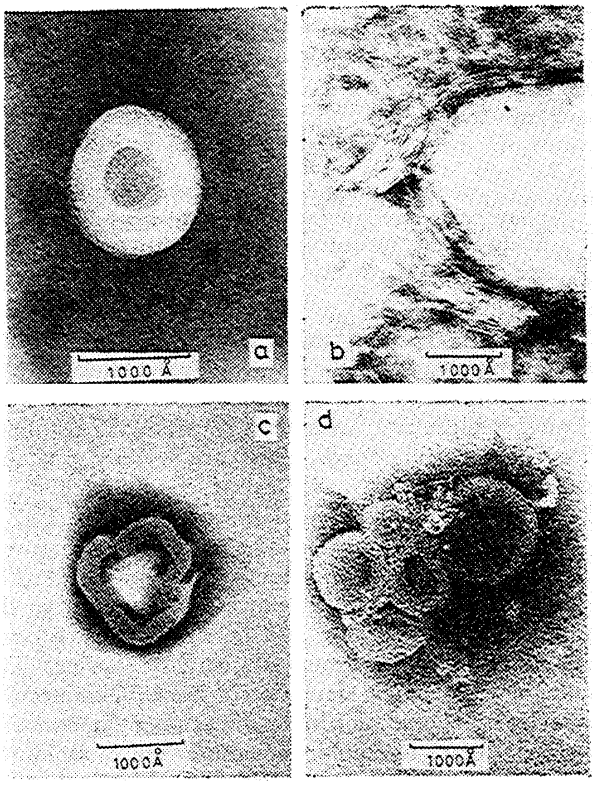

Fig. 1. Electron micrograph. a: $2C_{12}SO_3Na$, stained by phosphotungstic acid, ×300000. b: $2C_{16}SO_3Na$, stained by phosphotungstic acid, ×200000. c: $2C_{10}PONa$, stained by phosphotungstic acid, ×230000. d: $C_{18}C_{12}N^+2C_1$, stained by uranyl acetate, ×186000.

The present results obtained for the anionic dialkyl compound are similar to those obtained for dialkylammonium salts. Figure 1d shows an example of the aggregate structure of the latter salts. Both types of the amphiphile form molecular bilayers when dispersed in water. The aggregate structure (vesicle or lamella) commonly depends on the length of the alkyl chain. In the series of dialkyldimethylammonium bromides,[5] the didodecyl compound tends to form vesicles, whereas lamellar structures are produced readily with higher dialkyl compounds. A similar situation holds in the present study between $2C_{12}SO_3Na$ (Fig. 1a) and $2C_{16}$-SO_3Na (Fig. 1b). The difference in the nature of the hydrophilic head group may not change the aggregate structure drastically.

Cholesterol Binding. Cholesterol can be readily solubilized by these aggregates. Slightly turbid solutions were obtained when $2C_{12}SO_3Na$ or $2C_{12}POH$ and about one third molar cholesterol were suspended in deionized water (pH 8—9) and sonicated. Electron microscopic examination of these solutions indicates no definite structure formation. Bound cholesterol may destroy the regular aggregate structure. Only a turbid dispersion was obtained from $2C_{13}COOH$ and one third molar cholesterol.

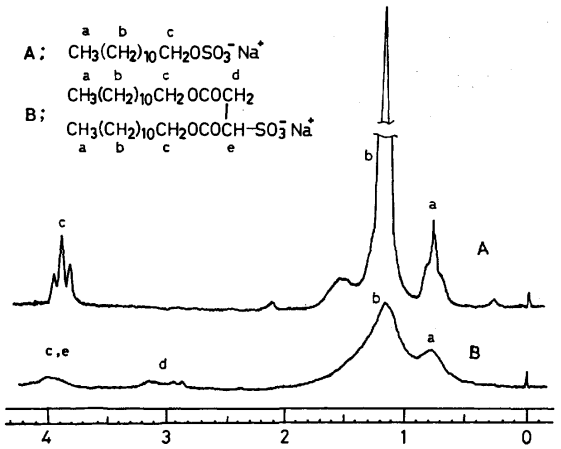

Fig. 2. ^{1}H-NMR spectra. 10 mM in D_2O. Internal reference, DSS.

NMR Spectroscopy. Figure 2 shows an ^{1}H-NMR spectrum of $2C_{12}SO_3Na$ (D_2O solution) obtained at an ambient temperature, in comparison with that of sodium dodecyl sulfate, the assignments being given. The methyl and methylene protons of the alkyl chain of the former compound are much broader than those of the latter. A similar broadening is seen for other protons. The extent of broadening is similar to that of the alkyl proton in the dipalmitoyllecithin vesicle at around the phase transition temperature (≈40 °C).[11] It is suggested that the molecular motion of the aggregated $2C_{12}SO_3Na$ is as restricted as that of the lecithin bilayer.

Comparisons of Lipid and Synthetic Bilayers. The major lipid constituent of biomembranes belongs to phospholipids. The hydrophilic head group of the phospholipid may bear a net negative charge or may be zwitterionic at neutral pH. In a very rare case, the head group is positively charged, since two positive groups (lysyl) and one negative group (phosphate) are present.[12]

The thermodynamic justification for the presence of two alkyl groups in the bilayer formation has been discussed.[13] However, how the head group structure is related to the bilayer formation was not explicitly stated, apart from the importance of its hydrophilic property.

Previous studies[4,5,14] have suggested that simple and modified ammonium groups can be the hydrophilic head group. The present study indicates that simple anionic groups such as phosphate, sulfonate and carboxylate can also be used as the head group. Thus, we conclude that the stable molecular bilayer can be produced from amphiphilic molecules if they contain two normal alkyl groups of appropriate chain length (C_{10}–C_{20}). The hydrophilic head group need not be as complex as those of biolipid molecules.

These synthetic bilayers possess characteristics very similar to that of biomembrane. In the first, they solubilize cholesterol of up to 40 mol% readily. Similar solubilization was observed for the dialkylammonium aggregate.[14] Secondly, considerable broadening of the proton NMR peak of the aggregate is observed, the extent of broadening being similar to that of the lecithin bilayer. This is also the case for the dialkylammonium bilayer.[4] The molecular motion of the synthetic bilayer might thus be as restricted as that of lipid bilayers.

In conclusion, some simple, synthetic amphiphiles, both cationic and anionic, can produce molecular bilayers in aqueous solutions. The structure and some properties of these bilayer aggregates are intrinsically the same as those of the biomembrane.

The authors are grateful to Prof. M. Takayanagi for use of the electron microscope, and to Union Giken Co. for use of the light scattering instrument.

References

1) H. T. Tien, Ed., "Bilayer Lipid Membranes," Marcel Dekker, New York (1974), Chap. 2.
2) J. M. Gebicki and M. Hicks, *Nature*, **243**, 232 (1973); *Chem. Phys. Lipids*, **16**, 142 (1976).
3) M. Okuyama, T. Yoshida, T. Tanii, M. Kunugi, and I. Ishizaki, *Bull. Chem. Soc. Jpn.*, **48**, 191 (1975).
4) T. Kunitale and Y. Okahata, *J. Am. Chem. Soc.*, **99**, 3860 (1977).
5) T. Kunitake, Y. Okahata, K. Tamaki, F. Kumamaru, and M. Takayanagi, *Chem. Lett.*, **1977**, 387.
6) Amercan Cyanamide Co., USP 2628091 (1936).
7) For detailed NMR analysis of Aerosol OT, see M. Ueno, H. Kishimoto, and Y. Kyogoku, *Chem. Lett.*, **1977**, 599.
8) DuPont Co., USP 2005619 (1935).
9) B. R. Harris, USP 2025984 (1935).
10) J. H. Fendler and E. J. Fendler, "Catalysis in Micellar and Macromolecular Systems," Academic Press, New York (1975), Chap 2.
11) M. P. Sheetz and S. I. Chan, *Biochemistry*, **11**, 4573 (1972).
12) C. Tanford, "The Hydrophobic Effect," Wiley-Interscience, New York (1973), Chap. 12.
13) Ref. 12, Chap. 9.
14) T. Kunitake and Y. Okahata, *Chem. Lett.*, **1977**, 1337.

Study on Solubilization by Electrophoresis and Diffusion

Keizo OGINO, MASAHIKO ABE, and Nobuo TAKESHITA

Faculty of Science and Technology, Science University of Tokyo, Yamazaki, Noda, Chiba 278

(Received August 1, 1977)

The difference in solubilization phenomena exhibited when polar and nonpolar oily materials are solubilized by Sodium dodecyl sulfate (SDS) has been investigated by measuring the electrophoresis, the diffusion, and the viscosity. Based on the assumption that the micelle is spherical the effective specific volume, the effective radius, the ζ-potential and the number of effective charges have been calculated. At the limit of solubilization all four quantities were larger for octanoic acid than for octane. The electrophoretic mobility of the micelle, $|U_M|$, increased when octanoic acid was solubilized, in contrast to a decrease observed in the solubilization of octane.

In the literature, we find a number of reports dealing with the electrophoresis, diffusion and light scattering of micelles composed of pure surfactant including SDS,[1] mixed ionic-nonionic surfactants[2] and polyether sulfate.[3] However, only a few are concerned with solubilizate-containing micelles. Among the ways of incorporating the solubilizate into the micelles are (a) adsorption on the surface of the micelles; (b) deep penetration in the palisade layer and (c) dissolution in the hydrocarbon core.

In this study, the mechanism of solubilization has been investigated. SDS micelles containing octanoic acid, a polar oily material, or octane, a nonpolar oily material, have been examined in terms of electrophoretic properties. The results indicate that octanoic acid is solubilized by deep penetration into the palisade layer whereas octane is solubilized by dissolution in the hydrocarbon core.

Experimental

Materials. Sodium dodecyl sulfate (SDS) of reagent grade was extracted with ether and recrystallized from ethanol. The octanoic acid and octane were supplied by Wako Pure Chemical Industries, LTD and were more then 99% pure.

Apparatus and Conditions. 0.3 and 1.5% SDS solutions, of above critical micelle concentration (CMC), were prepared with 0.2 mol dm^{-3} NaCl solutions. The procedure for the determination of the limits of solubilization was as follows. Into several 100-cm^3 glass-stoppered Erlenmeyer flasks, 50-cm^3 portions of 0.3 or 1.5% SDS solutoin were placed; varying amounts of oily materials were added to them, and the mixtures were stirred for 12 h in a thermostat at 25 °C, followed by settling for 36 h until equilibrium was established. After equilibrium had been established, the turbidity of the solution was measured with an Electro photocolorimeter of Hirama 2B type at wave length 655 nm, using a cell of 10.0 mm light path. The limit of solubilization was determined from the break point of the turbidity *vs.* solubilizate concentration curve. An amount of solubilizate, corresponding to 10, 30, 50, 80, 90, or 100% of the above-determined limit of solubilization in 0.3 and 1.5% SDS solutions. Two series of solutions with different degrees (10—100%) of solubilization were prepared by dissolving. The electrophoresis and diffusion measurements were carried out with a Hitachi, model HTB-2A Tiselius apparatus and a Tchukasa, Neurath cell immersed in a thermostat at 25 °C. A pair of 0.3 and 1.5% solutions with the same degree of solubilization were used as upper and lower layers, thus minimizing the boundary disturbance often encountered in electrophoresis and diffusion.

The relative viscosities of the solutions including solubilized oily substances were measured at 25 °C with an Ubbelohde viscometer with appropriate auxiliary equipment. The flow time was measured with a stopwatch of 0.1-s precision; the over-all fluctuations were within $\pm$0.1-s. The specific gravity gravity was determined using a pycnometer of 25-cm^3 capacity.

Results and Discussion

Relative Viscosity and Effective Specific Volume of the Micelle. Figure 1 shows the relative viscosity, η_r, of the solutions which were prepared by solubilizing octanoic acid using given concentrations of SDS.

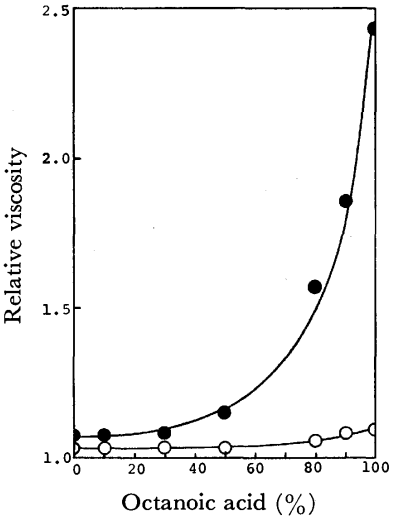

Fig. 1. Relative viscosity, η_r, of the solutions which were prepared by solubilizing octanoic acid using SDS of given concentrations.
○: 0.3% SDS, ●: 1.5% SDS.

From Guth and Simha's equation,[4-7] which is a form of Einstein's equation extended to more concentrated solutions,

$$\eta_r = 1 + 2.5\phi + 14.1\phi^2, \quad (1)$$

the volume fraction occupied by the spherical particles, ϕ, may be calculated from the relative viscosity, η_r. The effective specific volume of 1 g of SDS containing oily materials, V, is given by[5,8]

$$V = \phi/C, \quad (2)$$

where C is the concentration of the solution in g/cm^3.

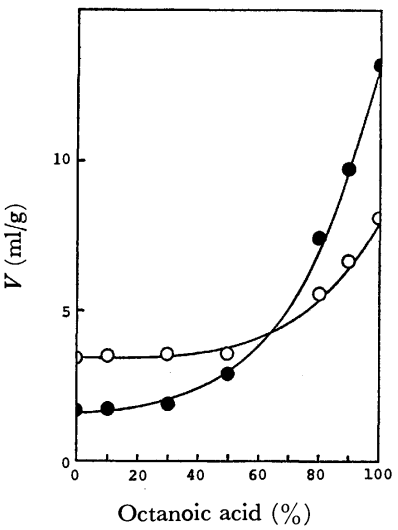

Fig. 2. Effective specific volume, V, plotted against the amount of octanoic acid.
○: 0.3% SDS, ●: 1.5% SDS.

Figure 2 shows the effective specific volume, V, plotted against the amount of octanoic acid. Nakagawa[9] suggested that the effective specific volume in various concentrations of the surfactant (0.3—3.0%) was approximately constant and did not tend to decrease or increase with increasing concentration of surfactant. For a solution of surfactant alone, it can be said that above the CMC the number of micelles increases with an increase in the amount of surfactant whilst the size of the micelle remains almost unchanged (aggregates of 50—100).[10] From Fig. 2, it is evident that the effective specific volume of 0.3 and 1.5% SDS solutions containing octanoic acid increases with an increase in the amount of octanoic acid.

Table 1. Micellar parameters for octanoic acid and octane

Octanoic acid (%)	$D\times10^7$ cm²/s	$a\times10^8$ cm	$-U_M\times10^4$ cm²/V s	$-\zeta$ mV	Q
0	9.33	25.2	2.56	45.3	23
30	8.76	26.9	3.01	52.9	30
50	6.22	37.9	3.06	52.0	54
80	3.88	60.7	3.15	51.0	126
90	2.78	84.7	3.22	50.3	233
100	2.15	109.5	3.26	49.7	376
Octane 100 %	5.59	42.1	1.49	25.1	32

Diffusion Coefficient and Effective Radius of the Solubilizate-containing Micelle. The diffusion coefficient of the SDS micelle containing solubilized octanoic acid was measured in 0.2 mol dm^{-3} NaCl. The diffusion of hydrophilic colloidal electrolyte usually becomes rapid, since the charged colloid is influenced by ionic atmosphere. This effect may be suppressed by keeping the concentration of the salt above 0.2 mol dm^{-3}.[10] Table 1 demonstrates the change in the diffusion coefficient and the effective radius of the micelle with an increase in the amounts of octanoic acid. This indicates that the diffusion coefficient of the micelle decreases with an increase in the amount of solubilized octanoic acid. Consequently, the effective radius of the micelle, a, increases as shown by the Stokes equation[11]

$$a = kT/6\pi\eta D, \tag{3}$$

where k is Boltzmann constant and η is the viscosity of the medium. The increase in the effective radius of the micelle is considered to be due to the deep penetration of octanoic acid into the micelle. This view is concordant with the results obtained for the relative viscosity and the effective specific volume measurements of the micelle. At the limit of solubilization of oily material, the diffusion coefficient of the micelle containing octanoic acid is smaller than that of octane-containing one. The effective radius of the micelle containing octanoic acid is larger than that of the micelle containing octane.

Electrophoresis. In the electrophoresis of the above mentioned surfactant solution, there exist Na^+, Cl^- and micelle, M^-, in both the upper and lower layers. Thus two boundaries appear when the current is applied.[12] (Since the concentrations of surfactant monomer and solubilizate are negligibly small compared with the concentration of the other ions, they may be neglected). One of the boundaries is an unmoving one named ζ and ε peak, which if the concentrations of NaCl and surfactant are correct do not appear.[13] With 0.2 mol dm^{-3} NaCl, the peak of the electrophoretic diagram was only one in both upper and lower sides. From the measurements at 25 °C of the velocities of the upper and lower boundaries, V_a and V_d, the electrophoretic mobility of the micelle, U_M, was calculated by the following equation:[2,12]

$$U_M = V_d\tau^\beta - (V_a\tau^\alpha - V_d\tau^\beta)/(T_M^\beta/T_M^\alpha) - 1, \tag{4}$$

where T_M is the transference number of the micelle, τ is the specific conductance of the solution, and the superscripts α and β refer to the upper and lower layers respectively. T_M^β/T_M^α in Eq. 4 is expressed as

$$T_M^\beta/T_M^\alpha = (C_M^\beta/\tau^\beta)/(C_M^\alpha/\tau^\alpha), \tag{5}$$

where C_M^α and C_M^β, which are the concentrations of M^- ions in α and β phases respectively, are given by

$$\begin{aligned} C_M^\alpha &= (C-\mathrm{CMC})_\alpha, \\ C_M^\beta &= (C-\mathrm{CMC})_\beta, \end{aligned} \tag{6}$$

where C is the concentration of the surfactant. Table 1 gives the data of the electrophoretic mobility of the micelle with corresponding amount of solubilized octanoic acid. The absolute value of the electrophoretic mobility of the micelle containing solubilized octanoic acid, $|U_M|$, increased a little with an increase in the amount of solubilized octanoic acid. The ζ-potential was calculated from U_M by the Henry equation[14]

$$\zeta = [6\pi\eta/\varepsilon f(\kappa a)] \times U_M, \tag{7}$$

where $f(\kappa a)$ is the Henry function; κ, the Debye-Hückel parameter; a, the radius of the micelle, and η and ε, the viscosity and dielectric constant of the medium respectively. Table 1 demonstrates that the ζ-potential of the micelle containing octanoic acid remained constant at about −50 mV, regardless of the amount of octanoic acid added. This may be responsible for the small

changes in U_M. At the limit of solubilization of oily material, the ζ-potential for octanoic acid is larger than that for octane. The value of U_M for octanoic acid, 3.26, is larger than that of the solubilizate-free micelle, 2.56, as compared to octane, 1.49, which is smaller. The effective micelle charge, Q, may be estimated by the following equation:[14]

$$Q = (1/e) \times [(1+\kappa a+\kappa r_i)/(1+\kappa r_i)] \times \varepsilon a\varphi, \quad (8)$$

where e is the elementary charge and r_i is the radius of the counter ion. (In the present study we have assumed 0.22 nm as its radius).[15] At the limit of solubilization of oily material, the effective charge of the octane-containing micelle is somewhat larger, and the octanoic acid-containing micelle much larger than that of the solubilizate-free micelle.

TABLE 2. DEGREE OF SOLUBILIZATION AND RELATIVE VISCOSITY FOR OCTANOIC ACID AND OCTANE

Concentration of SDS	Degree of solubilization (mol/l)		Relative viscosity	
	Octanoic acid	Octane	Octanoic acid	Octane
0.3%	0.53×10^{-2}	0.70×10^{-2}	1.09	1.03
1.5%	2.31×10^{-2}	2.80×10^{-2}	2.42	1.08

Table 2 demonstrates the degree of solubilization and relative viscosity of the solutions, prepared by solubilizing octanoic acid and octane up to the limit of solubilization. As is evident from Table 2, although the degree of solubilization of octanoic acid is smaller than that of octane, the relative viscosity of the solution containing octanoic acid is larger than that of the solution containing octane. This may be explained in terms that the effective specific volume is larger when the micelle is saturated with octanoic acid than when saturated with octane since octanoic acid carries a considerable amount of water of hydration, V (10.4), compared with octane, V (1.01). It is the carboxylic group that undergoes hydration. Since it is difficult energetically for this hydrated carboxylic acid to dissolve into the hydrocarbon core of the micelle, the carboxylic group of octanoic acid remains on the surface of the micelle, allowing the alkyl group of octanoic acid to penetrate into the palisade layer. Since octane does not undergo hydration, the whole molecule can dissolve into the hydrocarbon core of the micelle.

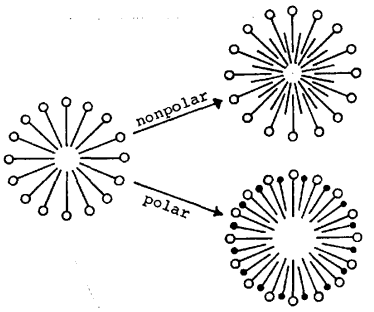

Fig. 3. Solubilization models of polar and nonpolar compounds.
○—— =Surfactant molecule, ●—— =polar molecule, —— =nonpolar molecule.

Thus, the solubilization model[16] shown in Fig. 3, which has been generally accepted, is consistent with the above results.

References

1) J. N. Phillips and K. J. Mysels, *J. Phys. Chem.* **59**, 325 (1955).
2) T. Nakagawa and H. Inoue, *Nippon Kagaku Zasshi*, **78**, 636 (1957).
3) F. Tokiwa and K. Ohiki, *Bull. Chem. Soc. Jpn.*, **42**, 1216 (1969).
4) E. Guth and R. Simha, *Kolloid Z.*, **74**, 147 (1936).
5) D. C. Robins and I. L. Thomas, *J. Colloid. Interface Sci.*, **26**, 415 (1968).
6) T. Ito and H. Mizutani, *Yakugaku*, **17**, 246 (1968).
7) K. Shinoda, T. Nakagawa, B. Tamamushi, and T. Isemura, "Colloidal Surfactants," Academic Press, New York (1963), p. 115.
8) Y. Iwadare and T. Suazwa, *Bull. Chem. Soc. Jpn.*, **43**, 2326 (1970).
9) G. S. Hartley, "Aqueous Solution of Paraffin Chain Salts," Hermann, Paris (1936).
10) H. R. Bruins, *Kolloid-z.*, **57**, 152 (1931).
11) F. Tokiwa and K. Ohki, *J. Phys. Chem.* **71**, 1343 (1967).
12) V. P. Dole, *J. Am. Chem. Soc.*, **67**, 1119 (1945); H. Svensson, *Ark, Kemi. Mineral, Geol.* **22A**, No. 10 (1945).
13) L. G. Longsworth, *J. Phys. Colloid Chem.*, **51**, 171 (1970).
14) D. C. Henry, *Proc. R. Soc., London, Ser. A*, **133**, 106 (1931).
15) C. B. Monk, "Electrolytic Dissociation," Academic Press, New York (1961), p. 271.
16) S. Riegelman, N. A. Allawala, M. K. Hrenoff, and L. A. Strait, *J. Colloid. Sci.*, **13**, 208 (1958).

NOTES

BULLETIN OF THE CHEMICAL SOCIETY OF JAPAN, VOL. 51 (6), 1883—1884 (1978)

Calorimetric Phenomena of Methanol Adsorption on Active Carbon

Ryoichi TSUNODA and Yoshiyuki FUKAZAWA

Industrial Research Institute of Kanagawa Prefecture, Showa-machi, Kanazawa-ku, Yokohama 236

(Received October 5, 1977)

Synopsis. The heats of immersion in methanol of active carbon which preadsorbed methanol from the vapor phase at a given equilibrium pressure were measured. The calorimetric phenomena of methanol adsorption on active carbon were interpreted by comparing them with the distribution of the adsorption potential of methanol on active carbon.

The adsorption of gas on active carbon is accompanied by exothermic and/or endothermic phenomena. However, the direct measurement of the calorimetric phenomena on the gas adsorption is difficult without employing a specific calorimeter for solid-gas measurements. In this study, the calorimetric phenomena of methanol adsorption on active carbon have been measured by means of a conventional calorimeter (for solid-liquid) and the observed heats of immersion have been interpreted by comparing them with the distribution of the adsorption potential of methanol on active carbon.

In a spherical Pyrex glass tube, about 12 mm in diameter, *ca.* 200 mg of commercially available Pittsburgh SGL-type active carbon, dried overnight at 110 °C, was outgassed at a pressure of 10^{-6} Torr at 30 °C for 14 h by means of a conventional adsorption apparatus, while the adsorption of methanol at a given pressure was carried out at 30 °C. After 45 min of methanol adsorption, the Pyrex glass tube was sealed. The sample was then subjected to the measurement of the heat of immersion in methanol at 30 °C by means of a twin-type calorimeter manufactured by Oyo Denki.

The adsorption isotherm,[1] the characteristic and distribution curves of the adsorption potential,[1] and the heats of immersion in methanol of active carbon which preadsorbed methanol from the vapor phase are shown in Figs. 1—3 respectively.

The net-heat of adsorption corresponding to the coverage of the monolayer was calculated from the adsorption isotherm using the BET equation:[2]

$$\frac{P/P_0}{V(1-P/P_0)} = \frac{1}{V_mC} + \frac{(C-1)P/P_0}{V_mC}, \quad (1)$$

where $C=\exp[(E_1-E_L)/RT]$ is the BET constant; E_1, the mean heat of adsorption in the first adsorption layer; E_L, the heat of condensation; E_1-E_L, the so-called net heat of adsorption corresponding to the coverage of the monolayer; V, the amount adsorbed at the relative pressure of P/P_0, and V_m, the monolayer capacity. The calculated parameters in the BET equation are shown

TABLE 1. PARAMETERS IN THE BET EQUATION

Active carbon	C[a]	E_1-E_L[b] (cal/mol)	V_m[c] (cm^3/g)
SGL	12.6	1527	0.320

a) The BET constant. b) The net-heat of adsorption corresponding to the coverage of the monolayer. c) The monolayer capacity.

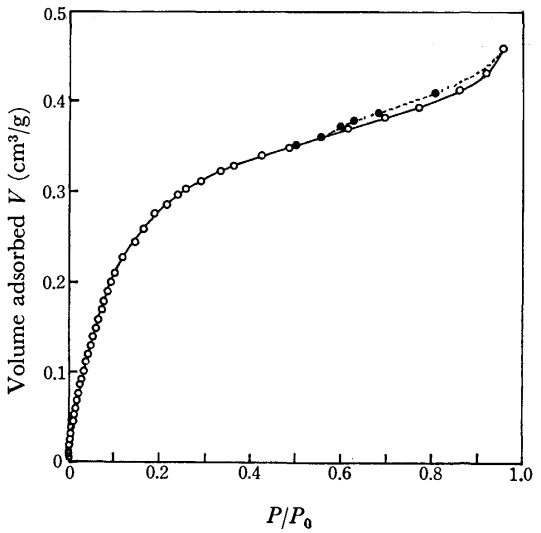

Fig. 1. Adsorption isotherm of methanol on SGL-type active carbon at 30 °C.[a]
Filled symbols indicate desorption. a) Ref. 1.

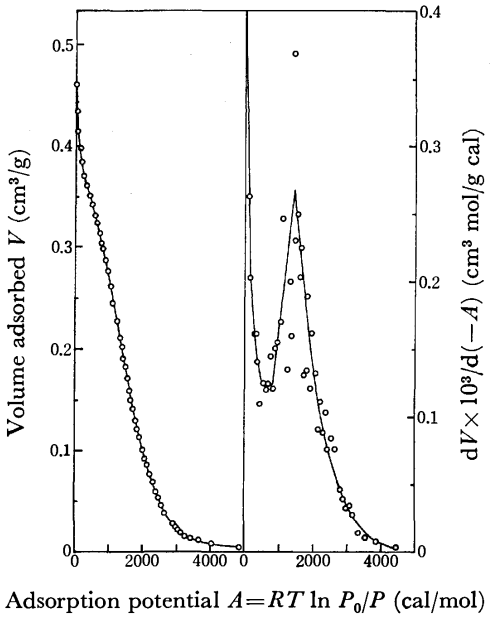

Fig. 2. Characteristic and distribution curves of adsorption potential of methanol on SGL-type active carbon at 30 °C.[a] a) Ref. 1.

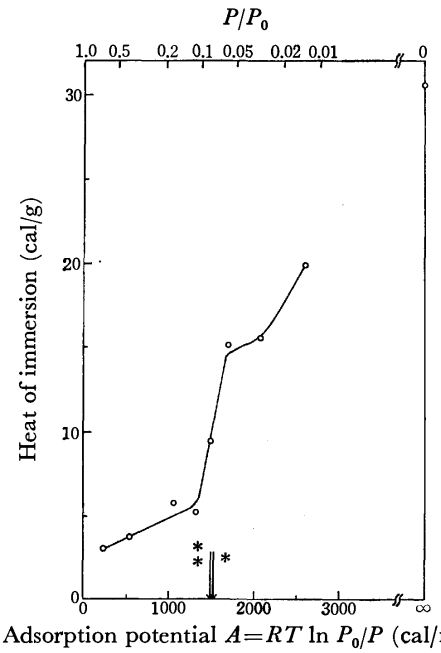

Fig. 3. Heat of immersion in methanol of SGL-type active carbon which preadsorbed methanol from the vapor phase at 30 °C.
The adsorption potential ($A=RT \ln P_0/P$) corresponds to the equilibrium partial pressure (P/P_0) at which the adsorption of methanol on active carbon was carried out at 30 °C. The heat of immersion in methanol of active carbon which preadsorbed methanol from the vapor phase was measured at 30 °C.
*: The adsorption potential corresponding to the net-heat of adsorption for the monolayer coverage.
‡: The adsorption potential corresponding to that at $dV/d(-A)$=maximum.

in Table 1.

The observed heats of immersion showed a drastic decrease at the adsorption potential ($A=RT \ln P_0/P$) corresponding to the net-heat of adsorption (1527 cal/mol) for the monolayer coverage (see Fig. 3). However, the BET constant, C, obtained form a simple fitting of the BET equation to the adsorption isotherm reflects only the average energy parameter of adsorption sites being filled in the region of the fitting, *i.e.*, usually in $0.05<P/P_0<0.3$.[3] Therefore, the so-called net-heat of adsorption, E_1-E_L, 1527 cal/mol, calculated from the value of C may also reflect the average energy of the net-heat of adsorption.

Meanwhile, the adsorption potential at the point of the drastic decrease in the heats of immersion corresponds also to the adsorption potential (*ca.* 1470 cal/mol) at $dV/d(-A)$=maximum on the distribution curve of the adsorption potential, as is shown in Fig. 2. The adsorption potential at 1470 cal/mol is equivalent to $P/P_0=0.0872$, indicating the adsorption volume of 0.195 cm^3/g, on the adsorption isotherm in Fig. 1. The adsorption volumes corresponding to the adsorption potentials at the * and ‡ marks in Fig. 3 are 0.181 and 0.195 cm^3/g respectively; therefore, the volume of methanol preadsorbed on active carbon, the drastic decrease of which in the heats of immersion is shown in Fig. 3, corresponds to a little more than half of the monolayer capacity of active carbon.

The observed heat of immersion in Fig. 3 corresponds to the heat of immersion of the uncovered part of the surface of the active carbon with methanol, although, strictly speaking, the observed calorimetric phenomena are accompanied by the heat of condensation of methanol adsorbed on the surface of carbon, and the decrease in the heat of immersion is proportional to the surface free-energy lowering. Moreover, taking into consideration the fact that the adsorption mechanism expressed in the relationship between $dV/d(-A)$ and A is changed at about 61% of the monolayer capacity of methanol adsorption, the observed lowering of the surface free energy seems to be due to the change in the adsorption state, *e.g.*, the change in the geometrical structure of the adsorbed methanol molecules.

References

1) R. Tsunoda, *Bull. Chem. Soc. Jpn.*, **50**, 2058 (1977).
2) S. Brunauer, P. H. Emmett, and E. Teller, *J. Am. Chem. Soc.*, **60**, 309 (1938).
3) L. M. Dormant and A. W. Adamson, *J. Colloid Interface Sci.*, **38**, 285 (1972).

BULLETIN OF THE CHEMICAL SOCIETY OF JAPAN, VOL. 51 (6), 1885—1886 (1978)

Location of the ν_1, ν_2, ν_3, and ν_5 Fundamental Vibrations of Ethylene-d_4

Nobukimi OHASHI, Tetsuo KYOGOKU, and Shin-ichi MATSUOKA

Institute for Spectroscopic Study of Matter, Faculty of Science, Kanazawa University, Maruno-uchi, Kanazawa 920

(Received November 15, 1977)

Synopsis. The ^{Q}Q branch peaks of the ν_1, ν_2, and ν_3 Raman active bands of ethylene-d_4 were located at ν_1= 2260.8±0.1 cm^{-1}, ν_2=1518.3±0.1 cm^{-1}, and ν_3=984.4±0.1 cm^{-1}, respectively. The band center of the ν_5 band which does not have a ^{Q}Q branch was determined to be ν_5=2315.6 ±0.3 cm^{-1} from the analysis in the symmetric top approximation.

While many Raman data have been presented for ethylene-d_0,[1-6] few Raman data have been published for ethylene-d_4. Though its pure rotational Raman spectrum was studied by Dowling *et al.*,[2] its vib-rotational Raman spectra have not been studied. Only the liquid state vibrational frequencies of the Raman active bands have been measured, by Hemptinne *et al.*[7] As a preliminary to the vib-rotational Raman study of ethylene-d_4, we report the ν_1, ν_2, ν_3, and ν_5 fundamental frequencies, since these data are considered to be important in the force constant calculation of this molecule.

Experimental

The experimental setup consisted of a He-Cd laser operated at 441.570 nm, a gas cell, and an Echelle grating monochromator. The scattered Raman radiation from a multi-reflection cell[8] placed inside the laser cavity was analyzed by the Echelle grating monochromator and detected by a cooled photomultiplier operated in conjunction with photon counting equipment. Ethylene-d_4 gas obtained from Merck, Sharp, and Dohme was used at a pressure of about 400 Torr. Wavelength calibration was made by using as standards the lines from an iron-neon hollow cathode lamp. A slit width of 0.4 cm^{-1} was used in the measurements of the ν_1 ^{Q}Q and the ν_2 ^{Q}Q branch peaks, and a slit width of 0.8 cm^{-1} was used in the measurements of the ν_3 ^{Q}Q branch peak and the ν_5 band.

Results

The ^{Q}Q branch peaks of the totally symmetric bands of ethylene-d_4 gas were determined to be ν_1=2260.8±0.1 cm^{-1}, ν_2=1518.3±0.1 cm^{-1}, and ν_3=984.4±0.1 cm^{-1}. The ν_1 value is larger than that in liquid state by 10 cm^{-1}, but the ν_2 and ν_3 fundamental frequencies are nearly equal to those in liquid state, as obtained by Hemptinne *et al.*[7] These circumstances are similar to those in ethylene-d_0.[9]

As the rotational structure of the ν_5 band was observed under low resolution (about 1.0 cm^{-1}), as shown in Fig. 1, this band was analyzed in the symmetric top approximation. In order to enable the K-assignment to be done exactly we made use of the simulated spectrum which was caculated using the calculation program for the asymmetric rotor. As the rotational constants in the v_5=1 state can not be obtained at the present stage, we calculated the spectrum with A_0=A_5=2.425 cm^{-1}, B_0=B_5=0.73630 cm^{-1}, and C_0=C_5=0.56355 cm^{-1}, where the ground state constants for ethylene-d_4 were taken from the paper of Duncan *et al.*[10] In the symmetric top approximation the $^{P,R}Q_k$ branches form a series of lines at the origins of subbands, if $\bar{B}_0$—$\bar{B}_5$ is negligibly small. From the least squares fit of the observed data we obtained the following quadratic equation for the subband origins:

$$\nu^{sub} = 2317.4 + 3.601K - 0.006K^2.$$

This equation gives ν_5=2315.6±0.3 cm^{-1} for the band

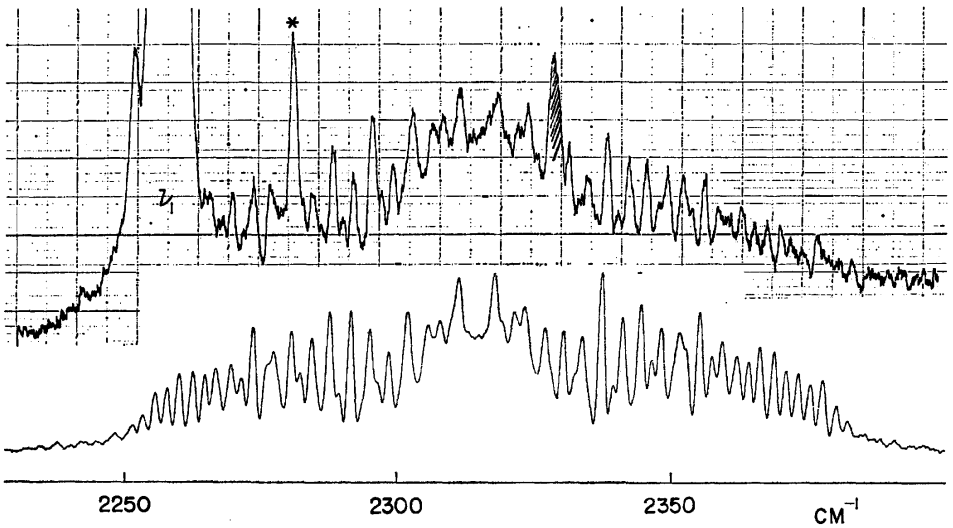

Fig. 1. Observed (top) and calculated (bottom) spectra of the ν_5 band of ethylene-d_4. The peak marked by * was attributed to ν_1 (C_2HD_3) and the peak with shadow was overlapped by N_2 line.

center, which is also about 11 cm^{-1} larger than that in liquid state. The negative value of the coefficient in K^2 is contradictory to $A_5-\bar{B}_5=1.801>A_0-\bar{B}_0=1.775$. It was perhaps caused by the circumstance that the correction for the term $(\bar{B}_5-\bar{B}_0)J(J+1)$ was not applied to the observed data and that the symmetric top approximation was used for an asymmetric top molecule.

References

1) J. Romanko, T. Feldman, E. J. Stransbury, and A. McKellar, *Can. J. Phys.*, **32**, 735 (1954).
2) J. M. Dowling and B. P. Stoicheff, *Can. J. Phys.*, **37**, 703 (1959).
3) T. Feldman, J. Romanko, and H. L. Welsh, *Can. J. Phys.*, **34**, 737 (1956).
4) L. Nemes and S. Suzuki, *J. Raman Spectrosc.*, **2**, 193 (1974).
5) G. W. Hills and W. J. Jones, *J. Chem. Soc., Faraday Trans. 2*, **71**, 812 (1975).
6) R. B. Foster, G. W. Hills, and W. J. Jones, *Mol. Phys.*, **33**, 1589 (1977).
7) M. de Hemptinne, J. Jungers, and J. M. Delfosse, *J. Chem. Phys.*, **6**, 319 (1938).
8) N. Ohashi, H. Watanabe, and S. Matsuoka, *Jpn. Appl. Phys.*, **12**, 1103 (1973).
9) G. Glocker and M. M. Renfrew, *J. Chem. Phys.*, **6**, 170 (1938); **6**, 409 (1938).
10) J. L. Duncan, I. J. Wright, and D. Van Lerberghe, *J. Mol. Spectrosc.*, **42**, 463 (1972).

BULLETIN OF THE CHEMICAL SOCIETY OF JAPAN, VOL. 51 (6), 1887—1888 (1978)

Carbon Deposition on Nickel from a Mixture of Ethylene and Hydrogen

Shozo KISHIMOTO, Noriyuki SOTANI,* Kazuyo NIIMI, and Toshiko URATA

Department of Chemistry, Faculty of Science, Kobe University, Nada, Kobe 657

**College of Liberal Arts, Kobe University, Nada, Kobe 657*

(Received December 20, 1977)

Synopsis. Two periods (acceleration and steady state period) were defined in the process of carbon deposition on cold-worked nickel from ethylene. From the dependence of the former period on annealing temperature, it was found that lattice defects in the crystal play a role in the creation of carbon nuclei and the separation of nickel atoms from the surface.

Carbon deposition on catalysts has been an important topic in connection with catalytic processes involving hydrocarbons. Recently Lobo *et al.*,[1,2] studying the kinetics of these reactions on nickel foils, have reported that, in general, there are three periods in the course of the reaction: an induction period, an acceleration period, and a steady state period. Furthermore, they suggested that the length of the induction period is strongly dependent on both the mode of pretreatment of the catalyst and the reaction temperature, but the rate of reaction in the steady state is independent of the catalyst history. Many studies[3] have shown that the catalytic activities of metals for various reactions are greatly influenced by pretreatments, such as cold-working, irradiation, and annealing, and that these changes in the activity are mainly ascribed to the generation or the annihilation of active sites during the treatments. It seems probable that a similar situation exists in the case of the reaction of carbon deposition on metals. Shirasaki *et al.*[4] observed the deposit of carbon from C_2H_4 on Ni crystals by an electron microscope and claimed that the boundaries of crystallites were much more active than their plane surfaces. Walker and Thomas[5] have suggested that the deposition of carbon from CO is favored at dislocations in metal catalysts, in agreement with the hypothesis previously presented by Gwathmey *et al.*[6] Emphasis in the present work is placed on the effect of the pretreatments of Ni catalysts on the initial stages of the carbon deposition by the decomposition of C_2H_4.

The reactions were carried out in a static system and a Cahn electrobalance (Venton Instr. Corp.) was used to record the weight change due to the carbon deposition. Well annealed Ni wire (Japan Lamp Industrial Co., Ltd.) with a diameter of 0.5 mm was rolled to a thickness of 0.1 mm at room temperature. Specimens used for the experiment were in the form of ribbons (surface area approximately 10 cm^2). After being carefully washed with solvents, they were suspended from the balance arm and then were annealed at different temperatures between 350 and 800 °C in H_2 for 1 h. After this, the H_2 was pumped out.

C_2H_4 obtained from Takachiho Co., Ltd. was purified by repeated freezing and vacuum distillation. H_2 made by electrolysis was used after passage through hot Cu powder and a molecular sieve column cooled by liquid N_2. A mixture of C_2H_4 and H_2, 1 : 1 molar ratio, was used for all experiments at a total pressure of 13.3 kPa. Under these experimental conditions the reaction occurred at conveniently measureable rates in the temperature range of 360—600 °C. Carbon deposited surfaces were examined by a scanning electron microscope (Japan Electronics LAB-JSM U3 Type).

Figure 1 shows the typical time course of the reaction at 400 °C for the specimens annealed at four different temperatures. The rates increase gradually with the progress of the reaction and attain a steady limiting value (about 4.5 $\mu g/cm^2$ min). Thus, two periods are evident: (a) acceleration and (b) steady state period. It is seen that the former is very dependent on the annealing temperature but the latter is not much effected by the treatment. Figure 2(A) shows the effect of the annealing temperature on the catalytic activities in the range of the acceleration period at a reaction temperature of 400 °C. (The activities are expressed as the time to effect equal increment in the amounts of deposition). Although the experimental values are very scattered, the decrease in the activity is apparent in a range of 400—550 °C. It is also shown in Fig. 2(B) that the change in hardness of cold-worked Ni was paralleled

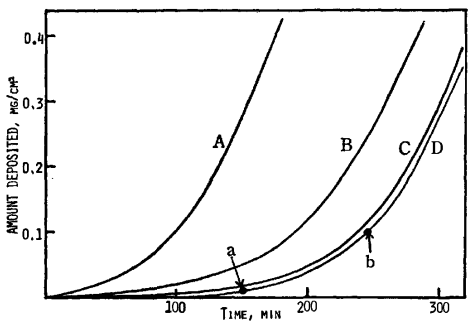

Fig. 1. Carbon deposition on Ni annealed at 400 (A), 450 (B), 550 (C), and 800 °C(D).

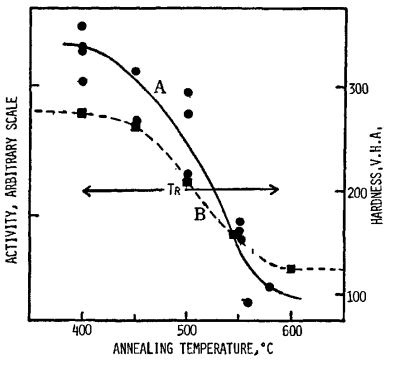

Fig. 2. Dependence of the catalytic activity in the acceleration period (A) and of hardness (B) on the annealing temperature.

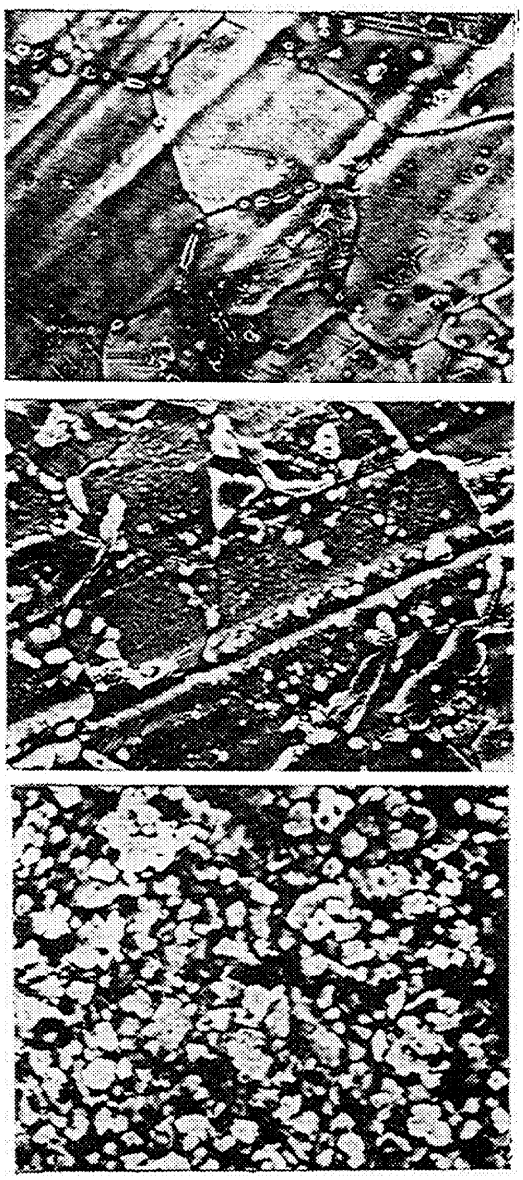

Fig. 3. Scanning electron micrographs (× 1000) of deposited carbon on Ni surfaces annealed at 800 °C.
(A) and (B) showing patterns at point a (10 μg/cm²) and b (100 μg/cm²) in Figure 1(D); (C), at a point in the steady state period.

by the change in the activity by annealing. According to our previous results,[7] this temperature range approximately corresponds to the recovery range (T_R) involving the migration and the annihilation of lattice defects (mainly dislocations) produced by cold-working. It has been already established that the acceleration period involves the creation of carbon nuclei and a subsequent growth process on the surface, and that the latter process is accompanied by the separation of Ni atoms from the surface.[1,8] From the facts presented above, it seems to be right to consider that the defects produced by cold-working in the crystals play a role in these processes in the acceleration period.

On the other hand, as the reaction temperature was raised, the reactions were always accompanied by the reduction in the acceleration period and the rates increased rapidly. At the temperatures above 450 °C, the acceleration periods were hardly discernible and the influence of the pretreatments on the catalytic activity was no longer detectable. These facts indicate that the contributions of normal surfaces to the catalytic activity overwhelm the effects which result from the special active sites responsible for the reactions at low temperatures.

In the case of the catalysts annealed at higher temperatures above 600 °C, the initial processes of deposit were examined with a scanning electron microscope. Figure 3 shows some typical examples observed at a reaction temperature of 400 °C. It is clear that the deposit occurs preferentially at special sites in a crystal face and at grain boundaries. These patterns are approximately similar to those of Shirasaki *et al.*[4] In conclusion, the present results suggest that on cold-worked catalysts the reaction is initiated at a large number of evenly distributed active sites formed by the pretreatment, while on the catalysts annealed at higher temperatures it proceeds on a localized region (*e.g.* grain boundaries) and on a small number of special sites which remain after annealing.

References

1) L. S. Lobo and D. L. Trimm, *J. Catal.*, **29**, 15 (1973).
2) C. A. Bernardo and L. S. Lobo, *J. Catal.*, **37**, 267 (1975).
3) J. M. Thomas and W. J. Thomas, "Introduction to the Principles of Heterogeneous Catalysis," Academic Press, New York (1967), Chap. 5.
4) T. Shirasaki, A. Kitahara, S. Sakamoto, T. Sukeno, and K. Morikawa, *Kogyo Kagaku Zasshi*, **68**, 596, 2297, 2300 (1965).
5) J. M. Thomas, *Adv. Catal.*, **19**, 293 (1969).
6) A. T. Gwathmey and R. E. Cunningham, *Adv. Catal.*, **10**, 57 (1958).
7) I. Uhara, S. Kishimoto, T. Hikino, Y. Kageyama, H. Hamada, and Y. Numata, *J. Phys. Chem.*, **67**, 996 (1963).
8) Y. Nishiyama and Y. Tamai, *J. Catal.*, **33**, 98 (1974).

BULLETIN OF THE CHEMICAL SOCIETY OF JAPAN, VOL. 51 (6), 1889—1890 (1978)

Gas-chromatographic Studies of the Thermal Decompositions of Carbonato-pentaammine-, Carbonatotetraammine-, and Dicarbonato-diamminecobalt(III) Complexes in the Solid State

Sukeo ONODERA*

Department of Chemistry, Faculty of Science, Science University of Tokyo, Kagurasaka, Shinjuku-ku, Tokyo 162

(Received November 8, 1977)

Synopsis. This paper will describe gas-chromatographic studies of the thermal decompositions of $[CoOCO_2(NH_3)_5]X\cdot H_2O$ (I), $(CoCO_3(NH_3)_4]X\cdot nH_2O$ (II), and $K[Co(CO_3)_2(NH_3)_2(NH_3)_2]\cdot H_2O$ (III) (where, X=Cl, NO_3, SO_4, and n=0, 0.5, 3). The GEA curves for these compounds show that the complexes lose water between 80 and 160 °C, and that the decomposition of the anhydrous compounds begins with an evolution of ammonia at about 140 °C (for I) and 180 °C (for II and III).

The thermal decompositions of the cobalt(III) carbonatoammine complexes are usually studied by means of thermogravimetric analysis (TG)[1-3] and differential thermal analysis (DTA).[4,5] These techniques give information concerning the weight-loss and thermal changes in the compounds during the thermal reactions, but they do not give information on the species and the composition of the gases produced. Thus, gas-evolution analysis (GEA) is required for the above reactions in order to obtain more exact information on the decomposition processes of the compounds.

Although gas-chromatographic (GC) analysis may be expected to be useful to ascertain the composition of the gaseous decomposition products of the metal ammine complexes, few papers have been published on GC studies of thermal dissociation, even in simple metal complexes.[6-8] The present work illustrates the applicability of pyrolysis-gas chromatography in elucidating the mechanism of the decomposition of the cobalt(III) carbonatoammine complexes.

Experimental

The complexes, $[CoOCO_2(NH_3)_5]X\cdot H_2O$, $[CoCO_3(NH_3)_4]X\cdot nH_2O$, and $K[Co(CO_3)_2(NH_3)_2]\cdot H_2O$ (where, X=Cl, NO_3, SO_4, and n=0, 0.5, 3), were prepared according to the methods given in the Literature.[1,9] They were identified by measurements of the infrared absorption spectra. Samples ranging in particle size between 100 and 200 mesh was used in the present work.

The GEA apparatus employed has been described previously.[8] The procedure used for the pyrolysis of the sample and the analysis of the gaseous products are essentially the same as those reported in our previous paper.[8] The GC patterns for various pure substances are shown in Fig. 1.

Results and Discussion

In a preliminary examination of the thermal decompositions of the cobalt(III) carbonatoammine complexes, the differential scanning calorimetric (DSC) curves for these complexes were measured using a Rigaku Thermoflex 8001 with a standard differential scanning calorimeter in a dynamic nitrogen atmosphere at a heating rate of 5 °C/min. The ΔT_{max} values observed

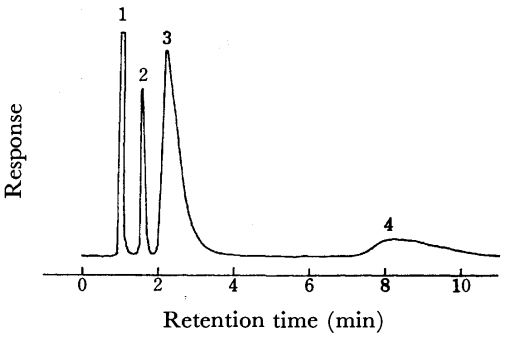

Fig. 1. Gas chromatogram of nitrogen (1), carbon dioxide (2), ammonia (3), and water (4) using 20% Silicon SF-96 on Fluoro Pack-80.

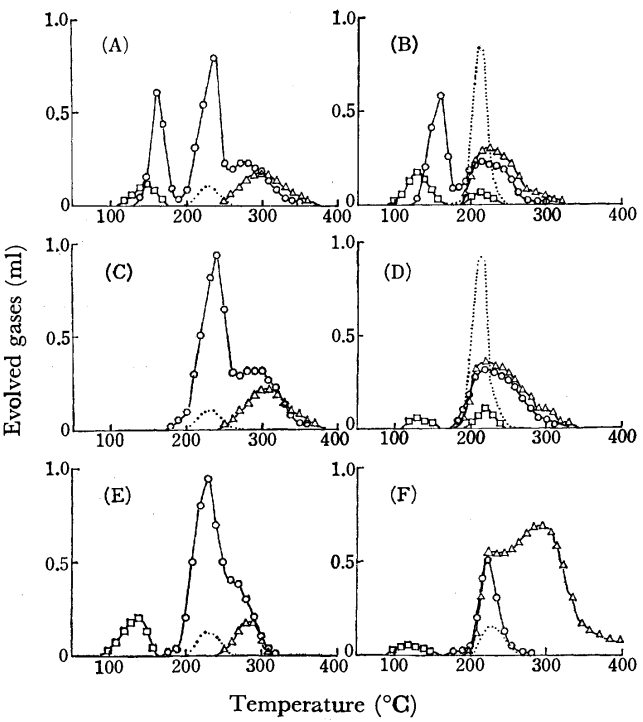

Fig. 2. GEA curves for $[CoOCO_2(NH_3)_5]Cl\cdot H_2O$ (A), $[CoOCO_2(NH_3)_5]NO_3\cdot H_2O$ (B), $[CoCO_3(NH_3)_4]Cl$ (C), $[CoCO_3(NH_3)_4]NO_3\cdot 0.5H_2O$ (D), $[CoCO_3(NH_3)_4]_2SO_4\cdot 3H_2O$ (E), and $K[Co(CO_3)_2(NH_3)_2]\cdot H_2O$ (F) in a helium atmosphere.
H_2O; -□-, NH_3; -○-, CO_2; -△-, N_2; ·····.

* Present address: Faculty of Pharmaceutical Science, Science University of Tokyo, Ichigaya-funagawara, Shinjuku-ku, Tokyo 162.

on the DSC curves for these compounds were (endo= endothermic peak, exo=exothermic peak): $[CoOCO_2(NH_3)_5]NO_3 \cdot H_2O$, endo 160, 210, exo 220 °C; $[CoOCO_2(NH_3)_5]Cl \cdot H_2O$, endo 165, 230, 280, and 350 °C; $[CoCO_3(NH_3)_4]NO_3 \cdot 0.5H_2O$, endo 140, 210, exo 220 °C; $[CoCO_3(NH_3)_4]Cl$, endo 230, 280, and 350 °C; $[CoCO_3(NH_3)_4]_2SO_4 \cdot 3H_2O$, endo 140 and 250 °C. The numbers of these endo- and exothermic peaks observed on the DSC curves are in agreement with those appearing on the DTA curves reported by earlier workers,[4,5] but the dissociation temperatures are somewhat different from those appearing on the DTA curves.

The GEA curves for the cobalt(III) carbonatoammine complexes in the 25—400 °C temperature range in a helium atmosphere are given in Fig. 2. The water in the gaseous products could not be exactly determined by means of the gas chromatography employed in the present work, because part of the water remained in the separation column even after a long time. Therefore, the amount of the evolved water given in the GEA curves is smaller than that estimated from the composition of these compounds.

The GEA curves for the cobalt(III) carbonatoammine complexes given in Fig. 2 show that the complexes lose water between 80 and 160 °C, and that the decomposition of the anhydrous compounds begins with an evolution of ammonia. The evolution of ammonia from the pentaammine complexes began at about 140 °C, while from the tetraammine and diammine complexes, it began at about 180 °C. Above 180 °C, both the pentaammine and tetrammine complexes decomposed in the same fashion. These temperature ranges and the number of peaks observed in the GEA curves are in agreement with those appearing on the DSC curves for the compounds obtained in the preliminary examination.

The thermally stable compounds as intermediate species, which may be formed by the evolution of 0.4—0.5 molar ammonia, were detectable in these GEA curves for the pentaammine complexes. However, no intermediate species were detectable in these GEA curves for the tetraammine and diammine complexes. In the GEA curves re-examined for the pentaammine complexes heated up to 170 °C, the first peak, which is due to the evolution of ammonia between 140 and 170 °C, disappeared. In addition, the IR spectra of the compounds heated up to 170 °C were characterized by the disappearance of the band at about 1490 cm^{-1} which was assigned to the CO_3^{2-} as an unidentate ligand, and by the appearance of new bands at about 840 and 770 cm^{-1} which were assigned to the CO_3^{2-} as bidentates.[10] As Yamada and Tada[5] concluded, this phenomenon indicates that most of the CO_3^{2-} as an unidentate ligand changed to a bidentate ligand when the pentaammine complexes were heated to 170 °C.

Based on the GEA curves for the cobalt(III) carbonatoammine complexes given in Fig. 2, it is confirmed that the endothermic peaks appearing on the DSC curves for the compounds obtained in the preliminary examination were caused by the evolution of water and ammonia, while, the exothermic peaks were caused by the oxidation of ammonia, with the nitrate anion as outer-ligand.

From the results described above and those obtained by earlier workers,[3,5] it may be seen that the processes of the thermal decomposition reactions of the cobalt(III) carbonatoammine complexes in a helium atmosphere take place by means of the following competition reactions:

$$[CoOCO_2(NH_3)_5]X \cdot H_2O \xrightarrow{140\text{—}170\,^\circ C} [CoCO_3(NH_3)_{4.5}]X + H_2O + 0.5NH_3$$

$$[CoCO_3(NH_3)_4]X \xrightarrow{180\text{—}200\,^\circ C} [CoXCO_3(NH_3)_3] + NH_3$$

$$[CoCO_3(NH_3)_4]X \xrightarrow{180\text{—}200\,^\circ C} \text{low ammine cobalt(II) complexes}$$

$$[CoCO_3(NH_3)_4]X \xrightarrow{200\text{—}300\,^\circ C} Co_2OX_2 + N_2 + NH_3 + CO_2$$

Since the evolution of ammonia and nitrogen during the decomposition of these compounds in the 180—250 °C temperature range was observed in these GEA curves, it may be concluded that the Co(III) in the compounds was reduced to Co(II) by ammonia, and that NH_4X was an intermediate dissociation product.

Although the peak maximum temperature is dependent upon the heating rate of the furnace, the flow rate of the carrier gas, the sample size, the furnace atmosphere, and so on, the combination of the above GEA curves with the results of TG and DTA (and DSC) studies allows a more complete interpretation of the thermal decomposition reactions of the cobalt(III) carbonatoammine complexes.

The author wishes to thank Professor Masaakira Iguchi, Tokyo University of Science, for his interest in this work, and also Dr. Hiroshi Ogino for his DSC analysis.

References

1) M. Mori, M. Shibata, E. Kyuno, and T. Adachi, *Bull. Chem. Soc. Jpn.*, **29**, 883 (1956).
2) M. Figlarz, *C. R. Acad. Sci.*, **249**, 2780 (1959); **250**, 3844 (1960).
3) W. W. Wendlandt and J. H. Woodlock, *J. Inorg. Nucl. Chem.*, **28**, 1485 (1966).
4) J. M. Amigo, J. Gracia-Gonzalez, and C. Miravilles, *J. Thermal Anal.*, **3**, 169 (1971).
5) M. Yamada and K. Tada, *Nippon Kagaku Kaishi*, **1974**, 1903.
6) K. Nagase, *Bull. Chem. Soc. Jpn.*, **46**, 144 (1973).
7) T. S. Rao and B. R. Gandhe, *J. Chromatogr.*, **88**, 407 (1974).
8) S. Onodera, *Bull. Chem. Soc. Jpn.*, **50**, 123 (1977).
9) E. G. Rochow, *Inorg. Synth.*, Vol. IV, 171; Vol. VI, 173, 174, 177 (1960); J. Kranig, *Ann. Chim.*, [*10*], *11*, 85 (1929).
10) J. Fujita, A. E. Martell, and K. Nakamoto, *J. Chem. Phys.*, **36**, 339 (1962).

BULLETIN OF THE CHEMICAL SOCIETY OF JAPAN, VOL. 51 (6), 1891—1892 (1978)

Electrochemical Fluorination of Thiols

Hajime BABA, Kazuo KODAIRA, Shunji NAGASE, and Takashi ABE

Government Industrial Research Institute, Nagoya, Hirate-machi, Kita-ku, Nagoya 462

(Received December 20, 1977)

Synopsis. Electrochemical fluorination of C_3 and C_4 thiols has been investigated. Perfluoroalkylsulfur pentafluoride derivatives including new compounds, together with fragmented fluorocarbons and sulfur hexafluoride, have been formed.

Our previous paper[1] showed that electrochemical fluorination of ethanethiol afforded a variety of fluoroalkyl sulfur compounds. As a continuation of this study, the electrochemical fluorination of C_3 and C_4 thiols including branched-chain compounds has been examined in the hope that the effects of branching on the products could be determined.

2-Propane- (I), 1-butane- (II), 2-methyl-1-propane- (III), 2-butane- (IV), and 2-methyl-2-propanethiols (V) have been subjected to the electrochemical fluorination. These were expected to yield perfluoroalkyl derivatives of sulfur hexafluoride, which have received considerable attention because of their unique inertness[2] and their usefulness as intermediates.[3]

The extensive breakdown of the thiols occurred, particularly in the carbon-sulfur bond during fluorination, and resulted in the formation of fluorocarbons and sulfur hexafluoride. Even so, a part of the starting materials was converted into the corresponding fully fluorinated analogs, perfluoroalkylsulfur pentafluorides. For example, II produced $CF_3(CF_2)_3SF_5$ (VI) in 12% yield. IV afforded a perfluoro compound which retained a sulfur pentafluoride group on the secondary carbon, $C_2F_5CF(CF_3)SF_5$[4] (VII), but the yield was poor (2%).

The physical constants and the ^{19}F and ^1H NMR spectral data of the isolated new compounds are shown in Table 1. These sulfur pentafluorides could be confirmed by their ^{19}F NMR spectra, which indicated the presence of two differently shielded types of fluorine nucleus bonded to the sulfur in the correct intensity ratio of 1 : 4 in the regions expected.[5] The molecular ion peaks for these compounds were undetectable, but such characteristic ions as $[M-SF_5]$ and $[SF_3]$ were always found.

In the electrochemical fluorination of a tertiary thiol, V, the formation of the fully fluorinated analog of the starting material could not be confirmed. It yielded the entirely rearranged products, VI and $(CF_3)_2CFCF_2SF_5$ (VIII) in low yields ($\approx$2%), together with perfluorobutane (42%) and perfluoro (2-methylpropane) (4%).

The secondary thiols also gave isomerized derivatives as well as perfluorinated analogs of the starting materials; $CF_3CF_2CF_2SF_5$ (IX), $(CF_3)_2CFSF_5$ (X), and $C_2F_5CH_2SF_5$ (XI) were isolated in the fluorination of I, and VI and VII in the fluorination of IV. The other branched-chain thiol, III, produced VIII and the straight-chain compound VI. In these cases the amounts of the straight-chain perfluoro derivatives were higher than those of the branched-chain isomers, the yields of the former being up to 12%. The isomerization by the migration of a methyl or an ethyl group located at a branching site of the chain has been observed in the electrochemical fluorination of branched organic compounds, *e.g.* amines.[6]

The low yields of the fluorinated products from the thiols may be attributable partly to the instability of the thiols in anhydrous hydrogen fluoride.[7] Considerable amounts of polymeric tarry materials and elemental sulfur were always found as deposits on the electrodes and at the bottom of the electrolytic cell.

Experimental

Materials and Apparatus. The thiols used were commercial chemicals. II (97%) contained a small amount of III. The others were more than 98% pure. The electrolytic fluorination apparatus[8] and operating procedures[1] were similar to the ones described previously. The mass spectra were recorded on a Hitachi RMU-7 instrument at 70 eV, the ^{19}F NMR spectra on a Hitachi R-20B instrument at 56.4 MHz, and the ^1H NMR spectra on a Hitachi R-22 instrument at 90 MHz.

Fluorination of 2-Propanethiol (I). I (25.0 g, 0.328 mol) was added to electrochemically purified anhydrous hydrogen fluoride (400 ml) in the cell. The resulting solution was electrolyzed under the following conditions: anodic current density, 2.6 A/dm^2 (effective surface area of anodes, 770 dm^2); cell voltage, 4.7—6.1 V; cell temperature, 8—10 °C; electricity supplied, 227 A h (670 min); helium flow rate, 60 ml/min.

The products collected in a series of cold traps immersed in ice and in liquid nitrogen were combined (71.3 g) and distilled into four fractions, and each fraction was then subjected to gas-chromatographic analysis (column: 2 m $\times$ 3 mm, silica gel; 4 m $\times$ 3 mm, Daifl oil 3 (20%) on Chromosorb P-AW). The following compounds were obtained (the compositions were calculated on the basis of the chromatographic peak areas): C_1 and C_2 fluorocarbons (0.9 g), SF_6 (18.8 g), C_3F_8 (30.1 g, 48.8%), *n*-C_4F_{10} (0.1 g), $CHF_2C_2F_5$ (1.1 g), $(CF_3)_2CHF$ (1.2 g), $CH_2FC_2F_5$ (6.4 g), $C_2H_5CF_3$ (0.9 g), $C_2F_5SF_5$ (0.2 g), IX (3.3 g, 3.4%), X (1.7 g, 1.8%), XI (0.8 g, 0.9%), others (unidentified complex mixtures, 5.6 g).

X, MS: *m/e* 169 $[M-SF_5]$, 131 $[C_3F_5]$, 127 $[SF_5]$, 119 $[C_2F_5]$, 100 $[C_2F_4]$, 89 $[SF_3]$, 70 $[SF_2]$, 69 $[CF_3]$. Found: C, 12.19; F, 76.5%. Calcd for $C_3F_{12}S$: C, 12.17; F, 77.0%. XI, MS: *m/e* 241 $[M-F]$, 191 $[M-CF_3]$, 133 $[M-SF_5]$, 131 $[C_3F_5]$, 127 $[SF_5]$, 119 $[C_2F_5]$, 113 $[C_3HF_4]$, 100 $[C_2F_4]$, 89 $[SF_3]$, 83 $[C_2H_2F_3]$, SF_2 [70], 69 $[CF_3]$. Found: C, 14.02; H, 0.84; F, 72.4%. Calcd for $C_3H_2F_{10}S$: C, 13.85; H, 0.78; F, 73.0%.

Fluorination of 1-Butanethiol (II). II (20.6 g, 0.288 mol) was fluorinated under the following conditions: 2.9 A/dm^2, 5.8—8.0 V, 14—15 °C, 151 A h (400 min), helium 60 ml/min. The following compounds were obtained: C_1, C_2, and C_3 fluorocarbons (0.9 g), SF_6 (5.9 g), CF_3SF_5 (0.2 g), $(CF_3)_3CF$ (0.8 g), *n*-C_4F_{10} (6.9 g, 10.6%), $C_2F_5SF_5$ (0.4 g), $(CF_3)_3CH$

Table 1. Fluoroalkyl sulfur compounds

Compound	Source[a]	Bp[b] (°C)	n_D^{20}	^{19}F and H^1 NMR spectral data[c,d]	
				Chemical shifts, ppm	Coupling constants, Hz
				$(CF_3^a)_2CF^tSF_5$	
$(CF_3)_2CFSF_5$	I	43.3	<1.28	F^a 72.2, F^t 150.5, SF_{eq} −55.8, SF_{ax} −65.4	F^a–SF_{eq} 12.8, F^a–F^t 6.2, SF_{ax}–F^t 3.3, SF_{ax}–F^a 1.5, SF_{ax}–SF_{eq} 140.6
				$CF_3^aCF_2^bCH_2SF_5$	
$C_2F_5CH_2SF_5$	I	60.0	<1.28	F^a 86.2, F^b 120.1 SF_{eq} −73.1, SF_{ax} −75.5 H 4.0	SF_{ax}–SF_{eq} 128 H–F^b 16, H–SF_{eq} 7
				$(CF_3^a)_2CF^tCF_2^bSF_5$	
$(CF_3)_2CFCF_2SF_5$	III V	69.0	<1.28	F^a 72.5, F^b 87.9, F^t 183.2 SF_{eq} −44.2, SF_{ax} −62.6	F^a–F^b 10.6, F^a–SF_{eq} 5.4, F^a–F^t 5.2, SF_{ax}–F^t 1.8, SF_{ax}–F^b 5.0, SF_{ax}–SF_{eq} 142.7
				$CF_3^aCF_2^bCF^t(CF_3^c)SF_5$	
$C_2F_5CF(CF_3)SF_5$	IV	71.0	<1.28	F^a 79.9, F^b 117.9, F^c 70.6 F^t 147.1, SF_{eq} −58.2, SF_{ax} −65.1	F^a–SF_{eq} 9.3, F^a–F^t 6.2, F^a–F^c 3.1, SF_{ax}–SF_{eq} 139.2

a) I: 2-Propanethiol, III: 2-methyl-1-propanethiol, IV: 2-butanethiol, V: 2-methyl-2-propanethiol. b) Recorded, uncorrected, at atmospheric pressure. c) CCl_4 solution. Chemical shifts are in δ values with respect to CCl_3F for ^{19}F and to TMS for ^1H as internal references. d) SF_{eq} and SF_{ax} indicate equatorial and axial fluorine atoms respectively.

(0.1 g), $CF_3CH_2C_2F_5$ (0.4 g), VI (9.7 g, 12.3%), others (1.0 g).

Fluorination of 2-Methyl-1-propanethiol (III). III (25.0 g, 0.277 mol) was fluorinated; 3.0 A/dm², 4.8—6.0 V, 10—11 °C, 174 A h (455 min), helium 60 ml/min. The following compounds were obtained: C_1, C_2, and C_3 fluorocarbons (0.3 g), SF_6 (7.6 g), $(CF_3)_3CF$ (2.3 g, 3.5%), n-C_4F_{10} (5.5 g, 8.4%), $(CF_3)_2C{=}CF_2$ (0.1 g), $CF_3CHFC_2F_5$ (0.2 g), $(CF_3)_3CH$ (0.2 g), $CF_3CH_2C_2F_5$ (0.2 g), IX (0.4 g), VIII (2.4 g, 2.5%), VI (11.7 g, 12.2%), others (0.6 g).

VIII, MS: *m/e* 219 [M−SF_5], 150 [C_3F_6], 131 [C_3F_5], 127 [SF_5], 119 [C_2F_5], 100 [C_2F_4], 89 [SF_3], 70 [SF_2], 69 [CF_3]. Found: C, 13.62; F, 76.7%. Calcd for $C_4F_{14}S$: C, 13.88; F, 76.9%.

Fluorination of 2-Butanethiol (IV). IV (25.0 g, 0.277 mol) was fluorinated; 3.1 A/dm², 4.8—7.5 V, 9—11 °C, 203 A h (510 min), helium 60 ml/min. The following compounds were obtained: C_1, C_2, and C_3 fluorocarbons (2.3 g), SF_6 (15.0 g), $(CF_3)_3CF$ (1.6 g), n-C_4F_{10} (32.3 g, 48.9%), $CF_3CHFC_2F_5$ (0.6 g), $(CF_3)_3CH$ (0.2 g), $CF_3CH_2C_2F_5$ (0.6 g), IX (0.2 g), VI (5.0 g, 5.3%), VII (1.9 g, 2.0%), $[CF_3(CF_2)_3]_2SF_4$ (0.1 g), others (1.5 g).

VII,[4] MS: *m/e* 219 [M−SF_5], 150 [C_3F_6], 131 [C_3F_5], 127 [SF_5], 100 [C_2F_4], 93 [C_3F_3], 89 [SF_3], 70 [SF_2], 69 [CF_3]. Found: C, 13.70; F, 77.1%. Calcd for $C_4F_{14}S$: C, 13.88; F, 76.9%.

Fluorination of 2-Methyl-2-propanethiol (V). V (24.0 g, 0.266 mol) was fluorinated; 3.2 A/dm², 5.1—6.6 V, 10—12 °C, 172 A h (420 min), helium 60 ml/min. The following compounds were obtained: C_1, C_2, and C_3 fluorocarbons (5.3 g), SF_6 (6.2 g), n-C_4F_{10} (26.4 g, 41.8%), $(CF_3)_3CF$ (2.6 g, 4.1%), $CF_3CHFC_2F_5$ (0.9 g), $CHF_2C_3F_7$ (0.2 g), $(CF_3)_3CH$ (0.4 g), $CF_3CH_2C_2F_5$ (2.9 g), n-C_5F_{12} (0.8 g), IX (0.1 g), VI (2.0 g, 2.2%), VIII (0.6 g, 0.7%), others (6.0 g).

References

1) H. Baba, K. Kodaira, S. Nagase, and T. Abe, *Bull. Chem. Soc. Jpn.*, **50**, 2809 (1977).

2) For example, Shin-Liang Yu, and J. M. Shreeve, *J. Fluorine Chem.*, **6**, 259 (1975).

3) Dow Corning Co., Fr. 1512068 (1967); L. A. Loree, U. S. 3456024 (1969).

4) The formula is listed in Ref. 3.

5) a) N. Muller, P. C. Lauterbur, and G. F. Svatos, *J. Am. Chem. Soc.*, **79**, 1043 (1957); b) M. T. Rogers and J. D. Graham, *ibid.*, **84**, 3666 (1962).

6) a) T. C. Simmons, F. W. Hoffmann, R. B. Beck, H. V. Holler, T. Katz, R. J. Koshar, E. R. Larsen, J. E. Mulvaney, K. E. Paulson, F. E. Rogers, B. Singleton, and R. E. Sparks, *J. Am. Chem. Soc.*, **79**, 3429 (1957); b) V. S. Plashkin, L. N. Pushkina, and S. V. Sokolov, *Zh. Org. Khim.*, **10**, 1215 (1974); c) K. Omori, S. Nagase, H. Baba, K. Kodaira, and T. Abe, *J. Fluorine Chem.*, **9**, 279 (1977).

7) J. H. Simons, "Fluorine Chemistry," Vol. 1, ed by J. H. Simons, Academic Press, New York (1950), p. 239.

8) S. Nagase, H. Baba, and T. Abe, *Bull. Chem. Soc. Jpn.*, **40**, 2358 (1967).

BULLETIN OF THE CHEMICAL SOCIETY OF JAPAN, VOL. 51 (6), 1893—1894 (1978)

The Preparation of a Seven-Coordinate Dimethyllead(IV) Complex, $(CH_3)_2Pb(gbha)(H_2O)$, and Ionic Dissociation of the Coordinated Water

Tetsuro MAJIMA and Yoshikane KAWASAKI

Department of Petroleum Chemistry, Osaka University, Yamadakami, Suita, Osaka 565

(Received December 22, 1977)

Synopsis. A seven-coordinate dimethyllead(IV) complex, $(CH_3)_2Pb(gbha)(H_2O)$, was prepared. From spectroscopic studies the water molecule in the complex was found to coordinate rather strongly to the lead atom as the seventh ligand. An interesting feature of the complex is that the dissociation of a proton from the coordinated water occurs in such coordinating solvents as DMSO and HMPA.

Although there are a great number of four- and six-coordinate dimethyllead(IV) complexes, seven-coordinate ones have not been reported. In a previous paper,[1] we reported on the interaction between a six-coordinate dimethyllead(IV) complex of *N,N'*-ethylenebis(salicylideneaminato); (saln), $(CH_3)_2Pb(saln)\cdot CH_3OH$, and donor-solvent molecules in solution. The formation of a seven-coordinate complex was assumed in the above experiments on the basis of the following data: 1) the $\delta(Pb-CH_3)$ value shifts to a higher magnetic field and 2) both the $^2J(^{207}Pb-CH_3)$ and $^3J(^{207}Pb-N=CH)$ values increase with an increase in the donor strength of the solvents. Similar observations have been reported for dimethyllead(IV) complexes of 8-qunolinolato,[2] β-diketonato,[3] and benzoato.[4]

We wish to report here on the first successful isolation of a seven-coordinate dimethyllead(IV) complex of bis(2-metidineaminophenolato); (gbha), $(CH_3)_2Pb(gbha)(H_2O)$; (**A**), and on the dissociation of a proton from the water molecule coordinated to the lead atom in such solvents as DMSO and HMPA.

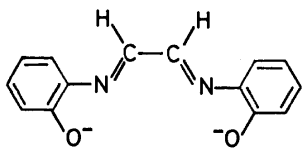

gbha

Experimental

Preparation of $(CH_3)_2Pb(gbha)(H_2O)$. Dimethyllead dichloride was prepared by the chlorination of tetramethyllead in ethyl acetate at about −10 °C.[5] The *N,N'*-di(2'-hydroxyphenyl)-1,2-ethanediimine, H_2gbha, was prepared by a method reported previously.[6] $(CH_3)_2Pb(gbha)(H_2O)$[7] was prepared by the reaction of dimethyllead dichloride (2.5 g, 10 mmol) and Na_2gbha (Na; 0.5 g, 20 mmol and H_2gbha; 2.4 g, 10 mmol in 20 dm of methanol) in about 20 dm of methanol. The precipitates were recrystallized from a CH_2Cl_2/hexane (large excess) mixture. The complex was obtained as a black crystalline solid in a 78% yield and did not melt below 300 °C. Found: C, 38.68; H, 3.38; N, 5.77; Pb, 41.89%. Calcd for $C_{16}H_{18}N_2O_3Pb$: C, 38.94; H, 3.68; N, 5.68; Pb, 41.98%.

Measurements. The molar weight of the complex in $CHCl_3$ (0.72 wt%), established using a Mechrolab vapor-pressure osmometer at 25 °C, was found to be 514 (calcd 493). The molar conductances were measured by means of a Yokogawa F-255A Universal Bridge and a cell (cell constant; 0.377 cm^{-1}). The specific conductances of the solvents used, CH_2Cl_2, $(CH_3O)_3PO$, pyridine, DMSO, and HMPA, are $<10^{-7}$, 9.5×10^{-7}, 8.9×10^{-7}, 4.2×10^{-7}, and 4.8×10^{-7} Ω^{-1} cm^{-1} respectively.

The IR and ^1H NMR spectra of about a 4 wt% solution were recorded with a Hitachi EPI-2G Spectrophotometer and a JEOL-PS-100 Spectrometer operating at 100 MHz respectively. The chemical shifts were measured relative to TMS as an internal standard.

Results and Discussion

The ^1H NMR and IR spectral data and the molar conductance of the (**A**) complex in several solvents are summarized in Table 1. The $^3J(^{207}Pb-N=CH)$ value of the complex was observed in all the solvents. The stretching frequencies of the C–N double bond of the complex in CH_2Cl_2 (1712 cm^{-1}) and HMPA (1695 cm^{-1}) are almost the same and are different from that of free gbha (1640 cm^{-1} in Na_2gbha[8]). Therefore, gbha in the complex may be supposed to coordinate to the lead atom as an ONNO quadridentate ligand in all the solvents, according to the similar discussion of $(CH_3)_2Pb(saln)\cdot CH_3OH$.[1] The $^2J(^{207}Pb-CH_3)$ and

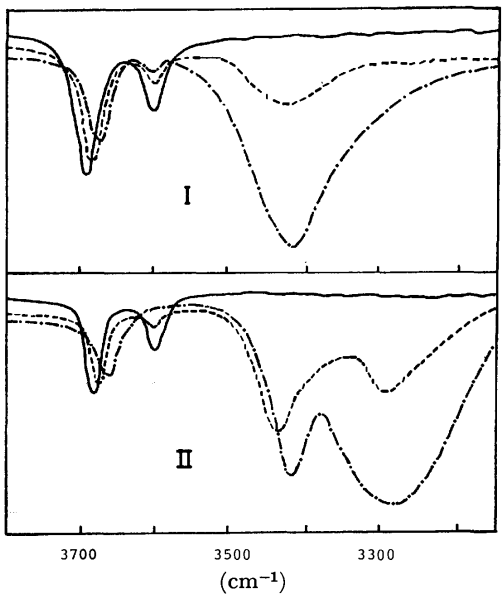

Fig. 1. IR spectra of free water molecule (I) and the gbha complex (II) in CH_2Cl_2–DMSO solutions (4 wt%). The concentration of DMSO added is 0(——), 0.8(——), and 7.8 wt%(-·-·-).

Table 1. The ^1H NMR and IR data and the molar conductance of $(CH_3)_2Pb(gbha)(H_2O)$ in several solvents

Solvent	δ(Pb–CH_3) (ppm)	δ(Pb–N=CH) (ppm)	$^2J(^{207}Pb–CH_3)$ (Hz)	$^3J(^{207}Pb–N=CH)$ (Hz)	ν(OH) (cm^{-1})	Λ_m[a] (Ω^{-1} cm^2 mol^{-1})
$CDCl_3$	1.96	8.65	176.4	37.8	—[b]	—[b]
CH_2Cl_2	1.94	8.67	178.9	37.9	3680 3600	0.1
$(CH_3O)_3PO$	1.75	8.68	177.6	36.8	3407 3270	10.0
Pyridine	1.85	8.66	180.5	38.4	3400[c] 3275	11.0
DMSO	1.68	8.84	179.0	38.0	3418 3280	15.2
HMPA	1.69	8.64	179.5	36.6	3425 3240	2.5

a) At 10^{-3} mol dm^{-3} (25±0.1 °C). b) Not measured. c) This peak may come from 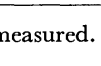 .

$^3J(^{207}Pb–N=CH)$ values in $CDCl_3$ are much larger than those of $(CH_3)_2Pb(saln)\cdot CH_3OH$ with the six-coordinate structure ($^2J(^{207}Pb–CH_3)=157.8$ Hz and $^3J(^{207}Pb–N=CH)=23.4$ Hz in $CDCl_3$) and do not change even in such highly coordinating solvents as DMSO and HMPA. The $^2J(^{207}Pb–CH_3)$ value of $(CH_3)_2$-(gbha)Pb(H_2O) is similar to that of $(CH_3)_2Pb(saln)\cdot CH_3OH$ in DMSO. The above results suggest that the water molecule coordinates, as the seventh ligand, to the lead atom rather strongly in the (**A**) complex.

The IR spectrum of the (**A**) complex in CH_2Cl_2 showed two peaks, at 3680 and 3600 cm^{-1}, assigned to the O–H antisymmetric and symmetric stretching vibrations respectively. Figure 1 shows the IR spectra for free water (I) and the gbha complex (II) in CH_2Cl_2–DMSO solutions of the O–H stretching vibrational region. The frequencies and shapes of the O–H bands change continuously with the concentration of DMSO added. The changing features of the spectra for (I) and (II) are quite different and suggest that the water molecule in the complex is not free.

The molar conductance shows that the complex is an electrolyte in the coordinating solvents, but not in CH_2Cl_2 (Table 1). On the other hand, the free water does not show any electric conductivity even in DMSO and HMPA. Therefore, the appearance of the conductances in the complex suggests the presence of an ionic species, $[(CH_3)_2Pb(gbha)(OH)]^-$; (**B**), in the coordinating solvents. The values of the conductances are smaller than those for usual 1:1 electrolytes (for example, 25—40 Ω^{-1} cm^2 mol^{-1} for 1:1 electrolytes in DMSO at a concentration of *ca.* 10^{-3} mol dm^{-3} [9]). Consequently, the following equilibrium may occur in coordinating solvents, in which the dissociation of a proton takes place instead of the replacement of the coordinated water molecule by a solvent molecule. The existence of the anionic hydroxo complex (**B**) and the protonated solvent molecule ($[HD]^+$) is substantiated by the appearance of two peaks (at *ca.* 3270 and *ca.* 3400 cm^{-1}) in the IR spectra of the complex in coordinating solvents.

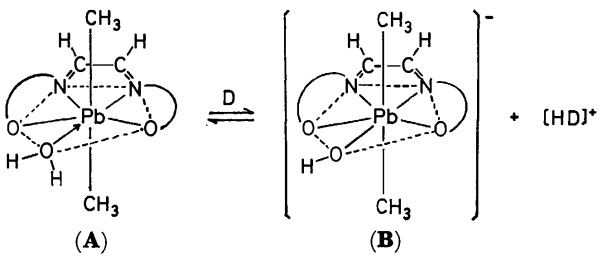

(**A**) (**B**)

D=HMPA, DMSO, pyridine, $(CH_3O)_3PO$.

In the conclusion, $(CH_3)_2Pb(gbha)(H_2O)$ may be supposed to take the seven-coordinate structure (**A**), with the water molecule coordinating to the lead atom rather strongly in non-coordinating solvents. On the other hand, in coordinating solvents, a partial dissociation of a proton from the coordinated water occurs, resulting in an equilibrium between **A** and the ionic species **B** and $[HD]^+$.

References

1) Y. Kawasaki and T. Majima, *Inorg. Nucl. Chem. Lett.*, **11**, 779 (1975).

2) M. Aritomi and Y. Kawasaki, *J. Organomet. Chem.*, **81**, 363 (1974).

3) M. Aritomi, Y. Kawasaki, and R. Okawara, *Inorg. Nucl. Chem. Lett.*, **8**, 69 (1972).

4) M. Aritomi and Y. Kawasaki, *J. Organomet. Chem.*, **90**, 185 (1975).

5) G. Grüttner and E. Kraus, *Chem. Ber.*, **49**, 1415 (1916).

6) E. Bayer and G. Schenk, *Chem. Ber.*, **93**, 1184 (1960).

7) Di Bianca *et al.* reported the preparation of $(CH_3)_2Pb$-(gbha) by almost the same procedure. However, no O–H stretching band was observed: F. Di Bianca, E. Rivarola, G. C. Stocco, and R. Barbieri, *Z. Anorg. Allg. Chem.*, **387**, 126 (1972).

8) G. O. Dudek and R. H. Holm, *J. Am. Chem. Soc.*, **83**, 2099 (1961).

9) D. G. Sears, R. R. Lester, and L. R. Pauson, *J. Phys. Chem.*, **60**, 1433 (1956).

BULLETIN OF THE CHEMICAL SOCIETY OF JAPAN, VOL. 51 (6), 1895—1896 (1978)

Magnetic Circular Dichroism Spectra of Amino Acid Complexes of the $[Co^{III}(N)_5(O)]^{n+}$ Type

Etsuyo UEDA, Nobuko MATSUOKA,* and Yoichi SHIMURA

Department of Chemistry, Faculty of Science, Osaka University, Toyonaka, Osaka 560

(Received February 7, 1978)

Synopsis. MCD spectra of amino acid complexes of $[Co(NH_3)_5(OCOCHRNH_3)]^{3+}$, $[Co(NH_2CHRCO_2)(NH_3)_4]^{2+}$, and $[Co(NH_2CHRCO_2)(en)_2]^{2+}$ types have been measured. The complexes belonging to a given type show nearly identical MCD curves irrespective of variation in their natural CD patterns. The complexes of D-, L-, and DL-alanine show identical MCD spectra.

In connection with our previous study[1] on magnetic circular dichroism (MCD) spectra of a series of racemic tris(chelate)cobalt(III) complexes, it seems worthwhile to investigate MCD spectra of optically active cobalt(III) complexes. Larcher and Gabriel compared MCD spectra of mono- and bis(L-valinato)nickel(II) complexes with their natural CD spectra.[2] We have made a comparison of the MCD and natural CD spectra of α-amino acid complexes of the $[Co^{III}(N)_5(O)]^{n+}$ type, the result of which are reported here. The complexes studied are classified into three types, namely, a pentaammine type $[Co(NH_3)_5(OCOCHRNH_3)]^{3+}$, in which the carboxylate end of amino acid ligand is attached to the central cobalt ion,[3] and a tetraammine and a bis(ethylenediamine) type, $[Co(NH_2CHRCO_2)(NH_3)_4]^{2+}$ and $[Co(NH_2CHRCO_2)(en)_2]^{2+}$, which contain the amino carboxylato ligand as chelate one. The natural CD spectra of a large part of these complexes were investigated previously in our laboratory.[4] The following abbreviations are used for the amino acid ligands: Hgly for glycine, Hala alanine, Hser serine, and Hphe phenylalanine.

Experimental

Preparations. The pentaammine (chloride or perchlorate) and tetraammine (sulfate) complexes were prepared by the methods described in previous papers.[3-5] The bis(ethylenediamine) complexes were prepared as follows.

$[Co(gly)(en)_2]Br_2 \cdot H_2O$ and $[Co(DL\text{-}ala)(en)_2]Br_2 \cdot H_2O$: A solution containing glycine (0.4 g) (or DL-alanine, 0.5 g) and $[Co(NH_3)(en)_2(OH_2)]Br_3$ (2.5 g) in 20 cm³ of water was evaporated together with powdered activated charcoal (0.1 g) to about 5 cm³ at 80 °C on a water-bath. The solution was cooled to room temperature, filtered, and 1 cm³ of methanol was added. After mixture was kept in a refrigerator overnight, the orange red deposit was filtered, washed with methanol and ether, and dried in air. The crude complex was dissolved in 5 cm³ of water (*ca.* 50 °C). The solution was filtered, and kept in a refrigerator overnight after 3 cm³ of methanol had been added. The crystalline powder deposited was filtered, washed with methanol and ether, and dried in air. The pure complex was obtained by repeated crystallizations. Found: C, 16.93; H, 5.28; N, 16.50%. Calcd for $C_6H_{20}N_5O_2Br_2Co$ H_2O: C, 16.72; H, 5.14; N, 16.25%. Found: C, 18.60; H, 5.44; N, 15.53%. Calcd for $C_7H_{22}N_5O_2Br_2Co \cdot H_2O$: C, 18.89; H, 5.44; N, 15.74%.

Measurements. The CD and MCD spectra were recorded with a JASCO MOE-1 spectropolarimeter. The MCD measurements were made in a magnetic field of 1.5 T(= 15000 G). The MCD intensity is expressed in terms of the molar circular dichroism per unit magnetic field in the direction of the light beam, $\Delta\varepsilon_M$, which has the units of $cm^{-1} \cdot mol^{-1}\ dm^3\ T^{-1}$. The visible and near-ultraviolet absorption spectra were measured using a Shimadzu UV-200 spectrophotometer. All measurements were made at room temperature in aqueous solutions.

Results and Discussion

Figure 1 shows the observed curves of absorption, natural CD and MCD spectra of $[Co(NH_3)_5(L\text{-}Hala)]^{3+}$ and the related complexes. The MCD spectrum of the optically active complex is observed in overlap with the natural CD. Therefore the true MCD spectrum ($\Delta\varepsilon_M$ curve) was obtained by calculating the difference between the observed MCD and the natural CD curves, assuming that the natural CD and MCD are additive. The MCD spectra which are obtained in this manner are shown in Fig. 2. The MCD extremum data of the complexes studied are shown in Table 1. It is most

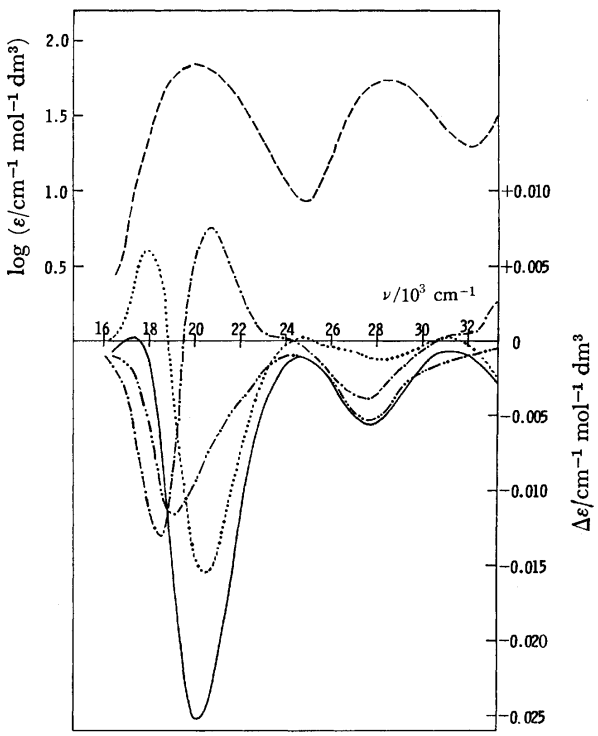

Fig. 1. The absorption (——) and CD (·····) spectra of $[Co(NH_3)_5(L\text{-}Hala)]^{3+}$, and overlapped curves of CD and MCD in a magnetic field of 1.5 T of $[Co(NH_3)_5(L\text{-}Hala)]^{3+}$ (——), $[Co(NH_3)_5(D\text{-}Hala)]^{3+}$ (—·—), and $[Co(NH_3)_5(DL\text{-}Hala)]^{3+}$ (-··-).

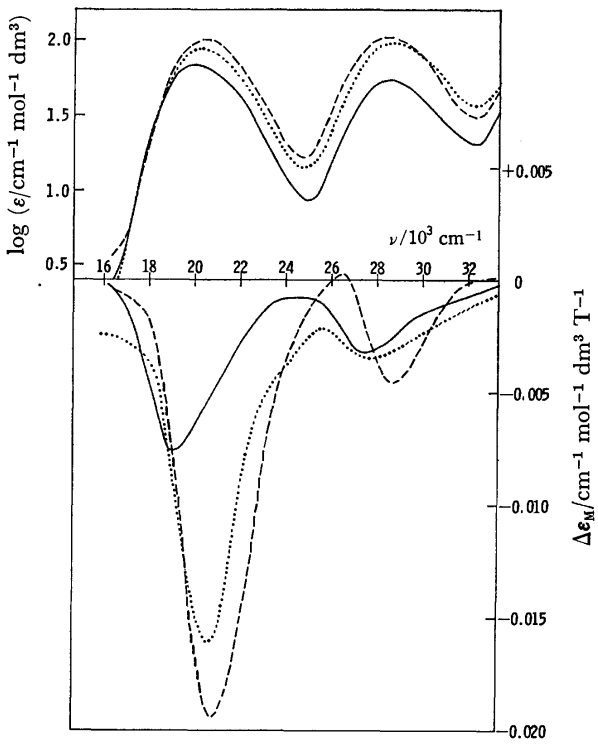

Fig. 2. The absorption and MCD spectra of $[Co(NH_3)_5$-(L-Hala)]$^{3+}$ (——), $[Co(L\text{-ala})(NH_3)_4]^{2+}$ (·····), and $[Co(DL\text{-ala})\ (en)_2]^{2+}$ (----).

remarkable that the D-, L- and DL-alanine complexes show strictly identical MCD spectra.

The MCD spectra of all the pentaammine type complexes are very similar, *viz.*, a negative band which may be mainly due to Faraday B term appears each in the first and the second absorption band region. Such a behavior in MCD is quite different from that in natural CD, which show a variety of patterns.[4] The natural CD curve of $[Co(NH_3)_5(L\text{-Hala})]^{3+}$ has two extrema, 18000 (+0.005) and 20600 cm^{-1} (−0.015), in the first d-d band region. In the same region the tetraammine complex $[Co(L\text{-ala})(NH_3)_4]^{2+}$ has three extrema, 18200 (−0.036), 19700 (+0.11), and 21900 cm^{-1} (−0.32). The $\Delta\varepsilon_M$ intensity in the first d-d band region is greater than that in the second band region as was also observed for tris(chelate) complexes.[1] The intensity increases in the order of pentaammine< tetraammine<bis(ethylenediamine) in both first and second band regions; this order is parallel to the increase of absorption intensity.

The pentaammine complex ion belongs approximately to the C_{4v} symmetry, and in the first absorption band region two components, $^1E \leftarrow {}^1A_1$ and $^1A_2 \leftarrow {}^1A_1$, are expected in 19600 and 21000 cm^{-1}, respectively, as is seen in Table 2. The observed MCD peak is located at 19100 cm^{-1}. Therefore the MCD peak is primarily due to the Faraday B term of the E transition. The fact that the peak is in longer wavelength than the expected position of the E transition may be rationalized in terms of the swamping of the Faraday A term having a negative wing in the longer wavelength region. In the tetraammine and bis(ethylenediamine) complexes the longer wavelength component (^1E in C_{4v} symmetry)

Table 1. Absorption maximum and MCD extremum data
(Wave numbers are given in 10^3 cm^{-1})

Complex ion	Absorption band ν (log ε)	MCD band ν ($\Delta\varepsilon_M$)
$[Co(NH_3)_5(Hgly)]^{3+}$	20.0(1.83) 28.6(1.74)	19.0(−0.007) 27.6(−0.003)
$[Co(NH_3)_5(L\text{-Hala})]^{3+}$ a)	20.0(1.84) 28.6(1.74)	19.0(−0.007) 27.5(−0.003)
$[Co(NH_3)_5(L\text{-Hser})]^{3+}$ b)	20.0(1.83) 28.6(1.73)	19.1(−0.009) 27.5(−0.003)
$[Co(NH_3)_5(L\text{-Hphe})]^{3+}$ c)	20.0(1.83) 28.7(1.74)	19.2(−0.012) 27.5(−0.003)
$[Co(NH_3)_5(\beta\text{-Hala})]^{3+}$	19.8(1.87) 28.3(1.76)	19.0(−0.008) 27.4(−0.004)
$[Co(gly)(NH_3)_4]^{2+}$	20.3(1.89) 28.5(1.98)	20.4(−0.013) 28.2(−0.003)
$[Co(L\text{-ala})(NH_3)_4]^{2+}$ a)	20.3(1.90) 28.7(1.94)	20.4(−0.015) 28.1(−0.003)
$[Co(gly)(en)_2]^{2+}$	20.3(2.02) 28.5(2.05)	20.8(−0.020) {26.0(+0.0003) {28.6(−0.005)
$[Co(DL\text{-ala})(en)_2]^{2+}$	20.3(2.00) 28.5(2.02)	20.8(−0.020) {26.2(+0.0003) {28.8(−0.005)

a) The complex of D or DL ligand also shows the identical spectra. b) The L-leucine and L-threonine complexes show the MCD spectra nearly identical to that of the L-serine complex. c) The L-valine and L-proline complexes show the MCD spectra nearly identical to that of the L-phenylalanine complex.

Table 2. Splitting of the first d-d band

Complex	Calcd position of component a)			MCD peak observed
	$E(C_{4v})$	$A_2(C_{4v})$	Weighted mean	
$[Co(NH_3)_5(OCOCHRNH_3)]^{3+}$	19.6	21.0	20.1	19.1
$[Co(NH_2CHRCO_2)(NH_3)_4]^{2+}$	19.8, 19.9	21.1	20.3	20.4
$[Co(NH_2CHRCO_2)(en)_2]^{2+}$	20.1, 20.1	21.4	20.5	20.8

a) The following values of Yamatera's parameters[6] are used: $\delta(NH_3)=0$ (the first band of hexaammine complex is in 21000 cm^{-1}), $\delta(en)=\delta$(N, amino carboxylate) = +400 cm^{-1}, δ(O, chelated amino carboxylate) = −4660 cm^{-1}, and δ(O, unidentate amino acid) = −5500 cm^{-1}, the latter two values of which were calculated from the data of the $E_g(D_{4h})$ bands of *trans*(*O*)-$[Co(gly)_2(en)]^+$ (18870 cm^{-1}) and *trans*(*O*)-$[Co(en)_2(L\text{-Hala})_2]^{3+}$ (18450 cm^{-1}).

splits into two components by the lowering of symmetry, and the Faraday A term is not expected. The MCD peaks of complexes of these types appeared near the mean position of the split components as is seen in Table 2. Thus it is concluded that the negative MCD peaks of these complexes are mainly due to the composed B terms of split components.

References

1) N. Matsuoka and Y. Shimura, *Bull. Chem. Soc. Jpn.*, **49**, 2118 (1976).
2) D. Larcher and M. Gabriel, *J. Inorg. Nucl. Chem.*, **37**, 2117 (1975).
3) J. Fujita, T. Yasui, and Y. Shimura, *Bull. Chem. Soc. Jpn.*, **38**, 654 (1965).
4) T. Yasui, J. Hidaka, and Y. Shimura, *Bull. Chem. Soc. Jpn.*, **39**, 2417 (1966).
5) Y. Shimura, *Bull. Chem. Soc. Jpn.*, **31**, 173 (1958).
6) H. Yamatera, *Bull. Chem. Soc. Jpn.*, **31**, 95 (1958).

BULLETIN OF THE CHEMICAL SOCIETY OF JAPAN, VOL. 51 (6), 1897—1898 (1978)

Esterification of *N*-(Benzyloxycarbonyl)amino Acids and Amino Acids Using BF_3-Etherate as Catalyst

Takashi YAMADA, Nobuyuki ISONO,* Akemi INUI, Toshifumi MIYAZAWA, Shigeru KUWATA, and Hiroshi WATANABE

Laboratory of Chemistry, Faculty of Science, Kōnan University, Okamoto, Higashinada-ku, Kobe 658

(Received August 16, 1977)

Synopsis. Methyl and ethyl esters of *N*-(benzyloxycarbonyl)amino acids were prepared conveniently in good yields using BF_3-etherate as catalyst. Esterification of free amino acids was also examined.

Methyl or ethyl esters of *N*-(benzyloxycarbonyl)amino acids are useful intermediates not only for the peptide syntheses,[1] but also for the preparation of amino aldehydes[2,3] *etc.* While these compounds are usually prepared by benzyloxycarbonylation of amino acid esters, esterification of *N*-(benzyloxycarbonyl)amino acids is also useful and often affords better results than the former.[2] In the latter category, methylation with diazomethane is most widely used. The reagent is, however, highly toxic and known to react with phenol as well as carboxylic acid. Therefore, it is still unsuitable for the large scale preparation. Recently, Meienhofer and his co-workers[4] reported the facile syntheses of

TABLE 2. ETHYL ESTERIFICATION OF *N*-(BENZYLOXYCARBONYL)AMINO ACIDS

Amino acid	Yield (%)	$[\alpha]_D^{20}$ Obsd	$[\alpha]_D^{20}$ Lit (c, solvent)
Gly	95[a]		
Ala	90[b]	−38.4	
Val	90[c]	−19.6	
Leu	91	−30.4	−27.5 (1.0 MeOH)[2]
Phe	99	−13.8	
		−11.2[d]	−10.1 (1.4 EtOH)[2]

a) Mp 35—35.5 °C; lit mp 35.5—36.5 °C.[15] b) Found C, 61.94; H, 6.96; N, 5.61%. c) Found C, 64.18; H, 7.66; N, 5.09%. d) c 1.4, EtOH.

TABLE 1. METHYL ESTERIFICATION OF *N*-(BENZYLOXYCARBONYL)AMINO ACIDS

Amino acid	Yield (%)	Mp (°C) Obsd	Mp (°C) Lit	$[\alpha]_D^t$ Obsd	$[\alpha]_D^t$ Lit (c, solvent, t °C)
Gly	88	oil[f]	24.5—25.5[7]		
Ala	89	46—47	45—46[8]	−36.5	−36.0 (1 MeOH 22)[8]
Val	97	55.5—56.5	54—55[9]	−21.9	−18.9 (1 MeOH 20)[9]
Leu	85	oil		−29.5	
Ile	94	oil		−15.5	−11.5 (1.1 MeOH 20)[2]
Phe	95	oil	oil[3]	−17.1	−15.6 (1.02 MeOH 19)[3]
Tyr	95	92—93	92—93[10]	− 9.7	
				−30.4[g]	−32.7 (2 DMF 23)[10]
Ser	93	oil	oil[11]	−14.2	−12.5 (1 MeOH 22)[11]
Thr	92	89—90	90—91[12]	−18.7	−17.3 (1 MeOH 21)[12]
Met	71	oil		−35.6	−34.1 (1.1 MeOH 20)[2]
Cys[a] | Cys	95	71—73	71—73[13]	−96.7	−105 (2 MeOH 22)[13]
Trp	95	oil		−11.8	−11.4 (1.1 MeOH 20)[2]
His[b]	57	75—77		−12.1	
Asp[c]	85	oil	oil[8]	−20.4	
				+27.5[h]	+29.4 (1 $CHCl_3$ 22)[8]
Asn	87	151—152	150[14]	−17.4	
				− 0.9[i]	− 2.0 (AcOH 20)[14]
Glu[c]	94	oil		−22.6	
Pro	94	oil		−64.0	−57.3 (1.0 MeOH 20)[2]
Lys[d]	85	oil		−13.3	−13.0 (1.1 MeOH 20)[2]
Arg[e]	59	oil		−16.0	

a) *N*,*N*′-Bis(benzyloxycarbonyl) derivative. b) Reaction time, 6 h. c) Dimethyl ester. d) α,ε-Bis(benzyloxycarbonyl) derivative. e) Reaction time, 6 h. Isolated as boron trifluoride monohydrate of the ester (Found: C, 44.28; H, 5.99; N, 13.16%). f) The structure was confirmed by comparing its IR and NMR spectra with those of the authentic sample prepared by methylating Z–Gly–OH with diazomethane. g) c 1, DMF, 20 °C. h) c 1, $CHCl_3$, 22 °C. i) c 1, AcOH, 20 °C.

* Present address: Daigo Nutritive Chemicals, Ltd., 12-44, Nonakakita-2-chome, Yodogawa-ku, Osaka.

Table 3. Methyl esterification of amino acids (esters were isolated as *p*-toluenesulfonates)

Amino acid	Yield (%)	Mp (°C)		$[\alpha]_D^t$		
		Obsd	Lit[16]	Obsd	Lit	(*c*, solvent, *t* °C)[16]
Gly	14	115—116	116—117			
Ala	44	105—106		+ 3.7		
Val	60	174—175	175—176	+12.7	+13.4	(10 MeOH 23)
Leu	71	173—174	175.5—176	+11.5	+11.6	(6.9 MeOH 19—23)
Phe	82	162—163	162—162.5	+10.2	+13.1	(7.5 MeOH 19—23)
Glu[a]	73	127—129	130—130.5	+14.5	+15.8	(8.0 MeOH 19—23)

a) Diester.

protected amino acid esters by alkylating their cesium salts.

In another attempt at finding a mild esterification method, we thus utilized the reaction of carboxylic acid with alcohol, using boron trifluoride–etherate as catalyst, which was reported by Kadaba and his coworkers.[5] This method has previously been applied to the preparation of ε-*N*-benzyloxycarbonyl-L-lysine ester by Coggins *et al.*[6] We could successfully extend this method to the esterification of a series of *N*-(benzyloxycarbonyl)amino acids. The results thus obtained are summarized in Tables 1 and 2. The method was very convenient and required neither special apparatus nor complicated manipulation: the alcoholic solution of *N*-(benzyloxycarbonyl)amino acid was refluxed for a short time in the presence of boron trifluoride–etherate. But the reactions of histidine and arginine were exceptionally slow (6 h-reflux was required) and the latter ester was isolated as boron trifluoride salt after the usual work-up.

Moreover, we tried to apply this method to free amino acids. The results are summarized in Table 3. While the results were not as good as in the cases of the *N*-protected amino acids, some lipophilic amino acids gave good results. It should be noted here that washing with water or a saturated aqueous sodium chloride solution, after neutralization of the reaction product, should be avoided, because any washing process markedly decreased the yield and the omission of this process had no influence upon the purity of the ester.

Experimental

The melting points are uncorrected. Optical rotations were measured on a Yanagimoto Polarimeter OR-10 for 1% solutions in methanol at 20 °C unless otherwise stated. The amino acids used in this experiment, except glycine, are all of L-configuration.

Esterification of N-*(Benzyloxycarbonyl)amino Acid.* A solution of *N*-(benzyloxycarbonyl)amino acid (4.76 mmol) in absolute methanol or ethanol (20 ml) was refluxed for 1 h in the presence of BF_3–etherate (10 mmol, 2.1 equivalent). After the solvent was evaporated, the residue was treated with ice–water (40 ml), and extracted with ethyl acetate. The extract was successively washed with water, 1M aqueous sodium hydrogencarbonate solution, and water, and dried over anhydrous sodium sulfate. After removal of the solvent under reduced pressure, almost analytically pure ester was obtained.

Esterification of Amino Acid. A mixture of a finely ground amino acid (2 mmol) and BF_3–etherate (10 mmol) in absolute methanol was refluxed for 24 h. After removal of the solvent, the residue was dissolved in ethyl acetate or ether, neutralized with a saturated aqueous solution of potassium carbonate, and dried over anhydrous sodium sulfate for 1 h. Into this solution was added *p*-toluenesulfonic acid (2 mmol) in ethyl acetate. After 1 h the separated crystals were collected.

References

1) M. Bodanszky, Y. S. Klausner, and M. A. Ondetti, "Peptide Synthesis," 2nd ed, John Wiley & Sons, New York (1976), p. 85.
2) A. Ito, R. Takahashi, and Y. Baba, *Chem. Pharm. Bull.*, **23**, 3081 (1975).
3) A. Ito, R. Takahashi, C. Miura, and Y. Baba, *Chem. Pharm. Bull.*, **23**, 3106 (1975).
4) S.-S. Wang, B. F. Gisin, D. P. Winter, R. Makofske, I. D. Kulesha, C. Tzougraki, and J. Meienhofer, *J. Org. Chem.*, **42**, 1286 (1977).
5) P. K. Kadaba, *Synth. Commun.*, **4**, 167 (1974), and references cited therein.
6) J. Coggins, R. Demayo, and N. L. Benoiton, *Can. J. Chem.*, **48**, 385 (1970).
7) G. Tadema, E. Harryvan, H. J. Panneman, and J. F. Arens, *Recl. Trav. Chim. Pays-Bas*, **83**, 345 (1964).
8) D. Keglević, A. Kornhauser, and Š. Valenteković, *Carbohyd. Res.*, **22**, 245 (1972).
9) M. Miyoshi, *Bull. Chem. Soc. Jpn.*, **46**, 1489 (1973).
10) M. Kinoshita and H. Klostermeyer, *Justus Liebigs Ann. Chem.*, **696**, 226 (1966).
11) E. Schröder, *Justus Liebigs Ann. Chem.*, **670**, 127 (1963).
12) E. Schröder and H. Gibian, *Justus Liebigs Ann. Chem.*, **656**, 190 (1962).
13) C. Zioudrou, M. Wilchek, and A. Patchornik, *Biochemistry*, **4**, 1811 (1965).
14) M. Bergmann and L. Zervas, *Ber.*, **65**, 1192 (1932).
15) A. E. Barkdoll and W. F. Ross, *J. Am. Chem. Soc.*, **66**, 951 (1944).
16) J. M. Theobald, M. W. Williams, and G. T. Young, *J. Chem. Soc.*, **1963**, 1927.

BULLETIN OF THE CHEMICAL SOCIETY OF JAPAN, VOL. 51 (6), 1899—1900 (1978)

Resolution of α-Formyl-ε-acyl-DL-lysines by Acylase

Yoshihiro MINEMATSU, Yasuyuki SHIMOHIGASHI, Michinori WAKI, and Nobuo IZUMIYA

Laboratory of Biochemistry, Faculty of Science 33, Kyushu University, Higashi-ku, Fukuoka 812

(Received August 16, 1977)

Synopsis. Taka-acylase hydrolyzed an α-formyl derivative of ε-acyl-L-lysine faster than the corresponding α-acetyl derivative. Preparative resolution by crude Taka-acylase afforded ε-formyl or ε-benzyloxycarbonyl-L-lysine from the corresponding α-formyl-ε-acyl-DL-lysine. The action of *p*-toluenesulfonic acid on α-formyl-ε-benzyloxycarbonyl-D-lysine under mild conditions afforded pure ε-benzyloxycarbonyl-D-lysine.

Many ε-acyl-L-lysines have been prepared by enzymatic resolution. For example, Chibata *et al.* prepared ε-benzoyl-L-lysine by the resolution of α-Ac-ε-benzoyl-DL-lysine[1] with Taka-diastase,[2] and Izumiya *et al.* ε-benzoyl-L-lysine from ε-benzoyl-DL-lysinamide by hog kidney amidase.[3] From recent findings that For-L-phenylalanine is hydrolyzed most rapidly among series of acyl-L-phenylalanines by Taka-acylase, we have undertaken the resolution of α-For-ε-acyl-DL-lysines by crude Taka-acylase. α,ε-Diformyl-DL-lysine was prepared by the action of formic anhydride[4] on free DL-lysine, and α-For-ε-Z-DL-lysine by that on ε-Z-DL-lysine.

Prior to the preparative resolution of α-For-ε-acyl-DL-lysines, their optimum pH values were determined by using reference compounds such as α-Ac-ε-Z-DL-lysine and Ac-DL-phenylalanine (Table 1). The hydrolytic rates of α-formyl derivatives and reference compounds at various concentrations were determined at each optimum pH, the relative hydrolytic rates at 0.005 M concentration being given in Table 1. The results indicate that α-For-ε-Z-L-lysine is more susceptible than the corresponding α-acetyl derivative. Although α,ε-diformyl-L-lysine is less susceptible than α-For-ε-Z-L-lysine, the resolution of α,ε-diformyl-DL-lysine might be achieved with a slightly increased amount of crude Taka-acylase. Actually, ε-For(or Z)-L-lysine and α-For-ε-For(or Z)-D-lysine were isolated in good yields from the incubation mixture of α-For-ε-For(or Z)-DL-lysine (see Experimental).

We have attempted selective removal of formyl group by a solution-phase procedure. α-For-ε-Z-D-lysine dissolved in aqueous dioxane was treated with one equivalent of *p*-toluenesulfonic acid at 50 °C, the reaction mixture being examined by TLC at selected intervals. After *ca.* 6 h an α-formyl group in the compound was removed, the ε-benzyloxycarbonyl group remaining intact. Wünsch and Fürst reported that by heating a suspension of α-For-*O*-benzyl-D-serine in 1 M hydrobromic acid until dissolution, *O*-benzyl-D-serine was isolated.[5]

Table 1. Optimum pH and relative hydrolytic rate of α-acylamino acids by crude Taka-acylase

Substrate[a]	Optimum pH	Relative hydrolytic rate
Ac-DL-Phe-OH	7.5	1.0
For-DL-Lys(For)-OH	7.1	1.25
For-DL-Lys(Z)-OH	7.4	2.9
Ac-DL-Lys(Z)-OH	7.6	0.72

a) Substrate concentration in respect to L-form, 0.005 M.

Experimental

The amino acid derivative was determined with a Hitachi amino acid analyzer KLA-5 with spherical resin under the following conditions: flow rate, 30 ml/h; jacket temperature, 55 °C.

For-DL-Lys(For)-OH. DL-Lysine monohydrochloride (3.65 g, 0.02 mol) dissolved in water (15 ml) was put on a column (2×10 cm) of Dowex 50X8 (H^+ form). The column was washed with water and eluted with 2 M NH_4OH (80 ml). The eluate was evaporated *in vacuo*. Evaporation was repeated several times by addition of water, and the residue was dissolved in 99% formic acid (84 ml). Acetic anhydride (28 ml, 0.28 mol) was added to the solution at 0 °C under stirring . After being stirred at 0 °C for 2 h and at room temperature overnight, the solution was evaporated, and the residual solid was recrystallized from EtOH–acetone; yield, 2.71 g (67%); mp 143—144 °C.

Found: C, 47.27; H, 6.96; N, 13.54%. Calcd for $C_8H_{14}O_4N_2$: C, 47.52; H, 6.98; N, 13.86%.

For-DL-Lys(Z)-OH. H-DL-Lys(Z)-OH[6] (0.02 mol) in 99% formic acid (42 ml) was treated with acetic anhydride (0.14 mol) as described above. The residual solid was recrystallized from EtOH–water; yield, 88%; mp 116—117 °C.

Found: C, 58.33; H, 6.56; N, 9.00%. Calcd for $C_{15}H_{20}O_5N_2$: C, 58.43; H, 6.54; N, 9.09%.

Ac-DL-Lys(Z)-OH. This was prepared by the following procedure in a better yield than in the previous synthesis, in which H-DL-Lys(Z)-OH was treated with acetic anhydride and sodium hydroxide.[6] A suspension of H-DL-Lys(Z)-OH (0.01 mol) in AcOH (10 ml) and acetic anhydride (0.014 mol) was refluxed for 10 min. The resulting solution was evaporated, evaporation being repeated several times by addition of water. The residual solid was recrystallized from EtOH–water; yield, 89%; mp 115—116 °C. Reported values; yield, 66%; mp 114 °C.[6]

Crude Taka-acylase. This was prepared by a procedure almost the same as that of Shimohigashi *et al.*[7] Takadiastase powder (200 g) was suspended in water (1100 ml), the insoluble material being filtered off at 0 °C. The filtrate was treated with $(NH_4)_2SO_4$ (165 g, 0.26 saturation) and centrifuged at 0 °C. The supernatant phase was brought to 0.85 saturation with $(NH_4)_2SO_4$ (375 g) and centrifuged. The sediment was suspended in 30% acetone (400 ml) at −5 °C and the suspension was centrifuged. The sediment was dissolved in a small amount of water, dialyzed, and lyophilized; yield of crude Taka-acylase, 1.21 g.

Determination of Optimum pH. To a solution of acyl-DL-amino acid (0.02 mmol) and 0.1 M NaOH (0.2 ml) in a 2-ml flask were added 1/7 M sodium barbital buffer (1 ml) with a specified pH, 1/80 M $CoCl_2$ (0.2 ml), and an aqueous enzyme

solution (0.2 ml) containing a specified weight. The solution was made up to 2.0 ml with water. The reaction mixture was incubated at 38 °C, an aliquot being withdrawn after 1 h. Appearance of L-amino acid was determined with an amino acid analyzer: column, 0.6×10 cm; buffer, standard 0.2 M sodium citrate at pH 3.25 for H-L-Lys(For)-OH, pH 4.25 for H-L-Phe-OH, and pH 5.28 for H-L-Lys(Z)-OH. Calculation of each L-amino acid produced was made on the basis of the color value determined for the corresponding authentic amino acid with the analyzer.

Determination of Relative Hydrolytic Rate of α-Acylamino Acids by Taka-acylase. A mixture of an acyl-DL-amino acid (0.02 mmol), 0.1 M NaOH (0.2 ml), 1/7 M sodium barbital buffer (1 ml) at optimum pH, 1/80 M $CoCl_2$ (0.2 ml) and an aqueous enzyme solution (0.2 ml) was made up to 2.0 ml with water. The rate of hydrolysis at 38 °C was followed by the analyzer under the conditions described above. The hydrolysis of substrates followed zero-order kinetics within experimental error. The relative hydrolytic rate was calculated by taking the hydrolytic rate of Ac-L-phenylalanine as 1.0.

Resolution of For-DL-Lys(For)-OH. H-L-Lys(For)-OH: For-DL-Lys(For)-OH (2.02 g, 10 mmol) was dissolved in aqueous triethylamine, the pH being adjusted to 7.1. To the solution were added crude Taka-acylase (80 mg), 1/80 M $CoCl_2$ (100 ml), and water. The solution (1000 ml) was left to stand at 38 °C, the pH of the solution being adjusted occasionally to 7.1. After 3 days, pH of the solution was adjusted to 5 with formic acid. A small amount of Norit was added, and the mixture was maintained at 50—60 °C for 10 min. To the filtrate was added Dowex 50X8 (H^+ form) (20 ml) at 0 °C. After a few minutes, the resin was collected and washed with cold water (the combined filtrates were used for the preparation of For-D-Lys(For)-OH). The resin was suspended in 2 M NH_4OH (60 ml) and stirred at room temperature for a few minutes. The filtrate was evaporated, and the residual solid was recrystallized from water–EtOH; yield, 0.79 g (91%); $[\alpha]_D^{20}$ +13.9° (*c* 2, saturated $NaHCO_3$). Reported value; $[\alpha]_D^{26}$ +15.5° (saturated $NaHCO_3$).[8]

For-D-Lys(For)-OH: The combined filtrates obtained above were evaporated, and the residual solid was recrystallized from water–acetone; yield, 0.80 g (75%); mp 119—121 °C; $[\alpha]_D^{20}$ +3.3° (*c* 2, H_2O).

Found: C, 45.64; H, 6.85; N, 13.14%. Calcd for $C_8H_{14}O_4N_2 \cdot 1/2H_2O$: C, 45.49; H, 7.16; N, 13.27%.

H-L-Lys-OH·HCl: To a solution of H-L-Lys(For)-OH (1 mmol) in a mixture (5 ml) of dioxane–water (1: 1, v/v) was added TosOH·H_2O (1.1 mmol). After being left to stand at 50 °C for 10 h, the solution was treated with 2 ml of Dowex 50X8 (H^+ form). The resin was eluted with 2 M NH_4OH. The eluate was evaporated, and the residue was dissolved in water, the pH being adjusted to 7 with 1 M HCl. The solution was evaporated, and the residual solid was recrystallized from water–EtOH; yield, 94%; $[\alpha]_D^{20}$ +20.8° (*c* 2, 5 M HCl). Reported value, $[\alpha]_D^{15}$ +20.5° (5 M HCl).[3]

H-D-Lys-OH·HCl: This was prepared from For-D-Lys-(For)-OH (0.5 mmol) with TosOH·H_2O (1.1 mmol) as described above; yield, 77%; $[\alpha]_D^{20}$ −20.1° (*c* 2, 5 M HCl).

Resolution of For-DL-Lys(Z)-OH. H-L-Lys(Z)-OH: For-DL-Lys(Z)-OH (0.77 g, 2.5 mmol) was dissolved in aqueous triethylamine, the pH being adjusted to 7.4. To the solution were added crude Taka-acylase (16 mg), 1/80 M $CoCl_2$ (25 ml), and water. After the solution (250 ml) had been left to stand at 38 °C for 3 days, the precipitate formed was collected and washed with water, and the combined filtrates were evaporated to a small volume. 6 M HCl was added to the solution until it reached a pH of 3. An oily product was extracted with EtOAc. The extract was used for the preparation of For-D-Lys(Z)-OH. The aqueous layer and the above precipitate dissolved in a small volume of 1 M HCl were put on a column (2.2×5 cm) of Dowex 50X8 (H^+ form). The column was eluted with 2 M NH_4OH (30 ml). The eluate was evaporated, and the residue was recrystallized from water–EtOH; yield; 0.28 g (80%); mp 233—235 °C (dec); $[\alpha]_D^{20}$ +16.7° (*c* 1, 5 M HCl). Reported value; $[\alpha]_D$ +17.3° (2 M HCl).[9]

For-D-Lys(Z)-OH: The extract obtained above was dried (Na_2SO_4) and evaporated. The residual solid was recrystallized from EtOH–water; yield, 0.31 g (79%); mp 93—95 °C; $[\alpha]_D^{20}$ −10.7° (*c* 2, EtOH). Reported values for the L-isomer; mp 74—78 °C; $[\alpha]_D^{24}$ +9.6° (EtOH).[8]

H-D-Lys(Z)-OH: To a solution of For-D-Lys(Z)-OH (0.3 mmol) in a mixture (10 ml) of dioxane–water (9: 1, v/v) was added TosOH·H_2O (0.33 mmol). After being left to stand at 50 °C for 6 h, aqueous triethylamine was added to the solution until its pH became 7, and the solution was evaporated. The residual solid was recrystallized from water–EtOH; yield, 75%; $[\alpha]_D^{20}$ −16.4° (*c* 1, 5 M HCl). Reported value for the L-isomer; $[\alpha]_D$ +17.3° (2 M HCl).[9]

References

1) Abbreviations used: Ac, acetyl; For, formyl; TosOH, *p*-toluenesulfonic acid; Z, benzyloxycarbonyl.

2) I. Chibata, S. Yamada, and S. Yamada, *Bull. Agric. Chem. Soc. Jpn.*, **20**, 174 (1956).

3) N. Izumiya, H. Uchio, and T. Kamata, *Bull. Chem. Soc. Jpn.*, **33**, 66 (1960).

4) J. S. Fruton and H. T. Clarke, *J. Biol. Chem.*, **106**, 667 (1934).

5) E. Wünsch and G. Fürst, *Z. Physiol. Chem.*, **329**, 109 (1962).

6) M. Muraoka and N. Izumiya, *Memoirs Fac. Sci. Kyushu Univ., C*, **7**, 133 (1970).

7) Y. Shimohigashi, S. Lee, and N. Izumiya, *Bull. Chem. Soc. Jpn.*, **49**, 3280 (1976).

8) K. Hofmann, E. Stutz, G. Spühler, H. Yajima, and E. T. Schwartz, *J. Am. Chem. Soc.*, **82**, 3727 (1960).

9) R. Ledger and F. H. C. Stewart, *Aust. J. Chem.*, **18**, 933 (1965).

BULLETIN OF THE CHEMICAL SOCIETY OF JAPAN, VOL. 51 (6), 1901—1902 (1978)

Studies of Quinazoline Pigments. II. Synthesis of Dimethyl Substituted Pyrido[2,1-*b*]pyrido[1′, 2′: 1, 2]pyrimido-[4,5-*g*]quinazoline-7,15-diones

Yasukazu YOKOYAMA

Central Research Laboratory, Toyo Soda Manufacturing Co., Ltd., Tonda, Shin-nanyo-shi, Yamaguchi 746

(Received October 17, 1977)

Synopsis. In the presence of alkali, 4,12-, 3,11-, 2,10-, and 1,9-dimethyl derivatives of 6, 14-dihydropyrido-[2,1-*b*]pyrido[1′,2′:1,2]pyrimido[4,5-*g*]quinazoline-7,15-dione reacted with nitrobenzene to give 2,5-bis(3-, 4-, 5-, and 6-methyl-2-pyridylamino) terephtharic acids. The intramolecular cyclization of 3-, 4-, and 5-methyl derivatives, gave 4,12-, 3,11-, and 2,10-dimethylpyrido[2, 1-*b*]pyrido[1′,2′: 1,2] pyrimido[4, 5-*g*]quinazoline-7,15-dione respectively, but the 6-methyl derivative did not give any cyclization product. The synthesis of the 1,9-dimethyl derivative was accomplished by the dehydrogenation of 1, 9-dimethyl-6, 14-dihydropyrido-[2,1-*b*]pyrido[1′,2′: 1,2]pyrimido[4,5-*g*]quinazoline-7, 15-dione with *p*-chloranil.

Recently, pyrido[2,1-*b*]pyrido[1′,2′: 1,2]pyrimido-[4,5-*g*]quinazoline-7,15-diones (**1**) have been reported to be valuable red pigments with excellent light-fastness and good tinctorial strength, but their published chemistry is still very limited. Although Wiedemann mentioned the synthesis of **1** by the dehydrogenation of 6, 14-dihydropyrido [2, 1-*b*] pyrido [1′, 2′: 1, 2] pyrimido-[4, 5-*g*] quinazoline-7, 15-diones (**2**), he reported no details.[1]

In our previous paper, we described that the dehydrogenation of **2a** with a nitro compound in the presence of alkali is accompanied by ring opening to give 2,5-bis(2-pyridylamino)terephthalic acid (**3a**), which is then cyclized by treatment with acid to form **1a**.[2] This paper will describe the dehydrogenation of **2b**—**e** under alkali conditions to give **1b**—**e**.

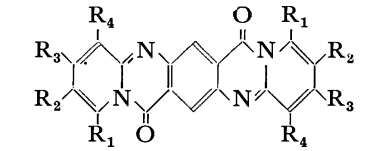

1

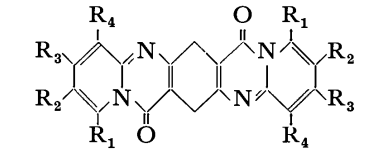

2

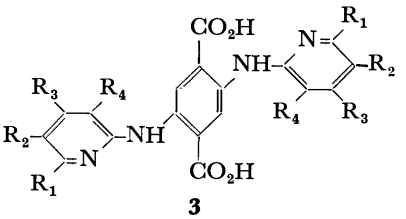

3

a : $R_1=R_2=R_3=R_4=H$
b : $R_1=R_2=R_3=H$, $R_4=CH_3$
c : $R_1=R_2=R_4=H$, $R_3=CH_3$
d : $R_1=R_3=R_4=H$, $R_2=CH_3$
e : $R_2=R_3=R_4=H$, $R_1=CH_3$

Results and Discussion

Diethyl 2,5-dioxocyclohexane-1,4-dicarboxylate reacts with 2-aminopyridine or substituted 2-aminopyridines under acid catalysis to give **2**.[1,3] In glacial acetic acid, **2a** was obtained in an 80% yield, but the yields of **2b**—**d** were 50—65%. In the case of **2e**, under the same reaction conditions, only a 16% conversion was observed (Table 1). The low yield of **2e** is attributable to the steric hindrance of the methyl group.

The reactions of **2b**—**d** with nitrobenzene in the

Table 1. Physical properties of compounds **2**, **3**, and **1**

Compound	**2** Yield %	**2** NMR (δ)[a] $H_{6,14}$	**2** NMR (δ)[a] CH_3	**3** Found (Calcd) N%	**3** IR (cm^{-1}) νC=O	**3** NMR (δ)[b] phenyl	**3** NMR (δ)[b] CH_3	**1** Yield[c] %	**1** Color	**1** Found (Calcd) N%	**1** IR (cm^{-1}) νC=O	**1** NMR (δ)[a] $H_{6,14}$	**1** NMR (δ)[a] CH_3
a	80	4.36 s 4H	—	15.97 (16.00)	1685	8.50 s 2H	—	97	red	17.79 (17.83)	1690	9.00 s 2H	—
b	50	4.39 s 4H	2.80 s 6H	14.81 (14.81)	1690	9.06 s 2H	2.30 s 6H	76	orange	16.52 (16.37)	1695	9.12 s 2H	2.87 s 6H
c	60	4.30 s 4H	2.78 s 6H	14.88 (14.81)	1680	8.43 s 2H	2.28 s 6H	97	red	16.46 (16.37)	1690	8.92 s 2H	2.80 s 6H
d	65	4.32 s 4H	2.67 s 6H	14.76 (14.81)	1680	8.41 s 2H	2.22 s 6H	97	red	16.18 (16.37)	1680	8.98 s 2H	2.68 s 6H
e	16	4.10 s 4H	3.22 s 6H	14.32 (14.81)	1670	8.04 s 2H	2.40 s 6H	69	orange	16.32 (16.37)	1690	8.72 s 2H	3.28 s 6H

a) Measured in CF_3COOH, with TMS as the internal standard. b) **3a**—**d**: in CD_3OD–NaOD; internal standard: TMS, **3e**: in D_2O–NaOD; internal standard: TSP. c) In overall yield from **2**.

presence of alkali gave **3b—d**, which cyclized easily to **1b—d** under acidic conditions. Since **3e** was not cyclized to **1e** under the same conditions, the synthesis of **1e** was achieved by heating **2e** with chloranil in glacial acetic acid. Some pertinent data on **1**, **2**, and **3** are compared in Table 1.

The hydrolytic ring opening of **1e** took place both in aqueous sulfuric acid and in alkali. On the other hand, **1a—d** were hydrolyzed in aqueous alkali, but not in acid. The ring opening of the same ring system has been studied. That is, it has been reported that the ring opening of 3-ethoxycarbonyl-6-methylpyrido[1,2-*a*]-pyrimidin-4-one is accelerated by the methyl group at the 6-position.[4]

Compounds **1b—e** are red to orange crystals, soluble in aqueous sulfuric acid but only sparingly soluble in organic solvents.

Experimental

The IR spectra were taken with a Shimadzu IR-27G spectrophotometer, while the NMR spectra were determined with a Varian HA-100 high-resolution NMR spectrometer.

*6,14-Dihydropyrido[2,1-*b*]pyrido[1',2': 1,2]pyrimido[4,5-*g*]quinazoline-7,15-diones (**2**).* The reactions of diethyl 2,5-dioxocyclohexane-1,4-dicarboxylate and 2-aminopyridines were carried out according to the methods reported by Wiedemann[1] and the products, **2a—e**, were characterized in the way described in the literature.[2] The yields of **2a—e** are listed in Table 1.

*Dimethylpyrido[2,1-*b*]pyrido[1',2': 1,2]pyrimido[4,5-*g*]quinazoline-7,15-diones (**1b—e**).* *a*): A mixture of 5.0 g of **2b**, 5.0 g of sodium *m*-nitrobenzenesulfonate, 10 g of a 50 wt% aqueous sodium hydroxide solution, and 100 ml of ethylene glycol was placed in a 500-ml round-bottomed flask equipped with a reflux condenser and a mechanical stirrer. The mixture was boiled and stirred under reflux for 2 h. The reaction mixture was allowed to cool to about 60 °C, diluted with 300 ml of cold water, and then neutralized with aqueous sulfuric acid. Pale yellow solids were collected on a filter, washed with water, and dried at 60 °C. IR, NMR, and analytical data are summarized in Table 1. These results proved that this compound was 2,5-bis(3-methyl-2-pyridylamino)terephthalic acid (**3b**).

Into 100 ml of 0.5 M-sulfuric acid, 5 g of **3b** was added after which the mixture was heated at 70—80 °C for 1 h. After cooling, the precipitate was collected by filtration, washed with water, and dried. The red product thus obtained was identified as **1b** on the basis of its IR, NMR, and analytical data. The total yield of **1b** was 3.8 g (76%).

Compounds **3c—e** were also obtained under the same reaction conditions. Compounds **3c—d** cyclized to give **1c—d**, except for **3e**. The yields, products, and analytical data for all the runs are listed in Table 1.

b): A mixture of **2e** (15 g) and chloranil (12 g) was refluxed in glacial acetic acid (300 ml) for 2 h. After the reaction mixture had been cooled, the resulting crystals were collected by filtration and dispersed in 300 g of a 2 wt% aqueous sodium hydroxide solution. The dispersion was filtered, and the resulting reddish orange crystals were thoroughly washed with water and dried to obtain 10.3 g of **1e**. Its IR, NMR, and analytical data are shown in Table 1.

*Ring Opening of **1a—e** (General Method).* Compound **1a** (5.0 g) was heated in a 1 M aqueous sodium hydroxide solution (100 ml) for 3 h. Then the solution was neutralized with aqueous sulfuric acid. The precipitated **3a** (5.3 g) was filtered off as pale yellow crystals.

References

1) W. Wiedemann, Ger. Offen., 2237679 (1974); *Chem. Abstr.*, **80**, 126755v (1974).

2) Y. Yokoyama and E. Iwamoto, *Nippon Kagaku Kaishi*, **1977**, 382.

3) Y. Yokoyama, K. Shibata, O. Fujii, and E. Iwamoto, *Bull. Chem. Soc. Jpn.*, **48**, 591 (1975).

4) G. Naray-Szabo, I. Hermecz, and Z. Meszaros, *J. Chem. Soc., Perkin Trans. I*, **1974**, 1753.

BULLETIN OF THE CHEMICAL SOCIETY OF JAPAN, VOL. 51 (6), 1903—1904 (1978)

Studies on Nucleosides and Nucleotides. VI.[1] A Facile Cleavage of the Anhydro Bond of 2′,3′-*O*-Isopropylidene-O^2,5′-cyclouridine with the Use of Proton Acid or Lewis Acid

Junji KIMURA and Oyo MITSUNOBU

Department of Chemistry, College of Science and Engineering, Aoyama Gakuin University, Chitosedai, Setagaya-ku, Tokyo 157

(Received November 9, 1977)

Synopsis. When 2′,3′-*O*-isopropylidene-O^2,5′-cyclouridine (**1**) was allowed to react with methanol in the presence of *p*-toluenesulfonic acid at room temperature, 5′-*O*-methyl-2′,3′-*O*-isopropylideneuridine was obtained in good yield. Similarly, with the use of boron trifluoride etherate, **1** reacted smoothly with diphenyl phosphate to give the corresponding 5′-phosphorylated product.

Cyclonucleosides are versatile reagents for the synthesis of nucleoside derivatives.[2] Except for a few cases, however, the reactions of cyclonucleosides with nucleophiles were carried out under rather drastic conditions.[3] It is, therefore, of interest to find out the conditions under which the anhydro bond of cyclonucleosides easily cleaves.[4]

We wish to report herewith a facile cleavage of 2′,3′-*O*-isopropylidene-O^2,5′-cyclouridine by nucleophiles in the presence of a proton acid or Lewis acid.

It is known that the cleavage of O^2,5′-cyclouridine occurs in two directions. As an example, 2′,3′-*O*-isopropylidene-O^2,5′-cyclouridine (**1**) reacts with methanol to form O^2-methyl-2′,3′-*O*-isopropylideneuridine.[5] On the other hand, it reacts with phosphate ester to give 5′-phosphorylated uridine.[3a,b]

These results suggest that, when N^3-position of uracil moiety is first protonated, 5′-substituted uridines are predominantly formed. For the sake of clarification, we examined the reaction of **1** with methanol in the presence of a proton acid.

When a solution of **1** in dry methanol was stirred with an equimolar amount of *p*-toluenesulfonic acid at room temperature for 1 day, 5′-*O*-methyl-2′,3′-*O*-isopropylideneuridine[6] was obtained as expected in 80% yield. The 5′-*O*-tosyl-2′,3′-*O*-isopropylideneuridine was treated with methanol at room temperature for 1 day. The starting material was recovered quantitatively. The possibility of intermediary formation of the tosylate in the above reaction was thus ruled out. The reaction seems to proceed through initial protonation of uracil moiety followed by the attack of methanol on the 5′-carbon atom.

The reaction was further applied to phosphorylation of uridine. When **1** was reacted with diphenyl phosphate in the presence of *p*-toluenesulfonic acid in tetrahydrofuran (THF) at room temperature, 5′-*O*-tosyl-2′,3′-*O*-isopropylideneuridine[7] was unexpectedly obtained in 81% yield. On the other hand, when the reaction was carried out in the presence of trifluoroacetic acid, 2′,3′-*O*-isopropylideneuridine 5′-(diphenyl)phosphate (**2**) was isolated in 58% yield. The yield of **2** increased to 77%, when a solution of **1** and diphenyl phsophate in THF was stirred with boron trifluoride etherate at room temperature for 2 h. This shows that boron trifluoride activates the O^2,5′-anhydro bond by interaction with N^3(or O^4)-position of uracil moiety.

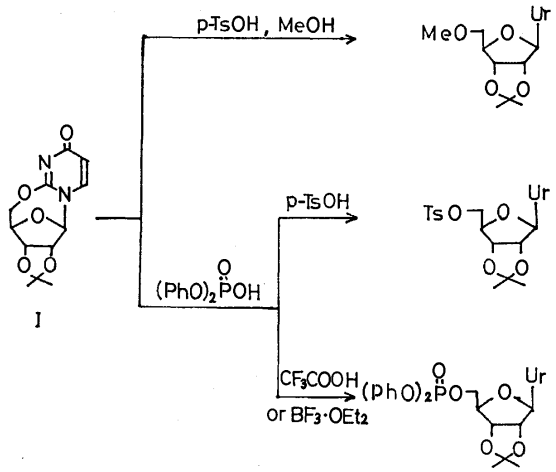

In order to obtain a carbon-carbon bond at the 5′-position of uridine, we studied the reaction of **1** with silyl enol ether in the presence of Lewis acid. A solution of 2′,3′-*O*-isopropylidene-O^2,5′-cyclouridine and cyclohexanone trimethylsilyl enol ether in THF was stirred with boron trifluoride at room temperature for 2 h. Examination by TLC revealed the formation of several products. No attempt was made to identify the products. Next, **1** was allowed to react with two molar equivalents of the silyl enol ether and titanium(IV) chloride[8] at 0 °C for 30 min. 5′-Chloro-5′-deoxy-2′,3′-*O*-isopropylideneuridine[9] was unexpectedly obtained in 84% yield.

2′,3′-*O*-Isopropylidene-O^2,5′-cyclouridine was allowed to react with benzylmagnesium bromide in THF at room temperature for 3 h to form 5′-bromo-5′-deoxy-2′,3′-*O*-isopropylideneuridine (79%).[9] So far no report seems to have appeared on halogenation with the use of Grignard reagents. The reason why no benzylation takes place is not obvious.

Experimental

5′-O-Methyl-2′,3′-O-isopropylideneuridine. A solution of **1** (266 mg, 1 mmol) in dry methanol (25 ml) was stirred with *p*-toluenesulfonic acid (190 mg, 1 mmol) in the presence of molecular sieve at room temperature for 1 day and the resulting mixture was evaporated *in vacuo*. The product was separated by preparative TLC (Merck silica gel PF_{254}, 20× 30 cm plate, developing solvent; ethyl acetate) to give 238 mg (80%) of 5′-*O*-methyl-2′,3′-*O*-isopropylideneuridine (foamy glass, λ_{max}^{MeOH} 262 nm λ_{min} 231 nm, NMR ($CDCl_3$–TMS) δ 10.22

(1H, br s, N^3H) 3.41 (3H, s, OCH_3).[6]

Reactions of **1** *with Diphenyl Phosphate. In the Presence of* p-*Toluenesulfonic Acid*: 2′,3′-*O*-Isopropylidene-O^2,5′-cyclouridine (1 mmol) was stirred with diphenyl phosphate (500 mg, 2 mmol) in the presence of *p*-toluenesulfonic acid (1 mmol) in THF (5 ml) at room temperature for 1 day. The reaction mixture was separated by preparative TLC (developing solvent; ethyl acetate). 5′-*O*-Tosyl-2′,3′-*O*-isopropylideneuridine was obtained in 81% yield (mp 152—154 °C, recrystallization from methanol, λ_{max}^{MeOH} 226 nm (ε 12500), 260 nm (ε 8500), λ_{min} 241 nm).[7] No phosphorylated product was obtained.

In the Presence of Trifluoroacetic Acid: When trifluoroacetic acid (*ca.* 2 mmol), instead of *p*-toluenesulfonic acid, was used in the above reaction, 2′,3′-*O*-isopropylidene 5′-(diphenyl)-phosphate (**2**) was isolated in 58% yield by preparative TLC (developing solvent; chloroform: methanol=10: 1). Rechromatography was carried out with ethyl acetate (colourless glass, λ_{max}^{MeOH} 261 nm, λ_{min} 230 nm, NMR($CDCl_3$–TMS) δ 10.10 (1H, s, N^3H) 7.19 (11H, PhO–, C^6H)).

In the Presence of Boron Trifluoride Etherate: The yield of **2** increased to 77% when a solution of **1** and diphenyl phosphate in THF was stirred with boron trifluoride etherate at room temperature for 2 h.

Attempts to form Carbon-Carbon Bond. Use of Titanium-(IV) Chloride: Titanium(IV) chloride (1 mmol) was added to a solution of 1 (1 mmol) and cyclohexanone silyl enol ether (170 mg, 2 mmol) in THF (5 ml) at 0 °C. After 30 min, satd. aqueous sodium hydrogen carbonate solution (2 ml) was added. The product was extracted with chloroform (5 ml×2) and separated by preparative TLC (developing solvent; ethyl acetate). 5′-Chloro-5′-deoxy-2′,3′-*O*-isopropylideneuridine was obtained in 84% yield (mp 178—179 °C, lit,[9] 175.5—176.5 °C) and 10% of 2′,3′-*O*-isopropylideneuridine was recovered.

Use of Grignard Reagent: A suspension of **1** (1 mmol) in THF (1 ml) was added to a freshly prepared solution of benzylmagnesium bromide (3 mmol) in THF (3 ml) at 0 °C. The reaction mixture was kept stirring at room temperature for 2 h and to it was added satd. aqueous ammonium chloride solution (20 ml). The solution was extracted with chloroform (20 ml×3) and the organic layer was evaporated *in vacuo*. 5′-Bromo-5′-deoxy-2′,3′-*O*-isopropylideneuridine was obtained in 79% yield (mp 187—189 °C, lit,[9] 184—186 °C) by preparative TLC (developing solvent; chloroform: ethyl acetate=1:1).

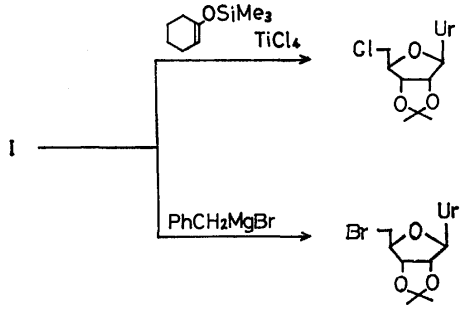

This work was carried out with financial support from the Ministry of Education.

References

1) Part V: S. Shimokawa, J. Kimura, and O. Mitsunobu, *Bull. Chem. Soc. Jpn.*, **49**, 3357 (1976).

2) J. J. Fox, *Pure Appl. Chem.*, **18**, 223 (1969); M. Ikehara, *Acc. Chem. Res.*, **2**, 47 (1969); M. Ikehara and T. Ueda, *Yuki Gosei Kagaku Kyokaishi*, **32**, 402 (1974).

3) a) J. Zemlicka and J. Smrt, *Tetrahedron Lett.*, **1964**, 2081; b) J. Nagyvary, *Biochemistry*, **5**, 1316 (1966); c) J. P. H. Verheyden, D. Wagner, and J. G. Moffatt, *J. Org. Chem.*, **36**, 250 (1971) and refs. therein.

4) 2′,3′-*O*-Isopropylidene-O^2,5′-cyclouridine reacts with tributylammonium salt of (*O*-benzyl phosphoric)benzoic anhydride at 37 °C in dioxane. Y. Mizuno, T. Sasaki, T. Kanai, and H. Igarashi, *J. Org. Chem.*, **30**, 1533 (1965).

5) D. M. Brown, A. R. Todd, and S. Varadarajan, *J. Chem. Soc.*, **1957**, 868.

6) J. T. Kusmierek, J. Giziewicz, and D. Shugar, *Biochemistry*, **12**, 194 (1973).

7) P. A. Levene and R. S. Tipson, *J. Biol. Chem.*, **106**, 113 (1934).

8) Mukaiyama *et al.* have extensively studied the reaction of silyl enol ether with various substrates in the presence of $TiCl_4$. *Cf. e. g.* K. Narasaka, K. Soai, Y. Aikawa, and T. Mukaiyama, *Bull. Chem. Soc. Jpn.*, **49**, 779 (1976).

9) J. P. H. Verheyden and J. G. Moffatt, *J. Org. Chem.*, **37**, 2289 (1972); Y. Fujisawa and O. Mitsunobu, *J. Chem. Soc., Chem. Commun.*, **1973**, 201.

BULLETIN OF THE CHEMICAL SOCIETY OF JAPAN, VOL. 51 (6), 1905—1906 (1978)

A Proton Magnetic Resonance Study of the Amide Configurations of 2-Acetoacetamido Derivatives of 4-Methylpyridine and Pyrimidine

Michio KONDO

Central Research Laboratories, Sankyo Co., Ltd., Hiromachi 1-2-58, Shinagawa-ku, Tokyo 140

(Received November 9, 1977)

Synopsis. It has been found by ^{1}H NMR spectroscopy that 2-acetoacetamido-4-methylpyridine (**1**) and 2-acetoacetamidopyrimidine (**2**) exist predominantly in keto forms in $CDCl_3$ and DMSO. The amide group of **1** seems to be in a *s-trans* configuration in both solvents, whereas that of **2** is in a *s-cis* form in $CDCl_3$, but predominantly in a *s-trans* isomer in DMSO at room temperature. Configurations of the enol forms are discussed.

It is well known that β-diketones and a number of derivatives of acetoacetic acid undergo keto-enol tautomerism in solution and that ^{1}H NMR spectroscopy has been used as a powerful tool to study such kinds of equilibrium.[1] However, only a few papers have been concerned with acetoacetamide derivatives, which have been proved to exist predominantly as keto forms.[2,3]

It is also familiar that *N*-monosubstituted amides undergo *cis-trans* rotational isomerism and that the isomers are almost all *s-trans* in the cases of acetylamino and higher acylamino derivatives.[4] For a few acetanilides with bulky ortho substituents, it has been reported that the *s-cis* isomers are appreciable.[5] The terms *s-cis* and *s-trans* refer to the relative location of the NH and CO group about the amide bond.

This paper will be concerned with 2-acetoacetamido-4-methylpyridine and 2-acetoacetamidopyrimidine, which undergo keto-enol tautomerism and *cis-trans* isomerism concurrently.

Experimental

2-Acetoacetamido-4-methylpyridine (**1**) was prepared according to the literature method.[6] Commercial 2-acetoacetamidopyrimidine (**2**) was purified by recrystallization from water.

The ^{1}H NMR spectra were recorded on A Varian XL-100A-15 spectrometer, using TMS as the internal standard. In all spectra, the pulsed Fourier transform (FT) operation was utilized. The concentrations were 0.3—0.5% w/v.

Results and Discussion

Signal Assignment. The ^{1}H NMR spectra of **1** and **2** in $CDCl_3$ and DMSO seem to be explainable in terms of two molecular species, a keto and an enol tautomer, with preponderance of the keto tautomer (85—92%). The olefinic and the methylene proton signals almost completely disappeared when **1** and **2** were dissolved in CD_3OD, as did the amide and the enolic proton, on account of the replacement of H by D at the methylene and olefinic sites. The ^{1}H NMR spectra of the aromatic protons were of the first order. Therefore, signal assignment could be done straightforwardly. The chemical shifts thus determined are collected in Table 1. The large magnitude of "acylation shift" observed for the ring proton 3 of **1** suggests a *s-trans* configuration of the amide group of this compound in these solvents, on the basis of extensive studies[4b] concerning the acylation shifts of a number of anilides. Unfortunately, this kind of information was not obtained for **2**, because of the absence of a proton ortho to the acetoacetamide substituent.

Keto Tautomers. The methylene protons of **1** resonate at about the same field in both $CDCl_3$ and DMSO solution (δ 3.59 and 3.63), whereas those of **2** resonate at a very low field in $CDCl_3$ (δ 4.00) and at δ 3.81 in DMSO. These results suggest that the amide configuration of **1** is the same (*s-trans*) in both solvents, but that of **2** is solvent dependent. Lower field resonances of the methylene protons of **2** suggest that these protons are close to an electronegative atom, *e.g.*, the ring nitrogen atom; this can be realized in the *s-cis* configuration (**2A**).

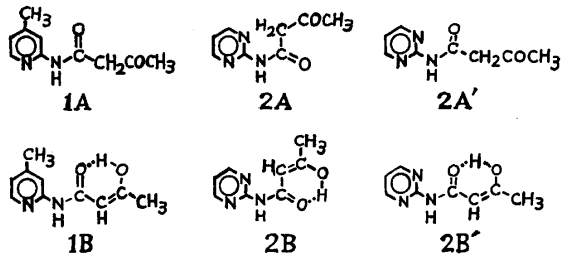

Enol Tautomers. The methyl signals for the enol tautomers are located at fields higher by about 0.25—0.35 ppm than those for the keto tautomers. This value of about 0.3 ppm is very close to that for ethyl acetoacetate, but it is clearly larger than that for acetylacetone.[7] The enolic OH proton resonates at δ 13.5—14.2, intermediate between those for acetylacetone and ethyl acetoacetate (δ 15.6 and 12.2 in pure liquid, respectively[7]). From these results, it is reasonable to explain the enol-spectrum of **1** in terms of structure **1B** or the alternate enol form (**1C**: Ar–HNC(OH)=CHC(=O)CH_3), rather than in terms of a rapidly interconverting state between **1B**⇄**1C**. The olefinic proton signal of **1** in DMSO was observed as a broad quartet (J=0.7 Hz). This favors the structure **1B**. The structures **2B** and **2B′** are preferable to **2C** and **2C′** ((2-pyrimidyl)HNC(OH)=CHC(=O)CH_3) for the same reason (J=0.7 Hz for the DMSO solution).

Other enol forms, Ar–HNCOCHC=(OH)CH_3; Ar: pyridyl or pyrimidyl, which have no intramolecular hydrogen bond between the amide carbonyl oxygen and the enolic OH, could be neglected because of the

Table 1. Chemical shifts (δ) of various protons of **1** and **2**

Compd.	Solvent	Form	CH_3	CH_2	=CH	NH	OH	H-3	H-4(CH_3)	H-5	H-6	p(%)[a]
1	$CDCl_3$	keto	2.33	3.59	—	9.17	—	7.99	2.36	6.88	8.15	88
		enol	1.98	—	5.00	b	13.5	b	b	b	b	12
	DMSO	keto	2.19	3.63	—	10.5	—	7.91	2.31	6.94	8.15	92
		enol	1.90	—	5.37	b	b	b	b	b	b	8
	CD_3OD	keto	2.29					7.94	2.34	6.97	8.12	90
		enol	1.94		(4.83)[c]			b	b	b	b	10
2	$CDCl_3$	keto	2.33	4.00	—	9.60	—	—	8.58	7.00	8.58	85
		enol	2.07	—	6.20	b	14.1	—	8.60	6.99	8.60	15
	DMSO	keto	2.20	3.81	—	10.6	—	—	8.62	7.15	8.62	91
		enol	1.95	—	5.79	10.4	14.2	—	8.64	b	8.64	9
	CD_3OD	keto	2.29						8.59	7.13	8.59	88
		enol	1.98		(4.83)[c]				b	b	b	12

a) Population was estimated from the methyl peak heights of the two isomers. These values are in good agreement with the values obtained from the integration value measured under the CW mode for much concentrated solutions. b) Not identified. c) Averaged signal of the methylene, olefinic, amide, and enolic protons.

results of the ^1H NMR spectroscopic study of ethyl 3-(methylamino)crotonate, where the corresponding species have been found to be minor components.[8]

The olefinic proton of **1** in $CDCl_3$ resonates at δ 5.00, this value being almost the same as those for ethyl acetoacetate and 2′,5′-dichloroacetoacetanilide.[3] This signal shifts downfield a little with the solvent change from $CDCl_3$ to DMSO, as in the case of *N*-(2,5-dichlorophenyl)-3-aminocrotonamides.[9] In contrast to this, the olefinic proton of **2** in $CDCl_3$ resonates at δ 6.20, a field lower by as much as 1.20 ppm than that for **1**; furthermore, this signal even demonstrates an upfield shift of 0.41 ppm upon changing solvents from $CDCl_3$ to DMSO. These facts strongly suggest a solvent dependence of the amide configuration of **2**.

^1H NMR Spectra at Low Temperatures. Because of the low solubility of **2** in $CDCl_3$, recording the ^1H NMR spectra at low temperatures was not attempted. In a mixed solvent of $CDCl_3$ and DMSO (6: 1 v/v), the methylene protons of **2** were observed at δ 3.89 as a singlet at room temperature. Lowering the temperature of this solution below −10 °C caused an appreciable broadening in the methylene-signal and at −40 °C the methylene signal split into a clear doublet (δ 4.11 and 3.74) with about equal intensity. The olefinic proton showed an upfield shift as well as signal-broadening with temperature decrease and at −40 °C it was observed around δ 5.55 as a very broad signal. Further decrease of the temperature caused significant reduction of spectral resolution, probably due to solidification of DMSO. The amide proton shifted downfield a little with temperature decrease and gave an asymmetric signal, due to the occasional overlapping of two signals corresponding to the two rotational isomers. The ring proton signals also showed the expected complexity.

In the case of an acetone solution of **2**, lowering the temperature did not cause any sign of splitting in the methylene signal, which was located at δ 4.01 at room temperature. These results indicate that the chemical shift of the methylene protons well reflects the amide configuration of **2** in the solvents tested. A similar solvent dependence of the amide configuration has been reported for 2-acetamidopyrimidine (**3**).[10]

Conclusion. Compound **2** exists almost exclusively in the *s-cis*-keto and *s-cis*-enol forms in $CDCl_3$, but predominantly in the *s-trans*-keto and *s-trans*-enol in DMSO, though some appreciable contribution of the *s-cis* form cannot be discounted on the basis of a rather large difference of about 0.5 ppm between the olefinic proton resonances of **1** and **2**. A DMSO molecule intermolecularly hydrogen bonded with the amide proton may induce electrostatic repulsion with the amide carbonyl group in the *s-cis* form. This may be one reason why **2** in DMSO favors the *s-trans* form. On the other hand, **1** exists in the *s-trans*-keto and *s-trans*-enol in both solvents, $CDCl_3$ and DMSO.

The electrostatic repulsion between two lone pair electrons on the ring nitrogen and on the carbonyl oxygen, which is unavoidable in the *s-trans* form of **2** but avoidable in **1**, may be responsible for the considerable *s-cis* contribution in **2**.

References

1) J. G. Dawber and M. M. Crane, *J. Chem. Educ.*, **44**, 150 (1967) and references cited therein.

2) R. F. Hobson, L. W. Reeves, and R. C. Shaddick, *Org. Magn. Reson.*, **6**, 129 (1974).

3) M. Kondo, *Bull. Chem. Soc. Jpn.*, **49**, 1719 (1976).

4) a) L. A. LaPlanche and M. T. Rogers, *J. Am. Chem. Soc.*, **85**, 3728 (1963); **86**, 337 (1964); b) R. F. C. Brown, L. Radom, S. Sternhell, and I. D. Rae, *Can. J. Chem.*, **46**, 2577 (1968); c) B. D. Andrews, I. D. Rae, and B. E. Reichert, *Tetrahedron Lett.*, **1969**, 1859.

5) a) H. Kessler and A. Rieker, *Z. Naturforsch.*, **22b**, 456 (1967); b) H. Kessler and A. Rieker, *Justus Liebigs Ann. Chem.*, **708**, 57 (1967).

6) M. Shur and S. S. Israelstam, *J. Org. Chem.*, **33**, 3015 (1968).

7) J. L. Burdett and M. T. Rogers, *J. Am. Chem. Soc.*, **86**, 2105 (1968).

8) A. G. Sanchez, M. T. Aldave, and U. Scheideggar, *J. Chem. Soc., C*, **1960**, 2570.

9) M. Kondo, *Bull. Chem. Soc. Jpn.*, **50**, 2961 (1977).

10) M. Kondo, *Bull. Chem. Soc. Jpn.*, **49**, 1443 (1976).

BULLETIN OF THE CHEMICAL SOCIETY OF JAPAN, VOL. 51 (6), 1907—1908 (1978)

The Fries Rearrangement of *bz*-Benzoyloxybenzofuran Derivatives and the Synthesis of the Furo Derivatives of 4-Phenyl-2*H*-chromen-2-one

Yoshiyuki KAWASE, Seiji YAMAGUCHI, Kumiko AOYAMA, and Michiyo MATSUDA
Department of Chemistry, Faculty of Science, Toyama University, Gofuku, Toyama 930
(Received December 2, 1977)

Synopsis. The Fries rearrangement of 4-, 5-, 6-, and 7-benzoyloxy-2,3-dimethylbenzofurans gave exclusively or mainly the corresponding *o*-hydroxy ketones, which were converted to the dimethylfuro derivatives of 4-phenyl-2*H*-chromen-2-one.

In a previous paper, the Fries rearrangement of *bz*-acetoxy-2,3-dimethylbenzofurans to the corresponding *o*-hydroxy ketones accompanied by small amounts of para isomers in some cases was reported.[1] In the present experiments, the reaction of *bz*-benzoyloxy-2,3-dimethylbenzofurans was studied. In order to investigate their spectra and biological activity, the products were converted into the dimethylfuro derivatives of 4-phenyl-2*H*-chromen-2-one.

In the Fries rearrangement of benzoyloxybenzofuran derivatives, Shah and Shah[2] reported that 6-benzoyloxy-3-methylbenzofuran-2-carboxylic acid gave the corresponding 7-benzoyl-6-hydroxy compound. Royer *et al.*[3] reported the synthesis of the furo derivatives of 4-phenyl-2*H*-chromen-2-one, some of which were prepared by the Pechmann reaction of 2,3-dimethyl-*bz*-hydroxybenzofurans and ethyl benzoylacetate.

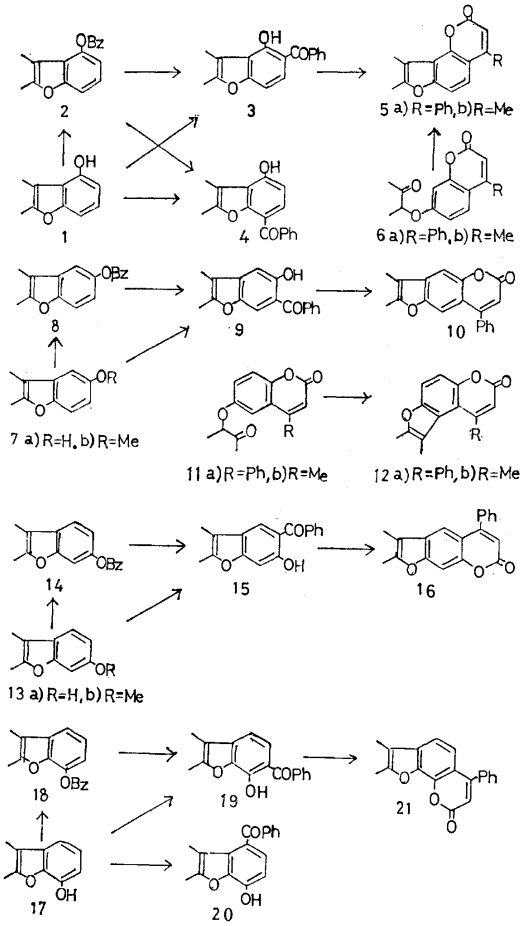

The Fries rearrangement of 4- (**2**), 5- (**8**), 6- (**14**), and 7-benzoyloxy-2,3-dimethylbenzofuran (**18**) was carried out at 120—130 °C. The reaction of **2** with aluminium chloride gave 5-benzoyl-4-hydroxy-2,3-dimethylbenzofuran (**3**) and some amounts of the 7-benzoyl isomer (**4**). The direct benzoylation of 4-hydroxy-2,3-dimethylbenzofuran (**1**) by benzoic acid and polyphosphoric acid (PPA) gave **2**, **3**, and a small amount of **4**. The Fries reaction of **8** and **14** gave 6-benzoyl-5-hydroxy- (**9**) and 5-benzoyl-6-hydroxy-2,3-dimethylbenzofuran (**15**), which were also prepared by the Friedel-Crafts benzoylation of 5- (**7b**) and 6-methoxy-2,3-dimethylbenzofuran (**13b**). The benzoylation of 5- (**7a**) and 6-hydroxy-2,3-dimethylbenzofuran (**13a**) with benzoic acid and PPA gave only **8** and **14**; in the case of acetylation or phenylacetylation, the hydroxy ketone was obtained.[4,5] The Fries reaction of **18** gave 6-benzoyl-7-hydroxy-2,3-dimethylbenzofuran (**19**) as compared to the benzoylation of 7-hydroxy-2,3-dimethylbenzofuran (**17**) with benzoic acid and PPA which gave **19** and some amounts of the para isomer (**20**).

The *o*-hydroxy ketones (**3**, **9**, **15**, and **19**) thus obtained were converted to the corresponding furo derivatives of 4-phenyl-2*H*-chromen-2-one (**5a**, **10**, **16**, and **21**) by the action of acetic anhydride and 1,8-diazabicyclo-[5.4.0]undecene-7 (DBU); in this reaction, anhydrous sodium acetate instead of DBU only gives the acetates. The cyclization of 7-(1-methyl-2-oxopropoxy)-4-phenyl-2*H*-chromen-2-one (**6a**) gave also **5a**. It is interesting to note that the furan ring formation of 6-(1-methyl-2-oxopropoxy)-4-phenyl-2*H*-chromen-2-one (**11a**) gave **12a** instead of the isomeric **10**, the furan ring having closed at the hindered position. The furo derivatives of 4-methyl-2*H*-chromen-2-one (**5b**[3] and **12b**) were also prepared through the analogous route in order to compare the spectra. Royer *et al.*[3] have reported the Pechmann reaction of the hydroxybenzofurans (**1** and **17**) gave the furochromenones (**5a**, **5b**, and **21**) compared to the reaction of **7a** which gave a mixture of **10** and **12a**. These were not however, separated into the pure components.

The structures of all the compounds were determined by means of IR, NMR spectroscopy and elemental analysis. In the NMR spectra, it was observed that the chemical shift of the 1-methyl protons of **12a** appeared at δ 1.01, a much higher magnetic field than that (δ 2.20) of the 3-methyl protons of **10**. This characteristic shift is analogous to the 4-phenyl-2*H*-chromen-2-one derivatives,[6,7] and appears due to the anisotropic shielding effect of the phenyl ring at the 9-position.[7] The chemical shift of the 1-methyl protons of **12b** appeared at δ 2.64, a lower field than those of

Table 1. The MP, IR, and elemental analysis of the new compounds

Compd	Mp °C (solv.a))	ν_{CO}^{KBr}	Found		Calcd	
			C%	H%	H%	C%
2	118—119(Et)	1745	76.44	5.13	76.67	5.30
3	87—88(Et)	1635	76.42	5.41	76.67	5.30
4	207.5—208.5(Et)	1645	76.44	5.58	76.67	5.30
6a	117—119(Et)	1725(broad)	73.86	5.28	74.01	5.23
6b	99—101(Et)	1725, 1710	68.08	6.00	68.28	5.73
8	84—85(Et)	1745	76.82	5.27	76.67	5.30
9	118—120(Et)	1650	76.45	5.12	76.67	5.30
10	164—165(Me)	1710	78.49	4.81	78.60	4.85
11a	117.5—120(Et)	1720(broad)	74.24	5.40	74.01	5.23
11b	78—79(Et)	1735, 1715	68.44	5.45	68.28	5.73
12a	168—171(Et)	1720	78.56	5.01	78.60	4.85
12b	218—219(Et)	1710	73.69	5.58	73.67	5.30
14	120—121(Et)	1730	76.55	5.01	76.67	5.30
15	153—154.5(Et)	1630	76.48	5.45	76.67	5.30
16	192—193(Et)	1710	78.88	4.93	78.60	4.85
18	65.5—66.5(Et)	1745	76.64	5.22	76.67	5.30
19	127—128(Me)	1655	76.41	5.02	76.67	5.30
20	195—196(Pr)	1615	76.71	5.50	76.67	5.30

a) Et: ethanol, Me: methanol, and Pr: propanol.

the corresponding methyl protons of other compounds; this appears due to the effect of the 9-methyl group.

Experimental[8]

The bz-*Benzoyloxy-2,3-dimethylbenzofurans (**2**, **8**, **14**, and **18**).* These compounds were prepared from *bz*-hydroxy-2,3-dimethylbenzofurans[9] (**1**, **7a**, **13a**, and **17**) by the benzoyl chloride-pyridine method (about 60% yields).

The Fries Rearrangement. A mixture of benzoyloxy-2,3-dimethylbenzofuran (1.3 g) and powdered anhydrous aluminium chloride (0.8 g) was heated for 1 h at 120—130 °C. The cooled mixture was decomposed with dilute hydrochloric acid, and extracted with ether. The ethereal solution was washed with 5% aqueous sodium hydroxide solution. The *o*-hydroxy ketones were obtained from the ethereal solution and the *p*-hydroxy ketone was obtained from the alkaline solution. Products(yields %): **3**(26.0) and **4**(8.3) from **2**, **9**(16.7)from **8**, **15**(15.4) from **14**, and **19**(15.0) from **18**.

The Benzoylation of bz-*Hydroxy-2,3-dimethylbenzofurans.* A mixture of the hydroxybenzofuran (4 g), benzoic acid (3.4 g), and PPA (n=1.5, 60 g) was heated for 1 h at 90—100 °C. The cooled mixture was decomposed with water, and extracted with chloroform. The chloroform solution was washed with 5% aqueous sodium hydroxide solution and the benzoyloxy compounds or/and the *o*-hydroxy ketones were obtained from the chloroform solution. In the case of **1**, **2**, and **3** were separated by chromatography on silica gel with benzene–hexane (1:9) as a solvent. The *p*-hydroxy ketones were obtained from the alkaline solution. Products(yields %): **2**(20.2), **3**(31.2), and **4**(1.1) from **1**, **8**(36.5) from **7a**, **14**(36.5) from **13a**, and **19**(15.5) and **20**(6.2) from **17**.

The Benzoylation of bz-*Methoxy-2,3-dimethylbenzofurans.* Anhydrous aluminium chloride (4.5 g) was added to a solution of methoxy-2,3-dimethylbenzofuran[9] (3.8 g) and benzoyl chloride (3.6 g) in benzene (30 ml) with cooling and stirring. The mixture stirred for 2 h at room temperature and then refluxed for 10 min. The usual treatment gave the *o*-hydroxy ketones. Products(yields %): **9**(44.6) from **7b**, and **15**(40.6) from **13b**.

The Preparation of the Furo Derivatives of Chromenone. A mixture of the hydroxy ketone (1 g), acetic anhydride (0.8 g), and DBU (0.4 g) was heated for 8 h at 180 °C. The cooled mixture was treated with water, allowed to stand overnight, and then extracted with chloroform. The chloroform solution was washed with 5% aqueous sodium hydroxide solution, and the product from the chloroform solution recrystallized. 8,9-Dimethyl-4-phenyl-2*H*-furo[2,3-*h*]chromen-2-one (**5a**); mp 124.5—125.5 °C (from ethanol), (lit,[3] mp 123 °C), ν_{CO}^{KBr} 1715 cm^{-1}, Anal. C, 78.45; H, 4.86%. Products(yields %): **5** (26.6) from **3**, **10**(40.4) from **9**, **16**(40.1) from **15**, and **21**(21.8) from **19**. 2,3-Dimethyl-6-phenyl-8*H*-furo[3,2-*h*]chromen-8-one (**21**); mp 151.5—152.5 °C (from methanol), (lit,[3] mp 146 °C), ν_{CO}^{KBr} 1725 cm^{-1}, Anal. C, 78.31; H, 4.64%.

The Preparation of the Furo Derivatives of Chromenones from Hydroxychromenones. *a*) Anhydrous potassium carbonate (3.5 g) was added to a mixture of hydroxy-2*H*-chromen-2-one[10] (2 g), 3-chloro-2-butanone (0.9 g), and acetone (10 ml), and the mixture was refluxed for 8 h. The cooled mixture was treated with water, extracted with chloroform, and the chloroform solution was washed with 5% aqueous sodium hydroxide solution. The product from the chloroform solution recrystallized to give 6- and 7-(1-methyl-2-oxopropoxy) derivatives of chromenones (**6a**, **6b**, **11a**, and **11b**), respectively (about 50% yields). *b*) A mixture of the alkoxychromenone (1 g) and PPA (n=2.5, 20 g) was heated for 4 h at 130 °C. The cooled mixture was treated with water, and the precipitates recrystallized to give the product. Products(yields %): **5a**(55.9) from **6a**, **5b**(67.3) from **6b**, **12a**(56.9) from **11a**, and **12b**(56.9) from **11b**. 4,8,9-Trimethyl-2*H*-furo[2,3-*h*]chromen-2-one (**5b**); mp 155—156 °C (from ethanol), (lit,[3] mp 155—156 °C), ν_{CO}^{KBr} 1710 cm^{-1}, Anal. C, 73.89; H, 5.43%.

References

1) M. Nanbu, S. Yamaguchi, Y. Sugimasa, T. Miyaura, and Y. Kawase, *Bull. Chem. Soc. Jpn.*, **48**, 3423 (1975).

2) N. M. Shah and P. M. Shah, *Chem. Ber.*, **92**, 2933 (1959).

3) J.-P. Lechartier, P. Demerseman, A. Cheutin, and R. Royer, *Bull. Soc. Chim. Fr.*, **1966**, 1716.

4) Y. Kawase, M. Nanbu, and F. Miyoshi, *Bull. Chem. Soc. Jpn.*, **41**, 2676 (1968).

5) Y. Kawase, S. Yamaguchi, N. Oki, and F. Okumura, *Bull. Chem. Soc. Jpn.*, **44**, 2163 (1971).

6) K. Kawazu, H. Ohigashi, and T. Mitsui, *Tetrahedron Lett.*, **1968**, 2383; S. K. Nigam, C. R. Mitra, G. Kunesch, B. C. Das, and J. Polonsky, *ibid.*, **1967**, 2633; G. D. Breck and G. H. Stout, *J. Org. Chem.*, **34**, 4203 (1969).

7) T. Matsui, S. Nishimura, M, Nakayama, S. Hayashi, and K. Fukui, *Bull. Chem. Soc. Jpn.*, **50**, 1975 (1977).

8) All the melting points are uncorrected.

9) R. Royer, E. Bisagni, C. Hudry, A. Cheutin, and M.-L. Desvoye, *Bull. Soc. Chim. Fr.*, **1963**, 1003.

10) S. Sethna and R. Phadke, "Organic Reactions," ed by R. Adams, Vol. 7, John Wiley and Sons, New York (1953), p. 1; R. D. Desai and C. K. Mavani, *Proc. Indian Acad. Sci.*, **25A**, 353 (1947).

BULLETIN OF THE CHEMICAL SOCIETY OF JAPAN, VOL. 51 (6), 1909—1910 (1978)

Application of Structure Construction Logic in CHEMICS for Determination of Amino Acid Sequence of Polypeptide by CI Mass Spectrometry

Yasuhiko YOTSUI, Hisashi NOMURA, Mitsuji SANO, Yoshihiro KUDO,* and Shin-ichi SASAKI*

Research Institute, Daiichi Seiyaku Co. Ltd., Edogawa-ku, Tokyo 132
**Miyagi University of Education, Aoba, Sendai 980*

(Received December 5, 1977)

Synopsis. The amino acid composition for each oligopeptide fragment in the hydrolysis mixture of polypeptides was determined using mass spectrometer with a CI source. The amino acid sequence was elucidated by structure construction logic in CHEMICS.

There have been several investigations[1-4] using mass spectrometry to determine the sequence of amino acids in polypeptide. Biemann *et al.*[4] developed a method in which di- or tripeptide fragments generated by the partial hydrolysis of the original peptide were determined by gas chromatography-mass spectrometry and reconstructed with the aid of a computer. This paper describes a new technique for the determination of the amino acid sequence in polypeptides using CI mass spectrometry and structure construction logic. The latter technique, established by two of the authors (S.S. and Y.K.) enumerates the isomers based on the molecular formula (*composition*) and probable partial structures (*components*) of an organic compound in the study of system CHEMICS.[5] The enumeration logic was thought applicable to the determination of the amino acid sequence of polypeptides, where the *composition* was the number and the kind of amino acids, and the *components* the nature of oligopeptides originated by the partial hydrolysis of the sample of an unknown polypeptide. In practice the *composition* may be determined by ordinary amino acid analysis and the *components* elucidated by CI mass spectrometry of the oligopeptide fragments generated by the partial acid hydrolysis of polypeptides.

The new determination method consists of six steps. Step 1: The composition of the unknown polypeptide was elucidated by amino acid analysis. Step 2: The sample was partially hydrolyzed with acid into oligopeptide fragments (mostly di- and tripeptides). The carboxylic and amino groups of all the fragments except the ε-amino group of lysine were converted into methoxycarbonyl and acetoamido groups, respectively, by the successive treatment of the mixture with CH_3OH–HCl and an equivalent mixture of acetic anhydride and acetic anhydride-d_6. Step 3: The CI mass spectrum for the esterified and acetylated mixture at step 2 was measured. This mixture was introduced into the spectrometer, *without any previous separation.* Each oligopeptide fragment may be detected as a doublet due to the acetylated molecule (M) and deuterioacetylated molecule (M+3). The execution of steps 4 through to 6 were performed by computer. Step 4: The constitution of amino acids in each oligopeptide was determined by comparing the mass with the composition of the sample determined at step 1. Step 5: The number of possible oligopeptides present in the sample were computed. The probable polypeptide structures (candidates) were constructed from the set of oligopeptides as executed in CHEMICS. Step 6: This routine involves the elimination of candidates which did not fulfil the necessary conditions. Compared with other methods, this method has the advantages of simplicity and high sensitivity brought about by the effective use of CI mass spectrometry and the computer logic of structure construction. Furthermore the logic can treat any type of peptide, either cyclic and branched.

PGL–LEU–TYR–GLU–ASP–LYS–PRO–ARG–ARG–PRO–TYR–ILE–LEU

Fig. 1. Neurotensin.

The present method was implemented for commercially available neurotensin[6] (Fig. 1). Ordinary amino acid analysis demonstrated that the polypeptide consisted of thirteen amino acids of nine types. One of two glutamic acids in the sample molecule was shown to be a pyroglutamic acid (PGL),** (there was no reaction of the sample with ninhydrin reagent) and this data was fed to the computer.

After hydrolyzing neurotensin with 6M-HCl (80 °C, 4 h), the hydrolysis mixture was treated with CH_3OH–HCl followed by a mixture of acetic anhydride and acetic anhydride-d_6. This was conducted at room temperature and overnight. The reaction mixture was introduced into a mass spectrometer with a CI source *without previous separative treatment.* The CI spectrum of the mixture suggested the presence of 14 oligopeptides (Nos. 1 through 10′) and the amino acid composition was computed by comparing the mass with the amino acid composition of the original polypeptide neurotensin, as shown in Table 1. In addition to these oligopeptides, FD mass spectrum demonstrated the presence of a dipeptide, ARG–ARG.

In order to construct the structure of neurotensin it is not necessary to use all the kinds of oligopeptides shown in Table 1. The reasons for this are as follows: No. 11 seems to be a fragment of No. 7, therefore No. 7 appears to be present in the form of either LYS–ASP–PRO or ASP–LYS–PRO. Paying attention to ASP, No. 7 may be connected to No. 4 to yield GLU–ASP–

** PGL was used for pyro-glutamic acid instead of P-GLU for the convenience of computer input and output.

Table 1. Peptide fragments of neurotensin analyzed by CI mass spectra

No.	*m/e*		Components
1	299	QM^+	LEU, PGL
2	301	QM^+	LEU, LEU
2′		QM^+	PRO, ASP
3	335	QM^+	PRO, TYR
4	347	QM^+	ASP, GLU
5	351	QM^+	LEU, TYR
6	381	QM^+	GLU, TYR
7	429	QM^+	PRO, LYS, ASP
7′		QM^+	LEU, LEU, LYS
8	464	QM^+	LEU, LEU, TYR
8′		QM^+	PRO, ASP, TYR
9	494	QM^+	LEU, GLU, TYR
10	561	QM^+	LEU, LEU, PRO, TYR
10′		QM^+	PRO, PRO, ASP, TYR
11	300	F	LYS, ASP
12	416	F	LEU, PRO, TYR
13	387	QM^+	ARG, ARG

QM^+: quasi-molecular ion of oligopeptide $(M+1)^+$
F: fragment ion ARG-ARG (No. 13): detected by FD mass spectrometry

LYS–PRO (No. 14). Nos. 2′, 7′, 8′, and 10′, which are not in agreement with No. 14, may be eliminated. Furthermore, two possible structures, ASP–GLU–TYR and TYR–GLU–ASP, are derived from Nos. 4 and 6. This structure is successively connected to No. 14 and 9 to give LEU–TYR–GLU–ASP–LYS–PRO (No. 15) as a longer partial structure of neurotensin.

Thus all the possible structures for neurotensin may be constructed from Nos. 1, 2, 3, 5, 8, 10, 12, 13, and 15. The number of structures (candidates) amounts to eight as shown in Fig. 2. In the present method, LEU cannot be distinguished from ILE, since both possess the same molecular weight. Consequently all the possible candidates amount to 24.

```
001 P PGL-LEU-LEU-TYR-PRO-LEU-TYR-GLU-ASP-LYS-PRO-ARG-ARG
002 P PGL-LEU-PRO-TYR-LEU-LEU-TYR-GLU-ASP-LYS-PRO-ARG-ARG
003 P PGL-LEU-ARG-ARG-PRO-TYR-LEU-LEU-TYR-GLU-ASP-LYS-PRO
004 P PGL-LEU-TYR-PRO-LEU-LEU-TYR-GLU-ASP-LYS-PRO-ARG-ARG
005 P PGL-LEU-TYR-GLU-ASP-LYS-PRO-PRO-TYR-LEU-LEU-ARG-ARG
006 P PGL-LEU-TYR-GLU-ASP-LYS-PRO-ARG-ARG-PRO-TYR-LEU-LEU
007 P PGL-LEU-TYR-GLU-ASP-LYS-PRO-TYR-LEU-LEU-PRO-ARG-ARG
008 P PGL-LEU-TYR-GLU-ASP-LYS-PRO-TYR-LEU-LEU-ARG-ARG-PRO

END
```

Fig. 2. Candidate polypeptides afforded by computer-aided CI mass spectrometry for neurotensin.

Experimental

Isobutane CI mass spectra were determined on a HITACHI RMU-6MG mass spectrometer with a combined EI-CI source under conditions of 100 eV ionizing potential and 80 μA ionizing current. FD mass spectra were obtained with a JEOL JMS-D100 mass spectrometer equipped with a combined FD-FI-EI source using an emitter current of 10—15 mA and a cathode potential of −5kV.

Partial hydrolysis of neurotensin: About 0.1 μmol of neurotensin was heated with 6M hydrochloric acid at 80 °C for 4 h in a sealed tube. Subsequently the hydrochloric acid was removed *in vacuo* and the residue used without purification.

Esterification: A solution of the partial hydrolysis product of neurotensin in 0.5 ml of methanol was allowed to stand overnight at room temperature.

Acetylation: To a solution of the methyl esters of the oligopeptides, 0.25 ml of acetic acid (d_0: d_3=1: 1) and 0.25 ml of acetic anhydride (d_0: d_6=1: 1) were added, then the mixture was allowed to stand overnight. Excess reagent was removed *in vacuo* and the residue used directly for the determination of CI spectrum.

Under these conditions, the ε-amino group of lysine appears resistant to acetylation. No mass peaks corresponding to oligopeptides including diacetamidolysine methyl ester were detected.

References

1) H. K. Wipf, P. Irving, M. McCamish, R. Venkataraghavan, and F. W. McLafferty, *J. Am. Chem. Soc.*, **95**, 3369 (1973).

2) G. M. Schier, B. Halpern, and G. W. A. Milne, *Biomed. Mass Spectrom.*, **1**, 212 (1974).

3) S. A. Poku, G. W. Wood and D. E. Schmidt Jr., *Biomed. Mass Spectrom.*, **2**, 121 (1975).

4) H. Nau and K. Biemann, *Anal. Biochem.*, **73**, 175 (1976).

5) S. Sasaki, H. Abe, Y. Kudo, and T. Yamasaki, 1977 ACS Symposium Series on Computer-assisted Structure Elucidation of Organic Compounds, No. 54, 108 (1977); Y. Kudo and S. Sasaki, *J. Chem. Inf. Comp. Sci.*, **16**, 43 (1976).

BULLETIN OF THE CHEMICAL SOCIETY OF JAPAN, VOL. 51 (6), 1911—1912 (1978)

Solvent Incorporation in Bromination of Acetylenes in Alcohols

Sakae UEMURA,* Hajime OKAZAKI, Masaya OKANO, Seiji SAWADA,**
Atsuko OKADA,** and Kimiko KUWABARA**

Institute for Chemical Research, Kyoto University, Uji, Kyoto 611
***Department of Chemistry, Kyoto University of Education, Kyoto 612*

(Received December 16, 1977)

Synopsis. The reactions of acetylenes with bromine in alcohols at 20—25 °C afford dibromodialkoxyalkanes in good yields together with variable amounts of dibromoalkenes. Similar treatment of phenylacetylene with copper(II) bromide gives only bromophenylacetylene and 2-phenyl-1,1,2-tribromoethylene, the latter being formed by dibromination of the former with copper(II) bromide.

Contrary to fluorination[1] and chlorination[2] of acetylenes in alcohols where solvent incorporation occurs, it has been reported that bromination of 1-hexyne in methanol gave only 1,2-dibromo-1-hexene and none of solvent incorporated products.[2] This seems to be strange since bromination of olefin in alcohols usually gives both dibromoalkanes and alkoxybromoalkanes.[3] During studies on halogenation of acetylenes by molecular halogen and metal halides,[4,5,6] we found that bromination of acetylenes in methanol actually gives dibromodimethoxyalkanes as well as dibromoalkenes. It should be noted that the reactions of acetylenes with *N*-bromosuccinimide in alcoholic solvents have been known to produce dibromo acetals.[7]

Results and Discussion

When the reactions of various acetylenes with equimolar amount of bromine were carried out by adding methanolic solution of bromine to that of acetylene (**1**) at 20—25 °C and by stirring the resulting solution for 0.5—3 h, dibromodimethoxyalkanes (**3**) were obtained in good yields together with minor amounts of isomeric dibromoalkenes (**2**) [Scheme (1)], leaving excess **1** unreacted. In the reactions of phenylacetylene the following facts were revealed: (i) The product ratio is not much changed by lowering the reaction temperature or increasing the amount of methanol. (ii) The use of excess of bromine to **1** results in a slight decrease of the amount of **3**. (iii) The reaction proceeds also in ethanol or ethylene glycol to give **2** and **3**-analogue, while almost only **2** is obtained in 2-propanol or *t*-butyl alcohol. In ethylene glycol the attack of second alkoxyl group occurred intramolecularly to give 2-(dibromomethyl)-2-phenyl-1,3-dioxolane. The reaction with 1-hexyne gave (**3**; R=*n*-Bu, R′=H) in 40—60% yield in contrast to the report by Hennion *et al.*,[2] though the reason for the discrepancy is not yet clear. Typical results are shown in Table 1. The formation of only **3** as the solvent-incorporated product without any appreciable amounts of bromomethoxyalkenes may suggest that enol ethers are more reactive to electrophilic addition than acetylenes in these cases.

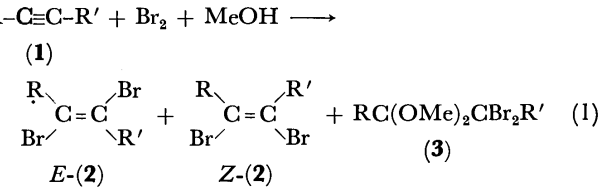

When phenylacetylene was treated with copper(II) bromide instead of bromine in methanol, bromophenylacetylene (**4**) and 2-phenyl-1,1,2-tribromoethylene (**5**) were obtained, none of (**3**; R=Ph, R′=H) being formed. Tribromination of terminal acetylenes with copper(II) bromide in refluxing methanol has been reported by Castro *et al.*[8] The mechanism which involves dibromination followed by tetrabromination and subsequent dehydrobromination has been proposed for this reaction. We would like to suggest another possible pathway for tribromination which consists of the initial formation of **4** followed by its dibromina-

Table 1. Bromination of acetylenes in alcohols

(**1**) R	(**1**) R′	(**1**) (mmol)	Br_2 (mmol)	Alcohol	(ml)	Temp (°C)	Time (h)	Products and yields[a] *E*-(**2**)	*Z*-(**2**)	(**3**)
Ph	H	2.5	2.5	MeOH	25	25	0.5	7	trace	65
Ph	H	2.5	5	MeOH	25	25	0.5	13	2	75[b]
Ph	H	5	5	MeOH	100	25	0.5	7	trace	79
Ph	H	2.5	2.5	MeOH	25	−60	0.5	7	trace	70
Ph	H	5	5	EtOH	100	20	3	28	0	39[c]
Ph	H	5	5	$HOCH_2CH_2OH$	100	20	3	trace	0	55[d]
Ph	Me	5	5	MeOH	100	20	3	37	0	63
n-Hexyl	H	5	5	MeOH	100	20	3	29	0	53
n-Bu	H	5	5	MeOH	100	20	3	29	0	52

a) Determined by NMR using a suitable internal standard; on the basis of a half mole of **1**. b) Yields are based on **1**; other product, a small amount of **4**. c) $PhC(OEt)_2CHBr_2$. d) $PhC(OCH_2CH_2O)CHBr_2$.

* To whom correspondence should be addressed.

$$PhC{\equiv}CH + CuBr_2 + MeOH \longrightarrow PhC{\equiv}CBr + Ph(Br)C{=}CBr_2 \quad (2)$$

(4) (5)

$CuBr_2$

MeOH

tion, since we confirmed separately that **4** reacted with copper(II) bromide in methanol to give **5** [Scheme (2)]. As to the formation of **4**, the direct exchange of hydrogen by bromine may be conceivable as one of the possible pathways, since *E*- and/or *Z*-**2** did not give any **4** by dehydrobromination under these reaction conditions.

Experimental

Phenylacetylene, 1-phenyl-1-propyne, and 1-phenyl-1-butyne were prepared by the literature method.[4] 1-Hexyne, 1-octyne, alcohols, bromine, and copper(II) bromide were commercial products and used without further purification. The purification of these reagents by distillation or drying *et al.* did not give any effects on the results. The GLC analyses were carried out on Shimadzu 4BMPF and 4CMPF apparatus using EGSS-X (1 and 3 m) columns (N_2 as the carrier gas). The NMR spectra were recorded with a Varian EM-360 and a JEOL JNM-MH-100 apparatus using CCl_4 solvent (TMS as an internal standard). Authentic samples of **2**,[6] **4**,[9] and **5**[8] were prepared by the reported methods.

Formation of (3; R=Ph, R'=H). To a stirred methanol (25 ml) solution of phenylacetylene (0.51 g, 5 mmol) was added a methanol (25 ml) solution of bromine (0.80 g, 5 mmol) drop by drop (*ca.* 3—5 min) at 20—25 °C and the resulting mixture was stirred for 0.5 h during which period the red color of bromine gradually disappeared. The mixture was then added with aqueous sodium thiosulfate (*ca.* 1%, 150 ml) and extracted with benzene (70 ml×3). The benzene extract was washed with water and dried over $MgSO_4$. This extract was revealed to contain phenylacetylene, *E*- and *Z*-(**2**; R=Ph, R'=H), (**3**; R=Ph, R'=H), and trace amounts of **4**, **5**, and an unidentified compound by GLC analysis. Evaporation of benzene left 0.6 g of a white solid which contained *E*-**2**, *Z*-**2**, and **3** of the ratio of 9:1:90 (by NMR). Recrystallization from ethanol afforded 0.4 g of pure (**3**; R=Ph, R'=H): mp 65—67 °C, NMR δ 3.27 (s, 6H), 5.91 (s, 1H), 7.15—7.75 (m, 5H). Found: C, 36.62; H, 3.53%. Calcd for $C_{10}H_{12}O_2Br_2$: C, 37.07; H, 3.73%.

Identification of other **3** which was isolated similarly as above or by column chromatography on alumina (hexane as an eluent) was as follows: (**3**: R=Ph, R=Me), mp 49—51 °C, NMR δ 2.27 (s, 3H), 3.48 (s, 6H), 7.0—7.7 (m, 5H). Found: C, 39.04; H, 4.11%. Calcd for $C_{11}H_{14}O_2Br_2$: C, 39.08; H, 4.17%. $PhC(OEt)_2CHBr_2$, mp 35—36 °C, NMR δ 1.22 (t, 6H), 3.54 (q, 4H), 5.84 (s, 1H), 7.1—7.6 (m, 5H). Found: C, 41.20; H, 4.66%. Calcd for $C_{12}H_{16}O_2Br_2$: C, 40.94; H, 4.58%. $PhC(OCH_2CH_2O)CHBr_2$, mp 69—72 °C, NMR δ 3.73—4.0 (m, 2H), 4.0—4.38 (m, 2H), 5.66 (s, 1H), 6.9—7.7 (m, 5H). Found: C, 37.25; H, 3.06%. Calcd for $C_{10}H_{10}O_2Br_2$: C, 37.30; H, 3.13%. The following two products were identified by NMR without isolation: (**3**; R=*n*-Bu, R'=H), δ 0.8—2.2 (m, 7H), 2.57 (t, 2H), 3.27 (s, 6H), 5.70 (s, 1H); (**3**; R=*n*-Hexyl, R'=H), δ 0.85—2.4 (m, 11H), 2.60 (t, 2H), 3.29 (s, 6H), 5.67 (s, 1H).

Formation of 4 and 5. A heterogeneous mixture of phenylacetylene (0.26 g, 2.5 mmol), copper(II) bromide (2.70 g, 12.5 mmol) and methanol (25 ml) was kept at 25 °C for 24 h with stirring. Water (100 ml) was added to the mixture and the resulting solution was extracted with benzene (70 ml×3). The benzene extract was treated as described above. The GLC analysis of the residue revealed the presence of **4** (0.31 g, 1.7 mmol, 68% yield on the basis of the acetylene charged), a trace amount of *E*-**2**, and **5** (0.12 g, 0.35 mmol, 14% yield).

Treatment of **4** (1 mmol) with $CuBr_2$ (3 mmol) in methanol (10 ml) at reflux temperature for 5 h afforded 69% yield of **5**. Similar reaction at 25 °C gave 11% yield of **5**, leaving 84% of **4** unreacted.

References

1) R. F. Merritt, *J. Org. Chem.*, **32**, 4124 (1967).
2) J. J. Verbanc and G. F. Hennion, *J. Am. Chem. Soc.*, **60**, 1711 (1938).
3) See for example, R. C. Fahey, "Topics in Stereochemistry," Vol 3, ed by E. L. Eliel and N. L. Allinger, Interscience, New York, N. Y. (1968), pp. 280—283.
4) S. Uemura, H. Okazaki, A. Onoe, and M. Okano, *J. Chem. Soc., Perkin Trans. 1*, **1977**, 676.
5) S. Uemura, A. Onoe, and M. Okano, *J. Chem. Soc., Chem. Commun.*, **1976**, 145.
6) S. Uemura, H. Okazaki, and M. Okano, *J. Chem. Soc., Perkin Trans. 1*, in press.
7) W. P. Pilgrim, Ph. D. Thesis, Queen's University, Kingston, Ontario, 1969; S. Wolfe, W. P. Pilgrim, T. F. Garrard, and P. Chamberlain, *Can. J. Chem.*, **49**, 1099 (1971).
8) C. E. Castro, E. J. Gaughan, and D. C. Owsley, *J. Org. Chem.*, **30**, 587 (1965).
9) S. I. Miller, G. R. Ziegler, and R. Wieleseck, *Org. Synth.*, Coll. Vol. V, 921 (1973).

BULLETIN OF THE CHEMICAL SOCIETY OF JAPAN, VOL. 51 (6), 1913—1914 (1978)

Conversion of Disilanes to Functional Monosilanes. IV.[1] Synthesis of Methyldichlorosilane and Dimethylchlorosilane by the Reaction of Methylchlorodisilanes with Hydrogen Chloride in the Presence of Tetrakis(triphenylphosphine)palladium(0)

Hideyuki MATSUMOTO, Tsuneo MOTEGI, Minoru HASEGAWA, and Yoichiro NAGAI

Department of Chemistry, Gunma University, Kiryu, Gunma 376

(Received December 19, 1977)

Synopsis. Methylchlorodisilanes such as 1,2-dimethyl-1,1,2,2-tetrachlorodisilane, 1,1,2-trimethyl-1,2,2-trichlorodisilane and 1,1,2,2-tetramethyl-1,2-dichlorodisilane were effectively cleaved by hydrogen chloride in the presence of tetrakis(triphenylphosphine)palladium(0) to give methylchlorohydrosilanes in good yields.

The cleavage of methylchlorodisilanes by hydrogen chloride constitutes one of the important routes to methyldichlorosilane and dimethylchlorosilane and considerable effort has been devoted to this reaction.[2] The transition metal-catalyzed cleavage, however, had been overlooked until 1973, when Atwell and Bokerman reported in a patent literature that the cleavage of a disilane mixture containing 1,2-dimethyl-1,1,2,2-tetrachlorodisilane, 1,1,2-trimethyl-1,2,2-trichlorodisilane and 1,1,2,2-tetramethyl-1,2-dichlorodisilane was effected by dichlorobis(phenyldimethylphosphine)palladium-(II).[3] In their experiment a low boiling mixture was obtained which consisted of methyldichlorosilane, dimethylchlorosilane, methyltrichlorosilane and dimethyldichlorosilane (yield was not given), indicating that all the disilanes had been cleaved to some extent.

During the course of our recent investigation on various cleavage reactions of methylchlorodisilanes,[1] we have found that disilanes such as 1,2-dimethyl-1,1,2,2-tetrachlorodisilane, 1,1,2-trimethyl-1,2,2-trichlorodisilane and 1,1,2,2-tetramethyl-1,2-dichlorodisilane were effectively cleaved by hydrogen chloride in the presence of tetrakis(triphenylphosphine)palladium-(0). The results are summarized in Table 1.

In the presence of this particular palladium catalyst, *sym*-dimethyltetrachlorodisilane was readily cleaved at 140 °C by hydrogen chloride to give a 1 : 1 mixture of methyldichlorosilane and methyltrichlorosilane in a 90% combined yield. It is apparent, therefore, that reaction 1

$$Cl_2MeSiSiMeCl_2 + HCl \xrightarrow{Pd(0)} MeSiHCl_2 + MeSiCl_3 \quad (50 : 50) \qquad (1)$$

provides a convenient method for preparation of methyldichlorosilane. The reaction of *sym*-tetramethyldichlorodisilane with hydrogen chloride was rather slow at 140 °C, but at 170 °C, the reaction with 0.4 mol% of the palladium(0) catalyst proceeded with a 32% conversion to afford a 1 : 1 mixture of dimethylchlorosilane and dimethyldichlorosilane in a 97% combined yield based on the disilane consumption. Thus, Reaction 2 is of some validity for the production of dimethylchlorosilane by a single route.

$$ClMe_2SiSiMe_2Cl + HCl \xrightarrow{Pd(0)} Me_2SiHCl + Me_2SiCl_2 \quad (50 : 50) \qquad (2)$$

1,1,2-Trimethyl-1,2,2-trichlorodisilane was found to be cleaved at 150 °C in two ways as shown below. The slightly preponderant occurrence of path A and path B suggests that attack of chlorine on the Me_2SiCl group in the disilane is somewhat favored over that on the $MeSiCl_2$ group.

$$Cl_2MeSiSiMe_2Cl + HCl \longrightarrow \begin{cases} MeSiHCl_2 + Me_2SiCl_2 \quad (28 : 40) & \text{[path A]} \\ Me_2SiHCl + MeSiCl_3 \quad (8 : 24) & \text{[path B]} \end{cases} \qquad (3)$$

Comparison of the reaction conditions for the cleavages 1, 2 and 3 finds the reactivity order of the disilanes to be $Me_2Si_2Cl_4 > Me_3Si_2Cl_3 > Me_4Si_2Cl_2$. This was further found to be the case by the competitive

TABLE 1. REACTION OF METHYLCHLORODISILANES WITH HYDROGEN CHLORIDE IN THE PRESENCE OF TETRAKIS(TRIPHENYLPHOSPHINE)PALLADIUM(0)[a]

Disilane	Conversion of disilane %[b]	Yield of monosilanes %[c]	Product distribution, %[d]			
			$MeSiHCl_2$	Me_2SiHCl	$MeSiCl_3$	Me_2SiCl_2
$Cl_2MeSiSiMeCl_2$[e]	100	90	50		50	
$ClMe_2SiSiMe_2Cl$[f]	32	97		50		50
$Cl_2MeSiSiMe_2Cl$[g]	100	80	28	8	24	40

a) The reactions were carried out by passing hydrogen chloride (50 ml/min) through a solution of a disilane (200 mmol), mesitylene (10 ml) and the Pd(0) complex. b) Conversion is meant by 100 × (mol of the disilane consumed)/(mol of the disilane charged). c) Isolated yield based on the disilane consumption. d) Determined by GLC and NMR analyses. e) Carried out at 140 °C for 4 h. The catalyst concentration is 0.2 mol% based on the disilane charged. f) Carried out at 150 °C for 5 h. The catalyst concentration is 0.2 mol%. g) Carried out at 170 °C for 8 h. The catalyst concentration is 0.4 mol%.

cleavage of pairs of three disilanes at 150 °C in the presence of the palladium(0) catalyst which gave the relative rates $Me_2Si_2Cl_4$ 16, $Me_3Si_2Cl_3$ 10, and $Me_4Si_2Cl_2$ 1. The reactivity order thus found is in keeping with that for ammonium chloride-catalyzed cleavage reaction previously reported[4] and suggests that the present reaction is likely to involve the nucleophilic attack of chlorine atom in hydrogen chloride on the Si–Si bond for which the direct interaction with the Pd(0) complex is expected.[1c,5]

Finally, catalyst efficiency was tested briefly with other common Group VIII metal-phosphine complexes using the reaction of *sym*-dimethyltetrachlorodisilane with hydrogen chloride as standard (140 °C, 5 h, 0.2 mol% of the catalyst). For example, dichlorobis(triphenylphosphine)palladium(II) also was found to initiate the cleavage of the disilane, but the reaction gave a 34: 66 mixture of methyldichlorosilane and methyltrichlorosilane only in a 21% combined yield. Further, the reaction in the presence of dichlorobis(triphenylphosphine)nickel(II) gave only a 21% combined yield of methylchlorosilanes consisting of 3% methyldichlorosilane and 97% methyltrichlorosilane.

Experimental

1,2-Dimethyl-1,1,2,2-tetrachlorodisilane,[6] 1,1,2-trimethyl-1,2,3-trichlorodisilane,[7] and 1,1,2,2-tetramethyl-1,2-dichlorodisilane[7] were prepared by literature procedures. Commercial anhydrous hydrogen chloride was uesd without further purification. Authentic methylchlorosilanes (*e.g.*, $MeSiHCl_2$, Me_2SiHCl, Me_2SiCl_2, and $MeSiCl_3$) were obtained commercially. Reagent grade mesitylene was freshly distilled prior to use. The complexes $NiCl_2(PPh_3)_2$,[8] $Pd(PPh_3)_4$,[9] and $PdCl_2(PPh_3)_2$[10] were prepared according to literature directions. Structural assignment for the methylchlorosilanes obtained was performed by comparing their physical properties (*e.g.*, NMR and IR spectra and GLC retention times, *etc.*) with those of authentic samples.

General Procedure for the Cleavage Reactions. All cleavage reaction were carried out in an apparatus consisting of a 30 ml three-necked round-bottomed flask equipped with a magnetic stirrer, a thermometer and an inlet tube for hydrogen chloride and topped by a distillation column filled with glass helices. The upper part of this column was connecteed with an even pressure reflux regulator to which a 100 ml flask was attached for collection of methylchlorosilanes. Effluent gaseous materials were trapped in a tube immersed in a Dry Ice–acetone bath.

A typical procedure is exemplified by the cleavage of 1,2-dimethyl-1,1,2,2-tetrachlorodisilane in the presence of tetrakis(triphenylphosphine)palladium(0). To a mixture of 45.5 g (200 mmol) of the disilane and 10 ml of mesitylene was added 0.452 g (0.4 mmol) of the Pd(0) complex. The stirred mixture was kept at 140 °C, and hydrogen chloride was bubbled through the solution at a rate of 50 ml/min. The reaction was complete in 4 h and 47.6 g (90% yield based on the disilane charged) of methylchlorosilanes were collected. GLC and NMR analyses showed the product to be a 50: 50 mixture of methyldichlorosilane and methyltrichlorosilane.

Procedure for Competitive Experiments. Hydrogen chloride was bubbled through a mixture of two different disilanes, mesitylene and the palladium(0) complex (0.2 mol%) at 150 °C. After 30—70% completion, unconverted disilanes were analyzed by GLC. Relative rates were calculated using the Ingold-Shaw equation,[11] where A_t and B_t are the initial concentrations of two disilanes,

$$\frac{k_1}{k_2} = \frac{\log [A]_t/[A]_f}{\log [B]_t/[B]_f}$$

A_f and B_f final concentrations, and k_1/k_2 the ratio of rate constants for the attack of hydrogen chloride on the two species. Relative rates are expressed by taking that for 1,1,2,2-tetramethyl-1,2-dichlorodisilane as standard.

References

1) For preceding papers of this series, see (a) H. Matsumoto, S. Nagashima, K. Yoshihiro, and Y. Nagai, *J. Organomet. Chem.*, **85**, Cl (1975); (b) H. Matsumoto, K. Yoshihiro, S. Nagashima, H. Watanabe, and Y. Nagai, *ibid.*, **128**, 409 (1977); (c) H. Matsumoto, T. Yako, T. Motegi, and Y. Nagai, *ibid.*, in press.

2) (a) K. Shiina and M. Kumada, *Kogyo Kagaku Zasshi*, **60**, 1395 (1967); (b) J. A. Barry and J. W. Gilkey, U.S. Patent 2681355 (1954); *Chem. Abstr.*, **49**, 6301 (1955); (c) B. A. Bluestein, U. S. Patent 2709176 (1955); *Chem. Abstr.*, **49**, 15284 (1955), (d) A. R. Gilbert and G. D. Cooper, U.S. Patent 2842580 (1958); *Chem. Abstr.*, **52**, 18216 (1958); (e) G. D. Cooper and A. R. Gilbert, *J. Am. Chem. Soc.*, **82**, 5402 (1960).

3) W. H. Atwell and G. N. Bokerman, U. S. Patent 37772347 (1973).

4) C. J. Wilkins, *J. Chem. Soc.*, **1953**, 3409.

5) K. Tamao, T. Hayashi, and M. Kumada, *J. Organomet. Chem.*, **114**, C19 (1976).

6) H. Watanabe, M. Kobayashi, Y. Koike, S. Magashima, H. Matsumoto, and Y. Nagai, *J. Organomet. Chem.*, **128**, 73 (1977).

7) H. Matsumoto, T. Motegi, M. Hasegawa, and Y. Nagai, *J. Orgnomet. Chem.*, **142**, 149 (1977).

8) L. M. Venanzi, *H. Chem. Soc.*, **1958**, 719.

9) D. R. Coulson, *Inorg. Synth.*, **13**, 121 (1972).

10) F. R. Hartley, *Organomet. Chem. Rev. A*, **6**, 119 (1970).

11) C. K. Ingold and F. R. Shaw, *J. Chem. Soc.*, **1927**, 2918.

BULLETIN OF THE CHEMICAL SOCIETY OF JAPAN, VOL. 51 (6), 1915—1916 (1978)

A Simple Synthetic Method for 2,15-Hexadecanedione from a Butadiene Telomer

Jiro TSUJI,* Mitsumasa KAITO, Toshiro YAMADA, and Tadakatsu MANDAI

Tokyo Institute of Technology, Meguro, Tokyo 152

(Received January 20, 1978)

Synopsis. The terminal double bond of 3,8-nonadienoate was oxidized to methyl ketone with a catalyst system of $PdCl_2/CuCl/O_2$ and the internal double bond was reduced to give 8-oxononanoate, which was hydrolyzed to 8-oxononanoic acid. The Kolbe electrolysis of the acid produced 2,15-hexadecanedione in a high yield.

Palladium compounds are useful reagents for organic synthesis. Particularly there are two useful synthetic reactions catalyzed by palladium compounds. They are oxidation of olefins catalyzed by $Pd(II)/Cu(II)/O_2$ system to carbonyl compounds,[1-3] and telomerization of butadiene with nucleophiles catalyzed by palladium-phosphine complexes.[4]

We now wish to report the application of these two palladium catalyzed reactions to the synthesis of 2,15-hexadecanedione (**3**). The conversion of this diketone to muscone by aldol condensation had been reported by Stoll.[5] One drawback of the Stoll method is a low yield of the intramolecular aldol condensation, which competes with the intermolecular reaction. In order to make this method more useful and make up for the low yield of the aldol condensation, it is essential to synthesize the diketone **3** as the precursor easily in high yield. We have already reported the synthesis of the diketone **3** by coupling a C_8 chain, which is easily available by the palladium catalyzed telomerization of butadiene with acetic acid.[6,7]

The present method shown below utilizes a C_9 acid **2b** which was coupled by the Kolbe reaction. The method is simpler and gave a higher overall yield.

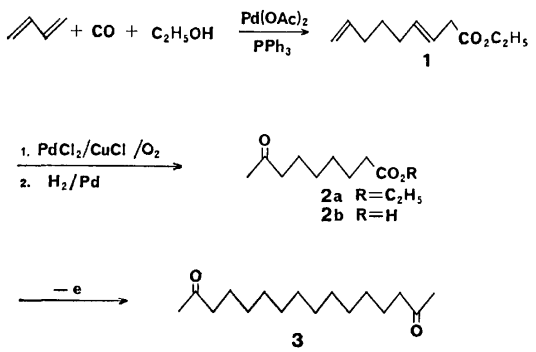

We have reported the dimerization-carbonylation of butadiene catalyzed by a system of palladium acetate and triphenylphosphine to give 3,8-nonadienoate (**1**) in a high yield.[8,9] In the present studies, this C_9 ester was converted into the C_{16} diketone as shown in the above scheme. The Kolbe coupling of 8-oxononanoic acid (**2b**) has been claimed by Tsuzuki and Motoki in a patent.[10] However, in their method, the acid **2b** was synthesized by the cross Kolbe reaction of adipic acid and levulinic acid, which gave inevitably a mixture of coupled products.[10,11] In the present method the easily available C_9 ester **1** is the starting material.

At first the terminal double bond of **1** was oxidized to a methyl ketone using $PdCl_2/CuCl/O_2$ as a catalyst system at room temperature in *N,N*-dimethylformamide.[12] Ethyl 8-oxo-3-nonenoate was isolated by distillation in 86.7% yield. The internal double bond which remained intact during the oxidation was hydrogenated by using palladium on carbon as a catalyst to give ethyl 8-oxononanoate in 98% yield. The ester was then hydrolyzed with methanolic KOH to give 8-oxononanoic acid as crystals in 92% yield. The final step of the synthesis is the Kolbe electrolysis. The sodium salt of the keto acid **2b** in methanol was subjected to Kolbe electrolysis using Pt electrode at 0° C. After the reaction, a neutral fraction was isolated by the usual work-up as a solid material which was recrystallized from methanol to afford the diketone **3** as colorless crystals in 63% yield. The diketone was identified by its mp and NMR spectral data.

Experimental

Melting points were measured on a Shibata (No. 297) melting point apparatus. The IR spectra were taken on a JASCO (IRA-2) spectrophotometer. The NMR spectra were taken on a HITACHI (R-24A) spectrometer (60 MHz) with tetramethylsilane as an internal reference.

Materials. Ethyl 3,8-nonadienoate (**1**) was prepared by the reaction of butadiene with carbon monoxide and ethanol using palladium acetate and triphenylphosphine as a catalyst under pressure of carbon monoxide,[8] bp 60—63 °C/4 Torr: IR (neat) 2980, 2920, 1740, 1640, 1160, 970, 910 cm^{-1}; NMR (CCl_4) δ 5.3—6.1 (m, 3H), 4.7—5.1 (m, 2H), 4.0 (q, J=7 Hz, 2H), 2.8—3.1 (m, 2H), 1.8—2.3 (m, 4H), 1.55 (t, J=6 Hz, 2H), 1.2 (t, J=7 Hz, 3H).

Oxidation of Ethyl 3,8-Nonadienoate. A mixture of $PdCl_2$ (877 mg, 4.95 mmol) and CuCl (4.90 g, 49.6 mmol) in aqueous *N,N*-dimethylformamide (25 ml, H_2O, 3 ml) was shaken in a 100 ml glass vessel under oxygen atmosphere for 1 h. Then the ester **1** (8.96 g, 49.2 mmol) was added and the mixture was shaken under oxygen atmosphere at room temperature for 5 h. The solution was poured into dilute hydrochloric acid and the resulting mixture was extracted with dichloromethane. Ethyl 8-oxo-3-nonenoate was isolated by distillation (8.44 g, 86.7%): bp 86—87 °C/5 Torr; NMR (CCl_4) δ 5.3—5.5 (m, 2H), 4.0 (q, J=7 Hz, 2H), 2.8—3.0 (m, 2H), 2.35 (t, J=6.5 Hz), 2.0 (s 3H), 1.4—2.1 (m, 4H), 1.2 (t, J=7 Hz, 3H); IR (neat) 2980, 2940, 1735, 1715, 1370, 1250, 1165, 1030, 970 cm^{-1}.

Hydrogenation of Ethyl 8-Oxo-3-nonenoate. Ethyl 8-oxo-3-nonenoate (2.88 g, 14.5 mmol) was dissolved in ethanol (20 ml) in a 50 ml flask and palladium on carbon (5%, 80 mg) was added. The resulting mixture was shaken under atmospheric pressure of hydrogen at room temperature for

3 h. The mixture was filtered and the solvent was removed to give crude ethyl 8-oxonoanoate (**2a**) (2.85 g, 98%): NMR (CCl_4) δ 4.0 (q, J=7 Hz, 2H), 2.2 (t, J=8 Hz, 4H), 2.05 (s, 3H), 1.0—1.7 (broad, 11H).

Hydrolysis of Ethyl 8-Oxononanoate. Ethyl 8-oxononanoate (17.7 g, 88.5 mmol) was dissolved in methanol (30 ml) in a 200 ml flask and an aqueous KOH solution (5.0 g, 89.3 mmol in 100 ml of H_2O) was added and the solution was stirred for 3 h. After the usual work-up, crude 8-oxononanoic acid (**2b**) (14.1 g, 82.0 mmol, 92%) was obtained. The acid **2b** was purified by recrystallization from hexane and benzene to give colorless needles, mp 42.5—44 °C (reported 40°C[13]): NMR (CCl_4) δ 11.3 (s, $-CO_2H$, 1H), 2.35 (t. J= 6 Hz, 2H), 2.30 (t, J=6 Hz, 2H), 2.1 (s, 3H), 1.0—1.9 (broad, 8H).

Kolbe Electrolysis. 8-Oxononanoic acid (6.28 g, 36.6 mmol) in sodium methoxide solution (50 mg of Na in 70 ml of MeOH) was placed in a 100 ml glass vessel equipped with a Pt electrode and a magnetic bar. The electrolysis was carried out with stirring at 0 °C under nitrogen atmosphere (65 volt, 0.2—0.6 ampere) for 2 h. After the reaction, precipitated white solid was filtered and the filtrate was concentrated. The residue was poured into an aqueous $NaHCO_3$ solution and the solution was extracted with dichloromethane. The dichloromethane solution was washed with brine and dried over $MgSO_4$. After removal of the solvent, white solid was obtained which was recrystallized from methanol to afford 2,15-hexadecanedione (**3**) as colorless crystals, 2.93 g, 63%, mp 83.5—85.0 °C, (reported 83—84 °C)[11]: NMR (CCl_4) δ 2.1—2.4 (t, J=7 Hz, 4H), 1.95 (s, 6H), 1.0—1.7 (broad, 20H); IR (KBr disk) 2900, 2830, 1710, 1460, 1160, 800, 720, 600 cm^{-1}.

References

1) J. Smidt, W. Hafner, R. Jira, R. Sieber, J. Sedlmeier, and A. Sabel, *Angew. Chem. Int. Ed. Engl.*, **1**, 80 (1962).

2) W. H. Clememt and C. M. Selwitz, *J. Org. Chem.*, **29**, 241 (1964).

3) D. R. Fahey and E. A. Zuech, *J. Org. Chem.*, **39**, 3276 (1974).

4) J. Tsuji, *Acc. Chem. Res.*, **6**, 8 (1973).

5) M. Stoll and A. Rouve, *Helv. Chem. Acta*, **30**, 2019 (1947).

6) J. Tsuji, K. Mizutani, I. Shimizu, and K. Yamamoto, *Chem. Lett.*, **1976**, 773.

7) J. Tsuji, M. Kaito, and T. Takahashi, *Bull. Chem. Soc. Jpn.*, **51**, 547 (1978).

8) J. Tsuji, Y. Mori, and M. Hara, *Tetrahedron*, **28**, 3721 (1972).

9) W. E. Billups, W. E. Walker, and T. C. Schields, *Chem. Commun.*, **1971**, 1067.

10) Y. Tsuzuki and S. Motoki, Jpn. Patent 6626 (1957); *Chem. Abstr.*, **52**, 9821e (1958).

11) M. Stoll, *Helv. Chim. Acta*, **34**, 1817 (1951).

12) J. Tsuji, I. Shimizu, and K. Yamamoto, *Tetrahedron Lett.*, **1976**, 2975.

13) H. Kamioka, K. Kinoshita, and N. Hirao, *Kogyo Kagaku Zasshi*, **72**, 1204 (1969), *Chem. Abstr.*, **71**, 80615h (1969).

A Molecular Orbital Study of the Electrophilicity of Hydroxyl Radical in Hydrogen Abstraction Reaction

Hiroyuki SHINOHARA*, Akira IMAMURA,** Takahiro MASUDA, and Masaharu KONDO

Department of Chemistry, Faculty of Science, Tokyo Metropolitan University, Fukasawa, Setagaya-ku, Tokyo 158

***Shiga University of Medical Science, Seta, Otsu, Shiga 520-21*

(Received June 11, 1977)

The electrophilicity of the hydroxyl radical in hydrogen abstraction from methane was studied by the CNDO/2 method. The stabilization energy due to the delocalization of the electrons (SEDE) between methane and the radical at a close distance was calculated. The electrophilicity defined by the SEDE from methane to the hydroxyl radical was larger than the nucleophilicity defined by that from the hydroxyl radical to methane. This result is consistent with the electrophilicity observed in hydrogen abstraction by the hydroxyl radical from a series of substituted methanes. For sulfhydryl radical, the electrophilicity was also suggested by the calculation for hydrogen abstraction from methane. The calculations were also carried out for various radicals which have low electron affinity (hydrogen atom and methyl radical), and the SEDE from methane to the radical was found to be large compared with that from the converse case.

Various kinds of radicals have been shown to react as electrophiles in reactions such as addition, substitution, or abstraction. A typical instance was given by Anbar *et al.*,[1,2] who determined the rate constants for reactions of hydroxyl radical with one series of aromatic and two series of aliphatic compounds (substituted methanes and acetate ions) in gamma-irradiated aqueous solutions. They concluded from the ρ values in the Hammett equation that the hydroxyl radical reacts as an electrophile in these reactions.

Recently, in order to explain the electrophilicity observed in radical reactions, theoretical attempts have been made by some workers. Nagase *et al.*[3] suggested the electrophilicity of a radical in hydrogen abstraction by an intermolecular perturbation approach and proposed a three-stage model which gives an insight into the mechanism of radical reactions.[4,5] Imamura has developed the molecular orbital (MO) method, which defines the polarity of the radical (nucleophilicity or electrophilicity) from the comparison of the stabilization energy due to delocalization of electrons (SEDE) between a substrate and the radical at a close distance.[6] According to this procedure, the nucleophilicity of the radical is evaluated by the SEDE from the occupied MO's of the radical to the vacant MO's of the substrate and the electrophilicity by that from the occupied MO's of the substrate to the vacant MO's of the radical. The electrophilicity of the hydroxyl radical in addition reactions with a series of mono-substituted benzenes was well understood by the differences in the SEDE.[6]

In the present work, as a first step in the investigation of the Hammett equation, we applied the MO method to hydrogen abstractions by the hydroxyl radical, sulfhydryl radical, hydrogen atom, and methyl radical from methane. The SEDE which corresponds to the electrophilicity is larger than that related to the nucleophilicity, and it can be concluded that these radicls react with methane as electrophiles.

Method of Calculation

The total energies for the reacting systems were calculated by the UHF method[7] in the CNDO/2 approximation.[8,9] The values of the parameters included in the CNDO-UHF calculation are the same as those used in the original papers.[8,9]

Procedure of Analysis. For the analysis of the polarity of a radical, a calculation should be carried out to obtain the MO's of substrate RH and radical X in the supposed model, in which they interact electrostatically with each other but are prohibited from any overlapping of MO's between them. Therefore the delocalization of electrons is prohibited in the model. These MO's can be obtained by the SCF calculation after dropping the resonance integrals I_{rs} between the atomic orbitals (AO's) of RH, χ_r, and AO's of X, χ_s, as given by

$$I_{rs} = \frac{1}{2}(\beta_r + \beta_s)S_{rs}. \tag{1}$$

Then the MO's for the reacting system [R···H···X] are classified into the MO's localized on RH and those localized on X:

$$\psi_{RHi} = \sum_r C_{RHi,r}\chi_r, \tag{2}$$

$$\psi_{Xj} = \sum_s C_{Xj,s}\chi_s. \tag{3}$$

ψ_{RHi} is the i-th MO localized on RH and $C_{RHi,r}$ is the coefficient of AO's in the i-th MO, and ψ_{Xj} and $C_{Xj,s}$ are for X. From Eq. 2, one obtains

$$\sum_i C_{RHi,r_1}\psi_{RHi} = \sum_r\sum_i C_{RHi,r_1}C_{RHi,r}\chi_r = \sum_r \chi_r \sum_i C_{RHi,r_1}C_{RHi,r}. \tag{4}$$

Since a set of ψ_{RHi},s is orthonormal,

$$\sum_i C_{RHi,r_1}C_{RHi,r} = \delta_{rr_1}, \tag{5}$$

and thus

$$\chi_r = \sum_i C_{RHi,r}\psi_{RHi}, \tag{6}$$

$$\chi_s = \sum_j C_{Xj,s}\psi_{Xj}. \tag{7}$$

From Eqs. 6 and 7, one obtains the relation between the I_{rs} represented by the AO basis of χ_r, χ_s, and the I_{ij} by the MO basis of ψ_{RHi}, ψ_{Xj}:

$$I_{rs} = \int \chi_r h^\circ \chi_s d\tau = \sum_i\sum_j C_{RHi,r}C_{Xj,s}\int \psi_{RHi}h^\circ\psi_{Xj}d\tau = \sum_i\sum_j C_{RHi,r}C_{Xj,s}I_{ij}. \tag{8}$$

Instead of Eq. 8, the I_{rs} in Eq. 9 is used in the SCF calculation in order to include the delocalization of electrons between particular orbital sets (i_1,j_1):

$$I_{rs} = \sum_{(i_1-j_1)} C_{RHi_1,r} C_{Xj_1,s} I_{i_1j_1}, \quad (9)$$

where $\sum_{(i_1-j_1)}$ denotes the summation over the sets (i_1,j_1). From Eq. 9, it is easily proved that the I_{ij} reduces to zero except for the $I_{i_1j_1}$ term, which has the same value as that obtained by using Eq. 8.

The procedure of the calculations is written as follows.
(i) The total energy of the reacting system without the delocalization of electrons is calculated by the SCF calculation after dropping the I_{rs} in Eq. 1. Thus we obtain the MO's in Eqs. 2 and 3.
(ii) By using the MO's obtained in the step (i), the modified resonance integrals between AO's are calculated according to Eq. 9 in order to take the delocalization of electrons between particular MO's into account.
(iii) The I_{rs} in Eq. 9 is employed to calculate the total energy of the reacting system with the delocalization of electrons, which corresponds to the nucleophilic or the electrophilic nature of the radical in question.
(iv) A measure of the nucleophilicity of the radical defined by the SEDE from the radical to the substrate, N, or the electrophilicity defined by the SEDE from the substrate to the radical, E, is evaluated by the difference between the two energies obtained in the steps (i) and (iii).

Results

Figure 1 shows a model for hydrogen abstraction by the hydroxyl radical from methane. The hydrogen atom of the hydroxyl radical lies at the opposite direction to the C^1–H^2 bond with regard to the C^1–H^5 bond. We examined the energy dependence of the CH_4–OH system upon the angle H^5OH in the intermolecular distance of 1.46 Å ;the result is given in Table 1. The minimum energy was situated at the angle between 100.45 and 104.45°. Therefore we assumed that the hydroxyl radical approaches to the H^5 atom of methane along the extension of the C^1–H^5 bond, maintaining the angle H^5OH at 104.45° (bond angle of water), and abstracts the H^5 atom.

Figure 2 shows the potential curves of the CH_4–OH system calculated by assuming that the HCH angle of the CH_3 group is not varied throughout the

TABLE 1. THE ENERGY DEPENDENCE OF CH_4–OH SYSTEM[a] UPON THE ANGLE H^5OH

H^5OH angle (°)	Total energy
96.45	−28.0226
100.45	−28.0229
104.45	−28.0229
108.45	−28.0227
112.45	−28.0226
180.00	−28.0056

a) The calculation was carried out at point A(1.09, 1.46) by the INDO method.[15] Atomic units.

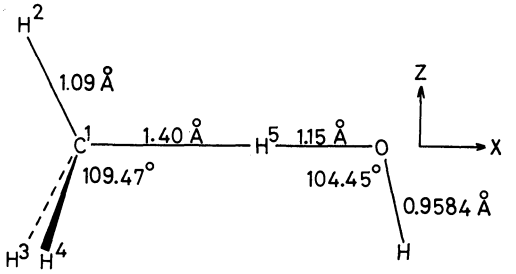

Fig. 1. Coordinate system for hydrogen abstraction by the hydroxyl radical from methane.

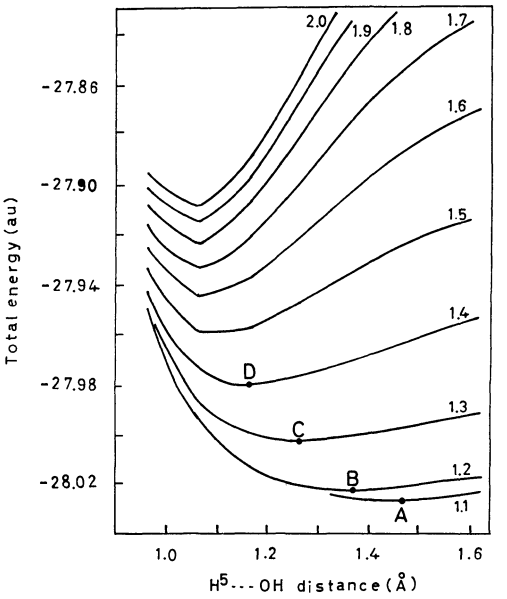

Fig. 2. Potential curves as a function of H^5–O distance at various C^1–H^5 distances in CH_4–OH system. 1.1 and others in figure correspond to C^1–H^5 distances in Å. INDO method.[15]

reaction. In this figure, we specify the reaction path with a notation (r_1,r_2), where r_1 is the distance (in Å) between C^1 and H^5 atoms and r_2 is that between H^5 and hydroxyl oxygen atoms in Fig. 1. As the energy of the system increases monotonously, the geometry of the transition state is not obvious. However, it can be assumed that a more favorable reaction path for H^5 atom abstraction goes through the following points: A, B, C, and D, which are specified respectively by the sets of r_1 and r_2 indicated in the parenthesis: A(1.09, 1.46), B(1.20, 1.35), C(1.30, 1.25), D(1.40, 1.15).

Table 2 shows the schematic representation of the intermolecular interaction between the MO's of RH and X obtained by dropping the I_{rs} in Eq. 1. Here, Occ and Vac represent occupied and vacant MO's respectively; N or E denotes the nucleophilicity or the electrophilicity of the radical defined previously. Among them, N_1, N_2, E_1, and E_2 include the effect of the delocalization of electrons only, while N_3, N_4, E_3, and E_4 include the interaction between occupied MO's in addition to the effect of the delocalization. It can be noticed from the electron distribution shown

Table 2. The schematic representation of the orbital interaction between substrate RH and radical X[a)]

	α-spin			β-spin		
Electrostatic interaction (Zero)	RH	Occ	Vac	RH	Occ	Vac
	X	Occ	Vac	X	Occ	Vac
Nucleophilicity-1 (N_1)	RH	Occ	Vac	RH	Occ	Vac
	X	Occ	Vac	X	Occ	Vac
Electrophilicity-1 (E_1)	RH	Occ	Vac	RH	Occ	Vac
	X	Occ	Vac	X	Occ	Vac
Nucleophilicity-2 (N_2)	RH	Occ	Vac	RH	Occ	Vac
	X	Occ	Vac	X	Occ	Vac
Electrophility-2 (E_2)	RH	Occ	Vac	RH	Occ	Vac
	X	Occ	Vac	X	Occ	Vac
Nucleophilicity-3 (N_3)	RH	Occ	Vac	RH	Occ	Vac
	X	Occ	Vac	X	Occ	Vac
Electrophilicity-3 (E_3)	RH	Occ	Vac	RH	Occ	Vac
	X	Occ	Vac	X	Occ	Vac
Nucleophilicity-4 (N_4)	RH	Occ	Vac	RH	Occ	Vac
	X	Occ	Vac	X	Occ	Vac
Electrophilicity-4 (E_4)	RH	Occ	Vac	RH	Occ	Vac
	X	Occ	Vac	X	Occ	Vac
All interactions (All)	RX	Occ	Vac	RH	Occ	Vac
	X	Occ	Vac	X	Occ	Vac

a) The symbol for the orbital interaction used in the text is given in the parentheses. The interaction which includes the $I_{i_1 j_1}$ is represented by a solid line.

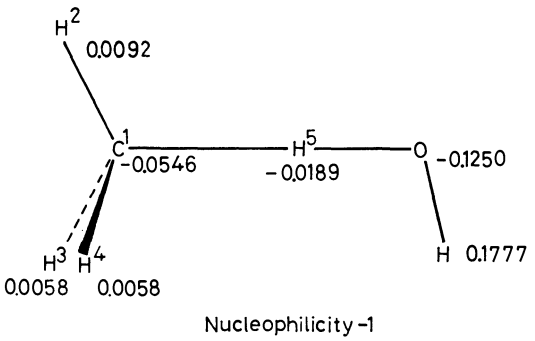

Nucleophilicity-1

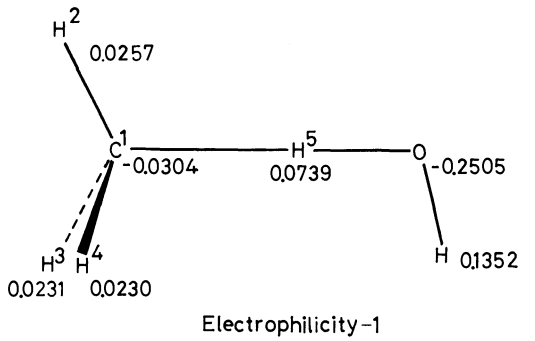

Electrophilicity-1

Fig. 3. The electron distribution of CH_4-OH system by the orbital interaction N_1 or E_1 defined in Table 2.

in Fig. 3 that the delocalization of electrons occurs from the hydroxyl radical to methane by the interaction N_1, while that from methane to the hydroxyl radical occurs by the interaction E_1. These results are summarized in Table 3. The ratios of E_1/N_1 are 2.7, 2.1, 1.8, and 1.5 at the points A, B, C, and D, respectively. As is shown in N_3 and E_3, the SEDE including the interaction of occupied MO's is larger than that including the delocalization of electrons only. This energy can be considered to include the redistribution energy as well as the delocalization energy. It should be noticed that the stabilization energy by delocalization is much larger than that by the redistribution effect, although the absolute magnitude of the latter is not negligibly small. Consequently, if we can determine the polarity of a radical from the viewpoint of the SEDE, it will be possible to conclude that the hydroxyl radical reacts as an electrophile in hydrogen abstraction from methane. The HOMO-LUMO interaction plays an important role in E_1 and the electrophilicity of the hydroxyl radical is closely related with this interaction.

As organic sulfur compounds are recognized to have high levels of HOMO and low levels of LUMO, it is interesting to determine the polarity of the sulfhydryl radical. Figure 4 shows a model for hydrogen abstraction by the sulfhydryl radical from methane.

TABLE 3. THE ELECTROPHILICITY OF THE HYDROXYL RADICAL IN HYDROGEN ABSTRACTION FROM METHANE

Path point	Orbital[a] interaction	Total[b] energy	Stabilization[b] energy	ET[c]
(A)	Zero	−29.0560	0	0
	N_1	−29.0667	0.0107	0.0114
	E_1	−29.0848	0.0288	−0.0423
	All	−29.1062	0.0502	−0.0372
(B)	Zero	−29.0253	0	0
	N_1	−29.0439	0.0186	0.0208
	E_1	−29.0646	0.0393	−0.0610
	All	−29.1031	0.0778	−0.0518
(C)	Zero	−28.9653	0	0
	N_1	−28.9943	0.0290	0.0341
	E_1	−29.0170	0.0517	−0.0845
	All	−29.0836	0.1183	−0.0736
(D)	Zero	−28.8765	0	0
	N_1	−28.9202	0.0437	0.0527
	HOMO-LUMO	−28.8998	0.0233	0.0378
	E_1	−28.9440	0.0675	−0.1253
	HOMO-LUMO	−28.9378	0.0613	−0.1095
	N_2	−28.9422	0.0657	0.0707
	E_2	−28.9445	0·0680	−0.1158
	N_3	−28.9591	0.0826	0.0659
	E_3	−28.9609	0.0844	−0.1561
	N_4	−28.9790	0.1025	0.0913
	E_4	−28.9720	0.0955	−0.1700
	All	−29.0620	0.1855	−0.1028

a) See Table 1. b) Atomic units. c) Electron transfer quantities due to delocalization of electrons. Positive values correspond to those from the radical to substrate and negatives, *vice versa*.

TABLE 4. THE ELECTROPHILICITY OF THE SULFHYDRYL RADICAL IN HYDROGEN ABSTRACTION FROM METHANE

Path point	Orbital[a] interaction	Total[b] energy	Stabilization[b] energy	ET[c]
(C)	Zero	−21.5850	0	0
	N_1	−21.5857	0.0007	0.0014
	E_1	−21.5871	0.0021	−0.0038
	N_2	−21.5860	0.0010	0.0015
	E_2	−21.5878	0.0028	−0.0048
	All	−21.5883	0.0033	−0.0033
(D)	Zero	−17.2002	0	0
	N_1	−17.2226	0.0224	0.0494
	E_1	−17.4292	0.2297	−0.3095
	N_2	−17.2354	0.0352	0.0673
	E_2	−17.4412	0.2410	−0.3459
	N_3	−17.4284	0.2282	−0.5974
	E_3	−17.6064	0.4062	−0.6706
	N_4	−17.4446	0.2444	−0.5321
	E_4	−17.6315	0.4313	−0.5184
	All	−17.7315	0.5313	−0.6110

a), b), c) See the notes in Table 3.

Figure 5 shows the energy dependence of the CH_4–SH system upon the intermolecular H^5–S distance, with the C^1–H^5 distance fixed at 1.09 Å, while Fig. 6 shows that upon the C^1–H^5 distance with variations of the C^1–S distance. The result of calculations (Table 4) at the points C (1.40, 2.74) and D(1.40, 1.524) in Fig. 6 confirms the electrophilicity of the sulfhydryl radical.

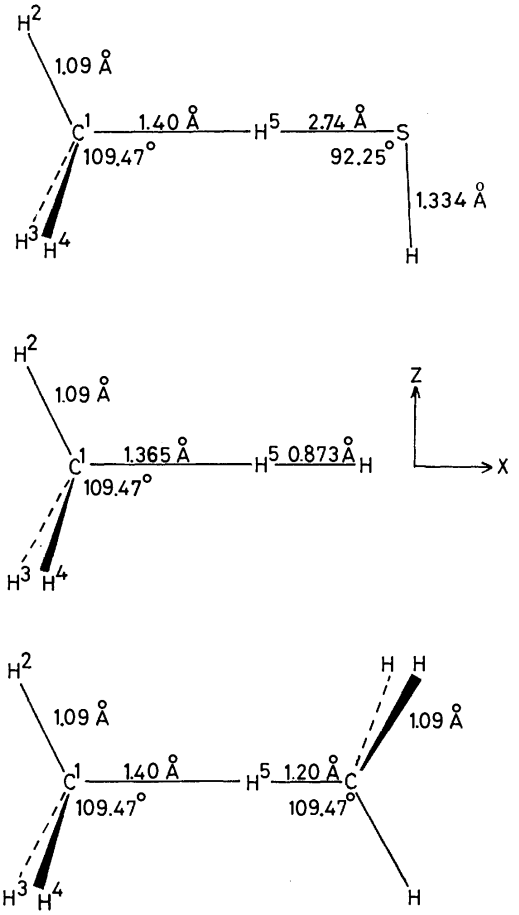

Fig. 4. Coordinate system for hydrogen abstraction by the doublet radical from methane.

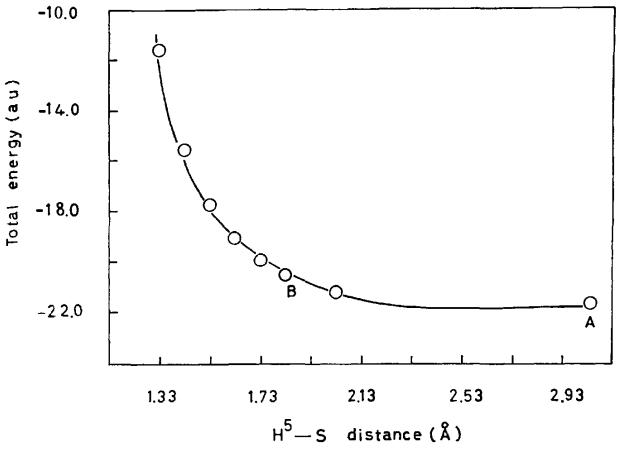

Fig. 5. Potential curve as a function of H^5–S distance in CH_4–SH system.

Calculations were carried out for the radicals of low electron affinities, such as hydrogen atom and methyl radical. For hydrogen atom, the result is given in Table 5. The ratio of E_1/N_1 calculated in the coordinate system (Fig. 4) which corresponds to the transition state deduced from *ab initio* MO method[10] represents the electrophilicity.

The electrophilicity of the methyl radical was clarified by Fujimoto *et al.*[11] using the semiempirical MO

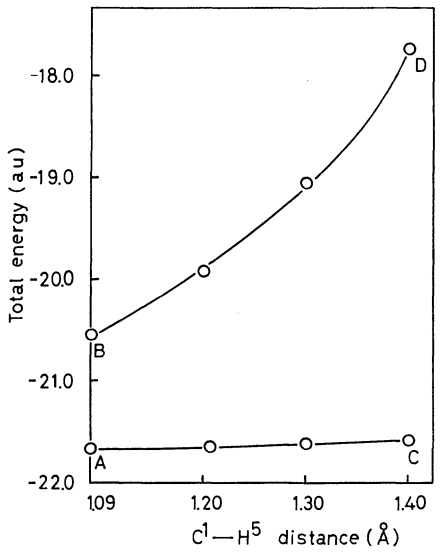

Fig. 6. Potential curves as a function of C^1-H^5 distance, with C^1-S distance varied in CH_3-SH system.

Table 5. The electrophilicity of the hydrogen atom in hydrogen abstraction from methane

Orbital[a] interaction	Total[b] energy	Stabilization[b] energy	ET[c]
Zero	−10.5959	0	0
N_1	−10.6078	0.0120	0.0249
E_1	−10.6723	0.0765	−0.1338
All	−10.7001	0.1043	−0.0953

a), b), c) See the notes in Table 3.

Table 6. The electrophilicity of the methyl radical in hydrogen abstraction from methane

Orbital[a] interaction	Total[b] energy	Stabilization[b] energy	ET[c]
Zero	−18.9894	0	0
N_1	−19.0358	0.0464	0.0822
E_1	−19.1336	0.1442	−0.2029
N_2	−19.0455	0.0561	0.0895
E_2	−19.1342	0.1448	−0.2036
N_3	−19.0758	0.0864	0.1836
E_3	−19.1438	0.1544	−0.2212
N_4	−19.0769	0.0875	0.1812
E_4	−19.1624	0.1730	−0.1980
All	−19.2782	0.2888	−0.0263

a), b), c) See the notes in Table 3.

method including overlap integrals; it is also confirmed by our analysis (Table 6), which was carried out in the strong interaction region, as is shown in Fig. 4.

Discussion

As the present analysis is based on the zero differential overlap approximation, the quantitative evaluation of the polarity of a radical is hardly possible because of the crudeness of the calculation. The aim of this work is to discuss qualitatively the polarity of a radical from the viewpoint of the SEDE between a substrate and a radical. Despite these inaccuracies, we believe that the results obtained here may still be useful as a working tool for understanding radical reactions. It is concluded that not only the hydroxyl radical but also the hydrogen atom or the methyl radical reacts as an electrophile in hydrogen abstraction from methane, in spite of its low electron affinity. The polarity of a radical is derived properly from the rate constants for reactions with a series of substrates. However, it is essentially dependent on the substrate, and thus a relative property given to individual reactions. The direction of the delocalization of electrons in an individual reaction may not necessarily accord with the electrophilicity defined by the ρ value.

Sakurai *et al.*[12] reported the linear relationship of the electron affinities of the radicals and the negative ρ values for hydrogen abstractions by various radicals from substituted toluenes. The electrophilicity defined in the present work is related to the electron affinity of the radical; therefore, the negative ρ values may be expected to correlate with the SEDE from a substrate to the radical calculated for individual reactions. Isopropyl and *t*-butyl radicals have recently been found to react as nucleophiles in hydrogen abstractions from substituted toluenes by Pryor *et al.*[13] The positive ρ value increases with a decrease in the ionization potential (*IP*) of the radical (i-C_3H_7: $\rho=0.8$, $IP=7.90$ eV, t-C_4H_9: $\rho=1.0$, $IP=7.07$ eV[14]). As the nucleophilicity defined in the present work is related with the ionization potential of the radical, SEDE from the radical to a substrate will provide a way to explain the reactions of positive ρ values. Further calculations of the SEDE are in progress for hydrogen abstractions by various kinds of radicals.

The authors are grateful to the Quantum Chemical Research Group in Kyoto University for helpful discussions.

The calculations were carried out on the FACOM 230-75 computer of the Computer Center of Kyoto University. The research was supported, in part, by Scientific Grants (139012 and 038012) from the Ministry of Education, Culture, and Sciences.

References

1) M. Anbar, D. Meyerstein, and P. Neta, *J. Phys. Chem.*, **70**, 2660 (1966).
2) M. Anbar, D. Meyerstein, and P. Neta, *J. Chem. Soc., B*, 742 (1966).
3) S. Nagase and T. Fueno, *Theoret. Chim. Acta (Berlin)*, **41**, 59 (1976).
4) S. Nagase, T. Takatsuka, and T. Fueno, *J. Am. Chem. Soc.*, **98**, 3838 (1976).
5) S. Nagase and T. Fueno, *Bull. Chem. Soc. Jpn.*, **49**, 2920 (1976).
6) A. Imamura and K. Hirao, to be published.
7) J. A. Pople and R. K. Nesbet, *J. Chem. Phys.*, **22**, 571 (1954).
8) J. A. Pople, D. P. Santry, and G. A. Segal, *J. Chem. Phys.*, **43**, s129 (1965); J. A. Pople and G. A. Segal, *ibid.*, **43**, s136 (1965).

9) J. A. Pople and G. A. Segal, *J. Chem. Phys.*, **44**, 3289 (1966).
10) K. Morokuma and R. E. Davis, *J. Am. Chem. Soc.*, **94**, 1060 (1972).
11) H. Fujimoto, S. Yamabe, T. Minato, and K. Fukui, *J. Am. Chem. Soc.*, **94**, 9205 (1972).
12) H. Sakurai and K. Tokumaru, *Kagaku No Ryoiki, Zokan*, **81**, 355 (1967).
13) W. H. Davis, Jr., and W. A. Pryor, *J. Am. Chem. Soc.*, **99**, 6365 (1977).
14) F. W. McLatterty, Ed, "Mass Spectrometry of Organic Ions," Academic Press, New York (1963), Chap. 5.
15) J. A. Pople and D. L. Beveridge, "Approximate Molecular Otbital Theory," McGraw-Hill, New York (1970).

The Effect of the Vibrational and Translational Energies of Ionic Reactant on the Reaction $C_3H_4^+ + NH_3 \rightarrow C_3H_3 + NH_4^+$

Kenji HONMA,* Inosuke KOYANO,† and Ikuzo TANAKA

Department of Chemistry, Tokyo Institute of Technology, Ohokayama, Meguro-ku, Tokyo 152

(Received August 12, 1977)

The effect of the internal and translational energies of ionic reactant on the rates of the reactions $C_3H_4^+ + NH_3 \rightarrow C_3H_3 + NH_4^+$ has been examined by producing the reactant ions from propyne, allene, and cyclopropene by photoionization at various wavelengths. The translational energy was varied by changing the repeller voltage in the ionization chamber. The cross sections for all the reactions decreased with an increase in the internal energy at all the translational energies studied. The results have been explained in terms of the complex mechanism.

The roles played by various forms of reactant energy in bimolecular reactions in the gas phase have been the subject of intensive study in recent years, both experimentally and theoretically.[1] In ion-molecule reactions, the effect of the vibrational energies of ionic reactants can be studied rather easily since the primary ions can be prepared in various vibrational states with known distributions. Photoionization is particularly suited for this purpose,[2] showing well-defined vibrational structure in the ionization efficiency curves. The distribution of ions among vibrational states can be determined precisely by photoelectron spectroscopy. In a favorable case, ions can be prepared in only one particular vibrational state (and even in a rotational state) selectively by making use of autionization[3,4]

Although many investigations have been performed from both experimental and theoretical viewpoints[5] on the proton transfer reactions:

$$\begin{aligned} XH^+ + Y &\rightarrow X + HY^+ \\ YH + X^- &\rightarrow Y^- + XH, \end{aligned} \qquad (2)$$

the main interest has centered on the comparison of the measured cross section with those predicted from the classical dipole theory; only a few works have been concerned with the effects of reactant vibration and translation. Chupka and Russell[6] studied this exothermic reaction:

$$NH_3^+ + NH_3 \rightarrow NH_2 + NH_4^+, \qquad (3)$$

by the use of a high-resolution photoionization technique and found that the cross section decreases as the vibrational energy increases at all the translational energies studied. On the other hand, by the use of a flow-drift tube technique, Lindinger *et al.*[7] measured the rate constants of the proton transfer reactions of several ions with NH_3 as a function of the relative kinetic energy. They found that the rate constants are generally in good agreement with those predicted by the ADO (average-dipole-orientation) theory in the thermal energy range.

In the present study, the photoionization technique has been applied to the study of the effects of the translational and internal energies on the probabilities of the proton transfer reactions:

$$C_3H_4^+ + NH_3 \rightarrow C_3H_3 + NH_4^+. \qquad (1)$$

As the sources of $C_3H_4^+$, three structural isomers of C_3H_4 (propyne, allene, and cyclopropene) were used. These systems constitute a favorable case for investigating the factors which govern the reaction probability, since, in these systems, the reduced masses and the polarizability and permanent dipole moment of the neutral reactant are identical.

Experimental

The experiments were carried out using a photoionization apparatus which has been described previously in considerable detail.[8] Briefly, it consists of a continuum light source, a Seya-Namioka-type vacuum monochromator, an ionization chamber, and a quadrupole mass spectrometer, these being combined together *via* a five-stage differential pumping system. Radiation from a Hinteregger-type hydrogen discharge lamp passed through the monochromator and irradiated the sample gas in the ionization chamber to produce reactant ions. Since the ionization potentials of allene and cyclopropene are 9.61 eV (corresponding to 129.0 nm) and 9.63 eV (corresponding to 128.3 nm) respectively, the radiation of wavelengths shorter than the respective IP, but longer than 121.7 nm (corresponding to the ionization potential of ammonia), produced only $C_3H_4^+$ ions as reactants in the mixture of C_3H_4 and NH_3, thus enabling one to study Reaction 1 by the single-source method. In the case of the propyne–ammonia system, however, the photons which can ionize propyne (IP=10.35 eV) always ionize ammonia in the mixture; thus there is a possibility that the secondary NH_4^+ ions were produced also by Reaction 3. This problem will be discussed in a later section.

Five or more wavelengths were used for each system to produce $C_3H_4^+$ ions in various vibrational states. Pressure studies were carried out at each wavelength, λ then to determine the phenomenological cross section, Q_λ. The results were this analyzed in terms of the "maximum excess internal energy," E, which is given by equation: E=(photon energy)−(ionization potential). The actual internal energy E_i, of the reactant ions produced by irradiation at λ ranges from 0 to E. The effect of the translational energy was studied by changing the ion-exit energy E_t, between 0.5 and 5.6 eV. The ions were detected by means of a pulse-counting technique using a 20-stage electron multiplier. The pressures of the 1 : 1 mixtures of C_3H_4 and NH_3 in the ionization chamber were typically less than 1×10^{-3} Torr, and the resolution width (FWHM) of the ionizing radiation was 0.23 nm.

Commercial pure propyne, allene, and ammonia were used without further purification. The cyclopropene was synthesized from allyl chloride and sodium amide by the method of Closs and Klantz;[9] it was then purified by bulb-to-bulb distillation.

† Present address: Institute for Molecular Science, Myodaiji, Okazaki 444.

Results and Discussion

General. In all the C_3H_4+NH_3 systems, the $C_3H_4^+$ ions react with C_3H_4 in addition to undergoing Reaction 1. These reactions have been studied by Myher and Harrison[10] in both pure propyne and pure allene. They found that Reactions 4 and 5 are dominant for propyne, while only Reaction 5 is dominant for allene:

$$C_3H_4^+ + C_3H_4 \rightarrow C_3H_5^+ + C_3H_3 \quad (4)$$

$$\rightarrow C_6H_7^+ + H. \quad (5)$$

In the present study, these results have been confirmed in runs with pure propyne and allene; in addition, similar reactions in pure cyclopropene have been examined. In the latter systems, it was found that the reaction

$$C_3H_4^+ + C_3H_4 \rightarrow C_3H_3^+ + C_3H_5, \quad (6)$$

is the dominant one, with the reaction

$$C_3H_4^+ + C_3H_4 \rightarrow C_6H_5^+ + H_2 + H, \quad (7)$$

occuring to a moderate extent and Reactions 4 and 5, to only a minor extent.[11] All these reactions were taken into account in all systems as the loss processes of the reactant $C_3H_4^+$ ion, in obtaining the relative cross sections for Reaction 1. That is, they were calculated by means of the equation

$$Q_J \cdot p_s \cdot d = I_{sJ}/(I_p + \sum_i I_{si}),$$

where I_p, I_{si}, p_s, and d are the intensity of the primary ion, the intensity of the secondary ion, the sample pressure, and the distance between the origin of the primary ion and the exit slit respectively.

Internal Energy Dependence. The experimental results for the cyclopropene–ammonia and allene–ammonia systems are shown in Figs. 1 and 2. In these figures, the relative cross sections (Q) at three ion-exit energies are plotted *vs.* the maximum excess internal energy. It may be seen from these figures that the reaction cross section decreases with an increase in the excess energy at all translational energies. This can be explained qualitatively in terms of the complex formation mechanism, as has been done in other reactions.[1,3,6] In the complex mechanism, the decrease in the reaction cross section with an increase in the internal energy can be predicted from the phase space theory of Light[12] if the cross section for complex formation is independent of the internal energy. According to this theory, the collision complex decomposes along all energetically available channels, including the backward reaction, the relative probabilities for the different decomposition channels depending on the energy content of the collision complex. When the vibrational energy of a reactant is low (*e.g.*, when all vibrational modes are in the ground state), only one backward decay channel (forming reactants with all modes in the ground state) would be energetically available for the collision complex. This channel is thermoneutral and would correspond to a very small volume of the phase space, resulting in a negligibly small probability for this channel compared with that

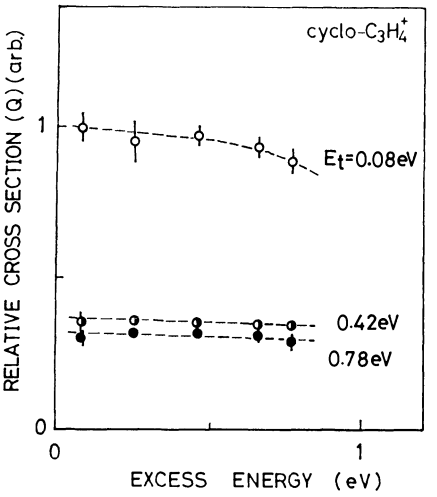

Fig. 1. Dependence of the cross section for the reaction $C_3H_4^+$(cyclopropene)+$NH_3 \rightarrow NH_4^+ + C_3H_3$ on the excess internal energy of $C_3H_4^+$. E_t indicates relative kinetic energies.

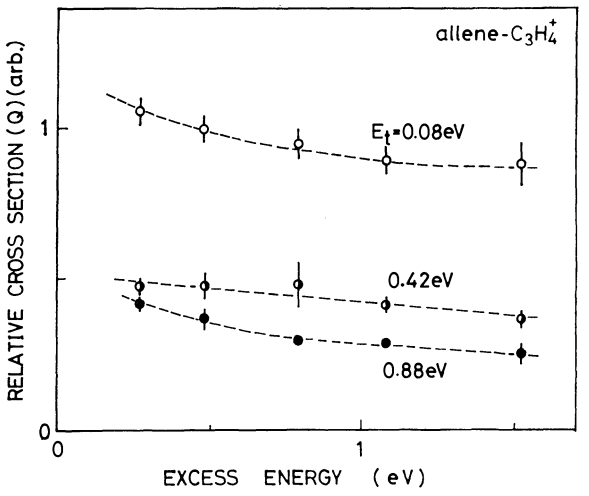

Fig. 2. Dependence of the cross section for the reaction $C_3H_4^+$(allene)+$NH_3 \rightarrow NH_4^+ + C_3H_3$ on the excess internal energy of $C_3H_4^+$. E_t indicates relative kinetic energies.

for the exothermic forward channels. As the excess energy of the reactant (and, accordingly, the energy content of the complex) increases, the exothermic backward decay channels, *i.e.*, the channels going back to the reactants which have lower vibrational quantum numbers than they had initially, become increasingly available. With complex molecular ions such as those used in the present study, the channels going back to the reactants which are excited in a different mode from the original one also become available at high excess energies. All these channels cause substantial increases in the relative volume of the phase space for the back reaction; thus, the reaction cross section decreases with an increase in the excess energy of the reactant ion.

Recently we have studied the translational and vibrational energy dependence of the cross section for the reaction:[1]

$$NO^+ + i\text{-}C_4H_{10} \rightarrow HNO + C_4H_9^+, \quad (8)$$

and have concluded that this reaction proceeds *via* complex formation at low translational energies, but the mechanism changes to a stripping type as the ionic translational energy increases. A similar mechanistic change has also been proposed by Chupka *et al.*[3] for the reaction

$$H_2^+ + H_2 \rightarrow H_3^+ + H. \quad (9)$$

These conclusions are based on the different vibrational energy dependence of the cross section at low and high translational energies. In contrast, all the present reactions show the same vibrational energy dependence at all the translational energies studied. The highest relative kinetic energy used here is much higher than the energy at which the mechanism change was observed in the previous system ($NO^+ + C_4H_{10}$). Thus, the above results indicate that the complex formation in the present system persists up to much higher energies than in Reactions 8 and 9. One of the origins of this difference might be the presence of a permanent dipole moment in the neutral reactant, NH_3. Because of the long-range interaction between the charge on the ion and the permanent dipole moment, the collisons in the present system are expected to be more "sticky" than those in Reactions 8 and 9. In this connection, it is to be noted that Reaction 3, which involves NH_3 as a neutral reactant, also shows a single-complex-type behavior at all the energies studied.[6]

Translational Energy Dependences. The translational energy dependences of Reaction 1 for the two $C_3H_4^+$ isomers with NH_3 are shown in Fig. 3. The solid and broken lines indicate the $E^{-1/2}$ and E^{-1} dependences respectively. In the ADO theory, the cross section for reaction between an ion and a polar molecule is given by

$$\sigma = \pi e[(2\alpha)^{1/2}E^{-1/2} + c\mu_D E^{-1}],$$

where E is the collision energy, α and μ_D, the polarizability and permanent dipole moment of the neutral molecule respectively, and c, a parameter characteristic of the neutral reactant. Thus, the cross-sections might be expected to show energy-dependence curves which lie between the solid and broken lines in Fig. 3. However the results were that the cross sections almost obey the $E^{-1/2}$ dependence.

The rate constants for several exothermic proton transfer reactions have recently been studied by Lindinger *et al.*[7] using a flow-drift tube. Their results show that the thermal-energy rate constants were given reasonably well by the Langevin (nonpolar) or the ADO(polar) collision rate constants in most cases. However, the translational-energy dependence of the reaction-rate constants was not that predicted by these theories; *i.e.*, the rate constants of all proton transfer reactions to NH_3, except that for the reaction $NH_3^+ + NH_3 \rightarrow NH_4^+ + NH_2$, decline with the relative kinetic energy less steeply than would be predicted from the ADO theory. These rate constants even show a Langevin-like behavior in a certain kinetic energy region above the thermal region. Thus, although no generalized conclusion can be drawn from this limited number of studies, the $E^{-1/2}$ dependence of the cross section observed in the present study is in line with the general trend observed by Lindinger *et al.* for the proton transfer reactions with NH_3.

Propyne–Ammonia System. In the propyne–ammonia system, the determination of the relative

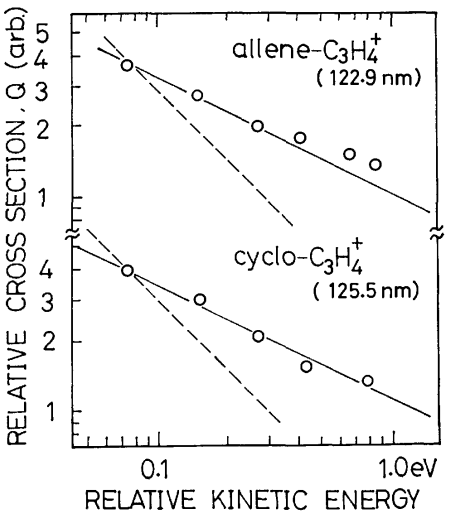

Fig. 3. Kinetic energy dependence of the cross sections for the reactions $C_3H_4^+ + NH_3 \rightarrow NH_4^+ + C_3H_3$. Allene and cyclopropene were ionized to produce $C_3H_4^+$ at 122.9 and 125.5 nm radiation, respectively. Solid and broken lines indicate the $E^{-1/2}$ and E^{-1} dependence, respectively.

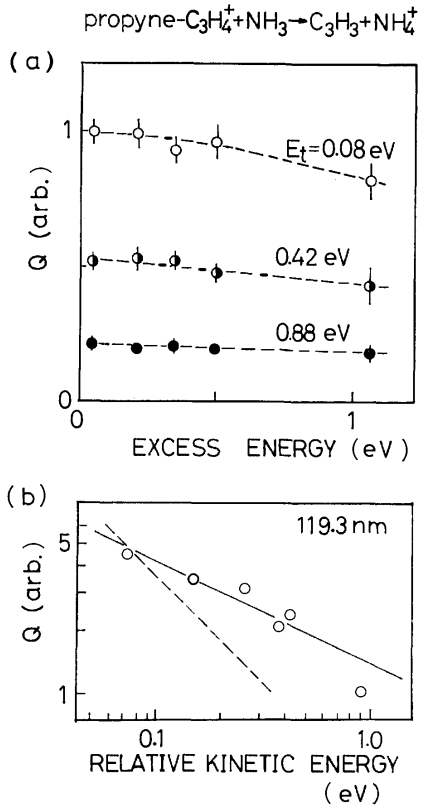

Fig. 4. Dependence of the cross section for the reaction $C_3H_4^+$(propyne) $+ NH_3 \rightarrow NH_4^+ + C_3H_3$ on the excess internal energy of $C_3H_4^+$ at 119.3 nm radiation. Solid and broken lines indicate the $E^{-1/2}$ and E^{-1} dependence, respectively.

cross section of Reaction 1 is not as straightforward as in the above two systems, since, as was mentioned earlier, ammonia is always ionized by the radiation which ionizes propyne. That is, the following reactions must also be taken into consideration:

$$NH_3^+ + NH_3 \rightarrow NH_4^+ + NH_2, \quad (10)$$

$$C_3H_4^+ + NH_3 \rightarrow NH_3^+ + C_3H_4, \quad (11)$$

$$NH_3^+ + C_3H_4 \rightarrow NH_4^+ + C_3H_3. \quad (12)$$

The extent to which Reaction 10 contributes to the formation of NH_4^+ could easily be estimated from the study with pure ammonia, thus, the NH_4^+ intensities obtained in the mixtures have been corrected for this contribution. However, it is difficult to assess the importance of Reactions 11 and 12 by the use of the present technique. We have examined the variation in the NH_3^+ intensity as a function of the pressure of the added C_3H_4, keeping the NH_3 pressure constant; no significant change was observed within the experimental error at any wavelength. The implication of this result may be either that both Reactions, 11 and 12, are negligible compared, respectively, with Reactions 1 and 10, or that both reactions are fast but proceed, fortuitously, at almost the same rate, leading to no net change in the NH_3^+ intensity. Although the latter possibility can not be ruled out completely, we dared to assume that both Reactions, 11 and 12, are negligible under the present experimental conditions and analyzed the data in the same way as in the allene–ammonia and cyclopropane–ammonia systems. The resulting relative cross sections for Reaction 1 are presented in Fig. 4 as a function of both the excess internal energy (Fig. 4a) and the relative kinetic energy (for the 119.3 nm irradiation). It is interesting to see that the cross sections obtained for the propyne-ammonia system with the above assumption show the same excess energy and translational energy dependence as those in the other two systems.

References

1) See, for example, K. Honma, K. Tanaka, I. Koyano, and I. Tanaka, *J. Chem. Phys.*, **65**, 678 (1976) and the references cited therein.

2) W. A. Chupka, "Ion-Molecule Reactions by Photoionization Techniques," in "Ion-Molecule Reactions," ed by J. L. Franklin, Plenum, New York (1972).

3) W. A. Chupka, M. E. Russell, and K. Refaey, *J. Chem. Phys.* **48,** 1518 (1968).

4) W. A. Chupka and M. E. Russell, *J. Chem. Phys.*, **49**, 5426 (1968).

5) See, for example, D. K. Bohme, "The Kinetics and Energetics of Proton Transfer," in "Interaction between Ions and Molecules," ed by P. Ausloos, Plenum, New York (1974).

6) W. A. Chupka and M. E. Russell, *J. Chem. Phys.*, **48**, 1527 (1968).

7) W. Lindinger, D. L. Albritton, F. C. Fehsenfeld, A. L. Schmeltekopf, and E. E. Ferguson, *J. Chem. Phys.*, **62**, 3549 (1975).

8) K. Tanaka and I. Tanaka, *J. Chem. Phys.*, **59**, 5042 (1973).

9) G. L. Closs and K. D. Krantz, *J. Org. Chem.*, **31**, 638 (1966).

10) J. J. Myher and A. G. Harrison, *J. Phys. Chem.*, **72**, 1905 (1966).

11) A. Nato, M. Niwa, K. Honma, I. Koyano, and I. Tanaka, to be published.

12) J. C. Light, *J. Chem. Phys.*, **40**, 3221 (1964).

The Mechanism of Oxygen Reduction at a $LaNiO_3$ Electrode

Yasumichi MATSUMOTO, Hiroshi YONEYAMA, and Hideo TAMURA*

Department of Applied Chemistry, Faculty of Engineering, Osaka University, Yamadakami, Suita, Osaka, 565

(Received September 7, 1977)

The reaction mechanism of the O_2 reduction at $LaNiO_3$ was studied by using a rotating ring-disc electrode, which consists of a $LaNiO_3$ disc and Pt ring electrodes. It was found that the O_2 was completely reduced to OH^- on the Hoare path. Oxygen vacancies seem to be required in the oxide surface for reduction of adsorbed O_2H^- to OH^-.

It was shown in previous studies[1,2] of the catalytic activity of transition metal oxides for the O_2 reduction that the band structure of oxides is a major factor in determining their catalytic activities. In order for the oxides to have a high catalytic activity, they must have a filled or partially filled σ^* band. $LaNiO_3$ satisfies this requisite, and hence shows high electrocatalytic activity for the O_2 reduction. It was also found that the O_2 reduction at $LaNiO_3$ and related oxides proceeded with the Hoare path and that the rate-determining electron transfer step, $O_2H+e\rightarrow O_2H^-$, was greately affected by the d-electron configuration in the σ^* band.

It is important to clarify the over-all reaction mechanism in order to elucidate the electrocatalysis of O_2 reduction. Especially important is the role which O_2H^- plays in the sequence of the reaction. The use of the rotating ring-disc electrode has been shown to be successful for this purpose.[3-7]

In the present study, therefore, the reaction mechanism of the O_2 reduction at $LaNiO_3$ is determined by using the rotating ring-disc electrode assembly, and the major factor which leads to O_2H^- formation is discussed.

Experimental

A rotating $LaNiO_3$ disc electrode with a Pt ring was prepared by the following method. A $LaNiO_3$ disc electrode of 6 mm diameter was prepared in the same manner as described in a previous paper,[8] and then assembled in a Teflon rod together with a Pt ring (6.7 mm in inner diameter and 9 mm in outer diameter). The area of the disc electrode was then 0.28 cm^2, and the geometric factor N was 0.39, as calculated from the dimension of the disc and ring electrodes.

The ring-disc electrode was set in a rotating ring-disc measurement system (Nikko Keisoku, model RRDE-1). The electrolytes were 1 M** NaOH and NaOH–Na_2SO_4 mixtures. The latter was prepared so as to give the same ionic strength as 2 M NaOH, but various pH values. A hydrogen electrode, H.E., in the test electrolytes was used as a reference electrode. The electrode potentials cited in this paper are referred to this electrode, unless otherwise stated.

As the pretreatment of the disc electrode, it was washed with acetone, followed by immersion in 0.5 M H_2SO_4 for 10 s, and then washed with distilled water.[9] The pretreatment of the Pt ring electrode was made electrochemically; it was polarized at 1.8 V for 30 s in the same solution as the test electrolyte in order to eliminate the adsorbed impurities on the surface, then at −0.1 V for 30 s to reduce an oxidized surface, and finally for about 3 h at 1.4 V, which was the same potential as that selected for detection of O_2H^-. The background current decreased to less than 0.2 μA by the final treatment, and thereby reproducible results could be obtained. Potential-current curves of the disc electrode were measured under a potentiostatic condition, and the oxidation current of O_2H^- at the ring electrode was measured at 1.4 V.[3]

** M=mol·dm^{-3}.

Results

Figure 1 shows the ring current, I_r, and the disc current, I_d, as a function of disc electrode potentials, E_d. The rotation rate, ω, was set at 2000 min^{-1}. A very small ring current was observed in the potential region less positive than 0.825 V.

$1/J$ *vs.* $\omega^{-1/2}$ plots are shown in Fig. 2 for the limiting current region, where $J=|I_d|+I_r/N$. As shown in Fig. 1, I_r was very small compared with I_d, and hence I_r negligibly contributed to J. The conclusion can be drawn, therefore, from the good linearities between J and $\omega^{-1/2}$ that the reaction order of O_2 is 1[10] in the potentials giving a saturated $|I_d|$ at which the rate detremining step is O_2 adsorption to the electrode surface[1].

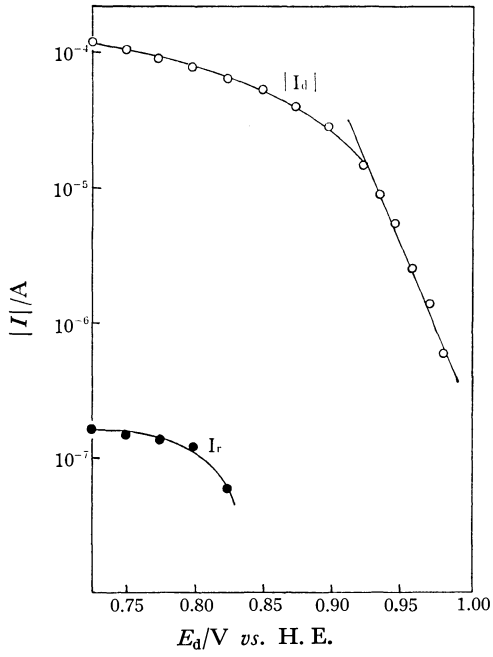

Fig. 1. Ring and disc currents in 1 M NaOH as a function of the disc potentials.

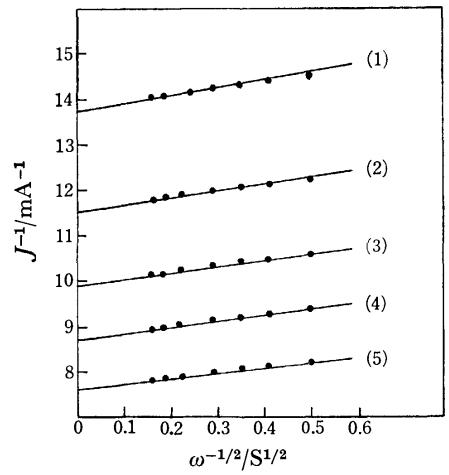

Fig. 2. $1/J$ *vs.* $\omega^{-1/2}$ plots in 1 M NaOH. E_d/V: (1) 0.825; (2) 0.8; (3) 0.775; (4) 0.75; (5) 0.725 (*vs.* H. E.).

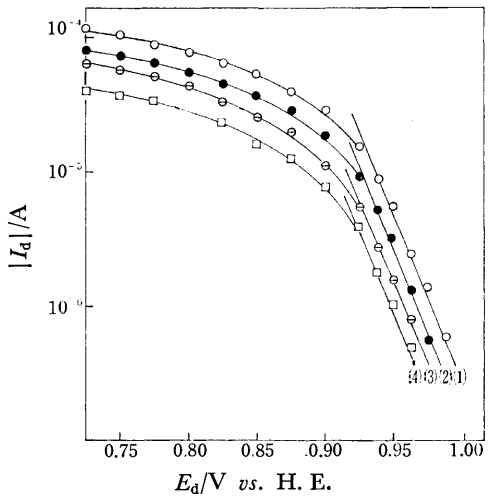

Fig. 3. Dependence of current-potential curve of O_2 reduction in 1 M NaOH on P_{O_2} at $\omega=2000\,\text{min}^{-1}$. P_{O_2}/atm: (1) 1; (2) 0.5; (3) 0.2; (4) 0.1.

Figure 3 shows an effect of introduced oxygen pressure, P_{O_2}, on the current-potential curves at the disc electrode. The relations between log P_{O_2} and log $|I_d|$ in the potentials giving the Tafel slope are shown in Fig. 4. The slope of the line in this figure is about 0.8, from which it is suggested that the reaction order of O_2 in the Tafel region is also 1.

Figure 5 shows $|I_d|$ in the Tafel region as a function of pH of the electrolytes. In this case, the disc potential values are converted into the normal hydrogen electrode scales so that the reaction order of OH^- can be directly obtained form the slope of log $|I_d|$ *vs.* pH plots.[11] It is noticed that good linearities were established between log $|I_d|$ and pH, and that the slope was about -0.8, although the points are a little scattered. This result implies that the reaction order of OH^- in this potential region is -1. Then the rate equation in the Tafel region can be written as follows with the rate constant k:

$$I_d = k[O_2][OH^-]^{-1}\exp(-\Delta G^*/RT), \qquad (1)$$

where ΔG^* is the electrochemical activation energy,

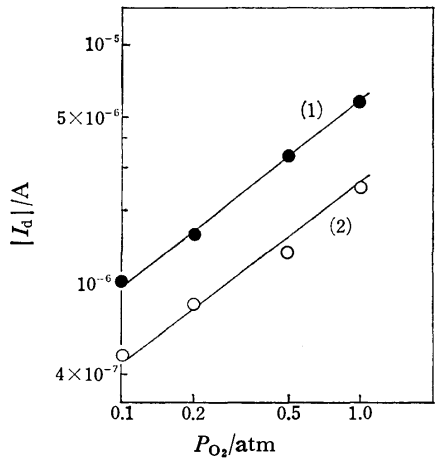

Fig. 4. log $|I_d|$ *vs.* log P_{O_2} plots in 1 M NaOH. E_d/V: (1) 0.95; (2) 0.9625 (*vs.* H. E.).

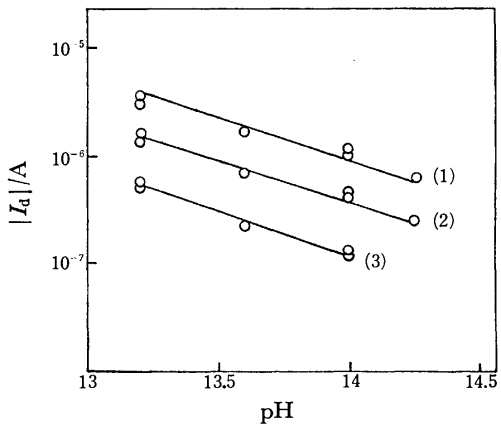

Fig. 5. log $|I_d|$ *vs.* pH plots in the Tafel region at $\omega=2000\,\text{min}^{-1}$. E_d/V: (1) 1.2; (2) 1.45; (3) 1.7 (*vs.* NHE).

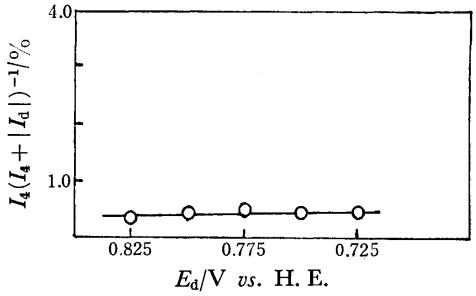

Fig. 6. $I_4/(I_4+|I_d|)$ at $\omega=2000\,\text{min}^{-1}$ in 1 M NaOH as a function of the disc potentials.

which was discussed in detail in Ref. 12. Equation 1 contains all the reaction steps preceeding to the rate determining step.

Figure 6 shows $I_4/(I_4+|I_d|)$ as a function of the disc potentials, where I_4 denotes the total current of OH^- diffusing away from the disc electrode to the solution (Fig. 7), and is given by I_r/N.[13] The I_1 path in Fig.7 means that O_2 is directly reduced to OH^- through a side-on type adsorption of O_2. The value of $I_4/(I_4+|I_d|)$ was 0.4% and almost equal to those observed at cobalt mixed oxides ($CoO+Co_2O_3$), Co_3O_4, and Co_2NiO_4 electrodes,[6,7] suggesting that

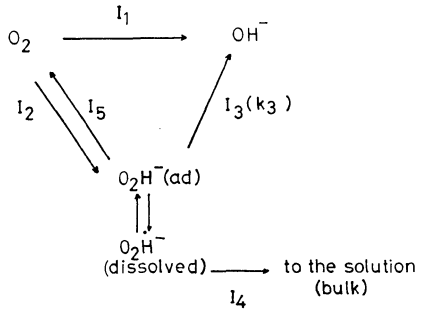

Fig. 7. A general scheme of O_2 reduction in alkaline solutions.

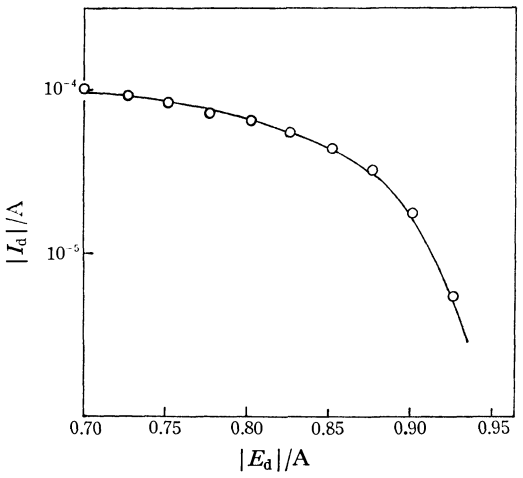

Fig. 8. Current-potential curves for reduction of O_2H^- at $\omega = 2000\ min^{-1}$.

O_2 is predominatnly reduced to OH^- at a $LaNiO_3$ electrode. The $|I_d|/I_r$ *vs.* $\omega^{-1/2}$ plots were so scattered that k_3 could not be determined. The small ring current seems to be responsible for the large scatter of the plots. In order to elucidate the role of OH^- in the reaction scheme of the Hoare path, the feasibility of the O_2H^- reduction was investigated in 1 M NaOH saturated with N_2. The O_2H^- concentration was 10^{-2} M. It was found that the reduction of O_2H^- proceeded easily at the disc electrode, as shown in Fig. 8.

As reported in a previous paper,[14] the NiO used as a starting material to synthesize $LaNiO_3$ remained as an isolated phase in $LaNiO_3$ if the preparation was made in a very short time or at a low temperature. Therefore, there is a possibility that the $LaNiO_3$ used in the present study contained a very small amount of isolated NiO, even though $LaNiO_3$ was prepared at 850 °C for 2 days. Bagotzky *et al.*[7] reported that O_2H^- ions were produced in the O_2 reduction on NiO at a potential region less positive than about 0.8 V and that the O_2H^- produced was not further reduced. This potential was in accord with that found in the present study for commencement of the very small ring current (see Fig. 1). Therefore, it seems reasonable to consider that NiO as an impurity in $LaNiO_3$ is responsible for the production of O_2H^- at the disc electrode. If this view is valid, then it can be concluded that O_2 is completely reduced to OH^- and that O_2H^- in solution is easily reduced to OH^- at $LaNiO_3$ with no isolated phase.

Discussion

The rate Eq. 1 holds for the Hoare path of the O_2 reduction at $LaNiO_3$, as described in previous papers.[1,2,14] Then the following reaction scheme will be valid:

$$O_2 \rightarrow O_2(ad), \quad (2)$$

$$O_2(ad) + e \rightarrow O_2^-(ad), \quad (3)$$

$$O_2^-(ad) + H_2O \rightarrow O_2H(ad) + OH^-, \quad (4)$$

$$O_2H(ad) + e \rightarrow O_2H^-(ad). \quad (5)$$

The rate determining step was found to be step (5) when the Tafel relation holds, and (2) for the limiting current case.[1] Presnov *et al.*[15] proposed the feasibility of a reaction scheme similar to that proposed here from a general treatment of oxide catalysts on the basis of a knowledge of coordination chemistry.

Any step subsequent to (5) has to conform to the experimental result of non-detection of O_2H^- in the electrolyte. The rearrangement of adsorbed O_2H^- on the electrode surface in a manner such as that shown in Eq. 6 seems to be feasible for the formation of OH^-:

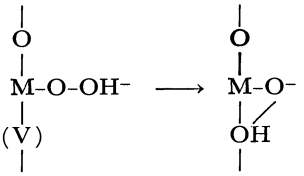

(6)

Here (V) denotes an O^{2-} ion vacancy on the oxide surface. If step (6) does rapidly occur, the desorption of O_2H^- (ad) will not take place, and hence no detection of dissolved O_2H^- is possible at the ring electrode. In this case the electron transfer from the electrode to the σ^* orbital of the adsorbed O_2H^-, which follows step (6), must destroy its σ bond and then OH^- will be produced. Such a mechanism seems to fit well for preferential reduction of O_2 to OH^- at $LaNiO_3$.

In the process of the rearrangement of the adsorbed O_2H^- (Eq. 6), an O_2^- ion vacancy is required at the oxide surface. In the case of $LaNiO_3$, the surface composition may be represented as $LaNiO_{3-\delta}$, where δ is the deficiency of O^{2-} from the stoichiometric composition and was about 0.2 to 0.3 in the O_2 reduction potential region[9] Therefore, step (6) is likely to take place. The results that O_2 was completely reduced to OH^- and that the reduction of O_2H^- proceeded quite easily at this oxide seem to be reasonable in the light of the mechanism proposed.

Co_2O_3, Co_3O_4, and Ni_3O_4 seem to have a fairly large number of O_2^- vacancies; but not so with NiO and CoO when these oxides are polarized in alkaline solutions in potentials less positive than about 0.9 V, in which the O_2 reduction proceeeds,[6,7] because thermodynamically NiO and CoO are very stable in this potential region. It was reported that the O_2 reduction at cobalt mixed oxides ($CoO+Co_2O_3$), Co_2O_3, and Co_2NiO_4 gave no appreciable amount of O_2H^- and that O_2H^-, when added to an electrolyte, was easily

reduced at these oxides.[6,7] On the contrary, the O_2 reduction at NiO gave O_2H^-, and O_2H^- was not reduced to OH^-.[6,7] These results, therefore, support the necessity of O^{2-} vacancies for the O_2 reduction. In the case of the mixed cobalt oxides, O_2H^- might be produced on the CoO phase but it must immediately be reduced further to OH^- on the co-existing Co_2O_3 phase. Because of this, the ring current is believed to have been detected only very faintly.[6,7]

It is predicted from the above discussion that O_2 is completely reduced to OH^- at $La_{1-x}Sr_xMnO_3$ and $La_{1-x}Sr_xCoO_3$ catalysts[16,17] in alkaline solutions, because these oxides have some O^{2-} vacancies in the potential region where the O_2 reduction proceeds.

References

1) Y. Matsumoto, H. Yoneyama, and H. Tamura, *J. Electroanal. Chem.*, **79**, 319 (1977).
2) Y. Matsumoto, H. Yoneyama, and H. Tamura, *J. Electroanal. Chem.*, **83**, 237 (1977).
3) A. Damjanovic, M.A. Genshaw, and J. O'M Bockris, *J. Electrochem. Soc.*, **114**, 1107 (1967).
4) A. Damjanovic, M.A. Genshaw, and J. O'M. Bockris, *J. Electroanal. Chem.*, **15**, 173 (1967).
5) H. S. Wroblowa, Yen-Chi-Pan, and G. Rajumney, *J. Electroanal. Chem.*, **69**, 195 (1976).
6) N. A. Shumilova, E. I. Khrushcheva, and O. V. Moravskaya, *J. Electrochem. Soc. Jap.*, **43**, 14 (1975).
7) V. S. Bagotzky, N. A. Schumilova, and E. I. Khrushcheva, *Electrochim. Acta*, **21**, 919 (1976).
8) Y. Matsumoto, H. Yoneyama, and H. Tamura, *Chem. Lett.*, **1975**, 661.
9) Y. Matsumoto, H. Yoneyama, and H. Tamura, *J. Electroanal. Chem.*, **80**, 115 (1977).
10) A. C. Riddiford, "Advances in Electrochemistry and Electrochemical Engineering," Vol. 4, ed by P. Delahey, Interscience Publishers (Wiley), New York (1966), p. 96.
11) J. O'M. Bockris, *J. Chem. Phys.*, **24**, 814 (1956).
12) D. S. Gnanamuthu and J. V. Petrocelli, *J. Electrochem. Soc.*, **114**, 1063 (1967).
13) A. Damjanovic, M. A. Genshaw, and J. O'M. Bockris, *J. Chem. Phys.*, **45**, 4057 (1966).
14) Y. Matsumoto, H. Yoneyama, and H. Tamura, *J. Electroanal. Chem.*, **83**, 167 (1977).
15) V. A. Presnov and A. M. Trunov, *Elektrokhimiya*, **11**, 71 (1975).
16) T. Kudo, H. Obayashi, and T. Genjo, *J. Electrochem. Soc.*, **122**, 159 (1975).
17) A. C. C. Tseung and H. L. Bevan, *J. Electroanal. Chem.*, **45**, 429 (1973).

A Theoretical Approach to the Rearranged Ion in the Mass Spectrum of Methyl Formate

Tsutomu TAKAGI* and Masayoshi OIWA

Department of Applied Chemistry, Faculty of Engineering, Kansai University, Suita, Osaka 564

(Received October 19, 1977)

The hydrogen-migration mechanism of the fragmentation of the methyl formate under electron impact has been discussed from the standpoint of the all-valence electron semi-empirical SCF-MO theory (CNDO/2-Unrestricted Hartree Fock), assuming the following models:

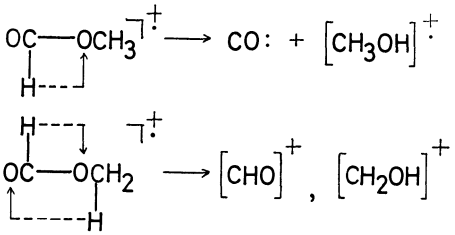

The model for the hydrogen migration and the possible driving force are presented based on the partition method. The localized MO calculation has been carried out, by the "energy localization" method of the MINDO MO's, for the origin and the terminus of the migration as an aid to the understanding of the migration. Although the possibility of the hydrogen migration in other models can not always be neglected, the hydrogen migration via Model 1 may be estimated to be energetically favorable, judging from the variation in the total energy and the conformation influence.

It is interesting to disclose the migration processes[1] involved in the fragmentation from the standpoint of the molecular orbital theory (MO theory), although the empirical speculations of the migration mechanisms based on a variety of mass spectral data have been presented by many investigators. The analyses of the mass spectral data of organic compounds has not been completely established because of the complexity of the driving factors governing the cleavage of the molecular ion $M^{\dagger}$ on electron-impact collision. In order to establish the rules governing fragmentation, it is important to clarify the mechanism of the intramolecular migration of hydrogen.

In a previous paper,[2] models for the hydrogen migration in butyl alcohol were reported. The results have been related to the ease of the cleavage of the $M^{\dagger}$ ion to the $[M-H_2O]^{\dagger}$ ion in the rearrangement process. This simple model employed was able to explain the mechanism.

In the mass spectrum of methyl formate, the peak thought to be the ion formed by the rearrangement was observed. Production of the ion with a *m/e* 32 involves hydrogen rearrangement from the formyl carbon to the oxygen atom. The base peak corresponds to the CH_2OH ion with a *m/e* 31 due to the loss of hydrogen[3] on the methyl group. The $[CH_2OH]^+$ ion is probably formed by the following mechanism:[4]

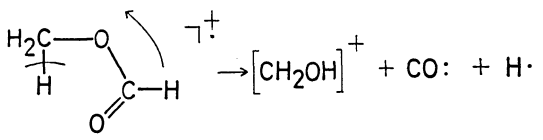

This migration mechanism has however not been fully elucidated, but only speculated from the mass spectral data.[5]

The present paper is concerned with the hydrogen-migration mechanism in methyl formate and the variation of energy in terms of the MO theory. In the model-process simulated, the migration points, the driving force in the hydrogen migration and the energy profiles obtained from the CNDO and MINDO calculations are reported. The bonding interaction along the migration path has also been examined.

Computation and Geometry

Computation. All computations were carried out on a NEAC 2200 Model 700 computer at Osaka University. The semi-empirical SCF-MO wave functions were computed with the CNDO-UHF method developed by Pople and coworkers.[6] The AO parameters used for CNDO were those originals[7] reported by the authors. The energy partitioning was obtained from the method reported by Fischer[8] and Gordon.[9] The LMO calculation was carried out using the "energy localization" method of Edmiston-Reudenberg.[10]

Geometry. The starting geometry for the migration requires a minimization of the total energy of the system with respect to all its independent internal coordinates, and the generation of a complete potential energy surface for the chemical reaction requires a path in the energy minimum. The problem is that the conformation and the electronic state of the $M^{\dagger}$ ion absorbing energy in the ionizing chamber have stable geometries and the migrating hydrogen has a path in the energy minimum.

For the rearrangement model, it is, therefore, important to clearly decide the geometry. However, under electron impact, it is difficult to absolutely determine the reaction coordinate passing through the equilibrium geometry. The instantaneous conformation of the $M^{\dagger}$ ion which had absorbed the energy could not be established. According to Franck-Condon,[11] it may

be assumed that the geometry of the M^+ ion is in the ground state. Consequently, the assumed models in the migration process are as shown in Fig. 1.

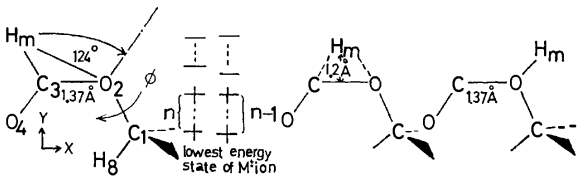

Fig. 1. Schematic representation of hydrogen-migration from carbon to oxygen.
n represents a number of the occupied MO and the numbering system of the atoms is that used in this paper.

Five points were chosen to form a path representing the hydrogen migration from the formyl carbon(C_3) to Oxygen(O_2). The terminus structure employed here was decided from the stability of the conformation of the CH_3OH. Point 3 in which angle $\angle C_3H_mO_2$ is 60° was also available for the intermediate structure and then the other points were situated in the middle of these points. The distance between the center of the C–O bond and the migrating hydrogen at Point 3 was assumed to be 1.2 Å; 1.2 Å was defined judging from the energy minimum state in which the conformation is energetically stable with 1.1 and 1.3 Å. The length of the O_2–C_3 bond with 1.37 Å was chosen as the terminus of the migration. As shown in Fig. 2, the total energy changed with the length of the O_2–C_3 bond at Points 4 and 5; thus the total energy was a minimum at 1.37 Å.

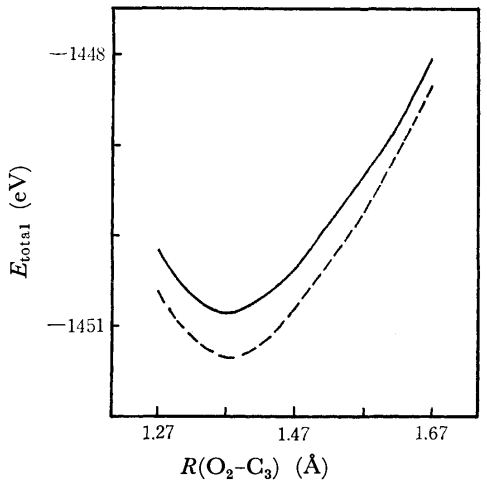

Fig. 2. Variation of the total energy with O-C bond length for Points 4 and 5.
——: Point 4, ----: Point 5.

The bond lengths and bond angles for the origin of the migration, with the exception of the C_2–O_3, were taken from the standard tables.[12]

The migrating hydrogen in the terminus is then situated in the XY plane as shown in Fig. 1 and the hydrogen atom migrates in this plane. The conformations in Models 1 and 2 were chosen to be planar with $\phi=0°$ and $\phi=180°$, respectively. The form of the CH_3OH in the terminus of the migration is an eclipsed one in Model 1, while in Model 2 it is a staggered one.

TABLE 1. MOLECULAR GEOMETRIES[a] FOR THE MIGRATING POINTS

Parameter[b]	1 Origin	2	3	4	5 Terminus
$\angle O_2C_3H_m$(°)	118.5	86.5	60.0	38.8	27.7
$R(O_2\text{-}H_m)$(Å)	2.119	1.736	1.382	1.052	0.960

a) The other parameters were described in Fig. 1.
b) Application of the law of cosines for a triangle.

In Model 3, the path synchronously representing the two hydrogenes (H_m and H_8) in the following figure was selected, in which the movement of H_8 was chosen with respect to the least-motion path from C_1 to the lone pair of O_4. The lengths between O_4 and H_8 in each point are 2.920, 1.753, 1.457, 1.184, and 0.960 Å, and then the others are the same as Model 1.

Finally, the electronic states of the M^+ ion are not the only states that loses an electron in the highest occupied orbital; the states in any part of the lower orbitals also lose electrons. However, the demotion step of an electron from the higher energy levels to the lower vacant level may occur before fragmentation.[13] Therefore, the electronic state of the M^+ ion employed has been the lowest energy state, as found in butyl alcohol.[2]

Results and Discussion

Energy Profile. The results of the CNDO calculation in methyl formate are summarized in Table 2. This treatment was found to give a good description of the cleavage of the C–H bond during the migration.

It is apparent from the shape of the curve in Fig. 3 that the transition state lies in the latter half of the reaction. Both the total energy profiles which were obtained from Models 1 and 2 show a maxima at Point 3 along the coordinate representing migration of the hydrogen from C_3 to O_2. The total energy tends to decrease after the transition state. These results suggest that the small potential energy easily

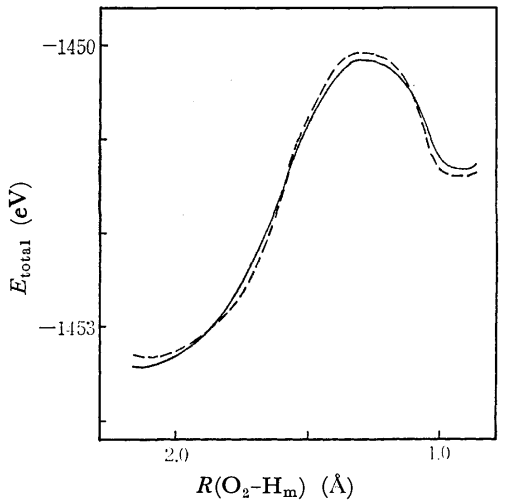

Fig. 3. Energy profiles in Models 1 and 2.
——: Model 1, ----: Model 2.

Table 2. Variation of the total energy and E_{AB}[a,b]

		1	2	3	4	5
				Model 1		
$R(O_2\text{-}H_m)$(Å)		2.119	1.736	1.382	1.052	0.960
E_{total}		−1453.416	−1452.608	−1450.156	−1450.829	−1451.319
E^U+E^R c)		−2372.164	−2372.885	−2385.868	−2392.275	−2388.718
		(−187.390)	(−185.609)	(−182.173)	(−185.234)	(−188.203)
E_{AB}	$C_1\text{-}O_2$	−24.706	−24.700	−24.121	−23.190	−23.666
	$O_2\text{-}C_3$	−33.145	−31.465	−28.468	−26.954	−27.597
	$C_3\text{-}O_4$	−33.782	−40.256	−45.030	−45.837	−46.099
	$C_3\text{-}H_m+O_2\text{-}H_m$	−18.677	−17.982	−15.552	−18.597	−18.501
				Model 2		
E_{total}		−1453.313	−1452.537	−1450.090	−1450.898	−1451.375
E^U+E^R		−2371.368	−2372.165	−2385.088	−2391.368	−2388.072
E_{AB}	$C_1\text{-}O_2$	−24.752	−24.751	−24.129	−23.222	−23.648
	$O_2\text{-}C_3$	−33.118	−31.388	−28.004	−23.062	−27.633
	$C_3\text{-}O_4$	−39.004	−40.529	−45.042	−45.948	−46.214
	$C_3\text{-}H_m+O_2\text{-}H_m$	−18.661	−17.874	−15.544	−18.584	−18.433

a) Energy in eV. b) The total energy, E, in the CNDO scheme, can be partitioned into chemically useful terms, $E=\sum_A^A E_A+\sum_{A<B} E_{AB}$; in which $E^U=\sum_r^A P_{rr}U_{rr}$ and $E^R=2\sum_r\sum_s P_{rs}S_{rs}\beta^\circ_{AB}$. There is a qualitative correspondence between E_{AB} and the bond length; thus the values of E_{AB} for the strong bonding interaction are very large and negative one.[14] c) Values in parentheses correspond to E^R.

initiated the migration. The potential energy, 3.3 eV in Model 1, is small in comparision with the ionization potential. Moreover, the variation of the total energy of the system is small in comparison with the appearance potentials of the fragment ions. The difference between the total energy of the ground state of the molecule and that of the M^+ ion is also smaller than the appearance potentials in the simple fragmentation. The potential energy, 3.3 eV, is thus small in comparision with the minimum energy required to bring about scission of the bonds. Then, the variation of the total energy in the origin of the migration in both Models, which is 2.4 kcal/mol, is the small difference. The difference in the terminus energies of both Models is smaller than that in the origin and this indicates that the migration by both Models is energetically favorable and that Model 1 is more favorable.

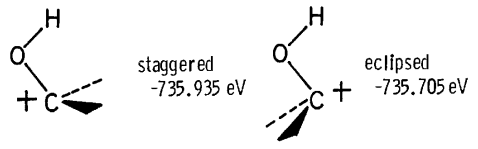

In the fragment ion, *i.e.*, CH_3OH ion, the calculation of methyl alcohol[15] in the cation radical state predicts the staggered form to be more stable energetically. In the calculation on the fragment ion, it is predicted that the CH_2OH ion in the cation state has the lower energy in the staggered form. The difference in the total energy is 5.3 kcal/mol. It seems that the terminus of the migration is favorable in the staggered form.

Here, the driving force in the hydrogen migration was interpreted using the partitioned energy. The variation of the one-center term $\Delta\sum E_A$, is 1.67 eV and that the two-center term $\Delta\sum E_{AB}$, 0.426 eV. The driving force from the origin to the terminus form is, therefore, found principally in the two-center term. As is shown in Table 2, it was found that the partitioned energy contributing to this migration was the resonance energy in which there was proportionality between the total energy and the E^R value. The resonance energy term (E^U+E^R) decreases with the hydrogen migration in both Models. It has been suggested that the decrease in energy is due to the resonance effect and that the decrease in total energy results from the steric effect.

The sum of the E_{AB} values of the two bonds ($C_3\text{-}H_m+O_2\text{-}H_m$) decreases along the latter half of the reaction. This decrease implies that the bonding interaction between oxygen and the approaching hydrogen becomes

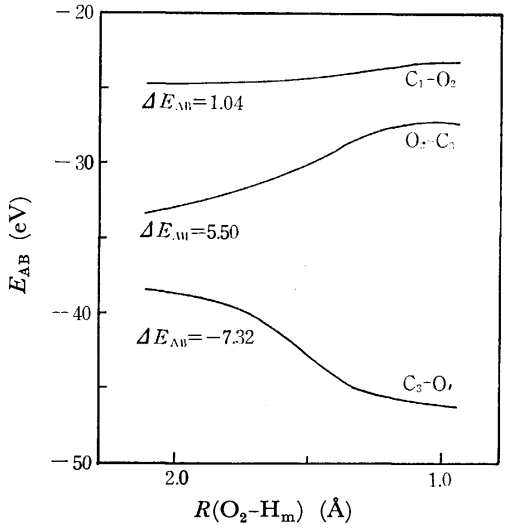

Fig. 4. Variation of E_{AB} of each bond to migration in Model 1.

stronger in this process. As shown in Fig. 4 the bonding interaction energy of the O_2–C_3 bond increases remarkably with the approach of hydrogen to O_2; this shows that the interaction between O_2 and C_3 is weakened by the hydrogen migration in Model 1. The variation of the E_{AB} value of the C_1–O_2 bond is smaller than that of the O_2–C_3 bond, whereas the E_{AB} value for the C_3–O_4 bond decreases remarkably. These results may be related to the ease of the cleavage from the M^+ ion to the CH_3OH ion.

Table 3 shows the energy profile calculated by the MINDO calculation in the hydrogen migration in Model 1; both predict the decrease of the E_{AB} value of the sum of the two bonds and the resonance energy, although there are some differences between the CNDO and MINDO. The total energy and the E_{AB} of the

TABLE 3. VARIATION OF E_{AB}[a)]

		Origin	Terminus
$R(O_2$-$H_m)$(Å)		2.119	0.960
E_{total}		−933.858	−933.619
E_{AB}	O_2-C_3	−22.392	−17.001
	C_3-H_m+O_2-H_m	−10.617	−13.809

a) Geometries are same as CNDO and energy in eV.

O_2–C_3 bond are more stable at the terminus of the migration. It is also shown that investigation for hydrogen should be esitmated from MINDO.[16)]

The energy barrier by rotation of the O_2–C_3 bond is 1.2 kcal/mol, which is small in comparison with that of the CH_3 group. So, the hydrogen migration in Model in such a conformation was considered. Consequently, the total energy changes from −1453.279 to −1443.630 eV in the CNDO and this variation is larger than in the models discussed previously. There are then, as many conformations existing as migration processes, but the most likely conformation is the planar form. In the terminus form in the model the migration hydrogen is out of the molecular plane in the figure. The angle between the two lone pairs and the O_2–H_m bond is 61.8°[17)] in this model. As a results, the variation of the total energy is 61.7 kcal/mol which compared with Model 1 decreases

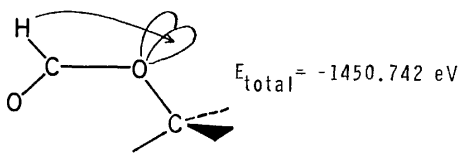

by more than 10 kcal/mol. It has been concluded this model that for the migration toward the lone pair of O_2 is energetically less favorable than Model 1. The formation of the CH_2OH ion has been discussed in terms of the synchronized migration model, *i.e.*, Model 3 in which the migration of hydrogen on the

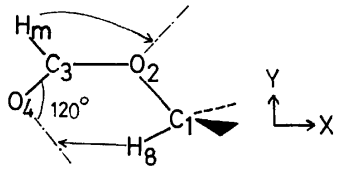

CH_3 group in the molecular plane was employed. The movement of H_m is the same as in Model 1 and H_8 synchronously migrated to O_4. Table 4 shows the variation of the energies with the migration. The total energy increases remakably with the migration, though there is a slight decrease at the end of the migration. The change of the bonding interaction of the O_2–C_3 bond shows the remarkably increasing trend. The sum of the E_{AB} values of the two bonds for H_m changes randomly, implying that the migration of H_m is prevented by H_8. Convertly, the length between O_4 and H_8 at the origin and the terminus of the migration, 2.920 Å, is larger than that for H_m. However, the E_{AB} value decreases during the migration from Point 3 to Point 4. Consequently, the migration of H_8 may be possible, judging from the variation of the E_{AB} value. These results are energetically in agreement with regard to the mass spectral data; the peaks of the CH_2OH ion and the CHO ion are in abundance, which shows that this process is possible.

It may be possible that H_8 migrates from C_1 to O_4 just like protonated formaldehyde.[18)] Thus, the process which H_8 migrates to the lone pair of O_4 was calculated, in which H_m was fixed at the origin of the migration. The variation of the sum of the two bonds was similar to that in Model 3. The total energy increases with the migration, but in the latter half tends to decrease. The E_{AB} values of the O_2–C_3 bonds in the origin and the terminus were −33.145 and −33.572 eV, respectively, implying that the bonding interaction of the O_2–C_3 bond does not weaken by the migration of H_8 alone. These results show that the peaks of HCO(H)[19)] ion and CH_2O ion with a *m/e* 30 is in less abundance. These peaks are, in fact, in less abundance in the mass spectrum of methyl formate.

Considering the variation of the total energy, the profile is as follows, (the values are the total energies of the systems). The variation of the toatl energy in each system predicts that the fragmentation

TABLE 4. VARIATION OF THE TOTAL ENERGY AND E_{AB}[a)]

		Model 3				
		1	2	3	4	5
$R(O_4$-$H_8)$(Å)		2.920	1.753	1.457	1.184	0.960
E_{total}		−1453.416	−1451.120	−1445.164	−1445.323	−1445.690
E_{AB}	O_2-C_3	−33.145	−32.054	−29.739	−26.036	−21.962
	C_3-H_m+O_2-H_m	−18.677	−17.968	−16.097	−18.919	−16.178
	C_1-H_8+O_4-H_8	−20.513	−19.248	−15.913	−17.508	−19.073

a) Energy in eV.

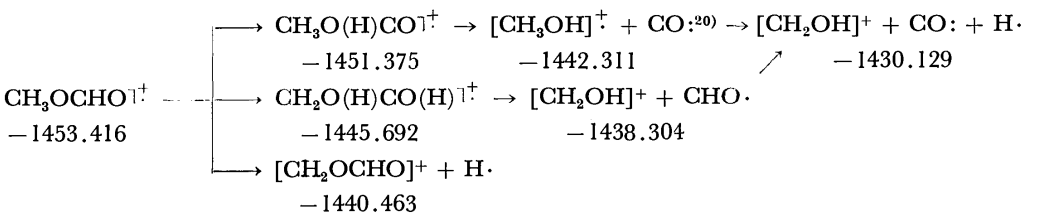

reaction in methyl formate would be *via* the $CH_3O(H)CO^+$; the fragment ion, $[CH_3OH]^+$, is produced by the elimination of CO from the terminus of the migration. Judging from the variation of the total energy the CH_2OH ion results from the elimination of hydrogen from the CH_3OH ion in methyl alcohol. In the case of methyl formate, the CH_3OH ion decomposes further, and one of the energetically most favorable paths appears to be α-cleavage[21] to give the stable CH_2OH ion. The bonding character of the particular bond, *i.e.*, the O_2–C_3 bond varies from bonding to antibonding with the migration. Moreover, the bonding character of the O_2–C_3 bond changed from bonding(0.232) to antibonding(−0.143), as the electron was excited from the single occupied MO to the lowest unoccupied MO; thus the O_2–C_3 bond was weakened by the migration and then by the excitation in the origin of the migration. There is then the possibility that hydrogen migrates to O_2 before scission of the O_2–C_3 bond.

Charge Distribution. The changes of the electron densities of the atoms along the reaction coordinates have been examined and the results of the calculation for Model 1 are summarized in Table 5. It is immediately apparent from the densities that the most significant electron density changes observed are on the atoms: *viz.* C_3 and O_4. There is an increase in the atomic population on C_3. This electron flow to C_3 and O_4 implies that the CO has a stabilizing radical in the migration process. There is the charge on the CHO side in the origin of the migration. However, when H_m migrates to O_2, the charge moves to the CH_3OH side;

$$[OHC]^+\text{-}OCH_3 \rightarrow CO\text{-}[HOCH_3]^+.$$

Thus, the elctron density of H_m decreases with the migration as is shown in Table 5. It seems the migrating hydrogen moves like a proton, judging from the variation of the density of H_m. From the results of the hydrogen migration, it appears that the charge of the system remains on the CO, suggesting the formation of the $[M-CO]^+$ ion with a *m/e* 32. A decrease of electron on H_8 and an increase on O_4, was seen, *i.e.*, H_8 in the methyl group is a movable hydrogen and in the same way as the rearrangement of hydrogen to oxygen in aldehydes, there is a good chance of migration from C_1 to O_4. The increase of the electron on O_4 interacts with H_8 and may be considered as a driving force. Therefore, the influence of the synchronized migration of H_8 on the migration of H_m should be discussed.

Table 5. Atomic populations

Atoms	1	2	3	4	5
C_1	3.8851	3.8864	3.8676	3.8287	3.8634
O_2	6.0781	6.0931	6.1412	6.0924	6.0460
C_3	3.5172	3.5537	3.6226	3.7396	3.6905
O_4	5.9044	5.8951	5.9679	6.0230	6.0233
H_m	0.8374	0.7855	0.6192	0.5938	0.6607
H_6	0.9162	0.9196	0.9227	0.9111	0.9114
H_7	0.9162	0.9196	0.9227	0.9111	0.9114
H_8	0.9453	0.9471	0.9360	0.9005	0.8933

Localized MO. The simplest relation between the origin and the terminus of the migration by the LMO representation is as follows. In the terminus of the migration the O_2–C_3 bond becomes the lone pair of oxygen and the radical orbital of carbon.The increase of LMO energy of the O_2–C_3 bond due to the migration results from the change to the weak C–O bond due to the conversion of the O_2–C_3 bond to the lone pair. However, the increase of this MO energy is considerably offset by the lone pairs.

Table 6. % s nature[a] in Model 1

	Origin	Terminus
C_3–O_2	34.12	7.98
O_2–C_3	16.25	25.37
O_2–C_1	23.09	21.21
C_3–O_4	18.47	20.05

a) Percent s nature determined by summing the squares of the coefficients of the AO contribution to the LMO and dividing this by the 2s AO coefficient.

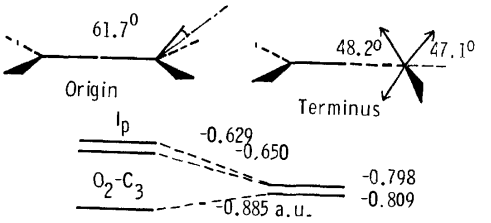

In Table 6, the values of the % s nature of the hybrid orbitals contributing to the localized orbitals are given. From this data, it seems that there is a remarkable decrease in % s in the C_3–O_2 bond. The % s of the C_3–O_2 bond decreases by 7.98 with the migration. This indicates that the electrons are highly localized in the C_3–O_4 bond and in the shape as the C_3 radical orbitals; since the s AO energy is lower than the p AO, the lower value of s nature leads to the more unstable state. This picture is more directly attainable than from the set of LMO.

Conclusion

There are many configurations in the M^+ ion produced by electron impact. The fragment ions and

the rearranged ions result from the fission of the M^+ ion produced. Therefore, it is difficult to absolutely determine the geometry and the electronic state of the M^+ ion which has absorbed the energy and the path of the hydrogen migration. As a model, the lowest energy state of the M^+ ion in the planar form and the terminus form of the migration which has the lower energy in the staggered form were employed . This indicates that the hydrogen on the formyl carbon migrates to O_2. This simple model gives a fairly good feature with respect to the CH_3OH ion and the CH_2OH ion in the mass spectrum. The treatment of the M^+ ion using the partitioning energy yielded results in the rearrangement reaction.

The authors wish to thank Professor Teijiro Yonezawa of Kyoto University for providing the program of LMO calculations.

References

1) a) F. P. Boer, T. W. Shannon, and F. W. McLafferty, *J. Am. Chem. Soc.*, **90**, 7239 (1968); b) H. Kollmar and H. O. Smith, *Tetrahedron Lett.*, **1970**, 1833; c) V. A. Stoute, M. A. Winnik, and L. G. Csizmadia, *J. Am. Chem. Soc.*, **96**, 6388 (1974); d) J. A. Altmann, I. G. Csizmadia, and K. Yates, *ibid.*, **97**, 5217 (1975).

2) T. Takagi and M. Oiwa, *Bull. Chem. Soc. Jpn.*, **48**, 2979 (1975).

3) a) J. H. Beynon, R. A. Saungers, and A. E. Williams, *Anal. Chem.*, **33**, 221 (1961); b) R. R. Bernecker and F. A. Long, *J. Chem. Phys.*, **39**, 253 (1963).

4) A. B. King and F. A. Long, *J. Chem. Phys.*, **29**, 374 (1958).

5) a) D. V. Raalts and A. G. Harrison, *Can. J. Chem.*, **41**, 2054 (1963); b) W. Sonnevelt, *J. Chem. Phys.*, **42**, 806 (1965).

6) a) J. A. Pople and P. K. Nesbet, *J. Chem. Phys.*, **27**, 571 (1955). b) J. A. Pople, D. P. Santry, and G. A. Segal, *J. Chem. Phys.*, **43**, s129 (1965).

7) J. A. Pople and G. A. Segal, *J. Chem. Phys.*, **44**, 3289 (1966).

8) H. Fischer and H. Kollmar, *Theoret. Chem. Acta*, **16**, 163 (1970).

9) M. S. Gordon, *J. Am. Chem. Soc.*, **91**, 3122 (1969).

10) K. Ruedenberg and C. Edmiston, *Rev. Mod. Phys.*, **35**, 457 (1963).

11) G. W. Robinson, "Experimental Methods of Physics," Vol. III, ed by L. Marton and D. Williams, Academic Press, New York (1962) p. 155 ff.

12) "Table of Interatomic Distances," Chem. Soc., Spec. Publs, No. 11 (1958); No. 18 (1965).

13) H. Nakata and A. Tatematsu, *Tetrahedron Lett.*, **1969**, 4303.

14) T. Yonezawa, H. Konishi, and H. Kato, *Bull. Chem. Soc. Jpn.*, **42**, 933 (1969).

15) a) L. Radom, W. J. Hehne, and J. A. Pople, *J. Am. Chem. Soc.*, **94**, 2371 (1972); b) P. Ros, *J. Chem. Phys.*, **49**, 4902 (1968).

16) M. J. S. Dewar and D. H. Lo, *J. Am. Chem. Soc.*, **93**, 7201 (1971).

17) This value results from the vector sum of the coefficients of P AO's in LMO.

18) K. F. Purcell and J. M. Collins, *J. Am. Chem. Soc.*, **92**, 465 (1970).

19) (H) in HCO(H) represents hydrogen migrated.

20) The energy value, −1442.311 eV, is the sum of the total energies of the $[CH_3OH]^+$ and CO:.

21) H. Budxikiewcz, C. Djerassi, and D. H. Williams, "Mass Spectrometry of Organic Compounds," Holden Day, San Francisco (1967), p. 94.

The Structure of Water in the Vicinity of Complex Ions of Transition Elements in Their Aqueous Solutions as Revealed by the Shift of the Temperature of Maximum Density of Water

Goro WADA*, Emiko NAGAO, Nagako KAWAMURA, and Kyoko KINUMOTO

Department of Chemistry, Faculty of Science, Nara Women's University, Nara 630

(Received October 20, 1977)

The temperature of the maximum density (TMD) of aqueous solutions was measured for twenty complex ions of transition metals. From the degrees of depression of TMD, Despretz's constant k_D^{ion} and the constant of excess depression of mixing Δk^{ion} were determined. These constants along with B^{ion} coefficient of viscosity give us information on the structure of water in the vicinity of ions. $[Co(H_2O)_6]^{2+}$, $[Ni(H_2O)_6]^{2+}$, $[Cu(H_2O)_6]^{2+}$, and $[Zn(H_2O)_6]^{2+}$ are electrostrictive structure-breakers in the natural order of Irving-Williams, Co(II)<Ni(II)<Cu(II)>Zn(II). Of the complexes $[Co(NH_3)_6]^{3+}$, $[Co(en)_3]^{3+}$, and $[Co(pn)_3]^{3+}$, the pn-complex is the strongest hydrophobic structure-maker due to the hydrophobic nature of its aliphatic constituent. Both $[Fe(CN)_6]^{3-}$ and $[Co(CN)_6]^{3-}$ are fairly strong electrostrictive structure-breakers, while $[Fe(phen)_3]^{2+}$, $[Co(phen)_3]^{2+}$, and $[Co(phen)_3]^{3+}$ are clathrate-like structure-makers. The EDTA and CyDTA complex ions of Co(II), Ni(II), Cu(II), and Zn(II) show no significant difference in k_D^{ion}, the situation being complicated by the hydrophobicity of the ligands and the radius effect of the complex ion. The actions of ions as structure-makers should be classified into three categories; electrostrictive, hydrophobic (iceberg formation), and hydrophobic (clathrate-like structure formation). The characteristic influence of the structure-making nature on k_D^{ion}, Δk^{ion}, and B^{ion} is discussed.

The phenomenon of the maximum density of water occurring at 3.98 °C is interpreted as evidence that water exists as an equilibriating mixture of an ice-like structure (a so-called "iceberg") and a denser one without hydrogen bondings; the iceberg, whose fraction in water diminishes with increasing temperature, gives a smaller coefficient of thermal expansion than that of the denser structure, and the apparent coefficient of thermal expansion of water results in negative values below 3.98 °C.[1] Addition of a solute to water generally influences the equilibrium between the two different forms of water causing the shift of the temperature of maximum density (TMD) of water from 3.98 °C. Many simple electrolytes are known to depress the TMD of water, θ, as expressed by the Despretz rule,[2]

$$-\Delta\theta = k_D x \tag{1}$$

by which it is shown that the degree of depression of TMD, $-\Delta\theta$, is proportional to the mole fraction of a solute, x, at least in low concentration range with the Despretz constant, k_D. The observed data for many simple electrolytes have been published.[3]

Since Wada and Umeda[4,5] treated the TMD of aqueous solutions of various nonelectrolytes quantitatively in view of water structure, many investigations dealing with this phenomenon as a clue for clarifying the solute-water interactions have been carried out.[6–20] Cause of the depression of TMD of an aqueous solution from 3.98 °C ($-\Delta\theta>0$) might be explained as follows. The state of water in the solution at 3.98 °C corresponds to a state of pure water at a temperature higher than 3.98 °C, at which water is composed of the iceberg with a smaller fraction and the denser structure with a larger fraction than at 3.98 °C, the latter being promoted in the close vicinity around the solute added.

The molar volumes of pure water V_1, pure solute V_2, and their mixture V at a given temperature t in centigrade, in a small temperature range close enough to 3.98 °C, can be given by the following equations.

$$V_1 = V_1^*[1+\beta(t-3.98)^2] \tag{2}$$

$$V_2 = V_2^\circ(1+\alpha t), \tag{3}$$

$$V = (1-x)V_1 + xV_2 + \Delta V_x^E, \tag{4}$$

where V_1^* and V_2° are the molar volumes of water at 3.98 °C and of the solute at 0 °C, α and β are the coefficients of thermal expansion of the solute and water ($\beta=7.81\times10^{-6}\,K^{-2}$), and ΔV_x^E is the molar excess volume of mixing at the mole fraction of the solute x. By differentiating V with respect to t and equating the result to zero, the degree of the elevation of TMD, $\Delta\theta$, is given by the following relation.[4–6]

$$\Delta\theta = \theta - 3.98 = -\frac{1}{2(1-x)\beta V_1^*}\left[x\alpha V_2^\circ + \frac{\partial \Delta V_x^E}{\partial t}\right] \tag{5}$$

If ΔV_x^E were either zero in the case of an ideal mixing or constant by chance in the small temperature range around 3.98 °C in a special case, the second term in the bracket on the right-hand side of Eq. 5 would disappear and the Despretz constant k_D would be reduced to k at the limiting dilute concentration.

$$k = \frac{\alpha V_2^\circ}{2\beta V_1^*} \tag{6}$$

It is clear from Eq. 6 that k is always positive (namely, $-\Delta\theta>0$), since normal substances have positive values for α. Accordingly, the excess depression of TMD of real aqueous solutions at infinitely low concentration is dependent upon the temperature variation of the excess volume of mixing as follows.

$$\Delta k = k_D - k = \frac{1}{2\beta V_1^*}\left[\frac{1}{x}\cdot\frac{\partial \Delta V_x^E}{\partial t}\right]_{x\to 0} \tag{7}$$

For most simple electrolytes, ΔV_x^E is negative and $\partial\Delta V_x^E/\partial t$ positive due to the electrostriction in the hydration sphere of ions. On the other hand, some alcohols with hydrophobic alkyl radicals such as *t*-butanol exhibit large negative Δk, so large that k_D ($=k+\Delta k$) becomes negative and consequently $\Delta\theta$ positive.[4]

In the present investigation, twenty coordinate com-

plexes of some transition elements are adopted as solutes, with ligands of either hydrophilic or hydrophobic nature towards the surrounding water in contact. The observed $\Delta\theta$ might give some clue to the structure of water around the complex ions.

Experimental

Materials. Pure water was made up by treating tap water with ion-exchange resin, followed by double distillation of its alkaline permanganate solution.

For the preparation of aqueous solutions of $[Co(H_2O)_6]Cl_2$, $[Ni(H_2O)_6]Cl_2$, $[Cu(H_2O)_6]Cl_2$, and $[Zn(H_2O)_6]Cl_2$, hydrous salts of $CoCl_2$, $NiCl_2$, $CuCl_2$, and $ZnCl_2$ of special grade reagents were used without further purification. The concentrations of salts in each solutions were determined by titration with $AgNO_3$ for Co, Ni, and Cu salts and with EDTA for Zn salt. In order to avoid the partial hydrolysis of $ZnCl_2$, HCl was added to the solution of $ZnCl_2$. The TMD values for the solution were obtained by subtracting the value for HCl solution from that for the mixed solute, by virtue of the nature of additivity rule of TMD.[4]

The crystals of $[Co(NH_3)_6]Cl_3$ and $[Co(en)_3]Cl_3$ were prepared by the usual method. The crystalline $[Co(pn)_3]Cl_3$ (pn: propylenediamine) was obtained by modifying the method for the preparation of $[Co(en)_3]Cl_3$; an aqueous HCl solution of pn containing $CoCl_2$ was oxidized by aeration and the complex was crystallized by addition of hydrochloric ethanol.

The crystals of $K_3[Fe(CN)_6]$ and $K_3[Co(CN)_6]$ were obtained from commercial reagents of special grade.

The crystal of $[Fe(phen)_3]Cl_2\cdot 7H_2O$ was prepared as follows. An HCl solution saturated with nitrogen gas was mixed with $FeCl_2$ in the presence of iron wire at 60 °C for 20 min in order to reduce Fe(III) which might be present in $FeCl_2$. Stoichiometric amount of 1,10-phenanthroline was added to the mixture for the formation of the Fe(II) complex to which was added NaCl. Then the complex was crystallized by cooling. The crystal of $[Co(phen)_3]Cl_2\cdot 8H_2O$ was prepared in a similar manner to the case of Fe-complex. $[Co(phen)_3]Cl_3\cdot 7H_2O$ was made up by passing Cl_2 gas through $[Co(phen)_3]Cl_2$ solution for the purpose of oxidation, the excess amount of Cl_2 being eliminated by vacuum pumping. The concentrations of $[Fe(phen)_3]Cl_2$[21] and $[Co(phen)_3]Cl_2$[22] in solution were determined spectrophotometrically.

For the preparation of solutions of EDTA and CyDTA complexes (CyDTA: 1,2-cyclohexanediamine-*N*,*N*,*N'*,*N'*-tetraacetic acid), solutions of sodium salts of EDTA and CyDTA were mixed with those of chloride salts of respective metals in equivalent molar quantity. Thus each solution contained $Na_2[M(edta)]+2NaCl$ or $Na_2[M(cydta)]+2NaCl$. The TMD values for pure complex salt solutions were obtained by subtraction of the values for NaCl according to the additivity rule. In the case of Zn complexes, in addition to NaCl, HCl was necessary in their aqueous solutions for the purpose of suppressing the partial hydrolysis of Zn^{2+} ion. The TMD values were determined by also applying the additivity rule to the three kinds of solutes.

Determination of TMD. For the determination of TMD, a specially designed dilatometer was used.[4]

Determination of Coefficients of Thermal Expansion of Solutes. For the determination of α for various solutes, a specific gravity bottle of ordinary shape was used. Details of procedure have been reported.[4] Determination of α was not necessarily performed for all the complexes adopted in the present investigation, because of the difficulty in obtaining some complexes in pure form and not in the form of aqueous solution. It was found that the contribution of k to k_D was not large enough for the order of Δk in the respective series of homologues of complexes to be altered when k_D itself was adopted instead. Thus, theoretical considerations will be made by a comparison of either k or Δk_D.

Determination of B-Coefficients of Aqueous Solutions. The viscosity of the aqueous solutions of $K_3[Fe(CN)_6]$ and $K_3[Co(CN)_6]$ at 25 °C was determined with an Ostwald-type viscometer. It took 164.5 s for water to flow down at 25 °C. Accoding to the Jones-Dole equation,[23]

$$\frac{\eta}{\eta_0} = 1 + A\sqrt{C} + BC, \tag{8}$$

B-coefficient can be obtained from the slope of the linear plot of $[(\eta/\eta_0)-1]/\sqrt{C}$ against $\sqrt{C}$, in which η and η_0 denote viscosity of solution and of pure water, respectively, and C concentration of the solute.

Results and Discussion

The linear relationships of the shift of TMD, $\Delta\theta$, against the mole fraction of solutes, x, following Eq. 1, can be seen from the straight lines for some examples given in Fig. 1. The case for the solution of mixed

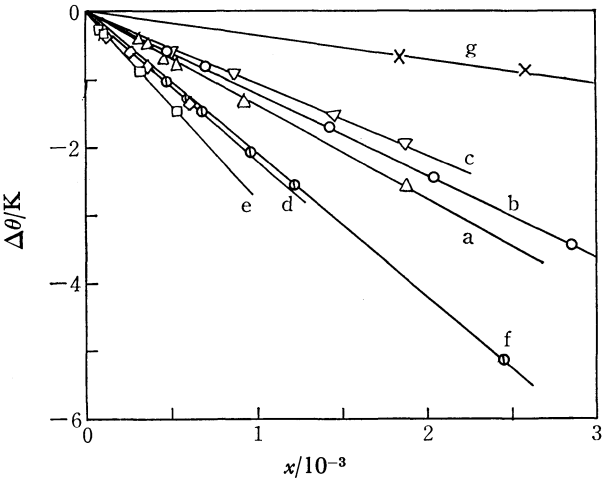

Fig. 1. Proportional relationship between shift of TMD, $\Delta\theta$, and mole fraction of solutes, x.
a: $[Co(NH_3)_6]Cl_3$, b: $[Co(en)_3]Cl_3$, c: $[Co(pn)_3]Cl_3$, d: $[Fe(phen)_3]Cl_2$, e: $[Co(phen)_3]Cl_2$, f: $K_3[Co(CN)_6]$, g: HCl.

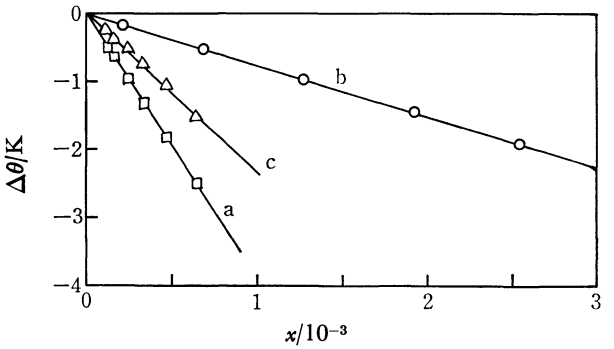

Fig. 2. $\Delta\theta$ *vs.* x plot for $Na_2[Co(edta)]$ obtained from the additivity rule.
a: $Na_2[Co(edta)]+2NaCl$, b: NaCl, c: $Na_2[Co(edta)]$.

TABLE 1. DESPRETZ CONSTANT k_D, THE COEFFICIENT OF THERMAL EXPANSION α, MOLAR VOLUME AT 0 °C V_2° OF VARIOUS SOLUTES, AND CONSTANT FOR IDEAL MIXING k AND THE EXCESS OF THE COASTANT Δk

Complex	k_D / 10^3 K	α / 10^{-4} K^{-1}	V_2° / cm^3·mol^{-1}	k / 10^3 K	Δk / 10^3 K
$[Co(H_2O)_6]Cl_2$	0.899				
$[Ni(H_2O)_6]Cl_2$	0.914				
$[Cu(H_2O_6)]Cl_2$	0.964				
$[Zn(H_2O)_6]Cl_2$	0.883				
$[Co(NH_3)_6]Cl_3$	1.344	4.14	155.67	0.229	1.115
$[Co(en)_3]Cl_3$	1.130	5.18	233.62	0.431	0.699
$[Co(pn)_3]Cl_3$	1.035	6.00	276.49	0.590	0.445
$[Fe(phen)_3]Cl_2$	2.207	1.26[a]	573.73[a]	0.514	1.693
$[Co(phen)_3]Cl_2$	2.727	0.60[b]	572.04[b]	0.244	2.483
$[Co(phen)_3]Cl_3$	2.224				
$K_3[Fe(CN)_6]$	2.150	3.87	173.36	0.223	1.927
$K_3[Co(CN)_6]$	2.105	5.19	172.31	0.318	1.787
$Na_2[Co(edta)]$	2.26				
$Na_2[Ni(edta)]$	2.30				
$Na_2[Cu(edta)]$	2.26				
$Na_2[Zn(edta)]$	2.32				
$Na_2[Co(cydta)]$	2.52				
$Na_2[Ni(cydta)]$	2.27				
$Na_2[Cu(cydta)]$	2.26				
$Na_2[Zn(cydta)]$	2.31				
HCl	0.354				
NaCl	0.740				
KCl	0.644	1.01	37.09	0.013	0.631

a) $7H_2O$ hydrate. b) $8H_2O$ hydrate.

solute, $Na_2[Co(edta)]+2NaCl$, is shown in Fig. 2. Subtraction of the slope of the straight line independently observed for NaCl from that observed for the mixed solute gives the slope for $Na_2[Co(edta)]$ only.

Thus, the values of $\Delta\theta$ obtained for various solutes at various x give values of k_D for each solute. They are given in Table 1, along with the observed data of α and V_2° and the calculated values of k and Δk. On the simple assumption that the individual contributions of K^+ and Cl^- ions to the total KCl value of k_D, k, and Δk are equal to each other, these constants for all salts can be divided into each component ion, k_D^{ion}, k^{ion}, and Δk^{ion}, using values of $k_D^{ion}(K^+)=k_D^{ion}(Cl^-)=0.322\times10^3$ K, $k^{ion}(K^+)=k^{ion}(Cl^-)=0.007\times10^3$ K, and $\Delta k^{ion}(K^+)=\Delta k^{ion}(Cl^-)=0.315\times10^3$ K. The values of the ionic constants for complex ions thus obtained are given in Table 2, ionic values of B-coefficient also being given, on the basis of $B^{ion}(Cl^-)=-0.00_7$ at 25 °C.[28] The constants assigned for individual ions can be compared with each other only among ions of the same electric charges. However, it is meaningless to compare them between ions of opposite signs or different charges.

(i) $[Co(H_2O)_6]^{2+}$, $[Ni(H_2O)_6]^{2+}$, $[Cu(H_2O)_6]^{2+}$, *and* $[Zn(H_2O)_6]^{2+}$. As regards alkaline earth metal ions, the value of k_D^{ion} increases in the order Mg^{2+} $(0.10\times10^3) < Sr^{2+}(0.56\times10^3) < Ba^{2+}(0.66\times10^3)$.[3] It seems that the stronger electrostrictive structure-breaker the ion, the greater its k_D^{ion} value. The aqua complexes of transition metal ions are comparatively weak electrostrictive structure-breakers in the order Co(II)< Ni(II)<Cu(II)>Zn(II) as is seen in Table 2. Such an order is frequently recognized in the chemical properties of complexes of high spins, the so-called Irving-Williams' natural order[29] based on the crystal field stabilization energies and ionic radii. This indicates that the aqua complex of copper(II) displays the largest electrostrictive structure-breaking, probably due to Jahn-Teller's distortion, and that the structure of water in contact with the coordinated shell might be destroyed to the greatest extent in the case of copper(II).

(ii) $[Co(NH_3)_6]^{3+}$, $[Co(en)_3]^{3+}$, *and* $[Co(pn)_3]^{3+}$. The value of both k_D^{ion} and Δk^{ion} of these cobalt(III) complexes decreases in the order NH_3-complex>en-complex>pn-complex (Table 2). The outer layers of these complex ions are covered with many hydrogen atoms; $[Co(NH_3)_6]^{3+}$ has 18 H-atoms, which are all bonded with 6 N-atoms; $[Co(en)_3]^{3+}$ has 24 H-atoms, 12 of which are bonded with 6 N-atoms and the other 12 with 6 C-atoms; $[Co(pn)_3]^{3+}$ has 30 H-atoms, 12 of which are bonded with 6 N-atoms and 18 with 9 C-atoms. Due to the difference in the electronegativity of N and C atoms, an H-atom bonded with a C-atom is more hydrophobic than one bonded with an N-atom. Part of the positive charges on cobalt(III) is rather scattered on H-atoms bonded with N-atoms, in the manner $Co{\overset{\curvearrowright}{\underset{\curvearrowright}{N}}}H^{\delta+}$, making the ammine complex to

TABLE 2. IONIC VALUES OF k_D^{ion}, k^{ion}, Δk^{ion}, AND B^{ion}

	Complex ion	k_D^{ion} / 10^3 K	k^{ion} / 10^3 K	Δk^{ion} / 10^3 K	B^{ion} / mol^{-1}
(i)	$[Co(H_2O)_6]^{2+}$	0.255			0.38[24] 0.36[25]
	$[Ni(H_2O)_6]^{2+}$	0.270			
	$[Cu(H_2O)_6]^{2+}$	0.320			
	$[Zn(H_2O)_6]^{2+}$	0.239			
(ii)	$[Co(NH_3)_6]^{3+}$	0.378	0.209	0.170	0.17[24]
	$[Co(en)_3]^{3+}$	0.164	0.411	−0.246	0.56[24]
	$[Co(pn)_3]^{3+}$	0.069	0.570	−0.500	0.88[24]
(iii)	$[Fe(phen)_3]^{2+}$	1.563	0.501	1.063	
	$[Co(phen)_3]^{2+}$	2.082	0.231	1.853	1.61[24]
	$[Co(phen)_3]^{3+}$	1.258			1.53[24]
(iv)	$[Fe(CN)_6]^{3-}$	1.184	0.203	0.982	0.27
	$[Co(CN)_6]^{3-}$	1.139	0.298	0.842	0.29
(v)	$[Co(edta)]^{2-}$	1.42			0.88[26]
	$[Ni(edta)]^{2-}$	1.46			0.86[26]
	$[Cu(edta)]^{2-}$	1.42			0.82[26]
	$[Zn(edta)]^{2-}$	1.48			0.86[26]
(vi)	$[Co(cydta)]^{2-}$	1.68			1.03[27]
	$[Ni(cydta)]^{2-}$	1.43			1.01[27]
	$[Cu(cydta)]^{2-}$	1.42			0.92[27]
	$[Zn(cydta)]^{2-}$	1.47			0.98[27]
	H^+	0.032			
	Na^+	0.418			
	Cl^-	0.322	0.007	0.315	0.007[28]

be very hydrophilic. Thus, the outer layer of the coordinate sphere of the complex ions is more hydrophobic in the reverse order of k_D^{ion} and Δk^{ion}, namely NH_3-complex < en-complex < pn-complex. Probably, the icelike structure with hydrogen bondings might be promoted in the vicinity of $[Co(pn)_3]^{3+}$ in spite of its electrostrictive structure-breaking effect caused by the electric charge on the central metal ion. It seems that the stronger hydrophobic structure-maker a complex ion, the smaller both Δk_D^{ion} and k^{ion} values. A similar trend has been noticed in the series of hydrophobic alcohols.[4]

The values of *B*-coefficients from viscosity of their aqueous solutions are in the order NH_3-complex<en-complex<pn-complex,[24] in line with the expectation from the physical interpretation of *B*-coefficient.

(iii) $[Fe(phen)_3]^{2+}$, $[Co(phen)_3]^{2+}$, *and* $[Fe(phen)_3]^{3+}$. These 1,10-phenanthroline-complexes have very large values of k_D^{ion}, Δk^{ion}, and B^{ion} as compared with other cations with the same electric charges, but it is clear that they are of hydrophobic nature on account of phen molecules surrounding the central metal ions. The hydrophobicity of phen-complex ions of iron and cobalt is well accounted for by the fact that R_f-value of thin layer chromatography with aqueous solutions is 1.0 for $[Co(NH_3)_6]^{3+}$, while it is zero for phen-complexes.[30] The abnormally large values of k_D^{ion} and Δk^{ion} might arise not from iceberg promotion but from the occurrence of a clathrate-like structure of water formed around the phen-complex ions. This is deduced by the fact that a similar phenomenon has been found in the case of tetrabutylammonium ion where k_D^{ion} value is outstandingly large as compared with other homologous tetraalkylammonium ions, since only $(n\text{-}C_4H_9)_4N^+$ is of suitable shape and size to fit in a clathrate-like cage structure of water.[9] Of the three complexes, $[Co(phen)_3]^{2+}$ may have the most favored conditions[31] for the clathrate-like cage to wrap the complex ion in, although only the dimension of $[Fe(phen)_3]^{2+}$ is known.[32]

On the other hand, the large value of B^{ion} [24] indicates that the formation of clathrate-like structure would interfere with smooth flow of the aqueous solution; this may be easily understood by taking the steric framework of hydrogen bondings in clathrate structure into consideration.

The extent of development of clathrate-like structure is thus supposed to be in the order $[Fe(phen)_3]^{2+}$< $[Co(phen)_3]^{2+}$>$[Co(phen)_3]^{3+}$.

(iv) $[Fe(CN)_6]^{3-}$ *and* $[Co(CN)_6]^{3-}$. The value of both k_D^{ion} and Δk^{ion} of cyano complexes which are of hydrophilic nature lies in the order Fe(III)-complex>Co(III)-complex but that of *B*-coefficient lies in the reverse order. This is consistent, indicating that $[Fe(CN)_6]^{3-}$ ion is a stronger electrostrictive structure-breaker than $[Co(CN)_6]^{3-}$ ion. Since both are of low spin complexes, Fe(III)-complex has a smaller crystal field stabilization energy with a ionic radius longer than that of Co(III)-complex, thus being a weaker electrostrictive structure-maker or a stronger electrostrictive structure-breaker.

(v) EDTA and CyDTA Complexes of Co(II), Ni(II), Cu(II), and Zn(II). The values of k_D^{ion} and B^{ion} [26,27] do not significantly differ from each other among these complex ions, with the exception of k_D^{ion} of $[Co(cydta)]^{2-}$ ion. CyDTA has a cyclohexane ring in its molecule, which is very hydrophobic and is large in dimension. Consequently, the stronger hydrophobicity of CyDTA, which would make the value of k_D^{ion} smaller as a hydrophobic structure-maker, might cancel the effect of the larger ionic radius of cydta-complex ion, making the value of k_D^{ion} larger as an electrostrictive structure-breaker, as compared with the cases of edta-complex ions. This might be due to the fact that almost no difference is seen between the edta- and cydta-complexes. According to Yasuda,[24,27] divalent metal chelates of EDTA and CyDTA are supposed to be partly present in penta-coordinated structure in aqueous solution. The various forms of these complexes make the systematic differences caused by the crystal field theory ambiguous. A similar result is also noticed in the values of B^{ion}.

Up to the present time, ions in aqueous solution have often been simply classified into two types, the structure-maker and the structure-breaker on the basis of the interactions between ions and water molecules as solvent. In view of the present considerations, however, the simple classification seems to be no longer sufficient for understanding the behavior of complex ions. The structure-making or -breaking nature can be divided into more detailed categories as shown in Table 3.

There are two causes for structure formation of water around ions; "electrostrictive" and "hydrophobic", the

Table 3. General trends of variation of Δk^{ion} (or k_D^{ion}) and B^{ion} caused by a structure-maker
In case of a structure-breaker, the trends should be reversed.

	Δk^{ion} or k_D^{ion}	B^{ion}	Examples
Electrostrictive	Decrease	Increase	Simple ion (alkali and alkaline earth metals) Aqua ion
Hydrophobic			
Iceberg	Decrease	Increase	$[Co(pn)_3]^{3+}$
Clathrate-like	Increase	Increase	$[Co(phen)_3]^{2+}$ $(n\text{-}C_4H_9)_4N^+$

latter being further divided into "iceberg" formation and "clathrate-like" formation. They give rise not necessarily to similar behavior but in quite opposite direction on the variation of Δk^{ion} or k_D^{ion}, according to their kind and type of hydrophobicity, while B^{ion} shows always the same tendency of variation, irrespective of the sort of structure formation. Hydrophobic structure formation is usually promoted by the presence of alkyl radicals, giving rise to icelike structure or so-called icebergs in the vicinity of the ions. If the shape, size, and certain other unknown conditions are satisfied for any hydrophobic ions by chance, water molecules would come together, wrapping ions in clathrate-like polyhedral cages connected with each other by hydrogen bondings. This structure makes the solution more viscous.

The partial molar entropy of the solution for an ion of a structure-maker also always shows a nagative value, being useless, as well as B^{ion}, for identifying the cause of structure formation. The measurement of TMD thus affords one convenient and effective method for finding the water structure in the close range outside the complex ions.

References

1) G. Wada, *Bull. Chem. Soc. Jpn.*, **34**, 955 (1961).
2) M. C. Despretz, *Ann. Chim. Phys.*, **70**, 49 (1839), **73**, 296 (1840).
3) "International Critical Tables," Vol. III, McGraw-Hill Book Co., New York (1933), p. 107.
4) G. Wada and S. Umeda, *Bull. Chem. Soc. Jpn.*, **35**, 646 (1962).
5) G. Wada and S. Umeda, *Bull. Chem. Soc. Jpn.*, **35**, 1797 (1962).
6) F. Franks and B. Watson, *Trans. Faraday Soc.*, **1967**, 329.
7) D. A. Armitage, M. J. Blandamer, K. W. Morcom, and N. C. Treloar, *Nature*, **219**, 718 (1968).
8) A. J. Darnell and J. Greyson, *J. Phys. Chem.*, **72**, 3021 (1968).
9) G. Wada and M. Miura, *Bull. Chem. Soc. Jpn.*, **42**, 2498 (1969).
10) J. L. Neal and D. A. I. Goring, *J. Phys. Chem.*, **74**, 658 (1970).
11) J. E. Garrod and T. M. Herrington, *J. Phys. Chem.*, **74**, 780 (1970).
12) D. D. Macdonald, M. D. Smith, and J. B. Hyne, *Can. J. Chem.*, **49**, 2817 (1971).
13) M. Sakurai, T. Komatsu, and T. Nakagawa, *Bull. Chem. Soc. Jpn.*, **45**, 1038 (1972).
14) K. R. Foster and E. D. Finch, *J. Phys. Chem.*, **78**, 2305 (1974).
15) S. V. Subrahmanyam and N. M. Moorthy, *Z. Phys. Chem. Neue Folge*, **88**, 116 (1974).
16) J. R. Kuppers, *J. Phys. Chem.*, **78**, 1041 (1974).
17) J. R. Kuppers, *J. Phys. Chem.*, **79**, 2105 (1975).
18) D. D. Macdonald and J. B. Hyne, *Can. J. Chem.*, **54**, 3073 (1976).
19) J. R. Kuppers, *Can. J. Chem.*, **55**, 798 (1977).
20) D. D. Macdonald, *Can. J. Chem.*, **55**, 800 (1977).
21) M. L. Moss and M. G. Mellon, *Ind. Eng. Chem., Anal. Ed.*, **14**, 826, 931 (1942).
22) K. Yamasaki, T. Hara, and M. Yasuda, *Proc. Jpn. Acad.*, **29**, 337 (1953).
23) G. Jones and M. Dole, *J. Am. Chem. Soc.*, **51**, 2950 (1929).
24) M. Yasuda, *Bull. Chem. Soc. Jpn.*, **41**, 139 (1968).
25) M. Kaminsky, *Disc. Faraday Soc.*, **24**, 171 (1957).
26) R. G. Charles, *J. Am. Chem. Soc.*, **78**, 3946 (1956).
27) M. Yasuda, *Bull. Chem. Soc. Jpn.*, **42**, 2547 (1969).
28) R. W. Gurney, "Ionic Processes in Solution," McGraw-Hill Book Co. Inc., New York (1953), p. 168.
29) H. Irving and R. J. P. Williams, *Nature*, **162**, 146 (1948).
30) H. Yoneda, *Kagaku*, **29**, 763, 865 (1974).
31) P. Sixou and P. Dansus, *Ber. Bunsenges. Phys. Chem.*, **80**, 364 (1976).
32) J. Lucie, D. R. Stranks, and J. Burgess, *J. Chem. Soc., Dalton Trans.*, **1975**, 245.

Molecular Motions in Sodium Tetrachloroaurate Dihydrate as Studied by the Proton and Chlorine Nuclear Relaxation Times

Kenshô Sagisawa, Hideko Kiriyama,* and Ryôiti Kiriyama

The Institute of Scientific and Industrial Research, Osaka University, Yamadakami, Suita 565

(Received November 25, 1977)

The ^{1}H and ^{35}Cl relaxation times in $NaAuCl_4 \cdot 2H_2O$ have been measured at temperatures between 79 and 350 K. The ^{1}H T_1 data revealed that the water molecule of crystallization reorients about its C_2 axis with an activation energy of 26 kJ mol^{-1}. The ^{35}Cl T_1 values of the four NQR absorptions indicated that the reorientation of the water molecule makes no important contribution to the chlorine T_1, in spite of the hydrogen bonds between them. A brief analysis of the ^{35}Cl T_1 led to a frequency of 58 cm^{-1} for the torsional vibration of the $AuCl_4^-$ ion.

It has been reported that vibrational and reorientational motions of a molecule containing resonant quadrupolar nuclei produce their nuclear relaxation. However, the relaxation resulting from random motions of atoms near the relaxing nucleus has received less attention. Woessner and Gutowsky suggested that the CH_3 reorientation in $(CH_3)_2CCl_2$ is responsible for not only the proton T_1 but also the chlorine T_1.[1] They estimated the chlorine T_1 by assuming that the electric field gradient at the chlorine nucleus fluctuates while the CH_3 reorientation is actually taking place, but their calculated value did not agree with the observed one even in order of magnitude.

Recently we measured T_1 of both the proton and chlorine nuclei in α-NH_4HgCl_3, and showed that the motion of the ammonium ion affects the chlorine T_1 as well as the proton T_1.[2] In α-NH_4HgCl_3 the ammonium ion reorients about its C_2 and C_3 axes, and flips by 90° about its S_4 axis. Obviously the former, C_2 and C_3 reorientations, do not change the orientation of the ammonium ion, whereas the latter, S_4 flip, does change it. In the preceding paper, we therefore proposed that only the flip mode should affect the chlorine T_1. In order to substantiate this proposal, our study was extended to $NaAuCl_4 \cdot 2H_2O$, in which one of the chlorine atoms is probably hydrogen-bonded to water molecules, whereas the other three do not participate in any hydrogen bonds. The comparison of these chlorine T_1 values will enable us to examine the influence of the reorientation of the water molecules on the chlorine T_1.

Experimental

A variable frequency pulsed spectrometer (Bruker, B-KR-322s) was employed to measure the ^{1}H and ^{35}Cl relaxation times. The spin-lattice relaxation time, T_1, was obtained by use of a 180°-τ-90° pulse sequence for ^{1}H, and a 90°-τ-90° sequence for ^{35}Cl. The ^{35}Cl spin phase-memory time, T_2, was measured by a 90°-τ-180° method, and the inverse line width parameter, T_2^*, was determined from the free induction decay following a 90° pulse. The ^{35}Cl signal after the r.f. pulses was often time-averaged because of its small signal to noise ratio. The temperature of the specimen was varied from 79 to 350 K by using liquid nitrogen or Dry Ice, and measured by means of a copper-constantan thermocouple with an accuracy of ±0.3 K. Polycrystalline $NaAuCl_4 \cdot 2H_2O$ was prepared from an equimolar solution of NaCl and $HAuCl_4 \cdot 4H_2O$, and identified by use of an X-ray diffractometer.

Results and Discussion

The orthorhombic crystal of $NaAuCl_4 \cdot 2H_2O$ contains one kind of planar complex ion, $AuCl_4^-$, the four chlorine atoms of which are crystallographically nonequivalent to one another.[3] The crystal structure shown in Fig. 1 suggests that only one of these four, Cl(1) atom, is hydrogen-bonded to four oxygen atoms; the distances between Cl(1) and the oxygen atoms (3.36 and 3.42 Å) are shorter than the van der Waals contact (4.0 Å). The lone-pair orbitals of the oxygen atom are probably directed to sodium atoms. The ^{35}Cl nuclear quadrupole resonance (NQR) gave four absorption lines corresponding to the four nonequivalent chlorine atoms, as listed in Table 1. Fryer and Smith and Sasane *et al.* have studied the temperature dependence of the resonance frequency, and suggested that the positive temperature coefficient of the lowest frequency line arises from the hydrogen bonds of the Cl(1) atom.[4,5]

In order to elucidate the orientation and motion of the water molecules of crystallization, the ^{1}H T_1 was measured at the resonance frequencies of 20 and 35 MHz. A plot of log T_1 *vs.* inverse temperature exhibited a minimum (0.44 s at 308 K for 20 MHz) as

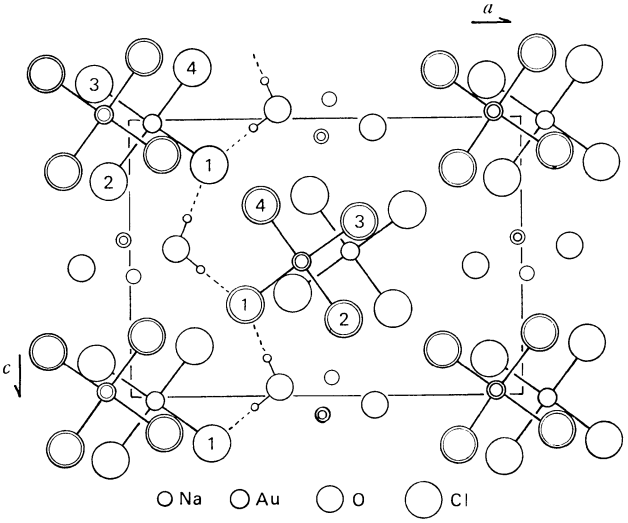

Fig. 1. The crystal structure of $NaAuCl_4 \cdot 2H_2O$ projected along the b axis. The tetrachloroaurate and sodium ions locate on the mirror plane at $y=1/4$ (single circle) or $y=3/4$ (double circle), while the oxygen atoms locate at $y \approx 0$ and $y \approx 0.5$.

Table 1. ^{35}Cl NQR frequencies and relaxation times in $NaAuCl_4 \cdot 2H_2O$

T/K		Frequency/MHz	T_1/s	T_2/μs	T_2^*/μs
79	ν_1	25.353	1.86	400	61
	ν_2	28.001	0.94	930	79
	ν_3	28.866	1.20	970	150
	ν_4	29.467	0.56	850	76
297	ν_1	25.702	0.065	470	150
	ν_2	27.376	0.040	870	190
	ν_3	28.345	0.049	820	260
	ν_4	28.737	0.034	820	170

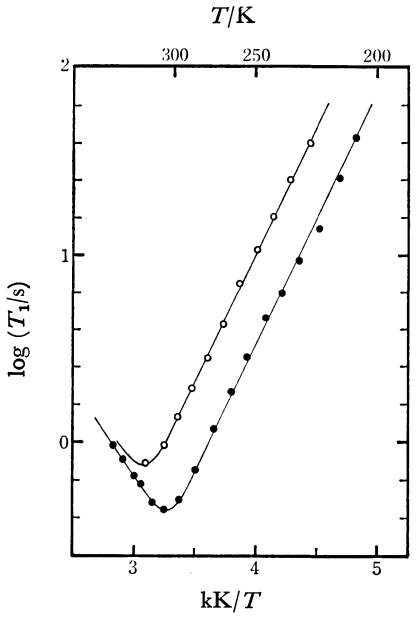

Fig. 2. The temperature dependence of ^1H T_1 in $NaAuCl_4 \cdot 2H_2O$.
●: 20 MHz, ○: 35 MHz.

shown in Fig. 2, and gave the activation energy of 26 kJ mol^{-1}. These results, together with the fact that the ^1H T_2 is almost unchanged in the temperature range studied, indicate clearly that the water molecule reorients about its C_2 axis.

The theoretical value of the ^1H T_1 for the reorienting water molecules was calculated as follows:[6]

$$\frac{1}{T_1} = \gamma^4\hbar^2 \frac{3I(I+1)}{16N} \sum_{i \neq j} \left[B_{ij}^{(1)} \frac{\tau_c}{1+(1/4)\omega_o^2\tau_c^2} + (2A_{ij}^{(1)} + B_{ij}^{(2)}) \frac{\tau_c}{1+\omega_o^2\tau_c^2} + 2A_{ij}^{(2)} \frac{\tau_c}{1+4\omega_o^2\tau_c^2} \right], \quad (1)$$

$$A_{ij}^{(q)} \equiv [F_{ij}^{(q)}(\beta,\beta) - F_{ij}^{(q)}(\delta,\delta)]^2 + [F_{ij}^{(q)}(\beta,\delta) - F_{ij}^{(q)}(\delta,\beta)]^2,$$

$$B_{ij}^{(q)} \equiv \frac{1}{2}[F_{ij}^{(q)}(\beta,\beta) + F_{ij}^{(q)}(\delta,\delta) - F_{ij}^{(q)}(\beta,\delta) - F_{ij}^{(q)}(\delta,\beta)]^2, \quad (2)$$

$$F_{ij}^{(o)}(\beta,\beta) \equiv r_{ij}^{-3}(\beta,\beta)[1-3\cos^2\theta_{ij}(\beta,\beta)],$$

$$F_{ij}^{(1)}(\beta,\beta) \equiv r_{ij}^{-3}(\beta,\beta)\sin\theta_{ij}(\beta,\beta) \times \cos\theta_{ij}(\beta,\beta)\exp[-i\phi_{ij}(\beta,\beta)],$$

$$F_{ij}^{(2)}(\beta,\beta) \equiv r_{ij}^{-3}(\beta,\beta)\sin^2\theta_{ij}(\beta,\beta)\exp[-2i\phi_{ij}(\beta,\beta)], \quad (3)$$

Table 2. Positional parameters of hydrogen atoms in $NaAuCl_4 \cdot 2H_2O$

		x/a	y/b	z/c
Model A	H (1)	0.1534	0.4327	0.3829
	H (2)	0.1776	0.5697	0.5199
Model B	H (1)	0.1553	0.4646	0.3728
	H (2)	0.1770	0.5378	0.5380

where N is the number of spins, $\omega_o = \gamma H_o$, and τ_c is the correlation time. The β and δ in parentheses refer to the two equilibrium lattice sites of a given proton. For polycrystalline specimens, one must take the spatial averages of the θ_{ij} and ϕ_{ij} terms.
Thus,

$$F_{ij}^{(o)}(\beta,\beta)^2 = \frac{4}{5} r_{ij}^{-6}(\beta,\beta),$$

$$F_{ij}^{(o)}(\beta,\beta) \cdot F_{ij}^{(o)}(\delta,\delta) = \frac{2}{5}[3\cos^2\alpha(\beta\beta,\delta\delta) - 1] \times r_{ij}^{-3}(\beta,\beta) r_{ij}^{-3}(\delta,\delta),$$

$$F_{ij}^{(1)}(\beta,\beta)^2 = \frac{2}{15} r_{ij}^{-6}(\beta,\beta),$$

$$F_{ij}^{(1)}(\beta,\beta) \cdot F_{ij}^{(1)}(\delta,\delta) = \frac{1}{15}[3\cos^2\alpha(\beta\beta,\delta\delta) - 1] \times r_{ij}^{-3}(\beta,\beta) r_{ij}^{-3}(\delta,\delta),$$

$$F_{ij}^{(2)}(\beta,\beta)^2 = \frac{8}{15} r_{ij}^{-6}(\beta,\beta),$$

$$F_{ij}^{(2)}(\beta,\beta) \cdot F_{ij}^{(2)}(\delta,\delta) = \frac{4}{15}[3\cos^2\alpha(\beta\beta,\delta\delta) - 1] \times r_{ij}^{-3}(\beta,\beta) r_{ij}^{-3}(\delta,\delta), \quad (4)$$

where $\alpha(\beta\beta,\delta\delta)$ is the angle between vector $\beta\beta$ and vector $\delta\delta$.

Prior to the T_1 calculation, the hydrogen atoms were located by assuming that: A) the H–H vector is parallel to the Cl(1)–Cl(1) vector or B) the H–H vector is normal to the Na–Na vector. In both cases the typical values ($\angle$H–O–H=106° and O–H=1.00 Å) were used for the geometry of a water molecule. The positional parameters of protons thus obtained (Table 2) yielded the T_1 minima of 0.28 s for model A, and 0.65 s for model B at the Larmor frequency of 20 MHz; both of these values are close to the experimental one. In both models the water molecule is hydrogen-bonded to the Cl(1) atoms, although the positions of the hydrogen atoms are slightly different from each other. Therefore, the agreement between the observed and calculated values of the T_1 minima supports the formation of the hydrogen bonds. Moreover, the hydrogen bonding is suggested from the fact that the spin phase-memory time, T_2, of the Cl(1) atom is shorter than those of the other chlorine atoms (Table 1). Presumably, the shorter T_2 of the Cl(1) atom is due to the magnetic dipole interaction with protons.

Figure 3 shows the temperature dependence of ^{35}Cl T_1 for the four absorptions. All ^{35}Cl T_1 decrease monotonously with an increase in temperature with the coefficients, $\Delta\log T_1/\Delta\log T$, ranging from −2.1 to −2.5. It should be noticed that the ^{35}Cl T_1 for the lowest frequency line is comparable to those for the other lines,

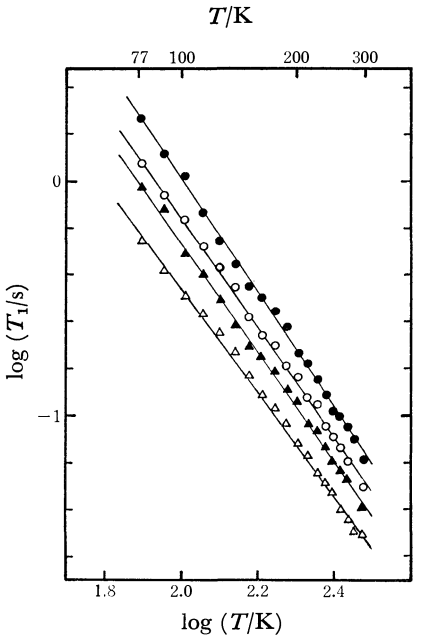

Fig. 3. The temperature dependence of ^{35}Cl T_1 in $NaAuCl_4 \cdot 2H_2O$.
●: ν_1, ▲: ν_2, ○: ν_3, △: ν_4.

and shows no anomalous temperature dependence. This finding, contrary to the suggestion of Woessner and Gutowsky,[1] permits us to conclude that the reorientation of the water molecule affects the chlorine T_1 very little, although the hydrogen bonds are formed between them. The very short T_1 observed in $(CH_3)_2CCl_2$ is probably caused not by the CH_3 reorientation but by molecular reorientations.

Then the chlorine T_1 in $NaAuCl_4 \cdot 2H_2O$ was interpreted on the basis of the torsional vibrations of the $AuCl_4^-$ ion. The quadrupole transition probabilities, $W_1(|\Delta m|=1)$ and $W_2(|\Delta m|=2)$, can be expressed by

$$W_1 = \frac{3}{2}\frac{\hbar\omega_Q^2}{I\omega_t^3}\frac{1}{\tau_a}\coth\left(\frac{x}{2}\right), \tag{5}$$

$$W_2 = \frac{3}{64}\left(\frac{\hbar\omega_Q}{I\omega_t}\right)^2\frac{\tau_a}{\sinh^4(x/2)}, \tag{6}$$

where ω_Q is the angular NQR frequency, ω_t is the angular torsional frequency, I is the moment of inertia, τ_a is the average life time of torsional levels, and $x=\hbar\omega_t/kT$. The T_1 for quadrupolar nuclei of spin 3/2 is given in terms of W_1 and W_2 by

$$\frac{1}{T_1} = 2(W_1+W_2). \tag{7}$$

Equations 5, 6, and 7 yield the following quadratic equation:

$$A_2\tau_a^2 - \frac{1}{2T_1}\tau_a + A_1 = 0, \tag{8}$$

where A_1 and A_2 are parameters determined by ω_Q, ω_t, I, and T.

In order to obtain ω_t, the Bayer approximation was used:[7]

$$\frac{(\Delta\nu_Q/\Delta T)}{\nu_Q} = -\frac{3}{2}\sum_i\frac{k}{(I\omega_t^2)_i}, \tag{9}$$

where the summation is taken over all effective modes.

Table 3. Calculated values of ν_t, τ_a, and $W_1=W_2$ at different temperatures

T/K	ν_t/cm^{-1}	τ_a/ps	$W_1=W_2$/s^{-1}
79	56.62	4.880	0.278
102	57.16	3.358	0.500
150	57.62	1.898	1.250
201	59.16	1.257	2.252
297	58.67	0.694	6.098

In the crystal lattice, the planar $AuCl_4^-$ ion may vibrate about the two Cl–Au–Cl axes and about the axis perpendicular to the plane. Supposing that these three rotary modes are degenerate, and taking account of the two effective modes, we estimated the value of $\nu_t(=\omega_t/2\pi)$ to be 38.1 cm^{-1} from the average temperature coefficient (-0.99×10^{-4} K^{-1}) of all the resonance frequencies except the lowest one. Substituting the value of ω_t and the average value of the experimental T_1 into Eq. 8, however, yielded imaginary values of τ_a at all temperatures of measurement. This means that the T_1 value predicted by the theory is shorter than the observed one. Such a discrepancy has also been pointed out in the chlorine relaxation study for *p*-dichlorobenzene.[1]

It is noteworthy that the ω_t dependence of the temperature coefficient of the resonance frequency is quite different from those of the transition probabilities of W_1 and W_2. If the approximation $e^x \approx 1+x+x^2/2$ is used, we obtain

$$W_1 = 3\sum_i\frac{\omega_Q^2 kT}{(I\omega_t^4\tau_a)_i}, \tag{10}$$

$$W_2 = \frac{3}{4}\sum_i\frac{\omega_Q^2 k^4T^4}{(\hbar^2I^2\omega_t^6)_i}(\tau_a)_i. \tag{11}$$

The powers of ω_t in Eqs. 10 and 11 are much smaller than that in Eq. 9. This means that high frequency modes contribute to the temperature coefficient of resonance frequency more strongly than to W_1 and W_2. Hence, a new attempt to evaluate the ω_t from the T_1 data was made by assuming

$$\left(\frac{1}{2T_1}\right)^2 = 4A_1A_2. \tag{12}$$

This predicts the minimum value of ω_t which will give a real τ_a. The quadratic equation then yields

$$\tau_a = \frac{1}{4T_1A_2} \tag{13}$$

and

$$W_1 = W_2 = \frac{1}{4T_1} \tag{14}$$

with the simplifying assumption of only one torsional mode, one finds

$$\omega_t = \sqrt[10]{36\frac{\omega_Q^4k^5T^5T_1^2}{\hbar^2I^3}}. \tag{15}$$

The calculated values of $\nu_t(=\omega_t/2\pi)$, τ_a, and W_1 $(=W_2)$ are summarized in Table 3. Though one has no justification for the use of Eq. 12, the resulting ratio of W_2/W_1 $(=1)$ is comparable to those obtained in *p*-dichlorobenzene (2—12 at 300K and 0.5—2 at 77K),[8] and the values of ν_t are approximately constant in the

temperature range studied. These results support the present model for the chlorine relaxation time. The ν_t value of about 58 cm^{-1} predicts a temperature coefficient of -0.28×10^{-4} K^{-1}, which is somewhat smaller than the average experimental one on the absolute scale. The residual part of the coefficient may be interpreted in terms of high frequency modes, as described above.

References

1) D. E. Woessner and H. S. Gutowsky, *J. Chem. Phys.*, **39**, 440 (1963).
2) K. Sagisawa, H. Kiriyama, and R. Kiriyama, *Chem. Lett.*, **1975**, 1285.
3) M. Bonamico, G. Dessy, and A. Vaciago, *Atti Accad. Naz. Lincei, Cl. Sci. Fis. Mat. Natur. Rend.*, **39**, 504 (1965).
4) C. W. Fryer and J. A. S. Smith, *J. Chem. Soc., A*, **1970**, 1029.
5) A. Sasane, T. Matuo, D. Nakamura, and M. Kubo, *J. Magn. Reson.*, **4**, 257 (1971).
6) D. C. Look and I. J. Lowe, *J. Chem. Phys.*, **44**, 2995 (1966).
7) H. Bayer, *Z. Phys.*, **130**, 227 (1951).
8) M. J. Weber, *J. Phys. Chem. Solids*, **17**, 267 (1961).

Vibrational Fine Structure of the Ligand Field Absorption Band of Halogenoammine Cobalt(III) Complexes

Kunimasa FUKUDA and Akio URUSHIYAMA*

Department of Chemistry, Faculty of Science, Rikkyo University, Nishiikebukuro, Toshima-ku, Tokyo 171

(Received December 13, 1977)

The crystal absorption spectra of some halogenoammine complexes of Co(III) were measured at liquid helium temperature. The vibrational fine structures observed for the spin-allowed ligand field bands were interpreted in terms of a vibronic intensity mechanism in comparision with the vibrational frequencies of the skeletons. It was found that all the vibrational fine structures consist of the uniquantal progression of totally symmetric Co–N stretching vibration. This suggests that the equilibrium Co–N distances of these complexes are elongated in the ligand field electronic excited state as compared with those in the ground state.

The vibrational fine structure of the ligand field absorption band of $[Co(NH_3)_6]^{3+}$ was studied by Wentworth.[1] He found in his low temperature optical study that the vibrational fine structure of the $^1T_{1g}\leftarrow{}^1A_{1g}$ band of the complex consists of the uniquantal progression correlated to the totally symmetric Co–N stretching vibration of the CoN_6 skeleton. Since then some reports concerning $[Co(en)_3]^{3+}$ have appeared.[2,3] A study was carried out for the mixed ligand complexes.[4] In the present study, the crystal absorption spectra of some halogenoammine complexes of Co(III) have been measured at liquid helium temperature, the vibrational fine structure of the ligand field bands of the complexes in reduced symmetries being of much interest. Complex fine structure could be observed for almost all the bands in the visible region. The observed fine structures were interpreted on the basis of the infrared and Raman data of the complexes assuming a vibronic intensity scheme.

Experimental

All the complex salts were prepared according to the procedures reported previously[5] except for *trans*-$[CoCl_2(NH_3)_4]_3[Co(CN)_6]$ and *trans*-$[CoBr_2(NH_3)_4]_3[Co(CN)_6]$. Excellent single-crystals of $[CoF(NH_3)_5]Cl_2\cdot 2H_2O$ for the transmission spectroscopy could be obtained by evaporation of the aqueous solution in a vacuum dessicator. In the cases of $[Co(NH_3)_6][Co(CN)_6]$, $[CoCl(NH_3)_5]Cl_2$, and $[CoBr(NH_3)_5]Br_2$, excellent crystals could be obtained when the aqueous solutions of $K_3[Co(CN)_6]$, 1M HCl, and 1M HBr, respectively, were dispersed extremely slowly into each of the solutions containing the corresponding complex cation. The fine crystalline powders of *trans*-$[CoCl_2(NH_3)_4]_3[Co(CN)_6]$ and *trans*-$[CoBr_2(NH_3)_4]_3[Co(CN)_6]$ were precipitated immediately from the freshly prepared aqueous solutions of *trans*-$[CoCl_2(NH_3)_4]Cl$ and *trans*-$[CoBr_2(NH_3)_4]ClO_4$, respectively, by adding an aqueous solution of $K_3[Co(CN)_6]$ at 0 °C. The diffuse reflectance spectra in the visible region and the infrared absorption spectra of the crystals suggest that the skeletons of the complexes are retained throughout these procedures. Found: Co, 29.1%. Calcd for *trans*-$[CoCl_2(NH_3)_4]_3[Co(CN)_6]$: Co, 29.1%. Found: Co, 22.0%. Calcd for *trans*-$[CoBr_2(NH_3)_4]_3[Co(CN)_6]$: Co, 21.9%.

The visible absorption spectra of the crystalline samples were measured with an apparatus (Fig. 1) consisting of a JASCO model CT-50 monochromater, a specially designed liquid helium optical cryostat, and a HTV model C767 photon counting system. The liquid helium flowed from the container of the cryostat to a specially designed cooling stage made of a copper block through a tunnel bored inside it. Single-crystals of appropriate size ($\sim 0.2\times\sim 0.2\times\sim 0.02$ mm) were mounted over a pinhole ($\phi=0.15$ mm) in an indium plate, which was then placed on the cooling stage of the cryostat. The sample crystals were made large enough to cover the pinhole completely for the measurements. Silicone grease ensured good thermal contact between the crystal, indium plate, and cooling stage. Silicone grease mulls of the powdered sample were mounted on a small glass plate, and placed on the cooling stage in a similar way to that for the single-crystal measurements. A thermocouple (gold-iron: chromel) indicated the cooling of samples to liquid helium temperature throughout the measurements. The values of transmission light recorded were corrected by those of the blank measurement adjusting the transmittance to unity in the lower wavenumber region where the samples could not absorb.

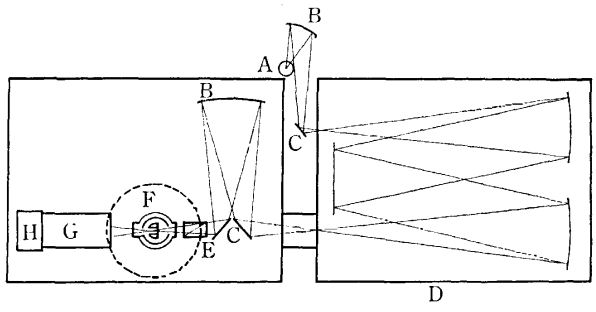

Fig. 1. Apparatus for low temperature optical study. A: Tungsten lamp, B: mirror, C: mirror, D: monochromater (CT-50), E: polarizer, F: cryostat, G: photomultiplyer (HTV R649S or R585S), H: pre. amp.

Results and Discussion

$[Co(NH_3)_6]^{3+}$. The single crystal absortpion spectrum of $[Co(NH_3)_6][Co(CN)_6]$ is shown in Fig. 2. Clear vibrational structure is superimposed on the $^1T_{1g}\leftarrow{}^1A_{1g}$ band of $[Co(NH_3)_6]^{3+}$ as reported by Wentworth.[1] However, no structure could be detected on the $^1T_{2g}\leftarrow{}^1A_{1g}$ band in the near-ultraviolet region. The crystal is hexagonal with the space group $R\bar{3}$ and the precise symmetry of $[Co(NH_3)_6]^{3+}$ is S_6.[7] However, the polarized absorption spectra with the light parallel and perpendicular to the crystal c axis appear to be almost identical.

Most of the lines can be explained in terms of the uniquantal progression of the $\nu_1(a_{1g})$ Co–N stretching vibration of the combination, $\nu_i+(N+n)\nu_1(a_{1g})$,

Table 1. Skeletal vibrational frequencies of Co(III) complexes[a)]

Compound	Vibrational frequency, cm^{-1}					
O_h symmetry	$\nu_1(a_{1g})$	$\nu_3(t_{1u})$	$\nu_4(t_{1u})$			
$[Co(NH_3)_6]^{3+}$	490[b)]	480[b)]	331[b)]			
D_{4h} symmetry	$\nu_1(a_{1g})$	$\nu_2(a_{1g})$	$\nu_9(e_u)$	$\nu_{10}(e_u)$	$\nu_{11}(e_u)$	
trans-$[CoCl_2(NH_3)_4]^+$	275[b)]	492[b)]	501[c)]	178[c)]	290[c)]	
trans-$[CoBr_2(NH_3)_4]^+$		482[d)]	486[c)]	140[c)]	295[c)]	
C_{4v} symmetry	$\nu_1(a_1)$	$\nu_3(a_1)$	$\nu_8(e)$	$\nu_9(e)$	$\nu_{10}(e)$	$\nu_{11}(e)$
$[CoF(NH_3)_5]^{2+}$		494[d)]	504[c)]	309[c)]	249[c)]	328[c)]
$[CoCl(NH_3)_5]^{2+}$	274[b)]	485[b)]	487[c)]	285[c)]	200[c)]	325[c)]
$[CoBr(NH_3)_5]^{2+}$		483[d)]	501[c)]			319[c)]

a) Normal modes are denoted according to Ref. 6a. b) Frequencies reported in Ref. 6a. c) Frequencies reported in Ref. 6b. d) Present work for the perchlorates.

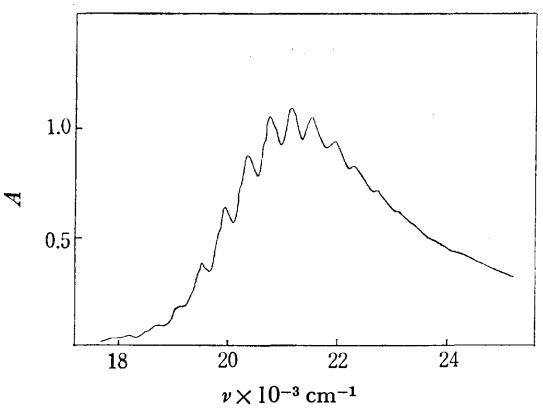

Fig. 2. Crystal absorption spectrum of $[Co(NH_3)_6]$-$[Co(CN)_6]$ at 4.2 K (with polarized light parallel to the crystal c axis).

where ν_i=ungerade vibration, N=integer, and n= 0, 1, 2, . . . , assuming a vibronic intensity scheme. The vibrational frequencies of the ammine complexes of Co(III) have been studied by several workers.[6)] The frequencies referred to in the present study are given in Table 1. The average spacing of 402 cm^{-1} seems to be reasonable for the $\nu_1(a_{1g})$ vibrational frequency at the $^1T_{1g}$ electronic excited state. It represents an 18% reduction in the $\nu_1(a_{1g})$ vibrational frequency as compared with the ground state value of 490 cm^{-1}. The electronic excitation into the antibonding e_g orbital may elongate the Co–N bond distances to some extent, giving rise to this frequency reduction. Each line could be resolved into two or more components. However, measurement with higher resolution is necessary for further discussion of the structure.

trans-$[CoCl_2(NH_3)_4]^+$ *and* trans-$[CoBr_2(NH_3)_4]^+$. The low temperature mull spectra of *trans*-$[CoCl_2(NH_3)_4]_3[Co(CN)_6]$ and *trans*-$[CoBr_2(NH_3)_4]_3[Co(CN)_6]$ are shown in Figs. 3 and 4, respectively. The bands in the 16000—18500 cm^{-1} region are assigned to the $^1E_g[^1T_{1g}(O_h)]\leftarrow{}^1A_{1g}$ transition and those in the 18500—22000 cm^{-1} region to the $^1A_{2g}[^1T_{1g}(O_h)]\leftarrow{}^1A_{1g}$ transition in D_{4h} symmetry. Some indistinct structure was found on the $^1E_g\leftarrow{}^1A_{1g}$ band of *trans*-$[CoCl_2(NH_3)_4]^+$, whereas no structure could be detected for the band of *trans*-$[CoBr_2(NH_3)_4]^+$. Due to its low resolution, no assignment of the structure is possible in the present study.

In the $^1A_{2g}\leftarrow{}^1A_{1g}$ band region, predominant progressions were found with average spacings of 422 and 411 cm^{-1}, for *trans*-$[CoCl_2(NH_3)_4]^+$ and *trans*-$[CoBr_2(NH_3)_4]^+$, respectively. These frequencies can naturally be correlated to the $\nu_2(a_{1g})$ Co–N stretch-

Table 2. Selection rule for the ligand field absorption band of Co(III) complexes in reduced symmetry

Transition	Electronic	Vibronic	
D_{4h}			Vibrational species
$^1E_g\leftarrow{}^1A_{1g}$	forbidden	allowed(xy)	a_{2u}
		allowed(xy)	b_{2u}
		allowed(xyz)	e_u
$^1A_{2g}\leftarrow{}^1A_{1g}$	forbidden	allowed(xy)	e_u
C_{4v}			
$^1E\leftarrow{}^1A_1$	allowed(xy)	allowed(xy)	b_1
		allowed(xy)	b_2
		allowed(z)	e
$^1A_2\leftarrow{}^1A_1$	forbidden	allowed(xy)	e

Table 3. Observed optical transitions and assignments for the $^1A_{2g}\leftarrow{}^1A_{1g}$ transition of *trans*-$[CoCl_2(NH_3)_4]^+$ at 4.2 K

Peak	Energy, cm^{-1}	Assignment
1c	18450	$^1A_{2g}+\nu_9+(N+1)\nu_2$
2c	18880	$+\nu_9+(N+2)\nu_2$
3a	19040	$+\nu_{10}+(N+3)\nu_2$
3b	19150	$+\nu_{11}+(N+3)\nu_2$
3c	19290	$+\nu_9+(N+3)\nu_2$
4b	19580	$+\nu_{11}+(N+4)\nu_2$
4c	19720	$+\nu_9+(N+4)\nu_2$
5b	19990	$+\nu_{11}+(N+5)\nu_2$
5c	20130	$+\nu_9+(N+5)\nu_2$
6b	20400	$+\nu_{11}+(N+6)\nu_2$
6c	20560	$+\nu_9+(N+6)\nu_2$
7b	20810	$+\nu_{11}+(N+7)\nu_2$
7c	20980	$+\nu_9+(N+7)\nu_2$
8b	21150	$+\nu_{11}+(N+8)\nu_2$
8c	21300	$+\nu_9+(N+8)\nu_2$

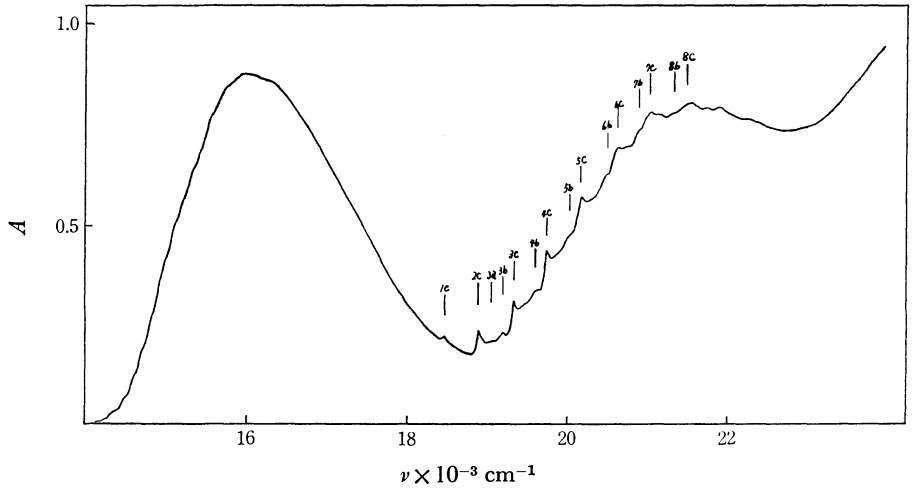

Fig. 3. Crystal absorption spectrum of *trans*-$[CoCl_2(NH_3)_4]_3[Co(CN)_6]$ at 4.2 K (mull method).

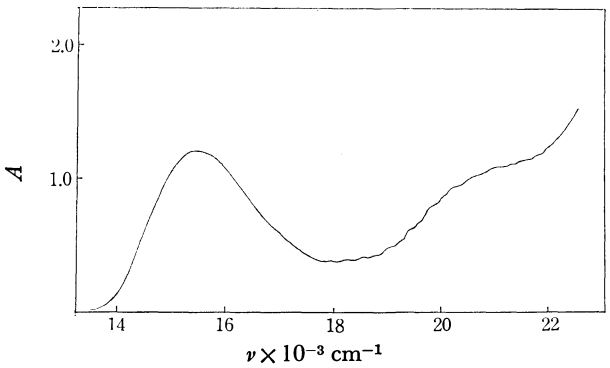

Fig. 4. Crystal absorption spectrum of *trans*-$[CoBr_2(NH_3)_4]_3[Co(CN)_6]$ at 4.2 K (mull method).

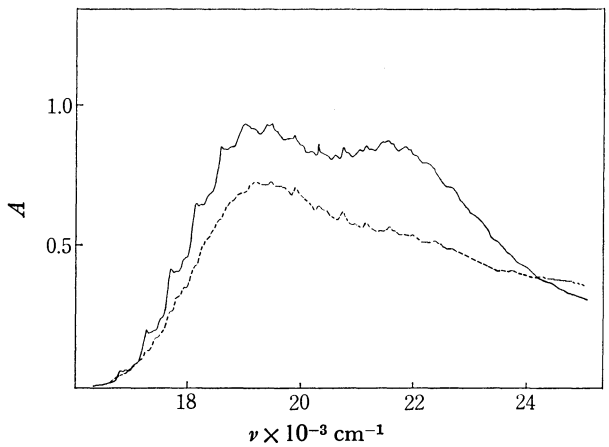

Fig. 5. Polarized absorption spectra of $[CoF(NH_3)_5]Cl_2 \cdot 2H_2O$ at 4.2 K.

ing vibration of the *trans*-CoX_2N_4 groups in the electronic excited state. The frequency reduction of the ν_2 vibration were estimated to be 14 and 15% for *trans*-$[CoCl_2(NH_3)_4]^+$ and *trans*-$[CoBr_2(NH_3)_4]^+$, respectively, as compared with the values in the ground state. These findings suggest that the complexes are displaced along the Q_2 normal coordinate in the $^1A_{2g}$ electronic excited state. The coordinate has been analysed to consist mainly of the symmetric Co–N bond length changes in these complexes.[6] The $^1A_{2g} \leftarrow {}^1A_{1g}$ transition corresponds to an electronic excitation from the d_{xy} orbital to the antibonding $d_{x^2-y^2}$ orbital. It can be surmised that the Co–N equilibrium distances are elongated to some extent in the $^1A_{2g}$ electronic excited state as compared with those in the ground state. This is in line with the present results.

The selection rules of the ligand field absorption bands are given in Table 2. For the $^1A_{2g} \leftarrow {}^1A_{1g}$ transition, only the e_u vibrational mode can couple with the electronic state to give a vibronically allowed transition. Thus, the vibronic patterns observed should be characterized by the $\nu_9(e_u)$: Co–N str., $\nu_{10}(e_u)$: Co–X bend., and $\nu_{11}(e_u)$: N–Co–N def. vibrations combined with the totally symmetric vibration. If we compare the energy differences between adjacent peaks with the infrared absorption energies, the assignments (Table 3) seem reasonable, although the excited state vibrational frequencies may somewhat differ from those in the ground state. The vibronic pattern of the $^1A_{2g} \leftarrow {}^1A_{1g}$ band of *trans*-$[CoBr_2(NH_3)_4]^+$ can be interpreted similarly, although the components of $\nu_{11}(e_u)$ were indistinct.

$[CoF(NH_3)_5]^{2+}$, $[CoCl(NH_3)_5]^{2+}$, and $[CoBr(NH_3)_5]^{2+}$. The polarized absorption spectra of $[CoF(NH_3)_5]Cl_2 \cdot 2H_2O$, $[CoCl(NH_3)_5]Cl_2$, and $[CoBr(NH_3)_5]Br_2$ are shown in Figs. 5, 6, and 7, respectively. They were measured by polarized light along the extinction directions perpendicular to the crystal face which exhibited the most distinct dichroism under a polarizing microscope. A distinct splitting of the $^1T_{1g}(O_h) \leftarrow {}^1A_{1g}(O_h)$ band was observed in each case. The bands at lower energy are assigned to the $^1E[^1T_{1g}(O_h)] \leftarrow {}^1A_1$ transition and the higher energy ones to the $^1A_2[^1T_{1g}(O_h)] \leftarrow {}^1A_1$ transition in C_{4v} symmetry. A good deal of vibrational structure was observed for almost all the bands.

In the $^1E \leftarrow {}^1A_1$ band region of $[CoCl(NH_3)_5]^{2+}$, distinct lines appeared apparently with progressional spacing of 200 cm^{-1}, weak components being found in the alternate gaps between these lines. However, by careful inspection of the relative intensities of the peaks,

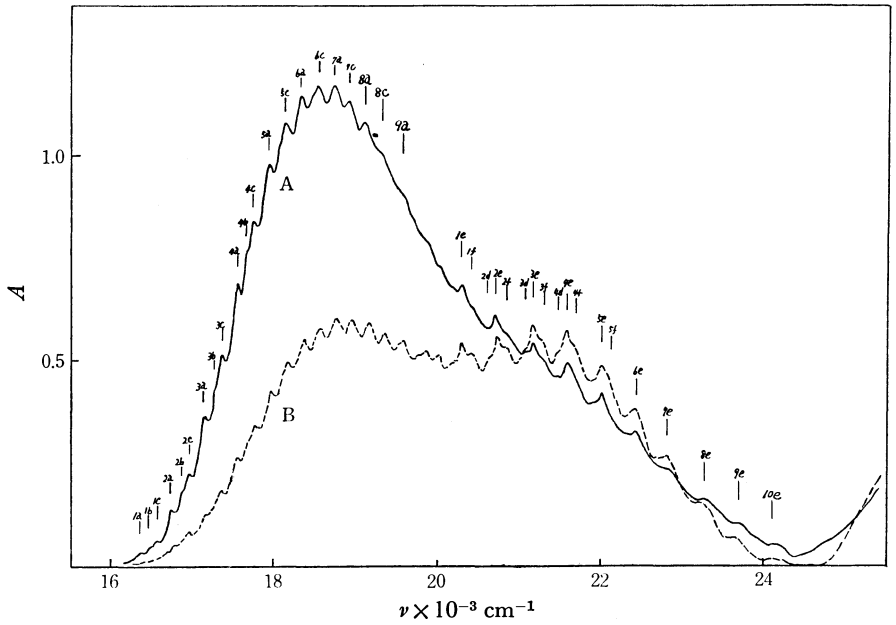

Fig. 6. Polarized absorption spectra of $[CoCl(NH_3)_5]Cl_2$ at 4.2 K.

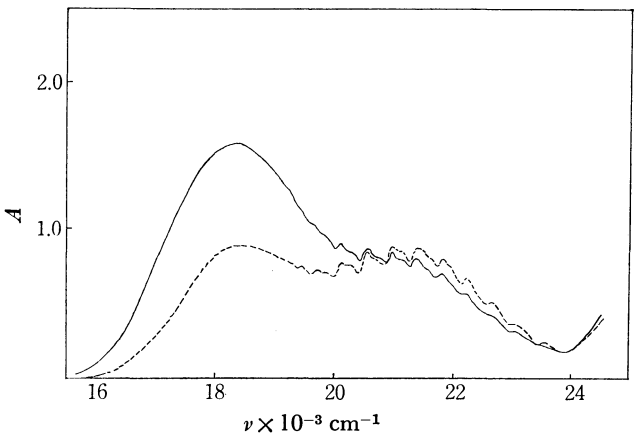

Fig. 7. Polarized absorption spectra of $[CoBr(NH_3)_5]Br_2$ at 4.2 K.

the vibronic pattern could be characterized to consist of the progression with average spacing of 397 cm^{-1} in three components. This frequency can be correlated to the $\nu_3(a_1)$: Co–N str. vibration in the ^1E electronic excited state, representing a 20% frequency reduction in comparision with the ground state value of 495 cm^{-1}. Stanko[4] studied the polarized absorption spectra of $[CoX(NH_3)_5]SiF_6$, where X=Cl, Br, CN, and concluded that the main features of the ligand field absorption bands of these complexes can be accounted for by a vibronic intensity mechanism. He also showed on the basis of intensity calculation that the $\nu_8(e)$: Co–N str., $\nu_{10}(e)$: Co–X bend., and $\nu_{11}(e)$: N–Co–N def. vibrational modes play an important role in the vibronic mechanism of the ^1E band of $[CoCl(NH_3)_5]^{2+}$. It was found in the present study that the A polarized spectrum (Fig. 6), which is thought to be rich with the xy-polarized spectrum of the complex because of the dominant emergence of the $^1A_2$ band, shows no vibrational component more than those observed in the B spectrum, which must be rich with the z-polarized spectrum of the complex (Table 2). The best fit to experimantal data when the energy differences between adjacent peaks are compared with the infrared frequencies of the e vibrational modes is shown in Table 4.

In the spectra of $[CoF(NH_3)_5]^{2+}$, the vibrational structure of the ^1E band appears in a different pattern for each polarization direction. This suggests that the a_2 and/or b_2 vibrational species responsible for the vibronic intensity along the xy axis of the complex are important for this band. However, the spacings of the progression were estimated to be 420 cm^{-1}. The frequency corresponds to the $\nu_3(a_1)$ vibration.

All the complexes in the present study show a complex fine structure in their $^1A_2 \leftarrow {}^1A_1$ band region.[4] Several components were found to form a progression for each complex. The intervals of the progression found in the spectra of $[CoF(NH_3)_5]Cl_2 \cdot 2H_2O$, $[CoCl(NH_3)_5]Cl_2$, and $[CoBr(NH_3)_5]Br_2$ were estimated to be 420, 419, and 429 cm^{-1}, respectively. These frequencies correspond to the $\nu_3(a_1)$ vibration in the $^1A_2$ excited state, representing frequency reductions of 15, 14, and 12%, respectively, as compared with the ground state values. The $^1A_2 \leftarrow {}^1A_1$ band of these complexes can be interpreted in terms of the vibronic intensity mechanism through the vibrations of e species (Table 2). The observed components can be assigned by considering the energy differences between adjacent peaks (Table 4). The vibronic patterns of the $^1A_2 \leftarrow {}^1A_1$ $[CoF(NH_3)_5]^{2+}$ and band of $[CoBr(NH_3)_5]^{2+}$ can be interpreted in a similar way to that for the chloro complex. The $\nu_{10}(e)$ components of $[CoBr(NH_3)_5]^{2+}$ are thought to be obscured due to the shift toward a position close to the $\nu_8(e)$ components because of the reduction in the $\nu_{10}(e)$ vibrational frequency of the complex.

The authors wish to express their thanks to Prof. Yukio Kondo, Rikkyo University, for his encouragement.

Table 4. Observed optical transitions and assignments in the 16000—24000 cm^{-1} region for $[CoCl(NH_3)_5]^{2+}$ at 4.2 K

Peak	Energy, cm^{-1}	Assignment	Peak	Energy, cm^{-1}	Assignment
1a	16300	$^1E+\nu_{10}+(N+1)\nu_3$	1e	20230	$^1A_2+\nu_{11}+(N+1)\nu_3$
1b	16400	$+\nu_{11}+(N+1)\nu_3$	1f	20360	$+\nu_8+(N+1)\nu_3$
1c	16500	$+\nu_8+(N+1)\nu_3$	2d	20530	$+\nu_{10}+(N+2)\nu_2$
2a	16700	$+\nu_{10}+(N+2)\nu_3$	2e	20660	$+\nu_{11}+(N+2)\nu_3$
2b	16820	$+\nu_{11}+(N+2)\nu_3$	2f	20790	$+\nu_8+(N+2)\nu_3$
2c	16900	$+\nu_8+(N+2)\nu_3$	3d	20970	$+\nu_{10}+(N+3)\nu_3$
3a	17100	$+\nu_{10}+(N+3)\nu_3$	3e	21080	$+\nu_{11}+(N+3)\nu_3$
3b	17220	$+\nu_{11}+(N+3)\nu_3$	3f	21220	$+\nu_8+(N+3)\nu_3$
3c	17310	$+\nu_8+(N+3)\nu_3$	4d	21390	$+\nu_{10}+(N+4)\nu_3$
4a	17500	$+\nu_{10}+(N+4)\nu_3$	4e	21480	$+\nu_{11}+(N+4)\nu_3$
4b	17610	$+\nu_{11}+(N+4)\nu_3$	4f	21600	$+\nu_8+(N+4)\nu_3$
4c	17710	$+\nu_8+(N+4)\nu_3$	5e	21910	$+\nu_{11}+(N+5)\nu_3$
5a	17890	$+\nu_{10}+(N+5)\nu_3$	5f	22030	$+\nu_8+(N+5)\nu_3$
5c	18090	$+\nu_8+(N+5)\nu_3$	6e	22330	$+\nu_{11}+(N+6)\nu_3$
6a	18290	$+\nu_{10}+(N+6)\nu_3$	7e	22730	$+\nu_{11}+(N+7)\nu_3$
6c	18480	$+\nu_8+(N+6)\nu_3$	8e	23180	$+\nu_{11}+(N+8)\nu_3$
7a	18670	$+\nu_{10}+(N+7)\nu_3$	9e	23600	$+\nu_{11}+(N+9)\nu_3$
7c	18870	$+\nu_8+(N+7)\nu_3$	10e	24020	$+\nu_{11}+(N+10)\nu_3$
8a	19070	$+\nu_{10}+(N+8)\nu_3$			
8c	19280	$+\nu_8+(N+8)\nu_3$			
9a	19470	$+\nu_{10}+(N+9)\nu_3$			

References

1) R. A. D. Wentworth, *Chem. Commun.*, **1965**, 532.
2) R. Dingle, *Chem. Commun.*, **1965**, 304.
3) R. G. Denning, *Chem. Commun.*, **1967**, 120.
4) J. A. Stanko, Ph. D. Thesis, University of Illinois, U. S. A. 1966. He studied single-crystals of $[CoCl(NH_3)_5]SiF_6$ and $[CoBr(NH_3)_5]SiF_6$ at liquid nitrogen temperature, and observed simple peaks with progressional spacings of 466 and 410 cm^{-1}, respectively, on the $^1A_2 \leftarrow {}^1A_1$ band.
5) "Gmelin Handbuch" **58**, Tl. B. 1964.
6) a) T. M. Loehr, J. Zinich, and T. V. Long II, *Chem. Phys. Lett.*, **7**, 183 (1970); b) L. Sacconi, A. Sabatini, and D. Gans, *Inorg. Chem.*, **3**, 1772 (1964); c) T. Shimanouchi and I. Nakagawa, *Spectrochim. Acta*, **18**, 89 (1966); e) T. Shimanouchi and I. Nakagawa, *Inorg. Chem.*, **3**, 1805 (1964).
7) M. Iwata and Y. Saito, *Acta Crystallogr., Sect. B*, **29**, 822 (1973).

Phase-shift Studies of Cadmium-photosensitized Luminescence of Ammonia and Some Aliphatic Amines

Hironobu UMEMOTO,* Shigeru TSUNASHIMA, and Shin SATO

Department of Applied Physics, Tokyo Institute of Technology, Ookayama, Meguro-ku, Tokyo 152

(Received December 13, 1977)

A phase-shift method was used to study the cadmium-photosensitized luminescence of ammonia and some aliphatic amines. The phase angles between the resonance fluorescence at 326.1 nm and the luminescence from the excited complexes have been measured at various modulation frequencies (10—99 kHz). The results could not be explained by means of the reaction mechanism proposed by analogy with the mercury-photosensitized luminescence of ammonia. In order to obtain a consistency, the equilibrium between the unstabilized and stabilized complexes: $CdNH_3^{\dagger}+NH_3 \rightleftarrows CdNH_3^*+NH_3$, had to be taken into account. The reverse reaction was not necessary to explain the results of the mercury-photosensitized luminescence of ammonia. This discrepancy may be ascribed to the difference in the energy gap between the $^3P_1$ and $^3P_0$ states of mercury and cadmium.

In the cadmium(5^3P_1)-photosensitized reactions of ammonia and some other electron-donor molecules, such as water and amines, broad, diffuse emission bands can be observed in the visible light region, while in the cases of mercury(6^3P_1)-photosensitization, similar emission bands are observed in the ultraviolet region.

To the studies of mercury-photosensitized luminescence, flash methods and modulation techniques have been applied by several groups.[1-6] The mercury–ammonia system has been especially well studied because of the high quantum yield of the luminescence. It is now well established that the sensitized luminescence arises from a charge-transfer complex formed between an ammonia molecule and an excited mercury atom, and that an $Hg(^3P_0)$ atom plays a significant role in the formation of this complex. The lifetime of the $HgNH_3^*$ complex has been measured by several groups.[1-6]

As for cadmium-photosensitized luminescence, however, there is only one example of such a measurement.[7] In the last several years, we have studied this cadmium-photosensitized luminescence by using a method of stationary excitation at 326.1 nm.[8-10] We have measured the steady-state intensities of the resonance fluorescence at 326.1 nm and of the sensitized luminescence as a function of the pressure of foreign gases. The quantum yield of the luminescence for ammonia was larger than those for other substrates.[9-10] In the photosensitization of ammonia, the ratio of the resonance fluorescence at 326.1 nm in the absence of ammonia to that in the presence of ammonia increased nonlinearly with an increase in the ammonia pressure in the low-pressure region, although it increased linearly in the high-pressure region.[8] In order to explain this nonlinearity, we considered the formation of an unstabilized complex which is in equilibrium with the excited cadmium atom and ammonia and which is stabilized by collisions with third bodies.

In the present study, in order to investigate the mechanism of the luminescence, we applied a phase-shift method to the cadmium–ammonia and cadmium–aliphatic amine systems.

Experimental

The experimental system was similar to that described previously for the study of the mercury-photosensitized luminescence,[6] except that the reaction vessel was kept in an electric furnace at 525±1 K. The vapor pressure of the cadmium in the cell was kept constant, 4.0×10^{-3} Torr (1 Torr≃133.3 Pa),[11] by maintaining the temperature of the cadmium reservoir at 519±1 K. The exciting resonance lamp was a home-made microwave-powered one containing about 10 Torr of helium as a carrier gas. This cadmium lamp was made of Pyrex glass, which cut off another resonance line at 228.8 nm. The emitting part of the lamp was covered with another Pyrex glass tube, and the intervening space was evacuated to prevent cadmium metal from depositing on the wall of the lamp. The reaction vessel was made of quartz.

The emission from the reaction system was focused by means of a quartz lens and detected with a 1P28 photomultiplier (Hamamatsu TV) in conjunction with a Shimadzu QV-50 monochromator. The phase angles of the photomultiplier signals relative to the internal reference signal of a lock-in amplifier (NF Circuit Design Block Co., LI-573) were measured. The pressures of the gases were measured with a Wallace & Tiernan model 61-050 pressure gauge.

The cadmium used was a high-purity sample (99.9999%) manufactured by the Osaka Asahi Metal Co. Pure-grade ammonia (Takachiho Shoji Co.) was used after being degassed at the temperature of liquid nitrogen. Pure-grade methylamine and dimethylamine (Takachiho Shoji Co.) were used after repeated trap-to-trap distillation. An aqueous solution of trimethylamine (Tokyo Kasei Co.) was used after repeated trap-to-trap distillation and drying with calcium hydride and with an alloy of sodium and potassium.

Results

In the cadmium–ammonia system, the phase difference between the resonance fluorescence at 326.1 nm and the sensitized emission from the excited complex at 432 nm decreased with the increase in the pressure of ammonia, as is shown in Fig. 1. It is well known that, in the case of a pseudo-first order reaction, the phase shift, ϕ, is related to the lifetime of the excited species, τ, by means of the following equation:

$$\frac{\tan\phi}{\omega}=\tau,$$

where ω is the angular frequency of modulation.[12] In the present case, although this value of $\tan\phi/\omega$ was independent of the frequency, it depended on the ammonia pressure and had a linear relation with the reciprocal of the pressure in the range of 15—200 Torr, as is shown in Fig. 2. The phase angle of the

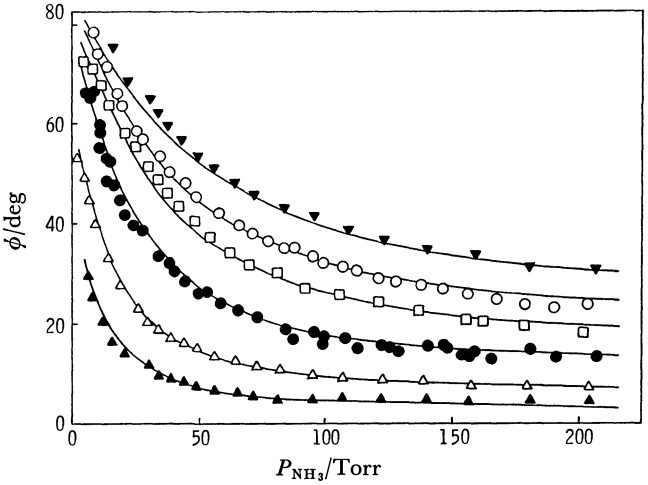

Fig. 1. Phase difference between the resonance fluorescence at 326.1 nm and the luminescence from $CdNH_3$* at 432 nm as a function of NH_3 pressure.
▲: 10 kHz, △: 20 kHz, ●: 40 kHz, □: 60 kHz, ○: 78 kHz, ▼: 99 kHz.
Solid lines show the values calculated according to Eq. 12.

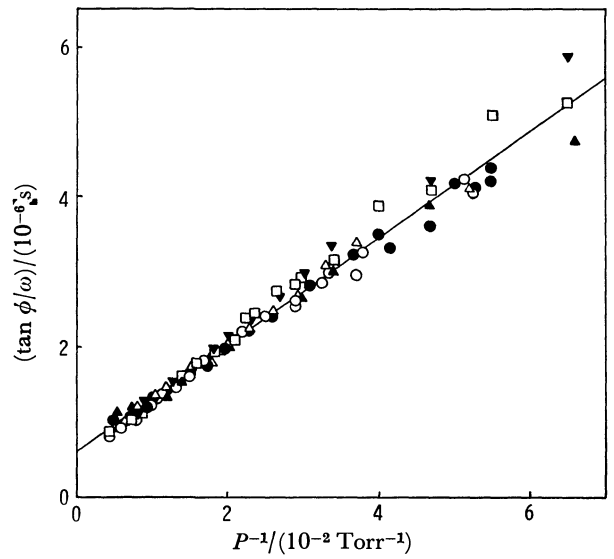

Fig. 2. Values of tan ϕ/ω as a function of the reciprocal of the NH_3 pressure.
▲: 10 kHz, △: 20 kHz, ●: 40 kHz, □: 60 kHz, ○: 78 kHz, ▼: 99 kHz.

sensitized emission was independent of the wavelength of the emission band of the complex. Similar results could also be obtained in the cases of methylamine, dimethylamine, and trimethylamine, which are illustrated in Figs. 3—5 and 6. The phase angle did not change when a UVD-25 filter, which removes visible light, was inserted between the exciting lamp and the cell. The intensity of the background scattered light at 326.1 nm was measured on the assumption that 100 Torr of hydrogen can quench the triplet cadmium completely;[13] it was estimated to be 0.2% of the emission intensity at 326.1 nm in the absence of quenching gases.

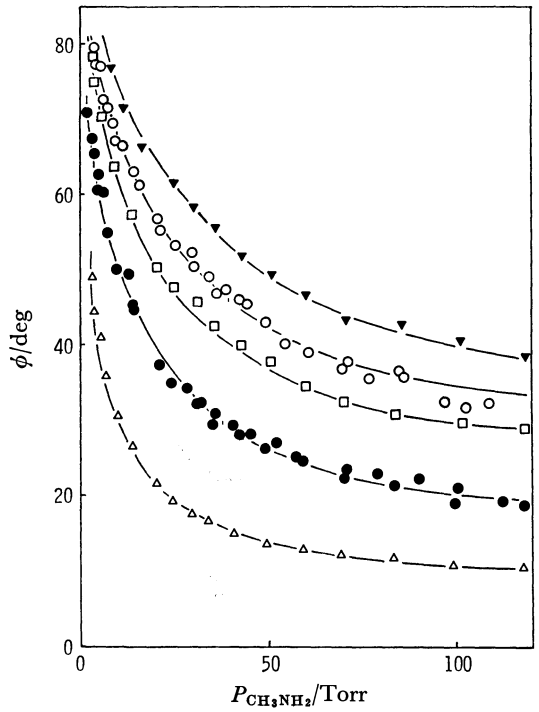

Fig. 3. Phase difference between the resonance fluorescence at 326.1 nm and the luminescence from $CdCH_3NH_2$* at 449 nm as a function of CH_3NH_2 pressure.
△: 20 kHz, ●: 40 kHz, □: 60 kHz, ○: 78 kHz, ▼: 99 kHz.

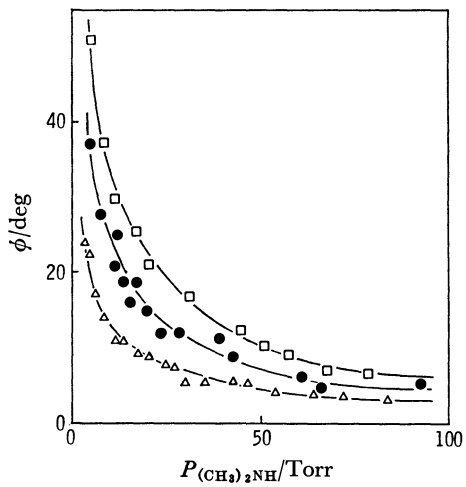

Fig. 4. Phase difference between the resonance fluorescence at 326.1 nm and the luminescence from $Cd(CH_3)_2NH$* at 450 nm as a function of $(CH_3)_2NH$ pressure.
△: 20 kHz, ●: 40 kHz, □: 60 kHz.

Discussion

In a recent phase-shift study of the reaction of ammonia with triplet mercury, we found that the phase angle between the resonance fluorescence at 253.7 nm and the luminescence from the excited complex varies with the wavelength of the emission band of the complex.[6] This finding suggests that there are at

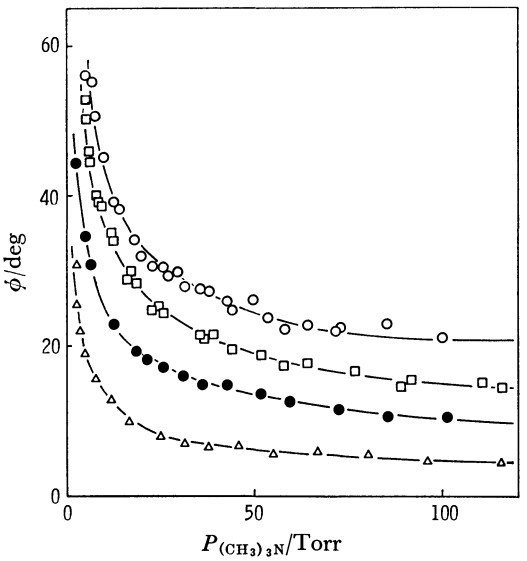

Fig. 5. Phase difference between the resonance fluorescence at 326.1 nm and the luminescence from $Cd(CH_3)_3N^*$ at 435 nm as a function of $(CH_3)_3N$ pressure.
△: 20 kHz, ●: 40 kHz, □: 60 kHz, ○: 78 kHz.

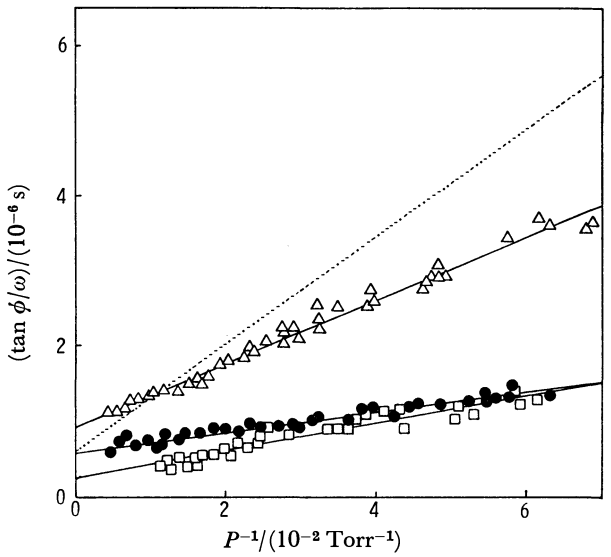

Fig. 6. Values of $\tan\phi/\omega$ as function of the reciprocal of the pressure.
△: CH_3NH_2, □: $(CH_3)_2NH$, ●: $(CH_3)_3N$.
The broken line shows the value for NH_3.

least two kinds of emitting species in this system. On the other hand, in the cadmium–ammonia system, the phase angle of the sensitized luminescence was found to be independent of the wavelength. In other words, the presence of an unstabilized complex could not be confirmed by the present measurements. However, as has been mentioned above, we have found nonlinearity in the Stern-Volmer plots for the quenching of the 326.1 nm resonance line.[8] This nonlinearity cannot be explained without assuming the presence of an unstabilized complex as a precursor of an emitting complex. Accordingly, at first, the following reaction mechanism, which is similar to the one proposed for the mercury–ammonia system, was considered:

$$Cd + h\nu \rightarrow Cd_1^*, \quad (1)$$

$$Cd_1^* \rightarrow Cd + h\nu, \quad (2)$$

$$Cd_1^* + NH_3 \rightarrow \text{Products}, \quad (3)$$

$$Cd_1^* + NH_3 \rightleftarrows CdNH_3^\dagger, \quad (4)$$

$$CdNH_3^\dagger \rightleftarrows Cd_0^* + NH_3, \quad (5)$$

$$CdNH_3^\dagger + NH_3 \rightarrow CdNH_3^* + NH_3, \quad (6)$$

$$CdNH_3^* \rightarrow Cd + NH_3 + h\nu'. \quad (7)$$

Here, Cd, Cd_1^*, and Cd_0^* stand for Cd atoms in the 5^1S_0, 5^3P_1, and 5^3P_0 states respectively, and $CdNH_3^\dagger$ and $CdNH_3^*$ stand for unstabilized and stabilized complexes. Since the energy difference between the $^3P_1$ and $^3P_0$ states is only 6.5 kJ/mol, the reverse reaction of Reaction 4, which was not considered in the mercury–ammonia system, was added. However, in consequence, we failed to explain the present experimental results in terms of this reaction mechanism. According to the above reaction scheme, the measured phase shift, ϕ, can be separated into two parts, the one associated with the finite rate of the removal of $Cd(^3P_0)$ and $CdNH_3^\dagger$ by Reactions 4—6, and the other, with the finite rate of Reaction 7. At limiting high pressures of ammonia, the former part of the phase delay can be ignored compared with the latter one, and the limiting value of $\tan\phi/\omega$ at high pressures, $\tan\phi_\infty/\omega$, becomes equal to the reciprocal of the emitting rate, which is identical to the lifetime of the complex. It should be noted that the rates for Reactions 1—3 make no contribution to the phase difference between the resonance fluorescence (Reaction 2) and the sensitized luminescence (Reaction 7). Once the value of ϕ_∞ has been estimated from the intercept of the linear relationship in Fig. 2, we can obtain the phase delay due to Reactions 4—6 in the low-pressure region by subtracting ϕ_∞ from ϕ. It can easily be verified that this value of $(\phi_\infty - \phi)$ corresponds to the phase difference between the a.c. component of the concentration of the unstabilized complex and that of Cd $(^3P_1)$. Figure 7 shows the the value of $\omega/\tan(\phi - \phi_\infty)$ increases linearly with the ammonia pressure. The fault of the above mechanism, Reactions 1—7, is that

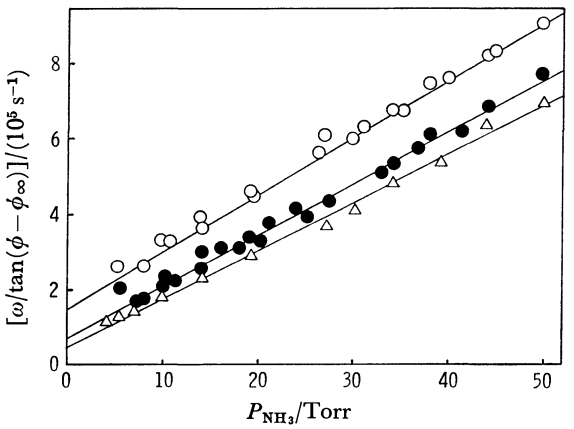

Fig. 7. Values of $\omega/\tan(\phi - \phi_\infty)$ as a function of NH_3 pressure.
△: 20 kHz, ●: 40 kHz, ○: 78 kHz.
Values for other modulation frequencies also showed similar pressure dependence.

the linear relation cannot be derived

Morten *et al.* also have presented a reaction mechanism for this system by analogy with the mercury–ammonia system; in this reaction mechanism a termolecular reaction is assumed in the formation of the complex.[7] However, the linear relationship shown in Fig. 7 cannot be interpreted in terms of their mechanism, either.

On the other hand, the following rather simple mechanism, in which only one intermediate complex is assumed, can explain the linear relations shown in Figs. 2 and 7:

$$Cd + h\nu \rightarrow Cd_1^*, \quad (1)$$

$$Cd_1^* \rightarrow Cd + h\nu, \quad (2)$$

$$Cd_1^* + NH_3 \rightarrow \text{Products}, \quad (3)$$

$$Cd_1^* + NH_3 \rightleftarrows CdNH_3^*, \quad (8)$$

$$CdNH_3^* \rightleftarrows Cd_0^* + NH_3, \quad (9)$$

$$CdNH_3^* \rightarrow Cd + NH_3 + h\nu'. \quad (7)$$

As will be shown in the Appendix, the phase difference between Reactions 2 and 7 is given by

$$\frac{\tan\phi}{\omega} = \frac{\omega^2 + k_{-9}^2[A]^2 + k_9k_{-9}[A]}{(k_9+k_7+k_{-8})\omega^2 + (k_7+k_{-8})k_{-9}^2[A]^2}, \quad (10)$$

where the rate coefficient for Reaction j is denoted by k_j, and the reverse reaction, by k_{-j}. The ammonia pressure is represented by [A]. If the following inequality is valid under the conditions that $\omega/2\pi<99$ kHz and [A]>15 Torr:

$$(k_7+k_{-8})k_{-9}^2[A]^2 \gg (k_9+k_7+k_{-8})\omega^2,$$

then Eq. 10 can be simplified as follows:

$$\frac{\tan\phi}{\omega} \simeq \frac{1}{k_7+k_{-8}} + \frac{k_9}{(k_7+k_{-8})k_{-9}}\frac{1}{[A]}. \quad (11)$$

Equation 11 corresponds to the linear plots in Fig. 2. The linear relation between $\omega/\tan(\phi-\phi_\infty)$ and [A] shown in Fig. 7 can also be derived under appropriate conditions such as

$$\omega^4 + \omega^2\{k_{-9}^2[A]^2 + (k_7+k_{-8})(k_7+k_{-8}+k_9)\} \ll \omega^2k_9k_{-9}[A] + (k_7+k_{-8})^2k_{-9}^2[A]^2$$

and

$$\omega^2 \ll k_{-9}[A](k_7+k_{-8}).$$

However, the value of $(\phi-\phi_\infty)$ as well as the value of $\tan\phi_\infty/\omega$ in this mechanism loses its simple physical meaning because of the presence of decay processes of the complex back into its initial components. Even though this scheme is consistent with the linear relations shown in Figs. 2 and 7, the nonlinearity in the Stern-Volmer plots for the quenching of the resonance line cannot be derived.

In order to overcome this discrepancy, we tried to combine these two reaction mechanisms. This was done by including the reverse reaction of Reaction 6 in the first mechanism, Reactions 1—7. Provided that the decay rate of the stabilized complex, $CdNH_3^*$, is much larger than the angular frequency of the modulation, ω, the phase difference between the concentrations of $CdNH_3^*$ and $CdNH_3^\dagger$ can be neglected and an equation similar to Eq. 11 can be obtained for the representation of $\tan\phi/\omega$. The exact expression of $\tan\phi/\omega$, according to the modified mechanism, is given by

$$\frac{\tan\phi}{\omega} = \frac{(k_{-4}+k_5+k_6[A]+k_{-6}[A]+k_7)\omega^2 + (k_{-4}+k_6[A]+k_{-6}[A]+k_7)k_{-5}^2[A]^2 + (k_{-6}[A]+k_7)k_5k_{-5}[A]}{-\omega^4 + \omega^2\{k_{-4}k_7+k_5k_7+(k_{-4}k_{-6}+k_5k_{-6}+k_6k_7-k_5k_{-5})[A]-k_{-5}^2[A]^2\} + \{k_{-4}k_7+(k_{-4}k_{-6}+k_6k_7)[A]\}k_{-5}^2[A]^2}. \quad (12)$$

If the following inequalities can be assumed

$$k_{-6}[A] \gg k_7, \ \frac{\omega^2}{k_{-4}}, \ \frac{k_5\omega^2}{k_{-4}k_{-5}[A]}, \quad (13)$$

$$k_{-5}^2[A]^2 \gg \frac{k_5\omega^2}{k_{-4}}, \ \left\{1+\frac{k_5}{k_{-4}+(k_6+k_{-6})[A]}\right\}\omega^2, \quad (14)$$

Eq. 12 can be approximated by the following equation:

$$\frac{\tan\phi}{\omega} \simeq \frac{k_6+k_{-6}}{k_{-4}k_{-6}+k_6k_7} + \frac{k_{-4}k_{-5}+k_5k_{-6}}{(k_{-4}k_{-6}+k_6k_7)k_{-5}}\frac{1}{[A]}. \quad (15)$$

The validity of Eqs. 13 and 14 will be checked in the Appendix. The intercept and the slope of the relationship shown in Fig. 2 correspond to the first and the second terms of the right-hand side of Eq. 15 respectively. The intercepts and the slopes in Fig. 6 also give the relations among the rate constants in the cases of the cadmium–aliphatic amine systems, which are summarized in Table 1.

TABLE 1. RELATIONS AMONG THE RATE CONSTANTS DEDUCED FROM Eq. 15

	$\frac{k_{-4}k_{-5}+k_5k_{-6}}{k_{-5}(k_{-4}k_{-6}+k_6k_7)}$/$10^{-5}$ s Torr	$\frac{k_6+k_{-6}}{k_{-4}k_{-6}+k_6k_7}$/$10^{-7}$ s
NH_3	7.1±0.1	6.0±0.3
CH_3NH_2	4.2±0.1	9.6±0.2
$(CH_3)_2NH$	1.8±0.2	2.9±0.8
$(CH_3)_3N$	1.4±0.1	5.7±0.2

It should be noted that, although the reaction mechanism proposed in this paper is a little different from that we presented in previous papers, where the reverse reaction of Reaction 6 is not considered,[8-9] this difference has no essential influence on the steady-state treatment. Tiny change in the meaning of the parameters has to be taken into account.

Because of the presence of the reverse reaction of Reaction 6, we could not determine the radiative lifetime of the complex, $CdNH_3^*$. The determination of the lifetime would be very difficult, even if the phase angle of the $Cd(^3P_0)$ absorption could be measured. In the mercury-photosensitized luminescence of ammonia, the radiative lifetime of $HgNH_3^*$ could be precisely determined to be (1.4±0.1) μs.[6] The difficulty in determining the radiative lifetime of $CdNH_3^*$ obviously results from the small energy difference between the $Cd(^3P_1)$ and $Cd(^3P_0)$ states.

Appendix

Derivation of Eq. 10. When the initial intensity of the resonance radiation from the lamp is modulated with the angular frequency, ω, the concentration of the excited species

oscillates with the same frequency. In the cases of Reactions 1—3 and 7—9, the concentration may be written as follows:

$$[Cd_1^*] = \bar{a} + \tilde{a}e^{i\omega t},$$
$$[Cd_0^* = \bar{b} + \tilde{b}e^{i(\omega t-\theta)},$$
$$[CdNH_3^*] = \bar{c} + \tilde{c}e^{i(\omega t-\phi)}.$$

Here, the d.c. and a.c. components of the concentration are respectively expressed by the first and the second terms of the right-hand sides. The phase angles of $[Cd_0^*]$ and $[CdNH_3^*]$ are denoted by θ and ϕ. On the basis of Reactions 1—3 and 7—9, the following differential equations can be obtained:

$$\frac{d[Cd_0^*]}{dt} = i\omega\tilde{b}e^{i(\omega t-\theta)}$$
$$= k_9(\bar{c}+\tilde{c}e^{i(\omega t-\phi)}) - k_{-9}[A](\bar{b}+\tilde{b}e^{i(\omega t-\theta)}),$$
$$\frac{d[CdNH_3^*]}{dt} = i\omega\tilde{c}e^{i(\omega t-\phi)}$$
$$= k_8[A](\bar{a}+\tilde{a}e^{i\omega t}) + k_{-9}[A](\bar{b}+\tilde{b}e^{i(\omega t-\theta)}) - (k_9+k_7+k_{-8})(\bar{c}+\tilde{c}e^{i(\omega t-\phi)}).$$

Separating the time-dependent parts, we obtain

$$(i\omega+k_{-9}[A])\tilde{b}e^{-i\theta} - k_9\tilde{c}e^{-i\phi} = 0,$$
$$-k_{-9}[A]\tilde{b}e^{-i\theta} + (i\omega+k_9+k_7+k_{-8})\tilde{c}e^{-i\phi} = k_8[A]\tilde{a}.$$

Equation 10 can easily be derived from these simultaneous equations. Equation 12 can also be obtained in a similar manner.

Validity of Eqs. 13 and 14. In order to explain theoretically the observed pressure dependence of the phase angle, ϕ, in Fig. 1, we tried to find a set of parameters according to the reaction mechanism proposed. The following values are some examples: $k_{-4}=5.5\times10^6$ s^{-1}, $k_5=3.8\times10^8$ s^{-1}, $k_{-5}=9.1\times10^5$ s^{-1} Torr^{-1}, $k_6=2.2\times10^7$ s^{-1} Torr^{-1}, $k_{-6}=8.6\times10^6$ s^{-1} Torr^{-1}, and $k_7=1.7\times10^5$ s^{-1}. The solid lines in Fig. 1 were drawn according to Eq. 12 by using these values. From these values, the validity of Eqs. 13 and 14 can easily be derived. Since the observable value is only the phase difference between the two kinds of emission, the resonance fluorescence at 326.1 nm and the luminescence from the excited complex, we cannot verify that the above set of parameters is unique.

References

1) C. G. Freeman, M. J. McEwan, R. F. C. Claridge, and L. F. Phillips, *Chem. Phys. Lett.*, **9**, 578 (1971); C. G. Freeman, M. J. McEwan, R. F. C. Claridge, and L. F. Phillips, *Trans. Faraday Soc.*, **67**, 2004 (1971).

2) A. B. Callear, J. H. Connor, and J. Koskikallio, *J. Chem. Soc., Faraday Trans. 2*, **70**, 1542 (1974); A. B. Callear and C. G. Freeman, *Chem. Phys.*, **23**, 343 (1977).

3) A. B. Harker and C. S. Burton, *J. Chem. Phys.*, **63**, 885 (1975).

4) K. Luther, H. R. Wendt, and H. E. Hunziker, *Chem. Phys. Lett.*, **33**, 146 (1975).

5) T. Hikida, M. Santoku, and Y. Mori, *Chem. Phys. Lett.*, **55**, 280 (1978).

6) H. Umemoto, S. Tsunashima, and S. Sato, *Chem. Phys. Lett.*, **53**, 521 (1978).

7) P. D. Morten, C. G. Freeman, M. J. McEwan, R. F. C. Claridge, and L. F. Phillips, *Chem. Phys. Lett.*, **16**, 148 (1972).

8) S. Yamamoto, S. Tsunashima, and S. Sato, *Bull. Chem. Soc. Jpn.*, **48**, 1172 (1975).

9) S. Yamamoto and S. Sato, *Bull. Chem. Soc. Jpn.*, **48**, 1382 (1975).

10) S. Yamamoto, K. Tanaka, and S. Sato, *Bull. Chem. Soc. Jpn.*, **48**, 2172 (1975).

11) "C. R. C. Handbook of Chemistry and Physics," **50**, D-167 (1969—1970).

12) L. F. Phillips, "Progress in Reaction Kinetics," Vol. 7, Pergamon Press, London (1973), Part 2.

13) W. H. Breckenridge and T. W. Broadbent, *Chem. Phys. Lett.*, **29**, 421 (1974).

The Mechanism of the CO Oxidation over Polycrystalline Platinum

Tatsuo MATSUSHIMA

The Research Institute for Catalysis, Hokkaido University, Sapporo 060

(Received December 15, 1977)

The kinetics of the CO oxidation has been studied on polycrystalline platinum at various partial pressures, total pressures, and temperatures; $0.1<P_{CO}/P_{O_2}<5$, $10^{-6}<P<10^{-3}$ Pa, and $300<T<900$ K. The reaction was first-order in CO and zero-order in O_2 for low pressures of CO, while it was inhibited by CO above a certain critical CO pressure, which increased with an increase in the O_2 pressure and temperature. Above that CO pressure, the reaction was first-order in O_2 and negative-order in CO. The amount of CO adsorbed was determined during the reaction with a flash-desorption technique. Above the critical CO pressure it was almost equal to that determined in the CO/Pt equilibrium system. It decreased sharply around the CO pressure and was very small at lower pressures. The kinetic behavior can be explained in terms of a Langmuir-Hinshelwood process and a change in the rate-limiting step.

Numerous investigations have been reported on CO oxidation over single-crystal and polycrystalline-platinum surfaces.[1–14] Different kinetic behavior at the steady state was observed below and above about 550 K, and the reaction orders with respect to O_2 and CO depend strongly on the partial pressure ratio.[1] Several transient techniques[5–14] have provided ample evidence that CO_2 is formed through two elementary processes: an Eley-Rideal process (E-R), CO(phys. ads.)+O(a)→CO_2, and a Langmuir-Hinshelwood process (L-H), CO(chem. ads.)+O(a)→CO_2. According to measurements with AES[10,11] and secondary-ion mass-spectroscopy,[15] CO(a) is much less than O(a) when $P_{CO}<P_{O_2}$, while the reverse is true for $P_{CO}>P_{O_2}$. Generally, the kinetics at the steady state has been explained in terms of the E-R process.[3–5] On the contrary, though, this work will report that the inhibitory region is narrowed with an increase in the temperature and will ascribe this to a contribution from the L-H process.

Experimental

The experimental apparatus and procedures were essentially the same as those reported previously.[16] A polycrystalline platinum foil ($30\times4\times0.05$ mm) was used as a catalyst. Prior to the experiments it was exposed to 1×10^{-4} Pa of oxygen at 1400 K for several hours, and then flashed to 1600 K for a few tens of minutes. Several repetitions of this treatment were sufficient to establish stable catalyst behavior. A Bayard-Alpert gauge was used for only the calibration of the sensitivity of the mass spectrometer. The observed $m/e=44$ signal was proportional to the CO_2 production rate, since the system was continuously pumped. All of these experiments utilize a hot-filament electron supply in the mass spectrometer. There is some background reaction on the filament, which was measured separately with the substrate at room temperature and subtracted from the results of measurements made at the operating temperatures.

Results

Since CO_2 is not adsorbed under the conditions used here[17] it is assumed that CO_2 interacts so weakly with the surface that the partial pressure exerts no influence on the rate of the reaction.

Temperature Dependence. The oxidation rate depended strongly on the substrate temperature. The profile was characterized by an optimum around the CO desorption temperature. Some typical results are shown in Fig. 1. For $P_{CO}<P_{O_2}$, the rate showed an increase similar to the other case below a certain critical temperature, where it increased discontinuously up to the maximum level, which was constant over a wide range of temperatures. The activation energies were estimated to be 55—84 kJ mol^{-1}, zero, and negative below, around, and above the optimum respectively.

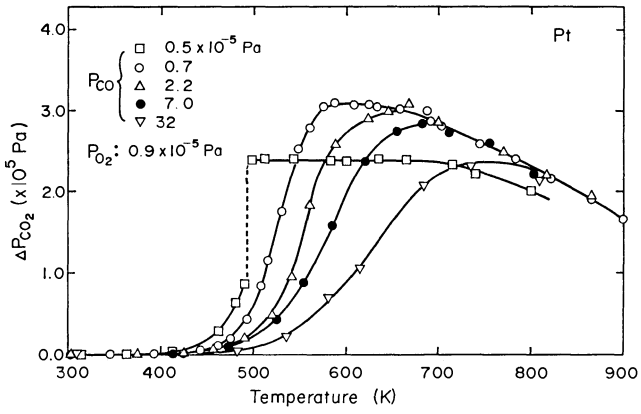

Fig. 1. Variation of the rate of CO_2 production at the steady state with temperature at various fixed pressures of CO and O_2. The vertical dotted line at 0.5×10^{-5} Pa of CO shows a discontinuous change of CO_2 production.

CO Pressure Dependence. The results are summarized in Figs. 2 and 3. These figures are both characterized by sharp transitions at a certain critical CO pressure. Below that pressure the reaction was first-order in CO and independent of the temperature, while above that pressure it was negative-order in CO and very sensitive to the temperature. The rate dropped discontinuously at the critical CO pressure, as is shown by the vertical dotted lines. The CO pressure shifted toward low values with a decrease in the temperature, and toward high values with an increase in the oxygen pressure.

O_2 Pressure Dependence. The results are displayed in Fig. 4. Like carbon monoxide, the oxygen-pressure dependence showed sharp transitions at some oxygen pressure. The rate showed first-order and zero-order behavior below and above the transition pressure respectively. Such sharp breaks in the CO and O_2 pres-

sure dependences were in general agreement with those reported by Bonzel and Ku for Pt (110), although they reported only turning points at a fixed high temperature.

CO Adsorption during the Catalyzed Reaction. The amount of CO adsorbed was determined in the course of the catalyzed reaction by means of flash desorption.[16] A steady-state $CO/O_2/Pt$ system was established at a fixed temperature, and then the substrate was heated while the CO peak was monitored. Afterward, the system was returned to the same steady state and the CO_2 peak was recorded during a second flash-desorption experiment. Figure 5 shows some typical transients of CO and CO_2 generated by flash desorption. The desorption of CO was complete around the final temperature, 900 K. The dashed lines in Fig. 5 are arbitrarily drawn as point-by-point reference lines for constructing a mirror image of the CO_2 production curve. Assuming that the only sink for CO, aside from the pump, is its conversion to CO_2, and that the only source of CO_2 is CO, it is clear as a result of the stoichiometry that the cross-hatched area gives the amount of CO adsorbed initially.[16,19] Figure 6 shows the CO adsorption at 468 and 526 K with 1.7×10^{-5} Pa of oxygen and without oxygen. Above the critical CO pressure, the coverage during the reaction equalled the value measured in the CO/Pt non-working system; *i.e.*, the adsorption-desorption process of CO was in equilibrium. It decreased sharply around the CO pressure and became very small under lower pressures. Note the marked difference between the CO/Pt non-working system and the $CO/O_2/Pt$ working system below the critical CO pressure. At a low temperature, the sharp drop occurred at lower CO pressures.

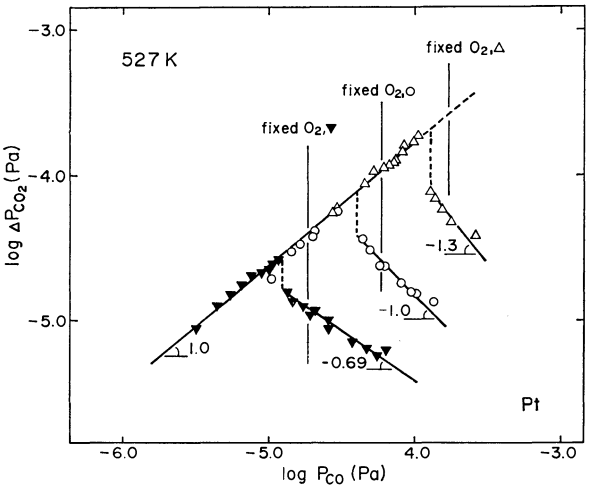

Fig. 2. Variation of the rate of CO_2 production with CO pressure at 527 K and various fixed oxygen pressures. The vertical bars indicate the fixed oxygen pressures. ▼: 1.9×10^{-5} Pa, ○: 6.0×10^{-5} Pa, △: 1.7×10^{-4} Pa. The reaction orders with respect to CO are indicated along the linear portion of each curve. The vertical dotted lines show sharp drops in the CO_2 production.

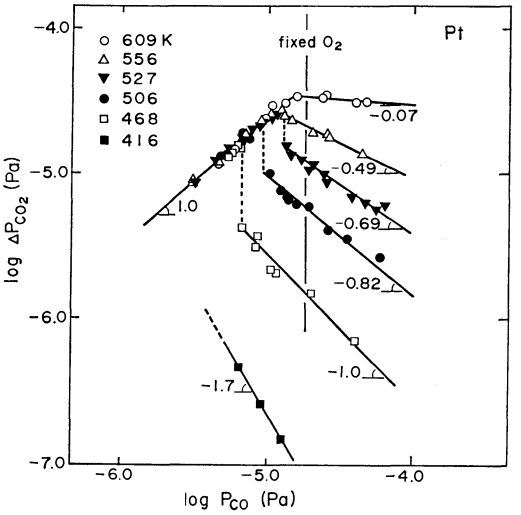

Fig. 3. Variation of the rate of CO_2 production with CO pressure at various temperatures, under a fixed O_2 pressure of 1.9×10^{-5} Pa. There are sharp transitions of the rate law at some critical CO pressure drawn by vertical dotted lines.

Discussion

The Activation Energy. The temperature dependence in Fig. 1 is qualitatively similar to the results reported on single-crystal ((100)[1] and (111)[12]) and on polycrystalline[2,13] platinum. Similar results have also been reported for other metal surfaces: Pd,[18,19] Ni,[26] Ir,[27–30] and Ru.[31,32] Below the optimum, Bonzel and Ku[1] concluded that the rate-limiting step was the desorption of CO(a) from the surface; they reached this conclusion by comparing the apparent activation energy with the enthalpy for the CO desorption. Recent studies of the L-H process[5] have shown that the rate at 415 K in the presence of 1×10^{-6} Pa of oxygen is comparable to that of CO thermal desorption. Under higher pressures of O_2, the former contributes more to the removal of CO(a). In general, under the experimental conditions employed here CO(a) can be removed mainly *via* the L-H process. The adsorption-desorption process of CO is in equilibrium below the optimum, and the surface area available for O_2 adsorption increases with the temperature. The apparent activation energy decreases with an increase in the CO pressure and becomes much less than the enthalpy of CO desorption, 120 kJ mol^{-1},[20–23,25] in contrast with the model, in which the CO desorption is rate-limiting. Around the optimum, the amount of CO(a) is much less than that in equilibrium with the CO partial pressure. The rate is limited by the CO collision frequency, and the reaction probability of CO is close to unity.[11] Thus, the activation energy is zero. Above the optimum, the surface is covered by O(a) and CO(a)≪O(a). When $P_{CO}>P_{O_2}$ the rate is limited by the O_2 adsorption; the decrease is attributed to the decrease in oxygen coverage through the thermal desorption.[11] When $P_{CO}<P_{O_2}$, the rate begins to decrease at temperatures as high as 730 K, since the CO collision is rate-limiting and the decrease in the surface oxygen near full coverage does not cause any decrease in the CO_2 production.[8]

Kinetic Behavior in Terms of Adsorbed Species. The

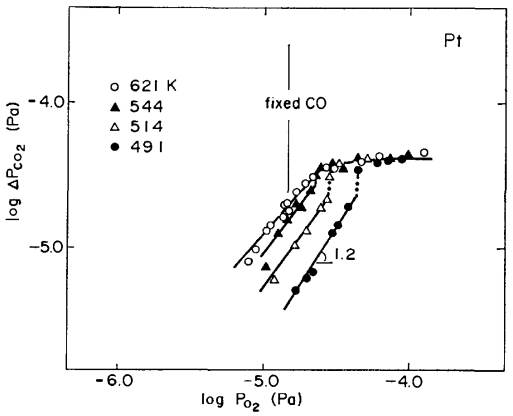

Fig. 4. Variation of the rate of CO_2 production with O_2 pressure at various temperatures under a fixed CO pressure of 1.3×10^{-5} Pa. The vertical dotted lines show sharp jumps in the CO_2 production.

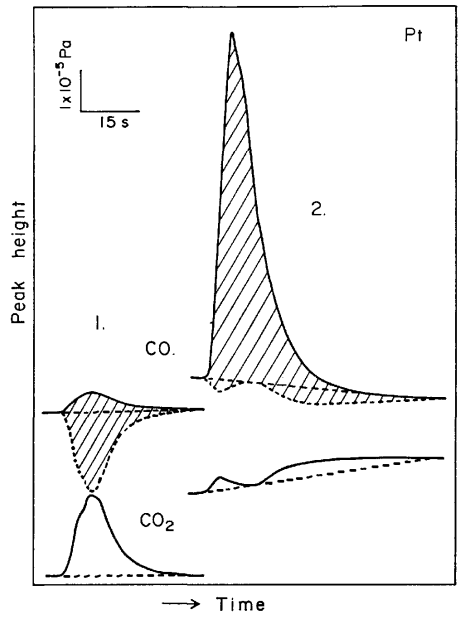

Fig. 5. Flash desorption peaks of CO and CO_2 induced by heating the substrate from a kinetic steady state at 468 K to a final temperature of 900 K. The steady state pressures (in pascals) of CO, O_2, and CO_2 for each pair of peaks are as follows in the form (P_{CO}, P_{O_2}, P_{CO_2}), (1) (4.8×10^{-6}, 1.7×10^{-5}, 1.3×10^{-5}): (2) (3.7×10^{-5}, 1.7×10^{-5}, 3.7×10^{-6}). Peaks are shifted with each other for easier viewing.

results shown in Figs. 2, 3, and 4 strongly suggest that a change in the rate-limiting step occurs around the critical CO pressure. At CO pressures below the critical value, CO(a) was not accumulated up to the equilibrium level. This fact shows that the L-H process plays a main role in eliminating CO(a) from the surface under working conditions and contributes to the CO_2 production. The rate-limiting step is the CO collision with the oxygen-covered surface. Thus, the reaction is first-order in CO and zero-order in O_2. On the other hand, above the critical CO pressure the amount of CO(a) was almost equal to that observed in the CO/Pt non-working system and O(a)≪CO(a).[11]

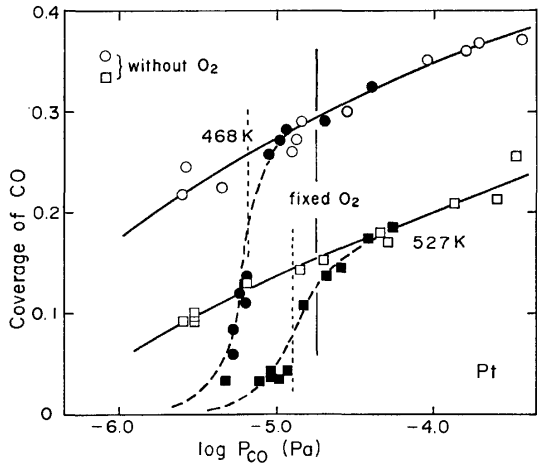

Fig. 6. CO adsorption isotherm determined by flash desorption in the presence and absence of oxygen. (○, □): without oxygen, (●, ■): with 1.7×10^{-5} Pa of oxygen. The coverage was defined as the CO peak area relative to the maximum area which was obtained by flashing from room temperature. The vertical dotted lines show CO transition pressures.

The rate is limited by the O_2 adsorption, which is severely retarded by CO(a). Thus, the reaction should be first-order in oxygen and negative-order in CO. The magnitude of the negative order should increase with an increase in the CO pressure and also with a decrease in the temperature, as was actually observed.

CO Inhibition Region. The inhibition becomes large as the temperature decreases, but not because the heat of adsorption of CO is larger than that of oxygen, since just the reverse is true.[20–22,25,34,36–39] Rather, it arises because the L-H process, which plays a role in eliminating CO(a) from the surface, is slower than the CO adsorption. The latter needs little activation energy, while at low temperatures the former requires a significant activation energy.[5] At temperatures as high as 550 K, where the L-H process is very fast, the boundary of the CO inhibition region is determined by the balance between the supply rates of oxygen and carbon monoxide onto the surface. At lower temperatures it can be ascertained by a comparison of the rate of the L-H process with the adsorption rate of CO. Below, a simple model will be used in the estimation of the boundary pressure. The four experimental situations involve different conditions with regard to the temperature, the relative collision frequency, and the rate of the L-H process. In the A(1) region the CO collision rate is greater than the maximum oxygen adsorption rate, while in the B(1) region the reverse is true. At relatively low temperatures the B(1) region is divided further into the A(2) and B(2) regions. In the A(2) region the CO collision rate is greater than the maximum rate of the L-H process, while in the B(2) region the reverse is true. We assume first of all that the reaction probability per CO collision is unity provided a steady-state oxygen coverage exists.[11] Second, we take the sticking probability of O_2 at zero coverage to be 0.36.[11] Finally, we assume that the variation in the sticking probability with the coverage

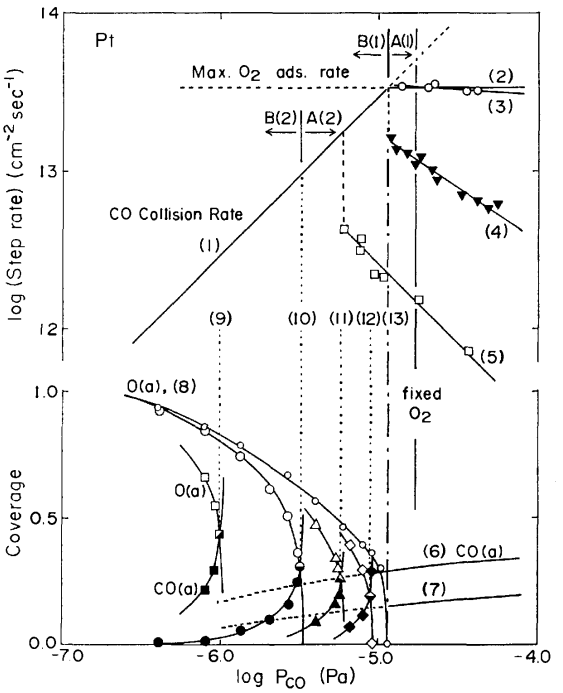

Fig. 7. A model of the reaction structure of the CO oxidation. At higher temperatures, the CO_2 production rate should follow line(1) and then line(2), as a function of CO pressure. At lower temperatures, the rate is retarded by CO(a) above critical CO pressure as shown by vertical dashed-dotted line(13) at relatively high temperatures and vertical dotted lines (9—12) at various lower temperatures. (1) CO collision rate, (2): maximum O_2 adsorption rate, (3)—(5): CO_2 production rates observed at 609, 527 and 468 K, (6), (7): CO adsorption isotherm observed at 468 and 526 K, (8): oxygen coverage when $CO(a) \ll O(a)$, (9)—(13): calculated boundary CO pressures at 313, 362, 400, 468, and above 500 K, respectively. Open and closed symbols in the lower panel show calculated coverages of O(a) and CO(a) at temperatures shown above.

is given by the data in Fig. 1 previously reported in Ref. 11. The results analyzed are presented in Fig. 7. For comparison with the experimental data, the rates observed in the inhibition region at 609, 527, and 468 K are also shown in the figure. The vertical position of the latter was shifted in such a way that the maximum CO_2 production observed was at the maximum O_2 adsorption rate calculated.

High Temperatures: The L-H process is very fast. The boundary between A(1) and B(1) occurs when $P_{CO}/P_{O_2}=0.6$. In the A(1) region the lifetime of O(a) is very short and no steady-state concentration of O(a) can accumulate. Kinetically, the adsorption of oxygen is rate-limiting. The reaction is zero-order in CO at temperatures where CO can not be adsorbed. At lower temperatures, where CO can be adsorbed, the CO_2 production drops when $P_{CO}/P_{O_2}=0.6$ and is negative-order in CO. In the B(1) region the rate at which oxygen atoms appear on the surface exceeds the CO collision rate. The reaction rate will be determined by the CO collision frequency. Since the O_2 pressure is known, the O_2 sticking probability can be determined,[11] and then the steady-state oxygen coverage can be predicted. The coverage calculated is shown as a function of the CO pressure in Fig. 7.

Low Temperatures: The rate of the L-H process is not fast enough to eliminate enough CO(a) for it to become negligible. The critical CO pressure should appear at the boundary between A(2) and B(2). Most of the CO(a) will be removed as CO_2 through the L-H process whenever the O_2 pressure is significant.[5] An upper boundary on the amount of CO(a) can be set by assuming that all the CO_2 arises from the L-H process and that the upper boundary is to be set by the CO collision frequency. As the rate constant of the L-H process has been deduced by Bonzel and Burton,[5] an upper boundary for the product, $\theta_{O(a)} \times \theta_{CO(a)}$, can be calculated ($\theta_1$ is defined as the coverage). The $\theta_{O(a)}+\theta_{CO(a)}$ sum can be estimated by using the procedures outlined in the former section, assuming that CO(a) influences the O_2 sticking probability in the same way as does O(a). The calculated coverages are shown in Fig. 7. After the two curves cross, the amounts change sharply to zero for O(a) and infinite for CO(a). Above that point the CO coverage must be equal to that at equilibrium with gaseous CO. Thus, the boundary CO pressure can be determined; it is shown by vertical dotted lines at various temperatures. In the A(2) region the adsorption of oxygen is still rate-limiting. Two adjacent empty sites are necessary for the dissociative adsorption of oxygen, and its rate is severely retarded as CO(a) increases. Therefore, the CO_2 production undergoes a very sharp drop in passing from the B(2) region to the A(2) region.

The sharp drop in the CO_2 production at 527 K occurred at the CO pressure predicted in the high-temperature region. The rate observed at 468 K, however, dropped at a CO pressure 30% less than that predicted. Generally, the criticalCO pressure predicted at low temperatures is 30—40% higher than that observed, as may be seen in Fig. 7. This discrepancy may be due to inadequacies in representing the coverage dependence of the sticking probability of oxygen as the same for O(a) and CO(a).

This work was supported in part by the Matsunaga Science Foundation.

References

1) H. P. Bonzel and R. Ku, *J. Vac. Sci. Technol.*, **9**, 663 (1972).
2) A. W. Sklyarov, J. Völter, and I. I. Tretjakov, *Z. Anorg. Allg. Chem.*, **396**, 129 (1973).
3) I. Langmuir, *Trans. Faraday Soc.*, **17**, 621 (1922).
4) H. Heyne and F. C. Tompkins, *Proc. R. Soc. London, Ser., A*, **292**, 460 (1966).
5) H. P. Bonzel and R. Ku, *Surf. Sci.*, **33**, 91 (1972); H. P. Bonzel and J. J. Burton, *Surf. Sci.*, **52**, 223 (1975).
6) Y. Nishiyama and H. Wise, *J. Catal.*, **32**, 50 (1974).
7) M. Alnot, J. Fusy, and A. Cassuto, *Surf. Sci.*, **57**, 651 (1976).
8) J. M. White and A. Golchet, *J. Chem. Phys.*, **66**, 5744 (1977).

9) R. Ducros and R. P. Merrill, *Surf. Sci.*, **55**, 227 (1976).
10) H. Hopster, H. Ibach, and G. Comsa, *J. Catal.*, **46**, 37 (1977).
11) T. Matsushima, D. B. Almy, and J. M. White, *Surf. Sci.*, **67**, 89 (1977).
12) R. L. Palmer and J. N. Smith, Jr., *J. Chem. Phys.*, **60**, 1453 (1974); *Catal. Rev. Sci. Eng.*, **12**, 279 (1975).
13) N. Pacia, A. Cassuto, A. Pentenero, and B. Weber, *J. Catal.*, **41**, 455 (1976).
14) W. L. Winterbotton, *Surf. Sci.*, **36**, 205 (1973).
15) V. L. Kuchayev, Abstr. No. A25, 6th Int. Congress on Catalysis, London, 1976.
16) T. Matsushima and J. M. White, *J. Catal.*, **39**, 265 (1975); T. Matsushima, D. B. Almy, D. C. Foyt, J. S. Close, and J. M. White, *ibid.*, **39**, 277 (1975); T. Matsushima and J. M. White, *ibid.*, **40**, 334 (1975); T. Matsushima, C. J. Mussett, and J. M. White, *ibid.*, **41**, 397 (1976).
17) P. R. Norton, *Surf. Sci.*, **44**, 624 (1974); P. R. Norton and P. J. Richards, *Surf. Sci.*, **49**, 567 (1975).
18) G. Ertl and P. Rau, *Surf. Sci.*, **15**, 443 (1969); G. Ertl and J. Koch, *Z. Phys. Chem. N. F.*, **69**, 323 (1970); G. Ertl and J. Koch, Proc. 5th Int. Congress on Catalysis (ed Hightower), North-Holland Elsevior, New York (1973), p. 969.
19) J. S. Close and J. M. White, *J. Catal.*, **36**, 185 (1975).
20) G. Ertl, M. Neumann, and K. M. Streit, *Surf. Sci.*, **64**, 393 (1977).
21) R. W. McCabe and L. D. Schmidt, *Surf. Sci.*, **66**, 101 (1977).
22) R. A. Shigeishi and D. A. King, *Surf. Sci.*, **58**, 379 (1976).
23) C. M. Comrie and R. M. Lambert, *J. Chem. Soc., Faraday Trans. 1*, **72**, 1659 (1976).
24) P. Kisliuk, *J. Phys. Chem. Solids*, **3**, 95 (1957).
25) W. H. Weinberg, C. M. Comrie, and R. M. Lambert, *J. Catal.*, **41**, 489 (1976).
26) H. H. Madden, J. Küppers, and G. Ertl, *J. Chem. Phys.*, **58**, 3401 (1973).
27) V. P. Ivanov, G. K. Boreskov, V. I. Savchenko, W. F. Egelhoff, Jr., and W. H. Weinberg, *Surf. Sci.*, **61**, 377 (1976); *J. Catal.*, **48**, 269 (1977).
28) D. I. Hagen, B. E. Nieuwenhuys, G. Rovida, and G. A. Somorjai, *Surf. Sci.*, **57**, 632 (1976).
29) K. Christmann and G. Ertl, *Z. Naturforsch., Teil A*, **28**, 1144 (1973).
30) J. Küppers and A. Plagge, *J. Vac. Sci. Technol.*, **13**, 259 (1976).
31) T. E. Madey, H. A. Engelhardt, and D. Menzel, *Surf. Sci.*, **48** 304 (1975).
32) P. D. Reed, C. M. Comrie, and R. M. Lambert, *Surf. Sci.*, **64**, 603 (1977).
33) G. Ertl and M. Neumann, *Z. Phys. Chem. N. F.*, **90**, 127 (1974).
34) Y. K. Peng and P. T. Dawson, *Can. J. Chem.*, **52**, 3507 (1974).
35) P. R. Norton, *Surf. Sci.*, **47**, 98 (1975).
36) G. Kneringer and F. P. Netzer, *Surf. Sci.*, **49**, 125 (1975).
37) D. M. Collins, J. B. Lee, and W. E. Spicer, *Surf. Sci.*, **55**, 389 (1976).
38) K. Schwaha and E. Bechtold, *Surf. Sci.*, **65**, 277 (1977).
39) M. Wilf and P. T. Dawson, *Surf. Sci.*, **65**, 399 (1977).

Electron Trapping in Irradiated NaOH Ices. Electrons Stabilized at 4 K in Shallow Traps Associated with Na^+ Cations

Jerzy KROH,** Shoji NODA, Kiyomi YOSHIDA, and Hiroshi YOSHIDA*

Faculty of Engineering, Hokkaido University, Kita-ku, Sapporo 060

(Received December 19, 1977)

Studies on electron trapping in 8 and 18 mol·dm^{-3} NaOH glassy ices were performed by means of 4 K γ-irradiation technique. The optical absorption spectra of e^-_t were found to be considerably red-shifted and broader compared with the spectra in the ices irradiated and examined at 77 K. This trend was more pronounced for the concentrated sample. The red part of the broad spectra was removed either by photobleaching with light of $\lambda > 800$ nm at 4 K or by thermally annealing at 77 K. These results, combined with electron spin resonance data, lead to the conclusion that the shallow electron traps responsible for the red part of the spectra are formed with the participation of Na^+ cations in the alkaline ices.

Electron stabilization in irradiated glassy alkaline ices has been commonly interpreted in terms of solvation of excess electrons by dipoles of H_2O molecules ("dipolar trap"), and the role of alkali metal cations has been ignored in most models.[1] However, taking into account the relatively high concentration of the cations in most experiments (usually *ca.* 20 mol%), such picture is hardly acceptable and does not appeal to chemical intuition. In 1964, Kevan, who examined the electron spin resonance (ESR) spectra of γ-irradiated 2—5 mol·dm^{-3} LiOH, NaOH, and KOH ices, indicated a contribution of the alkali metal cation interaction to the ESR line width and suggested that "the charge density of trapped electrons in alkaline ices encompasses several water molecules and one or more cations".[2]

Recently, Polewoj and one of the present authors (J. K.) reported optical absorption spectra of electrons trapped at 77 K in highly concentrated (up to 20 mol·dm^{-3}) NaOH ice.[3,4] The properties of the spectra were tentatively explained by the existence of relatively shallow and unstable traps due to the formation of a cation-electron pair ("cationic trap"), $(Na^+\cdots e^-)_t$, whose absorption maximum lay at *ca.* 750 nm, as compared with the maximum at 585 nm in 10 mol·dm^{-3} NaOH ice. Here we provide further data, based mainly on optical absorption measurements at 4 K, which demonstrate the increasing variety of trap depths at high NaOH concentrations.

Experimental

Glassy NaOH ice samples of two concentrations, 8 and 18 mol·dm^{-3}, of NaOH were prepared in the form of windowless discs, 0.2 cm thick, by rapid cooling in liquid nitrogen. A modified version of the liquid helium cryostat described previously[5] was used for measurements at 4 K. The irradiations were carried out in dark with ^{60}Co γ-rays at a dose rate of *ca.* 0.9 Mrad/h at 77 K or at *ca.* 0.25 Mrad/h at 4 K. The total dose applied was *ca.* 0.2 Mrad.

The optical absorption spectra were recorded using a double-beam recording spectrophotometer with a twin photodetection system (Shimadzu, Model MPS-5000). ESR experiments were carried out with a conventional X-band spectrometer (JEOL, Model JES-3M) for the ice sample sealed in thin quartz tubes.

The irradiated samples were photobleached with light from a 500 W Xe lamp through a 420±50 nm band-pass filter or an 800 nm cut-off filter. Typically the samples were photobleached for 3 min for optical absorption measurements and for 15 min for ESR measurements.

Results and Discussion

Effect of Temperature on Optical Absorption Spectra. The optical absorption spectra due to trapped electrons are presented in Figs. 1 and 2 for 18 M and 8 M ice samples (containing 18 mol·dm^{-3} and 8 mol·dm^{-3} NaOH) irradiated and also examined at 4 and 77 K. In each case, the spectrum at 4 K is wider and red-shifted compared with the spectrum at 77 K. At 4 K the 8 M sample displays the absorption maximum at 650 nm and the spectral halfwidth is 1.4 eV. The former value is in complete agreement with that reported by Hase *et al.*,[6] whereas the latter value is somewhat lower. The 18 M sample at 4 K has a maximum at 690 nm and a halfwidth of 1.65 eV. The halfwidths at 4 K are *ca.* 1.3 times larger than those at 77 K for both samples. On the other hand, however, no dependence on the temperature of measurement, when examined at 77 and 4 K, is seen in the spectra of the samples irradiated at 77 K. This con-

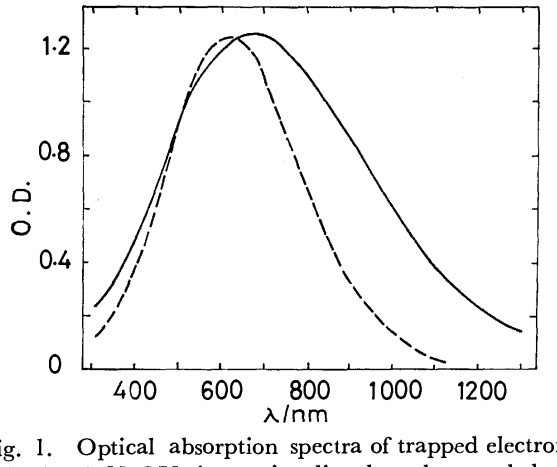

Fig. 1. Optical absorption spectra of trapped electrons in 18 M NaOH ices γ-irradiated and recorded at 4 K, —— and at 77 K, ----. The 77 K spectrum is normalized with the 4 K spectrum at peak height.

** Visiting Professor, sponsored by Japanese Society for Promotion of Science, from Technical University, Łódź, Poland.

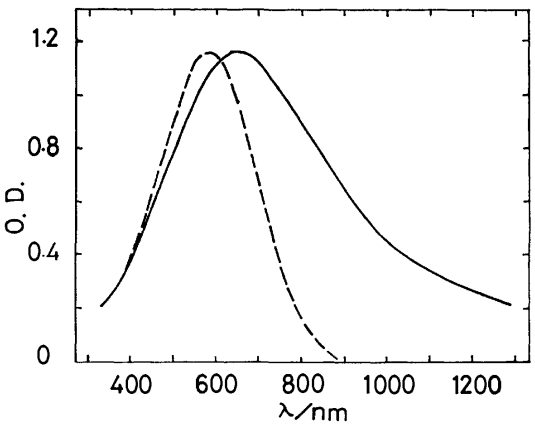

Fig. 2. Optical absorption spectra of trapped electrons in 8 M NaOH ices γ-irradiated and recorded at 4 K, —— and at 77 K, ----. The 77 K spectrum is normalized with the 4 K spectrum at peak height.

trast with blue-shift of the spectrum of trapped electrons in an ethanol glass observed upon cooling form 77 to 4 K after the irradiation at 77 K.[7]

Thermal bleaching, accomplished by transfer of the samples irradiated at 4 K into liquid nitrogen for 2 min and recording the spectra again at liquid helium temperature, led to the blue-shift and narrowing of the spectra. Thus, for the 18 M sample the absorption maximum shifts from 690 to 630 nm and the half-width decreases 1.1 times, whereas the 8 M sample shows the shift from 650 to 580 nm and the decrease in halfwidth of nearly 1.3 times. The effect of the thermal bleaching is more pronounced for the dilute sample than for the concentrated one.

Photobleaching of the Optical Absorption Spectra. The longer wavelength regions of the 4 K spectra are readily bleached by red light of $\lambda > 800$ nm, so that the absorption maxima effectively shift to the blue. The subsequent photo-bleaching with blue light of $\lambda \sim 420$ nm partially restores the longer wavelength regions and results in the red-shift of the maxima. The observed wavelength (transition energy) changes of the absorption maxima during the selective photo-bleaching for the 8 and 18 M samples are

$$\underset{(1.91\ \text{eV})}{650\ \text{nm}} \xrightarrow{\text{red light}} \underset{(2.16\ \text{eV})}{575\ \text{nm}} \xrightarrow{\text{blue light}} \underset{(1.98\ \text{eV})}{625\ \text{nm}}$$

and

$$\underset{(1.81\ \text{eV})}{685\ \text{nm}} \xrightarrow{\text{red light}} \underset{(2.10\ \text{eV})}{590\ \text{nm}} \xrightarrow{\text{blue light}} \underset{(1.77\ \text{eV})}{700\ \text{nm}}$$

respectively, and the shifts are more pronounced for the concentrated sample, whose recorded spectra are given in Fig. 3.

The changes of the spectral shape caused by photobleaching were first reported by Ershov *et al.*,[8] but they are not very distinct at 77 K. For 10 M NaOH ice, the shifts of the absortion maxima reported by Hase and Kevan do not exceed 35 nm.[9] For the 8 M sample at 77 K, photobleaching under the present experimental conditions did not change the spectral shape, though the total intensity decreased.

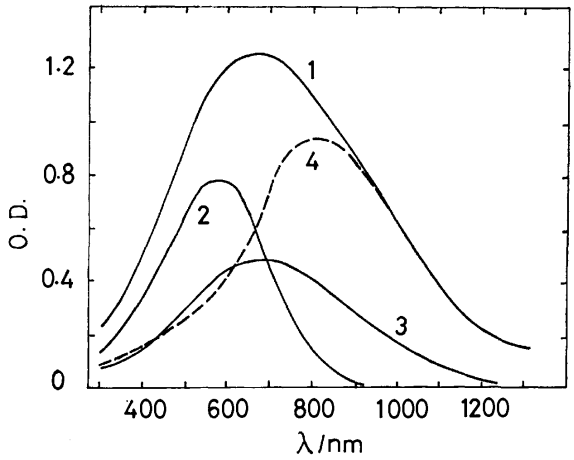

Fig. 3. The effects of selective photobleaching on the optical absorption spectrum of trapped electrons in 18 M NaOH ice irradiated and recorded at 4 K: 1, after γ-irradiation; 2, after photobleaching with 800 nm light; 3, after consecutive photobleaching with 400 nm light; 4, the spectrum bleached with the red light (1—2).

It is also interesting to note that the original 4 K spectrum can be generally reconstructed with respect to both absorption maximum and width by photobleaching at 4 K with the blue light the smaple which had been thermally bleached at 77 K.

The Nature of Shallow Electron Traps. All the above results of optical absortpion experiments seem to be consistent with the following picture: the trap depth distribution in NaOH ice shifts in favor of the shallow traps, responsible for the longer wavelength regions of the spectra, (a) with increasing NaOH concentration and (b) with decreasing temperature of irradiation. Point (a) suggests that the shallow traps may be of a cationic nature.

Electrons in the shallow traps are comparatively unstable and, in 18 M ice, were previously found to decay at 77 K.[3] It was suggested that about 15% of the trapped electrons generated in 18 M NaOH ice irradiated at 77 K are in "cationic" traps and are easily bleached.[4] At 4 K, the contribution of shallow traps significantly increases both for the 8 and 18 M samples. In contrast, the stable dipolar traps are responsible, in the 8 M sample irradiated at 77 K, for most trapped electrons, whose absorption spectra show very small shifts upon photobleaching.

Taking into account the fact that, at 77 K, the shallow trapped electrons still remain in the 18 M sample but not in the 8 M sample, it seems reasonable to expect that the thermal bleaching (4→77 K) effect may be larger for the dilute than for the concentrated sample. This has been found for both the shift of the absorption maxima and the narrowing of the spectral widths. It is suggested that no significant molecular rearrangements are required to allocate electrons in cationic traps and, therefore, they are more primary in nature. In the very early stage of electron trapping, probably in both the 8 and 18 M ices, a large number of electrons is stabilized by cations. The stabilization is

effective at 4 K, whereas it is short-lived at 77 K particularly in the 8 M ice.

Assuming that the spectral component bleached with red light at 4 K (curve 4 in Fig. 3) represents the electrons in the shallow, cationic traps, these electrons also have a very wide energy distribution. This may result from a variety of ion pairs more or less solvent separated, or more or less loose or tight, using the terminology of Seddon *et al.*[10] Their pulse radiolysis study indicated that the optical absorption bands of solvated electrons in amines and tetrahydrofuran are blue-shifted in the presence of alkali metal cations compared with those in neat solvents. Although the above results concerning liquid solutions bear a rather distant relation to the present work, they suggest that the cation-electon pairs form traps of intermediate depths between solvation wells in strongly (*e. g.* water) and weakly (*e. g.* tetrahydrofuran) polar media. It is also interesting to note that the solvated electron band in liquid ammonia shows a red-shift in the presence of metal ions, though this shift is not ascribed to the formation of a (M^+, e^-_s) pair.

The existence of two kinds of electron traps, the dipolar traps and the cationic ones, in the NaOH ice is also supported by more careful examination of the shape of the absorption spectra. None of the red parts of the spectra at 4 K fits a Gaussian distribution and all of them appear to be a superposition of two Gaussian components, as shown in Fig. 4. However, the spectral component in the longer wavelength region photobleached with red light at 4 K (curve 4 in Fig. 3) fits a single Gaussian shape (see curve 2 in Fig. 4) in agreement with the data reported for 77 K. The Gaussian form of the spectrum representing the ion-pairs should be also expected, judging from the results of Shubin *et al.*[11]

Electrons both in the shallow traps and in the deep ones are readily removable from their traps by photobleaching with light of a suitable wavelength (see Fig. 3). It is however worth noting that bleaching of the electrons in the shallow traps is not accompanied by any significant increase in the intensity of the shorter wavelength region of the spectra, corresponding to the electrons in the deep dipolar traps. The photobleached electrons probably disappear by reactions with O^- ions and impurities. On the other hand, the deep electrons are partially transformed into the shallow electrons by blue light. These results imply that an abundance of the shallow traps is available in the NaOH ice at 4 K.

ESR Evidence for the Shallow Traps Associated with Na^+ Cations. Additional evidence as to the wider variety of electron traps in the 18 M sample is provided by ESR measurements at 77 K. These results are shown in Fig. 5. The width of the initial trapped electron signal is 2.1 mT, in fairly good agreement with the data reported by Blandamer *et al.* for 20 M NaOH ice.[12] It decreases to 1.9 mT upon photobleaching with red light. The bleached component of the signal has the width of 2.4 mT, which is much broader than the width, 1.4 mT, of the ordinary trapped electrons in the dipolar traps in the alkaline ice

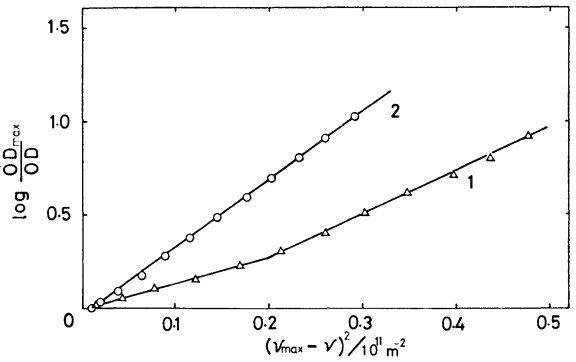

Fig. 4. The gaussian plots. The curve 1 for red parts of the spectrum of γ-irradiated 18 M NaOH ice at 4 K (Fig. 3, curve 1) and the curve 2 for the spectrum due to trapped electrons bleached with 800 nm light (Fig. 3, curve 4).

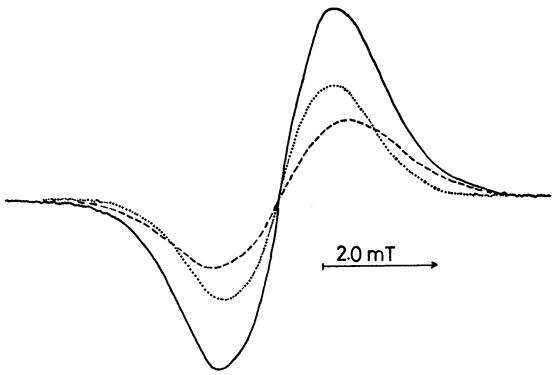

Fig. 5. ESR spectra of trapped electrons in γ-irradiated 18 M NaOH ice at 77 K: ——, after γ-irradiation; ·····, after photobleaching with 800 nm light; and ----, the spectrum bleached with the red light.

matrices of NaOH concentrations less than 10 M at 77 K.

It has been found that the ESR width of the trapped electrons in ethylene glycol–water mixed matrix is broadened from 0.3 to 1.4 mT when thermally annealed at 77 K after the irradiation at 4 K.[5] This change is accompanied by a tremendous blue-shift of the optical absorption spectrum of the trapped electrons.[5,6] This is interpreted in terms of the deepening of traps by the oriented matrix molecules with a polar hydroxyl group, which results in a closer distance between trapped electrons and neighboring protons and, therefore, a larger hyperfine broadening. However, the correlation between the ESR width and the optical absorption observed here is the reverse: when the absorption spectra effectively shift to the blue upon the photobleaching with red light, the ESR width becomes narrower. The present results strongly suggest that the deepening of traps (the blue-shift) in the 18 M sample is not due to the change in the orientational configuration of water molecular dipoles around the traps, but is due to the photorelease of electrons from the traps associated with Na^+ cations, leaving electrons in the dipolar traps.

The ESR width of 2.4 mT of the photobleached component of the signal can reasonably be under-

stood to be due to the hyperfine splitting of the Na nucleus, because it gives a non-negligible conctribution to the ESR width of electrons even in the ordinary dipolar traps in the NaOH ice of lower concentrations.[2] ESR spectra of 8 M and 18 M KOH glassy ice samples irradiated at 77 K have the same width of 1.2 mT. This is in good agreement with the reported data,[12] as reasonably expected from the small nuclear magnetic moment of the K nucleus.

Conclusion

The present data substantiate the results reported previously[3,4] and indicate the nature of shallow, cationic traps for excess electrons in irradiated NaOH ice. This kind of trap is abundant and contributes to the primary step in stabilizing and localizing the electrons.

In fact, the situation may be very complex. Dipolar traps themselves have a wide energy distribution and the contribution of shallow, unrelaxed dipolar traps probably increases at an early stage of the electron trapping process. Moreover, electrons in dipolar traps follow to some extent their own rearrangement pattern, when photo- or thermally bleached. The main purpose of the present work is to point out the possible importance of another type of electron stabilization, *i.e.*, by valence traps or in the form of ion pairs.

This work was performed by using the cryogenic facilities of the electron LINAC laboratory, Hokkaido University.

References

1) See for example, L. Kevan, Actions chimiques et biologiques des radiations, Vol. 13, ed by M. Haissinsky, Masson, Paris (1969), p. 57; *J. Phys. Chem.*, **76**, 3830 (1972); A. K. Pikaev, The solvated electron in radiation chemistry, transl. J. Schmorak, Keter Press, Jerusalem (1971), p. 243.
2) L. Kevan, *J. Am. Chem. Soc.*, **87**, 1481 (1965).
3) J. Kroh and P. Polewoj, *Radiat. Phys. Chem.*, in press.
4) P. Polewoj and J. Kroh, *Bull. Acad. Pol. Sci., Ser. Sci. Chim.*, **25**, 993 (1977).
5) T. Higashimura, M. Noda, T. Warashina, and H. Yoshida, *J. Chem. Phys.*, **53**, 1152 (1970).
6) H. Hase, M. Noda, and T. Higashimura, *J. Chem. Phys.*, **54**, 2975 (1971).
7) H. Hase, T. Warashina, M. Noda, A. Namiki, and T. Higashimura, *J. Chem. Phys.*, **57**, 1039 (1972).
8) B. G. Ershov, I. E. Makarov, and A. K. Pikaev, *Khim. Vys. Energ.*, **1**, 472 (1967).
9) H. Hase and L. Kevan, *J. Chem. Phys.*, **54**, 908 (1971).
10) W. A. Seddon, J. W. Fletcher, and R. Catterall, *Can. J. Chem.*, **55**, 2017 (1977).
11) V. N. Shubin, T. A. Frunze, and Yu. I. Sharanin, Kinetics investigation in pulse radiolysis, Nauka, Moscow, 1974 (in Russian); V. N. Shubin, L. F. Slepnera, and V. D. Mayboroda, *Int. J. Radiat. Phys. Chem.*, **7**, 371 (1975).
12) M. J. Blandamer, L. Shields, and M. C. R. Symons, *J. Chem. Soc.*, **1964**, 4352.

Direct Measurement of Interaction Energy between Solids and Gases. II. Microcalorimetric Studies on the Surface Acidity and Acid Strength Distribution of Solid Acid Catalysts

Tatsuo MASUDA,* Hitofumi TANIGUCHI, Kazuo TSUTSUMI, and Hiroshi TAKAHASHI

Institute of Industrial Science, The University of Tokyo, Roppongi, Minato-ku, Tokyo 106

(Received January 10, 1978)

The differential heats of adsorption of ammonia on several solid acids were measured by means of a twin conduction type microcalorimeter, and surface acid strength distribution and acidity were evaluated. Silica-alumina showed very high initial heats which were not observed in decationated zeolite and silica-magnesia. The acidity of zeolite was about 6 times as high as that of silica-alumina, showing very charactristic acid site distribution at 100 kJ/mol of adsorption energy, and suggesting the existence of homogeneous acid sites. The surface water modified surface acidic nature transforming strong acid sites into weaker ones. The poisoning of acid sites of silica-alumina with alkali occurred preferentially at sites on which adsorption energy of ammonia was 96—105 kJ/mol.

The measurement of the acidity and acid strength distribution of solid acid surfaces has been the subject of many researches, different methods being employed. The most common method is titration with amine in nonaqueous systems using various indicators. A number of reports have appeared on the adsorption of basic gases on solid acids.[1] Attempts were made to use a calorimeter for measurements of a surface acidic nature. Kevorkian and Steiner[2] measured heats of ammonia gas adsorption on alumina specimens from bayerite as a function of coverage. Hsieh[3] obtained the adsorption isotherms and heats of adsorption of ammonia at 0 °C on a series of commercial silica–alumina cracking catalysts and concluded that about one-tenth of the surface is heterogeneous with respect to ammonia adsorption. Similar measurements for alumina, silica–alumina, and X-type zeolite were carried out by Stone and Whalley.[4] None of these were satisfactory to account for the surface acidity and acid strength distribution of solid acids quantitatively. Tsutsumi *et al.*[5] have measured the differential heats of ammonia adsorption on several cation exchanged zeolites, obtaining a good correlation between the differential heats of adosrption and cumene-cracking activities.

In this work, the surface acidity and acid strength distribution were studied in detail with a twin conduction type microcalorimeter for several solid acids. The effects of surface water contents and sodium poisoning of silica–alumina were examined.

Experimental

Materials. Two types of silica-alumina catalyst(Al_2O_3 contents, 13 and 28%, SA-13 and SA-28, respectively) supplied by Shokubai Kasei Co., Ltd. were calcined at 500 °C for 3 h in the air. Sodium poisoned silica-alumina was obtained by impregnation with 0.1 M aqueous sodium acetate solution at 50 °C for 24 h, followed by washing with distilled water, drying at 110 °C and heating at 550 °C in the air (Na-1). Na-2 was obtained by repeated impregnation and washing 3 times under the same conditions as those of Na-1, followed by drying at 110 °C and heating at 550 °C in the air. Sodium contents were 0.38, 0.64 mmol/g in Na-1 and Na-2, respectively.

Y-type zeolite was supplied by Linde Co. in the sodium form. NH_4-Y zeolite was prepared by the conventional cation exchange procedure with NH_4NO_3 solution. The degree of ion-exchange determined by flame photometry was 69.78%.

Silica-magnesia and silica were supplied by Fuji Chem. Co. and Degussa Co., respectively. The magnesia content of silica-magnesia was 20.5 wt% on dry base.

All the substance were used as granules of 28—60 mesh in the calorimeter. The surface areas of these samples determined by N_2 adsorption at 77 K are given in Table 1. Ammonia was obtained from Matheson Co., and purified by the freezing and thawing method.

TABLE 1. SURFACE AREA OF SOLID ACIDS

	m^2/g		m^2/g
SA-13	557	$H\text{-}Y_{5.0}$	614
SA-28	511	Si-Mg[a]	450
Na-1,2	473	SiO_2	380

a) Silica-magnesia.

Apparatus and Procedure. The calorimeter and the procedure of measurement have been described.[6] In order to measure differential heats of adsorption, ca. 0.5 g of adsorbent was weighed into the sample cell and outgassed at several temperatures, mainly at 400 °C, under a pressure of 10^{-5} Torr for 5 h and set in the calorimeter. The calorimeter was maintained at 25±0.01 °C. The amount adsorbed was calculated from the pressure change before and after adsorption measured by a MKS capacitance manometer (below ≈10 Torr) and a mercury manometer (above ≈10 Torr). The amount of gas admitted was *ca.* 5×10^{-6} mol at low surface coverages, while at higher coverages some larger doses were admitted. The fraction of surface coverage was calculated by taking the cross-sectinal area of the ammonia molecules as 16 A^2 at 25 °C.

Results and Discussion

Differential Heats of Silica–Alumina and Silica. Differential heats of adsorption of ammonia on SA-13, SA-28, and silica are given in Fig. 1 as a function of surface coverage. The samples were pretreated at 400 °C *in vacuo*. Curve (c) shows the results of re-adsorption of ammonia on SA-13 which was NH_3-pre-adsorbed and evacuated at 25 °C for 6 h. In silica–alumina, the differential heats fall abruptly from

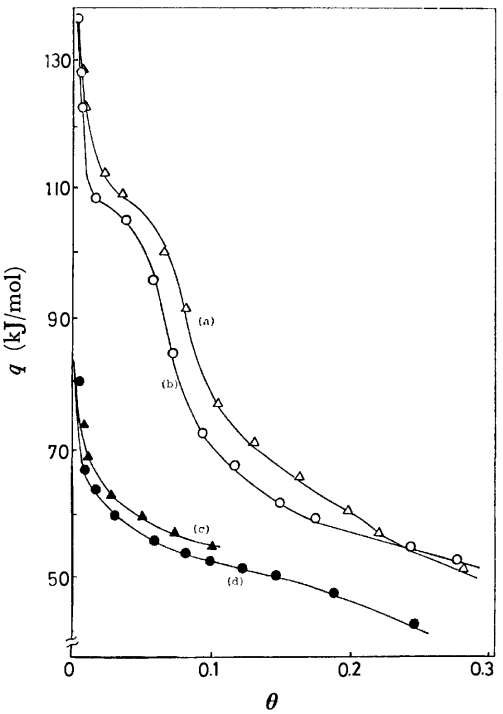

Fig. 1. Heats of adsorption of ammonia on silica-alumina and silica at 25 °C.
(a); SA-28, (b): SA-13, (c): NH_3-preadsorbed SA-13, (d): silica.

initial heat value of *ca.* 140 to 109 kJ/mol. The abrupt decrease in the differential heats indicates that the adsorption of ammonia molecules occurs on the strongest acid sites successively. Details of the q-θ curve in these regions were given previously.[6] After the abrupt decrease, the q-θ curve shows a stepped curve, differential heats decreasing gradually to 54.4 kJ/mol at 0.3 of θ. The stepped region in q-θ curve indicates that considerably homogeneous acid sites exist. The behavior of the q-θ curve is very similar in the two silica-alumina, but SA-28 has larger number of strong adsorption sites as compared with SA-13, especially over 105 kJ/mol. Clark and co-workers[7] studied the differential molar entropy for ammonia adsorbed on silica-alumina of various composition and reported that their values in the region of adsorbed amount smaller than 0.4 molecules/100 Å^2 are smaller than that of perfect two dimensional gas. This corresponds to the region of adsorption energy larger than about 96 kJ/mol, where no residual gas above 10^{-3} Torr was observed. This suggests that the mobilities of adsorbed ammonia are fairly restricted in this region.

Silica does not exhibit high intital heats of adsorption. the differential heats falling very slightly to *ca.* 41.8 kJ/mol at 0.25 of θ. From the fact that ammonia adsorbed on silica is easily desorbed by evacuation at 25 °C, the heat evolved during the course of adsorption is considered to be due to mainly hydrogen bonding and van der Waals interaction. The ammonia preadsorbed SA-13 shows a q-θ curve very similar to that of silica. However the former exhibits somewhat higher differential heat probably due to the interaction of ammonia molecules with the NH_4^+ ions. The

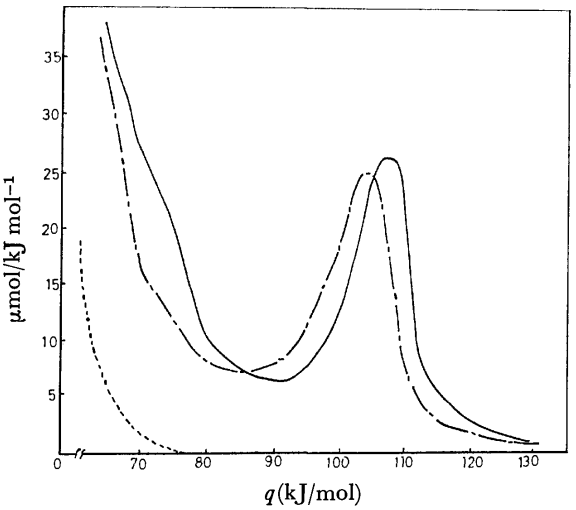

Fig. 2. Acid site distributions of silica-alumina and silica.
——: SA-28, ——: SA-13, ----: silica.

remaining amount of ammonia after evacuation at 25 °C on SA-13 measured by gravimetric methods is 0.6 mmol/g, corresponding to 0.1 of surface coverage. In comparison with the q-θ curve of SA-13 it can be concluded that the adsorbed ammonia with heat of adsorption lower than 70.0 kJ/mol can be desorbed by evacuation at 25 °C. The value nearly coincides with the initial heat of ammonia on preadsorbed SA-13.

The surface acid site distributions of silica-alumina and silica are given in Fig. 2. The maximum distributions are observed at 105 and 109 kJ/mol in SA-13 and SA-28, respectively. The region with a heat of adsorption between 75 and 92 kJ/mol shows relatively low distribution values, indicating that only a small amount of acid sites exists in these regions. Rouxhet and Sempls[8] observed two hydroxyl groups in silica-alumina; type 1, Si-OH groups identical with those present on the surface of silica; type 2, the sites responsible for the protonation of adsorbed ammonia whose acidity corresponds to the pK_a range from −4 to −8. The latter OH groups seem to be responsible for the maximum site energy distribution.

The distribution curve of silica has neither maximum nor minimum.

Effects of Outgassing Temperature on q-θ Curve of SA-13. The q-θ curves of SA-13 outgassed at various temperatures between 25 and 400 °C for 5 h are shown in Fig. 3. The initial heat obtained on the sample outgassed at 150 °C (curve b) is 159 kJ/mol, almost the same as that obtained on the sample outgassed at 400 °C (curve a). The sample outgassed at 25 °C exhibits no stronger adsorption energy than 110 kJ/mol. No apparent difference could be observed among all samples in the region below 70 kJ/mol. Similar results were also obtained in SA-28.

Figure 4 shows the acid strength distribution of the samples. The maximum at 105 kJ/mol in curve(a) shifted towards lower strength along with the lowering of outgassing temperature. The results indicate that the surface water modified the acidic nature and the strong acid sites were transformed into weak ones.

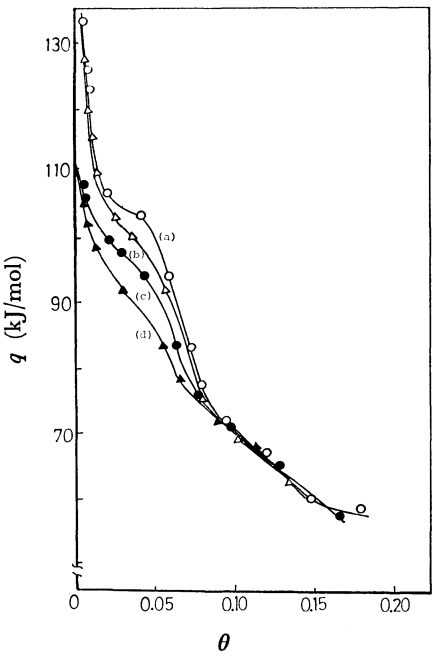

Fig. 3. Effects of outgassing temperature on q-θ curve of SA-13.
(a): 400 °C under 10^{-5} Torr, (b): 150 °C under 10^{-5} Torr, (c): 25 °C under 10^{-5} Torr, (d): 25 °C under 10^{-3} Torr.

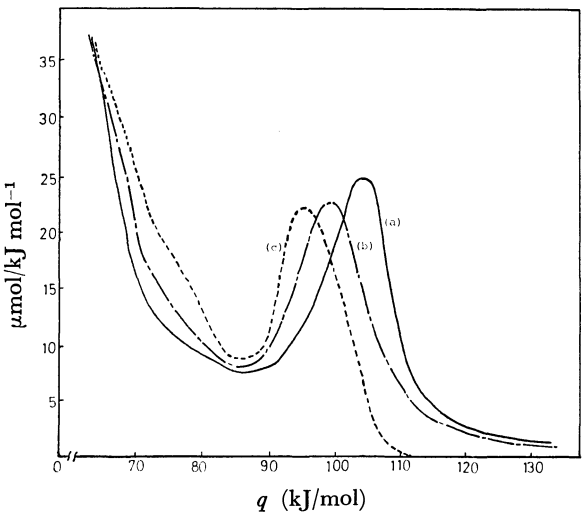

Fig. 4. Effects of outgassing temperature on acid site distributions of SA-13.
(a): 400 °C, (b): 150 °C, (c): 25°C under 10^{-5} Torr.

Gravimetric experiments showed that water released from SA-13 with an increase of evacuation temperature from 25 to 400 °C is *ca.* 3.1 mmol/g. The value is greater than the number of acid sites which were calculated to be *ca.* 0.6 mmol/g. This suggests that the surface water does not interact in a 1 : 1 molar ratio with acid sites. It should be pointed out that the infrared spectrum of pyridine adsorbed on SA-13 outgassed at 25 °C showed only pyridinium ion absorption band, suggesting the absence of Lewis acid sites. If protonic acid sites are formed by the interaction of water with Lewis acid sites, the adsorption energies

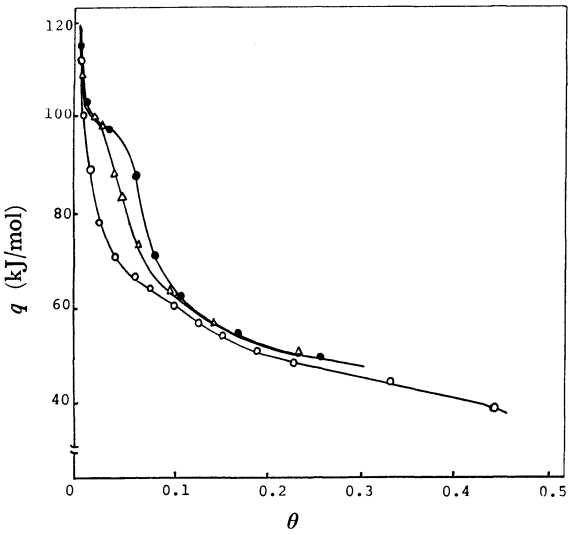

Fig. 5. Heats of adsorption of ammonia on sodium ion-exchanged silica-alumina at 25 °C.
-△-: Na-1, -○-: Na-2, -●-: SA-13.

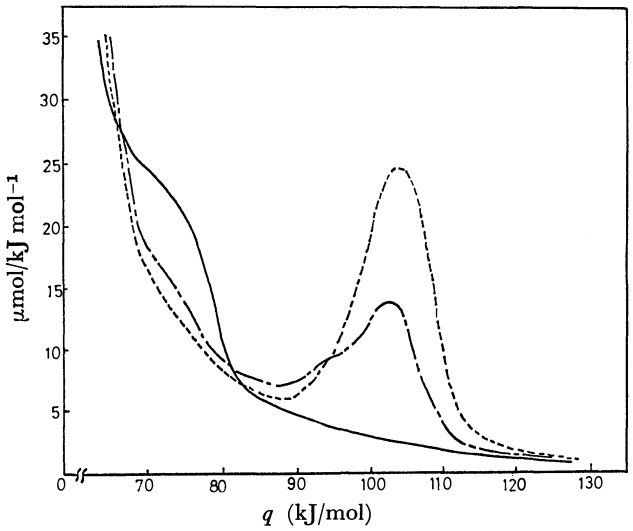

Fig. 6. Acid site distributions of sodium ion-exchanged silica-alumina.
——: Na-2, ———: Na-1, ----: SA-13.

of the resulting sites are probably lower than those of the original Lewis acid sites. The acid strength of the hydrated surface proton becomes less. The results given in Figs. 3 and 4 probably imply the circumstances of silica–alumina surface. It is noteworthy that the differential heats of the sample outgassed at 25 °C is greater than the heat of solution of ammonia in water, 35.6 kJ/mol.

The Effects of Alkali Metal Poisoning. The q-θ curves of sodium ion-exchanged SA-13 are shown in Fig. 5. These samples were pretreated at 400 °C *in vacuo*. The initial heat is almost the same as that of original SA-13. A remarkable difference from original SA-13 is a decrease of the number of the acid sites between 95 and 110 kJ/mol of adsorption heats. This is evident from the disappearance of a maximum in acid strength distribution of Na-2 shown in Fig. 6. In the region of adsorption heat lower than

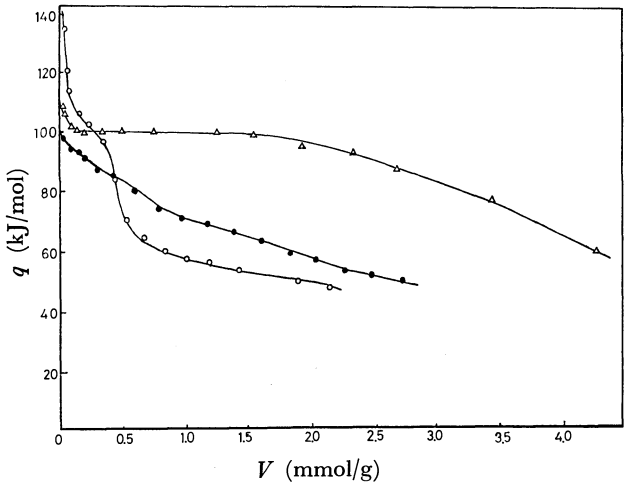

Fig. 7. Heats of adsorption of ammonia on H-$Y_{5.0}$ and silica-magnesia at 25 °C.
-△-: H-$Y_{5.0}$, -●-: silica-magnesia, -○-: SA-13.

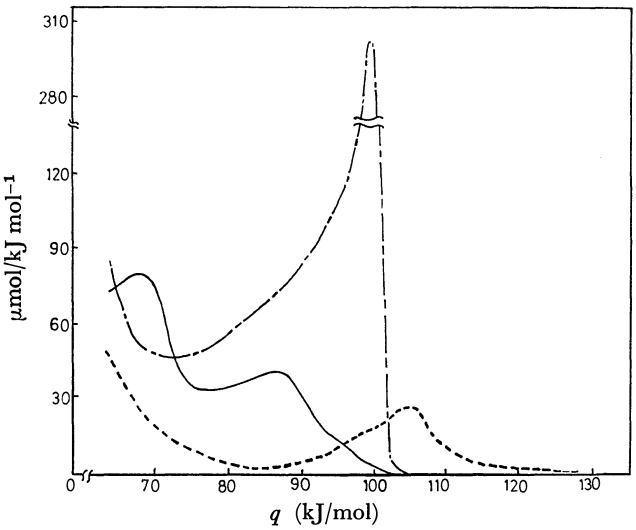

Fig. 8. Acid site distributions of H-$Y_{5.0}$ and silica-magnesia.
——: Silica-magnesia, ——: H-$Y_{5.0}$, ----: SA-13.

68 kJ/mol, however, the q-θ curve and acid strength distribution curve are little affected by sodium ion-exchange. This suggests that ammonia molecules probably interact physically with adsorption sites in this region An increase in the number of the acid sites between 68 and 80 kJ/mol implies that an exchanged Na^+ ion transforms a part of strong acid sites to weaker ones in line with the results of Hirshler.[9]

Flockhart and Pink[10] have reported that single base exchange-dehydration cycle can not poison all of the acid sites, especially Lewis acid sites. The infrared spectrum of ammonia adsorbed on Na-2 showed the presence of a very small amount of ammonium ions. This suggests that at low surface coverage, *i.e.*, in the region of high adsorption energy, ammonia molecules interact with Lewis acid sites on Na-2.

Differential Heats of H-$Y_{5.0}$ and Silica-Magnesia. The differential heats of H-$Y_{5.0}$ and silica-magnesia are shown in Fig. 7 together with the results of SA-13. Both samples were pretreated at 400 °C *in vacuo*. In H-$Y_{5.0}$, there are no acid sites with a value greater than 111 kJ/mol which can be seen in silica-alumina surface. The differential heats remain *ca.* 100 kJ/mol up to 1.5 mmol/g of the amount adsorbed and then smoothly decrease to 65 kJ/mol at 4.0 mmol/g. Those homogeneous acid sites giving about 100 kJ/mol of adsorption heats are probably protonic acid sites. The same results have been obtained in a series of H-Y zeolite with a different silica-alumina ratio.[5] The calculated number of protons which generated during the course of heat treatment of ammonium form zeolite at 400 °C is 2.27 mmol/g. This corresponds to the number of acid sites over 94 kJ/mol of adsorption heats.

The heat of adsorption on silica-magnesia is about 109 kJ/mol at an initial stage and then decreases gradually to 54 kJ/mol at 2.5 mmol/g of the amount adsorbed.

The acid strength distribution of these solid acids is shown in Fig. 8. Richardson[11] studied the effects of faujasite cations on acid sites by means of infrared spectroscopic measurements of several types of OH groups existing in the supercage and observed two kinds of centers with acid strength corresponding to pK_a=4.95 and −4.9, respectively. Although his model was not well defined, the shape of the distribution curve is very similar to ours. In comparison with the case of silica-alumina, maximum and minimum positions of site energy distribution of silica-magnesia differ greatly. At around 80—92 kJ/mol of the adsorption energy, silica-alumina has minimum distribution, and silica-magnesia a maximum one. Such a tendency is in line with the results of amine titration, *viz*, silica-magnesia has no stronger acid sites found in silica-alumina, its acid sites being more widely distributed from strong acid sites to weak acid sites as compared with the case of silica-alumina. More heterogeneous distributions observed for acid sites of amorphous silica-alumina and silica-magnesia in comparison with that of H-$Y_{5.0}$ might be probably due to a localization of their acid sites originated from surface Al and Mg, respectively.

Acid Distribution of Solid Acids. No estimation of the number of surface acid sites of solid from the measurements of differential heats of adsorption of basic molecules seems to have been made. The number and density of acid sites are shown as a function of adsorption energies (Table 2), calculated on the assumption that the effective acid sites are $q \geq 70$ kJ/mol and ammonia molecules interact in a 1:1 molar ratio with acid sites. The definition of the effective acid sites is somewhat arbitrary in this case. The results of acid distribution of silica-alumina measured with a Hammett indicator[12] show the existence of only very weak acids and very strong acids. However, our results show the existence of a considerable amount of medium strength acid sites between 75 and 95 kJ/mol, which is consistent with the results of H_R indicator[13] and ammonia desorption method.[14] The discrepancy might have resulted from the adsorption of Hammett

Table 2. Acid distribution of solid acids (mmol/g)

	$70 \leq q$	$80 \leq q$	$90 \leq q$	$100 \leq q$	$110 \leq q$	$120 \leq q$
SA-13	0.61 (1.09)[a)]	0.47 (0.84)	0.40 (0.70)	0.32 (0.57)	0.10 (0.18)	0.04 (0.07)
SA-28	0.72 (1.41)	0.52 (1.02)	0.44 (0.86)	0.35 (0.68)	0.18 (0.35)	0.06 (0.11)
Na-2	0.31 (0.61)	0.12 (0.25)	0.06 (0.13)	0.04 (0.08)	0.03 (0.06)	0.02 (0.04)
$H\text{-}Y_{5.0}$	3.78 (6.16)	3.23 (5.31)	2.45 (3.99)	1.55 (2.52)	0.01 (0.02)	— —
Si-Mg	0.97 (2.16)	0.62 (1.38)	0.22 (0.49)	0.04 (0.09)	— —	— —
SiO_2	0.03 (0.08)	0.01 (0.02)	— —	— —	— —	— —

a) ($mmol/m^2 \times 10^3$)

indicators on the acidic surfaces.[15] The surface acid density of SA-28 is larger than that of SA-13, its difference becoming greater in the region over 110 kJ/mol of adsorption energy. In comparison with silica–alumina, $H\text{-}Y_{5.0}$ possesses about 6 times the number of acid sites with q higher than 70 kJ/mol, which are rather homogeneous. The acidic properties of $H\text{-}Y_{5.0}$ probably support its high catalytic activity and selectivity in cracking reaction.

In Na-2, the reduction of the number of acid sites by base exchange is 0.3 mmol/g, which is smaller than the number of Na^+ ions on Na-2, suggesting that exchanged Na^+ ions do not correspond in a 1:1 molar ratio to acid sites or that they only decrease the strength of some acids.

The use of adsorption calorimetry and particularly the measurement of differential heats of basic gas molecules on solid acids seems to be useful for the determination of surface acidity and acid strength distribution. The method could be utilized in the measurements of very strong acid sites which can not be measured exactly by the conventional amine titration.

This work was partly supported by a Grant-in-Aid for Science Research from the Ministry of Education.

References

1) L. Forni, *Catal. Rev.*, **8**, 71 (1974).
2) V. Kevorkian and O. Steiner, *J. Phys. Chem.*, **67**, 545 (1963).
3) P. Y. Hsieh, *J. Catal.*, **2**, 211 (1963).
4) F. S. Stone and L. Whalley, *J. Catal.*, **8**, 173 (1967).
5) K. Tsutsumi, H. Q. Koh, S. Hagiwara, and H. Takahashi, *Bull. Chem. Soc. Jpn.*, **48**, 3576 (1975).
6) T. Masuda, H. Taniguchi, K. Tsutsumi, and H. Takahashi, *Bull. Chem. Soc. Jpn.*, **51**, 633 (1978).
7) A. Clark, V. C. F. Holm, and D. M. Blackburn, *J. Catal.*, **1**, 244 (1962).
8) P. G. Rouxhet and R. E. Sempls, *J. Chem. Soc., Faraday Trans. 1*, **70**, 2021 (1974).
9) A. E. Hirshler, *J. Catal.*, **2**, 428 (1963).
10) B. D. Flockhart and R. C. Pink, *J. Catal.*, **4**, 90 (1965).
11) J. T. Richardson, *J. Catal.*, **9**, 182 (1967).
12) H. Benesi, *J. Phys. Chem.*, **61**, 970 (1957).
13) A. E. Hirshler, *J. Catal.*, **6**, 1 (1966).
14) Y. Kubokawa, *J. Phys. Chem.*, **67**, 769 (1963).
15) M. Frenkel, *Anal. Chem.*, **47**, 598 (1975).

Direct Measurement of the Interaction Energy between Solids and Gases. III. Comparison of the Calorimetric Titration Method with the Amine Titration Method for the Determination of Acid Strength Distribution of Silica–Alumina Surface

Hitofumi TANIGUCHI,* Tatsuo MASUDA, Kazuo TSUTSUMI, and Hiroshi TAKAHASHI

Institute of Industrial Science, The University of Tokyo, Roppongi, Minato-ku, Tokyo 106

(Received January 11, 1978)

The acid strength distribution of silica–alumina catalyst (alumina content 13 wt%) evacuated at 400 °C for 5 h was determined by the measurement of heat of adsorption of ammonia, and compared with that determined by amine titration by use of a series of Hammett indicators. The heats of adsorption of ammonia on silica–alumina poisoned with Hammett indicators were also measured in order to obtain the relation between the dissociation constant of the acid (pK_a) and the heat of adsorption. When the dissociation constants of acid were equal to -5.6 and $+3.3$, the differential heats of adsorption of ammonia were observed to be 76.1 and 55.1 kJ/mol, respectively. The number of acid sites calculated from the heat *vs.* adsorbed amount curve was found to be about twice as large as that determined by amine titration. The discrepancy is discussed.

In previous papers, calorimetric titration with ammonia gas was reported for various solids (silica–alumina:alumina content 13 and 28 wt%, decationated zeolites and silica gel).[1,2] The adsorption energy distribution curve was derived for each sample from calorimetric data. The curve obtained shows a new aspect of the acid strength distribution of solid acid catalysts: the differential heat of adsorption of ammonia corresponds to the acid strength and the adsorbed amount of ammonia to the number of acid sites.

The acid strength is generally expressed by the Hammett acidity function, H_0, which is related to the dissociation constant of acid, pK_a, as

$$H_0 = pK_a + \log([B]/[BH^+]) \quad \text{(Brønsted acid)}$$

$$H_0 = pK_a + \log([B]/[BA]) \quad \text{(Lewis acid)}$$

where [B] and [BH^+] are the concentrations of the base and its conjugated acid, respectively, and [BA] is the concentration of the coordination compound of Lewis acid A and Lewis base B. The number and the strength of acid sites can be determined by butylamine titration by use of indicators with known pK_a values.[3] However, the method is unsuitable for colored samples. Moreover, indicator molecules are so large that they can scarcely migrate into micro pores of porous materials such as silica–alumina. Though silica–alumina has been known to have stronger acid sites than $pK_a = -8.2$, the color change of indicator corresponding to these regions can hardly be recognized with the naked eye.

Calorimetric method can overcome these disadvantages. However, the relationship between a differential heat of adsorption of basic gas and an acid strength or pK_a value has not been clarified as yet. The purpose of this study is to correlate the heat of adsorption of ammonia with the acid strength and to compare calorimetric titration with amine titriation.

Experimental

The solid acid catalyst used in this study was commercial FCC silica–alumina (alumina content 13 wt%, Catalysts & Chemicals Ind. Co., Ltd.). Each sample was pretreated at 400 °C under 10^{-5} Torr for 5 h before measurement. Butylamine titration was carried out before and after ammonia adsorption at different coverages in cyclohexane with use of a series of Hammett indicators: anthraquinone ($pK_a = -8.2$), benzylideneacetophenone ($pK_a = -5.6$), dicinnamylideneacetone ($pK_a = -3.0$), *p*-anilinoazobenzene ($pK_a = +1.5$), *p*-dimethylaminoazobenzene ($pK_a = +3.3$).

The heat of adsorption of ammonia was measured with a twin conduction type calorimeter.[1,2,4] In most cases, calorimetric measurement and ammonia titration in solid-gas phase with use of the indicators were carried out simultaneously. Specific surface area was determined by the BET nitrogen method. Surface coverage of ammonia gas was calculated by assuming a cross sectional area of ammonia molecule to be 16 Å^2.

Results and Discussion

Figure 1 shows the relation between the preadsorbed amount of ammonia and the subsequently titrated amount with butylamine for each indicator. The end point of butylamine titration changed with the preadsorbed amount of ammonia for every indicator; as an example, when the indicator was benzylidene-

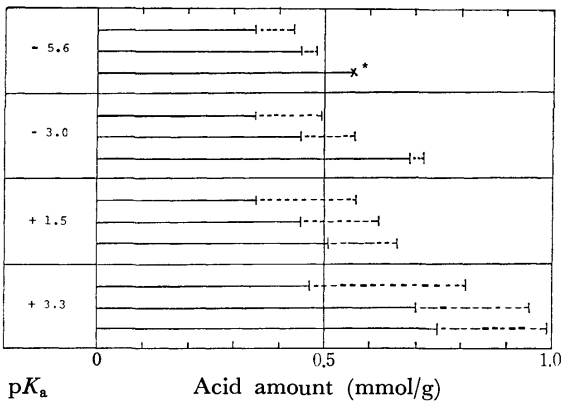

Fig. 1. Effect of ammonia poisoning on the acid amount titrated with butylamine.
Solid line: preadsorbed amount of ammonia.
Dashed line: titrated amount of butylamine after preadsorption of ammonia.
* Color change from the basic to the acidic was not observed.

Table 1. Calculated n value (on the basis of Fig. 1)

pK_a	−5.6	−3.0	+1.5	+3.3
n	2.0	2.8	2.0	2.6
		2.4	3.0	1.3
		(5.0)	1.8	1.6
Average		$n=2.2$		

Table 2. Acid amount determined by adsorbed amount of butylamine (1) and ammonia (2) (mmol/g)

pK_a	≦−5.6	≦−3.0	≦+1.5	≦+3.3
(1)	0.24	0.31	0.38	0.56
	0.24	0.33	0.39	0.57
			0.39	0.59
Average	0.24	0.32	0.38	0.57
(2)	0.52	0.68	0.83	1.21
	0.51	0.73	0.82	1.24
			0.84	1.27
Average	0.51	0.70	0.83	1.24

acetophenone($pK_a=-5.6$) and the preadsorbed amount of ammonia 0.45 mmol/g, the titrated amount of butylamine was 0.03 mmol/g, while the end point was 0.43 mmol/g at 0.35 mmol/g of preadsorbed ammonia. If butylamine molecules were adsorbed on acid sites in the same manner as ammonia, the end point would be independent of the preadsorbed amount of ammonia. However, this is not the case. The number of acid sites can be considered constant after pretreatment at the same temperature under the same pressure for the same period. Hence, the following simple equation should hold for every indicator:

$$x + ny = k, \quad (1)$$

where x is the preadsorbed amount of ammonia, y the titrated amount of butylamine, k the constant corresponding to the number of acid sites, and n the constant correlating the number of ammonia molecules with that of butylamine molecules adsorbed on silica–alumina surface. The values of n, calculated by means of Eq. 1 and on the basis of Fig. 1, are given in Table 1. Some scattering of values can be ascribed to the error of the titrated amount of butylamine. The average value, $n=2.2$, is considered to be reasonable as clarified in the following.

The numbers of acid sites calculated by use of conversion factor, $n=2.2$, are given in Table 2. They are constant within errors for a given pK_a value. Thus, if one ammonia molecule is adsorbed on one acid site, one butylamine molecule seems to occupy about two sites. The cross sectional area of ammonia molecule is 16 Å^2, and that of butylamine molecule 32 Å^2. Moreover, acid sites on silica–alumina surface seem to be localized due to localization of aluminum atom or ion.[5] The value of conversion factor, $n=2.2$, seems to depend mainly on the ratio of cross sectional areas, 32 Å^2/16 Å^2. Other factors such as the difference of basicity of amines may hardly affect the conversion factor.

In amine titration using Hammett indicators, butylamine in benzene or cyclohexane is generally used. In this study ammonia gas titration with a series of Hammett indicators was carried out, along with simultaneous calorimetric measurements for silica–alumina catalyst. Change from the basic to the acidic color was clearly observed as in amine titration in cyclohexane solution. The end points of gas titrations are shown in Table 3. These values are in good agreement with those in Table 2. The period required for adsorption equilibrium of ammonia was expected to be much shorter than that of butylamine in cyclohexane solution, since the diffusion rate of molecule in the gas phase is about ten thousand times as large as that in the liquid phase. The adsorption equilibrium seems to be attained within one or two hours, as estimated by simultaneous calorimetric measurement. Figure 2 shows the results of calorimetric measurement carried out simultaneously with gas titration. Each q-V (or q-θ) curve for the sample poisoned with indicator is similar in shape to that of the original sample. They are lower than the curve of the original sample by several kJ/mol in the low coverage range, coinciding with it in the higher coverage. The V values (adsorbed amount of am-

Table 3. Acid amount determined by ammonia gas titration by use of Hammett indicator and the corresponding q value

pK_a	≦−5.6	≦−3.0	≦+1.5	≦+3.3
V (mmol/g)	0.52	0.71	0.83	1.23
q (kJ/mol)	76.1	65.6	61.8	55.1

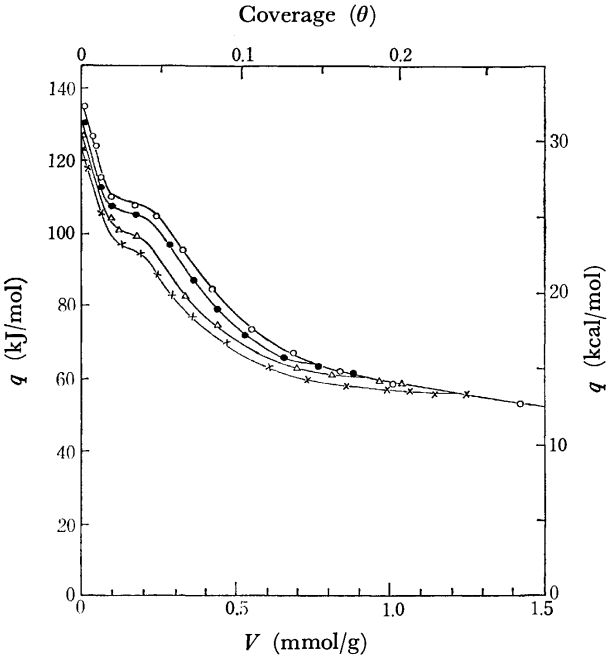

Fig. 2. Effect of poisoning with indicator on the differential heat of adsorption of ammonia.
(pretreatment temperature; 400 °C)
○: Original sample, ●: poisoned with dicinnamylideneacetone ($pK_a=-3.0$), △: poisoned with *p*-anilinoazobenzene ($pK_a=+1.5$), ×: poisoned with *p*-dimethylaminoazobenzene ($pK_a=+3.3$).

monia) at points where two curves coincide are in good agreement with those given in Tables 2 and 3 for all indicators. Smaller q values of the sample poisoned with the indicator, in the low coverage, can be ascribed to the desorption of the indicator. If we assume that the mechanism of ammonia titration consists of the desorption of indicator and the subsequent adsorption of ammonia, the observed heat of adsorption can be expressed by the following equation:

$$Q = nq_{(ads)} + mq_{(des)}, \quad (2)$$

where Q(kJ) is the observed heat, $q_{(ads)}$(kJ/mol) the heat of adsorption of ammonia, $q_{(des)}$(kJ/mol) the heat of desorption of indicator (negative value), n(mol) the adsorbed amount of ammonia, and m(mol) the desorbed amount of indicator. The q value in Fig. 2 derived from Eq. 2 is given by

$$q = Q/n = q_{(ads)} + (m/n)q_{(des)}. \quad (3)$$

The factor m/n represents the number of indicator molecules replaced by one ammonia molecule. Decrease in the q value, accompanied by poisoning with indicator, reflects the term $(m/n) \times q_{(des)}$ in Eq. 3.

In order to determine $q_{(des)}$, the heat of adsorption of indicator from indicator–cyclohexane solution was measured by a twin conduction type calorimeter. The adsorbed amount of indicator was determined spectroscopically before and after measurement. The adsorbed amounts of indicators, the heats of adsorption of indicators and the corresponding adsorbed amount of ammonia are given in Table 4. For *p*-dimethylaminoazobenzene, the ratio of the ammonia molecules adsorbed to the desorbed molecules of indicator, m/n in Eq. 3, is 0.21 on the assumption that the adsorbed amount of indicator is equal to its desorbed amount. Since the integral heat of adsorption of indicator is presumably equal to the integral heat of desorption, $(m/n) \times q_{(des)}$ in Eq. 3 can be equated to -19.0 kJ/mol for *p*-dimethylaminoazobenzene and -15.7 kJ/mol for *p*-anilinoazobenzene. A decrease in the q value induced by poisoning with indicator is sufficiently explained in terms of these values.

TABLE 4. THE HEAT OF ADSORPTION OF INDICATOR FROM INDICATOR–CYCLOHEXANE SOLUTION (1), THE ADSORBED AMOUNT OF INDICATOR (2), AND THE CORRESPONDING ADSORBED AMOUNT OF AMMONIA (3)

Indicator		$pK_a = +1.5$	$pK_a = +3.3$
(1)	(kJ/mol)	75.2	90.3
(2)	(mmol/g)	0.17	0.26
(3)	(mmol/g)	0.83	1.24

This work was partly supported by a Grant-in-Aid for Science Research from the Ministry of Education.

References

1) T. Masuda, H. Taniguchi, K. Tsutsumi, and H. Takahashi, *Bull. Chem. Soc. Jpn.*, **51**, 633 (1978).
2) T. Masuda, H. Taniguchi, K. Tsutsumi, and H. Takahashi, *Bull. Chem. Soc. Jpn.*, **51**, 1965 (1978).
3) H. A. Benesi, *J. Phys. Chem.*, **61**, 970 (1957).
4) K. Tsutsumi, H. Q. Koh, S. Hagiwara, and H. Takahashi, *Bull. Chem. Soc. Jpn.*, **48**, 3576 (1975).
5) T. Shiba, M. Sato, H. Hattori, and K. Yoshida, *Shokubai*, **6**, 80 (1964).

Gel Filtration Study of the Effect of Urea on the Dissolution State of Sodium Dodecyl Sulfate

Tsunetaka SASAKI,*† Hiroshi AMANO,†† and Hitoshi SUZUKI†††

Department of Chemistry, Faculty of Science, Tokyo Metropolitan University, Setagaya, Tokyo 158

(Received January 27, 1978)

Using gel columns of Sephadex G 50 Fine and CPG gel, gel filtration studies were made of the sodium dodecyl sulfate (SDS)–urea system. The results demonstrated that both the CMC and the elution volume of SDS were increased by the addition of urea. The increase of the elution volume indicates the decrease in micellar size, and this coupled with the increase of CMC indicates the increased difficulty of micelle formation by the addition of urea. The direct interaction between SDS and urea was also examined by the gel filtration method and such interaction was confirmed to be absent both below and above the CMC of SDS. Furthermore, the micellar weight of SDS was estimated by the gel filtration method and values of 23000 and 11000 were obtained for SDS solutions containing 0 and 3 mol dm^{-1} urea, respectively.

A number of studies have been reported of the effect of urea on the micelle formation of surfactants.[1–6] The addition of urea increases the critical micelle concentration (CMC) of surfactants. This effect has been explained in terms of the decrease of entropy of micellization due to the breakdown of the structure of water or the weakening of the hydrophobic bonding between the hydrophobic chains of surfactant molecules by the addition of urea.[4] Other explanations have also been presented.[1,2,5]

A similar effect has been discussed for the urea–protein system.[1,7,8] Here, the interaction between the protein and urea is suggested in addition to the interaction between water and urea.[8] Furthermore, urea–polyethlene glycol[9] and urea–fatty acid interactions[10] have been reported. In these studies, conductometric,[1,5] spectroscopic,[2] surface tension,[3] and membrane-potential[5] measurements have been employed.

In the present paper. the gel filtration method which enables a simple and direct measurement[11] has been adopted to study the effect of urea upon the aqueous solution of the ionic surfactant, sodium dodecyl sulfate (SDS). The discussion has been made upon both the water–urea and the SDS–urea interactions.

Experimental

Materials. SDS was prepared according to the Dreger method.[12]. It was purified by recrystalliztion from ethanol and washed with ethyl ether. Purity was confirmed by the absence of a minimum in the surface tension-concentration curve. The commercial SDS product from Nippon Surfactant Chemicals Co. was similarly purified and used. Commercial urea of a guaranteed grade was recrystallized from 95% ethanol. Substances used as a molecular weight standards were reagent grade sodium chloride, blue dextran (Pharmacia product), Pluronics F 68 and F 108 (Asahi Denka products), poly(vinyl alcohol) (PVA) (Nippon Gōsei Kōgyō product), and poly(sodium ethylenesulfonate) (PES) (commercial product). Gel used for packing columns were Sephadex G 50 Fine (Uppsala Pharmacia product) and CPG-10 (Electro-Nucleonic Inc. product). Distilled water was used after degassing by boiling.

Apparatus and Measurement. The apparatus used for the gel filtration was the same as reported in a previous paper.[11] Gel columns used were of 1.2 cm inner diameter and 32 and 80 cm in height for Sephadex G 50 Fine and CPG-10, respectively.

Measurement was made by charging 20 to 35 cm^3 of the sample solution onto the top of the gel column and the solution eluted at constant flow rates of 20 and 30 cm^3/h for Sephadex gel and CPG-10 gel, respectively. In the case of the SDS gel filtration, elution was made using water. For the SDS–urea gel filtration, the gel column was previously filled with urea solution of the same concentration as that of the sample solution. The sample solution was then charged and the solution eluted with urea solution of the same concentration. The eluted solutions were detected either by a conductometer or a differential refractometer (Mitsumi LDC Refractomonitor) and the elution curves obtained on a recorder.

All experiments were conducted at 30±1 °C.

Results and Discussion

Sephadex–Urea System. CMC vs. Urea Concentration: The elution curves of conductance *vs.* flow volume are shown in Fig. 1a and 1b which are similar to those of SDS below and above the CMC in the absence of urea, respectively.[11] Here, κ_T and κ_S represent conductances of the total solution and single ions, respectively and V_f, V_m, and V_s denote elution volumes of the elution front, SDS micelles and single ions, respectively. From these data, the CMC's of the SDS–urea system were obtained for 0, 1.5, and 3 mol dm^{-3} urea concentrations by plotting κ_T and κ_S against the concentration of SDS, as shown for instance in Fig. 2 for the SDS–urea system (3 mol dm^{-3} urea). Figure 3 shows the CMC *vs.* urea concentration curve. The CMC's are seen to increase with increasing concentration of urea. Figure 3 also gives the values calculated from the conductometric data of Emerson and Holtzer.[13]

Urea–SDS Interaction: The urea–SDS interaction has been explained indirectly as the breakdown of the structure of water by urea. However, urea has been reported to interact directly with protein,[8] surfactant,[9] and fatty acid monolayers,[10] and since there is no confirmation of the absence of such a direct interaction between urea and SDS, it was necessary to establish this point. For this purpose, the gel filtration measurement offers a simple and direct method.[14]

† Present address: Department of Chemistry, Faculty of Science, Tokai University, Kitakaname, Hiratsuka 259-12.

†† Present address: 2090-70 Andōyama, Fuse, Chiba 277.

††† Present address: 3-2-10 Honchō, Koganei, Tokyo 184.

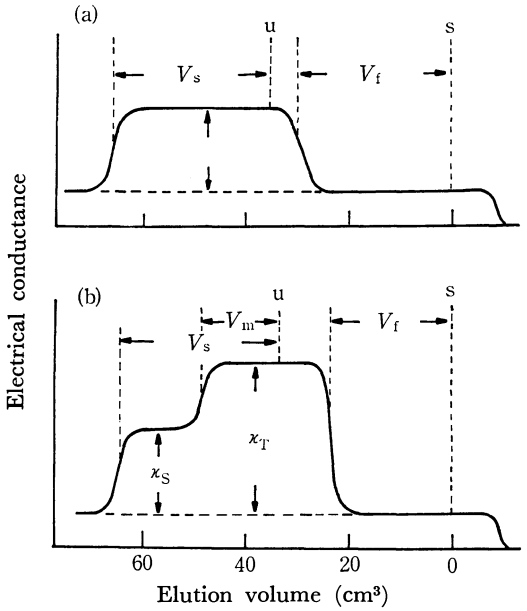

Fig. 1. Gel filtration of aq urea-SDS solution.
(a), (b); Elution curves below and above CMC, respectively. S, U; Points of urea and urea-SDS solution charge, respectively.

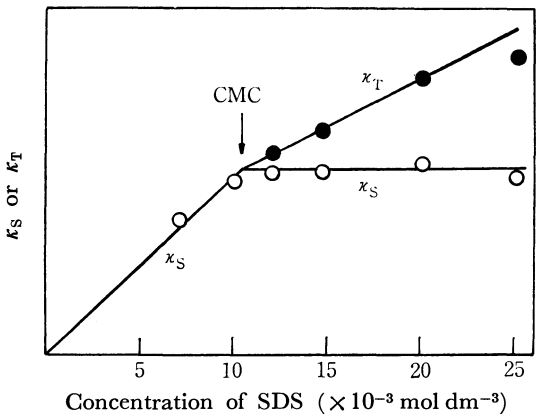

Fig. 2. Conductance of eluent *vs.* concentration of SDS plot.
Gel; Sephadex G 50 Fine, urea; 3 mol dm^{-3}, temperature; 30 °C, CMC; 10.5×10^{-3} mol dm^{-3}

Table 1. Gel filtration of SDS through Sephadex G 50

	Concn of SDS 10^{-3} mol dm^{-3}	Elution volume (cm³) Front V_f	Tail V_m	Tail V_s
Urea 0 mol dm^{-3}	6.7	35.0		35.0
	9.9	31.5	11.7	35.8
	12.0	29.1	11.8	35.5
	14.7	25.1	11.3	35.0
	20.5	22.1	13.6	34.7
Urea 3 mol dm^{-3}	7.1	33.4		33.6
	9.9	33.0		34.2
	12.0	30.1	11.0	33.8
	14.7	27.4	11.3	33.7
	20.0	24.3	14.3	33.8
	25.0	23.0	15.8	34.0

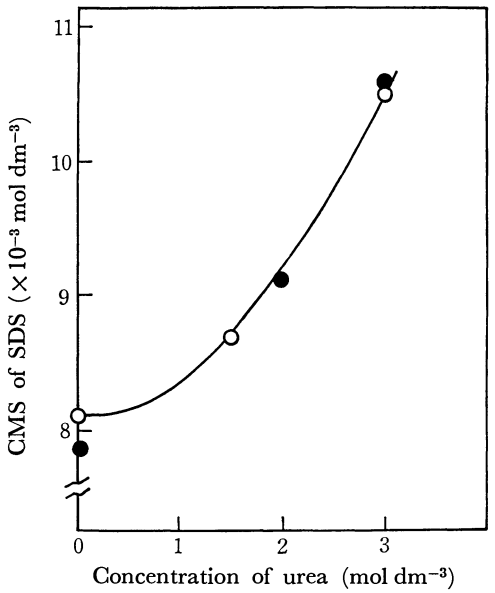

Fig. 3. CMC of SDS *vs.* concentration of urea plot.
○; Present experiment, ●; data of Emerson and Holtzer, temperature; 30 °C.

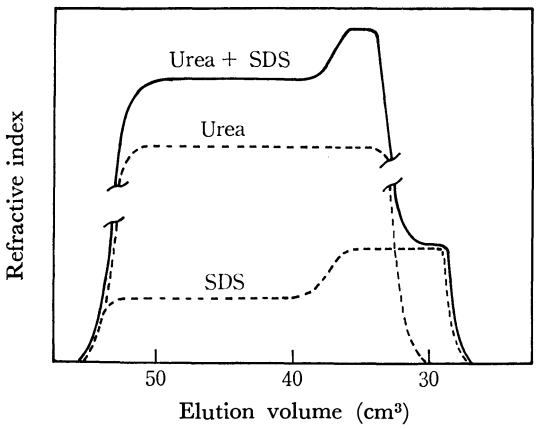

Fig. 4. Elution curve of aq urea-SDS solution.
Gel; Sephadex G 50 Fine, temperature; 30 °C.

Table 1 shows elution volumes V_f, V_m, and V_s of the urea–SDS system containing 0 and 3 mol dm^{-3} urea. Assuming that the urea–SDS complex is formed in the solution in equilibrium with single dodecyl sufate ions (DS^-) and urea, the complex will be eluted faster than DS^- or urea and thus V becomes smaller than V_s below the CMC as in the case of poly(vinyl acetate)–SDS complex formation.[14] However as seen in Table 1, V_f and V_s are equal to each other in the urea–SDS for a 3 mol dm^{-3} urea concentration below the CMC. Therefore the possibility of complex formation is excluded below the CMC. We also confirmed that the interaction of urea with SDS above the CMC or the solubilization was negligible, since the elution curve of the urea–SDS mixture above the CMC was obtained as a simple addition of the elution curves for the separate components as shown in Fig. 4. This differs from the complicated elution curve exhibited in the case of the solubilization of 1-dodecanol by SDS.[15] In Fig. 4, the broken lines show the elution curves of urea and

Table 2. Gel filtration of standard substances through Sephadex G 50

Substance	Urea concn (mol dm^{-3})	
	0	3
Pluronic F68 ($\bar{M}$=8350)	12.0	11.5
Pluronic F108 ($\bar{M}$=15500)	11.3	9.7
Blue dextran	10.2	9.2
NaCl	32.1	32.9

SDS above the CMC and the solid line denotes the elution curve of the urea–SDS system which is obtained by the addition of the ordinates of the former two curves. A similar absence of interaction has also been reported between urea and nonionic surfactant.[16]

V_m of SDS in Urea Solution: As seen from Table 1, the values of V_m show a complicated change with concentration of SDS and urea. Also the V_s values are not equal to each other for the systems of 0 and 3 mol dm^{-3} urea solutions. These facts may be attributed to the change of Sephadex gel matric produced by the addition ures and SDS. This has been confirmed by the change in the elution volumes of the substances of known molecular weight such as NaCl, Pluronics, and dextran by the addition of urea as shown in Table 2. Therefore, to estimate the micellar weight of SDS, it becomes necessary to measure the elution volume of the urea–SDS, system using a gel which is free from such a change. For this purpose CPG-10 gel was chosen.

CPG–Urea–SDS System. Preparation of CPG Gel Column: The CPG gel was superior to the Sephadex gel since the gel matrix was not affected by various solvents, but it showed less difference between V_m and V_s of SDS. A gel column more than twice as long as the Sephadex gel column was necessary to obtain a comparable separation efficiency.

The CPG gel was purified first by washing with distilled water and decantation. Then it was left free in concentrated nitric acid overnight, washed with distilled water, with a water ethanol mixture and finally with pure ethanol. The purified CPG was packed in a glass column mentioned already and care was taken to pack the column uniformly. The packed column was further washed with concentrated aqeous solutions of SDS and ethanol. The completeness of the washing was confirmed by absence of a peak in the elution curve of water obtained by refractometry.

Micellar Weight of SDS: Elution volumes of SDS, NaCl and blue dextran were measured in the absence and presence (3 mol dm^{-3}) of urea. In the latter case, the gel column was previously filled with 3 mol dm^{-3} urea and the same solution used for the elution of the sample solution. Table 3 and 4 show the results. It may be seen in the tables that the elutions volume of SDS single ions (V_s), NaCl and blue dextran are not affected by the addition of 3 mol dm^{-3} urea. Comparison of these results with Table 2 confirms that the CPG gel matrix is unaffected by the urea addition. Further, as seen in Table 3, the values of V_m of SDS are independent of SDS concentration

Table 3. Gel filtration of SDS through CPG-10

	Concn of SDS 10^{-3} mol dm^{-3}	Elution volume (cm^3)		
		Front V_f	Tail	
			V_m	V_s
Urea 0 mol dm^{-3}	18.0	45.0	39.1	50.0
	19.9	44.1	39.2	49.9
	24.7	42.9	39.2	49.5
Urea 3 mol dm^{-3}	18.0	46.5	40.8	50.1
	20.1	45.9	40.6	49.5
	25.2	44.2	40.6	50.2

Table 4. Elution volume of reference substances

Substance	Urea concn (mol dm^{-3})	
	0	3
Blue dextran	38.8	38.8
NaCl	47.1	47.2
PVS	39.5	39.5

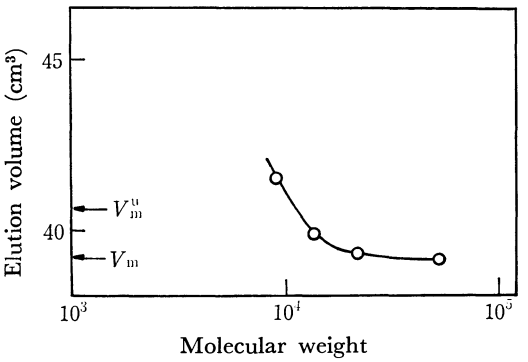

Fig. 5. Elution volume *vs.* molecular weight plot. Gel; CPG gel, V_m, V_m^u; Elution volumes of SDS micelles in water and in aq urea solution, respectively

both for the 0 and 3 mol dm^{-3} urea systems and the value of the 3 mol dm^{-3} urea solution is larger than that of the solution without urea. This evidently shows that the addition of urea decreases the size of the micelle independent of the SDS concentration.

To estimate the micellar weight or SDS, it was necessary to secure a series of substances of known molecular weight, which were used to construct a calibration curve of elution volume *vs.* molecular weight. A series of PVA of mean degrees of polymerization, 200, 300, 500, and 1200 were used as standard substances. The elution volume of PVA without urea is uncertain because of a marked tailing, whereas the tailing is reduced in the presence of 3 mol dm^{-3} urea and a distinct and identical elution volume is obtained for the front and the tail of PVA solution. This may indicate the absence of both CPG– and urea–PVA interactions and the elution volume was considered to be directly related to the molecular weight of PVA. Figure 5 shows the molecular weight *vs.* elution volume plot for 3 mol dm^{-3} urea solution, which was used as a calibration curve for the estimation of the micellar weight. It should be noted that the

range covered by this calibration curve is not satisfactory for the molecular weight determination, however it may be sufficient for the estimation of molecular weight as a whole. Thus, from this curve and the elution volumes of SDS micelles listed in Table 3, the micellar weights of 23000 and 11000 were obtained for SDS in 0 and 3 mol dm^{-3} urea solutions. The former value is comparable to the value of 25000 formerly reported.[17] Further, the micellar weight was confirmed to decrease by the addition of urea, which together with the increase of the CMC mentioned already may indicate the difficulty of micelle formation produced by the additon of urea. Contraty to this result, a slight increase of micellar aggregation number by the addition of urea has been reported for a nonionic surfactant.[18]

The above estimation of the micellar weight assumes a nearly equal weight ratio of hydration between PVA and SDS in the state of solution and the amount of hydration of SDS being independent of the addition of urea. The first point may be confirmed from the coincidence of unhydrated molecular weight *vs.* elution volume plots between PVA and SDS as estimated from the diagram of a previous paper.[17] The second point may be confirmed by comparison of the elution volumes of PES of nearly the same size (elution volume) as those of SDS micelles in 0 and 3 mol dm^{-3} urea solutions. This has been discussed in a previous paper.[19] From the data shown in Table 4, it may be seen that the elution volumes of PES measured in 0 and 3 mol dm^{-3} urea solution are equal to each other. From this we assumed that the amount of yhdration of PES and thereore SDS was not affected by the addition of urea.

References

1) W. Brunning and A. Holtzer, *J. Am. Chem. Soc.*, **83**, 4865 (1961).
2) P. Mukerjee and A. Ray, *J. Phys. Chem.*, **67**, 190 (1963).
3) M. J. Schick, *J. Phys. Chem.*, **68**, 3585 (1964).
4) J. A. Rupley, *J. Phys. Chem.*, **68**, 2002 (1964).
5) J. Piercy, M. N. Jones, and G. Ibbotson, *J. Colloid Interface Sci.*, **37**, 165 (1971).
6) W. U. Malik and S. P. Verma, *Kolloid Z. Z. Polym.*, **233**, 985 (1969).
7) I. M. Klotz and K. Shikama, *Arch. Biochem. Biophys.*, **123**, 551 (1968).
8) J. A. Gordon and W. P. Jencks, *Biochemistry*, **2**, 47 (1963).
9) G. G. Hammes and P. R. Schimmel, *J. Am. Chem. Soc.*, **89**, 442 (1967).
10) D. F. Sears, *J. Colloid Interface Sci.*, **29**, 288 (1969).
11) H. Suzuki and T. Sasaki, *Bull. Chem. Soc. Jpn.*, **44**, 2630 (1971).
12) E. E. Dreger, G. I. Keim, G. D. Miles, L. Schedlovsky, and J. Ross, *Ind. Eng. Chem.*, **36**, 610 (1944).
13) M. F. Emerson and A. Holtzer, *J. Phys. Chem.*, **71**, 3320 (1967).
14) T. Sasaki, K. Tanaka, and H. Suzuki, *Proc. 6th. Int. Congr. Surface Active Substnaces*, **2**, 849 (1972).
15) H. Suzuki, *Bull. Chem. Soc. Jpn.*, **49**, 381 (1976).
16) K. Tajima, *Bull. Chem. Soc. Jpn.*, **49**, 3403 (1976).
17) H. Suzuki, *Bull. Chem. Soc. Jpn.*, **49**, 375 (1976).
18) M. J. Schick, S. M. Atlas, and F. R. Erich, *J. Phys. Chem.*, **66**, 1326 (1962).
19) H. Suzuki, *Bull. Chem. Soc. Jpn.*, **49**, 1470 (1976).

Computation of the Correlation Functions for Fluids Composed of Diatomic Molecules by Means of the Method of Integral Equations

Kazumitsu KOJIMA and Kiyoshi ARAKAWA

Research Institute of Applied Electricity, Hokkaido University, Sapporo 060

(Received February 6, 1978)

Pair correlation functions and structure factors of molecular fluids were computed, based on the reference interaction site model (RISM) integral equation coupled with the Percus-Yevick (PY) and the hyper-netted chain (HNC) approximations. The system considered is a fluid of diatomic molecules consisting of two identical spheres of diameter σ with each center located at a distance L ($L<\sigma$). The total potential energy for the molecular fluid is assumed to be the sum of pair potentials of the Lennard-Jones type. It is shown that the pair correlation functions calculated are in agreement with results of molecular dynamics studies. The structure factors calculated by using two kinds of approximations (PY and HNC) are found to deviate from each other for small values of k (wave vector). Discussions are given on the behavior of the structure factors, $S(k)$. The rise of $S(k)$ at small k is ascribed to the effect of attractive forces between molecules.

It has become evident from studies on the properties of simple atomic fluids with use of the Percus-Yevick (PY) and the hyper-netted chain(HNC) equations that these equations are useful for fluids composed of spherical particles.[1] In the case of fluids composed of nonspherical molecules, however, solving the equations is difficult since the interactions between molecules depend on the mutual orientation of molecules as well as on their positions. Chen and Steel[2] applied the generalized PY equation to a system of diatomic molecules. In order to solve the equation, they transformed it into a set of coupled integral equations by expanding the correlation functions in a series of spherical harmonics. However, this treatment was laborious and not successful.

Chandler and Andersen[3] proposed the embedded site and the reference interaction site models for fluids consisting of polyatomic molecules. In these models, the total interaction between molecules is expressed as a sum of site-site interactions depending only on the separation between sites. In the embedded site model, each molecule is regarded as a hard sphere with embedded sites. This model was applied to a system of water-like particles.[4] In the reference interaction site model a molecule is composed of rigidly-connected hard spheres (the spheres within a molecule may overlap), where the centers of interaction sites are located at the centers of the spheres.

Lowden and Chandler[5,6] solved the reference interaction site model (RISM) integral equation for molecular fluids in which each molecule interacts through the hard sphere site-site repulsive potentials only. Ladanyi and Chandler[7,8] applied a topological reduction procedure to the new cluster expansion formula on the basis of the RISM theory, giving a relationship between the RISM equation for molecular fluids and the PY equation for simple atomic fluids. Hsu *et al.*[9] calculated the correlation functions for systems of homonuclear diatomic molecules using the method of the associated RISM model and intermolecular site-site cluster functions. They treated the attractive potential as a perturbation.

Recently, Johnson[10] has given a set of equations which are analogous to the RISM equation from the Ornstein-Zernike equation using Fourier-Wigner series. The equations using the PY approximation were applied to a system of molecules interacting through the Lennard-Jones site-site potential.

We have attempted to solve the RISM integral equation coupled with the PY and HNC approximations for the purpose of dealing with systems interacting through intermolecular site-site potentials without use of the perturbation technique. The results of our calculation are compared with those of molecular dynamics studies[11,12] and other calculations.[9,10]

Theory

Model. In the theory proposed by Chandler and Andersen,[3] a molecule is assumed to have m interaction sites. The location of the αth site on jth molecule is denoted by $\boldsymbol{r}_j^\alpha=\boldsymbol{R}_j+\boldsymbol{l}_j^\alpha$. Here, $\boldsymbol{R}_j$ denotes the location of the center of the jth molecule. The vector $\boldsymbol{l}_j^\alpha$ depends on the orientation of the molecule as described by the Eulerian angles. We assume that the molecule as shown in Fig. 1 is rigid so that the magnitude of $\boldsymbol{l}_j^\alpha$ and of the angles between different $\boldsymbol{l}_j^\alpha$ vectors within the same molecule become constant. The total potential energy for the molecular fluid is assumed to be the sum of pair potentials, where the pair interaction between molecule 1 and 2 is given by

$$w(1,2)=\sum_{\alpha=1}^{m}\sum_{\gamma=1}^{m}w_{\alpha\gamma}(\boldsymbol{r}_1^\alpha-\boldsymbol{r}_2^\gamma). \tag{1}$$

The pair interaction between α site of a molecule and γ site of another molecule is expressed as

$$w_{\alpha\gamma}(r)=4\varepsilon\left\{\left(\frac{\sigma}{r}\right)^{12}-\left(\frac{\sigma}{r}\right)^{6}\right\}. \tag{2}$$

Reference Interaction Site Model Equation.[3] The pair correlation function considered is the intermolecular site-site radial distribution function defined as

$$g_{\alpha\gamma}(r)=\rho^{-2}\left\langle\sum_{\substack{i=1\\(i\neq j)}}^{N}\sum_{j=1}^{N}\delta(\boldsymbol{r}_i^\alpha)\delta(\boldsymbol{r}_j^\gamma-\boldsymbol{r})\right\rangle, \tag{3}$$

where the bracket $\langle\cdots\rangle$ denotes an ensemble average, $\rho=\langle N/V\rangle$ the average density, and $\delta(\boldsymbol{r})$ the Dirac delta function. The structure of molecular fluid is given by the $g_{\alpha\gamma}(r)$ function where $4\pi r^2\rho g_{\alpha\gamma}(r)$ is a probability distribution for finding a site γ associated with one molecule at a distance r from an origin when a site α (in another molecule) is located at the origin.

The total correlation function is

$$h_{\alpha\gamma}(r) = g_{\alpha\gamma}(r) - 1, \tag{4}$$

which is a functional of site-site cluster functions, $f_{\alpha\gamma}(r)$ and intramolecular pair distribution functions, $s_{\alpha\gamma}(r)$. These quantities are defined as

$$f_{\alpha\gamma}(r) = \exp\{-\beta w_{\alpha\gamma}(r)\} - 1, \tag{5}$$

where β^{-1} is Boltzmann's constant times temperature and

$$\begin{aligned} s_{\alpha\gamma}(r) &= (1-\delta_{\alpha\gamma})\rho^{-1}\langle\sum_{i=1}^{N}\delta(\boldsymbol{r}_i^{\alpha})\delta(\boldsymbol{r}_i^{\gamma}-\boldsymbol{r})\rangle, \\ &= (1-\delta_{\alpha\gamma})(4\pi L_{\alpha\gamma})^{-1}\delta(r-L_{\alpha\gamma}). \end{aligned} \tag{6}$$

The second equality in Eq. 6 holds for rigid molecules only, where the distance between site α and γ within the same molecule is a constant $L_{\alpha\gamma}$.

The site-site total correlation function $h_{\alpha\gamma}(r)$ and the site-site direct correlation function $c_{\alpha\gamma}(r)$ are related by an Ornstein-Zernike type equation:

$$\hat{\boldsymbol{h}}(\boldsymbol{k}) = \hat{\boldsymbol{\omega}}(\boldsymbol{k})\hat{\boldsymbol{c}}(\boldsymbol{k})[\boldsymbol{1}-\rho\hat{\boldsymbol{\omega}}(\boldsymbol{k})\hat{\boldsymbol{c}}(\boldsymbol{k})]^{-1}\hat{\boldsymbol{\omega}}(\boldsymbol{k}), \tag{7}$$

where $\hat{\boldsymbol{h}}(\boldsymbol{k})$, $\hat{\boldsymbol{c}}(\boldsymbol{k})$, and $\hat{\boldsymbol{\omega}}(\boldsymbol{k})$ denote matrices with elements $\hat{h}_{\alpha\gamma}(k)$, $\hat{c}_{\alpha\gamma}(k)$, and $\hat{\omega}_{\alpha\gamma}(k)$,

$$\begin{aligned} \hat{h}_{\alpha\gamma}(k) &= \int d\boldsymbol{r}\, h_{\alpha\gamma}(r)e^{-i\boldsymbol{k}\boldsymbol{r}}, \\ \hat{c}_{\alpha\gamma}(k) &= \int d\boldsymbol{r}\, c_{\alpha\gamma}(r)e^{-i\boldsymbol{k}\boldsymbol{r}}, \\ \hat{\omega}_{\alpha\gamma}(k) &= \int d\boldsymbol{r}\, \omega_{\alpha\gamma}(r)e^{-i\boldsymbol{k}\boldsymbol{r}}, \end{aligned} \tag{8}$$

respectively. The $\omega_{\alpha\gamma}(r)$ is defined as

$$\omega_{\alpha\gamma}(r) = \delta_{\alpha\gamma}\delta(r) + s_{\alpha\gamma}(r). \tag{9}$$

PY and HNC Approximations. The RISM integral equation can be solved when the site-site direct correlation function $c_{\alpha\gamma}(r)$ is expressed in terms of the site-site total correlation function $h_{\alpha\gamma}(r)$.[3] According to Chandler[8] the $c_{\alpha\gamma}(r)$ on the RISM integral equation is expressed as

$$c_{\alpha\gamma}(r) = y_{\alpha\gamma}(r)f_{\alpha\gamma}(r), \tag{10}$$

where $y_{\alpha\gamma}(r)$ is

$$y_{\alpha\gamma}(r) = \exp\{\beta\omega_{\alpha\gamma}(r)\}g_{\alpha\gamma}(r). \tag{11}$$

He refers to Eq. 10 as a "PY like approximation." We propose here the application of a "HNC like approximation" defined as

$$c_{\alpha\gamma}(r) = h_{\alpha\gamma}(r) - \ln y_{\alpha\gamma}(r), \tag{12}$$

which is similar to the HNC approximation for simple atomic fluids.[13] A set of coupled non-linear integral equations is formed by combining Eq. 7 with the closure Eq. 10 or Eq. 12.

Computational Procedure

Computational Method. For a fluid composed of homonuclear diatomic molecules such as shown in Fig. 1, we have $h_{\alpha\gamma}(r)=h_{11}(r)$ and $c_{\alpha\gamma}(r)=c_{11}(r)$ for all (α,γ). The RISM integral equation (Ref. 5, Eq. 2.7) is

$$\hat{h}_{11}(k) = \{1+\hat{\omega}_{12}(k)\}^2\hat{c}_{11}(k)/[1-2\rho\{1+\hat{\omega}_{12}(k)\}\hat{c}_{11}(k)], \tag{13a}$$

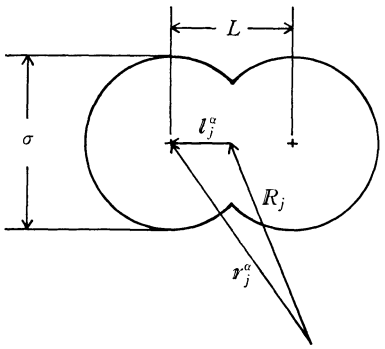

Fig. 1. The shape of RISM molecule.

$$\hat{\omega}_{12}(k) = (kL_{12})^{-1}\sin(kL_{12}), \tag{13b}$$

$$c_{11}(r) = y_{11}(r)f_{11}(r), \quad \text{(PY)} \tag{13c}$$

$$= h_{11}(r) - \ln y_{11}(r). \quad \text{(HNC)} \tag{13d}$$

An iteration procedure is carried out for solving Eqs. 13 numerically, the method of fast Fourier transformation (FFT) being used for the calculation.[14] The function $h_{11}(r)$ is discontinuous at $r=\sigma$ but the function $\gamma(r)=h_{11}(r)-c_{11}(r)$ is a continuous function of r.[5] With use of $\gamma(r)$, Eqs. 13a—d are written as

$$\rho\gamma(r) = \rho(2\pi)^{-3}\int d\boldsymbol{k}\left[\frac{\{1+\hat{\omega}_{12}(k)\}^2}{1-2\rho\{1+\hat{\omega}_{12}(k)\}\hat{c}_{11}(k)}-1\right]\hat{c}_{11}(k)e^{i\boldsymbol{k}\boldsymbol{r}} \tag{14}$$

and

$$\gamma(r) = y_{11}(r) - 1, \quad \text{(PY)} \tag{15a}$$

$$= \ln y_{11}(r), \quad \text{(HNC)} \tag{15b}$$

respectively. The iteraction procedure is carried out by means of Eqs. 14 and 15. The values of $\hat{c}_{11}(k)$ given by Lowden and Chandler[5] for the hard sphere intermolecular site-site interactions are taken as initial ones. The iteration has been continued until the self-consistency of

$$\left|\frac{y_{11}^{\text{out}}(r)-y_{11}^{\text{in}}(r)}{y_{11}^{\text{in}}(r)}\right| < 10^{-7} \tag{16}$$

is satisfied.

Structure Factor. Neutron scattering experiments determine the molecular structure factor, $S(k)$, which is defined as

$$S(k) = (\sum_{\alpha=1}^{m} b_{\alpha})^{-2}\sum_{\alpha,\gamma}^{m} b_{\alpha}b_{\gamma}\langle N^{-1}\sum_{i,j}^{N}\exp\{i\boldsymbol{k}\cdot(\boldsymbol{r}_i^{\alpha}-\boldsymbol{r}_j^{\gamma})\}\rangle. \tag{17}$$

In the calculation of $S(k)$ it is assumed that the interaction sites are located on the nuclei so that $\boldsymbol{r}_j^{\alpha}$ is the location of αth nucleus in the jth molecule. The coherent neutron scattering amplitude for a nucleus of type α is denoted by b_{α}. By performing the ensemble average in Eq. 17, the structure factor can be expressed in terms of site-site pair correlation functions:[6]

$$S(k) = (\sum_{\alpha=1}^{m} b_{\alpha})^{-2}\sum_{\alpha,\gamma}^{m} b_{\alpha}b_{\gamma}\{\hat{\omega}_{\alpha\gamma}(k)+\rho\hat{h}_{\alpha\gamma}(k)\}, \tag{18}$$

$$= \frac{1}{2}\{1+\hat{\omega}_{12}(k)\} + \rho\hat{h}_{11}(k). \tag{19}$$

The equality in Eq. 19 holds for fluids composed of homonuclear diatomic molecules. If the intermolecular

structure of a fluid is completely random (the ideal gas limit), the structure factor becomes

$$S_{\text{ideal}}(k) = \left(\sum_{\alpha=1}^{m} b_\alpha\right)^{-2} \sum_{\alpha,\gamma}^{m} b_\alpha b_\gamma \hat{\omega}_{\alpha\gamma}(k). \quad (20)$$

Molecular Parameters. We have carried out the calculation according to the procedure described above for liquid nitrogen. Barojas *et al.*[12] and Cheung and Powles[15] made a computer simulation for the homonuclear diatomic molecular liquid by means of a molecular dynamics method using the same potential as in the present paper. The parameters corresponding to liquid nitrogen are

$$L_{12} = |\boldsymbol{l}^1 - \boldsymbol{l}^2| = 1.100\,\text{A},$$
$$\sigma = 3.341\,\text{A},$$
$$\varepsilon/k = 44\,\text{K},$$

and

$$L^* = L_{12}/\sigma = 0.3,$$

where k is Boltzmann's constant. When these parameters are used, the values $\rho^*=\rho\sigma^3$ and $T^*=kT/\varepsilon$ at the triple point are 0.6964 and 1.437, respectively, and those at the critical point are $\rho^*=0.246$ and $T^*=2.86$. For the sake of comparison we have made a calculation of $S(k)$ for the same values of parameters. The values $\rho^*=0.6964$, $T^*=1.61$ used correspond to $T=71$ K, $\rho=0.868$ g/cm^3 for liquid nitrogen.[11]

Results and Discussions

Correlation Functions. Figures 2—5 show the site-site radial distribution functions calculated according to the procedure described in the preceding section. The $g_{11}(r)$ calculated are compared with the results of other theories[9,10] as well as those of molecular dynamics[11,12] in Figs. 2—4. The agreement between these results is satisfactory on the whole. The site-site pair correlation curve obtained from the RISM equation for the system with hard sphere site-site interactions is known to have two cusps appearing at $r^*=(r/\sigma)=1$ and $r^*=1+L^*$.[5] For the system with the Lennard-ones site-site potential, these cusps are supposed to be rounded off with a shoulder appearing instead at $r^*=1+L^*$. If one site is σ away from a site at the origin, then another site of the same molecule is located between σ and $\sigma+L_{12}$ from the site at the origin resulting in appearance of a shoulder at $r^*=1+L^*$. This feature distinguishes the structure of molecular fluids from

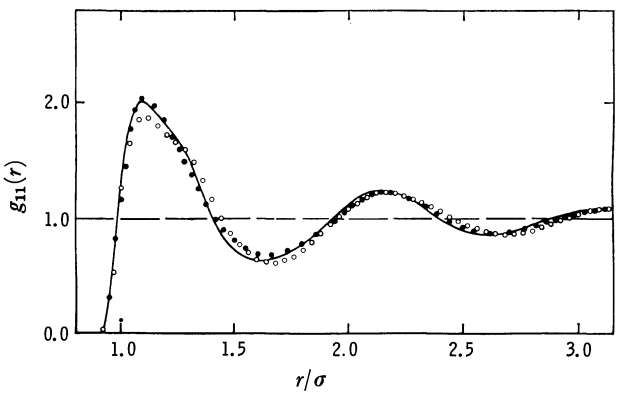

Fig. 2. Site-site radial distribution function, $g_{11}(r)$, for homonuclear diatomic fluids at $\rho^*=0.6964$ and $T^*=1.61$.
○: The molecular dynamics results of Ref. 11, ●: the calculated results of Ref. 10, ——: this work.

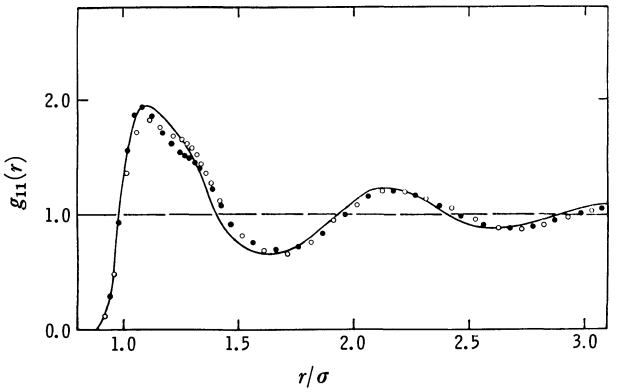

Fig. 3. Site-site radial distribution function, $g_{11}(r)$, for homonuclear diatomic fluids at $\rho^*=0.6964$ and $T^*=1.83$.
○: The molecular dynamics results of Ref. 12, ●: the calculated results of Ref. 9, ——: this work.

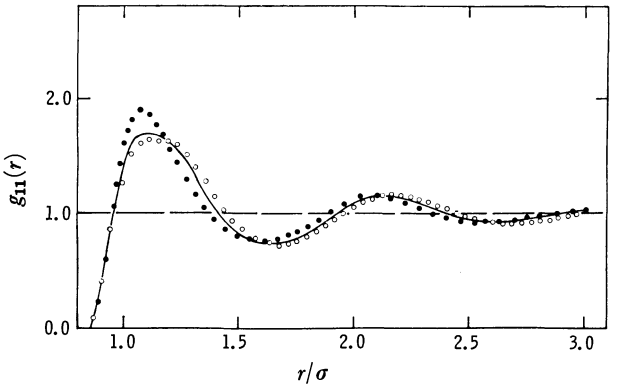

Fig. 4. Site-site radial distribution function, $g_{11}(r)$, for homonuclear diatomic fluids at $\rho^*=0.696$ and $T^*=4.03$.
○: The molecular dynamics results of Ref. 12, ●: the calculated results of Ref. 10, ——: this work.

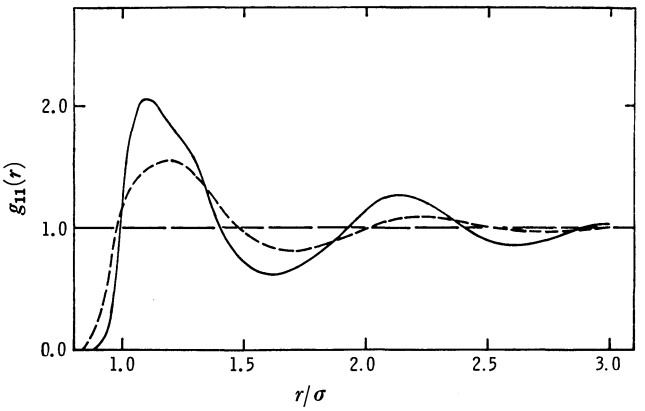

Fig. 5. Site-site radial distribution function, $g_{11}(r)$, for homonuclear diatomic fluids, ——: at $\rho^*=0.6964$ and $T^*=1.46$, ----: at $\rho^*=0.55$ and $T^*=4.03$.

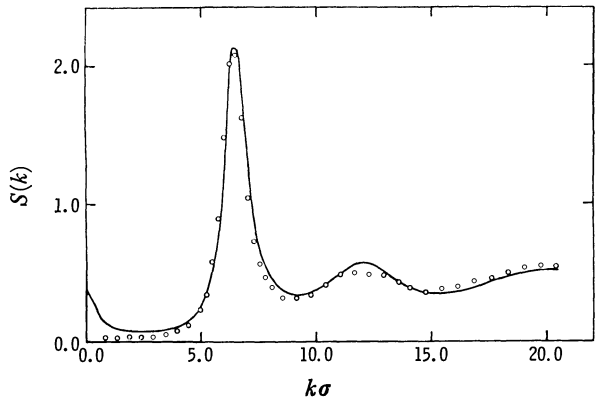

Fig. 6. Structure factor, $S(k)$, for homonuclear diatomic fluids at $\rho^*=0.6964$ and $T^*=1.61$.
○: The molecular dynamics results of Ref. 11, ——: this work.

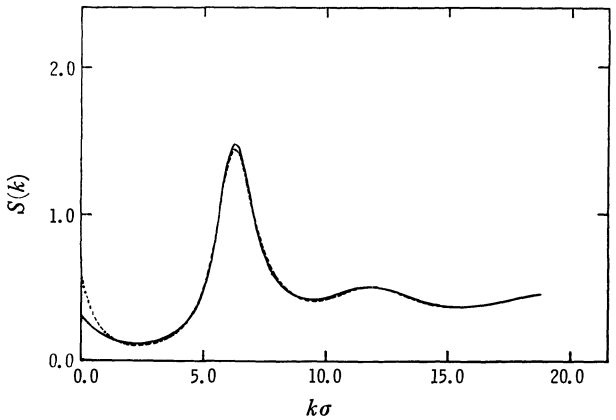

Fig. 7. Comparison of the structure factor, $S(k)$, calculated by using PY and HNC approximations at $\rho^*=0.60$ and $T^*=3.14$.
——: PY approximation, ----: HNC approximation.

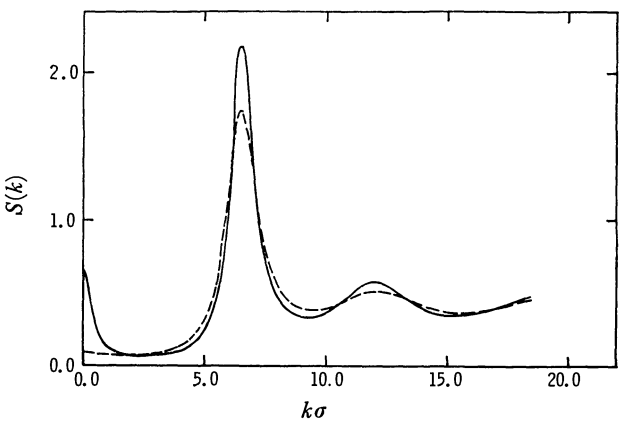

Fig. 8. Structure factor, $S(k)$, for homonuclear diatomic fluids.
——: At $\rho^*=0.6964$ and $T^*=1.51$, ----: at $\rho^*=0.6964$ and $T^*=3.14$.

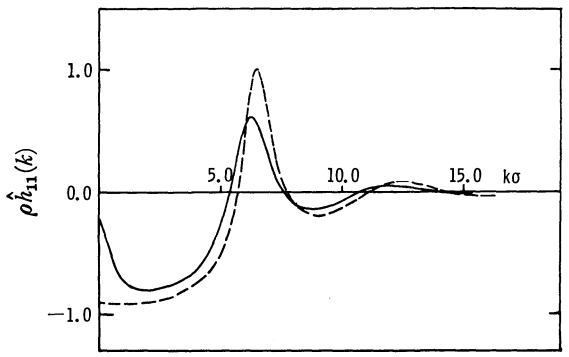

Fig. 9. Comparison of $\rho\hat{h}_{11}(k)$ between two different state.
——: At $\rho^*=0.55$ and $T^*=3.14$, ----: at $\rho^*=0.6964$ and $T^*=3.14$.

that of simple atomic fluids. The $g_{11}(r)$ obtained by Johnson[10] (Fig. 2) has no shoulder which is in sharp contrast to the result of our calculation as well as that of molecular dynamics.[11] The curve of Johnson deviates on the whole from the result of molecular dynamics[12] at higher temperatures (Fig. 4), while our curve is in a fairly good agreement. The shoulder disappears at higher temperatures, the $g_{11}(r)$ becoming similar to the radial distribution function for the fluid composed of spherical particles with the Lennard-Jones potential, as shown in Fig. 5.

Structure Factors. The structure factor calculated is compared with the results of molecular dynamics[11] in Fig. 6. Agreement is satisfactory except for small values of k. Figure 7 shows the structure factors calculated using the PY and HNC approximations, some difference appearing at small values of k. The difference appears also in structure factors calculated by use of the PY and HNC approximations for simple atomic fluids.[16] The structure factors we obtained for different temperatures at a fixed density are given in Fig. 8. The values of $S(k)$ increase in the small range of $k\sigma$ ($k\sigma<\pi$).[17] This has never been found in the results calculated by the method of a perturbation technique using blip function.[9] The behavior of the structure factors at small values of k seems to be due to the contribution of attractive potentials. In fact, at higher temperatures, the behavior of $S(k)$ becomes similar to that of $S(k)$ for the case of the hard sphere potential.

Weeks *et al.*[18] pointed out that the behavior of $\rho\hat{h}(k)$ is dominated by repulsive forces, and effect of the attractive forces is primarily manifested in the small wave vector portion as shown in Fig. 9. At lower densities, the contribution of the attractive forces becomes dominant at small values of k. On the other hand, at higher densities this contribution disappears and becomes similar to the behavior of $\rho\hat{h}(k)$ for the fluids consisting of hard sphere particles.

Concluding Remarks

The RISM integral equation coupled with the PY and HNC approximations has been applied to fluids consisting of homonuclear diatomic molecules interacting through the Lennard-Jones site-site potentials. Computation procedure and results are summarized as follows: (1) the RISM integral equation coupled with the PY and HNC approximations can be solved numer-

ically by means of a method of an iteration procedure with a fast Fourier transformation (FFT), (2) the site-site pair correlation function, $g_{11}(r)$, and structure factor, $S(k)$, are in agreement with the results of molecular dynamics, (3) the shoulder in $g_{11}(r)$ appears at $r^*=1+L^*$, which is considered to be characteristic of $g_{11}(r)$ for molecular fluids, not being present in $g(r)$ for simple atomic fluids, and (4) the behavior of $S(k)$ at small values of k is ascribed to the attractive part of potentials, the effect becoming more evident as compared with the results of the perturbation method.

The authers are much indebted to Dr. Yoshio Tago, Fujitsu Inc. Ltd., for preparation of the computer program used in the present paper.

References

1) K. Arakawa, *Kagaku Sosetsu*, **11**, 13 (1976); R. O. Watts, A Specialist Periodical Report, "Statistical Mechanics," Vol. 1, ed by K. Singer, The Chemical Society, London (1973), Chap. 1.
2) Yi-Der Chen and W. A. Steel, *J. Chem. Phys.*, **54**, 703 (1971).
3) D. Chandler and H. C. Andersen, *J. Chem. Phys.*, **57**, 1930 (1972); D. Chandler, *ibid.*, **59**, 2742 (1973).
4) F. Hirata, *Bull. Chem. Soc. Jpn.*, **50**, 1032 (1977).
5) L. J. Lowden and D. Chandler, *J. Chem. Phys.*, **59**, 6587 (1973).
6) L. J. Lowden and D. Chandler, *J. Chem. Phys.*, **61**, 5228 (1974).
7) B. M. Ladanyi and D. Chandler, *J. Chem. Phys.*, **62**, 4308 (1975).
8) D. Chandler, *Mol. Phys.*, **31**, 1231 (1976).
9) C. S. Hsu, D. Chandler, and L. J. Lowden, *Chem. Phys.*, **14**, 213 (1976).
10) E. Johnson, *J. Chem. Phys.*, **67**, 3194 (1977).
11) J. J. Weis and D. Levesque, *Phys. Rev. A*, **13**, 456 (1976).
12) J. Barojas, D. Levesque, and B. Quentrec, *Phys. Rev. A*, **7**, 1902 (1973); B. Quentrec and C. Brot, *ibid.*, **12**, 272 (1975).
13) In this paper we omit the term "like" since Eqs. 10 and 12 are identical in functional form with those of PY and HNC approximations used in usual statistical theory of fluids.
14) J. W. Cooley and J. W. Tukey, *Math. Comp.*, **19**, 297 (1965); F. Lado, *J. Comp. Phys.*, **8**, 417 (1971).
15) P. S. Y. Cheung and J. G. Powels, *Mol. Phys.*, **30**, 921 (1975).
16) The authors calculated $S(k)$ for simple atomic fluids by means of the PY and HNC equations. It was found that a difference appears in the small values of k.
17) P. A. Machin and J. Woodhead-Galloway, *J. Phys. C*, **3**, 2216 (1970).
18) J. D. Weeks, D. Chandler, and H. C. Andersen, *J. Chem. Phys.*, **54**, 5237 (1971); *ibid.*, **56**, 3812 (1972).

Pressure-Induced Metal-to-Ligand Electron Transfer and the Electrical Conductivity of Some Pt(II)-Glyoximes†

Yoji HARA* and Malcolm F. NICOL††

Department of Chemistry,††† University of California, Los Angeles, CA 90024, USA

(Received January 28, 1978)

Mid-infrared (900—1600 cm^{-1}), visible absorption spectra and electrical resistance of bis(benzil dioximato)-platinum(II) [abbreviated as $Pt(bz)_2$], bis(dimethylglyoximato)platinum(II) [$Pt(dmg)_2$], bis(1,2-cyclohexanedione dioximato)platinum(II) [$Pt(cd)_2$], and bis(pyruvaldehyde dioximato)platinum(II) [$Pt(pa)_2$] have been measured at high pressures. A decrease of the C=N frequency by -40.0 cm^{-1}, with reduction of the $d\pi\rightarrow\pi^*$ optical transition intensity by $\simeq 14\%$, show that $[Pt(bz)_2]$ enhances thermally its $d\pi\rightarrow\pi^*$ electron transfer at high pressures up to 35 kbar. No such changes are observed for $[Pt(dmg)_2]$, $[Pt(cd)_2]$, and $[Pt(pa)_2]$. This backbonding causes $[Pt(bz)_2]$ to release the instability, due to increasing overlapping of the electron clouds around Pt(II) at high pressures, that is the cause of the resistance minimum.

Many one-dimensional Pt(II) complexes exhibit minima of electrical resistance at high pressures.[1-4] These minima can be explained by calculations that identify two opposing effects on the $5d_{z^2}$—$6p_z$ energy gap. Compression of Pt–Pt separations to as little as 2.80 Å increases the $5d_{z^2}$—$6p_z$ overlap, decreasing the band gap,[5,6] while compression of the Pt-ligand separation usually increases the band gap as a result of ligand π-Pt p_z and ligand σ-Pt $\sigma(d_{x^2-y^2})$ interactions.[6] Exceptions to these generalizations are known. $MgPt(CN)_4\cdot 7H_2O$ has no detectable resistance minimum.[1] The behavior of $MgPt(CN)_4\cdot 7H_2O$ has been interpreted as the result of an additional electronic effect, strong enhancement of Pt $d\pi$-ligand π^* backbonding with compression, which reduces Coulombic repulsions between electrons in Pt orbitals, including orbitals on adjacent Pt atoms.

In a previous paper, Hara et al reported the electrical behavior under high pressure of several Pt(II) one-dimensional solids, including bis(benzil dioximato)platinum(II) [as $Pt(bz)_2$], bis(dimethylglyoximato)platinum(II) [as $Pt(dmg)_2$], bis(1,2-cyclohexanedione dioxomato)platinum(II) [as $Pt(cd)_2$], and bis(pyruvaldehyde dioximato)platinum(II) [as $Pt(pa)_2$].[2] When polycrystalline $[Pt(dmg)_2]$ is compressed, its resistance decreases continuously, by as much as 16 orders of magnitude, to 40 kbar; further compression causes the resistance to increase. $[Pt(bz)_2]$, however, has no resistance minimum; compression to 150 kbar continuously decreases its resistance, by as much as 13 orders of magnitude. In this respect, the high pressure electrical characteristics of $[Pt(bz)_2]$ resemble those of $MgPt(CN)_4\cdot 7H_2O$.

Since the pressure dependence of the C=N stretching vibration and $d\pi\rightarrow\pi^*$ optical transition of $[Pt(bz)_2]$ could be measured with our optical apparatus, we sought to establish whether the pressure dependence of the relevant spectra provided direct evidence that enhancement of the $d\pi\rightarrow\pi^*$ thermal electron transfer was responsible for the atypical resistance characteristics of $[Pt(bz)_2]$. For comparative purposes, infrared and visible absorption spectra of $[Pt(dmg)_2]$, $[Pt(cd)_2]$, and $[Pt(pa)_2]$, which have distinct resistance minima, also were studied. Compression of $[Pt(bz)_2]$ to 35 kbar had two effects on its spectra, the wavenumber of one C=N stretching band of the infrared spectrum decreased by an unusually large amount, and the intensity of the visible $d\pi\rightarrow\pi^*$ absorption band diminished. No such changes were observed for $[Pt(dmg)_2]$ or the other comparison compounds. The former effect indicates that metal-to-ligand $d\pi\rightarrow\pi^*$ thermal electron transfer in the ground state, which reduces the $d\pi\rightarrow\pi^*$ optical transition intensity, is greatly enhanced by compression of $[Pt(bz)_2]$, and demonstrate that enhancement of $d\pi\rightarrow\pi^*$ backbonding by electron acceptors such as the four phenyl groups of $[Pt(bz)_2]$ can be an important factor for reducing the electron repulsion terms on the Pt chain and increasing the conductivity of one-dimensional Pt complexes.

Experimental

For the infrared and visible spectral measurements, pressures to 35 kbar were generated by means of a high presuure optical bomb using a NaCl pressure medium.[7] The infrared technique has been described elsewhere,[8] except that these measurements were performed with a Perkin-Elmer 421 infrared double-beam spectrometer and were carried out in the range 900—1600 cm^{-1}. The visible spectral measurement was performed with a Bausch-Lomb grating spectrometer. The polycrystalline materials studied were prepared by the method used in the previous work.[2] The molecular structures of these samples are illustrated in Fig. 1.

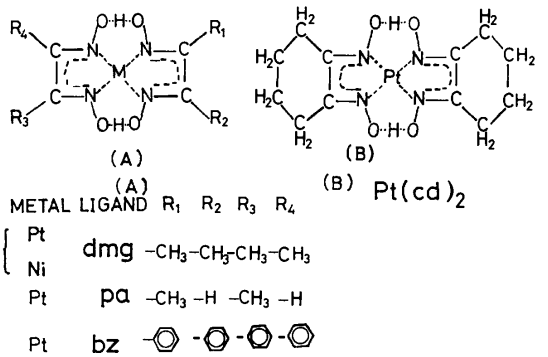

Fig. 1. Molecular structure of the samples.
(A) Bis(dimethylglyoximato)platinum(II) and nickel-(II); bis(pyruvaldehyde dioximato)platinum(II); bis(benzil dioximato)platinum(II).
(B) Bis(1,2-cyclohexanedione dioximato)platinum(II).

† Supported by NSF DMR 7308153.
†† Alfred P. Sloan Foundation Fellow, 1973—77.
††† Contribution No. 3824.

Results and Discussion

Figure 2 shows the effect of pressure on the electrical resistance of $[Pt(bz)_2]$, $[Pt(pa)_2]$, $[Pt(cd)_2]$, and $[Pt(dmg)_2]$. These effects are reversible and reproducible. The electrical resistance of $[Pt(dmg)_2]$, $[Pt(cd)_2]$ and $[Pt(pa)_2]$ show sharp resistance minima at 40, 90, and 120 kbar, respectively.

Infrared spectra of $[Pt(dmg)_2]$ at 0, 17, and 35 kbar are shown in Fig. 3. The C=N stretching modes are located at 1534 and 1482 cm^{-1}, and the N–O stretches at 1249 and 1078 cm^{-1}. The splitting of the C=N modes in $[Pt(dmg)_2]$ derives from the unequal C=N distance, 1.27 and 1.38 Å, respectively.[9] By way of comparison, $[Ni(dmg)_2]$ has single C=N stretching mode (1562 cm^{-1}) since its two distances are essentially identical, 1.30 and 1.29 Å.[10] Although the pressure effects are small, two are noteworthy. The C=N mode at 1482 cm^{-1}, corresponding to the 1.38 Å bond, disappears over 17 kbar, leaving single mode at 1533 cm^{-1}; this trend also is observed for $[Pt(cd)_2]$ and $[Pt(pa)_2]$. Also the degenerate and symmetric deformation modes of $C–CH_3$ between 1447—1330 cm^{-1} do not change much; thus, hyperconjugation must be less important than has been suggested.[2]

Comparable parts of the infrared spectra of $[Pt(bz)_2]$ at several pressures are reproduced in Fig. 4. Since two stretching bands are observed (at 1382 and 1430 cm^{-1}), the two C=N distances must be different. That these

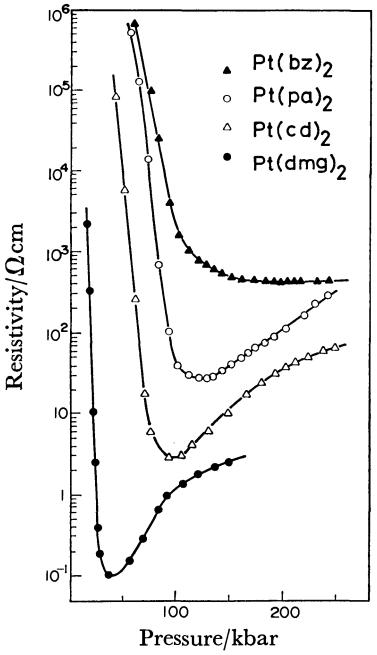

Fig. 2. Pressure effect on the electrical resistance of $[Pt(bz)_2]$, $[Pt(pa)_2]$, $[Pt(cd)_2]$, and $[Pt(dmg)_2]$.

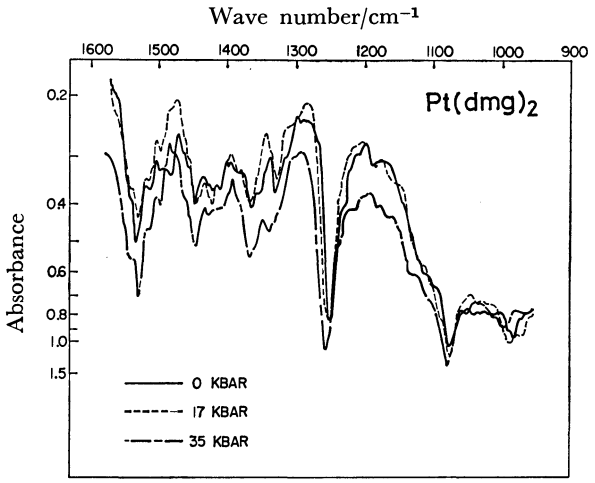

Fig. 3. Infrared spectra of $[Pt(dmg)_2]$ at 0, 17, and 35 kbar.

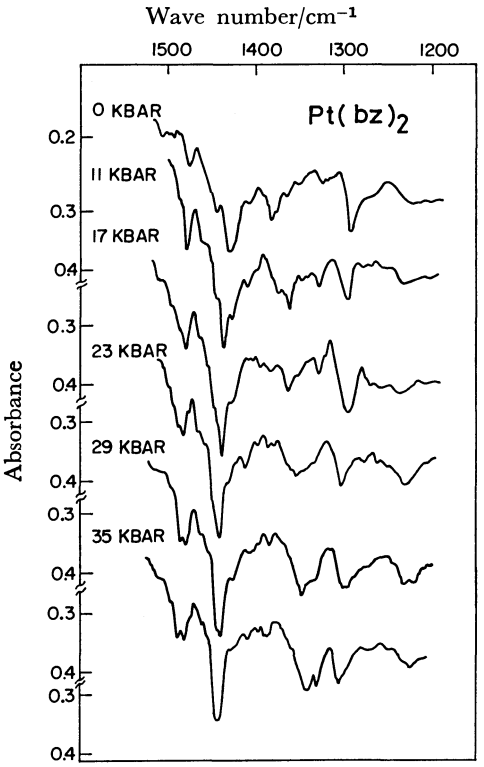

Fig. 4. Parts of the infrared spectra of $[Pt(bz)_2]$ at several pressures.

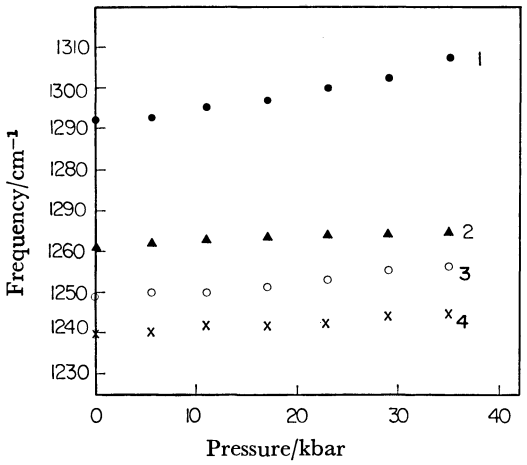

Fig. 5. Pressure-induced shifts of the N–O stretching bands of 1: $[Pt(bz)_2]$, 2: $[Pt(pa)_2]$, 3: $[Pt(dmg)_2]$, and 4: $[Pt(cd)_2]$.

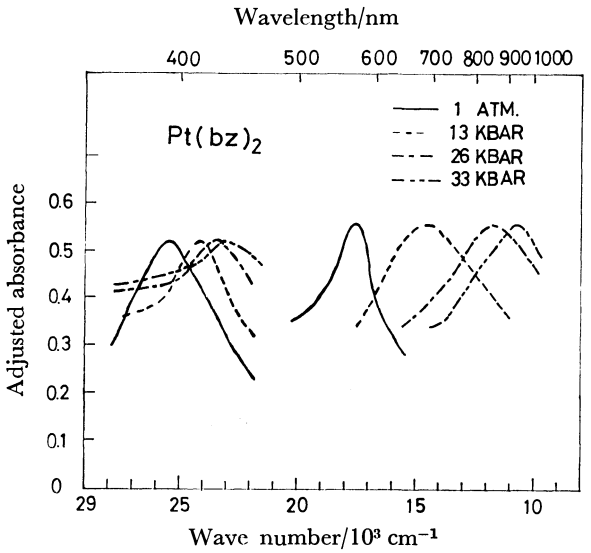

Fig. 6. Pressure dependence of the visible absorption spectra of $[Pt(bz)_2]$.
----: The peak intensities at higher pressures are normalized to the corresponding ones at 1 atm.

bands, and similar bands of $[Pt(dmg)_2]$, $[Pt(cd)_2]$, and $[Pt(pa)_2]$, have different pressure dependence is easily understood if one considers that the lower frequency band corresponds to the longer, more compressible C=N bond. However, this interpretation does not explain the anomalous shift of the 1382 cm^{-1} band to lower wavenumbers, by -40 cm^{-1} in 35 kbar. It is known that the frequencies of C=N stretching modes of metal-glyoximes decrease with increasing metal-to-ligand ($d\pi \rightarrow \pi^*$) backbonding.[11] The large frequency reduction of the C=N modes of $[Pt(bz)_2]$ suggests that $d\pi \rightarrow \pi^*$ backbonding is greatly enhanced at high pressures. As can be seen in Fig. 5, only small pressure-induced shifts of the N–O stretching bands (as well as C=N bands) are observed for $[Pt(dmg)_2]$, $[Pt(cd)_2]$, and $[Pt(pa)_2]$, indicating that backbonding is very minor in these complexes.

The pressure dependence of the visible absorption spectra of $[Pt(bz)_2]$, shown in Fig. 6, also indicates the importance of $d\pi \rightarrow \pi^*$ backbonding in this compound. Both the 25.4 kK band ($d\pi \rightarrow \pi^*$ charge transfer[12]) and the 18.0 kK band ($5d_{z^2} \rightarrow 6p_z$) shift to lower wavenumbers with compression, by -67 and -208 $cm^{-1} \cdot kbar^{-1}$ respectively. However, the $\simeq 14\%$ decrease of the intensity of the 25.4 kK band appears more significant; no similar fadeout of the $d\pi \rightarrow \pi^*$ transition is observed for $[Ni(dmg)_2]$ or $[Pt(dmg)_2]$.[13,14] This diminishing intensity is caused, in the ground state at high pressures, by occupation of ligand π^* orbitals by $d\pi$ electrons from the Pt atom. Thus, the four phenyl groups in $[Pt(bz)_2]$, which withdraw π-electrons from the C=N bonds, also induce significant electron transfer from the Pt $d\pi$ orbital to the ligand π system. In $[Pt(bz)_2]$, the central Pt(II) can compensate for the increasing overlap of the electron clouds at high pressures; which is the cause of the resistance minimum, by removing electrons outwards to the edge of the plane of the complex. These observations suggest that, by selecting even better electron acceptors than phenyl, one could make Pt-complexes that are significantly more conductive than $[Pt(bz)_2]$.

References

1) Y. Hara, I. Shirotani, and A. Onodera, *Solid State Commun.*, **17**, 827 (1975).
2) Y. Hara, I. Shirotani, and A. Onodera, *Solid State Commun.*, **19**, 171 (1976).
3) A. Onodera, N. Kawai, and T. Kobayashi, *Solid State Commun.*, **17**, 775 (1975).
4) L. V. Interrante and F. P. Bundy, *Inorg. Chem.*, **10**, 1169 (1971).
5) Y. Hara, I. Shirotani, Y. Ohashi, K. Asaumi, and S. Minomura, *Bull. Chem. Soc. Jpn.*, **48**, 403 (1975).
6) L. V. Interrante and R. P. Messmer, *Inorg. Chem.*, **10**, 1174 (1971).
7) M. Nicol, Y. Ebisuzaki, W. D. Ellenson, and A. Karim, *Rev. Sci. Instrum.*, **43**, 1368 (1972).
8) C. K. Wu, Ph. D. thesis, (University of California, Berkeley, 1972).
9) C. Panattoni, E. Terasson, and R. Zanetti, *Acta Crystallogr.*, **12**, 1027 (1959).
10) W. Pfab and R. Nast, *Z. Krist.*, **111**, 259 (1959).
11) K. Burge, I. Ruff, and F. Ruff, *J. Inorg. Nucl. Chem.*, **27**, 179 (1965).
12) Y. Ohashi, I. Hanazaki, and S. Nagakura, *Inorg. Chem.*, **9**, 2551 (1970).
13) With the increase in the $d\pi$-π^* interaction, the $d\pi \rightarrow \pi^*$ optical transition may borrow its intensity from $\pi \rightarrow \pi^*$ transition (see Ref. 14), then real rate of the decrease in $d\pi \rightarrow \pi^*$ intensity may be more than 14%.
14) I. Hanazaki and S. Nagakura, *J. Chem. Phys.*, **50**, 265, 276 (1969).

Fluorescence Spectra of 1,1′-Binaphthyl and Related Compounds at High Pressures

Yoji HARA* and Malcolm F. NICOL*

Department of Chemistry, University of California, Los Angeles, CA 90024, USA

(Received February 7, 1978)

Relative to the related compounds 2,2′-binaphthyl (I) and 2,2′-dimethoxy-1,1′-binaphthyl (II), the pressure dependence of the fluorescence of crystals of 1,1′-binaphthyl (III) is complex. Compression to 30 kbar at room temperature shifts the ^{1}La fluorescence spectra of all three compounds to longer wavelength but, for I and II does not change the intensity profile, except for some 0-0 reabsorption. For III, this red shift characteristic of ^{1}La fluorescence spectra is dominated by growth of new bands about 3.5 to 5.0×10^3 cm^{-1} to lower energy. Similar new bands are observed when 1,1′-binaphthyl crystals are compressed at 90 K or resolved crystals are compressed at room temperature, but are not found to 30 kbar for dilute solutions of 1,1′-binaphthyl in polyacrylonitrile. The planes of adjacent naphthyl residues along $\vec{b}$ in the crystal are parallel but offset, the normal distance between planes being 3.55 Å; Raman spectra provide no evidence for a structural phase transformation upon compression. These new bands are assigned as the binaphthyl excimer.

The molecular spectroscopy of 1,1′-binaphthyl is unusual in many respects due to the strong dependence of the energies of its excited electronic states on the angle, θ, between the planes of the two naphthyl residues. In the crystal or rigid matrices (methyltetrahydrofuran or methanol glass) at low temperatures, the fluorescence and first absorption band are mirror images and closely resemble comparable spectra of naphthalene.[1-4] These observations are interpreted to imply that the equilibrium value of θ for both the ground and lowest excited state is approximately $\pi/2$; the X-ray structure of the crystal suggests $\theta=68°$ at room temperature.[5] In fluid solutions, the structure of the fluorescence spectrum resembles more closely the ^{1}La absorption of naphthalene and the fluorescence decay rate ($\approx10^9$ s^{-1}) is more typical of the ^{1}La fluorescence of anthracence and larger linear polyacenes. This transformation of the fluorescence has been interpreted in terms of a thermally-activated crossing from the ^{1}Lb to a ^{1}La excited state which can be stabilized relative to ^{1}Lb by rotation of the naphthyl residues toward $\theta=0$ or $\theta=\pi$.[1,4]

This report describes yet another fluorescence transformation observed for crystalline 1,1′-binaphthyl, but not for dilute solutions of 1,1′-binaphthyl in polyacrylonitrile, for crystalline 2,2′-binaphthyl or for derivative such as 2,2′-dimethoxy-1,1′-binaphthyl. Upon compression of crystals of 1,1′-binaphthyl to pressures above 5 kbar, new bands appear in the fluorescence spectra about 3.5 to 5.0×10^3 cm^{-1} to lower wave numbers from the origin of the ^{1}La fluorescence. These bands increase in intensity with compression such that, at 30 kbar, they dominate the emission spectrum. This spectral transformation is completely reversible to compression at room temperature (nominally 295 K) and at 90 K. The new spectrum is assigned as an excimer fluorescence originating from pairs of binaphthyl molecules favorably disposed along the $\vec{b}$ axis of the crystal. Both dilute solution in polyacrylonitrile and substitution at the 2 and 2′ positions prevent similar intermolecular naphthyl residue interactions between 1,1′-binaphthyl molecules.

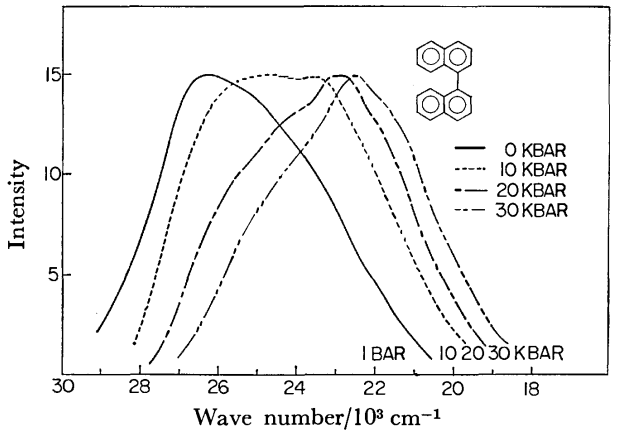

Fig. 1. Fluorescence spectra of 1,1′-binaphthyl at 295 K as a function of pressure.

Experimental

Commertially available reagent grade of 1,1′-binaphthyl from Eastman Kodak Co. was recrystallized from acetic acid and identified by infrared spectra.[6] 2,2′-dimethoxy-1,1′-binaphthyl were kindly provided by Dr. R. Helgesson of this department. The high pressure techniques for room[7,8] and low[9] temperatures are described elsewhere. The fluorescence from the samples which were excited at 3130 Å emission from 120W PEK Labs. Inc. high pressure mercury arc lamp was measured by means of front surface illumination in order to minimize reabsorption. The fluorescent intensities obtained at high pressures are normalized to that at 0 kbar. For Raman spectral measurement, a Spectra-Physics Model 165 argon laser was used for excitation. A Spex double monochrometer and photon-counting techniques were used to analyze the spectrum.

Results and Discussion

Fluorescence spectra of polycrystalline samples of 1,1′-binaphthyl at room temperature and 90 K at 1 bar, 10, 20, and 30 kbar are shown in Figs. 1 and 2. A typical pattern of other aromatics emerges from the spectra. The high wave number edge of the spectra appear to shift by -50 cm^{-1} kbar^{-1}, although reabsorption and the changing spectral profile make this value difficult to determine. For more important is the growth of intensity of new bands at low wave num-

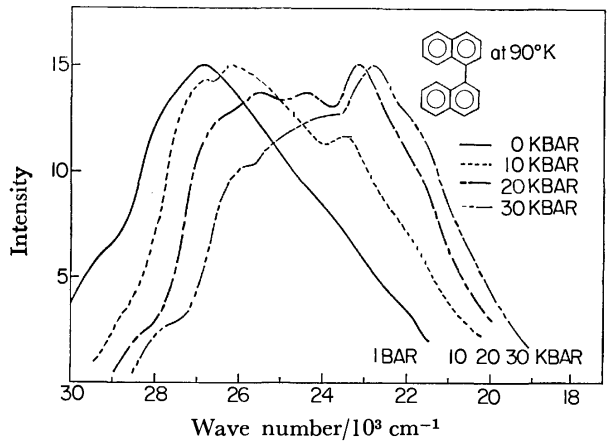

Fig. 2. Fluorescence spectra of 1,1′-binaphthyl at 90 K as a function of pressure.

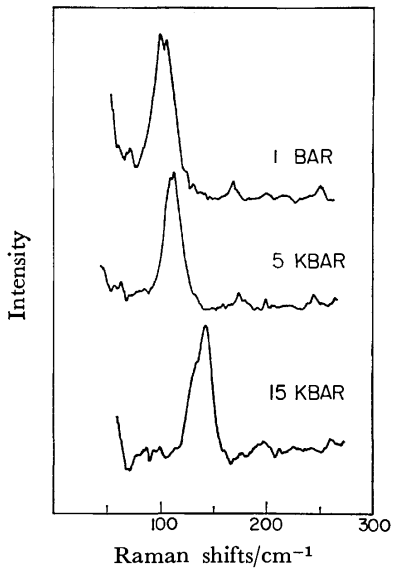

Fig. 3. Raman spectra of 1,1′-binaphthyl at 1 bar, 5 and 15 kbar.

bers, 3.5—5.0 × 10³ cm⁻¹ below the shifted 0-0. These transformation are completely reversible upon decompression. Similar new bands are observed when crystals of partially resolved 1,1′-binaphthyl are compressed.

Figure 3 shows the Raman spectra of polycrystalline 1,1′-binaphthyl at several pressures. These indicate that possibility of phase transition is very minor up to 15 kbar.

The new bands at low wave numbers in the fluorescence spectra of 1,1′-binaphthyl resemble in many respects new bands observed in the spectra of other crystalline aromatics at high pressures.[10–12] These spectra have been assigned to excimers formed by suitably oriented pairs of molecules at defect sites.

Figures 4 and 5 display the fluorescence spectra of 2,2′-binaphthyl and 2,2′-dimethoxy-1,1′-binaphthyl as a function of pressure. The primary effect of compression is to shift the fluorescence to lower wave numbers, by −30 cm⁻¹ kbar⁻¹ for 2,2′-binaphthyl and by about −40 cm⁻¹ kbar⁻¹ for 2,2′-dimethoxy-1,1′-binaphthyl. Except for some increased reabsorption of the 0-0

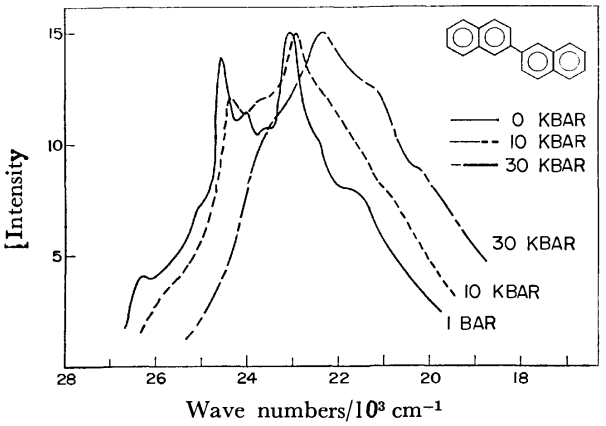

Fig. 4. Fluorescence spectra of 2,2′-binaphthyl at 1 bar, 10 and 30 kbar.

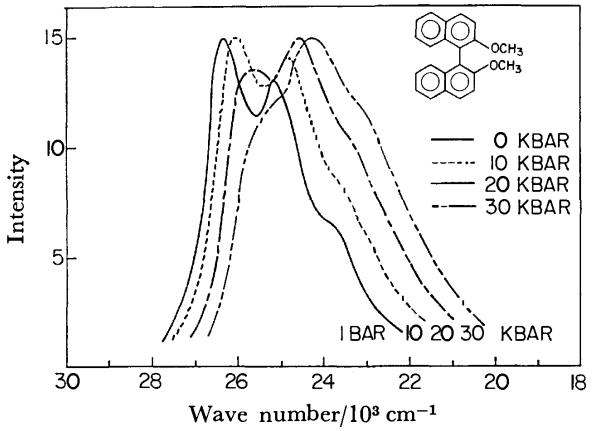

Fig. 5. Fluorescence spectra of 2,2′-dimethoxy-1,1′-binaphthyl at several pressures.

band at high pressures, the intensity profiles of these spectra change only slightly with compression which is the exception for aromatic hydrocarbons.[10–12] The interesting observation here is that the new bands are observed for 1,1′-binaphthyl but not for 2,2′-binaphthyl or 2,2′-dimethoxy-1,1′-binaphthyl. If the excimer fluorescence originated at defects, some excimer-like fluorescence would be anticipated from these compounds.

As steric hindrance between two naphthalene residues is at minimum in 2,2′-binaphthyl among various binaphthyls,[13] charge or excitonic resonance between two naphthyl residues should be maximized in 2,2′-binaphthyl. But no similar excimer fluorescence to 1,1′-binaphthyl was observed for 2,2′-binaphthyl. This indicates that the excimer fluorescence in 1,1′-binaphthyl is not originated from intramolecular interaction.

Figure 6 depicts the fluorescence spectra of dilute (≈ 10⁻³ M) solutions of 1,1′-binaphthyl in polyacrylonitrile at 1 bar and 30 kbar. No intensity redistribution is noted, which evidences the intermolecular nature of the excimer fluorescence.

An interesting explanation for the difference between 1,1′-binaphthyl and the other binaphthyls is suggested by examination of the structure of 1,1′-binaphthyl crystal.[5] Binaphthyl molecules with the same configuration are oriented with the planes of their naphthyl

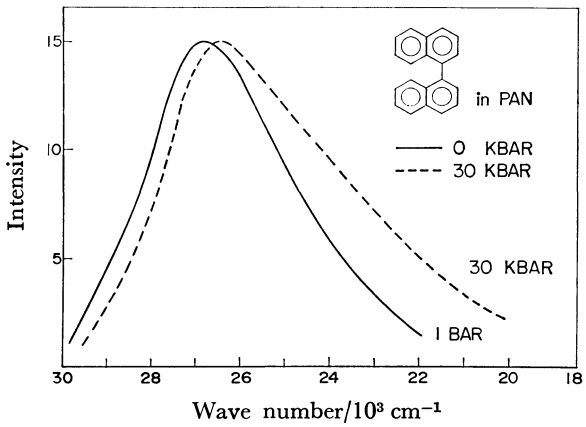

Fig. 6. Fluorescence spectra of dilute ($\approx 10^{-3}$ M) solutions of 1,1′-binaphthyl in polyacrylonitrile at 1 bar and 30 kbar.

residues parallel to each other and are separated by 6.35 Å along $\vec{b}$. For this geometry the normal distance between naphthyl planes of adjacent molecules is 3.55 Å, almost identical to the 3.53 Å separation between pyrene molecules in the dimeric structure of crystalline pyrene, the prototype excimer system.[14] Although the overlap of naphthyl residues is slightly less favorable for excimer emission, compression along $\vec{b}$ can compensate for this factor. However, substitution at the 2 position of the naphthyl residues necessarily increases the separation between binaphthyl molecules along this direction to a degree that should preclude excimer formation by this mechanism.

We are extremely grateful for the support provided by National Science Foundation and the binaphhtyl derivatives prepared by Dr. R. Helgesson.

References

1) R. M. Hochstrasser, *Can. J. Chem.*, **39**, 459 (1961).
2) H. Zimmermann and N. Joop, *Ber. Bunsenges. Phys. Chem.*, **64**, 1215 (1960).
3) M. F. M. Post, J. Langelaar, and J. D. W. VanVoorst, *Chem. Phys. Lett.*, **32**, 59 (1975).
4) M. F. M. Post, J. K. Eweg, J. Langelaar, J. D. W. Van Voorst, and G. TerMaten, *Chem. Phys.*, **14**, 165 (1976).
5) K. A. Kerr and J. M. Robertson, *J. Chem. Soc., B*, **1969**, 1146.
6) Y. Badar, C. C. K. Lings, A. S. Cooke, and M. M. Harris, *J. Chem. Soc.*, **1965**, 1543.
7) M. Nicol, *J. Opt. Soc. Am.*, **55**, 1176 (1965).
8) M. Nicol, S. M. Wild, and J. Yancey, *J. Chem. Phys.*, **58**, 4350 (1973).
9) M. Nicol, Y. Ebisuzaki, W. D. Ellenson, and A. Karim, *Rev. Sci. Instrum.*, **43**, 1368 (1972).
10) P. F. Jones and M. Nicol, *J. Chem. Phys.*, **48**, 5440 (1968).
11) M. Nicol, M. Vernon and J. T. Woo, *J. Chem. Phys.*, **63**, 1992 (1975).
12) H. W. Offen, "Organic Molecular Photophysics," Vol. 1, ed by J. B. Birks, Wiley, London (1973), p. 103.
13) R. A. Friedel, M. Orchin, and L. Reggel, *J. Am. Chem. Soc.*, **70**, 199 (1948).
14) J. B. Birks, A. A. Kazzaz, and T. A. King, *Proc. Soc. London, Ser. A*, **291**, 556 (1966).

Hydrogen-Deuterium Exchange Rate between a Peptide Group and an Aqueous Solvent as Determined by a Stopped-Flow Ultraviolet Spectrophotometry

Tetsuo TAKAHASHI, Mamoru NAKANISHI, and Masamichi TSUBOI*

Faculty of Pharmaceutical Sciences, The University of Tokyo, Hongo, Bunkyo-ku, Tokyo 113

(Received February 22, 1978)

When an ^1H_2O solution of *N*-methylacetamide was rapidly mixed with ^2H_2O, a time-dependent decrease of the ultraviolet absorbance at 227 nm was observed. This was not the case with *N,N*-dimethylacetamide. Hence, the time-dependent decrease in absorbance was attributed to be caused by the deuteration (NH→ND) reaction of *N*-methylacetamide. This provides an appropriate method for determining deuteration rate of the peptide group in a polypeptide or in a protein. By this method the deuteration rate of poly-D,L-alanine has been examined in the pH=5—8 and temperature=10—40 °C range. In this range, the deuteration was found to proceed always as a single first-order reaction, and the rate constant k_e is expressed within an experimental error as $k_e = 6.4 \times 10^{(6+pH-3850/T)}$. This is to be used as a standard rate-constant value in estimating the attenuation factor $\gamma_j = k_j/k_e$ of a given peptide group (j) in a protein molecule whose rate constant value is k_j.

When a protein or a polypeptide is placed in an aqueous medium, a proton exchange reaction takes place between the peptide NH group and the solvent H_2O. The rate of this exchange reaction depends upon the intramolecular environment of the peptide group in question, and a kinetic study of such an exchange reaction provides a useful piece of information of the protein or the polypeptide structure.[1-5] The kinetics has so far been examined mostly by an infrared spectrophotometric tracing of the deuteration process of the peptide groups of a protein molecule thrown into ^2H_2O.[6] The kinetics was also examined by tracing hydrogen-tritium exchange reaction by means of a radioactivity measurement in combination with the Sephadex column chromatography.[7] By these methods, however, the reactions faster than 0.1 s^{-1} are not easily traced.[7,8]

The scope of this paper is two-fold. First we report that the hydrogen-deuterium exchange reaction of the peptide NH group can be followed by a stopped-flow ultraviolet spectrophotometry.[9-11] It will be shown that, by this method, the exchange reaction as fast as 30 s^{-1} can readily be traced. Secondly, rate constant values (k_e) for a peptide group fully exposed to the solvent are given in the pH=5—8 and temperature=10—40 °C range. Each of these values is serviceable as a standard in estimating an attenuation factor γ_j for a given peptide group (j) in a given protein molecule. Thus,

$$\gamma_j = k_j/k_e, \quad (1)$$

where k_j is the hydrogen exchange rate constant of the j-th peptide group now in question at a given pH and temperature. The attenuation factor γ_j is a measure of how deeply the j-th peptide group is buried in the protein molecule, and $\ln \gamma_j$ is often considered to be proportional to the free energy required for bringing this j-th peptide group into a state fully exposed to the solvent. In the most useful range of pH (5—8) and temperature (10—40 °C), however, the k_e values are so high (or the exchange reaction of the peptide NH is so fast) that only the new method is applicable. By the former methods, the measurements were so far made only in the lower pH region and/or lower temperature region, and the k_e value in the range now in question was estimated only by an extrapolation.

Experimental

N-Methylacetamide was obtained from Aldrich Chemical Company, and *N,N*-dimethylacetamide from Wako Pure Chemical Industries, Ltd. Poly-D,L-alanine with an average molecular weight 3800 (average degree of polymerization=53) was purchased from Miles Chemical Company and purified by a Sphadex G25 column chromatography. ^2H_2O (deuterium atom content 99.8%) was purchased from CEA-CEN-SACLAY.

The fast deuterations were examined by the use of a Union Giken Stopped-Flow Spectrophotometer RA-401. This is equipped with a rapid mixing device of a dead time 0.5 ms, with two syringes operated with nitrogen gas pressure. A fast flow of the mixture goes through a cell of optical path-length 10 mm. At about 17 millisecond after the pressure is applied, the flow is stopped, and a time-dependent absorbance change starts in the cell. This is detected by an ultraviolet spectrophotometer of focal length 25 cm, and of sensitivity 0.0001 OD. The temperature of the solution was controlled by circulating ethylene glycol through a mantle from a Haake model KT41 circulator. The actual temperature of the solution was monitored by a thermocouple.

Slower exchange reactions were traced with another stopped-flow equipment and a Hitachi EPS-3T Recording Spectrophotometer.

The hydrogen ion concentration of the solution was determined with a Hitachi-Horiba F7SS pH meter. The pH values given in this paper were always those of the solutions after the mixing (*i.e.*, in 50% ^1H_2O+50% ^2H_2O). Here, the pH-metric readings are given without any correction.

Hydrogen-Deuterium Exchange in *N*-Methylacetamide

When *N*-methylacetamide is suddenly brought into a ^2H_2O medium, a time-dependent decrease in absorbance at 227 nm is observed as illustrated in Fig. 1(a). Such an absorbance change is not observed at all when this molecule is brought by the same equipment into pure ^1H_2O (see Fig. 1(b)). This is not observed also when *N,N*-dimethylacetamide, where no NH group remains, is brought into the same ^2H_2O medium (Fig. 1(c)). Therefore, the time-dependent absorbance decrease is attributable to the NH→ND

reaction in *N*-methylacetamide. As is shown in Fig. 2(a), *N*-methylacetamide has a strong absorption band at about 190 nm. It is probable that this band is shifted very slightly towards shorter wavelength on deuteration, such a shift is considered to cause a slight but appreciable absorbance drop at 227 nm.

A replot of the kinetic data such as that given in Fig. 1(a) shows that the absorbance decrease takes place as a single first-order process. By extrapolating this first-order process to zero time, we are able to determine the total absorbance change associated with this process (NH→ND). The absorbance changes

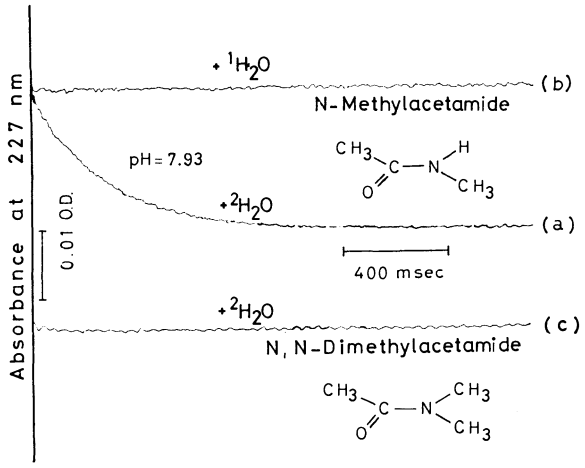

Fig. 1. (a) The time dependence of the decrease in absorbance at 227 nm observed when *N*-methylacetamide dissolved in ^1H_2O is mixed with ^2H_2O, so that final concentration of *N*-methylacetamide is 0.14 M and the solvent is 50% ^1H_2O+50% ^2H_2O of pH 7.93 at 22 °C. This is a photographic reproduction of the curve record on the plotter connected with a Union Giken stopped-flow spectrophotometer RA-401 and a data processor RA-450. This is a one scan datum; no accumulation was made. (b) The curve recorded in a control experiment, in which the same *N*-methylacetamide solution was mixed with pure ^1H_2O instead of ^2H_2O. (c) The curve recorded in another control experiment, in which a ^1H_2O solution of *N*,*N*-dimethylacetamide (instead of *N*-methylacetamide) was mixed with ^2H_2O.

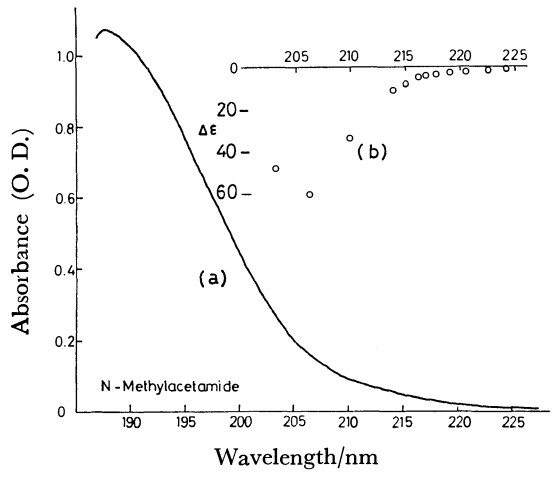

Fig. 2. (a) Ultraviolet absorption spectrum of 1.22×10^{-4} M *N*-methylacetamide in ^1H_2O at pH 5 and 25.2 °C. (b) A difference spectrum of *N*-methylacetamide *versus* *N*-methylacetamide-*d*, obtained from the kinetic measurement. Each point indicates the total absorbance change obtained for the first-order process observed on dilution with ^2H_2O to zero time. Ordinate scale $\Delta\varepsilon$ is the difference in the molar extinction coefficient ε.

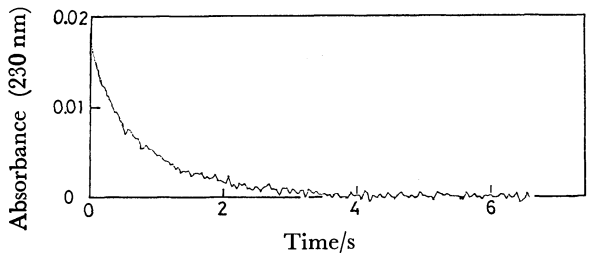

Fig. 3. The time dependence of the decrease in absorbance at 230 nm observed when poly-D,L-alanine dissolved in ^1H_2O is mixed with ^2H_2O, at pH 6.67 and at 13.5 °C. Final concentration of poly-D,L-alanine is 5.5 mM (for alanine residue).

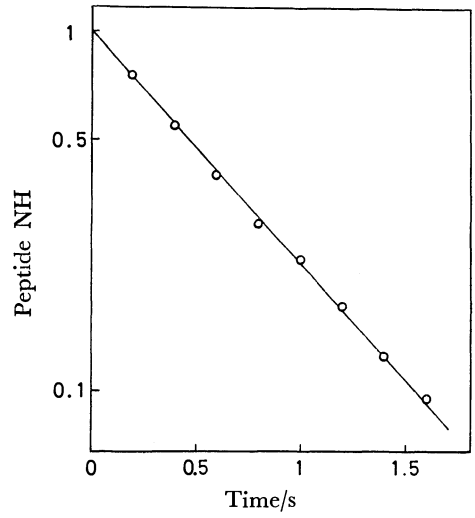

Fig. 4. Semilogarithmic plot of the data shown in Fig. 3.

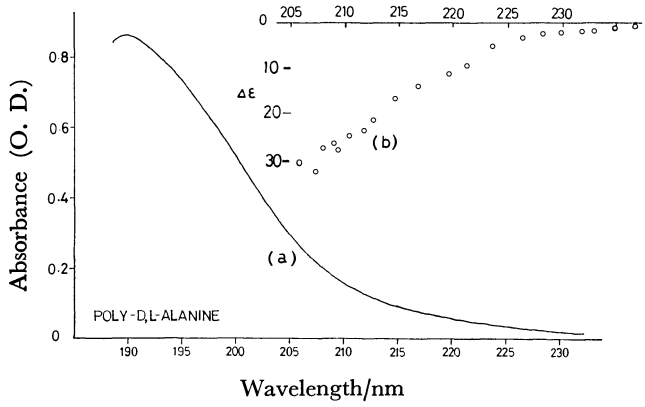

Fig. 5. (a) Ultraviolet absorption spectrum of poly-D,L-alanine in H_2O at pH 4 and 25.2 °C. (b) A difference spectrum of poly-D,L-alanine *versus* poly-D,L-alanine-*d*, obtained from the kinetic measurement, similar to what was described for Fig. 2(b).

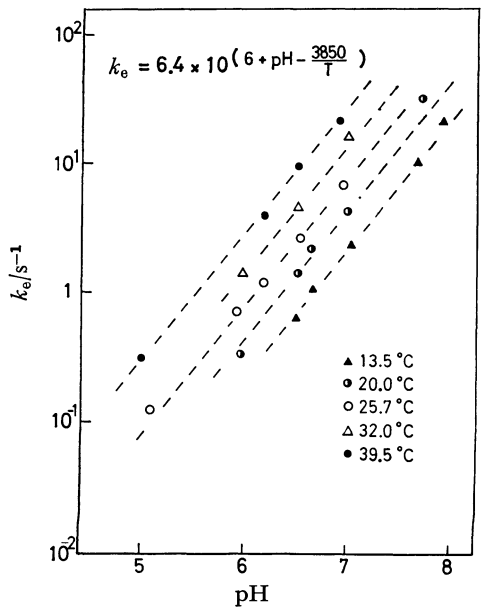

Fig. 6. The first-order rate constants k_e of the hydrogen-deuterium exchange reaction of poly-D,L-alanine, determined at various pHs and temperatures.

masured in this way at several different wavelengths generate a difference spectrum shown in Fig. 2(b). The rate constant of the NH→ND reaction is found to be 4.17 s^{-1} at pH 7.93 and at 22 °C and 0.31 s^{-1} at pH 6.83 and at 21 °C.

Hydrogen-Deuterium Exchange in Poly-D,L-alanine

Poly-D,L-alanine is an unfolded, non-helical polypeptide, and is soluble in H_2O. Every peptide group in this polypeptide is supposed to be "fully" exposed to the solvent at every pH and temperature in a proper range. This has been selected as a material, whose deuteration (NH→ND) rate (k_e) is used as a standard in estimating an attenuation factor γ_j with Eq. 1.

In Fig. 3, an example of the observed curve is given, which shows a time course of the absorbance change at 230 nm caused by the deuteration of poly-D,L-alanine. A replot of such a kinetic data on a logarithmic ordinate scale, as illustrated in Fig. 4, shows that the absorbance change takes place as a single first order process. The total absorbance change in such a process has been examined at various wavelengths. A difference spectrum of poly-D,L-alanine *versus* poly-D,L-alanine-*d*, thus obtained, is shown in Fig. 5.

The first-order rate constant k_e of the hydrogen-deuterium exchange reaction of poly-D,L-alanine has been determined in the pH range of 5—8 and temperature range of 10—40 °C. The results are graphically shown in Fig. 6. As may be seen in the figure, $\log_{10} k$ values fall on a single straight line at every pH, when they are plotted against reciprocal absolute temperature T. From the slope of this straight line the activation energy is estimated to be $\Delta H^* = 17.6 \pm 0.3$ kcal/mol, at every pH in the 5—8 range. When $\log_{10} k_e$ is plotted against pH, on the other hand, the points fall on a straight line of solpe=1, at every temperature. This fact indicates that in this pH range the reaction is catalyzed by OH^-. The empirical formula for the k_e value of poly-D,L-alanine is now given as

$$k_e = 6.4 \times 10^{(6+pH-3850/T)}. \quad (2)$$

It should be pointed out that what were previously given by an extrapolation[12–14] are slightly but appreciably different from the k_e values directly determined in our present work.

References

1) A. Hvidt and S. O. Nielsen, *Adv. Protein Chem.*, **21**, 287 (1966).
2) S. W. Englander, N. Downer, and H. Teitelbaum, *Ann. Rev. Biochem.*, **41**, 903 (1972).
3) M. Nakanishi, M. Tsuboi, and A. Ikegami, *J. Mol. Biol.*, **70**, 351 (1972).
4) M. Nakanishi, M. Tsuboi, and A. Ikegami, *J. Mol. Biol.*, **75**, 673 (1973).
5) M. Nakanishi and M. Tsuboi, *J. Mol. Biol.*, **83**, 379 (1974).
6) E. R. Blout, C. de Loze, and A. Asadourian, *J. Am. Chem. Soc.*, **83**, 1895 (1961).
7) S. W. Englander, *Biochemistry*, **2**, 798 (1963).
8) N. Suda, M. Nakanishi, and M. Tsuboi, *Rev. Sci. Instr.*, **45**, 680 (1974).
9) M. Nakanishi, H. Nakamura, A. Y. Hirakawa, M. Tsuboi, T. Nagamura, and Y. Saijo, *J. Am. Chem. Soc.*, **100**, 272 (1978).
10) M. Nakanishi and M. Tsuboi, *J. Am. Chem. Soc.*, **100**, 1273 (1978).
11) D. G. Cross, *Biochemistry*, **14**, 357 (1975).
12) S. O. Nielsen, *Biochim. Biophys. Acta*, **37**, 146 (1960).
13) W. P. Bryan and S. O. Nielsen, *Biochim. Biophys. Acta*, **42**, 552 (1960).
14) S. W. Englander and A. Poulsen, *Biopolymers*, **7**, 379 (1969).

The Crystal Structure of L-Asparaginato-D-aspartatocobalt(III) Monohydrate

Masao SEKIZAKI

College of Liberal Arts, Kanazawa University, Marunouchi, Kanazawa 920

(Received August 8, 1977)

The crystal structure of L-asparaginato-D-aspartatocobalt(III) monohydrate, $[Co(H_2NCOCH_2CHNH_2COO)(OCOCH_2CHNH_2COO)]\cdot H_2O$, has been determined by an X-ray diffraction method and refined by a block-diagonal least-squares method to give $R=0.033$ for 1517 non-zero reflections. The crystals are orthorhombic with the space group $P2_12_12_1$, $a=11.790(2)$, $b=17.059(2)$, $c=5.830(2)$ Å, and $Z=4$. The complex molecule has a slightly distorted octahedral coordination with *fac*(*N*) geometry. The amide group of L-asparaginate ion is coordinated through the nitrogen atom, and an enolic system of Co←NH=C(OH)–CH_2– is formed. The complex molecules are held together through hydrogen bonds which form two-dimensional networks parallel to the (010) plane. The networks are piled up through hydrogen bonds by water molecules to complete three-dimensional networks.

There are generally two coordination modes for an acid amide group: O-coordination(I)[1-5] and N-coordination (II),[6] the latter being accompanied by deprotonation of the amide group. Recently

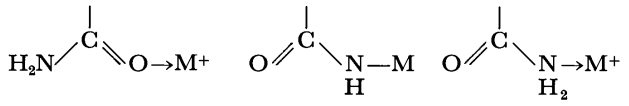

I II III

Takenaka and Shibata has suggested on the basis of infrared and visible spectra that the cobalt complex containing both L-asparaginate (L-2-aminosuccinamate, abbreviated as L-$aspNH_2^-$) ion and D-aspartate (D-2-aminosuccinate, D-asp^{2-}) ion, $[Co(L\text{-}aspNH_2)(D\text{-}asp)]\cdot H_2O$, has a *fac*(*N*) structure.[7] This means that the primary amide group of L-$aspNH_2^-$ is coordinated through the nitrogen atom without deprotonation, and the coordinating mode is neither I nor II. A third mode, like III, seems probable, although no example of this mode has been found to date. In order to investigate the coordination mode of this cobalt(III) complex, an X-ray single-crystal analysis has been undertaken.

Experimental

The crystals prepared and supplied by Professor Muraji Shibata of Kanazawa University are reddish-violet prisms. A crystal with dimensions of $0.2\times0.15\times0.15$ mm was selected, and the diffracted intensities were measured on a Philips PW 1100 four-circle diffractometer with Mo $K\alpha$ radiation monochromated by a graphite plate. The θ-2θ scan technique was used at a scan rate of 0.0668°/s in θ with a scan width of $(1.0+0.3\tan\theta)°$. The intensities of three reference reflections monitored every 2 h remained constant during data collection. A total of 2012 independent reflections was measured up to $2\theta=60°$, and 1517 of them with $|F|>3\sigma$ were used for the structure analysis. No corrections were made for absorption and extinction effects. Cell dimensions were obtained from the least-squares method based on 19 2θ values.

Crystal data:
$Co(H_2NCOCH_2CHNH_2COO)(OCOCH_2CHNH_2COO)\cdot H_2O$. *F. W.*=339.15. Orthorhombic, $a=11.790(2)$, $b=17.059(2)$, and $c=5.830(2)$ Å. $U=1173(1)$ Å^3. $\rho_x=1.921$ g·cm^{-3}, $Z=4$. Space group $P2_12_12_1$. $\mu=3.9$ cm^{-1} (Mo $K\alpha$, $\lambda=0.7107$ Å).

Determination and Refinement of the Structure

The coordinates of the cobalt atom were determined from the Patterson map; the successive Fourier synthesis phased by the cobalt atom gave an approximate skeletal structure shown in Fig. 1. In this figure, the four positions marked with * should be occupied by one nitrogen and three oxygen atoms, but, at this stage, it was impossible to distinguish these two kinds of atoms. Accordingly, the distinction between L-$aspNH_2^-$ and D-asp^{2-} was impossible. The block-diagonal least-squares refinement was carried out in expectation of getting a clue for the discrimination between oxygen and nitrogen. When all the four atoms marked with * (Fig. 1) were assumed to be oxygen, the *R*-value was 0.062. On the other hand when they were assumed to be nitrogen, *R* was 0.066. In both assumptions the isotropic temperature factors did not allow the two kinds of atoms to be distinguished. Anisotropic temperature factors were, then, introduced for all the atoms on the assumption that these four atoms were all oxygen. The *R*-value decreased to 0.050. The difference Fourier synthesis was calculated and gave the positions of all the 14 hydrogen atoms. The amide group could be distinguished at this stage from the carboxyl group. The obtained structure revealed the existence of both N–H and O–H bonds at the amide group, namely, the structure of the amide group is not I, II, nor III, but could be IV or V.

IV V

Several cycles of the refinements were carried out for these two modes IV and V, including the hydrogen atoms, the isotropic temperature factors of which were assumed to be 4.0 Å^2. Both modes, IV and V, gave the equivalent isotropic temperature factors (B_{eq})[8] 1.8—2.2 Å^2 for the coordinating atoms of the three carboxyl groups. The corresponding values for the non-coordinating oxygen atoms of these carboxyl groups were 2.8—3.2 Å^2. Similarly, those for the coordinating

TABLE 1. FINAL ATOMIC PARAMETERS AND THEIR ESTIMATED STANDARD DEVIATIONS IN PARENTHESES
Values for hydrogen atoms are multiplied by 10^3 and those for the others by 10^4.
Thermal parameters are in the form: $\exp[-(h^2\beta_{11}+k^2\beta_{22}+l^2\beta_{33}+hk\beta_{12}+hl\beta_{13}+kl\beta_{23})]$.

Atom	x	y	z	β_{11}	β_{22}	β_{33}	β_{12}	β_{13}	β_{23}
Co	246(1)	1565(1)	584(2)	28(1)	10(1)	84(2)	−1(1)	−8(2)	−5(2)
O(1c)	−867(3)	2377(2)	595(7)	31(3)	15(1)	154(9)	3(3)	8(10)	−13(7)
O(1)	−1138(3)	3584(2)	−741(8)	46(3)	21(2)	243(12)	19(3)	27(12)	7(8)
C(1)	−616(4)	2967(3)	−747(10)	29(3)	15(2)	151(13)	−0(3)	−33(13)	−18(9)
C(2)	463(4)	2846(3)	−2129(8)	33(4)	12(2)	115(12)	3(4)	−14(11)	11(7)
N(2)	663(4)	1990(3)	−2358(7)	39(3)	11(2)	111(10)	1(3)	9(10)	−4(6)
C(3)	1441(4)	3226(3)	−855(10)	31(3)	16(2)	182(15)	−5(4)	−10(12)	−11(8)
C(4)	1699(4)	2902(3)	1517(9)	30(3)	18(2)	149(13)	2(4)	29(12)	−19(8)
O(4)	2342(4)	3263(3)	2793(7)	55(3)	25(2)	195(12)	−32(4)	−39(11)	−20(7)
O(4c)	1276(3)	2237(2)	2146(7)	46(3)	15(2)	149(10)	−11(3)	−35(10)	2(6)
O(5c)	−302(3)	1199(2)	3497(6)	55(3)	15(1)	94(8)	−16(4)	18(10)	−14(5)
O(5)	−1047(4)	128(2)	5076(7)	103(4)	15(2)	134(11)	−24(4)	55(11)	0(6)
C(5)	−749(4)	508(3)	3412(8)	40(4)	16(2)	117(12)	−1(4)	15(12)	−22(8)
C(6)	−840(4)	170(3)	989(8)	40(4)	14(2)	104(13)	−5(4)	13(11)	−15(7)
N(6)	−834(3)	833(2)	−640(8)	28(3)	15(2)	114(10)	−2(3)	−1(11)	−13(8)
C(7)	163(5)	−368(3)	508(10)	46(3)	12(2)	170(12)	−1(4)	−25(16)	−11(9)
C(8)	1293(4)	32(3)	507(10)	42(3)	17(2)	103(11)	12(4)	9(14)	−9(9)
O(8)	2207(3)	−413(2)	456(9)	44(3)	19(2)	276(13)	15(3)	−22(13)	16(8)
N(8)	1401(3)	782(3)	515(8)	32(3)	16(2)	142(11)	1(3)	−27(12)	0(8)
O(H_2O)	1957(4)	−1949(2)	727(8)	68(3)	23(2)	167(11)	18(4)	74(13)	17(8)
H(C2)	36(7)	307(4)	−382(13)						
H(N2-a)	136(7)	191(5)	−278(14)						
H(N2-b)	22(7)	180(4)	−362(13)						
H(C3-a)	127(6)	379(4)	−61(15)						
H(C3-b)	202(7)	333(5)	−190(14)						
H(C6)	−153(6)	−15(4)	87(15)						
H(N6-a)	−151(6)	102(4)	−43(15)						
H(N6-b)	−69(7)	69(5)	−218(14)						
H(C7-a)	11(6)	−63(4)	−86(14)						
H(C7-b)	19(7)	−79(4)	159(13)						
H(O8)	205(6)	−94(4)	48(15)						
H(N8)	203(6)	97(4)	45(15)						
H(H_2O-a)	194(6)	−218(4)	−20(15)						
H(H_2O-b)	170(7)	−213(5)	201(14)						

TABLE 2. DETERMINATION OF THE ABSOLUTE CONFIGURATION

h	k	l	$F_c(hkl)$	Obsd	$F_c(h\bar{k}l)$	h	k	l	$F_c(hkl)$	Obsd	$F_c(h\bar{k}l)$
1	1	1	70	<	74	1	1	2	30	<	46
1	3	1	16	<	26	1	8	2	31	<	38
1	6	1	43	<	52	1	6	2	30	>	26
1	7	1	21	>	11	1	9	2	45	>	39
2	4	1	53	>	45	1	12	2	32	>	23
2	6	1	50	>	45	2	3	2	45	<	60
2	8	1	34	>	28	2	4	2	46	>	35
2	11	1	42	<	45	3	1	2	38	>	25
3	1	1	35	>	22	3	4	2	82	>	77
3	2	1	66	<	74	3	9	2	24	>	22
3	7	1	73	>	66	4	12	2	25	>	14
3	6	1	28	>	23	5	1	2	23	<	29
4	2	1	21	<	26	5	2	2	30	>	23
4	3	1	21	<	28	5	6	2	36	>	31
4	5	1	63	>	59						
5	1	1	60	>	51						
6	5	1	39	>	36						
7	1	1	22	>	14						
7	2	1	40	>	32						

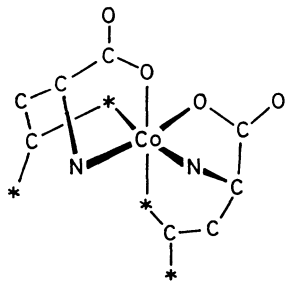

Fig. 1. Possible skeletal structure obtained from the Fourier synthesis.

and non-coordinating atoms of the amide group were 1.9 and 2.9 Å^2, respectively, for mode IV. But mode V gave reversed results: 3.1 and 1.9 Å^2, respectively. Usually, the thermal motions of binding atoms are smaller than those of terminal ones. Hence the structure of the amide group might be IV rather than V. Furthermore the R-value was 0.037 for IV while it was 0.042 for V. From a significance test,[9] the former might be prefered; this is in accordance with the suggestion of the spectroscopic investigation.[7]

The absolute configuration of the complex was obtained by comparing the absolute configurations of the two coordinating ligand ions with those of the respective free ligand molecules.

The anomalous scattering factor of the cobalt atom for Mo $K\alpha$ radiation was introduced into the refinement. The final R-value was 0.033 for the 1517 observed reflections. The final atomic parametes in a right-handed system of xyz-axes are listed in Table 1. The observed and calculated structure amplitudes are deposited with the Chemical Society of Japan (Document No. 7816).

To confirm the absolute configuration, equi-inclination Weissenberg photographs of the first and the second layers around the c axis were taken with Cu $K\alpha$ radiation. Differences between the intensities of 33 reflections and those of their counter-reflections were compared with the calculated intensity relations, as listed in Table 2.

The refinement of the structure and the drawing of thermal ellipsoids were carried out with the HBLS-IV[10] and ORTEP[11] programs, respectively. Other calculations were carried out with programs written by the author. The atomic scattering factors were taken from International Tables for X-Ray Crystallography.[12] The weights of reflections used in the refinements were 1.0 for $|F_o| \geqq 11.8$ and 0.5 for the others. A FACOM 230-75 computer at the Computation Center of Nagoya University and a FACOM 230-35 computer at the Data Processing Center of Kanazawa University were used.

Description of the Structure and Discussion

A projection of the structure along the c axis is shown in Fig. 2. The molecular structure and the

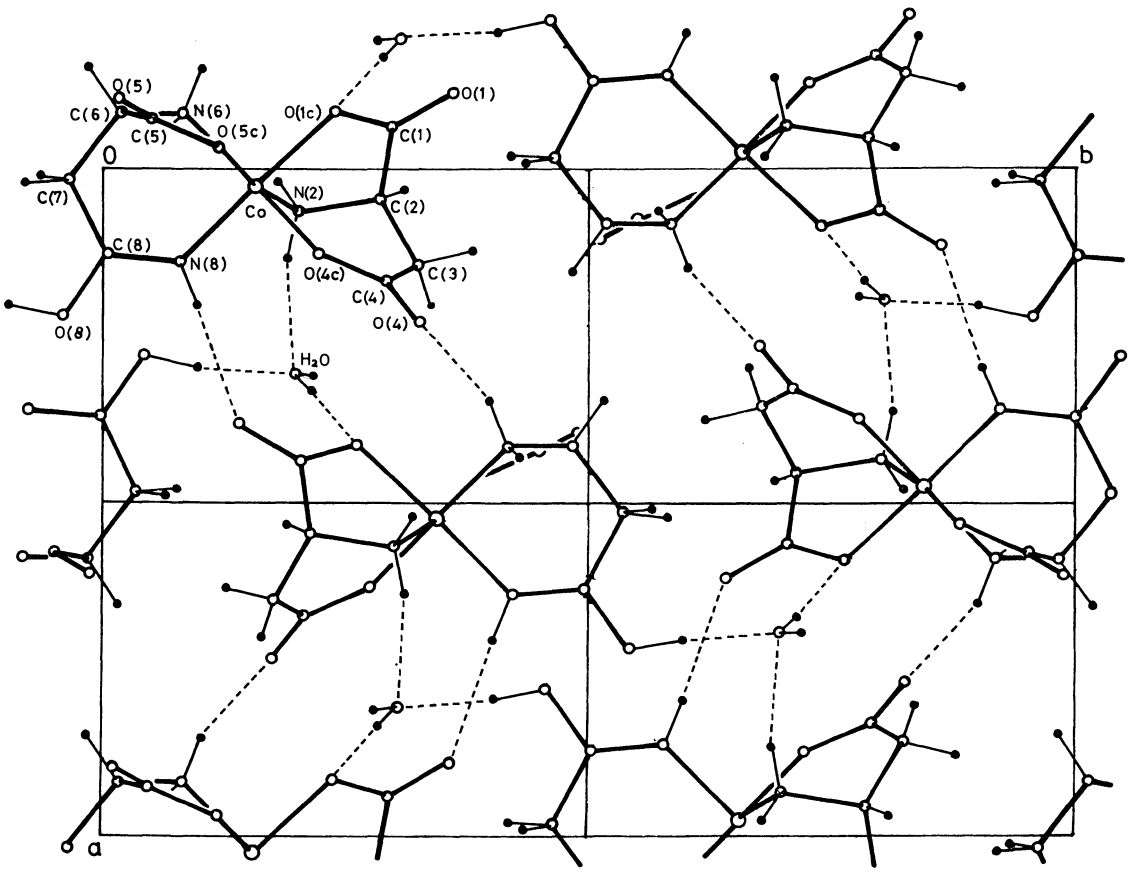

Fig. 2. Projection of the structure along the c axis.

Table 3. Interatomic distances and angles within the complex molecule

Co-O(1c)	1.908(4) Å	Co-O(5c)	1.921(4) Å
Co-N(2)	1.926(4)	Co-N(6)	1.921(4)
Co-O(4c)	1.902(4)	Co-N(8)	1.907(5)
O(1c)-C(1)	1.310(6)	O(5c)-C(5)	1.292(6)
O(1)-C(1)	1.220(7)	O(5)-C(5)	1.219(7)
C(1)-C(2)	1.521(7)	C(5)-C(6)	1.529(7)
C(2)-N(2)	1.485(6)	C(6)-N(6)	1.476(6)
C(2)-C(3)	1.517(7)	C(6)-C(7)	1.524(7)
C(3)-C(4)	1.520(7)	C(7)-C(8)	1.497(7)
C(4)-O(4)	1.228(6)	C(8)-O(8)	1.319(7)
C(4)-O(4c)	1.293(6)	C(8)-N(8)	1.286(7)
O(1c)-Co-N(2)	84.5(2)°	O(5c)-Co-N(6)	83.9(2)°
O(1c)-Co-O(4c)	90.0(2)	O(5c)-Co-N(8)	91.8(2)
N(2)-Co-O(4c)	92.1(2)	N(6)-Co-N(8)	90.6(2)
Co-O(1c)-C(1)	113.7(4)	Co-O(5c)-C(5)	113.6(4)
Co-N(2)-C(2)	104.5(3)	Co-N(6)-C(6)	105.2(3)
Co-O(4c)-C(4)	129.8(4)	Co-N(8)-C(8)	128.7(4)
O(1c)-C(1)-O(1)	123.3(5)	O(5c)-C(5)-O(5)	125.0(5)
O(1)-C(1)-C(2)	122.8(5)	O(5)-C(5)-C(6)	120.9(5)
O(1c)-C(1)-C(2)	113.6(5)	O(5c)-C(5)-C(6)	114.1(5)
C(1)-C(2)-C(3)	108.6(4)	C(5)-C(6)-C(7)	110.0(4)
C(1)-C(2)-N(2)	108.3(4)	C(5)-C(6)-N(6)	107.8(4)
C(3)-C(2)-N(2)	110.1(4)	C(7)-C(6)-N(6)	109.9(4)
C(2)-C(3)-C(4)	116.2(5)	C(6)-C(7)-C(8)	114.5(5)
C(3)-C(4)-O(4)	119.4(5)	C(7)-C(8)-O(8)	117.7(5)
C(3)-C(4)-O(4c)	120.1(5)	C(7)-C(8)-N(8)	122.8(5)
O(4)-C(4)-O(4c)	120.5(5)	O(8)-C(8)-N(8)	119.4(5)
C(2)-H	1.06(8) Å	C(7)-Ha	0.92(8) Å
N(2)-Ha	0.87(8)	C(7)-Hb	0.95(8)
N(2)-Hb	0.96(8)	O(8)-H	0.93(9)
C(3)-Ha	0.99(9)	N(8)-H	0.81(9)
C(3)-Hb	0.93(8)	$O(H_2O)$-Ha	0.67(9)
C(6)-H	0.98(9)	$O(H_2O)$-Hb	0.86(8)
N(6)-Ha	0.87(9)		
N(6)-Hb	0.95(8)		

Table 4. Intermolecular contacts through hydrogen bonds

Key to symmetry operations

i	x	y	z
ii	x	y	$-1+z$
iii	$1/2+x$	$1/2-y$	$-z$
iv	$-1/2+x$	$1/2-y$	$1-z$
v	$1/2-x$	$-y$	$-1/2+z$

A·····H———D[a]			A-D	A-H
$O^{i}(4)$	Ha	$O^{i}(H_2O)$	2.937(6) Å	2.34(9) Å
$O^{ii}(H_2O)$	Ha	$N^{i}(2)$	3.021(6)	2.16(8)
$O^{ii}(5c)$	Hb	$N^{i}(2)$	2.992(6)	2.06(8)
$O^{ii}(5)$	Hb	$N^{i}(6)$	2.784(6)	1.91(8)
$O^{iii}(1)$	H	$N^{i}(8)$	3.098(6)	2.30(9)
$O^{i}(4)$	Ha	$N^{iii}(6)$	2.929(6)	2.28(9)
$O^{i}(1c)$	Hb	$O^{iv}(H_2O)$	2.752(6)	1.90(8)
$O^{v}(H_2O)$	H	$O^{i}(8)$	2.643(6)	1.72(9)

a) A, Hydrogen acceptor; D, Hydrogen donor.

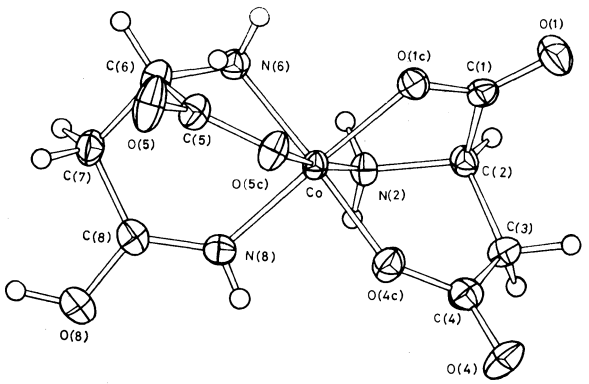

Fig. 3. The molecular structure and the absolute configuration with the anisotropic thermal ellipsoids of the atoms at 50% probability level.
Hydrogen atoms are drawn as spheres with a diameter of 0.1 Å.

absolute configuration are shown in Fig. 3, along with the thermal ellipsoids of the non-hydrogen atoms. The bond distances and angles are listed in Table 3 and the details of the hydrogen bonds in Table 4.

The asparaginate ion, L-aspNH_2^-, acts as a terdentate ligand coordinating through carboxyl oxygen,

TABLE 5. THE C–O AND C–N BOND DISTANCES OF THE AMIDE GROUPS OF SOME AMIDE COMPLEXES

Complex	C–O	C–N	Corrdinating atom	Ref.
$[Ni(H_2O)_2(piaH)_2]Cl_2$[a]	1.24 Å	1.31 Å	O	5
$[Ni(pia)_2]\cdot 2H_2O$[a]	1.24	1.27	Deprotonated N	6
$[Cu(pyaH)_2](ClO_4)_2$[b]	1.26	1.30	O	1
$[Cu\{HN(CH_2CONH_2)_2\}_2](ClO_4)_2$	1.265	1.31	O	2
$[Ni\{HN(CH_2CONH_2)_2\}_2](ClO_4)_2$	1.25	1.32	O	3
$[Cu(L\text{-}aspNH_2)_2]_n$	1.22	1.37	O	4
$[Co(D\text{-}asp)(L\text{-}aspNH_2)]\cdot H_2O$	1.32	1.29	Protonated N	Present work

a) piaH: pyridine-2-carboxamide. pia: deprotonated piaH. b) pya: pyrazine-2-carboxamide.

amino nitrogen, and amide nitrogen atoms. The amide group forms an enolic system on coordination. The aspartate ion, D-asp^{2-}, acts also as a terdentate ligand coordinating through two carboxyl oxygen atoms and one amino nitrogen atom. The cobalt atom is surrounded by these coordinating atoms in the *facial* $[Co(N)_3(O)_3]$ geometry. This structural feature agrees with the suggestion by Takenaka and Shibata.[7]

The coordination bond lengths are 1.902—1.926 Å, which agree with those of $[Co(L\text{-}asp)_2]^-$ within the estimated standard deviations.[17] The coordination bond angles around the cobalt atom are about 84° in the five-membered chelate rings, whereas they are 90—92° in the six- and seven-membered chelate rings. Hence the octahedron around the cobalt atom is slightly distorted.

The C–O and C–N bond lengths of L-aspNH$_2^-$ are listed in Table 5 along with those of other amide complexes. The C–N bond is longer than the C–O bond in the other complexes. But the present complex gives a reversed result, *i.e.* the C–N bond is slightly shorter (0.03 Å) than the C–O bond. This must be due to the difference between the enolic (the present complex) and keto (others) forms

Some other facts which support the N-coordination of the amide group are as follows:

1. Spectroscopic evidence supports the N-coordination.[7]

2. The complex is easily deprotonated in an alkaline solution.[7] This is explained by the following reaction:

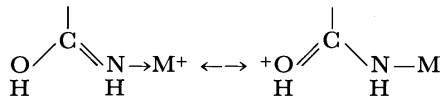

IV VI

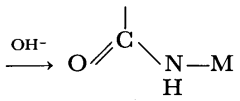

II

3. Several examples which have structure IV have been reported for the secondary amide groups based on the spectroscopic evidence.[13–15] Furthermore, one example of structure IV has been reported for a primary amide on the basis of NMR.[16]

4. No example of structure V has so far been found.

The complex molecules are connected with one another through hydrogen bonds $N^i(2)\cdots O^{ii}(5c)$, $N^i(6)\cdots O^{ii}(5)$, and $N^i(2)\cdots O^{ii}(H_2O)$, forming infinite chains along the c axis. These chains are connected with the adjacent ones through hydrogen bonds $N^i(8)\cdots O^{iii}(1)$, $O^i(1c)\cdots O^{iv}(H_2O)$, and $O^i(4)\cdots N^{iii}(6)$. Thus, two-dimensional networks are formed parallel to the (010) plane. Among these networks no contact shorter than 3.3 Å is observed, except for a hydrogen bond $O^i(8)\cdots O^v(H_2O)$. The networks are piled up through this hydrogen bond to complete three-dimensional networks.

The author is grateful to Professor Muraji Shibata of Kanazawa University for valuable advice, and to Professor Fumiyuki Marumo of Tokyo Institute of Technology for his helpful discussion. The author is also indebted to Professor Seiji Sugiura and Dr. Kuniaki Kihara, Department of Mineralogy, Kanazawa University, for the use of a Philips PW1100 automatic four-circle diffractometer.

References

1) M. Sekizaki, *Acta Crystallogr., Sect. B*, **29**, 327 (1973).
2) M. Sekizaki, *Bull. Chem. Soc. Jpn.*, **47**, 1447 (1974).
3) M. Sekizaki, *Acta Crystallogr., Sect. B*, **32**, 1568 (1976).
4) F. S. Stephens, R. S. Vagg, and P. A. Williams, *Acta Crystallogr., Sect. B*, **31**, 841 (1975).
5) A. Masuko, T. Nomura, and Y. Saito, *Bull. Chem. Soc. Jpn.*, **40**, 511 (1967).
6) Y. Nawata, H. Iwasaki, and Y. Saito, *Bull. Chem. Soc. Jpn.*, **40**, 515 (1967).
7) H. Takenaka and M. Shibata, *Chem. Lett.*, **1976**, 535.
8) W. C. Hamilton, *Acta Crystallogr.*, **12**, 609 (1959).
9) W. C. Hamilton, *Acta Crystallogr.*, **18**, 502 (1965).
10) T. Ashida, "Universal Crystallographic Computation Program System (UNICS)," ed by T. Sakurai, The Crystallographic Society of Japan, Tokyo (1967).
11) C. K. Johnson, Oak Ridge National Laboratory Report ORNL-3794 (1965).
12) "International Tables for X-Ray Crystallography," Vol. IV, Kynoch Press, Birmingham (1974).
13) M. Nonoyama, *Inorg. Chim. Acta*, **13**, 5 (1975).
14) M. T. Barnet, H. C. Freeman, D. A. Buckingham, I-nan Hsu, and D. van der Helm, *Chem. Commun.*, **1970**, 367.
15) E. B. Fleischer, D. Jeter, and R. Florian, *Inorg. Chem.*, **13**, 1042 (1974).
16) D. B. Brown, R. D. Burbank, and M. B. Robin, *J. Am. Chem. Soc.*, **91**, 2895 (1969).
17) I. Oonishi, M. Shibata, F. Marumo, and Y. Saito, *Acta Crystallogr., Sect. B*, **29**, 2448 (1973).

Chemical Shifts of Sulfur KLL Auger Electron Energies in Its Compounds

Shunichi NISHIKIDA and Shigero IKEDA*

Department of Chemistry, Faculty of Science, Osaka University, Toyonaka, Osaka 560

(Received August 13, 1977)

The sulfur 1s and 2p photoelectron spectra and $KL_{23}L_{23}$ Auger electron spectra in various sulfur compounds involving solid sulfur were measured by means of irradiation by Al $K\alpha$ and Cr $K\alpha$ X-rays. The chemical shifts of the S1s and S2p photoelectron spectra for compounds referred to the data for solid sulfur differ from each other in magnitude, but all are larger than that for the Auger electron spectra in the corresponding compound. The shift of the Auger electron spectra is different in fashion from those of the photoelectron spectra; the difference is largely attributable to the differences in relaxation energies. The extra-atomic relaxation energies due to core-electron emission were estimated by combining the atomic spectral data and the XPS and AES data of compounds; they were found not necessarily to depend upon the atomic charges. From the calculated sulfur $K\alpha$ X-ray spectra corresponding to the difference in the binding energy between 1s and 2p, the number of electrons on each sulfur atom was obtained by using the method derived from Coulson *et al.*, while the isolation was attempted on the basis of the contribution of polarization energies due to surrounding atoms to the extra-atomic relaxation energies.

Various arguments have been advanced during the last decade concerning the chemical shift of the kinetic energy of the Auger electron accompanied by the photoemission of the inner electrons of atoms in compounds.[1-7] Wagner[4] defined the difference in kinetic energy between an Auger line and a photoelectron line as the Auger parameter for an element. He attributed the difference in the Auger parameter to changes in the polarizabilities of the ligand ions. The first work concerning the chemical shift of the sulfur KLL Auger electron energy has been reported by Fahlman *et al.*[8,9] for two sulfur atoms with different oxidation numbers (+VI and −II respectively) in sodium thiosulfate. Recently Asplund *et al.*[10] and Keski-Rahkonen *et al.*[11] measured the sulfur $KL_{23}L_{23}(^1D)$ Auger energy in the free molecule.

With regard to the theoretical treatment for the Auger electron energy, Shirley[12,13] *et al.* introduced a static relaxation energy into the intermediate-coupling formulas given by Asaad and Burhop[14] in order to calculate the KLL Auger energies. This relaxation energy was derived by extending the concept of the polarization potential introduced by Hedin and Johansson[15] for photoemission to the case of the two-hole final state in the Auger electron emission process.

The present paper will report on the chemical shifts of the 1s and 2p photoelectron spectra and the $KL_{23}L_{23}$ ^1D Auger electron spectra for sulfur with various oxidation states in its compounds. The absolute values of the sums of the extra-atomic and outer relaxation energies are estimated from the total relaxation energies observed experimentally and the inner atomic relaxation energies obtained from the optical data for S^{6+} and S^{7+} ions.

Experimental

The measurements were performed by using an AEI ES-200-type electron spectrometer. Specimens were irradiated either with Cr $K\alpha_{1,2}$ radiation ($K\alpha_1$=5414.7 eV and $K\alpha_2$=5405.5 eV)[16] in order to obtain the S1s photoelectron line and the SKLL Auger line, or with Al $K\alpha_{1,2}$ radiation for the other photoelectrons. Because of the spin orbit interaction, two paired lines with an energy separation of 9.2 eV between Cr $K\alpha_1$ and Cr $K\alpha_2$ were always observed in the spectra.

For the purpose of the energy calibration of the spectrometer, in the case of alminium irradiation, the photoelectron peaks of four kinds of metals, Cu, Au, Pd, and Ag, which had been evaporated onto a stainless steel sample holder *in vacuo*, were used with the following binding energies,[17] and the spectrometer constant was determined.

$$Cu2p_{3/2} = 932.8,\ Au4f_{7/2} = 83.8,\ Pd4d = 0.0,$$
$$Pd3d_{3/2} = 335.2,\ Ag3d_{5/2} = 368.2.$$

In the case of Cr $K\alpha$ irradiation, however, the inner-shell photoelectron lines of the metals measured are not so strong in intensity because of the low ionization efficiency of such orbital electrons. Therefore, as is shown in Fig. 1, the calibration procedures were adjusted: the sodium 1s photoelectron and the $NaKL_{23}L_{23}$ ^1D Auger electron for freshly evaporated sodium chloride were measured by the irradiation of alminium $K\alpha_{1,2}$ and also by a chromium $K\alpha_1$ X-ray source. As the kinetic energy of the Auger line is independent of the excitation energies, the energy difference in the 1s photoelectron kinetic energies obtained by both methods must be equal to the energy difference between Al and Cr $K\alpha$

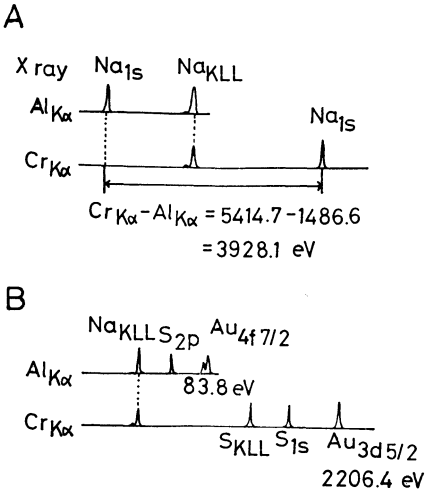

Fig. 1. Energy scale calibration for the case of Cr $K\alpha$ X-ray excitation.
A) i) Charging effect is calibrated by NaKLL Auger electron. ii) The energy difference of NaIs peaks obtained by Al $K\alpha$ and Cr $K\alpha$ excitation is calibrated with the energy difference of two X-ray sources.
B) The extent of charging is calibrated by the energy of $Au3d_{5/2}$ photoelectron peak of gold evaporated on the sample.

X-rays. Therefore, the spectrometer constant, the energy calibration for a scale reading, was calculated with the observed photoelectron energies and the energy difference between the two characteristic X-ray lines, 3928.1 eV.

The charging of the sample during each measurement was calibrated by the energy of the $Au4f_{7/2}$ photoelectron peak of the thin gold layer(83.8 eV) evaporated onto the sample from a tungsten filament. On the other hand, for Cr $K\alpha$ X-ray irradiation, not the $Au4f_{7/2}$ peak but the $Au3d_{5/2}$ photoelectron peak(2206.7 eV of the binding energy) was used to determine the extent of charging effects, except for sodium salts. For sodium salts, the Na_{KLL} Auger electron peak, whose energy was calibrated by the Al $K\alpha$-$Au4f_{7/2}$ method, was used for this purpose.

All the samples were powdered and placed onto a backing of double-backed cellophane tape at room temperature. All the chemicals were used without additional purification. Samples of the sodium salts were dried at 100 °C *in vacuo* for a few hours in order to remove any water of crystallization or any water adsorbed on the samples.

Results and Discussion

In Figs. 2a, b, and c, the spectra of the Sls and 2p photoelectrons and the $KL_{23}L_{23}$ ^1D Auger electron for sodium thiosulfate are shown. Sodium thiosulfate is a historic compound for which the chemical shift in the sulfur KLL Auger electron spectrum was first observed by the Uppsala group in 1966.[8,9] This compound has the structural formula of $2Na^+[S\text{-}SO_3]^{2-}$, containing two sulfur atoms in different chemical states, with oxidation numbers of +VI and −II. Three photoelectron peaks were observed for sulfur 1s in Fig. 2a; the central peak is an overlap of the other two peaks. The two kinds of sulfur in thiosulfate exhibit two peaks corresponding to the central and the ligand sulfur, each of which has two peaks due to the two strong energy sources of Cr $K\alpha$ X-rays used for the excitation, with a splitting energy of 9.2 eV. Therefore, there should be a total of four components, and the central one must be an overlapped peak for each of two different sulfur atoms. For the sulfur 2p photoelectron obtained by Al $K\alpha_{1,2}$ excitation and the $KL_{23}L_{23}$ ^1D Auger electron spectra, two peaks were observed corresponding to two kinds of different-oxidation-state sulfur. The magnitude of the chemical shift of the photoelectron line for two kinds of sulfur is different from those of the Auger electrons. That is, the chemical shift in the binding energy is 7.2 eV for the 1s orbital and 6.0 eV for the 2p orbital, while it is only 4.4 eV for the $KL_{23}L_{23}$ ^1D Auger electron.

Calculation of Extra-atomic Relaxation Energy. The $KL_{23}L_{23}$ Auger energy, $E_{KL_{23}L_{23}}$, can be expressed by the following relation;

$$E_{KL_{23}L_{23}} = E_K - E_L - E_L^*, \quad (1)$$

where E_K and E_L are the observed values of the binding energy for the K and L shells respectively. The E_L^* value is more complicated and does not correspond to the binding energy of the L shell. At the moment of the Auger electron ejection, one hole must have been in the L shell. Shirley *et al.*[12,13,18,19] presented the following formula for E_{KLL} by using the binding energy of E_L instead of E_L^*;

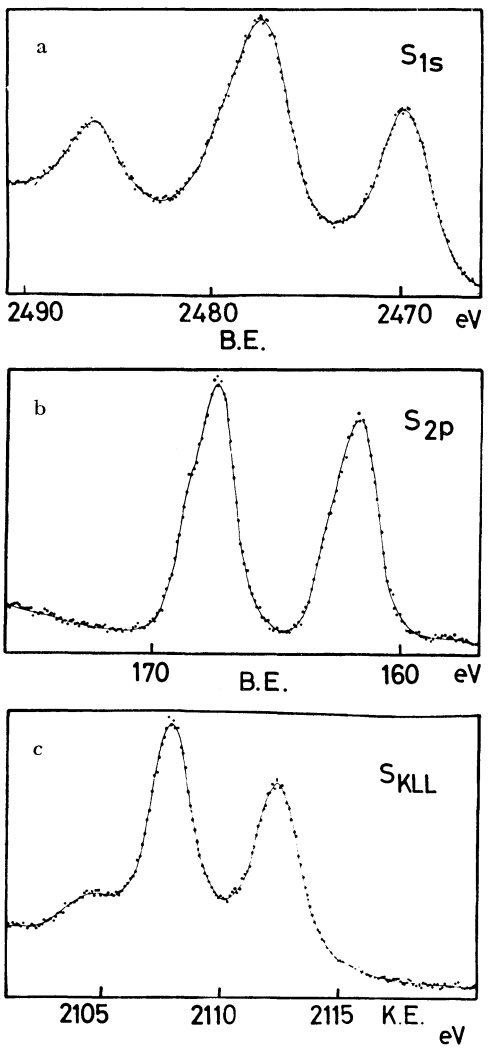

Fig. 2. Sulfur 1s and 2p photoelectron and $KL_{23}L_{23}$ Auger electron spectra in sodium thiosulfate.
a) 1s photoelectron (Cr $K\alpha$ excitation), b) 2p photoelectron (Al $K\alpha$ excitation), c) KLL Auger electron (Cr $K\alpha$ excitation).

$$E_{KL_{23}L_{23}} = E_K - 2E_L - \mathfrak{F} + E_R. \quad (2)$$

Here, the last two terms are the correction ones which result from substitution of E_L for E_L^*. $\mathfrak{F}$ is a final-state two-electron interaction term provided by the spin-orbit coupling.[14] Each final state interaction term can be evaluated from the values of Slater's integrals, F's and G's. E_R is a static relaxation energy. This term was derived from the work of Hedin and Johansson[15] on polarization energies for electron holes, by extending it to the two-hole final state resulting from the Auger process. The term is approximately twice the dynamic relaxation energy for a photoelectron ejection. Generally, the relaxation energy may be separated into two parts, atomic and extra-atomic relaxation energies.

It is difficult, however, to distinguish between the outer atomic relaxation energy and the extra-atomic relaxation energy, because the outer electrons participate in the bonding orbitals in the compound; that is, these electrons belong to both the central and the surrounding atoms. Here, for the analysis of the sulfur

$KL_{23}L_{23}$ Auger transition, we classified the 3s and 3p orbital electrons as contributing to the extra-atomic relaxation energy, together with the surrounding atoms. The 1s, 2s, and 2p orbital electrons are considered to contribute to the atomic relaxation energy.

Then, Eq. 2 is rewritten as follows;

$$E_{KLL} = E_K - 2E_L - \mathfrak{F} + E_R^A + E_R^{ex}, \quad (3)$$

where E_R^A and E_R^{ex} are the atomic and extra-atomic relaxation energies respectively. Here, it is a reasonable assumption* that the $-\mathfrak{F}+E_R^A$ term is independent of the oxidation numbers of the element to be investigated. The magnitude of the extra-atomic relaxation energy, E_R^{ex}, is a useful parameter for characterizing the bonding of ligand atoms in compounds.

The numerical value of $-\mathfrak{F}+E_R^A$ in Eq. 3 can be derived from the data for the atomic spectroscopy.[21] In the case of the sulfur ion with the oxidation number of +VI, there are no electrons in the 3s and 3p orbitals, so the contribution of the outer-orbital electrons to the relaxation energy for the ionization of the 2p electron is zero. Therefore, E(L) in Eq. 1 is equivalent to the ionization potential of S^{+6}, and E(L*), to that of S^{+7}. $-\mathfrak{F}+E_R^A$ can be obtained as the difference between these ionization potentials. The relative energy diagram for the total energies of the S^{6+}, S^{7+}, and S^{8+} ions, and also for the 1s hole state of the S^{6+} ion, is given in Fig. 3. In the Auger electron spectrum,

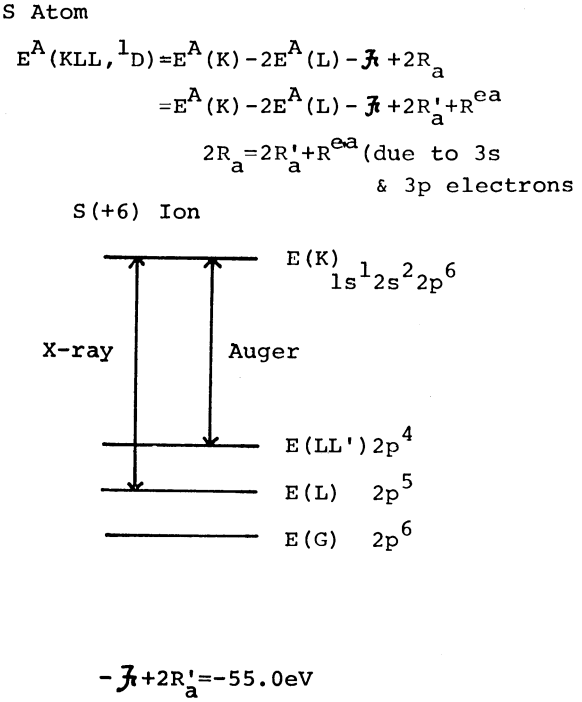

Fig. 3. Total energy level diagram of sulfur ions in various ionized states.
E(G): S^{6+} ground state, E(L): one 2p electron ionized state (S^{7+}), E(LL'): two 2p electrons ionized state (S^{8+}), E(k): one 1s electron ionized state.

* This assumption is supported by an atomic orbital calculation of the $-\mathfrak{F}$ term and of the relaxation energies of free atoms.[20]

TABLE 1. TOTAL ENERGY DIFFERENCES BETWEEN IONIZED STATES

	Change in electron configuration	Energy difference (eV)
S^{6+}	$1s^2 2s^2 2p^6$ —— $S^{7+} 1s^2 2s^2 2p^5$	280.99
S^{7+}	$1s^2 2s^2 2p^5$ —— $S^{8+} 1s^2 2s^2 2p^4({}^3P)$	328.80
S^{8+}	$1s^2 2s^2 2p^4({}^3P)$ —— $S^{8+} 1s^2 2s^2 2p^4({}^1D)$	7.19

the most intensive peak is assigned to the ^{1}D term, and it is necessary to add the energy difference between the ^{3}P and ^{1}D terms in the $2p^4$ configuration because the ^{3}P state in $2p^4$ is a ground state and the ionization energy of S^{7+} corresponds to the ^{3}P states in S^{8+}. The values for each state are obtained from the optical data[10] and are listed in Table 1. Consequently, from these data the value of −55.0 eV for $-\mathfrak{F}+2E_R^A$ is estimated. In Eq. 3, E_R^{ex} can be calculated by introducing the value for $-\mathfrak{F}+E_R^A$ and the measured values for the binding energy of 1s and 2p electrons and the Auger electron energy. In the gaseous state, the energy of the Auger electron is equal to the kinetic energy itself, and the binding energy of photoelectrons referred to the vacuum level can be obtained directly. In solid compounds, however, the energy reference used for photoelectrons is usually the Fermi level of the specimen. In order to evaluate E_{KLL} in Eq. 3, the Auger electron must be normalized with the same reference level as the photoelectron binding energies. When the Fermi level is used for the binding energy reference, the Auger electron kinetic energy should be estimated by referring to it. In this case, the kinetic energy of the electron ejected from the Fermi level is coincident with the X-ray source energy, 5414.7 eV for Cr $K\alpha_1$. This situation is shown schematically in Fig. 4.

In Table 2, the sulfur $KL_{23}L_{23}$ ^{1}D Auger electron

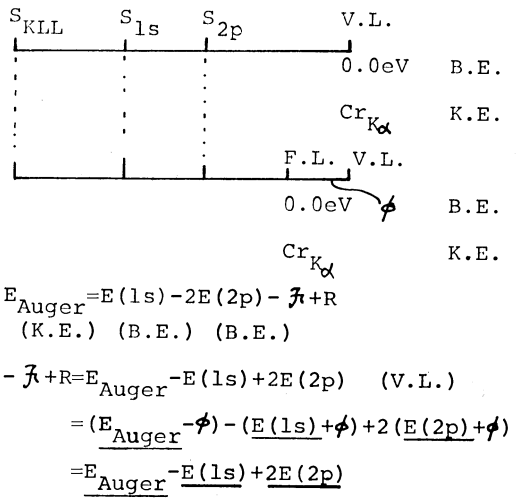

Fig. 4. The Auger electron energy referred to the Fermi level.
V. L.: vacuum level, F. L.: Fermi level,
$\underline{E(1s)}$, $\underline{E(2p)}$: binding energy referred to F. L.,
E_{Auger}: Auger electron energy referred to V. L.,
$E_{\underline{Auger}}$: Auger electron energy referred to F. L.,
ϕ: work function.

TABLE 2. CHEMICAL SHIFTS OF PHOTOELECTRON (E_b) AND AUGER ELECTRON (E_{Auger}) AND EXTRA-ATOMIC RELAXATION ENERGY (R^{ea})

Sample	E_b(S1s)	ΔE_b(S1s)	E_b(S2p)	ΔE_b(S2p)	E_{Auger}(SKLL)	ΔE_{Auger}	R^{ea}
S	2470.8	(0.0)	162.9	(0.0)	2114.2	(0.0)	24.2
ZnS	2469.4	−1.4	161.7	−0.8	2114.4	0.2	23.2
NaSCN	2470.1	−0.7	162.5	−0.4	2111.4	−2.8	21.3
NH_2CSNH_2	2469.4	−1.4	161.8	−1.1	2109.6	−4.6	18.8
Na_2SO	2475.9	5.1	167.9	4.3	2107.6	−6.6	21.1
Na_2SO_4	2478.2	7.4	169.1	6.2	2105.9	−8.3	21.1
$Na_2S_2O_3$(C)	2477.0	6.2	167.8	4.9	2107.9	−6.3	21.5
$Na_2S_2O_3$(L)	2469.8	−1.0	161.8	−1.1	2112.3	−1.9	21.1
BaS_2O_3(C)	2477.3	6.5	168.4	5.5	2108.2	−6.0	22.7
BaS_2O_3(L)	2470.1	−0.7	162.5	−0.4	2112.6	−1.6	22.5
44′-Dithio-bis(morpholine)	2470.7	−0.1	163.0	0.1	2114.0	−0.2	24.3

energies and binding energies for the sulfur 1s and 2p photoelectrons for various compounds are listed, together with their shifts from those of solid sulfur. A slight deviation in the magnitude of the chemical shifts between 1s and 2p photoelectron peaks is observed for each compound. Wagner's Auger parameter, which describes the energy difference between the kinetic energies of the photoelectron and the Auger electron, corresponds to the change in the extra-atomic relaxation energy, provided that the chemical shifts of two subshells associated with the Auger process are the same. This is not the case for the sulfur KLL Auger transition, however, and so the definition of the Auger parameter becomes ambiguous for these compounds. Ignoring the magnitude of the shifts, a similar tendency is observed in the energy gradation of the 1s and 2p photoelectrons for different samples. On the contrary, the Auger electron energy changes in a different fashion. It is necessary to note that, as photoelectron peaks are expressed with the binding energy scale, while Auger peaks are expressed in the kinetic energy scale, the signs of the chemical shifts are opposite to each other. The chemical shifts in the photoelectron binding energies increase with the increase in the formal charge of the corresponding sulfur atom in a compound. In the case of the S_{KLL} Auger electrons, though, the shift is not necessarily in the same direction as the photoelectron. That is, the chemical shift in photoelectron is largely the function of a charge distribution in the initial state, whereas the final state of electron ejection is largely responsible for the chemical shift of the Auger electron energy. Especially for a sulfur atom with a formal charge such as 0 or −2, the chemical shift is the reverse of that for photoelectrons. In thiourea, the S_{KLL} Auger electron shift is 4.6 eV in the opposite direction of the photoelectron shifts obtained by referring to the value for solid sulfur.

In the last column in Table 2, the extra-atomic relaxation energy, E_R^{ex}, derived from the method mentioned above is shown. The extra-atomic relaxation energy does not alter as much as the chemical shift in photoelectrons. These results predict that the chemical shift in the photoelectron for sulfur compound will follow a straight line against the calculated charge performed by ignoring the relaxation energy. The difference in the extra-atomic relaxation energy between two kinds of sulfur in thiosulfate is only 0.4 eV, while the chemical shift in the 1s photoelectron is 7.2 eV. It is apparent that less correlation was found between the extra-atomic relaxation energy and the charge density on the atom in these compounds. The fact that the extra-atomic relaxation energy of sulfur in thiourea is the least for the compounds investigated, while that in the sulfur molecule is the most, agrees with the results mentioned above, though the binding energies in the two compounds are not so different (only 1.4 eV).

Charge Density on the Sulfur Atom. As the difference in binding energies between the 1s and 2p orbitals corresponds to the energy of the $K\alpha$ X-ray, a difference in chemical shifts between the 1s and 2p binding energies would bring about a chemical shift in the $K\alpha$ X-ray. Sato *et al.*[22] have measured the $K\alpha$ X-ray energy shift for sulfur in various compounds in solid and liquid states, thus revealing the relationship between the formal oxidation number and the chemical shift from the sulfur molecule. The mean number of the valence electrons associated with the sulfur atom in compounds was calculated from the photoelectron energy shifts according to a theoretical correlation presented by Coulson *et al.*[23,24] According to Gianturco and Coulson,[24] the valence-electron density is calculated by using the self-consistent-field technique and by taking into account both parent and daughter systems for sulfur on the basis of Koopman's theorem model and the adiabatic model. In Fig. 5, the findings on the shifts of 1s and 2p photoelectrons for various oxidation numbers are shown. The two curves in Fig. 3 are adequately represented by

$$\Delta E = v(v+3)/11 \text{ for Koopman's theorem model, and} \quad (4)$$

$$\Delta E = v(v+4)/8 \text{ for adiabatic model,} \quad (5)$$

where ΔE is the chemical shift of the S$K\alpha$ X-ray fluorescence line at various oxidation numbers or degrees of ionization, v, from that for neutral sulfur. The energy shift in the $K\alpha$ fluorescence line of sulfur is attributed only to the electronic charge on the sulfur atom; therefore, the number of electrons, n, in the 3s and 3p orbitals of sulfur in a compound can be calculated by using Eq. 5, as $n=6-v$. This assumption seems reasonable, because the term which contributes

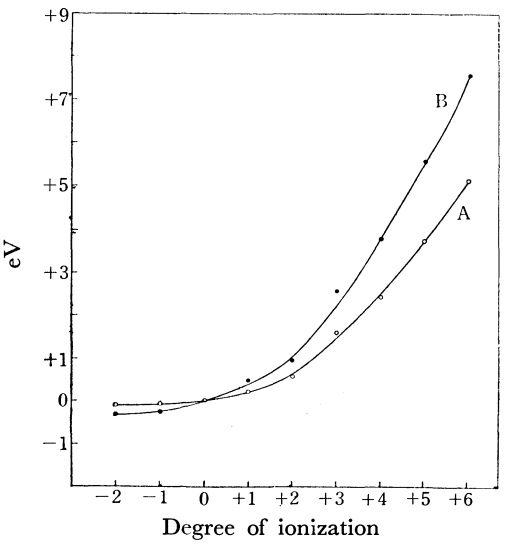

Fig. 5. Shifts in sulfur $K\alpha$ energy due to various degress of ionization.[24]
A) Koopmans' theorem model, B) Adiabatic model.

to the chemical shift in the binding energy is the same for each subshell except for the charge density on an atom. That is, the chemical shift in the $K\alpha$ X-ray energy is equal to the difference in the chemical shift between the binding energies of the two subshells. The chemical shifts for the binding energies of core electrons can be considered generally by dividing them into two parts——the inner atomic and the outer atomic parts. The inner atomic part is attributed to the charge density of the host atom and the relaxation energy due to the outer orbital electrons, while the outer atomic part is attributed to the potential energy and polarization energy due to the surrounding atoms which are bonding with the host atoms. The outer atomic part will contribute to the energy shift of orbital electrons homogeneously. Therefore, in the case of the chemical shift of the characteristic X-ray energy of inner orbitals, only the inner atomic part must be taken into account. In Table 3, the energy difference between the 1s and $2p_{3/2}$ photoelectron binding energies, which correspond to the calculated $K\alpha$ X-ray energy, are listed for various compounds. The shifts of these values from that for solid sulfur and the effective numbers of the electrons, n, in the 3s and 3p orbitals of the sulfur atom obtained from Eq. 5 for each compound are also listed in Table 3. Considering the core hole formation in the process of $K\alpha$ X-ray emission, Eq. 5 was adopted for the estimation of the relative atomic charge for sulfur in various compounds by referring to that in solid sulfur. It can easily be predicted that the relaxation energy due to outer-orbital electrons of sulfur atom is a function of the charge density on the outer orbital.

Extra-atomic Relaxation Energy Due to Ligand Atoms. Snyder[25] has recently shown that the relaxation from each shell is proportional to the population of each shell in the isolated atom. According to his investigation, the contribution of 3s and 3p electrons to the relaxation of the 2p core hole state in the sulfur atom is 1.09 eV per electron. For the Auger process, the

TABLE 3. ATOMIC CHARGE AND POLARIZATION ENERGY FOR SULFUR ATOMS

Sample	1s-2p (eV)	$\Delta K\alpha$[a] (calcd)	n[b]	$R^{ea'}$[c]	E_{pol}[c]
S	2307.9	(0.0)	6.0	13.2	11.0
ZnS	2307.7	−0.2	6.7	14.7	8.5
NaSCN	2307.6	−0.3	7.5	16.5	8.3
NH_2CSNH_2	2307.6	−0.3	7.5	16.6	2.3
Na_2SO_3	2308.7	0.8	4.6	10.1	11.0
Na_2SO_4	2309.1	1.2	4.0	8.8	12.1
$Na_2S_2O_3$(C)	2309.2	1.3	3.8	8.4	13.1
$Na_2S_2O_3$(L)	2308.0	0.1	5.8	12.8	8.3
BaS_2O_3(C)	2308.9	1.0	4.3	9.5	13.2
BaS_2O_3(L)	2307.6	−0.3	7.5	16.5	6.0
4,4'-Dithiobis(morpholine)	2307.7	−0.2	6.7	14.7	9.6

a) Energy shift in sulfur $K\alpha$ X-ray (calcd) from the sulfur molecule. The energy of $K\alpha$ X-ray (calcd) is equal to the difference between the 1s binding energy and 2p. b) Number of electrons on the sulfur 3s and 3p orbitals. c) Relaxation energy due to electrons on the 3s and 3p orbitals proportional to number of electrons(n). d) Polarization energy corresponding to the relaxation energy due to surrounding atoms.

static relaxation energy is approximately equivalent to twice that in the photoelectron process. Therefore, the static relaxation energy for the 2p hole state in the sulfur atom can be estimated as 2.2 eV per electron in the 3s and 3p orbitals. The static outer atomic relaxation energies for the S_{KLL} Auger electron calculated for various compounds are listed in the fourth column in Table 3. The static relaxation energy for a host atom due to only the surrounding atoms in a compound can be obtained by subtracting the static outer atomic relaxation energy from the static extra-atomic relaxation energy. The values for sulfur in various compounds are also listed in the fifth column in Table 3. The extra-atomic relaxation energy obtained above could be regarded as the polarization energy of surrounding atoms. The data in Table 3 indicate that these extra-atomic relaxation energies do not correlate with the chemical shift in the binding energy of the 1s and 2p photoelectrons. In sulfate, sulfite, and thiosulfate, the energy differences of the 2p photoelectron for the central sulfur atom from that in solid sulfur are appreciably large on the positive side, despite the large polarization energies for a core-hole formation, which generally decrease the binding energies. In these compounds, the largest polarization energy is found in the central sulfur of thiosulfate; the energies decrease from sulfate to sulfite. The central atom in thiosulfate bonds to three oxygen atoms and a sulfur atom, while the sulfur in the sulfate ion is surrounded by four oxygen atoms. Therefore, a sulfur atom bonded to a host atom may give a larger polarization energy than an oxygen atom. A slight difference in the polarization energies for the sulfur atom between sulfate and sulfite may be attributed to the decrease in the coordination number of the host atom. Therefore, the polarization energy is strongly correlated to the nature of the atoms

surrounding the sulfur, *e.g.*, the polarizability, the ionic radius, and the number of atoms. The terminal sulfur in thiosulfate, for which the photoelectron chemical shift of S2p is very small on the negative side, gets a little polarization energy. In this compound, the terminal sulfur atom adjoins only a sulfur atom and the distance from the nearest oxygen atom is twice that from a sulfur atom. It may be predicted that the polarization energy is mainly correlated to the nature of the nearest-neighboring atoms. Sulfur in zinc sulfide and sodium thiocyanate has small polarization energies, though the chemical shifts referred to the S2p energy for solid sulfur are negative. The polarizability of the bonding atoms also affect the polarization energy shifts of the host atom. For sodium thiocyanate, the sulfur atom is attached to the carbon atom, making only a little contribution to the polarization energy. This observation is further supported by the facts that the polarization energy of sulfur for 4,4′-dithio-bis(morpholine) is also very small and that no chemical shifts from the sulfur molecule are observable. In this case, considering the molecular structure of the morpholine group, the largest polarization energy can be expected for the core-hole formation of the sulfur atom. However, the results disagree with this prediction, presumably because of the small polarizability of the bonding carbon atoms.

Financial support for this research by the Toray Science Foundation is gratefully acknowledged.

References

1) E. Sokolowski, C. Nordling, and K. Siegbahn, *Phys. Rev.*, **110**, 776 (1958).
2) C. Nordling, E. Sokolowski, and K. Siegbahn, *Arkiv Fysik*, **13**, 483 (1958).
3) C. D. Wagner and P. Biloen, *Surface Sci.*, **35**, 82 (1973).
4) C. D. Wagner, *Discuss. Faraday Div., Chem. Soc.*, **60**, 291 (1975).
5) A. Barrie and F. J. Street, *J. Electron Spectrosc. Relat. Phenom.*, **7**, 1 (1975).
6) J. E. Castle and D. Epler, *Proc. R. Soc. London, Ser. A*, **339**, 49 (1974).
7) G. Schön, *J. Electron Spectrosc. Relat. Phenom.*, **2**, 75 (1973).
8) A. Fahlman, K. Hamrin, R. Norberg, C. Nordling, and K. Siegbahn, *Phys. Lett.*, **20**, 159 (1966).
9) S. Hagström, C. Nordling, and K. Siegbahn, *Z. Phys.*, **178**, 439 (1964).
10) L. Asplund, P. Kelfve, H. Siegbahn, O. Goscinski, H. Fellner-Feldegg, K. Hamrin, B. Lomster, and K. Siegbahn, *Chem. Phys. Lett.*, **40**, 353 (1976).
11) O. Keski-Rahkonen and M. O. Krause, *J. Electron Spectrosc. Relat. Phenom.*, **9**, 371 (1976).
12) D. A. Shirley, *Chem. Phys. Lett.*, **17**, 312 (1972).
13) D. A. Shirley, *Phys. Rev. A*, **7**, 1520 (1973).
14) W. N. Asaad and E. H. S. Burhop, *Proc. Phys. Soc. London*, **71**, 369 (1958).
15) L. Hedin and A. Johansson, *J. Phys. B*, **2**, 1336 (1969).
16) J. A. Bearden, *Rev. Mod. Phys.*, **39**, 78 (1967).
17) G. Johansson, J. Hedman, A. Berndtsson, M. Klasson, and R. Nilsson, *J. Electron Spectrosc. Relat. Phenom.*, **2**, 295 (1973).
18) S. P. Kowalczyk, R. A. Pollak, F. R. McFeely, L. Ley, and D. A. Shirley, *Phys. Rev. B*, **8**, 2387 (1973).
19) S. P. Kowalczyk, L. Ley, F. R. McFeely, R. A. Pollak, and D. A. Shirley, *Phys. Rev. B*, **9**, 381 (1974).
20) This result was obtained by using a copy of the program for non-relativistic $X\alpha$ calculations.
21) C. E. Moore, "Atomic Energy Levels as Derived from the Analysis of Optical Spectra," Natl. Bur, Stds. Circular No. 467 (U. S. GPO, Washington, D. C., 1949—1958), Vols. 1—3.
22) T. Sato, T. Takahashi, and K. Yabe, *Bull. Chem. Soc. Jpn.*, **40**, 298 (1967).
23) C. A. Coulson and C. Zauli, *Mol. Phys.*, **6**, 525 (1963).
24) F. A. Gianturco and C. A. Coulson, *Mol. Phys.*, **14**, 223 (1968).
25) L. C. Snyder, *J. Chem. Phys.*, **55**, 95 (1971).

The Temperature Dependence of the Solubilities of 1-Phenyl-1,3-butanedione and 4,4,4-Trifluoro-1-phenyl-1,3-butanedione in Water and Aqueous Electrolyte Solutions[1)]

Yasuki YOSHIMURA and Nobuo SUZUKI*

Department of Chemistry, Faculty of Science, Tohoku University, Aoba Sendai 980

(Received August 29, 1977)

The temperature dependence of the solubilities of 1-phenyl-1,3-butanedione (benzoylacetone) and 4,4,4-trifluoro-1-phenyl-1,3-butanedione (benzoyltrifluoroacetone) in water and in 1.0 mol l^{-1} aqueous solutions of $HClO_4$, HCl, $NaClO_4$, KCl, NaBr, NaCl, $BaCl_2$, and Na_2SO_4 was determined over the temperature ranges of 20 to 45 °C for benzoylacetone and of 15 to 30 °C for benzoyltrifluoroacetone. From these data, the thermodynamic quantities associated with the dissolution in water and with the transfer from water to the aqueous electrolyt solutions were estimated. Both the enthalpy and the entropy of solution of benzoyltrifluoroacetone in water were much smaller than those for benzoylacetone. This was interpreted by assuming a higher hydrophobic hydration for the less polar benzoyltrifluoroacetone. The thermodynamic quantities of the transfer of benzoyltrifluoroacetone from water to the aqueous perchloric acid solution showed characteristic features compared with those of the other electrolyte solutions. The overall salt effect on the dissolution of benzoylacetone and benzoyltrifluoroacetone is discussed in terms of the change in the thermodynamic quantities.

As the first step in clarifying the salt effect in the solvent extraction of metal chelates, we have investigated the salt effect on the liquid-liquid distribution of 1-phenyl-1,3-butanedione (benzoylacetone, abbreviated as BA) and 4,4,4-trifluoro-1-phenyl-1,3-butanedione (benzoyltrifluoroacetone, abbreviated as BFA).[2,3)] They are frequently used as extraction agents for various metal ions.[4)]

In the systems of the metal-chelate extraction, a system consists of an organic phase and an aqueous phase. Accordingly, in a thermodynamic study of the solvent extraction of metal chelates, it seems that the thermodynamic quantities of the dissolution of metal chelates in water give fundamental and important information. Because the solubilities of metal chelates in water are generally very low and metal chelates dissociate in water, few papers on the thermodynamic quantities of the dissolution of metal chelates in water have been published.

In view of the above points, in the present study the temperature dependence of the solubilities of BA and BFA in water and in several aqueous electrolyte solutions was measured. From the consequent data, the thermodynamic quantities of the dissolution of these β-diketones in water and of the transfer of these β-diketones from water to the aqueous electrolyte solutions were estimated. Such thermodynamic quantities of the transfer seem to give useful information relating to the salt effect.[5)]

Experimental

Materials. The benzoylacetone and BFA were purified as previously described.[2,3)] The stock solutions of the eight electrolytes used in this study were also prepared as previously described.[2,3)] The electrolytes used were as follows: perchloric acid, hydrochloric acid, sodium perchlorate, sodium chloride, sodium bromide, potassium chloride, barium chloride, and sodium sulfate. Redistilled water was used.

The Temperature Dependence of the Solubilities of Benzoylacetone and Benzoyltrifluoroacetone in Water and in 1.0 mol l^{-1} Aqueous Electrolyte Solutions. The solubility determination was made as follows: about 1—2 ml of a saturated solution of BA or BFA equilibrated with each solid phase at a desired temperature was transferred into a 25-ml volumetric flask which had been exactly weighed preliminarily (w_1 g). The saturated solution in the flask was allowed to stand for about 30 min at the constant room temperature of 25 °C, and then the total weight of the saturate solution and the flask was exactly weighed (w_2 g).

In an experiment at a temperature higher than room temperature, a modified procedure was applied to avoid any error due to recrystallization on standing in order to measure the weight. In this case, recrystallized BA or BFA was completely dissolved by adding 5 or 2.5 ml of 99.5% ethanol. Water was added to the mark, and then the absorbance was measured, if necessary, after appropriate dilution. To avoid any error due to the dissociation of BA and BFA, which are weak acids, the final solution was acidified to pH 3 with hydrochloric acid.

The addition of ethanol brought about a change in the content of the enol tautomer of BA in the solution; this was ascertained from the apparent extinction coefficient at 312 nm assigned to the enol tautomer of BA.[6)] Accordingly, in the case of the experiment for BA, the ethanol content in the final solution was adjusted to 20% (vol) by the further addition of ethanol. The concentration of BA in the equilibrated solution was then calculated from the absorbance at 312 nm. The apparent extinction coefficient of BA at 312 nm in the solution with the ethanol content of 20% (vol) was thus found to be 6860±27 l mol^{-1} cm^{-1} at 25 °C. This value was not affected by the electrolytes below 0.1 mol l^{-1}.

On the other hand, the extinction coefficient of BFA at the maximum absorption wave length of 249.5 nm was not affected by ethanol at contents below 10% (vol). In the case of BFA, the ethanol content in the final solutions was below 1% (vol), and so the concentration of BFA was simply determined as has previously been described.[3)] In the experiments at temperatures lower than room temperature for both BA and BFA, the addition of ethanol was not needed. Therefore, in these cases, too, the concentration of BA or BFA in the final sample solutions was measured as previously described.[2,3)]

The solubilities of BA and BFA in terms of the mole number in the saturate solution (1000 g), S, were calculated from

$$S = \frac{C \times (1/V_{dil}) \times 25}{w_2 - w_1}, \quad (1)$$

where C, V_{dil}, and $w_2 - w_1$ denote the measured concentration

of BA or BFA in the final sample solution (mol l^{-1}), the degree of dilution, and the weight of the saturated solution taken (g) respectively. The solubility measurements were made over the temperature ranges of 20 to 45 °C for BA and of 15 to 30 °C for BFA, and were made 4—8 times for the saturated solutions taken independently. The temperatures were kept at the desired temperatures within 0.2 °C.

The Temperature Dependence of the Keto-Enol Tautomerism Constants of Benzoylacetone in Water and in 1.0 mol l^{-1} Aqueous Electrolyte Solutions. The keto-enol tautomerism constants of BA at all the temperatures where its solubility was measured were estimated from the temperature dpendence of the apparent extinction coefficients at 310 nm of BA in water and in 1.0 mol l^{-1} aqueous electrolyte solutions.

The apparent extinction coefficients of BA in terms of the molarity at 310 nm in the respective solutions at 25 °C, which were measured in a previous work,[2] were converted into values in terms of molarity, $\varepsilon_{(m)}$, from the densities of the water and the 1.0 mol l^{-1} aqueous electrolyte solutions at 25 °C. The extinction coefficients for the enol tautomer, $\varepsilon_{(m)}$, were obtained from the above $\varepsilon_{(m)}$ and the enol contents estimated in the previous work.[2] The values for $\varepsilon_{(m)}$ estimated were as follows: 15058±69 (kg mol^{-1} cm^{-1}) in water (acidified to 0.001 mol l^{-1} HCl solution); 14787±87 in 1.0 mol l^{-1} HCl; 14276±140 in 1.0 mol l^{-1} $HClO_4$; 14775±10 in 1.0 mol l^{-1} NaCl, and 14458±91 in 1.0 mol l^{-1} $NaClO_4$.

The apparent extinction coefficients, $\varepsilon_{(m)}$, of BA at each temperature except 25 °C were determined as has been described above. In these measurements, the standard solutions of BA were immersed for about 30 min in a water bath kept at the desired temperature within 0.1 °C before the absorbance measurements at 310 nm. It was confirmed from a pre-experiment that the keto-enol tautomeric equilibrium of BA in an aqueous solution was attained within 10 min at a given temperature.

The keto-enol tautomerism constants of BA, K_{aq}, which were defined as the concentration ratios of the keto to the enol tautomers, were calculated by means of

$$K_{aq} = \frac{1-(\varepsilon_{(m)}/\varepsilon_{e(m)})}{\varepsilon_{(m)}/\varepsilon_{e(m)}}, \qquad (2)$$

where it was postulated that the values for $\varepsilon_{(m)}$ in the respective solutions were independent of the temperature.

The Densities of 1.0 mol l^{-1} Aqueous Electrolyte Solutions at 25 °C. The densities of 1.0 mol l^{-1} HCl, $HClO_4$, NaCl, KCl, NaBr, $BaCl_2$, and Na_2SO_4 solutions at 25 °C were obtained as follows. The densities of these aqueous electrolyte solutions at 25 °C have been listed in an earlier article as functions of the weight percent concentrations of these electrolytes.[7] For the respective electrolyte solutions, the plots of $W \times d$ against d, where W and d denote the weight-percentage concentrations of the electrolytes and the densities of the electrolyte solutions with the concentrations of W at 25 °C respectively, gave straight lines. Therefore the best-fit equations for these straight lines were obtained by the method of least squares. The densities of the above electrolyte solutions at 25 °C were calculated from the best-fit equations as has been described in the literature.[7]

The densities of aqueous $NaClO_4$ solutions at 25 °C have not yet been reported. Therefore, the density of the 1.0 mol l^{-1} $NaClO_4$ solution was measured with a pycnometer.

The densities of the 1.0 mol l^{-1} aqueous electrolyte solutions at 25 °C thus obatined were as follows: HCl, 1.0145 (g ml^{-1}); NaCl, 1.0368; KCl, 1.0426; $HClO_4$, 1.0455; NaBr, 1.0746; $NaClO_4$, 1.0754; Na_2SO_4, 1.1149; $BaCl_2$, 1.1741.

In the solubility experiments for the neutral electrolytes, the aqueous electrolyte solutions were acidified with HCl (0.001 M) to prevent the dissociation of BA and BFA. Therefore, contribution of added HCl to the densities of these solutions may be small enough to be neglected because of its low concentration.

Results and Discussion

The Thermodynamic Quantities of the Dissolution of Benzoylacetone and Benzoyltrifluoroacetone in Water.

(i) The Calculation of the Thermodynamic Quantities of the Dissolution in Water: The solubilities obtained by Eq. 1 were convereted to the value in terms of molality by using the densities of the respective electrolyte solutions at 25 °C.

The solubilities in terms of molality at different temperatures, $S_{(m)}$, are listed in Table 1 for BA and in Table 2 for BFA. In these tables, the addition of such small amounts of acids as 0.001 M to prevent the dissociation of BA and BFA does not introduce any error into the solubility determination.[2,3] The values quoted are the means of 4—8 independent experiments, and the deviations of the listed values denote mean errors,** in most cases, the relative mean errors did not exceed 0.6%.

In the case of BA, the solubilities tabulated in Table 1 are the apparent values for the mixtures of the enol and keto tautomers. The solubilities of the enol tau-

** The mean error, a, is given by

$$a = \frac{\sum_{i=1}^{n} |d_i|}{\sqrt{n(n-1)}},$$

where n and d indicate the times of measurement and the residue respectively.

Table 1. Temperature dependence of the solubility of benzoylacetone in water and 1.0 mol l^{-1} aqueous electrolyte solutions ($S_{(m)} \times 10^3$/mol kg^{-1})

Electrolyte	Temperature (°C)					
	20	25	30	35	40	45
Water[a]	$1.89_6 \pm 0.01_2$	$2.43_2 \pm 0.00_8$	$3.13_7 \pm 0.00_9$	$4.02_1 \pm 0.01_0$	$5.13_8 \pm 0.00_3$	$6.58_8 \pm 0.02_3$
HCl	$2.04_3 \pm 0.00_5$	$2.58_9 \pm 0.00_5$	$3.28_7 \pm 0.01_0$	$4.17_2 \pm 0.00_3$	$5.32_4 \pm 0.01_6$	$6.81^8 \pm 0.03_4$
$HClO_4$	$3.73_6 \pm 0.00_6$	$4.68_1 \pm 0.00_9$	$5.99_6 \pm 0.01_2$	$7.67_4 \pm 0.03_6$	$9.91_7 \pm 0.06_1$	$12.8_3 \pm 0.0_5$
NaCl[a]	$1.33_1 \pm 0.00_5$	$1.69_5 \pm 0.00_3$	$2.12_9 \pm 0.00_3$	$2.69_2 \pm 0.01_4$	$3.50_1 \pm 0.02_2$	$4.47_9 \pm 0.00_7$
$NaClO_4$[b]	$2.45_2 \pm 0.01_0$	$3.12_1 \pm 0.00_1$	$3.99_0 \pm 0.00_6$	$5.12_9 \pm 0.01_9$	$6.60_1 \pm 0.01_0$	$8.52_9 \pm 0.01_1$

a) Contains 10^{-3} mol l^{-1} HCl. b) Contains 10^{-3} mol l^{-1} $HClO_4$.

Table 2. Temperature dependence of the solubility of benzoyltrifluoroacetone in water and 1.0 mol l^{-1} aqueous electrolyte solutions ($S_{(m)} \times 10^3$/mol kg^{-1})

Electrolyte	Temperature (°C)			
	15	20	25	30
Water[a]	$12.8_9 \pm 0.0_1$	$13.6_7 \pm 0.0_2$	$13.8_3 \pm 0.0_3$	$14.1_2 \pm 0.0_3$
$HClO_4$	$14.7_0 \pm 0.1_3$	$15.1_7 \pm 0.0_5$	$15.7_3 \pm 0.0_1$	$16.4_0 \pm 0.0_5$
HCl	$10.6_2 \pm 0.0_2$	$10.6_4 \pm 0.0_2$	$10.8_7 \pm 0.0_4$	$11.1_5 \pm 0.0_4$
$NaClO_4$[a]	$10.2_8 \pm 0.0_4$	$10.6_8 \pm 0.0_3$	$11.0_2 \pm 0.0_7$	$11.4_1 \pm 0.0_2$
KCl[a]		$8.92_3 \pm 0.02_8$	$8.94_3 \pm 0.02_7$	$9.19_7 \pm 0.03_1$
NaBr[a]		$8.34_2 \pm 0.02_2$	$8.44_5 \pm 0.01_2$	$8.65_6 \pm 0.01_8$
NaCl[a]	$7.24_9 \pm 0.01_9$	$7.28_0 \pm 0.02_1$	$7.43_4 \pm 0.02_0$	$7.66_1 \pm 0.02_6$
$PaCl_2$[a]		$4.71_6 \pm 0.01_2$	$4.73_4 \pm 0.00_6$	$4.83_5 \pm 0.00_7$
Na_2SO_4[a]		$2.86_9 \pm 0.00_9$	$2.94_7 \pm 0.00_9$	$3.07_0 \pm 0.00_4$

a) Contains 10^{-3} mol l^{-1} HCl.

Table 3. Temperature dependence of the keto-enol tautomerism constant, K_{aq},[a] of benzoylacetone in water and 1.0 mol l^{-1} aqueous electrolyte solutions

Electrolyte	Temperature (°C)						
	15	20	25	30	35	40	45
Water[b]	1.70±0.01	1.80±0.01	1.93[d]	2.20±0.01	2.13±0.01	2.23±0.01	2.35±0.02
HCl		1.92±0.01	2.07±0.02	2.13±0	2.23±0.01	2.35±0.01	2.45±0.02
$HClO_4$		2.08±0.02	2.20±0.04	2.27±0.02	2.38±0.02	2.47±0.01	2.57±0.01
NaCl[b]		2.16±0.02	2.32±0.01	2.38±0.02	2.50±0	2.61±0.01	2.72±0.01
$NaClO_4$[c]		2.32±0.01	2.45±0.02	2.54±0.01	2.65±0.01	2.75±0.01	2.87±0.01

a) Estimated from the apparent extinction coefficient of BA at 310 nm measured at the respective temperature and defined as the concentration ratio of the keto to the enol tautomers. b) Contains 10^{-3} mol l^{-1} HCl. c) Contains 10^{-3} mol l^{-1} $HClO_4$. d) Literature value (M. L. Eidinoff, *J. Am. Chem. Soc.*, **67**, 2073 (1945); M. Bergon and J. P. Calmon, *Bull. Soc. Chim. Fr.*, **1972**, 1020).

tomer, $S_{e(m)}$, and those of the keto tautomer. $S_{k(m)}$, were estimated by using the keto-enol tautomerism constants of BA listed in Table 3.[2]

On the other hand, the solubilities of BFA tabulated in Table 2 can be regarded as those for the hydrate form of BFA previously reported.[3] Accordingly, in the following discussion of BFA, only the hydrate form will be considered.

Generally, the temperature dependence of the solubility of a solid nonelectrolyte can be written by

$$\ln S_{(m)} = -\frac{\Delta H_{soln}}{RT} + \text{const}, \quad (3)$$

where ΔH_{soln} indicates the heat of solution. The plots of $\ln S_{(m)}$ against $1/T$ grounded on Eq. 3 gave straight lines, as is shown in Fig. 1(a) for the enol tautomer of BA, in Fig. 1(b) for the keto tautomer of BA, and in Fig. 2 for BFA. The heats of solution in water, ΔH°_{soln}, were obtained from the slopes of the straight lines for the solubilities in water by the least-squares method. The free energies of solution in water, ΔG°_{soln}, were calculated by means of

$$\Delta G^\circ_{soln} = -RT \ln X^\circ_{sat}, \quad (4)$$

where X°_{sat} represents the solubilities in water in terms of the mole fraction. The values for $\ln X^\circ_{sat}$ were calculated from $\ln S^\circ_{(s)}$ at 25 °C obtained from the above straight lines. The entropies of solution in water, ΔS°_{soln}, were calculated from ΔH°_{soln} and ΔG°_{soln}. The activity coefficients of the enol and keto tautomers of BA, and of BFA in the saturated solutions are regarded as unity because of their quite low solubilities in water.[2,3] These results are tabulated in Table 4.

Table 4. Thermodynamic quantities of the dissolution of benzoylacetone and benzoyltrifluoroacetone at 25 °C in water

	ΔG°_{soln}[a] / cal mol^{-1}	ΔH°_{soln}[b] / cal mol^{-1}	ΔS°_{soln}[c] / cal mol^{-1} K^{-1}
Benzoylacetone (enol from)	6566±6	7913±5	4.5
Benzoylacetone (keto form)	6182±5	9840±4	12.2
Benzoyltrifluoroacetone (hydrate form)	4908±7	991±5	−13.1

a) Calculated by $\Delta G^\circ_{soln} = -RT \ln X^\circ_{sat}$. b) Obtained from the slopes of the plots of $\ln S^\circ_{(m)}$ *vs.* $1/T$. c) $\Delta S^\circ_{soln} = (\Delta H^\circ_{soln} - \Delta G^\circ_{soln})/T$.

(ii) A Comparison between the Thermodynamic Quantities of the Dissolution of Benzoylacetone and Those of Benzoyltrifluoroacetone: It has been confirmed by X-ray crystallography that BA exists in the enol form in the crystal.[8] Accordingly, it may be concluded that the thermodynamic quantities of the dissolution for the keto tautomer of BA are summations of those for the enol tautomer and the thermodynamic quantities of the ketonization in the saturated solution of BA.

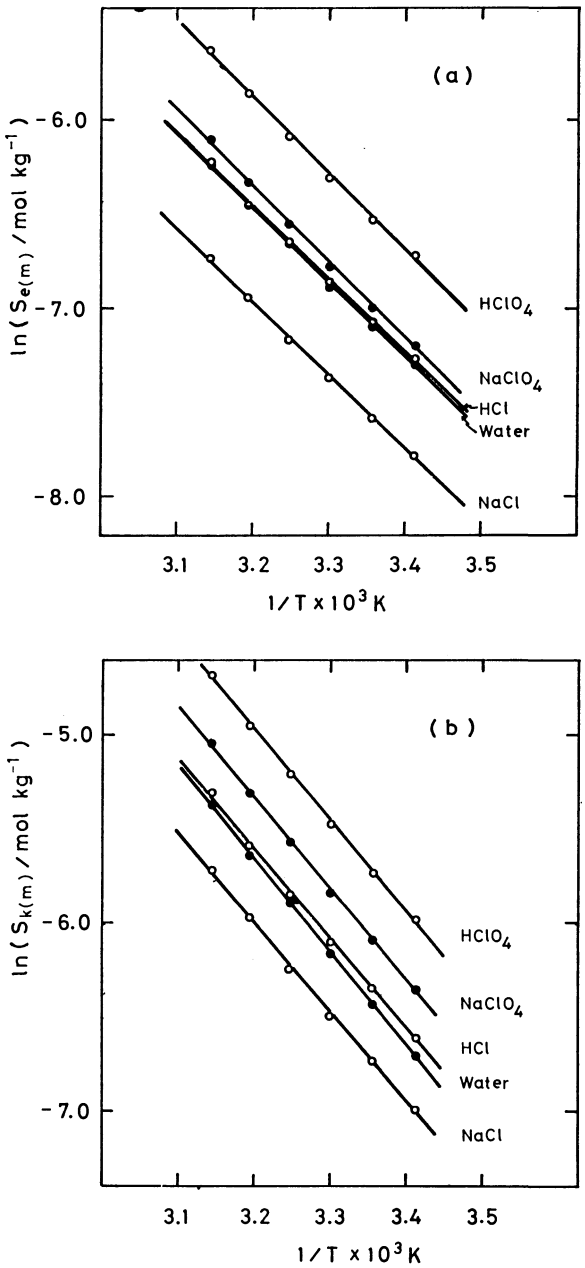

Fig. 1. Plot of $\ln S_{(m)}$ *vs.* $1/T$ for the solubilities of the respective tautomers of benzoylacetone in water and 1.0 mol l^{-1} aqueous electrolyte solutions.
Straight lines are drawn by method of least squares.
(a) For the enol tautomer,
(b) for the keto tautomer.

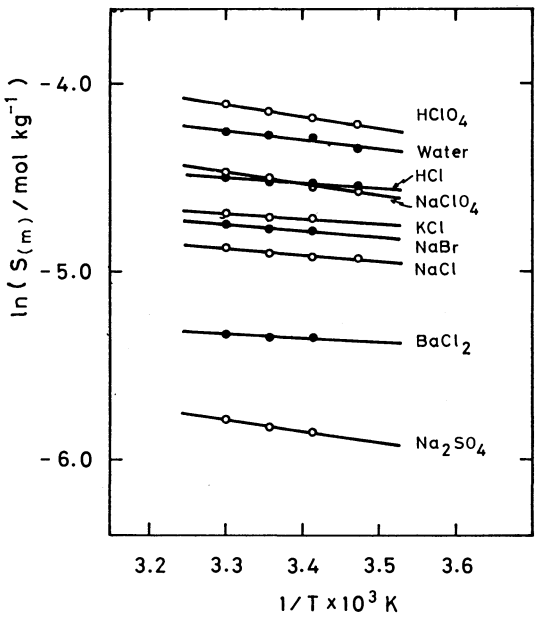

Fig. 2. Plot of $\ln S_{(m)}$ *vs.* $1/T$ for the solubilities of the hydrate form of benzoyltrifluoroacetone in water and 1.0 mol l^{-1} aqueous electrolyte solutions.
Straight lines are drawn by method of least squares.

Therefore, in the case of BA, the values for the enol tautomer ought to be discussed.

On the other hand, the reaction of 2-thenoyltrifluoroacetone (TTA) with water yields the crystal of its hydrate form.[9] Similarly, the solid phase of BFA equilibrated with its saturated solution seems to take the hydrate form. Thus, the solution equilibrium of BFA in the saturated solution may be established between the hydrate form in the aqueous phase and that in the solid phase. Therefore, the thermodynamic quantities of the dissolution of BFA do not involve the thermodynamic quantities of the hydrate formation.

The thermodynamic quantities of the dissolution of BFA in water are much smaller than those of BA. The smaller enthalpy of solution for BFA contributes to its smaller free energy of solution, and this results in its larger solubility in water. These results may be explained as follows, by assuming nearly identical volatilities for BA and BFA.[10] In water, the hydrophilic groups, such as the carbonyl and hydroxyl groups, can interact with water molecules through the electrostatic force and the hydrogen bond. On the other hand, the hydrophobic groups such as the alkyl group cause the formation of an "iceberg" structure of the water around them (hydrophobic hydration).[11] Our previous study suggests that the two hydroxyl groups and trifluoromethyl group in the hydrate form of BFA may behave as the hydrophobic groups rather than as the hydrophilic groups in its aqueous solution.[3] Thus, the higher hydrophobic hydration for BFA may cause a greater decrease in both the enthalpy and the entropy.

The above results give a useful suggestion regarding the dissolution behavior of metal chelates of BA and BFA in water. In these chelates, the hydrophilic parts in BA and BFA—that is, both the carbonyl group and the hydroxyl group—combine with the central metal ions, while the hydrophobic parts in BA and BFA mainly came in contact with water molecules in their aqueous solutions. This suggests that the hydrophobic hydration for their metal chelates may be higher than that for BA and BFA. This hydrophobic hydration of their chelates may contribute considerably to their thermodynamic quantities upon dissolution in water and a non-polar organic solvent.

The Thermodynamic Quantities of the Ketonization of Benzoylacetone in Water. The heat of ketoni-

Table 5. Thermodynamic quantities of the ketonization of benzoylacetone and acetylacetone at 25 °C in water

	ΔG_T° a) kcal mol^{-1}	ΔH_T° b) kcal mol^{-1}	ΔS_T° c) cal mol^{-1} K^{-1}
Benzoyl-acetone	−0.383±0.003	1.947±0.002	7.8
Acetyl-	−0.9	1.5	8

a) Calculated by $\Delta G_T^\circ = -RT \ln K_{aq}^\circ$. b) Obtained from the slope of the plot of $\ln K_{aq}^\circ$ *vs.* $1/T$. c) $\Delta S_T^\circ = (\Delta H_T^\circ - \Delta G_T^\circ)/T$. d) Literature values (Ref. 12).

zation of BA in water, ΔH_T°, was obtained from the plot of $\ln K_{aq}^\circ$ against $1/T$. K_{aq}° is the keto-enol tautomerism constant of BA in water. This plot gave a good straight line. The free energy, ΔG_T°, and the entropy of ketonization, ΔS_T°, were obtained in the ordinary manners. These results are listed in Table 5, along with the literature values[12] for those of acetylacetone (AA).

The entropies of ketonization for BA and AA are nearly identical, but the heat of ketonization of BA is larger than that of AA. It is this that mainly contributes to the smaller negative free energy of the ketonization of the former, that is to the higher enol content of the former in water. The difference in the heats of ketonization of BA and AA may be attributed mainly to a difference in the enthalpies of the enol tautomer of BA and AA; that is, the enthalpy of the enol tautomer of BA is lowered due to the resonance energy between the phenyl group and the enol ring.

The Thermodynamic Quantities of the Transfer of Benzoylacetone and Benzoyltrifluoroacetone from Water to 1.0 mol l^{-1} Aqueous Electrolyte Solutions. The free energies, ΔG_{tr}, and the enthalpies, ΔH_{tr}, of the transfer of one mole of BA or BFA from water to 1.0 mol l^{-1} aqueous electrolyte solutions at hypothetically identical solute concentrations were obtained by means of the following equations:[5]

$$\Delta G_{tr} = RT \ln (X_{sat}^\circ / X_{sat}), \quad (5)$$

$$\Delta H_{tr} = \Delta H_{soln} - \Delta H_{soln}^\circ. \quad (6)$$

In Eq. 5, X_{sat} indicates the solubilities in a mole fraction of BA or BFA in the 1.0 mol l^{-1} aqueous electrolyte solutions at 25 °C. The values for $\ln X_{sat}$ were calculated from $\ln S_{(m)}$ at 25 °C obtained from the best-fit equations for the plots shown in Figs. 1 and 2. The values for ΔH_{soln} in Eq. 6, which indicates the heats of solution in the aqueous electrolyte solutions, were also calculated from the slopes of the above best-fit equations. The entropies of transfer, ΔS_{tr}, were calculated from ΔH_{tr} and ΔG_{tr}. These results are listed in Table 6 for the hydrate form of BFA and in Table 7 for the enol and keto tautomers of BA.

Very few inorganic electrolytes are known to exhibit a so-called "salting-in" effect on non-polar nonelectrolytes. Table 6 shows that the thermodynamic quantities of the transfer of BFA to the aqueous perchloric acid solution show a characteristic feature in comparison with those to the other electrolyte solutions studied. That is, though the enthalpy of transfer to the perchloric acid solution is positive, the positive entropy contributes to the negative free energy, which results in the salting-in effect.

Table 6. Thermodynamic quantities of the transfer of benzoyltrifluoroacetone from water to 1.0 mol l^{-1} aqueous electrolyte solutions at 25 °C

Electrolyte	ΔG_{tr} a) cal mol^{-1}	ΔH_{tr} b) cal mol^{-1}	$T\Delta S_{tr}$ c) cal mol^{-1}
$HClO_4$	−67	270	337
$NaClO_4$	144	202	58
HCl	150	−413	−563
KCl	263	−462	−725
NaBr	300	−343	−643
NaCl	374	−347	−721
$BaCl_2$	641	−553	−1194
Na_2SO_4	922	197	−725

a) Calculated by $\Delta G_{tr} = RT \ln (X_{sat}^\circ / X_{sat})$. b) $\Delta H_{tr} = \Delta H_{soln} - \Delta H_{soln}^\circ$. c) $T\Delta S_{tr} = \Delta H_{tr} - \Delta G_{tr}$.

Table 7. Thermodynamic quantities of the transfer of benzoylacetone from water to 1.0 mol l^{-1} aqueous electrolyte solutions at 25 °C

Electrolyte	ΔG_{tr} a) cal mol^{-1}	ΔH_{tr} b) cal mol^{-1}	$T\Delta S_{tr}$ c) cal mol^{-1}
	Enol form		
$HClO_4$	−327	189	516
$NaClO_4$	−39	202	241
HCl	−1	−202	−201
NaCl	299	−128	−427
	Keto from		
$HClO_4$	−405	−209	196
$NaClO_4$	−181	−194	−13
HCl	−38	−397	−359
NaCl	195	−410	−605

a) Calculated by $\Delta G_{tr} = RT \ln (X_{sat}^\circ / X_{sat})$. b) $\Delta H_{tr} = \Delta H_{soln} - \Delta H_{soln}^\circ$. c) $T\Delta S_{tr} = \Delta H_{tr} - \Delta G_{tr}$.

The salt effect of tetraalkylammonium salts has been quite well studied,[13-17] and both the enthalpies and the entropies of transfer of various nonelectrolytes from water to the aqueous solutions of these ammonium salts have been found to be positive.[17,18] These results have been interpreted in terms of a so-called "hydrophobic interaction" between the nonelectrolyte solutes and the tetraalkylammonium cations.[17,19]

The positive enthalpy and entropy of transfer of BFA to the aqueous perchloric acid solution may also be interpreted in a similar way as follows. The perchlorate anion destroys the iceberg structure of water,[20] which may bring about the hydrophobic interaction with BFA, and this interaction in turn weakens the hydrophobic hydration for BFA. Thus, the decrease in the enthalpy and entropy of BFA through the hydrophobic hydration in the perchloric acid solution becomes smaller than that in water. This argument on the role of the perchlorate anion may offer a possible explanation of the well-known phenomenon that the perchlorate anion is markedly extracted into organic

solvents as ion pairs with large hydrophobic cations.[21]

For the transfer of BFA to the sodium sulfate solution, a negative entropy and a positive enthalpy are observed. This results in the largest positive free energy among the electrolytes studied. Both the enthalpies and the entropies of transfer to all the other electrolyte solutions, except for $HClO_4$, $NaClO_4$, and Na_2SO_4, are negative. Moreover, the larger negative entropies bring about positive free energies of transfer. However, it is very difficult at present to interpret the above results thoroughly.

The thermodynamic quantities of the transfer for the enol tautomer of BA in Table 7 show the same tendency as those for BFA. For all the electrolytes studied, the thermodynamic quantities of the transfer for the keto tautomer of BA are smaller than those for its enol tautomer. Probably these results may be ascribed to the stronger interaction between the more polar keto tautomer and its surroundings, such as water molecules and the electrolytes.

Very few papers on the salt effect in the solvent extraction of metal chelates have referred to the thermodynamic quantities. To clarify the very complicated salt in the solvent extraction of metal chelates, we consider the overall salt effect by dividing it into two stages, that is, the salt effect in chelate formation in the aqueous phase and that in the distribution of the metal chelates between aqueous and organic phases. In the former stage, the chemical reactions of metal ions with salt components must be taken into account; for example, the coordination of such anions as chloride and bromide ions to metal ions[22,24] and ion-pair formation between charged metal chelates and counter ions such as perchlorate anions[23,24] *etc.* Thus, the salt effect in this stage is very particular, and so it seems to be difficult to generalize about it. On the other hand, in the latter stage, the metal chelates distributed may be regarded as nonelectrolytes. Accordingly, the salt effect in this stage may described by analogy from the present results for the chelating agents. Thus, the present study gives useful suggestions for the generalized interpretation of the salt effect in the distribution of metal chelate compounds in the solvent extraction.

References

1) This paper is part of the Ph. D. thesis of Y. Yoshimura, Tohoku University, 1977.

2) Y. Yoshimura and N. Suzuki, *Anal. Chim. Acta*, **91**, 315 (1977).

3) Y. Yoshimura and N. Suzuki, *Talanta*, in press.

4) J. Stary and E. Hladky, *Anal. Chim. Acta*, **28**, 227 (1963).

5) A. Ben-Naim, "Water and Aqueous Solutions," ed by R. A. Horne, Wiley-Interscience, New York (1972), Chap. II.

6) R. A. Morton, A. Hassan, and T. C. Calloway, *J. Chem. Soc.*, **1934**, 883.
This extinction coefficient at 312 nm was calculated by using the total concentration of BA for the mixture of enol and keto tautomers. Therefore, even though this absorption was ascribed to the enol tautomer, the above extinction coefficient had to be called the "apparent" one.

7) "International Critical Tables," Vol. III, McGraw-Hill, New York (1928), p. 51.

8) D. Semmingsen, *Acta Chem. Scand.*, **26**, 143 (1972).

9) E. L. King and W. H. Reas, *J. Am. Chem. Soc.*, **73**, 1806 (1951).

10) The enthalpy and entropy of sublimation at 25 °C for the enol tautomer of BA were reported to be 20.0 kcal mol^{-1} and 43.2 e.u. respectibely. (A. Aihara, *Bull. Chem. Soc. Jpn.*, **32**, 1242 (1959).) The lower melting point of BFA suggests that BFA is somewhat more volatile than BA.

11) See, for example, H. S. Frank and M. W. Evans, *J. Chem. Phys.*, **13**, 507 (1945); H. S. Frank and W. Y. Wen, *Discuss. Farady Soc.*, **24**, 133 (1957); A. Ben-Naim, *J. Phys. Chem.*, **69**, 1922 (1965); *ibid.*, **69**, 3240 (1965); F. Franks and B. Watson, *Trans. Farady Soc.*, **63**, 329 (1967).

12) J. O. Hill and R. J. Irving, *J. Chem. Soc., A*, **1969**, 2759.

13) N. C. Deno and C. H. Spink, *J. Phys. Chem.*, **67**, 1347 (1963).

14) J. E. Desnoyers, G. E. Pelletier, and C. Tolicoeur, *Can. J. Chem.*, **43**, 3232 (1965).

15) J. E. Gordon and R. L. Thorne, *J. Phys. Chem.*, **71**, 4390 (1967).

16) H. E. Wirth and A. Losurdo, *J. Phys. Chem.*, **72**, 751 (1968).

17) W. Y. Wen and J. H. Hung, *J. Phys. Chem.*, **74**, 170 (1970).

18) R. Aveyard and R. Heselden, *J. Chem. Soc., Faraday Trans. 1*, **70**, 1953 (1974).

19) R. M. Diamond, *J. Phys. Chem.*, **67**, 2513 (1963).

20) G. R. Choppin and K. Buijs, *J. Chem. Phys.*, **39**, 2042 (1963).

21) See, for example, S. Uchikawa, *Bull. Chem. Soc. Jpn.*, **40**, 798 (1967); Y. Yamamoto, T. Tarumoto, and T. Tarui, *Chem. Lett.*, **1972**, 459; H. K. Biswas and B. M. Maudel, *Anal. Chem.*, **44**, 1636 (1972).

22) H. Moriya and T. Sekine, *Bull. Chem. Soc. Jpn.*, **45**, 1626 (1972).

23) S. Ōki and I. Terada, *Anal. Chim. Acta*, **61**, 49 (1972).

24) E. Sekido and Y. Yoshimura, *J. Inorg. Nucl. Chem.*, **38**, 1187 (1976).

Carbon-13 NMR Spectra of Benzene Mono- and Di-Carboxylic Acids and Their Analytical Applications

Yoshio KOSUGI* and Tsugio TAKEUCHI

Department of Synthetic Chemistry, Faculty of Engineering, Nagoya University, Nagoya 464

(Received September 28, 1977)

Carbon-13 NMR spectra of benzoic, and phthalic acids were compared both in D_2O with an excess of sodium hydroxide and in a mixture of DMSO-d_6 and H_2O (4:1). Tight ion pair forms of benzoate anion were considered. A simple additive rule for isomeric phthalic acids was employed to assign the spectral peaks. These carboxylic acids gave characteristic peaks and so can be distinguished from others in mixtures. Quantitative analyses of these carboxylic acids with calibration curves are also possible by a simple preparation of basic D_2O solutions. An example of the use of these data is the Henkel process (*cf.* Fig. 1) for the synthesis of terephthalic acid.

Better analyses of a mixture of benzoic acid (**1**) and isomeric phthalic acids (**6**—**8**) are highly desired not only in organic laboratories but also in polyester manufacturing industries. The most well-known method for the analyses of the benzenepolycarboxylic acids may be esterification, followed by gas-chromatographic separation. Ultraviolet spectroscopy is also of potential usefulness, but it is often interfered with by contamination.

Nuclear magnetic resonance (NMR) spectroscopic analysis is inferior to the gas-chromatographic method in accuracy and sensitivity, but it is still useful and of convenience in most cases when one needs to analyze a reaction mixture quickly or to follow its conversions as the reaction proceeds.

Unfortunately, the much more versatile ^1H NMR is often unsuitable for identifying structurally similar derivatives. On the other hand, the widely-ranging chemical shifts of ^{13}C NMR reflect a small difference in the structures.

Besides analytical purposes, the ^{13}C NMR data of aromatic carboxylic acids will be added to the data collections from which unambiguous empirical rules for the ^{13}C chemical shifts of substituted benzenes may be derived. The chemical shifts of carboxylic acids, however, often vary with the changes in solvent basicities, polarities, *etc.*, because the degrees of association and dissociation of carboxylic acids are solvent-dependent.[1] More generalized values of the chemical shifts of aromatic carboxylic acids are desirable.

Herein we will report some attempts to use ^{13}C NMR for comparing the differences among benzoic and benzenedicarboxylic acids.

Results and Discussion

Benzoic Acid. A few data on the ^{13}C NMR chemical shifts (δ^C) of benzoic acid have appeared in the literature.[2-4] The poor solubility of the acid in D_2O made it impossible to get a reasonable spectrum with an accumulation of 10000 transients at 26 °C. While no solubility problem is met with in aprotic polar solvents, such as DMSO-d_6, a small amount of water in the solvent often affects chemical shifts, especially when hydrogen bonding participates. Adding water in a 25 volume percentage to a DMSO-d_6 solution seems to be a successful way to eliminate the ill-defined effects of concentration changes and other factors which may vary the degrees of hydrogen bonding or dissociation of benzoic acid.[1] Species **1** seemed to be dominant in the possible equilibrations.

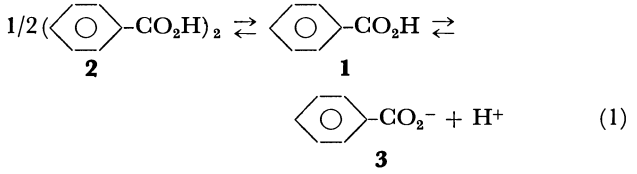

(1)

The peaks of the spectra are assigned with reference to the literature values, the off-resonance decoupled spectra, the gradual shift in peaks with different ratios of a mixed solvent, and the virtual peak intensities. The data are summarized in Table 1.

A large solvent dependency of the chemical shifts is evident in Table 1. The resonance-field change in δ_{CO} (the chemical shift of the carboxyl carbon atom) reaches *ca.* 5 ppm, this shift is attributable to the change in the association degree of benzoic acid.[1]

Benzoate Anion. Benzoic acid in a strong, basic heavy water shows a clean spectrum of the benzoate anion, the δ_{CO} of which shifts downfield by 11.4 ppm relative to δ_{CO} in DMSO-d_6, while the δ_{ipso} shifts by 8.8—10.1 ppm, compared to the values in DMSO-d_6 or $CDCl_3$ respectively. Essentially the same spectrum was obtained when sodium benzoate was dissolved in D_2O. This suggests that all the chemical shifts observed in a basic D_2O solution are attributable to the anion species, **3**. On the other hand, benzoic acid dissociated incompletely in the mixed solvent. The resulting chemical shifts were values between those of **1** and **3**. Similar chemical shifts were recorded when sodium benzoate was dissolved in the mixed solvent without adding sodium hydroxide (see

TABLE 1. CHEMICAL SHIFTS OF BENZOIC ACID IN VARIOUS SOLVENTS

$\delta^{C\,a)}$	$CDCl_3$[1]	CCl_4[b]	DMSO-d_6[1]	DMSO-d_6–H_2O(4 : 1)
Carboxyl	172.6	—	167.3	167.7
Ipso	129.4	130.6	130.7	130.3
Ortho	130.3	130.0	129.2	129.1
Meta	128.5	128.5	128.2	128.2
Para	133.8	133.6	132.5	132.7

a) Chemical shifts from TMS or DSS at a concentration of *ca.* 500 mg in a solvent of 3 ml (4 ml in the case of $CDCl_3$). b) Data from Ref. 3, in which data were converted using $\delta_c^{C_6H_6}$ 128.5.[3] 10% solution.

Table 2. Chemical shifts of benzoate anion

	Solvent	D_2O[1)]	Mixture[a)]	$CDCl_3$	DMSO-d_6	D_2O	Mixture[a)]
	Additive	NaOH	NaOH	Et_3N	Et_3N	b)	b)
δ^C	Carboxyl	178.7	171.4	172.2	170.2	178.7	171.2
	Ipso	139.5	138.2	136.7	135.6	139.7	138.3
	Ortho	132.1	129.0	129.2	129.0	132.2	129.6
	Meta	131.5	127.5	127.4	127.8	131.7	128.9
	Para	134.5	129.7	129.9	130.8	134.5	127.5

a) A mixture of DMSO-d_6 and H_2O in a ratio of 4 to 1. b) Sodium benzoate was used instead of benzoic acid.

Table 3. Chemical shifts of benzenedicarboxylic acids in two kinds of media

δ^C	In DMSO-d_6–H_2O (4 : 1)			In D_2O with *vs.* NaOH		
	6	**7**	**8**	**6**	**7**	**8**
Carboxyl	168.8	166.6	166.7	180.9	178.4	178.3
C_1	131.0	130.5	134.1	141.0	139.7	141.9
C_2	131.0	129.8	129.4	141.0	132.3	131.7
C_3	128.3	130.5	129.4	130.5	139.7	131.7
C_4	132.1	133.3	134.1	132.1	134.6	141.9
C_5	132.1	128.8	129.4	132.1	131.5	131.7
C_6	128.3	133.3	129.4	130.5	134.6	131.7

Table 4. Calculated chemical shifts of benzenedicarboxylic acids and their anions

δ^C	Dicarboxylic acids[a)]			Dicarboxylate anions[b)]		
	6	**7**	**8**	**6**	**7**	**8**
C_1	131.2	130.3	133.9	140.1	139.5	142.5
C_2	131.2	130.0	129.1	140.1	132.7	132.1
C_3	129.1	130.3	129.1	132.1	139.5	132.1
C_4	131.8	132.7	133.9	134.5	135.1	142.5
C_5	131.8	128.2	129.1	134.5	131.5	132.1
C_6	129.1	132.7	129.1	132.1	135.1	132.1

a) In DMSO-d_6–H_2O (4 : 1). b) In D_2O with an excess of sodium hydroxide.

the last column in Table 2).

Although an effort to record the spectrum of sodium benzoate in $CDCl_3$ was in vain, the benzoate anion in organic solvents was also generated by adding excess triethylamine. As may be seen in Table 2, the chemical shifts in $CDCl_3$ or DMSO-d_6 are independent of the solvent nature, but are different from those of the benzoate anion obtained in the D_2O solution. The downfield shifts of δ_{CO} and δ_{ipso} relative to those of benzoic acid in DMSO-d_6 were 2.9 ppm and 4.9 ppm respectively, smaller than those observed for the benzoate anion in D_2O (*vide ante*). That is, the chemical shifts of the benzoate anion in organic solvents are between these values of the free acid form, **1**, and of the completely ionized form, **3**. This may suggest that the negative charge on the carboxyl group is neutralized to some extent in a tight ion pair form, **4** or **5**.

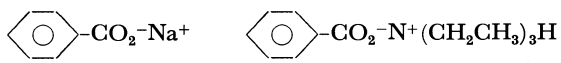

4 **5**

Benzenedicarboxylic Acids. The ^{13}C NMR spectra of phthalic acid (**6**), isophthalic acid (**7**), and terephthalic acid (**8**) were obtained in a mixed solvent (with the same ratio as above) and in D_2O with an excess of sodium hydroxide. The results are given in Table 3.

The assignment of the peaks was aided by the additive rule for disubstituted benzene derivatives. The usefulness of the calculation for several compounds had also been tested previously in this laboratory.[4–5)] Used for the additive calculation[6)] were the chemical shifts of benzoic acid in the mixed solvent (Table 1) and of the benzoate anion in D_2O saturated with sodium hydroxide (Table 2). In the calculation, the increments of the shifts can not be estimated by using the benzene standard for its chemical shifts in a D_2O solution are not available. Therefore, the δ^C of meta carbon was set for the standard both in the mixed solvent and in basic D_2O (Table 4).

The agreement between the observed and the calculated chemical shifts of phthalic acid and its anion was not perfect (the largest discrepancy was 0.8 ppm). Similar disagreements are common for ortho-substituted benzenes,[7)] where usually two bulky groups interact with one another. On the other hand, a fairly good agreement was established for isophthalic acid and terephthalic acid in two different solvents.

Analytical Applications. Terephthalic acid is in high demand as a material of polyester fibers and plastics. Numberless studies on synthesizing or manufacturing the material have been reported. One of the most successful findings is Henkel reaction[8)] by which terephthalic acid is produced from benzoic, phthalic, and isophthalic acids.

The pathways of the Henkel reaction are given below, although the acid forms represent the corresponding alkali salts in actual reactions where carbon dioxide and catalysts such as cadmium iodide are also present.

The most routine process of analysis may be the acidification of the reaction mixture, followed by the extraction of the acids, esterification and finally gas-chromatographic separation. However, NMR spectroscopy would be more convenient for the analysis if rigorous accuracy were not crucial, as it is not for usual organic reactions. Unfortunately, the more accessible ^1H NMR method does not seem appropriate for the present case because spectral overlaps are inevitable.

The proton signal of carboxyl groups of terephthalic acid (δ^H=10.5—11.7) is too broad and weak to be

used for the present analysis. One exception is the case when a reaction mixture composed of benzoic acid and terephthalic acid is made up in a DMSO solution. This happens in some related studies of benzenepolycarboxylic acids. When the method is applied to the crude reaction mixture of the Henkel process, acidification and extraction (and perhaps replacing the solvent with DMSO) are necessary because it contains exclusively water soluble alkali salts of the carboxylic acids.

Contrary to the ^1H NMR method, ^{13}C Fourier-transform NMR spectra with ^1H noise-decoupling give narrow, single peaks whose resonance frequencies are printed out from an attached computer memory.

Surveying Tables 1—3, it seems that one can distinguish the peaks of terephthalic aicd from the others. In fact, the spectra of mixtures of terephthalic acid with either benzoic acid (Fig. 2a) or phthalic acid and isophthalic acid (Fig. 2b) in basic D_2O demonstrate

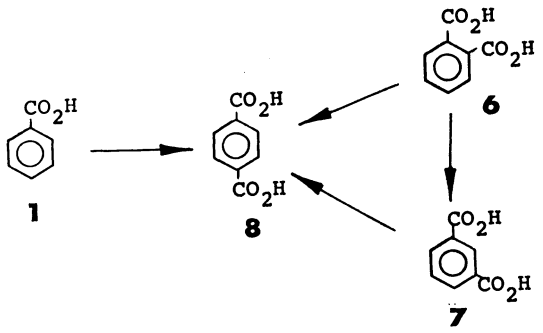

Fig. 1. Reaction paths of Henkel process.

applicable analyses of the Henkel process (Fig. 1)

When all these carboxylic acids are mixed, the only ambiguous distinction is the peak difference between benzoic acid and isophthalic acid. However, the mixed solvent instead of basic D_2O may be used for such a purpose.

Problems in Quantitative Determination. The application of ^{13}C NMR spectroscopy to quantitative analysis has recently been reported frequently.[9] Unlike the ^1H NMR, the ^{13}C peak intensity is affected by any nuclear Overhauser effects (NOE). Therefore, a simple integration of the peak intensity does not give quantitative amounts of carbon atoms. However, the amount of NOE on a particular carbon is usually independent of the sample concentrations, because the dipole-dipole (of proton) interaction dominates the ^{13}C relaxation. To confirm this accepted idea, benzoic acid was chosen to test the possibility of quantitative analysis.

A certain amount of benzoic acid was dissolved in basic D_2O with propionic acid (0.58 M). At lower concentrations, the peaks of carboxyl and ipso carbons were hidden in the noise levels. The relative peak intensities of the other ring carbons against methylene carbon of propionic acid (internal standard) were on fairly good straight lines in the range of 0.33—2.67M of benzoic acid (dotted lines in Fig. 3). These calibration lines, which had been expected to be straight are sufficient proof for the quantitative determination of other carboxylic acids, including therephthalic acid.

In connection with the NOE problem in the present analysis, pure oxygen, a paramagnetic substance, was saturated in the sample solutions. No improve-

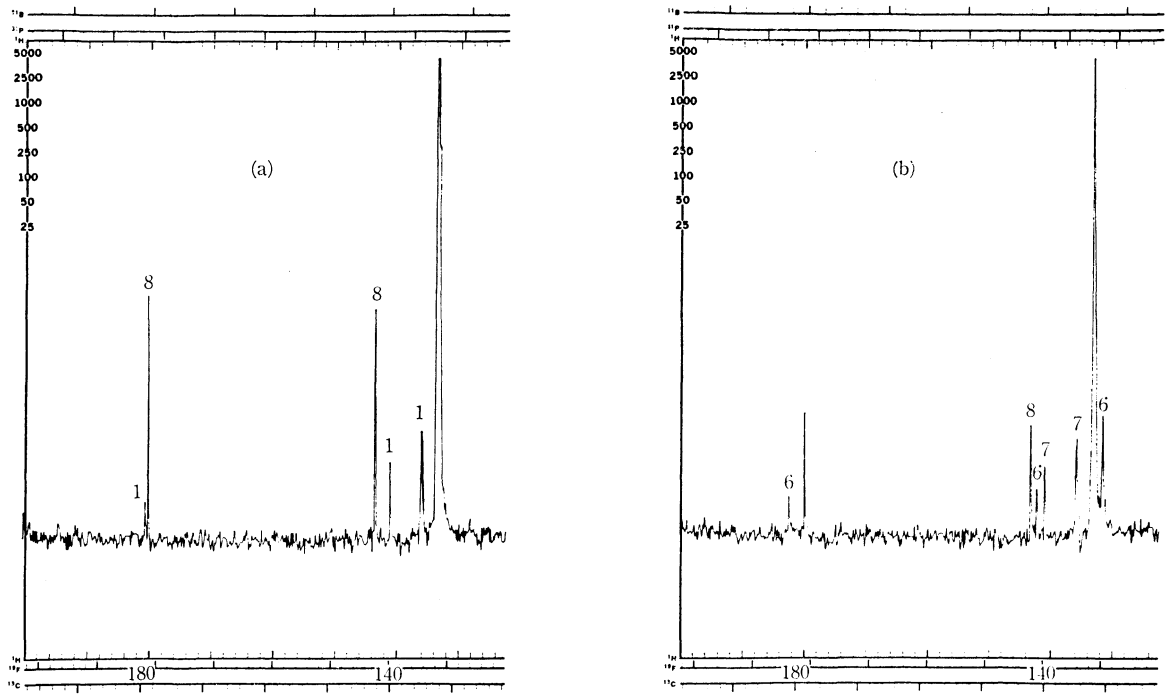

Fig. 2. ^{13}C NMR spectra of mixture samples.
(a) A mixture of terephthalic acid (**8**) of 200 mg and benzoic acid (**1**) of 100 mg in D_2O (3.3 ml) with sodium hydroxide of 300 mg.
(b) A mixture of **8** of 200 mg, phthalic acid (**6**) of 100 mg and isophthalic acid (**7**) of 100 mg in D_2O (4.3 ml) with sodium hydroxide 300 mg.

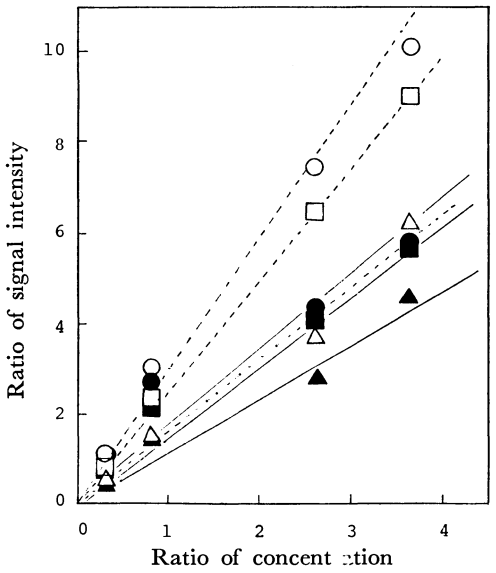

Fig. 3. Signal intensity ratios *versus* concentration ratios of sodium benzoate to methylene carbon atom of sodium propionate (0.58 M) either in aqueous solutions (open symbols with dotted lines) or in the solutions saturated with oxygen (blackened symbols with solid lines). Symbols are corresponding to ortho (circle), meta (square), and para (triangle) carbons of the benzoate.

ment for the determination was found, in spite of extra pretreatment before measurements.

Experimental

NMR Measurements. All the ^{13}C NMR spectra were recorded on a Varian XL-100-15 NMR spectrometer operating at 25.16 MHz in the pulsed Fourier transform mode with ^{1}H noise-decoupling with the 2 kHz band width at 8 mW. The pulse width of 60 μs (*ca.* 45° flip angle), with a pulse delay of 3 s, was applied. Spectral widths of 5000 Hz were swept with 4096 data points using a Varian DATA 620i computer with 8 K memory produced spectra with accuracies of better than 0.1 ppm. Normally 1000 transients were accummulated. Unless specified, a compound of *ca.* 500 mg and sodium hydroxide, when necessary, was dissolved in a solvent (3—5 ml) in a 12 φmm sample tube at a spinning rate of 10—16 rps at 26°. Tetramethylsilane (TMS) or sodium 2,2-dimethyl-2-silapentane-5-sulfonate (DSS, δ_C 0.015) was the internal standard. Carbonyl carbon of methyl acetate (82% benzene-d_6 solution) showed a peak at 171.4 ppm, which was the exact mean value of those obtained on 65 different C-13 NMR machines throughout the country.[10]

Chemicals. All the aromatic carboxylic acids and sodium benzoate were of a guaranteed grade, while the triethylamine and sodium hydroxide were of a reagent grade. Dimethyl sulfoxide (DMSO) of a reagent grade was distilled from calcium hydride and stored over molecular sieves of Type 4 A. The deuterated solvents (D_2O, $CDCl_3$, and DMSO-d_6) for NMR spectroscopy were purchased from Merck Japan, Ltd. TMS and DSS were also of a NMR spectroscopic grade. Except for DMSO, none of them, including oxygen gas, was purified before use. A mixture of DMSO-d_6 and H_2O in a volume ratio of 4 to 1 was used in the present study (mixed solvent).

The authors wish to thank Mr. K. Okada for his technical assistance. Partial financial support from the Ministry of Education is acknowledged.

References

1) Detailed discussions on the hydrogen bonding and dissociation will be made elsewhere.[11]

2) L. F. Johnson and W. C. Jankowski, Carbon-13 NMR Spectra, Wiley-Interscience, New York (1972), p. 230.

3) G. L. Nelson, G. C. Levy, and J. D. Cargioli, *J. Am. Chem. Soc.*, **94**, 3089 (1972).

4) M. Yamazaki, T. Usami, and T. Takeuchi, *Nippon Kagaku Kaishi*, **1973**, 2135.

5) M. Yamazaki, T. Takeuchi, and K. Matsushita, *Kogyo Kagaku Zasshi*, **74**, 656 (1971).

6) G. S. Savitsky, *J. Phys. Chem.*, **67**, 2723 (1963).

7) W. R. Woolfenden and D. M. Grant, *J. Am. Chem. Soc.*, **88**, 1496 (1966).

8) B. Raecke and H. Schirp to Henkel & Co., Ger. Patent, 945627 (1954); 1004602 (1957).

9) An example from this laboratory is C. Shibata, M. Yamazaki, and T. Takeuchi, *Bull. Chem. Soc. Jpn.*, **50**, 311 (1977).

10) A survey of ^{13}C NMR machinery errors was conducted throughout this country by NMR Data Subcommittee of the Chemical Society of Japan in 1976. The reports appeared in *Kagaku To Kogyo*, **29**, 589 (1976).

11) Y. Kosugi and T. Takeuchi, *J. Magn. Reson.*, in press.

Preparation and Reactivities of Phenylethynyl[1,1,1-tris(diphenylphosphinomethyl)ethane]copper(I) Complex

Katsuma HIRAKI,* Yoshio FUCHITA,* and Yasushi MORITA

Department of Industrial Chemistry, Faculty of Engineering, Nagasaki University, Bunkyo-machi, Nagasaki 852

(Received December 5, 1977)

Phenylethynyl[1,1,1-tris(diphenylphosphinomethyl)ethane]copper(I), [Cu(C≡CPh)(tdpme)]{tdpme=1,1,1-tris(diphenylphosphinomethyl)ethane}, has been prepared in good yield by a reaction between phenylethynylcopper(I), [{Cu(C≡CPh)}$_n$], and tdpme. From physicochemical and spectroscopic studies the complex is considered to have a monomeric tetrahedral structure. It reacts with *p*-cresol to give [Cu(O-C_6H_4-CH_3-*p*)(tdpme)] and also with highly active hydrogen compounds, methyl cyanoacetate and methyl nitroacetate, to give [Cu{CH(CN)-CO_2CH_3}(tdpme)] and [Cu{CH(NO_2)CO_2CH_3}(tdpme)], respectively. However, moderately active hydrogen compounds, such as acetonitrile, dimethyl malonate, and nitromethane, do not react with [Cu(C≡CPh)(tdpme)]. The reactivities of the complex with active hydrogen compounds are discussed in correlation with the pK_a values of the latter compounds.

Recently, the syntheses of organocopper compounds have been widely investigated in view of the fact that copper compounds play important roles in various copper-assisted organic reactions.

Alkyl-[1] and arylcopper(I)[2,3] complexes containing uni- or bidentate phosphorus ligand have been prepared and converted into substituted alkylcopper(I) complexes by reactions with active hydrogen compounds.[4,5] Coates and Parkin,[6] and Camus and Marsich[3] prepared tertiary phosphine-bonded phenylethynylcopper(I) complexes, which have complicated compositions depending on the phosphine or molar ratio of phosphine/copper, such as [Cu(C≡CPh)$(PR_3)_n$] (R=Me, n=1,2,3; R=Et and Ph, n=1) and [(CuC≡CPh)$_m${$Ph_2P(CH_2)_kPPh_2$}$_n$] (k=1, m/n=4/3; k=2, m/n=1/1,2/3,4/3).

A triphosphine ligand, 1,1,1-tris(diphenylphosphinomethyl)ethane, (tdpme), has a three-fold axis of symmetry (Fig. 1) and serves as a bidentate or a tridentate ligand in tetrahedral,[7-9] square pyramidal,[7] and octahedral[10] complexes. As for copper(I) complexes, the ligand afforded the tetrahedral complexes, [CuX(tdpme)] (X=halogen,[8] ONO_2, and $OClO_3$[9]) and a complex, [Cu(BH_4)(tdpme)], which seems to have a very distorted square pyramidal structure.[11]

In this paper, we report the preparation and characterization of [Cu(C≡CPh)(tdpme)] **1**, and its reactivities towards active hydrogen compounds.

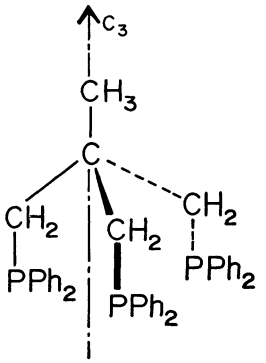

Fig. 1. Configuration of tdpme.

Experimental

Materials and Procedures. All the experiments were carried out in an atmosphere of dry nitrogen. Solvents were dried by the usual procedure and distilled.

1,1,1-Tris(diphenylphosphinomethyl)ethane (tdpme)[12] and phenylethynylcopper(I) [{Cu(C≡CPh)}$_n$][13] were prepared according to published procedures. Methyl nitroacetate was also prepared and purified by distillation under reduced pressure.[14]

General Procedures. IR spectra were measured on a Hitachi 285 spectrophotometer and ^{1}H-NMR spectra on a JEOL JNM-MH-100 spectrometer. Conductivity measurements were carried out for 1.0×10^{-3} M acetone solution at 25 °C on a Toa Electronics CM-6A conduct meter. Melting points were determined with a Yanaco micro melting point apparatus and are uncorrected. Molecular weight was determined in benzene by means of a cryoscopic method.

*Preparation of [Cu(C≡CPh)(tdpme)] **1**.* To a suspension of phenylethynylcopper(I) (158 mg, 0.96 mmol) in 20 ml of benzene was added tdpme (600 mg, 0.96 mmol) in 20 ml of benzene at room temperature. After the resulting pale yellow solution had been stirred for 24 h, the solvent was removed under reduced pressure. Recrystallization from toluene–hexane gave 637 mg of pale yellow crystals of **1** (yield 84%).

*Reaction of **1** with* p-*Cresol.* *p*-Cresol (30.2 mg, 0.28 mmol) in 5 ml of THF was added to a solution of **1** (200 mg, 0.25 mmol) in 30 ml of THF at room temperature. After being stirred for 5 h, the solvent was removed under reduced pressure. Recrystallization from benzene–hexane gave 80 mg of pale yellow crystals, [Cu(O-C_6H_4-CH_3-*p*)(tdpme)] **2** (yield 40%).

*Reaction of **1** with Methyl Cyanoacetate.* Methyl cyanoacetate (57.1 mg, 0.58 mmol) in 5 ml of THF was added to a solution of **1** (455 mg, 0.58 mmol) in 20 ml of THF at 0 °C. After being stirred for 5 h at 0 °C, the solvent was removed under reduced pressure and the resulting solid was washed with benzene. Recrystallization from dichloromethane–hexane gave 210 mg of white crystals, [Cu{CH(CN)CO_2CH_3}-(tdpme)] **3** (yield 46%).

*Reaction of **1** with Methyl Nitroacetate.* This reaction was carried out at 0 °C in the same way as described for **3**, and pale yellow crystals, [Cu{CH(NO_2)CO_2CH_3}(tdpme)] **4** were produced (yield 33%).

*Reaction of **1** with Other Active Hydrogen Compounds.* Complex **1** did not react with other moderately active hydrogen

Table 1. Some properties of the complexes **1**—**4**

No.	Mp (°C)	Elemental analyses[a] (%)			^{1}H-NMR (δ ppm)[b]			
					tdpme		≡CH	other
		C	H	N	$-CH_3$	$-CH_2$		CH_3
1	207—208	73.92 (74.56)	5.70 (5.62)	—	1.56	2.40	—	—
2	130—132 (dec)	73.42 (72.49)	6.11 (5.83)	—	1.50	2.40	—	2.24
3	159—164 (dec)	68.57 (68.74)	5.52 (5.51)	1.46 (1.78)	1.58	2.42	0.64	3.74
4	144—147.5 (dec)	65.55 (65.54)	5.59 (5.38)	1.69 (1.74)	1.34	2.38	0.90	3.67

a) Calculated values in parentheses. b) In $CDCl_3$ (TMS as the internal standard).

compounds, *i.e.*, acetonitrile, dimethyl malonate, and nitromethane in THF either at 0 °C, room temperature, or 65 °C (refluxing conditions), only the starting complex **1** being recovered.

Results and Discussion

*Preparation and Properties of [Cu(C≡CPh)(tdpme)] **1**.* Complex **1** was prepared by the reaction of phenylethynylcopper(I) with tdpme in benzene at room temperature. The complex is considerably stable in air and soluble in common organic solvents.

$$[\{Cu(C{\equiv}CPh)\}_n] + n\,\text{tdpme} \xrightarrow[\text{r. t.}]{\text{benzene}} n[Cu(C{\equiv}CPh)(\text{tdpme})]\ \mathbf{1}$$

The IR spectrum of **1** shows a ν(C≡C) band at 2030 cm^{-1}, higher (*ca.* 100 cm^{-1}) than that of phenylethynylcopper(I), and is assigned to the ethynyl group bonded to copper. Such shift of the ν(C≡C) band was observed in other phenylethynylcopper(I) complexes containing phosphine ligands.[3] Molecular weight determination revealed that **1** is monomeric in benzene: Found: 828 (2.25 wt%). Calcd for $C_{49}H_{44}CuP_3$: 789.4. Conductivity of **1** (Λ=5.75 Ω^{-1} cm^2 mol^{-1}) in acetone solution did not change significantly on addition of excess methyl iodide. This indicates that tdpme serves as a tridentate ligand, leaving no uncoordinated phosphine group expected to yield a phosphonium salt on addition of methyl iodide,[7] and that **1** has a tetrahedral structure as shown in Fig. 2.

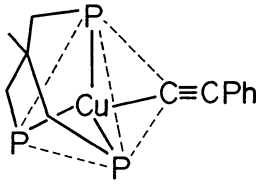

Fig. 2. Configuration of [Cu(C≡CPh)(tdpme)] **1**.

*Reactivities of [Cu(C≡CPh)(tdpme)] **1**.* Complex **1** reacted with *p*-cresol, methyl cyanoacetate, and methyl nitroacetate in THF to give new tdpme-copper complexes, [Cu(O–C_6H_4–CH_3-*p*)(tdpme)] **2**, [Cu{CH(CN)CO_2CH_3}(tdpme)] **3**, and [Cu{CH(NO_2)-CO_2CH_3}(tdpme)] **4**, respectively, which were characterized by elemental analyses, IR and ^{1}H-NMR spectroscopy. Some properties of the complexes are summarized together with those of **1** in Table 1.

$$[Cu(C{\equiv}CPh)(\text{tdpme})] + BH \xrightarrow[\text{THF}]{} [CuB(\text{tdpme})] + HC{\equiv}CPh$$

B: Conjugated base

Complexes **2**, **3**, and **4** show considerable thermal stability, and are moderately stable in air; they can be stored for a long time in dry nitrogen atmosphere. Their IR spectra show no ν(C≡C) band, which is found in the starting complex **1**.

A tetrahedral structure can be ascribed also to complex **2** in view of its ^{1}H-NMR showing only one methylene resonance for tdpme moiety.

The IR spectrum of **3** shows a ν(C≡N) band at 2155 cm^{-1} and a ν(C=O) band at 1610 cm^{-1}. The ^{1}H-NMR spectrum of **3** shows methine signal at a considerably high field (δ=0.64) and one methylene resonance at δ 2.42, indicating that the three methylene groups of tdpme moiety are equivalent. This indicates that **3** assumes a tetrahedral complex containing a copper-carbon σ-bond.

The conjugated base of methyl nitroacetate in **4** should be coordinated to copper either with methine carbon (structure A) or with an *aci*-nitro group (structure B), as shown in Fig. 3. In fact, [Cu(O_2NCH_2)-

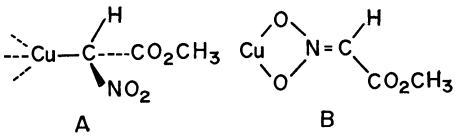

Fig. 3. Possible configurations of **4**.

(PPh_3)$_2$][15] and [Cu{O_2NCPh(NO_2)}(PPh_3)$_2$][16] were confirmed by X-ray analysis to be tetrahedral complexes, in which the nitro group is coordinated to copper with the *aci*-nitro form. Methylene protons in the *aci*-nitro group of [Cu(O_2NCH_2)(PPh_3)$_2$] show resonance at a very low field (δ=4.35).[15] On the other hand, the ^{1}H-NMR spectrum of **4** exhibits methine resonance at a considerably high field (δ=0.90), and only one methylene resonance at δ 2.38, similar to the respective one of **3**. This indicates that **4** has structure A, in which copper is coordinated with tdpme at three sites of phosphine groups. In order to confirm whether

TABLE 2. COMPARISON BETWEEN pK_a VALUE AND REACTIVITY

Compound	Reactivity of **1**	pK_a value	Ref.[a]
$C_6H_5C{\equiv}CH$	—	21	17
CH_3CN	No	25	17
$CH_2(CO_2CH_3)_2$	No	13.5	18
$CH_2(CN)_2$	Yes	11.2	17, 18
CH_3NO_2	No	10.2	17, 18
$NCCH_2CO_2CH_3$	Yes		
$O_2NCH_2CO_2CH_3$	Yes	5.8	18
$HO\text{-}C_6H_4\text{-}CH_3\text{-}p$	Yes	10.2	19

a) See references presented in the last part of this paper.

4 contains an uncoordinated phosphine group, conductivity of an acetone solution of **4** containing excess methyl iodide was measured. The experiment was unsuccessful owing to the immediate precipitation of a white solid , which was ascribed to [CuI(tdpme)][8] on the basis of elemental analysis and IR spectrum. Complex **4** seems to prefer structure A to B, owing to the chelating effect of the tridentate phosphine group which prevents the bidentate *aci*-nitro group from coordinating to copper. As for the IR spectrum of **4**, bands at 1440, 1620, and 1680 cm^{-1} were ascribed to $\nu_a(NO_2)$, $\nu_{as}(NO_2)$, and $\nu(C{=}O)$, respectively.

No reaction took place between **1** and other moderately active hydrogen compounds, *i.e.*, acetonitrile, dimethyl malonate, and nitromethane, even under refluxing conditions of THF. Malononitrile reacted with **1** to give yellow powder, which could not be isolated in a pure state.

As a whole, it appears that the reaction between **1** and active hydrogen compounds depends on the pK_a values of the latter[17-19] (Table 2). Complex **1** reacts with highly active hydrogen compounds having a pK_a value below 10, but not with less active hydrogen compounds with pK_a above 13. **1** shows fairly complicated reactivity towards the active hydrogen compounds with pK_a values in the range 10—13, while **1** reacts smoothly with *p*-cresol, a week Brönsted acid having a pK_a of 10.2. Such hydrogen activity is important for a similar exchange reaction with the phenylcopper(I)–triphenylphosphine system.[4]

References

1) A. Miyashita and A. Yamamoto, *Bull. Chem:. Soc. Jpn.*, **50**, 1102 (1977).
2) G. Costa, A. Camus, N. Marsich, and L. Gatti, *J. Organomet. Chem.*, **8**, 339 (1967).
3) A. Camus and N. Marsich, *J. Organomet. Chem.*, **21**, 249 (1970).
4) N. Marsich and A. Camus, *J. Organomet. Chem.*, **81**, 87 (1974).
5) A. Yamamoto, A. Miyashita, and T. Yamamoto, Preprints p. 23, Symposium on the chemical use of carbon dioxide, Tokyo, September 1975.
6) G. E. Coates and C. Parkin, *J. Inorg. Nucl. Chem.*, **22**, 59 (1961).
7) R. Davis and J. E. Fergusson, *Inorg. Chim. Acta*, **4**, 23 (1970).
8) L. Sacconi and S. Midollini, *J. Chem. Soc., Dalton Trans.*, **1972**, 1213.
9) R. J. Restivo, A. Costin, G. Ferguson, and A. J. Carty, *Can. J. Chem.*, **53**, 1949 (1975).
10) R. Davis and J. E. Fergusson, *Inorg. Chim. Acta*, **4**, 16 (1970).
11) P. Dapporto, S. Midollini, A. Orlandini, and L. Sacconi, *Inorg. Chem.*, **15**, 2768 (1976).
12) W. Hewertson and H. R. Watson, *J. Chem. Soc.*, **1962**, 1490.
13) R. D. Stephens and C. E. Castro, *J. Org. Chem.*, **28**, 3313 (1963).
14) S. Zen, M. Koyama, and S. Koto, *Kogyo Kagaku Zasshi*, **74**, 70 (1971).
15) A. Camus, N. Marsich, G. Nardin, and L. Randaccio, *Inorg. Chim. Acta*, **17**, L33 (1976).
16) A. Camus, N. Marsich, G. Nardin, and L. Randaccio, *J. Chem. Soc., Dalton Trans.*, **1975**, 2560.
17) H. Iida, "Yuki Gosei Kagaku," Baifukan, Tokyo (1975), p. 13.
18) J. B. Hendrickson, D. J. Cram, and G. S. Hammond, "Organic Chemistry," 3rd ed, McGraw-Hill Book Company, New York (1970), pp. 304—307.
19) W. Bartok, P. J. Lucchesi, and N. S. Snider, *J. Am. Chem. Soc.*, **84**, 1842 (1962).

Ligand Isotopic Exchange of Tris(acetylacetonato)germanium(IV) Perchlorate in Organic Solvents

Akira NAGASAWA and Kazuo SAITO*

Chemistry Department, Faculty of Science, Tohoku University, Aoba, Aramaki, Sendai 980

(Received December 8, 1977)

The ligand isotopic exchange between tris(acetylacetonato)germanium(IV) perchlorate and acetylacetone[^{14}C] has been studied in 1,1,2,2-tetrachloroethane (TCE), nitromethane (NM), and acetonitrile (AN), at 100—120 °C. In these solvents, the rate formula was $R=k[H_2O][complex]$; the concentrations of the complex, free ligand, and water in solution were in the ranges from 0.01 to 0.1 mol dm^{-3}. The activation enthalpies and entropies for the k's are 105, 98, and 90 kJ mol^{-1}; and −25, −53, and −69 J K^{-1} mol^{-1}, in TCE, NM, and AN, respectively. Influence of acid and base concentrations, and deuterium isotope effect on the rate in AN suggest that the rate controlling step of the exchange is governed by the ease of the proton transfer between the leaving and the incoming acac$^-$ in an intermediate.

Little information is collected concerning dynamic behavior of octahedral germanium(IV) compounds. We resolved tris(acetylacetonato)germanium(IV) [Ge(acac)$_3$]$^+$ and postulated an intramolecular mechanism for its racemization involving an intermediate with a unidentate acetylacetonate. The ligand isotopic exchange with free acetylacetone[^{14}C] (Hacac[^{14}C]) was much slower than the racemization, but the kinetics was left unknown.[1] This paper deals with kinetic studies of ligand isotopic exchange between [Ge(acac)$_3$]ClO$_4$ and Hacac[^{14}C] in dehydrated organic solvents at 100 to 120 °C. The mechanism is discussed with reference to the solvent effect, and compared with those of related reactions including the racemization.

Experimental

Materials. Tris(acetylacetonato)germanium(IV) Perchlorate: The complex was prepared by the reported procedure,[1] and recrystallized from acetonitrile (AN) by adding diethyl ether. Found: C, 38.58; H, 4.53%. Calcd for $C_{15}H_{21}O_{10}ClGe$: C, 38.38; H, 4.51%. The pattern of the absorption spectrum and the peak ($\tilde{\nu}$, 34700 cm^{-1}; ε, 35500 dm^2 mol^{-1}) in UV region coincided with those in the reference.

Acetylacetone: Commercially available Hacac was distilled under reduced pressure, dried with anhydrous calcium sulfate, and distilled at *ca.* 15 mmHg at 60 °C. The Hacac[^{14}C] was prepared by the Claisen condensation between acetone[^{14}C] (15 cm^3, 0.25 mCi) and ethyl acetate,[2] and distilled three times to yield ≈5 g of Hacac[^{14}C] with a specific activity ≈10 μCi g^{-1}. Acetylacetone[*methylene*-$^2H_2$] (Hacac[D]) was prepared by refluxing Hacac with deuterium oxide (D_2O) in dichloromethane, and fractionally distilled twice. The proton NMR spectrum indicated *ca.* 90% deuteration of methylene hydrogens. The purities of these reagents were checked by gas chromatography to be >99.99%.

Solvent for Kinetic Runs: Acetonitrile (AN) was dried by refluxing with diphosphorus pentaoxide (*ca.* 5 g for 1 dm^3) for *ca.* 3 h, and fractionally distilled at 81.6 °C. These procedures were repeated until ≲0.003 M (M=mol dm^{-3}) water remained on Karl Fischer titration. Nitromethane (NM) was distilled, frozen under a reduced pressure three times, dried with Molecular Sieve 4A Zeolite, and distilled at ≈15 mmHg. The product contained <10^{-2} M water, and ≈10^{-5} M nitroethane and nitropropanes. 1,1,2,2-Tetrachloroethane (TCE) was washed with concentrated sulfuric acid until the water layer remained colorless, and then with water, fractionally distilled at ≈15 mmHg at 60 °C in the dark, and aerated with dry air. 1,2-Dichloroethane (DCE) was washed successively with sodium hydroxide in water, dilute sulfuric acid, and water, and then fractionally distilled in the dark.

Other Reagents: Trichloroacetic acid was sublimed *in vacuo* at 60—70 °C. Trichloroacetic acid[^2H] (CCl_3COOD) was prepared by evaporating D_2O solution of trichloroacetic acid to dryness, and sublimed *in vacuo*. Pyridine was purified by recrystallizing pyridinium perchlorate, treating with solid potassium hydroxide, and distilling at 114—115 °C. Extra pure reagents of 2,6-lutidine and sodium perchlorate were used without further purification. Diethyl ether was dried over calcium chloride overnight, and distilled.

Kinetic Procedure. Ligand Isotopic Exchange: The solution of Hacac[^{14}C] (0.08 to 1 M) in a given solvent was prepared at least 48 h in advance to attain the keto-enol equilibrium. The complex solution (≈0.05 M) in the same solvent was mixed with the ligand solution at room temperature. Whenever required, given amounts of water and/or any other reagents were introduced and the final volume was adjusted to 10 cm^3. Several 1 to 2 cm^3 portions were sealed in Pyrex-glass tubes (10 cm in height and 0.8 cm in diameter) and placed in a thermostatted (±0.2 °C) silicone oil bath at 100—120 °C to let the exchange reaction start.

The ampoules were picked up one by one at proper time intervals and cooled in cold water for 1 min. The content of each ampoule was poured into diethyl ether (30—50 cm^3) and set aside for 30 min at *ca.* 10 °C. The crystallized complex was filtered off, washed with diethyl ether, and dried. It was dissolved in AN (3 to 10 mg in 3 cm^3). A one cm^3 portion was mixed with toluene containing *p*-terphenyl and *p*-bis(5-phenyl-2-oxazolyl)benzene to produce 15 cm^3 solution containing their 0.4 and 0.01%, respectively, and submitted to liquid scintillation counting. Another one cm^3 portion was diluted 100 to 500 fold with AN and the extinction was measured at 288 nm to find the concentration of the original solution in AN. The specific β-activity of the recovered complex, x, was known from these data.

The water content of the reaction mixture was determined by Karl Fischer titration. The UV absorption spectrum of the reaction mixture was recorded to find any change in composition during the kinetic runs.

Calculation of the Exchange Rate: The rate of isotopic exchange was calculated by the McKay formula,

$$R = -[3ab/(3a+b)][\ln(1-F)]/t, \quad (1)$$

where a and b are the concentrations of the complex and the free ligand, respectively, and t and F are the lapse of time and the extent of the reaction at time t, respectively. The F values were given by $(x_0-x_t)/(x_0-x_\infty)$, where the suffix denotes the time lapse from the initiation until the quenching of the exchange reaction.

Acetylacetone is present in tautomeric keto-enol equilibrium in TCE, NM, and AN. The percentages of the enolic form were estimated from the intensities of NMR signals for the enol and keto forms in deuterated solvents ([Hacac] = 10^{-2} M) to be 69, 50, and 58%, respectively at 110 °C. The rate of the keto-enol tautomerization was much greater (*ca.* 10^{-4} s^{-1}) than that of the exchange at >100 °C, and the *b* was taken as the gross concentration of free Hacac.[13]

Apparatuses. Hitachi 323 Spectrophotometer was used for recording the UV absorption spectra. The β-activity of ^{14}C was recorded with Nuclear Chicago Unilux II-A Liquid Scintillation Counter. Varian A-60 Spectrometer was employed for NMR spectroscopy.

Results

Ligand isotopic exchange was studied in acetonitrile, nitromethane, and TCE. The complex decomposed at >120 °C in TCE, whereas even at 100 °C in DCE.

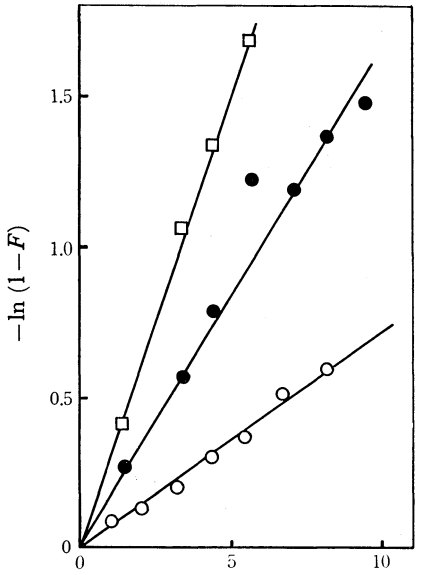

Fig. 1. McKay plot, $\ln(1-F)$ *vs.* *t*. The extent of reaction (*F*) was calculated from the specific activity of $[Ge(acac)_3]ClO_4$ in acetonitrile at 110.2 °C. Complex, 0.010 M; Hacac[^{14}C], 0.062 M; water, 0.013 M (○), 0.033 M (●), 0.047 M (□).

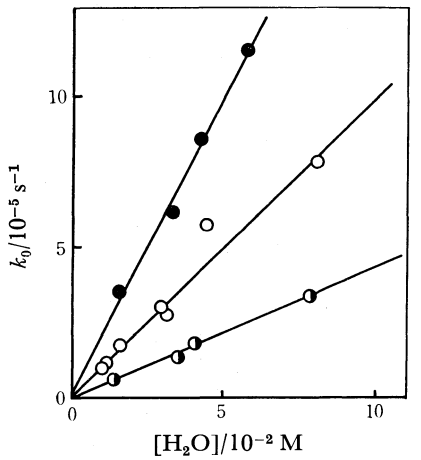

Fig. 2. Exchange rate constant k_0 *vs.* water content in acetonitrile, at 100.3 °C (◑), 110.2 °C (○), and 119.3 °C (●); [Hacac] ≈ 0.06 M, [complex] = 0.01 M.

General Aspect. McKay's *R* remained constant until *F* reached 0.7 (see Fig. 1) at 100—120 °C, and the UV absorption of the reaction mixture remained unchanged during these periods. Hence the following ligand exchange between the complex and the free ligand should take place exclusively.

$$[Ge(acac)_3]^+ + Hacac^* \rightleftharpoons [Ge(acac)_3{}^*]^+ + Hacac \quad (2)$$

The rate *R* was proportional to the complex concentration from 0.005 to 0.015 M, and the observed rate constant k_0 was calculated by the following equation:

$$R = k_0\,[complex], \quad (3)$$

while the free ligand concentration (0.03 to 0.09 M) gave very little influence, the plot of k_0 against water concentration (0.01 to 0.1 M) is linear as exemplified in Fig. 2 in AN, and the k_0 is expressed by

$$k_0 = k_x[H_2O]. \quad (4)$$

The k_x values in various solvents are given in Table 1. Ionic strength in acetonitrile solution (≤0.109 M, $NaClO_4$) gave very little influence on the rate at 110 °C.

Acid and Base Catalysis. Trichloroacetic acid enhanced the exchange in acetonitrile; also the separation-induced exchange became appreciable. The effect approached saturation when the acid concentration reached that of water (0.015 M) in the reaction mixture.

Pyridine and 2,6-lutidine caused change in UV absorption spectra of the reaction mixture in acetonitrile and gave precipitate after *ca.* 100 min at 110 °C even at a concentration lower than 0.01 M. A side reaction may have taken place. However, the original complex was partly recovered without decomposition to enable approximate measurement of its specific activity. The rate of exchange appeared to be smaller than in the absence of pyridine base.

Deuterium Isotope Effect. The rate of proton exchange between Hacac[^{14}C] and water is much greater than the ligand isotopic exchange rate of the complex. Hence the deuterium isotope effect should be reckoned as the gross influence of these protic species. Three kinetic runs were performed in solutions containing 0.010 M complex, 0.060 M Hacac, and 0.0060, 0.024, and 0.058 M water, the gross [H]/[D] ratios being 0.48, 0.60, and 0.71, respectively. The observed k_x's were smaller than those in the absence of excessive deuterium. Since the influence of proton and deuteron should be additive, the result was extrapolated to the purely deuterated system to find $k_{x(D)}$ 0.73 $M^{-1}\,s^{-1}$ at 110 °C. The gross $k_{x(H)}/k_{x(D)}$ ratio is therefore 1.4. Deuterated trichloroacetic acid also gave smaller rate than the ordinary trichloroacetic acid did.

Discussion

A plausible mechanism of the ligand exchange of $[Ge(acac)_3]^+$ is visualized in Fig. 3.

Catalytic Action of Water and Acid. If the solvent had contained no water, no ligand isotopic exchange

TABLE 1. RATE CONSTANTS OF LIGAND ISOTOPIC EXCHANGE OF $[Ge(acac)_3]ClO_4$[a)]

Solvent	Temp	[Ge]	[Hacac]	$[H_2O]$	k_x [b)]	Notes
	°C	10^{-2} M	10^{-2} M	10^{-2} M	10^{-3} M^{-1} s^{-1}	
CH_3CN (AN)	100.3	1.00	5.97	1.4—7.8	0.45±0.03	4 runs
	110.2	1.05	3.12	0.91	1.03	
		1.05	3.04	0.96	1.00	Aged Hacac[c)]
		1.00—1.05	6.24	1.0—8.2	0.99±0.10	7 runs
		1.00	6.24	1.1—3.2	1.00±0.03	$[NaClO_4] \leq 0.099$ M, 4 runs
		1.00	6.24	1.7—1.9	1.61±0.03	$[CCl_3COOH] = (0.0059$—0.035 M), 4 runs
		1.00	6.24	1.1	0.34	$[C_5H_5N] = 0.0051$ M
		1.05	9.36	1.2	0.97	
	119.3	1.00	5.97	1.6—5.8	1.94±0.23	4 runs
CH_3NO_2 (NM)	100.3	0.997	2.91—9.65	2.2—10	0.24±0.06	9 runs
	110.2	0.997	5.81—9.65	3.7—9.3	0.51±0.06	4 runs
	119.3	0.997	5.81	2.6—7.1	1.18±0.09	4 runs
$CHCl_2CHCl_2$	100.3	1.01	5.97	2.4—7.7	0.51±0.06	4 runs
(TCE)	110.2	1.01	2.89—8.68	1.7—6.3	1.26±0.16	4 runs

a) Rate law: $R = k_x[Ge][H_2O]$. b) Figures without error ranges represent those obtained by one kinetic run each.
c) Used after aging as a solution in AN for 1000 min at 110 °C.

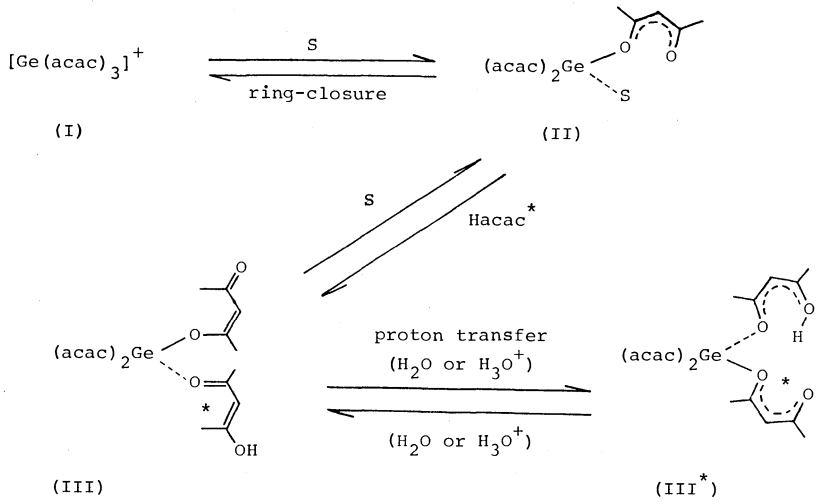

Fig. 3. Plausible mechanism of ligand isotopic exchange of $[Ge(acac)_3]ClO_4$ in organic solvents.[4)]
S: Solvent molecule. Asterisks indicate labelling with ^{14}C.

would have occured below 120 °C. Water in organic solvents can act as either a nucleophile or a proton donor of a moderate strength. It can also bring about indirect influence including change of permittivity of the bulk environment, and that of the degree of intermolecular association of the complex (*e.g.*, ion-pair formation with perchlorate). Since the ionic strength in acetonitrile gave very little effect on the exchange rate under the experimental conditions, intermolecular association should not give a dominant effect. Permittivity of the solvent can change with increase in water content, but neither this effect is important, because no exchange takes place in the absence of water in the given temperature range. Proton transfer from free Hacac to coordinated $acac^-$ is essential for the ligand exchange to take place, and proton donors such as protic acid and water can directly assist such a transfer. Acid as well as water accelerated the exchange, but bases did not. Catalytic activity of a protic acid seemed to saturate when the acid concentration reached a certain level. These observations as well as the deuterium isotope effect suggest that the water molecule serves as proton carrier, and that the proton transfer participates in the rate limiting step.[5)]

Reaction Mechanism. We postulated a plausible mechanism of racemization of $[Ge(acac)_3]^+$[1)]; *i.e.*, one of the Ge–O bonds of the original *Δ*-complex is broken with the aid of nucleophilic action of the solvent molecule to give an intermediate (II in Fig. 3, with a unidentate $acac^-$), which successively undergoes inversion to give *Λ*-isomer. The solvent-assisted break of Ge–O bond was reckoned as the rate limiting step.

The rate laws and the activation parameters of the present exchange differ considerably from those of the racemization(see Table 2). The racemization rate is insensitive to the water concentration, largely affected by the donor number[6)] of the solvent, and not

TABLE 2. RATE CONSTANTS AND ACTIVATION PARAMETERS OF RACEMIZATION AND LIGAND ISOTOPIC EXCHANGE OF $[Ge(acac)_3]ClO_4$ IN ORGANIC SOLVENTS

Solvents	ε[a]	DN[b]	Racemization			Ligand isotopic exchange		
			k_r [c]	ΔH^*	ΔS^*	k_x [d]	ΔH^*	ΔS^*
			10^{-5} s^{-1}	kJ mol^{-1}	J K^{-1} mol^{-1}	10^{-4} M^{-1} s^{-1}	kJ mol^{-1}	J K^{-1} mol^{-1}
$CHCl_2CHCl_2$ (TCE)	8.2	($\simeq$0)	0.58	117± 4	+16±12	5.1	105±20	−20±50
CH_3NO_2 (NM)	36	2.7	0.42	111± 4	− 5±14	2.4	98±15	−53±40
CH_3CN (AN)	38	14.1	2.9	102± 2	−18± 6	4.5	90±12	−69±32
$(CH_3)_2NCHO$ (DMF)	37	26.6	10	97±11	−21±36			
C_5H_5N (pyridine)	12	33.1	27 M^{-1} [e]	99±12	− 7±42			

a) Relative permittivity at *ca.* 20 °C. b) Donor number in ref. 6. c) Rate$=k_r$[complex], where [complex]$\approx 10^{-3}$ M at 50 °C. d) Rate$=k_x[H_2O]$[complex], at 100 °C. e) k_2 in *rate*$=(k_1+k_2$[pyridine])[complex], in acetonitrile at 50 °C.

changed in the presence and the absence of excessive Hacac, while the exchange rate is sensitive to the water content, and the solvent effect is small as compared with that in the racemization. All these facts support that the ligand isotopic exchange has a different feature from that of the racemization.

The racemization equilibrium must have been readily reached at >100 °C where the isotopic exchange was observed. The solvent molecule in the sixth coordination site of intermediate II may be replaced by the free ligand, Hacac[^{14}C], to give intermediate III. Since the concentration of free Hacac overwhelms that of II, change in Hacac concentration would not affect the concentration of III. The solvent molecules, especially nitromethane and acetonitrile, can give stable second sphere coordination towards III, to make III more stable than II. Whenever originally coordinated acac$^-$ in III undergoes ring-closure to give I, no ligand exchange takes place. On the other hand, when proton is transferred from the incoming Hacac [^{14}C] to the originally coordinated acac$^-$, this is protonated and leaves the coordination site to result in ligand exchange; the deprotonated (acac[^{14}C])$^-$ undergoes ring-closure to restore $[Ge(acac[^{14}C])_3]^+$. The observed proton catalysis should operate in the proton transfer stage. The aprotic solvents used in this work can hardly assist the proton transfer, and the exchange is very slow in the absence of water or trichloroacetic acid, which assists the transfer. [Autoprotolysis constants (pK_i at 25 °C) of nitromethane and acetonitrile are 19.5 and 28.5, respectively.]

The activation enthalpies decrease and the activation entropies become more negative in the sequence 1,1,2,2-tetrachloroethane < nitromethane < acetonitrile, although the experimental errors remain rather large. The nucleophilicity of the solvent molecules (*e.g.*, Donor number) is well correlated with this sequence, which seems to reflect the ease with which the intermediate II is formed.

The large minus ΔS^* values (which are responsible for making the isotopic exchange slow) seem to reflect the steric difficulty with which the two unidentate moieties in III have their mutual orientations favorable for proton transfer. Especially in nitromethane and acetonitrile, these molecules in the second coordination sphere would prevent the tenure of favorable orientations to make ΔS^* values more negative.

The differences in ΔH^*, $\approx$10 kJ mol^{-1} regardless of the solvents, between the racemization and the isotopic exchange are significant beyond the experimental errors, and ΔH^*'s of the isotopic exchange are smaller than those of the racemization. This observation suggests that the activation enthalpies in a given solvent consist mostly of those for the formation of the intermediates II and III, *i.e.*, that for the break of one Ge–O bond. The smaller ΔH^*'s for isotopic exchange than those for racemization are explained by the larger stability of III than II, because Hacac is more nucleophilic than acetonitrile, nitromethane, and 1,1,2,2-tetrachloroethane,[7] to give stronger interaction at the sixth coordination site of the intermediate. The extent of the stabilization of III brought about by the substitution of Hacac for the solvent molecules in II's is smaller to one another for the three kinds of solvent. The differences in nucleophilicities between Hacac and the solvent molecules may be partly compensated by the stabilization coming from the second sphere coordination of the solvent molecules.

The donor number of water (18) is larger than those of the solvents (<14), and comparable with that of Hacac. The concentration of water is much lower than those of the sovents by a factor $\approx 10^2$, and water may be unable to assist the formation of intermediate II. However, the activity of water should be large enough in the vicinity of III, to assist the proton transfer. β-Diketones have large affinity with water; even crystalline hydrates are known with hexafluoroacetylacetone. Water can have loose association with free Hacac in these solvents. Hence, water molecules can be present in the neighborhood of III when free Hacac interacts with II to give III, and facilitate the proton transfer between two unidentate acac$^-$ ligands.

Comparison with Related Compounds. Silicon(IV), tin(IV), and titanium(IV), the other members of Family IV of the periodic table also give octahedral complexes of the type $[M(\beta\text{-dik})_3]^+$ and *cis*-[M(β-

$dik)_2X_2]$ with various β-diketones in enolate form. Since no ligand field effect can be expected for these d^0 and d^{10} ions, the contribution of the ionic radius should be important in interpreting the different kinetic behavior of these complexes. Silicon(IV)[8] and germanium(IV)[1] complexes of the type $[M(\beta\text{-dik})_3]^+$ are inert towards ligand exchange and hydrolysis. Their racemization was measured in the temperature range 30 to 70 °C, and the mechanism was claimed to be intramolecular involving a unidentate β-diketonate. Their ligand isotopic exchange is measurable at ≥ 100 °C, and the unidentate ligand must resist against break of the remaining bond. The central metal ion possesses a high charge, +4, and the partial charge separation caused by break of one M–O bond on unidentate formation will increase the effective charge of M(IV) furt er to make the remaining bond stronger.

Corresponding tin V)[9] and titanium(IV)[10] complexes are much more labile and their ligand isotopic exchange was measured only below −10 °C. In both cases water seems to play an important part in the rate determining step, presumably as a nucleophile. Particularly the tin(IV) complex gave a partially hydrated product $[Sn(OH)(H_2O)(acac)_2]ClO_4$, which was reckoned as a common intermediate for the hydrolysis and the isotopic exchange. Tin(IV) with a large ionic radius must be more readily subject to the nucleophilic attack of water even at a low temperature to result in rapid substitutions. Water acts as a proton carrier for germanium(IV) with a smaller ionic radius, (*loc. cit.*); overwhelming amount of donor solvent molecules can assist the break of one Ge–O bond only at a high temperature. Similar consideration was applied to octahedral complexes of aluminium, gallium, and indium, $[M(\beta\text{-dik})_3]^0$.[11]

Intramolecular site exchange process was observed by dynamic NMR technique in *cis*-$[M(\beta\text{-dik})_2X_2]^0$ complexes of Family IV metal ions.[12] There seems to be remarkable difference in the rate and in the activation parameters among these complexes. In the complexes of titanium(IV),[13] these values are centered around in the following ranges: rate constant k at 25 °C, 10^1—10^3 s^{-1}; Arrhenius activation energy E_A, 25—60 kJ mol^{-1}; activation entropy ΔS^*, −10—−150 J K^{-1} mol^{-1}. The tin(IV) complexes have the values: k, 10^{-1}—10^1 s^{-1}; E_A, 50—70 kJ mol^{-1}; ΔS^*, −40—−60 J K^{-1} mol^{-1}.[14] On the other hand the germanium(IV) complex $[Ge(dpm)_2X_2]$ (dpm=2,2,6,6-tetramethyl-3,5-heptanedionate, X=Cl, Br, and I) rearranges intramolecularly with $k \approx 10^{-6}$ s^{-1}, $E_A \approx 105$ kJ mol^{-1} and $\Delta S^* \approx 0$ J K^{-1} mol^{-1}.[15] These observations are very similar to those in the intermolecular ligand exchange and hydrolysis of $[M(\beta\text{-dik})_3]^+$ (although the total charges of the complexes are different) suggesting significant influence of the radius of the central ion.

The present octahedral germanium(IV) complex is as inert as cobalt(III) and chromium(III) complexes, and should be included in the group of "inert complex." The source of such an inertness seems to consist in, at least partly, the stability of the Ge–O bond between germanium(IV) and unidentate $acac^-$.

The authors wish to thank the Ministry of Education for the Grant-in-Aid.

References

1) A. Nagasawa and K. Saito, *Bull. Chem. Soc. Jpn.*, **47**, 131 (1974).
2) F. W. Swamer and C. R. Hauser, *J. Am. Chem. Soc.*, **72**, 1352 (1950).
3) H. Kido and A. Nagasawa, unpublished results.
4) It is claimed that the unidentate $acac^-$ assumes trans form around the C_1–C_2 axis (where carbons in β-diketonate are: C_1, carbonyl; C_2, methylidyne; C_3, enol) in the homologous complex $[Si(\beta\text{-dik})_3]^+$ in TCE or AN at 40—80 °C. (Ref. 8) Pinnavaia *et al.* also found that allylic and acetyl methyl group on the unidentate $acac^-$ moiety in tetrahedral $R(CH_3)_2Si(acac)$ ($R=CH_3$, C_2H_5, C_6H_5, *etc.*) gives rapid interchange between the cis and trans form around C_1–C_2 and/or C_2=C_3 axis, in chlorobenzene at −20 to 0 °C: T. J. Pinnavaia, W. T. Collins, and J. J. Howe, *J. Am. Chem. Soc.*, **92**, 4544 (1970).
5) The intramolecular proton transfer between two coordinated $acac^-$ was found to be important in determining the rate of ligand exchange of $[Cr(acac)_3]^0$: H. Kido and K. Saito, *Inorg. Chem.*, **16**, 397 (1977).
6) V. Gutmann, "Coordination Chemistry in Non-aqueous Solutions," Springer, Wien (1968).
7) The donor number of Hacac was calculated to be ca. 18 from its association constant with $[VO(acac)_2]^0$ in 1,2-dichloroethane. M. Nishizawa, private communication.
8) T. Inoue and K. Saito, *Bull. Chem. Soc. Jpn.*, **46**, 2417 (1973); **48**, 1228 (1975).
9) A. Nagasawa and K. Saito, *Bull. Chem. Soc. Jpn.*, **49**, 3079 (1976).
10) M. Nishizawa, H. Kido, I. Kinoshita, Y. Soma, and K. Saito, *Bull. Chem. Soc. Jpn.*, **49**, 819 (1976).
11) K. Saito and K. Masuda, *Bull. Chem. Soc. Jpn.*, **43**, 119 (1970); K. Matsuzawa and K. Saito, *ibid.*, **46**, 2777 (1973); C. Chatterjee, K. Matsuzawa, H. Kido, and K. Saito, *ibid.*, **47**, 2809 (1974).
12) N. Serpone and D. G. Bickley, *Progr. Inorg. Chem.*, **17**, "Inorganic Reaction Mechanisms: Part II," 391 (1972).
13) R. C. Fay and R. N. Lowry, *Inorg. Chem.*, **6**, 1512 (1967); D. C. Bradley and C. E. Holloway, *J. Chem. Soc.*, *A*, **1969**, 282; J. F. Harrod and K. Taylor, *Chem. Commun.*, **1971**, 696.
14) R. W. Jones, Jr., and R. C. Fay, *Inorg. Chem.*, **12**, 2599 (1973).
15) R. W. Jones, Jr., Ph. D. Dissertation, Cornell University, Ithaca, N. Y., 1971.

Flameless Atomic Fluorescence Spectrometry of Mercury by Dispersive and Nondispersive Systems in Combination with Cold-vapor Technique

Taketoshi NAKAHARA,* Toshiaki TANAKA, and Sôichirô MUSHA

Department of Applied Chemistry, College of Engineering, University of Osaka Prefecture, Mozu-umemachi, Sakai 591

(Received December 14, 1977)

An atomic fluorescence spectrometer with dispersive and nondispersive systems has been designed and constructed. A flameless atomic fluorescence spectrometric method with the newly constructed spectrometer is described for the determination of mercury at the nanogram level. Mercury is reduced by tin(II) chloride and released from solution by a stream of argon into a quartz fluorescence cell. The fluorescence signal is measured by dispersive and nondispersive systems. Linear analytical working curves covering the mass range of mercury from the detection limits to approximately 10 and 1 μg have been established with dispersive and nondispersive systems, respectively. With the nondispersive system a detection limit of 0.003 ppb or 0.05 ng of mercury could readily be obtained. The present method was satisfactorily applied to the determination of mercury in wastewater samples.

As with atomic absorption spectrometry, atomic fluorescence spectrometry of mercury has been carried out both with flame and flameless vaporization(atomization) techniques. Atomic fluorescence spectrometric determination has some advantages over atomic absorption spectrometry, for example, a wider dynamic range not limited by the Lambert-Beer law, less susceptibility to interferences from spurious vapors, and a much greater possibility for simultaneous multi-element determination.

Mercury determination using atomic fluorescence spectrometry have been described by Winefordner and co-workers,[1-6] West and co-workers,[7-10] Vickers and co-workers,[11-13] Larkins,[14] and Vitkun *et al.*[15] using a flame as an atom reservoir. Muscat and co-workers,[16,17] Thompson and co-workers,[18,19] Shimomura and Hiroto,[20] Hawley and Ingle,[21] Cavalli and Rossi,[22] and Caupeil *et al.*[23] used a flameless cold-vapor technique. In the latter instances, the mercury reduced from solution has been excited in a fluorescence cell(quartz or quartz-windowed);[16,17,21] some workers[18-20,22,23] have eliminated the cell completely and vented the mercury vapor into the atmosphere where fluorescence excitation occured. Some authors[24,25] have used a flameless method of pulsed thermal atomization. For fluorescence measurements, a nondispersive system for atomic fluorescence spectrometry has certain advantages over a dispersive system such as greater energy throughput, simpler instrumentation, and simultaneous measurement of multiple lines of the analyte. In the case of flameless methods for mercury a nondispersive system might be preferable to a dispersive system, since mercury is mostly separated from the interfering matrix in the solution prior to fluorescence measurements. However a satisfactory detection limit for a nondispersive system has not always been substantiated in the literature concerning mercury.[1-25] Some authors[19,22,23] have reported the detection limits of 0.02—0.05 ng of mercury by using a cold-vapor technique. Until recently, the best reported detection limits[21] were 0.005 ppb or 0.005 ng of mercury, obtained with a dispersive system and a cold-vapor technique.

The present authors have designed and constructed an atomic fluorescence spectrophotometer which can be used with both dispersive and nondispersive systems. This paper describes the performance of the newly constructed atomic fluorescence spectrometer with which the atomic fluorescence of mercury has been measured using a cold-vapor technique. The present method has been successfully applied to the determination of mercury at the ppb level in wastewater samples.

Experimental

Chemicals. The mercury stock solution of Hg(II), 1000 ppm, was prepared from analytical-reagent grade $HgCl_2$, nitric acid and distilled water. Each mercury solution was prepared just before use from a 10-ppm solution of mercury which was prepared daily from the stock solution. The tin(II) chloride solution was prepared by dissolving tin(II) chloride (10 g) in hydrochloric acid(50 ml) and then by diluting to 100 ml with distilled water. The tin(II) chloride solution was bubbled with mercury-free argon, nitrogen or air to remove any mercury contamination. Magnesium perchlorate was used for drying the mercury vapor produced and granular activated charcoal for removing any trace amounts of mercury from argon, nitrogen or air. All the chemicals used in this study were obtained from Wakô

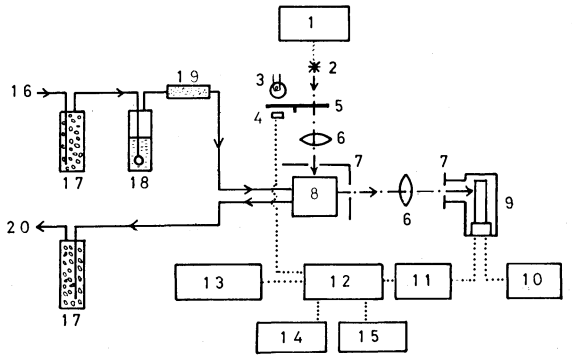

Fig. 1. Block diagram of the nondispersive atomic fluorescence spectrometer.
1: Power supply, 2: light source, 3: small lamp, 4: photocell, 5: light chopper, 6: lenses, 7: diaphragms, 8: fluorescence cell, 9: photomultiplier and its housing, 10: high voltage power supply, 11: preamplifier, 12: lock-in amplifier, 13: power stabilizer 14: recorder, 15: oscilloscope, 16: carrier gas inlet, 17: activated charcoal traps, 18: reduction vessel, 19: drying tube, 20: carrier gas outlet, ——: carrier gas flow, ——: optical path, ·····: electrical line.

Table 1. Experimental components used in this study

Item	Description (model No.) and supplier
Power stabilizer	A-133, NF Circuit Design Block
Light source	
Hg pen lamp	11SC-2, Ultra-Violet
Power supply	SCT-1, Ultra-Violet
Hg electrodeless	Hg metal (12 mg), Ar 6.7×10^2 Pa, 8 mm
discharge lamp	i. d. $\times$ 50 mm long (Suprasil), Laboratory-made
Power supply	Microtron 200, Electro-Medical Supplies
Resonant cavity	Model 211L, Electro-Medical Supplies
Lens	30-mm diameter, 75-mm focal length, quartz
Fluorescence cell	$25\times25\times30$ mm^3 and $12\times12\times30$ mm^3, quartz
Monochromator	JE-30, Nippon Jarrell-Ash
Entrance slit width	0.5 mm
Exit slit width	0.5 mm
Photomultiplier	R-166 (for nondispersive system), R-106 UH (for dispersive system), Hamamatsu TV
High voltage power supply	412B, John Fuke
Preamplifier	JP 406, Nippon Jarrell-Ash
Operational amplifier	2F/4539B, Aikoh Electric
Power supply	$\pm$15 V, Laboratory-made
Lock-in amplifier	572B, NF Circuit Design Block
Oscilloscope	CS-1351, Trio
Recorder	QPD_{54}, Hitachi
Flow regulator	LAS-S301, Nippon Tokushu Keiki
Reduction vessel	Volume 30 ml, Kinoshita

Pure Chemicals Co.

Apparatus. The block diagram of the newly constructed atomic fluorescence apparatus for a nondispersive system is shown in Fig. 1. The specific components employed are summarized in Table 1. The right half of Fig. 1 shows an atomic fluorescence spectrometer with a fluorescence cell. For a dispersive system the photomultiplier and its housing in Fig. 1 are replaced by the monochromator equipped with another type of photomultiplier.

Fluorescence Cell. Two fluorescence cells, being similar to that previously reported,[16] were made from transparent quartz. The square cells have 1.2×3- and 2.5×3-cm^2 quartz windows on two adjacent sides. The other two-adjacent sides of the cells were blackened by lusterless paint. The fluorescence cell was heated to approximately 120 °C by a ribbon heater to prevent the deposition of water onto the inner surface of the cell. For inlet and outlet ports, the glass tubing of 6 mm inside diameter was connected to the top and bottom of the cell. The connections between the fluorescence cell, magnesium perchlorate drying tube, reduction vessel, and activated charcoal bottles(Fig. 1) were made from silicon rubber tubing of 5 mm inside diameter.

Preparation of Mercury Electrodeless Discharge Lamps. A microwave-excited electrodeless discharge lamp(EDL) is known to be one of the most useful spectral line sources for atomic fluorescence spectrometry.[26-29] The authors prepared a number of Hg-EDLs using a vacuum line as illustrated in Fig. 2. The EDL-blank was made from transparent quartz ("suprasil") tubing of 8-mm internal diameter and 1-mm wall thickness. A 15-cm length of quartz tubing was sealed at one end and a constriction made between 1 and 7 cm from the end to give a tube from 1 to 7 cm in length. The tubing, the other end of which had a 12/20 mm ground glass socket, was attached to one of the outlets on the vacuum line and pumped down to a pressure of approximately 9.3×10^{-2} Pa. Argon was then introduced into the system and it was again pumped down to a similar pressure. The quartz tube(EDL-blank) was then heated to just below its melting point for about 5 min, during which time argon was again introduced into the system and pumped out. This procedure was repeated three times. The tube was allowed to cool under vacuum and then removed from the line. Between 5 and 20 mg of mercury metal was introduced into the tube, which was then reconnected to the vacuum line. The tube was evacuated as before, flushed out with argon, and re-evacuated to a pressure of about 9.3×10^{-2} Pa. Very gentle heating was then applied to the tubing to drive off any moisture or occluded gases in the mercury. The system was flushed twice more with argon and finally a given pressure was introduced into the vacuum system and the constriction sealed by an

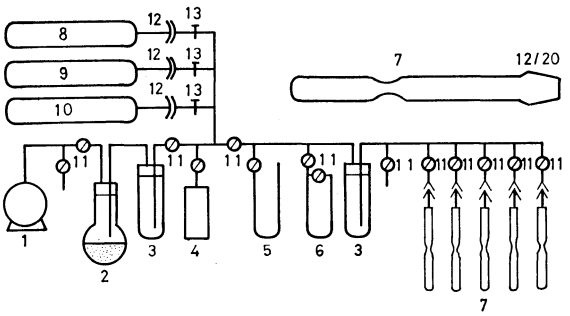

Fig. 2. Vacuum system used for preparation of electrodeless discharge lamps.
1: Mechanical pump, 2: diphosphorus pentaoxide trap, 3: liquid-nitrogen cold trap, 4: vacuum gauge, 5: mercury manometer, 6: oil manometer, 7: lamp blanks, 8: argon reservoir, 9: neon reservoir, 10: helium reservoir, 11: vacuum stopcocks, 12: ball-type joints, 13: needle valves.

Table 2. Optimum experimental conditions

Light source	Hg electrodeless discharge lamp
Microwave power	19 W (incident power, 25 W; reflected power, 6 W)
RC time constant	1.0 s
High voltage for photomultiplier	800 V
Load resistor	470 kΩ
Modulation frequency	90 Hz (for nondispersive system), 240 Hz (for dispersive system)
Fluorescence cell	$25 \times 25 \times 30$ mm^3
Diaphragms	
For cell	20×20 mm^2
For detection system	8×15 mm^2 (for dispersive system), 2×5 mm^2 (nondispersive system)
Carrier gas	Argon
Flow rate	1.0 l min^{-1}
Drying tube	9 cm long × 3 cm diameter
Volume of sample	20 ml
Volume of reductant	1.0 ml (10% $SnCl_2$-6 M HCl)

oxygen-propane hand torch.

Initiation of the discharge in the resonant cavity was achieved with a simple Tesla coil vacuum tester. The most useful Hg-EDL employed throughout this study is shown in Table 1.

General Procedure. A fixed volume(20 ml) of a mercury solution was introduced into the reduction vessel where the ionic mercury was reduced to mercury vapor by tin(II) chloride. The mercury vapor was then quickly carried by a stream of mercury-free argon, nitrogen or air through a glass tube with a spherically sintered glass end, which was connected to the fluorescence cell *via* a magnesium perchlorate drying tube (Fig. 1). There, a fluorescence signal was instantaneously generated. The height of the recorded peak was a measure of the mercury concentration.

Table 2 shows the optimum oprating conditions for the flameless atomic fluorescence spectrometry of mercury with both the dispersive and nondispersive systems.

Results and Discussion

Effect of Diaphragms in the Optics. The constant background level was mainly attributed to direct specular reflection and scattering of light from the mercury lamp into the fluorescence measuring entry aperture. This background was carefully minimized by placing diaphragms in front of two adjacent windows of the fluorescence cell and the entrance slit of the monochromator for the dispersive system and the photomultiplier housing for the nondispersive system. For maximum sensitivity it was essential to minimize the background level. In this study a number of rectangular or square diaphragms were used; at the same time the fluorescence signal and the background level were measured with each diaphragm to maximize the signal-to-noise ratio for the mercury determination. The optimum sizes of the diaphragms employed are shown in Table 2.

Effect of Modulation Frequencies of Source Radiation. In this study two types of light choppers were used for modulation of the source radiation; one was for 14.4 and 28.8 Hz and the other for 90, 150, 240, 480, and 960 Hz. The former had a synchronous motor (Japan Servo Co., Type HM6P2D1) of 30 Hz with a 1/12.5 reduction gear (Japan Servo Co., Type 6G12.5 H). The latter had a synchoronous motor (Yokogawa Sertec Co., Type SM-D3N) of 30 Hz. The relationships between relative fluorescence intensities and modulation frequencies were obtained for both the dispersive and the nondispersive systems and are shown in Table 3. The differences in relative fluorescence intensities may be attributed to the frequency characteristics of the photomultipliers and to the precision of the sectors, especially at the higher frequencies. The sectors used in the light choppers were all handmade. The optimum frequencies were 90 and 240 Hz for the dispersive and the nondispersive systems, respectively.

Table 3. Effect of modulation frequencies on fluorescence signals

Frequency (Hz)	Relative fluorescence signal[a]	
	Nondispersive system	Dispersive system
14.4	0.91	0.75
28.8	0.77	0.55
90	1.00	0.79
150	0.84	0.69
240	0.84	1.00
480	0.70	0.69
960	0.11	0.05

a) Mercury of 20 ng.

Table 4. Effect of carrier gas on fluorescence signals

Carrier gas[a]	Relative fluorescence signal[b]	
	Dispersive system	Nondispersive system
Air	1.00	1.00
Nitrogen	5.67	5.57
Argon	20.3	19.5

a) Flow rate of 1.0 l min^{-1}. b) Mercury of 10 ng.

Effect of Carrier Gas. Fluorescence measurements were made using argon, nitrogen, and air as the carrier gas. The enhancement of the fluorescence signals obtained by use of argon, compared with air, was approximately greater by a factor of 20, as shown in Table 4. Argon was the most useful carrier gas for fluorescence measurements taking advantage of its small cross section for the quenching of fluorescence, consequently argon was used throughout this study unless otherwise stated. The effect of carrier gas flow rates was also investigated. The flow rates between 0.4 and 1.4 l min^{-1} did not adversely affect the fluorescence measurements. However a decrease in flow rates caused an increase in half-widths of the fluorescence peaks. An optimum flow rate of 1.0 l min^{-1} was chosen in the following study.

Effect of Microwave Power on Source Radiation and Fluorescence Intensities. In atomic fluorescence spectrometry it is theoretically known that the fluo-

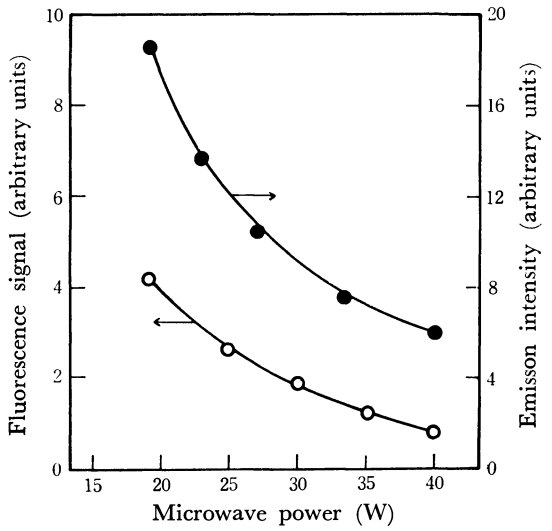

Fig. 3. Effect of microwave power on fluorescence signal and emission intensity of Hg-EDL.
○: Fluorescence signal at 253.7 nm, ●: emission intensity of Hg 253.7-nm line.

Table 5. Effect of organic solvents on fluorescence signals

Amount added (μg)	Relative fluorescence signal[a]		
	Benzene	Acetone	Ethanol
0	1.00	1.00	1.00
500	1.01	0.97	1.02
1000	0.68	0.80	0.96
2000	0.66	0.76	0.87
5000	0.68	0.86	0.86
10000	0.77	0.80	0.80

a) With the nondispersive system for mercury of 20 ng.

rescence intensity is directly proportional to the source radiation intensity.[30-32] The characteristics of the Hg-EDLs prepared were studied in terms of emission intensities and fluorescence signals at various microwave powers. The results obtained are shown in Fig. 3. The microwave power is a net power for discharge, that is, the reflected power is subtracted from the incident power. The optimum power for the Hg-EDL was 19 W; *i.e.*, an incident power of 25 W and a reflected power of 6 W. The Hg-EDL described in Table 1 gave a stable intensity after a warming-up time of *ca.* 30 min during this work and could be used for further experiments.

Quenching of Organic Solvents. The excited atoms are subject to radiationless deactivation due to bimolecular collision with the other species present in the atom reservoir, resulting in a decrease of fluorescence signal.[33] In this study the effect of some organic solvents, *e.g.*, acetone, benzene, and ethanol, was examined in their range of 500 to 10000 μg at a constant mercury level of 20 ng. The results obtained are shown in Table 5. The decrease in fluorescence signals may be attributed mainly to the quenching of fluorescence. The organic solvents(compounds) of more than 1000 μg are thus able to decrease the fluorescence signals, and so the effect of such quenching by organic solvents of higher vapor pressures should be corrected for in the determination of mercury in practical samples.

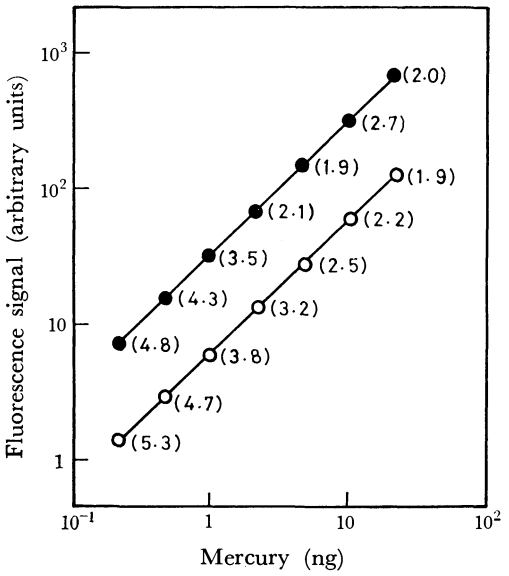

Fig. 4. Analytical working curves for mercury.
●: With nondispersive system, ○: with dispersive system, ( ): relative standard deviations(%).

Table 6. Detection limits for mercury by atomic fluorescence

Carrier gas	Detection limit[a]			
	Nondispersive system		Dispersive system	
	Hg-EDL	Hg pen lamp	Hg-EDL	Hg pen lamp
Air	1.0 ng	2.0 ng	12.9 ng	23 ng
	0.05 ppb	0.1 ppb	0.65 ppb	1.2 ppb
Argon	0.05 ng	0.1 ng	0.5 ng	2.0 ng
	0.003 ppb	0.05 ppb	0.03 ppb	0.1 ppb

a) $S/N=2$.

Analytical Working Curves, Sensitivity, and Presicion. Analytical working curves were obtained by using mercury standard solutions freshly prepared from a 1000-ppm mercury stock solution with both dispersive (at 253.7 nm) and nondispersive systems. A mercury pen lamp was used instead of Hg-EDL because of the much easier operation of the pen lamp. Two typical working curves obtained under the optimum conditions are shown in Fig. 4. The detection limits, expressed as the mass or concentration which produces a fluorescence signal equal to twice the noise level ($S/N=2$), are showed in Table 6. The analytical working curves were linear from the detection limits to approximately 10 and 1 μg of mercury with dispersive and nondispersive systems, respectively. The relative standard deviations for 10 measurements are shown in parentheses for the individual plots in Fig. 4. A blank value was negligible compared with instrumental limitations. The difference in sensitivities between with the Hg-EDL and with the mercury pen

TABLE 7. DETERMINATION OF MERCURY IN WASTEWATERS BY ATOMIC FLUORESCENCE AND ATOMIC ABSORPTION

Sample[a)]	Atomic fluorescence	Atomic absorption
A	7.6 ppb	7.3 ppb
B	23.0	22.5
C	3.0	2.8
D	2.2	2.1
E	18.0	16.8
F	21.0	20.8
G	4.0	3.8
H	1.6	2.1

a) Sample taken: 20 ml.

lamp may be explained by the fact that the Hg 253.7-nm line of the former was more intensive by a factor of 1.5 than that of the latter and that in atomic absorption measurements at 253.7 nm the sensitivity for 1% absorption with the former was higher by a factor of 1.4 than that with the latter.

Application of the Present Method to the Determination of Mercury in Wastewaters. The present method was applied to the determination of traces of mercury in wastewaters which were taken at the inlet of the Wastewater Treatment Facility of the University of Osaka Prefecture. The more sensitive nondispersive atomic fluorescence measurements were made using a mercury electrodeless discharge lamp and argon as an excitation source and carrier gas, respectively, under the optimum conditions as is shown in Table 2. The samples were acidified with a few drops of high-purity nitric acid. For atomic absorption spectrometry a quartz absorption cell of 1.8 cm internal diameter and 20 cm length was used as an atom reservoir instead of a fluorescence cell. The procedures for both methods were the same as already mentioned. The results are shown in Table 7. All the analytical results were obtained by referring to each calibration graph and 7 determinations taken and averaged for individual samples. The organic solvents(substances), being soluble in hexane, in the samples were not so much that they produced quenching of fluorescence in the measurements. The results by the present method are in good agreement with those by flameless atomic absorption spectrometry.

Conclusion

The present nondispersive and dispersive atomic fluorescence spectrometer which has been constructed has proved to be sensitive and reliable for the determination of trace amounts of mercury. The detection limits obtained with the nondispersive system were comparable with those obtained by recent authors.[19,21-23] The present detection limits would be improved by decreasing the scattering and reflection of light from the excitation souce into the measuring aperture and by developing the efficiency in light-gathering of the mercury lamp and the fluoresence of mercury vapor. It was impossible to measure the 184.9-nm mercury line of resonance fluoresence with the dispersive system due to appreciable atmospheric absorption at this wavelength. The present system is useful for the determination of traces of mercury in water samples.

References

1) J. D. Winefordner and R. A. Staab, *Anal. Chem.*, **36**, 165 (1964).
2) J. M. Mansfield, J. D. Winefordner, and C. Veillon, *Anal. Chem.*, **37**, 1049 (1965).
3) K. E. Zacha, M. P. Bratzel, Jr., J. D. Winefrodner, and J. M. Mansfield, *Anal. Chem.*, **40**, 1733 (1968).
4) J. M. Mansfield, M. P. Bratzel, Jr., H. O. Norgordon, D. O. Knapp, K. E. Zacha, and J. D. Winefordner, *Spectrochim. Acta, Part B*, **23**, 389 (1968).
5) M. Shull and J. D. Winefordner, *Anal. Chem.*, **43**, 799 (1971).
6) R. C. Elser and J. D. Winefordner, *Appl. Spectrosc.*, **25**, 345 (1971).
7) R. F. Browner, R. M. Dagnall, and T. S. West, *Anal. Chim. Acta*, **45**, 163 (1969).
8) G. B. Marshall and T. S. West, *Anal. Chim. Acta*, **51**, 179 (1970).
9) M. S. Cresser and T. S. West, *Anal. Chim. Acta*, **51**, 530 (1970).
10) D. O. Cooke, R. M. Dagnall, B. L. Sharp, and T. S. West, *Spectrosc. Lett.*, **4**, 91 (1971).
11) T. J. Vickers and S. P. Merrick, *Talanta*, **15**, 873(1968).
12) T. J. Vickers and R. M. Vaught, *Anal. Chem.*, **41**, 1476 (1969).
13) T. J. Vickers, P. J. Slevin, V. I. Muscat, and L. T. Farias, *Anal. Chem.*, **44**, 930 (1972).
14) P. L. Larkins, *Spectrochim. Acta, Part B*, **26**, 477 (1971).
15) R. A. Vitkun, N. S. Poluektov, and Yu. V. Zelyukova, *Zh. Anal. Khim.*, **25**, 474 (1970).
16) V. I. Muscat and T. J. Vickers, *Anal. Chim. Acta*, **57**, 23 (1971).
17) V. I. Muscat, T. J. Vickers, and A. Andren, *Anal. Chem.*, **44**, 218 (1972).
18) K. C. Thompson and G. D. Reynolds, *Analyst (London)*, **96**, 771 (1971).
19) K. C. Thompson and R. G. Godden, *Analyst (London)*, **100**, 544 (1975).
20) S. Shimomura and R. Hiroto, *Anal. Lett.*, **6**, 613 (1973).
21) J. E. Hawley and J. D. Ingle, Jr., *Anal. Chim. Acta*, **77**, 71 (1975).
22) P. Cavalli and G. Rossi, *Analyst (London)*, **101**, 272 (1976).
23) J. E. Caupeil, P. W. Hendrikse, and J. S. Bongers, *Anal. Chim. Acta*, **81**, 53 (1976).
24) A. M. Pchelintsev, Yu. I. Belyaev, A. V. Karyakin, and T. A. Koveshnikova, *Zh. Anal. Khim.*, **26**, 1355 (1971).
25) J. W. Robinson and Y. E. Araktingi, *Anal. Chim. Acta*, **63**, 29 (1973).
26) J. P. S. Haarsma, G. J. de Jong, and J. Agterdenbos, *Spectrochim. Acta, Part B*, **29**, 1 (1974).
27) S. Musha and T. Nakahara, *Kagaku*, **27**, 998 (1972).
28) G. F. Kirkbright and M. Sargent, "Atomic Absorption and Fluorescence Spectroscopy," Academic Press, London (1974), p. 145.
29) V. Sychra, V. Svoboda, and I. Rubeška, "Atomic Fluorescence Spectroscopy," translated by M. Cresser, Van Nostrand Reinhold, London (1975), p. 80.
30) J. D. Winefordner, M. L. Parsons, J. M. Mansfild, and W. J. McCarthy, *Spectrochim. Acta, Part B*, **23**, 37 (1967).
31) P. J. T. Zeegers, R. Smith, and J. D. Winefordner, *Anal. Chem.*, **40**, 26A (1968).
32) J. D. Winefordner and R. C. Elser, *Anal. Chem.*, **43**, 24A (1971).
33) J. D. Winefordner, ed, "Spectrochemical Methods of Analysis," Wiley-Interscience, New York (1971), pp. 3—125.

Reactions of Bis(acetylacetonato)oxovanadium(IV) with Phenol and Its *para*-Substituted Derivatives

Hiroshi TAGUCHI, Kiyoshi ISOBE, Yukio NAKAMURA,* and Shinichi KAWAGUCHI

Department of Chemistry, Faculty of Science, Osaka City University, Sumiyoshi-ku, Osaka 558

(Received December 16, 1977)

Bis(acetylacetonato)oxovanadium(IV) reacts with phenol or its *para*-substituted derivatives in methanol, affording stable adducts with the composition of $VO(acac)_2(p\text{-}XC_6H_4OH)$, where X=H, NO_2, CHO, COOH, Cl, or CH_3. The magnetic and spectral data reveal that these are vanadium(IV) complexes containing the phenol as a neutral ligand. They show an unusually low $\nu(V{=}O)$ frequency of ≈ 900 cm^{-1} as compared with the value of 1000 cm^{-1} for the parent complex, and are presumed to have a polymeric structure with an infinite chain of V=O···V=O···. The phenol is connected by a hydrogen bond to one oxygen atom of an acetylacetonate ligand. The behavior of the complex in solution is also discussed. The addition of 1,10-phenanthroline or 2,2′-bipyridine to a reaction mixture of $VO(acac)_2$ and nitrophenols results in phenolato complexes $VO(OC_6H_{5-n}X_n)(acac)$(phen or bpy), where $X=NO_2$ and $n=1$, 2, or 3. Two isomers of $VO(OC_6H_2(NO_2)_3)(acac)(bpy)$ are isolated and characterized.

Acetylacetone usually acts as a monoionic bidentate ligand in complexes with a variety of metal ions.[1] In recent years there have been reported several metal complexes which contain the acetylacetone molecule as a neutral ligand.[2] As one of the preparative methods, the reaction of the enolate chelates with dry hydrogen bromide was effective in obtaining $CrBr_2(acac)(acacH)$, $MnBr_2(acacH)_2$, $CoBr_2(acacH)$, and $NiBr_2(acacH)_2$.[2a] With the aim of extending the method to the preparation of similar oxovanadium(IV) complexes, the reactions of bis(acetylacetonato)oxovanadium(IV), $VO(acac)_2$, with phenol and its derivatives have now been examined. Although their acidities are appreciably different, neither phenol nor *p*-nitrophenol, afforded the desired complexes such as VO(acac)(acacH)(phenolate), but produced molecular adducts instead.

It is well known that the square pyramidal $VO(acac)_2$ forms 1:1 adducts in solution with a variety of bases, filling the sixth coordination site,[3] but little is known as to the interaction with acids. This paper will report on the phenol adducts and the phenolato complexes produced by these reactions.

Experimental

Bis(acetylacetonato)oxovanadium(IV) was prepared according to the method reported by Rowe and Jones.[4] Acetylacetone and methanol were distilled before use. Dichloromethane and diethyl ether were also distilled over phosphorus pentoxide and metallic sodium respectively. Commercially available phenols, 1,10-phenanthroline, and 2,2′-bipyridine were used without further purification.

Reactions of $VO(acac)_2$ with the Phenols in Methanol: Preparation of the $VO(acac)_2$(p-X-C_6H_4OH) Adducts (X=H, NO_2, CHO, COOH, Cl, or CH_3). To a solution of $VO(acac)_2$(1 g, 3.8 mmol) in methanol (30 ml) was added a methanol solution (10 ml) containing an equimolar amount of phenol or its *para*-substituted derivatives, and the mixture was kept at 70 °C for about 1 h in order to vaporize the solvent slowly. The concentrated dark brown mixture (*ca.* 5 ml) was then cooled to room temperature to deposit reddish brown needles. The yields and analytical data are summarized in Table 1.

Preparation of the Phenolato Complexes $VO(OC_6H_{5-n}X_n)(acac)$(phen or bpy) (X=NO_2; n=1, 2, or 3). To a solution of $VO(acac)_2$(1 g, 3.8 mmol) in methanol (30 ml) was added a methanol solution (10 ml) containing an equimolar amount of 4-nitro-, 2,4-dinitro- or 2,4,6-trinitrophenol, after which the mixture was kept at 70 °C in order to vaporize the solvent slowly. The resulting dark brown mixture (*ca.* 5 ml) was cooled to 0 °C. The addition of a methanol solution ($\approx$5 ml) containing an equimolar amount of a bidentate nitrogen base, phen or bpy, gave a crystalline product. The picrato complexes were also deposited from the dichloromethane solution of the 4-nitrophenolato complex containing an excess of picric acid when the solution stood at room temperature for a few hours. Two kinds of products, yellow and yellow-green, with the same composition of $VO(OC_6H_2(NO_2)_3)(acac)(bpy)$ were obtained by these alternative routes. The phenolato complexes were all stable in air. The analytical data and some physical properties are listed in Table 2.

Measurements. The absorption spectra in solution and the reflectance spectra were obtained using a Hitachi EPS-3T recording spectrophotometer. The IR spectra of solid specimens were measured by means of JASCO IR-E (4000—700 cm^{-1}) and Hitachi EPI-L (700—200 cm^{-1}) infrared spectrophotometers.

The electric conductance of 10^{-3} M solutions of the phenolato complexes in methanol was measured at 25 °C by using a Yanagimoto-type MY conductivity apparatus. Tetraethylammonium iodide was used as the standard of the uni-univalent electrolytes. The molecular weight was determined by means of vapor-pressure osmometry in a dichloromethane solution [(1—2)$\times 10^{-2}$M] with an apparatus manufactured by Knauer, Berlin, Germany.

The magnetic susceptibility was measured at room temperature on a Shimadzu automatically recording magnetic balance by the Faraday method. Mercury(II) tetraisothiocyanatocobaltate(II) was used as the reference.

Results and Discussion

Recently Aly[5] examined the reactions of neutral acetylacetonato complexes of Zn(II), Ni(II), Co(II), Al(III), and Fe(III) with nitrophenols in a refluxing mixture (1:1 by volume) of benzene and ethanol. In most of the reactions with 2,4,6-trinitro- and 2,4-dinitrophenols, cationic complexes of the $[M(acac)_n(H_2O)_m]$(nitrophenolate)type were obtained, although 4-nitrophenol did not react. On the contrary, the neutral adducts $VO(acac)_2(p\text{-}X\text{-}C_6H_4OH)$ are the only products in the reactions of $VO(acac)_2$ with phenol and its *para*-substituted derivatives in methanol, in spite of the

Table 1. Analytical data[a] of the $VO(acac)_2(p\text{-}XC_6H_4OH)$ adducts

Adduct	Mp/°C	C/%	H/%	N/%	Yield/%
$VO(acac)_2(p\text{-}NO_2C_6H_4OH)$	118	47.23(47.54)	4.66(4.74)	3.42(3.46)	43
$VO(acac)_2(p\text{-}CHOC_6H_4OH)$	114	52.65(52.72)	5.19(5.21)		69
$VO(acac)_2(p\text{-}COOHC_6H_4OH)$	153	50.18(50.63)	5.00(5.00)		34
$VO(acac)_2(p\text{-}ClC_6H_4OH)$	91	48.88(48.81)	4.80(4.86)		42
$VO(acac)_2(C_6H_5OH)\cdot 1/2H_2O$	65	52.28(52.18)	5.75(5.75)		39
$VO(acac)_2(p\text{-}CH_3C_6H_4OH)$	80	54.56(54.70)	5.87(5.94)		25

a) Calculated values in parentheses.

Table 2. Analytical data[a] and some physical properties of the phenolato complexes

Complex[b]	Color	Mp/°C	C/%	H/%	N/%	Yield/%
$VO(OC_6H_4NO_2)(acac)phen$	red-violet	191	56.36(57.03)	4.12(3.95)	8.52(8.68)	80
$VO(OC_6H_4NO_2)(acac)bpy$	red-brown	187	54.33(54.79)	4.25(4.16)	8.96(9.13)	84
$VO(OC_6H_3(NO_2)_2)(acac)phen$	orange	186	51.45(52.18)	3.26(3.43)	10.84(10.53)	89
$VO(OC_6H_3(NO_2)_2)(acac)bpy$	orange	170	49.66(49.91)	3.51(3.59)	11.22(11.09)	87
$VO(OC_6H_2(NO_2)_3)(acac)phen$	yellow-green	187	47.37(48.10)	3.57(2.98)	12.00(12.19)	89
$VO(OC_6H_2(NO_2)_3)(acac)bpy$						
Yellow isomer	yellow	180	45.45(45.83)	3.12(3.11)	12.63(12.73)	93
Yellow-green isomer	yellow-green	193	46.28(45.83)	3.17(3.11)	12.04(12.73)	49

a) Calculated values in parentheses. b) $OC_6H_4NO_2$: 4-nitrophenolate; $OC_6H_3(NO_2)_2$: 2,4-dinitrophenolate; $OC_6H_2(NO_2)_3$: 2,4,6-trinitrophenolate=picrate.

Table 3. The magnetic, spectral, and mol wt[a] data of the $VO(acac)_2(p\text{-}XC_6H_4OH)$ adducts

X	Magnetic moment	ν(V=O) [b]	ν(V···O)[b]	Reflectance spectra		Mol wt
	B. M.	cm^{-1}	cm^{-1}	$\nu_{max}/10^3\ cm^{-1}$		in CH_2Cl_2
NO_2	1.74	910	280	12.8	17.9	230(404)
CHO	1.75	905	280	12.7	18.4	227(387)
COOH	1.68	901	283	12.8	18.0	—
Cl	1.74	908	281	13.1	18.0	210(393)
H	1.76	904	281	12.9	17.9	186(359)
CH_3	1.76	910	278	13.0	17.9	213(373)
No adduct	1.73	1000	—	14.6	16.8	

a) Calculated values in parentheses. b) In Nujol.

widely different acidities of the phenols. Moreover, 2,4-dinitro- and 2,4,6-trinitrophenols do not react with $VO(acac)_2$ under the same reaction conditions. 2,2′-Bipyridine and 1,10-phenanthroline, however, induce reactions with the nitrophenols, resulting in the phenolato complexes $VO(X_nC_6H_{5-n}O)(acac)$(phen or bpy) ($X=NO_2$; $n=1$, 2 or 3).

The Phenol Adducts $VO(acac)_2$(p-X-C_6H_4OH). The magnetic, spectral, and molecular-weight data of the $VO(acac)_2(p\text{-}X\text{-}C_6H_4OH)$ complexes are shown in Table 3. The observed magnetic moments correspond to those of the vanadium(IV) state.

A crystal of $VO(acac)_2$ consists of discrete molecules of a square-pyramidal structure, with the vanadium atom near its center of gravity.[6] On the contrary, the present 4-nitrophenol adduct was disclosed by preliminary X-ray analysis[7] to have a polymeric structure of an infinite chain of square-pyramidal molecules connected by V=O···V=O··· bonds, as is depicted in Fig. 1. The phenol molecule is connected to one oxygen atom of an acetylacetonate ligand *via* the hydrogen bond with the OH···O distance of 2.68 Å. Our attempts to isolate the 1:1 adducts of $VO(acac)_2$ with anisole and sodium phenolate were unsuccessful. Thus, the presence of the phenolic hydrogen atom might be essential for making such a 1:1 adduct bearing a polymeric chain.

The ν(V=O) band of $VO(acac)_2$ appears at 1000 cm^{-1}, but the frequency decreases on adduct formation.[3] Caira *et al.*[8] reported that the ligation of a substituted pyridine to vanadium at the position cis to the oxo ligand lowers the ν(V=O) frequency by 42±4 cm^{-1}, while the trans ligation by 29±4 cm^{-1}. As may be seen in Table 3, the observed ν(V=O) frequencies for the present compounds are too low to be taken as those for simple phenol adducts. Such a low ν(V=O) frequency is characteristic of the oxovanadium(IV) complex bearing V=O···V=O··· bonds. For example, bis(trifluoroacetylacetonato)- and bis(thenoyltrifluoroacetonato)oxovanadium(IV) complexes display the ν(V=O) band at 1015 and 1012 cm^{-1} in dichloromethane, but at 932 and 900 cm^{-1} in Nujol, respectively, and so may be presumed to have the polymeric structure[9] in a solid. A similar polymeric structure has been

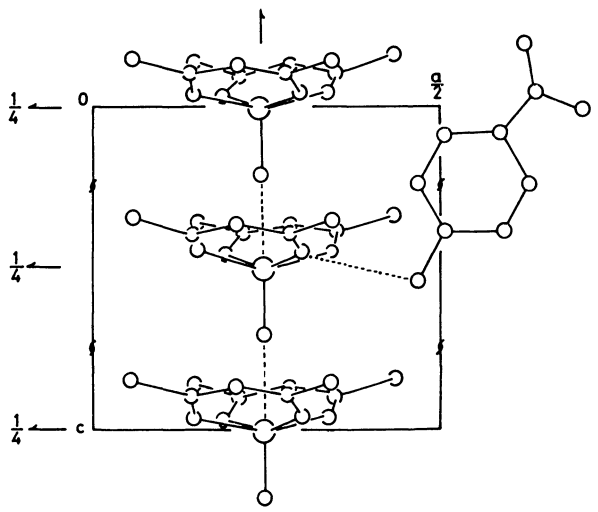

Fig. 1. The structure of $VO(acac)_2(p\text{-}NO_2C_6H_4OH)$ (from Ref. 7).

established by the X-ray analysis for (*N,N'*-disalicylidene-1,3-propanediaminato)oxovanadium(IV), VO(sal)$_2$tn,[10] the ν(V=O) vibration of which appears at 854 cm^{-1} in a solid.

We may now assign the new band at 280 cm^{-1}, which is not involved in the spectra of the parent complex and the free phenol, to the stretch of the bridging V···O linkage in the polymeric structure, according to the literature.[9] On the basis of the similarity of the IR spectra, the other adducts seem also to have an analogous chain structure. The anomalous orange-brown color of these complexes also supports the chain structure.[10–12]

It is worth noting that the order of each V=O bond length in $VO(acac)_2$ (1.56 Å, Ref. 6), $VO(acac)_2(p\text{-}NO_2C_6H_4OH)$ (1.60 Å, Ref. 7), and VO(sal)$_2$tn (1.633 Å, Ref. 10) is reflected in the ν(V=O) frequencies: 1000, 910, and 854 cm^{-1} in series. The reverse order of the V···O distance in $VO(acac)_2(p\text{-}NO_2C_6H_4OH)$ (2.32 Å) and VO(sal)$_2$tn (2.213 Å) is also reasonable.

The parent complex, $VO(acac)_2$, exhibits two d-d absorption maxima in non-coordinating media at 15000 and 16800 cm^{-1}, with a shoulder at 11500 cm^{-1}; those maxima are shifted to around 13000 and 17000 cm^{-1} in coordinating media.[13] As may be seen in Table 3, the reflectance spectra of the present phenol adducts have distinct maxima at around 13000 and 18000 cm^{-1}, indicating the formation of hexa-coordinate complexes. This is compatible with the polymeric structure discussed above. In dichloromethane, however, these two maxima for, *e.g.*, the 4-nitrophenol adduct are observed at 14700 and 16800 cm^{-1}. These shifts imply the V···O bond cleavage and the release of the phenol molecule, resulting in monomeric penta-coordinate species, even in such a non-coordinating medium. In methanol, these maxima revert again to 12700 and 17200 cm^{-1} due to the formation of the hexa-coordinate species by the ligation of a solvent molecule.

Such a dissociation of the adduct in solution is also indicated by the molecular-weight and IR data. The molecular weight determined in dichloromethane at 25 °C (Table 3) is close to half the value calculated for

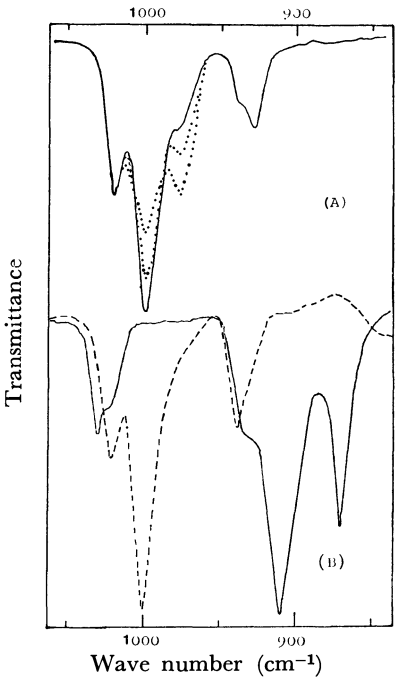

Fig. 2. IR spectra in CH_2Cl_2 (A) and in Nujol (B): $VO(acac)_2(p\text{-}NO_2C_6H_4OH)$ (——), $VO(acac)_2(p\text{-}NO_2C_6H_4OH)$ + $p\text{-}NO_2C_6H_4OH$ (·····), and $VO(acac)_2$ (----).

the monomeric adduct, revealing the extensive liberation of the phenol in solution in addition to the V···O bond cleavage. The IR spectrum of the 4-nitrophenol adduct in dichloromethane is quite different from that in Nujol and nearly coincides with that of $VO(acac)_2$ (Fig. 2), in accordance with the dissociation scheme noted before. If successive portions of 4-nitrophenol are added to the solution, the shoulder at 980 cm^{-1} grows gradually to a new absorption band at the expense of the 1000 cm^{-1} band. According to the assignment by Selbin *et al.*,[14] the new band can be assigned to the ν(V=O) vibration of the phenol adduct, in which the site trans to the exo ligand of $VO(acac)_2$ is occupied by the phenol molecule.

In the case of β-diketonato complexes, the driving force for the V=O···V=O stacking has been attributed mainly to the inductive effect of electron-withdrawing groups introduced in the parent acetylacetonate ligand.[9] The present case, however, involves only $VO(acac)_2$, in which the β-diketonate ligand does not bear any substituent exerting an electron-withdrawing effect on the metal acidity. It is not clear how the hydrogen bonding between the phenol and an acetylacetonate oxygen can exert an electronic and/or steric effect to make possible the V=O···V=O stacking in crystals.

The Phenolato Complexes $VO(OC_6H_{5-n}X_n)(acac)(phen$ or bpy) ($X=NO_2$; $n=1$, 2, or 3). The magnetic, spectral, molecular-weight, and conductance data of the phenolato complexes are shown in Table 4. The observed magnetic moments correspond to the d^1 spin state of the vanadium ion, indicating that no redox process of vanadium occurs during these reactions.

Caira *et al.*[8] examined the IR spectra of the substituted pyridine adducts $VO(acac)_2L$, as has been de-

Table 4. The magnetic, spectral, mol wt,[a] and conductance data of the $VO(OC_6H_{5-n}X_n)(acac)L$ complexes

$X_nC_6H_{5-n}O^-$	L	Magnetic moment / B. M.	ν(V=O) / cm^{-1} (in Nujol)	Visible spectra in CH_2Cl_2, ν_{max} / 10^3 cm^{-1}		Mol wt in CH_2Cl_2	Molar conductance in CH_3OH / ohm^{-1} cm^2 mol^{-1}
$4\text{-}NO_2C_6H_4O^-$	phen	1.74	970	12.3	17.0	509(484)	18
	bpy	1.67	968	12.5	17.1	414(460)	8
$2,4\text{-}(NO_2)_2C_6H_3O^-$	phen	1.70	965	12.5	16.9	d)	50
	bpy	1.74	962	12.4	17.4	539(505)	41
$2,4,6\text{-}(NO_2)_3C_6H_2O^-$	phen	1.72	972	13.0	17.1	584(574)	95
	bpy[b]	1.71	901	d)		d)	80
	bpy[c]	1.72	973	13.0	16.9	555(550)	81[e]

a) Calculated values in parentheses. b) Yellow isomer. c) Yellow-green isomer. d) Not determined because of poor solubility. e) This complex behaves in the same manner as the yellow isomer in methanol.

scribed previously. For the *cis* configuration, the ν(V=O) frequency showed no appreciable dependence upon the electronic nature of the pyridine substituent, whereas for the *trans* one the electron release by the substituent caused a reduction in the frequency. All of the present nitrophenolates except the yellow isomer of picrate (*vide infra*) display ν(V=O) bands in the 962—973 cm^{-1} region which are higher than those for the phenol adducts and which are almost constant, irrespective of the great difference in the pK_a's of the nitrophenols (pK_a=7.149, 4.110, and 0.708 at 25 °C for 4-nitro-, 2,4-dinitro-, and 2,4,6-trinitrophenols respectively). If the above IR criterion for the geometrical structure of $VO(acac)_2L$ is also applicable to the present complexes, the *cis* arrangement of the phenolate to the oxo ligand would be more probable. However, at the present stage it is not clear which atom, oxygen (acac) or nitrogen (bpy), occupies the position *trans* to the oxo ligand.

As may be seen in Table 4, the present phenolato complexes exhibit two d-d absorption maxima in dichloromethane at around 12500 and 17000 cm^{-1}, with a shoulder at around 21000 cm^{-1}. These spectra are similar to those of the phenol adducts in a solid and are typical ones for octahedral oxovanadium(IV) complexes. The two band positions are almost constant for these complexes and do not relate to the change in the pK_a's of the nitrophenols, again indicating no electronic effect of the substituted phenol on vanadium.

The observed molecular weight in dichloromethane at 25 °C is close to the calculated value, indicating that these complexes exist intact in solution without liberating the phenolate ligand. This contrasts with the cationic complex derived by Aly.[5] The conductance measured in methanol, on the contrary, depends on the nature of the nitrophenol contained in these complexes. The 4-nitrophenolato complex exists as a non-electrolyte even in methanol, while the picrato complex behaves practically as a uni-univalent electrolyte in this solution, presumably with the release of the picrate ion. The conductance of the 2,4-dinitrophenolato complex is intermediate between those of the 4-nitro- and the 2,4,6-trinitrophenolato complexes, suggesting partial ionization to a complex cation and a 2,4-dinitrophenolate ion in solution. The enhanced ionization with the increase in the number of the nitro substituent on the phenol ring appears to reflect the increase V–O(phenolate)-bond instability in these complexes resulting from the electronic and/or steric effect of the substituent.

Two kinds of $VO(OC_6H_2(NO_2)_3)(acac)(bpy)$ complexes were produced by different synthetic routes. The yellow-green isomer was prepared by the picrate substitution of the 4-nitrophenolato complex in dichloromethane, while the yellow isomer was obtained by the direct reaction of $VO(acac)_2$, 2,4,6-trinitrophenol, and bpy in methanol. However, it is likely that the difference in kind was caused by the difference in the donor abilities of the solvents used rather than by that in the synthetic routes, since the yellow-green isomer could also be prepared by means of a direct reaction in dichloromethane.

The ν(V=O) frequency of the yellow isomer lies at 901 cm^{-1} abnormally lower than those of other phenolato complexes, and is close to those of the phenol adducts. Thus, it is suggested that the isomer also has a V=O···V=O chain structure in a solid and is formulated by [VO(acac)(bpy)](picrate). The low solubility of the complex in nonpolar solvents may be due to its polymeric and ionic character. On the other hand, the complex dissolves in methanol and behaves as a uni-univalent electrolyte, as does the yellow-green isomer.

The existence of two isomers for the picrato complex containing bpy appears to be caused by a delicate balance among the coordinating abilities of a picrate ion, an adjacent vanadyl oxygen atom, and a methanol molecule, toward the sixth coordination site of a particular vanadium cation $[VO(acac)(bpy)]^+$. The yellow-green isomer is stable in dichloromethane, but releases the picrate ion in methanol, depositing the yellow isomer on evaporation. Why a pair of isomers of the phen derivative can not be derived is a question left to be solved.

The authors are grateful to Mr. Junichi Gohda for the elemental analysis. Financial aid by the Ministry of Education is also acknowledged.

References

1) J. P. Fackler, Jr., *Prog. Inorg. Chem.*, **7**, 361 (1966).

2) (a) Y. Nakamura, K. Isobe, H. Morita, S. Yamazaki, and S. Kawaguchi, *Inorg. Chem.*, **11**, 1573 (1972) and the references cited therein; (b) J. Hillis, J. Francis, M. Ori, and M. Tsutsui, *J. Am. Chem. Soc.*, **96**, 4800 (1974); R. F. Cramer, S. W. Cramer, K. F. Cramer, M. A. Chudyk, and K. Seff, *Inorg. Chem.*, **16**, 219 (1977).

3) J. Selbin, *Chem. Rev.*, **65**, 153 (1965); *Coord. Chem. Rev.*, **1**. 293 (1966).

4) R. A. Rowe and M. M. Jones, *Inorg. Synth.*, **5**, 114 (1957).

5) M. M. Aly, *J. Inorg. Nucl. Chem.*, **35**, 537 (1973).

6) R. P. Dodge, D. H. Templeton, and A. Zalkin, *J. Chem. Phys.*, **35**, 55 (1961).

7) K. Isobe, H. Taguchi, S. Ooi, and H. Kuroya, Abst. No. 2M02, 26th National Conference on Coordination Chemistry of Japan, Sapporo, August, 1976.

8) M. R. Caira, J. M. Haigh, and L. R. Nassimbeni, *J. Inorg. Nucl. Chem.*, **34**, 3171 (1972).

9) N. S. Al-Niaimi, A. R. Al-Karaghouli, S. M. Aliwi, and M. G. Jalhoom, *J. Inorg. Nucl. Chem.*, **36**, 283 (1974).

10) M. Mathew, A. J. Carty, and G. J. Palenik, *J. Am. Chem. Soc.*, **92**, 3197 (1970).

11) A. Pasini and M. Gullotti, *J. Coord. Chem.*, **3**, 319 (1974).

12) B. J. McCormick and R. A. Bozis, *Inorg. Chem.*, **10**, 2806 (1971).

13) J. Selbin, G. Maus, and D. L. Johnson, *J. Inorg. Nucl. Chem.*, **29**, 1735 (1967).

14) J. Selbin, H. R. Manning, and G. Cassac, *J. Inorg. Nucl. Chem.*, **25**, 1253 (1963).

cis-Dioxovanadium(V) and Mixed-Valence Divanadium(IV, V) Complexes Containing β-Diketonate and Heterocyclic Nitrogen-base Ligands

Hiroshi TAGUCHI, Kiyoshi ISOBE, Yukio NAKAMURA,* and Shinichi KAWAGUCHI

Department of Chemistry, Faculty of Science, Osaka City University, Sumiyoshi-ku, Osaka 558

(Received December 16, 1977)

Diamagnetic dioxovanadium(V) complexes, VO_2(β-dik)(phen or bpy),† were prepared by the direct reactions of VO(β-dik)$_2$ with 1,10-phenanthroline and 2,2′-bipyridine in dichloromethane under aerobic conditions as well as by two other methods. These compounds were concluded to have a *cis* configuration on the basis of the IR and Raman data. These complexes are solvolyzed to afford the di-μ-methoxo- or di-μ-hydroxo-divanadium(V) species, and are reduced by hydrogen bromide to the oxovanadium(IV) species in dichloromethane. In methanol instead of dichloromethane, $VO(acac)_2$ reacted with 2,2′-bipyridine to produce a novel mixed-valence divanadium-(IV, V) complex, $V_2O_3(acac)_3$(bpy), which was revealed by the magnetic, spectral, and polarographic data to be a trans adduct of $VO(acac)_2$ with VO_2(acac)(bpy) *via* an oxide ligand.

Bis(acetylacetonato)oxovanadium(IV), $VO(acac)_2$, acts as an effective and highly selective catalyst for the epoxidation of olefins[1] and olefinic alcohols[2] by *t*-butyl hydroperoxide. Gould *et al.*[1] provided some evidence showing that a vanadium(V) hydroperoxide complex produced by the reaction of $VO(acac)_2$ with a hydroperoxide served as an effective catalyst for the epoxidation. The intermediary vanadium(V) complex, however, was neither isolated nor characterized.

Solid $VO(acac)_2$ is stable in air for a long period, but in solution it is slowly oxidized by atmospheric oxygen to some as yet unknown quinquevalent species.[3] In general, VO^{2+} ions are stable for 6 months or more in concentrated strong acids, but they are rapidly oxidized above pH 2.45, especially in alkaline solutions.[4]

The reaction of $VO(acac)_2$ with a slight excess of 1,10-phenanthroline in methanol yielded a mixed ligand V(IV) complex with the composition of VO(acac)$_2$(phen)·2MeOH,[5] but the same reaction in dichloromethane under aerobic conditions resulted in a V(V) complex, VO_2(acac)(phen).[6] We wish now to report more detailed results on the reactions of several bis(β-diketonato)oxovanadium(IV) complexes with 1,10-phenanthroline and 2,2′-bipyridine under the latter reaction conditions to afford diamagnetic VO_2(β-dik)(phen or bpy).

Experimental

Materials. The oxovanadium(IV) complexes, $VO(acac)_2$,[7] $VO(tfac)_2$,[8] and $VO(bzac)_2$,[9] were prepared by the methods described in the literature and gave satisfactory elemental analyses and IR spectra. Commercially available β-diketones, 1,10-phenanthroline, and 2,2′-bipyridine were used without further purification. The organic liquids were dried and distilled before use. A stock solution of hydrogen bromide was prepared by dissolving in dichloromethane the gas which had been generated by the reaction of tetralin with bromine and by then drying through a tube containing calcium bromide.

Preparation of the Diamagnetic cis-*Dioxovanadium(V) Complexes.* These complexes were prepared by the following methods.

† β-dikH (β-diketone)=acacH(acetylacetone), bzacH (benzoylacetone), tfacH (trifluoroacetylacetone), dbmH (dibenzoylmethane), and hfacH (hexafluoroacetylacetone); phen and bpy stand for 1,10-phenanthroline and 2,2′-bipyridine respectively.

Method A: Direct Reaction of Bis(β-diketonato)oxovanadium-(IV) with 1,10-Phenanthroline and 2,2′-Bipyridine under Aerobic Conditions. cis-*Dioxo(acetylacetonato)(1,10-phenanthroline)-vanadium(V),* cis-VO_2(acac)(phen) (**1**): To a dichloromethane solution (40 ml) of $VO(acac)_2$ (1.0 g, 3.8 mmol) we added a solution of an excess of 1,10-phenanthroline monohydrate in dichloromethane (40 ml); oxygen was bubbled through the mixture for about 5 h to deposit reddish brown crystals. They were then filtered off, washed with diethyl ether, and dried *in vacuo*, but they still contained dichloromethane as the solvent of crystallization. Recrystallization from a mixture (1:1 by volume) of methanol and acetylacetone freed the complex from the solvent of crystallization.

Compounds **2**, **3**, **4**, and **6** in Table 1 were prepared by similar methods, but the oxidation was continued for 7—9 h. In the preparation of 2,2′-bipyridine derivatives the solution after oxidation was concentrated to 10 ml to deposit crystals.

Method B: Replacement Reactions of VO_2(acac)(phen or bpy) by Other β-Diketonate Ligands. The VO_2(acac)(phen or bpy) complex (1 mmol) was added to a methanol solution (20 ml) containing twice the molar amounts of a β-diketone other than acetylacetone, and the mixture was heated to dissolve the complex. The solution was then filtered and cooled to room temperature to separate out crystals of the corresponding β-diketonate complex, VO_2(β-dik)(phen or bpy).

This method was useful for the preparation of *cis*-dioxo complexes **3**—**10**. The low yield of *cis*-dioxo(2,2′-bipyridine)-(dibenzoylmethanido)vanadium(V) monohydrate *cis*-VO_2(dbm)(bpy)·H_2O is caused by partial methanolysis. Thus, a reddish brown methanolysis product was first precipitated and analyzed to fit $VO(OCH_3)_2$(dbm) (Found: C, 57.84; H, 4.85. Calcd for $C_{17}H_{17}O_5V$: C, 57.96; H, 4.86%). The desired red compound separated out from the filtrate.

Method C: Replacement of the 2,2′-Bipyridine in VO_2(β-dik)-(bpy) by 1,10-Phenanthroline. A methanol solution (10 ml) of 1,10-phenanthroline (3 mmol) was added to a methanol solution (25 ml) containing VO_2(β-dik)(bpy) (1 mmol) and the same kind of β-diketone ligand (3 mmol). The mixture was heated to 60 °C for 1 h, and then kept at room temperature to precipitate the phen complex.

Compounds **1**, **3**, and **5** were prepared according to this method. The analytical data, decomposition temperatures, and yields (by each synthetic method, A, B, or C) of these dioxovanadium(V) complexes are listed in Table 1.

Solvolysis Reactions of cis-VO_2(β-dik)(phen or bpy). When the *cis*-VO_2(β-dik)(phen or bpy) complex (1 mmol) was heated to dissolve it in methanol (20 ml), a solvolytic reaction occurred and a product with the composition of $V_2O_4(OCH_3)_2$(phen or bpy) was separated out on cooling

Table 1. Analytical data,[a] dec temp, and yields

No.	Compound	C/%	H/%	N/%	Dec temp °C	Yield/% A[b]	B[b]	C[b]
1	VO_2(acac)(phen)	55.67(56.36)	4.39(4.17)	7.45(7.73)	143—144	36		63
2	VO_2(acac)(bpy)	53.09(53.27)	4.45(4.47)	8.01(8.28)	170—171	63		
3	VO_2(bzac)(phen)	61.60(62.27)	4.13(4.04)	6.76(6.60)	191—193	86	80	45
4	VO_2(bzac)(bpy)·1/2H_2O	58.93(58.69)	4.45(4.43)	6.93(6.84)	167—168	86	91	
5	VO_2(tfac)(phen)	49.06(49.06)	2.91(2.91)	6.83(6.73)	177—179		82	29
6	VO_2(tfac)(bpy)	45.08(45.94)	3.00(3.08)	6.89(7.14)	176—177	54	31	
7	VO_2(dbm)(phen)	66.52(66.67)	3.95(3.94)	5.52(5.76)	215—217		88	
8	VO_2(dbm)(bpy)·H_2O	62.97(62.51)	4.58(4.41)	5.61(5.83)	200—203		6	
9	VO_2(hfac)(phen)	43.26(43.24)	1.94(1.92)	5.77(5.93)	167—168		70	
10	VO_2(hfac)(bpy)	40.82(40.38)	2.23(2.03)	6.25(6.28)	159—161		42	
11	VOBr(acac)(phen)·2H_2O	43.64(44.18)	4.11(4.14)	6.12(6.06)	203—204		42	
12	VOBr(acac)(bpy)·2H_2O	40.91(41.12)	4.32(4.37)	6.30(6.39)	191—193		62	
13	VOBr(bzac)(phen)·1/2H_2O	53.78(53.14)	3.81(3.65)	5.68(5.63)	170—172		57	
14	VOBr(bzac)(phen)·H_2O	50.15(49.81)	3.90(3.55)	5.71(5.81)	149—151		40	
15	V_2O_3(acac)$_3$(bpy)	49.75(49.76)	4.90(4.84)	4.46(4.64)	165—167	55		62[c]

a) Calculated values in parentheses. b) Yield by each synthetic method (A, B or C) described in Exptl Section. c) Yield by an equimolar reaction between $VO(acac)_2$ and VO_2(acac)(bpy).

to room temperature. The yields were 54% for $V_2O_4(OCH_3)_2$(phen) (Found: C, 40.67; H, 3.37; N, 6.83. Calcd for $C_{14}H_{14}N_2O_6V_2$: C, 41.20; H, 3.46; N, 6.86%. Dec 179—180 °C), and 63% for $V_2O_4(OCH_3)_2$(bpy) (Found: 37.17; H, 3.70; N, 7.12. Calcd for $C_{12}H_{14}N_2O_6V_2$: C, 37.52; H, 3.67; N, 7.29%. Dec 169—170 °C). The latter compound was also prepared by stirring for a few days a suspension of vanadium(V) pentoxide in methanol containing 2,2′-bipyridine. The subsequent heating of the complex in other organic solvents, such as chloroform, dichloromethane, acetone, and nitromethane, resulted in $V_2O_4(OH)_2$(phen)·3/2H_2O or $V_2O_4(OH)_2$(bpy)·2H_2O. The yield was 67% for $V_2O_4(OH)_2$(phen)·3/2H_2O (Found: C, 35.38; H, 2.49; N, 6.55. Calcd for $C_{12}H_{13}N_2O_{7.5}V_2$: C, 35.37; H, 3.22; N, 6.88%. Dec 194—196 °C). The yield was 48% for $V_2O_4(OH)_2$(bpy)·2H_2O (Found: C, 30.97; H, 2.74; N, 6.60. Calcd for $C_{10}H_{14}N_2O_8V_2$: C, 30.89; H, 3.60; N, 7.14%. Dec 156—158 °C). The products of methanolysis and hydrolysis were all unstable in air and were insoluble in most solvents, thus precluding physical measurements.

Reduction of cis-*VO_2(acac)(phen or bpy) with Hydrogen Bromide.* The *cis*-VO_2(acac)(phen or bpy) complex (2 mmol) was dissolved in dichloromethane (60 ml) containing acetylacetone (9 mmol), and to the mixture we then added, drop by drop, a solution (0.16 M, 25 ml) of hydrogen bromide in dichloromethane. The resultant white-green precipitate was found to be dibromooxo(1,10-phenanthroline)vanadium(IV) $VOBr_2$(phen) or dibromo(2,2′-bipyridine)oxovanadium(IV) $VOBr_2$(bpy) on the basis of elemental analysis. The filtrate was concentrated to 20 ml to deposit yellow-green crystals with the composition of VOBr(acac)(phen)·2H_2O (**11**) or VOBr(acac)(bpy)·2H_2O (**12**). The corresponding VOBr(bzac)(phen)·1/2H_2O (**13**) and VOBr(bzac)(bpy)·H_2O (**14**) complexes were produced in a similar manner and gave satisfactory analyses (Table 1).

*Preparation of the Mixed-Valence Divanadium(IV, V) Complex. Tris(acetylacetonato)(2,2′-bipyridine)trioxo-divanadium(IV, V), V_2O_3(acac)$_3$(bpy) (**15**):* A methanol solution (30 ml) containing $VO(acac)_2$ (1.6 g, 6.2 mmol) and 2,2′-bipyridine (1.0 g, 6.4 mmol) was concentrated to about 10 ml at 60 °C on a water bath and then cooled to room temperature to deposit green crystallites of $V_2O_3(acac)_3$(bpy). The complex was also prepared by simple adduct formation between $VO(acac)_2$ and **2**: equimolar amounts of $VO(acac)_2$ (0.58 g, 2.2 mmol) and VO_2(acac)(bpy) (0.74 g, 2.2 mmol) were dissolved in methanol (50 ml) containing acetylacetone (2 ml), and then the mixture was concentrated to 20 ml to separate $V_2O_3(acac)_3$(bpy).

The analytical data, decomposition temperature, and yield of the complex are listed in the last row of Table 1.

Measurements. Each specimen of the complexes was dried *in vacuo* at room temperature before being subjected to elemental analysis. The absorption spectra of the solutions and the reflectance spectra of the solid specimen were measured by means of a Hitachi EPS-3T autorecording spectrophotometer equipped with an RIO reflectance attachment. The infrared spectra were taken in Nujol on JASCO IR-E (4000—700 cm^{-1}) and Hitachi EPI-L (700—200 cm^{-1}) infrared spectrophotometers. The Raman spectra were recorded with the aid of a JRS-S1 Laser Raman spectrophotometer by exciting a solid specimen in a rotating cell with a 5145 Å Argon laser.

The magnetic susceptibility was measured by means of a Shimadzu MB-2 automatically recording magnetic balance, employing mercury tetraisothiocyanatocobaltate(II) as a reference. The electric conductivities of compounds **11** and **12** were measured in methanol by means of an MY-7 apparatus of the Yanagimoto Seisakusho, Ltd.

Results and Discussion

As has been described in the Experimental Section, each VO_2(β-dik)(phen or bpy) complex could be prepared by one or more of three synthetic methods. The complexes are all yellow to red crystals. The magnetic susceptibilities of the representative compounds, **1** and **2**, were measured at room temperature. They are both diamagnetic, χ_M being -1.52×10^{-4} and -4.72×10^{-5} c.g.s. unit respectively. This implies that the vanadium atom is in a quinquevalent state with the d^0 configuration in these complexes,

Table 2. The characteristic IR bands of the $VO_2(\beta\text{-dik})$(phen or bpy) complexes (cm^{-1})

No.	Compound	ν_s(C=O)	ν_{as}(C=C=C)	$\nu_s(VO_2)$	$\nu_{as}(VO_2)$	$\delta(VO_2)$
1	VO_2(acac)(phen)	1613	1515	916	891	340
2	VO_2(acac)(bpy)	1613	1513	911	886	344
3	VO_2(bzac)(phen)	1612	1515	915	891	337
4	VO_2(bzac)(bpy)·1/2H_2O	1615	1516	914	881	336
5	VO_2(tfac)(phen)	1653	1545	923	900	326
6	VO_2(tfac)(bpy)	1651	1537	922	901	328
7	VO_2(dbm)(phen)	1600	1515	918	892	327
8	VO_2(dbm)(bpy)·H_2O	1610	1518	915	887	337
9	VO_2(hfac)(phen)	1662	1554	932	907	322
10	VO_2(hfac)(bpy)	1663	1555	939	912	327

The diamagnetism of the other dioxo complexes can also be inferred by analogy with **1** and **2**.

Geometrical Structure. To our knowledge, only the *cis* arrangement of two oxide ligands has been elucidated by X-ray analysis for octahedral dioxovanadium(V) complexes, such as ammonium salts of dioxobis(oxalato)vanadate(V)[10] and (dihydrogenethylenediaminetetraacetato)dioxovanadate(V),[11] and trisodium (ethylenediaminetetraacetato)dioxovanadate-(V) tetrahydrate.[12] Hence, it is of interest to explore whether or not the two oxo groups in the present complexes are in a *cis* configuration. As has been described in a preliminary communication,[6] the *cis* structure was also established by a single crystal X-ray analysis of compound **1**.

Griffith and Wickins[13,14] proposed that the strong π-donor effect of the oxo ligand in octahedral complexes will make the d^0 species of the $[MO_2X_4]^{n-}$ type take the *cis* configuration. From the theoretical treatment of the vibrational modes they[14] showed that, for the *cis* form, the three vibrational modes of $\nu_s(MO_2)$, $\nu_{as}(MO_2)$, and $\delta(MO_2)$ are active in both IR and Raman spectra, while for the trans form only the symmetric stretching mode is Raman-active, with the other modes being IR-active only. They examined the IR and Raman spectra of a number of d^0 species of the $[MO_2X_4]^{n-}$ type (Mo^{VI}, W^{VI}, or V^V; X=F, Cl, or ½ox). All of them exhibited three bands due to the vibrational modes described above at around 950, 900, and 370 cm^{-1} respectively in either the IR or Raman spectra. Thus, these d^0 complexes were concluded to have a *cis* rather than a *trans* arrangement of the oxo ligands.

The IR spectrum of compound **1** in Nujol shows two strong bands assignable to the V–O (oxide) stretching vibration at 916 and 891 cm^{-1}, together with a band due to the O–V–O bending mode at 340 cm^{-1} (Table 2). The Raman spectrum also exhibits two stretching bands, although the O–V–O bending mode is indiscernible because of the intense background. These results are compatible with the conclusion drawn from the theoretical treatment. As may be seen in Fig. 1, the higher-frequency $\nu(VO_2)$ band is weaker in IR, but is much stronger in Raman than the lower-frequency one, revealing that the former band is attributable to the symmetric vibration, and the latter, to the anti-symmetric vibration. In many bent triatomic molecules the ν_{as} band is observed in a higher-

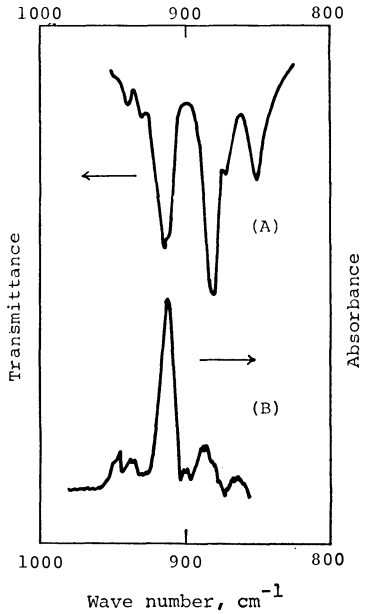

Fig. 1. The IR (in Nujol) (A) and Raman (in solid state) (B) spectra of VO_2(acac)(phen) in the V–O (oxide) stretching region.

frequency region than the ν_s band, but compound **1** shows an opposite pattern. A similar situation is also observed in $(NH_4)_3[VO_2(ox)_2]\cdot 2H_2O$,[14] while VO_2Cl, VO_2F and VO_2SbF_6[15] show the $\nu_{as}(VO_2)$ band in a higher-frequency region than the $\nu_s(VO_2)$ band. The presence of the ν_s band at a higher frequency in the oxalato complex and the present compound **1** might be attributable to the enhanced repulsion between the oxide ligands as compared with the other three compounds. Such a reversion of ν_{as} and ν_s frequencies is also observed for triatomic molecules with an isosceles-triangular structure such as O_3 and OF_2 because of the large repulsion between the two atoms on the base.[16] As may be seen in Table 2, all the dioxo complexes other than compound **1** also exhibit three IR bands assignable to the $\nu_s(VO_2)$, $\nu_{as}(VO_2)$, and $\delta(VO_2)$ vibrations, although Raman spectra of these complexes were not examined. By analogy with compound **1**, the *cis* configuration of the two oxide ligands in these complexes can also be inferred with confidence.

Other Characteristics. It has been well established that the β-diketonate chelates exhibit their ν_s(C=O) and

ν_{as}(C=C=C) bands in the 1500—1600 cm^{-1} region.[17] On the contrary, the present dioxo complexes display the carbonyl band at frequencies higher than 1600 cm^{-1}, as may be seen in Table 2. A similar situation was noticed when a bidentate nitrogen base, such as ethylenediamine, 1,10-phenanthroline, or 2,2′-bipyridine, was added so as to coordinate it to a neutral metal β-diketonate.[18] The increase in frequency was attributed to the weakening of the metal-oxygen(β-dik) bond by donation of electron from the base to the metal center. In the present case, it is most likely that the strong π-donor ability of oxide ligands weakens the V–O(β-dik) bond. Such a *trans* influence of two oxide ligands essentially resulted in the elongation of one of the two V–O(acac) bonds and of one of the two V–N bonds which are *trans* to the two oxide ligands in VO_2(acac)(phen)[6] (V–O: 2.177(4) and 1.949(4) Å, V–N: 2.300(4) and 2.148(4) Å). An additional weakening of the V–O(β-dik) bond is effected when an electron-withdrawing substituent is introduced into the acetylacetonate ligand of compounds **1** and **2**. In the trifluoro- and hexafluoroacetylacetonato complexes (**5**, **6**, **9**, and **10**) the carbonyl band is, in fact, observed at still higher frequencies than those of **1** and **2**, with concomitant shifts of $\nu_s(VO_2)$ and $\nu_{as}(VO_2)$ to the higher-frequency region (Table 2). It is also of interest that compound **5** was not prepared by Method A. This is probably because the reaction of $VO(tfac)_2$ with 1,10-phenanthroline gave the stable *cis*-adduct $VO(tfac)_2$(phen),[5] which hindered oxidation to the *cis*-dioxo complex.

The reflectance spectra of all the dioxo complexes prepared in this paper exhibit no band assignable to the d-d transitions in the visible region, in conformity with d^0 configuration. A similar feature is also observed in the solution spectra in methanol containing a small quantity of β-diketone to prevent decomposition.

Solvolysis Products. The solvolysis products, $V_2O_4(OCH_3)_2$ (phen or bpy) and their dihydroxo counterparts, include a $V_2O_4^{2+}$-moiety in these complexes. Although many binuclear molybdenum(V) complexes containing a $Mo_2O_4^{2+}$-moiety are known,[13] scarcely no corresponding vanadium(V) complexes with $V_2O_4^{2+}$-moiety have been found. Very recently, (2,2′-bipyridine)fluorodioxovanadium(V), VO_2F(bpy) was prepared[19] and its structure was found by X-ray analysis to have one V=O(terminal) bond on each vanadium(V) atom and asymmetric oxygen bridges (V 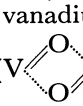 V).[20] The IR spectrum of this compound shows three V–O stretching bands, at 954, 938, and 872 cm^{-1}, while the present dimethoxo complexes exhibit two bands in the 940—960 cm^{-1} region, together with a broad band in the 700—720 cm^{-1} region. The lower frequency of the last band might be indicative of the presence of more symmetric oxygen bridges (V V).[21] However, these solvolysis products are unstable in air and insoluble in any solvents, thus precluding further examination.

Reduction of VO_2(β-dik)(phen or bpy) Complexes. The VO_2(acac) (phen or bpy) complexes were easily reduced by hydrogen bromide in dichloromethane to produce the vanadium(IV) species, VOBr(acac)(phen or bpy)·$2H_2O$, which show the magnetic moments of 1.75 and 1.73 B.M. per vanadium atom. The complexes are very similar in composition to the corresponding nitrophenolato complexes, $VO(OC_6H_{5-n}X_n)$(acac)(phen or bpy) (X=NO_2; n=1—3), previously isolated by us.[22] One of the latter complexes, the 4-nitrophenolato derivative, reacted with sodium bromide to afford VOBr(acac)(phen or bpy)·$2H_2O$. The reactions of complexes **3** and **4** with hydrogen bromide also gave the corresponding benzoylacetonato vanadium(IV) complexes, **13** and **14**. The ν(V=O) bands of these bromo complexes appear in the 960—980 cm^{-1} region, just as do those of the nitrophenolato complexes which have the *cis* configuration,[22] indicating the cis arrangement of the bromide and oxo ligands.

The absorption spectra of VOBr(acac)(phen or bpy)·$2H_2O$ in dichloromethane showed two bands near 13000 and 16000 cm^{-1}, together with a shoulder around 21000 cm^{-1}. These frequencies are very close to those of the nitrophenolato complexes (12500, 17000, and 21000 cm^{-1}),[22] suggesting the octahedral monomeric structure of the bromo complexes in dichloromethane. On the contrary, the complexes behave as uni-univalent electrolytes in methanol, as evidenced by the Λ_M values of 99(phen) and 91(bpy) ohm^{-1} cm^2 mol^{-1}.

The Mixed-valence Divanadium(IV, V) Complex. Unlike the reaction with 1,10-phenanthroline in methanol leading to $VO(acac)_2$(phen)·$2CH_3OH$,[5] $VO(acac)_2$ reacts with 2,2′-bipyridine in the same solvent to afford green crystals with the composition of $V_2O_3(acac)_3$(bpy) (**15**). The magnetic moment of **15** was found at room temperature to be 1.70 B.M. per divanadium unit, nearly corresponding to the value for a single spin. Thus, complex **15** seems to consist of two vanadium atoms in different oxidation states, V(IV)

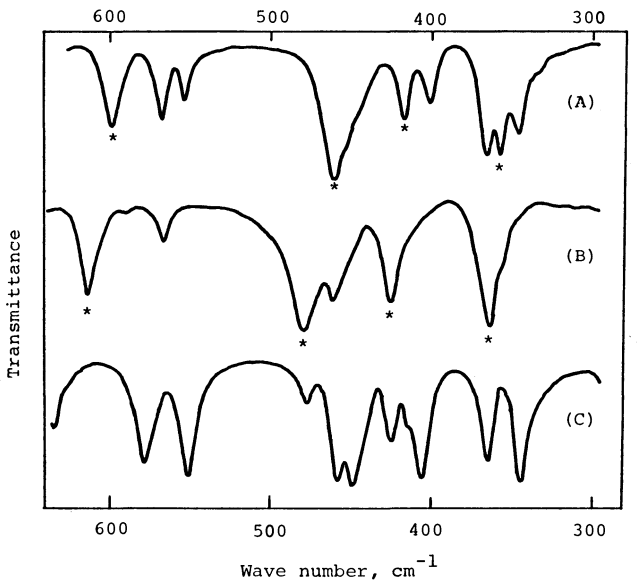

Fig. 2. The far IR spectra of $V_2O_3(acac)_3$(bpy) (A), $VO(acac)_2$ (B) and VO_2(acac)(bpy) (C) in Nujol. Asterisks denote V–O sensitive bands according to the assignment by Caira *et al.* [28].

and V(V).

It has been well established that the ν(V=O) band of $VO(acac)_2$ at 1000 cm^{-1} is shifted to the lower-frequency region on adduct formation, and that the extent of the frequency reduction varies in the range of 20 to 60 cm^{-1} according to the variation in the bases.[23-29] The IR spectrum of the present mixed-valence complex **15** exhibits three intense bands in the ν(V=O) region of 850 to 1000 cm^{-1}. The first band, at 960 cm^{-1}, is just in the range of the ν(V=O) frequencies of the base adducts, and the other two, at 930 and 883 cm^{-1} are very close to the $\nu_s(VO_2)$ and $\nu_{as}(VO_2)$ frequencies of $VO_2(acac)(bpy)$ (**2**) derived earlier in this paper. Hence, a simple adduct of $VO(acac)_2$ and **2** with one of the oxo ligands in **2** intervening between two vanadium atoms may be presumed for complex **15** ((I) or (II)):

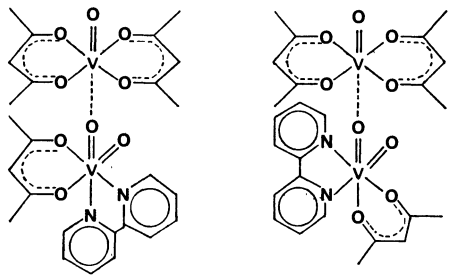

(I) (II)

In Fig. 2, the IR spectrum of **15** in the lower-frequency region is shown, together with those of $VO(acac)_2$ and **2** for comparison. The spectrum of **15** (Spectrum A) is very similar to a superposition of those for the latter two (Spectra B and C), supporting the proposed structure of **15**. Four bands, at 611, 488, 425, and 367 cm^{-1} of $VO(acac)_2$ previously assigned by Caira *et al.*[28] to the V–O sensitive modes, are lowered to 600, ≈460, 420, and 360 cm^{-1} respectively in complex **15**. Such a lowering without splitting of those bands has also been noted for the *trans* adducts of $VO(acac)_2$ with substituted pyridines[28] and substituted pyridine *N*-oxides.[29] Thus, these data again support the idea that complex **15** is a *trans* adduct of $VO(acac)_2$ with **2**. In fact, complex **15** could be synthesized by an equimolar reaction of $VO(acac)_2$ and $VO_2(acac)(bpy)$ in methanol containing excess acetylacetone. However, it is not possible at the present stage of investigation to discriminate the above two possible structures.

In Table 3 the reflectance and solution spectral data of **15** are shown, together with those of $VO(acac)_2$. As has been described earlier, $VO_2(acac)(bpy)$ exhibits no d-d band in the visible region. Hence, it is likely that the two bands in the reflectance spectrum of complex **15** at 13000 and 17200 cm^{-1}, along with a shoulder at around 22700 cm^{-1}, were brought about by the shift of the absorption bands of $VO(acac)_2$ at 14600 and 16800 cm^{-1} and a shoulder 25000 cm^{-1} respectively. Such shifts of the first and second bands of $VO(acac)_2$ to the lower and higher frequencies respectively are caused by the attainment of the octahedral environment around the vanadium(IV) ion on adduct formation.[30] If a dilute solution of **15** in methanol containing a small quantity of acetylacetone is left standing, $VO_2(acac)(bpy)$ is deposited from the mixture. These results may indicate that complex **15** dissociates in this solvent to $VO(acac)_2$ and $VO_2(acac)(bpy)$. The absorption spectrum of **15** in methanol containing acetylacetone in a large excess to prevent the decomposition of the complex exhibits two bands, at 22700 (ε=1670) and 12700 (ε=45) cm^{-1}, as is shown in Table 3. Because of the low solubility of **15** in this solution, a 10 cm-cell was used for the measurement of the low intensity band. The former band corresponds essentially to the absorption band at 22200 cm^{-1} (ε=1690) of $VO_2(acac)(bpy)$ in methanol containing acetylacetone in a large excess, while the latter corresponds to the first band of $VO(acac)_2$ in the same solvent. The other bands of $VO(acac)_2$ are masked by the tails of the strong ligand bands of $VO_2(acac)(bpy)$.

Table 3. The reflectance (in solid) and absorption (in methanol) spectra of $V_2O_3(acac)_3(bpy)$ and $VO(acac)_2$ (ν_{max}, 10^3 cm^{-1})

Compound	Reflectance spectra	Absorption spectra[a]
$V_2O_3(acac)_3(bpy)$	13.0	12.7 (45)[b]
	17.2	
	22.7	22.7 (1670)[b]
$VO(acac)_2$	14.6	13.0 (40)
	16.8	17.3 (16)
	25.0	25.0 (91)

a) ε values in parentheses.
b) In the presence of acetylacetone (0.503 M).

Another support for the presence of the $VO_2(acac)(bpy)$ species in methanol was obtained polarographically. The current-voltage curves of **15** and $VO_2(acac)(bpy)$ in methanol containing acetylacetone in 6.6×10^{-3} M were recorded using tetrabutylammonium perchlorate as a supporting electrolyte. In addition to the similarity of both the wave-shape and the wave-height, the half-wave potential of −0.02 V *vs.* SCE obtained for **15** is very close to that of −0.03 V *vs.* SCE for $VO_2(acac)(bpy)$, indicating the presence of $VO_2(acac)(bpy)$ in the solution.

The authors are grateful to Mr. Junichi Gohda and Mr. Akio Ichimura for the elemental analysis and polarographic measurements respectively. The measurements of the Raman spectrum at JOEL, Ltd., and a financial aid from the Ministry of Education are also acknowledged.

References

1) E. S. Gould, R. R. Hiatt, and K. C. Irwin, *J. Am. Chem. Soc.*, **90**, 4573 (1968); C.-C. Su, J. W. Reed, and E. S. Gould, *Inorg. Chem.*, **12**, 337 (1973).
2) K. B. Sharpless and R. C. Michaelson, *J. Am. Chem. Soc.*, **95**, 6136 (1973); S. Tanaka, H. Yamamoto, H. Nozaki, K. B. Sharpless, R. C. Michaelson, and J. D. Cutting, *ibid.*, **96**, 5254 (1974).
3) T. R. Ortolano, J. Selbin, and S. P. McGlynn, *J. Chem. Phys.*, **41**, 262 (1964).
4) J. Selbin, *Chem. Rev.*, **65**, 153 (1965).

5) K. Isobe, Y. Nakamura, and S. Kawaguchi, *J. Inorg. Nucl. Chem.*, **40**, 607 (1978).
6) K. Isobe, S. Ooi, Y. Nakamura, S. Kawaguchi, and H. Kuroya, *Chem. Lett.*, **1975**, 35.
7) R. A. Rowe and M. M. Jones, *Inorg. Synth.*, **5**, 114 (1957).
8) R. L. Carlin and F. A. Walker, *J. Am. Chem. Soc.*, **87**, 2128 (1965).
9) M. M. Jones, *J. Am. Chem. Soc.*, **76**, 5995 (1954).
10) W. R. Scheidt, C.-C. Tsai, and J. L. Hoard, *J. Am. Chem. Soc.*, **93**, 3867 (1971).
11) W. R. Scheidt, D. M. Collins, and J. L. Hoard, *J. Am. Chem. Soc.*, **93**, 3873 (1971).
12) W. R. Scheidt, R. Countryman, and J. L. Hoard, *J. Am. Chem. Soc.*, **93**, 3878 (1971).
13) W. P. Griffith, *Coord. Chem. Rev.*, **5**, 459 (1970).
14) W. P. Griffith and T. D. Wickins, *J. Chem. Soc., A*, **1968**, 400.
15) K. Dehnicke and J. Weidlein, *Angew. Chem. Int. Ed. Engl.*, **5**, 1041 (1966).
16) G. Herzberg, "Molecular Spectra and Molecular Structure, II. Infrared and Raman Spectra of Polyatomic Molecules," Lancaster Press, New York (1945), p. 272.
17) K. Nakamoto, "Infrared Spectra of Inorganic and Coordination Compounds" 2nd ed, Wiley-Interscience, New York (1970), p. 247.
18) Y. Nishikawa, Y. Nakamura, and S. Kawaguchi, *Bull. Chem. Soc. Jpn.*, **45**, 155 (1972); T. Kurauchi, M. Matsui, Y. Nakamura, S. Ooi, S. Kawaguchi, and H. Kuroya, *ibid.*, **47**, 3049 (1974).
19) J. Sala-pala and J. E. Guerchais, *J. Mol. Struct.*, **20**, 169 (1974).
20) A. J. Edwards, D. R. Slim, J. E. Guerchais, and J. Sala-Pala, *J. Chem. Soc., Dalton Trans.*, **1977**, 984.
21) Ref. 13, p. 476.
22) H. Taguchi, K. Isobe, Y. Nakamura, and S. Kawaguchi *Bull. Chem. Soc. Jpn.*, **51**, 2025 (1978).
23) K. Nakamoto, Y. Morimoto, and A. E. Martell, *J. Am. Chem. Soc.*, **83**, 4533 (1961).
24) J. Selbin, H. R. Manning, and G. Cessac, *J. Inorg. Nucl. Chem.*, **25**, 1253 (1963).
25) R. G. Garvey and R. O. Ragsdale, *Inorg. Chim. Acta*, **2**, 191 (1968).
26) C. J. Poppe, J. H. Nelson, and R. O. Ragsdale, *J. Am. Chem. Soc.*, **91**, 610 (1969).
27) J. J. R. Fraústo da Silva and R. Wootton, *Chem. Commun.*, **1969**, 421.
28) M. R. Caira, J. M. Haigh, and L. R. Nassimbeni, *J. Inorg. Nucl. Chem.*, **34**, 3171 (1972).
29) N. S. Al-Niaimi, A. R. Al-Karaghouli, S. M. Aliwi, and M. G. Jalhoom, *J. Inorg. Nucl. Chem.*, **36**, 283 (1974).
30) J. Selbin, G. Maus, and D. L. Johnson, *J. Inorg. Nucl. Chem.*, **29**, 1735 (1967).

Synthesis and Oxygenation Reaction of Cobalt(II) Complexes with Jäger-Type Open-Chain Ligands[1)]

Koichi KUBOKURA, Hisashi OKAWA,* and Sigeo KIDA
Department of Chemistry, Faculty of Science, Kyushu University, Hakozaki, Higashi-ku, Fukuoka 812

(Received December 22, 1977)

Cobalt(II) complexes with Jäger-type open-chain ligands, H_2(J-R) (R=en, pn, ph, and tn), were prepared. It was found that Co(J-en), Co(J-pn), and Co(J-ph) are in low-spin state, and Co(J-tn) in high-spin state with a pseudo-tetrahedral configuration. The formation constant of pyridine adduct of Co(J-en)was spectrophotometrically determined to be 2.70, 2.18, and 1.90 M^{-1} at 0, 20, and 30 °C, respectively. Co(J-en)py forms oxygen adducts, Co(J-en)pyO_2 and [Co(J-en)py]$_2O_2$, in a 1,2-dichloroethane solution at room temperature, exhibiting a characteristic band at 525 nm. The ease of oxygenation and the characteristic absorption in the visible region were interpreted in terms of the electron-withdrawing ability of acetyl group in the ligand.

The copper(II) and nickel(II) complexes of the quadridentate ligands (Fig. 1) were synthesized and characterized by Wolf and Jäger.[2)] These ligands are abbreviated as H_2(J-R) in this paper, where R is en(ethylene), pn(propylene), ph(*o*-phenylene), or tn(trimethylene), representing the bridging chain in Fig. 1. One of the characteristics of Jäger's complexes is the ability of forming a macrocyclic ring when it is reacted with diamines.[2,3)] The cyclization is facilitated by the electron-withdrawning ability of the acetyl group attached to the γ-position of the ligand. The acetyl group of the coordinated ligand is also expected to exert the electron-withdrawing effect on the coordination geometry, the reactivity, and the electronic configuration of the complex. In this study we have prepared cobalt(II) complexes of H_2(J-R) in order to examine their pyridine- and oxygen-adduct formation in relation to the electronic configuration of the cobalt ion, which may adopt either the $(d_{xy})^2(d_{z^2})^1$ or $(d_{xy})^2(d_{yz})^1$ configuration depending on its ligand.

Experimental

Syntheses. Syntheses of H_2(J-R) (R=en, pn, ph, and tn) were carried out following the method of Wolf and Jäger.[2)]

Co(J-en): A mixture of H_2(J-en) (10 g), cobalt(II) acetate tetrahydrate (9 g) and sodium hydroxide (2.9 g) in ethanol (150 ml) was stirred at 60 °C for 1 h in nitrogen atomosphere in order to avoid the reaction with oxygen. After being left to stand overnight, the product was collected and recrystallized from chloroform to give orange needles.

Found: C, 49.89; H, 5.38; N, 8.38%. Calcd for $C_{14}H_{18}N_2O_4Co$: C, 49.86; H, 5.38; N, 8.31%.

Co(J-en)py: Co(J-en) was recrystallized from pyridine in an atmosphere of nitrogen, the complex being obtained as brown crystals.

Found: C, 55.19; H, 5.63; N, 10.16%. Calcd for $C_{19}H_{23}N_3O_4Co$: C, 54.81; H, 5.57; N, 0.10%.

Co(J-en)py$O_2 \cdot 1/4C_6H_5CH_3$: Co(J-en) was dissolved in toluene containing pyridine (*ca.* 5%), and oxygen or air was bubbled through the solution until black-purple prisms separated.

Found: C, 52.53; H, 5.52; N, 8.86%. Calcd for $C_{19}H_{23}N_3O_6Co \cdot 1/4C_6H_5CH_3$: C, 52.88; H, 5.35; N, 8.92%.

Co(J-en): This complex was obtained as orange needles in the same way as that for Co(J-en) except for the use of H_2(J-pn) instead of H_2(J-en).

Found: C, 51.20; H, 5.71; N, 8.03%. Calcd for $C_{15}H_{20}N_2O_4Co$: C, 51.29; H, 5.74; N, 7.97%.

Co(J-pn)py: Co(J-pn) was recrystallized from pyridine to afford the complex as brown crystals.

Found: C, 55.41; H, 5.86; N, 9.67%. Calcd for $C_{20}H_{25}N_3O_4Co$: C, 55.83; H, 5.86; N, 9.77%.

Co(J-pn)py$O_2 \cdot 1/4C_6H_5CH_3$: This complex was obtained as dark purple prisms when oxygen or air was passed through a solution of Co(J-pn) in toluene–pyridine (95:5) mixture.

Found: C, 53.49; H, 5.76; N, 8.66%. Calcd for $C_{20}H_{25}N_3O_6Co \cdot 1/4C_6H_5CH_3$: C, 53.83; H, 5.60; N, 8.66%.

Co(J-ph): This complex was obtained as deep red needles by reacting H_2(J-ph) and cobalt(II) acetate tetrahydrate in ethanol. The product was recrystallized from ethanol.

Found: C, 55.79; H, 5.15; N, 6.85%. Calcd for $C_{18}H_{18}N_2O_4Co \cdot 1/2C_2H_5OH$: C, 55.89; H, 5.18; N, 6.86%.

Co(J-ph)py: This complex was obtained as deep red prisms by recrystallizing Co(J-ph) from pyridine.

Found: C, 59.29; H, 5.04; N, 8.96%. Calcd for $C_{23}H_{23}N_3O_4Co$: C, 59.49; H, 4.99; N, 9.05%.

Co(J-tn): H_2(J-tn), cobalt(II) acetate tetrahydrate, and sodium hydroxide were reacted in ethanol at 70—75 °C to afford the complex as reddish brown crystals. The product was throughly washed with warm ethanol in order to separate sodium acetate.

Found: C, 50.98; H, 5.72; N, 7.89%. Calcd for $C_{15}H_{20}N_2O_4Co$: C, 51.29; H, 5.74; N, 7.97%.

Determination of Pyridine Adduct Formation Constants. Absorption spectra of Co(J-en) in 1,2-dichloroethane containing pyridine were measured at 0, 20, and 30 °C by successively altering the pyridine content (0—1 M), where the concentration of the complex was kept constant (3×10^{-4} M). Equilibrium constants were determined from the absorbance at 375 nm by the method of Marzilli *et al.*[4)]

Determination of Oxygen Adduct Formation Equilibrium. A thermostatted three necked flask (200 ml, filled with dry nitrogen) was fitted with a dropping funnel containing a solution of Co(J-en) (4×10^{-4} M) in deoxygenated 1,2-dichloroethane–pyridine (99.7:0.3), a tube connected to the cell for spectral measurement and a tube connected to the apparatus for controlling the partial pressure of oxygen (Fig. 2). The temperature of the flask was maintained at 0 °C by means of ice–water. The pressure in the flask was then partially reduced and oxygen introduced until it reached 760 mmHg. The partial pressure of oxygen was manometrically determined. A solution of the complex was then dropped into the flask and vigorously stirred for about 15 min. After equilibrium had been reached, the solution was introduced into the cell. Spectrophotometric measurements were carried out at 0 °C.

Other Physical Measurements. Electronic spectra on solid

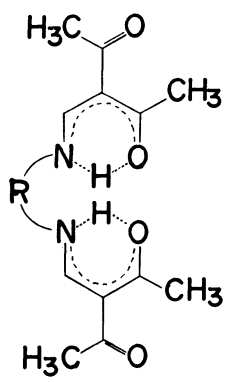

Fig. 1

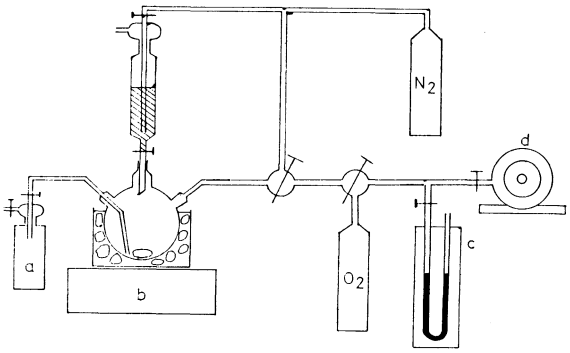

Fig. 2. Apparatus for the spectroscopic measurements under various oxygen pressures. a: Cell, b: magnetic stirrer, c: manometer, d: pump.

and in solution were measured with a Shimazu Multipurpose Spectrophotometer Model MSP-5000. Magnetic susceptibility was measured by the Faraday method, diamagnetic correction being carried out by means of Pascal's constants. ESR spectra (X-band) were measured on powder and in solutions with a JES-ME-3 spectrometer.

Results and Discussion

Effective magnetic moments of Co(J-en), Co(J-pn), Co(J-ph), and Co(J-tn) at room temperature are 2.24, 2.43, 2.56, and 4.36 BM, respectively. It is evident that the complexes except for Co(J-tn) are in low-spin state. ESR spectra of Co(J-R) (R=en, pn, and ph) diluted in the cooresponding Ni(J-R) were measured by X-band at 78 K. The spectra are similar to each other, showing a rhombic pattern. A typical example is shown in Fig. 3a. A band at $g=3.10$ shows an eight-lined hyperfine structure due to $^{59}Co(I=7/2)$ hyperfine coupling, from which A is determined to be 150 G. On the other hand two bands around $g=1.78$—1.85 are not well resolved because of their similar g and A values. The spectra of this type have been interpreted by Nishida and Kida[5] in terms of the $(d_{xy})^2(d_{yz})^1$ ground state for cobalt(II) ion. Electronic spectra of the present complexes exhibit one absorption around 1200 nm characteristic of low-spin cobalt(II) complexes.

The effective magnetic moment of Co(J-tn) is much larger as compared with other complexes, the electronic spectrum showing a complicated pattern with absorption bands at 1550, 695, 570, and 460 nm. Judging

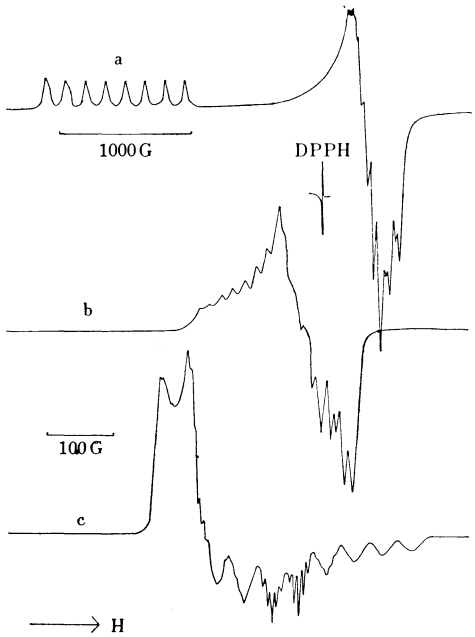

Fig. 3. Esr spectra at 78 K of a) Co(J-en) doped in Ni(J-en), b) oxygenated species of Co(J-en) in dichloroethane-pyridine, and c) pyridine adduct of Co(J-en) in dichloroethane-pyridine.

from the fact that the moment falls in the values of tetrahedral cobalt(II) ions and that the spectrum resembles that of *N,N'*-disalicylidenetrimethylenediaminatocobalt(II),[6] whose configuration was found to be pseudo-tetrahedral, we may conclude that the coordination geometry of Co(J-tn) is pseudo-tetrahedral.

The pyridine adducts Co(J-R)py (R=en, pn, and ph) were obtained when Co(J-R) was recrystallized from pyridine. They are also low-spin complexes (Co(J-en)-py, 1.94; Co(J-pn)py, 2.09; Co(J-ph)py, 2.04 BM). It is supposed that the pyridine adducts have a square-pyramidal structure with a pyridine molecule at the apex.

The orange colored solution of Co(J-en) in 1,2-dichloroethane or toluene containing a small amount of pyridine turned purple when air or oxygen was bubbled through the solution at room temperature. Orange color was recovered when nitrogen was passed through the solution or the solution was warmed at *ca.* 60 °C. It seems that this process is reversible. The purple colored solution exhibited a well defined ESR spectrum indicating two signals of $g_{//}=2.081$ and $g_{\perp}=2.005$ (Fig. 3b). Each signal consists of eight lines due to hyperfine splitting of ^{59}Co nucleus, $A_{//}$ and $A_{\perp}$ being estimated at 18 and 12 G, respectively. The eight-lined hyperfine structure with the very small hyperfine splitting indicates that the 1:1 oxygen adduct is formed in the purple solution.

The equilibrium between Co(J-en) and pyridine was studied in order to elucidate the oxygenation reaction of Co(J-en). A solution of Co(J-en) in 1,2-dichloroethane exhibits an absorption band at 377 nm. By addition of pyridine to this solution the band gradually disappeared and two isosbestic points were observed at 365 and 400 nm (Fig. 4). The spectrum converged when pyridine concentration exceeded 1M.

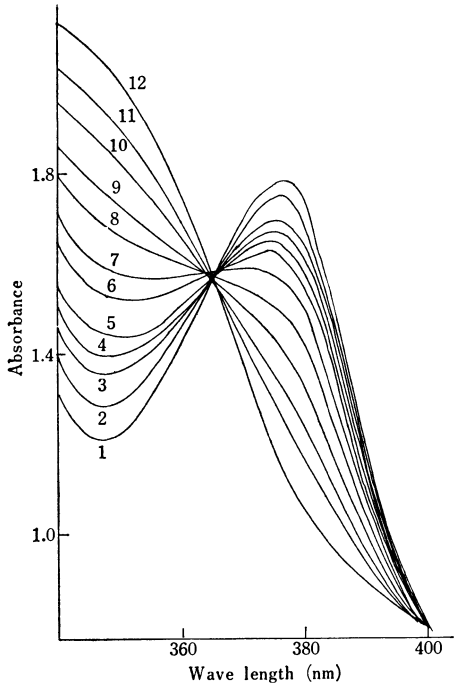

Fig. 4. Electronic spectra of Co(J-en) in dichloroethane with various contents of pyridine: 1), 0; 2), 5×10^{-4}; 3), 1.0×10^{-3}; 4), 1.5×10^{-3}; 5), 2.0×10^{-3}; 6), 3.0×10^{-3}; 7), $4.\times10^{-3}$; 8), 6.0×10^{-3}; 9), 9.0×10^{-3}; 10), 1.5×10^{-2}; 11), 2.4×10^{-1}; 12), 1.0 M. The concentration of Co(J-en) is maintained constant (3×10^{-4} M).

The equilibrium constant of the equation, Co(J-en)+ $n$py$\rightleftarrows$Co(J-en)$(py)_n$, is given by the relation,

$$K_{py} = [Co(J\text{-en})(py)_n]/[Co(J\text{-en})][py]^n. \quad (1)$$

If we denote the absorbances of Co(J-en) at 377 nm in the absence of pyridine, in the presence of large excess of pyridine, and in the presence of proper amount of pyridine by A_0, A_∞, and A, respectively, the equilibrium constant is given by

$$\log K_{py} = \log [(A_0-A)/(A-A_\infty)] - n \log[py]. \quad (2)$$

Absorption spectra of Co(J-en) were determined at 0, 20, and 30 °C at various concentrations of pyridine and $\log [A_0-A/(A-A_\infty)]$ was plotted against log [py] (Fig. 5). The plot gives a straight line with a slope nearly equal to 1. This indicates that the main species formed in the solution is Co(J-en)py and the formation of Co(J-en)$(py)_2$ is negligibly small even at the concentration of pyridine higher than 1M. This seems to contradict the fact that the ESR spectrum of the solution of Co(J-en) in 1,2-dichloroethane–pyridine (99 : 1) at 77.4 K displays the five-lined superhyperfine structure in addition to the eight-lined hyperfine structure, indicating that the unpaired electron interacts with two $^{14}N(I=1)$ nuclei in apical positions (Fig. 3c). This can be explained by assuming that Co(J-en)$(py)_2$ is preferred to Co(J-en)py at liquid nitrogen temperature, while Co(J-en)py is preferred at room temperature. The equilibrium constants ($\log K_{py}$) were evaluated to be 2.70, 2.18, and 1.90 M^{-1} at 0, 20, and 30 °C, respectively, by extraporating log[py] to zero. The equilibrium

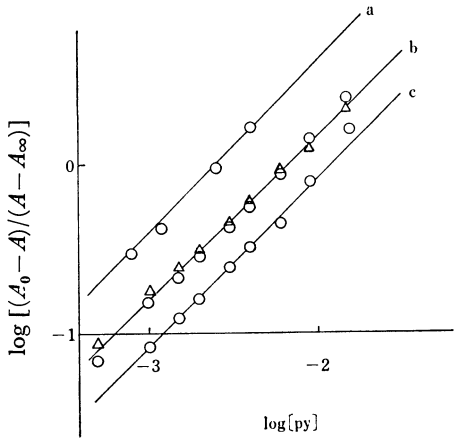

Fig. 5. Plots of $\log [(A_0-A)/(A-A_\infty)]$ *versus* log [py] at a) 0, b) 20, and c) 30 °C, based on the absorbance at 375 nm (○) and at 350 nm (△).

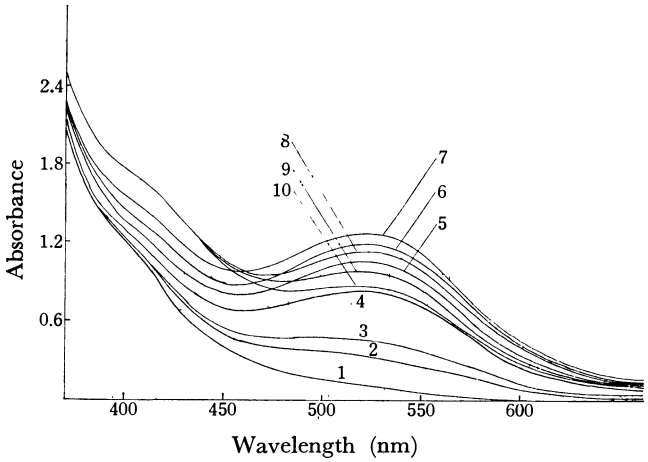

Fig. 6. Electronic spectra of Co(J-en) (4×10^{-4} M) in dichloroethane containing pyridine (0.3%) at 0 °C under various oxygen pressures: 1), 0; 2), 5; 3), 7; 4), 15; 5), 36; 6), 75; 7), 190; 8), 400; 9), 620; 10), 760 mmHg.

constant of Co(J-en)py is a little lower than that of *N,N'*-disalicylidene-*o*-phenylenediaminatocobalt(II).[4]

The electronic spectra of Co(J-en) in 1,2-dichloroethane containing 0.3% pyridine were measured under various oxygen partial pressures. As is shown in Fig. 6 a new absorption was observed when the complex was oxygenated. The intensity of this band reached maximum when the partial pressure of oxygen was *ca.* 200 mmHg and then gradually decreased with the increase in oxygen pressure. This implies that there are at least two oxygenated species in the solution. The species formed under high oxygen partial pressure may be the 1 : 1-type complex, Co(J-en)pyO_2, since this solution exhibits the absorption spectrum similar to the reflectance spectrum of Co(J-en)py$O_2\cdot1/4C_6H_5CH_3$ and ESR spectrum characteristic of the 1:1 oxygenated cobalt(II) complexes. Thus, it can be concluded that the species formed under low oxygen pressure is the 2 : 1-type "peroxo-bridged" complex. The oxygenation reaction of Co(J-en) is represented as follows:

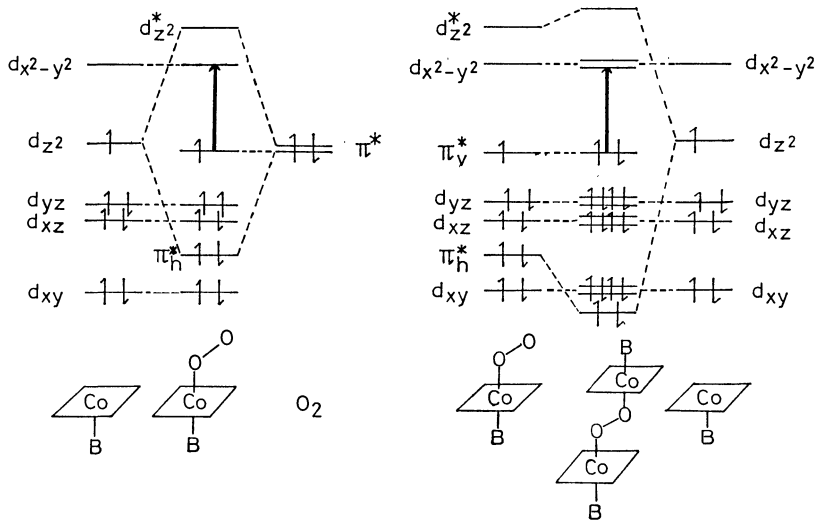

Fig. 7. Qualitative molecular orbital diagrams for Co(J-en)pyO_2 (left) and $[Co(J\text{-en})py]_2O_2$ (right).

$$Co(J\text{-en}) + py \rightleftharpoons Co(J\text{-en})py$$
$$2Co(J\text{-en})py + O_2 \rightleftharpoons [Co(J\text{-en})py]_2O_2$$
$$[Co(J\text{-en})py]_2O_2 + O_2 \rightleftharpoons 2Co(J\text{-en})pyO_2.$$

It is to be noted that Co(J-en)py forms "μ-peroxo-bridged" species even in dilute solution (4×10^{-4}M). In contrast, the formation of the 2:1 oxygen adduct for *N,N'*-disalicylidenealkanediaminatocobalt(II) complexes is negligibly small in dilute solution (less than 10^{-3} M).

Only a few cobalt(II) complexes showing absorption in the visible region upon oxygenation are known.[7,8] Oxygenation reactions of the cobalt(II) complexes with the quadridentate Schiff bases, in general, occur at low temperature.[9] Thus, Co(J-en) is characterized by 1) oxygenation at room temperature, 2) resistance against oxidation to cobalt(III), and 3) a new absorption in the visible region. These characteristics are closely connected with the electron-withdrawing effect of acetyl groups.

The metal-oxygen bond is interpreted in terms of the σ-type overlapping between the d_{z^2} orbital of cobalt(II) and the antibonding orbital (π^*_h) of molecular oxygen.[10] The d_{z^2} orbital in five-coordinated cobalt(II) complexes is generally higher in energy than the antibonding π^* orbital of oxygen. This often causes the irreversible oxidation of cobalt(II) to cobalt(III) during the course of oxygenation. The fact that the oxygen adducts of synthetic iron(II) complexes are obtainable only under a selected conditions, at low temperature and in aprotic solvents, and that the oxygen adduct of *meso*-tetraphenylporphyrinmanganese(II) is barely obtained at low temperature without sixth donor[11] can also be explained in terms of the correlation of the energies of the metal d_{z^2} orbital and the molecular oxygen π^* orbital (electronegativity increases in the order Mn(II)<Fe(II)<Co(II)).

Recently, Pillsbury and Busch[12] studied electrochemical properties of a series of nickel(II) complexes of the fifteen-membered N_4-macrocycles and found that the oxidation potential of Ni(II)→Ni(III) becomes higher when the γ-substituent is replaced by the more electron-attracting group. This suggests that in the present complexes the electron-attracting effect of the acetyl group lowers the energy of the cobalt d-orbitals. In this case the d_{z^2} orbital of Co(J-en)py might be low-lying as compared to the molecular oxygen π^*_h orbital, thereby forming a stable cobalt-oxygen bond even at room temperature without oxidation to cobalt(III) (Fig. 7).

Miskowski *et al.*[13] and McLendon *et al.*[14] studied the characteristic band around 500 nm for the μ-superoxo complex, $[Co(CN)_5\text{–}O_2\text{–}Co(CN)_5]^{5-}$, and the 1:1 oxygen adduct, $[Co(CN)_5O_2]^{3-}$, and assigned this band to the charge-transfer transition from the metal d_π orbital to the π^*_v orbital of oxygen. However, the assignment is invalid for the present complexes, since the π^*_v orbital of $[Co(J\text{-en})py]_2O_2$ is occupied. For the origin of the band at 525 nm of Co(J-en)pyO_2 and $[Co(J\text{-en})py]_2O_2$ it seems reasonable to assign it to the charge-transfer transition from the π^*_v orbital to the vacant $d_{x^2-y^2}$ orbital (Fig. 7). The $\pi^*_v(O_2)\rightarrow d_{x^2-y^2}(Co)$ charge-transfer transition is expected at a wavelength less than 400 nm for most cobalt oxygen carriers.[10] It can be concluded that in the present complexes the electron-attracting effect of the acetyl group lowers the energy of metal d orbital, so that the $\pi^*_v\rightarrow d_{x^2-y^2}$ charge-transfer band appears in the visible region.

References

1) Presented at the 27th Symposium of Coordination Chemistry, Matsumoto, November 28, 1977.
2) L. Wolf and E. Jäger, *Z. Anorg. Allg. Chem.*, **346**, 76 (1966).
3) E. Jäger, *Z. Chem.*, **8**, 30 (1968); *ibid.*, **8**, 392 (1968).
4) L. G. Marzilli, P. A. Marzilli, and J. Helpern, *J. Am. Chem. Soc.*, **93**, 1374 (1971).
5) Y. Nishida and S. Kida, *Chem. Lett.*, **1973**, 57.
6) M. Haribaram and F. L. Urbach, *Inorg. Chem.*, **8**, 556 (1968).

7) G. N. Schrauzer and L. P. Lee, *J. Am. Chem. Soc.*, **92**, 1551 (1970).
8) D. A. White, A. S. Solodar, and M. Baizer, *Inorg. Chem.*, **11**, 2160 (1972).
9) G. McLendon and A. E. Martell, *Coord. Chem. Rev.*, **19**, 1 (1976).
10) B. S. Tovrog, D. T. Kitko, and R. S. Drago, *J. Am. Chem. Soc.*, **98**, 5144 (1976).
11) B. M. Hoffman, C. J. Weschler, and F. Basolo, *J. Am. Chem. Soc.*, **98**, 5473 (1976).
12) D. G. Pillsbury and D. H. Busch, *J. Am. Chem. Soc.*, **98**, 7836 (1976).
13) V. M. Miskowski, J. L. Robbins, I. M. Teitel, and H. B. Gray, *Inorg. Chem.*, **14**, 2318 (1975).
14) G. McLendon, S. R. Pickens, and A. E. Martell, *Inorg. Chem.*, **16**, 1551 (1977).

Molecular and Crystal Structure of Hydrido(tricarbonyl)-bis(triphenylphosphine)manganese(I), $HMn(CO)_3[P(C_6H_5)_3]_2$

Hiroshi HAYAKAWA,** Hiroaki NAKAYAMA,*** Akiko KOBAYASHI, and Yukiyoshi SASAKI*

Department of Chemistry, Research Centre for Spectrochemistry, Faculty of Science, The University of Tokyo, Hongo, Bunkyo-ku, Tokyo 113

(Received December 26, 1977)

The crystal structure of the title compound has been determined by single crystal X-ray diffraction techniques. The compound crystallizes in the space group C2/c with unit-cell dimensions $a=23.54(1)$, $b=9.672(3)$, $c=15.941(7)$ Å, $\beta=114.90(4)°$, and $Z=4$. The manganese atom is octahedrally coordinated by two triphenylphosphines in the trans positions, three equatorial carbonyl ligands, and a hydrido hydrogen. The Mn–H bond has a normal covalent length, 1.46(8) Å. The molecule has C_2 symmetry, and Mn, O(1), C(1), and H_h are on special positions of (0, y, 1/4).

The crystal structure of hydrido(tricarbonyl)-bis(triphenylphosphine)manganese(I), $HMn(CO)_3[P(C_6H_5)_3]_2$, has been studied in order to obtain quantitative data on the Mn–H bond and interactions of hydrido hydrogen with other ligands.

Experimental

The compound was prepared by the reaction of manganese carbonyl and triphenyl phosphine in the presence of metallic sodium in dioxane.[1] The samples used for the X-ray diffraction studies were obtained by recrystallization from a mixture of benzene-petroleum ether. A specimen, a transparent yellow rhombus, stable in the air, of dimensions *ca.* $0.2\times0.2\times0.25$ mm, was used for collection of diffraction intensity data and for measurement of the unit cell dimensions. A Rigaku automated four-circle diffractometer with Mo $K\alpha$ radiation, ($\lambda=0.71069$ Å) monochromated by a graphite crystal was used. Unit cell dimensions were calculated by a least-squares refinement of 14 reflection data obtained for $20°<2\theta<40°$.

Crystal data: $C_{39}H_{31}O_3MnP_2$, $M=664.56$, monoclinic, C2/c, $a=23.54(1)$, $b=9.672(3)$, $c=15.941(7)$ Å, $\beta=114.90(4)°$ $U=3292.1$ Å^3, $D_c=1.34$ g cm^{-3}, $D_m=1.32$ g cm^{-3}, $Z=4$, μ(Mo $K\alpha$)$=6.5$ cm^{-1}.

The diffraction intensities were measured with the 2θ-ω scan technique and 1945 independent reflections for which $|F_{abs}|\geq19$ and $|F_o|\geq3\sigma(|F_o|)$ up to $2\theta=60°$ were obtained at 23 ± 1 °C. The intensity data were corrected for the Lorenz and the polarization effects, but not for absorption. The structure was solved by the heavy atom method. The atomic parameters and the temperature factors were refined by the block-diagonal least-squares method, the function minimized being $\Sigma w(|F_o|-K|F_c|)^2$ where $w=1$ for all the reflections. The atomic scattering factors used were taken from "International Tables for X-Ray Crystallography" Vol. IV (1974).[2]

Two possible space groups, Cc and C2/c, deduced from the extinction rule (hkl: $h+k=2n+1$, $h0l$: $l=2n+1$) gave almost the same R-values (6.6 and 6.4%) for all the non-hydrogen atoms. However, Cc was ruled out since it gave unreasonable bond lengths and angles in the structure of phenyl groups. All the 16 independent hydrogen atoms were found as 0.35—0.52 eÅ^{-3} peaks in difference Fourier maps. The final R-value converged to 4.83%, all the hydrogen atoms being included in the calculation, and no peak higher than 0.26 e Å^{-3} was found in the last difference Fourier maps.

All the calculations were performed on a HITAC 8700/8800 computer at the Computer Centre of the University of Tokyo using a local version of UNICS[3] and the ORTEP[4] program.

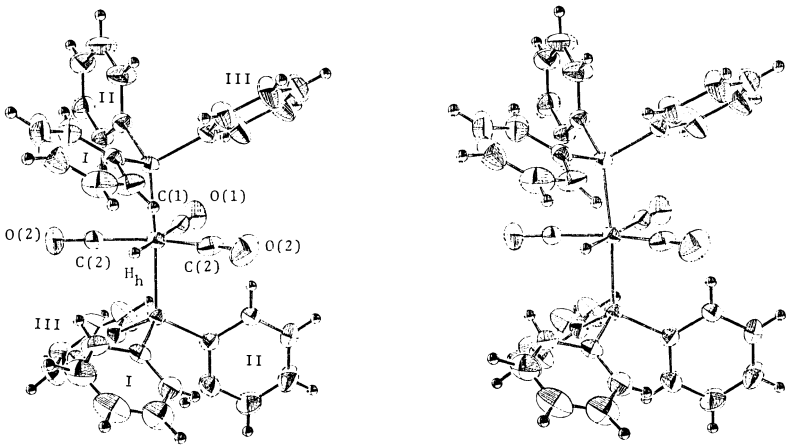

Fig. 1. Stereoscopic drawing of the molecule of $HMn(CO)_3[P(C_6H_5)_3]_2$. The non-hydrogen atoms are represented by their thermal ellipsoids with 50% probability, while the hydrogen atoms are represented by arbitrary spheres.

** National Chemical Laboratory for Industry, Honcho, Shibuya-ku, Tokyo 151.
*** Kagawa Nutrition College, 251 Chiyoda, Sakado, Saitama, 350-02.

Table 1. Final atomic coordinates ($\times 10^4$) and thermal factors ($\times 10^3$ Å^2)

The anisotropic thermal factors are of the form:

$$\exp[-2\pi^2(U_{11}h^2a^{*2}+U_{22}k^2b^{*2}+U_{33}l^2c^{*2}+2U_{12}hka^*b^*+2U_{13}hla^*c^*+2U_{23}klb^*c^*)]$$

The isotropic temperature factor is of the form $\exp[-B(\sin\theta/\lambda)^2]$.

Atom	X	Y	Z	U_{11}	U_{22}	U_{33}	U_{12}	U_{13}	U_{23}
Mn	0	2034(1)	2500	29(0)	27(0)	30(0)	0	15(0)	0
P	918(1)	1823(1)	2368(1)	29(1)	29(1)	30(1)	−2(1)	15(0)	−2(1)
O(1)	0	5077(6)	2500	75(4)	34(3)	50(4)	0	19(3)	0
O(2)	648(2)	1398(5)	4496(3)	61(3)	99(4)	44(2)	1(3)	11(2)	32(2)
C(1)	0	3889(7)	2500	29(4)	36(4)	34(4)	0	7(3)	0
C(2)	400(2)	1684(6)	3730(4)	32(3)	45(3)	47(3)	5(2)	19(2)	14(3)
C(11)	1192(2)	25(5)	2505(4)	39(3)	35(3)	38(3)	4(2)	24(2)	3(2)
C(12)	1756(3)	−408(7)	3196(4)	51(4)	52(4)	42(3)	10(3)	19(3)	3(3)
C(13)	796(3)	−984(6)	1933(4)	35(3)	42(3)	74(4)	0(3)	25(3)	−5(3)
C(14)	1913(3)	−1786(7)	3310(4)	82(5)	67(5)	51(4)	31(4)	29(3)	27(3)
C(15)	967(3)	−2368(6)	2056(5)	64(4)	37(3)	94(5)	−5(3)	44(4)	−8(3)
C(16)	1520(4)	−2774(7)	2740(5)	99(5)	40(4)	85(5)	15(4)	61(4)	19(3)
C(21)	1593(2)	2802(5)	3158(3)	31(2)	39(3)	33(2)	−4(2)	12(2)	−2(2)
C(22)	2146(3)	2830(8)	3040(4)	47(3)	89(5)	50(3)	−15(4)	30(3)	−23(4)
C(23)	1572(2)	3567(6)	3881(4)	36(3)	42(3)	38(3)	−2(2)	18(2)	−6(2)
C(24)	2661(3)	3579(8)	3635(5)	40(3)	106(6)	63(4)	−22(4)	29(3)	−15(4)
C(25)	2089(3)	4312(7)	4472(4)	43(3)	56(4)	37(3)	−8(3)	7(3)	−11(3)
C(26)	2631(3)	4312(8)	4348(4)	43(3)	78(5)	46(3)	−26(3)	11(3)	−8(3)
C(31)	904(2)	2380(5)	1255(3)	35(3)	39(3)	30(2)	−5(2)	19(2)	0(2)
C(32)	992(3)	1513(6)	646(4)	69(4)	50(3)	46(3)	11(3)	33(3)	1(3)
C(33)	786(4)	3762(7)	1024(5)	117(6)	40(4)	67(4)	−1(4)	62(4)	4(3)
C(34)	965(3)	2027(8)	−188(4)	91(5)	67(4)	39(3)	12(4)	38(3)	−4(3)
C(35)	770(4)	4254(7)	200(5)	132(7)	51(4)	98(6)	29(4)	84(6)	36(4)
C(36)	847(3)	3384(7)	−408(4)	74(4)	73(5)	47(3)	13(4)	37(3)	22(3)

Atom	X	Y	Z	B	Atom	X	Y	Z	B
H_h	0	52(9)	250	2.1(1.9)	H(24)	302(3)	353(8)	355(4)	4.9(1.9)
H(12)	202(2)	21(5)	347(3)	1.0(1.1)	H(25)	207(3)	489(7)	492(4)	3.0(1.5)
H(13)	41(2)	−77(6)	158(4)	1.4(1.2)	H(26)	296(3)	478(7)	473(4)	3.1(1.5)
H(14)	228(3)	−198(7)	377(4)	3.8(1.6)	H(32)	107(3)	53(7)	76(4)	3.8(1.7)
H(15)	67(3)	−297(7)	165(4)	3.4(1.5)	H(33)	76(3)	432(7)	144(4)	3.8(1.7)
H(16)	164(2)	−376(6)	289(4)	1.6(1.2)	H(34)	103(3)	150(7)	−56(4)	3.8(1.7)
H(22)	219(2)	236(5)	260(3)	0.7(1.0)	H(35)	66(3)	512(7)	7(4)	3.1(1.5)
H(23)	119(2)	355(5)	398(3)	1.0(1.1)	H(36)	84(3)	366(6)	−92(4)	2.5(1.4)

Table 2. Bond distances (standard deviations in parentheses)

Mn-P	2.267(2) Å	C(21)-C(22)	1.393(9) Å	C(11)-C(12)	1.386(7)		
Mn-C(1)	1.794(7)	C(22)-C(24)	1.389(9)	C(12)-C(14)	1.375(10)	C(31)-C(32)	1.363(9)
Mn-C(2)	1.815(5)	C(24)-C(26)	1.367(11)	C(14)-C(16)	1.373(9)	C(32)-C(34)	1.395(10)
Mn-H_h	1.46(8)	C(25)-C(26)	1.371(11)	C(15)-C(16)	1.357(9)	C(34)-C(36)	1.357(10)
		C(23)-C(25)	1.387(7)	C(13)-C(15)	1.387(8)	C(35)-C(36)	1.353(12)
C(1)-O(1)	1.150(9)	C(21)-C(23)	1.387(8)	C(11)-C(13)	1.391(7)	C(33)-C(35)	1.382(12)
C(2)-O(2)	1.143(7)					C(31)-C(33)	1.383(8)
		C(22)-H(22)	0.88(6)	C(12)-H(12)	0.85(5)		
P-C(11)	1.836(5)	C(23)-H(23)	0.96(6)	C(13)-H(13)	0.87(5)	C(32)-H(32)	0.97(7)
P-C(21)	1.823(5)	C(24)-H(24)	0.90(8)	C(14)-H(14)	0.89(6)	C(33)-H(33)	0.88(7)
P-C(31)	1.842(6)	C(25)-H(25)	0.92(7)	C(15)-H(15)	0.93(6)	C(34)-H(34)	0.84(8)
		C(26)-H(26)	0.88(6)	C(16)-H(16)	0.99(6)	C(35)-H(35)	0.88(7)
						C(36)-H(36)	0.85(7)

Results and Discussion

The atomic parameters and standard deviations are given in Table 1. The F_o-F_c Table is kept at the Office of the Chemical Society of Japan as Document No. 7825.

The molecular geometry $HMn(CO)_3[P(C_6H_5)_3]_2$ is shown in Figs. 1 and 2, the packing in the unit cell in Fig. 4. The molecule has C_2 symmetry, Mn, O(1), C(1), and H_h lying on special positions of (0, y, 1/4). The manganese atom is octahedrally coordinated by one hydrogen (H_h), three carbonyl ligands on the equator, and two phosphorus atoms of triphenylphosphine in trans positions. However, the octahedron is deformed. The eight atoms, Mn, H_h, two C(2), two O(2), C(1), and O(1), lie exactly on a plane, $0.99790x-0.06478z+1.90852=0$, and six atoms, Mn, H_h, C(1), O(1), and two P, form another plane, $-0.08441x-0.99643z+3.4603=0$; x, y, and z, are orthogonal coordinates in Å along a, b, and c^*, respectively. These two planes are almost perpendicular to each other. The two phosphorus atoms and two carbonyl ligands bend down toward H_h to deform the octahedron, the angle Mn–C(2)–O(2) not being linear. The bond distances and angles are given in Tables 2 and 3, respectively.

The Mn–H_h distance was determined to be 1.46(8) Å. The length is quite normal as a covalent bond length as compared to the value calculated from the covalent atomic radii of manganese (1.171 Å) and hydrogen (0.30 Å).[5] Concerning the Mn–H bond length, very few data are available. In the case of $HMn(CO)_5$, the distance 1.601(16) Å was found by neutron diffraction techniques.[6] The value 1.5 Å was reported in the crystal structure determination of $HMn(CO)_3[PCH_3(C_6H_5)_2]_2$.[7]

However, this value does not seem to be refined by the least-squares method. Interactions of the hydrido

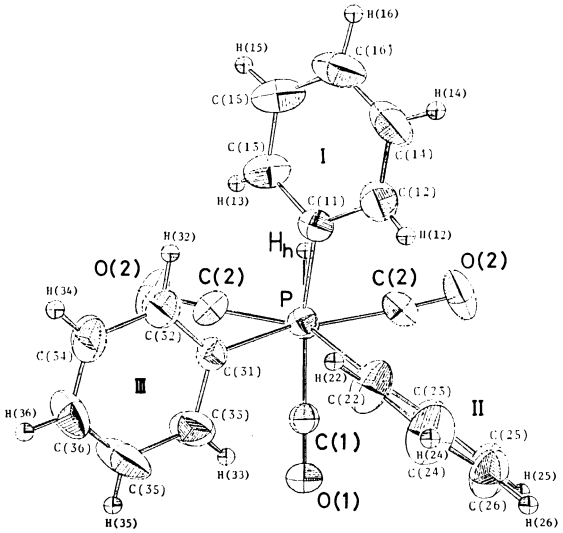

Fig. 2. Conformation of one of the triphenylphosphine ligand in the molecule of $HMn(CO)_3[P(C_6H_5)_3]_2$.

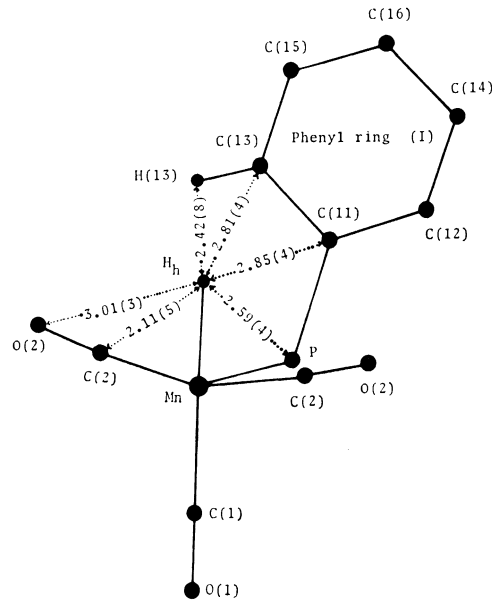

Fig. 3. Short contacts (in Å) around the hydrido hydrogen.

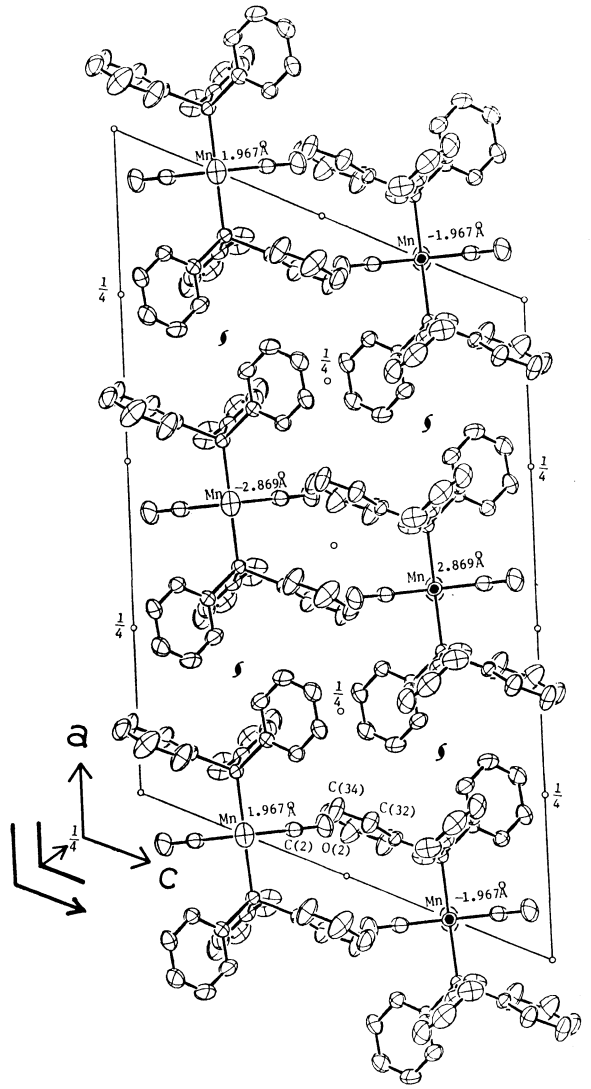

Fig. 4. Projection of the crystal structure along the b axis. The y coordinates (Å) of the Mn atoms are indicated.

Table 3. Bond angles (standard deviations in parentheses)

H_h	- Mn	- C (1)	180 (3)°	Mn	- C (2)	- O (2)	176.8 (5)	C (21)	- C (23)	- C (25)	120.9 (5)
H_h	- Mn	- C (2)	79 (3)	P	- C (11)	- C (12)	123.5 (4)	C (22)	- C (24)	- C (26)	120.2 (7)
P	- Mn	- P	169.66 (8)	P	- C (11)	- C (13)	118.8 (4)	C (23)	- C (25)	- C (26)	120.4 (6)
P	- Mn	- C (1)	95.2 (3)	P	- C (11)	- C (16)	175.1 (3)	C (24)	- C (26)	- C (25)	119.8 (6)
P	- Mn	- C (2)	90.1 (2)	C (12)	- C (11)	- C (13)	117.6 (5)	P	- C (31)	- C (32)	124.1 (5)
Mn	- P	- C (11)	112.1 (2)	C (11)	- C (12)	- C (14)	120.8 (5)	P	- C (31)	- C (33)	117.4 (5)
Mn	- P	- C (21)	118.5 (2)	C (12)	- C (14)	- C (16)	121.2 (6)	C (32)	- C (31)	- C (33)	118.6 (6)
Mn	- P	- C (31)	115.6 (2)	C (13)	- C (15)	- C (16)	121.0 (6)	C (31)	- C (32)	- C (34)	120.0 (6)
C (11)	- P	- C (21)	104.5 (2)	P	- C (21)	- C (22)	120.6 (5)°	C (31)	- C (33)	- C (35)	120.5 (8)
C (11)	- P	- C (31)	104.7 (3)	P	- C (21)	- C (23)	121.7 (4)	C (32)	- C (34)	- C (36)	120.9 (7)
C (21)	- P	- C (31)	99.8 (2)	C (22)	- C (21)	- C (23)	117.7 (5)	C (33)	- C (35)	- C (36)	120.6 (7)
Mn	- C (1)	- O (1)	179.9 (7)	C (21)	- C (22)	- C (24)	121.0 (6)	C (34)	- C (36)	- C (35)	119.4 (7)

Table 4. Best planes of three phenyl groups expressed by the formulae, $Ax+By+Cz+D=0$, and deviations of carbon atoms from the planes. x, y, and z are orthogonal coordinates in Å along a, b, and c^*

Phenyl ring	A	B	C	D
(I)	0.77429	0.09698	−0.62535	1.39021
(II)	−0.08213	0.79778	−0.59732	0.69332
(III)	−0.87985	−0.18445	−0.43799	2.35041

Phenyl ring	(I)	(II)	(III)
C-1	−0.0010 Å	−0.0058 Å	0.0000 Å
C-2	−0.0007	0.0040	−0.0025
C-3	0.0029	0.0037	0.0070
C-4	−0.0023	0.0009	−0.0018
C-5	−0.0021	0.0010	−0.0115
C-6	0.0032	−0.0036	0.0089

hydrogen with the surrounding atoms are discussed below.

The atom C(1) which is in the position trans to H_h is nearer to the manganese atom than the two other carbon atoms C(2) in *cis* positions, the C(1)–O(1) bond being shorter than C(2)–O(2). As shown in Fig. 2, three carbon atoms, C(11), C(21), and C(31), attached to the phosphorus do not form an equilateral triangle. The conformation of the triphenylphosphine ligand looks like a propeller with three blades having different pitches. The angles between the $Mn(CO)_3H$ plane and the three phenyl rings, (I), (II), and (III), are 35.6, 92.5, and 148°, respectively.

The phenyl ring (I) is nearest to H_h, having hardly any van der Waals contact with any carbonyl or other ligand. The bond angle Mn–P–C(11) (Table 3) is the smallest among the corresponding angles of three phenyl groups, the phosphorus atom P being bent towards H_h. Moreover, (I) is also declined to the same direction by 5°, the angle between the plane of the phenyl ring (I) and the P–C(11) vector being 175°. The phenyl group (II) seems to be balanced between carbon atoms of two carbonyl ligands, the distances C(1)–C(23) and C(2)–C(23) being 3.43 and 3.23 Å, respectively. In the case of the phenyl ring (III), a fairly short distance of 3.15 Å is found between C(31) and C(2), and an oxygen atom of the neighbor molecule O(2) is close to H(32) with the distance of 2.61 Å. These interactions might have stabilized the phenyl group (III) at the present position.

Figure 3 shows the interatomic distances from the hydrido hydrogen to the surrounding atoms. The distance to H(13) agrees with the sum of the van der Waals radii of two hydrogen atoms. The H_h–C(11) and H_h–C(13) distances are understood as the sum of the half thickness of an aromatic ring and the van der Waals radius of hydrogen atom. The two C(2) atoms of carbonyl groups and the two phosphorus atoms of triphenylphosphine ligands are found close to H_h, the distances being 2.11 and 2.59 Å, respectively. Such short contacts have been reported also in $HMn(CO)_5$[6] and $HMn(CO)_3[PCH_3(C_6H_5)_2]_2$.[7] The short contacts shown in Fig. 3 might give rise to the stability of the present hydrido complex.

The equations of the best planes for the three aromatic rings and deviations of each carbon atoms from these planes are given in Table 4. The average of all the C–C bonds is 1.378(13) Å and that of the C–H bonds 0.90(5) Å. The C–C–C angles are 120° within 1.2°. It is worthwhile to note that C(33), C(35), and C(36) having the largest deviations from the best plane (III) for an unknown reason have also the largest temperature factors (Fig. 2). Van der Waals contacts were found between O(2)···H(32) [2.61(7) Å] and H(25)···H(12) [2.54(10) Å]; there is no other intermolecular distance smaller than 2.7 Å. The crystal volume per each triphenylphosphine molecule is 411.6 Å^3. This volume is near 418 Å^3 of $Os(CO)_3[P(C_6H_5)_3]_2$[8], 423 Å^3 of $Mn(NO)(CO)_2[P(C_6H_5)_3]_2$[9] and $Ir(CO)Cl(SO_2)[P(C_6H_5)_3]_2$,[10] and 404 Å^3 of $ReNCl_2[P(C_6H_5)_3]_2$.[11] Triphenylphosphine itself has a molecular volume of 364 Å^3 in its crystals, the ligand occupying about 90% of the space in the solid of the present complex.

References

1) H. Nakayama, to be published.
2) "International Tables for X-Ray Crystallography," Kynoch Press, Vol. IV, Birmingham (1974).
3) The Universal Crystallographic Computation Program System, Crystallographic Society of Japan (1967).

4) C. K. Johnson, Oak Ridge National Laboratory Report ORNL-3794.
5) L. Pauling, "The Nature of the Chemical Bond and the Structure of Molecules and Crystals," Cornell University Press, Ithaca, N. Y. (1960), pp. 227, 256.
6) S. J. LaPlaca, W. C. Hamilton, J. A. Ibers, and L. Davidson, *Inorg. Chem.*, **8**, 1928 (1969).
7) M. Laing, E. Singleton, and G. Kruger, *J. Organomet. Chem.*, **54**, C30 (1973).
8) J. K. Stalick and J. A. Ibers, *Inorg. Chem.*, **8**, 419 (1969).
9) J. H. Enemark and J. A. Ibers, *Inorg. Chem.*, **6**, 1575 (1967).
10) S. J. LaPlaca and J. A. Ibers, *Inorg. Chem.*, **5**, 405 (1966).
11) R. J. Doedens and J. A. Ibers, *Inorg. Chem.*, **6**, 204 (1967).

Nondispersive and Dispersive Atomic Fluorescence Spectrometry of Arsenic by Utilizing the Arsine-generation Technique

Taketoshi NAKAHARA,* Toshiaki TANAKA, and Sôichirô MUSHA

Department of Applied Chemistry, College of Engineering, University of Osaka Prefecture, Mozu-umemachi, Sakai 591

(Received January 5, 1978)

Atomic fluorescence spectrometry with nondispersive and dispersive systems by utilizing the arsine-generation technique is described for the determination of arsenic at the nanogram level, where the premixed argon (entrained air)– and nitrogen(entrained air)–hydrogen flames and a microwave-excited electrodeless discharge lamp were used. For the low-temperature flames, a newly designed burner has been constructed. The best detection limits obtained for arsenic are 2.3 ng in mass and 0.12 ppb in concentration with a nondispersive system in argon(entrained air)–hydrogen flame. Linear analytical working curves covering the mass range of arsenic from 30 ng to around 1000 ng have been obtained with nondispersive and dispersive systems at 193.7 and 197.2 nm in both the hydrogen flames. Several elements including other hydride-forming elements, such as antimony, bismuth, selenium, and tellurium, have caused a decrease in fluorescence signals. The present method, with the most sensitive nondispersive system and argon(entrained air)–hydrogen flame, can be applied to the determination of trace amounts of arsenic in wastewaters.

In atomic fluorescence spectrometry by the direct nebulization of solutions into flame, some authors[1–6] have reported detection limits of 0.2—25 ppm of arsenic with a dispersive system, mostly at 189.0, 193.7, 197.2, and 235.0 nm, while others[7–9] have obtained the detection limits of 0.3—6 ppm of arsenic with a nondispersive system. For both systems they have used an arsenic electrodeless discharge lamp as the radiation source and air–acetylene, oxygen–, argon(entrained air)–, and nitrogen(entrained air)–hydrogen flames as the atom reservoir. Dagnall *et al.*[10] have applied the atomic fluorescence method to the determination of arsenic in nickel-base alloys and obtained a detection limit of 1.4 ppm of arsenic at 193.7 nm with a nitrogen (entrained air)–hydrogen flame and an arsenic electrodeless discharge lamp.

On the other hand, in atomic absorption spectrometry the sensitivity for arsenic has been remarkably improved by using an arsine-generation technique based on the reduction of arsenic to arsine and the introduction of the generated arsine into an atom reservoir (flame, heated quartz tube, or heated graphite furnace). As the reductant, zinc,[11–17] sodium tetrahydroborate,[17–24] and titanium trichloride and magnesium rod[25] have been used. Especially for arsenic, zinc has been recommended as a reductant.[15,17]

Tsujii and Kuga[26] have reported a detection limit of 2 ng of arsenic by nondispersive atomic fluorescence spectrometry with an arsine-generation technique in which arsenic is reduced by zinc to arsine. Thompson[27] has described a dispersive atomic fluorescence method at 193.7 nm in conjunction with an arsine-generation technique using sodium tetrahydroborate as a reductant; by using this method he obtained a detection limit of 0.1 ng of arsenic for a sample volume of 1.0 ml.

Recently the present authors have designed and constructed an atomic fluorescence spectrometer which can be used with both dispersive and nondispersive systems. They have demonstrated the performance of the newly constructed spectrometer by measuring mercury atomic fluorescence signals with dispersive and nondispersive systems combined with the cold-vapor technique.[28] This paper will describe the nondispersive and dispersive atomic fluorescence spectrometric determination of arsenic by using the arsine-generation technique and the premixed argon(entrained air)– and nitrogen(entrained air)–hydrogen flames produced with a new burner constructed in this laboratory. The interference effects of acids and diverse elements on the fluorescence signals of arsenic were examined. The most sensitive nondispersive atomic fluorescence method was also applied to the determination of arsenic in wastewater samples with satisfactory results.

Experimental

Reagents. All the reagents used were of an analytical reagent grade. The stock solution of arsenic, 1000 ppm, was prepared by dissolving 1.320 g of diarsenic trioxide in 20 ml of 2.5 mol dm^{-3} sodium hydroxide and by diluting to 1000 ml with a 5% sulfuric acid–20% hydrochloric acid solution. The diluent for the stock solution was a 5% sulfuric acid–20% hydrochloric acid solution. Diluted arsenic standard solutions were prepared immediately before use by dilution of the stock solution with the diluent.

Also used were: tin(II) chloride (10% $SnCl_2 \cdot 2H_2O$ in 6 mol dm^{-3} hydrochloric acid), potassium iodide (20% in distilled water), and zinc tablets. Zinc tablets were prepared as has previously been described.[17] Each tablet was 10 mm in diameter, 3 mm thick, and approximately 0.6 g in weight.

Apparatus. All the measurements were made with a laboratory-constructed atomic fluorescence spectrometer,[28] equipped with a Nippon Jarrell-Ash Model ASD-1A arsenic measurement unit and a newly constructed burner (*vide infra*). The atomic fluorescence instrument used contained the specific components shown in Table 1.

Burner. The present authors have reported the performance of a "multi-flame" burner of the slot type for atomic absorption spectrometry.[29] Based on a similar concept for premixed hydrogen flames, we designed and constructed a nitrogen-sheathed, water-cooled burner which can produce premixed argon (entrained air)– and nitrogen(entrained air)–hydrogen flames for atomic fluorescence measurements; the burner is shown in Fig. 1. It consists of a burner top and its holder, both of which are made of brass. To ensure the adequate entrainment of secondary air, the outer surface of the nozzle is tapered. Inside the burner is placed a porous

ceramic plate which contains about 50 holes(0.5 mm in diameter) per cm^2 and is 1.25 cm thick, to maintain the stability of the hydrogen flames of a higher burning velocity. In this study the new burner was fitted to a Techtron nebulizer chamber. A schematic diagram of the apparatus used in this work is shown in Fig. 2. The right half of the figure represents a nondispersive atomic fluorescence spectrometer. For a dispersive measuring system, the photomultiplier and its housing (10 in Fig. 2) are replaced by a monochromator equipped with a photomultiplier. The fluorescence radiation is measured at right angles to the axis of the optical path from the light source to the flame.

Procedures. The optimum instrumental variable settings used for the atomic fluorescence measurements are shown in Table 2. The arsine generated by the procedure previously reported for the atomic absorption spectrometry of arsenic[17] was introduced into premixed argon(entrained air)- and nitrogen(entrained air)-hydrogen flames in which argon and nitrogen respectively were used as the carrier gas as well as the auxiliary gas. The fluorescence signal was recorded on the pen recorder for the peak-height measurement throughout this work.

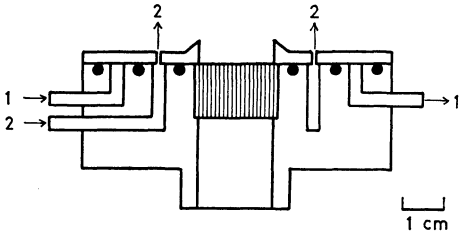

Fig. 1. Cross-sectional diagram of nitrogen-sheathed, water-cooled burner for atomic fluorescence measurements with premixed argon (entrained air)- and nitrogen (entrained air)-hydrogen flames.
1: Cooling water, 2: sheath gas, ▥: ceramic plate, ●: O-rings.

Table 1. Experimental components of the atomic fluorescence instrument used in this study

Item	Description (model No.) and supplier
Power stabilizer	A-133, NF Circuit Design Block
Light source and power	
Lamp	As electrodeless discharge lamp, EMI
Power supply	Microtron 200, Electro-Medical Supplies
Resonant cavity	Model 211 L, Electro-Medical Supplies
Light chopper	Laboratory-made
Lens	30-mm diameter, 75-mm focal length, quartz
Burner	Laboratory-made
Monochromator	JE-30, Nippon Jarrell-Ash
Photomultiplier	R-166 ("solar-blind" type, for nondispersive system) and R-106 UH (for dispersive system), Hamamatsu TV
High-voltage power supply for photomultiplier	412 B, John-Fluke
Preamplifier	JP 406, Nippon Jarrell-Ash
Operational amplifier	2F/4539B, Akikoh Electric
Power supply	±15 V, Laboratory-made
Lock-in amplifier	572B, NF Circuit Design Block
Oscilloscope	CS-1351, Trio
Recorder	QPD_{54}, Hitachi
Arsine-generating unit	ASD-1A, Nippon Jarrell-Ash

Results and Discussion

Atomic Fluorescence Spectrum of Arsenic. The spectral characteristics of all 15 lines of arsenic have been found by the solution-nebulization technique to exhibit atomic fluorescence in air–acetylene and argon- and nitrogen–hydrogen flames.[1] With the dispersive system, the spectral characteristics of the emission and fluorescence of all 15 lines of arsenic were examined in this study. The results obtained are shown in Table 3. With the present instrument, the 193.7 nm line gave the highest sensitivity in both the hydrogen flames. The values shown in Table 3 were not corrected for the photomultiplier spectral response.

Effect of Microwave Power. The present authors have previously described the relationship between the emission intensity of the arsenic 193.7 nm line and the microwave power applied for an arsenic electrodeless discharge lamp used for atomic absorption spectrometry.[30] In atomic fluorescence spectrometry for arsenic with the same arsenic electrodeless discharge lamp, the effect of microwave power ranging 18 to 40 W on the fluorescence signals was examined with the dispersive system at 193.7 nm. The results obtained were analogous to those previously reported in atomic absorption spectrometry.[30] This phenomenon can be easily explained on the base of the theoretical concept that the atomic fluorescence energy is directly proportional to the spectral irradiance of the light source.[31–33] The optimum power used is shown in Table 2.

Effect of Flame Composition and Flame Height. Tsujii and Kuga[26] have reported that the flame composition was not a critical factor with regard to the fluorescence

Table 2. Optimum experimental conditions

Microwave power applied	24 W (Incident power, 35 W; Reflected power, 11 W)
RC time constant	1.0 s
High voltage for photomultiplier	700 V
Load resistance	470 kΩ
Modulation frequency	90 Hz (for nondispersive system) and 240 Hz (for dispersive system)
Volume of sample	20 ml
Zinc tablet	One piece (Zn 0.6 g)
Potassium iodide solution	1.0 ml
Tin(II) chloride solution	1.0 ml
Hydrogen flow rate	3.6 l min^{-1}
Argon or nitrogen flow rates	Carrier 4.0 l min^{-1} Auxiliary 2.0 l min^{-1}
Nitrogen flow rate for flame sheathing	1.0 l min^{-1}
Flame height	4 cm (for argon (entrained air)-hydrogen flame) and 5 cm (for nitrogen (entrained air)-hydrogen flame)

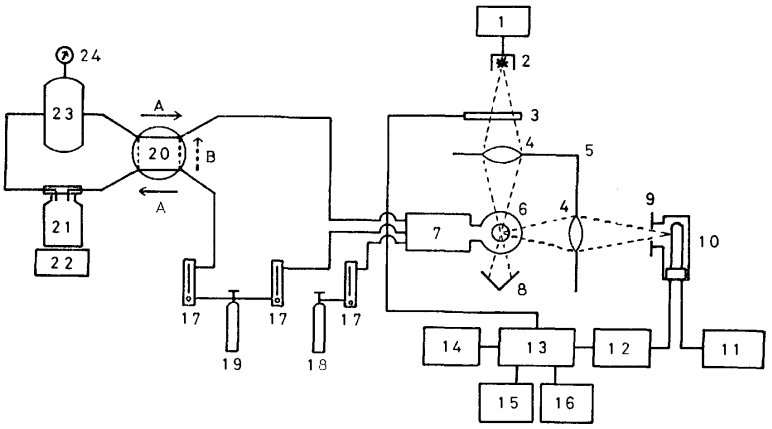

Fig. 2. Schematic diagram of the nondispersive atomic fluorescence instrument employed in this work.
1: Microwave generator, 2: electrodeless discharge lamp and resonant cavity, 3: light chopper, 4: lenses, 5: panel, 6: burner, 7: nebulizer chamber, 8: light trap, 9: diaphragm, 10: photomultiplier and its housing, 11: high-voltage power supply, 12: preamplifier, 13: lock-in amplifier, 14: line-power stabilizer, 15: oscilloscope, 16: pen recorder, 17: flowmeters, 18: hydrogen cylinder, 19: argon or nitrogen cylinder, 20: four-way stopcock, 21: reaction flask, 22: magnetic stirrer, 23: collection vessel, 24: pressure gauge, A: "sweep" gas flow, B: "by-pass" gas flow.

TABLE 3. ATOMIC FLORESCENCE SPECTRUM OF ARSENIC

Wavelength (nm)	Emission intensity of As electrodeless discharge lamp[a]	Fluorescence signal[b]	
		Ar(air)-H_2[c]	N_2(air)-H_2[d]
189.0[e]	7.9	13.0	5.6
193.7[e]	14.0	22.0	6.2
197.2[e]	14.7	18.0	5.0
228.8[f]	48.0	0.5	0.2
235.0[f]	54.0	0.8	1.5
238.1[g]	88.5	1.5	1.3
243.7[g]	20.5	1.0	0.6
245.7[g]	80.0	2.6	3.1
249.3[g]	62.5	4.2	5.0
274.5[f]	8.5	N. D.[h]	N. D.[h]
278.0[f]	25.0	1.2	0.8
286.0[f]	17.2	1.0	0.7
289.9[f]	3.8	N. D.[h]	N. D.[h]
303.3[g]	13.0	1.5	1.0
312.0[g]	5.2	N. D.[h]	N. D.[h]

a) Scale reading for each line from the lamp discharged at 24 W. b) Scale reading for 100-ng arsenic at the same measuring conditions. c) Argon (entrained air)-hydrogen flame. d) Nitrogen (entrained air)-hydrogen flame. e) Resonance fluorescence. f) Thermally-assisted direct-line fluorescence. g) Direct-line fluorescence. h) Not detected.

intensity, but that the noise level remarkably affected by the flame composition in the argon(entrained air)-hydrogen flame.

In argon(entrained air)- and nitrogen(entrained air)-hydrogen flames, the effects of the flame composition and the flame height on the fluorescence signals of arsenic were examined over the range of hydrogen flow rate of 1.8—4.5 l min^{-1}, with the flow rate of argon or nitrogen kept constant. The results obtained in

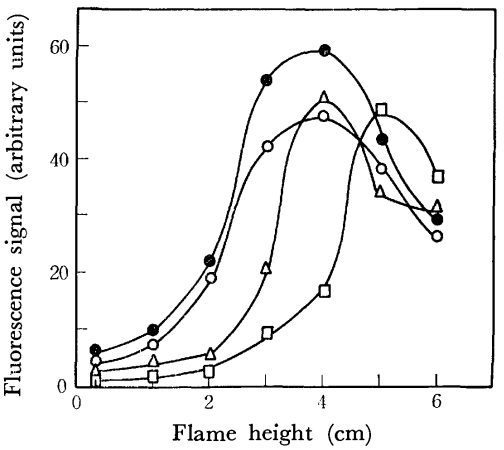

Fig. 3. Effect of flame composition and flame height on the fluorescence measurements.
Flame: argon (entrained air)-hydrogen flame, arsenic: 400 ng, argon flow rate for carrier gas: 4.0 l min^{-1}, argon flow rate for auxiliary gas: 2.0 l min^{-1}, hydrogen flow rates: ○ 1.8 l min^{-1}, ● 2.7 l min^{-1}, △ 3.6 l min^{-1}, □ 4.5 l min^{-1}.

the argon(entrained air)-hydrogen flame with the nondispersive system are shown in Fig. 3. Similar results were obtained in the nitrogen(entrained air)-hydrogen flame. As is shown in Fig. 3, the fluorescence signals varied remarkably with the variations in the flame composition and the flame height above the burner top. Taking account of noise levels, the optimum conditions for the flames were determined to be as is shown in Table 2. The flow rate of nitrogen as a sheath gas was fixed at 1.0 l min^{-1} throughout this work, because the flow rate did not affect the fluorescence signals in the range of 1.0 to 5.0 l min^{-1}.

Effect of Flow Rate of Carrier Gas. The fluorescence signals with the nondispersive system increased

Table 4. Effect of various other elements

Element[a]	Relative fluorescence signal[b]	Reaction time for 30 kPa (s)
None	1.00	90
B[c]	1.15	90
V[d]	1.07	75
Rb[e]	1.07	100
W[f]	1.07	75
In[e]	1.04	120
K[e]	1.02	90
Cu[g]	1.02	35
Au[e]	1.01	60
Si[f]	1.01	75
Y[g]	0.99	115
Mn[e]	0.98	120
Mg[e]	0.97	90
Cs[e]	0.94	80
Na[e]	0.94	95
Zn[e]	0.93	75
Ag[g]	0.90	40
Co[e]	0.89	20
Be[h]	0.89	80
Fe[e]	0.88	60
Ni[e]	0.88	20
Tl[g]	0.87	120
Zr[e]	0.86	65
Cd[e]	0.85	90
Bi[g]	0.84	300
La[e]	0.81	100
Ca[e]	0.81	90
Al[e]	0.80	80
Cr[e]	0.78	60
Se[f]	0.76	40
Li[e]	0.72	80
Ba[e]	0.71	60
Sb[e]	0.51	10
Mo[d]	0.47	90
Hg[e]	0.44	165
Te[e]	0.41	20
Pt[e]	0.07	10
Pd[e]	0.05	20

a) The amount added, 400 μg. b) Relative to atomic fluorescence signal for 400-ng arsenic. c) Added as boric acid. d) Added as ammonium vanadate or molybdate respectively. e) Added as chloride. f) Added as sodium tungstate, silicate, or selenite respectively. g) Added as nitrate. h) Added as sulfate.

with an increase in the flow rates of the carrier gas up to 4.0 l min^{-1} when the total flow rate of argon or nitrogen as the carrier and auxiliary gases was kept constant, but the presence of carrier gas for over 5.0 l min^{-1} caused a gradual decrease in the reproducibilities of the fluorescence signals. Below 3.0 l min^{-1} of the carrier gas the fluorescence signal was broadened because of the slower introduction of arsine into the flame. The optimum flow rate is shown in Table 2.

Effect of Pressure in Collection Vessel. The pressure of the arsine and hydrogen generated in the reaction flask (21 in Fig. 2) was indicated with a pressure gauge (24 in Fig. 2). The effect of the pressure in the range from 10 to 40 kPa on the fluorescence signals for arsenic was examined with the nondispersive system in the argon(entrained air)–hydrogen flame. The optimum pressure was found to be 30 kPa. The pressure increased proportionally with an increase in the reaction time. In this work it was considered to be preferable to allow the reaction to continue until the pressure had attained to 30 kPa rather than to monitor the reaction time. At higher pressures, the precision in the fluorescence measurements became poor because the higher pressures resulted in unstability in the flame because of the disturbance of the carrier gas stream.

Effect of Acids. The effects of nitric, perchloric, phosphoric, and sulfuric acids in the range from 0.05 to 2.0 mol dm^{-3} on the fluorescence signal of arsenic were examined. As a consequence, it was found that perchloric, phosphoric, and sulfuric acids did not interfere, but nitric acid caused a large depressing interference. This interference may be attributed to the strong oxidizing action of nitric acid depressing the generation of arsine.

Effect of Various Other Elements. With the arsine-generation technique, most of the interference might be related to the process of reducing arsenic to arsine in both the atomic absorption and atomic fluorescence methods. The effects of 37 elements at the level of a 1000-fold excess were examined in a solution containing 400 ng of arsenic with the nondispersive system and the argon(entrained air)–hydrogen flame. The results are summarized in Table 4, in which the reaction time required to reach a pressure of 30 kPa is also shown for the elements investigated. A large number of elements including other hydride-formimg elements, such as antimony, bismuth, selenium, and tellurium, had great depressing interferences.

It has been reported that bismuth fluorescences at 206.170, 269.7, and 302.5 nm excited with the iodine line at 206.163 nm can be observed.[34,35] A strong emission of the iodine line was observed in the arsenic electrodeless discharge lamp used. However, no enhancement in the fluorescence signal with the nondispersive system was observed in the presence of bismuth. This means that hardly no bismuth hydride(bismuthine) is produced by the zinc reduction method under the conditions suitable for arsenic.

Analytical Working Curve, Sensitivity, and Precision. Analytical working curves were obtained by using arsenic standard solutions freshly prepared from a 1000 ppm stock solution with both the nondispersive and dispersive systems in both the hydrogen flames. Figure 4 shows the analytical working curves thus obtained. The lower limits of the linear range in the curves were severely restricted by the relatively high background due to the reagent blank, as is shown in Fig. 4. The reagent blank was approximately 20 ng of arsenic in 20 ml of a sample. As has previously been reported by Dagnall *et al.*,[1] the 193.7 nm line was more sensitive at lower concentrations of arsenic than the 197.2 nm line.

The detection limits, expressed by the mass or concentration which produces a fluorescence signal equal

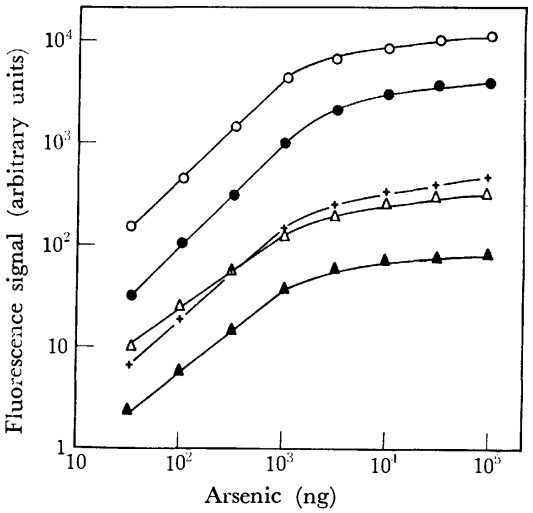

Fig. 4. Analytical working curves for arsenic in atomic fluorescence spectrometry.
○: With nondispersive system in argon (entrained air)-hydrogen flame, ●: with nondispersive system in nitrogen (entrained air)-hydrogen flame, △: with dispersive system at 193.7 nm in argon (entrained air)-hydrogen flame, +: with dispersive system at 197.2 nm in argon (entrained air)-hydrogen flame, ▲: with dispersive system at 193.7 nm in nitrogen (entrained air)-hydrogen flame.

TABLE 5. DETECTION LIMITS OF ARSENIC BY ATOMIC FLUORESCENCE

Flame	Detection limit[a]			
	Nondispersive system		Dispersive system[b]	
	ng	ppb	ng	ppb
Ar(air)-H_2[c]	2.3	0.12	15.2	0.76
N_2(air)-H_2[d]	4.8	0.24	31.1	1.56

a) Signal-to-noise ratio=2. b) At 193.7 nm. c) Argon (entrained air)-hydrogen flame. d) Nitrogen (entrained air)-hydrogen flame.

to twice the noise level(signal-to-noise ratio=2), are shown in Table 5. The detection limits with the dispersive system were obtained at 193.7 nm.

Standard solutions containing 30, 100, 300, and 1000 ng of arsenic were prepared, and the fluorescence signals were repeatedly measured with the nondispersive system in the argon(entrained air)-hydrogen flame. The relative standard deviations, calculated from seven measurements, were 11.5, 8.9, 4.2, and 2.7% for 30, 100, 300, and 1000 ng of arsenic respectively.

Application to the Determination of Arsenic in Wastewaters. The present method was also applied to the determination of arsenic in wastewaters. The wastewater samples were taken at the inlet of the Wastewater Treatment Facility of the University of Osaka Prefecture. The most sensitive nondispersive atomic fluorescence measurements were made with the argon (entrained air)-hydrogen flame under the optimum conditions shown in Table 2. The samples were diluted by a factor of 2 to adjust the concentrations of sulfuric and hydrochloric acids to 5 and 20% respectively. The results

TABLE 6. DETERMINATION OF ARSENIC IN WASTEWATERS

Sample	Arsenic (ppb)[a]	
	Atomic fluorescence spectrometry[b]	Atomic absorption spectrometry
1	11	12
2	14	16
3	18	21
4	10	9
5	469	453
6	28	30
7	116	124
8	22	24
9	90	83
10	58	54

a) Average for five determinations. b) With the nondispersive system in argon (entrained air)-hydrogen flame.

thus obtained are shown in Table 6. The atomic absorption measurements at 193.7 nm in the argon(entrained air)-hydrogen flame with a long-path "multiflame" burner[29,30,36-38] instead of the burner newly constructed for the atomic fluorescence measurements were made by means of the same procedures as in the atomic fluorescence method. The results obtained by the atomic fluorescence method were in good agreement with those obtained by the atomic absorption method.

Conclusion

The present nondispersive and dispersive atomic fluorescence spectrometers have been proved to be sensitive and reliable for the determination of arsenic at the nanogram order. The detection limits obtained with the nondispersive system and the argon(entrained air)-hydrogen flame produced by using a newly constructed burner were comparable with those reported by other authors.[26,27] In this study the sensitivity obtained by the nondispersive system was about one order of magnitude better than that obtained by the dispersive system at 193.7 nm. The former system requires a considerably simpler and less expensive instrumentation than the latter system. Moreover, there is little or no spectral interference except for the presence of the other hydride-forming elements examined in the present study, because of the separation of the analyte from the solution prior to atomization in the flame.

It was verified that the most sensitive nondispersive atomic fluorescence spectrometry can give a lower detection limit and a much larger linear dynamic range for arsenic than the corresponding atomic absorption spectrometry. With respect to interference, however, the present system was similar to the atomic absorption spectrometry.

An improvement in the sensitivity and linear dynamic range of arsenic might be made with a nonflame atomizer as an atom reservoir and/or the sodium tetrahydroborate($NaBH_4$) reduction method, which gives a much lower reagent blank than the zinc tablet reduc-

tion combined with tin(II) chloride and potassium iodide. Work is currently under way in this laboratory to investigate this possibility.

References

1) R. M. Dagnall, K. C. Thompson, and T. S. West, *Talanta*, **15**, 677 (1968).
2) R. M. Dagnall and T. S. West, *Appl. Opt.*, **7**, 1287 (1968).
3) R. M. Dagnall, M. R. G. Taylor, and T. S. West, *Spectrosc. Lett.*, **1**, 397 (1968).
4) K. C. Thompson and P. C. Wildy, *Analyst(London)*, **95**, 776 (1970).
5) A. Fulton, K. C. Thompson, and T. S. West, *Anal. Chim. Acta*, **51**, 373 (1970).
6) M. S. Cresser and T. S. West, *Anal. Chim. Acta*, **51**, 530 (1970).
7) T. J. Vickers, P. J. Slevin, V. I. Muscat, and L. T. Farias, *Anal. Chem.*, **44**, 930 (1972).
8) W. B. Barnett and H. L. Kahn, *Anal. Chem.*, **44**, 935 (1972).
9) P. L. Larkins, *Spectrochim. Acta, Part B*, **26**, 477 (1971).
10) R. M. Dagnall, M. R. G. Taylor, and T. S. West, *Lab. Pract.*, **20**, 209 (1971).
11) W. Holak, *Anal. Chem.*, **41**, 1712 (1969).
12) E. F. Dalton and A. J. Malonoski, *At. Absorpt. Newsl.*, **10**, 92 (1971).
13) R. C. Chu, G. P. Barron, and P. A. Baumgarner, *Anal. Chem.*, **44**, 1476 (1972).
14) Y. Yamamoto, T. Kumamaru, Y. Hayashi, and T. Kamada, *Bunseki Kagaku*, **22**, 876 (1973).
15) T. Maruta and G. Sudoh, *Anal. Chim. Acta*, **77**, 37 (1975).
16) S. Terashima, *Anal. Chim. Acta*, **86**, 43 (1976).
17) Y. Yamamoto and T. Kumamaru, *Z. Anal. Chem.*, **281**, 353 (1976).
18) F. J. Schmidt and J. L. Royer, *Anal. Lett.*, **6**, 17 (1973).
19) F. J. Fernandez, *At. Absorpt. Newsl.*, **12**, 93 (1973).
20) K. C. Thompson and D. R. Thomerson, *Analyst (London)*, **99**, 595 (1974).
21) A. E. Smith, *Analyst(London)*, **100**, 300 (1975).
22) F. D. Pierce, T. C. Lamoreux, H. R. Brown, and R. S. Fraser, *Appl. Spectrosc.*, **30**, 38 (1976).
23) J. Agget and A. C. Aspell, *Analyst(London)*, **101**, 341 (1976).
24) F. D. Pierce and H. R. Brown, *Anal. Chem.*, **49**, 1417 (1977).
25) E. N. Pollock and S. J. West, *At. Absorpt. Newsl.*, **12**, 6 (1973).
26) K. Tsujii and K. Kuga, *Anal. Chim. Acta*, **72**, 85 (1974).
27) K. C. Thompson, *Analyst(London)*, **100**, 307 (1975).
28) T. Nakahara, T. Tanaka, and S. Musha, *Bull. Chem. Soc. Jpn.*, **51**, 2020 (1978).
29) T. Nakahara, H. Date, M. Munemori, and S. Musha, *Bull. Chem. Soc. Jpn.*, **46**, 637 (1973).
30) T. Nakahara, H. Nishino, M. Munemori, and S. Musha, *Bull. Chem. Soc. Jpn.*, **43**, 1706 (1973).
31) P. J. T. Zeegers, R. Smith, and J. D. Winefordner, *Anal. Chem.*, **40**, 26A (1968).
32) J. D. Winefordner and R. C. Elser, *Anal. Chem.*, **43**, 24A (1971).
33) G. F. Kirkbright and T. S. West, *Chem. Brit.*, **8**, 428 (1972).
34) R. M. Dagnall, K. C. Thompson, and T. S. West, *Talanta*, **14**, 1467 (1967).
35) R. S. Hobbs, G. F. Kirkbright, and T. S. West, *Talanta*, **18**, 859 (1971).
36) T. Nakahara and S. Musha, *Anal. Chim. Acta*, **75**, 305 (1975).
37) T. Nakahara and S. Musha, *Anal. Chim. Acta*, **80**, 47 (1975).
38) T. Nakahara and S. Musha, *Appl. Spectrosc.*, **29**, 352 (1975).

Photoaddition Reaction of 9,10-Phenanthrenequinone with Alicyclic Olefins.[1] Product Distribution

Kazuhiro MARUYAMA,* Tatsuaki IWAI,** Yoshinori NARUTA, Tetsuo OTSUKI, and Yo MIYAGI***

Department of Chemistry, Faculty of Science, Kyoto University, Kyoto 606

(Received July 21, 1977)

The phtoaddition reaction of 9,10-phenanthrenequinone (**1**) with several alicyclic olefins (**6**) has been investigated. In addition to the expected products, dihydrodioxin(**2**) and keto oxetane (**3**), the hydroxydihydrofuran derivative (**4**, **5**) were found. Product distribution was shown to be deeply dependent on the structure of the olefins. Product **4** has been shown to be produced *via* the photorearrangement of **3**.

9,10-Phenanthrenequinone (PQ) **1** photochemically adds to olefins to give several products. Schönberg and Mustafa reported first the photochemical reaction of **1** with olefins gave dihydrodioxin **2**. The subsequent reaction has been investigated by many workers.[2-6] According to the literature[7] the product distribution is dependent on the olefins used in the reaction. For example, dihydrodioxin **2**, a common product in the reaction with acyclic olefins, is the exclusive product in the reaction of **1** with either *cis*- or *trans*-stilbens.[8] In contrast, the reactions with benzofuran,[9] isocumarin,[9] and vinylene carbonate[5,10] afforded keto oxetanes as the major products.

In this investigation the chemical reaction of **1** with alicyclic olefin **6** of various ring sizes from six to twelve membered has been examined. A novel type of product **4** has been isolated and the amounts of **4** were found to be dependent on the structure of the olefins.

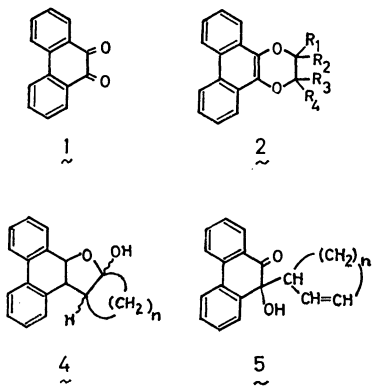

Results

Photochemical Reactions of 9,10-Phenanthrenequinone ***1*** *with Alicyclic Olefins* ***6a—g.*** Irradiation of a benzene solution of **1** and **6a—g** in a Pyrex tube using a 300W high pressure Hg lamp gave three kinds of products **7**, **8**, and **9**. Under these conditions no keto oxetane was found. The keto oxethane was obtained (yield 18%), however, using light of wavelength longer than 400 nm in the reaction of **1** with **6c**.

The formation of dihydrodioxin **7** has been reported in many photochemical reactions of **1** with olefins.[2-6] However, the products of adduct **8** type have been found only in a few cases.[11] So far hydroxydihydrofuran **9** has never been described in the literature. The structure of these products has been determined on the basis of their spectral data and yields are given in Table 1. Although the dihydrodioxins **7a—g** consisted of a mixture of the *cis*- and *trans*-isomers, the two isomers were separated in some cases by fractional crystallization. The isomer ratios were determined, in general, by means of ^{1}H-NMR spectroscopy taking advantage of the bridge-head methine protons exhibiting two distinct signals. The ^{1}H-NMR signal at lower field has been assigned to the *cis*-isomer and that at higher field to the *trans*-isomer.[12] It has been found that, in the conformational equilibrium that the bridge-head proton of the *trans*-isomer is advantageous to take axial position (Fig. 1); The *cis*-isomer favors the equatorial position, where it is affected strongly by the anisotropic effect of the dihydrodioxin ring.

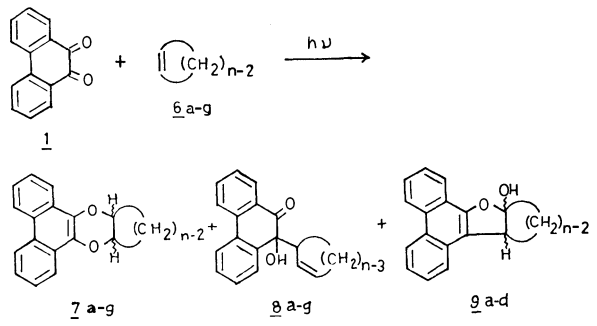

a; $n=6$, **b**; $n=7$, **c**; $n=8$, **d**; $n=9$, **e**; $n=10$, **f**; $n=11$ **g**; $n=12$.

As a result, the bridge-head proton of the *cis*-isomer appears at lower field. Table 2 shows the isomer ratios of the dihydrodioxins **7a—g**.

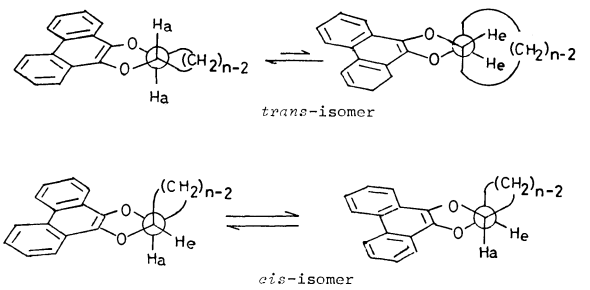

Fig. 1. The conformational equilibrium of *cis*- and *trans*-dihydrodioxins.

** Present address: Sun-Star Co. Ltd. Osaka.

*** Present address: Kanazawa University, Kanazawa.

Table 1. The yields of photoproducts[a)]

Olefin	Products		
	7[b)]	8[c)]	9
6a; $n=6$	46%	42% (mp 75—76 °C)	2% (mp 142—143 °C)
b 7[e)]	54%	23% (mp 90—93 °C)	8% (mp 154—155 °C)
c 8[e)]	66%	6% (oil)	20% (mp 149—150 °C)
d 9[e)]	59%	8% (oil)	7% (mp 129—130 °C)
e 10[e)]	42%	32% (mp 115—118 °C)	—[d)]
f 11[e)]	35%	38% (oil)	—[d)]
g 12[f)]	42%	40% (oil)	—[d)]

a) Yields were calculated on the basis of PQ used. b) Mixture of two isomers. c) Mixture of two or four isomers. d) Hydroxydihydrofuran was not isolated. e) *cis*-Isomer was used in the reaction. f) A mixture of *cis*- and *trans*-isomers was used in the reaction.

Table 2. The isomer ratios of dihydrodioxin **7**

Dihydro-dioxin	Ring size of alicyclic olefin	*cis*-Isomer (%)	*trans*-Isomer (%)
7a	6	85 (4.08[a)], oil[b)])	: 15 (3.48, oil)
b	7	69 (4.25, oil)	: 31 (3.70, mp 189.5—192 °C)
c	8	70 (4.41, mp 93.5—96 °C)	: 30 (4.00, oil)
d	9	88 (4.56, mp 124—6 °C)	: 12 (4.20, oil)
e	10	82 (4.61)[e)]	: 18 (4.24)[e)]
f	11	49 (4.56, mp 170—2 °C)	: 51 (4.24, mp 236.5—237.5 °C)
g	12	48 (4.52, mp 185—191 °C[d)])	: 52 (4.24, mp 220 °C[d)])

a) Chemical shifts of bridge-head methine protons. b) Physical properties. c) *cis*- and *trans*-mixture, mp 145—152 °C. d) A small amount of another isomer was contained. e) Not isolated.

Adducts **8a—c**, which arose from the α-hydrogen abstraction from the olefinic double bond, are mixtures of two diastereomers. Therefore, **8a** and **8b** show two distinguishable ^{1}H-NMR absorption signals which can be assigned to each of the diastereomer's. In the case of **8c**, the two diastereomers could not be distinguished by ^{1}H-NMR spectroscopy. Such phenomena have been observed by other investigators in the photochemical reactions of 1,1,4,4-tetramethyltetralin-2,3-dione, 1,1,4,4-tetramethylcyclohexane-2,3-dione, and 1,1-dimethylindan-2,3-dione with cyclohexene.[13] Adducts **8d—g** were isolated respectively as a mixture of four geometrical isomers in cycloalkene moiety. Hydroxydihydrofurans **9c** and **9d** can be easily dehydrated in the presence of a trace amount of acid. Dehydration in acidified methanol gave **10c** and **10d** in nearly quantitative yield. The dehydration strongly supports the structure of **9**. Under neutral conditions **9c, d** are fairly stable, but **9a, b** are not, decomposing to yield unidentifiable products.

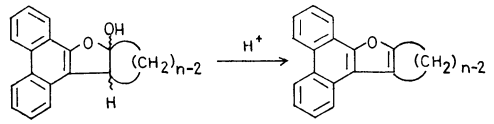

9 c,d 10 c,d

Photochemical Reaction of ***1*** *with Norbornene* ***11***.
The major products of the photoreaction of **1** with cycloalkenes **6a—g** as described above are the dihydrodioxines **7a—g**. In the photoreaction of **1** with norbornene **11** only the oxetane **12** was produced (yield: 75%), consequently the structure of the oxetane product has to be either **12A** or **B**. The configuration of the obtained oxetane **12** was determined by ^{1}H-NMR spectrocsopy: H_1' proton (δ 4.8, d, J=5 Hz) couples with H_2' proton (δ 2.42, d, J=5 Hz) and *vice versa*. However, the *endo* protons, H_1' and H_2', do not couple with the bridge-head protons, H_6' and H_3', respectively. It has been shown by Kumpler[14] that the coupling constants between the *endo* protons and the bridge-head protons in bicyclo[2.2.1]heptane system are very small (J=*ca.* 0). This phenomenon has been applied to determine the configuration of *exo*- and *endo*-oxetanes which were obtained from the photochemical reaction of norbornene with acetylcyanide.[15] From this evidence the configuration of the obtained oxetane **12** has been set as *exo*, *cis*. The orientation of the bicyclo[2.2.1]heptane ring to the C=O group in **12** has been determined from lantanide induced shift data. The shifts of the proton signals due to complex formation with tris(dipivalometanato)europium(III) [Eu(DPM)$_3$][16] are given in Table 3. The signals of the protons, H_1', H_6', and H_{7s}' underwent larger shifts than those of the protons, H_2', H_3', and H_{7a}', respectively. In addition, the same induced shift values were observed for each of the *endo* protons, H_{4N}' and H_{5N}'.

Phenanthrenequinone **1** + Nornene **11** ⟶ **12A** + **12B**

Similarly, the two *exo* protons, H_{4x}' and H_{5x}', showed the same induced shift. The induced shift values of the oxetane ring α- and β-protons are small compared with the corresponding oxetane ring protons of **15**. In the investigation of the structure of **15** it has been shown that the Eu^{3+} ion in the complex predominantly

TABLE 3. Eu(DPM)$_3$ INDUCED SHIFTS[a] IN THE ^{1}H-NMR SPECTRUM OF **12**[c]

Proton	H_1'	H_2'	H_3'	H_{4X}' and H_{5X}'	H_{4N}' and H_{5N}'	H_6'	H_{7s}'	H_{7a}'
Chemical shift[b] ppm	4.80	2.42	2.55	1.08	0.77	2.55	1.78	1.30
Induced shift ppm	18.4	15.0	2.1	1.2	3.9	7.2	7.0	3.7

a) Determined from the slopes of the plots of shifts (in ppm) *vs.* molar ratio of Eu(DPM)$_3$: **12** by least-squares method; concentration of **12**, *ca.* 0.125 M in CCl_4. b) CCl_4 was used as the solvent. c) The Chemical shifts and the induced shifts of aromatic protons are omitted in this table.

associates with the ethereal oxygen rather than with the alcohlic oxygen.[5] Moreover, in **12** the C-8 proton undergoes a smaller shift than that of the C-8 proton of **15**. Consequently, it has been concluded that by complexing with **12** the Eu^{3+} is situated at an equilibrium position between the ethereal oxygen and the carbonyl oxygen and the bicyclo[2.2.1]heptane ring is located *trans* to the carbonyl group; the isolated one corresponds to **12A**. The same conclusion may be drawn on the basis of the down-field shift of the *syn* proton H_{7s}', compared with the *anti* proton, H_{7a}', interpreted in terms of the benzene ring current.

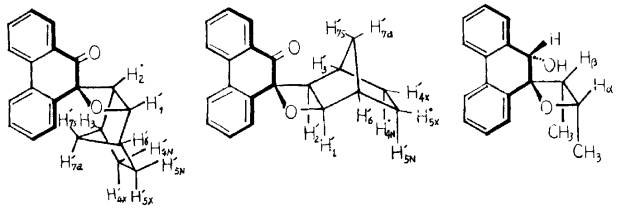

12A **12B** **15**

Photorearrangement of Oxetanes. Irradiation of a benzene solution of **1** with cyclooctene **6c** (300W high pressure Hg lamp) gave a mixture of **7c**, **8c**, and **9c** as described above. When the reaction was stopped at a relatively low conversion (irradiating light of a wavelength longer than 400nm), the corresponding oxetane **13** (18%) was isolated from the reaction mixture together with **7c** (39%, *cis*: *trans*=64: 36) and **8c** (5%). **9c** was not isolated. Further irradiation of **13c** dissolved in benzene using all the light of the high pressure lamp demostrated that **13c** easily photorearranged to **7c** and **9c** (relative ratio; 9 : 1). Since **7c** is photostable, the above results lead to the conclusion that **9a**—**d** and a part of **7a**—**d** are the photorearraged products of **13a**—**d**.

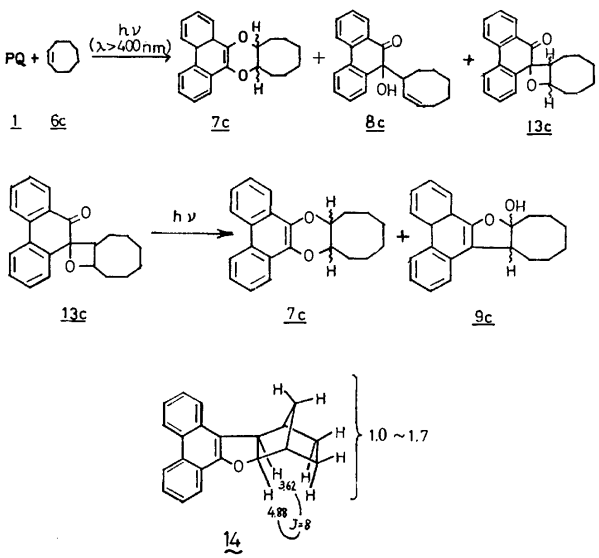

The oxetane **12** derived from norbornene, in comparison, was comparatively photostable, being ultimately decomposed under prolonged irradiation to give rather intractable products. After repeated column chromatography dihydrofuran **14** (*ca.* 12%) was isolated. On the basis of the ^{1}H-NMR spectrum the configuration of **14** was determined to be *exo*.[20]

Discussion

Using cycloalkenes with a *cis*-configuration,[22] a mixture of the *cis*- and *trans*-dihydrodioxins were obtained in every reaction (Table 2). These results suggest that each of the dihydrodioxins was formed in a stepwise fashion, perhaps *via* a biradical intermediate. Similar experimental results have been reported in the reaction of **1** with *cis*-2-butane,[17] *trans*-2-butene,[17] and *trans*-stilbene.[18]

In the formation of oxetane the present investigation gives no unambiguous information. However, the results published strongly indicate the contribution of a biradical intermediate.[9,10] Possible reaction pathways compatible with the present results are shown in Scheme 1. Photoexcited phenanthrenequinone reacts with a olefin in two competitive manners; addition to the olefin to give II (path a) and hydrogen abstraction from the olefin resulting in the formation of a radical pair I (path b). As shown in Tables 1 and 2, cyclo-

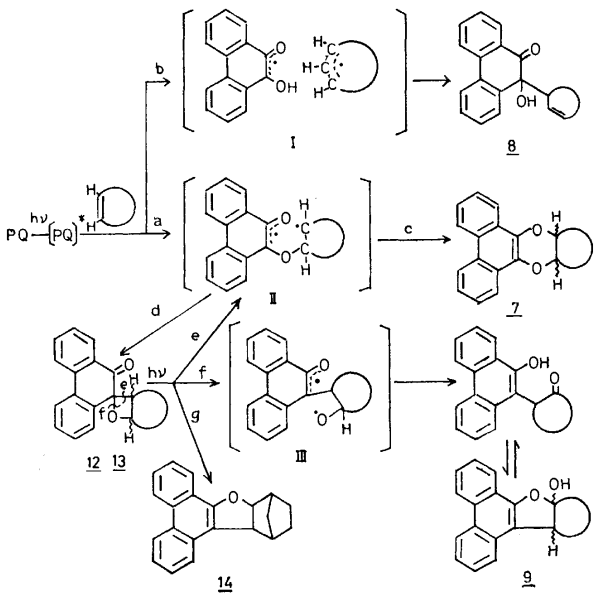

Scheme 1.

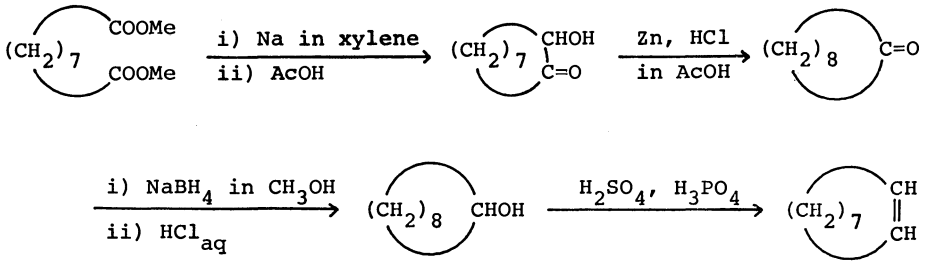

Scheme 2.

octene is most reactive for path a and least for path b for the examined monocycloolefins, because the yield of **8** is least in this case. In addition, the resulting biradical II is likely to be of rather a longer lifetime compared with those derived from other monocycloolefins;[22] this has been deduced from the relatively high yield of the corresponding *trans*-dihydrodioxin, *i.e.*, *trans*-**7e**, since the *cis*- and *trans*-dihydrodioxins are photostable in general. Thus, the difference in energy barriers between path a and path b could be highest in the case of cyclooctene of the examined mono-cycloolefins. In the case of norbornene the difference is thought to be so large that path b can not contribute to the reaction, being coincident with the fact that the α-hydrogen atom to the double bond of norbornene corresponds to the bridge-head one. The difference in cycloolefin behavior may be attributed to the cumulative effect of the internal strain and the restricted freedom of the ring fluctuation (depending on the ring size).

The resulting biradical II is stablized to give **7** and **13** (or **12**). Further irradiation of **13** with the light from a high pressure Hg lamp gave two biradicals II and III, finally resulting in the formation of **7** and **9**. The relative preference of path c or path d was found to be strongly dependent on the structure of olefins. In the case of norbornene, path d was the exclusive course. In the case of cyclooctene there may be a comparatively high contribution of path d, since the highest yield of **9** was attained in the reaction. The high selectivity for path d in the cases of norbornene and cyclooctene is likely to be correlated with the lesser yield of **8** in the reactions. Although the mechanism still remains ambiguous, the relative preference for path d seems to be connected with the higher *s*-charactor of the relating orbitals in the ring closure, especially of the orbital in the olefin moiety. The special behavior of norbornene and other highly strained cycloolefins in photocycloadditions with 1,4-naphthoquinone have been reported by the present auther and co-workers.[21] The higher *s*-charactor of the relating orbitals will result in the stronger σ-bond and this may be the reason for the stable isolation of oxetanes **12** and **13** derived from norbornene and cyclooctene respectively. In the other cases, isolation of the corresponding oxetanes was unsuccessful, perhaps due to the lack of stability.

As described in the previous section, the oxetane **12** photochemically rearranges to hydroxydihydrofuran **9** and dihydrodioxin **7**. The photorearrangement of **12** to **9** is of novel type. Farid has isolated an oxetane in the reaction of phenanthrenequinone with 1,2-di-*t*-butylethylene. Investigation of the photorearrangement yielded a mixture of dihydrodioxin, furan, and dioxole. However, the hydroxydihydrofuran derivative has not been isolated.[19]

Experimental

Instrumentation. ^{1}H-NMR spectra were recorded with JEOL PS-100 spectrometer and chemical shifts have been recorded in δ units using tetramethylsilane as an internal standard. Infrared spectra were taken with a JASCO IR-G spectrometer. Ultraviolet and visible spectra were obtained with a Shimadzu UV-200 spectrometer. Mass spectra were recorded with a Hitachi M-52 mass spectrometer. Elemental analyses were performed at the Microanalysis Center of Kyoto University. VPC was carried out using a JEOL JGC-20K equipped with a flame ionization detector using a column of 5% Ucon oil LB 550X on 80—100 mesh Diasolid L. Melting points and boiling points of materials or products have not been corrected.

Materials. 9,10-Phenanthrenequinone (**1**) was prepared by the oxidation of phenanthrene[23]; mp 209—210 °C (lit, mp 208.5—210 °C). Cyclohexene (**6a**), cycloheptene (**6b**), *cis*-cyclooctene (**6c**), cyclododecene (**6g**), and bicyclo-[2.2.1]hept-2-ene (norbornene) (**11**) were commercially available (reagent grade) and used without further purification. Analyzed by VPC, cyclododecene (**6g**) proved to be a mixture of 30% *cis*- and 70% *trans*-isomer. Cyclononene (**6d**) was synthesized from diethyl azelate according to the route described above (Scheme 2); bp 160—172 °C (lit,[26] bp 167—169 °C/740 mmHg for the *cis*-isomer, 73—74 °C/30 mmHg for the *trans*-isomer); ^{1}H-NMR (CCl_4) δ 1.0—2.4 (14H, m), 5.56 (2H, m); IR (NaCl) 2910, 2840, 717, 728 cm^{-1}. Analysis by VPC and IR indicated that the synthesized cyclononene (**6d**) contained mainly the *cis*-isomer.

Cyclododecene (**6e**) and cycloundecene (**6f**) were synthesized from cyclodecanone and cycloundecanone, respectively. Cyclodecanone and cycloundecanone were synthesized from cyclododecanone in good yield by the method of Garbish and Wohlleke.[25] Cyclodecene (**6e**); bp 87—92 °C/42 mmHg (lit,[24] bp 194—195 °C/740 mmHg for the *cis*-isomer, 68—70 °C/10 mmHg for the *trans*-isomer); ^{1}H-NMR (CCl_4) δ 1.2—2.4 (16H, m), 5.48 (2H, m); IR (NaCl) 2900, 2840, 980 cm^{-1}. Analysis by VPC and IR indicated that the synthesized cyclodecene (**6e**) contained approximately 45% of the *cis*- and 55% of the *trans*-isomer. Cycloundecene (**6f**); bp 110—111 °C/40 mmHg; ^{1}H-NMR (CCl_4) δ 1.0—2.4 (18H, m), 5.30 (2H, m); IR (NaCl) 2905, 2840, 970 cm^{-1}. Analysis by VPC and IR indicated that the synthesized cycloundecene (**6f**) contained about 28% of the *cis*- and 72% of the *trans*-isomer.

Irradiation of PQ (1) with Cycloalkene(6a—g) and Norbornene (11). Pyrex test tubes were charged with PQ (**1**)

TABLE 4. ^{1}H-NMR SPECTRAL DATA OF PHOTOPRODUCTS (solv. CCl_4 or $CDCl_3$)

Compd	δ, ppm		
	Ring proton	Bridge-head methine proton	Aromatic proton
7a	1.2—2.3 (8H, m)	3.48 (m) (2H) 4.08 (bd)	7.40 (4H, m) 8.04 (2H, m) 8.46 (2H, m)
7b	1.4—2.2 (10H, m)	3.70 (m) (2H) 4.25 (bd)	7.47 (4H, m) 8.16 (2H, m) 8.46 (2H, m)
7c	1.4—2.3 (12H, m)	4.00 (m) (2H) 4.41 (bd)	7.48 (4H, m) 8.12 (2H, m) 8.48 (2H, m)
7d	1.3—2.4 (14H, m)	4.20 (m) (2H) 4.56 (m)	7.50 (4H, m) 8.10 (2H, m) 8.54 (2H, m)
7e	1.4—2.4 (16H, m)	4.24 (m) (2H) 4.61 (m)	7.48 (4H, m) 8.08 (2H, m) 8.48 (2H, m)
7f	1.2—2.3 (18H, m)	4.22 (m) (2H) 4.56 (m)	7.60 (4H, m) 8.24 (2H, m) 8.64 (2H, m)
7g	1.2—2.1 (20H, m)	4.24 (m) (2H) 4.52 (m)	7.62 (4H, m) 8.26 (2H, m) 8.68 (2H, m)

Compd	δ, ppm			
	Ring proton	OH proton	Olefinic proton	Aromatic proton
8a	1.0—2.0 (6H, m) 2.3—2.5 (1H, m)	3.76 (s) (1H) 3.87 (s)	5.1—5.8 (2H, m)	7.2—8.0 (8H, m)
8b	1.0—2.6 (9H, m)	3.90 (s) (1H) 3.91 (s)	5.2—6.0 (2H, m)	7.2—8.1 (8H, m)
8c	1.0—2.9 (11H, m)	4.06 (1H, s)	5.1—5.7 (2H, m)	7.1—7.9 (8H, m)
8d	0.8—1.8 (12H, m) 2.6—2.9 (1H, m)	3.86 (1H, bs)	5.0—5.6 (2H, m)	7.1—8.0 (8H, m)
8e	0.8—2.0 (14H, m) 2.8—3.1 (1H, m)	3.84 (1H, s)	4.9—5.4 (2H, m)	7.2—8.0 (8H, m)
8f	0.8—2.8 (17H, m)	3.84 (1H, bs)	4.8—5.4 (2H, m)	7.0—8.0 (8H, m)
8g	0.8—2.8 (19H, m)	3.98 (1H, bs)	4.8—5.4 (2H, m)	7.0—8.0 (8H, m)

Compd	δ, ppm		
	Ring proton	OH proton	Aromatic proton
9a	1.0—2.2 (6H, m) 2.2—2.6 (2H, m) 3.40 (1H, m)	broadened	7.60 (5H, m) 8.14 (1H, m) 8.66 (2H, m)
9b	1.0—2.6 (10H, m) 3.72 (1H, m)	2.80 (1H, bs)	7.64 (5H, m) 8.13 (1H, m) 8.72 (2H, m)
9c	1.1—2.1 (10H, m) 2.1—2.7 (2H, m) 3.26 (1H, m)	3.02 (1H, bs)	7.54 (5H, m) 8.10 (1H, m) 8.68 (2H, m)
9d[a]	1.2—3.4 (m) 3.60 (bd) 5.18 (bd)	3.08 (bs) 10.28 (s)	7.60 (m) 8.07 (m) 8.58 (m)
12	0.77 (2H, m) 1.08 (2H, d) 1.30 (1H, m) 1.78 (1H, bs) 2.42 (1H, d) 2.55 (2H, d) 4.80 (1H, d)	——	7.1—7.8 (8H, m)

a) Compound **9d** showed the complicated ^{1}H-NMR spectrum because hemiacetal ring was somewhat dissociated. Phenolic OH proton was observed at δ 10.28 ppm.

(1 mmol), cycloalkene (**6a—g**) (2 mmol) or norbornene (**11**) and reagent grade benzene (30 ml) (dried over sodium). The solutions were irradiated with a 300 W high-pressure mercury lamp and during irradiation, the test tubes were often shaken. The course of the reactions was followed by TLC. When the PQ had mostly disappeared the solvent was evaporated, and products separated by preparative silica gel TLC eluted with hexane–benzene or by florisil column chromatography eluted with hexane–benzene. The yield of products were determined from the weight of the corresponding fractions. The structures of each fraction were confirmed by means of ^{1}H-NMR technique. The crystalline products were recrystallized from hexane, benzene, or cyclohexane. The spectral data and the results of elementa analyses are summarized in Tables 4—6.

Dehydration of ***9c, 9d.*** In a solution of hydroxydihydro-

Table 5. IR spectral data of photoproducts

Compd	ν, cm^{-1}		
	OH	C=O	C=C
7a			1620, 1600
7b			1620, 1600
7c			1620, 1600
7d			1620, 1600
7e			1620, 1600
7f			1620, 1600
7g			1625, 1600
8a	3450	1680	1600
8b	3450	1680	1600
8c	3470	1690	1600
8d	3470	1690	1600
8e	3450	1680	1600
8f	3450	1680	1600
8g	3450	1680	1600
9a	3400		1640, 1605
9b	3400		1640, 1605
9c	3400		1635, 1600
9d	3400		1640, 1605
12		1690	1600

Table 6. Elemental analyses of photoproducts

Compd	Calcd Formula			Calcd (%)		Found (%)	
	C	H	O	C	H	C	H
7a	20	18	2	82.73	6.25		
7b	21	20	2	82.86	6.62	82.79	6.79
7c	22	22	2	82.98	6.96	82.97	7.19
7d	23	24	2	83.10	7.28	82.89	7.18
7e	24	26	2	83.20	7.56	83.32	7.67
7f	25	28	2	83.29	7.83	83.15	7.83
7g	26	30	2	83.38	8.07	83.45	8.09
8a	20	18	2	82.73	6.25	82.44	6.19
8b	21	20	2	82.86	6.62	82.85	6.62
9c	22	22	2	82.98	6.96	82.75	7.20
12	21	18	2	83.41	6.00	83.55	6.15

furane **9c,d** (20 mg) in methanol (20 ml), one drop of concd HCl was added. After standing for 1 h at room temperature, TLC analysis indicated that hydroxydihydrofurane (**9c**) had disappeared and furan (**10c**) exclusively formed. After evaporation of the solvent, product **10c** was recrystallized from pentane; mp 141—142 °C, which showed the following spectral data; ^{1}H-NMR (CCl_4) δ 1.2—2.1 (8H, m), 2.96, 3.10 (4H, two overlapped t), 7.50 (4H, m), 8.22 (2H, m), 8.61 (2H, m); IR (KBr) 1620, 1605, 1575 cm^{-1}; mass spcetrum *m/e* 300 (M^+). Found: C, 87.86; H, 6.51%. Calcd for $C_{22}H_{20}O$: C, 87.96; H, 6.71%.

Similarly, **10d** was obtained from **9d**. **10d**, mp 151.5—153 °C, gave the following spectral data; ^{1}H-NMR (CCl_4) δ 1.2—2.0 (14H, m), 2.92 (2H, t), 3.10 (2H, t), 7.42 (4H, m), 8.16 (2H, m), 8.52 (2H, m); IR (KBr) 1620, 1605, 1575 cm^{-1}; mass spectrum *m/e* 314 (M^+).

Irradiation through a Filter. A solution containing PQ (**1**) (216 mg, 1.04 mmol) and cyclooctene (**6c**) (219 mg, 1.99 mmol) in reagent grade benzene (30 ml) was irradiated with a 300W high-pressure mercury lamp through a filter (Toshiba color glass filter V-Y 42) to exclude light below 400 nm. After the usual work-up the products were separated by preparative TLC eluted with benzene. Products; dihydrodioxin (**7c**) (128 mg) (*cis*: *trans*=64:36), detectable amounts of α-hydrogen abstracted adduct **8c**, and oxetane **13c** (61 mg) were isolated. **13c**, mp 190—191 °C, slightly yellowish leaflets gave the following spectral data; ^{1}H-NMR ($CDCl_3$) δ 1.0—2.4 (12H, m), 2.88 (1H, ddd, J=2,8,8 Hz), 5.00 (1H, dd, J=8,14 Hz), 7.2—8.2 (8H, m); IR (KBr) 1680, 1600 cm^{-1}; UV λ_{max} ($CHCl_3$) 245 nm (ε 25000), 281 (2700), 327 (2900); mass spectrum *m/e* 318 (M^+). Found: C, 82.98; H, 6.96%. Calcd for $C_{22}H_{22}O_2$: C, 82.70; H, 6.72%. Under similar conditions, a benzene solution of PQ (**1**) with cyclododecene (**6g**) was irradiated, but no oxetane could be isolated.

*Photorearrangement of Oxetane **13c**.* A solution of oxetane **13c** (62 mg) in reagent grade benzene (10 ml) (dried over sodium) was irradiated with a 300W high-pressure mercury lamp for 25 h. The TLC analysis indicated that dihydrodioxin (**7c**) and hydroxydihydrofurane (**9c**) were formed. After evaporation of solvent, the residue was dissolved in methanol (10 ml) and one drop of concd HCl added. After standing for 1 h at room temperature, dihydrodioxin (**7c**) and furane (**9c**) were isolated after the usual work-up. The ratio of **6c** to **9c** was determined as 10:1 by means of ^{1}H-NMR spectroscopy utilizing the bridge-head methine protons of **6c** and methine protons adjecent to furane ring of **9c** as their indices.

*Photorearrangement of Oxetane **12**.* A solution of oxetane (**12**) (215 mg) in benzene (30 ml) was irradiated with a 300W high pressure Hg lamp for about 10 days. The TLC analysis indicated that oxetane (**12**) almost disappeared. After evaporation of the solvent, dihydrofurane (**14**) (24 mg) was isolated from the residue. The other products were an intractable matter. **14** was recrystallized from hexane, mp 136—138 °C, which gave the following spectral data; ^{1}H-NMR (CCl_4) δ 1.0—1.7 (6H, m), 2.66 (2H, bs), 3.62 (1H, d, J=8 Hz), 4.88 (1H, d, J=8 Hz), 7.40 (5H, m), 7.92 (1H, m), 8.48 (2H, m); IR (KBr) 1640, 1615 cm^{-1}; mass spectrum *m/e* 286(M^+). Found: C, 87.99; H, 6.22%. Calcd for $C_{21}H_{18}O$: C, 88.08; H, 6.34%.

References

1) A preliminaly report: K. Maruyama, T. Iwai, and Y. Naruta, *Chem. Lett.*, **1975**, 1219.

2) A. Schönberg and A. Mustafa, *J. Chem. Soc.*, **1944**, 387.

3) J. M. Bruice, "The Chemistry of the Quinonoid Compounds," ed by S. Patai, John Wiley & Sons, London (1973), p. 456.

4) J. M. Bruice, *Quart. Rev.*, **21**, 405 (1967).

5) S. Farid and K.-H. Scholz, *J. Org. Chem.*, **37**, 481 (1972).

6) G. Pfundt and G. O. Schenck, "1,4-Cycloaddition Reaction," ed by J. Hamer, Academic Press, New York (1967), p. 345.

7) A. Schönberg, "The Preparative Organic Photochemistry," Springer, New York (1968), p. 119.

8) S. Farid, *Chem. Commun.*, **1967**, 1268.

9) S. Farid and K.-H. Scholtz, *Chem. Commun.*, **1968**, 412.

10) C. H. Crauch, S. Farid, and G. O. Schenck, *Chem. Ber.*, **98**, 3102 (1965). S. Farid, D. Hess, G. Pfundt, K. -H, Scholz, and G. Steffen, *Chem. Commun.*, **1968**, 638.

11) S. Farid and D. Hess, *Chem. Ber.*, **102**, 3747 (1969).

12) G. Pfundt and S. Farid, *Tetrahedron*, **22**, 2237 (1966).

13) G. E. Gream, M. Mular and J. C. Paice, *Tetrahedron Lett.*, **1970**, 3479.
14) W. D. Kumplar, *J. Am. Chem. Soc.*, **80**, 2533 (1958).
15) J. Shigematsu, Y. Odaira and S. Tsutsumi, *Tetrahedron Lett.*, **1967**, 55.
16) R. E. Sievers ed, "Nuclear Magnetic Resonance Shift Reagents," Academic, New York (1973) and references therein.
17) Y. L. Chow and T. C. Joseph, *J. Chem. Soc., Chem. Commun.*, **1968**, 604.
18) J. J. Bohning and K. Weiss, *J. Am. Chem. Soc.*, **88**, 2893 (1966).
19) S. Farid and K.-H. Sholz, *J. Chem. Soc., Chem. Commun.*, **1969**, 572.
20) Details are given in experimental section.
21) K. Maruyama, Y. Naruta, and T. Otsuki, *Bull. Chem. Soc. Jpn.*, **48**, 1553 (1975).
22) In this discussion cyclododecene (**6 g**) should be excluded, since a mixture of *cis*- and *trans*-isomers was submitted to the reaction.
23) *Org. Synth.*, Coll. Vol. 4, 757 (1963).
24) A. T. Blomquist, L. H. Liu and J. C. Bohrer, *J. Am. Chem. Soc.*, **74**, 3636, 3643 (1952).
25) E. W. Garbish, Jr., and J. Wohlleke, *J. Org. Chem.*, **33**, 2157 (1968).

Reduction of Acetals with $TiCl_4$–$LiAlH_4$

Hiroshi ISHIKAWA* and Teruaki MUKAIYAMA†

Laboratories of Medicinal Chemistry, Otsuka Pharmaceutical Co., Ltd., Kagasuno, Kawauchi-cho, Tokushima 771-01

† *Department of Chemistry, Faculty of Science, The University of Tokyo, Hongo, Bunkyo-ku, Tokyo 113*

(Received October, 12, 1977)

The reduction of dialkyl acetals derived from aromatic aldehydes and ketones with $TiCl_4$–$LiAlH_4$ in THF or diethyl ether at room temperature afforded the coupling products, pinacol ethers or olefins, in high yields. On the other hand, when acetals derived from aliphatic aldehydes and ketones were treated with $TiCl_4$–$LiAlH_4$ in diethyl ether, the reductive dealkoxylation took place and the corresponding ethers were isolated in good yields. As to the reaction mechanism we propose that Ti(II) is the reactive species in reductive coupling reaction of acetals derived from aromatic aldehydes and ketones, and that Ti(0)–H_2AlCl complex may be the reactive species in reductive dealkoxylation of acetals derived from aliphatic aldehydes and ketones.

The reactivity of $LiAlH_4$ can be greatly modified by addition of metal salts. $LiAlH_4$–$AlCl_3$ has been found to have an unusual applicability in epoxide reductrion[1] and in reduction of acetals to the corresponding ethers.[2–7] Further, $LiAl(OCH_3)_3H$–CuI can effect reductive removal of halo and mesyloxy groups,[8] and $LiAlH_4$–$TiCl_3$ has been found to be a coupling reagent.[9] Recently Ashby *et al.* have reported that 1,4-reduction of α,β-unsaturated ketones by using $LiAlH_4$–CuI proceeds with almost complete functional selectivity.

During the course of our investigation on the exploration of various synthetic reaction by the use of $TiCl_4$, we reported in the previous paper[11] that various olefins were prepared in good ylieds by the treatment of allyl methyl ethers with $TiCl_4$–$LiAlH_4$ in THF or diethyl ether.

Recently, it has been shown[12] that a low valent titanium compound, prepared from $TiCl_4$ and Zn, reduces aldehydes or ketones to afford the corresponding pinacols or olefins in high yields and that the selectivity of the reaction depends on the reaction conditions.

In the present work the reduction of various acetals using $TiCl_4$ and $LiAlH_4$ was studied, and it was found that reductive coupling or dealkoxylation took place depending on the types of starting acetals and on the solvents employed.

At first the reaction of benzaldehyde diethyl acetal (**1**) with the low valent titanium compound was examined under various conditions. For example, benzaldehyde diethyl acetal (**1**) was added to a mixture of equimolar amounts of $TiCl_4$ and $LiAlH_4$ in THF at room temperature, and after stirring at room temperature for 3 h, the mixture was quenched with aqueous potassium carbonate. Purification by column chromatography (silica gel) gave 1,2-diethoxy-1,2-diphenylethane (**2**) and stilbene (**3**) [trans: 86%, cis: 14%] in 85 and 10% yields, respectively.

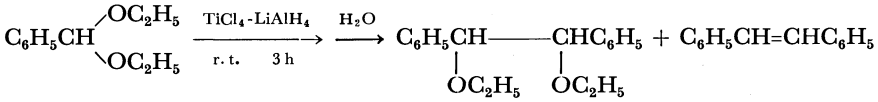

(**1**) (**2**) 85 (**3**) 10%

As shown in Table 1, when the ratio $LiAlH_4$ to $TiCl_4$ was decreased, the yield of products decreased. On the other hand, no difference in yields was observed when molar ratio of $LiAlH_4$ was increased.

The reaction of various acetals derived from aromatic aldehydes or ketones with equimolar amounts of $TiCl_4$–$LiAlH_4$ was tried in THF at room temperature, and the corresponding pinacol ethers and olefins were obtained in high yields as shown in the following equations; (1)-(4).

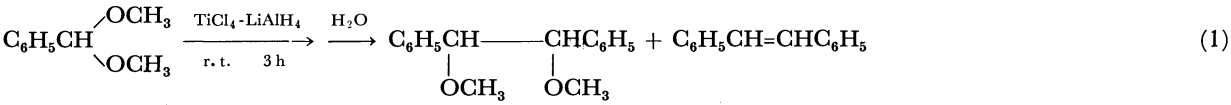

(**4**) (**5**) 77% (**3**) 15% (1)

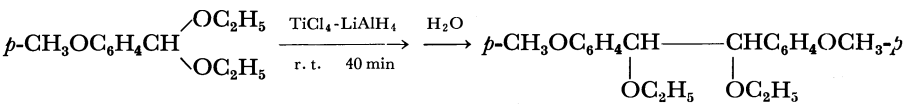

(**6**) (**7**) 98% (2)

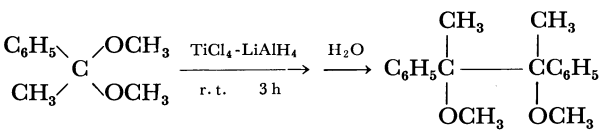

(**9**) (**10**) 97% (3)

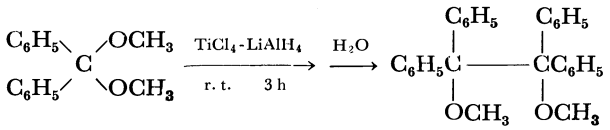

(4)

(11) (12) quant.

Table 1. Reductive coupling of benzaldehyde diethyl acetal with different ratio of the reagents in THF

Acetal	Molar ratio		Yield (%)	
	$LiAlH_4$	$TiCl_4$	Pinacol ether	Stilbene
1	0.5	1	41	5
1	1	1	85	10
1	2	1	83	9

As shown in the above equations, pinacol ethers were obtained in high yields by the reaction of acetals derived from aromatic aldehydes and ketones with $TiCl_4$–$LiAlH_4$. The yields of the two kinds of products, pinacol ether and olefins, markedly depended on the solvents used. For example, when *p*-methoxybenzaldehyde diethyl acetal (**6**) was treated with $TiCl_4$–$LiAlH_4$ in THF at room temperature, 4,4′-dimethoxystilbene (**8**) could not be detected and pinacol ether was obtained exclusively. In sharp contrast with this, when diethyl ether was used as solvent, olefins, (**8**) were isolated in 36% yield together with pinacol ether (**7**). However the reductive coupling did not proceed in benzene.

The results are show in Table 2.

Further, it was found that pinacol ether (**7**) reacted with two molar amounts of $TiCl_4$–$LiAlH_4$ in diethyl ether at room temperature to afford the corresponding olefins (**8**) in 57% yield.

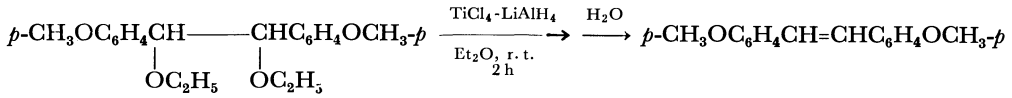

(7) (8) 57%

On the other hand, the reduction of acetals derived from aliphatic aldehydes and ketones such as 3-phenylpropanal dimethyl acetal (**13**) with $TiCl_4$–$LiAlH_4$ did not take place in THF. But when, the acetal (**13**) was treated with $TiCl_4$ and two molar amounts of $LiAlH_4$ in diethyl ether, the acetal was reduced to the corresponding ether, 1-methoxy-3-phenylpropane (**14**), in 87% yield.

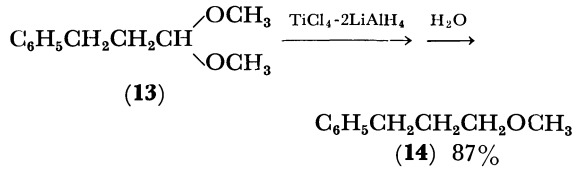

(13) (14) 87%

The generality of the reaction was examined by the use of various acetals such as 3-phenylpropanal diethyl acetal, benzylacetone dimethyl acetal, benzylacetone diethyl acetal, cyclohexanone dimethyl acetal, cyclohexanone ethylene acetal, and in all cases the corresponding ethers were obtained in good yield (see Table 3).

Although a detailed understanding of the reaction mechanism must wait knowledge of the nature of the reagent, Eq. 5, shows a possible explanation for the observation of a black precipitate and gas evolution in the first step of this reaction.

$$TiCl_4 + LiAlH_4 \longrightarrow TiCl_2 + LiCl + H_2AlCl + H_2 \quad (5)$$

McMurry[9] has suggested that Ti(II) is the reactive species in reductive coupling reactions. Recently, Corey[15] has proposed that Ti(II) is the reactive species in the intermolecular and intramolecular pinacolic coupling reaction of aldehydes and ketones. Based on these assumptions a possible mechanism of the reductive coupling reaction is proposed (Scheme 1).

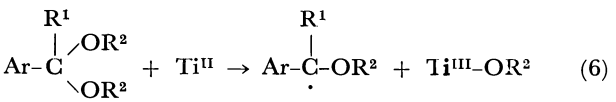

(6)

Scheme 1.

Table 2.

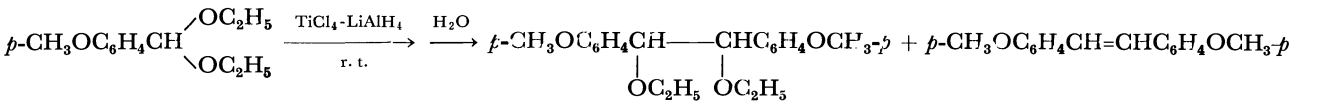

(6) (7) (8)

Solvent	Molar ratio			Reaction time (min)	Yield (%)		Recovery (%)
	(7)	$LiAlH_4$	$TiCl_4$		(7)	(8)	(6)
Benzene	1	1	1	120	0	0	91
THF	1	1	1	40	98	0	—
Ether	1	1	1	60	58	36	—
	1	2	1	60	53	42	—
	1	3	1	60	38	54	—

Table 3. Reduction of acetals derived from aliphatic aldehydes and ketones with $TiCl_4$-$2LiAlH_4$

Acetal	Ether	Yield (%)	Bp (°C/mmHg)
$C_6H_5CH_2CH_2CH(OCH_3)_2$ (**13**)	$C_6H_5CH_2CH_2CH_2OCH_3$ (**14**)	87	98—100/20[a]
$C_6H_5CH_2CH_2CH(OC_2H_5)_2$ (**15**)	$C_6H_5CH_2CH_2CH_2OC_2H_5$ (**16**)	76	104—107/20[b]
$C_6H_5CH_2CH_2CCH_3(OCH_3)_2$ (**17**)	$C_6H_5CH_2CH_2CHCH_3OCH_3$ (**18**)	69	100—102/12
$C_6H_5CH_2CH_2CCH_3(OC_2H_5)_2$ (**19**)	$C_6H_5CH_2CH_2CHCH_3OC_2H_5$ (**20**)	67	106—110/12
cyclo-$C_6H_{10}(OCH_3)_2$ (**21**)	cyclo-$C_6H_{11}OCH_3$ (**22**)	72	127—129/760[c]
cyclo-C_6H_{10} 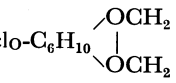 (**23**)	cyclo-$C_6H_{11}OCH_2CH_2OH$ (**24**)	75	100—101/14[d]

a) Lit,[13] 92—94 °C/12 mmHg. b) Lit,[14] 90—95°C/10 mmHg. c) Lit,[3] 122 °C/754 mmHg. d) Lit,[3] 100 °C/14 mmHg.

Table 4. Physical properties and analytical data of the products

Product	IR (cm^{-1})	NMR (δ)	Found (%) (Calcd) C	H
2	b) 700, 1100	c) 1.14(t, J=7 Hz, 3H), 3.40(q, J=7 Hz, 2H), 4.38(s, 1H), 7.07(s, 5H)	79.81 (79.96)	8.15 (8.20)
5		c) 3.08(s, 3H), 4.10(s, 1H), 7.22(s, 5H)	79.20 (79.31)	7.52 (7.49)
7	b) 1090, 1245	d) 1.14(t, J=7 Hz, 3H), 3.35(q, J=7 Hz, 2H), 3.66(s, 3H), 4.23(s, 3H), 6.72(q, J=9 Hz, 4H)	72.58 (72.70)	8.05 (7.93)
10	b) 700, 1110, 1118	c) 1.67(s, 3H), 3.08(s, 3H), 6.60—7.12(m, 5H)	79.79 (79.96)	8.23 (8.20)
12		c) 3.11(s, 3H) 6.90—7.70(m, 10H)	85.02 (85.24)	6.81 (6.64)
14	a) 1090	c) 1.80(m, 2H), 2.60(m, 2H), 3.26(s, 3H), 3.30(t, J=6 Hz, 2H), 7.17(s, 5H)		
16		c) 1.20(t, J=7 Hz, 3H), 1.92(m, 2H), 2.67(m, 2H), 3.49(q, J=7 Hz, 4H), 7.29(s, 5H)		
18	a) 1090	c) 1.10(d, J=6 Hz, 3H), 1.72(m, 2H), 2.65(m, 2H), 3.21(m, 3H), 3.27(s, 3H), 7.19(s, 5H)	80.31 (80.44)	9.92 (9.83)
20	a) 1095	c) 1.10(d, J=6 Hz, 3H), 1.70(m, 2H), 2.62(m, 2H), 3.39(m, 3H), 7.17(s, 5H)	80.62 (80.85)	10.23 (10.18)
22	a) 1080	c) 1.42(m, 10H), 3.28(s, 3H), 3.34(m, 1H)		
24	a) 3450, 1110	c) 1.53(m, 10H), 2.75(m, 1H),[e] 3.55(m, 5H)		

a) Neat, b) KBr disk, c) in CCl_4, d) in $CDCl_3$, e) exchanged with D_2O.

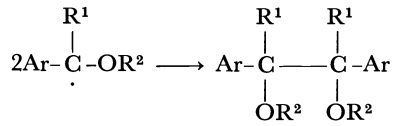

(7)

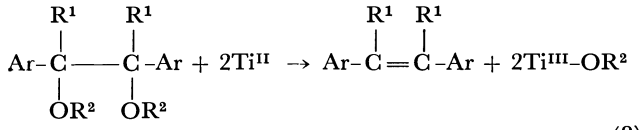

(8)

Reductin of acetals derived from aromatic aldehydes and ketones by the Ti(II) reagent may give a radical intermediate (Eq. 6), which dimerizes into pinacol ethers. Further reaction of the pinacol ether with Ti(II) reagent may give olefins.

In order to certify the hypothesis embodied in Scheme 1, we examined the reductive coupling using well-defined Ti(II) species. We have found Ti(II) complexes of known structure which are capable of

effecting the reduvtive coupling of acetal derived from aromatic aldehyde. The complex [**A**],[16] prepared by the reaction of Al–$AlCl_3$, $TiCl_4$, and hexamethylbenzene is especially effective: 1,2-diethoxy-1,2-bis (*p*-methoxyphenyl)ethane (**7**) was obtained in 52% yield by the reaction of [**A**] with *p*-methoxybenzaldehyde diethyl acetal (6).[17]

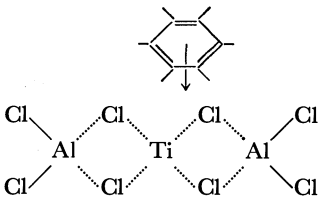

[**A**]

The observed solvent effects may reflect the different coordination ability of Ti(II) species with THF from that with diethyl ether.

On the other hand, the mechanism of the reduction of acetals derived from aliphatic aldehydes and ketones by $TiCl_4$–$2LiAlH_4$ could not be made clear. However, when $TiCl_4$ is treated with two molar amounts of $LiAlH_4$, titanium metal is supposed to be formed (Eq. 9). In fact, the formation of titanium metal was observed in this reaction.

$$TiCl_4 + 2LiAlH_4 \rightarrow Ti(0) + 2LiCl + H_2AlCl + H_2 \quad (9)$$

It is well known that the low valent titanium compound form complexes with organic or inorganic aluminum compounds[16,18] and with alkyl halides.[19]

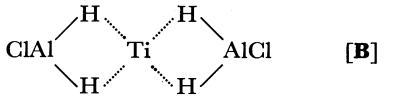

[**B**]

Accordingly, we assume that the reactive intermediate is complex [**B**] in the reduction of acetals derived from aliphatic aldehydes and ketones by using $TiCl_4$–$2LiAlH_4$.

We are continuing the mechanistic study on the intermediates of the titanium complex [**B**] in this reductive dealkoxylation.

In conclusion, it has been made clear that the combination of $TiCl_4$ and $LiAlH_4$ is effectively applied to the reduction of acetal like $AlCl_3$–$LiAlH_4$. It is characteristic that when the acetals derived from aromatic aldehydes and ketones are treated with $TiCl_4$–$LiAlH_4$ in THF, pinacol ethers are obtained in high yields.

Experimental

Materials. Commercially available $TiCl_4$ was distilled under argon atmosphere before use. Various acetals were prepared according to the procedures described in the literature[20] and purified by distillation. All boiling points and melting points were uncorrected. The IR spectra were recorded with a Hitachi 215 grating infrared spectrophotometer. The proton NMR spectra were recorded using Varian EM360 spectrometer and Hitachi R-20B high resolution spectrometer with TMS as an internal standard. The physical properties and analytical data of the products are shown in Table 4.

*Reductive Coupling of Benzaldehyde Diethyl Acetal (**1**).* To a stirred suspension of $TiCl_4$ (0.95 g, 5 mmol) in 15 ml of THF was added a suspension of $LiAlH_4$ (0.19 g, 5 mmol) in 10 ml of THF at room temperature under argon atmosphere. During the addition of $LiAlH_4$ hydrogen evolved vigorously and the reaction mixture turned to black, which indicated the formation of a low valent titanium compound. After stirring the mixture for 30 min at room temperature, benzaldehyde diethyl acetal (0.90 g, 5 mmol) in 10 ml of THF was added dropwise to the reaction mixture during 10 min at room temperature, and the reaction mixture was stirred for 3 h. The reaction was quenched by the addition of 10 ml of 10% aqueous potassium carbonate, and a dark brown precipitate appeared was filtered off. The filtrate was extracted with ether. The ether extract was washed with saturated sodium chloride solution and dried over sodium sulfate. After removal of the solvent under reduced pressure, 1,2-diethoxy-1,2-diphenylethane (**2**) and stilbene (**3**) were isolated by column chromatography (silica gel) using hexane–dichloromethane (1:1) as an eluent in 85% (0.75 g) and 10% (0.045 g) yields, respectively.

*Reduction of 1,2-Diethoxy-1,2-bis(p-methoxyphenyl)ethane (**7**) with $TiCl_4$–$LiAlH_4$.* To a sirred suspension of $TiCl_4$ (0.38 g, 2 mmol) in 5 ml of diethyl ether was added a suspension of $LiAlH_4$ (0.08 g, 2 mmol) in 8 ml of diethyl ether at room temperature under argon atmosphere. After stirring the mixture for 20 min at room temperature, pinacol ether (**7**) (0.33 g, 1 mmol) in 5 ml of diethyl ether was added at room temperature during the period of 5 min. The mixture was stirred at room temperature for 2 h. The reaction mixture was worked up as mentioned in the previous case. After removal of the solvent and purification by preparative TLC (silica gel) using dichloromethane to give 0.13 g (57%) of 4,4′-dimethoxystilbene (**8**).

*Reduction of 3-Phenylpropanal Dimethyl Acetal (**13**).* To a stirred suspension of $TiCl_4$ (0.95 g, 5 mmol) in 15 ml of diethyl ether was added a suspension of $LiAlH_4$ (0.38 g, 10 mmol) in 10 ml of diethyl ether at room temperature under argon atmosphere. After stirring the mixture for 30 min at room temperature, 3-phenylpropanal dimethyl acetal (0.90 g, 5 mmol) in 15 ml of diethyl ether was added at room temperature. The mixture was stirred at room temperature for 2 h, then refluxed for an additional 1 h, and worked up as mentioned in the previous procedure. After removal of the solvent and purification by column chromatography (silica gel), 1-methoxy-3-phenylpropane (**14**) was isolated in 87% (0.65 g) yield. The NMR and IR spectra of the product (**14**) are shown in Table 4.

*Reduction of Cyclohexanone Ethylene Acetal (**23**).* To a stirred suspension of $TiCl_4$ (9.5 g, 50 mmol) in 150 ml of diethyl ether was added a suspension of $LiAlH_4$ (3.8 g, 100 mmol) in 100 ml of diethyl ether at room temperature under argon atmosphere. After stirring the mixture for 1 h at room temperature, cyclohexanone ethylene acetal (7.1 g, 50 mmol) in 100 ml of diethyl ether was added during the period of 40 min. The mixture was stirred at room temperature for 2 h. After the usual work-up, 2-(cyclohexyloxy)ethanol (**24**) (5.4 g, 75%) was collected by distillation.

References

1) E. C. Ashby and B. Cooke, *J. Am. Chem. Soc.*, **90**, 1625 (1968), and references cited therein.

2) R. A. Daignault and E. L. Eliel, *Org. Syn.*, Coll. Vol. 5, 303 (1973).

3) E. L. Eliel, V. G. Badding, and M. N. Rerick, *J. Am. Chem. Soc.*, **84**, 2371 (1962).

4) E. L. Eliel, B. E. Nowak, R. A. Daignault, and V. G. Badding, *J. Org. Chem.*, **30**, 2441 (1965).

5) B. E. Leggetter and R. K. Brown, *Can. J. Chem.*, **41**, 2671 (1963).
6) W. W. Zajac, Jr., and K. Byrne, *J. Org. Chem.*, **35**, 3375 (1970).
7) E. L. Eliel, *Rec. Chem. Progr.*, **22**, 129 (1961).
8) S. Masamune, P. A. Rossy, and G. S. Bates, *J. Am. Chem. Soc.*, **95**, 6452 (1973).
9) J. E. McMurry and M. P. Fleming, *J. Am. Chem. Soc.*, **96**, 4708 (1974).
10) E. C. Ashby, J. J. Lin, and R. Kovar, *J. Org. Chem.*, **41**, 1939 (1976).
11) H. Ishikawa and T. Mukaiyama, *Chem. Lett.*, **1976**, 737.
12) T. Mukaiyama, T. Sato, and J. Hanna, *Chem. Lett.*, **1973**, 1041.
13) Eyre and Spottiswoode, "Dictionary Organic Compounds," Vol. 14, Great Britain by The Chaucer Press (1965), p. 2714.
14) L. Summers and M. L. Larson, *J. Am. Chem. Soc.*, **74**, 4498 (1952).
15) E. J. Corey, R. L. Danheiser, and S. Chandrasekaran, *J. Org. Chem.*, **41**, 260 (1976).
16) R. Giezynski, S. Dziergowski, and S. Pasynkiewicz, *J. Organomet. Chem.*, **87**, 295 (1975).
17) The reagent [**A**] is inferior to $TiCl_4$–$LiAlH_4$ for preparative reaction as the large amount of hexamethylbenzene which is produced during the reaction complicates the isolation of the product.
18) G. Natta, D. Pino, G. Mazzanti, U. Giannini, *J. Am. Chem. Soc.*, **79**, 2976 (1957).
19) D. S. Breslow *et al.*, *J. Polym. Sci.*, *A-1*, **3**, 2852 (1965).
20) S. R. Sandler and W. Karo, "Organic Functional Group Preparation, III," Academic Press, New York (1972), p. 2.

Branched-chain Sugars. XI. Synthesis of 2,3,6-Trideoxy-3-*C*,4-*O*-dimethyl-3-nitro-D-*arabino*-hexopyranose (D-Evernitrose)[1]

Juji YOSHIMURA,* Masafumi MATSUZAWA, and Masuo FUNABASHI
Laboratory of Chemistry for Natural Products, Faculty of Science, Tokyo Institute of Techgnology, Nagatsuta, Midori-ku, Yokohama 227
(Received October 31, 1977)

2,3,6-Trideoxy-3-*C*, 4-*O*-dimethyl-3-nitro-D-*arabino*-hexopyranose was synthesized by the oxidation of methyl α-glycoside of the corresponding 3-amino derivative with *m*-chloroperbenzoic acid followed by hydrolysis. The 3-amino derivative was synthesized from methyl 4,6-*O*-benzylidene-2-deoxy-α-D-*erythro*-hexopyranosid-3-ulose by introduction of the amino-branching function according to the method of Bourgeois, followed by 6-deoxygenation and 4-*O*-methylation.

Evernitrose (**1**) is a natural nitro-sugar first found by Ganguly *et al.* in oligosaccharide antibiotics, everninomicin B, C, and D.[2] The structure of **1** was deduced from spectroscopic evidence and chemical degradation[3] to be 2,3,6-trideoxy-3-*C*,4-*O*-dimethyl-3-nitro-L-*ribo*-hexophyranose (**2**). However, this was revised to L-*arabino* configuration by X-ray analysis of methyl β-glycoside of the corresponding 3-acetamido derivative (**3**).[4] Brimacombe and Doner attempted the sysnthesis of **1** by the nitroethane cyclization of dialdehyde obtained from methyl α-L-rhamnopyranoside, the product with the revised configuration at nitro-branching position being converted into 4-*epi*-vancosaminide (**4**).[5] However, this process is unsuitable for the synthesis of **1**, because of the poor yield (12%) and the difficulty of selective 4-*O*-methylation of the cyclization product, and the inevitable reduction of the nitro group in the subsequent 2-deoxygenation. Bourgeois reported a new method for the introduction of methyl and amino groups into C-3 position of 1,2 : 5,6-di-*O*-isopropylidene-α-D-*ribo*-hexofuranos-3-ulose by subsequent reactions of cyano-mesylation, reduction into spiro-aziridine and hydrogenolysis of the aziridine ring.[6] The steric course of the aziridine ring formation was proved by Brimacombe *et al.* to proceed by the intramolecular S_N2 mechanism[7] from the fact that identical amino-branched derivative was obtained by addition of azide to the corresponding 3-methylene derivative followed by hydrogenation.

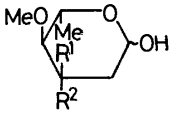

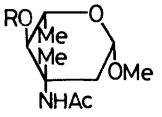

(**1**) R^1=Me, R^2=NO_2 (**3**) R=Me
(**2**) R^1=NO_2, R^2=Me (**4**) R=Ac

We have synthesized the enantiomer (**27**) of **1** from methyl 4,6-*O*-benzylidene-2-deoxy-α-D-*erythro*-hexopyranoside-3-ulose (**5**)[9] *via* the oxidation of the amino group of the corresponding amino-branched derivative into a nitro group. Since the method of Brimacombe *et al.*[7] was unsuccessful for the pyranoside ring, the amino-branched sugar was synthesized by that of Bourgeois.

Results and Discussion

Reaction of **5** with hydrogen cyanide in pyridine gave cyanohydrin (**6**) in *ca.* 50% yield. However, subsequent addition of trimethylsilyl chloride to the reaction mixture gave the corresponding ether (**7**) quantitatively. The configuration of **7** was determined to be D-*ribo* from the fact that the hydrogenation of **7** with lithium aluminium hydride(LAH) gave the corresponding 3-aminomethyl derivative (**8**) which was identical with the product obtained from known methyl 4,6-*O*-benzylidene-2-deoxy-3-*C*-nitromethyl-α-D-*ribo*-hexopyranoside[9] by hydrogenation. This indicates that cyanide anion attacks the carbonyl function of **5** from the upper side of the pyranoside ring selectively.

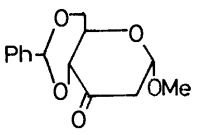

(**5**)

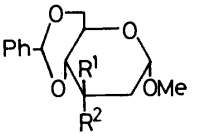

(**6**) R^1=CN, R^2=OH
(**7**) R^1=CN, R^2=OTMS
(**8**) R^1=CH_2NH_2, R^2=OH
(**9**) R^1=CN, R^2=OMs
(**10**) R^1=OMs, R^2=CN
(**13**) R^1=NH_2, R^2=Me
(**14**) R^1=NHAc, R^2=Me
(**25**) R^1=NO_2, R^2=Me

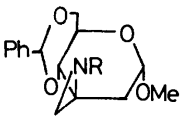

(**11**) R=H (**12**) R=Ac

Cyano-mesylation of **5** in a similar manner afforded the corresponding 3-*C*-cyano-3-*O*-mesyl derivative of D-*ribo* (**9**) and D-*arabino* (**10**) configuration in 64% and 3% yields, respectively. Compound **9** was converted into the corresponding spiro-aziridine (**11**) in 81% yield by reduction with LAH, which was then characterized as the *N*-acetyl derivative (**12**). Catalytic hydrogenation of **11** in the presence of Raney nickel gave the amino-branched derivative (**13**) in 93% yield, which was also characterized as the *N*-acetyl derivative (**14**). The two characteristic singlets (δ 2.24 and 2.70) of the methylene protons of aziridine ring in the NMR spectrum of **12** turned into a singlet of methyl protons (δ 1.59) in that of **14**. Treatment of **14** with *N*-bromosuccinimide and barium carbonate gave methyl 3-acetamido-4-*O*-benzoyl-6-bromo-2,3,6-trideoxy-3-*C*-methyl-α-D-*arabino*-hexopyranoside (**15**) in 60% yield, 6-bromine atom of which was hydrogenolyzed with Raney nickel to give the corresponding 6-deoxy derivative (**16**) as a sirup.

On the other hand, attempted dehydrobromination of **15** with silver fluoride[10] in pyridine or with 1,8-diazabicyclo[5.4.0]undec-7-ene in boiling benzene

unexpectedly gave a bicyclo pyrrolidine (**17**) quantitatively. The structure of **17** was distinguished from the possible seven-membered oxazolidine derivative by de-*O*-benzoylation with methanolic ammonia, followed by successful de-*N*-acetylation with aqueous potassium hydroxide. The 1C conformation of the pyranoside ring was confirmed by the NMR spectrum of de-*O*-benzoylated prodect (**18**: $J_{1,2a}=9.0$, $J_{1,2e}=4.0$ Hz). The conversion confirmed the configuration of the branching point of **15**—**16**, and also the steric course of the aziridine formation.

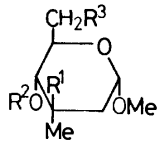

(**15**) R^1=NHAc, R^2=Bz, R^3=Br
(**16**) R^1=NHAc, R^2=Bz, R^3=H
(**20**) R^1=NHAc, R^2=H, R^3=H
(**21**) R^1=NHAc, R^2=Me, R^3=H
(**23**) R^1=NH_2, R^2=Me, R^3=H
(**26**) R^1=NO_2, R^2=Me, R^3=H

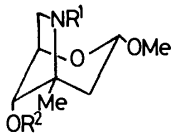

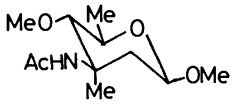

(**17**) R^1=Ac, R^2=Bz
(**18**) R^1=Ac, R^2=H
(**19**) R^1=H, R^2=H

(**22**)

Compound **16** was de-*O*-benzoylated and then methylated with equimolar sodium hydride and methyl iodide to give 4-*O*-methyl derivative (**21**) in 93% yield. It is interesting that **21** anomerized to the β-anomer (**22**) by treatment with cation exchanger (IR-120) in boiling methanol for 17 h, due to the 1,3-diaxial interaction between 3-*C*-Me and 1-OMe groups. Treatment of **21** with potassium hydroxide in hot aqueous ethanol gave a sirupy de-*N*-acetyl derivative (**23**) in 52% yield. In order to examine the oxidation of an amino group at the branching point, potassium permanganate and magnesium sulfate[11] were used for 3-amino-3-deoxy-1,2:5,6-di-*O*-isopropylidene-3-*C*-methyl-α-D-*gluco*-hexofuranose[5] and **13** in aqueous acetone, but the yields of the corresponding 3-nitro derivatives (**24** and **25**) were very poor (18% and 7.6%, respectively). However, *m*-chloroperbenzoic acid oxidation[12] of **13** in chloroform improved the yield (41%) of **25**. Thus, **23** in dichloromethane was successfully oxidized into the corresponding 3-nitro derivative (**26**) in 77% yield. The final hydrolysis of **26** with 0.05M sulfuric acid in aqueous dioxane at 90—95 °C gave D-evernitrose (**27**) in 72% yield.

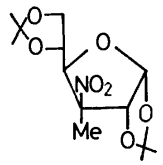

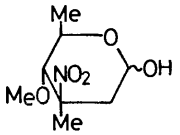

(**24**) (**27**)

Experimental

All the melting points are uncorrected. The solutions were evaporated under reduced pressure at a bath temperature not exceeding 45 °C. Specific rotations were measured in a 0.5-dm tube with a Carl Zeiss LEP-Al polarimeter with use of chloroform as the solvent unless otherwise stated. The IR spectra were recorded with a Hitachi Model EPI-G2 spectrometer. The NMR spectra were taken with a JEOL PS-100 spectrometer using tetramethylsilane as an internal standard in deuteriochloroform unless otherwise stated. Chemical shifts and coupling constants were recorded in δ and Hz units and IR frequencies in cm^{-1}.

*Methyl 4,6-O-Benzylidene-3-C-cyano-2-deoxy-α-D-ribo-hexopyranoside (**6**).* Hydrogen cyanide (1 ml, 25 mmol) was added to an ice-cooled solution of methyl 4,6-*O*-benzylidene-2-deoxy-α-D-*erythro*-hexopyranosid-3-ulose (**5**: 5 g, 18.9 mmol) in anhydrous pyridine (40 ml), and the resulting solution was kept at room temperature for one day. Appearance of a new spot was detected on TLC. Evaporation of the reaction mixture gave crystals which were fractionally recrystallized to give **6** in 50% (2.7 g) yield. Mp 156—159 °C, $[\alpha]_D^{22}$ +55.2° (*c* 1.0), IR: 3450 (OH), 2240 (CN), NMR: 7.64—7.24 (Ph; m, 5.65 (PhCH, s), 4.78 (H_1: q, $J_{1,2e}=1.6$, $J_{1,2a}=4.0$), 4.40—3.60 (H_4, H_5, H_6, H_6': m), 3.40 (OMe), 2.53 (H_{2e}: q, $J_{gem}=15.0$), 2.26 (H_{2a}: q).

Found: C, 61.73; H, 5.88; N, 4.86%. Calcd for $C_{15}H_{17}NO_5$: C, 61.85; H, 5.88; N, 4.81%.

*Methyl 4,6-O-Benzylidene-3-C-cyano-2-deoxy-3-O-trimethylsilyl-α-D-ribo-hexopyranoside (**7**).* Trimethylsilyl chloride (0.37 g, 3.4 mmol) was added to a reaction mixture of **5** (0.5 g, 1.9 mmol) and hydrogen cyanide (1 ml, 25 mmol) in pyridine (5 ml) as described above, and the resulting solution was kept at room temperature for one day. After evaporation of the mixture, the residue was extracted with toluene. Evaporation of the extracts gave pure crystals (0.65 g, 95%). Mp 88—91 °C, $[\alpha]_D^{22}$ +67.6° (*c* 1.0), IR: 2250 (CN), NMR: 0.24 (Me_3Si: s).

Found: C, 59.46; H, 6.86; N, 3.71%. Calcd for $C_{18}H_{25}NO_5Si$; C, 59.48; H, 6.93; N, 3.85%.

*Methyl 3-Aminomethyl-4,6-O-benzylidene-2-deoxy-α-D-ribo-hexopyranoside (**8**).* A suspension of **7** (0.5 g, 1.4 mmol) and excess LAH (75 mg) in ether was stirred at room temperature for 2 h, then poured gradually into ice-water containing acetic acid. The resulting mixture was extracted with chloroform and then worked up in the usual way to give **8** as crystals in 60% (0.24 g) yield. Mp 138—139 °C (ethanol-hexane), $[\alpha]_D^{22}$ +94.0° (*c* 1.0), IR: 3500—3000 (NH and OH), NMR: 7.6—7.1 (Ph: m), 5.57 (PhCH), 4.82 (H_1; q, $J_{1,2e}=1.0$, $J_{1,2a}=4.3$), 4.62—3.5 (H_4, H_5, H_6, and H_6': m), 3.36 (OMe), 2.96 and 2.62 (CH_2: each d, $J_{gem}=13.5$), 2.35 (OH), 2.12 (NH_2), 2.03 (H_{2e}: q, $J_{gem}=14.0$), 1.84 (H_{2a}: q).

Found: C, 60.81; H, 7.17; N, 4.54%. Calcd for $C_{15}H_{21}NO_5$: C, 61.00; H, 7.17; N, 4.74%.

The same compound was also obtained from methyl 4,6-*O*-benzylidene-2-deoxy-3-nitromethyl-α-D-*ribo*-hexopyranoside by catalytic reduction with Raney nickel.

*Methyl 4,6-O-benzylidene-3-C-cyano-2-deoxy-3-O-methylsulfonyl-α-D-ribo- (**9**) and D-arabino-Hexopyranoside (**10**).* Methylsulfonyl chloride (70 ml, 0.9 mol) was added dropwise at 0 °C to a reaction mixture of **5** (40 g, 0.15 mol) and hydrogen cyanide (10 ml, 0.25 mol) in pyridine, and the resulting solution was kept at 0 °C for 2 days. The mixture was poured into ice–water and extracted with chloroform. The usual work-up of the extract gave a half-crystalline mass which was triturated with ethanol to give crystals (34 g, 62%). **9**: Mp

161—162 °C (from dichloromethane-hexane), $[\alpha]_D^{22}$ +38.1° (*c* 1.0), IR: 2230 (CN), 1370 and 1190 (OMs), NMR: 7.56—7.24 (Ph: m), 5.66 (PhCH), 4.81 (H_1: q, $J_{1,2e}=1.0$, $J_{1,2a}=4.0$), 4.42—3.60 (H_4, H_5, H_6, and $H_{6'}$: m), 3.46 (OMs), 3.41 (OMe), 3.20 (H_{2e}: q, $J_{gem}=15.0$), 2.28 (H_{2a}: q).

Found: C, 51.92; H, 5.19; N, 3.65; S, 8.52%. Calcd for $C_{16}H_{19}NO_7S$: C, 52.03; H, 5.19; N, 3.79; S, 8.66%.

Chromatographic separation of the sirup obtained from the mother liquor of the above experiment gave **9** (0.2 g, 0.5%) and the 3-epimer, **10** (1.13 g, 3%). **10**: Mp 151—151.5 °C, $[\alpha]_D^{22}$ +102.1° (*c* 1.0), IR: 1360 and 1180 (OMs).

Found: C, 52.03; H, 5.18; N, 3.76; S, 8.50%. Calcd for $C_{16}H_{19}NO_7S$: C, 52.03; H, 5.19; N, 3.79; S, 8.60%.

*Spiro[aziridine-2,3'-(methyl 4,6-*O*-benzylidene-2,3-dideoxy-α-*D*-arabino-hexopyranoside)] (**11**) and Its* N*-Acetyl Derivative (**12**).* A suspension of **9** (30 g, 82 mmol) and LAH (4.6 g, 121 mmol) in ether (500 ml) was stirred at room temperature for 4 h, and then poured into water containing ethyl acetate to decompose excess LAH. The usual work-up of the resulting mixture gave unstable **11** in 81% (18.42 g) yield. Base-catalyzed acetylation of a part of this sirup gave **12** quantitatively. Mp 112—113 °C, $[\alpha]_D^{22}$ +34.6° (*c* 1.0), IR: 1680 (amido), NMR: 7.32 (Ph: s), 5.54 (PhCH), 4.82 (H_1: q, $J_{1,2e}=1.0$, $J_{1,2a}=4.0$), 4.36—3.64 (H_4, H_5, H_6, and $H_{6'}$: m), 3.35 (OMe), 2.70 and 2.24 (CH_2: each s), 2.56 (H_{2a}: q), 2.03 (NAc), 1.62 (H_{2e}: q, $J_{gem}=14.0$).

Found: C, 63.48; H, 6.65; N, 4.15%. Calcd for $C_{17}H_{21}NO_5$: C, 63.93; H, 6.63; N, 4.39%.

*Methyl 3-Amino-4,6-*O*-benzylidene-2,3-dideoxy-3-*C*-methyl-α-*D*-arabino-hexopyranoside (**13**) and Its* N*-Acetyl Derivative (**14**).* Hydrogenation of a suspension of **11** (18 g, 65 mmol) and Raney nickel (30 g) in methanol (400 ml) in an autoclave at 40 °C under 100 kg/cm² hydrogen atmosphere, and then the usual work-up gave a sirupy **13** in 93% (16.8 g) yield. Base-catalyzed acetylation of **13** and purification of the sirupy product on a silica gel column (benzene–acetone) gave pure **14** as an amorphous solid. The yield from **9** was 49%. $[\alpha]_D^{22}$ +38.6° (*c* 1.0), IR: 3300 (NH), 1650 and 1540 (amide), NMR: 7.60—7.28 (Ph: m), 5.56 (PhCH), 5.50 (NH: broad s), 4.72 (H_1: q, $J_{1,2a}=4.0$), 4.40—3.60 (H_4, H_5, H_6, and $H_{6'}$: m), 2.69 (H_{2a}: q), 2.35 (H_{2e}: q, $J_{gem}=14.0$), 1.93 (NAc), 1.59 (Me).

Found: C, 63.25; H, 7.22; N, 4.14%. Calcd for $C_{17}H_{23}NO_5$: C, 63.52; H, 7.21; N, 4.36%.

*Methyl 3-Acetamido-4-*O*-benzoyl-6-bromo-3-*C*-methyl-2,3,6-trideoxy-α-*D*-arabino-hexopyranoside (**15**).* A suspension of **14** (10 g, 31 mmol), *N*-bromosuccinimide (6.6 g, 37 mmol) and barium carbonate (7.3 g, 37 mmol) in dried carbon tetrachloride (400 ml) was refluxed for 4—5 h under normal room light until the colour changed from red to yellow, and then filtered. The filtered mass was washed with dichloromethane. The filtrate and washings were combined and washed in turn with aqueous sodium hydrogensulfite (5%), sodium hydrogencarbonate and water, and then dried. Evaporation of the solution gave a sirup (9.86 g) which was purified on a silica gel column (benzene–acetone) to give pure **15** in 60% (7.4 g) yield. The sirup gradually crystallized in a desiccator. Mp 71—72 °C, $[\alpha]_D^{22}$ +81.0° (*c* 1.0), IR: 3400 (NH), 1720 (ester), 1650 and 1530 (amide), NMR: 8.2—7.3 (Ph: m), 6.26 (NH: broad s), 5.48 (H_4: d, $J_{4,5}=10.0$), 4.85 (H_1: t, $J_{1,2e}=J_{1,2a}=3.0$), 4.18 (H_5: dt, $J_{5,6}=3.0$), 3.64—3.44 (H_6 and $H_{6'}$: m), 3.42 (OMe), 2.56 (H_{2e} and H_{2a}: d), 1.85 (NAc), 1.64 (Me).

Found: C, 50.55; H, 5.99; N, 3.08%. Calcd for $C_{17}H_{22}NO_5Br$: C, 51.01; H, 5.54; N, 3.50%.

*Methyl 3-Acetamido-4-*O*-benzoyl-3-*C*-methyl-2,3,6-tridoxy-α-*D*-arabino-hexopyranoside (**16**).* Catalytic hydrogenation of a suspension of **15** (0.36 g, 0.9 mmol) and triethylamine (0.11 g, 1.1 mmol) and Raney nickel (0.83 g) in methanol (100 ml) in an autoclave under 95 kg/cm² hydrogen atmosphere for 2 days and the usual work-up for the separation of the product from the amine salt gave sirupy **16** in 95% (0.28 g) yield. IR: 3400 (NH), 1720 (ester), 1650 and 1540 (amide), NMR: 8.18—7.30 (Ph: m), 6.20 (NH: s), 5.14 (H_4: d, $J_{4,5}=10.0$), 4.71 (H_1: q, $J_{1,2e}=1.6$, $J_{1,2a}=4.0$), 4.05 (H_5: dq, $J_{5,6}=7.2$), 3.37 (OMe), 2.68 (H_{2e}: q, $J_{gem}=15.0$), 2.36 (H_{2a}: q), 1.86 (NAc), 1.66 (Me), 1.24 (H_6: d).

Found: C, 62.94; H, 7.02; N, 4.41%. Calcd for $C_{17}H_{23}NO_5$: C, 63.53; H, 7.21; N, 4.36%.

Methyl N*-Acetyl-3,6-epimino-4-*O*-benzoyl-2,3,6-trideoxy-3-*C*-methyl-α-*D*-arabino-hexopyranoside (**17**) and Its De-*O*-benzoyl Derivative (**18**).* A solution of **15** (4.4 g, 11.0 mmol) and 1,8-diazabicyclo[5.4.0]undec-7-ene (1.84 g, 12.1 mmol) in dried benzene (70 ml) was refluxed for 3 h, and the crystals deposited were filtered off. A sirup obtained by evaporation of the filtrate was purified on a silica gel column to give **17** in 82% (2.9 g) yield. Mp 169—174 °C, $[\alpha]_D^{22}$ −111.3° (*c* 1.0), IR: 1720 (ester), 1622 (amide).

Found: C, 63.49; H, 6.49; N, 4.16%. Calcd for $C_{17}H_{21}NO_5$: C, 63.93; H, 6.63; 4.39%.

Treatment of **17** with methanolic ammonia in the usual manner gave **18** in 66% yield. Mp 109—111 °C, $[\alpha]_D^{22}$ −74° (*c* 1.0), IR: 3300 (OH), 1640 (amide), NMR (in CD_3OD): 4.62 (H_1: q, $J_{1,2e}=4.0$, $J_{1,2a}=9.0$), 4.23 (H_5: dt, $J_{5,6}=J_{5,6'}=2.0$), 3.50 (H_4: d, $J_{4,5}=3.0$), 3.46 (OMe), 3.67 (H_6 and $H_{6'}$: d, $J_{gem}=0$), 3.50 (H_4: d, $J_{4,5}=3.0$), 3.46 (OMe), 2.08 (H_{2a}: q), 2.05 (NAc), 1.74 (H_{2e}: q, $J_{gem}=13.0$), 1.52 (Me).

Found: C, 55.56; H, 7.93; N, 6.53%. Calcd for $C_{10}H_{17}NO_4$: C, 55.80; H, 7.96; N, 6.51%.

*Methyl 3,6-Epimino-3-*C*-methyl-2,3,6-trideoxy-α-*D*-arabino-hexopyranoside (**19**).* A solution of **18** (60 mg, 0.28 mmol) in 2 M potassium hydroxide (4 ml) was refluxed for 4 days. The starting material was still detected on TLC, but the solution was neutralized with acetic acid and evaporated. The residue was extracted with chloroform and the product obtained was separated on TLC to give sirupy **19** (15 mg, 31%). NMR: 4.24 (H_5: q, $J_{5,6}=2.7$), 4.88 (H_1: q, $J_{1,2e}=5.0$, $J_{1,2a}=8.1$), 3.51 (OMe), 3.45 (H_4: d, $J_{4,5}=3.8$), 3.19 (H_6 and $H_{6'}$: d, $J_{gem}=0$), 2.51 (NH and OH: s), 1.99 (Me), 1.80 (H_{2a}: q), 1.61 (H_{2e}: q, $J_{gem}=14.0$).

Found: C, 55.02; H, 8.16; N, 8.00%. Calcd for $C_8H_{15}NO_3$: C, 55.47; H, 8.73; N, 8.09%.

*Methyl 3-Acetamido-3-*C*-methyl-2,3,6-trideoxy-α-*D*-arabino-hexopyranoside (**20**).* A solution of **16** (120 mg, 0.37 mmol) in saturated methanolic ammonia (5 ml) was kept at room temperature overnight, evaporated, and the residual sirup was purified on TLC to give pure **20** (60 mg, 72%). $[\alpha]_D^{22}$ +73.8° (*c* 1.0, 50% MeOH–H_2O), IR: 3700—3150 (OH and NH), 1650 and 1540 (amide), NMR: 6.05 (OH), 5.84 (NH: broad s), 4.66 (H_1: q, $J_{1,2e}=1.6$, $J_{1,2a}=4.0$), 3.61 (H_5: dq, $J_{5,6}=6.0$), 3.38 (H_4: d, $J_{5,4}=9.4$), 3.32 (OMe), 2.01 (H_{2e}: q, $J_{gem}=15.8$), 2.00 (NAc), 1.85 (H_{2a}: q), 1.52 (Me), 1.31 (H_6: d).

Found: C, 56.08; H, 8.87; N, 6.16%. Calcd for $C_{10}H_{19}NO_4$: C, 55.28; H, 8.82; N, 6.45%.

The positive rotational change of this compound in cuprammonium solution ($[M]_{436}^{22}$ +254° → $[M]_{436}^{cuprA}$ +296°) also supports the configuration.

*Methyl 3-Acetamido-2,3,6-trideoxy-3-*C*,4-*O*-dimethyl-α-*D*-arabino-hexopyranoside (**21**).* To a solution of **20** (1.2 g, 5.4 mmol) in *N*,*N*-dimethylformamide (20 ml) was subsequently added equimolar sodium hydride (0.27 g) and methyl iodide (0.8 g) with stirring at room temperature. After

30 min, the reaction mixture was poured into ice-water and extracted with ether. The usual work-up of the extracts gave crystals (1.18 g, 93%), a part of which was recrystallized from hexane. Mp 136—138 °C, $[\alpha]_D^{22}$ +73° (*c* 1.0), NMR: 5.36 (NH: broad s), 4.68 (H_1: d, $J_{1,2a}$=4.5), 3.90 (H_4: d, $J_{4,5}$=10.0), 3.64 (H_5: dq, $J_{5,6}$=6.0), 3.49 and 3.28 (2×OMe), 2.97 (H_{2a}: q, J_{gem}=13.6), 1.94 (NAc), 1.77 (H_{2e}: d), 1.35 (Me), 1.28 (H_6: d).

Found: C, 56.50; H, 8.98; N, 5.90%. Calcd for $C_{11}H_{21}NO_4$: C, 57.12; H, 9.15; N, 6.06%.

Anomerization of ***21***. A suspension of **21** (0.1 g) and IR-120 (0.3 g) in absolute methanol (10 ml) was refluxed for 17 h and filtered, the filtrate then being evaporated to give a sirup (65 mg). Separation of the sirup on TLC (benzene: acetone=4:1) gave the β-anomer (**22**, 35 mg). Mp 159—160 °C, $[\alpha]_D^{22}$ −57° (*c* 1.0), NMR: 5.54 (NH: s), 4.50 (H_1: q, $J_{1,2e}$=2.5, $J_{1,2a}$=8.9), 3.75 (H_4: d, $J_{4,5}$=8.8), 3.54 (H_5: dq, $J_{5,6}$=6.0), 3.49 and 3.44 (2×OMe), 2.55 (H_{2a}: q, J_{gem}=13.5), 1.95 (H_{2e}: q), 1.93 (NAc), 1.34 (H_6: d), 1.30 (Me).

Found: C, 56.76; H, 9.00; N, 5.95%. Calcd for $C_{11}H_{21}NO_4$: C, 57.12; H, 9.15; N, 6.06%.

*Methyl 3-Amino-2,3,6-trideoxy-3-*C*,4-*O*-dimethyl-α-*D*-arabino-hexopyranoside (**23**).* A solution of **21** (630 mg, 2.73 mmol) and potassium hydroxide (612 mg) in 70% aqueous ethanol (3 ml) was refluxed under nitrogen atmosphere at 100—105 °C (bath temperature) for 4 days, neutralized with acetic acid, and then extracted with chloroform. The usual work-up of the extracts gave a sirup which was separated on a silica gel column to give sirupy **23** (113 mg) and the starting material (360 mg). NMR: 4.65 (H_1: q, $J_{1,2e}$=1.5, $J_{1,2a}$=4.0), 3.64 (H_5: dq, $J_{5,6}$=6.4), 3.57 and 3.29 (2×OMe), 2.67 (H_4: d, $J_{4,5}$=9.6), 1.82 (H_{2e}: q, J_{gem}=13.5), 1.70 (H_{2a}: q), 1.69 (NH_2: s), 1.28 (H_6: d), 1.24 (Me).

Found: C, 56.85; H, 10.22; N, 7.15%. Calcd for $C_9H_{19}NO_3$: C, 57.11; H, 10.12; N, 7.40%.

*3-Deoxy-1,2:5,6-di-*O*-isopropylidene-3-*C*-methyl-3-nitro-α-*D*-glucofuranose (**24**) and Methyl 2,3-Dideoxy-4,6-*O*-benzylidene-3-*C*-methyl-3-nitro-α-*D*-arabino-hexopyranoside (**25**). By Permanganate Oxidation*: A suspension of 3-amino-3-deoxy-1,2 : 5,6-di-*O*-isopropylidene-3-*C*-methyl-α-D-glucofuranose[5] (150 mg, 0.55 mmol), potassium permanganate (0.6 g, 3.8 mmol), and magnesium sulfate 7 hydrate (0.18 g) in acetone (4 ml) and water (1 ml) was stirred at room temperature for 29 h. Inorganic substances were precipitated by addition of acetone, and then filtered. The filtrate was evaporated and the residual sirup was extracted with chloroform. The usual work-up of the extract gave a sirup which was purified on a silica gel column to give **24** (30 mg, 18%). Mp 58—60 °C, $[\alpha]_D^{22}$ +52.6° (*c* 1.0), IR: 1550 (NO_2).

Found: C, 50.90; H, 6.86; N, 4.42%. Calcd for $C_{13}H_{21}NO_7$: C, 51.48; H, 6.98; N, 4.62%.

In a similar manner, **13** was oxidized to give **25** in 7.6% yield. Mp 131—132 °C (from ethanol), $[\alpha]_D^{22}$ +57.9° (*c* 1.0), IR: 1540 (NO_2).

Found: C, 57.95; H, 6.02; N, 4.23%. Calcd for $C_{15}H_{19}NO_6$: C, 58.24; H, 6.19; N, 4.53%.

By Peroxide Oxidation: A solution of **13** (0.2 g, 0.72 mmol) in chloroform (10 ml) was added dropwise over a period of 20 min to a refluxing solution of *m*-chloroperbenzoic acid (0.98 g, 5.7 mmol) in chloroform (10 ml). Heating was continued for 30 min. The resulting solution was then washed thoroughly with aqueous sodium sulfite (10%), saturated potasium hydrogencarbonate and water. Evaporation of the organic layer gave crystals which were fractionated on a silica gel column to give **25** in 41% (91 mg) yield.

*Methyl 2,3,6-Trideoxy-3-*C*,4-*O*-dimethyl-3-nitro-α-*D*-arabino-hexopyranoside (**26**).* Oxidation of **23** (112 mg) in dichloromethane with *m*-chloroperbenzoic acid in a similar way gave sirupy **26** in 77% (99 mg) yield. $[\alpha]_D^{22}$ +95.4° (*c* 1.9), IR: 1540 (NO_2), NMR: 4.74 (H_1: q, $J_{1,2e}$=1.5, $J_{1,2a}$=4.5), 3.78 (H_4: d, $J_{4,5}$=9.5), 3.64 (H_5: dq, $J_{5,6}$=5.4), 3.40 and 3.31 (2×OMe), 2.46 (H_{2a}: q, J_{gem}=13.5), 2.14 (H_{2e}: q), 1.75 (Me), 1.34 (H_6: d).

Found: C, 49.05; H, 7.78; N, 6.02%. Calcd for $C_9H_{17}NO_5$ C, 49.30; H, 7.82; N, 6.39%.

*2,3,6-Trideoxy-3-*C*,4-*O*-dimethyl-3-nitro-α-*D*-arabino-hexopyranose (*D*-Evernitrose) (**27**).* A solution of **26** (97 mg, 0.44 mmol) in 0.05 M sulfuric acid of dioxane-water (50%, 3 ml) was heated at 90—95 °C for 8 h, neutralized with excess barium carbonate and then filtered. The filtrate was evaporated to give a sirup which was purified on TLC. The sirup thus obtained (65 mg, 72%) was crystallized from benzene-hexane. Mp 84—88 °C, $[\alpha]_D^{22}$ +23.6° (*c* 0.9, ethanol) [lit,[3] the enantiomer: mp 88—93 °C, $[\alpha]_D$ −19.4°], IR: 3400 (OH), 1550 (NO_2). NMR spectrum showed the presence of α-(H_1: δ 5.33, q, $J_{1,2e}$=1.5, $J_{1,2a}$=4.0) and β-anomers (H_1: δ 4.88, q, $J_{1,2e}$=4.4, $J_{1,2a}$=7.2) in the ratio 1:1.

Found: C, 46.68; H, 7.33; N, 6.65%. Calcd for $C_8H_{15}NO_5$: C, 46.82; H, 7.37; N, 6.83%.

The authors are indebted to Mr. H. Matsumoto for NMR measurements and to the members of the Laboratory of Organic Analysis for microanalysis.

References

1) Part X. Submitted to *Carbohydr. Res.*

2) A. K. Ganguly and A. K. Saksena, *J. Antibiot.*, **28**, 707 (1975); A. K. Ganguly and S. Szmulewicz, *ibid.*, **28**, 710 (1975); A. K. Ganguly, O. Z. Sarre, D. Greeves, and J. Morton *J. Am. Chem. Soc.*, **97**, 1982 (1975).

3) A. K. Ganguly, O. Z. Sarre, and H. Reimann, *J. Am. Chem. Soc.*, **90**, 7129 (1968).

4) A. K. Ganguly, O. Z. Sarre, A. T. Mcphail, and K. D. Onan, *J. Chem. Soc., Chem. Commun.*, **1977**, 313.

5) J. S. Brimacombe and L. W. Doner, *J. Chem. Soc., Perkin Trans. 1*, **1974**, 62.

6) J. M. Bourgeois, *Helv. Chim. Acta*, **57**, 2553 (1974); **58** 363 (1975); **59**, 2214 (1976).

7) J. S. Brimacombe, J. A. Miller, and U. Zakir, *Carbohydr. Res.*, **41**, C3 (1975); **44**, C9 (1975); **49**, 233 (1976).

8) A. Klemer and G. Rodemeyer, *Chem. Ber.*, **107**, 2612 (1974); A. Rosenthal and P. Catsoulacos, *Can. J. Chem.*, **46**, 2868 (1968).

9) A. Rosenthal, K.-S. Ong., *Can. J. Chem.*, **48**, 3034 (1970).

10) D. Horton and W. Weckerle, *Carbohydr. Res.*, **44**, 227 (1975).

11) N. Kornblum, R. J. Clutter, and W. J. Jones, *J. Am. Chem. Soc.*, **78**, 4003 (1956).

12) C. H. Robinson, L. Milewich, and P. Hofer, *Tetrahedron*, **31**, 524 (1966).

Furan Derivatives. III. Some Electrophilic Substitution Reactions and Hydrogenation of 4,5-Dihydro-3*H*-naphtho[1,8-*bc*]furans

Takaaki HORAGUCHI* and Teishiro ABE†

Department of Chemistry, Faculty of Science, Niigata University, Ikarashi, Niigata 950-21

† *Department of General Education, Niigata University, Ikarashi, Niigata 950-21*

(Received November 4, 1977)

4,5-Dihydro-3*H*-naphtho[1,8-*bc*]furans (**1a—d**) reacted with a variety of electrophilic reagents to give the corresponding 2-substituted 4,5-dihydro-3*H*-naphtho[1,8-*bc*]furans. Hydrogenation of **1a—d** gave the corresponding 2*a*,3,4,5-tetrahydro-2*H*-naphtho[1,8-*bc*]furans. 2*H*-Naphtho[1,8-*bc*]furans (**7a—c**) which were prepared from **1a—c** were gradually converted to the 8-hydroxynaphthalene-1-carbaldehydes in air. The facile cleavage of the ether bond of **7a—c** is thought due to ring strain in the 2*H*-naphtho[1,8-*bc*]furan ring system.

In a previous paper,[1] the synthetic methods for 4,5-dihydro-3*H*-naphtho[1,8-*bc*]furans (**1a—d**) were reported. Since the novel ring system of **1a—d** possesses a furan ring at the *peri*-position of a partially saturated naphthalene ring, there may be some ring strain[1b] and so a difference in reactivity between **1a—d** and benzofurans is expected. In the present study, several reactions of **1a—d** have been examined and compared with those of the benzofurans.

Electrophilic substitution reactions and dimerization of **1a—d** are summarized in Table 1. Bromination of **1a—d** was carried out with bromine in carbon tetrachloride. Although **1b** and **1d** gave the corresponding 2-bromo compounds (**2b** and **2d**) in 89 and 74% yields, respectively, **1c** gave the corresponding 2-bromo compound (**2c**) in low yield (21%). The low yield was attributed to the formation of a resinous product. **1a** gave a complex mixture and the expected bromide was not isolated. Formylation of **1a,c,d** with *N,N*-dimethylformamide and phosphoryl chloride gave the corresponding 2-formyl compounds (**3a,c,d**). The yields of **3a** and **3c** were good (74 and 65% respectively), but **3d** gave only a 27% yield and the starting material (**1d**) was recovered; the low reactivity of **1d** is thought due to the strong inductive effect of the chlorine atom. Friedel-Crafts reaction of **1a** and **1c** was carried out with benzoyl chloride and tin(IV) chloride in carbon disulfide. The expected 2-benzoyl compounds (**4a** and **4c**) were obtained in low yields (27 and 25%, respectively) due to the formation of a resinous product. It appears that the 4,5-dihydro-3*H*-naphtho[1,8-*bc*]furan ring is appreciably unstable under the reaction conditions. When **1a—d** were treated with sulfuric acid in ethanol, **1a—c** gave the corresponding dimers (**5a—c**) in good yields (56—90%), but the dimerization of **1d** did not occur. Again, the strong inductive effect of the chlorine atom of **1d** reduces the electron deisity at the 2-position in the furan ring.

These results suggest that the position of electrophilic substitution reactions of **1a—d** are similar to those of the benzofurans. Thus, bromination, formylation, and acylation of the 3-alkylbenzofurans occur at the 2-position of the furan ring[3] and the dimerization of the

TABLE 1. ELECTROPHILIC SUBSTITUTION REACTIONS AND DIMERIZATION OF **1a—d**

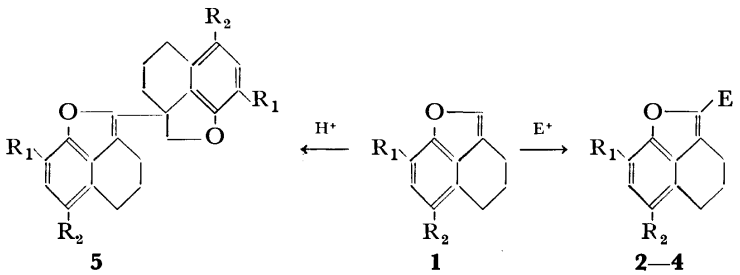

5 **1** **2—4**

a) R_1=H, R_2=H
b) R_1=CCH_3, R_2=H
c) R_1=H, R_2=OCH_3
d) R_1=CCH_3, R_2=Cl

Starting furan	Reagent	Product		Yield %
1a	Br_2	complex mixture		—
1b		**2** (E=Br)	**b**	89
1c			**c**	21
1d			**d**	74
1a	$HCON(CH_3)_2$ / $POCl_3$	**3** (E=CHO)	**a**	74
1c			**c**	65
1d			**d**	27
1a	C_6H_5COCl / $SnCl_4$	**4** ($E=C_6H_5CO$)	**a**	27
1c			**c**	25
1a	H_2SO_4	**5**	**a**	84
1b			**b**	56
1c			**c**	90
1d		no reaction		—

Table 2. Hydrogenation and dehydrogenation reactions of **1a—d** and **7a—c**

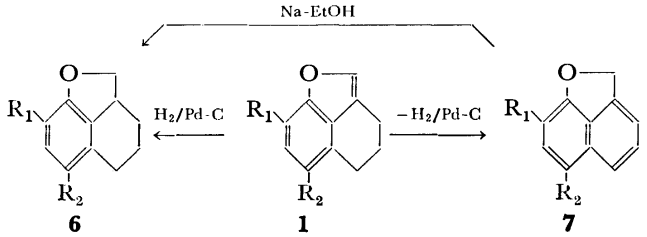

6 **1** **7**

a) R_1=H, R_2=H **c**) R_1=H, R_2=OCH_3
b) R_1=OCH_3, R_2=H **d**) R_1=OCH_3, R_2=Cl

Starting furan	Reagent	Product	Yield %
1a	H_2/Pd-C	**6a**	98
1b		**6b**	92
1c		**6c**	97
1d		**6b**	90
1a	Pd-C	**7a**	41
1b		**7b**	58
1c		**7c**	47
1d		no reaction	—
7a	Na-EtOH	**6a**	78
7b		**6b**	73
7c		**6c**	88

3-alkylbenzofurans is achieved readily by acid catalysis.[2] However, **1a—d** are significantly less stable compared with the benzofurans under vigorous conditions such as acylation.

Hydrogenation and dehydrogenation reactions of **1a—d** are summarized in Table 2. Palladium on charcoal catalyzed hydrogenation of **1a—c** in ethanol at ambient temperature and pressure gave the corresponding tetrahydro compounds (**6a—c**) in good yields (92—98%). In the case of **1d**, the chlorine atom was subjected to hydrogenolysis along with hydrogenation of the furan ring to give **6b** (90% yield). The benzofurans subjected to hydrogenation gave the corresponding 1,2-dihydrobenzofurans under the same conditions[1a,4] and the rate of hydrogen consumption of **1a—d** was comparable with that of the benzofurans. If **1a—d** contains a larger strain compared to that of the benzofurans, the former should be more readily hydrogenated than the latter. The above results suggest that **1a—d** contain little strain compared with the benzofurans.

When **1a—c** were heated with palladium on charcoal in *p*-cymene, the corresponding 2*H*-naphtho[1,8-*bc*]-furans (**7a—c**) were obtained in fairly good yields (41—58%). However **1d** could not be dehydrogenated to the corresponding 2*H*-naphtho[1,8-*bc*]furan and the starting material was recovered. Thus, the reactivity of **1d** is affected by the strong inductive effect of the chlorine atom. Reduction of **7a—c** with sodium and ethanol gave the corresponding tetrahydro compounds (**6a—c**) in good yields (73—88%). Colorless compounds of **7a—c** are appreciably unstable and turned yellow or red upon storage; the liqiud compound **7b** gave a particullarly prominent coloration. Berry *et al.*[5] have suggested that the coloration of **7a** is due to the formation of 8-hydroxynaphthalene-1-carbaldehyde (**8a**). The cause of the coloration of both **7b** and **7c** was examined; **7b** was chromatographed over silica gel and **8b** isolated as the main colored product. Similarly, the colored material of **7c** was confirmed to be **8c**. Thus the compounds of the general type **7a—c** are easily subjected to cleavage of the ether bond. It has been pointed out that acenaphthene (**9**) which possesses a similar ring skeleton with **7a—c** contains a strain in the fused ring system.[6] Therefore, the facile cleavage of the ether bond of **7a—c** is thought due to ring strain in the 2*H*-naphtho[1,8-*bc*]furan ring system.

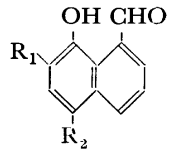

8

a) R_1=H, R_2=H
b) R_1=OCH_3, R_2=H
c) R_1=H, R_2=OCH_3

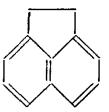

9

Experimental

All the melting points are uncorrected. The column chromatography was performed on silica gel (Wakogel C-200). Unless otherwise stated, anhydrous sodium sulfate was employed as the drying agent. The infrared absorption spectra were determined with a JASCO Model DS 402 G infrared spectrophotometer. The ultraviolet absorption spectra were determined with a Shimadzu Model UV-200 spectrophotometer. The nuclear magnetic resonance spectra were determined at 100 MHz with a JEOL Model 4H-100 NMR spectrometer, using tetramethyl silane as the internal standard.

*Bromination of 4,5-Dihydro-3H-naphtho[1,8-bc]furans (**1a—d**).* Bromine (0.85 g) in carbon tetrachloride (10 ml) was added dropwise to **1b** (1.0 g) in carbon tetrachloride (10 ml) with stirring at ambient temperature and the mixture further stirred for 30 min. After the removal of the solvent, the resulting oil was chromatographed and eluted with benzene to give **2b** (1.2 g, 89%). Colorless oil; bp 135 °C/1.5 Torr (partially decomposed). NMR(CCl_4): δ 1.85—2.09 (2H, m), 2.55—2.80 (4H, m), 3.96 (3H, s), 6.51 (1H, d, J=8 Hz), 6.71 (1H, d, J=8 Hz). Found: C, 53.88; H, 4.26%. Calcd for $C_{12}H_{11}O_2Br$: C, 53.96; H, 4.15%.

Similarly, **1c** and **1d** were brominated to give **2c** and **2d** (21 and 74%), respectively; **1a** was brominated to give a complex mixture and the simple bromide was not isolated.

2c: Colorless needles; mp 52—53 °C (from hexane). NMR(CCl_4): δ 1.85—2.08 (2H, m), 2.61 (2H, t, J=6 Hz), 2.73 (2H, t, J=6 Hz), 3.79 (3H, s), 6.61 (1H, d, J=8 Hz), 7.01 (1H d, J=8 Hz).
Found: C, 53.85; H, 4.20%. Calcd for $C_{12}H_{11}O_2Br$: C, 53.96; H, 4.15%.

2d: Colorless needles; mp 109—110 °C (from hexane). NMR (CCl_4): δ 1.87—2.11 (2H, m), 2.61 (2H, t, J=6 Hz), 2.75 (2H, t, J=6 Hz), 3.97 (3H, s), 6.55 (1H, s). Found: C, 47.68; H, 3.46%. Calcd for $C_{12}H_{10}O_2BrCl$: C, 47.79; H, 3.34%.

*Formylation of 4,5-Dihydro-3H-naphtho[1,8-bc]furans (**1a,c,d**).* Phosphoryl chloride (2.7 g) in *N,N*-dimethylformamide (4.5 g) was added to **1a** (1.5 g) in *N,N*-dimethylformamide (6.0 g) and the mixture heated at 90 °C for 3 h. The reaction mixture was then poured into ice water and allowed to stand overnight. The resulting precipitates were collected by filtration to give **3a** (1.3 g, 74%), which was purified by recrys-

tallization. Yellow needles; mp 88—89 °C (from methanol). IR(KBr): ν_{max} 1680 (CHO) cm^{-1}. NMR($CDCl_3$): δ 1.97—2.22 (2H, m), 2.93 (2H, t, J=6 Hz), 3.10 (2H, t, J=6 Hz), 6.98—7.48 (3H, m), 9.87 (1H, s). UV(EtOH): λ_{max} (ε) 203 (14300), 233^{sh} (9100), 238 (10000), 304 nm (22300). Found: C, 77.13; H, 5.41%. Calcd for $C_{12}H_{10}O_2$: C, 77.40; H, 5.41%.

Similarly, **1c** and **1d** were formylated to give **3c** and **3d** (65 and 27%), respectively.

3c: Yellow needles; mp 154—155 °C (from ethanol). IR(KBr): ν_{max} 1680 (CHO) cm^{-1}. NMR($CDCl_3$): δ 1.93—2.18 (2H, m), 2.86 (2H, t, J=6 Hz), 3.06 (2H, t, J=6 Hz), 3.86 (3H, s), 7.03 (1H, d, J=9 Hz), 7.22 (1H, d, J=9 Hz), 9.85 (1H, s). UV(EtOH): λ_{max} (ε) 206 (19500), 224^{sh} (10300) 306 nm (24000). Found: C, 72.02; H, 5.68%. Calcd for $C_{13}H_{12}O_3$: C, 72.21; H, 5.59%.

3d: Yellow needles; mp 171—172 °C (from methanol). IR(KBr): ν_{max} 1675 (CHO) cm^{-1}. NMR($CDCl_3$): δ 1.95—2.20 (2H, m), 2.85 (2H, t, J=6 Hz), 3.07 (2H, t, J=6 Hz), 4.00 (3H, s), 6.87 (1H, s), 9.92 (1H, s). UV(EtOH): λ_{max} (ε) 206 (28900), 247 (17000), 301 nm (19700). Found: C, 62.07; H, 4.52%. Calcd for $C_{13}H_{11}O_3Cl$: C, 62.29; H, 4.42%.

*Benzoylation of 4,5-Dihydro-3*H*-naphtho[1,8-*bc*]furans (**1a** and **1c**).* Tin(IV) chloride (2.0 g) was added to a solution of **1a** (1.0 g) and benzoyl chloride (1.1 g) in carbon disulfide (10 ml) under cooling with ice water and stirring, and the mixtures was further stirred at ambient temperature for 3 h. After the addition of diluted hydrochloric acid, the mixture was extracted with ether, ethereal layer washed successively with aqueous sodium hydrogencarbonate and water, and dried. After removal of the solvent, the resulting oil was chromatographed and eluted with benzene to give **4a** (0.44 g, 27%), which was identical with the sample previously prepared[1b] from the melting points and infrared spectra. Similarly, **1c** was benzoylated to give **4c** (25%).

4c: Colorless prisms; mp 90—91 °C (from ethanol). IR(KBr): ν_{max} 1625 (C=O) cm^{-1}. NMR($CDCl_3$): δ 1.89—2.13 (2H, m), 2.85 (2H, t, J=6 Hz), 3.00 (2H, t, J=6 Hz), 3.85 (3H, s), 7.02 (1H, d, J=9 Hz), 7.25 (1H, d, J=9 Hz), 7.38—7.58 (4H, m), 8.01—8.11 (2H, m). UV(EtOH): λ_{max} (ε) 207 (25500), 257 (7900), 322 nm (21700). Found: C, 78.01; H, 5.64%. Calcd for $C_{18}H_{16}O_3$: C, 78.06; H, 5.52%.

*Dimerization of 4,5-Dihydro-3*H*-naphtho[1,8-*bc*]furans (**1a—d**).* Sulfuric acid (6.0 g) was added dropwise to **1a** (1.0 g) in ethanol (4 ml) under cooling with ice water and stirring, and the mixture further stirred at ambient temperature for 3 h. The reaction mixture was then poured into ice water and the mixture extracted with ether. The ethereal layer was treated, in the usual manner, to give **5a** (0.84 g, 84%) which was purified by recrystallization. Colorless plates; mp 158—159 °C (from benzene-hexane). NMR(CCl_4): δ 1.60—1.90 (7H, m), 2.58—2.78 (5H, m), 4.18 (1H, d, J=8 Hz), 4.85 (1H, d, J=8 Hz), 6.52—7.13 (6H, m). UV(EtOH): λ_{max} (ε) 208 (40300), 215^{sh} (34100), 256 (16500), 286 nm (3500). Found: C, 83.40; H, 6.38%. Calcd for $C_{22}H_{20}O_2$: C, 83.51; H, 6.37%. Similarly, **1b** and **1c** were dimerized to give **5b** and **5c** (56 and 90%), respectively; **1d** was not dimerized and the starting material was recovered.

5b: Colorless plastic solid. NMR(CCl_4): δ 1.57—1.90 (7H, m), 2.53—2.78 (5H, m), 3.85 (3H, s), 3.94 (3H, s), 4.20 (1H, d, J=8 Hz), 4.92 (1H, d, J=8 Hz), 6.49 (1H, d, J=8 Hz), 6.53 (1H, d, J=8 Hz), 6.66 (1H, d, J=8 Hz), 6.70 (1H, d, J=8 Hz). UV(EtOH): λ_{max} (ε) 216 (46400), 249 (16300), 357 (15500), 280 (3900), 290 nm (3000). Found C, 76.80; H, 6.60%. Calcd for $C_{24}H_{24}O_4$: C, 76.57; H, 6.43%.

5c: Colorless plates; mp 182—183 °C (from benzene-hexane). NMR($CDCl_3$): δ 1.55—2.00 (7H, m), 2.60—2.70 (5H, m), 3.81 (6H, s), 4.21 (1H, d, J=8 Hz), 4.90 (1H, d, J=8 Hz), 6.64 (2H, s), 6.74 (1H, d, J=8 Hz), 7.10 (1H, d, J=8 Hz). UV(EtOH): λ_{max} (ε) 215^{sh} (34400), 260 (15900), 291 nm (7900). Found: C, 76.75; H, 6.54%. Calcd for $C_{24}H_{24}O_4$: C, 76.57; H, 6.43%.

*Catalytic Hydrogenation of 4,5-Dihydro-3*H*-naphtho[1,8-*bc*]furans (**1a—d**).* **1a** (1.0 g) in ethanol (50 ml) was hydrogenated in the presence of 10% palladium on charcoal (0.8 g) at ambient temperature and pressure for 10 h. After the removal of the catalyst by filtration, the solvent was evaporated to give **6a** (1.0 g, 98%), which distilled off at 101 °C/1 Torr and the distilate solidified in a short time. Colorless solid; mp 33—34 °C. NMR(CCl_4): δ 1.10—1.86 (2H, m), 1.90—2.20 (2H, m), 2.53—2.90 (2H, m), 3.00—3.37 (1H, m) 3.85 (1H, dd, J=8 and 12 Hz), 4.63 (1H, t, J=8 Hz), 6.42 (1H, d, J=8 Hz), 6.46 (1H, d, J=8 Hz), 6.88 (1H, t, J=8 Hz). Found: C, 82.21; H, 7.56%. Calcd for $C_{11}H_{12}O$: C, 82.46; H, 7.55%. Similarly, **1b** and **1c** were hydrogenated to give **6b** and **6c** (92 and 97%), respectively; **1d** was hydrogenated to give **6b** (92%) instead of **6d**.

6b: Colorless oil; bp 106 °C/1.5 Torr. NMR(CCl_4): δ 1.15—1.82 (2H, m), 1.92—2.20 (2H, m), 2.32—2.85 (2H, m), 3.00—3.40 (1H, m), 3.80 (3H, s), 3.86 (1H, dd, J=8 and 10 Hz), 4.67 (1H, t, J=8 Hz), 6.40 (1H, d, J=8 Hz), 6.53 (1H, d, J=8 Hz). Found: C, 75.54; H, 7.34%. Calcd for $C_{12}H_{14}O_2$: C, 75.76; H, 7.42%.

6c: Colorless oil; bp 112 °C/2 Torr. NMR(CCl_4): δ 1.00—1.85 (2H, m), 1.93—2.22 (2H, m), 2.35—2.81 (2H, m), 2.95—3.35 (1H, m), 3.68 (3H, s), 3.80 (1H, dd, J=2 and 8 Hz), 4.59 (1H, t, J=8 Hz), 6.35 (2H, s). Found: C, 75.60; H, 7.31%. Calcd for $C_{12}H_{14}O_2$: C, 75.76; H, 7.42%.

*Dehydrogenation of 4,5-Dihydro-3*H*-naphtho[1,8-*bc*]furans (**1a—d**).* A mixture of **1a** (1.8 g) and 10% palladium on charcoal (1.5 g) in *p*-cymene (20 ml) was heated at 180 °C for 4 h under a nitrogen atmosphere. The reaction mixture, after the usual treatment, was chromatographed and eluted with benzene-hexane (1:1) to give **7a** (0.73 g, 41%). Colorless plates; mp 53.5—54.5 °C (from methanol) (lit,[5] 53—54 °C). NMR(CCl_4): δ 5.60 (2H, s), 6.56 (1H, d, J=7 Hz), 6.97—7.50 (5H, m). UV(EtOH): λ_{max} (ε) 202 (14200), 251 (7700), 312 (8800), 340 nm (4200). Found: C, 84.44; H, 5.09%. Calcd for $C_{11}H_8O$: C, 84.59; H, 5.16%. Similarly, **1b** and **1c** were dehydrogenated to give **7b** and **7c** (58 and 47%), respectively; **1d** was not dehydrogenated and the starting material was recovered.

7b: Colorless oil; bp 96 °C/0.9 Torr. NMR(CCl_4): δ 4.00 (3H, s), 5.65 (2H, s), 7.01 (3H, s), 7.16 (1H, d, J=8 Hz), 7.41 (1H, d, J=8 Hz). UV(EtOH): λ_{max} (ε) 213 (21400), 238 (44000), 303 (3600), 334 nm (3200). Found: C, 77.38; H, 5.52%. Calcd for $C_{12}H_{10}O_2$: C, 77.40; H, 5.41%.

7c: Colorless needles; mp 46—47 °C (from benzene-hexane). NMR(CCl_4): δ 3.84 (3H, s), 5.61 (2H, s), 6.47 (1H, d, J=7 Hz), 6.50 (1H, d, J=7 Hz), 7.05 (1H, d, J=7 Hz), 7.33 (1H, t, J=7 Hz), 7.69 (1H, d, J=7 Hz). UV(EtOH): λ_{max} (ε) 207 (39300), 242 (24200), 246 (23600), 325 (7200), 339 nm (7500). Found: C, 77.13; H, 5.29%. Calcd for $C_{12}H_{10}O_2$: C, 77.40; H, 5.41%.

*Reduction of 2*H*-Naphtho[1,8-*bc*]furans (**7a—c**).* Sodium (2.0 g) was added, in limited amounts over 30 min, to **7a** (0.2 g) in ethanol (15 ml) with stirring at 80 °C and th mixture refluxed for an additional 1 h. The reaction mixture was poured into ice water, acidified with dilute hydrochloric acid and then extracted with ether. After evaporation of the ether, the resulting oil was chromatographed and eluted with benzene to give **6a** (0.16 g, 78%). Similarly, **7b** and **7c**

were reduced to give **6b** and **6c** (73 and 88%), respectively.

Examination of the Coloration of 2H-Naphtho[1,8-bc]furans (7b and 7c). The deeply reddish **7b** (1.0 g) was chromatographed and eluted with benzene–ether (9:1) to give **8b** (60 mg, 6%). Orange needles; mp 85—87 °C (from benzene–hexane). IR(KBr): ν_{max} 1660 (CHO), 3290 (Ar-OH) cm^{-1}. NMR($CDCl_3$): δ 4.00 (3H, s), 7.29—7.46 (3H, m), 7.95 (2H, d, J=8 Hz), 10.08 (1H, s), 10.75 (1H, s). Found: C, 71.39; H, 5.05%. Calcd for $C_{12}H_{10}O_3$: C, 71.28; H, 4.99%.

The colored material of **7c** was identical, by TLC analysis, with **8c** which was prepared from **7c** as below. A solution of **7c** (0.5 g) and lead tetraacetate (1.3 g) in acetic acid (60 ml) was stirred at ambient temperature for 4 h. The reaction mixture, after the usual treatment, was chromatographed to give **8c** (50 mg, 9%). Orange needles; mp 96—98 °C (from benzene–hexane). IR(KBr): ν_{max} 1665 (CHO) cm^{-1}. NMR ($CDCl_3$): δ 3.95 (3H, s), 6.93 (1H, d, J=8 Hz), 7.11 (1H, d, J=8 Hz), 7.55 (1H, t, J=7 Hz), 8.05 (1H, dd, J=1 and 6 Hz), 8.67 (1H, dd, J=1 and 6 Hz), 9.87 (1H, s), 10.97 (1H, s). Found: C, 71.38; H, 5.08%. Calcd for $C_{12}H_{10}O_3$: C, 71.28; H, 4.99%.

The authors wish to thank Mr. Yoshiaki Takahashi for the elemental analyses and Mr. Takao Oono for the nuclear magnetic resonance analyses.

References

1) (a) T. Horaguchi, T. Shimizu, and T. Abe, *Bull. Chem. Soc. Jpn.*, **49**, 738 (1976); (b) T. Horaguchi, T. Shimizu, and T. Suzuki, *ibid.*, **48**, 1249 (1975).

2) T. Abe and T. Shimizu, *Nippon Kagaku Zasshi*, **91**, 753 (1970).

3) (a) R. Stoemer, *Chem. Ber.*, **44**, 1853 (1971); (b) E. W. Smith, *Iowa State Coll. J. Sci.*, **12**, 155 (1937) [*Chem. Abstr.*, **32**, 2938 (1938)]; (c) D. S. Deorha and P. Gupta, *Chem. Ber.*, **97**, 3578 (1964); (d) M. Bisagni, Ng.Ph. Buu-Hoï, and R. Royer, *J. Chem. Soc.*, **1955**, 3688.

4) J. S. H. Davies, D. A. McCrea, W. L. Norris, and G. R. Ranage, *J. Chem. Soc.*, **1950**, 3206.

5) D. Berry and D. C. C. Smith, *J. Chem. Soc., Perkin Trans. 1*, **1972**, 699.

6) (a) H. W. W. Ehrlich, *Acta. Crystallogr.*, **10**, 699 (1957); (b) A. G. Anderson, Jr., and Robert H. Wade, *J. Am. Chem. Soc.*, **74**, 2274 (1952).

Calculation of the Carbon-13 NMR Chemical Shifts of Some Organic Compounds Using the Improved Virtual Orbital Method

Masahiro KONDO and Isao ANDO*

Department of Polymer Chemistry, Tokyo Institute of Technology, Ookayama, Meguro-ku, Tokyo 152

(Received November 28, 1977)

Using the wavefunction obtained from the improved virtual orbital (IVO) method proposed by Huzinaga, the ^{13}C NMR chemical shifts in some organic compounds (acetylene, ethylene, ethane, pentane, benzene, pyridine and acetone) have been calculated and compared with those obtained from the ordinary SCF-MO method. If the molecule considered is small, highly symmetric and non-polar, it can be expected that there is little difference in the calculated values between these two methods. If the molecule considered is rather large or polar, modification of the calculated values are apt to be induced by the IVO method. As far as qualitative tendencies of the chemical shifts of carbon in a molecule are concerned, both methods give similar results.

The carbon-13 NMR chemical shifts have been calculated by many methods[1,2] for organic compounds using various molecular orbital theories. The sum-over-state method[3,4] is one of such theories. In this method, not only the wavelfunctions for occupied orbitals but also those for virtual (or unoccupied) orbitals are needed in the calculation of the paramagnetic contribution. It is known[5] that in the system of 2N electrons the wavefunctions obtained by the ordinary Hartree-Fock operator are appropriate to the occupied orbitals but not to the virtual orbitals. These wavefunctions for the virtual orbitals are appropriate to the system of 2N+1 electrons rather than 2N electrons because an electron virtually involved in any virtual orbital suffers from the potentials of all the 2N electrons involved in the occupied orbitals. Thus, it is preferable to correct the wavefunctions for virtual orbitals so that they are appropriate for the system of 2N electrons as well as those for occupied orbitals. In an attempt to improve the situation, Huzinaga *et al.*[6,7] reported the improved virtual orbital (IVO) method in which a projection operator is introduced to modify the Hartree-Fock orperator for the virtual orbitals.

The carbon-13 chemical shifts and their tensors in some organic compounds have been calculated by the sum-over-state method without any improvement of the wavefunctions for virtual orbitals.[8,9] It appears that the calculated values systematically deviate from experimental values with relation to the size of the molecules;[9] in saturated hydrocarbons, as the number of carbons increase the paramagnetic contribution to the shielding constant tends to decrease. This trend makes it difficult to compare the relative shifts among the carbons in different molecules. Such a systematic deviation might come from an approximation adopted there, for example, the neglect of the overlap integral or the inexact wavefunction for virtual orbitals described above. This paper will focus on the latter case, *i.e.* the inexact wavefunction for virtual orbitals. The carbon-13 shielding constants will be calculated by the sum-over-state method using the wavefunctions obtained by the IVO method and these will be compared with the calculated results obtained by the ordinary SCF method.

Theoretical

In the sum-over-state method, one of the diagonal components of the paramagnetic shielding tensor of nucleus A, $\sigma^{p}_{\alpha\alpha}$ (α=x, y, or z), is expressed as follows:[3]

$$\sigma^{p}_{xx} = -\frac{2e^2\hbar^2}{m^2c^2}\langle r^{-3}\rangle_{2p}\sum_{i}^{occ}\sum_{k(\neq i)}^{unocc}(\Delta E_{i-k})^{-1}(C_{iy_A}C_{kz_A}-C_{iz_A}C_{ky_A}) \times\sum_{B}(C_{iy_B}C_{kz_B}-C_{iz_B}C_{ky_B}). \quad (1)$$

In these formulas, C_{ix_A} is the coefficient of the $2p_x$ atomic orbital on atom A of the i-th molecular orbital in the LCAO MO theory, ΔE_{i-k} the singlet-singlet excitation energy from the occupied orbital ϕ_i to the unoccupied orbital ϕ_k and $\langle r^{-3}\rangle_{2p}$ the mean inverse cubic radius of a 2p electron. The molecular orbitals are obtained from the IVO method[5-7] based on the MINDO/2 method.[10]

According to Huzinaga *et al.*[5-7] a new Fock operator $\mathbf{F}'_i$ in one-electron excitation from an occupied orbital ϕ_i is given by

$$\mathbf{F}'_i = \mathbf{F} + \mathbf{V}'_i \quad (2)$$

where

$$\mathbf{V}'_i = (\mathbf{1}-\mathbf{P})\Omega_i(\mathbf{1}-\mathbf{P}).$$

Here $\mathbf{F}$ is the ordinary Fock operator, $\mathbf{P}$ the projection operator, Ω_i the correction operator for the energy level of the virtual orbitals and these operators are given as follows:

$$\mathbf{F} = \mathbf{H}^{core} + \sum^{occ}(2\mathbf{J}_j-\mathbf{K}_j), \quad (3)$$

$$\mathbf{P} = \sum^{occ}|\phi_j\rangle\langle\phi_j|, \quad (4)$$

$$\Omega_i = -\mathbf{J}_i + 2\mathbf{K}_i, \quad (5)$$

where $\mathbf{J}_i$ and $\mathbf{K}_i$ are the Coulomb and Exchange operators, respectively. In the case of the new Fock operator $\mathbf{F}'_i$, for the occupied orbitals ϕ_j's

$$\mathbf{F}'_i|\phi_j\rangle = \mathbf{F}|\phi_j\rangle = \varepsilon_j|\phi_j\rangle \quad (6)$$

and for the virtual orbitals ϕ_k's

$$\mathbf{F}'_i|\phi_k\rangle = (\mathbf{F}+\Omega_i-\mathbf{P}\Omega_i)|\phi_k\rangle, \quad (7)$$

$$\varepsilon_k = \langle\phi_k|\mathbf{F}+\Omega_i|\phi_k\rangle. \quad (8)$$

That is, the operator $\mathbf{F}'_i$ gives an alteration of the eigenvalues and eigenfunctions for the virtual orbitals. A molecular orbital ϕ_j is given by a linear combination

of atomic orbitals χ_p's as follows:

$$\phi_j = \sum_p C_{jp}\chi_p. \quad (9)$$

Then a matrix representation of the operator $\mathbf{V}_i$ in Eq. 2 based on these atomic orbitals is given as

$$\mathbf{V}_i = (\mathbf{1}-\mathbf{D})\Omega_i'(\mathbf{1}-\mathbf{D}), \quad (10)$$

where $\mathbf{D}$ is the density matrix, Ω_i' the correction operator on the basis of atomic orbitals, which are given by

$$\mathbf{D} \equiv D_{pq}\sum_j^{occ} C_{ip}C_{jq} = \sum_j^{occ} D_{i,pq}, \quad (11)$$

$$\Omega_i' \equiv \Omega_{i,pq}' = \langle\chi_p|\Omega_i'|\chi_q\rangle = \sum_{v,w}\{-(pq|vw)+2(pw|vq)\}D_{i,vw}. \quad (12)$$

In these equations, (pq | vw) and (pw | vq) correspond to the Coulomb and Exchange integrals, respectively. Adopting the semi-empirical molecular orbital method, *i.e.* the MINDO/2 method,[10] the integrals may be estimated by the Slater-Condon parameters.[11] For the numerical values of bond lengths and bond angles the standard values determined by Pople and Gordon[12] were used. The numerical calculation was carried out by an HITAC-8800 computer at the Computer Center of the University of Tokyo.

Results and Discussion

The ^{13}C paramagnetic shielding constants of some organic compounds (acetylene, ethylene, ethane, pentane, benzene, pyridine, and acetone) were calculated using the wavelfunctions obtained from the ordinary Hartree-Fock method and the IVO method.[5-7] The calculated values by both methods are shown in Table 1. The characteristic feature in each compound is as follows:

A. Acetylene. The symmetry of the acetylene molecule belongs to the $D_{\infty h}$ point group and its electronic structure is composed of molecular orbitals with symmetry as shown in Table 2, in which the molecular orbitals were calculated by the MINDO/2 method.[10] According to the IVO method, the wavefunctions for the virtual orbitals are modified by the introduction of the correction operator $\mathbf{V}_i$ given in Eq. 2 while those for the occupied orbitals are not modified. This modification in virtual orbitals is responsible for the mixing among the virtual orbitals by the operator $\mathbf{V}_i$. From the viewpoint of the symmetry of the unoccupied orbitals, it is to be expected that the operator $\mathbf{V}_i$ causes the mixing between ϕ_6 and ϕ_{10} and between ϕ_7 and ϕ_8. ϕ_9 is not mixed because of orthogonality with the other unoccupied orbitals. From a considration of symmetry of the occupied and unoccupied orbitals it is possible to predict which transition can contribute to the paramagnetic shielding. As is seen from Eq.1, non-vanishing values of σ_{xx}^p, σ_{yy}^p and σ_{zz}^p are obtained if the transitions obey the selection rule that a direct product representation between the occupied and unoccupied orbitals contains representations of E_{1g}, E_{1g} and E_{2g}, respectively. Thus, two types of transitions can contribute to the σ_{xx}^p and σ_{yy}^p; one is the transition from the occupied orbital with a_{1g} symmetry to the unoccupied orbital with e_{1g} symmetry (σ-π^* transition), and the other is that from the e_{1u} occupied orbital to the a_{2u} unoccupied orbital (π-σ^* transition). Any transition does not contribute to σ_{zz}^p because any direct product representation between the occupied and unoccupied orbitals does not contain the representation of E_{2j}.

Focus will now be made on the molecular orbitals

Table 1. Calculated ^{13}C shielding constants in some organic compounds with and without IVO method

	Calculated without IVO					Calculated with IVO					Observed[a]	
	σ_{xx}^p	σ_{yy}^p	σ_{zz}^p	σ^p [b]	$\Delta\sigma$[c]	σ_{xx}^p	σ_{yy}^p	σ_{zz}^p	σ^p [b]	$\Delta\sigma$[c]	δ[d]	$\Delta\delta$[e]
Acetylene	−356.5	−356.5	0.0	−237.7		−356.5	−356.5	0.0	−237.7			
Ethylene	−528.7	−207.0	−348.4	−361.4		−528.7	−207.0	−348.4	−361.4		122.8	
Ethane	−238.2	−238.2	−221.2	−232.5		−239.0	−239.5	−221.5	−233.2		5.9	
Pentane												
C-1	−199.4	−203.7	−190.2	−197.7	20.0	−194.6	−202.0	−185.8	−194.2	36.1	13.7	20.8
C-2	−211.2	−225.9	−195.1	−210.7	7.0	−215.7	−238.1	−198.7	−217.5	12.8	22.6	11.9
C-3	−217.2	−239.4	−196.5	−217.7	0	−228.2	−255.9	−206.9	−230.3	0	34.5	0
Benzene	−306.2	−194.7	−436.6	−312.5		−310.7	−194.8	−441.2	−315.5		128.7	
Pyridine												
C-2	−449.7	−205.4	−342.2	−332.5	0	−490.0	−205.8	−349.9	−348.5	0	150.6	0
C-3	−391.5	−190.6	−330.8	−304.3	28.2	−392.8	−190.1	−338.3	−307.1	41.4	124.5	26.1
C-4	−304.0	−199.4	−445.0	−316.1	16.4	−297.9	−204.8	−460.0	−320.9	27.6	136.4	14.2
Acetone												
CH_3	−200.0	−224.7	−218.1	−214.3	140.1	−205.5	−224.2	−234.8	−221.5	162.1	30.2	174.9
CO	−445.0	−235.3	−382.8	−354.4	0	−477.3	−237.7	−435.9	−383.6	0	205.1	0

a) Collected from Ref. [1]. b) $\sigma^p=(\sigma_{xx}^p+\sigma_{yy}^p+\sigma_{zz}^p)/3$. c) The most deshielded carbon in each molecule is the reference. d) ppm from TMS. e) The most downfield carbon in each molecule is the reference.

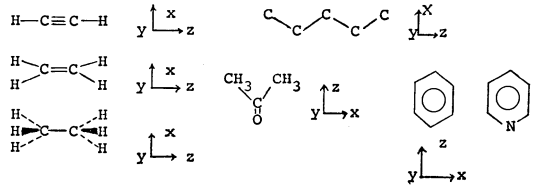

relating to the allowed transitions. New virtual orbitals ϕ_7' and ϕ_8' calculated by the IVO method are expressed as a linear combiantion of unoccupied orbitals ϕ_7 and ϕ_8 which are calculated by the ordinary Hartree-Fock method. When one electron is excited from the occupied orbital ϕ_1 to the unoccupied orbital ϕ_7 or ϕ_8, the wavefunctions of ϕ_7 and ϕ_8 are modified as follows:

$$\phi_7' = 0.7934\phi_7 - 0.6087\phi_8, \quad (13\text{-}1)$$

$$\phi_8' = 0.6087\phi_7 + 0.7934\phi_8, \quad (13\text{-}2)$$

and when one electron is excited from the occupied orbital ϕ_3 to the unoccupied orbital ϕ_7 or ϕ_8,

$$\phi_7'' = 0.7789\phi_7 - 0.6272\phi_8, \quad (14\text{-}1)$$

$$\phi_8'' = 0.6272\phi_7 + 0.7789\phi_8. \quad (14\text{-}2)$$

As the orbitals ϕ_7 and ϕ_8 degenerate with each other as shown in Table 2, the mixing between them by the operator $\mathbf{V}_i$ becomes large. However, if the excitation energy from the occupied orbital ϕ_1 or ϕ_3 to the unoccupied orbital ϕ_7 or ϕ_8 is not modified, induced modifications in the wavefunctions for orbitals ϕ_7 and ϕ_8 will not cause any change in the value of the paramagnetic shielding constant because of the degeneracy between these orbitals. The excitation energy, ΔE_{i-k}, can be simply calculated as a separation in energy levels between the virtual and occupied orbitals in the IVO method. If the excitation energy in the ordinary Hartree-Fock method is calculated from Eq. 15 taking into account Coulomb and Exchange integrals, little difference in the excitation energies with and without the IVO method is seen:

$$\Delta E_{i-k} = \varepsilon_k - \varepsilon_i - J_{ki} + 2K_{ki}. \quad (15)$$

For the other type of transition, when one electron is excited from the occupied orbital ϕ_4 or ϕ_5 to the unoccupied orbitals ϕ_6 and ϕ_{10}, modified wavefunctions for these virtual orbitals are expressed as follows:

$$\phi_6' = 0.9999\phi_6 - 0.0070\phi_{10}, \quad (16\text{-}1)$$

$$\phi_{10}' = 0.0070\phi_6 + 0.9999\phi_{10}. \quad (16\text{-}2)$$

The mixing between the orbitals ϕ_6 and ϕ_{10} by the operator $\mathbf{V}_i$ is very small. Thus, it is expected that there will be little difference in the contribution through these transitions whether the IVO method is used or not. For acetylene, it is seen that the improvement of the wavefunction for the virtual orbital by the IVO method induces little change in the magnetic shielding constant.

B. Ethylene. The ethylene molecule has the symmetry of the D_{2h} point group and has molecular orbitals with symmetry as shown in Table 3. Therefore, the wavefunctions for only two virtual orbitals ϕ_8 and ϕ_{12} are modified by the operator $\mathbf{V}_i$ because the other unoccupied orbitals are orthogonal to one another. The allowed transitions in the expression of σ_{xx}^p, σ_{yy}^p, and σ_{zz}^p are given by the selection rule that direct product representation between the occupied and unoccupied orbitals contains the representation of B_{3g}, B_{2g}, and B_{1g}, respectively; they are $\phi_1 \rightarrow \phi_7$, $\phi_4 \rightarrow \phi_7$, $\phi_6 \rightarrow \phi_8$, and $\phi_6 \rightarrow \phi_{12}$ for σ_{xx}^p, $\phi_5 \rightarrow \phi_7$ and $\phi_6 \rightarrow \phi_{10}$ for σ_{yy}^p, and $\phi_1 \rightarrow \phi_{11}$, $\phi_4 \rightarrow \phi_{11}$, $\phi_2 \rightarrow \phi_{10}$, $\phi_3 \rightarrow \phi_8$, $\phi_3 \rightarrow \phi_{12}$, and $\phi_5 \rightarrow \phi_9$ for σ_{zz}^p. The results on a part of the virtual orbitals ϕ_8 and ϕ_{12} are as follows: when one electron is excited from the occupied orbital ϕ_3 to the unoccupied orbital ϕ_8 or ϕ_{12}, modified wavefunctions ϕ_8' and ϕ_{12}' are expressed as

$$\phi_8' = 0.9854\phi_8 - 0.1705\phi_{12}, \quad (17\text{-}1)$$

$$\phi_{12}' = 0.1705\phi_8 + 0.9854\phi_{12}, \quad (17\text{-}2)$$

and when one electron is excited from the occupied orbital ϕ_6 to the unoccupied orbital ϕ_8 or ϕ_{12}, modified wavefunctions ϕ_8'' and ϕ_{12}'' are

$$\phi_8'' = 0.9997\phi_8 + 0.0255\phi_{12}, \quad (18\text{-}1)$$

$$\phi_{12}'' = -0.0255\phi_8 + 0.9997\phi_{12}. \quad (18\text{-}2)$$

The transition from ϕ_3 to ϕ_8 or ϕ_{12} corresponds to $\sigma \rightarrow \sigma^*$ and that from ϕ_6 to ϕ_8 or ϕ_{12} to $\pi \rightarrow \sigma^*$. It should be noted that the mixing by the operator $\mathbf{V}_i$ for the former type of transition is larger than that for the latter type. However, as the contributions to the paramagnetic shielding constant from the former transitions are vanishingly small, it is expected that the calculated value for σ_{zz}^p is hardly changed by modification of the virtual orbitals, ϕ_8 and ϕ_{12}. On the contrary, for the latter transitions, although a portion of these contributions to σ_{xx}^p is larger, the mixing between the orbitals ϕ_8 and ϕ_{12} due to the operator $\mathbf{V}_i$ is very small. For ethylene the result is similar to that of acetylene, namely the magnetic shielding constant is hardly changed by the IVO method.

C. Acetone. The acetone molecule has the symmetry of the C_{2v} point group and has molecular orbitals with the symmetry shown in Table 4. This compound is different from the above two compounds in that it contains an electronegative oxygen atom. The selection rules for the allowed transitions in the expressions of σ_{xx}^p, σ_{yy}^p, and σ_{zz}^p are, respectively, given by the terms of the direct product representations, B_2, B_1, and A_2, between the occupied and unoccupied orbitals. It is

TABLE 2. SYMMETRY OF MOLECULAR ORBITALS IN ACETYLENE

Occupied orbitals		Virtual orbitals	
ϕ_5	e_{1u} (π)	ϕ_{10}	a_{2u}
ϕ_4	e_{1u} (π)	ϕ_9	a_{1g}
ϕ_3	a_{1g}	ϕ_8	e_{1g} (π^*)
ϕ_2	a_{2u}	ϕ_7	e_{1g} (π^*)
ϕ_1	a_{1g}	ϕ_6	a_{2u}

Acetylene molecule has $D_{\infty h}$ symmetry. The molecular orbitals were calculated by MINDO/2 method.

TABLE 3. SYMMETRY OF MOLECULAR ORBITALS IN ETHYLENE

Occupied orbitals		Virtual orbitals	
ϕ_6	b_{1u} (π)	ϕ_{12}	b_{2u}
ϕ_5	b_{1g}	ϕ_{11}	b_{1g}
ϕ_4	b_{1g}	ϕ_{10}	b_{3u}
ϕ_3	b_{3u}	ϕ_9	a_{1g}
ϕ_2	b_{2u}	ϕ_8	b_{2u}
ϕ_1	a_{1g}	ϕ_7	b_{3g} (π^*)

Ethylene molecule has D_{2h} symmetry. The molecular orbitals were calculated by MINDO/2 method.

Table 4. Symmetry of molecular orbitals in acetone

Occupied orbitals		Virtual orbitals	
ϕ_{12}	b_1 (n)		
ϕ_{11}	a_1 (n)		
ϕ_{10}	b_2 (π)	ϕ_{22}	a_1
ϕ_9	b_1	ϕ_{21}	b_1
ϕ_8	a_2 (π')	ϕ_{20}	a_2 (π'*)
ϕ_7	a_1	ϕ_{19}	b_1
ϕ_6	b_1	ϕ_{18}	a_1
ϕ_5	b_2 (π')	ϕ_{17}	b_2 (π'*)
ϕ_4	a_1	ϕ_{16}	a_1
ϕ_3	b_1	ϕ_{15}	b_1
ϕ_2	a_1	ϕ_{14}	b_2 (π*)
ϕ_1	a_1	ϕ_{13}	a_1

Acetone molecule has C_{2v} symmetry. The molecular orbitals were calculated by MINDO/2 method. (π') denotes the pseudo-π orbitals due to the methyl group.

well-known that the n-π* transition gives a larger contribution to the paramagnetic shielding because of its low excitation energy. So, attention will be focused on the n-π* transitions. Some of the n-π* transitions give the contribution to σ^p_{xx} and σ^p_{zz}, *i.e.* $\phi_{11}\rightarrow\phi_{14}$, $\phi_{11}\rightarrow\phi_{17}$, and $\phi_{12}\rightarrow\phi_{20}$ to σ^p_{xx} and transitions $\phi_{11}\rightarrow\phi_{20}$, $\phi_{12}\rightarrow\phi_{14}$, and $\phi_{12}\rightarrow\phi_{17}$ to σ^p_{zz}. The unoccupied orbitals ϕ_{14} and ϕ_{17} are mixed with each other by the operator $\mathbf{V}_i$ while the unoccupied orbital ϕ_{20} is not mixed. When one electron is excited from the occupied orbital ϕ_{11} to the unoccupied orbital ϕ_{14} or ϕ_{17}, the modified orbitals ϕ'_{14} and ϕ'_{17} are expressed as

$$\phi'_{14} = 0.9809\phi_{14} + 0.1947\phi_{17}, \quad (19\text{-}1)$$

$$\phi'_{17} = -0.1947\phi_{14} + 0.9809\phi_{17}, \quad (19\text{-}2)$$

and when one electron is excited from the occupied orbital ϕ_{12} to the unoccupied orbital ϕ_{14} or ϕ_{17},

$$\phi''_{14} = 0.9843\phi_{14} + 0.1777\phi_{17}, \quad (20\text{-}1)$$

$$\phi''_{17} = -0.1777\phi_{14} + 0.9843\phi_{17}. \quad (20\text{-}2)$$

The virtual orbitals ϕ_{14} and ϕ_{17} are mainly located in the region of the carbonyl and methyl groups in acetone, respectively. Modification of these virtual orbitals decreases their delocalization in this case; the coefficients of the wavefunctions ϕ'_{14} and ϕ''_{14} at the carbonyl carbon are larger than that of ϕ_{14}. Therefore for the paramagnetic shielding of the carbonyl carbon, the values of σ^p_{xx} and σ^p_{zz} calculated by the IVO method are larger than those calculated by the ordinary method. As n-π* transitions do not largely contribute to the shielding constant of the methyl carbon, the corresponding increase in this contribution by the modification of the virtual orbitals is not so large compared to the case of the carbonyl carbon. For σ^p_{yy}, differences between the values calculated with the two methods is hardly the recognized in both of the methyl and carbonyl carbons, since the n-π* transition does not contribute to σ^p_{yy} at all. Ultimately, as far as a difference in the chemical shifts between the methyl and carbonyl carbons is concerned, the value obtained from the IVO method is larger than that from the ordinary method and it is noted that the former becomes closer to the observed one.

D. Other Compounds(ethane, pentane, benzene and pyridine). One of the aims of this paper was to examine whether the systematic deviation from the observed data described above could be avoided by the IVO method. In consequence the paramagnetic shielding constants calculated by the two methods in ethane and pentane will be compared. As shown in Table 1, for the ordinary method, the calculated value for any carbon of pentane is considerably underestimated if ethane is considered as a reference. For ethane, a difference between the calculated values with and without the IVO method is hardly observed. For pentane the contribution to the paramagnetic shielding in the most de-shielded carbon(C-3) increases by the modification of the virtual orbitals while that of the most shielded carbon (C-1) decreases. However, it may be seen that even for the C-3 carbon the underestimation of σ^p is still large. Thus, it does not seem that the IVO method serves to avoid the systematic deviation described above.

A brief examination of the calculated values for aromatic compounds will now be discussed. For benzene, it is seen that a small difference in the value of σ^p_{xx} or σ^p_{zz} is induced by the modification of the virtual orbitals while a small change is induced in the value of σ^p_{yy}. For pyridine, the value of σ^p_{xx} for C-2 carbon bonded to the nitrogen atom is considerably increased by the modification of the virtual orbitals, while the values of σ^p_{yy} and σ^p_{zz} do not increase as much because the n-π* transitions can contribute to only σ^p_{xx}. As far as differences in the chemical shifts among the carbons in pyridine are concerned, the IVO method gives rather poor agreement between the calculated observed results.

Conclusion

Using the wavefunction obtained from the improved virtual orbital (IVO) method proposed by Huzinaga, the ^{13}C NMR chemical shifts in some organic compounds have been calculated and compared with those obtained from the ordinary SCF-MO method. The following points were noted: If the molecule considered is small, highly symmetric and non-polar, it can be expected that there is little difference in the calculated values between these two methods because the mixings among the virtual orbitals are unlikely to be induced except for degenerate orbitals. If the molecule considered is rather large or polar, modification of the calculated values are apt to be induced by the IVO method. As far as qualitative tendencies of the chemical shifts of carbon in a molecule are concerned, both methods give similar results.

The authors wish to thank Professor A. Nishioka and Associate Professor R. Chujo of this Department and Dr. E. Hiroike of The University of Tohoku for their many helpful suggestions and discussions.

References

1) J. B. Stothers, "Carbon-13 NMR Spectroscopy," Academic Press, New York (1972).

2) R. Ditchfield and P. D. Ellis, "Topics in Carbon-13 NMR Spectroscopy," ed by G. C. Levy John Wiley & Sons, New York (1974).
3) J. A. Pople, *J. Chem. Phys.*, **37**, 53 (1962); **37**, 60 (1962); *Mol. Phys.*, **7**, 301 (1964).
4) A. B. Strong, D. Ikenberry, and D. M. Grant, *J. Magn. Reson.*, **9**, 145 (1973).
5) S. Huzinaga, D. McWilliams, and A. A. Cantu, "Advances in Quantum Chemistry," ed by P. O. Löwdin Vol. 7, p. 187, Acadimic Press, New York (1973).
6) S. Huzinaga and C. Arnau, *Phys. Rev.*, *A*, **1**, 1285 (1970); *J. Chem. Phys.*, **54**, 1948 (1971).
7) S. Huzinaga and A. A. Cantu, *J. Chem. Phys.*, **55**, 5543 (1971).
8) I. Ando, A. Nishioka, and M. Kondo, *Chem. Phys. Lett.*, **25**, 212 (1974).
9) I. Ando, A. Nishioka, and M. Kondo, *Bull. Chem. Soc. Jpn.*, **47**, 1097(1974); **48**, 1987 (1975).
10) M. J. S. Dewar and E. Haselbach, *J. Am. Chem. Soc.*, **92**, 590 (1970).
11) J. C. Slater, "Quantum Theory of Atomic Structure," Vol. 1, McGraw-Hill, New York (1960), p. 339.
12) J. A. Pople and M. Gordon, *J. Am. Chem. Soc.*, **89**, 4253 (1967).

Total Synthesis of (±)Variotin and Its Analogs

Akihiko ISHIDA* and Teruaki MUKAIYAMA†

Organic Chemistry Research Laboratory, Tanabe Seiyaku Co. Ltd., Kawagishi, Toda, Saitama 335

†*Department of Chemistry, Faculty of Science, The University of Tokyo, Hongo, Bunkyo-ku, Tokyo 113*

(Received December 1, 1977)

1-Sorboyl-2-pyrrolidone was prepared from sorbic acid and 2-ethoxy-1-pyrroline using 1-methyl-2-chloropyridinium iodide as a coupling reagent. Variotin and its analogs were similarly synthesized from lactim ethers and (2*E*, 4*E*, 6*E*)-8-hydroxy-2,4,6-dodecatrienoic acids without protecting the hydroxyl group at C-8. (2*E*,4*E*,6*E*)-8-Hydroxy-6-methyl-2,4,6-dodecatrienal, a precursor of trienoic acid, was synthesized by the elimination of methanol from (2*E*,6*E*)-8-acetoxy-5-methoxy-6-methyl-2,6-dodecadienal prepared from the reaction of 1-trimethylsiloxy-1,3-butadiene with (2*E*)-4-acetoxy-2-methyl-2-octenal dimethyl acetal.

The structure of variotin (**1b**), an antifungal antibiotic isolated from Pacecilomyces variotin Bainier var. antibioticus,[1] has been established by Yonehara and Takeuchi.[2]

Recently, a method for the preparation of polyenals[3] has been reported and applied to the synthesis of the naturally occurring polyolefinic compounds, vitamin A[4] and β-carotene.[5] Also, the synthesis of variotin (**1b**) has been reported briefly in a previous communication.[6b] This paper describes the experimental details employed for the synthesis of (±) **1b** and its analogs (**1a** and **1c**).

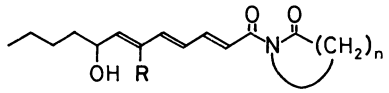

1 a) R=H n=3
b) R=CH$_3$ n=3
c) R=CH$_3$ n=4

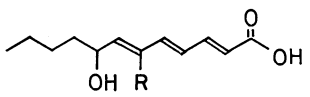

2 a) R=H
b) R=CH$_3$

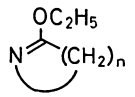

3 a) n=3
b) n=4

In the synthetic approach towards **1b**, the molecule was regarded as a condensation product of trienoic acid (**2b**) and lactim ether (**3a**). In the preliminary experiment, the reaction between sorbic acid (**4**) and 2-ethoxy-1-pyrroline (**3a**) was studied, employing 1-methyl-2-chloropyridinium iodide (**5**) as a coupling reagent (Scheme 1).

The hydroxytrienoic acids, **2a** and **2b**, may be derived from the corresponding polyenals (**20a** and **20b**).[3]

Results and Discussion

The Reaction of Sorbic Acid (4) and 2-Ethoxy-1-pyrroline (3a).[6a] The preparation of *N*-acyl lactam (**6**) in the presence of **5** and a tertiary amine was investigated under several conditions (Scheme 1).

The distribution of products depended on the method of addition (A, or B) as summarized in Table 1. An undesired acyl anhydride (**7**) was obtained as the major product when a solution of triethylamine in 1,2-dichloroethane was added immediately to a mixture of **3a**, **4**, and **5** at 0 or 50 °C (method A). In contrast, 1-sorboyl-2-pyrrolidone (**6**) was formed (63% yield) when a solution of **4** and tributylamine in toluene was added dropwise to a mixture of **3a** and **5** in toluene at 90 °C (method B). In addition to the small amount of **7**, ethyl 4-(sorboylamino)butanoate (**8**) was obtained (18% yield) as a side product identical to that prepared by the reaction of **6** and sodium ethoxide (Scheme 1).

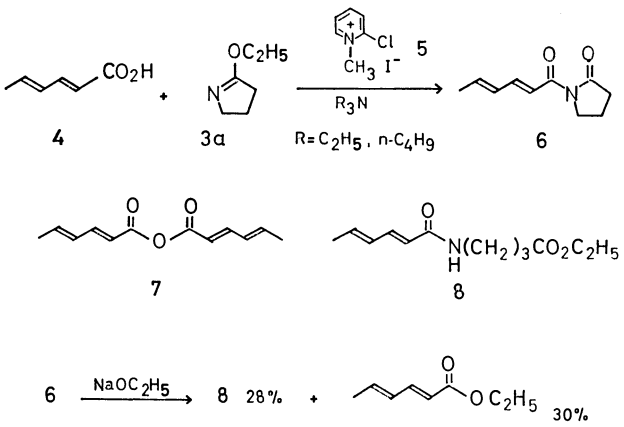

Scheme 1.

The reactions may be explained by assuming the initial formation of an active intermediate **4a**, which in turn reacted with nucleophiles (**3a** or **4**) to afford an intermediate **4b** and acyl anhydride (**7**). Subsequent elimination of ethyl halide from **4b** gave the

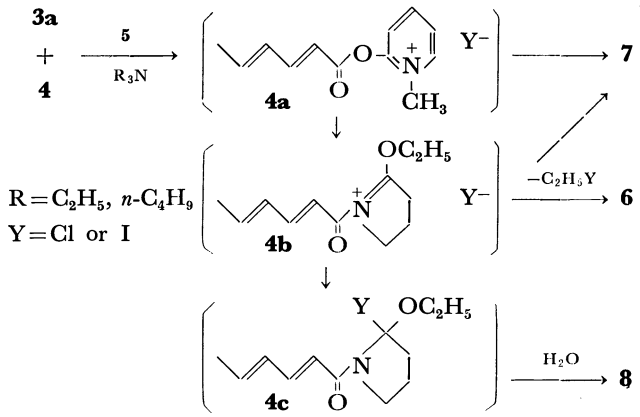

Scheme 2.

Table 1. The reaction of sorbic acid (**4**) and 2-ethoxy-1-pyrroline (**3a**) in the presence of 1-methyl-2-chloropyridinium iodide (**5**) and a base

Base	Reaction conditions			Addition method	Yield (%)		
	Solvent	Temp	Time (h)		**6**	**7**	**8**
$(C_2H_5)_3N$	$ClCH_2CH_2Cl$	0 °C	1.0	A[a]	—	93	—
$(C_2H_5)_3N$	$ClCH_2CH_2Cl$	50 °C	1.0	A	11	70	—
$(C_2H_5)_3N$	$ClCH_2CH_2Cl$	50 °C	4.0	B[b]	59	8	17
$(C_2H_5)_3N$	CH_3CN	50 °C	4.0	B	61	8	14
$(C_2H_5)_3N$	CH_3CN	refl.	4.0	B	60	6	14
n-Bu_3N	toluene	90 °C	2.0	B	63	7	18

a) The base was added immediately to the mixture of **3a**, **4**, and **5**.
b) The base and **4** were added dropwise to the mixture of **3a** and **5**.

desired acyl lactam (**6**). The amide (**8**) may be formed though an intermediate **4c** produced by the attack of an anion Y^- at the N^+=C bond of **4b** (Scheme 2).

Synthesis of Hydroxytrienoic Acid (2a and 2b). (2*E*)-4-Acetoxy-2-methyl-2-octenal (**11b**) was a key intermediate for the synthesis of **2b**. 3-Methyl-2-butenal (**9b**) was chosen as the starting material for the preparation of **11b** (Scheme 3).

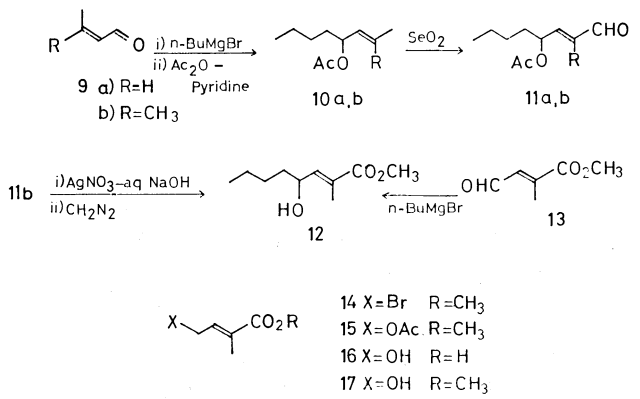

Scheme 3.

The reaction of **9b** with butylmagnesium bromide in ether, followed by acetylation with acetic anhydride–pyridine, gave 4-acetoxy-2-methyl-2-octene (**10b**). The yield was 81% after purification by distillation. The allylic oxidation of **10b** with 1.5 molar amounts of selenium dioxide[7] in refluxing xylene resulted in (2*E*)-4-acetoxy-2-methyl-2-octenal (**11b**) (43% yield). In order to determine the configuration of the C_2-double bond in **11b**, the aldehyde (**11b**) was converted into methyl 4-hydroxy-2-methyl-2-octenoate (**12**) by oxidation with silver oxide under basic conditions and subsequent treatment with ethereal diazomethane in 76% yield based on **11b**. Authentic methyl (2*E*)-4-hydroxy-2-methyl-2-octenoate (**12**) was derived from methyl (2*E*)-4-bromo-2-methyl-2-butenoate (**14**)[8] as follows. Treatment of **14** with potassium acetate in refluxing ethanol[9] afforded acetoxy ester (**15**). Hydrolysis of **15** with 20% KOH solution–methanol afforded (2*E*)-4-hydroxy-2-methyl-2-butenoic acid (**16**) (59% yield based on **14**). Treatment of **16** with diazomethane gave the hydroxy methyl ester (**17**) (85% yield), which on oxidation with pyridinium chlorochromate[10] in dichloromethane afforded methyl (2*E*)-2-methyl-4-oxo-2-butenoate (**13**) (75% yield). The reaction of **13** with butylmagnesium bromide in ether gave authentic (2*E*)-octenoate (**12**) (60% yield). The spectral data, the TLC and the GC behavior of the hydroxy ester (**12**) derived from **11b** were identical with those of the authentic sample obtained by the above route.

(2*E*,4*E*,6*E*)-8-Hydroxy-6-methyl-2,4,6-dodecatrienoic acid (**2b**) was derived from **11b** as depicted in Scheme 4. (2*E*)-Octenal (**11b**) was readily converted into its dimethyl acetal (**18b**) on treatment with trimethyl orthoformate–methanol in the presence of a catalytic amount of *p*-toluenesulfonic acid (89% yield). The reaction of 1-trimethylsiloxy-1,3-butadiene with the acetal (**18b**) in the presence of titanium tetrachloride and titanium tetraisopropoxide proceeded smoothly at −40 °C to (2*E*,6*E*)-8-acetoxy-5-methoxy-6-methyl-2,6-dodecadienal (**19b**). Preparative TLC gave a yield of 85%. The δ-methoxyl group of **19b** was readily eliminated with 4 molar amounts of 1,8-diazabicyclo[5.4.0]undec-7-ene (DBU) at room temperature in the presence of 3A molecular sieves to give (2*E*,4*E*,6*E*)-8-acetoxy-6-methyl-2,4,6-dodecatrienal (**20b**) (75% yield). The acetoxy aldehyde (**20b**) was converted into **2b** on oxidation with silver oxide at room temperature for 24 h (93% yield). (2*E*,4*E*,6*E*)-8-Hydroxy-2,4,6-dodecatrienoic acid (**2a**) was also prepared from crotonaldehyde (**9a**) through a similar synthetic route as described for **2b**.

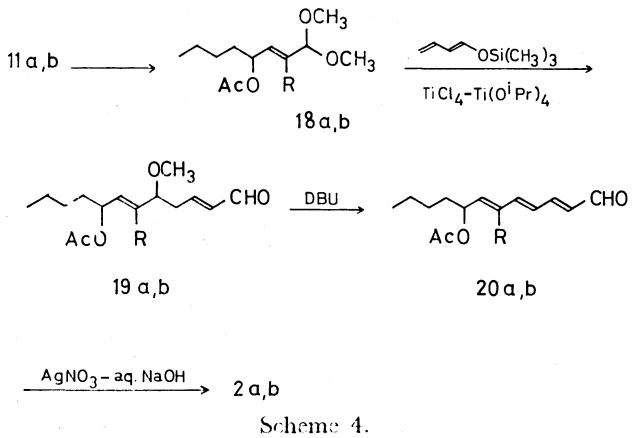

Scheme 4.

Condensation of Hydroxytrienoic Acid (2) and Lactim Ether (3). For the final step of the synthesis of **1b**, the condensation of **2b** and **3a** in the presence of tributylamine and **5** was conducted under similar conditions used for the preliminary reaction (Scheme 5). The reaction proceeded along a similar path without protecting the hydroxyl group of **2b**, and the yield of (±) variotin (**1b**) was improved (30—37%),[11b] together with ethyl 4-[(2*E*,4*E*,6*E*)-8-hydroxy-6-methyl-2,4,6-dodecatrienamido]butanoate (**21b**) (10—18% yield).

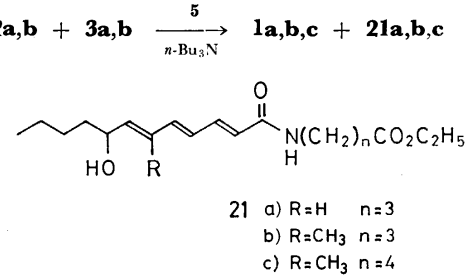

Scheme 5.

Similarly, **1a** and **1c** were prepared from **2** and **3** (36 and 27% yields, respectively). The spectral data of synthetic **1b** and **1c** were identical with those reported in the literature.[11,12] The potency of **1b**, thus obtained, against Trichophyton Asteroides was half that of the optically active natural variotin.

Experimental[13]

Reaction of Sorbic Acid (4) and 2-Ethoxy-1-pyrroline (3a). A solution of **4** (112 mg, 1.0 mmol) and tributylamine (195 mg, 1.05 mmol) in toluene (2 ml) was added dropwise to a mixture of 1-methyl-2-chloropyridinium iodide (614 mg, 2.4 mmol) and **3a** (208 mg, 2.4 mmol) in toluene (1 ml) over a period of 1 h at 85—90 °C under an argon atmosphere. After stirring for 1 h ethyl acetate (30 ml) was added. The resulting mixture was washed with dil HCl, 10% $NaHCO_3$ solution and water, dried and the organic layer concentrated under reduced pressure. The residue, subjected to preparative TLC on silica gel [hexane–ethyl acetate (1:1)] yielded four bands. The first band (highest R_f) consisted of ethyl sorbate (3 mg). IR(neat) 1710, 1640, 1620 cm^{-1}. NMR($CDCl_3$) δ 7.1—7.6 (1H, m), 6.1—6.25(2H, m), 5.82(1H, d, J=16Hz), 4.24 (2H, q), 1.86(3H, d, J=5Hz), 1.30(3H, t). The second band consisted of sorbic anhydride (**7**) (14 mg, 7%). IR(neat) 1780, 1710, 1640, 1610 cm^{-1}. NMR($CDCl_3$) δ 7.2—7.7 (2H, m), 6.25—6.45 (4H, m), 5.90(2H, d, J=16Hz), 1.90 (6H, d, J=5Hz). The third band consisted of 1-sorboyl-2-pyrrolidone (**6**) (113 mg, 63%), mp 122—123 °C (recrystallized from ethyl acetate) (lit,[14] mp 124—125 °C). IR (Nujol) 1730, 1660, 1630, 1590 cm^{-1}. NMR($CDCl_3$) δ 7.15—7.5 (2H, m), 6.1—6.4(2H, m), 3.87(2H, t), 2.60(2H, t), 2.00 (2H, quasi q), 1.87(3H, d, J=5Hz). The fourth band (lowest R_f) consisted of ethyl 4-(sorboylamido)butanoate (**8**) (41 mg, 18%), mp 63—64 °C (recrystallized from ether–petroleum ether). IR (Nujol) 3350, 1730, 1660, 1630, 1610 cm^{-1}. NMR($CDCl_3$) δ 6.95—7.45 (1H, m), 6.35—6.70(1H, br), 6.0—6.3(2H, m), 5.80(1H, d, J=16Hz), 4.10(2H, q), 3.40(2H, quasi q), 2.40(2H, quasi t), 1.8—2.2 (2H, m),1.90(3H, d, J=5Hz), 1.22(3H, t). Found: C, 64.26; H, 8.53; N, 6.02%. Calcd for $C_{12}H_{19}NO_3$: C, 63.97; H, 8.50; N, 6.22%.

Reaction of 1-Sorboyl-2-pyrrolidone (6) with Sodium Ethoxide. To a mixture of sodium ethoxide (1 mmol) and abs C_6H_6 (5 ml) was added a solution of **6** (180 mg, 1 mmol) in abs C_6H_6 (4 ml) at room temperature under an argon atmosphere. After stirring for 10 min ethyl acetate (10 ml) and acetic acid (66 mg, 1.1 mmol) were added. The resulting mixture was washed with water and dried over anhydrous Na_2SO_4. The solvent was removed and the residual oil chromatographed on silica gel. Elution with hexane–ethyl acetate (4:1) afforded 52 mg (30%) of ethyl sorbate. Further elution with hexane–ethyl acetate (1:1) gave 63 mg (28%) of ethyl 4-(sorboylamido) butanoate (**8**).

4-Acetoxy-2-methyl-2-octene (10b). The Grignard reagent was prepared from Mg (1.6 g, 66 mg-atom) and butyl bromide (9.32 g, 68 mmol) in dry ether (25 ml). To this was added a solution of **9b** (5.04 g, 60 mmol) in ether (30 ml) at −30 °C under an argon atmosphere. The mixture was stirred fro 30 min at −30 °C and brought to room temperature. After 2 h, the reaction was quenched by adding sat NH_4Cl solution, the mixture extracted with ether and the extract dried over anhydrous Na_2SO_4 and concentrated under reduced pressure. The residual oil was distilled to afford 7.70 g (90%) of 4-hydroxy-2-methyl-2-octene, bp 100—102 °C /27 mmHg. IR(neat) 3350, 1680 cm^{-1}. NMR($CDCl_3$) δ 5.20(1H, br d), 4.10—4.60 (1H, br), 1.72(6H, s), 1.1—1.7 (6H), 0.89(3H). A mixture of the above alcohol (7.70 g, 54.2 mmol) and acetic anhydride (10 g, 100 mmol) in pyridine (40 ml) was stirred for 15 h at room temperature. The reaction mixture was poured into ice-cold water, extracted with ether and the extract was washed with dil HCl, 10% $NaHCO_3$ solution, and water, dried over anhydrous $MgSO_4$, and evaporated to give an oil. The oil was distilled to yield 9.02 g (90%) of **10b**, bp 99—102 °C/20 mmHg. IR(neat) 1740, 1680 cm^{-1}. NMR($CDCl_3$) δ 5.30—5.70(1H, m), 5.10(1H, br d), 2.01(3H, s), 1.71, 1.73(6H, 2s), 1.1—1.7 (6H), 0.9(3H).

In the same manner, 4-acetoxy-2-octene (**10a**) was obtained from **9a** (81% yield), bp 105—107 °C/45 mmHg. IR(neat) 1740, 1670, 1235 cm^{-1}. NMR(CCl_4) δ 5.45—5.9(2H, m), 5.0—5.4 (1H, br), 2.04 (3H, s), 1.70(3H, d), 1.1—1.7(6H), 0.9(3H).

(2E)-4-Acetoxy-2-methyl-2-octenal (11b). The acetate (**10b**) (7.4 g, 40 mmol) in xylene (30 ml) was refluxed with SeO_2 (6.6 g, 60 mmol) for 40 min under an argon atomsphere. The black precipitates were removed by filtration, and the filtrate evaporated to give an oil. The oil was purified by column chromatography on silica gel [hexane–ethyl acetate (4:1) as an eluent] to yield 3.40 g (43%) of **11b**, bp 80 °C/0.05 mmHg. IR(neat) 1740, 1690, 1650, 1240 cm^{-1}. NMR ($CDCl_3$) δ 9.45(1H, s), 6.31 (1H, br d), 5.5—5.8(1H, br), 2.07(3H, s), 1.84(3H, s), 1.2—1.8(6H), 0.95(3H).

(2*E*)-4-Acetoxy-2-octenal (**11a**) was obtained in 45% yield by treating **10a** with SeO_2 under similar conditions. Bp 104—105 °C/1 mmHg. IR(neat) 1740, 1690, 1640, 1235 cm^{-1}. NMR(CCl_4) δ 9.55(1H, d, J=8Hz), 6.75 (1H, dd, J=6,16Hz), 6.10 (1H, dd, J=8,16Hz), 5.30—5.65(1H, br), 2.10(3H, s), 1.10—1.90(6H), 0.95(3H).

Methyl (2E)-4-Acetoxy-2-methyl-2-butenoate (15). A mixture of methyl (2*E*)-4-bromo-2-methyl-2-butenoate (1.93 g, 10 mmol) and potassium acetate (1.18 g, 12 mmol) in abs ethanol (13 ml) was refluxed for 3 h under a nitrogen atmosphere. The mixture was cooled to 0 °C, the precipitates filtered off and the filtrate evaporated to give an oil. The oil was distilled to yield 1.54 g (90%) of **15**, bp 140 °C/28 mmHg. IR(neat) 1740, 1720, 1660 cm^{-1}. NMR($CDCl_3$) δ 6.75 (1H, quasi t), 4.75(2H, quasi d),2.05(3H, s), 1.87(3H, s).

*(2E)-4-Hydroxy-2-methyl-2-butenoic Acid (**16**).* To a solution of **15** (372 mg, 2.16 mmol) in methanol (10 ml) was added 20% KOH solution (1.5 ml) at 0 °C. The mixture was stirred for 15 h at room temperature and methanol removed under reduced pressure. The aqueous solution was acidified with dil HCl, extracted with ethyl acetate and the extract dried over anhydrous Na_2SO_4 and evaporated to give an oil. The oil was purified by column chromatography on silica gel [hexane–ethyl acetate (1:2) as an eluent] to yield 163 mg (65%) of **16**, mp 78—80 °C. IR(KBr) 3200, 1670, 1630 cm^{-1}. NMR($CDCl_3$) δ 6.7—7.3(3H, br s), 4.33(2H, d, J=6Hz), 1.82(3H, s).

*Methyl (2E)-4-Hydroxy-2-methyl-2-butenoate (**17**).* To a solution of **16** (314 mg, 2.71 mmol) in abs ether (5 ml) was added a solution of diazomethane (excess) in ether at 0 °C. The mixture was kept at 0 °C for 1 h and the solvent removed under reduced pressure. The resulting oil was distilled to afford 298 mg (85%) of **17**, bp 124 °C/7 mmHg. IR(neat) 3400, 1720, 1660, 1260 cm^{-1}. NMR($CDCl_3$) δ 6.85(1H, quasi t), 4.35(2H, quasi d), 3.70(3H, s), 3.01(1H, s), 1.83 (3H, s).

*Methyl (2E)-4-Oxo-2-methyl-2-butenoate (**13**).* A solution of **17** (650 mg, 5 mmol) in dichloromethane (5 ml) was added in one portion to the stirred suspension of pyridinium chlorochromate (1.62 g, 7.5 mmol) and sodium acetate (125 mg, 1.52 mmol) in dichloromethane (5 ml). After 2 h, the reaction mixture was conducted according to Corey and Suggs.[10] Distillation of the crude oil gave 480 mg (75%) of **13**, bp 89 °C/15 mmHg (lit,[15] bp 76—78 °C/12 mmHg). IR(neat) 1720, 1680, 1630, 1260 cm^{-1}. NMR($CDCl_3$) δ 10.28(1H, d, J=8Hz), 6.85(1H, quasi d), 3.88(3H, s), 2.35 (3H, d, J=1.5Hz).

2,4-Dinitrophenylhydrazone, mp 206—207 °C (lit,[15] mp 204—205 °C).

*Methyl (2E)-4-Hydroxy-2-methyl-2-octenoate (**12**). From Methyl (2E)-4-Oxo-2-methyl-2-butenoate (**13**):* To a solution of the Grignard reagent prepared from Mg (59 mg, 2.4 mg atom) and butyl bromide (357 mg, 2.6 mmol) in ether (1 ml) was added a solution of **13** (256 mg, 2 mmol) in ether (1 ml) at −30 °C under an argon atmosphere. The mixture was stirred for 2 h at room temperature. After the usual work-up a crude oil was obtained. This oil was purified by preparative TLC on silica gel [hexane–ethyl acetate (4:1) as an eluent] to yield 227 mg (60%) of **12**, bp 95 °C/0.04 mmHg. IR(neat) 3400, 1720, 1650 cm^{-1}. NMR($CDCl_3$) δ 6.68(1H, br d), 4.3—4.8(1H, br). 3.74(3H, s), 2.64 (1H, br s), 1.87(3H, d, J=1.5Hz), 1.1—1.8(6H), 0.90(3H).

*From (2E)-4-Acetoxy-2-methyl-2-octenal (**11b**):* To a solution of silver nitrate (408 mg, 2.4 mmol) in water (4 ml) was added a solution of **11b** (396 mg, 2 mmol) in ethanol (8 ml) and aqueous NaOH (368 mg in 5 ml of H_2O). The mixture was stirred for 24 h at room temperature in the dark. The precipitates filtered off and ethanol removed under reduced pressure. The residual aqueous solution was acidified with dil HCl, extracted with ethyl acetate and the extract was dried over anhydrous Na_2SO_4 and concentrated under reduced pressure to give a crude acid (324 mg). This was treated with a small excess of ethereal diazomethane at 0 °C for 1 h. After evaporation of ether, the residual oil was purified by column chromatography on silica gel [hexane–ethyl acetate (2:1) as an eluent] to afford 282 mg (76%) of **12**, bp 95 °C/0.04 mmHg. The ester (**12**) was identified by comparison of its GLC retention time,[16] IR and NMR spectrum with those of an authentic sample (**12**) prepared from **13**.

*(2E)-4-Acetoxy-2-methyl-2-octenal Dimethyl Acetal (**18b**).* To a solution of **11b** (2.80 g, 14 mmol) and trimethyl orthoformate (4.5 g, 42 mmol) in abs methanol (7 ml) was added a catalytic amount of *p*-toluenesulfonic acid at −10 °C under an argon atmosphere. The mixture was stirred for 10 min at the same temperature and brought to room temperature. After stirring for a further 3 h, the reaction was quenched by adding anhydrous K_2CO_3. The solvent was removed under reduced pressure at 20 °C, the residue dissolved in petroleum ether (bp 30—60 °C), filtered and the filtrate evaporated to give an oil which distilled to give 3.04 g (89%) of **18b**, bp 85 °C/0.04 mmHg. IR(neat) 1740, 1240 cm^{-1}. NMR($CDCl_3$) δ 5.55(1H, br s), 5.45—5.70(1H, br), 4.52(1H, s), 3.30(6H, s), 2.01(3H, s), 1.71(3H, s), 0.9—1.8(9H).

(2*E*)-4-Acetoxy-2-octenal dimethyl acetal (**18a**) was obtained by treating **11a** with trimethyl orthoformate–methanol as described above (85% yield). Bp 98—100 °C/0.5 mmHg. IR(neat) 1740, 1240 cm^{-1}. NMR(CCl_4) δ 5.5—5.8(2H, m), 5.0—5.4(1H, m), 4.70 (1H, br d), 3.20(6H, s), 2.00(3H, s), 1.1—1.7(6H), 0.95(3H).

*(2E,6E)-8-Acetoxy-5-methoxy-6-methyl-2,6-dodecadienal (**19b**).* To a mixture of $Ti(O^iPr)_4$ (8 mmol) and $TiCl_4$ (8 mmol) in dichloromethane (40 ml) was added a solution of **18b** (976 mg, 4 mmol) and 1-trimethylsiloxy-1,3-butadiene (680 mg, 4.8 mmol) in dichloromethane (10 ml) at −40 °C under an argon atmosphere. After stirring for 30 min at −40 °C, the reaction was quenched by adding K_2CO_3 (7 g in 10 ml of H_2O). The resulting precipitates were removed by filtration and the filtrate extracted with ether and the extract was washed with water, dried over anhydrous $MgSO_4$ and evaporated. The residual oil was purified by preparative TLC on silica gel [hexane–ethyl acetate (4:1) as an eluent] to yield 959 mg (85%) of **19b**. Bp 135 °C/0.04 mmHg. IR (neat) 1740, 1690, 1640, 1240 cm^{-1}. NMR ($CDCl_3$) δ 9.55 (1H, d, J=8Hz), 6.83(1H, ddd, J=16.8, 8Hz), 6.13(1H, dd, J=16,8Hz), 5.2—5.6(2H, br), 3.64(1H, t), 3.22(3H, s), 2.5—2.7(2H, m), 2.01 (3H, s), 1.70(3H, s), 1.1—1.8(6H), 0.9(3H).

(2*E*,6*E*)-8-Acetoxy-5-methoxy-2,6-dodecadienal (**19a**) was obtained by reacting **18a** with dienoxysilane in the presence of $TiCl_4$ and $Ti(O^iPr)_4$ (83% yield). Bp 125 °C/0.08 mmHg. IR(neat) 1735, 1690, 1640, 1240 cm^{-1}. NMR (CCl_4) δ 9.40(1H, d, J=8Hz), 6.70(1H, ddd, J=16,8,8Hz), 6.00(1H, dd, J=8,16Hz), 5.45—5.60 (2H, m), 4.9—5.3 (1H, br), 3.5—3.8(1H, br), 3,20(3H, s), 2.3—2.7 (2H), 1.05—1.70(6H), 0.9(3H).

*(2E,4E,6E)-8-Acetoxy-6-methyl-2,4,6-dodecatrienal (**20b**).* To a mixture of **19b** (282 mg, 1 mmol) and molecular sieves 3A (500 mg) in dichloromethane (8 ml) was added a solution of DBU (304 mg, 2 mmol) in dichloromethane (2 ml) at room temperature under an argon atmosphere. After stirring for 1 h, a solution of DBU (2 mmol) in acetonitrile (3 ml) and molecular sieves 3A (500 mg) were added. The mixture was stirred for 2 h and poured into ice-cold brine containing acetic acid, the organic layer separated, washed with brine and dried over anhydrous Na_2SO_4. After removal of the solvent, the residual oil was purified by preparative TLC on silica gel [hexane–ethyl acetate (4:1) as an eluent] to yield 193 mg (77%) of **20b**. IR(neat) 1735, 1680, 1610, 1240 cm^{-1}. NMR($CDCl_3$) δ 9.63(1H, d, J=8Hz), 7.00 —7.50(1H, m), 6.5—7.0(2H, m), 6.20(1H, dd, J=16, 8Hz), 5.5—5.8(2H, br), 2.04(3H, s), 1.93(3H, s). 1.1—1.9(6H), 0.9(3H).

(2*E*,4*E*,6*E*)-8-Acetoxy-2,4,6-dodecatrienal (**20a**) was obtained by treating **19a** with DBU under similar conditions (75% yield). IR(neat) 1740, 1680, 1615, 1240 cm^{-1}. NMR ($CDCl_3$) δ 9.50 (1H, d, J=8Hz), 5.7—7.3(6H, m), 5.05—5.40(1H, br), 2.05(3H, s), 1.10—1.75(6H), 0.9(3H).

*(2E,4E,6E)-8-Hydroxy-6-methyl-2,4,6,-dodecatrienoic Acid (**2b**).* To a solution of silver nitrate (646 mg, 3.80 mmol) in water (5 ml) were added a solution of **20b** (791 mg, 3.16 mmol) in ethanol (13 ml) and NaOH (581 mg in 8 ml of H_2O). The mixture was stirred for 24 h at room temperature in the dark. After the usual work-up, **2b** (661 mg) was obtained (93% yield). IR(neat) 3300, 1690, 1620 cm^{-1}. NMR ($CDCl_3$) δ 7.2—7.7(1H, m), 6.3—6.8 (3H, m), 5.90(1H, d, J=16Hz), 5.70(1H, br d), 4.3—4.7(1H, br d), 1.86(3H,), 1.1—1.8(6H), 0.85(3H). UV $\lambda_{max}^{C_2H_5OH}$ 296 nm (ε 2.6×10). MS *m/e* 225(M^++1), 206, 139, 121. Found: C, 69.88; H, 9.02%. Calcd for $C_{13}H_{20}O_3$: C, 69.61; H, 8.99%.

(2*E*,4*E*,6*E*)-8-Hydroxy-2,4,6,-dodecatrienoic acid (**2a**) was obtained by treating **20a** with silver oxide under similar conditions (90% yield). Mp 85—86 °C (recrystallized from ethyl acetate-hexane). IR(Nujol) 3400—3300, 1700, 1610 cm^{-1}. NMR(CCl_4) δ 7.1—7.4(3H, m), 5.7—5.6 (4H, m), 4.0—4.3(1H, br), 1.1—1,7(6H), 0.9(3H). UV $\lambda_{max}^{C_2H_5OH}$ 296 nm(ε 2.9×10⁴). MS *m/e* 210(M^+), 192, 125. Found C, 68.41; H, 8.51%. Calcd for $C_{12}H_{18}O_3$: C, 68.54; H, 8.63%.

*Reaction of (2E,4E,6E)-8-Hydroxy-6-methyl-2,4,6,-dodecatrienoic Acid (**2b**) with 2-Ethoxy-1-pyrroline (**3a**).* A solution of **2b** (112 mg, 0.5 mmol) and tributylamine (102 mg, 0.55 mmol) in toluene (1 ml) was added dropwise to a mixture of 1-methyl-2-chloropyridinium iodide (307 mg, 1.2 mmol) and **3a** (136 mg, 1.2 mmol) in toluene (1 ml) over a period of 30 min at 85 °C under argon atmosphere. The mixture was stirred for an additional 10 min and the solvent removed under reduced pressure and the residue chromatographed on silica gel. Elution with dichloromethane-ether (4:1) afforded 44 mg (30%) of **1b**. Further elution with dichloromethane-ether (1:1) gave 17 mg (10%) of **21b**. In another experiment under the same conditions, **1b** (54 mg) and **21b** (30 mg) were obtained in 37% and 18% yields, respectively. **1b**: IR(neat) 3400, 1740, 1670, 1600 cm^{-1}. NMR ($CDCl_3$) δ 7.3—7.7(2H, m), 6.4—6.7(2H, m), 5.70(1H, br d), 4.3—4.8 (1H, br), 3.90(2H, t), 2.65(2H, quasi t), 2.50(1H,s), 1.8—2.4 (2H, m), 1.75(3H, s), 1.1—1.8(6H), 0.9(3H). UV $\lambda_{max}^{C_2H_5OH}$ 320 nm (ε 2.61×10⁴). MS *m/e* 291(M^+), 273, 206. Found: C, 70.03; H, 8.41; N, 4.66%. Calcd for $C_{17}H_{25}NO_3$: C, 70.07; H, 8.65, N, 4.81%. **20b**: IR(neat) 3300, 1740, 1650, 1610 cm^{-1}. NMR($CDCl_3$) δ 7.1—7.6(1H, m), 6.10—6.10(3H, m), 5.95(1H, d, J=16Hz), 5.65(1H, br d), 4.15(2H, q), 4.2—4.7(1H, br), 3.15—3.89(3H, m). 2.2—2.6(2H, m), 1.85(3H, s), 1.25(3H, t), 1.1—2.2(8H), 0.9(3H). UV $\lambda_{max}^{C_2H_5OH}$ 294 nm (ε 4.0×10⁴). MS *m/e* 337(M^+). Found: C, 67.91; H, 9.45; N, 4.09%. Cacld for $C_{19}H_{31}NO_4$: C, 67.62; H, 9.26; N, 4.15%.

In a similar manner, **1a** was obtained from **2a** and **3a** (36% yield), together with **21a** (16%). Similarly, **1c** (27%) and **21c** (28%) were obtained from **2b** and **3b**. Compound **1a**: IR(neat) 3400, 1730, 1660, 1600 cm^{-1}. NMR($CDCl_3$) δ 7.3—7.6(2H, m), 5.9—6.7(4H, m), 3.9—4.5(1H, br), 3.90 (2H, t), 2.3—2.8(3H, m), 1.8—2.3(2H, br q), 1.1—1.8(6H), 0.9(3(H). UV $\lambda_{max}^{C_2H_5OH}$ 324 nm (ε 2.68×10⁴). MS *m/e* 278(M^+), 193. Found: C, 69.51; H, 8.38; N, 5.25%. Calcd for $C_{16}H_{23}NO_3$: C, 69.28; H, 8.36; N, 5.05%. Compound **21a**: Mp 87—89 °C. IR(KBr) 3400, 3300, 1725, 1615, 1580, 1530 cm^{-1}. NMR($CDCl_3$) δ 7.0—7.5 5.7—6.8(7H, m), 4.0—4.5(1H, br), 4.10 (2H, q), 3.2—3.6(2H, m), 2.35 (1H, s), 2.1—2.7(2H, m), 1.20(3H, t), 1.2—2.2(8H), 0.9(3H). UV $\lambda_{max}^{C_2H_5OH}$ 295 nm(ε 4.46×10⁴). MS *m/e* 323(M^+), 305, 233. Found: C, 66.59; H, 9.15; N, 4.55%. Cacld for $C_{18}H_{29}NO_4$: C, 66.84; H, 9.04; N, 4.33%. Compound **1c**: IR(neat) 3400, 1690, 1670, 1600 cm^{-1}. NMR($CDCl_3$) δ 6.4—7.7(4H, m), 5.70(1H, br d), 4.3—4.8(1H, br), 3.6—4.0 (2H, m), 2.53(1H, s), 2.2—2.8 (2H, m), 1.83(3H,s), 1.1—2.2(10H), 0.9(3H). UV $\lambda_{max}^{C_2H_5OH}$ 317 nm (ε 2.23×10⁴). MS *m/e* 350(M^+), 297, 220. Found: C, 71.05; H, 8.98; N, 4.73%. Calcd for $C_{18}H_{27}NO_3$: C, 70.79; H, 8.91; N, 4.59%. Compound **21c**: IR(neat) 3270, 1740, 1650, 1610 cm^{-1}. NMR($CDCl_3$) δ 7.28(1H, dd, J=16, 8Hz), 6.2—6.6(3H, m), 5.95 (1H, d, J=16Hz), 5.63(1H, br d), 4.2—4.7(1H, br), 4.12(2H, q), 3.2—3.6 (2H, m), 2.2—2.7(2H, m), 2.90(1H, s), 1.80(3H, s), 1.23(3H, t), 1.1—1.8(10H), 0.9(3H). UV $\lambda_{max}^{C_2H_5OH}$ 295 nm (ε 4.1×10⁴). MS *m/e* 351 (M^+) 343, 266. Found: C, 68.54; 9.44; N, 4.11%. Calcd for $C_{20}H_{33}NO_4$: C, 68.34; H, 9.46; N, 3.99%.

References

1) H. Yonehara, S. Takeuchi, H. Umezawa, and Y. Sumiki, *J. Antibiot., Ser. A.*, **12**, 109(1959).

2) S. Takeuchi and H. Yonehara, *J. Antibiot.*, **22**, 179 (1969).

3) a) T. Mukaiyama and A. Ishida, *Chem. Lett.*, **1975**, 319; b) A. Ishida and T. Mukaiyama, *ibid.*, **1975**, 1167; c) A. Ishida and T. Murakaiyam, *Bull. Chem. Soc. Jpn.*, **50**, 1171 (1977).

4) T. Mukaiyama and A. Ishida, *Chem. Lett.*, **1975**, 1201.

5) A. Ishida and T. Mukaiyama, *Chem. Lett.*, **1976**, 1127.

6) a) A. Ishida, T. Bando, and T. Mukaiyama, *Chem. Lett.*, **1976**, 711; b) A. Ishida and T. Mukaiyama, *ibid.*, **1977**, 467.

7) U. T. Bhalerao and H. Rapoport, *J. Am. Chem. Soc.*, **93**, 4835 (1971).

8) a) A. Löffler, R. J. Pratt, H. P. Rüesch, and A. S. Dreiding *Helv. Chim. Acta*, **53**, 383 (1970); b) A. Löffler, F. Norris. W. Taub, K. L. Svanholt, and A. S. Dreiding, *ibid.*, **53**, 403 (1970).

9) G. Eletti-Bianchi, F. Centini, and L. Re, *J. Org. Chem.*, **41**, 1648 (1976).

10) E. J. Corey and J. W. Suggs, *Tetrahedron Lett.*, **1975**, 2647.

11) a) S. Takeuchi, H. Yonehara, a H. Shoji, *J. Antiobot., Ser. A*, **17**, 267 (1964); b) M. Sakakibara, T. Okami, T. Kitahara, and M. Matsui, *Agr. Biol. Chem.*, **37**, 903 (1973).

12) M. Sakakibara and M. Matsui, *Agr. Biol. Chem.*, **37**, 1131 (1973).

13) All melting and boiling points have not been corrected.

14) M. Sakakibara and M. Matsui, *Agr. Biol. Chem.*, **37**, 1179 (1973)

15) Y. Inouye, T. Sugita, and M. Ohno, *Bull. Agr. Chem. Soc. Jpn.*, **21**, 222 (1957).

16) Gas chromatography analysis was performed with Shimadzu GC-4B under the following conditions (1.5 m×3 mm, 3% OV-17 on chromosorb W (60—80 mesh) column, at 120 °C with 60 ml/min of N_2).

Boron Trifluoride Hydrate-catalyzed Competitive Benzylation of Benzene and Toluene with Benzyl and Substituted Benzyl Chlorides

Akiko TAKEMATSU, Kyoko SUGITA, and Ryohei NAKANE*

The Institute of Physical and Chemical Research, Wako-Shi, Saitama 351

(Received December 8, 1977)

The competitive benzylation of benzene and toluene catalyzed by boron trifluoride hydrate was carried out with benzyl, chlorobenzyl, alkylbenzyl, and alkoxybenzyl chlorides in boron trifluoride hydrate and hexane solutions. The relative rates of toluene to benzene were smaller than 1 in the benzylation with benzyl and chlorobenzyl chlorides, while they were larger than 1 with alkylbenzyl and alkoxybenzyl chlorides. Competitive benzylation catalyzed by boron trifluoride was also carried out in a nitromethane solution. The relative rates were reduced by from several to ten times in the former solutions as compared to the latter solution; the k_T/k_B value became smaller than 1 when the electrophile was such a very strongly electron-deficient reagent as the benzyl or chlorobenzyl cation. On the other hand, the k_T/k_B value was still larger than 1 when the electrophilicity was lower, as in the alkylbenzyl or alkoxybenzyl cation. The isomer distribution was insensitive to the nature of the solvents. The formation of the meta isomer was always only a small percentage. These results substantiate our previous conclusions obtained in the ethylation and isopropylation catalyzed by boron trifluoride hydrate.

Boron trifluoride-catalyzed ethylation with ethyl-2-^{14}C fluoride carried out in nonpolar organic solvents has indicated that an electrophile is not a donor:acceptor complex, but an ethyl cation.[1] Stock and Brown[2] suggested that, in aromatic substitution involving an ultimate powerful electrophile, the rate of toluene relative to benzene is 5/6 and that the orientation in the alkylation of toluene is 40% ortho, 40% meta, and 20% para isomer (statistical value). However, we found that the formation of the meta isomer of ethyltoluene or cymene is much lower than the statistical value, though the rate of toluene relative to benzene is smaller than 5/6, when the electrophile is such a very strongly electron-deficient reagent as the ethyl[3] or isopropyl[4] cation. The results do not agree with Brown's Selectivity Relationship.

Recently, some criticisms have been posed about such anomalous substrate selectivity that toluene is less reactive than benzene in spite of the electrophilic aromatic substitution. Carter *et al.*[5] carried out an ethylation of benzene and toluene with ethyl bromide under the influence of aluminium bromide in a hexane solution and concluded that the disproportionation and isomerization of products which occurred in the layer separation cause the reverse in the k_T/k_B value. Olah[6] suggested that, because of the secondary intermolecular rearrangement, the k_T/k_B value may apparently become smaller than 1 in the ethylation and the isopropylation, in which the *m*-isomer of ethyltoluene or isopropyltoluene usually is formed in a quantity of more than 20%.

In this work the benzylation catalyzed by boron trifluoride hydrate has been carried out with benzyl and substituted benzyl chlorides in order to substantiate our previous suggestion concerning the reaction mechanism of aromatic substitution involving the ultimate powerful electrophile.

Results and Discussion

Water dissolves small amounts of benzene and methylbenzenes.[7] Liquid boron trifluoride hydrate, which is formed when boron trifluoride is placed in contact with water, can also dissolve small amounts of benzene and methylbenzenes. When a boron trifluoride hydrate solution in which *o*-xylene and benzene have been dissolved is allowed to stand for many hours, both isomerization and disproportionation are observed to progress very slowly. When benzyl chloride is added to the boron trifluoride hydrate solution, dissolving the aromatics, the benzylation, accompanied by a little polymerization, occurs. The reaction is very rapid. The competitive benzylation of benzene and toluene with benzyl, *o*-, *m*-, *p*-chlorobenzyl, *p*-methyl-, *p*-ethyl-, *p*-isopropyl-, and *p*-methoxybenzyl chlorides was carried out in the boron trifluoride hydrate solution. The reaction proceeded in a homogeneous system. The data obtained are shown in Table 1. The rates of toluene relative to benzene, k_T/k_B, were smaller than 1 in the reactions with benzyl and chlorobenzyl chlorides, while they were larger than 1 in the reactions with *p*-alkyl- and *p*-alkoxybenzyl chlorides. No dibenzyltoluene was found. The benzylation catalyzed by boron trifluoride was also carried out in hexane. The data obtained are shown in Table 2. The results obtained were almost the same as those obtained in the boron trifluoride hydrate solution. Therefore, it appears that the catalyst in the hexane solution is not boron trifluoride itself, but boron trifluoride hydrate, as was suggested in previous works.[3,4] For comparison, a boron trifluoride-catalyzed benzylation was

Table 1. Boron trifluoride hydrate-catalyzed benzylation in boron trifluoride hydrate solutions at room temperature

R of $RC_6H_4CH_2Cl$	k_T/k_B	Isomer distribution (%)			$\frac{1}{2}o/p$
		o-	*m*-	*p*-	
o-Cl	0.5	46.5	16.1	37.4	0.62
m-Cl	0.8	47.2	15.5	37.3	0.63
p-Cl	0.5	46.8	6.1	47.1	0.50
H	0.9	43.6	6.1	50.3	0.43
p-CH_3	4.4	29.1	2.6	68.3	0.21
p-C_2H_5	5.6	28.1	2.9	69.0	0.20
p-*i*-C_3H_7	4.4	25.4	2.2	72.4	0.18
p-CH_3O	34	27.4	1.3	71.3	0.19

Table 2. Boron trifluoride hydrate-catalyzed benzylation in hexane at room temperature

R of $RC_6H_4CH_2Cl$	k_T/k_B	Isomer distribution (%)			$\frac{1}{2}o/p$
		o-	*m*-	*p*-	
o-Cl[a]	(0.7)	(42.2	16.0	41.8)	(0.53)
m-Cl	—	—	—	—	—
p-Cl	0.7	45.5	4.3	50.3	0.45
H	0.7	43.1	4.6	52.3	0.41
p-CH_3	4.4	24.4	2.1	73.4	0.17
p-C_2H_5	5.7	24.3	1.8	73.9	0.16
p-*i*-C_3H_7	3.1	21.3	1.8	76.9	0.14
p-CH_3O	23	28.4	3.8	67.8	0.21

a) The yield is very low.

Table 3. Boron trifluoride-catalyzed benzylation in nitromethane at room temperature

R of $RC_6H_4CH_2Cl$	k_T/k_B	Isomer distribution (%)			$\frac{1}{2}o/p$
		o-	*m*-	*p*-	
o-Cl	2.8	38.2	15.8	46.0	0.42
m-Cl	3.5	37.8	10.2	52.0	0.36
p-Cl	2.8	44.6	7.4	48.0	0.46
H	3.7	40.5	6.5	53.0	0.38
p-CH_3	36	29.8	2.3	67.9	0.22
p-C_2H_5	38	27.6	2.7	69.6	0.20
p-*i*-C_3H_7	37	26.4	2.4	71.2	0.18
p-CH_3O	106	29.8	1.4	68.8	0.22

carried out in nitromethane. The results obtained were similar to those obtained by others,[8] as is shown in Table 3. The finding that the formation of the *m*-isomer is only a small percentage in most of the reactions indicates that few thermodynamical side reactions (*i.e.*, isomerization and transalkylation) occur. The isomer distribution was almost independent of the nature of the solvent, while the k_T/k_B value was very sensitive to the reaction conditions.

Electrophile in Boron Trifluoride Hydrate-catalyzed Benzylation. The hydrates of $SnCl_2$, $SnCl_3$, $SnCl_4$, $ZnCl_2$, $FeCl_3$, $SbCl_3$, $SbCl_5$, $BiCl_2$, and $TiCl_4$ catalyze the benzylation of aromatics with benzyl chloride in aqueous media.[9] Olah[10] suggested that the investigated hydrates of metallic halides possess certain proton-acid catalytic activity and that the hydrolysis of benzyl chloride itself must proceed through a cation-type intermediate, capable under suitable conditions of effecting concurrent benzylation. The boron trifluoride hydrate is also a strong proton acid of a trifluorohydroxoboric or difluorodihydroxoboric acid type. The molar ratio of boron trifluoride to water in the boron trifluoride hydrate used for the benzylation is 0.77. In the solution there exists no free boron trifluoride which forms with benzyl chloride a polar donor:acceptor complex, $C_6H_5\overset{\delta+}{C}H_2Cl\cdot\overset{\delta-}{B}F_3$. The reaction of benzyl chloride with the boron trifluoride hydrate cannot give a donor:acceptor complex, since benzyl chloride is a much weaker donor than water. Therefore, in the boron trifluoride hydrate solution a benzyl cation-type intermediate is formed. Benzyl cation polymerizes when aromatics are not dissolved in the solution, but it becomes the electrophile of the benzylation in the presence of aromatics.

$$H_2O + BF_3 \rightleftharpoons H^+BF_3OH^-$$

$$H^+BF_3OH^- + C_6H_5CH_2Cl \longrightarrow C_6H_5CH_2{}^+BF_3OH^- + HCl$$

$$C_6H_5CH_2{}^+BF_3OH^- + ArH \longrightarrow C_6H_5CH_2Ar + H^+BF_3OH^-$$

The above presumption is also supported by the observations that an ethyl cation is the electrophile in the ethylation carried out with ethyl-1-^{13}C fluoride and ethyl-1,1-d_2 fluoride in the boron trifluoride hydrate solution.[11]

Effect of Electrophilicity of Reagents on Selectivity. Olah, *et al.*[8] concluded that intermolecular selectivity (rate ratio) is inversely related to the amount of polarization of the polar complex, while intramolecular selectivity (isomer distribution) is insensitive to the nature of the alkylating agent in the benzylation of benzene and toluene with benzyl and substituted benzyl halides in the presence of various Lewis acid catalysts. The explanation was made that the transition state can vary from a late one resembling an intermediate (σ complex) to an early one resembling the starting material (π complex), whereas the isomer distribution is related to the stability of the σ complex. The results obtained in this work showed effects similar to those found by Olah. The electrophile is the cation in the boron trifluoride hydrate-catalyzed benzylation, while it is the polar complex in the boron trifluoride-catalyzed benzylation. Since the electron deficiency of the former is much higher than that of the latter, the k_T/k_B values are reduced by as much as ten times in the boron trifluoride hydrate and hexane solutions as compared to the nitromethane solution. When the boron trifluoride-catalyzed benzylation was carried out with benzyl and chlorobenzyl chlorides in the latter solution, the k_T/k_B value was about 3. Consequently, the k_T/k_B value became smaller than 1 in the boron trifluoride hydrate and hexane solutions. On the other hand, the isomer distribution is less sensitive to the nature of the catalyst.

Rate-determining Step in the Boron Trifluoride Hydrate-catalyzed Benzylation. In the benzylation catalyzed by the boron trifluoride hydrate, the rupture of the C–Cl bond in benzyl or substituted benzyl chloride is complete before the reaction with the aromatics. The question arises whether or not an S_N1-type mechanism is applicable. If the rupture of the C–Cl bond determines the rate of the benzylation, the relative rate should always become 1, whether a substituted group of benzyl chloride is electron-attractive or electron-donative. The fact that the k_T/k_B values in the benzylation with *p*-alkyl- and *p*-alkoxybenzyl chlorides are from 4 to 34 indicates that the formation of *p*-alkyl- and *p*-alkoxybenzyl cations is not involved in the rate-determining step. On the other hand, the k_T/k_B values in the benzylation with chlorobenzyl chlorides are much smaller than 1. These values also suggest that the

rate-determining step is not the rupture of the C–Cl bond in chlorobenzyl chlorides.

The benzylation proceeds in the homogeneous system, and few thermodynamical side reactions occur. However, since the reaction is very rapid, there are the possibilities that the reaction takes place at a point of entrance of benzyl or substituted benzyl chlorides into the boron trifluoride hydrate solution in which aromatics are dissolved and that the diffusion of aromatics in the solution determines the rate of the benzylation. If so, the k_T/k_B value should be nearly 1, but it may change from 0.5 to 34 depending on the electrophilicity of the substituted benzyl cations.

Consequently, the benzylation catalyzed by the boron trifluoride hydrate involves an electrophilic attack on aromatics by the benzyl or substituted benzyl cation. When the electron deficiency of the cation is very high, benzene is more reactive than toluene, but only a small percentage of the meta isomer of benzyltoluene is formed. This substantiates our previous suggestions[4] that the rate-determining transition state formed in the substitution of toluene closely resembles the oriented π complex, that the difference in rates between benzene and toluene is due primarily to the difference in the entropies of activation, which can be negative, since the difference in the activation energies between the two aromatics is very small, and that the isomerization of benzyltoluene is mainly determined by the stability of the intermediate (σ complex).

Experimental

Material. The benzene, toluene, *p*-methoxybenzyl chloride, and nitromethane were obtained from the Wako Pure Chemical Co. (Osaka, Japan). The benzyl chloride, chlorobenzyl chlorides, *p*-alkylbenzyl chlorides, and hexane were obtained from the Tokyo Kasei Co. (Tokyo, Japan). The boron trifluoride gas was obtained from the Hashimoto Kasei Co. (Osaka, Japan). They all were commercially available materials of the highest purity and were used without further purification.

Benzylation in Boron Trifluoride Hydrate Solution. Preparation of a Boron Trifluoride Hydrate Solution Saturated with Aromatics: Boron trifluoride gas was introduced into an ice-cooled and stirred mixture composed of 20 mol of distilled water, 1 mol of benzene, and 1 mol of toluene. The amount of boron trifluoride absorbed in the mixture was estimated by means of the flow speed of the boron trifluoride gas (6.2 l/min). The molar ratio of boron trifluoride to water in the mixture was 0.77. After the introduction of boron trifluoride gas had finished, the mixture was allowed to stand overnight and was then separated into two liquid-phase layers. The lower layer was the boron trifluoride hydrate solution saturated with benzene and toluene. It was a clear, colorless, viscous solution, and its specific gravity was 1.73 at 30 °C. Small amounts of aromatics dissolved in the boron trifluoride hydrate solution were extracted with hexane and analyzed by gas chromatography. About 5 mg of aromatics[11] were dissolved in 10 g of the boron trifluoride hydrate solution, the molar ratio of toluene to benzene was from 0.8 to 1.2, according to the preparative conditions.

Preparation of a Boron Trifluoride Hydrate Solution Saturated with Benzyl or Substituted Benzyl Chlorides: Boron trifluoride gas was absorbed into an ice-cooled and stirred mixture of 20 mol of water and 0.05 mol of benzyl chloride or substituted benzyl chloride. The reactivity of benzyl chloride varied greatly with the substituent group. Therefore, the molar ratio of boron trifluoride to water in a boron trifluoride hydrate solution in which benzyl chlorides were dissolved was changed in order to obtain such appropriate reaction conditions that less than 15% of the combined aromatics were alkylated and no side reactions proceeded. The amount of boron trifluoride gas blown into the mixture was estimated by means of the flow speed (6.2 l/min). The molar ratio of boron trifluoride to water was 0.20 for *o*- and *m*-chlorobenzyl chlorides, 0.10 for benzyl chloride, *p*-chloro-, *p*-ethyl-, *p*-isopropyl-, and *p*-methoxybenzyl chlorides, and 0.01 for *p*-methylbenzyl chloride. Benzyl or substituted benzyl chlorides do not polymerize in a boron trifluoride hydrate solution in which the ratio of boron trifluoride to water is small. Benzyl or substituted benzyl chlorides dissolved in a boron trifluoride hydrate solution were used for benzylation after filterings out the crystals of boric acid which were produced by the hydrolysis of boron trifluoride, and after separating out any excess benzyl or substituted benzyl chlorides. Gas-chromatographic analysis showed no isomerization of benzyl or substituted benzyl chlorides dissolved in the boron trifluoride hydrate solution.

Competitive Benzylation in Boron Trifluoride Hydrate Solution. From 10 to 80 g of boron trifluoride hydrate, in which benzyl chloride or substituted benzyl chlorides had been dissolved, were added to a glass beaker containing 20 g of a boron trifluoride hydrate solution saturated with benzene and toluene. The reaction mixture, which was a clear, colorless solution, was stirred at room temperature and then instantly quenched by adding 70 g of icewater. The organic layer was extracted with 1 ml of hexane, washed with water, and dried with calcium chloride. It was analyzed by gas chromatography. Benzylation proceeded for about 15% of the combined aromatics.

Competitive Benzylation in Hexane. Competitive benzylation was carried out by blowing boron trifluoride gas into a mixture of benzene, toluene, benzyl chloride, and hexane which had been saturated with water. The molar ratio of reactants was as follows; C_6H_6: $C_6H_5CH_3$: $C_6H_5CH_2Cl$: C_6H_{14}: BF_3=5 : 5 : 3 : 30 : 2. The flow speed of the boron trifluoride gas was 230 ml/min. The mixture was stirred at room temperature, it was quenched with water after 5 to 60 min, and then it was washed with water, dried with calcium chloride, and analyzed by gas chromatography.

Competitive Benzylation in Nitromethane. Competitive benzylation was carried out in a solution with the following molar ratio: C_6H_6 : $C_6H_5CH_3$: $C_6H_5CH_2Cl$: CH_3NO_2 : BF_3 =5 : 5 : 3 : 30 : 2. The flow speed of the boron trifluoride gas was 230 ml/min. After from 5 to 60 min, the reaction mixture was quenched with water, extracted with diethyl ether, and dried with calcium chloride. It was then analyzed by means of gas chromatography.

Gas-chromatographic Analysis. The reaction products were analyzed with a Hitachi 163-type gas chromatograph using a hydrogen flame-ionization detector and a 3380A Reporting Integrator of Hullet Packard. A glass capillary column(length, 30 m; i.d., 0.28 mm) coated with sillicon OV-101 was used at 180 °C for benzylated products, while one with Ucon 550X was used at 150 °C for the analysis of the isomer of *o*-chlorobenzyltoluene.

References

1) A. Natsubori and R. Nakane, *J. Org. Chem.*, **35**, 3372 (1970).

2) L. M. Stock and H. C. Brown, *Adv. Phys. Org. Chem.*, **1**, 45 (1963).
3) R. Nakane, O. Kurihara, and A. Natsubori, *J. Am. Chem. Soc.*, **91**, 4528 (1969).
4) R. Nakane, O. Kurihara, and A. Takematsu, *J. Org. Chem.*, **36**, 2753 (1971).
5) B. J. Carter, W. D. Covey, and F. P. Dehaan, *J. Am. Chem. Soc.*, **97**, 4783 (1975).
6) Private discussion.
7) R. L. Bohon and W. F. Claussen, *J. Am. Chem. Soc.*, **73**, 1571 (1951); E. F. G. Herington, *ibid.*, **73**, 5883 (1951).
8) G. A. Olah, S. Kobayashi, and M. Tashiro, *J. Am. Chem. Soc.*, **94**, 7448 (1972).
9) R. Jenny, *C. R. Acad Sci.*, **246**, 3477 (1958); **248**, 3555 (1959); **250**, 1659 (1960).
10) G. A. Olah, "Friedel-Crafts and Related Reactions," Vol. 1, ed by G. A. Olah, Interscience, New York, N.Y. (1963), p 308.
11) T. Oyama, T. Hamano, K. Nagumo, and R. Nakane, *Bull. Chem. Soc. Jpn.*, **51**, 1441 (1978).

Carbon-13 NMR Spectra of Octahydro-1,4-naphthoquinones and of Their Derivatives

Hajime IRIKAWA* and Yasuaki OKUMURA

Department of Chemistry, Faculty of Science, Shizuoka University, Oya, Shizuoka 422

(Received December 15, 1977)

The ^{13}C NMR spectra are reported for hexahydro- and octahydro-1,4-naphthoquinones and their derivatives. The shielding trends of the methyl group are utilized for conformational analysis. A comparison of octahydro-1,4-naphthoquinones with the corresponding decalins reveals that the effects of the carbonyl group are the large downfield shift of the α-carbons and the upfield shifts of the β- and γ-carbons.

^{13}C NMR spectroscopy is a powerful method for clarifying stereochemical problems. Systematic studies of methyldecalins and decahydroquinolines have provided useful parameters for signal assignments.[1,2] This paper deals with a ^{13}C NMR study of *cis*-2,3,4a,5,8,8a-hexahydro- and *cis*-octahydro-1,4-naphthoquinones (**1a,b—5a,b**), *trans*-octahydro-1,4-naphthoquinones (**1c—3c**), and a number of derivatives (**6a,b, 7—13, 14a,b**).

Natural-abundance 15.04 MHz ^{13}C FT-NMR spectra were obtained by use of the ^{1}H noise-decoupling technique. The signals of methyl, methylene, and methine carbons were identified by a combination of off-resonance decoupling and partially relaxed FT spectra.[3]

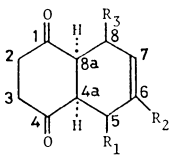

1a—5a

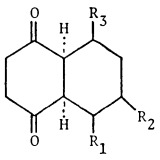

1b—5b

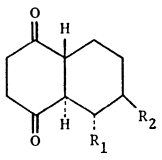

1c R_1, R_2=H
2c R_1=Me R_2=H
3c R_1=H R_2=Me

1a,b R_1, R_2, R_3=H
2a,b R_1=Me R_2, R_5=H
3a,b R_2=Me R_1, R_5=H
4a,b R_1=COOMe R_2, R_5=H
5a,b R_1=COOMe R_2=H R_3=Me

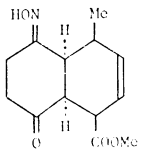

6a

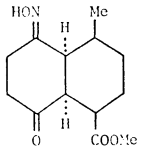

6b

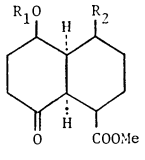

7 R_1, R_2=H
8 R_1=H R_2=Me
9 R_1=Ac R_2=H
10 R_1=Ac R_2=Me

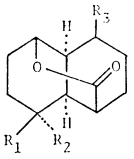

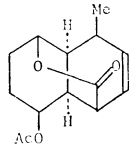

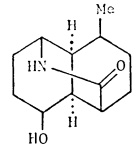

11 R_1, R_2=O R_3=H
12 R_1, R_2=O R_3=Me
13 R_1=OH R_2=H R_3=Me
14b R_1=OAc R_2=H R_3=Me

14a

15

Results and Discussion

Materials. Compounds **1a—5a** were prepared from the Diels-Alder adduct[4-8] of *p*-benzoquinone and the corresponding diene by zinc reduction, respectively. Catalytic hydrogenation of **1a—5a** provided **1b—5b**, respectively.[4,8,9] The configuration of the methyl group in **3b** was estimated to be *cis-syn* because of the hydrogenation from less hindered side. Compound **2b** was isomerized into *trans*-**2c** by acid treatment and **3b** into *trans*-**3c** by alumina column. Hydrogenation of **6a**, derived from **5a**, with platinum oxide in methanol provided the dihydro keto oxime (**6b**), whereas that in acetic acid afforded the δ-lactam (**15**). The ^{13}C NMR spectrum of **15** was similar to that of **13** except for C-1, supporting the position of the hydroxyimino group and the cis ring junctions in **6a** and **6b**. Compounds **10** and **14b** were obtained by acetylation of **8** and **13**, respectively.[8]

The chemical shifts of the $\Delta^{6,7}$-compounds (**1a—6a, 14a**) are summarized in Table 1, those of the octahydro-compounds (**1b—6b, 1c—3c**) in Table 2, and those of **7—13** and **14b** in Table 3.

Signal Assignments. Assignments for the signals in **2b, 3b,** and **4b** were made on their preferred conformations shown below. The methylene signal at 26.62 ppm in **4b** was assigned to C-8, since it was shifted upfield upon reduction of the C-1 carbonyl to the hydroxyl group (to **7**). Accordingly, the signal at 26.01 ppm in **2b** was assigned to C-8, which seems to be little affected by the substituent. Carbons α to the double bond in cyclohexenes are characteristically shielded ($\Delta\delta = \delta_C^{alkane} - \delta_C^{alkene} > 0$).[10] The shielding trends of the double bonds for C-5 in **2a** and **4a** ($\Delta\delta$ 2.23 ppm between **2a** and **2b**; $\Delta\delta$ 1.22 ppm between **4a** and **4b**) support the assignments for C-8 in **2b** and **4b** ($\Delta\delta$ 3.45 ppm between **2a** and **2b**; $\Delta\delta$ 2.80 ppm between **4a** and **4b**). Saturation of the double bonds in **1a—6a** causes the downfield shifts of C-4a and -8a. The trend is in agreement with the

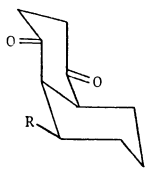

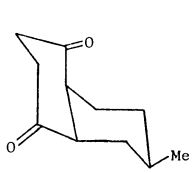

2b R=Me
4b R=COOMe

3b

Table 1. ^{13}C NMR chemical shifts of the $\Delta^{6,7}$-compounds[a)]

Compound	**1a**	**2a**	**3a**	**4a**	**5a**	**6a**[b)]	**14a**[c)]
C-1	209.24	209.96*	208.83*	208.75*	207.85*	155.38	75.07
C-2	35.79	35.34	35.95	35.18	34.73	26.09	30.31
C-3	35.79	37.13	35.95	36.32	37.61	35.87	22.07
C-4	209.24	209.64*	209.15*	207.04*	210.29*	209.48	72.35
C-4a	44.76	48.69	45.53**	46.62	46.05	45.08	39.60
C-5	23.49	30.96	28.20	40.01	39.44	38.26*	37.17*
C-6	124.42	130.95	131.72	125.03	121.37	121.42	125.35
C-7	124.42	122.95	118.41	123.20	131.27	130.71	135.90
C-8	23.49	22.56	24.06	23.82	30.55	28.08	34.77
C-8a	44.76	45.20	44.84**	45.00	48.33	37.65*	37.78*
C-Me		17.65	23.37		17.40	17.40	16.51
COO				171.98	172.06	171.98	171.98
O-Me				52.10	52.10	51.25	

a) Asterisks indicate that assignments are not unambiguous. b) In DMSO-d_6. c) Acetyl signals: 21.14 and 170.19.

Table 2. ^{13}C NMR chemical shifts of the octahydro-1,4-naphthoquinones[a)]

Compound	**1b**	**2b**	**3b**	**4b**	**5b**	**6b**[b)]	**1c**	**2c**	**3c**
C-1	210.37	210.77*	208.91*	209.56*	208.91*	155.50	209.24	208.66	208.91
C-2	36.36	36.44	36.92	35.83	35.10	26.82	36.76	38.26*	36.84
C-3	36.36	37.25	36.07	36.56	37.41	36.15	36.76	37.65*	36.84
C-4	210.37	209.80*	210.61*	207.85*	209.80*	211.26	209.24	208.66	208.91
C-4a	48.04	51.17**	50.03	49.22	47.68	46.26	49.75	56.00	49.71*
C-5	25.85	33.19	36.23	41.23	41.35	40.50*	26.45	31.32	34.77
C-6	23.45	29.42	32.18	23.98**	20.08	17.53	24.75	34.00	31.36
C-7	23.45	23.49	30.35	23.49**	30.47	30.92	24.75	24.22	33.39
C-8	25.85	26.01	23.74	26.62	31.45	26.82	26.45	26.66	26.37
C-8a	48.04	50.52**	46.01	48.41	51.13	40.86*	49.75	51.25	49.46*
C-Me		18.54	22.23		15.82	15.25		21.02	22.23
COO				173.60	173.52	173.36			
O-Me				51.82	51.78	51.05			

a) Asterisks indicate that assignments are not unambiguous. b) In DMSO-d_6.

Table 3. ^{13}C NMR chemical shifts of **7**—**13** and **14b**[a)]

Compound	**7**	**8**	**9**[b)]	**10**[c)]	**11**	**12**	**13**	**14b**[d)]
C-1	70.45	70.20	72.31	72.07	79.57	74.14	74.70	74.22
C-2	29.21	31.61	25.97	28.36	30.63*	30.92*	30.59*	30.63*
C-3	38.51	37.90	38.30	37.82	32.99	33.43	25.68	22.40
C-4	209.48	210.94	207.85	209.56	208.66	208.59	70.36	72.72
C-4a	49.75	47.27	49.42	47.15	52.95	54.13	44.80	42.16
C-5	42.56	42.69	42.36	42.48	40.50	40.25	36.40	37.25
C-6	23.98*	19.55	23.65*	18.95	31.32*	31.45*	31.57*	31.53*
C-7	24.83*	34.04	24.63*	34.00	19.15	27.79	28.93	28.77
C-8	21.18	27.67	21.91	28.04	29.05	33.84	34.85	34.98
C-8a	45.69	47.56	42.36	44.15	34.33	40.25	39.81	39.85
C-Me		17.12		17.00		19.23	19.15	19.11
COO	174.57	174.57	173.85	173.93	172.30	172.39	175.84	174.41
O-Me	51.70	51.61	51.61	51.57				

a) Asterisks indicate that assignments are not unambiguous. b) Acetyl signals: 21.14 and 170.19. c) Acetyl signals: 21.06 and 170.28. d) Acetyl signals: 21.18 and 170.19.

downfield shifts of the carbons β to the double bond in cyclohexenes.[10] Assignment for C-5 in **3b** is based on the β_e parameter (9.03 ppm) of the methyl group[1a] and the chemical shift of C-8 in **2b**, since both carbons seem to be similarly affected by the 1,4-cyclohexanedione ring. The situation of C-6 in **2b** is similar to that of C-7 in **3b**, their signals being observed at 29—30 ppm.

Of the two signals for C-2 and -3 in **5a** and **5b**, the signals at lower fields were assigned to C-3, respectively, since they were slightly shifted upfield upon replacement of the C-1 carbonyl with the hydroxyimino group (to **6a** and **6b**). In the spectra of **7** and **8**, the signals shifted upfield upon acetylation were assigned to C-2 and -8a, and the C-8 signals appearing upfield were compared with those in **4b** and **5b** by the γ-gauche effects of the hydroxyl groups, respectively.[11]

Assignments for C-4a, -7, -8, and -8a in **11** and **12** are based on the Dalling-Grant parameters.[1] The effects of the equatorial methyl group on C-7 and -8a in **12** are in line with the predicted values (C-7: $\beta_e+\beta_e\alpha_a=8.2$ ppm; C-8a: $\beta_e+\alpha_a\beta_e=5.6$ ppm), although the effect on the α-carbon is larger than the predicted value (C-8: $\alpha_e+\alpha_e\beta_a=3.1$ ppm) (Table 4). The relatively large downfield shift of C-4a might come from the $\beta_g\gamma_t$ effect. In the spectrum of **13**, the signals shifted upfield upon acetylation (to **14b**) were assigned to C-3 and -4a, and the C-5 signal appearing upfield was compared with that in **12** by the γ-gauche effect of the hydroxyl group.

As shown in Fig. 1, the large downfield shift of the α-carbon of the hydroxyl group in **7** upon lactonization (to **11**) seems due to the characteristic deshielding effect of the lactone group, since the similar trend was observed between methyl *cis*-3-hydroxycyclohexanecarboxylate and 1,3-cyclohexanecarbolactone.[12]

Conformational Analysis. The shielding trends of the methyl substituent (Table 4) are useful for conformational analysis. The γ-effects on C-4a and -6 found in **8** and **10** suggest the axial orientation of the methyl group. The δ-effects observed for C-2 indicate the *syn*-diaxial Me–CH_2(C-2) interaction.[13] In contrast to the large upfield shift of C-1 in **12**, the characteristically small γ-gauche effects of the methyl group on C-1 in **8** and **10** are in line with the observation that the γ-gauche effects of the hydroxyl group are reduced whenever it is *syn*-diaxial to a δ-carbon.[14] Thus **8** and **10** are thought to exist in a form bearing

TABLE 4. METHYL SUBSTITUENT EFFECTS[a]

Compound	C-1	C-2	C-4a	C-5	C-6	C-7	C-8	C-8a
5b	−0.65	−0.73	−1.54	0.12	−3.90	6.98	4.83	2.72
8	−0.25	2.40	−2.48	0.13	−4.43	9.21	6.49	1.87
10	−0.24	2.39	−2.27	0.12	−4.70	9.37	6.13	1.79
12	−5.43	0.29	1.18	−0.25	0.13	8.64	4.79	5.92
2c	−0.58	1.50	6.25	4.87	9.25	−0.53	0.21	1.50
3c	−0.33	0.08	−0.04	8.32	6.61	8.64	−0.08	−0.29

a) Values obtained from $\delta_c^{R=Me}-\delta_c^{R=H}$ for the corresponding carbons in each case.

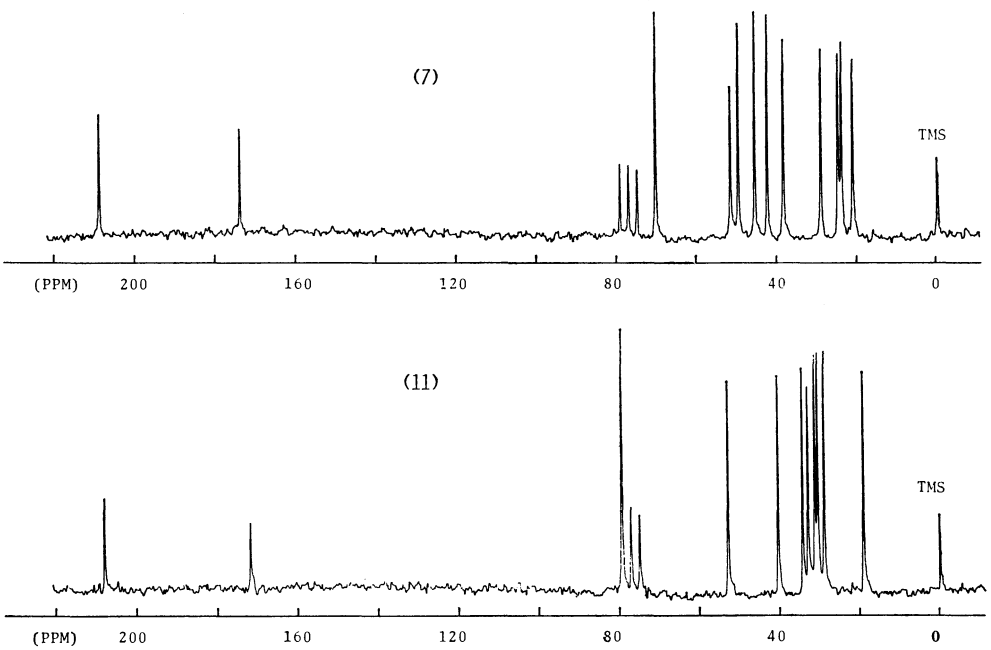

Fig. 1. Proton noise decoupled natural abundance FT ^{13}C NMR spectra of **7** and **11** in $CDCl_3$ at 15.04 MHz: pulse width, 25 μs (45°); repetition time 3 s; number of scans, 1000; spectral width, 5000 Hz; data points, 8192; acquisition time, 0.82 .

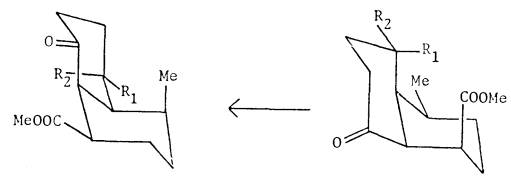

5b R_1, R_2=O
8 R_1=OH R_2=H
10 R_1=OAc R_2=H

the axial methyl group, as shown above. The estimation is in line with the ^1H NMR of **8**.[8]

Conformation of **5b** bearing two substituents in cis relation is of interest, since the conformational distribution of methyl *cis*-4-methylcyclohexanecarboxylate is estimated to be 67% of the equatorial methyl conformer by conformational free energy of a methyl and a methoxycarbonyl group.[12] In **5b**, the γ-effects of the methyl group are observed on C-4a and -6, the β-effect on C-8a being smaller than those on C-8a in **12** and C-4a in **2c**. Saturation of the $\Delta^{6,7}$-double bond causes upfield shift of the methyl signal in **5a**, in contrast to the downfield shifts of those in **2a** and **14a**. The chemical shift of C-5 in **5b** is similar to that in **4b** bearing equatorial methoxycarbonyl group. These data indicate that **5b** also exists in a form similar to that of **8** and **10**. Absence of the δ-effect on C-2 might be due to the nonchair conformation of the 1,4-cyclohexanedione ring.[15]

Comparison with Carbocyclic Analogues. It is of interest to compare **1c**—**3c**, **2b**, and **3b** with the corresponding decalins (X=CH_2).[1b] The chemical shift differences are summarized in Table 5. The ^{13}C NMR spectra of decalins were recorded as neat substance, whereas the spectra reported here were obtained in $CDCl_3$. A comparison of the shift values of *trans*-decalin in $CDCl_3$ (26.86, 34.37, and 43.70 ppm) with the literature values of the neat substance (27.17, 34.74, and 44.22 ppm) indicates that the solvent effect is not large.

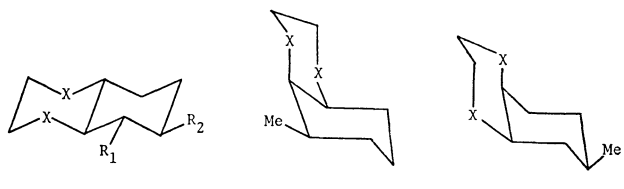

1c X=CO R_1, R_2=H
2c X=CO R_1=Me R_2=H
3c X=CO R_1=H R_2=Me

2b X=CO

3b X=CO

The strong shieldings for C-5 and -8 in **1c**—**3c**, and for C-8 in **3b** are similar to that for the methyl group (−9.4 ppm) in 2-methylcyclohexanone,[16] and mainly ascribed to the β-effect of the carbonyl group. Although the effects of the axial carbonyl group on cyclohexane ring are not clear, the fact that C-7 in **2b** and C-6 in **3b** are shielded indicates the presence of the γ-effect of the carbonyl group similar to that of oxygen and nitrogen on *anti*-periplanar γ-carbons.[17] The upfield shifts of C-5 and -7 in **5b** compared with those in **8** might be rationalized by the shielding effect of the C-1 carbonyl group. Accordingly, the upfield shifts of C-6 and -7 in **1c**—**3c** seem to be mainly due to the effect of the carbonyl group at the γ-position.

On the other hand, C-6 and -8 in **2b**, and C-5 and -7 in **3b** are little affected. The feature might be explained by two opposing effects: shielding by the two carbonyl groups and deshielding due to the absence of the γ_{HH} interaction,[1b] the latter being in line with the small chemical shift differences between C-2 and -3 in **2b**—**5b**.

Experimental

Melting points are uncorrected . The IR spectra were recorded on a Hitachi Infrared Spectrometer EPI-G_3 in Nujol. The ^{13}C NMR spectra were obtained on a JEOL JNM-PFT-60 (15.04 MHz) at 27 °C. Samples were observed in 10 mm spinning tubes at *ca.* 20% solution in $CDCl_3$, unless otherwise stated. The solvent provided the internal lock signal. The measurement conditions are shown in Fig. 1. All the chemical shifts are expressed in terms of δ(ppm downfield from internal TMS). Each observed chemical shift is estimated to be accurate to $\delta \pm 0.08$.

Preparation of ***2a***. A crude adduct[5] formed by 1.00 g of *trans*-1,3-pentadiene and 0.80 g of *p*-benzoquinone was reduced with 5 g of zinc in 20 ml of AcOH at room temperature for 1 h. Work-up in the usual way afforded 1.16 g of **2a**: mp 84—85 °C (from diisopropyl ether); IR 1708 cm^{-1}. Found: C,74.08; H, 7.99%. Calcd for $C_{11}H_{14}O_2$: C, 74.13; H,7.92%.

Compound ***3a***. In a similar way to the preparation of **2a**, a crude adduct[6] formed by 6.81 g of isoprene and 7.00 g of *p*-benzoquinone was reduced with zinc to afford 6.52 g of **3a**: mp 86—87 °C (from hexane); IR 1714 cm^{-1}. Found: C, 74.09; H, 8.04%. Calcd for $C_{11}H_{14}O_2$: C, 74.13; H, 7.92%.

Compound ***4a***. In a similar way to the preparation of **2a**, 2.00 g of the adduct[7] of methyl 2,4-pentadienoate and *p*-benzoquinone was reduced with zinc to afford 0.92 g of **4a**: mp 130—131 °C (from benzene-hexane); IR 1733 and 1709 cm^{-1}. Found: C, 64.64; H, 6.32%. Calcd for $C_{12}H_{14}O_2$: C, 64.85; H, 6.35%.

TABLE 5. SHIFT DIFFERENCES[a] BETWEEN OCTAHYDRO-1,4-NAPHTHOQUINONES (X=CO) AND DECALINS (X=CH_2)

Compound	C-4a	C-5	C-6	C-7	C-8	C-8a	Me
1c	5.53	−8.29	−2.42	−2.42	−8.29	5.53	
2c	5.40	−7.10	−3.12	−3.23	−8.73	7.20	1.28
3c	6.22	−8.54	−1.70	−2.27	−7.93	6.07	−0.62
2b	8.19	−3.99	−0.12	−3.93	0.24	11.82	−1.24
3b	13.05	0.60	−2.04	0.02	−9.48	9.54	−0.93

a) Values obtained from $\delta_c^{X=CO} - \delta_c^{X=CH_2}$ for the corresponding carbons in each case.

Compound ***2b***. Hydrogenation of 1.10 g of **2a** with 117 mg of 5% Pd-C in 100 ml of AcOEt afforded 0.84 g of **2b**: mp 55—56 °C (from diisopropyl ether); IR 1718 and 1704 cm^{-1}. Found: C, 73.25; H, 9.07%. Calcd for $C_{11}H_{16}O_2$: C, 73.30; H, 8.95%.

Compound ***2c***. Treatment of 149 mg of **2b** with 2 ml of 6% methanolic hydrogen chloride at room temperature overnight afforded 48 mg of **2c**: mp 62—63 °C (from petroleum ether); IR 1705 cm^{-1}. Found: C, 73.12; H, 9.05%. Calcd for $C_{11}H_{16}O_2$: C, 73.30; H, 8.95%.

Compounds ***3b*** *and* ***3c***. Hydrogenation of 1.14 g of **3a** with 165 mg of 5% Pd-C in 80 ml of AcOEt afforded 0.78 g of **3b**: mp 66—67 °C (from diisopropyl ether); IR 1705 cm^{-1}. Found: C, 73.44; H, 9.08%. Calcd for $C_{11}H_{16}O_2$: C, 73.30; H, 8.95%. The mother liquor was chromatographed on 5 g of Al_2O_3. Elution with benzene afforded 0.20 g of **3c**: mp 119—120 °C (from hexane); IR 1707 cm^{-1}. Found: C, 73.27; H, 9.16%. Calcd for $C_{11}H_{16}O_2$: C, 73.30; H, 8.95%.

Preparation of ***6a***. A mixture of 17.56 g of **5a**,[8] 5.54 g of $NH_2OH \cdot HCl$, and 6.67 g of NaOAc in MeOH–H_2O (400 ml–100ml) was refluxed for 2 h. Concentration of the solution afforded 16.41 g of **6a**: mp 208—209 °C (from MeOH); IR 3480, 1731, and 1708 cm^{-1}. Found: C, 61.97; H, 6.84; N, 5.51%. Calcd for $C_{13}H_{17}O_4N$: C, 62.14; H, 6.82; N, 5.57%.

Compound ***6b***. Hydrogenation of 2.54 g of **6a** with 65 mg of PtO_2 in 300 ml of MeOH afforded 1.55 g of **6b**: mp 211—213 °C (from MeOH); IR 3490, 1736, and 1701 cm^{-1}. Found: C, 61.66; H, 7.65; N, 5.49%. Calcd for $C_{13}H_{19}O_4N$: C, 61.64; H, 7.56; N, 5.53%.

Compound ***15***. Hydrogenation of 2.89 g of **6a** with 195 mg of PtO_2 in 150 ml of AcOH afforded 1.46 g of **15**: mp 199—200 °C (from AcOEt); IR 3430, 3190, and 1668 cm^{-1}; ^{13}C NMR 19.47(Me), 26.17(C-3), 28.52(C-7), 30.80(C-2*), 32.09(C-6*), 35.26(C-8), 36.88(C-5), 40.17(C-8a), 45.16 (C-4a), 46.91(C-1), 71.54(C-4), and 176.69 ppm (C=O). Found: C, 68.84; H, 9.31; N, 6.95%. Calcd for $C_{12}H_{19}O_2N$: C, 68.86; H, 9.15; N, 6.69%.

The Acetate ***10***. Treatment of 310 mg of **8**[8] with 3 ml of Ac_2O and 4 ml of pyridine at room temperature overnight afforded 339 mg of **10**: mp 115—117 °C(from AcOEt-hexane); IR 1737, 1710, and 1249 cm^{-1}. Found: C, 63.72; H, 8.00%. Calcd for $C_{15}H_{22}O_5$: C, 63.81; H, 7.85%.

The Acetate ***14b***. In a similar way to the preparation of **10**, 216 mg of **13**[8] was acetylated to afford 229 mg of **14b**: mp 97.5—99 °C (from benzene-hexane); IR 1740, 1717, and 1241 cm^{-1}. Found: C, 66.59; H, 8.07%. Calcd for $C_{14}H_{20}O_4$: C, 66.64; H, 7.99%.

References

1) (a) D. K. Dalling and D. M. Grant, *J. Am. Chem. Soc.*, **94**, 5318 (1972); (b) D. K. Dalling, D. M. Grant, and E. G. Paul, *ibid.*, **95**, 3718 (1973).

2) (a) E. L. Eliel and F. W. Vierhapper, *J. Org. Chem.*, **41**, 199 (1976); (b) F. W. Vierhapper and E. L. Eliel, *ibid.*, **42**, 51 (1977).

3) G. C. Levy and G. L. Nelson, "Carbon-13 Nuclear Magnetic Resonance for Organic Chemists," Wiley Interscience, New York (1972), Chap. 9.

4) W. Hückel and W. Kraus, *Chem. Ber.*, **92**, 1158 (1959).

5) C. A. Grob and H. Wicki, *Helv. Chim. Acta*, **31**, 1706 (1948).

6) H. v. Euler, H. Hasselquist, and A. Glaser, *Arkiv Kemi*, **3**, 1 (1950).

7) R. B. Woodward, F. E. Bader, H. Bickel, A. J. Frey, and R. W. Kierstead, *Tetrahedron*, **2**, 1 (1958).

8) H. Irikawa and Y. Okumura, *Bull. Chem. Soc. Jpn.*, **51**, 657 (1978).

9) A. C. Ghosh, K. Mori, A. C. Rieke, S. K. Roy, and D. M. S. Wheeler, *J. Org. Chem.*, **32**, 722 (1967).

10) J. B. Stothers, "Carbon-13 NMR Spectroscopy," Academic Press, New York (1972), p. 80.

11) H. J. Reich, M. Jautelat, M. T. Messe, F. J. Weigert, and J. D. Roberts, *J. Am. Chem. Soc.*, **91**, 7445 (1969).

12) Y. Senda, J. Ishiyama, and S. Imaizumi, *Bull. Chem. Soc. Jpn.*, **49**, 1359 (1976).

13) S. H. Grover and J. B. Stothers, *Can. J. Chem.*, **52**, 870 (1974).

14) H. Eggert, C. L. VanAntwerp, N. S. Bhacca, and C. Djerassi, *J. Org. Chem.*, **41**, 71 (1976).

15) G. M. Kellie and F. G. Riddell, "Topics in Stereochemistry," Vol. 8, ed by E. L. Eliel and N. L. Allinger, Wiley Interscience, New York (1974), p. 238.

16) F. J. Weigert and J. D. Roberts, *J. Am. Chem. Soc.*, **92**, 1347 (1970).

17) E. L. Eliel, W. F. Bailey, L. D. Kopp, R. L. Willer, D. M. Grant, R. Bertrand, K. A. Christensen, D. K. Dalling, M. W. Duch, E. Wenkert, F. M. Schell, and D. W. Cochran, *J. Am. Chem. Soc.*, **97**, 322 (1975).

A Novel Type of Polycondensation Utilizing Transition Metal-Catalyzed C–C Coupling. I. Preparation of Thermostable Polyphenylene Type Polymers

Takakazu YAMAMOTO,* Yasuhiro HAYASHI, and Akio YAMAMOTO

Research Laboratory of Resources Utilization, Tokyo Institute of Technology, Nagatsuta-cho, Midori-ku, Yokohama 227

(Received January 21, 1978)

Transition metal compounds including $NiCl_2$(bpy) (bpy=2,2′-bipyridine), $NiBr_2(PPh_3)_2$ (PPh_3=triphenylphosphine), $PdCl_2$(bpy), $NiCl_2$, $CoCl_2$, $FeCl_2$, and $FeCl_3$ catalyze polycondensation of di- and polyhalogenated organic aromatic compounds by dehalogenation with magnesium under mild conditions. Poly(*p*-phenylene), poly(*m*-phenylene), poly(oxybiphenylene), and poly(phenylenemethylene) were prepared from *p*-dihalobenzene, *m*-dichlorobenzene, bis(*p*-bromophenyl) ether, and α,*p*-dichlorotoluene. They have a high degree of polymerization and high thermal stability. Poly(*p*-phenylene), poly(oxybiphenylene), and poly(phenylenemethylene) have regularly repeated structures as proved by IR spectroscopy and X-ray powder diffraction. Polymerization of polyhalogenated aromatic compounds (1,3,5-trichlorobenzene and hexachlorobiphenyl) in tetrahydrofuran (THF) gave copolymers having aromatic nuclei and THF units. Polymerization of the haloaromatic compounds is considered to proceed through a mechanism in which consecutive cycles of oxidative addition of haloaromatic compounds (R–X) to the transition metal catalyst take place so as to cause alkylation (arylation) by the Grignard reagent formed in the system (R′MgX) and elimination of R–R′ from an active transition metal compound having R and R′ groups.

Polyphenylene type polymers consisting of coupled aromatic nuclei have high heat-resistance. Some of them have been utilized as material for rocket nozzles, electrical insulation, and fabrics which must withstand high temperatures.[1] Numerous reactions which produce the polyphenylene-type polymers have been developed over the past 15 years. The preparative methods include: (1) oxidative cationic polymerization of aromatic compounds by use of Friedel-Crafts type catalysts,[2] (2) dehalogenation of di- and poly-halogenated aromatic compounds with metals such as copper (Ullmann reaction)[3] and alkali metals (Wurtz-Fittig reaction),[4] (3) denitrogenation polymerization of diazonium compounds.[5] Of these methods the dehalogenation of di- and poly-halogenated aromatic compounds with metals such as copper[3] and alkali metals[4] serve as one of the most convenient and versatile routes for the preparation of the polyphenylene type polymers. However, the dehalogenation reaction by metals generally requires high temperatures, the polymers obtained having some structural irregularity and/or branching due to the radical nature of the conventional dehalogenation reactions by metals.

It was recently reported that transition metals or their compounds catalyze the coupling of Grignard reagents with aryl halides.[6]

$$RMgX + R'X \xrightarrow{\text{Transition metal}} R\text{-}R' + MgX_2 \qquad (1)$$

Since the transition metal-catalyzed coupling reaction proceeds selectively and quantitatively under mild conditions, it has been applied to the preparation of various organic aromatic compounds.[6]

Extension of the principle of the transition metal catalyzed coupling led us to its application to the preparation of polyphenylene-type polymers having regular recurring units by starting from dihalogenated aromatics. *p*-Dihalobenzene, for example, can be readily dehalogenated by coupling on reaction with magnesium which is promoted by transition metal catalysts, a linear polyphenylene being formed.

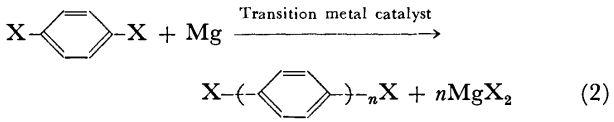

$$\qquad + nMgX_2 \qquad (2)$$

The net reaction resembles the conventional dehalogenation polymerization of haloaromatic compounds with Cu and Na. However, the reaction by the new method proceeds under much milder conditions, and can be applied more widely. A part of the results was reported previously.[7]

Results and Discussion

Polymerization of Halo Aromatic Compounds. The results of polymerization of di- and poly-halogenated aromatic compounds are given in Table 1. Although the halo aromatic compounds are not polymerized with magnesium alone in the absence of transition metal catalyst (Exp. No.1, Table 1), addition of a catalytic amount of a suitable transition metal compound to the reaction mixtures initiates very smooth polymerization to yield polyphenylene-type polymers in high yields.

Dihalo Aromatic Compounds: A variety of transition metal compounds catalyze the polymerization of *p*-dibromobenzene. Of the transition metal complexes, $NiCl_2$(bpy) (bpy=2,2′-bipyridine) acts as one of the most effective catalysts. Even a minor amount of the compound (*e.g.*, 5 mg of the complex with Ni/monomer of 3.4×10^{-4} in Exp. No. 3) gives a polymer in a high yield in 4 h at refluxing temperature of tetrahydrofuran (THF).

The polymerization proceeds most smoothly in THF under reflux conditions. However, since the catalytic activity of the complex is very high, it proceeds even at 0 °C (No. 4) though there is some induction period in this case. Employment of other ethereal solvents such as dibutyl ether (No. 5) and diglyme

TABLE 1. DEHALOGENATION POLYMERIZATION OF HALO ALOMATIC COMPOUNDS WITH MAGNESIUM IN THE PRESENCE OF TRANSITION METAL CATALYSTS[a]

No.	Monomer	g (mmol)	Mg g (mmol)	Catalyst[b] (mg)	Solvent[c] (ml)	Time h	Yield[d] g(%)	Remarks
1	*p*-Dibromobenzene	11.8(50)	1.22(50)	none	THF	4.0	0	
2	*p*-Dibromobenzene	11.8(50)	1.22(50)	$NiCl_2$(bpy) (51)	THF	4.0	3.8(95)	
3	*p*-Dibromobenzene	11.8(50)	1.22(50)	$NiCl_2$(bpy) (5)	THF	4.0	2.7(64)	
4	*p*-Dibromobenzene	11.8(50)	1.22(50)	$NiCl_2$(bpy) (50)	THF	6.0	4.0(94)	e)
5	*p*-Dibromobenzene	11.8(50)	1.22(50)	$NiCl_2$(bpy) (50)	Bu_2O	4.5	2.8(68)	
6	*p*-Dibromobenzene	11.8(50)	1.35(56)	$NiBr_2(PPh_3)_2$ (50)	THF	4.0	2.7(64)	
7	*p*-Dibromobenzene	11.8(50)	1.22(50)	$PdCl_2$(bpy) (50)	THF	4.0	4.1(95)	
8	*p*-Dibromobenzene	11.8(50)	1.35(56)	$FeEt_2(bpy)_2$ (100)	THF	6.0	0.8(18)	
9	*p*-Dibromobenzene	11.8(50)	1.35(56)	$CrMeCl_2(THF)_3$ (50)	THF	7.0	0.5(11)	
10	*p*-Dibromobenzene	11.8(50)	1.22(50)	$Ni(cod)(PPh_3)_2$ (50)	THF	4.0	3.8(86)	
11	*p*-Dibromobenzene	11.8(50)	1.22(50)	$NiCl_2$ (54)	THF	4.0	4.0(83)	
12	*p*-Dibromobenzene	11.8(50)	1.22(50)	$FeCl_2$ (50)	THF	4.0	3.2(76)	
13	*p*-Dibromobenzene	11.8(50)	1.22(50)	$FeCl_3$ (50)	THF	4.0	3.0(68)	
14	*p*-Dibromobenzene	11.8(50)	1.22(50)	$CoCl_2$ (50)	THF	4.0	3.2(77)	
15	*p*-Dichlorobenzene	7.4(50)	1.32(54)	$NiCl_2$(bpy) (70) (50)	THF	6.0	2.5(60)	
16	*p*-Diiodobenzene	3.3(10)	0.24(10)	$NiCl_2$(bpy) (8)	THF	4.0	0.4(50)	
17	*m*-Dichlorobenzene	7.2(49)	1.22(50)	$NiCl_2$(bpy) (50)	THF	6.0	3.6(92)	
18	Bis(*p*-bromophenyl)ether	12.8(40)	1.33(55)	$NiCl_2$(bpy) (100)	THF	5.0	4.0(60)	
19	Bis(*p*-bromophenyl)ether	11.9(36)	1.33(55)	$NiBr_2(PPh_3)_2$ (55)	THF	9.0	2.4(39)	
20	α,*p*-Dichlorotoluene	8.09(50)	1.28(53)	$NiCl_2$(bpy) (50)	THF	7.0	3.3(69)	
21	2,5-Dibromopyridine	11.9(50)	1.22(50)	$NiCl_2$(bpy) (50)	THF	8.0	3.9(62)	
22	2,5-Dibromopyridine	11.9(50)	1.22(50)	$NiBr_2(PPh_3)_2$ (50)	THF	8.0	4.5(64)	
23	2,5-Dibromopyridine	11.9(50)	1.22(50)	$NiCl_2$ (50)	THF	8.0	1.4(23)	
24	9,10-Dibromoanthracene	8.4(25)	0.64(26)	$NiCl_2$(bpy) (50)	THF	6.0	1.25(22)	
25	1,3,5-Trichlorobenzene	9.07(50)	3.65(150)	$NiCl_2$(bpy) (50)	THF	15	2.15	f)
26	1,3,5-Trichlorobenzene	4.53(25)	1.83(75)	$NiCl_2$(bpy) (50)	Diglyme	10.5	1.76(72)	
27	Hexachlorobiphenyl	18.0(50)	3.65(150)	$NiCl_2$(bpy) (50)	THF	15.0	8.2	f)

a) Under reflux except for No. 4. b) bpy=2,2′-bipyridine, PPh_3=triphenylphosphine, cod=1,5-cyclooctadiene, Me=methyl, Et=ethyl. c) THF=tetrahydrofuran, Bu_2O=dibutyl ether. d) Based on the amount of carbon taken into the polymer. e) At 0 °C. f) Copolymer with THF (see the text).

gives similar results.

Other nickel and palladium complexes such as $NiBr_2(PPh_3)_2$ (PPh_3=triphenylphosphine) and $PdCl_2$-(bpy) also show high catalytic activities, but the catalytic activities of iron and chromium complexes, $Fe(C_2H_5)_2(bpy)_2$ and $CrCl_2(CH_3)(THF)_3$, are relatively low. Simple transition metal compounds such as $NiCl_2$, $FeCl_2$, and $CoCl_2$ catalyse the polymerization as well. In contrast to these transtion metal compounds metallic Pd and Ni, $PdCl_2$, $CuBr_2$, Cu(acetylacetonato)$_2$, and $MnCl_2$ have negligible or no catalytic activity for the polymerization, although Pd metal and $PdCl_2$ are known to act as effective catalysts for the preparation of low molecular weight aromatic compounds by Reaction 1.[6d,6e] Cuprous halides do not catalyze the polymerization of halo aromatic compounds, either, but they catalyze the polymerization of halo aliphatic compounds to yield aliphatic polymers having high molecular weight. *p*-Dichlorobenzene and *p*-diiodobenzene are also polymerized by the transition metal catalysts, the yields being lower than in the polymerization with *p*-dibromobenzene.

Polymerization is not restricted to *p*-dihalobenzene. *m*-Dichlorobenzene (No. 17, Table 1) and other dihalo aromatic compounds such as bis(*p*-bromophenyl) ether and α,*p*-dichlorotoluene can be polymerized by using the transition metal catalysts.

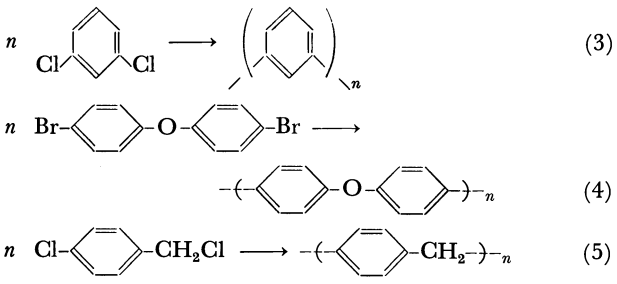

(3)

(4)

(5)

Some transition metal compounds catalyze the coupling between organolithiums and organic halides:[8]

$$RLi + R'X \xrightarrow{[M]} R\text{-}R' + LiX \quad (6)$$

However, attempts to utilize lithium instead of magnesium as the dehalogenating reagent in the preparation of polyphenylene type polymers from aromatic halides were unsuccessful.

Polyhalo Aromatic Compounds: When the dehalogenation polymerization of aromatic compounds having three or more halogen atoms is carried out in THF (Nos. 25 and 27, Table 1), the polymers obtined

Table 2. Properties of the polyphenylene type polymers

No.[a]	Polymer	Color	Mp (°C)	Soluble fraction in hot toluene (%)[b]
2	$-(-p\text{-}C_6H_4-)-_n$	light yellow	550 dec	20
6	$-(-p\text{-}C_6H_4-)-_n$	light yellow	550 dec	16
14	$-(-p\text{-}C_6H_4-)-_n$	light yellow	550 dec	35
17	$-(-m\text{-}C_6H_4-)-_n$	white	190—200[c] 280—295[d]	39
18	$-(-C_6H_4\text{-}O\text{-}C_6H_4-)-_n$	white	250—280	18
20	$-(-C_6H_4CH_2-)-_n$	white	230—235[c] >400[d]	52
21	$-(-C_5H_3N-)-_n$	brown	260	e)
25	$C_6H_3Cl_3$-THF copolymer[f]	yellow	190—195	
26	$-(-C_6H_3-)-_n$	brown	290 dec	
27	$C_{12}H_4Cl_6$-THF copolymer[f]	brown	185—200	

a) Numbers correspond to those in Table 1. b) Extracted with hot toluene in a Soxhlet extractor for 50 h. c) For polymers soluble in hot toluene. d) For polymers insoluble in hot toluene. e) Soluble in acidic water. f) See the text.

contain both the aromatic nuclei and THF units. The IR spectra show bands characteristic of not only aromatic compounds but also of polytetrahydrofuran $-(-O\text{-}CH_2\text{-}CH_2\text{-}CH_2\text{-}CH_2-)-_n$. The NMR spectra show signals of aromatic protons at δ 7—8 ppm and those of THF-protons at δ 1.8 ppm $-(-CH_2\text{-}C\underline{H}_2\text{-}CH_2-)-$, δ 2.4 ppm $-(-C_6H_4\text{-}C\underline{H}_2-)-$, δ 3.7 ppm $-(-O\text{-}C\underline{H}_2-)-$, and δ 4.1 ppm $-(-C_6H_4\text{-}O\text{-}C\underline{H}_2-)-$. The polymers are not soluble in THF, which dissolves polytetrahydrofuran, but soluble in chloroform, which does not dissolve polyphenylene type polymers. The resutls suggest that the polymers are copolymer such as

$$-(-A-)_m-(-O\text{-}CH_2\text{-}CH_2\text{-}CH_2\text{-}CH_2-)-_n,$$

where A represents the aromatic units.

In the case of hexachlorobiphenyl polymerized with magnesium in THF, the NMR spectrum indicates that the copolymer contains the two monomer units in about 1:1 ratio in line with the analytical data. The peak areas of methylene protons at δ 2.4 ppm and δ 4.1 ppm contained in the THF units adjacent to the aromatic unit are considerably small, although the copolymer contains the two monomer units in about 1:1 ratio. This suggests that the copolymer has a block structure rather than a random structure.

The copolymers of polyhaloaromatic compounds and THF melt without decomposition at considerably high temperatures (Table 2). The polymerization of polyhalogenated aromatic compounds in other ethereal solvents such as dibutyl ether and diglyme gives normal dehalogenated homopolymers of the polyhalogenated aromatic compounds (No. 26).

Properties of Polymers. Physical Properties: The color, melting point, and solubility of the polymers obtained are given in Table 2. The polymers prepared by the present method are much less colored than those prepared by conventional methods such as oxidative cationic polymerization of benzene and dehalogenation polymerization of halo aromatic compounds. For example, poly(*p*-phenylene) prepared by the present method is light yellow, whereas the one prepared by conventional methods is brown or black.[1-5] Poly(*m*-phenylene) prepared by the Wurtz-Fittig reaction[4b] of $m\text{-}C_6H_4Br_2$ and poly(oxybiphenylene) prepared by the polycondensation of potassium *p*-(*p*-bromophenyl)phenoxide[9] were reported to be yellow and gray, respectively.

The polymers prepared here generally have high thermal stability. The thermal stability of poly(*p*-phenylene) prepared by the present method is comparable with that prepared by the oxidative cationic polymerization of benzene. It does not melt up to 550 °C, where it begins to decompose in the air. Differential thermoanalysis (DTA) of poly(*p*-phenylene) in the air showed an exothermic peak at 580 °C due to the oxidation of the polymer. Poly(*m*-phenylene), poly(oxybiphenylene), poly(phenylenemethylene), and poly(2,5-pyridinediyl) melt above 200 °C. Poly(1,3,5-benzene-triyl)(No. 26) which appears to have a three dimentional structure decomposes at 290 °C without melting. The copolymers with THF melt at relatively low temperatures, their melting points being much higher than the melting point of the THF homopolymer.

The solubility of the polyphenylene-type polymers is low. Poly(*p*-phenylene), poly(*m*-phenylene), poly(oxybiphenylene), and poly(phenylenemethylene) are partially extracted by hot toluene as shown in Table 2, but the extracted fractions do not dissolve in toluene at room temperature. Poly(pyridinediyl) (No. 21—23) is soluble in an aqueous solution containing HCl with the concentration higher than 3 M. Dilution or neutralization of the solution caused precipitation of the polymer. The copolymers with THF are soluble in chlorinated hydrocarbons such as $CHCl_3$ and CCl_4.

IR Spectra and Molecular Weight: Figute 1 shows IR spectra of typical polymers. The IR spectrum of poly(*p*-phenylene) prepared by the present method is essentially of poly(*p*-phenylene)s prepared by conventional methods such as oxidative cationic polymerization of benzene. The out-of-plane vibration of *p*-phenylene units, δ(para), in poly(*p*-phenylene)s prepared under various conditions appears in the region 805±

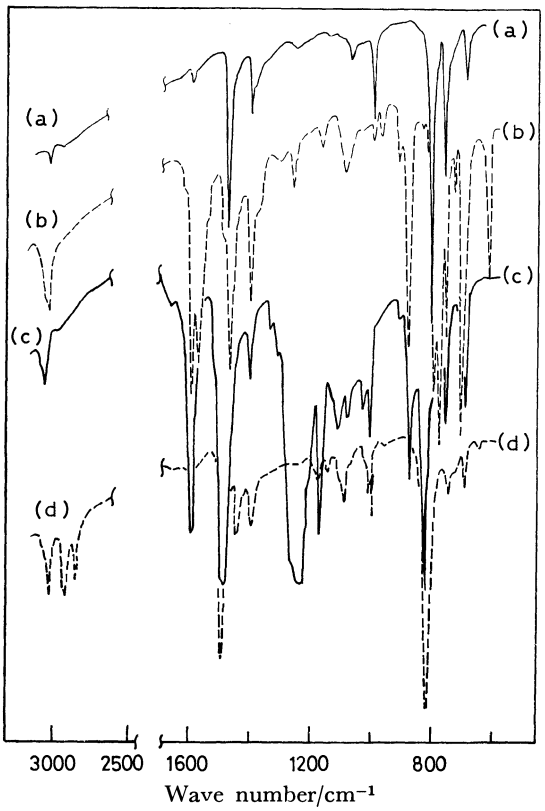

Fig. 1. IR spectra of (a) poly(*p*-phenylene) prepared from *p*-dibromobenzene, (b) poly(*m*-phenylene), (c) poly(oxybiphenylene), and (d) poly(phenylenemethylene).

5 cm^{-1}. Weak ν(C–Cl), ν(C–Br), and ν(C–I) bands of terminal *p*-halophenyl groups are observed at 1085, 1065, and 1055 cm^{-1}, respectively, in the IR spectra of poly(*p*-phenylene)s prepared from the corresponding *p*-dihalobenzenes. In addition to the δ(para) band at 805±5 cm^{-1} assignable to the *p*-phenylene units the IR spectrum of poly(*p*-phenylene) shows two out-of-plane vibration bands due to terminal phenyl group at 760 cm^{-1} (δ(mono$_1$)) and 690 cm^{-1} (δ(mono$_2$)).[2b] These IR spectroscopic data suggest that the poly(*p*-phenylene) has both *p*-halophenyl and phenyl groups as the terminal groups:

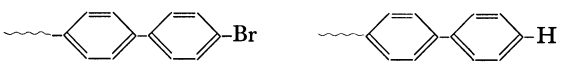

The fact that the intensities of the bands due to the terminal phenyl group (δ(mono$_1$) and δ(mono$_2$)) are much greater than the ν(C–X) band suggests that the proportion of the terminal group bearing the halogen is not so high.

Kovacic and Oziomek took the relative intensity of δ(para) to that of δ(mono$_1$) and δ(mono$_2$), $A(\delta(\text{para}))/\{A(\delta(\text{mono}_1))+A(\delta(\text{mono}_2))\}$ (A=absorbance of the peak), as a measure for the degree of polymerization.[2b,2c] The value $A(\delta(\text{para}))/\{A(\delta(\text{mono}_1)+A(\delta(\text{mono}_2))\}$ for poly(*p*-phenylene) prepared from dibromobenzene with various catalysts lies between 1.92 (No. 2, Table 1) and 3.85 (No. 7, Table 1), indicating that poly(*p*-phenylene)s obtained have considerably high degrees of polymerization, comparable to that

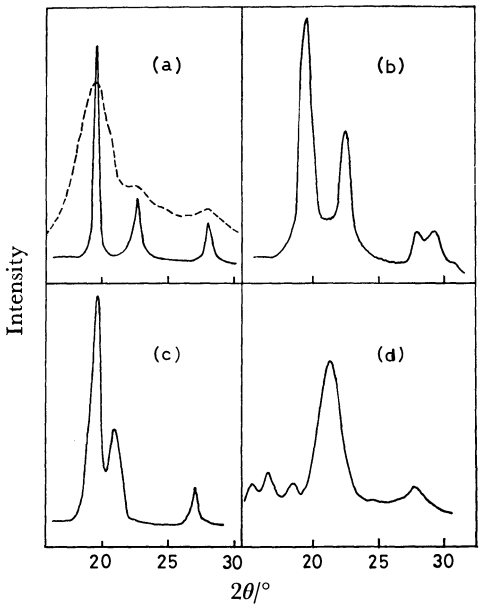

Fig. 2. X-Ray diffraction patterns of (a) poly(*p*-phenylene), (b) poly(oxybiphenylene), (c) poly(phenylenemethylene), and (d) poly(*m*-phenylene). See the text for the broken line in Fig. 2a.

prepared by Kovacic and Oziomek through oxidative cationic polymerization of benzene.[2b]

The IR spectra of types of polymers other than poly(*p*-phenylene) are also in line with the expected structures as represented in Eqs. 3—5. The absorptions in the region of the out-of-plane vibration of poly(*m*-phenylene) are more complicated than those of poly(*p*-phenylene) since each *m*-phenylene unit has both isolated δ(C–H) and three adjacent δ(C–H)'s. Poly(oxybiphenylene) has strong ν(C–O) band at 1245 cm^{-1} and poly(phenylenemethylene) has aliphatic ν(C–H) bands at 2860 and 2960 cm^{-1}. Poly(oxybiphenylene) and poly(phenylenemethylene) have ν(C–X) (1050—1090 cm^{-1}) band of terminal halophenyl group and δ(C–H) (680—770 cm^{-1}) bands of terminal phenyl group. The fact that the relative intensities of these bands assignable to terminal phenyl and halophenyl groups are considerably weaker than those of δ(C–H) bands due to the inner repeating aromatic units (800—900 cm^{-1}) indicates that these polymers have high degree of polymerization.

X-Ray Diffraction: Figure 2 shows X-ray diffraction patterns of the powdery polymers prepared by polycondensation with magnesium. The X-ray diffraction spectrum of poly(*p*-phenylene) shows strong and sharp peaks even before annealing of the polymer, indicating that the polymer has high crystallinity due to the polymer structure having regularly repeated units in the polymer chain produced by highly selective condensation reaction between the Grignard reagents and aryl halides (Eq. 1). The poly(*p*-phenylene) prepared by the oxidative cationic polymerization of benzene shows only broad signals as represented by the broken line in Fig. 2a when it is not annealed; sharp peaks appear only after the annealing of the polymer.[2d]

The X-ray diffraction patterns of poly(oxybiphenylene) and poly(phenylenemethylene) also show sharp

peaks before annealing. Formation of the following three units is possible in the polymerization of α,*p*-dichlorotoluene:

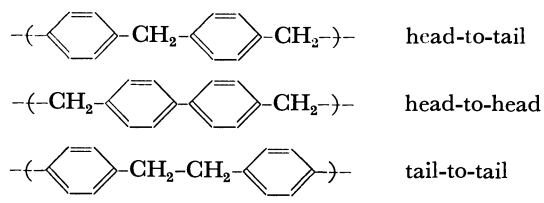

However, the sharp X-ray diffraction peaks of the polymer as well as the simple IR pattern in the region of the out-of-plane vibration suggest that the polymer contains mainly one of the three units, presumably the head-to-tail structure.

The X-ray diffraction pattern of poly(*m*-phenylene) shows broad peaks and that of poly(2,5-pyridinediyl) shows no clear peaks. The broadness of the peaks in the X-ray pattern of poly(*m*-phenylene) might be due to the irregularities caused by the presence of both *cis-trans* and *trans-trans* configurations:

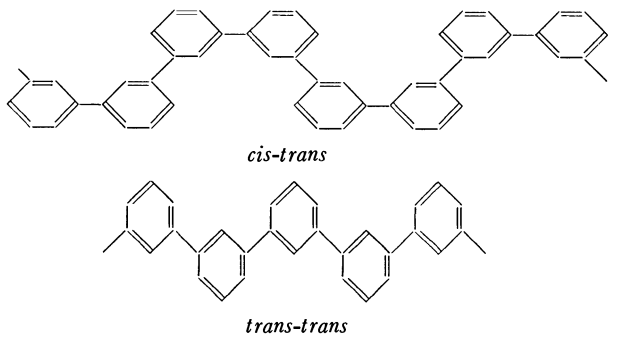

3. Polymerization Mechanism: The coupling between a Grignard reagent RMgX and an aryl halide R'X catalyzed by a dihalonickel complex NiX_2L_2 (L= ligand) (Eq. 1) seems to proceed through a mechanism comprised of

(a) formation of NiR_2L_2 by the reaction of NiX_2L_2 with RMgX,

(b) reaction of NiR_2L_2 with R'X to yield R–R and $NiR'(X)L_2$,

(c) alkylation of $NiR'(X)L_2$ with RMgX to yield $NiR(R')L_2$, and

(d) elimination of R–R' with formation of $NiR'(X)L_2$ in the reaction of $NiR(R')L_2$ with R'X:[6b]

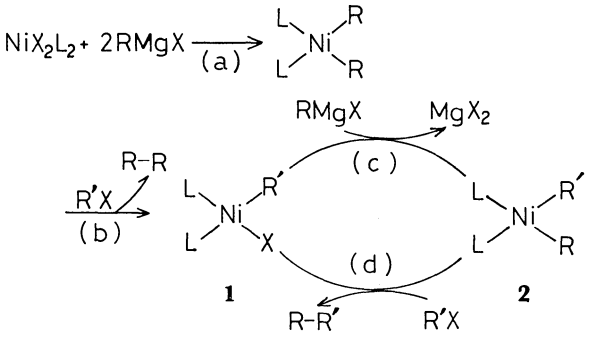

In the mechanism the starting complex NiX_2L_2 is converted into the active species $NiR'(X)L_2$ by reactions (a) and (b). The catalytic formation of R–R' then proceeds through the key intermediates $NiR'(X)L_2$ and $NiR'(R)L_2$.

If the same mechanism can be applied to the present polymerization of *p*-$C_6H_4Br_2$, it seems to proceed as follows:

$$\mathrm{BrNiL_2\text{–}(\text{–}C_6H_4\text{–})_{n_1}MgBr} + \mathrm{Br\text{–}(\text{–}C_6H_4\text{–})_{n_2}MgBr}$$
$$\mathbf{1}(n_1) \qquad\qquad \mathbf{P}(n_2)$$
$$\xrightarrow{\text{(c) type reaction}} \mathrm{Br\text{–}(\text{–}C_6H_4\text{–})_{n_2}NiL_2\text{–}(\text{–}C_6H_4\text{–})_{n_1}MgBr} + \mathrm{MgBr_2}$$
$$\mathbf{2}(n_1, n_2)$$
$$\mathbf{2}(n_1, n_2) + \mathrm{Br\text{–}(\text{–}C_6H_4\text{–})_{n_3}MgBr}$$
$$\mathbf{P}(n_3)$$
$$\xrightarrow{\text{(d) type reaction}} \mathrm{BrNiL_2\text{–}(\text{–}C_6H_4\text{–})_{n_3}MgBr} + \mathrm{Br\text{–}(\text{–}C_6H_4\text{–})_{\overline{n1+n2}}MgBr}$$
$$\mathbf{1}(n_3) \qquad\qquad \mathbf{P}(n_1+n_2)$$
$$\mathbf{1}(n_3) + \mathbf{P}(n_4) \rightarrow \mathbf{2}(n_3, n_4)$$
$$\mathbf{2}(n_3, n_4) + \mathbf{P}(n_5) \rightarrow \mathbf{1}(n_5) + \mathbf{P}(n_3+n_4)\cdots etc.$$

Scheme 1.

where $\mathbf{P}(n)$ stands for the polymer having n phenylene units and $\mathbf{P}(1)$ represents the monomer *p*-BrC_6H_4MgBr which is the main product of the reaction between *p*-$C_6H_4Br_2$ and Mg. $\mathbf{1}(n_1)$, $\mathbf{2}(n_1,n_2)$... represent intermediate nickel complexes **1** and **2** having phenylene groups bonded to nickel. We have examined the time course of the polycondensation by following the disappearance of the mono-Grignard reagent Br–C_6H_4–MgBr, di-Grignard reagent BrMg–C_6H_4–MgBr and intact dibromobenzene formed by the reaction of dibromobenzene with Mg in a 1:1 ratio by means of gas chromatography. The amounts of the di- and mono-Grignard reagents were measured as benzene and bromobenzene after hydrolysis of the reaction mixture.

Figure 3 shows time-course of the decrease of species in the $NiCl_2$(bpy)-catalyzed dehalogenation polymerization of *p*-$C_6H_4Br_2$ with Mg at 3±1 °C where the rate of polymerization is not very high. As shown in Fig. 3 the reaction of *p*-$C_6H_4Br_2$ with Mg in a 1:1 molar ratio gives a mixture of *p*-$C_6H_4(MgBr)_2$, *p*-BrC_6H_4MgBr, and intact *p*-$C_6H_4Br_2$. The rate of consumption of these chemical species is low at the early stage, becoming higher after the induction period. The dihalonickel complex $NiCl_2$(bpy) seems to be converted into the active species (*e.g.*, Ni(C_6H_4MgBr)(Br)(bpy), **1**(1)) during the induction period.

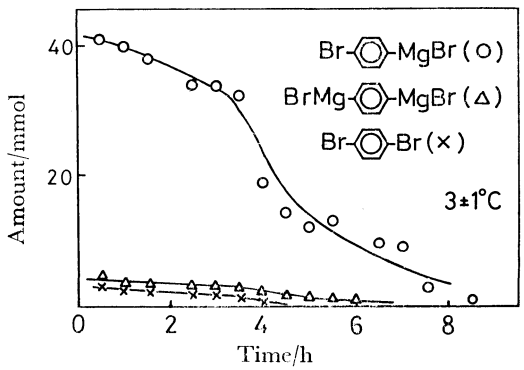

Fig. 3. Time course of mnomer consumption during the polymerization of p-$C_6H_4Br_2$ (11.8 g, 50 mmol) in THF (50 ml) at 3±1 °C; p-BrC_6H_4MgBr (○), p-$C_6H_4(MgBr)_2$ (△), and p-$C_6H_4Br_2$ (×), Catalyst = $NiCl_2$(bpy) (50 mg).

According to Scheme 1 the polymer should have both $-C_6H_4MgBr$ and $-C_6H_4Br$ terminals. The phenyl terminal of poly(p-phenylene) was thought to be formed from the $-C_6H_4MgBr$ terminal during the work-up of the polymer. However, reactions of the raw polymer with D_2O or CO_2 did not introduce D or carboxyl group into the polymer. This excludes the presence of the $-C_6H_4MgBr$ terminal in the polymer. The phenyl terminal can be formed through the incorporation of mono-functional species such as C_6H_5MgBr and C_6H_5Br formed by the reactions of p-$C_6H_4(MgBr)_2$ and p-BrC_6H_4MgBr with trace amounts of water in the solvent. If these nomo-functional species should participate, the polymerization would be terminated with formation of the phenyl terminal(s). Under certain conditions the polymerization might be terminated mainly through this process, and most of the polymer end would be the phenyl group. The infrared spectra of some polymers suggest the formation of polymers with phenyl end group(s). Addition of C_6H_5Br or C_6H_5MgBr into the polymerization system decreases the degree of polymerization as judged from the increase in the intensities of $\delta(\text{mono}_1)$ and $\delta(\text{mono}_2)$ in the IR spectrum of the polymer obtained.

When an aromatic compound having three or more halogen atoms is employed for the polymerization, it may act as an electron acceptor, coordinating with the transition metal complex. Coordination of the electron acceptor to the transition metal would enhance the Lewis acidity of the transition metal and initiate the ring-opening polymerization of THF, which is usually catalyzed by Lewis acid, producing the copolymer with THF units:

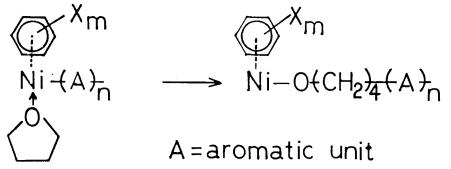

Experimental

Material. Commercial haloaromatic compounds except for hexachlorobiphenyl were used. Hexachlorobiphenyl was supplied by Prof. Emeritus S. Kambara. Solvents were dried over sodium wire and distilled under nitrogen. $NiCl_2$(bpy),[10] $NiBr_2(PhP_3)_2$,[11] $PdCl_2$(bpy),[12] $Fe(C_2H_5)_2$-(bpy)$_2$,[13] $Cr(CH_3)Cl_2(THF)_3$,[14] and (1,5-cyclooctadiene)bis-(triphenylphosphine)nickel[15] were prepared according to the literature. Commercial products were used for simple transition metal compounds.

Polymerization. When 51 mg of $NiCl_2$(bpy) was added to a mixture of the products obtained by the reaction of 11.8 g (50 mmol) of p-dibromobenzene with 1.22 g (50 mg-atom) of magnesium in dry tetrahydrofuran (50 ml), smooth polymerization started. Polymerization was almost completed after refluxing the mixture for 1 h. After further refluxing for 4 h the reaction mixture was poured into 500 ml of ethyl alcohol. The polymer precipitated was collected over a glass filter, washed with dilute hydrochloric acid and ethyl alcohol, and dried in a vacuum to yield 3.8 g (95%) of light yellow poly(p-phenylene) (No. 2, Table 1). Extraction of the polymer by hot toluene with Soxhlet extractor for 50 h gave 0.70 g of the extractable fraction. Polymerization of p-dibromobenzene catalyzed by other transition metal compounds and that of other haloaromatic compounds were carried out in a similar manner. Analytical data of the polymers agreed with the structures given in the text. Percent yields in Table 1 are calculated based on the amount of carbon taken into the polymer.

The polyphenylene type polymers were also prepared by stirring the mixture of halo aromatic compound, magnesium, and the catalyst added before formation of the Grignard reagent. The yields and spectral data of the polymers prepared by this method were almost the same as those prepared by the method described above.

Kinetics. The reaction of p-dibromobenzene (11.8 g, 50 mmol) and magnesium (1.22 g, 50 mg-atom) was carried out in 50 ml of THF at room temperature. After completion of the reaction the reaction vessel was immersed in thermostatted water. Toluene (2.00 g) was added to the reaction mixture as an internal standard of gas chromatography and then 50 mg of $NiCl_2$(bpy) was added with stirring. The reaction mixture was occasionally pipetted out and treated with dil HCl. The amounts of p-$C_6H_4(MgBr)_2$, p-BrC_6H_4MgBr, and p-$C_6H_4Br_2$ were determined by measuring the amounts of benzene, bromobenzene, and p-dibromobenzene with a Shimadzu GC-3BT Gas Chromatogram.

Spectral Measurement and Analyses. IR spectra were recorded on a Hitachi Model 295 spectrometer. NMR spectra were taken with a Japan Electron Optics Laboratory SP-100 NMR spectrometer. Differential thermoanalyses were performed with a Shimadzu DT-30 thermal analyzer. X-Ray diffraction spectra were obtained with a Phillips PW-1051 X-Ray Diffractometer. Microanalyses of the polymers were performed by Mr. T. Saito with a Yanagimoto CHN Type MT-2 autocorder.

References

1) Review articles: (a) G. K. Noren and J. K. Stille, *Makromol. Reviews*, **5**, 385 (1971); (b) J. G. Speight, P. Kovacic and F. W. Koch, *Rev. Makromol. Chem.*, **6**, 295 (1971); (c) M. Kinoshita, "New Polymerization Reactions," ed by T. Saegusa, Kagaku-Dojin (in Japanese) (1971), p. 31.

2) (a) P. Kovacic and C. Wu, *J. Polym. Sci.*, **47**, 45 (1960); (b) P. Kovacic and J. Oziomek, *J. Org. Chem.*, **29**, 100 (1964); (c) P. Kovacic and L. C. Hsu, *J. Polym. Sci., A-1*, **4**, 5 (1966); (d) P. Kovacic, M. B. Feldman, J. P. Kovacic, and J. B. Lando, *J. Appl. Polym. Sci.*, **12**, 1735 (1968); (e) P. Kovacic and A. Kyriaskis *J. Am. Chem. Soc.*, **85**, 454 (1963); (f) Y.

M. Paushkin, L. S. Polak, O. Y. Omarov, and I. I. Patalakh, *J. Polym. Sci.*, **C16**, 2615 (1967); (g) J. E. Durham and P. Kovacic, *J. Polym. Sci. Polym. Lett.*, **14**, 347 (1976).

3) (a) A. A. Berlin, *J. Polym. Sci.*, **55**, 621 (1961); (b) J. C. Dacons, U. S. Patent 3450778 (1969); (c) E. Ibuki, S. Ozasa, and K. Murai, *Bull. Chem. Soc. Jpn.*, **48**, 1868 (1975).

4) (a) G. Goldschmidt, *Monatsh. Chem.*, **7**, 40 (1886); (b) A. A. Berlin, Z. V. Popova, and D. M. Yanovskii, *Vysokomol. Soedin.*, **7**, 623 (1965).

5) (a) A. A. Berlin, V. I. Liogonskii, and V. P. Parini, *J. Polym. Sci.*, **55**, 675 (1961); (b) S. Hayama, S. Nuno, and H. Kobamatsu, *Kogyo Kagaku Zasshi*, **72**, 608 (1969); (c) S. Hayama, S. Nuno, and H. Kobamatsu, *ibid.*, **72**, 1589 (1969); (d) S. Hayama and S. Nuno, *J. Polym. Sci., Polym. Chem. Ed.*, **12**, 357 (1974).

6) (a) K. Tamao, K. Sumitani, and M. Kumada, *J. Am. Chem. Soc.*, **94**, 4374 (1972); (b) K. Tamao, K. Sumitani, Y. Kiso, M. Zembayashi, A. Fujioka, S. Kodama, I. Nakajima, A. Minato, and M. Kumada, *Bull. Chem. Soc. Jpn.*, **49**, 1958 (1976); (c) D. G. Morrell and J. K. Kochi, *J. Am. Chem. Soc.*, **97**, 7262 (1975); (d) A. Sekiya and N. Ishikawa, *J. Organomet. Chem.*, **118**, 349 (1976); (e) A. Sekiya and N. Ishikawa, *ibid.*, **125**, 281 (1977); (f) M. Uchino, A. Yamamoto, and S. Ikeda, *J. Organomet. Chem.*, **24**, C63 (1970); (g) M. Uchino, K. Asagi, A. Yamamoto, and S. Ikeda, *ibid.*, **84**, 93 (1975).

7) T. Yamamoto and A. Yamamoto, *Chem. Lett.*, **1977**, 353.

8) M. Yamamura, I. Moritani, and S. Murahashi, *J. Organomet. Chem.*, **91**, C39 (1975).

9) J. H. J. Golden, *Soc. Chem. Industr. Monogr.*, **13**, 231, 303 (1961).

10) (a) J. A. Broomhead and F. P. Dwyer, *Aust. J. Chem.*, **14**, 250 (1961); (b) T. Yamamoto, A. Yamamoto, and S. Ikeda, *J. Am. Chem. Soc.*, **93**, 3350 (1971).

11) L. M. Venanzi, *J. Chem. Soc.*, **1958**, 718.

12) (a) S. E. Livingston, *J. Proc. Roy. Soc. New South Wales*, **86**, 32 (1952); (b) P. M. Gidney, R. O. Gillard, and B. T. Heaton, *J. Chem. Soc. Dalton*, **1973**, 132.

13) A. Yamamoto, K. Morifuji, S. Ikeda, T. Saito, Y. Uchida, and A. Misono, *J. Am. Chem. Soc.*, **87**, 4652 (1965).

14) K. Nishimura, H. Kuribayashi, A. Yamamoto, and S. Ikeda, *J. Organomet. Chem.*, **37**, 317 (1972).

15) (a) G. Wilke, E. W. Muller, and M. Kroner, *Angew. Chem.*, **73**, 33 (1961); (b) G. Wilke, E. M. Muller, M. Kroner, P. Heimbach, and H. Breil, German Patent 1191375 (1965).

Medium Effects on Stereochemistry of Acid-Catalyzed Ethanolysis of *trans*-2,3-Diphenyloxirane

Masashi INOUE,* Yoshio TAGUCHI, Toshio SUGITA, and Katsuhiko ICHIKAWA

Department of Hydrocarbon Chemistry, Faculty of Engineering, Kyoto University, Yoshida, Kyoto 606

(Received January 23, 1978)

The acid catalyzed ethanolysis of *trans*-2,3-diphenyloxirane was examined in a wide variety of binary ethanolic solvent systems. The reaction proceeded with 26% retention and 74% inversion of configuration in pure ethanol at 50 °C. The dilution of ethanol by hexane or benzene produced almost no change in stereochemistry of the ethanolysis. The addition of acetonitrile, nitromethane, or sulfolane to the ethanolic solution resulted in increased degrees of retention. In binary ethanolic mixtures containing DMSO, DMF, or HMPA, increased ratios of inverted product were obtained. The steric course of the ethanolysis could be controlled from 85% retention–15% inversion (CH_3NO_2:ethanol=20:2 by volume) to 10% retention–90% inversion (HMPA:ethanol=10:12) by the choice of co-solvent. The results are discussed in terms of the solvation-shell concept.

Reaction media have an enormous effect on organic reactions, and many papers have been published on the solvent effects of reaction kinetics. Since the physical properties can be varied continuously by changing the composition of the solvents, binary solvent systems are particularly interesting, and a number of papers have discussed the reaction kinetics in binary solvent mixtures. Arnett and his co-workers have reported that the rates of solvolysis of *t*-butyl chloride in aqueous mixture are determined by changes in the stability of the *ground state* and not of the transition state.[1]

Although the effects of the composition of the binary solvent mixture on the steric course of reaction seem to be interesting, only a few papers have dealt with this problem. The results of the solvolysis of optically active 1-methylheptyl *p*-bromobenzenesulfonate by Weiner and Sneen[2] are the most famous and have been quoted in many texts. The reaction in 75% aqueous dioxane gave inverted 2-octanol in 77% optical purity, whereas the solvolysis in pure water resulted in 100% inversion of configuration. The results were explained by assuming an intermediate, an oxonium ion formed by the S_N2 attack by dioxane.

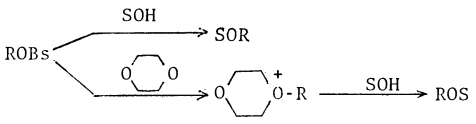

(1)

A similar mechanism was proposed by Streitwieser for the solvolysis of optically active 1-butyl-1-*d* *p*-nitrobenzenesulfonate in the mixtures of dibutyl ether and acetic acid.[3]

Okamoto and his co-workers found that the butyrolysis of optically active α-methylbenzyl chloride in pure butanoic acid gave α-methylbenzyl butanoate with 3.5% net inversion. The reaction proceeded faster in the binary solvent system of butanoic acid and acetonitrile than in pure butanoic acid to yield the product with 2.9% net retention. A small amount of *N*-(α-methylbenzyl)acetamide was also isolated with net (3.2%) inversion.[4] The results were explained by the following reaction scheme, which includes a nucleophilic solvation of the ion-pair intermediate from the side opposite to that of the leaving group, *i.e.* a shielding from the back mechanism.

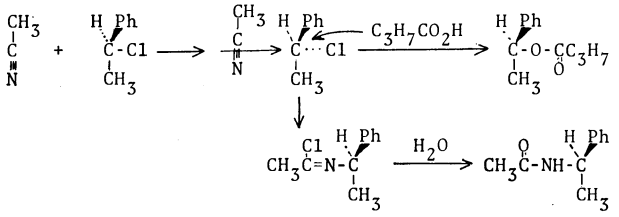

(2)

The largest variation in the steric course of solvolytic reactions with the variation of the composition of binary solvent mixture was found in the acid-promoted methanolysis of 1,3-dimethyl-1-ethylbutyl hydrogen phthalate.[5]

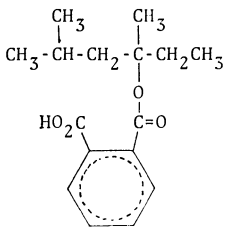

In pure methanol, the steric course of the reaction was 60% net inversion, whereas the result was 100% racemization in a mixture of 20% methanol and 80% nitromethane. The complete discussion and experimental details have not yet been published.

In the steric course of epoxide ring-opening, Italian workers have proposed a shielding from the back mechanism for the trichloroacetolysis of aryl-substituted epoxycyclohexanes.[6] Ito reported that the dielectric constant of the medium is an important factor affecting the steric course of the hydrolysis of 2,3-diphenyloxirane.[7] However, these workers did not explore the effects of the composition of the binary solvent mixture.

Aryloxiranes are interesting compounds for the stereochemical investigations on the medium effects in binary solvent systems. This present paper reports the experimental results of the acid-catalyzed ethanolysis of *trans*-2,3-diphenyloxirane (**1**) in binary ethanolic mixtures containing various kinds of co-solvents (solvents added to ethanol), and discusses the relationship between the steric course of the reaction and the nature of solvation in binary solvent mixtures.

Table 1. Ethanolysis of **1** in pure ethanol at 50 °C

1	$[H^+]$ [a]	Total yield	Product distribution			Ret.[c]
			Rearr.[b]	*threo*-**2**	*erythro*-**2**	
mmol l^{-1}	mmol l^{-1}	%	%	%	%	%
9.1	0.91	92	10	23	67	26
23.2	0.91	93	11	23	66	26
46.4	0.91	99	12	23	65	26
92.7	0.91	93	11	23	66	26
46.4	7.85	89	12	23	65	26
46.4	0.78	92	12	23	65	26

a) H_2SO_4 was used. b) **4**+**5**. c) (*threo*-**2**/**2**)×100.

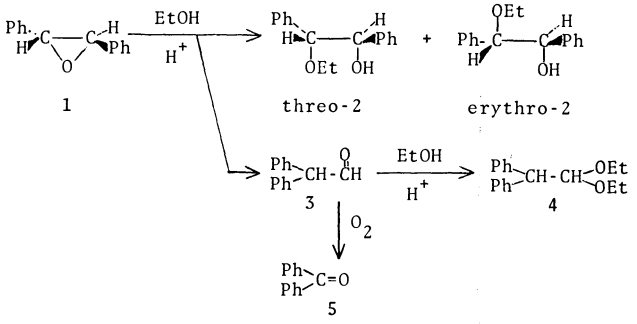

Scheme 1.

Results

The acid-catalyzed ethanolysis of **1** in pure ethanol gave *threo*- and *erythro*-2-ethoxy-1,2-diphenylethanols (*threo*- and *erythro*-**2**), diphenylacetaldehyde (**3**), and the diethyl acetal of **3** (**4**) as shown in scheme 1. The total yields of the four compounds were more than 90 per cent by GLC analysis and more than 80 per cent after isolation.

The autoxidation catalyzed by potassium carbonate,[8] which was added to neutralize the catalyst acid, converted completely **3** into benzophenone (**5**) (see experimenatl section). Therefore, the yields of **5** were presumed to be those of **3**. To check the possibility of the formation of **5** during the ethanolysis, the reaction mixture was subjected to GLC analysis directly without potassium carbonate treatment. The yield of **5** was less than 0.5 per cent, which would be attributed to the oxidation of **3** under the ethanolysis conditions. As the authors were mainly concerned with the steric course of the ethanolysis of **1**, the detailed processes of the oxidation were not examined.

Table 1 shows the effects of concentrations both of acid and of **1** on the product distribution of the ethanolysis in pure ethanol at 50 °C. The ratio of the two ethanolysis products, *threo*- and *erythro*-**2**, was not affected within experimental error, whereas the reaction rate increased with the increase of acid concentration. This demonstrates that both of the stereoisomers **2** are formed through a common intermediate, *i.e.* the conjugate acid of **1** (**1**-H^+). At high acid-concentrations, 1-ethoxy-2,2-diphenylethylene (**6**) was observed in the latter stage of the reaction and seems to be formed by the elimination of ethanol from **4**.

Table 2. Ethanolysis of **1** in ethanol–CH_3CN at 70 °C

CH_3CN	Yield (%)					Ret.[a]
				threo-	*erythro*-	
vol%	**1**	**4**	**5**	**2**	**2**	%
0	0	15	tr	25	54	31
9	0	19	tr	28	48	37
23	0	21	3	32	41	44
36	0	18	10	35	35	50
46	0	18	12	36	32	53
68	5	10	23	34	18	65
91[b]	33	4	32	21	4	85

a) See foot-note of Table 1. b) Several other products were detected, see text.

Table 2 shows the variation in yield of products with variation of the composition of the ethanol–acetonitrile system at 70 °C. With an increasing percentage of acetonitrile, the reaction rate decreased and the proportion of the retained product (*threo*-**2**) increased, though the yields of the rearranged products, **4** and **5**, also increased. The formation of products other than those listed in Table 2 was negligible except in the case of the solvent system composed of 91% acetonitrile by volume. The products were detected by GLC analysis in the experiment of 91% acetonitrile, and isolation of the products was carried out by column chromatography. The isolated products were as follows: *threo*-**2**, 28%; *erythro*-**2**, 8%; **5**, 21%; **3**, trace; **4**, 13%; **6**, 7%; benzyl phenyl ketone (**7**), 1%; 2-hydroxy-1,2-diphenylethanone (**8**), 4%; diphenylethanedione (**9**), trace; 1,2-diphenylethanol (**10**), 2%; 2,2-diphenylethanol (**11**), 3%. The compound **7** is another rearranged product of **1**, and a trace of **7** was always observed in GLC analyses in all experiments throughout this paper. The last four are the redox-reaction products.

Table 3 shows the results of ethanolysis at 50 °C in the ethanol–acetonitrile system. Similar results to those in Table 2 are observed, but the proportion of the retained product *threo*-**2** at 70 °C was always higher, as compared with the result of the same solvent composition at 50 °C.

Table 4 shows the variation of the product distribution with different times of reaction. As shown in Table 4, **4** seems to be formed by a successive reaction

TABLE 3. ETHANOLYSIS OF **1** IN ETHANOL–CH_3CN AT 50 °C

CH_3CN	Yield (%)					Ret.[a]
vol%	**1**	**4**	**5**	*threo*-**2**	*erythro*-**2**	%
0	0	11	1	22	63	26
9	0	12	2	25	55	31
23	0	12	7	30	48	38
36	7	6	14	32	40	44
46	12	4	14	31	34	48
68	38	2	16	26	17	60
91[b]	73	1	16	14	3	83

a) See foot-note of Table 1. b) Trace amounts of 1,2-diphenylethanol (**10**) and benzyl phenyl ketone (**7**) were observed.

of **3**, and therefore, the mechanism that **4** is a primary reaction product may be ruled out.

Figure 1 shows the effect of the composition of benzene or dioxane systems on the steric course of the ethanolysis at 70 °C. The proportion of retained product increased with an increase in the composition of co-solvents as is the case of acetonitrile, but the effect of benzene or dioxane was smaller than that of acetonitrile. The yields of the rearranged products were found to increase with an increasing proportion of co-solvent in the same manner as acetonitrile.

Figure 2 shows the effects of the composition of various solvent systems at 50 °C. With an increasing percentage of nitromethane, the proportion of the retained product increased as is the case of acetonitrile, while the stereochemical outcome of the ethanolysis was virtually unchanged when hexane was added to the solvent system. Aromatic hydrocarbons and dioxane had slightly retentive effects. In every solvent system, large amounts of the retained product were formed at higher reaction temperatures.

In Table 5 are presented the data of the ethanolysis of **1** in binary solvent systems, ethanol–co-solvent

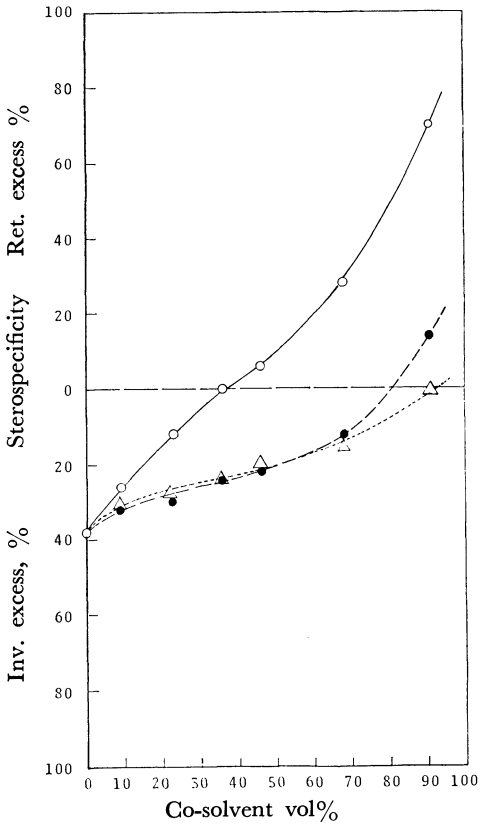

Fig. 1. Co-solvents on stereospecificity of the ethanolysis of **1** in binary solvent systems at 70 °C.
—○—: Acetonitrile, ——●——: dioxane, ---△---: benzene.

(12:10 by volume). Different stereochemical results were observed with change in co-solvent. As the reaction in DMSO, HMPA, and DMF proceeds quite slowly, higher concentrations of acid (10 times) than in the other experiments were used. The nature of these co-solvents was such that **1** gave larger amounts of inverted **2** in these systems than in pure ethanol. In all cases except those of these three co-solvents, the total yield of the four compounds in Scheme 1 was

TABLE 4. ETHANOLYSIS OF **1** AT 50 °C

Solvent[a]	Time	Yield (%)						Ret.
	h	**1**	*threo*-**2**	*erythro*-**2**	**4**	**5**	Others	%
I	0.17	84	4	11	0	2		26
I	0.5	49	10	27	tr	4		27
I	1.0	27	16	44	0.6	7		26
I	1.33	16	19	54	1	7		26
I	1.67	8	20	56	2	7		26
I	3.0	1	21	60	3	6		26
I	3.3	tr	21	60	5	5		26
II	1.0	56	12	36	1	5	b)	24
II	2.0	17	19	53	6	7	b)	27
II	3.0	17	18	54	7	6	b)	25
II	4.0	9	20	56	9	5	b)	26
II	5.0	3	21	60	11	3	b)	26
II	7.0	tr	21	60	13	2	b)	27

a) I, pure ethanol; II, ethanol/hexane=2 : 20 by volume. b) Trace amounts of **7** were observed.

Table 5. Ethanolysis of **1** at 50 °C in ethanol–co-solvent (10 : 12 by volume) mixtures[a]

Co-solvent	Reaction time	Yield (%)[b]					Others[c]	Ret.
	h	**1**	*threo*-**2**	*erythro*-**2**	**4**	**5**		%
Ethanol	8	0	22	63	11	1		26
Hydrocarbons								
Hexane	4	tr	23	64	11	2		26
Cyclohexane	6	0	22	64	11	3		25
Benzene	5	6	26	49	16	tr	**a**	35
Toluene	6	0	26	54	16	4		33
m-Xylene	4	tr	25	54	19	tr	**a**	32
Mesitylene	6	tr	23	55	12	5	**a**	30
Halides								
CCl_4	1	2	25	68	4	9	**a, b, c, e**	27
$CHCl_2CHCl_2$	6	34	11	21	2	2	**a, b**	33
Ethers								
Bu_2O	6	0	22	63	12	3		25
THF	6	0	17	43	25	11	**a, b**	28
Dioxane	7	48	11	23	7	9		32
DME	6	0	22	45	15	12	**a, b**	33
Diglyme	6	10	18	34	16	13	**a, b**	34
Ketone								
Acetone	6	0	26	40	18	2	**a, b**	40
Nitrogen compounds								
CH_3NO_2	4	0	39	29	32	tr		57
$PhNO_2$	6	39	13	16	1	8	**a, b, c**	44
CH_3CN	8	12	31	34	4	14	**c, e**	48
PhCN[d]	6	—	—	—	—	—	—	41
DMF	72	32	2	10	0	2	**a, b, e**	19
Sulfur compounds								
DMSO	72	0	4	16	10	5	**a, b, c, d, e**	16
Sulfolane[d]	16	—	—	—	—	—	—	44
Phosphorus compound								
HMPA	16	24	3	29	0	7		10

a) Reactions were conducted with **1** (200 mg) in mixtures of ethanol (10 ml) and co-solvent (10 ml), and 2 ml, of 0.01 N sulfuric acid solution in ethanol. When DMSO, DMF, and HMPA were used as co-solvent, 0.1 N sulfuric acid solution was used instead of 0.01 N solution. b) Yields were calcd on the basis of **1** used. c) The other products were as follows: **a**, benzyl phenyl ketone (**7**); **b**, 1-ethoxy-2,2-diphenylethylene (**6**); **c**, 1,2-diphenylethanol (**10**); **d**, 2-hydroxy-1,2-diphenylethanone (**8**), diphenylethanedione (**9**), and/or 2,2-diphenylethanol (**11**); **e**, unidentified products. d) Due to the difficulty of separation of solvent from internal standard on GLC analysis, product yields could not be calculated.

Table 6. Ethanolysis of **1** at 50 °C in ethanol-substituted nitrobenzene mixtures[a]

Nitrobenzene (mmol)	Yield (%)					Ret.
	1	*threo*-**2**	*erythro*-**2**	**4**	**5**	%
Nitrobenzene (0.05)	0	28	44	9	9	39
Nitrobenzene (0.02)	0	27	56	16	1	32
p-Nitrotoluene (0.05)	0	28	47	9	9	37
p-Nitrotoluene (0.02)	0	26	55	16	1	32
m-Nitrotoluene (0.02)	0	26	54	16	1	32
m-Chloronitrobenzene (0.05)	0	27	44	7	9	38
m-Chloronitrobenzene (0.02)	0	26	55	17	1	32
p-Nitroanisole (0.02)	0	27	54	17	1	34

a) Reactions were conducted with **1** (200 mg) in mixtures of ethanol (10 ml) and nitrobenzenes (0.02 mmol or 0.05 mmol), and 2 ml of 0.1 M ethanolic solution of sulfuric acid. The amount of nitrobenzenes are given in parentheses.

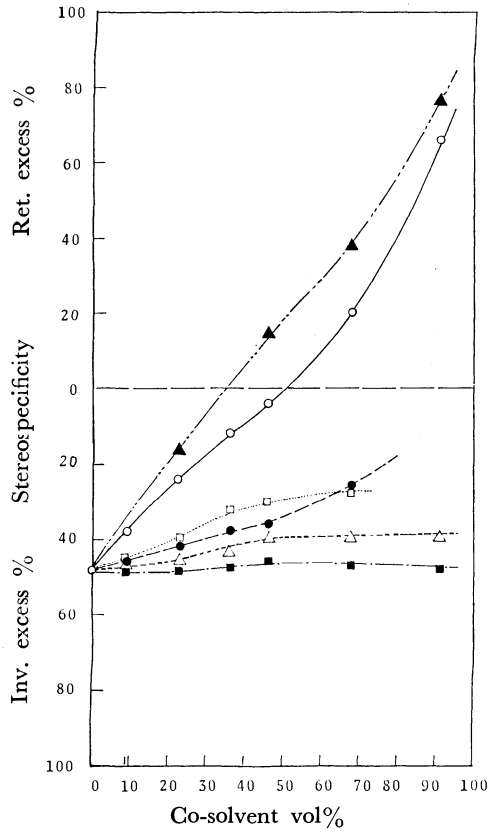

Fig. 2. Co-solvent effects on stereospecificity of the ethanolysis of **1** in binary solvent systems at 50 °C.
—○—: Acetonitrile, ——●——: dioxane, ···□···: benzene, ----▲----: nitromethane, ---△---: mestylene, ——■——: hexane.

greater than 80 per cent. By-products, **6**–**11** were formed in some solvent systems. but the yield of these by-products was less than 2 per cent. When DMSO was used as the co-solvent, the total yield decreased unexpectedly, but no products other than described above could be isolated.

In Table 6 are presented the results of the ethanolysis of **1** in mixtures composed of ethanol and substituted nitrobenzenes. As many of nitrobenzenes are solid and it was difficult to determine the volume ratios, experiments were carried out with fixed mol fractions.

Discussion

Several kinds of mechanisms have been proporsed to explain the solvent effects on the steric course of solvolysis and these will be examined here in the light of the results reported. From the application of Sneen's mechanism[2] to the reaction, it may be deduced that the co-solvent reacts from the back of the epoxide ring at an ionizing stage of the epoxide C–O bond, as shown in Scheme 2.

Upon closer examination of the experimental results (see Appendix), this scheme meets a difficulty in that the co-solvent should have a stronger nucleophilicity to the conjugate acid of **1** than ethanol. However, the scheme involves the assumption that the co-solvent has no nucleophilicity to co-solvent-participating intermediate (**12**).

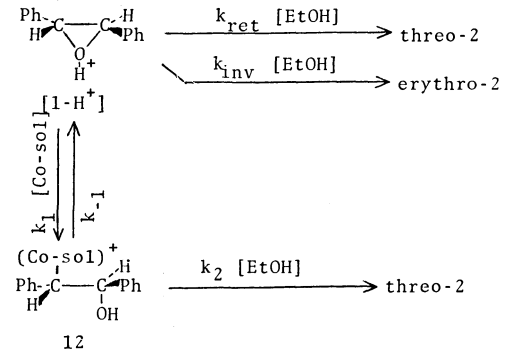

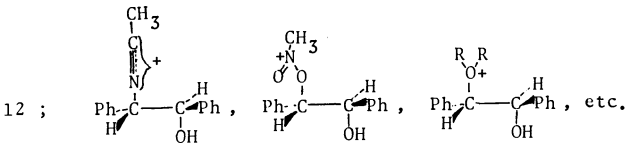

Scheme 2.

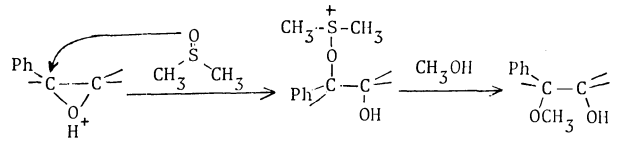

Scheme 3.

The results reported involve several kinds of data which conflict with the shielding from the back mechanism. For example: 1. The proportion of the retained product decreased in the following orders of co-solvent; benzene>toluene>*m*-xylene>mesitylene; nitrobenzene>*p*-nitrotoluene, which is inverse to the order of nucleophilicity.

2. Swern and his co-workers reported that DMSO reacts with epoxide to yield the alkoxysulfonium salt which is the same type of ion as the assumed intermediate **12** and that this sulfonium ion reacts with alcohol to yield *β*-alkoxy alcohol (Scheme 3).[9] However, the reaction of DMSO with epoxide requires a much higher acid concentration than the ethanolysis experiments reported here. When DMSO was used as co-solvent in our experiment, larger amounts of inverted product were formed than in pure ethanol. These facts make it difficult to assume the alkoxysulfonium ion as an intermediate of the ethanolysis of **1** in DMSO.

3. Acetonitrile, nitromethane, and sulfolane, in which the ethanolysis of **1** yielded large amounts of the retained product, are known as relatively weak bases. Although no data are available to compare directly the nucleophilicity of the solvents toward a carbonium ion, their coordination abilities to metal cations may afford some insight. The coordinating abilities of acetonitrile and nitromethane are much weaker than those of DMSO and DMF. Since the nucleophilic participation of DMSO has been dis proved (see above), it is improbable that acetonitrile or nitromethane, which are poorer nucleophiles than DMSO, participate in the ionizing stage of **1**.

None of the mechanisms proposed for solvolytic

reaction can explain the experimental results reported here.

In the epoxide reactions, the mechanism of the ring-opening leading to the formation of stereoisomeric products has been reviewed by Parker and Isaacs. They discussed the reaction kinetics and stereochemistry and concluded that the reactions took place concurrently in these reactions, one of which gave the retained product and the other the inverted one.[10] This proporsal has been widely accepted, and the results of the reaction of aryl-substituted epoxycyclohexanes reported by Italian workers also supports this concurrent reaction mechanism.[11] The results presented in this paper, that the stereospecificity of the reaction varied widely from 80% inversion excess to 76% retention excess by changing the co-solvent, appear to support Parker and Isaacs' conclusion, in that the results can not be explained by a single mechanism.

A short comment against the S_N1 mechanism for the epoxide reaction is necessary. By examining the entropies of activation in the acid-catalyzed methanolysis of aryloxiranes, Chapman and his co-workers suggested that the reaction does not proceed *via* an unimolecular mechanism except in the case of 2.2-diphenyloxirane which shows a deviation towards an S_N1 mechanism.[12]

Two mechanisms have been proporsed for the retention reaction, one of the concurrent reactions. Brewster explained the retentive acetolysis of *trans*-2-methyl-2,3-diphenyloxirane in terms of an ion pair in a "cage" of solvent molecules (S_Ni mechanism, Scheme 4).[13]

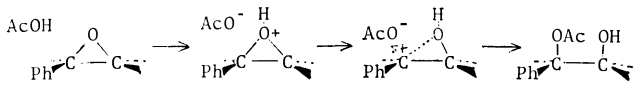

Scheme 4.

Another mechanism is a double inversion or a phenonium-ion mechanism (Scheme 5),[10] and was proporsed as a possible explanation for the results of the acetolysis of 2-(*p*-methoxyphenyl)-3-phenyloxirane.[14] Recently Ito found, however, that the position attacked by acetic acid is not benzyl carbon but *p*-anisyl one of that compound.[15] To explain this by a phenonium-ion mechanism, the participating group should not be a methoxyphenyl but a phenyl group, which is an unlikely process.

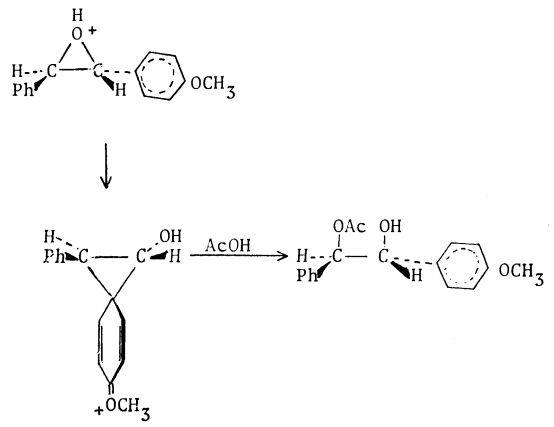

Scheme 5.

Although the phenonium-ion mechanism has been employed by many workers, there is no clear evidence to confirm the existence of the phenonium ion substituted by heteroatoms. If the double inversion mechanism were valid here, the phenonium ion (**13**) depicted below should exist as an intermediate and react with ethanol. The existence of this intermediate appears to be unlikely, when the following processes are taken into account. When the bridging phenyl group moves from the center of two carbon atoms (C_1, C_2) towards the C_1 atom, a developing p-orbital on the C_2 carbon atom can conjugate with a lone pair of oxygen atom adjacent to the C_2 carbon atom, and the cation gains additional stabilization energy. At the end of this drift, an oxonium ion or the conjugate acid of the aldehyde is formed which is well established as more stable than the phenonium ion by kinetic evidence.[16] Consequently, the phenonium ion, if it were to be formed, is not an intermediate of the retentive solvolysis but the transition state of the rearrangement to **3**.

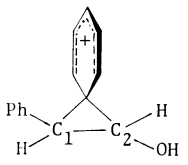

(**13**)

As summarized in Table 7, the stereochemical results of the acid-catalyzed solvolysis of **1** are closely related to those of the optically active 2-phenyloxirane. Here, the phenonium ion cannot be an intermediate of the solvolysis of 2-phenyloxirane, since nucleophiles attack the benzyl carbon atom. Therefore, it is unreasonable to consider that the phenonium ion is the intermediate in the solvolysis of **1**, and thus the conclusion drawn is that an S_Ni (ion pair) mechanism opperates in the retentive ethanolysis which is one of the concurrent reactions of **1** (Scheme 6).

As indicated by Parker and Isaacs,[10] the transition state depicted by Brewster is similar to the borderline S_N2 mechanism with the added proviso that the reagent is held close to the epoxide oxygen by electrostatic forces. However, the authors consider that the transition state of retentive ethanolysis of **1** has a stronger

Table 7. Stereochemical results of the acid-catalyzed solvolysis of aryloxiranes

	Alcoholysis	Hydrolysis
2-Phenyloxirane	11% ret-89% inv[a]	50% ret-50% inv[b]
trans-2,3-Diphenyloxirane	26% ret-73% inv[c]	60% ret-40% inv[d]

a) Methanoylsis at 22.8 °C, J. Biggs, N. B. Chapman, and V. Wray, *J. Chem. Soc., B*, **1971**, 71. b) Suspension; C. Dupin and J.-F. Dupin, *Bull. Soc. Chim. Fr.*, **1970**, 249. c) Ethanolysis at 50 °C; this work. d) Extrapolation value from the results on hydrolysis in the mixtures of water and various kinds of co-solvents; unpublished work of this laboratory.

TABLE 8. CO-SOLVENT EFFECTS ON ETHANOLYSIS OF **1**[a] AND PHYSICAL PROPERTIES OF CO-SOLVENTS

Co-solvent	Ret.[b] %	Rearr.[b] %	ε	pK_a of conjugate acid	E_T	
CH_3NO_2	56	32	35.87	−11.7	46.3	group 1
CH_3CN	48	22	37.5	−10.13	46.0	group 1
Sulfolane	44	23	43.3		44.0	group 1
$PhNO_2$	44	24	34.82	−10.39	42.0	group 1
PhCN	41		25.2	−10.45	42.0	group 1
Acetone	40	23	20.7	−6.5	42.2	
Benzene	35	17	2.275		34.5	group 2
Diglyme	34	36				group 2
DME	33	29	7.20	−3.27	38.2	group 2
$CHCl_2CHCl_2$	33	12	8.20			group 2
Toluene	33	20	2.379		33.9	group 2
Dioxane	32	32	2.207	−3.22	36.0	group 2
m-Xylene	32	19	2.374			group 2
Mesitylene	30	17	2.279			group 2
THF	28	38	7.85	−2.08	37.4	group 2
CCl_4	27	12	2.238		32.5	group 2
Hexane	26	12	1.8799		30.9	group 2
Bu_2O	25	15	3.083	−5.40		group 2
Cyclohexane	25	14	2.023			group 2
DMF	20		52.1	(−0.19)[c]	43.8	group 3
DMSO	16		44.68	0	45.0	group 3
HMPA	10	21	30			group 3
Ethanol	26	12	24.55	(−2.2)[d]	51.9	

a) See foot-note a) of Table 5. b) See foot-notes b) and c) of Table 1. c) pK_a of the conjugate acid of *N,N*-dimethylacetamide. d) pK_a of the conjugate acid of methanol.

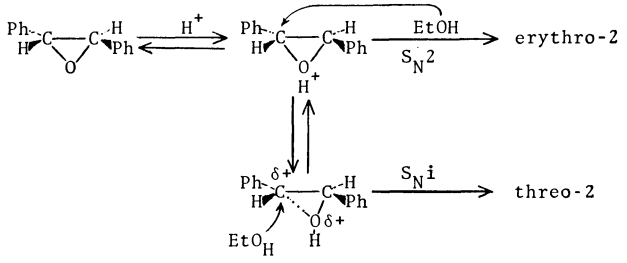

Scheme 6.

tendency toward an S_N1 mechanism than that of the borderline S_N2 reaction giving the inverted product, and this will be discussed in a separate paper.

In Table 8, the stereochemical results in binary solvent systems are given together with the dielectric constants, the pK_a of conjugate acids,[17] and the E_T values[18] of the co-solvents. No direct relationship has been established between the stereochemical results and the physical properties of the co-solvents. However, a detailed examination of Table 8 suggests that the co-solvents can be classified into three groups. The first group (group 1) contains acetonitrile, nitromethane, sulfolane,[19] *etc.*, which have poor basicities and high dielectric constants in which the ethanolysis of **1** yields large amounts of retained product. The second group (group 2) solvents have poor basicities and low dielectric constants, and these co-solvent have no effect or a slightly retentive effect on the ethanolysis of **1**. The third group (group 3) contains aprotic polar solvents such as DMSO, DMF, and HMPA. The difference between the aprotic polar solvents and those of the first group is that the former have a much more basic character, therefore, higher coordinating abilities than those of the first group.

To discuss the function of co-solvents in ethanolysis of **1**, the nature of the solvation has to be known. Solvation shells are most often discussed in terms outlined by Gurney[20] as regions A, B, and C. Region A is one of high order imposed by the influence of the solute on nearby solvent molecules. Region C is a region of unaltered bulk solvent. Region B is a "disordered" compromise region which is influenced comparably both by the forces exerted by the solute which produce region A near the solute and by the solvent-solvent forces which produce region C in the bulk far from the solute.[21]

A modification of Gurney's classification will be made,[22] extended to the solvation of protons in binary solvent mixtures, and used here. Region A is defined as a primary coordination sphere. In region A, the proportion of the solvent with strong basicity, *i.e.* high coordinating ability to a proton, should be larger than in the whole solvent system. For example, in the ethanol–acetonitrile system, the proportion of ethanol in region A should be larger than that in the bulk solution, since ethanol is a stronger base than acetonitrile. In the ethanol–DMSO system, the proportion of DMSO in region A is larger, since DMSO is a

stronger base than ethanol. Region C is a bulk region, in which the composition of solvents is the same as the compostition of the whole solvent system. Region B is defined as a transition region between region A and region C, and influenced by many kinds of forces. Among them, charge-dipole interaction which is a long range intermolecular force appears to be the most important in the present case. It is difficult to estimate the composition of solvents in region B of the binary solvent systems, since the nature of charge-dipole interactions in solution is not yet clear. However, it may be pointed out that the proportion of the solvent of high dielectric constant should be higher in region B than in the bulk solution, since the effects of the dielectric field of the proton can be relaxed by the dielectric polarizability of the solvent. The discussion is clearly oversimplified, but is able to explain the stereochemical results.

It is well established that initial protonation is a fast reversible step in the acid-catalyzed ring-opening reaction of epoxides. Around the proton of the protonated epoxide, solvent molecules build up region A,[23] and the back of the epoxide ring borders on region B.[24,25] Ethanol proportions in the two regions A and B differ by the influence of basicity and dielectric polarizability of co-solvent, and therefore, the effective concentrations of ethanol on both sides of epoxide differ in the *ground state* of ethanolysis. In other words, the effective concentrations[26] of ethanol for S_Ni and S_N2 reactions differ from each other and this difference results in the changes of the steric course of ethanolysis of **1**.

On the basis of the above discussion, the stereochemistry of the ethanolysis can be explained as follows. In binary ethanolic mixtures containing group 1 co-solvents, effective concentration of ethanol to the front of the epoxide is much higher than to the back of the epoxide, since the proportion of co-solvent in region B and that of ethanol in region A are higher than those in the whole solvent system. Consequently, the ethanolysis of **1** in these solvent system yields larger amounts of the retained product than in pure ethanol.[27] In binary ethanolic mixture containing group 3 co-solvents, the strong basicity of the co-solvent results in an increase of co-solvent proportion in region A, and in a decrease of effective concentration of ethanol to the front of the epoxide. Consequently, the ethanolysis of **1** in ethanol-group 3 co-solvent mixtures yields larger amounts of the inverted product. In binary ethanolic mixtures containing group 2 co-solvents, which have low dielectric constants, the probability of the existence of group 2 co-solvents in regions A and B is low, since the two regions are in a dielectric field of positive charge. As a results, the steric course of the ethanolysis of **1** in these solvent mixtures is similar to that in pure ethanol.

The discussion mentioned above may not be limited to the epoxide reaction, and Streitwieser and Doering's results quoted at the beginning of this paper may be explained using this theory.

The medium effects on the steric course of acid-catalyzed solvolitic reactions of **1** and optically active 2-phenyloxirane are now being investigated.

Experimental

Materials. *trans*-2,3-Diphenyloxirane (**1**) was prepared by the *m*-chloroperbenzoic acid oxidation of *trans*-stilbene and recrystallized from hexane and then from benzene, mp 68.5—69.5 °C (lit,[28] 69.0—69.5 °C). Ethanol was dried by Lund and Bjerrum's method.[29] All the co-solvents were dried by the most efficient ways reported in the literature[30] and distilled before use.

erythro-*2-Ethoxy-1,2-diphenylethanol* (erythro-**2**). A mixture of *meso*-1,2-diphenyl-1,2-ethanediol[31] (2.0 g) and triethyloxonium tetrafluoroborate (2.66 g) in dry ether (100 ml) was stirred for 24 h at room temperature, poured into water, and extracted with ether. The ether layer was dried over sodium carbonate and removal of the solvent gave 1.3 g of a white solid. GLC analysis indicated that it contained three products. After separation of the products by column chromatography, *erythro*-**2** (117 mg) was obtained from the middle fraction, mp 52.5—53.5 °C (lit,[32] 45—50 °C). NMR ($CDCl_3$) δ: 1.1[0] (3H, t, J=7 Hz), 2.4[7] (1H, d, J=4 Hz, OH), 3.3[7] (2H, AB part of ABX_3 coupling), 4.4[0] (1H, d, J=5 Hz), 4.8[3] (1H, d d, J=4 and 5 Hz), and 7.1[3] (10H, phenyl). Found: C, 79.47; H, 7.56%. Calcd for $C_{16}H_{18}O_2$: C, 79.31; H, 7.49%.

The other products were the starting material and *meso*-1,2-diethoxy-1,2-diphenylethane.

threo-*2-Ethoxy-1,2-diphenylethanol* (threo-**2**). 2-Ethoxy-1,2-diphenylethanone was reduced with sodium borohydride in the usual way. GLC analysis indicated that the crude product was composed of two components with a ratio of 87:13. The crude product was purified by column chromatography. The major product consisted of *erythro*-**2**, and *threo*-**2** was obtained as the minor one which did not crystallize even after several months. NMR ($CDCl_3$) δ: 1.2[1] (3H, t, J=7 Hz), 1.7 (1H, s, OH), 3.3[9] (2H, q, J=7 Hz), 4.1[8] (1H, d, J=8 Hz), 4.5[8] (1H, d, J=8 Hz), and 7.0[7] (10H, phenyl). Found: C, 79.32; H, 7.52%. Calcd for $C_{16}H_{18}O_2$: C, 79.31; H, 7.49%.

Ethylation of *dl*-1,2-diphenyl-1,2-ethandiol by the oxonium salt gave no reaction.

1,1-Diethoxy-2,2-diphenylethane (**4**). To a solution of **3**[33] (2.0 g) in abs ethanol (70 ml), a drop of concd sulfuric acid was added. The reaction mixture was stirred for 24 h at room temperature. GLC analysis of the reaction mixture indicated 97% conversion to **4**. Distillation of the neutralized reaction mixture gave 1.6 g of **4**: bp 117—119 °C/2.5 mmHg: IR: 1060 and 1120 cm^{-1}; NMR ($CDCl_3$) δ: 1.0[3] (6H, t, J=7 Hz), 3.5 (4H, AB part of ABX_3 coupling $\Delta\nu$=10 Hz, J_{AB}=9.3 Hz, J_{AX}=6.8 Hz, J_{BX}=7.2 Hz), 4.2[3] (1H, d, J=7.8 Hz), 5.0[5] (1H, d, J=7.8 Hz), and 7.3[0] (10H, phenyl).

When anhydrous copper(II) sulfate was used for the acetallization instead of sulfuric acid, initially formed **4** was converted into **6**[34] before acetallization was completed.

Ethanolysis of **1** *in Pure Ethanol.* To a 20 ml ethanolic solution of weighed quantities of **1** and dibenzyl ether (internal standard) held in a controlled-temperature block, acidified (H_2SO_4) ethanol (2 ml) was added with vigorous shaking. After a definite period, the reaction mixture (0.5 ml) was pipetted into a sampling tube containing a small amount of potassium carbonate and the tube shaken vigorously. The quenched sample was kept at room temperature for a day and analyzed by GLC.

Ethanolysis of **1** *in Binary Solvent Systems.* To a 10 ml ethanolic solution of **1** (200 mg) and dibenzyl ether (30—50 mg, weighed), co-solvent (10 ml) was added and the mixture held in a controlled temperature block. Ethanolic solu-

tion of sulfuric acid (2 ml, *ca* 0.01 N)[35] was added to the mixture and then treated as reported above.

GLC Analysis. The GLC analyses (Hitachi 163 gas chromatograph) were carried out successfully on a 4 m column of 5% PEG-20M on Shimalite W at a column temperature of 205 °C. For example, the retention times of dibenzyl ether, **4**, **5**, **6**, **3**, *threo*-**2**, **7**, *erythro*-**2**, **8**, and three compounds (**9**, **10**, and **11**) were 9.3, 11.4, 12.3, 14.6, 15.2, 18.2, 20.3, 23.8, 25.8, and 31.2 min respectively.

Autoxidation of **3**. To a solution of freshly prepared **3** (10 mg) in ethanol (10 ml), a catalyst was added. The reaction mixture was kept at room temperature for 24 h and subjected to GLC analysis. The conversions of **3** to **5** (catalyst; a small amount of potassium carbonate, a small amount of sodium carbonate, 0.1 ml of 0.1 N sulfuric acid solution in ethanol) were 100, 53, and 0.3%. Only a trace of **5** was found when the ethanolic solution of **3** was allowed to stand for a day without catalyst.

Appendix

From the reaction sequence described in Scheme 1, the following equations may be obtained:

$$\frac{d[\textit{threo}\text{-}\mathbf{2}]}{dt} = k_{ret}[EtOH][\mathbf{1}\text{-}H^+] + \frac{k_1k_2[\text{co-sol}][\mathbf{1}\text{-}H^+][EtOH]}{k_2[EtOH]+k_{-1}},$$

$$\frac{d[\textit{erythro}\text{-}\mathbf{2}]}{dt} = k_{inv}[EtOH][\mathbf{1}\text{-}H^+].$$

Therefore,

$$\frac{[\textit{threo}\text{-}\mathbf{2}]}{[\textit{erythro}\text{-}\mathbf{2}]} = \frac{k_{ret}}{k_{inv}} + \frac{\frac{k_1}{k_{inv}}[\text{co-sol}]}{[EtOH]+\frac{k_{-1}}{k_2}}.$$

If the effective concentrations in reaction kinetics are the same as the molar concentration of the medium, the values 0.48, 2.04, and 0.55 for k_{ret}/k_{inv}, k_1/k_{inv}, and k_{-1}/k_2 respectively can satisfy the experimental results presented in Table 2 except in the case of 91 vol % of acetonitrile concentration.

However, the value 2.04 for k_1/k_{inv} indicates that the nucleophilicity of acetonitrile to the conjugate acid of **1** (**1**-H^+) is stronger than that of ethanol, whereas the reaction scheme includes an assumption that the co-solvent, as compared with ethanol, has a negligibly small nucleophilicity to the intermediate **12**.

It is difficult to consider that the two orders of the nucleophilicities of ethanol and acetonitrile toward **1**-H^+ and **12** have been reversed. The nucleophilicity of co-solvent to **12** is assumed, which leads to the following reaction scheme (Scheme 7).

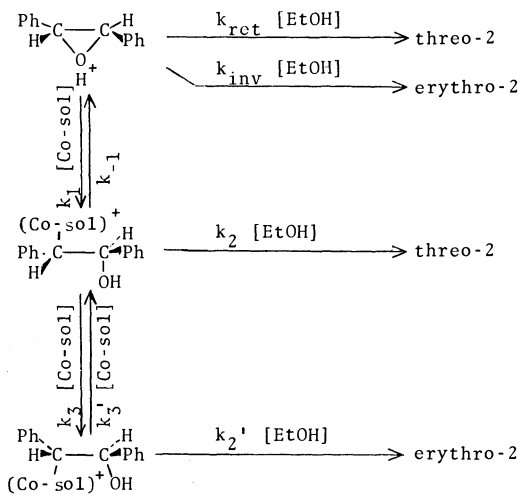

Scheme 7.

The implications of this reaction-scheme are similar to Streitwieser's. However, a solution of the reaction kinetics using the steady state method leads to the same difficulties as mentioned above since the experimental results are satisfied only when $k_1 > k_{inv}$ and $k_2 > k_3$.

References

1) E. M. Arnett, W. G. Bentrude, J. J. Burke, and P. M. C. Duggleby, *J. Am. Chem. Soc.*, **87**, 1541 (1965).
2) H. Weiner and R. A. Sneen, *J. Am. Chem. Soc.*, **87**, 287 (1965).
3) A. Streitwieser, Jr. and S. Andreades, *J. Am. Chem. Soc.*, **80**, 6553 (1958).
4) K. Okamoto, I. Nitta, and H. Shingu, *Bull. Chem. Soc. Jpn.*, **44**, 3220 (1971).
5) W. von E. Doering and A. Streitwieser, Jr., unpublished work cited in Ref 5a).
5a) A. Streitwieser, Jr., *Chem. Rev.*, **56**, 571 (1956).
6) A. Balsamo, P. Crotti, B. Macchia, and F. Macchia *Tetrahedron*, **29**, 199 (1973).
7) S. Ito and N. Nomura, *Nippon Kagaku Kaishi*, **1972**, 1985.
8) J. W. Huffman and R. P. Elliott, *Chem. Ind. (London)*, **1963**, 650; J. Bornstein, M. A. Joseph, and J. E. Shields, *J. Org. Chem.*, **30**, 801 (1965).
9) T. M. Santosusso and D. Swern, *J. Org. Chem.*, **40**, 2764 (1975); M. A. Khuddus and D. Swern, *J. Am. Chem. Soc.*, **95**, 8393 (1973).
10) P. E. Parker and N. S. Isaacs, *Chem. Rev.*, **59**, 737 (1959).
11) C. Battistini, P. Crotti, and F. Macchia, *Tetrahedron Lett.*, **1975**, 2091; C. Battistini, A. Balsano, G. Berti, P. Crotti, B. Macchia, and F. Macchia, *J. Chem. Soc., Chem. Commun.*, **1974**, 712.
12) J. Biggs, N. S. Chapman, A. F. Finch, and V. Wray, *J. Chem. Soc., B*, **1971**, 55; J. Biggs, N. S. Chapman, and V. Wray, *ibid.*, **1971**, 63, 66.
13) J. H. Brewster, *J. Am. Chem. Soc.*, **78**, 4061 (1956).
14) D. Y. Curtin, A. Bradley, and Y. G. Hendrickson, *J. Am. Chem. Soc.*, **78**, 4064 (1956).
15) S. Ito, *Nippon Kagaku Kaishi*, **1972**, 1758.
16) L. Summers, *Chem. Rev.*, **55**, 301 (1955); H. Gross and E. Hoeft, *Angew. Chem.*, **79**, 358 (1967).
17) E. M. Arnett, "Quantitative Comparison of Weak Organic Bases" in "Progress in Physical Organic Chemistry," Vol. 1, ed by S. G. Cohen, A. Streitwieser. Jr., and R. W. Taft, Interscience, New York (1963).
18) K. Dimroth, C. Reichardt, T. Siepmann, and F. Bohlmann, *Ann. Chem.* **661**, 1 (1963); *ibid.*, **669**, 95 (1963).
19) E. M. Arnett and C. F. Douty, *J. Am. Chem. Soc.*, **86**, 409 (1964).
20) R. W. Gurney, "Ionic Processes in Solution," McGraw-Hill, New York (1953), Chap. 16.
21) C. H. Langford and J. P. K. Tong, *Acc. Chem. Res.*, **10**, 258 (1977).
22) A similar modification was proposed; E. M. Kosower, "An Introduction to Physical Organic Chemistry," John Wiley & Sons, New York (1968).
23) Major parts of solvation energies should come from hydrogen bonding from acidic hydrogen of the conjugate acid of epoxide to "bulk ethanol,"

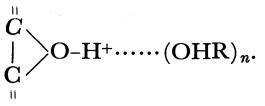

For a detailed discussion of hydrogen bonding from the hydrogen of onium ion to "bulk water," see for example; E. M. Arnett, B. Chawla, L. Bell, M. Taagepera, W. J. Hehre, and R. W. Taft, *J. Am. Chem. Soc.*, **99**, 5729 (1977).

24) A variety of the values for the solvation number of proton have been reported; 1—2,[a] 2.5,[b] 3.9,[c] 5,[d] and 10.[e] The oxonium ion (**1**-H$^+$) in solution can be considered to be formed by substitution of one of the solvent molecules in solvation shell of proton (region A) for the epoxide.

As the first solvation shell of proton (region A) is small, the side opposite to that of the epoxide oxygen of **1** borders on region B.

24a) A. Pasynskii, *Zhur. Fiz. Khim.*, **11**, 608 (1938); b) B. F. J. Vorgin, P. S. Knapp, W. L. Flint, A. Anton, G. Highberger, and E. R. Malinowski, *J. Chem. Phys.*, **54**, 178 (1971); c) E. Glueckauf, *Trans. Faraday Soc.*, **51**, 1235 (1955); d) H. Ulich, *Z. Phys. Chem.*, **168**, 141 (1934); e) J. B. Hasted, D. M. Riston, and C. H. Collie, *J. Chem. Phys.*, **16**, 1 (1948).

25) These structures of solution are easily fading, but have enough life time for epoxide to be attacked in these solution structures, because acidic hydrogen should exist at the epoxide oxygen during the reaction.

26) A similar concept has been discussed in terms of preferential solvation, see Ref 21.

27) If ethanol molecules in region A are completely oriented by the effect of charge of proton, nucleophilicity of the ethanol should be much lower than that of ethanol in region C. However, this problem can be solved by Backrins-Saluja's model for solvation, in which coordination number is always larger than solvation number.[a] In other words, they pointed out the existence of non-solvated coordinated molecules in region A. In the present case, the non-solvated coordinated ethanols in region A have ordinary nucleophilicity to **1** to yield the retained product (*threo*-**2**).

27a) J. O'M. Bockrins and P. P. S. Saluja, *J. Phys. Chem.*, **76**, 2140, 2298 (1972).

28) D. Y Curtin and D. B. Kellom, *J. Am. Chem. Soc.*, **75**, 6011 (1953).

29) H. Lund, J. Bjerrum, *Ber.*, **64**, 210 (1931); H. Lund, *J. Am. Chem. Soc.*, **74**, 3188 (1952).

30) J. A. Riddick and W. B. Bunger, "Organic Solvents," 3rd ed, Wiley Interscience, New York (1970).

31) L. F. Fieser, "Organic Experiments," D. C. Heath & Co., Boston (1964), p. 216, 229.

32) J. Read and I. G. Campbell, *J. Chem. Soc.*, **1930**, 2377.

33) D. J. Reif and H. O. House, *Org. Synth.*, Coll. Vol. IV, 375 (1963).

34) E. F. Silversmith and D. Smith, *J. Org. Chem.*, **23**, 427 (1958).

35) A definite concentration of sulfuric acid solution in ethanol (0.01 N) was prepared initially, but the correction factor decreased gradually on storage. However, the stereochemical results of ethanolysis of **1** in binary solvent systems were not affected by the acid concentration.

A New Synthesis of α-Phenylsulfonyl-γ-lactones and Their Use for Syntheses of Actinidiolide Derivatives[1)]

Kenji UNEYAMA, Manabu KUYAMA, and Sigeru TORII*

Department of Industrial Chemistry, School of Engineering, Okayama University, Okayama 700

(Received January 25, 1978)

The acid-catalyzed cyclization of 2-phenylsulfonyl-4,8-dimethyl-3,7-nonadienoic acid (**5**) was performed by treatment with sulfuric acid-acetic acid and/or boron trifluoride in various aprotic solvents to afford 2,2,6-trimethyl-9-phenylsulfonyl-7-oxabicyclo[4.3.0]nonan-8-one (**4**) in 70—75% yield. Similarly, 2-phenylsulfonyl-2-(2,6,6-trimethyl-1,3-cyclohexadienyl)acetic acid provided 2,2,6-trimethyl-9-phenylsulfonyl-7-oxabicyclo[4.3.0]non-4-en-8-one (**7**) in 62% yield. The lactones **4a**, **4b**, and **7** were converted into dihydroactinidiolide, tetrahydroactinidiolide, and 4,5-dihydroactinidiolide. The reaction conditions and mechanism of the cyclization of **5** are discussed.

In connection with syntheses of terpenoids, the acid-catalyzed cyclization of functionalized polyisoprenoids has been reviewed.[2)] However, in spite of need for obtaining naturally occurring γ-lactones, very few satisfactory results have been obtained concerning one-step lactonization of acyclic polyolefinic carboxylic acids.[3)]

Reports have been given on a convenient preparation of 2-phenylsulfonyl-1,3,3-trimethylcyclohexene (**1a**) by the acid-catalyzed cyclization of 1-phenylsulfonyl-3,7-dimethylocta-2,6-diene (**2a**), as well as its use for the syntheses of terpenoids such as deoxytrisporone, vitamin A acid and ferruginol.[4)] On the cyclization of **2**, it was assumed that the reaction proceeds *via* the carbonium ion **3** which would undergo deprotonation or ring closure by intramolecular nucleophilic attack of another carbon-carbon double bond. This assumption prompted us to carry out one-step preparation of 2,2,6-trimethyl-9-phenylsulfonyl-7-oxabicyclo[4.3.0]nonan-8-one (**4**) from 2-phenylsulfonyl-4,8-dimethyl-3,7-nonadienoic acid (**5**). The presence of a phenylsulfonyl group at the terminal position of polyolefin chain allows the introduction of carboxyl group at the α-position, affording both α,β-unsaturated and saturated γ-lactones by either thermal elimination or reductive removal of the phenylsulfonyl group.

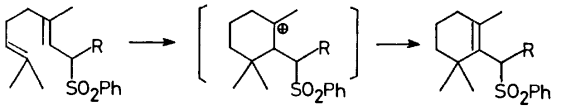

2a R=H
b R=Alkyl

3

1a
b

This paper gives details on cyclization[5)] of **5** and 2-phenylsulfonyl-2-(2,6,6-trimethyl-1,3-cyclohexadienyl)-acetic acid (**6b**) along with a novel transformation of lactones **4a**, **4b**, and 2,2,6-trimethyl-9-phenylsulfonyl-7-oxabicyclo[4.3.0]non-4-en-8-one (**7**) into dihydroactinidiolide (**8**), isolated from Actinidia polygama Mig. (Matatabi),[6,7)] tetrahydroactinidiolide (**9a** and **9b**),[8)] and 4,5-dihydroactinidiolide (**10**).[9)]

Results and Discussion

Acid-catalyzed Lactonization of the Carboxylic Acids 5 and 6b. The carboxylic acids **5** and **6b** were easily prepared from the corresponding sulfones **2a** and **6a** by carboxylation.[10)] Treatment of **2a** with 2 equiv. of butyllithium in tetrahydrofuran at −70 °C followed with dry carbon dioxide yielded **5** in 99% yield. Similarly, **6b** was obtained in 96% yield.

Table 1. Cyclization of 5 with sulfuric acid

Entry	Ratio of acids[a)] H_2SO_4/AcOH	Temp[b)] °C	Product, %	
			4 (*cis*/*trans*)	**11**
1	1/1	12	64 (1.6)	26
2	4/1	5	66 (2.3)	3
3	4/1	20	66 (6.0)	0
4	1/0	5	75 (∞)[c)]	0

a) v/v. b) Reaction time 0.5 h. c) No *trans*-isomer obtained.

The acid-catalyzed lactonization of **5** was performed using protonic or Lewis acid (Table 1). Treatment of **5** with sulfuric and acetic acids (1:1) at 12 °C for 0.5 h provided **4** (64%) and **11** (26%). The product **4** consists of a mixture of *cis*- and *trans*-fused γ-lactones, which were separated by column chromatography and identified by a comparison with spectral data and also conversion of **4a** and **4b** into the corresponding tetrahydroactinidiolides **9a** and **9b** by reductive removal of the phenylsulfonyl group. The structure of **11** was confirmed by a comparison of the spectral data with those of the authentic sample prepared by the carboxylation of **1a**.

Increase of the concentration of sulfuric acid and/or the higher reaction temperature (Table 1, Runs 3—4) facilitates the formation of *cis*-lactone **4a**. In particular, the reaction of **5** in concd sulfuric acid at 5 °C gave **4a** in 75% yield as the sole product.

The carboxylic acid **11** was converted into **4** (**4a**/**4b**=4/1) in 45% yield on treatment with sulfuric and acetic acids (1:1) for 4 h. The *trans*-lactone **4b** undergoes complete isomerization to *cis*-lactone **4a** on treatment with sulfuric acid at 5 °C for 1 h. In strong acidic media the thermodynamically more stable *cis*-lactone **4a** would be produced preferentially to *trans*-isomer **4b**. Thus, it is assumed that the intermediate **12** would suffer either deprotonation to afford monocyclic carboxylic acid **11** (Path A in Scheme 1) or intramolecular nucleophilic attack by carboxyl group to produce a mixture of *cis*- and *trans*-lactones (Path B), although the mechanism of the concerted lactonization of **5** to *trans*-**4b** followed by isomerization of **4b** to **4a** *via* **12** could not be ruled out.

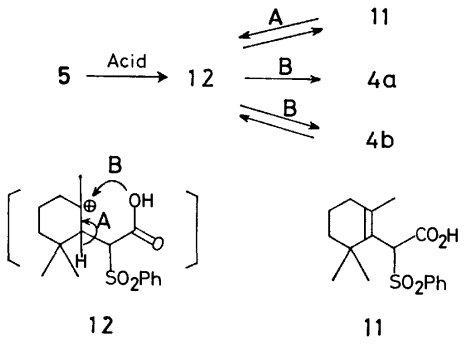

Scheme 1.

Among Lewis acids, boron trifluoride gave satisfactory results as shown in Table 2. Treatment of **5** with boron trifluoride in refluxing benzene for 1 h provided **4** (75%) and **11** (20%). Changes of solvents did not seriously affect the yield of **4**. Only carbon tetrachloride slightly improved the yield of *trans*-lactone **4b**.

Cyclization of the carboxylic acid **6b** with sulfuric and acetic acids (1:6) afforded *cis*-lactone **7** (62%). The stereochemistry of **7** was confirmed by the fact that hydrogenation of **7** with PtO_2 affords **4a** exclusively.

Preparation of Actinidiolide Derivatives. Many attempts have been made to synthesize **8** and related compounds **9a** and **9b**, because of its significant biological activity and importance as a strong fragrance for tea and tobacco. Photochemical oxidation of β-ionone derivatives,[11] β-carotenoids,[12] and retinal[13] gives **8** in poor yield. Another approach includes lactonization of homogeranic acid derived from 2,2,6-trimethylcyclohexanone resulting in unsatisfactory total yield.[14]

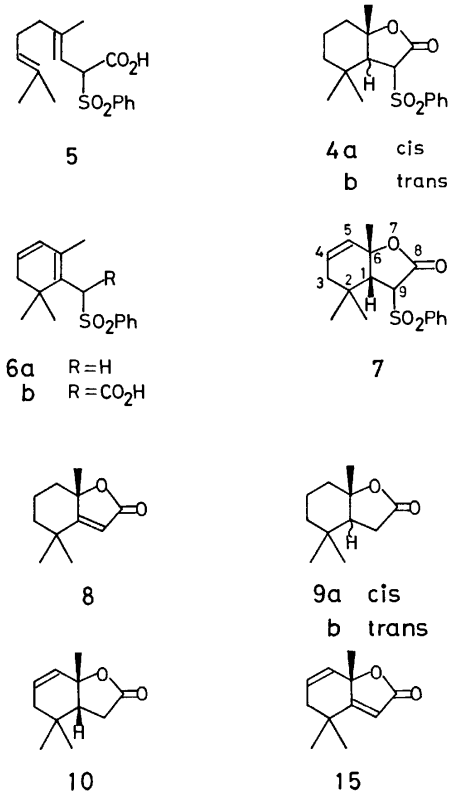

Table 2. Cyclization of **5** with boron trifluoride in various solvents

Entry	Solvent	Temp °C	Time h	Product, %	
				4 (*cis*/*trans*)	**11**
1	Toluene	reflux	1	73 (2.4)	3
2	Benzene	reflux	1	75 (2.4)	20
3	$CHCl_3$	reflux	1	71 (2.3)	26
4	CH_2Cl_2	reflux	1	70 (2.0)	21
5	CH_2Cl_2	0—4	168	71 (2.3)	21
6	CCl_4	reflux	1	55 (1.7)	12

The present attempt deals with a straightforward preparation of **8**, **9a**, **9b**, and **10** *via* the lactones **4** and **7**. Thermolysis of the lactone **4a** at *ca.* 300 °C afforded **8** (67%) and diphenyl disulfide (66%). The spectral data of **8** are in line with those reported.[6,9] Reduction of **4a** with Raney Ni W-2 in ethanol afforded *cis*-tetrahydroactinidiolide (**9a**) (84%). Similarly, **4b** yielded the *trans*-isomer **9b** (81%). The structure of both **9a** and **9b** were identified by a comparison of their spectral data.[15,16]

Reduction of **7** with potassium metal in liquid ammonia at −70 °C afforded **10** (91%)[9] and **13** (4%).[14e] Hydrogenation of the lactone **10** with Pd/C in methanol gave **9a** in 91% yield.

In contrast to the thermal elimination of phenylsulfonyl group of **4**, the lactone **7** gave **14** (75%) and diphenyl disulfide (65%) instead of actinidiolide (**15**), when **7** was heated to 225 °C. The thermal reaction of **7** can be initiated by the preferential 1,4-elimination of phenylsulfonyl group and allylic proton on C-3 as shown in Scheme 2. The incipient intermediate **16** might undergo recyclization producing **17**, which would be transformed into the stable aromatic compound **14** by subsequent Wagner-Meerwein rearrangement followed by deprotonation and aromatization.

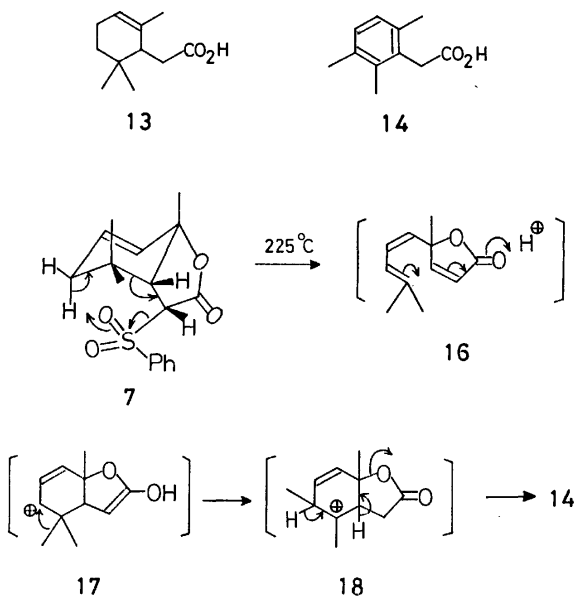

Scheme 2.

Experimental

Melting points are uncorrected. IR spectra were determined with a JASCO IRA-1 infrared spectometer. NMR spectra were obtained at 60 MHz with a Hitachi R-24 spectrometer, chemical shift values being expressed in δ value (ppm) relative to Me_4Si in $CDCl_3$.

*2-Phenylsulfonyl-4,8-dimethyl-3,7-nonadienoic Acid (**5**).* To a stirred solution of 56 mg (0.2 mmol) of **2a** in 4 ml of dry THF was added dropwise 0.8 ml (0.4 mmol) of BuLi at −70 °C under N_2. After stirring at −70 °C for 5 min, dry CO_2 was introduced into the solution with vigorous stirring for 2.5 h. The mixture was concentrated to 1 ml under reduced pressure. The residue was dissolved in ether, the acidic products being extracted with saturated $NaHCO_3$. The combined $NaHCO_3$ extracts were acidified with 10% HCl. The organic material was extracted with AcOEt. The extracts were washed with brine, dried (Na_2SO_4) and concentrated *in vacuo*. The residue was chromatographed (SiO_2, hexane and then EtOH–CH_2Cl_2=4/1) to give 64 mg (99%) of **5** as a colorless liquid. Esterification of **5** with diazomethane gave 66 mg of the corresponding methyl ester. Methyl ester of **5**: IR (neat): 1745 (C=O), 1580, 1327, 1149 (SO_2) cm^{-1}; NMR : δ 7.32—7.99(m, 5, ArH), 5.26 (d, 1, J=11 Hz, CH=), 5.03(m, 1, CH=), 4.78 (d, 1, J=11Hz, $CHSO_2$), 3.75(s, 3, CH_3O), 1.90—2.19 (m, 4, CH_2), 1.70 (s, 3, CH_3), 1.60 (s, 3, CH_3), 1.51 (s, 3, CH_3). Found: C, 64.52; H, 7.30%. Calcd for $C_{18}H_{24}O_4S$: C, 64.26; H, 7.19%.

*2-Phenylsulfonyl-2-(2,6,6-trimethyl-1,3-cyclohexadienyl)acetic Acid (**6b**).* The carboxylic acid **6b** was obtained in 96% yield as a slight yellow oil by a procedure similar to that for **5**. Methyl ester of **6b**: IR(neat): 1741 (C=O), 1320, 1145 (SO_2) cm^{-1}; NMR: δ 7.37—8.12 (m, 5, ArH), 5.79 (br s, 2, CH=), 4.89 (s, 1, CH), 3.66 (s, 3, CH_3O), 1.96—2.28 (m, 2, CH_2), 1.81 (s, 3, CH_3), 1.16 (s, 3, CH_3), 1.01 (s, 3, CH_3). Found: C, 64.93; H, 6.55%. Calcd for $C_{18}H_{22}O_4S$: C, 64.65: H, 6.63%.

*2-Phenylsulfonyl-2-(2,6,6-trimethyl-1-cyclohexenyl)acetic Acid (**11**).* Mp 182—182.5 °C; IR (Nujol): 1706 (C=O), 1325, 1150 (SO_2) cm^{-1}; NMR of methyl ester of **11**: δ 7.35—8.08 (m, 5, ArH), 4.70 (s, 1, CH), 3.70 (s, 3, CH_3O), 1.98—2.30 (m, 2, CH_2C=), 1.88 (s, 3, CH_3), 1.47—1.78 (m, 4, CH_2), 1.08(s, 3, CH_3), 0.89 (s, 3, CH_3). Found: C, 63.51; H, 6.92%. Calcd for $C_{17}H_{22}O_4S$: C, 63.33; H, 6.88%.

*2,6,6-Trimethyl-9-phenylsulfonyl-7-oxabicyclo[4.3.0]nonan-8-one (**4**).* To a refluxing solution of 161 mg (0.5 mmol) of **5** in 6 ml of freshly distilled CH_2Cl_2 under N_2 was added BF_3 etherate (150 mg). After the mixture had been refluxed for 30 min, 100 mg of BF_3 etherate and after 30 min an additional 30 mg were added. The mixture was further refluxed for 1 h. After being cooled to room temperature and quenched with saturated $NaHCO_3$, the mixture was washed with brine, dried (Na_2SO_4), and concentrated *in vacuo*. The residual crystalline product was chromatographed (SiO_2, benzene–AcOEt=10:1) to give 121 mg (75%) of **4** (**4a**/**4b**=2.4/1) as colorless crystals. The $NaHCO_3$ solution was acidified with 5% HCl, the organic material being extracted with AcOEt. The extracts were washed with brine, dried (Na_2SO_4), and concentrated *in vacuo* to yield 32 mg (20%) of **11** as crystals.

(**4a**): Mp 173.5—174.5 °C; IR (Nujol): 1770 (C=O), 1317, 1150 (SO_2) cm^{-1}; NMR: δ 7.35—8.07 (m, 5, ArH), 4.01 (d, 1, J=6 Hz, CHCO), 2.76 (d, 1, J=6 Hz, CH), 1.31—2.00 (m, 6, CH_2), 1.60(s, 3, CH_3), 1.14 (s, 3, CH_3), 1.06 (s, 3, CH_3). Found: C, 63.50; H, 7.03%. Calcd for $C_{17}H_{22}O_4S$: C, 63.33; H, 6.88%.

(**4b**): Mp 131—132 °C; IR (Nujol): 1770 (C=O), 1305, 1145 (SO_2) cm^{-1}; NMR: δ 7.30—8.00 (m, 5, ArH), 4.17 (d, 1, J=13 Hz, CHCO), 2.78 (d, 1, J=13 Hz, CH), 1.25—2.05 (m, 6, CH_2), 1.41 (s, 3, CH_3), 1.34(s, 3, CH_3), 1.15 (s, 3, CH_3). Found: C, 63.16; H, 6.83%. Calcd for $C_{17}H_{22}O_4S$: C, 63.33; H, 6.88%.

*Cyclization of **4** with H_2SO_4.* 1 ml of ice-cooled concd H_2SO_4 was added dropwise to 75 mg (0.23 mmol) of **5**. After vigorous stirring at 0 °C for 1 h, the mixture was poured into 10 ml of ice water. The organic layer was extracted with AcOEt. The extracts were washed with brine, dried (Na_2SO_4), and concentrated *in vacuo*. The residue was chromatographed (SiO_2, benzene) to give 56 mg (75%) of **4a**.

*2,2,6-Trimethyl-9-phenylsulfonyl-7-oxabicyclo[4.3.0]non-4-en-8-one (**7**).* To 50 mg (0.16 mmol) of **6b** was added dropwise 3.5 ml of an ice-cooled mixture of H_2SO_4 (0.5 ml) and AcOH (3 ml). After being stirred at room temperature for 18 h, the mixture was poured into 15 ml of ice water and the organic layer was extracted with AcOEt. The extracts were washed with brine, dried (Na_2SO_4), and concentrated *in vacuo*. The residue was chromatographed (SiO_2, benzene–AcOEt=10/1) to give 31 mg (62%) of **7** as colorless crystals: mp 134—134.5 °C (benzene–hexane); IR (Nujol): 1769 (C=O), 1321, 1150 (SO_2) cm^{-1}; NMR: δ 7.35—8.10 (m, 5, ArH), 5.80 (br s. 2, CH=), 4.00 (d, 1, J=4 Hz, CHCO), 2.91 (d, 1, J=4 Hz, CH), 1.85—2.07 (m, 2, CH_2), 1.63 (s, 3, CH_3), 1.09 (s, 3, CH_3), 0.95 (s, 3, CH_3). Found: C, 63.58; H, 6.16%. Calcd for $C_{17}H_{20}O_4S$: C, 63.73; H, 6.29%.

*Isomerization of **4b** to **4a**.* 1 ml of ice-cooled concd H_2SO_4 was added dropwise to 35 mg (0.11 mmol) of **4** (**4a**/**4b**=1/2.3). After vigorous stirring at 0 °C for 1 h, the mixture was poured into ice water and the organic layer was extracted with AcOEt. The extracts were washed with brine, dried (Na_2SO_4), and concentrated *in vacuo*. The residue was chromatographed (SiO_2, benzene) to give 31 mg (89%) of **4a** as colorless crystals.

*Hydrogenation of **7** to **4a**.* A suspension of 32 mg (0.1 mmol) of **7** and 10 mg of PtO_2 in 2 ml of dry MeOH was stirred vigorously at room temperature under H_2 for 12 h. The usual work-up and chromatography (SiO_2, benzene–AcOEt=10/1) yielded 31 mg (96%) of **4a** as colorless crystals.

*2,2,6-Trimethyl-7-oxabicyclo[4.3.0]non-9-en-8-one (Dihydroactinidiolide) (**8**).* Sulfone **4a** (40 mg, 0.12 mmol) in a glass tube (7ϕ, 25 cm) was refluxed in an air bath at 300—320 °C for 12 min, the volatile oil being collected. The oil was chromatographed (SiO_2, hexane–AcOEt=2/1) to give 15 mg (67%) of **8** as a colorless oil and 9 mg (66%) of diphenyl disulfide.

trans-*Tetrahydroactinidiolide (**9b**).* A suspension of 120 mg of Raney Ni W-2 and 37 mg (0.11 mmol) of **4b** in a mixture of 1.5 ml of EtOH and 1.5 ml of distilled water was refluxed at 110—120 °C for 10 h. After separation of Raney Ni through a short column, the organic phase was concentrated and chromatographed (SiO_2, benzene–AcOEt=10/1) to yield 17 mg (81%) of **9b** as a colorless oil.

cis-*Tetrahydroactinidiolide (**9a**).* Similarly, reduction of **4a** with Raney Ni W-2 provided **9a** in 84% yield.

*2,2,6-Trimethyl-7-oxabicyclo[4.3.0]non-4-en-8-one (**10**).* A few pieces of potassium metal (29 mg, 0.75 mmol) were added to a solution of **7** (80 mg, 0.25 mmol) in 1 ml of dry THF and 20 ml of liq ammonia at −70 °C. After 1 min, saturated NH_4Cl was added and then liq ammonia was evaporated at room temperature for 2 h. The residue was combined with 2 ml of 5% HCl and the organic substances were extracted with AcOEt. The extracts were washed with

brine, dried (Na_2SO_4), and concentrated under reduced pressure to yield 44 mg of colorless liquid which was chromatographed (SiO_2, benzene–AcOEt=30/1) to give 41 mg (91%) of **10** as a colorless liquid and 2 mg (4%) of **13**.

Hydrogenation of ***10***. A suspension of 7 mg of Pd/C and 37 mg (0.21 mmol) of **10** in 2 ml of dry MeOH was stirred under H_2 at room temperature for 12 h. After the usual work-up and chromatograph (SiO_2, benzene), 34 mg (91%) of **9a** was obtained as a colorless oil.

*2,3,6-Trimethylphenylacetic Acid (****14****)*. Lactone **7** (48 mg, 0.15 mmol) was heated to 225 °C in a glass tube settled in a Kugelrohr distillation apparatus for 3 h. During the course of heating, 45 mg of a dark colored oil was distilled out and chromatographed (SiO_2, benzene) to give 20 mg (75%) of **14**, 10 mg (61%) of diphenyl disulfide, and 8 mg (17%) of **7**. The carboxylic acid **14** was esterified with CH_2N_2 and subjected to preparative GLC (SE-30) to show a single peak: IR ($CHCl_3$) 3400—2400 (OH), 1697 (C=O) cm^{-1}; NMR: δ 9.59 (s, 1, CO_2H), 6.94 (s, 2, ArH), 3.72 (s, 2, CH_2), 2.28 (s, 3, CH_3), 2.24 (s, 3, CH_3), 2.20 (s, 3, CH_3). Methyl ester of **14**; Found: C, 74.90; H, 8.55%. Calcd for $C_{12}H_{16}O_2$: C, 74.97; H, 8.39%.

References

1) Alicyclic Terpenoids from Cyclocitryl Phenyl Sulfides VIII. Part VII. S. Torii, K. Uneyama, I. Kawahara, and M. Kuyama, *Chem. Lett.*, **1978**, 455.

2) W. S. Johnson, *Acc. Chem. Res.*, **1**, 1 (1968); E. E. van Tamelen, *ibid.*, **1**, 111 (1968); T. Kato and S. Kumazawa, *Yuki-goseikagaku Kyokaishi*, **33**, 223 (1975); W. S. Johnson, *Angew. Chem. Int. Ed. Engl.*, **15**, 9 (1976).

3) The cyclization of homogeranic acid with $SnCl_4$ in nitromethane yielded 51% of *cis*-**9a**: a) T. Kato, S. Kumazawa, and Y. Kitahara, *Synthesis*, **1972**, 573; b) S. Kumazawa, T. Kato, and Y. Kitahara, *Chem. Lett.*, **1973**, 633.

4) a) S. Torii, K. Uneyama, and M. Ishihara, *Chem. Lett.*, **1975**, 479; b) K. Uneyama and S. Torii, *Tetrahedron Lett.*, **1976**, 443; c) K. Uneyama and S. Torii, *Chem. Lett.*, **1977**, 39; d) S. Torii, K. Uneyama, and H. Hamada, *Bull. Chem. Soc. Jpn.*, **50**, 2503 (1977).

5) S. Torii, K. Uneyama, and M. Kuyama, *Tetrahedron Lett.*, **1976**, 1513.

6) T. Sakan, S. Isoe, and S. B. Hyeon, *Tetrahedron Lett.*, **1967**, 1623.

7) a) W. C. Bailey, Jr., A. K. Bose, R. M. Ikeda, R. H. Newman, H. V. Secor, and C. Varsel, *J. Org. Chem.*, **33**, 2819 (1968); b) S. Fukushima, Y. Akahori, and T. Tsuneya, *Yakugaku Zasshi*, **88**, 646 (1968); c) H. Kaneko and K. Ijichi, *Agric. Biol. Chem.*, **32**, 1337 (1968); d) E. von Sydow and K. Anjou, *Lebensm. Wiss. Technol.*, **2**, 78 (1969); e) S. Fukushima, Y. Akahori, and T. Tsuneya, *Yakugaku Zasshi*, **89**, 1729 (1969); f) K. Ina, Y. Sakato, and H. Fukami, *Tetrahedron Lett.*, **1968**, 2777; g) T. Fujimori, R. Kasuga, H. Matsushima, H. Kaneko, and M. Noguchi, *Agric. Biol. Chem.*, **40**, 303 (1976).

8) H. Kaneko and K. Hoshino, *Agric. Biol. Chem.*, **33**, 969 (1969).

9) E. Demole and P. Enggist, *Helv. Chim. Acta*, **51**, 481 (1968).

10) E. A. Lehto and D. A. Shirley, *J. Org. Chem.*, **22**, 989 (1957).

11) a) M. Mousseron-Canet, J. C. Mani, and J. P. Dalle, *Bull. Soc. Chim. Fr.*, **1967**, 608; b) S. Isoe, S. B. Hyeon, H. Ichikawa, S. Katsumura, and T. Sakan, *Tetrahedron Lett.*, **1968**, 5561; c) K. Ina, T. Takano, Y. Imai, and Y. Sakato, *Agric. Biol. Chem.*, **36**, 1033 (1972); d) B. R. von Warburg, H. R. Wolf, and O. Jeger, *Helv. Chim. Acta*, **56**, 1948 (1973); e) S. Kurata, Y. Inouye, and H. Kakisawa, *Tetrahedron Lett.*, **1973**, 5153; f) S. Kurata, T. Kusumi, Y. Inouye, and H. Kakisawa, *J. Chem. Soc. Perkin Trans 1*, **1976**, 532.

12) a) S. Isoe, S. B. Hyeon, and T. Sakan, *Tetrahedron Lett.*, **1969**, 279; b) U. Schwieter, W. Arnold, W. E. Oberhänsli, N. Rigassi, and W. Vetter, *Helv. Chim. Acta*, **54**, 2447 (1971); c) S. Isoe, S. B. Hyeon, S. Katsumura, and T. Sakan, *Tetrahedron Lett.*, **1972**, 2517; d) K. Kawashima and T. Yamanishi, *Nippon Nogei Kagaku Kaishi*, **47**, 79 (1973).

13) D. Lerner, J. C. Mani, and M. Mousseron-Canet, *Bull. Soc. Chim. Fr.*, **1970**, 1968.

14) a) Ref. 6; b) Ref. 7a; c) Ref. 9; d) Z. Horii, M. Ito, I. Minami, M. Yamauchi, M. Hanaoka, and T. Monose, *Chem. Pharm. Bull.*, **18**, 1967 (1970); e) M. Stoll, P. Bolle, and L. Ruzicka, *Helv. Chim. Acta*, **33**, 1510 (1950); f) Ref. 16.

15) M. Robi and C. H. Engster, *Helv. Chim. Acta*, **52**, 1732 (1969).

16) T. Matsumoto, G. Sakata, Y. Tachibana, and K. Fukui, *Bull. Chem. Soc. Jpn.*, **45**, 1147 (1972).

The Synthesis of Tetrakisdehydrotetraazaannulenes. Tetramethyl[32]-, [40]-, and Tetrabenzo[32]annulene

Jūro Ojima,* Yūji Shiroishi, and Masamitsu Fujiyoshi

Department of Chemistry, Faculty of Science, Toyama University, Gofuku, Toyama 930

(Received January 25, 1978)

The conjugate aldehydes, containing terminal acetylenes, were converted to the corresponding conjugated azines **6a**—**c** and **8a**—**c**, respectively. Oxidative couplings of these azines were attempted. The azines **6b**, **6c**, and **8b** afforded the corresponding cyclic dimers **9**, **10**, and **11**, respectively. Examination of ^{1}H NMR spectra indicates that the tetraazaannulenes are atropic.

In 1974, Yamamoto and Sondheimer attempted the oxidative couplings of the conjugated azines of type **1** to obtain the corresponding cyclic monomer and/or dimer, which are the macrocyclic analogues of pyridazine **2** and 1,2,4,5-tetrazine **3**, respectively.[1] In attempted oxidative couplings, they obtained the cyclic dimer **4** from the azine **1b** using copper(II) acetate monohydrate in ether and pyridine under relatively dilute concentrations. Also, quite recently, Darby *et al.* found that oxidative coupling of terminal diacetylenes to macrocyclic 1,3-diacetylenes usually proceeds in higher yield when anhydrous copper(II) acetate instead of the monohydrate is employed.[2]

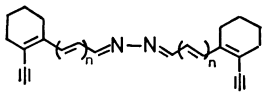

1

1a : n=0
b : n=1
c : n=2

2

3

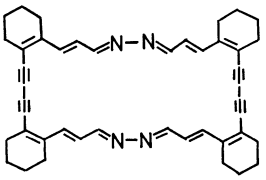

4

Bearing these results in mind and expecting to obtain the cyclic monomeric compounds using the conditions reported by Darby *et al.*, we undertook to examine oxidative couplings of the conjugated azines of types **6** and **8**. In practice, we obtained no cyclic monomeric compounds, but the respective cyclic dimers **9**, **10**, **11**, from the azines **6b**, **6c**, and **8b**.

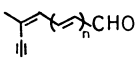

5

5a : n=0
b : n=1
c : n=2

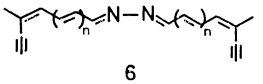

6

6a : n=0
b : n=1
c : n=2

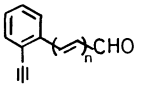

7

7a : n=0
b : n=1
c : n=2

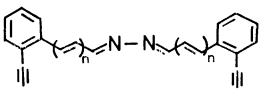

8

8a : n=0
b : n=1
c : n=2

Table 1. Yields and melting points of the azines **6** and **8**

	Azines	
	Yield (%)	Mp (°C)
6a	82	110 (dec)
6b	76	160 (dec)
6c	87	110 (dec)
8a	85	140 (dec)
8b	64	169—170
8c	64	199—200

The trienyne aldehyde **5c** was prepared from its lower homologue, the dienyne aldehyde **5b** in 50% yield by condensation with ethyl vinyl ether according to the Isler's method[3,4] or by Wittig condensation with (1,3-dioxolan-2-ylmethyltriphenyl)phosphonium bromide.[5,6]

Treatment of the aldehydes **5a**—**c** and **7a**—**c** in ethanol with aqueous hydrazine, as described by Yamamoto and Sondheimer,[1] yielded the corresponding conjugated azines **6a**—**c** and **8a**—**c**, respectively. The yields and melting points of the azines are summarized in Table 1.

All of attempted oxidative couplings of these azines (**6a**—**c**, **8a**—**c**) were carried out with anhydrous copper(II) acetate in pyridine and ether at 50 °C as reported by Darby *et al.*[2] The azines **6b**, **6c**, and **8b** afforded the corresponding cyclic dimers **9** (14%), **10** (17%), **11** (20%), and they formed red needles (122 °C (dec)), purple needles (*ca.* 95 °C (dec)), yellow needles (170 °C (dec)), respectively; the compound **10** was a rather unstable material. Under the same conditions as above, the yellow crystals were isolated from the azine **8c**, but the structure of the material is not yet established. In the cases of **6a** and **8a**, the oxidative couplings were also investigated under several different conditions (see Experimental), but no desired cyclic product could be obtained.

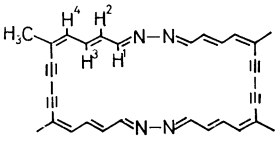

9

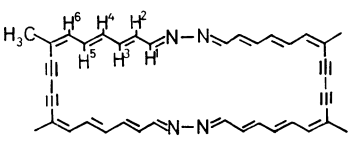

10

The dimeric structure of the product from **6b**, **6c**, and **8b** was established by the mass spectra. The mass spectral measurement of **10** using direct inlet system were not satisfactory owing to decomposition

Table 2. ^{1}H-NMR parameters of **9**, **10**, and **11** in $CDCl_3$ at 100 MHz
(τ-Values; internal standard, TMS; J values in Hz in parentheses)

Proton	**9**	**10**	**11**
H^1	2.30 (d, 9)	2.03 (d, 9)	1.86 (d, 9)
H^2	3.51 (dd, 15, 9)	2.6—3.6 (m)	2.92 (dd, 16, 9)
H^3	2.86 (dd, 15, 11)		2.51 (d, 16)
H^4	3.45 (d, 11)		
H^5, H^6			
CH_3	7.98 (s)	7.96 (s), 7.99 (s)	
benzenoid H			2.3—2.6 (m)

during measurement. However, the mass spectrum obtained by field desorption technique was satisfactory one, revealing a molecular ion peak (mol wt, 573) clearly. The UV spectra of **9**, **10**, and **11** are illustrated

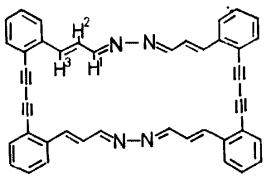

11

in Fig. 1. These spectra are similar as those of **4**,[1] and shows characteristic feature of [4*n*]annulene.[7] The ^{1}H-NMR data of **9**, **10**, and **11** are given in Table 2. The chemical shifts of the olefinic and methyl protons of these compounds suggest that the compounds **9**, **10**, and **11** are atropic molecules.

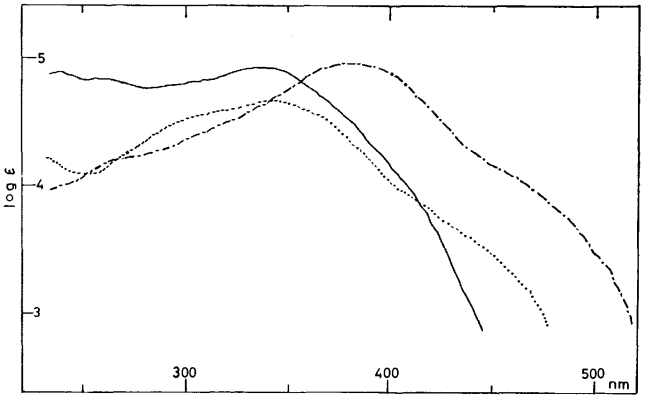

Fig. 1. Electronic spectra of tetrakisdehydrotetraazaannulenes **9** (----), **10** (——-), and **11** (——) in THF.

In conclusion, although we expected that the cyclic monomers, which are the macrocyclic analogues of pyridazine **2**, might also result from the azines by using the procedure reported by Darby *et al.*, the compounds obtained are dimeric ones.

Experimental

All melting points are uncorrected. The IR spectra were measured on Hitachi EPI-S2 or Unicam SP 200 spectrophotometer: only significant maxima are reported. The electronic spectra obtained on Hitachi 124 or Unicam SP-800 spectrophotometer were recorded in nm. The ε-values are given in parentheses, the shoulder being denoted by sh. The mass spectra were measured with JEOL JMS-OI-SG-2, AEI MS-12 or JEOL JMS-D equipped with field desorption system. The ^{1}H-NMR spectra were obtained on Varian EM-930, Varian T-60 or Varian XL-100 spectrometer, and refer to solutions in $CDCl_3$, in τ-values with TMS as an internal standard at 90 MHz unless otherwise stated. The coupling constants (J) are given in Hz. The individual assignments are made on the basis of the multiplicity and coupling constants. The number indicated in the by-line starts from the carbon adjacent to nitrogen atom of the azine group, as shown in the formulae of **9**, and in **5c** the number starts from the carbon of the aldehyde group. Alumina (Act. II—III) was used for column chromatography unless otherwise indicated. Progress of most reactions was followed by TLC using Merck precoated alumina. Evaporation of the solvents was carried out at water aspirator pressure.

7-Methyl-2,4,6-nonatrien-8-ynal **5c**.[4] A 1% soln of *p*-toluenesulfonic acid monohydrate in absolute ethanol (15 drops) was added to a soln of the aldehyde **5b**[3] (6.1 g, 0.05 mol) and ethyl orthoformate (9.2 g, 0.06 mol) in absolute ethanol (10 ml). After being stirred at room temperature overnight, the mixture was treated with pyridine (1 ml) and poured into 2% aqueous $NaHCO_3$ (100 ml). Extraction with ether, drying over $MgSO_4$, and evaporation of the solvents yielded the crude diethyl acetal of **5b** as a red liquid. The liquid was dissolved in ethyl acetate (10 ml) and warmed to 35 °C in a flask equipped with two dropping funnels, a condenser, and a magnetic stirrer. A 10% soln of zinc chloride in ethyl acetate (20 drops) was added, and then the same soln (10 ml) and ethyl vinyl ether (40 ml) were added simultaneously during 5 min under stirring at 35 °C. The mixture was stirred for 2 h at room temperature, stoppered, and allowed to stand overnight. A soln of sodium acetate (15 g) in water (10 ml) and acetic acid (150 ml) was then added, and the mixture was heated to 90 °C for 2 h. Dilution with water (700 ml), extraction with ether, drying over $MgSO_4$, and evaporation gave a residue, which was chromatographed on alumina (200 g, Woelm, Act. III). Elution with pentane-ether (96:4—90:10) and evaporation of the solvents gave the aldehyde **5c** (3.6 g, 50%) as solid. Recrystallization from ether-hexane gave pure **5c** as orange needles, mp 64—65 °C; MS: *m/e* 146 (M^+), 131 (M^+-15), 117 (M^+-29); mol wt, 146.2; IR ($CHCl_3$): 3290 (-C≡CH), 2100 (-C≡C-), 1670, 1600 (C=O, C=C), 995 cm^{-1} (*trans* C=C); UV (ether): λ_{max} 234 (14600), 305 sh (32900), 324 (47500), 337 nm (44900); NMR (60 MHz): 0.41 (d, 8, 1H, CH^1O), 2.80 (dd, 15, 11, 1H, H^5), 2.87 (dd, 15, 11, 1H, H^3), 3.41—3.67 (m, 2H, H^4 and H^6), 3.82 (dd, 15, 8, 1H, H^2), 6.54 (s, 1H, -C≡CH), 7.99 (s, 3H, $-CH_3$).

Found: C, 82.42; H, 6.71%. Calcd for $C_{10}H_{10}O$: C, 2.16; H, 6.90%.

The compound **5c** was also prepared in 42% yield by Wittig condensation with (1,3-dioxolan-2-ylmethyl) triphenyl-

phosphonium bromide as reported for the preparation of **7b**,[6] except the use of lithium ethoxide instead of lithium methoxide as a base.[5]

Azine ***6a***. A soln of **5a**[8] (2.0 g, 2.1 mmol) in ethanol (20 ml) was added to a soln prepared from hydrazine sulfate (1.5 g), Na_2CO_3 (2.0 g), and H_2O (15 ml), with stirring at ambient temperature. After the reaction was continued for 2 h at the same temperature, the reaction mixture was poured into aqueous $NaHCO_3$ soln (200 ml), and extracted with benzene, washed with aqueous $NaHCO_3$ and dried over K_2CO_3. The residual red liquid, after solvent removal, was chromatographed on alumina (120 g) with light petroleum–ether (80:20) to give **6a** (1.6 g, 82%). Recrystallization from chloroform–ethanol afforded yellow needles, mp *ca.* 110 °C (dec), MS: *m/e* 184 (M^+, 50), 183 (100); mol wt, 184.2; IR (KBr disk): 3200 (–C≡CH), 2100 (–C≡C–), 1610 (N=C); UV (EtOH): λ_{max} 302 sh (19900), 315 (26700), 328 (27100), 344 sh (18200); NMR: 1.38 (d, 10, 2H, H^1), 3.40 (broad d, 10, 2H, H^2), 6.55 (s, 2H, –C≡CH), 7.90 (s, 6H, $-CH_3$).

Found: C, 78.05; H, 6.30; N, 15.00%. Calcd for $C_{12}H_{12}N_2$: C, 78.23; H, 6.57; N, 15.21%.

Azine ***6b***. In a similar manner, **6b** was prepared from **5b**[3] (1.4 g, 12 mmol) in EtOH (15 ml) and hydrazine sulfate (0.79 g), Na_2CO_3 (0.98 g), and H_2O (8.1 ml). Elution with light petroleum–ether (20:80—5:95) from the column of alumina (130 g) gave **6b** (1.05 g, 76%), obtained as yellow needles from benzene–hexane, mp *ca.* 160 °C (dec), MS: *m/e* 236 (M^+, 44), 193 (100); mol wt, 236.3; IR (KBr disk): 3300 (–C≡CH), 2100 (–C≡C–), 1615 (N=C), 1600 (C=C), 980 cm^{-1} (*trans* C=C); UV (THF): λ_{max} 231 (11400), 239 sh (9710), 247 sh (6380), 280 sh (6420), 292 (7600), 322 sh (22400), 341 sh (42500), 357 (57200), 373(57700), 392(36800); NMR (100 MHz): 1.79 (d, 10, 2H, H^1), 2.84 (dd, 15, 11, 2H, H^3), 3.52 (dd, 15, 11, 2H, H^2), 3.53 (d, 11, 2H, H^4), 6.56 (s, 2H, –C≡CH), 7.99 (s, 6H, $-CH_3$).

Found: C, 81.42; H, 6.86; N, 11.65%. Calcd for $C_{16}H_{16}N_2$: C, 81.32; H, 6.83; N, 11.86%.

Azine ***6c***. This substance was similarly prepared from **5c** (430 mg, 2.94 mmol) in EtOH (3.8 ml) and hydrazine sulfate (199 mg), Na_2CO_3 (247 mg), and H_2O (2 ml). Elution with ether–chloroform (1:1) from the column of alumina (120 g) gave **6c** (370 mg, 87%), obtained as brownish yellow needles from chloroform, mp *ca.* 110 °C (dec), MS: *m/e* 288 (M^+, 100); mol wt, 288.3; IR (KBr disk): 3280 (–C≡CH), 2100 (–C≡C–), 1620 (N=C), 1590 (C=C), 995 cm^{-1} (*trans* C=C); UV (THF): λ_{max} 260 (6460), 271 sh (5590), 281 sh (4020), 312 sh (5460), 325 sh (7070), 396 (40000), 413 (40900), 434 (25200); NMR: 1.81 (d, 9. 2H, H^1), 3.0—3.7 (m, 10H, olefinic H), 6.63 (s, 2H, –C≡CH), 8.03 (s, 6H, $-CH_3$).

Found: C, 83.27; H, 6.72; N, 9.87%. Calcd for $C_{20}H_{20}N_2$: C, 83.29; H, 6.99; N, 9.71%.

Azine ***8a***. Similarly, **8a** was prepared from **7a**[9] (3.0 g, 2.3 mol) in EtOH (30 ml) and hydrazine sulfate (1.6 g), Na_2CO_3 (1.9 g), and H_2O (16 ml). Elution with light petroleum–ether (85:15—60:40) from the column of alumina (150 g) gave **8a** (2.5 g, 85%), obtained as yellow needles from benzene–hexane, mp *ca.* 140 °C (dec), MS: *m/e* 256 (M^+, 75), 255 (100); mol wt, 256.2; IR (KBr disk): 3200 (–C≡CH), 2100 (–C≡C–), 1625 cm^{-1} (N=C); UV (THF): λ_{max} 232 (31400), 248 sh (25700), 255 sh (19900), 302 sh (26200), 315 (29200). 332 sh (24500), 349 sh (11300); NMR: 0.83 (s, 2H, H^1), 1.66—1.85 (m, 2H, benzenoid H), 2.36—2.75 (m, 6H, benzenoid H), 6.60 (s, 2H, –C≡CH).

Found: C, 84.27; H, 4.92; N, 10.66%. Calcd for $C_{18}H_{12}N_2$: C, 84.35; H, 4.72; N, 10.93%.

Azine ***8b***. This material was similarly prepared from **7b**[6] (1.8 g, 0.12 mmol) in EtOH (20 ml) and hydrazine sulfate (0.97 g), Na_2CO_3 (0.98 g), and H_2O (1.1 ml). The resulting precipitates were collected and washed with EtOH, giving **8b** (1.14 g, 64%), obtained as yellow needles from benzene–ethanol, mp 169—170 °C, MS: *m/e* 308 (M^+, 30), 280 (100); mol wt, 308.3; IR (KBr disk): 3250 (–C≡CH), 2100 (–C≡C–), 1635 (N=C), 1590 (C=C), 980 cm^{-1} (*trans* C=C); UV (THF): λ_{max} 290 sh (8260), 339 sh (44600), 353 (52900), 370 sh (47400), 390 sh (24000); NMR: 1.67 (d, 9, 2H, H^1), 2.43 (d, 16, 2H, H^3), 2.97 (dd, 16, 9, 2H, H^2), 2.32—2.90 (m, 8H, benzenoid H), 6.68 (s, 2H, –C≡CH).

Found: C, 86.43; H, 5.33; N, 8.83%. Calcd for $C_{22}H_{16}N_2$: C, 86.69; H, 5.23; N, 9.09%.

Azine ***8c***. This substance was similarly prepared from **7c**[10] (1.0 g, 5.5 mmol) in EtOH (7.1 ml) and hydrazine sulfate (371 mg), Na_2CO_3 (460 mg), and H_2O (3.7 ml). Fractions eluted with light petroleum–ether (50:50) from the column of alumina (150 g) gave **8c** (623 mg, 64%), obtained as yellow plates from chloroform, mp 199—200 °C. Attempts to obtain a satisfactory elemental analysis were unsuccessful in our hands, but the Mass (*m/e* 360 (M^+, 45), 180 (100); mol wt, 360.4), the IR (KBr disk) (3300 (–C≡CH), 2100 (–C≡C–), 1615 (N=C), 995 cm^{-1} (*trans* C=C)), the UV (THF) λ_{max} 276 sh (14300), 368 sh (54000), 389 (67000), 405 sh (62000), 430 sh (15000)), and the NMR (1.75 (d, 9, 2H, H^1), 2.35—3.48 (m, 16H, benzenoid and olefinic H), 6.65 (s, 2H, –C≡CH)) were found to be consistent with the assigned structure.

Oxidative Coupling of ***6b*** *to the Tetrakisdehydrotetraaza[32]annulene* ***9***. A soln of **6b** (950 mg, 4.02 mmol) in pyridine (63 ml) and dry ether (21 ml) was added dropwise during 4 h to a stirred soln of anhydrous copper(II) acetate (5.1 g) in pyridine (140 ml) and dry ether (47 ml) kept at 50 °C; the mixture was stirred for further 2 h at the same temperature. Then the mixture was chilled, diluted with benzene (100 ml), and filtered through Hyflo Super-Cel. The precipitates formed were washed with benzene (100 ml × 4). The filtrate was washed with H_2O thirteen times to remove pyridine, and dried over K_2CO_3. After solvent removal, the residual red liquid was chromatographed on alumina (200 g). Fractions eluted with light petroleum–ether (65:35)—ether–benzene (30:70) contained **9**. The slightly crude **9** was dissolved in ether and chromatographed on alumina (140 g) with ether to give **9** (129 mg, 14%), obtained as orange needles from benzene–hexane, mp 122 °C (dec); MS: *m/e* 470 (M^+, 8), 324 (100); mol wt, 470.5; IR (KBr disk): 2150 (–C≡C–), 1610 (N=C), 1600 (C=C), 975 cm^{-1} (*trans* C=C); UV (THF): (see Fig. 1) λ_{max} 232 (14000), 269 sh (15700), 312 sh (33000), 339 nm (45000): NMR: see Table 2.

Oxidative Coupling of ***6c*** *to the Tetrakisdehydrotetraaza[40]annulene* ***10***. To a stirred soln of anhydrous copper(II) acetate (1.3 g) in pyridine (36 ml) and dry ether (12 ml) kept at 50 °C was added with stirring a soln of **6c** (300 mg, 1.04 mmol) in pyridine (40 ml) and dry ether (10 ml) during 2.5 h: the mixture was stirred for further 2.5 h at 45—50 °C (bath temp). Then the mixture was worked up as in the preparation of **9**. Elution with benzene from the column of alumina (200 g) gave **10** (50 mg, 17%), obtained as purple microcrystals from chloroform mp *ca.* 95 °C (dec); MS (field desorption method): *m/e* 573 (M^+), 574 ($M^+ + 1$); mol wt, 572.6; IR (KBr disk): 2200 (–C≡C–), 1620 (N=C), 1580 (C=C), 995 cm^{-1} (*trans* C=C), UV (THF): (see Fig. 1) λ_{max} 238 sh (10100), 258 sh (14900), 381 (87500), 468 sh (9630); NMR: see Table 2.

Oxidative Coupling of ***8b*** *to the Tetrakisdehydrotetraaza[32]annulene* ***11***. A soln of azine **8b** (710 mg, 2.30 mmol) in pyridine (42 ml) and dry ether (14 ml) was added during

2 h to a stirred soln of anhydrous copper(II) acetate (2.9 g) in pyridine (80 ml) and dry ether (27 ml) at 50 °C; the mixture was stirred for further 3 h. Then the product was worked up as in the preparation of **9**. The residual liquid, after solvent removal, was chromatographed on alumina (150 g) with ether–benzene (50:50—90:10) to give **11** (144 mg, 20%), obtained as yellow microcrystals from chloroform, mp 168—170 °C (dec): MS: *m/e* 613 (M^+, 27), 307 (100); mol wt, 612.7; IR (KBr disk): 2200, 2150 (–C≡C–), 1635 (N=C), 1595 (C=C), 980 cm^{-1} (*trans* C=C); UV (THF): (see Fig. 1) λ_{max} 287 sh (60200), 303 sh (65400), 333 (83400); NMR: see Table 2.

The yield of **11** was only 8% when the coupling of **8b** was carried out with copper(II) acetate monohydrate in pyridine and ether at 70 °C according to the procedure described for the preparation of **4**.[1)]

*Oxidative Coupling of **6a** and **8a**.* These oxidative couplings were carried out under the following conditions: a) with conditions as described for the preparation of **9**; b) with copper(II) acetate monohydrate in pyridine and ether as reported for the preparation of **4** (Ref. 1); c) with copper(II) acetate monohydrate in pyridine under concentrate conditions.[11)] In all attempted runs, only polymeric products were obtained.

*Oxidative Coupling of **8c**.* In a run performed under similar conditions as the preparation of **9**, the yellow crystals (260 mg) were obtained from the azine **8c** (690 mg, 1.91 mmol) in pyridine (50 ml) and dry ether (16 ml), and anhydrous copper(II) acetate (2.4 g) in pyridine (66 ml) and dry ether (22 ml). After chromatographic purification, they formed yellow microcrystals from chroloform, mp 180 °C (dec). However, the structure of the material is not established.

The authors wish to thank Prof. Franz Sondheimer, University College London, for permitting us to publish some experimental data. We also thank Dr. Fumio Ogura and Prof. Masazumi Nakagawa, Osaka University, for measurement of NMR spectra at 100 MHz, and Mr. Tetsuo Higuchi, Nippon Denshi Co., for the measurement of mass spectrum using field desorption technique. Financial aid by the Ministry of Education (Grant-in-Aid 054103, 1975) is acknowledged.

References

1) K. Yamamoto and F. Sondheimer, *Tetrahedron*, **30**, 4229 (1974).
2) N. Darby, T. M. Cresp, and F. Sondheimer, *J. Org. Chem.*, **42**, 1960 (1977).
3) J. Ojima, M. Ishiyama, and A. Kimura, *Bull. Chem. Soc. Jpn.*, **50**, 1584 (1977).
4) This experiment was carried out in Prof. Sondheimer's laboratory at University College London.
5) R. L. Wife and F. Sondheimer, *Tetrahedron Lett.*, **1974**, 195; The details of preparation was given from Prof. Sondheimer.
6) J. Ojima, A. Kimura, Y. Yokoyama, and T. Yokoyama, *Bull. Chem. Soc. Jpn.*, **48**, 367 (1975).
7) I. C. Calder, Y. Gaoni, and F. Sondheimer, *J. Am. Chem. Soc.*, **90**, 4946 (1968); Y. Yoshikawa, S. Nakatsuji, F. Iwatani, S. Akiyama, and M. Nakagawa, *Tetrahedron Lett.*, **1977**, 1737.
8) J. Ojima, T. Katakami, G. Nakaminami, and M. Nakagawa, *Bull. Chem. Soc. Jpn.*, **49**, 292 (1976).
9) J. Ojima, T. Yokomachi, and A. Kimura, *Bull. Chem. Soc. Jpn.*, **49**, 2840 (1976).
10) J. Ojima, M. Enkaku, and M. Ishiyama, *J. Chem. Soc., Perkin Trans. 1*, **1977**, 1548.
11) *Inter alia*, a) P. D. Howes, E. LeGoff, and F. Sondheimer, *Tetrahedron Lett.*, **1972**, 3691; b) J. Ojima, Y. Yokoyama, and M. Enkaku, *Bull. Chem. Soc. Jpn.*, **50**, 1522 (1977).

Branched-chain Sugars. XII. The Stereoselectivities in the Reaction of Methyl 4,6-*O*-Benzylidene-α- and -β-D-hexopyranosid-3-uloses with Diazomethane[1]

Ken-ichi SATO and Juji YOSHIMURA*

Laboratory of Chemistry for Natural Products, Faculty of Science, Tokyo Institute of Technology, Nagatsuta, Midoriku, Yokohama 227

(Received February 7, 1978)

The stereoselectivities in the diazomethane reaction of methyl 4,6-*O*-benzylidene-2-*O*-methyl-α-D-*ribo*-hexopyranosid-3-ulose (**2**), its 2-epimer (**3**), β-anomer of **2** and the corresponding 2-*O*-Benzoyl derivative were examined, in comparison with those in the Grignard reaction and sodium borohydride reduction. The complemental stereoselectivity of diazomethane reaction in the case of **2** and **3** indicated that the electrostatic attractive effect in the transition state between diazomethyl cation and the axial methoxyl oxygen at the α-position to carbonyl function in **3** is much stronger than that at β-position which is predominat in the case of **2**. In cases of β-anomers having no axial oxygen, stereoselectivies were preferentially controlled by the usual steric factors.

In previous papers, we examined the stereoselectivities in nucleophilic reactions of methyl 2-*O*-Benzyl-4,6-*O*-benzylidene-α-D-*ribo*-hexopyranosid-3-ulose (**1**)[2] and other uloses,[3,4] and found the complemental stereoselectivity between the Grignard and diazomethane reactions. The abnormality of the latter reaction was deduced to be controlled predominantly by the electrostatic attractive interaction between vicinal or neighboring hydroxyl oxygens and diazomethyl cation in the zwitterionic intermediate.

In order to confirm the above hypothesis, the stereoselectivities in the Grignard and diazomethane reactions and in sodium borohydride reduction of 2-*O*-methyl derivative (**2**)[5] of **1**, its 2-epimer (**3**),[6] β-anomer (**4**)[7] of **1** and its 2-*O*-methyl derivative (**5**)[8] were examined in this paper. Compound **5** was obtained by the dimethyl sulfoxide–trifluoroacetic anhydride oxidation[6,9] of methyl 4,6-*O*-benzylidene-2-*O*-methyl-β-D-altropyranoside which was synthesized by the preferential ring-opening of the corresponding 2,3-epoxide[10] of D-allo configuration with methanol. Epimerization at C-2 position during the oxidation could not be suppressed in this case.

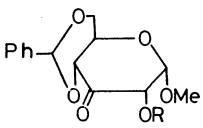

(**1**) R=Bz
(**2**) R=Me

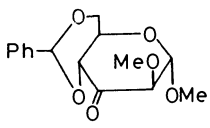

(**3**)

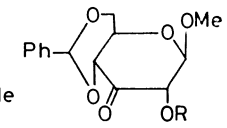

(**4**) R=Pz
(**5**) R=Me

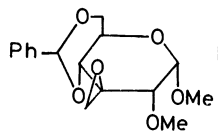

(**6**)

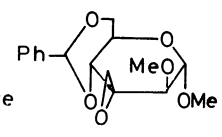

(**11**)

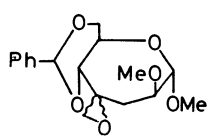

(**12**)

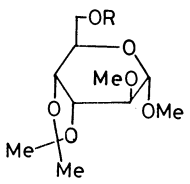

(**14**) R=H
(**15**) R=Ac

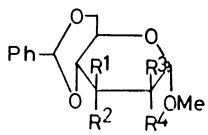

	R¹	R²	R³	R⁴
(**7**)	OH	Me	H	OMe
(**8**)	Me	OH	H	OMe
(**9**)	Me	OMe	H	OMe
(**10**)	OMe	Me	H	OMe
(**13**)	Me	OH	OMe	H
(**16**)	Me	OAc	H	OMe
(**17**)	Me	OAc	OMe	H
(**18**)	OAc	Me	H	OMe

Results

In general, diazomethane reaction was carried out in less polar solvent than benzene–ether–ethanol (1:1:1) to suppress the accompanying ring-expansion, and the Grignard reaction in benzene–ether at room temperature.

Reaction of **2** with diazomethane gave the corresponding spiro epoxide (**6**) in 73% yield which was reduced with lithium aluminium hydride to give the corresponding 3-*C*-methyl derivative (**7**), quantitatively. Besides, the reaction of **2** with methylmagnesium iodide gave the epimeric 3-*C*-methyl derivative (**8**) of **7** in a good yield which was methylated with sodium hydride and methyl iodide to give 3-*O*-methyl derivative (**9**). The same compound was obtained by *O*-methylation of known methyl 4,6-*O*-benzylidene-3-*C*-methyl-α-D-allopyranoside[3,11] which is the Grignard reaction product of **1**. The 3-*O*-methyl derivative (**10**) of **7** was not identical with **9**. These results indicate that the stereoselectivities in the both reactions of **2** are complemental as was depicted in the case of **1**.[2]

Diazomethane reaction of **3** gave the corresponding spiro epoxide (**11**) and ring-expansion product (**12**) in 41 and 36.9% yields, respectively, by the separation on a TLC. Reduction of **11** gave a 3-*C*-methyl derivative (**13**) which was identical with that obtained by the Grignard reaction of **3**. The configuration of **13** was determined to be D-altro from the following conversions. De-*O*-benzylidenation of **13** with 70% acetic acid and subsequent acetonation gave the corresponding 3,4-*O*-isopropylidene derivative (**14**) which gave the 6-*O*-acetate (**15**) by base-catalyzed acetylation. These results indicate that the tertiary hydroxyl group in **13** was protected by the acetonation, and consequently in *cis*-interrelation to the 4-hydroxyl group.

Chemical shifts of tertiary acetoxyl groups of 3-*O*-acetate of **8** (**16**: δ 2.04) and **13** (**17**: δ 2.00) in the region of axial one (δ 2.07—1.96) supported also the above configurational assignment, but, that of 3-*O*-acetate of **7** (**18**: δ 2.04) was not in agreement with equatorial one (δ 1.93—1.88).[12] Such instances were also reported in the case of nitromethyl-branching derivatives.[13] The position of ring methylene in ring-expanded **12** was determined to be C-3 from the coupling constants ($J_{1,2}$=6.2, $J_{2,3}$=11.0, $J_{2,3'}$=1.8, and $J_{3,3'}$=14.0 Hz) of ring protons.[14]

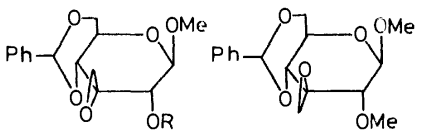

(**19**) R=Bz (**24**)

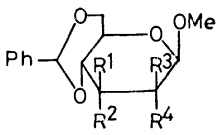

	R¹	R²	R³	R⁴
(**20**)	Me	OH	H	OH
(**21**)	Me	OH	H	OBz
(**22**)	OH	Me	H	OBz
(**25**)	Me	OH	H	OMe
(**23**)	Me	OMe	H	OMe
(**27**)	H	OH	H	OMe

The configuration of the spiro epoxide (**19**) predominantly obtained by the diazomethane reaction of **4** was determined to be D-allo by the rotational change of the corresponding reductively cleaved product (**20**) in cupraammonium solution ($[M]_{436}$ −329.2°→ $[M]_{436}^{\text{cupra A}}$ +77.4°). The Grignard reaction of **4** gave a mixture of epimeric pair of 2-*O*-benzoates (**21** and **22**) and their de-*O*-benzoylated products from which **21**, **22**, and **20** were separated in a pure state on a TLC. The configuration of **21** was determined from the fact that partial benzoylation of **20** gave **21**. The ratio of epimers was measured after de-*O*-benzoylation with a densitometer. Diazomethane reaction of **5** gave the corresponding epimeric spiro epoxides (**23** and **24**) by the separation on a TLC, and the predominant product (**23**) was reduced into the 3-*C*-methyl derivative (**25**). The configuration of **25** was determined to be D-allo from the identity of 2,3-di-*O*-methyl derivative of **20** and 3-*O*-methyl derivative (**26**) of **25**. The Grignard reaction of **5** gave preferentially **25**.

As a standard for the comparison of stereoselectivities, reduction of **2**, **3** and **5** with sodium borohydride in methanol was also carried out. The configuration and the ratio of products were determined with NMR and/or densitomer, after conversion of the products into the corresponding 3-*O*-acetate. In all cases, a product caused by the equatorial attack (from the less-hindered upper side of the pyranose-ring) of the reagent was preferentially obtained, as is known in the cases of cyclohexanone derivatives.[15]

Table 1. Yields of products and the attacking direction of nucleophiles to the pyranose-ring in the reaction with methyl 4,6-*O*-benzylidene-α- and -β-D-hexopyranosid-3-uloses

3-Uloses	Yields (%) of products in CH_2N_2 (upper rows), CH_3MgI (down rows in parentheses), and $NaBH_4$ (down rows) reactions	
	axial attack	equatorial attack
(**1**)	77.3	
		55—90[a] (74.2)
(**2**)	73.0	
		82.0, 94[a] (93.2)
(**3**)		41.0[b]
		77.9 (95.4)
(**4**)		90.2
	45[a] (34.8)	48[a] (52.2)
(**5**)	17.6	76.5
	16.6, 6[a]	75.1, 83[a] (94.2)

a) *Cf.* Y. Kondo, *Carbohydr. Res.*, **30**, 386 (1973). b) A ring-expansion product (**12**) was obtained in 36.9% yield.

Discussion

Coupling constants ($J_{1,2}$ and $J_{4,5}$) of ring protons in starting materials used here [**2** (4.5 Hz and unclear), **3** (0 and 9.0 Hz), **4** (7.5 and 9.5 Hz), and **5** (7.5 and 9.5 Hz)] indicate that the pyranose ring of these compounds is in C_1 chair conformation flattened slightly by the introduction of the carbonyl group. Consequently, it is reasonable that nucleophiles preferentially attack the carbonyl group from the equatorial direction, unless any special factors control the stereoselectivity strongly. As shown in Table 1, compound **2** afforded similar results to that of **1** in which the Grignard reaction gave the normal product and diazomethane reaction showed an abnormal stereoselectivity by the electrostatic attractive effect of the oxygen atom in axial C_1-methoxyl group.

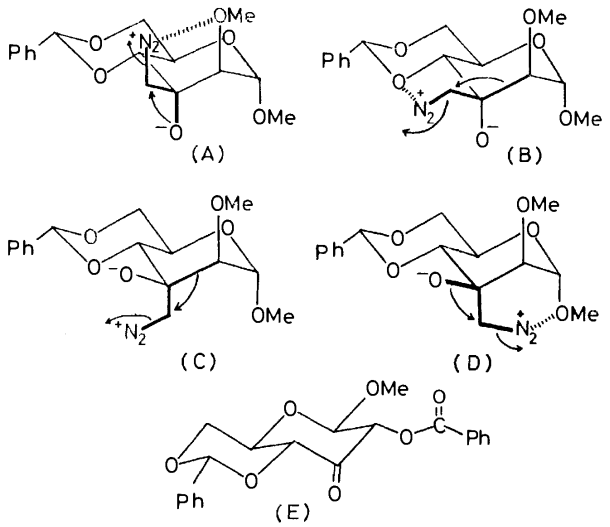

In the diazomethane reaction of **3**, three typical transition states (A, B, and C) will be considered for the formation of **11** and **12**. The state (A) in which

the conformation of diazomethylene cation is stabilized by the electrostatic attractive effect of axial C_2-methoxyl oxygen will give smoothly **11**. For the formation of **12** the state (B) in which the conformation of diazomethylene cation is stabilized by C_4-oxygen will be more probable than (C) in which no stabilizing effect can be expected. If diazomethane attacks the carbonyl group of **3** from axial direction as seen in (C), rather stable conformation (D) would afford the 3-epimer of **11**, and actually, a similar transition state should play the essential role in the formation of **6** from **2**. Thus, it will be concluded that **12** was formed *via* (B) and that the complemental stereoselectivity in diazomethane reaction of **2** and **3** is attributed to the more effective electrostatic attractive force of axial oxygen in α-position than β-position to the carbonyl group.

On the other hand, it is known that in reduction of alicyclic six-membered ketones, sodium borohydride produces more axial alcohol than lithium aluminum hydride, reflecting a greater effective size of the reagent.[16] Although there are no remarkable differences in the stereoselectivities of the Grignard reaction and sodium borohydride reduction, the differences in the results of **4** and **5** should be explained by C_2-substituents. However, results in the both reactions of **4** can not compare in the same sense with others, because 2-*O*-benzoyl group is hydrolzyed in reduction and reacts with the Grignard reagent. Nevertheless, it is common that the stereoselectivities in the both reactions of 2-*O*-benzoyl derivatives, **1** and **4**, are lower than those of 2-*O*-methyl derivatives. Higher stereoselectivity in diazomethane reaction of **4** than that of **5** may suggest an attractive effect of carbonyl oxygen of benzoyl group which is placed in the upper region of the pyroanosering as shown in (E).

From the results mentioned above, the followings will be concluded. 1) Diazomethane having zwitterionic structure attacks 3-uloses from the side of axial alkoxyl group nearer to the carbonyl group by the electrostatic attractive force of oxygen atom which is also stabilize the conformation of diazomethyl cation in the transition state. Thus, the stereoselectivity in diazomethane reaction of **1** and **2** is complemental to that in usual reactions, whereas, it is the same in the reactions of **3**. 2) When a 3-ulose has no axial substituent, the stereoselectivity in the diazomethane reaction is controlled by the same steric factors as in other reactions.

Experimental

All melting points were uncorrected. The solutions were evaporated under reduced pressure at a bath temperature not exceeding 50 °C. Optical rotations were measured in a 0.2-dm tube with Carl Zeiss LEP-Al polarimeter in chloroform unless otherwise stated. IR spectra were recorded with Hitachi Model EPI-G2 spectrometer. NMR spectra were taken with JEOL SP-100 spectrometer in deuteriochloroform containing TMS as an internal reference. Chemical shifts and coupling constants were recorded in δ and Hz units, and IR frequencies in cm^{-1}.

*Methyl 4,6-O-Benzylidene-2-O-methyl-β-D-*ribo*-hexopyranosid-3-ulose (5).* A solution of methyl 2,3-anhydro-4,6-*O*-benzylidene-β-D-allopyranoisde[8] (2 g, 7.6 mmol) and sodium (2 g) in methanol (50 ml) was refluxed for 24 h, poured into water, and then extracted with chloroform. An usual work up of the extract and fractional crystallization of the product from ethanol–hexane and ether–hexane gave the corresponding 2-*O*-methyl-β-D-altropyranoside [mp 122—124 °C; $[\alpha]_D^{22}$ −60.5° (*c* 1.0); Found: C, 59.96; H, 6.91%. Calcd for $C_{15}H_{20}O_6$: C, 60.80; H, 6.80%; coupling constants ($J_{1,2}=1.2$, $J_{2,3}=J_{3,4}=3.0$, $J_{4,5}=9.0$) in the NMR spectrum of the corresponding 3-*O*-acetate supported the structure] and 3-*O*-methyl-β-D-glucopyranoside [mp 168—170 °C; $[\alpha]_D^{22}$ −50.0° (*c* 1.4); lit,[17] mp 172—173 °C, $[\alpha]_D^{14}$ −40.0° (*c* 0.3). Found: C, 60.28; H, 6.77%. Calcd for $C_{15}H_{20}O_6$; C, 60.80; H, 6.80%; coupling constants ($J_{1,2}=J_{2,3}=8.0$, $J_{3,4}=J_{4,5}=7.5$) in the NMR spectrum of the corresponding 2-*O*-acetate supported the structure] in 45 and 8% yields, respectively.

Oxidation of the above β-D-altropyranoside with dimethyl sulfoxide–trifluoroacetic anhydride under a similar condition reported before[6] afforded **5**, accompanying with the epimerization of 2-*O*-methoxyl group, in 89% yield which was recrystallized from ethanol. Mp 217—219 °C; $[\alpha]_D^{22}$ −110.5° (*c* 0.9) (lit,[8] mp 178—180 °C, $[\alpha]_D^{22}$ −128.2°); IR: 1735 (C=O); NMR: 7.60—7.25 (Ph: m); 5.54 (PhCH); 4.51 (H_1: d, $J_{1,2}=7.5$), 4.49 (H_6: q, $J_{5,6}=4.5$), 4.28 (H_4: q, $J_{4,5}=9.6$, $J_{2,4}=1.5$), 3.89 ($H_{6'}$: t, $J_{5,6'}=J_{6,6'}=9.8$), 3.78 (H_2: q), 3.64 (H_5: sex), 3.60 (2×OMe).

Found: C, 61.21; H, 6.18%. Calcd for $C_{15}H_{18}O_6$: C, 61.21; H, 6.17%.

Reaction of 3-Uloses (2—5) and Diazomethane. To a suspension of **2** (294 mg, 1.0 mmol) in ethanol (30 ml) was added dropwise a solution of diazomethane (2.0 mmol) in ether (10 ml) at 0 °C. With proceeding of the reaction, the mixture turned to homogeneous. After keeping the mixture at room temperature for 12 h, the solution was evaporated to give a crystalline methyl 3,3′-anhydro-4,6-*O*-benzylidene-3-*C*-hydroxymethyl-2-*O*-methyl-α-D-glucopyranoside (**6**), which was recrystallized from benzene–hexane. The diazomethane reaction did not proceed in the benzene–ethanol (30 ml, 1:1) in this case. Yield, 167 mg (57%); mp 131—133 °C, $[\alpha]_D^{22}$ +76.5° (*c* 0.6), NMR: 7.44—7.20 (Ph: m), 5.45 (PhCH), 4.89 (H_1: d, $J_{1,2}=4.0$), 4.35—4.17 (H_5: m), 3.84 ($H_{6'}$:t, $J_{5,6'}=J_{6,6'}=9.0$), 3.84—3.67 (H_4, H_5 and H_6: m), 3.61 (H_2: d), 3.05 (epoxy CH_2: s), 3.49 and 3.44 (2×OMe).

Found: C, 62.10; H, 6.57%. Calcd for $C_{16}H_{20}O_6$: C, 62.32; H, 6.54%.

A similar reaction of **3** (294 mg. 1.0 mmol) in benzene–ethanol (30 ml, 1:1) with diazomethane, and sepatartion of two products on a preparative TLC (ether:hexane=1:1) gave methyl 3,3′-anhydro-4,6-*O*-benzylidene-3-*C*-hydroxymethyl-2-*O*-methyl-α-D-altropyranoside (**11**) and a ring-expanded product (**12**) in 41.0% and 36.9% yields, respectively.

11: Mp 141—143 °C (from ether–hexane), $[\alpha]_D^{22}$ +76.1° (*c* 2.1), NMR: 7.55—7.27 (Ph: m), 5.55 (PhCH), 4.76 (H_1: s), 4.44—4.12 (H_4, H_6, and $H_{6'}$: m), 3.86 (H_5: m), 3.18 and 2.75 (epoxy CH_2: ABq, $J=4.8$), 3.44 (2×OMe), 3.06 (H_2: s).

Found: C, 61.58; H, 7.05%. Calcd for $C_{16}H_{20}O_6$: C, 62.32; H, 6.54%.

12: Mp 157—160 °C (from ether–hexane), $[\alpha]_D^{22}$ +91.6 °C (*c* 0.5), NMR: 7.55—7.27 (Ph: m), 5.46 (PhCH), 4.48 (H_1: d, $J_{1,2}=6.2$), 4.72 (H_7: q, $J_{6,7}=4.4$), 4.04 (H_6: m), 3.85 (H_5: d, $J_{5,6}=9.0$), 3.67 (H_2: octet), 3.62 ($H_{7'}$: t, $J_{7,7'}=J_{6,7'}=8.8$), 3.23 and 2.73 (epoxy CH_2: ABq, $J=5.6$), 2.34 (H_3: q, $J_{2,3}=11.0$), 1.45 ($H_{3'}$: q, $J_{2,3'}=1.8$, $J_{3,3'}=14.0$), 3.44 and 3.37 (2×OMe).

Found: C, 63.31; H, 6.84%. Calcd for $C_{17}H_{22}O_6$: C, 63.34; H, 6.88%.

Reaction of **4** and diazomethane in a similar manner as above gave methyl 3,3′-anhydro-2-*O*-benzoyl-4,6-*O*-benzylidene-3-*C*-hydroxymethyl-β-D-allopyranoside (**19**) as a sirup in 90.2% yield. $[\alpha]_D^{27}$ −32.6° (*c* 1.9), NMR: 8.13—7.95 and 7.60—7.24 (Ph: m), 5.54 (PhCH), 5.42 (H_1: d, $J_{1,2}$=7.5), 4.83 (H_2: d), 4.43 (H_5: m), 3.58—4.03 (H_4, H_6, and $H_{6'}$: m), 3.10 and 2.72 (epoxy CH_2: ABq, J=4.5), 3.55 (OMe).

Found: C, 65.95; H, 5.46%. Calcd for $C_{22}H_{22}O_7$: C, 66.32; H, 5.57%.

A similar reaction of **5** (294 mg, 1.0 mmol) in benzene-ethanol (10 ml, 1:1) with diazomethane and the separation of two products in a similar way gave the epimeric pair of spiro epoxides, methyl 3,3′-anhydro-4,6-*O*-benzylidene-3-*C*-hydroxymethyl-2-*O*-methyl-β-D-allopyranoside (**23**) and the corresponding β-D-glucopyranoside (**24**) in 76.5 and 17.6% yields, respectively.

23: Mp 157—158 °C, $[\alpha]_D^{22}$ −63.8° (*c* 1.1), NMR: 7.56—7.23 (Ph: m), 5.51 (PhCH), 4.58 (H_1: d, $J_{1,2}$=7.5), 4.23—4.47 (H_6: m), 3.95—3.60 (H_4, H_5, and $H_{6'}$: m), 3.37 (H_2: d), 3.10 and 3.01 (epoxy CH_2: ABq, J=5.7), 3.59 and 3.55 (2×OMe).

Found: C, 62.53; H, 6.47%. Calcd for $C_{16}H_{20}O_6$: C, 62.32; H, 6.54%.

24: Mp 150—151 °C, $[\alpha]_D^{22}$ −74.9° (*c* 1.0), NMR: 7.55—7.20 (Ph: m), 5.46(PhCH), 4.35 (H_6: q, $J_{5,6}$=5.0), 4.34 (H_1: d, $J_{1,2}$=7.6), 3.83 (H_4: d, $J_{4,5}$=9.5), 3.77 ($H_{6'}$: t, $J_{5,6'}$=$J_{6,6'}$=10.4), 3.65—3.35 (H_5: m), 3.36 (H_2: d), 3.06 (epoxy CH_2: s), 3.47 and 3.55 (2×OMe).

Found: C, 62.22; H, 6.51%. Calcd for $C_{16}H_{20}O_6$: C, 62.32; H, 6.54%.

*Hydrogenation of Spiro Epoxides (**6**, **11**, **19**, and **23**) with Lithium Aluminium Hydride.* To a solution of **6** (150 mg, 0.52 mmol) in tetrahydrofuran (THF, 20 ml) was added lithium aluminium hydride (LAH, 50 mg), and then the mixture was stirred at room temperature for 1 h. The excess hydride was carefully decomposed with water, and then filtered. The water layer was extracted with chloroform. The combined extract was washed with water, dried with anhydrous magnesium sulfate, and evaporated to give a colorless sirup of methyl 4,6-*O*-benzylidene-3-*C*:2-*O*-dimethyl-α-D-glucopyranoside (**7**). The sirup was purified with preparative TLC (benzene:acetone=8:1, R_f=0.25). Yield 92%, $[\alpha]_D^{22}$+67.4° (*c* 1.2), NMR: 7.60—7.20 (Ph: m), 5.49 (PhCH), 4.84 (H_1: d, $J_{1,2}$=4.0), 4.28 (H_5: m), 3.80—3.30 (H_2, H_4, H_6, and $H_{6'}$: m), 3.42 and 3.30 (2×OMe), 2.43 (OH: s), 1.46 (Me).

Found: C, 61.87; H, 7.16%. Calcd for $C_{16}H_{22}O_6$: C, 61.92; H, 7.15%.

A similar reduction of **11** (150 mg, 0.52 mmol) in THF (10 ml) as above gave methyl 4,6-*O*-benzylidene-3-*C*:2-*O*-dimethyl-α-D-altropyranoside (**13**) in quantitative yield, which was crystallized from ether-hexane. Mp 88—91 °C, $[\alpha]_D^{22}$ +26.6° (*c* 2.1), IR: 3530 (OH), NMR: 7.60—7.20 (Ph: m), 5.58 (PhCH), 4.79 (H_1: broad s), 4.33 (H_6: q), 4.06 (H_5: sex), 3.80 ($H_{6'}$: t, $J_{5,6'}$=$J_{6,6'}$=8.6), 3.67 (H_4: d, $J_{4,5}$ =9.0), 3.15 (H_2: s), 3.49 and 3.46 (2×OMe), 1.38 (Me).

Found: C, 61.99; H, 7.19%. Calcd for $C_{16}H_{22}O_6$: C, 61.92; H, 7.15%.

A similar hydrogenation of **19** (150 mg) in THF (5 ml) as above gave methyl 4,6-*O*-benzylidene-3-*C*-methyl-β-D-allopyranodise (**20**) in 87% yield. Mp 123—125 °C (from benzene-hexane). $[\alpha]_D^{22}$ −53.2° (*c* 1.2), IR: 3480 (OH), NMR: 7.50—7.16 (Ph: m), 5.47 (PhCH), 4.47 (H_1: d, $J_{1,2}$=8.0), 4.33 (H_6: q, $J_{5,6}$=3.6), 3.67 ($H_{6'}$: t, $J_{5,6'}$=$J_{6,6'}$=10.0), 3.30 (H_4: d, $J_{4,5}$=9.6), 3.20 (H_2: d), 3.50 (OMe), 1.40 (Me).

Found: C, 60.52; H, 6.73%. Calcd for $C_{15}H_{20}O_6$; C, 60.80; H, 6.80%.

A similar hydrogenation of **23** (100 mg) in THF (5 ml) afforded methyl 4,6-*O*-benzylidene-3-*C*:2-*O*-dimethyl-β-D-allopyranoside (**25**) in 92% yield, which was crystallized from ethanol hexane. Mp 150—151 °C, $[\alpha]_D^{22}$ −79.8° (*c* 1.3), IR: 3525 and 3400 (OH), NMR: 7.50 —7.16(Ph: m), 5.47 (PhCH), 4.47 (H_1: d, $J_{1,2}$=8.0), 4.43 (H_6: q, $J_{5,6}$ =3.6), 3.67 ($H_{6'}$: t, $J_{5,6'}$=10.0), 3.30 (H_4: d, $J_{4,5}$=9.6), 3.20 (H_2: d), 3.50 (OMe), 1.40 (Me).

Found: C, 61.91; H, 7.05%. Calcd for $C_{16}H_{22}O_6$: C, 61.92; H, 7.15%.

*Reaction of 3-Uloses (**2**—**5**) with Methylmagnesium Iodide.* To a solution of methylmagnesium iodide in ether (5 ml)-benzene (5 ml) prepared from magnesium turnings (60 mg, 2.47 mmol) and methyl iodide (1 ml) was added **2** (294 mg, mmol) in benzene (5 ml), and the reaction mixture was kept at room temperature for 1.5 h, poured into cold ammonium chloride solution. The resulting solution was extracted with dichloromethane. The extract was washed with water and evaporated to give a white powder of methyl 4,6-*O*-benzylidene-3-*C*:2-*O*-dimethyl-α-D-allopyranoside (**8**) which was crystallized from ethanol-hexane. Yield, 93.2%, mp 140—142° C, $[\alpha]_D^{22}$ +85.0° (*c* 1.5), IR: 3530 (OH), NMR: 7.65—7.27 (Ph: m), 5.55 (PhCH), 4.94 (H_1: d, $J_{1,2}$=3.8), 4.37 (H_6: q, $J_{5,6}$=4.8), 4.10 (H_5: sex), 3.72 ($H_{6'}$:t, $J_{5,6'}$=$J_{6,6'}$=9.8), 3.37 (OH), 3.30 (H_4: d, $J_{4,5}$=9.0), 3.15 (H_2: d), 3.55 and 3.49 (2×OMe), 1.42 (Me).

Found: C, 61.60; H, 7.06%. Calced for $C_{16}H_{22}O_6$: C, 61.92, H, 7.15%.

A similar reaction of **3** and methylmagnesium iodide as above gave **13** in 95.4% yield, which was identical with the authentic sample obtained *via* the diazomethane reaction of **3**.

Reaction of **4** and methyl magnesium iodide in a similar manner as above and separation of three products on a preparative TLC (benzene: acetone=8:1) gave methyl 2-*O*-benzoyl-4,6-*O*-benzylidene-3-*C*-methyl-β-D-allopyranodide (**21**), its 3-epimer (**22**) and de-benzoylated product, **20** in 33, 8, and 19% yields, respectiviely.

21: Mp 180—181 °C (from benzene-hexane), $[\alpha]_D^{22}$ −40.3° (*c* 1.7), IR: 3540 and 3475 (OH), 1724 and 1690 (ester), NMR: 8.15—8.00 and 7.60—7.20 (Ph: m), 5.65(PhCH), 5.02 and 4.86 (H_1 and H_2: each d, $J_{1,2}$=8.0), 4.35 (H_4: d, $J_{4,5}$=8.0), 4.00 (H_5: sex), 4.40 (H_6: q, $J_{5,6}$=4.0), 3.77 ($H_{6'}$: t, $J_{5,6}$=$J_{6,6'}$=10.0), 3.47 (OMe), 2.07 (OH), 1.35 (Me).

Found: C, 65.15; H, 5.93%. Calcd for $C_{22}H_{24}O_7$: C, 65.99; H, 6.04%.

22: $[\alpha]_D^{22}$ −37.2° (*c* 1.5), IR: 3500 (OH), 1735 (ester), NMR: 8.20—8.04 and 7.70—7.27 (Ph: m), 5.58 (PhCH), 5.18 (H_2: d, $J_{1,2}$=8.0), 4.57 (H_1: d), 4.39 (H_6: q, $J_{5,6}$=4.2), 3.82 ($H_{6'}$: t, $J_{5,6'}$=$J_{6,6'}$=10.0), 3.82—3.54 (H_4 and H_5: m), 3.49 (OMe), 2.60 (OH: broad s), 1.50 (Me).

20: all phisical constants were identical with the authentic sample which was derived from the reaction of **4** and diazomethane.

Grignard reaction of **5** in a similar way as above gave **25** in 94.2% yield, which was identical with the authentic sample obtained *via* the diazomethane reaction of **5**.

*O-Methylation of 3-C-Methyl Derivatives (**7**, **8**, **20**, and **25**) with Sodium Hydride and Methyl Iodide.* To a solution of **7** (50 mg. 0.16 mmol) and sodium hydride (10 mg, 0.42 mmol) in DMF (1 ml) was added methyl iodide (0.1 ml) at

0 °C. After keeping the mixture at room temperature for 30 min, the solution was poured into cold water, and the water layer was extracted with ether. The extract was evaporated to gave sirupy methyl 4,6-*O*-benzylidene-3-*C*-methyl-2,3-di-*O*-methyl-α-D-glucopyranoside (**10**) in a good yield. $[\alpha]_D^{22}$ +56.4° (*c* 1.7), NMR: 7.60—7.24 (Ph: m), 5.54 (PhCH), 4.82 (H_1: d, $J_{1,2}$=4.0), 4.28 (H_6: m), 3.87—3.60 (H_4, H_5, and $H_{6'}$: m), 3.34 (H_2: d), 3.52, 3.43, and 3.40 (3×OMe), 1.47 (Me).

Found: C, 62.31; H, 7.66%. Calcd for $C_{17}H_{24}O_6$: C, 62.95; H, 7.46%.

A similar methylation of **8** gave methyl 4,6-*O*-benzylidene-3-*C*-methyl-2,3-di-*O*-methyl-α-D-allopyranoside (**9**) in a quantitative yield which was recrystallized from hexane. Mp 91—92 °C, $[\alpha]_D^{22}$ +95.6° (*c* 2.1), NMR: 7.60—7.20 (Ph: m), 5.41 (PhCH), 4.85 (H_1: d, $J_{1,2}$=4.0), 4.45—4.10 (H_5 and H_6: m), 3.80—3.35 (H_4 and $H_{6'}$: m), 3.09 (H_2: d), 3.45, 3.44 and 3.43 (3×OMe), 1.46 (Me).

Found: C, 63.00; H, 7.43%. Calcd for $C_{17}H_{24}O_6$: C, 62.95; H, 7.46%.

A similar methylation of methyl 4,6-*O*-benzylidene-3-*C*-methyl-α-D-allopyranoside[2] gave also **9** in a good yield.

Methylation of **20** in a similar manner as above gave sirupy methyl 4,6-*O*-benzylidene-3-*C*-methyl-2,3-di-*O*-methyl-β-D-allopyranoside (**26**) in 89% yield which was crystallized from ether-hexane. Mp 94—95 °C, $[\alpha]_D^{22}$ −45.1° (*c* 1.7), NMR: 7.56—7.27 (Ph: m), 5.39 (PhCH), 4.72 (H_1: d, $J_{1,2}$=8.0), 4.36 (H_6: q, $J_{5,6}$=4.5), 3.90 (H_5: m), 3.68 ($H_{6'}$: t, $J_{5,6'}=J_{6,6'}$=9.8), 3.34 (H_4: d, $J_{4,5}$=9.0), 2.78 (H_2: d), 3.56, 3.52, and 3.47 (3×OMe), 1.49 (Me).

Found: C, 62.82; H, 7.88%. Calcd for $C_{17}H_{24}O_6$: C, 62.95; H, 7.46%.

Methylation of **25** gave also compound **26** in a good yield.

Determination of the Configuration of ***13***. To a solution of **13** (150 mg, 0.48 mmol) in 70% aqueous acetic acid was refluxed until the starting material disappeared on TLC (benzene:acetone=8:1). Then the solution was evaporated to give a sirup which was chromatographically homogeneous.

A solution of the sirup and anhydrous copper(II) sulfate (300 mg) in acetone (10 ml) containing one drop of sulfuric acid was stirred for 24 h at room temperature, neutralized with barium carbonate, filtered, and the filtrate was evaporated to give a sirupy methyl 3,4-*O*-isopropyliden-3-*C*-2-*O*-dimethyl-α-D-altropyranoside (**14**) in 73% yield, which was purified on TLC (ether:hexane=1:1). $[\alpha]_D^{22}$ +112.3° (*c* 1.4), IR: 3480 (OH), NMR: 4.37 (H_1: d, $J_{1,2}$=6.0), 4.00—4.30 (H_4, H_5, H_6 and $H_{6'}$: m), 3.30 (H_2: d), 3.60 and 3.46 (2×OMe), 2.15 (OH: broad s), 1.52 and 1.43 (isopropylidene-Me), 1.37 (Me).

Found: C, 54.98: H, 8.35%. Calcd for $C_{12}H_{22}O_6$: C, 54.95; H, 8.45%.

Base-catalyzed acetylation of **14** gave a sirupy methyl 6-*O*-acetyl-3,4-*O*-isopropylidene-3-*C*,2-*O*-dimethyl-α-D-altropyranoside (**15**) in a quantitative yield. $[\alpha]_D^{22}$ +101.9° (*c* 1.0). IR: 1740 (ester), NMR: 4.35 (H_1: d, $J_{1,2}$=6.0), 4.50—3.87 (H_5, H_6, and $H_{6'}$: m), 3.83 (H_4: d, $J_{4,5}$=9.0), 3.28 (H_2: d), 3.57 and 3.28 (2×OMe), 2.12 (OAc), 1.49 and 1.40 (isopropylidene-Me), 1.35 (Me).

Found: C, 55.33; H, 7.98%. Calcd for $C_{14}H_{24}O_7$: C, 55.25; H, 7.95%.

Acid-catalyzed Acetylation of Tertiary Hydroxyl Gruop in ***7***, ***8***, *and* ***13***. A solution of **7** (100 mg) and *p*-toluensulfonic acid (10 mg) in acetic anhydride (3 ml) was stirred at room temperature for 1.5 h, poured into ice-water, and the resulted solution was extracted with chloroform. The extracts were washed with sodium hydrogencarbonate and then water, dried and evaporated to give methyl 3-*O*-acetyl-4,6-*O*-benzylidene-3-*C*:2-*O*-dimethyl-α-D-glucopyranoside (**18**) which was recrystallized from ethanol-hexane. Yield, 92%; mp 111.5—112.5 °C; $[\alpha]_D^{22}$ +11.9° (*c* 1.4) IR: 1720 (ester), NMR: 7.60—7.25 (Ph: m), 5.53 (PhCH), 4.90 (H_1: d, $J_{1,2}$=4.2), 4.78 (H_4: d, $J_{4,5}$=9.0), 4.62 (H_2: d), 4.45—4.15 and 3.95—3.60 (H_5, H_6 and $H_{6'}$: m), 3.51 and 3.43 (2×OMe), 2.04 (OAc), 1.55 (Me).

Found: C, 59.86; H, 6.69%. Calcd for $C_{18}H_{24}O_7$: C, 61.35; H, 6.86%.

Acid-catalyzed acetylation of **8** in a similar way as above gave methyl 3-*O*-acetyl-4,6-*O*-benzylidene-3-*C*:2-*O*-dimethyl-α-D-allopyranoside (**16**) in 94% yield, which was crystallized from ethanol-hexane. Mp 192—194 °C, $[\alpha]_D^{22}$ +39.2° (*c* 0.6), IR: 1738 (ester), NMR: 7.60—7.27 (Ph: m), 5.53 (PhCH), 4.86 (H_1: d, $J_{1,2}$=4.0), 4.33 (H_6: q, $J_{5,6}$=5.0), 4.22 (H_5: m), 3.68 ($H_{6'}$: t, $J_{5,6'}=J_{6,6'}$=9.0), 3.32, (H_4: d, $J_{4,5}$=9.2), 3.14 (H_2: d), 3.56 and 3.46 (2×OMe), 2.04 (OAc), 1.94 (Me).

Found: C, 61.49; H, 6.32%. Calcd for $C_{18}H_{24}O_7$: C, 61.35; H, 6.86%.

A similar acetylation of **13** as above gave methyl 3-*O*-acetyl-4,6-*O*-benzylidene-3-*C*:2-*O*-dimethyl-α-D-altropyranoside (**17**) in 91% yield, which was crystallized from benzene-hexane. Mp 189—191 °C, $[\alpha]_D^{22}$ +34.9° (*c* 0.7), IR: 1730 (ester), NMR: 7.64—7.28 (Ph: m), 5.55 (PhCH), 4.68 (H_1: d, $J_{1,2}$=1.4) 4.34 (H_2: d), 4.45—4.10 and 3.90—3.60 (H_4, H_5, H_6 and $H_{6'}$: m), 3.52 and 3.38 (2×OMe), 2.00 (OAc), 1.70 (Me).

Found: C, 61.55; H, 6.85%. Calcd for $C_{18}H_{24}O_7$: C, 61.35; H, 6.86%.

Partial Benzoylation of ***20*** *with Benzoic Anhydride.* A solution of **20** (150 mg, 0.51 mmol) and benzoic anhydride (175 mg, 0.77 mmol) in pyridine (2 ml) was stirred at room temperature for 12 h, poured into ice-water, and the resulting solution was extracted with chloroform. The usual work up of the extracts gave **21** which was identical with that obtained by the reaction of **4** with methylmagnesium iodide.

*Hydrogenation of 3-Uloses (****2****, ****3****, and* ***5****) with Sodium Borohydride in Mathenol.* To a vigorously stirring solution of **2** (100 mg) in methanol (15 ml) was added dropwise a solution of sodium borohydride (400 mg) in methanol (8 ml). After the reduction was continued for 10 min at room temperature, acetic acid was added to the reaction mixture to decompose the excess hydride, and the resulting solution was evaporated. An aqueous solution of the crude product was extracted with chloroform in a usual manner to give sirupy product. The configuration and the ratio of products were examined with NMR spectrometer and/or densitomether after conversion into the corresponding *O*-acetate by a usual method. In this case, only methyl 3-*O*-acetyl-4,6-*O*-benzylidene-2-*O*-methyl-α-D-allopyranoside was obtained in 82% yield. Mp 116—117 °C, (from ethanol-hexane), IR: 1738 (ester), $[\alpha]_D^{22}$ +78.8° (*c* 0.7), NMR: 7.60—7.25 (Ph: m), 5.90 (H_3: t, $J_{2,3}=J_{3,4}$=3.0), 4.83 (H_1: d, $J_{1,2}$=4.0), 4.30 (H_5: m, $J_{4,5}$=9.6), 4.16 (H_6: q, $J_{5,6}$=5.0), 3.70 ($H_{6'}$: t, $J_{5,6'}=J_{6,6'}$=9.6), 3.62 (H_4: q, $J_{4,5}$=9.6), 3.47 and 3.45 (2×OMe), 2.17 (OAc).

Found: C, 60.36; H, 6.61%. Calcd for $C_{17}H_{22}O_7$: C, 60.34; H, 6.55%.

A similar reduction of **3** and subsequent acetylation of the product gave sirupy methyl 3-*O*-acetyl-4,6-*O*-benzylidene-2-*O*-methyl-α-D-altropyranoside in 77.9% yield. $[\alpha]_D^{22}$ +113.1° (*c* 1.9), NMR: 7.65—7.20 (Ph: m), 5.57 (PhCH), 5.27 (H_3: t, $J_{2,3}=J_{3,4}$=3.2), 4.66 (H_1: s), 3.49 and 3.88 (2×OMe), 2.09 (OAc).

Reduction and acetylation of **5** as above gave epimeric mixture of methyl 3-*O*-acetyl-4,6-*O*-benzylidene-2-*O*-methyl-β-D-glucopyranoside and -allopyranoside in 75.1 and 16.6%

yields, respectively. NMR data of the mixture was the following: major product: 7.60—7.24 (Ph: m), 5.85 (H_3: t, $J_{2,3}=J_{3,4}=3.0$), 5.50 (PhCH), 4.62 (H_1: d, $J_{1,2}=9.0$), 4.37 (H_6: q, $J_{5,6}=3.4$, $J_{6,6'}=8.4$), 4.03—3.46 (H_4, H_5 and $H_{6'}$: m), 3.20 (H_2: q), 3.55 and 3.44 (2×OMe), 2.14 (OAc). Minor product: 5.45 (PhCH), 5.24 (H_3: t, $J_{2,3}=J_{3,4}=9.4$), other protons could not be assigned.

The authors are indebted to the members of the Laboratory of Organic Analysis for microanalysis and to Mr. H. Matsumoto for NMR measurements.

References

1) Part XI: J. Yoshimura, M. Matsuzawa, and M. Funabashi, *Bull. Chem. Soc. Jpn.*, **51**, 2067 (1978).
2) J. Yoshimura, K. Sato, K. Kobayashi, and C. Shin, *Bull. Chem. Soc. Jpn.*, **46**, 1515 (1973).
3) J. Yoshimura, K. Kobayashi, K. Sato, and M. Funabashi, *Bull. Chem. Soc. Jpn.*, **45**, 1806 (1972).
4) J. Yoshimura, K. Mikami, K. Sato, and C. Shin, *Bull. Chem. Soc. Jpn.*, **49**, 1686 (1976).
5) P. M. Collins, P. Gupta, and R. Lyer, *J. Chem. Soc., Perkin Trans. 1*, **1972**, 1670.
6) J. Yoshimura, K. Sato, and H. Hashimoto, *Chem. Lett.*, **1977**, 1327.
7) P. M. Collins, D. Gardiner, S. Kumar, and W. G. Overend, *J. Chem. Soc., Perkin Trans. 1*, **1972**, 2596.
8) Y. Kondo, *Agr. Biol. Chem.*, **39**, 2251 (1975).
9) S. L. Huang, K. Omura, and D. Swern, *J. Org. Chem.*, **41**, 957, 3329 (1976).
10) R. D. Guthrie, A. M. Prior, and S. E. Creasey, *J. Chem. Soc. C*, **1970**, 9761.
11) F. A. Carey and K. O. Hodgson, *Carbohydr. Res.*, **12**, 463 (1970).
12) F. W. Lichtenthaler, *Fortschr. Chem. Forsch.*, **14**, 556 (1970); F. W. Lichtenthaler and P. Emig, *Tetrahedron Lett.*, **1976**, 577.
13) J. H. Jordaan, J. J. Nieuwenhuis, and C. J. Lourens, *Carbohydr. Res.*, **51**, 195 (1976).
14) T. D. Inch, G. J. Lewis, R. P. Peel, and N. Williams, *J. Chem. Soc., Chem. Commun.*, **1970**, 1549.
15) E. C. Ashby and J. T. Laemmle, *Chem. Rev.*, **75**, 521 (1975).
16) W. G. Dauben, G. J. Fonken, and D. S. Noyce, *J. Am. Chem. Soc.*, **78**, 2579 (1956); M. Milikovic, M. Gligorijevic, and D. Milikovic, *J. Org. Chem.*, **39**, 2118 (1974).
17) Y. Kondo, *Agr. Biol. Chem.*, **39**, 1879 (1975).

Synthesis of 6-*O*-Acyl Derivatives of Immunoadjuvant Active *N*-Acetylmuramyl-L-alanyl-D-isoglutamine[1]

Shoichi KUSUMOTO, Satoshi OKADA, Koji YAMAMOTO, and Tetsuo SHIBA*

Department of Chemistry, Faculty of Science, Osaka University, Toyonaka, Osaka 560

(Received December 26, 1977)

Seven acyl derivatives of *N*-acetylmuramyl-L-alanyl-D-isoglutamine, which had previously been shown to be a minimum structure required for the immunoadjuvant activity, were synthesized in order to evaluate the significance of lipophilicity on the adjuvant activity and on the possible antitumor effect. Among them, are included 6-*O*-docosanoyl, stearoyl, lauroyl, octanoyl, butyryl, acetyl, and 4,6-di-*O*-acetyl derivatives. Some of these compounds were found to serve an improvement in the administration method to living body.

Synthetic studies by us[2] as well as Merser *et al.*[3] had established that a minimum structure required for the "immunoadjuvant activity" of bacterial cell walls is *N*-acetylmuramyl-L-alanyl-D-isoglutamine (**1**), which corresponds to a common building unit of the cell wall peptidoglycans. The synthetic muramyl dipeptide (**1**) enhanced distinctly both humoral and cellular immunities of living bodies towards various antigens. Since that time, it became possible to discuss the immunopotentiating activity in a sense of molecular level. Meanwhile, we have already reported a synthesis of the labelled compound of **1** for the purpose of an elucidation of the action mechanism of such unique molecule.[4] Relationships between structure and activity of the muramyl peptides were also investigated by syntheses of various analogs of **1**.[2,5]

Our synthetic effort was next brought in focus on the following two subjects, namely, i) an improvement in the administration method of the muramyl dipeptide (**1**) which exhibited the adjuvant activity in the injection only in an emulsified form of water in mineral oil; ii) a possible appearance of an antitumor activity in derivatives of the muramyl peptides on an extended line of the adjuvant activity. It has long been known that even bacterial cell walls must be injected in a form of water in mineral oil emulsion for test of the adjuvant activity.[6] Synthetic muramyl dipeptide (**1**) also requires such physical form. These facts may indicate that the physical state predominates over the chemical entity in this biological action. Furthermore, the mineral oil emulsion causes a severe tissue reaction like the skin swelling in tested animals and may not be applicable to human beings. Therefore, a derivative of the muramyl peptide which can be used in a form other than emulsion to the living bodies has been desired not only for a clarification of physical character of the adjuvant active material, but also for the therapeutic purpose.[7] It could be assumed that the immunoactive substance must be anyhow transported to a lipophilic region in lymph system. A role of the mineral oil in the emulsion may be related to an importance of the lipophilicity in this action, although it is not quite clear.[8] Therefore, we anticipated that the use of the mineral oil could be avoided if enough lipophilicity is given to the molecule of muramyl dipeptide (**1**).

On the other hand, an antitumor effect of BCG cell wall has been understood on the basis of the immunoadjuvant activity.[9] Although the distinct adjuvant activity was observed in *N*-acetylmuramyl-L-alanyl-D-isoglutamine (**1**) as mentioned before, it did not show any antitumor activity so far.[10] One of the big differences between BCG cell wall and **1** itself must be in a lack of the lipophilicity in the latter, since the BCG cell wall is covered with a long-chain fatty acid, *i.e.*, mycolic acid, on the surface. Now, an assumption is made that the lipophilicity in the molecule may be required for the antitumor effect, if the muramyl peptide moiety is also essential to this activity.

In these respects, we planned to prepare several acyl derivatives of the muramyl dipeptide (**1**) for investigation of the biological activities. For the synthesis, the primary hydroxyl group at C-6 of muramic acid moiety in **1** was chosen for introduction of various acyl groups.[11]

Two alternative pathways for the synthesis of 6-*O*-acyl-*N*-acetylmuramyl-L-alanyl-D-isoglutamines (**2**) were tested in terms of 6-*O*-stearoyl derivative (**2e**) to elucidate whether the muramic acid moiety should be first condensed with the acyl group (route A) or with the peptide moiety (route B).

The synthesis *via* route A was carried out by an introduction of stearoyl group to benzyl *N*-acetyl-α-muramide (**3**) prior to coupling with the peptide moiety. Selective stearoylation of the primary hydroxyl group in **3** was performed by use of mixed anhydirde with trifluoroacetic acid[12] though in a rather low yield. Thus, two monostearoyl products were isolated from the reaction mixture after silica gel column chromatography. From elemental analyses and spectral data, the slower moving product was assumed to be the desired 1-α-*O*-benzyl-6-*O*-stearoyl-*N*-acetylmuramic acid (**4**) while the faster one, without free carboxyl group in it, was determined to be an intramolecular ester (**5**) of the former. The 6- rather than 4-*O*-acyl structure for the compound **4** was deduced by its conversion into **5** by treatment with dicyclohexylcarbodiimide. Use of stearoyl chloride in the above acylation did not improve the yield of **4**. Condensation of stearoyl muramic acid (**4**) with L-alanyl-D-isoglutamine benzyl ester[2b] with dicyclohexylcarbodiimide–*N*-hydroxysuccinimide gave the protected stearoyl muramyl dipeptide (**7e**), *i.e.*, 1-α-*O*-benzyl-6-*O*-stearoyl-*N*-acetylmuramyl-L-alanyl-D-isoglutamine benzyl ester, in a good yield. Hydrogenolytic deprotection of **7e** in acetic acid afforded 6-*O*-stearoyl-*N*-acetylmuramyl-L-alanyl-D-isoglutamine (**2e**).

Synthesis of the stearoyl derivative (**2e**) *via* route B

Table 1. Physical properties and analytical data of protected *O*-acyl-*N*-acetylmuramyl dipeptides obtained *via* route B

Compd	Yield from **6** (%)	Mp (°C)	$[\alpha]_D^{22}$ a)	Molecular formula	Found (Calcd) C%	H%	N%
7b	52	174—175	+72.8°	$C_{37}H_{50}O_{12}N_4 \cdot 1/2H_2O$	59.18 (59.11	6.80 6.84	7.52 7.45)
7cb)	66	175—177	+67.3°	$C_{41}H_{58}O_{12}N_4$	61.27 (61.64	7.30 7.32	7.00 7.01)
7d	55	172—175	+62.4°	$C_{45}H_{66}O_{12}N_4$	63.14 (63.20	7.85 7.78	6.40 6.55)
7f	58	171.5—173.5	+54.4°	$C_{55}H_{86}O_{12}N_4$	66.17 (66.37	8.69 8.71	5.43 5.63)

a) *c* 0.5 in $CHCl_3$. b) Recrystallized from acetone–ether.

Table 2. Physical properties and analytical data of *O*-acyl-*N*-acetylmuramyl dipeptides (**2a—f, 9**)a)

Compd	Mp (dec, °C)	$[\alpha]_D^{16}$ b)	R_fc)	Partitiond) coefficient $H_2O/CHCl_3$	Molecular formula	Found (Calcd) C%	H%	N%
2a	132—134	+38.6°	0.14	148	$C_{21}H_{34}O_{12}N_4 \cdot 1/2H_2O$	46.14 (46.40	6.31 6.49	10.17 10.31)
2b	105—107	+35.6°	0.18	56	$C_{23}H_{38}O_{12}N_4 \cdot 1/2H_2O$	48.47 (48.33	6.76 6.88	9.62 9.80)
2c	66— 72	+32.6°	0.22	45	$C_{27}H_{46}O_{12}N_4 \cdot H_2O$	51.22 (50.93	7.39 7.60	8.85 8.80)
2d	107—110	+35.6°	0.29	14 (13)	$C_{31}H_{54}O_{12}N_4 \cdot H_2O$	54.00 (53.74	7.94 8.15	8.07 8.09)
2e	133—136	+29.3°	0.35	27 (2)	$C_{37}H_{66}O_{12}N_4 \cdot 2H_2O$	55.99 (55.90	8.57 8.88	7.09 7.05)
2f	153—155	+37.0° e)	0.49	—	$C_{41}H_{74}O_{12}N_4 \cdot 1/2H_2O$	59.52 (59.75	9.28 9.18	6.54 6.80)
9	111—116	+31.2°	0.17	(55)	$C_{23}H_{36}O_{13}N_4 \cdot 1/2H_2O$	46.86 (47.17	6.17 6.37	9.55 9.57)

a) These values are obtained for substances isolated by lyophilization. b) *c* 0.5 in H_2O, 2 days after dissolution. c) Silica gel G, $CHCl_3$–CH_3OH–CH_3CO_2H (100 : 20 : 1). d) See experimental section. e) In THF–H_2O (10 : 1).

was then examined starting from the protected muramyl dipeptide,[2b] *i.e.*, 4,6-*O*-benzylidene-1-α-*O*-benzyl-*N*-acetylmuramyl-L-alanyl-D-isoglutamine benzyl ester. The benzylidene group of this compound was selectively removed in the usual manner with 60% acetic acid to afford 1-α-*O*-benzyl-*N*-acetylmuramyl-L-alanyl-D-isoglutamine benzyl ester (**6**), which was then treated with stearoyl chloride in a mixture of pyridine and tetrahydrofuran (THF). For the selective acylation of the primary hydroxyl group, a short reaction time and use of large excess of the chloride were preferable. When the reaction was stopped just after the disappearance of the starting material in the reaction mixture, **7e** was obtained as a practically sole product. The structure of **7e** was identified with the compound prepared above *via* route A by means of NMR and TLC. It was then converted into free stearoyl muramyl dipeptide (**2e**) similarly as described above.

Ample solubilities of 6-*O*-stearoyl derivative (**2e**) thus obtained both in chloroform and in water may indicate a detergent-like property of this compound, and actually its aqueous solution showed vigorous foaming in a procedure of evaporation *in vacuo*.[13] Since **2e** showed enough adjuvant activity in a preliminary test, we then synthesized various acyl derivatives of **1**, *i.e.*, acetyl, butyryl, octanoyl, lauroyl, and docosanoyl derivatives, in order to compare the effect of the acyl groups on the activity.

For the syntheses of these acyl derivatives, we adopted the route B rather than A, since the muramyl dipeptide derivative (**6**) can be used as a common synthetic intermediate in the former route and the intramolecular ester formation, which was observed in the route A, could be avoided by a prior introduction of the peptide moiety. On acetylation of **6** with acetic anhydride, 6-*O*-monoacetate (**7a**) was obtained at 0 °C and 4,6-di-*O*-acetate (**8**) at above room temperature. The protected 6-*O*-butyryl, octanoyl, lauroyl, and docosanoyl derivatives (**7b—d, f**) were prepared by use of the corresponding acid chlorides on the muramyl dipeptide (**6**) in a similar manner to that described for the stearoyl derivative (**7e**). Hydrogenolysis of **7a—d, f** and **8** afforded pure 6-*O*-acyl and 4,6-di-*O*-acetyl-*N*-acetylmuramyl-L-alanyl-D-isoglutamine (**2a—d, f** and **9**) in quantitative yields, respectively. The physical properties and results of elemental analyses of the protected and free acyl muramyl dipeptides are summarized in Tables 1 and 2.

As shown in Table 2, the R_f values of the compounds increase with the carbon number of the acyl groups, indicating the augmentation in lipophilicity in this order. However, the partition coefficients of the series

of the compounds between water and chloroform showed a peculiar phenomenon at the stearoyl derivative (**2e**). In Table 2, the values obtained by extraction from their aqueous solutions with chloroform are shown without parentheses, and those obtained reversely by extraction from chloroform solutions with water were indicated in parentheses. Whereas both values were practically equal in the case of lauroyl derivative (**2d**), the stearoyl derivative (**2e**) gave different values depending on the procedure used. This fact may suggest that **2e** could exist as micelles of different type of association either in chloroform or in water, thus resulting in the unusual behavior on extraction. The following observation also supports this assumption. In the NMR spectrum of **2e** in chloroform-*d*, no distinct signals were observed at all in the regions of protons due to the sugar peptide moiety around at δ 3—5, while those of fatty acid moiety were clearly recognized. However, when methanol-d_4 was added to the same solution, the former signals appeared instantaneously and a spectrum expected from the structure was finally obtained. This indicates that methanol could destroy the micellar structure of **2e** in chloroform, where the fatty acid moiety can interact with the solvent or can fluoctuate freely whereas the sugar peptide are rigidly fixed. The partition coefficient of docosanoyl derivative (**2f**) could not be determined by the above extraction procedure because of facile emulsion formation of the two phases. This might indicate the most effective detergent activity of this compound of all the acyl derivatives prepared.

The adjuvant activities of the 6-*O*-acyl-*N*-acetylmuramyl-L-alanyl-D-isoglutamine (**2a**—**f**, **9**) thus obtained were investigated by Kotani *et al.* of our collaborative group.[14] Thus, 6-*O*-acetyl and 6-*O*-stearoyl derivatives (**2a** and **2e**) have activities comparable to that of the original *N*-acetylmuramyl dipeptide (**1**) while the other derivatives showed somewhat less activities when administered in a form of water in oil emulsion. The relatively high activity of **2e** seems to reflect an adequate balance of lipophilicity and hydrophilicity in the molecule, although the details of this relation are not yet clear. Furthermore, Kotani *et al.* found that highly lipophilic congeners, **2e** and **2f**, can manifest their adjuvant activities even if they are applied in liposomes to animals.[14] This finding will give an ample hope for the therapeutic use of these substances in the future.

Unfortunately, no antitumor activity was found even in **2e**, which showed the maximum adjuvant activity among those prepared in this study. However, we further extended the study along this line and finally reached the synthesis of 6-*O*-mycoloyl derivative of the muramyl dipeptide (**1**)[15] which exhibited a distinct antitumor activity in the animal test. The results were already reported in a preliminary form.[16]

Experimental

Melting points are uncorrected. All fatty acids were of commercial sources and purified by fractional distillation of their methyl esters if necessary. The purities of the acids were guaranteed over 99.9% by means of gas chromatography.

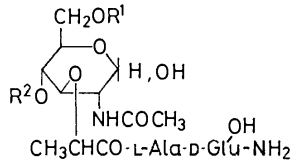

1 $R^1=R^2=H$
2a—**f** R^1=acyl, $R^2=H$
9 $R^1=R^2=CH_3CO$

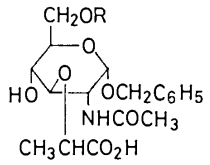

3 R=H
4 R=stearoyl

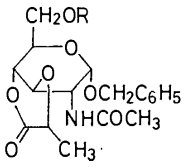

5 R=stearoyl

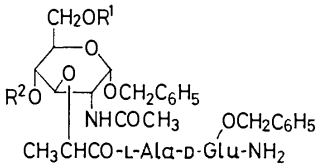

6 $R^1=R^2=H$
7a—**f** R^1=acyl, $R^2=H$
8 $R^1=R^2=CH_3CO$

2 and **7**
a: R^1=acetyl, **b**: R^1=butyryl,
c: R^1=octanoyl, **d**: R^1=lauroyl,
e: R^1=stearoyl, **f**: R^1=docosanoyl.

Acid chlorides were prepared by refluxing the corresponding acids in thionyl chloride followed by distillation as usual. Silica gel 60 (0.063—0.2 mm) and G, Merck, were used for column chromatography and TLC, respectively.

Benzyl N-*Acetyl-α-muramide (3).* Benzyl 4,6-*O*-benzylidene-*N*-acetyl-α-muramide[17] (2.0 g, 4.2 mmol) was heated in 60% aqueous acetic acid (150 ml) at 100 °C for 35 min. After evaporation of the solvent *in vacuo*, benzene and ethanol were added to the residue and agin evaporated *in vacuo*. The residual colorless solid was recrystallized from ethyl acetate; yield, 1.35 g (84%); mp 156—157 °C; $[\alpha]_D^{22}$ +163° (*c* 0.5, methanol), (lit,[18] mp 160—161 °C; $[\alpha]_D^{20}$ +168° (*c* 1.25, methanol)).

Found: C, 56.22; H, 6.56; N, 3.66%. Calcd for $C_{18}H_{25}O_8N$: C, 56.39; H, 6.57; N, 3.65%.

1-α-O-Benzyl-6-O-stearoyl-N-acetylmuramic Acid (4). A mixture of stearic acid (0.90 g, 3.2 mmol) and trifluoroacetic anhydride (1.0 ml) was heated at 50 °C for 15 min and then dissolved in anhydrous THF (2 ml). This solution was added with pyridine (2 ml) to a stirred solution of **3** (1.0 g, 2.6 mmol) in anhydrous THF (8 ml) at −14 °C. After 35 min, the mixture was poured into 10% aqueous K_2CO_3 solution (25 ml) and set aside for 10 min. The solution was brought to pH 4 by addition of 6 M HCl and extracted with $CHCl_3$ (25 ml×2). The $CHCl_3$ layer was dried ($MgSO_4$), and evaporated *in vacuo*. The residue was subjected to silica gel column chromatography. Elution with benzene–ethyl acetate (1:1 v/v) gave a mixture of stearic acid and the intramolecular ester (**5**). Recrystallization from ether afforded pure **5**; yield, 0.45 g (27%); mp 122—123 °C.

Found: C, 67.92; H, 9.15; N, 2.24%. Calcd for $C_{36}H_{57}O_8N$: C, 68.43; H, 9.09; N, 2.22%.

Successive elution with $CHCl_3$–methanol–acetic acid (20:1:0.05 v/v) afforded a syrup, which was dissolved in 0.3 M aqueous NaOH (4 ml) and acidified with 1 M HCl to give **4** as a waxy solid; yield, 0.43 g (25%); mp 62—65 °C; $[\alpha]_D^{22}$ +61.6° (*c* 0.5, $CHCl_3$).

Found: C, 66.70; H, 9.39; N, 1.96%. Calcd for $C_{36}H_{59}O_9N$: C, 66.53; H, 9.15; N, 2.16%.

Conversion of 4 into 5. Dicyclohexylcarbodiimide (16 mg, 0.076 mmol) was added to a solution of **4** (48 mg,

0.074 mmol) in anhydrous THF (2 ml) and the mixture was stirred at room temperature overnight. *N,N'*-Dicyclohexylurea was filtered off, the solvent was evaporated *in vacuo* and the residue was recrystallized from ether; yield, 44 mg (94%); mp 121—123 °C. This product was identified with the intramolecular ester (**5**) obtained above by means of IR, NMR and TLC ($CHCl_3$–methanol–acetic acid 30:1:0.3 v/v).

*1-α-O-Benzyl-N-acetylmuramyl-L-alanyl-D-isoglutamine Benzyl Ester (**6**).* 1-α-*O*-Benzyl-4,6-*O*-benzylidene-*N*-acetylmuramyl-L-alanyl-D-isoglutamine benzyl ester[2b] (2.72 g, 3.6 mmol) was heated in 60 % aqueous acetic acid (270 ml) on a boiling water bath for 30 min. After the procedure as described for **3**, the product was recrystallized from methanol–ether; yield, 1.77 g (71%); mp 221.5—223 °C (dec); $[\alpha]_D^{22}$ +93.6° (*c* 0.5, methanol).

Found: C, 58.42; H, 6.55; N, 8.27%. Calcd for $C_{33}H_{44}O_{11}N_4 \cdot 1/2CH_3OH$: C, 58.42; H, 6.73; N, 8.14%.

*1-α-O-Benzyl-6-O-stearoyl-N-acetylmuramyl-L-alanyl-D-isoglutamine Benzyl Ester (**7e**).* *i) From **4** (*via *route A*)*: To an ice-cooled solution of **4** (125 mg, 0.19 mmol) in anhydrous THF (5 ml), *N*-hydroxysuccinimide (45 mg, 0.39 mmol) and dicyclohexylcarbodiimide (39 mg, 0.19 mmol) were added. After the mixture had been stirred in an ice bath for 2 h, *N,N'*-dicyclohexylurea formed was filtered off. The filtrate was again cooled, L-alanyl-D-isoglutamine benzyl ester hydrochloride[2b] (66 mg, 0.19 mmol) and triethylamine (0.027 ml, 0.22 mmol) were added, and the final mixture was stirred overnight. After the usual work-up the product was recrystallized from ethyl acetate; yield, 122 mg (68%); mp 167—169 °C; $[\alpha]_D^{15}$ +58.9° (*c* 1, $CHCl_3$).

Found: C, 64.97; H, 8.35; N, 5.96%. Calcd for $C_{51}H_{78}O_{12}N_4$: C, 65.21; H, 8.37; N, 5.97%.

*ii) From **6** (route B)*: Stearoyl chloride (3.0 g, 10 mmol) in anhydrous THF (30 ml) was added to a solution of **6** (1.34 g, 2.0 mmol) in pyridine (100 ml) and anhydrous THF (90 ml) with stirring, The reaction mixutre was kept at 12 °C and further amount of stearoyl chloride (4.2 g, 14 mmol) was added within 3 h. The remaining chloride was destroyed with addition of ice. After evaporation of the solvent *in vacuo*, the mixture was diluted with water and extracted with $CHCl_3$. The $CHCl_3$ layer was washed with 1 M HCl and aqueous NaCl solution. It was then dried ($MgSO_4$) and evaporated *in vacuo*. The residue was extracted with hot hexane to remove excess stearic acid. The insoluble material was subjected to silica gel column chromatography. Elution with $CHCl_3$–methanol (20:1 v/v) followed by recrystallization from methanol afforded **7e**, which was identical with the sample obtained above in (i) by means of NMR and TLC ($CHCl_3$–methanol 9:1 v/v); yield, 1.03 g (55%); mp 174.5—175.5 °C.

Found: C, 65.13; H, 8.40; N, 5.86%.

*6-O-Stearoyl-N-acetylmuramyl-L-alanyl-D-isoglutamine (**2e**).* A solution of **7e** (253 mg, 0.27 mmol) in acetic acid (20 ml) was hydrogenolyzed at room temperature in the presence of palladium black. After the catalyst had been filtered off and washed with water, the filtrate and the washing were combined and then subjected to lyophilization to afford colorless solid; yield, 204 mg (95%); mp 133—136 °C (dec); $[\alpha]_D^{16}$ +29.3° (*c* 1, H_2O, 2 days after dissolution).

Found: C, 55.99; H, 8.57; N, 7.09%. Calcd for $C_{37}H_{66}O_{12}N_4 \cdot 2H_2O$: C, 55.90; H, 8.88; N, 7.05%.

*6-O-Acetyl-1-α-O-benzyl-N-acetylmuramyl-L-alanyl-D-isoglutamine Benzyl Ester (**7a**).* Acetic anhydride (0.20 ml, 2.1 mlmo) was added to a stirred solution of **6** (200 mg, 0.30 mmol) in pyridine (4 ml) under ice-cooling. After 1 h, ice was added and the mixture was worked up as usual. Recrystallization was effected from methanol; yield, 130 mg (59%); mp 184—185 °C; $[\alpha]_D^{22}$ +72.3° (*c* 0.5, $CHCl_3$).

Found: C, 57.14; H, 6.58; N, 7.65%. Calcd for $C_{35}H_{46}O_{12}N_4 \cdot H_2O$: C, 57.36; H, 6.60; N, 7.65%.

*4,6-Di-O-acetyl-1-α-O-benzyl-N-acetylmuramyl-L-analyl-D-isoglutamine Benzyl Ester (**8**).* Acetic anhydride (0.20 ml, 2.1 mmol) was added to a stirred solution of **6** (160 mg, 0.24 mmol) in pyridine (3 ml) under ice-cooling. The mixture was then stirred at 45 °C for 3.5 h, worked up as usual and the product was recrystallized from ethanol; yield, 118 mg (65%); mp 219—220 °C; $[\alpha]_D^{22}$ +78.7° (*c* 0.5, $CHCl_3$).

Found: C, 58.87; H, 6.45; N, 7.45%. Calcd for $C_{37}H_{48}O_{13}N_4$: C, 58.72; H, 6.39; N, 7.40%.

*6-O-Acyl-1-α-O-benzyl-N-acetylmuramyl-L-alanyl-D-isoglutamine Benzyl Ester (**7b—d, f**).* These compounds were prepared from the corresponding acid chlorides and **6** in similar manners to that described for **7e** (route B). Selective monoacylation with excess of butyryl, octanoyl and lauroyl chlorides were better carried out under ice-cooling, whereas reaction with stearoyl and docosanoyl chlorides were performed at 12—15 °C. The latter two chlorides were not dissolved sufficiently in a mixture of THF and pyridine at low temperature. In all cases, the products were pure enough after single recrystallization from ethyl acetate, so that no chromatographic purification was needed. The yields, physical constants and results of elemental analyses of the products are summarized in Table 1.

*6-O-Acyl and 4,6-Di-O-acetyl-N-acetylmuramyl-L-alanyl-D-isoglutamine (**2a—d, f, and 9**).* These compounds were prepared by catalytic hydrogenolysis of **7a—d, f** and **8** in acetic acid followed by lyophilization as described above for **2e**. The yields, physical constants and results of elemental analyses are summarized in Table 2.

*Determination of Partition Coefficients of **2a—f** and **9**.* The compound **2a—f** and **9** (2 mg each) were dissolved in water (5.0 ml) in a test tube (1.2 × 15.5 cm), respectively. After $CHCl_3$ (5.0 ml) had been added, the tube was stoppered, gently rotated upside down 50 times, and then set aside overnight. The aqueous phase was withdrawn with a pipette. The $CHCl_3$ layer was once evaporated *in vacuo*, and the residue was dissolved in an exact amount of water. The relative amounts of the substances in aqueous and $CHCl_3$ layer were determined colorimetrically by modified Morgan-Elson method[19] described for *N*-acetylglucosamine. In some cases the substances were first dissolved in $CHCl_3$ and then extracted with water. The results are summarized in Table 2.

References

1) This work was supported by a Grand-in-Aid for Scientific Research from the Ministry of Education and was presented at the 34th National Meeting of the Chemical Society of Japan, Kanagawa, April 1976; *cf.* Abstract, p. 701.

2) a) S. Kotani, Y. Watanabe, F. Kinoshita, T. Shimono, I. Morisaki, T. Shiba, S. Kusumoto, Y. Tarumi, and K. Ikenaka, *Biken J.*, **18**, 105 (1975); b) S. Kusumoto, Y. Tarumi, K. Ikenaka, and T. Shiba, *Bull. Chem. Soc. Jpn.*, **49**, 553 (1976).

3) C. Merser, P. Sinaÿ, and A. Adam, *Biochem. Biophys. Res. Commun.*, **66**, 1316 (1975)

4) S. Kusumoto, K. Ikenaka, and T. Shiba, *Tetrahedron Lett.*, **1977**, 4055.

5) S. Kotani, F. Kinoshita, Y. Watanabe, I. Morisaki, T. Shimono, K. Kato, T. Shiba, S. Kusumoto, K. Ikenaka, and Y. Tarumi, *Biken J.*, **20**, 125 (1977). A similar work

was also reported by French authors: A. Adam, M. Devys, V. Souvannavong, P. Lefrancier. J. Choay, and E. Lederer, *Biochem. Biophys. Res. Commun.*, **72**, 339 (1976).

6) J. Freund and K. McDermott, *Proc. Soc. Expt. Biol. Med.*, **49**, 548 (1942).

7) Chedid *et al.* reported that synthetic **1** and its several derivatives are capable to stimulate the humoral immune responses in mice even if administered in a form of saline solution; L. Chedid, F. Audibert, P. Lefrancier, J. Choay, and E. Lederer, *Proc. Natl. Acad. Sci. U. S. A.*, **73**, 2472 (1976). L. Chedid, M. Parant, F. Parant, P. Lefrancier, J. Choay, and E. Lederer, *ibid.*, **74**, 2089 (1977). However, cellular immunity, which seems to be important for antitumor activity, can not be enhanced by this recipe.

8) Another important role of the mineral oil emulsion seems to be in keeping the antigen and the adjuvant together long enough until they are recognized in lymph system. The liposome recipe by Kotani *et al.*[14] might be a very good substitution of this function.

9) B. Zbar, J. Rapp, and E. Ribi, *J. Natl. Cancer Inst.*, **48**, 831 (1972).

10) I. Azuma, K. Sugimura, T. Taniyama, M. Yamawaki, Y. Yamamura, S. Kusumoto, S. Okada, and T. Shiba, *Infect. Immun.*, **14**, 18 (1976).

11) In natural cell wall peptidoglycans, most of the corresponding hydroxyl groups of muramic acid moieties do not exist in free states but are linked to polysaccharides through phosphodiester. Thus, modification of the hydroxyl group in **1** is expected not to lead to loss of adjuvant activity.

12) E. J. Bourne, M. Stacey, J. C. Tatlow, and J. M. Tedder, *J. Chem. Soc.*, **1949**, 2976.

13) The docosanoyl derivative (**2f**) described below also showed a similar property.

14) S. Kotani, F. Kinoshita, I. Morisaki, T. Shimono, T. Okunaga, H. Takada, M. Tsujimoto, Y. Watanabe, K. Kato, T. Shiba, S. Kusumoto, and S. Okada, *Biken J.*, **20**, 95 (1977).

15) S. Kusumoto, S. Okada, T. Shiba, I. Azuma, and Y. Yamamura, *Tetrahedron Lett.*, **1976**, 4287.

16) Y. Yamamura, I. Azuma, K. Sugimura, M. Yamawaki, M. Uemiya, S. Kusumoto, S. Okada, and T. Shiba, *Proc. Jpn. Acad.*, **53**, 63 (1977).

17) H. M. Flowers and R. W. Jeanloz, *J. Org. Chem.*, **28**, 2983 (1963).

18) Flowers[17] prepared this compound *via* its methyl ester.

19) J. L. Reissig, J. L. Strominger, and L. F. Leloir, *J. Biol. Chem.*, **217**, 959 (1959).

Studies of Peptide Antibiotics. XXXIX.[1] Syntheses of Gramicidin S Analogs Containing L-Histidine in Place of L-Ornithine

Kazuhiko NONAKA,† Kazuki SATO, Shigeyuki TERADA, Tetsuo KATO, and Nobuo IZUMIYA*

Laboratory of Biochemistry, Faculty of Science 33, Kyushu University, Higashi-ku, Fukuoka 812

(Received February 10, 1978)

Two analogs of gramicidin S, [2-L-histidine]-gramicidin S (**14**) and [2,2′-di-L-histidine]-gramicidin S (**19**), were synthesized to compare the biological role of δ-amino groups in L-ornithine residues in the antibiotic with that of weakly basic imidazolyl groups in L-histidine residues. Compound **14** exhibited identical activity to that of gramicidin S, but **19** was only 1/8 as active. The optical rotatory dispersions of these analogs and gramicidin S were nearly the same: molecular conformation of these peptides must be very similar. Compounds **14** and **19** showed esterolytic activity against *p*-nitrophenyl acetate. The activity of **14** was higher than that of imidazole, **14** being more active than **19**.

There is ample evidence that the presence of charged amino groups in ornithine residues is essential to the antibacterial activity of gramicidin S (GS). Change in the length of the methylene chain in basic amino acid residues does not alter the activity.[2,3] Conversion of the amino group into strongly basic guanidino group afforded similarly active [Arg$^{2,2'}$]-GS.[4] On the other hand, acylation of the amino groups caused drastic decrease in activity.[5] However, no attempt seems to have been made to substitute the ornithine residues with weakly basic histidine residues and to examine the role of amino and imidazolyl groups for antimicrobial activity. This paper deals with the syntheses, antibacterial properties, and ORD measurements of [His^2]-GS (namely, [His^2]-hybrid GS) and [His$^{2,2'}$]-GS, in which the L-ornithyl residues in 2 and 2′ positions are replaced, singly or together, by L-histidine residues (Fig. 1). Possible esterolytic activity of these analogs was tested, because histidine is known to constitute a part of the catalytic site in several esterolytic enzymes such as α-chymotrypsin and subtilisin.

The syntheses of [His^2]-GS and [His$^{2,2'}$]-GS are outlined in Figs. 2 and 3.[6] The principle of the syntheses is to locate the leucyl residue at the *C*-terminal.[7]

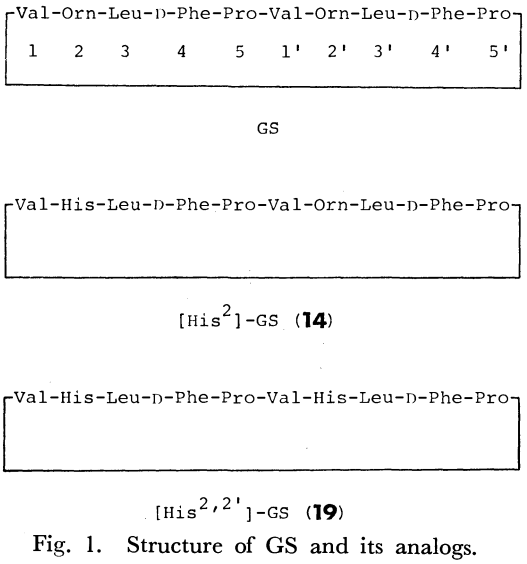

Fig. 1. Structure of GS and its analogs.

† Present address: Teikoku Hormone Mfg. Co., Ltd., Takatsu-ku, Kawasaki 213.

The imidazolyl function of histidine is protected by the benzyloxycarbonyl group only in the first coupling step, and unprotected in later steps, because azide coupling is known to proceed without affecting imidazolyl function, and because there is no suitable and conveniently cleavable protecting group for imidazolyl function.

For the synthesis of [His^2]-GS (**14**), Boc-pentapeptide ester (**7**) was perpared by the coupling of Boc-tripeptide hydrazide (**6**) with dipeptide ester (**2**) which was obtained by mixed anhydride coupling of Z–His(Z)–OH and H–Leu–OEt and subsequent hydrogenation. Boc–Pro–Val–OEt (**3**) and Boc–D-Phe–Pro–Val–OEt (**5**) were obtained similarly. A part of **7** was converted into Boc-pentapeptide hydrazide (**8**). Coupling of **8** and **9**, which was derived from Boc–D-Phe–Pro–Val–Orn(Z)–Leu–OEt,[8] afforded Boc-decapeptide ester (**10**). This was converted into the corresponding hydrazide (**11**) which was then subjected

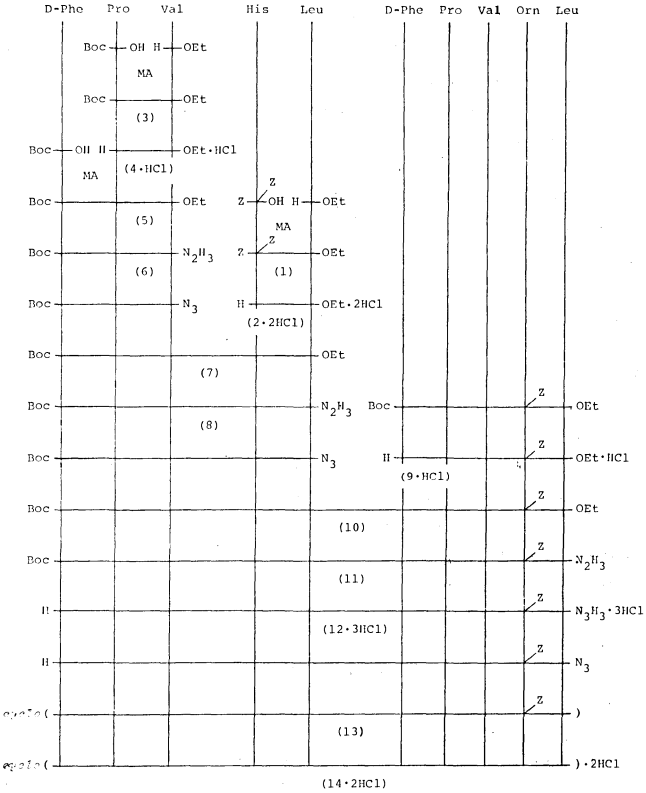

Fig. 2. Synthesis of [His^2]-GS.

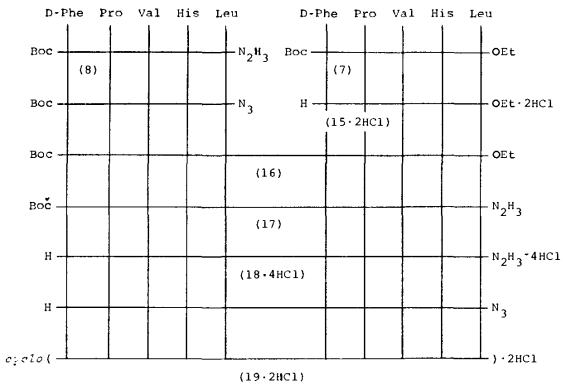

Fig. 3. Synthesis of [His$^{2,2'}$]-GS.

TABLE 1. ANTIBACTERIAL ACTIVITY OF GS AND ITS ANALOGS
(Minimum inhibitory concentration, μg/ml)

Strain	GS	[His^2]-GS (**14**)	[His$^{2,2'}$]-GS (**19**)
Staphylococcus aureus	3.12	3.12	50
Staphylococcus epidermidis	3.12	3.12	25
Bacillus subtilis	1.56	1.56	12.5
Escherichia coli	>100	>100	>100

to cyclization. The protected cyclodecapeptide (**13**) was obtained in 54% yield. A product **14** was obtained by hydrogenation of **13** in 75% yiled. Another product **19** was synthesized from cyclization of linear decapeptide precursor (**16**) instead of doubling cyclization with use of pentapeptide precursor (**7**). Synthesis of **19** was carried out thus because the results of previous experiments suggested that cyclization from **7** could give a mixture of cyclic penta- and decapeptides and, furthermore, the content of the cyclic pentapeptide might be considerably high.[9]

The homogeneity of **14** and **19** was confirmed by paper and thin-layer chromatography, paper electrophoresis and elemental analysis. Intermediates containing histidine such as **7** and **13** and the final product **19** were purified by silica gel column chromatography, and intermediates **10** and **16** by Sephadex LH-20, instead of the usual acid washing in order to avoid loss of the basic peptides. Satisfactory results were obtained for elemental analyses of all the crystalline compounds.

Table 1 shows antibacterial activities of **14**, **19**, and GS. Activity of **14** was exactly the same as that of GS, the presence of one amino and additional one imidazolyl groups apparently being enough to exhibit full activity. In contrast, **19** was only 1/8 or 1/16 times active as compared with GS. This result is interesting but somewhat unusual, because many amino acid-substituted analogs gradually change their activity from mono- to di-substitution. We tentatively explain the apparent discrepancy as follows: [His^2]-GS can gain access to bacterial membrane by ionic interaction between amino group and phospholipid.[5] A weakly basic imidazolyl group also can make a salt-like linkage

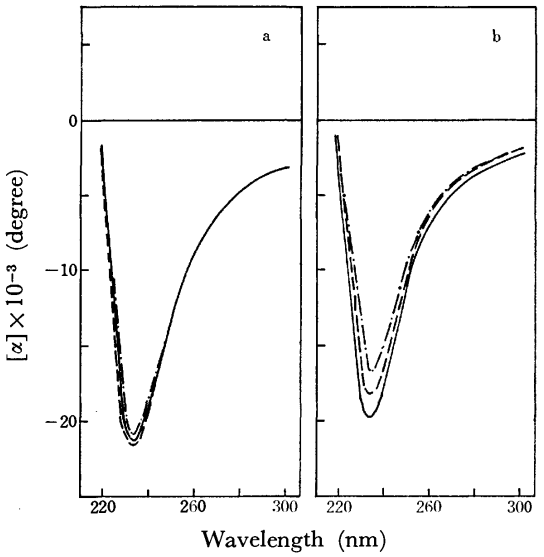

Fig. 4. ORD curves of GS and its analogs.
Solvent: a, EtOH; b, 8 M urea. Curve: ——, GS; – – –, [His^2]-GS; —•—, [His$^{2,2'}$]-GS.

TABLE 2. HYDROLYSIS OF *p*-NITROPHENYL ACETATE WITH CATALYSTS[a]

Catalyst	Second order rate constant ($M^{-1} \cdot min^{-1}$)	
	20% EtOH	50% EtOH
[His^2]-GS (**14**)	38	12
[His$^{2,2'}$]-GS (**19**)	22	7
Boc-pentapeptide-OEt (**7**)	10	10
GS	0	0
Imidazole	22	13

a) Buffer, 1/30 M phosphate at pH 7.86 containing EtOH. Temp, 25 °C. Concentrations, 1.4×10^{-5} M and 6×10^{-5} M for *p*-nitrophenyl acetate and each catalyst, respectively.

with the phospholipid, when the antibiotic sufficiently approaches the membrane. However, ionic interaction between [His$^{2,2'}$]-GS and the membrane may be so weak that it is difficult for the antibiotic to come near the lipid membrane, thus causing weakening of its antimicrobial activity.

Figure 4-a shows the ORD curves of **14**, **19**, and GS measured in ethanol, all the curves being superimposable. In 8 M urea, which causes denaturation of various polypeptides, a slight deviation was observed, the trough at 233 nm being slightly shallower in the case of **14** and **19** (Fig. 4-b). The results of ORD measurements indicate that the conformation of the analogs must be very similar to that of GS but the stability of the analogs decreases with the number of the substitution. Dygert *et al.* proposed the presence of intramolecular hydrogen bondings between δ-amino groups in ornithine and carbonyl groups in D-phenylalanine.[10] Loss of these hydrogen bondings might cause slight instabilization in the peptide backbone of the analogs.

Table 2 shows catalytic activities of **14** and **19** on

the hydrolysis of *p*-nitrophenyl acetate. Experimental conditions are similar to those described by Katchalski *et al.*[11] In 1/30 M phosphate buffer, pH 7.86, containing 20% ethanol, catalytic activity of **14** was enhanced, but the enhancement disappeared in a more hydrophobic solvent, 50% ethanol. This suggests that the enhancement was caused by the hydrophobic interaction between the peptides and the substrate. Nakajima and Okawa reported a similar enhanced catalytic activity of cyclo(–L-His–L-Glu–L-Cys–D-Phe–Gly–)$_2$ on the hydrolysis of *p*-nitrophenyl acetate.[12] Imanishi *et al.* observed strongly enhanced catalytic activity of cyclo(–L-His–D-Leu–) on *p*-nitrophenyl laurate.[13] Since **7** shows no enhancement on the catalysis, the mere presence of an imidazolyl group in a peptide does not give high catalytic activity. Rigid β-sheet backbone conformation of **14** and **19** and hydrophobic environment derived from this conformation should be responsible for the activity. The high activity of **14** is interesting because it contains only one histidine residue. The presence of a free amino group in ornithine might cause additional accelerating effect.

Experimental

All the melting points are uncorrected. TLC was carried out on silica gel G (Merck) with the following solvent systems, the ratio in parentheses after each solvent system being indicated by vol: R_f^1, $CHCl_3$–MeOH (5:1); R_f^2, $CHCl_3$–MeOH–AcOH (95:5:1); R_f^3, *n*-BuOH–AcOH–pyridine–H_2O (4:1:1:2). Optical rotations were measured on a Union high sensitivity polarimeter PM-71. Amino acid analyses were performed with a Hitachi amino acid analyzer KLA-5.

*Z-His(Z)-Leu-OEt (**1**).* To a chilled solution of Z-His(Z)-OH·EtOH (5.84 g, 12.4 mmol) and NMM (1.36 ml, 12.4 mmol) in THF (10 ml) was added isobutyl chloroformate (1.36 ml, 12.4 mmol) at −15 °C. After 10 min, a chilled solution of H–Leu–OEt·TsOH (4.10 g, 12.4 mmol) and NMM (1.62 ml, 12.4 mmol) in CH_2Cl_2 (10 ml) was added. The mixture was stirred at 0 °C for 1 h and at room temperature overnight, evaporated *in vacuo*, and the residue was dissolved in EtOAc. The solution was washed successively with 4% $NaHCO_3$, 10% citric acid and water, dried (Na_2SO_4), and evaporated. The resulting solid was recrystallized from EtOH–ether; yield, 5.60 g (80%); mp 116—118 °C; $[\alpha]_D^{20}$ −6.4° (*c* 0.5, EtOH); R_f^1 0.75, R_f^2 0.46.

Found: C, 63.78; H, 6.39; N, 9.96%. Calcd for $C_{30}H_{36}O_7N_4$: C, 63.81; H, 6.43; N, 9.92%.

*H–His–Leu-OEt·2HCl (**2**·2HCl).* Compound **1** (3.95 g, 7 mmol) dissolved in 0.2 M hydrogen chloride in EtOH (70 ml) was hydrogenated using palladium black as a catalyst. After 5 h, the filtrate from the catalyst was evaporated. Addition of ether to the oily residue gave hygroscopic crystals, which were recrystallized from EtOH–ether; yield, 2.09 g (81%); R_f^1 0.17.

*Boc–Pro–Val-OEt (**3**).* This was prepared from Boc–Pro–OH (6.46 g, 30 mmol) and H–Val–OEt·TsOH (9.52 g, 30 mmol) as described for **1**. The product was recrystallized from EtOH–ether–petroleum ether; yield, 7.50 g (73%); mp 72—75 °C; $[\alpha]_D^{20}$ −70.1° (*c* 0.5, EtOH); R_f^1 0.88, R_f^2 0.66.

Found: C, 59.35; H, 8.80; N, 8.06%. Calcd for $C_{17}H_{30}O_5N_2$: C, 59.62; H, 8.83; N, 8.18%.

*H–Pro–Val-OEt·HCl (**4**·HCl).* Compound **3** (3.60 g, 10.5 mmol) was dissolved in 2.8 M hydrogen chloride in EtOAc (75 ml). The solution was allowed to stand at room temperature for 30 min and then evaporated to leave an oil; yield, 2.93 g (100%); R_f^1 0.32.

*Boc–D-Phe–Pro–Val-OEt (**5**).* This was prepared from Boc–D-Phe–OH (2.79 g, 10.5 mmol) and **4**·HCl (2.93 g, 10.5 mmol) as described for **1**. The product was obtained as an oil; yield, 4.63 g (90%); R_f^1 0.82.

*Boc–D-Phe–Pro–Val–N_2H_3 (**6**).* A solution of **5** (4.63 g, 9.46 mmol) and hydrazine hydrate (9.18 ml, 189 mmol) in MeOH (40 ml) was allowed to stand at room temperature for 3 days. The solution was evaporated and the residue was dissolved in $CHCl_3$ (200 ml). The solution was washed with water, dried (Na_2SO_4), and evaporated. The residual oil was solidified by the addition of ether, and the product was recrystallized from EtOH–ether; yield 3.59 g (80%); mp 158—160 °C; $[\alpha]_D^{20}$ −86.8° (*c* 0.5, EtOH); R_f^1 0.65, R_f^2 0.31.

Found: C, 60.40; H, 7.82; N, 14.58%. Calcd for $C_{24}H_{37}O_5N_5$: C, 60.61; H, 7.84; N, 14.73%.

*Boc–D-Phe–Pro–Val–His–Leu-OEt (**7**).* To a solution of **6** (1.76 g, 3.7 mmol) in DMF (70 ml) were added 2.8 M hydrogen chloride in EtOAc (3.96 ml) and isopentyl nitrite (0.57 ml, 4.07 mmol) at −60 °C. After being left to stand at −20 °C for 10 min, the solution was cooled again to −60 °C and neutralized with TEA (1.55 ml, 11.1 mmol). To this solution was added a chilled solution of **2**·2HCl (2.05 g, 5.55 mmol) and TEA (1.55 ml, 11.1 mmol) in DMF (30 ml). The reaction mixture was stirred at 0 °C for 48 h and then evaporated. The residue was dissolved in EtOAc and the solution was washed successively with 4% $NaHCO_3$ and water, dried (Na_2SO_4), and evaporated. The oily product was applied to a column (5×50 cm) of silica gel (Merck) and the column was washed with $CHCl_3$–EtOH–AcOH (95:5:1) (3200 ml). The product was then eluted with a mixture (1500 ml) of $CHCl_3$–EtOH (5:1). Each fraction was assayed by TLC, and the fractions containing the desired product were evaporated to leave an oil which was crystallized by the addition of ether and petroleum ether; yield, 2.14 g (78%); mp 89—92 °C; $[\alpha]_D^{20}$ −74.5° (*c* 0.5, EtOH); R_f^1 0.66, R_f^2 0.07.

Found: C, 58.83; H, 7.61; N, 12.48%. Calcd for $C_{33}H_{57}O_8N_7\cdot 2H_2O$: C, 58.82; H, 7.92; N, 12.64%.

*Boc–D-Phe–Pro–Val–His–Leu–N_2H_3 (**8**).* Compound **7** (601 mg, 0.81 mmol) was treated with hydrazine hydrate (1.58 ml, 32.5 mmol) as described for **6**; yield, 498 mg (84%); mp 170—175 °C; $[\alpha]_D^{20}$ −69.4° (*c* 0.5, EtOH); R_f^1 0.53, R^2 0.04.

Found: C, 58.15; H, 7.58; N, 16.92%. Calcd for $C_{36}H_{55}O_7N_9\cdot H_2O$: C, 58.13; H, 7.72; N, 16.95%.

*H–D-Phe–Pro–Val–Orn(Z)–Leu-OEt·HCl (**9**·HCl).* This was prepared from Boc–D-Phe–Pro–Val–Orn(Z)–Leu–OEt[8] (2.21 g, 2.6 mmol) as described for **4**·HCl. The oily product was crystallized by the addition of ether and petroleum ether; yield, 1.85 g (91%); mp 111—120 °C; $[\alpha]_D^{20}$ −120° (*c* 0.5, EtOH); R_f^1 0.67, R_f^2 0.14.

Found: C, 60.80; H, 7.71; N, 10.45%. Calcd for $C_{40}H_{58}O_8N_6\cdot HCl$: C, 61.01; H, 7.55; N, 10.67%.

*Boc–D-Phe–Pro–Val–His–Leu–D-Phe–Pro–Val–Orn(Z)–Leu-OEt (**10**).* This was prepared from **8** (327 mg, 0.45 mmol) and **9**·HCl (425 mg, 0.54 mmol) as described for **7**. The crude product dissolved in MeOH (5 ml) was applied to a column (2.8×156 cm) of Sephadex LH-20. The column was developed with MeOH, the fractions with the desired product were evaporated, and the oily residue was crystallized by the addition of ether; yield, 408 mg (63%); mp 135—138 °C; $[\alpha]_D^{20}$ −106° (*c* 0.3, EtOH); R_f^1 0.69, R_f^2 0.13.

Found: C, 62.01; H, 7.63; N, 12.42%. Calcd for $C_{76}H_{109}O_{15}N_{13}\cdot 3/2H_2O$: C, 62.02; H, 7.67; N, 12.37%.

Boc–D-Phe–Pro–Val–His–Leu–D-Phe–Pro–Val–Orn(Z)–Leu–

*N_2H_3 (**11**).* Compound **10** (387 mg, 0.27 mmol) was treated with hydrazine hydrate (0.26 ml, 5.4 mmol) as described for **6**; yield, 359 mg (94%); mp 140—145 °C; $[\alpha]_D^{20}$ −82.1° (*c* 0.5, MeOH); R_f^1 0.49, R_f^2 0.05.

Found: C, 60.45; H, 7.55; N, 14.38%. Calcd for $C_{74}H_{107}O_{14}N_{15}\cdot 2H_2O$: C, 60.60; H, 7.63; N, 14.32%.

*H-D-Phe-Pro-Val-His-Leu-D-Phe-Pro-Val-Orn(Z)-Leu-N_2H_3·3HCl (**12**·3HCl).* Compound **11** (341 mg, 0.24 mmol) was treated with 0.1 M hydrogen chloride in formic acid (7.4 ml) as described for **4**·HCl and the oily product was crystallized by the addition of ether; yield, 330 mg (96%); mp 174—178 °C; $[\alpha]_D^{20}$ −154° (*c* 0.5, MeOH); R_f^1 0.22.

Found: C, 56.81; H, 7.17; N, 14.51%. Calcd for $C_{69}H_{99}O_{12}N_{15}\cdot 3HCl\cdot H_2O$: C, 56.84; H, 7.19; N, 14.41%.

*cyclo(-D-Phe-Pro-Val-His-Leu-D-Phe-Pro-Val-Orn(Z)-Leu-) (**13**).* To a solution of **12**·3HCl (310 mg, 0.22 mmol) in DMF (4 ml) were added 2.8 M hydrogen chloride in EtOAc (0.24 ml) and isopentyl nitrite (0.031 ml, 0.22 mmol) in DMF (0.3 ml) at −30 °C. After 15 min, the reaction mixture was added to pyridine (66 ml) at 0 °C. After being stirred at 5 °C for 4 days, the solution was evaporated and the addition of water afforded a white precipitate, which was filtered and washed with water. The crude product was purified with a column (3.3×42 cm) of silica gel using a mixture of $CHCl_3$–EtOH (5:1) as a developing agent as described for **6**; yield, 151 mg (54%); mp 238—240 °C; $[\alpha]_D^{20}$ −295° (*c* 0.5, MeOH); R_f^1 0.66, R_f^2 0.05.

Found: C, 61.07; H, 7.28; N, 13.25%. Calcd for $C_{65}H_{95}O_{12}N_{13}\cdot 3H_2O$: C, 61.26; H, 7.53; N, 13.46%.

*cyclo(-D-Phe-Pro-Val-His-Leu-D-Phe-Pro-Val-Orn-Leu-)·2HCl ([His^2]-GS·2HCl) (**14**·2HCl).* Compound **13** (78 mg, 0.06 mmol) dissolved in 0.05 M hydrogen chloride in MeOH (2.7 ml) was hydrogenated as described for **2**·2HCl. The product was recrystallized from EtOH–ether; yield, 56 mg (75%); mp 274—275 °C (dec); $[\alpha]_D^{20}$ −283° (*c* 0.5, EtOH); R_f^1 0.35, R_f^3 0.81. Amino acid ratios in acid hydrolyzate; Phe 2.10, Pro 2.05, Val 1.96, His 1.06, Orn 1.08, Leu 2.00.

Found: C, 56.37; H, 7.40; N, 13.55%. Calcd for $C_{61}H_{89}O_{10}N_{13}\cdot 2HCl\cdot 4H_2O$: C, 55.95; H, 7.62; N, 13.91%.

*H-D-Phe-Pro-Val-His-Leu-OEt·2HCl (**15**·2HCl).* This was prepared from **7** (592 mg, 0.8 mmol) as described for **4**·HCl. The oily product was crystallized by the addition of ether and petroleum ether; yield, 520 mg (91%); mp 190—200 °C; $[\alpha]_D^{20}$ −147° (*c* 0.5, EtOH); R_f^1 0.26.

Found: C, 54.64; H, 7.44; N, 13.16%. Calcd for $C_{33}H_{49}O_6N_7\cdot 2HCl\cdot H_2O$: C, 54.24; H, 7.31; N, 13.42%.

*Boc-(D-Phe-Pro-Val-His-Leu)$_2$-OEt (**16**).* This was prepared from **8** (363 mg, 0.5 mmol) and **15**·2HCl (428 mg, 0.6 mmol) as described for **7**. The crude product was purified by a column (2.8×156 cm) of Sephadex LH-20 as described for **10**; yield, 213 mg (32%); mp 150—156 °C; $[\alpha]_D^{20}$ −123° (*c* 0.3, EtOH); R_f^1 0.61.

Found: C, 59.45; H, 7.37; N, 13.97%. Calcd for $C_{69}H_{100}O_{13}N_{14}\cdot 3H_2O$: C, 59.72; H, 7.70; N, 14.13%.

*Boc-(D-Phe-Pro-Val-His-Leu)$_2$-N_2H_3 (**17**).* Compound **16** (200 mg, 0.15 mmol) was treated with hydrazine hydrate (0.15 ml, 3 mmol) as described for **6**; yield, 181 mg (91%); mp 190—192 °C (dec); $[\alpha]_D^{20}$ −111° (*c* 0.4, MeOH); R_f^1 0.30.

Found: C, 59.16; H, 7.41; N, 16.31%. Calcd for $C_{67}H_{99}O_{12}N_{16}\cdot 2H_2O$: C, 59.31; H, 7.65; N, 16.52%.

*H-(D-Phe-Pro-Val-His-Leu)$_2$-N_2H_3·4HCl (**18**·4HCl).* Compound **17** (166 mg, 0.13 mmol) was treated with 0.1 M hydrogen chloride in formic acid (5.2 ml) as described for **4**·HCl and the oily product was crystallized by the addition of ether; yield, 158 mg (92%); mp 239—240 °C; $[\alpha]_D^{20}$ −164° (*c* 0.5, MeOH); R_f^1 0.06.

Found: C, 53.36; H, 7.04; N, 15.60%. Calcd for $C_{62}H_{90}O_{10}N_{16}\cdot 4HCl\cdot 2H_2O$: C, 53.13; H, 7.05; N, 15.99%.

*cyclo(-(D-Phe-Pro-Val-His-Leu)$_2$-)·2HCl ([$His^{2,2'}$]-GS·2HCl) (**19**·2HCl).* Compound **18**·4HCl (137 mg, 0.1 mmol) dissolved in DMF (3 ml) was treated with 2.8 M hydrogen chloride in EtOAc (0.14 ml) and isopentyl nitrite (0.014 ml, 0.1 mmol) in DMF (0.1 ml) as described for **13**. The crude product was purified with a column (3.3×30 cm) of silica gel as described for **13**; yield, 41 mg (32%); mp 262—263 °C (dec); $[\alpha]_D^{20}$ −276° (*c* 0.5, EtOH); R_f^1 0.28, R_f^3 0.85. Amino acid ratios in acid hydrolyzate; Phe 1.04, Pro 0.98, Val 0.96, His 1.10, Leu 1.00.

Found: C, 57.53; H, 7.05; N, 14.73%. Calcd for $C_{62}H_{86}O_{10}N_{14}\cdot 2HCl\cdot 2H_2O$: C, 57.44; H, 7.15; N, 15.12%.

Paper Electrophoresis. This was carried out with Toyo Roshi No. 52 paper and with a solvent system of HCOOH–AcOH–MeOH–H_2O (1:3:6:10, pH 1.8) for 2.5 h at 500 V/30 cm. Each of the peptides (**14** and **19**) revealed a single spot, the mobility being the same as that of GS.

Microbiological Assays and ORD Measurements. Measurements were carried out as described in a previous paper,[7] the results being shown in Table 1 and Fig. 4.

Kinetic Measurements. The esterolytic reaction was initiated by the addition of an ethanolic solution of *p*-nitrophenyl acetate (10 μl) to an aqueous ethanolic solution of catalyst (2.99 ml). Hydrolysis by the action of the catalyst was monitored by the increase in absorbance at 400 nm on a Hitachi 124 spectrophotometer; light path, 1 cm.

References

1) Part XXXVIII of this series: K. Sato, K. Ueda, M. Kondo, H. Aoyagi, and N. Izumiya, *Bull. Chem. Soc. Jpn.*, **51**, 1830 (1978).

2) R. Schwyzer and P. Sieber, *Helv. Chim. Acta*, **41**, 2186 (1958).

3) M. Waki, O. Abe, R. Okawa, T. Kato, S. Makisumi, and N. Izumiya, *Bull. Chem. Soc. Jpn.*, **40**, 2904 (1967).

4) A. B. Silaev and V. M. Stepanov, *Dokl. Akad. Nauk SSSR*, **112**, 297 (1957).

5) A. S. Kaprel'yants, V. V. Nikiforov, A. I. Miroshnikov, L. G. Sneshkova, V. A. Eremin, and O. N. Ostrovski, *Biochemistry (translated from Russian)*, **42**, 252 (1977).

6) Abbreviations recommended by the IUPAC-IUB Commission of Biochemical Nomenclature (*J. Biol. Chem.*, **247**, 977 (1972)) have been used throughout. Additional abbreviations: DMF, *N*,*N*-dimethylformamide; MA, mixed anhydride; NMM, *N*-methylmorpholine; TEA, triethylamine; THF, tetrahydrofuran.

7) M. Ohno, K. Kuromizu, H. Ogawa, and N. Izumiya, *J. Am. Chem. Soc.*, **93**, 5251 (1971).

8) H. Abe, K. Sato, T. Kato, and N. Izumiya, *Bull. Chem. Soc. Jpn.*, **49**, 3113 (1976).

9) K. Nonaka, K. Kamekawa, K. Sato, M. Waki, T. Kato, and N. Izumiya, "Peptide Chemistry 1977," ed by T. Shiba, Protein Res. Foundation, Osaka, pp. 135—138.

10) M. Dygert, N. Go, and H. A. Scheraga, *Macromolecules*, **8**, 750 (1975).

11) E. Katchalski, G. D. Fasman, E. Simons, E. R. Blout, F. R. N. Gurd, and W. L. Koltun, *Arch. Biochem. Biophys.*, **88**, 361 (1960).

12) K. Nakajima and K. Okawa, *Bull. Chem. Soc. Jpn.*, **46**, 1811 (1973).

13) Y. Imanishi, M. Tanihara, T. Sugihara, and T. Higashimura, *Biopolymers*, **16**, 2203 (1977).

The Sensitized Photooxidation of Cycloheptatriene (Tropilidene). Isolation and Thermal Isomerization of $(4\pi+2\pi)$ Cycloadduct, 8,9-Dioxabicyclo-[3.2.2]-2,6-nonadiene, and Preparation of Tropone[1]

Toyonobu Asao,* Morio Yagihara,†,[2] and (the late) Yoshio Kitahara†

Department of Chemistry, College of General Education, Tohoku University, Kawauchi, Sendai 980

† *Department of Chemistry, Faculty of Science, Tohoku University, Aramaki Aoba, Sendai 980*

(Received February 20, 1978)

The sensitized photooxidation of cycloheptatriene (tropilidene) in methanol afforded $(4\pi+2\pi)$ cycloadduct; 8,9-dioxabicyclo[3.2.2]-2,6-nonadiene (**1**), 6-hydroxy-2,4-cycloheptadienone and 6-oxoheptadienal presumably derived from $(6\pi+2\pi)$ cycloadduct, and small amounts of tropone and benzaldehyde. Mechanism of their formation are discussed. It was found that the treatment of the photooxidation mixture with triethylamine afforded tropone in about 50% yield. Thermal isomerization of **1** in refluxing xylene afforded *cis*-3,9-dioxatricyclo-[6.1.0.0^{2,4}]-5-nonene, 8-oxabicyclo[5.1.0]-4-octen-3-one and 4-hydroxy-2,6-cycloheptadienone.

Kende and Chu have reported evidence that the oxidation of tropilidene by photochemically generated singlet oxygen gave $(4\pi+2\pi)$ and $(6\pi+2\pi)$ cycloadducts and hydroperoxide by isolating their hydrogenation products including cycloheptanol, 3-hydroxycycloheptanone and *cis*-1,4-cycloheptanediol.[3] However, they could not isolate any direct oxidation products. Meanwhile, the oxidation of tropilidene with peracetic acid gave monoepoxide, 8-oxabicyclo[5.1.0]-2,4-octadiene,[4] and its further oxidation with excess peracid afforded a mixture of diepoxides and triepoxides.[5]

We have studied the similar photooxidation reaction for the purpose of the isolation of the oxidation products and the preparation of tropone *via* photooxidation of tropilidene,[6] and we have isolated a $(4\pi+2\pi)$ cycloadduct; 8,9-dioxabicyclo[3.2.2]-2,6-nonadiene, 6-hydroxy-2,4-cycloheptadienone and 6-oxoheptadienals presumably derived from a $(6\pi+2\pi)$ cycloadduct, and have discussed the mechanisms of the formation of these products. We have also obtained tropone in considerable yield by the base treatment of the photooxidation mixture. Furthermore, it was found that the thermal reaction of $(4\pi+2\pi)$ cycloadduct in refluxing xylene afforded three isomeric rearranged products. The results are reported in this paper.

Results and Discussion

When a 1.5% solution of tropilidene in methanol was irradiated with visible light (6×20 W) in the presence of methylene blue for 2 days[7] while oxygen was slowly passed through the solution, $(4\pi+2\pi)$ cycloadduct (8,9-dioxabicyclo[3.2.2]-2,6-nonadiene) (**1**) (8.4%), 6-hydroxy-2,4-cycloheptadienone (**2**) (23.4%), tropone (**3**) (trace), benzaldehyde (**4**) (trace), *trans,trans*-6-oxoheptadienal (**5**) (0.4%), *trans,trans*-6-oxoheptadienal dimethylacetal (**6**) (0.63%) and a mixture of stereoisomer of 6-oxoheptadienal dimethylacetal (**7**) (0.55%) were isolated after repeated purification by column chromatography on silica gel.

When the photooxidation of tropilidene was performed in acetone in the presence of hematoporphyrin, benzaldehyde was obtained in 51% yield, and the reaction in a mixture of methanol and acetone (1:1) afforded the compound (**1**) in 15% yield.

The structures of the products were determined mainly by their spectroscopic data as well as some chemical transformations. ^{1}H-NMR spectrum of **1**, and ^{1}H-NMR parameter of the compounds (**1**, **2**, **5**, and **6**) were shown in Fig. 1, and Table 1, respectively.

Kende and Chu have reported[3] that catalytic hydrogenation of the total crude photooxidation mixture in ethyl acetate in the presence of 10% Pd–C afforded a mixture of cycloheptanone (**8**), cycloheptanol (**9**), 3-hydroxycycloheptanone (**10**), 4-hydroxycycloheptanone (**11**) and *cis*-1,4-cycloheptanediol (**12**). We have also isolated the same products[8] by the catalytic hydrogenation of the photooxidation mixture in the presence of 5% Pd–C, and furthermore we have obtained **11** and **12**, and **10** by the catalytic hydrogenation of **1**, and **2**, respectively.

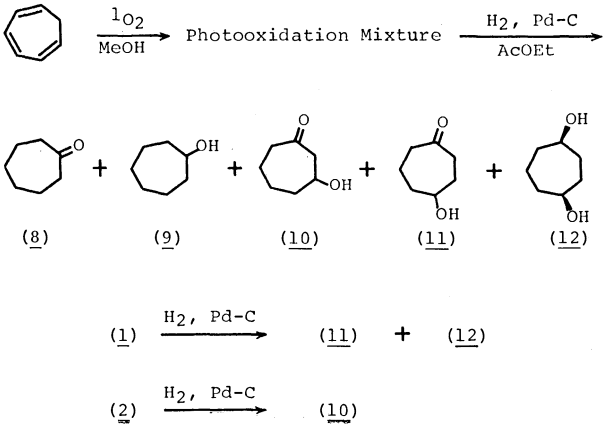

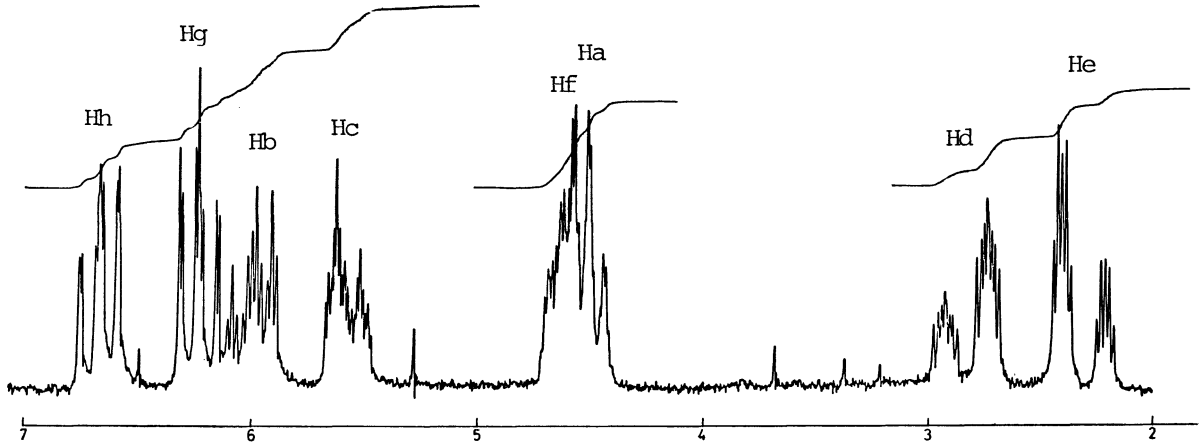

Fig. 1. ^{1}H-NMR spectrum of **1** in $CDCl_3$ (100 MHz).

Table 1. ^{1}H-NMR parameters of **1**, **2**, **5**, **6**, **15**, **27**, and **28**

Compound	^{1}H-NMR parameters (δ-values, J in Hz)[a]
1[b]	2.30 (He), 2.83 (Hd), 4.48 (Ha), 4.65 (Hf), 5.59 (Hc), 5.98 (Hb), 6.25 (Hg), 6.66 (Hh) $J_{ab}=7.0$, $J_{ac}=1.1$, $J_{ag}=1.2$, $J_{ah}=7.0$, $J_{bc}=10.5$, $J_{bd}=2.0$, $J_{be}=2.0$, $J_{bh}=0.5$, $J_{cd}=4.0$, $J_{ce}=4.0$, $J_{cf}=1.5$, $J_{de}=19.0$, $J_{df}=5.0$, $J_{ef}=2.0$, $J_{fg}=7.0$, $J_{fh}=1.2$, $J_{gh}=9.0$
2[b]	2.76 (Hf), 3.50 (Hg), 3.97 (OH), 4.73 (He), 6.00 (Hc), 6.05 (Ha), 6.55 (Hd), 6.65 (Hb) $J_{ab}=2.2$, $J_{af}=1.5$, $J_{bc}=7.6$, $J_{cd}=11.4$, $J_{ce}=2.0$, $J_{de}=4.0$, $J_{df}=3.0$, $J_{ef}=4.6$, $J_{eg}=12.8$, $J_{fg}=15.8$
5[b]	2.29 (CH_3), 6.3—6.6 (m, 2H), 6.9—7.3 (m, 2H), 9.63 (CHO)
6[b]	2.20 (CH_3), 3.25 (OCH_3), 4.82 (He), 5.92 (Hd), 6.07 (Ha), 6.40 (Hc), 6.98 (Hb) $J_{ab}=15.4$, $J_{bc}=10.7$, $J_{cd}=15.4$, $J_{ce}=1.2$, $J_{de}=4.0$
15[c]	2.3—2.9 (m, Hf, Hg), 2.90 (m, Hh), 3.07 (m, Ha), 3.35 (m, Hc), 3.48 (m, Hb), 5.68 (m, Hd, He)
27[c]	2.3—3.4 (m, 6H), 5.90 (d,d, J=12.0, 2.0, Ha), 6.47 (d,d,d, J=12.0, 7.0, 5.0, Hb)
28[b]	2.61 (He), 2.82 (Hd), 3.08 (OH), 4.69 (Hc), 6.03 (Ha), 6.14 (Hg), 6.61 (Hf), 6.71 (Hb) $J_{ab}=12.5$, $J_{ac}=2.0$, $J_{ag}=2.0$, $J_{bc}=2.5$, $J_{bd}=1.0$, $J_{cd}=11.0$, $J_{ce}=5.0$, $J_{cf}=0.5$, $J_{de}=17.0$, $J_{df}=4.5$, $J_{dg}=2.0$, $J_{ef}=7.0$, $J_{eg}=1.0$, $J_{fg}=12.0$

a) Refer the text for proton numberings. b) In $CDCl_3$. c) In CCl_4.

Hydrolysis of **6** with hydrochloric acid afforded the corresponding aldehyde (**5**), which can be converted to 6-oxoheptanal (**13**) upon catalytic reduction. Acid hydrolysis of **7** afforded **5** as one of the products.

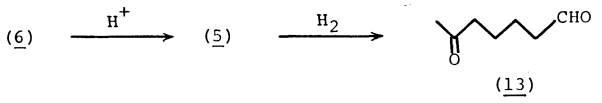

The compound (**2**) must be resulted from the cleavage of dioxide ring of ($6\pi+2\pi$) adduct (**14**). But as less likely mechanism, Kende and Chu have pointed out that **2** could be arised by multiple rearrangement of ($4\pi+2\pi$) adduct (**1**) through an allylic diepoxide intermediate (**15**) or *via* S_N'-hydrolysis of **1** to 6-hydroperoxy-2,4-cycloheptadien-1-ol (**16**) in the reaction condition.

As will be described later, thermal isomerization of the adduct (**1**) did not give **2**, but gave diepoxide (**15**) as one of the products, and it was found that **15** does not change to **2**, but gradually changed to 4-hydroxy-2,6-cycloheptadienone on column of silica gel. Furthermore, the compound (**1**) did not change in aqueous methanol in the presence or absence of

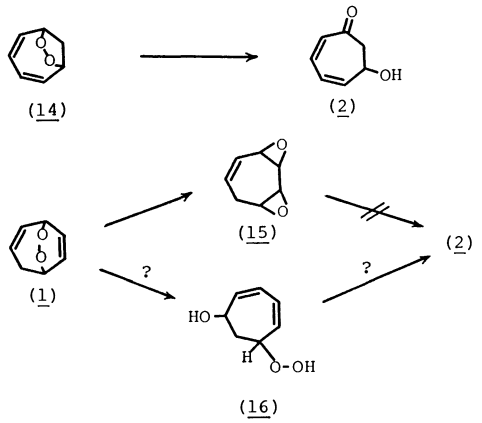

diluted perchloric acid by standing at room temperature for 5 days. Therefore, it is assumed that the compound (**2**) must not be resulted from ($4\pi+2\pi$) adduct (**1**), but must be resulted from the initially formed ($6\pi+2\pi$) adduct (**14**) as has been posturated by Kende.[3]

The formation of acyclic compounds (**5**—**7**) can be explained by the following three processes. Path (a) involves a retro-Aldol cleavage of the compound (**2**).

Path (b) involves a rearrangement of ($6\pi+2\pi$) adduct (**14**) to epoxyaldehyde (**17**) followed by isomerization to the aldehyde (**5**) *via cis,cis*-6-oxoheptadienal (**18**). Path (c) proceeds through the direct new peroxide rearrangement of **14** to **18** followed by *cis-trans* isomerization.

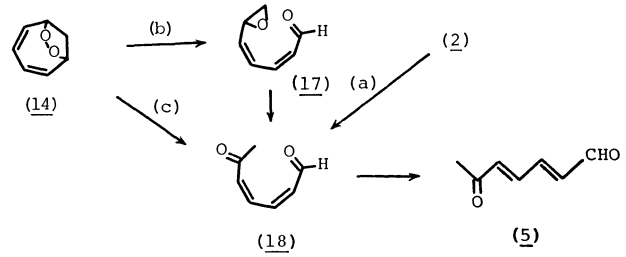

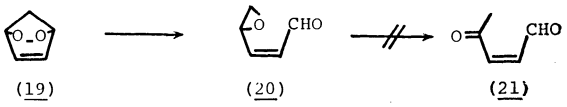

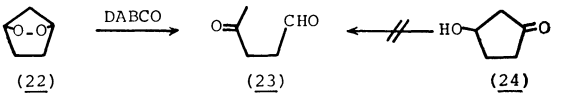

The possibility of path (a) may be ruled out since **2** does not change on standing in methanol. Ohloff *et al.*, and Adams *et al.* have isolated a epoxide (**20**) derived from 1,4-epidioxy-2-cyclopentene (**19**) during photooxidation of cyclopentadiene, however, they did not observe the formation of 4-oxopentenal (**21**).[9] Therefore, the path (c) is assumed to be more plausible for the formation of **5**—**7**, although further study is needed to establish a mechanism. Recently, it has been reported that 5,6-dioxabicyclo[2.2.1]heptane (**22**) underwent a rearrangement upon exposure to 1,4-diazabicyclo[2.2.2]octane to give levlinaldehyde (**23**) and that the possibility might arise *via* retro-aldol cleavage of 3-hydroxycyclopentanone (**24**) was ruled out.[10] The both rearrangements to ketoaldehydes (**5** and **23**) may proceed by the similar mechanism.

The mechanism of the formation of benzaldehyde can be explained by the rearrangement of the initially formed hydroperoxide (**25**) *via* norcaradiene intermediate (**26**). The formation of tropone can also be explained by the dehydration of **25**[3] and/or 6-hydroxy-2,4-cycloheptadienone (**2**).

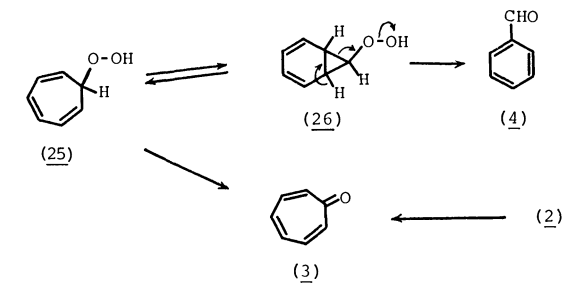

When the compounds (**1** and **2**) were treated with triethylamine, tropone was formed in quantitative yields, respectively. Furthermore, it was found that when the crude photooxidation mixture was allowed to stand in the presence of triethylamine at room temperature for 12 h, tropone was obtained in about 50% yield from tropilidene. Therefore, the photooxidation of tropilidenes will become a useful synthetic method of tropone and its derivatives.

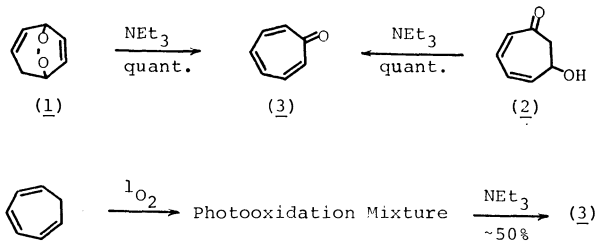

Since it has long been known that some epidioxy compounds are thermally and photochemically labile, and many interesting rearranged products have been derived from the epidioxy compounds, the thermal reaction of the compound (**1**), isolated for the first time, was studied. Heating of **1** in refluxing xylene afforded three isomeric products; *cis*-3,9-dioxatricyclo-[6.1.0.0^{2,4}]-5-nonene (**15**), 8-oxabicyclo[5.1.0]-4-octen-3-one (**27**) and 4-hydroxy-2,6-cycloheptadienone (**28**), in the yield of 25, 20, and 18%, respectively. The structure of the products including a stereochemistry of **15** was determined by the analyses of their NMR (Table 1) and the comparison of the NMR with those of their phenyl and methoxy derivatives obtained from phenyl- and methoxytropilidenes,[11] and general mechanistic consideration of the rearrangement of epidioxides.[12] Catalytic hydrogenation and acetylation of **28** afforded 4-hydroxycycloheptanone (**11**) and 4-acetoxy-2,6-cycloheptadienone (**29**).

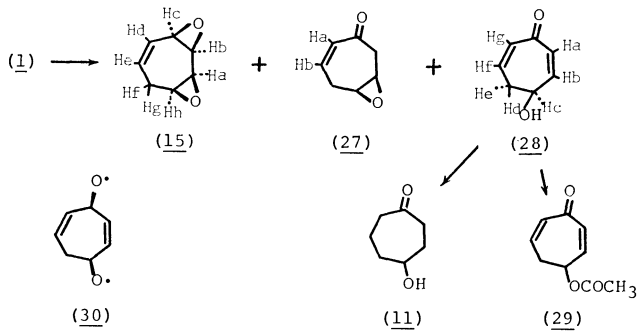

Although Prinzbach and Rücker have already reported[5] the synthesis of *cis*-diepoxide (**15**) as a mixture with other epoxides the present work is the first time to isolate **15** in pure state.

During the purification of the compounds (**15** and **27**) using column chromatography on silica gel, they gradually changed to the hydroxyketone (**28**). Therefore, **28** may be formed as secondary product by the rearrangement of **15** and/or **27** which may be formed as primary rearranged products of **1** *via* biradical intermediate (**30**). It would also be considered that epoxyketone (**27**) also results from the rearrangement of the diepoxide (**15**),[13] however, **27** could not be detected during the purification of **15**. Upon treatment of these isomers with triethylamine, tropone was obtained in quantitative yields.

Experimental

The mp values are uncorrected. The IR spectra were recorded with Hitachi EPI 510 and Hitachi 215 grating spectrophotometer and for the UV spectra Hitachi EPS 035 and Hitachi 323 spectrophotometers. The mass spectra were obtained with a Hitachi RMU 60 mass spectrometer. The NMR spectra were recorded on Varian HA-100, A-60 and Hitachi R-22 spectrometers.

Sensitized Photooxidation of Cycloheptatriene. A solution of cycloheptatriene (3.5 g, 0.038 mol) and Methylene Blue (100 mg) in methanol (250 ml) was irradiated by visible light (6×20 watt) for 2 days at around 25 °C by cooling with water while oxygen was slowly passed through the solution. The solvent was removed under reduced pressure, the residue was extracted with ether and an oil (2.13 g) was obtained from the extract. The oil was submitted to column chromatography on silica gel (60 g) and eluted with chloroform. From the effluents, benzaldehyde (trace), adduct (**1**) (402.5 mg, 8.4%), a mixture of ring opening products, tropone (**3**) (trace), and 6-hydroxy-2,4-cycloheptadienone (**2**) (1.09 g, 23.4%) were obtained by the order of the effluents. A mixture of ring opening products were further purified by a column chromatography on silica gel using a mixture of benzene and ethyl acetate as solvent, and *trans,trans*-6-oxoheptadienal dimethylacetal (**6**) (40.6 mg, 0.63%), a mixture of stereoisomer of 6-oxoheptadienal dimethylacetal (**7**) (35.3 mg, 0.55%), and *trans,trans*-6-oxoheptadienal (**5**) (18.5 mg, 0.4%) were obtained. **1**; Colorless oil; IR (neat) 1640, 1058, 995, 975, 905, 880, 750 cm^{-1}; MS *m/e* 124 (M^+, 22), 106 (92), 105 (100), 96 (29), 95 (49), 81 (28), 78 (37), 77 (96). Found: C, 67.53; H, 6.62%. Calcd for $C_7H_8O_2$: C, 67.73; H, 6.50%. **2**; Pale yellow oil; IR (CCl_4) 3430, 1658, 1640 cm^{-1}; UV λ_{max}^{MeOH} 240 nm (log ε, 3.38), 291 (3.66); MS *m/e* 124 (M^+, 23), 82 (27), 78 (15), 54 (100). Found: C, 67.83; H, 6.65%. Calcd for $C_7H_8O_2$: C, 67.73; H, 6.50%.
5; Colorless needles, mp 40—42.5 °C; IR (CCl_4) 2820, 2740, 1690, 1590 cm^{-1}; UV λ_{max}^{MeOH} 274 nm (log ε, 4.44), 352 (2.54), 341 (2.52); MS *m/e* 124 (M^+, 96), 109 (100), 81 (96), 58 (86), 41 (91). Found: C, 67.78; H, 6.66%. Calcd for $C_7H_8O_2$: C, 67.73; H, 6.50%. **6**; Colorless oil; IR (CCl_4) 1690, 1675, 1600 cm^{-1}; UV λ_{max}^{MeOH} 265.5 nm (log ε, 4.48), 330 (2.70); MS *m/e* 170 (M^+, 9), 139 (32), 127 (23), 95 (24), 81 (22), 75 (36), 44 (100). Found: C, 63.45; H, 8.18%. Calcd for $C_9H_{14}O_3$: C, 63.51; H, 8.29%. **7**; Colorless oil; IR (CCl_4) 1690, 1580 cm^{-1}; MS *m/e* 170 (M^+).

Catalytic Hydrogenation of 1, 2, and 5. a) A solution of **1** (200 mg, 1.61 mmol) in ethyl acetate (20 ml) was submitted for a catalytic hydrogenation in the presence of 5% Pd–C (10 mg) at room temperature and atmospheric pressure, and about 120 ml of hydrogen was absorbed. The catalyst was filtered off, the solvent was removed under reduced pressure, the residue was purified by column chromatography on silica gel using ethyl acetate as solvent. From the effluents, 4-hydroxycycloheptanone (**11**) (158 mg, 1.23 mmol, 76.4%) and 1,4-cycloheptanediol (**12**) (40 mg, 0.31 mmol, 19.3%) were obtained.[8]
b) A solution of **2** (100 mg, 0.8 mmol) in ethyl acetate (10 ml) was hydrogenated in the presence of 5% Pd–C (5 mg), and worked up the same as in the above procedure. 3-Hydroxycycloheptanone (**10**) was obtained in almost quantitative yield.[8]
c) A solution of 5 (30 mg) in ethyl acetate was hydrogenated in the presence of 5% Pd–C, and 6-oxoheptanal (**13**) was obtained as colorless oil in almost quantitative yield by purification using column chromatography on silica gel. The compound showed bp 100 °C/0.1 mmHg; IR (CCl_4) 2930, 1715, 1370 cm^{-1}; MS *m/e* 128 (M^+), and was identified by the comparison of its IR and NMR spectra with those of 6-oxoheptanal obtained by oxidation of 1-methylcyclohexene with ozone.

Formation of Tropone from the Photooxidation Products. a) A crude photooxidation mixture (2.62 g) obtained by oxidation of cycloheptatriene (3.5 g) in methanol (250 mg) in the presence of Methylene Blue (90 mg) was dissolved in methanol (50 ml) containing triethylamine (1 ml), and the solution was allowed to stand at room temperature for 12 h. The solvent was removed under reduced pressure, the residue was purified by column chromatography on silica gel using a mixture of chloroform and 3% methanol as solvent, and tropone (2.01 g, *ca.* 50%) was obtained. b) A solution of **1** (200 mg) and triethylamine (0.5 ml) in methanol (30 ml) was allowed to stand at room temperature for 12 h. The solvent was removed under reduced pressure, and tropone was obtained in almost quantitative yield.

Thermal Reaction of 1. A solution of **1** (602 mg, 4.86 mmol) in anhydrous xylene (30 ml) was refluxed under nitrogen atmosphere for 2 days. The solvent was removed under reduced pressure, the residue was submitted to column chromatography on silica gel (40 g) and eluted with a mixture of benzene and ethyl acetate (9:1), and in the order of the effluents, diepoxide (**15**) (150.5 mg, 1.21 mmol, 24.9%), ketoepoxide (**27**) (119.5 mg, 0.96 mmol, 19.8%), and ketoalcohol (**28**) (107 mg, 0.86 mmol, 17.8%) were obtained. The compounds (**15** and **27**) were gradually changed to **28** during further purification by chromatography on silica gel. **15**; Colorless crystals, mp 23—25 °C; IR (neat) 940, 915, 905, 840 cm^{-1}; MS *m/e* 124 (M^+, 4), 95 (35), 68 (87), 67 (47), 66 (100). Found: C, 67.50; H, 6.60%. Calcd for $C_7H_8O_2$: C, 67.73; H, 6.50%. **27**; Colorless oil; IR (neat) 1670, 820 cm^{-1}; UV λ_{max}^{MeOH} 228 nm (log ε, 3.89), 275 (2.63); MS *m/e* 124 (M^+, 5.5), 96 (42), 95 (29), 81 (28), 68 (100), 67 (26). Found: C, 68.02; H, 6.30%. **28**; Colorless oil; IR (CCl_4) 3430, 1650, 1615, 1430 cm^{-1}; UV λ_{max}^{MeOH} 232.5 nm (log ε, 4.06), 240 (3.97), 303 (3.11), 312 (3.08); MS *m/e* 124 (M^+, 28), 106 (47), 96 (54), 95 (91), 78 (77), 55 (54), 28 (100). Found: C, 67.94; H, 6.55%.
Acetate (**29**); Colorless oil; IR (neat) 1745, 1650, 1615 cm^{-1}.

References

1) This work was presented partly at the 6th symposium on the chemistry of non-benzenoid aromatic compounds, Fukuoka, October, 1973, and at the National Meeting of the Chemical Society of Japan, Tokyo, April, 1975.
2) Present address; Fuji Photofilm Co., Minami-ashigara, Kanagawa.
3) A. S. Kende and Y. C. Chu, *Tetrahedron Lett.*, **1970**, 4837.
4) P. Schiess and M. Wisson, *Helv. Chim. Acta*, **57**, 980, 1692 (1974).
5) H. Prinzbach and C. Rücker, *Angew. Chem.*, **88**, 611 (1976); *Angew. Chem. Int. Ed. Engl.*, **15**, 559 (1976).
6) a) Schenck had reported without any description of the condition and the yield that the photooxidation of cycloheptatriene gave tropone; G. O. Schenck, *Angew. Chem.*, **69**, 579 (1957); b) Many general synthetic methods of tropone have been reported; *cf.* T. Nozoe *et al.*, "Daiyuki Kagaku (Comprehensive Organic Chemistry)," ed by M. Kotake, Vol. 13, Tokyo (1960); F. Pietra, *Chem. Rev.*, **73**, 293 (1973); K. Takase, "Shin-Gikken Kagaku Koza," ed by Chemical Society of Japan, Vol. 14, (1977), p. 901.
7) Progress of the reaction was monitored by GLC analysis

on an SE-30 column, and at the end of the reaction, color of the solution was still deep blue.

8) IR and NMR of **10** were in agreement with those of 3-hydroxycycloheptanone kindly provided by Prof. H. Nozaki, Kyoto University; H. Nozaki, M. Kurita, and R. Noyori, *Tetrahedron Lett.*, **1968**, 2025. Authentic *cis*-1,4-cycloheptanediol and 4-hydroxycycloheptanone were prepared by the reduction of 8,9-dioxabicyclo[3.2.2]-6-nonene and 4-hydroxy-2,6-cycloheptadienone (**28**), respectively.

9) K. H. Schulte-Elte, B. Willhalm, and G. Ohloff, *Angew. Chem.*, **81**, 1049 (1969); *Angew. Chem. Int. Ed. Engl.*, **8**, 985 (1969); W. R. Adams and D. J. Trecker, *Tetrahedron*, **27**, 2631 (1971); N. Harada, S. Suzuki, H. Uda, and H. Ueno, *J. Am. Chem. Soc.*, **94**, 1777 (1972).

10) R. G. Solomon and M. F. Solomon, *J. Am. Chem. Soc.*, **99**, 3501 (1977).

11) M. Yagihara, Y. Kitahara, and T. Asao, unpublished results.

12) W. Adam, *Angew. Chem.*, **86**, 683 (1974); *Angew. Chem. Int. Ed. Engl.*, **13**, 619 (1974).

13) K. K. Maheshevari, P. de Mayo, and D. Wiegand, *Can. J. Chem.*, **48**, 3265 (1970).

Studies on Diazo Type Process. VI. Physico-chemical Studies on 1-(*p*-Dimethylaminophenylazo)-2-naphthol-3,6-disulfonic Acid in Aqueous Solutions

Shin SUZUKI,* Rebati C. DAS, and Kieko HARADA
Department of Image Science and Engineering, Faculty of Engineering, Chiba University, Yayoi-cho, Chiba-shi, Chiba 280
(Received January 5, 1978)

1-(*p*-Dimethylaminophenylazo)-2-naphthol-3,6-disulfonic acid is formed in many important commercial "dry process" diazo-printing. Some physico-chemical properties of this dye in solutions have been investigated. Its absorption spectra in various solvents and in water at various acidities have been discussed on the basis of azo-quinone hydrazone tautomeric and acid-base equilibria respectively. The dissociation constants of the acid-base equilibria in the pH range of 1—14 in aqueous solutions have been determined at 25 °C and 1.0 M ionic strength. Conductivities of aqueous solutions at various concentrations and temperatures have been interpreted on the basis of the colloidal nature of the dye. The polarograms of the compound have been drawn at various pH's and discussed. Polarographic method indicates complex formation between Zn(II) salt and the dye in the mole ratio of 1:2.

The authors are presently engaged in the study of the physico-chemical properties of azo dyes formed in "diazo-printing" processes. *p*-Dimethylaminobenzenediazonium chloride and 2-naphthol-3,6-disulfonic acid (R-acid) are very commonly used in many commercial "two-component" diazo papers as the photosensitive "diazo" and "coupler" components respectively for "dry process" printing.[1] The present paper reports the behaviour in aqueous solutions of the important azo dye formed by reaction between the above two components.

Experimental

Materials. *p*-Dimethylaminobenzenediazonium salt was prepared from the corresponding amine (analytical grade), precipitated as fluoroborate and then coupled with R-acid. The dye so prepared was recrystallized from water and stored in the absence of light. The other materials used were of analytical grade.

Methods. A Shimadzu (Model UV-180) spectrophotometer was used for absorbancy measurements. Conductance measurements were taken with a Yokokawa Denki universal bridge in conjunction with a Kikusui Denshi-Kogyo (Model 537) oscilloscope. A TOA Electronics Ltd. pH-meter (digital type, Model HM 20B) was used for pH measurement. Polarographic measurements were taken with a recording polarograph (Yanagimoto, Model PG-5). The DC current-voltage curves were obtained by measuring against saturated calomel electrode. Nitrogen gas was bubbled through the solution for 20—25 min immediately before measurement to remove dissolved oxygen. 0.02% gelatin was used as "suppressor," without which good polarographic waves were not obtained. The capillary characteristics of the dropping mercury electrode were $m=1.116$ mg s^{-1} and $\tau=3.49$ s at a mercury head of 74 cm. 1M solution of potassium nitrate was used as the supporting electrolyte.

Results and Discussion

Tautomerism. Azo dyes with a hydroxyl group located ortho- or para- to azo link are well known to exhibit azophenol-quinone hydrazone tautomerism.[2] This has been the subject of study of many workers[3–18] by various physico-chemical means *e.g.* IR, UV-Vis and NMR spectroscopies. Most of the works have been done in nonaqueous solvents or in the solid state and the tautomerism of the present compound has not been studied. It was thought necessary to study in greater detail the extent of tautomerism of the compound in aqueous solution.

Azo form Quinone hydrazone form

(A)

The absorption spectrum of the dye has been drawn in different polar and nonpolar solvents and shown in Fig. 1. In nonaqueous solvents, the dye derived from β-naphthol in stead of R-acid was used because the presence of sulfonate groups in R-acid makes the dye insoluble in nonaqueous solvents. The presence of $-SO_3H$ group is irrelevant in spectral analysis. Two characteristic features of the spectrum are (a) a band, usually appearing as a shoulder, at ≈430 nm and (b) a strong band at ≈500 nm whose shape and position are markedly dependent upon the solvent. The two bands at ≈430 and ≈500 nm can be unequivo-

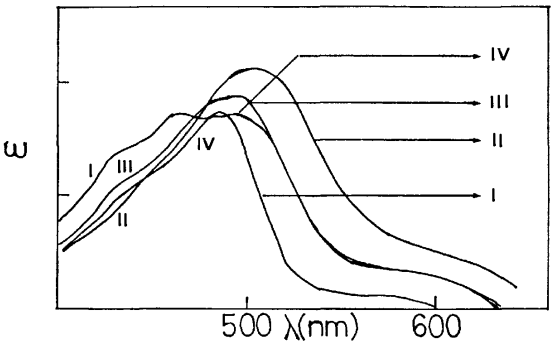

Fig. 1. Absorption spectrum of 1-(*p*-dimethylaminophenylazo)-2-naphthol in different solvents. I: Hexane, II: formamide, III: methanol, IV: chloroform. Molar absorptivity coefficents are arbitrary.

cally assigned to azo and quinone hydrazone forms respectively.[5,6,10,13,14] The band due to the hydrazone form is a split one which is clearly observed in non-polar solvents. The split bands coalesce and move to higher wavelength region in more polar solvents due to greater solute-solvent interaction. Similar splittting of bands have been observed at low temperatures.[7] It is clear that the polarity of the solvent has a greater influence on the shape and position of the spectrum of the quinone hydrazone tautomer which has a more polar structure of the two forms. As observed in the figure, the proportion of the quinone hydrazone form increases with the increase of the polarity of the solvent.[7,12] For the purpose of quantitative interpretation, the following ratio proposed by Ospenon[9] may be used,

$$\varepsilon_{quin}/\varepsilon_{azo} + \varepsilon_{quin},$$

where ε_{azo} and ε_{quin} are molar absorptivity of the azo and quinone hydrazone bands respectively, deduced from Gaussian analysis of the spectra. Table 1 gives the value of this ratio for different solvents. In water, this ratio is 0.80 which corresponds to 80% of the quinone hydrazone form in the tautomeric mixture, if the molar absorptivity of both the forms are nearly equal. This very high proportion of the quinone hydrazone form in aqueous solution of the dye may be ascribed to (i) strong polar nature of the solvent favoring more polar quinone hydrazone form[7,12] and (ii) intramolecular hydrogen bond between the hydroxyl oxygen** and the azo nitrogen atoms facilitating hydrogen transfer fom O- to N-atom,[12] which more than compensate the opposite influence of the highly electron donating $-N(CH_3)_2$ group.[15]

Table 1. Proportion of azo tautomer present in different solvents

Solvent	Hexane	Chloroform	Methanol	Water	Formamide
% Azo	33.3	24.5	23.8	20.5	17.9

The color of the dye in aqueous solutions is markedly dependent upon the pH of the solution as can be seen in Fig. 2. In highly acidic solutions (pH<1.5) the color is yellow-orange. At intermediate (7—9) and high (>12.0) pH's, the colors are violet and red respectively. The spectra of the dye at different pH's pass through clear isobestic points characteristic of equilibria (not shown in the figure). The following acid-base equilibria are obviously operative in aqueous solution.

$$RH_2^- \underset{H_2O}{\overset{K_1}{\rightleftharpoons}} RH^{2-} + H_3O^+$$

$$K_2 \uparrow\downarrow H_2O$$

$$R^{3-} + H_3O^+$$

Identification of the species, RH_2^-, RH^{2-} and R^{3-}, responsible for different colors, is clearly necessary.

** The term hydroxyl oxygen is used in keeping with the general practice, although in this compound it is actually a quinonic oxygen.

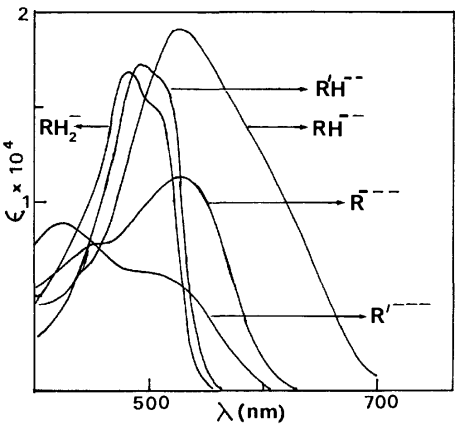

Fig. 2. Absorption spectra of different species of 1-phenylazo-2-naphthol-3,6-disulfonic acid and 1-(*p*-dimethylaminophenylazo) - 2 - naphthol - 3,6 - disulfonic acid in aqueous solutions. RH_2^-: Structure VI, RH^{2-}: structure II, R^{3-}: structure III, $R'H^{2-}$: structure VI without *p*-NR_2 group. R'^{3-}: structure III without *p*-NR_2 group.

In neutral medium the dye (RH^{2-}) may have structures I and/or II.

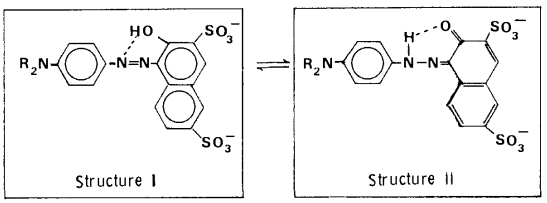

(B)

The aforesaid discussion has clearly indicated that RH^{2-} predominantly exists in sturcture II.

In highly alkaline medium (pH>12) where the phenolic group is completely dissociated (R---),*** the compound exists as structure III. The azo and quinone hydrazone structures are the different canonical forms of structure III.

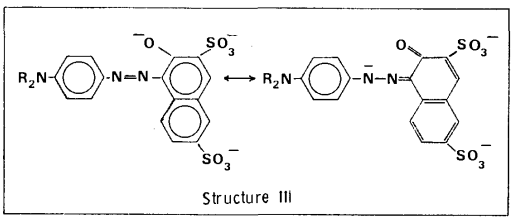

(C)

The spectrum of R^{3-} contains clear bands at ≈420 and ≈520 nm.

In acidic medium (pH<1.5), the species RH_2^-, may be formed by protonation of the N-atom of the tertiary amino group or the O-atom of the phenolic group.[19] Protonation of the amino group of the azo form causes the possibility of resonance between ammonium (structure IV) and azonium (structure V) forms, the azonium form being stabilized by reson-

*** Strictly speaking, the hydrogen belongs to the N-atom in the quinone hydrazone structure.

ance as shown.[20,21] Suggestion that proton could be bonded preferentially to the α-azo nitrogen in the protonated structure[22] is too untenable from theoretical argument and spectroscopic evidence[20,23] to warrant detailed discussion.

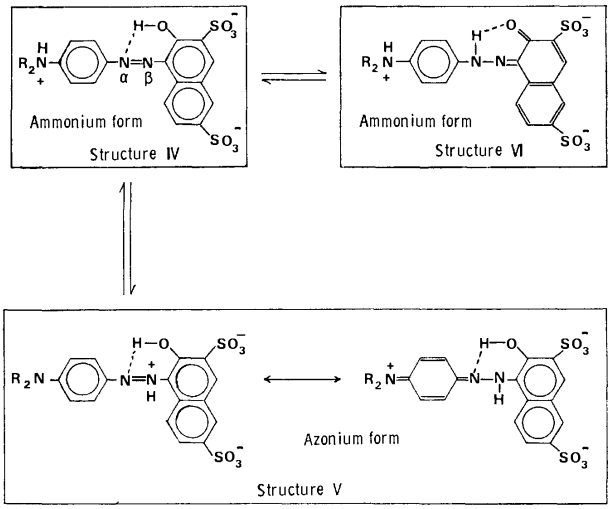

(D)

The possible azonium form of the quinone hydrazone structure (VI) lacks the resonance stabilization as in structure V and hence, may not be existing in solution, but the possibility cannot be completely ruled out. A suitable choice of structure for RH_2^- between structures IV, V, and VI can be made by comparison of the spectrum with that of the dye without the $-N(CH_3)_2$ group (1-phenylazo-2-naphthol-3,6-disulfonic acid). Figure 2 also shows the spectrum of 1-phenylazo-2-naphthol-3,6-disulfonic acid. At all pH's below 6.5 (spectrum measured upto pH 0.4) only one spectrum is observed which is similar with that of RH_2^- of the present dye. Similarly at pH's above 12, its spectrum remains unchanged. One may conclude that 1-phenylazo-2-naphthol-3,6-disulfonic acid only exists in two species containing undissociated and dissociated phenolic group (denoted as $R'H^{2-}$ and R'^{3-} respectively) at the pH range studied. The striking similarity of the spectra of RH_2^- and $R'H^{2-}$ is not surprising as it is well known that although aniline and *N*-substituted anilines in neutral solutions absorb at longer wavelengths and have higher intensities than benzene, the absorption characteristics of the anilinium ions are very similar to those of benzene.[24] From this it may be concluded that, in very acidic solutions, the protonation of the present dye takes place at the amino nitrogen atom and structure V is not present in any appreciable amount (this structure is not possible with $R'H^{2-}$) and consequently, RH_2^- probably exists predominantly in the quinone hydrazone from (structure VI). However, at very highly acidic media, there may be possibilities of protonation at other sities, particularly at the phenolic oxygen,[19] which has not been investigated in the present work.

Aggregation. Aggregation of some arylazonaphthols having formulae,† in aqueous solutions have

† Only the structure of the azo tautomers are presented.

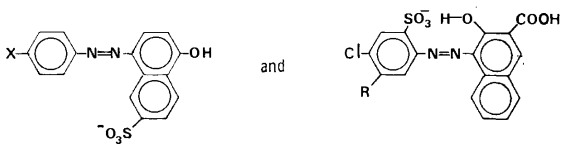

(E)

been reported from the non-Beer's law behavior of the solution spectra by Zollinger[25] and Monahan[26,27] *et al.* respectively. This may be due to intermolecular H-bonding through the phenolic or carboxylic hydrogen atom. In the present compound the hydroxyl group, which is present at ortho position, is H-bonded with the azo nitrogen atom (intramolecular H-bonding) and there would be less possibility of intermolecular hydrogen bonding. It is found that Beer's law is followed in dilute aqueous solutions (0.5×10^{-5} to 3×10^{-4} M). But addition of some electrolytes to a concentrated solution of the dye causes precipitation. It was, therefore, thought necessary to check the aggregation by another physical method.

Whereas the plots of equivalent conductance, Λ (ohm^{-1} cm^2 g equiv^{-1}) *vs.* $C^{1/2}$ (C=g eqiv dm^{-3})of a pure strong electrolyte follows Debye-Hückel-Onsager theory, the same in the case of a colloidal electrolyte has two conspicuous features: (a) a sudden deviation at low concentrations from theoretical Debye-Hückel-Onsager theory and (b) almost a constant value of Λ, or sometimes a weak minimum, at high concentrations.[28] Similar plot as prescribed for colloidal electrolytes was obtained as can be seen in Fig. 3.

Mushran and Prakash[29] have studied the conductance of several colloidal systems and have found that, in general, the "temperature of zero conductance" of a true electrolyte lies at about −40 °C, whereas in colloidal systems, this temperature ranges between −15 and −35 °C. This has been further verified by Srivastava, Seth, and Dey.[30] Conductances of three solutions of the present dye were determined at different temperatures. The plots of specific conductance, k (ohm^{-1} cm^{-1}) *vs.* temperature (°C) were linear and are shown in Fig. 4. The extrapolated value of the "temperature of zero conductance" was found to be −23 °C lending further evidence about the colloidal nature.

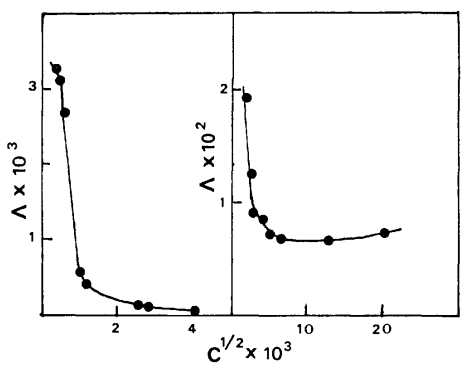

Fig. 3. Variation of equivalent conductance of 1-(*p*-dimethylaminophenylazo)-2-naphthol-3,6-disulfonic acid with square root of equivalent concentration.

TABLE 2. RESULTS OF pK_1 AND pK_2 OF THE AZO DYE AT 25 °C AND I=1.0 M

Concn of azo[a] $\times 10^5$		3.019	3.321	3.623	3.925	4.227	2.717	3.623	3.019	
$[H^+]$[a] $\times 10^5$		8.510	8.700	8.700	12.880	13.800	7.240	5.880	6.910	
580 nm	Abs	0.331	0.351	0.389	0.370	0.383	0.303	0.421	0.337	
	pK_1	3.68	3.72	3.70	3.69	3.71	3.72	3.74	3.74	
620 nm	Abs	0.237	0.252	0.279	0.268	0.279	0.219	0.299	0.240	
	pK_1	3.64	3.68	3.66	3.65	3.66	3.67	3.72	3.71	
Concn of azo[a] $\times 10^5$		1.811	2.415	2.717	3.019	3.623	3.321	3.925	2.113	3.019
$[H^+]$[a] $\times 10^{11}$		3.890	2.884	3.236	3.548	1.778	2.630	2.570	3.981	1.318
540 nm	Abs	0.299	0.375	0.423	0.482	0.535	0.510	0.599	0.345	0.430
	pK_2	10.63	10.53	10.49	10.54	10.56	10.53	10.52	10.58	10.56
600 nm	Abs	0.154	0.191	0.221	0.260	0.250	0.260	0.310	0.186	0.175
	pK_2	10.53	10.57	10.56	10.59	10.62	10.59	10.61	10.57	10.55

Av pK_1=3.69±0.03 : Av pK_2=10.56±0.03.

The molar absorptivities of different species as determined by separate sets of experiments are $\varepsilon_{RH^{2-}(580)}=69\pm1$, $\varepsilon_{RH^{2-}(620)}=0$, $\varepsilon_{RH^{2-}(540)}=19270\pm120$, $\varepsilon_{RH^{2-}(580)}=15380\pm98$, $\varepsilon_{RH^{2-}(600)}=13069\pm98$, $\varepsilon_{RH^{2-}(620)}=10772\pm82$, $\varepsilon_{R^{3-}(540)}=11864\pm94$, $\varepsilon_{R^{3-}(600)}=2367\pm18$

a) mol dm^{-3}.

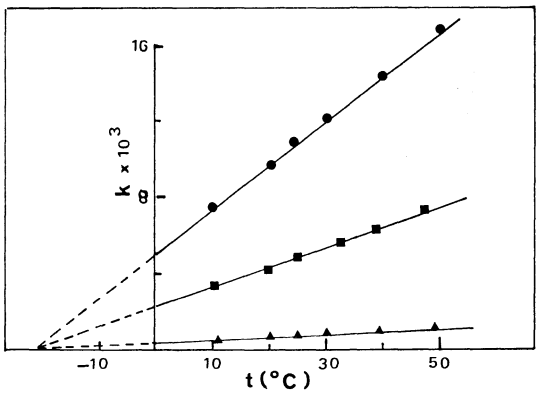

Fig. 4. Variation of specific conductance of 1-(*p*-dimethylaminophenylazo)-2-naphthol-3,6-disulfonic acid with temperature (centigrade).
Concentrations: ● 7.81×10^{-4} M, ■ 3.12×10^{-4} M, and ▲ 0.39×10^{-4} M.

From the foregoing observations one may be tempted to conclude that in the case of the aqueous solutions of the present dye, the dye-dye interaction through hydrogen bonding may not be responsible for the aggregation. More detailed study is necessary to throw light on the cause of aggregation of azo dyes in aqueous solutions.

In view of the colloidal nature of the dye, all equilibrium studies reported in the subsequent part of this paper have been carried out in as dilute solutions as possible.

Dissociation Constants. It was thought useful to determine the dissociation constants of the two dissociation processes existing in aqueous solutions. The following method was followed.

The pH's and absorbances at appropriate wavelengths of a series of solutions were measured. The pK_1 was calculated from the data of solutions at pH's where only RH_2^- and RH^{2-} exist in equilibrium. Similarly pK_2 was calculated from the data where RH^{2-} and R^{3-} co-exist. The molar absorptivity (ε) of RH_2^-, RH^{2-}, and R^{3-} species at appropriate wavelengths were determined separately by measuring absorbances of the dye solutions at suitable pH's where singular species exist. The method of calculation is shown below.

As a general case, where the following equilibrium is operative,

$$\underset{(1-\alpha)C}{HA} + H_2O \rightleftharpoons H_3O^+ + \underset{\alpha C}{A^-}$$

(for convenience the charge on the different species are omitted, α is the degree of dissociation and C is the molar concentration), absorbancy of the solution is given by the equation,

$$A = \varepsilon_{HA}(1-\alpha)Cl + \varepsilon_A Cl. \quad (1)$$

ε_{HA} and ε_H are molar absorptivity of HA and A respectively and l is the length of the light path. It follows from Eq. 1 that

$$\alpha C = \frac{A-\varepsilon_{HA}Cl}{(\varepsilon_A-\varepsilon_{HA})}. \quad (2)$$

Knowing α, K can be calculated from Eq. 3.

$$K = \frac{[H^+]\alpha}{1-\alpha}. \quad (3)$$

For the calculation of pK_1, absorbancies at wavelengths 580 and 620 nm were measured. Similarly data at 540 and 600 nm were used for calculation of pK_2. Table 2 gives pK_1 and pK_2 values at 25 °C and 1 M KNO_3 solution. The values are 3.69±0.03 and 10.56±0.03 respectively. The corresponding free energy changes (ΔG) of the first and second dissociation processes are 21.1 and 60.3 kJ mol^{-1} respectively. (1 J=0.2392 cal)

Reaction with Metal Salts. It has been reported that the presence of zinc salts during diazo-printing improves the image area and in some cases, the prints can be used as "intermediate prints on a transparent base."[31] Zinc chloride is also often used as "stabilizer" for diazonium salts.[32] It was, therefore, thought useful to study the complexation reaction of the dye with Zn(II). Spectrophotometric method was found unsuitable as it was observed that the absorption spectrum

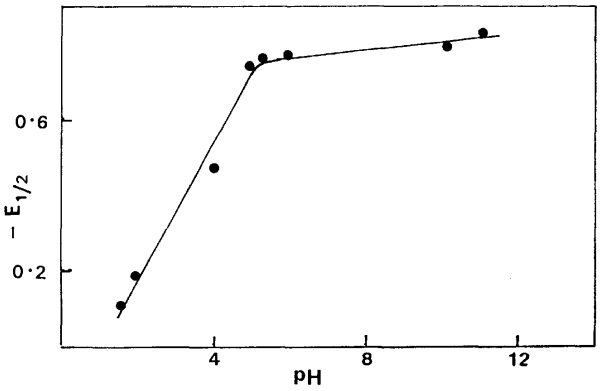

Fig. 5. Variation of half-wave potential of 1-(*p*-dimethylaminophenylazo)-2-naphthol-3,6-disulfonic acid with pH of solution. [azo]$=2.963\times10^{-4}$ M.

of the dye is not sufficiently altered in the presence of zinc(II) salts to make any quantitative study possible. Hence, polarographic method was tried.

In the preliminary runs in water, the polarograms of the dye indicated a two electron process reduction as calculated from the famous Heyrovsky-Ilkovic equation,[33]

$$E_{de} = E_{1/2} - \frac{RT}{zF}\log\frac{i}{i_d - i}, \qquad (4)$$

where E_{de} is the potential at the dropping mercury electrode, $E_{1/2}$ is the half-wave potential of the dye in solution, z is the number of electrons involved in the electrode reaction, i_d is the limiting diffusion current, i is the current corresponding to the potential E_{de}, and R, T, and F have their conventional meanings. A plot of the half-wave potential of the dye against pH, as shown in Fig. 5, indicate that $E_{1/2}$ is dependent on pH of the solution. The variation of $E_{1/2}$ with pH is not surprising in view of the fact that the nature of the species existing in solution is also dependent upon the hydrogen ion concentration.

The half-wave potential of zinc nitrate changed to more negative values in the presence of the azo dye, clearly indicating complex-formation between them. The shift of half-wave potential and the overall stability constant (β_n) of the complex, ML_n, formed is related by the following equation,

$$\Delta E_{1/2} = \frac{2.303RT}{zF}\log\beta_n + \frac{2.303RT}{zF}n\log[L]. \qquad (5)$$

([L]=concentration of the ligand in solution)

Figure 6 shows the plot of $\Delta E_{1/2}$ *vs.* log[L]. The slope of the plot gives $n\approx2$. Unfortunately, it was not possible to work at high concentrations of the ligand (azo dye) because, at high concentrations, it precipitates in the presence of the zinc salt. For this reason calculation of β_2 was not attempted. Essential condition for the calculation of β is that the concentration of the ligand should be much greater than that of the metal ion.[35] Qualitative conclusion regarding the metal: ligand ratio in the complex can, however, be made from our experimental plots.[36]

The authors are grateful to the Japan Society for the Promotion of Science for financial support. The

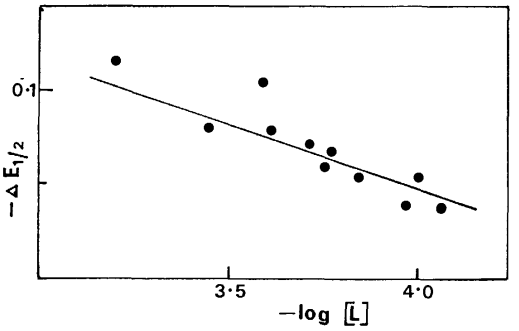

Fig. 6. Change of half-wave potential of zinc nitrate in the presence of the azo dye. Temperature: 25 °C, Medium: 1 M KNO_3, $[Zn^{2+}]=6.803\times10^{-5}$ M.

valuable discussions and suggestions of Dr. Stephen Stojanov, UNESCO Fellow, Tokyo Institute of Technology, and the help rendered during the experimental work of Mr. Thai Anh Tuan and Dr. Osamu Koga of this department are acknowledged (with thanks). Thanks are also due to Professor Rokuro Kuroda and Dr. Kouichi Oguma of Chiba University for permitting the use of the polarograph belonging to their laboratory.

References

1) J. Kosar, "Light Sensitive Systems," John Wiley & Sons, Inc. (1964), p. 252.
2) C. V. Stead, "The Chemistry of Synthetic Dyes," Vol. III, ed by K. Venkataraman, Academic Press (1970), p. 250.
3) D. Hadzi, *J. Chem. Soc.*, **1956**, 2143.
4) J. Morgan, *J. Chem. Soc.*, **1961**, 2151.
5) A. Burawoy, A. G. Salem, and A. R. Thompson, *J. Chem. Soc.*, **1952**, 4793.
6) E. Fischer and Y. F. Frei, *J. Chem. Soc.*, **1959**, 3159.
7) G. Gabor, Y. Frei, D. Gegiou, N. Kaganowitch, and E. Fischer, *Israel J. Chem.*, **5**, 193 (1967).
8) L. Reeves and R. S. Kaiser, *J. Org. Chem.*, **35**, 3670 (1970).
9) J. N. Ospenson, *Acta Chem. Scand.*, **4**, 1351 (1950); **5**, 491 (1951).
10) L. Skulski, *Bull Pol. Acad. Sci., Ser. Sci. Chim.*, **14**, 29, 37 (1966).
11) A. Burawoy and J. T. Chamberlain, *J. Chem. Soc.*, **1952**, 3734.
12) A. Burawoy, and A. R. Thompson, *J. Chem. Soc.*, **1953**, 1443.
13) A. H. Cook, P. G. Jones, and J. B. Polja, *J. Chem. Soc.*, **1949**, 1315.
14) D. Simov and St. Stojanov, *J. Mol. Struct.*, **19**, 255 (1973).
15) J. E. Kuder, *Tetrahedron*, **28**, 1973 (1972).
16) J. Griffiths, *J. Soc. Dyers Colour.*, **1972**, 106.
17) V. Bekarek, K. Rothschein, P. Vetesnik, and M. Vecera, *Tetrahedron Lett.*, **1968**, 3711.
18) A. H. Berric, P. Hampson, S. W. Longworth, and A. Mathias, *J. Chem. Soc., B*, **1968**, 1308.
19) R. W. Bigelow, *J. Phys. Chem.*, **80**, 2694 (1976).
20) G. E. Lewis, *Tetrahedron*, **10**, 129 (1960).
21) M. Isaks and H. H. Jaffe, *J. Am. Chem. Soc.*, **86**, 2209 (1964).
22) S. E. Sheppard and P. T. Newsome, *J. Am. Chem. Soc.*, **64**, 2937 (1942).

23) G. M. Badger, R. G. Buttery, and G. E. Lewis, *J. Chem. Soc.*, **1954**, 1888.
24) A. Wohl, *Bull. Soc. Chim. Fr.*, **6**, 1312 (1939).
25) H. Zollinger, "Azo and Diazo Chemistry," Interscience, New York (1961), p. 311.
26) A. R. Monahan and D. F. Blossey, *J. Phys. Chem.*, **74**, 4014 (1970).
27) A. R. Monahan, N. J. Germano, and D. F. Blossey, *J. Phys. Chem.*, **75**, 1227 (1971).
28) A. E. Alexander and P. Johnson, "Colloid Science," Oxford Univ. Press, London (1950), p. 677.
29) S. P. Mushran and S. Prakash, *J. Phys. Chem.*, **50**, 251 (1946).
30) S. C. Srivastava, R. L. Seth, and A. K. Dey, *J. Colloid Sci.* **17**, 86 (1962).
31) S. Suzuki, K. Harada, and M. Kurokawa, *Chiba Univ. Rep.*, **3**, 55 (1970).
32) Same as Ref. 1, p. 195.
33) J. Heyrovsky and D. Ilkovic, *Collect. Czech. Chem. Commun.*, **7**, 198 (1935).
34) T. Iijima, *Rev. of Polarography (Japan)*, **14**, 317 (1967).
35) J. J. Lignane, *Chem. Rev.*, **29**, 1 (1941).
36) R. M. Keefer, *J. Am. Chem. Soc.*, **68**, 2329 (1946).

A Convenient Method for the Synthesis of Dihydropyranobenzopyrandiones and Their Sulfur Analogs

J. R. MERCHANT* and S. Y. DIKE

Organic Chemistry Department, Institute of Science, Madame Cama Road, Bombay 400032, India

(Received May 23, 1977)

A general and convenient synthesis is described of a number of 2,3-dihydro-4*H*,5*H*-pyrano[3,2-*c*][1]benzopyran-4,5-diones and 2,3-dihydro-4*H*,5*H*-pyrano[2,3-*b*][1]benzothiopyran-4,5-diones. It involves the condensation of 4-hydroxycoumarin derivatives and their thioanalogs with different α,β-unsaturated acids in the presence of PPA. Assignments of the structures in both the cases are based on analytical and spectroscopic evidence.

The well-known anticoagulant activity of dicoumarol has led to the synthesis of large number of 4-hydroxycoumarin derivatives. Recently, a number of 3-[3-(*p*-substituted phenyl)-1,2,3,4-tetrahydro-1-naphthyl]-4-hydroxycoumarins have been reported, many of which show outstanding activity against both warfarin sensitive and warfarin resistant rats.[1]

A major degradation product of the fungal metabolite citromycetin has also a 4-hydroxycoumarin skeleton.[2]

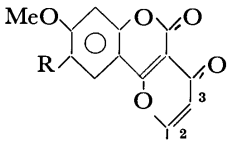

I R=OMe

II R=H; 2,3-dihydro

One of the common methods for the synthesis of such type of compounds is to treat the appropriate 4-hydroxycoumarin derivative with ethyl acetoacetate.[3] Also, in connection with the synthesis of radicinin and (±)-dihydroradicinin, Kato and coworkers[4] have reported the formation of similar types of compounds from the reaction of 4-hydroxy-2-pyranone and crotonoyl chloride in the presence of titanium tetrachloride in 1,1,2,2-tetrachloroethane. Using the same method, Whalley and coworkers[5] have synthesised di-*O*-methylcitromycinone (I).

The synthetic method described in the present work is a new route to a variety of 2,3-dihydro-4*H*,5*H*-pyrano-[3,2-*c*][1]benzopyran-4,5-diones which involves the reaction of 4-hydroxycoumarin derivatives with α,β-unsaturated acids in the presence of polyphosphoric acid. Besides acrylic acid other acids such as methcrylic, crotonic, β,β-dimethylacrylic and cinnamic acids could be used. Generally, the products were separated after quenching the reaction mixture with water, but in some cases, extraction with chloroform becomes necessary. Mechanistically the reaction follows a Friedel-Crafts acylation route. The reaction conditions used are compatible with a variety of substituents. The yields of the diones range from 35 to 40%. Hydroxycoumarins could be recoverred to the extent of 20 to 25%. In this context it is pertinent to mention that the cyanoethylation of 4-hydroxycoumarin derivative with acrylonitrile does not take place either in the presence of acidic or basic catalyst.

The structures of the compounds **1**—**17** were established on the basis of spectral and analytical data. In general dihydropyranobenzopyrandiones exhibit characteristic UV bands at λ_{max}^{MeOH} 215, 220, 280—290 (>C=O, lactonic), 315 nm (>C=O chromanone). The IR (Nujol or CH_2Cl_2) spectra of these compounds showed two bands: 1720—1740, 1660—1680. In the ^1H NMR spectra in $CDCl_3$ the aromatic protons appeared in the region δ 7.3—7.8 but in trifluoroacetic acid they were observed at δ 8.0.

Further, all of them readily gave 2,4-dinitrophenylhydrazones, which rule out the possibility of the acryloyloxy derivatives. As a model compound for the synthesis of I, 4-hydroxy-7-methoxycoumarin was reacted with crotonic acid in the presence of PPA to yield a crystalline solid (II) which readily gave 2,4-dinitrophenylhydrazone (mp 264 °C) and was found to be identical (mmp) with the compound previously reported.[5]

The above reaction was extended to 4-hydroxythiocoumarin and its derivatives. The chemistry of the latter is of interest since they also show the same pharmacological properties as the oxygen analogs. The activity of the sulfur analog of dicoumarol is 1/10th that of parent compound but the sulfur analog of warfarin has the same activity as that of dicoumarol.[6]

When 4-hydroxy(thiocoumarin) was allowed to reacted with α,β-unsaturated acids in the presence of polyphosphoric acid, the dihydropyranobenzothiopyrandiones were obtained in good yields (55—70%). However, the spectral data of these compounds revealed that they are not the expected 2,3-dihydro-4*H*,5*H*-pyrano[3,2-*c*][1]benzothiopyran-4,5-diones (III) but rather the isomeric chromanones (IV) as follows:

Firstly, their UV_{max}^{MeOH} showed only two principal bands namely at λ 225—230 nm and λ 305—315 nm indicating that absorption due to carbonyl group of the coumarin is absent.

The IR (CH_2Cl_2) of some typical compounds of this type showed bands at 1680 and 1610 cm^{-1} corresponding to CO frequencies at 4 and 5 positions.

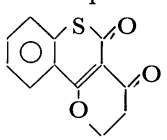

III

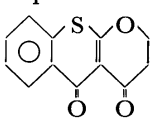

IV

Additional and convincing proof of the above structures was deduced from their NMR spectra.

In the latter, the aromatic protons were shifted much downfield to δ 8.7—9.1 whereas in the expected dihydropyrano[3,2-*c*][1]benzothiopyrandiones the signals for aromatic protons would have come to δ 7.4—7.8.

It would be expected that the hydrogen nucleus proximate to the carbonyl group *i.e.* at the position 6,

would be the most pertubed of aromatic hydrogen atoms of the 2,3-dihydro-4*H*,5*H*-pyrano[2,3-*b*][1]-benzothiopyran-4,5-diones. These aromatic protons constitute a complex system wherein the proton at position '6' produces a quartet at unusually low field. In contrast the aromatic protons of the angular 2,3-dihydro-4*H*,5*H*-pyrano[3,2-*c*][1]benzothiopyran-4,5-diones would absorb around δ 7.4—7.8 as observed by us as well as by Berndt and Holzer[7] in their work on the Beckmann rearrangement of oximes of thiochromanones.

This difference helps in distinguishing angular and linear pyranobenzothiopyrandione structures.

The general applicability of this reaction was demonstrated by reacting 4-hydroxy-8-methyl, 7-methyl; 6-methylcoumarins as well as thiocoumarins with α,β-unsaturated acids in presence of PPA.

Experimental

^{1}H NMR spectra were recorded for solutions in deuteriochloroform and trifluoroacetic acid with a Varian A-60 instrument (tetramethylsilane as an internal reference). IR spectra were measured for Nujol mulls and for solutions in dichloromethane with a Perkin-Elmer spectrophotometer. UV spectra were measured for solutions in methanol with a Hilger instrument. Melting points were determined in a sulfuric acid bath. Purity of compounds was tested by TLC in all cases.

General procedure for the condensation of 4-hydroxycoumarin or thiocoumarin with α,β-unsaturated acids.

To a freshly prepared mixture of phosphorus pentaoxide (20 g) and phosphoric acid (10 ml) preheated to 100° for 30 min, 4-hydroxycoumarin or thiocoumarin (0.01 mol) and α,β-unsaturated acid (0.01 mol) were added. Temperature of the reaction mixture was maintained at 120 °C for 5 h. Reaction mixture was then cooled and cold water added and it was kept overnight. The product that separated was collected by filtration and washed well with sodium hydrogencarbonate solution to remove unreacted hydroxycoumarin and then with water, dried and crystallized from appropriate solvents. In cases of extraction with chloroform, the solvent layer was thoroughly washed with sodium hydrogen carbonate solution, water and dried. Evaporation of the solvent yielded a solid in most cases, crystallised from suitable solvent.

a) From 4-Hydroxycoumarin:

1 Mp 196—197 °C (ethanol), brown needles. UV λ_{max} (MeOH) 215, 295 and 315 nm. NMR ($CDCl_3$+DMSO-d_6) δ: 2.9 (2H, t, CH_2 next to C=O, J=3 Hz); 4.95 (2H, t, CH_2 next to O, J=3 Hz); 7—8 (4H, m, ar.). Found: C, 66.5; H, 3.4%. Calcd for $C_{12}H_8O_4$: C, 66.7; H, 3.1%. 2,4-DNP, mp 258—260 °C. Found: N, 14.2%. Calcd for $C_{18}H_{12}N_4O_7$: N, 14.2%. Yield: 800 mg.

2 Mp 213—214 °C (methanol-acetone); brown plates. UV λ_{max} (MeOH) 215, 295, and 320 nm. IR (Nujol) cm^{-1}: 1750 (>C=O, coumarin); 1675 (>C=O, chromanone); 1600, 1550, and 1500 (ar.). NMR ($CDCl_3$+DMSO-d_6) δ: 1.2 (3H, d, CH_3, J=3.5 Hz); 2.8 (1H, m, <CH); 4.6—4.8 (2H, d, O-CH_2-, J=3 Hz); 7—8 (4H, m,ar.). Found: C, 67.5; H, 4.5%. Calcd for $C_{13}H_{10}O_4$: C, 67.8; H, 4.3%. 2,4-DNP, mp 254—255 °C. Found: 14.0%. Calcd for $C_{19}H_{14}N_4O_7$: N, 13.7%. Yield: 830 mg.

3 Mp 209—210 °C (ethanol), yellow plates. IR(Nujol) cm^{-1}: 1740 (>C=O, counarim); 1660 (>C=O, chromanone); 1600, 1550, 1500 (ar.). NMR (CF_3CO_2H) δ: 1.83 (3H, d, CH_3, J=6 Hz), 3.0 (2H, broad s, CH_2); 5.1—5.4 (1H, broad, m, >CH); 7.4—8.4 (4H, m, ar.). MS: *m/e* 230, 215 (M−15). Found: C, 67.8; H, 4.6%. Calcd for $C_{13}H_{10}O_4$: C, 67.8; H, 4.3%. 2,4-DNP, mp 264—265 °C. Found: N, 13.8%. Calcd for $C_{19}H_{14}N_4O_7$: N, 13.7%. Yield: 740 mg.

4 Mp 184—185 °C (ethanol), pale yellow needles. Found: C, 68.6; H, 5.1%. Calcd for $C_{14}H_{12}O_4$ C, 68.9; H, 4.9%. 2,4-DNP, mp 249—251 °C. Found: N, 13.5%. Calcd for $C_{20}H_{16}N_4O_7$: N, 13.7%. Yield: 840 mg.

5 Mp 258—260 °C (ethanol–chloroform), brown plates. Found: C, 73.9; H, 4.2%. Calcd for $C_{18}H_{12}O_4$: C, 74.0; H, 4.1%. Yield: 860 mg.

6 Mp 203—204 °C (acetic acid–water); brown needles. Found: C, 68.1; H, 4.0%. Calcd for $C_{13}H_{10}O_4$: C, 67.8; H, 4.3%. Yield: 835 mg.

7 Mp 209—210 °C (ethanol), brown needles. Found:

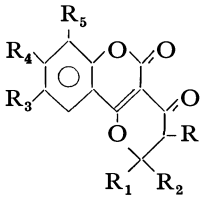

2,3-Dihydro-4*H*,5*H*-pyrano[3,2-*c*][1]benzopyran-4,5-diones.

1 R=R$_1$=R$_2$=R$_3$=R$_4$=R$_5$=H
2 R=Me; R$_2$=R$_5$=H
3 R=H; R$_1$=Me; R$_2$—R$_5$=H
4 R=H; R$_1$=R$_2$=Me; R$_3$—R$_5$=H
5 R=H; R$_1$=Ph; R$_2$—R$_5$=H
6 R=R$_1$=R$_2$=R$_4$=R$_5$=H; R$_3$=Me
7 R=R$_3$=Me; R$_1$=R$_2$=R$_4$=R$_5$=H
8 R$_1$=R$_3$=Me; R=R$_2$=R$_4$=R$_5$=H
9 R$_1$=R$_2$=R$_3$=Me; R=R$_4$=R$_5$=H
10 R=R$_1$=R$_2$=R$_3$=R$_5$=H; R$_4$=Me
11 R=R$_4$=Me; R$_1$=R$_2$=R$_3$=R$_5$=H
12 R$_1$=R$_4$=Me; R=R$_2$=R$_3$=R$_5$=H
13 R$_1$=R$_2$=R$_4$=Me; R=R$_3$=R$_5$=H
14 R=R$_1$=R$_2$=R$_3$=R$_4$=H; R$_5$=Me
15 R=R$_5$=Me; R$_1$=R$_2$=R$_3$=R$_4$=H
16 R$_1$=R$_5$=Me; R=R$_2$=R$_3$=R$_4$=H
17 R$_1$=R$_2$=R$_5$=Me; R=R$_3$=R$_4$=H

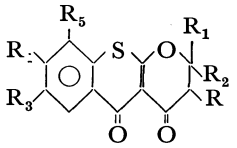

2,3-Dihydro-4*H*,5*H*-pyrano[2,3-*b*][1]benzothiopyran-4,5-diones.

18 R—R$_5$=H
19 R=Me; R$_1$—R$_5$=H
20 R$_1$=Me; R=R$_2$=R$_5$=H
21 R$_1$=R$_2$=Me; R=R$_2$—R$_5$=H
22 R$_3$=Me; R=R$_1$=R$_2$=R$_4$=R$_5$=H
23 R=R$_3$=Me; R$_1$=R$_2$=R$_4$=R$_5$=H
24 R$_2$=R$_3$=Me; R=R$_1$=R$_4$=R$_5$=H
25 R$_1$=R$_2$=R$_3$=Me; R=R$_4$=R$_5$=H
26 R$_1$=R$_4$=Me; R=R$_2$=R$_3$=R$_5$=H
27 R$_1$=R$_2$=R$_4$=Me; R=R$_3$=R$_5$=H
28 R—R$_4$=H; R$_5$=Me
29 R=R$_5$=Me; R$_1$—R$_4$=H
30 R$_1$=R$_5$=Me; R=R$_2$—R$_4$=H
31 R$_1$=R$_2$=R$_5$=Me; R=R$_3$=R$_4$=H

C, 68.7; H, 5.1%. Calcd for $C_{14}H_{12}O_4$: C, 68.9; H, 4.9%. 2,4-DNP, mp >280 °C. Found: N, 14.3%. Calcd for $C_{20}H_{16}N_4O_7$: N, 14.2%. Yield: 810 mg.

8 Mp 192—194 °C (benzene–acetone), brown cubes. IR (CH_2Cl_2) cm^{-1}: 1760 (>C=O, coumarin); 1650 (>C=O, chromanone); 1600, 1550, and 1500 (ar.). NMR ($CDCl_3$) δ: 1.7 (3H, d, CH–C<u>H</u>$_3$; J=6.5 Hz); 2.5 (3H, s, CH_3); 2.8 (2H, d, CH_2, J=7 Hz); 4.9—5.2 (1H, m, C<u>H</u>–); 7.2—7.8 (3H, m, ar.). Found: C, 69.1; H, 4.9%. Calcd for $C_{14}H_{12}O_4$: C, 68.9; H, 4.9%. Yield: 850 mg.

9 Mp 199—201 °C (ethanol), yellowish brown needles. Found: C, 69.6; H, 5.5%. Calcd for $C_{15}H_{14}O_4$: C, 69.8; H, 5.4%. 2,4-DNP, mp 268—270 °C. Found: N, 12.6%. Calcd for $C_{21}H_{18}N_4O_7$: N, 12.8%. Yield: 820 mg.

10 Mp 168 °C (ethanol–chloroform), brown needles. Found: C, 67.9; H, 4.4%. Calcd for $C_{13}H_{10}O_4$: C, 67.8; H, 4.3%. Yield: 790 mg.

11 Mp 183—185 °C (ethanol), pale brown needles. Found: C, 68.6; H, 5.2%. Calcd for $C_{14}H_{12}O_4$: C, 68.9; H, 4.9%. 2,4-DNP, mp —320 °C. Found: N, 14.2%. Calcd for $C_{20}H_{18}N_4O_7$: N, 14.2%. Yield: 800 mg.

12 Mp 170—171 °C (aqueous ethanol), yellow prisms. Found: C, 69.2; H, 4.9%. Calcd for $C_{14}H_{12}O_4$: C, 68.9; H, 4.9%. 2,4-DNP, mp 265—266 °C. Found: N, 14.4%. Calcd for $C_{20}H_{16}N_4O_7$: N, 14.2%. Yield: 780 mg.

13 Mp 158—160 °C (ethyl acetate–petroleum ether), yellow needles. IR (KBr) cm^{-1}: 1725 (>C=O, coumarin); 1680 (>C=O, chromanone) 1600, 1550, and 1500 (ar.). NMR ($CDCl_3$) δ: 1.63 $\left(6H, s, C\langle^{CH_3}_{CH_3}\right)$; 2.8 (2H, s, CH_2); 7.1—7.8 (3H, m, ar.). Found: C, 69.6; H, 5.6%. Calcd for $C_{15}H_{14}O_4$: C, 69.8; H, 5.4%. 2,4-DNP, mp 274—275 °C. Found: N, 15.9%; Calcd for $C_{21}H_{18}N_4O_7$: N, 15.7%. Yield: 720 mg.

14 Mp 221—223 °C (ethanol–chloroform), pale yellow needles. Found: C, 68.1; H, 4.2%. Calcd for $C_{13}H_{10}O_4$: C, 67.8; H, 3.9%. Yield: 680 mg.

15 Mp 225—227 °C (ethanol–chloroform), pale orange needles. Found: C, 69.2; H, 4.7%. Calcd for $C_{14}H_{12}O_4$: C, 68.9; H, 4.9%. 2,4-DNP, mp >290 °C. Found: N, 14.4%. Calcd for $C_{20}H_{16}N_4O_7$: N, 14.2%. Yield: 790 mg.

16 Mp 170—172 °C (ethanol–chloroform), brown needles. Found: C, 69.1; H, 5.2%. Calcd for $C_{14}H_{12}O_4$: C, 68.9; H, 4.9%. Yield: 900 mg.

17 Mp 165—167 °C (ethyl acetate–petroleum ether), brown prisms. Found: C, 69.6; H, 5.5%. Calcd for $C_{15}H_{14}O_4$: C, 69.8; H, 5.4%. 2,4-DNP, mp 279—280 °C. Found: N, 12.9%. Calcd for $C_{21}H_{18}N_4O_7$: N, 12.8%. Yield: 750 mg.

b) From 4-Hydroxy(thiocoumarin):

18 Mp 178—180 °C (ethanol–chloroform), pale yellow needles. UV (MeOH) λ_{max}: 230 and 315 nm. IR (CH_2Cl_2) cm^{-1}: 1710 (>C=O, chromanone); 1615 (>C=O, chromone), 1600, 1500 (ar.). NMR (CF_3CO_2H) δ: 3.9 (2H, t, CH_2 next to >C=O); 5.15 (2H, t, CH_2– next to –O–), 8.1—8.5 (3H, m, ar.), 8.83—9.1 (1H, m, ar.); MS: *m/e* 232, 204 (M−CO). Found: C, 62.4; H, 3.8%. Calcd for $C_{12}H_8O_3S$: C, 62.1; H, 3.5%. 2,4-DNP, mp 254—256 °C. Found: N, 13.4%. Calcd for $C_{18}H_{12}O_4$: N, 13.6%. Yield: 900 mg.

19 Mp 199—201 °C (ethanol), brown prisms. UV (MeOH) λ_{max} 230, 305 nm. Found: C, 63.3; H, 4.3%. Calcd for $C_{13}H_{10}O_3S$: C, 63.4; H, 4.1%. 2,4-DNP, mp 275—277 °C. Found: N, 13.1%. Calcd for $C_{19}H_{14}O_6N_4S$: N, 13.1%. Yield: 1.1 g.

20 Mp 203—205 °C (methanol), yellow prisms. IR (Nujol) cm^{-1}; 1700 (>C=O, chromanone); 1610 (>C=O, chromone), 1600, 1500 (ar.). NMR (CF_3CO_2H) δ: 1.9 (3H, d, CH_3, J=5 Hz); 3.2 (2H, broad t, CH_2– next to >C=O); 5.4 (2H, broad t, CH_2– next to –O–); 8.0 (3H, broad s, ar.); 8.75 (1H, broad d, ar. J=10 Hz). Yield: 1.3 g.

21 Bp 180—190 °C/2.5 mmHg, yellow oil. Found: C, 64.9; H, 4.7%. Calcd for $C_{14}H_{12}O_3S$: C, 64.6; H, 4.6%. 2,4-DNP, mp 220—221 °C. Found: N, 12.9%. Calcd for $C_{20}H_{16}N_4O_6S$: N, 12.7%). Yield: 900 mg.

22 Mp 194—195 °C (aqueous ethanol), brown prisms. Found: C, 63.6; H, 4.4%. Calcd for $C_{13}H_{10}O_3S$: C, 63.4; H, 4.1%. 2,4-DNP, mp 264—265 °C. Found: N, 13.6%. Calcd for $C_{19}H_{14}N_4O_6S$: N, 13.8%. Yield: 1.32 g.

23 Yellow oil. Found: C, 64.5; H, 4.8%. Calcd for $C_{14}H_{12}O_3S$: C, 64.6; H, 4.6%. 2,4-DNP, mp 205—207 °C. Found: N, 12.8%. Calcd for $C_{20}H_{16}N_4O_6S$: N, 12.7%. Yield: 1.1 g.

24 Mp 159—161 °C (aqueous ethanol), yellow prisms. Found: C, 64.4; H, 4.7%. Calcd for $C_{14}H_{12}O_3S$: C, 64.6; H, 4.6%. 2,4-DNP, mp 268—270 °C. Found: N, 12.8%. Calcd for $C_{20}H_{16}N_4O_6S$: N, 12.7%. Yield: 1.45 g.

25 Yellow oil. Found: C, 65.9; H, 5.4%. Calcd for $C_{15}H_{14}O_3S$: C, 65.7; H, 5.1%. 2,4-DNP, mp 260—261 °C. Found: N, 12.2%. Calcd for $C_{21}H_{18}N_4O_5S$: N, 12.3%. Yield: 1.2 g.

26 Mp 164—165 °C (benzene–petroleum ether), pale yellow needles. Found: C, 64.9; H, 4.8%. Calcd for $C_{14}H_{12}O_3S$: C, 64.6; H, 4.6%. Yield: 1.43 g.

27 Yellow oil. Found: C, 65.5; H, 4.9%. Calcd for $C_{15}H_{14}O_3S$: C, 65.7; H, 5.1%. 2,4-DNP, mp 205—207 °C. Found: N, 12.5%. Calcd for $C_{21}H_{18}N_4O_6S$: N, 12.3%. Yield: 1.2 g.

28 Mp 214—215 °C (acetic acid), pale yellow prisms. Found: C, 63.6; H, 4.3%. Calcd for $C_{13}H_{10}O_3S$: C, 63.4; H, 4.1%. Yield: 1.38 g.

29 Mp 226—228 °C (acetic acid), pale black needles. Found: C, 64.7; H, 4.9%. Calcd for $C_{14}H_{12}O_3S$: C, 64.6; H, 4.6%. Yield: 1.25 g.

30 Mp 203—204 °C (ethanol), pale brown needles. Found: C, 64.3; H, 4.5%. Calcd for $C_{14}H_{12}O_3S$: C, 64.6; H, 4.6%. Yield: 1.47 g.

31 Yellow oil. Found: C, 65.5; H, 5.1%. Calcd for $C_{15}H_{14}O_3S$: C, 65.7; H, 5.1%. Yield: 1.3 g.

We thank Dr. K. Nagarajan, Ciba-Geigy Research Centre, for IR and NMR spectra. Senior Research Fellowship from Council of Scientific and Industrial Research to (S.Y.D.) is gratefully acknowledged.

References

1) M. R. Hadler and R. S. Shadbolt, *Nature*, **253**, 275, (1975). M. R. Hadler, R. Radfern, and F. P. Rowe, *J. Hygiene*, **74**, 441 (1975). M. R. Hadler, and R. B. Rennison, *J. Hygiene*, **74**, 449 (1975).

2) G. W. K. Cavill, A. Robertson, and W. B. Whalley, *J. Chem. Soc.*, **1950**, 1031.

3) G. G. Badcock, F. M. Dean, A. Robertson, and W. B. Whalley, *J. Chem. Soc.*, **1950**, 903.

4) K. Kato, Y. Hirata, and S. Yamamura, *Chem. Commun.*, **1968**, 319.

5) S. A. Ali, J. W. Powell, and W. B. Whalley, *J. Chem. Soc., Perkin Trans. 1*, **1973**, 173.

6) P. S. Jamkhandi, S. Rajagopal, and S. M. Sirsi, *Ind. J. Exp. Biol.*, **6**, 224 (1968).

7) E. Berndt and G. Holzer, *Chem. Ber.*, **129**, 3462 (1976).

Studies on the Cannabinoid Field: Synthesis of New Cannabinoids from 4-Hydroxycoumarin and 4-Hydroxythiocoumarin by Pyridine-catalysed Condensation of Citral and Citronellal

S. Y. Dike and J. R. Merchant*

Department of Organic Chemistry, Institute of Science, Madame Cama Road, Bombay 400032, India

(Received June 27, 1977)

The reaction of 4-hydroxycoumarin and 4-hydroxythiocoumarin with citral in basic as well as acidic conditions led to the formation of tetrahydrocannabiol derivatives. With citronellal, the above hydroxycoumarins afforded the corresponding hexahydrocannabiol derivatives in moderate yields. The structures and the stereochemistry of the compounds obtained are established on the basis of spectral-analytical evidence.

In connection with studies[1] on the synthesis of cannabinoid analogs, we have investigated the reaction of 4-hydroxycoumarin (**1**) and 4-hydroxythiocoumarin (4-hydroxy-2*H*-1-benzothiopyran-2-one)(**2**) with citral and citronellal under different conditions. This work was prompted by the fact that both **1** and **2** can exist in tautomeric forms and that the hydroxyl group in them is highly acidic as indicated by their easy solubility in aqueous hydrogen carbonate solution. Another point of interest is the fact that the 4-hydroxycoumarin structure exists in a number of naturally occurring as well as physiological active compounds, such as the antibiotics novobiocin,[2] coumarmycin[3] and the well-known anticoagulants like dicoumarol[4] and warfarin.[5]

The reaction of **1** with citral in the presence of pyridine at 140 °C for 8 h or at 45—50 °C for 15 h gave a mixture of products, from which two compounds **3** and **4** could be isolated by careful chromatographic procedure. Their structural assignment is based on spectroscopic data, especially on NMR analysis.

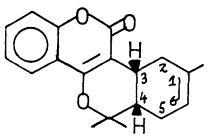

3

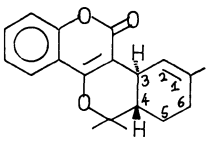

4

These compounds exhibit similar spectral features. The mass spectrum of both shows the molecular ion peak at *m/e* 296. It also shows an M−43 peak which suggests that they are not the normal chromene derivatives in which this peak is invariably absent. The elemental analysis indicates their molecular formula as $C_{19}H_{20}O_3$. The UV spectra of **3** and **4** are also similar and show λ_{max} at 215, 280, and 300 nm, indicating that the reaction occurred with the retention of the coumarin ring and thus ruling out the alternate chromone structure. This assumption is supported by their IR spectra which show a carbonyl band at 1720 cm^{-1} corresponding to the coumarin ring.

The analysis of NMR spectra of **3** and **4** is fully consistent with their assigned structures. The presence of a broad doublet for one olefinic proton at 5.19 and of a signal at 3.7 for one proton rules out other isomeric structures with a double bond in different positions in the cyclohexane ring. The four aromatic protons appeared as complex multiplet at 7.35—7.85. The assignment of *cis* configuration to **3** follows from the signal in the NMR at 3.7 due to the C_3 proton and the olefinic proton observed at 5.19 confirms that it is the Δ^6 isomer. A signal for the olefinic proton in **4** at 6.35 indicates that the compounds **3** and **4** should differ in the relative position of the double bond and the position of the C_3 proton at 3.25 supports a trans ring fusion. Hence **4** is a Δ^1-*trans* isomer. The NMR values we obtained are in perfect agreement with those obtained for Δ^1- and Δ^6-3,4-*cis*- and *trans*-tetrahydrocannabiol (abbreviated to THC) by Taylor[6] as well as by Archer and co-workers.[7]

It has been reported that the reaction of citral with *m*-benzenediols in the presence of pyridine generally leads to the synthesis of either chromene or cannabicyclol derivatives whereas, under acidic conditions, the formation of THC is observed.[8] The formation of THC in the presence of pyridine does not seem to have been reported so far.

In view of the above observations, the reaction of **1** which citral under mild acid conditions was studied. Compounds **3** and **4** were obtained after chromatography over silica gel (superimposable IR and NMR spectral).

Mechanistically, the formation of **3** and **4** in acid medium could be explained in the same way as that described by Crombie and Ponsford[8] for the acid-catalyzed reaction of citral and olivetol. In pyridine medium the formation of **3** and **4** is somewhat surprising. Our findings can be explained by the earlier observations of Berkoff and Crombie[9] who, in their work on citrylidenemalonic acid involving the reaction of citral with malonic acid in pyridine, reported that whenever "weak proton sources are available, the reaction seems to be so catalyzed." In our case strongly acidic 4-hydroxycoumarin is a good proton source and the reaction follows the acid-catalyzed pathway described above giving **3** and **4**.

Due to the ready reaction of citral with **1** leading to the formation of **3** and **4**, we investigated the reaction of **1** with citronellal in the presence of pyridine (molar proportions) at 140 °C. The reaction has not been studied so far and this is the first report of its use in the work connected with synthesis of cannabinoids. After purification by chromatography over silica gel only one compound **5** was isolated as a crystalline solid.

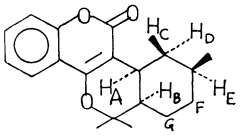

5

The mass spectrum of **5** showed a molecular ion peak at *m/e* 298. Comparison of the mass spectra of **3** and **5** revealed that the fragmentation pattern in both is very similar. The above observation and the analytical data show that **5** has the molecular composition $C_{19}H_{22}O_3$. Its UV showed λ_{max} at 215 and 300 nm whereas in the IR spectrum the carbonyl frequency was observed at 1725 cm^{-1}. The NMR spectrum of **5** revealed four aromatic protons at 7.1—7.7 in addition to other signals. The 100 MHz NMR ($CDCl_3$) spectrum provided additional proof for the structure as well as its stereochemistry.

The proton H_D unusually appears upfield at 0.66 as a quartet and is coupled to protons H_C (geminal), H_A, and H_E. The analysis of the system (three J_s of 11 Hz) requires the proton to be axial in order to have two ax-ax and one geminal couplings. This makes protons H_A, H_E, and H_D axial as H_D is diaxially coupled to H_A and H_E. Hence CH_3 at C_8 is equatorial. Arnone *et al.*[10] have also observed that the most stable conformation is the one where the Me group is disposed equatorially. The fact permits the assignment 1,3-*trans* configuration (Me-eq, H_B–A_X) to compound **5**. The chemical shifts of the methyl group on C_1 of **5** in the ^{13}C NMR spectrum (22.0 ppm, $CDCl_3$) confirms its equatorial orientation[11]. Similarly, the proton H_C appears unusually low field at 3.14 as a doublet of tripletes (J=11,3,3Hz). The samll values of coupling constants require the H_C proton to be equatorial. The abnormal downfield shift exhibited by the proton H_C as well as the upfield shift of the proton H_D are presumably due to the effect of a carbonyl functionality on the γ-methylene hydrogen and is well documented in the work of Williams *et al.*[12] on 11-keto steroids. Further, such methylene units are characterized by a marked upfieild shift of H axial and a very marked downfield shift of H equatorial. A triplet of doublet signals at 2.39 is attributed to the tertiary H_A proton as the protons oriented 1,3-diaxial to the methyl groups are deshielded. The H_A proton is coupled to H_B and H_D (J=11 Hz) diaxially. This defines the realtive stereochemistry of all the chiral centres in **5**.

Mechanistically the formation of **5** can be explained as shown in the upper part of the next column.

The pyridine catalysed condensation of citral and citronellal was studied with 4-hydroxythiocoumarin **2**.

The chemistry of the latter is equally interesting in that it possesses the same physiological and chemical properties as **1**. Citral on condensation with **2** afforded a yellow oil which after chromatography over silica gel was found to contain a mixture of isomers in the ratio 1:1 as evident from the NMR spectrum. Its IR showed only a strong carbonyl band at 1610 cm^{-1} indicating that the coumarin ring was not present.

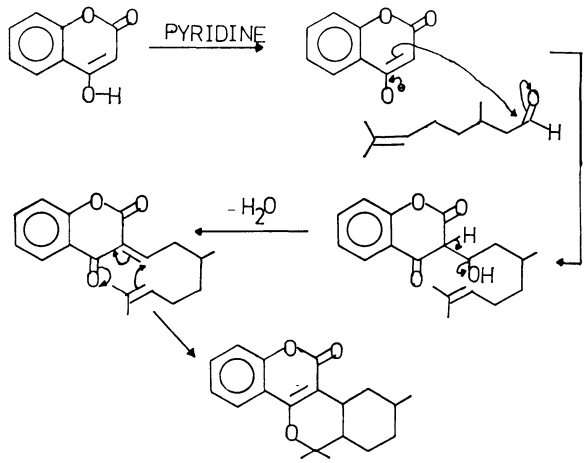

Further, in the NMR spectrum, the aromatic protons gave two different signals at 7.4 and 8.15 integrating for three and one proton, respectively, The latter downfield shift of the aromatic proton can be explained on the basis of structure **7** in which the C_5 proton is deshielded due to its proximity to the carbonyl group of the chromone ring whereas in **6** the aromatic protons would have shown signals at 7.3—7.8 as observed in **5**. The position of the olefinic protons at 6.2 and 5.4 of nearly equal intensity suggests that the compound is a mixture of stereoisomers, the difference being only in the position of double bond. The mass spectrum also favours the THC structure as, in addition to M^+ peak at 312, it shows M—43 peak due the loss of a C_3H_7 unit from the molecule.

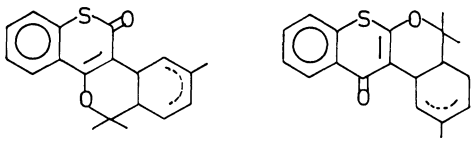

6 7

The reaction of **2** with citronellal in the presence of pyridine yielded after purification by chromatography only a single crystalline compound which was assigned the structure **8** on the basis of spectral-analytical evidence. Its UV spectrum showed only two bands at λ_{max} 225 and 305 nm and the IR gave a NMR spectrum was also in line with the structure **8** and the various proton positions indicated its stereochemistry as shown. In the mass spectrum prominent peaks were obtained at *m/e* 314, 299 (M—15), and 271 (M—43).

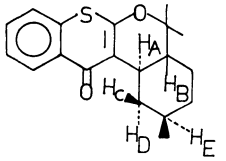

8

Experimental

Melting points are uncorrected. UV spectra were measured in MeOH solutions. The IR spectra were measured

with a Perkin Elmer instrument, NMR (values in δ, J in Hz, TMS as internal standard, $CDCl_3$ as solvent unless otherwise stated) with a Varian A-60 spectrophotometer, and NMR 100 MHz with a Varian XL-15-100 spectrometer. Chromatography was performed with silica gel.

General procedure for the condensation of hydroxycoumarins with citral and citronellal.

4-Hydroxycoumarin or 4-hydroxythiocoumarin (0.01 mol) in dry pyridine (0.01 mol) was heated to 120 °C, and pure citral or citronellal (0.01 mol) was added slowly in 10 min. The resulting reaction mixture was refluxed at 140 °C for 7 h and then extracted with chloroform. The solvent layer was washed with dilute HCl and water to remove pyridine. Further washing of aqueous $NaHCO_3$ solution was carried out in order to remove unreacted 4-hydroxycoumarin or thiocoumarin. The organic phase was dried (Na_2SO_4) followed by removal of the solvent to yield a gummy mass which was subjected to chromatography over silica gel.

(a) Compound **3** (0.2 g), mp 113—114 °C. Found: C, 77.2; H, 7.1%. Calcd for $C_{19}H_{20}O_3$: C, 77.0; H, 6.8%. IR (Nujol) cm^{-1}: 1720(CO), 1600, 1560 (ar.). NMR ($CDCl_3$) δ: 1.2 (3H, s, CH_3), 1.35 (3H, s, CH_3), 1.65 (3H, s, CH_3), 0.9—2.2 (4H, m), 2.89 (1H, br, d, C_2H), 3.7 (1H, m, C_3H), 5.19 (1H, s, olefinic-H), 7.35—7.8 (4H, m, ar.), MS *m/e*: 296, 281, 253, 213.

(b) Compound **4** (180 mg), a viscous oil. Found: C, 76.8; H, 6.9%. Calcd for $C_{19}H_{20}O_3$: C, 77.0; H, 6.8%. IR (CH_2Cl_2) cm^{-1}: 1720 (CO), 1600, 1500 (ar.). NMR ($CDCl_3$)δ: 1.2 (3H, s, CH_3), 1.55 (1H, s, CH_3), 1.66 (1H, s, CH_3), 0.9—2.5 (4H, m), 3.2 (1H, br, m, C_3H), 6.35 (1H, br, d, olefinic-H), 7.3—7.85 (4H, m, ar.). MS *m/e*: 296, 281, 253, 213. Compound **5** from citronellal (600 mg), mp 113—114 °C (light petroleum ether (40—60 °C)). Found: C, 76.7; H, 7.4%. Calcd for $C_{19}H_{22}O_3$: C, 76.5; H, 7.4%. IR (CH_2Cl_2) cm^{-1}: 1725 (CO), 1600, 1500 (ar.). NMR ($CDCl_3$: 60 MHz) δ: 0.66 (1H, q, J=11 Hz, 11 Hz, and 11 Hz, H_D), 1.0 (3H, d, CH_3), 1.2 (3H, s, CH_3), 1.55 (3H, s, CH_3), 1.8—2.0 (6H, m), 2.4 (1H, 3d, H_A), 3.1 (1H, m, H_C), 7.35—7.8 (4H, m, ar.). NMR ($CDCl_3$, 100 MHz) δ: 0.66 (1H, q, $J_{DC}=J_{DE}$=11.5 Hz), 0.96 (3H, d, CH_3), 1.2 (1H, s, CH_3), 1.54 (1H, s, CH_3), 0.90—2.00 (6H, br, m, CH_{2F}, CH_{2G}, H_E, H_B), 2.39 (1H, 3d, $J_{AD}=J_{CE}$=3 Hz), 7.35—7.78 (4H, m, ar.). ^{13}C NMR: 19.47 (q, C_{12} or C_{13}), 22.00 (q, C_8), 35.07 (T, C_5), 37.2 (T, C_9), 26.91 (T, C_6), 27.35 (q, C_{12}, C_{13}), 32.13 (d, C_7), 34.15 (d, C_{10}), 48.2 (d, C_{11}), 81.05 (s, C_4) ppm.

(c) Compound **7**, from 4-hydroxythiocoumarin and citral viscous oil, 1 : 1 mixture. Found: C, 73.1; H, 6.5%; Calcd for $C_{19}H_{28}O_2S$: C, 73.4; H, 6.7%. IR (CH_2Cl_2) cm^{-1}: 1610 (>C=O), 1600, 1500 (ar.). NMR (CCl_4) δ: 1.25 (3H, s, CH_3), 1.4 (1H, s, CH_3), 1.65 (1H, d, CH_3), 1.8—2.5 (5H, m), 3.2 (1H, m, CH), 5.4 (1H, br, m, olefinic H), 6.2 (1H, d, olefinic H), 7.42 (3H, s, ar.), 8.15 (1H, broad, ar.).

(d) Compound **8**, from 4-hydroxythiocoumarin and citronellal (400 mg), mp 172—175 °C (ethyl acetate). Found C, 72,6; H, 7.0%; Calcd for $C_{19}H_{22}O_2S$: C, 72.8; H, 7.1%. IR (KBr) cm^{-1}: 1610 (>C=O), 1600, 1500 (ar.). NMR ($CDCl_3$) δ: 0.56 (1H, q, J=11.5, 11.5, 11.5 Hz, H_D), 1.0 (3H, d, CH_3), 1.2 (3H, s, CH_3), 1.5 (3H, s, CH_3), 1.8—2.2 (5H, m), 2.51 (1H, 3d, J=11.5 Hz, 3.5 Hz, 3.5 Hz, H_A), 3.0 (1H, 2t, J=11.5, 11.5, 11.5 Hz, H_C), 7.35 (3H, m, ar.), 8.15 (1H, m, ar.), MS *m/e*: 314, 299, 271.

We are grateful to Dr. V. V. Kane, Ortho Pharmaceutical Corporation, U.S.A., for providing ^1H NMR and ^{13}C NMR data as well as for valuable suggestions. We wish to thank the staff of Ciba-Geigy Research Centre and the Hoechst Research Centre, Bombay, for IR, NMR, and mass spectral data. One of us (S.Y.D.) wishes to thank the C.S.I.R., New Delhi for financial assistance.

References

1) S. Y. Dike, M. S. Kamath, and J. R. Merchant, *Experientia*, **33**, 985 (1977).

2) B. K. Vaterlaus, K. Doebel, J. Kiss, A. I. Rachlin, and H. Spiegelberg, *Experientia*, **19**, 383 (1963).

3) H. Kawaguchi, T. Miyaki, and H. Tsukiura, *J. Antibiot. Ser. A*, **18**, 220 (1965); *Chem. Abstr.*, **64**, 3462 (1966).

4) K. P. Link, *Harvey Lect.*, **39**, 162 (1943—1944); *Chem. Abstr.*, **39**, 3856 (1945).

5) M. A. Stahmann, M. Ikawa, and K. P. Link, U. S. Pat., 2427578 (1947); *Chem. Abstr.*, **42**, 603 (1948).

6) E. C. Taylor, K. Lenard, and Y. Shvo, *J. Am. Chem. Soc.*, **88**, 367 (1966).

7) R. A. Archer, D. B. Boyd, P. V. Demurco, I. J. Tyminski, and N. L. Allinger, *J. Am. Chem. Soc.*, **92**, 5200 (1970).

8) L. Crombie and R. Ponsford, *J. Chem. Soc., C*, **1971**, 800.

9) C. E. Berkoff and L. Crombie, *J. Chem. Soc.*, **1960**, 3740.

10) A. Arnone, L. Merlini, and S. Servi, *Tetrahedron*, **31**, 3093 (1975).

11) J. B. Stothers, "^{13}C NMR Spectroscopy," Academic Press, London (1972), p. 66.

12) D. H. Williams, N. S. Bhacca, and C. Djerassi, *J. Am. Chem. Soc.*, **85**, 2810 (1963).

Phthalimides. III.[1,2] Ammonolysis, Aminolysis, Hydrazinolysis, Pyrolysis, and Action of Grignard Reagents on Phthalimide Derivatives

A. F. M. Fahmy,* N. F. Aly, and M. O. Orabi
Faculty of Science, Ain Shams University, Abbassia, Cairo, Egypt

(Received September, 14 1977)

N-Hydroxyphthalimide undergoes ammonolysis to give phthalimide. *N*-(Aroyloxy)phthalimides undergo alcoholysis followed by ammonolysis to give mixtures of phthalimide and ester. *N*-(Arylsulfonyloxy)phthalimides undergo ammonolysis, followed by Lossen rearrangement to give mixtures of 2,4-quinazolinedione and ammonium salts of arenesulfonic acids. *N*-Hydroxyphthalimide undergoes aminolysis to give the corresponding *N*-arylphthalimides. *N*-Hydroxyphthalimide reacts with hydrazine hydrate and/or phenylhydrazine in acetic acid or ethanol to give the corresponding 1,4-phthalazinedione, or by fusion to give phthalimide and *N*-phenylphthalimide, respectively. Pyrolysis of *N*-hydroxyphthalimide gives phthalimide, and *N*-(aroyloxy)phthalimides give mixtures of phthalimide and carboxylic acids. *N*-(Arylsulfonyloxy)phthalimides give mixture of phthalimide and arenesulfonic acids. However, pyrolysis of *N*-(arylcarbamoyloxy)phthalimides gave *N*-arylphthalimides. *N*-Hydroxyphthalimide reacts with phenylmagnesium bromide to give 1,1-diphenyl-3-(phenylimino)-1,3-dihydroisobenzofuran *via* ring opening followed Beckmann rearrangement, while *N*-(arylsulfonyloxy)phthalimides react with arylmagnesium bromide to give mixtures of [*O*-(arylamino)phenyl]diarylmethanols, and arenesulfonic acids *via* ring opening followed by Lossen rearrangement.

In a previous publication[1] *N*-(arylsulfonyloxy)phthalimides were reported to undergo base-catalyzed Lossen rearrangement with amines and acid-catalyzed Beckmann rearrangement with anhydrous aluminium chloride in the presence of aromatic substrates. We have reinvestigated the problem imide rearrangement and ring opening with different types of imides under different reaction conditions.

I. Ammonolysis. The hitherto unknown reaction of *N*-hydroxyphthalimide, and its *O*-arylsulfonyl and *O*-aroyl derivatives with ammonia was investigated. *N*-Hydroxyphthalimide (**1**) reacts with ethanolie ammonia to give phthalimide (**2**).

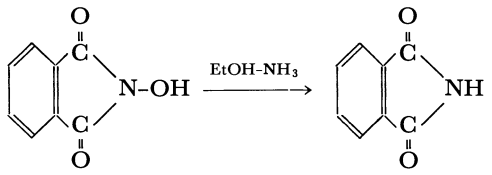

(**1**) (**2**)

N-(Aroyloxy)phthalimides (**3**) undergo ammonolysis to give mixtures of phthalimide (**2**), esters (**4a**—**d**) *via* the intermediate *N*-hydroxyphthalimide (**1**).

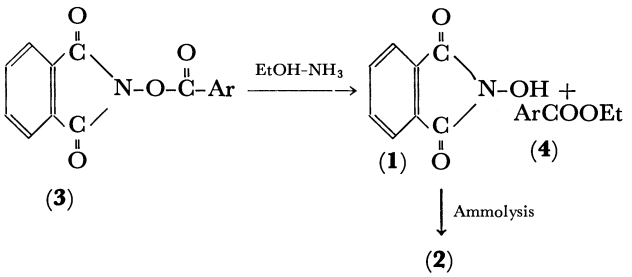

(**3**) (**1**) (**4**) (**2**)

a: Ar=C_6H_5; **b**: Ar=$C_6H_4CH_3$(*p*-);
c: Ar=$C_6H_4OCH_3$(*p*-); **d**: Ar=C_6H_4Cl(*p*-).

The reaction is actually alcoholysis, followed by ammonolysis. It was found that *N*-(arylsulfonyloxy)-phthalimides (**5a** and **b**) undergo ammonolysis *via* Lossen-rearrangement to give mixture of 2,4-quinazolinedione (**6**) and ammonium salts of arenesulfonic acids (**7a** and **b**).

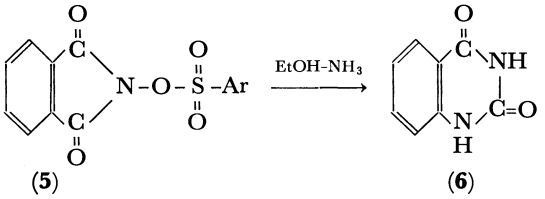

(**5**) (**6**) + $ArSO_3^+NH_4$ (**7**)

a: Ar=C_6H_5; **b**: Ar=$C_6H_4CH_3$(*p*-)

The reaction probably takes place according to Scheme 1.

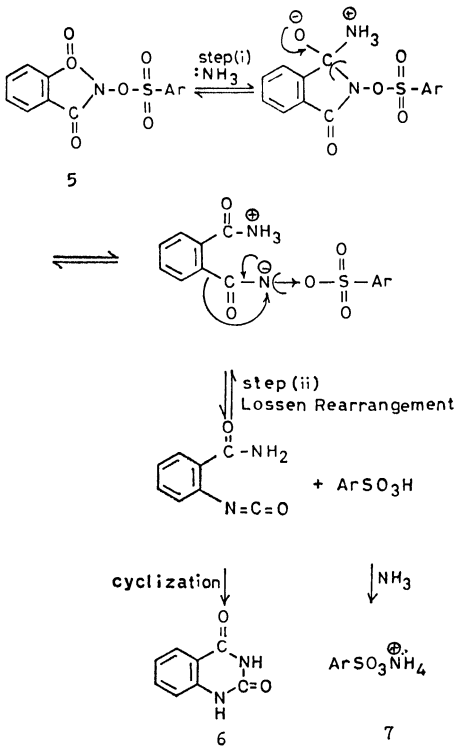

Scheme 1.

II. Aminolysis. When **1** is allowed to react with aromatic amines, and/or amino acids, it undergoes aminolysis to give *N*-arylphthalimides (**8a**—**m**).

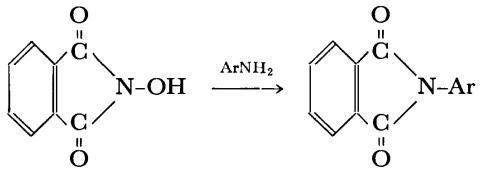

(1) (8)

a: Ar=C_6H_5, **b**: Ar=$C_6H_4CH_3(o)$, **c**: Ar=$C_6H_4CH_3(p)$, **d**: Ar=$C_6H_4OCH_3(o)$, **e**: Ar=$C_6H_4OCH_3(p)$, **f**: Ar=$C_6H_4Cl(o)$, **g**: Ar=$C_6H_4Cl(m)$, **h**: Ar=$C_6H_4Cl(p)$, **i**: Ar=$C_6H_4Br(p)$, **j**: Ar=$C_6H_5NO_2(p)$, **k**: $C_6H_4COOH(o)$, **l**: Ar=$C_6H_4COOH(m)$, **m**: Ar=$C_6H_4COOH(p)$

III. Hydrazinolysis. A novel reaction of **1** with hydrazines was found to occur under different conditions.

N-Hydroxyphthalimide (**1**) reacts with hydrzaines in acetic acid or ethanol to give the corresponding 1,4-phthalazinedione (**9a** and **b**)

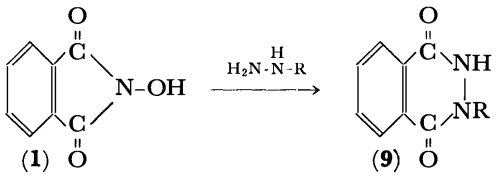

(1) (9)

a: R=H **b**: R=C_6H_5

It was also found that **1** reacts with hydrazine hydrate, and/or phenylhydrazine by fusion at 400 °C to give phthalimide (**2**), and *N*-phenylphthalimide (**8a**), respectively

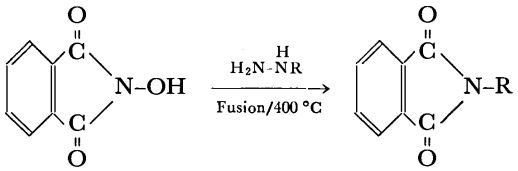

(1) **2**: R=H **8a**: R=C_6H_5

The reaction takes place according to Scheme 2.

This was confirmed by the fact that heating of *N*-anilinophthalimide (**10b**) at 200 °C for 2 h gives 2-phenyl-1,4-phthalazinedione (**9b**) in 67% yield, and the latter on pyrolysis at 400 °C giving *N*-phenylphthalimide (**8a**) in 65% yield.

The results shows that **9b** and **10b** are intermediates in Scheme 2.

IV. Pyrolysis. It was found that **1** gives **2** on pyrolysis quantitatively. We studied the thermal decomposition of *N*-hydroxyphthalimide derivatives to see the effect of substituents on the mode of pyrolysis.

Pyrolysis of (**3a—d**) give mixtures of **2** and the corresponding acids (**11a—d**)

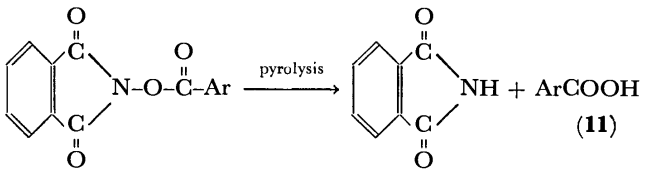

(3) (2) (11)

a: Ar=C_6H_5, **b**: Ar=$C_6H_4CH_3(p)$, **c**: Ar=$C_6H_4OCH_3(p)$, **d**: Ar=$C_6H_4Cl(p)$

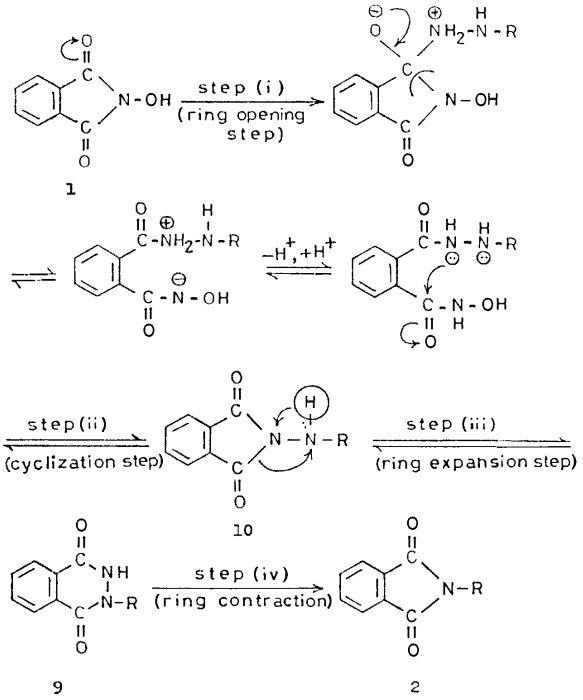

Scheme 2.

Similarly **5a** and **b** undergo pyrolysis to give mixtures of **2** and the corresponding arenesulfonic acids (**12**).

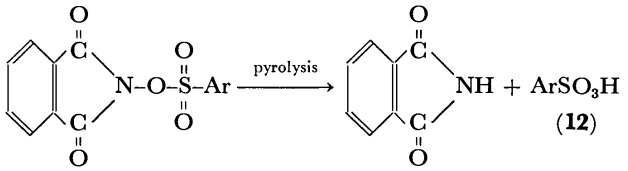

(5) (2) (12)

a: Ar=C_6H_5, **b**: Ar=$C_6H_4CH_3(p)$

However, *N*-(arylcarbamoyloxy)phthalimides (**13a—d**) give *N*-arylphthalimides (**8a, e, h, j**) by pyrolysis.

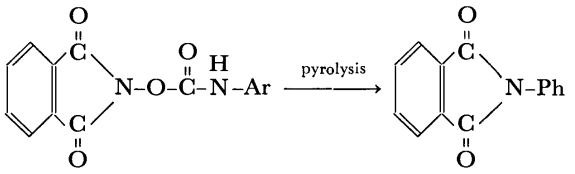

(13) (8)

a: Ar=C_6H_5, **e**: Ar=$C_6H_4OCH_3(p)$, **h**: Ar=$C_6H_4Cl(p)$, **j**: Ar=$C_6H_4NO_2(p)$

V. Addition of Grignard Reagents. A novel reaction of **1** and **5** with Grignard reagents was studied.

N-Hydroxyphthalimides reacts with phenylmagnesium bromide to give 1,1-diphenyl-3-(phenylimino)-1,3-dihydroisobenzofuran (**14**).

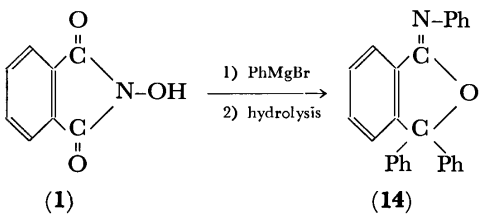

(1) (14)

The reaction might be the ring opening followed by

Beckmann rearrangement, and cyclization.

N-(Arylsulfonyloxy)phthalimides (**5**) were used instead of *N*-hydroxyphthalimide (**1**) in order to see the effect of the introduction of arylsulfonyl group on the imide reaction with Grignard reagent.

N-(Arylsulfonyloxy)phthalimide (**5a** and **b**) react with arylmagnesium bromide to give mixtures of [*O*-(arylamino)phenyl]diphenylmethanols (**15a—d**), and (**12a** and **b**).

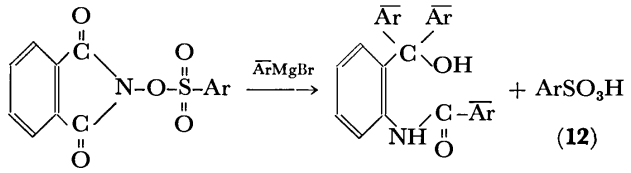

(**5**) (**15**) (**12**)

a: $\overline{Ar}=C_6H_5$, **b**: $\overline{Ar}=C_6H_4CH_3(p)$,

c: $\overline{Ar}=C_6H_4OCH_3(o)$, **d**: $\overline{Ar}=C_6H_4OCH_3(p)$

Structures of products (**15a—d**) were confirmed from their identity with products obtained by the reaction of arylmagnesium bromides with the corresponding 2-aryl-3,1-benzoxazin-4-ones (**16**).

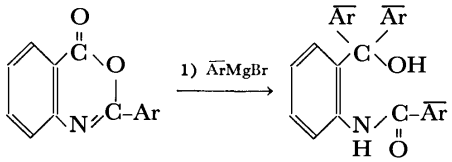

(**16**) (**15**)

The reaction is actually the ring opening of the phthalimide ring with Grignard reagents followed by Lossen rearrangement.

Experimental

All the melting points are not corrected. IR spectra were measured on a Unicam Sp 1200 spectrophotometer using KBr wafer technique. Mass spectrum was measured with A.E.I.M.S. 12 single focusing mass spectrophotometer at a beam energy of 70 eV. and accelerating voltage of 8 kV. The sample was introduced to the sources *via* a direct inlet system the operating temperature being 270 °C.

I. Ammonolysis of N-*Hydroxyphthalimide and Its Derivatives.*

A. Action of Ethanolic Ammonia on N-*Hydroxyphthalimide (1); Formation of 2*: A mixture of *N*-hydroxyphthalimide (**1**) (prepared *via* phthalic anhydride and hydroxylamine)[3] (0.005 mol) and concd ethanolic ammonia (40 ml) was heated under reflux for about 3 h, then concentrated, and cooled. The solid obtained was filtered off, and recrystallised from methanol to give **2** as white crystals (mp 231—232 °C, yield 82%). It was confirmed to be phthalimide **2** by comparison of mp and mixture mp with those of an authentic sample[4] and its IR spectrum.[5,6]

B. Action of Ethanolic Ammonia on N-*(Aroyloxy)phthalimides (3a—d); Formation of 2*: A mixture of *N*-(aroyloxy)phthalimides (**3**) (prepared from *N*-hydroxyphthalimide and aroyl halides)[7] (0.005 mol), and concd ethanolic ammonia (50 ml) was heated under reflux for 3 h, then cooled to afford white crystals. It was filtered off, and recrystallized from ethanol to give white crystals (mp 230—231 °C, yield 71%). It was confirmed to be phthalimide by comparison of mp and mixture mp with authentic sample.[4]

The filtrate was heated under reflux with KOH for 30 min, cooled and acidified with hydrochloric acid to yield the corresponding acids (**11a—d**) which were proved by mp and mixture mp.[8]

C. Action of Ethanolic Ammonia on N-*(Arylsulfonyloxy)phthalimides (5a, b); Formation of 6 and 7*: A mixture of *N*-(arylsulfonyloxyl)phthalimides (**5a** and **b**) (0.01 mol) and ethanolic ammonia (60 ml) was heated under reflux for 2 h, then cooled. The solid obtained was filtered off, and recrystallised from acetic acid to give **6** as white needles (mp >350°, yield 74%).

It was found to be 2,4-quinazolinedione (**6**) by mp and mixture mp with authentic sample[9,10], and IR spectrum which showed ν_{NH} in the region 3280—3080 cm^{-1}, and coupling carbonyl bands in the regions 1740—1700 and 1680—1660 cm^{-1}.

The mother liquor was concentrated to low bulk to give the corresponding ammonium salts of arenesulfonic acids (**7**) which was confirmed by means of mp and mixture mp.

II. Aminolysis of N-*Hydroxyphthalimide. Action of Primary Amines and Amino Acids on* N-*Hydroxyphthalimide (1); Formation of* N-*Arylphthalimides (8a—m)*: A mixture of 1 (0.01 mol), and aromatic amines and/or aminoacids (0.04 mol) in ethanol (20 ml) was heated under reflux for 3 h, then concentrated, and cooled. The solid products were filtered off and recrystallized from suitable solvent to give (**8a—m**), *cf.* Table 1. It was found to be *N*-arylphthalimides by means of mp and mixed mp[11-17] and IR spectra.[5,6]

III. Hydrazinolysis of N-*Hydroxyphthalimide.*

A. Action of Hydrazines on N-*Hydroxyphthalimide in Acetic Acid or Ethanol: Formation of 9*: A mixture of **1** (0.01 mol) and hydrazine (0.03 mol), in acetic acid or ethanol (10 ml) was heated under reflux for about 12 h, then cooled. The solid obtained was filtered off, and recrystallized from acetic acid to give **9** (*cf.* Table 1).

It was found to be 1,4-phthalazinediones (**9a** and **b**) by means mp and mixture mp[18,19] and IR spectra which showed $\nu_{C=O}$ (1640—1630 cm^{-1}) and ν_{NH} (3180—3170 cm^{-1}).

B. Reaction of Hydrazine Hydrate with N-*Hydroxyphthalimide by Fusion (1); Formation of 2*: A mixture of **1** (0.01 mol), and hydrazine hydrate (0.05 mol) was heated at (400 °C) on a sand bath for 1.5 h. The solid product was extracted with hot ethanol, and recrystallized from ethanol to give **2** as white crystals (mp 230—231 °C, yield 65%).

It was proved to be phthalimide (**2**) by means of mp, mixture mp[4], and IR spectrum.[5,6]

C. Action of Phenylhydrazine on N-*Hydroxyphthalimide (1) and/or Phthalic Anhydride; Formation of 8a*: A mixture of **1** (0.01 mol) and/or phthalic anhydride (0.01 mol) and phenylhydrazine (0.03 mol) was heated at (400 °C) on a sand bath for 2 h, then cooled. The product was extracted with hot ethanol and recrystalized from the same solvent to yield a white crystals mp 204—205°; yield 65%. It was found to be *N*-phenylphthalimide (**8a**) by means of mp and mixture mp,[11] and IR spectrum.[5,6]

IV. Pyrolysis of N-*Hydroxyphthalimide and Its Derivatives.*

A. Pyrolysis of N-*Hydroxyphthalimide (1); Formation of Phthalimide (2)*: *N*-Hydroxyphthalimide (**1**) was heated above its mp on a sand bath for 1 h. The solid product was obtained in sublimed needles; collected in an air condenser, mp 231—232 °C, yield 60%. It was found to be phthalimide (**2**) by means of mp and mixture mp,[4] and IR spectrum.[5,6]

B. Pyrolysis of N-*(Aroyloxy)phthalimides (3a—d); Formation of Phthalimide (2) and Benzoic Acids (11a—d)*: *N*-(Aroyloxy)-phthalimides (**3a—d**) were heated at 300 °C in a sand bath for 3 h. After cooling the solid product obtained was recrystallized from ethanol and charcoalized to give solid (**2**) (mp 230—231 °C, yield 70%). It was found to be phthalimide (**2**) by means of mp and mixture mp,[4] and IR spectra.[5,6]

Table 1. Formation of *N*-arylphthalimides (**8a—m**), 1,4-phthalazinediones (**9**), and phthalimides (**2**)

Base added	Product No.	Mp °C	Mixed mp °C	Yield %	Ref.
Aniline	**8a**	204—205[a]	204	79	11
o-Toluidine	**b**	180[a]	179—180	76	12
p-Toluidine	**c**	201—202[a]	201	58	13
o-Anisidine	**d**	155—156[a]	155	79	14
p-Anisidine	**e**	155[a]	153—155	78	15
o-Chloroaniline	**f**	140[a]	140	76	16
m-Chloroaniline	**g**	183—184[a]	183	82	16
p-Chloroaniline	**h**	194—195[a]	195	76	16
p-Bromoaniline	**i**	203—204[a]	203	68	17
p-Nitroaniline	**j**	271[a]	270—271	77	11
Anthranilic acid	**k**[c]	217[b]	216	65	17
m-Aminobenzoic acid	**l**	281—282[b]	281	69	17
p-Aminobenzoic acid	**m**	289—290[b]	290	72	2
Hydrazine hydrate	**9a**	340[b]	339	80	18
Phenylhydrazine	**b**	210[b]	210	79	19

a) Recrystallized from ethanol. b) Recrystallized from acetic acid. c) Reflux in the presence of a few drops of pyridine.

Table 2. Formation of benzoic acids (**11**)

Product	Mp °C	Mixed mp °C	Yield %	Ref.
11a	118—119	118—120	62	8
b	176	175—176	68	8
c	176—177	175—177	66	8
d	225	224—225	52	8

Table 3. Formation of *N*-arylphthalimides (**8**)

Compound No.	Mp °C	Mixed mp °C	Yield %	Ref.
8a	204—205	204	65	11
e	155	154	69	15
h	194—195	195	60	16
j	271—272	271	72	11

Table 4. Formation of [*O*-(aroylamino)phenyl]diarylmethanols (**15a—d**)

Product	Mp °C	Yield %	Formula	Annlysis (%)		IR		
				Found	Calcd	ν_{OH} cm^{-1}	ν_{NH} cm^{-1}	$\nu_{C=O}$ cm^{1}
15a	232	61	$C_{26}H_{21}NO_2$	C 81.32 H 5.54 N 3.60	82.34 5.54 3.69	3400	3290	1640
b	200—203	63	$C_{29}H_{27}NO_2$	C 81.75 H 6.45	82.66 6.40	3360	3320	1680
c	155	60	$C_{29}H_{27}NO_5$	C 74.21 H 5.94	74.20 5.75	3500	3300	1660
d	163	66	$C_{29}H_{27}NO_5$	C 75.17 H 6.22	74.20 5.75	3400	3360	1680

The mother liquors were concentrated by evaporation to give the corresponding benzoic acids,[11] identified by means of mp and mixture mp[8] (*cf.* Table 2).

C. Pyrolysis of N-*(Arylsufonyloxy)phthalimides (**5a** and **b**); Formation of **2** and Arenesulfonic Acids (**12a**, **b**)*: *N*-(Arylsulphonyloxy)phthalimides (**5**) were heated at (400 °C) on a sand bath for *ca.* 2 h, The solid products were recrystallized from ethanol with charcoalization to give white crystals mp 230—231 °C, yield 71%. It was found to be phthalimide (**2**) by means of mp and mixture mp[4] and IR spectrum.

The mother liquors were evaporated to dryness to give the corresponding arenesulfonic acids[20] (**12**).

D. Pyrolysis of N-*(Arylcarbamoyloxy)phthalimides (**13**); Formation of* N-*Arylphthalimides (**8a**, **e**, **h**, **j**)*: *N*-(Arylcarbamoyloxy)phthalimides (**13a—d**) were heated on a sand bath for 3 h. The products were extracted with hot ethanol and recrystalized from the same solvent. They were proved to be the corresponding *N*-arylphthalimides (**8**) by means of mp and mixture mp with authentic samples and IR spectra (*cf.* Table 3).

V. Action of Grignard Reagent on N-*Hydroxyphthalimide and Its Derivatives.*

A. Action of Phenylmagnesium Bromide on N-*Hydroxyphthalimide (**1**); Formation of 1,1-Diphenyl-3-phenylimino-1,3-dihydrobenzofuran (**14**)*: A solution of phenylmagnesium bromide (0.6 mol) in dry ether was added to a solution of *N*-hydroxyphthalimide (**1**) (0.1 mol) in dry ether. The reaction mixture was refluxed on a boiling water bath for 6 h and left to stand overnight. The reaction mixture was decomposed with ice-cold concentrated solution of ammonium chloride. The ethereal layer was separated, dried over anhydrous sodium sulfate, and the solvent was distilled off.

The solid product was filtered off and recrystallized from ethanol to give 1,1-diphenyl-3-(phenylimino)-1,3-dihydrobenzofuran (**14**) as colourless crystals (mp 188—190 °C, yield 68%). (Found: C, 86.4; H, 5.2%; Calcd for

$C_{26}H_{19}NO$: C, 86.4; H, 5.2%).

Structure **14** was confirmed by IR spectrum showing $\nu_{C=N}$ (1600 cm^{-1}), and MS showing [M^{+}; at (*m/e* 361); and $M^{+}-16$; at *m/e*=345].

B. Action of Grignard Reagents on N-*(Arylsulfonyloxy)phthalimides (**5a, b**); Formation of* [O-*(Arylamino)phenyl*] *Diarylmethanols (**15a—d**), and Arenesulfonic Acids (**13a, b**)*: The solution of arylmagnesium bromide (0.6 mol) in dry ether was added to a solution of *N*-(arylsulfonyloxy)phthalimides (**5**) (0.1 mol) in dry ether. The reaction mixture was heated under reflux on a boiling water bath for 6 h, and then allowed to stand overnight at room temperature. It was poured onto ice-cold concentrated solution of ammonium chloride. The ethereal layer was separated, dried over anhydrous sodium sulphate, and the solvent was distilled off. The solid product was filtered off and recrystalized from ethanol to give [*O*-(aroylamino)phenyl]diarylmethanols (**15a—d**) as white crystals (*cf.* Table 4). The mother liquor was concentrated by evaporation to give the corresponding arenesulfonic acids (**12**).[20]

References

1) A. F. M. Fahmy, N. F. Aly, A. Nada, and N. Y. Aly, *Bull. Chem. Soc. Jpn.*, **50**, 2678 (1977).
2) A. F. M. Fahmy, N. F. Aly, and M. H. Arief, *Indian J. Chem.*, (accepted for publication).
3) H. Gross, and J. Keitel, *J. Prakt. Chem.*, **311**, 692 (1969).
4) W. A. Noyes, and P. K. Porter, *Org. Synth.*, Coll. Vol. I, 457 (1932).
5) F. G. Baddar, A. F. M. Fahmy, and N. F. Aly, *J. Chem. Soc.*, **1973**, 2448.
6) W. R. Roderick and W. G. Brown, *J. Am. Chem. Soc.*, **79**, 5196 (1957).
7) L. A. Carpino, *J. Am. Chem. Soc.*, **79**, 38 (1957).
8) W. S. Emerson, V. E. Lucas, and R. A. Heimsch, *J. Am. Chem. Soc.*, **71**, 1742 (1949).
9) A. N. Lange, and F. E. Sheibley, *Org. Synth.* Coll. Vol. II, 79 (1943).
10) F. M. Sheibley, *J. Org. Chem.*, **12**, 743 (1947).
11) C. I. Butler, and R. Adams, *J. Am. Chem. Soc.*, **47**, 2610 (1925).
12) F. D. Chattaway, C. L. Cumming, and B. H. Wilson, *J. Chem. Soc.*, **99**, 1950 (1911).
13) O. L. Brady, W. G. E. Quick, and W. F. Welling, *J. Chem. Soc.*, **127**, 2265 (1925).
14) A. Piutti, *Gazz. Chim.*, **40**, I, 555.
15) A. Piutti, and U. Abati, *Ber.*, **36**, 1000 (1903).
16) M. L. Sherrill, F. L. Schaeffer, and E. P. Shoyer, *J. Am. Chem. Soc.*, **50**, 474 (1928).
17) S. Gabriel, *Ber.*, **11**, 2261 (1878).
18) H. A. Foersterling, *J. Prakt. Chem.*, [2], **51**, 376 (1895).
19) B. Hotte, *J. Prakt. Chem.*, [2], **35**, 285 (1887).
20) I. Vogel, "Practical Organic Chemistry," Longmans, Green and Co. Ltd., London (1956), pp. 549, 552.

Kinetics and Mechanism of the Oxidation of the Esters of Mandelic Acid by Lead Tetraacetate

Kalyan K. BANERJI,* Sudheer K. BANERJEE,** and Rama SHANKER**

Department of Chemistry, University of Jodhpur, Jodhpur 342001, India

** *Department of Chemistry, University of Udaipur, Udaipur 313001, India*

(Received November 7, 1977)

The oxidation of eight esters of mandelic acid by lead tetraacetate in benzene solution has been studied. The product of the oxidation is the corresponding phenylglyoxylic ester. The oxidation is of first order with respect to the oxidant and second order to the ester. The reaction is catalysed by pyridine, the catalysed reaction being first order in pyridine. In the presence of pyridine, the reaction is first order with respect to each the oxidant and the ester. The oxidation of ethyl α-deuteriomandelate indicated a kinetic isotope effect. The activation parameters have been determined. The results have been interpreted in terms of a slow decomposition of lead tetraalkoxide derivative involving heterolysis of Pb–O bond.

Oxidation of organic compounds by lead tetraacetate (LTA) is known to involve both homolytic and heterolytic reactions.[1] The mechanism depends mainly on the nature of the compound and the reaction conditions. Baer and Kates[2] observed that the yield of pyruvic ester in the oxidation of methyl lactate varies with the solvent used. The oxidation of methyl mandelate in boiling benzene by LTA yields 70% methyl phenylglyoxylate.[2] Little kinetic data are available on the oxidation of mandelic esters by LTA. Oxidation of mandelic acid has earlier been reported from this laboratory.[3] However, hydroxy acids and their esters are known to react by different mechanisms.[4,5] The present communication reports the oxidation of some esters of mandelic acid by LTA, both uncatalysed and pyridine-catalysed.

Results

The rate laws and other experimental data were obtained for the oxidation of eight esters of mandelic acid. Since results are similar, only those of methyl mandelate (MM) are reproduced here.

The oxidation of mandelic esters by LTA, both uncatalysed and catalysed, yields carbonyl products as evidenced by the isolation of their 2,4-dinitrophenylhydrazones (2,4-DNP). However, no data were available on the 2,4-DNP of phenylglyoxylic esters. The esters of phenylglyoxylic acid were therefore, prepared by the reported mehtods.[6] Then the esters were converted into their 2,4-DNP. The 2,4-DNP of phenylglyoxylic esters and those of the oxidation products had identical mp. Mixed mp and mixed TLC confirmed that 2,4-DNP obtained by both the methods are identical. 2,4-DNP of the oxidation products of butyl and isopropyl mandelates showed correct analysis for C, H, and N. The mp of 2,4-DNP of the phenylglyoxylic esters are recorded in Table 1, along with the results of elemental analysis.

Stoichiometry. Excess of LTA was allowed to react with 0.0025 M of isopropyl mandelate in the presence of varying amounts of pyridine and the unreacted oxidant estimated. The ester and LTA react in 1 : 1 ratio. For some runs, the carbonyl product was estimated as its 2,4-DNP, using an excess of the ester. The carbonyl product is isolable in 80±3% yield. The overall reaction is as follows:

$$PhCH(OH)COOR + Pb(OAc)_4 \rightarrow PhCOCOOR + Pb(OAc)_2 + 2\,AcOH. \quad (1)$$

Rate Laws. When the ester is in excess, the rate of disappearence of LTA follows first order rate laws. The rate constant is independent of the initial concentration of LTA (Table 2) confirming that the order with respect to LTA is one. In uncatalysed reactions the order with respect to the ester is two (Table 3), In the presence of pyridine, the order with respect to LTA remains unchanged but the reaction becomes first order with respect to the substrate also (Table 4). The catalysed reaction is of first order in pyridine (Table 5).

An attempt was made to detect the formation of free radicals, during these oxidation in benzene, using acrylonitrile in an atmosphere of nitrogen. No free

TABLE 1. ANALYTICAL DATA FOR THE 2,4-DINITROPHENYLHYDRAZONES OF ALKYL PHENYLGLYOXYLATE

Alkyl group	Formula	Mp °C	Found (%)			Calcd (%)		
			C	H	N	C	H	N
Me	$C_{15}H_{12}N_4O_6$	169	—	—	—	—	—	—
Et	$C_{16}H_{14}N_4O_6$	152	—	—	—	—	—	—
n-Pr	$C_{17}H_{16}N_4O_6$	162	—	—	—	—	—	—
i-Pr	$C_{17}H_{16}N_4O_6$	171	50.04	4.35	14.99	54.83	4.30	15.05
n-Bu	$C_{18}H_{18}N_4O_6$	120	55.89	4.80	15.16	55.95	4.66	14.50
i-Bu	$C_{18}H_{18}N_4O_6$	138	—	—	—	—	—	—
s-Bu	$C_{18}H_{18}N_4O_6$	134	—	—	—	—	—	—
Benzyl	$C_{21}H_{16}N_4O_6$	189	—	—	—	—	—	—

radicals could be detected.

To ascertain the importance of α-C–H bond rupture in the rate-determining step, the oxidation of ethyl α-deuteriomandelate (PhCD(OH)COOEt) was investigated. The results are summarised in Table 6.

Tables 7 and 8 record the data on the effect of temperature on the uncatalysed and the catalysed oxidation respectively. The average error limits in the values of ΔH^*, ΔS^*, and ΔF^* are ±5 kJ mol^{-1}, ±10 J mol^{-1}·K^{-1}, and ±7 kJ mol^{-1}, respectively.

Table 2. Oxadation of methyl mandelate: oxidant dependence of the reaction rate

[MM] 0.05 M, Temp 318 K.

10^2[Pb(IV)]M	0.50	0.61	1.00	1.25	2.00
$10^5 k_1$ s^{-1}	3.17	3.30	3.30	3.00	3.17

Table 3. Oxidation of methyl mandelate: substrate dependence of the reaction rate

[PV(IV)] 0.005 M, Temp 318 K.

10^2[MM]M	3.12	5.00	7.50	10.0	12.5
$10^5 k_1$ s^{-1}	1.27	3.17	7.87	13.0	20.3
$10^2 k_1$/[MM]^2	1.31	1.27	1.39	1.30	1.31

Table 4. Dependence of the reaction rate on the concentration of methyl mandelate, in the presence of pyridine

[Pb(IV)] 0.005 M, [Pyridine] 0.20 M, Temp 298 K.

10^2[MM]M	1.87	3.12	5.00	6.25	10.0
$10^5 k_1$ s^{-1}	5.18	8.74	14.2	17.5	28.0

Discussion

The constancy of ΔF^* values indicates that the esters are oxidised by the same mechanism. Data in Tables 7 and 8 indicate the rate of oxidation of various esters do not differ markedly and a random variation becomes apparent when these rates are compared at different temperatures. This suggests that the structural changes in the alcohol moiety of the ester fail to affect the reaction rate. This is not surprising considering that at least four sigma bonds intervene between the reaction site and the substituent. Similar effects have been observed in many Ce(IV) oxidations.[7] Another possibility is that the reaction has been studied

Table 5. Dependence of the reaction rate on pyridine concentration

[Pb(IV)] 0.005 M, [MM] 0.05 M, Temp 293 K.

[Pyridine] M	0.10	0.20	0.30	0.40	0.50
$10^5 k_1$ s^{-1}	4.60	9.98	13.9	20.0	25.2

Table 6. Kinetic isotope effect in the oxidation of ethyl mandelate

[Pb(IV)] 0.005 M, [Ester] 0.05 M, Temp 308 K.

[Pyridine] M	$10^5 k_1$ s^{-1}		k_H/k_D
	α-H	α-D	
0.00	7.40	3.10	2.39
0.20	25.3	5.00	5.60

Table 7. Rate constants at difeerent temperatures and the activation parameters for the uncatalysed oxidation of alkyl mandelates by Pb(IV)

Alkyl group	$10^3 k$ l^2 mol^{-2} s^{-1}				ΔH^* kJ mol^{-1}	$-\Delta S^*$ J mol^{-1} K^{-1}	ΔF^* kJ mol^{-1}
	308	313	318	323 K			
Me	5.18	7.26	13.0	22.9	74.7	50.3	91.6
Et	7.40	9.60	18.0	25.4	68.7	66.7	91.1
n-Pr	8.44	12.7	15.4	21.5	50.8	124	91.6
i-Pr	7.29	11.5	13.4	16.9	50.0	127	92.4
n-Bu	9.21	11.9	21.1	27.6	61.2	89.0	90.7
s-Bu	6.52	8.83	18.0	23.8	72.6	55.0	91.6
i-Bu	8.44	11.9	19.9	29.2	68.9	65.0	90.7
Benzyl	3.72	6.14	8.80	11.7	64.3	86.7	93.2

Table 8. Rate constants at different temperatures and the activation parameters for the pyridine-catalysed oxidation of alkyl mandelates by Pb(IV)

Alkyl group	$10^3 k$ l^2 mol^{-2} s^{-1}				ΔH^* kJ mol^{-1}	$-\Delta S^*$ J mol^{-1} K^{-1}	ΔF^* kJ mol^{-1}
	293	298	303	308 K			
Me	9.98	14.2	21.1	27.3	48.7	121	85.7
Et	11.5	13.4	19.6	25.3	51.2	147	86.1
n-Pr	10.7	11.1	18.4	23.0	36.4	163	86.5
i-Pr	11.9	15.0	18.8	24.9	37.3	159	86.1
n-Bu	11.5	15.4	19.6	24.9	38.3	155	86.1
s-Bu	11.1	14.2	19.8	25.1	41.2	146	86.1
i-Bu	9.98	13.0	17.3	24.9	44.9	134	86.1
Benzyl	12.3	16.1	21.5	30.7	44.1	135	85.7

at or very near the isokinetic temperature. A plot of ΔH^* and ΔS^* ($r=0.986$) of the uncatalysed reaction gives an isokeintic temperature 312 K. Since the rates were determined close to the isokeintic temperature, consideration of rates alone could lead to erroneous conclusion about the nature of the reaction.

The formation of the keto ester in good yield and a second order dependence on substrate concentration indicate that the oxidation takes place through the decomposition of dialkoxylead(IV) derivative, the monoalkoxylead(IV) derivative being kinetically insignificant. The oxidation of alcohols is known to proceed through the disproportionation of such derivatives.[8,9]

The disproportionation of the dialkoxy derivative may either involve a heterolysis of Pb–O bond (and a C–H bond rupture) or a rapid sequential two successive one electron processes. The presence of kinetic isotope effect and failure to induce polymerisation of acrylonitrile suggest that the disproportionation is a two-electron process. It may be mentioned here that homolytic oxidation of alcohols by LTA in nonpolar solvents results in cyclisation and fragmentation products—tetrahydrofurans and tetrahydropyrans.[1,10] Absence of such products also indicate a two-electron process.

$$Pb(OAc)_4 + 2\,PhCH(OH)COOR \rightleftharpoons 2\,AcOH + (PhCH(COOR)O)_2Pb(OAc)_2 \quad (2)$$

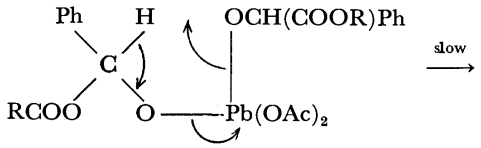

$$PhCOCOOR + PhCOCOOR + Pb(OAc)_2 + PhCHOH\cdot COOR \quad (3)$$

The observed negative entropies of activation also favour this mechanism over homolysis of Pb–O bond. The following transition state could be envisaged.

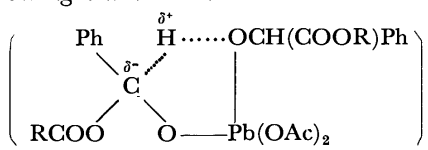

Due to partial positive charge created in the transition state in a nonpolar solvent like benzene, the solvent molecules will acquire induced dipoles and ion-dipole forces will restrict the movements of many benzene molecules. Further, since the dielectric constant is small, the lines of force will go far out into the solvent and a great many solvent molecules will be involved. The immobilisation of a large number of benzene molecules reduces the partition function of the transition state as compared to the reactant states. This would result in a large negative entropy of activation.

The reaction in the presence of pyridine is a neat one involving heterolysis of Pb–O bond.[8] The first order dependence on the ester concentration shows that pyridine coordinates with LTA to form a complex. Such a complex has been isolated from benzene by Partch and Monthony.[8] The increased polarisation interaction in Pb–N as compared to Pb–O bond renders the complex more labile and electrophilic. When [pyridine]$\gg$[Pb(IV)] the effective concentration of species like LTA-Py will be fairly constant and catalysis due to bases like pyridine seems to be quite profound. Further, a high kinetic isotope effect in pyridine-catalysed oxidation also requires a catalysis by pyridine. It therefore, appears that pyridine also acts as a base in facilitating the rupture of α-C–H bond. Lowering of ΔF^* in all cases in going from the uncatalysed to catalysed reaction is expected.

Experimental

Esters of mandelic acid, prepared by the reported methods,[11] were purified by distillation under reduced pressure and crystallization. Their mp and bp agreed with the literature values.[12] Solvents and other reagents were purified and dried in the usual manner. Ethyl mandelate (α-D, 90±5% deuterated) was prepared by the esterification of α-deuteriomandelic acid, which itself was prepared by the method of Kemp and Waters.[13] LTA was prepared by the reported method[14] (purity=98%).

Kinetic Measurements. The solvent used was benzene. AcOH (1% v/v) was added to each reaction mixture to avoid phase separation and to keep $Pb(OAc)_2$ in solution. Conductivity measurements showed that there was no appreciable interaction between pyridine and AcOH in this medium, hence no correction was applied to the initial concentration of pyridine. The reaction was studied under pseudo-first-order conditions by keeping a large excess the ester over LTA and were followed by the method of Cordner and Pausacker.[15] A parallel blank was always run to account for the decomposition of LTA, if any. The observed rates of pyridine-catalysed reactions were corrected for the rate of uncatalysed reaction. Similarly the rate of oxidation of the deuterated ester was corrected for the ordinary ester present. The first order rate constant, k_1, was evaluated from the plots of log[LTA] against time by a least square method and were reproducible within ±4%.

References

1) R. O. C. Norman and R. A. Watson, *J. Chem. Soc., B*, **1968**, 692.
2) E. Baer and M. Kates, *J. Am. Chem. Soc.*, **67**, 1482 (1945).
3) R. Shanker, S. K. Banerjee, and O. P. Sachdeo, *Z. Naturforsch.*, **28b**, 375 (1973).
4) S. L. Sharma, R. Shanker and G. V. Bakore, *Indian J. Chem.*, **14A**, 82 (1976).
5) D. S. Jha and G. V. Bakore, *J. Chem. Soc. B*, **1971**, 1161.
6) H. Gilman, *Org. Synth.*, Coll. Vol. 1, 241 (1961).
7) K. K. Banerji, *J. Indian Chem. Soc.*, **52**, 573 (1975).
8) R. Partch and J. Monthony, *Tetrahedron Lett.*, **1967**, 4427.
9) K. K. Banerji, S. K. Banerjee, and R. Shanker, *Indian J. Chem.*, **15A**, 702 (1977).
10) M. L. Mihailovic, J. Bosnjak, Z. Maksimovic, Z. Cekovic, and L. Lorence, *Tetrahedron*, **21**, 955 (1966).
11) E. Fisher and A. S. Spencer, *Ber. dt. Chem. Ges.*, **1895**, 3255.
12) J. Phloi, "Dictionary of Organic Compounds," Vol. 4, Oxford University Press, Oxford (1965), p. 2052.
13) T. J. Kemp and W. A. Waters, *J. Chem. Soc.*, **1964**, 1194.
14) J. C. Blair, Jr., *Inorg. Synth.*, **1**, 47 (1930).
15) J. P. Cordner and K. H. Pausacker, *J. Chem. Soc.*, **1953**, 102.

Preparation, Infrared and Mass Spectral Studies of 6-Substituted 6,7-Dihydro-5*H*-dibenzo[*d*,*f*][1,3,2]diazaphosphepine 6-Oxides

M. S. R. Naidu*,† and C. Devendranath Reddy

Department of Chemistry, Post-Graduate Centre, Sri Venkateswara University, Anantapur 515003, India

(Received November 1, 1976)

Several 6-substituted 6,7-dihydro-5*H*-dibenzo[*d*,*f*][1,3,2]diazaphosphepine 6-oxides have been synthesized and their structures were confirmed by IR and mass spectra. The existence of hydrogen bonding between the amidic hydrogens and the phosphoryl oxygen in theses compounds is indicated by the IR spectra. Under electron impact, the splitting pattern of these compounds takes about four major fragmentation pathways. The stability of dibenzodiazaphospheine cyclic system is indicated by the appearence of ions at *m/e* 229 and 211 corresponding to the species $C_{12}H_{10}N_2OP^+$ and $C_{12}H_8N_2P^+$, respectively, in all the spectra of the compounds except in the methyl and ethyl substituted compounds.

Considerable interest in organophosphorus compounds has been sustained by medical and commercial applications of their biological properties. The syntheses of these compounds containing benzodiazaphosphole ring have acquired much importance recently as these compounds have been investigated for their insecticidal, bactericidal, antiviral and anticarcinogenic properties.[1] The search for a satisfactory drug for cancer produced many new phosphorus heterocyclic compounds[2-5] and many of them possessed significant antitumour activity. These laboratories have reported[6] earlier the synthesis of several 2-(4-chloro-3-methylphenoxy)-2,3-dihydro-1*H*-1,3,2-benzodiazaphosphole 2-oxides, and the present paper describes the synthesis, infrared and mass spectral studies of 6-substituted 6,7-dihydro-5*H*-dibenzo[*d*,*f*][1,3,2]diazaphosphepine 6-oxides (**1**—**8**).

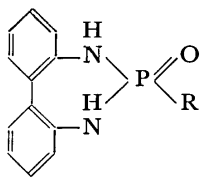

	R		R
1	CH_3	**5**	C_6H_5
2	C_2H_5	**6**	O-$C_6H_4CH_3$(*p*-)
3	$(CH_2)_2CH_3$	**7**	O-$C_6H_4NO_2$(*p*-)
4	$CH(CH_3)_2$	**8**	O-$C_6H_3ClCH_3$(4,3-)

These cyclizations were accomplished by reacting equimolar quantities of various phosphonic dichlorides and phosphorodichloridates with 2,2'-diaminobiphenyl in refluxing benzene or toluene under nitrogen atmosphere. The yields of diazaphosphepines obtained (see Table 1) indicate that nucleophilic substitution of the amino groups proceeds more easily leading to the completion of cyclization with phosphorodichloridates than with phosphonic dichlorides. This may be explained by the fact that substituted phenoxyl groups attached to the phosphorus atom renders it more electrophilic. The lowest yield is obtained in the case of methylphosphonic dichloride. This may be due to the electron donating effect of methyl group by hyperconjugation which renders the phosphorus atom of the dichloride less electrophilic. All these compounds are crystalline solids with high melting points and are also easily soluble in organic solvents. They appear to be more stable than benzodiazaphosphole 2-oxides.[6]

The infrared frequencies associated with the major functional groups of the compounds in the present investigation are plotted in Table 2. All the compounds have exhibited P=O and P–NH vibrations in the regions 1210—1140 cm^{-1} and 3400—3080 cm^{-1}. The free P=O and NH stretching vibrations would give rise to bands around 1300—1250 cm^{-1} and 3350—3210 cm^{-1} [7,8] respectively. Bellamy[8] has also assigned 1250—1150 cm^{-1} for P=O stretching vibrations in the compounds which involve hydrogen bonding. The frequencies exhibited by P=O and P–NH groups indicate that they have involved in the hydrogen bond formation. All the compounds exhibited characteristic infrared frequencies for P–O–C_{aryl}[9-13], P–N_{phenyl}[14], P–N[14], aryl C–NO_2[15-17] and aryl C–Cl[18] groups.

To confirm the configuration of the cyclic system present in these molecules and also to study the splitting patterns and fragmentation pathways of this system, the mass spectra of these compounds (**1**—**8**) have been studied. As a general representation of this series, the splitting pattern and the fragmentation pathways of (*p*-methylphenoxy)dibenzodiazaphosphepine (**6**) under electron impact are shown in Scheme 1 (Fig. 1). The molecular ion, $C_{19}H_{17}N_2O_2P^+$, (*m/e* 336) itself appears as the most abundant ion for this compound. The initial fragmentation of the molecular ion occurs by ejecting the C_7H_7O radical attached to the phosphorus atom with the formation of the ion $C_{12}H_{10}N_2OP^+$ at *m/e* 229 (20%). This ion loses a water molecule to form the ion, $C_{12}H_8N_2P^+$ at *m/e* 211 (15%).

The ions at *m/e* 182 (16%) and 181 (24%) corresponding to the species $C_{12}H_{10}N_2^+$ and $C_{12}H_9N_2^+$ might

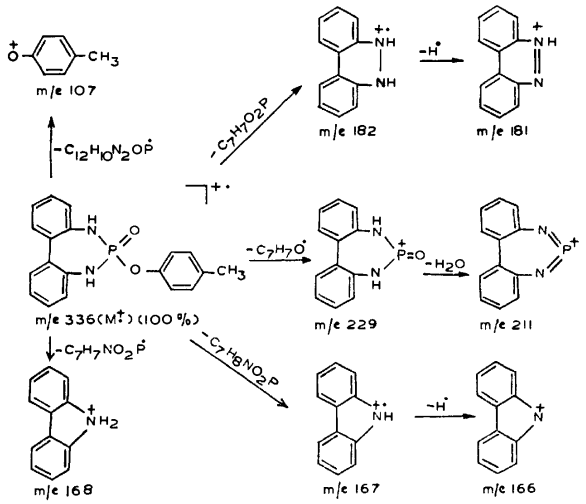

Scheme 1.

† Present address: S.V. University, Tirupati 517502, India.

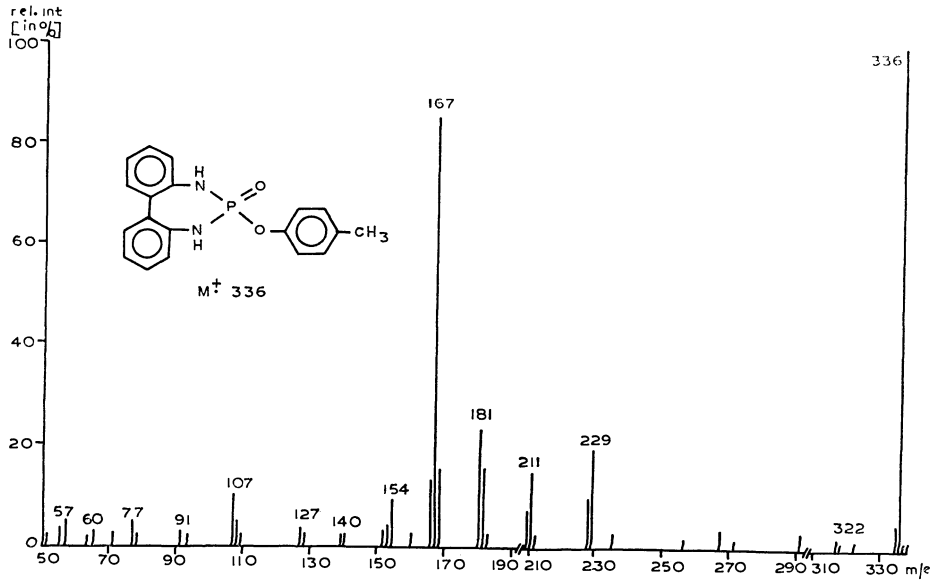

Fig. 1. Mass spectrum of 6-(4-methylphenoxy) 6,7-dihydro-5*H*-dibenzo[*d*,*f*][1,3,2]diazaphosphepine 6-oxide at 70 eV.

Table 1. Synthesis of 6-substituted 6,7-dihydro-5*H*-dibenzo[*d*,*f*][1,3,2]diazaphosphepine 6-oxides

Compound	Phosphonic dichloride or phosphorodichloridate	Yield (%)[a]	Reaction time (min)[b]	Mp (°C)	Molecular formula	Found (%) C	H	N	Calcd (%) C	H	N
	With 2,2′-diaminobiphenyl										
1	Methylphosphonic dichloride	47[c]	115	252—255[e]	$C_{13}H_{13}N_2OP$	63.78	5.41	11.32	63.93	5.36	11.48
2	Ethylphosphonic dichloride	58[c]	120	226—228[f]	$C_{14}H_{15}N_2OP$	65.02	5.94	10.82	65.10	5.85	10.85
3	Propylphosphonic dichloride	84[c]	120	225—228[g]	$C_{15}H_{17}N_2OP$	66.29	6.25	10.49	66.15	6.29	10.29
4	Isopropylphosphonic dichloride	68[c]	120	205—210[e]	$C_{15}H_{17}N_2OP$	66.08	6.35	10.19	66.15	6.29	10.29
5	Phenylphosphonic dichloride	89[c]	115	330—333[h]	$C_{18}H_{15}N_2OP$	70.71	5.27	8.95	70.60	4.94	9.15
6	*p*-Tolyl phosphorodichloridate	80[c]	120	255—257[h]	$C_{19}H_{17}N_2O_2P$	67.69	4.95	8.36	67.85	5.09	8.47
7	*p*-Nitrophenyl phosphorodichloridate	92[c]	120	255—257[i]	$C_{18}H_{14}N_3O_4P\frac{1}{2}H_2O$	57.38	4.00	10.94	57.46	4.02	11.12
8	4-Chloro-3-methylphenyl phosphorodichloridate	88[d]	120	234—238[i]	$C_{19}H_{16}N_2O_2ClP$	61.43	4.42	7.43	61.55	4.35	7.56

a) Product isolated after one crystallization. b) As the reagents were mixed at about 40—60 °C and then heated to reflux, the times recorded are approximate. Reactions were carried out in refluxing, c) benzene and d) toluene. Products recrystallized from e) methanol–ether, f) ethanol–ether, g) chlorobenzene, h) 95% ethanol, and i) methanol.

Table 2. Infrared spectra of 6-substituted 6,7-dihydro-5*H*-dibenzo[*d*,*f*][1,3,2]diazaphosphepine 6-oxides

Compound	P=O (cm^{-1})	P-NH (cm^{-1})	P-N-C aromatic: P-N-C (aryl) (cm^{-1})	P-N-C aromatic: P-N (cm^{-1})	*ortho*-Disubstituted benzenes (cm^{-1})	P-O-C aromatic (cm^{-1})		
1	1140	3250	1310	950	760	—		
2	1140	3375	1300	945	760	—		
3	1175	3150	1280	930	760	—		
4	1140	3400	1290	940	765	—		
5	1190	3080	1280	930	750	—		
6	1210	3150	1285	925	760	1220	950	
7	1205	3150	1285	935	758	1235	980	aryl C-NO_2 1510 cm^{-1} 1340 cm^{-1}
8	1160	3150	1280	938	755	1220	978	aryl C-Cl 1060 cm^{-1}

Table 3. Mass spectral data

Compound No.	*m/e* (% relative abundance)
1	181(100), 180(45), 179(12), 167(9), 166(39), 165(58), 164(23), 91(15).
2	182(24), 181(19), 180(81), 179(21), 167(17), 166(78), 165(100), 164(43), 139(12), 138(16), 92(13), 91(28), 90(70), 79(35), 77(16), 65(11), 51(11).
3	272($M^{\ddagger}$, 50), 244(14), 230(62), 229(8), 213(22), 211(12), 182(17), 181(21), 180(10), 168(20), 167(100), 166(23), 93(16).
4	272($M^{\ddagger}$, 14), 244(4), 184(79), 183(35), 182(8), 168(42), 167(59), 166(25), 138(11), 137(12), 129(10), 127(11), 126(10), 92(45), 91(100), 90(21), 89(24), 78(28), 77(58), 65(48), 64(23), 63(37), 52(30), 51(47).
5	307(13), 306($M^{\ddagger}$, 62), 290(25), 211(4), 182(7), 181(11), 168(15), 167(100), 166(8), 153(19), 93(10), 67(11), 55(11).
7	367($M^{\ddagger}$, 22), 337(18), 336(61), 292(10), 291(59), 229(21), 211(18), 182(20), 181(28), 168(20), 167(100), 166(18), 154(14), 153(41), 152(11), 114(15), 113(13), 109(22), 108(12), 107(18), 93(11), 91(11), 78(22), 77(14), 66(15), 64(25), 58(12), 57(13), 55(18), 51(8).
8	372(20), 371(14), 370(60), 229(33), 228(13), 211(19), 182(21), 181(26), 168(14), 167(100), 166(17), 154(11).

have been formed from the molecular ion by the cleavage of P–N bonds followed by the loss of hydrogen atom.

The ion at *m/e* 168 (16%) might have resulted by the loss of $C_7H_7NO_2P^{\cdot}$ from the molecular ion. In another mode of decomposition, the molecular ion might have lost $C_7H_8NO_2P$ resulting with the formation of a cation radical at *m/e* 167 (92%) corresponding to the species $C_{12}H_9N^{\ddagger}$. This ion on further loss of a hydrogen radical leads to the formation of the ion $C_{12}H_8N^{+}$ at *m/e* 166 (13%). The loss of $C_{12}H_{10}N_2OP^{\cdot}$ from the molecular ion by the rupture of the P–O bond results with the formation of the ion at *m/e* 107.

This general fragmentation pattern is observed for all other compounds in this series. The mass spectral data of the other compounds (**1**—**5**, **7**, and **8**) are presented in Table 3. An examination of all their spectra indicates that 6-aryl substituted compounds are more stable under electron impact than the 6-alkyl substituted compounds. The methyl and ethyl substituted dibenzodiazaphosphepines (**1** and **2**) do not show any peaks corresponding to their molecular ions. The mass spectra of **4**, **7**, and **8** show uniformly the ion at *m/e* 167 as their base peak. Even for **6** this ion appears with an intensity of 92 per cent.

The ions at *m/e* 229 and 211 corresponding to the species $C_{12}H_{10}N_2OP^{+}$ and $C_{12}H_8N_2P^{+}$ respectively (refer Scheme 1) are present as characteristic peaks in all the compounds except for methyl- and ethyl-substituted compounds (**1** and **2**). The ions at *m/e* 182 and 181 derived from the diamine fragment of the molecular ions are found to appear in the spectra of all the compounds.

Apart from these general peaks present in the spectra of all these molecules, the peaks can be explained as follows: the ion at *m/e* 337 in the spectrum of **7** might have been formed by the loss of NO from the NO_2 of the compound.[20] The ion at *m/e* 244 is observed in the spectra of both **3** and **4** and it might have been formed by the ejection of C_2H_4 from the alkyl substituents of their molecular ions.[21]

Experimental

All melting points were determined on a Mel-Temp apparatus and are uncorrected. The elemental analyses were performed by Dr. R. D. MacDonald, Australian Microanalytical Service. IR spectra were recorded on a Perkin-Elmer Model 700 in Nujol mulls. Mass spectra were determined using a Varian Mat CH7, electron energy 70 eV and trap current 100 μA at Indian Institute of Technology, Madras.

2,2′-Diaminobiphenyl. It was prepared by reduction of 2,2′-dinitrobiphenyl,[22] mp 78—79 °C (lit,[23] mp 77—78 °C).

Methyl-, ethyl-, propyl-, and isopropylphosphonic dichlorides were obtained from Speciality Organics, Inc., U. S. A. and phenylphosphonic dichloride was procured from Fluka. 4-Chloro-3-methylphenyl phosphorodichloridate[6], *p*-tolyl phosphorodichloridate,[6] *p*-nitrophenyl phosphorodichloridate[24] were prepared according to the procedures reported in the literature.

*6-Phenyl 6,7-Dihydro-5*H*-dibenzo*[d,f][*1,3,2*]*diazaphosphepine 6-Oxide (5).* A solution of phenylphosphonic dichloride (3.9g, 0.02 mol) in dry benzene (20 ml) was added drowise to a warm (40—50 °C) and stirred solution of 2,2′-diaminobiphenyl (3.7g 0.02 mol) in dry benzene (30 ml). A slow stream of nitrogen was bubbled through the reaction mixture and the progress of the condensation was followed by titrating the evolved HCl gas with standard alkali. The reaction mixture was brought to reflux temperature and the evolution of the calculated amount of HCl was complete in 95 min. The reaction mixture was refluxed with vigorous stirring for an additional 20 min and cooled. On working up, the reaction mixture yielded 5.4g (89%) of the product which on recrystallization from 95% ethanol four times afforded an analytical samples of 6-phenyl-6,7-dihydro-5*H*-dibenzo[*d,f*]-[1,3,2]diazaphosphepine 6-oxide (**5**), mp 330—333 °C (dec).

This typical procedure was used as a general method for the preparation of all other compounds (**1**—**4**, **6**—**8**) reported and their relevant details are summarized in Table 1.

The authors would like to express their sincere appreciation to Dr. K. L. Loening, Nomenclature Director, Chemical Abstract Service, for his advice in naming

the heterocyclic compounds in this article. The authors are also thankful to the University Grants Commission, for the award of a Junior Research Fellowship to one of them (CDR).

References

1) Chugai Pharmaceutical Co., Jpn. Patent 26819 (1965); *Chem. Abstr.*, **64**, 9737 (1966).
2) H. Arnold, F. Bourseaux, and N. Brock, *Arzenimittel. Forsch.*, **11**, 143 (1961).
3) O. M. Friedman, Z. B. Papanastassiou, and R. S. Levi, *J. Med. Chem.*, **6**, 82 (1963).
4) H. Zimmer and A. Sill, *Progr. Drug. Res.*, **5**, 150 (1964).
5) P. Hsu, I. S. Kao, J. S. Tsai, C. H. Chou, M. C. Liu, M. L. Sheu, T. Y. Meug, Y. F. Jeu, R. C. Pan, and S. W. Li, *Sci. Sinica (Peking)*, **13**, 789 (1964).
6) M. S. R. Naidu and C. D. Reddy, *Indian J. Chem.*, **12**, 349 (1974).
7) K. Nakanishi, "Infrared Absorption Spectroscopy," Holden-Day, SanFrancisco (1962), pp. 38, 56.
8) L. J. Bellamy, "The Infrared Spectra of Complex Molecules," Methuen, London (1958), pp. 249, 311.
9) L. J. Bellamy and L. Beecher, *J. Chem. Soc.*, **1952**, 475, 1701.
10) L. J. Bellamy and L. Beecher, *J. Chem. Soc.*, **1953**, 728.
11) D. E. C. Corbridge, *J. Appl. Chem.*, **6**, 456 (1976).
12) R. A. Nyquist, *Appl. Spectrosc.* **11**, 161 (1957).
13) A. C. Chapman and R. Harper, *Chem. Ind. (London)*, 985 (1962).
14) N. B. Colthup, L. H. Daly, and S. E. Wiberley, "Introduction to Infrared and Raman Spectroscopy," Academic Press, New York (1964), p. 305.
15) R. J. Francel, *J. Am. Chem. Soc.*, **74**, 1265 (1952).
16) J. F. Brown, Jr., *J. Am. Chem. Soc.*, **77**, 6341 (1955).
17) R. D. Kross and V. A. Fassel, *J. Am. Chem. Soc.*, **78**, 4224 (1956).
18) N. B. Colthup, L. H. Daly, and S. E. Wiberley, "Introduction to Infrared and Raman Spectroscopy," Academic Press, New York (1964), p. 317 and relevant references cited therein.
19) Q. N. Porter and J. Baldas, "Mass Spectrometry of Heterocyclic Compounds," Wiley-Interscience, New York (1971), p. 420.
20) R. A. W. Johnstone, "Mass Spectrometry for Organic Chemists," Cambridge University Press, London (1972), p. 94.
21) J. H. Beynon, R. A. Saunders, and A. E. Williams, "The Mass Spectra of Organic Molecules," Elservier Publishing Company, Amsterdam (1968), p. 101.
22) R. C. Fuson and E. A. Cleveland, *Org. Synth.*, Coll. Vol. III, p. 339 (1955).
23) J. L. Evertt and W. C. J. Ross, *J. Chem. Soc.*, **1972**, 1949.
24) A. F. Turner and H. G. Khorona, *J. Am. Chem. Soc.*, **81**, 4651 (1959).

Intermolecular Chelate Linkage Isomerism of the Hydroxyimino Group in the Nickel(II), Copper(II), and Palladium(II) Complexes of Quadridentate Schiff-base Ligands

N. S. Dixit, B. P. Sudha, and C. C. Patel*

Department of Inorganic and Physical Chemistry, Indian Institute of Science, Bangalore 560012, India

(Received February 21, 1977)

The C-nitrosation of bivalent quadridentate β-imino ketone complexes of nickel(II), copper(II), and palladium(II), with nitrosating reagents has been investigated. The chemical analysis and spectroscopic results reveal that one of the α-CH groups of the coordinated lignad undergoes selective nitrosation forming mono(hydroxyimino) derivative. The hydroxyimino group introduced coordinates through either N- or O- atom to metal(II) by dislodging the carbonyl group already coordinated. This gives rise to two linkage isomers, one with N-bonded and the other with O-bonded hydroxyimino group in the case of nickel(II) (except for **1d**) and palladium(II), and a single isomer with O-bonded hydroxyimino group in copper(II) complexes. The isomers obtained from **1b** and **1i** have been separated by column chromatography. In chloroform each of the isomers of nickel(II) isomerizes to give an equilibrium mixture of two isomers, but not those of copper(II) and palladium(II).

The α-CH proton of coordinated β-diketones[1–3] and β-imino ketones[4–9] can be substituted by a variety of electrophiles. However, reports on the nitrosation of these chelates are scanty.[10–12] Nitrosation reactions of coordinated β-diketones and its nitrogen analogs assume special importance, for in these reactions the α-CH group is generally converted into hydroxyimino group. The latter being potentially ambidentate can coordinate to metal(II) through either nitrogen or oxygen giving chelate linkage isomers.

The linkage isomers of monooximato complex have been isolated by nitrosation of [*N*,*N*′-bis(1-methyl-3-oxobutylidene)ethylenediaminato]nickel(II) (**1a**) and a single isomer (hydroxyimino O-bonded) for the corresponding copper(II) complex.[13–14] The structure of the latter compound has been confirmed by X-ray diffraction studies.[15]

In continuation of our work on the linkage isomerism of the hydroxyimino group, we report here the preparation and characterization of a series of monooximato Ni(II), Cu(II), and Pd(II) complexes (**2b**—**2i**) from corresponding complexes of quadridentate β-imino ketones(**1b**—**1i**). The linkage isomers of the hydroxyimino group in Pd(II) complexes has been isolated for the first time.

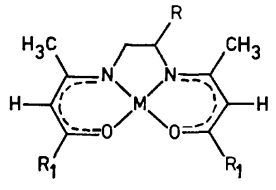

1a — 1i

	M(II)	R	R_1
1a	Ni	H	CH_3
1b	Ni	CH_3	CH_3
1c	Ni	CH_3	C_6H_5
1d	Ni	H	C_6H_5
1e	Cu	CH_3	CH_3
1f	Cu	H	C_6H_5
1g	Cu	CH_3	C_6H_5
1h	Pd	H	CH_3
1i	Pd	CH_3	CH_3

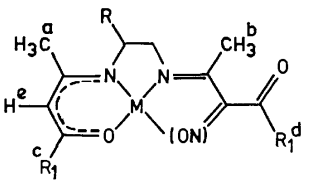

2a — 2i

Schiff-base ligands of the monooximato complexes, **2a**—**2i** corresponding to **1a**—**1i** are listed below:

- **a, h**: 3-hydroxyimino-4,9-dimethyl-5,8-diaza-4,8-dodecadiene-2,11-dione
- **b, e, i**: 3-hydroxyimino-4,7,9-trimethyl-5,8-diaza-4,8-dodecadiene-2,11-dione
- **d, f**: 2-hydroxyimino-3,8-dimethyl-1,10-diphenyl-4,7-diaza-3,7-decadiene-1,10-dione
- **c, g**: 2-hydroxyimino-3,6,8-trimethyl-1,10-diphenyl-4,7-diaza-3,7-decadiene-1,10-dione.

Experimental

Materials and Physical Techniques. The quadridentate Schiff-base ligands and their complexes (**1b**—**1i**) were prepared by the reported methods.[16] Nitrogen monoxide was generated by the method of Blanchard.[17] Nickel(II) acetate tetrahydrate, copper(II) acetate monohydrate, sodium nitrite (A.R. grade) and palladium(II) chloride (Johnson Mathey, Ltd.) were used. Alumina (neutral, Brockmann activity,1) was obtained from National Chemical Laboratory, Poona, India. Silica gel (60—120 mesh, BDH) was used for chromatographic separation. All the organic solvents used were of A.R. grade.

The conductivity, magnetic susceptibility, and spectral measurements of the complexes were carried out according to the reported procedure.[18] The molecular weights of the nickel(II) complexes which are soluble in benzene were determined by cryoscopic method, while those of Pd(II) complexes were determined by mass spectrometry using an Atlas Mat Breman Massen CH4 spectrometer. ESR spectra of the Cu(II) complexes in chloroform were recorded at 28 °C on a spectrometer, constructed at TIFR, Bombay, operating at 9.52 GHz klystron frequency. Proton probe was used to measure the magnetic field.

Palladium and nickel in their complexes were estimated as their dimethylglyoximates, and copper(II) by iodometry.[19] C, H, and N were analyzed by microanalytical methods.

Preparation of Complexes. All the complexes (Table 1) were prepared by two methods. In both methods, limited quantities of nitrosating reagents were used to avoid the formation of dioximato complexes, indicated by their precipitation due to low solubility as compared to that of monooximato complexes. Qualitatively, the rate of nitrosation of the complexes was found to be in the order Ni>Cu>Pd.

Method I. A solution of a Schiff-base complex (**1b**—

TABLE 1. COLORS, MELTING POINTS, MAGNETIC MOMENTS (μ_{eff}), AND ANALYTICAL DATA OF THE COMPLEXES

Metal	Complex	Color	Mp °C	μ_{eff}. BM	Found (%)			
					C	H	N	Metal
Ni	**2d**							
	Isomer A	Dark red	174	Dia.	48.12 (48.18)	6.01 (5.91)	12.81 (12.96)	18.02 (18.11)
	Isomer B	Red	179	Dia.	48.10 (48.18)	6.82 (5.91)	12.79 (12.96)	17.79 (18.11)
Ni Ni	**2d** **2c**	Red	150	Dia.	60.82 (60.86)	4.59 (4.87)	9.52 (9.67)	13.41 (13.52)
	Isomer(A+B)	Red	—	Dia.	61.69 (61.64)	5.11 (5.17)	9.25 (9.37)	13.02 (13.10)
Pd	**2h** Isomer(A+B)	Bright yellow	—	Dia.	40.33 (40.29)	4.56 (4.76)	11.66 (11.75)	29.71 (29.77)
Pd	**2i**							
	Isomer A	Yellow	300 (dec)	Dia.	41.98 (42.00)	4.89 (5.10)	11.26 (11.31)	28.61 (28.65)
	Isomer B	Orange yellow	300 (dec)	Dia.	41.89 (42.00)	4.82 (5.10)	11.18 (11.31)	28.55 (28.65)
Cu	**2e**	Red violet	188	1.90	47.36 (87.48)	5.79 (5.82)	12.62 (12.77)	19.15 (19.22)
Cu	**2f**	Chocolate red	235	1.91	60.08 (60.19)	4.73 (4.82)	9.52 (9.57)	14.41 (14.47)
Cu	**2g**	Chocolate red	200 (dec)	1.90	60.92 (60.89)	4.98 (5.11)	9.15 (9.27)	13.98 (14.02)

Abbreviations: dec=decomposes; Dia.=diamagnetic.
Calculated analytical values are in the parentheses.

1i) in 100 ml chloroform was degassed at 0 °C by bubbling nitrogen. Gaseous nitrogen monoxide, dried over sodium hydroxide pellets was then passed through the above solution for 30—50 min at a rate of 10 bubbles per minute. The resulting solution was concentrated *in vacuo* to obtain a crystalline product. The crystals were separated by filtration, washed with ether or benzene to remove the unreacted compound. The complexes were recrystallized from benzene, methanol, or chloroform. Yields, 80—90%.

Method II. A solution containing copper(II) acetate, or nickel(II) acetate or palladium(II) chloride (0.01 mol) and sodium nitrite (0.5 mol) in 150 ml water was treated with an appropriate Schiff-base ligand (10 mmol). The reaction mixture was stirred at ambient temperature for about 1 h in the case of Ni(II) and Cu(II) complexes, and 2—3 days in the case of Pd(II) complexes. The crystals of the complexes (80—95%) deposited were filtered, washed with water and recrystallized as before. The rate of nitrosation was found to be catalyzed in the presence of a few drops of glacial acetic acid.

Preliminary TLC experiments showed the presence of two components for Ni(II) and Pd(II) complexes of **1b**, **1c**, **1h**, and **1i** indicating the presence of two isomers, and a single component in the Ni(II) complex of **1d** and all the Cu(II) complexes.

*Separation of the Isomers of the Reaction Product of **1i**.* A concentrated solution of the nitrosation product of **1i** (250 mg) dissolved in a chloroform–methanol mixture (9 : 1 v/v) was poured into a silica gel column. Elution with the same solvent mixture gave a rapidly moving yellow band followed by a slowly moving orange yellow band. Collection of yellow and orange-yellow eluates and removal of the solvent at room temperature yielded yellow (isomer A) and orange-yellow (isomer B) crystals, respectively. The crystals were recrystallized from cold benzene.

The isomers obtained from **1b** were separated by the same procedure using an alumina column instead of silica gel column. Isomer A was more rapidly eluted than the isomer B. Attempts to separate the isomers derived from **1c** and **1h** were not successful. However, isomer A of oximato nickel complex from **1c** was obtained in pure form by fractional crystallization from ethanol.

Results and Discussion

Colors, melting points, and analytical data of the complexes are given in Table 1. The elemental analyses of the complexes indicate that they are monooximato complexes (**2b**—**2i**). The molar conductances ($\Lambda_M < 1\ \Omega^{-1}\ cm^2\ mol^{-1}$) in acetone show that they are non-electrolytes. The complexes with $R_1=CH_3$ are more soluble in common organic solvents as compared to those with $R_1=C_6H_5$. Molecular weights of the isomers of nickel complex **2b** in benzene [calcd for $NiC_{13}H_{19}O_3N_3$ 328; found 324] indicate their monomeric nature. The mass spectra of the isomer A or B of palladium complex **2i** and the mixture of isomers of **2h** show ion peaks at m/e=371 and 357 corresponding to the parent molecular ions $C_{13}H_{19}N_3O_3Pd^+$ and $C_{12}H_{17}O_3N_3Pd^+$, respectively. Insufficient solubility of the remaining complexes in benzene preclude their molecular weight determination by cryoscopic method. Ni(II) and Pd(II) complexes are diamagnetic suggesting square-planar geometry around the metal(II), while Cu(II) complexes are paramagnetic with $\mu_{eff} \approx 1.90$ B.M., a value expected for monomeric Cu(II) complexes without any magnetic coupling.

Table 2. Principal IR bands[a] (in cm^{-1}) of the monooximato Cu(II), Ni(II), and Pd(II) complexes in Nujol mull and in chloroform

Metal	Complex	$\nu_{C=O}$ (bonded)	$\nu_{C=O}$ (non-bonded)		ν_{N-O} (O-bonded)
			In mull	In $CHCl_3$	
Cu	**2e**	1520(s)	1680(s)	1680(s)	1162(s)
Cu	**2f**	1520(s)	1650(s)	1650(s)	1165(s)
Cu	**2g**	1520(s)	1652(s)	1650(s)	1160(s)
Ni	**2b**				
	Isomer A	1520(s)	1682(s)	1680(s)	1180(s)
	Isomer B	1520(s)	1645(s)	1644(s)	—
Ni	**2d**	1510(s)	1650(s)	1650(s)	1152(s)
Ni	**2c**				
	Isomer A	1522(s)	1658(s)	1650(s)	1160(s)
	Isomer B	1522(s)	1640(s)	1635(s)	—
Pd	**2h**				
	Isomer A	1515(s)	1690(s)	1688(s)	1125(s)
	Isomer B	1515(s)	1665(s)	1660(s)	—
Pd	**2i**				
	Isomer A	1512(s)	1688(s)	1688(s)	1135(w)
	Isomer B	1512(s)	1665(s)	1650(s)	—

a) Abbreviations: s=strong; w=weak.

The electronic absorption spectra of isomers of the Ni(II) complexes in chloroform display a shoulder around 23300 cm^{-1}, assignable to the d-d transition of the square-planar Ni(II) complexes. Similarly Cu(II) complexes exhibit a broad absorption band in the 18000—25000 cm^{-1} region (ε=400—500 l mol^{-1} cm^{-1}). The isomers of Pd(II) complexes, on the other hand, show an intense band at 25000 cm^{-1}. Since the intensity of this band (ε=4000—6000 l mol^{-1} cm^{-1}) is rather high, it appears to be a charge-transfer transition, which has obsured the possible d-d transition of the planar Pd(II) complexes.

Structure of Nickel(II) and Palladium(II) Complexes. Since the hydroxyimino group can coordinate to a metal ion ambidentatively, two structures, **2A** and **2B**, are expected for the monooximato complexes. The relevant IR frequencies along with their assignments are given in Table 2. The IR spectra of all the complexes show an intense band in the region 1645—1690 and 1520 cm^{-1}, assignable to the non-coordinated and coordinated CO vibrations, respectively. They further show the characteristic bands around 760(s) and 1185(vw) cm^{-1} attributable to the out-of-plane and in-plane vibrations of α-CH, respectively.

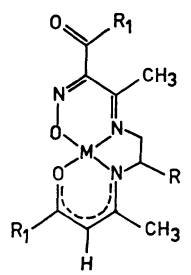

2A

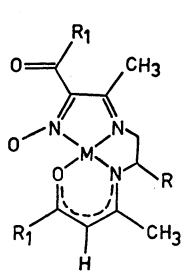

2B

The position of the non-coordinated ν_{CO}, sensitive to the bonding site of the hydroxyimino group, has been used as a probe for differentiating the structures **2A** and **2B**.[13-14] For example, ν_{CO} of N- and O-bonded isomers of nickel complex **2a** occurs at 1644 and 1684 cm^{-1}, respectively. The IR spectra of isomers A of **2b**, **2h**, and **2i** are very close to that of the hydroxyimino O-bonded isomer of Ni(II) complex **2a** and corresponding Cu(II) complex. Based on these results, the structure of type **2A** has been assigned to the isomers A. Similar structures have been suggested for nickel complex **2d** and isomer A of **2c**. The IR spectra of these complexes display the non-coordinated ν_{CO} around 1658 cm^{-1}. Furthermore, the occurrence of an intense band in the 1125—1180 cm^{-1} region, which is characteristic of coupled O-bonded ν_{CO} vibration[13] also supports the hydroxyimino O-coordination for the isomers A.

The IR spectra of isomers B of **2b**, **2c**, **2h**, and **2i** display the non-bonded ν_{CO} in the range expected for the hydroxyimino N-bonded moiety.[13-14] The structure of type **2B** has thus been proposed for the isomer B. However, it has not been possible to identify the N-bonded ν_{CO}. It is evident that isomers A and B differ only in bonding site of the hydroxyimino group. The dual modes of bonding of donor atoms of the hydroxyimino group are displayed in two different molecules. The isomerism of this type has been referred to as "intermolecular chelate linkage isomerism."

The available spectroscopic data of the isomers of the complexes led us to draw a significant conclusion about the non-bonded ν_{CO} vibrational frequency. For a given isomeric pair, the ν_{CO} of isomer A appears at a higher frequency (by $\approx$25—30 cm^{-1}) than that of isomer B. However, the dependence of ν_{CO} on the mode of attachment of hydroxyimino group is not yet clear. It is plausible that the resonance form **3A** contributes more to the structure of isomer

TABLE 3. PMR SIGNALS[a] (δ, in ppm) OF THE MONOOXIMATO COMPLEXES ALONG WITH THEIR ASSIGNMENTS

Metal	Complex	a	b	c	d	e	Diamine skeleton protons		
							CH_3	CH_2	CH
Ni	**2b**								
	Isomer A	1.88(s, 3)	2.00(s, 3)	2.18(s, 3)	2.38(s, 3)	4.98(s, 1)	1.18(d, 3) (J=6.0 Hz)	3.45(m, 4)	4.00(m, 1)
	Isomer B	1.94(s, 3)	2.04(s, 3)	2.30(s, 3)	2.48(s, 3)	5.02(s, 1)	1.36(d, 3) (J=6.0 Hz)	3.40(m, 2)	4.05(m, 1)
Ni	**2c**								
	Isomer A	1.97(s, 3)	2.06(s, 3)	2.68(m, 5)	2.56(m, 5)	5.80(s, 1)	8.61(d, 3) (J=6.0 Hz)		
	Isomer B	2.01(s, 3)	2.10(s, 3)	2.27(m, 5)	2.16(m, 5)	5.95(s, 1)	8.55(d, 3) (J=6.0 Hz)		
Pd	**2h**								
	Isomer A	2.03(s, 3)	2.26(s, 3)	1.95(s, 3)	2.38(s, 3)	4.85(s, 1)		3.70(m, 4)	
	Isomer B	2.03(s, 3)	2.32(s, 3)	1.97(s, 3)	2.54(s, 3)	4.90(s, 1)		3.42(m, 4)	
Pd	**2i**								
	Isomer A	2.05(s, 3)	2.23(s, 3)	1.96(s, 3)	2.40(s, 3)	4.86(s, 1)	1.31(d, 3) (J=6.0 Hz)	3.40(m, 2)	4.10(m, 1)
	Isomer B	2.05(s, 3)	2.35(s, 3)	2.00(s, 3)	2.43(s, 3)	4.92(s, 1)	1.40(d, 3) (J=6.0 Hz)	3.38(m, 2)	4.02(m, 1)

a) Key: s=singlet; d=doublet; m=complex multiplet.
Complexity and relative peak intensities of the signals are in parentheses.

A than of isomer B.

$$R_1\text{-}\underset{\underset{O}{\|}}{C}\text{-}C{=}N\text{-}O^- \longleftrightarrow R_1\text{-}\underset{\underset{O^-}{|}}{C}{=}C\text{-}N{=}O$$

3A **3B**

As expected the PMR spectra of **2b**, **2h**, and **2i** show four distinct methyl signals of the chelate ring, the assignments of which are given in Table 3. It can be seen that the proton signals of isomer A except $COCH_3$ protons and α-CH proton of isomer A are more shielded than those of isomer B. Similar spectral features are found in the isomers of nickel complex **2c**.

Chelate Linkage Isomerization. In the solid state, isomer A of **2b** is hydroxyimino O-bonded, while isomer B is hydroxyimino N-bonded. In chloroform at 40 °C, each of these isomerizes giving an equilibrium mixture of A and B isomers. The transformation is irreversible. This is due to the fact that

$$\text{Nickel complex } \mathbf{2b} \text{ isomer A or B} \xrightarrow[40\,^\circ C]{CDCl_3} \text{isomers(A+B)} \quad (1)$$

the IR as well as PMR spectra of the complexes obtained by refluxing each isomer in chloroform at 40 °C, corresponded to those containing mixture of the isomers A and B. Similarly isomer A of **2c** also isomerizes in $CDCl_3$. Its room temperature PMR spactrum displays two methyl signals and a complex multiplet due to phenyl protons with intensity ratio of 3 : 3 : 10, respectively. However, the spectrum of

$$\text{Nickel complex } \mathbf{2c} \text{ isomer A} \xrightarrow[50\,^\circ C]{CDCl_3} \text{isomers(A+B)} \quad (2)$$

isomer A, which was previously refluxed at 50 °C in $CHCl_3$, showed a pattern corresponding to the mixture of isomers A and B. In Eqs. 1 and 2, the isomers are produced by the reorganization in the donor sites of the hydroxyimino group of the same ligand. This phenomenon may be referred to as "chelate linkage isomerization," the occurrence of which is rare in organic chelating ligands. It is, however, common in the case of inorganic ligands, particularly the complexes of chalcogenocyanates.[20] The isomerization is not favoured in **2d** (hydroxyimino O-bonded), Pd(II) and Cu(II) complexes under similar conditions. Probably, the high activation energies associated with these complexes appear to be responsible for their failure to isomerize.

Structure of the Copper(II) Complexes. In contrast to Ni(II) and Pd(II) complexes, a single isomer is obtained by nitrosation of the Cu(II) Schiff-base complexes. The ν_{CO} (non-bonded) and ν_{NO} in the Cu(II) complexes appear in the region 1650—1680 cm^{-1} and at 1160 cm^{-1}, respectively. The positions of these bands are compatible with those of the corresponding isomer A of the Ni(II) complexes. Hence, the bonding of the hydroxyimino group in all the Cu(II) complexes is suggested to be through oxygen.

The first derivative ESR spectra of the Cu(II) complexes consist of four main groups of equally spaced lines, which result from the coupling of ^{63}Cu (I=3/2) with the unpaired electron. The hyperfine structure of the first two high field signals consists of five peaks of intensity ratio 1 : 2 : 3 : 2 : 1. These peaks result from the splitting by two nitrogens (I=1) of the diamine skeleton. Thus, the hyperfiine structure of the main peaks suggests that the coordination sphere around Cu(II) is N_2O_2. This conclusion is in line

with that derived from IR data. The average values of ESR parameters are 2.07(g), 90.0 G (A_{Cu}), 12.5 G (A_N) and 7.6 (covalency factor α^2). These values are compatible with the square-planar Cu(II) complexes with N_2O_2 ligational environment.[21-24]

In conclusion, nitrosation of **1b—1i** gives monooximato complexes under the experimental conditions employed, unlike the conventional substitution reactions. Further, the hydroxyimino group introduced at the ring CH carbon dislodges the coordinated carbonyl group and coordinates to metal ion either through nitrogen or oxygen, giving rise to chelate linkage isomers. The preferential mode of coordination of the hydroxyimino group essentially depends upon the metal ion.

References

1) D. H. Busch, *Am. Chem. Soc. Adv. Chem. Ser.*, No. 37 (1963).
2) J. P. Collman, "Transition Metal Chemistry" ed by R. L. Carlin, Vol. 2, Marcel Dekker, Inc., New York (1966), p. 1.
3) J. P. Collman, *Angew, Chem. Int. Ed. Engl.*, **4**, 132 (1965).
4) R. W. Kluiber, *J. Am. Chem. Soc.*, **82**, 4839 (1960).
5) J. P. Collman and E. T. Kittleman, *Inorg. Chem.*, **1**, 499 (1962).
6) Y. Fujii, *Bull. Chem. Soc. Jpn.*, **43**, 1722 (1970).
7) A. Kasahara and T. Izumi, *Bull. Chem. Soc. Jpn.*, **41**, 2185 (1968).
8) C. J. Hipp and D. H. Busch, *Inorg. Chem.*, 737 (1972).
9) C. J. Hipp and D. H. Busch, *Inorg. Chem.*, **12**, 894 (1973).
10) I. Masuda, M. Tamaki, and K. Shinra, *Bull. Chem. Soc. Jpn.*, **42**, 157 (1969).
11) K. S. Bose and C. C. Patel, *J. Inorg. Nucl. Chem.*, **33**, 2947 (1971).
12) D. A. White, *J. Chem. Soc., A*, **1971** 233.
13) M. J. Lacey, C. G. Mcdonald, and J. S. Shannon, *Aust. J. Chem.*, **26**, 263 (1973).
14) N. S. Dixit, Ph. D. Thesis, Indian Institute of Science, Bangalore (1976).
15) C. M. Biagini, V. A. Chiesi, M. A. Gaetani, and M. Nardelli, *Acta Crystallogr., Sect. B*, **28**, 1075 (1972).
16) P. J. McCarthy, R. J. Hovey, K. Ueno, and A. E. Martell, *J. Am. Chem. Soc.*, **77**, 5820 (1955).
17) A. Blanchard, *Inorg. Synth.*, **2**, 126 (1946).
18) R. R. Iyengar, K. S. Bose, and C. C. Patel, *Inorg. Chim. Acta*, **7**, 3 (1973).
19) A. I. Vogel, "A Text Book of Quantitative Analysis," 2nd ed, Longmans Green, New York (1951).
20) A. H. Norbury, "Advances in Inorganic and Radiochemistry," ed by H. J. Emeleus and H. G. Sharpe, Academic Press, New York (1975) No. 17, p. 231.
21) B. R. McGarrey, *J. Phys. Chem.*, **60**, 71 (1956).
22) G. M. Larvin, G. V. Panova, and E. G. Rudhadze, *Russ. J. Str. Chem. (Eng. Transl.)*, **6**, 664 (1965).
23) H. A. Kuska and M. J. Rogers, *J. Chem. Phys.*, **43**, 1744 (1965).
24) E. M. Roberts and W. S. Koski, *J. Am. Chem. Soc.*, **82**, 3006 (1960).

NOTES

BULLETIN OF THE CHEMICAL SOCIETY OF JAPAN, VOL. 51 (7), 2165—2166 (1978)

Chemical Equilibria of Methyl-, Ethyl-, and Propylmercury(II) Chlorides and Their Complexes with L-Cysteine in Liquid-Liquid Distribution Systems

Masaru NIITSU,* Teruo MANRI, and Nobuhiko IRITANI

Faculty of Pharmaceutical Sciences, Josai University, Sakado, Saitama, 350-02

(Received August 11, 1977)

Synopsis. The distribution constants for methyl-, ethyl-, and propylmercury(II) chlorides (RHgCl) between aqueous 1 mol dm^{-3} (H, Na)Cl and benzene were determined to be $10^{1.04}$, $10^{1.60}$, and $10^{2.20}$ respectively. The formation constants for the complexes of these organomercury(II) chlorides with L-cysteine (R'SH), $K=[RHgSR'][H^+][Cl^-][RHgCl]^{-1}[R'SH]^{-1}$, were determined to be $10^{1.71}$ $10^{1.55}$, and $10^{1.49}$ respectively.

The formation of highly stable complex with L-cysteine has been employed in analytical procedures for methylmercury(II),[1,2] on the basis that organomercury(II) is highly extractable into organic solvents as halides but the extractability disappears in an exchange of the halide ion with L-cysteine.[3,4]

In the present study, the distribution equilibria of methyl-, ethyl-, and propylmercury(II) chlorides and the exchange equilibria of the chloride ion in these compounds with L-cysteine in the aqueous phase were studied in systems containing two liquid-phases, aqueous 1 mol dm^{-3} (H, Na)Cl and benzene.

Experimental

The methyl-, ethyl-, and propylmercury(II) chlorides were obtained from Mitsuwa Chemical Co. and Soekawa Rikagaku Co., and the L-cysteine from Wako-Pure Chemical Co. The other reagents were of an analytical grade.

All the procedures were carried out at 25 °C. Benzene containing a certain amount of an organomercury(II) chloride was washed with 0.1 mol dm^{-3} hydrochloric acid and used. A portion of the benzene solution and the same volume of an aqueous 1 mol dm^{-3} (H, Na)Cl solution containing none or 1×10^{-3} mol dm^{-3} of L-cysteine were placed in a stoppered glass tube, agitated vigorously for 2 min and centrifuged. The organomercury(II) in the aqueous phase was extracted into carbon tetrachloride containing diphenyl thiocarbazone and the absorption of the organic phase at 620 nm was measured.[5]

Results and Discussion

For the analysis of the distribution data, the following equations were employed:

$$D = [RHgCl]_{org}([RHgCl]+[RHgSR'])^{-1} \quad (1)$$

$$RHgCl \rightleftharpoons RHgCl(org)$$

$$K_d = [RHgCl]_{org}[RHgCl]^{-1} \quad (2)$$

$$RHgCl + R'SH \rightleftharpoons RHgSR' + H^+ + Cl^-$$

$$K = [RHgSR'][H^+][Cl^-][RHgCl]^{-1}[R'SH]^{-1} \quad (3)$$

where R denotes an alkyl group, and R'SH denotes L-cysteine. The subscript "org" and the lack of subscript denote the chemical species in the organic and aqueous phases respectively. The formation constant K was calculated by introducing Eqs. 1 and 2 into the following equations:

$$[RHgSR'] = [RHg(II)]_{total} - [RHgCl] \quad (4)$$

$$[R'SH] = [R'SH]_{total} - [RHgSR'] \quad (5)$$

In the preliminary experiments, it was found that the distribution ratios of these organomercury(II) chlorides were independent of both the hydrogen-ion concentration in the aqueous phase and their own concentration in the organic phase in ranges of 3×10^{-3} to 1 mol dm^{-3} and 3×10^{-4} to 2×10^{-2} mol dm^{-3} respectively. The effect of the chloride ion on the distribution of methyl-, ethyl-, and propylmercury(II) chlorides was also measured when the aqueous phase was 1 mol dm^{-3} (H, Na)(Cl, ClO_4) containing 0.1 mol dm^{-3} of hydrogen-ion and the initial concentration of methyl-, ethyl-, and propylmercury(II) chlorides was 5.0×10^{-4}, 1.1×10^{-3}, and 5.7×10^{-3} mol dm^{-3} respectively. It was found that the distribution ratio was independent of the chloride ion concentration in the range 10^{-3} to 1 mol dm^{-3}. The distribution constants, K_d, between 1 mol dm^{-3} (H, Na)Cl and benzene were thus determined to be $10^{1.04}$, $10^{1.60}$, and $10^{2.20}$ respectively for methyl-, ethyl-, and propylmercury(II) chlorides.

The distribution ratio of these organomercury(II) as a function of the hydrogen-ion concentration was

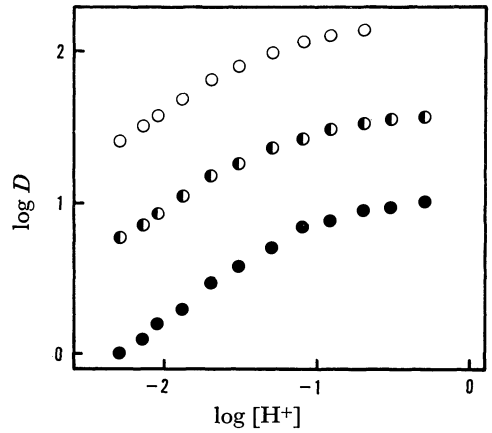

Fig. 1. Distribution ratio of methyl- (●), ethyl- (◐), and propyl (○) mercury(II) between benzene and 1 mol dm^{-3} (H, Na)Cl containing 10^{-3} mol dm^{-3} L-cysteine as a function of the hydrogen-ion concentration in the aqueous phase.

Table 1. The formation constants for the complexes of methyl-, ethyl-, and propylmercury(II) chlorides with L-cysteine in the 1 mol dm^{-3} (H,Na)Cl in Eq. 3

[H$^+$]	log K (CH_3Hg(II))	log K (C_2H_5Hg(II))	log K (C_3H_7Hg(II))
5.0×10^{-1}	1.62	1.58	
3.0×10^{-1}	1.70	1.53	
2.0×10^{-1}	1.65	1.59	1.51
1.2×10^{-1}	1.72	1.57	1.48
8.0×10^{-2}	1.66	1.61	1.48
5.0×10^{-2}	1.77	1.56	1.49
3.0×10^{-2}	1.74	1.55	1.48
2.0×10^{-2}	1.73	1.51	1.48
1.3×10^{-2}	1.75	1.53	1.49
9.0×10^{-3}	1.70	1.54	1.49
7.0×10^{-3}	1.70	1.54	1.48
5.0×10^{-3}	1.72	1.51	1.47
mol dm^{-3}	Av 1.71	Av 1.55	Av 1.49

also measured in the presence of L-cysteine and illustrated in Fig. 1.

For the analysis of the data, no extraction of organomercury(II) as a L-cysteine complex was assumed.[1-4] The values of K calculated on this assumption in Table 1 were reasonably constant.

From these results, it can be concluded that K_d of these organomercury(II) chlorides increases by a factor of four by the addition of one $-CH_2-$ into the alkyl chain. This is an observation similar to that found among a series of organic compounds.[6] Simpson reported[4] a value of K_d of methylmercury(II) chloride between water and toluene to be $10^{1.04}$, and Budevsky, *et al.*[7] reported the value between 1 mol dm^{-3} (Na, H)ClO_4 and *o*-xylene to be $10^{1.07}$; they are similar to the present value.

The value of K is somewhat greater in the order of propylmercury(II) < ethylmercury(II) < methylmercury(II). This order may correspond with the basicity order of these organomercury(II).

It is readily seen that the electron density of the oxygen in the carboxyl group of L-cysteine (pK_a=1.96)[8] is affected by a change in the hydrogen-ion concentration but that of the sulfur in the thiol group (pK_a=10.28)[8] should remain constant. This seems to indicate coordination of the central mercury(II) in the complexes with the sulfur in the thiol group since the formation constant, K, was not affected by changes in the hydrogen-ion concentration. This agrees with the general tendency that mercury(II) is a soft acid which interacts with sulfur stronger than oxygen.

References

1) S. Nishi and Y. Horimoto, *Bunseki Kagaku*, **17**, 1247 (1968).
2) S. Fukui, K. Tanaka, S. Kanno, and T. Ukita, Adv. water pollution Res. 6th Int. Conf. Jerusalem, 819 (1973).
3) M. L. Anson, K. Bailey, and J. T. Edsall, "Advance in Protein Chemistry," Vol. XI, Academic Press Inc. New York (1956) p. 366.
4) R. B. Simpson, *J. Am. Chem. Soc.*, **83**, 4711 (1961).
5) E. B. Sandell, "Colorimetric Determination of Trace of Metals," Interscience, New York (1965).
6) A. A. Collander, *Acta Chem. Scand.*, **3**, 717 (1949).
7) O. Budevsky, F. Ingman, and D. H. Liem, *Acta Chem. Scand.*, **27**, 1277 (1973).
8) A. Albert, *Biochem. J.*, **50**, 690 (1952).

BULLETIN OF THE CHEMICAL SOCIETY OF JAPAN, VOL. 51 (7), 2167—2168 (1978)

Reactivity of Organic Ions by Chemical Ionization Mass Spectrometry. II. Chemical Ionization Mass Spectra of Alkylbenzenes with Methane by Using a Quadrupole Mass Spectrometer

Kozo Iseda

Government Industrial Research Institute, Nagoya, Hirate-machi, Kita-ku, Nagoya 462

(Received September 13, 1977)

Synopsis. The titled spectra have been determined at 75 °C. The $(M+H)^+$ ion intensities for methylbenzenes decrease linearly with the number of methyl substituents. The $(M+H)^+$ ion intensities for dialkylbenzenes decrease in the order *o*->*m*->*p*-, while those of trimethylbenzenes decrease in the order 1,2,3->1,3,5->1,2,4-, and those of tetramethylbenzenes decrease in the order 1,2,3,4->1,2,3,5->1,2,4,5-.

In the previous paper the author reported chemical ionization mass spectra (CIMS) of alkylbenzenes with isobutane as reactant gas.[1] The result has been interpreted as showing that the order of the $(M+H)^+$ ion intensities of alkylbenzenes is dependent on the basicities of these compounds.

Since the $C_2H_5^+$ ion from methane is a stronger Brønsted acid than the t-$C_4H_9^+$ ion from isobutane,[2] in the case of methane some different results can be expected. No study has been reported on the CIMS of alkylbenzenes with three isomers with methane except that on diethylbenzenes by Munson and Field.[3] Methylbenzenes are suited for the study of the relationship between the number of methyl groups and the ion intensity of the formed ions, because of their small dealkylation.

The purpose of this paper is to explore the difference of reactivity due to the difference of properties between the two reactant gases.

Experimental

The mass spectra were measured with a Finnigan Model 3000 GC mass spectrometer which has been modified to operate under chemical ionization conditions.[1] The experimental conditions are the same as those used previously, which were as follows: ion source pressure, 1 mmHg; ion source temperature, 75 °C; electron energy, 90 eV. Low boiling samples were admitted to the ion source with a Nupro bellows metering valve SS-4BMG. High boiling and solid samples were admitted with the solid probe equipped with a heater. All values used in this work are the average of more than three measurements.

Methane (99.7%) obtained from Tokyo Methane Co., Ltd. was employed without further purification as the reagent gas. The following alkylbenzenes (Tokyo Kasei Kogyo Co., Ltd., extra pure or more) were studied: benzene (B), toluene(T), xylenes(X), ethyltoluenes(ET), diethylbenzenes(DEB), diisopropylbenzenes(DIPB), trimethylbenzenes(TrMB), tetramethylbenzenes(TeMB), pentamethylbenzene(PMB), and hexamethylbenzene(HMB).

Table 1. CIMS of benzene and hexamethylbenzene (CH_4 reactant = 1 mmHg)

Benzene		Hexamethylbenzene	
Ion	RI(%Σ)[a]	Ion	RI(%Σ)[a]
$(M-15)^+$		$(M-15)^+$	2.7±0.3
$(M-1)^+$		$(M-1)^+$	25.8±0.4
M^+	5.1±0.2	M^+	18.0±0.4
$(M-1)^+$	79.9±0.3	$(M+1)^+$	42.1±0.3
$(M+29)^+$	5.5±0.1	$(M+29)^+$	3.1±0.0
$(M+41)^+$	1.6±0.0	$(M+41)^+$	0.6±0.1

a) Average of four replicates±average deviation.

Results and Discussion

Table 1 shows the reproducibility of the intensities for benzene and hexamethylbenzene. Such a good reproducibility is adequate for the purpose of this study. The spectra of 21 alkylbenzenes with methane are given in Table 2. The intensities of $(M+H)^+$ ions tend to decrease from benzene to *p*-diisopropylbenzene as the number of alkyl carbon atoms in the aromatic molecule increases. For methyl-substituted compounds there is a decrease in intensity of $(M+H)^+$ ions with increasing the number of methyl substituents on the benzene ring, that is, the protonated hydrocarbons decrease with increasing electron density on the benzene ring. These results are not consistent with those of usual chemical reactions and of reactions with isobutane. The $(M+H)^+$ intensities of dialkylbenzenes decrease in the order *o*->*m*->*p*-, while those of trimethylbenzenes decrease in the order 1,2,3->1,3,5->1,2,4,-, and those of tetramethylbenzenes decrease in the order 1,2,3,4->1,2,3,5->1,2,4,5-. These orders also are not the same as those obtained with isobutane.

As shown in Table 2, the $(M-H)^+$ ion intensities tend to increase from toluene to *p*-diethylbenzene with increasing the carbon number of the side chain. The $(M-H)^+$ intensities for methylbenzenes also increase with the methyl substituents on the benzene ring. The intensities of $(M-H)^+$ ions increase in the order *o*-<*m*-<*p*- in the disubstituted compounds, 1,2,3-<1,3,5-<1,2,4- in the trimethylbenzenes, and 1,2,3,4-<1,2,3,5-<1,2,4,5- in the tetramethylbenzenes. The order of the $(M-H)^+$ ion intensities for all the isomers is obviously opposite to that of the $(M+H)^+$ ion intensities.

As can be seen from Table 2, the intensities of $(M+29)^+$ ions for toluene, xylenes, ethyltoluenes, diethylbenzenes, and trimethylbenzenes are higher than that of benzene. This seems to be a result of the hyperconjugation effect due to the alkyl groups. On the contrary, the intensities of the $(M+29)^+$ ions for the compounds which have four or more methyl substituents are lower than that of benzene, and decrease

Table 2. CIMS (CH_4 reactant = 1 mmHg), RI (%Σ) of ions in alkylbenzenes

	$(M-43)^+$	$(M-41)^+$	$(M-29)^+$	$(M-15)^+$	$(M-1)^+$	M^+	$(M+1)^+$	$(M+29)^+$	$(M+41)^+$
B						5.1	79.9	5.5	1.6
T					3.9	5.1	74.5	7.1	1.9
o-X				1.2	6.1	5.4	69.7	8.0	1.9
m-X				1.2	8.0	5.4	68.7	7.6	2.0
p-X				1.2	10.6	6.0	66.7	6.9	1.6
o-ET				4.3	6.5	5.1	60.5	8.7	2.5
m-ET				4.3	8.1	5.7	59.6	7.3	2.4
p-ET				5.3	11.3	5.4	57.8	6.5	1.6
o-DEB	1.2	0.9	4.1	6.7	8.2	5.8	51.2	6.8	1.8
m-DEB	1.2	0.8	3.2	6.5	9.7	6.9	50.1	6.2	1.8
p-DEB	1.4	0.8	3.3	7.7	11.4	6.7	46.9	7.0	1.7
m-DIPB	2.3	16.5	2.8	9.1	6.7	3.2	19.1	0.3	0.6
p-DIPB	3.0	19.6	1.1	11.9	9.3	4.3	18.7	0.3	0.6
1,2,3-TrMB				1.4	10.0	5.9	66.9	6.5	1.8
1,3,5-TrMB				1.3	13.1	6.3	62.7	7.1	1.9
1,2,4-TrMB				1.4	14.7	6.5	62.4	6.4	1.5
1,2,3,4-TeMB				1.7	15.6	8.1	59.1	4.3	1.2
1,2,3,5-TeMB				1.8	19.7	8.9	56.4	4.9	1.1
1,2,4,5-TeMB				1.8	21.3	9.8	53.7	4.7	0.9
PMB				2.4	23.5	13.2	48.7	4.2	0.7
HMB				2.7	25.8	18.0	42.1	3.1	0.6

with the methyl substituents. This decrease results from the steric hindrance due to the methyl substituents. There is also a nearly similar tendency for the $(M+41)^+$ ions. Both $(M+29)^+$ and $(M+41)^+$ ions formed in all compounds in contrast with the $(M+57)^+$ ion observed in the case of isobutane; this can be explained on the basis of the differences of ionic volume.

The relationship between the $(M+H)^+$ ion intensities and the number of methyl substituents is different from the results with isobutane; this can be ascribed to the difference of Brøsted acid strength between the ion from methane and the ion from isobutane. The ion from methane is $C_2H_5^+$, which is a stronger Brønsted acid than t-$C_4H_9^+$ from isobutane,[2] so the $C_2H_5^+$ ion is both a stronger proton addition and hydride abstraction reactant than t-$C_4H_9^+$.[2] Actually the $(M+H)^+$ ion intensity of benzene is higher than that with the isobutane,[1] and the $(M-H)^+$ ion intensities of tetramethylbenzenes are higher than those with the isobutane.[1] The attack by a strong acid, such as $C_2H_5^+$ ions, is not appreciably affected by the basicity of aromatics in contrast with the attack by the weaker acid of t-$C_4H_9^+$ ions. Therefore, in this case, the basicity for the aromatics is not necessary for the proton addition. Since the $C_2H_5^+$ ion can abstract hydride in proportion to the number of methyl substituents, as described above, because of its strong acidity, the formation of $(M+H)^+$ ion is affected rather by the formation of the $(M-H)^+$ ion than the basicity of aromatics. That is to say, in the proton addition reaction, a strong Brønsted acid, such as the $C_2H_5^+$ ion, counteracts any effect resulting from the electron density on the benzene ring. Accordingly, in the case of a methane reactant, the order of the proton addition reactions is not consistent with the order of the basicities for alkylbenzenes.

In spite of the higher basicity of *m*-xylene compared with *o*-xylene,[4] the $(M+H)^+$ intensity for *m*-xylene is lower than that for *o*-xylene, which is opposite to the result with isobutane.[1] This discrepancy also may be explained in the same way as ascribed above: that is, in the case of a methane reactant, the formation of $(M+H)^+$ is affected rather by the formation of $(M-H)^+$ ion than by the basicity of aromatics. However, in this case, while each xylene has the same methyl number, the reason why the hydride is easily abstracted from *m*-xylene is not known at present. Thus, it can be considered that the stability of the ions can not be determined only from the order of formation for the ions, for that order depends on the kind of reactant gas. The alkylbenzene isomers can be identified by the exchange of reactant gas.

References

1) K. Iseda, *Nippon Kagaku Kaishi*, **4**, 627 (1976).
2) M. S. B. Munson and F. H. Field, *J. Am. Chem. Soc.*, **88**, 2621 (1966); B. Munson, *Anal. Chem.*, **43**, 28A (1971).
3) M. S. B. Munson, and F. H. Field, *J. Am. Chem. Soc.*, **89**, 1047 (1967).
4) H. C. Brown and J. D. Brady, *J. Am. Chem. Soc.*, **71**, 3573 (1949); *ibid.*, **74**, 3570 (1952); L. J. Andrews and R. M. Keefer, *ibid.*, **71**, 3644 (1949); D. A. McCaulay and A. P. Lien, *ibid.*, **73**, 2013 (1951).

BULLETIN OF THE CHEMICAL SOCIETY OF JAPAN, VOL. 51 (7), 2169—2170 (1978)

The Preparation of Phosphonic Acids Having Labile Functional Groups

Tsuyoshi MORITA,* Yoshiki OKAMOTO, and Hiroshi SAKURAI

The Institute of Scientific and Industrial Research, Osaka University, Yamada-kami, Suita, Osaka 565

(Received September 19, 1977)

Synopsis. Phosphonic acids having labile functional groups have been prepared quantitatively by the hydrolysis of bis(trimethylsilyl) phosphonates, were prepared by the reaction under mild conditions of the corresponding dialkyl phosphonates with bromotrimethylsilane.

The biological activity of phosphonic acids has become of interest in recent years.[1] Phosphonic acids may be capable of inhibiting or perturbing the regular metabolism.[2] The phosphonic acid esters need re-examination as the corresponding acids which may be more readily assimilated by organisms. A convenient method for the preparation of phosphonic acids from dialkyl phosphonates (**1**) has been recently reported, which includes the reaction of **1** with chloro- or bromotrimethylsilane (**2**) and the subsequent hydrolysis under mild conditions of the resulting bis(trimethylsilyl) phosphonates (**3**).[3,4] Dialkyl phosphonates react more readily with **2** to give **3** than with chlorotrimethylsilane. The limitation for silylation of **1** with **2** has not yet been reported. The conditions for silylation were investigated by the reaction of **1** having different labile functional groups with **2**, a modification of the procedures of Mckenna[3] and Rabinowitz.[4]

The silylation of **1** with double the molar quantity of **2** was carried out at room temperature for 1 h to give **3** in good yields. The reaction, which was monitored by the NMR of the reaction mixture, was completed within 1 h. The results are summarized in Table 1.

$$\underset{(1)}{RP(O)(OR')_2} + 2\underset{(2)}{Me_3SiBr} \longrightarrow \underset{(3)}{RP(O)(OSiMe_3)_2} + 2R'Br$$

1a R=$(MeO)_2CH$, R'=Me
1b R=MeCO, R'=Et
1c R=Me_2NCO, R'=Et
1d R=$MeOCOCH_2$, R'=Et
1e R=$PhOCOCH_2$, R'=Et
1f R=MeOCO, R'=Et
1g R=$NCCH_2$, R'=Et
1h R=H_2NCOCH_2, R'=Et
1i R=EtOCH=CH, R'=Me

For the silylation of **1h**, different conditions were required, namely, a slight excess of **2** (2.3 times). In the reaction of diethyl 2,3-epoxypropylphosphonate with an equimolar amount of **2**, diethyl 2-bromo-3-trimethylsiloxypropylphosphonate was produced instead of bis(trimethylsilyl) 2,3-epoxypropylphosphonate. The reaction appears to proceed *via* an onium type intermediate formed by the attack of phosphinyl sp^3 oxygen on the silicon atom of **2**, which in turn decomposes to the trimethylsilylated esters of phosphonic acid and alkyl bromide.

The hydrolysis of **3** was carried out with a water–ether mixture at room temperature for a few minutes to afford the phosphonic acids (**4**), which were isolated as the anilinium or cyclohexylammonium salts in good yields. These salts were recrystallized from a mixture of methanol–acetone. The results are summarized in Tables 2 and 3.

$$\underset{(3)}{RP(O)(OSiMe_3)_2} + H_2O \longrightarrow \underset{(4)}{RP(O)(OH)_2} + Me_3SiOSiMe_3$$

TABLE 1. YIELDS AND PHYSICAL PROPERTIES OF **3**

	Yield (%)	Bp (°C/mmHg)	IR (cm^{-1})	^1H NMR δ in CCl_4 (ppm)
3a	99	116—119/10	1248(P=O)	3.14 (6H, s, CH_3O), 4.34 (1H, d, J=6.0 Hz, CHP), 0.26 (16H, s, $OSiMe_3$),
3b	91	60—62/0.1	1690(C=O) 1245(P=O)	2.38 (3H, d, J=4.8 Hz, CH_3C), 0.30 (18H, s, $OSiMe_3$)'
3c	92	80—82/0.1	1616(C=O) 1240(P=O)	2.92 (3H, s, CH_3N), 3.30 (3H, s, CH_3N), 0.28 (18H, s, $OSiMe_3$)
3d	90	123—124/8	1732(C=O) 1244(P=O)	3.65 (3H, s, CH_3O), 2.74 (2H, d, J=21.6 Hz, CH_2P), 0.28 (18H, s, $OSiMe_3$)
3e	90	133—135/0.5	1760(C=O) 1256(P=O)	3.00 (2H, d, J=21.6 Hz, CH_2P), 7.23 (5H, m, C_6H_5), 0.29 (18H, s, $OSiMe_3$)
3f	91	60—62/0.1	1724(C=O) 1250(P=O)	3.78 (3H, s, CH_3O), 0.30 (18H, s, OSiMe)
3g	93	129—130/7	2250(C≡N) 1250(P=O)	2.84 (2H, d, J=21.6 Hz, CH_2P), 0.32 (18H, s, $OSiMe_3$)
3h	> 99[a]	—	—	3.21 (2H, d, 21.0 Hz, CH_2P), 0.33 (18H, s, $OSiMe_3$)
3i	92	71—73/0.01	1600(C=C) 1245(P=O)	1.30 (3H, t, CH_3C), 3.84 (2H, q, CH_2O), 4.69 (1H, dd, J=9.6 Hz, CHP, J=13.2 Hz, HCCH), 7.02 (1H, t, J=13.2 Hz, HCCP), 0.26 (18H, s, $OSiMe_3$)

a) The reaction was carried out in $CHCl_3$ and the silyl ester was not isolated. Yield was estimated on the reaction mixture by NMR in $CDCl_3$. A broad signal of $CONH_2$ was observed at δ=6.5−8.0.

Table 2. Yields and physical properties of salts of **4**

	Yield (%)	Mp (°C)	^{1}H NMR δ in D_2O (ppm)
4a	96	135—137 (dec)	3.47 (6H, s, CH_3O), 4.45 (1H, d, J=4.2 Hz, CHP), 7.50 (5H, m, C_6H_5N)
4b	92	159—162 (dec)	2.34 (3H, d, J=4.2 Hz, CH_3C)
4c	93	148—150	2.91 (3H, s, CH_3N), 3.32 (3H, s, CH_3N), 7.44 (5H, m, C_6H_5N)
4d	94	145—146	3.68 (3H, s, CH_3O), 2.84 (2H, d, J=19.2 Hz, CH_2P), 7.45 (5H, m, C_6H_5N)
4e	89	157—159	3.21 (2H, d, J=19.8 Hz, CH_2P), 7.52 (10H, m, C_6H_5O, C_6H_5N)
4f	95	160—162	3.72 (3H, s, CH_3O), 7.30 (10H, m, C_6H_5N)
4g	97	172—174	2.85 (2H, d, J=19.2 Hz, CH_2P), 7.50 (5H, m, C_6H_5N)
4h	92	131—133	2.74 (2H, d, J=20.4 Hz, CH_2P), 7.51 (5H, m, C_6H_5N)
4i	90	164—167 (dec)	1.23 (3H, t, CH_3C), 3.85 (2H, q, CH_2O), 4.90 (1H, dd, J=9.6 Hz, CHP, J=13.8 Hz, HCCH), 6.84 (1H, dd, J=11.4 Hz, HCCP)

Table 3. Elemental analysis of salts of **4**

	Formula	Found (%)				Calcd (%)			
		C	H	N	P	C	H	N	P
4a	$C_9H_{16}O_5NP$[a]	43.64	6.64	5.80	12.17	43.37	6.43	5.62	12.45
4b	$C_{14}H_{31}O_4N_2P$[d]	48.85	9.58	8.98	9.89	52.17	9.63	8.70	9.63
4c	$C_9H_{15}O_4N_2P$[a]	44.08	6.31	11.37	12.51	43.90	6.10	11.38	12.60
4d	$C_9H_{14}O_5NP$[a]	43.69	5.88	5.73	12.34	43.72	5.67	5.67	12.55
4e	$C_{14}H_{16}O_5NP$[a]	54.04	5.50	4.81	10.12	54.37	5.18	4.53	10.03
4f	$C_{14}H_{19}O_5N_2P$[b]	51.70	6.03	8.69	9.24	51.53	5.83	8.59	9.51
4g	$C_8H_{11}O_3N_2P$[a]	45.12	5.37	13.13	14.90	44.86	5.14	13.08	14.49
4h	$C_8H_{13}O_4N_2P$[a]	41.30	5.94	12.23	13.10	41.38	5.60	12.07	13.36
4i	$C_{10}H_{22}O_4NP$[c]	47.90	9.13	5.81	12.46	47.81	8.76	5.58	12.35

a) Monoanilinium salt. b) Dianilinium salt. c) Monocyclohexylammonium salt. d) Dicyclohexylammonium salt.

Experimental

All the melting and boiling points are uncorrected. NMR spectra were obtained by a JNM-TS-100 spectrometer with TMS or DSS as an internal reference. IR spectra were obtained by a Shimadzu IR-400.

*Preparation of Dialkyl Phosphonates (**1**).* The phosphonates (**1b**—**1h**) were prepared by the Arbuzov reaction of the corresponding chlorides with triethyl phosphite. The phosphonate (**1a**) was prepared from PCl_3 and trimethyl orthoformate accroding to the method of Gross and Freiberg.[5] The phosphonate (**1i**) was prepared from ethyl vinyl ether and PCl_5 according to the method of Anisimov and Nesmeynov.[6]

*Preparation of Bromotrimethylsilane (**2**).* Bromotrimethylsilane (**2**) was prepared from hexamethyldisiloxane and PBr_3 according to the method of Gilliam *et al.*[7]

*Preparation of Bis(trimethylsilyl) Phosphonates (**3**).* Bromotrimethylsilane (**2**) (20 mmol) was added dropwise to **1** (10 mmol) with stirring at room temperature for 1 h. After the removal of the resulting methyl or ethyl bromide, **3** was obtained by distillation.

*Preparation of Phosphonic Acids (**4**).* Compound **3** (10 mmol) was dissolved in ether (50 ml) and the solution extracted with three portion of water (3×30 ml). The combined aqueous solution was neutralized by the addition of aniline or cyclohexylamine (20 mmol) and concentrated to dryness under reduced pressure to give a solid. The solid was recrystallized from a mixture of methanol-acetone (1:5 v/v) to afford the salt of **4**.

References

1) D. Redmore, *Chem. Rev.*, **71**, 351 (1971).
2) R. Engel, *Chem. Rev.*, **77**, 349 (1977).
3) C. E. Mckenna, M. T. Higa, N. H. Cheug, and M. Mckenna, *Tetrahedron Lett.*, **1977**, 155.
4) R. Rabinowitz, *J. Org. Chem.*, **28**, 2975 (1963).
5) H. Gross and J. Freiberg, *Chem. Ber.*, **101**, 1250 (1968).
6) K. N. Anisimov, and A. N. Nesmeyanov, *Bull. Acad. Sci. U.S.S.R. Div. Chem. Sci.*, **1954**, 521; *Chem. Abstr.*, **49**, 11541b (1955).
7) W. F. Gilliam, R. N. Meals, and R. O. Sauer, *J. Am. Chem. Soc.*, **68**, 1161 (1946).

BULLETIN OF THE CHEMICAL SOCIETY OF JAPAN, VOL. 51 (7), 2171—2172 (1978)

Asymmetric Synthesis of Alanine by Alkylation of Optically Active *N*-Alkyl-*N*-formylaminoacetonitriles[1)]

Kaoru HARADA,* Minoru TAMURA, and Shinnichiro SUZUKI
Department of Chemistry, The University of Tsukuba, Ibaraki 300-31

(Received November 30, 1977)

Synopsis. Optically active *N*-alkyl-*N*-formylaminoacetonitriles were prepared and the nitriles were alkylated with methyl iodide. The products were hydrolyzed and hydrogenolyzed to form optically active alanine. The optical yields of alanine ranged from 2 to 18%. The effects of the reaction temperature and of the asymmetric moieties on the optical yields were examined. The optical yields were also determined by the NMR spectra of the resulting diastereomers.

So far numerous asymmetric syntheses of α-amino acids have been reported.[2)] However, only a few papers deal with the asymmetric synthesis of α-amino acids by alkylation.[3)] An asymmetric synthesis of aspartic acid through β-lactams using optically active *N*-(alkylamino)acetonitriles[4)] has been reported.

In the present paper, sterically controlled synthesis of alanine from opitcally active *N*-alkyl-*N*-formylaminoacetonitriles(**3a—e**) by asymmetric alkylation with methyl iodide is described(Scheme 1). After hydrolysis and subsequent hydrogenolysis of the products, alanine was obtained. The *N*-(alkylamino)acetonitriles(**2a—e**) were prepared from racemic and optically active amines(**1a—e**) and chloroacetonitrile. The **2a—e** were converted in to the corresponding formylated compounds(**3a—e**). They were treated with sodium hydride and methyl iodide in DMF at various temperatures. The products were hydrolyzed with 6 M hydrochloric acid without isolation. The resulting *N*-alkyl-alanines(**4a—e**) were isolated by the use of a Dowex 50 column and were hydrogenolyzed with palladium hydroxide on charcoal to yield alanine. Yields of the synthesized alanine were in the range 2—66%, and the optical yields in the range 2—18%. When (*S*)-(−)-amines were used, (*R*)-(−)-alanine was obtained for all reaction temperatures. When α-methylbenzylamine was used, the optical yield of the resulting alanine was low. The use of 1-(1-naphthyl)-ethylamine slightly increased the optical yield of alanine. However, when α-ethylbenzylamine was used, the optical purity of alanine clearly increased. This suggests that the small(S) and the middle(M) groups among the large(L), M, and S groups of the asymmetric center might play an important role in the asymmetric synthesis.

The temperature effect on the optical yield was observed; the lower the reaction temperature, the higher the optical yield of alanine. However, the temperature effect was not so large. The results are summerized in Table 1.

In some cases, the optical yields of the asymmetric syntheses could be estimated by the NMR spectra of the resulting mixture of diastereomers.[5)] In the NMR spectrum of **4c**, the two sets of doublet signals observed are referred to (*S*-*R*) and (*S*-*S*) isomeric methyl protons (H_a, Scheme 1). The lower doublet

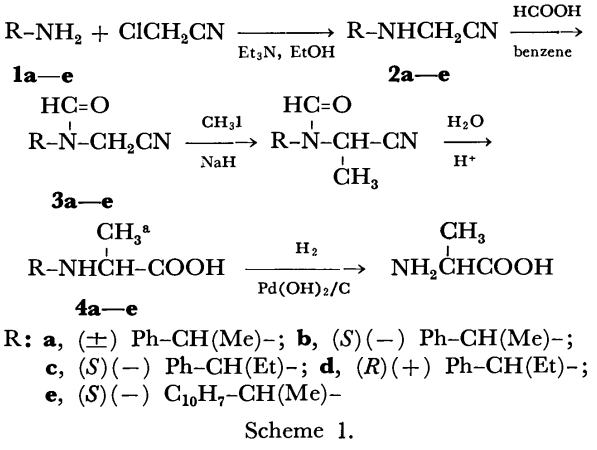

R: **a**, (±) Ph-CH(Me)-; **b**, (*S*)(−) Ph-CH(Me)-; **c**, (*S*)(−) Ph-CH(Et)-; **d**, (*R*)(+) Ph-CH(Et)-; **e**, (*S*)(−) $C_{10}H_7$-CH(Me)-

Scheme 1.

TABLE 1. ASYMMETRIC SYNTHESIS OF ALANINE

Starting material **3**	Config. of asymmetric moiety	Temp (°C)	Synthesized Ala		DNP-Ala	
			Config.	Yield (%)[a)]	$[\alpha]_D^{25}$ (*c*)[b)]	Optical yield (%)[c)]
a	±	−15	±	62		
b	(*S*)(−)	−15	*R*	61	− 2.1(0.70)	2
c	(*S*)(−)	−15	*R*	66	−14.0(1.00)	10
		−25	*R*	60	−18.4(1.25)	13 [d)]
d	(*R*)(+)	−25	*S*	54	+20.0(1.05)	14 [d)]
		−45	*S*	2	+24.0(0.13)	17
e	(*S*)(−)	−15	*R*	23	− 7.8(0.83)	5
d	(*R*)(+)	−78	*S*	35	+26.8(0.35)	18 [e)]

a) Calculated from **3**. b) Specific rotation of DNP-alanine measured in 1 M NaOH. c) Defined ($[\alpha]_D$ obsed/$[\alpha]_D$ of the compound) × 100. DNP-(*S*)-(+)-alanine, $[\alpha]_D^{25}$ +143.9° (1 M NaOH). d) Also calculated from the NMR spectra of **4**. (Table 2). e) Lithium diisopropylamide (4.94 mmol), HMPA (4.94 mmol), and methyl iodide (2.47 mmol) treated with **3d** (2.47 mmol) in THF.

Table 2. Optical yields calculated from the NMR spectra of **4**[a]

Starting material **3**	Config. of asymmetric moiety	Reaction temp (°C)	δ of H^a (ppm)	Ratio	Optical[b] yield (%)
c	(*S*)(−)	−25	1.45(*S-S*) 1.55(*S-R*)	*S-R*/*S-S* =57/43	14
d	(*R*)(+)	−25	1.45(*R-R*) 1.55(*R-S*)	*R-S*/*R-R* =56/44	12

a) The NMR spectra measured in D_2O with a 60 MHz spectrometer using DSS as an internal standard. b) Defined as $[(S\text{-}R)-(S\text{-}S)/(S\text{-}R)+(S\text{-}S)]\times 100$, or $[(R\text{-}S)-(R\text{-}R)/(R\text{-}S)+(R\text{-}R)]\times 100$.

signal with larger area was assigned to the methyl proton (H_a) of (*S-R*) isomer, from which (*R*)-alanine was obtained by hydrolysis and hydrogenolysis. The optical yield was determined by the ratio of the doublet signals of the diastereomers. The optical yield of **4d**, was also determined in the same way. The optical yields of **4c,d** determined by the NMR spectra(Table 2) agreed with those determined by the specific rotation of 2,4-dinitrophenyl(DNP)-alanine (Table 1).

Experimental

The amino acid analyses were carried out with a Yanagimoto LC-5S instrument. The NMR spectra were obtained with Hitachi H-60 and R-24 A instruments. The specific rotations were measured with a JASCO ORD-CD 20 C spectropolarimeter using a 10 mm cell. The boiling points and melting points were uncorrected. The optically active amines used were as follows. **1b**($[\alpha]_D^{25}$ −41.3°, benzene),[6,7] **1c**($[\alpha]_D^{25}$ −21.0°, benzene),[7,8] **1d**($[\alpha]_D^{25}$ +23.3°, benzene),[7,8] **1e**($[\alpha]_D^{25}$ −90.9°, benzene).[9] *N*-alkylaminoacetonitriles (**2a—d**) were prepared as described.[4]

(S)-(−)-N-α-Ethylbenzyl-N-formylaminoacetonitrile (3c). Compound **2c**(4.77 g, 27.4 mmol) and formic acid (6.30 g, 0.137 mol) were dissolved in 100 ml of dry benzene. The solution was stirred at room temperature for 2 h and then refluxed for 3 h with use of a Dean Stark distillation tube. After the reaction was over, the benzene solution was washed with 3% sodium hydrogencarbonate. The benzene solution was dried with anhydrous sodium sulfate and the solvent was evaporated. Compound **3c** was obtained by distillation under reduced pressure, yield, 3.42 g, 61.8%, bp 142—143 °C/1 Torr, $[\alpha]_D^{25}$ −99.3° (*c* 0.826, benzene). After distillation the nitrile **3c** crystallized. This was recrystallized from ethanol; mp, 56—57 °C, Found: C, 71.37; H, 6.91; N, 13.94%. Calcd for $C_{12}H_{14}N_2O$: C, 71.26; H, 6.98; N, 13.85%. IR(KBr): 2950, 1655, and 1390 cm^{-1}; $\delta(CDCl_3)$: 1.05(3H, t, J=7.2 Hz), 2.15(2H, quintet, J=7.2 Hz), 2.94(2H, ABq, J=17.4 Hz), 4.59(1H, t, J=7.2 Hz), 7.39(5H, s), 8.45(1H, s). Other nitriles were prepared in a similar way. The physical properties were as follows: **3a**; bp 156—157 °C/2 Torr, Found: C, 69.93; H, 6.48; N, 14.95%. Calcd for $C_{11}H_{12}N_2O$: C, 70.19; H, 6.43; N, 14.88%. **3b**; bp 157—158 °C/2 Torr, $[\alpha]_D^{25}$ −63.7°(*c* 0.97, benzene). Found: C, 70.12; H, 6.45; N, 14.82%. Calcd for $C_{11}H_{12}N_2O$: C, 70.19; H, 6.43; N, 14.88%. **3d**; bp 164—165 °C/3 Torr, $[\alpha]_D^{25}$ +103.1°(*c* 0.62, benzene); Found: C, 71.28; H, 6.98; N, 13.88%. Calcd for $C_{12}H_{14}N_2O$: C, 71.26; H, 6.98; N, 13.85%. **3e**; bp 195—197 °C/1 Torr, $[\alpha]_D^{25}$ −76.1°(*c* 0.18, benzene). Found: C, 75.49; H, 5.99; N, 11.72%. Calcd for $C_{15}H_{14}N_2O$: C, 75.61; H, 5.92; N, 11.76%.

N-[(S)-α-Ethylbenzyl]-(R)-alanine (4c). The formylated nitrile **3c**(0.510 g, 2.52 mmol) and methyl iodide(0.526 g, 3.71 mmol) were dissolved in 15 ml of anhydrous DMF. The solution was cooled to −25 °C and sodium hydride(0.140 g, 2.74 mmol, 47%, suspension in mineral oil) was added with stirring. The reaction mixture was stirred for 24 h at −25 °C. After the reaction was over the solvent was evaporated at 30 °C under reduced pressure. The residue was refluxed with 20 ml of 6 M hydrochloric acid for 20 h. After evaporation of hydrochloric acid, the hydrolyzate was applied on a Dowex 50 column(H^+ form). The column was eluted with 3 M aqueous ammonia and the solution was evaporated to dryness under reduced pressure. A part of **4c** was dissolved in 3 M hydrochloric acid and the solvent was removed under reduced pressure to crystallize **4c** hydrochloride. The salt was subjected to NMR analysis $\delta(D_2O)$: 0.80(3H, t, J=7.2 Hz), 1.45(3H, d, J=7.2 Hz), 1.55(3H, d, J=7.2 Hz), 2.10(2H, quintet, J=7.2 Hz), 7.50(5H, s).

(R)-Alanine (5). Compound **4c** was dissolved in a mixture of water(10 ml) and ethanol(10 ml) and was hydrogenolyzed with palladium hydroxide on charcoal(0.5 g) for 24 h at 1 atm. After the reaction was over the catalyst was removed by filtration. A part of the solution was diluted appropriately and analyzed with an automatic amino acid analyzer to determine the yield of alanine(60%). A part of alanine was converted to 2,4-dinitrophenyl(DNP)-alanine in the usual way,[4] and the resulting DNP-alanine was purified with use of a celite column treated with a citrate-phosphate buffer(pH 4 and pH 7).[10] The DNP-alanine was further confirmed by thin layer chromatography using ether-AcOH-H_2O(100 : 1 : 1 v/v) solvent system. DNP-(*R*)-alanine, $[\alpha]_D^{25}$ −18.4°(*c* 1.25, 1 M NaOH); optical purity 13%.

This work was partially supported by a Grant-in-Aid for Scientific Research from the Ministry of Education. The authors wish to express their thanks to Dr. Takenori Kusumi for his valuable discussions and for taking some of the NMR spectra.

References

1) Sterically Controlled Synthesis of Opticaly Active Organic Compounds. XXIII; Part XXII: K. Harada and I. Nakamura, *Chem. Lett.*, **1978**, 9.

2) J. D. Morrison and H. S. Mosher, "Asymmetric Organic Reactions," Prentice-Hall, Englewood Cliffs, New Jersey (1971), Chap. 7; J. W. Scott and D. Valentine, Jr., *Science*, **184**, 943 (1974).

3) S. Yamada, T. Oguri, and T. Shioiri, *J. Chem. Soc., Chem. Commun.*, **1976**, 136.

4) T. Okawara and K. Harada, *J. Org. Chem.*, **37**, 3286 (1972).

5) J. C. Fiaud and A. Horeau, *Tetrahedron Lett.*, **1972**, 2565; S. Yamada and S. Hashimoto, *ibid.*, **1976**, 997.

6) W. Theilacker and H. Hinker, *Chem. Ber.*, **87**, 690 (1954).

7) "Stereochemistry, Fundamental and Methods," H. B. Kagan ed, Col. 4, Georg Thieme Publishers, Stuttgart (1977), p. 103.

8) M. E. Warren, Jr., and H. E. Smith, *J. Am. Chem. Soc.*, **87**, 1757 (1965).

9) Ref. 7, p. 106.

10) K. Matsumoto and K. Harada, *J. Org. Chem.*, **31**, 1956 (1966).

BULLETIN OF THE CHEMICAL SOCIETY OF JAPAN, VOL. 51 (7), 2173—2174 (1978)

Photochemical Oxidation of Toluene with Nitrogen Dioxide in Gas Phase. "Effects of Oxygen"

Hiroshi ISHIKAWA, Kazuo WATANABE, and Wataru ANDO*

Department of Chemistry, The University of Tsukuba, Niiharigun, Ibaraki 300-31

(Received December 22, 1977)

Synopsis. The products and mechanism of the reaction of toluene with nitrogen dioxide have been investigated in the presence of oxygen. The volatile products observed were benzaldehyde, *o*-, *m*-, and *p*-nitrotoluene, along with 6-nitro-*o*- and 2-nitro-*p*-cresol.

Myriad descriptions of the mechanism of photochemical oxidation of aromatic hydrocarbons with nitrogen oxides have appeared over the last ten years.[1-4] These reviews have been accompanied by an even greater number of discriptions of the properties of reactive intermediates and of reaction rates. While much work has been carried out on the products and mechanism of the gas phase reaction of alkylbenzene with NO_2, mainly by Kato[5] and Akimoto *et al.*,[6] the major part of the reaction products was unfortunately a material of low volatility which could not be characterized. The present work was undertaken in the hope of obtaining additional information about the photooxidative products from the reaction of toluene with nitrogen dioxide in the presence of oxygen.

Experimental

A conventional high vacuum apparatus utilizing Teflon stopcocks was employed. A cylindrical reaction vessel made of Pyrex glass (22.5 liter), 1.5 m long and 16 cm in diameter, was connected to the storage bulbs for the reactants, to the trapping system equipped with gas-chromatographic take off bulbs, and to the high vacuum system.

Commercially available toluene was dried completely and distilled with rejection of appropriate first and last fraction until it was gas-chromatographically pure. Nitrogen dioxide dried by phosphorus pentaoxide was purified by repeated trap to tarp distillation under vacuum. The gases used were Nihon Tokushu Gas Co. extra dry grade nitrogen and oxygen, and Nihon Sanso Co. special grade air.

Known amounts of toluene and nitrogen dioxide were admitted to the reaction vessel and diluted with dry nitrogen or air to atmospheric pressure. The samples were irradiated for periods of 10 h with four Toshiba fluorescent light-bulbs, FLR40SBL-A(wavelength 300—420 nm, maximum at 360 nm, light intensity range of 4—8 $\mu W/cm^2$). The irradiated products were fractionally collected in a sample tube for gas-chromatographic analysis cooled at Dry Ice temperature. The products which were non-condensable in the Dry Ice trap were condensed in liquid nitrogen. The GLC analyses were carried out using a Hitachi 163 flame ionization detector with a 20 m long OV-101 capillary glass column. In all cases, the gas chromatographic evaluation of product yield was based on the internal standard 1-methylnaphthalene. There was an appreciable scatter in the quantitative yields of benzaldehyde and benzyl nitrate, perhaps because of some spurious loss of these highly oxidizable substances. The yields of these two compounds reported in the present work must therefore be regarded as only approximate. A maximum error of $\pm 10\%$ in the product yields was expected in all other cases.

Non-volatile products in the reaction vessel were washed out with methanol and analyzed by GLC; they were mainly 4,6-dinitro-*o*-cresol.

Results and Discussion

Photolysis of Nitrogen Dioxide in Toluene and Nitrogen or Air System. The reaction was studied extensively at 25—30 °C at the concentration of 1000 ppm of nitrogen dioxide and toluene, respectively, for irradiation times ranging from 2—10 h. The reaction products observed were benzaldehyde(1), *o*-nitrophenol(2), *o*-nitrotoluene(3), benzylnitrate(4), α-nitrotoluene(5), *m*-nitrotoluene(6), *p*-nitrotoluene(7), 6-nitro-*o*-cresol(8), 2-nitro-*p*-cresol(9), and 4,6-dinitro-*o*-cresol(10). The yields of major products are given in Table 1.

No benzyl alcohol, *o*-, *m*-, or *p*-cresol were detected under these reaction conditions. In addition, a small amount of methane and ethane was observed for non-condensable products at 196 °C. On the other hand, there was some formation of *o*- and *p*-nitrotoluene without irradiation, but the yields are less than 1 ppm.

It can be seen that there is a general agreement in the product yields under the reaction conditions.

The available evidence suggests that in the photolysis of toluene with nitrogen dioxide in nitrogen atmosphere, nitrogen dioxide is the major light absorbing species in the region of less than 398 nm, forming nitric oxide and ground state oxygen atoms. Thus it seems likely that atomic oxygen is the predominant agent involved in the initial attack on the aromatic ring to form biradical [A], followed by isomerization of phenolic compounds, which then react with nitrogen dioxide to form nitrocresol. On the other hand, the intermediate biradical [A] and [B] may react with nitrogen dioxide, followed by dehydration to give *o*-, *m*-, and *p*-nitrotoluene. A possible reaction sequence is shown in Scheme 1.

The formation of *o*-nitrophenol could be explained by the ipso-attack of oxygen atom at the position of methyl group to form phenol, which then reacts with nitrogen dioxide to give nitrophenol. By analogy with the formation of nitrocresol, the formation of 4,6-

TABLE 1. YIELDS (ppm) OF THE REACTION PRODUCTS IN THE REACTION OF TOLUENE AND NITROGEN DIOXIDE IN ATOMOSPHERE OF NITROGEN[a)]

Product	1	2	3	4	5	6	7	8	9	10
Run 1	trace	0.8	0.3	0.3	4.2	9.5	2.2	27	14.4	5.2
Run 2	trace	0.6	0.3	0.2	3.2	10.5	2.3	26	13.2	5.2

a) 10 h irradiation for 1000 ppm toluene and 1000 ppm No_2.

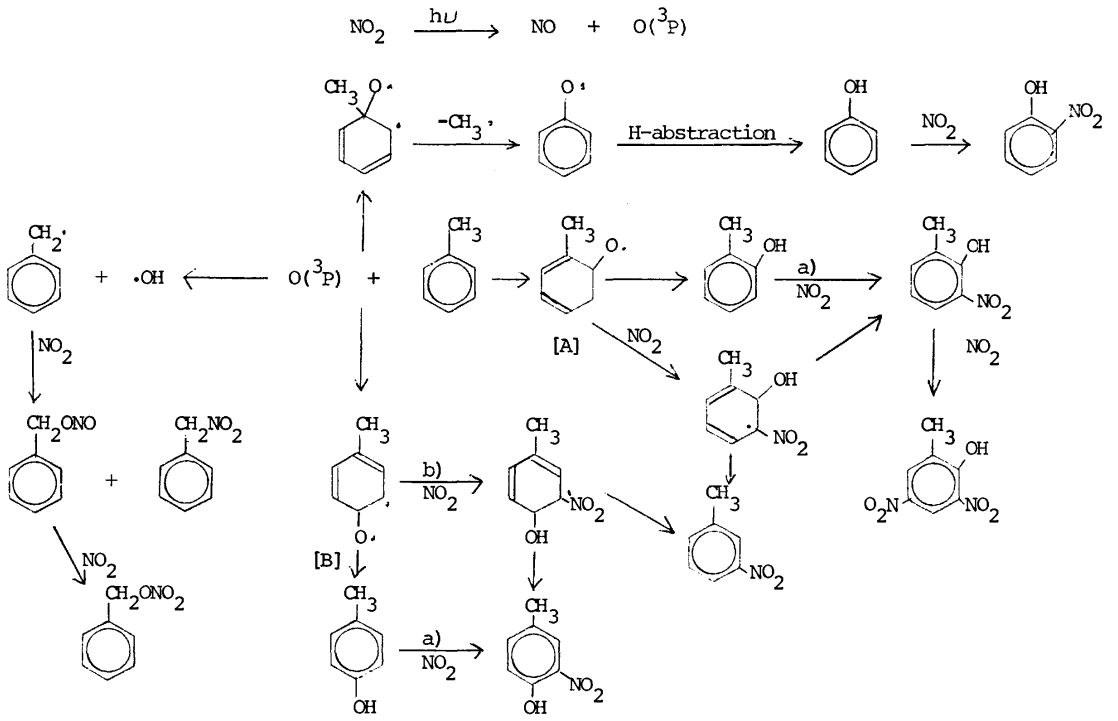

Scheme 1.

dinitro-*o*-cresol presumably proceeds by addition of nitrogen dioxide to 6-nitro-*o*-cresol to give an encounter pair, followed by intramolecular nitro group attack on the paraposition and subsequent aromatization to produce the 4,6-dinitro-*o*-cresol.

Although the activation energy of hydrogen abstraction is generally much higher than that for addition, and there is no report of the hydrogen abstraction of toluene with oxygen atom, one anticipates that in the reaction of nitrogen dioxide with toluene hydrogen abstraction may occur in view of the formation of α-nitrotoluene and benzyl nitrate. The presence of methane and ethane suggests the formation of methyl and phenyl radicals which can abstract a hydrogen atom to form methane and benzene, or recombine to form ethane.

The Role of Oxygen in the Photochemical Reaction of Toluene and Nitrogen Dioxide. In the presence of air, the products distribution for the photolysis of nitrogen dioxide and toluene was studied; the results are given in Table 2. There is a drastic increase in the yield of the products, in comparison to the oxygen free system. This is readily understandable in terms of the conversion of nitric oxide to nitrogen dioxide by oxygen. Oxygen must play an especially important role in the formation of benzyl nitrate. Benzyl nitrate may be formed from the strong interaction of the intermediate of the benzyl radical with oxygen, followed by a reaction most likely with nitric oxide or nitrogen dioxide.

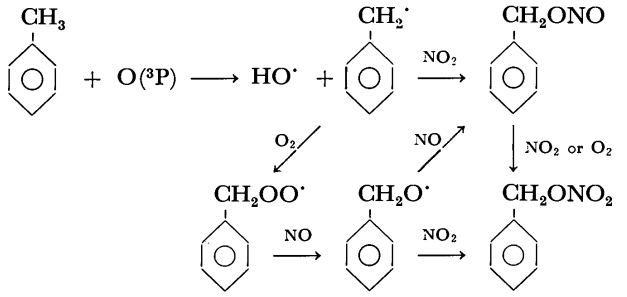

From this and previous work, the reaction of the aromatic hydrocarbons with nitrogen dioxide can be satisfactory explained in terms of the general reaction mechanism of an oxygen atom with an aromatic ring. The difference in the yield of products between nitrogen and air systems arises because of the recyclization of nitric oxide to nitrogen dioxide.

Table 2. Effects of oxygen on product yields (ppm) (NO_2 1000 ppm, toluene 1000 ppm, irradiation time 10 h, temperature 25—30 °C.)

Product	1	2	3	4	5	6	7	8	9	10
Run 1	2.5	2.9	0.5	9.9	0.6	2.7	2.0	49.4	16.3	38.0
Run 2	2.8	2.9	0.6	7.1	0.7	2.6	1.1	46.4	18.4	55.1
Run 3	2.3	3.0	0.9	6.0	0.9	2.3	1.3	44.6	16.3	60.8

References

1) S. L. Kopczynski, *Int. J. Air Wat. Poll.*, **8**, 107 (1964).
2) D. L. Dunburg, *Can. J. Chem.*, **43**, 1714 (1965).
3) A. P. Altshuller, C. R. Cohen, S. F. Sleva, and S. L. Kopczynski, *Science*, **138**, 442 (1962).
4) A. P. Altshuller, S. L. Kopczynski, W. A. Lonneman, F. D. Sulterfield, and D. L. Wilson, *Env. Soc. Tech.*, **4**, 44 (1970).
5) T. Kato and Y. Hanai, *Env. Soc. Rep. Yokohama Univ.*, **3**, 1 (1976).
6) (a) M. Hoshino, N. Washida, H. Akimoto, G. Inoue, and M. Okuda, Symp. Photochemistry Kyushu, 1976. (b) H. Akimoto, G. Inoue, M. Okuda, M. Hoshino, and N. Washida, Symp. Photochemistry Tokyo 1975.

BULLETIN OF THE CHEMICAL SOCIETY OF JAPAN, VOL. 51 (7), 2175—2176 (1978)

Preparation and Reactions of Di-1,3,5-triazinyl Ethers. I. Preparation of Di-1,3,5-triazinyl Ethers

Ryuta SAKURAI, Yoji HASHIDA, and Kohji MATSUI*
Faculty of Engineering, Gunma University, Kiryu, Gunma 376

(Received January 6, 1978)

Synopsis. Di-1,3,5-triazinyl ethers have been prepared by the condensation of 2-chloro-1,3,5-triazines with potassium 1,3,5-triazin-2-olate in acetonitrile in the presence of a small amount of cyclic polyether. Di-1,3,5-triazinyl ether was also prepared by the reaction of 2-chloro-1,3,5-triazine with potassium nitrite.

A number of derivatives of 1,3,5-triazine have been prepared by the condensation of 2-chloro-1,3,5-triazines with various nucleophiles.[1] Among the compounds investigated amines[2] and sulfides[3,4] containing two or three triazine nuclei on the same N or S atom are of particular interest because of their unique chemical behavior. This paper reports two preparative methods for di-1,3,5-triazinyl ethers.

Results and Discussion

Reaction of 2-Chloro-1,3,5-triazines with 1,3,5-Triazin-2-ol. The Williamson synthesis which involves the reaction of sodium alkoxide with an alkyl halide was considered applicable to the synthesis of di-1,3,5-triazinyl ethers. 1,3,5-Triazine nuclei are electron-withdrawing, and therefore the di-1,3,5-triazinyl ethers would be expected to have properties similar to those of acid anhydrides. Consequently a proper choice of solvent is important in the preparation of di-1,3,5-triazinyl ethers, because a solvent of high nucleophilicity will react with the di-1,3,5-triazinyl ethers formed to afford derivatives of the mono triazine nucleus.

Among the solvents investigated acetonitrile was found to be the most suitable. In acetonitrile, reaction took place very slowly when potassium 4,6-dimethoxy-1,3,5-triazin-2-olate (**1**, Scheme 1) was heated with an equimolecular amount of 2-chloro-4,6-dimethoxy-1,3,5-triazine (**3c**); after heating for 48 h, di-1,3,5-triazinyl ether (**4c**) was obtained (yield 44%; No. 4, Table 1). The addition of a small amount of 18-crown-6 accelerated the reaction; chlorotriazine (**3c**) disappeared within 30 min to give di-1,3,5-triazinyl ether (**4c**) (yield 58%; No. 5). From the mechanism[5] generally accepted, the catalytic effect of the cyclic polyether can be explained in terms of the presence of a "bared" triazinolate anion which attacks chlorotriazine much more readily.

The product (**4c**) had a parent mass peak of 296 and a PMR signal for the methyl protons was observed as a sharp singlet at δ 4.09. In addition, the IR spectrum of **4c** did not show the presence of C=O group. 1,3,5-Triazin-2-ol is known to exist as a tautomeric mixture of (**1**) and (**2**); thus, there is a possible isomer (**5**) as shown in Scheme 1. However, from the evidence the indication is that the product has the structure (**4**). The yield of di-1,3,5-triazinyl ether was found to be sensitive to the amount of cyclic polyether employed, *e.g.*, when dibenzo-18-crown-6 was used, yield of di-1,3,5-triazinyl ether (**4c**) increased to 65% (No. 6).

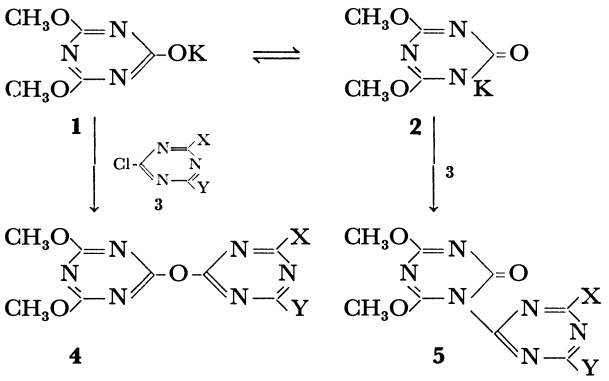

a: X=Y=Cl
b: X=Cl, Y=OCH_3
c: X=Y=OCH_3
d: X=OCH_3, Y=NEt_2
e: X=Y=NEt_2

Scheme 1.

The condensation of triazinol with chlorotriazine is affected by the substituents in the triazine nucleus. In the reaction with **1**. chlorotriazines having electron-withdrawing substituents such as Cl– (**3a**, **3b**) and/or CH_3O– (**3c**) afforded the di-1,3,5-triazinyl ether (**4a**—**c**). However, chlorotriazines (**4d**, **4e**) containing electron-donating substituents such as dialkylamino groups gave only the starting materials, and no desired di-1,3,5-triazinyl ether (No. 7, 8). When chlorotriazine possessed more than one active halogen atom, ditriazinyl ethers involving more than one ether oxygen atom were obtained. For example, in the reaction of potassium 4,6-dimethoxy-1,3,5-triazin-2-olate (**1**) with cyanuric chloride (**4a**) in a molar ratio of 2:1, 2-chloro-4,6-bis(4,6-dimethoxy-2-triazinyloxy)-1,3,5-triazine was obtained (No. 1). When the reaction was carried out in a molar ratio of 3:1, all active chlorine atoms were replaced by dimethoxytriazinyloxy groups (No. 2).

Di-1,3,5-triazinyl ether was also prepared by treating chlorotriazine with potassium nitrite. In the attempt to prepare the nitrous acid ester of triazinol by treating chlorotriazine (**3c**) with potassium nitrite, instead of nitrous acid ester, di(triazinyl)ether (**4c**) was obtained. In this case, the presence of the cyclic polyether (18-crown-6) greatly accelerated the reaction (see, Experimental Section).

Although the mechanism of this reaction is not still clear, the reaction is assumed to proceed by the fol-

Table 1. Reaction of potassium 4,6-dimethoxy-1,3,5-triazin-2-olate with 4,6-disubstituted 2-chloro-1,3,5-triazines

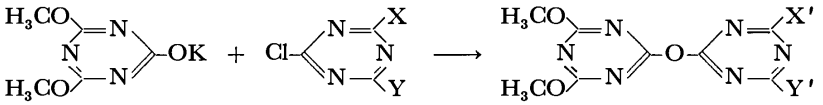

No.	Substitnent X	Substitnent Y	Product X'	Product Y'	Yield %	Mp °C	Recryst. solvent	Found (Calcd) % C	H	N	Cl
1	Cl	Cl	OT	Cl	47[a]	162—163	Benzene	40.31 (40.54	3.98 4.08	28.39 28.37)	
2	Cl	Cl	OT	OT	57[a]	167—168	Benzene	36.88 (36.67	2.91 2.84	29.46 29.61	8.10 8.33)
3	Cl	OCH_3	Cl	OCH_3	59[a]	128—129	Benzene	36.19 (35.98	3.05 3.02	28.29 27.97	11.91 11.80)
4	OCH_3	OCH_3	OCH_3	OCH_3	44[b]	157—158	Benzene	39.93 (39.57	3.50 3.32	31.03 30.76)	
5	OCH_3	OCH_3	OCH_3	OCH_3	58[a]	—	—	—	—	—	—
6	OCH_3	OCH_3	OCH_3	OCH_3	65[c]	—	—	—	—	—	—
7	OCH_3	NEt_2	No ditriazinyl ether was formed.								
8	NEt_2	NEt_2									

T = 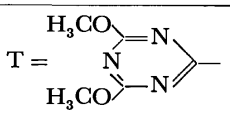

a) The reaction was carried out in the presence of 1/5 equimolar amount of 18-crown-6. b) The reaction was carried out in the absence of cyclic polyether. c) The reaction was carried out in the presence of 1/5 equimolar amount of dibenzo-18-crown-6.

lowing sequence (Scheme 2), analogous to the reaction of active chlororbenzene derivatives with potassium nitrite.[6] This reaction did not occur in the triazine derivatives bearing electron-donating substituents. For instance, in the reaction of 2-chloro-4,6-bis(diethylamino)-1,3,5-triazine (**3e**) with potassium nitrite in the presence of cyclic polyether, only the starting material was recovered even after long heating (120 h). This indicates that the first step in Scheme 2 did not occur.

$$\mathbf{3c} + 2KNO_2 \longrightarrow \mathbf{1} + N_2O_3 + KCl$$

$$\mathbf{1} + \mathbf{3c} \longrightarrow \mathbf{4c} + KCl$$

Scheme 2.

This method is limited to the preparation of the symmetric ditriazinyl ether, while the synthetic method by condensation of chlorotriazine with triazinol is applicable for the preparation of symmetric and unsymmetrical derivatives.

Experimental

All the melting points are uncorrected.

Preparation of Di-triazinyl Ethers by Condensation of Chlorotriazines with Triazinol. A example is shown of the reaction of 2-chloro-4,6-dimethoxy-1,3,5-triazine (**3c**) with potassium 4,6-dimethoxy-1,3,5-triazin-2-olate (**1**). A solution of **3c**(3.00 g, 17.1 mmol) in acetonitrile (50 ml) was added, drop by drop, into a solution of a mixture of **1** (3.37 g, 17.1 mmol) and 18-crown-6 (0.90 g, 3.41 mmol) in acetonitrile (50 ml) at room temperature. After stirring for 1 h under reflux, the solvent was removed *in vacuo*. The residue was chromatographed on a silica gel column with benzene–acetone (10:1, v/v) as eluent to give a crude product of di-1,3,5-triazinyl ether (**4c**). The recrystallization from benzene gave the pure material.

The reaction in the absence of cyclic polyether was carried out in a similar way as described above.

Reaction of 2-Chloro-4,6-dimethoxy-1,3,5-triazine (3c) with Pottassium Nitrite. To a solution containing potassium nitrite (2.01 g, 23.6 mmol) and 18-crown-6 (1.03 g, 3.88 mmol) in acetonitrile (50 ml) was added dropwise a solution of **3c** (2.50 g, 14.3 mmol) in acetonitrile (50 ml) and the mixture stirred for 3 h at room temperature. After removal of the solvent, the residue was chromatographed on a silica gel column with benzene–acetone (10:1, v/v) as eluent to give di-1,3,5-triazinyl ether (**4c**); yield, 1.27 g (61%).

The reaction in the absence of cyclic polyether was carried out in a similar way in refluxing acetonitrile for 48 h to afford the same product (45%) and starting triazine derivative (18%).

References

1) E. M. Smolin, and L. Rapoport, "*s*-Triazine and Derivatives," Interscience Publishers (1959).

2) N. Nohara, S. Sekiguchi, and K. Matsui, *J. Heterocyclc. Chem.*, **7**, 519 (1970).

3) G. A. Loughran, G. F. L. Ehlers, and J. L. Burkett, *J. Heterocycl. Chem.*, **3**, 137 (1966).

4) G. A. Loughran, G. F. L. Ehlers, and J. L. Burkett, *J. Heterocycl. Chem.*, **3**, 143 (1966).

5) J. H. Fendler and E. J. Fendler, "Catalysis in Micellar and Macromolecular Systems," Academic Press, New York (1975), Chap. 11.

6) T. J. Broxton, D. M. Muir, and A. J. Parker, *J. Org. Chem.*, **40**, 2037 (1975).

BULLETIN OF THE CHEMICAL SOCIETY OF JAPAN, VOL. 51 (7), 2177—2178 (1978)

The Reaction of Ethylbenzene with Methylbenzene–$AlCl_3$–HCl Complex

Nobuyoshi NAMBU, Sawako HAMANAKA, and Masaya OGAWA*

Department of Applied Chemistry, Faculty of Engineering, Kansai University, Senriyama, Suita, Osaka 564

(Received January 12, 1978)

Synopsis. Toluene, *m*-xylene, and mesitylene complexes prepared with $AlCl_3$ and HCl, were separated from the upper hydrocarbon layer and allowed to react with ethylbenzene at 2 and 30 °C. The proton exchange between methylbenzenium ions and ethylbenzene, and the transalkylation of ethylbenzene were investigated by ^{13}C NMR spectroscopy.

In a previous paper,[1] it was reported that methylbenzenes–$AlCl_3$–HCl complexes give fairly stable methylbenzenium ions even at room temperature due to the extraordinary stability of the methyl group for rearrangement. However, NMR spectroscopic studies[2] indicate that proton exchange between the methylbenzenium ions and their parent methylbenzenes takes place in these complex layers.

In order to clarify the behavior of the proton exchange in these complex layers, we have studied the reactions of the methylbenzenes complexes with ethylbenzene which is easily transalkylated in a strong acid.

Reaction with m-*Xylene Complex.* Equimolar ethylbenzene to *m*-xylene was added as an upper layer to a *m*-xylene complex layer prepared by the same procedure as reported.[1] The mixture was then agitated vigorously at 2 and 30 °C for 1 h. The reaction attained equilibrium. After the reaction was completed, the hydrocarbon and complex layers obtained were analyzed separately by VPC. The results are given in Table 1.

In the reaction at 2 °C no transalkylated products were obtained, no proton transfer from *m*-xylenium ion to ethylbenzene taking place in the complex layer. However, proton transfer proceeded in the reaction at 30 °C, giving di- and trisubstituted products. 5-Ethyl-*m*-xylene was obtained in a substantial amount in the complex layer. The complex layers were studied by ^{13}C NMR spectroscopy. The spectra measured at 2 and 30 °C are shown in Fig. 1.

The spectrum of the *m*-xylene complex layer (Fig. 1(a)) gave a set of fused ring signals[1] resulting from *m*-xylenium ion and *m*-xylene, indicating that fast proton exchange between *m*-xylenium ion and *m*-xylene takes place in the complex layer, as follows.[3]

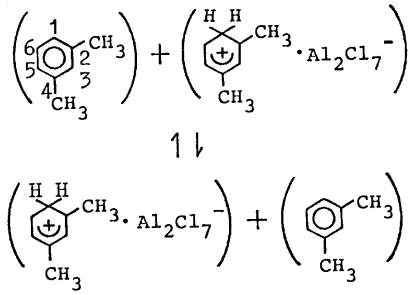

The protonation of *m*-xylene probably occurs at 1- and 5-positions. The formation of 3-protonated *m*-xylene is also expected, but no evidence of the 3-protonated *m*-xylene was obtained in the spectrum.[4]

Figure 1(b) shows a spectrum of the *m*-xylene complex layer in the reaction with ethylbenzene at 2 °C. When ethylbenzene was added to the *m*-xylene complex layer, some parts of ethylbenzene were dissolved into the complex layer and some parts of unprotonated *m*-xylene were transferred to the upper hydrocarbon layer. However, no transalkylated products were obtained in the complex layer. The spectrum indicates that ethylbenzene dissolved is not protonated by proton exchanging with *m*-xylenium ion and that a set of fused ring signals of *m*-xylenium ion is found in a slightly broader range of field than that of Fig. 1(a), *viz.*, the signals of (1—1°, 5—5°) and (3—3°) are shifted to higher field, and the signals of (2—2°, 4—4°) and (6—6°) to lower field. This is because the content of unprotonated *m*-xylene in the complex layer is less than that of the initial complex layer and hence the relative intensity of ring signals of *m*-xylenium ion is enhanced in the fused signals.

On the other hand, the spectrum of the complex layer obtained at 30 °C (Fig. 1(c)) shows that the ring signals of the *m*-xylene complex have disappeared and a new set of ring signals is observed besides those of *m*-xylene and ethylbenzene.

In order to investigate the new signals, 5-ethyl-*m*-xylene was prepared with *m*-xylene and ethyl bromide by the Friedel-Crafts reaction and allowed to react with an equimolar amount of HAl_2Cl_7. The complex thus obtained consists of only 5-ethyl-*m*-xylenium ion. The NMR spectra of 5-ethyl-*m*-xylene and its complex are shown in Figs. 1(d) and (e), respectively. All the signals of 5-ethyl-*m*-xylenium ion in Fig. 1(c) show almost the same chemical shifts as those in Fig. 1(e) except for the ring methylene signal (1'') which broadens, becoming obscure (Fig. 1(c)). This indicates that no proton exchange between 5-ethyl-*m*-xylenium ion and the other alkylbenzenes occurred in the complex layer. Consequently, almost all 5-ethyl-*m*-xylene found in the complex layer was protonated, giving benzenium ion. It is of interest that no 5-ethyl-*m*-xylene was found in the upper hydrocarbon layer. On the other hand, di- and triethylbenzene were not

TABLE 1. REACTION OF ETHYLBENZENE WITH *m*-XYLENE COMPLEX LAYER (Reaction time: 1 h)

Reaction temp (°C)	Layer	Reaction products (mol%)					
		$C_6H_4Me_2$-(1,3-)	C_6H_5Et	C_6H_6	$C_6H_4Et_2$	$Me_2(1,3-)$-$C_6H_3Et(5-)$	$C_6H_3Et_3$-(1,3,5-)
2	Hydrocarbon	45.1	54.9	—	—	—	—
	complex	54.1	45.9	—	—	—	—
30	Hydrocarbon	42.2	36.4	15.1	6.3	—	—
	complex	33.2	26.5	15.0	2.6	22.4	0.3

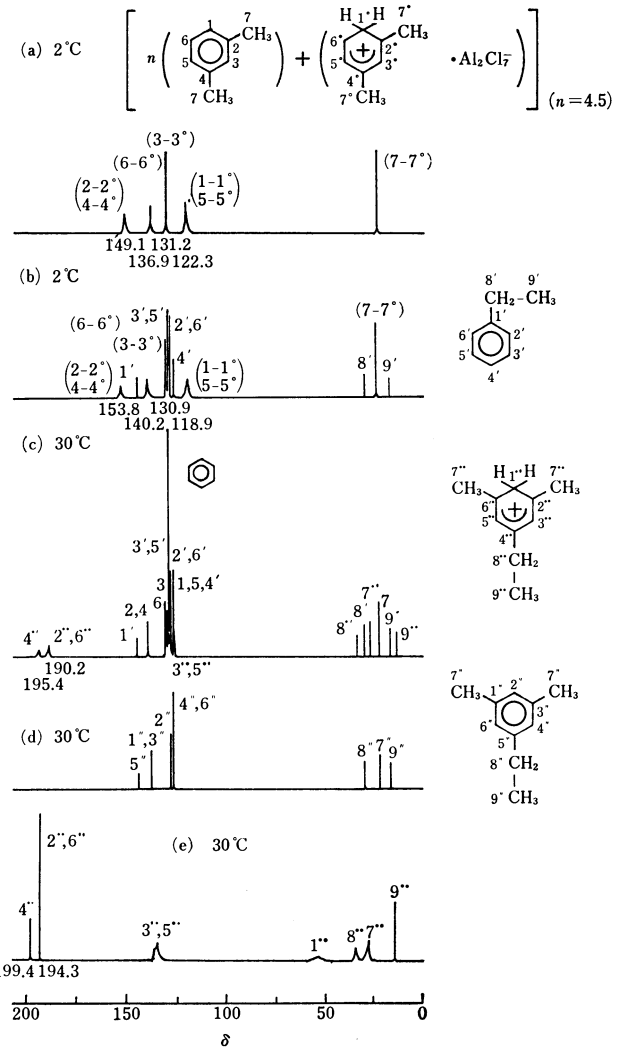

Fig. 1. ^{1}H decoupled ^{13}C NMR spectra of *m*-xylene complex layer (a), the complex layer treated with ethylbenzene for 1 h at 2 °C (b) and at 30 °C (c), 5-ethyl-*m*-xylene (d), and 5-ethyl-*m*-xylene(1 mol)-Al_2Cl_6(1 mol)-HCl complex (e).

detected in the NMR spectra owing to the small contents. Probably, the former was unprotonated and the latter gave a benzenium ion[5] such as 5-ethyl-*m*-xylene. However, the content of triethylbenzene might be too small to have serious influence on the spectrum.

Reaction with Toluene Complex. The reaction products are given in Table 2. In both the reactions at 2 and 30 °C for 1 h (equilibrium conditions), transalkylated products were obtained as in the reaction with *m*-xylene at 30 °C.

In the reaction at 2 °C, trisubstituted products were obtained in a negligible amount, disubstituted products being found predominantly in the toluene complex layer. This indicates the formation of disubstituted benzenium ions. Proton exchange occurred probably between the disubstituted benzenium ions and their parent disubstituted benzenes.

However, in the reaction at 30 °C, substantial amounts of trisubstituted products were obtained in the complex layer. Almost all the benzenium ions might arise from trisubstituted benzenes as in the reaction

Table 2. Reaction of ethylbenzene with toluene complex layer (Reaction time: 1 h)

Reaction temp (°C)	Layer	Reaction products (mol%)						
		C_6H_5Me	C_6H_5Et	C_6H_6	MeC_6H_4Et	$C_6H_4Et_2$	$MeC_6H_3Et_2$(3,5-)	$C_6H_3Et_3$-(1,3,5-)
2	Hydrocarbon	38.8	35.3	16.0	7.8	2.1	—	—
	complex	37.1	27.8	15.1	15.0	3.0	2.0	trace
30	Hydrocarbon	35.6	22.2	27.4	12.2	2.6	—	—
	complex	31.3	15.3	26.8	10.0	2.3	11.5	2.8

with the *m*-xylene complex at 30 °C. All the results were confirmed by NMR spectroscopy.

Reaction with Mesitylene Complex. No transalkylation took place in both the reactions at 2 and 30 °C. Ethylbenzene was partly dissolved into the mesitylene complex layer and mesitylene was also partly transferred into the upper layer. The NMR spectrum of the complex layer shows a set of fused signals resulting from mesitylene and its ion. Proton exchange between mesitylene and mesitylenium ion then took place, but ethylbenzene remained unchanged in the complex layer. The reaction of ethylbenzene with the mesitylene complex layer was initiated at about 50 °C (for 1 h), giving a small amount of transalkylated products.

All the present reactions provide the following order in the relative stability of the methylbenzenium ions: toluenium ion<*m*-xylenium ion<mesitylenium ion. This is in line with the basicity of the parent methylbenzenes: toluene<*m*-xylene<mesitylene.[6] Thus the reactivity of the methylbenzenium ions for transalkylation shows the opposite trend.

Experimental

All alkylbenzenes used in the reaction were dried over metallic sodium and distilled prior to use. VPC analyses were performed on a Shimadzu GC-3AF chromatograph using a 3 m × 3 mm column packed with Apiezon grease L (10 wt%). All the reaction mixtures were treated with water before VPC analyses. NMR spectra were obtained on a JEOL JNM-PS-100/EC-100 spectrometer equipped with a Fourier transform unit at 25.15 MHz under complete proton decoupling. The spectra were observed at 6250 Hz (data point 8191), the pulse width 12 μs (about π/4 pulse), and repetition time 6 s. The sample was placed in a 10 mmφ tube with an internal lock standard (acetone-d_6 and TMS) in a coaxially centered capillary tube (3 mmφ). All chemical shifts are referred to TMS standard.

References

1) Y. Okami, N. Otani, D. Katoh, S. Hamanaka, and M. Ogawa, *Bull. Chem. Soc. Jpn.*, **46**, 1860 (1973).

2) G. A. Olah, R. H. Schlosberg, R. D. Porter, Y. K. Mo, D. P. Kelly, and G. D. Mateescu, *J. Am. Chem. Soc.*, **94**, 2034 (1972); G. A. Olah and Y. K. Mo, *ibid.*, **94**, 9241 (1972).

3) A protic acid from $AlCl_3$ and HCl is HAl_2Cl_7 as was known in our previous paper. N. Nambu, N. Hiraoka, K. Shigemura, S. Hamanaka, and M. Ogawa, *Bull. Chem. Soc. Jpn.*, **49**, 3637 (1976).

4) The protonation of *m*-dichlorobenzene at 3-position was estimated about 5%. D. M. Brouwer, *Recl. Trav. Chim. Pays-Bas*, **87**, 342 (1968).

5) G. A. Olah, R. J. Spear, G. Messina, and P. W. Westerman, *J. Am. Chem. Soc.*, **97**, 4051 (1975).

6) D. A. McCaulay and A. P. Lien, *J. Am. Chem. Soc.*, **73**, 2013 (1951).

BULLETIN OF THE CHEMICAL SOCIETY OF JAPAN, VOL. 51 (7), 2179—2180 (1978)

Electroorganic Chemistry. XXVI.[1] Electrooxidation of Enamines, Haloolefins, and Enol Ethers

Tatsuya SHONO,* Yoshihiro MATSUMURA, Hiroshi HAMAGUCHI, Tamotsu IMANISHI, and Kaoru YOSHIDA

Department of Synthetic Chemistry, Faculty of Engineering, Kyoto University, Yoshida, Sakyo, Kyoto 606

(Received October, 31 1977)

Synopsis. Electrooxidation of enamines in methanol afforded two types of methoxylated enamines. Similar treatment of enol ethers gave trimethoxylated compounds. The products formed by the electrolysis of haloolefins in acetic acid were α-acetoxy haloolefins and α-acetoxy ketones.

Because of mild reaction conditions and non-polluting nature, anodic oxidation is a highly promising method for the oxidation of organic compounds. The electrooxidation of some alkenes[2] or enol esters[3] has been studied from both synthetic and mechanistic points of view. The utility of electrooxidation in organic synthesis prompted us to extend it to the oxidation of such olefinic systems as enamines, haloolefins, and enol ethers.

Anodic Oxidation of Enamines. As shown in Scheme 1 the anodic oxidation of enamines **1a** and **1b** gave two types of enamine, namely, the methoxylated compounds at the vinylic **2** and allylic **3** positions of the starting enamine, though the two compounds were hardly separated from each other by distillation or gas chromatography. A mixture of the products **2b**+**3b** was identified by comparison of its NMR and IR spectra with those of the mixture of enamines **2b**+**3b** prepared independently from 2-methoxy-1-cyclohexanone[4] by the standard method.[5] Furthermore, the hydrolysis[5] of the mixture of products gave 2-methoxy-1-cyclohexanone in 80% yield. The elemental analysis of the product mixture **2a**+**3a** or **2b**+**3b** gave a satisfactory result.

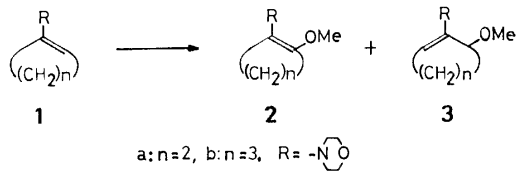

Scheme 1.

Anodic Oxidation of Haloolefins. Haloolefins **4a—d** were anodically oxidized to afford haloolefins **5** acetoxylated at the allylic position and the α-acetoxyketones **6** as shown in Scheme 2.

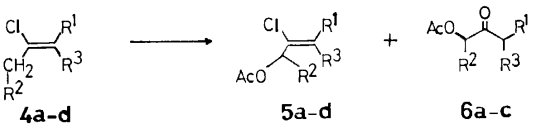

a: R^1=H, R^2, R^3=$-(CH_2)_2-$,
b: R^1=H, R^2, R^3=$-(CH_2)_3-$,
c: R^1=H, R^2=*n*-C_5H_{11}, R^3=H,
d: R^1=Cl, R^2, R^3=$-(CH_2)_3-$

Scheme 2.

Anodic Oxidation of Enol Ethers. Enol ethers **7a** and **7b** were electrooxidized to give the trimethoxylated compounds **8**. Upon hydrolysis with aqueous hydrochloric acid, compound **8b** gave 2-methoxy-1-cyclohexanone[4] in 73% yield. Furthermore, **8b** could be anodically oxidized easily to the acetal ester **9**, which can hardly be obtained by the conventional chemical methods.

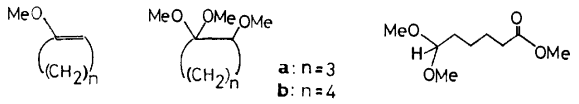

Reaction Pathway. The reaction pathways might be as shown in Scheme 3 in which the initiation step is the electron-transfer to the anode from the conjugating olefinic system involving a hetero atom and a double bond. Further reactions of the first intermediate **10** can be controlled by several factors such as the nature of substituent Y and solvents, and reaction conditions. The products determining intermediates, however, would be allylic cations **11** and **12**, and a cation **13**. No product was formed from the allylic cation **11** formation, of which has been observed in the anodic oxidation of alkenes.[2] This method of oxidation of such olefinic compounds is promising for the synthesis of ketone derivatives hardly obtainable by other methods.

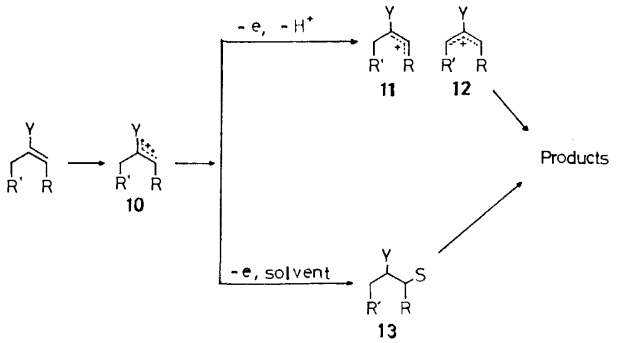

Scheme 3.

Experimental

Materials. Enamines, haloolefins and enol ethers were prepared from the corresponding ketones by reported methods.[5-7] The spectroscopic data of NMR and IR and the result of elemental analysis of the compounds (**2**, **3**, **5**, **6**, **8**, and **9**) are summarized in Table 1.

Electrooxidation of Enamines. Anodic oxidation of an enamine (50 mmol) in methanol (50 ml) containing sodium

Table 1. Spectroscopic data of NMR and IR, and the results of elemental analysis of compounds (**2**, **3**, **5**, **6**, **8**, **9**)

Product	IR cm^{-1}	NMR (CCl_4) δ	Calcd for:	Calcd (Found) (%) C	H	N
2a+**3a**	1645, 1120	1.65—2.50 (m), 2.94 (m, $-NCH_2-$), 3.28 (s, $-OCH_3$), 3.49 (t, $-OCH_3$), 3.72 (t, $-OCH_2$), 4.44 (m, 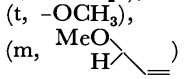)	$C_{10}H_{17}NO_2$	65.54, (65.44,	9.35, 9.45,	7.63 7.70)
2b+**3b**	1650, 1111	1.75—2.10 (m), 2.80 (m, $-NCH_2-$), 3.33 (s, $-OCH_3$), 3.57 (s, $-OCH_3$), 3.72 (t, $-OCH_2-$), 4.56 (m), 4.65 (t)	$C_{11}H_{19}NO_2$	66.97, (66.77,	9.71, 9.95,	7.10 7.13
Product	IR	NMR		C	H	Cl
5a	1730, 1620, 1240	2.10 (s, 3H, acetyl), 1.7—2.9 (m, 8H), 5.30 (t, 1H, H+OAc), 5.93 (b.s, 1H, olefinic)	$C_7H_9O_2Cl$	52.35, (52.37,	5.65, 5.78,	22.08 22.30)
6a	1740, 1715, 1240	2.20 (s, 3H, acetyl), 1.57—2.63 (m, 6H), 5.00 (t, 1H, H+OAc)	$C_7H_{10}O_3$	59.99, (59.98,	5.75 6.01)	
5b	1740, 1650, 1240	2.0 (s, 3H, acetyl), 1.4—2.4 (m, 6H), 5.2 (t, 1H, H+OAc), 6.0 (t, 1H, olefinic)	$C_8H_{12}O_2Cl$	55.04, (55.14,	6.35, 6.45,	20.31 20.19)
6b	1730, 1715, 1240	2.05 (s, 3H, acetyl), 1.5—2.6 (m, 8H), 5.0 (t, 1H, H+OAc)	$C_8H_{12}O_3$	61.52, (61.32,	8.63 8.55)	
5c	1740, 1640, 1240	0.80—1.50 (m, 9H), 2.00 (s, 3H, acetyl), 5.35 (b.s, 1H, H+OAc), 5.30 (m, 2H, olefinic)	$C_9H_{15}O_2Cl$	56.69, (56.58,	7.93, 8.01,	18.59 18.63)
6c	1730, 1720, 1240	0.70—1.50 (m, 9H), 2.00 (s, 3H, acetyl), 2.10 (s, 3H, acety), 4.80 (t, 1H)	$C_9H_{10}O_3$	62.76, (62.86,	9.36 9.50)	
5d	1740, 1640, 1240	1.70—2.00 (m, 9H), 2.05 (s, 3H, acetyl), 2.30—2.70 (m, 2H, allylic), 4.6 (t, 1H)	$C_8H_{10}O_2Cl_2$	49.96, (50.02,	4.82, 4.70,	33.92 33.92)
Materials	IR	NMR		C	H	
8a	2840, 1280, 1100	1.23—2.50 (m, 6H), 3.13 (s, 6H, methoxy), 3.33 (s, 3H, methoxy), 3.20—3.35 (m, 1H, H+OAc)	$C_8H_{16}O_3$	59.98, (60.05,	10.07 9.97)	
8b	2840, 1250, 1100	1.20—2.00 (m, 8H), 3.16 (s, 6H, methoxy), 3.30 (s, 3H, methoxy), 3.20—3.30 (m, 1H, H+OAc)	$C_9H_{18}O_3$	62.04, (62.14,	10.41 10.29)	
9	2840, 1730, 1170, 1130	1.20—2.25 (m, 8H), 3.33 (s, 6H, methoxy), 3.70 (s, 3H, methoxy), 4.30 (t, 1H, H-C$(CH_3)_2$)	$C_9H_{18}O_4$	56.82, (56.77,	9.54 9.39)	

methoxide (50 mmol) as a supporting electrolyte was carried out with carbon rod electrodes at room temperature. After 3 *F*/mol of electricity had been passed, methanol was removed by evaporation, and the residue was washed with three portions of ether. The combined ethereal solution was filtrated and distilled.

Electrolysis of ***1a*** (7.65 g, 50 mmol) at the anode potential of 1.65—1.75 V *vs.* SCE gave a mixture of **2a** and **3a** (6.95 g); bp 101—104 °C/mmHg.

*Enamine (**1b**) (8.35 g, 50 mmol) was electrooxidized* at the anode potential of 1.90—2.20 V *vs.* SCE to give a mixture of **2b** and **3b** (7.29 g); bp 121—124 °C/mmHg.

Electrolysis of Haloolefins. Electrolysis of a haloolefin (50 mmol) in acetic acid containing potassium acetate was carried out according to the reported method.[8] The amount of electricity passed through the cell was 5.5 *F*/mol. The product was analyzed after it had been separated by gas chromatography.

Anodic Oxidation of ***4a*** (5.125 g, 50 mmol) gave **5a** (2.81 g) and **6a** (0.945 g). **5a** and **6a**: Bp 100—120 °C/20 mmHg.

Electrolysis of Enol Ethers. A solution of an enol ether (50 mmol) in methanol (50 ml) containing sodium methoxide (50 mmol) as a supporting electrolyte was electrooxidized with carbon rod electrodes at room temperature until 3.5 *F*/mol of electricity was passed. After the usual work-up, the product was obtained by distillation.

Anodic oxidation of **7a** yielded **8a** (3.60 g). **8a**: Bp 71—73 °C/11 mmHg.

Electrolysis of ***7b*** gave **8b**: Bp 83—85 °C/13 mmHg.

1,1,2-Trimethoxycyclohexane (**8b**) (1.74 g, 10 mmol) was anodically oxidized according to the reported method[9] to give **9**, yield being 75%. **9**: Bp 121—123 °C/18 mmHg.

References

1) Part XXV: T. Shono, I. Nishiguchi, and M. Nitta, *Chem. Lett.*, **1976**, 1319.

2) T. Shono and A. Ikeda, *J. Am. Chem. Soc.*, **94**, 7892 (1972); T. Shono, A. Ikeda, J. Hayashi, and S. Hakozaki, *J. Am. Chem. Soc.*, **97**, 4261 (1975).

3) T. Shono, Y. Matsumura, and Y. Nakagawa, *J. Am. Chem. Soc.*, **96**, 3532 (1974); T. Shono, I. Nishiguchi, and M. Nitta, *Chem. Lett.*, **1976**, 1319.

4) H. W. Dürbech, C. G. B. Frischkorn, and K. Hilpert, *Tetrahedron*, **27**, 2927 (1971).

5) S. Hünig, E. Lücke, and W. Breninger, *Org. Synth.*, Coll. Vol. V, 808.

6) E. A. Braude and J. A. Coles, *J. Chem. Soc.*, **1950**, 2014; G. B. Bachman and A. J. Hill, *J. Am. Chem. Soc.*, **56**, 2730 (1934); M. Mousseron and R. B. Jacoquier, *C. R. Acad. Sci.*, **226**, 256 (1948),

7) R. A. Wohl, *Synthesis*, **1974**, 38.

8) T. Shono, M. Okawa, and I. Nishiguchi, *J. Am. Chem. Soc.*, **97**, 6144 (1975).

9) T. Shono, H. Hamaguchi, Y. Matsumura, and K. Yoshida, *Tetrahedron Lett.*, **1977**, 3625.

BULLETIN OF THE CHEMICAL SOCIETY OF JAPAN, VOL. 51 (7), 2181—2182 (1978)

Electroorganic Chemistry. XXXIV. Novel Intramolecular Cyclization through Anodic Oxidation of Enol Acetates

Tatsuya SHONO,* Ikuzo NISHIGUCHI, Shigenori KASHIMURA, and Masahisa OKAWA

Department of Synthetic Chemistry, Faculty of Engineering, Kyoto University, Yoshida, Sakyo, Kyoto 606

(Received January 25, 1978)

Synopsis. The anodic oxidation of 1-acetoxy-1,6-heptadiene homologues in acetic acid gave mainly intramolecular cyclization products, cyclohexenyl ketones. The cyclization takes place through the electrophilic attack of the cationic center generated from the enol ester moiety to the double bond.

It has been demonstrated by our recent studies[1,2] that the anodic oxidation of enol acetates leads to the selective formation of α,β-unsaturated enones or α-acetoxy ketones under suitably arranged conditions. Although the nature of radical cations, the first intermediates formed from the starting esters, is not necessarily clear, the product determining intermediate in the reaction may possess cationic character at the β-carbon atom of the enol acetate moiety. Thus, it seems interesting to examine the intramolecular cycloaddition between the cationic species generated by anodic oxidation of enol acetates and an olefinic bond in a reasonable position, and the formation of new carbon–carbon bond at the adjacent position to the carbonyl group.

Results and Discussions

Anodic oxidation of enol acetates **1a—f** in acetic acid containing tetraethylammonium *p*-toluenesulfonate as a supporting electrolyte was carried out in an undivided cell equipped with carbon rod electrodes under constant current conditions. After 4 *F*/mol of electricity was passed, the usual work-up and distillation afforded three types of products, namely the expected cyclized ketones **2a—f**, the conjugated enones **3c, d**, and the ketones **4a—f**[3] formed by hydrolysis of the starting enol acetates.

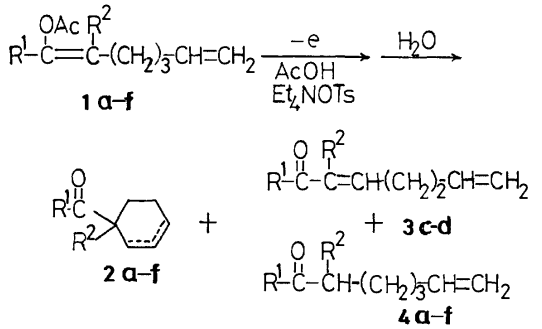

The results are summarized in Table 1. All the products were isolated by preparative gas chromatography, and characterized through IR, NMR, and MS analyses. Further identification of **2a—e** was accomplished by the comparison of spectroscopic and gas chromatographic behaviors of the corresponding saturated ketones **5a—e** obtained by the hydrogenation of **2a—e** with those of authentic samples.[4-8] Although the position of the double bond in the cyclohexenyl ring of **2a—f** was not definitely determined, spectroscopic and gas chromatographic analyses clearly indicated that each of **2a—f** was a single isomer.

Table 1. Anodic oxidation of enol acetates **1a—f**

	Enol acetates **1** R^1	R^2	Anodic potential (V *vs.* SCE)	Product (Yield[a,b] %) **2**	**3**	**4**
a	CH_3	H	1.8—1.9	35(47)	—	25
b	CH_3	CH_3	1.8—1.9	40(47)	—	15
c	$-(CH_2)_3-$		1.8—2.0	25(28)	33(37)	10
d	$-(CH_2)_4-$		1.8—2.0	19(22)	12(14)	13
e	$-(CH_2)_5-$		1.6—1.8	18(32)	—	44
f	$-(CH_2)_6-$		2.2—2.4[c,d]	30(50)	—	40

a) Isolated. b) The number in the parentheses shows the yield calculated on the basis of the consumed **1**. Unconsumed starting esters were recovered as the ketones **4**. c) The reaction was continued until 10 *F*/mol of electricity was passed. d) Anodic oxidation of **1f** in a divided cell gave a mixture of **2f** and **4f** in 35 and 53% yields, respectively.

Extensive studies[9-11] have already been carried out on the intermolecular anodic coupling of electron-rich olefins, though the nature of the key intermediate has been not always clear. It has well been established, however, that in the intramolecular cyclization of 5-hexenyl cations or radicals, electrophilic reaction gives predominantly six-membered ring[12] products, while five-membered ring products are the main products in homolytic reaction.[13,14]

Hence, the exclusive formation of **2a—f** rather than **6a—f** from **1a—f** may indicate that the cyclization takes place through the electrophilic attack of the cationic center generated from the enol ester moiety to the double bond.[15]

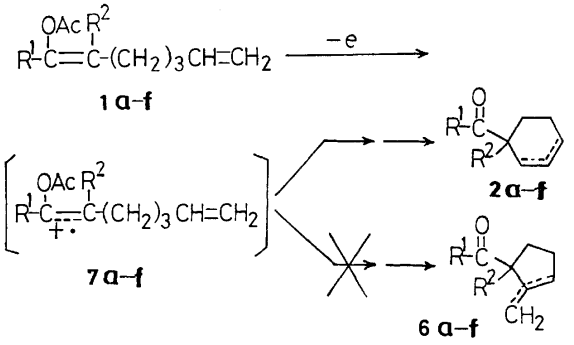

This result may also suggest that the radical cations **7a—f** generated by the first electron transfer from **1a—f**, do not show any reactivity as a free radical.

Experimental

Preparation of Enol Acetates ***1a—f.*** Nonconjugated olefinic ketones, 7-octen-2-one (**4a**),[17] 3-methyl-7-octen-2-one (**4b**),[18] 2-(4-pentenyl)cyclopentanone (**4c**),[19] 2-(4-pentenyl)-cyclohexanone (**4d**),[20] 2-(4-pentenyl)cycloheptanone (**4e**), and 2-(4-pentenyl)cyclooctanone (**4f**), were prepared through β-keto ester condensation.[21,22] Enol acetates **1a—f** were prepared from the corresponding ketones **4a—f** according to the procedure similar to the method of Bedoukian[23] or House.[24] Satisfactory NMR, IR, and mass spectra were obtained for **1a—f** as shown below. **1a**, bp 90 °C/30 Torr; IR (neat), 3080, 3010, 1750, 1640, 1160, 910 cm^{-1}; NMR (CCl_4), δ 6.1—4.9 (3H, m, $-CH=CH_2$), 4.7—4.5 (1H, m, $>C=CH-$), 2.10 (3H, s, $COCH_3$), 2.4—1.3 (9H, m, $-CH_3$ and $-CH_2-$); MS, *m/e* 168 (M^+). **1b**, bp 110 °C/35 Torr; IR (neat), 3080, 1750, 1640, 1140, 910 cm^{-1}; NMR (CCl_4), δ 6.2—4.6 (3H, m, $-CH=CH_2$), 2.10 (3H, s, $COCH_3$), 1.75 (3H, s, $-CH_3$), 1.7—0.9 (6H, m, $-CH_2-$); MS, *m/e* 182 (M^+). **1c**, bp 90 °C/2 Torr; IR (neat), 3080, 1750, 1640, 1220, 910 cm^{-1}; NMR (CCl_4), δ 6.2—4.6 (3H, m, $-CH=CH_2$), 2.05 (3H, s, $COCH_3$), 2.7—1.0 (12H, m, $-CH_2-$); MS, *m/e* 194 (M^+). **1d**, bp 85—87 °C/20 Torr; IR (neat), 3080, 1750, 1630, 1220, 910 cm^{-1}; NMR (CCl_4), δ 6.2—4.7 (3H, m, $-CH=CH_2$), 2.05 (3H, s, $COCH_3$), 2.0—1.9 (14H, m, $-CH_2-$); MS, *m/e* 208 (M^+). **1e**, bp 100—102 °C/2 Torr; IR (neat), 3080, 1740, 1630, 1210, 900 cm^{-1}; NMR (CCl_4), δ 6.3—4.8 (3H, m, $-CH=CH_2$), 2.10 (3H, s, $COCH_3$), 2.6—1.1 (16H, m, $-CH_2-$); MS, *m/e* 222 (M^+). **1f**, bp 95—98 °C/0.7 Torr; IR (neat), 3080, 1750, 1640, 1220, 910 cm^{-1}; NMR (CCl_4), δ 6.2—4.8 (3H, m, $-CH=CH_2$), 2.10 (3H, s, $COCH_3$), 2.5—1.1 (18H, m, $-CH_2-$); MS, *m/e* 236 (M^+).

General Procedure for the Anodic Oxidation of Enol Acetates ***1.*** Into a 30 ml undivided electrolysis cell equipped with carbon rod electrodes and a reference electrode (SCE) was placed a solution of 0.01 mol of an enol acetate and 0.01 mol of tetraethylammonium *p*-toluenesulfonate in 10 ml of glacial acetic acid. Stirred with a magnetic bar and cooled with running water, the solution was electrochemically oxidized at the constant current of 200 mA. After 4 *F*/mol of electricity was passed, the reaction mixture was poured into 100 ml of a cold saturated potassium carbonate solution and extracted with three 50 ml portions of ether. The combined ethereal solution was dried over anhydrous magnesium sulfate and evaporated. The residue was distilled *in vacuo*. The isolated yield of the products, **2a—f**, **3c**, **d**, and **4a—f**, are summarized in Table 1. **2a**, bp 90—93 °C/30 Torr; IR (neat), 3020, 1710, 735 cm^{-1}; NMR (CCl_4), δ 5.6—5.5 (2H, m, $-CH=CH-$), 2.10 (3H, s, $-COCH_3$), 2.3—1.4 (7H, m, $-CH_2-$ and $>CH-$); MS, *m/e* 124 (M^+). **2b**, bp 80—83 °C/20 Torr; IR (neat), 3020, 1705, 740 cm^{-1}; NMR (CCl_4), δ 5.6—5.5 (2H, m, $-CH=CH-$), 2.10 (3H, s, $-COCH_3$), 2.4—1.2 (6H, m, $-CH_2-$), 1.09 (3H, s, $-CH_3$); MS, *m/e* 138 (M^+). **2c**, 60—62 °C/2.0 Torr; IR (neat), 3020, 1725, 760 cm^{-1}; NMR (CCl_4), δ 5.5—5.4 (2H, m, $-CH=CH-$), 2.5—1.3 (12H, m, $-CH_2-$); MS, *m/e* 150 (M^+). **2d**, bp 60—63 °C/0.5 Torr; IR (neat), 3020, 1700, 760 cm^{-1}; NMR (CCl_4), δ 5.6—5.5 (2H, m, $-CH=CH-$), 2.5—1.4 (14H, m, $-CH_2-$); MS, *m/e* 164 (M^+). **2e**, bp 81—83 °C/0.5 Torr; IR (neat), 3010, 1700, 770 cm^{-1}; NMR (CCl_4), δ 5.7—5.5 (2H, m, $-CH=CH-$), 2.7—1.2 (16H, m, $-CH_2-$); MS, *m/e* 178 (M^+). **2f**, bp 91—93 °C/0.5 Torr; IR (neat), 3020, 1695, 760 cm^{-1}; NMR (CCl_4), δ 5.7—5.5 (2H, m, $-CH=CH-$), 2.7—1.2 (18H, m, $-CH_2-$); MS, *m/e* 192 (M^+). **3c**, bp 120 °C/25 Torr; IR (neat), 3080, 1690, 1630, 910 cm^{-1}; NMR (CCl_4), δ 7.1—7.0 (1H, m, =CH– of enone), 6.0—4.7 (3H, m, $-CH=CH_2$), 2.6—0.9 (10H, m, $-CH_2-$); MS, *m/e* 150 (M^+). **3d**, bp 130 °C/20 Torr; IR (neat), 3080, 1670, 1640, 910 cm^{-1}; NMR (CCl_4), δ 7.2—7.1 (1H, m, =CH– of enone), 6.1—4.9 (3H, m, $-CH=CH_2$), 2.7—1.0 (12H, m, $-CH_2-$); MS, *m/e* 162 (M^+).

Hydrogenation of ***2a—f*** was carried out by a standard method. The products, saturated ketones **5a—e** showed identical spectroscopic and gas chromatographic behavior with authentic samples.[4-8] Spiro[5.7]tridecan-6-one (**5f**) was characterized by IR, NMR, MS, and elemental analyses. **5f**, bp 85—87 °C/0.5 Torr; IR (neat), 1700 cm^{-1}; NMR (CCl_4), δ 2.5—2.2 (2H, m, $-COCH_2-$), 2.1—0.9 (20H, m, $-CH_2-$); MS, *m/e* 194 (M^+). Found: C, 80.18; H, 11.42%. Calcd for $C_{13}H_{22}O$: C, 80.35; 11.41%.

References

1) T. Shono, M. Okawa, and I. Nishiguchi, *J. Am. Chem. Soc.*, **97**, 6144 (1975).
2) T. Shono, Y. Matsumura, and Y. Nakagawa, *J. Am. Chem. Soc.*, **96**, 3532 (1974).
3) Some (5—6%) of the starting enol acetate were hydrolyzed during the electrolysis.
4) H. G. Walker, *J. Am. Chem. Soc.*, **68**, 1386 (1946).
5) M. Mousseron, *Bull. Chim. Soc. Fr.*, **1947**, 459.
6) H. Christol and R. Jacquier, *Bull. Chim. Soc. Fr.*, **1957**, 1027.
7) R. K. Hill and R. T. Conley, *J. Am. Chem. Soc.*, **82**, 645 (1960).
8) M. Mousseron and R. Jacquier, *Bull. Chim. Soc. Fr.*, **1957**, 346.
9) H. Schäfer, *Chem. Eng. Tech.*, **42**, 164 (1970).
10) (a) H. Schäfer and E. Steckhan, *Angew. Chem. Int. Ed. Engl.*, **8**, 518 (1969); (b) B. Belleau and Y. K. Au-Young, *Can. J. Chem.*, **47**, 2117 (1969).
11) H. Schäfer and E. Steckhan, *Tetrahedron Lett.*, **1970**, 3835.
12) (a) W. S. Johnson, *Acc. Chem. Res.*, **1**, 1 (1968); (b) E. E. van Tamelen, *ibid.*, **8**, 152 (1975); (c) P. D. Bartlett, *Justus Liebigs Ann. Chem.*, **653**, 45 (1962); (d) W. S. Johnson, D. M. Bailey, R. Owyang, R. A. Bell, B. Jacques, and J. C. Crandall, *J. Am. Chem. Soc.*, **86**, 1959 (1964), and other cited therein.
13) (a) M. Julia, *Acc. Chem. Res.*, **4**, 386 (1971); *Pure Appl. Chem.*, **15**, 167 (1967); (b) C. Walling and M. S. Pearson, *J. Am. Chem. Soc.*, **86**, 2262 (1964); (c) C. Walling, J. H. Cooley, A. A. Ponaras, and E. J. Racah, *ibid.*, **88**, 5361 (1966), and other cited therein.
14) T. Shono, I. Nishiguchi, H. Ohmizu, and M. Mitani, *J. Am. Chem. Soc.*, **100**, 545 (1978).
15) Oxidation of the terminal vinyl group may be negligible under the reaction conditions as the half-wave oxidation potentials ($E_{1/2}$) of enol acetates are +1.44—+2.09 V *vs.* SCE in acetonitrile[2] while those of 1-alkene are +2.70—+2.90 V *vs.* Ag/0.01 N $AgClo_4$ in acetonitrile.[16]
16) K. Fleischman and D. Pletcher, *Tetrahedron Lett.*, **1968**, 6255.
17) C. L. Feugeas, *Bull. Soc. Chem. Fr.*, **1963**, 2568.
18) F. Rauessac, *Tetrahedron Lett.*, **1965**, 3313.
19) G. Opitz and H. Mildenberges, *Justus Liebigs Ann. Chem.*, **650**, 115 (1961).
20) J. M. Conia, *Bull. Soc. Chim. Fr.*, **1967**, 818.
21) U. Ravid and R. Ikan, *J. Org. Chem.*, **39**, 2637 (1974).
22) D. S. Breslow, E. Baumgarten, and C. R. Hauser, *J. Am. Chem. Soc.*, **66**, 1286 (1944).
23) P. Z. Bedoukian, *J. Am. Chem. Soc.*, **67**, 1430 (1945).
24) H. O. House, M. Gall, and H. D. Olinstead, *J. Org. Chem.*, **36**, 2361 (1971).

BULLETIN OF THE CHEMICAL SOCIETY OF JAPAN, VOL. 51 (7), 2183—2184 (1978)

A Simple Preparative Method of Alkylthiotrimethylsilanes

Isao KUWAJIMA* and Toru ABE

Department of Chemistry, Tokyo Institute of Technology, Ookayama, Meguro-ku, Tokyo 152

(Received February 2, 1978)

Synopsis. Treatment of *sym*-disulfides with metallic sodium in the presence of trimethylchlorosilane in an appropriate solvent affords the corresponding alkylthiotrimethylsilanes in high yield.

The utility of alkylthiotrimethylsilanes has recently been recognized. They can be efficiently used for conversion of the carbonyl group into the corresponding thioacetal or (1-alkylthioalkyl)trimethylsilanes.[1,2] Several methods have been developed, including silylation of lead mercaptides,[3] silylation of thiols with trialkylsilane catalyzed by transition metal[4] or with hexamethyldisilazane catalyzed by imidazole.[5]

In this paper we wish to describe a convenient method of preparation, starting from disulfides. As a part of studies on the reductive silylation reactions with metallic sodium and trimethylchlorosilane,[6] we have examined the reaction of disulfides with this reductive system.[7] *sym*-Disulfide was added to a solution of trimethylchlorosilane in an appropriate sodium suspension. After stirring or heating for an appropriate length of time, the substance deposited was filtered off. Removal of the solvent, followed by fractional distillation, afforded the corresponding alkylthiotrimethylsilane. By this procedure, various disulfides can be converted into the thiosilane derivatives, including primary, secondary, or tertiary alkyl, and phenyl groups, in high yield and with high purity.

$$(R\text{-}S)_2 \xrightarrow{Na\text{--}Me_3SiCl} \begin{cases} \longrightarrow 2R\text{-}S\text{-}SiMe_3 \\ \longrightarrow R\text{-}S\text{-}R + (Me_3Si)_2S \end{cases}$$

For the preparation of *n*-alkylthio derivatives, choice of solvent is important. Non-polar ones such as pentane or hexane should be used for efficient conversion. When ether was employed, the corresponding dialkyl sulfide was formed in sufficient amount along with alkylthiotrimethylsilane. For *s*- or *t*-alkylthio and phenylthio derivatives, ether can be used equally well as pentane, hexane and benzene.

In the cases of dimethyl and dibenzyl disulfides, carbon–sulfur bond cleavage took place predominantly or competitively and they could not be converted into the corresponding thiosilanes, giving instead, bis(trimethylsilyl) sulfide as the major product with any solvent. The reductive silylation procedure of dimethyl disulfide affords one of the most convenient methods for the preparation of bis(trimethylsilyl) sulfide,[8,9] since it can be isolated with high purity through simple fractional distillation.

$$(R\text{-}S)_2 \xrightarrow[R=CH_3 \text{ or } C_6H_5CH_2]{Na\text{--}Me_3SiCl} 2(Me_3Si)_2S + 2R\text{-}SiMe_3$$

Experimental

Materials. Disulfides were used after purification of commercial products by distillation. Trimethylchlorosilane was purified by distillation over CaH_2. Solvents were purified shortly before use by drying and distillation over sodium or sodium-benzophenone. Sodium dispersion was prepared in xylene in the usual way and used after complete removal of xylene.

General Procedure. Disulfide (17.5 mmol) and trimethylchlorosilane (4.2 g, 38.7 mmol) in an appropriate solvent (30 ml) was added to a sodium suspension (0.97 g, 0.422 g atom) in the same solvent (60 ml) over a period of 5 min at room temperature under argon atmosphere. After being stirred at room temperature or under refluxing for an appropriate time, the dark-purple colored reaction mixture was filtered through a pad of Celite and washed with the solvent (30 ml). The solvent was removed under atmo-

TABLE 1. REACTIONS OF *sym*-DISULFIDE, $(R\text{-}S)_2$, WITH $Na\text{--}Me_3SiCl$

R	Reaction conditions: Solvent	Temp	Period (h)	Product (yield %, bp)
CH_3[a]	ether	reflux	3	$(Me_3Si)_2S$[b] (67, 87—92°/80 Torr)
C_2H_5	pentane	R. T.	1	$C_2H_5SSiMe_3$[c] (83, 127—129 °C)
$(CH_3)_2CH$	pentane	R. T.	1	$(CH_3)_2CHSSiMe_3$[c] (80, 140—142 °C)
$(CH_3)_3C$	ether	R. T.	3	$(CH_3)_3CSSiMe_3$[c] (86, 155—159 °C)
	benzene	R. T.	2	$(CH_3)_3CSSiMe_3$ (72)
	hexane	R. T.	1	$(CH_3)_3CSSiMe_3$ (80)
n-C_6H_{13}	ether	R. T.	2	$C_6H_{13}SSiMe_3$[d] (60, 110—115 °C/30 Torr), $(C_6H_{13})_2S$ (30)
	benzene	reflux	1	$C_6H_{13}SSiMe_3$ (55), $(C_6H_{13})_2S$ (40)
	benzene	R. T.	9	$C_6H_{13}SSiMe_3$ (78)
C_6H_5	benzene	R. T.	0.5	$C_6H_5SSiMe_3$[c] (95, 120—122 °C/50 Torr)
$C_6H_5CH_2$[e]	benzene	reflux	3	$C_6H_5CH_2SiMe_3$ (50), $(Me_3Si)_2S$ (40)[f]

a) Carried out with Na (10 eq) and Me_3SiCl (10 eq). b) *Cf.* E. W. Abel, *J. Chem. Soc.*, **1961**, 4933. c) Ref. 4. d) *Cf.* J. D. Citron, *J. Organomet. Chem.*, **30**, 21 (1971). e) Carried out with Na (4.4 eq) and Me_3SiCl (4.0 eq). f) *Ca.* 50% of starting disulfide recovered.

spheric pressure and the residual oil was distilled, giving the corresponding thiosilane. The results are given in Table 1.

References

1) D. A. Evans, L. K. Truesdale, K. G. Grimm, and S. L. Nesbitt, *J. Am. Chem. Soc.*, **99**, 5009 (1977).

2) For other synthetic reactions using thiosilanes, see; E. W. Abel, D. J. Walker, and J. N. Wingfield, *J. Chem. Soc., A*, **1968**, 1814; E. W. Abel and D. J. Walker, *ibid.*, **1968**, 2338; K. Itoh, K. Matsuzaki, and Y. Ishii, *J. Chem. Soc., C*, **1968**, 2709; I. Ojima and Y. Nagai, *J. Organomet. Chem.*, **57**, C42 (1973); T. Mukaiyama, T. Takeda, and K. Atsumi, *Chem. Lett.*, **1974**, 187; T. Mukaiyama, T. Takeda, and K. Atsumi, *ibid.*, **1974**, 1013.

3) E. W. Abel, *J. Chem. Soc.*, **1960**, 4406.

4) I. Ojima, M. Nihonyanagi, and Y. Nagai, *J. Organomet. Chem.*, **50**, C26 (1973).

5) R. S. Glass, *J. Organomet. Chem.*, **61**, 83 (1973).

6) I. Kuwajima, T. Sato, N. Minami, and T. Abe, *Tetrahedron Lett.*, **1976**, 1591; I. Kuwajima, K. Atsumi, and I. Azegami, *J. Chem. Soc., Chem. Commun.*, **1977**, 76.

7) Silylation of sodium alkanethiolates is reported to give the corresponding thiosilanes in only low yields; S. H. Langer, S. Connell, and I. Wender, *J. Org. Chem.*, **23**, 50 (1958).

8) Silylation of sodium methanethiolate gave bis(trimethylsilyl) sulfide in a moderate yield; K. A. Hooton and A. L. Allred, *Inorg. Chem.*, **4**, 671 (1965).

9) For synthetic reactions using bis(trimethylsilyl) sulfide, see; H. S. D. Soysa and W. P. Weber, *Tetrahedron Lett.*, **1978**, 235.

BULLETIN OF THE CHEMICAL SOCIETY OF JAPAN, VOL. 51 (7), 2185—2186 (1978)

Reactive Troponoids and *o*-Aminophenol. I. Synthesis of Cyclohepta[*b*][1,4]benzoxazine[1)]

Tetsuo NOZOE,* Harue OKAI, and Taichi SOMEYA†

Tokyo Reseach Laboratory of Kao Soap Co., Ltd., Bunka, Sumida-ku, Tokyo 131

† *Central Reseach Laboratory of Takasago Perfumery Co., Ltd., Kamata, Ohta-ku, Tokyo 144*

(Received December 15, 1977)

Synopsis. Cyclohepta[*b*][1,4]benzoxazine and 2-(*o*-hydroxyanilino)tropone were obtained by the reactions of 2-chloro- and 2-methoxytropone with *o*-aminophenol. A similar reaction with *o*-methoxylaniline gave 2-(*o*-methoxyanilino)tropone and 1-(*o*-methoxyanilino)-7-(*o*-methoxyphenylimino)-1,3,5-cycloheptatriene. The chemical and physical properties of cyclohepta[*b*][1,4]benzoxazine were discussed.

Benzotropazine (**2a**)[2)] and cyclohepta[*b*][1,4]benzothiazine (**3**),[3)] which are heterocyclic compounds containing two hetero atoms, with a 6,6,7-ring system, were obtained by the reactions of 2-chloro- (**1a**) or 2-methoxytropone (**1b**) with *o*-phenylenediamine and with *o*-aminobenzenethiol, respectively.

The correct structure of 6*H*-cyclohepta[*b*]quinoxaline (**2b**) was proposed for **2a** by means of NMR.[4,5)] We wish to report on the reaction of **1a**, **b** with *o*-aminophenol giving cyclohepta[*b*][1,4]benzoxazine (**5**), which is a heterocyclic compound with a 6,6,7-ring system containing an oxazine ring, and its chemical and physical properties.

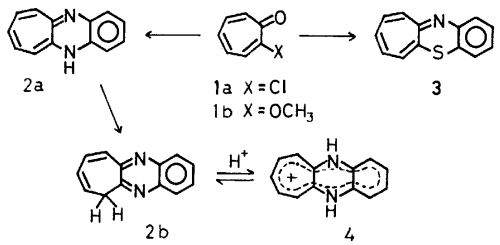

Results and Discussion

Heating of **1a** with *o*-aminophenol in acetic acid under reflux yielded two condensation products **5** and **6** in 48 and 40% yields, respectively. In a similar manner, the reaction of **1b** with *o*-aminophenol also gave **5** and **6** in 16 and 70% yields, respectively. When these reactions were carried out in ethanol, the product was almost solely **6**. This indicates that **5** is formed from **6** in acidic medium. In fact, heating of **6** in acetic acid, in the presence of concd sulfuric acid, afforded **5** in a quantitative yield. Heating of **5** in ethanol with dilute alkali gave **6** quantitatively. However, longer heating with exess alkali resulted in its decomposition into tropolone and *o*-aminophenol. The results reveal that **6** is 2-(*o*-hydroxyanilino)tropone and **5** is cyclohepta[*b*][1,4]benzoxazine. The structures were also supported by elemental analyses and mass and IR spectra.

The reactions of **1a** and **1b** with *o*-methoxyaniline chiefly gave **7**, with 1—3% of **8**. Since **7** was also obtained by the methylation of **6**, **7** was identified as 2-(*o*-methoxyanilino)tropone, and **8** was identified as 1-(*o*-methoxyanilino)-7-(*o*-methoxyphenylimino)-1,3,5-cycloheptatriene by elemental analysis and spectral data. Moreover, **8** gave a copper(II) chelate as brown crystals, mp 234—236 °C, by the known method for 2-aminotropone imines.[6)] Formation of **8** suggests that, in the reaction of **1** with *o*-aminophenol in acidic conditions, the amino group of the reagent reacts not only at the carbon atom with leaving group but also at the carbonyl group of **1**.

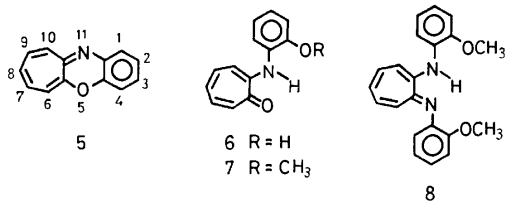

Fukunaga reported that tetrafluoroborate (**4**) of **2b** is a resonance stabilized (aromatic) $4n\pi$ system by comparison of the NMR spectrum of **4** in acetonitrile-d_3 with the related compounds.[4)] On the other hand, measurement of the NMR spectra of **3** in trifluoroacetic acid and chloroform-*d*, shows that the seven-membered ring protons of the cation (**9**) derived from **3** shift about 1.0 ppm towards lower magnetic field, while the benzene ring protons hardly shows any shift. Thus the positive charge of the cation (**9**) is not thought to be delocalized over the benzene ring.[7)]

The NMR data of **5** measured in trifluoroacetic acid and chloroform-*d*, show shift of the seven-membered ring protons by 1.22—1.40 ppm and that of the benzene ring protons by 0.10—0.22 ppm towards lower magnetic field. This indicates that the positive charge of the cation (**10**) derived from **5** is also delocalized over both the seven-membered ring and the heterocyclic part as in the case of **9**.

Experimental

All the melting points are uncorrected. TLC and preparative TLC were carried out on Kiesel gel 60 F_{254} (Merck) and Wakogel BF 5 (Wako), respectively, developed with benzene, spots being detected with a UV lamp. IR and UV spectra were taken on Hitachi EPI-G2 and Hitachi 124 spectrometers, respectively. UV spectra of acidic or basic medium were measured by adding three drops of 1 M HCl or 1 M NaOH to the sample solution. NMR spectra were

recorded on 60 MHz Hitachi R-24A and 100 MHz Varian HA-100 spectrometers with TMS as an internal standard. Mass spectra were recorded on a Hitachi RMU-6M mass spectrometer operating at 75 eV.

2-(o-Hydroxyanilino)tropone (6). A mixture of **1a** (1.0 g, 7.1 mmol), *o*-aminophenol (1.0 g, 9.2 mmol), and acetic acid (15 ml) was refluxed for 75 min. After removal of acetic acid under reduced pressure, water (30 ml) was added to the residue and precipitate A was separated from filtrate B. Recrystallization of A from benzene gave 0.16 g (40%) of **6** as yellow needles: mp 163 °C; λ_{max}^{MeOH} nm (log ε): 205 (4.40), 231 (4.40), 342 (4.00), and 404 (4.18); $\lambda_{max}^{MeOH+HCl}$ nm (log ε): 239 (4.36) and 382 (4.03); $\lambda_{max}^{MeOH+NaOH}$ nm (log ε): 231 (4.48), 340 (3.95), and 411 (4.06); IR (KBr): 3260 (NH), 3100 (OH), and 1610 cm^{-1} (C=O); NMR ($CDCl_3$, 60 MHz); δ 9.50 (br s, 1H, OH), 8.70 (br s, 1H, NH), and 6.50—7.40 ppm (m, 9H). Found: C, 72.95; H, 5.19; N, 6.51%; M^+, 213. Calcd for $C_{13}H_{11}NO_2$: C, 73.22; H, 5.20; N, 6.57%; M, 213.

Cyclohepta[b][1,4]benzoxazine (5). Filtrate B was extracted with chloroform. After removal of the solvent, the residue was dissolved in ethanol and treated with picric acid to precipitate the picrate. The picrate was washed with ether, and decomposed with 2 M NaOH in ethanol. The solution was extracted with benzene. The extract was washed with water, dried over Na_2SO_4, and evaporated to give 0.66 g (48%) of **5** as dark brown needles. Recrystallization from hexane gave an analytical sample: mp 93 °C; λ_{max}^{MeOH} nm (log ε): 215 (4.33), 262 (4.38), 270^{sh} (4.35), and 410 (4.05); $\lambda_{max}^{MeOH+HCl}$ nm (log ε): 225 (4.34), 265^{sh} (4.35), 273 (4.38), 320 (3.87), and 435 (3.93); NMR ($CDCl_3$, 100 MHz): δ 6.73 (m, 3H, $C_{1,2,3}$–H), 6.36 (m, 1H, C_4–H), 6.03 (m, 2H, $C_{6,7}$–H), 5.92 (d d, 1H, J=11.0 and 9.0 Hz, C_9–H), 5.77 (m, 1H, C_8–H), and 5.36 ppm (d d, 1H, J=9.0 and 1.0 Hz, C_{10}–H); NMR (CF_3COOH, 100 MHz): δ 6.83 ($C_{1,2,3}$–H), 6.58(C_4–H), 7.35 ($C_{6,7}$–H), 7.17 (C_9–H), 7.00 (C_8–H), and 6.76 ppm (C_{10}–H). Found: C, 80.13; H, 4.80; N, 7.14%; M^+, 195. Calcd for $C_{13}H_9NO$: C, 79.98; H, 4.65; N, 7.11%; M, 195. Picrate: dark red needles (from EtOH), mp 203.5—204 °C (dec); Found: C, 53.88; H, 3.09; N, 13.34%. Calcd for $C_{19}H_{12}N_4O_8$ C, 53.78; H, 2.85; N, 13.21%.

Reaction of 2-Methoxytropone (1b) with o-Aminophenol. A mixture of **1b** (1.0 g, 7.3 mmol), *o*-aminophenol (1.0 g, 9.2 mmol), and acetic acid (15 ml) was refluxed for 2 h. After the same treatment as described above, 1.1 g (70%) of **6** and 0.23 g (16%) of **5** were obtained.

Reactions of 1a and 1b with o-Aminophenol in Ethanol. A mixture of **1a** or **1b** and *o*-aminophenol was refluxed in ethanol for 3 h. The reaction mixture was found to be a mixture of **6** and *o*-aminophenol by TLC.

Conversion of 6 into 5. A solution of **6** (200 mg) in 5 ml of acetic acid and one drop of concd H_2SO_4 was refluxed for 30 min. After removal of acetic acid, the residue was dissolved in benzene, washed with aq $NaHCO_3$ and water, dried and evaporated. Recrystallization of the residue from hexane gave 175 mg (95%) of **5.**

Conversion of 5 into 6. A solution of **5** (150 mg) in 8 ml of ethanol and 1 M NaOH (4 ml) was refluxed for 30 min. After removal of ethanol, the residue was dissolved in water (10 ml) and neutralized with 1 M HCl. The resulting precipitate was filtered and dried in a desicater. Recrystallization from benzene gave 155 mg (95%) of **6**. A solution of **6** in ethanol and large excess 1 M NaOH was refluxed for 2 h. The neutralized solution was found to be a mixture of tropolone and *o*-aminophenol by TLC.

2-(o-Methoxyanilino)tropone (7). A mixture of **1a** (1.5 g, 10.7 mmol), *o*-methoxyaniline (2.5 g, 20.3 mmol), and acetic acid (6 ml) was refluxed for 1.5 h. The solution was concentrated to dryness and the residue was recrystallized from benzene to yield 2.2 g (91%) of **7** as yellow prisms, mp 117 °C; λ_{max}^{MeOH} nm (log ε): 205 (4.70), 231 (4.69), 344 (4.38), and 404 (4.56); $\lambda_{max}^{MeOH+HCl}$ nm (log ε): 205 (4.70), 240 (4.71), and 382 (4.47); IR (KBr): 3270 (NH), 1610 (C=O), 2850, 1240, and 1025 cm^{-1} (OMe); NMR ($CDCl_3$, 60 MHz): δ 8.75 (br s, 1H, NH), 6.50—7.45 (m, 9H), and 3.78 ppm (s, 3H, OMe). Found: C, 73.99; H, 5.86; N, 6.11%; M^+, 227. Calcd for $C_{14}H_{13}NO_2$: C, 73.99; H, 5.77; N, 6.16%; M, 227.

1-(o-Methoxyanilino)-7-(o-methoxyphenylimino)-1,3,5-cycloheptatriene (8). From the mother liquor of the recrystallization of **7**, 35 mg (1%) of **8** was obtained by preparative TLC as orange red oil; λ_{max}^{MeOH} nm (log ε): 213 (4.89), 236 (4.89), 285 (4.54), 370 (3.60), and 415 (3.68); $\lambda_{max}^{MeOH+HCl}$ nm (log ε): 215 (4.89), 252 (4.88), and 415 (3.75); IR (neat): 3230 (NH), 2850, 1250 and 1025 cm^{-1} (OMe); NMR ($CDCl_3$, 60 MHz): δ 9.20 (br s, 1H, NH), 6.85—7.30 (m, 8H, brezene ring protons), 6.05—6.75 (m, 5H, cycloheptatriene ring protons), and 3.76 ppm (s, 6H, OMe); MS *m/e* (rel intensity): 332 (M^+, 10), 224 (36), 181 (37), 167 (46), 155 (38), 92 (58), 77 (100), 65 (70), and 51 (80). Picrate: yellow prisms, mp 193 °C (dec). Found: C, 57.48; H, 3.94; N, 12.21%. Calcd for $C_{27}H_{23}N_5O_9$: C, 57.75; H, 4.12; N, 12.47%.

Reaction of 1b with o-Methoxyaniline. A mixture of **1b** (1.5 g, 11.0 mmol), *o*-methoxyaniline (2.0 g, 16.2 mmol), and acetic acid (6 ml) was refluxed for 1.5 h. By the same procedure as described above, **7** (2.1 g, 85%) and **8** (0.1 g, 3%) were obtained.

The authors wish to express their thanks to Dr. Tadamichi Fukunaga, E. I. Du Pont de Nemours & Co. U.S.A. and Dr. Kazuko Takahashi, Tohoku University for their kind communications. Thanks are also due to Dr. Masao Sugimura and Sankyo Co., Ltd. for the measurements of mass spectra, 100 MHz NMR spectra and elemental analyses.

References

1) A part of this work was presented at the 34th National Meeting of the Chemical Society of Japan, Kanagawa, April 1976, II, p. 738.

2) T. Nozoe, Y. Kitahara, K. Takase, and T. Sasaki, *Proc. Jpn. Acad.*, **32**, 349 (1956).

3) T. Nozoe, T. Asao, and K. Takahashi, *Bull. Chem. Soc. Jpn.*, **34**, 146 (1961).

4) a) T. Fukunaga, XXIII IUPAC Congress, Boston (July 1971), Abstracts p. 102; b) T. Fukunaga, private communication.

5) Fukunaga considered that the earlier reported benzotropazine[2] was in fact a dimer of **2a**.[4]

6) W. R. Brasen, H. E. Holmquist, and R. E. Benson, *J. Am. Chem. Soc.*, **83**, 3125 (1961).

7) Kindly measured by Dr. K. Takahashi (Tohoku University).

BULLETIN OF THE CHEMICAL SOCIETY OF JAPAN, VOL. 51 (7), 2187—2188 (1978)

Dissociation Constants of the Cyanohydrins of Substituted Acetonaphthones

P. Ananthakrishna NADAR,* C. GNANASEKARAN, and J. CHANDRASEKARAN
Post-graduate Department of Chemistry, V.H.N.S.N. College, Virudhunagar 626002, India

(Received February 27, 1978)

Synopsis. The dissociation constants of the cyanohydrins of 4-substituted 1-acetonaphthones and 6-substituted 2-acetonaphthones were determined at 30 °C in 80% dioxan-water(v/v). 1-Acetonaphthone Cyanohydrin has a greater dissociation constant than 2-acetonaphthone cyanohydrin due to steric interaction between the reaction centre and *peri*-H. The Hammett equation is well obeyed by both the series. The ρ values are found to be -1.18 and -2.36 for the 1-series and the 2-series respectively. The significant difference in the ρ values suggests that the electronic transmission is different in these two cases.

The position of equilibrium in the reversible dissociation of cyanohydrins of aralkyl ketones (Eq. 1) is governed by both steric and electronic effects. Steric

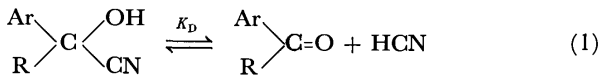

(1)

strain in the cyanohydrin favours the dissociation since there is a change in the coordination of the reaction centre from tetrahedral to trigonal.[1] The carbonyl group can mesomerically conjugate with the aryl group and stabilise the product. Hence electron-donating substituents in the aromatic ring favour the dissociation while the reverse is the case for electron-attracting substituents.[2] This is borne out by the negative ρ value obtained for the dissociation of the cyanohydrins of *meta*- and *para*-substituted benzaldehydes.[3] In an attempt to understand the degree of electronic transmission in substituted acetonaphthones, we measured the dissociation constants of the cyanohydrins of 4-substituted 1-acetonaphthones and 6-substituted 2-acetonaphthones. We report herein our results.

Experimental

Material. The substituted acetonaphthones were prepared by known methods.[4] Commercial dioxan was refluxed with 1M hydrochloric acid (100 ml for 1 litre of dioxan) with occasional passing of air, treated with excess sodium hydroxide and distilled. It was finally fractionated over sodium.[5] Doubly distilled water was used for all purposes. Solutions of HCN were obtained by mixing equal volumes of equimolar solutions of potassium cyanide and perchloric acid in the reaction medium and decanting the clear solution from precipitated potassium perchlorate.

Determination of Equilibrium Constants. The titrimetric method of Lapworth and Manske[6] was followed. The required quantity of the ketone was weighed into a volumetric flask (50 ml), dissolved in a small amount of the solvent and treated with exactly 20.0 ml of the stock solution of HCN. A 2% solution of piperidine (1 ml) was then added and the volume was made up to 50 ml. The flask was stoppered, sealed with paraffin wax and kept in a thermostat at 30 °C for 36 h. At the end of this period, the unreacted hydrogen cyanide was estimated by pipetting out aliquots (10 ml) into a known excess of silver nitrate containing 1% HNO_3 and back titrating with ammonium thiocyanate. A blank run was carried without the ketone in order to determine the initial concentration of HCN. The dissociation constant K_D, was calculated from the relation,

$$K_D = \frac{(a-x)(b-x)}{x},$$

where a is the initial concentration of ketone, b is that of HCN and x is the equilibrium concentration of cyanohydrin.

Results and Discussion

In Tables 1 and 2 are given the dissociation constants of the cyanohydrins of 4-substituted 1-acetonaphthones and 6-substituted 2-acetonaphthones respectively.

The data indicate that the cyanohydrin of 1-acetonaphthone (I) dissociates to a greater extent than that of 2-acetonaphthone (II). In the case of I, interaction

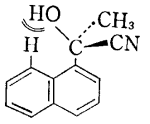

I

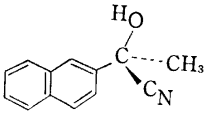

II

with adjacent *peri*-H is relieved on dissociation leading to a higher K_D value; such an interaction is absent in II. Based on the electronic effect of the 2,3-benzo group($\sigma=0.5$) and 3,4-benzo group($\sigma=0.04$)[7] alone, one would expect the cyanohydrin of 2-acetonaphthone to dissociate to a greater extent. Our present results obviously indicate that steric effect outweighs the electronic effect in this reaction.

The Hammett equation is obeyed both by 1- and 2-series (Figs. 1 and 2). The ρ value is found to be -1.18($r=0.997$) for the dissociation of the cyanohydrins of 4-substituted 1-acetonaphthones and -2.36 ($r=0.991$) for the dissociation of 6-substituted 2-acetonaphthone cyanohydrins. For the Hammett plots, the

TABLE 1. DISSOCIATION CONSTANTS OF THE CYANOHYDRINS OF 4-SUBSTITUTED 1-ACETONAPHTHONES IN 80% DIOXAN-WATER(V/V) AT 30 °C

Substituent	$K_D \times 10^2$ mol/l
H	19.1
F	16.0
Cl	11.4
Br	10.8
CH_3	28.5
OCH_3	52.2

Table 2. Dissociation constants of the cyanohydrins of 6-substituted 2-acetonaphthones in 80% dioxan-water (v/v) at 30 °C

Substituent	$K_D \times 10^2$ mol/l
H	9.59
F	7.55
Cl	6.00
Br	5.35
SCH_3	8.44
SO_2CH_3	1.55
CH_3	21.9
OCH_3	31.5

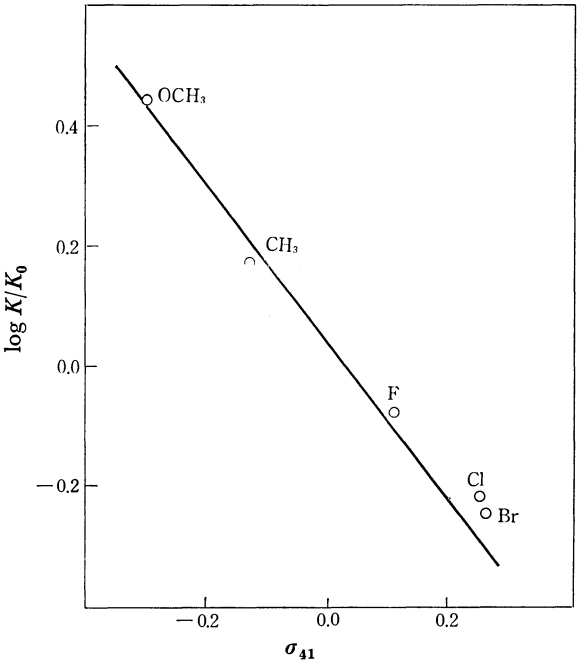

Fig. 1. Hammett plot of 4-substituted 1-acetonaphthones.

σ constants derived by Baliah and Ananthakrishna Nadar[4] were used. In 1-acetonaphthone the acetyl group has a difinite tendency[8] to go out the plane of the aromatic ring due to the *peri*-H. Owing to the difficulty in attaining coplanarity the mesomeric interaction of the acetyl group with the ring will be less in 1-acetonaphthones than in 2-acetonaphthones. This is reflected in a smaller ρ value for the 1-series than that for 2-series. A similar result was obtained by

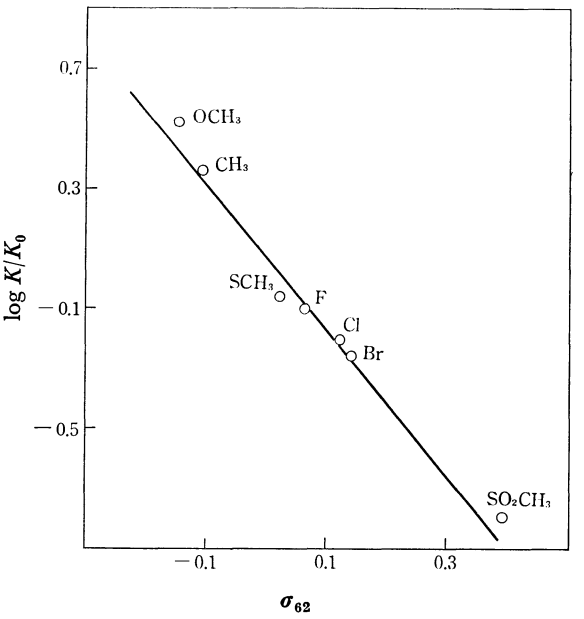

Fig. 2. Hammett plot of 6-substituted 2-acetonaphthones.

us in the reduction of substituted acetonaphthones by sodium tetrahydroborate[9].

The authors gratefully thank the managing board of the V.H.N.S.N. College, Virudhunagar for the research facilities.

References

1) H. C. Brown, R. S. Fletcher, and R. B. Johannesen, *J. Am. Chem. Soc.*, **73**, 212 (1951).
2) J. W. Baker and H. B. Hopkins, *J. Chem. Soc.*, **1949**, 1089.
3) H. H. Jaffe, *Chem. Rev.*, **53**, 191 (1953).
4) V. Baliah and P. Ananthakrishna Nadar, *Indian J. Chem.*, **9**, 671, 1241 (1971).
5) V. Baliah and J. Chandrasekaran, *Indian J. Chem.*, **15B**, 826 (1977).
6) A. Lapworth and R. H. F. Manske, *J. Chem. Soc.*, **1928**, 2535; **1930**, 1976.
7) G. B. Barlin and D. D. Perrin, *Quart. Rev.*, **20**, 75 (1966).
8) P. H. Gore, J. A. Hoskins, C. K. Thadani, R. J. W. Le Fevre, L. Radom and G. L. D. Ritchie, *J. Chem. Soc. B*, **1969**, 426.
9) P. Ananthakrishna Nadar, C. Gnanasekaran, and J. Chandrasekaran, *J. Chem. Soc., Perkin Trans. 2*, communicated.

BULLETIN OF THE CHEMICAL SOCIETY OF JAPAN, VOL. 51 (7), 2189 (1978)

Bromate Ion Specific Adsorption at Hg/$KBrO_3$(aq) Interface

M. V. RAMANAMURTI,* A. QAYUM, and R. K. SINGH

Department of Chemistry, Faculty of Science, Banaras Hindu University, Varanasi 221005, India

(Received May 20, 1977)

Synopsis. Adsorption analysis at polarized Hg/$KBrO_3$ (aq) interface through capacity measurements at 25 °C indicates bromate ion specific adsorption by the cathodic shift of zero charge potential with bulk electrolyte activity confirmed by means of q^1 (charge due to specifically adsorbed anions) *vs.* q^m(electrode charge) curves. At any concentration, $q^1 > q^m$ revealed bromate ion superequivalent adsorption. At fixed q^m, q^1 increases with electrolyte activity.

It was confirmed by Grahame and Soderberg[3] that the specific adsorption of inorganic oxoanions, *e.g.* nitrate,[1] perchlorate,[2] at Hg/solution interface is more complex than that of simpler halide ions. This communication presents evidence (both qualitative and quantitative) of specific adsorption of BrO_3^- (an oxoanion) at Hg/$KBrO_3$ (aq) interface through capacity measurements.

Experimental

Differential capacity measurements were made on an a.c. bridge, described by Grahame[4,5] using a dropping mercury electrode (DME) with a thin walled capillary and drop time *ca.* 8s at zero charge potential (E_{pzc}) of mercury in 0.10 mol·kg^{-1} KCl-solution. The a.c. frequency used was 1000 Hz with an amplitude less than 5 mV across the cell. An electronic magnetic drop detacher helped to knock off the drop at about two-thirds of its natural life. The time between two successive knocks was determined with a stop watch, measuring time-interval up to 0.05 s. The bridge was balanced at the instant of drop detachment. The out of balance of the bridge amplified by a multistage transistor preamplifier (Marconi Type TM6591A) was displayed on a Dumont Oscillograph (Type 274). A large mercury pool electrode and 1 M KCl calomel electrode (NCE) were used as auxiliary and reference electrodes, respectively. Direct contact was made between the reference electrode and the test solution by a saturated-KCl salt bridge which minimized the liquid junction potential to be negligible. The potential applied, measured on a portable potentiometer (Pye-Cambridge), was accurate up to one millivolt. Differential capacities were measured in the potential range from −0.10 to −1.40 V *vs.* NCE. The zero charge potential was determined separately, using streaming mercury electrode.[6] All the measurements were carried out in an air-thermostat controlled at 25±0.1 °C.

Mercury was purified by the procedure described by Trasatti.[7] Twice crystallized $KBrO_3$ (BDH/AnalaR) was used. Solutions at required molalities were prepared in conductivity water and deoxygenated with purified and presaturated nitrogen gas before the experiments were carryied out.

Results and Discussion

The differential capacities of the double layer as a function of ploarization potential, for eight concentrations of $KBrO_3$ in the range 0.025—0.500 mol kg^{-1}, are shown in Fig. 1. The characteristic capacity-hump occurs at anodic polarization with respect to E_{pzc} which shifts towards more negative potential with bulk electrolyte activity. Activity values were derived from graphical interpolation of the reported data.[8] A clear diffuse layer minimum appears for 0.025 mol kg^{-1} at more cathodic potential than E_{pzc}, due to the effect of superimposed steeply rising inner layer capacity. Complete disappearance of diffuselayer minimum in the capacity curves as the concentration approaches 0.10 mol kg^{-1} gives a clear indication of anionic specific adsorption.[9]

The shift of E_{pzc} (from its value *viz.*, −0.476 V *vs.* NCE in systems with no specific adsorption, *e.g.*, fluoride solution) for the anion under investigation to more cathodic values with the increase in bulk electrolyte activity (*cf.* Fig. 2) can be taken as a semi-quantitative estimate of the extent of specific adsorption; $|\Delta E_{pzc}|$ is an approximate measure of the specific adsorption (Esin Markov effect[10]).

The charge on the electrode surface (q^m) was obtained by integration of capacity curves. Knowledge of E_{pzc} facilitated the evaluation of integration constant. The charge due to specifically adsorbed bromate ions (q^1) has been calculated from the equations developed by Grahame and Soderberg[3] following diffuse layer theory. q^1 thus obtained, accurate up to ±1 μC cm^{-2}, has been plotted against q^m at four concentrations in the range 0.05—0.40 mol kg^{-1} (*cf.* Fig. 3). At any concentration the magnitude of q^1 is greater than $q^m(>0)$, indicating superequivalent adsorption of bromate ions. At the highest concentration studied, there exists a finite value of q^1 even at $q^m = -6$ μC cm^{-2}, revealing a strong affinity of BrO_3^- to the metal. At any electrode charge, the magnitude of q^1 increases with increase in electrolyte activity.

Grateful thanks are due to CSIR, Government of India, for financial assistance to one of the authors (RKS).

References

1) R. Payne, *J. Electrochem. Soc.*, **113**, 999 (1966).
2) R. Payne, *J. Phys. Chem.*, **70**, 204 (1966).
3) D. C. Grahame and B. Soderberg, *J. Chem. Phys.*, **42**, 337 (1965).
4) D. C. Grahame, *J. Am. Chem. Soc.*, **63**, 207 (1941).
5) D. C. Grahame, *J. Am. Chem. Soc.*, **71**, 2975 (1949).
6) D. C. Grahame, R. P. Larsen, and M. A. Path, *J. Am. Chem. Soc.*, **71**, 2978 (1949).
7) S. Trasatti, *J. Electroanal. Chem.*, **28**, 257 (1970).
8) R. A. Robinson and R. H. Stokes, "Handbook of Electrochemical Constants," ed by Roger Parsons, Butterworths, London (1959), p. 22.
9) R. Parsons, "Modern Aspects of Electrochemistry," Vol. 1, ed by J. O'M. Bockris and B. E. Conway, Butterworths, London (1954), p. 103.
10) O. A. Esin and B. F. Markov, *Acta Physicochim, U. R. S. S.*, **10**, 353 (1939).

BULLETIN OF THE CHEMICAL SOCIETY OF JAPAN, VOL. 51 (7), 2190 (1978)

Dizirconium Trioxide Sulfate——$Zr_2O_3SO_4$

G. V. JERE,* V. RAMAN, and M. T. SANTHAMMA
Department of Chemistry, Indian Institute of Technology, New Delhi 110029, India

(Received August 16, 1977)

Synopsis. Dizirconium trioxide sulfate $Zr_2O_3SO_4$ has been isolated and characterised. It is obtained as a thermally degraded product of peroxosulfatozirconium(IV) complex, $Zr_2(O_2)_3SO_4 \cdot 8—10H_2O$, around 400—500 °C. It contains zirconium, oxide oxygen and sulfate in its lattice.

The TGA curve[1] of peroxosulfatozirconium(IV) complex, $Zr_2(O_2)_3SO_4 \cdot 8—10H_2O$, shows a relatively flat plateau in the region 350—600 °C. This indicates the formation of a stable intermediate compound. The present note deals with isolation and characterisation of this intermediate compound.

Experimental

The peroxosulphatozirconium(IV) complex — $Zr_2(O_2)_3SO_4 \cdot 8—10H_2O$— was prepared by the method reported.[1,2] The dried solid was heated in a muffle furnace at *ca.* 450 °C for an hour in order to obtain the stable intermediate product. Several samples were prepared and analyzed for zirconium and sulfate contents. The difference in percentage, after subtracting the total value for zirconium and sulfate was assigned to the oxide oxygen. The analytical results are given below:

Composition (%)			Molar ratio		
Zr	SO_4^{2-}	O^{2-}	Zr :	SO_4^{2-} :	O^{2-}
55.92	28.60	15.48	1	0.49	1.58
56.69	28.78	14.53	1	0.48	1.46
56.44	29.02	14.54	1	0.49	1.47
		Average composition			
56.35	28.80	14.85	1	0.49	1.50

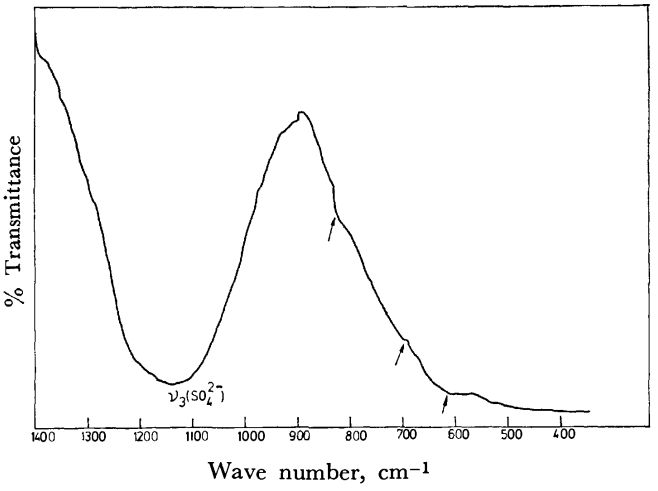

Fig 1. Salient features of the IR spectrum of $Zr_2O_3SO_4$.

The IR spectra of the samples were recorded in Nujol mull, on a Perkin Elmer double beam IR spectrophotometer, model 225. Salient features of the spectrum are given in Fig.1. TGA was carried out on a Stanton recording thermobalance, HT-D, with a 6 °C/min heating rate.

Discussion

We see that the molar composition of the species approximates $Zr : SO_4^{2-} : O^{2-}$ as 1 : 0.5 : 1.5. The compound is formulated as $Zr_2O_3SO_4$. The formation of this compound as a thermally degraded product of the parent peroxo complex can be visualized as follows:

$$\underset{\text{(peroxo compound)}}{Zr_2(O_2)_3SO_4 \cdot 8—10\,H_2O} \xrightarrow{400—450\,^\circ C} \underset{\text{(loss of water + peroxo oxygen)}}{} \underset{\text{(oxide sulfate)}}{Zr_2O_3SO_4}$$

This was indicated earlier also by Tikhomirov *et al.*[2] The molar ratio zirconium to sulphate (1 : 0.5)remains the same both in the intermediate and its parent peroxo compound. It is seen from TGA study that the decomposition of sulfate group from the oxide sulfate commences at *ca.* 600 °C, showing that the sulfate is intact in it. In the IR spectrum of the compound (Fig.1), the ν_3 (SO_4) and ν_4 (SO_4) appear as strong and broad absorptions in the region 1200—1000 cm^{-1} and around 600 cm^{-1} respectively. These two degenerate modes show no splitting. ν_1 and ν_2 do not appear in the IR spectrum. This indicates that sulfate is ionic in nature[3] in the oxide sulfate, unlike the case of the parent peroxo compound where it is of coordinated and bridging type.[1] The sulfate group might have undergone some internal rearrangement during the thermal decomposition of the parent peroxo compound. It is seen that $Zr_2O_3SO_4$ characterised for the first time is an oxide sulfate of zirconium containing zirconium, oxide oxygen and sulfate in its lattice.

One of the authors (M.T.S.) is grateful to the Council of Scientific and Industrial Research (India) for a research fellowship.

References

1) G. V. Jere and G. D. Gupta, *J. Inorg. Nucl. Chem.*, **32**, 537 (1970).
2) V. I. Tikhomirov, B. V. Lenin, V. V. Mironova, and V. M. Solovaya, *Russ. J. Inorg. Chem., Engl. Transl.*, **7**, 960 (1962).
3) K. Nakamoto and R. J. McCarthy, "Spectroscopy and Structure of Metal Chelate Compounds," John Wiley & Sons, New York (1968), p. 216.

The Radiolysis of Binary Mixtures of Tetrahydrofuran with Benzene, Thiophene, Pyridine, and Nitrobenzene

Masao MATSUI* and Masashi IMAMURA†

Department of Pharmacy, Hokuriku University, Kanagawa-machi, Kanazawa-shi, Ishikawa 920-11

†*The Institute of Physical and Chemical Research, Wako-shi, Saitama 351*

(Received January 17, 1978)

Binary mixtures of tetrahydrofuran (THF) with benzene, thiophene, and nitrobenzene were subjected to radiolysis with γ-rays. The THF–benzene mixture was also irradiated with 28.6 MeV ^{4}He- and 90.9 MeV ^{12}C-ions. For THF–benzene mixtures, similar deviations of $G(H_2)$ from the mixture law were observed for all the radiolyses; these results are regarded as being due to energy transfer from THF^+, the precursor of hydrogen, to benzene. The total ionization yield of THF was calculated as 3.0—3.3 in G-units, irrespective of radiation and additives. This is on the basis of Hardwick's procedure, in which the deviations of $G(H_2)$ are divided by the efficiency of the energy transfer. This result also indicates that the total ionization yield is independent of the nature of radiation, whose LET range is from 0.02 to 49.2 eV/Å.

In the radiolysis of binary mixtures of organic liquids, a deviation from the mixture law[1] is sometimes observed. This deviation has been interpreted as a result of an energy or charge transfer from one component to the other.

Hardwick[2] has shown that the efficiency of an energy or charge transfer can be estimated from these deviations. When a radiolysis product is formed from an ionic precursor which can transfer its charge to the other component of the binary mixture, one can calculate a total ionization yield by combining the limiting efficiency of the charge transfer with the deviation of the product yield from the expected one.

One of the present authors[3] has previously reported that the hydrogen yield from a binary mixture of tetrahydrofuran (THF) and furan shows a deviation from the mixture law in the γ radiolysis and that the decrease in $G(H_2)$ is due to the charge transfer from THF to furan.

In the present study, binary mixtures of THF with benzene, thiophene, pyridine, and nitrobenzene as well as furan were subjected to irradiation with γ rays; the THF–benzene mixture was also irradiated with He- and C-ions. Moreover, the total ionization yields of THF, calculated by Hardwick's procedure, were compared with that of γ radiolysis.

Experimental

Materials. The THF was purified as has been described in a previous paper.[4] The thiophene (Tokyo Kasei Guaranteed Reagent) and benzene (Junsei Pure Chem. Guaranteed Reagent) were purified gas-chromatographically using a 3-m column of PEG-1000 at 100 °C. The pyridine (Wako Pure Chem. Extra Pure Reagent) and nitrobenzene (Wako Pure Chem. Guaranteed Reagent) were kept on sodium hydroxide and calcium chloride respectively for several days before rectifying.

Irradiation. γ-irradiation was carried out with a 10-kCi ^{60}Co source at a dose rate of 5.85×10^{17} eV $g^{-1}min^{-1}$ (9370 rad min^{-1}), which was determined by using a Fricke dosimeter on the basis of $G(Fe^{3+})=15.6$. The G-values were calculated after the correction of the absorbed dose for the electron densities of the solutions used. The He-(28.6 MeV) and C-(90.9 MeV) ions were accelerated with the cyclotron at the Institute of Physical and Chemical Research. The current intensity and total dose for charged particles were $\approx$1 nA and $(3.6—5.0)\times10^{19}$ eV respectively. The samples were vigorously stirred with a magnetic stirrer during irradiation at an ambient temperature.

The details of the irradiation arrangement and experimental procedures for charged-particle radiolysis were the same as those described previously.[5]

Analysis of Products. The gaseous fraction at −196 °C was determined on a conventional calibrated gas burette and a Toepler pump. The hydrogen and carbon monoxide were determined by gas chromatography using a Molecular Sieve 5A.

Results and Discussion

γ Radiolysis of THF–Benzene and THF–Thiophene Mixtures. The yield of hydrogen from pure liquid THF was $G=3.5$ in the present study, in agreement with several values previously reported.[4,6] The hydrogen yields for the binary mixtures of THF–benzene and THF–thiophen are plotted as a function of the electron fractions of benzene and thiophene respectively in Figs. 1 and 2. In both cases, the yields are lower than those to be expected from the mixture law. A similar trend of $G(H_2)$ has been observed for the THF–furan mixture,[3] whose concave variation of $G(H_2)$ was interpreted as being due to charge transfer from THF cations to furan molecules. For the THF–benzene and THF–thiophene mixtures, the deviation from straight

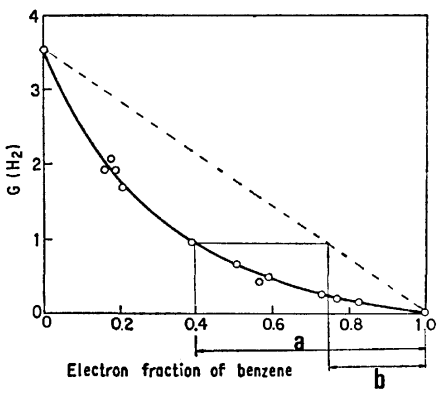

Fig. 1. Hydrogen yields from THF–benzene mixtures in γ radiolysis.

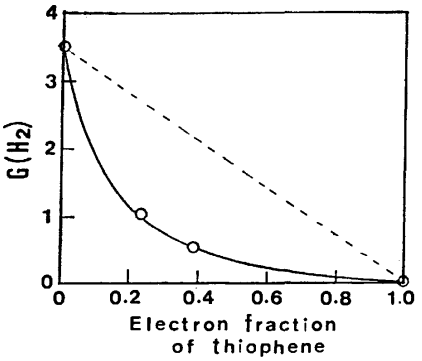

Fig. 2. Hydrogen yields from THF–thiophene mixtures in γ radiolysis.

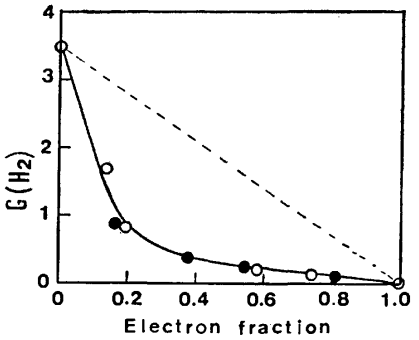

Fig. 3. Hydrogen yields from THF–pyridine (○) and THF–nitrobenzene (●) mixtures in γ radiolysis.

lines connecting the $G(H_2)$'s of THF and additives may also be explained on the same basis. In the γ radiolysis of THF, hydrogen was found to be produced molecularly; *i.e.*, the $G(H_2)$ was not affected by adding radical scavengers.[3] Most of the hydrogen is considered to be formed by rapid ion-molecule reactions of THF^+.[7] Therefore, the deviation of $G(H_2)$ from the mixture law may reasonably be explained in terms of charge transfer from THF^+ to the additives whose hydrogen yields are lower than that of THF.

This argument is supported by the facts that the ionization potentials[8] of benzene, thiophene, and furan are lower (9.25, 8.86, and 8.89 eV respectively) than that of THF (9.54 eV) and that the maximum deviations of $G(H_2)$, which appear at an electron fraction of about 0.25 for the above three additives, are in the order of the ionization potentials of the additives.

A similar relation has been observed in the production of D_2 and HD for the liquid-phase radiolysis of several binary mixtures of ethane-d_6, propane-d_8, and butane-d_{10} in liquid hydrocarbons at 195 K. That is, solvents with higher ionization potentials enhance the production of D_2 and HD from deuterated solutes with lower ionization potentials. There is also a great deal of evidence indicating that charge transfer to, or the positive-ion scavenging of, benzene takes place in liquid and glassy solutions.[10-18]

The occurrence of the charge transfer from THF^+ to benzene is further supported by the fact that the $\Delta G(H_2)$ of the THF–benzene mixture was reduced on the addition of triethylamine, that is, a positive-ion scavenger. For example, $\Delta G(H_2)=1.10$ in the THF–benzene ($a=0.2$) mixture was reduced to 0.55 on the addition of both benzene ($a=0.12$) and triethylamine ($a=0.08$) to THF. Since the $G(H_2)$ from pure triethylamine is higher than that of THF, the $G(H_2)$ for the THF–triethylamine mixture is increased by transferring the charge from THF^+ to triethylamine.

In contrast to $G(H_2)$, $G(CO)$ varies linearly with the electron fraction of the additives. Carbon monoxide has been shown to be produced from excited THF,[3] therefore, its yield is expected not to be affected by the presence of charge scavengers.

γ Radiolysis of THF–Pyridine and THF–Nitrobenzene Mixtures. Concave variations in $G(H_2)$ apparently similar to those observed for the THF–benzene and THF–thiophene mixtures described in the previous section were also observed for THF–pyridine and THF–nitrobenzene mixtures. It should be noted, however, that no substantial difference was observed between the two mixtures, as is shown in Fig. 3.

Either of these two additives has not only an ionization potential higher than that of THF, but also a high rate-constant toward hydrated electrons: $k(\text{pyridine}+e^-_{aq})=3.7\times10^9\ M^{-1}\ s^{-1}$ and $k(\text{nitrobenzene}+e^-_{aq})=3.0\times10^{10}\ M^{-1}\ s^{-1}$,[19] which are 10^2—10^3 times those of benzene ($k=1.4\times10^7\ M^{-1}\ s^{-1}$), thiophene ($k=3.0\times10^6\ M^{-1}\ s^{-1}$), and furan ($k=6.5\times10^7\ M^{-1}\ s^{-1}$).[19]

These facts indicate that, in the THF–pyridine and THF–nitrobenzene mixtures, the additives could act as efficient electron scavengers to reduce $G(H_2)$ from THF. Hydrogen is produced from THF by the reaction of electrons with the $THFH^+$ produced by the ion-molecule reaction ($THF^+ + THF$) as well as by the decomposition of excited THF molecules within spurs. Therefore, insofar as additives react with solvated electrons at a diffusion-controlled rate, the variation in $G(H_2)$ with the electron fraction should be independent of the nature of the additive. In fact, the $G(H_2)$-values from THF–pyridine solutions containing carbon tetrachloride were found to fit the curve in Fig. 3 when plotted *vs.* the sum of the electron fractions of pyridine and carbon tetrachloride.

He- and C-ion Radiolysis of THF–Benzene Mixture. The radiolysis of the THF–benzene mixture was carried out with 28.6 MeV He- and 90.9 MeV C-ions. The results are shown in Fig. 4, where the observed $G(H_2)$'s are plotted as a function of the electron fraction of benzene. Although the hydrogen yields from both THF and benzene are higher than those in the γ radiolysis, the variations in the $G(H_2)$ are qualitatively similar to those in the γ radiolysis. Thus, the charge transfer from THF^+ to benzene can be assumed to explain the concave variation in $G(H_2)$ in the He- and C-ion radiolysis.

Total Ionization Yields and Their LET-Dependence. Assuming that the additives act as charge acceptors (benzene, thiophene, and furan) or electron acceptors (pyridine and nitrobenzene) in the THF solutions, and that hydrogen is produced only from THF^+ and excited THF, one can calculate the total ionization yields in γ and heavy-ion radiolyses by using the procedure proposed by Hardwick.[2]

When a stands for the electron fraction of THF in the

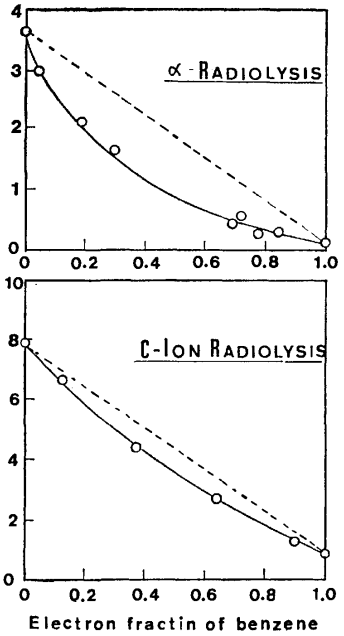

Fig. 4. Hydrogen yields from THF–benzene mixtures in He- and C-ion radiolysis.

mixture, and b, the apparent fraction of THF, as indicated by the measured value of $G(H_2)$ (see Fig. 2), the amount of THF which transfers energy is given by $(1-b)-(1-a)=a-b$. The fraction of THF molecules transferring a charge to acceptor molecules is, therefore, $(a-b)/a$.

The limiting values of $(a-b)/a$ can be obtained by plotting $(a-b)/a$ as a function of the electron fractions of the additives. In the γ radiolysis, such plots gave the limiting values of 0.70—0.75, identical within the range of experimental error for the THF–benzene, THF–thiophene, and THF–furan mixtures; these results are in accord with those obtained for alkane mixtures.[2] As Hardwick has stated, the identical limiting values for these mixtures may indicate that the characteristics of the donor molecule rather than those of the acceptor molecule govern the transfer process.

The limiting values of $(a-b)/a$ obtained with THF–benzene mixtures for He- and C-ion radiolysis were 0.65 and 0.50 respectively. Since THF in the THF–benzene, THF–thiophene, and THF–furan mixtures has an ionization potential lower than those of the additives, the energy transfer taking place in these systems may be regarded as a charge transfer. This assumption may also support the above findings as to the very close limiting values of $(a-b)/a$ for these mixtures. The remaining molecules, which do not transfer but decompose to give products, may, as Hardwick argued, be considered to be electronically excited. As has been mentioned above, in the He- and C-ion radiolyses the limiting values of $(a-b)/a$ were found to be 0.65 and 0.50 respectively for the THF–benzene mixtures. These values are lower than that obtained in γ radiolysis and show a substantial LET dependence. This fact, on the assumption mentioned above, indicates that the relative yield of electronically excited states which decompose to give products is substantially increased in high LET radiolyses.

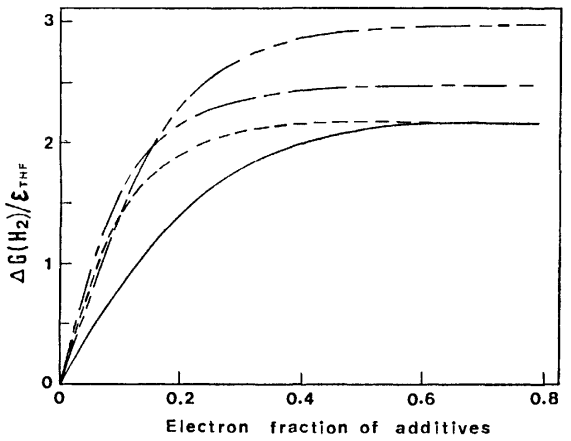

Fig. 5. Effectiveness of additives in γ radiolysis. Benzene (——), thiophene (– – –), furan (– – – –), pyridine and nitrobenzene (— — —).

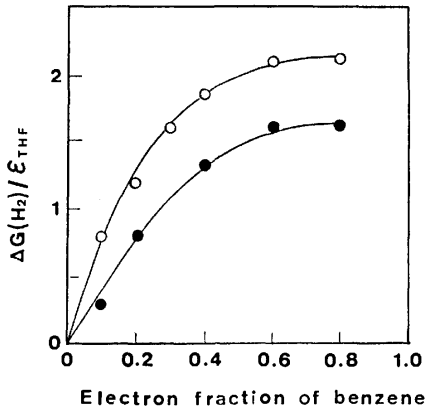

Fig. 6. $\Delta G(H_2)/\varepsilon_{THF}$ against the electron fraction of benzene for He- (○) and C- (●) ion radiolysis.

The effectiveness of additives may be seen from the curves shown in Fig. 5, where the deviations of $G(H_2)$ from the mixture law divided by the electron fraction of THF are plotted against the electron fraction of additives. For the He- and C-ion radiolyses, the deviations from the mixture law divided by the electron fraction of THF, $\Delta G(H_2)/\varepsilon_{THF}$, are shown in Fig. 6 as a function of the electron fraction of benzene. From Figs. 5 and 6 it is apparent that the limiting values of $\Delta G(H_2)$ corresponding to the limiting fraction of the THF-transferring charge are 2.2—2.5 for γ radiolysis and 2.1 and 1.6 for He- and C-ion radiolyses respectively.

On the other hand, a limiting $\Delta G(H_2)$-value of 2.9 is obtained by a similar treatment of the results observed for the γ radiolysis of THF–pyridine and THF–nitrobenzene mixtures in Fig. 5. Since these additives are thought to act as electron scavengers to reduce $G(H_2)$ from THF, and since the limiting value of $\Delta G(H_2)$ obtained is much the same as that of $G(e^-)$ reported by Baxendale *et al.*,[20] this value may represent the yield of electrons. They have determined the G(ion pair) values of 2.6 and 2.7 for the pulse radiolysis of THF–pyrene (5 mM)–$LiAlH_4$ (maximum$\simeq$0.45 M) and the γ radiolysis of THF–carbon tetrachloride (maximum$\simeq$ 0.1 M) mixtures respectively.

Shaede *et al.*[21] have also observed a total ionization yield of 3.75 for the nanosecond pulse radiolysis of a THF–pyrene mixture. The difference between $G(THF^+)$ and $G(e^-)$ estimated by the above-described treatment is probably attributable to the discrepancy of the efficiency between electron transfer and electron capture.

If one can assume that benzene acts solely as a charge acceptor in the present binary mixtures, the "total ionization yield" may be obtained by dividing the limiting value of $\Delta G(H_2)$ by that of $(a-b)/a$. The value of 3.0—3.1 is obtained for the γ radiolysis systems and that of 3.2—3.3 for the heavy-ion radiolysis systems. No substantial difference in the total ionization yield is seen between the two systems. These results reflect the fact that the ionization yield of liquid THF is independent of LET over a wide range and that the increased yields of hydrogen observed for heavy-ion-radiolysis systems may be attributable to the increased yields of the excited states.

The author's thanks are due to Messrs. Kazuo Otsuka and Yasuo Harata, who helped us throughout this work.

References

1) The mixture law states that energy is initially absorbed in a mixture in proportion to the electron fraction's relationship to the components. *Cf.* J. P. Manion and M. Burton, *J. Phys. Chem.*, **56**, 560 (1952); R. A. Holroyd, in "Fundamental Processes in Radiation Chemistry," ed by P. Ausloos, Interscience, New York (1968), Chap. 7, p. 493.
2) T. J. Hardwick, *J. Phys. Chem.*, **66**, 2132 (1962).
3) M. Matsui, *Bull. Chem. Soc. Jpn.*, **39**, 1640 (1966).
4) M. Matsui and M. Immamura, *Bull. Chem. Soc. Jpn.*, **42**, 3362 (1969).
5) M. Matsui and M. Imamura, *Bull. Chem. Soc. Jpn.*, **47**, 1113 (1974).
6) F. S. Dainton and G. A. Salmon, *Proc. R. Soc. London, Ser. A*, **285**, 319 (1965).
7) J. H. Baxendale, D. Beaumond, and M. A. J. Rodgers, *Int. J. Radiat. Phys. Chem.*, **2**, 39 (1970).
8) K. Watanabe, T. Nakayama, and J. Mottl, *J. Quant. Spectrosc. Radiat. Transfer*, **2**, 369 (1962).
9) J. A. Stone, A. R. Quirt, and O. A. Miller, *Can. J. Chem.*, **44**, 1175 (1966).
10) L. I. Bone and J. H. Futrell, *J. Chem. Phys.*, **47**, 4366 (1967).
11) L. Y. Wei and L. I. Bone, *J. Phys. Chem.*, **75**, 2272 (1971).
12) K. N. Jha and G. R. Freeman, *Can. J. Chem.*, **49**, 2651 (1971).
13) M. G. Kennedy and J. A. Stone, *Can. J. Chem.*, **51**, 149 (1973).
14) J. K. Thomas and I. Mani, *J. Chem. Phys.*, **51**. 1834 (1969).
15) T. Shida and W. H. Hamill, *J. Chem. Phys.*, **44**, 2375, 4372 (1966).
16) A. Ekstrom, *J. Phys. Chem.*, **74**, 1705 (1970).
17) F. W. F. Louwrier and W. H. Hamill, *J. Phys. Chem.*, **74**, 1418 (1970).
18) P. S. Rudolph and C. E. Melton, *J. Chem. Phys.*, **32**, 586 (1960).
19) M. Anbar, M. Bambenek, and A. B. Ross, "Selected Specific Rates of Reactions of Transients from Water in Aqueous Solution. 1. Hydrated Electron," NSRDS-NBS 43, Washington, D. C. (1973).
20) J. H. Baxendale, D. Beaumond, and H. A. J. Rodgers, *Trans. Faraday Soc.*, **66**, 1966 (1970).
21) E. A. Shaede, H. Kurihara, and L. M. Dorfman, *Int. J. Radiat. Phys. Chem.*, **6**, 47 (1974).

Carrier Effect on the Nature of V^{4+} and Active Oxygen Species in Vapor-phase Oxidation of Butadiene over Supported Divanadium Pentaoxide Catalysts

Masamichi AKIMOTO,* Masahiro USAMI, and Etsuro ECHIGOYA

Department of Chemical Engineering, Tokyo Institute of Technology, Ookayama, Meguro-ku, Tokyo 152

(Received January 13, 1978)

The reactivity of V^{4+} with gaseous oxygen formed on various kinds of supported V_2O_5 catalysts has been investigated by ESR. The results are discussed as carrier effect in relation to the selectivity for maleic anhydride formation during the course of the vapor-phase oxidation of butadiene. V^{4+} formed on Al_2O_3 (V/Al$\leq$10/90 atom ratio) and MgO (V/Mg$\leq$30/70) showed a hyperfine ESR structure and was hardly oxidized whereas V^{4+} formed on SiO_2 (V/Si$\geq$5/95) had the singlet ESR signal and was easily oxidized. Formation of these two kinds of V^{4+} was observed on V_2O_5–Al_2O_3 (V/Al$\geq$20/80). They were similarly observed in the case of V_2O_5–TiO_2, but some portion of V^{4+} having the hyperfine structure was also oxidized. The selectivity was high over the catalysts forming the reactive V^{4+} as compared with those forming the unreactive one. The reactive V^{4+} was shown by X-ray diffraction to be preferentially formed in crystalline V_2O_5. Study of the reduction and reoxidation of unsupported crystalline V_2O_5 by means of IR and the effect of addition of alkali metal oxide on the catalytic activity of the supported V_2O_5 were discussed. The important role of double bond type lattice oxygen V=O in maleic anhydride formation was proposed.

In heterogeneous catalysis, a carrier is generally used for supporting the active component. However, the nature of the active site is strongly influenced by the kind of carrier, the supporting not always leading to better result. Thus, there are some observations which imply a chemical interaction between active component and carrier which may give rise to a carrier effect.[1-3] In heterogeneous oxidation of hydrocarbons, in which use of a carrier is strongly desirable, the role of carrier is not fully understood. In a previous paper,[4] a report was given on the carrier effect on the nature of supported molybdena catalyst in vapor-phase oxidation of butadiene. It was shown that the catalyst forming Mo^{5+} which is easily oxidized by gaseous oxygen has higher selectivity to maleic anhydride formation than that giving Mo^{5+} which is not oxidized. We have carried out a detailed investigation of carrier effect in the same catalytic oxidation using various supported V_2O_5 catalysts. Alumina, silica, titania, and magnesia were used as carrier, and the physical and chemical properties of these catalysts were investigated by X-ray analysis, ESR and IR spectroscopy in relation to the selectivity for maleic anhydride formation. Oxygen species, which is active and selective for the production of maleic anhydride, was also studied.

Experimental

The apparatus and procedure used for the oxidation were the same as those reported.[4] Pure butadiene (99.9% up) was used. Various supported V_2O_5 catalysts were prepared by mechanically kneading either alumina gel, silica gel, titania gel, or magnesium hydroxide with an aqueous solution of ammonium metavanadate for 3 h, evaporating the cake to dryness on a water bath and sieving the dried mass obtained into particles of 32—60 mesh. The catalysts were then calcined in an air current at 550 °C for 3 h. Titania gel was prepared by hydrolysis of titanium tetrachloride of reagent grade. Supported V_2O_5 catalysts modified with alkali metal oxide were prepared similarly. As a source of the metal oxide, extra pure alkali metal nitrates were used.

The gaseous effluent from the reactor was analyzed by gas chromatography. PEG 20M 20 wt% on Neopak 1A (60 °C, furan, acrylaldehyde, acetaldehyde), propylene carbonate 40 wt% on Celite 545 (room temp, butadiene, CO_2) and molecular sieve 13X (room temp, CO, N_2, O_2) were used as separating columns. Since maleic anhydride was the only acid obtained, the product was absorbed into water followed by titration with an aqueous solution of sodium hydroxide (0.1 M) after boiling off carbon dioxide. The structure of the catalysts was investigated by X-ray diffraction using nickel-filtered Cu $K\alpha$ radiation. The surface area of the catalysts was determined by the BET method using nitrogen as an adsorbate. A JEOL JES-PE-2X ESR spectrometer was used, in which microwave frequency was the X band and 100 kHz modulation was adopted. The amount of V^{4+} was measured using Mn^{2+} and DPPH as an internal standard. A Hitachi EPI-G3 spectrometer was used for IR studies.

Results

The Oxidation of Butadiene over Various Supported V_2O_5 Catalysts. Alumina, silica, titania, and magnesia showed negligible activity in the oxidation of butadiene. The carriers promoted only complete combustion of butadiene without formation of maleic anhydride. Figure 1 shows the result of oxidation over V_2O_5–Al_2O_3 catalyst. The catalyst containing V_2O_5 at V/Al=5/95 atom ratio had a negligible activity. However, further addition of V_2O_5 enhanced the activity to reach a maximum value at V/Al=20/80. The selectivity to maleic anhydride was low, *i.e.*, 6.5% over the catalyst of V/Al=10/90 in contrast to those (30—35%) over the catalysts of V/Al$\geq$20/80.

The catalytic activity of V_2O_5–SiO_2 increased with increase in the content of V_2O_5 (Fig. 2). V_2O_5–TiO_2 showed a tendency similar to that of V_2O_5–Al_2O_3 (Fig. 3). However, in contrast to the latter catalyst, the former two catalysts had an ability of producing maleic anhydride in spite of the low content of V_2O_5, *i.e.*, V/Si=5/95 and V/Ti=5/95. V_2O_5–MgO (V/Mg$\leq$30/70) formed no maleic anhydride; conversion of butadiene and yield of CO_2 and CO were 24.9, 24.2% (V/Mg=5/95), 39.6, 33.7% (10/90), 58.9, 55.4%

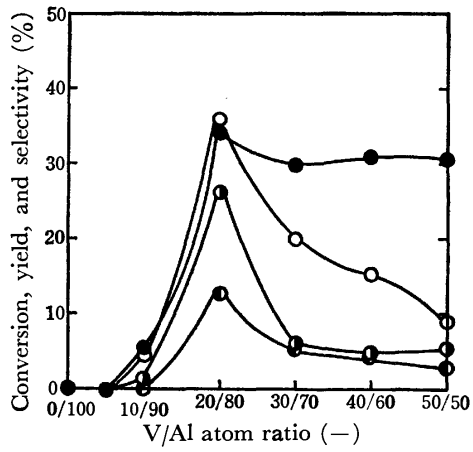

Fig. 1. The oxidation of butadiene over various V_2O_5–Al_2O_3 catalysts. Reaction temp (bath): 310 °C, feed: butadiene 1.45 vol% in air, contact time: W/F=0.373 g-cat·h/g-mol.
○: Conversion of butadiene, ◑: yield of CO_2+CO, ◐: yield of maleic anhydride, ●: selectivity to maleic anhydride.

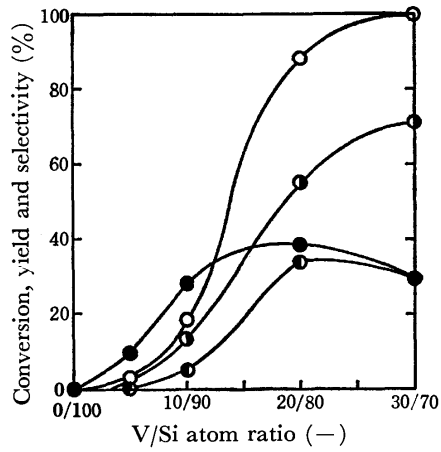

Fig. 2. The oxidation of butadiene over various V_2O_5–SiO_2 catalysts. Reaction temp (bath): 380 °C, feed: butadiene 1.45 vol% in air, contact time: W/F=0.373 g-cat·h/g-mol. Symbols are the same as those in Fig. 1.

(20/80), and 57.0, 57.4% (30/70), respectively, at 425 °C, contact time W/F=1.490 g-cat·h/g-mol and butadiene 1.45 vol% in air.

Based on the selectivity to maleic anhydride formation, these catalysts can be divided into the following three groups;

(A) V_2O_5–Al_2O_3 (V/Al=5/95 and 10/90), V_2O_5–MgO (V/Mg≤30/70).

The selectivity is negligible or very low.

(B) V_2O_5–SiO_2 (V/Si=5/95), V_2O_5–TiO_2 (V/Ti=5/95).

The selectivity is 10—16%.

(C) V_2O_5–Al_2O_3 (V/Al≥20/80), V_2O_5–SiO_2 (V/Si≥10/90), and V_2O_5–TiO_2 (V/Ti≥10/90).

The selectivity is 30—39%.

X-Ray Studies on the Supported V_2O_5 Catalysts. Al_2O_3 and SiO_2 were almost amorphous, the former showing weak X-ray diffraction at 2θ=46.0 and 67.0°. Thus, Al_2O_3 was γ-type. In the case of V_2O_5–Al_2O_3, the diffraction due to crystalline V_2O_5 appeared from

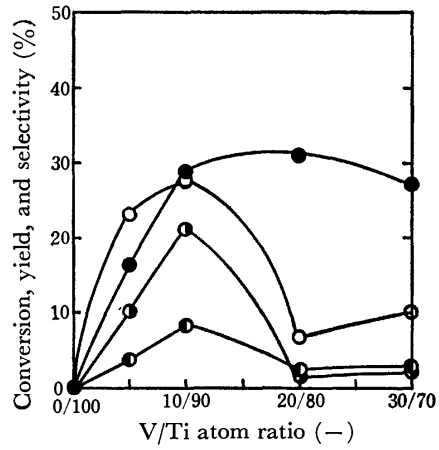

Fig. 3. The oxidation of butadiene over various V_2O_5–TiO_2 catalysts. Reaction temp (bath): 300°C, feed: butadiene 1.32 vol%, oxygen 9.11 vol%, diluent–nitrogen, contact time: W/F=0.325 g-cat·h/g-mol. Symbols are the same as those in Fig. 1.

V/Al=20/80 (2θ=25.6°), its strength increasing with rise in the content of V_2O_5; *i.e.*, V_2O_5–Al_2O_3 (V/Al=40/60) showed diffraction at 2θ=20.5, 26.1, 31.0° (strong), 15.5, 21.8, 32.4, and 34.4° (medium). On the other hand, the presence of crystalline V_2O_5 was observed from V/Si=10/90 (2θ=15.4, 26.0, and 32.2°), its amount increasing with rise in content. TiO_2 was of anatase-type (2θ=25.2, 37.9, 48.0, and 54.0°), formation of the V_2O_5 being distinctly observed at V/Ti≥20/80 (2θ=15.2, 20.2, 26.2, and 31.3°). In contrast, V_2O_5–MgO (V/Mg≤30/70) showed strong X-ray diffraction due to periclase-type MgO at 2θ=36.9, 42.7, and 62.1° with a very weak diffraction due to V_2O_5 at 2θ=35.1° (V/Mg≥10/90). Thus, the group C catalysts contain crystalline V_2O_5 in contrast to groups A and B.

ESR Spectrum of V^{4+} and Its Reactivity to Gaseous Oxygen. Formation of paramagnetic species in various V_2O_5 catalysts preevacuated at 450 °C under 10^{-5} mmHg was investigated by means of ESR. V_2O_5–SiO_2 (V/Si=5/95) gave a singlet spectrum, its g-factor being 1.98 and the linewidth expressed by maximum slope separation 107G. The line shape was nearly Lorentzian. This spectrum agreed with that of V^{4+} which forms a cluster in pure V_2O_5 and on Alundum carrier.[5] However, the linewidth increased with further rise in the content of V_2O_5 (V/Si=20/80, ΔH_{msl}=213G).

A completely different spectrum was observed for V_2O_5–Al_2O_3 (V/Al≤10/90), V_2O_5–TiO_2 (V/Ti=5/95), and V_2O_5–MgO (V/Mg≤30/70), which clearly showed hyperfine splitting caused by the nuclear magnetic moment of vanadium I=7/2 (Fig. 4, V/Al=5/95). V_2O_5–Al_2O_3 (V/Al≥20/80) and V_2O_5–TiO_2 (V/Ti≥10/90) gave ESR spectra consisting of hyperfine structure and singlet. Analysis of the complicated spectrum having the hyperfine structure was carried out by the method developed by Hecht and Johnstone.[6] The spectrum was analyzed with an axial symmetric spin Hamiltonian[7]

$$\mathcal{H} = \beta(g_{\parallel}H_zS_z + g_{\perp}H_xS_x + g_{\perp}H_yS_y) + A_{\parallel}S_zI_z + A_{\perp}S_xI_x + A_{\perp}S_yI_y, \quad (1)$$

where β is the Bohr magneton, $g_{\parallel}$ and $g_{\perp}$ are the parallel and perpendicular principal components, respectively, of the g-tensor; $A_{\parallel}$ and $A_{\perp}$ are the parallel and perpendicular principal components, respectively, of the hyperfine-coupling tensor; H_x, H_y, H_z are the components of the magnetic field; S_x, S_y, S_z, and I_x, I_y, I_z are the components of spin operators of the electron and nucleus, respectively, the coordinate system being fixed to the molecule. The absorption peaks are related to $2I+1$ values of m_I, the peaks appearing in the field of

$$H_{\parallel} = 2H_0/g_{\parallel} - (A_{\parallel}/g_{\parallel}\beta)m_I \quad (\text{for } \theta = 0), \qquad (2)$$

$$H_{\perp} = 2H_0/g_{\perp} - (A_{\perp}/g_{\perp}\beta)m_I \quad (\text{for } \theta = \pi/2), \qquad (3)$$

where θ is the angle spanning between H_0 and the axial symmetry axis of the ion site. Plotting the magnetic field of the observed peaks corresponding to either $H_{\parallel}$ or $H_{\perp}$ against the nuclear quantum number m_I, we obtain a linear relation. The slopes and the intercepts with the $m_I=0$ line can be used to obtain values of the parameters, $g_{\parallel}$, $A_{\parallel}$, $g_{\perp}$, and $A_{\perp}$. Assignment of the peaks of the observed spectrum was attained according to the method used by Takahashi *et al.*[5] The result is illustrated as two sets of octets as shown in Fig. 4 (V/Al=5/95). The values of the parameters are given in Table 1. The observed components of the g-factor show that the g-tensor of V^{4+} ion has axial symmetry. The observed parameters agree with those of the V^{4+} formed separately on Neobead carrier.[5]

Reactivity of V^{4+} with gaseous oxygen was investigated by introduction of 20 mmHg O_2 followed by heating at various temperatures for 30 min. The amount of V^{4+} existing after the reaction was determined at room temperature. V^{4+} in V_2O_5–Al_2O_3 (V/Al≤10/90) was scarcely oxidized even at 450 °C, but a large portion of V^{4+} in V_2O_5–Al_2O_3 (V/Al≥20/80) was oxidized to V^{5+} above 200 °C with simultaneous appearance of the hyperfine structure. V^{4+} in V_2O_5–MgO (V/Mg≤30/70) was also hardly oxidized at 450 °C whereas that in V_2O_5–SiO_2 (V/Si≤30/70) was easily oxidized. Thus,

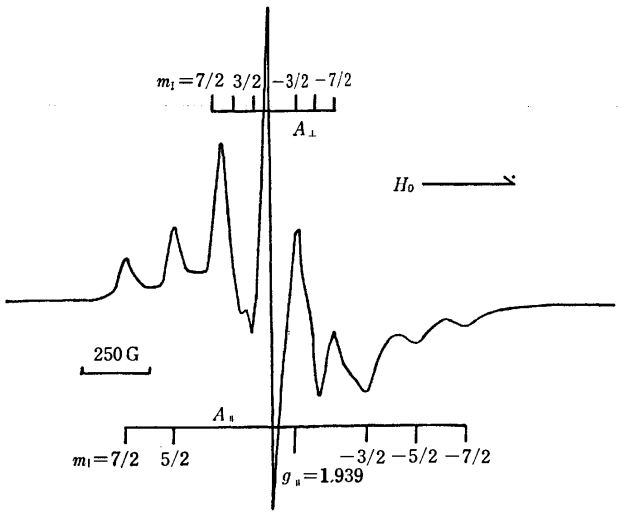

Fig. 4. ESR spectrum of V^{4+} formed in V_2O_5–Al_2O_3(V/Al=5/95). Catalyst: evacuated at 450 °C and 10^{-5} mmHg for 2 h. ESR: measured at room temperature.

V^{4+} having the singlet spectrum is reactive to oxygen, but not the one having hyperfine structure. However, some portion of V^{4+} formed in V_2O_5–TiO_2 (V/Ti=5/95) was easily oxidized irrespective of the hyperfine structure. V^{4+} in V_2O_5–TiO_2 (V/Ti≥10/90) showed a reactivity similar to that in V_2O_5–Al_2O_3 (V/Al≥20/80). The observations are summarized in Table 2. The catalysts forming reactive V^{4+} have high selectivity as compared with those having unreactive V^{4+}. The reactive V^{4+} is preferentially formed in crystalline V_2O_5.

Correlation Existing between the Amount of V^{4+} and the Catalytic Activity. The amount of V^{4+} formed by the evacuation of various V_2O_5–Al_2O_3 at 450 °C and decreased on contact with gaseous oxygen at 350 °C were determined (Table 3). 0.4—1.2% of vanadium present in the catalyst is V^{4+}, in line with the other catalysts. The amount of V^{4+} which is reactive to

Table 1. Spin Hamiltonian parameters of the spectrum of V^{4+} on various carriers

Catalyst(atom ratio)	$\lvert A_{\parallel}\rvert$	$\lvert A_{\perp}\rvert$	$\lvert A_0\rvert$	$g_{\parallel}$	$g_{\perp}$	g_0	$H_{\parallel}(m_I=0)$	$H_{\perp}(m_I=0)$
V_2O_5–Al_2O_3 (V/Al=5/95)	161×10^{-4}cm^{-1} 178G	56×10^{-4}cm^{-1} 61G	91×10^{-4}cm^{-1} 100G	1.939	1.983	1.968	3399G	3324G
V_2O_5–Al_2O_3 (V/Al=10/90)	161×10^{-4}cm^{-1} 177G	57×10^{-4}cm^{-1} 62G	92×10^{-4}cm^{-1} 100G	1.944	1.976	1.965	3383G	3328G
V_2O_5–TiO_2 (V/Ti=5/95)	167×10^{-4}cm^{-1} 180G	56×10^{-4}cm^{-1} 61G	93×10^{-4}cm^{-1} 101G	1.922	1.983	1.963	3427G	3324G
V_2O_5–MgO (V/Mg=20/80)	160×10^{-4}cm^{-1} 177G	59×10^{-4}cm^{-1} 64G	93×10^{-4}cm^{-1} 102G	1.936	1.976	1.963	3408G	3339G

$|A_0|$, g_0: calculated values.

Table 2. Summary of the characteristics of various supported V_2O_5 catalysts

Catalyst group	Selectivity to MA (%)	Presence of crystalline V_2O_5	Nature of V^{4+}	
			ESR spectrum	Reactivity to O_2
A	≈0	no	h.f.s.	no
B	10—16	no	singlet (V/Si=5/95) h.f.s. (V/Ti=5/95)	yes
C	30—39	yes	singlet (V/Si≥10/90) singlet+h.f.s. (V/Al, V/Ti≥20/80)	no (h.f.s.) yes (singlet)

Table 3. The amount of V^{4+} formed in V_2O_5–Al_2O_3 catalysts

V/Al atom ratio(—)	Surface area (m^2/g)	V^{4+}formed (spins/g-cat)[a]	V^{4+}/total V(%)	Reactive V^{4+} [b]
0/100	—	0.00	—	0.00
5/95	338	0.71×10^{19}	1.27	neg.
10/90	353	0.67×10^{19}	0.61	neg.
20/80	77	1.55×10^{19}	0.69	0.61×10^{19}
30/70	68	1.15×10^{19}	0.40	0.35×10^{19}
40/60	59	1.42×10^{19}	0.39	0.34×10^{19}
50/50	66	2.80×10^{19}	0.66	0.31×10^{19}

a) Evacuated at 450 °C and 10^{-5} mmHg for 2 h. b) The amount of V^{4+} (spins/g-cat.) decreased on contact with gaseous oxygen (20 mmHg) at 350 °C for 30 min.

oxygen increased suddenly with increase in the content of V_2O_5, reaching a maximum value at V/Al=20/80, decreasing gradually with further increase. The amount is not that of reactive V^{4+} existing on the surface. However, increase in the yield of maleic anhydride with increase in amount also indicates the important role of the reactive V^{4+} in the anhydride formation.

IR Studies on the Reduction and Reoxidation of V_2O_5. The above results reveal that the reactive V^{4+} formed in crystalline V_2O_5 is important for anhydride formation. In order to clarify the kind of lattice oxygen participating in the reduction-oxidation of V_2O_5, unsupported crystalline V_2O_5 was used in IR studies instead of the group C catalysts. Absorption bands were obtained at about 1020 cm^{-1} ($\nu_{V^{5+}=O}$) and 830 cm^{-1} (ν_{V-O-V}).[8-10] Effect of the reduction of this V_2O_5 with a current of hydrogen at 512 °C on the ratio of the peak area of these absorption bands was investigated. Gradual decrease in the ratio with rise in the reduction time was observed, a small lower shift of these bands taking place

Table 4. Change in the ratio of IR absorption peak area ($\nu_{V^{5+}=O}/\nu_{V-O-V}$) with the reduction of unsupported V_2O_5[a]

Reduction time/min	$\nu_{V^{5+}=O}$ / cm^{-1}	ν_{V-O-V} / cm^{-1}	Ratio of the peak area ($\nu_{V^{5+}=O}/\nu_{V-O-V}$)
0	1017	830	—
5	1014	820	0.473
10	1008	825	0.454
15	1005	825	0.403

a) KBr disk technique: Reduction temp: 512 °C, V_2O_5: 0.5 g, Flow rate of hydrogen: *ca.* 50 NTPml/min.

(Table 4). Formation of V^{4+}=O or VO_2 was confirmed by the appearance of a new absorption band at 980 cm^{-1},[8,11] its intensity increasing with increase in reduction time. The results are the same as those reported.[12,13] The original absorption bands were easily recovered by the reoxidation of the reduced V_2O_5 with a current of air at the same temperature. Thus, double bond type lattice oxygen V^{5+}=O in crystalline V_2O_5 is first reduced to give reactive V^{4+} and is recovered by reoxidation.

Effect of the Addition of Alkali Metal Oxide on the Catalytic Activity of Supported V_2O_5 Catalysts. The effect of addition of alkali metal oxide on the formation of maleic anhydride was studied using V_2O_5–Al_2O_3 (V/Al=20/80) and V_2O_5–SiO_2 (V/Si=20/80). The rate of maleic anhydride formation per unit surface area measured by means of a differential reactor was enhanced with a decrease in the electronegativity of the metal ion added (Table 5).

Table 5. Effect of the addition of alkali metal oxide on the catalytic activity of supported V_2O_5 in the oxidation of butadiene

Alkali metal oxide	Electronegativity of alkali metal element[a]	Rate of maleic anhydride formation (g-mol/m^2-cat·h)	
		V_2O_5–Al_2O_3 (V/Al=20/80)[b]	V_2O_5–SiO_2 (V/Si=20/80)[c]
Cs_2O	0.7	5.88×10^{-5}	5.20×10^{-5}
Rb_2O	0.8	3.81×10^{-5}	4.89×10^{-5}
K_2O	0.8	4.89×10^{-5}	4.61×10^{-5}
Na_2O	0.9	3.36×10^{-5}	4.26×10^{-5}
Li_2O	1.0	1.92×10^{-5}	3.98×10^{-5}

a) Pauling. b) Cat.: V/Al=20/80 atom ratio, alkali metal/V=1/100 atom ratio, Reaction temp: 315 °C, Feed: butadiene 1.45 vol% in air. c) Cat.: V/Si=20/80 atom ratio, alkali metal/V=0.5/100 atom ratio, Reaction temp: 340 °C, Feed: butadiene 1.45 vol% in air.

Discussion

The change in catalytic activity of V_2O_5–Al_2O_3 can be attributed not to that in the surface area but to the formation of active species by the addition of V_2O_5 to Al_2O_3 (Table 3). The active species is V^{4+}, which is the case in the other catalysts. However, the results obtained indicate that the nature of V^{4+} formed has strong effect on the selectivity to maleic anhydride formation. The catalysts having reactive V^{4+} had high selectivity to the anhydride, this kind of V^{4+} being formed preferentially in the crystalline V_2O_5 (Tables 2 and 3).

During the catalytic oxidation, V^{5+}=O in the crystalline V_2O_5 is first reduced to give V^{3+} as shown by IR studies (Table 4). The V^{3+} then forms V^{4+} and V^{4+}=O by donation of its one electron to a neighbouring V^{5+}=O, *i.e.*, $V^{3+}+V^{5+}=O\rightarrow V^{4+}+V^{4+}=O$. The V^{4+}=O is further reduced or recovered into original V^{5+}=O when V^{4+} is oxidized to V^{5+}=O. On the reactive V^{4+}, various electronegative oxygen species such as O_2^- and O^- are formed when gaseous oxygen is adsorbed.[14] At elevated temperature, these oxygen species change rapidly to lattice oxygen O^{2-}, instead V^{4+} being oxidized to V^{5+}. The lattice oxygen formed is of double bond type as shown by IR studies on the reoxidation of reduced V_2O_5. The high selectivity of V_2O_5 catalysts forming the reactive V^{4+} strongly suggests a very important role of the negatively charged oxygen species formed by the oxidation of V^{4+}. The reactive V^{4+} plays a role of a precursor which forms the oxygen species.

Generally, the strength of metal-oxygen bond increases in proportion to the electronegativity of metal ion.[15,16] Thus the reactivity of lattice oxygen decreases with rise

in the electronegativity of metal ion. In contrast, the amount of oxygen species adsorbed increases with rise in electronegativity, rate of catalytic oxidation increasing when oxygen species adsorbed is important. This was confirmed by the oxidation of various hydrocarbons over MoO_3,[17] TiO_2,[18] and Bi_2O_3[19] catalysts modified with oxide of 5B group element or of alkali metal. The electronegativity of these metal ion was shown to have changed in proportion to that of the metal ion added. On the analogy of the rsults, it can be expected that the electronegativity of vanadium ion modified with alkali metal oxide is $Li^+>Na^+>K^+>Rb^+>Cs^+$ as a sequence of alkali metal ion added, the reactivity of its lattice oxygen being $Cs^+>Rb^+>K^+>Na^+>Li^+$. Thus, increase in the rate of maleic anhydride formation with decrease in the electronegativity of alkali metal ion (Table 5) strongly supports participation of lattice oxygen rather than the adsorbed oxygen species in maleic anhydride formation over these catalysts. This lattice oxygen is considered to be of double bond type V=O as shown by IR studies. This is in line with the important role of Mo=O in the oxidation of butadiene to maleic anhydride over MoO_3 catalyst[4] and with the special activity of the double bond type lattice oxygen proposed.[10,20-22]

Lattice oxygen of transition metal oxide serves to abstract hydrogen irrespective of the type of metal-oxygen bonding (σ- and double bond one).[20,23] However, the former lattice oxygen is not always incorporated into selective oxidation product.[23] Maleic anhydride is formed from butadiene by the repetition of oxygen addition and hydrogen abstraction.[24,25] Thus, it was considered that V=O is requisite as oxygen species incorporated into the anhydride. Possibly, this lattice oxygen also plays a role of hydrogen abstraction from intermediates leading to maleic anhydride. The oxygen species participating in the complete oxidation over the group A catalysts was not clarified. However, it is apparent that the electronegative oxygen species were hardly formed during the course of catalytic oxidation, as suggested by the unreactivity of V^{4+} to oxygen. Oxygen species participating in maleic anhydride formation over V_2O_5–SiO_2 (V/Si=5/95) seems to be the same as that over the group C catalysts as judged from the similarity in the ESR spectrum of V^{4+}. Those over V_2O_5–TiO_2 (V/Ti=5/95) were not clarified.

Structures of the catalysts are discussed. V^{4+} formed in a cluster has a singlet ESR spectrum and that formed separately a hyperfine structure, the distance between the nearest neighbour V^{4+} being <5 Å in the former V^{4+} and ≈ 9 Å in the latter.[5] Vanadium ions in V_2O_5–MgO (V/Mg$\leq$30/70) are finely dispersed in the carrier whereas V_2O_5 on SiO_2 (V/Si$\geq$5/95) forms cluster. In the case of V_2O_5–Al_2O_3 and V_2O_5–TiO_2, vanadium ions are finely dispersed when the content of V_2O_5 is low (V/Al$\leq$10/90, V/Ti$\leq$5/95). Formation of V_2O_5 cluster takes place with increase in the content, thus giving the spectra made by overlap of these two kinds of ESR spectra. This explanation is in line with the observation of crystalline V_2O_5 by X-ray studies. V^{4+}, which is not oxidized with oxygen, is possibly formed from finely dispersed vanadium ions by a solid-phase reaction when the catalysts were prepared. V^{4+}, on the other hand, formed at the sites where lattice oxygen in V_2O_5 cluster is lost by evacuation, appears to be easily oxidized. The reactive nature of V^{4+} formed in V_2O_5–TiO_2 (V/Ti=5/95) to oxygen irrespective of the hyperfine structure is presumably attributed to a relatively large mobility of lattice oxygen in the titania as compared with the other carriers.

References

1) I. J. Adadurov, *J. Phys. Chem., USSR*, **6**, 206 (1935).
2) P. W. Selwood, "Advances in Catalysis," Vol. 3, Academic Press, New York (1951), p. 28.
3) F. Solymosi, "Catalysis Reviews," Vol. 1, Marcel Dekker Inc., New York (1968), p. 233.
4) M. Akimoto and E. Echigoya, *J. Catal.*, **29**, 191 (1973).
5) H. Takahashi, M. Shiotani, H. Kobayashi, and J. Sohma, *J. Catal.*, **14**, 134 (1969).
6) H. G. Hecht and T. S. Johnstone, *J. Chem. Phys.*, **46**, 23 (1967).
7) B. Bleaney, *Phil. Mag.*, **42**, 441 (1951).
8) L. D. Frederickson and D. M. Hansen, *Anal. Chem.*, **35**, 818 (1963).
9) B. E. Zeitsev and I. I. Ioffe, *Kinet. Katal.*, **7**, 755 (1966).
10) Y. Kera and K. Hirota, *J. Phys. Chem.*, **73**, 3973 (1969).
11) M. E. Brown and B. V. Sewart, *J. Thermal. Anal.*, **2**, 287 (1970).
12) S. Hasegawa, N. Miyazawa, S. Kitamori, and T. Kawaguchi, *Nippon Kagaku Kaishi*, **1975**, 246.
13) A. Miyamoto, Y. Yamazaki, and Y. Murakami, *Nippon Kagaku Kaishi*, **1977**, 619 (1977).
14) V. A. Shvets and V. B. Kazansky, *Kinet. Katal.*, **10**, 356 (1969): *J. Catal.*, **25**, 123 (1972).
15) A. F. Clifford, *J. Am. Chem. Soc.*, **79**, 5404 (1957); *J. Phys. Chem.*, **63**, 1227 (1959).
16) Y. Moro-oka, Y. Morikawa, and A. Ozaki, *J. Catal.*, **7**, 23 (1967).
17) M. Akimoto and E. Echigoya, *J. Catal.*, **35**, 278 (1974).
18) M. Akimoto and E. Echigoya, *J. Chem. Soc., Faraday Trans. 1*, **73**, 193 (1977).
19) M. Akimoto, K. Ichikawa, and E. Echigoya, *Nippon Kagaku Kaishi*, **1977**, 320.
20) F. Trifiro and I. Pasquon, *J. Catal.*, **12**, 412 (1968).
21) K. Tarama, S. Teranishi, and S. Yoshida, Proc. 3rd Int. Congr. Catal., Vol. 1, 3rd ed, North-Holland, Amsterdam (1964), p. 282.
22) K. Hirota, Y. Kera, and S. Teratani, *J. Phys. Chem.*, **72**, 3133 (1968).
23) T. Seiyama, M. Egashira, T. Sakamoto, and I. Aso, *J. Catal.*, **24**, 76 (1972); H. E. Swift, J. E. Bozik, and J. A. Ondrey, *J. Catal.*, **21**, 212 (1971) *etc.*
24) M. Ai, K. Harada, and S. Suzuki, *Kogyo Kagaku Zasshi*, **73**, 524 (1970).
25) M. Akimoto and E. Echigoya, *Bull. Chem. Soc. Jpn.*, **48**, 3518 (1975).

The Crystal and Molecular Structure of *N*-Carboxy-γ-benzyl-L-glutamate Anhydride

Hitoshi KANAZAWA,* Tohru KAWAI, Yuji OHASHI,** and Yoshio SASADA**

Department of Polymer Technology, Tokyo Institute of Technology, O-okayama, Meguro-ku, Tokyo 152
***Laboratory of Chemistry for Natural Products, Tokyo Institute of Technology, Nagatsuta, Midori-ku, Yokohama 227*

(Received January 26, 1978)

The structure of *N*-carboxy-γ-benzyl-L-glutamate anhydride has been determined by X-ray analysis. The crystal is orthorhombic; space group, $P2_12_12_1$; $Z=4$ with $a=7.766(1)$, $b=27.470(4)$, and $c=5.948(1)$ Å. The structure was deduced by the direct method and refined to a final R value of 0.057 for 1504 observed reflections by the block-diagonal least-squares method. The hydrogen bond is formed between the imino group and the carbonyl group of the side chain. The dimension of the five-membered ring is affected by the intermolecular hydrogen bond as compared with the crystal structures of the other *N*-carboxy anhydrides of α-amino acid.

The *N*-carboxy anhydrides of α-amino acids (amino acid NCAs) are often used for the syntheses of polypeptides. The polymerization mechanism differs with the kind of initiator. When a primary amine is used as an initiator, polymerization is considered to proceed as follows,[1] the first step being the formation of an amino acid derivative by interaction of the NCA and the initiator.

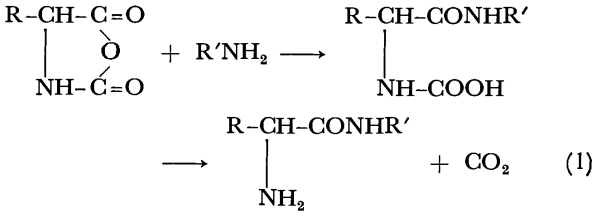

The amino acid derivative formed in (1) can react successively with amino acid NCA in a similar manner, leading to polymeric products. The over-all process is written as follows.

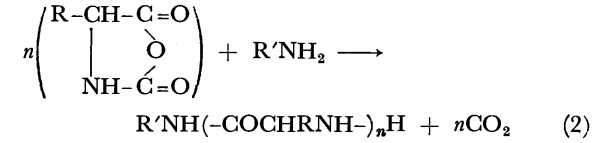

The polymerization of amino acid NCA was carried out not only in the homogeneous system but also in the heterogeneous system and in crystalline state. When butylamine (an initiator) is added into the suspension of the crystals of amino acid NCA in hexane, polymerization occurs in the solid state and a polypeptide of a considerably high molecular weight can be obtained. Polymerizability differs a great deal from that in a heterogeneous system using acetonitrile as a solvent of NCA.[2] In order to interpret the polymerization of amino acid NCAs in the solid state, we have attempted to analyze their crystal structures. In previous studies, the crystal structures of glycine NCA[3] and L-alanine NCA[4] were reported. This paper deals with the crystal structure of γ-benzyl-L-glutamate NCA, which is most extensively used for the study of synthetic polypeptides.

Experimental

γ-Benzyl-L-glutamate NCA (BLG NCA) was synthesized in the same way as that for glycine NCA, and purified by crystallization with ethyl acetate–hexane several times. BLG NCA thus obtained (about 100 mg) was dissolved in an appropriate vessel with 5 ml of ethyl acetate. The vessel was placed in a covered bottle containing hexane and allowed to stand at room temperature for a few days. Colorless plate crystals were obtained. The unit-cell dimensions were determined by the least-squares refinement with 25 high-angle reflections. The crystal data are summarized in Table 1.

Table 1. Crystal data

$C_{13}NO_5H_{13}$	Space group: $P2_12_12_1$
$M.W.$: 263	$Z=4$
Orthorhombic	$D_x=1.40$ g·cm^{-3}
$a=7.766(1)$ Å	$D_m=1.38$ g·cm^{-3}
$b=27.470(4)$	μ(Mo $K\alpha$)$=1.30$ cm^{-1}
$c=5.948(1)$	
$U=1268.9(4)$ Å^3	

With use of a $0.3\times0.4\times0.4$ mm crystal, intensity data up to $2\theta=55°$ were collected on a Rigaku four-circle diffractometer with graphite monochromated Mo $K\alpha$ radiation. The usual ω-2θ scan technique was employed with a scan speed 4° (2θ)min^{-1}. A total of 1735 independent reflections were obtained, in which 231 with $|F_o|<3\sigma(|F_o|)$ were regarded as zero reflections. The usual Lorentz and polarization corrections were made. Absorption was uncorrected.

Structure Determination

The structure was determined by the direct method using the program MULTAN. Refinement of the structure was carried out by the block-diagonal least-squares method. After several cycles of refinement, two strong reflections, 020 and 060, were excluded since they seem to undergo secondary extinction. All the hydrogen atoms were revealed on a difference map. The final refinement was performed including these hydrogen atoms with isotropic temperature factors. The weighting scheme: $w=0.25$ for $|F_o|<1.95$ and $|F_o|>15.62$, and $w=(5.959-1.127|F_o|+0.0642|F_o|^2)^{-1}$ for the other reflections. The final R value became 0.057 for all the non-zero reflections. In the final stage, no peaks higher than 0.2 eÅ^{-3} were found on the difference map. The atomic scattering factors were taken from "International Tables for X-Ray Crystallography."[5] The final atomic parameters and their standard devia-

Table 2. Final atomic coordinates and thermal parameters for γ-benzyl-L-glutamate NCA with their estimated standard deviations

Anisotropic thermal parameters ($\times 10^5$) are in the form: $\exp\{-(B_{11}h^2+B_{22}k^2+B_{33}l^2+B_{12}hk+B_{13}hl+B_{23}kl)\}$.

Atom	x	y	z	B_{11}	B_{22}	B_{33}	B_{12}	B_{13}	B_{23}
C(1)	0.4302(4)	0.2372(1)	0.1049(5)	1443(55)	126(4)	1930(84)	1(3)	89(127)	163(32)
C(2)	0.2635(3)	0.2530(1)	0.4070(5)	1207(47)	82(3)	1988(77)	46(2)	−230(116)	106(31)
C(3)	0.2523(3)	0.1989(1)	0.3630(4)	1057(46)	83(3)	1740(75)	−53(2)	−107(112)	6(28)
C(4)	0.3077(4)	0.1702(1)	0.5698(5)	1448(54)	84(3)	1776(76)	6(2)	−136(126)	125(29)
C(5)	0.3144(4)	0.1153(1)	0.5284(5)	1789(61)	86(4)	2213(88)	−8(3)	−440(138)	56(31)
C(6)	0.3813(4)	0.0888(1)	0.7299(5)	1572(54)	84(3)	2535(91)	3(2)	186(142)	155(32)
C(7)	0.4930(5)	0.0149(1)	0.8678(6)	2589(82)	119(5)	2505(106)	294(3)	25(171)	175(37)
C(8)	0.5531(4)	−0.0340(1)	0.7847(6)	1664(59)	81(4)	2864(104)	−23(2)	95(146)	287(33)
C(9)	0.6522(5)	−0.0614(1)	0.9291(7)	2319(80)	113(4)	3998(134)	54(3)	−1689(204)	40(44)
C(10)	0.7050(5)	−0.1078(1)	0.8708(7)	2399(80)	112(4)	5278(170)	274(3)	−2123(224)	180(48)
C(11)	0.6611(5)	−0.1272(1)	0.6674(7)	2251(81)	96(4)	4855(152)	135(3)	151(212)	−67(44)
C(12)	0.5623(5)	−0.1005(1)	0.5230(7)	3164(98)	132(5)	3573(124)	192(4)	−480(214)	230(45)
C(13)	0.5080(5)	−0.0538(1)	0.5815(6)	2871(87)	126(5)	3110(119)	235(3)	−1051(196)	20(42)
N(1)	0.3655(3)	0.1945(1)	0.1706(4)	1637(46)	91(3)	1565(61)	40(2)	311(109)	−124(25)
O(1)	0.5216(3)	0.2473(1)	−0.0494(4)	2246(51)	195(4)	2761(81)	−103(3)	1850(117)	353(33)
O(2)	0.3727(3)	0.2735(1)	0.2533(3)	1439(35)	87(2)	2493(61)	−57(2)	275(91)	156(23)
O(3)	0.1968(3)	0.2765(1)	0.5499(4)	2040(46)	98(3)	2639(67)	123(2)	855(106)	−179(26)
O(4)	0.3992(4)	0.1053(1)	0.9147(4)	3690(66)	102(3)	2148(64)	362(2)	−556(132)	−61(24)
O(5)	0.4221(3)	0.0426(1)	0.6818(4)	2550(54)	83(3)	2450(64)	208(2)	−606(116)	70(23)

Table 3. Final atomic coordinates and thermal parameters B(Å^2) for the H atoms with their estimated standard deviations

Atom	x	y	z	B
H(1)	0.382(4)	0.166(1)	0.097(5)	4.6(7)
H(2)	0.138(3)	0.192(1)	0.329(4)	2.6(5)
H(3)	0.418(4)	0.182(3)	0.616(4)	3.0(6)
H(4)	0.231(4)	0.177(1)	0.694(5)	4.5(7)
H(5)	0.200(4)	0.104(1)	0.499(6)	6.2(9)
H(6)	0.399(4)	0.110(1)	0.408(6)	6.2(9)
H(7)	0.398(4)	0.011(1)	0.968(5)	4.5(7)
H(8)	0.589(4)	0.034(1)	0.938(6)	5.6(8)
H(9)	0.688(4)	−0.046(1)	1.078(6)	5.5(8)
H(10)	0.783(4)	−0.124(1)	0.964(6)	7.4(10)
H(11)	0.702(5)	−0.161(1)	0.614(6)	7.3(10)
H(12)	0.541(4)	−0.112(1)	0.376(6)	7.5(10)
H(13)	0.451(4)	−0.038(1)	0.473(7)	6.7(9)

tions for non-hydrogen atoms and hydrogen atoms are given in Tables 2 and 3, respectively. A list of the observed and calculated structure factors is kept in the office of the Chemical Society of Japan (Document No. 7821). Computation was carried out on the HITAC 8700 computer at this Institute.

Description of the Structure

Bond distances and angles are shown in Fig. 1, together with the numbering system. The dimensions involving hydrogen atoms are given in Table 4. There is a significant difference between the distances of C(1)–O(2) and C(2)–O(2) in the *N*-carboxy anhydride ring (NCA ring). This feature is similar to that of L-alanine NCA[4] but differs from that of glycine NCA[3] and L-leucine NCA,[6] in which C(1)–O(2) has nearly the same distance as C(2)–O(2). The other bond distances, C(2)–C(3), C(1)–N(1), and C(3)–N(1), are comparable to the corresponding lengths in glycine NCA, L-alanine NCA, and L-leucine NCA. The characteristic dimensions in the NCA ring of the present compound are discussed in detail and compared with those of the other amino acid NCAs. The fluctuation of the distances in the benzene ring can be explained by the thermal vibration around C(8)–C(11).

Table 4. Bond lengths and angles involving hydrogen atoms in γ-benzyl-L-glutamate NCA

The estimated standard deviations are 0.03—0.04 Å in distances and 2—3° in angles.

Bond lengths (l/Å)			
N(1)–H(1)	0.91	C(7)–H(8)	1.00
C(3)–H(2)	0.93	C(9)–H(9)	1.02
C(4)–H(3)	0.96	C(10)–H(10)	0.93
C(4)–H(4)	0.97	C(11)–H(11)	1.03
C(5)–H(5)	0.96	C(12)–H(12)	0.95
C(5)–H(6)	0.99	C(13)–H(13)	0.90
C(7)–H(7)	0.95		

Bond angles (ϕ/°)			
C(1)–N(1)–H(1)	124	C(4)–C(5)–H(5)	109
C(3)–N(1)–H(1)	123	C(6)–C(5)–H(6)	106
C(2)–C(3)–H(2)	107	C(8)–C(7)–H(7)	111
N(1)–C(3)–H(2)	113	O(5)–C(7)–H(8)	109
C(3)–C(4)–H(4)	110	C(11)–C(12)–H(12)	120
H(3)–C(4)–H(4)	106	C(10)–C(11)–H(11)	123
C(4)–C(5)–H(6)	107	C(8)–C(13)–H(13)	124
H(5)–C(5)–H(6)	116	C(8)–C(7)–H(8)	112
C(3)–C(4)–H(3)	108	H(7)–C(7)–H(8)	112
C(5)–C(4)–H(3)	111	C(10)–C(9)–H(9)	122
C(6)–C(5)–H(5)	108	C(11)–C(10)–H(10)	120
O(5)–C(7)–H(7)	104	C(12)–C(11)–H(11)	117
C(5)–C(4)–H(4)	109	C(12)–C(13)–H(13)	115
		C(13)–C(12)–H(12)	120

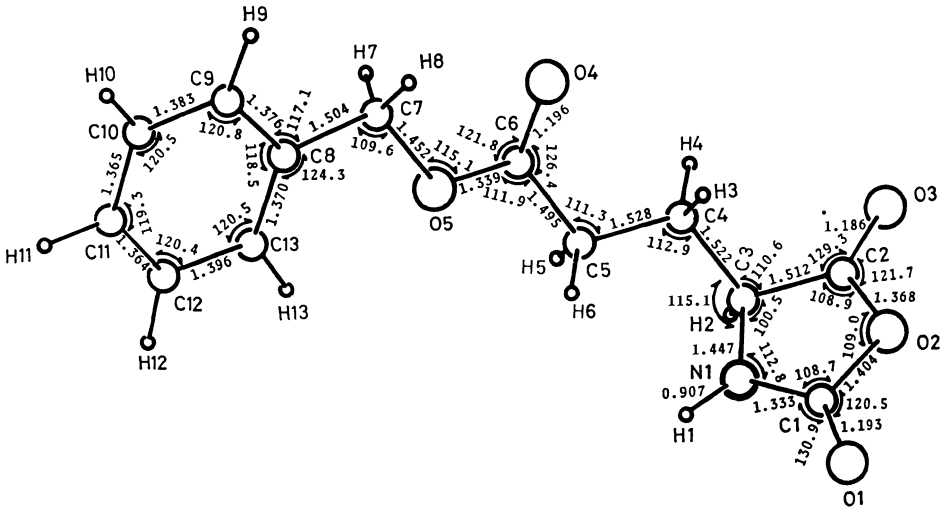

Fig. 1. A perspective view of γ-benzyl-L-glutamate NCA along the c axis with the numbering of the atoms, bond lengths(l/Å), and angles(ϕ/°). The estimated standard deviations are 0.004—0.006Å in distances and 0.2—0.4° in angles.

The equations of the least-squares planes, plane I through the NCA ring, plane II through the carbonyl group and plane III through the benzene ring, are given in Table 5, together with the deviations of the atoms from the planes. Three oxygen atoms, O(1), O(2), and O(3) deviate distinctly from plane I. This is also the case in the other amino acid NCA crystals. Plane I makes angles of 56.8 and 69.7° with planes II and III, respectively. Plane II makes an angle of 13.0° with plane III.

Conformations of the side chain by Newman projections are shown in Fig. 2. Both of the conformations about C(4)–C(3) and C(5)–C(4) are trans.

A stereoscopic view of the crystal structure is shown in Fig. 3. The hydrogen bond (broken lines) is formed between N(1)–H(1)···O(4′). The length of N(1)···O(4′)

TABLE 5. EQUATION OF THE LEAST-SQUARES PLANES AND THE DEVIATIONS OF ATOMS FROM THE PLANES

Coordinates X, Y, Z are in Å referred to a, b, and c.

Plane I: $-0.7834X+0.1448Y-0.6044Z+2.0546=0$	
Atom	Deviation
C(1)	0.005
C(2)	−0.004
C(3)	0.007
N(1)	−0.008
*O(1)	0.044
*O(2)	−0.035
*O(3)	−0.019
*H(1)	0.043
*C(4)	−1.188
Plane II: $-0.9305X-0.2835Y+0.2322Z+2.4389=0$	
Atom	Deviation
C(5)	−0.000
C(6)	0.001
O(4)	−0.001
O(5)	−0.000
Plane III: $-0.8289X-0.3821Y+0.4087Z+1.2926=0$	
Atom	Deviation
C(8)	−0.002
C(9)	−0.001
C(10)	0.004
C(11)	−0.004
C(12)	0.001
C(13)	0.002
*C(7)	0.074

*Atoms not included in the least-squares caluculations.

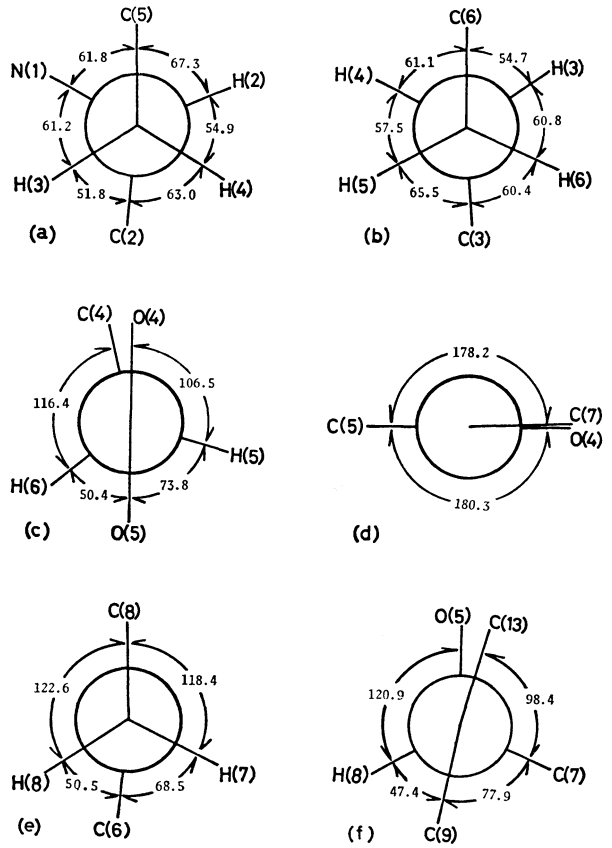

Fig. 2. Newman projection along the bonds of (a) C(4)–C(3), (b) C(5)–C(4), (c) C(6)–C(5), (d) O(5)–C(6), (e) C(7)–O(5), and (f) C(8)–C(7) in the side chain.

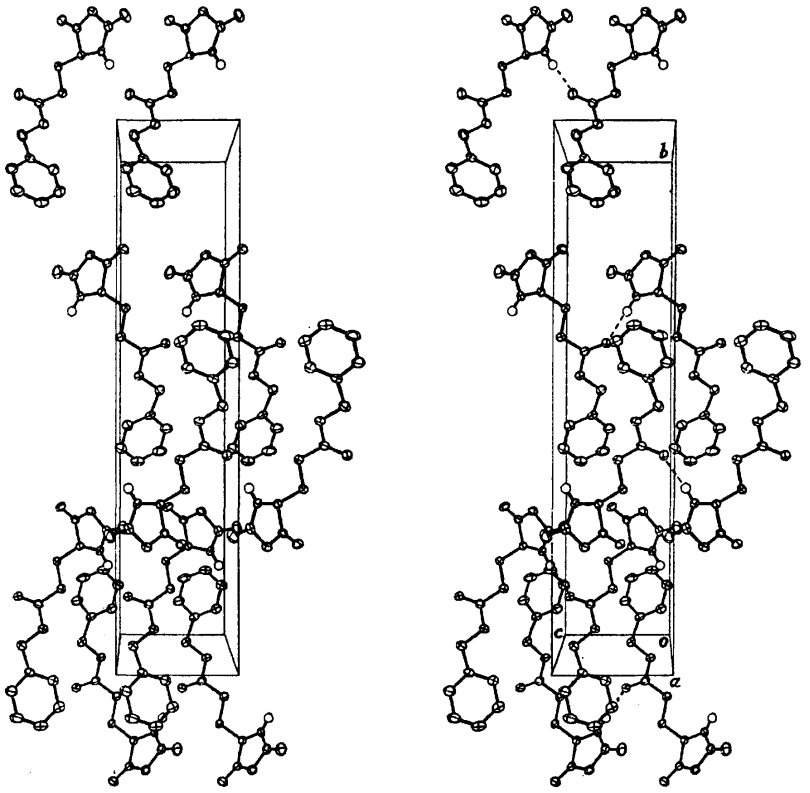

Fig. 3. Stereoscopic drawing of the crstal structure of γ-benzyl-L-glutamate NCA viewed along the a axis. The thermal ellipsoids are drawn at 50% probability level. Hydrogen atoms are omitted for clarity except for H(1) with circles. Hydrogen bond are shown by broken lines.

and the angle of N(1)–H(1)···O(4′) are 2.898(4) Å and 174(3)°, respectively. This type of hydrogen bond is in marked contrast to that in the crystals of the other amino acid NCAs, in which the oxygen atom of either carbonyl group in the NCA ring participates in the hydrogen bond. There is no unusually short contact among the other intermolecular distances.

Discussion

The bond distances in the NCA rings of four amino acid NCAs are given in Table 6. A significant difference in the distances C(1)–O(2) and C(2)–O(2) is seen among these compounds. In glycine NCA and L-leucine NCA, the distances of two bonds are similar to each other. On the other hand, C(1)–O(2) is significantly greater than C(2)–O(2) in L-alanine NCA and BLG NCA. The difference in L-alanine NCA is more distinct than that in BLG NCA. It is plausible that the difference is caused by the hydrogen bond in the crystalline state.

The hydrogen bonds of these amino acid NCA crystals are divided into three types:

(1) N(1)–H(1)···O(1′) as observed in glycine NCA and L-leucine NCA,

(2) N(1)–H(1)···O(3′) in L-alanine NCA,

(3) N(1)–H(1)···O(4′) in BLG NCA.

Since no oxygen atoms of carbonyl groups in the NCA ring form the hydrogen bond with N(1)–H(1) in BLG NCA, it is reasonable to take the dimensions of this NCA ring as the standard ones.

It was pointed out by Leiserowitz and Nader[7] that the oxygen atom of the amide group is more negative than that of the carbonyl group in the amide-dicarboxylic acid complexes. This implies that the limiting structure (II), shown in Fig. 4, might contribute to the resonance state in the NCA ring. However, in BLG NCA, C(2)–O(2) is shorter than C(1)–O(2), C(1)–O(1) having the same distance as C(2)–O(3). This suggests that the limiting structures (II) and (IV), which is given in a simplified form by (V), should contribute to the state in the NCA moiety.

Table 6. Comparison of the bond distances (Å) in the four NCAs
Estimated standard deviations are in parentheses.

NCA	C(1)–O(2)	C(2)–O(2)	C(2)–C(3)	C(1)–N(1)	C(3)–N(1)	C(1)–O(1)	C(2)–O(3)
Glycine	1.394(2)	1.381(2)	1.502(3)	1.326(3)	1.449(3)	1.212(3)	1.188(2)
L-Alanine	1.412(5)	1.354(4)	1.514(5)	1.327(5)	1.449(5)	1.203(5)	1.188(5)
L-Leucine	1.394(5)	1.380(5)	1.490(5)	1.319(5)	1.456(5)	1.199(5)	1.194(5)
BLG	1.404(4)	1.368(4)	1.512(4)	1.333(4)	1.447(4)	1.193(4)	1.186(4)

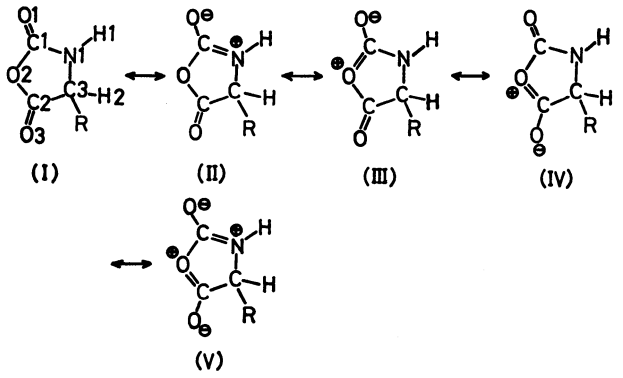

Fig. 4. The limiting canonical structures.

When O(1) forms the hydrogen bond with N(1)–H(1) as observed in glycine NCA and L-leucine NCA, the limiting structure (III) could contribute to the resonance state, on the assumption that the negative charge is attracted to the N–H···O hydrogen bond. In the glycine NCA and L-leucine NCA crystals, C(1)–O(2) is shorter and C(2)–O(2) is longer than the corresponding ones in BLG NCA. When O(3) forms the hydrogen bond with N(1)–H(1), the limiting structure (IV) would contribute for the same reason. In L-alanine NCA, C(1)–O(2) is longer and C(2)–O(2) shorter than the corresponding bonds in BLG NCA.

As for the C–O distances of carbonyl group and the N–C length, the difference is made obscure owing to the contribution of the limiting structure (II), except for the C–O distances in glycine NCA.

In the course of the polymerization process, the bonds of C(2)–O(2) and C(1)–N(1) are cleaved to release CO_2. Since the limiting structure (III) contributes to the resonance state in glycine NCA and L-leucine NCA, it is quite adequate to consider that the C(2)–O(2) bond of these amino acid NCAs should be more easily cleaved than that of the other amino acid NCAs. Contrary to such expectation, glycine NCA shows very low reactivity in the crystalline state, although the crystal of L-leucine NCA is observed to have the highest polymerizability.[2] This implies that the other factors should be taken into account. In the succeeding paper,[6] the effect of the crystalline field will be discussed.

References

1) C. H. Bamford, A. Elliot, and W. H. Hanby, "Synthetic Polypeptides," Academic Press, New York (1956), p. 62.
2) H. Kanazawa and T. Kawai, to be published.
3) H. Kanazawa, Y. Matsuura, N. Tanaka, M. Kakudo, T. Komoto, and T. Kawai, *Bull. Chem. Soc. Jpn.*, **49**, 954 (1976).
4) H. Kanazawa, Y. Matsuura, N. Tanaka, M. Kakudo, T. Komoto, and T. Kawai, *Acta Crystallogr., Sect. B*, **32**, 78 (1976).
5) "International Tables for X-Ray Crystallogaphy," Vol. IV, The Kynoch Press, Birmingham (1974), p. 72.
6) H. Kanazawa, T. Kawai, Y. Ohashi, and Y. Sasada, *Bull. Chem. Soc. Jpn.*, **51**, 2208 (1978).
7) L. Leiserowitz and F. Nader, *Acta Crystallogr., Sect. B*, **32**, 2719 (1977).

The Crystal and Molecular Structure of *N*-Carboxy-L-leucine Anhydride at −70 °C

Hitoshi KANAZAWA,* Tohru KAWAI, Yuji OHASHI,** and Yoshio SASADA**

Department of Polymer Technology, Tokyo Institute of Technology, O-okayama, Meguro-ku, Tokyo 152

***Laboratory of Chemistry for Natural Products, Tokyo Institute of Technology, Nagatsuta, Midori-ku, Yokohama 227*

(Received January 26, 1978)

The crystal structure of *N*-carboxy-L-leucine anhydride has been determined by means of X-ray. The crystal is orthorhombic; space group, $P2_12_12_1$; $Z=4$ with $a=6.527(1)$, $b=23.920(4)$, and $c=5.527(1)$ Å. The structure was deduced by the direct method and refined to the final R value 0.049 for 624 observed reflections by the block-diagonal least-squares method. The *N*-carboxy anhydride rings are arranged in a layer form sandwiched by hydrophobic side chains. The highest polymerizability of this compound in the crystalline state is due to the sandwich structure.

The *N*-carboxy anhydrides of α-amino acids (amino acid NCAs) are the most useful for preparing polypeptides with high degree of polymerization. Serial crystal structures of amino acid NCAs[1-3] were reported for interpreting their polymerization in the crystalline state. Of the various amino acid NCAs, the title compound is the most reactive in the solid state, polymerizing more rapidly in the crystalline state than in the heterogeneous system using acetonitrile as the solvent of NCA.[4] In a previous paper,[3] we proposed that the charge distribution of the five-membered ring of the amino acid NCA affects its polymerizability. However, this factor alone is not sufficient to explain the high reactivity. We have examined other factors, especially the crystalline field.

Experimental

The title compound was synthesized in the same way as glycine NCA,[1] and purified by recrystallization several times with ethyl acetate–hexane and diisopropyl ether–hexane. L-Leucine NCA thus obtained (*ca.* 100 mg) was dissolved in an appropriate vessel with 20 ml of diisopropyl ether. The vessel was placed in a covered bottle containing hexane and allowed to stand overnight at about 6 °C. Colorless rod-like crystals suitable for X-ray work were obtained.

Since the crystal decomposes easily owing to polymerization at room temperature, data collection was carried out at −70 °C, using a cooling equipment with liquid nitrogen. The unit cell dimensions were determined by the least-squares refinement with 25 high-angle reflections at −70 °C and room temperature. The crystal data are summarized in Table 1.

TABLE 1. CRYSTAL DATA OF L-LEUCINE NCA AT −70 °C (a) AND AT ROOM TEMPERATURE 20 °C (b)

(a)	(b)
$C_7NO_3H_{11}$	
M.W.: 157	
Orthorhombic	
$a=6.527(1)$ Å	$a=6.518(4)$ Å
$b=23.920(4)$	$b=23.983(14)$
$c=5.527(1)$	$c=5.531(5)$
$U=862.9(3)$ Å^3	$U=864.7(11)$ Å^3
Space group: $P2_12_12_1$	
$Z=4$	
$D_x=1.21$ g·cm^{-3}	$D_x=1.21$ g·cm^{-3}
$D_m=\cdots$	$D_m=1.21$ g·cm^{-3}
μ(Mo $K\alpha$)$=1.13$ cm^{-1}	

The intensities for the reflections with $2\theta\leqq 40°$ were collected on a Rigaku automated diffractometer with graphite monochromated Mo $K\alpha$ radiation. The usual ω-2θ scan technique was employed with a scan speed $4°(2\theta)\text{min}^{-1}$. A total of 693 reflections were observed, in which 69 with $|F_o|<3.0\sigma(|F_o|)$ were considered as zero reflections. The usual Lorentz and polarization corrections were made. Absorption was uncorrected.

Structure Determination

The structure was determined by the direct method using the program MULTAN. Refinement of the structure was carried out by the block-diagonal least-squares method. All the hydrogen atoms were revealed on a difference map. The final refinement was performed including these hydrogen atoms with isotropic temperature factors. The weighting scheme, $w=0.3$ for $|F_o|<2.52$ and $|F_o|>37.75$, and $w=(4.0476-0.3027|F_o|+0.00758|F_o|^2)^{-1}$ for the other reflections. The final R value became 0.049 for all the non-zero reflections. At the final stage, no peaks higher than 0.11 eÅ^{-3} were found on the difference map. The atomic scattering factors were taken from "International Tables for X-Ray Crystallography."[5] The final atomic parameters and their standard deviations are given in Table 2. A list of the observed and calculated structure factors is kept in the office of the Chemical Society of Japan (Document No. 7822). Computation was carried out on the HITAC 8700 computer at this institute.

Description of the Structure

The bond lengths and angles and the numbering of the atoms are shown in Fig. 1. The distances of C(1)–O(2) and C(2)–O(2) are in good agreement with the corresponding ones in glycine NCA and distinct from the corresponding ones in L-alanine NCA and γ-benzyl-L-glutamate NCA (BLG NCA). Other bond distances in the five-membered ring are close to the corresponding ones in these three NCAs. The C(4)–C(5) and C(5)–C(6) bonds are slightly shorter probably due to ignoring of the high-angle reflections. The angles in the five-membered ring are also in good agreement with the corresponding ones of the other three NCAs. The bond lengths and angles involving the hydrogen atoms are

TABLE 2. FINAL ATOMIC COORDINATES AND THERMAL PARAMETERS FOR L-LEUCINE NCA WITH THEIR ESTIMATED STANDARD DEVIATIONS

The anisotropic thermal parameters ($\times 10^5$) are in the form: $\exp\{-(B_{11}h^2+B_{22}k^2+B_{33}l^2+B_{12}hk+B_{13}hl+B_{23}kl)\}$.

Atom	x	y	z	B_{11}(or B)	B_{22}	B_{33}	B_{12}	B_{13}	B_{23}
C(1)	0.4151(6)	0.2272(1)	0.2778(7)	4919(144)	192(7)	3808(153)	−376(57)	1809(310)	−277(64)
C(2)	0.3703(6)	0.1577(1)	0.5481(7)	3712(120)	259(8)	3830(157)	−328(58)	1555(287)	4(66)
C(3)	0.1946(5)	0.1548(1)	0.3764(7)	2670(99)	202(7)	3190(131)	−12(47)	727(249)	111(57)
C(4)	0.1755(5)	0.0979(1)	0.2562(7)	2632(98)	174(6)	4215(152)	39(44)	581(257)	−7(59)
C(5)	0.0003(6)	0.0934(1)	0.0779(7)	2756(93)	209(7)	5716(197)	−113(56)	−640(316)	−34(69)
C(6)	−0.2078(6)	0.1041(2)	0.1873(11)	2636(116)	427(12)	11067(345)	−155(69)	−250(424)	−394(127)
C(7)	0.0031(8)	0.0353(1)	−0.0458(10)	5538(163)	239(9)	8418(273)	−387(76)	−3956(488)	−560(87)
N(1)	0.2482(5)	0.2001(1)	0.2119(5)	4016(94)	159(5)	3739(120)	−273(44)	−370(230)	−70(49)
O(1)	0.5001(5)	0.2669(1)	0.1909(5)	7020(117)	228(5)	6715(143)	−1225(48)	4732(322)	−215(51)
O(2)	0.4933(4)	0.2024(1)	0.4863(5)	3998(79)	319(5)	4713(103)	−815(45)	−29(218)	−350(50)
O(3)	0.4119(5)	0.1282(1)	0.7150(5)	5211(102)	425(7)	4373(122)	−448(51)	−1415(239)	662(57)
H(1)	0.162(6)	0.211(1)	0.084(7)	10.6(11)					
H(2)	0.081(4)	0.167(1)	0.468(6)	5.5(7)					
H(3)	0.304(5)	0.089(1)	0.174(7)	8.0(9)					
H(4)	0.145(5)	0.068(1)	0.407(5)	7.2(8)					
H(5)	0.021(5)	0.122(1)	−0.053(6)	6.7(8)					
H(6)	−0.343(6)	0.091(1)	0.088(7)	11.5(11)					
H(7)	−0.197(5)	0.084(1)	0.342(7)	8.9(9)					
H(8)	−0.200(5)	0.145(1)	0.243(7)	8.6(9)					
H(9)	−0.129(6)	0.038(1)	−0.163(8)	11.5(12)					
H(10)	−0.019(6)	0.005(1)	0.105(6)	9.6(10)					
H(11)	0.146(6)	0.026(1)	−0.089(7)	11.6(13)					

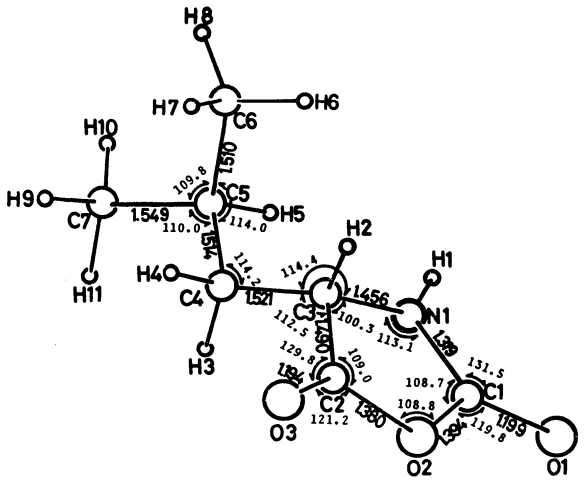

Fig. 1. A perspective drawing of L-leucine NCA viewed along the c axis with the numbering of the atoms, the bond distances (l/Å) and angles (ϕ/°). The estimated standard deviations are 0.004—0.006Å in distances and 0.2—0.4° in angles.

given in Table 3.

Both conformations around C(3)–C(4) and C(4)–C(5) are of stable staggered forms (Fig. 2).

The mean plane consisting of four atoms, C(1), C(2), C(3), and N(1), and the deviations of the atoms from the plane are given in Table 4. The three oxygen atoms, O(1), O(2), and O(3), are significantly displaced from the plane. These features are close to those of the other NCAs.

A stereoscopic drawing of the crystal structure viewed along the c axis is shown in Fig. 3. The hydrogen bonds, N(1)–H(1)···O(1′), connect the molecules to form a ribbon along the a axis (broken lines). The distance of N(1)···O(1′) and the angle of N(1)–H(1)···O(1′) are 2.864(5) Å and 176(3)°, respectively. The ribbons are stacked along the c axis. A pile of ribbons looks like a hydrophilic layer of the five-membered rings sandwiched by hydrophobic side chain layers. These sandwiches are in contact with each other at $y=0$ and $y=1/2$. This

TABLE 3. BOND LENGTHS (l/Å) AND ANGLES (ϕ/°) INVOLVING HYDROGEN ATOMS

The standard deviations are 0.03—0.04 Å in lengths and 2—3° in angles.

Bond lengths			
N(1)–H(1)	0.94	C(6)–H(7)	0.99
C(3)–H(2)	0.95	C(6)–H(8)	1.02
C(4)–H(3)	0.98	C(7)–H(9)	1.08
C(4)–H(4)	1.12	C(7)–H(10)	1.12
C(5)–H(5)	1.01	C(7)–H(11)	0.99
C(6)–H(6)	1.09		
Bond angles			
C(1)–N(1)–H(1)	125	C(5)–C(6)–H(6)	119
C(3)–N(1)–H(1)	122	C(5)–C(6)–H(7)	102
C(2)–C(3)–H(2)	104	C(5)–C(6)–H(8)	104
C(4)–C(3)–H(2)	116	H(6)–C(6)–H(7)	111
N(1)–C(3)–H(2)	107	H(6)–C(6)–H(8)	117
C(3)–C(4)–H(3)	109	H(7)–C(6)–H(8)	102
C(3)–C(4)–H(4)	106	C(5)–C(7)–H(9)	101
C(5)–C(4)–H(3)	109	C(5)–C(7)–H(10)	105
C(5)–C(4)–H(4)	108	C(5)–C(7)–H(11)	108
H(3)–C(4)–H(4)	111	H(9)–C(7)–H(10)	113
C(4)–C(5)–H(5)	109	H(9)–C(7)–H(11)	128
C(6)–C(5)–H(5)	107	H(10)–C(7)–H(11)	99
C(7)–C(5)–H(5)	108		

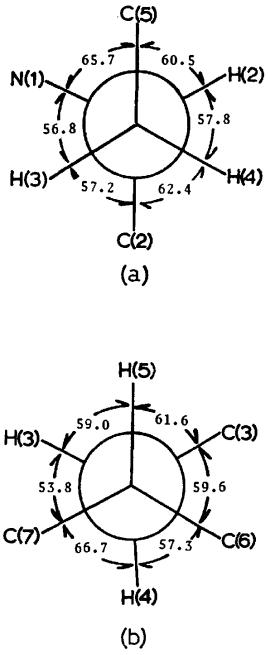

Fig. 2. Newman projection along the bonds (a) C(4)–C(3) and (b) C(5)–C(4).

explains the fact that polymerization cannot proceed along the b axis, the cleavage plane of the crystal being perpendicular to the b axis.

Discussion

The hydrogen bonding schemes differ for the four amino acid NCA crystals so far determined. The distances and angles are summarized in Table 5. The hydrogen bonds are fairly strong.[6] In the crystal of glycine NCA, the molecules form dimers through two hydrogen bonds around the center of symmetry. In the crystals of L-alanine NCA, L-leucine NCA and BLG NCA, the hydrogen bonds extend as linear chains along the b, a, and c axes, respectively.

When the amino acid NCA molecules polymerize progressively, N(1) should attack the C(2) atom of the neighboring molecule nucleophilically.[7] This indicates that in the crystal the C(2) atom of the amino acid NCA molecule contiguous to the terminal amino group of the polymer comes close to the amino group. The distance of the movement required to make a bond is 2.0—5.0 Å for these amino acid NCA crystals.

The dimer structure, as found in the glycine NCA crystal, is unfavorable for progressive polymerization, since two hydrogen bonds should be broken or two molecules as a dimer should move in the crystal. Low reactivity was thus observed for the glycine NCA crystal.

Table 4. The equation of the least-squares plane

Equation	Atom	Deviation/Å
$0.5342X-0.6218Y-0.5727Z$	C(1)	−0.012
$+2.799=0$	C(2)	0.010
$(X=ax,\ Y=by,\ Z=cz)$	C(3)	−0.017
	N(1)	0.019
	*O(1)	−0.030
	*O(2)	−0.030
	*O(3)	0.066
	*C(4)	1.145
	*H(1)	−0.035

* Atoms not included in the least-squares calculation.

Table 5. Hydrogen-bond distances and angles of four NCAs

Standard deviations are in parentheses.

NCA	D–H···A	Distance (D···A)	Angle (D–H–A)
Glycine	N(1)–H(1)···O(1′)	2.915(2) Å	162(2)°
L-Alanine	N(1)–H(1)···O(3′)	3.034(5)	170(3)
L-Leucine	N(1)–H(1)···O(1′)	2.864(5)	176(3)
BLG[a)]	N(1)–H(1)···O(4′)[b)]	2.898(4)	174(3)

a) γ-Benzyl-L-glutamate NCA. b) An oxygen atom of carbonyl group in the side chain of γ-benzyl-L-glutamate NCA.

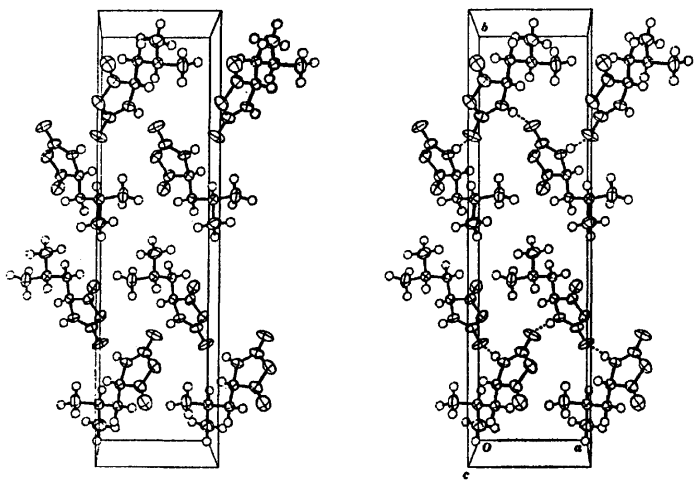

Fig. 3. Stereoscopic drawing of the crystal structure of L-leucine NCA viewed along the c axis. The thermal ellipsoids are drawn at a 50% probability level and the hydrogen atoms are shown in circles.

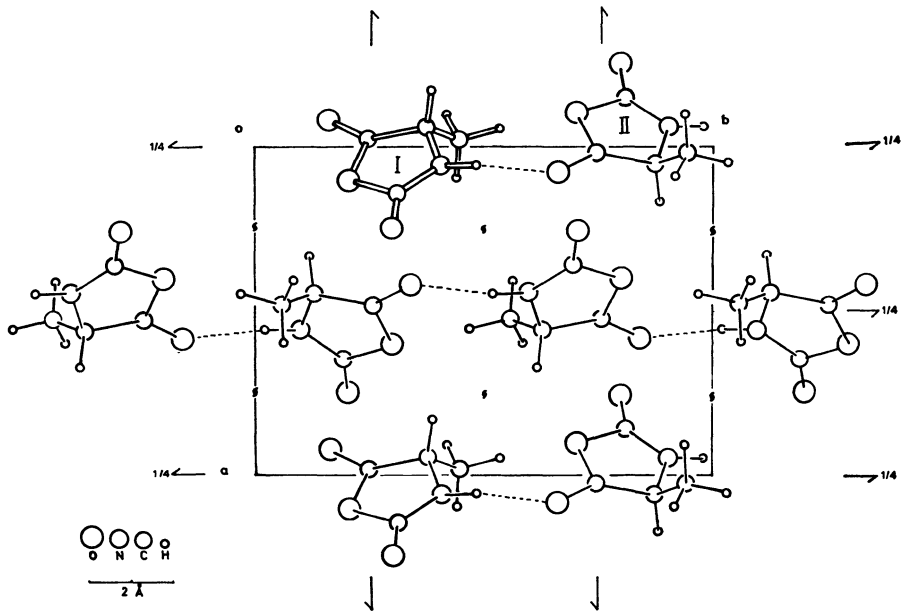

Fig. 4. Projection of the crystal structure of L-alanine NCA viewed along the c axis. I,(x,y,z); II, $(-x,1/2+y,1/2-z)$. Hydrogen bonds are shown by broken lines.

In the BLG NCA crystal, the hydrogen bond is formed between N(1)–H(1) and the oxygen atom of the carbonyl group in the side chain of the neighboring molecule. Since the five-membered ring would drag the side chain of the neighboring molecule, polymerization cannot occur easily. The reactivity of BLG NCA in the crystalline state is not so high as in the heterogeneous system.[4]

On the other hand, the crystal of L-leucine NCA has the following favorable conditions:

(1) because of the sandwiched layer structure, the polymerization proceeds within one sandwich and would not destroy the molecular arrangement in the neighboring sandwich, (2) within a sandwich, the side chains do not hinder the five-membered rings from approaching each other, (3) the side chain can move easily since it does not entwine with side chains of the neighboring molecules and relatively loose contacts are observed between them (compare the structure and the density of the L-leucine NCA crystal with the corresponding ones of the BLG NCA crystal), and (4) in the process of polymerization, the crystal should be easily cloven between sandwichs, leaving a gap between them, and carbon dioxide goes out through the gap without deteriorating the alignment of the amino acid NCA molecules.

The crystal of L-alanine NCA, whose structure viewed along the c axis is shown in Fig. 4, has no such favorable conditions as a result of the N(1)–H(1)···C(3′) hydrogen bond. For example, the shortest distance 3.591 Å of N(1)···C(2), is found between molecules I and II. However, the methyl group prevents molecule II from approaching I. Polymerization does not seem to proceed without destroying the arrangement of the monomers. The L-alanine NCA crystal is very stable in the air, having very low reactivity.

The type of hydrogen bond, N(1)–H(1)···O(1′), is the most favorable for polymerization, taking into account the charge distribution of the five-membered ring and facility of the ring opening.[3] However, high reactivity cannot be attained only by this factor, as suggested by the low reactivity of the glycine NCA crystal. Thus, it is quite reasonable that the sandwich structure accelerates the reactivity in the crystalline state. Because of the sandwich structure and the charge distribution in the NCA ring, L-leucine NCA is more reactive in the crystalline state than in the solution state, and even in the molten state.

Recently a Weissenberg photograph of a polymer crystal formed by keeping an L-leucine NCA crystal on the goniometer head for a few days, indicated that the polymer has the α-helical structure elongated along the c axis. This can be interpreted easily on the basis of the present crystal structure.

References

1) H. Kanazawa, Y. Matsuura, N. Tanaka, M. Kakudo, T. Komoto, and T. Kawai, *Bull. Chem. Soc. Jpn.*, **49**, 954 (1976).

2) H. Kanazawa, Y. Matsuura, N. Tanaka, M. Kakudo, and T. Kawai, *Acta Crystallogr., Sect. B*, **32**, 78 (1976).

3) H. Kanazawa, T. Kawai, Y. Ohashi, and Y. Sasada, *Bull. Chem. Soc. Jpn.*, **51**, 2200 (1978).

4) H. Kanazawa and T. Kawai, to be published.

5) "International Tables for X-Ray Crystallography," Vol. IV, The Kynoch Press, Birmingham (1974), p. 72.

6) G. C. Pementel and A. L. McClellan, "The Hydrogen Bond," W. H. Freeman and Company, San Francisco and London (1960), p. 286.

7) C. H. Bamford, A. Elliot, and W. H. Hanby, "Synthetic Polypeptides," Academic Press, New York (1956), p. 62.

A Stereoselective Rule for the Cross-bicyclization in Linear Conjugated Polyenes

Kazuyoshi TANAKA and Kenichi FUKUI*

Department of Hydrocarbon Chemistry, Faculty of Engineering, Kyoto University, Sakyo-ku, Kyoto 606

(Received January 27, 1978)

A concept of the cross-bicyclization complementary to that of the cycloaddition is defined for interpreting the mechanism of the simultaneous bicyclizations in linear conjugated polyenes based on the perturbation treatment in the frame of Hückel MO's. Stereoselective modes in thermal and photo-induced reactions are shown to depend on the sign of the bond-bond-polarizability, $\Pi_{rs,tu}$, of the concerned polyene, where r, s, t, and u refer to the atomic positions at which the bicyclization occurs. From the properties of $\Pi_{rs,tu}$ of linear conjugated polyenes, these modes are simply determined by the relationship among r, s, t, and u in thermal cases, but not in photo-induced ones. The predicted stereoselective modes are discussed in line with experimental observations. It is demonstrated that the "symmetry-disfavored" reactions inferred from the usual cycloaddition mechanism can be interpreted as the concerted cross-bicyclization reactions.

The stereoselective rules from the concept of the concerted cycloaddition reactions by Woodward and Hoffmann[1] or those from the orbital interaction approach, particularly among the highest occupied (HO)MO, the lowest unoccupied (LU)MO, and the singly occupied (SO)MO, by the present authors' group[2] have clearly interpreted steric control modes of both thermal and photo-induced (2+2) or (4+2) cycloadditions and so on. These rules have also been applied to most of the intramolecular cases without hesitation. Some of the recent experimental informations, however, have shown discrepancies with the predictions issued from the above rules with regard to the stereoselections in photo-induced (2+2) and (4+2) cycloadditions in the conjugated dienes and trienes, respectively. For instance, Padwa *et al.* have essentially provided (4_s+2_a) photoisomerizations of **1** and **2** in accordance with the rules of cycloadditions,[3]

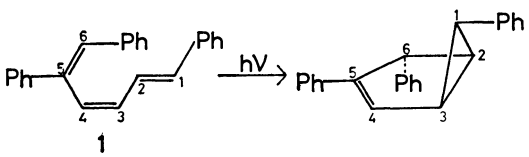

1

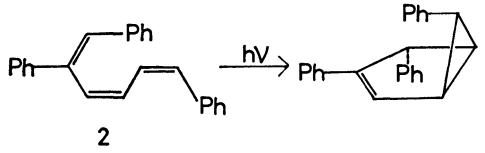

2

while, on the contrary, Courtot *et al.* have unambiguously observed disfavoured (4_a+2_a) modes in those of **3**, **4**, and **5** with monitoring by NMR.[4]

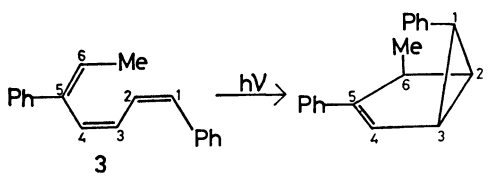

3

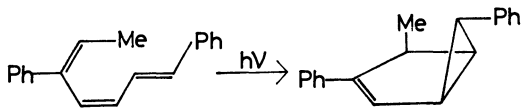

4

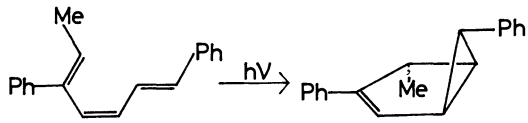

5

Other examples of disfavored modes in photoisomerizations of dienes or trienes have also been found out[5-8] as will be shown later. Almost all of these "troublesome" reactions within the category of the usual cycloadditions have been excluded out from the concerted reactions. But why concerted in **1** and **2**, and non-concerted in **3**, **4**, and **5**? Can we not interpret the concertedness and the stereoselective modes of these bicyclizations in conjugated polyenes? The answer is yes. At first it should be pointed out that the stereoselective rules of the cycloaddition mentioned above are suitable for merely cyclic additions between two separate conjugated polyene parts whichever they are in different molecules or in a molecule. Therefore, from the theoretical point of view, one had better distinguish the nature of the bicyclizations in a conjugated polyene from the usual cyclic additions. In this paper, we will present a new theoretical interpretation, which is complementary to the concept of the concerted cycloaddition reactions, so that one might comprehend the concertedness and the stereoselective rules of the above reactions with "disfavored" mode.

We define a simultaneous bicyclization between the r-th and the s-th and between the t-th and the u-th carbons (**6**→**7**) in a linear conjugated polyene containing $2n$ π electrons as a $[r,s/t,u]$ *cross-bicyclization* under the condition that r and s are odd and t and u are even or *vice versa*, where the numbering of carbons is counted from the end of conjugated carbon chain and $r<t<s<u$ holds.

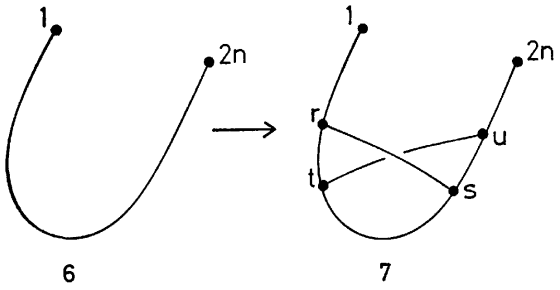

6 7

In the cross-bicyclization thus defined, the conjugation between the s-th and the t-th carbons generally exists throughout the process of reaction. This is the point of essential importance. If this conjugation does not exist, the reaction would turn out as a usual cycloaddition. In what follows, we try to establish a simple but reasonable method in such reactions employing the perturbation theory in the scheme of the Hückel MO approach.[9] Similar method has been used successfully to treat the stereospecific ring-closure of conjugated polyenes.[10] Then the predicted stereoselective rules will be applied to interpret the latest several experimental results.

Formulation

Consider two simultaneous conjugations, $k\beta$ and $l\beta$, appearing as a perturbation as indicated in **6'**.

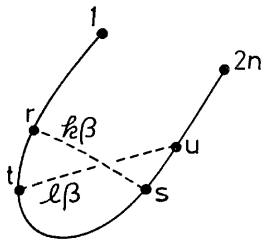

6'

The quantity β is the resonance integral between two adjacent 2pπ atomic orbitals (AO's). Hence, $k\beta$, for instance, is adopted to be the resonance integral between ϕ_r and ϕ_s when σ-like overlapping of these two AO's in the distorted π electron system occurs, where ϕ_r denotes 2pπ AO of the r-th carbon. The signs of $k\beta$ and $l\beta$ concern the mode of overlap stabilization as indicated below.

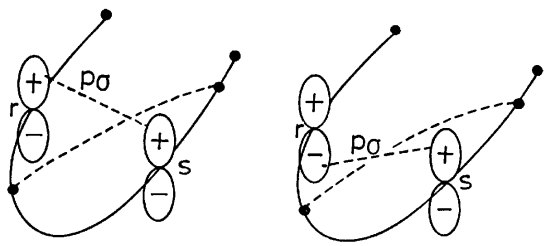

$k\beta<0(k>0)$; Disrotatory $k\beta>0(k<0)$; Conrotatory

Letting α be the Coulomb integral of 2pπ AO, the perturbed secular determinant in the present case becomes as follows.

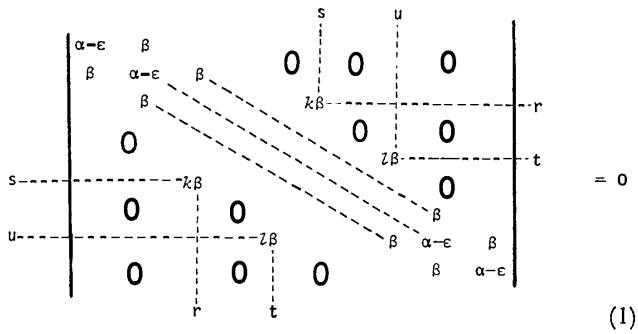

(1)

According to the procedure previously reported ("method of perturbed secular determinant"),[11] we get the following formula within the second-order perturbation treatment.

$$\frac{\Delta E}{\beta} = 2kP_{rs} + 2lP_{tu} + k^2\Pi_{rs,rs} + 2kl\Pi_{rs,tu} + l^2\Pi_{tu,tu} \qquad (2)$$

Here ΔE represents the change in the π-electronic energy, and P_{rs} and $\Pi_{rs,tu}$ are the same quantities as the usual bond-order and bond-bond-polarizability, respectively, defined as

$$P_{rs} = \sum_i^{\text{all}} n_i C_r^i C_s^i, \qquad (3)$$

$$\Pi_{rs,tu} = \frac{1}{2}\sum_i^{\text{all}}\sum_{j(\neq i)}^{\text{all}} \times n_i(2-n_j)\frac{(C_r^iC_s^j + C_r^jC_s^i)(C_t^iC_u^j + C_t^jC_u^i)}{x_i - x_j} \left(x_i = \frac{\varepsilon_i - \alpha}{\beta}\right) \qquad (4)$$

where n_i, ε_i, and C_r^i represent the occupation number, the orbital energy, and the coefficient of ϕ_r, respectively, of the i-th MO of the unperturbed system **6**. Since the sign of β is negative, the overlap stabilization is brought about in the system when the sign of the right hand side in Eq. 2 becomes positive. We have only to judge the sign of the next formula, because the required values of P_{rs} and P_{tu} vanish in the case of the present $2n$ conjugated polyene.

$$\frac{\Delta E}{\beta} = k^2\Pi_{rs,rs} + 2kl\Pi_{rs,tu} + l^2\Pi_{tu,tu} \qquad (2')$$

It is easily shown that this quadratic form is positive by the Cauchy-Schwartz' inequality. According to the sign of the $\Pi_{rs,tu}$ value, the mode of cross-bicyclization may be classified into the following four types of rotations in the direction of increasing value of $\Delta E/\beta$.

$\Pi_{rs,tu}$	k	l	Rotating mode
positive	positive	positive	A(disrotatory-disrotatory)
	negative	negative	B(conrotatory-conrotatory)
negative	positive	negative	C(disrotatory-conrotatory)
	negative	positive	D(conrotatory-disrotatory)

No distinction can be made of mode A from B, nor of

mode C from D within the present second-order perturbation treatment. However, in some favorable cases, consideration of steric circumstances, which is important in such cases as the cross-bicyclization, may assist in predicting the more probable mode. It is not difficult to show that, in thermal case, the sign of $\Pi_{rs,tu}$ is positive or negative according as $(s-r)+(u-t)$ is equal to $4m+2$ or $4m$, respectively, from the integral representation for $\Pi_{rs,tu}$ obtained by Coulson and Longuet-Higgins.[9c] On the contrary, in photo-induced case, there is no such a simple relationship between the sign of $\Pi_{rs,tu}$, which is calculated in regard to the first excited configuration, and r, s, t, and u. Hence one has to examine the numerical value of the concerned $\Pi_{rs,tu}$ in order to predict the mode of photo-induced cross-bicyclization.

Stereoselective Modes of Cross-bicyclization and Cycloaddition

For the cases of diene, triene, and tetraene, we show all kinds of rotating modes in thermal and photo-induced cross-bicyclizations in Table 1 along with the numerical values of $\Pi_{rs,tu}$. Interestingly, it is seen that the predicted stereoselective modes make no difference in both thermal and photo-induced reactions in each cross-bicyclization of diene, triene, and tetraene.[12] These predictions are remarkably different from those issued from the concept of the cycloaddition by Woodward and Hoffmann or from the frontier orbital interaction approach. It should also be emphasized that modes A and B are favored when $(s-r)+(u-t)$ is equal to $4m+2$, while modes C and D are favoured when it is $4m$ in these polyenes. The cases of longer polyenes could also be treated by a simple extension of the present calculations, with which we will not further deal in this study.

Let us treat here some of the usual cycloadditions with our formulation for the sake of comparison. In the case of the (4+2) cycloaddition, for instance, the triene is divided into a diene and an olefin and thus the conjugation between C_2 and C_3 is cut off as shown in Fig. 1(A). In this case, the amplitudes of the frontier orbitals on C_1, C_2, C_3, and C_6 are large and the orbital energy differences among them are small as a matter of fact, so $\Pi_{rs,tu}$ defined by Eq. 4 mainly depends on the expansion terms of $(i,j)=(2,4)$ and $(3,5)$ in the thermal process, while of $(i,j)=(2,3)$ and $(4,5)$ in the photo-induced process. In other words, the HOMO-LUMO interactions in the former process and the HOMO-SOMO and the SO'MO-LUMO interactions in the latter between a diene and an olefin shown in Figs. 1(B) and (C), respectively, are essentially important in order to predict the distinct stereoselective mode in

Table 1. Rotating modes in cross-bicyclization

Polyene	$[r,s/t,u]$	Thermal ($\Pi_{rs,tu}$)	Photo-induced ($\Pi_{rs,tu}$)
Diene	[1,3/2,4][a]	C,D(−0.3578)	C,D(−0.1789)
Triene	[1,3/2,6][b]	A,B(0.2352)	A,B(0.0762)
	[1,3/2,4]	C,D(−0.2906)	C,D(−0.0694)
	[1,5/2,6]	C,D(−0.3597)	C,D(−0.1661)
	[3,5/2,4]	C,D(−0.0274)	C,D(−0.2072)
Tetraene	[1,3/2,4]	C,D(−0.2659)	C,D(−0.0410)
	[1,3/2,6]	A,B(0.2013)	A,B(0.0053)
	[1,3/2,8][c]	C,D(−0.1809)	C,D(−0.0029)
	[1,5/2,6]	C,D(−0.2998)	C,D(−0.1269)
	[1,5/2,8]	A,B(0.2359)	A,B(0.0725)
	[1,5/4,6]	A,B(0.1863)	A,B(0.0830)
	[1,5/4,8][d]	C,D(−0.1685)	C,D(−0.1135)
	[1,7/2,8]	C,D(−0.3548)	C,D(−0.1965)
	[3,5/4,6]	C,D(−0.2270)	C,D(−0.0878)
	[3,5/2,4]	C,D(−0.0311)	C,D(−0.1626)
	[3,7/2,6]	C,D(−0.0515)	C,D(−0.1649)
	[3,7/2,4]	A,B(0.0054)	A,B(0.0801)

a), b), c), and d) have been classified into (2+2), (4+2), (6+2), and (4+4) cycloaddition, respectively, up to now.

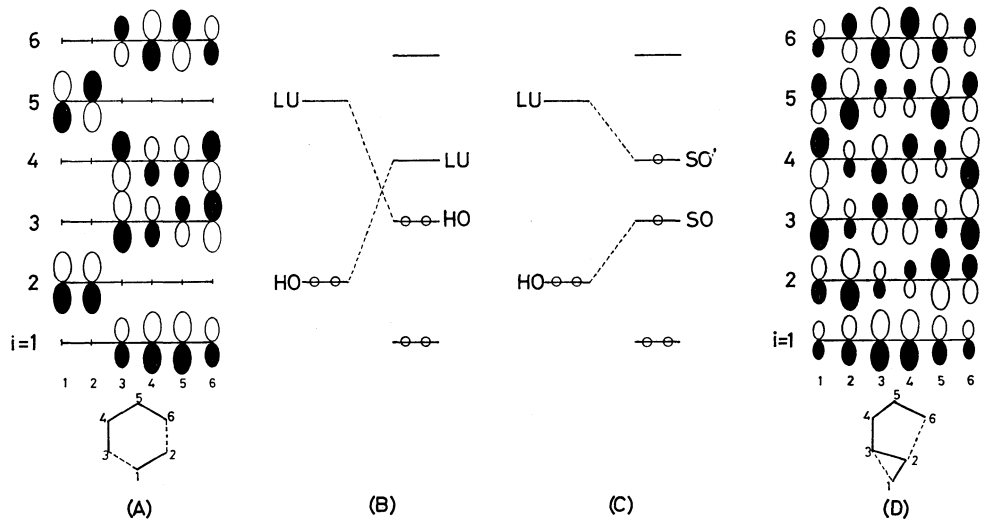

Fig. 1. Orbital patterns of the systems composed of (A) an olefin and a diene, and (D) a triene. (B) and (C) show the frontier orbital interactions in (A) in thermal and photo-induced processes, respectively. It should be noted that σ bond between C_2 and C_3 may remain in (A).

TABLE 2. STEREOSELECTIVE MODES IN CYCLOADDITION THROUGH THE TREATMENT OF THE PRESENT FORMULATION

Type of Cycloaddition	Thermal ($\Pi_{rs,tu}$; its main term[a])	Photo-induced ($\Pi_{rs,tu}$; its main term[b])
2+2	C,D(−0.5000; −0.5000) (2_s+2_a or 2_a+2_s)	A,B(+∞; +∞) (2_s+2_s or 2_a+2_a)
4+2	A,B(0.3416; 0.4472) (4_s+2_s or 4_a+2_a)	C,D(−0.8292; −0.9472) (4_a+2_s or 4_s+2_a)
6+2	C,D(−0.2588; −0.3759) (6_a+2_s or 6_s+2_a)	A,B(0.4185; 0.4893) (6_s+2_s or 6_a+2_a)
4+4	C,D(−0.2683; −0.4236) (4_s+4_a or 4_a+4_s)	A,B(+∞; +∞) (4_s+4_s or 4_a+4_a)

a) Contribution to $\Pi_{rs,tu}$ from the HOMO-LUMO interactions between two separate polyene parts. b) Contribution to $\Pi_{rs,tu}$ from the HOMO-SOMO and the SO'MO-LUMO interactions between two separate polyene parts.

each process of the cycloaddition. On the contrary, in the case of the cross-bicyclization in a triene, the same criterion would no longer serve because of the alterations of the amplitudes in the MO's with i=2, 3, 4, and 5 on the concerned carbons as shown in Fig. 1(D). In this sense one can not always expect a conspicuous difference of the stereoselective mode between the thermal and photo-induced processes and has to sum up extending over all MO's such as in Eq. 4 in order to judge the signs of $\Pi_{rs,tu}$'s in the cross-bicyclization apart from the cycloaddition.

The values of $\Pi_{rs,tu}$ and the predicted stereoselective modes for cycloadditions in the cases of (2+2), (4+2), (6+2), and (4+4) are listed in Table 2 along with the main terms in $\Pi_{rs,tu}$ arising from the frontier orbital interactions. For cycloaddition reactions, the required $\Pi_{rs,tu}$'s are formally evaluated on the basis of the secular determinant in Eq. 1 with setting the resonance integral to be zero at the position where the conjugation is cut off. In photo-induced (2+2) and (4+4) cases, the degeneracies between the HOMO and the SOMO and between the SO'MO and the LUMO invalidate to evaluate the required $\Pi_{rs,tu}$. Actually, however, these degeneracies would be reduced by the energetical splittings between these MO's on account of the presence of the electron correlation as illustrated in Fig. 2.[13] Therefore, we tentatively set here the

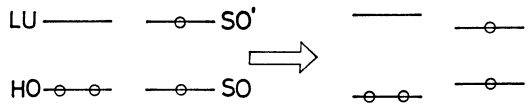

Fig. 2. The splittings of the levels between the HOMO and the SOMO and between the SO'MO and the LUMO.

values of ($x_{HO}-x_{SO}$) and ($x_{SO'}-x_{LU}$) in Eq. 4 to be infinitely small positive, from which the concerned $\Pi_{rs,tu}$'s are positive infinite. This means that photo-induced [1,3/2,4] cross-bicyclization of diene or [1,5/4,8] case of tetraene might rather favour the (2+2) or (4+4) cycloaddition, respectively, from the viewpoint of the energetical stabilization, as will be seen in the next section.

Application

[1,3/2,4] Cross-bicyclization of Diene. Dauben and Ritscher have early obtained the photoproducts **9**, **11**, and **12** from ethylidenecyclooctenes **8** and **10**.[5]

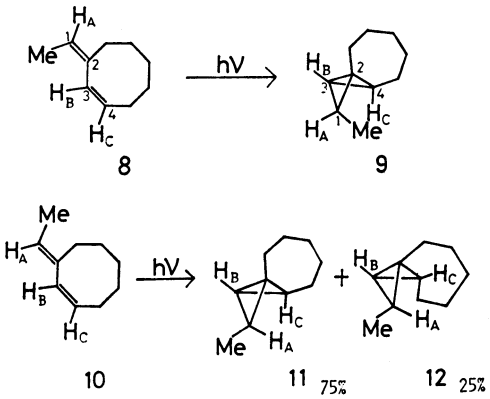

Both **9** and **11** are the results of mode B and compatible with the usual (2_a+2_a) cycloaddition. However, **12** is the result of the disfavoured mode C or D ((2_s+2_a) or (2_a+2_s)), so they have supposed an anomalous concerted reaction from a vibrationally relaxed singlet having an electronic configuration composed of an allyl anion and a methyl cation, while, from the standpoint of the cross-bicyclization, **12** is a reasonable product but **9** and **11** are not. The reason why these reactions rather favor these products can be explained by not a little energetical stabilizations in the photo-induced (2+2) cycloadditions as has been stated above. Furthermore, some steric hindrance in connection with the cyclooctene ring might play a role in separating the C_2–C_3 conjugation. Therefore, the photo-induced [1,5-/4,8] case of tetraene, which has not been reported, would also be of interest because of the possibility of the competition with (4+4) cycloaddition.

[1,3/2,6] Cross-bicyclization of Triene. In the photoinduced [1,3/2,6] case of triene, mode A or B is favored, which predicts exactly the products from **3**, **4**, and **5** provided by Courtot *et al.*[4] The products from **1** and **2** by Padwa *et al.*,[3] however, show the opposite mode of stereoselection in the sense of the cross-bicyclization. In order to examine these discrepancies, we have evaluated $\Pi_{13,26}$ values as functions of the resonance integrals between C_2 and C_3 (β_{23}) of **1** or **2**, and **3**, **4**, or

TABLE 3. THE VALUES OF $\Pi_{13,26}$ AS FUNCTIONS OF β_{23} IN **1** OR **2**, AND **3**, **4**, OR **5** IN THEIR FIRST EXCITED CONFIGURATIONS

β_{23}	**1** or **2**	**3**, **4**, or **5**
β	0.0382	0.0859
0.7β	0.0042	0.0822
0.6β	−0.0219	0.0686
0.5β	−0.0599	0.0391

5 in their first excited configurations taking phenyl groups into considerations as listed in Table 3. It is evidently seen that the $\Pi_{13,26}$ of **3**, **4**, or **5** used by Courtot *et al.* is less sensitive to the weakening of β_{23}, while that of **1** or **2** by Padwa *et al.* is the smaller at $\beta_{23}=\beta$ and changes its sign at $\beta_{23}=0.6\beta$. That is, the stereoselective modes in photo-induced [1,3/2,6] cases of **1** and **2** will more easily change into that issued from the (4+2) cycloaddition than those of **3**, **4**, and **5**, according to the weakening of the conjugation between C_2 and C_3, if it takes place for some reason. We infer that these situations are reflected in the reactions of Padwa *et al.* to a certain extent, although more detailed calculation including σ electrons is requisite to provide a definite information on these species. An example as to the hexatriene free from the conjugated substituents has also been shown. Dauben and Kellogg have obtained the photoproduct *via* (4_a+2_a) cycloaddition from 1,3,5-cycloundecatriene,[6]

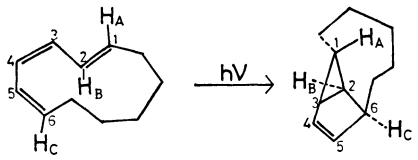

and supposed that the cyclization is initiated from the vibrationally relaxed first excited singlet state like the above case of ethylidenecyclooctene. But this stereoselective mode is easily explained by the cross-bicyclization of triene.

There have been other examples of the cross-bicyclizations that are found out in the photoisomerizations of benzohexatrienes reported by Seeley,[7]

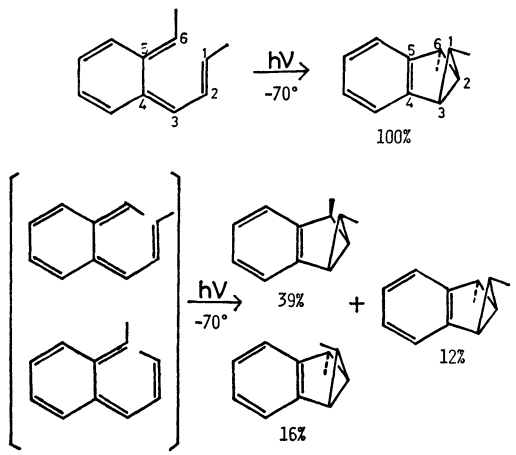

and by Sieber *et al.*[8]

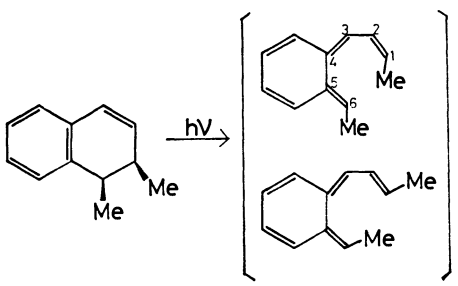

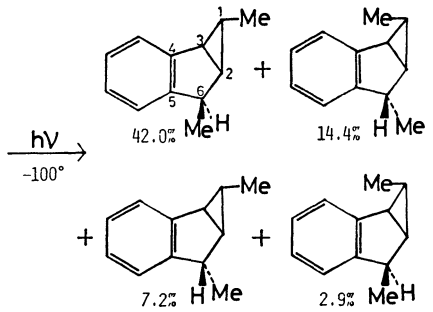

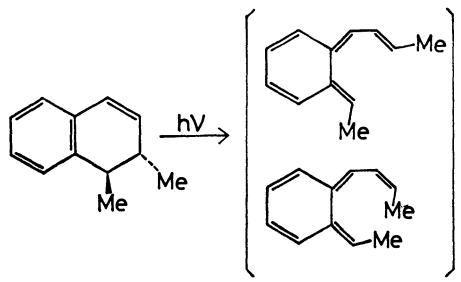

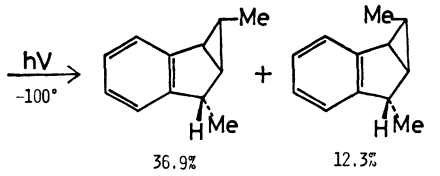

Since the major products of these reactions are not controlled by the stereoselective modes from the cycloaddition, these authors have ascribed these results to non-concerted reactions. But we are now in a position to tell that these reactions are concerted as well with the aid of the concept of the cross-bicyclization.

Summary

We have defined the concept of the cross-bicyclization complementary to that of the cycloaddition and pointed out the essential difference between these two. The predicted stereoselective modes from the cross-bicyclization are in reasonable agreement on the whole with the experimental observations that have been discarded from the category of the concerted reactions because of the faith in the cycloaddition rules. However, one should pay attention to the application of the rules to photo-induced [1,3/2,4] case of diene or [1,5/4,8] case of tetraene as well as to the case of polyene with conjugated substituents. To the authors' knowledge, any stereospecific bicyclizations in a conjugated polyene treated by the concept of the cycloaddition up to the present have been probed in this study.

It is also an interesting conclusion, in diene, triene, and tetraene, that the thermal and photo-induced processes happen to yield quite identical results and that there occurs a distinct difference in the stereoselective mode according as $(s-r)+(u-t)$ is equal to $4m+2$ or $4m$. Further experimental observations are desirable in order to assess the utility of the present concept of the cross-bicyclization.

This work was supported by Grant-in-Aid for Scientific Research from the Ministry of Education of Japan (No. 139012). One of the authors (K.F.) wishes to thank Prof. P. Courtot for letting him know interesting photochemical results.

References

1) a) R. Hoffmann and R. B. Woodward, *J. Am. Chem. Soc.*, **87**, 2046 (1965); b) R. Hoffmann and R. B. Woodward, *Acc. Chem. Res.*, **1**, 17 (1968); c) R. B. Woodward and R. Hoffmann, *Angew. Chem.*, **81**, 797 (1969); d) R. B. Woodward and R. Hoffmann, "The Conservation of Orbital Symmetry," Academic Press, New York (1969).

2) a) K. Fukui, *Acc. Chem. Res.*, **4**, 57 (1971); b) K. Fukui, "Theory of Orientation and Stereoselection," Springer-Verlag, Berlin (1975).

3) a) A. Padwa and S. Clough, *J. Am. Chem. Soc.*, **92**, 5803 (1970); b) A. Padwa, L. Brodsky, and S. Clough, *ibid.*, **94**, 6767 (1972).

4) P. Courtot, J. Salaün, and R. Rumin, *Tetrahedron Lett.*, **1976**, 2061.

5) W. G. Dauben and J. S. Ritscher, *J. Am. Chem. Soc.*, **92**, 2925 (1970).

6) W. G. Dauben and M. S. Kellogg, *J. Am. Chem. Soc.*, **94**, 8951 (1972).

7) D. A. Seeley, *J. Am. Chem. Soc.*, **94**, 4378 (1972).

8) W. Sieber, H. Heimgartner, H. J. Hansen, and H. Schmid, *Helv. Chim. Acta*, **55**, 3005 (1972).

9) a) C. A. Coulson and H. C. Longuet-Higgins, *Proc. R. Soc. London, Ser. A*, **191**, 39 (1947); b) *ibid.*, **192**, 16 (1947); c) *ibid.*, **193**, 447 (1948).

10) K. Fukui, *Bull. Chem. Soc. Jpn.*, **39**, 498 (1966).

11) a) K. Fukui, C. Nagata, T. Yonezawa, H. Kato, and K. Morokuma, *J. Chem. Phys.*, **31**, 287 (1959); b) K. Fukui, K. Morokuma, T. Yonezawa, and C. Nagata, *Bull. Chem. Soc. Jpn.*, **33**, 963 (1960).

12) The identity of the predicted stereoselective modes in thermal cases with those in photo-induced ones is quite accidental. For instance, $\Pi_{13,210}$ of pentaene is positive (0.1491) in thermal case, whereas it is negative (−0.0341) in photo-induced case. Therefore, thermal and photo-induced [1,3/2,10] cases of pentaene will show different stereoselective modes each other.

13) For example, see p. 48 of Ref. 2b and references therein.

Potential of Hydrocarbons for Photochemical Conversion of NO to NO_2

Nobuaki WASHIDA,* Gen INOUE, Hajime AKIMOTO, and Michio OKUDA
The National Institute for Environmental Studies, P.O. Yatabe, Tsukuba, Ibaraki 300-21
(Received January 31, 1978)

The factor F, the number of NO molecules which are converted photochemically into NO_2 when one hydrocarbon molecule is consumed, was determined for fourteen different hydrocarbons in the photochemical oxidation process. Experiments were carried out in a 67 dm^3 Pyrex reaction chamber in which a mixture of hydrocarbon, NO, H_2O, and air was irradiated by a xenon short arc lamp. In the range from low to middle conversion, hydrocarbons and NO decayed nearly exponentially, NO being converted into NO_2. The observed value of F was approximately two for most of the hydrocarbons studied. The value is in line with the long chain mechanism involving OH radicals predicted by Heicklen *et al.* Only *m*-xylene gave a larger F value. Reaction sequences of the long chain mechanism caused by OH radicals were discussed, a generalized kinetic model for the chain mechanism being proposed. This will be useful for the atmospheric modeling of photochemical smog.

When mixtures of hydrocarbons and nitrogen oxides (NO and NO_2) in air are irradiated with ultraviolet radiation, NO is converted into NO_2 as hydrocarbons are consumed.[1,2] After the concentration of NO_2 passes through a maximum, O_3 and other oxidants such as PAN are produced as the NO_2 is consumed.

Heicklen *et al.*[3] proposed a long chain mechanism involving OH radicals for the photochemical conversion of NO into NO_2 in urban atmospheres. According to their mechanism, the conversion is promoted by the reaction of NO with $RO_2\cdot$ radicals which are formed in the reaction of organic free radicals and O_2.

$$RO_2\cdot + NO \longrightarrow RO\cdot + NO_2 \quad (1)$$

In the reaction with propylene,[4] 2-methylpropene,[3] and butane,[3] Heicklen *et al.* proposed the following overall reactions.

$$C_3H_6 + 2NO + 2O_2 \longrightarrow CH_3CHO + CH_2O + 2NO_2 \quad (2)$$

$$C_4H_8 + 2NO + 2O_2 \longrightarrow C_3H_6O + CH_2O + 2NO_2 \quad (3)$$

$$C_4H_{10} + 2NO + 2O_2 \longrightarrow C_4H_8O + H_2O + 2NO_2 \quad (4)$$

According to their suggestion, two NO molecules should be converted into NO_2 when one hydrocarbon molecule is consumed. However, if the intermediate radicals degrade further to form simpler aldehydes such as CH_2O in Reactions 2, 3, and 4, three to five NO molecules should be converted into NO_2 when one hydrocarbon molecule is consumed.[2]

This report deals with the measurement of the number of NO molecules (factor F) which would be converted into NO_2 when one hydrocarbon molecule is consumed.

Experiments were carried out for fourteen different hydrocarbons. The results would be useful for the computer simulation studies of atmospheric photooxidation processes.

Experimental

Experiments were carried out with use of a Pyrex cylinder as the reaction chamber, inner diam 240 mm, length 1660 mm and volume 67 dm^3, which can be evacuated to less than 1×10^{-6} Torr. Each end of the reaction chamber was sealed with a Pyrex window 20 mm thick. The light source was a 500 W xenon short arc lamp and a parallel light beam of 200 mm ϕ was obtained with an elliptic mirror, a lens, and an off-axis parabolic mirror. The effective light intensity for the primary photo-decomposition rate of NO_2 was 0.08 min^{-1}.

An oil free pumping system consisting of an ion pump, titanium getter pump, cryo-sorption pump, and oil rotary pump with a liquid nitrogen cooled foreline trap was used in order to avoid oil contamination of the reaction chamber.

Hydrocarbons and NO were first subjected to pressure reading in a 105 ml flask, and then expanded to the reaction chamber. After that, water vapor and air were introduced through four inlets. In order to verify that all the gases had been mixed homogeneously, four sampling outlets were attached to the chamber, at the center, at one-fourth the distance from one end, and at both ends. After one and a half hours, the contents of sample gases from the four different ports reached the constant values. After this, sampling was done through the center port.

The decay of hydrocarbons were measured by a F.I.D. gas chromatograph, and the concentrations of NO and NO_2 were monitored by a chemiluminescent NO_x analyzer (Monitor Labs. Model 8440). The analyzer is capable of measuring simultaneously the concentrations of NO and total NO_x, where total NO_x is the sum of NO, NO_2, and other nitrogen containing compounds which can be reduced to NO by a molybdenum converter.

The concentration of reactants was 0.5—2 ppm of hydrocarbons and 1—2 ppm of NO in 1 atm of air, the relative humidity being about 60%. The mixture was irradiated until 50—60% of NO was converted into NO_2. In the case of T.M.E. (2,3-dimethyl-2-butene), the reaction proceeded too fast for consecutive GC analysis. Mesh screens were placed between the chamber and the light source in order to reduce the light intensity. The reaction mixture was drawn first into a constant volume glass bulb (700 cm^3) and then concentrated in a GC sampling tube cooled by liquid nitrogen. After being subjected to the concentration process, the sampling tube was heated and the sample was fed into the gas chromatograph directly.

Sampling to the GC and to the NO_x analyzer was done every 20 or 30 min. When sampling had been carried out 7—10 times, the pressure of the reaction chamber decreased to *ca.* 600 Torr. The pressure drop effect on the measurements was calibrated in advance and all the data are corrected for the pressure change.

Chemicals (research grade, Wako Pure Chemical Ind.) were used without further purification except degassing. The gases, propylene and *cis*-2-butene (research grade, Takachiho

Kogyo Co.), pure air (pure gas B, Nippon Sanso), and NO (research grade, Matheson) were used without purification.

Before irradiation, the initial concentrations of NO and NO_2 in the mixture were measured by a NO_x analyzer. Usually, *ca.* 0.1 ppm of NO_2 was detected in a mixture containing *ca.* 1 ppm of NO.

The impurity of air and organic compounds adsorbed on the wall of the reaction chamber might convert NO into NO_2 by irradiation. In order to check the impurity effect a mixture of NO, water, and air was irradiated. The effect was found to be negligible.

Results and Discussion

When a dry mixture of hydrocarbon and NO with a small amount of NO_2 is irradiated, the initial decay of hydrocarbon and NO is very slow, showing an induction period, then the decay becomes faster as the reaction proceeds.[1,2] The time dependency of the concentrations of hydrocarbon and NO could not be followed by an exponential decay. On the other hand, if water vapor is added to the mixture, for example, at a humidity of 50%, the decrease of hydrocarbon and NO is much faster than for the dry mixture and is well approximated by an exponential decay up to the middle conversion region.[5] This could be explained by an equilibrium reaction between NO, NO_2, and H_2O and HONO.[6]

$$NO + NO_2 + H_2O \rightleftarrows 2HONO \qquad (5)$$

The HONO formed is photolyzed, giving OH radicals.[7]

$$HONO + h\nu(290\text{—}400\ \text{nm}) \longrightarrow OH + NO \qquad (6)$$

Thus, in the wet system the reaction can be initiated by OH radicals and is followed by long chain reactions involving-OH radicals.[3] In this case the steady state concentration of OH radicals will be reached in a shorter reaction time.[8]

The result in the $C_3H_6/NO/H_2O$/air system is shown in Fig. 1. Propylene and NO decay nearly exponentially except for a few points after starting, the total NO_x remaining unchanged. According to reports by Winer *et al.*[9] and Spicer and Miller,[10] the commercial chemiluminescent NO_x analyzer responds to nitrogen containing compounds such as PAN, nitrates and nitrites. Thus we cannot state that all the amount of NO consumed was converted into NO_2. However, since the production of nitrates and nitrites could not be observed by F.I.D. gas chromatography and the conversion of C_3H_6 is not large (30%), the formation of nitrates and nitrite is thought to be very small and the great part of NO consumed would be NO_2. The ratio of the NO consumed to the C_3H_6 consumed is about 2. The net photochemical loss of the NO_2 formed is also negligibly small due to the following reaction sequences:

$$NO_2 + h\nu \longrightarrow NO + O \qquad (7)$$

$$O + O_2 + M \longrightarrow O_3 + M \qquad (8)$$

$$O_3 + NO \longrightarrow NO_2 + O_2 \qquad (9)$$

Figure 2 shows the results of the *m*-xylene/NO/H_2O/air system. In this case the amount of the total NO_x decreases as *m*-xylene and NO are consumed. This could be explained by the formation of nitrates and nitrocompounds which was observed by F.I.D. gas chromatography. NO report seems to have appeared on the response of commercial chemiluminescent NO_x analyzer to aromatic nitrates and nitrocompounds. However, the result in Fig. 2 shows that it should be much lower than that to NO and NO_2. The ratio of the NO consumed to *m*-xylene consumed is *ca.* 3.2.

The amount of NO_2 produced (total NO_x—NO) was almost equal to that of NO consumed in the system of alkenes and alkanes. On the other hand, in the system of aromatic compounds, the amount of NO_2 produced

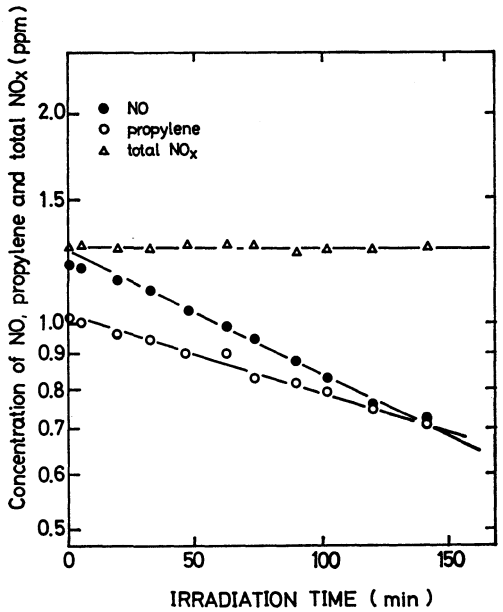

Fig. 1. Concentrations of NO (●), propylene (○), and total NO_x(△) *vs.* irradiation time. The concentration of NO_2 is the difference between total NO_x and NO.

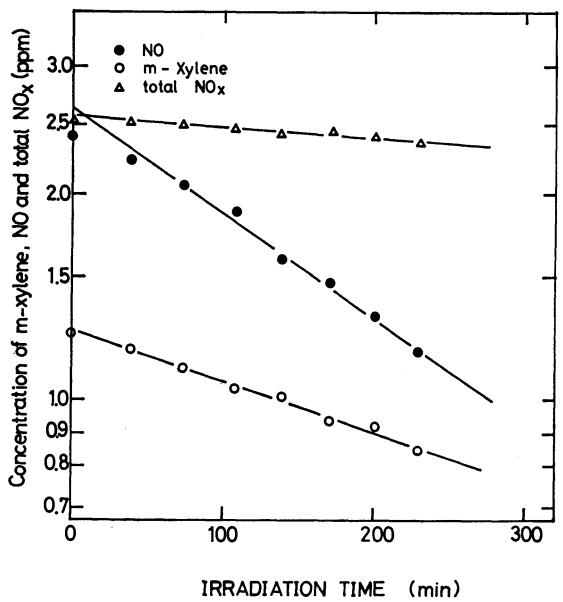

Fig. 2. Concentrations of NO (●), *m*-xylene (○), and total NO_x (△) are plotted against irradiation time.

was always smaller than that of NO consumed. Benzyl nitrate and *m*-nitrotoluene are produced in the photooxidation of the toluene/HONO/air system.[11,12] These nitrates and nitrocompounds are produced in other aromatic compounds. This would account for the loss of NO_2 as compared to the NO consumed in the reaction system involving these compounds.

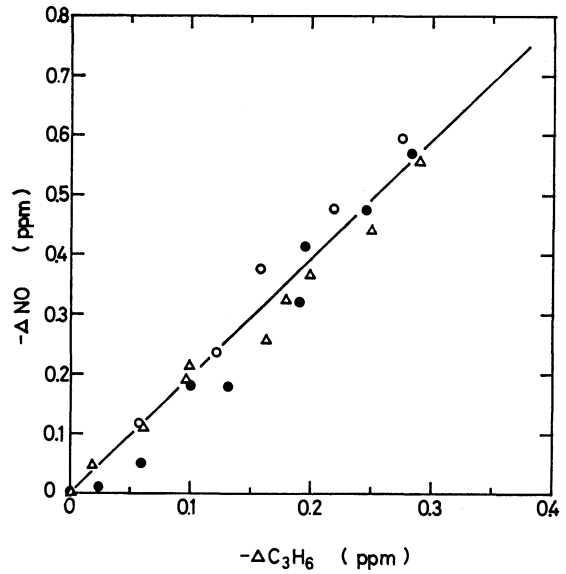

Fig. 3. Consumed NO, $-\Delta NO$, is plotted against comsumed propylene, $-\Delta C_3H_6$, for three different conditions.
Initial conditions are: (○) $[C_3H_6]=1.06$ ppm, $[NO]=1.85$ ppm; (△) $[C_3H_6]=1.01$ ppm, $[NO]=1.20$ ppm; (●) $[C_3H_6]=0.68$ ppm, $[NO]=2.20$ ppm.

In order to obtain the ratio of the NO consumed ($-\Delta NO$) to the hydrocarbons consumed ($-\Delta H.C.$), $-\Delta NO$ was plotted against $-\Delta H.C.$ Figure 3 shows an example of propylene. The results under three different initial conditions lie on a straight line. The least-squares method was used in order to obtain factor *F*, *i.e.*, the number of NO molecules converted into NO_2 when one propylene molecule is consumed. The factors thus obtained are given in Table 1. Numbers in parentheses give the error limits, ±, calculated by the least squares standard deviation (5%).

Taking into consideration the error limits, the *F* value is found to be approximately 2 for most of the compounds studied. This value was predicted by Heicklen *et al.* for propylene,[4] 2-methylpropene,[3] and butane[3] and by Niki *et al.* for propylene.[1] Although there is a small difference between the mechanisms proposed by Heicklen *et al.* and Niki *et al.*, the overall reaction for propylene can be described by Reaction 2 in both mechanisms. Referring to the mechanism of Heicklen *et al.* and also that of Niki *et al.*, the reactions for *cis*-2-butene can be explained by the following:

$$C_4H_8 + OH \longrightarrow \cdot C_4H_8OH \quad (10)$$
$$\cdot C_4H_8OH + O_2 \longrightarrow HOC_4H_8O_2\cdot \quad (11)$$
$$HOC_4H_8O_2\cdot + NO \longrightarrow HOC_4H_8O\cdot + NO_2 \quad (12)$$
$$HOC_4H_8O\cdot \longrightarrow CH_3CHO + \cdot C_2H_4OH \quad (13)$$
$$\cdot C_2H_4OH + O_2 \longrightarrow HOC_2H_4O_2\cdot \quad (14)$$
$$HOC_2H_4O_2\cdot + NO \longrightarrow HOC_2H_4O\cdot + NO_2 \quad (15)$$
$$HOC_2H_4O\cdot \longrightarrow OH + CH_3CHO \quad (16)$$

The overall reaction is

$$C_4H_8 + 2NO + 2O_2 \longrightarrow 2CH_3CHO + 2NO_2 \quad (17)$$

Table 1. *F* factors for organic compounds

Compound	Run number	Initial conditions Hydrocarbon(ppm)	NO(ppm)	Final concentration of hydrocarbon(ppm)	$F(\pm)$
Propylene	1	1.06	1.85	0.08	1.8 (0.2)
	2	1.01	1.20	0.70	2.2 (0.2)
	3	0.68	2.20	0.44	2.3 (0.3)
cis-2-Butene	4	0.92	2.03	0.67	2.0 (0.1)
	5	0.55	1.93	0.34	2.1 (0.3)
T.M.E.[a] (2,3-Dimethyl-2-butene)	6	1.11	1.99	0.78	2.0 (0.3)
Cyclopentene	7	1.08	2.02	0.40	1.9 (0.1)
Cyclohexene	8	1.26	1.71	0.70	2.3 (0.6)
Pentane	9	1.31	2.20	0.93	2.2 (0.3)
Hexane	10	2.00	2.21	1.60	2.0 (0.4)
Cyclopentane	11	0.84	1.83	0.61	2.2 (0.4)
Cyclohexane	12	1.21	2.03	0.92	2.3 (0.5)
	13	1.43	1.67	0.78	1.8 (0.1)
Toluene	14	1.34	1.69	1.00	2.2 (0.2)
	15	1.07	1.72	0.82	2.3 (0.3)
Ethylbenzene	16	1.46	1.96	1.05	1.9 (0.3)
o-Xylene	17	1.00	2.79	0.51	2.3 (0.2)
m-Xylene	18	0.97	2.18	0.76	3.4 (0.5)
	19	1.25	2.42	0.83	3.2 (0.3)
p-Xylene	20	0.91	1.83	0.57	2.4 (0.1)
	21	0.96	1.70	0.50	2.1 (0.3)
Mesitylene	22	0.92	1.75	0.56	2.3 (0.1)

a) Irradiation light intensity reduced to 1/8. Irradiation time 2—4 h for all measurements.

In the case of *cis*-2-butene, Demerjian *et al.*[2] proposed a reaction, which forms formic acid, instead of Reaction 16.

$$HOC_2H_4O\cdot \longrightarrow CH_3\cdot + HCOOH \quad (18)$$

The reaction sequence is

$$CH_3\cdot + O_2 \longrightarrow CH_3O_2\cdot \quad (19)$$

$$CH_3O_2\cdot + NO \longrightarrow CH_3O\cdot + NO_2 \quad (20)$$

$$CH_3O\cdot + O_2 \longrightarrow H_2CO + HO_2\cdot \quad (21)$$

$$HO_2\cdot + NO \longrightarrow OH + NO_2 \quad (22)$$

In this case four NO molecules should be converted into NO_2 as one *cis*-2-butene molecule is consumed. Our results, (F=2 for *cis*-2-butene), support the mechanism of Heicklen *et al.* and Niki *et al.*, and refute that of Demerjian *et al.* The results for T.M.E. could also be explained by the following overall reaction:

$$(CH_3)_2C_2(CH_3)_2 + 2NO + 2O_2 \longrightarrow 2(CH_3)_2CO + 2NO_2 \quad (23)$$

For cyclopentene, the sequence would be

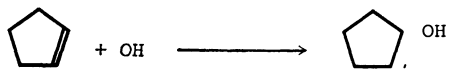
(24)

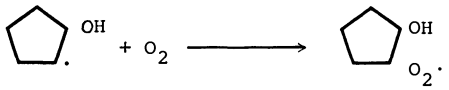
(25)

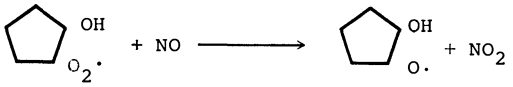
(26)

(27)

$$OCH(CH_2)_3\dot{C}H(OH) + O_2 \longrightarrow OCH(CH_2)_3CH(OH)O_2\cdot \quad (28)$$

$$OCH(CH_2)_3CH(OH)O_2\cdot + NO \longrightarrow OCH(CH_2)_3CH(OH)O\cdot + NO_2 \quad (29)$$

$$OCH(CH_2)_3CH(OH)O\cdot \longrightarrow OCH(CH_2)_3CHO + OH \quad (30)$$

The overall reaction is

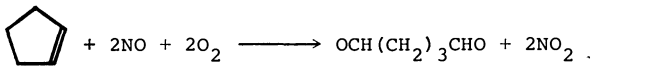
(31)

The photooxidation of cyclohexene could be explained in a similar way.

For alkanes, Heicklen *et al.*[3] proposed a mechanism for butane.[3] In a similar manner, the sequence for pentane is

$$C_5H_{12} + OH \longrightarrow C_5H_{11}\cdot + H_2O \quad (32)$$

$$C_5H_{11}\cdot + O_2 \longrightarrow C_5H_{11}O_2\cdot \quad (33)$$

$$C_5H_{11}O_2\cdot + NO \longrightarrow C_5H_{11}O\cdot + NO_2 \quad (34)$$

$$C_5H_{11}O\cdot + O_2 \longrightarrow C_5H_{11}O + HO_2\cdot \quad (45)$$

$$HO_2\cdot + NO \longrightarrow NO_2 + OH \quad (22)$$

The overall reaction is

$$C_5H_{12} + 2NO + 2O_2 \longrightarrow C_5H_{10}O + H_2O + 2NO_2 \quad (36)$$

For hexane, the overall reaction is

$$C_6H_{14} + 2NO + 2O_2 \longrightarrow C_6H_{12}O + H_2O + 2NO_2 \quad (37)$$

Carter *et al.*[14] suggested an isomerization mechanism in the alkane reaction. In the case of pentane, $C_5H_{11}O\cdot$ formed in Reaction 34 can be isomerized in part *via* the following reaction:

$$C_5H_{11}O\cdot \longrightarrow \cdot C_5H_{15}(OH) \quad (38)$$

The reaction might proceed *via*

$$\cdot C_5H_{10}(OH) + O_2 \longrightarrow \cdot O_2C_5H_{10}(OH) \quad (39)$$

$$\cdot O_2C_5H_{10}(OH) + NO \longrightarrow \cdot OC_5H_{10}(OH) + NO_2 \quad (40)$$

$$\cdot OC_5H_{10}(OH) + O_2 \longrightarrow (OH)C_5H_9O + HO_2 \quad (41)$$

$$HO_2 + NO \longrightarrow OH + NO_2 \quad (22)$$

In this case, the value of factor F should be between 2 and 3, according to the competition between Reactions 35 and 38. Considering the error limit in Table 1, the mechanism proposed by Carter *et al.* is also acceptable in the case of pentane and hexane. In the case of cyclopentane, the sequence might be as follows:

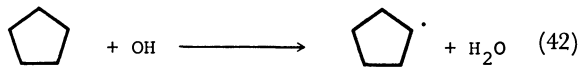
(42)

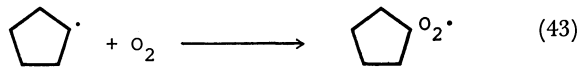
(43)

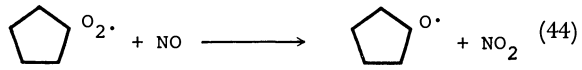
(44)

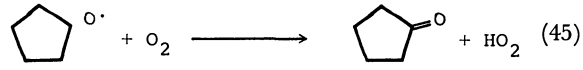
(45)

$$HO_2 + NO \longrightarrow NO_2 + OH \quad (22)$$

The overall reaction for cyclohexane is

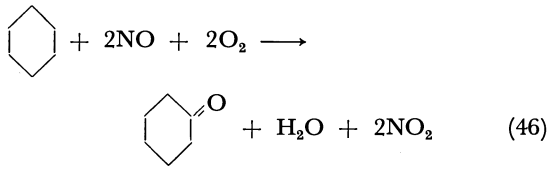
(46)

The above mechanisms might explain the fact that factor F is usually about 2 for alkenes and alkanes.

In the reaction of aromatic hydrocarbons the mechanism is not so simple. For example, for toluene the reaction mechanism[11,12] might be

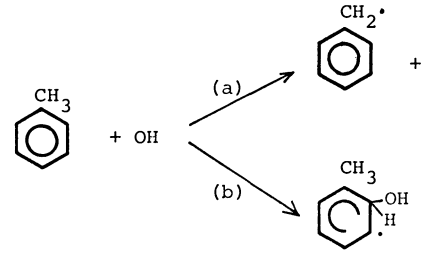

(47)

(48)

For path (a)

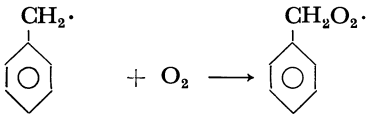

(49)

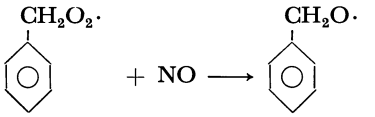

(50)

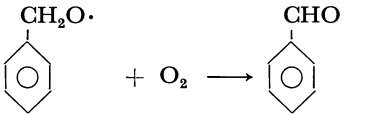

(51)

$$HO_2\cdot + NO \longrightarrow NO_2 + OH \qquad (22)$$

The overall reaction for path (a) is

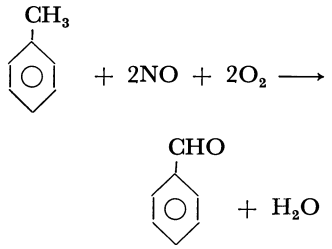

(52)

For path (b)

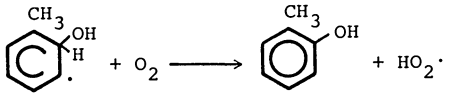

(53)

$$HO_2\cdot + NO \longrightarrow NO_2 + OH \qquad (22)$$

and

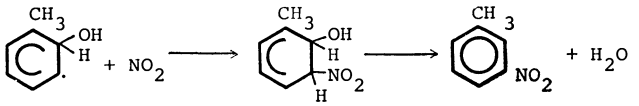

(54)

The formation of benzaldehyde, cresols, and *m*-nitrotoluene has been reported[11,12] in the photooxidation of the toluene/HONO/air system. According to the above mechanism, factor F for toluene should be less than two. However, small amounts of glyoxal and methylglyoxal have been detected in the photooxidation of the toluene/NO_2 system.[15] These products are also found in the photooxidation of the toluene or xylene/NO/H_2O/air systems.[13] The formation mechanism of these compounds is not yet clear, but it is most probable that they are formed after the aromatic ring is opened. Probably factor F for toluene becomes about 2 due to the radicals which are formed by the ring rupture.

The reaction mechanism of other aromatic compounds might be similar to that of toluene. The F factors for aromatic compounds are generally a little larger than 2, except for *m*-xylene. It is not known why the F factor of only *m*-xylene is larger than 3. Among the reaction rate constants of OH with xylene, only *m*-xylene is about twice faster than other *o*- and *p*-xylenes.[16] Probably the fraction of aromatic ring opening is larger in *m*-xylene.

In addition to the compounds listed in Table 1, determination of factor F was made for ethylene, which is of theoretical interest as the simplest alkene. Due to the poor efficiency of liquid nitrogen trapping of ethylene, the value for F scattered from 1.0 to 3.0, and is therefore not given in Table 1.

It has been suggested[17,18] that OH is the most important intermediate species during the initial stages of smog chamber experiments and that the contribution to attack on hydrocarbons by OH is much larger than O_3, HO_2, and $O(^3P)$. The contribution of O_3 to the consumption of hydrocarbons in the present study can be estimated as follows.

According to Reactions 7—9, the final steady state concentration of O_3 in our experiments is given by

$$[O_3]_{ss}^{final} = \frac{k_7[NO_2]^{final}}{k_9[NO]^{final}} \qquad (I)$$

where the value of k_7 is 0.08 min^{-1} except for the case of T.M.E. where it is 0.01 min^{-1}. The most recent value for k_9 is 26.5 $ppm^{-1}\ min^{-1}$.[19] The ratio of NO_2 to NO in the final measurement could be obtained experimentally, assuming that the concentration of NO_2 is equal to the value of total NO_x minus NO. The calculated final steady state concentrations of O_3 for several selected hydrocarbons are given in Table 2.

If hydrocarbons are consumed by OH and O_3, the concentration of hydrocarbons is given by the following equation, assuming that the concentrations of OH and O_3 are constant:

$$\frac{\ln[\text{hydrocarbon}]_0 - \ln[\text{hydrocarbon}]}{t} = k_a[OH] + k_b[O_3] \qquad (II)$$

where $[\text{hydrocarbon}]_0$ refers to the initial concentration of hydrocarbons, and k_a and k_b are the rate constants for the reaction of OH and O_3, respectively, with hydrocarbons. Since the initial and final concentrations for hydrocarbons and irradiation time, which is 2—3 h for alkenes, are known, the left hand side of Eq. II can be calculated. The values for k_b are reported for propylene,[20] *cis*-2-butene,[21] and T.M.E.[21] as 1.56×10^{-2}, 1.85×10^{-1}, and 1.55 $ppm^{-1}\ min^{-1}$, respectively. Therefore, the contribution of O_3 to the consumption of hydrocarbons at the final point of measurement can be

TABLE 2. CALCULATED VALUES FOR $[O_3]_{ss}^{final}$, $k_b\,[O_3]_{ss}^{final}$ AND THE LEFT HAND SIDE OF EQ. II FOR SELECTED ALKENES GIVEN IN TABLE 1

Compound	Run number in Table 1.	Irradiation time (min)	Calculated $[O_3]_{ss}^{final}$ (ppm)	$k_b\,[O_3]_{ss}^{final}$ (min^{-1})	$\frac{1}{t}\cdot\ln\frac{[hydrocarbon]_0}{[hydrocarbon]}$ (min^{-1})
Propylene	1	180	1.64×10^{-3}	2.6×10^{-5}	1.6×10^{-3}
	2	140	2.50	3.9	2.6
	3	140	1.29	2.0	3.1
cis-2-Butene	4	135	1.11	21	2.3
	5	150	1.05	19	3.2
T.M.E.[a] (2,3-Dimethyl-2-butene)	6	160	0.16	25	2.2
Cyclopentene	7	115	4.06	85[b]	8.6

a) Irradiation light intensity reduced to 1/8. b) Calculated using the rate constant for *cis*-2-butene+O_3 as k_b.

calculated by the form of $k_b[O_3]_{ss}^{final}$. The experimental decay rate of hydrocarbons and the calculated contributions of O_3 are given in Table 2 for propylene, *cis*-2-butene and T.M.E. The contribution of O_3 is less than 2 and 10% for propylene and *cis*-2-butene, respectively, and for T.M.E. nearly 10% at the final points in the measurements. These contributions of O_3 to other measured points would be much smaller, since ozone increases exponentially with irradiation time. The value for k_b is unknown for cycloalkanes. The effect on cyclopentene was calculated with use of the value of k_b for *cis*-2-butene. In this case the contribution by O_3 was also less than 10% (Table 2).

The contribution by O_3 should be very small in the case of alkanes and aromatics, because the reaction of ozone with alkanes and aromatics is extremely slow.

The results in Table 1 show that the long chain mechanism proposed by Heicklen *et al.*[3] and by Niki *et al.*[1] may be right and the value of factor F nearly equal to 2 can be used in computer simulation studies of the photooxidation process of a hydrocarbon and NO mixture.

The finding that factor F is approximately 2 regardless of the type and carbon number of hydrocarbons might allow us to propose a generalized oxidation chain mechanism which would be useful for the mathematical modeling of photochemical air pollution in an urban airshed. For alkenes the NO oxidation mechanism could be generalized as follows, referring to the mechanism given for *cis*-2-butene,

$$\text{(A)}\quad RH + OH \xrightarrow{+O_2} RO_2\cdot + H_2O$$
$$RO_2\cdot + NO \longrightarrow RO\cdot + NO_2$$
$$RO\cdot + O_2 \longrightarrow R'_2CO + R''O_2\cdot$$
$$R''O_2\cdot + NO \longrightarrow R'''_2CO + NO_2 + OH$$

where R'_2CO and R''_2CO represent aldehydes or ketones. Similarly, a generalized model for alkanes can be written as

$$\text{(B)}\quad RH + OH \xrightarrow{+O_2} RO_2\cdot + H_2O$$
$$RO_2\cdot + NO \longrightarrow RO\cdot + NO_2$$
$$RO\cdot + O_2 \longrightarrow RCHO + HO_2\cdot$$
$$HO_2\cdot + NO \longrightarrow OH + NO_2$$

Model (B) is equivalent to model (A) if $HO_2\cdot$ is recognized as $R'O_2\cdot$ and the difference in the type and the stoichiometric number of carbonyl compounds formed in the chain is ignored. In the case of aromatic hydrocarbons, path (a) initiated by H atom abstraction can be generalized just as for paraffins. However path (b) initiated by the OH addition and aromatic ring rupture path is difficult to be generalized at this stage since the reaction mechanism is far from being clarified. Nevertheless, from the evidence that the overall factor F is approximately 2 for most of the aromatic compounds, it is reasonable to adopt the generalized model of reaction (A) or (B) even for these compounds if the difference in the stoichiometric number and the type of oxidized compounds is ignored.

Thus, we propose a generalized kinetic model (A) or (B) for the NO oxidation chain processes in the presence of alkanes, alkenes, and aromatic hydrocarbons commonly present in the polluted urban atmosphere. This would be useful for the development of atmospheric photochemical air pollution modeling. Sveral reports[22–24] have appeared on the mathematical modeling of photochemical air pollution in an urban airshed. The mathematical modeling requires a kinetic reaction model for atmospheric reactions as well as models for atmospheric diffusion and transport processes. A kinetic model must satisfy certain requirements to be applicable to the atmospheric simulations. First, the model should predict the behavior of a complex mixture of hydrocarbons since a polluted urban atmosphere contains various hydrocarbon species. Second, since an atmospheric simulation model consists of a set of partial differential equations for diffusion and transport, the kinetic model must be compact enough to avoid excessive computation time for numerical integration. Model (A) or (B) satisfies these requirements. Since the models are common for various types of hydrocarbons, the chemical behavior of various hydrocarbon species is characterized only by the reaction rates with OH, O, and O_3. Thus, if it is combined with other typical reactions among NO, NO_2, O_3, RH, OH, and $RO_2\cdot$, the atmospheric simulation could be made by model (A) or (B).

References

1) H. Niki, E. E. Daby, and B. Weinstock, *Adv. Chem.*

Ser., **113**, 16 (1972).

2) K. L. Demerjian, J. A. Kerr, and J. G. Calvert, *Adv. Environ. Sci. Technol.*, **4**, 1 (1974).

3) J. Heicklen, K. Westberg, and N. Cohen, "Chemical Reactions in Urban Atmospheres," ed by C. Tuesday, Elsevier (1971) p. 55.

4) A. Gitchell, R. Simonaitis, and J. Heicklen, *J. Air Pollut. Control Assoc.*, **24**, 357 (1974).

5) A. C. Lloyd, K. R. Darnall, A. M. Winer, and J. N. Pitts, Jr., *J. Phys. Chem.*, **80**, 789 (1976).

6) W. H. Chan, R. J. Nordstrom, J. G. Calvert, and J. H. Shaw, *Environ. Sci. Technol.*, **10**, 674 (1976).

7) R. A. Cox and R. G. Derwent, *J. Photochem.*, **6**, 23 (1976/77).

8) C. H. Wu, C. C. Wang, S. M. Japar, L. I. Davis, Jr., M. Hanabusa, D. Killinger, H. Niki, and B. Weinstock, *Int. J. Chem. Kinet.*, **8**, 765 (1976).

9) A. M. Winer, J. W. Peters, J. P. Smith, and J. N. Pitts, Jr., *Environ. Sci. Technol.*, **8**, 1118 (1974).

10) C. W. Spicer and D. F. Miller *J. Air Pollut. Control Assoc.*, **26**, 45 (1976).

11) H. Akimoto, M. Hoshino, G. Inoue, M. Okuda, and N. Washida, Proceedings of International Conference on Photochemical Oxidant Pollution and Its Control, EPA-600/3-77-001a (1977).

12) M. Hoshino, H. Akimoto, and M. Okuda, *Bull. Chem. Soc. Jpn.*, **51**, 718 (1978).

13) H. Takagi, N. Washida, H. Akimoto, and M. Okuda, "Photooxidation of *o,m,p*-Xylene in the NO/H_2O/Air System," Paper presented at the National Meeting, Japan Society of Air Pollution, Fukuoka, November 1977.

14) W. P. L. Carter, K. D. Darnall, A. C. Lloyd, A. M. Winer, and J. N. Pitts, Jr., *Chem. Phys. Lett.*, **42**, 22 (1976).

15) K. Nojima, K. Fukaya, S. Fukui, and S. Kanno, *Chemosphere*, **4**, 77 (1975).

16) D. A. Hansen, R. Atkinson, and J. N. Pitts, Jr., *J. Phys. Chem.*, **79**, 1763 (1975).

17) E. D. Morris and H. Niki, *J. Phys. Chem.*, **75**, 3640 (1971).

18) G. J. Doyle, A. C. Lloyd, K. R. Darnall, A. M. Winer, and J. Pitts, Jr., *Environ. Sci. Technol.*, **9**, 237 (1975).

19) J. W. Birks, B. Schoemaker, T. J. Leck, and D. M. Hinton *J. Chem. Phys.*, **65**, 5181 (1976).

20) J. T. Herron and R. E. Huie, *J. Phys. Chem.*, **78**, 2085 (1974).

21) R. E. Huie and J. T. Herron, *Int. J. Chem. Kinet., Symp.*, **1**, 165 (1975).

22) S. D. Reynols, P. M. Roth, and J. H. Seinfeld, *Atmos. Environ.*, **7**, 1033 (1973).

23) A. Q. Eschenroeder and J. R. Martinez, *Adv. Chem. Ser.*, **113**, 101 (1972).

24) K. Takeuchi and F. Kimura, *Meterol. Geophys.*, **27**, 41 (1976).

The Crystal and Molecular Structures of Three (Acetylacetonato)-organoantimony(V) Compounds, [(acac)R_nSbX_{4-n}]

Nobuko KANEHISA, Kenichi ONUMA,** Shinzo UDA,*** Kiyoshi HIRABAYASHI,†
Yasushi KAI, Noritake YASUOKA, and Nobutami KASAI*

Department of Applied Chemistry, Faculty of Engineering, Osaka University, Yamadakami, Suita, Osaka 565

(Received February 13, 1978)

X-Ray crystal structure analyses of three (acetylacetonato)organoantimony(V) compounds have been conducted. Crystals of [(acac)$MeSbCl_3$] belong to the tetragonal system: $a=13.865(1)$, $c=24.935(5)$ Å, space group $I4_1/a$ with $Z=16$. [(acac)Me_2SbBr_2] forms monoclinic crystals: $a=9.247(1)$, $b=7.695(1)$, $c=9.104(1)$ Å, $\beta=106.94(1)°$, space group $P2_1/m$ with $Z=2$. Crystals of [(acac)Ph_2SbCl_2] (high-melting point form) belong to the monoclinic system: $a=14.733(11)$, $b=7.541(1)$, $c=16.014(13)$ Å, $\beta=92.66(1)°$, space group $P2_1/c$ with $Z=4$. All structures have been elucidated by the heavy atom method and refined by the block-diagonal least-squares procedure. Through the three compounds, the antimony atoms have a slightly distorted octahedral geometry with substituents on apical positions, slightly bent towards the planar acetylacetonato groups.

The chemistry of (acetylacetonato)organoantimony-(V) compounds of the type [(acac)R_nSbCl_{4-n}] ($n=1$ and R=Me, Et, or Ph; $n=2$ and R=Me, Et, or Ph; $n=3$ and R=Ph; and $n=4$ and R=Me, Et, or Ph)†† has been the subject of a number of recent papers.[1-6] Among them there are two possible configurations for [(acac)-$RSbCl_3$], and three for [(acac)R_2SbCl_2] (Fig. 1). Spectroscopic studies of these two types of compound left some ambiguities on their molecular structures.[2,4,5,7] In order to determine the exact configuration of these molecules by X-ray diffraction, (acetylacetonato)methyltrichloroantimony(V) [(acac)$MeSbCl_3$], (acetylacetonato)dimethyldibromoantimony(V) [(acac)Me_2SbBr_2], and (acetylacetonato)diphenyldichloroantimony(V) [(acac)Ph_2SbCl_2] have been chosen as typical examples of [(acac)$RSbCl_3$] and [(acac)R_2SbCl_2]. As [(acac)-Me_2SbCl_2] was untsable in the solid state, crystals of [(acac)Me_2SbBr_2] which were considered to have the same configuration as [(acac)Me_2SbCl_2] were subjected to X-ray structure analysis. Recrystallization of ([acac)-Ph_2SbCl_2] from benzene gave two kinds of crystals in different forms: long prismatic (mp 192 °C) and rhombohedral (mp 184.5 °C) crystals (Table 1). This promoted the crystal structure analysis of two forms which may consist of molecules of different configurations. Kroon[8] determined the X-ray molecular structure of the low-melting point form, independently, which agrees well with the results obtained by the present authors.[9] Therefore, the crystal structure analysis of only the high-melting point form will be described. Brief accounts of the X-ray molecular structure of the above-mentioned compounds have been published.[10-12]

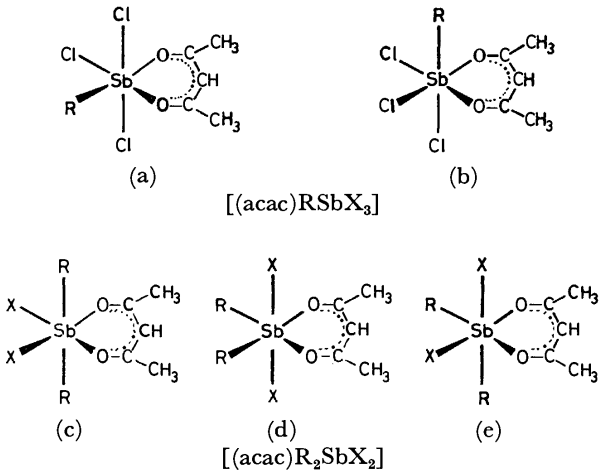

Fig. 1. Possible configurations of [(acac)$RSbX_3$] ((a) and (b)) and [(acac)R_2SbX_2] ((c), (d), and (e)). X=Cl or Br.

Experimental

Crystal Data. Crystals were all supplied by Professor R. Okawara and co-workers of this university. The unit-cell dimensions of [(acac)$MeSbCl_3$] and [(acac)Me_2SbBr_2] were determined by the least-squares fit of 2θ values of high angle reflections measured on a G. E. Single Crystal Orienter equipped on a Rigaku SG-2 goniometer. Those of [(acac)-Ph_2SbCl_2] were determined from Weissenberg photographs taken around the b and c axes, on which the Debye lines of tungsten were superimposed for calibration. In all cases nickel-filtered Cu $K\alpha$ radiation ($\lambda=1.5418$ Å) was used. Density measurements were carried out by the flotation method. Crystal data are given in Table 1.

Crystal structure analysis of [(acac)Me_2SbCl_2] instead of [(acac)Me_2SbBr_2] had been first intended, however, it was found during the preliminary X-ray work that all the [(acac)-Me_2SbCl_2] single crystals examined readily decomposed at room temperature to give powder patterns. Approximate unit-cell parameters were determined from oscillation and Weissenberg photographs: $a=9.00$, $b=7.59$, $c=9.05$ Å, $\beta=107.4°$, $U=590$ Å^3, space group $P2_1$ or $P2_1/m$, $D_c=1.82$ g·cm^{-3} for $Z=2$. These facts suggest that [(acac)Me_2SbCl_2] is isomorphous or at least iso-structural with [(acac)Me_2SbBr_2].

Intensities. *[(acac)$MeSbCl_3$] and [(acac)Me_2SbBr_2]:* Intensities were measured on a Rigaku automated, four-circle-

** Present address: Central Research Laboratory, Ajinomoto and Co., Ltd., Suzukicho, Kawasaki-ku, Kawasaki, Kanagawa 210.

*** Present address: Otake Factory, Daicel and Co., Ltd., Toei, Otake, Yamaguchi 739-06.

† On leave from Faculty of Textile Science and Technology, Shinshu University; Present address: Department of Filature, Faculty of Technology, Tokyo University of Agriculture and Technology, Nakamachi, Koganei, Tokyo 184.

†† acac: acetylacetonato group, Me: methyl group, Et: ethyl group, and Ph: phenyl group.

Table 1. Crystal data

Compound	[(acac)MeSbCl$_3$]	[(acac)Me$_2$SbBr$_2$]	[(acac)Ph$_2$SbCl] High-melting point form	[(acac)Ph$_2$SbCl] Low-melting point form[a]
F.W.	342.5	410.74	445.98	445.98
Crystal	colorless polyhedral	colorless square bipyramidal	colorless long prismatic	colorless rhombohedral
Crystal system	tetragonal	monoclinic	monoclinic	monoclinic
Systematic absence of reflections	$h+k+l=2n$ $00l$, $l=4n$ $hk0$, $h=2n$ $k=2n$	$0k0$, $k=2n$	$00k$, $k=2n$ $h0l$, $l=2n$	$0k0$, $k=2n$ $h0l$, $l=2n$
Space group	$I4_1/a$	$P2_1/m$	$P2_1/c$	$P2_1/c$
a [Å]	13.685(1)	9.247(1)	14.733(11)	13.24
b [Å]		7.695(1)	7.541(1)	9.22
c [Å]	24.935(5)	9.104(1)	16.014(3)	15.49
β [°]		106.94 (1)	92.66 (1)	109.24
U [Å^3]	4669.8	619.7 (1)	1777.2	1785.3
D_m [g·cm^{-3}]	1.95 ($ZnBr_2$ aq solution)	2.21 (CH_3Br/C_2H_5OH)	1.66 (ZnI_2 aq solution)	—
Z	16	2	4	4
D_x [g·cm^{-3}]	1.95	2.20	1.67	1.66
μ [cm^{-1}]	30	91	156	161

a) Our observation.

diffractometer using zirconium-filtered Mo $K\alpha$ radiation. The θ-2θ scan technique was employed, scan rate being 4° min^{-1}. The scan width in 2θ was from $-1.0°$ from the $K\alpha_1$ to 1.0° from $K\alpha_2$ peak, where θ_c is the calculated value of the Bragg angle using λ(Mo $K\alpha_1$) (=0.70926 Å). Backgrounds were measured for 10 s before and after the scan of each peak. Totals of 2270($\sin\theta/\lambda \leqq 0.64$) and 1454($\sin\theta/\lambda \leqq 0.64$) independent reflections were collected, of which 206 and 72 reflections were classified as unobserved, respectively. Two and three standard reflections (004 and 080, and 400, 005, and 040) were measured after every 25 and 50 reflections for [(acac)MeSbCl$_3$] and [(acac)Me$_2$SbBr$_2$], respectively. Lorentz and polarization corrections were made by the AICOM-C$_2$ computer attached to the diffractometer. Absorption correction was made for the [(acac)Me$_2$SbBr$_2$] data.

[*(acac)Ph$_2$SbCl$_2$*]: Using nickel-filtered Cu $K\alpha$ radiation, layers from 0 through 4 around the b axis were recorded by the multiple-film Weissenberg technique. Reflections of the layers from 0 through 2 around the c axis were also collected mainly for the interlayer scaling. Intensities were estimated visually by using a calibrated standard scale. A total of 1720 (1453 non-zero) independent reflections were obtained. Lorentz and polarization effects were corrected but no absorption correction was made.

Elucidation of the Structure

All the structures of the three complexes have been elucidated by the heavy atom method.

[*(acac)MeSbCl$_3$*]: The position of the antimony atom was readily reduced from a three-dimensional Patterson map, and the positions of the non-hydrogen atoms by the successive Fourier syntheses.

[*(acac)Me$_2$SbBr$_2$*]: The systematic absence of reflection determined the corresponding space group as either $P2_1/m$ or $P2_1$. Since the unit-cell contains two molecules, the following three possible cases have been examined: (1) $P2_1/m$, with the acac ligand positioned on the mirror plane, (2) $P2_1/m$, with the acac perpendicular to the mirror plane, or (3) $P2_1$, with the molecule itself having no symmetry. Approximate positions of the antimony and two bromine atoms obtained from the three-dimensional Patterson function excluded case (2). All the non-hydrogen atoms were located by the successive Fourier syntheses.

[*(acac)Ph$_2$SbCl$_2$*]: From the three-dimensional Patterson map, two sets of possible locations were obtained for the antimony and two chlorine atoms; (1) Sb (0.24, 0.25, 0.43), Cl (1) (0.30, 0.07, 0.53) and Cl(2) (0.14, 0.03, 0.39), or (2) Sb (0.24, 0.25, 0.43), Cl (1) (0.30, 0.43, 0.53), and Cl (2) (0.14, 0.03, 0.39). The successive two sets of Fourier syntheses favored the former parameters set, and located the non-hydrogen atoms.

Refinement

The structures determined were all refined by the block-diagonal least-squares procedure, the function minimized being $\Sigma w(\Delta F)^2$ using the HBLS V program.[13] Neutral atomic scattering factors used were taken from those of Hanson and co-workers.[14]

[*(acac)MeSbCl$_3$*]: The final $R_1=\sum||F_o|-|F_c||/\sum|F_o|=0.059$ and $R_2=\sum w(|F_o|-|F_c|)^2/\sum w|F_o|^2=0.059$ for 2064 non-zero reflections. The weighting scheme applied was: $w=(|F_{max}|/|F_o|)^2$ for $|F_o| \geqq 40.0$, $w=1.0$ for $40.0 \geqq |F_o| \geqq 15.0$, and $w=0.2$ for $|F_o|<15.0$.

[*(acac)Me$_2$SbBr$_2$*]: Two possible space group struc-

tures, $P2_1$ and $P2_1/m$ were refined isotropically, and a reasonable result obtained for $P2_1/m$. At the final stage of the refinement $F(020)$ was omitted from the calculation since it was largely affected by the extinction. Final anisotropic refinements with unit weight gave $R_1=0.076$ for 1381 non-zero reflections.

[(acac)Ph_2SbCl_2]: Anisotropic temperature factors were applied for the antimony and two chlorine atoms and w was taken as unity. The final $R_1=0.12$ for 1453 non-zero reflections.

The final positional and thermal parameters are given in Tables 2 and 3,[†††] respectively.

TABLE 2. THE ATOMIC FRACTIONAL COORDINATES ($\times 10^4$) ALONG WITH THEIR ESTIMATED STANDARD DEVIATION IN PARENTHESES

Atom	x	y	z
[(acac)$MeSbCl_3$]			
Sb	2161 (4)	3193 (4)	188 (2)
Cl (1)	3089 (21)	3749 (19)	917 (10)
Cl (11)	1519 (21)	1870 (21)	688 (12)
Cl (21)	2978 (19)	4271 (21)	−411 (11)
O (1)	3328 (39)	2295 (46)	42 (24)
O (2)	1508 (45)	2570 (48)	−478 (23)
C (1)	4387 (66)	1166 (71)	−348 (46)
C (2)	3441 (61)	1687 (59)	−347 (34)
C (3)	2762 (74)	1487 (67)	−740 (37)
C (4)	1833 (65)	1919 (59)	−793 (33)
C (5)	1164 (81)	1634 (82)	−1237 (42)
C (6)	927 (69)	272 (43)	4134 (72)
[(acac)Me_2SbBr_2]			
Sb	5352 (1)	25	2618 (1)
Br (1)	7257 (2)	25	993 (2)
Br (2)	7388 (2)	25	5285 (2)
O (1)	3583 (15)	25	550 (15)
O (2)	3618 (16)	25	3759 (16)
C (1)	1136 (26)	25	−1333 (23)
C (2)	2158 (25)	25	381 (23)
C (3)	1480 (24)	25	1542 (26)
C (4)	2171 (22)	25	3060 (26)
C (5)	1235 (28)	25	4184 (28)
C (11)	5282 (21)	5285 (23)	2606 (18)
[(acac)Ph_2SbCl_2] (high-melting point form)			
Sb	2365 (1)	2417 (5)	4338 (1)
Cl (1)	3077 (8)	585 (15)	5431 (6)
Cl (2)	1198 (7)	345 (16)	3876 (7)
O (1)	3333 (17)	4413 (39)	4686 (16)
O (2)	1877 (14)	4273 (32)	3443 (12)
C (1)	4330 (27)	6905 (59)	4581 (24)
C (2)	3534 (26)	5750 (60)	4239 (24)
C (3)	3154 (27)	6389 (59)	3465 (25)
C (4)	2311 (19)	5597 (47)	3144 (18)
C (5)	1888 (27)	6469 (62)	2344 (25)
C (11)	3318 (21)	1527 (49)	3446 (20)
C (12)	2908 (25)	1149 (58)	2624 (23)
C (13)	3550 (27)	488 (60)	1970 (24)
C (14)	4481 (30)	245 (67)	2196 (27)
C (15)	4808 (27)	595 (61)	3077 (25)
C (16)	4216 (26)	1270 (58)	3668 (23)
C (21)	1483 (22)	3618 (52)	5247 (20)
C (22)	1394 (27)	5469 (62)	5194 (24)
C (23)	807 (26)	6277 (60)	5740 (24)
C (24)	362 (24)	5204 (57)	6336 (22)
C (25)	500 (30)	3418 (70)	6396 (27)
C (26)	1032 (23)	2547 (72)	5788 (21)

Results and Discussion

Molecular Structure. The atom numbering scheme is given in Fig. 2. A stereoscopic drawing of the molecules are shown in Fig. 3. Bond lengths and bond angles are listed in Table 4. Least-squares planes of various groups are presented in Table 5.

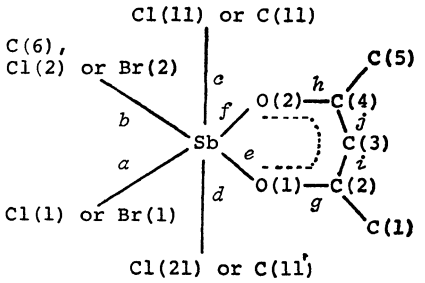

Fig. 2. The numbering scheme of atoms.

As seen in Fig. 3, the antimony atoms have slightly distorted octahedral geometries through the three compounds. In all cases the substituents are on apical positions, slightly bend towards the acetylacetonato groups.

In [(acac)$MeSbCl_3$] the methyl group has been located on the basal plane: of the two possible configurations in Fig. 1, (a) has been established. In [(acac)-Me_2SbBr_2] and [(acac)Ph_2SbCl_2] the alkyl or aryl groups occupy the apical positions: the (c) configuration being found among the three possible ones in Fig. 1. From the PMR study[5] it has been concluded that both phenyl groups in [(acac)Ph_2SbCl_2] are approximately perpendicular to the bisector of the Cl–Sb–Cl angle. In the high-melting point form, one phenyl ring (C(11)–C(16)) is approximately perpendicular [89°] to the bisector, however, the other (C(21)–C(26)) is approximately parallel [3°]: the dihedral angle between two rings being 92° (Fig. 4). In the low-melting point form, both phenyl rings are neither perpendicular nor parallel to the bisector: each phenyl ring makes an angle of about 65 or 77° to the bisector, and the dihedral angle between them is about 38° (Fig. 4).[8] This appears to be the main difference between the molecular structures of the two isomers.

Among the three Sb–Cl bond lengths in [(acac)-$MeSbCl_3$] those on apical positions [2.380(3) and 2.366(3) Å] are slightly longer than those on the basal plane [2.345(3) Å]. The Sb–Cl bond lengths in the high- and low-melting point forms are equal [av. 2.42 Å]. All of these Sb–Cl lengths are significantly longer than those in other antimony compounds.[15–20] The Sb–Br bond lengths in [(acac)$MeSbBr_2$] are 2.610(3) and 2.603(3) Å, which are slightly longer than those in $SbBr_3$ [2.52(3) Å].[21]

††† The observed and calculated structure factors are kept at the Chemical Society. Document No. 7824.

TABLE 3. THERMAL PARAMETERS ALONG WITH THEIR ESTIMATED STANDARD DEVIATIONS IN PARENTHESES
Anisotropic thermal parameters ($\times 10^5$) are of the form: $\exp[-(\beta_{11}h^2+\beta_{22}k^2+\beta_{33}l^2+\beta_{12}hk+\beta_{23}kl+\beta_{13}hl)$, and isotropic ones are B (in Å^2).

Atom	β_{11} or B	β_{22}	β_{33}	β_{12}	β_{23}	β_{13}
[(acac)MeSbCl$_3$]						
Sb	399 (1)	482 (1)	136 (1)	144 (1)	−61 (1)	−45 (1)
Cl (1)	890 (2)	618 (2)	179 (4)	44 (3)	−130 (1)	−309 (2)
Cl (11)	709 (2)	742 (2)	287 (1)	−277 (3)	228 (2)	−2 (2)
Cl (21)	628 (2)	889 (2)	209 (1)	−51 (3)	299 (2)	22 (1)
O (1)	419 (3)	710 (4)	209 (1)	432 (7)	−106 (4)	−174 (3)
O (2)	592 (4)	712 (4)	193 (1)	257 (7)	−294 (4)	−230 (4)
C (1)	466 (5)	611 (6)	355 (3)	464 (10)	−144 (7)	−43 (6)
C (2)	466 (5)	408 (5)	178 (2)	112 (8)	15 (5)	69 (5)
C (3)	725 (7)	547 (6)	185 (2)	272 (10)	−103 (5)	−6 (6)
C (4)	608 (6)	401 (5)	155 (2)	−7 (9)	−47 (5)	−84 (5)
C (5)	866 (8)	876 (8)	224 (2)	159 (14)	−317 (7)	−457 (7)
C (6)	587 (6)	662 (7)	290 (2)	635 (11)	−151 (7)	95 (7)
[(acac)Me$_2$SbBr$_2$]						
Sb	988 (1)	1836 (2)	838 (1)	0	0	436 (2)
Br (1)	1195 (3)	3117 (6)	1230 (3)	0	0	959 (5)
Br (2)	1333 (3)	2767 (5)	996 (3)	0	0	133 (4)
O (1)	1096 (18)	3271 (41)	1037 (18)	0	0	734 (30)
O (2)	1141 (19)	4695 (56)	1040 (19)	0	0	947 (32)
C (1)	1333 (32)	4680 (88)	822 (26)	0	0	−377 (46)
C (2)	1525 (32)	2693 (54)	1035 (27)	0	0	585 (48)
C (3)	961 (27)	5118 (96)	1302 (32)	0	0	239 (48)
C (4)	798 (24)	4468 (82)	1470 (33)	0	0	836 (46)
C (5)	1572 (36)	4856 (94)	1574 (37)	0	0	2006 (62)
C (11)	2678 (33)	1933 (32)	1695 (25)	501 (56)	605 (49)	2704 (49)
[(acac)Ph$_2$SbCl$_2$] (high-melting point form)						
Sb	377 (10)	939 (48)	265 (8)	142 (69)	−43 (57)	−5 (12)
Cl (1)	780 (69)	1624 (262)	298 (38)	942 (228)	590 (177)	75 (81)
Cl (2)	567 (58)	1610 (256)	529 (52)	−628 (210)	−551 (209)	166 (87)
O (1)	4.3 (6)					
O (2)	2.7 (4)					
C (1)	4.7 (9)					
C (2)	4.1 (8)					
C (3)	4.3 (9)					
C (4)	2.2 (6)					
C (5)	4.6 (9)					
C (11)	2.6 (6)					
C (12)	3.9 (8)					
C (13)	4.4 (9)					
C (14)	5.4 (10)					
C (15)	4.5 (9)					
C (16)	4.0 (8)					
C (21)	2.9 (7)					
C (22)	4.3 (9)					
C (23)	4.2 (8)					
C (24)	3.5 (7)					
C (25)	5.3 (10)					
C (26)	4.2 (7)					

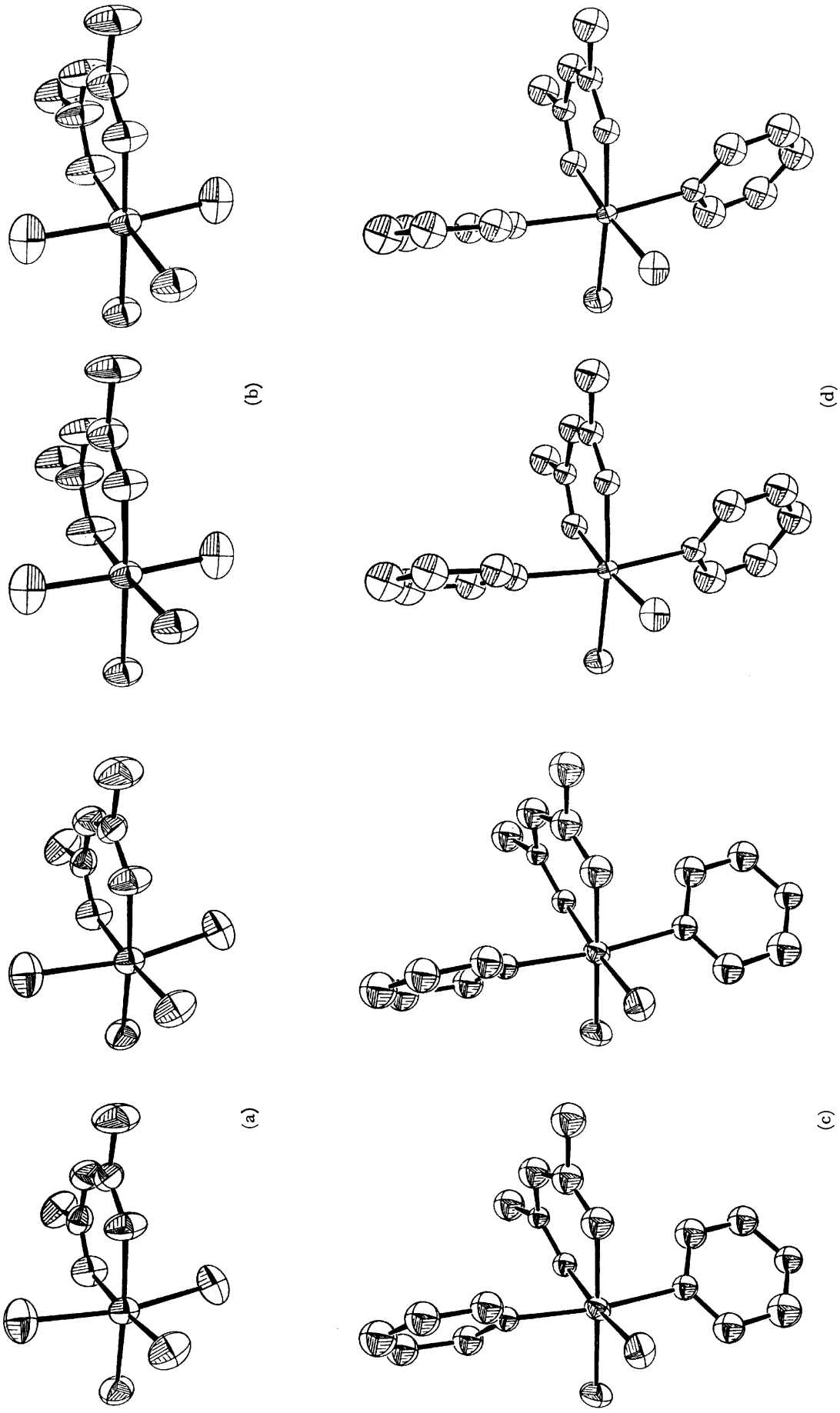

Fig. 3. The stereoscopic drawing of (a) [(acac)$MeSbCl_3$], (b) [(acac)Me_2SbBr_2], (c) [(acac)Ph_2SbCl_2](high-melting point form) and (d)[(acac)Ph_2SbCl_2] (low-melting point form).

TABLE 4. BOND LENGTHS AND BOND ANGLES (E.s.d.'s in parentheses)
The names of the bonds, *a*, *b*, *c*,..., and *l*, are the same as those given in Fig. 2.

	[(acac)·MeSbCl$_3$]	[(acac)·Me$_2$SbBr$_2$]	[(acac)Ph$_2$SbCl$_2$] High-melting point form	[(acac)Ph$_2$SbCl$_2$] Low-melting point form[8]
(a) Bond lengths (l/Å)				
Sb–X (X=Cl or Br)				
a	2.345(3)	2.610(3)	2.249(12)	2.415(3)
b		2.603(3)	2.414(12)	2.421(3)
c	2.366(3)			
d	2.380(3)			
Sb–C(R) (R=Me or Ph)				
b	2.134(11)			
c		2.144(20)	2.16 (4)	2.132(12)
d		2.144(20)	2.19 (4)	2.127(12)
Acetylacetonato group				
e	2.048(6)	2.104(14)	2.13 (3)	2.116(10)
f	2.069(7)	2.150(15)	2.11 (3)	2.117(10)
g	1.288(11)	1.28 (3)	1.28 (5)	1.26 (2)
h	1.269(11)	1.30 (3)	1.29 (4)	1.26 (2)
i	1.378(13)	1.38 (3)	1.42 (6)	1.38 (2)
j	1.408(13)	1.34 (3)	1.45 (6)	1.40 (2)
k	1.478(14)	1.57 (3)	1.54 (6)	1.50 (2)
l	1.489(14)	1.52 (4)	1.55 (6)	1.53 (2)
O(1)···O(2)	2.833 (9)	2.91 (2)	2.86 (4)	2.900[a]

	[(acac)·MeSbCl$_3$]	[(acac)·Me$_2$SbBr$_2$]	[(acac)Ph$_2$SbCl$_2$] High-melting point form	[(acac)Ph$_2$SbCl$_2$] Low-melting point form[8]
(b) Bond angles(ϕ/°)				
Around Sb				
a,*b*	99.0(3)	96.0(1)	97.5(4)	95.7(1)
a,*c*	92.4(1)	91.2(5)	91.6(10)	93.4(4)
a,*d*	91.8(1)	91.2(5)	90.5(11)	91.9(4)
a,*e*	84.8(2)	88.3(4)	87.3(8)	88.2(3)
a,*f*	171.8(2)	174.7(4)	172.2(7)	173.6(3)
b,*c*	96.7(3)	91.0(5)	94.1(10)	91.3(4)
b,*d*	93.4(3)	91.0(5)	92.0(11)	94.5(4)
b,*e*	175.4(3)	175.7(4)	175.1(9)	175.2(3)
b,*f*	89.2(3)	89.3(4)	90.3(7)	89.7(3)
c,*d*	168.4(1)	176.7(7)	173.3(14)	171.6(5)
c,*e*	85.7(2)	88.9(7)	86.8(13)	84.9(9)
c,*f*	87.0(2)	88.7(7)	88.2(12)	88.8(9)
d,*e*	83.9(2)	88.9(7)	86.9(13)	88.9(9)
d,*f*	87.4(2)	88.7(7)	88.9(12)	85.3(9)
Acetylacetonato group				
e,*f*	87.0(3)	86.4(5)	84.9(10)	86.5(4)
i,*j*	126.3(9)	127.1(23)	117.8(38)	120.7(15)
e,*g*	128.0(6)	127.7(14)	125.5(28)	127.9(9)
f,*h*	129.4(6)	124.7(14)	127.4(22)	126.5(9)
g,*i*	125.7(8)	126.2(21)	131.6(42)	125.2(15)
h,*j*	123.6(8)	128.0(22)	128.2(34)	126.7(15)
g,*k*	114.7(8)	114.8(19)	116.0(38)	114.1(15)
h,*l*	115.4(8)	112.1(20)	116.7(32)	113.5(15)
k,*i*	119.6(9)	119.0(21)	112.4(38)	120.8(15)
j,*l*	121.0(9)	119.9(22)	115.1(34)	119.7(15)

a) Calculated from the data of Kroon *et al.*[8]

TABLE 5. LEAST-SQUARES PLANES AND ATOM DEVIATIONS
Plane equations are of the form $AX+BY+CZ+D=0$, where X, Y, Z, and D are measured in Å units: $X=ax$, $Y=by$, and $Z=cz$ for [(acac) MeSbCl$_3$] and $X=ax+cz\cos\beta$, $Y=by$, and $Z=cz\sin\beta$ for both [(acac)Me$_2$SbBr$_2$] and [(acac)Ph$_2$SbCl$_2$].

Acetylacetonato group							
[(acac)MeSbCl$_3$]	$-0.3954X+0.5724Y-0.7183Z+4.0109=0$						
	O(1)	O(2)	C(1)	C(2)	C(3)	C(4)	C(5)
	0.015	−0.014	−0.005	−0.004	−0.002	0.001	0.009
[(acac)Me$_2$SbBr$_2$]	$Y=0.25$ (mirror plane)						
[(acac)Ph$_2$SbCl$_2$]	(high-melting point form) $0.5973X-0.5924Y-0.5407Z+3.3379=0$						
	0.039	−0.050	−0.103	0.024	0.108	0.012	−0.022
[(acac)Ph$_2$SbCl$_2$]	(low-melting point form)[a] $0.0263X-0.8640Y-0.5029Z+1.8036=0$						
	0.031	−0.039	−0.056	0.022	0.056	−0.001	−0.009
Phenyl rings							
[(acac)Ph$_2$SbCl$_2$]	(high-melting point form)						
Ring(i)	$-0.2109X-0.9411Y+0.2643Z+0.5903=0$						
	C(11)	C(12)	C(13)	C(14)	C(15)	C(16)	
	−0.014	0.022	0.004	−0.021	0.023	−0.012	
Ring(ii)	$-0.0749X-0.1134Y-0.6520Z+7.1140=0$						
	C(21)	C(22)	C(23)	C(24)	C(25)	C(26)	
	−0.008	−0.021	0.019	0.014	−0.045	0.042	

a) Calculated from the data of Kroon *et al.*[8] The original numbering scheme of atoms are converted into as those given in Fig. 2.

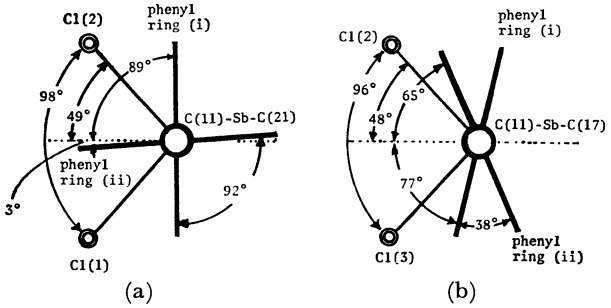

Fig. 4. The dihedral angles between the bisector(dotted line) of chloro substituents and phenyl groups in [(acac)-Ph_2SbCl_2]. (a) high-melting point form, and (b) low-melting point form.

The Sb–C(Me) bond lengths in [(acac)$MeSbCl_3$] and [(acac)Me_2SbBr_2] are standard values [2.134(11) and 2.144(20) Å, respectively] compared with those in hexa-coordinated antimony compounds: 2.10 and 2.14 Å in $Sb(CH_3)_3$[22] and 2.02(5) Å in $Me_3SbFe(CO)_4$.[23] The Sb–C(Ph) bond lengths in the high-melting point form of [(acac)Ph_2SbCl_2] are also standard values [2.16(4) and 2.19(4) Å] compared with those in the low-melting point form [2.132(12) and 2.127(12) Å] and also in $Ph_4Sb_2Cl_6$ [2.125(9) Å].[24]

The Sb–O bond lengths in [(acac)$MeSbCl_3$] [2.069(7) and 2.048(6) Å] are shorter than those in [(acac)Me_2-$SbBr_2$] [2.104(14) and 2.150(15) Å] and [(acac)Ph_2-$SbCl_2$] [2.13(3) and 2.11(3) Å].

The acetylacetonato groups are planar: in [(acac)-Me_2SbBr_2] being exactly planar because it lies on a crystallographic mirror plane together with the antimony and two bromine atoms. In [(acac)$MeSbCl_3$] and [(acac)Ph_2SbCl_2] (low-melting point from) the acetylacetonato groups are also planar: maximum deviations of atoms from the plane, Δ_{max} being 0.02 and 0.06 Å, respectively. The mean planes are almost coplanar with the plane defined by Sb, O(1), and O(2) atoms, the dihedral angles between them being 1.2 and 1.4°, respectively. However, the planarity of the acetylacetonato group in [(acac)Ph_2SbCl_2] (high-melting point form) is not standard [Δ_{max}=0.11 Å], the mean plane being bent by 15.0° away from the plane made by Sb, O(1), and O(2) atoms. This kind of bending has been found in other acetylacetonato compounds, [$Zr(acac)_4$][25] [22.6°] and [$Y(acac)_3 \cdot 3H_2O$][26] [18.9°]. In all cases the bond lengths and bond angles around the acetylacetonato ligands are standard compared with those of Lingafelter's standard data.[27]

The average bond length of the phenyl groups in [(acac)Ph_2SbCl_2] is 1.42 Å (high-melting point form)

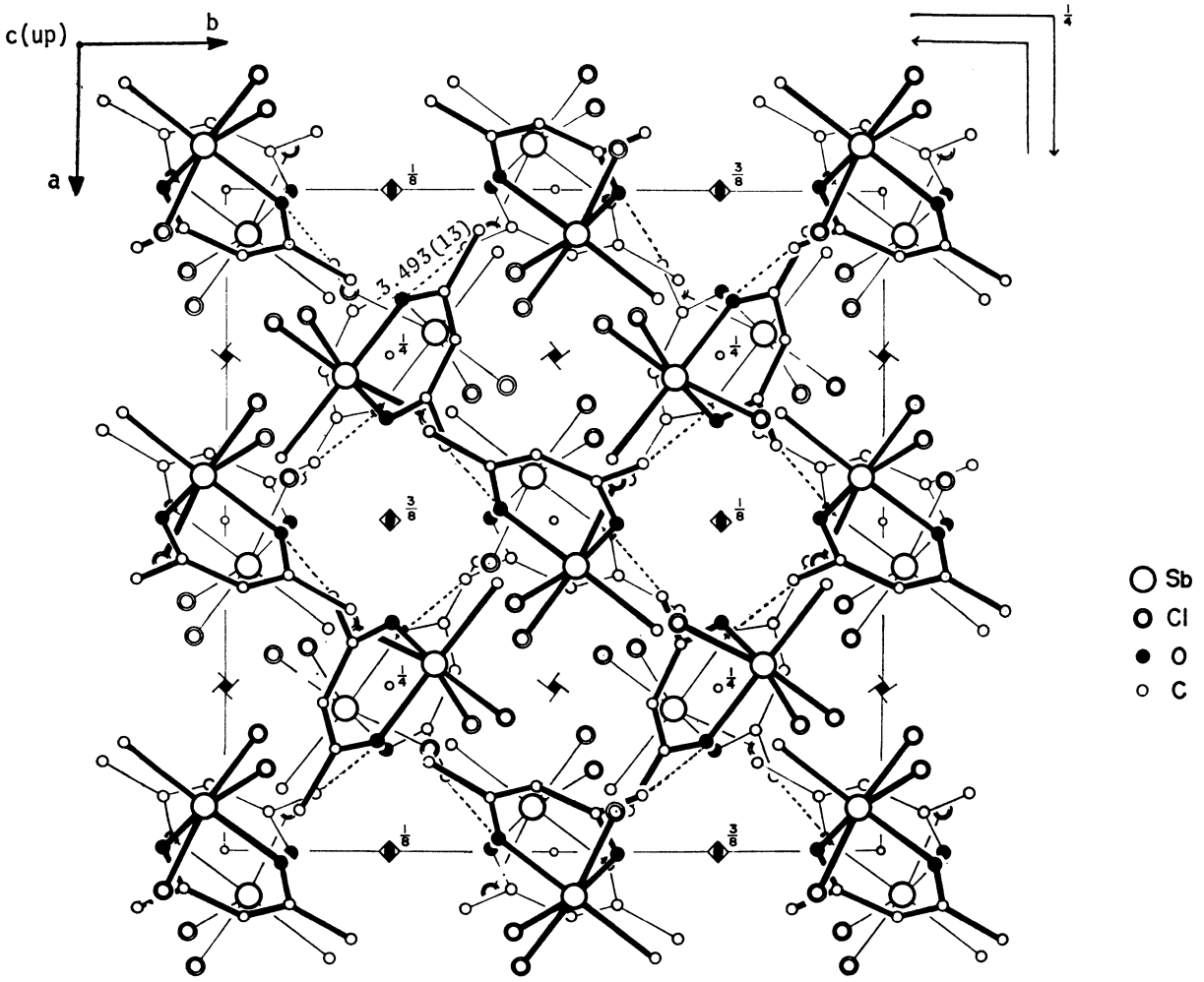

Fig. 5. The crystal structure of [(acac)$MeSbCl_3$] projected along the c axis.

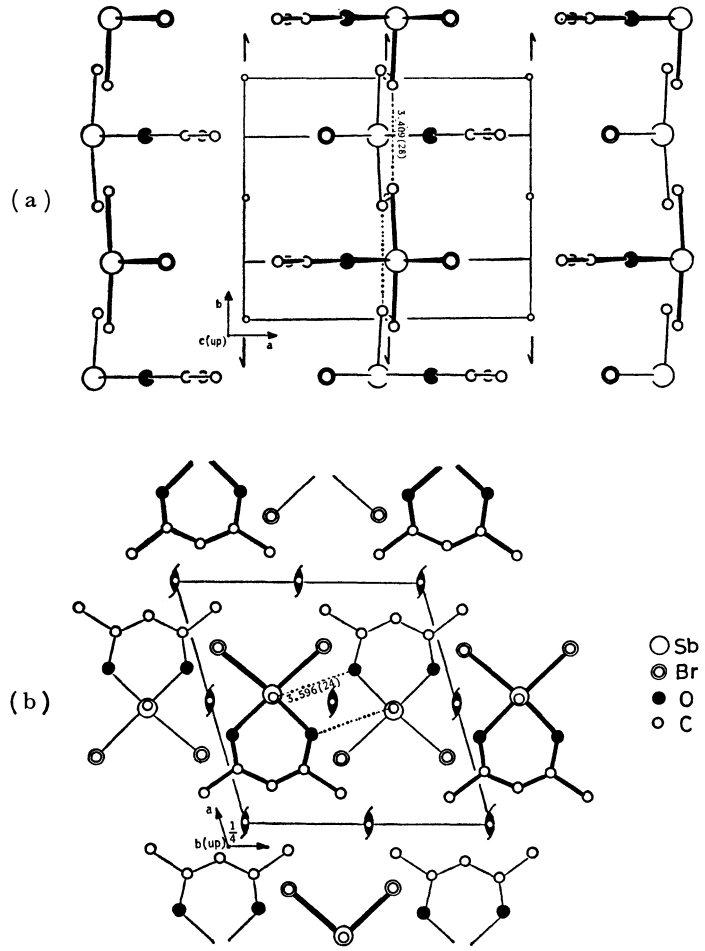

Fig. 6. (a) The crystal structure of [(acac)Me_2SbBr_2] projected along the c axis.
(b) The crystal structure of [(acac)Me_2SbBr_2] projected along the b axis.

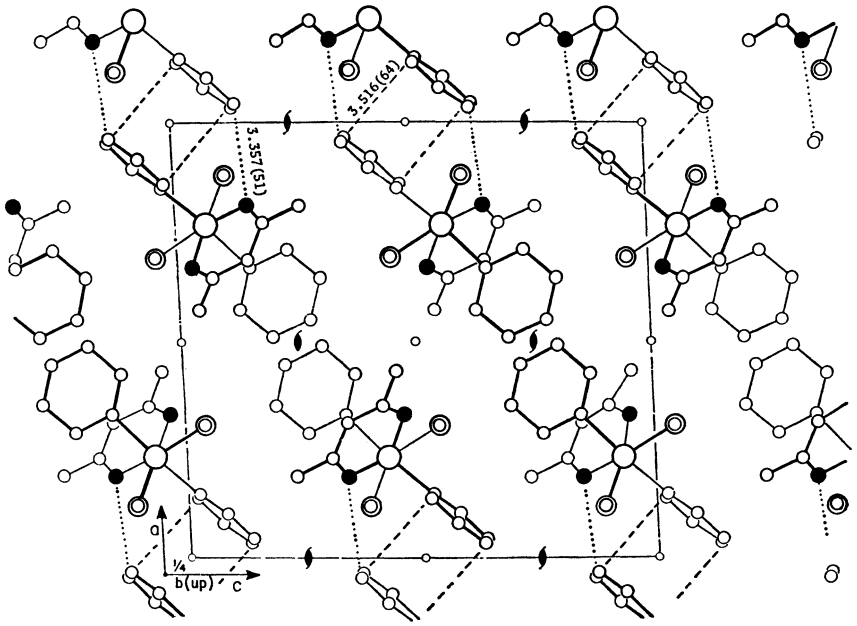

Fig. 7. The crystal structure of [(acac)Ph_2SbCl_2] (high-melting point form) projected along the b axis.

TABLE 6. SHORT INTERMOLECULAR ATOMIC CONTACTS LESS THAN 3.8 Å [*l*/Å] (E.s.d.'s in parentheses)

[(acac)$MeSbCl_3$]

Cl(1)···Cl(21)[a]	3.764(4)	Cl(11)···C(6)[e]	3.763(11)	key:			
Cl(1)···O(2)[a]	3.750(7)	C(6)···Cl(11)[e]	3.763(11)	a	0.75−y,	0.25+x,	0.25+z
Cl(21)···Cl(1)[b]	3.764(4)	Cl(1)···C(1)[f]	3.701(12)	b	−0.25+y,	0.75−x,	−0.25+z
O(2)···Cl(1)[b]	3.750(7)	O(1)···C(5)[f]	3.493(13)	e	0.25−y,	−0.25+x,	−0.25+z
C(1)···Cl(1)[c]	3.701(12)			d	−x,	1−y,	−z
C(5)···O(1)[c]	3.493(13)			c	−x,	0.5 −y,	z
C(6)···C(6)[d]	3.726(22)			f	0.25+y,	0.25−x,	0.25+z

[(acac)Me_2SbBr_2]

C(11)···C(11′)[a]	3.409(28)	O(2)···C(11′)[g]	3.596(24)	key:			
C(11′)···C(11)[b]	3.409(28)	C(12)···O(2)[h]	3.596(24)	a	x,	1+y,	z
C(3)···Br(1)[c]	3.789(24)	O(2)···C(11)[h]	3.596(24)	b	x,	−1+y,	z
Br(1)···C(3)[d]	3.789(24)			c	−1+x,	y,	z
C(11)···O(1)[e]	3.744(24)			d	1+x,	y,	z
O(1)···C(11′)[e]	3.744(24)			e	1−x,	0.5+y,	−z
C(11′)···O(1)[f]	3.744(24)			f	1−x,	−0.5+y,	−z
O(1)···C(11)[f]	3.744(24)			g	1−x,	0.5+y,	1−z
C(11)···O(2)[g]	3.596(24)			h	1−x,	−0.5+y,	1−z

[(acac)Ph_2SbCl_2] (high-melting point form)

O(1)···C(13)[a]	3.657(54)	O(2)···C(24)[h]	3.357(51)	key:			
C(1)···Cl(1)[b]	3.632(46)	C(21)···C(23)[h]	3.656(59)	a	x,	0.5−y,	0.5+z
C(1)···C(15)[b]	3.769(64)	C(21)···C(24)[h]	3.731(59)	b	x,	1+y,	z
C(1)···C(16)[b]	3.603(62)	C(22)···C(23)[h]	3.746(65)	c	x,	−1+y,	z
Cl(1)···C(1)[c]	3.632(46)	C(22)···C(24)[h]	3.516(64)	d	x,	0.5−y,	−0.5+z
C(15)···C(1)[c]	3.769(64)	C(22)···C(25)[h]	3.783(70)	e	1−x,	0.5+y,	0.5−z
C(16)···C(1)[c]	3.603(62)	C(23)···C(21)[h]	3.656(59)	f	−x,	−y,	1−z
C(13)···O(1)[d]	3.657(54)	C(23)···C(22)[h]	3.746(65)	g	1−x,	1−y,	1−z
C(1)···C(14)[e]	3.630(67)	C(23)···C(26)[h]	3.675(70)	h	−x,	1−y,	1−z
C(15)···C(14)[e]	3.699(68)	C(24)···O(2)[h]	3.357(51)	i	1−x,	−0.5+y,	0.5−z
C(3)···C(14)[e]	3.786(67)	C(24)···C(21)[h]	3.731(59)				
Cl(2)···C(25)[f]	3.794(54)	C(24)···C(22)[h]	3.516(64)				
C(25)···Cl(2)[f]	3.794(54)	C(25)···C(22)[h]	3.783(70)				
O(1)···C(1)[g]	3.721(53)	C(26)···C(23)[h]	3.675(70)				
C(1)···O(1)[g]	3.721(53)	C(14)···C(1)[i]	3.630(67)				
C(1)···C(1)[g]	3.702(89)	C(14)···C(3)[i]	3.786(67)				
C(1)···C(16)[g]	3.713(62)	C(14)···C(15)[i]	3.699(68)				
C(16)···C(1)[g]	3.713(62)						

[(acac)Ph_2SbCl_2] (low-melting point form)[a)]

O(1)···C(25)[a]	3.673	C(3)···C(24)[c]	3.673	key:			
O(1)···C(26)[a]	3.572	C(14)···C(22)[c]	3.780	a	−x,	−y,	−z
C(1)···C(26)[a]	3.700	C(22)···C(14)[d]	3.780	b	x,	0.5−y,	0.5+z
C(25)···O(1)[a]	3.738	C(24)···C(1)[d]	3.789	c	x,	1+y,	z
C(26)···O(1)[a]	3.572	C(24)···C(3)[d]	3.673	d	x,	−1+y,	z
C(26)···C(1)[a]	3.700	C(1)···Cl(1)[e]	3.756	e	x,	0.5−y,	−0.5+z
Cl(1)···C(1)[b]	3.756	C(3)···C(12)[e]	3.695	f	1−x,	0.5+y,	0.5−z
C(12)···C(3)[b]	3.695	C(25)···C(14)[e]	3.790	g	e1−x,	−0.5+y,	0.5−z
C(14)···C(25)[b]	3.790	C(15)···O(2)[f]	3.639				
C(1)···C(24)[c]	3.789	O(2)···C(15)[f]	3.639				

a) Calculated from the data of Kroon *et al.*,[8)] in which e.s.d.'s are not given. The original numbering scheme of atoms are converted into as those given in Fig. 2.

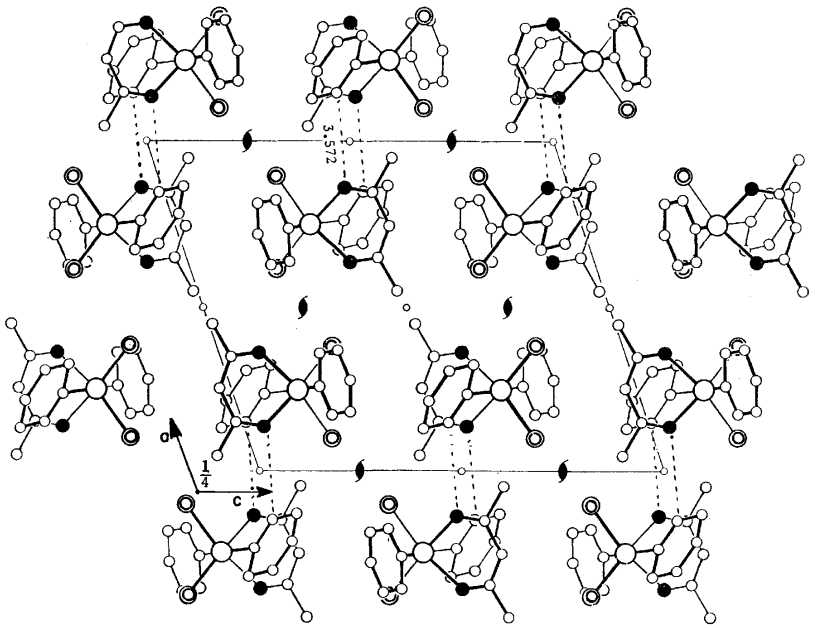

Fig. 8. The crystal structure of [(acac)Ph_2SbCl_2] (low-melting point form) projected along the b axis. (Drawn by using the data of the present authors.[9])

and 1.39 Å (low-melting point form[8]) respectively.

Crystal Structure. Crystal structures of the three compounds are respectively shown in Figs. 5, 6, and 7. In Fig. 8 the crystal structure of [(acac)Ph_2SbCl_2] (low-melting point form) is given using the data of Kroon *et al.*[8] Figures 9 shows a stereoscopic drawing of the packing of the former three crystals. Short intermolecular atomic contacts less than 3.8 Å are listed in Table 6.

[*(acac)$MeSbCl_3$*]: As seen in Fig. 5, in the tetragonal unit-cell molecules are arranged in helical manner along the crystallographic 4_1 screw axis, and each of these molecules is paired by the center of symmetry with a molecule to form a double helical arrangement along the c axis. In the four-fold helical arrangement of molecules, the closest atomic contacts occur between the methyl groups and the oxygen atoms of the acetylacetonato groups of the adjacent molecules of upper and lower steps [C(5)···O(1)=3.493(13) Å, Fig. 5].

[*(acac)Me_2SbBr_2*]: Along the b axis a pile of molecules forms a column, in which both methyl groups in apical positions of the molecule have the closest contacts with the other molecules above and below [C(11)···C(11′)^a =C(11′)···C(11)^b=3.409(28) Å, Fig. 6(a)]. Each molecule in the column has close contact with molecules in the adjacent column, related by the two-fold screw axis [C(11)···O(2)^g and O(2)···C(11′)^g, both 3.596 (24) Å, Fig. 6(b)], by which the two columns are tied. An infinite sheet parallel to the b and c axes is formed by rather close contacts with the adjacent tied columns along the c axis, and the parallel stack of these infinite sheets produces the crystal (Fig. 6(b)).

[*(acac)Ph_2SbCl_2] (High-melting point form)*: Figure 7 shows that the molecules lie approximately parallel to the (101) plane. There are many close atomic contacts, the closest one being [O(2)···C(24)^h or C(24)···O(2)^h, 3.357(51) Å] between a pair of molecules related by the center of symmetry. Along the b axis each molecule has rather close contacts with the other molecules above and below: the shortest distance being 3.603(62) Å [C(1)···C(16)^b or C(16)···C(1)^c]. Molecules related by the center of symmetry have additional close contacts between the acetylacetonato and phenyl carbon atoms.

(Low-melting point form): Molecules lie approximately parallel to the (100) plane (Fig. 8). There are several close atomic contacts including the closest one [O(1)··· C(26)^a or C(26)···O(1)^a, 3.572 Å] between a pair of molecules related by the center of symmetry. Comparison of the crystal structures of the two forms indicates that the low-melting poing form has a looser packing and smaller number of short inter-atomic contacts than the high-melting point form (Table 6). These facts possibly contribute to the difference in melting point between the two forms.

Computations throughout the present study were carried out on a NEAC 2200-700 computer at Osaka University. Figures 3, and 9 were drawn on a NUMERICON 7000 system at Osaka University using a local version of ORTEP.[28]

The authors wish to express their deep thanks to Professor Rokuro Okawara and his co-workers for many helpful discussions and kindess in supplying crystals.

References

1) N. Nishii, M. Shindo, Y. Matsumura, and R. Okawara, *Inorg. Nucl. Chem. Lett.*, **5**, 529 (1969).

2) Y. Kawasaki and R. Okawara, *Bull. Chem. Soc. Jpn.*, **40**, 428 (1967).

3) H. A. Meinema and J. G. Noltes, *J. Organomet. Chem.* **16**, 257 (1969).

4) N. Nishii, Y. Matsumura, and R. Okawara, *Inorg. Nucl.*

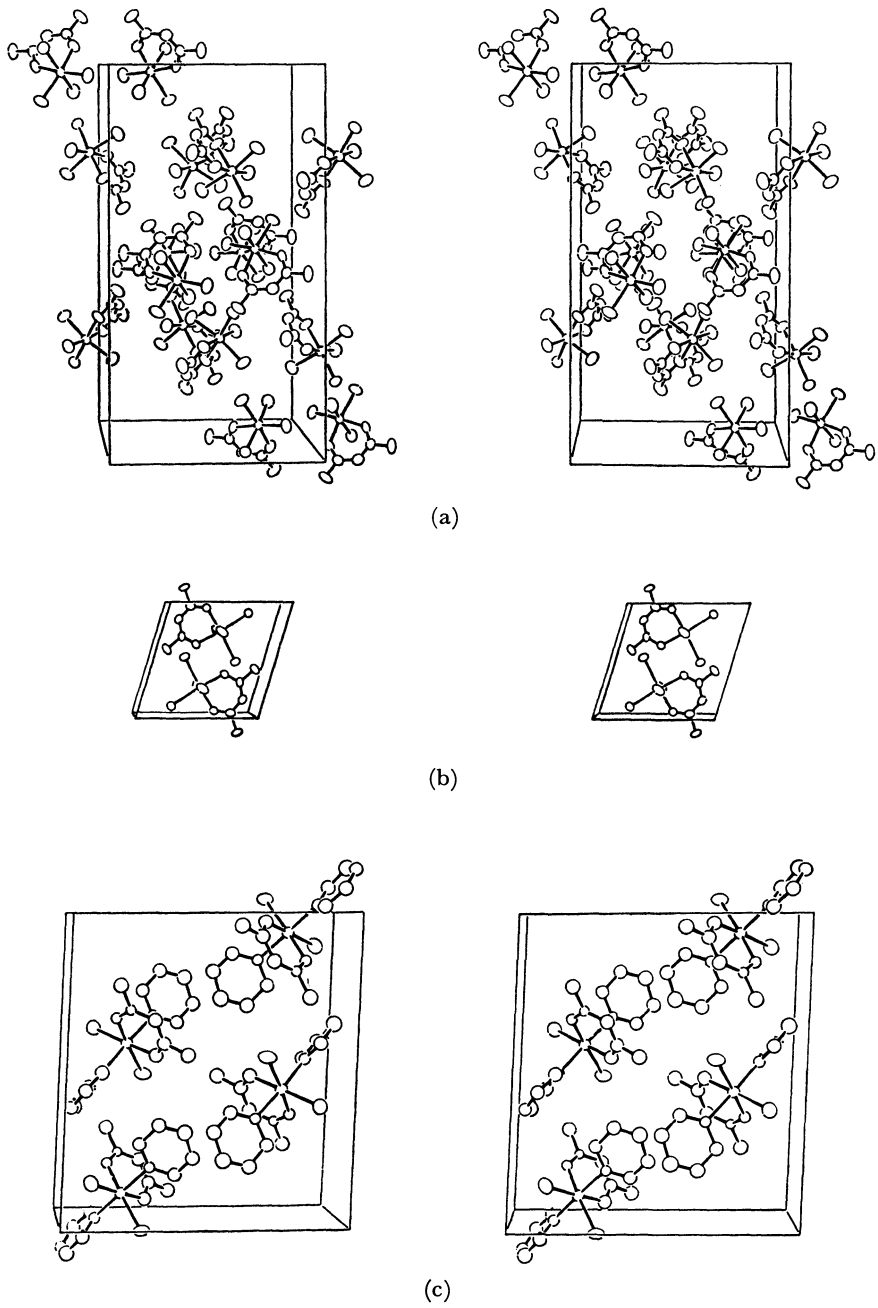

Fig. 9. Stereoscopic drawing of the molecular packings of (a) [(acac)$MeSbCl_3$], (b) [(acac)Me_2SbBr_2], and (c) [(acac)Ph_2SbCl_2] (high-melting point form).

Chem. Lett., **5**, 703 (1969).

5) H. A. Meinema, A. Mackor, and J. G. Noltes, *J. Organomet. Chem.*, **37**, 285 (1972).

6) Y. Matsumura and R. Okawara, *Inorg. Nucl. Chem. Lett.*, **4**, 521 (1968).

7) R. Okawara, Y. Matsumura, and N. Nishii, Abstracts, 4th International Conference on Organometallic Chemistry, Bristol, Z8 (1969).

8) J. Kroon, J. B. Hulscher, and A. F. Peerdeman *J. Organomet. Chem.*, **37**, 297 (1972).

9) S. Uda, Y. Kai, N. Yasuoka, and N. Kasai, unpublished data.

10) K. Onuma, Y. Kai, and N. Kasai, *Inorg. Nucl. Chem. Lett.*, **8**, 143 (1972).

11) N. Kanehisa, Y. Kai, and N. Kasai, *Inorg. Nucl. Chem. Lett.*, **8**, 375 (1972).

12) S. Uda, Y. Kai, N. Yasuoka, and N. Kasai, *Cryst. Struct. Commun.*, **3**, 257 (1974).

13) T. Ashida, The Universal Crystallographic Compuing System, Osaka. The Computation Center, Osaka University, (1973), p. 55.

14) H. P. Hanson, F. Herman, J. D. Lea, and S. S. Skillman., *Acta Crystallogr.*, **17**, 1040 (1964).

15) M. A. Bush, P. F. Lindley, and P. Woodward, *J. Chem. Soc., A.*, **1967**, 221.

16) P. Kisliuk, *J. Chem. Phys.*, **22**, 86 (1954).

17) L. Brun and C.-I. Brändén, *Acta Crystallogr.*, **20**, 749 (1966).

18) B. L. Patton and K. N. Raymon, *Inorg. Chem.* **8**. 2426 (1969).

19) J.-M. Le Carpentier and R. Weiss, *Acta Crystallogr., Sect. B*, **28**, 1442 (1972).
20) B. Chevrier, J.-M. Le Carpentier, and R. Weiss., *Acta Crystallogr., Sect. B*, **28**, 2667 (1972).
21) N. W. Lister and L. E. Sutton, *Trans. Faraday Soc.*, **37**, 393 (1941).
22) F. Di Bianca, E. Rivarola, A. L. Spek, H. A. Meinema, and J. G. Noltes, *J. Organomet. Chem.*, **63**, 293 (1973).
23) J.-J. Legendre, C. Girard, and M. Huber, *Bull. Soc. Chim. Fr.*, **6**, 1998 (1971).
24) J. Bordner, G. O. Doak, and John R. Peters, Jr., *J. Am. Chem. Soc.*, **96**, 6763 (1974).
25) J. V. Silverton and J. L. Hoard, *Inorg. Chem.*, **2**, 243 (1963).
26) J. A. Cunningham, D. E. Sands, and W. F. Wagner, *Inorg. Chem.*, **6**, 499 (1967).
27) E. C. Lingafelter and R. L. Braun, *J. Am. Chem. Soc.*, **88**, 2957 (1966).
28) C. K. Johnson, *ORTEP, Report ORNL-3794*, Oak Ridge National Laboratory, Tennesee (1965).

Solubility and Diffusion Coefficient of Sulfur in Copper

Kazuo FUEKI* and Yasumasa OUCHI

Department of Industrial Chemistry, Faculty of Engineering, The University of Tokyo, Hongo, Bunkyo-ku, Tokyo 113

(Received March 3, 1978)

The solubility and diffusion coefficient of sulfur in copper were determined by a new method, wherein a thin copper(I) sulfide film was formed on the surface of a copper specimen and the decrement of its thickness after diffusion annealing was determined coulometrically. It was found that the solubility C_s could be represented by

$$\log C_s \text{ (ppm)} = -0.616 - 0.410 \ (10^4/T),$$

and the diffusion coefficient is given by

$$D = 0.834 \times \exp(-40900/RT) \text{ cm}^2 \text{ s}^{-1}.$$

When a binary alloy is oxidized in an oxygen atmosphere, oxygen diffuses into the alloy and forms dispersed oxide particles with the less noble component. This phenomenon, called internal oxidation, has a significant effect on the oxidation rate of the alloy. Therefore, the solubility and diffusion coefficient of oxygen in the metal are most important for the elucidation of internal oxidation. Similarly, the solubility and diffusion coefficient of sulfur in metals are necessary in order to elucidate the mechanism and rate of alloy sulfidation.

The concentration of non-metallic elements in metals is usually determined by the vacuum fusion method, and in some cases by the combustion method or the tracer method. If physical properties such as resistivity and hardness are known as a function of the concentration of non-metallic elements, the solubility can be determined from the break point in the slope of the plot of physical quantity against concentration.

The diffusion coefficient of non-metallic elements is usually determined by the tracer method. In some cases, it is determined by the chemical relaxation method, which utilizes the change of physical property with time after the step-like change of ambient conditions.

The purpose of the present work is to determine the solubility and diffusion coefficient of sulfur in copper by a new method, wherein a thin copper(I) sulfide film is formed on the surface of high purity copper specimen and the decrement of the surface film after the diffusion annealing is determined by the coulometric method.

Theoretical

When a copper specimen covered with a thin copper(I) sulfide film on its surface is annealed *in vacuo* at a high temperature the copper(I) sulfide decomposes into sulfur and copper by the reaction

$$Cu_2S = 2Cu + S(\text{in Cu}), \quad (1)$$

and the sulfur diffuses inwards. If the concentration of sulfur is represented by $C(x,t)$, its differential with respect to time can be given by

$$\frac{\partial C}{\partial t} = D\frac{\partial^2 C}{\partial x^2}, \quad (2)$$

where D is the diffusion coefficient. Solving the differential equation with the boundary conditions

$$C(0,t) = C_s, \quad (3)$$

$$C(l,t) = C_s, \quad (4)$$

and

$$C(x,0) = 0 \quad \text{for } 0 < x < l, \quad (5)$$

one obtains[1]

$$C = C_s - \frac{4C_s}{\pi}\sum_{j=0}^{\infty}\frac{1}{2j+1}\sin\frac{(2j+1)\pi}{l} \times \exp\left[-\left(\frac{(2j+1)\pi}{l}\right)^2 Dt\right], \quad (6)$$

where C_s is the solubility and j is an integer. The mean concentration $\bar{C}(t)$ is

$$\bar{C}(t) = \frac{1}{l}\int_0^l C(x,t)\mathrm{d}x = C_s - \frac{8C_s}{\pi^2}\sum_{j=0}^{\infty}\frac{1}{(2j+1)^2}\exp\left[-\left(\frac{(2j+1)\pi}{l}\right)^2 Dt\right]. \quad (7)$$

In the present study, $\bar{C}(t)$ is determined by the difference in sulfide film thickness between time zero and time t. For $\bar{C} \geq 0.2C_s$ the first term of the series is an excellent approximation. Therefore, Eq. 7 can be simplified to

$$\bar{C} = C_s - \frac{8C_s}{\pi^2}\exp\left(\frac{-\pi^2 Dt}{l^2}\right). \quad (8)$$

Accordingly, from the saturation value of the $\bar{C}$-t/l^2 curve, the solubility C_s is determined. Equation 8 is rewritten into

$$\frac{C_s - \bar{C}}{C_s} = \frac{8}{\pi^2}\exp\left(-\frac{\pi^2 Dt}{l^2}\right). \quad (9)$$

Taking the logarithm of both sides of this equation, one gets

$$\log\frac{C_s - \bar{C}}{C_s} = \log\frac{8}{\pi^2} - \frac{\pi^2 D}{2.303}\cdot\frac{t}{l^2}. \quad (10)$$

Equation 10 indicates that the diffusion coefficient D is determined from the slope of the plot of $\log(C_s - \bar{C})/C_s$ against (t/l^2).

Experimental

Copper Specimens. Electrolytic copper, 99.999% pure and 5 mm thick, was used for samples. The result of chemical

TABLE 1. RESULT OF CHEMICAL ANALYSIS

Impurity	Content
Pb	1 ppm
As	1
Sb	1
Fe	1
Ni	1
S	6

analysis of the copper is given in Table 1. The electrolytic copper was cut into rectangular specimens with a small knob at one corner. The size of each specimen was 15 mm × 7 mm × (0.2—1)mm. The copper specimens were polished with emery paper and then with alumina polishing powder of 10, 5, 0.5, and 0.3μ successively. The size of polished specimens was measured by means of a vernier caliper and the thickness was calculated from the weight and the surface area. In order to remove the strain and non- metallic elements dissolved in copper, the specimens were placed in a Vycor basket, suspended in a tube kept at 600 °C, and heat-treated in a 5% H_2–95% N_2 gas mixture for 5 h.

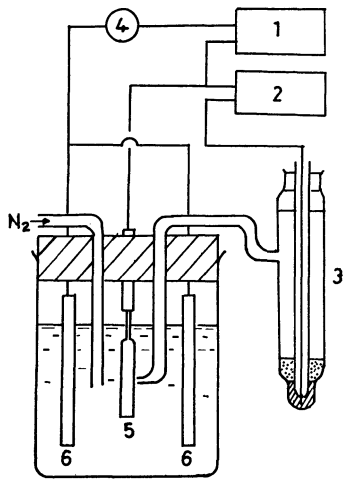

Fig. 1. Schematic drawing of electrolytic cell and electrical circuit.
1: Galvanostat, 2: recorder, 3: S.C.E., 4: ammeter, 5: test electrode, 6: counter electrode.

Formation and Determination of Surface Sulfide. The essential point of the present work is the determination of $\bar{C}(t)$, in other words, the determination of sulfide film thickness at time zero and time t. The sulfide film was as thin as about 1000 Å, so the electrochemical method was employed for the formation of sulfide film and the determination of its thickness. Figure 1 shows the drawing of the electrochemical cell and the electrical circuit for these purposes. In the first cell a 0.1 M KCl-solution was used as electrolyte. The solution was deaerated by passing nitrogen gas bubbles for 10 min and a heat-treated copper specimen was immersed in the solution. The current was made to flow between the specimen and two counter electrodes to reduce the surface oxide on the copper. The cathodic current density was 1 mA/cm². Then the specimen was taken out of the cell, washed with water, and transferred to the second cell which contained a 6.3×10^{-3} M Na_2S solution as electrolyte. The specimen was anodized at a current density of 0.1 mA/cm² for 10 to 20 min to form thin sulfide films of the desired thickness on both surfaces of copper. Usually, the thickness was chosen to be about twice or three times greater than the thickness after the diffusion annealing. Then, the specimen was taken out and washed with pure water.

The sulfide film thickness was determined by means of the coulometric method. The specimen was immersed in a 0.1 M KCl solution and the surface sulfide was reduced cathodically at a constant current density of 0.1 mA/cm². The potential with reference to S. C. E. was recorded. The potential was constant while the residual sulfide existed on the metal surfaces, shifted to a less noble value in an instant where the sulfide was completely removed, and remained at another constant value which corresponded to the potential of hydrogen evolution on the bare metal surface. From the reflection of the potential-time curve, the electric charge necessary for the reduction of sulfide was calculated. The charge determined from the reduction of sulfide was found to be always about 10% larger than that determined from the formation of sulfide. It was considered that the difference might be due to the reaction of copper with polysulfide ions contained in the Na_2S solution as an impurity. So the Na_2S solution of the same concentration was used for the formation of sulfide, and the film thickness formed by the reaction of copper with polysulfide ions was taken into account for the determination of the initial film thickness.

Diffusion Annealing. The copper specimen covered with copper(I) sulfide film was placed in a Vycor tube in which nitrogen gas was made to flow for 10 min to replace the air in it. Then the tube was evacuated to 10^{-4} Torr and sealed by means of a hydrogen-oxygen torch. Care was taken so that the sample would not be heated. The sealed tube was placed in an electric furnace kept at a desired annealing temperature within ±2 °C, and after a pre-determined length of time the tube was taken out from the furnace. The thickness of the remaining sulfide film was determined coulometrically and the mean concentration $\bar{C}$ in copper was calculated.

Results and Discussion

Soubility of Sulfur in Copper. The plot of $\bar{C}$ *vs.* t/l^2 is given in Figs. 2 and 3. As is seen in these figures, $\bar{C}$ approaches to a saturation value C_s with the increase of t/l^2. Figure 4 shows the plot of log C_s *vs.* $1/T$. Clearly, a linear relationship exists between log C_s and $1/T$. The equation is

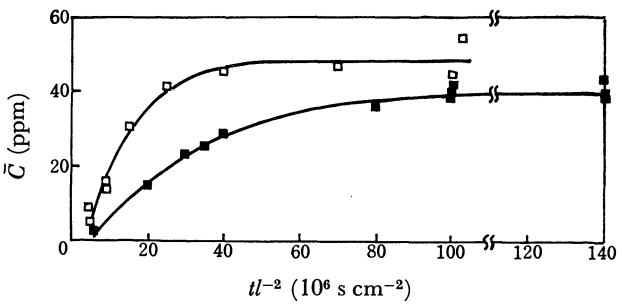

Fig. 2. Change of $\bar{C}$ with time.
■: 800 °C, □: 850 °C.

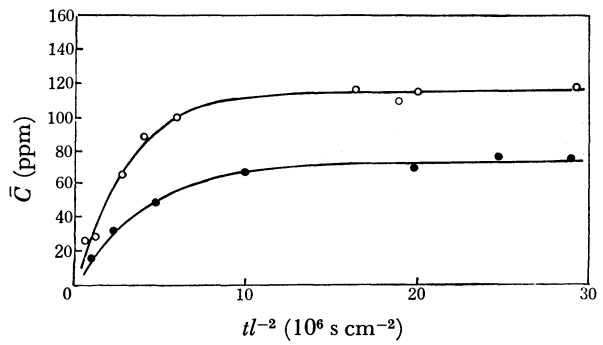

Fig. 3. Change of $\bar{C}$ with time.
●: 900 °C, ○: 950 °C.

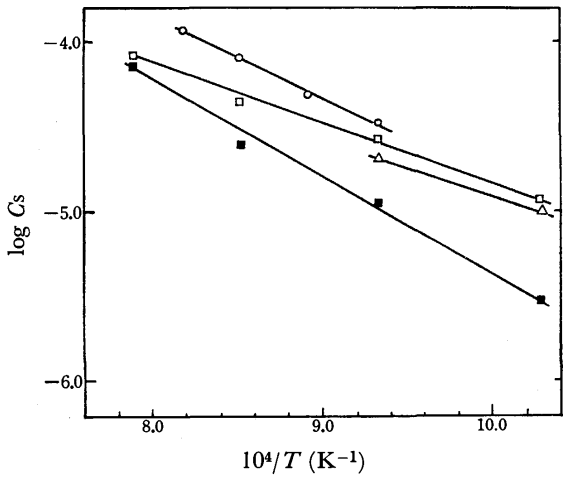

Fig. 4. Plot of log C_s *vs.* $1/T$.
○: This work, □: (Oudar): HPCu, ■: (Oudar): OFHC, △: Smart *et al.*

$$\log C_s(\text{ppm}) = -0.616 - 0.410\left(\frac{10^4}{T}\right). \qquad (11)$$

If the solubility is represented in terms of mole fraction N,

$$\log N(\text{ppm}) = -0.319 - 0.410\left(\frac{10^4}{T}\right). \qquad (12)$$

For comparison, Oudar's result[2] obtained by the tracer method and Smart's result[3] obtained from the relationship between sulfur content and resistivity of copper are also given in this figure These results are in good agreement with each other. The enthalpy and entropy of sulfur dissolution in copper in accordance with Eq. 1 are calculated to be 18.7 and −1.46 cal/mol·deg, respectively. The small entropy is probably due to the transfer of sulfur from solid to solid, as given by Eq. 1.

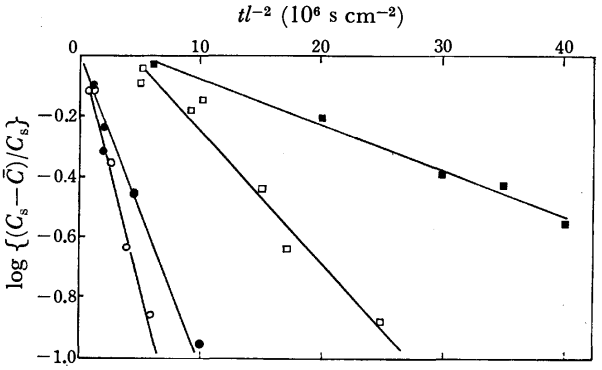

Fig. 5. Plot of log $\{(C_s-\bar{C})/C_s\}$ *vs.* t/l^2.
■: 800 °C, □: 850 °C, ●: 900 °C, ○: 950 °C.

Diffusion Coefficient. Figure 5 gives the relationship between log $(C_s-\bar{C})/C_s$ and t/l^2. A good linear relationship indicates that Eq. 9 holds for the present case and the diffusion coefficient D can be determined from the slope of the plot. The Arrhenius plot for D is given in Fig. 6. For comparison, Moya's result[4,5] obtained by the tracer method and the result obtained

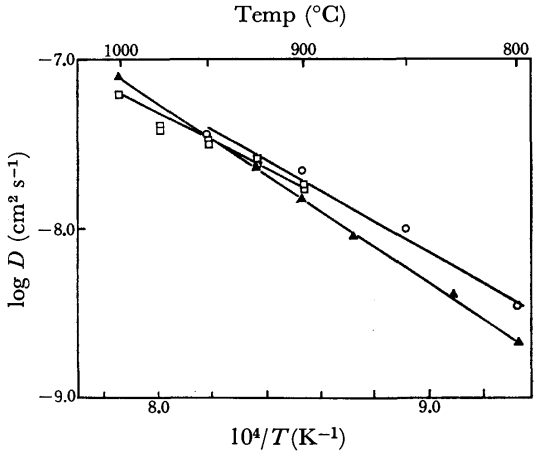

Fig. 6. Arrhenius plot for D.
○: This work, □: Wang and Grabke, ▲: Hoya.

by Wang and Grabke[6] by means of the relaxation method are shown in the same figure. These results agree with each other. The Arrhenius equation for the present work is

$$D = 0.834 \times \exp\left(-\frac{40900}{RT}\right)\text{cm}^2\,\text{s}^{-1}. \qquad (13)$$

Summary

(1) For the determination of solubility and diffusion coefficient of non-metallic elements in metals a new method was proposed. A thin compound film was formed on the metal surface and the film thicknesses before and after diffusion annealing were determined by the coulometric method.

(2) The solubility of sulfur in copper determined by the new method was given in terms of mole fraction by the equation

$$\log N_s(\text{ppm}) = -0.319 - 0.410\left(\frac{10^4}{T}\right).$$

This result was in good agreement with those obtained by other methods.

(3) The diffusion coefficient of sulfur in copper in the present investigation was represented by

$$D = 0.834 \times \exp\left(-\frac{40900}{RT}\right)\text{cm}^2\,\text{s}^{-1}.$$

This result agreed with the previous results obtained by other methods.

References

1) P. G. Shewmon, "Diffusion in Solids," McGraw-Hill (1963).
2) J. Oudar, *C. R. Acad. Sci.*, **249**, 259 (1959).
3) J. S. Smart, Jr., and A. A. Smith, Jr., *Trans. AIME*, **166**, 144 (1946).
4) F. Moya and F. Cabane-Brouty, *C. R. Acad. Sci., Paris, Ser. C*, **264**, 1543 (1969).
5) F. Moya, G. E. Moya-Fontier, and F. Cabane-Brouty, *Phys. Status Solidi.*, **35**, 893 (1969).
6) S. J. Wang and H. J. Grabke, *Z. Metallk.* **61**, 597 (1970).

Molecular Structure and Conformation of Ethyl Methyl Ether as Studied by Gas Electron Diffraction

Kazuko OYANAGI and Kozo KUCHITSU*

Department of Chemistry, Faculty of Science, The University of Tokyo, Bunkyo-ku, Tokyo 113

(Received March 20, 1978)

The bond distances (r_g) and angles (r_a) in ethyl methyl ether have been determined by gas electron diffraction as follows: average of C(methyl)–O and C(methylene)–O=1.418±0.002 Å, C–C=1.520±0.004 Å, C–H=1.118±0.004 Å, ∠C–O–C=111.9±0.5°, ∠O–C–C=109.4±0.3°, ∠H–C–H=109.0±0.4°, where uncertainties represent estimated limits of experimental error. The two r_g(C–O) distances have been estimated independently with the aid of the rotational constants for the *trans* conformer reported by Hayashi *et al.*: C(methyl)–O=1.413±0.009 Å and C(methylene)–O=1.422±0.007 Å. The dihedral angle for the *gauche* conformer, 84±6°, and the relative abundance of the *trans* and *gauche* conformers in the gas phase at 20 °C, $n_t/(n_t+n_g)=0.80\pm0.08$, have also been determined.

The conformation and the barrier to internal rotation about a C–O axis are of great importance in wide fields of chemistry, such as in polymer chemistry, and have been studied extensively by vibrational spectroscopy.[1–8] Ethyl methyl ether (Fig. 1) is one of the simplest molecules enabling such a study. This molecule is known to be a mixture of two conformers in the gas phase.[5–8] The infrared spectra observed by Kitagawa and Miyazawa[5] indicated that the more stable conformer was *trans*, and the enthalpy difference in the gas phase was measured to be 1.5±0.2 kcal/mol. The rotational constants for the *trans* conformer have been determined by Hayashi *et al.* by microwave spectroscopy, from which the r_s atomic coordinates have been derived.[9] On the other hand, the conformation of the less stable conformer has only been inferred by vibrational spectroscopy to be *gauche*. Since electron diffraction provides direct information on interatomic distances, it is one of the most powerful methods for determining the mixing ratio of the conformers and the dihedral angle for the less stable conformer.[10]

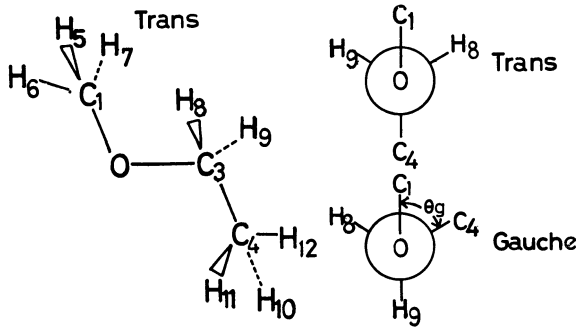

Fig. 1. Ethyl methyl ether. The dihedral angle for the *gauche* conformer measured from *cis* position is denoted by θ_g.

There are two non-equivalent C–O bonds in ethyl methyl ether. Though the average of these bond lengths can be obtained by electron diffraction, they cannot be determined individually. The moment of inertia I_a depends sensitively on these distances. Therefore, a joint analysis of electron diffraction intensity and the rotational constants can determine these nearly equal C–O distances separately, though the moments of inertia alone are not sufficient to determine a complete structure.

In the present study, the structure of ethyl methyl ether is determined first by use of the electron diffraction data alone. Then the difference of the two C–O distances is estimated by the use of the diffraction data and the rotational constants. Finally, the conformation is investigated and the structure of this molecule is compared with those of related molecules.

Experimental

The sample for spectroscopic use was supplied by Dr. Kitagawa.[7] Diffraction patterns were taken with an r^3-sector at camera lengths of 243.3 and 107.7 mm with 40 kV electrons. The electron wavelength was calibrated with reference to the r_a(C=O) distance of carbon dioxide (1.1646 Å) within 0.10%.[11] The sample reservoir was held in a Dry Ice–acetone bath in order to control the pressure of the sample at about 40 Torr during the experiment, and the sample gas was introduced into the diffraction chamber through a nozzle of 0.2 mm i.d. The exposure times were about 60 and 100 s for the long and short camera lengths, respectively. Other experimental conditions are described elsewhere.[11,12]

Four photographic plates taken at each camera length were selected for the intensity measurement by means of automated microdensitometry and data processing.[13] The optical densities (0.2—0.5) were assumed to be proportional to electron intensities. Molecular intensities in the ranges s=3.1—18.8 and 9.4—37.3 Å^{-1} were obtained from the long and short distance data, respectively, by use of hand-drawn backgrounds.

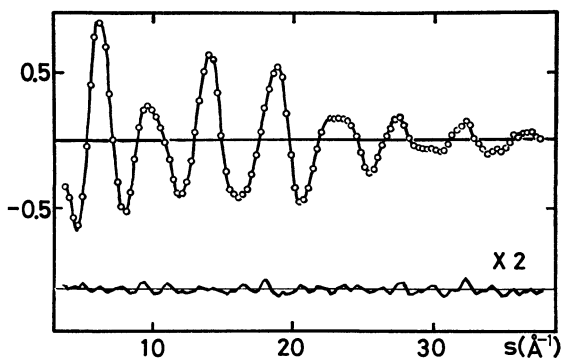

Fig. 2. Molecular intensities for ethyl methyl ether. Observed values are shown as open circles, and the solid curves represent the best-fit theoretical intensities. The lower solid curve represents the residuals.

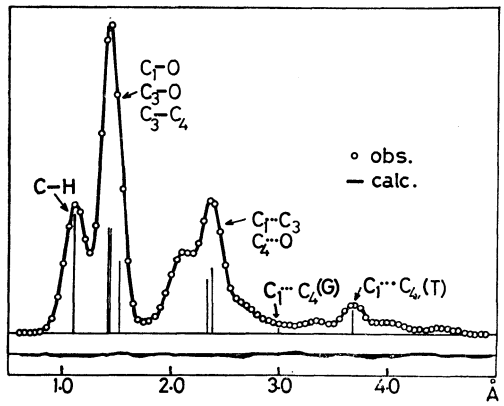

Fig. 3. Experimental and theoretical radial distribution curves. Damping factor, $\exp(-0.0016\,s^2)$, was used. The residuals are shown below in the same scale.

Since they agreed with each other in the overlapping region within experimental error, they were joined at $s=12.6$ Å^{-1}. Four independent molecular intensity curves covering the whole s range were obtained by arbitrary combinations of four intensity curves for each camera length. The elastic and inelastic scattering factors and the phase shifts were taken from the tables prepared by Schäfer *et al.*[14] The molecular intensity and the corresponding radial distribution curve are shown in Figs. 2 and 3, respectively.[15] Most of the calculations were carried out on a HITAC 8800/8700 in the Computer Center of the University of Tokyo.

Analysis

The essential information on the conformation is contained in the distance of the C(methyl)···C(methyl) nonbonded pair. This distance for the *trans* conformer appears in the radial distribution curve (Fig. 3) as a peak at 3.7 Å, while the small shoulder at 3.0 Å consists of the corresponding distance for the *gauche* conformer. The relative abundance of the two conformers can be derived from the heights of the peak and the shoulder. By comparing the observed radial distribution curve with the curves calculated assuming various mixing ratios, the *trans* conformer was found to be dominant, being in agreement with the results from vibrational spectroscopy.[4,6] The shape of the shoulder at 3.0 Å carries information on the dihedral angle for the *gauche* form. The conformational analysis is discussed in detail in a later section.

In order to obtain a more precise skeletal structure, the molecular intensities were analyzed by a least-squares method with an empirical diagonal weight matrix[16] on the assumption that no stable conformer other than the above two existed in the gas phase at room temperature. The following additional assumptions were made so as to reduce the number of independent parameters without significant loss of accuracy:

1) The *trans* conformer has C_s symmetry in the r_α structure.

2) The *trans* and *gauche* conformers have identical bond distances and angles except for the dihedral angle about the C(methylene)–O bond. (This assumption was modified in the conformational analysis described in a later section).

3) All the C–H bond distances are equal.

4) The difference in the C(methyl)–O and C(methylene)–O bond distances is 0 ± 0.01 Å, on the basis of the structural data for dimethyl ether[17] and ethyl alcohol.[18] (The need for this assumption was removed in the joint analysis of the molecular intensities and the rotational constants).

5) The H–C(methylene)–H plane is perpendicular to the O–C–C plane, and each angle is bisected by the plane defined by the other angle at the methylene carbon atom.

6) Each of the methyl groups has local C_{3v} symmetry and no tilt. With these assumptions, the geometrical parameters were restricted to seven: the C–C, $(C-O)_{av}$, $(C-H)_{av}$ bond distances, the C–O–C, O–C–C, $(H-C-H)_{av}$ bond angles and the dihedral angle for the *gauche* conformer. The dihedral angle for the *trans* conformer was set equal to 180° by assumption 1). In addition, the

Table 1. Mean amplitudes (l_{ij}) and shrinkage corrections (r_a-r_α) for ethyl methyl ether[a] (in 10^{-4} Å)

	l_{ij}	r_a-r_α		l_{ij}	r_a-r_α
i) *trans* form					
C_1–H_5	787	59	$C_3\cdots H_{11}$	1089	8
C_1–H_6	787	51	$C_1\cdots C_3$	645	−6
C_3–H_8	789	74	$C_4\cdots O$	664	−10
C_4–H_{10}	786	72	$C_1\cdots H_8$	1407	10
C_4–H_{11}	786	65	$C_3\cdots H_6$	1365	−3
C_1–O	480	5	$O\cdots H_{11}$	1426	−15
C_3–O	483	4	$C_3\cdots H_5$	1275	78
C_3–C_4	527	3	$O\cdots H_{10}$	1015	−24
$O\cdots H_8$	1022	7	$C_1\cdots C_4$	693	−51
$O\cdots H_5$	1012	13	$C_1\cdots H_{11}$	1474	−105
$O\cdots H_6$	1014	9	$C_4\cdots H_6$	1365	42
$C_4\cdots H_8$	1078	5	$C_4\cdots H_5$	1157	−68
$C_3\cdots H_{10}$	1084	11	$C_1\cdots H_{10}$	1147	−65
ii) *gauche* form					
C_1–H_5	787	58	C_1–H_7	787	50
C_1–H_6	787	55	C_3–H_8	789	89
C_3–H_9	789	86	$C_1\cdots C_3$	649	−12
C_4–H_{10}	786	66	$C_4\cdots O$	657	−14
C_4–H_{11}	786	60	$C_4\cdots H_7$	1564	−46
C_4–H_{12}	786	66	$C_1\cdots H_{11}$	1607	−137
C_1–O	481	0	$C_1\cdots H_8$	1482	−41
C_3–O	483	7	$C_3\cdots H_6$	1447	−49
C_3–C_4	529	−5	$C_3\cdots H_7$	1351	−40
$O\cdots H_8$	1023	29	$O\cdots H_{11}$	1399	−42
$O\cdots H_9$	1022	29	$O\cdots H_{12}$	1513	−43
$O\cdots H_5$	1013	9	$C_1\cdots C_4$	939	−25
$O\cdots H_6$	1015	6	$C_1\cdots H_{12}$	1665	19
$O\cdots H_7$	1014	−1	$C_4\cdots H_6$	1717	67
$C_4\cdots H_8$	1079	7	$C_1\cdots H_9$	1002	41
$C_4\cdots H_9$	1044	10	$C_3\cdots H_5$	1006	33
$C_3\cdots H_{10}$	1086	0	$O\cdots H_{10}$	1018	27
$C_3\cdots H_{11}$	1090	−5	$C_4\cdots H_5$	1148	42
C_3–H_{12}	1090	0	$C_1\cdots H_{10}$	1145	32

a) Calculated at 20°C. See Fig. 1 for the numbers of atoms. Nonlinear shrinkages due to the C(methylene)–O torsion and the methyl torsions are included. (See text.) The values for H···H pairs are not listed.

mixing ratio of the two conformers was taken as a variable parameter.

The mean amplitudes and the vibrational corrections for all interatomic distances,[19,20] listed in Table 1, were calculated with the force constants based on the valence force field.[4] Since the skeletal and methyl torsions were large-amplitude motions, contributions to the vibrational corrections from these motions were estimated by Karle's method[21,22] with the barrier heights (V_3) obtained from far infrared spectroscopy.[7] The contribution from the skeletal torsion to the vibrational correction for the C(methyl)···C(methyl) nonbonded pair, about 0.003 Å, had some influence on the dihedral angle, while those from the methyl torsions affected the corrections for the nonbonded C···H and O···H pairs by about 0.004 Å, and the H–C–H angle was influenced consequently. The asymmetry parameter κ for the bonded C–H distance was estimated to be 1.3×10^{-5} Å^3,[23,24] and the rest of the κ parameters were assumed to be zero, since they had little effect on molecular geometry. Since the C–C bond and two C–O bonds form a single peak in the radial distribution curve, the amplitudes for the C–O and C–C bonds could not be varied independently. Therefore, the amplitudes for the C–H and C–O bonds were taken as parameters and the rest of the mean amplitudes were fixed to the calculated values. The structure obtained in this analysis (average of the structures derived from the four molecular intensities mentioned above) is listed in Table 2. The error limits in the molecular parameters were estimated from random and systematic errors including the uncertainties originating from those in the amplitudes and the vibrational corrections.[25,26] The relative uncertainties in the amplitudes and the vibrational corrections for bonded pairs were tentatively estimated to be 5%. The mean amplitudes and the vibrational corrections for nonbonded pairs consist of the contributions from the small-amplitude and large-amplitude modes. The former contributions were estimated to have relative uncertainties of ±10%, while the latter contributions calculated by Karle's method were estimated to have uncertainties of 100% of the contributions. The uncertainties caused by the assumptions mentioned above were also estimated roughly and included in the errors given in Table 2. A typical error matrix is shown in Table 3.

Table 2. Molecular structure and mean amplitudes for ethyl methyl ether determined by electron diffraction[a]

r(C–C)	1.520(4)	∠C–O–C	111.9(5)
r(C–O)$_{av}$	1.418(2)	∠O–C–C	109.4(3)
r(C(methyl)–O)	1.413(9)[b]	∠H–C–H	109.0(4)
r(C(methylene)–O)	1.422(7)[b]	θ_g[d]	84(6)
r(C–H)$_{av}$	1.118(4)	$n_t/(n_t+n_g)$[e]	80(8)
l(C–O)$_{av}$[c]	0.050(3)		
l(C–H)$_{av}$[c]	0.082(5)		

a) Bond distances (r_g) are in Å units. Angles (r_α) are in degrees. The numbers in parentheses represent estimated limits of error attached to the last significant digits. b) These distances were separately determined by the joint analysis. The other parameters obtained by the joint analysis were essentially equal to those given in this table. c) Observed mean amplitudes. d) The dihedral angle for the *gauche* conformer measured from the *cis* position. e) % *trans* form. $\Delta G=1.23\pm0.27$ kcal/mol.

Electron Diffraction and Microwave Data. The r_α structure derived from the electron diffraction data was used to calculate the rotational constants. For this purpose the r_α distances were extrapolated to zero kelvin by estimating the difference $r_\alpha^0-r_\alpha$.[19] The rotational constants, A_α^0, B_α^0, and C_α^0, for the *trans* conformer were calculated from the average r_α^0 structure, and are listed in Table 4. On the other hand, the zero-point average rotational constants, A_z, B_z, and C_z, for the *trans* conformer were derived by making vibrational corrections[27] from the A_0, B_0, and C_0 determined by microwave spectroscopy.[9] The uncertainties in A_z,

Table 3. Error matrix[a] and correlation matrix[b] for ethyl methyl ether[c]

	k_1	k_2	x_1	x_2	x_3	x_4	x_5	x_6	x_7	x_8	l_1	l_2
a)	73	186	343	16	4	10	51	39	45	420	12	5
k_1	100	23	−27	50	29	−39	−16	−30	44	12	0	−5
k_2		100	−35	71	−55	64	−73	62	28	13	87	85
x_1			100	−30	16	−24	23	−20	−19	−29	−31	−29
x_2				100	50	45	−56	−40	56	1	65	−22
x_3					100	−30	7	−64	45	−15	−43	−67
x_4						100	−46	39	49	−2	52	54
x_5							100	−80	−35	18	−65	−56
x_6								100	−53	−22	51	72
x_7									100	10	30	−7
x_8										100	10	14
l_1											100	65
l_2												100

a) Diagonal elements of error matrix. Units ($\times10^{-4}$) for the distances and mean amplitudes are Å, those for the indices and the relative abundance of the *trans* form are dimensionless. b) Correlation matrix. Units ($\times10^{-2}$) are all dimensionless. c) k_1,k_2=indices of resolution for the long and short distance data, (0.94±0.02 and 1.03±0.07) respectively, x_1=relative abundance of the *trans* form, $x_2=r$(C–C), $x_3=r$(C–O)$_{av}$, $x_4=r$(C–H)$_{av}$, $x_5=\angle$C–O–C, $x_6=\angle$O–C–C, $x_7\angle=$H–C–H, x_8=dihedral angle for the *gauche* form, $l_1=l$(C–H)$_{av}$ and $l_2=l$ (C–O)$_{av}$.

Table 4. Observed and calculated rotational constants for *trans* ethyl methyl ether (in cm^{-1})

	0[b]	z[c]	α^0 [d]	av[e]
A	0.933712(1)	0.941(3)	0.940(4)	0.937(4)
B	0.138745(1)	0.1388(3)	0.1375(12)	0.1383(5)
C	0.129796(1)	0.1298(2)	0.1289(10)	0.1295(4)

a) Uncertainties attached to the last significant digits are given in parentheses. b) Observed rotational constants for the ground vibrational state, Ref. 9. c) Zero-point average rotational constants calculated from A_0, B_0, and C_0 with corrections for vibrational effects. d) Rotational constants calculated from the r_α^0 parameters which are compatible with the structure given in Table 2 determined in the analysis of electron diffraction intensities. Uncertainties are estimated from those in the r_α parameters. e) Best fit rotational constants obtained by the combined analysis of diffraction and microwave data. The structural parameters (r_{av}) which reproduce these constants are essentially equal to those given in Table 2 if the distances are transformed into r_g. Uncertainties represent 2.5 times the estimated standard deviations.

B_z, and C_z were estimated from the following sources: a) Uncertainties in the corrections for the large-amplitude modes were estimated to be $\pm 100\%$ of the corrections. b) The uncertainties in the corrections for all the small-amplitude modes were estimated to be $\pm 10\%$ of the corrections. The rotational constants, A_α^0, B_α^0, and C_α^0, calculated from the r_α^0 structure agreed with the zero-point average rotational constants, A_z, B_z, and C_z, within their uncertainties. This suggests that the frame structures of the *trans* and the *gauche* conformers do not differ greatly.

The rotational constants, A_z, B_z, and C_z, were thus combined with diffraction intensities into a joint least-squares analysis.[23,28] The weights for A_z, B_z, and C_z used in the analysis were so chosen that 2.5 times their standard deviations were approximately equal to the estimated uncertainties in the rotational constants. They were 1×10^3, 1×10^5, and 1×10^5, respectively, where a unit weight was assigned to the molecular intensities from $s=6.3$ to 26.7 $Å^{-1}$ taken at $\pi/10$ $Å^{-1}$ intervals. The r_{av} structure agreed with the r_α^0 structure, and the mean amplitudes also converged to essentially the same values as those obtained in the analysis of the electron diffraction data alone. The assumption 4) made in the analysis of the diffraction intensities was now excluded, and the two C–O bond distances were varied independently. The average of the two C–O bond lengths determined separately in the present analysis (listed in Table 2) is equal to that obtained from electron diffraction.

Rotational Isomerism. The differences in the geometrical parameters for the *trans* and *gauche* conformers have influence on the conformational analysis. For this molecule the dihedral angle for the *gauche* conformer is derived from the bonded distances, the skeletal angles and the nonbonded C(methyl)···C(methyl) distance. Among their uncertainties those in the skeletal angles have much influence on that of the dihedral angle. Since at present there are no experimental data on the differences of the geometrical parameters for the *trans* and *gauche* conformers, the O–C–C and C–O–C angles were assumed to be 0—3° larger in the *gauche* form than in the *trans* form on the basis of the structural data for analogous molecules.[29,30] The error limit in the dihedral angle listed in Table 2 includes the influence of these uncertainties.

The effective temperature of the sample system at the scattering point must be defined when the "thermal-equilibrium" fractions of rotational isomers are discussed. The following assumptions were made: When the sample gas leaves the jet, it has reached thermal equilibrium with the nozzle throat. With our nozzle design the cooling of the gas in the passage from the nozzle tip to the scattering point is negligible.[31] Therefore, the effective vibrational temperature was assumed to be equal to the room temperature. The population of the *trans* conformer given in Table 2, $80\pm8\%$, then implies that the *gauche-trans* free energy difference ΔG is 1.23 ± 0.27 kcal/mol, the uncertainty including that in the effective temperature. This estimate is compatible with the enthalpy difference ΔH, 1.5 ± 0.2 kcal/mol, obtained by the temperature dependence of spectral intensities.[5]

In order to further examine the rotational isomerism in ethyl methyl ether, the molecular intensities in the range from $s=3.5$ to 8.2 $Å^{-1}$ were analyzed by the method of background function.[32,33] The background functions $I_b(s)$ were derived from the experimental total intensities $I_t(s)$ and from the theoretical molecular intensities $sM(s)$ based on models. The smoothness of the $I_b(s)$ function, *i.e.* the absence of systematic fluctuations with periods similar to that of the molecular terms, was taken as a criterion for the choice of a proper conformational model. The theoretical molecular intensities $sM(s)$ were calculated with the structural parameters determined in the preceding section, and the mixing ratio and the *gauche* dihedral angle were varied. Typical I_b curves for a number of models are illustrated in Fig. 4. The I_b curve corresponding to a *trans* population of 80% and a *gauche* dihedral angle of 85° is acceptable since it has no fluctuation exceeding 0.5% of I_b, whereas all the other models shown in the figure are unacceptable because they result in systematic oscillations in the I_b curves.

The limit of uncertainty in the background function was estimated from two principal sources of error:[32,33] the random and systematic errors in the intensity measurement and the uncertainties in the structural

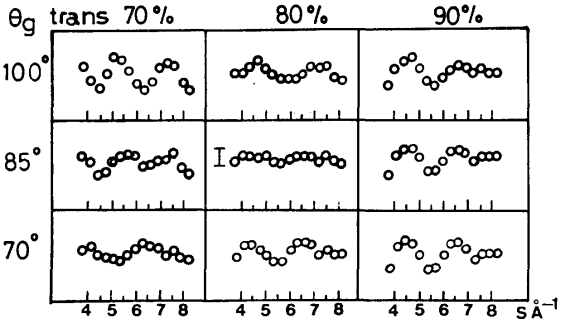

Fig. 4. Background functions I_b for different compositions of the *trans* and *gauche* conformers and dihedral angle (θ_g) for the *gauche* form. The vertical bar represents 0.5% of I_b. See text.

parameters assumed in this background analysis. The effect of the former was estimated by checking the reproducibility of the intensities obtained from different photographic plates and by examining various sources of systematic error.[26] The systematic error originating from the error in the frame structure was checked by calculating the background function with sets of the geometrical parameters varied within the limit of their estimated uncertainties. The limit of uncertainty in the background function was thus estimated to be $\pm 0.5\%$. This value corresponds to the limit of uncertainty of less than 10% in the mixing ratio and that of less than 10° in the dihedral angle. Consequently, the conformational parameters determined by the method of background function agree with those obtained from the least-squares method.

Comparison with Related Molecules

The skeletal structure of ethyl methyl ether is compared with those of analogous molecules (Table 5). The $(C-O)_{av}$ bond length and the C–O–C bond angle agree with those in dimethyl ether [17] within their uncertainties. The C–C bond distance (1.520 ± 0.004 Å) is significantly shorter than that in butane (1.531 ± 0.004 Å).[29] The C–H bond length is very similar to that in butane. The r_g C–C bond length and the C–O–C and H–C–H bond angles in the r_α structure are nearly equal to those in the r_s structure,[9] while the C–H and $(C-O)_{av}$ bond distances (r_g) are slightly larger than the corresponding r_s distances. In view of the known differences in the r_g and r_s structures for analogous molecules,[34] these r_g and r_s distances seem to correspond well. On the other hand, there seems to be a slight discrepancy between the r_g and r_s structures in regard to the difference of the C(methyl)–O and C(methylene)–O bond lengths: The r_g structure indicates a *positive* difference of the order of 0.01 Å, whereas the r_s structure indicates a *negative* difference of the same order of magnitude. However, neither trend can be regarded as conclusive, since these distance parameters have large uncertainties (particularly the r_s structure has systematic error because the oxygen coordinates were determined with the aid of the first-moment equation).

Table 5. Comparison of related molecules

	$CH_3OCH_2CH_3$[b]	CH_3OCH_3	CH_3CH_2-CH_2CH_3[d]
C–C	1.520(4)	—	1.531(2)
C–O	1.418(2)[e]	1.418(3)[f]	—
C–H	1.118(4)	1.100(6)[f]	1.117(5)
∠C–O–C	111.9(5)	111.5(15)	—
θ_g[g]	84(6)	—	65(6)
$n_t/(n_t+n_g)$[h]	80(8)	—	54(9)
ΔG[i]	1.23(27)	—	0.50(22)

a) Distances in r_g and angles r_α (r_a for c). Uncertainties represent estimated limits of error attached to the last significant digits. b) Present study. c) Ref. 17. d) Ref. 29. e) Average value of the two C–O bond lengths. f) Estimated from the r_a distance reported in the literature by addition of l^2/r_a. g) The dihedral angle for the *gauche* conformer measured from *cis* position. h) % *trans* form. i) Free energy difference (kcal/mol): $\Delta G = G_{gauche} - G_{trans}$.

The *gauche* dihedral angle in ethyl methyl ether ($84 \pm 6°$) obtained in the present study is significantly larger than that in butane ($65 \pm 6°$).[29]

Structures of a number of polyether crystals were recently determined by X-ray diffraction.[35-37] The C–C bond lengths adjacent to C–O bonds, determined to be about 1.48—1.52 Å, are shorter than the usual C–C bond distances. This trend is similar to that observed in the C_1–C_2 bond lengths in ethyl methyl ether. The conformation about the C–O bonds in polyethers is found to be most commonly *trans*. However, some intra- and intermolecular forces make the *gauche* conformation stable in some parts of a polymer, and in this case the dihedral angles about the C–O bonds for the *gauche* conformation are about 70—90°. This trend is analogous to that observed for small molecules in the gas phase by electron diffraction.

The authors are indebted to Professor Tatsuo Miyazawa, Professor Michiro Hayashi, and Dr. Teizo Kitagawa for helpful discussions, to Dr. Tsutomu Fukuyama for his technical assistance in the diffraction experiment and analysis, and to Miss Mami Mikami for her assistance in the initial stage of the present study.

References

1) H. Wieser, W. G. Laidlaw, P. J. Kreuger, and H. Fuhrer, *Spectrochim. Acta, Part A*, **24**, 1055 (1968); J. P. Perchard, J. C. Monier, and P. Dizabo, *ibid.*, **27**, 447 (1971).

2) T. Yoshihara, H. Tadokoro, and S. Murahashi, *J. Chem. Phys.*, **41**, 2902 (1964).

3) T. Shimanouchi, Y. Ogawa, M. Ohta, H. Matsuura, and I. Harada, *Bull. Chem. Soc. Jpn.*, **49**, 2999 (1976).

4) R. G. Snyder and G. Zerbi, *Spectrochim. Acta, Part A*, **23**, 391 (1967).

5) T. Kitagawa and T. Miyazawa, *Bull. Chem. Soc. Jpn.*, **41**, 1976 (1968).

6) J. P. Perchard, *Spectrochim. Acta, Part A*, **26**, 707 (1970); J. P. Perchard, *J. Mol. Struct.*, **6**, 457 (1970).

7) T. Kitagawa, K. Ohno, H. Sugeta, and T. Miyazawa, *Bull. Chem. Soc. Jpn.*, **45**, 969 (1972).

8) T. Kitagawa, K. Kusaki, and T. Miyazawa, *Bull. Chem. Soc. Jpn.*, **46**, 3685 (1973).

9) M. Hayashi, H. Imaishi, K. Ohno, and H. Murata, *Bull. Chem. Soc. Jpn.*, **44**, 299 (1971); M. Hayashi and K. Kuwada, *J. Mol. Struct.*, **28**, 147 (1975).

10) R. K. Bohn, "Electron Diffraction Studies of Molecular Conformation" in "Molecular Structure by Diffraction Methods," in Specialist Periodical Reports, Vol. 5, ed by G. A. Sim and L. E. Sutton, (1977), Chap. 2.

11) Y. Murata, K. Kuchitsu, and M. Kimura, *Jpn. J. Appl. Phys.*, **9**, 591 (1970).

12) M. Tanimoto, K. Kuchitsu, and Y. Morino, *Bull. Chem. Soc. Jpn.*, **43**, 2776 (1970).

13) The authors are indebted to Mr. Kunio Kohata for his technical assistance in the microdensitometry. The procedure was presented at the 36th National Meeting of the Chemical Society of Japan, Osaka, April 1977 (Abstr. No. 1M02), and in the Symposium on Molecular Structure, Sapporo, August 1977 (Abstr. No. 1C04).

14) L. Schäfer, A. C. Yates, and R. A. Bonham, *J. Chem. Phys.*, **55**, 3055 (1971).

15) Numerical experimental data of the leveled intensity and the background have been deposited with the Chemical Society of Japan. (Document No. 7829)
16) Y. Morino, K. Kuchitsu, and Y. Murata, *Acta Crystallogr.*, **18**, 549 (1965).
17) K. Kimura and M. Kubo, *J. Chem. Phys.*, **30**, 151 (1959).
18) Y. Sasada, M. Takano, and T. Satoh, *J. Mol. Spectrosc.*, **38**, 33 (1971).
19) K. Kuchitsu and S. Konaka, *J. Chem. Phys.*, **45**, 4342 (1966).
20) K. Kuchitsu and S. J. Cyvin, "Molecular Structure and Vibrations" ed by S. J. Cyvin, Elsevier, Ambsterdam (1972), Chap. 12.
21) J. Karle, *J. Chem. Phys.*, **22**, 1246 (1954).
22) J. Karle and H. Hauptman, *J. Chem. Phys.*, **18**, 875 (1950).
23) K. Kuchitsu, *Bull. Chem. Soc. Jpn.*, **40**, 498 (1967).
24) K. Kuchitsu and Y. Morino, *Bull. Chem. Soc. Jpn.*, **38**, 806 (1965).
25) K. Kuchitsu, T. Fukuyama, and Y. Morino, *J. Mol. Struct.*, **1**, 463 (1968).
26) K. Kuchitsu, "Molecular Structures and Vibrations," ed by S. J. Cyvin, Elsevier, Amsterdam (1972), Chap. 10.
27) M. Toyama, T. Oka and Y. Morino, *J. Mol. Spectrosc.*, **13**, 193 (1964).
28) K. Kuchitsu, in G. Allen (editor), MTP International Review of Science, A. Biennial Series, Physical Chemistry, Vol. 2, Medical and Technical Publisher, Oxford (1972), Chap. 6.
29) W. F. Bradford, S. Fitzwater, and L. S. Bartell, *J. Mol. Struct.*, **38**, 185 (1977).
30) S. Fitzwater and L. S. Bartell, *J. Am. Chem. Soc.*, **98**, 8338 (1976).
31) R. R. Ryan and K. Hedberg, *J. Chem. Phys.*, **50**, 4986 (1969).
32) Y. Morino and K. Kuchitsu, *J. Chem. Phys.*, **28**, 175 (1958).
33) M. M. Abe, K. Kuchitsu, and T. Shimanouchi, *J. Mol. Struct.*, **4**, 295 (1969).
34) K. Kuchitsu, T. Fukuyama, and Y. Morino, *J. Mol. Struct.*, **4**, 41 (1969).
35) I. Goldberg, *Acta Crystallogr., Sect. B*, **33**, 472 (1977).
36) R. Iwamoto and H. Wakano, *J. Am. Chem. Soc.*, **98**, 3764 (1976).
37) S. Pérez and F. Brisse, *Acta Crystallogr., Sect. B*, **33**, 1673 (1977).

Molecular Structure and Conformation of Ethyl Methyl Sulfide as Studied by Gas Electron Diffraction

Kazuko OYANAGI and Kozo KUCHITSU*

Department of Chemistry, Faculty of Science, The University of Tokyo, Bunkyo-ku, Tokyo 113

(Received April 21, 1978)

The bond distances (r_g) and angles (r_a structure) in ethyl methyl sulfide have been determined by gas electron diffraction as follows: average of C(methyl)–S and C(methylene)–S=1.813±0.004 Å, C–C=1.536±0.008 Å, C–H=1.111±0.008 Å, ∠C–S–C=97.1±1.1°, ∠S–C–C=114.0±0.5°, ∠H–C–H=109.6±1.4°, where uncertainties represent estimated limits of experimental error. The two C–S lengths have been estimated independently with the aid of the rotational constants for the *trans* conformer reported by Hayashi *et al.*: C(methyl)–S=1.806±0.027 Å, C(methylene)–S=1.818±0.027 Å. The dihedral angle for the *gauche* conformer (66±9°) and the relative abundance of the *trans* and *gauche* conformers in the gas phase at 20 °C, $n_t/(n_t+n_g)=0.25\pm0.15$, have also been determined.

In the preceding paper,[1] the conformation of ethyl methyl ether was studied by gas electron diffraction, and the *trans* conformer was found to be more stable than the *gauche* conformer. The conformations of normal alkanes have also been investigated in detail by this method.[2,3] Electron diffraction is an important tool for such a conformational analysis,[4,5] since it provides, in principle, information on all interatomic distances in a molecule. However, conformations about the C–S bond in saturated compounds have never been studied by gas electron diffraction except for that in ethyl methyl disulfide.[6] Ethyl methyl sulfide is one of the simplest compounds that have internal rotation about the C–S bond. The vibrational spectra of this molecule have been observed and the conformation has been discussed.[7–11] The conformation was also investigated by a calculation based on molecular mechanics.[12] These studies have shown that there exist two conformers, the *gauche* and *trans* forms, in the gas and liquid phases. Spectroscopic experiments concluded that the two conformers had nearly the same energy in the gas phase,[8] the *gauche* conformer being 30±50 cal/mol more stable.[11]

In the present study, the frame structure and the mixing ratio of the two conformers have been derived from electron diffraction. In addition, the rotational constants of the *trans* conformer of the normal species determined by microwave spectroscopy[13] were used with our electron diffraction data to estimate the individual C–S bond lengths.

Experimental

A commercial sample (Tokyo Kasei Co., Ltd.) was purified by distillation. The purity was checked by gas chromatography, and the sample was found to be more than 99% pure.

Diffraction photographs were taken at camera lengths of 107.7 and 243.3 mm with an apparatus equipped with an r^3-sector.[14] The accelerating voltage was about 40 kV and was stabilized within 0.01% during the experiment. The sample was maintained at thermal equilibrium with its liquid phase at room temperature. The vapor pressure was about 100 Torr, and the exposure times were about 15 and 30 s for the long and short camera lengths, respectively. The scale factors of the diffraction patterns were calibrated with reference to the C=O distance (r_a) of carbon dioxide (1.1646 Å) measured under the same experimental conditions. Other experimental details are described elsewhere.[14,15]

Three photographic plates at each camera length were selected for the analysis. The optical density (0.15—0.45) was measured by a microphotometer and an integrating digital voltmeter, and it was assumed to be proportional to the molecular intensities. After correction for the imperfections of the r^3-sector shape and hand drawing of a smooth background, molecular intensities were obtained in the range s=3.7—18.8 (long) and 7.9—34.5 Å (short) at intervals of $s=\pi/10$ Å^{-1}.[16]

Since they agreed with each other in the overlapping region within their experimental errors, they were joined at s=11 Å^{-1}. The elastic and inelastic scattering factors and the phase shifts, which were required to remove the atomic and inelastic scattering, were taken from the tables prepared by Schäfer *et al.*[17] A typical molecular intensity and the corresponding

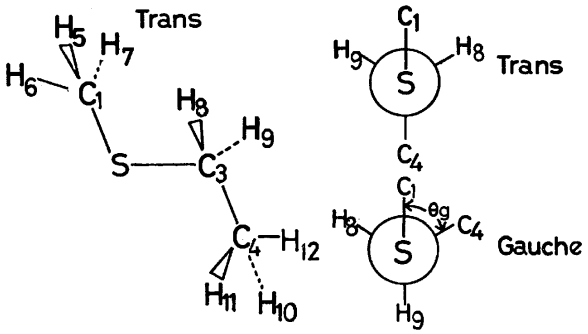

Fig. 1. Ethyl methyl sulfide. The dihedral angle for the *gauche* conformer measured from *cis* position is denoted by θ_g.

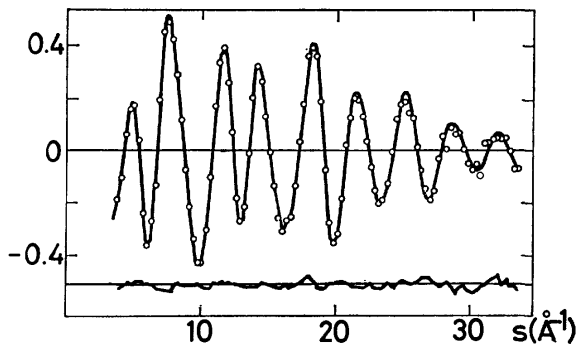

Fig. 2. Molecular intensities for ethyl methyl sulfide. Observed values are shown as open circles, and the solid curve represents the best-fit theoretical intensity. The lower solid curve represents the residuals.

radial distribution curve are illustrated in Figs. 2 and 3, respectively. Most of the calculations were carried out on a HITAC 8800/8700 in the Computer Center of the University of Tokyo.

Results and Discussion

Analysis of the Diffraction Data. The radial distribution curve has the following features: All the distances are contained in the 1.0—2.0 Å region. The peak at 1.1 Å is due to the C–H distance, and the C–C distance makes a small peak at 1.5 Å. The prominent peak contains the two C–S distances. The peaks at 2.4 and 2.9 Å are due to the nonbonded distances independent of the torsion about the C(methylene)–S axis. The shoulder at 3.2 Å and the small peak at 4.2 Å are due to the torsion-dependent C(methyl)···C(methyl) distances; the former shoulder and the latter peak come from the *gauche* and the *trans* conformers, respectively. Thus, their relative populations in the gas phase are determined from the contour of these peaks, *i.e.*, from the contributions of the C(methyl)···C(methyl) distances. On the basis of this analysis, it was concluded that two principal conformers existed in the gas phase at room temperature. By comparing the observed radial distribution curve with the curves calculated from various mixing ratios, the *gauche* conformer was inferred to be dominant. This is consistent with the conclusion derived from spectroscopy. The mean amplitudes for the C(methyl)···C(methyl) nonbonded pairs are so large that the intensity contributions from these pairs fade out in larger scattering angles. Therefore, the ratio of the two conformers is determined by the molecular intensities in the range of $s<5$ Å^{-1}. On the other hand, the r_α structure of the skeleton is determined by a least-squares analysis of molecular intensities in the larger s range ($s>5$ Å^{-1}), since in this range correlation between the parameters for the frame structure and the mixing ratio is not significant.

In this least-squares analysis the following approximations were made in order to decrease the number of the structural parameters:

1) Each of the methyl groups has C_{3v} symmetry and has no tilt.

2) For the methylene group, the bisectors of the H–C–H angle and the S–C–C angle are colinear.

3) All the C–H bond lengths are equal.

4) The difference in the two C–S bond distances is 0 ± 0.01 Å, on the basis of the structural data for dimethyl sulfide,[18] 1,2-ethanedithiol.[19] (The need for this assumption was removed in a later stage).

5) The geometrical parameters of the two conformers are equal except for the dihedral angles about the C(methylene)–S bond. (This assumption was examined in a later stage).

6) The *trans* conformer has C_s symmetry.

With these assumptions, the molecular structure is described by six parameters: the C–C bond length, the average of the C–S bond lengths, the C–H bond length, the S–C–C angle, the C–S–C angle, the weighted average of the H–C–H angles, and the dihedral angle about the C(methylene)–S bond for the *gauche* conformer. The corresponding dihedral angle for the *trans* conformer was fixed to 180° according to assumption 6).

Table 1. Mean amplitudes (l_{ij}) and shrinkage corrections (r_a-r_α) for *trans* and *gauche* ethyl methyl sulfide[a] (in 10^{-4} Å)

trans	l_{ij}	r_a-r_α		l_{ij}	r_a-r_α
C_1–H_5	786	78	S···H_8	1104	2
C_1–H_6	786	66	S···C_4	727	−10
C_3–H_8	786	87	C_1···C_3	890	−16
C_4–H_{10}	786	76	C_1···H_8	2099	−68
C_4–H_{11}	786	63	S···H_{11}	1706	114
C_3–C_4	525	10	S···H_{10}	1011	−67
C_1–S	522	8	C_3···H_5	1099	−149
C_3–S	535	−4	C_1···C_4	855	−244
C_3···H_{10}	1067	24	C_4···H_6	2018	251
C_3···H_{11}	1066	18	C_1···H_{11}	1790	−339
C_4···H_8	1070	19	C_1···H_{10}	1326	−249
S···H_5	1073	19	C_4···H_5	1145	−341
S···H_6	1071	13	C_3···H_6	2049	−53
gauche	l_{ij}	r_a-r_α		l_{ij}	r_a-r_α
C_1–H_5	786	69	C_1–H_7	786	62
C_1–H_6	786	65	C_3–H_8	786	97
C_3–H_9	786	96	C_1···H_{11}	2476	443
C_4–H_{10}	786	113	C_4···H_7	2792	405
C_4–H_{11}	786	89	C_4···S	728	−16
C_4–H_{12}	786	106	C_1···C_3	892	−22
C_3–C_4	526	6	C_3···H_6	2045	26
C_1–S	522	−5	C_3···H_7	1957	38
C_3–S	535	4	C_1···H_8	2086	41
C_3···H_{10}	1067	53	S···H_{11}	1706	4
C_3···H_{11}	1066	9	S···H_{12}	1936	−19
C_3···H_{12}	1066	36	C_1···C_4	1956	25
C_4···H_8	1070	22	C_4···H_6	3448	−58
C_4···H_9	1070	26	C_1···H_{12}	3608	−136
S···H_5	1073	0	S···H_{10}	1011	−72
S···H_6	1071	−2	C_3···H_5	1101	−164
S···H_7	1071	−6	C_1···H_9	1773	8
S···H_8	1104	19	C_4···H_5	1944	−120

a) Calculated at 20 °C. See Fig. 1 for the numbering of the atoms. Nonlinear shrinkages due to the C (methylene) –S torsion and the methyl torsions are included. (See text.) The values for H···H pairs are not listed.

The asymmetry parameter κ[20] for the C–H bond was estimated to be 1.3×10^{-5} Å^3 from the anharmonicity parameter a_3 for the C–H bond, which was assumed to be 1.98 Å^{-1}.[21] The asymmetry parameters for other atom pairs were ignored, since they did not contribute to molecular intensities significantly. The mean amplitudes and the shrinkage corrections (r_a-r_α)[22,23] for all the atom pairs were calculated on the basis of the modified Urey-Bradley force field,[9] as listed in Table 1. The frequencies of the skeletal and methyl torsions may be so low that a large-amplitude treatment is necessary. Since the frequencies and the potential functions for the skeletal torsions were not known, the contributions from these vibrational modes were estimated by Karle's method.[24-26] The three-fold potential barrier for the C(methylene)–S torsion was estimated to be about 500 cm^{-1} from those of methanethiol[27] and ethanethiol[28] assuming additivity of the contributions from substituted atoms or atom groups to the potential barrier.[29] The mean amplitudes estimated from the barrier height

turned out to be smaller than those estimated by the usual approximation of infinitesimal displacements. Karle's correction had the largest effect on the mean amplitude of the C(methyl)···C(methyl) nonbonded pair for the *gauche* conformer. The only significant effect of this torsion on the $r_a - r_\alpha$ is that for the C(methyl)···C(methyl) nonbonded atom pair, 0.0094 Å. The effect of the methyl torsions was estimated from the threefold potential barrier of about 700 cm^{-1} for the C(methyl)–S group and about 1400 cm^{-1} for the C(methyl)–C group, which were assumed from those of related molecules.[28,30] The uncertainties in the mean amplitudes and the shrinkage corrections were assumed to be 100% for the contributions from the C(methylene)–S and methyl torsions and 10% for those from the other modes.

The mean amplitudes of the C–C, the average of the C–S amplitudes and the weighted average of the C–H amplitudes were varied as parameters in the subsequent analysis. Other mean amplitudes were fixed to the values listed in Table 1. A conventional diagonal weight matrix was used in the analysis.[31] In this stage, the structural parameters obtained were the weighted *trans* and *gauche* parameters. The r_α structure and the r_g distances derived from the r_α structure are listed in Table 2. The error limits listed in this table were estimated from random and systematic errors including those originating from the approximations mentioned above.[32,33]

Table 2. Structure and mean amplitudes for ethyl methyl sulfide derived from electron diffraction data (in Å and degrees)

	r_α	r_g	ε[a]
$(C-S)_{av}$	1.811	1.813	0.004
$C_{methyl}-S$[b]	1.804	1.806	0.027
$C_{methylene}-S$[b]	1.816	1.818	0.027
C–C	1.534	1.536	0.008
C–H	1.096	1.111	0.008
∠C–S–C	97.1		1.1
∠S–C–C	114.0		0.5
∠H–C–H	109.6		1.4
θ_g[c]	66		9
$n_t/(n_t+n_g)$[d]	0.25		0.10
l(C–H)	0.079		0.005
l(C–C)	0.058		0.007
$l(C-S)_{av}$	0.054		0.004

a) Estimated limits of error. b) These distances were determined separately by a joint analysis. The rest of the parameters obtained by the joint analysis were essentially equal to those given in this Table. c) The dihedral angle for the *gauche* conformer measured from the *cis* position. d) Relative abundance of the *trans* conformer at room temperature estimated by the method of background function. See text.

Analysis of Diffraction Data with Supplementary Use of the Rotational Constants. The observed diffraction intensity carries information on the structures of the two conformers. On the other hand, the rotational constants are known only for the less abundant *trans* conformer, but the structure of this conformer has not been determined from the rotational constants. In order to take these rotational constants into the analysis as additional experimental information, the difference in the geometrical parameters for the *trans* and the *gauche* conformers had to be assumed. In the analysis of normal alkanes,[34] the C–C–C angle in the *gauche* conformer was estimated to be $0.1 \pm 1°$ larger than the corresponding angle in the *trans* conformation on account of the *gauche* C–C interaction, while their C–C bond lengths were assumed to be equal. Since existing spectroscopic data[11] and calculations based on molecular mechanics[12] suggest little enthalpy difference between the two conformers, it seems unlikely that intramolecular strain in the *gauche* conformer causes its skeletal structure to differ greatly from that of the *trans* conformer. Therefore, the possible differences in the skeletal C–C–S and C–S–C angles in the *gauche* and *trans* conformers were assumed to be 0—2°. It was also assumed that all the bond lengths were equal in the two conformers. Since the rotational constants for the *trans* conformer have different dependence on the two C–S bond lengths, it was possible to treat these distances as independent parameters in the joint analysis.

Table 3. Observed and calculated rotational constants for *trans* ethyl methyl sulfide[a] (in cm^{-1})

	B_0[b]	B_z[c]	$B_\alpha{}^0$[d]	B_{av}[e]
A	0.5342879	0.537(5)	0.526(15)	0.533(5)
B	0.106293	0.1063(2)	0.1056(20)	0.1058(8)
C	0.0933749	0.0934(1)	0.0923(12)	0.0930(5)

a) Uncertainties attached to the last significant digits are given in parentheses. b) Observed rotational constants for the ground vibrational state. Uncertainties are not listed in the original reference. Ref. 13. c) Zero-point average rotational constants calculated from A_0, B_0, and C_0 with corrections for vibrational effects. d) Rotational constants calculated from r_α parameters given in Table 2 determined in the analysis of electron diffraction intensities. Uncertainties are estimated from those in the r_α parameters. e) Best-fit rotational constants corresponding to the r_α sturcture, listed in Table 2, derived from the combined analysis of diffraction and microwave data. Uncertainties represent 2.5 times the estimated standard deviations.

The rotational constants for the ground vibrational states, A_0, B_0, and C_0, were converted to the zero-point average rotational constants, A_z, B_z, and C_z, by the harmonic corrections[35] listed in Table 3. The uncertainties in these corrections were assumed to be 100% for the contributions from the C–S and methyl torsions and 10% for those from all the other small amplitude modes. The uncertainties in the average rotational constants originate mainly from these corrections. The r_α structure determined by electron diffraction was extrapolated to zero kelvin by estimating the difference $r_\alpha - r_\alpha{}^0$.[23] In order to check the consistency of the diffraction data and the rotational constants, the rotational constants, $A_\alpha{}^0$, $B_\alpha{}^0$, and $C_\alpha{}^0$ for the *trans* conformer were calculated from the $r_\alpha{}^0$ structure and compared with A_z, B_z, and C_z. The agreement was

Table 4. Error matrix[a] and correlation matrix[b] for ethyl methyl sulfide[c]

	k_1	k_2	x_1	x_2	x_3	x_4	x_5	x_6	x_7	l_1	l_2	l_3
	102	358	31	6	16	76	36	100	567	19	24	14
k_1	100	52	−23	−16	32	−57	48	46	19	57	10	58
k_2		100	83	−58	61	−65	−34	58	18	82	78	96
x_1			100	−51	54	−52	−69	56	24	62	66	77
x_2				100	−41	33	−27	−45	−19	−47	−42	−55
x_3					100	−37	−25	53	−6	46	46	60
x_4						100	−48	−76	−42	−55	−47	−64
x_5							100	15	−29	−19	−34	−27
x_6								100	43	50	43	56
x_7									100	12	16	16
l_1										100	61	80
l_2											100	71
l_3												100

a) Error matrix. Units ($\times 10^{-4}$) for the distances and mean amplitudes are Å, those for the angles are rad, and those for the indices are dimensionless. b) Correlation matrix ($\times 10^{-2}$). c) k_1,k_2=indices of resolution for the long and short distance data, respectively, $x_1=r$(C–C), $x_2=r$(C–S)$_{av}$, $x_3=r$(C–H)$_{av}$, $x_4=\angle$C–S–C, $x_5=\angle$S–C–C, $x_6=\angle$H–C–H, x_7=dihedral angle for the *gauche* conformer, $l_1=l$(C–H), $l_2=l$(C–S), and $l_3=l$(C–C).

within the experimental uncertainties of A_α^0, B_α^0, and C_α^0, as shown in Table 3. Hence, these constants were used with the diffraction intensities as subsidiary observables. The weights for the rotational constants used in this analysis were estimated by the procedure mentioned in Ref. 1; they are 1×10^3, 1×10^4, and 1×10^4 for A_z, B_z, and C_z, respectively, where a unit weight was assigned to the molecular intensities from $s=10.5$ to 25.1 Å^{-1} taken at $s=\pi/10$ Å^{-1} intervals. A typical error matrix is shown in Table 4. The r_{av} structure[23] agreed with the r_α^0 structure, and the mean amplitudes also converged to essentially the same values as those obtained in the analysis of the electron diffraction data alone. The assumption 4) made in the analysis of the diffraction intensities was now removed, and the two C–S bond distances were varied independently. The two C–S bond lengths estimated separately in the present analysis are listed in Table 2. Their limits of uncertainty include the systematic uncertainties caused by the various assumptions described above, the main origin of the uncertainties being the assumed differences in the skeletal C–C–S and C–S–C angles in the *gauche* and *trans* conformers. The average of the C–S distances is equal to that obtained from electron diffraction.

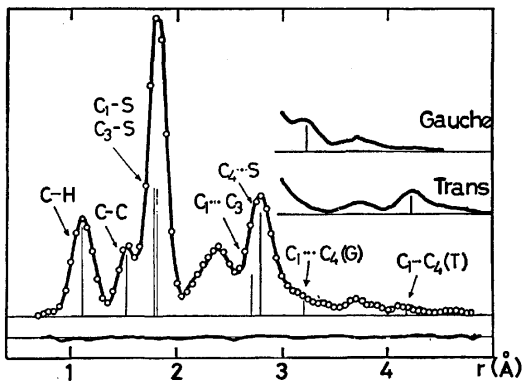

Fig. 3. Experimental and theoretical radial distribution curves. Damping factor, exp(−0.0016 s^2), was used. The residuals are shown below in the same scale.

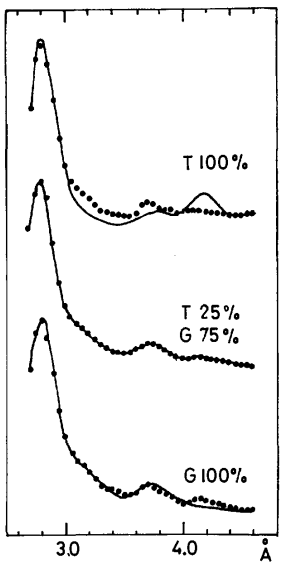

Fig. 4. Experimental and theoretical radial distribution curves illustrating the dependence on internal rotation.

Rotational Isomerism. The experimental radial distribution curve is compared in Fig. 4 with the theoretical radial distribution curves based on several different compositions of the *gauche* and *trans* conformers. The peaks from 3 to 4 Å^{-1} in the experimental curve show that in the gas phase at room temperature** the *gauche* form occupies more than 60% of the total population.

The essential experimental information about the conformation is contained in the molecular intensities from $s=2.2$ to 5.0 Å. The molecular intensity in this range is slightly influenced by the electron distributions forming chemical bonds. However, this effect[36] is less

** As discussed in Ref. 1, the above estimate of the sample temperature is based on the assumption that the thermal equilibrium at the temperature of the nozzle (room temperature) was retained in the gas jet when the electron beam was diffracted by the gas molecules.

than the error limits estimated below. The molecular intensities in this range measured at intervals of $s=\pi/10$ Å^{-1} were analyzed by the method of background function.[37,38] This method makes use of a background function $I_b(s)$ derived from the experimental total intensities $I_t(s)$ and the molecular intensities $sM(s)$ calculated from a structural model. If the structural model is correct, the I_b function should be free from fluctuations with a period similar to that of the molecular term. In other words, whether or not the I_b function oscillates with an amplitude exceeding a certain noise level is a sensitive criterion for selecting an acceptable conformation model. The I_b functions based on several different assumptions of the mixing ratio are shown in Fig. 5. Theoretical molecular intensities based on the

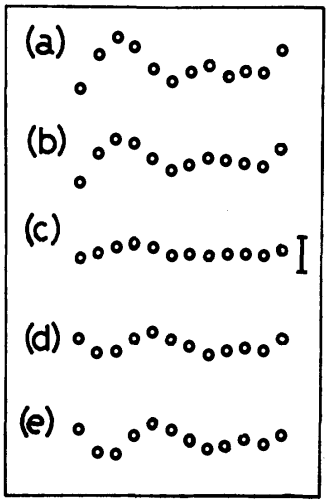

Fig. 5. Background functions I_b for different compositions of the *gauche* and *trans* isomers. (a) 60%, 40%, (b) 70%, 30%, (c) 75%, 25%, (d) 80%, 20%, and (e) 90%, 10%. The vertical bar represents 0.8% of I_b. See text.

geometrical parameters determined in the preceding section were used for the calculation of I_b. Models of A, B, C, D, and E correspond to the *trans* fractions of 40, 30, 25, 20, and 10%, respectively. A nearly flat I_b function is obtained for Model C. On the other hand, systematic fluctuations with a period of 1.6 Å^{-1} corresponding to the C_1–C_3 distance in the *trans* conformer appear in A, B, D, and E. They demonstrate that these models contain unacceptable assumptions regarding the *trans* fraction.

The limit of uncertainty of this background-function method depends on two sources: uncertainties in the model used for calculating the molecular terms, and random and systematic errors in the experimental intensities. In order to check the former uncertainties, background functions were calculated with various sets of the geometrical parameters. The effect of the latter was estimated by checking the reproducibility of the intensities obtained from the three different photographic plates and by examining various sources of systematic error. As a consequence, the limit of uncertainty in the background function is estimated to be $\pm 0.8\%$. This leads to the uncertainties of 15% in the estimates of the *gauche* and the *trans* fractions in the gas phase at room temperature, 75 and 25%, respectively.

Comparison of Structures. The skeletal structure of ethyl methyl sulfide is compared with those of related molecules in Table 5. The average of the two C–S bond lengths is nearly equal to those in dimethyl disulfide[6] and ethyl methyl disulfide.[6] There has been little information about the difference of the C(methyl)–S and C(methylene)–S distances. The present analysis suggests that the C(methylene)–S distance is slightly larger than the C(methyl)–S distance, which is nearly equal to those of dimethyl sulfide[18] and methyl vinyl sulfide.[39] This trend is similar to that observed in the C(methyl)–O and C(methylene)–O bond distances in ethyl methyl ether.[1] The C–C bond length is equal to those in normal alkanes[40,41] within the limits of error. This bond length is not affected by the adjacent sulfur atom, whereas the C–C bond in ethyl methyl ether[1] is shortened by the adjacent oxygen atom. The C–S–C angle is nearly equal to that in dimethyl sulfide and 6° smaller than that in methyl vinyl sulfide.

The population of the *gauche* conformer of ethyl methyl sulfide, $75\pm15\%$ in the gas phase at room temperature, implies that the *gauche* conformer is slightly more stable than the *trans* conformer by ΔG of 0.18 ± 0.35 kcal/mol. This conclusion is compatible with that obtained from recent Raman spectroscopy. The energy difference between the conformers may be contrasted with those for butane[2] and ethyl methyl ether,[1] where the *trans* conformer is more stable than the *gauche* conformer by 0.50 ± 0.22 and 1.23 ± 0.26 kcal/mol, respectively. The stability of the *gauche* conformer for ethyl methyl sulfide is the largest among these molecules.

Table 5. Comparison of the structures of related molecules[a]

	C–S	C–C	C–S–C	$n_t/(n_t+n_g)$[l]	ΔG[m]
CH_3–S–CH_2–CH_3[b]	1.813(4)[j]	1.536(8)	98.0(7)	25(15)	−0.18(35)
CH_3–S–CH_3[c]	1.807(2)	—	99.05(4)	—	—
CH_3–S–S–CH_3[d]	1.816(3)	—	—	—	—
CH_3–S–S–CH_2–CH_3[e]	1.817(4)[j]	1.540(7)	—	—	—
CH_3–S–CH=CH_2[f]	1.808(3)[k]	1.532(3)	104.6(8)	—	—
CH_3–CH_2–CH_3[g]	—	1.532(3)	—	—	—
CH_3–O–CH_2–CH_3[h]	—	1.520(4)	—	80(8)	1.23(27)
CH_3–CH_2–CH_2–CH_3[i]	—	1.531(2)	—	54(9)	0.50(22)

a) Distances (Å) in r_g and angles (deg) in r_{av} (r_a for f)). b) Present study. c) Ref. 18. d) Ref. 6. e) Ref. 6. f) Ref. 39. g) Ref. 40. h) Ref. 1. i) Ref. 2. j) Average of C_{methyl}–S and $C_{methylene}$–S distances. k) C_{methyl}–S distance. l) % *trans* form. m) Free energy difference (kcal/mol): $\Delta G=G_{gauche}-G_{trans}$.

The H···H nonbonded distances among the two methyl groups in these molecules make a reverse order; those in ethyl methyl ether are the smallest, and those in ethyl methyl sulfide are the largest. Steric effect of the rotors seems to play a dominant role in determining the relative stability of the conformers.

The authors are indebted to Professor Tatsuo Miyazawa and Professor Michiro Hayashi for their helpful comments and to Dr. Tsutomu Fukuyama for his technical assistance in the experiment and analysis.

References

1) K. Oyanagi and K. Kuchitsu, *Bull. Chem. Soc. Jpn.*, **51**, 2237 (1978).
2) W. F. Bradford, S. Fitzwater, and L. S. Bartell, *J. Mol. Struct.*, **38**, 185 (1977).
3) S. Fitzwater and L. S. Bartell, *J. Am. Chem. Soc.*, **98**, 8338 (1976).
4) O. Bastiansen, H. M. Seip, and J. E. Boggs, "Perspectives in Structural Chemistry," Vol. IV, ed by J. D. Dunitz and J. A. Ibers, Wiley, New York (1971).
5) R. K. Bohn, "Electron Diffraction Studies of Molecular Conformation," in "Molecular Structure by Diffraction Methods," Specialist Periodical Reports, Vol. 5, ed by G. A. Sim and L. E. Sutton, (1977), Chap. 2.
6) A. Yokozeki and S. H. Bauer, *J. Phys. Chem.* **80**, 618 (1976).
7) D. W. Scott, H. L. Finke, J. P. McCullough, M. E. Gross, K. D. Williamson, G. Waddington, and H. M. Huffman, *J. Am. Chem. Soc.*, **73**, 261 (1951).
8) M. Hayashi, T. Shimanouchi, and S. Mizushima, *J. Chem. Phys.*, **26**, 608 (1957).
9) M. Ohsaku, Y. Shiro, and H. Murata, *Bull. Chem. Soc. Jpn.*, **46**, 1399 (1973).
10) N. Nogami, H. Sugeta, and T. Miyazawa, *Bull. Chem. Soc. Jpn.*, **48**, 3573 (1975).
11) M. Sakakibara, H. Matsuura, I. Harada, and T. Shimanouchi, *Bull. Chem. Soc. Jpn.*, **50**, 111 (1977).
12) N. L. Allinger and M. J. Hickey, *J. Am. Chem. Soc.*, **97**, 5167 (1975).
13) H. Imaishi and M. Hayashi, *J. Sci. Hiroshima Univ., Ser. A*, **38**, 21 (1974).
14) Y. Murata, K. Kuchitsu, and M. Kimura, *Jpn. J. Appl. Phys.*, **9**, 591 (1970).
15) M. Tanimoto, K. Kuchitsu, and Y. Morino, *Bull. Chem. Soc. Jpn.*, **43**, 2776 (1970).
16) Numerical experimental data of the leveled intensity and the background have been deposited with the Chemical Society of Japan (Document No. 7831).
17) L. Schäfer, A. C. Yates, and R. A. Bonham, *J. Chem. Phys.*, **55**, 3055 (1971).
18) T. Iijima, S. Tsuchiya, and M. Kimura, *Bull. Chem. Soc. Jpn.*, **50**, 2564 (1977).
19) G. Schultz, I. Hargittai, *Acta Chim. Acad. Sci. Hung.*, **75**, 381 (1973).
20) K. Kuchitsu, *Bull. Chem. Soc. Jpn.*, **40**, 498 (1967).
21) K. Kuchitsu and Y. Morino, *Bull. Chem. Soc. Jpn.*, **38**, 805 (1965).
22) K. Kuchitsu and S. Konaka, *J. Chem. Phys.*, **45**, 4342 (1966).
23) For definition of the structural parameters used in the present study, see K. Kuchitsu and S. J. Cyvin, "Molecular Structures and Vibrations," ed by S. J. Cyvin, Elsevier, Amsterdam (1972) Chap. 12.
24) J. Karle and H. Hauptman, *J. Chem. Phys.*, **18**, 875 (1950).
25) J. Karle, *J. Chem. Phys.*, **22**, 1246 (1954).
26) M. Kitano, T. Fukuyama, and K. Kuchitsu, *Bull. Chem. Soc. Jpn.*, **46**, 384 (1973).
27) B. Kirtman, *J. Chem. Phys.*, **37**, 2516 (1962).
28) F. Inagaki, I. Harada, and T. Shimanouchi, *J. Mol. Spectrosc.*, **46**, 381 (1973).
29) O. L. Stiefvater and E. B. Wilson, *J. Chem. Phys.*, **50**, 5385 (1969).
30) A. S. Manocha, W. G. Fateley, and T. Shimanouchi, *J. Phys. Chem.*, **77**, 1977 (1973).
31) Y. Morino, K. Kuchitsu, and Y. Murata, *Acta Crystallogr.*, **18**, 549 (1965).
32) K. Kuchitsu, T. Fukuyama, and Y. Morino, *J. Mol. Struct.*, **1**, 463 (1968).
33) K. Kuchitsu, "Molecular Structures and Vibrations," ed by S. J. Cyvin, Elsevier, Amsterdam (1972), Chap. 10.
34) L. S. Bartell and D. A. Kohl, *J. Chem. Phys.*, **39**, 3097 (1963).
35) M. Toyama, T. Oka, and Y. Morino, *J. Mol. Spectrosc.*, **13**, 193 (1964).
36) T. Iijima, R. A. Bonham, C. Tavard, M. Roux, and M. Cornille, *Bull. Chem. Soc. Jpn.*, **38**, 1757 (1965).
37) Y. Morino and K. Kuchitsu, *J. Chem. Phys.*, **28**, 175 (1958).
38) M. M. Abe, K. Kuchitsu, and T. Shimanouchi, *J. Mol. Struct.*, **4**, 245 (1969).
39) S. Samdal and H. M. Seip, *J. Mol. Struct.*, **28**, 193 (1975).
40) T. Iijima, *Bull. Chem. Soc. Jpn.*, **45**, 1291 (1972).
41) T. Iijima, *Bull. Chem. Soc. Jpn.*, **46**, 2311 (1973).

Correlation between Relative Sensitivities for Electron Capture Detector and Chemical Structure of Aromatic Halogeno and Nitro Compounds

Yukikazu HATTORI,* Yoshio KUGE, and Shigeru NAKAGAWA
Environmental Pollution Control Center of Osaka Prefecture, Nakamichi, Higashinari-ku, Osaka-shi, Osaka 537
(Received July 13, 1977)

Relative sensitivities of an electron capture detector (ECD, ^{63}Ni) for aromatic halogeno and nitro compounds were measured at detector temperatures of 230, 290, and 320 °C. The effects of various substituents on the sensitivity of ECD were determined. A good correlation was recognized between the relative sensitivities of ECD and the positions of substituents for aromatic chloro, bromo, and nitro compounds. The plotted logarithm values of ECD sensitivities for aromatic chloro and bromo compounds *vs.* Hammett's σ values of various substituents are not linear, but the plots for aromatic nitro compounds follow a straight line. Modified σ values (σ_H) were determined on the basis of the relative sensitivities of aromatic chloro compounds. Plots of aromatic chloro, bromo, and nitro compounds *vs.* σ_H values gave straight lines. The temperature dependence of electron capture coefficients for these compounds was determined using D.C. mode. The electron capture spectra obtained are similar to those using pulsed mode.

Various organic compounds containing a halogen, oxygen, and sulfur atom exhibit electron capture sensitivities. Many reports of ECD sensitivities for these compounds have been published.[1-5] Lovelock and others reported the electron absorption coefficients for polychlorinated benzenes using a ^{3}H detector (pulsed mode).[1] The correlation between the sensitivity of various pesticides and their molecular structure was examined by Zielinski and others[2-4] using a ^{3}H detector. But in these studies the complete rule of the correlation could not be established and the temperature dependence of the sensitivity was not considered.

Wentworth *et al.*[6-12] have studied the thermal electron attachment to various compounds using the pulse-sampling technique. In their reports, the temperature dependence of electron capture coefficients (K values) was elucidated. Activation energies for electron capture reactions and the electron affinities of these compounds were also calculated.

Vessman *et al.*[13] investigated the correlation of the temperature dependence of sensitivities with the molecular structure for benzophenone derivatives by using a ^{3}H detector (D.C. mode).

Recently, Kojima and Satouchi *et al.*[14-19] investigated minutely the temperature dependenc of K values by using a ^{63}Ni detector which could operate at a higher detector temperature than the ^{3}H detector used by Wentworth *et al.* They pointed out that electron capture reactions for aromatic halogeno compounds were similar to bimolecular nucleophlic substitution.

In this work, sensitivities of ECD for aromatic halogeno and nitro compounds at three different detector temperatures were determined by using a ^{63}Ni detector. Moreover, the temperature dependence of electron capture coefficients was investigated. The relationships between ECD response and the molecular structure of these compounds were studied with D.C. mode. We intend to use this relationship for prediction of ECD sensitivity and for identification of unknown samples.

Experimental

Apparatus and Materials. A Varian aerograph 2100 type gas chromatograph with an electron capture detector (^{63}Ni, 8.5 mCi) was used in this experiment. Applied voltage was supplied with D. C. mode. The glass column (2 mm$\phi \times$ 1.5 m) was packed with Gaschrom Q (100—120 mesh) coated with 5% Bentone 34 and 5% Silicone DC-200. Nitrogen gas was used as a carrier gas; the flow rate was 30 ml/min. The temperature of the sample injection part was kept at 200 °C. The column temperature was set ordinarily at 100 °C. The temperature of the detector cell (foil temperature) was changed from 150 (130) to 350 °C (290 °C). The reagents used were all commercially available (special and guaranteed grade from Tokyo Chemical Co.). All reagents were checked by gas chromatography and distilled before use if necessary.

Procedure. The relative sensitivity (hereafter abbreviated to *R.S.*) was obtained by calculating the relative peak area per mole of the compound, using *p*-dichlorobenzene as a standard. The sample size was so chosen as to keep the peak area within a linear range on the calibration curve. The area under the chromatographic peak was obtained by multiplying the peak height by the width at half point of peak height. The relative retention time (hereafter abbreviated to *R.R.T.*) was also obtained by using *p*-dichlorobenzene as a standard, ordinarily at a column temperature of 100 °C. The electron capture coefficient (K value) was calculated from the following equation 1 derived by Wentworth:

$$K = (F/S \cdot N)\int (I_b - I_e)/I_e \cdot dx, \quad (1)$$

where F is the carrier gas flow rate (l/min), S is the chart speed (cm/min), N is the amount of sample injected (mol), and I_b and I_e are the detector current without and with capturing species in the detector, respectively. Since the detector signal is proportional to $(I_b - I_e)$, we can convert the term of $(I_b - I_e)/I_e$ to $(I_b - I_{ep})/I_{ep}$. $(I_b - I_{ep})$ is the recorder response corresponding to the maximum peak height; I_{ep} can be obtained by subtracting $(I_b - I_{ep})$ from I_b. So Eq. 1 can be converted to

$$K = (F/S \cdot N)\{(I_b - I_{ep})/I_{ep}\} \cdot W. \quad (2)$$

The integral in the Eq. 1 corresponds to the peak area on the chromatogram in Eq. 2, where W is the width at the half peak height.

TABLE 1. RELATIVE SENSITIVITY FOR ECD AND RELATIVE RETENTION TIME OF AROMATIC CHLORO COMPOUNDS

Compound	Relative sens. (230 °C)	Relative sens. (290 °C)	Relative sens. (320 °C)	Relative retention time
Chlorobenzene	0.0013	0.00170	0.00140	0.526
p-Dichlorobenzene	1.00	1.00	1.00	1.00
m-Dichlorobenzene	2.18	2.16	1.91	1.31
o-Dichlorobenzene	1.76	1.57	1.88	2.21
1,2,3-Trichlorobenzene	27.2	21.6	21.6	7.21
1,2,4-Trichlorobenzene	11.0	12.6	12.4	3.07
1,3,5-Trichlorobenzene	22.3	19.1	18.2	1.88
1,2,3,4-Tetrachlorobenzene	82.1	42.6	63.6	9.79[a]
1,2,3,5-Tetrachlorobenzene	84.0	44.4	51.8	5.41[a]
1,2,4,5-Tetrachlorobenzene	36.2	24.5	28.9	5.75[a]
Pentachlorobenzene	642.0	109.7	232.4	11.6[b]
Hexachlorobenzene	498.9	102.2	217.6	25.5[b]

a) Determined at a column temperature of 120 °C.
b) Determined at a column temperature of 140 °C.

Results and Discussion

Relative Sensitivity for ECD and Relative Retention Time. *R.S.* for ECD and *R.R.T.* of polychlorinated benzenes are tabulated in Table 1. *R.S.* of ECD becomes larger as the number of chlorine atoms increases, except that the result of *R.S.* for pentachlorobenzene (PCB) is larger than that of hexachlorobenzene (HCB). This tendency is similar to that of the electron absorption coefficient determined with a ^3H detector by Lovelock *et al.*[1] Shimokawa *et al.*[20] measured the relative electron capture efficiencies of halobenzenes, compared with biphenyl as a reference material, in glassy 2-methyltetrahydrofuran at 77 K by absorption spectrometry. They defined the relative electron capture efficiency (K_s/K_{ϕ_1}) as follows:

$$OD°/OD = 1 + (K_s/K_{\phi_1}) \cdot ([s]/[\phi_2]),$$

where $OD°$ and OD represent the optical densities of biphenyl anion (410 nm) in the absence and presence of solute, K_s and K_{ϕ_1} are the electron capture coefficients of the given solute and of biphenyl, and [s] and $[\phi_2]$ are the concentrations of given solute and of biphenyl. $OD°$ and OD correspond to I_b and I_e, respectively, in our report. Their report also shows that the relative electron capture efficiency becomes larger with increasing the number of chlorine atoms. The relative electron capture efficiency of PCB is also larger than that of HCB. They attributed this fact to the shielding effect of the π-orbital system by the substituent chlorine atom on the benzene ring. The same effect was observed in the electron capture reaction of polychlorinated benzenes in our gas chromatographic study.

R.R.T. values of polychlorinated benzenes ordinarily become larger as the number of chlorine atoms increases.

TABLE 2. RELATIVE SENSITIVITY FOR ECD AND RELATIVE RETENTION TIME OF AROMATIC CHLORO, BROMO, AND NITRO COMPOUNDS

Compound	Relative sens. (230 °C)	Relative sens. (290 °C)	Relative sens. (320 °C)	Relative retention time
p-Chlorotoluene	0.00116	0.00068	0.00135	0.90
m-Chlorotoluene	0.00117	0.00081	0.00105	0.89
o-Chlorotoluene	0.00134	0.00120	0.00160	0.87
p-Bromochlorobenzene	31.6	21.6	18.9	1.76
m-Bromochlorobenzene	46.7	28.9	26.2	2.48
o-Bromochlorobenzene	47.1	29.1	27.1	3.04
p-Chloronitrobenzene	63.6	31.4	26.2	9.55
m-Chloronitrobenzene	89.1	42.3	43.9	13.03
o-Chloronitrobenzene	102.7	53.8	43.7	28.44
Bromobenzene	0.540	0.430	0.444	0.97
p-Dibromobenzene	88.9	50.0	31.4	2.99
m-Dibromobenzene	141.8	69.8	45.0	3.79
o-Dibromobenzene	219.3	117.6	56.6	6.00
p-Bromotoluene	0.293	0.193	0.220	1.60
m-Bromotoluene	0.108	0.0980	0.0997	1.60
p-Bromonitrobenzene	80.4	38.7	20.6	16.4
m-Bromonitrobenzene	144.8	65.5	44.6	23.9
o-Bromonitrobenzene	148.2	68.2	46.4	—
Nitrobenzene	15.8	7.36	3.48	6.32
p-Nitrotoluene	18.8	5.64	2.61	15.50
m-Nitrotoluene	15.0	6.52	3.29	11.76
o-Nitrotoluene	25.4	5.49	2.49	8.91

R.S. for ECD and *R.R.T.* of aromatic chloro, bromo, and nitro compounds with diverse substituents are summarized in Table 2. *R.S.* of monosubstituted benzenes are in the order of NO_2>Br>Cl. *R.S.* of nitrobenzene becomes higher with decreasing detector temperature. *R.S.* of disubstituted benzenes are in the order of Br(dibromobenzene)>Cl(dichlorobenzene). This order is in accordance with that of the ECD reactivity of disubstituted benzenes which was investigated with plasma chromatography by Karasec *et al.*[21] *R.S.* for ECD of these compounds varies greatly with the kind of substituents. The effects on *R.S.* of ECD with changing substituents for disubstituted compounds are clearly recognizable in Table 2. *R.S.* for ECD of a methyl-substituted compound which was derived from a monosubstituted one becomes lower than that of the original one. For example, *R.S.* for ECD of bromotoluene is smaller than that of bromobenzene. The same result was obtained for chlorotoluene. An exceptional result was observed for nitrotoluene only at a detector temperature of 230 °C. *R.S.* for ECD of the compound which was derived from an electron donative substituent such as a methyl group becomes smaller than the

original one. On the other hand, if a chloro, bromo, or nitro group which is an electron attractive substituent is introduced into the monosubstituted compound, *R.S.* for ECD of the compound becomes higher than that of the original. *R.S.* for ECD of the compound into which a nitro substituent was introduced becomes larger as the detector temperature decreases.

In order to investigate the effect of substituents on the ECD sensitivity in more detail, logarithm values of *R.S.* for these compounds were plotted against varying isomeric (*o*-, *m*-, and *p*-) positions and various kinds of substituents. The correlation between *R.S.* for ECD of aromatic chloro compounds ($Cl-C_6H_4-X$, X: substituent) and bromo compounds ($Br-C_6H_4-X$, X: substituent) is shown in Fig. 1 (a). The line was drawn by the least squares procedure. The correlation coefficient was 0.9813. Good correlation was obtained. The correlation between *R.S.* of aromatic chloro compounds ($Cl-C_6H_4-X$) and nitro compounds ($O_2N-C_6H_4-X$) is shown in Fig. 1 (b). Excellent correlation was given between chloro and nitro compounds. At detector temperatures of both 230 and 320 °C excellent correlations were observed. From these facts, the substituted effect for the electron capture reaction can be deduced. Logarithm values of *R.S.* for disubstituted compounds *vs.* Hammett's σ values were also plotted (Figs. 2 (a), (b), (c)). In Figs. 2 (a) and (b), most of plots deviate from the straight lines which were drawn using the average method. But the plots for the original compounds (chlorobenzene and bromobenzene) and the *meta*-substituted compounds are found to be linear, except for *m*-Br and *m*-NO_2 in Fig. 2(a) and *m*-NO_2 in

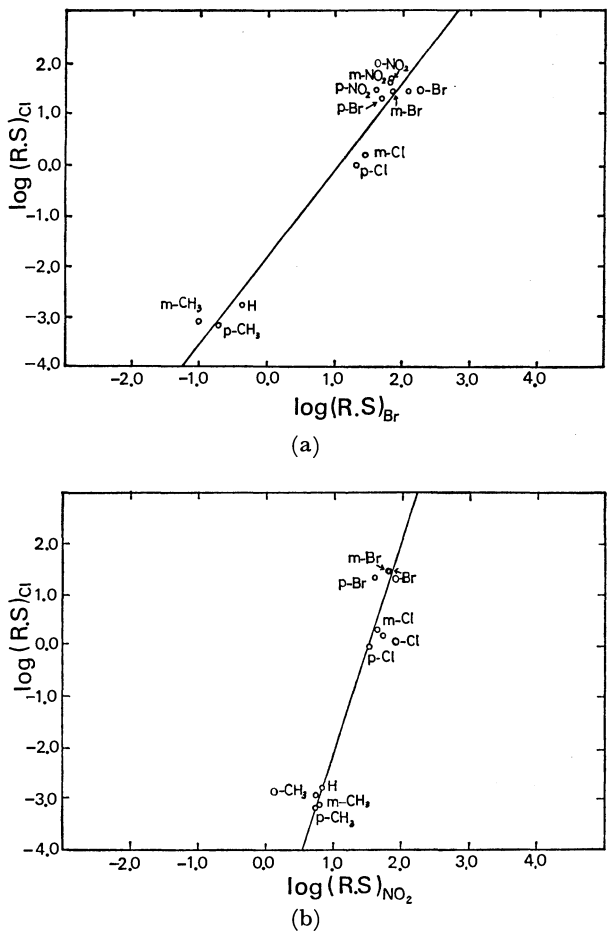

Fig. 1. (a) Correlation between *R.S.* for ECD of aromatic chloro compounds ($Cl-C_6H_4-X$) and bromo compounds ($Br-C_6H_4-X$) with varying substituents X. (*D.T.*: 290 °C). (b) Correlation between *R.S.* for ECD of aromatic chloro compounds and nitro compounds ($O_2N-C_6H_4-X$) with varying substituents X. (*D.T.*: 290 °C).

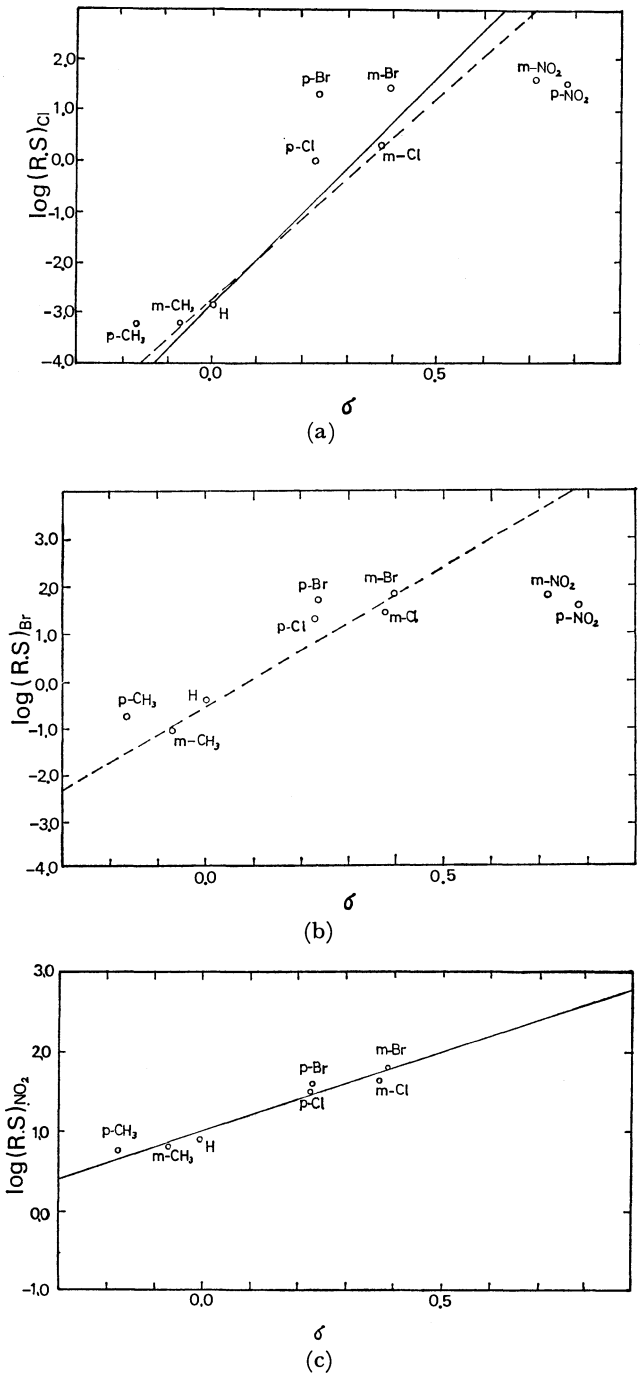

Fig. 2. (a) *R.S.* for ECD of aromatic chloro compounds *vs.* Hammett's σ values. (*D.T.*: 290 °C). (b) *R.S.* for ECD of aromatic bromo compounds *vs.* Hammett's σ values. (*D. T.*: 290° C). (c) *R. S.* for ECD of aromatic nitro compounds *vs.* Hammett's σ values. (*D.T.*: 290 °C).

Fig. 2(b). The plot of *m*-Br lies above the dotted straight line in Fig. 2(a), because the reactivity of bromo substituent is greater than that of the chloro substituent. The plots of *para*-substituted compounds are also above the dotted line. These facts suggest, as noted by Satouchi *et al.*,[17,18] that the electron capture reaction of these compounds seems to be the radical reaction. The plot of Hammett's σ values *vs.* *R.S.* of aromatic nitro compounds are shown in Fig. 2(c). Each plot was found to be almost linear by calculating with the least-squares procedure. The electron capture reactions of aromatic nitro compounds seem to obey Hammett's law and thus seem to take place in a different way from other aromatic halogeno compounds. Generally, the reactions of aromatic nitro compounds in an electron capture detector are described as taking place by the non-dissociative mechanism. Since those reactions obey Hammett's law, it is considered that a polar effect by substituents has a direct effect on the first stage of reaction, namely, on the stage of electron attachment. The modified σ values (σ_H) which are suitable for *R.S.* of these aromatic chloro and bromo compounds were determined at a detector temperature of 290 °C. These values were calculated from the line in Fig. 2(a) which was drawn by the average method as $\sigma_H=0$ for the hydrogen atom. The σ_H values are listed in Table 3.

TABLE 3. SIGMA σ_H VALUES[a]

Substituent	σ_H value	Substituent	σ_H value
p-CH_3	−0.044	*p*-Br	+0.454
m-CH_3	−0.035	*m*-Br	+0.469
o-CH_3	−0.017	*o*-Br	+0.469
p-Cl	+0.307	*p*-NO_2	+0.473
m-Cl	+0.343	*m*-NO_2	+0.487
o-Cl	+0.329	*o*-NO_2	+0.499

a) σ_H values were determined at a detector temperature of 290 °C.

The plots of σ_H values *vs.* the logarithm values of *R.S.* of aromatic bromo compounds are shown in Fig. 3 (a) Every plot gives a straight line. The plots of σ_H values *vs.* the logarithm values of *R.S.* of aromatic nitro compounds are shown in Fig. 3(b). Each plot also gives a straight line. At detector temperatures of 230 and 320 °C, the plots of σ_H values *vs.* the logarithm values of *R.S.* of these compounds also give straight lines. Even for *ortho*-substituted compounds, the plots fit a straight line, too. It seems that the steric effect does not take part in the electron capture reaction at least for *ortho*-substituted compounds. Then, if *R.S.* for ECD of a few compounds are known, *R.S.* of other compounds can be predicted from σ_H values. The plots of σ_H value *vs.* sigma values which were determined for ESR nitrogen coupling constants[22] of *para*-substituted derivatives of nitrobenzene are shown in Fig. 4. Except for NO_2 substituent, good correlation is shown. This fact suggests that the σ_H values are parameters related to the stability of anion radicals for these compounds. The plot of the activation energy E^*(kcal/mol) in electron capture reactions reported by Satouchi *et al.* *vs.* the values of $\rho^*\sigma_H$ are shown in Fig. 5. The values

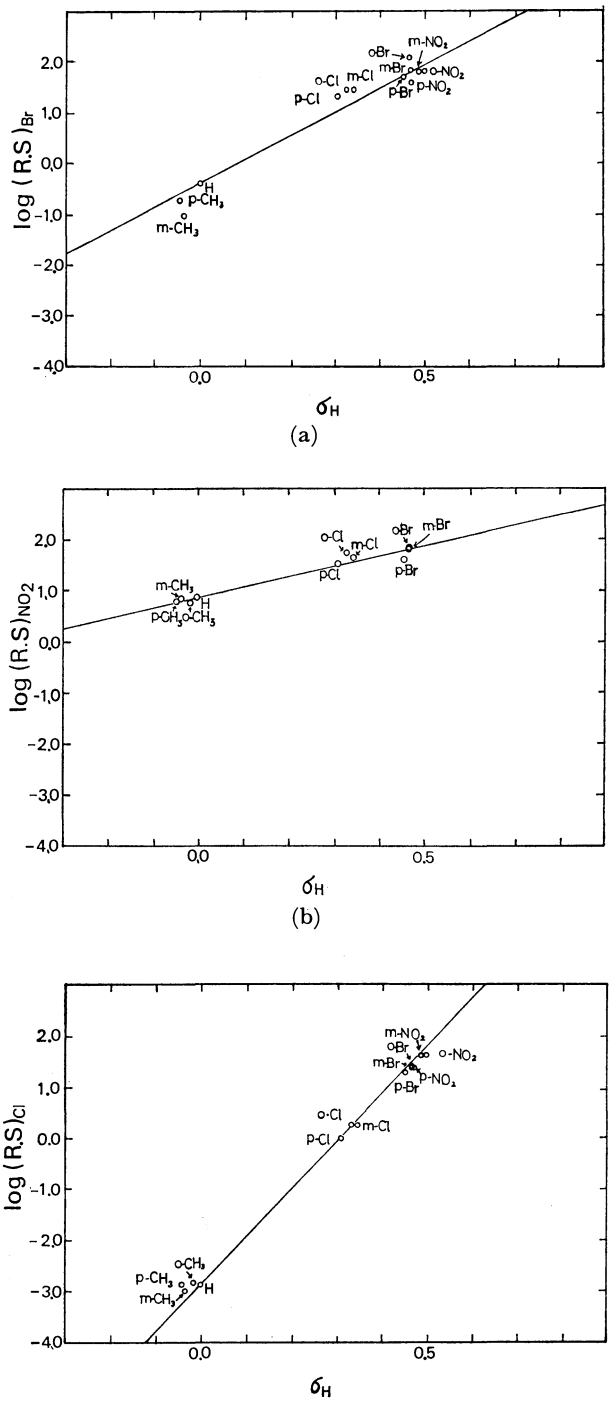

Fig. 3.(a) *R.S.* for ECD of aromatic bromo compounds *vs.* modified σ value (σ_H). (*D.T.*: 290 °C). (b) *R.S.* for ECD of aromatic nitro compounds *vs.* σ_H value. (*D.T.*: 290 °C). (c) *R.S.* for ECD of aromatic chloro compounds *vs.* σ_H value. (*D.T.*: 320 °C).

of $\rho^*\sigma_H$ are directly proportional to the E^* values. The ρ^* value represents the slope of the plot of the logarithm values of *R.S.* *vs.* σ_H. Thus $\rho^*\sigma_H$ values represent log *R.S.*

Temperature Dependence of Electron Capture Coefficients. The temperature dependence of electron capture coefficients (*K* values) was examined to investigate more

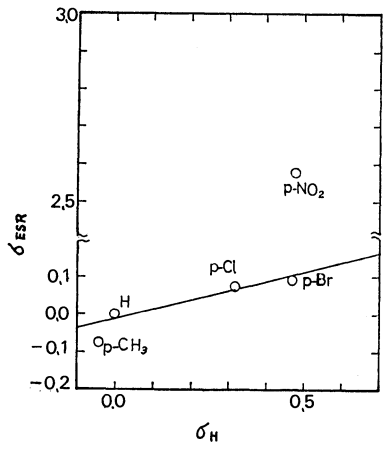

Fig. 4. σ_H values *vs.* Sigma constants determined from ESR nitrogen coupling constant of aromatic nitro compounds.

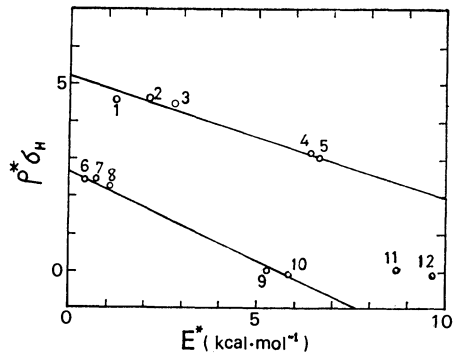

Fig. 5. $\rho^*\sigma_H$ (*D.T.*: 290 °C) *vs.* the activation energies reported by Satouchi *et al.*[17]
1: *m*-Chloronitrobenzene, 2: *o*-chloronitrobenzene, 3: *p*-chloronitrobenzene, 4: *m*-dichlorobenzene, 5: *o*-dichlorobenzene, 6: *m*-bromonitrobenzene, 7: *o*-bromonitrobenzene, 8: *p*-bromonitrobenzene, 9: bromobenzene, 10: *o*-bromotoluene, 11: chlorobenzene, 12: *o*-chlorotoluene.

minutely the mechanism of electron capture reaction by D.C. mode. The temperature dependences of K values for aromatic chloro, bromo, and nitro compounds are shown in Figs. 6(a) and (b). They were measured at a column temperature of 100 °C. The temperature dependences of K values which were measured at a column temperature of 140 °C are shown in Fig. 6(c). The temperature dependences of mono, di, tri, and tetrachlorobenzene have negative slopes. The magnitude of the negative slope becomes smaller with increasing numbers of chlorine atoms. For PCB and HCB, the temperature dependences of K values have positive slopes. The slope of PCB is larger than that of HCB. The temperature dependences of these chlorobenzenes show inflection points which are not observed in pulsed mode. For aromatic nitro compounds, the temperature dependences of K values show the positive slopes at the higher detector temperatures. Wentworth *et al.*[10] suggested that information on electron capture reaction mechanisms can be obtained from the temperature dependence of K values by not only pulsed mode but also D.C. mode. They gave the formula for $\{(b-[e^-])/[e^-]\}$ by assuming only either a non-dissociative reaction or a dissociative reaction. They expected that the magnitude of the slope given by D.C. mode would be smaller than that of pulsed mode. The values of apparent activation energies E^* and electron affinities EA' are tabulated in Table 4. They were calculated from the magnitude of slopes.

The patterns of temperature dependence of K values were classified into the following three types (Fig. 7).

A) Chlorobenzene type (chlorobenzene and chlorotoluene isomers)

The temperature dependence of K value shows a negative slope at the higher temperature and zero or a small

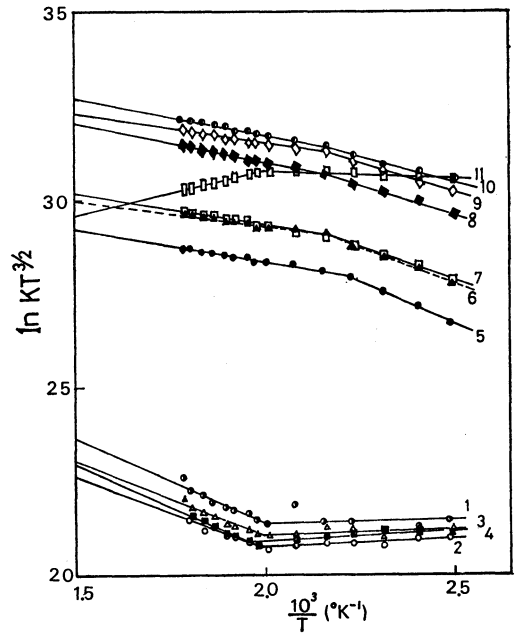

Fig. 6 (a).

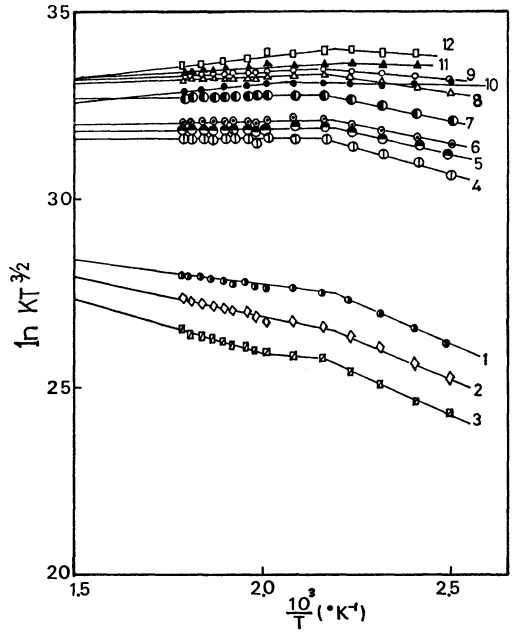

Fig. 6 (b).

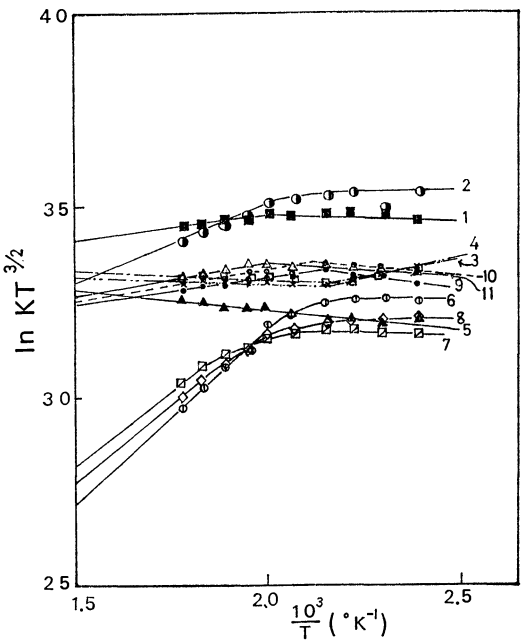

Fig. 6 (c)

Fig. 6 (a). Temperature dependence of electron capture coefficients (K values) measured at a column temperature of 100 °C.
1: Chlorobenzene, 2: *p*-chlorotoluene, 3: *m*-chlorotoluene, 4: *o*-chlorotoluene, 5: *p*-dichlorobenzene, 6: *m*-dichlorobenzene, 7: *o*-dichlorobenzene, 8: 1,2,4-trichlorobenzene, 9: 1,3,5-trichlorobenzene, 10: 1,2,3-trichlorobenzene, 11: nitrobenzene.
(b). Temperature dependence of K values measured at a column temperature of 100 °C. (*compounds were measured at 140 °C)
1: Bromobenzene, 2: *p*-bromotoluene, 3: *m*-bromotoluene, 4: *p*-bromochlorobenzene, 5: *m*-bromochlorobenzene, 6: *o*-bromochlorobenzene, 7: *p*-dichlorobenzene, 8: *m*-dibromobenzene, 9: *o*-dibromobenzene, 10*: *p*-bromonitrobenzene, 11*: *o*-bromonitrobenzene, 12*: *m*-bromonitrobenzene.
(c). Temperature dependence of K values measured at a column temperature of 140 °C.
1: Hexachlorobenzene, 2: pentachlorobenzene, 3: 1,2,3,4-tetrachlorobenzene, 4: 1,2,3,5-tetrachlorobenzene, 5: 1,2,4,5-tetrachlorobenzene, 6: *o*-nitrotoluene, 7: *m*-nitrotoluene, 8: *p*-nitrotoluene, 9: *p*-chloronitrobenzene, 10: *o*-chloronitrobenzene, 11: *m*-chloronitrobenzene.

positive slope at the lower detector temperature. This type of compound appears to undergo mainly dissociative electron attachment at the higher detector temperature. The magnitude of the negative slope in D.C. mode is smaller than in pulsed mode.

B) Dichlorobenzene type (dichlorobenzene, trichlorobenzene, bromobenzene, and bromotoluene isomers)
The temperature dependence of K value shows a negative slope which has an inflection point. The magnitude of the negative slope at the lower detector temperature is smaller than at the higher temperature. The reaction of this type may proceed chiefly according to dissociative electron attachment. The E^* values calculated from the magnitude of slopes at the higher

TABLE 4. APPARENT ELECTRON AFFINITIES (EA') AND ACTIVATION ENERGIES (E^*) FOR AROMATIC CHLORO, BROMO, AND NITRO COMPOUNDS IN D.C. MODE

Compound	EA' (kcal/mol)	$-\text{Slope} \times R$ [a] (kcal/mol)	E^* [b] (kcal/mol)
Chlorobenzene		9.17	5.96
p-Dichlorobenzene		3.60	1.33
m-Dichlorobenzene		2.84	1.15
o-Dichlorobenzene		3.43	1.61
1,2,3-Trichlorobenzene		3.97	2.48
1,2,4-Trichlorobenzene		3.97	2.70
1,3,5-Trichlorobenzene		3.06	2.31
1,2,3,4-Tetrachlorobenzene		0.84	
1,2,3,5-Tetrachlorobenzene		0.71	
1,2,4,5-Tetrachlorobenzene		2.01	0.41
Pentachlorobenzene	7.54		
Hexachlorobenzene	2.55		
p-Chlorotoluene		7.29	6.30
m-Chlorotoluene		9.09	6.19
o-Chlorotoluene		8.17	6.22
m-Chloronitrobenzene	2.61		
o-Chloronitrobenzene	2.31		
Bromobenzene		2.55	1.06
p-Bromotoluene		3.97	2.75
m-Bromotoluene		5.74	4.84
p-Bromonitrobenzene	1.99		
m-Bromonitrobenzene	2.26		
o-Bromonitrobenzene	1.14		
Nitrobenzene	4.81		
p-Nitrotoluene	15.79		
m-Nitrotoluene	14.90		
o-Nitrotoluene	18.06		

a) Calculated from $\ln KT^{2/3}$ *vs.* $1/T$ in kcal/mol.
b) Calculated from $\ln K$ *vs.* $1/T$.

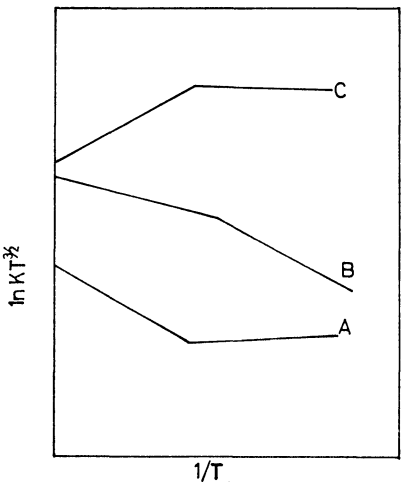

Fig. 7. Types of temperature dependence of K values.
A: Chlorobenzene type, B: dichlorobenzene type, C: nitrobenzene type.

detector temperature with D.C. mode are smaller than those with pulsed mode. The inflection points, whose physical meaning is not obvious, could be used for identification of unknown samples.

C) Nitrobenzene type (nitrobenzene, nitrotoluene isomers, PCB, HCB, and other nitro compounds) The temperature dependence of K value gives a positive slope at the higher temperature and a negative or zero slope at the lower temperature. In pulsed mode, this type of compound undergoes non-dissociative electron capture reaction. Similarly they seem to undergo non-dissociative electron attachment in D.C. mode. But for bromonitrobenzene and chloronitrobenzene isomers the magnitude of the positive slope is smaller than that in pulsed mode at the higher temperature. At the lower detector temperature, a negative slope is observed. Therefore, it is considered that these compounds undergo both dissociative and non-dissociative electron capture reactions. Since plots of both σ_H values and of Hammett's σ values *vs.* *R.S.* of aromatic nitro compounds give straight lines, the stage of electron attachment and elimination of the halogen atom may be important in the electron capture reaction of nitro compounds such as chloronitrobenzene isomers.

As mentioned above, the temperature dependence of K value in D.C. mode was similar to that in pulsed mode. Ordinarily, the magnitude of the slope, which corresponds to the calculated value of apparent activation energy (E^*) or electron affinity (EA'), was smaller than in pulsed mode. For example, the E^* value of chlorobenzene was found to be 5.96 kcal/mol in D.C. mode and 8.6 kcal/mol in pulsed mode by Satouchi *et al.*[17] As pointed out by Wentworth *et al.*,[10] this result may be attributed to the fact that electrons in the detector of D.C. mode have an additional energy given by the applied voltage. With this applied voltage in D.C. mode, the negatively charged ion of a sample molecule moves to the anode and discharges an electron. This effect is also observed in the case of disubstituted compounds containing electron attractive substituents. As regards this effect, an interesting phenomenon was observed. At the tailing part of the peak, some shape deformation (negative dip) was observed, as shown in

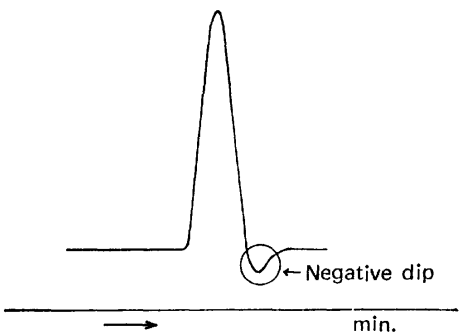

Fig. 8. Negative dip in the peak of gaschromatogram.

Fig. 8. This phenomenon was not caused by detector contamination. This deformation could not be observed at higher temperatures. The reason for the appearance of the negative dip is not obvious, but the following experimental results were obtained. This negative dip can be observed in electron capture response of dissociative type compounds such as chlorobenzene, but is not observed or is less observed in non-dissociative type compounds such as nitrobenzene and other nitro compounds. The depth of negative dip for *meta*-substituted compounds is larger than for *para*- and *ortho*-substituted compounds.

Summary

The mechanism in electron capture reaction can be determined by measuring the temperature dependence of K value in D.C. mode as well as in pulsed mode. We have used chromatographic data such as shape, slope, and inflection point in the curve of the temperature dependence of K value along with the data of retention time for identification of unknown substances.

The authors are very grateful to Dr. M. Satouchi for his valuable advice and useful suggestions.

References

1) J. E. Lovelock, "Gas Chromatography," ed by N. Brenner, Academic Press, New York, London (1962), p. 219.
2) W. L. Zielinski, Jr., and L. Fishbein, *J. Chromatogr.*, **28**, 293 (1967).
3) W. L. Zielinski, Jr., L. Fishbein, and R. O. Thomas, *J. Chromatogr.*, **30**, 77 (1967).
4) W. L. Zieliski, Jr., L. Fishbein, and L. Martin, Jr., *J. Gas Chromatogr.*, **5**, 552 (1967).
5) Girenko D. B. and Klisenko M. A., *Ukr. Khim. Zh. (Russ. Ed.)*, **41**, 422 (1975).
6) W. E. Wentworth, E. Chen, and J. E. Lovelock, *J. Phys. Chem.*, **70**, 445 (1966).
7) W. E. Wentworth, R. S. Becker, and Roberta Tung, *J. Phys. Chem.*, **71**, 1652 (1967).
8) W. E. Wentworth and E. Chen, *J. Phys. Chem.*, **71**, 1929 (1967).
9) D. C. Fenimore, A. Zlatkis, and W. E. Wentworth, *Anal. Chem.*, **40**, 1594 (1968).
10) W. E. Wentworth and E. Chen, *J. Gas Chromatogr.*, **5**, 170 (1967).
11) W. E. Wentworth and W. Ristau, *J. Phys. Chem.*, **73**, 2126 (1969).
12) W. E. Wentworth, L. W. Kao, and R. S. Becker, *J. Phys. Chem.*, **79**, 1161 (1975).
13) J. Vessman and P. Hartvig, *Reprint from Acta Pharm. Sucic.*, **8**, 235 (1971).
14) M. Satouchi and T. Kojima, *Anal. Lett.*, **5**, 931 (1972).
15) T. Kojima and M. Satouchi, *Bunseki Kagaku*, **22**, 1428 (1973).
16) T. Kojima and M. Satouchi, *Jpn. Analyst, Note*, **23**, 79 (1974).
17) M. Satouchi and T. Kojima, *Bunseki Kagaku*, **25**, 764 (1976).
18) T. Kojima, M. Satouchi, and Y. Tanaka, 36th National Meeting of the Chemical Society of Japan, Osaka, April 1977, I, p. 558.
19) T. Kojima, Y. Tanaka, and M. Satouchi, *Anal. Chem.*, **48**, 1760 (1976).
20) T. Shimokawa and T. Sawai, *Bull. Chem. Soc. Jpn.*, **50**, 365 (1977).
21) F. W. Karasek, O. S. Tatone, and D. M. Kane, *Anal. Chem.* **45**, 1210 (1973).
22) K. W. Bowers, "Radical Ions," ed by Kaiser Kevan, John Wiley, New York (1968), pp. 211—232.

A Redetermination of Diphenanthro[5,4,3-*abcd*: 5′,4′,3′-*jklm*]perylene

Isao Oonishi, Shoji Fujisawa,* Junji Aoki, and Takaaki Danno
Department of Chemistry, Faculty of Science, Toho University, Funabashi, Chiba 274
(Received September 14, 1977)

It has been shown that the true unit cell of diphenanthro[5,4,3-*abcd*: 5′,4′,3′-*jklm*]perylene consists of three subcells in which the atomic arrangements differ slightly from each other. The model for the ordered structure has been deduced from the consideration of weak reflections. The average structure of the subcell with $a=30.80$, $b=3.837$, $c=19.87$ Å, $\beta=112.5°$, and $Z=4$ has been redetermined. The final R value is 0.103 for 1244 independent reflections. The two naphthanthrone planes in the molecule make an angle of 36°, which shows a large distortion from a planar structure.

Recently, the photoconductivities of tetrabenzo-[*a*,*cd*,*j*,*lm*]perylene (hereafter TBP) and diphenanthro-[5,4,3-*abcd*: 5′,4′,3′-*jklm*]perylene (hereafter DPP) have been observed.[1] DPP was found to have a very high photoconductivity.

In order to discuss the relation between such high photoconductivities and the intramolecular electronic states or molecular arrangement, the details of molecular geometries must be known.

The crystal structure of TBP has been determined by Kohno *et al.*[2] The R value is 0.056. That of DPP has been determined by Robertson and Trotter,[3] but the R values reported by them were rather high (0.111 for $h0l$ and 0.26 for $h1l$ reflections), which suggests that the y coordinates were not accurate. Therefore, we have attempted a redetermination of this material.

Experimental

The DPP crystals used in the present investigation were obtained by condensation of naphthanthrone with copper powder, zinc chloride, and sodium chloride, by a method similar to that described by Aoki *et al.*[5] The method of preparation was different from that used by Robertson and Trotter.[4]

The crude product was dissolved in toluene and passed through a column of alumina to obtain the pure crystals. Small orange-red needles elongated along the b axis were grown by slow sublimation in a glass tube under a nitrogen atomosphere (5 mmHg).

The cross section of the crystal used for X-ray work (normal to the b axis) is 0.02×0.2 mm, which is smaller than that of 0.25×0.18 mm used by Robertson and Trotter.[3] The lattice constants of the crystal reported by Robertson and Trotter are: $a=30.73$, $b=3.855$, $c=19.87$ Å, and $\beta=113.0°$. Weissenberg photographs of the crystal used in the present investigation showed that the true a axis length is three times the above length. We observed essentially the same diffraction patterns for 10 different crystals. However, when very weak reflections are not taken into account, the unit cell corresponds to that of Robertson and Trotter (see below). This means that the true unit cell is divided into three parts, and the atomic arrangements in these subcells differ only slightly from each other. In the work by Robertson and Trotter, such weak reflections were not found, but diffuse streaks parallel to a* through Bragg reflections were found. On the contrary, such diffuse streaks are negligibly weak on our Weissenberg photographs (Plates 1 and 2). However, intense reflections corresponding to the subcell show the same features in the crystals used by both us and Robertson and Trotter. These facts suggest that there are different disorders in the two crystals, which seem to have been caused by a difference of purity.

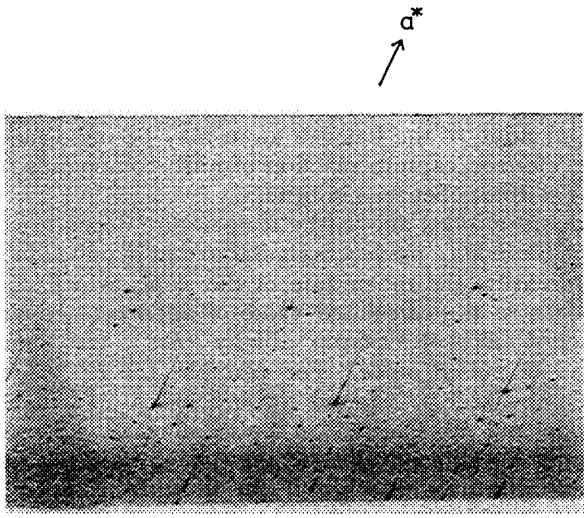

Plate 1. Weissenberg photograph of (h01).

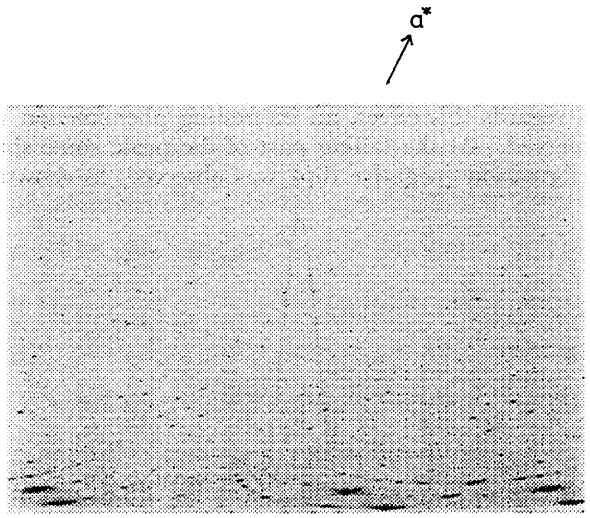

Plate 2. Equi-inclination Weissenberg photograph of ($h1l$).

Crystal Data for Subcell. $C_{38}H_{22}$, $M=478.60$, mp 340 °C, Space group: C2, $Z=4$; $a=30.80\pm0.04$, $b=3.837\pm0.005$, $c=19.87\pm0.03$ Å, $\beta=112.5\pm0.2°$, $v=2169.4$ Å^3; $D_x=1.465$, $D_m=1.45$ g cm^{-3}; $F(000)=1000$; μ(Cu $K\alpha$)$=6.3$ cm^{-1}. These values agree with those given by Robertson and Trotter within the experimental errors.[3]

Sets of multiple-film equi-inclination Weissenberg photographs were taken about the b axis (0th to 3rd layers) and about the c axis (0th layer). Cu $K\alpha$ radiation was employed throughout. The intensities were estimated by means of a

Rigaku photometer MP3. Weak intensities were visually estimated with a standard film strip. They were corrected for Lorentz and polarization factors, but no absorption correction was applied. The range of relative intensities was from 1 to 50000. 1244 independent reflections fell within this range, whereas 869 others were too weak to be observed.

The Model of Ordered Structure

When weak reflections have been taken into consideration, the extinction rules for the true unit cell are $h+k=2n$ in hkl reflections; $h=6n$ when $l=2n$ and $h=2$ when $l=2n+1$ in $h0l$ reflections. The latter cannot be explained with ordinary symmetry elements.

On the other hand, the distribution of intense reflections is $h=3(2n)$ when $k=0$, $h=3(2n+1)$ when $k=1$, $h=3(2n)$ when $k=2$, and so on. Thus, the only extinction rule for the subcell is $h'+k=2n$ in $h'kl$ reflections where $h'=h/3$. Both the true unit cell and the subcell are **C**-base centered lattices. The total intensity of weak reflections (281 in number) is less than 1% of that of the intense reflections.

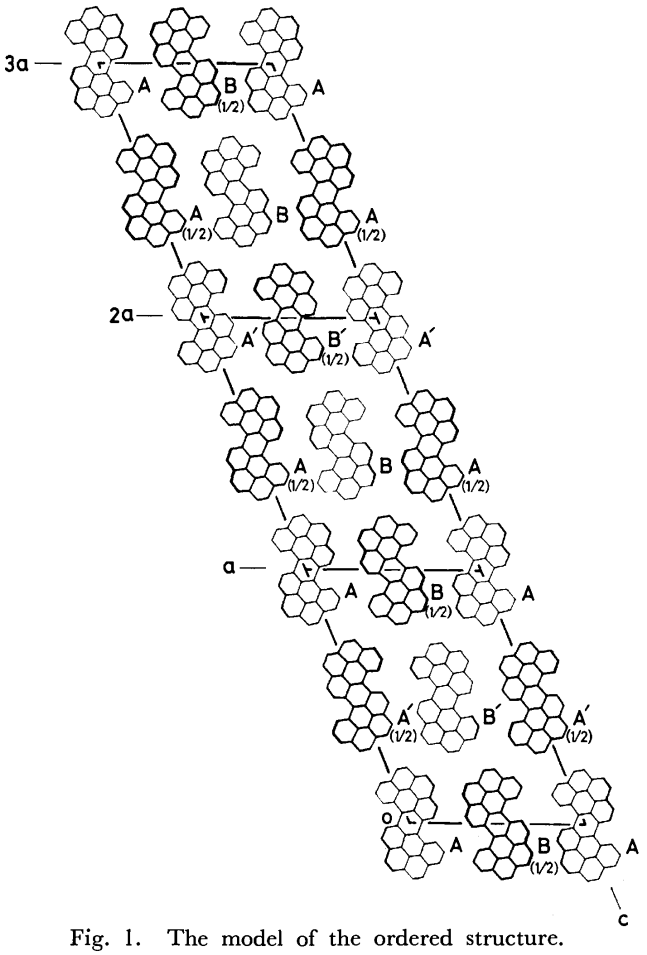

Fig. 1. The model of the ordered structure.

We have deduced the model pictured in Fig. 1 to explain the extinctions. In Fig. 1, a and c correspond to the subcell. A and B are enantiomer, and A′ and B′ are related to A and B by an approximate twofold rotation perpendicular to the ab-plane and a following translation of (3a/6, b/2), respectively. A and B′ (A′ and B) have the same shape when projected along the b axis. The molecules with the subscript of (1/2), for example A′(1/2) and B(1/2), have the height of b/2 relative to the ones without subscript.

In the true unit cell, the 4A molecules and 2B′ molecules (4B and 2A′) are in the positions of (x, z), $(1/6+x, z)$, $(3/6+x, z)$, $(4/6+x, z)$, $(2/6+x, 1/2+z)$ and $(5/6+x, 1/2+z)$, respectively. Only such a relative configuration is able to explain the extinction rules described above.

The structure is built of two kinds of energetically equivalent layers parallel to the bc-plane. Along the a direction, the two kinds of layers exist laterally in the ratio of 2: 1. The former can be expressed as ABAB— and the latter as A′B′A′B′—. They are related by a reflection on the ac-plane and a following translation of (3a/6, b/2, c/2).

According to the model of Robertson and Trotter, the two kinds of layers mentioned above exist randomly in the ratio of 1: 1 along the a direction. However, they have reported that this model cannot explain the appearance of $h0l$ reflections with l odd.

Refinement of the Average Structure

The average structure is a superposition of three subcells. The overlappings of the molecules in the average structure are AAA′ and BBB′. Thus, molecules A and B are given 2/3 factors, and A′ and B′ are given 1/3 factors.

We started refinement with the parameters given by Robertson and Trotter.[3] In the least squares calculations, molecules A and B were independently refined with isotropic temperature factors. After three cycles of least squares calculations, the R value converged to 19%. The three dimensional electron density map, calculated at this stage, revealed peaks with about 1/3 the height of a carbon atom, which have also been found on the two dimensional electron density given by Robertson and Trotter.[3] We assigned 1/3 factors to the peaks according to the model described above. At the same time, the factors of C(4) and C(5) atoms were changed to 2/3 (see the numbering scheme in Fig. 2). Hydrogen atoms except H(C4), H(C5), H(4′), and H(C5′) have also been found on the electron density map. However, since the shapes of the molecules A and A′ (B and B′) are very similar, only C(4), C(4′), C(5), and C(5′) atoms were separated on the electron density map.

After the introduction of anisotropic temperature factors for carbon atoms, six more cycles of refinement were carried out. The following weighting scheme was employed: $w=0.3$ if $F_o<F_{\min}$ (4.0), $w=1.0$ for the others. The final R value was 10.3% for all observed reflections. The atomic scattering factors were taken from International Tables for X-Ray Crystallography.[6] The final atomic parameters and their estimated standard deviations are given in Table 1(a) for carbon atoms and in Table 1(b) for hydrogen atoms. The positional and thermal parameters except those of the separated atoms need to be considered as the weighted average values of the overlapped atoms of molecules A and A′ (B and B′).

Table 1. Atomic parameters

(a) Positional and thermal parameters for non-hydrogen atoms ($\times 10^4$), with e.s.d.'s in parentheses ($\times 10^3$ for y, β_{22}, β_{12}, β_{23}).

The β_{ij}'s are defined by $\exp[-(h^2\beta_{11}+k^2\beta_{22}+l^2\beta_{33}+2hk\beta_{12}+2hl\beta_{13}+2kl\beta_{23})]$.

	x	y	z	β_{11}	β_{22}	β_{33}	β_{12}	β_{13}	β_{23}
Molecule A									
C(1)	1867(5)	169(4)	2078(8)	12(2)	72(14)	37(5)	−4(3)	15(5)	1(4)
C(2)	1483(5)	220(4)	2274(8)	14(2)	87(16)	36(6)	−3(3)	17(6)	−4(5)
C(3)	1020(4)	144(4)	1769(7)	10(2)	81(14)	30(5)	−2(3)	11(5)	4(4)
C(4)	621(6)	162(5)	1985(11)	11(3)	43(17)	34(7)	1(3)	16(7)	−3(6)[a]
C(4′)	311(15)	−272(13)	−1571(17)	23(7)	127(54)	13(10)	−14(10)	38(14)	−19(13)[b]
C(5)	191(6)	87(5)	1506(11)	12(2)	28(16)	46(7)	−4(3)	19(7)	−2(6)[a]
C(5′)	99(10)	−210(10)	1458(16)	9(3)	29(34)	24(9)	−14(6)	9(9)	−5(9)[b]
C(6)	83(4)	−33(4)	761(7)	11(2)	80(14)	32(5)	4(3)	17(5)	3(4)
C(7)	464(4)	−31(4)	529(7)	8(2)	62(12)	29(4)	0(2)	14(4)	2(4)
C(8)	394(4)	−73(4)	−194(7)	9(2)	45(11)	39(5)	−2(2)	17(5)	−1(4)
C(9)	790(4)	−163(4)	−416(7)	12(2)	68(13)	34(5)	0(3)	21(5)	3(4)
C(10)	735(5)	−290(5)	−1081(8)	11(2)	105(18)	39(5)	1(3)	18(6)	1(5)
C(11)	1121(5)	−379(5)	−1333(11)	13(2)	119(19)	78(10)	2(4)	30(8)	0(8)
C(12)	1572(5)	−307(4)	−764(9)	15(2)	90(17)	51(7)	2(3)	35(7)	3(5)
C(13)	1648(5)	−186(5)	−81(9)	13(2)	73(14)	52(7)	2(3)	27(6)	3(5)
C(14)	2114(5)	−116(5)	485(9)	10(2)	88(16)	57(7)	−1(3)	26(6)	2(6)
C(15)	2190(4)	0(4)	1145(8)	9(2)	93(16)	44(6)	−1(3)	14(6)	−2(5)
C(16)	1798(4)	65(4)	1367(8)	10(2)	76(14)	44(6)	−4(3)	16(6)	−2(5)
C(17)	1259(4)	−110(4)	133(8)	10(2)	65(13)	42(6)	−2(2)	22(5)	−1(4)
C(18)	1334(4)	−6(4)	848(7)	10(2)	56(12)	35(5)	0(2)	14(5)	3(4)
C(19)	938(4)	32(4)	1063(7)	9(2)	64(13)	29(4)	−1(2)	13(4)	−1(4)
Molecule B									
C(1)	1580(5)	632(4)	4226(8)	13(2)	83(14)	44(6)	−3(3)	28(6)	−2(5)
C(2)	1134(5)	683(4)	3739(7)	14(2)	96(15)	25(4)	−1(3)	23(5)	3(4)
C(3)	735(5)	603(5)	3893(8)	11(2)	97(15)	35(5)	1(3)	17(5)	0(5)
C(4)	268(8)	607(7)	3354(12)	18(4)	107(26)	36(8)	7(5)	25(9)	16(8)[a]
C(4′)	643(12)	199(10)	6970(14)	11(5)	84(36)	0(7)	−4(6)	3(9)	12(8)[b]
C(5)	−132(7)	491(7)	3526(12)	13(2)	103(26)	59(9)	5(4)	22(8)	−3(8)[a]
C(5′)	−207(12)	258(12)	3496(20)	15(5)	49(41)	53(13)	3(7)	33(13)	7(13)[b]
C(6)	−72(4)	425(4)	4262(7)	12(2)	65(12)	28(4)	3(2)	16(5)	3(4)
C(7)	391(4)	433(4)	4783(7)	9(2)	44(10)	30(4)	0(2)	15(4)	−3(4)
C(8)	465(4)	387(4)	5525(7)	9(2)	72(14)	33(5)	−2(2)	12(5)	4(4)
C(9)	944(4)	302(4)	6069(8)	12(2)	71(13)	35(5)	0(3)	16(5)	−1(4)
C(10)	1030(5)	174(5)	6750(8)	13(2)	105(18)	40(6)	0(3)	20(6)	−2(5)
C(11)	1479(6)	93(6)	7278(10)	18(3)	117(18)	51(7)	2(4)	17(7)	6(7)
C(12)	1865(5)	159(5)	7054(9)	13(2)	94(17)	47(6)	7(3)	16(6)	0(5)
C(13)	1794(5)	274(4)	6366(9)	12(2)	77(14)	45(6)	4(3)	18(6)	−1(5)
C(14)	2174(5)	345(5)	6145(10)	11(2)	100(17)	56(8)	5(3)	16(7)	1(6)
C(15)	2118(5)	464(4)	5456(9)	11(2)	80(15)	50(7)	0(3)	20(6)	−1(5)
C(16)	1653(4)	527(4)	4935(8)	11(2)	58(13)	41(5)	0(2)	22(5)	−3(4)
C(17)	1333(4)	350(4)	5823(8)	9(2)	63(13)	44(6)	1(2)	13(5)	0(5)
C(18)	1260(4)	460(4)	5132(7)	10(2)	55(11)	32(5)	1(2)	16(5)	−3(4)
C(19)	799(4)	498(4)	4594(7)	11(2)	57(12)	34(5)	2(2)	21(5)	1(4)

a) Population 2/3. b) Population 1/3.

(b) Positional parameters for hydrogen atoms ($\times 10^3$)

Mean isotropic temperature factor for hydrogen atoms is 4.0 Å^2.

Molecule A	x	y	z	Molecule B	x	y	z
H(C1)	224	225	247	H(C1)	192	−325	404
H(C2)	153	323	256	H(C2)	109	−275	316
H(C4)	67	288	242[a]	H(C4)	23	703	283[a]
H(C4′)	26	−356	−209[b]	H(C4′)	65	88	739[b]
H(C5)	−15	94	168[a]	H(C5)	−46	439	313[a]
H(C5′)	−41	−244	−189[b]	H(C5′)	−2	193	672[b]

H(C10)	41	−325	−176	H(C10)	76	140	686
H(C11)	107	−490	−196	H(C11)	153	−20	783
H(C12)	191	−344	−92	H(C12)	220	125	747
H(C14)	238	−144	26	H(C14)	248	288	654
H(C15)	253	37	149	H(C15)	246	519	526

a) Population 2/3. b) Population 1/3.

The observed and calculated structure factors are listed in Table 2.**

Description and Discussion

Figure 2 shows the average structure projected along the b axis and at the same time the bond lengths and angles in the molecules. When the atoms C(4) and C(5) are changed to the atoms C(4′) and C(5′), the molecules A and B change to the molecules A′ and B′, respectively. Since A and A′ (B and B′) have not been separated, as explained above, we cannot discuss the details of the bond lengths and angles, but only the shapes of molecules A and B.

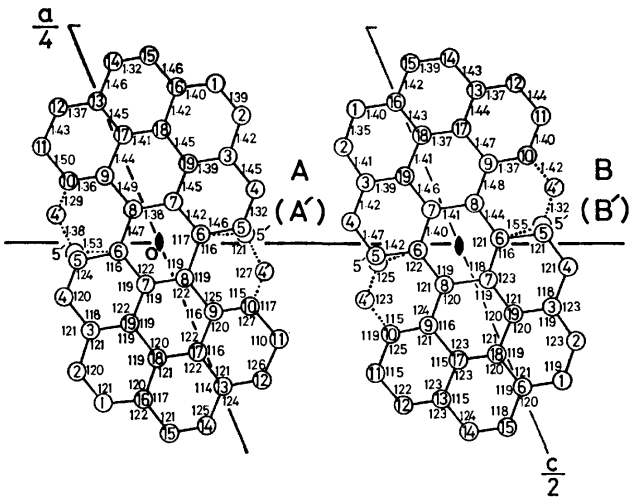

Fig. 2. The projection of the average structure along the b axis, and the bond lengths and bond angles.

Figure 3 shows the diagrams of DPP and TBP. In the molecule A, the downward naphthanthrone is twisted in a clockwise direction and the upper one is twisted in a counterclockwise direction around the arrow in Fig. 3. Figure 4 shows the perspective drawing of the molecule A, looking down along the arrow in Fig. 3 which runs through the two carbon atoms of the central ring. The molecules A and B are significantly distorted from a planar structure due to repulsions between the hydrogen atoms at the positions denoted with * in Fig. 3. Such distortion forces the central ring to adopt a twisted boat form. The molecules A and B are left- and right-handed propeller-shaped respectively. There exist short contacts at the positions marked * in Fig. 3. The

** Table 2 has been deposited with the office of Chemical Society of Japan, 1-5 Kanda-Surugadai, Chiyoda-ku, Tokyo 101 (Document No. 7826).

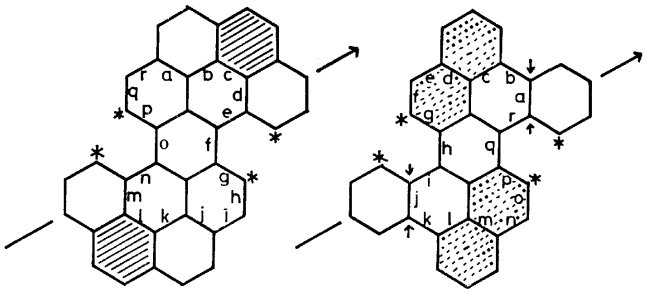

Fig. 3. The diagrams of DPP and TBP.

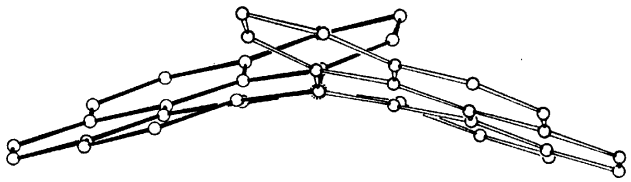

Fig. 4. A perspective drawing of DPP.

distances of C(5)···C(10) are 3.01 Å in the molecule A, and 2.87 Å in the molecule B. They correspond to the mean value of 2.953 Å reported by Robertson and Trotter, and are comparable to 2.971 and 2.944 Å in TBP.

The molecule DPP consists of two naphthanthrone skeletons. The deviations of the atoms from the mean planes through naphthanthrone moieties range from −0.11 to 0.34 Å in the molecule A, and from −0.31 to 0.12 Å in the molecule B. The two planes in the molecule A (B) make an angle of 36° (36°), which are larger than 30.5° in the molecule TBP described below.

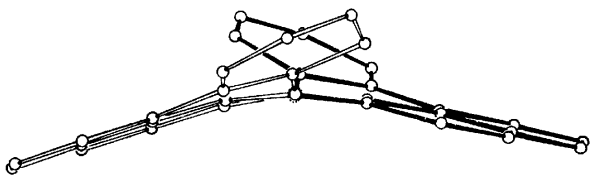

Fig. 5. A perspective drawing of TBP.

To compare DPP with TBP, the right-handed propeller-shaped TBP is drawn in Fig. 5, according to the parameters given by Kohno *et al.*[2] It is taken looking down along the large arrow in Fig. 3. The molecule TBP consists of two benzanthrone skeletons. The two naphthalene moieties, shaded with the dotted lines in Fig. 3, are planar within ±0.05 Å, and the two planes make an angle of 30.5°. On the other hand,

the atoms in the [*a*]- and [*j*]-benzene rings significantly deviate from the planes. The largest deviations are 0.670 and 0.624 Å, respectively. Thus, the benzanthrone moieties in TBP are largely bent in the parts indicated with the small arrows in Fig. 3. Twisting of the central ring is partially relaxed due to such bending, compared to the twisting in DPP.

However, in the naphthanthrone moieties of DPP such a large bending is prevented by an additional benzene ring, shaded with the solid lines in Fig. 3. The strain distributes over the whole molecule.

Thus, the distortions of DPP and TBP are clearly different, and the overlappings of molecules in the DPP and TBP crystals are different as well. These differences seem to be the reason why the photoconductivity of DPP is larger than that of TBP.

In order to give a detailed discussion of the mechanism of photoconduction, we need to gather more data of photoconductivity and crystal structure for polycyclic aromatic hydrocarbons where there are repulsions between hydrogen atoms.

All these calculations were carried out on a HITAC 8700/8800 at the Computer Center of University of Tokyo with a local version of the Universal Crystallographic Computation Program System, UNICS (1967).

References

1) Y. Kamura, H. Inokuchi, J. Aoki, and S. Fujisawa, *Chem. Phys. Lett.*, **46**, 356 (1977).
2) Y. Kohno, M. Konno, Y. Saito, and H. Inokuchi, *Acta Crystallogr., Sect. B*, **31**, 2076 (1975).
3) T. M. Robertson and J. Trotter, *J. Chem. Soc.*, **1959**, 2614.
4) E. Clar, W. Kelley, J. M. Robertson, and M. G. Rossmann, *J. Chem. Soc.*, **1956**, 3878.
5) J. Aoki, M. Takekawa, S. Fujisawa, and S. Iwashima, *Bull. Chem. Soc. Jpn.*, **50**, 1017 (1977).
6) "International Tables for X-Ray Crystallography," Vol. III, Birmingham, Kynoch Press (1962).

The Application of a Modified Dubinin-Radushkevich Equation to Adsorption on Active Carbon with Heterogeneous Micropore Systems

Ryoichi TSUNODA

Industrial Research Institute of Kanagawa Prefecture, Showa-machi, Kanazawa-ku, Yokohama 236

(Received September 20, 1977)

The Dubinin-Radushkevich plots of active carbons, curved concavely for a high value of $\log^2 P_0/P$, on methanol adsorption at 30 °C have been characterized by using a modified Dubinin-Radushkevich equation, *i.e.*:

$$V = CV_0 \exp [- B_0A^2] \exp [A^4\Delta^2/2] [1 - \mathrm{erf}(X)]/2,$$

where $\mathrm{erf}(X)$ is the error function, $A=RT \ln P_0/P$, V_0 is the micropore volume, C is the correcting coefficient for fitting the equation to the experimental data, and $X=(A^2-B_0/\Lambda^2)\Delta/\sqrt{2}$, with B_0 being the average value of a measure of the micropore size and Λ, the heterogeneity parameter of the micropore size. The significance of the equation was discussed, and it was shown that the equation can describe the heterogeneous micropore systems of active carbons with suitable parameters.

The Dubinin-Radushkevich equation,[1]

$$V = V_0 \exp [- k(A/\beta)^2], \quad (1)$$

has been used to characterize microporous carbons. In this equation, V is the volume adsorbed at a relative pressure of P/P_0; V_0 is the micropore volume, $A=RT \ln P_0/P$, and k and β are constants. The linear form of the Dubinin–Radushkevich equation,

$$\log V = \log V_0 - D \log^2 P_0/P, \quad (2)$$

where $D=2.303\, kR^2T^2/\beta^2$, is usually used to plot the adsorption data.

However, although the plot may show a linear range, it is rarely linear over a wide pressure range.[2-5] Rand[4] has recently reported three general types of Dubinin-Radushkevich plots which show deviations from linearity. These three types are designated as Type A, B, and C Dubinin-Radushkevich curves. The Type A, curve has two linear sections with a gentle slope for low values of $\log^2 P_0/P$. The Type B curve is curved concavely over the whole range of $\log^2 P_0/P$. The Type C curve shows two inflection points, indicating a bimodal distribution of the adsorption potential. Especially in the case of the Type B curve, the plots can be linearized by means of the Dubinin-Astakhov equation,

$$V = V_0 \exp [- k(A/\beta)^n], \quad (3)$$

with a suitable value of n, and the micropore volume is obtained by extrapolation of the plot.

However, the characterization of the Dubinin-Radushkevich plot by use of the Dubinin-Astakhov equation is contrary to the original nature of the Dubinin-Radushkevich equation, and the Dubinin-Radushkevich plot should be characterized by an equation maintaining the original nature of the Dubinin-Radushkevich equation.

Stoeckli[7] has recently proposed an adsorption equation maintaining the nature of the Dubinin-Radushkevich equation. Assuming that the Dubinin-Radushkevich equation has a general validity, but applies to homogeneous systems of micropores, he has described adsorption by heterogeneous micropore systems by means of a sum of the Dubinin-Radushkevich equation:

$$V = \sum_j V_{pj} \exp [- B_jA^2], \quad (4)$$

where $B_j=k_j/\beta^2$.

Equation 4 may be replaced by the integral,

$$V(A^2) = \int_0^\infty V_p f(B) \exp [- BA^2]\, dB, \quad (5)$$

where $f(B)$ is the normalized Gaussian distribution and is described as follows:

$$f(B) = \frac{1}{\sqrt{2\pi}\,\Delta} \exp [- (B - B_0)^2/2\Delta^2], \quad (6)$$

with B_0 being the avarage value of B, and Δ, the standard deviation, *i.e.*, the heterogeneity parameter.

Moreover, Eq. 5 leads to,

$$V(A^2) = V_p \exp [- B_oA^2] \times \exp [A^4\Delta^2/2] [1 - \mathrm{erf}(X)]/2, \quad (7)$$

where $X=(A^2-B_0/\Delta^2)\Delta/\sqrt{2}$ and $\mathrm{erf}(X)$ is the error function. Equation 7 is expected to be applied to the Type B curve of the Dubinin-Radushkevich plot.

Meanwhile, as to the determination of the micropore volume from the non-linear Dubinin-Radushkevich plots, the present author[5,6] has previously reported that the adsorption volume (V) corresponding to the adsorption potential (A), at which the plot of $dV/d(-A)$ *vs.* A has its minimum value, is the value of the micropore volume (V_0) in cases where the extrapolation of the Dubinin-Radushkevich plot cannot be applied because of the non-linearity of the plot.

In this paper, micropore systems of active carbon showing Type B curve by Rand's classification[4] or plots gradually curved concavely for a high value of $\log^2 P_0/P$ on methanol adsorption have been characterized by means of the modified Dubinin-Radushkevich equation, and the significance of the modified Dubinin-Radushkevich equation discussed.

Experimental

Active Carbons. Commercially available Pittsburgh Filtrasorb 100- and SGL-type active carbons and Hokutan active carbon were used. For the SGL-type active carbon, the adsorption isotherm reported in a previous paper[5] was used.

Methanol Adsorption. The adsorption of methanol on active carbons at 30 °C was measured gravimetrically by means

of a conventional quartz spring balance. Prior to the adsorption measurement, active carbon dried overnight at 110 °C was outgassed at a pressure of 10^{-6} Torr at 30 °C for 14 h. In all cases, the adsorption equilibrium was established within 45 min.

Results and Discussion

Micropore Volume. The adsorption isotherms, Dubinin-Radushkevich plots, and characteristic curves are sown in Figs. 1—3.

The micropore volumes (V_0) of active carbons were obtained by the method[5,6] described above; they are listed in Table 1.

Modified Dubinin-Radushkevich Equation and Its Application to the Experimental Data. In this paper, following Stoeckli,[7] the micropore systems of active carbon are classified into "homogeneous" and "heterogeneous" micropore systems. Actually, active carbon with a homogeneous surface does not exist. However, when the structural constitution of micropores is considered as a system, the micropore system determined by a given constant, k, in Eq. 1 can be said to be a homogeneous micropore system, and, in this case, the Dubinin-Radushkevich plot is strictly linear in form. On the

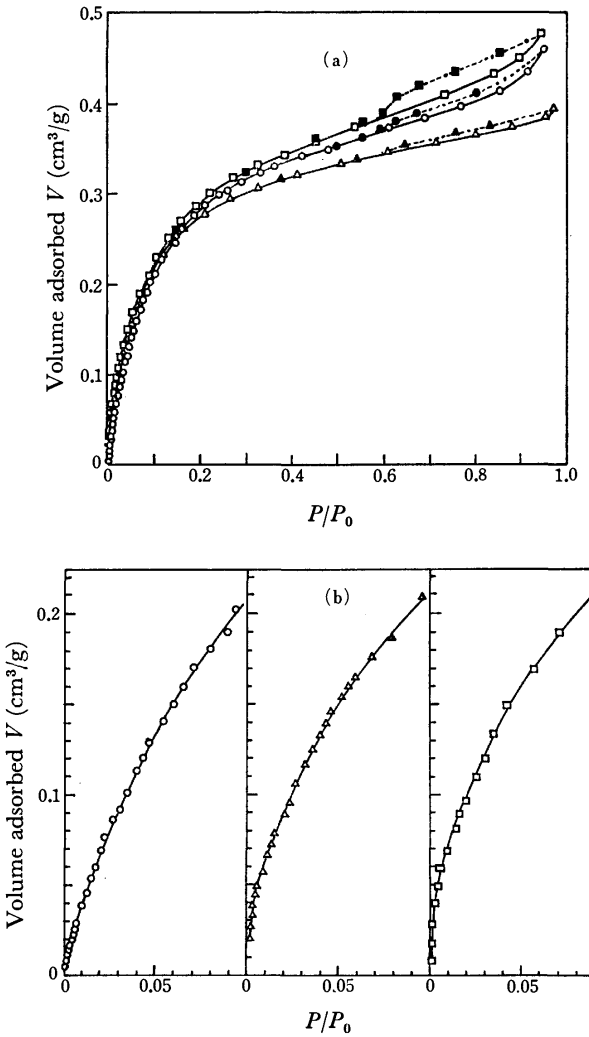

Fig. 1. Adsorption isotherms of methanol at 30 °C on active carbons.
○ SGL, △ Filtrasorb 100, □ Hokutan.
Filled symbols indicate desorption.

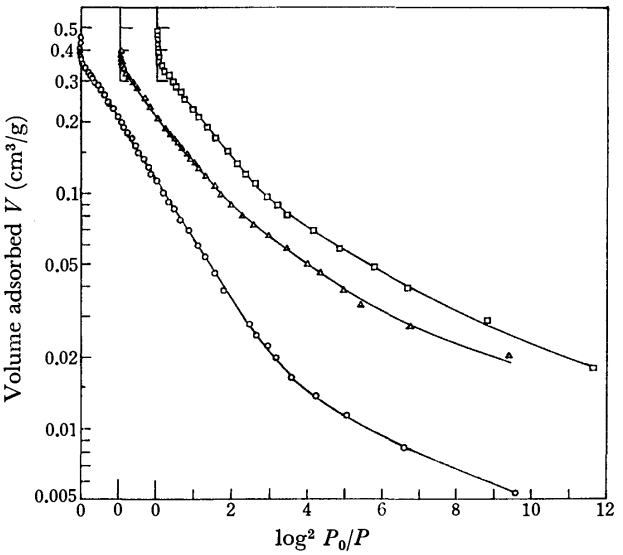

Fig. 2. Dubinin-Radushkevich plots of methanol adsorption at 30 °C on active carbons.
○ SGL, △ Filtrasorb 100, □ Hokutan.

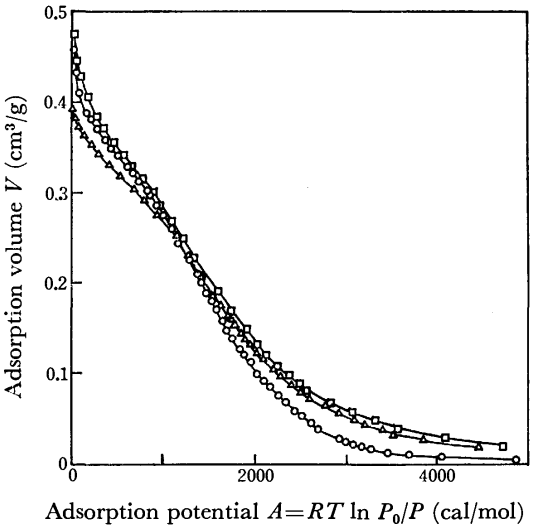

Fig. 3. Characteristic curves of methanol adsorption at 30 °C on active carbons.
○ SGL, △ Filtrasorb 100, □ Hokutan.

Table 1. Parameters in Eqs. 10, 11, and 11′

Active carbon	V_0 (cm³/g)	$B_0\times10^6$ (mol²/cal²)	$A\times10^6$ (mol²/cal²)	C	C'
SGL	0.305	0.35	0.10	1.19	1.001
Filtrasorb 100	0.305	0.27	0.135	1.17	1.023
Hokutan	0.325	0.27	0.15	1.27	1.037

The micropore volume, V_0, is the experimental value determined from the adsorption volume (V) at the $dV/d(-A)$=minimum on the distribution curve of the adsorption potential ($A=RT\ln P_0/P$). The parameters, B_0, A, and C, are values so determined that Eq. 11 fits the adsorption data obtained using V_0.

other hand, in the case of the non-linear Dubinin-Radushkevich plot, k is not constant and the micropore system can be designated as a heterogeneous micropore system.

According to Dubinin,[1] the k constant in Eq. 1 is a measure of the average micropore size, while the β constant is the relative differential molar work of vapor adsorption with the chosen standard substance, often called the affinity coefficient of the characteristic curve. Therefore, as to the heterogeneous micropore systems, the $B_j=k_j/\beta^2$ expression in Eq. 4 has validity. However, B_j is a positive value; therefore, using the distribution function, $f(B)$ (Eq. 6), in Eq. 5 is not adequate. In order to integrate the distribution function over $B>0$, we must use a new distribution function, $g(B)=C'f(B)$, instead of $f(B)$; C' is defined by the following equation:

$$\int_0^\infty g(B)\mathrm{d}B = \int_0^\infty C'f(B)\,\mathrm{d}B = 1 \tag{8}$$

and Eq. 7 is written as follows:

$$V(A^2) = C'V_0 \exp[-B_0A^2] \times \exp[A^4\Delta^2/2]\,[1-\mathrm{erf}(X)]/2. \tag{9}$$

The coefficient C''s are listed in Table 1. However, in order to fit Eq. 9 to the experimental data of the micropore-volume range, the C' coefficient must be multiplied by the correcting coefficient, C'', to give

$$C = C' \times C''. \tag{10}$$

The following equation is written in order to describe the experimental data:

$$V(A^2) = CV_0 \exp[-B_0A^2] \times \exp[A^4\Delta^2/2]\,[1-\mathrm{erf}(X)]/2 \tag{11}$$

or

$$\log V = \log V_0 - 2.303\,B_0R^2T^2\log^2 P_0/P + \frac{1}{2}2.303^3\Delta^2R^4T^4\log^4 P_0/P + \log\frac{1-\mathrm{erf}(X)}{2} + \log C,$$

where

$$X = (2.303^2R^2T^2\log^2 P_0/P - B_0/\Delta^2)\Delta/\sqrt{2}. \tag{11'}$$

The application of the modified Dubinin-Radushkevich equation (Eq. 11') with the best-fit parameters, listed in Table 1, to the experimental data is shown in Fig. 4. The value of B_0 is a measure of the average value of the micropore size, and at the same time, a measure of the higher adsorptive capacity for a smaller value of B_0 at a low relative pressure (see Figs. 1(b), 2, and 3). The heterogeneity parameter, Δ, is the standard deviation of B, and also a factor influencing the pore-size distribution at a given value of B_0, with a larger value of Δ giving a broader shape of the pore-size distribution. Moreover, both parameters, B_0 and Δ, are responsible for the pore-size distribution and for the adsorptive capacity on the Dubinin-Radushkevich plots at a high value of $\log^2 P_0/P$.

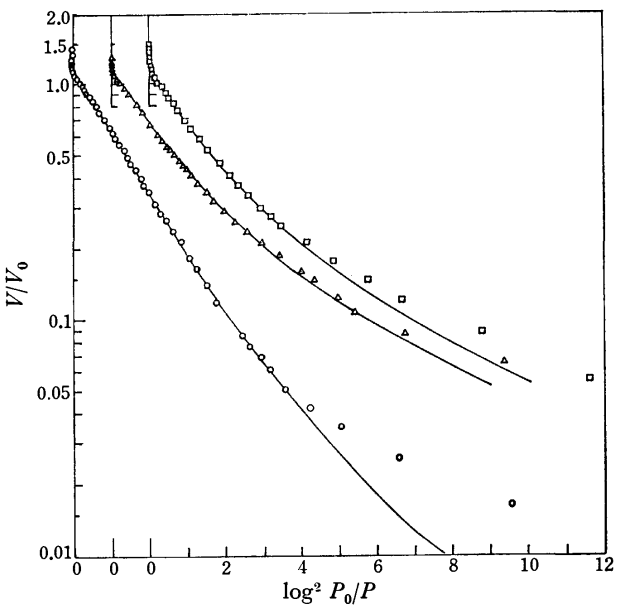

Fig. 4. Application of the modified Dubinin-Radushkevich equation (Eq. 11') to the Dubinin-Radushkevich plots.
○ SGL, △ Filtrasorb 100, □ Hokutan.
The solid curves were calculated by use of Eq. 11'.

From these results, the modified Dubinin-Radushkevich equation can be said to have the following characteristics:

Equations 11 and 11' are based on the original Dubinin-Radushkevich equation, and they maintain their general validity. Although the Dubinin-Astakhov equation is successful in linearizing the Dubinin-Radushkevich plots, it is empirical, and so it is more difficult to make a physical interpretation of the Dubinin-Radushkevich plots compared with the use of Eqs. 11 and 11'. On the other hand, the modified Dubinin-Radushkevich equation enables us to describe the heterogeneous micropore systems of active carbon on the Dubinin-Radushkevich plots by means of 4 parameters, V_0, B_0, Δ, and C.

The author wishes to express his thanks to Mr. Yoshiyuki Fukazawa for his helpful discussions.

References

1) M. M. Dubinin, "Chemistry and Physics of Carbon," ed by P. L. Walker, Jr., Vol. 2, Marcell Dekker, N. Y. (1966), p. 51.
2) P. Chiche, H. Marsh, and S. Prégermain, *Fuel*, **46**, 341 (1967).
3) H. Marsh and B. Rand, *J. Colloid Interface Sci.*, **33**, 101 (1970).
4) B. Rand, *J. Colloid Interface Sci.*, **56**, 337 (1976).
5) R. Tsunoda, *Bull. Chem. Soc. Jpn.*, **50**, 2058 (1977).
6) R. Tsunoda, *Bull. Chem. Soc. Jpn.*, **51**, 341 (1978).
7) H. F. Stoeckli, *J. Colloid Interface Sci.*, **59**, 184 (1977).

The Two n,π^* Transitions of Monohalogenoanthraquinones

Sanae Y. MATSUZAKI* and Akira KUBOYAMA

National Chemical Laboratory for Industry, Shibuya-ku, Tokyo 151

(Received October 3, 1977)

The n,π^* absorption and phosphorescence spectra of 1-fluoro-, 2-fluoro, 1-chloro-, 2-chloro-, 1-bromo-, and 2-bromoanthraquinones were studied in solutions, mainly at 77 K. These phosphorescence spectra and their lifetimes resemble those of anthraquinone (AQ), except for those of 1-F-AQ. The phosphorescence spectrum of 1-F-AQ is at longer wavelengths than that of AQ, and its lifetime is 0.8 ms in the methylcyclohexane solution, much shorter than that of AQ. All of the 1-halogenoanthraquinones showed two distinct n,π^* singlet-singlet absorption bands at 77 K, and 1-Br-AQ showed an additional band of the n,π^* singlet-triplet transition at 492 nm. The low-energy n,π^* singlet and triplet states of these compounds are discussed on the basis of these experimental results.

The lowest excited singlet and triplet states of carbonyl compounds including quinones are generally assigned to the n,π^* states. These n,π^* states are thought to be largely localized at the carbonyl groups, because of the strong Coulomb attraction between the excited electron and the remaining non-bonding positive hole. In quinones which have two carbonyl groups, each of the lowest excited singlet and triplet states is expected to consist of two n,π^* states close to each other in energy, as in the case of *p*-benzoquinone.[1] Previously, we have studied the n,π^* phosphorescence spectra of AQ in solutions at 77 K.[2] Recently, high-resolution n,π^* phosphorescence spectra of AQ in crystals and in solutions have been reported on by many authors.[3] In 1-halogenoanthraquinones, as the lone electron-pair of the oxygen and halogen atoms are close to each other, the interaction between them should be large. Therefore, it is very interesting how the n,π^* singlet and triplet levels would be affected by the halogen atom introduced to the 1-position of anthraquinone. Shcheglova *et al.*[4] have already discussed this problem on the basis of the emission spectra obtained by the photographic method, but some problems have remained to be clarified. For instance, no actual n,π^* absorption and emision spectra of monohalogenoanthraquinones have been reported. We have, therefore, studied the n,π^* absorption and emission spectra of monohalogenoanthraquinones at 77 K and discussed the above-mentioned problem.

Experimental

Measurements. The emission spectra and their lifetimes were measured in the methylcyclohexane solutions at 77 K by the way described in our previous paper.[2] A Cary Model 14 spectrophotometer was used to measure the absorption spectra. In the measurement of the absorption spectra at 77 K, the 1-cm cell and the Dewar vessel used in our previous work[5] were used again.

The absorption spectra were obtained in the heptane solutions at room temperature (R. T.) and at 77 K, in the benzene and heptane solutions, which were poly-crystalline at this temperature. Using these poly-crystalline solutions at 77 K, clear and about ten-times-intensified spectra were obtained in comparison with those at R. T., when the concentrations of solutes were regulated for their absorbances so as not to exceed 0.1 at R. T. This enhancement in absorbance is based on a mechanism similar to that which holds in the case of the diffuse-reflectance spectra. Both the benzene and heptane solutions gave almost the same spectra, but the spectra of the former were clearer than those of the latter.

Materials. 1-F-AQ and 2-F-AQ were synthesized from 1- and 2-aminoanthraquinones by diazotization and by the substitution of the diazo group by a fluorine atom[6] respectively. The other monohalogenoanthraquinones were commercially available. All of these quinones were refined by the two methods of vacuum sublimation and liquid column chromatography on alumina (the developer; toluene). The refined sample were melted within 1 °C of their melting points, as is shown in Table 1. The solvents—hexane, methylcyclohexane, benzene, and toluene—were all commercially available spectrograde reagents.

TABLE 1. MELTING POINTS OF MONOHALOGENOANTHRAQUINONES (°C)

1-F-AQ	232.0—233.0 (226—227[5])
1-Cl-AQ	160.5—161.5 (162[7])
1-Br-AQ	190.0—191.0 (188[7])
2-F-AQ	199.0—200.0 (203—204[5])
2-Cl-AQ	208.5—209.5 (208—209[7])
2-Br-AQ	208.4—209.1 (204—205[7])

Results

The observed n,π^* absorption spectra of monohalogenoanthraquinones are shown in Figs. 1 and 2. The spectra of 2-F-AQ and 2-Cl-AQ, which are not shown in these figures, quite resemble that of 2-Br-AQ. The wavelengths of the peaks and shoulders in these absorption spectra are listed in Table 2. The emission spectra of 1- and 2-halogenoanthraquinones in solutions at 77 K are shown in Figs. 3, 4, and 5, while the wave-

TABLE 2. WAVELENGTHS (nm) OF THE ABSORPTION PEAKS AND SHOULDERS

A) Heptane solutions at R.T. (the values in parentheses are molar absorption coefficients)					
1-F-AQ	376,		392.5,		419 (67)
1-Cl-AQ	377,		397.5,		419 (76)
1-Br-AQ	377,		396.5,		419(110[a])
2-F-AQ	374,	376.5,	396.5,	402,	421
2-Cl-AQ	376,	378,	397.7,	405,	424.5
2-Br-AQ	376.5,	379,	398,	405.5,	424 (70[a])
B) Benzene solutions at 77K					
1-F-AQ	400,	410,	413.5,	421.5,	436
1-Cl-AQ	416,	450,			
1-Br-AQ	416.5,	435,	460,	492	
2-Br-AQ	406,	416.5			

a) Values in the toluene solutions.

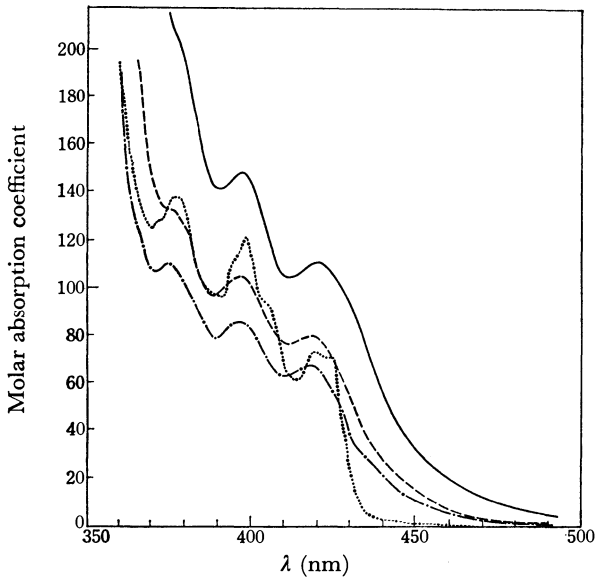

Fig. 1. Absorption spectra in the heptane solutions at R.T.
——: 1-Br-AQ, ——: 1-Cl-AQ, -·-·-: 1-F-AQ, and ····: 2-Br-AQ. The scale of the ordinate for 1-Br- and 2-Br-AQ's is arbitrary.

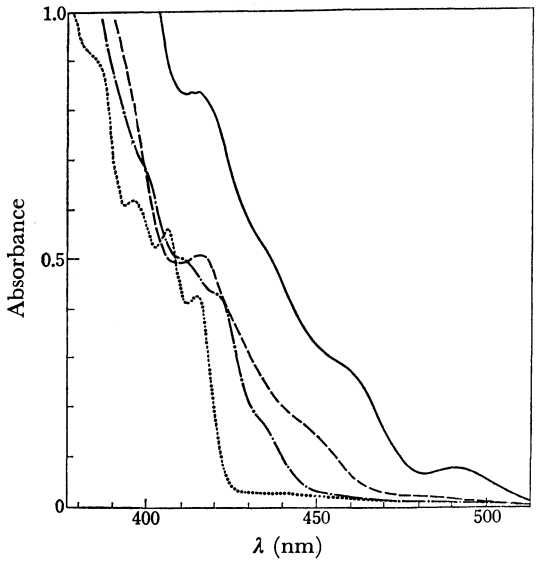

Fig. 2. Absorption spectra in the benzene solutions at 77 K.
——: 1-Br-AQ, ——: 1-Cl-AQ, -·-·-: 1-F-AQ, and ····: 2-Br-AQ. The scale of the ordinate is arbitrary.

Table 3. Wavelengths (nm) of the emission peaks in the methylcyclohexane solutions at 77 K

1-F-AQ	476.6	517.2	565.5	622.5	
1-Cl-AQ	456.5	493.7	537.5	589.3	(515, 560)[a]
1-Br-AQ	456.8	493.7	538.0	589.4	
2-F-AQ	454.4	492.1	535.5	587.1	
2-Cl-AQ	458.2	495.4	539.7	592.7	
2-Br-AQ	458.4	496.0	540.5	593.2	

a) Those of the shorter-lifetime component.

Table 4. Lifetimes (ms) of the phosphorescence bands in the methylcyclohexane solutions at 77 K

1-F-AQ	0.8
1-Cl-AQ	3.5, $\lesssim$0.1
1-Br-AQ	3.5
2-F-AQ	3.2
2-Cl-AQ	3.3
2-Br-AQ	2.5

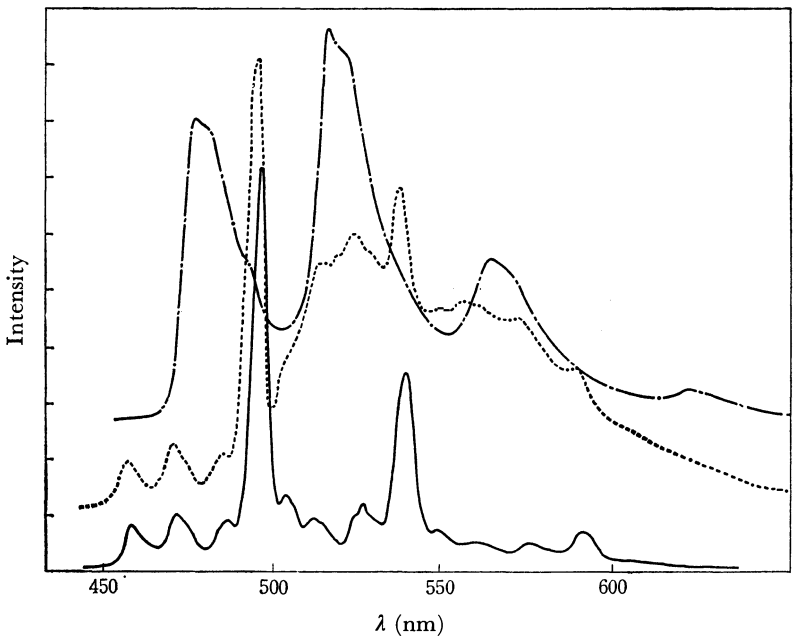

Fig. 3. Phosphorescence spectra of 1-halogeno AQ's in the methylcyclohexane solutions at 77 K, ——: 1-Br-AQ, ——: 1-Cl-AQ, and -·-·-: 1-F-AQ.

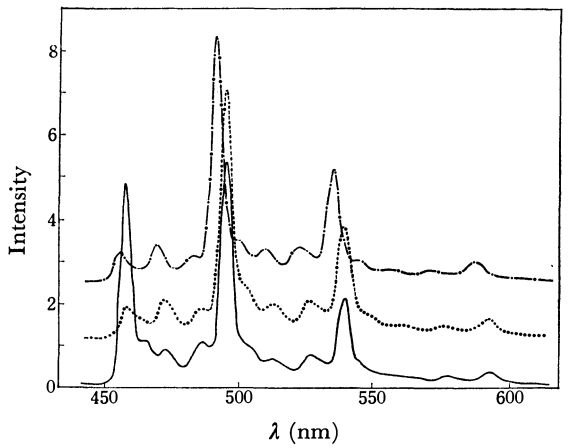

Fig. 4. Phosphorescence spectra of 2-halogeno AQ in the methylcyclohexane solutions at 77 K, ——: 2-Br-AQ, ——: 2-Cl-AQ, and -·-·-: 2-F-AQ.

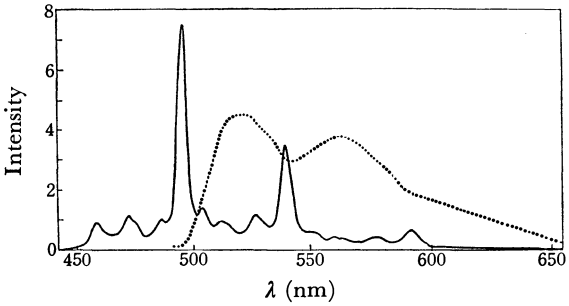

Fig. 5. The two components of the phosphorescence of 1-Cl-AQ in the methylcyclohexane solution at 77 K, ——: the phosphorescence with longer lifetime, and ····: that with shorter lifetime.

lengths of their peaks and their lifetimes are listed in Tables 3 and 4 respectively. The shoulder at 493 nm in the emission spectrum of 1-F-AQ became smaller and smaller as the sample was refined repeatedly, and its position was the same as those of the highest peaks of 1-Cl-AQ and AQ (see Fig. 3). Therefore, it may be considered to be due to some impurities.

The total emission of 1-Cl-AQ consists of two components which are different in lifetime. The emission spectrum with the longer lifetime of 3.5 ms could be observed separately with a sector, while that with the shorter lifetime was obtained as the difference between the total spectrum and the spectrum obtained with the sector. This shorter lifetime was too short to be measured. The intensity ratio of the longer-lifetime spectrum to the shorter-one was about 1 : 2. These two spectra are shown in Fig. 5.

Discussion

In 1-halogenoanthraquinones, one of the two carbonyl groups is adjacent to the halogen atom, and the lone electron-pair orbital of its oxygen atom is thought to overlap considerably with that of the halogen atom. 1-Halogenoanthraquinones may be destabilized by this overlapping in the ground state, and stabilized by the charge-transfer interaction between the vacant n-orbital of the carbonyl group and the occupied n-orbital of the halogen atom in the n,π^* excited state. Therefore, one of these two lowest-energy n,π^* states, which is mainly localized at the carbonyl group adjacent to the halogen atom, may be considerably lower in energy than the other, which is mainly localized at the other carbonyl group. The order of the magnitudes of the separations between these two n,π^* levels is thought to be equal to the order of the van der Waals radii of the halogen atoms; Br>Cl>F.

As may be seen in Fig. 1, the n,π^* absorption spectra of the 1-halogenoanthraquinones at R.T. are similar to that of 2-Br-AQ, which in form is very similar to that of AQ, except for the long tails in the region of 430—500 nm. These tails and the shorter-wavelength absorption bands are considered to be due to the transition from the ground state to the above-mentioned lower and higher n,π^* singlet excited states respectively. As for the n,π^* absorption spectra at 77 K, which are shown in Fig. 2, the spectra of the 1-halogenoanthraquinones show structures up to 500 nm; the spectrum of 1-Br-AQ, for example, has three shoulders, at 416.5, 435, and 460 nm, and one peak, at 492 nm. The shoulder at 416.5 nm may be assigned to the shorter-wavelength n,π^* band, and the shoulders at 435 and 460 nm, to the longer-wavelength n,π^* bands. The absorption peak at 492 nm may be assigned to the n,π^* singlet-triplet absorption band intensified by the internal heavy-atom effect of the bromine atom, since the corresponding absorption in 1-Cl-AQ and 1-F-AQ cannot be found. This absorption peak may not be assigned to the π,π^* singlet-triplet absorption band, because a corresponding absorption cannot be observed in 2-Br-AQ. Since the n,π^* bands and the tails of the lowest π,π^* band of monohalogenoanthraquinones shift toward blue and red to a considerable extent at 77 K compared with those at R.T. (see Figs. 1 and 2), the spectra at 77 K are thought to be those of aggregates. In general, the n,π^* states in aggregates may be considered to be similar to those in solutions because of their localizing character. In this discussion, the electronic structures of the n,π^* states in these aggregates were assumed to be similar to those in isolated molecules, except for small energy shifts.

The emission spectra of the monohalogenoanthraquinones in solutions at 77 K can all safely be assigned to the n,π^* phosphorescence, since they have, as may be seen in Figs. 3, 4, and 5, the principal vibrational structure of the carbonyl stretching frequency (*ca.* 1640 cm^{-1}) and the short lifetime of the order of a millisecond (see Table 4). These phosphorescence spectra quite resemble that of AQ in position, shape, and lifetime, except for that of 1-F-AQ and the shorter lifetime spectrum of 1-Cl-AQ.

As for the phosphorescence spectrum of 1-F-AQ, it lies at longer wavelengths (the energy difference is *ca.* 900 cm^{-1}) and has a shorter lifetime, than the spectra of the other monohalogenoanthraquinones. The phosphorescence quantum yields of 1-F-AQ, 1-Cl-AQ (total), and 1-Br-AQ were roughly estimated to be in the ratio of 3 : 1 : 1 by considering the relative absorbances at 420 nm of the n,π^* S_1-S_0 bands in nearly

saturated methylcyclohexane solutions at R.T. and the relative intensities of the phosphorescences with excitations at 420 nm in the same solutions. According to this estimation, the phosphorescence of 1-F-AQ would have a much shorter natural lifetime than the others. The shorter-lifetime spectrum of 1-Cl-AQ, which has the vibrational structure of the C–O stretching and which lies at an energy lower by *ca.* 1000 cm^{-1} than that of 1-F-AQ is too broad to discuss in detail, but it may be assigned to the same kind of emission as that of 1-F-AQ.

On the basis of these facts, it may be concluded that the phosphorescence of 1-F-AQ and the shorter-lifetime emission of 1-Cl-AQ correspond to the emission from the above-mentioned lower n,π* triplet state, and that the phosphorescence of 1-Br-AQ and the longer-lifetime emission of 1-Cl-AQ correspond to that from the upper n,π* triplet state. In 1-Br-AQ and 1-Cl-AQ, the internal conversion between the two n,π* triplet states may be slow, since these states are considered, as has been mentioned before, to be mainly localized on the two carbonyl groups separately, far from each other and with a large energy difference between them. Therefore, the phosphorescence from the upper state can be observed in these molecules. However, this internal conversion may be faster in 1-F-AQ because of the small energy difference between these two states, so the emission from the upper state cannot be observed.

As for the phosphorescence of 1-F-AQ and the shorter-lifetime emission of 1-Cl-AQ, their lifetimes may be shortened by the relatively fast, radiationless process from the phosphorescent lower n,π* triplet state, which is due to the before-mentioned interaction between lone-pair orbitals of the oxygen atom and the adjacent halogen atom. In the case of 1-Br-AQ, the emission from the lower state may not be observed because of the slow internal conversion between the two n,π* states and the fast radiationless process from the lower n,π* state to the ground state, mainly due to the heavy atom effect of the bromine atom.

The n,π* singlet and triplet levels of 1-halogenoanthraquinones and the phosphorescent processes, considered on the basis of the above discussion, are shown in Fig. 6.

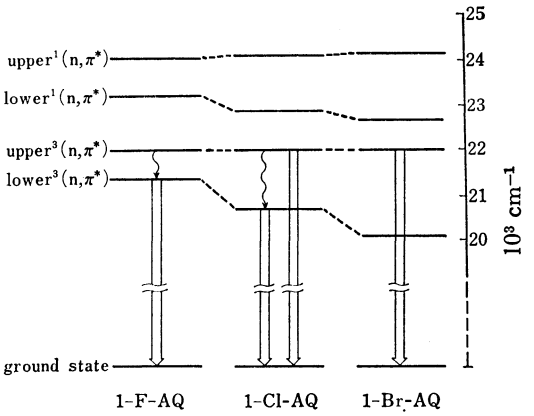

Fig. 6. Energy levels and phosphorescent processes of 1-halogeno AQ's, ⟹; phosphorescence, ⇝; internal conversion.

Shcheglova *et al.* have given a similar discussion of the two n,π* triplet states of the 1-halogenoanthraquinones based on their experimental results, and they have claimed that lower n,π* states of 1-Cl-AQ and 1-Br-AQ are not discrete but continuous states. This explanation may be rejected on the basis of this work.

References

1) H. P. Trommsdorff, *J. Chem. Phys.*, **50**, 5358 (1972); H. Veenvliet and D. A. Wiersma, *Chem. Phys.*, **8**, 432 (1975); Y. Miyagi, M. Koyanagi, and Y. Kanda, *Chem. Phys. Lett.*, **40**, 98 (1976).

2) A. Kuboyama and S. Yabe, *Bull. Chem. Soc. Jpn.*, **40**, 2475 (1967); A. Kuboyama, *ibid.*, **43**, 3373 (1970).

3) K. E. Drabe, H. Veenvliet, and D. A. Wiersma, *Chem. Phys. Lett.*, **35**, 469 (1975); T. Narisawa, M. Sano, and Y. I'Haya, *Chem. Lett.*, **1975**, 1289; O. S. Khalil and L. Goodman, *J. Phys. Chem.*, **80**, 2170 (1976); J. P. Galaup, J. Megel, and H. P. Trommsdorff, *Chem. Phys. Lett.*, **41**, 397 (1976).

4) N. A. Shcheglova, D. N. Shigorin, and N. S. Dokunikhin, *Russ. J. Phys. Chem.*, **36**, 1045 (1962).

5) A. Kuboyama, R. Yamazaki, S. Yabe, and Y. Uehara, *Bull. Chem. Soc. Jpn.*, **42**, 10 (1969).

6) G. Valkanas and H. Hopff, *J. Org. Chem.*, **27**, 3680 (1962).

7) "Daiyuukikagaku," Vol. 12, Asakura Shoten, Tokyo (1960), p. 248.

Catalysis by Supported Metal Crystallites from Carbonyl Clusters. I. Catalytic Methanol Synthesis under Mild Conditions over Supported Rhodium, Platinum, and Iridium Crystallites Prepared from Rh, Pt, and Ir Carbonyl Cluster Compounds Deposited on ZnO and MgO

Masaru ICHIKAWA

Sagami Chemical Research Center, Nishi-Ohnuma, Sagamihara, Kanagawa 229

(Received December 6, 1977)

Methanol synthesis by the catalytic hydrogenation of carbon monoxide proceeded under atmospheric pressure and at 150—250 °C over rhodium, platinum and iridium crystallite catalysts, prepared from well-defined Rh, Pt, and Ir carbonyl cluster compounds highly dispersed on ZnO and MgO. The activity and selectivity of methanol formation depended considerably on the kind of metal carbonyl clusters and metal oxides employed as inorganic carriers. The catalysts prepared by the pyrolysis of smaller Rh, Pt, and Ir carbonyl clusters on ZnO, MgO, CaO, and BeO exhibited a higher selectivity of methanol synthesis. A small amount of ethanol was also produced besides methanol in CO–H_2 reaction over the pyrolysed catalysts of Rh carbonyl clusters on MgO, CaO, and BeO. Other metal oxides such as SiO_2 gel, γ-Al_2O_3, SnO_2, and WO_2 were employed for preparation of the dispersed Rh catalysts from carbonyl clusters, which catalysed mainly formation of methane and higher hydrocarbons with negligible selectivity of the oxygenated products under the reaction conditions.

The dispersion of metal plays, in many cases, an important role in exhibiting high activity and selectivity of metal supported catalysts. The proportion and fraction of metal atoms in the dispersed metal aggregates present on surface depend on the system and conditions of catalyst preparation. Various devices have been proposed for the preparation of highly dispersed metal, such as in the conventional impregnation methods and ion exchange methods.[1] In some cases, molecular metallic cluster compounds have been used as specific precursors for the generation of dispersed metal aggregates.[2] The pyrolysed Pt_3–Pt_{15} carbonyl clusters deposited on γ-Al_2O_3 or silica gel catalyse the selective dehydrocyclization of hexane, the particle size of which being conventionally estimated to be down to 10 Å.[3]

The work has been extended to rhodium, platinum and iridium crystallites similarly prepared on ZnO and MgO from the corresponding carbonyl clusters which catalysed selective methanol synthesis from CO and H_2 under atmospheric pressure. The rates and selectivity of methanol formation have been measured by changing the reaction conditions and preparation of the catalysts uning various carbonyl clusters and metal oxides as inorganic carriers.

Experimental and Procedures

The catalyst preparation and reaction of CO and H_2 were carried out in a closed circulating glass reactor (total volume 420 ml) operating in a continuous circulating flow mode. Analysis of the products was based on gas chromatography using Porapak Q 4 m (200 °C He carrier) and Polyethylene glycol 1500 2 m (80 °C He carrier) columns for alcohol and water, alumina–DMF (38 wt%) 4 m (0 °C He carrier) for C_2—C_5 hydrocarbons and active carbon 1 m (25 °C) for CH_4, CO, and H_2 in the gas phase. Highly pure hydrogen and CO were used from the respective cylinders. Alcohols and water produced were separately obtained at the cooling part equipped with a Dry Ice trap in the circulating reaction systems. $Rh_4(CO)_{12}$ was synthesized by the method of Chini and Matinengo[4] and identified by the IR carbonyl absorption of its hexane solution and by mass spectrometry. $Rh_2(\pi\text{-}C_5H_5)_2(CO)_3$ was prepared from $Rh(\pi\text{-}C_5H_5)(CO)_2$ by prolonged UV illumination (with a high pressure Hg lamp) of hexane solution at 25 °C under N_2 atmosphere, and purified by recrystallization.[5] The deep-red crystal was identified with with $Rh_2(\pi\text{-}C_5H_5)_2(CO)_3$ from its IR spectra in solid and solution, and by mass spectrometry. $Rh_6(CO)_{16}$ and $Ir_4(CO)_{12}$ (Strem Chem. Co.,) were used without purification. The trigonal prismatic carbonyl cluster salts $[Pt_3(\mu_2\text{-}CO)_3(CO)_3]_n 2NR_4$ (n=3, 4, and 5, R=C_2H_5 and n-C_4H_9) were separately obtained by the reaction with alkaline–methanol solution of $PtCl_6^{2-}$ under CO atmosphere in a similar way to that described[3] and isolated as tetra-alkylamine salts, which were stored under inert atmosphere in ampoules. $Rh_{13}(CO)_{23}H_{2-3}2N(C_4H_9)_4$ was synthesized by the method of Albano *et al.*[6] by the reaction with $Rh_{12}(CO)_{30}2N(C_4H_9)_4$ under hydrogen atmosphere and identified by IR carbonyl absorption of is tetrahydrofuran solution. The carbonyl clusters were deposited in high dispersion from the solution onto the metal oxides such as ZnO, MgO, CaO, BeO, SiO_2 gel and γ-Al_2O_3 powders. The entire procedure was performed in a vacuum or inert atmosphere of He and N_2. Pyrolysis of each dispersed metal carbonyl cluster compound on various oxides proceeded in a vacuum or hydrogen atmosphere by raising the temperature up to 180—200 °C in order to remove CO and the pyrolysed organic residues. The infrared spectra of the Rh and Pt carbonyl clusters on metal oxides were recorded in the range 2200—1600 cm^{-1} with a Hitachi EPI-G3 grating spectrometer.

Results and Discussion

Catalytic Hydrogenation of CO over the Supported Rh Crystallites on ZnO and MgO Prepared by Pyrolysis of $Rh_4(CO)_{12}$. $Rh_4(CO)_{12}$ was deposited from hexane solution onto zinc oxide (Kadox 25 ZnO from New Jersey Co. 22 m^2/g) and magnesium oxide powders, (MgO Merck Chem. Co., 99.9%, 34 m^2/g) evacuated at 320 °C for 15 h prior to use. The solvent was removed by evaporation at room temperature. Removal of CO was accomplished by heating the material charged in a Pyrex-reactor at 160 °C for 2 h *in vacuo* (10^{-3}—10^{-4}

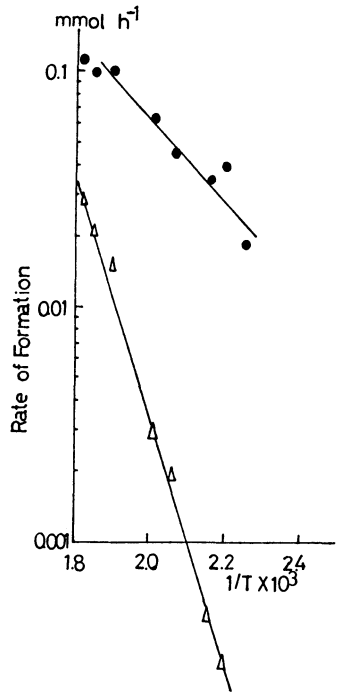

Fig. 1a. Arrhenius plots of methanol and methane formation over the pyrolysed catalyst on ZnO prepared from $Rh_4(CO)_{12}$. $Rh_4(CO)_{12}$ 0.11 g (0.15 mmol) and ZnO (Kadox 25) 20 g, 0.75% Rh wt dispersion. The volume of the reactor was 320 ml. CO: H_2=15 cmHg: 45 cmHg.
-●-: Formation of methanol (mmol/h),
-△-: formation of methane (mmol/h).

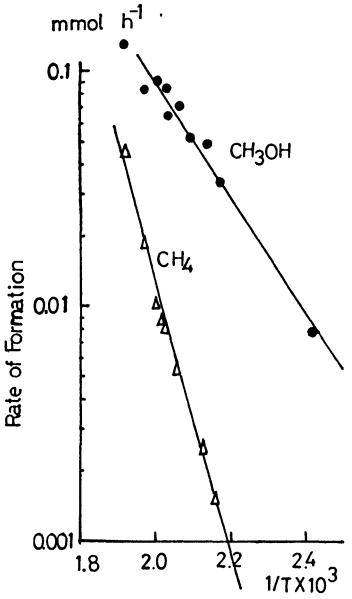

Fig. 1b. Arrhenius plots of methanol and methane formation over the pyrolysed catalyst on MgO prepared from $Rh_4(CO)_{12}$. $Rh_4(CO)_{12}$ 0.11 g (0.15 mmol) and MgO 20 g, 0.75% Rh wt dispersion. The volume of the reactor was 320 ml. CO: H_2=20 cmHg and 45 cmHg.
-●-: Formation of methanol (mmol/h),
-△-: formation of methane (mmol/h).

mmHg). The desorption of CO from the dispersed $Rh_4(CO)_{12}$ on ZnO and MgO proceeded sharply under He flow (1 atm 45 ml/min) in the temperature range 125—135 °C. This was confirmed by temperature-programmed technique using gas chromatography with active-carbon 1 m column. The infrared spectra of $Rh_4(CO)_{12}$ dispersed on ZnO were measured before and after the heattreatment *in vacuo*, and by introducing CO onto it. The sample wafer for infrared study was prepared by pressing the supported $Rh_4(CO)_{12}$ on Kadox 25 ZnO (1.8 Rh wt% dispersion) in a 2 cm diameter die and area force of 500 kg/cm². The IR spectra of the sample showed strong bands at 2050 and 1845 cm^{-1}, assigned to the terminal and bridged carbonyl absorptions, respectively, of the corresponding carbonyl cluster in solution and in crystal.[7] Both carbonyl bands completely disappeared by evacuation of the sample wafer at 120—150 °C for 1 h, probably due to desorption of CO. After evacuation 10—250 mmHg of CO was admitted at 25 °C, a broad and intense bands at 2000 and 1840—1870 cm^{-1} being observed. After pyrolysis, a mixture of CO and H_2 (molar ratio 1: 2 under total pressure of 45—65 cmHg) was introduced onto the pyrolysed catalysts at 150—250 °C, methanol being catalytically obtained after some induction period (*ca.* 5 h) in Dry-Ice cooling part of the circulating reactor. A small amount of methane was formed in gas phase. Carbon dioxde and C_2—C_5 hydrocarbons were detected in a minute quantity in the reaction products over these catalysts. The material balance of the methanol and methane produced was confirmed by means of the total amount of consumed CO through the reaction. The rates of methanol and methane formation over the pyrolysed catalysts were found to obey approximately the first order kinetics in each run, after the stationary state of the reaction was realized. The initial rates of methanol and methane formation (mmol/h) over the pyrolysed $Rh_4(CO)_{12}$ on ZnO and MgO were plotted against the reaction temperature (Figs. 1a and 1b). The apparent activation energies of methanol and methane formation were estimated at 11—12 kcal/mol and 32—37 kcal/mol, respectively, in the given temperature range. The selectivity of methanol synthesis over the catalysts was over 90% per CO consumed at 180—220 °C. Magnesium oxide was completely inactive for methanol synthesis under the reaction conditions. A small amount of methanol and methane was only detected over ZnO powder (Kadox 25 or 99.9% purity zinc oxide from Kishida Chem. Reagent Co.) at 260 °C in 125 h when CO (20 cmHg) and H_2 (45 cmHg) was admitted onto it, after the prolonged hydrogen reduction. A small amount of ethanol besides methanol was catalytically produced in CO–H_2 reaction over the pyrolysed $Rh_4(CO)_{12}$ catalyst dispersed on MgO. At temperatures above 220 °C, methane formation proceeded considerably, the proportion of ethanol and C_2—C_4 hydrocarbons slightly increasing (Table 1). Methane and C_2—C_4 hydrocarbons were markedly suppressed by increasing the CO/H_2 molar ratio from 0.2 to 2.0 under a constant total pressure.

Selectivity of Methanol Synthesis over the Rh Crystallite

Table 1. Product distribution in CO–H_2 reaction over pyrolysed catalysts on MgO prepared from $Rh_4(CO)_{12}$

CO	H_2 (cmHg)	T (°C)	CO conv. in 10 h (%)	Product distribution (mmol in 10 h)[a]							Methanol[b] select. (%)
				CH_3OH	C_2H_5OH	O.P.	CH_4	C_2	C_3	C_4	
20	45	195	18.9	0.69	0.002	—	0.026	—	—	—	95.8
20	45	220	25.7	0.88	0.008	—	0.076	+	+	—	91.7
20	45	235	32.9	0.98	0.023	—	0.18	0.008	0.006	0.001	78.4
20	45	245	49.7	1.3	0.035	—	0.45	0.01	0.008	0.002	69.5
30	38	220	20.9	1.1	0.006	—	0.045	—	—	—	96.0
40	22	220	5.7	0.40	0.003	—	0.025	—	—	—	94.1
10	35	220	57.4	0.96	0.010	—	0.12	+	+	—	89.0

a) O.P.: other oxygenated products. $C_2=C_2H_4+C_2H_6$, $C_3=C_3H_6+C_3H_8$, $C_4=C_4H_8+C_4H_{10}$ (+) less than 0.001 mmol (—) negligible. b) (Methanol)/(CO consumed) $\times 100$ (%).

Catalysts Prepared from Various Rh Carbonyl Clusters Deposited on ZnO. Rhodium carbonyl clusters such as $Rh_2(\pi\text{-}C_5H_5)_2CO)_3$, $Rh_6(CO)_{16}$ and $Rh_{13}(CO)_{23}H_{2-3}2N(C_4H_9)_4$ were employed instead of $Rh_4(CO)_{12}$ to disperse Rh crystallite on ZnO. $Rh_2(\pi\text{-}C_5H_5)_2(CO)_3$ (0.10 g) was deposited from a hexane solution on ZnO (20 g from Kishida Chem. Reagent Co.,) and pyrolysed under hydrogen atmosphere at 180 °C for 2 h in order to remove CO and cyclopentadiene residue. $Rh_6(CO)_{16}$ and $Rh_{13}(CO)_{23}H_{2-3}2N(C_4H_9)_4$ were dispersed from tetrahydrofuran solutions onto ZnO powders (Kadox 25 and Kishida Chem. Reagent Co.,) and pyrolysed *in vacuo* by raising the temperature up to 180 °C and treated with hydrogen at 200 °C for 2 h. When a CO–H_2 mixture reactant was admitted onto the pyrolysed catalysts, methanol was catalytically produced with a small amount of methane at 180 and 250 °C. The rates and selectivity of methanol formation over the Rh crystallite catalysts prepared from various Rh carbonyl clusters were measured in the stationary state of reaction. The results are summarized in Table 2. The optimal yield of methanol was obtained over the catalysts by pyrolysis of $Rh_4(CO)_{12}$ and $Rh_6(CO)_{16}$. The relative activity of methanol formation (mmol/h·g_{Rh}, g_{Rh}=Rh weight) varied with the kind of rhodium carbony cluster employed:

$$Rh_3(\pi\text{-}C_5H_5)_2(CO)_3 < Rh_4(CO)_{12} < Rh_6(CO)_{16} < Rh_{13}(CO)_{23}H_{2-3}2N(C_4H_9)_4$$

For comparison, the conventional Rh metal catalyst was prepared from impregnated $RhCl_3 3H_2O$ on ZnO (Kadox 25) in 1.0 and 2.5 Rh wt% loading followed by hydrogen reduction (1 atm 350 °C 10 h). The resulting Rh catalyst catalysed mainly methane formation with less than 15% selectivity.

Catalytic Hydrogenation of CO over the Rh Crystallites Deposited on Various Metal Oxides. A number of metal oxides were found to act as alternative carriers such as BeO and CaO. $Rh_4(CO)_{12}$ was deposited from a hexane solution over BeO (Merck Co., 99.99% purity) and CaO powders, (Merck Co., 99.9%) which were preheated *in vacuo* at 320 °C for 15 h. After pyrolysis of the substance *in vacuo* at 160 °C, the CO–H_2 reaction was carried out in the circulating reactor. Methanol was selectively, obtained but with lower CO conversion, over the pyrolysed catalyst on CaO at 200—260 °C. Over the Rh crystallites on BeO, methanol and a trace of ethanol were formed but with lower methanol selectivity. Typical results of catalytic hydrogenation of CO over the catalysts on CaO, and BeO are summarized in Table 3. For comparison, other metal oxides such as SiO_2 gel (AEROSIL-300, Yokohama Aerosil Co., 300 m^2/g), γ-Al_2O_3 (A-11, Harshaw Co.,

Table 2. Methanol synthesis over pyrolysed catalysts on ZnO prepared from various Rh carbonyl cluster compounds

Catalyst	T (°C)	Product distribution (mmol in 10 h)						CO conversion (% in 10 h)	Methanol selectivity (%)
		CH_3OH	C_2H_5OH	CH_4	C_2	C_3	C_4		
$Rh_2Cp_2(CO)_3$–ZnO(I) (0.10 g) (20 g)	220	0.23	0	0.006	0	0	0	6.2	97.4
	250	0.48	0	0.03	0	0	0	13.4	94.1
$Rh_4(CO)_{12}$–ZnO(I) (0.11 g) (20 g)	220	0.63	0	0.03	0	0	0	17.4	95.4
	250	1.12	0	0.27	0	0	0	36.5	80.6
$Rh_4(CO)_{16}$–ZnO(I) (0.10 g) (20 g)	220	0.56	0	0.006	0	0	0	14.8	98.9
	250	0.84	0	0.18	0	0	0	26.8	82.4
$Rh_6(CO)_{16}$–ZnO(II) (0.10 g) (20 g)	220	0.42	0	0.01	0	0	0	11.3	97.6
	250	0.68	0	0.15	0	0	0	21.8	81.9
$Rh_{13}(CO)_{23}H_{2-3}2NBu_4$ –ZnO(I) (0.12 g) (20 g)	220	0.25	0	0.08	0	0	0	8.7	75.7
	250	0.36	0	0.35	0	0	0	18.7	50.7

ZnO(I) Kadox 25 New Jersey Co. ZnO(II) Kishida Chem. Reagent Co. CO (20 cmHg) and H_2 (45 cmHg). The volume of the closed circulating reactor was 320 ml.

Table 3. Product di stribution in $CO-H_2$ reaction over pyrolysed catalysts of $Rh_4(CO)_{12}$ dispersed on various metal oxides

Catalyst	T (°C)	Product distribution (mmol in 10 h)							CO conv. (% in 10h)	Methanol select. (%)
		CH_3OH	C_2H_5OH	O.P.[a]	CH_4	C_2	C_3	C_4		
$Rh_4(CO)_{12}$–BeO (0.12 g) (20 g)	225	0.36	0.01	–	0.20	–	–	–	15.4	68.3
	240	0.45	0.04	–	0.44	–	–	–	24.3	49.2
$Rh_4(CO)_{12}$–CaO (0.12 g) (20 g)	232	0.30	0.001	–	0.003	–	–	–	8.0	98.6
	250	0.51	0.003	–	0.010	–	–	–	14.2	98.1
$Rh_4(CO)_{12}$–SiO_2 (0.12 g) (5 g)	220	0.005	0.023	+	0.49	0.015	0.035	0.006	23	0.6
	235	0.026	0.013	+	0.57	0.039	0.038	0.010	27	3
$Rh_4(CO)_{12}$–γ-Al_2O_3 (0.12 g) (20 g)	220	0.004	0.002	–	1.18	0.16	0.13	0.053	54.6	0.2
	250	+	+	–	2.2	0.20	0.16	0.05	86	—

CO: H_2=(15 cmHg: 50 cmHg). The volume of the reactor was 420 ml. a) A trace of CH_3CHO, C_3H_7OH, and C_4H_9OH was detected in the oxygenated products.

280 m^2/g), SnO_2 (Nakarai Chem. Co., 99.9% purity) WO_3 (Nakarai Chem. Co., 99.9%) and V_2O_5 (Kishida Chem. Reagent Co., 99.9% purity) were employed to prepare the dispersed Rh catalysts by the pyrolysis of $Rh_4(CO)_{12}$. All the pyrolysed catalysts produced mainly methane with lower CO conversion in $CO-H_2$ reaction. Over the catalysts on SiO_2 and γ-Al_2O_3, a trace of methanol and ethanol was detected in the condensed products at temperatures above 200 °C. The pyrolysed catalysts on other metal oxides such as SnO_2, WO_3, and V_2O_5 yielded a negligible amount of methanol or other oxygenated products. At elevated temperatures methane was obtained in a large amount over these catalysts. The metal oxides used in the experiments were completely inactive for CO hydrogenation. This suggests that the reactivities of the supported Rh crystallites from carbonyl clusters are markedly dependent on the kind of metal used as inorganic carrier. The basic metal oxides such as ZnO, MgO, CaO, and BeO were found to be the optimal carriers to prepare highly selective Rh crystallite catalysts for methanol synthesis under mild reaction conditions.

Catalytic Hydrogenation of CO over the Supported Platinum and Iridium Crystallites on ZnO and MgO Prepared by Pyrolysis of the Carbonyl Cluster Compounds. Pt carbonyl cluster anion salts such as $Pt_9(CO)_{18}2NEt_4$ and $Pt_{15}(CO)_{30}2NEt_4$ were dispersed from tetrahydrofuran solutions onto ZnO and MgO powders in 0.5—1.0 Pt wt% loading. After removal of the solvent at room temperature, the resulting substance charged in the closed circulating Pyrex-reactor (*ca.* 420 ml) was heated *in vacuo* up to 180 °C. The desorption of CO from each dispersed Pt carbonyl cluster salt proceeds almost completely in a vacuum or H_2 flow (1 atm).[3] This was confirmed by temperature-programmed technique using gas chromatography and mass spectrometry. The desorption temperatures of the Pt clusters on γ-Al_2O_3 and ZnO were 150 °C for $Pt_{15}(CO)_{30}2NEt_4$ and 165 °C for $Pt_9(CO)_{18}2NEt_4$, respectively. The hydrogenation of CO took place reproducibly at 180—250 °C by introducing a $CO-H_2$ (1 : 2 molar ratio) gas onto the pyrolysed catalysts. Methanol was also catalytically produced with a small amount of methane. Ethanol and higher hydrocarbons (C_2—C_4) were detected in a negligible amount in the reacton. The methanol yields per Pt weight over the catalyst on MgO were higher than that on ZnO under similar reaction conditions. For comparison, the conventional Pt metal catalyst was prepared from the impregnated H_2PtCl_6 on ZnO (Kadox 25) in 2.5 Pt wt% loading, followed by hydrogen reduction at 350 °C for 15 h. The resulting catalyst showed considerably lower CO conversion, producing mainly methane with less than 5% selectivity of methanol formation in $CO-H_2$ reaction under atmospheric pressure.

$Ir_4(CO)_{12}$ was dissolved in tetrahydrofuran, and

Table 4. Product distribution in $CO-H_2$ reaction over pyrolysed catalysts on ZnO and MgO prepared from Pt and Ir carbonyl cluster compounds

Catalyst	T (°C)	CO conv. (% in 10 h)	Product distribution (mmol 10 h)						Methanol select. (%)
			CH_3OH	C_2H_5OH	CH_4	C_2	C_3	C_4	
$Pt_9(CO)_{18}2NEt_4$–ZnO (0.17 g) (20 g)	220	5.7	0.19	–	0.01	–	–	–	95
	260	6.9	0.24	–	0.015	–	–	–	94
$Pt_{15}(CO)_{30}2NEt_4$–ZnO (0.15 g) (20 g)	240	3.2	0.12	–	+	–	–	–	99
	260	5.4	0.20	–	0.005	–	–	–	98
$Pt_{15}(CO)_{30}2NEt_4$–MgO (0.28 g) (20 g)	170	13.9	0.48	+	0.006	–	–	–	98
	200	26.3	0.89	0.003	0.012	–	–	–	98
$Ir_4(CO)_{12}$–ZnO (0.10 g) (20 g)	240	2.2	0.072	–	0.011	–	–	–	87
	270	8.6	0.18	–	0.051	–	–	–	78
$Ir_4(CO)_{12}$–ZnO (0.10 g) (20 g)	270	0.5	0.005	–	0.015	–	–	–	25
	305	1.2	0.006	–	0.037	–	–	–	14

CO: H_2=15: 45 cmHg. The volume of the reactor was 420 ml. (+) denotes less than 0.001 mmol.

deposited on 20 g of ZnO or MgO powder. On coming in contact with MgO powder, the pale-yellow solution of $Ir_4(CO)_{12}$ turned deep-red, probably due to the formation of Ir_6-carbonyl clusters such as $Ir_6(CO)_{15}^{2-}$ salt[8] completely adsorbed on MgO. Removal of CO, after evaporating the solvent, was accomplished *in vacuo* at 180 °C for 2 h. Methanol was catalytically produced at higher temperatures above 240 °C after a long induction period over the pyrolysed Ir crystallite catalyst on ZnO. No ethanol and higher hydrocarbons were obtained in CO–H_2 reaction over Ir crystallite catalyst. The catalyst prepared by pyrolysis of $Ir_4(CO)_{12}$ on MgO gave a trace of methanol for the oxygenated product, and mainly methane from CO–H_2 mixture reactant. Typical results of methanol synthesis over the Pt and Ir crystallite catalysts are summarized in Table 4. It is suggested that the pyrolysed catalysts of Pt and Ir carbonyl clusters on ZnO and MgO also catalyse methanol synthesis under atmospheric pressure, although the specific methanol conversions were relatively lower than those from Rh carbonyl clusters. The activity and selectivity of methanol formation in CO–H_2 reaction depend on the catalyst preparation by selecting metal carbonyl clusters as well as metal oxides as inorganic carriers.

References

1) J. H. Sinfelt, *J. Catal.*, **29**, 308 (1973), *Acc. Chem. Res.*, **10**, 15 (1977).

2) J. K. Anderson and D. M. Mainwaring, *J. Catal.*, **35**, 162 (1974); M. Ichikawa, *J. Chem. Soc., Chem. Commun.*, **1976**, 11, 26.

3) M. Ichikawa, *Chem. Lett.*, **1976**, 335.

4) P. Chini and S. Martinengo, *Inorg. Chim. Acta*, **3**, 315 (1969).

5) O. S. Mills and E. F. Paulus, *Chem. Commum.*, **1966**, 815. J. P. Nice and E. F. Paulus, *J. Organomet. Chem.*, **10**, 337 (1976).

6) V. G. Albano, A. Ceriotti, P. Chini, G. Ciani, S. Martinengo, and W. Anker, *J. Chem. Soc., Chem. Commun.*, **1975**, 859. From the Ir carbonylabsorption spectra, the synthesized product was presumed to be a mixture of $Rh_{13}(CO)_{23}H_x2N(C_4H_9)_4$, where $x=2$ and 3.

7) P. Chini and S. Martinengo, *J. Chem. Soc., Chem. Commun.*, **1976**, 251.

8) L. Malatesta, G. Caglio, M. Anguletta, *Chem. Commum.*, **1970**, 532. $Ir_4(CO)_{12}$ is readily converted in alkaline solution into $Ir_6(CO)_{15}^{2-}$ and $Ir_6(CO)_{16}$ as deep-red complexes.

Catalysis by Supported Metal Crystallites from Carbonyl Clusters. II. Catalytic Ethanol Synthesis from CO and H_2 under Atmospheric Pressure over Supported Rhodium Crystallites Prepared from Rh Carbonyl Clusters Deposited on TiO_2, ZrO_2, and La_2O_3

Masaru ICHIKAWA

Sagami Chemical Research Center, Nishi-Ohnuma, Sagamihara, Kanagawa 229

(Received December 6, 1977)

Ethanol was catalytically produced in the CO–H_2 reaction under atmospheric pressure and at 150—250 °C over rhodium crystallite catalysts prepared from Rh carbonyl cluster compounds highly dispersed on La_2O_3, TiO_2, and ZrO_2. The activity and selectivity of ethanol formation depend on the kind of metal carbonyl cluster and metal oxide used as inorganic carriers. The catalysts prepared by the pyrolysis of smaller Rh carbonyl clusters such as $Rh_2(C_5H_5)_2(CO)_3$, $Rh_4(CO)_{12}$, and $Rh_6(CO)_{16}$ on La_2O_3, TiO_2, and ZrO_2 show higher selectivity of the oxygenated products containing ethanol (main), acetaldehyde, and methanol. The ethanol contents in the oxygenated products increased considerably above 200 °C over the catalysts. CeO_2 and ThO_2 were also employed in the preparation of the pyrolysed catalysts to disperse the Rh carbonyl clusters, which catalyses the ethanol formation in the CO–H_2 reaction at atmospheric pressure.

The catalytic synthesis of hydrocarbons and oxygen-containing compounds from CO and H_2 (Fischer-Tropsch synthesis and synthesis of alcohols) is of interest from both a practical and theoretical point of view.[1] The conventional metal catalysts containing Fe and Co are not selective, exhibiting considerably broad spectra of the product distribution. The formation of hydrocarbons and alcohols from CO–H_2 mixture is thermodynamically favorable, although higher pressures (in excess of 1 atm) are necessary to facilitate the formation of higher molecular weight products. It is important to study the surface reactions in catalytic hydrogenation of CO over supported metal catalysts to control rates and selectivity for the possible products in connection with the surface composition of the catalysts. The purpose of this study is to correlate the reactivities of highly dispersed noble metal catalysts in the CO–H_2 reaction with their chemical compositions, being associated with the dispersion of metal and composition on the surface, which depend on the systems and conditions of ctalyst preparations. The author has developed a method for the preparation of the dispersed metal crystallites on various metal oxides by using molecular metallic cluster compounds as specific precursors.[2] Recently, Muetterties and others[3] demonstrated that the metal carbonyl clusters such as $Ru_3(CO)_{12}$ and $Ir_4(CO)_{12}$ slowly produce methane and higher hydrocarbons in homogeneous hydrogenation of CO at 140—200 °C and 1—2 atm. The supported Rh, Pt, and Ir crystallites on ZnO and MgO prepared from the carbonyl clusters catalyse a selective methanol synthesis in catalytic hydrogenation of CO under atmospheric pressure.[4] In this paper, a report is given on the direct catalytic ethanol formation from CO–H_2 mixture at atmospheric pressure over the Rh crystallites prepared from the carbonyl clusters deposited on specific metal oxides such as TiO_2, ZrO_2, and La_2O_3. The rates and product distribution in the CO–H_2 reaction over the supported Rh crystallite catalysts were observed by changing the reaction conditions and catalyst preparation using various Rh carbonyl cluster compounds and metal oxides as inorganic carriers.

Experimental

The catalyst preparation and CO–H_2 reaction were carried out in a closed circulating glass-reactor. Experiments were performed under atmospheric pressure in a pyrex glass tubular reactor operating in continuous flow in order to measure the one-path yields and selectivity of the reaction through the fixed-bed catalysts. Analysis of the oxygenated products and hydrocarbons was carried out by gas chromatography using Porapak Q, PEG 1500, alumina–DMF and active carbon columns, as reported.[4] The oxygenated products in the CO–H_2 reaction were separately obtained in the condensed part with a Dry-Ice cooling trap in the circulating reactor. In the continuous flow reaction system, the gaseous product was collected at intervals in a glass flask containing water and analyzed by FID (Hitachi-FD6) gas chromatography with a 4 m PQ column. The rhodium carbonyl cluster compounds such as $Rh_2(C_5H_5)_2(CO)_3$, $Rh_4(CO)_{12}$, $Rh_6(CO)_{16}$ and Rh_{13}-$(CO_{23}H_{2-3}2NBu_4$ were obtained.[4] $Rh_7(CO)_{16}3NEt_4$ was synthesized in the reaction with $Rh_4(CO)_{12}$ under CO atmosphere by the method of Martinengo and Chini[5] and isolated as tetra ethylammonium salt, which was stored in a glass ampoule under He atmosphere. The Rh carbonyl clusters were deposited in high dispersion from their solutions onto the metal oxides such as La_2O_3, CeO_2, TiO_2, ZrO_2, and ThO_2. The removal of CO and residual organics (amines and cyclopentadiene) was accomplished in a vacuum or H_2 atmosphere by heat treatment of the supported samples. The procedure of catalyst preparation was carried out *in vacuo* or under an inert atmosphere of He and N_2 because of air-sensitivity of the carbonyl cluster compounds.

Results and Discussion

Catalytic Etanol Formation from CO and H_2 over the Rh Crystallites on La_2O_3 Prepared from $Rh_4(CO)_{12}$. 0.11 g of $Rh_4(CO)_{12}$ was deposited from a hexane solution onto 20 g of lanthanum oxide (La_2O_3, 99.9% purity, Nakarai Chem. Reagent Co.,) which was evacuated at 320 °C for 13 h prior to use. The solvent was then removed by evaporation at room temperature. The sample pellets

Table 1. Product distribution in $CO-H_2$ reaction over the pyrolysed catalyst on La_2O_3 prepared from $Rh_4(CO)_{12}$

CO (cmHg)	H_2	T (°C)	CO conv. (% in 5 h)	Product distribution (mmol in 10 h)							
				CH_3OH	C_2H_5OH	CH_3CHO	CH_3COOCH_3	CH_4	C_2	C_3	C_4
20	45	170	7.2	0.165	0.036	—	—	0.10	+	+	—
20	45	195	11.3	0.38	0.19	+	—	0.068	0.002	0.008	+
20	45	205	15.2	0.62	0.36	+	—	0.17	0.005	0.013	+
20	45	225	36.4	0.74	1.12	+	—	0.56	0.026	0.082	0.026
15	48	195	14.6	0.32	0.21	+	—	0.11	+	0.008	+
30	35	195	5.9	0.20	0.19	+	—	0.038	+	+	+

The volume of the reactor was 320 ml. + denotes less than 0.001 mmol in 10 h.

(*ca.* 5—10 mesh) for the $CO-H_2$ reaction were prepared by pressing the supported material under pressure of 400 kg/cm², and charged in a Pyrex glass reactor. Desorption of CO from the supported $Rh_4(CO)_{12}$ sample proceeded under evacuation (10^{-3}—10^{-4} mmHg) by raising the temperature upto 180 °C for 2 h. After pyrolysis, a mixture of CO and H_2 (molar ratio 1 : 1—2 under total pressure of 45—65 cmHg) was circulated with *ca.* 50 ml/min flow rate through the catalyst pellets. The oxygenated products containing C_2H_5OH, CH_3CHO, and CH_3OH were catalytically obtained in a certain induction period (*ca.* 5 h) at 150—250 °C. Methane and a small amount of C_2—C_4 hydrocarbons were also formed in gas phase. The reproducible rates of the oxygenated products and hydrocarbons were measured by changing the reaction temperatures and ratios of CO to H_2 partial pressure in a wide range. Typical results are summarized in Table 1. The carbon efficiency of oxygenated products per CO consumed was between 60 and 90% over the pyrolysed catalyst in the temperature range 150—200 °C. At temperatures below 190 °C, methanol contents in the oxygenated products were relatively high, the yields of ethanol increasing considerably with temperature rise above 200 °C. The apparent activation energy of methanol, ethanol and methane formation was estimated at 11, 20, and 28 kcal/mol, respectively. At higher CO/H_2 ratios of the mixture gas, the formation of C_1—C_4 hydrocarbons was suppressed and ethanol selectivity increased comparatively, although total CO conversion decreased. It should be noted that lanthanum oxide as an inorganic support was completely inactive for the $CO-H_2$ reaction at 120—320 °C, even after prolonged heat treatment under hydrogen.

Hydrogenation of CO over the Rh Crystallites on La_2O_3 Prepared from Various Rh Carbonyl Clusters. A number of Rh carbonyl cluster compounds, such as $Rh_2(C_5H_5)_2(CO)_3$, $Rh_6(CO)_{16}$, $Rh_7(CO)_{16}3NEt_4$, and $Rh_{13}(CO)_{23}2NBu_4$ were employed instead of $Rh_4(CO)_{12}$, as precursors in the preparation of pyrolysed catalysts on lanthanum oxide. Each carbonyl cluser compound (0.10 g) was deposited onto the La_2O_3 powder (20 g) from the solution of tetrahydrofuran ($Rh_6(CO)_{16}$ and $Rh_{13}(CO)_{23}H_{2-3}2NBu_4$) and of acetone ($Rh_7(CO)_{16}3NEt_4$). The supported material was loaded in the reactor of the closed circulating reaction system (total volume 420 ml). After pyrolysis at 180 °C for 2 h and hydrogen treatment at 200 °C for 1 h, the $CO-H_2$ reaction took place by circulation of a mixture gas (CO/H_2=*ca.* 0.5, 65 cmHg) over the catalysts. $Rh_2(C_5H_5)_2(CO)_3$ was dispersed on La_2O_3 from the hexane solution.

Decomposition of the supported cluster was accomplished under H_2 atmosphere (60 cmHg) at 180 °C for 2 h and evacuated for a few minutes. The rates and product distribution in a catalytic hydrogenation of CO were measured over these pyrolysed catalysts in the temperature range 150—250 °C. The reproducible results are given in Table 2. It was suggested that the pyrolysed catalysts from smaller Rh clusters such as Rh_2—Rh_6 exhibit a relatively higher selectivity of oxygenated products containing mainly ethanol and methanol. On the contrary, C_2—C_4 hydrocarbons were produced at higher contents of the products over the catalysts prepared from larger carbonyl clusters such as Rh_7—Rh_{13}. The composition in the oxygenated products exhibited almost the same spectra over all the pyrolysed Rh cluster catalysts. With a rise in the reaction temperature above 200 °C, the content of acetaldehyde in the products increased a little and C_2—C_4 hydrocarbons were produced with higher yields over the catalysts from larger Rh carbonyl clusters. It is of interest that the catalyst based on $Rh_2(C_5H_5)_2(CO)_3$ and La_2O_3 produced catalytically methyl acetate in the $CO-H_2$ reaction above 200 °C. The catalysts kept almost the same rates and selectivity of ethanol formation in prolonged runs of about 20 days. Accordingly, with Rh carbonyl clusters as precursors, the relative yields of ethanol per unit Rh weight changed over the pyrolysed catalysts on La_2O_3 in the order:

$$Rh_2(C_5H_5)_2(CO)_3 < Rh_4(CO)_{12} > Rh_6(CO)_{16} > Rh_7(CO)_{12}3NEt_4 > Rh_{13}(CO)_{23}H_{2-3}2NBu_4.$$

For comparison, the Rh catalyst was prepared conventionally by hydrogen reduction (350 °C 15 h) of the impregnated $RhCl_3$ on La_2O_3 (2.5% Rh weight loading) from the aqueous solution. When a $CO-H_2$ mixture was admitted onto the catalyst at 200 °C, a small amount of the oxygenated products containing ethanol and methanol was obtained after a long induction period of several days. The reproducible results in the $CO-H_2$ reaction over the catalyst showed relatively smaller CO conversion and lower selectivity of the oxygenated products. Methane and higher hydrocarbons were preferentially produced above 200 °C (Table 2). The results suggest that the Rh carbonyl clusters play the role of specific precursor to prepare the supported catalyst on La_2O_3, which catalyses the selective formation of oxygenated products in a CO hydrogenation

Table 2. Product distribution in $CO-H_2$ reaction over the pyrolysed catalysts on La_2O_3 prepared from various Rh carbonyl cluster compounds

Catalyst	T (°C)	CO conv. (% in 5h)	Product distribution in carbon efficiency[a] (%)							
			CH_3OH	C_2H_5OH	CH_3CHO	CH_3COOCH_3	CH_4	C_2	C_3	C_4
$Rh_2Cp_2(CO)_3$-La_2O_3 (0.08g) (20 g)	220	1.9	25.6	54.8	3.0	0.8	13.3	1.0	2.2	+
	250	8.5	2.9	50.3	2.4	4.4	29.4	9.6	6.6	1.5
$Rh_4(CO)_{12}$-La_2O_3 (0.10 g) (20 g)	205	14.9	41.7	48.3	+	−	17.4	0.3	2.3	0.2
	224	36.4	20.2	61.1	+	+	11.9	0.8	4.4	1.3
$Rh_6(CO)_{16}$-La_2O_3 (0.10 g) (20 g)	220	16.4	17.7	46.6	3.6	+	18.9	3.8	4.9	3.3
	242	25.5	10.3	45.8	1.5	+	25.9	6.5	7.9	2.0
$Rh_7(CO)_{16}3NEt_4$-La_2O_3 (0.10 g) (20 g)	220	14.8	8.9	32.8	4.6	+	13.5	14.0	19.4	6.8
	240	20.1	4.6	13.8	3.0	+	26.0	18.6	26.0	8.2
$Rh_{13}(CO)_{23}H_{2-3}2NBu_4$-$La_2O_3$ (0.16 g) (20 g)	225	15.5	6.4	28.9	2.4	+	22.5	19.8	19.8	6.6
	255	20.7	+	15.4	1.8	+	24.6	24.8	24.2	9.5
$RhCl_3$[b]-La_2O_3 (0.13 g) (20 g)	220	4.7	10.7	17.1	+	+	65.4	6.2	7.9	1.4
	240	6.5	8.1	8.5	+	+	45.7	12.8	19.0	5.7

$CO:H_2=20:45$ cmHg. a) Carbon efficiency $=(i\,Ci/\sum i\,Ci)\times 100$: i=carbon number of the product. b) The catalyst was reduced by hydrogen at 350 °C.

under mild reaction conditions.

Ethanol Formation in $CO-H_2$ Reaction over the Pyrolysed Catalysts of $Rh_4(CO)_{12}$ and $Rh_6(CO)_{16}$ Deposited on TiO_2, ZrO_2, CeO_2, and ThO_2. Other metal oxides such as TiO_2, ZrO_2, CeO_2, and ThO_2 were found to act as promoters for ethanol formation in catalytic hydrogenation of CO over the supported Rh crystallite catalysts. $Rh_4(CO)_{12}$ and $Rh_6(CO)_{16}$ (0.10 g) were similarly deposited onto each metal oxide (TiO_2 99.9% Merck Co., ZrO_2 99.9% Nakarai Chem. Reagent Co., CeO_2 99.9% Wako Pure Reagent Co., and ThO_2 99.9% Kishida Chem. Reagent Co.,)[6] 20 g from the solutions. The pressed pellets of the supported materials were charged in the closed circulating reactor (320 ml). After pyrolysis *in vacuo* at 180 °C for 2 h, a mixture of CO and H_2 was introduced and circulated at 150 and 250 °C. The oxygenated products containing mainly ethanol were produced in a wide temperature range over the pyrolysed catalysts. The reproducible rates and product distribution in the $CO-H_2$ reaction are given in Table 3. The product distribution illustrates a remarkable specificity for ethanol formation in the oxygenated products. The selectivity of the oxygenated products was relatively higher over the catalyst on ZrO_2 than that on TiO_2 and CeO_2, and gave comparatively smaller formation of C_1–C_4 hydrocarbons. The olefinic products of C_2—C_4 hydrocarbons increased considerably by employing the liquid nitrogen trap, instead of Dry-Ice cooling, to collect the hydrocarbon products at higher temperatures. The CO—H_2 reaction readily proceeded over the pyrolysed Rh carbonyl cluster catalysts on ThO_2 at 150—180 °C to produce the oxygenated products containing methanol and ethanol. By raising the temperature above 190 °C, the higher hydrocarbons such as C_5H_{12}, C_6H_{14}, and C_7H_{16}[7] were considerably formed, and the yields of the oxygenated products decreased although CO conversion was very high. TiO_2 and ThO_2 may accelerate the condensation and dehydration of the oxygenated products at a catalyst surface. The product distribution and rates in the $CO-H_2$ reaction over the Rh crystallite catalysts markedly depend on the kind of metal oxide.[4] The pyrolysed catalysts prepared from Rh carbonyl clusters on ZnO, MgO, BeO, and CaO (Ia and IIa metal

Table 3. Product distribution in $CO-H_2$ reaction over the pyrolysed catalysts on various metal oxides prepared from $Rh_4(CO)_{12}$

Catalyst	T (°C)	CO conv. (% in 5 h)	Product distribution in carbon efficiency (%)							
			CH_2OH	C_2H_5OH	CH_3CHO	O.P.[a]	CH_4	C_2	C_3	C_4
$Rh_4(CO)_{12}$-TiO_2 (0.10 g) (20 g)	195	42.2	8.2	47.1	+	+	19.9	6.1	11.7	6.9
	210	45.6	3.9	22.8	+	+	42.2	9.6	14.8	6.8
$Rh_6(CO)_{16}$-TiO_2 (0.10 g) (20 g)	195	29.4	4.6	39.6	3.5	+	20.2	10.2	21.9	1.2
	210	38.4	4.8	33.3	0.8	+	29.9	4.5	16.2	9.8
$Rh_4(CO)_{12}$-ZrO_2 (0.10 g) (20 g)	180	5.2	25.1	57.7	0.3	−	17.1	+	0.5	+
	215	23.3	14.8	47.0	0.6	−	34.3	0.8	1.2	0.7
$Rh_4(CO)_{12}$-ThO_2 (0.10 g) (20 g)	160	15.2	9.6	50.9	+	+	12.5	4.6	17.7	4.6
	175	39.5	12.7	39.1	+	+	21.9	2.7	13.2	10.0
$Rh_4(CO)_{12}$-CeO_2 (0.10 g) (20 g)	205	8.4	26.4	35.0	2.0	−	22.1	3.1	9.7	1.8
	238	19.5	10.4	38.8	2.2	−	27.1	6.8	10.2	4.4

$CO:H_2=20:45$ cmHg. The volume of the reactor was 320 ml. a) O.P.=other oxygenated products containing a small amount of C_3H_7OH and C_4H_9OH.

oxides) selectively produced methanol in the reaction. Ethanol and C_2-oxygenated products were obtained over the catalysts dispersed on La_2O_3 and CeO_2 (IIIa metal oxides) and TiO_2, ZrO_2, and ThO_2 (IVa metal oxides). In contrast, C_1—C_5 hydrocarbons (mainly methane) were preferentially produced with less than 5% selectivity of the oxygenated products (mainly ethanol) over the Rh crystallites on SiO_2 gel and γ-Al_2O_3 (IIIb and IVb metal oxides). Methane was selectively formed with lower CO conversion over the catalyst on SnO_2, V_2O_5, and P_2O_5 in the CO–H_2 reaction. It seems that the half-hydrogenated intermediates in catalytic hydrogenation of CO are influenced by the surface properties of the metal oxides dispersing Rh crystallites. Surface properties such as acidity or basicity of metal oxides might be correlated with product distribution in the CO–H_2 reaction over those supported Rh crystallite catalysts.

CO–H_2 Reactions in Continuous Flow System under Atmospheric Pressure over the Pyrolysed Catalysts Prepared from $Rh_4(CO)_{12}$ on La_2O_3 and TiO_2. The CO–H_2 reaction was carried out operating the continuous flow mode using a 50 cm Pyrex glass tubular reactor, 18 mm in diameter. A pellet catalyst (*ca.* 20 ml) of the supported $Rh_4(CO)_{12}$ on La_2O_3 or TiO_2 (in 0.5% Rh loading) was charged in the reactor, and 2 mm glass beads were packed above and below the catlayst bed. The reactor was placed vertically in an electric furnace. CO and

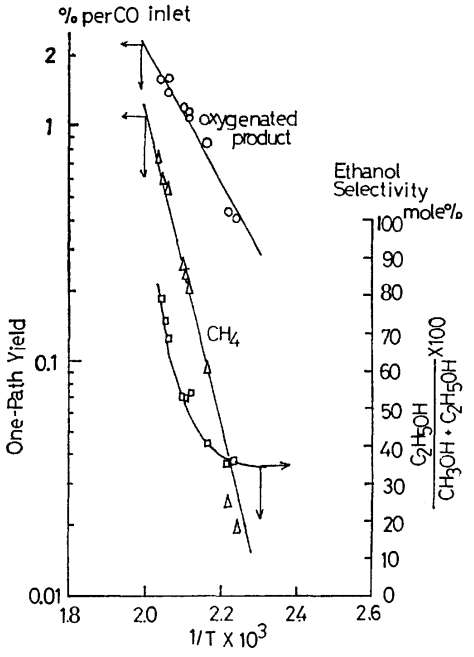

Fig. 1. Temperature dependency of methanol, ethanol, and methane formation over the pyrolysed catalyst on La_2O_3 prepared from $Rh_4(CO)_{12}$. $Rh_4(CO)_{12}$ 0.30 g (0.40 mmol) and La_2O_3 38 g, 0.43% Rh wt dispersion. Activated under hydrogen stream (1 atm, 40 ml/min) at 200 °C. CO(15 ml/min) and H_2 (40 ml/min). -○-: One-path yield (% per CO inlet) of the oxygenated products containing methanol and ethanol, -△-: one-path yield (% per CO inlet) of methane, -□-: mol % of ethanol in the oxygenated products produced. (ethanol)/(methanol)+(ethanol) × 100.

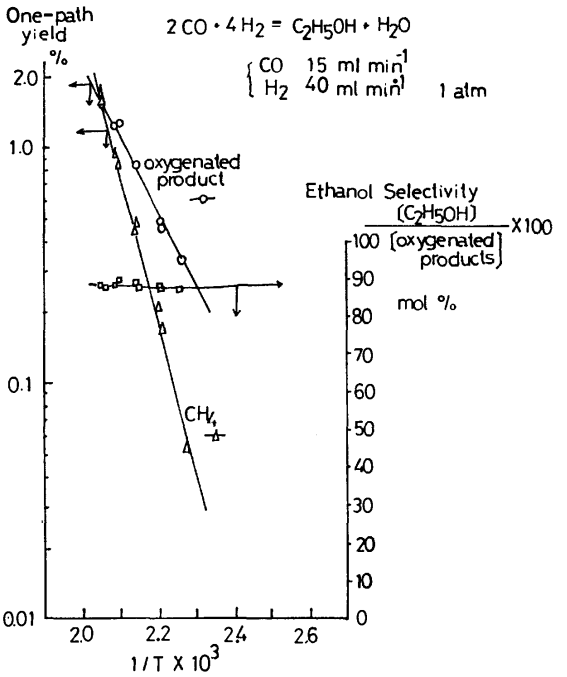

Fig. 2. Temperature dependency of the formation of oxygenated products and methane over the pyrolysed catalyst on TiO_2 prepared from $Rh_4(CO)_{12}$. $Rh_4(CO)_{12}$ 0.35 g (0.47 mmol) and TiO_2 38 g in 0.50 Rh wt % dispersion. Activated under hydrogen stream (1 atm, 40 ml/min). CO(15 ml/min) and H_2 (40 ml/min). -○-: One-path yield (% per CO inlet) of the oxygenated products containing ethanol, methanol and acetaldehyde, -△-: one-path yield (% per CO inlet) of methane, -□-: mol % of ethanol in the oxygenated products formed.

hydrogen were supplied from the respective cylinders. After measuring the flow rates of CO and H_2 separately, the gases were mixed and brought to contact with the catalyst bed at the flow rates 30—100 ml/min. The gaseous product was transferred from the bottom of the reactor in a 100 ml flask containing water. The oxygenated products collected at intervals were analyzed by FID gas chromatography using PQ column, and C_1—C_4 hydrocarbons by alumina–DMF and active carbon columns. Removal of CO was accomplished by slow heating of the catalysts at 180—200 °C in a stream of pure hydrogen for 2 h. The 1:1—2 mixture of CO and H_2 was reacted at 180—250 °C. The stationary rates and product distribution of the reaction were attained in the continuous flow for 10 h at 200 °C. The one-path yields of methanol, ethanol, and methane were measured at various temperatures under constant space velocity. The results are shown in Figs. 1 and 2. The formation of other C_2-oxygenated products and C_2—C_4 hydrocarbons was negligibly small. The ethanol content in the oxygenated products was found to be almost constant over the pyrolysed catalyst on TiO_2 in a wide temperatures range. On the other hand, the ethanol content was markedly dependent on the reaction temperature over the catalyst on La_2O_3, increasing with rise in temperature. By increasing the ratios of CO/H_2 the selectivity of the oxygenated products increased and the C_1—C_4 hydrocarbon forma-

tion was suppressed considerably, as measured over the catalysts in the closed circulating reactor system.

References

1) H. Stortch, N. Golumbic, and R. Anderson, "The Fischer-Tropsch Synthesis," Wiley N. Y. (1951); Y. T. Eidus, *Russ. Chem. Rev.*, **36**, 338 (1967).

2) M. Ichikawa, *J. Chem. Soc., Chem. Commun.*, **1976**, 11, **26**, *Chem. Lett.*, **1976**, 335.

3) G. C. Demitres and E. L. Muetteries, *J. Am. Chem. Soc.*, **99**, 2796 (1977); M. G. Thomas, B. F. Beier, and E. L. Muetterties, *ibid.*, **98**, 296 (1976).

4) M. Ichikawa, *Bull. Chem. Soc. Jpn.*, **51**, 2268 (1978).

5) S. Martinengo and P. Chini, *Gazz. Chim. Ital.*, **102**, 344 (1972).

6) The metal oxides employed gave in a negligible amount the oxygenated products and hydrocarbons in the CO–H_2 reaction at elevated temperatures above 250 °C.

7) The oily products were analyzed by temperature-programmed gas chromatography using Polapak Q column.

Structures of Lanthanoid Complexes of Glyceric Acid, Gluconic Acid, and Lactobionic Acid from the Lanthanoid-Induced ^{1}H NMR Shifts: pH Dependence of the Lanthanoid-Substrate Equilibria

Tooru TAGA,* Yoshihiro KURODA, and Makoto OHASHI
Faculty of Pharmaceutical Sciences, Kyoto University, Sakyo-ku, Kyoto 606
(Received December 8, 1977)

Lanthanoid-induced ^{1}H NMR shifts of glyceric acid, gluconic acid, and lactobionic acid were observed in D_2O. Stoichiometric analysis using the shift data at various pH values indicated that the concentration of a 1:1 complex between substrates and lanthanoid ions was higher than that of a 2:1 complex at a low pH. The structure of an axially symmetric 1:1 complex was obtained on the assumption of a predominant pseudo-contact interaction between a europium ion and the ligand nuclei. All the title glycosidic acids were found to chelate the cation with α-carboxy, α-hydroxy, and β-hydroxy oxygens. The relative position of β-hydroxy oxygen is particularly important for the complex formation between β-hydroxy carboxylic acids and metal ions.

In previous papers[1,2] dealing with calcium binding to polyhydroxy dicarboxylic acid, DL-glucaric acid, we have reported that the α-carboxyl group chelates the cation with α-carboxy, α-hydroxy, and β-hydroxy oxygens in an aqueous solution, while the δ-carboxyl group is not bound to the cation either in solution or in the crystalline state. The configuration about the carbon chain of glyceric acid, **1**, gluconic acid, **2**, and lactobionic acid, **3**, is the same as that of glucaric acid, **4**, with respect to the α-carboxyl part (Fig. 1). We were, therefore, interested in the chelating geometry of Compounds **1**, **2**, and **3** to a lanthanoid ion in relation to that of glucaric acid, **4**. It has been known that acidic and neutral carbohydrates occasionally well chelate a metal ion with hydroxyls.[3] The chelating stability depends on the steric arrangement of hydroxyls

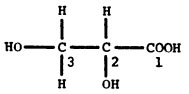
(1)

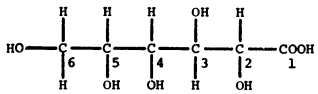
(2)

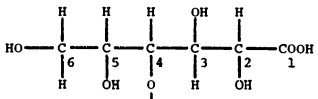
(3)

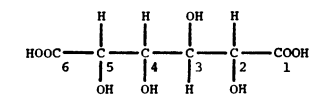
(4)

Fig. 1. Structural formulas of D-glyceric acid (**1**), D-gluconic acid (**2**), D-lactobionic acid (**3**), and D-glucaric acid (**4**).

in the substrate and on the size of the cation. For instance, an axial-equatorial-axial hydroxyl arrangement about a six-membered ring of inositol or pyranose sugar is suitable for the chelation to an alkaline-earth ion, as has been pointed out by Angyal.[4] X-Ray and neutron diffraction studies[5–8] have revealed that **1** and **2** have two different conformations in the crystalline states, and that Compounds **1**, **2**, and **3** have a large flexibility. However, it is possible for them to have a conformation suitable for the stable complexing with a lanthanoid ion in solution. Thus, we studied the structures of the lanthanoid complexes of these compounds in D_2O by the lanthanoid probe method of ^{1}H NMR.

Since the "fast exchange" assumption for complexing between the substrate and the lanthanoid ion in D_2O may be correct, and since complexes with three or more substrates may be negligible, the paramagnetic lanthanoid-induced shift of the ith nucleus in the substrate should conform to the following equation:[9]

$$\Delta\delta_i = \frac{1}{S_0}(x\Delta_{1i} + 2y\Delta_{2i}), \quad (1)$$

where Δ_{1i} and Δ_{2i} are the shifts depending intrinsically on 1:1 and 2:1 complexes respectively, where x and y are the concentrations of the corresponding complexes, and where S_0 is the total concentration of substrates in solution. The Δ_{1i} and Δ_{2i} shifts have usually been derived from chemical shifts observed by changing the molar ratio, ρ, between lanthanoid ions and substrates or by changing the total concentration, S_0, at a constant ρ.[10–12] However, the present complexes are precipitated in an aqueous alkaline solution, and the chemical shift below pK_a depends largely on the pH of the solution. Hence, the evaluation of Δ_{1i} and Δ_{2i} from the data given by the pH change of a solution is desirable.

This paper will describe a treatment of the pH dependence of the lanthanoid-induced shift and will show an application of this method for the cases of three carboxylate complexes. The pseudo-contact shift for an axially symmetric cmoplex is given by the McConnell-Robertson equation:[13]

$$\Delta\nu_i/\nu_0 = A\cdot(3\cos^2\theta_i - 1)/r_i^3, \quad (2)$$

where A is a constant for a lanthanoid ion at a given temperature, where r_i is the distance between the

paramagnetic ion and the ^1H nucleus, and where θ_i is the angle between the principal magnetic axis of the complex and the vector, r_i. As has been reported by many authors,[14,15] the application of Eq. 2 in establishing the ligand conformation in a lanthanoid complex has been successful. The structure can be determined by minimizing the square errors between observed and calculated shifts for trial complex models.

Experimental

The ^1H NMR spectra were recorded on a VARIAN HA-100D spectrometer in the frequency-sweep mode at 100 MHz, using HDO or tetramethylsilane sealed in a capillary tube as an internal lock signal. The probe temperature was kept at 30 °C. The chemical shifts were measured from the acetone peak as an internal standard. The D_2O stock solution of 0.5 M glyceric acid was prepared from *ca.* 70% DL-glyceric acid, whose exact concentration was determined by the titration of 1 M NaOH. The D_2O solutions of sodium gluconate and lactobionic acid were prepared from commercial reagents supplied by the Tokyo Kasei Company. Europium nitrate, $Eu(NO_3)_3 \cdot 6H_2O$, and praseodymium nitrate, $Pr(NO_3)_3 \cdot 6H_2O$, were used as paramagnetic shift reagents, while lanthanum nitrate, $La(NO_3)_3 \cdot 6H_2O$, was used as a diamagnetic shift reagent. The pH of the solution was adjusted by adding concd DCl and NaOD, using a CE-150A glass electrode (Toko Chemical Laboratory Co. LTD) connected with a Hitachi-Horiba M-7E pH meter.

Calculations of the stoichiometry and structures of lanthanoid-substrates complexes were performed on a NOVA 1200 computer operating in connection with a DIABLO-31 disk drive, using the FORTRAN IV programs written by the present authors.

Results and Discussion

Stoichiometry of Lanthanoid-Substrate Complexes. Figures 2, 3, and 4 show the pH dependence of Eu(III)-induced shifts for Compounds **1**, **2**, and **3** respectively in D_2O solutions. Since diamagnetic effects may be included in the Eu(III)-induced shifts,[16,17] the effect was corrected by means of La(III)-induced shifts observed under the same experimental conditions, on the assumption that Eu(III) and La(III) form complexes with similar structures in solution. All the protons bonded to the carbons in **1** and **2**, and three protons of H(2), H(3), and H(1') in **3** were assigned to the observed signals. The other protons of **3** could not be assigned because of the heavy overlapping of the peaks. When the pH value increases, the peaks of H(2) and H(3) for all compounds were shifted upfield, while the other peaks were shifted downfield. The J values given in Table 1 do not change greatly in this experimental pH range.

The pH dependence of the concentrations, x and y, corresponding respectively to the 1 : 1 and 2 : 1 complexes

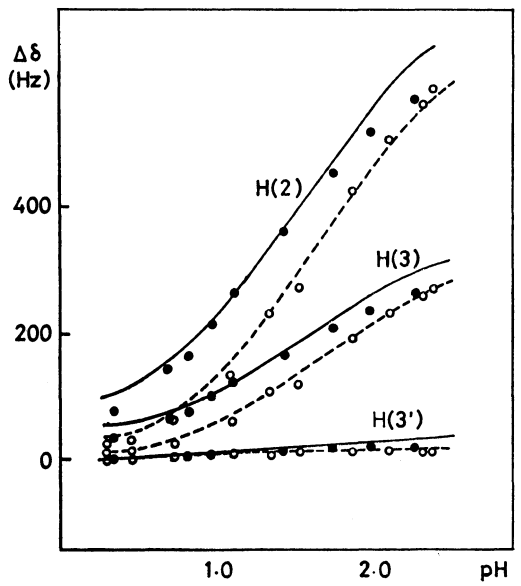

Fig. 2. Eu(III)-induced shifts ($\Delta\delta_{obsd}$) of DL-glyceric acid observed by successive pH changes. ●, $\rho=0.5$, $S_0=0.5$ M; ○, $\rho=2.0$, $S_0=0.05$ M. The curves were obtained by theoretical fitting (see text).

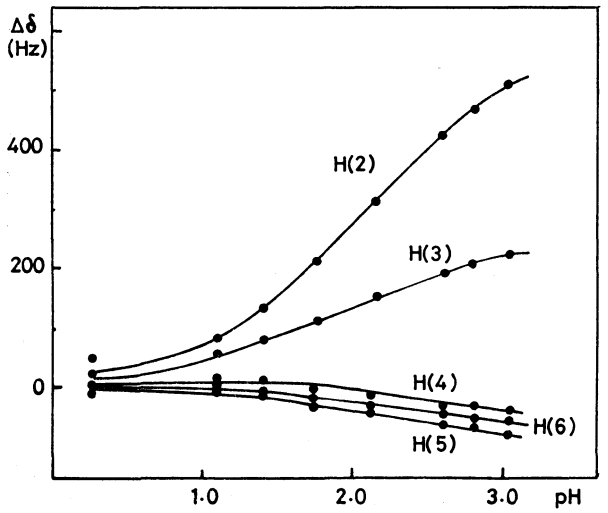

Fig. 3. Eu(III)-induced shifts ($\Delta\delta_{obsd}$) of D-gluconic acid observed by successive pH changes. ○, $\rho=0.5$, $S_0=0.1$ M. The curves were obtained by theoretical fitting (see text).

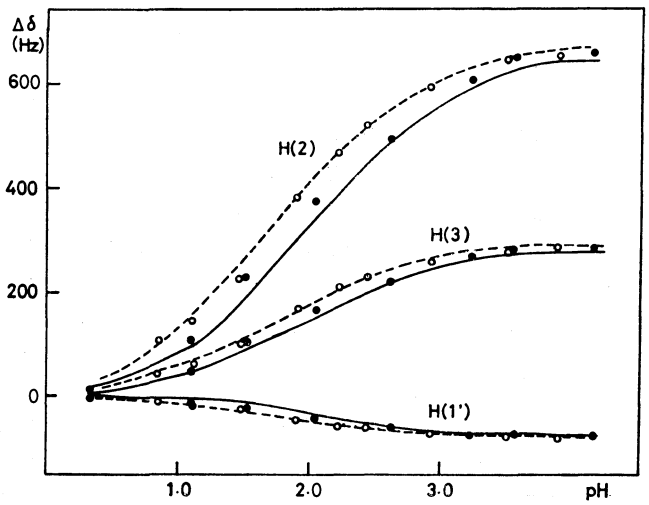

Fig. 4. Eu(III)-induced shifts ($\Delta\delta_{obsd}$) of D-lactobionic acid observed by successive pH changes. ●, $\rho=0.5$, $S_0=0.1$ M; ○, $\rho=0.5$, $S_0=0.2$ M. The curves were obtained by theoretical fitting (see text).

TABLE 1. COUPLING CONSTANTS (±0.2 Hz) OBSERVED FOR LANTHANOID COMPLEXES

Glycerate		Gluconate		Lactobionate	
J_{2-3}	4.1	J_{2-3}	3.5	J_{2-3}	2.7
$J_{2-3'}$	3.0	J_{3-4}	3.0	J_{3-4}	3.7
$J_{3-3'}$	12.1	J_{4-5}	7.6	$J_{1'-2'}$	9.5
		J_{5-6}	3.0		

can be derived from the following stoichiometric consideration. If we denote the lanthanoid ion as L, the protonated carboxylic acid as SH, and the unprotonated carboxylate anion as S, the following equilibria may exist in solution:

$$SH \overset{K_a}{\rightleftharpoons} S + H, \quad (3)$$

$$L + S \overset{K_s}{\rightleftharpoons} LS, \quad (4)$$

$$L + SH \overset{K_{sh}}{\rightleftharpoons} LSH, \quad (5)$$

$$LS + S \overset{K_{ss}}{\rightleftharpoons} LSS, \quad (6)$$

$$LSH + S \overset{K_{shs}}{\rightleftharpoons} LSHS, \quad (7)$$

$$LS + SH \overset{K_{ssh}}{\rightleftharpoons} LSSH, \quad (8)$$

$$LSH + SH \overset{K_{shsh}}{\rightleftharpoons} LSHSH, \quad (9)$$

where K_a is a dissociation constant of carboxylic acid given as

$$K_a = [S]\cdot[H]/[SH], \quad (10)$$

and where K_s, K_{sh}, K_{ss}, K_{shs}, K_{ssh}, and K_{shsh} are association constants corresponding to each complex. Since the total concentration of lanthanoid ions, $L_0 = [L]+x+y$, and that of substrates, $S_0 = [S]+[SH]+x+2y$, the concentrations for each complex are expressed in terms of x and y by using Eq. 10 as follows:

$$[LS] = K_s(L_0 - x - y)(S_0 - x - 2y)/(1 + h), \quad (11)$$

$$[LSH] = K_{sh}(L_0 - x - y) \times (S_0 - x - 2y)h/(1 + h), \quad (12)$$

$$[LSS] = K_{ss}K_s(L_0 - x - y) \times (S_0 - x - 2y)^2/(1 + h)^2, \quad (13)$$

$$[LSHS] = K_{shs}K_{sh}(L_0 - x - y) \times (S_0 - x - 2y)^2h/(1 + h)^2, \quad (14)$$

$$[LSSH] = K_{ssh}K_s(L_0 - x - y) \times (S_0 - x - 2y)^2h/(1 - h)^2, \quad (15)$$

$$[LSHSH] = K_{shsh}K_{sh}(L_0 - x - y) \times (S_0 - x - 2y)^2h^2/(1 + h)^2, \quad (16)$$

where $$h = [H]/K_a = 10^{(pK_a - pH)}. \quad (17)$$

The following quadratic equations are obtained from Eqs. 11—16 by using the $x=[LS]+[LSH]$ and $y=[LSS]+[LSHS]+[LSSH]+[LSHSH]$ relations:

$$x = \eta(L_0 - x - y)(S_0 - x - 2y), \quad (18)$$

$$y = \xi x(S_0 - x)/(\eta + 2\xi x), \quad (19)$$

where $$\eta = (K_s + hK_{sh})/(1 + h), \quad (20)$$

$$\xi = \{(K_{ss} + hK_{ssh})K_s + (K_{shs} + hK_{shsh})hK_{sh}\}/(1 + h)^2. \quad (21)$$

From Eqs. 18 and 19,

$$x^3 + Ax^2 + Bx + C = 0, \quad (22)$$

where $$A = \{-2\rho S_0 + \eta/\xi - 4/\eta\}/\{1 - 4\xi/\eta^2\}, \quad (23)$$

$$B = \{(2\rho - 1)S_0^2 - (\rho + 1) \times (\eta/\xi)S_0 - 1/\xi\}/\{1 - 4\xi/\eta^2\}, \quad (24)$$

$$C = \{\rho(\eta/\xi)S_0^2\}/\{1 - 4\xi/\eta^2\}. \quad (25)$$

Equations 22—25, which are similar to the Shapiro-Johnston equations,[9] are a general expression including the pH dependence for the "two-step mechanism." If the pK_a of the carboxylate in D_2O is known, and if a suitable value of the association constant is assumed, the concentration, x, at a given pH can be obtained by solving Eq. 22, while y can be given by Eq. 19. If the induced shifts of the proton signals of the LS and LSH complexes are the same, and if those of the LSS, LSSH, LSHS, and LSHSH complexes are also the same, (the total lanthanoid-induced shift of the ith nucleus can be calculated by means of Eq. 1. The best fit parameters, Δ_{1i} and Δ_{2i}, can be obtained by the least-squares method, minimizing the sum of errors between the observed and calculated induced shifts.[9]

TABLE 2. ASSOCIATION CONSTANTS ASSIGNED FOR 1:1 AND 2:1 COMPLEXES, AND THE pK_a OF EACH ACID

		Glyceric acid	Gluconic acid	Lactobionic acid
K_s	(mol^{-1})	980	1180	600
K_{sh}	(mol^{-1})	0.001	0.001	0.001
K_{ss}	(mol^{-2})	180	185	100
K_{shs}	(mol^{-2})	0.0	0.0	0.0
K_{ss}	(mol^{-2})	0.0	0.0	0.0
K_{shsh}	(mol^{-2})	0.0	0.0	0.0
pK_a		3.553	3.60	3.60

The full and dotted lines in Figs. 2, 3, and 4 are the best-fit curves obtained by means of the least-squares calculation. The association constants used for the calculations are listed in Table 2, while the parameters, Δ_1 and Δ_2, determined through the procedure are given in Table 3. The agreement factors defined by $\sum(||\Delta\delta_{obsd}| - |\Delta\delta_{calcd}||)/\sum|\Delta\delta_{obsd}|$ are 0.082, 0.068,

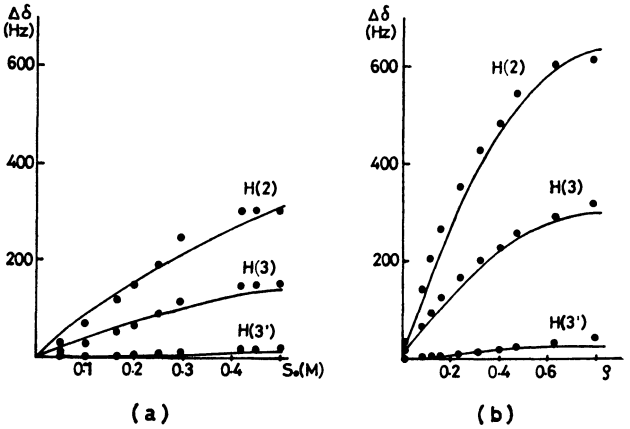

Fig. 5. Eu(III)-induced sflifts ($\Delta\delta_{obsd}$) of DL-glyceric acid observed by successive S_0 changes at $\rho=2.0$, pH=0.45 (a), and by successive ρ changes at $S_0=0.42$ M, pH=2.0 (b).

Table 3. Lanthanoid-induced shifts, Δ_1 and Δ_2 (± 0.05 ppm)[a] depending intrinsically on 1: 1 and 2: 1 complexes

	Glycerate			Gluconate			Lactobionate	
	Δ_1	Δ_2		Δ_1	Δ_2		Δ_1	Δ_2
H(2)	6.41	9.91	H(2)	5.07	7.76	H(2)	10.43	7.58
H(3)	2.96	4.73	H(3)	3.44	2.91	H(3)	4.69	3.31
H(3′)	0.21	0.41	H(4)	0.77	−1.09	H(1′)	−1.20	−0.82
			H(5)	−0.51	−1.24			
			H(6)	−0.15	−0.97			

a) A minus sign denotes a downfield shift.

and 0.042 for the cases of Compounds **1**, **2**, and **3** respectively. Figure 5 shows the ρ and S_0 dependences of the Eu(III)-induced shifts in the case of glyceric acid, **1**. The full curves were theoretically calculated from the association constants assumed in the case of the pH dependence. Since the observed points lie approximately on the curves, the data obtained by analysis based on the pH dependence will be consistent with those obtained on the basis of the ρ and S_0 dependences. Figure 6 shows the pH dependence of the concentrations of 1: 1 and 2: 1 complexes. For all compounds, the concentration of the 1: 1 complex is higher than that of the 2:1 complex at low pH's. When the pH value increases to pK_a, the concentration of the 2: 1 complex increases markedly. A large amount of lanthanoid ions in solution results in a high concentration of the 1: 1 complex, as is indicated in the case of glyceric acid (Fig. 6a). The concentrations, [LSH], [LSHS], [LSSH] and [LSHSH], calculated by means of Eqs. 12 and 14—16 are negligible for all cases. Only an unprotonated carboxyl substrate is bound to the lanthanoid ion; they form a stable complex.

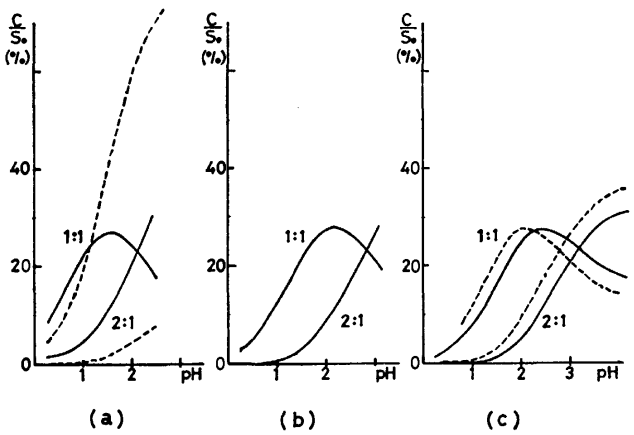

Fig. 6. PH dependence of concentrations of 1: 1 and 2: 1 complexes in D_2O solutions; (a) for glyceric acid, where the full curves are for ρ=0.5 and S_0=0.5 M, and the dotted curves are for ρ=2.0 and S_0=0.05 M, (b) for gluconic acid, where the full curves are for ρ=0.5 and S_0=0.1 M, and (c) for lactobionic acid, where the full curves are for ρ=0.5 and S_0=0.1 M, and the dotted curves are for ρ=0.5 and S_0=0.2 M.

Structure of the 1: 1 Complex. The Δ_1 and Δ_2 shifts generally include two different interactions, contact and pseudo-contact. The contact interaction is usually strong at the nucleus, which is only a few bonds away from the complexing sites, and the shift value depends on the kind of paramagnetic ion.[18] When praseodymium nitrate was added to a glyceric acid solution, ^{1}H peaks were shifted in the direction opposite to that in the case of europium nitrate. The shift ratios of each signal observed in both cases agree within an error of 10%. Thus, the effect of europium ions on the present ^{1}H signals should be attributed mainly to the pseudo-contact interaction.[16] Thus, Eq. 2 can be used in the structure determination of axially symmetiric complexes. Figure 7 shows the structures of 1: 1 complexes obtained by the application of Eq. 2, and Table 4 lists the observed and calculated shifts for each complex; the agreement factors are 0.009, 0.090, and 0.092 for **1**, **2**, and **3** respectively. The carboxyl parts of the ligand anions have similar conformations for all com-

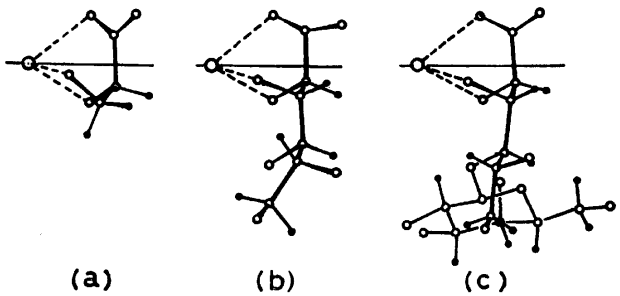

Fig. 7. Structures of 1: 1 complexes between Eu(III) and substrates; (a) for glyceric acid, (b) for gluconic acid, and (c) for lactobionic acid.

Table 4. Observed and calculated induced-shifts (± 0.05 ppm)[a] of ^{1}H peaks of 1: 1 complexes

	Glycerate			Gluconate			Lactobionate	
	obsd	calcd		obsd	calcd		obsd	calcd
H(2)	6.41	6.41	H(2)	5.07	4.95	H(2)	10.43	10.00
H(3)	2.96	2.95	H(3)	3.44	3.39	H(3)	4.69	5.50
H(3′)	0.21	0.28	H(4)	0.77	1.28	H(1′)	−1.20	−1.15
			H(5)	−0.51	−0.62			

a) A minus sign denotes a downfield shift.

TABLE 5. Eu···O DISTANCES IN THE 1:1 COMPLEX BETWEEN β-HYDROXY CARBOXYLIC ACID AND THE EUROPIUM ION (±0.05 Å)

	Glycerate	Gluconate	Lactobionate
Eu···O(1)	2.53	2.55	2.54
Eu···O(2)	2.42	2.39	2.43
Eu···O(3)	2.33	2.35	2.36

plexes, α-hydroxy oxygen being approximately on the same plane as the four carboxy atoms and β-hydroxy oxygen being *gauche-gauche* to the α-substituents. The anions chelate a europium ion through three oxygens, α-carboxy, α-hydroxy, and β-hydroxy oxygens. The Eu–O distances are given in Table 5. The magnetic axis of the complex is assumed as the mean direction of the three Eu–O vectors. Two β-protons of glyceric acid **1**, were nonequivalent in the experimental pH range, and the glycerate anion may have two or more stable conformations in D_2O.[19] Two favorable conformations, of **1** have been found in the crystal structure of calcium glycerate dihydrate.[5] The β-protons in one conformer are *gauche-gauche* to the α-proton, while those in other conformer are *trans-gauche*. The ligand conformation of the 1:1 complex established here (Fig. 7a) is similar to the former. The C(1)–C(2)–C(3)–O(3) torsion angle is 30°, compared with that of 48° in the crystal structure. Two stable conformations of the gluconate anion, **2**, have also been found as dimorphic crystals in the potassium salts.[6] One has a straight chain conformation stabilized by the intramolecular hydrogen bond between the two *syn* axially related hydroxyls, while the second has a bent chain conformation. The present ^1H NMR study indicates that the gluconate anion in the 1:1 complex (Fig. 7b) has the latter bent conformation. The torsion angles are −60 and −144° for H(3)–C(3)–C(4)–H(4) and H(4)–C(4)–C(5)–H(5) respectively. The gluconic acid moiety of lactobionic acid **3** also has a bent conformation in solution (Fig. 7c). Not only is the conformation of the lactobionate anion similar to that observed in the crystal structure[8] as a whole, but also the chelating structure to the cation is similar to that in the crystal, the cation being bound to the gluconic acid moiety rather than to the neutral galactoside moiety. The torsion angles about the glycosidic bond in the complex are 133 and −167° for C(3)–C(4)–O(1′)–(1′) and C(4)–O(1′)–C(1′)–C(2′) respectively.

As has previously been described, the three carboxylates have the same type of "three O atoms" chelation. The chelating structure is similar to that of glucaric acid, **4**, reported previously.[2] The difference in calcium affinities between the two carboxyl groups in glucaric acid, **4**, may be due to the configurations of hydroxyls about the C–C bonds located near each carboxyl group. The configuration given in Fig. 8a, corresponding to the cases of the present three compounds and the α-carboxyl part of glucaric acid, is favored for the complex formation with a cation, while the configuration given in Fig. 8b, corresponding to the case of the δ-carboxyl part of glucaric acid, is not favored for the chelation because of repulsion between parallel C(1)–O(1′) and C(3)–C(4) bonds. Hence, the relative arrangement of hydroxyl groups, particularly that of

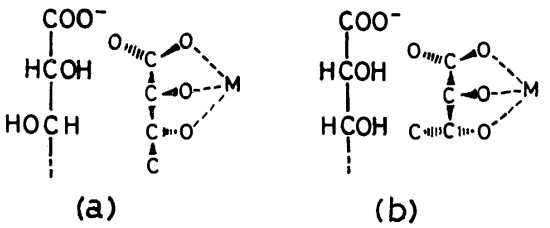

Fig. 8. Two types of configurations and possible 'three O atoms' chelations to a metal ion M.

β-hydroxyl, is important for a stable complex formation. Generally, the carboxylic acid of acyclic polyol, which has the Fig. 8a configuration, forms a stable chelating complex with a metal ion.

In conclusion, the data analysis based on the pH dependence of lanthanoid-induced NMR shifts is useful for the structural study of lanthanoid–carboxylates complexes in D_2O. The application of this method to the three carboxylates showed that glycosidic acids of acyclic polyol form a stable complex with a lanthanoid ion in the "three O atoms" chelation including the β-hydroxy oxygen.

We wish to thank Professor Kenji Osaki for his kind support of this work and Miss Ritsuko Yamaguchi for her experimental assistance. This work was supported in part by a Grant-in-Aid for Scientific Research from the Ministry of Education.

References

1) T. Taga and K. Osaki, *Bull. Chem. Soc. Jpn.*, **49**, 1517 (1976).
2) T. Taga, Y. Kuroda, and K. Osaki, *Bull. Chem. Soc. Jpn.*, **50**, 3083 (1977).
3) J. A. Rendleman, *Adv. Carbohydr. Chem.*, **21**, 209 (1966).
4) S. J. Angyal, *Tetrahedron*, **30**, 1695 (1975),.
5) T. Taga, M. Ohashi, and K. Osaki, *Bull. Chem. Soc. Jpn.*, **51**, 1697 (1978).
6) N. C. Panagiotopoulos, G. A. Jeffrey, S. J. La Placa, and W. C. Hamilton, *Acta Crystallogr., Sect. B*, **30**, 1421 (1974).
7) G. A. Jeffrey and E. J. Fasiska, *Carbohydr. Res.*, **21**, 187 (1972).
8) W. J. Cook and C. E. Bugg, *Acta Crystallogr., Sect. B*, **26**, 215 (1973).
9) B. L. Shapiro and M. D. Johnston, *J. Am. Chem. Soc.*, **94**, 8185 (1972).
10 F. Inagaki, S. Takahashi, M. Tasumi, and T. Miyazawa, *Bull. Chem. Soc. Jpn.*, **48**, 853 (1975).
11) F. Inagaki, S. Takahashi, M. Tasumi, and T. Miyazawa, *Bull. Chem. Soc. Jpn.*, **48**, 1590 (1975).
12) F. Inagaki, S. Tasumi, and T. Miyazawa, *Bull. Chem. Soc. Jpn.*, **48**, 1427 (1975).
13) H. M. McConnell and R. E. Robertson, *J. Chem. Phys.*, **29**, 1361 (1958).
14) O. Hofer, *Top. Stereochem.*, **9**, 111 (1976).
15) J. D. Roberts, G. E. Hawkes, J. Husar, A. W. Roberts, and D. W. Roberts, *Tetrahedron*, **30**, 1833 (1974).
16) B. Bleaney, C. M. Dobson, B. A. Lavine, R. B. Maetine, R. J. P. Williams, and A. V. Xavier, *J. Chem. Soc., Chem. Commun.*, **1972**, 791.
17) K. Tori, Y. Yoshimura, M. Kainosho, and K. Ajisaka, *Tetrahedron Lett.*, **1973**, 3127.
18) K. Ajisaka and M. Kainosho, *J. Am. Chem. Soc.*, **97**, 330 (1975).
19) D. T. Sawyer and J. R. Brannan, *Anal. Chem.*, **38**, 192 (1966).

Electron Configuration Analysis for Many-System Interactions. Electron Delocalization in Pyracylene, Acepleiadylene, and Dipleiadiene

Satoshi INAGAKI* and Yoshio HIRABAYASHI

Department of Synthetic Chemistry, Faculty of Engineering, Gifu University, Kakamigahara, Gifu 504

(Received December 21, 1977)

The method of electron configuration analysis for many-system interactions (ECAMSI) has been developed and applied to the π electronic structures of polycyclic molecules. The HMO-ECAMSI calculations have been carried out on acenaphthylene, pleiadiene, pyracylene, acepleiadylene, and dipleiadiene. Electron delocalization in the naphthalene core predominates in these molecules and remains unchanged from acenaphthylene to dipleiadiene; the central cross-linked π bond is not a small perturbation. There are four electron-delocalizing modes for the cyclic peripheral conjugation in acepleiadylene which give rise to an additional but appreciable delocalization, while the peripheral delocalization in pyracylene and dipleiadiene is almost completely depressed. The substituent effects on the delocalization have been predicted on the basis of the ECAMSI results and on the concept of the continuity-discontinuity of cyclic conjugation which has recently been developed.

The Hückel $4n+2\pi$ rule[1] is not directly applicable to polycyclic π conjugation. More than two decades ago two theoretical proposals[2,3] appeared about the "aromaticity" of the polycyclic systems. Platt[2] assumed that many polycyclic molecules were composed of peripheral polyene and intraannular cross-links. Assuming the cross-links are small perturbations, the Hückel rule may be applied to the peripheral polyenes. Craig's rules[3] predict the valence bond wavefunction of a given polycyclic system to be totally symmetric (aromatic) or not (pseudoaromatic). The qualitative evidence and the simple conclusions drawn stimulated many organic synthesists, but there are limitations.[4] The concept of resonance energy has frequently been used in both the LCAO and the VB methods for estimating the stabilities.[5-7] The improvement and the development of the methods are developing spheres of theoretical chemistry. A recent noticeable development has been the application of the graph theory.[8-12] The question of bond alternation, a measure of the electron delocalization is another property discussed for conjugated systems.[13,14]

In this paper a method for the electron configuration analysis for many-system interactions (ECAMSI) as an extension of the method of Baba *et al.* for two-system interactions has been presented.[15] The ECAMSI calculation enables the investigation of the constitution rather than the gross properties of the π electronic structures. The eigenfunctions have been analyzed from the point of view that polycyclic π conjugated molecules are composite systems of constituent ethylenic π subsystems. The main Kekulé structure of a given polycyclic system is uniquely determined and the mode of electron delocalization is visualized by investigating the mixing of electron-transferred configurations into the "zero" configuration which corresponds to the main Kekulé structure. The ECAMSI method has been applied to acenaphthylene (**1**), pleiadiene (**2**), pyracylene (**3**), acepleiadylene (**4**), and dipleiadiene (**5**). The tetracyclic nonbenzenoid hydrocarbons, **3**—**5**, were of theoretical interest.[16-19] The ECAMSI calculations have numerically solved such interesting questions as to whether the peri-bridges conjugate with the naphthalene core such that the intrinsic conjugation in the naphthalene substantially breaks down; the vinyl cross-links are involved almost exclusively in a naphthalene-like conjugation or the electrons are delocalized on the periphery without disturbing the naphthalene conjugation.

Theoretical

The total wavefunction of polycyclic π electron systems may be expressed as a linear combination of a basis set of electron configuration functions constructed as Slater determinants from the orbitals of the constituent subsystems. An electron configuration is denoted by the zero-configuration, Φ_0, where neither electron transter from one ethylenic unit to another nor electron promotion within any unit takes place. The second type of configuration is the electron-transferred configuration, $\Phi_{K\to L}$, in which an electron is shifted from the π bonding orbital of one ethylenic unit (K) to the π^* antibonding orbital of another (L). The third type of configuration is the locally excited configuration, Φ_{K^*}, in which an electron is promoted from the π orbital to the π^* orbital within the same unit (K). The other configurations have been neglected for simplicity in this study. The total wavefunction is then approximated as

$$\Psi \simeq C_0\Phi_0 \sum_{K,L} C_{K\to L}\Phi_{K\to L} + \sum_K C_{K^*}\Phi_{K^*}, \qquad (1)$$

where

$$\Phi_0 = N_0|a\bar{a}b\bar{b}\cdots z\bar{z}|,$$

$$\Phi_{K\to L} = \frac{1}{\sqrt{2}}N_{K\to L}\{|a\bar{a}b\bar{b}\cdots k\bar{l}^*\cdots z\bar{z}| + |a\bar{a}b\bar{b}\cdots l^*\bar{k}\cdots z\bar{z}|\},$$

$$\Phi_{K^*} = \frac{1}{\sqrt{2}}N_{K^*}\{|a\bar{a}b\bar{b}\cdots k\bar{k}^*\cdots z\bar{z}| + |a\bar{a}b\bar{b}\cdots k^*\bar{k}\cdots z\bar{z}|\}.$$

The normalization factors for Φ are denoted by N with the subscript. The π and π^* orbitals of A, B,···Z are denoted by a, b,···z with and without an asterisk. The total wavefunction,

$$\Psi = N|\phi_1\bar{\phi}_1\phi_2\bar{\phi}_2\cdots\phi_n\bar{\phi}_n|,$$

can be expanded by applying the following relation,

$$\phi_i = \sum_X(\lambda_{ix}x + \lambda_{ix^*}x^*).$$

The occupied MO's of the whole system are denoted by ϕ's and x and x* are the bonding and antibonding molecular orbitals of the subsystem, X, λ being the coefficient. The coefficients of the configurations are

then (the overlap integrals having been neglected):

$$C_0 = D_0^2,$$

$$C_{K\to L} = \sqrt{2}\, D_0 D_{K\to L},$$

$$C_K^* = \sqrt{2}\, D_0 D_K^*,$$

where

$$D_0 = \begin{vmatrix} \lambda_{1a} \cdots \lambda_{1k} \cdots \lambda_{1z} \\ \vdots \quad \vdots \quad \vdots \\ \lambda_{na} \cdots \lambda_{nk} \cdots \lambda_{nz} \end{vmatrix},$$

$$D_{K\to L} = \begin{vmatrix} \lambda_{1a} \cdots \lambda_{1l}^* \cdots \lambda_{1z} \\ \vdots \quad \vdots \quad \vdots \\ \lambda_{na} \cdots \lambda_{nl}^* \cdots \lambda_{nz} \end{vmatrix},$$

$$D_K^* = \begin{vmatrix} \lambda_{1a} \cdots \lambda_{1k}^* \cdots \lambda_{1z} \\ \vdots \quad \vdots \quad \vdots \\ \lambda_{na} \cdots \lambda_{nk}^* \cdots \lambda_{nz} \end{vmatrix}.$$

Polycyclic π conjugated molecules have usually many Kekulé structures. Each of them can be a basis set of ethylenic units in the ECAMSI calculations. The use of the main Kekulé structure as a basis set is, however, chemically the most acceptable. The main Kekulé structure may be defined as a set of ethylenic units of which the corresponding zero-configuration represents the most appropriate electronic structure, that is, a Kekulé structure which has the largest C_0. In this sense the coefficient of the zero-configuration can be used as an index demonstrating the degree of contribution from a given Kekulé structure.

The degree of electron delocalization in a molecule has been examined by investigating the magnitude of the coefficients, $C_{K\to L}$. Direct comparison between the coefficients of the different molecules may, however, make no chemical sense since a large molecule usually has a large number of possible configurations and then a small C_0. Reasonable comparison is made in terms of the absolute value of the coefficient ratio (CR), $|C_K/C_0|$.

A relative value as the criterion to determine the significant configurations has been proposed. The comparable units in **1**—**5** have been denoted by the same letters, A, B,···I (see **1a**—**5a**). The value, δ, has been defined as the difference between the maximum and the minimum of the CR's for a set of the configurations represented by the same symbol, K→L or K*. One or more significant configurations may then be found in the set of the configurations with a large δ. Tentatively 0.05 was chosen as the critical value, δ_c. A second critical value, CR_c, has been used. Whether $\delta > \delta_c$ is not important if each configuration in a set has a small CR or contributes little to the corresponding molecule. No account has been taken of the sets of configurations in which all CR's are smaller than $CR_c(=0.2)$, even if $\delta > \delta_c$.

Results

The main purpose of this paper has been to present a procedure which allows a numerical examination of the qualitative many-system interaction theory[20,21] applicable to polycyclic π conjugated molecules where many subsystems interact with one another. A sophisticated molecular orbital calculation was not necessary. The HMO method was employed.

TABLE 1. KEKULÉ INDICES[a]

	a	b	c
1	0.299	0.257	
2	0.255	0.219	
3	0.264	0.225	0.000
4	0.159	0.140	0.098
5	0.185	0.160	0.000

a) See the definition in the text.

The Kekulé indices of the possible structures of **1**—**5** were calculated and are listed in Table 1. The values show that the main Kekulé structures contain benzenoid ones, **1a**, **2a**, **3a**, **4a**, and **5a**, in both six-membered rings of the naphthalene cores. The contribution from any quinonoid structure is small. A further important implication is found in the Kekulé indices of **3c**, **4c**, and **5c**. These structures should contribute more or less if the molecules enjoy the peripheral delocalization of electrons; a complete delocalization gives the equivalent Kekulé indices for **a** and **c**. The zero values for **3c** and **5c** indicate the absence of peripheral delocalization in **3** and **5**, while a non-zero value (0.098) implies that the electrons in **4** delocalize to some degree.

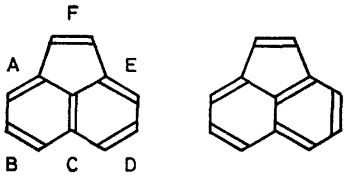

1a **1b**

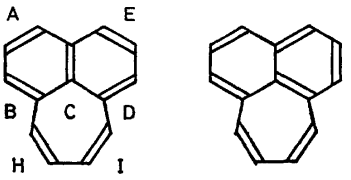

2a **2b**

The CR's of the transferred configurations are listed in Table 2; those of the locally excited configurations have been omitted since they are much smaller (<0.069) than CR_c. Table 2 shows that the degree of electron shift depends on the distance between the ethylenic units where the shift occurs. The CR's for the adjacent-unit shifts range from 0.265 (F→A of **3**) to 0.547 (B→A of **4**) while the maximum for the nonadjacent-unit shifts is 0.260 (H→A of **4**). This result may be explained in terms of the perturbation theory for many-system interactions.[20,21] The adjacent-unit shifts correspond to first-order mixing of the transferred configurations while the nonadjacent-unit shifts correspond to higher-order mixing.

In the Platt model, the intraannular cross-links in **3**—**5** are assumed to be small perturbations and the electron shifts from and to the central double bond are negligibly small. In the first-order approximation of the naphthalene-core conjugation the delocalization is

Table 2. Absolute values of the coefficient ratios[a)]

	1	2	3	4	5	δ[b)]
A → B	0.431	0.437	0.455	0.430	0.466	0.036
A → C	0.444	0.420	0.453	0.431	0.409	0.044
B → A	0.485	0.480	0.455	0.547	0.466	0.092
B → C	0.436	0.416	0.453	0.421	0.409	0.044
C → A	0.407	0.431	0.397	0.408	0.437	0.040
C → B	0.415	0.434	0.397	0.418	0.437	0.040
A → F	0.373		0.345	0.402		0.057
F → A	0.275		0.265	0.288		0.023
B → H		0.289		0.294	0.294	0.005
H → B		0.364		0.399	0.347	0.052
H → I		0.367		0.383	0.358	0.025
A → D	0.181	0.154	0.109	0.230	0.103	0.127
A → E	0.137	0.029	0.091	0.178	0.049	0.149
B → D	0.044	0.082	0.091	0.142	0.049	0.098
B → E	0.029	0.057	0.109	0.057	0.103	0.080
A → H		0.145		0.163	0.154	0.018
A → I		0.077		0.119	0.058	0.042
B → F	0.174		0.126	0.246		0.120
B → I		0.109		0.139	0.096	0.043
C → F	0.000		0.000	0.000		0.000
C → H		0.088		0.075	0.089	0.014
F → B	0.148		0.132	0.173		0.041
F → C	0.148		0.133	0.114		0.034
H → A		0.182		0.260	0.164	0.096
H → C		0.039		0.040	0.037	0.003
H → D		0.205		0.249	0.182	0.067
H → E		0.101		0.189	0.058	0.131
F → G			0.000			
F → H				0.112		
H → F				0.202		
H → J					0.011	
H → K					0.060	

a) $|C_M/C_O|$. b) The difference between the maximum and the minimum values in the row (see the text).

discussed in terms of the adjacently transferred configurations. These configurations contain A→B, A→C, B→A, B→C, C→A, C→B, and the eqivalents. Each set of configurations has δ smaller than δ_c except in the case of B→A. The large δ value for B→A is due to an extraordinarily large CR for **4**. These results show that the electrons in **1**—**5** delocalize in the naphthalene cores to a similar degree although the B→A shift in **4** is appreciably enhanced. This argues against the Platt assumption that the intraannular cross-links are small perturbations.

Secondly, adjacent-unit transfer has been restricted to five- and seven-membered rings, *i.e.*, A⇄F, B⇄H, and H⇄I. The CR's of these configurations are smaller (0.265—0.402) than those of the configurations corresponding to the electron shifts in the naphthalene cores (0.397—0.547). This shows that electrons delocalize in the five- and seven-membered rings to a lesser extent than in the naphthalene cores. The peri-bridge double bond, F, in the five-membered ring was found to accept rather than donate electrons (compare the CR's between A→F and F→A in **1**, **3**, and **4**). The butadienic parts (H or I) in the seven-membered ring tended to release electrons (compare the CR's between B→H and H→B in **2**, **4**, and **5**). An important observation was that the electron shifts to the five-membered ring and from the seven-membered ring were enhanced in **4** and depressed in **3** and **5** to an appreciable degree. Both A→F and H→B have δ values larger than δ_c while the others do not. The CR of A→F is largest in **4** and smallest in **3**, and the CR of H→B is largest in **4** and smallest in **5**.

Some distantly transferred configurations characterize the electronic structures of **3**—**5**. The B→F, H→A, H→D, and A→D configurations have δ larger than δ_c. They are enhanced in **4** but depressed in **3** and **5**. A significant difference in the transfers between the peri-bridges should also be noted. The H→F in **4** has a large CR while the F→G transfer in **3**, the H→J and H→K transfers in **5** have small ones. The ECAMSI results are summarized in **6**—**8**. The characteristic transfers are all enhanced in **4** (→) and depressed in **3** and **5** (⇢).

Now the cyclic electron delocalization on the molecular periphery will be examined. A cyclic delocalization among n units is described as a set of n−1 modes of transfer which have particular relations with one another.[21)] Firstly, an adjacent-unit transfer mode is necessary. The transferred electron in the acceptor should be shifted further to a neighboring acceptor,

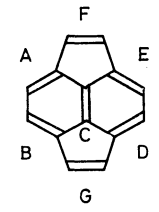

3a

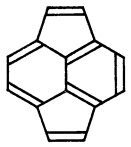

3b

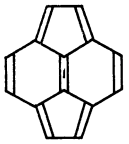

3c

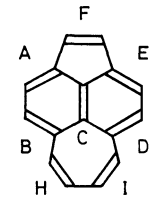

4a

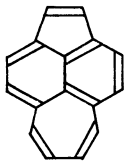

4b

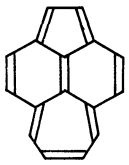

4c

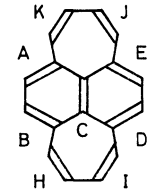

5a

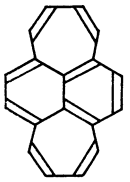

5b

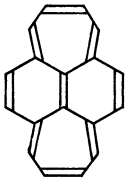

5c

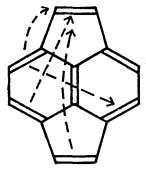

6

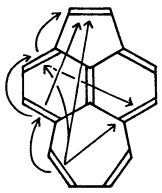

7

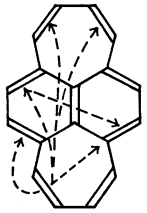

8

or the resulting hole in the donor should be supplied with an electron by a neighboring donor. These processes are expressed as the interaction of the first transferred configuration with the second configuration where an electron is shifted from the first donor to the second acceptor or from the second donor to the first acceptor. The second configuration is required to interact with the third one which satisfies a similar condition. The complete description ends with another adjacently transferred configuration. For **4** four electron-delocalizing modes (**9**—**12**)[21] can be constructed from the enhanced transfers (**7**). The shadow and the blank represent the orbital phase relation. The coupled shadow-blank and the single shadow or blank stand for the LUMO and the HOMO of the ethylenic π-bond units, respectively. It may be seen that **9**—**12** meet the orbital-phase continuity requirements for electron delocalization among many systems.[20,21] As a result, the peripheral delocalization is unequivocally confirmed by the ECAMSI calculations while the delocalization is depressed in **3** and **5**.

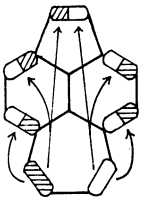

9

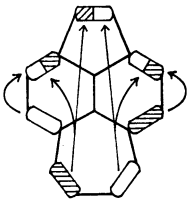

10

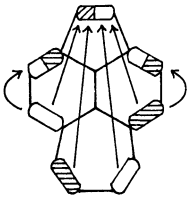

11

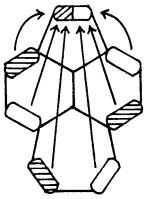

12

From this the effects of electron-releasing (R) and -withdrawing (W) substituents on the stabilities of **3**—**5** may be predicted. The delocalization in the naphthalene core has been found to be insensitive to the peri-bridges and is probably so to other substituents. The stabilities are, therefore, expected to depend on the peripheral delocalization. All electron-delocalizing modes, **9**—**12**, of **4** contain the diene bridge as a donor and the monoene as an acceptor, the peripheral parts on the naphthalene playing the dual roles. This suggests that the introduction of R into the diene and of W into the monoene (**14**) enhances the delocalization. In **3** the peri-bridges tend to accept electrons. The derivatives with R on the naphthalene core and with W on the bridges (**13**) may be more stable than the parent molecule. The electron-donability of the diene parts in **5** suggests that R-substituents on the dienes and W-substituents on the naphthalene core (**15**) stabilize the derivatives. Fortunately, the donor and acceptor groups arrange alternately along the periphery in the substituted molecules, **13** and **15**. Such alternation has recently been shown to make the cyclic conjugation discontinuous.[21] The degree of delocalization is not restricted by the Hückel rule; **13** and **15** avoid the disadvantage of 4n π periphery.

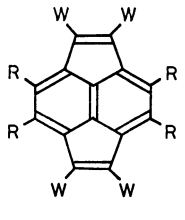

13

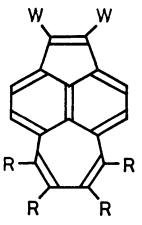

14

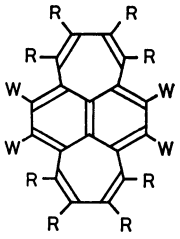

15

Discussion

Pullman *et al.*[16] calculated the HMO delocalization energy which predicted that **4** would be aromatic.

Zahradnik *et al.*[17] also drew a similar conclusion. Boekelheide and Vick[22] synthesized **4** and showed that **4** did not react with maleic anhydride under the conditions under which maleic anhydride gave the Diels-Alder adduct with **2**. Afterwards Jones *et al.*[23] concluded from the relatively narrow carbon-13 chemical shift range and the high-field shifts of the intraannular quarternary carbon atoms that **4** was highly conjugated on the periphery. The properties of **4**, predicted theoretically and suggested by the observed chemical reactivity and NMR shifts, seem to substantially confirm Platt's peripheral conjugation of $4n+2\pi$ electrons.

Yamaguchi and Nakajima,[18] using the semiempirical SCF LCAO-π-MO method, showed that the bond lengths of the naphthalene core of **4** were almost the same as those of the free naphthalene molecule, and that there was a marked bond fixation in the remainder of the periphery although the extent was smaller in **4** than in **3** and **5**. This implication is in good agreement with the ECAMSI results: (1) the degree and the mode of electron delocalization in the naphthalene core remains almost unchanged on the peri-bridging, (2) the degree of electron delocalization is smaller between the naphthalene core and the peri-bridges than in the naphthalene core, (3) electrons delocalize on the molecular periphery to an appreciable degree. As a result, the peripheral delocalization is significant but additional to the naphthalene-core delocalization.

The application of Platt's peripheral conjugation model suggests a description of **3** and **5** as antiaromatic perturbed [12]annulenes. This contradicts the prediction made by Craig's rules that they are aromatic. Using the HMO method, Zahradnik *et al.*[17] predicted that **3** and **5** were unstable. Pyracylene has been synthesized by Trost and Bright[24] while **5** is not yet known. The up-field shift of the NMR spectrum and the unusually low value of the first half wave potential were found and from this the conclusion drawn was that the peripheral model was a better representation than the peri-bridged naphthalene core model. Comparison of carbon-13 NMR spectra of **3** and its dihydro derivatives supported the indication that **3** exhibits paratropism.[25] The relative instability was suggested from the failure to isolate **3** and the reluctance of pyracene into **3**.[26] These results are compatible with Platt's model.

Lo and Whitehead[19] concluded from PPP-MO calculations that the most stable configuration of **3** corresponds to the peri-bridged naphthalene core model, a result similar to that of Yamaguchi and Nakajima.[18] The ECAMSI calculations also support this model. The degree and mode of electron delocalization in the naphthalene core are very similar to those in other molecules, the peripheral delocalization being appreciably depressed.

Conclusion

The ECAMSI calculations contribute to the understanding of the electronic properties of molecules as well as the nature of the interactions of many molecules. In this paper the polycyclic nonbenzenoid aromatics have been investigated. The ECAMSI calculations numerically showed how the polycyclic molecules were composed of the constituent ethylenic π bond units, *i.e.*, the kinds of electronic rearrangements occuring among the subsystems in the molecules. The calculations were successful in disclosing the mode of electron delocalization on the periphery and in estimating the degree of it.

The authors would like to thank Professor Ichiro Murata of Osaka University for his visit to this laboratory which, as well as his article with Dr. Kagetoshi Yamamoto [*Kagaku Sosetsu*, **15**, 211 (1977)], directed the authors attention to the polycyclic π conjugation. The present work was partially supported by a Grant-in-Aid from the Ministry of Education (No. 139012). The calculations were carried out by the FACOM 230-28 computer of Gifu Univesity, the FACOM 230-75 computer of the Nagoya University Computer Center, and FACOM M-190 computer of the Data Processing Center, Kyoto University.

References

1) E. Hückel, *Z. Phys.*, **70**, 204 (1931); **76**, 628 (1932).
2) J. R. Platt, *J. Chem. Phys.*, **22**, 1448 (1954).
3) D. P. Craig, *J. Chem. Soc.*, **1951**, 3175.
4) For example see A Streitwieser, Jr., "Molecular Orbital Theory for Organic Chemists," Wiley, New York, N.Y. (1961), Chap. 10.
5) a) R. G. Parr, *J. Chem. Phys.*, **19**, 799 (1951); b) R. S. Mulliken and R. G. Parr, *ibid.*, **19**, 1271 (1951).
6) a) M. J. S. Dewar, "Molecular Orbital Theory of Organic Chemistry," McGraw-Hill, New York, N. Y. (1969), Chap. 5; b) A. L. Chung and M. J. S. Dewar, *J. Chem. Phys.*, **42**, 756 (1965); c) M. J. S. Dewar and G. J. Gleicher, *J. Am. Chem. Soc.*, **87**, 685 (1965); d) M. J. S. Dewar and C. Llano, *ibid.*, **91**, 789 (1969).
7) L. J. Schaad and B. A. Hess, Jr., *J. Chem. Educ.*, **51**, 640 (1974); b) B. A. Hess, Jr., and L. J. Schaad, *J. Am. Chem. Soc.*, **93**, 305 (1971).
8) a) H. Hosoya, *Theor. Chim. Acta*, **25**, 215 (1972).
9) I. Gutman and N. Trinajstić, *Topics Curr. Chem.*, **42**, 49 (1973).
10) W. C. Herndon, *J. Chem. Educ.*, **51**, 10 (1974).
11) J. Aihara, *Bull. Chem. Soc. Jpn.*, **48**, 517 (1975).
12) M. Randić, *J. Chem. Soc., Faraday Trans. 2*, **72**, 232 (1976).
13) a) G. Binsch, E. Heilbronner, and J. N. Murrell, *Mol. Phys.*, **11**, 305 (1966); b) G. Binsch, "Aromaticity, Pseudo-Aromaticity, Anti-Aromaticity," ed by E. D. Bergmann and B. Pullman, The Israel Academy of Sciences and Humanities, Jerusalem (1971), p. 25.
14) T. Nakajima, *Topics Curr. Chem.*, **33**, 1 (1972).
15) a) H. Baba and S. Suzuki, *Bull. Chem. Soc. Jpn.*, **40**, 2457 (1967); b) H. Baba, S. Suzuki, and T. Takemura, *J. Chem. Phys.*, **50**, 2078 (1969). See also the application; c) H. Fujimoto, S. Kato, S. Yamabe, and K. Fukui, *J. Chem. Phys.*, **60**, 572 (1974); d) S. Kato, H. Fujimoto, S. Yamabe, and K. Fukui, *J. Am. Chem. Soc.*, **96**, 2024 (1974).
16) B. Pullman, A. Pullman, G. Berthier, and J. Pontis, *J. Chim. Phys.*, **49**, 20 (1952).
17) R. Zahradnik, J. Michl, and J. Pancir, *Tetrahedron*, **22**, 1355 (1966).
18) H. Yamaguchi and T. Nakajima, *Bull. Chem. Soc. Jpn.*, **44**, 682 (1971).

19) D. H. Lo and M. A. Whitehead, *Chem. Commun.*, **1968**, 771.
20) a) K. Fukui and S. Inagaki, *J. Am. Chem. Soc.*, **97**, 4445 (1975); b) S. Inagaki, H. Fujimoto, and K. Fukui, *ibid.*, **98**, 4693 (1976).
21) S. Inagaki and Y. Hirabayashi, *J. Am. Chem. Soc.*, **99**, 7418 (1977).
22) V. Boekelheide and G. K. Vick, *J. Am. Chem. Soc.*, **78**, 653 (1956).
23) A. J. Jones, P. D. Gardner, D. M. Grant, W. M. Litchman, and V. Boekelheide, *J. Am. Chem. Soc.*, **92**, 2395 (1970).
24) B. Trost and G. M. Bright, *J. Am. Chem. Soc.*, **89**, 4244 (1967).
25) B. M. Trost and W. B. Herdle, *J. Am. Chem. Soc.*, **98**, 4080 (1976).
26) B. M. Trost, G. M. Bright, C. Frihart, and D. Brittelli, *J. Am. Chem. Soc.*, **93**, 737 (1971).

Isomerization of Carvomenthene Oxide over Solid Acids and Bases[1)]

Kazushi ARATA, Susumu AKUTAGAWA,† and Kozo TANABE*,††

Department of Chemistry, Hokkaido University of Education, Hachiman-cho, Hakodate 040
†*Central Research Laboratory, Takasago Perfumery Co., Kamata 5, Ohta-ku, Tokyo 144*
††*Department of Chemistry, Faculty of Science, Hokkaido University, Sapporo 060*

(Received December 26, 1977)

The reaction of carvomethene oxide (a mixture of *cis*- and *trans*-forms) over solid acids and bases gives *trans*- and *cis*-1-methyl-3-isopropyl-1-cyclopentanecarbaldehyde (III), carvomenthone (IV), 1(7)-*p*-menthen-2-ol of *trans*-(V) and *cis*-form and carvotanacetol of *trans*-(VI) and *cis*-form. A large amount of III was formed together with IV over SiO_2–Al_2O_3, SiO_2–TiO_2 and zeolite H-F9. $LiClO_4$, H_2SO_4/SiO_2, $FeSO_4$, and solid H_3PO_4 gave preferentially IV, while TiO_2–ZrO_2 formed mainly V and VI. With respect to aluminas, carbonyl compounds (III and IV) were predominantly formed over Al_2O_3D, while allylic alcohols (V and VI) were preferentially given by Al_2O_3 A and B.

Several workers have studied the isomerization reaction of terpene epoxides such as α-pinene, limonene, carvomenthene, and caryophyllene oxides,[2)] some products being valuable as raw material for perfume, flavor cosmetic and pharmaceutical materials. Settine and his co-workers found that, in the case of carvomenthene oxide, the oxide in the presence of zinc bromide rearranges with ring contraction to 1-methyl-3-isopropyl-1-cyclopentanecarbaldehyde and methyl (3-isopropylcyclopentyl) ketone, undergoing isomerization to carvomenthone.[3)] Eschinasi reported that the rearrangement of the oxide in the presence of a catalytic amount of aluminum isopropoxide is utilizable for selective preparation of allylic alcohols (carvotanacetol and 1(7)-*p*-menthen-2-ol) in high yields.[4)]

Previous studies disclosed that the isomerization of *d*-limonene oxide catalyzed by solid acids and bases shows strikingly different selectivity depending on the type of catalyst.[5)] Since the studies on the isomerization of carvomenthene oxide were performed in a homogeneous system, the oxide in the present experiment has been isomerized over solid acid and base catalysts under heterogeneous conditions.

Experimental

Carvomenthene oxide (Takasago Perfumery Co., a 1:1 mixture of *cis*- and *trans*-forms, purity 97%) and toluene of guaranteed grade were used. The latter was purified by distillation over sodium metal.

Standard Reaction Procedure. The reaction was carried out in the presence of toluene as a solvent at 80 °C for 75 min. A mixture of 0.5 ml of the epoxide, 2.5 ml of toluene, and about 0.3 g of catalyst ground to below 100 mesh, was stirred in a reaction vessel with a magnetic stirrer. At appropriate time intervals, a small amount of the sample was taken out with a 1 ml syringe, separated from the catalyst by centrifugation, and analyzed with a gas-liquid chromatograph with a TCD detector using a 3 m column of 20% polyethylene glycol 20 M on Celite 545 SK (150 °C; He, 1.0 kg/cm²). For the separation of two peaks of III, a 45-m capillary column of Ucon LB-550-X (112 °C; N_2, 2.0 kg/cm²) was used. The yields of products were based on the unreacted epoxide and calculated by measurement of GLC peak areas (uncorrected.)

Catalysts. SiO_2–Al_2O_3 [N361(L)(Al_2O_3; 15 wt%) of Nikki Chemical Co.] was calcined at 500 °C. SiO_2–TiO_2 (molar ratio=1:1) was prepared by coprecipitation of a mixed solution of ethyl orthosilicate and titanium tetrachloride with aqueous ammonia. The precipitate was aged over a water bath for 1 h, washed with distilled water until no chloride ion was detected, dried at 100 °C for 20 h and calcined at 500 °C. Zeolite H-F9 was prepared from zeolite F-9 (Tekkosha Co.,) by a conventional ion-exchange method using NH_4Cl and by calcination at 500 °C. $LiClO_4 \cdot 3H_2O$ (guaranteed grade, Nakarai Chemical Co.) was dried at 120 °C for 3 days. H_2SO_4/SiO_2 was prepared as follows. 10 g of granular silica gel was immersed in 12 ml of 0.5 M H_2SO_4, evaporated, dried and then calcined at 150 °C. $FeSO_4$ and $NiSO_4$ were prepared by calcining their heptahydrates (guaranteed grade) at 600 and 350 °C, respectively. Solid phosphoric acid, N501 (Nikki Chemical Co.) was calcined at 400 °C. TiO_2–ZrO_2 (molar ratio=1:1) was prepared by thermal decomposition at 500 °C of H_4TiO_4–$Zr(OH)_4$, precipitated by heating a mixed aqueous solution of titanium tetrachloride, zirconium oxychloride and an excess amount of urea on a boiling water bath, followed by thorough washing of the precipitate with distilled water until no chloride ions were detected in the filtrate, and drying in air at 110 °C. ThO_2 was prepared by thermal decomposition at 500 °C of $Th(OH)_4$, precipitated by hydrolysis of $Th(NO_3)_4$ with 28% ammonia. Al_2O_3 A (KAT 6, Nishio Chemical Co.) was subjected to heat-treatment at 500 °C. Al_2O_3 B, C, and D, *viz.*, Albes FF, Albes FE, and Albes C (Showa Tansan Kaisha, Ltd.) were calcined at 500 °C before use. All the catalysts were heat-treated in the air for 3 h and stored in sealed ampoules.

Identification of Products. Catalytic activities of various solid acids and bases and the product distributions are given in Tables 1 and 2. The reaction products are given in the order of elution (Table 1) on a GLC PEG 20 M column at 150 °C. Product IV, a mixture of V and VI, and VII, was isolated from the isomerized mixture catalyzed by solid H_3PO_4 by column chromatography using silica gel and eluting with petroleum ether–diethyl ether (1:1). IV was identified as carvomenthone by its IR, NMR, and MS:** IR (neat): 1710 cm^{-1} ketone, 1380, 1360 cm^{-1}, isopropyl;[6)] NMR (δ): 1.8—1.1 (m, 6H, CH_2), 0.8—1.0 ppm (m, 9H, CH_3–); MS: important ions at *m/e* 154 (M^+), 111 (100%), 55 (70%), 41 (43%), 83 (27%) (Lit,[6)]: 154 (M^+), 111 (100%) 55 (51%), 41 (33%), 83 (23%)). VII was identified as carvotanacetol by its IR, NMR, and MS:** IR (neat): 1385, 1370 cm^{-1} isopropyl, 1060, 1035 cm^{-1} secondary alcohol, 915 cm^{-1} vinyl; NMR (δ): 5.5 (t, 1H, C=CH), 4.2 (s, 1H, OH), 1.8 (s, 3H, $C=CCH_3$), 0.9 ppm (d, 6H, $C(CH_3)_2$); MS: important ions at *m/e* 154 (M^+), 84 (100%), 82 (83%), 43 (67%), 93 (65%), 69 (63%), (lit,[7)]:

** Obtained by combined gas chromatography-mass spectrometry, Hitachi RM50GC, using a 2-m column of PEG 20-M at 70 eV of ionization voltage.

TABLE 1. ISOMERIZATION OF CARVOMENTHENE OXIDE OVER VARIOUS SOLID ACID AND BASE CATALYSTS AT 80 °C FOR 75 min

Catalyst	Catalyst amount g	Total conversion %	Products (%) II	III (a, b)	IV	V	VI	VII+VIII
SiO_2–Al_2O_3[a]	0.46	100	3	50 (41, 9)	40			
SiO_2–Al_2O_3[b]	0.46	100	4	60	32			
SiO_2–TiO_2	0.39	100	8	70 (36, 34)	22			
SiO_2–TiO_2[c]	0.39	100	7	68	22			
Zeolite H-F9[d]	0.29	100	1	50 (29, 21)	38	4		1
$LiClO_4$	0.38	97	3	12 (8, 4)	77			1
H_2SO_4/SiO_2	0.25	54	3	6	37	1	2	2
H_2SO_4/SiO_2[b]	0.25	19	1	3	10	1	1	1
$FeSO_4$	0.25	98	1	19 (15, 4)	61	4	5	5
$FeSO_4$[b]	0.25	84	1	20	45	4	6	4
$NiSO_4$	0.32	44		9	13	12	5	4
$NiSO_4$[b]	0.32	28	0.5	5	9	5	3	2
Solid H_3PO_4[e]	1.09	100		24 (15, 9)	41	10	11	11
TiO_2–ZrO_2	0.39	59	1	6	4	16	22	7
TiO_2–ZrO_2[b]	0.39	28		4	2	6	12	2
ThO_2	0.29	3						

a) Temperature, 70 °C; time, 1 h. b) Time, 10 min. c) Time, 25 min. d) Mixture of 1 ml epoxide and 5 ml toluene reacted at 100 °C for 1 h. e) Mixture of 5.5 ml epoxide and 30 ml toluene reacted at 100 °C for 1 h.

TABLE 2. ISOMERIZATION OF CARVOMENTHENE OXIDE OVER ALUMINAS AT 80 °C FOR 75 min

Catalyst	Catalyst amount g	Total conversion %	Products (%) II	III (a, b)	IV	V	VI	VII+VIII
Al_2O_3 A[a]	0.22	31		4	2	12	4	6
Al_2O_3 B	0.22	66		15 (10, 5)	7	21	9	10
Al_2O_3 C	0.32	65		24 (17, 7)	16	9	10	
Al_2O_3 C[b]	0.32	43		15	12	5	7	
Al_2O_3 D	0.17	100	2	33 (25, 8)	45	4	6	6
Al_2O_3 D[c]	0.17	100	2	36	43	3	8	7

a) Temperature, 70 °C. b) Time, 25 min. c) Time, 10 min.

154 (M^+), 82 (100%), 84 (88%), 43 (75%), 69 (72%)). A mixture of V and VI was revealed to consist of 1(7)-*p*-menthen-2-ol and carvotanacetol by IR, NMR, and MS: IR (neat): 1380, 1370 cm^{-1} isopropyl, 1070, 1050, 1030 cm^{-1} secondary alcohol, 900 cm^{-1} methylene;[7] NMR (δ): 5.5 (C=CH), 4.8 (C=CH_2), 4.4 and 4.1 (OH), 1.8 (C=CCH_3), 0.85 ppm ($C(CH_3)_2$); MS of V: 154 (M^+), 82 (100%), 111 (91%), 93 (83%), 55 (80%), 41 (80%), 43 (70%); MS of VI: 154 (M^+), 84 (100%), 82 (78%), 43 (73%), 93 (71%) [Lit,[7]: *trans*-1(7)-*p*-menthen-2-ol: 154 (M^+), 111 (100%), 93 (95%), 55 (84%), 82 (83%), 43 (80%)]. V, VI, and VII were recognized to be *trans*-1(7)-*p*-menthen-2-ol, *trans*- and *cis*-carvotanacetol, respectively, from the following experimental results: (1) the mass spectra of VI and VII are identical, indicating the *cis-trans* relationship, (2) the GLC column gives the elution order of *trans-exo*-carveol, *trans-endo*-carveol, *cis-endo*-carveol and *cis-exo*-carveol for the isomerized products of *d*-limonene oxide.[5] The same order of elution was also obtained on a Carbowax 20 M column for the allylic alcohols selectively prepared from *d*-limonene and carvomenthene oxides by aluminum isopropoxide. Nearly the same isomeric ratio was observed in both reactions.[4] The catalytic selectivity of the present catalysts (Tables 1 and 2) is also analogous to that expected from the results in the case of *d*-limonene oxide.[5]

For the identification of III, a mixture of *cis*- and *trans*-carvomenthene oxide (50 g) was reacted with 5 g of Davison silica-alumina (W. R. Grace Company, Grade 160) at 70—150 °C with vigorous stirring, a sufficient amount of III for analysis being obtained. The two compounds (IIIa and IIIb), bp 76 °C/10 mmHg could not be separated on a 61 cm Nester-Faust spinning band column. However, the mixture showed NMR and IR spectra in line with the structure of *cis*- and *trans*-1-methyl-3-isopropyl-1-cyclopentanecarbaldehyde. The mass spectra of the two compounds were identical. IR (neat): 1715 cm^{-1} aldehyde, 1377, 1357, 934 cm^{-1} isopropyl; NMR (δ): 9.36 (s, 1H, CHO), 2.3—1.2 (m, 6H, $>CH_2$), 1.13 (s, 3H, $-CH_3$), 0.89 ppm (d, 6H, $C(CH_3)_2$; MS: seven most intense peaks at *m/e*, 154 (M^+), 69, 55, 41, 83, 43, 125, 57 for IIIa and IIIb.

Results and Discussion

The reaction products of carvomenthene oxide (*cis* and *trans* in a 1:1 ratio) (I) catalyzed by solid acids and bases were 1-methyl-3-isopropyl-1-cyclopentanecarbaldehyde (III), carvomenthone (IV), *trans*-1(7)-*p*-menthen-2-ol (V), *trans*-carvotanacetol (VI), *cis*-carvotanacetol (VII) and unidentified compound (II).

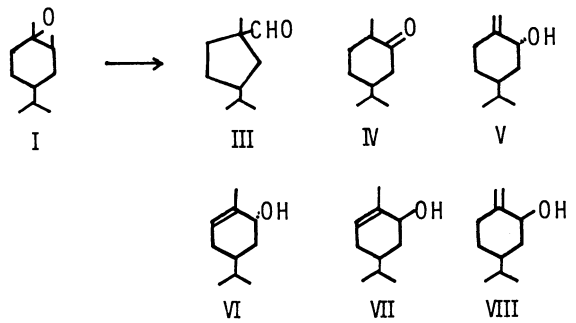

The products are given in the order of elution on a GLC column. II is the first eluted compound of the products, *i.e.*, immediately after toluene as a solvent. It might be a diene formed by the dehydration of the allylic alcohols, since cymene formation was observed in the rearrangement of *d*-limonene oxide.[5] The mass spectrum of II was not identical with that of cymene, 1,3-*p*-menthadiene or 1,4-*p*-menthadiene. Thus II is considered to be a compound with double bonds in other positions.

A minor compound observed immediately after VII in GLC is supposed to be *cis*-1(7)-*p*-menthen-2-ol (VIII) from the elution order of four allylic alcohols produced from carvomenthene and *d*-limonene oxide (see Experimental). No detailed analysis was performed, it being a minor product. Since VII and VIII were not separated satisfactorily, summation of their percentage is given in Tables 1 and 2.

III consists of two compounds, *cis*- and *trans*-form. The aldehyde was identified by Settine and McDaniel from the reaction of zinc bromide with carvomenthene oxide.[8] However, they made no mention of using a mixture of *cis*- and *trans*-oxides or the kind of aldehyde obtained (*cis*-, *trans*- or the mixture). In our case, two aldehydes were neither separated nor identified spectroscopically, but IIIa, eluted earlier, and IIIb are considered to be *trans*- and *cis*-forms, respectively, from the view point that *trans*-forms of allylic alcohols and ketones in the rearrangement of *d*-limonen[5] and carvomenthene[4] oxides were eluted earlier in high yields on a GLC column. The formation of IIIa is shown to predominate over the catalysts used in this investigation. From the product distribution, *trans*-oxide seems to be more reactive than *cis*-one (Tables 1 and 2). Similar observations were reported in the case of *d*-limonene oxide.[5b] The higher reactivity of *trans*-oxides was also observed by Eschinasi for the rearrangement of limonene and menthene oxides catalyzed by aluminum isopropoxide.[4] A large amount of ring-contracted aldehydes (III) was formed together with ketone (IV) over SiO_2–Al_2O_3, SiO_2–TiO_2, and zeolite H-F9, the selectivity for the carbonyl compounds (III+IV) being 90%. SiO_2–Al_2O_3 and SiO_2–TiO_2 are known to have exceedingly strong acid sites on their surfaces, *viz.*, 0.34 mmol/g at $H_0=-8.2$ for SiO_2–Al_2O_3[9] and the analogous acidic properties for SiO_2–TiO_2.[10] Thus, the remarkable activity for isomerization as well as high selectivity for the carbonyl formation of these catalysts can be explained by the formation of a tertiary carbonium ion intermediate *via* the breaking of α-bond of oxygen adsorbed on the strong acid sites.

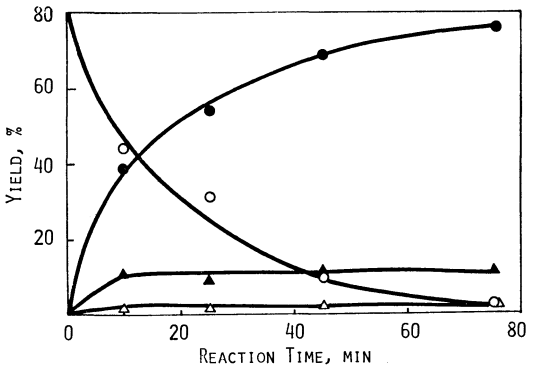

Fig. 1. Isomerization of carvomenthene oxide over $LiClO_4$ at 80 °C.
I (○), II (△), III (▲), IV (●).

The reaction mechanism for the preferential formation of carbonyl compounds is illustrated as follows.

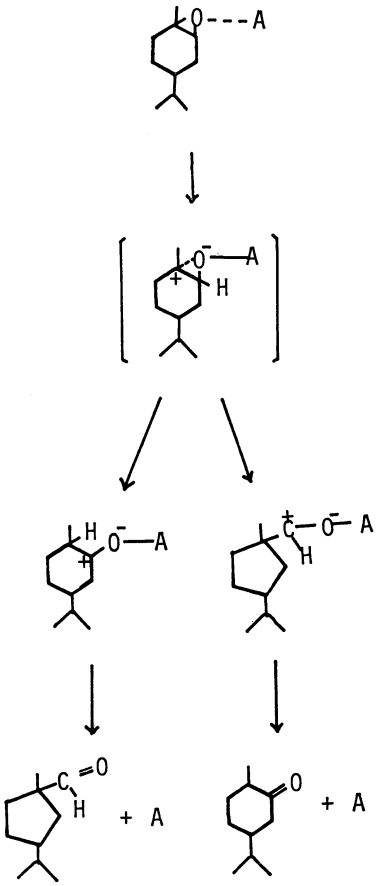

A: acid site on catalyst surface, protonic (Brönsted) or Lewis acid.

Lithium perchlorate, H_2SO_4/SiO_2 and $FeSO_4$ gave preferentially ketone (IV). The high activity of $LiClO_4$ for the ketone formation is similar to the observation of Rickborn and Gerkin that 80% of 2-methylcyclohexanone is formed from 1-methylcyclohexene oxide over $LiClO_4$.[11] The relation of the product distribution *vs.* reaction time over $LiClO_4$ is shown in Fig. 1. The yield of ketone increases remarkably following almost first-order reaction kinetics with respect to oxide

concentration. Since the partial dissolution of the catalyst was observed, Li^+ is considered to be catalytically significant. The ketone formation over $LiClO_4$ is interpreted by a process *via* tertiary carbonium ion produced with Li^+, as was shown by Rickborn and Gerkin.

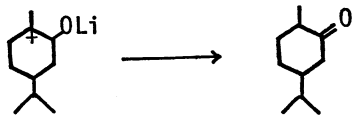

Sulfuric acid mounted on silica gel gave only a small amount of II which was formed by the dehydration of carvomenthene oxide, though it gave a large amount of *p*-cymene formed by dehydration in the case of *d*-limonene oxide. The difference might be due to high stability of *p*-cymene. The preferential formation of ketone (IV) was observed over H_2SO_4/SiO_2, $FeSO_4$, $NiSO_4$, and solid phosphoric acid. The tertiary carbonium ion formed by the breaking of α-bond of oxygen adsorbed on strong acid sites of SiO_2–Al_2O_3 and SiO_2–TiO_2 should be strong enough to be attached to the 3-position of cyclohexane ring to form a five-membered ring, while the carbonium ion formed by relatively weak acid sites[12] on H_2SO_4/SiO_2, $FeSO_4$, $NiSO_4$ or solid phosphoric acid does not seem to be so. A hydrogen at the 2-position of ring seems to migrate as a hydride ion to the cleaved tertiary center, 1-position, during the course of formation of a weak carbonium ion, probably a partially ionized cation.

Titania-zirconia shows a remarkable activity for the allylic alcohol formation. TiO_2–ZrO_2 is known to have both acidic acid basic sites, acting as an acid-base bifunctional catalyst.[13] Epoxide opening to allylic alcohols can be illustrated in terms of the bifunctional character of TiO_2–ZrO_2 as follows.

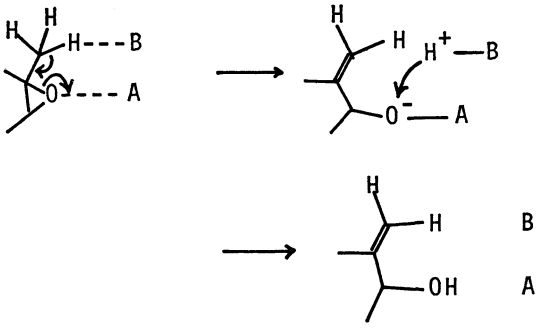

B: basic site.

In the formation of allylic alcohols over TiO_2–ZrO_2, VI exceeded V. According to electronic considerations, the preferential formation of V is expected due to the more enhanced acidity of primary hydrogen. Such observations were reported by Eschinasi; isomerization of menthene oxide catalyzed by aluminum isopropoxide gives 70% of V and 30% of VI.[4] From the above acid-base bifunctional mechanism, the acidic and basic properties of TiO_2–ZrO_2 seem to be quite specific.

Thorium oxide, which is known to produce selectively 1-alkene in the dehydration of secondary alcohol,[14,15] is almost inactive in the reaction of carvomenthene oxide.

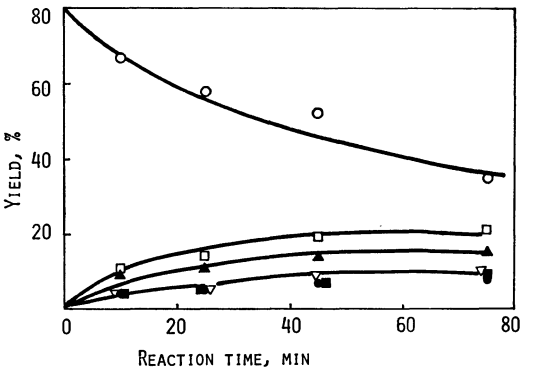

Fig. 2. Isomerization of carvomenthene oxide over Al_2O_3 B at 80 °C.
I (○), III (▲), IV (●), V (□), VI (■), VII+VIII (▽).

This catalyst would become active at higher reaction temperature.

It is of interest that the selectivity of aluminas differs a great deal with the type of alumina (Table 2). Carbonyl compounds (III) and (IV) were predominantly formed over Al_2O_3 D, the yield being about 80%. Allylic alcohols (V) and (VI) were preferentially given by Al_2O_3 A and B. It is remarkable that Al_2O_3 D is extremely active for the isomerization. Thus, Al_2O_3 A and B are expected to have both acidic and basic sites, while Al_2O_3 D is expected to have high acidity on its surface. In this respect Al_2O_3 C falls into the intermediate category of acid-base property. An example of time-variation of the products is shown in Fig. 2, where the catalyst is Al_2O_3 B. The yields of all products increase almost parallel to each other during the course of reaction. A similar time-variation of product was observed over other catalysts, suggesting that they are not precursors of each other and that there is little possibility of interconversion after the formation.

The authors are indebted to Dr. J. O. Bledsoe, the Organic Chemical Division, SCM Corp., for his assistance in the identification of compound III.

References

1) Epoxide Rearrangement X. Part IX: K. Arata, J. O. Bledsoe, and K. Tanabe, *Tetrahedron Lett.*, **1976**, 3861.
2) a) I. C. Nigam and L. Levi, *Can. J. Chem.* **46**, 1944 (1968); b) V. S. Joshi, N. P. Damodaran, and S. Dev, *Tetrahedron*, **27**, 475 (1971); c) J. P. Monthéard and Y. Chrétien-Bessiére, *Bull. Soc. Chim. Fr.*, **1968**, 336; d) M. P. Hartshorn, D. N. Kirk, and A. F. A. Wallis, *J. Chem. Soc.*, **1964**, 5494.
3) R. L. Settine, G. L. Parks, and G. L. K. Hunter, *J. Org. Chem.*. **29**, 616 (1964).
4) E. I. Eschinasi, *Isr. J. Chem.*, **6**, 713 (1968).
5) a) K. Arata, S. Akutagawa, and K. Tanabe, *J. Catal.*, **41**, 173 (1976); b) K. Arata, H. Takahashi, and K. Tanabe, *Rocz. Chem.*, **50**, 2101 (1976).
6) J. Iwamura, K. Beppu, and S. Hirao, *Bunseki Kiki*, **14**, 112 (1976).
7) J. Iwamura, K. Beppu, and S. Hirao, *Bunseki Kiki*, **14**, 162 (1976).
8) R. L. Settine and C. McDaniel, *J. Org. Chem.*, **32**, 2910 (1967).

9) H. A. Benesi, *J. Phys. Chem.*, **61**, 970 (1957).
10) M. Itoh, H. Hattori, and K. Tanabe, *J. Catal.*, **35**, 225 (1974).
11) B. Rickborn and M. Gerkin, *J. Am. Chem. Soc.*, **93**, 1963 (1971).
12) K. Tanabe, "Solid Acids and Bases," Kodansha, Tokyo, Academic Press, New York, London (1971).
13) K. Arata, S. Akutagawa, and K. Tanabe, *Bull. Chem. Soc. Jpn.*, **49**, 390 (1976).
14) A. J. Lundeen and R. Van Hoozer, *J. Am. Chem. Soc.*, **85**, 218 (1963).
15) B. H. Davis and W. S. Brey, Jr., *J. Catal.*, **25**, 81 (1972).

Differential Pulse Polarographic Determination of *N*-Nitroso-2-pyrrolidinemethanol

Kiyoshi HASEBE*,** and Janet G. OSTERYOUNG***

Department of Civil Engineering and Microbiology, Colorado State University, Fort Collins, Colorado, 80523, U.S.A.

(Received March 29, 1977)

The pulse polarographic behavior of a new *N*-nitroso compound, *N*-nitroso-2-pyrrolidinemethanol, in buffered solutions has been studied. The effects of temperature, mercury pressure, modulation amplitude, surfactant concentration and solvent, and supporting electrolyte have been investigated. The reduction process is complicated and pH-dependent. In acid solutions, *N*-nitroso-2-pyrrolidinemethanol gives one irreversible reduction wave over a wide pH range below 7. The reduction of the *N*-nitroso compound is diffusion-controlled in d.c. and of normal pulse polarographic modes. In basic solutions, the reduction is also diffusion-controlled. The 10^{-7} mol dm^{-3} content of *N*-nitroso-2-pyrrolidinemethanol has been determined.

In recent years, interest in the electrochemical behavior of biologically important compounds such as nitrosamines and derivatives of hydantoin has increased since some of these compounds are carcinogenic, mutagenic, or teratogenic.[1-5] We are interested in the electrochemical behavior of nitrosamine, *N*-nitroso derivatives of pyrrolidine skeleton. Of many analytical techniques,[6-17] differential pulse (DP) polarography provides both qualitative and quantitative information on both non-volatile and volatile *N*-nitroso compounds.[17] The kinetics and mechanism of the electrochemical process have been discussed.[15-19] L-2-Pyrrolidinemethanol is an important inhibitor of protein synthesis in biochemistry and biology.[20] L-2-Pyrrolidinemethanol (prolinol) reacts in the presence of acid with nitrite to form the relatively non-volatile compound, *N*-nitroso-2-pyrrolidinemethanol (NOProlinol). No determination of the product of prolinol nitrosation seems to have been described. Sensitivity and detection limits for this compound were determined.

Experimental

Apparatus. Polarograms were recorded with a Model 174 Polarographic Analyzer with a Model 174/70 Drop Timer. The measurement conditions were the same as those reported.[17] Measurements of pH were made with a Corning Model 110 expanded scale digital pH meter. Except for temperature dependence studies, all the measurements were carried out at room temperature (20±1) °C.

Materials. The chemicals used were of reagent grade and were dissolved in deionized water. NOProlinol was prepared from L-2-pyrrolidinemethanol (Aldrich Chemical Company, Inc.). A stock solution of 1.95×10^{-2} mol dm^{-3} NOProlinol was prepared in 0.1 mol dm^{-3} HCl and kept in a refrigerator. This solution was found to be stable for over 5 months by means of polarography. The pH of the polarographic solutions was adjusted with Britton-Robinson buffer in the pH range 1.82—11.5. Measurements were made in HCl or H_2SO_4 below pH 1 and in NaOH above pH 12.

Results and Discussion

Effects of pH on the NOProlinol Reduction. The effect of pH on the reduction wave is shown in Fig. 1. The results are in line with those on other nitrosamines, supporting the mechanism of reduction of the protonated form in acid solution. Free NOProlinol like *N*-nitrosopyrrolidine is directly reduced in basic solutions since NOProlinol is present in the solution as a neutral molecule. The slopes of the potential *vs.* pH curves indicate involvement of one proton per electron in the rate determining step in the pH range 3—7 (*ca.* −65 mV/pH). The larger slope below pH 3 (*ca.* −116 mV/pH) seems to indicate involvement of two proton per electron. Complications of adsorption and the double layer structure make it difficult to interpret these data and account for values of the slope which differ from integral multiples of 58 mV.

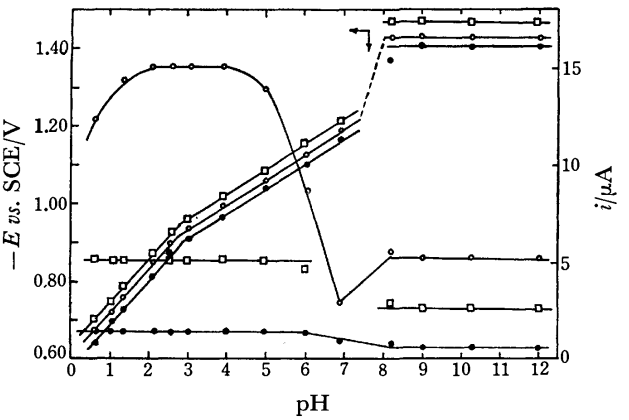

Fig. 1. Effect of pH on the wave height and half-wave or peak potentials for *N*-nitroso-2-pyrrolidinemethanol in 0.1 mol dm^{-3} LiCl containing 50% (volume fraction) B-R buffer.
Concentration: 9.75×10^{-5} mol dm^{-3}; scan rate, v: 2 mV s^{-1}; modulation amplitude, ΔE: −50 mV; ●: d.c. mode; □: NP mode; ○: DP mode.

NP and d.c. current for NOProlinol were constant over a wide range of pH as in the case of *N*-nitrosopyrrolidine.[17] This might be due to the presence of neutral molecules of both *N*-nitroso compounds in basic solu-

** Present address: Department of Chemistry, Faculty of Science, Hokkaido University, Sapporo 060.
*** Present address: National Science Foundation, Washington DC, 20550.

tions. On the other hand, the decrease in the DP current at low pH might be due to a decrease in the reduction rate, whereas the NP and d.c. current remains constant (Fig. 1). When the concentration of the B-R buffer was less than 50%, the peak potential shifted to more negative values with decreasing buffer concentration, DP peak height and NP and d.c. waves remaining constant. Therefore, it is desirable to use at least a 50% B-R buffer.

In acid solutions, the dependence on modulation amplitude of DP peak height and peak potential showed the same tendency as in basic solutions. This dependence is similar to that of *N*-nitrosopyrrolidine. It is advantageous to work at larger pulse amplitudes to get better sensitivity when the electrode process is irreversible.

Reversibility. The NP and d.c. polarographic waves were analyzed logarithmically in order to obtain $n_a\alpha$, where n_a is the number of electron involved in potential-determining step and α transfer coefficient. Typical results for the d.c. waves are given in Table 1. In acid solutions, the $n_a\alpha$ values were 0.75. However, the values in basic solutions were 0.58. In ethanol–water mixtures, the same tendency was also observed (Tables 3 and 4). The irreversible reduction gives the DP current theoretically less than the reversible DP current, the current-concentration relation depending on rate parameters. The peak resolution is measured by the peak width at half height, $W_{1/2}$. The results for $W_{1/2}$ are given in Tables 2, 3, and 4. The values are larger than the theoretical values for reversible reductions, indicating that the reduction is irreversible.

Table 1. Polarographic characteristics of NOProlinol in aqueous solution

pH	Slope of *i-t* value[a]	$n_a\alpha$[b]	p of h_{corr} d.c.	Dependence[c] NP
1.12[d]	0.20	0.72	0.45	0.65
2.59	0.19	0.91	0.50	0.70
4.96	0.20	0.77	0.50	0.66
6.06	0.22	0.66	0.48	—
8.16	0.24	0.57	—	0.72
9.03	0.21	0.58	—	—
10.26	0.22	0.57	0.50	0.70
12.04	0.22	0.59	0.47	0.72
13.11[e]	0.22	0.58	0.48	0.70

Supporting electrolyte: 0.1 mol dm^{-3} LiCl containing 50% B-R buffer solution. a) Slope=d lg i/d lg t. b) $n_a\alpha=(2.303RT/F)\mathrm{d}[\lg(i_d-i)/i]/\mathrm{d}E$. i_d=limiting current. c) p=d lg i_d/d h_{corr}. d) 0.1 mol dm^{-3} HCl. e) 0.1 mol dm^{-3} NaOH.

Table 2. Relative temperature coefficients at 20 °C and peak half width ($W_{1/2}$)

pH	Relative temp coeff, (% K^{-1}) d.c.	NP	DP[a]	$W_{1/2}$;[a] (mV)
2.11	1.73	1.49	1.19	110[b]
10.03	1.84	1.66	1.12	145[c]

Supporting electrolyte is 0.1 mol dm^{-3} LiCl containing 50% B-R buffer. a) $\Delta E=-50$ mV. b) Observed in the pH range 1.12—6.06. c) Observed in the pH range. 8.16—13.11.

Table 3. Polarographic characteristics of NOProlinol in ethanol–water mixture (apparent pH 2.10)

Ethanol, % (volume fraction)	Slope of *i-t* value[a]	$n_a\alpha$[b]	$W_{1/2}$[c] (mV)
0	0.19	0.88	110
10	0.20	0.79	105
20	0.19	0.93	100
30	0.19	0.84	100
40	0.18	0.87	100

Supporting electrolyte is 0.1 mol dm^{-3} $NaClO_4$ containing 50% B-R buffer. a) Slope=d lg i/d lg t. b) $n_a\alpha=(2.303RT/F)\mathrm{d}[\lg(i_d-i)/i]/\mathrm{d}E$. c) $\Delta E=-50$ mV.

Table 4. Polarographic characteristics of NOProlinol in ethanol–water mixture (apparent pH 9.53)

Ethanol, % (volume fraction)	Slope of *i-t* value[a]	$n_a\alpha$[b]	$W_{1/2}$[c] (mV)
0	0.20	0.58	145
10	0.20	0.58	145
20	0.22	0.59	135
30	0.22	0.53	130
40	0.19	0.52	125

Supporting electrolyte is 0.1 mol dm^{-3} $NaClO_4$ containing 50% B-R buffer. a) Slope=d lg i/d lg t. b) $n_a\alpha=(2.303RT/F)\mathrm{d}[\lg(i_d-i)/i]/\mathrm{d}E$. c) $\Delta E=-50$ mV.

Diffusion Control. For diffusion-controlled waves, the wave height in d.c. mode is approximately proportional to $h_{corr}^{1/2}$ when the natural drop time is used, and that in NP mode is approximately proportional to $h_{corr}^{2/3}$ with a mechanically drop time; h presents the height of the mercury reservoir. The values of p, the power of h_{corr}, obtained by logarithmic plots (Table 1), indicate that the limiting currents are diffusion-controlled. The relative standard deviation of these values is 0.019, lying in the range of reported values.[21] The results in ethanol–water or methanol–water mixtures are almost the same as those for aqueous solutions. The diffusion-controlled character was confirmed according to the criteria of the time dependence of the limiting currents of the first drops and the agreement of the ratio of limiting currents in d.c. and NP modes with the theoretical value. The diffusion coefficients of NOProlinol were estimated by using the d.c. polarographic data and the Ilkovič equation and checked by the value of the diffusion coefficient of thallium(I) ions measured under the same conditions; the latter was in agreement with the reported value 2.00×10^{-5} cm^2 s^{-1}.[21] The diffusion coefficient of NOProlinol in 0.1 mol dm^{-3} LiCl containing 50% B-R buffer solution was $(7.90\pm0.35)\times10^{-6}$ cm^2 s^{-1} at pH 2.59, and that in the same supporting electrolytes was $(7.55\pm0.30)\times10^{-6}$ cm^2 s^{-1} at pH 9.03 with a 99% probability.

Temperature Dependence. Half-wave potentials of reversible processes are known to be nearly independent of temperature. Although NOProlinol is reduced

irreversibly, its half-wave potential, $E_{1/2}$ and peak potential, E_p, observed in the mixtures containing 40% (volume fraction) ethanol (apparent pH 2.10) were independent of temperature within experimental error as those in mixtures containing 40% (volume fraction) ethanol (apparent pH 9.13). $E_{1/2}$ or E_p of NOProlinol in aqueous solutions was also temperature independent. This result supports the view that the reduction rate depends on adsorption of reactants.[17,22]

Some of the relative temperature coefficients of the current for NOProlinol reduction in the temperature range 1—45 °C are given in Table 2. The results correspond to activation energies of diffusion. The relative temperature coefficients of the limiting current in ethanol–water mixture also lie in the range 1.0—2.0% K^{-1}.

Effect of Organic Solvents. If miscible organic solvents are present in the polarographic solution without specific chemical effects, the limiting current should decrease due to changes in the drop time and the diffusion coefficient with changing ionic strength and the viscosity of the medium. Figure 2 shows the effect of ethanol on the limiting current and $E_{1/2}$ or E_p for the reduction of NOProlinol in the polarographic solutions of apparent pH 9.13. A similar behavior was observed in a solution of apparent pH 2.10 as well as in a methanol–water mixture. Current change in the DP mode becomes more pronounced than in the d.c. or NP mode. However, the reduction of NOProlinol is also diffusion-controlled in ethanol– or methanol–water mixtures (Tables 2 and 3). This is not surprising, since the rate determining step for the reduction involves reactant adsorption,[17] *i.e.*, the alcohol molecules compete with the reactant for adsorption sites easier than water molecules do. Therefore, the decrease in the reaction rate would decrease the DP peak current.

Presence of Surfactants and i-t Curve. The effects of peptone (an enzyme of digest of proteins), Triton X-100, and gelatin were studied. These compounds are reasonable model surfactants, and important matrices to protein synthesis. None of them affected the DP peak current at concentrations less than 10^{-3}%, the slopes of lg *i*-lg *t* being in the range 0.19—0.20. At higher concentrations than 10^{-3}%, they were strongly adsorbed at the dropping mercury electrode, DME, the reaction mechanism being affected.

Choice of Supporting Electrolyte. Cation adsorption would lower the reaction rate by competition with reactant adsorption and by reduction of the proton activity in the reaction layer. Several supporting

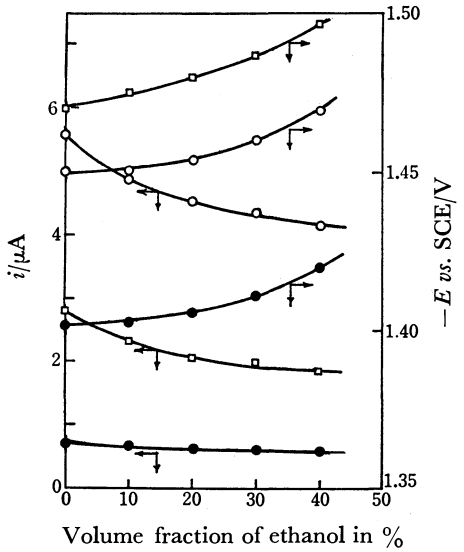

Fig. 2. Effect of the volume fraction of ethanol on the wave or peak height and half-wave or peak potentials for NOProlinol. Apparent pH=9.13; other conditions and symbols same as Fig. 1.

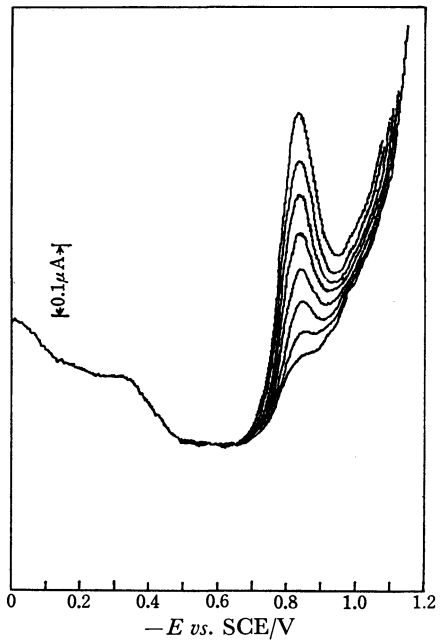

Fig. 3. Differential pulse polarograms of *N*-nitroso-2-pyrrolidinemethanol in 0.1 mol dm^{-3} $NaHSO_4$–Na_2SO_4 (pH 2.06).
Concentration=0, 1.00, 3.00, 5.00, 7.00, 9.00, 11.00, and 13.00×10^{-7} mol dm^{-3} NOProlinol; *v*: 2 mV s^{-1}; ΔE: −100 mV.

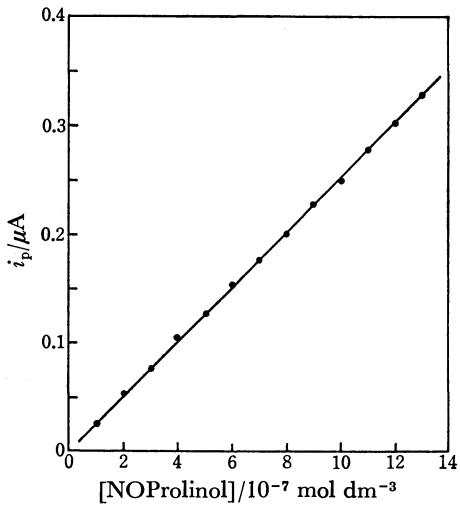

Fig. 4. Calibration curve of *N*-nitroso-2-pyrrolidinemethanol by DP mode.
Conditions same as Fig. 3.

electrolytes were studied in the pH range 2—4, there being no change in current with pH (Fig. 1). Sodium hydrogensulfate–sodium sulfate (0.1 mol dm^{-3}) is suitable for the determination of NOProlinol (Figs. 3 and 4). Potassium chloride (0.1 mol dm^{-3})–hydrochloric acid medium is also suited as supporting electrolyte.

Calibration Curve and Detection Limit. Figure 3 shows typical DP polarograms at the 10^{-7} mol dm^{-3} content of NOProlinol in 0.1 mol dm^{-3} sodium hydrogensulfate and 0.1 mol dm^{-3} sodium sulfate. The DP peak height is proportional to the concentration of NOProlinol between 8×10^{-8} and 1.4×10^{-6} mol dm^{-3} (Fig. 4). The detection limit for NOProlinol under the same conditions shown in Fig. 4 was 6×10^{-8} mol dm^{-3}, as estimated statistically.[23] The detection limit for NOProlinol is somewhat lower than that for the other carcinogenic nitrosamines.

In a sample containing NOProlinol and *N*-nitrosoproline 10^{-7} mol dm^{-3} (pH 4.0), we can determine NOProlinol quantitatively because the difference of E_p of NOProlinol from that of *N*-nitrosoproline is *ca.* 120 mV at $\Delta E=-50$ mV. In the mixture of NOProlinol and *N*-nitrosopyrrolidine, these nitrosamines could not be determined separately since both the compounds show a similar behavior in both acid and basic solutions, and the difference between the two E_p is insignificant.

This work was supported in part by NIH Grant 1-ROl-CA 15028. The authors thank Prof. R. A. Osteryoung, Colorado State University, for useful suggestions and discussions, and Prof. H. Suginome, Hokkaido University, for his comments.

References

1) P. N. Magee and J. Barnes, *Brit. J. Cancer*, **10**, 114 (1956).
2) P. N. Magee and J. Barnes, *Adv. Cancer Res.*, **10**, 163 (1967).
3) H. Druckrey, R. Preussmann, S. Ivankovič, and D. Schmahl, *Z. Krebsforsch.*, **69**, 103 (1967).
4) A. Wolff and A. E. Wasserman, *Science*, **177**, 15 (1972).
5) T. Aune, *Nord. Veterinaermed.*, **24**, 356 (1972).
6) B. Gowenlock and W. Luttke, *Quart. Rev.*, **12**, 321 (1958).
7) R. H. White, D. C. Havery, E. L. Roseboro, and T. Fazio, *J. Assoc. Off. Anal. Chem.*, **57**, 1380 (1974).
8) E. T. Huxel, R. A. Scanlan, and L. M. Libbey, *J. Agric. Food Chem.*, **22**, 698 (1974).
9) D. H. Fine, D. P. Rounbehler, and N. P. Sen, *J. Agric. Food Chem.*, **24**, 980 (1976).
10) M. Castegnaro, B. Pignatelli, and E. A. Walker, *Analyst*, **99**, 156 (1974).
11) E. A. Walker, M. Castegnaro, and B. Pignatelli, *Analyst*, **100**, 817 (1975).
12) M. J. Downes, M. W. Edwards, T. S. Elsey, and C. L. Walters, *Analyst*, **101**, 742 (1976).
13) L. S. Hwang and J. D. Rosen, *J. Agric. Food Chem.*, **24**, 1152 (1976).
14) D. H. Fine, R. Ross, D. P. Rounbehler, A. Silvergleid, and L. Song, *J. Agric. Food Chem.*, **24**, 1069 (1976).
15) S. K. Chang and G. W. Harrington, *Anal. Chem.*, **47**, 1857 (1975).
16) W. F. Smyth, P. Watkiss, J. S. Burmicz, and H. O. Hanley, *Anal. Chim. Acta*, **78**, 81 (1975).
17) K. Hasebe and J. G. Osteryoung, *Anal. Chem.*, **47**, 2412 (1975).
18) J. G. Osteryoung and K. Hasebe, *Rev. Polarog. (Kyoto)*, **22**, 1 (1976).
19) I. M. Kolthoff and J. J. Lingane, "Polarography," Vol. 2, 2nd ed, Interscience, New York, N. Y. (1952), p. 765.
20) Aldrich Chem. Co. Inc., *Aldrichimica Acta*, **7**, 54 (1974).
21) I. M. Kolthoff and J. J. Lingane, "Polarography," Vol. 1, 2nd ed, Interscience, New York, N. Y. (1952), pp. 86, 95.
22) J. H. Christie, J. G. Osteryoung, and R. A. Osteryoung, *Anal. Chem.*, **45**, 210 (1973).
23) R. K. Skogerboe and C. L. Grant, *Spectrosc. Lett.*, **3**, 215 (1970).

Use of Ion Microanalyzer in the Analysis of Passive Layers on Stainless Steel

Yoshiaki OKAJIMA,* Yukiyoshi AIZAWA, and Yasushi SUGAWARA
Hitachi Research Laboratory, Hitachi Ltd., Kuzi-machi, Hitachi-shi, Ibaraki 319-12
(Received September 6, 1977)

Passive layers on various stainless steels were studied with an ion microanalyzer. An argon ion beam was directed on the specimen surface in an oxygen atmosphere. The use of oxygen atmosphere effectively minimized the difference in ion yields of the elements in the oxidized layers and matrices, making it possible to determine these elements with good reproducibility. 18% Cr–8% Ni and 18% Cr–8% Ni–0.4% Ti stainless steel was exposed to neutral water containing 8 ppm oxygen at 289 °C. The passive layers contained larger amounts of iron and smaller amounts of chromium than the matrices.

The remarkable resistance of stainless steel to corrosion in various atmospheres is due to the protective nature of the passive layers on the surface. Studies of passive layers have been carried out by means of electrochemistry,[1] impedance and capacitance measurements,[2,3] ellipsometry,[4,5] and infrared spectroscopy.[2] However, no quantitative analyses can be carried out. In order to clarify the nature of passive layer, it is necessary to determine the concentration of elements in the layer, but passive layers are too thin to make analysis by conventional means possible. Recently, Auger electron spectroscopy (AES)[6] and X-ray photoelectron spectroscopy (XPS)[2,6–8] have been used for the determination of the composition of passive layers. The mean escape depth of Auger electrons or photoelectrons from a surface is about 20 Å or less. Thus these methods can be used for the analysis of surface elements. The compositional depth profiles in a thin layer are obtained by ion bombardment. Since these methods are not quantitative, comparison of variations in the ratio of chromium and nickel to iron in specimens is only used for the analyses of passive layers.

The composition profiles of thin layers can be obtained with an ion microanalyzer (IMA) just as with AES and XPS. A quantitative method using an IMA has been examined with calibration[9] and thermodynamical techniques.[10] However, the techniques were developed for elements in matrices.

An oxidized layer, such as a passive layer, gives off much larger quantities of secondary ions than those of a matrix when argon ions are used as primaries. This is due to the difference in the ion yields of elements in oxidized layers and those in matrix. In order to estimate the difference in the concentration of an element between oxidized layer and matrix, it is necessary that the ion yield of the element is the same in both places.

Oxygen ions have been used as primary ions. Andersen and Hinthorne[11] and Nishimura and Okano[12] reported that the difference in the relative sensitivities of element is smaller in the case of oxygen primary ions than in the case of argon primary ions. This seems to result from the oxidation and temperature rise at specimen surface.

We have carried out bombardment by argon ions in an oxygen-atmosphere in order to minimize the difference in the ion yields of elements in the oxidized layers and matrices. The results are applied to analyses of passive layers on stainless steel.

Experimental

Materials. The specimens used in quantitative study of element concentration in a matrix were Japanese Standards of Stainless Steel. Table 1 gives the composition of the main constituents. The specimens were cut into 5 mm cubes, polished with diamond paste and cleaned ultrasonically in alcohol and ether.

The specimens used for the study of element concentration in passive layers were commercial AISI type 304 and 321 stainless steel. The specimens were treated in neutral water containing 8 ppm oxygen. The temperature and time of passivation treatment were 289 °C and 2000 h, respectively.

TABLE 1. CONTENTS OF MAIN CONSTITUENTS OF STAINLESS STEEL SPECIMENS

Specimen	Concentration (%)				
	Fe	Cr	Ni	Mn	Si
No. 650	82.1	16.45	0.24	0.37	0.66
No. 651	69.7	18.65	8.86	1.73	0.47
No. 652	65.5	17.44	11.79	1.94	0.54
No. 654	53.0	24.71	19.80	1.54	0.70

TABLE 2. WORKING CONDITIONS FOR DETERMINATION

Ionic species	Ar^+
Accel. voltage for primary ions	10 kV
Current density of primary ions	0.1 mA/cm^2
Beam diameter	0.8 mm
Sample chamber pressure	
without oxygen	27 μPa
with oxygen	5.3 mPa
Accel. votage for secondary ions	3 kV

Experimental Procedure. An Hitachi type IMA-2 Ion Microanalyzer was used. Typical working conditions are given in Table 2. Argon ionized by duoplasmatron was accelerated at 10 kV. The current density of the primary ions was 0.1 mA/cm^2, making the analysis of a very thin layer satisfactory. The sputtering rate of the stainless steel was 0.04 nm/s.

Figure 1 shows the apparatus for the introduction of oxygen gas into the sample chamber. Oil particles in oxygen gas were removed by means of a filter. The sample chamber was evacuated with a diffusion pump and liquid nitrogen trap. Pressure of the sample chamber was 27 μPa in the absence of oxygen gas. Oxygen gas was introduced with a pressure of up

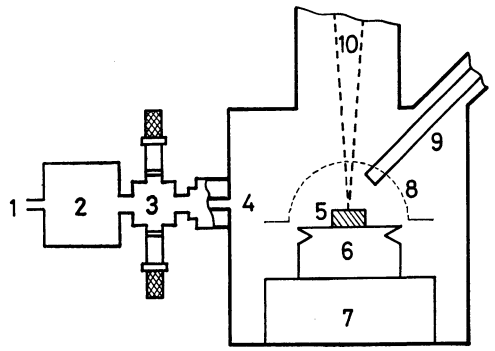

Fig. 1. Apparatus for introduction of oxygen gas into the sample chamber.
1. Oxygen gas inlet; 2. filter; 3. needle valve; 4. sample chamber; 5. specimen; 6. specimen holder; 7. plate for shifting samples; 8. hemispherical shield made of wire gauze; 9. extracting electrode; 10. argon ion beam.

to 5.3 mPa by controlling with a needle valve.

Principle of Quantitative Analysis. The secondary ion current I_X of a specific isotope of element X is given by[9]

$$I_x = \eta_x S_x^+ C_x I_p, \quad (1)$$

where η_X is the transmission coefficient of the instrument between the sample and the collector, S_X^+ the ion yield of element X, C_X the concentration of element X and I_P the current density of the primary ions. Thus the ratio of the secondary ion current of an element X to a reference element (matrix) R is given by

$$\frac{I_x}{I_R} = S(\mathrm{rel})^+ \frac{C_x}{C_R}, \quad (2)$$

where I_R is the secondary ion current of reference element R, C_R the concentration of a reference element R and $S(\mathrm{rel})^+$ the ratio of the ion yield of element X to a reference element R. This can be used for the determination of the constituents of stainless steel, when a straight line is obtained for I_X/I_R plotted as a function of C_X/C_R.

Results

Effect of Oxygen Atmosphere on Sputtering. Figure 2 shows the texture of the surface of a nickel specimen sputtered by argon ion bombardment. The results were obtained by surface roughness measurement. There is pronounced surface unevenness under a pressure of 27 μPa (without oxygen). On the other hand, the surface resulting from the sputtering in oxygen atmosphere under pressure of 5.3 mPa is very smooth. When the other conditions are the same, the sputtering rates are 0.2 and 0.03 nm/s under pressure of 27 μPa and 5.3 mPa, respectively. The sputtering rate of the stainless steel was 0.04 nm/s under pressure of 5.3 mPa.

The results demonstrate that bombardment by argon ions in oxygen atmosphere is effective for the analysis of a very thin layer such as the passive layers on the surface of stainless steel.

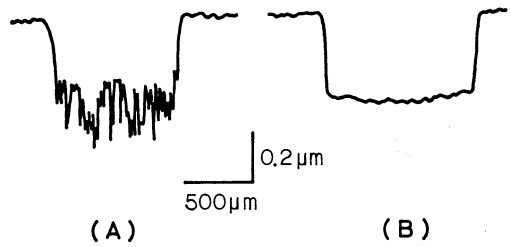

Fig. 2. Texture of surface sputtered by argon ion. Accelerating voltage and current density of argon ion were 10kV and 0.1 mA/cm², respectively. (A) Sample chamber pressure was 27 μPa and nickel bombardment time was 30 min. (B) Sample chamber pressure was 5.3 mPa and nickel bombardment time was 180 min.

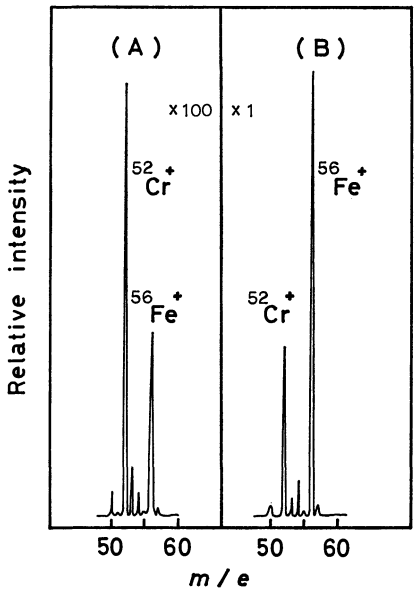

Fig. 3. Mass spectra of chromium and iron ion sputtered from stainless steel. Sample chamber pressure was (A) 27 μPa (without oxygen) and (B) 5.3 mPa(with oxygen).

Effect of Oxygen Atmosphere on Intensity of Secondary Ions. Figure 3 shows the mass spectra of chromium and iron ions. The pressure in the sample chamber is 27 μPa (without oxygen) for the specimens on the left side and 5.3 mPa (with oxygen) for the specimens on the right side. The specimen contained 82% Fe and 16% Cr. The peaks of $^{52}Cr^+$ and $^{56}Fe^+$ in the case with oxygen are *ca.* 40 and 240 times that in the case without oxygen, respectively. The other elements contained in stainless steel also show the same tendency. However, the peak height multiple differs from one element to the other. The relative ion yield of each element as compared to iron was calculated in the cases of pressure 27 μPa and 5.3 mPa. Table 3 gives the results where the secondary

Table 3. Relative ion yield of each element to iron

Element	Relative ion yield[a] (A)	(B)
Fe	1.0	1.0
Cr	8.6	2.7
Ni	0.3	0.4
Mn	5.6	2.1
Si	1.8	0.4

a) Sample chamber pressure 27 μPa for (A) (without oxygen) and 5.3 mPa for (B) (with oxygen).

ion intensity of each element is divided by the concentration and the value of each element is divided by the value of iron. The relative ion yield of elements is in the range 0.3—8.6 for 27 μPa, and in the range 0.4—2.7 for 5.3 mPa. The results show that the introduction of oxygen into the sample chamber causes increase in the sensitivity of elements and decrease in the difference in the relative ion yield of elements.

Selection of Reference Element. Iron is used as a reference element for analyses of steels containing more than 90% Fe. Thus the secondary ion peak of iron does not vary even when the secondary ion peak values of other elements vary. However, in the analysis of stainless steel containing less than 80% Fe, the percentage varies from specimen to specimen, and neither iron nor any other element can be used as a reference element.

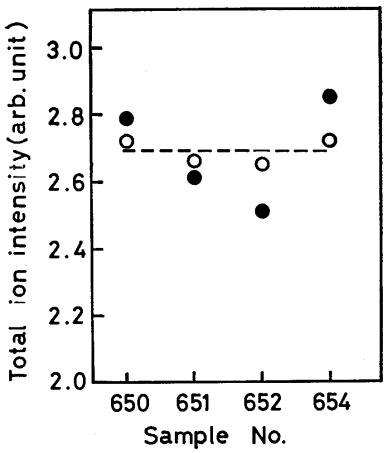

Fig. 4. Variations in total ion intensity with different specimens. Sample chamber pressure was (●) 27 μPa (without oxygen) and (○) 5.3 mPa(with oxygen).

Equation 2 cannot be used without a reference element. The secondary ion peak values of all the elements in steel are summed and the value obtained is assumed to be a composite reference. Figure 4 shows variations in the sums of the secondary ion peak values (total ion intensity) with different specimens. The total ion intensity varies widely with specimen when no oxygen is introduced into the sample chamber, but varying very little when it is introduced.

Figure 5 shows the relation between the ratio of secondary ion peak value to total ion intensity and concentration. A linear relation is obtained in an oxygen atmosphere. The total ion intensity could be used as a reference. The reproducibility of the method when the total ion intensity is used as a reference is given in Table 4.

Analysis of Passive Layers. Figure 6 shows the variation of total ion intensity below the surface of a specimen with a passive surface layer. In the case without oxygen, there is a large difference in total ion intensity between the passive layer and the matrix, while in an oxygen atmosphere, total ion intensity is the same for both. Consequently, the calibration curve shown in Fig. 5 can be used in the quantitative analysis of sub-surface concentration profiles in specimens with passive surface layers.

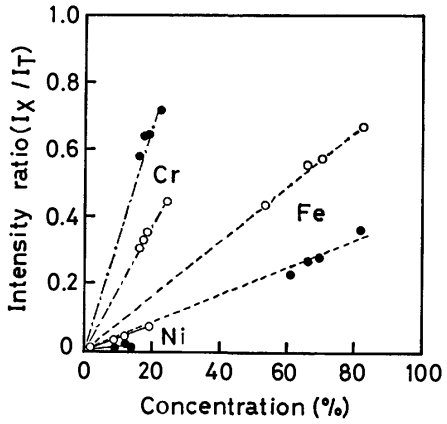

Fig. 5. Relation between the ratio of secondary ion intensity to total ion intensity and concentration. Sample chamber pressure was (●) 27 μPa(without oxygen) and (○) 5.3 mPa(with oxygen). -•-•-: Chromium,----: iron,——: nickel.

TABLE 4. REPRODUCIBILITY OF IMA METHOD

No.	With oxygen (%)			Without oxygen (%)		
	Fe	Cr	Ni	Fe	Cr	Ni
1	69.7	18.62	9.00	70.9	18.95	9.00
2	70.0	18.60	9.22	71.3	18.43	8.32
3	69.7	18.60	9.22	70.9	18.95	7.71
4	70.0	18.60	8.93	69.5	19.00	8.18
5	70.1	18.62	9.20	68.1	19.38	8.85
6	69.6	18.65	9.20	70.4	18.48	9.71
7	69.6	18.62	9.00	69.3	19.00	7.82
8	70.0	18.65	9.21	72.3	18.33	7.88
9	69.7	18.62	8.90	69.3	18.95	8.53
10	69.7	18.65	8.92	69.1	18.76	9.12
Av.	69.8	18.62	9.08	70.1	18.82	8.52
Std. val.	69.7	18.65	8.86	69.7	18.65	8.86
Std. dev.	0.19	0.21	0.14	1.2	0.31	0.63
C. v. (%)	0.27	0.11	1.5	1.7	1.6	7.4

Analyses were carried out with specimen 651, Table 1.

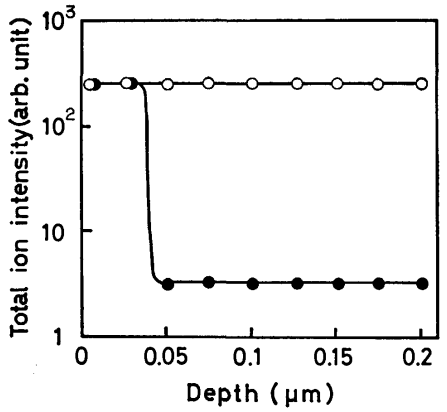

Fig. 6. Sub-surface variations in total ion intensity in specimens with passive surface layers. Sample chamber pressure was (●) 27 μPa(without oxygen) and (○) 5.3 mPa(with oxygen).

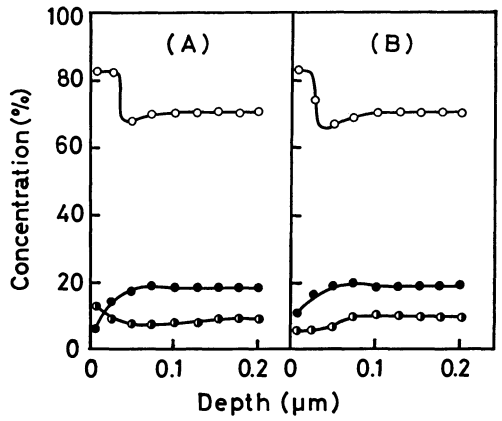

Fig. 7. Indepth concentration profiles for (A) 304 and (B) 321 stainless steels treated in neutral water containing 8 ppm oxygen. Specimens were treated for 2000 h at 289 °C.
○: Fe, ●: Cr, ◑: Ni.

The present method has been used to determine the concentration profiles in the surface layer of 304 and 321 stainless steel specimens treated in neutral water containing 8 ppm oxygen. Figure 7 shows the results obtained with specimens treated at 289 °C for 2000 h. The passive layers on the surfaces of 304 and 321 stainless steel are about 20 and 10 nm in thickness, respectively. These layers contain a larger amount of iron and a smaller amount of chromium than the matrices of the same steel.

It was found by carbon furnace atomic absorption spectrometry that iron, chromium, and nickel dissolve in water in a concentration of 239, 320, and 48.7 ppb, respectively. The concentration ratios of chromium and nickel to iron are 0.24 and 0.18 in matrices and 1.34 and 0.20 in water, respectively. The amount of nickel in water was nearly equal to that in the matrices, but the amount of chromium in water was much greater than that in matrices.

Thus, the decrease in the amount of chromium in passive layers corresponds to the increase in the amount of chromium in water.

A number of studies have been carried out on the composition of the passive film on 18% Cr–8% Ni stainless steel. Castle and Clayton[8] analyzed the passive film by X-ray photoelectron spectroscopy. They reported that the passive film prepared in low temperature (313 and 353 K), neutral, de-oxygenated water has a duplex layer structure, the outer layer being rich in iron and inner layer rich in chromium. A duplex layer structure was reported by Kowaka and Nagata,[13] and Bittel *et al.*[14] They prepared the passive layer in steam at temperatures 600—650 °C[13] and 1200—1300 °C, and analyzed the cross section of passive film with an electron probe microanalyzer. The results show that the passive layer consists of an outer layer of hematite rich in iron and inner layer of spinel and fcc metal rich in chromium.

Our result shows that the passive layer is rich in iron, corresponding to the composition of the outer layer.

References

1) G. Okamoto and T. Shibata, *Corros. Sci.*, **10** 371 (1970).
2) G. Okamoto, *Corros. Sci.*, **13**, 471 (1973).
3) J. S. Leach, *J. Inst. Metals*, **88**, 24 (1959).
4) K. N. Goswami and R. W. Staehle, *Electrochim. Acta*, **16**, 1895 (1971).
5) Z. Szklarska-Smialowska, *Corros. Sci.*, **16**, 355 (1976).
6) Y. Takasu, H. Shimizu, S-I. Maru, M. Tomori, and Y. Matsuda, *Corros. Sci.*, **16**, 159 (1976).
7) K. Asami, K. Hashimoto, and S. Shimodaira, *Corros. Sci.*, **16**, 387 (1976).
8) J. E. Castle and C. R. Clayton, *Corros. Sci.*, **17**, 7 (1977).
9) K. Sato and K. Tsunoyama, *Oyo Butsuri*, **45**, 828 (1976).
10) C. A. Andersen and J. R. Hinthorne, *Anal. Chem.*, **45**, 1421 (1973).
11) C. A. Andersen and J. R. Hinthorne, *Science*, **175**, 853 (1972).
12) H. Nishimura and J. Okano, *Mass Spect.*, **23**, 9 (1975).
13) M. Kowaka and S. Nagata, *J. Jpn. Inst. Metals*, **36**, 486 (1972).
14) J. T. Bittel, L. H. Sjodahl, and J. R. White, *Corrosion-NACE*, **25**, 7 (1969).

Studies on the Ammonium Form of Crystalline Zirconium Phosphate. II.[1,2] Ammonium–Lithium Ion-exchange Isotherms

Yoshitsugu HASEGAWA* and Yoshimitsu KOMIYAMA†

Department of Industrial Chemistry, Faculty of Technology, Tokyo University of Agriculture and Technology, Koganei Tokyo 184

(Received October 3, 1977)

The ion-exchange isotherms for the NH_4^+–Li^+ system on crystalline zirconium phosphate have been determined at 25 °C, and the structural change and water content of the exchanger have also been investigated by means of X-ray diffraction and thermal analysis. The isotherms showed that the ion-exchange reaction took place in one stage, that is, the ammonium-form was converted into the lithium-form in the forward process, and *vice versa* in the reverse process. However, the results of X-ray diffractometry indicated that the ion-exchange reactions proceeded in three stages in each direction. The isotherms also showed a hysteresis loop. This phenomenon can be ascribed to the difference in the water content of the exchangers, because the X-ray powder patterns of the exchanger phases were essentially identical at similar ionic mole fraction of lithium ion in the exchangers of the two processes.

Many inorganic ion-exchangers have been extensively investigated in the field of nuclear energy, water desalination, analytical chemistry, *etc.* Crystalline zirconium bis(monohydrogen orthophosphate) monohydrate, $Zr(HPO_4)_2 \cdot H_2O$, generally called α-zirconium phosphate, is one of the most studied materials. α-Zirconium phosphate as well as its cation-exchanged form has a layered structure, and the ion-exchange reaction is strongly influenced by the interlayer distance of the exchanger and by the ionic radius of an exchanging cation.[3] Also, the hydration and dehydration of cations affect the ion-exchange. Of alkali metal cations, lithium ion has the largest standard free energy for hydration and dehydration,[4,5] and its ionic radius is the smallest. When lithium ion exchanges on a cation-exchanged form with a cation having a larger ionic radius, not all the water molecules bound to the lithium ion are dehydrated.

During an investigation of the ammonium–hydrogen ion-exchange on α-zirconium phosphate prepared by the reflux method, the pH titration curves indicate that the solid phase of $Zr(NH_4PO_4)_{4/3} \cdot (HPO_4)_{2/3} \cdot nH_2O$ is present instead of $Zr(NH_4PO_4)(HPO_4) \cdot n'H_2O$.[6] The interlayer distance of the ammonium-form is shorter than that to be expected from the ionic radius of ammonium ion.[7,8] The behavior of the ammonium–hydrogen ion-exchange is similar to that observed in the hydrogen–lithium ion-exchange.[9]

Thus, it is of interest to study how the relatively short interlayer distance of the ammonium-form exchanger affects its selectivity from the points of view of the mechanism of the ion-exchange and the application to the recovery of metals, and how the ionic hydration and the similar behavior of the ion-exchange reactions affect the ammonium–lithium ion-exchange.

In the present work, the ammonium–lithium ion-exchange isotherms at 25 °C, the structural change, and the water content per mole of the exchanger will be reported.

† Present address: 4-13-5 Sengen-cho, Fuchu, Tokyo 183.

Experimental

Reagents and Preparation of Exchangers. All the chemicals were of reagent grade and were used without purification.

The ammonium-form exchanger, $Zr(NH_4PO_4)_2 \cdot H_2O$, was prepared according to Hasegawa and Aoki.[6] The lithium-form exchanger, $Zr(LiPO_4)_2 \cdot 4H_2O$, was prepared by the continuous percolation of a 0.1 mol dm^{-3} lithium chloride solution through a column filled with the ammonium-form exchanger. Both the exchangers were dried over a saturated sodium chloride solution (with a relative humidity of about 75% at room temperature). The identification of the exchanger was made by means of the X-ray diffraction pattern and the loss of ignition.

Analytical Procedure. The concentration of ammonium ions in the solution was determined gravimetrically.[10] The concentration of lithium ions was determined by atomic absorption spectrophotometry with a Hitachi atomic absorption spectrophotometer 208. In order to determine the structural change in the exchanger phase during the ion-exchange, X-ray powder patterns were obtained with nickel-filtered Cu $K\alpha$ radiation with a Geigerflex (Rigaku Denki Co., Ltd.). The exchanger was conditioned before measurement over a saturated sodium chloride solution at room temperature.

TABLE 1. DEPENDENCE OF X_{Li} ON THE TIME

Time (day)	0.25	0.5	1	2	3
X_{Li}[a)]	0.93	0.94	0.93	0.94	0.93

a) X_{Li}=the mole fraction of lithium ion in the solution of F8 in Fig. 1.

Ion-exchange Isotherms. A weighed amount of the exchanger (100 mg) was shaken continuously with 10.0 cm^3 of a solution containing a total of 0.100 M of ammonium and lithium chlorides at 25 °C. In order to select the reaction time, the concentration of lithium ions in the solution was determined after a given period of time for the F8 sample in Fig. 1. The concentration of lithium ions varied within the limits of experimental error (Table 1). A reaction of at least 48 h was thus chosen. Near the end point (the mole fraction of lithium or ammonium ion, X_{Li} or $X_{NH_4}=1.0$) the volume of the solution was increased and/or the amount of the exchanger was decreased to prompt the reaction, and also a shaking period longer than 48 h was taken.

Results and Discussion

In order to investigate the effect of the pH's of solutions on the ion-exchange isotherms and to calculate the ionic fraction of exchanging cations in the exchanger phase, the concentrations of ammonium and lithium ions and pH values in the solution phase were determined separately. As is shown in Table 2, the sum of the ionic fraction of the solution phase for ammonium and lithium ions was equal to unity in all cases, within the limits of experimental error. The pH values were slightly higher than the pH's which were determined for the solutions containing the same ionic fraction of ammonium and lithium ions and no exchanger. The difference in the hydrogen-ion concentration was very small, and it is possible to neglect the effect of the pH value of the solution on the ion-exchange reaction.

Table 2. Mass balance data for NH_4^+/Li^+ exchange

	X_{Li}	X_{NH4}	Total ionic fraction	pH	
				Initial	Final
F1	0.78	0.19	0.97	5.78	5.75
F2	0.81	0.19	1.00	5.80	6.05
F3	0.84	0.18	1.02	5.80	6.18
F4	0.85	0.16	1.01	5.80	6.25
F5	0.90	0.13	1.03	5.80	6.20
F6	0.91	0.11	1.02	5.80	6.58
F7	0.95	0.06	1.01	5.80	6.80
F8	0.97	0.03	1.00	5.80	6.90
R1	0.98	0.33	1.01	5.78	6.50
R2	0.94	0.08	1.02	5.71	6.35
R3	0.86	0.14	1.00	5.65	6.20
R4	0.79	0.22	1.01	5.60	6.45
R5	0.72	0.32	1.04	5.50	6.20
R6	0.66	0.36	1.02	5.52	5.95
R7	0.59	0.42	1.01	5.52	6.00
R8	0.51	0.49	1.00	5.48	5.95
R9	0.44	0.59	1.03	5.50	5.35
R10	0.23	0.75	0.98	5.50	5.40

F and R denote the forward and reverse processes respectively. F1...R10 correspond to those in Fig. 1. X_{Li} and X_{NH4} represent the mole fractions of the respective ions.

Forward Process (The Ammonium-form→the Lithium-form). The ion-exchange isotherm is shown in Fig. 1(a). It was found that the isotherm showed a steep sloping when the mole fraction of lithium ion in the solution, X_{Li}, was larger than 0.7. No clear plateaus or vertical portions were observed in the isotherm. These facts indicate that the ammonium-form was converted into the lithium-form without the formation of an intermediate, half-exchanged form, $Zr(NH_4PO_4)(LiPO_4)\cdot mH_2O$. Since it took a long time to prepare the lithium-form, perfect conversion seems to be difficult.

It is known that α-zirconium phosphate and its sodium-form have a layered structure and that the first reflection in the X-ray powder pattern corresponds to the interlayer spacing.[3] This means that when two solid phases coexist, two reflections are observed at lower diffraction angles. As the ammonium-form has a layered structure,[8] similar phenomena can be expected. Based on this hypothesis, it has been possible to deduce the structural change of the exchanger phase during the ion-exchange. The precise estimation of the intensity of two peaks is difficult in this case, however, because two peaks overlapped at lower diffraction angles. Hence, the intensity ratio in Table 3 is only approximate.

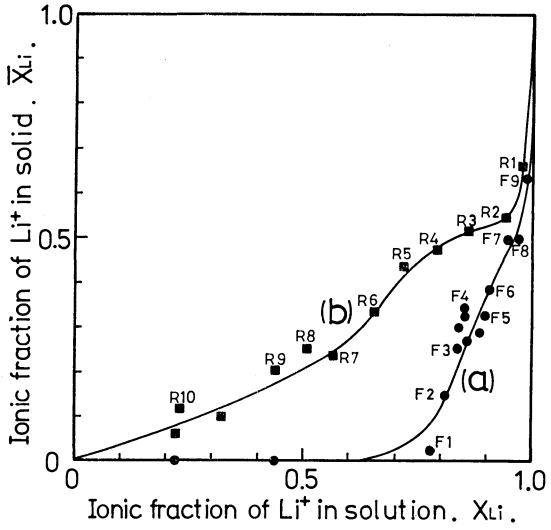

Fig. 1. Ion-exchange isotherms, (a) forward and (b) reverse process. X_{Li}: the mole fraction of lithium ion in the solution phase. $\bar{X}_{Li}$: the mole fraction of lithium ion in the solid phase.

Table 3. Relative intensities of the interlayer distances in the forward process

Symbol[a]	Interlayer distances		
$\bar{X}_{(Li)}$	9.4 Å	10.0 Å	10.5 Å
F1 (0.03)	10	—	—
F2 (0.15)	10	1.1	—
F3 (0.25)	3.0	10	—
F4 (0.35)	—	10	3.5
F5 (0.33)	—	10	5.1
F6 (0.38)	—	10	7.2
F7 and F8 (0.50)	—	—	10
F9 (0.63)	—	3.0	10
Li form (1.0)	—	10	—

a) Symbols correspond to those in Fig. 1(a).

In the region of the mole fraction of lithium ion in the exchanger phase $\bar{X}_{Li}=0-0.03$, the interlayer distance remained constant (9.4 Å), corresponding to that of the ammonium-form. When $\bar{X}_{Li}$ was above 0.15, a peak appeared at 10.0 Å, and its intensity increased with an increase in $\bar{X}_{Li}$. Between F3 and F4 ($\bar{X}_{Li}\fallingdotseq 0.3$), the

peak at 9.4 Å diminished and another peak appeared at 10.5 Å. This change in the exchanger phase indicates that a new phase with an interlayer distance of 10.0 Å was present in the very narrow region of X_{Li}.

Two peaks, at 10.0 and 10.5 Å, were observed in the region of $\bar{X}_{Li}$=0.3—0.4. The intensity of the former decreased with an increase in $\bar{X}_{Li}$, and only the peak at 10.5 Å was present at F7 and F8 ($\bar{X}_{Li} \fallingdotseq 0.5$).

Above $\bar{X}_{Li}$=0.5 the peak at 10.5 Å disappeared gradually, and the intensity of the peak at 10.0 Å increased again. This peak at 10.0 Å should be considered as a different one from that observed in the region of $\bar{X}_{Li}$=0.15—0.4, because it is not probable that the same phase exists in another region of $\bar{X}_{Li}$. The interlayer distance of 10.0 Å was identical to that of the lithium-form reported by Alberti *et al.*[11] It can thus be inferred from the X-ray studies that the ion-exchange reaction took place in three stages, while the isotherm showed no clear stages.

In order to determine the water content per mole of the exchanger, the solid obtained during the ion-exchange process was heated to 420 °C and the weight loss was measured. The molecular formula of the exchanger can be assumed to be $Zr(NH_4PO_4)_a \cdot (LiPO_4)_{2-a} \cdot nH_2O$. Since the exchanger loses its water of hydration and ammonia in the temperature range of 100—420 °C, the water content is calculated by means of the following equation:

$$n = [295.0p + (11.0p - 17.0)a]/18.0(1 - p), \quad (1)$$

where a and n are moles of NH_4^+ and H_2O per formula weight of the exchanger, as shown above, and p is the portion of weight loss to the molecular weight.

The relationship between the water content per mole of the exchanger (n) and $\bar{X}_{Li}$ is shown in Fig. 2(a). The value of n increased linearly with $\bar{X}_{Li}$. The change in n can be represented as follows;

$$n = 3(\bar{X}_{Li}) + 1$$
$$= (3/2)(2 - a) + 1. \quad (2)$$

Equation 2 shows that the net water molecules diffusing with a lithium ion into the crystal lattice of the exchanger were equal to 1.5. The water content of the ion-exchanger of the lithium-form was equal to $3.9H_2O$/mol, less than that previously reported.[11,12] This is due to the tendency of the lithium-form to lose the water of hydration.[11]

Reverse Process (the Lithium-form→the Ammonium-form). The ion-exchange isotherm of the reverse process is shown in Fig. 1(b). In contrast with the forward process, this ion-exchange reaction took place at $X_{NH_4} < 0.03$. The isotherm showed an almost vertical sloping in the region of $\bar{X}_{Li}$=1.0—0.5. Near R2 and R3 ($\bar{X}_{Li} \fallingdotseq 0.5$) the curve tended to have a plateau, and then it again sloped below $\bar{X}_{Li}$=0.5.

Table 4 shows the change in the peaks in the powder patterns at lower diffraction angles. Even at the beginning of the reaction the peak at 10.5 Å appeared and two phases coexisted. The peak at 10.5 Å showed its maximum intensity at R2, while the peak at 10.0 Å was present as a shoulder. The intensity of the peak at 10.0 Å increased again at R3. This peak after R3 should be regarded as another, separate one, as has been

TABLE 4. RELATIVE INTENSITIES OF THE INTERLAYER DISTANCES IN THE REVERSE PROCESS

Symbol[a]	Interlayer distances		
($\bar{X}_{Li}$)	9.4 Å	10.0 Å	10.5 Å
R1			
(0.67)	—	8	10
R2			
(0.54)	—	s	10
R3			
(0.52)	—	5.2	10
R5			
(0.44)	—	8.2	10
R6			
(0.34)	—	10	8.0
R7			
(0.22)	10	8.1	—
R9			
(0.20)	10	8.6	—
R10			
(0.12)	10	s	—

a) Symbols correspond to those in Fig. 1(b).
s: Shoulder.

stated above. The findings indicate that the phase with the interlayer distance of 10.5 Å was formed at the narrow region of X_{Li} between R2 and R3. In the region of $\bar{X}_{Li}$=0.5—0.3, two peaks at 10.0 and 10.5 Å were observed. The intensity of the 10.0 Å peak increased with a decrease in $\bar{X}_{Li}$ and showed its maximum at R6. The peaks at 10.0 and 9.4 Å coexisted below $\bar{X}_{Li}$=0.3. The latter corresponds to the interlayer distance of the ammonium-form. Near the end point (X_{Li} and $\bar{X}_{Li}$=0), only the ammonium-form was present. The results showed that the ion-exchange reaction proceeded in three stages.

The change in the water content per mole of the exchanger, n, calculated by means of Eq. 1 is shown in Fig. 2(b). The value of n was approximately represented as follows above $\bar{X}_{Li}$=0.3:

$$n = 2(\bar{X}_{Li}) + 2$$
$$= (2 - a) + 2. \quad (3)$$

Below this point the equation changes to approximately:

$$n = 5(\bar{X}_{Li}) + 1$$
$$= 5/2(2 - a) + 1$$

(the dashed line in Fig. 2). Equation 3 shows that one water molecule migrates with a lithium ion and that the water content of the exchanger phase was higher in the reverse direction than in the forward one.

The X-ray powder patterns of the exchanger phase with a similar $\bar{X}_{Li}$ were essentially identical and made no noticeable difference in the crystal structure. The water content of the exchanger in the forward process was different from that in the reverse one at the same $\bar{X}_{Li}$. Consequently, the hysteresis phenomenon can be ascribed to the difference in the number of water molecules involved in the ion-exchange reactions.

At the first stage in both processes, the interlayer distance of the exchanger expanded, though the change was larger in the forward process than in the reverse one. This indicates that more energy is needed and that

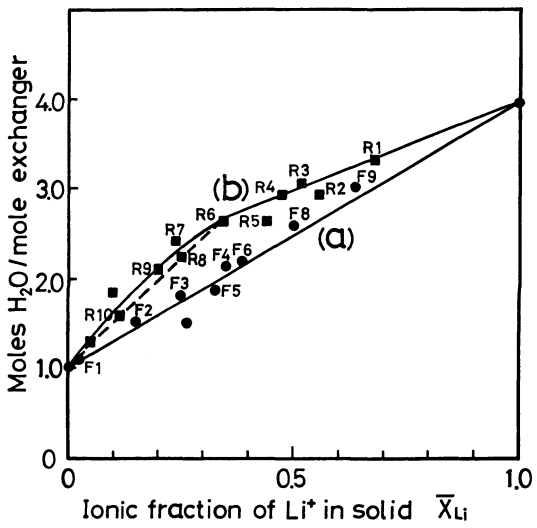

Fig. 2. Change in the water content per one mole of the exchanger phase (n). (a) forward and (b) reverse process.

it is more difficult for the ion-exchange reaction to take place in the forward process. In the second stage, the interlayer distance expanded in the forward process, but contracted in the reverse one. Hence, the ion-exchange reaction in the forward process may need a higher X_{Li}.

While hydration in the exchanger phase is an important factor in affecting the ion-exchange reaction,[6,10] ionic hydration in the solution phase must also be taken into account. During the ion-exchange process, bare or partially hydrated cations diffuse into the exchanger because of the steric factor.[3,8] Ions must lose hydrated water molecule(s) in order to exchange. Kim and Rubin calculated the activation energy for dehydration of alkali cations.[5] Though the activation energy for ammonium ion has not been estimated, it can be considered, according to the model employed by them, that the activation energy for dehydration of ammonium ion will be less than that for lithium ion, mainly because of the crystal ionic radius and the mass of ammonium ion. Thus, it is easier for ammonium ion than lithium ion to diffuse into the exchanger. The activation energy for dehydration of primary hydrated lithium ion was estimated to be greater than that of sodium ion if each ion loses the same number of bound water molecules.[5] A comparison with the obtained isotherms for NH_4^+–Li^+ and NH_4^+–Na^+ systems suggests that the lithium ion is partially dehydrated,[10] for the ion-exchange reaction took place at a low ionic fraction of lithium ion in the solution.

The relationship between the formation of a new phase and the absence of the step-by-step change in the isotherm can be explained by the following factors: (1) the two ion-exchange reactions ocurred in a very narrow X_{Li} region, as shown in the NH_4^+–Na^+ systems, and (2) two phases formed the solid solution over a wide range of composition, because the exchanger used showed a good crystallinity but was not fully crystalline, as was pointed out in the case of the Li^+–H^+ exchange.[13]

The authors would like to thank Professor Isao Tomita, the University of Tsukuba, for his many helpful discussions. The authors are also much indebted to Professor Shuji Abe for his valuable discussions.

References

1) Part I. Y. Hasegawa, *J. Inorg. Nucl. Chem.*, **38**, 319 (1976).
2) A part of this paper was presented at the 34th National Meeting of the Chemical Society of Japan, Hiratsuka, April, 1976.
3) A. Clearfield, W. L. Duax, A. S. Medina, G. D. Smith, and J. R. Thomas, *J. Phys. Chem.*, **73**, 3424 (1969).
4) S. Goldman and R. G. Bates, *J. Am. Chem. Soc.*, **84**, 1476 (1972).
5) S. H. Kim and R. T. Rubin, *J. Phys. Chem.*, **77**, 1245 (1973).
6) Y. Hasegawa and H. Aoki, *Bull. Chem. Soc. Jpn.*, **46**, 836 (1973).
7) A. Clearfield and J. A. Stynes, *J. Inorg. Nucl. Chem.*, **26**, 117 (1964).
8) A. Clearfield and J. M. Troup, *J. Phys. Chem.*, **77**, 243 (1973).
9) A. Clearfield and J. Troup, *J. Phys. Chem.*, **74**, 314 (1970).
10) Y. Hasegawa, *J. Inorg. Nucl. Chem.*, **38**, 319 (1976).
11) G. Alberti, U. Costantino, S. Allulli, M. A. Massucci, and N. Tomassini, *J. Inorg. Nucl. Chem.*, **36**, 653 (1974).
12) E. Torracca, *J. Inorg. Nucl. Chem.*, **31**, 1189 (1969).
13) A. Clearfield and D. A. Tuhtar, *J. Phys. Chem.*, **80**, 1296 (1976).

Studies of Inorganic Ion Exchangers. II.[1] Effects of Sulfuric Acid on the Synthesis of $Ti(HPO_4)_2 \cdot 0—1/2H_2O$

Etsuro KOBAYASHI

National Chemical Laboratory for Industry, Hon-machi, Shibuya-ku, Tokyo 151

(Received December 8, 1977)

In order to develop an inorganic ion exchanger for industrial use, sulfuric acid has been added to the reaction system of amorphous titanium(IV) phosphate and phosphoric acid. The effects of the additive on the formation of titanium(IV) hydrogenphosphate, a compound observed to have ion exchange affinities towards K^+ and Cs^+, have been investigated. $Ti(HPO_4)_2 \cdot 0—1/2H_2O$ has been synthesized using the sulfuric acid solution of $TiOSO_4$, an intermediate in the production process of titanium dioxide. The addition of sulfuric acid to phosphoric acid and a resulting mole ratio of H_2SO_4/H_3PO_4 greater than 0.14, produced a borderline in the formation of the monohydrate and hemihydrate within the temperature range of 148—155 °C. Titanium(IV) hydrogenphosphate crystallized as fine particles (1—3 μ) by the double decomposition between the sulfuric acid solution of $TiOSO_4$ and phosphoric acid. The X-ray diffraction pattern of the product obtained using the sulfuric acid solution of $TiOSO_4$ above 160 °C compared favourably with that of the hemihydrate already reported. The composition was shown by the formula of $Ti(HPO_4)_2 \cdot 0—1/2H_2O$. In the X-ray diffraction pattern of $Ti(HPO_4)_2 \cdot 0—1/2H_2O$, two characteristic diffraction lines appeared at 11.6 and 9.21 Å; thus it has been assumed that the product is not a pure crystallite but a mixture of two or more species.

Some phosphates of polyvalent metals have been known as inorganic ion exchangers, zirconium phosphate being especially useful in analytical chemistry.[2,3] Previous investigations of the ion exchange properties of some phosphates,[4,5] lead to this investigation of titanium phosphate. The crystalline titanium(IV) bis(hydrogenphosphate) monohydrate, $Ti(HPO_4)_2 \cdot H_2O$, can absorb Li^+ and Na^+,[6,7] but not the ions of larger radius, such as K^+ and Cs^+. In a previous work,[1] titanium(IV) bis(hydrogenphosphate) hemihydrate, $Ti(HPO_4)_2 \cdot 1/2H_2O$, was formed by refluxing amorphous titanium(IV) phosphate with concentrated phosphoric acid. The X-ray diffraction pattern of the hemihydrate differed considerably from that of the monohydrate, and larger *d*-values appeared. It has been observed that this compound has ion exchange capacities towards K^+ and Cs^+. In the present work, an attempt has been made to prepare $Ti(HPO_4)_2 \cdot 1/2H_2O$ by the reaction of concentrated phosphoric acid with the sulfuric acid solution of titanium oxide sulfate, $TiOSO_4$, the intermediate in the production process of titanium dioxide. The effects of sulfuric acid on the formation of titanium phosphate have been investigated by refluxing amorphous titanium(IV) phosphate with a mixture of H_2SO_4 and H_3PO_4. Subsequently, $Ti(HPO_4)_2 \cdot 0—1/2H_2O$ has been synthesized using the sulfuric acid solution of $TiOSO_4$ or titanium(IV) oxide monohydrate (metatitanic acid, $TiO_2 \cdot H_2O$).

Experimental

Starting Materials. Amorphous titanium(IV) phosphate has been prepared by the method described in a previous paper.[1] Synthesising conditions and analytical data are given in Table 1.

The sulfuric acid solution of $TiOSO_4$, which is the polish for titanium dioxide as a white pigment and does not contain iron as an impurity, was obtained from Ishihara Sangyo Kaisha Ltd. The composition is shown as a footnote in Table 2. $TiO_2 \cdot H_2O$ used was a commercial grade powder.

Preparation of Titanium(IV) Bis(hydrogenphosphate). An appropriate quantity of titanium compound and other materials (amorphous titanium(IV) phosphate, H_2SO_4 soln of $TiOSO_4$, $TiO_2 \cdot H_2O$: 25 g, 30 ml, 9.18 g) were placed in a three-necked flask, and H_3PO_4–H_2SO_4 solution (900 ml) was added. The mixture was refluxed for 50 h after which a condenser and a thermometer were connected to the flask. The resulting precipitate was separated centrifugally from the mother liquor, water added, the mixture vigorously shaken up, and the precipitate was separated centrifugally. This procedure was repeated several times, and the product finally dried at 50—60 °C for 24 h.

Analysis. The components of the product, P_2O_5, TiO_2, and H_2O, were determined by previously reported methods.[1] The quantity of H_2SO_4 in the mother liquor was determined gravimetrically as barium sulfate. The X-ray diffraction patterns were obtained using a Rigaku-Denki model 2001 diffractometer with Ni-filtered Cu *Kα* radiation, with 20 kVP and 15 mA, or 30 kVP and 20 mA.

Results and Discussion

Reaction of Amorphous Titanium(IV) Phosphate with H_3PO_4–H_2SO_4 Solution. The effects of sulfuric acid on the formation of titanium(IV) bis(hydrogenphosphate) have been investigated by using amorphous titanium(IV) phosphate as the starting material. The conditions of synthesis and the results of analysis are summarized in Table 1.

Proportion of Titanium Compound with Mother Liquor. When the quantity of amorphous titanium(IV) phosphate is small compared with the volume of mother liquor, the reflux is smooth; this production is, however, commercially unprofitable. When a large amount of the titanium compound is refluxed with the mother liquor, the operation is not smooth, and the growth of the crystal of titanium(IV) bis(hydrogenphosphate) is obstructed. As may be seen from Table 1(Nos. 1—4), the quantity of amorphous titanium(IV) phosphate mixed with H_3PO_4 as the mother liquor was varied. The X-ray diffraction patterns of the products thus obtained are shown in Fig. 1. It is evident that the crystallinities of the products increase in the order Nos. 1, 2, and 3. The ratios (*R*) of the volume of mother liquor to the

TABLE 1. SYNTHESIZING CONDITIONS OF TITANIUM(IV) BIS(HYDROGENPHOSPHATE) BY THE ADDITION OF SULFURIC ACID, AND ANALYTICAL DATA

No.	Reaction conditions[a]							Reaction product				
	Amorphous titanium-(IV) phosphate (g)	Mother liquor H_3PO_4 (mol/l)	Mother liquor H_2SO_4 (mol/l)	Mother liquor $\frac{H_2SO_4}{H_3PO_4}$	Mother liquor Volume (ml)	Temp (°C)	Time (h)	TiO_2 (%)	P_2O_5 (%)	H_2O (%)	$TiO_2:P_2O_5:H_2O$ (Mole ratio)	Estimated formula
1	20.0	15.1	0	0.00	300	175	12	32.7	57.0	10.3	1.02:1.00:1.43	$Ti(HPO_4)_2 \cdot 1/2H_2O$
2	4.0	15.1	0	0.00	96	175	12	32.5	56.9	10.6	1.02:1.00:1.47	$Ti(HPO_4)_2 \cdot 1/2H_2O$
3	3.0	15.1	0	0.00	96	175	12	32.0	58.1	10.9	0.98:1.00:1.48	$Ti(HPO_4)_2 \cdot 1/2H_2O$
4	2.0	14.9	0	0.00	97	175	12	31.6	58.0	10.4	0.97:1.00:1.41	$Ti(HPO_4)_2 \cdot 1/2H_2O$
5	3.0	12.9	1.8	0.14	101	175	12	31.6	57.4	11.0	0.98:1.00:1.51	$Ti(HPO_4)_2 \cdot 1/2H_2O$
6	3.0	12.4	5.1	0.41	96	175	12	32.5	57.2	10.4	1.01:1.00:1.43	$Ti(HPO_4)_2 \cdot 1/2H_2O$
7	3.0	9.1	7.5	0.82	88	175	12	31.7	57.1	11.2	0.99:1.00:1.54	$Ti(HPO_4)_2 \cdot 1/2H_2O$
8	3.0	12.1	1.7	0.14	108	140	15	30.9	54.8	14.5	1.00:1.00:2.08	$Ti(HPO_4)_2 \cdot H_2O$
9	3.0	12.8	1.8	0.14	102	148	15	30.7	54.7	14.6	1.01:1.00:2.11	$Ti(HPO_4)_2 \cdot H_2O$
10	3.0	14.3	2.0	0.14	91	155	12	32.2	56.8	11.1	1.01:1.00:1.54	$Ti(HPO_4)_2 \cdot 1/2H_2O$
11	3.0	16.5	2.3	0.14	79	160	12	32.3	57.0	10.7	1.01:1.00:1.48	$Ti(HPO_4)_2 \cdot 1/2H_2O$
12	3.0	9.9	4.1	0.41	110	148	12	31.5	54.5	14.0	1.03:1.00:2.03	$Ti(HPO_4)_2 \cdot H_2O$
13	3.0	10.4	4.3	0.41	105	155	12	33.6	57.8	8.7	1.03:1.00:1.18	$Ti(HPO_4)_2 \cdot 0—1/2H_2O$
14	3.0	7.3	6.0	0.82	120	148	12	32.2	54.9	13.0	1.04:1.00:1.86	$Ti(HPO_4)_2 \cdot 1/2—1H_2O$
15	3.0	7.7	6.4	0.83	113	155	12	33.2	55.8	11.0	1.06:1.00:1.56	$Ti(HPO_4)_2 \cdot 1/2H_2O$
16	25.0	13.0	1.8	0.14	880	160	24	32.4	56.2	11.4	1.02:1.00:1.60	$Ti(HPO_4)_2 \cdot 1/2H_2O$
17	25.0	13.0	1.8	0.14	880	160	50	32.0	56.4	10.1	1.01:1.00:1.43	$Ti(HPO_4)_2 \cdot 1/2H_2O$
								42.7	33.8	23.3	2.24:1.00:5.42	

a) The mixture of amorphous titanium(IV) phosphate and mother liquor was refluxed at boiling point.

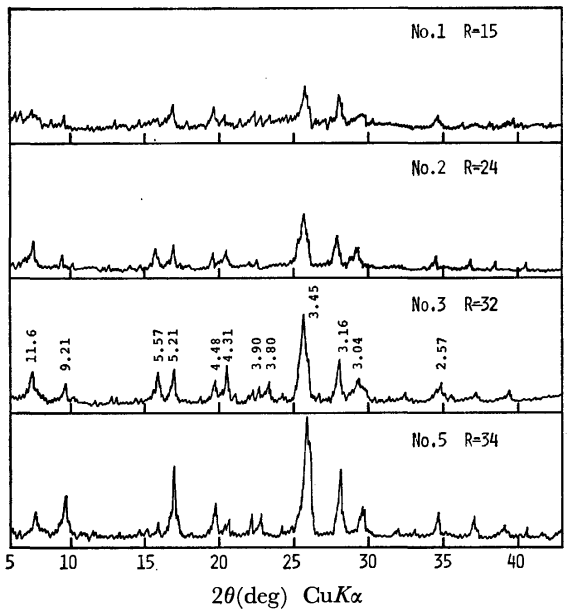

Fig. 1. X-Ray diffraction patterns of $Ti(HPO_4)_2 \cdot 1/2H_2O$. Effect of amount of amorphous titanium(IV) phosphate to mother liquor.
R: Mother liquor(ml)/amorphous titanium(IV) phosphate(8). Nos. 1, 2, and 3: H_3PO_4 used as mother liquor, No. 5: H_3PO_4–H_2SO_4 mixed solution used as mother liquor. Numerals near peaks indicate corresponding *d* values.

weight of titanium compound were found suitable within 32 to 50 (ml/g). In No. 5 the H_3PO_4–H_2SO_4 solution was used as the mother liquor, and the crystallinity of product improved more than in the case of only H_3PO_4.

Effect of Concentration of H_2SO_4. The effect of concentration of H_2SO_4 added to the mother liquor was examined (Nos. 5—7). The initial volume ratios of 18 M H_2SO_4 to 14.5 M H_3PO_4 were 1: 9, 2.5: 7.5, and 4: 6 in Nos. 5, 6, and 7, respectively. In these cases, the concentrations of H_3PO_4 and H_2SO_4 in the mother liquor after reflux are shown in Table 1. In the product X-ray diffraction patterns, the intensities decreased slightly with increase in H_2SO_4. However, the compositions of products and X-ray diffraction patterns were all the same with those of $Ti(HPO_4)_2 \cdot 1/2H_2O$. Therefore, an obstacle to the formation of the hemihydrate did not appear until a volume ratio of 4: 6 was reached. But the existence of a different phosphate was recognized from the X-ray diffraction pattern and analytical data (TiO_2: 35.2%, P_2O_5: 35.6%, SO_3: 19.5%, H_2O: 8.5%) of the product formed in the case of a volume ratio 9: 1 of H_2SO_4 to H_3PO_4.

Effect of Reaction Temperature. As previously reported, $Ti(HPO_4)_2 \cdot 1/2H_2O$ was formed by refluxing amorphous titanium(IV) phosphate with H_3PO_4 containing more than 64% P_2O_5 at above 170 °C.[1] $Ti(HPO_4)_2 \cdot H_2O$ was also formed as the solid phase in equilibrium with the mother liquor containing 13—64% P_2O_5. Variations in the mixing ratio of H_2SO_4 to H_3PO_4 and the refluxing temperature were conducted (Nos. 5 and 8—15). From the results of analysis and the X-ray diffraction data, the species of titanium phosphate are shown in Fig. 2. As seen from the figure a mother liquor consisting of only phosphoric acid

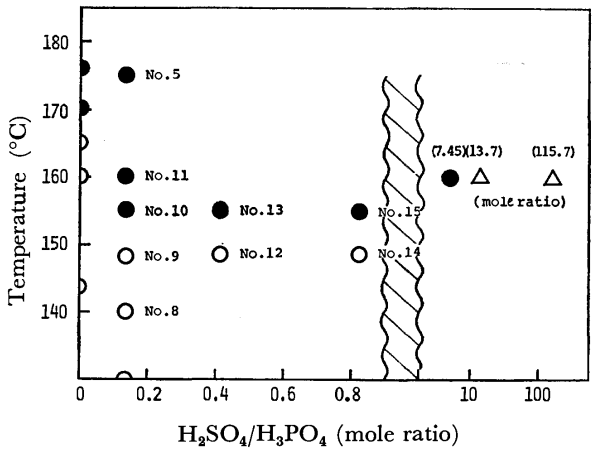

Fig. 2. Effects of sulfuric acid in mother liquor and reaction temperature on formed salts.
●: $Ti(HPO_4)_2 \cdot 1/2H_2O$, ○: $Ti(HPO_4)_2 \cdot H_2O$, △: unknown salt.

produced a border in the formation of the monohydrate and the hemihydrate between 160 and 170 °C. When the mole ratio of H_2SO_4 to H_3PO_4 exceeded 0.14, a borderline appeared in the range of 148—155 °C, *i.e.* the reaction temperature for formation of the hemihydrate was lowered by about 15 °C by the addition of H_2SO_4. Since the fraction of water in the mother liquor decreased by the addition of 18 M H_2SO_4, the water required for the formation of the monohydrate was not sufficient, and the resulting hemihydrate was formed as the stable solid phase in equilibrium with the mother liquor. It is possible that the sulfuric acid in the heated mother liquor dehydrated the water of crystallization.

Determination of Reaction Time. The effects of reaction time in the synthesis of $Ti(HPO_4)_2 \cdot 1/2H_2O$ have been examined (Nos. 11(12h), 16(24h), and 17(50h)). With the H_3PO_4–H_2SO_4 solution as mother liquor, the X-ray diffraction patterns showed the crystallinity of product improved until a reaction time of 24 h. The reaction time in the synthesis of the monohydrate has been reported to be 50[6] and 200 h.[7] Therefore, in terms of hemihydrate formation as an ion exchanger and the commercialization of the process the reaction time has been set at 50 h.

Synthesis of $Ti(HPO_4)_2 \cdot 0$—$1/2H_2O$ Using the Sulfuric Acid Solution of $TiOSO_4$. The synthesizing conditions of titanium(IV) bis(hydrogenphosphate) and their analytical results are summarized in Table 2.

The reaction between $TiOSO_4$ and H_3PO_4 is shown in the following equation

$$TiOSO_4 + 2H_3PO_4 \longrightarrow Ti(HPO_4)_2 \cdot H_2O + H_2SO_4.$$

Titanium(IV) bis(hydrogenphosphate) crystallizes in the mother liquor, and then sulfuric acid is newly formed. When the $TiOSO_4$–H_2SO_4 solution was used as the starting material, a gelatinous product of undefined composition was initially produced. To avoid aggregation of the gel, the $TiOSO_4$–H_2SO_4 solution was added little by little to the stirred H_3PO_4–H_2SO_4 solution. A second method was to stir the reaction mixture without refluxing in a mother liquor having the boilling point higher than the appointed reaction temperature. This method is called the precipitate method compared with the previous one, the refluxing method. In No. 18, which used a mother liquor of boilling point 160 °C, the monohydrate was formed by the precipitate method at 100 °C. The diameter of the product thus obtained was 10—30 μ, and appeared larger than that of the product formed by the refluxing method. Upon investigation through a microscope the product was shown to be an aggregation of fine particles. This aggregation gradually separated into fine particles as the temperature of the mother liquor rose. In Nos. 19—21 (precipitate method) and Nos. 22—25 (refluxing method) the monohydrate, hemihydrate and anhydride were obtained as fine particles with a diameter of about 1—3 μ. The X-ray diffraction patterns of $Ti(HPO_4)_2 \cdot H_2O$ formed by the precipitate method and $Ti(HPO_4)_2 \cdot 0$—$1/2H_2O$ formed by the refluxing method are shown in Fig. 3.

The X-ray diffraction patterns of the products obtained using the sulfuric acid solution of $TiOSO_4$ at

Table 2. Synthesizing conditions of titanium(IV) bis(hydrogenphosphate) using $TiOSO_4$–H_2SO_4 solution or $TiO_2 \cdot H_2O$, and analytical data

No.	Reaction conditions: Raw material $TiOSO_4$[a] (ml)	Raw material $TiO_2 \cdot H_2O$ (g)	Mother liquor H_3PO_4 (mol/l)	Mother liquor H_2SO_4 (mol/l)	Mother liquor Volume (ml)	Temp (°C)	Time (h)	Reaction product: Method[b]	TiO_2 (%)	P_2O_5 (%)	H_2O (%)	TiO_2:P_2O_5:H_2O (Mole ratio)	Estimated formula
18	20	—	8.60	2.82	600	100	50	PPT	31.4	57.4	13.6	0.97:1.00:1.87	$Ti(HPO_4)_2 \cdot H_2O$
19	30	—	6.76	3.08	900	135	50	PPT	32.1	54.4	14.5	1.05:1.00:2.10	$Ti(HPO_4)_2 \cdot H_2O$
20	30	—	8.03	3.40	900	150	50	PPT	31.2	54.6	14.2	1.01:1.00:2.05	$Ti(HPO_4)_2 \cdot H_2O$
21	30	—	8.03	3.40	900	160	50	PPT	32.6	57.7	9.0	1.01:1.00:1.23	$Ti(HPO_4)_2 \cdot 0$—$1/2H_2O$
22	20	—	8.60	2.82	600	163	50	REF	32.4	57.5	8.85	1.01:1.00:1.22	$Ti(HPO_4)_2 \cdot 0$—$1/2H_2O$
23	30	—	10.9	3.06	900	165	50	REF	32.4	60.7	7.6	0.95:1.00:0.99	$Ti(HPO_4)_2$
24	—	9.18	8.31	1.59	900	140	50	REF	29.9	54.9	14.5	0.97:1.00:2.08	$Ti(HPO_4)_2 \cdot H_2O$
25	—	9.18	9.26	3.83	900	168	50	REF	32.8	56.8	8.2	1.02:1.00:1.14	$Ti(HPO_4)_2$

a) Solution containing 250 g TiO_2 and 1044 g/l H_2SO_4. b) PPT: precipitate method, REF: refluxing method.

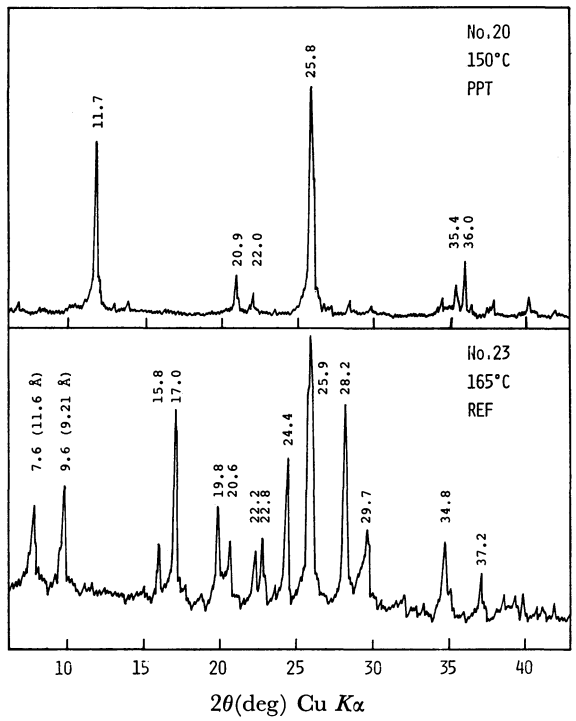

Fig. 3. X-Ray diffraction patterns of $Ti(HPO_4)_2 \cdot H_2O$ (No. 20) and $Ti(HPO_4)_2 \cdot 0—1/2H_2O$ (No. 23). No. 20: 15 mA, 20 kVP, No. 23: 20 mA, 30 kVP.

above 160 °C were almost the same with those of the hemihydrate obtained using amorphous titanium(IV) phosphate. However, from the results of analysis, the compositions of product were shown by $Ti(HPO_4)_2 \cdot 0—1/2H_2O$, and the products (Nos. 23, 25) corresponding to the anhydride were also formed at times. In the X-ray diffraction pattern of $Ti(HPO_4)_2 \cdot 0—1/2H_2O$ the intensity was lower than that of the monohydrate, two characteristic diffraction lines appearing at 11.6 and 9.21 Å. The lines also differed slightly in the 2θ values. It may be assumed from these X-ray diffraction patterns that $Ti(HPO_4)_2 \cdot 0—1/2H_2O$ is not a pure crystallite, but consists of two or more species. Generally, it is considered that the diffusion of phosphoric acid on the solid of titanium(IV) oxide monohydrate ($TiO_2 \cdot H_2O$) is the rate determining step. The powders of $TiO_2 \cdot H_2O$ were clearly dissolved with sulfuric acid, and therefore, the rate of formation of $Ti(HPO_4)_2 \cdot 0—1/2H_2O$ would be accelerated using a H_3PO_4–H_2SO_4 solution as compared with the pure phosphoric acid solution. The refluxing method, in which the suspended TiO_2–H_2O actively reacts with the mother liquor, is more suitable than the precipitate method.

References

1) a) The paper was presented at the 36th National Meeting of the Chemical Society of Japan, Osaka, April 1977; b) Part I of this series: E. Kobayashi, *Bull. Chem. Soc. Jpn.*, **48**, 3114 (1975); *Tokyo Kogyo Shikensho Hokoku*, **72**, 177 (1977).

2) C. B. Amphlett, "Inorganic Ion Exchangers,"Elsevier Publishing Company, Amsterdam (1964), p. 92.

3) M. Abe, *Bunseki Kagaku*, **23**, 1561 (1974).

4) E. Kobayashi and T. Goto, *Kogyo Kagaku Zasshi*, **73**, 692 (1970); *Tokyo Kogyo Shikensho Hokoku*, **66**, 313 (1971).

5) E. Kobayashi, *Kogyo Kagaku Zasshi*, **73**, 1797 (1970); *Tokyo Kogyo Shikensho Hokoku*, **66**, 326 (1971).

6) G. Alberti, P. Cardini-Gallt, U. Costantino, and E. Torracca, *J. Inorg. Nucl. Chem.*, **29**, 571 (1967).

7) K. Takaguchi and I. Tomita, *J. Chromatogr.*, **118**, 263 (1976).

Solubility of Hexaamminenickel(II) Complexes in Aqueous Ammonia Solution and the Thermal Decomposition of Ammine Complexes of Nickel(II)

Tsugio SATO,* Takeshi SUDA, Hideki UCHIDA, and Taijiro OKABE

Department of Applied Chemistry, Faculty of Engineering, Tohoku University, Aramaki, Sendai 980

(Received December 20, 1977)

The solubility of hexaamminenickel(II) complexes in aqueous ammonia solution (0 to 37 g-free NH_3/100 g-solv.) was investigated at temperatures 0—55 °C. It rapidly decreases with increase in free ammonia concentration but increases with rise in temperature. Hexaamminenickel(II) carbonate, sulfate, and chloride are slightly soluble at ammonia concentration above 30 g-free NH_3/100 g-solv., but nitrate is considerably soluble even at ammonia concentration of 35 g-free NH_3/100 g solv. The thermal decomposition of ammine complexes of nickel(II) was also investigated by means of TG and DTA under a streaming nitrogen gas atmosphere. Ammine complexes of nickel(II) decompose as shown in the following, the reaction orders and activation energies for steps a, b, c, and d being 0.5, 1.5, 1.0, and 0.5, and 16.5, 38.8, 25.3, and 79.4 kcal/mol, respectively.

$$[Ni(NH_3)_6](NO_3)_2 \xrightarrow{a} [Ni(NH_3)_4](NO_3)_2 \xrightarrow{b} [Ni(NH_3)_{2.5}](NO_3)_2 \longrightarrow NiO$$

$$[Ni(NH_3)_6]SO_4\cdot 2H_2O \longrightarrow [Ni(NH_3)_6]SO_4 \longrightarrow [Ni(NH_3)_2]SO_4 \xrightarrow{c} [Ni(NH_3)_{0.5}]SO_4 \longrightarrow$$

$$[Ni(NH_3)_5]SO_4\cdot H_2O \longrightarrow$$

$$NiSO_4 \xrightarrow{d} NiO$$

$$[Ni(NH_3)_6]CO_3\cdot 4H_2O \longrightarrow [Ni(NH_3)_4]CO_3\cdot 3H_2O \longrightarrow [Ni(NH_3)]CO_3\cdot H_2O \longrightarrow$$

$$[Ni(NH_3)]CO_3 \longrightarrow NiCO_3 \longrightarrow NiO$$

X-Ray diffraction data for $[Ni(NH_3)_6]Cl_2\cdot 0.5H_2O$, $[Ni(NH_3)_6](NO_3)_2$, $[Ni(NH_3)_5]SO_4\cdot H_2O$, and $[Ni(NH_3)_2]SO_4$ powder are given.

Various processes have been developed for the extraction of nickel from ores. Recently hydrometallurgical processes have drawn attention, since the recovery of nickel from low grade ores and non-sulfide ores is possible without any pollution problem. They are classified into two processes, leaching by an acid solution and that by an ammoniacal alkaline solution. The latter process has an advantage of little contamination by iron and magnesium. Some commercial operations based on the ammonia leaching process have been established, such as the Sherritt-Gordon process[1] of leaching sulfide ore, and the Nicaro process[2] of leaching laterite ore. In both processes, nickel is first leached as ammine complexes of nickel(II), but the subsequent steps differ a great deal. In the Sherritt-Gordon process, nickel metal is recovered by the reduction of hexaamminenickel(II) sulfate solution with compressed hydrogen. In the Nicaro process, nickel(II) oxide is recovered by the thermal decomposition of basic nickel(II) carbonate produced by heating the hexaamminenickel(II) carbonate solution and purging ammonia. In the present study it was found that the solubility of hexaamminenickel(II) complexes decreases rapidly with increase in free ammonia concentration in solution, and that the complexes decompose by releasing ammonia at considerably low temperature. This paper deals with studies of the solubility of hexaamminenickel(II) complexes in aqueous ammonia solution, and the thermal decomposition of solid ammine complexes of nickel(II) for the purpose of recovering highly purified nickel(II) salts or oxide by the thermal decomposition of solid ammine complexes separated by blowing ammonia gas into the leaching solution containing ammine complexes of nickel(II). Ammine complexes of nickel(II) are produced by blowing ammonia gas into aqueous nickel(II) salt solutions.[3-6] However, nickel has not been found to be completely recovered as hexaamminenikel(II) complex powder by an extreme increase of the free ammonia concentration. No report seems to have appeared on the solubility of hexaamminenikel(II) complexes in aqueous ammonia solution. Although several studies of thermal decomposition of hexaamminenickel(II) chloride,[7-12] nitrate,[7-9] and sulfate[7-9] have been reported, the thermal decomposition processes of hexaamminenickel(II) nitrate and sulfate are not clarified. No investigation of the thermal decomposition of hexaamminenickel(II) carbonate seems to have been carried out.

Part I. Solubility of Hexaamminenickel(II) Complexes in Aqueous Ammonia Solution

Experimental

Chemicals. Basic nickel(II) carbonate ($2NiCO_3\cdot 3Ni(OH)_2\cdot 3H_2O$) of reagent grade was used. All other chemicals were of analytical reagent grade.

Preparation of Hexaamminenickel(II) Complexes. Hexaamminenickel(II) carbonate was prepared as follows. Ten grams of ammonium carbonate and 19.5 g of basic nickel(II) carbonate were mixed in 100 ml of 16.5 wt% aqueous ammonia solution with a magnetic stirrer for 24 h. After the mixture had been filtered, ammonia gas was blown into the filtrate while being cooled with ice to precipitate hexaamminenickel(II) carbonate. Hexaamminenickel(II) chloride, sulfate, and nitrate were prepared by blowing ammonia gas into saturated aqueous solutions of nickel(II) chloride, sulfate, and nitrate, respectively. These complexes were washed with liquid ammonia and then kept in a

Table 1. Compositions of hexaamminenickel(II) complexes

Compound	Ni(wt%)		NH_3(wt%)	
	Found	Calcd	Found	Calcd
$[Ni(NH_3)_6]CO_3 \cdot 4H_2O$	20.5	20.0	33.5	34.9
$[Ni(NH_3)_6]SO_4 \cdot 2H_2O$	20.0	20.1	34.2	34.8
$[Ni(NH_3)_6](NO_3)_2$	19.4	20.6	36.4	35.8
$[Ni(NH_3)_6]Cl_2 \cdot 0.5H_2O$	23.9	24.4	41.9	42.4

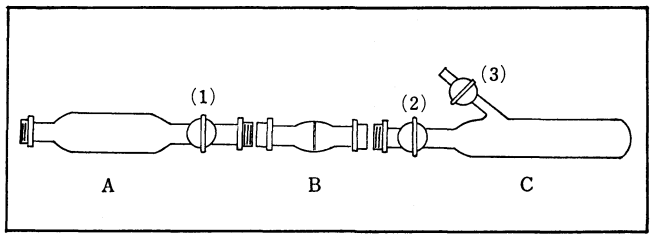

Fig. 1. Apparatus for solubility measurement.
A: Sealed glass tube, B: glass filter, C: sampling tube, 1,2,3: stopcock.

desiccator under ammonia atmosphere. The compositions of these complexes are given in Table 1.

Procedure. The apparatus for measurement of the solubility is shown in Fig. 1. The solubility of hexaamminenickel(II) complexes was determined as follows. Each 25 ml of sealed glass tube(A) was sealed soon after the transfer of 15 ml of aqueous ammonia solution of the desired concentration and excess amount of the sample complex, placed in a thermostat and agitated at 15 r.p.m. for 1 h. The sealed glass tube(A), glass filter(B) and sampling tube(C) were connected with each other. After the pressure of sampling tube(C) was reduced with an aspirator, stopcock(3) was closed, and stopcocks(1) and (2) were opened. A clear supernatant solution was withdrawn.

Analysis. Sampling tube(C) was separated from glass filter(B) and weighed. The sampling solution was acidified with excess standard sulfuric acid solution, diluted to a suitable concentration and subjected to the analysis of nickel(II) and ammonia. The amount of nickel(II) was determined by reacting nickel(II) with excess standard disodium ethylendiaminetetraacetate solution, and back-titrating the excess disodium ethylendiaminetetraacetate with standard zinc(II) chloride solution using Eriochrome Black T for end point detection. The total amount of nickel(II) and ammonia was determined by titrating excess sulfuric acid with standard sodium hydroxide solution using methylred for end point detection. The amount of ammonia was determined by subtracting the amount of nickel(II).

Results and Discussion

The solubility of hexaamminenickel(II) carbonate, chloride, sulfate, and nitrate in aqueous ammonia solution at temperatures 0—55 °C is given in Tables 2, 3, 4, and 5, respectively. The solubility of hexaamminenickel(II) carbonate and of sulfate linearly decreases with increase in free ammonia concentration up to 20 g free NH_3/100 g solvent. The complexes are slightly soluble at the free ammonia concentration above 30 g free NH_3/100 g solvent. The solubility of hexaamminenickel(II) carbonate increases with temperature when the free ammonia concentration is kept constant. The solubility at 55 °C is about twice that at 0 °C. The solubility of hexaamminenickel(II) sulfate

Table 2. Solubility of $[Ni(NH_3)_6]CO_3$ in aqueous ammonia solution

Temp (°C)	Free NH_3 concn (g-free NH_3/100 g-solv.)	Solubility (g/100 g-solv.)	Temp (°C)	Free NH_3 concn (g-free NH_3/100 g-solv.)	Solubility (g/100 g-solv.)
	3.5	39.85		7.4	56.72
	7.3	29.82		9.5	48.56
	10.0	22.12		14.0	34.01
0	11.8	16.76	45	18.8	24.78
	18.6	4.86		21.9	15.55
	20.0	4.14		26.8	6.09
	25.7	1.64		34.1	1.34
	33.2	0.11			
	6.9	49.50		0.2	88.88
	13.7	29.56		4.1	72.86
	17.7	18.27		6.2	64.11
25	21.8	8.64	55	9.6	56.72
	26.3	3.19		12.4	64.11
	28.3	2.03		25.0	12.97
	37.9	0.89		26.9	9.16
	41.0	0.22		33.8	2.03
	6.4	56.18			
	8.9	49.50			
	9.9	44.26			
35	11.9	38.95			
	17.6	22.76			
	19.2	17.05			
	28.6	2.95			
	33.7	1.34			

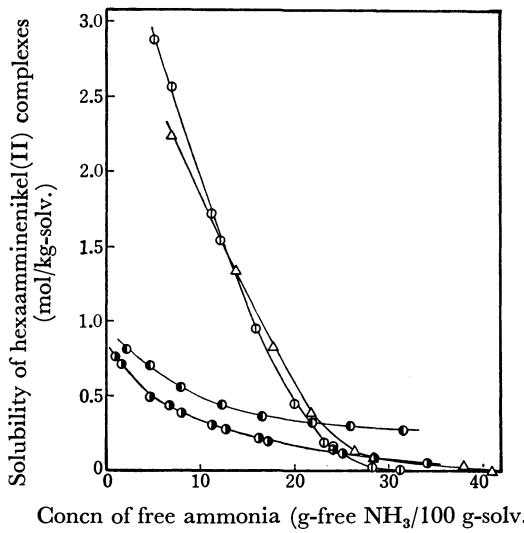

Fig. 2. Solubility of hexaamminenickel(II) complexes in aqueous ammonia solutions at 25 °C.
-⊖-: $[Ni(NH_3)_6]SO_4$, -△-: $[Ni(NH_3)_6]CO_3$, -◐-: $[Ni(NH_3)_6](NO_3)_2$, -◑-: $[Ni(NH_3)_6]Cl_2$.

TABLE 3. SOLUBILITY OF $[Ni(NH_3)_6]Cl_2$ IN AQUEOUS AMMONIA SOLUTION

Temp (°C)	Free NH_3 concn (g-free NH_3/100 g-solv.)	Solubility (g/100 g-solv.)	Temp (°C)	Free NH_3 concn (g-free NH_3/100 g-solv.)	Solubility (g/100 g-solv.)
	0.7	9.13		1.5	23.81
	3.0	7.37		2.7	19.43
	4.5	6.05		4.4	17.12
	6.6	4.30		8.6	12.66
0	8.1	3.60	45	12.9	9.24
	10.9	3.03		15.4	7.41
	14.5	2.62		19.4	5.71
	16.8	2.40		22.6	4.76
	22.3	1.94		25.9	3.85
	33.5	0.54		32.2	2.32
				37.1	1.65
	1.0	17.63			
	1.7	16.50		0.2	31.27
	4.7	11.52		6.0	17.12
	6.8	10.18		10.1	13.73
	8.1	8.93	55	15.9	9.04
25	11.3	7.12		19.3	6.76
	12.7	6.54		30.6	3.06
	16.2	5.34			
	17.1	4.73			
	24.1	3.20			
	25.1	2.88			
	28.5	2.23			
	36.1	1.39			
	0.7	22.46			
	1.1	21.51			
	3.3	16.40			
	4.5	14.55			
35	5.2	13.61			
	5.7	12.84			
	6.6	12.37			
	9.9	9.85			
	14.8	7.12			
	21.6	4.25			
	23.3	4.08			
	32.8	2.03			

TABLE 4. SOLUBILITY OF $[Ni(NH_3)_6]SO_4$ IN AQUEOUS AMMONIA SOLUTION

Temp (°C)	Free NH_3 concn (g-free NH_3/100 g-solv.)	Solubility (g/100 g-solv.)	Temp (°C)	Free NH_3 concn (g-free NH_3/100 g-solv.)	Solubility (g/100 g-solv.)
	1.9	56.18		6.6	77.56
	5.4	36.61		7.5	69.23
	8.7	24.15	35	9.6	61.71
0	11.7	14.64		13.2	45.52
	17.0	3.35		20.8	11.57
	21.3	1.43		25.4	3.92
	22.8	0.96			
	29.6	0.08		6.3	75.81
				6.9	73.13
	3.2	72.00		9.0	63.35
	7.9	49.77		15.0	35.35
	13.5	25.17	45	15.4	33.72
15	20.4	6.34		21.1	12.45
	25.7	2.31		24.7	4.42
	28.5	0.73		26.0	3.51
	33.7	0.28		31.2	0.88
	5.1	73.67		4.8	82.05
	6.9	65.84		10.3	57.98
	11.2	44.22	55	12.6	32.59
	12.1	39.76		19.9	15.25
25	15.9	24.36		24.5	4.45
	20.0	11.48		31.3	0.99
	23.0	5.19			
	24.0	4.37			
	28.2	0.93			
	31.2	0.54			

also increases with temperature up to 35 °C, remaining constant above 35 °C. The solubility of hexaamminenickel(II) chloride and of nitrate also decreases with increase in free ammonia concentration, but increases with rise in temperature. However, the decrements of solubility of these complexes with increase in free ammonia concentration are less than those of carbonate and sulfate. On the other hand, the increments of solubility of the former with temperature are larger than those of the latter; the solubility of hexaamminenickel(II) chloride and of nitrate at 55 °C is about four times as much as that at 0 °C.

Figure 2 shows the solubility of each hexaamminenickel(II) complex in aqueous ammonia solution at 25 °C. It is clear that the solubility of hexaamminenickel(II) carbonate and of chloride at low free ammonia concentration is similar to that of sulfate and nitrate respectively. The solubility of hexaamminenickel(II) carbonate and of sulfate is 3—4 times as much as that of chloride and nitrate at low free ammonia concentration. On the other hand, hexaamminenickel(II) carbonate, sulfate, and chloride are slightly soluble for free ammonia concentration above 30 g free NH_3/100 g solvent, nitrate, however, being considerably soluble even for free ammonia concentration of 35 g free NH_3/100 g solvent.

Part II. Thermal Decomposition of Ammine Complexes of Nickel(II)

Experimental

Preparation of Ammine Complexes of Nickel(II). Ammine complexes of nickel(II) except hexaamminenickel(II) complexes were prepared as follows. Tetraamminenickel(II) carbonate trihydrate: hexaamminenickel(II) carbonate tetrahydrate was left to stand in a desiccator under dilute ammoia atmosphere for at least 24 h. Monoamminenickel(II) carbonate monohydrate: hexaamminenickel(II) carbonate tetrahydrate was heated at 60 °C for 2 h. Pentaammine-

Table 5. Solubility of $[Ni(NH_3)_6](NO_3)_2$ in aqueous ammonia solution

Temp (°C)	Free NH_3 concn (g-free NH_3/100 g-solv.)	Solubility (g/100 g-solv.)	Temp (°C)	Free NH_3 concn (g-free NH_3/100 g-solv.)	Solubility (g/100 g-solv.)
	0.2	14.48		3.1	27.06
	3.9	6.85		9.6	18.76
	4.1	6.52		14.1	14.17
	5.6	5.53	45	17.2	12.68
0	10.4	4.22		23.3	10.93
	15.2	3.72		27.1	9.30
	17.7	3.32		35.0	8.70
	20.0	3.23			
	24.1	3.20		3.6	32.12
	27.4	2.88		8.9	22.16
	31.8	2.66		12.9	18.68
			55	17.6	15.57
	2.2	18.57		23.1	12.78
	4.7	15.59		29.0	10.89
	7.9	12.42		36.6	10.08
25	12.3	10.40			
	16.6	8.62			
	21.9	7.27			
	25.9	6.81			
	31.5	6.03			
	1.7	24.98			
	9.4	14.77			
35	15.8	11.50			
	20.6	9.81			
	24.4	8.86			
	27.3	7.76			
	30.7	7.67			

nickel(II) sulfate monohydrate: hexaamminenickel(II) sulfate dihydrate was washed with ammoniacal ethyl alcohol and ether. Diamminenickel(II) sulfate:hexaamminenickel(II) sulfate dihydrate was heated at 110 °C for 2 h. The compositions of ammine complexes prepared are given in Table 6.

Table 6. Compositions of ammine complexes of nickel(II)

Compound	Ni(wt%)		NH_3(wt%)	
	Found	Calcd	Found	Calcd
$[Ni(NH_3)_4]CO_3 \cdot 3H_2O$	16.2	16.9	30.7	29.4
$[Ni(NH_3)]CO_3 \cdot H_2O$	38.5	38.2	11.4	11.1
$[Ni(NH_3)_5]SO_4 \cdot H_2O$	21.7	21.3	30.3	30.8
$[Ni(NH_3)_2]SO_4$	30.1	31.1	16.6	18.0

Apparatus. A Rigaku Denki Thermoflex high temperature type TG-DTA instrument was used for TG and DTA studies. Samples, 10—20 mg in weight, were pyrolyzed under a streaming nitrogen gas atmosphere. The flow rate of nitrogen gas was 40 ml/min. The heating rate of the furnace was 10 and 20 deg/min. Ignited alumina was used as a reference material in the DTA sample block. X-Ray diffraction patterns were recorded over the range $2\theta = 10$—60° with an X-ray diffractometer, Rigaku Denki Geigerflex, using nickel filtered Cu $K\alpha$ radiation at 30 kV and 15 mA as the X-ray diffraction source, with a 2°/min scanning speed, a 1 s time constant, a 1° divergency slit and 0.2 mm receiving slit.

Results and Discussion

Thermal Decomposition Process. The TG and DTA curves, in nitrogen, for hexaamminenickel(II) sulfate dihydrate and pentaamminenickel(II) sulfate monohydrate are shown in Fig. 3.

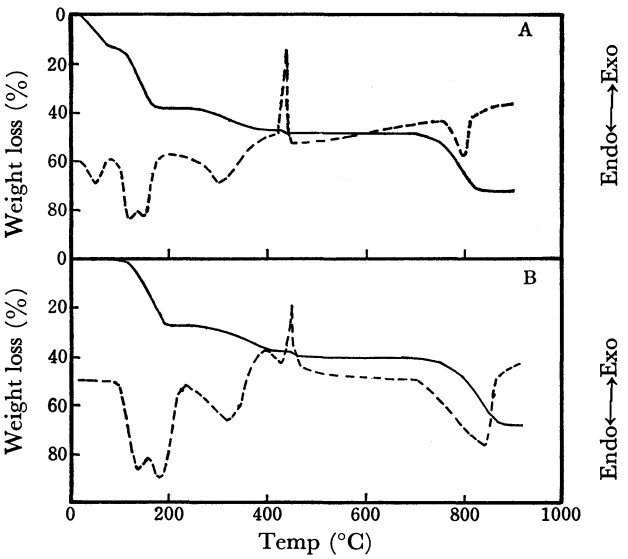

Fig. 3. TG and DTA curves of hexaamminenickel(II) sulfate dihydrate and pentaamminenickel(II) sulfate monohydrate under a nitrogen gas atmosphere.
A: $[Ni(NH_3)_6]SO_4 \cdot 2H_2O$, B: $[Ni(NH_3)_5]SO_4 \cdot H_2O$, flow rate of nitrogen gas: 40 ml/min, heating rate of furnace (deg/min)—A: 10, B: 20, amount of sample (mg)—A: 13.4, B: 16.6, —: TG, ---: DTA.

Hexaamminenickel(II) sulfate dihydrate appears to decompose in five steps as follows:

(I) $[Ni(NH_3)_6]SO_4 \cdot 2H_2O \longrightarrow [Ni(NH_3)_6]SO_4 + 2H_2O$

(II) $[Ni(NH_3)_6]SO_4 \longrightarrow [Ni(NH_3)_2]SO_4 + 4NH_3$

(III) $[Ni(NH_3)_2]SO_4 \longrightarrow [Ni(NH_3)_{0.5}]SO_4 + 1.5NH_3$

(IV) $[Ni(NH_3)_{0.5}]SO_4 \longrightarrow NiSO_4 + 0.5NH_3$

(V) $NiSO_4 \longrightarrow NiO + SO_2 + (1/2)O_2$

The complex, $[Ni(NH_3)_6]SO_4 \cdot 2H_2O$, begins to decompose at room temperature and loses two moles of water of crystallization per mole of compound to form $[Ni(NH_3)_6]SO_4$ up to 80 °C. The second step, corresponding to the loss of four moles of ammonia per mole of compound, begins immediately after the first step at *ca.* 80 °C, showing a definite break in the TG curve at *ca.* 180 °C. The third step of the decomposition results in the gradual loss of one and half moles of ammonia per mole of compound up to 350 °C. The fourth step of the decomposition begins at *ca.* 350 °C to gradually form $NiSO_4$ up to 450 °C. $NiSO_4$ begins to decompose at *ca.* 650 °C, resulting in the formation of NiO up to 820 °C. Endothermic peaks in the DTA curve at

50, 120—140, 300, 426, and 790 °C seem to correspond to steps I, II, III, IV, and V, respectively. The following studies have been performed on the thermal decomposition process of hexaamminenickel(II) sulfate.

(1) Paris:[8] $[Ni(NH_3)_6]SO_4 \longrightarrow [Ni(NH_3)_2]SO_4 \longrightarrow [Ni(NH_3)]SO_4 \longrightarrow [Ni(NH_3)_{0.5}]SO_4 \longrightarrow NiSO_4$

(2) Ephraim:[9] $[Ni(NH_3)_6]SO_4 \longrightarrow [Ni(NH_3)_4]SO_4 \longrightarrow [Ni(NH_3)_2]SO_4 \longrightarrow [Ni(NH_3)]SO_4 \longrightarrow [Ni(NH_3)_{0.5}]SO_4 \longrightarrow NiSO_4$

(3) Viltange:[10] $[Ni(NH_3)_6]SO_4 \xrightarrow{80-230\,^\circ C} [Ni(NH_3)_2]SO_4 \xrightarrow{230-350\,^\circ C} [Ni(NH_3)_{0.5}]SO_4 \xrightarrow{350-450\,^\circ C} NiSO_4$

(4) George and Wendlandt:[7] $[Ni(NH_3)_6]SO_4 \xrightarrow{100-190\,^\circ C} [Ni(NH_3)_2]SO_4 \xrightarrow{190-500\,^\circ C} NiSO_4$

Our results agree with the thermal decomposition process given by Viltange,[10] although the temperature we obtained for DTA peaks is lower by 10—20 degrees. A sharp exothermic peak in the DTA curve at 420—440 °C does not seem to have been reported so far.

Pentaamminenickel(II) sulfate monohydrate appears to decompose in four steps. The first step begins at *ca.* 110 °C, showing a definite break in the TG curve at *ca.* 180 °C. The weight loss up to this point corresponds to the loss of three moles of ammonia and one mole of water of crystallization per mole of compound. The thermal decomposition proceeds afterward in a similar manner to that after the third step of hexaamminenickel(II) sulfate dihydrate. The reason why the peaks in DTA curve of pentaamminenickel(II) sulfate monohydrate are situated at higher temperature region than those of hexaamminenickel(II) sulfate dihydrate seems to be due to the fact the heating rate of the furnace in the thermal decomposition of the former is faster than that of the latter.

Figure 4 shows the results of the thermal decomposition of hexaamminenickel(II) nitrate and carbonate tetrahydrate and tetraamminenickel(II) carbonate trihydrate. Tetraamminenickel(II) carbonate trihydrate and monoamminenickel(II) carbonate monohydrate (Table 6) are formed by the isothermal decomposition of hexaamminenickel(II) carbonate tetrahydrate at room temperature under a dilute ammonia atmosphere and at 60 °C in the air, respectively. Hexaamminenickel(II) carbonate tetrahydrate appears to decompose in five steps as follows:

(I) $[Ni(NH_3)_6]CO_3 \cdot 4H_2O \longrightarrow [Ni(NH_3)_4]CO_3 \cdot 3H_2O + 2NH_3 + H_2O$

(II) $[Ni(NH_3)_4]CO_3 \cdot 3H_2O \longrightarrow [Ni(NH_3)]CO_3 \cdot H_2O + 3NH_3 + 2H_2O$

(III) $[Ni(NH_3)]CO_3 \cdot H_2O \longrightarrow [Ni(NH_3)]CO_3 + H_2O$

(IV) $[Ni(NH_3)]CO_3 \longrightarrow NiCO_3 + NH_3$

(V) $NiCO_3 \longrightarrow NiO + CO_2 + (1/2)O_2$

Although no clear distinction is found between the first step and the second step from the TG curve, the

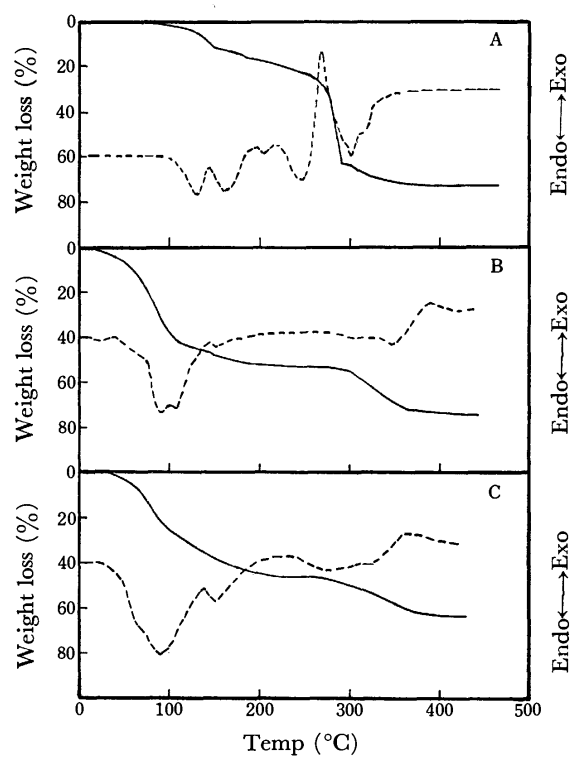

Fig. 4. TG and DTA curves of hexaamminenickel(II) nitrate and carbonate tetrahydrate and tetraamminenickel(II) carbonate trihydrate under a nitrogen gas atmosphere.
A: $[Ni(NH_3)_6](NO_3)_2$, B: $[Ni(NH_3)_6]CO_3 \cdot 4H_2O$, C: $[Ni(NH_3)_4]CO_3 \cdot 3H_2O$, flow rate of nitrogen gas: 40 ml/min, heating rate of furnace (deg/min)—A, B: 10, C: 20, amount of sample (mg)—A: 13.6, B: 16.6, C: 15.6, —: TG, ---: DTA.

complex, $[Ni(NH_3)_6]CO_3 \cdot 4H_2O$, seems to decompose *via* the complex, $[Ni(NH_3)_4]CO_3 \cdot 3H_2O$, because two endothermic peaks are found in the DTA curve at a temperature between 25 and 140 °C, and because $[Ni(NH_3)_4]CO_3 \cdot 3H_2O$ is produced from $[Ni(NH_3)_6]CO_3 \cdot 4H_2O$ at room temperature under a dilute ammonia atmosphere and is comparatively stable. Namely, $[Ni(NH_3)_6]CO_3 \cdot 4H_2O$ begins to decompose at room temperature and becomes $[Ni(NH_3)]CO_3 \cdot H_2O$ up to 140 °C *via* $[Ni(NH_3)_4]CO_3 \cdot 3H_2O$. The third step, corresponding to the loss of remaining water of crystallization, begins immediately after the second step at 140 °C to form $[Ni(NH_3)]CO_3$ up to 220 °C. The fourth step of the decomposition results in the gradual loss of remaining ammonia with the formation of $NiCO_3$ up to 300 °C. The fifth decomposition step begins at *ca.* 300 °C and results in abrupt weight loss with the formation of NiO up to 400 °C. The endothermic peaks in DTA curve at 95, 105, 153, and 345 °C seem to correspond to steps I, II, III, and IV, respectively.

The decomposition of tetraamminenickel(II) carbonate trihydrate seems to proceed in four steps. The first step of the decomposition begins at *ca.* 40 °C, showing a definite break in the TG curve at *ca.* 140 °C. The weight loss up to this point corresponds to the loss of three moles of ammonia and two moles of water of crystallization per mole of compound. The next steps

are similar to the processes after the third step of hexaamminenickel(II) carbonate tetrahydrate.

Hexaamminenickel(II) nitrate seems to decompose in three steps as follows:

$$\text{(I)}\quad [Ni(NH_3)_6](NO_3)_2 \longrightarrow [Ni(NH_3)_4](NO_3)_2 + 2NH_3$$

$$\text{(II)}\quad [Ni(NH_3)_4](NO_3)_2 \longrightarrow [Ni(NH_3)_{2.5}](NO_3)_2 + 1.5NH_3$$

$$\text{(III)}\quad [Ni(NH_3)_{2.5}](NO_3)_2 \longrightarrow NiO$$

The complex $[Ni(NH_3)_6](NO_3)_2$ begins to decompose at *ca.* 80 °C, showing a definite break in the curve at *ca.* 145 °C. The weight loss up to this point corresponds to the loss of two moles of ammonia per mole of compound. The second step begins immediately after the first step, losing one and half moles of ammonia per mole of compound up to 200 °C. The third step of the decomposition results in the abrupt weight loss with the formation of NiO at *ca.* 380 °C. Endothermic peaks at 140 and 160 °C, and exothermic peak at 250 °C seem to correspond to steps I, II, and III, respectively. George and Wendlandt[7] indicated that the ratio of evolved ammonia to nickel up to 180 °C is 2.76: 1. However, the ratio of that up to 200 °C has been found to be 3.5: 1 in the present study. Since the third step of the decomposition does not seem to be a single elementary reaction and is difficult to analyze, the detailed mechanism of the reaction has not been clarified. George and Wendlandt[7] observed that only nitrogen, water and oxygen are present in the decomposition gases above 260 °C by mass spectrographic analysis, and considered that the reaction between nitrate and ammonia should proceed. This conclusion has been confirmed on the basis of the appearance of the large exothermic peak at 250 °C.

Kinetics. The methods of Freeman-Carroll[13] and Coats-Redfern[14] were used to study the kinetics. The methods can be used only when the reaction is a single elementary reaction. Thus the kinetics was studied only for the first and second steps of hexaamminenickel(II) nitrate decomposition, and the third and the fifth steps of hexaamminenickel(II) sulfate dihydrate decomposition. The formula of the Freeman-Carroll method can be written as

$$\Delta \log (dW/dt)/\Delta \log W_r = x - E\Delta(1/T)/2.303RT(\Delta \log W_r), \quad (1)$$

where dW/dt is the weight change in mg·per minute, x the order of the reaction, T the absolute temperature and $W_r = W - W_c$, where W is the weight (mg) at time T, and W_c the weight (mg) of the sample at the end of the reaction. E is the energy of activation. If the plot of the ratio $\Delta \log (dw/dt)/\Delta \log W_r$ values *vs.* $\Delta(1/T)/\log W_r$ lie on a straight line, the activation energy and the reaction order will be given by its slope and intercept, respectively. This is illustrated in Figs. 5 and 6 for the decomposition of hexaamminenickel(II) nitrate and sulfate dihydrate, respectively.

The formula of the Coats-Redfern method can be written as

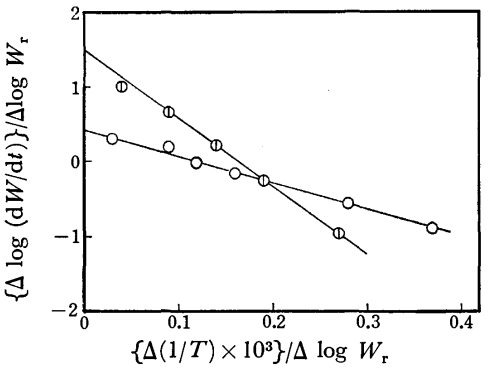

Fig. 5. Freeman-Carroll straight line for the I and II steps of hexaamminenickel(II) nitrate decomposition.
-○-: Step I, -◑-: Step II.

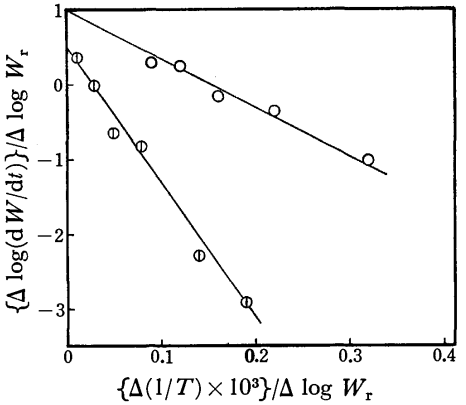

Fig. 6. Freeman-Carroll straight line for the III and V steps of hexaamminenickel(II) sulfate dihydrate decomposition.
-○-: Step III, -◑-: Step V.

$$\left.\begin{aligned} x \neq 1: &\log\{1-(1-\alpha)^{1-x}/(1-x)T^2\} \\ x = 1: &\log\{-\log(1-\alpha)/2.303T^2\} \end{aligned}\right\}, \\ = \log(AR/\phi E)(1-2RT/E) - E/2.303RT, \quad (2)$$

where α is the fraction of reaction, ϕ the heating rate of furnace and A the frequency factor. Graphic repre-

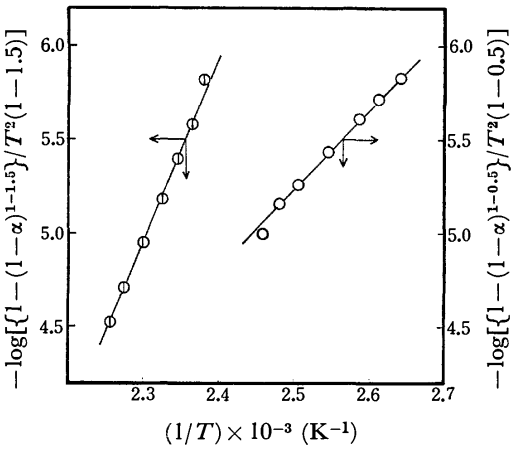

Fig. 7. Coats-Redfern straight line for the I and II steps of hexaamminenickel(II) nitrate decomposition.
-○-: Step I, -◑-: Step II, x— -○-: 0.5, -◑-: 1.5.

TABLE 7. REACTION ORDERS AND ACTIVITION ENERGIES OF THE THERMAL DECOMPOSITION OF NICKEL(II) AMMINE COMPLEXES

Nickel(II) ammine complexes	Decomposition step	E_1	E_2	E_{av}	x_1	x_2	x_{av}
$[Ni(NH_3)_6](NO_3)_2$	I	16.2	16.8	16.5	0.4	0.5	0.5
	II	38.2	39.4	38.8	1.5	1.5	1.5
$[Ni(NH_3)_6]SO_4 \cdot 2H_2O$	III	27.9	22.6	25.3	1.0	1.0	1.0
	V	80.6	78.2	79.4	0.5	0.5	0.5

E_1, x_1: determined by the Freemann-Carroll method, E_2, x_2: determined by the Coats-Redfern method, E_1, E_2: activation energy (kcal/mol), x_1, x_2: reaction order.

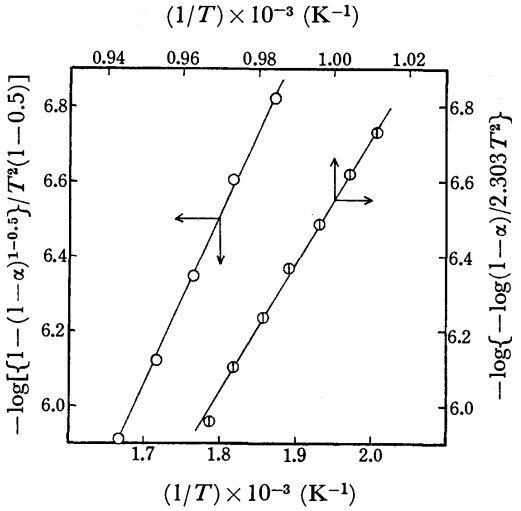

Fig. 8. Coats-Redfern straight line for the III and V steps of hexaamminenickel(II) sulfate dihydrate decomposition.
-○-: Step III, -⊕-: Step V.

sentation of the $\log\{1-(1-\alpha)^{1-x}/(1-x)\,T^2\}$ or $\log\{-\log(1-\alpha)/2.303T^2\}$ values as a function of $1/T$ gives a straight line of slope $-E/2.303R$ for the correct value of x. This is illustrated in Figs. 7 and 8 for the decomposition of hexaamminenickel(II) nitrate and sulfate dihydrate, respectively. The results are given in Table 7.

X-Ray Diffraction Data for Nickel(II) Ammine Complexes Powders. X-Ray diffraction data of four kinds of nickel(II) ammine complexes powders are given in Table 8. Hexaamminenickel(II) carbonate tetrahydrate and sulfate dihydrate decompose so rapidly in the air even at room temperature that their X-ray diffraction data have not been investigated.

This study is a part of studies on *Gasification of Coals Treated with Non-aqueous Solvents* being carried out by Coal Gasification Research Group (representative, Prof. Y. Tamai) in the Chemical Research Institute of Non-aqueous Solutions, Tohoku University. The object of the study is the recovery of nickel used as a catalyst in the coal gasification process.

TABLE 8. X-RAY DIFFRACTION DATA OF NICKEL(II) AMMINE COMPLEXES POWDERS

d(Å)	I/I_1	d(Å)	I/I_1
$[Ni(NH_3)_6]Cl_2 \cdot 0.5H_2O$		$[Ni(NH_3)_6](NO_3)_2$	
5.83	100	6.28	100
3.56	30	3.85	31
3.04	8	3.29	9
2.91	23	3.14	8
2.52	16	2.72	7
2.06	9	2.43	3
1.94	6	2.09	4
1.78	6	1.92	3
1.70	6		
1.59	6		
$[Ni(NH_3)_5]SO_4 \cdot H_2O$		$[Ni(NH_3)_2]SO_4$	
6.07	53	5.57	100
5.61	77	4.93	50
5.34	32	3.60	25
5.19	45	3.24	38
4.42	100	2.59	31
4.19	69	1.93	21
4.02	57	1.77	20
3.47	30		
3.15	24		
3.00	30		

References

1) F. A. Forward, C. S. Samis, and V. Kudryk, *Trans. Can. Inst. Min. Met.*, **51**, 350 (1948).
2) P. Queneau, "Extractive Metallurgy of Copper, Nickel, and Cobalt," New York (1961), p. 347.
3) G. Andre, *C. R. Acad. Sci.*, **106**, 936 (1888).
4) F. Kocsis, *Magy. Kem. Folyr.*, **34**, 33 (1928).
5) F. Ephraim, *Ber. Deut. Chem. Ges.*, **45**, 1322 (1912).
6) M. Grandperrin, *Bull. Soc. Chim. Fr.*, **5**, 1712 (1938).
7) T. D. George and W. W. Wendlandt, *J. Inorg. Nucl. Chem.*, **25**, 395 (1963).
8) R. Paris, *Ann. Chim. (Paris)*, **10**, 363 (1955).
9) F. Ephraim, *Ber. Deut. Chem. Ges.*, **46**, 3103 (1913).
10) M. Viltange, *Mikrochim. Acta*, 609 (1965/4).
11) I. G. Murglescu and E. Segal, *Rev. Roum. Chim.*, **11**, 13 (1966).
12) I. G. Murglescu and E. Segal, *Rev. Roum. Chim.*, **11**, 291 (1966).
13) F. S. Freeman and B. Carroll, *J. Phys. Chem.*, **62**, 394 (1958).
14) A. W. Coats and J. P. Redfern, *Nature*, **201**, 68 (1964).

Kinetic Studies of the Aluminium Acetate Complex Formation Reaction in Aqueous Solutions by the Pressure-Jump Method

Michinori HIRAISHI,* Shoji HARADA,** and Tatsuya YASUNAGA**

Department of Chemistry, Faculty of Education, Miyazaki University, Funatsuka, Miyazaki 880
***Department of Chemistry, Faculty of Science, Hiroshima University, Higashisenda-machi, Hiroshima 730*

(Received December 26, 1977)

The pressure-jump method was applied to aqueous solutions of aluminium acetate. Relaxation effects were observed in ms and s regions. Both relaxation times depend a great deal on the pH of solution. They were ascribed to the following complex formation reactions.

$$Al^{3+} \underset{Ac^-}{\overset{\text{slow}}{\rightleftharpoons}} AlAc^{2+} \underset{Ac^-}{\overset{\text{fast}}{\rightleftharpoons}} AlAc_2^+$$

Detailed studies on the fast relaxation effect revealed that the hydrolyzed ionic species accelerate the overall reaction. The mechanism of the fast reaction was discussed, the kinetic parameters being obtained.

The relaxation method mainly developed by Eigen *et al.*[1] has made it possible to study kinetically the fast metal complex formation reaction. Considerable kinetic information now exists on the complexations of metal ions with organic and inorganic ligands.[2,3] Many relaxation phenomena can be interpreted by the step-by-step association picture.

On the complexation of aluminium ion, a few kinetic studies have so far been reported, such as pressure-jump studies of aluminium sulfate[4,5] and aluminium ferricyanide.[6] The present study was undertaken in order to obtain kinetic information on the complex formation reaction of aluminium ion with acetate ion by means of the pressure-jump method at different concentrations, acidities and temperatures.

Experimental

Chemicals of reagent grade were used without purification. A stock solution of aluminium acetate was prepared by mixing a stoichiometric amount of $Al_2(SO_4)_3$ with barium acetate and removing the $BaSO_4$ produced by centrifugation. Barium acetate was prepared by neutralizing acetic acid with $Ba(OH)_2$. The concentration of aluminium in the resulting solution was gravimetrically determined by means of oxine precipitation. Each solution was prepared by diluting the standard solution with an acetic acid solution of known concentration to the desired concentration and pH. No supporting electrolyte was added in order to avoid a decrease in relaxation amplitude.

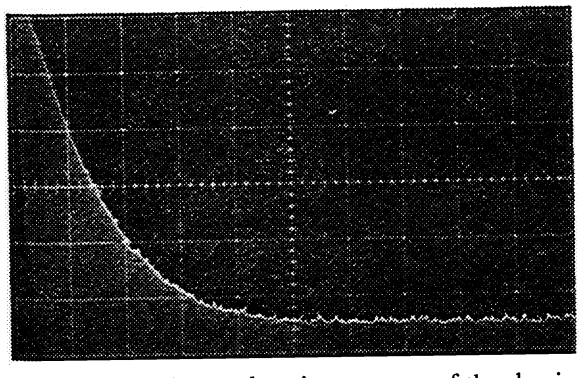

Fig. 1. Pressure-jump relaxation spectrum of the aluminium acetate system at 25 °C: $\sum Al = 2.46 \times 10^{-3}$ M, $\sum Ac = 0.105$ M, pH=3.76; sweep 20 ms/div.

The measurement of the relaxation effect was carried out by pressure-jump technique with a conductivity readout. A representative relaxation spectrum in ms region is shown in Fig. 1. The apparatus realizes a pressure jump of about 100 atm within 100 μs.[7] The temperature of the sample was controlled to ±0.1 °C by circulating thermostated water around the pressure-jump cell.

Results and Discussion

Two relaxation phenomena were observed in all the aluminium acetate solutions: a fast reaction with ms order time constant and a slow reaction with s order time constant. Both relaxation times depend a great deal on the pH of the solution.

In the blank test, neither $Al(NO_3)_3$ nor acetic acid aqueous solution showed relaxation phenomena under the same experimental conditions and in the same time region. This indicates that the relaxation effects observed in the aluminium acetate system can be ascribed to the complex formation reaction of aluminium ion with acetate ion, and are not directly associated with either the hydrolysis reaction of aluminium ion or the dissociation reaction of acetic acid.

In comparison with the rate constants of the water exchange reaction of aluminium ion measured by NMR[8,9] and those of the complex formation reaction of other aluminium complexes,[4-6] the relaxation effects observed in the present experiment are attributed to the following reactions.

$$Al^{3+} \underset{Ac^-}{\overset{\text{slow}}{\rightleftharpoons}} AlAc^{2+} \underset{Ac^-}{\overset{\text{fast}}{\rightleftharpoons}} AlAc_2^+ \qquad (1)$$

Two series of measurements were performed: (i) variation of pH by the addition of acetic acid, the total concentration of aluminium being kept constant (Table 1) and (ii) variation of the total concentrations of aluminium and acetic acid, the pH being kept at 3.76 (Table 2). The reciprocal relaxation times represent an average of at least four runs, the maximum errors being less than ±10%.

In the present study, the following equilibria are assumed to be present.

$$Al^{3+} + Ac^- \overset{K_1}{\rightleftharpoons} AlAc^{2+} \qquad (2)$$

TABLE 1. RECIPROCAL RELAXATION TIMES AND EXPERIMENTAL CONDITIONS FOR THE ALUMINIUM ACETATE SYSTEM AT CONSTANT $\sum$Al OF 0.99×10^{-2} M

$\sum$Ac, M	pH	τ^{-1}, s^{-1}		
		20 °C	25 °C	30 °C
0.0670	4.43	109.5	179.2	349.8
0.0839	4.25	77.18	135.3	277.1
0.1069	4.15	64.06	120.6	213.0
0.1452	4.02	45.77	85.68	162.0
0.1834	3.90	37.46	71.18	146.8
0.2599	3.78	29.89	58.01	115.2
0.3365	3.61	25.84	47.34	103.0
0.4895	3.50	20.80	40.01	73.61
0.6043	3.28	18.72	35.38	74.16
1.2295	3.13	16.04	29.07	57.54
1.4293	3.06	15.86	32.05	55.35

TABLE 2. RECIPROCAL RELAXATION TIMES AND EXPERIMENTAL CONDITIONS FOR THE ALUMINIUM ACETATE SYSTEM AT CONSTANT pH OF 3.76

$\sum$Al, 10^{-2} M	$\sum$Ac, M	τ^{-1}, s^{-1}	
		20 °C	25 °C
1.98	0.4605	32.00	60.24
0.981	0.2763	24.93	48.30
0.487	0.1770	22.10	44.89
0.246	0.1054	19.66	39.98
0.124	0.0808	15.10	32.90
0.0625	0.0468		24.11

$$AlAc^{2+} + Ac^- \overset{K_2}{\rightleftharpoons} AlAc_2^+ \quad (3)$$

$$Al^{3+} + H_2O \overset{K_3}{\rightleftharpoons} AlOH^{2+} + H^+ \quad (4)$$

$$AlOH^{2+} + Ac^- \overset{K_4}{\rightleftharpoons} Al(OH)Ac^+ \quad (5)$$

$$HAc \overset{K_5}{\rightleftharpoons} Ac^- + H^+ \quad (6)$$

In order to analyze the kinetic data and elucidate the reaction mechanism, it is necessary to evaluate the equilibrium concentrations of each ionic species in solution. For this purpose, the equilibrium constants of Eqs. 2—6 should be known. However, no stability constants of aluminium acetate complexes are found in literature. The equilibrium constants of equilibria 2 and 3 were evaluated to be the same as those of the propionate ligand,[10] *i.e.*, $K_1=60$ M^{-1} and $K_2=43$ M^{-1}. The other equilibrium constants were taken from literature as follows. $K_3=10^{-5.0}$ M,[11] $K_4=10^{2.4}$ M^{-1} [12] and $K_5=10^{-4.7}$ M.[13] The result of calculations revealed that the concentrations of the hydrolyzed species $AlOH^{2+}$ and $Al(OH)Ac^+$ are very small as compared to those of unhydrolyzed complex ions and can be neglected.

If we take account of the fact that the relaxation times in the present system depend a great deal on the concentration of the hydrogen ion, the overall mechanism of Eq. 3 can be expressed by the following reaction scheme.

$$\begin{array}{ccccc} & & HL & & \\ & & +H\uparrow\downarrow -H\ K_5 & & \\ L+LM & \overset{K_{12}}{\rightleftharpoons} & LMO\begin{matrix}H\\ \diagup\\ \diagdown\\ H\end{matrix}L & \overset{k_{23}}{\underset{k_{32}}{\rightleftharpoons}} & ML_2 \\ +H\uparrow\downarrow -H & & +H\uparrow\downarrow -H & & +H\uparrow\downarrow -H \\ L+LM(OH) & \overset{K_{45}}{\rightleftharpoons} & LM(OH)O\begin{matrix}H\\ \diagup\\ \diagdown\\ H\end{matrix}L & \overset{k_{56}}{\underset{k_{65}}{\rightleftharpoons}} & L_2M(OH) \end{array} \quad (7)$$

where L is the ligand (=acetate ion), LM the metal complex ion (=$AlAc^{2+}$), K_{12} and K_{45} are the outer-sphere complex formation constants.

All the vertical steps are protolytic reactions and very fast, while in the horizontal steps the outer-sphere complex formation reactions (①⇌② and ④⇌⑤) are fast as compared to the inner-sphere complex formation reactions. Thus, the reactions within the coordination sphere (②⇌③ and ⑤⇌⑥) are the rate-determining steps of the complex formation. The reciprocal relaxation time for this system, then, is given by

$$\tau^{-1} = A(k_{32} + k_{65}K_{36}/C_H), \quad (8)$$

where K_{36} is the hydrolysis constant of inner-sphere complex and

$$A = 1 + K_{23}\cdot\frac{K_{12}\{C_{LM}/(1+\alpha)+C_L\}}{1+K_{12}\{C_{LM}/(1+\alpha)+C_L\}}, \quad (9)$$

with

$$\alpha = \frac{C_H}{K_5 + C_L}. \quad (10)$$

From calculation of ionic concentrations, α was found to be smaller than unity under the present experimental conditions. Thus, Eq. 9 becomes

$$A = 1 + K_{23}\cdot\frac{K_{12}(C_{LM}+C_L)}{1+K_{12}(C_{LM}+C_L)}. \quad (11)$$

In order to use this equation, the values of K_{23} and K_{12} should be known. K_{12} was estimated by means of the Fuoss equation.[14,15] K_{23} is related to K_{12} as regards

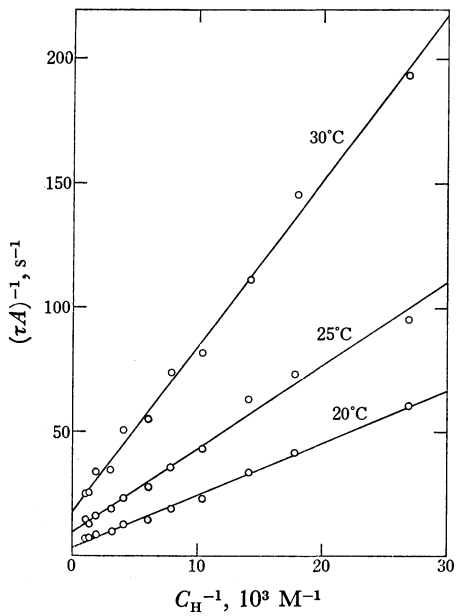

Fig. 2. $(\tau A)^{-1}$ *vs.* C_H^{-1} plot at various temperatures. $\sum$Al was kept constant to be 0.99×10^{-2} M.

the conventional stability constant K_2 as follows:

$$K_2 = K_{12}(1 + K_{23}). \quad (12)$$

In the pH variation measurement, the values of $(\tau A)^{-1}$ are plotted against C_H^{-1} to give k_{32} and $k_{65}K_{36}$ from the intercept and the slope of the line, respectively. Plots of values in Table 1 lie on straight lines for each temperature (Fig. 2). Taking into account the small variation of A, *i.e.*, 1.8—2.3, τ^{-1} depends predominantly on the concentration of the hydrogen ion and only slightly on those of other ionic species. Thus, k_{32} and $k_{65}K_{36}$ were obtained from Fig. 2 and k_{23} was calculated by means of the relation $K_{23}=k_{23}/k_{32}$. The values obtained are given in Table 3.

Table 3. Kinetic data for the aluminium acetate complex formation reaction of mechanism (7) at 25 °C and $\mu=0.03$

K_{12}	M^{-1}	2.9
K_{23}		13.9
k_{23}	s^{-1}	132
k_{32}	s^{-1}	9.5
$\Delta E_{32}^{\ddagger}$	kcal mol^{-1}	29.9
$\Delta H_{32}^{\ddagger}$	kcal mol^{-1}	29.3
$\Delta S_{32}^{\ddagger}$	cal deg^{-1} mol^{-1}	46.6
$k_{65}K_{36}$	$M\,s^{-1}$	0.0034

In the pH constant measurement, the terms in parenthesis of Eq. 8 remain constant, τ^{-1} being affected only by A. Under the present conditions of pH 3.76, the ratio of $k_{65}K_{36}/C_H$ to k_{32} was found to be 2.0 at 25 °C (Fig. 2). Applying this ratio to Eqs. 8 and 11, the following equation is obtained as an empirical formula at pH 3.76 and 25 °C:

$$\tau^{-1} = 3.0\left\{k_{32} + k_{23}\cdot\frac{K_{12}(C_{LM} + C_L)}{1 + K_{12}(C_{LM} + C_L)}\right\}. \quad (13)$$

The values of τ^{-1} in Table 2 are plotted against $K_{12}(C_{LM}+C_L)/\{1+K_{12}(C_{LM}+C_L)\}$ and are shown in Fig. 3. The intercept and the slope of the straight line gave k_{32} and k_{23} to be 7.4 and 112 s^{-1} respectively, K_{23} being calculated to be 15.0 by means of the relation $K_{23}=k_{23}/k_{32}$. The values are comparable to those in Table 3. The fact that the values of the rate constants obtained in two different measurements coincide approximately indicates that reaction mechanism 7 and the relaxation formulas are reasonable.

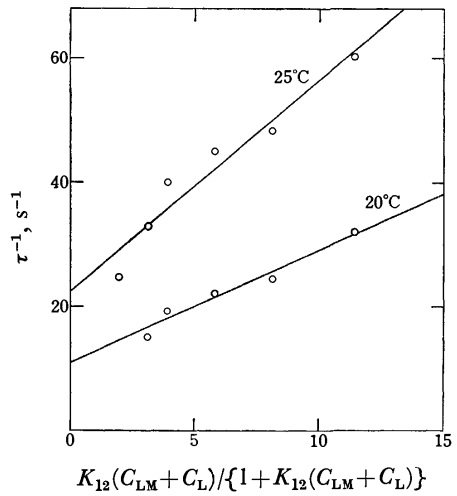

Fig. 3. τ^{-1} *vs.* $K_{12}(C_{LM}+C_L)/\{1+K_{12}(C_{LM}+C_L)\}$ plot at 25 °C. pH was kept constant to be 3.76.

In the aqueous solutions of aluminium ion and its complex ions, the rate constant of the coordinated water exchange, k_{H_2O}, has also been measured by means of NMR. The value of k_{H_2O} of Al^{3+} is about 1 s^{-1}, [8] smaller by a factor of 10^2 than that of k_{23}. This is why the slow relaxation effect was attributed to equilibrium 2 and the fast to equilibrium 3. Although k_{23} should be discussed in comparison with k_{H_2O} of $AlAc^{2+}$ ion, the value of the latter has not been found in literature. In the DMF solutions of Al^{3+} and $Al(acac)^{2+}$, the rate constants of the coordinated solvent molecule exchange have been reported. The value of $Al(acac)^{2+}$ [16] is accelerated by a factor of 10^2 as compared to that of Al^{3+}. [17] This increment may be caused by the instabilization of the coordinated solvent molecule owing to the electrostatic charge effect. Applying the same idea to the aqueous solution system of aluminium acetate, the value of k_{23} may be recognized as the rate constant of the coordinated water exchange of $AlAc^{2+}$.

The temperature dependence of the rate constants, k_{32}, gave the Arrhenius energy of activation, $\Delta E_{32}^{\ddagger}$, enthalpy of activation, $\Delta H_{32}^{\ddagger}$, and entropy of activation, $\Delta S_{32}^{\ddagger}$ (Table 3).

It is predicted that the slow relaxation effect in the present observation can be ascribed to the reaction of equilibrium 2.

References

1) M. Eigen and L. DeMaeyer, "Technique of Organic Chemistry," Vol. VIII, ed by W. P. Mason, Academic Press, New York (1963).

2) M. Eigen and R. G. Wilkins, *Adv. Chem. Ser.*, **49**, 55 (1964).

3) D. J. Hewkin and R. H. Prime, *Coord. Chem. Rev.*, **5**, 45 (1970).

4) B. Behr and H. Wend, *Ber. Bunsenges. Phys. Chem.*, **66**, 223 (1962).

5) C. Kalidas, W. Knoche, and D. Paradoulos, *Ber. Bunsenges. Phys. Chem.*, **75**, 106 (1971).

6) M. Matušek and H. Strehlow, *Ber. Bunsenges. Phys. Chem.*, **73**, 427 (1969).

7) W. Knoche, "Techniques of Chemistry," Vol. VI, Part II, 3rd ed, ed by G. G. Hammes, A Wiley-Interscience Publication, New York (1974), p. 187.

8) D. Fist and R. E. Connick, *J. Am. Chem. Soc.*, **90**, 608 (1968).

9) R. E. Schuster and A. Fratiello, *J. Chem. Phys.*, **47**, 1554 (1967); A. Fratiello, R. E. Lee, V. M. Nishida, and R. E. Schuster, *ibid.*, **47**, 4951 (1967).

10) P. H. Tedesco and V. B. De Rumi, *J. Inorg. Nucl. Chem.*, **37**, 1833 (1975).

11) L. G. Sillén and A. E. Martell, "Stability Constants," the Chemical Society, London (1964), p. 65.

12) A. S. Kereichuk and L. M. Il'cheva, *Zh. Neorg. Khim.*, **21**, 380 (1976); *Chem. Abstr.*, **84**, 141429t (1976).

13) R. C. Weast, "Handbook of Chemistry and Physics," the Chemical Rubber Co., Cleveland (1964).
14) R. M. Fuoss, *J. Am. Chem. Soc.*, **80**, 5059 (1958).
15) G. G. Hammes and J. I. Steinfeld, *J. Am. Chem. Soc.*, **84**, 4639 (1962).
16) N. A. Matwiyoff and W. G. Movius, *J. Am. Chem. Soc.*, **90**, 5452 (1968).
17) W. G. Movius and N. A. Matwiyoff, *Inorg. Chem.*, **61**, 847 (1967); *J. Phys. Chem.*, **72**, 3063 (1968).

Trimethylenediamine Complexes. V.[1] Preparative and Kinetic Studies on the Reactions of (Ethylenediamine)tetranitro- and Tetranitro(trimethylenediamine)-cobaltates(III) with Several Nucleophiles

Yoshiaki Ito and Shinichi Kawaguchi*

Department of Chemistry, Faculty of Science, Osaka City University, Sumiyoshi-ku, Osaka 558

(Received January 9, 1978)

Substitution reactions of a nitrite ligand in $Co(NO_2)_4(en \text{ or } tn)^-$ with NH_3, py, N_3^-, and NCS^- have been investigated. The product trinitro complexes were isolated and their geometrical structures were assigned on the basis of NMR data. The preparation method for the two conformational isomers of *mer*-$Co(NO_2)_3NH_3(en)$ was established. The kinetic data of substitution with azide were analyzed according to the **D** mechanism. The relative nucleophilicity of ligands towards $Co(NO_2)_3(AA)$ is in the order: $OH^- \gg N_3^- > NO_2^-$, CH_3COO^-, $NCS^- \gg H_2O > Cl^-$, I^-. Dinitro complexes, $[Co(NO_2)_2(phen)(en \text{ or } tn)]NO_2 \cdot H_2O$ and $K[Co(NO_2)_2(ox)(tn)]$ were also prepared.

In a previous paper[1] the acid and base hydrolysis reactions of (diamine)tetranitrocobaltates(III), $Co(NO_2)_4(AA)^-$, where AA is ethylenediamine (en) or trimethylenediamine (tn), were reported to proceed *via* the **D** mechanism with $Co(NO_2)_3(AA)$ as a common intermediate, and the relative reactivity towards the five-coordinate intermediate was found to be in the order: $OH^- \gg NO_2^- \gg H_2O$. The present paper is concerned with preparation and characterization of $Co(NO_2)_3X(AA)$ ($X = NH_3$, py, N_3^-, or NCS^-) and other related complexes, and also with competitive reactions of some nucleophiles with $Co(NO_2)_3(AA)$.

Experimental

Preparation of Complexes. Potassium Tetranitro(ethylenediamine or trimethylenediamine)cobaltate(III), K[Co(NO$_2$)$_4$(AA)]: These complexes were prepared by the literature method[2] and recrystallized twice from water–methanol. The trimethylenediamine complex was obtained as a hemihydrate in a 46% yield.[1]

Trinitro(pyridine)(ethylenediamine or trimethylenediamine)cobalt(III), Co(NO$_2$)$_3$(py)(AA): In an aqueous solution (20 ml) $K[Co(NO_2)_4(en)]$ (1.0 g) was allowed to react with pyridine (0.25 ml) at 60 °C for 1 h. The mixture was then cooled with ice–water and a precipitate (monohydrate) was filtered and washed with methanol. The yield was 19% (0.2 g). The tn complex (anhydrous) was also obtained by a similar reaction at 60 °C for 30 min in a 42% (0.4 g) yield.

The Yellow Form and Brown Form of Ammine(ethylenediamine)-trinitrocobalt(III), Co(NO$_2$)$_3$NH$_3$(en): To a solution (20 ml) of $K[Co(NO_2)_4(en)]$ (1 g) was added 28% aqueous ammonia (0.41 ml) and the mixture was stirred at 60 °C. After *ca.* 45 min white amorphous powder began to deposit on the wall around the liquid surface. On further heating yellow crystallites gradually increased. After reaction for about 2 h the mixture was cooled with ice. The precipitate was filtered and washed with methanol. The yield was 25% (0.2 g).

When the above reaction mixture was cooled with ice before the white powder appeared, a brown precipitate was produced, which was filtered and washed with methanol. The yield was also 25% (0.2 g).

Amminetrinitro(trimethylenediamine)cobalt(III), Co(NO$_2$)$_3$NH$_3$(tn): The reaction of $K[Co(NO_2)_4(tn)] \cdot 1/2H_2O$ with ammonia in the same composition as above at 60 °C for about 20 min afforded a yellow precipitate. Only one kind of product was obtained in a 38% (0.3 g) yield in this case.

Potassium Azido(ethylenediamine)trinitrocobaltate(III), K[Co(NO$_2$)$_3$(N$_3$)(en)]: $K[Co(NO_2)_4en]$ (1 g) was allowed to react with sodium azide (0.19 g) in aqueous solution (55 ml) at 60 °C for 75 min. After cooling in ice–water, potassium iodide (*ca.* 5 g) was added to the solution, and a small amount of precipitate was filtered. Ethanol (*ca.* 10 ml) was added to the filtrate, and the solution was kept in a refrigerator for several days. Crude crystals of Isomer A (0.3 g) was separated and recrystallized from methanol–water (5: 1) in a refrigerator (below 0 °C). The final yield was 8% (0.08 g).

After the prolonged reaction in aqueous solution (25 ml) at 60 °C for 2 h and addition of potassium iodide at 0 °C as described above, an equal volume (*ca.* 25 ml) of methanol was added to the solution and the mixture was kept in a refrigerator overnight. A red powder (0.1 g), which gave Isomer A on recrystallization, was filtered and the filtrate was kept in a refrigerator for 2—3 months to deposit dark red crystals of Isomer B, which were separated and washed with methanol. The yield was 35% (0.35 g).

Potassium Azidotrinitro(trimethylenediamine)cobaltate(III) K[Co(NO$_2$)$_3$N$_3$(tn)]: In aqueous solution (15 ml) at 60 °C $K[Co(NO_2)_4(tn)] \cdot 1/2H_2O$ (1.0 g) was allowed to react with sodium azide (0.18 g) for 20 min. After filtration, potassium iodide (*ca.* 0.5 g) was added to the filtrate followed by 15 ml of methanol and the mixture was kept in a refrigerator for a week. A dark red precipitate was recrystallized from methanol–water (5: 1 by volume). The final yield was 19% (0.2 g) and the compound was analyzed to contain two molecules of lattice water and proved to be a mixture of fac and mer isomers (Table 2). When the filtrate, which had been separated from the crude reaction product, was kept in a refrigerator for a few weeks, dark red crystals deposited on the glass wall in a 10% yield (0.1 g). This specimen was a monohydrate of the mer isomer as will be described in Results. Then the separation of a mixture of the geometrical isomers was tried. A solution of $K[Co(NO_2)_3N_3(tn)] \cdot 2H_2O$ was passed through a column ($\phi 1 \times 10$ cm) containing an anion exchanger QAE-Sephadex A-25 which was cooled by ice–water circulating in a jacket. Two adsorbed bands were observed and eluted with an aqueous solution (0.4 mol·l^{-1}) of sodium chloride. The early portion of eluates containing the lower band showed an absorption spectrum which is identical with that of $K[Co(NO_2)_3N_3(tn)] \cdot H_2O$, and is concluded to be the mer isomer. The upper adsorbed band may be attributed to the fac isomer and showed an absorption maximum at 470 nm with $\varepsilon = 380$ l·mol^{-1}·cm^{-1}. The cobalt content in the eluate was deter-

mined by the photochemical reduction to cobalt(II) followed by the spectrophotometric analysis of the latter as the tetrakis (isothiocyanato)cobaltate(II) complex.[3]

Potassium Isothiocyanatotrinitro(trimethylenediamine)cobaltate(III) Monohydrate, $K[Co(NO_2)_3NCS(tn)]\cdot H_2O$: The reaction of $K[Co(NO_2)_4(tn)]\cdot 1/2H_2O$ (0.5 g) with potassium thiocyanate (0.133 g) in aqueous solution (20 ml) at 60 °C was conducted for 15—20 min. To the solution cooled in ice–water was added potassium iodide (*ca.* 5 g) followed by an equivolume of methanol and the mixture was kept in a refrigerator for 2—3 days to precipitate small reddish plates in a 15% (0.08 g) yield.

Dinitro(1,10-phenanthroline)(ethylenediamine or trimethylenediamine)cobalt(III) Nitrite Monohydrate, $[Co(NO_2)_2(phen)(AA)]NO_2\cdot H_2O$: To an aqueous solution (20 ml) of $K[Co(NO_2)_4(AA)]$ (1 g) at 60 °C was added a small quantity of methanol solution containing 1,10-phenanthroline (0.579 g) and the mixture was stirred for about 5 min to deposit red-brown (AA=en) or brown (AA=tn) crystals in a 60% (0.8 g) or a 70% (0.9 g) yield, respectively.

Potassium Dinitro(oxalato)(trimethylenediamine)cobaltate(III), $K[Co(NO_2)_2(ox)(tn)]$: A solution (20 ml) of oxalic acid (2 g) was added to a suspension of $K[Co(NO_2)_4(tn)]\cdot 1/2H_2O$ (5 g) in water (30 ml), and the mixture was kept at 60 °C under reduced pressure to vaporize the solvent. The concentrate was filtered during hot and the filtrate was kept standing at room temperature. The product was filtered and recrystallized from water containing potassium nitrite. The method is an extension of that used for preparation of the corresponding en complex,[4] and the yield was 4% (0.2 g) in the present tn case.

Measurements. The hydrogen ion activity in solution was determined by means of a Beckman "Century" SS-1 pH meter with a Beckman 39301 glass electrode and a Beckman 39400 calomel electrode, and converted to the hydrogen ion concentration by virtue of the activity coefficient $f_H=0.83$ at 25 °C and $\mu=0.1$.[5] Absorption spectra were recorded on a Hitachi EPS-3T spectrophotometer and NMR spectra on a JEOL C-60HL with tetramethylsilane as an internal reference. IR spectra were measured in Nujol with JASCO IR-E (4000—600 cm^{-1}) and Hitachi EPI-L (700—200 cm^{-1}) Infrared Spectrophotometers.

The kinetic measurement was performed by the spectrophotometric method. In a dark measuring flask were placed desired amounts of a sodium nitrite solution and a NaX solution ($X^-=Cl^-$, I^-, N_3^-, NCS^-, or CH_3COO^-). Solutions of perchloric acid and sodium perchlorate were added to the mixture to adjust pH and maintain the ionic strength at 0.1. Into the flask kept in a thermostat at 25 °C was poured a solid specimen of $K[Co(NO_2)_4(AA)]$ by the help of thermostated pure water, and a 100 ml reaction mixture was made up. The complex was rapidly dissolved on agitation and the reaction started. Aliquots were pipetted at appropriate time intervals and spectra were recorded over the 400—550 nm region.

Results and Discussion

In order to examine the possibility of studying the competitive reactions of some nucleophiles with the five-coordinate species $Co(NO_2)_3(AA)$ postulated as an intermediate in the hydrolysis reactions of $Co(NO_2)_4(AA)^-$, the reaction products $Co(NO_2)_3X(AA)$ ($X=NH_3$, py, N_3^-, or NCS^-) and the related complexes $Co(NO_2)_2(BB)(AA)$ (BB=phen or an oxalate anion) were prepared (Table 1).

Characterization of Newly Prepared Complexes. $K[Co(NO_2)_3N_3(en)]$, A-form and B-form: As was described in Experimental section, two forms of the azido(ethylenediamine)trinitrocobaltate(III) were obtained. Each of them shows a single absorption maximum in the visible region in aqueous solution at 2 °C, but the exact position is a little different: A, $\lambda_{max}=466$ nm ($\varepsilon=508$); *B*, $\lambda_{max}=480$ nm ($\varepsilon=480$). The spectra in the ultraviolet region are also different: A, $\lambda_{max}=346$ ($\varepsilon=8.10\times10^3$) and 258 nm ($\varepsilon=1.59\times10^4$); B, $\lambda_{max}=316$ ($\varepsilon=1.09\times10^4$) and 259 nm ($\varepsilon=1.94\times10^4$). The most remarkable difference in the IR spectra is noticed on the $\delta(NH_2)$ band. A-form shows a broad band at 1574 cm^{-1}, while B-form two distinct bands at 1593 and 1571 cm^{-1}. Thus the two forms seem to constitute a couple of geometrical isomers, *viz.* facial and meridional, such as depicted in Fig. 1.

The chelate rings in both ethylenediamine and trimethylenediamine complexes are known to undergo a rapid interconversion among possible conformations

Table 1. Newly prepared complexes

Compound	Found (%)			Calcd (%)		
	C	H	N	C	H	N
$K[Co(NO_2)_3N_3(en)]$				7.10	2.38	33.14
A-form	7.18	2.64	32.58			
B-form	7.11	2.56	33.52			
$Co(NO_2)_3NH_3(en)$				8.77	4.05	30.66
Yellow form	8.79	4.06	30.39			
Brown form	8.59	4.08	30.59			
$Co(NO_2)_3(py)(en)\cdot H_2O$	22.99	3.84	24.07	23.74	4.27	23.73
$[Co(NO_2)_2(phen)(en)]NO_2\cdot H_2O$	36.91	3.95	21.95	36.94	3.98	21.55
$K[Co(NO_2)_3N_3(tn)]\cdot 2H_2O$	9.72	2.97	28.70	9.28	3.64	28.86
$K[Co(NO_2)_3N_3(tn)]\cdot H_2O$	9.19	3.27	30.18	9.73	3.27	30.27
$K[Co(NO_2)_3NCS(tn)]\cdot H_2O$	11.92	3.07	21.56	12.44	3.13	21.76
$Co(NO_2)_3NH_3(tn)$	12.64	4.53	29.63	12.51	4.55	29.17
$Co(NO_2)_3(py)(tn)$	26.75	4.28	23.81	27.44	4.32	23.99
$[Co(NO_2)_2(phen)(tn)]NO_2\cdot H_2O$	38.17	4.22	21.40	38.39	4.30	20.89
$K[Co(NO_2)_2(ox)(tn)]$	16.73	2.98	15.69	17.05	2.86	15.91

Table 2. Absorption maxima (the first band) and NMR data[a)]

Compound	λ_{max} nm	ε $l \cdot mol^{-1} \cdot cm^{-1}$	Chemical shift/ppm NH_2[b)]	$CH_2(\alpha)$[b)]	$CH_2(\beta)$[b)]	Others	Proposed structure
$K[Co(NO_2)_4(en)]$	430	494	4.27	c)			
$K[Co(NO_2)_3N_3(en)]$							
A-form	466	508	4.06	2.40			fac
B-form	480	480	4.19, 4.25	2.43			mer
$Co(NO_2)_3NH_3(en)$	430	282	4.43(1),[d)] 4.73(1)[e)]	c)		3.58(NH_3)	mer
$Co(NO_2)_3(py)(en)\cdot H_2O$	439	437	4.73	2.63		7.5—8.7(py)	fac
$[Co(NO_2)_2(phen)(en)]NO_2\cdot H_2O$	425	345(sh)	4.28, 4.55, 4.83	c)		7.6—9.3(phen)	cis
$K[Co(NO_2)_4(tn)]\cdot 1/2H_2O$	435	438	4.20(2)	2.31(2)	1.43(1)		
$K[Co(NO_2)_3N_3(tn)]\cdot 2H_2O$	481	432	3.93(2/3), 4.23(4/3)	2.26+2.32(2)	1.40+1.46(1)		fac+mer
$K[Co(NO_2)_3N_3(tn)]\cdot H_2O$	481	487	3.93(1), 4.23(1)	2.26(2)	1.40(1)		mer
$K[Co(NO_2)_3NCS(tn)]\cdot H_2O$	454	379	4.24(2)	2.34(2)	1.45(1)		fac
$Co(NO_2)_3NH_3(tn)$	437	256	4.30(1),[d)] 4.58(1)[e)]	2.18(2)	1.51(1)	3.60(NH_3)	mer
$Co(NO_2)_3(py)(tn)$	450	302	f)				
$[Co(NO_2)_2(phen)(tn)]NO_2\cdot H_2O$	450	278(sh)	4.12, 4.40	2.03(1), 2.33(1)	1.44(1)	7.5—9.3(phen)	cis
$K[Co(NO_2)_2(ox)(tn)]$	483	202					

a) The electronic spectra were measured in aqueous solutions at 2 °C, and NMR spectra in DMSO-d_6 at room temperature with TMS as an internal reference. b) Figures in parentheses show the relative area. c) Masked by the impurity band. d) NH_2 trans to the NO_2 ligand. e) NH_2 trans to the NH_3 ligand. f) Not stable in DMSO at room temperature.

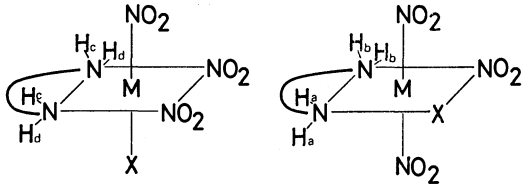

Fig. 1. Geometrical isomers of the $Co(NO_2)_3X(AA)$ complex.

in solution.[6)] Then both of the (diamine)tetranitrocobaltates(III) have a pseudo C_2 axis and the amine protons are all equivalent. However, the trinitro complex has a lower symmetry and the amine protons are no longer equivalent. In *mer*-$Co(NO_2)_3X(AA)$ one amine group occupies a site trans to a nitro ligand and the other to X. Different chemical shifts will be observed for $NH_2{}^a$ and $NH_2{}^b$ protons and the separation between them will depend on the nature of X.

In the case of *fac*-$Co(NO_2)_3X(AA)$ both amine groups are trans to the nitro ligands, but the magnetic environments of H^c and H^d are not strictly equal due to non-equivalence of the nitro and X ligands, although the difference in chemical shifts of the two type of protons will be smaller than in the mer form. Thus when a couple of the geometrical isomers are available, the proton NMR spectra will be helpful in identifying them.

As is listed in Table 2, the spectrum of A-form in DMSO-d_6 exhibits a broad band of amine protons at 4.06 ppm from TMS, whereas the amine signal of B-form shows two maxima at 4.19 and 4.25 ppm, suggesting that A-form is facial and B-form is meridional. Interconversion between the two forms cannot be studied since the complex is liable to hydrolysis and other ligand substitution reactions.

The corresponding tn complex, $K[Co(NO_2)_3N_3(tn)]\cdot 2H_2O$ seems to be a mixture of mer and fac isomers, since the amine protons show two resonances at 3.93 and 4.23 ppm with the area ratio of 1 : 2. The signals assignable to the $CH_2(\alpha)$ and $CH_2(\beta)$ protons in NH_2-$CH_2(\alpha)CH_2(\beta)CH_2(\alpha)NH_2$ also have two double maxima at 2.26, 2.32 ppm and 1.40, 1.46 ppm, respectively, maintaining the area ratio of 2 : 1. On the other hand the monohydrate species which separated from the mother liquor exhibits a simpler spectrum, the amine protons resonating at 3.93 and 4.23 ppm in the area ratio of 1 : 1 and the methylene protons at 2.26 and 1.40 ppm in the area ratio of 2 : 1. Then the monohydrate is considered to be meridional, and the fac isomer, which has not been isolated, may be responsible for the signals at 4.23 (NH_2), 2.32 (α-CH_2) and 1.46 (β-CH_2) ppm. These chemical shifts nearly coincide with those for $K[Co(NO_2)_3NCS(tn)]\cdot H_2O$.

$Co(NO_2)_3NH_3(en)$: The compound exists in two forms which have different crystal habits, colors and IR spectra in Nujol, but give identical absorption spectra in solution. Both of the brown and yellow forms were concluded by MacDermott and Barfoed[7a)] to be meridional on the basis of NMR spectra. This conclusion was ascertained by X-ray analysis.[8)] The essential difference is the conformations of the nitro groups, and the two forms were termed rotational or conformational isomers.

This interesting compound was prepared by other methods and a mixture of two forms in an unfixed ratio was obtained in each case.[7a)] The reproducible synthetic method to prepare each isomer exclusively has not been established.[7b)] Now it is possible to obtain either form selectively by controlling the temperature of crystallization. As was described in Experimental section, if a solution containing $K[Co(NO_2)_4(en)]$ and ammonia is kept at 60 °C to allow deposition of the product, the yellow form is obtained solely. On the other hand, when he reaction mixture is rapidly cooled with ice prior to deposition of crystallites, the brown form is produced exclusively. The yellow form looks more stable than

the brown form, and it is easier to convert the brown form into the yellow isomer than the opposite transformation in the recrystallization processes.

The corresponding tn complex, $Co(NO_2)_3NH_3(tn)$ was prepared under various conditions, but only one form has been isolated so far. The NMR spectra were assigned by reference to those of $Co(NO_2)_3NH_3(en)$,[7a] and the meridional structure is inferred.

K[Co(NO$_2$)$_3$NCS(tn)]·H$_2$O: The linkage isomerism displayed by the thiocyanate ion in metal complexes has been amply documented,[9] and IR spectra are utilized as the convenient and useful technique for structural assignments.[10] In the case of cobalt(III) complexes, $[CoNCS(NH_3)_5](ClO_4)_2$[11] and $K_3[CoNCS(CN)_5]$[12] exhibit broad ν(CN) bands at 2125 and 2065 cm^{-1}, and the ν(CS) bands at 806 and 810 cm^{-1}, respectively, whereas $[CoSCN(NH_3)_5](ClO_4)_2$[11] and $K_3[CoSCN(CN)_5]$[13] show sharp ν(CN) bands at 2100 and 2110 cm^{-1}, and weak ν(CS) bands at 710 and 719 cm^{-1}, respectively. In the IR spectrum of $K[Co(NO_2)_3NCS(tn)]\cdot H_2O$, a strong band at 2120 cm^{-1} assignable to the ν(CN) band is broad in the lower frequency side and a small peak at 825 cm^{-1} accompanying a sharp strong $\delta(NO_2)$ band at 835 cm^{-1} may be attributed to the ν(CS) vibration. Thus the thiocyanate ligand in $K[Co(NO_2)_3NCS(tn)]\cdot H_2O$ is considered to be N-bonded rather than S-bonded.

The NMR spectrum of this complex in DMSO-d_6 shows a single broad peak at 4.24 ppm which is ascribed to the amine protons, suggesting that the complex has a facial structure. The reaction of $K[Co(NO_2)_4(en)]$ with an equimolar amount of potassium thiocyanate in water has been carried out to prepare $K[Co(NO_2)_3NCS(en)]$, but a product of satisfactory purity has not yet been obtained.

Other Complexes: $[Co(NO_2)_3py(en)]\cdot H_2O$ shows a single peak of amine protons at 4.73 ppm and seems to have a facial structure. The corresponding tn complex is not stable enough in DMSO to allow the NMR measurement at room temperature. For the $CoX_2(AA)_2$ complexes too, the NMR spectra are usually most helpful in assigning the geometrical structure. The amine protons of a trans isomer will resonate as a single peak, whereas those of a cis isomer will exhibit two or more peaks.[14-16] Both of $[Co(NO_2)_2(phen)(en)]NO_2\cdot H_2O$ and $[Co(NO_2)_2(phen)(tn)]NO_2\cdot H_2O$, which were produced by the reactions of the tetranitro(diamine) complexes with 1,10-phenanthroline, show two broad bands attributable to the amine protons, and seem to have the cis structure. Recently properties of *cis*-$K[Co(NO_2)_2(ox)(en)]$ were reported by Ito and Shibata.[17] The structural assignment of $K[Co(NO_2)_2(ox)(tn)]$ now prepared is not unambiguous as yet.

In Table 2 are collected the absorption maxima (the first band) together with the NMR data. As was noted in previous papers,[18] the first band of each trimethylenediamine complex lies at a little longer wavelength side than that of the corresponding ethylenediamine complex, indicating that the ligand field of trimethylenediamine is weaker than that of ethylenediamine.

Kinetic Studies. The Reactions of (Diamine)tetranitrocobaltates(III) with Azide Ions: The absorption spectra in the 400—550 nm region of $K[Co(NO_2)_4(en)]$, $Co(NO_2)_3(H_2O)(en)$, *fac*- and *mer*-$K[Co(NO_2)_3N_3(en)]$ in aqueous solutions at 2 °C are displayed in Fig. 2. The spectral change accompanying the reaction of $Co(NO_2)_4(en)^-$ with excess azide ions exhibits two isosbestic points at 424 and 443 nm up to about 70% conversion. These two wavelengths correspond to the isosbestic points of $Co(NO_2)_4(en)^-$ and *fac*-$Co(NO_2)_3N_3(en)^-$, indicating that the facial isomer is primarily produced in this substitution reaction. The reaction was followed spectrophotometrically by measuring the

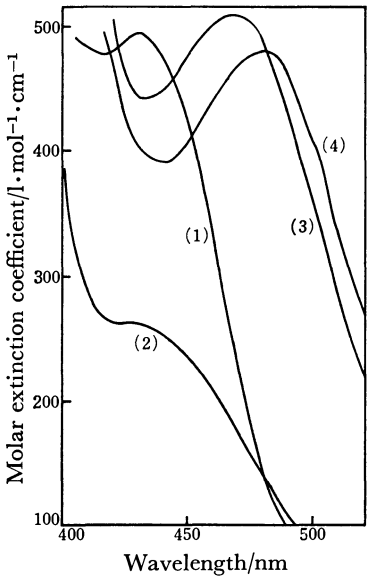

Fig. 2. The absorption spectra in the 400—550 nm region of $K[Co(NO_2)_4(en)]$ (1), $Co(NO_2)_3(H_2O)(en)$ (2), *fac*-$K[Co(NO_2)_3N_3(en)]$ (3), and *mer*-$K[Co(NO_2)_3N_3(en)]$ (4) in aqueous solutions at 2 °C.

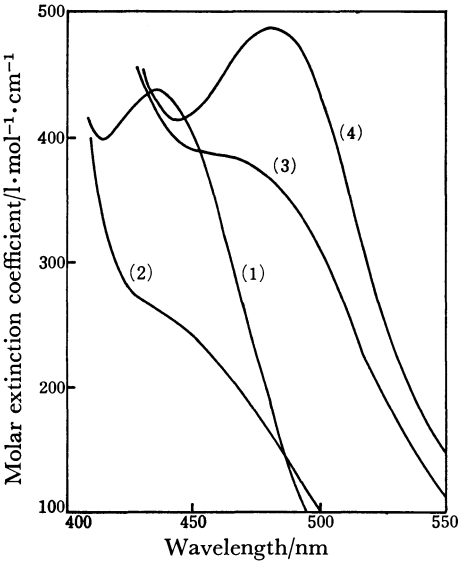

Fig. 3. The absorption spectra in the 400—550 nm region of $K[Co(NO_2)_4(tn)]\cdot 1/2H_2O$ (1), $Co(NO_2)_3(H_2O)(tn)$ (2), *fac*-$Co(NO_2)_3N_3(tn)^-$ (3), and *mer*-$K[Co(NO_2)_3N_3(tn)]\cdot H_2O$ (4) in aqueous solutions at 2 °C.

absorbance at 476 nm. The first order rate law was obeyed up to *ca.* 70% conversion in the presence of excess nitrite and azide ions.

Figure 3 shows the visible absorption spectra of *mer*-$K[Co(NO_2)_3N_3(tn)]\cdot H_2O$ and *fac*-$Co(NO_2)_3N_3(tn)^-$ which was isolated in solution, together with those of $K[Co(NO_2)_4(tn)]\cdot 1/2H_2O$ and $Co(NO_2)_3(H_2O)(tn)$. The change of spectrum accompanying the reaction of $Co(NO_2)_4(tn)^-$ with excess azide ions shows two isosbestic points at 432 and 452 nm up to *ca.* 80% conversion which coincide exactly with the isosbestic points of $Co(NO_2)_4(tn)^-$ and *fac*-$Co(NO_2)_3N_3(tn)^-$, revealing that the facial isomer of the trinitroazido complex is produced specifically in the case of the trimethylenediamine complex, too. The pseudo first order plot based on the absorbance at 484 nm also gives a good straight line through the duration of 80% reaction.

$$Co(NO_2)_4(AA)^- + N_3^- \xrightarrow{k_{obsd}} Co(NO_2)_3N_3(AA)^- + NO_2^- \quad (1)$$

The pseudo first order rate constants (k_{obsd}) of Reaction 1 decrease with increase in the nitrite ion concentration. According to the mechanism proposed in a previous paper,[1] the ligand substitution reactions of $Co(NO_2)_4(AA)^-$ should proceed *via* a five-coordinate intermediate.

$$Co(NO_2)_4(AA)^- \underset{k_{NO_2}}{\overset{k_{-NO_2}}{\rightleftharpoons}} Co(NO_2)_3(AA) + NO_2^- \quad (2)$$

$$Co(NO_2)_3(AA) + H_2O \underset{k_{-H_2O}}{\overset{k_{H_2O}}{\rightleftharpoons}} Co(NO_2)_3(H_2O)(AA) \quad (3)$$

$$Co(NO_2)_3(AA) + OH^- \xrightarrow{k_{OH}} Co(NO_2)_3(OH)(AA)^- \quad (4)$$

$$Co(NO_2)_3(AA) + N_3^- \xrightarrow{k_{N_3}} Co(NO_2)_3(N_3)(AA)^- \quad (5)$$

Since the isosbestic points of the tetranitro, and trinitroazido complexes are maintained in the present experimental conditions, the concentration of trinitroaqua complexes, of which spectra are included in Figs. 2 and 3, is negligible and the reverse step of Eq. 3 may be ignored. Assuming a steady state for $Co(NO_2)_3(AA)$, the pseudo first order rate constant of the azide complex formation may be expressed by

$$k_{obsd} = \frac{k_{-NO_2}k_{N_3}[N_3^-]}{k_{H_2O} + k_{OH}[OH^-] + k_{NO_2}[NO_2^-] + k_{N_3}[N_3^-]}, \quad (6)$$

which is transformed into Eq. 7.

$$\frac{k_{-NO_2}}{k_{obsd}} = 1 + \frac{k_{H_2O} + k_{OH}[OH^-]}{k_{N_3}[N_3^-]} + \frac{k_{NO_2}[NO_2^-]}{k_{N_3}[N_3^-]}. \quad (7)$$

In a previous paper,[1] the value of k_{-NO_2} was obtained as $(2.08\pm0.01)\times10^{-4}$ and $(9.27\pm0.03)\times10^{-4}$ s^{-1} for AA=en and tn, respectively, at 25 °C and μ=0.1. Thus, if k_{obsd} is determined at various nitrite concentrations with constant azide and hydrogen ion concentrations, the plot of k_{-NO_2}/k_{obsd} against the nitrite concentration will give a straight line with

$$\text{slope} = k_{NO_2}/k_{N_3}[N_3^-], \quad (8)$$

$$\text{intercept} = 1 + (k_{H_2O} + k_{OH}[OH^-])/k_{N_3}[N_3^-]. \quad (9)$$

In fact the observed rate data give rise to straight lines which are shown in Fig. 4. Since nitrite and azide ions were used in large excess as compared with the complex anions, the concentrations of added nitrite and azide, c_{NO_2} and c_{N_3}, were used for the calculation instead of $[NO_2^-]$ and $[N_3^-]$. From the slopes of the straight lines, the values of k_{NO_2}/k_{N_3} were calculated to be 0.65 ± 0.02 and 0.25 ± 0.04 for AA=en and tn, respectively, at 25 °C and μ=0.1.

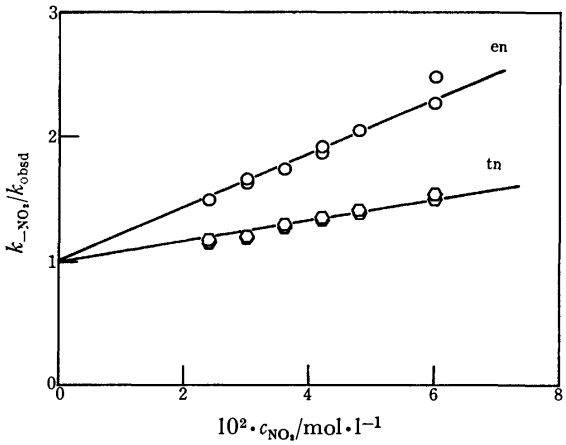

Fig. 4. The linear plots of rate data for the reaction (1) referring to Eq. 7: $c_M = 1.169\times10^{-3}$ mol·l^{-1} (in the case of AA=en) or 1.369×10^{-3} mol·l^{-1} (AA=tn), $c_{N_3} = 3.000\times10^{-2}$ mol·l^{-1}, pH=6.5—6.7, μ=0.1, 25 °C.

In Fig. 4 both of the two straight lines intercept the ordinate at 1.0, indicating that for both systems

$$(k_{H_2O} + k_{OH}[OH^-])/k_{N_3}[N_3^-] \ll 1. \quad (10)$$

In the studies on the hydrolysis reactions of $Co(NO_2)_4(AA)^-$, k_{H_2O}/k_{NO_2} was reported to be $(2.15\pm0.14)\times10^{-3}$ and $(1.79\pm0.13)\times10^{-2}$ mol·l^{-1} for AA=en and tn, respectively, at 25 °C and μ=0.1.[1] Thus $k_{H_2O}/k_{N_3} = (1.39\pm0.13)\times10^{-3}$ and $(4.4\pm1.0)\times10^{-3}$ mol·l^{-1} for AA=en and tn, respectively. The concentration of azide added, c_{N_3}, is 3×10^{-2} mol·l^{-1} and hence $k_{H_2O}/k_{N_3}[N_3^-]=0.046$ (AA=en) and 0.14 (AA=tn), nearly satisfying a part of Eq. 10.

Since pK_a of hydrazoic acid is 4.44 at 25 °C and μ=1 mol·l^{-1}($NaClO_4$),[19] pH of the reaction system was kept in the 6.5—6.7 region in order to prevent participation of HN_3, and thus contribution of the base hydrolysis (Eq. 4) must be taken into account. In the previous studies of hydrolysis,[1] k_{OH}/k_{NO_2} was estimated to be $\gg5\times10^3$ for both the en and tn systems. Now Eq. 10 gives the upper limit of k_{OH}. In order to satisfy Eq. 10, the condition $k_{OH}\leq0.1\ k_{N_3}[N_3^-]/[OH^-]$ must be met. Since $[N_3^-]/[OH^-]\fallingdotseq6\times10^5$ in the present experiments, $k_{OH}/k_{N_3}\leq6\times10^4$, leading to the estimation: $9.3\times10^4\geq k_{OH}/k_{NO_2}\gg5\times10^3$ for AA=en and $2.4\times10^5\geq k_{OH}/k_{NO_2}\gg5\times10^3$ for AA=tn. In this way the relative nucleophilicity of OH^-, NO_2^-, and N_3^- toward $Co(NO_2)_3(AA)$ is estimated as listed in Table 3 with reference to H_2O.

The Reactions of (Diamine)tetranitrocobaltates(III) with Other Nucleophiles: In the presence of excess nitrite and azide ions, substitution of a nitrite ligand in $Co(NO_2)_4(AA)^-$ with an azide ion seems to proceed to completion, although displacement of the second nitrite ligand

Table 3. Relative nucleophilicity of some ligands toward $Co(NO_2)_3(AA)$ at 25 °C and $\mu=0.1$

AA	H_2O	NO_2^-	N_3^-	OH^-
en	1	$(2.59\pm0.17)\times10^4$	$(4.02\pm0.37)\times10^4$	$\gg1.3\times10^8$ and $\leq2.4\times10^9$
tn	1	$(3.11\pm0.23)\times10^4$	$(1.25\pm0.29)\times10^4$	$\gg1.6\times10^7$ and $\leq7.8\times10^8$

contributes in a later stage of the reaction. On the contrary halide ions such as chloride and iodide cannot replace the nitrite ligand, but give rise to the aqua complex alone. The thiocyanate and acetate ions can compete with water and yields the trinitro(aniono) complex besides the trinitro(aqua) complex, but the quantitative competition ratios are not obtained. The relative nucleophilicity of ligands examined towards $Co(NO_2)_3(AA)$ is in the order: $OH^-\gg N_3^->NO_2^-$, CH_3COO^-, $NCS^-\gg H_2O>Cl^-$, I^-. The order coincides with that of the proton affinity of these ions (except the thiocyanate ion), suggesting that $Co(NO_2)_3(AA)$ is a hard acid.

The authors are grateful to Mr. J. Gohda for the elemental analysis and to Dr. T. Kinoshita for the NMR measurements. The financial aid by the Ministry of Education is also acknowledged.

References

1) Part IV: Y. Ito and S. Kawaguchi, *Bull. Chem. Soc. Jpn.*, **51**, 1083 (1978).
2) M. Shibata, M. Mori, and E. Kyuno, *Inorg. Chem.*, **3**, 1573 (1964).
3) R. G. Hughes, J. F. Endicott, M. Z. Hoffman, and D. A. House, *J. Chem. Educ.*, **46**, 440 (1969).
4) E. Kyuno, *Nippon Kagaku Zasshi*, **80**, 722 (1959).
5) J. Kielland, *J. Am. Chem. Soc.*, **59**, 1675 (1937).
6) T. G. Appleton and J. R. Hall, *Inorg. Chem.*, **9**, 1807 (1970); J. E. Sarneski and C. N. Reilley, *ibid.*, **13**, 977 (1974).
7) (a) T. E. MacDermott and S. Barfoed, *Acta Chem. Scand.*, **24**, 924 (1970); (b) In this paper a "latitude effect" was suggested to be operating. It was said that the brown isomer predominates in Denmark, while the yellow form is obtained almost exclusively in Australia.
8) K. G. Jensen, H. Soling, and N. Thorup, *Acta Chem. Scand.*, **24**, 908 (1970).
9) A. H. Norbury, *Adv. Inorg. Chem. Radiochem.*, **17**, 232 (1975).
10) R. A. Bailey, S. L. Kozak, T. W. Michelsen, and W. N. Mills, *Coord. Chem. Rev.*, **6**, 407 (1971).
11) D. A. Buckingham, I. I. Creaser, and A. M. Sargeson, *Inorg. Chem.*, **9**, 655 (1970).
12) I. Stotz, W. K. Wilmarth, and H. Haim, *Inorg. Chem.*, **7**, 1250 (1968); D. F. Gutterman and H. B. Gray, *J. Am. Chem. Soc.*, **91**, 3105 (1969).
13) J. L. Burmeister, *Inorg. Chem.*, **3**, 919 (1964).
14) C. J. Hawkins, "Absolute Configuration of Metal Complexes," Wiley, New York (1971), Chap. 6.
15) I. R. Jonasson, S. F. Lincoln, and D. R. Stranks, *Aust. J. Chem.*, **23**, 2267 (1970).
16) H. Kawaguchi and S. Kawaguchi, *Bull. Chem. Soc. Jpn.*, **46**, 3453 (1973).
17) T. Ito and M. Shibata, *Inorg. Chem.*, **16**, 108 (1977).
18) H. Kawaguchi, N. Yano, and S. Kawaguchi, *Bull. Chem. Soc. Jpn.*, **42**, 136 (1969); H. Kawaguchi and S. Kawaguchi, *ibid.*, **43**, 2103 (1970).
19) F. Maggio, V. Romano, and L. Pellerito, *Ann. Chim. (Italy)*, **57**, 191 (1967).

Inter- and Intramolecular Rhodium-Rhodium Interactions in Bis-(bidentate isocyanide)rhodium(I) Hexafluorophosphates

Katsuhiko KAWAKAMI, Masaki OKAJIMA, and Toshio TANAKA*

Department of Applied Chemistry, Faculty of Engineering, Osaka University, Yamada-kami, Suita, Osaka 565,

(Received February 4, 1978)

The reaction of $[RhCl(1,5\text{-}C_8H_{12})]_2$ with the stoichiometric amount of bidentate isocyanide followed by metathesis affords complexes of the types $[Rh(L\text{–}L)_2]PF_6$ (L–L=$CN(CH_2)_8NC$ (**1**), $CN(CH_2)_7NC$ (**2**)) and $[Rh_2(L\text{–}L)_4](PF_6)_2$ (L–L=$CN(CH_2)_6NC$ (**3**), $CN(CH_2)_4NC$ (**4**)). The electronic spectra at various concentrations reveal that in dilute solutions **1** and **2** exist as monomers with chelating isocyanides, while **3** and **4** form dimers with bridging isocyanides through intramolecular rhodium–rhodium interactions as the smallest unit. On the other hand, in concentrated solutions **1** and **2** form dimers and **4** tetramers through intermolecular Rh–Rh interactions.

Much attention has been paid to one-dimensional inorganic complexes in order to synthesize materials of anisotropic electrical conductivity. One of the most promising compounds is square planar d^8 metal complexes, the representative example of which is $K_2Pt(CN)_4\cdot Br_{0.30}\cdot 3H_2O$.[1] In this respect tetrakis(isocyanide)rhodium(I) and -iridium(I) cations are interesting because of their deep coloration.[2] Actually they have been found to exhibit oligomerization in solution.[3–5] Rhodium(I) complexes containing monodentate isocyanides are well known,[2,6] however, studies are relatively sparse on those containing bidentate isocyanides.[5] This paper reports the synthesis of some rhodium(I) complexes coordinated by bidentate isocyanides, $CN(CH_2)_nNC$ (n=4, 6, 7, or 8) and their electronic spectra, which reveal the presence of rhodium–rhodium interactions in these complexes in solution.

Experimental

Materials. Rhodium trichloride trihydrate was of reagent grade and used as supplied. Di-μ-chlorobis(1,5-cyclooctadiene)dirhodium(I), $[RhCl(1,5\text{-}C_8H_{12})]_2$, was prepared according to the literature.[7] The bidentate isocyanides $CN(CH_2)_nNC$ (n=4, 6, 7, or 8) were prepared by slightly modifying the literature method.[8] Dimethyl sulfoxide (DMSO) was distilled twice under reduced pressure after drying over $CaSO_4$ to give specific conductance, $k=1.1\times10^{-6}$ $ohm^{-1}\,cm^{-1}$.

Physical Measurements. Physical data were obtained in DMSO solutions. Infrared spectra (1×10^{-2} M) were measured on a Hitachi Perkin-Elmer 225 Spectrophotometer, electric conductivity (1×10^{-3} M) by using a Yokogawa F-255A universal bridge and a cell with the cell constant of 0.322 cm^{-1}, and electronic spectra on a Hitachi 124 Spectrophotometer by using 1, 0.1, and 0.01 cm quarz cells.

*Preparation of $[Rh(L\text{–}L)_2]PF_6$ (L–L=$CN(CH_2)_8NC$ (**1**), $CN(CH_2)_7NC$ (**2**)) and $[Rh_2(L\text{–}L)_4](PF_6)_2$ (L–L=$CN(CH_2)_6NC$ (**3**), $CN(CH_2)_4NC$ (**4**)).* An ethanol (10 ml) solution of hexamethylene diisocyanide (0.32 g, 2.4 mmol) was added dropwise to a stirred suspension of $[RhCl(1,5\text{-}C_8H_{12})]_2$ (0.29 g, 0.58 mmol) in ethanol (10 ml). The mixture was stirred for 1 h, followed by the addition of NH_4PF_6 (2.30 g, 1.4 mmol) in water (5 ml). The resulting product was reprecipitated from a mixture of dichloromethane and heptane to give a dark blue powder of **3** (60%): ν(NC), 2169 cm^{-1}; Λ_M=62 $cm^2\,ohm^{-1}\,mol^{-1}$. Found: C, 36.84; H, 4.78; N, 10.71%. Calcd for $C_{32}H_{48}F_{12}N_8P_2Rh_2$: C, 36.94; H, 4.65; N, 10.77%.

Other complexes were similarly prepared. **1** was reprecipitated from acetonitrile–water (73%): ν(NC), 2165 cm^{-1}; Λ_M=31 $cm^2\,ohm^{-1}\,mol^{-1}$. Found: C, 41.81; H, 5.78; N, 9.82%. Calcd for $C_{20}H_{32}F_6N_4PRh$: C, 41.68; H, 5.60; N, 9.72%. **2** was purified as **3** and contains a half molecule of dichloromethane (82%): ν(NC), 2170 cm^{-1}; Λ_M=34 $cm^2\,ohm^{-1}\,mol^{-1}$. Found: C, 37.71; H, 4.89; N, 9.23%. Calcd for $C_{18.5}H_{29}ClF_6N_4PRh$: C, 37.61; H, 4.95; N, 9.48%. **4** was purified as **3** (81%): ν(NC), 2175 cm^{-1}; Λ_M=58 $cm^2\,ohm^{-1}\,mol^{-1}$. Found: C, 31.77; H, 3.97; N, 11.80%. Calcd for $C_{24}H_{32}F_{12}N_8P_2Rh_2$: C, 31.05; H, 3.47; N, 12.07%.

Results and Discussion

The complexes obtained exhibit dark violet or blue color in the solid state, which is reminicent of metal-metal interactions. Conductivity measurements indicated that they are all electrolytes in DMSO. Infrared spectra of the complexes in DMSO showed only one strong band in the ν(N≡C) region, implying the equivalence of four isocyanide groups coordinated to the rhodium atom.

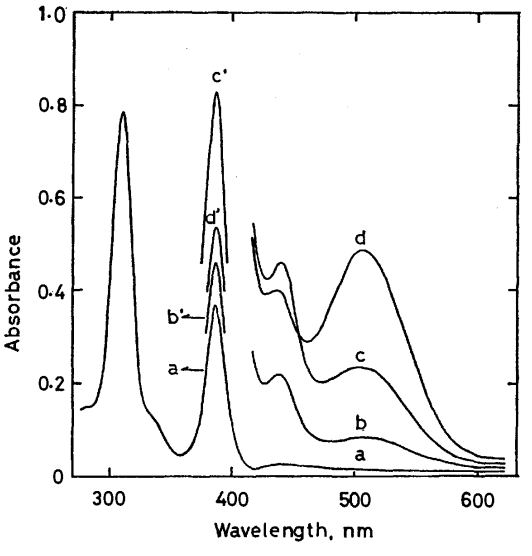

Fig. 1. Electronic spectra of $[Rh(CN(CH_2)_7NC)_2]PF_6$ (**2**) in DMSO at various concentrations at 25 °C (cell length, cm): a (1), 3.5×10^{-5} M; b (1) and b′ (0.1), 5.1×10^{-4} M; c (1) and c′ (0.1), 1.2×10^{-3} M; d (0.1) and d′ (0.01), 8×10^{-3} M.

TABLE 1. THE WAVELENGTHS AND MOLAR EXTINCTION COEFFICIENTS OF THE ABSORPTION MAXIMA OF THE CATIONS

No.	Cation	λ_{max}, nm($\varepsilon \times 10^{-4}$)						
1	$[Rh(CN(CH_2)_8NC)_2]^+$	312 (2.7)	338	sh	387 (1.2)	440 (<0.1)	505[b]	
2	$[Rh(CN(CH_2)_7NC)_2]^+$	311 (2.3)	338	sh	387 (1.1)	440 (<0.1)	505[b]	
3	$[Rh_2(CN(CH_2)_6NC)_4]^{2+}$	313 (4.2)	338	sh	386 (0.3)[a]		526 (1.5)	
4	$[Rh_2(CN(CH_2)_4NC)_4]^{2+}$	314 (2.2)	340	sh	383 (0.2)[a]		564 (1.9)	765[b]

a) See text. b) Observable only in concentrated solutions.

Electronic spectra of these complexes in DMSO show concentration dependence, which is illustrated by the spectra of **2** in DMSO at various concentrations (Fig. 1). A dilute solution (3.5×10^{-5} M) exhibit four absorption bands. The wavelengths and molar extinction coefficients of these bands (Table 1) are close to the charge transfer bands of tetrakis(ethyl isocyanide)-rhodium(I) perchlorate observed in acetonitrile (308 (ε 24000), 333[sh], 380 (8400), 435 nm (260)). This complex was reported to exist as the discrete rhodium(I) cation.[9] In addition, a molecular model suggests that the methylene chain of $CN(CH_2)_7NC$ is long enough for chelation to the rhodium(I) ion. Thus, the four absorption bands observed in dilute solutions are due to monomeric $[Rh(CN(CH_2)_7NC)_2]^+$. A more concentrated solution of **2** exhibits a new broad band at 505 nm, which is intensified relatively at the expense of the 387 and 440 nm bands as the concentration increases. The 505 nm band may therefore be assigned to dimeric $[Rh(CN(CH_2)_7NC)_2]_2^{2+}$ by analogy with $[Rh(C_6H_5NC)_4]^+$, which was reported to exhibit an absorption arising from its dimer at 568 nm in concentrated acetonitrile solutions.[4] If one can assume that an equilibrium exists between monomeric $[Rh(CN(CH_2)_7NC)_2]^+$ and its dimeric dication, the equilibrium constant, K_1, is expressed by the following equation (Eq. 1), where C, A, and ε stand for the concentration, absorbance, and molar extinction coefficient of the monomeric and dimeric species denoted by the subscripts M and D, respectively.

$$K_1 = \frac{C_D}{C_M^2} = \frac{A_D/\varepsilon_D}{(A_M/\varepsilon_M)^2} \quad (1)$$

Equation 1 can be transformed as follows:

$$A_M^2 = \frac{\varepsilon_M^2}{K_1 \varepsilon_D} \times A_D. \quad (2)$$

This equation predicts a linear relationship between A_M^2 and A_D. In fact, a plot of the absorbance at 505 nm *vs.* the square of that at 387 nm[10] gave a straight line shown in Fig. 2. It is therefore suggested that **2** exists as an equilibrium mixture of the monomeric and dimeric species in concentrated solutions. The association of $[Rh(CN(CH_2)_7NC)_2]^+$ may be formed through Rh–Rh interactions as illustrated in **A**. A similar result

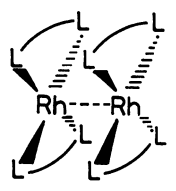

A

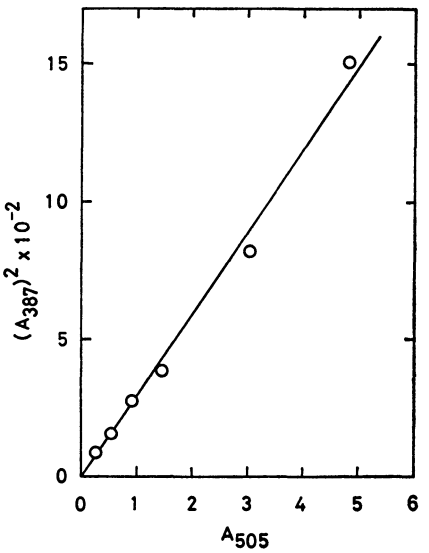

Fig. 2. A plot of the absorbance at 505 nm, A_{505}, *vs.* the square of that at 377 nm, $(A_{387})^2$, for $[Rh(CN(CH_2)_7NC)_2]PF_6$ (**2**) in DMSO at 25 °C.

was obtained for **1** (see Table 1). Unfortunately, the K_1 and ε_D values have not been determined in the present study, because limited solubilities of **1** and **2** have precluded the spectral measurements over a concentration range wide enough to warrant the least squares analysis[11] to calculate these two values.

Figure 3 displays electronic spectra of **4** in DMSO at various concentrations. A dilute solution (4.2×10^{-4} M) exhibits four absorption bands. These wavelengths

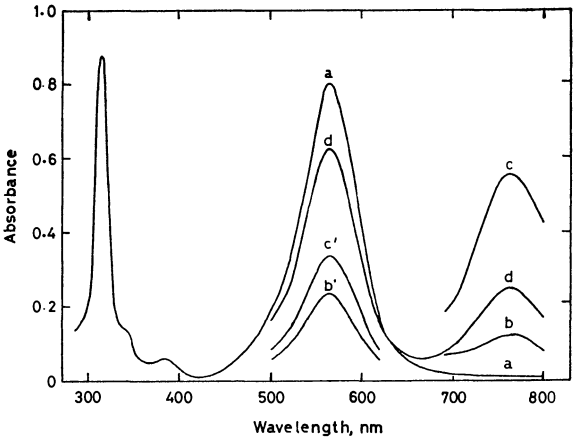

Fig. 3. Electronic spectra of $[Rh_2(CN(CH_2)_4NC)_4](PF_6)_2$ (**4**) in DMSO at various concentrations at 25 °C (cell length, cm): a (0.1), 4.2×10^{-4} M; b (0.1) and b′ (0.01), 8.4×10^{-4} M; c (0.1) and c′ (0.01), 1.7×10^{-3} M; d (0.01), 3.5×10^{-3} M.

(Table 1) except 383 nm (*vide infra*) are close to those of absorptions of the $CN(CH_2)_3NC$ analog in a dilute methanol solution (318, 342, 555 nm), for which a dimeric structure with bridging isocyanides has recently been suggested.[5] A molecular model indicates that $CN(CH_2)_4NC$ will not be able to chelate to the rhodium(I) ion. Therefore, **4** probably contains bridging isocyanides to form a dimer with an intramolecular Rh–Rh interaction as the smallest unit in dilute solutions, **B**. The intensity of the rather weak band at 383

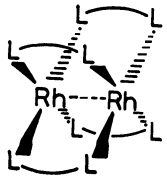

B

nm decreases considerably on addition of $CN(CH_2)_4NC$ to its Rh(I) complex in DMSO. In view of this result and the fact that monomeric **1** and **2** show absorptions at 387 nm (Table 1), the band may arise from such a monomeric species as, for example, $[Rh(CN(CH_2)_4NC)_2(DMSO)_2]^+$ involving unidentate $CN(CH_2)_4NC$. Thus, the 314 and 340 nm bands of **4** (Table 1) may be contributed from the monomeric species to some extent, since monomeric **1** and **2** exhibit absorptions at similar wavelengths. A more concentrated solution of **4** exhibits a new broad band at 765 nm, which is intensified at the expense of the 564 nm band as the concentration increases. The 765 nm band can be assigned to tetrameric $[Rh_2(CN(CH_2)_4NC_4]_2^{4+}$ by analogy with the $CN(CH_2)_3NC$ analog.[5] Moreover, a linear relationship was obtained between the absorbance at 765 nm *vs.* the square of that at 564 nm (the dimer band), supporting the assignment. It is therefore suggested that in concentrated solutions the dimeric **4** undergoes an intermolecular association to form the tetramer **C**. No similar association of **3** has been observed

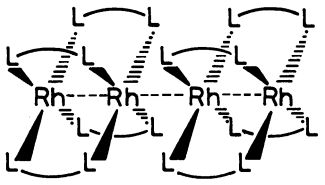

C

in the electronic spectrum because of its poor solubility, although in dilute solutions it exhibited a spectrum similar to that of **4** (Table 1). The absorptions at long wavelengths of these four complexes will be explained to be due to the dimeric and tetrameric species by a simple MO diagram proposed by Gray *et al.*[4,5]

References

1) J. S. Miller and A. J. Epstein, *Prog. Inorg. Chem.*, **20**, 1 (1976).
2) L. Malatesta and F. Bonati, "Isocyanide Complexes of Metals," Wiley (Interscience), New York, N. Y. (1969).
3) K. Kawakami, M. Haga, and T. Tanaka, *J. Organomet. Chem.*, **60**, 363 (1973).
4) K. R. Mann, J. G. Gordon II, and H. B. Gray, *J. Am. Chem. Soc.*, **97**, 3553 (1975).
5) N. S. Lewis, K. R. Mann, J. G. Gordon II, and H. B. Gray, *J. Am. Chem. Soc.*, **98**, 7461 (1976).
6) J. W. Dart, M. K. Lyoyd, R. Mason, and J. A. McCleverty, *J. Chem. Soc., Dalton Trans.*, **1973**, 2039 and references cited therein.
7) J. Chatt and L. M. Venanzi, *J. Chem. Soc.*, **1957**, 4735.
8) J. Casanova, N. D. Werner, and E. R. Schuster, *J. Org. Chem.*, **31**, 3473 (1966).
9) H. Isci and W. R. Mason, *Inorg. Chem.*, **14**, 913 (1975).
10) The 387 nm band was used for the monomer in place of the 440 nm band, which is somewhat overlapped by the new band at 505 nm.
11) H. Hosoya, J. Tanaka, and S. Nagakura, *J. Mol. Spectrosc.*, **8**, 257 (1962).

The Crystal Structures of Bis(*cis*-1,3-diaminocyclohexane)palladium(II) Chloride and Its Platinum(II) Analogue

Keiko KAMISAWA, Keiji MATSUMOTO, Shun'ichiro OOI,* Hisao KUROYA, Reiko SAITO,** and Yoshinori KIDANI***

Department of Chemistry, Faculty of Science, Osaka City University, Sumiyoshi-ku, Osaka 558
***Aichi Junior College of Nursing, Kamishidanmi, Moriyama-ku, Nagoya 463*
***Faculty of Pharmaceutical Sciences of Nagoya City University, Tanabedori, Mizuho-ku, Nagoya 467*

(Received February 6, 1978)

The structure of bis(*cis*-1,3-diaminocyclohexane)palladium(II) chloride has been determined from X-ray diffraction data collected by the counter method. The crystal is orthorhombic with space group Pnnm, $a=17.728(5)$, $b=6.418(4)$, $c=6.914(2)$ Å, and $Z=2$. The crystal structure has been determined by Patterson and Fourier techniques and refined by a least-squares method to $R=0.026$ for 1151 independent reflections for which $F_o^2>3\sigma(F_o^2)$. The Pd atom has a planar coordination of 4 N atoms and the complex cation has a crystallographically imposed C_{2h} symmetry, the two *cis*-1,3-diaminocyclohexane ligands being related to each other by a two fold axis. The six-membered chelate ring Pd–NH_2–CH–CH_2–CH–NH_2 (with a $-(CH_2)_3-$ bridge) is of the envelope conformation.

The structural features of the ligating *cis*-1,3-diaminocyclohexane have been described. The crystal of bis(*cis*-1,3-diaminocyclohexane)platinum(II) (orthorhombic, $a=17.727(8)$, $b=6.371(3)$, $c=6.965(2)$ Å) was found to be isomorphous with that of the palladium analogue.

The *cis*-1,3-diaminocyclohexane (1,3-dach) molecule usually exists in the diequatorial conformation in which the disposition of the two NH_2 groups is highly unfavorable to chelation. However, the molecule is capable of chelating to the metal ion when it assumes the diaxial conformation.

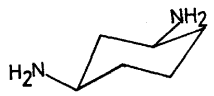

The diequatorial conformation

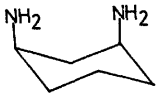

The diaxial conformation

Two of the authors (R. S. and Y. K.) have found that 1,3-dach reacts with some transition metal ions and have synthesized several Pd(II) and Pt(II) chelates of 1,3-dach with the formula $[MX_2(1,3\text{-dach})]$ and $[M(1,3\text{-dach})_2]Cl_2$, where M stands for Pd(II) or Pt(II) and X for Cl or Br.[1] Thus the presence of a metal ion which has a strong affinity towards the N atom promotes the interconversion from the diequatorial to the diaxial conformation, giving rise to a metal chelate of 1,3-dach. With these complexes it was found that the electronic spectra were indicative of a planar 4-coordinate configuration, and furthermore, the ^1H NMR and IR spectra suggested the diaxial conformation of the 1,3-dach ligand. In order to investigate the structural features of the ligating 1,3-dach molecule in detail, the single crystal X-ray structure analysis of $[Pd(1,3\text{-dach})_2]Cl_2$ has been performed.

Experimental

The preparations of $[Pd(1,3\text{-dach})_2]Cl_2$ and $[Pt(1,3\text{-dach})_2]Cl_2$ have been reported elsewhere.[1]

Crystal Data. $[Pd(1,3\text{-dach})_2]Cl_2$: $C_{12}H_{28}N_4Cl_2Pd$, $F.W.=405.7$, Orthorhombic, $a=17.728(5)$, $b=6.418(4)$, $c=6.914(2)$ Å, $U=786.7(6)$ Å^3, $D_m=1.71$, $D_c=1.71$ g/cm^3, $Z=2$, μ(Mo $K\alpha$)$=16.1$ cm^{-1}, space group Pnnm or Pnn2 from systematic absences: $h0l$ when $h+l$ is odd, $0kl$ when $k+l$ is odd. The former space group was used in the structure analysis and confirmed by the successful refinement of the structure.

$[Pt(1,3\text{-dach})_2]Cl_2$: $C_{12}H_{28}N_4Cl_2Pt$, $F.W.=494.4$, Orthorhombic, $a=17.727(8)$, $b=6.371(3)$, $c=6.965(2)$ Å, $U=786.7(3)$ Å^3, $D_m=2.08$, $D_c=2.09$ g/cm^3, $Z=2$, μ(Mo $K\alpha$)$=105.6$ cm^{-1}, space group Pnnm or Pnn2; X-ray diffraction pattern showed the same space-group extinctions as those of the Pd analogue.

The Laue symmetries, space groups, and the approximate unit-cell dimensions were determined from oscillation and Weissenberg photographs taken with Cu $K\alpha$ radiation. The unit cell dimensions of the respective compounds were refined by the least-squares analyses of the θ values (16 reflections for the Pd- and 14 for the Pt-compound) measured on a Philips PW 1100 four-circle diffractometer with Mo $K\alpha$ radiation.

Data Collection. Intensity data for one octant of the reciprocal space were collected by the ω-2θ scan technique with graphite-monochromated Mo $K\alpha$ radiation. The specimen size was $0.14\times0.12\times0.15$ mm. A scan speed of 0.017° s^{-1} in ω and a scan range $(0.8+0.2\tan\theta)°$ were chosen. The background was counted for half of the scan time at each end of the scan range. Three standard reflections (200, 040, 002), monitored every 3 h throughout the data collection, showed no significant variation in intensity. Of the 1752 reflections collected in the range of $2\theta\leq66°$, 1151 reflections having $F_o^2>3\sigma(F_o^2)$ were used in the structure analysis. Intensity data were processed by the computer program of Hornstra and Stubbe.[2] A spherical absorption correction ($r=0.07$ mm) was applied.

Structure Determination and Refinement. The crystal structure of $[Pd(1,3\text{-dach})_2]Cl_2$ was solved by the heavy-atom technique. Of the two possible space groups, Pnnm and Pnn2, the former was chosen. The positional and thermal parameters were refined by the block-diagonal least-squares method. The minimized function was $\sum w(|F_o|-|F_c|)^2$. The weighting scheme, $w=p$ for $|F_o|<F_{min}$, $w=1.0$ for $F_{min}\leq|F_o|\leq F_{max}$, and $w=(F_{max}/F_o)^2$ for $|F_o|\geq F_{max}$, was used. The p, F_{min} and F_{max} were varied as indicated by F_o and $(\sin\theta/\lambda)$ analysis of $\sum w\Delta F^2$. The difference Fourier map, calculated after the refinement of the parameters for the nonhydrogen atoms by the use of anisotropic temperature factors, clearly showed the peaks of all H atoms. These H atoms were

Table 1. Positional and thermal parameters

Atomic coordinates ($\times 10^4$).

	x	y	z
Pd	0	0	0
Cl	4129.9(5)	2313(1)	0
N	575(1)	1481(3)	2191(3)
C(1)	1971(2)	−134(6)	0
C(2)	1954(1)	1218(4)	1806(4)
C(3)	1282(1)	2696(4)	1847(4)
C(4)	1220(2)	3972(5)	0

Anisotropic temperature factors ($\times 10^4$) in the form $\exp[-(B_{11}h^2+B_{22}k^2+B_{33}l^2+B_{12}hk+B_{13}hl+B_{23}kl)]$.

	B_{11}	B_{22}	B_{33}	B_{12}	B_{13}	B_{23}
Pd	12.62(7)	136.7(6)	78.3(4)	6.6(6)	0	0
Cl	22.5(2)	163(2)	146(2)	−32(1)	0	0
N	16.3(5)	175(5)	98(3)	7(3)	0000(2)	−39(7)
C(1)	16.5(7)	116(7)	129(5)	26(5)	0	0
C(2)	16.5(6)	163(5)	125(5)	2(3)	−12(3)	−5(9)
C(3)	18.7(6)	135(5)	127(4)	−1(3)	−3(3)	−71(8)
C(4)	24.3(11)	101(7)	197(9)	5(5)	0	0

Atomic coordinates ($\times 10^3$) and isotropic temperature factros of H atoms.

	x	y	z	B/Å^2
H(1N)	25(1)	222(5)	275(5)	3.1(7)
H(2N)	66(2)	49(4)	305(5)	2.7(7)
H(1C1)	153(2)	−115(7)	0	2.4(9)
H(2C1)	244(2)	−95(7)	0	2.6(9)
H(1C2)	240(2)	206(4)	180(5)	3.0(7)
H(2C2)	193(1)	40(4)	298(5)	2.8(7)
H(C3)	133(1)	359(4)	295(4)	2.3(6)
H(1C4)	79(3)	472(7)	0	3.3(10)
H(2C4)	163(2)	490(7)	0	3.0(10)

included in the following least-squares calculation, isotropic temperature factors being used. The convergence was attained at R 0.026 ($R'=[\sum w\Delta F^2/\sum wF_o^2]^{1/2}=0.030$). In the final cycle of the refinement all parameter shifts were less than 0.2σ. The $F_{min}=8.7$, $F_{max}=42.0$ and $p=0.4$ were found to be optimum.

The atomic scattering factors of Pd^0, Cl^-, N, and C were taken from Ref. 3 and that of H from Ref. 4. Real parts of the anomalous dispersion corrections were applied for Pd^0 and Cl^-. Atomic coordinates and temperature factors are given in Table 1. A complete list of the observed and calculated structure factors is preserved by the Chemical Society of Japan (Document No. 7823). All the computations were carried out on a FACOM 230-60 computer of Osaka City University, by the use of the RSSFR-5, HBLS-IV, and DAPH programs in the UNICS.[5]

Results and Discussion

The perspective drawing of the complex cation is shown in Fig. 1. The complex has a crystallographically imposed two fold axis and a symmetry plane; the two fold axis runs through the Pd atom and bisects the N–Pd–N″ angle, whereas the symmetry plane is perpendicular to the two fold axis and passes through the Pd, C(1) and C(4) atoms. The primed atoms are related to the unprimed ones by the symmetry plane. Thus

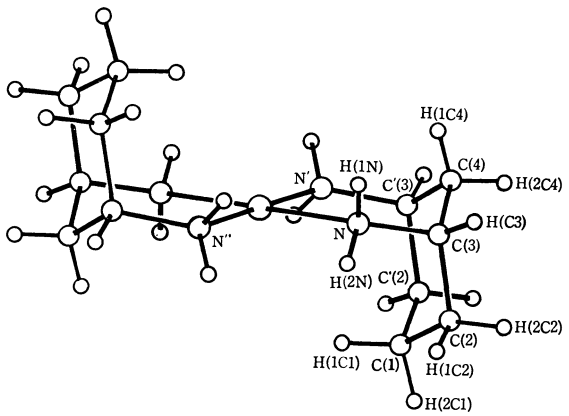

Fig. 1. Structure of $[Pd(1,3\text{-dach})_2]^{2+}$.

the complex has an exact C_{2h} symmetry, the Pd atom being located at the center of inversion.

The six-membered chelate ring composed of the Pd, N, C(3), C(4), C′(3), and N′ is of the envelope conformation. However, the [Pd, N, N′] plane is not exactly coplanar with the [N,C(3),C′(3),N′] plane; as can be seen in the elevation of the complex (Fig. 2), the latter plane is slightly bent away from the former plane so as to deform the chelate ring toward the chair conformation. The interplanar angle is 169.2° (Table 3).

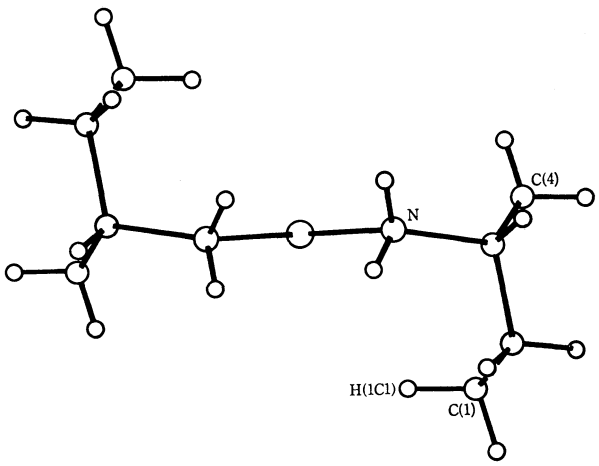

Fig. 2. Elevation of $[Pd(1,3\text{-dach})_2]^{2+}$.

Bond lengths and angles are given in Table 2. The Pd–N bond length (2.058(2) Å) is slightly longer than those in $[Pd(en)_2]Cl_2$ (2.030(6) and 2.043(7) Å),[6] $[PdCl_2(meso\text{-}2,3\text{-diaminobutane})]$ (2.029(6) Å),[7] and $[Pd(N^1\text{-Me-}(S)\text{-pn})_2]Cl_2\cdot 2H_2O$ (2.040(5) Å),[8] although the magnitude of elongation is not "highly significant." The electronic spectra of the present complex shows two bands at 27000 cm^{-1} (shoulder) and 34200 cm^{-1}.[1] These bands are displaced slightly to a lower energy relative to the corresponding bands of $[Pd(R\text{-pn})_2]Cl_2$ (29000 and 34800 cm^{-1}).[9] As the Pd–N bond length in the *R*-pn complex should presumably not be different from those in the en and *meso*-2,3-diaminobutane complexes, the slight elongation of the Pd–N bond in the 1,3-dach complex seems to be responsible for the low energy shift of the d→d bands.

TABLE 2. INTERATOMIC DISTANCES (l) AND BOND ANGLES (ϕ)

	l/Å		ϕ/°
Pd–N	2.058(2)	N–Pd–N′	94.8(2)
N–C(3)	1.494(3)	Pd–N–C(3)	122.6(2)
C(1)–C(2)	1.521(5)	C(2)–C(1)–C′(2)	110.4(4)
C(2)–C(3)	1.523(4)	C(1)–C(2)–C(3)	112.7(2)
C(3)–C(4)	1.521(5)	C(2)–C(3)–C(4)	112.1(2)
		C(3)–C(4)–C′(3)	114.2(4)
C(2)···C′(2)	2.497(5)	N–C(3)–C(4)	110.8(2)
C(3)···C′(3)	2.554(5)	N–C(3)–C(2)	109.5(2)
N···N′	3.029(4)		
N–H(1N)	0.84(3)	H(1C1)–C(1)–H(2C1)	108(4)
N–H(2N)	0.89(3)	H(1C1)–C(1)–C(2)	111(2)
C(1)–H(1C1)	1.02(4)	H(2C1)–C(1)–C(2)	109(2)
C(1)–H(2C1)	0.99(4)	H(C3)–C(3)–N	105(2)
C(2)–H(1C2)	0.95(3)	H(C3)–C(3)–C(2)	109(2)
C(2)–H(2C2)	0.97(3)	H(C3)–C(3)–C(4)	110(2)
C(3)–H(C3)	0.96(3)	H(1C4)–C(4)–H(2C4)	108(4)
C(4)–H(1C4)	0.90(4)	H(1C4)–C(4)–C(3)	110(3)
C(4)–H(2C4)	0.94(4)	H(2C4)–C(4)–C(3)	107(3)
Pd···H(1C1)	2.81(4)	Pd···H(1C1)–C(1)	125(3)
Pd···H(1C4)	3.34(4)	Pd···H(1C4)–C(4)	83(3)
N···Cl*[a]	3.347(2)		
H(2N)···Cl*	2.47(3)	Cl*···H(2N)–N	170(3)
N″···Cl*	3.307(2)		
H(1N″)···Cl*	2.54(3)	Cl*···H(1N″)–N″	152(3)

a) The Cl* denotes the chloride anion at the equivalent position $(1/2-x, y-1/2, 1/2+z)$.

TABLE 3. INTERPLANAR AND TORSION ANGLES

Interplanar angles (ϕ)

Plane (1)	Pd, N, N′
Plane (2)[a]	N, C(3), C′(3), N′
Plane (3)	C(3), C(4), C′(3)
Plane (4)[a]	C(2), C(3), C′(3), C′(2)
Plane (5)	C(2), C(1), C′(2)

Plane	Plane	ϕ/°
(1)	(2)	168.9
(2)	(3)	114.4
(2)	(4)	109.6
(3)	(4)	136.1
(5)	(4)	130.5

Torsion angles (τ)

Fragment	τ/°
Pd–N–C(3)–C(4)	40.9
Pd–N–C(3)–C(2)	−83.3
N–C(3)–C(2)–C(1)	71.2
N–C(3)–C(4)–C′(3)	−74.2
C′(2)–C(1)–C(2)–C(3)	55.6
C(1)–C(2)–C(3)–C(4)	−52.1
C(2)–C(3)–C(4)–C′(3)	48.5

a) All four atoms lie exactly on one plane.

The N–Pd–N′ bond angle (94.8(2)°) is significantly larger than those in the Pd complexes with five-membered chelate rings of diamines (82.9—83.6°).[6-8] Although the Pd–N–C bond angle (122.6(2)°) is fairly larger than the tetrahedral angle, it is comparable to those in the metal chelates with six-membered chelate rings.[10]

The cyclohexane ring is of the diaxial conformation, as inferred from ^{1}H NMR and IR spectra.[1] Bond lengths and angles are in reasonable agreement with those in the cyclohexane II,[11] *trans*-1,2-diaminocyclohexane,[12] and *trans*-1,4-diaminocyclohexane.[13] However, the C(3)–C(4)–C′(3) bond angle (114.2(4)°) is larger than any C–C–C angles (≈112.3°) in the molecules cited for comparison.

Various torsion angles are also given in Table 3. The torsion angles of the –C–C–C–C– fragments are generally smaller than those in the cyclohexane and its substituted derivatives (55.4—58.4°)[11-13] and particularly, that of the –C(2)–C(3)–C(4)–C′(3)– is the smallest (48.5°) among them. This value is comparable to that (47.0°) found in the $-CH_2-CH(COOH)-CH(COOH)-CH_2-$ portion of the *trans*-1,2-cyclohexanedicarboxylic acid,[14] the small value of which has been ascribed to the steric repulsion between the two carboxyl groups.[15] Interpretation for the present case of –C(2)–C(3)–C(4)–C′(3)– is as follows. In the scaled model of the diaxial 1,3-dach molecule, the distance between N and N′ is 2.7 Å[16] (the same atom numbering as the one given for coordinating 1,3-dach (Fig. 1) is used for the scaled model but expressed in bold-faced type). In order to increase the **N**···**N′** distance to 3.029 Å as found in the present 1,3-dach ligand it is necessary to synchronously rotate the –**C(3)**(**N**)(**C(4)**) and –**C′(3)**(**C(4)**)(**N′**) segments about **C(2)**–**C(3)** and **C′(2)**–**C′(3)** axes, respectively. Such rotations give rise to i) decrease of torsion angle in the –**C(2)**–**C(3)**–**C(4)**–**C′(3)**– fragment, ii) increase of the interplanar angle between [**C(2)**, **C(3)**,**C′(3)**,**C′(2)**] and [**C(3)**,**C(4)**,**C′(3)**] planes, and iii) increase of **C(3)**–**C(4)**–**C′(3)** bond angle. Actually, in ligating 1,3-dach the corresponding interplanar angle is larger by 5.6° than the [C(2),C(3),C′(3),C′(2)]–[C(2),C(1),C′(2)] interplanar angle which is in agreement with the average value in cyclohexane II (130.3°). Moreover, the C(3)–C(4)–C′(3) bond angle is the largest among the C–C–C bond angles. In the intermolecular contacts in which the H atoms of the cyclohexane group participate, none of the interatomic distances is less than the sum of the van der Waals

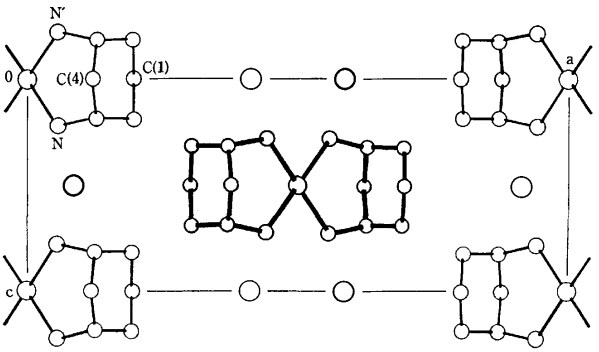

Fig. 3. Crystal structure viewed down the b axis. Complexes drawn by thin lines lie at $y=0$, while that shown by thick lines is located at $y=1/2$. For Cl anions thin circles have $y\approx0.23$, and thick ones $y\approx0.73$.

radii. Therefore, the structural features of the cyclohexane ring found in ligating 1,3-dach should be regarded as arising from an intramolecular potential energy but not from an intermolecular one.

Figure 3 shows the crystal structure. All H atoms of the NH_2 groups participate in the N–H···Cl hydrogen bonding. Data concerning the hydrogen bonds are listed in Table 2.

The unit-cell dimensions of $[Pt(1,3\text{-dach})_2]Cl_2$ are very close to those of $[Pd(1,3\text{-dach})_2]Cl_2$ and furthermore, the intensity distribution in the reciprocal space of the former has similar features to that of the latter. Accordingly the crystal in the former case may be regarded as isomorphic with the present Pd compound.

The H(1Cl) atom has a short contact with the Pd atom. The Pd···H distance is comparable with that found in the bis(L-ornithinato)palladium(II) (2.79 Å).[17] In the ^1H NMR spectrum of the $[Pt(1,3\text{-dach})_2]Cl_2$ it was found that one of the eight methylene protons resonates at lower field than those for the remainders. The spectrum of the Pd analogue is almost identical with that of the Pt complex.[1] The proton which shows down-field shift is thought to be the H(1Cl) atoms, although in solution the M···H distance varies as the ligand molecules make some motion, *e.g.*, the rapid oscillation of the 1,3-dach ligand about N···N′ axis.

This research was supported by a Grant-in-Aid for Scientific Research from the Ministry of Educatiosn.

References

1) R. Saito and Y. Kidani, *Chem. Lett.*, **1977**, 1141.
2) J. Hornstra and B. Stubbe, PW 1100 Data Processing Program, Philips Research Laboratories, Eindhoven, Holland.
3) "International Tables for X-Ray Crystallography," Vol. IV, Kynoch Press, Birmingham (1974), pp. 71, 148.
4) R. F. Stewart, E. R. Davidson, and W. T. Simpson, *Chem. Phys.*, **42**, 3175 (1965).
5) "The Universal Crystallographic Computation Program System," Crystallographic Society of Japan, (1969).
6) J. R. Wiesner and E. C. Lingafelter, *Inorg. Chem.*, **5**, 1770 (1966).
7) T. Ito, F. Marumo, and Y. Saito, *Acta Crystallogr., Sect. B*, **27**, 1695 (1971).
8) Y. Nakayama, S. Ooi, and H. Kuroya, Proceedings of the 34th National Meeting of the Chemical Society of Japan, I, p. 28 (1976). N^1-Me-(*S*)-pn, 1-methylamino-2(*S*)-aminopropane.
9) H. Ito, J. Fujita, and K. Saito, *Bull. Chem. Soc. Jpn.*, **40**, 2584 (1967).
10) F. A. Jurnak and K. N. Raymond, *Inorg. Chem.*, **13**, 2387 (1974), and references therein.
11) R. Kahn, R. Fourme, D. André, and M. Renaud, *Acta Crystallogr., Sect. B*, **29**, 131 (1973).
12) M. D. Morse and J. P. Chesick, *Acta. Crystallogr., Sect. B*, **32**, 954 (1976).
13) J. D. Dunitz and P. Stricker, *Helv. Chim. Acta*, **49**, 2502 (1966).
14) E. Benedetti, P. Corradini, C. Pedone, and B. Post, *Chem. Commun.*, **1968**, 1626.
15) E. Beneditti, C. Pedone, and G. Allegra, *J. Phys. Chem.*, **74**, 512 (1970).
16) The coordinates of C atoms in the cyclohexane II[11] were utilized in the estimation of the N···N′ distance in the scaled model. The coordinates of the two axial N atoms, each of which is bonded to C(2) or C′(1) atom of the cyclohexane II (C′(1), C(1) at equivalent position $1/2-x,1/2-y,-z$), were calculated on the assumption that the C–N bond length is 1.494 Å and each C atom has sp^3 hybridization with C_{2v} symmetry. From such a model the N···N′ distance was calculated to be 2.68 Å.
17) Y. Nakayama, K. Matsumoto, S. Ooi, and H. Kuroya, *J. Chem. Soc., Chem. Commun.*, **1973**, 170.

Studies on Mixed Valence Complexes of Platinum and Palladium. I. Preparation and Characterization of Pt(II)-Pt(IV), Pd(II)-Pt(IV), and Pd(II)-Pd(IV) Complexes of the General Formula, $[M(AA)_2][M'X_2(AA)_2]Y_4$

Naohide MATSUMOTO, Masahiro YAMASHITA, and Sigeo KIDA*

Department of Chemistry, Faculty of Science, Kyushu University 33, Hakozaki, Fukuoka 812

(Received February 6, 1978)

A series of deeply colored mixed valence complexes of the general formula $[M(AA)_2][M'X_2(AA)_2]Y_4$ were prepared and characterized, where M–M′=Pt(II)–Pt(IV), Pd(II)–Pt(IV), and Pd(II)–Pd(IV); (AA)=ethylenediamine, propylenediamine, and trimethylenediamine; X=Cl, Br, and I; Y=ClO_4, BF_4. The relationships between the reflection spectra and the nature of the constituents (X, (AA), Y and M–M′) of the compounds were studied. The value of $\bar{\nu}_{max}$ of the main absorption band in the visible region decreases in the order: Cl→Br→I, pn→tn→en, ClO_4→BF_4, Pd(II)–Pt(IV)→Pt(II)–Pt(IV)→Pd(II)–Pd(IV). On the basis of dichroism of the crystals, it can be predicted that the X–M′(IV)–X···M(II) atoms in these complexes are arrayed in a straight line parallel to the crystal needle.

Of a group of platinum compounds which appear to contain Pt(III), the most typical ones are PtA_2X_3 and PtA_4X_3, where A represents ammonia or organic monoamine, and X halogen or other monovalent anions.[1] These compounds are not simple Pt(III) compounds, but mixed valence compounds containing Pt(II) and Pt(IV) in 1 : 1 ratio, since they are diamagnetic and display strong color.[2] This was verified by sigle-crystal X-ray analysis.[3–8] It was found that they consist of square planar Pt(II) and tetragonal bipyramidal Pt(IV) complexes arrayed in lines as shown in Fig. 1.

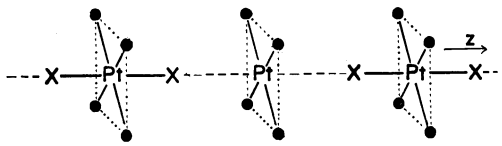

Fig. 1. The skeletal structure of Pt(II)–Pt(IV) mixed-valence complexes.

Yamada and Tsuchida studied the polarized single-crystal spectra of these compounds and attributed the strong absorption to the charge transfer transition from Pt(II) to Pt(IV), assuming a considerable electron exchange interaction between Pt(II) and Pt(IV) through the intervening halogen atom.[9] Recently, Clark *et al.* have shown on the basis of resonance Raman study that such an interaction actually exists between Pt(II) and Pt(IV) through the halogen atom.[10]

In spite of an increasing interest in the Pt(II)–Pt(IV) mixed valence compounds,[11] only a limited number of such compounds are known so far. Wolffram's red salt $[Pt(ea)_4][PtCl_2(ea)_4]Cl_4\cdot 4H_2O$ (ea=ethylamine) is known to be of the PtA_4X_3 type. However, no other homologs were known except the bromo derivative,[1] until Kida reported the synthesis of $[Pt(en)_2][PtCl_2(en)_2](ClO_4)_4$, suggesting the possibility of the synthesis of other homologous compounds.[12]

We have synthesized numerous Pt(II)–Pt(IV) compounds of the type, $[Pt(AA)_2][PtX_2(AA)_2]Y_4$ (AA= ethylenediamine(en), propylenediamine(pn), or trimethylenediamine(tn); X=Cl, Br, or I; Y=ClO_4 or BF_4). We have succeeded in the preparation of Pd(II)–Pt(IV) and Pd(II)–Pd(IV) compounds of similar type. We measured powder reflectance spectra of the compounds in order to elucidate the relationship between the band positions and the constituents of the compounds such as diamine, halogen, counter ion, and metal ion.

Experimental

Starting Materials. $[Pt(AA)_2]Cl_2$,[13] $[Pd(AA)_2]Cl_2$,[14] and $[PtX_2(AA)_2]X_2$[15] (AA=en, pn, tn; X=Cl, Br) were prepared according to the reported methods.

Pt(II)–Pt(IV) Compounds. Compounds of this type were prepared by a procedure similar to that for $[Pt(en)_2][PtCl_2(en)_2](ClO_4)_4$.[12] The tetrafluoroborates were prepared by the same method as that for the perchlorate except for use of a 42% tetrafluoroboric acid solution instead of a 60% perchloric acid solution. Some typical examples are shown below. The procedure of Bekaroglu *et al.* was employed[16] for iodo derivatives.

i) $[Pt(en)_2][PtBr_2(en)_2](BF_4)_4$: Equimolar amounts of $[Pt(en)_2]Cl_2$(386 mg) and $[Pt(en)_2Br_2]Br_2$(635 mg) were dissolved in 20 ml of water. To this solution was added dropwise a 42% tetrafluoroboric acid solution to yield dark green needles with metallic luster, which were filtered and then washed with a small amount of water and then acetone. Recrystallization was carried out from a dilute tetrafluoroboric acid solution.

ii) $[Pt(tn)_2][PtI_2(tn)_2](ClO_4)_4$: One millimole of $[Pt(tn)_2]Cl_2$(414 mg) was dissolved in 20 ml of water. To this solution was added an excess amount of I_2 dissolved in ethanol. The solution was evaporated almost to dryness in a rotary evaporator under reduced pressure in order to remove unreacted I_2. To this residue were added 414 mg (1 mmol) of $[Pt(tn)_2]Cl_2$, 440 mg of $NaClO_4$, and 5 ml of 42% tetrafluoroboric acid. Golden needles with metallic luster were separated from the solution. They were filtered and recrystallized from a dilute perchloric acid solution.

Pd(II)–Pt(IV) Compounds. The compounds were obtained by a procedure similar to that for the Pt(II)–Pt(IV) compounds using $[Pd(AA)_2]Cl_2$ instead of $[Pt(AA)_2]Cl_2$.

Pd(II)–Pd(IV) Compounds. $[PdX_2(AA)_2]X_2$ was not isolated because of its low stability. However, in the mixed valence state Pd(IV) is much stabilized. Hence, $[Pd(AA)_2]^{2+}$ was oxidized by X_2 to form $[PdX_2(AA)_2]^{2+}$, which immediately reacted with the remaining $[Pd(AA)_2]^{2+}$ in a perchloric acid solution. Preparation of iodo homologs of this series was

not successful. Typical examples of the procedure are shown below.

i) $[Pd(en)_2][PdCl_2(en)_2](ClO_4)_4$: One half gram of $[Pd(en)_2]Cl_2$ was dissolved in 10 ml of water. Ten millilitres of 60% perchloric acid was added to this solution, and chlorine gas was passed into the solution under ice-cooling. Dark green fine needles with metallic luster immediately separated out. The crystals were dissolved in a small amount of cold water and filtered. To the filtrate was added 60% $HClO_4$ under ice-cooling in order to obtain the crystals, which were filtered and washed with water and acetone. It should be noted that the Pd(IV) oxidation state is stable only in the crystal lattice of the mixed valence compound. Thus, recrystallization was carried out as quikly as possible.

ii) $[Pd(en)_2][PdBr_2(en)_2](ClO_4)_4$: This was prepared by a procedure similar to that described above except for use of Br_2 instead of Cl_2.

Measurement. Powder reflectance spectra were obtained with a Shimadzu Multipurpose Spectrophotometer Model MSP-5000.

Results and Discussion

The results of elemental analyses are given in Table 1. All the compounds crystallized from aqueous solutions forming strongly colored needles or long prisms, exhibiting remarkable dichroisms, *i.e.*, strongly colored for the

Table 1. Elemental analysis of $[M(AA)_2][M'X_2(AA)_2]Y_4$

M	M′	(AA)	X	Y	%C		%H		%N	
					Found	Calcd	Found	Calcd	Found	Calcd
Pt	Pt	en	Cl	ClO_4	8.94	8.74	2.89	2.93	10.26	10.19
Pt	Pt	pn	Cl	ClO_4	12.40	12.47	3.48	3.49	9.68	9.70
Pt	Pt	tn	Cl	ClO_4	12.47	12.47	3.52	3.49	9.68	9.70
Pt	Pt	en	Cl	BF_4	9.16	9.16	2.96	3.08	10.66	10.69
Pt	Pt	pn	Cl	BF_4	12.95	13.05	3.75	3.65	9.92	10.14
Pt	Pt	tn	Cl	BF_4	13.13	13.05	3.74	3.65	10.17	10.14
Pt	Pt	en	Br	ClO_4	8.21	8.09	2.72	2.71	9.61	9.43
Pt	Pt	pn	Br	ClO_4	11.77	11.58	3.20	3.24	9.09	9.01
Pt	Pt	tn	Br	ClO_4	11.62	11.58	3.25	3.24	9.08	9.01
Pt	Pt	en	Br	BF_4	8.52	8.45	2.95	2.84	9.92	9.85
Pt	Pt	pn	Br	BF_4	12.01	12.08	3.44	3.38	9.30	9.39
Pt	Pt	tn	Br	BF_4	12.00	12.08	3.55	3.38	9.27	9.39
Pt	Pt	en	I	ClO_4	7.58	7.49	2.49	2.52	8.66	8.74
Pt	Pt	pn	I	ClO_4	10.73	10.77	2.94	3.01	8.30	8.37
Pt	Pt	tn	I	ClO_4	10.93	10.77	3.01	3.01	8.47	8.37
Pt	Pt	pn	I	BF_4	10.37	10.60	3.42	3.53	8.30	8.24
Pt	Pt	tn	I	BF_4	11.06	10.60	3.29	3.53	8.47	8.24
Pd	Pt	en	Cl	ClO_4	9.45	9.50	3.15	3.19	10.86	11.09
Pd	Pt	pn	Cl	ClO_4	13.38	13.50	3.75	3.78	10.47	10.51
Pd	Pt	tn	Cl	ClO_4	13.45	13.50	3.72	3.78	10.43	10.51
Pd	Pt	en	Cl	BF_4	10.14	10.00	3.34	3.35	11.42	11.67
Pd	Pt	pn	Cl	BF_4	14.11	14.18	4.02	3.96	10.97	11.03
Pd	Pt	tn	Cl	BF_4	14.27	14.18	3.93	3.96	10.96	11.03
Pd	Pt	en	Br	ClO_4	8.83	8.73	2.94	2.93	10.26	10.19
Pd	Pt	pn	Br	ClO_4	12.51	12.46	3.47	3.49	9.71	9.70
Pd	Pt	tn	Br	ClO_4	12.56	12.46	3.55	3.49	9.79	9.70
Pd	Pt	en	Br	BF_4	9.31	9.50	3.16	3.06	10.81	10.69
Pd	Pt	pn	Br	BF_4	13.17	13.03	3.70	3.65	10.29	10.14
Pd	Pt	tn	Br	BF_4	12.93	13.03	3.88	3.65	9.94	10.14
Pd	Pt	pn	I	ClO_4	11.12	11.53	3.05	3.23	8.62	8.97
Pd	Pt	tn	I	ClO_4	11.70	11.53	3.25	3.23	9.12	8.97
Pd	Pd	en	Cl	ClO_4	10.36	10.42	3.42	3.50	11.49	12.15
Pd	Pd	pn	Cl	ClO_4	14.68	14.74	4.07	4.12	11.49	11.46
Pd	Pd	tn	Cl	ClO_4	14.56	14.74	4.12	4.12	11.27	11.46
Pd	Pd	en	Cl	BF_4	10.92	11.03	3.71	3.70	12.65	12.86
Pd	Pd	pn	Cl	BF_4	15.35	15.54	4.34	4.35	11.88	12.08
Pd	Pd	tn	Cl	BF_4	15.44	15.54	4.52	4.35	12.05	12.08
Pd	Pd	en	Br	ClO_4	9.69	9.51	3.12	3.19	11.24	11.09
Pd	Pd	pn	Br	ClO_4	13.52	13.51	3.77	3.78	10.59	10.50
Pd	Pd	tn	Br	ClO_4	13.60	13.51	3.77	3.78	10.59	10.50
Pd	Pd	en	Br	BF_4	10.04	10.01	3.26	3.36	11.56	11.67
Pd	Pd	pn	Br	BF_4	14.24	14.18	4.02	3.97	10.74	11.03
Pd	Pd	tn	Br	BF_4	14.31	14.18	4.00	3.97	10.93	11.03

Table 2. Color and spectral data (10^3 cm^{-1})

	Pt(II)–Pt(IV)			Pd(II)–Pt(IV)			Pd(II)–Pd(IV)		
	ClO_4	BF_4	Color	ClO_4	BF_4	Color	ClO_4	BF_4	Color
en-Cl	22.73	20.00		24.69	23.81		15.63	15.04	
tn-Cl	22.96	20.62	red	24.69	23.81	yellow	16.39	15.34	dark green[a]
pn-Cl	23.53	21.51		26.32	25.64		19.42	17.30	
en-Br	15.15	14.08		21.28	20.41		13.0[b]	13.0[b]	
tn-Br	16.53	14.08	dark green[a]	20.83	19.61	red	13.0[b]	13.0[b]	golden yellow[a]
pn-Br	17.70	15.87		22.22	21.74		13.0[b]	13.0[b]	
en-I	12.3[b]	—		—	—		—	—	
tn-I	12.3[b]	12.3[b]	golden yellow[a]	13.5[b]	—	golden yellow[a]	—	—	
pn-I	12.3[b]	12.3[b]		13.5[b]	—		—	—	

a) With metallic luster. b) Broad band.

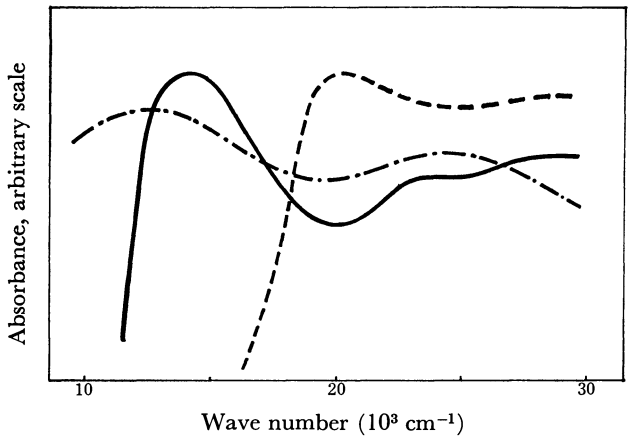

Fig. 2. Powder reflectance spectra of $[Pt(tn)_2][PtX_2(tn)_2](BF_4)_4$; —— X=Cl, —— X=Br, -·-·- X=I.

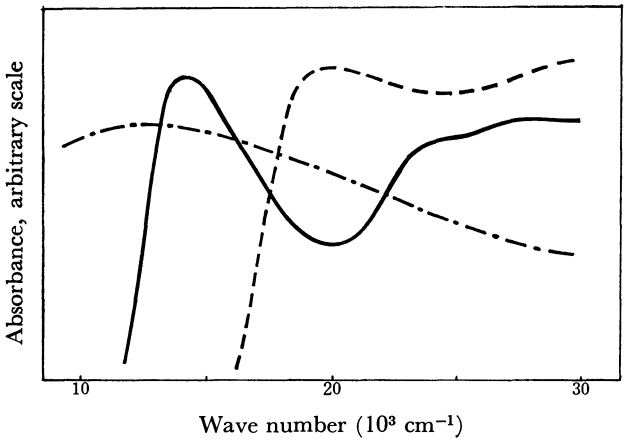

Fig. 3. Powder reflectance spectra of $[M(tn)_2][M'Br_2(tn)_2](BF_4)_4$; —— M–M'=Pt–Pt, —— M–M'=Pd–Pt, -·-·- M–M'=Pd–Pd.

light polarized along the needle and only slightly colored for the light polarized perpendicular to the needle. The colors and band maxima of the powder reflectance spectra in the visible region are given in Table 2. Some spectra are shown in Figs. 2 and 3. Since no intense coloration of the crystals is observed in aqueous solutions and in either of the constituent complexes $[M(AA)_2]Y_2$ and $[MX_2(AA)_2]Y_2$, the strong absorption in the visible region should be attributed to the charge transfer transition from M(II) to M(IV) (M=Pt or Pd) effected by the interaction between M(II) and M(IV) through the halogen atom.[9] Thus, the band can be assigned to the transition from d_{z^2}-{M(II)} to the molecular orbital consisting of p_z (halogen) and d_{z^2}-{M(IV)}, assuming the model depicted in Fig. 1. Since this transition corresponds to the $^1A_1 \leftarrow {}^1A_1{}^*$ in the model (C_{2v} symmetry), it is only allowed for the z axis. Thus, from the fact that the crystals absorb light polarized along the crystal needle only, we can predict that the –Pt–X···Pt··· axis is arrayed parallel to the crystal needle.

On the basis of the theory of charge-transfer complex[2,17] we can assume that the position of the visible band is a measure of the interaction between M(II) and M(IV), *i.e.* the lower the wave-number of the band the stronger the interaction. From the data given in Table 2, it is seen that the $\tilde{\nu}_{max}$ of the main absorption band decreases in the order: 1) Cl→Br→I, 2) pn→tn→en, 3) $ClO_4 \rightarrow BF_4$, 4) Pd^{II}–$Pt^{IV} \rightarrow Pt^{II}$–$Pt^{IV} \rightarrow Pd^{II}$–$Pd^{IV}$.

References

1) "Gmelins Handbuch," Platin Teil A (1957), pp. 616—624.
2) M. B. Robin and P. Day, *Adv. Inorg. Chem. Radiochem.*, **10**, 247 (1967).
3) B. M. Craven and D. Hall, *Acta Crystallogr.*, **14**, 475 (1961).
4) J. Wallen, C. Brosset, and N. Vannerberg, *Arkiv Kemi*, **18**, 541 (1961).
5) T. A. Ryan and R. E. Rundle, *J. Am. Chem. Soc.*, **83**, 2814 (1961).
6) B. M. Craven and D. Hall, *Acta Crystallogr.*, **21**, 177 (1966).
7) K. L. Brown and D. Hall, *Acta Crystallogr., Sect. B*, **32**, 279 (1976).
8) C. Brosset, *Arkiv Kemi Min. Geol.*, **25A**, (1948).
9) R. Tsuchida and S. Yamada, *Nature*, **174**, 1064 (1954); S. Yamada and R. Tsuchida, *Bull. Chem. Soc. Jpn.*, **29**, 894 (1956); *ibid.*, **29**, 421 (1956); *Nippon Kagaku Zasshi*, **8**, 753 (1965).
10) R. J. H. Clark, M. L. Franks, and W. R. Trumble, *Chem. Phys. Lett.*, **41**, 287 (1976); R. J. H. Clark and M. L. Franks, *J. Chem. Soc., Dalton*, **1977**, 198.

11) L. V. Interrante, K. W. Browall, and F. P. Bundy, *Inorg. Chem.*, **13**, 1158 (1974); *ibid.*, **13**, 1162 (1974); *J. Inorg. Nucl. Chem.*, **39**, 1333 (1977).
12) S. Kida, *Bull. Chem. Soc. Jpn.*, **38**, 1804 (1965).
13) R. N. Keller, *Inorg. Synth.*, **2**, 250 (1946).
14) F. G. Mann, D. Crawfoot, D. C. Gattiker and H. Wooster, *J. Chem. Soc.*, **1935**, 1642.
15) F. Basolo, J. C. Bailar, and B. R. Tark, *J. Am. Chem. Soc.*, **72**, 2433 (1950).
16) Ö. Bekaroglu, H. Breer, H. Endres, H. J. Keller, and H. Namgung, *Inorg. Chim. Acta*, **21**, 183 (1977).
17) R. S. Mulliken, *J. Am. Chem. Soc.*, **74**, 811 (1952).

The Oxidative Amination of Tropone and Tropolone

Katsuo KIKUCHI,* Yuji MAKI, and Kazuo SATO

Department of Chemistry, Faculty of Science, Yamagata University, Koshirakawa-cho, Yamagata 990

(Received March 22, 1978)

The reaction of tropone with aniline, *p*-toluidine, *p*-anisidine, and *p*-chloroaniline in the presence of copper(II) acetate gave 2-arylaminotropones and 2-arylamino-*N*-aryltroponeimines. However, when *o*-toluidine and *o*-anisidine were used, only the corresponding 2-arylaminotropones were obtained. The reaction of tropolone with methylamine, ethylamine, and isopropylamine afforded 3-aminotropolone derivatives, while the reaction with dimethylamine, pyrrolidine, and morpholine gave 3- and 5-aminotropolone derivatives, the latter being minor products.

Aminotropones and aminotropolones have usually been obtained 1) by the nucleophilic substitution of 2-alkoxy, 2-halo, and 2-tosyloxytropones; 2) by the reduction of the appropriate nitro, nitroso, or arylazotropolones; 3) by the hydrolysis of 3-(arylsulfonylamido)tropolones; and 4) by the reaction of 3-iodotropolone with liquid ammonia to give 4-aminotropolone.[1] Recently, however, a novel nuclear amination of 3-dialkylaminotropones and 3-alkoxytropones under mild conditions to give 7-aminated tropone derivatives was reported.[2] Also, previously one of the present authors reported that the reaction of tropone and 2-phenyltropone with ammonia, methylamine, and dimethylamine in the presence of copper(II) salt gave 2-aminotropone derivatives and/or salicylaldehyde derivatives.[3] As one of a series of systematic investigations of the oxidative amination of seven-membered aromatics, the reaction of tropone with aromatic primary amines, and the reaction of tropolone with several kinds of primary and secondary amines in the presence of copper(II) salt were investigated; these results will be reported in this paper.

Results and Discussion

When tropone was treated in a closed vessel with a solution of copper(II) acetate and *p*-toluidine in methanol at room temperature for several days, 2-*p*-toluidinotropone (**1a**) and 1-(*p*-toluidino)-7-(*p*-tolylimino)-1,3,5-cycloheptatriene (**2a**)[4] were obtained in about 39 and 17% yields respectively. That the reaction must involve an oxidation step was suggested by the observations that the color of the solution gradually turned greenish brown from deep greenish blue, and that, in some instances, copper(I) oxide was separated on the wall of the reaction vessel. The yields of **1a** and **2a** *versus* the reaction times are listed in Table 1. The ratio of **1a** to **2a** remained almost constant after 5 days' reaction time. Moreover, the reaction of **1a** with *p*-toluidine in the presence or absence of copper(II) acetate was investigated, but in both cases **2a** was not obtained at all. Therefore, the possibility that **1a** was an intermediate for **2a** was eliminated. 7-*p*-Tolylimino-1,3,5-cycloheptatriene,[5] which formed at a slow and reversible step, is considered to be aminated to give **2a**, though the reaction of tropone and *p*-toluidine in the absence of copper(II) salt did not afford a detectable amount of the 7-*p*-tolylimino compound. A similar treatment of tropone with aniline, *p*-anisidine, and *p*-chloroaniline gave the corresponding 2-arylaminotropones (**1b**, **1c**, and **1d**) and, in addition, 1-arylamino-7-arylimino-1,3,5-cycloheptatrienes (**2b**, **2c**, and **2d**). However, the reaction of tropone with *o*-toluidine and *o*-anisidine afforded only the corresponding 2-arylaminotropone derivatives (**1e** and **1f**).

Table 1. The yields of **1a** and **2a** *versus* the reaction times[a]

Reaction time (day)	Temp (°C)	Yields (%)[b] **1a**		**2a**	
1.0	22—24	25.1	(21.4)	4.8	(3.8)
5.0	22—24	42.1	(36.8)	21.0	(16.1)
10.0	22—24	45.2	(39.1)	22.6	(16.6)
20.0	22—24	49.1	(41.1)	26.1	(18.2)

a) Tropolone (5 mmol), *p*-toluidine (20 mmol), copper(II) acetate (10 mmol), and methanol (10 ml) were used. b) The yields of **1a** and **2a** were estimated by the TLC separation of a known amount of the reaction product, followed by the measurement of the absorbance at 407 nm for **1a** and at 417 nm for **2a**. The isolated yields are indicated in parentheses.

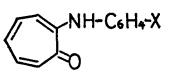

1a: X=*p*-CH_3
1b: X=H
1c: X=*p*-CH_3O
1d: X=*p*-Cl
1e: X=*o*-CH_3
1f: X=*o*-CH_3O

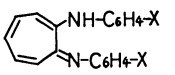

2a: X=*p*-CH_3
2b: X=H
2c: X=*p*-CH_3O
2d: X=*p*-Cl

When tropolone and aqueous methylamine was allowed to react for a long period of time, 2-methylaminotropone (**3**) was obtained in a moderate yield. On the other hand, when tropolone was treated with methylamine in the presence of copper(II) sulfate in water, 3-methylaminotropolone (**4a**) and yellow prisms (**5**) were obtained besides **3**. The UV spectrum of **5** showed maxima at 229 (4.32), 277 (4.35), 360 (4.37), and 433 nm (log ε 3.88). In the IR spectrum, a carbonyl absorption appeared at 1595 cm^{-1}. A sharp *N*-methyl singlet (6H) appeared at 2.98 ppm besides the aromatic and NH protons in the NMR spectrum, indicating the symmetrical structure of **5**. The benzoylation of **5** gave monobenzoyl (**6**) and dibenzoyl compound (**7**). The alkaline hydrolysis of **6** gave 3-(*N*-benzoylmethylamino)-tropolone (**8**), which was also obtained by the benzoyla-

Table 2. The yields of **3**, **4a**, and **5** *versus* the reaction temperature[a)]

Reaction temp (°C)	Reaction time (day)	Yields (%)			
		3	**4a**	**5**	Recovery
8—10	30	0	6	23	34
18—20	10	0	3	21	18
30—32	10	11	15	21	8
50—52	2	13	25	5	8
70—72	1	27	25	0	0

a) Tropolone (20 mmol), copper(II) sulfate (40 mmol), and aqueous methylamine (30%, 25 ml) were allowed to react. The yields were based on the tropolone used.

tion of **4a**, followed by the alkaline hydrolysis of the resulting product. These results indicate that **5** is 2,7-bis(methylamino)tropone. It is interesting here to note that raising the reaction temperature increases the yields of **3** and **4a**, and that at 70 °C **5** was not isolated at all (see Table 2). The further treatment of **3** or **4a** under similar conditions did not afford **5**; it is thought that **5** must be formed through a different reaction pathway. The reaction of tropolone with ethylamine and isopropylamine under similar conditions gave 3-ethylaminotropolone (**4b**) and 3-isopropylaminotropolone (**4c**) respectively.

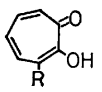

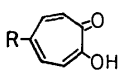

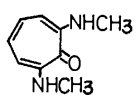

4a: R=CH_3NH **9a**: R=1-pyrrolidinyl **5**
4b: R=C_2H_5NH **9b**: R=morpholino
4c: R=*i*-C_3H_7NH **9c**: R=$(CH_3)_2N$
4d: R=1-pyrrolidinyl
4e: R=morpholino
4f: R=$(CH_3)_2N$

The reactions of tropolone and secondary amines have also been investigated. When tropolone was allowed to react with pyrrolidine in the presence of copper(II) sulfate, yellow prisms (**4d**) ($C_{11}H_{13}O_2N$, mp 98—99 °C) and yellow plates (**9a**) ($C_{11}H_{13}O_2N$, mp 236—238 °C (decomp.)) were obtained; the latter was a minor product. The elemental analysis and UV spectrum of **4d** showed it to be 3-(1-pyrrolidinyl)tropolone. The compound (**9a**) was also confirmed to have a tropolone nucleus from its UV spectrum and its characteristic iron(III) chloride test. The compound (**9a**) was also obtained when 5-bromotropolone was allowed to react with pyrrolidine in the presence of copper(II) acetate, though the yield was poor. Therefore, **9a** must be 5-(1-pyrrolidinyl)tropolone. Similar treatment of tropolone with morpholine and dimethylamine gave 3-(and 5-)-morpholinotropolones (**4e** and **9b**) and 3-(and 5-)-dimethylaminotropolones (**4f** and **9c**) respectively. The reaction of 5-chlorotropolone wtih pyrrolidine in the presence of copper(II) acetate gave 5-chloro-3-(1-pyrrolidinyl)tropolone (**10**), while the reaction of 3-bromotropolone with methylamine under similar conditions afforded 3-methylaminotropolone (**4a**).

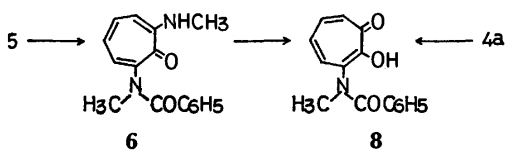

6 **8**

Experimental

The Reaction of Tropone with Aniline, p-Toluidine, p-Anisidine, p-Chloroaniline, o-Toluidine, and o-Anisidine in the Presence of Copper(II) Acetate. Into a suspension of copper(II) acetate (2.00 g) in methanol (10 ml), *p*-toluidine (2.14 g) and tropone (0.530 g) were added successively with stirring. After several minutes, voluminous precipitates were separated. The mixture was allowed to stand for 10 days at 22—24 °C in an atmosphere of nitrogen. The reaction mixture was diluted with water, neutralized with dilute hydrochloric acid, and extracted thoroughly with chloroform. Hydrogen sulfide was passed through the chloroform solution, the copper(II) sulfide was filtered off, the filtrate was washed with water, and the solution was diluted with chloroform to 100 ml. A one-thousandth portion of this solution was separated on thin-layer chromatography using Merck Silica Gel PF_{254}. The fractions corresponding to 2-*p*-toluidinotropone (**1a**) and 1-(*p*-toluidino)-7-(*p*-tolylimino)-1,3,5-cycloheptatriene (**2a**) were eluted with methanol (10.0 ml), and the yields of **1a** and **2a** were estimated spectrophotometrically using the absorbances at 407 nm (for **1a**) and at 417 nm (for **2a**).

For the isolation of **1a** and **2a**, the solvent was removed under reduced pressure, and the residue was dissolved in a mixture of benzene and cyclohexane (1:1) and chromatographed on a column containing 10 g of silica gel. The fraction eluted with the same solvent mixture gave orange crystals, which were subsequently recrystallized from the same solvent mixture to give 250 mg (17%) of **2a** as orange prisms; mp 139—140 °C (lit,[4)] mp 143—144 °C). The fractions eluted with benzene and chloroform gave yellow crystals. Recrystallization from cyclohexane gave 415 mg (39%) of **1a**, mp 108—109 °C (lit,[6)] mp 108.5—109.5 °C).

The reaction of tropone with aniline, *p*-anisidine, *p*-chloroaniline, *o*-toluidine, and *o*-anisidine was carried out in a similar manner to give the following 2-arylaminotropones and 2-arylamino-*N*-aryltroponeimines:

2-Anilinotropone (**1b**), oil, picrate; mp 141—142 °C (lit,[6)] oil, picrate, mp 141—142 °C).

1-Anilino-7-phenylimino-1,3,5-cycloheptatriene (**2b**); mp 84—86 °C (lit,[4)] mp 86—88 °C); yield, 22%.

2-*p*-Anisidinotropone (**1c**); mp 90—91 °C (lit,[7)] mp 91—92 °C); yield, 22%.

1-(*p*-Anisidino)-7-(*p*-anisylimino)-1,3,5-cycloheptatriene (**2c**); mp 110.5—111.5 °C (lit,[4)] mp 112.5—113.5 °C); yield, 31%.

2-*p*-Chloroanilinotropone (**1d**); mp 143—144 °C (lit,[4)] 147 °C); yield, 37%.

1-(*p*-Chloroanilino)-7-(*p*-chlorophenylimino)-1,3,5-cycloheptatriene (**2d**); mp 165—166 °C (lit,[4)] mp 168—170 °C); yield, 14%.

2-*o*-Toluidinotropone (**1e**). Recrystallization from cyclohexane gave yellow prisms; mp 52—53 °C; yield, 14%. UV (methanol) max: 238 (log ε 4.36), 341 (4.09), and 404 nm (4.19). Found: C, 79.61; H, 6.16; N, 6.45%. Calcd for $C_{14}H_{13}ON$: C, 79.59; H, 6.20; N, 6.63%.

2-*o*-Anisidinotropone (**1f**). Recrystallization from a mixture of benzene and cyclohexane gave yellow prisms; mp 111—113 °C; yield, 44%. UV (methanol) max: 234 (log ε 4.33), 345 (4.04), and 406 nm (4.21). Found: C, 74.19; H, 5.80; N 6.02%. Calcd for $C_{14}H_{13}O_2N$: C, 73.99; H, 5.77; N, 6.16%.

The Reaction of Tropolone with Methylamine Tropolone (1.22 g) was dissolved in aqueous methylamine (40%, 10 ml), and the mixture was allowed to react at room temperature for 15 days. The reaction mixture was diluted with water, neutralized with dilute hydrochloric acid, and extracted with chloroform. The chloroform solution was extracted with a sodium hydroxide solution and dilute hydrochloric acid successively. The alkaline solution gave 475 mg of tropolone (mp 48—50 °C), while the acidic solution afforded 683 mg (51%) of 2-methylaminotropone (**3**) (mp 80—82 °C). A similar reaction of tropolone with aqueous pyrrolodine, however, did not afford 2-(1-pyrrolidinyl)tropone.

The Reaction of Tropolone with Primary Amines in the Presence of Copper(II) Salt. The example to be cited is the reaction of tropolone with methylamine. A deep blue solution obtained by dissolving tropolone (2.44 g) and copper(II) sulfate (10.0 g) in aqueous methylamine (30%, 25 ml) was heated at 50—52 °C for 48 h, during which time the color of the solution turned greenish brown and brown crystals began to separate. Water (75 ml) was then added to the reaction mixture, and the precipitate was collected by filtration.

The precipitate was dried and dissolved in chloroform, and hydrogen sulfide was passed through the solution. The copper(II) sulfide was filtered off, and the filtrate was washed successively with an excess of a dilute sodium hydroxide solution and dilute hydrochloric acid. The alkaline solution was acidified with acetic acid, and the yellow crystals (**A**, 850 mg, mp 100—110 °C) that separated were collected by filtration. The filtrate was extracted with chloroform, the chloroform solution was washed with water and dried, and the solvent was evaporated to give a red oil (**B**, 164 mg).

The acid solution was neutralized with sodium hydrogencarbonate, and the yellow crystals that separated were collected, washed, and dried. These crystals were dissolved in a mixture of benzene and chloroform (1:1) and chromatographed on an alumina column to obtain yellow crystals (**C**, 154 mg, mp 117—127 °C). The aqueous solution was extracted with chloroform, the chloroform solution was washed with water and dried, and the solvent was removed to give brown crystals (505 mg). These crystals were dissolved in a mixture of benzene and cyclohexane and treated with a copper(II) acetate solution. The copper(II) complex that was thus obtained was again treated with hydrogen sulfide to regenerate copper-free yellow crystals (**D**, 400 mg, mp 74—80 °C). The portion which did not afford copper(II) salt gave further crops of yellow crystals (**C**, 40 mg; mp 115—124 °C).

The aqueous solution, obtained at first by the dilution of the reaction mixture and the filtration of the precipitate, was acidified with dilute hydrochloric acid and extracted with chloroform, while the chloroform solution was similarly treated to give yellow crystals (**A**, 10 mg), a red oil (**B**, 380 mg), and a small amount of yellow crystals (a mixture of **C** and **D**).

The recrystallization of **A** from ethanol gave 3-methylaminotropolone (**4a**) as yellow plates; mp 113.5—115 °C (lit,[8] mp 113—114 °C; yield, 765 mg (25.3%). (Found: C, 63.67; H, 6.04; N, 8.94%).

The recrystallization of **C** from ethanol gave 2,7-bis(methylamino)tropone (**5**) as yellow needles; mp 128—130 °C; yield, 4.8%. Found: C, 65.67; H, 7.50; N, 16.92%. Calcd for $C_9H_{12}ON_2$: C, 65.83; H, 7.37; N, 17.06%.

The recrystallization of **D** from a mixture of benzene and cyclohexane gave 2-methylaminotropone (**3**); mp 81—82 °C; yield, 13%.

The red oil (**B**) was dissolved in chloroform and washed with dilute hydrochloric acid to remove the basic compounds. The chloroform solution was washed with water and dried, and the solvent was removed. The recrystallization of the crystalline residue from cyclohexane gave 205 mg of tropolone as pale yellow crystals.

The reaction of tropolone with ethylamine and isopropylamine was carried out in a similar manner.

3-Ethylaminotropolone (**4b**); yellow plates (from ethanol); mp 57—58 °C (lit,[8] mp 51—53 °C); yield, 20%. (Found: C, 65.75; H, 6.82; N, 8.42%).

3-Isopropylaminotropolone (**4c**); yellow prisms (from dilute methanol); mp 72—73.5 °C (lit,[8] 72—73 °C); yield, 23%. (Found: C, 66.48; H, 7.28; N, 7.75%).

Benzoylation of 2,7-Bis(methylamino)tropone (5). Into a solution of **5** (600 mg) in pyridine (5 ml), benzoyl chloride (2.5 ml) was added under ice cooling and with stirring. After 1 h, the reaction mixture was poured into water, acidified with hydrochloric acid, and extracted with chloroform. The solution was washed with water, the solvent was removed, and the crystalline residue was washed with benzene. The crystals were recrystallized from 1-butanol to give 2,7-bis(*N*-benzoylmethylamino)tropone (**7**) as yellow prisms; mp 230—232 °C. UV (methanol) max: 282 (log ε 4.00), and 355 nm (3.81). Found: C, 73.70; H, 5.51; N, 7.31%. Calcd for $C_{23}H_{20}O_3N_2$: C, 74.17; H, 5.41; N, 7.52%.

The benzene solution was chromatographed on a silica gel column, and the fraction eluted with chloroform was recrystallized from benzene to give 2-(*N*-benzoylmethylamino)-7-methylaminotropone (**6**) as yellow prisms; mp 183—184 °C; yield, 202 mg. UV (methanol) max: 253 (log ε 4.25) 345 (4.04), and 420 nm (4.20). Found: C, 71.40; H, 6.10; N, 10.34%. Calcd for $C_{16}H_{16}O_2N_2$: C, 71.62; H, 6.01; N, 10.44%.

Alkaline Hydrolysis of 6. A solution of **6** (150 mg) in ethanol (3 ml) was refluxed with 10% aqueous sodium hydroxide (0.6 ml) for 4 h. The reaction mixture was then diluted with water, acidified with acetic acid, and extracted with chloroform. The evaporation of the solvent gave a crystalline residue, which was recrystallized from a mixture of benzene and cyclohexane to give 65 mg of 3-(*N*-benzoylmethylamino)-tropolone (**8**) as pale yellow prisms; mp 115—116 °C. UV (methanol) max: 331 (log ε 3.79) and 368 nm (3.78). Found: C, 70.52; H, 5.12; N, 5.32%. Calcd for $C_{15}H_{13}O_3N$: C, 70.58; H, 5.13; N, 5.49%.

3-(N-Benzoylmethylamino)tropolone (8) from 4a. Into a solution of **4a** (100 mg) in pyridine (1 ml), benzoyl chloride (0.6 ml) was added under ice cooling and with stirring. After 1 h, the mixture was poured into water, and a viscous oily product was separated from the water. This oil was, without further purification, dissolved in ethanol (5 ml) and refluxed with an excess of an aqueous sodium hydroxide solution for 2 h. The mixture was then diluted with water, acidified with acetic acid, and extracted with chloroform. The solvent was removed, and the residue was chromatographed on a silica gel column. The fraction eluted with chloroform gave **8** (58 mg); mp 114—116 °C, which was identical with that obtained from **5**.

The Reaction of Tropolone with Secondary Amines in the Presence of Copper(II) Salt. The example cited will be for the reaction of tropolone with pyrrolidine. A deep blue solution obtained by dissolving copper(II) sulfate (5.00 g), ammonium chloride (3.00 g), and tropolone (1.22 g) in a mixture of pyrrolidine (12 ml), and water (12 ml) was heated at 50—55 °C for 5 days. Water (150 ml) was added to the reaction mixture, neutralized with hydrochloric acid, and the precipitate was collected by filtration. The filtrate was extracted with chloroform, the precipitate and chloroform extract were combined, and hydrogen sulfide was passed through the solution. The copper(II) sulfide was removed, and the filtrate was washed with a dilute sodium hydroxide solution. The aqueous layer was acidified with acetic acid, and the precipitate (**A**)

was filtered and washed with water. The filtrate was extracted with chloroform, and the chloroform solution was washed with water and dried. The subsequent evaporation of the solvent and distillation of the residue under reduced pressure afforded 496 mg of tropolone; mp 48—51 °C.

The crystals (**A**, 763 mg) were distilled under reduced pressure (2 Torr). The **B** fraction (distilled at a bath temperature of 120—130 °C) was recrystallized from methanol to give 552 mg (29%) of 3-(1-pyrrolidinyl)tropolone (**4d**), while the **C** fraction (sublimed under a free flame) was recrystallized from methanol, followed by dimethylformamide, to give 95 mg (5%) of 5-(1-pyrrolidinyl)tropolone (**9a**).

3-(1-Pyrrolidinyl)tropolone (**4d**); yellow prisms (from methanol); mp 98—99 °C. UV (methanol) max: 269 (log ε 4.34), 361 (4.19), and 422 nm (3.79). Found: C, 69.26; H, 7.18; N, 7.48%. Calcd for $C_{11}H_{13}O_2N$: C, 69.09; H, 6.85; N, 7.33%.

5-(1-Pyrrolidinyl)tropolone (**9a**); yellow plates (from dimethylformamide); mp 236—238 °C (dec). UV (methanol) max: 240 (log ε 4.32), 286 (3.51), 374 (4.29), and 394 nm (sh, 4.23). Found: C, 69.30; H, 7.09; N, 7.40%. Calcd for $C_{11}H_{13}O_2N$: C, 69.09; H, 6.85; N, 7.33%.

The reaction of tropolone with morpholine and dimethylamine was carried out in a manner similar to that described above, and the following 3- and 5-aminotropolone derivatives were obtained.

3-Morpholinotropolone (**4e**); yellow plates (from cyclohexane); mp 84—86 °C; yield, 21%. UV (methanol) max: 226 (log ε 4.24), 273 (4.19), and 355 nm (4.03). Found: C, 64.17; H, 6.42; N, 6.99%. Calcd for $C_{11}H_{13}O_3N$: C, 63.75; H, 6.32; N, 6.76%.

5-Morpholinotropolone (**9b**); yellow prisms (from dioxane); mp 201—202 °C; yield, 2%. UV (methanol) max: 236 (log ε 4.32), 283 (3.54), and 363 nm (4.12). Found: C, 63.39; H, 6.39; N, 6.95%. Calcd for $C_{11}H_{13}O_3N$: C, 63.75; H, 6.32; N, 6.76%.

3-Dimethylaminotropolone (**4f**); yellow prisms (from cyclohexane); mp 54.5—56 °C; yield, 24%. UV (methanol) max: 226 (log ε 4.14), 271 (4.26), and 360 nm (4.04). Found: C, 65.62; H, 6.95; N, 8.44%. Calcd for $C_9H_{11}O_2N$: C, 65.44; H, 6.71; N, 8.48%.

5-Dimethylaminotropolone (**9c**); yellow needles (from ethanol); mp 163—164.5 °C (lit,[9] 160—162 °C); yield, 2%. (Found: C, 65.36; H, 6.73; N, 8.66%).

The Reaction of 5-Chlorotropolone and 5-Bromotropolone with Pyrrolidine in the Presence of Copper(II) Salt. 5-Chlorotropolone (0.64 g) was added to a solution obtained by dissolving copper(II) acetate (1.60 g) in pyrrolidine (4 ml) and ethanol (10 ml), and the mixture was heated at 55—60 °C for 24h. The mixture was then diluted with water, and the precipitate was collected by filtration. The filtrate was neutralized with dilute hydrochloric acid and extracted with chloroform. The precipitate and the chloroform extract were then combined, and hydrogen sulfide was passed through the solution. Copper(II) sulfide was filtered off, and the filtrate was treated with a dilute sodium hydroxide solution. The separated sodium salt and the aqueous solution were combined, acidified with acetic acid, and extracted with chloroform, and the chloroform solution was again treated with 6M-hydrochloric acid. The acid-insoluble portion gave 232 mg of 5-chlorotropolone. The acid-soluble portion was neutralized with sodium hydrogencarbonate to give 215 mg of yellow crystals. These crystals were recrystallized from ethanol to give 5-chloro-3-(1-pyrrolidinyl)tropolone (**10**) as yellow crystals; mp 90—92 °C; yield, 190 mg (21%). UV (methanol) max: 277 (log ε 4.38), 368 (4.19), and 430 nm (3.82). Found: C, 58.68; H, 5.53; N, 6.19%. Calcd for $C_{11}H_{12}O_2NCl$: C, 58.54; H, 5.37; N, 6.21%.

A solution of copper(II) acetate (1.60 g), pyrrolidine (6 ml), methanol (6 ml), and 5-bromotropolone (0.80 g) was heated at 55—60 °C for 24 h, after which the reaction mixture was treated much as above. The portion soluble in both the sodium hydroxide solution and 6M-hydrochloric acid gave 30 mg of 5-(1-pyrrolidinyl)tropolone (**9a**) as yellow crystals (mp 235—237 °C (dec)) identical with the sample obtained by the reaction of tropolone and pyrrolidine described above.

The Reaction of 3-Bromotropolone with Methylamine in the Presence of Copper(II) Salt. To a deep blue solution obtained by dissolving copper(II) acetate (2.00 g) in methanol (10 ml) and methylamine (30%, 5 ml), 3-bromotropolone (1.00 g) was added, after which the mixture was heated at 60—65 °C for 20 h. The precipitate was then removed, and the filtrate was concentrated under reduced pressure. The residue was diluted with water, and hydrochloric acid was added to the solution to adjust the pH at about 3. The precipitate that formed was filtered and washed with water, while the filtrate was extracted with chloroform. The precipitate and chloroform extract were then combined, hydrogen sulfide was passed through, and the copper(II) sulfide was filtered off. The filtrate was washed with 4M-hydrochloric acid, and the acid-soluble portion was neutralized with sodium hydrogencarbonate. The crystals that separated out were recrystallized from ethanol to give yellow scales (mp 111—113 °C; 85 mg) which were identical with 3-methylaminotropolone (**4a**).

References

1) a) T. Nozoe, K. Takase, and H. Matsumura, "Dai-Yuki Kagaku," Vol. 13, Asakura Publishing Co., Tokyo (1960), Chaps., 7, 8, and 11; b) F. Pietra, *Chem. Rev.*, **73**, 293 (1973).

2) B. Ricciarelli, R. Cabrino, F. D. Cima, C. A. Veracini, and F. Pietra, *J. Chem. Soc., Chem. Commun.*, **1974**, 723.

3) K. Kikuchi, *Bull. Chem. Soc. Jpn.*, **40**, 385 (1967).

4) W. R. Brasen, H. E. Holmquist, and R. E. Benson, *J. Am. Chem. Soc.*, **83**, 3125 (1961).

5) a) Y. Kitahara, T. Asao, and M. Funamizu, Japanese Patent 17824 and 17825 (1964); b) K. Sanechika, S. Kajigaeshi, and S. Kanemasa, *Synthesis*, **1977**, 202.

6) T. Nozoe, Y. Kitahara, T. Ando, S. Masamune, and H. Abe, *Sci. Repts. Tohoku Univ. Ser. I.* **36**, 166 (1952).

7) a) T. Mukai and M. Kimura, *Tetrahedron Lett.*, **1970**, 717; b) M. Kimura, Ph. D. Thesis, Tohoku University, Sendai, Japan, 1969.

8) K. Takase, M. Yasunami, and H. Okino, unpublished results.

9) K. Takase, M. Yasunami, and T. Yamatani, unpublished results.

Constituents of the Essential Oil of *Chrysanthemum japonense*. Nojigiku Alcohol and Its Acetate

Yasuto UCHIO

Department of Chemistry, Faculty of Science, Hiroshima University, Higashisenda, Hiroshima 730

(Received November 24, 1977)

The essential oil of *Chrysanthemum japonense* has been analyzed to isolate a new monoterpenoid named nojigiku alcohol together with its acetate, the structure of which has been elucidated as (5*R*)-2,2-dimethyl-3-methylenebicyclo[2.2.1]heptan-5-ol. In addition, fifteen monoterpenoids including (+)-α-pinene, (+)-camphene, β-pinene, sabinene, 1,8-cineole, *p*-cymene, filifolone, (+)-chrysanthenone, (+)-camphor, (+)-borneol, (−)-*cis*- and (+)-*trans*-chrysanthenyl acetate, *cis*- and *trans*-carveyl acetate, (+)-bornyl acetate and nine sesquiterpenoids including α-copaene, β-elemene, β-caryophyllene, germacrene-D, γ-cadinene, calamenene, β-caryophyllene oxide, T-muurolol and α-cadinol were identified in the essential oil.

In Japan about twenty species of the *Genus Chrysanthemum* (the *family* of *Compositae*) are distributed as native plants. The plants are known to be a typical group, the chromosome number of which are the multiple such as $2n=18$, 36, 54, 72, and 90.[1] Consequently, they have been investigated by many workers in the field of the botany, especially taxonomy, morphology, cytology and genetics. However, there has been little chemical investigation on the constituents of the essential oils except for the isolation of chrysanthenone from *Chrysanthemum sinense* Sabin, (an agricultural species) and its structural elucidation by Kotake and Nonaka.[2]

The present author is continuing the investigation on the essential oils of the species, and has already reported the structural elucidations of (+)-*trans*-chrysanthenyl acetate,[3] two new acetylenic compounds,[4] and also the analyses of the essential oils of *Ch. boreale* Makino ($2n=18$),[5] *Ch. makinoi* Matsum. *et* Nakai ($2n=18$),[5] *Ch. shiwogiku* Kitam. ($2n=54$)[3] and *Ch. japonense* var. *devile* Kitam. ($2n=54$).[6] In the present work, the essential oil of *Ch. japonense* (Makino) Nakai ($2n=54$) has been analyzed and a new monoterpene alcohol isolated of good aroma, (5*R*)-2,2-dimethyl-3-methylenebicyclo[2.2.1]heptan-5-ol (**1**), together with its acetate (**2**). The alcohol has been named nojigiku alcohol and its structure elucidated as 5-hydroxycamphene. This is the first example of an oxygenated derivative of camphene having been isolated in nature. The details of the structural elucidation and the analytical results on other mono and sesquiterpenoids are described. Part of the work has been presented in a prelininary report.[7]

Results and Discussion

Structural Elucidation of Nojigiku Alcohol and Its Acetate. Nojigiku alcohol (**1**), mp 52.0—53.0 °C, $[\alpha]_D^{25}$ +12.0° (*c* 1.10, $CHCl_3$), has been isolated, together with an oily acetate, $[\alpha]_D^{25}$ +20.9° (*c* 0.58, $CHCl_3$) from the essential oil by a combination of fractional distillation and elution chromatography.

The alcohol has been analyzed for $C_{10}H_{16}O$ (M^+ 152) and afforded a crystalline 3,5-dinitrobenzoate, mp 107.0—108.0 °C. The IR and ^{1}H-NMR spectra revealed the alcohol to contain a secondary hydroxyl group (δ 3.71, 1H, dd, $J=7.0$ and 3.0 Hz; ν 3350 and 1050 cm^{-1}), a *gem*-dimethyl (δ 0.91 and 1.01, each 3H, s; ν 1380, 1375, and 1360 cm^{-1}), an allylic methine (δ 2.63, 1H, br s), and an *exo*-methylene group (δ 4.60 and 4.81, each 1H, s; ν 3060, 1655, and 885 cm^{-1}).

Examination of the ^{13}C-NMR spectrum showed a close resemblance to that of camphene, which is a bicyclic monoterpene hydrocarbon containing all the functional groups mentioned above except the secondary hydroxyl group. The chemical shifts and the signal multiplicities are shown in Table 1. In the catalytic hydrogenation over Adams catalyst in AcOH, the alcohol took up one molar equivalent of hydrogen to afford two saturated alcohols attributable to the *endo*- and *exo*-methyl isomers in a ratio of 4: 1, a similar reaction to that of camphene; the major product (**4**), $C_{10}H_{18}O$ (M^+ 154), after isolation by preparative GLC, exhibited a doublet due to the newly formed secondary methyl group at δ 0.90. These results suggested the alcohol to be a bicyclic monoterpene alcohol. The alcohol was oxidized with Jones reagent to give a nonconjugated cyclopentanone derivative (**3**), $C_{10}H_{14}O$ (M^+ 150.1049); mp 47.0—48.0 °C (semicarbazone, mp 189.0—190.0 °C); ν 1755 cm^{-1}, leaving the *exo*-methylene group unaffected (δ 4.82 and 5.06, each 1H, s; ν 3075, 1655, and 899 cm^{-1}). In the spectra of this ketone, an absorption band attributable to the newly formed active methylene appeared at ν 1420 cm^{-1} and the broad singlet of the allylic methine showed a much lower shift (δ 3.00) owing to the anisotropic effect of the carbonyl group compared with the original alcohol. Thus, nojigiku alcohol was characterized as a camphene derivative bearing the hydroxyl group on the C-5 position, that is, the planar structure of nojigiku alcohol was determined as 2,2-dimethyl-3-methylenebicyclo-[2.2.1]heptan-5-ol.

On treatment with acetic anhydride in pyridine, the

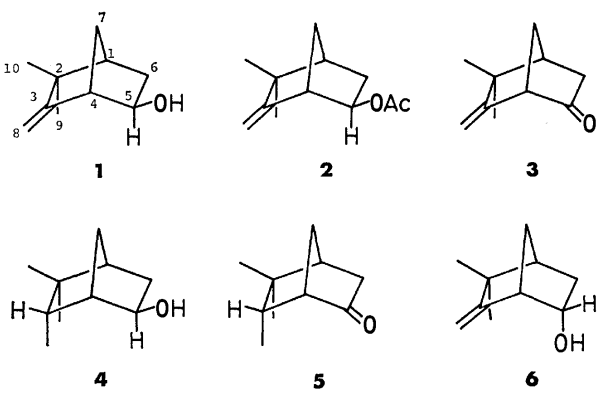

Table 1. ^{13}C-NMR spectral data[a] of nojigiku alcohol (**1**), its acetate (**2**) and camphene (**7**), and shielding differences

Carbon atom	**1**	**2**[b]	**7**[c]	$\Delta\delta$(**1**—**7**)[d]	$\Delta\delta$(**2**—**7**)[d]
1	48.4(d)	47.5(d)	48.8(d)	−0.4(γ)	−1.3(γ)
2	41.5(s)	41.2(s)	42.3(s)	−0.8(δ)	−1.1(δ)
3	163.2(s)	159.7(s)	167.9(s)	−4.7(γ)	−8.2(γ)
4	56.4(d)	52.5(d)	47.6(d)	8.8(β)	4.9(β)
5	74.4(d)	76.3(d)	29.2(t)	45.2(α)	47.1(α)
6	36.9(t)	34.2(t)	24.1(t)	12.8(β)	10.1(β)
7	33.9(t)	34.2(t)	37.9(t)	−4.0(γ)	−3.7(γ)
8	104.2(t)	104.5(t)	100.3(t)	3.9	4.2
9	29.6(q)	29.2(q)	29.9(q)	−0.3	−0.7
10	25.7(q)	25.4(q)	26.2(q)	−0.5	−0.8

a) The spectra were measured in $CDCl_3$ with an internal standard of TMS. Multiplicities given in parentheses were determined by off-resonance ^{1}H decoupled spectra. b) For the additional $-COCH_3$ 170.6(s) and 21.4(q) were given. c) The assignment depended upon Ref. 14. d) Effects of hydroxy or acetoxy group are reported at designated position relative to camphene (**7**).

alcohol gave an oily monoacetate, $C_{12}H_{18}O_2$ (M^+ 194); ν 1740 and 1250 cm^{-1}, which was identical with the co-occurring acetate in IR, ^{1}H-NMR, and MS spectra. The reduction of the co-occurring acetate with $LiAlH_4$ afforded an alcohol showing the same TLC behavior as nojigiku alcohol.

With regard to the ^{13}C-NMR spectra of nojigiku alcohol and its acetate the shielding differences of the carbon atoms ($\Delta\delta$ in Table 1) were calculated for those of camphene. In this case the differences showed the same trend as in the case of 5-*exo*-hydroxynorbornane towards norbornane.[8] In the ^{1}H-NMR spectra of the alcohol, its acetate, and dihydro alcohol the carbinyl protons uniformly showed a double doublet (J=7.0 and 3.0 Hz) at δ 3.71, 4.55, and 3.97, which indicated the protons on C-5 to have the *endo* configuration.[9] Furthermore, the cyclopentanone derivative (**3**) was reduced with $LiAlH_4$ to give two epimeric alcohols in a ratio of 9: 1. Of these products the minor alcohol was identical with nojigiku alcohol in IR, ^{1}H-NMR, and MS spectra. The major alcohol could be characterized as its epimer (**6**) holding the hydroxyl group in the *endo* configuration based on the fact that a broad doublet (δ 2.67) of the allylic bridgehead proton had a coupling constant of about J=4.0 Hz as well as that of (J=3.8 Hz) in *endo*-norborneol.[9] These facts clearly designated the hydroxyl group of nojigiku alcohol to have the *exo* configuration. The proposed structure for nojigiku alcohol, however, has been reported to a chlorination product of camphene by some workers.[10a–d] For confirmation of the identity, the compound was synthesized from *dl*-camphene according to the reports;[10b,d] the IR, ^{1}H-NMR, and MS spectra were respectively coincident with those of nojigiku alcohol.

In order to determine the absolute configuration of nojigiku alcohol, its dihydro alcohol (**4**) was oxidized with Jones reagent to a saturated ketone (**5**) which showed a negative Cotton effect ($[\phi]_{297}$ −4690, $[\phi]_{265}$ +1600, *c* 0.039, MeOH) on the ORD curve. This indicated, according to the relation between the Cotton effect and stereostructure in a bicyclo[2.2.1]heptan-2-one system,[11] that the saturated ketone had an absolute configuration as shown by (**5**). Consequently, the absolute configuration of nojigiku alcohol and its acetate isolated from *Ch. japonense* may be represented as formulae (**1**) and (**2**) holding the chirality of *d*-camphene. The configuration of the hydroxyl group in this formula (**1**) agreed with the determination by Horeau's method.[12]

Other Constituents of the Essential Oil. From the essential oil of *Ch. japonense* fifteen monoterpenoids and nine sesquiterpenoids were identified other than nojigiku alcohol and its acetate as shown in Table 2. The composition, calculated from the relative GLC peak areas and identification methods are also listed. Total amounts of the monoterpenoids and sesquiterpenoids were *ca.* 87 and 13%, respectively, in the oil. The monoterpenoids thus identified have been classified into the camphane type ((+)-camphene, (+)-camphor, nojigiku alcohol and its acetate, (+)-borneol, and (+)-bornyl acetate), the pinane type ((+)-α-pinene, β-pinene, (+)-chrysanthenone, (+)-*trans*- and (−)-*cis*-chrysanthenyl acetate), *p*-menthane type (1,8-cineole, *p*-cymene, *trans*- and *cis*-carveyl acetate), and others (sabinene and filifolone). The camphane, pinane and *p*-menthane types were respectively 74.8, 6.5, and 5.5% of the total oil. Thus, the major part of the oil consisted of bicyclic monoterpenoids, in which (+)-camphor was the main (60.0%), and the other monoterpenoids were in trace amounts except for 1,8-cineole. As to the pinane type, (+)-*trans*-chrysanthenyl acetate has been previously isolated from the essential oil of *Ch. shiwogiku*[3] by the present author *et al.*, and (−)-*cis*-chrysanthenyl acetate has been reported as the main component of *Centipeda Cunninghami*[13] by Pinhey and Southwell. Both isomers, however, co-occurred in this essential oil. (+)-Chrysanthenone, (+)-*trans*- and (−)-*cis*-chrysanthenyl acetate should be counted in the series of (−)-α-pinene in the chirality, but any oxygenated derivative of (+)-α-pinene could not be identified in the oil.

The essential oil of *Ch. japonense* remarkably differed from that of *Ch. japonense var. devile*,[6] which contains borneol and bornyl acetate as major components but not nojigiku alcohol and its acetate, although the latter has been classified as a variety of the former.

Table 2. Constituents of the essential oil of *Ch. japonense*

	Compound	Content (% in total oil)		Method of identification
Monoterpenoids				
Camphane type	(+)-Camphene	2.3		IR, NMR, MS
	(+)-Camphor	60.0		IR, NMR, MS
	(+)-Nojigiku alcohol	5.4	74.8	IR, NMR, MS
	(+)-Borneol	1.5		IR, NMR, MS
	(+)-Bornyl acetate	4.3		IR, NMR, MS
	(+)-Acetate of nojigiku alcohol	1.3		IR, NMR, MS
Pinane type	(+)-α-Pinene	1.4		IR, MS
	β-Pinene	0.6		IR, MS
	(+)-Chrysanthenone	2.4	6.5	IR, NMR, MS
	(+)-*trans*-Chrysanthenyl acetate	1.3		IR, NMR, MS
	(−)-*cis*-Chrysanthenyl acetate	0.8		IR, NMR, MS
p-Menthane type	1,8-Cineole	4.8		IR, NMR, MS
	p-Cymene	0.4	5.5	IR, MS
	trans-Carveyl acetate	0.2		IR, NMR, MS
	cis-Carveyl acetate	0.1		IR, NMR, MS
Other	Sabinene	0.2	0.6	IR, MS
	Filifolone	0.4		IR, NMR, MS
Sesquiterpenoids				
Hydrocarbons	α-Copaene	0.1		IR, NMR, MS
	β-Elemene	1.0		IR, NMR, MS
	β-Caryophyllene	1.2	9.6	IR, NMR, MS
	Germacrene-D	6.7		IR, NMR, MS
	γ-Cadinene	0.3		IR, NMR, MS
	Calamenene	0.2		IR, MS
Oxygenated compounds	β-Caryophyllene oxide	1.1		IR, NMR, MS
	T-Muurolol	1.6	3.5	IR,[15] NMR, MS
	α-Cadinol	0.1		IR,[15] NMR, MS
	Unidentified	0.7		

Experimental

All melting and boiling points are uncorrected. The IR spectra were measured in CCl_4. The ^{1}H-NMR spectra were obtained on a Hitachi R-20 or Varian T-60 spectrometer in CCl_4 using TMS as the internal standard. The ^{13}C-NMR spectra were recorded on a JEOL-PFT-100 spectrometer operating at 25.5 MHz. The mass spectra were measured on a Hitachi RMS-4 spectrometer, and the high mass measurements on a Hitachi RMU-7L spectrometer. The TLC was carried out using a Merck Kiesel Gel G, and the elution chromatography using a Merck Kiesel Gel Type 60. The analytical GLC was performed with a separation column (3 mm×2 m) packed with 3% PEG-6000, PEG-20M, DEGS, and SE-30 on Chromosorb AW (60—80 mesh) under the flow rate of 20 ml/min of N_2, and preparative GLC with a separation column (6 mm×2 m) packed with 10% PEG-6000, PEG-20M, DEGS, and SE-30 on Chromosorb AW (60—80 mesh) using He as a carrier gas (30 ml/min).

Separation and Fractionation of the Essential Oil[1] *Ch. japonense* used in the experiment was collected at the sea side of Suzaki city in Kochi prefecture in October prior to efflorescence. After being dried in the shade for one day, the plant (8.1 kg) was steam distilled to obtain the essential oil (6.0 g, yield 0.07%), $[\alpha]_D^{25}$ −1.86°, n_D^{25} 1.4800, d_4^{25} 0.9388, including an ether extract from the distilled water. The essential oil showed twenty six GLC peaks using a SE-30 column under a temperature programme of 3 °C/min from 80 to 200 °C.

The oil was fractionated through a small size-spinning band distillation column (6×500 mm) under reduced pressure and separated into the following fractions and residue (2.4 g). Fr. 1 (bp 40—60 °C/30 Torr): 1.2 g; fr. 2 (60—80 °C/20 Torr): 1.0 g; fr. 3 (80—100 °C/20 Torr): 0.9 g. The residue was then eluted stepwise over a silica gel column by hexane (100 ml), a hexane and ethyl acetate mixture (v/v, 3: 1, 200 ml), and diethyl ether (100 ml) to give three additional fractions, R-1, R-2, and R-3, respectively.

Isolation of Nojigiku Alcohol (1) and Its Acetate (2). Fraction R-2 was again eluted over a silica gel column with a mixed solvent of hexane and ethyl acetate (v/v, 5: 1) and nojigiku alcohol isolated from the last eluate in a homogeneous state for GLC (SE-30 and PEG-20M). MS *m/e* 152 (M^+, $C_{10}H_{16}O$, 0.5%), 137 (M−CH_3, 3%), 135 (M−OH, 4%), 134 (M−H_2O, 3%), 108 (base), 119 (14), 93 (62), 91 (39), 81 (13), 79 (29), 67 (21), and 41 (34). 3,5-Dinitrobenzoate, Found: C, 58.97; H, 5.23; N, 8.06%. Calcd for $C_{17}H_{18}N_2O_6$: C, 58.95; H, 5.24; N, 8.09%.

Acetylation of the alcohol (30 mg) with Ac_2O (1 ml) in pyridine (1 ml) gave an oily monoacetate (35 mg). $[\alpha]_D^{25}$ +11.6° (*c* 1.20, $CHCl_3$). The IR, ^{1}H-NMR, and MS spectra were respectively superimposable on those of the co-occurring acetate described in the following.

The early eluate in the column chromatography of fraction R-2 afforded an oily mixture of monoterpene acetates showing six GLC peaks, the fourth peak of which was characterized, after isolation by preparative GLC (PEG-20M, 110 °C), as the acetate (**2**) of nojigiku alcohol based on the following data.

MS *m/e* 194.1309 (M^+, 1.9%, calcd for $C_{12}H_{18}O_2$, 194.1312), 179 (3), 150 (35), 134 (4), 119 (12), 107 (58), 93 (13), 91 (13), 89 (17), 79 (11), 77 (7), 67 (8), 65 (5), 53 (8), 43 (base), and 41 (18); IR *ν* 3075, 1740, 1655, 1375, 1365, 1250, 1035, and 895 cm^{-1}; ^{1}H-NMR *δ* 1.07 (6H, s), 1.95 (3H, s), 2.73 (1H, br s), 4.55 (1H, dd, *J*=7.0 and 3.0 Hz), 4.73 (1H, s), and 4.99 (1H, s). Found: C, 74.35; H, 9.41%. Calcd for $C_{12}H_{18}O_2$: C, 74.19; H, 9.34%.

The acetate was applied to the TLC plate, and some drops of an ethereal solution of $LiAlH_4$ applied. After standing for a times, the plate was developed with $CHCl_3$ and a mixture of hexane and ethyl acetate (v/v, 5: 1), giving an R_f 0.30 or 0.35. This mobility agreed with that of nojigiku alcohol.

Catalytic Hydrogenation of Nojigiku Alcohol. The alcohol (70 mg) was subjected to hydrogenation over Adams catalyst (5 mg) in AcOH (3 ml) at room temperature until the uptake of H_2 ceased. The hydrogenated mixture was treated in the usual manner to give a product showing two peaks attributable to two diastereoisomers of dihydronojigiku alcohol in GLC (DEGS) with a relative peak intensity of about 4: 1. The major product was isolated by preparative GLC (DEGS) to give the 3-*endo*-methyl isomer (**4**) as colorless needles, mp 68.0—69.0 °C. MS *m/e* 154 (M^+, $C_{10}H_{18}O$, 3%), 139 (5), 121 (6), 110 (6), 95 (29), 84 (14), 81 (12), 71 (22), 67 (30), 55 (47), and 41 (base); IR *ν* 3620, 3320, 1390, 1375, 1365, and 1040 cm^{-1}; ^{1}H-NMR *δ* 0.75 (3H, s), 0.87 (3H, s), 0.90 (3H, d, *J*=6.0 Hz), 1.70 (1H, br s, OH exchanged with D_2O), and 3.97 (1H, dd, *J*=7.0 and 3.0 Hz).

*Oxidation of 3-*endo*-Methyl Alcohol (**4**).* The 3-*endo*-methyl alcohol (45 mg) was oxidized with Jones reagent (1 ml) in acetone (5 ml) at room temperature. After the usual work up, the mixture gave a crystalline ketone (**5**) (30 mg), mp 58.0—59.0 °C. MS *m/e* 152 (M^+, 21%), 137 (10), 123 (4), 119 (12), 117 (14), 110 (34), 95 (96), 83 (20), 81 (29), 69 (41), 67 (32), 55 (59), and 41 (base); IR *ν* 1750, 1420, 1390, 1380, and 1365 cm^{-1}; ^{1}H-NMR *δ* 0.83 (3H, d, *J*=6.0 Hz), 0.92 (3H, s), 1.17 (3H, s), and 2.35 (1H, br d, *J*=4.0 Hz).

*Oxidation of Nojigiku Alcohol (**1**).* To the alcohol (120 mg) in acetone (10 ml) Jones reagent (2 ml) was added drop by drop at room temperature. After the brown color of the reaction mixture disappeared, it was treated according to the usual procedure and purified over a silica gel column with $CHCl_3$ to give an unsaturated ketone (**3**) as a colorless solid. $[\alpha]_D^{25}$ +33.7° (*c* 0.86, $CHCl_3$). MS *m/e* 150.1049 (M^+, 27%, calcd for $C_{10}H_{14}O$, 150.1044), 135 (17), 121 (11), 107 (81), 106 (86), 91 (77), 79 (69), 77 (41), 67 (25), 65 (24), 53 (44), and 41 (base); IR *ν* 3075, 1755, 1665, 1420, 1390, 1370, 1150, and 899 cm^{-1}; ^{1}H-NMR *δ* 1.13 (3H, s), 1.22 (3H, s), 3.00 (1H, br s), 4.82 (1H, s), and 5.06 (1H, s).

*Reduction of the Unsaturated Ketone (**3**).* To a suspention of $LiAlH_4$ (20 mg) in dry diethyl ether (5 ml) an ethereal solution of the ketone (**3**) (75 mg/2 ml) was added drop by drop and the mixture stirred at room temperature for 3 h. After the excess reagent was decomposed by adding H_2O (1 ml), the ethereal layer was separated, washed with 1% H_2SO_4 and H_2O, dried over Na_2SO_4 and concentrated to give a colorless oil (69 mg). GLC (DEGS) showed two peaks with an intensity ratio of 9: 1, which were eluted over a silica gel column with $CHCl_3$. The major compound thus obtained gave an R_f 0.37 in TLC using $CHCl_3$ as a solvent and it was thus characterized as the *endo*-hydroxy isomer (**6**) of nojigiku alcohol. mp 67.5—68.5 °C. MS *m/e* 152.1189 (M^+, 1%, calcd for $C_{10}H_{16}O$, 152.1200), 137 (4), 135 (3), 134 (2), 119 (14), 108 (87), 93 (54), 91 (34), 81 (15), 79 (20), 77 (32), 67 (35), 65 (22), 55 (34), 53 (44), 51 (22), 43 (30), and 41 (base); IR *ν* 3540, 3075, 1660, 1398, 1380, 1125, 1045, and 895 cm^{-1}; ^{1}H-NMR *δ* 1.12 (6H, s), 2.68 (1H, br d, *J*=4.0 Hz), 4.03 (1H, m), and 4.93 (2H, s). 3,5-Dinitrobenzoate, mp 136.5—138.0 °C.

The minor compound gave R_f 0.30 in TLC which was identical with nojigiku alcohol in IR, ^{1}H-NMR, and MS spectra.

Absolute Configuration of the Hydroxyl Group in Nojigiku Alcohol by Horeau's Method.[12] α-Phenylbutylic anhydride was prepared by refluxing racemic α-phenylbutylic acid with acetic anhydride for 5 h and evaporation of the solvent *in vacuo*. The racemic anhydride (1.2 mmol) was added to a solution of the alcohol (0.4 mmol) in pyridine (2 ml), and the mixture allowed to stand for 20 h at room temperature. After the excess anhydride was decomposed with H_2O (1.0 ml), the mixture was diluted with benzene and titrated with 0.1 M NaOH using phenolphthalein as indicator. The aqueous layer was separated, acidified with 0.5 M H_2SO_4 and extracted with benzene. The benzene solution was dried and evaporated under reduced pressure to give an oily α-phenylbutylic acid. The acid thus recovered was dissolved in benzene (5 ml), and the optical rotation measured in a 0.5 dm cell as $[\alpha]_D^{25}$ +10.0°. Thus the optical yield was calculated as +56.3%.

Synthesis of Nogigiku Alcohol. Camphene (1.0 g) was sealed in a pyrex tube with *t*-butyl hypochlorite (1.2 g) and irradiated with a tungsten lamp (40 W) for 9 h in an ice bath.[10b] The mixture was fractionated under reduced pressure (70 °C/1 Torr) to give a distillate, which separated by preparative GLC (PEG-20M, 125 °C) to afford *exo*-6-chlorocamphene. MS *m/e* 172 and 170 (7 and 19%, M^+ for $C_{10}H_{15}Cl$), 157 (9), 155 (24), 135 (37), 121 (30), 119 (27), 107 (50), 93 (base), 91 (50), 79 (40), 77 (47), 67 (27), 53 (20), and 41 (45); IR *ν* 3060, 1660, 1385, 1360, 1300, 1095, 890, and 770 cm^{-1}; ^{1}H-NMR *δ* 0.98 (3H, s), 1.06 (3H, s), 2.81 (1H, br s), 3.80 (1H, dd, *J*=7.0 and 3.5 Hz), 4.68 (1H, s), and 4.93 (1H, s).

The chlorocamphene (120 mg) was then refluxed[10d] with Li_2CO_3 (60 mg) in water for 10 h. The resulting alcohol was extracted with ether, and purified by preparative GLC (PEG-20M, 125 °C). The compound thus synthesized was identical with nojigiku alcohol in IR, ^{1}H-NMR, and MS spectra.

Identification of Other Monoterpenoids in the Essential Oil. Fraction 1 and 2, which were separated by fractional distillation from the oil, were further treated by preparative GLC (PEG-6000, 80 °C) to isolate six hydrocarbons which were identified on the spectra listed in Table 2. Among them, (+)-α-pinene: $[\alpha]_D^{25}$ +17.1° (*c* 0.80, $CHCl_3$), (+)-camphene: $[\alpha]_D^{25}$ +82.7° (*c* 1.60, $CHCl_3$).

Fraction R-2, which was separated from the fractional distillation residue of the oil by elution chromatography, was again chromatographed over silica gel with hexane and ethyl acetate (v/v, 5: 1). The first eluate was treated with preparative GLC (SE-30, 120 °C and PEG-20M, 110 °C) to give six monoterpene acetates including the acetate of nojigiku alcohol, identified as shown in Table 2. From the middle eluate, three ketones and an alcohol were isolated by a combination of additional chromatography (hexane and ethyl acetate, v/v, 5: 1) and preparative GLC (PEG-20M, 120 °C). Spectral data of these compounds were as follows.

(+)-trans-*Chrysanthenyl Acetate*: $[\alpha]_D^{25}$ +36.7° (*c* 1.40, $CHCl_3$); MS *m/e* 194 (M^+, 1.5%), 179 (1), 151 (5), 137(8), 135 (29), 119 (24), 93 (17), 91 (28), 81 (23), 69 (10), 67 (12), 59 (14), and 43 (base); IR *ν* 3025, 1740, 1375, 1360, 1250, 1180, 1033, and 791 cm^{-1}; ^{1}H-NMR *δ* 0.89 (3H, s), 1.25 (3H, s), 1.57 (3H, q, *J*=2.0 Hz), 1.88 (3H, s), 4.87 (1H, t, *J*=6.0 Hz), and 5.30 (1H, m).

(−)-cis-*Chrysanthenyl Acetate*: $[\alpha]_D^{25}$ −25.5° (*c* 1.10, $CHCl_3$); MS *m/e* 194 (M^+, 1%), 179 (2), 137 (9), 135 (26), 119 (61), 109 (27), 91 (26), 81 (25), 69 (15), 67 (14), 59 (21), 43 (base)

and 41 (37); IR ν 3030, 1740, 1375, 1360, 1240, 1040, and 720 cm^{-1}; ^{1}H-NMR δ 0.91 (3H, s), 1.43 (3H, s), 1.70 (3H, q, J=2.0 Hz), 2.01 (3H, s), 4.45 (1H, s), and 5.23 (1H, m) (IR and ^{1}H-NMR values in agreement with authentic spectra provided by professor J. T. Pinhey, University of Sydney).

trans-*Carveyl Acetate*: ^{1}H-NMR δ 1.67 (3H, m), 1.70 (3H, br s), 1.97 (3H, s), 4.70 (2H, m), 5.18 (1H, m), and 5.65 (1H, br d, J=6.0 Hz).

cis-*Carveyl Acetate*: ^{1}H-NMR δ 1.64 (3H, m), 1.74 (3H, br s), 2.00 (3H, s), 4.73 (2H, br s), and 5.30 (1H, m).

(+)-*Bornyl Acetate*: $[\alpha]_D^{25}$ +20.7° (*c* 5.70, $CHCl_3$)

Filifolone: MS *m/e* 150 (M^+, 30%), 135 (14), 122 (35), 107 (base), 93 (35), 91 (65), 85 (43), 80 (83), 79 (63), 70 (61), 57 (43), 55 (32), 43 (48), and 41 (72); IR ν 1779 cm^{-1}; ^{1}H-NMR δ 1.08 (3H, s), 1.17 (3H, s), 1.75 (3H, br s), 2.53 (3H, m), 4.00 (1H, m), and 5.35 (1H, m) (IR and ^{1}H-NMR spectra in agreement with authentic ones provided by Professor R. B. Bates, University of Arizona).

(+)-*Chrysanthenone*: $[\alpha]_D^{25}$ +61.0° (*c* 1.50, $CHCl_3$); MS *m/e* 150 (M^+, 1.7%), 135 (7), 122 (20), 107 (base), 91 (57), 79 (30), 69 (17), 55 (12), 53 (14), 43 (10), and 41 (32), IR ν 1780 cm^{-1}; ^{1}H-NMR δ 1.18 (3H, s), 1.20 (3H, s), 1.70 (3H, q, J=2.0 Hz), 2.51 (2H, m), and 5.30 (1H, m).

(+)-*Camphor*: Mp 178 °C; $[\alpha]_D^{25}$ +25.4° (*c* 3.10, $CHCl_3$). Oxime: Mp 118.0—118.5 °C. Semicarbazone: Mp 236.0—237.0 °C.

(+)-*Borneol*: Mp 204.0—205.0 °C; $[\alpha]_D^{25}$ +10.8° (*c* 1.80, EtOH). 3,5-Dinitrobenzoate: mp 155.5—156.0 °C.

Identification of Sesquiterpenoids in the Essential Oil. The hexane eluate in the chromatography of fr. R-2 was further treated by preparative GLC (PEG-20M, 150 °C) to give six sesquiterpene hydrocarbons. Fr. R-3 was also treated in combination of silica gel column chromatography (petroleum ether and diethyl ether, v/v, 3: 1) and preparative GLC (SE-30, 200 °C) to give three oxygenated sesquiterpenes. These compounds thus isolated, were identified on the basis of the IR, ^{1}H-NMR, and MS spectra, are listed in Table 2.

The author wishes to express his gratitude to Professor Shûichi Hayashi, Hiroshima University, for many helpful discussions and suggestions in the course of this work. Thanks are also due to Professor Ryuso Tanaka, Botanical Institute, Hiroshima University, for the collection and identification of the plant material.

References

1) R. Tanaka, *The Heredity (Tokyo)*, **21** (10), 9 (1967).
2) M. Kotake and H. Nonaka, *Ann. Chem.*, **607**, 153 (1957).
3) A. Matsuo, Y. Uchio, M. Nakayama, and S. Hayashi, *Bull. Chem. Soc. Jpn.*, **46**, 1565 (1973).
4) A. Matsuo, Y. Uchio, M. Nakayama, and S. Hayashi, *Tetrahedron Lett.*, **1974**, 1885.
5) A. Matsuo, Y. Uchio, M. Nakayama, and S. Hayashi, *Nippon Kagaku Kaishi*, **1975**, 2188.
6) A. Matsuo, M. Nakayama, T. Nakamoto, Y. Uchio, and S. Hayashi, *Agric. Biol. Chem.*, **37**, 925 (1973).
7) A. Matsuo, Y. Uchio, M. Nakayama, Y. Matsubara, and S. Hayashi, *Tetrahedron Lett.*, **1974**, 4219.
8) "Topics in Stereochemistry," ed by E. L. Eliel and N. L. Allinger, John Wiley & Sons, Vol. 8, New York (1974). p. 1.
9) J. I. Musher, *Mol. Phys.*, **6**, 93 (1963).
10) a) M. Juria, D. Mansuy, and P. Detraz, *Tetrahedron Lett.*, **1976**, 2141; b) B. H. Jennings and G. B. Herschbach, *J. Org. Chem.*, **30**, 3902 (1965); c) H. G. Richey, J. E. Grant, T. J. Garbacik, and D. L. Dull, *J. Org. Chem.*, **30**, 3909 (1965); d) M. Gaitonde, P. A. Vatakencherry, and S. Dev, *Tetrahedron Lett.*, **1964**, 2007.
11) G. Jacob, G. Ourrison, and A. Rasat, *Bull. Soc. Chim. Fr.*, **1959**, 1374.
12) A. Horeau, *Tetrahedron Lett.*, **1961**, 506.
13) J. T. Pinhey and J. A. Southwell, *Aust. J. Chem.*, **24**, 1311 (1971).
14) L. F. Johnson and W. C. Jankowski, "Carbon-13 NMR Spectra," Wiley Interscience, New York (1972), spectrum no. 393.
15) The IR spectra of α-cardinol and T-murrolol were kindly supplied by Dr. Yoshio Hirose, The Institute of Food Chemistry, Mishima, Osaka.

Carboxylation of Olefins with Carbon Monoxide Using Various Strong Acids-H_2O-Group 1B Metal Carbonyl Catalyst Systems

Norihiko YONEDA,* Tsuyoshi FUKUHARA, Yukio TAKAHASHI, and Akira SUZUKI

Department of Applied Chemistry, Faculty of Engineering, Hokkaido University, Sapporo 060

(Received December 1, 1977)

Carboxylation of 2,4,4-trimethyl-1-pentene and 1-octene with carbon monoxide was studied in the presence of various strong acids–H_2O–Cu(I) carbonyl catalyst systems in an attempt to find a practical method for the preparation of carboxylic acids. The reaction takes place smoothly at room temperature to give tertiary acids in higher yields than that with the use of sulfuric acid. The procedure is preferable for the ready separation of products from the catalyst layer without quenching by water.

An interesting carboxylation procedure of olefins and alcohols using Cu(I) carbonyl catalyst in the presence of concentrated sulfuric acid has been demonstrated by Souma *et al.*[1] The procedure gives tertiary carboxylic acids in high yields under milder conditions than those of the Koch-Haaf reaction.[2] However, in order to isolate the products, it is necessary to quench the reaction system by adding a large amount of water which leads to the destruction of the catalyst. It was considered that the reaction in strong acids having a water molecule as its component might facilitate the formation of carboxylic acid without the addition of a water molecule at the end of the reaction. We thus investigated extensively the catalytic behavior of Cu(I) carbonyl in the presence of strong acids such as BF_3–H_2O, BF_3–H_3PO_4–H_2O, HF–H_2O and so on. Some of these catalyst systems were found not only to show very high activity on the carboxylation of olefins but also to separate products readily from the reaction mixture with use of a co-solvent such as cyclohexane and chlorobenzene without quenching by intentional addition of water.[3]

Further details of these reaction behaviors will be described hereinafter.

Experimental

Materials. Commercial copper(I) oxide, silver monoxide, boron trifluoride and carbon monoxide of the highest purity were used without further purification. Olefins and organic solvents were purified in the usual way. Distilled hydrogen fluoride was used. BF_3–H_2O complex was prepared by introducing BF_3 gas into water cooled with ice. The desired complexes with given BF_3/H_2O mole ratios could be obtained by adjusting the amount of BF_3 absorbed.[4]

General Procedure of Carboxylation. A solution of Cu_2O (2 g, 14 mmol) in 40—50 g of strong acid was placed in a 200 ml galss reaction vessel fitted with a thermometer and a reflux condenser. Carbon monoxide was then introduced into the reaction mixture under thorough stirring with a magnetic stirrer at a constant flow rate of 20 ml/min to obtain Cu(I) carbonyl at the desired temperature. After complete carbon monoxide absorption, *i.e.*, the completion of cuprous carbonyl formation, 100 mmol of olefin (2,4,4-trimethyl-1-pentene or 1-octene) with or without 50 ml of an appropriate organic solvent was added dropwise by introducing an excess amount of carbon monoxide at a fixed temperature.

A polyethylene reaction vessel was used in the case of HF. All the work was conducted in a well-shielded fume hood.

After completion of the reaction, the reaction mixture separated into two layers, the upper usually being an organic layer and the lower a catalyst layer. The catalyst layer was then hydrolyzed with ice–water and organic materials were extracted with ether. In the case of a recycle experiment of the catalyst, the catalyst layer separated out from the organic layer was subjected to the next run without any treatment.

The yield of individual acids such as 2,2-dimethylpropanoic, tertiary C_6—C_8, tertiary C_9 and polymeric (mainly C_{13} acids) was determined by VPC.[4] The analysis was carried out with a Shimadzu 3AH apparatus, fitted with a 3 m × 3 mm column packed with ethylene glycol succinate–H_3PO_4 at 170 °C. C_9 and C_{13} acids produced by Shell Oil Company were used as references. Tertiary C_6—C_8 acids were synthesized by the Grignard reaction from the corresponding alkyl halides.

The amount of Cu^+ in the organic layer was analyzed as Cu^{2+} after oxidation with the air by the atomic absorption spectroscopic method.

Results and Discussion

Group IB Metal Carbonyl Complex Formation in Various Acid Systems. A Stream of Carbon monoxide was

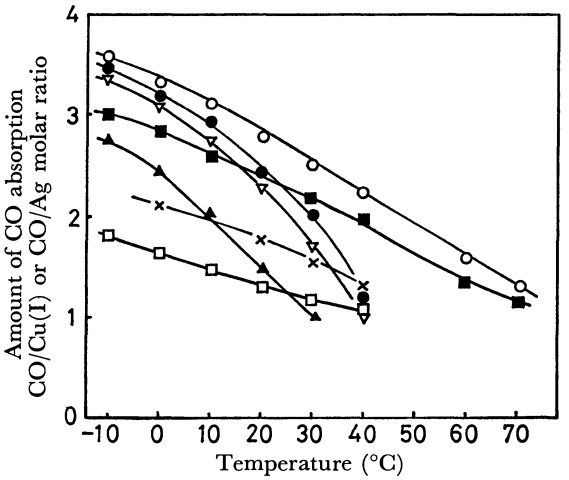

Fig. 1. Temperature dependence of CO absorption in various strong acid–H_2O–Cu_2O (Ag_2O) system.
Amount of Cu_2O; 14 mmol.
Amount of Ag_2O; 14 mmol.
Amount of acid–H_2O; 40 g.
-○- BF_3–H_3PO_4(85%)–H_2O–Cu_2O; $BF_3/H_3PO_4/H_2O$ = 1/1.1/1. -●- BF_3–HF–H_2O–Cu_2O; $BF_3/HF/H_2O$ = 0.9/6.8/1. -▽- HF–H_2O–Cu_2O; HF/H_2O = 9/1. -■- BF_3–H_2O–Cu_2O; BF_3/H_2O = 0.9/1. -▲- HF–H_2O–Cu_2O; HF/H_2O = 6/1. -×- BF_3–H_2SO_4(70%)–H_2O–Cu_2O; $BF_3/H_2SO_4/H_2O$ = 1/0.4/1. -□- BF_3–H_2O–Ag_2O; BF_3/H_2O = 0.9/1.

Table 1. Carboxylation of trimethylpentene using strong acid–H_2O–$M(CO)_n^+$ [a] system

Strong acid–H_2O–$M(CO)_n^+$ system	Reaction temp (°C)	Organic solvent	Product distribution (%)		Total yield of acid (%)
			In org. layer	In cat. layer	
BF_3–H_2O–Cu_2O 0.9: 1	30	Cyclohexane	53	47	96
BF_3–H_2O–Cu_2O 0.9: 1	30	Chlorobenzene	88	12	93
BF_3–H_2O–Cu_2O 0.7: 1	30	Cyclohexane	90	10	55
BF_3–85%H_3PO_4–Cu_2O	20	Cyclohexane	21	79	77
BF_3–85%H_3PO_4–Cu_2O	20	Chlorobenzene	30	70	80
BF_3–50%H_2SO_4–Cu_2O	30	Cyclohexane	28	72	81
BF_3–50%H_2SO_4–Cu_2O	30	Chlorobenzene	71	29	83
HF–H_2O–Cu_2O[b] 11.4: 1	18	Cyclohexane	45	55	98
HF–H_2O–BF_3–Cu_2O 6.8: 1: 0.9	18	Cyclohexane	12	88	99
HF–H_2O–BF_3–Cu_2O 6.8: 1: 0.9	18	Chlorobenzene	15	85	95
BF_3–H_2O–Ag_2O 0.9: 1	20	Chlorobenzene	95	5	78
BF_3–H_2O–Ag_2O[c] 0.9: 1	20	Cyclohexane	44	56	80
96% H_2SO_4–Cu_2O[d]	20	Cyclohexane	7	93	40
96% H_2SO_4–Cu_2O[d]	20	Chlorobenzene	30	70	40
BF_3–H_2O–Cu_2O[e] 0.9: 1	20	Cyclohexane	100	—	73

a) Reaction conditions: BF_3, 0.50 mol; Cu_2O, 14 mmol; organic solvent, 50 ml; trimethylpentene, 0.1 mol.
b) H_2O, 0.55 mol. c) Ag_2O, 7 mmol. d) 96% H_2SO_4, 40 g. e) 1-Octene, 0.10 mol.

passed through a solution of Cu_2O in various acids at −10—70 °C. The results are shown in Fig. 1.

Remarkable absorption of carbon monoxide was observed in acid media such as BF_3–H_3PO_4–H_2O (molar ratio, 1: 0.9: 0.1), BF_3–HF–H_2O (0.9: 6.8: 1), HF–H_2O (9: 1) and BF_3–H_2O (0.9: 1), as compared with that in concentrated sulfuric acid.[1] Even in HF–H_2O of molar ratio 6: 1, about 3 mol of carbon monoxide was absorbed per one mol of Cu(I) at −10 °C.

As described by Souma and Sano,[1,5] the unstable tricarbonylcopper(I) cation $Cu(CO)_3^+$ formed in acid media acts as a catalyst for the carboxylation of olefins under atmospheric pressure. The active species $Cu(CO)_3^+$ can be considered to show the following equilibrium. The species carbonylcopper(I) cation, $Cu(CO)^+$, shows no catalytic behavior for the carboxylation reaction.[1]

$$Cu(CO)_3^+ \rightleftarrows Cu(CO)^+ + 2CO$$

The value of CO(absorbed)/Ag(I) becomes 2 in the H_2SO_4–1/4SO_3 at −10 °C under a carbon monoxide pressure of 20 kg/cm² for silver carbonyl, which is also expected to have the same catalytic activity for the carboxylation of olefins.[6] However, such dicarbonyl silver(I) cation was readily prepared in BF_3–H_2O (0.9: 1 molar ratio) under atmospheric pressure (Fig. 1).

The Cu(I) carbonyl cation with high carbon monoxide coordination can be expected to show a much higher catalytic activity in the carboxylation reaction of olefins. Matsushima *et al.* first reported[7] the formation of tetracarbonylcopper(I) cation, $Cu(CO)_4^+$, in BF_3–H_2O (1: 1.06 molar ratio) solution. However, no investigation seems to have been carried out on the carboxylation of olefins using such acid media involved Ib group metal carbonyl cation before we presented our data.[3]

Reaction of 2,4,4-Trimethyl-1-pentene (Diisobutylene) with Carbon Monoxide in Various Acids–H_2O Containing Copper or Silver Carbonyl Cations. Carboxylation of 2,4,4-trimethyl-1-pentene (TMP) with carbon monoxide was carried out in the presence of BF_3–H_2O, BF_3–H_3PO_4–H_2O, BF_3–H_2SO_4–H_2O, BF_3–HF–H_2O and HF–H_2O having copper carbonyl cation with cyclohexane or chlorobenzene as a co-solvent at 18—30 °C. The results are summarized in Table 1.

The reaction took place in two liquid phase system (upper solvent layer and lower catalyst layer). The carboxylic acids produced were usually present in both layers. The total yield of carboxylic acids, *i.e.*, the sum of yields in both layers, was found to be considerably higher than that obtained in 96% H_2SO_4.

The carboxylic acids thus obtained consist of 2,2-dimethylpropanoic acid and C_9 acids together with small amounts of C_6—C_8 and other acids. Thus, the reaction of TMP with carbon monoxide in the presence of acid–H_2O–group Ib metal carbonyl, is considered to proceed as shown in the following scheme.

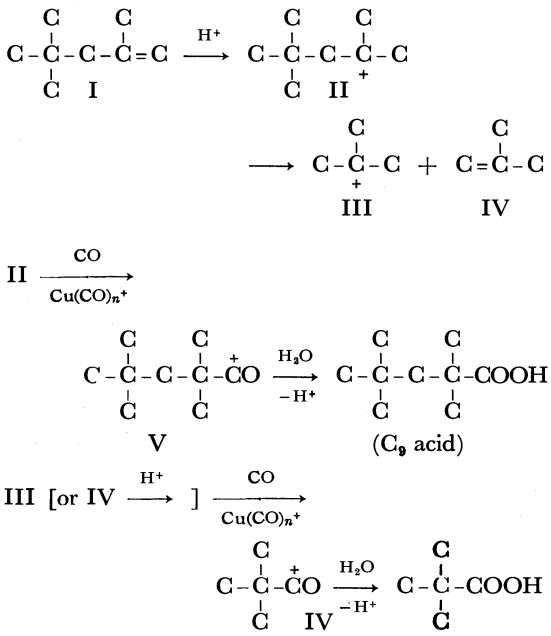

$$I + III(\text{or } II + IV) \longrightarrow C_{12}^{+}$$

$$C_{12}^{+} \xrightarrow[Cu(CO)_n^+]{CO} t\text{-}C_{13} \text{ acids}$$

$$C_{12}^{+} \longrightarrow C_5^{+}(\text{or } C_5^{=}) + C_7^{=}(\text{or } C_7^{+})$$

$$C_5^{+} \xrightarrow[Cu(CO)_n^+]{CO} t\text{-}C_6 \text{ acid}$$

$$C_7^{+} \xrightarrow[Cu(CO)_n]{CO} t\text{-}C_8 \text{ acids}$$

The tertiary C_9 acids of various skeletal structures were found in the products, since skeletal isomerization of C_8 carbenium ion (II) takes place easily under such reaction conditions.

The carboxylic acids existing in the solvent layer seem to be produced by the reaction of alkanoyl cations such as V and VI with water in the catalyst, *i.e.*, acid–H_2O–$Cu(CO)_n^+$. Such carboxylic acids were obtained in a high yield in the presence of BF_3–H_2O–$Cu(CO)_n^+$ catalyst. Despite the fact that an almost quantitative total yield of carboxylic acid was obtained in the presence of HF–H_2O–$Cu(CO)_n^+$ or HF–H_2O–BF_3–$Cu(CO)_n^+$, an insufficient amount of carboxylic acids separated into the organic layer under the conditions employed.

Carboxylation of Trimethylpentene Using BF_3–H_2O–$Cu(CO)_n^+$ Catalyst. Carboxylation of TMP with carbon monoxide was studied in the presence of BF_3–H_2O–$Cu(CO)_n^+$ with various BF_3/H_2O molar ratios. The results are given in Table 2.

Table 2. Effect of BF_3/H_2O molar ratio of BF_3–H_2O on the reaction

BF_3–H_2O / BF_3/H_2O Molar ratio	Total yield of acid, % (acid value)	Product distribution (%)	
		Yield of acid found separately from cat. layer (acid value)	Yield of acid found in cat. layer (acid value)
0.6	12.7(366)	97.0(366)	3.0(—)
0.7	47.8(362)	93.8(356)	6.2(461)
0.8	79.0(371)	86.5(356)	13.5(467)
0.9	76.9(395)	62.7(347)	37.3(478)
1.0	80.4(375)	59.9(344)	40.1(440)

Reaction conditions: BF_3, 0.50 mol; Cu_2O, 14 mmol: reaicton temperature, 30 °C, trimethylpentene, 0.10 mol.

The total yield of carboxylic acids increased with increase in the BF_3/H_2O molar ratio of the catalyst. An important feature is that the reaction takes place with the release of a large portion of the carboxylic acids as products from the catalyst layer without addition of water at the end of the reaction. The portion of carboxylic acids thus obtained was found to be over 90% of all the products in the presence of the catalyst having a BF_3/H_2O molar ratio less than 0.7. However, this portion tends to decrease with increase in the BF_3/H_2O molar ratio of the catalyst.

The BF_3–H_2O complex with BF_3/H_2O molar ratio of 1 is known as a stronger acid than concentrated sulfuric acid (96%) and can be described as $H^+BF_3OH^-$. The Ho value of this acid was reported to be −11.4 (Ho of 100% H_2SO_4 is −11.2).[8] The complexes with BF_3/H_2O molar ratio in the range 0.5—1.0 are mainly mixture of $H^+BF_3OH^-$ and $H_3^+OBF_3OH^-$.[9] The latter species (boron trifluoride dihydrate) should be a weaker acid than the former.

$$BF_3 + H_2O \rightleftharpoons H^+BF_3OH^-$$

$$H^+BF_3OH^- + H_2O \rightleftharpoons H_3^+OBF_3OH^-$$

The content of $H^+BF_3OH^-$ increases with increase in BF_3/H_2O.[10] $H^+BF_3OH^-$ appears to have a stronger affinity for carboxylic acids than $H_3^+OBF_3OH^-$. Hence, in the case of a catalyst rich in $H^+BF_3OH^-$, most of the carboxylic acids produced would be readily protonated to form $RCOOH_2^+BF_3OH^-$ and remain in the catalyst layer. However, when we use catalysts rich in $H_3^+OBF_3OH^-$, most of the carboxylic acids are present in the form of free acid and can be found separately from the catalyst layer.

Higher carboxylic acids such as C_9 and C_{13} acids might have smaller affinity for the catalyst as compared with lower ones such as 2,2-dimethylpropanoic acid, since the mean acid value of the products found in the catalyst layer is always higher than that of those obtained separately from the catalyst layer (Table 2).

The reaction may be expected to occur effectively by separating the products and catalyst from each other with heterogeneous use of co-existing organic solvents.

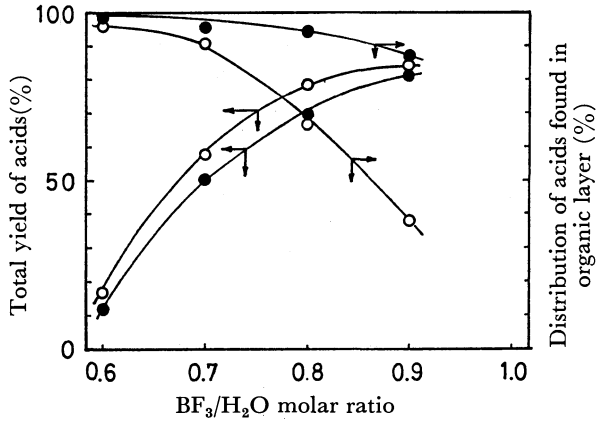

Fig. 2. The effect of BF_3/H_2O molar ratio of BF_3–H_2O on the total yield of acids and distribution of acids found in organic layer.
Reaction conditions: BF_3, 0.50 mol; Cu_2O, 14 mmol; reaction temperature, 30 °C; trimethylpentene, 0.10 mol; organic solvent, 50 ml.
–●–: Chlorobenzene, –○–: cyclohexane.

A solution of TMP in cyclohexane or chlorobenzene was added dropwise to the BF_3–H_2O–$Cu(CO)_n^+$ catalyst with a 0.6—0.9 BF_3/H_2O molar ratio, carbon monoxide being introduced at 30 °C. The results are shown in Fig. 2. All the reactions took place in the heterogeneous liquid phase to give products present in the organic and catalyst layers. The total yield of acids was found to be almost the same as in the case where no organic solvent was used. However, the amount of acids found in the organic layer was greatly affected by the BF_3/H_2O molar ratio in the catalyst, particularly in the case of cyclohexane.

TABLE 3. EFFECT OF ORGANIC SOLVENTS ON THE CARBOXYLATION OF TRIMETHYLPENTENE

Organic solvent	Total yield of acids %	Acids found in organic layer %	Composition of acid products											
			Acids in total				Acids in org. layer				Acids in cat. layer			
			C_5	C_{6-8}	C_9	C_{others} [a]	C_5	C_{6-8}	C_9	C_{others} [a]	C_5	C_{6-8}	C_9	C_{others} [a]
Non	76.9	62.7	31.7	13.3	36.1	18.9	16.6	11.6	42.0	29.8	57.0	16.2	26.1	0.7
Cyclohexane	82.1	36.5	41.0	13.9	35.5	9.6	8.9	8.6	59.0	24.0	62.5	17.6	20.2	—
Mesitylene	84.6	69.0	26.1	10.9	50.4	12.6	12.8	10.1	60.4	16.7	56.3	12.7	27.7	3.3
Chloro-Cyclohexane	49.8	82.3	13.5	11.1	35.5	39.9	8.6	11.0	37.1	43.3	35.6	11.8	28.1	24.5
Fluorobenzene	80.4	79.9	40.7	9.9	40.6	8.8	30.8	10.4	48.4	10.4	80.2	7.8	9.3	2.7
Chlorobenzene	80.1	84.5	44.2	10.7	36.1	9.0	37.1	11.4	41.0	10.5	83.1	7.0	9.3	0.6
Bromobenzene	71.2	82.5	34.9	12.0	44.0	9.1	26.6	12.4	50.2	10.8	73.3	9.7	15.6	1.4
CCl_4	72.9	—	44.4	11.4	34.7	9.5	—	—	—	—	—	—	—	—
$CHCl_3$	66.7	94.4	40.3	7.7	40.4	11.6	38.0	7.7	42.2	12.1	78.5	7.5	10.4	3.6
CH_2Cl_2	46.4	96.5	30.6	19.5	36.3	13.6	29.2	19.7	13.1	14.0	69.7	13.6	13.7	3.0
CH_2ClCH_2Cl	54.1	93.5	35.8	15.1	42.2	6.9	33.0	15.4	44.7	6.9	76.5	11.6	4.4	7.5

a) Polymeric acids. b) Reaction conditions: BF_3–H_2O, 40 g; BF_3/H_2O molar ratio, 0.9; Cu_2O, 14 mmol; reaction temperature, 30 °C; olefin, 0.10 mol; organic solvent, 50 ml.

Other organic solvents were also examined by using the BF_3–H_2O complex with a 0.9 BF_3/H_2O molar ratio (Table 3). The products were again found in both layers except for the case using tetrachloromethane which resulted in an emulsion. The product distribution between both layers was greatly affected by the kind of solvent.

A significant quantity of the product was found to be distributed in organic solvents such as polyhalogenated alkyl compounds. However, the total yield of carboxylic acid produced was rather low as compared with the case in which no solvent reaction took place. In the course of the reaction using these solvents, the formation of copper carbonyl chloride Cu(CO)Cl, which has no catalytic activity, was observed. This is shown in the following scheme for the case of chloroform.

$$CHCl_3 \rightleftharpoons \overset{+}{C}HCl_2 + Cl^-$$

$$Cu(CO)_n^+ + Cl^- \longrightarrow Cu(CO)Cl + (n-1)CO$$

Although chloroform is known to easily undergo hydrolysis in basic solution, hardly any report is available on its behavior in acidic media.[11,12] However, the reaction of chloroform with aromatic compounds forming triarylmethane is known to be induced by a Lewis acid such as aluminum chloride, iron(III) chloride and so on. Thus the free form of BF_3 liberated in the BF_3–H_2O solution can also be considered to be a catalyst which induces the formation of active species as shown in the following.

$$CHCl_3 + BF_3 \longrightarrow \overset{+}{C}HCl_2BF_3Cl^-$$

This species might be considered to be the source of chloride anion and $\overset{+}{C}HCl_2$ cation.

We examined the behavior of chloroform in BF_3–H_2O solution by adding silver nitrate. In a solution allowed to stand at room temperature with stirring, the formation of silver chloride was observed with the evolution of carbon monoxide.[12] From the results, it seems that chloroform in the BF_3–H_2O liberates chloride anion and $\overset{+}{C}H_2Cl$ cation which undergo hydrolysis to give formic acid and then decompose into water and carbon monoxide.

$$\overset{+}{C}HCl_2 \xrightarrow[-HCl]{H_2O} \begin{matrix} H \\ \diagdown \\ C=O \\ \diagup \\ Cl \end{matrix} \xrightarrow[-HCl]{H_2O} \begin{matrix} O \\ \| \\ HC-OH \end{matrix} \longrightarrow CO + H_2O$$

In the presence of cyclohexane, mesitylene or halobenzenes, the reactions give satisfactory high yields of carboxylic acids (Table 3).

The amount of products in the cyclohexane layer is extremely low as compared with the cases using other organic solvents. This is puzzling. The amount of acid products in the organic layer would be affected by the product composition obtained by the reaction. Namely, the reactions producing rather long chain carboxylic acids with less affinity for the catalyst should give large amounts of products in the organic solvent layer. Although C_5 acids and C_9 acids are the main products in each case, C_6, C_8 and longer chain acids than C_{13} were produced. These carboxylic acids are formed as follows. TMP is depolymerized by acid to give 2-methylpropene and *t*-butyl cation which in turn reacted with another molecule of TMP to form C_{12}^+ or higher cations. On the other hand, C_5^+ and C_7^+ ions are produced by the depolymerization of C_{12}^+ (Scheme 1). In the case of the reaction using a higher acidic catalyst such as one with a 0.9 BF_3/H_2O molar ratio, it is particularly easy to form C_{12}^+ and longer chain carbocations which would be sources of long chain carboxylic acids.

Thus, dilution of the alkene by an organic solvent would more or less prevent the formation of longer acids. This is the case where the reaction in the presence of cyclohexane gave rise to the formation of C_{13} and higher acids in rather low yields in the composition, most of the 2,2-dimethylpropanoic acid in high yields remaining in the catalyst layer.

Such a tendency was clearly seen in the reactions using BF_3–H_2O acid systems with large BF_3/H_2O molar ratios. The reaction in the presence of lower acidic

catalyst of BF_3–H_2O with BF_3/H_2O molar ratio of 0.7 or less gave C_9 acids as the main products which were in the organic solvent layer as shown in Fig. 2.

However, as seen in Table 3, although almost the same composition of products was obtained when cyclohexane and halobenzenes were used as the solvent, the amount of products found in the halobenzene layer was always higher. The solubility of carboxylic acids in such organic solvents may be different. In fact, we found that cyclohexane shows a lower solubility for 2,2-dimethylpropanoic acid at 10 °C (1.07 g/ml) than other solvents (chlorobenzene, 1.34 g/ml; chloroform, 1.44 g/ml). Thus, chlorocyclohexane which has a high solubility for 2,2-dimethylpropanoic acid (1.8 g/ml) should dissolve acid products. However, a remarkable formation of other acids was observed. This might be due to the occurrence of a side-reaction, as shown in the following equation. Cl^- liberated in the course of the reaction should deteriorate the catalyst.

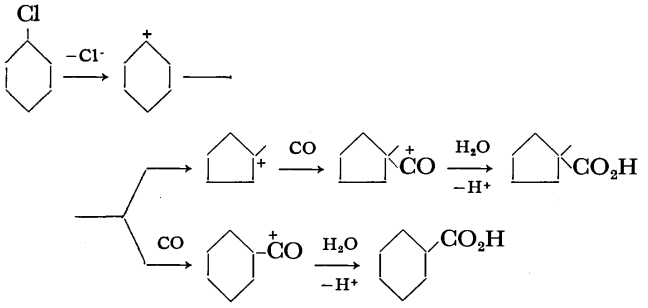

The effect of reaction temperature on the yield of carboxylic acids was also examined. The results are shown in Figs. 3 and 4.

The reaction using 96% H_2SO_4 gave a 56% maximum total yield of products at 40 °C, the catalytic activity decreasing thereafter rapidly because of the decomposition of Cu(I) carbonyl cation. On the other hand, the reaction using BF_3–H_2O complex gave the products in *ca.* 20% yield even at 70 °C. This seems also to indicate

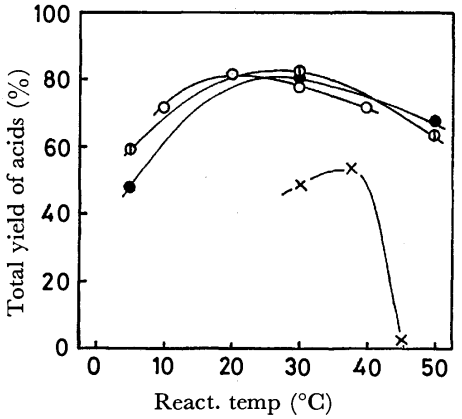

Fig. 3. The effect of reaction temperature on the total yield of acids.
Reaction conditions: BF_3–H_2O, 24 g; BF_3/H_2O molar ratio, 0.90; 96% H_2SO_4, 40 g; Cu_2O, 14 mmol; reaction time, 30 min; amount of solvent, 50 ml; trimethylpentene, 0.10 mol.
-×-: 96% H_2SO_4, -○-: without solvent, -●-: chlorobenzene, -ⓓ-: cyclohexane.

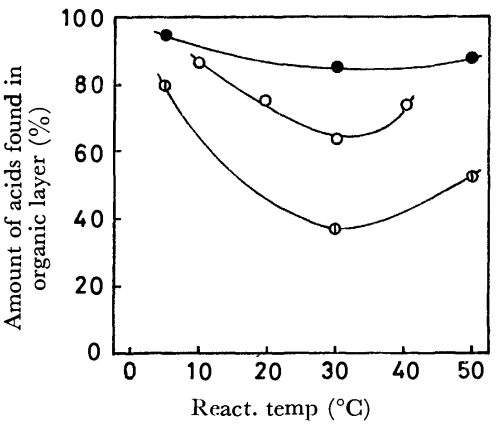

Fig. 4. The effect of reaction temperature on the amount of acids found in organic layer.
Reaction conditions: BF_3–H_2O, 24 g; BF_3/H_2O molar ratio, 0.9; Cu_2O, 14 mmol; reaction time, 30 min; amount of solvent, 50 ml; trimethylpentene, 0.10 mol.
-○-: Without solvent, -●-: chlorobenzene, -ⓓ-: cyclohexane.

the high stability of active species as catalyst, *i.e.*, $Cu(CO)_3^+$ in the BF_3–H_2O complex in a wide range of temperature.

The reaction using BF_3–H_2O complex in the presence of chlorobenzene showed no large difference in yield of acid products found in the organic layer over the entire range of reaction temperature (Fig. 4). However, in the presence of cyclohexane, or in the absence of organic solvent, the amount of such products found to be remarkably decreased at 30 °C. The reactions under these conditions have a tendency to form products rich in 2,2-dimethylpropanoic acid with a high affinity to the catalyst layer. In the reactions carried out at low reaction temperatures, polymerization and depolymerization of TMP resulting in the formation of C_{13} or higher carboxylic acids would be predominant. These long chain carboxylic acids clearly have less affinity to the catalyst and should exist apart from the catalyst layer. In reactions at a temperature higher than 40 °C, the rate of reaction of carbon monoxide with 1,1,3,3-tetramethylbutyl cation derived from initial protonation of TMP would cause a β-cleavage of the cation to give *t*-butyl cation and 2-methylpropene. Hence, the reaction gave products rich in C_9 acids, most of them being observed in the organic layer because of the low affinity of C_9 acids to the catalyst layer.

Repeated Use of the Catalyst. In order to show the advantage of a Cu(I)–carbonyl catalyst in the BF_3–H_2O solution, we have extended our investigation to recycling of the used catalyst. The carboxylation of olefins in various organic solvents was conducted in the same way as described in the previous section. After completion of the reaction, the recovered catalyst layer which had been added to the corresponding amount of water consumed in the first run was used for the second run under the same conditions. The upper organic solvent layer separated out from the reaction mixture was subjected to work-up for the product and analysis for the amount of copper ion as Cu^{2+} after oxidation with

TABLE 4. REPEATED USE OF THE CATALYST (BF_3/H_2O= 0.9) IN THE CARBOXYLATION OF TRIMETHYL-PENTENE (solvent; cyclohexane)

No. of repeated expt.	Yield of acid[a,d] %	Product distribution[a] %				Cu^{2+} mg
		C_5	C_{6-8}	C_9	C_{others}	
1	24	17	8	56	19	trace
2	30	—	—	—	—	trace
3	41	11	9	45	35	trace
4	32	—	—	—	—	trace
5	49	14	11	43	32	trace
	(—[c])	44	16	28	12)[b]	

a) Found in organic layer in each expt. b) Product distribution found in catalyst layer in the 5th expt. c) The acids found in the catalyst layer was 55% of total yields of acids. d) Total yield of acids 77%. Reaction conditions: initial amount of BF_3–H_2O, 62 g; Cu_2O, 14 mmol; react. temp 30 °C; olefin 0.1 mol; solvent, 50 ml, in each run.

TABLE 5. REPEATED USE OF THE CATALYST (BF_3/H_2O= 0.7) IN THE CARBOXYLATION OF TRIMETHYL-PENTENE (solvent; cyclohexane)

No. of repeated expt.	Yield of acid[a,d] %	Product distribution[a] %				Cu^{2+} mg
		C_5	C_{6-8}	C_9	C_{others}	
1	54	22	16	56	6	trace
2	56	26	15	52	7	trace
3	45	25	13	56	6	trace
4	57	21	14	56	9	trace
5	56	25	15	50	10	trace
	(—[c])	66	17	16	1)[b]	

a) Found in organic layer in each expt. b) Product distribution found in catalyst layer in the 5th expt. c) The acids found in the catalyst layer was 6% of total yield of acids. d) Total yield of acids, 57%. Reaction conditions: initial amount of BF_3–H_2O, 68 g; Cu_2O, 14 mmol; react. temp, 30 °C; olefin, 0.1 mol; solvent 50 ml in each run.

TABLE 6. REPEATED USE OF THE CATALYST (BF_3/H_2O= 0.9) IN THE CARBOXYLATION OF 1-OCTENE (solvent; cyclohexane)

No. of repeated expt.	Yield of acid[a,d] %	Product distribution[a] %				Cu^{2+} mg
		C_5	C_{6-8}	C_9	C_{others}	
1	73	3	0.2	97	—	trace
2	69	1	—	99	—	trace
3	72	1	—	99	—	trace
4	67	—	—	100	—	trace
5	65	—	—	100	—	trace
	(—[c])	11	1	88	—)[b]	

a) Found in organic layer in each expt. b) Product distribution found in catalyst layer in the 5th expt. c) The acids found in the catalyst layer was 1.5% of total yield of acids. d) Total yield of acids, 70%. Reaction conditions: initial amount of BF_3–H_2O, 62 g; Cu_2O, 14 mmol; react. temp, 30 °C; olefin, 0.1 mol; solvent, 50 ml in each run.

TABLE 7. REPEATED USE OF THE CATALYST (BF_3/H_2O= 0.9) IN THE CARBOXYLATION OF TRIMETHYL-PENTENE (solvent, chlorobenzene)

No. of repeated expt.	Yield of acid[a,d] %	Product distribution[a] %				Cu^{2+} mg
		C_5	C_{6-8}	C_9	C_{others}	
1	64	38	21	41	1	69
2	69	—	—	—	—	105
3	73	—	—	—	—	330
4	83	32	13	40	15	340
5	98	—	—	—	—	475
6	68	25	14	39	22	375
	(—[c])	43	19	33	5)[b]	

a) Found in organic layer in each expt. b) Product distribution found in catalyst layer in the 6th expt. c) The acids found in the catalyst layer was 1.5% of total yield of acids. d) Total yield of acids, 77%. Reaction conditions: initial amount of BF_3–H_2O, 62 g; Cu_2O, 14 mmol; react. temp, 30 °C; olefins, 0.1 mol; solvent, 50 ml in each run.

air by the usual atomic absorption spectroscopic method.[13] Some typical results are given in Tables 4—7.

In the reaction of TMP using cyclohexane as a solvent, the activity of catalyst remained unchanged. Only a negligible amount of copper ion was present in the organic solvent layer (Tables 4 and 5).

A gradual accumulation of carboxylic acid was observed in the catalyst layer with successive use of the catalyst. In the case of BF_3–H_2O with a 0.9 molar ratio (Table 4), *ca.* 55% of the total yield of carboxylic acids was found in the catalyst layer after five repeated runs. However, this accumulation of products in the catalyst layer was remarkably decreased when a catalyst with 0.7 BF_3/H_2O molar ratio was used. Only 6% of carboxylic acids was present (Table 5).

In the reaction of 1-octene, there was no accumulation of products in the catalyst layer even in the case of BF_3–H_2O with 0.9 molar ratio (Table 6). Since no cleavage of carbon-carbon bonds in the olefin takes place, almost all the carboxylic acids produced were C_9-acids which have less affinity to the catalyst layer.

On the other hand, in the reaction of TMP using chlorobenzene as a solvent, almost complete recovery of products into the solvent layer was observed even in the presence of the catalyst with 0.9 BF_3/H_2O molar ratio (Table 7). In contrast, the amount of copper ion found in the organic layer was considerably high. This might decrease the concentration of the active species by successive use of the catalyst layer.[14]

The present procedure seems to have a great advantage in the practical preparation of carboxylic acids by carboxylation of olefins with carbon monoxide.

References

1) Y. Souma, H. Sano, and J. Iyoda, *J. Org. Chem.*, **38**, 2016 (1973); Y. Souma and H. Sano, *Bull. Chem. Soc. Jpn.*, **46**, 3237 (1973).

2) H. Koch, *Brennstoff-Chemie*, **36**, 321 (1955); H. Koch and W. Haaf, *Justus Liebigs Ann. Chem.*, **618**, 251 (1958); K. E. Möller, *Brennstoff-Chemie*, **47**, 10 (1966).

3) N. Yoneda, T. Fukuhara, Y. Takahashi, and A. Suzuki, *Chem. Lett.*, **1974**, 607.
4) M. Matsubara, Y. Matsushima, N. Yoneda, and H. Ohtsuka, *Kogyo Kagaku Zasshi*, **73**, 2147 (1970); N. Yoneda, Y. Matsushima, M. Matsubara, and H. Ohtsuka, *Bull. Jpn. Petrl. Inst.*, **14**, 178 (1972).
5) H. Sano, *Nippon Kagaku Kaishi*, **1970**, 630.
6) Y. Souma and H. Sano, *Chem. Lett.*, **1973**, 1059.
7) Y. Matsushima, T. Koyano, T. Kitamura, and S. Wada, *Chem. Lett.*, **1973**, 433.
8) N. Yoneda and Y. Takahashi, *J. Jpn. Petrl. Inst.*, **20**, 468 (1977).
9) N. N. Greenwood and R. L. Martin, *J. Chem. Soc.*, **1951**, 1915.
10) N. Yoneda and H. Ohtsuka, *Kogyo Kagaku Zasshi*, **72**, 1743 (1969).
11) J. March, "Advanced Organic Chemistry," McGraw-Hill Book Co. (1968), p. 304.
12) $CHCl_3$ in concentric sulfuric acid with silver nitrate did not react under such conditions.
13) T. Takeuchi and M. Suzuki, "Genshikyuko Bunko Bunseki," Nankodo (1972).
14) When the organic layer thus obtained was treated with aqueous alkaline solution, yellow precipitate of copper hydroxide was formed, the amount of which corresponds to that of Cu^{2+} determined by atomic absorption spectroscopy. Cu(I) carbonyl solubilized into organic layer could be recovered as cuprous oxide after calcination of copper hydroxide in the absence of oxygen.

Modification of Aminocyclitol Antibiotics. 6. Preparation of 5-Deoxykanamycin B

Tetsuo SUAMI,* Shigeru NISHIYAMA, Yasuhide ISHIKAWA, and Eijiro UMEMURA

Department of Applied Chemistry, Faculty of Engineering, Keio University, Hiyoshi, Yokohama 223

(Received December 14, 1977)

Aminocyclitol antibiotic kanamycin B has been modified as regards the aminocyclitol moiety by removing a hydroxyl group on C-5. 5-Deoxykanamycin B thus obtained was tested against several microorganisms. The structure of 5-deoxykanamycin B was established by mass and ^{13}C NMR spectrometry. 5,6,3′,4′-Tetradeoxyneamine was prepared as a reference compound for ^{13}C NMR spectrometry.

In connection with the preceding paper,[1] antibiotic kanamycin B[2-5] has been modified as regards the aminocyclitol moiety. It has been disclosed that removal of the hydroxyl group on C-5 of neamine enhances the antimicrobial activity relative to the parent neamine against kanamycin resistant strains.[6]

Recently, 5-deoxygentamicin complex[7] has been prepared by means of bioconversion[8] using 2,5-dideoxystreptamine[9] as a precursor in the culture medium. The antibiotic exhibits improved activity against gentamicin-acetylating strains of resistant bacteria. 5-Deoxysisomicin: Mutamicin 2[10] and 5-deoxykanamycin A[11] have also been prepared by means of bioconversion.

Since removal of the hydroxyl group on C-5 of kanamycin B might enhance its antimicrobial activity, we have attempted to prepare 5-deoxykanamycin B by using analogous reactions employed in the preparation of 5-deoxyneamine.[6]

When 1,3,2′,6′,3″-pentakis-*N*-(ethoxycarbonyl)kanamycin B[12] (**1**) was treated with 22 molar equivalents of benzoyl chloride in pyridine, penta-*O*-benzoyl derivative (**2**) was obtained in 63% yield. As the hydroxyl group on C-5 of **1** is sterically highly hindered, compound **2** was deduced to be 3′,4′,2″,4″,6″-penta-*O*-benzoyl derivative. The proposed structure was rationalized by the fact that successive reactions gave 5-deoxykanamycin B. Chlorination of **2** with sulfuryl chloride in pyridine afforded chloro-deoxy compound (**3**) in which the chlorination occurred on C-5 with an inversion of configuration.[13] Dehalogenation of **3** was performed with tributylstannane[14] in toluene solution, giving deoxykanamycin B derivative (**4**) in 86% yield. Compound **4** was converted into deoxykanamycin B (**5**) by removing the protecting groups. *N*-Acetylation of **5** gave penta-*N*-acetyl-deoxykanamycin B (**6**).

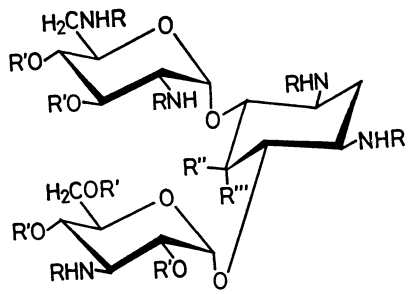

1 R=Cbe, R′=R‴=H, R″=OH
2 R=Cbe, R′=Bz, R″=OH, R‴=H
3 R=Cbe, R′=Bz, R″=H, R‴=Cl
4 R=Cbe, R′=Bz, R″=R‴=H
5 R=R′=R″=R‴=H
6 R=Ac, R′=R″=R‴=H
Cbe=COOEt

Scheme 1.

The structure of **5** was determined by mass and ^{13}C NMR spectra as follows. The mass spectrum reveals the molecular ion and $[M+1]^+$ peak at *m/e* 467 and 468, respectively, equivalent to M−O and M+1−O ions of kanamycin B.[15] The peaks at *m/e* 335 and 336 are in line with protonated formyl ions. The amino sugar fragments reveal the peaks at *m/e* 161 and 162, observed in the spectrum of kanamycin B.[15] The aminocyclitol fragment ions appear at *m/e* 175, 157, 147, and 129. The results indicate that the aminocyclitol moiety of **5** has been deoxygenated, supporting the proposed structure. The structure of **5** was confirmed by ^{13}C NMR spectroscopy. The spectrum was determined at pD above 11, showing eighteen carbon signals. The signals are assigned in accordance with the data for kanamycin B,[16] neamine, 5-, 6-, 5,6-di- and 5,6,3′,4′-tetradeoxyneamine (**11**). Compound **11** was prepared by a five step reaction from neamine.

When the spectrum of **5** is compared with that of kanamycin B, it is obvious that deoxygenation causes no appreciable shifts of the signals of carbons in the amino sugar moieties, except for anomeric carbon C-1′. In contrast, the signals of the carbons in the aminocyclitol moiety are more or less shifted by deoxygenation.

In fact, the signal of C-1′ shifts toward a higher field by 4.3 ppm. An analogous upfield shift of the signal of C-1′ has been observed in the spectra of 5-, 5,6-dideoxyneamine, and **11**. However, no such shift of the signal of C-1′ was observed in the spectrum of 6-deoxyneamine.

The signals of C-4 and 6 shift upfield by 9.3 and 4.5 ppm, respectively. This is in line with the fact that the signals of C-2 and 4 of methyl 3-deoxy-α-D-glucopyranoside appear in a higher field, as compared to those of methyl α-D-glucopyranoside.[17] The signals of C-1 and 3 shift to a lower field by 2.9 and 2.3 ppm, respectively. This is elucidated by the antiperiplanar arrangement of Eliel *et al.*[18]

The spectra were then determined at pD 1 in order to observe the N-protonation effect, which will supply valuable evidences for structure analysis.[16,19] At pD 1, the signal of C-2 of **5** shifts upfield a great deal (7.8 ppm), that of C-4 and 6 moderately (6.4 and 5.5 ppm) and that of C-5 toward a higher field (2.0 ppm) as compared

Table 1. The ^{13}C NMR chemical shifts[a] of 5-deoxykanamycin B, kanamycin B, and neamine derivatives

	5-Deoxykanamycin B (**5**)		Kanamycin B		5-Deoxyneamine[6]		6-Deoxyneamine[6]		5,6-Dideoxyneamine[6]		5,6,3′,4′-Tetradeoxyneamine (**11**)		Neamine	
	pD 11	pD 1	pD 11	pD 1	pD 11	pD 1	pD 11	pD 1	pD 11	pD 1	pD 11	pD 1	pD 11	pD 1
C-1	53.4	52.2	50.5	50.5	54.9	53.5	45.6	45.3	48.6	48.0	48.7	48.2	51.8	50.7
C-2	36.9	29.1	36.5	28.6	37.0	29.3	42.1	32.6	41.9	32.9	41.9	32.9	36.9	29.0
C-3	52.6	51.7	50.3	49.3	53.0	52.0	50.7	50.0	53.1	52.4	53.3	52.7	50.3	49.5
C-4	78.1	71.7[c]	87.4	77.5	78.7	71.8[g]	91.1	80.4	80.4	73.8	80.5	73.1	88.9	77.7
C-5	34.9	32.9	75.2[d]	75.1	37.6	34.6	72.1	70.9	27.6	25.7	28.0	25.8	77.4	75.9
C-6	84.1	78.6	88.6	84.5	73.7	68.1	41.6	37.2	33.6	27.8	33.7	27.9	78.6	73.3
C-1′	96.2	91.4	100.5	96.2	96.4	91.6	102.3	96.6	96.2	91.5	96.6	90.5	102.2	96.1
C-2′	55.9	54.0	56.3	54.4	56.2	54.0	56.6	54.5	56.3	54.0	50.2	49.1	56.8	54.5
C-3′	75.4	69.6	74.9[d]	69.0	75.9[f]	69.5[h]	75.3[i]	69.2	76.0	69.5[j]	27.2	21.8	75.6	69.0
C-4′	73.0[b]	71.3[c]	73.3[e]	71.8	73.3	71.6[g]	73.2	71.7	73.4	71.6	28.4	26.6	73.4	71.7
C-5′	74.4	69.8	74.7	70.1	75.1[f]	69.7[h]	75.0[i]	69.9	75.2	69.6[j]	71.0	66.3	75.6	69.9
C-6′	42.7	41.1	42.8	41.2	42.9	41.1	42.9	41.3	43.0	41.0	46.0	43.7	43.0	41.3
C-1″	101.8	100.2	101.4	101.4										
C-2″	72.8[b]	68.8	73.0[e]	69.0										
C-3″	55.9	55.7	56.5	55.8										
C-4″	71.5	67.0	71.3	66.3										
C-5″	73.8	73.3	74.0	73.7										
C-6″	62.3	61.4	62.0	60.8										

a) In parts per million downfield from tetramethylsilane. b—j) The signals may be reversed.

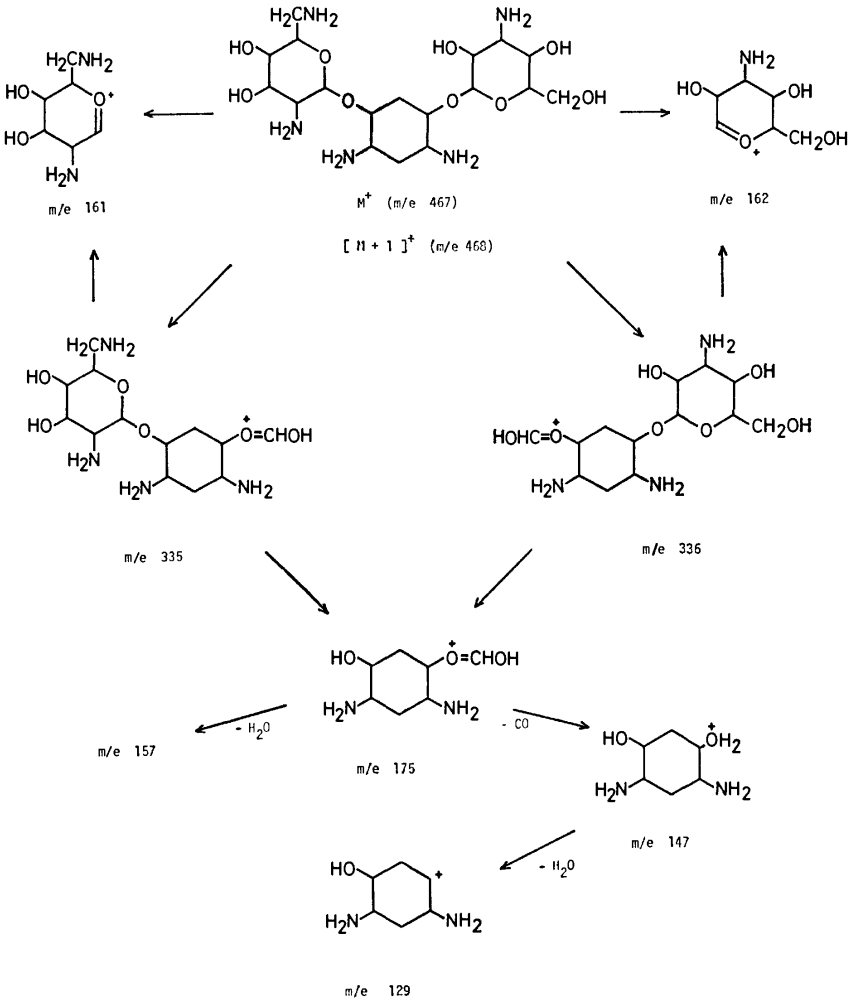

Scheme 2.

TABLE 2. ANTIMICROBIAL ACTIVITY OF 5-DEOXYKANAMYCIN B (**5**)

Test organisms	MIC (mcg/ml)
Staphylococcus aureus ATCC 6538P	0.78
Staphylococcus epidermidis ATCC 12228	0.39
Diplococcus pneumoniae Type 3	0.2
Bacillus subtilis ATCC 6633	0.2
Escherichia coli NIHJC-2	3.12
Klebsiella pneumoniae 602	3.12
Pseudomonas aeruginosa IAM 1007	100
Proteus vulgaris OX-19	0.39
Salmonella paratypin A 1015	1.56
Salmonella paratyphi B	12.5
Shigella flexneri 2a·SH-74-1	6.25

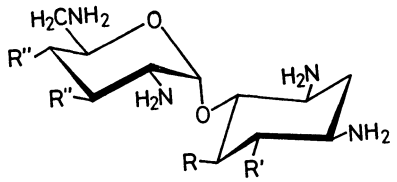

5-Deoxyneamine[6] R=H, R′=R″=OH
6-Deoxyneamine[6] R=R″=OH, R′=H
5,6-Dideoxyneamine[6] R=R′=H, R″=OH
5,6,3′,4′-Tetradeoxyneamine (**11**) R=R′=R″=H
Neamine R=R′=R″=OH

Scheme 3.

to those determined at pD 11. This is in line with the fact that the effect of N-protonation appears strongly on a β-carbon and weakly on a γ-carbon.[19] Thus, the proposed structure of **5** has been confirmed.

Antimicrobial activities of **5** were determined against several microorganisms. The MIC (minimum inhibition concentration) values, given in Table 2, are similar to those of kanamycin B against most of the microorganisms tested so far.

Experimental

General Methods. Melting points were determined in capillary tubes and are uncorrected. Solutions were concentrated under reduced pressure below 40 °C. Optical rotations were measured on a Japan Spectroscopic DIP-SL polarimeter. ^{1}H NMR spectra were recorded on a Varian A-60D spectrometer at 60 MHz. Deuteriochloroform was used as a solvent with an internal standard of tetramethylsilane. The peak positions are given in δ values. ^{13}C NMR spectra were determined on a Varian FT-80 spectrometer at 20 MHz. Deuterium oxide was used as a solvent with an internal standard of dioxane. The resonance signals are expressed in ppm downfield from the signal of tetramethylsilane (δ_C for dioxane= −67.4). Mass spectrum was recorded with a Hitachi RMU-6M single focusing mass spectrometer. TLC was performed on Wakogel B-10 plates (Wako Pure Chemical Co., Ltd.), and silica gel (Wakogel C-300) was employed for column chromatography.

*3′,4′,2″,4″,6″-Penta-*O*-benzoyl-1,3,2′,6′,3″-pentakis-*N*-(ethoxycarbonyl)kanamycin B (2).* Benzoyl chloride (1.5 ml) was added gradually to a solution of 1,3,2′,6′,3″-pentakis-*N*-(ethoxycarbonyl)kanamycin B[12] (**1**, 500 mg) in pyridine (15 ml) with stirring under ice cooling. After 18 h at ambient temperature, the solution was poured into 2.5% $NaHCO_3$ solution. The aqueous mixture was extracted with chloroform repeatedly, and the combined chloroform solution was washed with water. After being dried over Na_2SO_4, the solution was concentrated. The residue was purified on a silica-gel column using 7: 1 (v/v) benzene–methanol. Fractions homogeneous on TLC (R_f 0.32) in the same solvent were combined and concentrated to dryness. The residue was washed with ether and the product **2** (512 mg, 63%) was precipitated from a benzene solution by addition of hexane. Mp 137—143 °C, $[\alpha]_D^{25}$ +82.7° (*c* 0.4, chloroform).

Found: C, 59.61; H, 5.67; N, 5.08%. Calcd for $C_{68}H_{77}N_5O_{25}$: C, 59.86; H, 5.69; N, 5.13%.

*1D-4-*O*-(3,4-Di-*O*-benzoyl-2,6-dideoxy-2,6-bisethoxycarbonylamino-α-D-glucopyranosyl)-6-*O*-(2,4,6-tri-*O*-benzoyl-3-deoxy-3-ethoxycarbonylamino-α-D-glucopyranosyl)-5-chloro-1,2,3,5-tetradeoxy-1,3-bisethoxycarbonylamino*-neo-*inositol (3).* Sulfuryl chloride (0.8 ml) was added to a solution of **2** (868 mg) in pyridine (15 ml) with agitation under ice cooling. After being stirred at 0 °C overnight, the solution was poured into ice-cold water (100 ml). The aqueous solution was extracted with chloroform and the chloroform solution was washed with $NaHSO_4$ solution, $NaHCO_3$ solution and water successively. After being dried over Na_2SO_4, the solution was concentrated. The residue was purified on a silica gel column using 10: 1 (v/v) benzene–methanol. Fractions homogeneous on TLC (R_f 0.29) in the same solvent were combined and concentrated to give 735 mg (84%) of **3**, mp 111—116 °C, $[\alpha]_D^{21}$ +80.8° (*c* 0.4, chloroform).

Found: C, 58.61; H, 5.61; N, 5.00; Cl, 2.90%. Calcd for $C_{68}H_{76}N_5O_{24}Cl$: C, 59.06; H, 5.54; N, 5.06; Cl, 2.56%.

*3′,4′,2″,4″,6″-Penta-*O*-benzoyl-5-deoxy-1,3,2′,6′,3″-pentakis-*N*-(ethoxycarbonyl)kanamycin B (4).* Tributylstannane[3] (1 ml) and bis(α-cyanoisopropyl)diazene (26 mg) were added to a solution of **3** (643 mg) in toluene (30 ml). The reaction mixture was heated at 78 °C for 1.5 h under nitrogen stream. The mixture was concentrated and the residue was washed with hexane. The crude product was purified on a silica-gel column using 7: 1 (v/v) benzene–methanol as an eluant. Fractions showing a single spot at R_f 0.32 in the same solvent were combined and concentrated to give 538 mg (86%) of **4**, mp 134—137 °C, $[\alpha]_D^{20}$ +81.5° (*c* 1.1, chloroform).

Found: C, 60.28; H, 5.65; N, 5.17%. Calcd for $C_{68}H_{77}N_5O_{24}$: C, 60.57; H, 5.76; N, 5.19%.

5-Deoxykanamycin B (5). A solution of **4** (529 mg) in methanol (6 ml) was added to a solution of barium hydroxide octahydrate (4 g) in water (14 ml). The mixture was heated under reflux for 8 h. Carbon dioxide was bubbled into the mixture and the precipitates were filtered off. The filtrate was concentrated and the residue was purified on a column of Amberlite CG-50(NH_4^+) resin. After being washed with water and 0.05 M aqueous ammonia, the column was eluted with 0.3 M aqueous ammonia to give 47 mg (26%) of **5**, mp 179—185 °C (dec), $[\alpha]_D^{22}$ +124° (*c* 0.7, water). The product showed a single spot on TLC (R_f 0.27) in 5: 8: 10: 7 (v/v) 28% ammonia–1-butanol–ethanol–water.

*1,3,2′,6′3,″-Penta-*N*-acetyl-5-deoxykanamycin B (6).* Compound **5** (15 mg) was acetylated with acetic anhydride (0.1 ml) in methanol (2 ml) to give 18 mg (81%) of **6**, mp above 260 °C, $[\alpha]_D^{21}$ +108° (*c* 0.4, water). ^{1}H NMR (D_2O): δ 1.96 (s, 3, NAc), 1.99 (s, 3, NAc), 2.03 (s, 9, 3×NAc), 4.96 (d, 1, J=3 Hz, anomeric H), 5.01 (d, 1, J=3.5 Hz, anomeric H).

Found: C, 48.54; H, 6.85; N, 10.01%. Calcd for $C_{28}H_{47}N_5O_{14}\cdot H_2O$: C, 48.33; H, 7.10; N, 10.07%.

*1,3,2′,6′-Tetrakis-*N*-(ethoxycarbonyl)neamine (7).* The compound was prepared by a similar reaction to that employed in the preparation of 1,3,2′,6′-tetrakis-*N*-(methoxycarbonyl)-neamine.[20] The product, mp 224—227 °C, $[\alpha]_D^{18}$ +45.2° (*c*

0.5, DMF), was obtained in 61% yield.

Found: C, 47.12; H, 6.77; N, 8.81%. Calcd for $C_{24}H_{42}N_4O_{14}$: C, 47.21; H, 6.93; N, 9.18%.

1,3,2',6'-Tetrakis-N-*(ethoxycarbonyl)-5,6,3',4'-tetra*-O-*mesyl-neamine (8).* Compound **7** (2.0 g) was treated with methanesulfonyl chloride (2.0 ml) in pyridine (20 ml). The product was recrystallized from 3: 1 (v/v) acetone–ether to give 1.96 g (65%) of **8**, mp 192—193 °C, $[\alpha]_D^{21}$ +22.5° (*c* 1.06, chloroform). ^1H NMR: δ 3.06 (s, 3, SO_2CH_3), 3.11 (s, 3, SO_2CH_3) 3.24 (s, 3, SO_2CH_3), 3.27 (s, 3, SO_2CH_3), 5.21 (d, 1, J=3.5 Hz, H-1').

Found: C, 36.27; H, 5.47; N, 5.90; S, 13.62%. Calcd for $C_{28}H_{50}N_4S_4O_{22}$: C, 36.27; H, 5.47; N, 5.90; S, 13.62%.

5,6,3',4'-Tetradeoxy-1,3,2',6'-tetrakis-N-*(ethoxycarbonyl)neamine-5,3'-diene (9).* Compound **8** (1.44 g) was heated with zinc powder (11 g) and sodium iodide (20 g) in DMF (35 ml) at 95°C for 2.5 h. The mixture was diluted with chloroform, the insoluble matter being filtered off. The filtrate was washed with sodium chloride solution, sodium thiosulfate solution and water successively. After being dried over Na_2SO_4, the solution was concentrated. The residue was recrystallized from 1: 4 (v/v) ether–methanol to give 0.38 g (45%) of **9**, mp 223—224 °C. From the mother liquor, a second crop of **9** (84 mg, 10%) was obtained. A part of the product was recrystallized for elemental analysis, mp 225—226 °C, $[\alpha]_D^{20}$ +73.6° (*c* 0.84, DMF). ^1H NMR (DMSO-d_6): δ 1.22 (*t*, 12, J=7.0 Hz, 4×$CO_2CH_2C\underline{H}_3$), 5.32 (d, 1, J=3.5 Hz, H-1'), 5.84 (broad s, 4, H-5, 6, 3' and 4').

Found: C, 53.20; H, 7.02; N, 10.20%. Calcd for $C_{24}H_{38}N_4O_{10}$: C, 53.15; H, 7.06; N, 10.33%.

1,3,2',6'-Tetrakis-N-*(ethoxycarbonyl)-5,6,3',4'-tetradeoxyneamine (10).* Compound **9** (306 mg) was hydrogenated in the presence of palladium black in aqueous dioxane (15 ml) in hydrogen atmosphere (3.4 kg/cm²) for 26 h. The product was purified on a silica-gel column using 14: 1 (v/v) benzene–isopropyl alcohol. Fractions homogeneous on TLC (R_f 0.49) in 15: 1 (v/v) chloroform–ethanol were combined and concentrated to give 277 mg (90%) of **10**, mp 196—198 °C, $[\alpha]_D^{20}$ +97.9° (*c* 0.88, chloroform).

Found: C, 52.68; H, 7.62; N, 10.19%. Calcd for $C_{24}H_{42}N_4O_{10}$: C, 52.74; H, 7.74; N, 10.25%.

5,6,3',4'-Tetradeoxyneamine (11). Compound **10** (430 mg) was hydrolyzed in aqueous barium hydroxide solution as in the preparation of **5** to give 94 mg (46%) of **11**, mp 204 °C (dec), $[\alpha]_D^{19}$ +123.8° (*c* 0.63, water). The product was homogeneous on a paper chromatogram (R_f neamine 2.4) in 1: 6: 4: 3 (v/v) acetic acid–1-butanol–pyridine–water. Lit,[21] the sulfate, mp 253—265 °C, $[\alpha]_D^{27}$ +80° (*c* 1, water).

N-Acetylation of **11** (18 mg) with acetic anhydride in methanol afforded 27 mg (91%) of tetra-*N*-acetyl derivative (**12**), mp above 264 °C (dec), $[\alpha]_D^{21}$ +138.3° (*c* 0.94, methanol). ^1H NMR (D_2O): δ 1.95 (s, 3, NAc), 1.96 (s, 6, 2×NAc), 2.01 (s, 3, NAc), 4.93 (d, 1, J=4 Hz, H-1').

Found: C, 56.02; H, 7.91; N, 12.89%. Calcd for $C_{20}H_{34}N_4O_6$: C, 56.32; H, 8.03; N, 13.14%.

The authors would like to express their sincere thanks to Mr. Saburo Nakada for the elemental analyses and to Mr. Kiyoshi Aoki for the determination of ^{13}C NMR spectra. This work was supported by a grant from the Asahi Glass Foundation for Contribution to Industrial Technology.

References

1) S. Nishiyama, Y. Ishikawa, M. Yamazaki, and T. Suami, *Bull. Chem. Soc. Jpn.*, in press.
2) H. Schmitz, O. B. Fardig, F. A. O'Herron, M. A. Rousche, and I. R. Hooper, *J. Am. Chem. Soc.*, **80**, 2911 (1958).
3) T. Wakazawa, Y. Sugano, M. Abe, S. Fukatsu, and S. Kawaji, *J. Antibiot. (Tokyo)*, **A14**, 180 (1961).
4) T. Wakazawa, M. Abe, Y. Sugano, and S. Kawaji, *J. Antibiot. (Tokyo)*, **A14**, 187 (1961).
5) M. Hichens and K. L. Rinehart, Jr., *J. Am. Chem. Soc.*, **85**, 1547 (1963).
6) T. Suami, S. Nishiyama, Y. Ishikawa, and S. Katsura, *Carbohydr. Res.*, **53**, 239 (1977).
7) D. Rosi, W. A. Goss, and S. J. Daum, *J. Antibiot. (Tokyo)*, **30**, 88 (1977).
8) W. T. Shier, K. L. Rinehart, Jr., and D. Gottlieb, *Proc. Nat. Acad. Sci.*, **63**, 198 (1969).
9) T. Suami, S. Ogawa, H. Uchino, and Y. Funaki, *J. Org. Chem.*, **40**, 456 (1975).
10) M. J. Weinstein, F. J. L. Daniels, G. H. Wagman, and R. Testa, Jpn. Patent 75-42092 (1975): D. B. Patent, 2437, 159 (1975).
11) T. Suami, T. Ishikawa, S. Umezawa, and H. Umezawa, Jpn. Patent 76-109385 (1976).
12) S. Umezawa, H. Umezawa, Y. Okazaki, and T. Tsuchiya, *Bull. Chem. Soc. Jpn.*, **45**, 3624 (1972).
13) H. Jennings and J. K. N. Jones, *Can. J. Chem.*, **43**, 2372 (1965).
14) G. J. M. Van der Kerk, J. G. Noltes, and J. G. A. Lujiten, *J. Appl. Chem.*, **7**, 366 (1957); H. Arita and Y. Matsushima, *J. Biochem. (Tokyo)*, **70**, 795 (1971).
15) P. J. L. Daniels, M. Kugelman, A. K. Mallams, R. W. Tkach, H. F. Vernay, J. Weinstein, and A. Yehaskel, *Chem. Commun.*, **1971**, 1629; P. J. L. Daniels, A. K. Mallams, J. Weinstein, J. J. Wright, and G. W. A. Milne, *J. Chem. Soc., Perkin Trans. 1*, **1976**, 1078.
16) G. Kotowycz and R. U. Lemieux, *Chem. Rev.*, **73**, 669 (1973).
17) E. Conway, R. D. Guthrie, S. D. Gero, G. Lukacs, A.-M. Sepolchre, E. W. Hagaman, and E. Wekert, *Tetrahedron Lett.*, **1972**, 4879.
18) E. L. Eliel, W. F. Bailey, L. D. Kopp, R. L. Willer, D. M. Grant, R. Bertrand, K. A. Christensen, D. K. Dalling, M. W. Duch, E. Wenkert, F. M. Schell, and D. W. Cochran, *J. Am. Chem. Soc.*, **97**, 322 (1975).
19) K. F. Kocv, J. A. Rhoades, E. W. Hagaman, and E. Wenkert, *J. Am. Chem. Soc.*, **96**, 3300 (1974).
20) S. Umezawa, Y. Okazaki, and T. Tsuchiya, *Bull. Chem. Soc. Jpn.*, **45**, 3619 (1972).
21) A. Canas-Rodrinuez and S. G. Ruiz-Poveda, *Carbohydr. Res.*, **58**, 379 (1977).

Conformational Analysis of Some Benzyl *t*-Butyl Sulfoxides by Measurement of Their Dipole Moments

Minoru HIROTA,* Yoshiyuki TAKAHASHI, Motohiro NISHIO,** and Ken NISHIHATA**

Department of Applied Chemistry, Faculty of Engineering, Yokohama National University, Minami-ku, Yokohama 232

***Central Research Laboratories, Meiji Seika Kaisha Ltd., Kohoku-ku, Yokohama 222*

(Received December 27, 1977)

Favored conformations of benzyl *t*-butyl sulfoxides and their α-methyl derivatives in solutions were determined from their dipole moments and compared with those in crystals.

In connection with studies on stereochemistry of the reactions involving α-sulfinyl carbanion, the conformations of the related sulfoxides have been investigated.[1-4] Some of the present authors investigated the methylation and deuteration of benzyl alkyl sulfoxides *via* carbanion intermediates, a highly stereospecific nature of the reaction being revealed.[5-8] Furthermore, the conformations of the above sulfoxides in crystalline states were determined by means of X-ray crystal analysis. The results show that *p*-bromobenzyl *t*-butyl sulfoxide (1b) takes conformation III (where Ar=*p*-BrC_6H_4 and $R_1=R_2=H$),[9] and (*RR*/*SS*)-*t*-butyl 1-(*p*-bromophenyl)-ethyl sulfoxide (2b; $R_1=CH_3$, $R_2=H$)[10] and its (*RS*/*SR*) isomer (3b; $R_1=H$, $R_2=CH_3$)[11] conformations II and I, respectively, in crystalline state. On the other hand, benzyl *t*-butyl sulfoxide (1a) takes conformation II in which the *t*-butyl and phenyl groups are gauche to each other as shown by LIS and ASIS measurements.[12] The stereochemistry of its deuteration was again best rationalized by assuming conformation II.

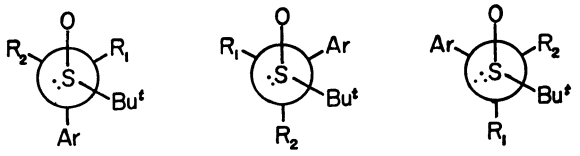

(I) ϕ 180° (II) 300°(−60°) (III) 60°

Thus, another more decisive evidence on their conformations in solution is necessary to settle this apparent disagreement. Since the dipole moment often offers a very conclusive evidence for the conformation in solution of a molecule carrying two polar substituents at suitable positions, their dipole moments were determined.

Experimental

Materials. The sulfoxides were prepared according to known methods. The new compounds were identified by spectral and elementary analyses. Benzene for the solvent was carrefully purified and dried.

Dielectric Measurement. Dielectric constants of the benzene solution of the sulfoxides were determined at 25 °C with a heterodyne-beat apparatus. The dipole moments were calculated according to the method of Halverstadt and Kumler[13,14] from the observed dielectric constants and densities of the benzene solution at varying concentrations. The molar refraction was calculated from the bond refraction values.[14]

Results and Discussion

The dipole moments of substituted benzyl *t*-butyl sulfoxides are given in Table 1. The substituent effect on the (*RS*/*SR*), or threo, series (3) is apparently anomalous since the dipole moment of *p*-bromo derivative is lower than that of both unsubstituted and *p*-nitro derivatives. Since the conformations of the molecules are governed by the steric circumstances around the bond in question and insensitive to the electronic effect of the substituents far from the bond, the sulfoxide molecules appear to take a similar conformation irrespective of the para-substituents when the configuration is the same. Thus, the anomalous substituent effect is reasonable only when the angle between the C–X (X=Br or NO_2) and the S–O bond moment vectors are larger than a right angle, which is only possible in confor-

TABLE 1. OBSERVED DIPOLE MOMENTS (μ) OF THE SULFOXIDES AND RELATED COMPOUNDS

Compound	R_1	R_2	Ar	No.	μ/D
(*R*/*S*)Benzyl *t*-butyl sulfoxide	H	H	C_6H_5	1a	3.90
(*R*/*S*)*p*-Bromobenzyl *t*-butyl sulfoxide	H	H	*p*-BrC_6H_4	1b	4.72
(*R*/*S*)*p*-Nitrobenzyl *t*-butyl sulfoxide	H	H	*p*-$NO_2C_6H_4$	1c	6.44
(*RR*/*SS*) 1-Phenylethyl *t*-butyl sulfoxide	CH_3	H	C_6H_5	2a	3.84
(*RR*/*SS*) 1-(*p*-Bromophenyl)ethyl *t*-butyl sulfoxide	CH_3	H	*p*-BrC_6H_4	2b	4.23
(*RR*/*SS*) 1-(*p*-Nitrophenyl)ethyl *t*-butyl sulfoxide	CH_3	H	*p*-$NO_2C_6H_4$	2c	5.69
(*RS*/*SR*) 1-Phenylethyl *t*-butyl sulfoxide	H	CH_3	C_6H_5	3a	3.86
(*RS*/*SR*) 1-(*p*-Bromophenyl)ethyl *t*-butyl sulfoxide	H	CH_3	*p*-BrC_6H_4	3b	3.42
(*RS*/*SR*) 1-(*p*-Nitrophenyl)ethyl *t*-butyl sulfoxide	H	CH_3	*p*-$NO_2C_6H_4$	3c	4.26
Methyl phenyl sulfoxide					3.88
p-Bromobenzyl *t*-butyl sulfone					4.90

mation I (see Figs. 1 and 2). The above qualitative assignment of the conformation agrees with the results of its X-ray crystal analysis and is rationalized by a more quantitative computation on the conformation dependence of dipole moments. From a similar discussion on the (*RR*/*SS*) series (2), the privileged conformation can not be determined uniquely, and both conformers II and III are suspected. However, operation of a considerable repulsive force is expected when methyl and *t*-butyl groups are located gauche to each other, as realized in the conformer III of (2). Conformer II should thus be the more stable of the two.

Table 2. Bond and group moment values[16,17]

Bond or group (+) (−)	*m*/D
H − C	0.0
C − S	0.90
C − C_6H_5	0.35
C − $C_6H_4Br(p)$	1.53
C − $C_6H_4NO_2(p)$	4.00
S − O	3.00

In order to estimate the dipole moments of these molecules quantitatively, they were calculated as the sum of the component bond moments by taking the values in Table 2 and the bond lengths and bond angles reported by Kodama and co-workers.[15] The S–O bond moment was re-evaluated by measuring the dipole moments of some sulfoxides. The observed dipole moment of phenyl methyl sulfoxide gives a larger S–O bond moment (3.2 D) than that reported.[16] The best fit value of S–O bond moment is 3.0 D (Table 2) for this series of sulfoxides, which is employed as the bond moment for the present calculations.

Table 3. Dipole moments of the sulfoxides (1a—3c) calculated by assuming the conformations in crystals

Ar	R_1 R_2	Benzyl series (1) H H	(*RR*/*SS*) series (2) CH_3 H	(*RS*/*SR*) series (3) H CH_3
C_6H_5(a)		3.85	3.75(4.03)	3.28(3.53)
p-BrC_6H_4(b)		4.61	4.23(4.87)	2.31(2.68)
p-$NO_2C_6H_4$(c)		6.62	5.91(6.96)	1.70(2.29)
The conformation in crystal		III	II	I

a) The dipole moments calculated by employing the modified bond moments[17] (m_{S-O}=2.70 D, m_{C-S}= 1.47 D) are given in parentheses.

Dipole moments for the conformations in crystals[10,11] were calculated first. Benzyl *t*-butyl sulfoxides are assumed to exist exclusively in conformation III in which the bulky phenyl and *t*-butyl groups are located anti to each other.[9] The results are given in Table 3. The calculated values for the series of (1)[18] and (2) agree very closely with the observed ones (Table 2). However, those for the series of (3) do not agree with the observed ones at all. The dipole moments of the series of (*RR*/*SS*) (2) and (*RS*/*SR*) (3) were then calculated as the function of dihedral angle around C_{benzyl}–S bond. The results are shown in Figs. 1 and 2, where the abscissa represents the dihedral angle (ϕ) between the S–O and C–Ar bonds. The best fit values for the (*RR*/*SS*) series (2) are attained when the dihedral angle ϕ is near 300° (−60°). This is in line with the conclusion from X-ray and other evidences. However, no dihedral angle reasonable for the (*RS*/*SR*) series (3) could be found (Fig. 2). The dipole moment of (*RS*/*SR*) sulfoxides (3) is interpreted by assuming the conformational equilibria between (or among) conformers I and III (or II). Again conformer II should be excluded since the *t*-butyl and methyl groups are gauche to each other (as in conformer III of the (*RR*/*SS*) series). When the mole fraction of conformer I is *X*, the dipole moment of the mixture (μ) is given by the equation,

$$\mu = \{X\mu_I^2 + (1 - X)\mu_{III}^2\}^{1/2},$$

where μ_I and μ_{III} refer to the dipole moments of conformer I and III, respectively. The calculated dipole moments for the conformational mixtures are given as the function of *X* in Table 4. Near *X*=0.7, the dipole moments of the (*RS*/*SR*) sulfoxides are reproduced almost quantitatively, and the order of magnitude of dipole moments is in line with the observed values in the range of *X*=0.8—0.65.[17] Thus the (*RS*/*SR*) sulfoxides are concluded to exist as a mixture of confor-

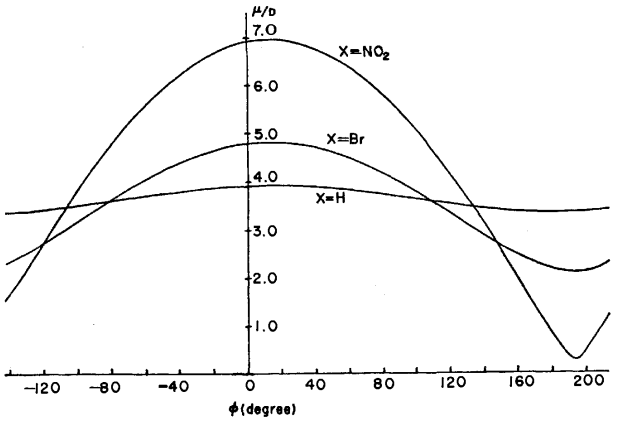

Fig. 1. Dihedral angular dependency of the dipole moments of (*RR*/*SS*)-*t*-butyl 1-phenylethyl sulfoxides.

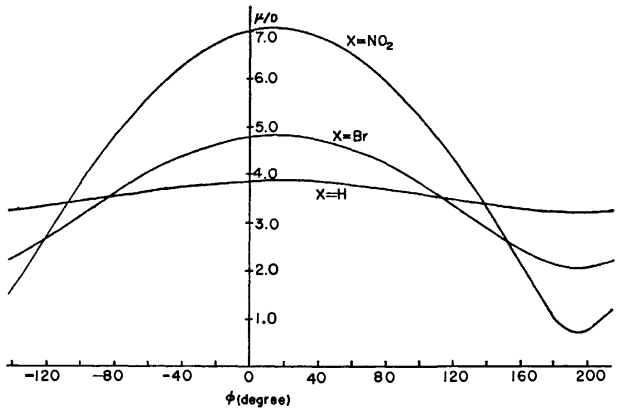

Fig. 2. Dihedral angular dependency of the dipole moments of (*RS*/*SR*)-*t*-butyl 1-phenylethyl sulfoxides.

TABLE 4. DIPOLE MOMENTS OF (3)'S CALCULATED BY ASSUMING THE COEXISTENCE OF CONFORMERS I AND III IN VARYING PROPORTIONS

Ar	X[a]					
	0.85	0.80	0.75	0.70	0.65	0.60
C_6H_5	3.38	3.41	3.44	3.46	3.49	3.51
p-BrC_6H_4	2.91	3.04	3.16	3.28	3.40	3.51
p-$NO_2C_6H_4$	3.28	3.57	3.84	4.10	4.34	4.56

a) Mole fraction of conformer I. Sice the existence of conformer II and other conformers are neglected, the mole fraction of the III should be $1-X$.

mers in which conformer I predominates in benzene solutions.

In conclusion, both the (*RR*/*SS*) and (*RS*/*SR*) isomers of *t*-butyl 1-phenylethyl sulfoxides are shown to take conformations in which bulky *t*-butyl and phenyl groups approach closely. From these observations on dipole moments, the participation of a specific attractive force between the phenyl and the *t*-butyl groups might take place. On the other hand, an alternative explanation in which the repulsive force between the methyl and *t*-butyl groups plays an important role is also possible. In order to decide which of the above effect is more predominant, the conformation of a benzyl *t*-butyl sulfone was determined by measurement of their dipole moments.

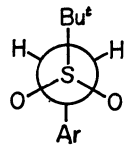

(IV)

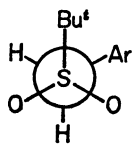

(V)

The observed dipole moment for *p*-bromobenzyl *t*-butyl sulfone (4) is 4.90 D, while the calculated values for conformers IV and V (where Ar=C_6H_4Br-*p*) are 5.2 and 3.7 D, respectively, and the result favors the anti-conformation in which phenyl and *t*-butyl groups are located farthermost to each other. In view of this, the repulsive force is supposed to play an important role in determining the conformations of these sulfoxides. However, a similar attractive interaction between the alkyl and aromatic groups was reported recently.[12] The conformations of these sulfoxides may also be determined by the cooperation of the repulsive force caused by steric hindrance, the specific attractive force, and other forces in their molecules.

References

1) A. Rauk, E. Buncel, R. Y. Moir, and S. Wolfe, *J. Am. Chem. Soc.*, **87**, 5498 (1965).
2) A. Rauk, S. Wolfe, and G. Csizmadia, *Can. J. Chem.*, **47**, 113 (1969).
3) M. D. Brown, M. J. Cook, B. J. Huchinson, and A. R. Katritzky, *Tetrahedron*, **27**, 593 (1971).
4) U. Folli, F. Montanari, and G. Torre, *Tetrahedron Lett.*, **1966**, 5037.
5) M. Nishio, *Chem. Commun.*, **1968**, 562.
6) K. Nishihata and M. Nishio, *Chem. Commun.*, **1971**, 958; *J. Chem. Soc., Perkin Trans. 2*, **1972**, 1730.
7) K. Nishihata and M. Nishio, *Tetrahedron Lett.*, **1972**, 4839.
8) K. Nishihata and M. Nishio, *Tetrahedron Lett.*, **1976**, 1695.
9) Y. Kodama and Y. Iitaka, to be published.
10) Y. Kodama, K. Nishihata, M. Nishio, and Y. Iitaka, *J. Chem. Soc., Perkin Trans. 2*, **1976**, 1490.
11) Y. Iitaka, Y. Kodama, K. Nishihata, and M. Nishio, *J. Chem. Soc., Chem. Commun.*, **1974**, 389.
12) Kodama, K. Nishihata, M. Nishio, and N. Nakagawa, *Tetrahedron Lett.*, **1977**, 2105.
13) a) I. F. Halverstadt and W. D. Kumler, *J. Am. Chem. Sic.*, **64**, 2988 (1942); b) C. P. Smyth, "Dielectric Behavior and Structure," McGraw-Hill Book Co., Inc., N. Y. (1955).
14) T. Shimozawa, "Yudenritsu-no-kaishaku(Intepretation of the Dielectric Behavior)," Kyoritsu Publ. Co., Tokyo (1967).
15) Y. Kodama, K. Nishihata, and M. Nishio, *J. Chem. Res. (S)*, **1977**, 102.
16) "Kagaku Benran" 2nd ed, ed by Chemical Society of Japan, Maruzen, Tokyo (1975), pp. 1404—1407, p. 1260.
17) A large C–S bond moment (1.46 D) and a smaller S–O bond moment (2.70 D) are proposed by Saito and coworkers, [S. Saito, *Bull. Chem. Soc. Jpn.*, **42**, 663 (1969) and S. Saito and F. Makino, *ibid.*, **45**, 92 (1972)]. The dipole moments of the (*RR*/*SS*) and (*RS*/*SR*) sulfoxides are also calculated on the basis of these bond moments (see Table 3). The calculated values also explain the observed dipole moments qualitatively. However, the agreements is less satisfactory. Calculation by these bond moments on the (*RS*/*SR*) series also suggests the conformation equilibria, the composistion for the best fit dipole moments containing about 40% of the conformer I. (The order of the dipole moment values agrees in the range X= 0.55—0.30).
18) Conformer II is also compatible with the observed dipole moment.

Synthesis of 11-Methyl- and 11,11-Dimethylprostaglandins *via* the Wittig Reaction of α-Dienol[1]

Kenji INOUE, Junya IDE, and Kiyoshi SAKAI*

Central Research Laboratories, Sankyo Co., Ltd., 1-2-58 Hiromachi, Shinagawa-ku, Tokyo 140

(Received January 9, 1978)

The key intermediates for 11-methyl- and 11,11-dimethylprostaglandins corresponding to Corey's lactone were synthesized *via* the Wittig reaction of dimethyl 2-substituted-4,5-dioxocyclopentane-1,3-dicarboxylate with stable ylides. 11,11-Dimethylprostaglandin E_2 was then synthesized.

Recently, a number of groups have done research on the synthesis of methylprostaglandins (PGs) whose biological activities resemble those of PGEs. 11-Methyl-PGE_2[2] was synthesized by 1,4-addition of ate-complex or diazomethane to the natural PGA_2. We have previously reported the synthesis of 11-deoxy- and natural prostaglandins intermediates[1,3] by the Wittig reaction from enolized α-diketone. We wish to describe the synthesis of the intermediates (**8a** and **8b**) for 11-methylated PGs and a total synthesis of 11,11-dimethyl-PGE_2 (**1b**) starting from **8b**.

The Wittig reaction of one equivalent of dimethyl 4,5-dioxo-2-methylcyclopentane-1,3-dicarboxylate (**2a**) (α-dienol) with two equivalents[4] of (methoxycarbonylmethylene)triphenylphosphorane (**3a**) in chloroform under reflux for 24 h afforded a mixture of the corresponding olefins (**4a**, **4b**, and **4d**). This reaction, however, seemed to proceed differently from the usual Wittig reaction. On addition of the ylide **3a** to α-dienol **2a** in chloroform at room temperature, **2a** was rapidly transformed into a polar intermediate (as monitored by TLC), which was gradually converted into the final olefinic products **4a**, **4b**, and **4d** under reflux. Since the starting material **2a** was quantitatively recovered from the polar intermediate by acid (8% HCl) treatment, the polar intermediate seems to be a phosphonium salt. The formation of the phosphonium salt might be due to the relatively strong acidity[5] of **2a** (pK_{a_1} 6.26 and pK_{a_2} 11.1). The reaction mechanism from the salt to olefins remains unsolved. It is noteworthy that the Wittig reaction proceeded in the case of acidic α-dienols,[3] although under the same conditions cyclopentanone, β-keto ester (**13**), and α-keto enol ethers (**14**) and (**15**) with **3a** gave no products.

The purification of the products was effected by silica gel chromatography and successive fractional recrystallization to give the *exo*-olefins **4a** (mp 82—83.5 °C) and **4b** (mp 96—97.5 °C) in a 25.3% total yield, and the oily *endo*-isomer **4d**[6] in a 25.6% yield. In the NMR spectra vinyl protons of **4a** and **4b** appeared at 6.39 and 6.38 ppm, respectively. The methyl group in **4b** was observed at 1.13 ppm as a doublet, due to a shielding effect of the adjacent methoxycarbonyl group which was larger than that of **4a** at 1.31 ppm. These observations support the stereochemical assignments of the methyl group to the methoxycarbonyl group in **4a** and **4b** as *trans* and *cis*, respectively, except for the geometry of the *exo* double bond. Further confirmation of the stereochemistry of **4a** was made in connection with the stereochemistry of the *trans-trans*-keto diester (**5a**) derived from **4a** by successive catalytic hydrogenation and decarboxylation (*vide infra*). The *endo*-isomer **4d** contains no vinyl proton, but the methyl group appeared at 2.35 ppm as a singlet assignable to an olefinic methyl group. The *endo*-isomer **4d** would be obtained from **4a** and/or **4b** by the migration of the *exo* double bound under the employed reaction conditions.

Catalytic hydrogenation of the *trans-exo*-olefin **4a** over 10% Pd–C in methanol, followed by treatment with NaI–AcOH–diglyme,[7] afforded stereoselectively the *trans-trans*-keto diester **5a** in a 72.7% yield. Its stereochemical assignment was based on the following observations: i) No epimerization of **5a** occurred after treatment with sodium methoxide in methanol, which suggested that **5a** was thermodynamically stable in its configuration. ii) In the NMR spectra the *trans*-methyl group on the cyclopentane ring was generally observed at a lower field than the corresponding *cis*-methyl group, as shown in Table. 1[8] The methyl signal of **5a** at 1.20 ppm was also observed at a lower field than the other two isomers, *i.e.* the *cis-trans*-keto diester (**5b**) (1.13 ppm) and the *cis-cis*-keto diester (**5d**) (0.96 ppm) (*vide infra*). Further chemical transformation of **5a** into 11-methylprostaglandin E_2 confirmed its stereochemical features. On the other hand, for both **4b** and **4d**, catalytic hydrogenation followed by decarboxylation gave a stereoisomeric mixture of **5a** (*trans-trans*), **5b** (*cis-trans*), and **5d** (*cis-cis*), in the ratio of 5: 2: 3.

TABLE 1. NMR OF METHYL CYCLOPENTANES CHEMICAL SHIFT AND J VALUE OF METHYL SIGNALS

trans δ (JHz)	cis δ (JHz)	trans δ (JHz)	cis δ (JHz)
1.20 (5)	1.04 (6)	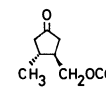 1.17 (5)	1.03 (6)
1.10 (5)	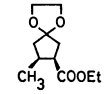 0.97 (7)	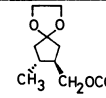 1.06 (4)	0.98 (6)
1.07 (4)	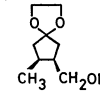 0.97 (6)	1.21 (6)	1.15 (6)
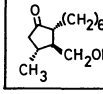 1.14 (6)	1.00 (6)	—	1.09 (6)

The *cis-exo*-olefin **4b** was found to be isomerized to the *endo* double bond in **4d** by treatment with activated 10% Pd–C in methanol under argon atmosphere. The formation of the mixture of **5a**, **5b**, and **5d** from **4b** was thus explained on the assumption that **4b** was

isomerized to **4d** prior to hydrogenation.

Separation of these isomers by silica gel or alumina column chromatography was unsuccessful. HPL chromatography, however, gave the pure isomer **5b** and a mixture of **5a** and **5d**. In the NMR spectra, methyl signals of **5a**, **5b**, and **5d** appeared at 1.20 (doublet, J=5 Hz), 1.13 (doublet, J=8 Hz), and 0.96 ppm (doublet, J=8 Hz). These NMR data indicate that the methyl group of **5d** was more shielded by other substituents on the cyclopentane ring, *i.e.*, methoxycarbonyl and methoxycarbonylmethyl groups, than were the methyl groups of **5a** and **5b**. Therefore, the less shielded isomer **5b** may be assigned as *cis-trans* and the most shielded one **5d** as *cis-cis*.

These assignments are supported by the facts that the *cis-trans*-isomer **5b** readily isomerizes to an equilibrium mixture of **5b** and **5d** in the ratio of 2: 3 under decarboxylation conditions, *i.e.*, NaI–AcOH–diglyme at 120 °C, whereas the *trans-trans*-isomer **5a** underwent no isomerization under the same conditions. The equilibration between *cis-trans*- and *cis-cis*-isomers on the cyclopentanone ring has already been observed: *cis-trans*-PGE_1s and/or *cis-cis*-PGE_1s underwent isomerization to their equilibrium mixture by treatment with bases such as K_2CO_3 or NaOH.[9]

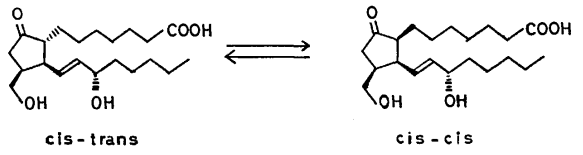

Scheme 1.

Treatment of a stereoisomeric mixture of **5** with a strong base such as NaOMe furnished predominantly the *trans-trans*-isomer **5a**. Ultimately, the stable isomer **5a** was obtained in a 46.4% yield starting from the α-dienol **2a**, without separation of the products in each step.

The reduction of the keto diester **5a** with potassium tri-*s*-butylborohydride gave the lactone (**6a**) in a 67.8% yield. By hydrolysis with concd hydrochloric acid, crystalline lactone acid (**7a**) (65.5%, mp 116—117 °C) was obtained. On reduction with $NaBH_4$ after conversion into the mixed anhydride ($ClCOOEt$–Et_3N), **7a** gave the key intermediate lactone alcohol (**8a**), which may be easily converted into 11-methyl-PGs by established methods.

11,11-Dimethyl-PGE_2 (**1b**) was obtained from the α-dienol (**2b**) by the same method. The Wittig reaction of **2b** (pK_{a_1} 6.61 and pK_{a_2} 11.1) with stable ylide (**3b**) gave a mixture of the corresponding olefins (**4c** and **4e**) (*ca.* 3: 7) in a 25.4% yield. Catalytic hydrogenation of the mixture over 10% Pd–C, followed by treatment with concd hydrochloric acid, gave the decarboxylated product. This was reesterified with diazomethane to give the keto diester (**5c**) in a 78.5% yield. The keto diester **5c** was stereoselectively reduced with potassium tri-*s*-butylborohydride to give the lactone ester (**6b**) (46.7%, mp 69.5—71 °C). Acid-hydrolysis of **6b** with hydrochloric acid gave the lactone acid (**7b**) (71%, mp 179.5—181 °C); this was reduced *via* the mixed anhydride to the lactone alcohol (**8b**) in a 73.6% yield.

Both side chains required for the prostaglandins were introduced into **8b** by the usual method. The Collins oxidation of **8b** followed by the Wittig reaction gave the enone (**9**), which was reduced with $NaBH_4$ to an epimeric mixture of (**10**) and its 15-OH epimer. By preparative layer chromatography the less polar compound **10** was obtained. This was tentatively assigned as the 15α-OH(*S**) epimer. Treatment of **10** with dihydropyran in the presence of *p*-TsOH, followed by reduction with diisobutylaluminium hydride, provided the lactol (**11**). The Wittig reaction of **11** with sodium 5-(triphenylphosphoranylidene)pentanoate, followed by the oxidation with the Collins reagent, afforded 15-tetrahydropyranyloxy-11,11-dimethyl-PGE_2 (**12**). Removal of the protecting group of **12** with aqueous AcOH afforded 11,11-dimethyl-PGE_2 **1b**.

11,11-Dimethyl-PGE_2 **1b** showed *anti*-ulcer activity

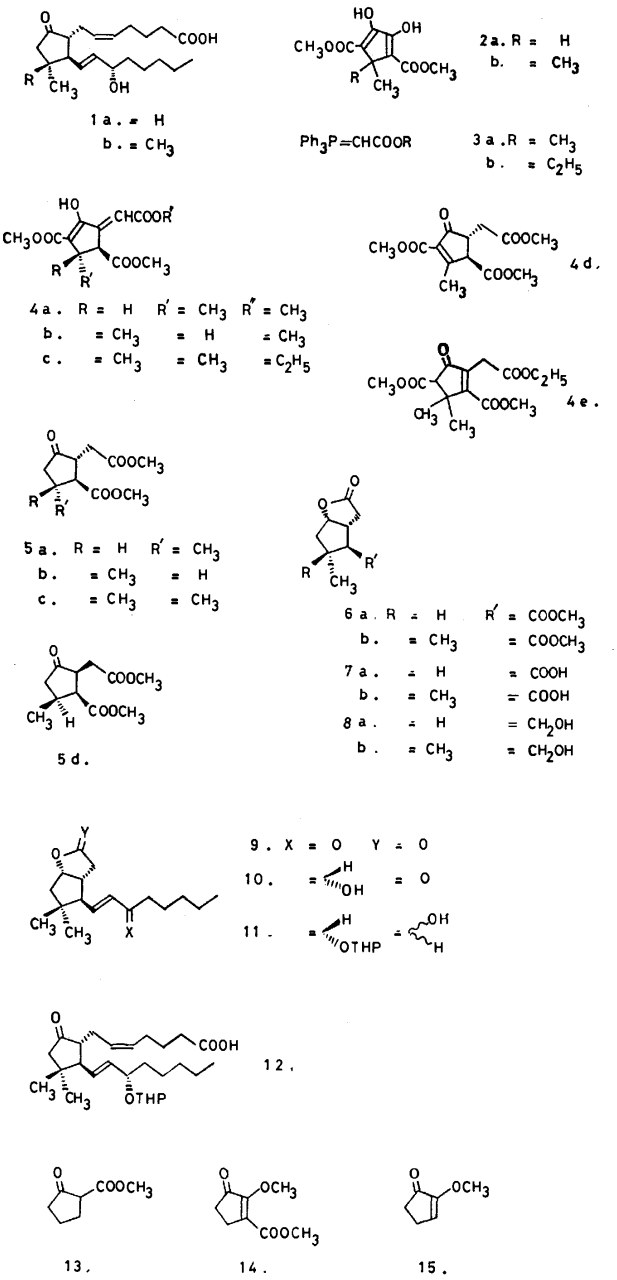

nearly equal to 11-methyl-PGE_1.

Experimental

The melting points were determined on a Micro Melting Point Apparatus (Yanagimoto) and are uncorrected. The infrared spectra were recorded in Nujol mull or neat on a JASCO Model A-2. The NMR spectra were obtained on a Varian T-60 spectrometer with TMS as an internal standard.

The starting materials **2a** and **2b** were prepared from oxalyl ester and dimethyl 3-methyl- or 3,3-dimethylglutarate.[10]

*Dimethyl 2-Hydroxy-3-methoxycarbonylmethylene-*trans*-5-methyl-1-cyclopentene-1,4-dicarboxylate* ***4a****, Its* cis*-Isomer* ***4b****, and* endo*-Olefinic Isomer* ***4d****.* A solution of **2a** (9.15 g) and **3a** (26.8 g) in chloroform was stirred at 60 °C for 24 h. The reaction mixture was washed with 8% HCl and the solvent was evaporated *in vacuo*. The residue was added to hexane–benzene and extracted well with 10% aqueous K_2CO_3. The basic aqueous extracts were combined, acidified with dil HCl, and extracted with ether. The ethereal extracts were washed with water, dried over Na_2SO_4, and evaporated to give a dark oil. The crude product was chromatographed on an acid-washed silica gel to give a mixture of crystalline *exo*-olefins as the less polar fraction, which consisted of two stereoisomers **4a** and **4b** (2.86 g ratio **4a**: **4b**=1: 1), and an oily *endo*-olefin as the more polar fraction **4d**. Recrystallization from ethanol afforded pure **4a** and **4b**. **4a**: Mp 82—83.5 °C; MS: *m/e* 284 (M^+); IR: 3350, 1715, 1705, 1645, and 1610 cm^{-1}; NMR ($CDCl_3$): 9.98 (1H, bs, OH), 6.39 (1H, d, J=2 Hz, olefin), 3.7 (1H, m, >CH–COO), 3.06 (1H, dq, J=2 and 6 Hz, >CH–Me), and 1.31 (3H, d, J=6 Hz, CH_3). Found: C, 54.87; H, 5.57%. Calcd for $C_{13}H_{16}O_7$: C, 54.93; H, 5.67%. **4b**: mp 96—97.5 °C; IR: 3360, 1735, 1715, 1710, 1645, and 1610 cm^{-1}; NMR ($CDCl_3$): 10.02 (1H, s, OH), 6.38 (1H, d, J=2 Hz, olefin), 4.20 (1H, q, J=8 Hz, >CH–COO), 3.36 (1H, dq, J=7 and 8 Hz, >CH–Me), and 1.13 (3H, d, J=7 Hz, CH_3). Found: C, 54.64; H, 5.38%; Calcd for $C_{13}H_{16}O_7$: C, 54.93; H, 5.67%. **4d**: oil; IR: 1730 and 1630 cm^{-1}; NMR ($CDCl_3$): 3.77, 3.66, and 3.60 (3× 3H, s, $COOCH_3$), 3.7 (1H, m, >CH–COO), 3.2—2.6 (3H, m), and 2.35 (3H, s, CH_3). Found: C, 54.75; H, 5.43%. Calcd for $C_{13}H_{16}O_7$: C, 54.93; H, 5.67%.

Hydrogenation and Decarboxylation of ***4a****,* ***4b****, and* ***4c*** *to* ***5****.* A solution of **4a** (0.426 g) in methanol was hydrogenated in the presence of 5% Pd–C under hydrogen atmosphere at room temperature. After removal of the catalyst and evaporation of the solvent, the hydrogenated product was heated at 120—140 °C for 1 h in a mixture of diglyme (6 ml), acetic acid (0.4 ml), and sodium iodide (0.2 g). The reaction mixture was poured into water and extracted with ether. The ethereal extracts were evaporated to dryness and the residue was chromatographed on silica gel to give **5a** (0.27 g), which was homogeneous in TLC, gas chromatography, and HPLC. **5a**; IR: 1740 cm^{-1}; NMR ($CDCl_3$): 3.63 and 3.73 (2× 3H, s, $COOCH_3$) and 1.20 (3H, d, J=5 Hz, CH_3); Found: C, 58.18; H, 7.14%. Calcd for $C_{11}H_{16}O_5$: C, 57.88; H, 7.07%.

Similarly, **4b** and **4c** were hydrogenated and decarboxylated. In each case there was only one spot on TLC, but the NMR spectra of the methyl group showed three components. These mixtures were separated into two fractions by HPLC. The first fraction showed a doublet signal at 1.13 ppm assignable to the methyl of **5b**, the second fraction two doublet signals at 1.20 and 0.96 ppm, to which were assigned **5a** and **5d**, respectively.

A Mixture of Dimethyl 5,5-Dimethyl-3-ethoxycarbonylmethylene-2-hydroxy-1-cyclopentene-1,4-dicarboxylate ***4c*** *and Its Olefinic Isomer* ***4e****.* A solution of **2b** (25.1 g) and **3b** (72.3 g) in chloroform was stirred at 60 °C for 5 days. After evaporation of the solvent *in vacuo*, the residue was added to ether and the precipitate of the unreacted **3b** was filtered off. The filtrate was washed with 8% HCl and then 10% aqueous K_2CO_3, and evaporated *in vacuo*. The residue was redissolved in diisopropyl ether and stored in a refrigerator to give triphenylphosphine oxide. After removal of Ph_3PO by filtration, evaporation of the filtrate gave a reddish oil which was chromatographed on acid-washed silica gel to give a mixture of **4c** (*exo*) and **4e** ((*endo*)(8.21 g). MS: *m/e* 312 (M^+); IR: 1740, 1710, and 1655 cm^{-1}; NMR ($CDCl_3$): 10.5 (s, OH) and 6.4 (d, olefin).

Methyl t*-2-Methoxycarbonyl-*c*-3-methyl-5-oxocyclopentane-*r*-1-acetate* ***5a*** *and 3,3-Dimethyl Derivative* ***5c****.* A solution of the crude Wittig products, obtained from α-dienol **2a** (6.84 g) and 10% Pd–C (4.0 g) in methanol was hydrogenated under atmospheric pressure. After filtration and evaporation *in vacuo*, the oily residue was refluxed in concd HCl for 3 h. The reaction mixture was evaporated to dryness *in vacuo*, and reesterified with CH_2N_2 in ether to give crude **5a** which was equilibrated with NaOMe in methanol at room temperature for 12 h. The chromatography of the crude oil on a silica gel column gave the oil **5a** (3.17 g). MS: *m/e* 228 (M^+); IR: 1740 cm^{-1}; NMR ($CDCl_3$): 3.75 and 3.66 (2× 3H, s, $COOCH_3$) and 1.20 (3H, d, J=5 Hz, CH_3). Found: C, 57.69; H, 7.14%; Calcd for $C_{11}H_{16}O_5$: C, 57.88; H, 7.07%.

A similar procedure starting from the crude Wittig products **4c** and **4e** (8.20 g) afforded **5c** (5.03 g), which was homogeneous in TLC; no isomerization was observed after the treatment of **5c** with NaOMe–methanol. MS: *m/e* 242 (M^+); IR: 1740 cm^{-1}; NMR ($CDCl_3$): 1.40 and 1.00 (2× 3H, s, CH_3). Found: C, 59.23; H, 7.42%. Calcd for $C_{12}H_{18}O_5$: C, 59.49; H, 7.49%.

c*-5-Hydroxy-*t*-2-methoxycarbonyl-*c*-3-methylcyclopentane-*r*-1-acetic Acid γ-Lactone* ***6a*** *and 3,3-Dimethyl Derivative* ***6b****.* To a stirred solution of **5a** (2.28 g) in tetrahydrofuran at 0 °C under argon was added dropwise a solution of 0.5 M/L potassium tri-*s*-butylborohydride in tetrahydrofuran (22 ml). The mixture was stirred at 0 °C for 30 min. The reaction was quenched by addition of 4% HCl. The resulting mixture was diluted with brine and extracted with ethyl acetate. The combined extracts were washed with brine, dried over Na_2SO_4, and evaporated *in vacuo* to give a crude oil. The oil was chromatographed on silica gel to give **6a** (1.34 g). IR: 1775, 1740, and 1735 cm^{-1}; NMR ($CDCl_3$): 5.0 (1H, m, lactone), 3.71 (3H, s, $COOCH_3$), and 1.10 (3H, d, J=5.5 Hz, CH_3). Found: C, 60.37; H, 7.25%. Calcd for $C_{10}H_{14}O_4$: C, 60.59; H, 7.12%.

A similar procedure starting from **5c** (5.53 g) afforded **6b** (2.27 g). Mp 69.5—71 °C; MS: *m/e* 212 (M^+); IR: 1775, 1765, and 1730 cm^{-1}; NMR ($CDCl_3$): 4.96 (1H, dt, J=7 and 5 Hz, lactone), 3.70 (3H, s, $COOCH_3$), 1.24 and 0.90 (2× 3H, s, CH_3). Found: C, 62.40; H, 7.61%. Calcd for $C_{11}H_{16}O_4$: C, 62.25; H, 7.60%.

t*-2-Carboxy-*c*-5-hydroxy-*c*-3-methylcyclopentane-*r*-1-acetic Acid γ-Lactone* ***7a*** *and 3,3-Dimethyl Derivative* ***7b****.* A solution of **6a** (1.32 g) in concd HCl was refluxed for 2 h. The resulting solution was evaporated *in vacuo* and the residue was recrystallized from benzene–diisopropyl ether to give the lactone acid **7a** (0.803 g). Mp 116—117 °C; NMR ($CDCl_3$): 10.7 (1H, s, COOH), 5.00 (1H, m, lactone), and 1.17 (3H, d, J=5 Hz, CH_3). Found: C, 58.43; H, 6.35%. Calcd for $C_9H_{12}O_4$: C, 58.69; H, 6.57%.

Similarly, **6b** (2.27 g) was converted by the same procedure into **7b** (1.51 g). Mp 179.5—181 °C; MS: *m/e* 198 (M^+); NMR (acetone-d_6): 8.2 (1H, bs, COOH), 5.0 (1H, dt, J=7 and 5 Hz, lactone), 1.32 and 0.93 (2× 3H, s, CH_3). Found: C, 60.34; H, 7.17%. Calcd for $C_{10}H_{14}O_4$: C, 60.59; H, 7.12%.

c*-5-Hydroxy-*t*-2-hydroxymethyl-*c*-3-methylcyclopentane-*r*-1-Acid*

γ-Lactone 8a and 3,3-Dimethyl Derivative 8b. To a solution of **7a** (0.75 g) and triethylamine (0.572 g) in tetrahydrofuran at 0 °C under argon was added ethyl chloroformate (0.61 g) in tetrahydrofuran. After 1 h, the precipitate was filtered off from the reaction mixture. To the filtrate was added dropwise a solution of $NaBH_4$ (0.643 g) in water at 0 °C and the mixture was stirred at ambient temperature for an additional 1 h. After cooling to 0 °C, 8% HCl was added to the reaction mixture, and extraction was carried out with ethyl acetate. The combined extracts were washed with brine, dried over Na_2SO_4, and evaporated *in vacuo* to give a crude oil. This was chromatographed on silica gel to afford the lactone alcohol **8a** (0.552 g). MS: *m/e* 170 (M^+); IR: 3500 and 1770 cm^{-1}; NMR ($CDCl_3$): 4.90 (1H, m, lactone), 3.4—4.0 (3H, m), and 1.07 (3H, d, J=6 Hz, CH_3). Found: C, 63.47; H, 8.18%; Calcd for $C_9H_{14}O_3$: C, 63.51; H, 8.29%.

Similarly, **7b** (1.50 g) was converted by the same procedure into the oil **8b** (1.03 g). MS: *m/e* 184 (M^+); IR: 3450 and 1770 cm^{-1}; NMR ($CDCl_3$): 4.92 (1H, dt, J=7 and 5 Hz, lactone), 3.3—4.0 (3H, m), 1.16 and 0.82 (2× 3H, s, CH_3). Found: C, 65.03; H, 8.72%; Calcd for $C_{10}H_{16}O_3$: C, 65.19; H, 8.75%.

*3,3-Dimethyl-*c*-5-hydroxy-*t*-2-(3-oxo-*trans*-1-octenyl)cyclopentane-*r*-1-acetic Acid γ-Lactone 9.* To a stirred solution of the Collins reagent prepared from CrO_3 (4.04 g) and pyridine (6.25 ml) in dichloromethane at 0 °C under argon was added a solution of **8b** (1.03 g) in dichloromethane. The resulting solution was stirred at 0 °C for 5 min and then at ambient temperature for 20 min, and added to ether. The precipitate was filtered and the filtrate was washed with 4% sodium hydroxide, water, 4% HCl, water, 3% $NaHCO_3$, and water, dried over Na_2SO_4, and evaporated to give a crude aldehyde (0.92 g). To the solution of this aldehyde in ether was added a solution of (2-oxoheptylidene)tributylphosphorane (2.32 g) in dry ether. The mixture was stirred at ambient temperature for 6 h under argon. After evaporation of the solvent, the residual oil was chromatographed on silica gel to give the enone **9** (1.18 g). IR: 1775, 1700, 1675, and 1630 cm^{-1}; NMR ($CDCl_3$): 6.7 (1H, dt, J=16 and 8 Hz, olefin), 6.1 (1H, d, J=6 Hz, olefin), 5.0 (1H, dt, lactone), and 0.9 (2X 3H, s, CH_3). Found: C, 73.37; H, 9.44%. Calcd for $C_{17}H_{26}O_3$: C, 73.34; H, 9.41%.

*3,3-Dimethyl-*c*-5-hydroxy-*t*-2-[(3S*)-hydroxy-*trans*-1-octenyl)]-cyclopentane-*r*-1-acetic Acid γ-Lactone 10.* A solution of **9** (1.37 g) and $NaBH_4$ (0.205 g) in absolute methanol was stirred at 0 °C for 1 h under argon. The reaction mixture was quenched by addition of aqueous acetic acid. The resulting solution was extracted with ethyl acetate. The combined extracts were washed with brine, dried over Na_2SO_4, and evaporated to give a crude oil. The oil was separated into a less polar oil (0.655 g) and a more polar crystalline part (mp 53—54 °C) (0.562 g) by preparative thin layer chromatography. The former was assigned tentatively as the 15*S**-hydroxy lactone **10** and the latter as the 15*R**-hydroxy epimer. **10**: MS: *m/e* 280 (M^+); IR: 3450 and 1770 cm^{-1}; NMR ($CDCl_3$): 5.4—5.6 (2H, m, olefin), 5.0 (1H, m, lactone), 4.1 (1H, m, >CH–O), 1.0 and 0.8 (2× 3H, s, CH_3). Found: C, 72.88; H, 9.91%; Calcd for $C_{17}H_{28}O_3$: C, 72.82; H, 10.06%.

*3,3-Dimethyl-*c*-5-hydroxy-*t*-2-[(3S*)-(tetrahydropyranyloxy)-trans-1-octenyl]cyclopentane-*r*-1-acetaldehyde γ-Lactone 11.* A solution of **10** (0.641 g), dihydropyran (0.5 ml), and a catalytic amount of *p*-toluenesulfonic acid in dry dichloromethane was stirred at 0 °C for 20 min. After the addition of a few drops of pyridine, the reaction mixture was extracted with ether. The combined extracts were washed with brine, dried over Na_2SO_4, and evaporated to give an oil. This oil was chromatographed on aluminum oxide (Woelum grade III) to give a tetrahydropyranylated lactone (0.864 g). NMR ($CDCl_3$): 4.6 (1H, m, O–CH–O). To a stirred solution of the tetrahydropyranylated lactone in toluene at −70 °C under argon was added a solution of 25% diisobutylaluminium hydride (4 ml) in toluene. After 1.5 h the reaction was quenched by addition of methanol. The resulting mixture was allowed to warm to ambient temperature with stirring and water was added. The mixture was filtered through celite, and washed with ethyl acetate. The organic layer was separated and the aqueous layer was extracted with ethyl acetate. The combined extracts were washed with brine, dried over Na_2SO_4, and evaporated *in vacuo* to give a crude oil. The oil was chromatographed on silica gel to give **11** (0.612 g). MS: *m/e* 366 (M^+); IR: 3425 cm^{-1}; NMR ($CDCl_3$): 5.2—5.7 (3H, m), 1.0 and 0.8 (2× 3H, s, CH_3). Found: C, 71.78; H, 10.48%; Calcd for $C_{22}H_{38}O_4$: C, 72.09; H, 10.45%.

11,11-Dimethyl-15-(tetrahydropyranyloxy) prostaglandin E_2 12. To a solution of sodium 5-(triphenylphosphoranylidene) pentanoate prepared from (4-carboxybutyl)triphenylphosphonium bromide (3.82 g) and NaH (0.78 g) in DMSO under argon was added **11** (0.592 g) in DMSO. The mixture was allowed to stand at room temperature for 2 h. The reaction mixture was poured into ice–water, acidified with acetic acid, and extracted with ether. The combined extracts were washed with brine, dried over Na_2SO_4, and evaporated to give a crude oil. To a solution of the Collins reagent (2.32 g) in dichloromethane at 0 °C under argon was added a solution of the crude oil in dichloromethane. The resulting mixture was stirred at ambient temperature for 30 min and added to ether. The mixture was then filtered through celite. The filtrate was washed with 4% HCl and evaporated to give an oily residue. The residue was chromatographed on silica gel to give **12** (0.467 g). IR: 1740, 1710, and 1020 cm^{-1}; NMR ($CDCl_3$): 10.0 (1H, bs, COOH), 5.0—5.7 (4H, m, olefin), 1.2 and 0.9 (2× 3H, s, CH_3). Found: C, 71.99; H, 9.92%; Calcd for $C_{27}H_{44}O_5$: C, 72.28; H, 9.89%.

11,11-Dimethylprostaglandin E_2 1b. A solution of **12** (0.467 g) in acetic acid, water, and tetrahydrofuran (20: 10: 3) was heated at 40 °C for 6 h. The solvent was evaporated azeotropically with toluene *in vacuo*. The residue was added to water and extracted with ethyl acetate. The combined extracts were washed with brine, dried over Na_2SO_4, and evaporated to give an oily residue. The crude product was chromatographed on an acid-washed silica gel to give **1b** (0.267 g). MS: *m/e* 364 (M^+); IR: 3450 and 1740 cm^{-1}; NMR ($CDCl_3$): 6.9 (2H, bs, COOH and OH), 5.1—5.7 (4H, m, olefin), 4.1 (1H, m, $C_{15}H$), 1.1 and 0.9 (2× 3H, s, CH_3). Found: C, 72.62; H, 9.80%; Calcd for $C_{22}H_{36}O_4$: C, 72.49; H, 9.96%.

References

1) Synthetic studies on prostanoids XV. Part XIV: K. Inoue and K. Sakai, *Tetrahedron Lett.*, **1977**, 4063.

2) Ch. V. Grudzinskas and M. J. Weiss, *Tetrahedron Lett.*, **1973**, 141; A. Guzman and P. Crabbe, *Chem. Ind. (London)*, **1973**, 635; A. Guzman, M. Vera, and P. Crabbe, *Prostaglandins*, **8**, 85 (1974).

3) K. Inoue and K. Sakai, *Tetrahedron Lett.*, **1976**, 4107.

4) The reaction of the α-dienol and ylide in a 1: 1 molar ratio afforded the same olefinic products as **2** molar equivalents of the ylide was employed, although the yield was comparatively low.

5) K. Aghoramurthy and P. M. Lewis, *Tetrahedron Lett.*, **1969**, 1415.

6) The structure of **4d** was confirmed by an unambiguous

alternative synthesis,: J. Ide. K. Inoue, and K. Sakai, *Chem. Lett.*, **1978**, 747.

7) L. J. Dolby, C. A. Elliger, S. Esfandiari, and K. S. Marshall, *J. Org. Chem.*, **33**, 4508 (1968).

8) The syntheses of the compounds listed in the Table 1 were reported by our group: K. Sakai, S. Amemiya, O. Odal, and J. Ide, Abstr. No. 5B 2—3, 95th Annual Meeting of the Pharmaceutical Society of Japan, Nishinomiya, April 1975.

9) J. Ide and K. Sakai, *Tetrahedron Lett.*, **1976**, 1367.

10) J. P. Scheafer and J. J. Bloomfield, *Org. React.*, **15**, 1 (1967).

Catalytic Activities of Salicylaldehyde Derivatives. VIII. Kinetic Studies of the Catalytic Racemization of L-Glutamic Acid at 25 °C

Makoto Ando* and Sakae Emoto

The Institute of Physical and Chemical Research, Wako-shi, Saitama 351

(Received January 10, 1978)

The racemization of L-glutamic acid catalyzed by 15 kinds of salicylaldehyde derivatives has been kinetically studied at 25 °C and pH 10 in the presence of copper(II) ion. When 4- and 5-substituted salicylaldehydes were used as the catalyst, Hammett's plots for the racemization against σ^- were found to be linear with fewer points deviating from the line than the plots against σ. This fact has not been observed previously, since the salicylaldehyde derivatives tested having a substituent of different value between σ and σ^- were degraded during the course of reaction at 80 °C. Hammett's plots for the reaction catalyzed by 3-substituted salicylaldehydes indicated no linear relation with either σ or σ^-. These catalytic racemizations, including the case of the 6-substituted salicylaldehydes have been discussed.

In previous papers,[1-4] the racemization of L-glutamic acid catalyzed by various salicylaldehyde derivatives has been kinetically studied in the presence of copper(II) ion at pH 10 and 80 °C. Eighty degrees has been adopted as the temperature in order to observe the slow catalytic racemization throughout these studies. Hammett's plots for the racemization catalyzed by 4- and 5-substituted salicylaldehydes indicated a linear relation against Hammett's constant, σ.[2,3] It was difficult sometimes to determine the observed rate constants for the catalytic racemization of some salicylaldehyde derivatives such as the dimethylsulfonio derivatives, because of degradation of the catalysts at 80 °C.[4,5]

This paper deals with the determination of the observed rate constants, k_{obsd}, for the catalytic racemization at 25 °C and with the relation between $\log k_{obsd}$ and Hammett's constant. The following 15 salicylaldehyde derivatives were used as the catalysts: salicylaldehyde (SAL), 3-bromo- (3-BR), 5-bromo- (5-BR), 3-nitro- (3-NI), 4-nitro- (4-NI), 5-nitro- (5-NI), 6-nitro-salicylaldehyde (6-NI), 3-trimethylammonio- (3-TA), 4-trimethylammonio- (4-TA), 5-trimethylammonio- (5-TA), 6-trimethylammonio- (6-TA), 3-dimethylsulfonio- (3-DS), 4-dimethylsulfonio- (4-DS), 5-dimethylsulfonio- (5-DS), and the 6-dimethylsulfonio-derivative of salicylaldehyde (6-DS).

As described previously,[1-4] the catalytic racemization of L-glutamic acid has been carried out in the presence of copper(II) ion (L-glutamic acid: copper(II) ion: the catalyst = 1: 0.02: 0.02 in molar ratio) at pH 10 and 25 °C, under which conditions no side reaction such as transamination was observed. Since it is well documented that the catalytic racemization obeys a first-order kinetic law, the catalytic activity, $(\log \alpha_0 - \log \alpha_t)/t$, should be a constant, where t is the time and α_t is the observed optical rotation at t. The observed rate constant, k_{obsd}, has been calculated from the following equation:

$$k_{obsd} = \frac{2.30 \times (\log \alpha_0 - \log \alpha_t)}{t}.$$

Experimental

Preparation of the Catalysts. Commercially available SAL was purified by vacuum distillation. 3-BR,[2] 5-BR,[2] 3-NI,[2] 4-NI,[6] 5-NI,[2] 6-NI,[7] 3-TA,[3] 4-TA,[1] 5-TA,[3] 6-TA,[8] 3-DS,[5] 4-DS,[5] 5-DS,[5] and 6-DS[4] were prepared by methods described in the literature.

Procedure of the Racemization.[1] In a tightly stoppered test tube a mixture of a pH-adjusted solution (pH 10, 2 ml) of sodium L-glutamate (2 mmol) containing copper(II) sulfate (0.04 mmol) and a pH-adjusted 0.05 M borate buffer solution (pH 10, 2 ml) of the catalyst (0.04 mmol) was kept at 25 °C for the required time. After the reaction time as described in Table 1, 6 M hydrochloric acid (5 ml) was added to the mixture in order to stop the reaction. The optical rotation of the resulting solution was measured with a Perkin-Elmer model 141 polarimeter (direct reading, 0.001° with an error of ±0.002°; $\alpha_0 = +1.02°$).

Results and Discussion

As Table 1 shows, the mode of the catalytic activity may be classified into three categories according to the kind of the catalyst used; in the first case, the catalytic activity is nearly constant throughout the reaction (SAL, 3-BR, 5-BR, 3-NI, 5-NI, 3-TA, 4-TA, 5-TA, 3-DS, and 5-DS); in the second one, it is approximately constant only at the early stage of the reaction and then gradually falls (4-NI, 6-TA, 4-DS, and 6-DS); in the last case, it lacks constancy even at the early stage of the reaction (6-NI). The decrease in the catalytic activity has been accompanied by a simultaneous decrease in the absorption maximum of the reaction mixture at *ca.* 380 nm, which has been attributed to the chelation of the Schiff base of glutamic acid with the catalyst and copper(II) ion,[9] as previously reported.[3,10] From these constant values of the catalytic activities, the observed rate constants, k_{obsd}, have been calculated as shown in Table 2. For comparison, k_{obsd} for the reaction catalyzed by pyridoxal has also been calculated from the data in Ref. 10.

It has been found that the plots of $\log k_{obsd}$ against Hammett's constant, σ,[11] were on a straight line for the reaction catalyzed by SAL, 5-BR, 5-NI, 4-TA, 5-TA, and 5-DS except 4-NI and 4-DS. In the cases of 4-NI and 4-DS, $\log k_{obsd}$ were abnormally large against the corresponding σ.

As Fig. 1 shows, the plots of $\log k_{obsd}$ against Hammett's constant, σ^-,[12] indicate a linear relation for all of the 4- and 5-substituted salicylaldehydes

Table 1. Catalytic activity at 25 °C

Time h	Catalytic activity $(\log \alpha_0 - \log \alpha_t) \times 10^5/t$, (min^{-1})														
	SAL	3-BR	5-BR	3-NI	4-NI	5-NI	6-NI	3-TA	4-TA	5-TA	6-TA	3-DS	4-DS	5-DS	6-DS
2					26.7								22.9		20.9
4					29.5		11.4					10.5	23.9	14.3	21.2
6					29.6								23.3		22.0
8				8.06	26.6	9.10	10.5	4.64	10.2	10.7	6.74	11.6	23.5	14.1	21.1
16				8.13	16.6	9.11	8.6	4.72	10.4	11.0	6.80	11.1	22.5	14.2	19.6
24	1.57	3.71	3.92	8.25	11.3	8.73	7.4	4.44	10.1	10.8	6.67	11.4	21.6	14.0	18.5
32				8.14	8.6	8.47	6.8	4.54	10.3	10.8	5.98	11.1	21.3	13.1	16.9
40				8.05	7.4	8.37	6.2	4.59	10.2	10.8	6.28	10.9	21.0	13.7	16.3
48	1.68	3.70	3.79	7.93	6.4	8.50	5.9	4.52	10.2	10.8	6.06	11.0	19.9	13.5	16.1
72	1.59	3.61	3.62	7.73	4.5	8.44	5.0	4.69	10.1	10.8	5.61	11.2	18.8	13.9	14.8
96	1.59	3.59	3.89	7.81	3.8	8.13	4.3	4.67	10.1	10.6	5.22	10.9	17.5	13.5	14.5
120	1.62	3.63	3.76	7.57	3.3	8.10	3.9	4.66	10.0	10.7	5.08	10.7	17.3	13.2	13.6
168	1.67	3.47	3.61	7.77	2.8	8.10	3.2	4.57	9.8	10.3	4.84	10.7	15.6	13.3	11.8
240	1.58	3.45	3.68												
360	1.57	3.34	3.60												
480	1.57	3.33	3.64												

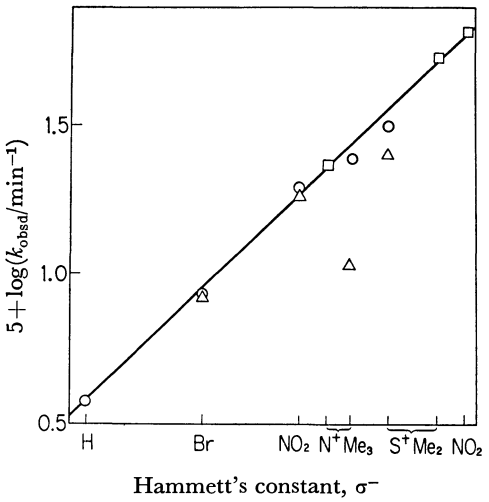

Fig. 1. Relation between the obsd rate const, k_{obsd}, and Hammett's const, σ^-.
△: 3-, □: 4-, ○: 5-substituted salicylaldehyde.

tested including 4-NI and 4-DS. The reaction constant, ρ, has been determined as 0.99. As it has been well documented, σ^- is determined by the ionization constants of substituted phenols or anilines, whereas σ is based on the ionization constants of substituted benzoic acids. Therefore the σ^--values of some substituents such as *p*-nitro and *p*-dimethylsulfonio groups, which can conjugate with hydroxyl or amino groups through quinonoidal-conjugate rings, are considerably larger than the corresponding σ-values. This means that Hammett's constants of *m*- and *p*-substituents such as trimethylammonio group having a negligible quinonoidal-conjugate effect are of no difference between σ and σ^-, since there are two cases, whether the σ^--value includes only an electron-withdrawing effect or a combination of electron-withdrawing and conjugate effects. Probably, this conjugate effect is expected to act between formyl group and nitro or dimethylsulfonio group in the para position on the benzene ring.

The Braunstein-Snell mechanism for non-enzymatic reactions of amino acids catalyzed by pyridoxal in the presence of a metal ion[13] has been generally accepted. When the mechanism is applied to the salicylaldehyde system, the presence of the intermediates, **1**, **2**, and **3** shown in Scheme have to be considered. The contribution of a substituent such as *p*-nitro or *p*-dimethylsulfonio group to the resonance of the quinonoidal form conjugated with a formyl group would stabilize **2**, resulting in an increase in the rate of racemization. Consequently, it is reasonable that in the cases of 4-NI and 4-DS, Hammett's plots against σ^- are linear although those against σ are not.

Table 2. Observed rate constant, k_{obsd}

	k_{obsd}, (min^{-1})		k_{obsd}, (min^{-1})
SAL	3.7×10^{-5}	5-TA	24.7×10^{-5}
3-BR	8.4	6-TA	14.8
5-BR	8.6	3-DS	25.3
3-NI	18.2	4-DS	53.8
4-NI	65.4	5-DS	31.5
5-NI	19.6	6-DS	49.0
3-TA	10.6		
4-TA	23.3	pyridoxal	64.8

As shown in Table 2, The observed rate constants for 5-substituted salicylaldehydes are larger than those for the corresponding 3-isomers in spite of having the same σ^--value. Possibly, the 3-substituents sterically hinder the formation of the chelate ring of the adjacent phenol group with copper(II) ion. Similar phenomena have also been observed at 80 °C.[2,3] The differences in k_{obsd} between 3-TA and 5-TA and 3-DS and 5-DS are considerably larger than those between other 3- and 5-substituted salicylaldehydes. Apparently 3-TA, 5-TA, 3-DS, and 5-DS have a bulky and positively charged substituent, therefore, in the racemization by 3-TA and 3-DS, the formation of the chelate ring is inhibited and this is assumed due to the effects of simple steric hindrance and additional strong ionic repulsion

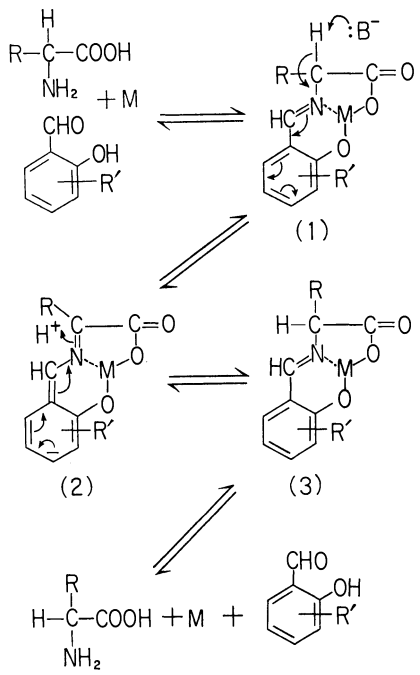

between the substituent and copper(II) ion.

Since steric effects of the 6-substituents on the adjacent formyl group would not be straightforward and Hammett's constants of the *o*-substituent have not been determined, the evaluation of Hammett's constant of an *o*-substituent based on the racemization catalyzed by 6-substituted salicylaldehyde has not been attempted. The larger catalytic activities of 6-NI and 6-DS compared to the corresponding 5-isomers are thought due to a similar case of *p*-substituents of 4-NI and 4-DS.

As Table 1 shows the orders of the catalytic activities at the early stage of the reaction are 4-NI>6-NI>5-NI>3-NI, 4-DS>6-DS>5-DS>3-DS, and 5-TA>4-TA>6-TA>3-TA. As described above, this order is reasonable qualitatively considering the electron-withdrawing effect, the resonance effect through the conjugate system, and the steric hindrance of a substituent including ionic repulsion. These results show that the steric effect of the 3-substituent on the phenol group seems to be larger than that of the corresponding 6-substituent on the formyl group and that the formation of the chelate ring of the hydroxyl group in the salicylaldehyde with copper(II) ion plays an important role in the catalytic racemization.

The work was supported partially by a Research Grant for Biosciences given by this Institute.

References

1) M. Ando and S. Emoto, *Bull. Chem. Soc. Jpn.*, **42**, 2624 (1969).
2) M. Ando and S. Emoto, *Bull. Chem. Soc. Jpn.*, **42**, 2628 (1969) and earlier references cited therein.
3) M. Ando and S. Emoto, *Bull. Chem. Soc. Jpn.*, **51**, 2433 (1978).
4) Part VII of this series: M. Ando and S. Emoto, *Bull. Chem. Soc. Jpn.*, **51**, 2437 (1978).
5) M. Ando and S. Emoto, *Bull. Chem. Soc. Jpn.*, **51**, 2435 (1978).
6) J. Segesser and M. Calvin, *J. Am. Chem. Soc.*, **64**, 852 (1942).
7) M. Ando and S. Emoto, *Bull. Chem. Soc. Jpn.*, **46**, 2903 (1973).
8) M. Ando and S. Emoto, *Bull. Chem. Soc. Jpn.*, **47**, 501 (1974).
9) A. Nakahara, *Bull. Chem. Soc. Jpn.*, **32**, 1195 (1959).
10) M. Ando and S. Emoto, *Bull. Chem. Soc. Jpn.*, **48**, 1655 (1975).
11) D. H. Mc Daniel and H. C. Brown, *J. Org. Chem.*, **23**, 420 (1958).
12) a) "Riron-yukikagaku (Hanno-hen)," ed by Y. Yukawa, Kagakudojin, Kyoto (1974), p. 63; b) S. Oae, "Yuki-iou No Kagaku," Kagakudojin, Vol. 2, Kyoto (1969), p. 226.
13) a) D. E. Metzler, M. Ikawa, and E. E. Snell, *J. Am. Chem. Soc.*, **76**, 648 (1954); b) A. E. Braunstein and M. M. Shemykin, *Biokhimiya*, **18**, 393 (1953).

Coordination of Alkanethiolate Anion to Ruthenium(II) Carbonyl Complex of Octaethylporphine: Model for Carbonyl Adduct of Cytochrome P-450

Hisanobu Ogoshi*, Hiroshi Sugimoto, and Zen-ichi Yoshida
Department of Synthetic Chemistry, Kyoto University, Kyoto 606
(Received January 12, 1978)

Absorption, infrared, and ^{1}H-NMR spectra of the ruthenium(II) octaethylporphine carbonyl complex [Ru(II)-OEP·CO] were studied in the presence of alkanethiolate anion ($^-$SR) as a model system for the reduced cytochrome P-450 carbonyl complex. The ^{1}H-NMR spectra reveal that alkanethiolate anions coordinte toa the central metal atom of Ru(II)OEP·CO as the sixth ligand. The hexaccordinated complex [Ru(II)OEP·CO·$^-$SR] has anomalous features as compared with the pentacoordinated complex [Ru(II)OEP·CO]: (1) the Soret band is splitted into two peaks, one in the near UV 363—365 nm region and the other in the 419—428 nm region, (2) the carbonyl stretching frequency is shifted by 25 cm^{-1} to lower wave number, (3) the proton signals of porphyrin ligand are shifted to higher magnetic field. Similarity of absorption and infrared spectra of the hexacoordinated complex to those of the reduced cytochrome P-450 carbonyl complex supports the axial ligation of the cysteinate to the central iron atom of the heme-proteins. The low wave number shifts of carbonyl stretching vibration and high field shifts of protons in the ^{1}H-NMR spectra suggest the charge transfer interaction from 3p lone pair electrons of sulfur atom of alkanethiolate anion to the central metal and/or the porphyrin ligand.

Cytochrome P-450 found in bacteria and lever microsomes are a kind of heme-enzymes which activate the molecular oxygen to catalyze the hydroxylation of the organic compounds in drug metabolism.[1,2] Recent investigations have been focused on elucidation of the structure of the active site of the heme enzymes. Simulation to the moiety of the prothetic protoheme in the enzyme by use of model compounds has provided a plausible explanation for the properties of axial ligand to the heme in P-450.[3-6] Spectroscopic studies showed similarity between the oxidized cytochrome P-450 and model compounds.[7-11] Addition of CO to the reduced cytochrome P-450 shows an anomalous red-shifted Soret band at *ca.* 450 nm.[12] This anomalous electronic spectrum has been successfully duplicated with synthetic heme in the presence of alkanethiolate anion and CO.[3,4,6] This gives strong evidence of axial coordination of the cysteinate to the heme-CO complex in P-450.

Divalent and trivalent ruthenium porphyrin complexes have been prepared by Whitten and his coworkers.[13] It is noted that the ruthenium(II) carbonyl porphyrin is isolable as a stable complex with or without the sixth ligand such as amine tetrahydrofuran and alcohol. These Ru(II)porphyrin·CO·L complexes are d^6-metal complexes of diamagnetic low spin state. Thus the electronic structure of the ruthenium(II) carbonyl complex is considered to be similar to that of the ferrous carbonyl porphyrin complex. The divalent metal ions of Ru(II)porphyrin·CO·(base) and Os(II)-porphyrin·CO·(base) are highly insensitive to oxygen as compared with the heme-CO adduct at ambient temperature.[13,14] The advantage of high stability of the ruthenium(II) complexes enables us to study the axial ligation of the alkanethiolate anion to the metal carbonyl porphyrin. Replacement of the iron atom of ferrous carbonyl porphyrin with ruthenium atom might afford an alternative model for the carbonyl adduct of the reduced cytochrome P-450. We wish to report spectroscopic evidence of the interaction between the alkanethiolate anion and the Ru(II) porphyrin·CO.

Experimental

Ruthenium(II) carbonyl octaethylporphine [Ru(II)OEP·CO] and ruthenium(II) carbonyl mesoporphyrin IX dimethyl ester were obtained by the reaction of octaethylporphine and mesoporphyrin IX dimethyl ester with $Ru_3(CO)_{12}$ in dry benzene, respectively.[13] The other chemicals and solvents were purified. Solutions of sodium alkanethiolates (RS$^-$Na$^+$, R=$-CH_2CH_2CO_2CH_3$, $-CH_2CH_3$, and $-C(CH_3)_3$) were prepared by the following procedure. Pulverized sodium hydride was washed with pentane several times and dried in a vacuum. Mercaptan (RSH, R=$-CH_2CH_2CO_2CH_3$, $-CH_2CH_3$, and $-C(CH_3)_3$) was added to NaH under argon atmosphere. After stirring for 15 min, the mixture was evacuated in order to remove excess mercaptan. To the deaerated solvents (benzene, ether, acetonitrile, *N,N*-dimethylformamide, dimethyl sulfoxide; 1 ml containing dibenzo-18-crown-6 (12 mg, 0.032 mmol) was added an equimolar amount of sodium alkanethiolate. The mixture was stirred until the sodium alkanethiolate dissolved completely. To the solution was added Ru(II)OEP·CO (20 mg, 0.032 mmol) and the solution was stirred for 1 h. The red solution turned to yellowish orange gradually. Disappearance of the Soret band due to Ru(II)-OEP·CO was monitored by measurement of the visible

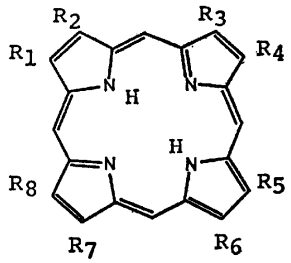

$R_1=R_2=R_3=R_4=R_5=R_6=R_7=R_8=CH_2CH_3$ octaethylporphine

$R_1=R_3=R_5=R_8=CH_3$, $R_2=R_4=$vinyl, $R_6=R_7=CH_2CH_2CO_2CH_3$ protoporphyrin IX dimethyl ester

$R_1=R_3=R_5=R_8=CH_3$, $R_2=R_4=CH_2CH_2$, $R_6=R_7=CH_2CH_2CO_2CH_3$ mesoporphyrin IX dimethyl ester

spectra. Spectral measurements were carried out under argon atmosphere. Infrared spectra were measured on a Hitachi Model G-3 spectrophotometer in NaCl liquid cells with 0.1 mm optical path. Absorption spectra were measured with a Hitachi EPS-3T spectrophotometer in 0.1 mm quartz cells. Proton NMR were obtained with JEOL FX-60 and Varian HA-100 D spectrometers in CD_3CN and referred to tetramethylsilane (TMS) or hexamethyldisiloxane (HMDS).

Results and Discussion

Absorption Spectra. The visible spectra of Ru(II)-OEP·CO in various solvents are summarized in Table 1. The ruthenium complex shows characteristic absorptions of the divalent metalloporphyrin at *ca.* 550 and 520 nm (the α-, β-bands) assigned to the first $\pi\rightarrow\pi^*$ transitions splitted by vibronic interaction and the Soret band at 395 nm due to the second $\pi\rightarrow\pi^*$ transitions.[15] The transition energy for the absorption shows small dependency on polarity of solvent molecule. Slight red shifts of these absorptions were observed in DMF. Nucleophilicities of alkanethiolate anion can be enhanced by the incorporation of alkaline metal ion to crown ether. Addition of an equimolar amount of alkanethiolate anion thus generated (*e.g.* RS^-, R=$-CH_2CH_2CO_2CH_3$, $-CH_2CH_3$, and $-C(CH_3)_3$) to Ru(II)OEP·CO caused the splitting of the Soret band into two bands at 363—366 and 419—428 nm. The absorption strength of both α- and β-bands decreased considerably, a new band appearing at 540 nm. On the other hand, addition of an equimolar amount of mercaptan (*e.g.* RSH, R=$-CH_2CH_2CO_2CH_3$, $-CH_2CH_3$, and $-C(CH_3)_3$) gave no marked change in the transition energies and the absorption strength.

Table 1. Absorption maxima of Ru(II)OEP·CO·L

Solvent	L	Soret	β	α (nm)
Benzene	none	396	517	549
CH_3CN	none	393	518	549
DMF	none	407	529	560
DMSO	none	396	520	551
Benzene	^-SR[a]	363, 419	535	
CH_3CN	^-SR	364, 423	538	
DMF	^-SR	365, 428	540	
DMSO	^-SR	366, 428	540	
	Absorption maxima of Fe(II)OEP·CO·L			
Benzene	^-SR[b]	357, 436	540	
DMF	^-SR	370, 447	540	

a) R=$-CH_2CH_2CO_2CH_3$, alkanethiolate anion was solubilized by dibenzo-18-crown-6. [Ru(II)OEP·CO]=0.032 mM, [^-SR]=0.032 mM. b) [Fe(II)-OEP·CO]=0.032 mM, [^-SR]=0.32 mM. The 408 nm peak assignable to the pentacoordinated complex [Fe(II)OEP·CO] did not completely disappear even in the presence of the 100 eq. amount of alkanethiolate anion.

The hexacoordinated complex of ferrous carbonyl porphyrin[Fe(II)OEP·CO·(^-SR)] was obtained by treatment of the ferric porphyrin OEP·Fe(III)Cl with a large excess of alkanethiolate anion in the presence of carbon monoxide.[5,6] Coordination of alkanethiolate anion to Fe(II)OEP·CO in benzene solution caused the appearance of new bands at 357 and 436 nm. However, the absorption at 408 nm due to the pentacoordinated complex [Fe(II)OEP·CO] was observed even in the presence of ten times molar amounts of alkanethiolate anion.[5,6,16] Spectral change due to ligation of alkanethiolate anion was quite similar to that of the ferrous carbonyl complex of protoporphyrin IX dimethyl ester.[5,6] Two vinyl groups at the peripheral positions of protoheme may cause bathochromic shifts of those absorption maxima as compared with the complex of octaethylporphine. Complete formation of the hexacoordinated complex [Fe(II)OEP·CO·(^-SR)] requires large excess amounts (10^5—10^6 eq.) of the alkanethiolate anion.[5,6,16] Splitting of the Soret band of these hexacoordinated complexes depends a great deal on polarity of solvent molecule. In more polar solvent such as DMF the absorptions shift to longer wave length.

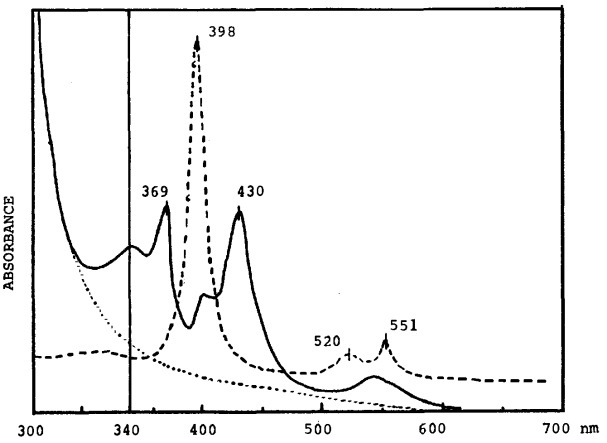

Fig. 1. Absorption spectra of Ru(II) carbonyl mesoporphyrin IX dimethyl ester, (——) with an equimolar amount of $HSCH_2CH_2CO_2CH_3$ in DMF; (——) with equimolar amount of $^-SCH_2CH_2CO_2CH_3$ solubilized by dibenzo-18-crown-6 in DMF; (····) base line.

Similar anomalous absorption spectra can be duplicated by using the ruthenium(II) carbonyl complex of mesoporphyrin IX dimethyl ester with an equimolar amount of the alkanethiolate anion as shown in Fig. 1. Axial ligation of alkanethiolate anion to ruthenium(II) carbonyl porphyrin causes clear splitting of the Soret band to two peaks as has been found for ferrous carbonyl porphyrin. Recently, Hanson and his co-workers have reported that[17] splitting of the Soret band into two bands of the reduced cytochrome P-450 carbonyl adduct and its model compounds can be attributed to the charge transfer transition from the 3p lone pair electrons of the sulfur atom to the lowest vacant π^* orbitals of the porphyrin ring and that the transition may cause strong interaction with the $\pi\rightarrow\pi^*$ (a_{1u}, $a_{2u}\rightarrow e_g^*$) transitions. Recent MCD studies of the cytochrome P-450 and its model compounds seem to support their theoretical interpretation.[11]

Infrared Spectra. The carbonyl stretching vibrations[14] of Ru(II)OEP·CO were observed in various solvents (Table 2). Figure 2 shows the infrared spectra

Table 2. Carbonyl stretching vibrations of Ru(II)OEP·CO·L

Solvent	L	ν_{CO} (cm^{-1})
Ether	PPh_3	1966
Ether	none	1942
THF	none	1938
Pyridine	none	1931
Benzene	none	1946
Benzene	$-SR$[a]	1917
DMF	none	1917
DMF	$-SR$	1889
	Carbonyl stretching vibrations of Fe(II)OEP·CO·L	
Benzene	none	1975
Benzene	$-SR$[b]	1950
DMF	none	1948
DMF	$-SR$	1923

a) R=$-CH_2CH_2CO_2CH_3$, alkanethiolate anion was solubilized by dibenzo-18-crown-6. [Ru(II)OEP·CO]=0.032 mM, [$^-$SR]=0.032 mM. b) [Fe(II)-OEP·CO]=0.032 mM, [$^-$SR]=0.32 mM.

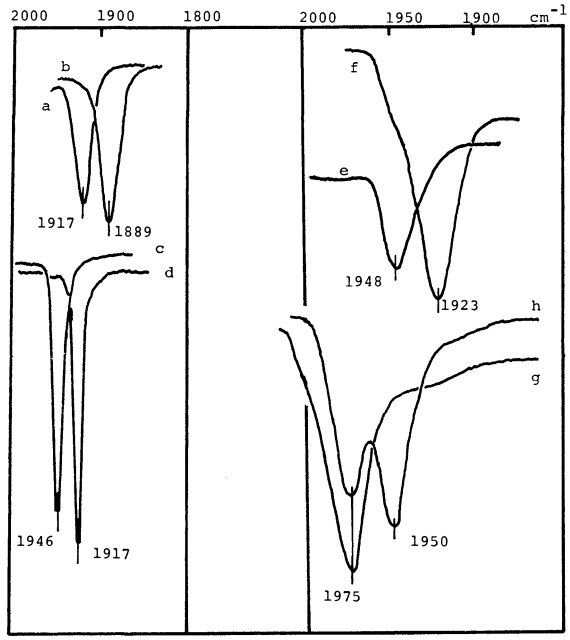

Fig. 2. Infrared spectra of M(II)OEP·CO·L in the carbonyl stretcfling region of; (a) M=Ru, L=none in DMF, (b) M=Ru, L=$^-$SR in DMF, (c) M=Ru, L=none in benzene, (d) M=Ru, L=$^-$SR in benzene, (e) M=Fe, L=none in DMF, (f) M=Fe, L=$^-$SR in DMF, (g) M=Fe, L=none in benzene, (h) M=Fe, L=$^-$SR in benzene. R=$-CH_2CH_2CO_2CH_3$. The conditions of measurements are described in Table 2.

of these complexes in the region of carbonyl stretching. Addition of alkanethiolate anion reduced the wave number of the carbonyl stretching by 28—29 cm^{-1} for the ruthenium complex and 25 cm^{-1} for a ferrous complex.[16] In the case of Fe(II)OEP·CO with excess amounts of alkanethiolate anion in benzene, two carbonyl stretching vibrations were observed at 1975 and 1950 cm^{-1}. This provides further evidence of the coexistence of the pentacoordinated complex (**2**) (1975 cm^{-1}) and the hexacoordinated complex (**4**) (1950 cm^{-1}) for the iron complex as has been found for the absorption spectra. These trends can be explained in terms of

$$\text{M(II)OEP·CO} + {}^-\text{SR} \rightleftarrows \text{M(II)OEP·CO·}({}^-\text{SR})$$

M=Ru (**1**) M=Ru (**3**)

M=Fe (**2**) M=Fe (**4**)

π-back donation from dπ-orbitals of metal to the *anti*-bonding π^*-orbitals of the carbonyl. Divalent ruthenium in the pentacoordinated complex (**1**) is considered to be a stronger π-base than ferrous ion in the pentacoordinated complex (**2**) on the basis of the shift of the carbonyl stretching vibration. Enhanced back donation from the dπ-orbitals of ruthenium to the anti-bonding π^*-orbitals of the carbonyl decreases electron density on the ruthenium atom. On the other hand, addition of a strong π-acceptor ligand such as PPh_3 shows appreciable increase of the carbonyl stretching frequency. A similar trend has been found for the osmium(II) carbonyl porphyrin complexes by Buchler and Rohback.[14] These results suggest that ligation of alkanethiolate anion to central metal facilitates charge transfer to the central metal from sulfur atom.[11d] Furthermore, it is noted that carbonyl stretching frequencies are very sensitive to polarity of solvent molecule. Increasing of polarity of solvent from benzene to DMF reduces the frequencies of the carbonyl stretching by 28—29 cm^{-1} for the ruthenium complex and 17 cm^{-1} for the ferrous complex. The carbonyl stretching frequency (1923 cm^{-1}) of the hexacoordinated complex (**4**) in DMF is the same as that (1923 cm^{-1}) of Fe(II) protoporphyrin IX dimethyl ester in *N*,*N*-dimethylacetamide in the presence of both carbon monoxide and 1-butanethiolate.[6] Polar solvent molecules may stabilize the polarization along the axial direction due to the charge transfer from alkanethiolate

Table 3. Proton chemical shifts (60 MHz, ppm from TMS) of Ru(II)OEP·CO·L

	Assignment			
L	meso	α-CH_2–	β-CH_3	Alkanethiolate
none[a]	0.06 (s, 4H)	6.16 (q, 16H)	8.03 (t, 24H)	
$-SCH_2CH_3$[b]	0.35 (s, 4H)	6.03 (q, 16H)	8.05 (t, 24H)	11.59 (t, 3H, $-CH_2\underline{CH_3}$)
				13.00 (q, 2H, $-\underline{CH_2}CH_3$)
$-SC(CH_3)_3$	0.36 (s, 4H)	6.04 (q, 16H)	8.03 (t, 24H)	11.99 (s, 9H, $-C(\underline{CH_3})_3$

a) Measured in $CDCl_3$ at 31.5 °C. b) Measured in CD_3CN at 31.5 °C, [Ru(II)OEP·CO]=0.032 mM, [$^-$SR]=0.032 mM.

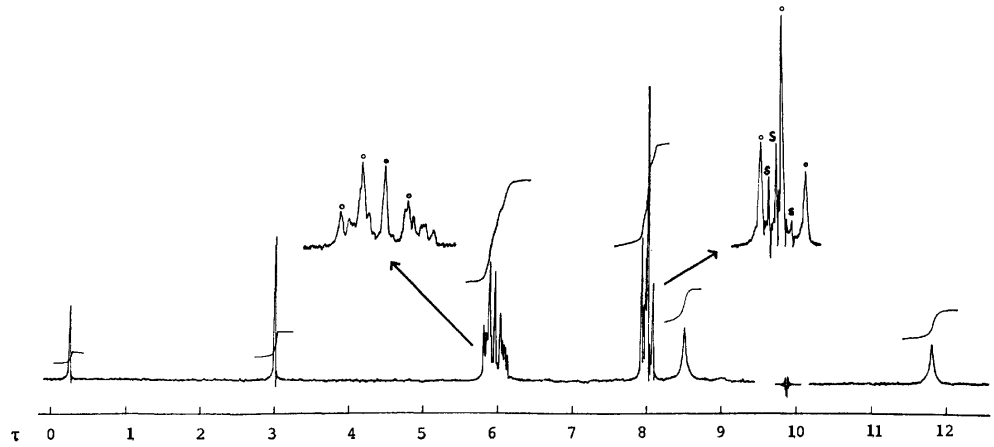

Fig. 3. 100 MHz NMR spectrum of Ru(II)OEP·CO with twice molar amounts of $^{-}SC(CH_3)_3$ solubilized by dibenzo-18-crown-6 in CD_3CN at 31.5 °C. Symbols (o) and (s) denote signals due to ethyl protons of porphyrin ligand and solvent, respectively. Singlet at τ 3 and multiplet at τ 6 are assigned to protons of crown ether. The chemical shifts are calculated from the outernal rock signal of hexamethyldisiloxane (HMDS) to τ values.

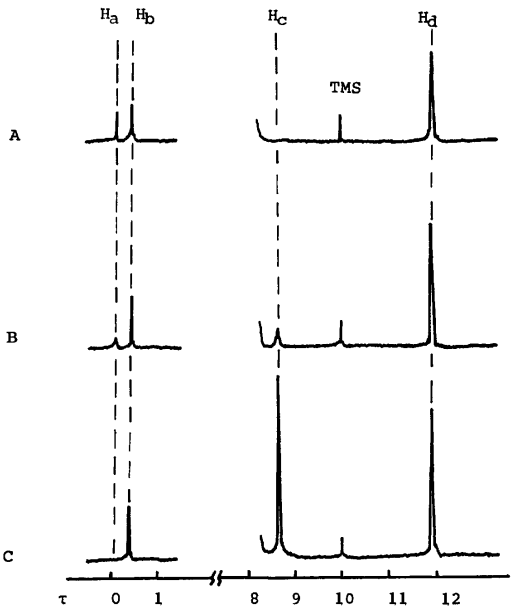

Fig. 4. 60 MHz NMR spectra of Ru(II)OEP·CO at various concentrations of alkanethiolate anion in CD_3CN in the low and high magnetic field regions. [Ru(II)OEP·CO]=0.032 mM, A [$^{-}$SR]=0.016 mM, B [$^{-}$SR]=0.032 mM, and C [$^{-}$SR]=0.045 mM. R=$-C(CH_3)_3$. H_a, H_b, H_c, and H_d are assignable to meso protons of Ru(II)OEP·CO, meso protons of Ru(II)OEP·CO·($^{-}$SR), *tert*-butyl protons of the free alkanethiolate anion, and *tert*-butyl protons of the coordinated alkanethiolate anion, respectively.

anion to the carbonyl group.

^{1}H-NMR Spectra. ^{1}H-NMR spectroscopic study on diamagnetic ruthenium(II) carbonyl porphyrin enables us to obtain insight into the interaction between the divalent metalloporphyrin and the alkanethiolate anion. The ^{1}H-NMR spectra of Ru(II)OEP·CO and the complexes with an equimolar amount of alkanethiolate anions are given in Table 3. In the presence of alkanethiolate anion the signals of the meso protons appear at higher magnetic field than those of Ru(II)-OEP·CO. The up-field shifts might be explained in terms of the increased electron density at the ruthenium atom because of the charge transfer of the negatively charged alkanethiolate anion to the central metal.[11,17] Axial ligation of alkanethiolate anion was rationalized by marked up-field shifts of alkyl protons of alkanethiolate anion due to the diamagnetic ring current of porphyrin ring. For ethanethiolate anion, the signals of the α-methylene and β-methyl group were found at τ 13.00 (quartet 2H) and 11.59 (triplet 3H), respectively. Figure 3 shows 100 MHz ^{1}H-NMR spectrum of Ru(II)OEP·CO with twice molar amounts of 2-methyl-2-propanethiolate anion ($^{-}SC(CH_3)_3$) in CD_3CN. Two signals at τ 8.68 and 11.94 are assignable to the methyl protons of the free $^{-}SC(CH_3)_3$ and those of the coordinated $^{-}SC(CH_3)_3$ to Ru(II)OEP·CO, respectively. Strong affinity of ruthenium atom for alkanethiolate anion was confirmed by ^{1}H-NMR spectra. Figure 4 shows 60 MHz ^{1}H-NMR spectra of Ru(II)OEP·CO with various concentrations of alkanethiolate anion. When a half molar amount of the alkanethiolate anion was added, no signal (H_c) of the free $^{-}S(CH_3)_3$ could be observed. Two meso proton signals appear at τ 0.06 (H_a) and 0.30 (H_b) (Fig. 4A). The former signal appearing at lower magnetic field is due to the meso protons of the Ru(II)OEP·CO. The assignment was confirmed by the measurement in the absence of alkanethiolate anion. The NMR spectrum of the Ru(II)OEP·CO (**1**) with an equimolar amount of the alkanethiolate anion indicates predominant existence of the hexacoordinated complex [Ru(II)OEP·CO·($^{-}$SR)] (**3**) (Fig. 4B). Thus, the affinity of Ru(II)OEP·CO (**1**) to the alkanethiolate anion is much higher than that of the ferrous carbonyl complex (**2**). Figure 5 shows the 100 MHz ^{1}H-NMR spectra of Ru(II)carbonyl mesoporphyrin IX dimethyl ester and its alkanethiolate complex.

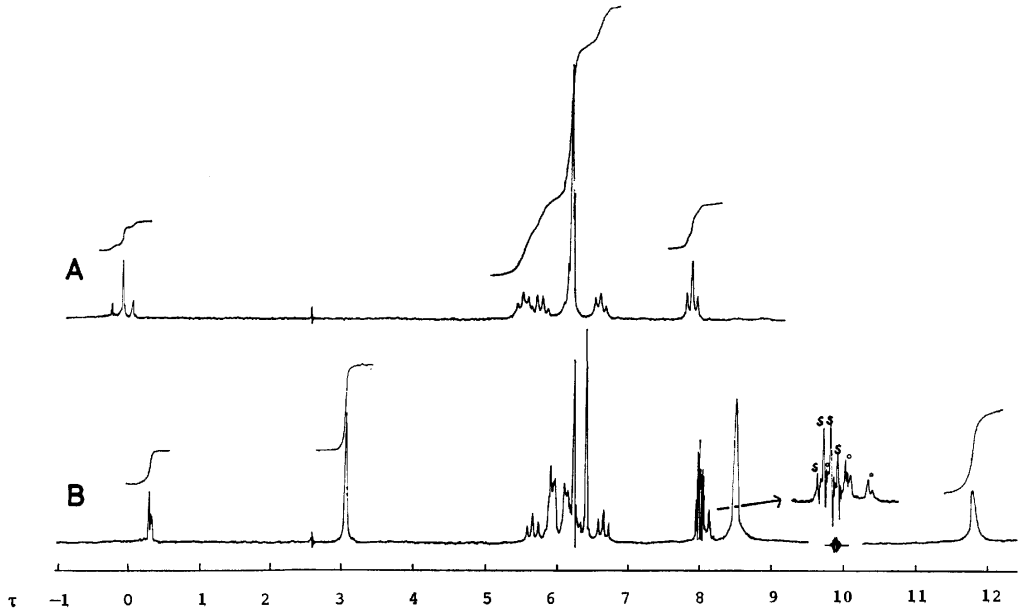

Fig. 5. 100 MHz NMR spectra of CD_3CN solution of (A) Ru(II) carbonyl mesoporphyrin IX dimethyl ester, and (B) Ru(II) carbonyl mesoporphyrin IX dimethyl ester with three equivalents of $^-SC(CH_3)_3$ solubilized by dibenzo-18-crown-6. Symbol (o) denotes the methyl protons of ethyl groups of porphyrin ligand. Singlet at τ 3 and multiplet at τ 6 are assigned to crown ether. The chemical shifts are calculated from the outernal rock signal of hexamethyldisiloxane (HMDS) to τ values.

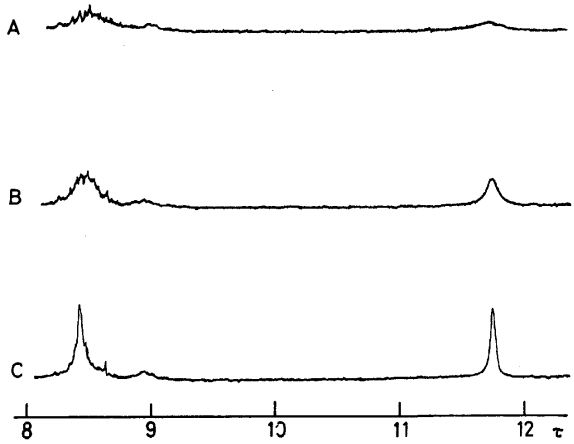

Fig. 6. The high field part of 100 MHz NMR spectra for Ru(II)OEP·CO with twice molar amounts of $^-SC(CH_3)_3$ solubilized by dibenzo-18-crown-6 in CD_3CN; (A) at 80 °C, (B) at 50 °C, and (C) at 32 °C.

Similar up-field shifts were observed for the meso protons, the methyl protons of 1, 3, 5, and 8-positions and the α-methylene protons of 6 and 7-positions of the complex. As shown in Figs. 3 and 5, the broad signals due to the free and coordinated alkanethiolate anion suggest existence of exchange between them. Figure 6 shows the signals of $^-SC(CH_3)_3$ at elevated temperature. The methyl proton resonance is broadened with rise in temperature owing to rapid exchange of ligand. The coalescence temperature could not be determined.

^{1}H-NMR studies of the hexacoordinated complex [Ru(II)OEP·CO·($^-$SR)] show unequivocally that the ligation of the alkanethiolate anion to the ruthenium increases electron density at the central metal. The effect is in line with the observation of anomalous splitting of the Soret band and reduction in the carbonyl stretching vibrations.[11d]

On the other hand, addition of the alkanolate anion to Ru(II)OEP·CO shows no significant changes in absorption and infrared spectra as has been reported for ferrous complexes.[6] The trend was also confirmed by ^{1}H-NMR measurement. Figure 7 shows the 60 MHz ^{1}H-NMR spectrum of Ru(II)OEP·CO in the presence of three equimolar amounts of 2-methyl-2-propanolate anion. Signals of *t*-butyl protons of the free alcoholate anion were observed at τ 8.70.

Strong ligation of alkanethiolate anion might be ascribed to more polarizable 3p lone pair electrons of sulfur atom of alkanethiolate anion than 2p lone pair electrons of oxygen of alkanolate anion. Energy levels of lone pair electrons of the alkanethiolate anion seem to be closer to the anti-bonding orbitals $\pi^*(e_g^*)$ of the porphyrin ring than those of the alkanolate anion.[17] Consequently the lone pair electrons of alkanethiolate anion may be allowed to interact strongly with $\pi^*(e_g^*)$ orbitals of porphyrin ring. In conclusion, NMR, infrared, and absorption studies on the present model systems provide strong evidence to support the axial ligation of the alkanethiolate (cysteinate) to the central iron metal of the heme in the cytochrome P-450, which causes considerable charge transfer from cysteinate to iron and/or porphyrin ring.

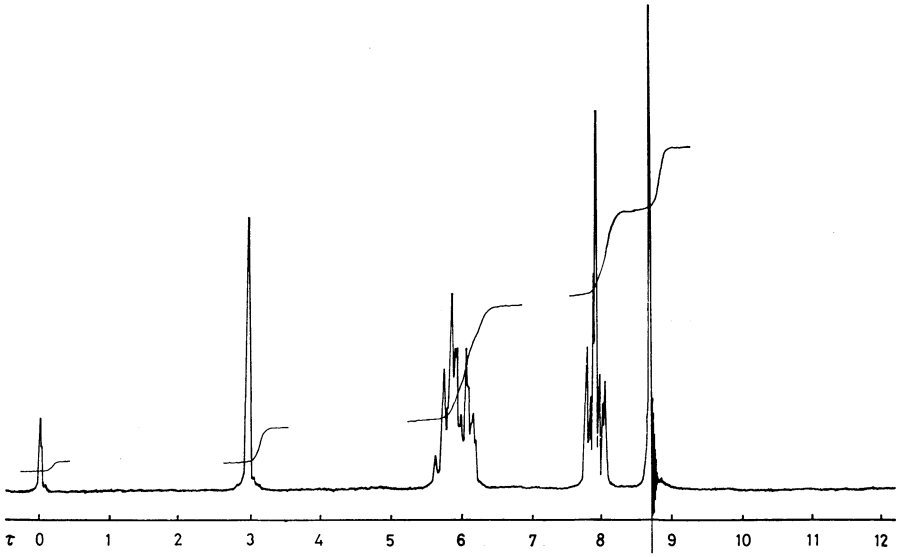

Fig. 7. 60 MHz NMR spectrum of Ru(II)OEP·CO with three amounts of $^{-}OC(CH_3)_3$ solubilized by dibenzo-18-crown-6 in CD_3CN. Singlet at τ 3 and multiplet at τ 6 are assigned to crown ether.

References

1) D. Y. Cooper, O. Rosenthal, R. Snyder, and C. Witmer, "Cytochrome P-450 and b_5," Plenum Press, New York (1975), pp. 1—339.

2) I. C. Gunsalus, J. R. Meek, J. D. Lipscomb, P. Debrunner, and E. Munk, "Molecular Mechanisms of Oxygen Activation," ed by O. Hayaishi, Academic Press, New York (1974), pp. 559—613.

3) J. O. Stern and J. Peisach, *J. Biol. Chem.*, **249**, 7495 (1974).

4) J. P. Callman and T. N. Sorell, *J. Am. Chem. Soc.*, **97**, 4133 (1975).

5) C. K. Chang and D. Dolphin, *J. Am. Chem. Soc.*, **98**, 1607 (1976).

6) C. K. Chang and D. Dolphin, *Proc. Natl. Acad. Sci. U.S.A.*, **73**, 3338 (1976).

7) R. Tsai, C. A. Yu, I. C. Gunsalus, J. Peisach, W. Blumberg, W. H. Orme-Johnson, and H. Beinert, *Proc. Natl. Acad. Sci. U.S.A.*, **66**, 1157 (1970).

8) J. P. Callman, T. N. Sorell, and B. M. Hoffman, *J. Am. Chem. Soc.*, **97**, 913 (1975).

9) S. Koch, S. C. Tang, R. H. Holm, R. B. Frankel, and J. A. Ibers, *J. Am. Chem. Soc.*, **97**, 916 (1975).

10) H. Ogoshi, H. Sugimoto, and Z. Yoshida, *Tetrahedron Lett.*, **1975**, 2285.

11) (a) J. H. Dawson, J. R. Trudell, G. Barth, R. E. Linder, E. Bunnenberg, C. Djerassi, M. Gouterman, C. R. Connell, and P. Sayer, *J. Am. Chem. Soc.*, **99**, 641 (1977); (b) J. H. Dawson, R. H. Holm, J. R. Trudell, G. Barth, R. E. Linder, E. Bunnenberg, C. Djerassi, and S. C. Tang, *J. Am. Chem. Soc.*, **98**, 3708 (1976); (c) J. H. Dawson, T. R. Trudell, G. Barth, R. E. Linder, E. Blunnenberg, C. Djerassi, R. Chiang, and L. P. Hager, *J. Am. Chem. Soc.*, **98**, 3709 (1976); (d) J. P. Collman, T. N. Sorell, J. H. Dawson, J. R. Trudell, E. Bunnenberg, and C. Djerassi, *Proc. Natl. Acad. Sci. U.S.A.*, **73**, 6 (1976).

12) T. Omura and R. Sato, *J. Biol. Chem.*, **239**, 2370, 2379 (1964).

13) (a) E. B. Fleisher, *Chem. Commun.*, **1965**, 475; B. C. Chow and I. A. Cohen, *Bioinorg.*, **1**, 57 (1971); (b) M. Tsutui, D. Ostfeld, and L. M. Hoffman, *J. Coord. Chem.*, **1**, 115 (1971); (c) G. W. Sovocool, F. R. Hopf, and D. G. Whitten, *J. Am. Chem. Soc.*, **94**, 4350 (1972).

14) J. W. Buchler and K. Rohback, *J. Organomet. Chem.*, **65**, 223 (1974).

15) J. E. Falk, "Porphyrins and Metalloporphyrins," Elsevier, Amsterdam (1964), p. 72.

16) J. P. Callman and T. N. Sorell, *J. Am. Chem. Soc.*, **97**, 4133 (1975).

17) L. K. Hanson, W. A. Eaton, S. G. Sliger, I. C. Gunsalus, M. Gouterman, and C. R. Connell, *J. Am. Chem. Soc.*, **98**, 2672 (1976).

Incorporation of CO_2 in Butadiene Dimerization Catalyzed by Palladium Complexes. Formation of 2-Ethylidene-5-hepten-4-olide

Yoshio INOUE,* Yoshiyuki SASAKI, and Harukichi HASHIMOTO
Department of Applied Chemistry, Faculty of Engineering, Tohoku University, Sendai 980
(Received January 30, 1978)

Reaction of carbon dioxide with butadiene catalyzed by palladium–phosphine complexes was studied. When the reaction was carried out in certain polar, aprotic solvents, such as dimethylformamide (DMF), 2-ethylidene-5-hepten-4-olide was formed in about 5% yield by the incorporation of CO_2 together with the formation of butadiene linear dimers. The main dimer was 1,3,7-octatriene. The ditertiary phosphines, $R_2PCH_2CH_2PR_2$ where R is methyl or phenyl, were found to be suitable as the ligand for the olide synthesis. A possible mechanism involving the intermediate of π-allyl, σ-allyl form from two moles of butadiene and the palladium complex is proposed.

There has been much attention in recent years to the fixation of CO_2, but catalytic reaction is rare. In a preliminary communication[1] we have reported that CO_2 can react with butadiene in the presence of plladium–phosphine complexes to give a small amount of 2-ethylidene-5-hepten-4-olide together with butadiene oligomers in certain polar, aprotic solvents such as DMF. This is the first example of the catalytic formation of a new C–C bond between CO_2 and an organic compound.

The dimerization of butadiene catalyzed by transition metal complexes is well known and it has been shown recently that not only the catalytic activity of metal complexes but also the catalytic properties can be altered when the dimerization reaction is carried out under CO_2 pressure.[2-5] For example, $Pt(PPh_3)_3$ converts butadiene to 4-vinylcyclohexene in 90—97% yield under nitrogen or argon atmosphere, however with CO_2 present, the product is mainly 1,3,7-octatriene with higher conversion of butadiene.[2] Though the role of CO_2 in these reactions is not clear yet, a direct effect on the catalyst has been suggested.

In this paper we wish to report the studies of the factors which affect the incorporation of CO_2 in butadiene dimer catalyzed by palladium–phosphine complexes.

Results and Discussion

The catalytic activity of the following transition metal complexes on butadiene–CO_2 reaction was examined at 120 °C in DMF; $Pd(dpe)_2$, $Pt(dpe)_2$, $Ni(dpe)_2$, $HCo(dpe)_2$, $H_2Fe(dpe)_2$, $Pt(PPh_3)_4$, $RhCl(PPh_3)_3$, $H_2Ru(PPh_3)_4$, and $H_3Ir(PPh_3)_3$, where dpe stands for 1,2-bis(diphenylphosphino)ethane $[Ph_2PCH_2CH_2PPh_2]$. Among these complexes, only the $Pd(dpe)_2$ system afforded a CO_2-incorporated product, *i.e.*, 2-ethylidene-5-hepten-4-olide. Henceforth the catalytic activity of the palladium complex was examined in detail.

When butadiene was reacted with CO_2 in the presence of $Pd(dpe)_2$, butadiene linear dimers (**1**), (**2**), and (**3**) were obtained as the main products together with a small amount of the lactone (**4**).

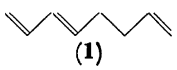
(1)

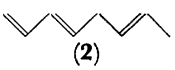
(2)

TABLE 1. EFFECT OF SOLVENT
Solvent 10 ml, $Pd(dpe)_2$ 0.2 mmol, butadiene 7.3 g, CO_2 50 atm; 120 °C, 20 h.

Solvent	Product yield (%)				
	1	**2**	**3**	**4**	Others[b]
None	2.4	3.6	58.0	trace	18.5
DMF	26.8	21.9	13.9	4.0	15.1
DMSO	55.7	12.3	4.5	4.2	9.3
t-Butylalcohol	44.3	17.9	6.6	0.5	15.0
Triethylamine	74.8	8.2	trace	0.5	7.7
Tetramethylurea	35.5	22.5	12.0	1.6	11.9
1-Methyl-2-pyrrolidone	41.1	16.4	5.0	5.4	ND[a]
Benzonitrile	51.0	17.6	5.7	1.9	ND
HMPA	2.9	trace	0	0	ND
Dichloromethane	0.8	trace	0	0	1.3
Anisole	24.6	3.6	0	0.5	2.2
Toluene	ND	ND	trace	1.8	8.5
Benzene	35.7	21.8	17.7	0.4	18.1
Chlorobenzene	33.5	7.0	0	0.2	1.9
Nitrobenzene	60.9	2.2	0	0	ND

a) Not determined. b) "Others" mainly consists of butadiene trimers.

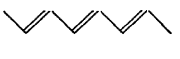
(3)

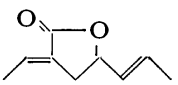
(4)

It was found that the distribution of the products depends on the solvent used. The effects of the solvents are summarized in Table 1. In the solvent-free system, 2,4,6-octatriene was the main product whereas 1,3,7-octatriene was the main one in certain solvents. The isomerization of 1,3,7-octatriene to 2,4,6-isomer has been reported to be affected by several palladium(0) phosphine complexes under CO_2 atmosphere.[4] Table 1 shows that polar, aprotic solvents such as DMF, dimethyl sulfoxide (DMSO), and 1-methyl-2-pyrrolidone are suitable for the lactone formation. But in case of hexamethylphosphoric triamide (HMPA), which is a typical polar, aprotic solvent, the decomposition of the catalyst was observed. The yield of the lactone (**4**) was rather small in benzene.

The yield of the lactone (**4**) increased with the increase in the amount of solvent DMF as shown in

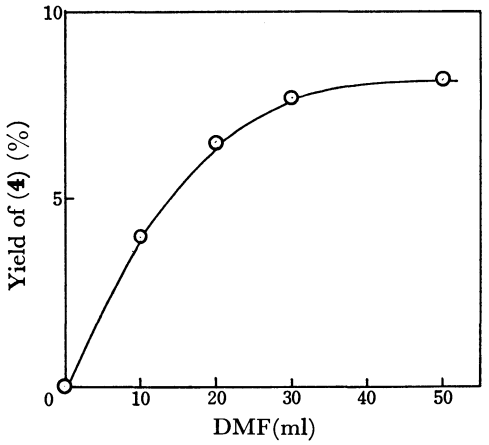

Fig. 1. Effect of the amount of DMF. $Pd(dpe)_2$ 0.2 mmol, butadiene 7.3 g, CO_2 50 atm; 120 °C, 20 h.

Fig. 1. This may be ascribed to the increase in the relative concentration of CO_2 to butadiene, because CO_2 concentration in the solvent is almost constant whereas that of butadiene is lowered with the increase in the amount of the solvent.

When the reaction was carried out at temperature below 100 °C and terminated before the complete conversion of butadiene, then the organic acids, (**5**) and (**6**), were isolated in up to 10% together with the lactone (**4**). Both acids were easily converted into the lactone (**4**) under the conditions given in Table 1, indicating that these acids were the precursors of the lactone (**4**). The CO_2-incorporated products were obtained in the highest yield from the catalyst system involving $Pd(dpe)_2$ in DMF at 84 °C as shown in Fig. 2.

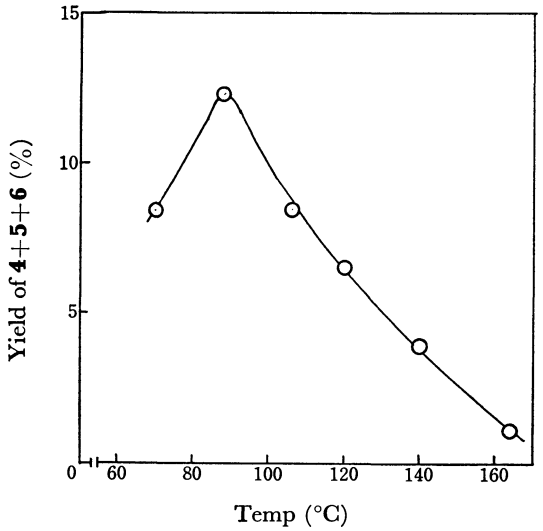

Fig. 2. Effect of temperature on the yield of **4**+**5**+**6** $Pd(dpe)_2$ 0.2 mmol, butadiene 7.3 g, DMF 20 ml, CO_2 50 atm; 20 h.

A study has been made of the effect of ligands on the yield of the lactone (**4**) using a catalyst system derived from $Pd(dba)_2$ (dba=dibenzylideneacetone) and a ligand. Results of the effects of unidentate and bidentate ligands are summarized in Table 2. Linear dimerization was also the main reaction in this catalyst system, and in some cases the activity for the dimerization was lost on addition of certain ligands, *e.g.*, arsines. The yield of the lactone (**4**) was very poor in the monodentate ligand systems in general, though basic ligand systems, *e.g.*, tributylphosphine system, brought about slightly higher yields than less basic ligand ones, *e.g.*, triphenylphosphine system. Among the bidentate ligands, $Ph_2PCH_2CH_2PPh_2$ and $Me_2PCH_2CH_2PMe_2$ appear to be suitable for the lactone formation. The $Ph_2P(CH_2)_3PPh_2$ system catalyzed the dimerization of butadiene in much less conversion. This ligand has such a high coordination ability that it may form a stable six membered chelate ring and occupies the active sites of the metal to stop the reaction.

Table 2. Effect of ligand

$Pd(dba)_2$ 0.2 mmol, ligand (unidentate 0.8 mmol, bidentate 0.4 mmol), butadiene 7.3 g, DMF 20 ml, CO_2 50 atm; 120 °C, 20 h.

Ligand	Product yield (%)[a]		
	Octatrienes	**4**	Others[b]
$P(OEt)_3$[c]	65.9	0	14.1
PPh_3[c]	72.5	0.5	11.3
$BuPPh_2$	56.8	1.6	12.6
Bu_2PPh	58.5	1.2	11.9
Bu_3P	67.8	2.5	9.9
$AsPh_3$	trace	0	4.3[d]
$Ph_2PCH_2CH_2OH$	71.6	0.7	8.0
$Ph_2PCH_2CH_2NEt_2$	72.6	1.4	8.6
$Ph_2P(CH_2)_2PPh_2$	74.4	5.4	9.7
$Ph_2P(CH_2)_3PPh_2$	1.3	0.1	5.0[d]
$Ph_2P(CH_2)_4PPh_2$	58.8	0.8	11.2
$Ph_2P(CH_2)_6PPh_2$	55.6	2.0	9.9
$Me_2P(CH_2)_2PMe_2$	49.5	4.8	12.3
$Ph_2As(CH_2)_2AsPh_2$	trace	0	3.4[d]
$Me_2N(CH_2)_2NMe_2$	56.4	0.7	3.1

a) Yield is based on the butadiene charged. b) "Others" mainly consists of butadiene trimers. c) $Pd(ligand)_4$ complex was used. d) Mainly 4-vinylcyclohexene.

Wilke,[6] Hagihara[7] and their co-workers have proposed π-allyl intermediates, **7** and **8**, for the palladium-catalyzed linear dimerization of butadiene. It has been assumed that the size of the palladium atom precludes the cyclization, and that a rapid hydrogen transfer occurs.

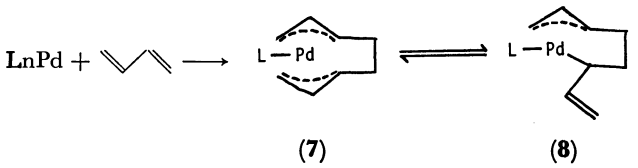

(**7**) (**8**)

We have proposed the following mechanism for this reaction, which involves the CO_2 insertion at the palladium-carbon bond followed by the transfer of hydrogen to give the acid (**5**).[1]

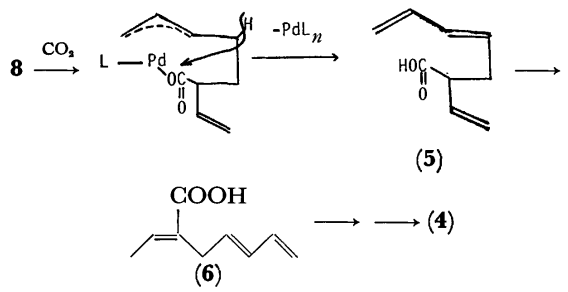

The distribution of the products is determined by the concentration and reactivity of these intermediates, **7** and **8**, which are influenced, in turn, by the reaction conditions and the steric and electronic properties of the ligands. Similar intermediates have often been proposed for the dimerization of butadiene catalyzed by nickel-phosphine complexes, and it is said that basic ligands stabilize the π-allyl, σ-allyl form, and that less basic ones stabilize the bis-π-allyl form. If this inspection is applicable to the palladium system, the experimental results for the monodentate ligands are in agreement with this hypothesis as can be seen from Table 2. This suggests that the catalyst is behaving as a nucleophile toward CO_2. Ditertiary phosphine-$[Ph_2P(CH_2)_nPPh_2]$ with $n=2$ may have the adequate stabilizing effect on the active intermediate (**8**) by the formation of a five membered chelate ring.

The suitability of polar, aprotic solvents for the lactone synthesis may be ascribable partly to the higher solubility of CO_2 in these media, and partly to their solvation effects; the nucleophilic nature of the intermediate (**8**) is supposed to be enhanced by the solvation of these solvents.

As an extention of the study we investigated the reaction of isoprene with CO_2. In the absence of CO_2, $Pd(dpe)_2$ complex catalyzed the dimerization of isoprene only in low conversions. In the presence of CO_2, the catalytic activity of the palladium complex was enhanced to yield considerable amounts of isoprene dimers. The major dimer was 2,7-dimethyl-1,3,7-octatriene, a tail-to-tail dimer. Several CO_2-incorporated products of five membered lactone structures were also formed in very low yields (about 1%). The detailed results may be published elsewhere.

Experimental

GLC analyses were performed on a Shimadzu GC-3AH instrument [20% Silicone DC 550 (2 m) on Diasolid M (60—80 mesh) and 10% FFAP (2 m) on Chromosorb W (60—80 mesh) (He as the carrier gas)]. The measuring conditions were as follows: for the lactone (**4**); at 205 °C on the FFAP column with benzophenone as an internal standard: for the butadiene dimers; at 145 °C on the Silicone DC 550 column with *t*-butylbenzene as an internal standard. Preparative GLC for the CO_2-incorporated products was performed on a Shimadzu GC-2H instrument at 180 °C using H_2 as the carrier gas [10% FFAP (2.5 m) on Chromosorb W (60—80 mesh)]. The PMR spectra were recorded on a Hitachi R-24 apparatus (60 MHz), using the proton decouple method at the same time. IR and UV spectra were recorded on a Shimadzu IR 430 and a Shimadzu UV 200 apparatus, respectively.

Reagents. Solvents were dried by appropriate drying agents and distilled under nitrogen atmosphere. Butadiene (purity 99.99%) and CO_2 (purity 99.50%) were used without further purification. $BuPPh_2$,[8] Bu_2PPh,[9] $Ph_2PCH_2CH_2OH$,[10] $Ph_2PCH_2CH_2NEt_2$,[11] and $Me_2PCH_2CH_2PMe_2$[12] were prepared according to the published methods. The ditertiary phosphines $[Ph_2P(CH_2)_nPPh_2$ ($n=2$, 3, 4, and 6)] were prepared according to the method described by Hewertson and Watson.[8] The other ligands were commercially obtained. $Pd(dpe)_2$,[13] $Pt(dpe)_2$,[13] $Ni(dpe)_2$,[13] $HCo(dpe)_2$,[14] $H_2Fe(dpe)_2$,[15] $Pd(PPh_3)_4$,[16] $Pt(PPh_3)_4$,[17] $RhCl(PPh_3)_3$,[18] $H_2Ru(PPh_3)_4$,[19] $H_3Ir(PPh_3)_3$,[19] $Pd[P(OEt)_3]_4$,[20] and $Pd(dba)_2$,[21] were synthesized by the reported methods.

Procedure. A typical procedure was as follows. Into a 100 ml stainless steel autoclave equipped with an inductive rotary agitator, $Pd(dpe)_2$ (0.2 mmol), DMF (10 ml), and butadiene (7.3 g) were added under nitrogen atmosphere, then CO_2 was introduced to the pressure of 50 atm. The autoclave was heated to 120 °C and stirred for 20 h. The products were analyzed by GLC.

Identification. The octatrienes (bp ≈90 °C/100 mmHg) and the lactone (**4**) (bp ≈138 °C/5—6 mmHg) were distilled from the reaction mixture and purified by preparative GLC. The acids (**5**) and (**6**) were isolated from the reaction mixture by extraction with aqueous NaOH and after acidification were purified by preparative GLC.

1,3,7-Octatriene (1). PMR (CCl_4): δ 2.0—2.3 (m, 4H, $-CH_2-$), 4.7—5.2 (m, 4H, $CH_2=$), and 5.3—6.8 (m, 4H, CH=).

1,3,6-Octatriene (2). PMR (CCl_4): δ 1.6 (d, 3H, CH_3), 2.5—2.9 (m, 2H, $-CH_2-$), 4.6—5.1 (m, 2H, $CH_2=$), and 5.2—6.7 (m, 5H, CH=).

2,4,6-Octatriene (3). PMR(CCl_4): δ 1.7 (d, 6H, CH_3) and 5.2—6.2 (m, 6H, CH=).

2-Ethylidene-5-hepten-4-olide(4). Found: C, 71.20; H, 8.12%. Calcd for $C_9H_{12}O_2$: C, 71.03; H, 7.95%. IR (neat): 1755 (C=O), 1675, and 970 cm^{-1} (*trans* CH=CH). PMR (CCl_4): δ 1.6—1.9 (m, 6H, $CH_3C=$), 2.1—3.3 (m, 2H, CH_2), 4.5—4.9 (m, 1H, HC), 5.1—6.0 (m, 2H, CH=CH), and 6.3—6.7 (m, 1H, $CH_3C\underline{H}=$). UV (EtOH): λ_{max} 217 nm (ε16,300). The methyl proton peaks separated into two parts, centered at δ 1.70 and at δ1.80, which were assigned by PMR spin decoupling method to the methyl group at position 7 and to the one in the ethylidine moiety, respectvely. The ordinal chemical shift value of the methyl group in ethylidine moiety (δ 1.80) indicates that the methyl group is *trans* position to the carbonyl group, becauce if it is *cis* position, the peak might appear in the lower field due to the anisotropy from the carbonyl group. The geminal protons in position 3 are non-equivalent due to the ring formation and give a typical AB pattern signal. In order to confirm this structure, the lactone (**4**) was hydrolyzed by aqueous NaOH. White solid (mp 101—103 °C) was obtained after acidification, which was identified to be a hydroxyl acid, 2-ethylidene-4-hydroxy-5-heptenoic acid (**9**), by the following data. Found:

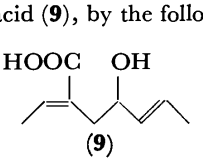

(**9**)

C, 63.18; H, 8.54%. Calcd for $C_9H_{14}O_3$: C, 63.51; H, 8.29%. IR(KBr): 3400—3200 (OH), 3000—2500 (COOH), 1680 (C=C-COOH), and 960 cm^{-1} (*trans* CH=C$\underline{H}$). UV (EtOH): λ_{max} 213 nm (ε10480). PMR (CD_3COCD_3): δ 1.61 (m, 3H, CH_3-position 7), 1.82 (d, 3H, CH_3 in ethylidine moiety), 2.51 (d, 2H, CH_2), 4.16 (m, 1H, CH), 5.3—5.6 (m, 2H, CH=CH), 6.93 (q, 1H, $CH_3C\underline{H}=$), and 7.00 (b, 2H,

COOH and OH). The methyl group in the ethylidene moiety confirmed to be *trans* position to the carbonyl group on the basis of the value of its PMR chemical shift.

2-Vinyl-4,6-heptadienoic Acid (5). IR (neat): 3200—2400 (COOH), 1705 (C=O), 1418 (COOH), 1005 and 905 cm^{-1} (CH_2=CH). PMR (CCl_4): δ 2.2 (q, 2H, $-CH_2-$), 2.8 (t, 1H, CH), 4.7—5.2 (m, 2H, CH_2=), 5.3—6.4 (m, 4H, CH=), and 11.2 (s, 1H, COOH).

2-Ethylidiene-4,6-hept-dienoic Acid (6). Found: C, 71.06, H; 7.88%. Calcd for $C_9H_{12}O_2$: C, 71.03, H; 7.95%. IR (neat): 3200—2400 (COOH), 1680 (C=C–COOH), 1635 ($C=CH_2$), 1420 and 1280 (COOH), and 1005 and 900 cm^{-1} (CH_2=CH). PMR(CCl_4): δ 1.80 (d, 3H, CH_3), 3.00 (d, 2H, $-CH_2-$), 4.94 (m, 2H, CH_2=), 5.4—6.2 (m, 3H, CH=), 6.94 (q, 1H, $CH_3C\underline{H}$=), and 11.65 (s, 1H, COOH). UV (EtOH): λ_{max} 209 nm (ε 4900).

We thank the Ministry of Education, for the financial support.

References

1) Y. Sasaki, Y. Inoue, and H. Hashimoto, *J. Chem. Soc., Chem. Commum.*, **1976**, 605.
2) J. F. Kohnle, L. H. Slaugh, and K. L. Nakamaye, *J. Am. Chem. Soc.*, **91**, 5904 (1969).
3) K.E. Atkins, W. E. Walker, and R. M. Manyik, *Chem. Commun.*, **1971**, 330.
4) A. Musco and A. Silvani, *J. Organomet. Chem.*, **88**, C41 (1975).
5) A. Musco, *J. Mol. Catal.*, **1**, 443 (1975).
6) G. Wilke, B. Bodganovic, P. Hardt, P. Heimbach, W. Keim, M. Kroner, W. Oberkirch, K. Tanaka, D.E. Steinrucke, D. Walter, and D. H. Zimmermann, *Angew. Chem. Int. Ed. Engl.*, **5**, 151 (1966).
7) S. Takahashi, H. Yamazaki, and N. Hagihara, *Bull. Chem. Soc. Jpn.*, **41**, 254 (1968).
8) W. Hewertson and H. R. Watson *J. Chem. Soc.*, **1962**, 1490.
9) W. C. Davis and W. J. Jones, *J. Chem. Soc.*, **1929**, 33.
10) K. Issleib and H. M. Möbius,. *Chem. Ber.*, **94**, 102(1961).
11) K. Issleib and R. Rieschel, *Chem. Ber.*, **98**, 2086 (1965).
12) H. Niebergall and B. Langenfeld, *Chem. Ber.*, **95**, 64 (1962). K. Issleib and A. Tzshach, *Chem. Ber.*, **93**, 1852 (1960).
13) J. Chatt, F. A. Hart, and H. R. Watson, *J. Chem. Soc.*, **1962**, 2537.
14) A. Sacco and R. Ugo, *J. Chem. Soc.*, **1964**, 3274.
15) G. Peet and D. H. Gerlach, *Inorg. Synth.*, **15**, 38 (1974).
16) D. R. Coulson, *Inorg. Synth.*, **13**, 121 (1972).
17) R. Ugo, F. Cariati, and G. La Monica, *Inorg. Synth.*, **11**, 105 (1968).
18) J. A. Osborn and G. Wilkinson, *Inorg. Synth.*, **10**, 67 (1967).
19) J. J. Levison and S. D. Robinson, *J. Chem. Soc., A*, **1970**, 2947.
20) M. Meier and F. Basolo, *Inorg. Synth.*, **13**, 112 (1972).
21) Y. Takahashi, T. Ito, S. Sakai, and Y. Ishii, *Chem. Commun.*, **1970**, 1065.

The Effect of Leaving Group Orientation on Solvolytic Cope Rearrangements. A Study of *exo*-Tricyclo[4.4.1.1^{2,5}]dodeca-3,7,9-trien-11-yl Tosylates and Derivatives

Shô Itô,* Isamu Itoh, Yutaka Fujise, Tetsuo Nakatsu,
C. A. Senkler,**,† and P. v. R. Schleyer***,†
Department of Chemistry, Tohoku University, Sendai 980
†*Department of Chemistry, Princeton University, Princeton, N.J. 08540, U.S.A.*
(Received February 3, 1978)

Synthesis and solvolytic behavior of derivatives of the highly hindered title compounds are described. *exo*-Tricyclo[4.4.1.1^{2,5}]dodeca-3,7,9-trien-*syn*-yl tosylate (*syn*-**18**-OTs) and the corresponding perhydro derivative, *syn*-**23**-OTs, solvolyze at rates that are in reasonable agreement with those predicted by Foote-Schleyer calculations. *syn*-**18**-OTs, and its dihydro derivatives, *syn*-**19**-OTs and *syn*-**20**-OTs, give completely rearranged products on solvolysis in acetic acid and 75% dioxane, 80% acetone, and 75% dioxane, respectively (Table 2). These products can be explained by normal cationic rearrangements, probably occurring after ionization. On the other hand, *anti*-**18**-OTs and *anti*-**23**-OTs solvolyze at rates *ca.* 10^2 times slower than those predicted by Foote-Schleyer calculations. Presumably the *anti* derivatives of **18**-OTs, **20**-OTs, **23**-OTs, and the tetrahydro tosylate (**22**-OTs) suffer steric hindrance to ionization. Product formation from *anti*-**18**-OTs (Table 3) and *anti*-**19**-OTs in acetic acid and 75% dioxane, respectively, is explained as a [3_S+3_S] sigmatropic shift induced by ionization, with formation of an allylic ion providing the driving force for rearrangement.

Molecular topologies which induce solvolysis by prior thermal rearrangement, or conversely in which thermal rearrangement is induced by ionization, have not been fully elucidated. Studies of such systems should help to clarify the relationship between reactivity and the orientation of the orbitals and the magnitude of their overlap. We now report the synthesis and solvolytic behavior of a number of derivatives of one such topology, the *exo*-tricyclo[4.4.1.1^{2,5}]dodeca-3,7,9-trien-11-yl system, **1**.††

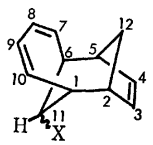

1

Several papers provide a foundation for understanding the interplay of thermal and ionic processes. In many cases, thermal process occurs prior to the ionization. (2,4,6-Cycloheptatrienyl)methyl 3,5-dinitrobenzoate solvolyzes 5.5×10^5 times faster than its fully saturated analog in 80% acetone yielding unrearranged alcohol and styrene.[1] For the rearrangment to styrene, the valence tautomerism to norcaradiene systems, **2a** and/or **2b** followed by the ionization was suggested. The similar rates of solvolysis for **3** and **4** ($k_{(4/3)}=3.4$) indicate that the 10^5 cyclopropyl-assisted rate acceleration dampens any kinetic effect due to the orientation of the leaving group with respect to the 1,3-diene system.[2] Thus, the influence of geometry, **2a** or **2b**, on the rates of solvolysis of (2,4,6-cycloheptatrienyl)methanol derivatives is probably too small to be important kinetically.[3]

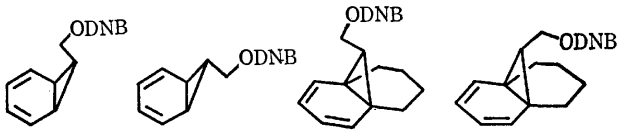

2a **2b** **3** $k_{rel}=1.0$ **4** $k_{rel}=3.4$

1-, 2-, and 3-Chlorocycloheptatrienes rearrange to benzyl compounds, but the 1-chloro derivative reacts faster.[4] In addition, the rate increases with solvent polarity is slower in 80% ethanol than the rate of solvolysis of benzyl chloride. Hence, the rate determining step, though ionic, is not ionization of benzyl chloride. A probable mechanism is tautomerism to the norcaradienyl isomer, **5**, which ionizes *via* disrotatory ring opening to give the benzyl cation in the rate determining step. This mechanism accounts for the slower rates of the 2- and 3-chloro derivatives since they must first rearrange *via* 1,5-hydrogen shifts to the 1-chloro isomer. Another possible mechanism, not excluded but highly unlikely,[5] is σ participation to give the benzyl cation directly. The transition state for this process would probably not benefit from benzyl delocalization.

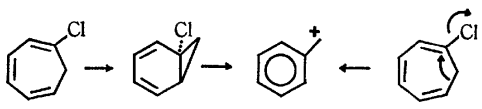

5

**Apart of this paper is taken from C. A. Senkler's Ph. D. Thesis, Princeton University, 1974.

***Present address: Institut für Organische Chemie der Universität Erlangen-Nürnberg, D-8520, Erlangen, West Germany.

†† Although the tosylates could be named as *cis*-1-*transoid*-1,2-*cis*-2-tricyclo[4.4.1.1^{2,5}]dodeca-3,7,9-trien-11(a)-yl and -11(e)-yl *p*-toluenesulfonates following IUPAC Tentative Rules in their most extended application (IUPAC Tentative Rules for Nomenclature of Organic Chemistry, Section E: Fundamental Stereochemistry, *IUPAC Bulletin*, No. 35), we use in this paper the *exo-endo* (for carbon skeleton) and *syn-anti* (for functional groups) nomenclature for the sake of simplicity.

The rearrangement of halo- and acetoxycyclooctatetraenes **6** to the corresponding *trans*-β-halostyrenes[6] was shown to occur *via* an electrocyclic reaction to **7** followed by ionization and conrotatory ring opening.[7-9] For chloro- and acetoxycyclooctatetraenes (**6**: X=Cl or OAc), the rate determining step is ionization, **7**→**8**. For bromocyclooctatetraene (**6**: X=Br), however, ionization is rate determining in solvents of low polarity, $E_T<42$, while the electrocyclic reaction **6**→**7** is rate determining in more polar solvents. Fluorocyclooctatetraene gives a 12% yield of *trans*-β-fluorostyrene upon heating at 100 °C for 35 h, but the mechanism of this transformation has not been determined.[10]

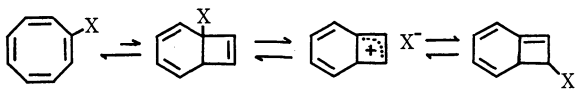

6 **7** **8**

The rate of acetolysis of 2-(2-cyclobutenyl)ethyl tosylate, **9**, reflects a competition between solvent displacement and conrotatory ring opening to a butadiene derivative, which then goes on to product.[11] The estimated rate of ring opening, 1×10^{-5} s^{-1}, in this case is greater than the rate of solvent displacement, 3×10^{-6} s^{-1}.

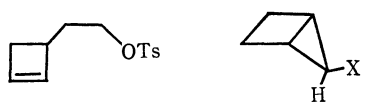

9 **10**

Investigations of the solvolysis kinetics of *anti*-5-bicyclo[2.1.0]pentyl derivatives, **10** (X=OTs, or OPNB),[12] have revealed a remarkable insensitivity to solvent polarity and leaving group. The products, however, are cyclopentadiene and 2-cyclopentenol, typical of cationic intermediates. The expalanation involves rate-limiting epimerization of **10** to the corresponding *syn* isomers, presumably *via* diradical.[13] *syn* Isomers then undergo disrotatory solvolytic ring opening to give the observed products.

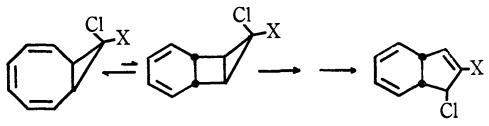

11 **12** **13**

In agreement with Vogel's original proposal,[14] both 9,9-dichlorobicyclo[6.1.0]nonatriene (**11**: X=Cl), and *syn*-9-chlorobicyclo[6.1.0]nonatriene-9-*d* (**11**: X=D), rearrange at a rate independent of solvent to give dihydroindenyl chlorides **13**.[15] An attractive mechanistic proposal is a rate determining electrocyclic reaction to a tricyclo[6.1.0.0^{2,7}]nonadiene ring system **12** followed by rapid disrotatory solvolytic ring opening to an allylic dihydroindenyl cation which gives the observed products. *anti*-9-Chlorobicyclo[6.1.0]nonatriene, **14**, also solvolyzes at a rate independent of solvent to give the same dihydroindenyl chloride. However, the reaction of **14**-*d* revealed the complete deuterium scrambling.[15] This result eliminates an epimerization mechanism similar to that found in **10**, and culminates to a mechanism which involves the rate-determining rearrangement of **14** to 9-chlorocyclononatetraene, **15**, followed by rapid solvolysis *via* the cyclononatetraenyl cation. The mechanism is consistent with the observation that 9-chlorocyclononatetraene **15** behaves exactly same way at −60° in SO_2 while **14** is inert at −20 °C in SO_2.[16]

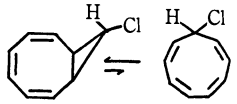

14 **15**

Apart from these instances in which isomerization takes place prior to solvolysis, Breslow's work on derivatives of dicyclopentadiene has provided an interesting example of the converse process, an electrocyclic reaction induced by solvolysis (Scheme 1).[17] The ionization of **16** to ion pair weakens the β bonds antiparallel to the leaving group and induces a Cope rearrangement (transition state; **17**), the driving force being formation

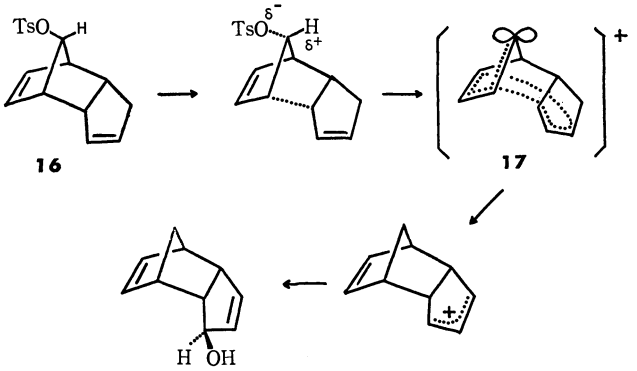

16 **17**

Scheme 1.

of an allylic ion. Supporting evidence for this mechanism is the fact that the C-8 ketones related to **16** undergo relatively rapid Cope rearrangement which are facilitated by protonation of the carbonyl oxygen.[18]

After the completion of the present study, Haywood-Farmer *et al.* published their preliminary result on the acetolysis of very similar brosylates, with no implication on product analysis.[19] The paper includes the kinetic data of brosylate of our *anti*-**23**-OH (*vide infra*).

Results

Synthesis of Substrates. Ketone **18**-O, the product of [6+4] cycloaddition of tropone with cyclopentadiene,[20] underwent Meerwein-Ponndorf reduction to give 21% of *syn*-**18**-OH and 74% of *anti*-**18**-OH. The conjugated double bonds of these alcohols were selectively reduced by Na/*n*-BuOH to give alcohols, *syn*- and *anti*-**19**-OH and *syn*- and *anti*-**20**-OH. Allowing *syn*- and *anti*-**18**-OH to react with two moles of hydrogen each gave four alcohols, *syn*- and *anti*-**21**-OH and *syn*- and *anti*-**22**-OH, while complete hydrogenation resulted in *syn*- and *anti*-**23**-OH (Scheme 2). Tosylates of these alcohols were obtained by the standard procedure.

Configuration of the alcohols were assigned by correla-

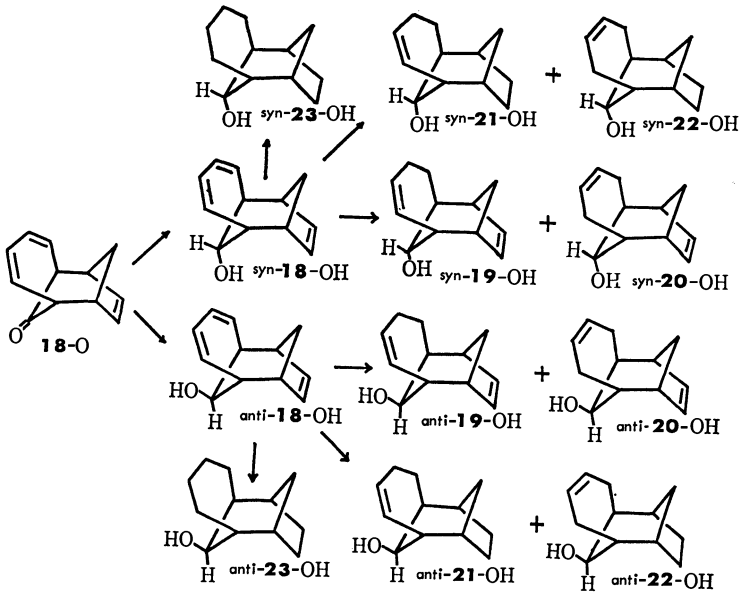

Scheme 2.

Table 1. Molecular mechanics calculations[21]

Structure	Engler force field				Allinger force field			
	ΔH_f (kcal/mol)	Strain (kcal/mol)	Steric energy (kcal/mol)	ϕ (°) H_1–C_1–C_{11}–H_{11} H_6–C_6–C_{11}–H_{11}	ΔH_f (kcal/mol)	Strain (kcal/mol)	Steric energy (kcal/mol)	ϕ (°) H_1–C_1–C_{11}–H_{11} H_6–C_6–C_{11}–H_{11}
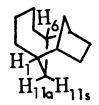	−16.71	32.97	41.61	H_{11a} {72.3 70.8	−16.63	33.51	34.15	H_{11a} {72.5 71.0
				H_{11s} {41.8 43.3				H_{11s} {40.5 41.9
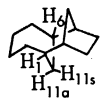	−18.20	31.48	40.12	H_{11a} {64.8 64.8	−21.03	29.11	29.75	H_{11a} {63.7 63.6
				H_{11s} {48.0 47.8				H_{11s} {47.1 47.0
anti-**23**-OH (a-form)	—	—	43.88	H_{11s} {43.5 44.5	—	—	—	—
anti-**23**-OH (b-form)	—	—	44.37	H_{11s} {49.8 49.8	—	—	—	—
syn-**23**-OH (a-form)	—	—	44.42	H_{11a} {74.8 73.7	—	—	—	—
syn-**23**-OH (b-form)	—	—	43.63	H_{11a} {66.7 66.7	—	—	—	—
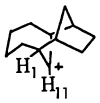	—		37.35	16.1	—	—	—	—
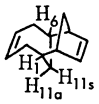	—		—	—	—	—	21.19	H_{11a} {78.1 78.2
								H_{11s} {37.0 36.9
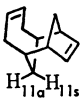	—		—	—	—	—	25.66	H_{11a} {64.2 64.2
								H_{11s} {46.6 46.6

tion of the magnitude of $J_{\underline{C}HOH\text{-bridgehead }\underline{H}}$ with dihedral angle. Molecular mechanics calculations[21] on alcohols *syn*-**23**-OH and *anti*-**23**-OH (Table 1) reveal both the dihedral angles, ϕ, and preferred conformations. *anti*-**23**-OH is less strained by 0.5 kcal/mol in the chair (a) than the boat-like (b) conformation, while *syn*-**23**-OH is less strained by 0.8 kcal/mol in b- form than in

a b

a-form. Thus, both conformers are likely present in each alcohol and tosylate. Dihedral angles for *anti*-**23**-OH range from 43 to 50°, for which J=3.5—4.0 Hz is expected, while dihedral angles of 66° to 75° for *syn*-**23**-OH suggest J=0—0.8 Hz.[22] NMR data described in experimental part agree with the expectations, showing a broad singlet for *syn* compounds and a triplet (J=4—7 Hz) for *anti* compounds.

That the ketone **18**-O is somewhat sterically hindered was evidenced by its failure to react with sodium borohydride or sodium in ethanol. However, reduction by lithium aluminium hydride in tetrahydrofuran yielded a single alcohol *syn*-**18**-OH.[20a] The result is supported by calculations. Thus, hindrance calculations[23] suggest that both *anti* and *syn* sides of the ketone are quite hindered. However, congestion is substantially larger on the *syn* side (116.1) than on the *anti* side (77.5), and therefore kinetically-controlled reduction would be expected to give *syn*-**18**-OH.

Solvolysis. *anti*-**18**-OTs was heated at 110 °C in acetic acid buffered with sodium acetate for 24 h. The resulting acetate mixture (75% yield) was reduced with lithium aluminium hydride and then oxidized with chromium(VI) oxide–pyridine. The products, separated by column chromatography, consisted of known ketones: **24**-O[24a] and **25**-O.[24b] Thus, the original acetates must have been **24**-OAc and **25**-OAc (Table 2).

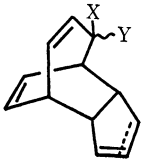

24-O: X, Y=O
24-OAc: X=H, Y=OAc
24-OH: X=H, Y=OH,

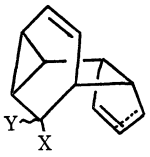

25-O: X, Y=O
25-OAc: X=H, Y=OAc
25-OH: X=H, Y=OH

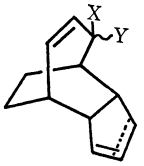

26-O: X, Y=O
26-OH: X=H, Y=OH

A mixture of *anti*-**19**-OTs and *anti*-**20**-OTs was heated at 90 °C for 5 h in 75% aqueous dioxane. The latter was unreactive under these conditions and was recovered quantitatively. The alcohol product from *anti*-**19**-OTs was oxidized to give a mixture of α,β-unsaturated ketones, **26**-O, ν_{CO}=1657 cm^{-1}. The NMR spectrum of the mixture featured absorptions at δ 5.5 (m) and 5.83 ppm (dt, J=6.0 and 2.0 Hz), due to the isolated double bond, and δ 6.15 (d, J=11.0 Hz) and 7.25 ppm (dd, J=11.0 and 9.0 Hz), due to the conjugated double bond. Catalytic hydrogenation of the mixture gave the corresponding, fully saturated ketone.[24a,c] Thus, the original alcohol products consist of **26**-OH.

syn-**19**-OTs was heated for 4.5 h in 80% aqueous acetone. The resulting alcohol, **27**-OH, was oxidized to a single ketone, **27**-O, ν_{CO}=1727 cm^{-1}, whose NMR featured a 2H multiplet at δ 6.01 ppm. Dehydrogenation of **27**-O gave the known ketone **28**.[25]

Refluxing *syn*-**20**-OTs in 75% aqueous dioxane resulted in three alcohols. The major alcohol, *syn*-**29**-OH, and the minor alcohol, *anti*-**29**-OH, showed NMR absorptions for two vinyl hydrogens and were oxidized

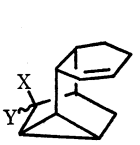

27-O: X, Y=O
27-OH: X=H, X=OH

28

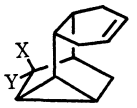

29-O: X, Y=O
syn-**29**-OH: X=H, Y=OH
anti-**29**-OH: X=OH, Y=H

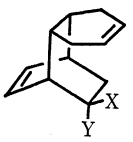

30-O: X, Y=O
30-OH: X=OH, Y=H

31

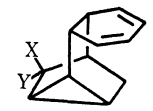

syn-**32**-OAc: X=H, Y=OAc
anti-**32**-OAc: X=OAc, Y=H

to the same ketone, **29**-O, ν_{CO}=1729 cm^{-1}. Dehydrogenation of this ketone gave **28**. The structure of *syn*-**29**-OH was assigned on the basis of the singlet at δ 4.00 ppm for the >CHOH proton, while that of *anti*-**29**-OH was based on a quartet nature of the same proton at δ 4.46 ppm (dd, J=5.5 and 3.2 Hz). The third alcohol, **30**-OH, featured a carbinyl proton, δ 3.87 ppm, split into a multiplet and vinyl absorptions integrating for four protons: δ 6.08 (2H, m), 6.23 (1H, t, J=5.0 Hz) and 6.37 ppm (1H, t, J=5.0 Hz). Oxidation to a ketone, **30**-O, caused a significant shift only in the last two vinyl absorptions: δ 6.25 (1H, tt, J=7.0 and 1.5 Hz) and 6.67 ppm (1H, tt, J=7.0 and 1.2 Hz). Dehydrogenation of **30**-O gave the aromatic compound **31**.

The solvolysis of *syn*-**18**-OTs afforded *syn*- and *anti*-**32**-OAc and **33**-OAc. While the result of acetolysis has been published,[25] hydrolysis also gave the major product, *syn*-**32**-OH with no trace of fragmentation product. Product data for all compounds are summarized in Table 2. Rates of solvolysis in 60% aqueous acetone with *syn*/*anti* rate ratios and relative rates are presented in Table 3.

Table 2. Solvolysis products

Compound	Condition	Product
anti-**18**-OTs	HOAc, NaOAc 110 °C, 24 h	**24**-OAc (55%) **25**-OAc (12%)
anti-**19**-OTs	75% aq dioxane 90 °C, 5 h	**26**-OH (51%) Cycloheptatriene (trace)
syn-**18**-OTs	HOAc, NaOAc 110 °C, 3 h	*syn*-**32**-OAc (80%) *anti*-**32**-OAc (10%) **33**-OAc (6%)
	75% aq dioxane 95 °C, 5 h	*syn*-**32**-OH (95%) (as *N*-Phenylmaleimide adduct)
syn-**19**-OTs	80% aq acetone reflux, 4.5 h	**27**-OH (80%)
syn-**20**-OTs	75% aq dioxane reflux, 18 h	*syn*-**29**-OH (42%) *anti*-**29**-OH (10%) **30**-OH (24%)

Table 3. Rates of solvolysis[a] and relative rates

Compound	k[b] (s^{-1})	T (°C)	$\Delta H^{\neq}$ (kcal/mol)	$\Delta S^{\neq}$ (e.u.)	k(*syn*/*anti*) (75 °C)	k_{rel} (75 °C) *anti*	k_{rel} (75 °C) *syn*
syn-**23**-OTs	$(5.23\pm0.14)\times10^{-4}$	30.0	17.8	−14.8	122	—	1.0
	$(3.48\pm0.05)\times10^{-3}$	50.0					
	3.13×10^{-4} c)	25.0					
	2.76×10^{-2} c)	75.0					
anti-**23**-OTs	$(2.25\pm0.04)\times10^{-4}$	74.9	23.2	−8.9	1.0	1.0	—
	$(2.16\pm0.10)\times10^{-3}$	100.1					
	$(2.97\pm0.05)\times10^{-3}$	102.2					
	7.03×10^{-7} c)	25.0					
	2.27×10^{-4} c)	75.0					
syn-**22**-OTs	$(6.32\pm0.32)\times10^{-5}$	49.9	25.3	0.3	580	—	4.2×10^{-2}
	$(1.18\pm0.06)\times10^{-3}$	75.2					
	1.16×10^{-3} c)	75.0					
	2.17×10^{-6} c)	25.0			980		
anti-**22**-OTs	$(2.04\pm0.40)\times10^{-6}$	75.2	27.4	−6.1	1.0	8.8×10^{-3}	—
	$(3.81\pm0.35)\times10^{-5}$	102.2					
	2.00×10^{-6} c)	75.0					
	2.20×10^{-9} c)	25.0					
syn-**20**-OTs	$(8.19\pm0.25)\times10^{-5}$	49.7	25.9	2.9	400	—	6.1×10^{-2}
	$(1.72\pm0.02)\times10^{-3}$	75.3					
	1.67×10^{-3} c)	75.0					
	2.67×10^{-6} c)	25.0					
	$(7.58\pm0.35)\times10^{-5}$	102.0					
anti-**20**-OTs	$(6.79\pm0.21)\times10^{-4}$	125.3	27.2	−5.4	1.0	1.8×10^{-2}	—
	4.16×10^{-6} c)	75.0					
	4.89×10^{-9} c)	25.0					
syn-**18**-OTs	$(1.40\pm0.15)\times10^{-4}$	75.0	23.8	−8.2	53	—	5.1×10^{-3}
	$(1.52\pm0.15)\times10^{-3}$	100.2					
	3.75×10^{-7} c)	25.0					
anti-**18**-OTs	$(4.86\pm0.20)\times10^{-5}$	100.2	29.0	−1.0	1.0	1.2×10^{-2}	—
	$(6.04\pm0.20)\times10^{-4}$	125.2					
	2.66×10^{-6} c)	75.0					
	2.00×10^{-9} c)	25.0					
anti-**21**-OTs	$(3.18\pm0.30)\times10^{-4}$	75.3	25.4	−1.9	—	1.4	—
	$(8.32\pm0.03)\times10^{-4}$	84.4					
	3.07×10^{-4} c)	75.0					
	5.56×10^{-7} c)	25.0					

a) 60% acetone, 2,6-lutidine buffer. b) Determined conductimetrically, rate is average of at least two determinations. c) Calculated from data at other temperatures.

Discussion

Using the Foote-Schleyer treatment,[26] the unassisted rates of solvolysis for *syn*-**18**-OTs, *anti*-**18**-OTs, *syn*-**23**-OTs and *anti*-**23**-OTs in 60% acetone, along with several related compounds, can be calculated (Table 4). The difference in strain between chair and boat conformers for both *syn*- and *anti*-**23**-OH is less than 1 kcal/mol[21] (Table 1). Since the effect on conformer population of replacing -OH with -OTs should be small, it seems reasonable that both *syn*- and *anti*-**23**-OTs exist as a chair–boat mixture. Thus, as a crude estimate, rates were calculated for both chair and boat conformers. Dihedral angles for the chair conformation of the hydrocarbon **20**-H were used to approximate those of *syn*- and *anti*-**18**-OTs. The chair form of **20**-H is more stable than the boat form by 4.5 kcal/mol.[21a]

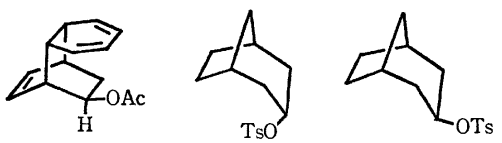

33-OAc **34** **35**

Table 4 reveals that the observed rate of *syn*-**23**-OTs in 60% acetone is $10^{1.4}$ and $10^{0.8}$ times slower than the rates calculated for the chair and boat conformations, respectively. *syn*-Bicyclo[3.2.1]oct-3-yl tosylate, **34**, which lacks only the four-carbon bridge of *syn*-**23**-OTs, would seem to be a plausible model. Jefford, *et al.*,[27] have observed that **34** undergoes acetolysis *ca.* 6 times slower than calculated, perhaps due to the "reflex" effect[28] or steric hindrance to ionization by the ethylene bridge. Although the Foote-Schleyer parameters used in Table 4 differ somewhat from those of Jefford, *et al.*,[27]

Table 4. Foote-schleyer calculations[26]

Compd	Ketone ν_{CO} (cm^{-1})	ϕ, deg	GS-TS (kcal/mol)	log k_{rel} (reference: cyclohexyl OTs) Calcd Foote-Schleyer (25 °C)	Obsd 60% acetone[f] (25 °C)
syn-**23**-OTs (a-form)	1705	36, 35[a]	0.8	+3.73	+2.34
syn-**23**-OTs (b-form)	1705	40, 40[a]	0.8	+3.16	
anti-**23**-OTs (a-form)	1705	50, 48[a]	0.6[i]	+2.91	−0.31
anti-**23**-OTs (b-form)	1705	56, 56[a]	0.8	+1.89	
anti-**18**-OTs	1715	37, 37[b]	0.3	−0.82[g]	−2.85
syn-**18**-OTs	1715	38, 38[b]	0.4	−0.87[g]	−0.58
					Obsd AcOH (25°)
34	1714[d]	45, 45[c]	3.8[d]	+3.59	+2.04[d]
35	1714[d]	45, 45[c]	0.6[i]	+1.31	+1.00[d]
36	1700[e]	45, 45[c]	0.6[i]	+1.16[h]	+0.46[e]
37	1700[e]	45, 45[c]	1.9	+3.09[h]	+1.86[e]

a) Determined by molecular mechanics calculations on the alcohol. b) Dihedral angles of the chair conformation of **20**-H, used as approximation, see text. c) Determined by molecular mechanics calcuations on bicyclo[3.2.1]-octane. d) Ref. 27. e) Ref. 32. f) Rate of cyclohexyl tosylate in AcOH (0.001 M Ac_2O) $k=4.88\times10^{-8}$ s^{-1}: S. Winstein, B. K. Morse, E. Grunwald, H. W. Jones, J. Corse, D. Trifan, and H. Marshall, *J. Am. Chem. Soc.*, **74**, 1127 (1952). This was converted to the reference rate constant in 60% acetone, $k=1.42\times10^{-6}$, using $m=0.6$, $Y_{60\%\ acetone}=+0.80$, $Y_{AcOH}=-1.64$: S. Winstein and A. H. Fainberg, *ibid.*, **78**, 2770 (1956). g) Includes inductive factor 3/8, Ref. 26b. h) Includes inductive factor 1/8, Ref. 26b. i) Axial cyclohexyl strain energy, E. L. Eliel, "Stereochemistry of Carbon Compounds," McGraw Hill Book Co., New York, N. Y. (1962), p. 236.

the indication is similar: **34** is $10^{1.5}$ times slower than expected.[29] Hence neither *syn*-**23**-OTs nor **34** solvolyzes *via* σ participation, and both may be somewhat slowed by steric interactions. The rates of *syn*-**23**-OTs and **34** in 60% acetone at 25 °C are quite comparable; $k_{syn\text{-}23\text{-}OTs}/k_{34}=2.0$.[30]

Inclusion of a Δ^8 double bond (*syn*-**22**-OTs), causes a 24 fold rate decrease relative to *syn*-**23**-OTs at 75 °C (Table 3). This seems large for an inductive effect of a γ double bond, as β double bonds usually cause only a 10 fold decrease in rate.[26b] In any case, the double bond in *syn*-**22**-OTs does not seem to be participating.

The observed rate for *anti*-**23**-OTs is $10^{2.2}$ and $10^{3.2}$ times slower than the rates calculated for the boat and chair conformers, respectively. Calculations by Jefford, *et al.*,[27] and those in Table 4 reveal that model compound **35** solvolyzes at a normal, largely unassisted rate in acetic acid. Comparison of the relative rates for *anti*-**23**-OTs and **35** in 60% acetone at 25 °C, $k_{anti\text{-}23\text{-}OTs}/k_{35}=0.003$, seems to indicate that steric hindrance to ionization by the four-carbon bridge in the former may be responsible for its slow rate. Steric effects of a similar magnitude have been observed in crowded norbornanes.[31]

Hindrance calculations[23] on the ketone **23**-O formed on oxidation of *syn*- or *anti*-**23**-OH show a pronounced reversal of congestion, relative to unsaturated ketone **18**-O. Attack by a nucleophile from the *syn* direction is much less hindered (62.4) than attack from the *anti* direction (1441.1). In fact, the ketone **23**-O yielded *anti*-**23**-OH quantitatively on the reduction with lithium aluminium hydride. The value of 1441.1 is quite large; therefore H_{9a} must be displaced 0.7 Å to allow attack of the nucleophile from the *anti* direction.[23] Clearly these observations support the idea that steric hindrance to ionization is a major contributor to the rate deceleration observed in *anti*-**23**-OTs.

Inclusion of a Δ^8 double bond (*anti*-**22**-OTs) causes a rate decrease relative to *anti*-**23**-OTs by a factor of 0.0088 which again seems quite large for an inductive effect (Table 3). This deceleration might be due to steric hindrance to ionization as in the case of *anti*-**23**-OTs. One of the two most hindering atoms in the ketone **23**-O, H_{9a} and H_{7a},[23] remains intact in *anti*-**22**-OTs, while the other has become vinylic. Since molecular mechanics calculations indicate that the twisted form of **22**-O, a similar system, is more stable than the boat by 4.5 kcal/mol,[21] it would seem that the preference for the twisted form in *anti*-**22**-OTs might be even larger due to substitution of -OTs for=O. In contrast, the Δ^7 double bond in *anti*-**21**-OTs causes a rate enhancement of 1.4 over *anti*-**23**-OTs. The actual rate enhancement is probably *ca.* 14 if one assumes that a β-double bond in a nonparticipating system should slow the rate by a factor of 10.[26b] In this case, migration of one of the σ bonds *trans* to the leaving group

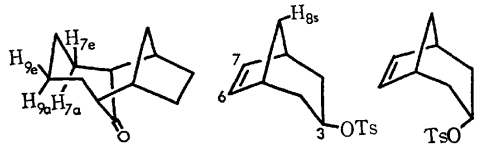

23-O **36** **37**

results in formation of an allyl cation. This is likely the mode of participation. However, products were not determined for this compound.

The rates of *anti*-**22**-OTs, *anti*-**20**-OTs and *anti*-**18**-OTs are within a factor of 2.1 of one another at 75 °C. Since the last tosylate reacts 10^2 times slower than the Foote-Schleyer calculation predicts, and the calculation estimates for the first two should be faster than for *anti*-**18**-OTs, all three seem to be anomalously slow. Since a model compound for *anti*-**18**-OTs and *anti*-**20**-OTs, bicyclic **36** also solvolyzes at a rate which agrees with that calculated by the Foote-Schleyer equation (Table 4), the distance between the double bond and the carbon containing the leaving group in **36** has been postulated to be too far to permit participation.[32] In the *endo* conformation with the 6-membered ring in a chair form of bicyclo[3.2.1]octane, molecular mechanics calculations indicate the distances C-3 to C-6 and C-3 to C-7 to be 2.999 and 2.997 Å, respectively,[21b] while, in the olefin, these would probably be *ca.* 0.1 Å shorter. On the other hand, participation by a double bond has occurred over greater distances. For example, in (*endo*-bicyclo[3.3.1]non-6-en-3-yl)methyl tosylate, in which the rate enhancement is *ca.* 10^4, [33] the distances between the olefinic carbons and the carbon bearing the leaving group are 3.313 and 3.280 Å.[21b] Therefore, it seems also possible that **36** solvolyze from the *exo* conformation (boat form), for which the distances in bicyclo[3.2.1]octane are 3.425 and 3.437 Å.[21b] This conformation would probably not allow "edge-on" interaction[34] of the double bond with the developing cationic center. The *exo* conformation in bicyclo[3.2.1]octane, however, is less stable than the *endo* by ≈5 kcal/mol.[21b] Replacing -H by -OTs should provide increased steric interaction with the H_{8s}, thus accentuating the energy difference between *endo* and *exo*. Compounds *anti*-**18**-OTs and *anti*-**20**-OTs, however, do not have such conformational freedom and the distance from the double bond carbons to C–OTs is only 2.854 Å. Thus, it seems likely that the source of the decelerations for *anti* unsaturated derivatives also lies in the four-carbon bridge.

The rate of *syn*-**18**-OTs shows good agreement with that calculated at 25 °C in 60% acetone. The 12.0 fold rate acceleration of *syn*-**20**-OTs (Table 3) is generally consistent with its having one less double bond than *syn*-**18**-OTs. Thus, neither compound seems to be benefiting from participation to a large degree, as in the model compounds **37**.[32]

Table 2 shows that *anti*-**18**-OTs gives completely rearranged products on acetolysis. Kinetic analysis seems to indicate that rearrangement occurs after ionization. Scheme 3 depicts possible rearrangement pathways available to the ion pair **38**. Breaking the σ bond *trans* to the leaving group (**a**) gives allylic ion **39**. Rotation about the bond joining the two rings of **39** permits reclosure six ways (**c**—**h**) to give six isomeric resonance stabilized cations, **40**—**45**. Ion **40** may also result from **38** directly *via* a Wagner-Meerwein rearrangement or a [1,5] sigmatropy (**b**). Both **38** and **39** may undergo fragmentation (**i**, **j**) to give tropylium ion and cyclopentadiene, which can undergo [4+2] cycloaddition giving **45**.[24b] Finally, **38** can undergo a Cope rearrangement (**o**) also giving **45**. Ions **44** and **45** can be interconverted through vinyl–cyclopropylcarbinyl rearrangements (**l**—**m**—**n**).

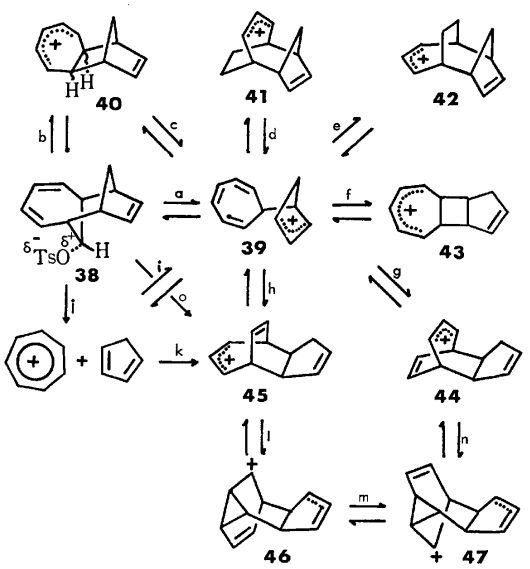

Scheme 3.

According to Table 2, however, products form only from **45** and **46**. Formation of **45** *via* reclosure of **39** (**h**) requires a *ca.* 180° rotation about the σ bond joining the rings of the initially formed ion. Since **45** should be similar in stability to **40**—**44**, the failure to observe products deriving from these latter ions argues against reclosure of **39** *via* **h**.

The tropylium ion and cyclopentadiene undergo [4+2] cycloaddition in 66% dioxane or acetic acid to give, after reduction of the acetates in the latter case, **24**-OH and **25**-OH in a ratio of 4.6 to 1.0.[24b] Notably, this is the same ratio in which **24**-OAc and **25**-OAc are formed on acetolysis of *anti*-**18**-OTs (Table 2). Therefore, both the fragmentation-recombination sequences (**j**—**k**) and the Cope rearrangement (**o**) can account for the stereospecific formation of **45**, which in turn forms **46** *via* path **l**.

In order to establish the fragmentation–recombination pathway for *anti*-**18**-OTs, trapping experiments were carried out. Acetylacetone trapped the tropylium ion as tropylacetylacetone (86% in hydrolysis and 51% in acetolysis) and *N*-phenylmaleimide captured cyclopentadiene as its cycloadduct (91%) in acetolysis. Furthermore, acetolysis with constant addition of methylcyclopentadiene resulted in a 6% incorporation of the latter, although this figure is somewhat inaccurate because of extensive polymerization of methylcyclopentadiene during the reaction. Thus, the pathway **j**—**k** was established.

Since the partially hydrogenated derivative, *anti*-**19**-OTs, can react *via* the Cope mechanism but cannot form the highly stable tropylium ion *via* fragmentation, its solvolysis products should help reveal the former pathway (**o**). In this case, fragmentation of the ion corresponding to **39** would form the cycloheptadienyl cation and cyclopentadiene which are incapable of cycloaddition reaction. Furthermore, the fragmentation

would have a driving force comparable to that of the bond rotation-recombination pathways. Accordingly, a mixture of products with various carbon skeleton is expected from *anti*-**19**-OTs, if *anti*-**18**-OTs were reacting by the fragmentation-recombination mechanism. The fact that tricyclic product derived only from **48** (Table 2) implied that the Cope rearrangement path is operative. In addition, the detection of cycloheptariene which is the deprotonation product of cycloheptadienyl cation implied the fragmentation process is also operative to some extent.

Thus, *anti*-**18**-OTs and *anti*-**19**-OTs solvolyze through the Cope rearrangement and fragmentation, the difference between these cases being that, in the former, the fragmentation products cycloadd to give the same products with those of internal process, while in the latter the fragmentation products are incapable of recombination and are detected as such.

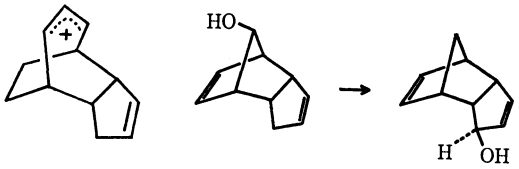

48 **49**

An alternative pathway for the intramolecular rearrangement is initial Cope rearrangement of these tosylates to the allyl tosylate followed by rapid solvolysis. The thermal Cope rearrangement of a similar systems **49**, is rapid only above 140 °C [17b] and *anti*-**18**-OH and its tosylate are stable at 120 °C. Thus, the rate of solvolysis of *anti*-**18**-OTs, if is were indicative of a thermal rate-determining step, should be much slower than that of *anti*-**20**-OTs or *anti*-**22**-OTs which do not contain the 1,5-diene system. At 75 °C, however, the rates of solvolysis for these three are within a factor of 2.1 (Table 3).

Thus, one of the rearrangement pathway for both *anti*-**18**-OTs and *anti*-**19**-OTs appears to be a rather remarkable $[3_s+3_s]$ sigmatropic shift induced by ion pair formation[35] which weakens the σ bonds *trans* to the leaving group.[36] This bond weakening may permit the skew orientation of the 1,5-diene system to distort towards the preferred chair orientation.[37] The aromatic Cope transition state **50** can conjugate with the external carbenium ion, thus stabilizing both;[38] this is similar to the stabilization of an adjacent carbonium ion by a benzene ring.

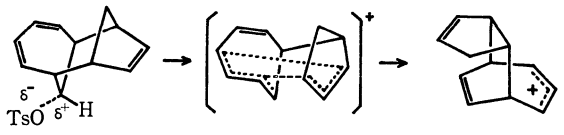

38 **50** **45**

If the facility with which the *anti* compounds, *anti*-**18**-OTs and *anti*-**19**-OTs, undergo the Cope rearrangement and fragmentation is due chiefly to the weakening of the σ bonds *trans* to the leaving group, then the *syn* compounds should not rearrange in this manner. The data in Table 2 confirm this premise. *syn*-**18**-OTs, *syn*-**19**-OTs, and *syn*-**20**-OTs rearrange completely to the products of the same tetracyclic skeleton and, for *syn*-**18**-OTs, essentially no difference was observed by the change of the solvent. Furthermore, any attempt to trap cyclopentadiene or the tropylium ion failed. The Foote-Schleyer treatment has implied that the *syn* compounds solvolyze at an unassisted rate. To account for >99% rearranged products due to σ participation, a rate enhancement of at least 100 over the calculated unassisted rate is necessary.[39] Clearly such a rate enhancement is lacking. Hence, *syn* compounds likely rearrange after ionization. A possible rearrangement path for *syn*-**18**-OTs is given below. Participation of the Δ^3 double bond gives the cyclopropylcarbinyl ion derivative **51**, solvent capture of which accounts for both tetracyclic *syn*- and *anti*-**32**-OAc as well as tricyclic *anti*-**33**-OAc.

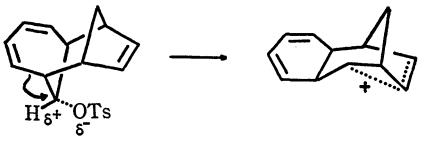

51

Conclusion

Comparison of the kinetic data in Table 3 with the rates calculated *via* the Foote-Schleyer equation and the rates of model compounds seems to indicate that the *anti* compounds solvolyze anomalously slow. In the case of *anti*-**23**-OTs, this is probably due to steric hindrance to ionization by the four-carbon bridge. Steric hindrance to ionization also seems to be a factor also for unsaturated *anti* derivatives. *syn* Compounds solvolyze at rates which agree with those predicted by Foote-Schleyer calculation. Since *syn*-**18**-OTs, *syn*-**19**-OTs and *syn*-**20**-OTs give completely rearranged products but a very small rate enhancement, it seems probable that rearrangement follows ionization. Products from these *syn* tosylates result from normal carbenium ion rearrangements.

anti-**18**-OTs and *anti*-**19**-OTs undergo both fragmentation and a $[3_s+3_s]$ sigmatropic rearrangement induced by ionization. The ease of the latter process results from two factors: (1) The σ bond *trans* to the leaving group, which is weakened on ionization, is also the σ bond broken in the Cope rearrangement; and (2) the Cope transition state can conjugate with the external carbenium ion, thus allowing for mutual stabilization.

Experimental

General. Infrared spectra were taken in a film for liquids and KBr pellets for solids using Hitachi EPI-S2 IR spectrometer. All NMR spectra were measured in $CDCl_3$ solution with TMS internal standard using a Varian HA-100 or A-60D instrument. Tosylation of alcohols was carried out by the standard method.[40]

Rate Measurement. All rates were determined in 60% acetone conductimetrically with a Wayne-Kerr Model B331 Impedence Bridge capable of 0.1% accuracy. The acetone

was purified by refluxing with potassium permanganate, drying with Drierite, and distilling through a 60 cm Vigreux column prior to use. The conductivity cells used had bright platium electrodes, cell constants of 0.2—0.4 and volumes of *ca.* 25 ml. In a typical run, enough tosylate to make a 10^{-3} M solution was placed in the conductivity cell and 20 ml of 60% acetone was added. The cell was sealed and equilibrated with shaking for 4 min in the constant temperature bath. The usual number of measurements was 35. Each reaction was run at least in duplicate, and was followed for at least two half-lives. Good first-order rate plots were obtained in all cases.

Synthesis. Meerwein-Ponndorf Reduction of exo-*Tricyclo*-[*4.4.1.1*^{2,5}]*dodeca-3,7,9-trien-11-one* (**18**-O). *Preparation of* syn-***18**-OH and* anti-***18**-OH*: Ten grams of **18**-O[20] in 200 ml of 2-propanol was heated unser reflux with 10 g of aluminium isopropoxide for 10 h and 100 ml of solvent was distilled during further refluxing for 10 h. The reaction mixture was poured into 50 ml of 2M HCl and extracted with ether. After the ether solution was washed with water and dried, the solvent was removed to yield 10 g of a semisolid material which was recrystallized from petroleum ether to give 5.7 g of *anti*-**18**-OH.

anti-**18**-OH: Mp 80—82 °C. IR: 3500 cm^{-1}. NMR (δ): 1.18 (1H, m), 1.53 (1H, d, J=11 Hz), 1.80 (1H, br. d, $J\approx$ 9 Hz), 2.7—3.0 (4H, complex)[41], 4.10 (1H, m),[41] 5.7—6.3 ppm (6H, complex). Found: C, 82.30; H, 7.99%. Calcd for $C_{12}H_{14}O$: C, 82.72; H, 8.10%.

anti-**18**-OTs: Mp 114—115 °C. NMR (δ): 1.18 (1H, m), 1.65 (1H, d, J=11 Hz), 2.44 (3H, s), 2.60—3.00 (4H, complex), 5.05 (1H, t, J=5.5 Hz), 5.5—6.2 (6H, complex), 7.33 (1H, d, J=8.5 Hz), 7.70 ppm (1H, d, J=8.5 Hz). Found: C, 69.51; H, 6.08%. Calcd for $C_{19}H_{20}O_3S$: C, 69.49; H, 6.14%.

The filtrate from the recrystallization of *anti*-**18**-OH was subjected to silica gel chromatography. Elution with a mixed solvent system of petroleum ether–ether gave 1.7 g of *anti*-**18**-OH and 2g of *syn*-**18**-OH.

syn-**18**-OH: Mp 32.5—34.5 °C. UV (MeOH) λ_{max}: 243 nm (ε=4552, sh), 252 (5720), 262 (5668), 273 (3173). IR: 3490 cm^{-1}. NMR (δ): 1.49 (1H, m), 2.21 (1H, d, J=10.4 Hz), 2.74 (5H, br.m), 3.90 (1H, br.s), 5.83 (4H, m), 6.21 ppm (2H, br.s). Found: C, 82.48; H, 8.16%. Calcd for $C_{12}H_{14}O$: C, 82.72; H, 8.10%.

syn-**18**-OTs: Mp 138—139.5 °C. NMR (δ): 1.40 (1H, m), 1.98 (1H, d, J=11 Hz), 2.43, (3H, s), 2.70 (4H, m), 4.76 (1H, br.s), 5.90 (6H, m), 7.30 (1H, d, J=9 Hz), 7.68 ppm (1H, d, J=9 Hz). Found: C, 69.23; H, 6.04%. Calcd for $C_{19}H_{20}O_3S$: C, 69.49; H, 6.14%.

Bouveault-Blanc Reduction of exo-*Tricyclo*[*4.4.1.1*^{2,5}]*dodeca-3,7,9-trien*-syn-*11-ol* (syn-***18**-OH). *Preparation of* syn-***19**-OH and* syn-***20**-OH*: To 3.63 g of *syn*-**18**-OH in 100 ml of 1-butanol were added, in several portions, 2 g of sodium at room temperature. The reaction mixture was refluxed gently and 3 g of sodium was added over 0.5 h. The cooled solution was diluted with water, neutralized with 5% HCl and extracted with ether. After the ether solution was washed with water and dried, the solvent was removed to yield 4.5 g of oil. The oil was separated by silica gel chromatography. Elution with a mixture of hexane and ether gave 1.0 g of *syn*-**19**-OH and 1.5 g of *syn*-**20**-OH.

syn-**19**-OH: Oil. IR: 3560, 3460 cm^{-1}. NMR (δ): 4.03 (1H, d, J=10 Hz),[41] 5.65 (2H, complex), 6.39 ppm (2H, m). Found: C, 81.58; H, 9.18%. Calcd for $C_{12}H_{16}O$: C, 81.77; H, 9.15%.

syn-**19**-OTs: Mp 96 °C (dec). NMR (δ): 1.60 (1H, dt, J=12 and 5 Hz), 2.45 (3H, s), 4.90 (1H, br.s), 5.60 (2H, m), 6.03 (2H, m), 7.32 (2H, d, J=8.5 Hz), 7.73 ppm (2H, d, J=8.5 Hz). Found: C, 68.91; H, 6.82%. Calcd for $C_{19}H_{22}O_3S$: C, 69.06; H, 6.71%.

syn-**20**-OH: Mp 37—38 °C. IR: 3586, 3450 cm^{-1}. NMR (δ): 1.45 (1H, dt, J=11 and 5.5 Hz), 3.85 (1H, s,) 5.50 (2H, br.s), 6.40 ppm (2H, br.s). Found: C, 81.71; H, 9.12%. Calcd for $C_{12}H_{16}O$: C, 81.77; H, 9.15%.

syn-**20**-OTs: Mp 126.5—128 °C. NMR (δ): 1.45 (1H, dt, J=11 and 5 Hz), 2.45 (3H, s), 4.70 (1H, br.s), 5.45 (2H, br.s), 6.10 (2H, d, J=1 Hz), 7.32 (2H, d, J=8.5 Hz), 7.55 ppm (2H, d, J=8.5 Hz), Found: C, 68.89; H, 6.65%. Calcd for $C_{19}H_{22}O_3S$: C, 69.06; H, 6.71%.

Bouveault-Blanc Reduction of exo-*Tricyclo*[*4.4.1.1*^{2,5}]*dodeca-3,7,9-trien*-anti-*11-ol* (anti-***18**-OH). *Preparation of* anti-***19**-OH*: The alcohol *anti*-**18**-OH was reduced similarly to 1: 1 mixture of *anti*-**19**-OH and *anti*-**20**-OH. Separation of these alcohols was unsuccessful. A mixture of *anti*-**19**-OH and *anti*-**20**-OH was also prepared by sodium reduction of **18**-O. As the solvolysis rates of tosylates of *anti*-**19**-OH and *anti*-**20**-OH differ greatly, the mixture was used without separation. The mild solvolysis yielded pure *anti*-**20**-OTs, $LiAlH_4$ reduction of which produced *anti*-**20**-OH.

anti-**20**-OH: Mp 101.5—103 °C. IR: 3450 cm^{-1}. NMR (δ): 1.40 (1H, dt, J=11 and 5 Hz), 4.00 (1H, t, J=6.5 Hz), 5.60 (2H, t, J=2 Hz), 6.02 ppm (2H, m). Found: C, 81.00; H, 8.97%. Calcd for $C_{12}H_{16}O$: C, 81.77; H, 9.15%.

anti-**20**-OTs: Mp 132—133 °C. NMR (δ): 1.38 (1H, dt, J=10 and 6 Hz), 2.44 (3H, s), 4.98 (1H, t, J=7 Hz), 5.48 (2H, br.s), 6.03 (2H, d, J=1 Hz), 7.32 (2H, d, J=8.5 Hz), 7.76 ppm (2H, d, J=8.5 Hz). Found: C, 68.93; H, 6.65%. Calcd for $C_{19}H_{22}O_3S$: C, 69.06; H, 6.71%.

Catalytic Reduction of exo-*Tricyclo*[*4.4.1.1*^{2,5}]*dodeca-3,7,9-trien*-syn-*11-ol* (syn-***18**-OH). *Prepartaion of* syn-***21**-OH and* syn-***22**-OH*: Two grams of *syn*-**18**-OH was hydrogenated in 50 ml of methanol with 10% Pd–C catalyst (200 mg) at room temperature. After 2.1 mol of hydrogen uptake, the catalyst and the solvent were removed, giving 2 g of an oil. *syn*-**21**-OH and *syn*-**22**-OH were partly separated by silica gel chromatography eluted with a mixture of hexane and ether.

syn-**21**-OH: Oil. IR: 3300 cm^{-1}. NMR (δ): 1.0 (1H, m), 4.13 (1H, br.s), 5.62 ppm (2H, m). Found: C, 81.02; H, 10.06%. Calcd for $C_{12}H_{18}O$: C, 80.85; H, 10.18%.

syn-**21**-OTs: Mp 121—122 °C. NMR (δ): 1.0 (1H, m), 2.44 (3H,s), 4.85 (1H, br.s), 5.60 (2H, complex), 7.46 (2H, d, J=8 Hz), 7.90 ppm (2H, d, J=8 Hz). Found: C, 68.75; H, 7.16%. Calcd for $C_{19}H_{24}O_3S$: C, 68.64; H, 7.28%.

syn-**22**-OH: Oil. IR: 3300 cm^{-1}. NMR (δ): 1.0 (1H, m), 1.5—2.4 (14H, complex), 3.95 (1H, br.s), 5.45 ppm (2H, br.s). Found: C, 80.88; H, 10.08%. Calcd for $C_{12}H_{18}O$: C, 80.85; H, 10.18%.

syn-**22**-OTs: Mp 113—114.5 °C. NMR (δ): 1.0 (1H, m), 2.44 (3H, s), 4.73 (1H, br.s), 5.50 (2H, br.s), 7.44 (2H, d, J=8.5 Hz), 7.90 ppm (2H, d, J=8.5 Hz). Found: C, 68.68; H, 7.35%. Calcd for $C_{19}H_{24}O_3S$: C, 68.64; H, 7.28%.

Catalytic Reduction of exo-*Tricyclo*[*4.4.1.1*^{2,5}]*dodeca-3,7,9-trien*-anti-*11-ol* (anti-***18**-OH). *Preparation of* anti-***21**-OH and* anti-***22**-OH*: Compound *anti*-**18**-OH was reduced similarly to a 1: 1 mixture of *anti*-**21**-OH and *anti*-**22**-OH. These alcohols were partly separated by silica gel chromotography.

anti-**21**-OH: Oil. IR 3370 cm^{-1}. NMR (δ); 1.05 (1H, m), 1.4—2.7 (14H, complex), 4.03 (1H, t, J=5.2 Hz), 5.65 (1H, ddd, J=11, 6.5, and 2.5 Hz), 6.90 ppm (1H, dd, J=11 and 4.5 Hz). Found: C, 81.02; H, 10.07%, Calcd for $C_{12}H_{18}O$: C, 80.85; H, 10.18%.

anti-**21**-OTs: Mp 99—100.5 °C. NMR (δ): 1.05 (1H, m), 2.46 (3H, s), 4.90 (1H, t, J=5 Hz), 5.10 (1H, ddd, J=12, 5, and 2 Hz), 5.88 (1H, dt, J=12 and 4.5 Hz), 7.47

(2H, d, J=8 Hz), 7.89 ppm (2H, d, J=8 Hz). Found: C, 68.62; H, 7.25%. Calcd for $C_{19}H_{24}O_3S$: C, 68.64; H, 7.28%.

anti-**22**-OH: Oil. IR: 3350 cm^{-1}. NMR (δ): 1.00 (1H, m), 1.55 (4H, m), 2.1—2.50 (9H, complex), 4.05 (1H, t, J=5.5 Hz), 5.54 ppm (2H, t, J=2 Hz). Found: C, 81.00; H, 10.10%. Calcd for $C_{12}H_{18}O$: C, 80.85; H, 10.18%.

anti-**22**-OTs: Mp 120—121 °C. NMR (δ): 1.0 (1H, m), 1.45—2.20 (13H, complex), 2.42 (3H, s), 4.92 (1H, t, J=5.5 Hz), 5.48 (2H, t, J=2 Hz), 7.35 (2H, d, J=8 Hz), 7.80 ppm (2H, d, J=8 Hz). Found: C, 68.54; H, 7.37%. Calcd for $C_{19}H_{24}O_3S$: C, 68.64; H, 7.28%.

Catalytic Reduction of syn-***18-OH*** *and* anti-***18-OH***. *Preparation of* syn-***23-OH*** *and* anti-***23-OH***: 500 mg of *syn*-**18**-OH was hydrogenated in methanol (10 ml) with 10% Pd-C catalyst (100 mg) at room temperature for two days and the catalyst and solvent were removed. Recrystallization of the residue from petroleum ether yielded 450 mg of *syn*-**23**-OH.

syn-**23**-OH: Mp 80—81 °C. IR: 3350 cm^{-1}. NMR (δ): 0.8—2.3 (18H, complex), 3.92 ppm (1H, s). Found: C, 79.67; H, 11.19%. Calcd for $C_{12}H_{20}O$: C, 79.94; H, 11.18%.

syn-**23**-OTs: NMR (δ): 2.46 (3H, s), 4.68 (1H, br.s), 7.43 (2H, d, J=8 Hz), 7.88 ppm (2H, d, J=8 Hz). Unstable in air.

Catalytic reduction of *anti*-**18**-OH was performed exactly the same way to give *anti*-**23**-OH.

anti-**23**-OH: Mp 73—75 °C. IR: 3400 cm^{-1}. NMR (δ): 1.0 (1H, br.d, J=11 Hz), 1.2—2.2 (18H, complex), 4.15 ppm (1H, br.t, J=4 Hz). Found: C, 79.26; H, 10.99%. Calcd for $C_{12}H_{20}O$: C, 79.94; H, 11.18%.

anti-**23**-OTs: Mp 96.5—97.5 °C. NMR (δ): 0.95 (1H, br.d, J=12 Hz), 1.2—2.2 (17H, complex), 2.45 (3H, s), 4.87 (1H, t, J=5 Hz), 7.35 (2H, d, J=8.7 Hz), 7.80 ppm (2H, d, J=8.7 Hz). Found: C, 68.34; H, 7.89%. Calcd for $C_{19}H_{26}O_3S$: C, 68.23; H, 7.84%.

Solvolysis of anti-***18-OTs***. *anti*-**18**-OTs (4 g) was heated at 110 °C for 24 h in acetic acid (150 ml) with sodium acetate (1.3 g). The resulting cooled solulon was neutralized with sodium hydrogencarbonate and extracted with a mixed solvent of ether and benzene. After the extract was washed with water and dried, the solvent was removed to yield 2 g of an oil. The residue was chromatographed on silica gel (100 g) to give an acetate mixture (1.73 g). No product originated from fragmentation was detected.

The acetate (1.73 g) in dry ether (40 ml) was treated at room temperature for 5 h with $LiAlH_4$ (250 mg) in dry ether (30 ml). After excess reagent was decomposed, the reaction mixture was washed with 2 M HCl and water, dried, and the solvent was removed to give an alcohol mixture (1.16 g).

The alcohol (1.16 g) in dry pyridine (50 ml) was oxidized overnight at room temperature with chromium(VI) oxide-pyridine (1.2 eqv.), poured into ice water (50 ml), neutralized with 2 M HCl and extracted with ether. The extract was washed with water, dried and evaporated, leaving an oil (1.06 g). The residue was chromatographed on silica gel (600 g) to give a mixture of **24**-O[24a] (760 mg), and **25**-O (165 mg).[24b] **24**-O was further chromatographed on silica gel impregnated with $AgNO_3$ afforded the two previously known ketones.[24a]

Solvolysis of anti-***19-OTs***. The mixture of *anti*-**19**-OTs and *anti*-**20**-OTs (550 mg) was solvolyzed in 75% dioxane (20 ml) at 90° for 5 hr. After addition of water (20 ml), the reaction mixture was extracted with a mixed slvent of benzene and ether. The extract was washed with water, dried and evaporated, leaving an oil (400 mg). The residue was chromatographed on silica gel (250 g) to give hydrocarbons (20 mg), *anti*-**20**-OTs (220 mg) and alcohols (120 mg).

The alcohols (100 mg) in dry pyridine (5 ml) were oxidized with chromium(VI) oxide-pyridine complex (2.0 eqv.) to give an oily ketone (90 mg). The oil was purified by chromatography on silica gel (5 g) to give **26**-O (75 mg).

26-O: Oil. MS m/e: 174 (M^+). IR: 1657 cm^{-1}. NMR (δ): 1.4—2.2 (5H, m), 2.5—2.9 (5H, m), 5.5 (1H, m), 5.83 (1H, dt, J=6 and 2 Hz), 6.15 (1H, d, J=11 Hz), 7.25 ppm (1H, dd, J=11 and 9 Hz). Found: C, 82.68; H, 8.16%. Calcd for $C_{12}H_{14}O$: C, 82.72; H, 8.10%. Cycloheptatriene was identified by GLC examination of the hydrocarbon fraction.

Catalytic Hydrogenation of ***26-O***. A methanol (10 ml) solution of **26**-O (20 mg) was hydrogenated with 10% Pd-C catalyst (10 mg) at room temperature and the catalyst and the solvent were removed to give previously konwn saturated ketone quantitatively.[24]

Solvolysis of syn-***19-OTs*** *and Oxidation of the Product to* ***27-O***. The mixture of *syn*-**19**-OTs and *syn*-**20**-OTs (2.2 g) was heated for 4.5 h under reflux in 80% acetone (37 ml), and poured into ice water (20 ml), leaving a crystalline substance (720 mg) which was unchanged *syn*-**20**-OTs. The filtrate was extracted with a mixed solvent of benzene and ether, washed with water, dried and evaporated the solvent to give 800 mg of an oil. The oil was chromatographed on silica gel (40 g) to give *syn*-**20**- OTs (100 mg) and an oil (570 mg).

The oil (320 mg) was oxidized (10 min) at room temperature with chromium(VI) oxide-pyridine complex (6 eqv.) in dichlormethane (30 ml), and filtered through silica gel layer, evaporated the solvent to give **27**-O (300 mg).

27-O: Oil. MS m/e: 174 (M^+). IR: 1727 cm^{-1}. NMR (δ): 1.7—2.3 (12H, m), 6.08 ppm (2H, m). Found: C, 82.81; H, 8.06%. Calcd for $C_{12}H_{14}O$: C, 82.72; H, 8.10%.

Dehydrogenation of ***27-O***. **27**-O (50 mg) and DDQ (10 eqv.) were heated for 2 days in dry benzene (10 ml), under reflux. The reaction mixture was filtered through alumina layer, evaporated to give semicrystalline material (40 mg). Purification by recrystallization yielded the ketone **28** (38 mg).

28: Mp 70.5—71 °C. NMR (δ): 1.5 (1H, d, J=10.5 Hz), 1.8 (1H, ddd, J=7, 4.5, and 1.4 Hz), 2.3—2.7 (2H, complex), 2.8 (1H, t, J=7 Hz), 3.1 (1H, d, J=6 Hz), 7.0—7.3 ppm (4H, AA'BB').

Solovolysis of syn-***20-OTs***. *syn*-**20**-OTs (720 mg) in 75% dioxane (20 ml) was heated for 18 h under reflux and cooled reaction mixture was extracted with ether. The extract was dried and evaporated to give an oil (490 mg). The residue was chromatographed on silica gel (300 g) to yield *syn*-**29**-OH (162 mg), *anti*-**29**-OH (40 mg) and **30**-OH (90 mg).

syn-**29**-OH: Mp 80—81 °C. MS m/e: 176 (M^+). IR: 3300 cm^{-1}. NMR (δ): 0.94 (1H, tt, J=8 and 1.5 Hz), 1.2—2.0 (12H, m), 4.00 (1H, s), 5.97 ppm (2H, m). Found: C, 81.62; H, 9.20%. Calcd for $C_{12}H_{16}O$: C, 81.77; H, 9.15%.

anti-**29**-OH: Oil. MS m/e: 176 (M^+). IR: 3350 cm^{-1}. NMR (δ): 0.81 (1H, tt, J=7 and 1.5 Hz), 1.2—2.3 (12H, m), 4.46 (1H, dd, J=5.5 and 3.2 Hz), 6.05 ppm (2H, m). Found: C, 81.81; H, 9.15%. Calcd for $C_{12}H_{16}O$: C, 81.77; H, 9.15%.

30-OH: Mp 86—87 °C. MS m/e: 158 (M^+-H_2O). IR: 3300 cm^{-1}. NMR (δ): 1.6—2.6 (11H, m), 3.87 (1H, m), 6.08 (2H, m), 6.23 (1H, t, J=5 Hz), 6.37 ppm (1H, t, J=5 Hz). Found: C, 81.98; H, 9.21%. Calcd for $C_{12}H_{16}O$: C, 81.77; H, 9.15%.

Oxidation of ***30-OH*** *to* ***30-O***. **30**-OH (50 mg) in dichloromethane (13 ml) was oxidized for 10 min. at toom temper-

ature with chromium(VI) oxide–pyridine complex (6 eqv.) and filtered through silica gel layer, evaporated to give the ketone **30**-O (45 mg).

30-O: Oil. MS *m/e*: 174 (M^+). IR: 1723 cm^{-1}. NMR (δ): 1.5—3.0 (10H, m), 6.00 (2H, m), 6.25 (1H, tt, $J=7$ and 1.5 Hz), 6.67 ppm (1H, tt, $J=7$ and 1.2 Hz). Found: C, 82.66; H, 8.14%. Calcd for $C_{12}H_{14}O$: C, 82.72; H, 8.10%.

Dehydrogenation of ***30***-O. **30**-O (30 mg) was dehydrogenated to the known ketone **31**[25] (27 mg), by the same procedure as for **27**-O.

Oxidation of syn-***29***-*OH and* anti-***29***-*OH*. *syn*-**29**-OH (10 mg) and *anti*-**29**-OH (110 mg) were oxidized to the same ketone **29**-O by the oxidation with chromium(VI) oxide-pyridine complex under the conditions described previously.

29-O: Oil. MS *m/e*: 174 (M^+). IR: 1729 cm^{-1}. NMR (δ): 1.7—2.4 (12H, m), 6.03 (2H, m). Found: C, 82.88; H, 8.09%. Calcd for $C_{12}H_{14}O$: C, 82.72; H, 8.10%.

29-O was oxidized to **28**[25] with DDQ in refluxing benzene for 48 h.

Solvolysis of anti-***18***-*OTs in the Presence of Trapping Reagents. Hydrolysis in the Presence of Acetylacetone*: *anti*-**18**-OTs (135 mg) was heated at 130 °C for 10 days in dioxane–H_2O (3: 1) with sodium acetate (38 mg) and acetylacetone (2 ml). After cooling, sodium *p*-toluenesulfonate (66 mg) was filtered off and the solvent was evaporated. Tropylacetylacetone[42] mp 126—126.5 °C (8 mg) was obtained from the concentrated mixture. NMR spectrum of mother liquor shows to contain *anti*-**18**-OTs (51%), tropylacetylacetone (44%) and acetylacetone (4.5%). Thus, total yield of tropylacetylacetone was 57% with 33% recovery of *anti*-**18**-OTs.

Acetolysis in the Presence of Acetylacetone. *anti*-**18**-OTs (200 mg) was heated at 105 °C for 24 h in acetic acid (10 ml) with sodium acetate (62 mg) and acetylacetone (2 ml). The resulting solution was neutralized with sodium hydrogencarbonate to pH 6, extracted twice with chloroform, washed with brine and dried over sodium sulfate. Removal of solvents under reduced pressure gave 127 mg of oil, NMR spectrum of which revealed the presence of 51% of tropylacetylacetone[42] and 41% of acetate mixture correspond to **24**-OAc.

Acetolysis in the Presence of N-*Phenylmaleimide*. *anti*-**18**-OTs (202 mg) was heated at 105 °C for 15 h in acetic acid (10 ml) with sodium acetate (63 mg) and *N*-phenylmaleimide (500 mg). The resulting reaction mixture was neutralized with sodium hydrogencarbonate and extracted 3 times with chloroform. Organic layer was washed twice with water, once with brine and dried over sodium sulfate. Removal of solvents under reduced pressure, followed by column chromatography on silica gel, gave 134 mg (91%) of cyclopentadiene-*N*-phenylmaleimide adduct.[43]

Acetolysis in the Presence of Methylcyclopentadiene. *anti*-**18**-OTs (500 mg) was solvolyzed for 13 h as in the previous section, with the dropwise addition of methylcyclopentadiene (500 mg) in acetic acid (10 ml). The reaction mixture turned dark immediately. The work up, treatment with $LiAlH_4$ and chromic acid oxidation, carried out exactly as in the previous section, furnished 65 mg of an α,β-unsaturated ketone mixture. NMR spectra of the mixture showed small broad singlet at 1.69 ppm. Mass spectrum (at 15 eV) showed *m/e* 172 with the 1/15 intensity of *m/e* 158.

Solvolysis of syn-***18***-*OTs*. *syn*-**18**-OTs (204 mg) was heated in 75% aq dioxane in the presence of *N*-phenylmaleimide (525 mg) and sodium acetate (62 mg) for 5 h at 95 °C yielded *N*-phenylmaleimide adduct of *syn*-**32**-OH (667 mg) in 95% yield. No cyclopentadiene adduct was detected.

We are indebted to Mrs. Hinako Ando, Mr. Yuji Ikegami and Mr. Akira Nakamura for their technical assistance. Dr. John B. Collins performed the molecular mechanics and Dr. Peter Gund the hindrance calculations. The work at Princeton was supported by grants from the National Science Foundation and the National Institute of Health.

References

1) G. D. Sargent, N. Lowry, and S.D. Reich, *J. Am. Chem. Soc.*, **89**, 5985 (1967).
2) L. A. Paquette and G.L. Thompson, *J. Am. Chem. Soc.*, **95**, 2364 (1973).
3) P. v. R. Schleyer, G. W. Van Dine, U. Schöllkopf, and J. Paust, *J. Am. Chem. Soc.*, **88**, 2868 (1966).
4) B. Föhlish and W. Vodrazka, *Tetrahedron Lett.*, **1971**, 1207.
5) D. R. Kelsey and R. G. Bergman, *J. Am. Chem. Soc.*, **93**, 1953 (1971).
6) A. C. Cope and M. Burg, *J. Am. Chem. Soc.*, **74**, 168 (1952).
7) R. Huisgen and W. E. Konz, *J. Am. Chem. Soc.*, **92**, 4102 (1970).
8) W. E. Konz, W. Hechtl, and R. Huisgen, *J. Am. Chem. Soc.*, **92**, 4104 (1970).
9) R. Huisgen, W. E. Konz, and G. E. Gream, *J. Am. Chem. Soc.*, **92**, 4105 (1970).
10) G. Schröder, G. Kirsh, J. F. M. Oth, R. Huisgen, W. E. Konz, and U. Schregg, *Chem. Ber.*, **104**, 2405 (1971).
11) R. N. McDaonald and E. P. Lyznicki, Jr., *J. Am. Chem. Soc.*, **93**, 5290 (1971).
12) K. Fellenberger, U. Schöllkopf, C. A. Bahn, and P. v. R. Schleyer, *Tetrahedron Lett.*, **1972**, 359; J. J. Tufariello, A. C. Baker, and J. J. Spadaro, Jr., *ibid.*, **1972**, 363.
13) J. J. Tufariello and A. C. Bayer, *Tetrahedron Lett.*, **1972**, 3551.
14) E. Vogel, *Angew. Chem.*, **73**, 548 (1961); H. Kiefer, Dissertation, Köln, 1962; E. Vogel, *Angew. Chem.*, **74**, 829 (1962); *Angew. Chem., Int. Ed. Engl.*, **2**, 1 (1963).
15) J. C. Barborak, T. -M. Su, P. v. R. Schleyer, G. Boche, and G. Schneider *J. Am. Chem. Soc.*, **93**, 279 (1971) and the references cited therein.
16) A. G. Anastassiou and E. Yakali, *Chem. Commum.*, **1972**, 92.
17) (a) R. Breslow and J. M. Hoffman, Jr., *J. Am. Chem. Soc.*, **94**, 2110 (1972); (b) R. Breslow and J. M. Foffman, Jr., *ibid.*, **94**, 2111 (1972).
18) R. B. Woodward and T. J. Katz, *Tetrahedron*, **5**, 70 (1959); P. Yates and P. Eaton, *Tetrahedron Lett.*, **1960**, No 11, 5; R. C. Cookson, J. Hudec, and R. O. Williams, *ibid.*, **1960**, No. 22, 29.
19) J. Haywood-Farmer, B. T. Friedlander, A. Crawford, L. M. Thompson, and W. Wetzer, *Can. J. Chem.*, **53**, 3078 (1975).
20) (a) S. Itô, Y. Fujise, T. Okuda, and Y. Inoue, *Bull. Chem. Soc. Jpn.*, **39**, 1351 (1966); (b) R. C. Cookson, B. V. Drake, J. Hudec, and A. Morrison, *Chem. Commum.*, **1966**, 15.
21) (a) Calculations performed by Mr. John B. Collins; (b) For a critical evalutaion, see: E. M. Engler, J. D. Andose, and P. v. R. Schleyer, *J. Am. Chem. Soc.*, **95**, 8005 (1973); E. M. Engler, Ph. D. Thesis, Princeton University, Prieceton, N. J. (1973).
22) M. Karplus *J. Chem. Phys.*, **30**, 11 (1959).
23) W. T. Wipke and P. Gund, *J. Am. Chem. Soc.*, **96**, 299 (1974).

24) (a) S. Itô, K. Sakan, and Y. Fujise, *Tetrahedron Lett.*, **1970**, 2873; (b) S. Itô and I. Itoh, *ibid.*, **1971**, 2969: (c) S. Itô, K. Sakan and Y. Fujise, *ibid.*, **1969**, 775.

25) S. Itô, T. Otomo, Y. Fujise, and K. Sakan, *Chem. Commum.*, **1968**, 782.

26) (a) C. S. Foote, *J. Am. Chem. Soc.*, **86**, 1853 (1964); (b) P. v. R. Schleyer, *ibid.*, **86**, 1855, 1856 (1964).

27) C. W. Jefford, D. T. Hill, and J. Gunsher, *J. Am. Chem. Soc.*, **89**, 6881 (1967).

28) C. Sandris and G. Ourisson, *Bull. Soc. Chim. Fr.*, **1958**, 1524.

29) Calculations by Jefford, *et al.*[27] apparently did not include torsional terms. Also the (GS-Ts) term used by them for **35** was 1.8 kcal/mol (the solvolytic value).

30) The rate constant of **34** in Ref. 27 was converted to that in 60% acetone, $k=1.55\times10^{-4}$, and compared with the value in Table 3.

31) D. Faulkner, M. A. McKervey, D. Lenoir, C. A. Senkler, and P. v. R. Schleyer, *Tetrahedron Lett.*, **1973**, 705 and the references cited therein.

32) N. A. LeBel and R. J. Maxwell, *J. Am. Chem. Soc.*, **91**, 2307 (1969).

33) D. J. Raber, G. J. Kane, and P. v. R. Schleyer, *Tetrahedron Lett.*, **1970**, 4117.

34) P. G. Gassman, J. Seter, and F. J. Williams, *J. Am. Chem. Soc.*, **93**, 1673 (1971); P. G. Gassman and F. J. Williams, *ibid.*, **93**, 2704 (1971).

35) For our definition of ion pair, see T. W. Bentley and P. v. R. Schleyer, *J. Am. Chem. Soc.*, **98**, 7658 (1976). F. L. Schadt, T. W. Bentley, and P. v. R. Schleyer, *ibid.*, **98**, 7667 (1976).

36) T. G. Traylor, W. Hanstein, H. J. Berwin, N. A. Clinton, and R. S. Brown, *J. Am. Chem. Soc.*, **93**, 5715 (1971) and the references cited therein; R. Hoffmann, L. Radom, J. A. Pople, P. v. R. Schleyer, W. J. Hehre, and L. Salem, *ibid.*, **94**, 6221 (1972).

37) W. von E. Doering and W. R. Roth, *Tetrahedron*, **18**, 67 (1962); A. Brown, M. J. S. Dewar, and W. Schoeller, *J. Am. Chem. Soc.*, **92**, 5516 (1970); M, J. S. Dewar, "Quantitative SCF MO Studies of Reaction Mechanisms," XXIIIrd International Congress of Pure and Applied Chemistry, Butterworths, Vol. 1, London (1971), pp. 1—30.

38) M. J. Goldstein and R. Hoffmann, *J. Am. Chem. Soc.*, **93**, 6193 (1971).

39) P. v. R. Schleyer and C. J. Lancelot, *J. Am. Chem. Soc.*, **91**, 4297 (1969).

40) L. F. Fiser and M. Fiser, "Reagents for Organic Synthesis," John Wiley and Sons, Vol. 1, New York (1967), p. 1180.

41) This is due to the coupling with OH, as acertained by its change upon addition of acidic D_2O; *syn* compounds to a broad singlet and *anti* compounds to a triplet ($J=\approx5$ Hz).

42) K. Conrow, *J. Am. Chem. Soc.*, **81**, 5461 (1959).

43) H. Hopff and C. W. Rautenstrauch, *Chem. Abstr.*, **36**, 1046 (1942).

A Remarkable Solvent Effect on the Reductive Silylation of Carboxylic Esters. Preparation of 1,1-Bis(trimethylsilyl)-1-alkanols

Isao KUWAJIMA,* Naoki MINAMI, Toru ABE, and Toshio SATO†

Department of Chemistry, Tokyo Institute of Technology, Ookayama, Meguro-ku, Tokyo 152

†*Department of Chemistry, Faculty of Science, The University of Tokyo, Hongo, Bunkyo-ku, Tokyo 113*

(Received February 4, 1978)

1,1-Bis(trimethylsilyl)-1-alkanols were obtained in good yields when ethyl esters of the corresponding carboxylic acids were treated with sodium suspension and chlorotrimethylsilane in refluxing tetrahydrofuran followed by acidic hydrolysis.

Various carboxylic esters undergo facile reductive dimerization to afford the corresponding 1,2-bis(trimethylsiloxy)alkenes **1** on treatment with alkali metals such as lithium, sodium, or potassium–sodium alloy in the presence of chlorotrimethylsilane.[1] Bloomfield and Owsley who have studied this type of reaction extensively,[2] suggested that the conventionally adopted mechanism involving dimerization of the radical species is not operative, the reaction proceeding through the nucleophilic attack of the radical anion **3** (Scheme 1) initially formed on the carboxylic ester, followed by several steps. In connection with these reactions, we have found that trimethylsilyl carboxylates give the trimethylsilyl ethers of the corresponding 1,1-bis(trimethylsilyl)-1-alkanols **2** exclusively by a similar treatment in refluxing tetrahydrofuran (THF);[3] several synthetic reactions with use of 1,1-bis(trimethylsilyl)-1-alkanols[4] were developed. In order to establish a precise procedure for the preparation of such kind of alcohols, reductive silylation reactions of various esters have been studied in detail.

$$R\text{-}CO_2R' \longrightarrow \begin{cases} \longrightarrow Me_3SiO\text{-}CR{=}CR\text{-}OSiMe_3 & \mathbf{1} \\ \longrightarrow R\text{-}C(SiMe_3)_2\text{-}OSiMe_3 & \mathbf{2} \end{cases}$$

For studying the difference between reaction paths **1** and **2**, trimethylsilyl and ethyl esters of 3-methylbutyric acid were employed as substrates, and their reactions with metallic sodium in the presence of chlorotrimethylsilane were examined by using benzene, ether, tetrahydrofuran (THF), or 1,2-dimethoxyethane (DME) as the reaction solvent, since benzene and ether are usually employed for the preparation of 1,2-bis(trimethylsiloxy)-alkenes **1**. The reactions were performed with commercial sodium suspension in order to eliminate the effect due to the difference in the grade of dispersion of reducing agent. It was found that the solvent plays a crucial role in deciding the reaction path and **1** or **2** can be prepared selectively through a similar procedure simply by changing the reaction solvent (Table 1). Thus, when tetrahydrofuran or dimethoxyethane was used as a solvent, the type **2** product, silyl ether of 1,1-bis(trimethylsilyl)-3-methyl-1-butanol, was obtained exclusively from both of the starting esters, whereas the reactions with the same esters in benzene or ether afforded the type **1** product, 4,5-bis(trimethylsiloxy)-2,7-dimethyl-4-octene, as the major products. In the latter case, addition of dibenzo-18-crown-6 to the reaction system resulted in appreciable enhancement of the formation of **2**, both types of products being obtained in fair yields. No marked difference in product distribution was observed between the reactions of trimethylsilyl and ethyl esters when the same solvent was employed.

The results indicate that the predominant factor for determining the reaction paths is attributable mainly to the different behavior of the anion radical **3** depending on the solvent. In a non-polar solvent such as benzene or ether, the anion radical **3** seems to react with the parent carboxylic ester preferentially to yield the 1,2-disiloxyalkene type of product **1** *via* the reaction paths proposed by Bloomfield and Owsley.[2] On the contrary, chlorotrimethylsilane seems to be a more efficient anion acceptor in a polar solvent such as tetrahydrofuran or 1,2-dimethoxyethane, trapping the anion radical **3** to afford the corresponding 1-alkoxy-1-(trimethylsiloxy)-alkyl radical **4**. Radical **4** thus formed can not participate in the formation of the 1,2-disiloxyalkene **1**, according to the mechanism of Bloomfield and Owsley, which accounts for exclusive formation of **2**. The only available reaction path for radical **4** is expected to be a further one electron reduction with metallic sodium which yields the anionic species **5** (Scheme 1). Silylation of **5** with the chlorosilane would lead to the formation of 1-alkoxy-1-(trimethylsiloxy)alkyltrimethylsilane **6**.

TABLE 1. SOLVENT DEPENDENCE OF THE REDUCTIVE SILYLATION OF ESTER

$$(CH_3)_2CHCH_2\overset{O}{\overset{\|}{C}}OR \xrightarrow{Na\text{–}Me_3SiCl} \underset{(1)}{(CH_3)_2CHCH_2\overset{Me_3SiO}{\overset{|}{C}}{=}\overset{OSiMe_3}{\overset{|}{C}}CH_2CH(CH_3)_2} + \underset{(2)}{(CH_3)_2CHCH_2\overset{OSiMe_3}{\overset{|}{C}}(SiMe_3)_2}$$

R	Product	THF	DME	Benzene[a]	Benzene	Ether
$SiMe_3$	**1**	—	—	36	62	65
	2	91	88	52	4	2
Et	**1**	5	—	48	68	68
	2	93	91	41	—	—

a) The reaction was performed in the presence of dibenzo-18-crown-6 (an equimolar amount with the ester).

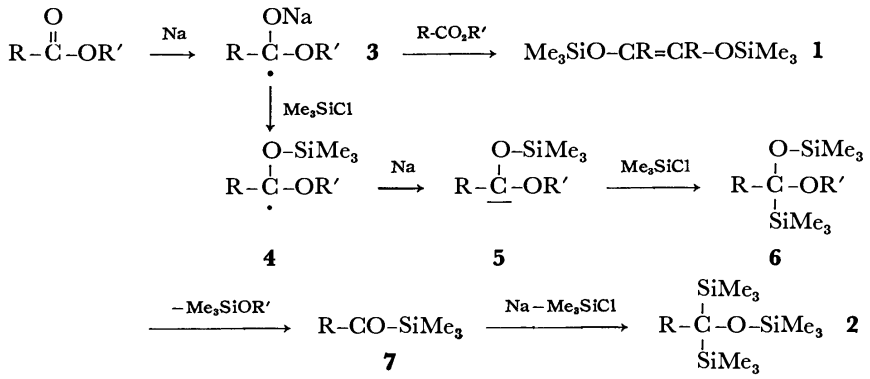

Scheme 1.

This type of product was isolated by Picard *et al.* through the reaction of the corresponding ester with metallic lithium–chlorotrimethylsilane system at low temperature.[5] At a temperature of refluxing tetrahydrofuran, **6** would decompose through removal of alkyl trimethylsilyl ether to yield the corresponding acyltrimethylsilane **7**, which undergoes further reductive silylation to give **2** as the final product. Actually, 3-methylbutyltrimethylsilane was converted into the corresponding **2** by a separate experiment under similar reaction conditions.[6]

We examined the reductive silylation reactions of ethyl esters of various carboxylic acids. All the reactions were performed in a preparative scale (*ca.* 0.2 mol) with a sodium suspension prepared in the usual manner. The results are given in Table 2. All the mono-esters examined afford the corresponding **2** in good yields, without appreciable concomitant formation of type **1** product, when the reactions are carried out at the temperature of refluxing tetrahydrofuran. As compared with the results in Table 1, the yields of the products are smaller, the corresponding acyltrimethylsilanes **7**

TABLE 2. PREPARATION OF 1,1-BIS(TRIMETHYLSILYL)-1-ALKANOL, $R-C(SiMe_3)_2OH$, FROM ETHYL CARBOXYLATE, $R-CO_2C_2H_5$

R	Bp °C/mmHg	Yield	IR (neat) cm^{-1}; NMR (CCl_4)	Molecular formula
C_2H_5	85—87/15	62	3500, 1240, 820; 0.10 (18H, s, $SiCH_3$), 0.80 (1H, s, OH), 0.85 (3H, t, J=8 Hz, CH_3) 1.80 (2H, q, J=8 Hz, CH_2).	$C_9H_{24}OSi_2$
n-C_3H_7	93—95/10	65	3500, 1250, 840; 0.10 (18H, s, $SiCH_3$), 0.80 (1H, s, OH), 0.87 (3H, t, J=8 Hz, C–CH_3) 1.10—2.10 (4H, m, aliphatic CH)	$C_{10}H_{26}OSi_2$
n-C_5H_{11}	105—107/5	65	3440, 1235, 840; 0.06 (18H, s, $SiCH_3$), 0.85 (1H, s, OH), 0.95 (3H, t, J=6 Hz, C–CH_3), 1.10—1.85 (8H, broad, aliphatic CH).	$C_{12}H_{30}OSi_2$
n-C_7H_{15}	106—108/3	65	3450, 1240, 840; 0.05 (18H, s, $SiCH_3$), 0.85 (1H, s, OH), 0.97 (3H, t, J=6 Hz, C–CH_3), 1.10—1.87 (12H, broad, aliphatic CH)	$C_{14}H_{34}OSi_2$
$C_6H_5CH_2CH_2$	127—130/2	64	3430, 1245, 845; 0.13 (18H, s, $SiCH_3$), 0.95 (1H, s, OH), 1.80—2.20 (2H, m, $PhCH_2$), 2.60—2.95 (2H, m, $PhCH_2$), 7.20 (5H, s, aromatic CH)	$C_{15}H_{28}OSi_2$
CH_2=$CH(CH_2)_8$	139—142/3	70	3420, 1250, 845; 0.05 (18H, s, $SiCH_3$), 0.85 (1H, s, OH), 1.05—1.80 (14H, broad, aliphatic CH), 2.05 (2H, m, C=C–CH_2), 4.87 (1H, d, J_{ac}=11 Hz, H_a of H_a\ /H_c C=C, H_b/ \C), 4.92 (1H, d J_{bc}=16 Hz, H_b), 5.12—6.00 (1H, m, H_c)	$C_{17}H_{38}OSi_2$
$(CH_3)_2CHCH_2$	120—122/20	66	3500, 1260, 850; 0.10 (18H, s, $SiCH_3$), 0.82 (1H, s, OH), 1.00 (6H, d, J=6 Hz, CH ($C\underline{H}_3)_2$), 1.10 (1H, m, $CH_2C\underline{H}$ $(CH_3)_2$), 1.60 (2H, d, J=5 Hz, $C\underline{H}_2CH(CH_3)_2$)	$C_{12}H_{28}OSi_2$
$(CH_3)_2CH$	114—115/30	66	3500, 1250, 860, 840; 0.10 (18H, s, $SiCH_3$), 0.80 (1H, s, OH), 1.00 (6H, d, J=7 Hz, CH ($C\underline{H}_3)_2$), 1.60 (1H, m, $C\underline{H}(CH_3)_2$)	$C_{10}H_{26}OSi_2$
n-$C_4H_9(C_2H_5)CH$	98—101/0.25	68	3450, 1250, 840; 0.13 (18H, s, $SiCH_3$), 0.70 (1H, s, OH), 0.95 (3H, t, J=7 Hz, C–CH_3), 1.00 (3H, t, J=7 Hz, C–CH_3), 1.15—2.10 (9H, m, aliphatic CH).	$C_{14}H_{34}OSi_2$
$-(CH_2)_8-$	173—176/0.3	56	3450, 1245, 840; 0.03 (36H, s, $SiCH_3$), 0.73 (2H, s, OH), 1.10—1.85 (16H, broad, aliphatic CH).	$C_{22}H_{54}O_2Si_2$

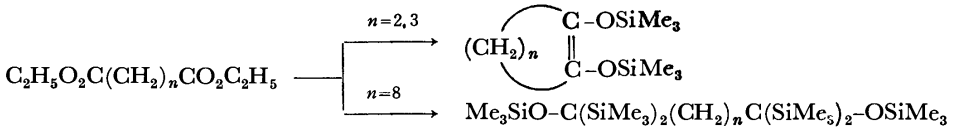

Scheme 2.

being formed as by-products. This can be attributed to the decreased activity of sodium suspension. Silyl ethers **2** usually undergo facile acidic hydrolysis to afford the corresponding 1,1-bis(trimethylsilyl)-1-alkanols in high yields. The only exceptional case was that with the silyl ether of 2,2-dimethyl-1,1-bis(trimethylsilyl)-1-propanol,[7] which could not be hydrolyzed even under severe reaction conditions.

In the reactions with diesters, succinic and glutaric esters gave type **1** products exclusively even when the reactions were carried out in tetrahydrofuran. This can be explained by assuming that the internal nucleophilic attack of the radical anion on the remaining ester carbonyl takes place preferentially since the favorable five- and six-membered intermediates are involved in these processes. In contrast, further elongation of the carbon chain dissecting two ester sites makes the above process less favorable, the corresponding **2** being obtained in good yield. For example, diethyl ester of decane-1,10-dicarboxylic acid could be converted into 1,1,10,10-tetrakins(trimethylsilyl)-1,10-decanediol in 56% yield through the reductive silylation reaction followed by acidic hydrolysis.

Organo-silicon compounds have recently been employed for synthetic purposes in various aspects.[8] The present procedure which provides a simple method for introducing two silyl groups into the same carbon is useful for the preparation of several other types of organo-silicon compounds.[4d-f]

Experimental

All the boiling points are uncorrected. IR spectra were recorded on a Hitachi 260-10 or a Hitachi EPIG3 spectrometer. NMR spectra were taken in a Vatian T-60 spectrometer, using dichloromethane as an internal standard. Elementary compositions of 1,1-bis(trimethyllsilyl)alkyl trimethylsilyl ethers were determined by means of high mass spectra, using a Hitachi RMU-7M mass spectrometer.

Materials. Tetrahydrofuran (THF), 1,2-dimethoxyethane (DME), ether, and benzene were purified shortly before use by drying and distillation over sodium–benzophenone or sodium. Chlorotrimethylsilane was purified by distillation over CaH_2. Esters were purified by distillation. Trimethylsilyl 3-methylbutyrate was prepared by treating the corresponding carboxylic acid with chlorotrimethylsilane in the presence of sidium hydride in tetrahydrofuran in 85% yield.

Two kinds of sodium suspensions were used. (A), a commercial, product (Alfa Ventron), was used after washing three times with hexane and then drying under reduced pressure. (B) was prepared in xylene, according to the usual procedure and was used after xylene had been removed by decantation and then evaporation under reduced pressure.

Reductive Silylation Reactions of Ehtyl or Trimethylsilyl 3-Methylbutyrate in Various Solvents. The ester (3 mmol) and bibenzyl (220 mg) in an appropriate solvent (3 ml) was added dropwise to sodium suspension A (0.03 g atom) suspended in the same solvent (5 ml) containing chlorotrimethylsilane (24 mmol) during a period of 45 min at room temperature under argon atmosphere. Exothermic reaction took place immediately and the temperature rose nearly to the refluxing point of solvent. After being stirred for 1.5 h, the yields were determined by GLC analysis [3 mm×1 m column of 10% SE30 on Diasolid L, column temperature 110 °C] by comparison with the internal standard (bibenzyl). The results are given in Table 1.

Preparation of 1,1-Bis(trimethylsilyl)-1-aklanol. General Procedure: A tetrahydrofuran solution (100 ml) of an ethyl ester (0.2 mol) and chlorotrimethylsilane (174 g, 1.6 mol) was added to sodium suspension B (36.8 g, 1.6 g atom) suspended in boiling tetrahydrofuran (300 ml) during a period of 1 h under argon atmosphere. After addition had been completed, the reaction mixture was heated to refluxing for 30 min under stirring. The materials deposited were filtered off and the solvent was removed under reduced pressure. The residual oil was treated with 10 ml of 6 M hydrochloric acid in 200 ml of dioxane at 50 °C for 1 h, and was neutralized with aq $NaHCO_3$. The corresponding 1,1-bis(trimethylsilyl)-1-alkanol was obtained from the ether extracts after removal of the solvent, followed by distillation using Vigreux column (*ca.* 2×30 cm). Yields, boiling points, and spectral data are given in Table 2.

The authors wish to thank the Ministry of Education, for Grant-in-Aid 247017.

References

1) For reviews, see; K. Ruhlmann, *Synthesis*, **1971**, 236; J. J. Bloomfield, D. C. Owsley, and J. M. Nelke, *Org. React.*, **23**, 259 (1976).

2) J. J. Bloomfield and D. C. Owsley, *J. Org. Chem.*, **40** 393 (1975).

3) I. Kuwajima, T. Sato, N. Minami, and T. Abe, *Tetrahedron Lett.*, **1976**, 1591.

4) For synthetic reactions by the use of the alcohol, see; a) I. Kuwajima, T. Sato, M. Arai, and N. Minami, *Tetrahedron Lett.*, **1976**, 1817; b) I. Kuwajima, N. Minami, and T. Sato, *ibid.*, **1976**, 2253; c) I. Kuwajima, T. Abe, and N. Minami, *Chem. Lett.*, **1976**, 993; d) N. Minami and I. Kuwajima, *Tetrahedron Lett.*, **1977**, 1423; e) I. Kuwajima M. Arai, and T. Sato, *J. Am. Chem. Soc.*, **99**, 4181 (1977); f) N. Minami, T. Abe, and I. Kuwajima, *J. Organomet. Chem.*, **145**, C1 (1978).

5) J. P. Picard, A. Ekouya, J. Dunogues, N. Duffaut, and R. Calas, *J. Organomet. Chem.*, **93**, 51 (1975).

6) In this experiment, a small amount of trimethylsilyl enol ether of the corresponding acyltrimethylsilane[4e] was also formed. The formation is attributable to the existence of sodium hydroxide formed on the surface of metallic sodium.

7) Trimethylsilyl 2,2-dimethylpropionate also afforded the corresponding type **2** product. We are indebted to Dr. J. P. Picard for his correction of our mistake in the preliminary report.[3]

8) I. Fleming, *Chem. Ind. (London)*, **1975**, 449; P. F. Hudrlik, "New Applications of Organometallic Reagents in Organic Synthesis," ed by D. Seebach, Elsevier, Amsterdam (1976), p. 127.

The Reaction of Azidotriazines with Pyridines and Triphenylphosphine

Kenji FUJINUMA, Yoji HASHIDA, and Kohji MATSUI*

Department of Synthetic Chemistry, Faculty of Engineering, Gunma University, Kiryu, Gunma 376

(Received February 6, 1978)

2-Azido-4,6-dimethoxy-1,3,5-triazine (**1a**) gave an adduct with pyridine in a molar ratio of 1:1. On the contrary, 2-azido-4,6-bis(dimethylamino)-1,3,5-triazine (**1b**) did not react with pyridine. Similarly, **1a** gave an adduct with 3-methylpyridine, whereas in the reactions of **1a** with 2-methyl-, 4-methyl-, and 2,6-dimethylpyridines, 2-amino-4,6-dimethoxy-1,3,5-triazine was obtained instead of the adduct. On the other hand, **1a** and **1b** gave the corresponding triazinyliminophosphoranes with triphenylphosphine.

Organic azides are well known to react with organic bases to yield the corresponding ylides.[1] During the course of our study of the reactions of azido-1,3,5-triazines, it has become apparent that azido-1,3,5-triazines have unique properties situated between those of ordinary aryl and acyl azides.[2] Thus, triazinyl ylides, if prepared, are expected to have different characters from those of ordinary acyl and aryl ylides. On the other hand, even though the reaction of azidotriazine with an organic base can be expected to be one of the general routes for the preparation of triazinyl ylides, this reaction has not yet been investigated. This paper will report the thermal reactions of azidotriazines with several pyridine derivatives and triphenylphosphine.

Results and Discussion

Reactions of Azido-1,3,5-triazines with Pyridine. When 2-azido-4,6-dimethoxy-1,3,5-triazine (**1a**) was heated in pyridine (**2**) under reflux, an 1:1 adduct (**3**) was obtained in a quantitative yield (Scheme 1). On the basis of the spectral data, one of the methyl groups of the adduct was found to be located at the ring nitrogen atom. For the adduct, **3** and **3'** are suggested as possible; of the two, **3** may be more stable. Among three possible structures (**3a**, **3b**, and **3c**), **3a** is most probable, because the highest stabilization by the delocalization of the negative charge can be expected in this case.[3] **3** is considered to result from an intermediate (**A**) produced by the addition of azidotriazine to pyridine, followed by the O→N migration of one methyl group. The facile migration of the methyl group in the intermediate (**A**) is probably due to a decrease in the aromaticity of the triazine ring because of a large contribution of the $\mathbf{A}_2$ formula.

On the other hand, when 2-azido-4,6-bis(dimethylamino)-1,3,5-triazine (**1b**) was refluxed in pyridine, most of the starting material was recovered. The intertness of this azidotriazine is probably due to the weak electrophilic reactivity of the azido group in the presence of two electron-donating dimethylamino groups in the triazine nucleus.

Reaction of Azido-1,3,5-triazine (1a) with Methylpyridines. When 2-azido-4,6-dimethoxy-1,3,5-triazine (**1a**) was refluxed in methylpyridines, the reaction was found to occur in different manners depending upon the position of the methyl group in the pyridine nucleus (Scheme 2). In the reaction with 3-methylpyridine (**4b**), an similar (**5**)[4] adduct to that found in the case of pyridine was formed. However, in the cases of 2-methyl- (**4a**), 4-methyl- (**4c**), and 2,6-dimethylpyridine (**4d**), **1a** gave 2-amino-4,6-

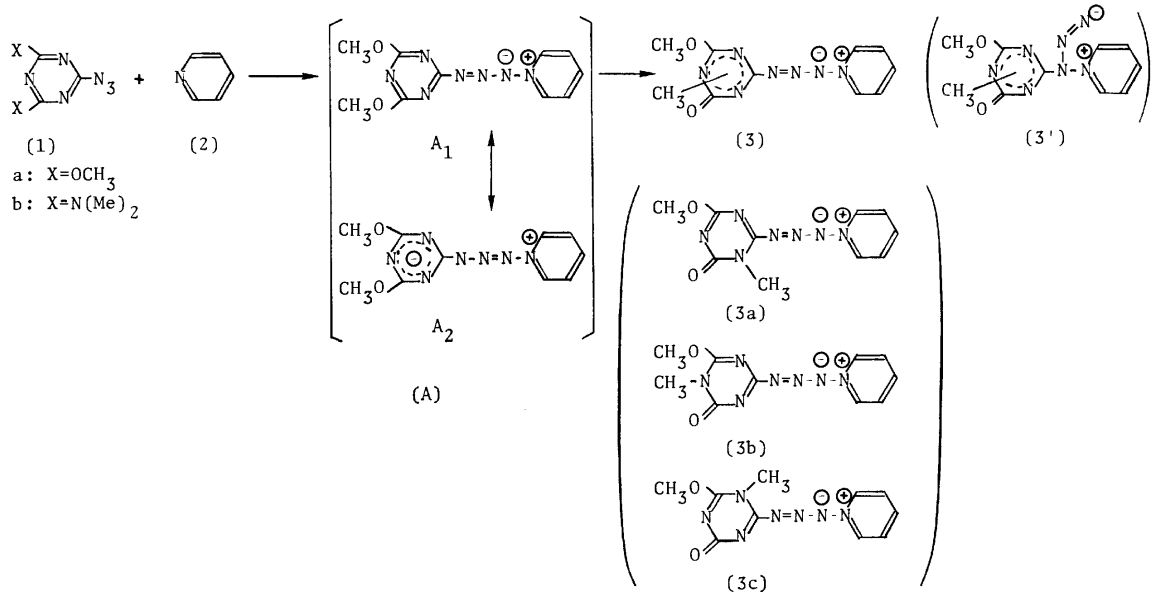

Scheme 1.

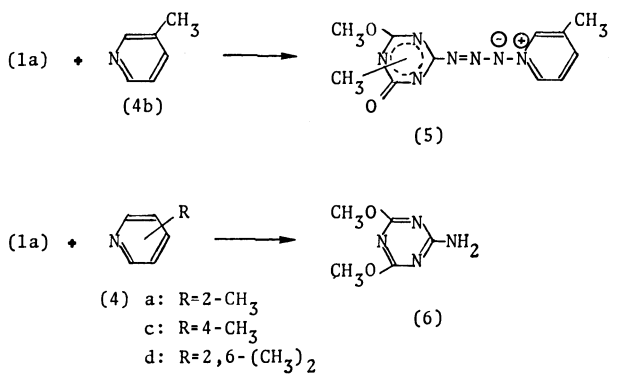

Scheme 2.

dimethoxy-1,3,5-triazine (**6**) as the major product. Aminotriazine (**6**) seems to be produced by the hydrogen abstraction of triazinylnitrene formed by the decomposition of azidotriazine (**1a**). However, monoazidotriazines are thermally stable and do not decompose up to 195 °C.[5] Therefore, a process involving triazinylnitrene as a reactive intermediate is improbable. Moreover, azidotriazine (**1a**) was found to decompose slowly in 2-methylpyridine, even at room temperature, to afford the same aminotriazine (**6**). This evidence suggests the existence of another intermediate which can give aminotriazine rather than triazinylnitrene. It would seem reasonable to consider that the adducts which are formed by the combination of azidotriazine with methylpyridine or dimethylpyridine decompose to give aminotriazine when the methyl group is attached at the 2- and/or 4-position (Scheme 3).

In the adducts to 2- and 4-methylpyridines, methyl hydrogen atoms are readily removable as protons because of the cationic character of the ring nitrogen of pyridine. Thus, in these cases, methyl hydrogen would be abstracted by the α-nitrogen of the adduct as a proton, intra- (in the cases of 2-methyl- and 2,6-dimethylpyridine) or intermolecularly (in the case of 4-methylpyridine), to give *N*-triazinyltriazenes. Ordinary 1,3-diaryltriazenes are known to be thermally not very stable and are known to decompose homolytically at about 140—150 °C, even in the absence of acid.[6] Therefore, if *N*-triazinyltriazene is produced, it can be expected to decompose, even at the boiling points of methylpyridines, to afford pyridylmethyl and triazinylamino radicals. The latter may react with the solvent to give aminotriazine (**6**).

As has been described before, in the case of 3-methylpyridine, the reaction stopped at the stage of adduct formation, because the proton transfer from the methyl group to the α-nitrogen was difficult because of the weak acidity of the methyl hydrogen atoms. In other words, in the reactions of azidotriazines with pyridine derivatives, the initial product was the 1 : 1 adduct in every case. However, a difference was observed in the subsequent process of the reaction depending upon the stability of the adduct. In the cases of pyridine and 3-methylpyridine, the adducts underwent the O→N migration of the methyl group to afford the rearranged product, while in the cases of 2-methyl-, 4-methyl-, and 2,6-dimethylpyridine, the adducts decomposed to give aminotriazine as the final product.

Although various adducts of organic azides to bases have been known, no adducts resulting from organic azides and amines have yet been reported. Thus, it may be said that the **3** and **5** adducts are novel examples of isolable adduct of azide and amine.

The adducts from pyridine and 3-methylpyridine were thermally stable; they did not decompose upon heating at the boiling point of pyridine or methylpyridine. By means of differential thermal analysis, no decomposition was observed below 190 °C; above this temperature, the adducts showed a slight weight loss. The TG curve of the adducts showed a weight loss corresponding to the loss of the pyridine component when they were heated at 220 °C. However, when the adducts were heated at 200—230 °C for 1 h, the resulting products were dark polymeric substances which were insoluble in most of organic solvent; from the reaction mixture *N*-(1-pyridinio)triazinylaminide could not be isolated.

Reaction of Azido-1,3,5-triazines with Triphenylphosphine. The reaction of organic azides with tertiary phosphines

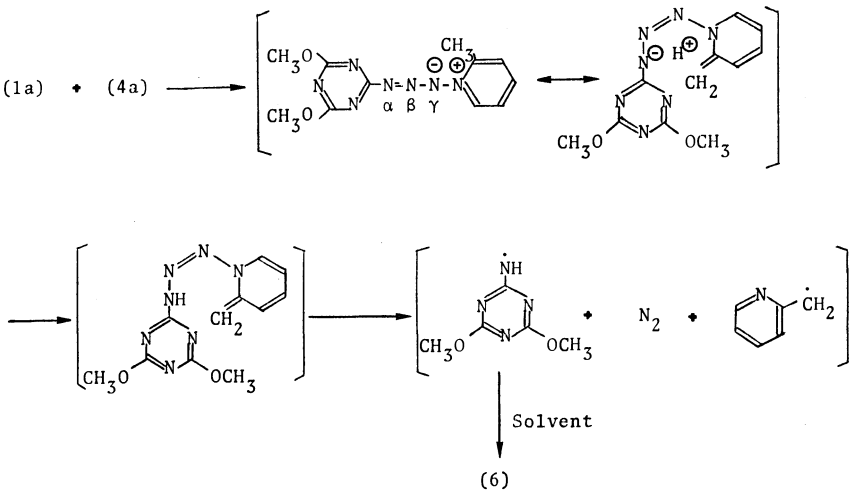

Scheme 3.

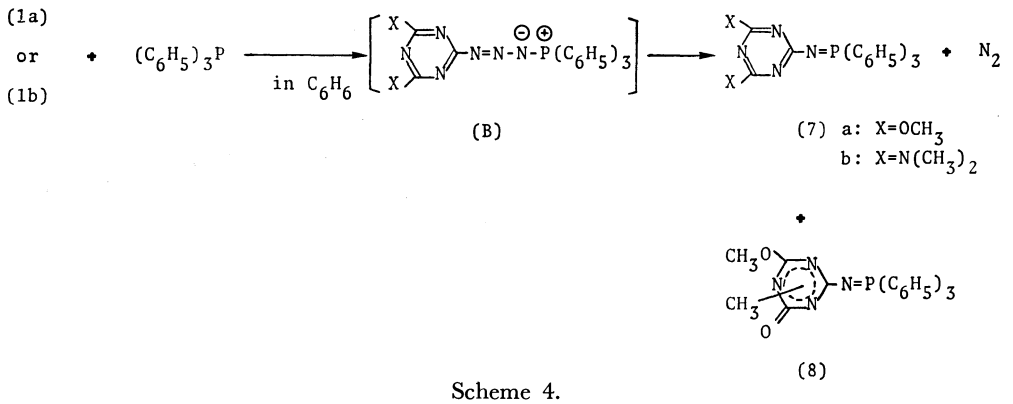

Scheme 4.

is known to be the oldest method for the preparation of iminophosphoranes; in some cases, the 1 : 1 adduct of azide with phosphine is isolated as an intermediate.[7-9] However, these adducts are thermally not very stable and afford iminophosphoranes, with the loss of nitrogen, upon heating.

When a solution of 2-azido-4,6-dimethoxy-1,3,5-triazine (**1a**) in benzene was added to a cold benzene solution of triphenylphosphine, the colorless solution soon became yellow. However, the color disappeared within a few minutes, with an evolution of nitrogen, and colorless crystals seperated out before long. The crystals, obtained in a good yield, were found to be *N*-(4,6-dimethoxy-1,3,5-triazin-2-yl)iminophosphorane (**7a**) (Scheme 4). Along with this major product, a product (**8**) resulting from an O→N migration of one of the methyl groups was also obtained. A similar reaction took place between 2-azido-4,6-bis(dimethylamino)-1,3,5-triazine (**1b**) and triphenylphosphine to give *N*-[4,6-bis(dimethylamino)-1,3,5-triazin-2-yl]iminophosphorane (**7b**) as the sole major product.

Even though attempts to isolate the initial adduct were unsuccessful, the progress of the reaction suggests that the reaction to give iminophosphorane proceeded *via* an 1 : 1 adduct (**B**); since the monoazidotriazines do not decompose under the reaction conditions employed, it may be reasonable to assume that they are not monoazidotriazines, but 1 : 1 adducts (**B**) that decomposed with an evolution of nitrogen.

In summary, it has been shown that the azidotriazine gave the stable 1 : 1 adducts in reactions with pyridines (**2**, **4b**). On the other hand, azidotriazines gave iminophosphoranes with triphenylphosphine, in contrast to the behavior of common organic azides, which give isolable 1 : 1 adducts with tertiary phosphine.[7-9] Although the reasons for the high stability of the **3** and **5** adducts are still ambiguous, one of the general factors may be given here. In the **3** and **5** adducts, the flow of

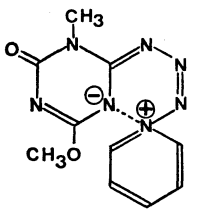

(**3a**)

the negative charge into a triazine ring is undoubtedly to be expected. Therefore, the adducts could be effectively stabilized by means of the electrostatic attraction between opposite charges, as is shown in the bottom of the left column.

On the other hand, in the 1 : 1 adducts (**B**) of azidotriazines with triphenylphosphine, the presence of three bulky phenyl groups at the phosphorus atom would hinder the approach of the phosphorus and ring nitrogen atoms; consequently, the stabilization by the attraction between the opposite charges would be weakened, and decomposition would take place much more easily.

Experimental

All the melting points are uncorrected.

Materials. The azidotriazines were prepared according to the procedures given in the previous paper.[5] The organic solvents were purified by the standard methods. Commercial pyridines were distilled before use. Triphenylphosphine of a reagent grade was used without purification.

*Reaction of 2-Azido-4,6-dimethoxy-1,3,5-triazine (**1a**) with Pyridine.* A solution of **1a** (17.1 g, 93.7 mmol) in pyridine (20 ml) was refluxed for 3 h. After cooling, the precipitate which resulted was collected by filtration. The recrystallization of the precipitate from EtOH and then from *i*-PrOH gave a pure adduct (**3**): mp 133—134 °C; yield, 17.9 g (73.0%); λ_{max} [EtOH], 242 nm; IR (KBr), 1700 cm^{-1} (C=O): PMR (DMSO-d_6), δ 3.88 (2H, s), 4.48 (3H, s), 8.00—9.30 (5H, m). Found: C, 45.94; H, 4.26; N, 37.52%. Calcd for $C_{10}H_{11}O_2N_7$: C, 45.97; H, 4.24; N, 37.42%.

*Reaction of 2-Azido-4,6-dimethoxy-1,3,5-triazine (**1a**) with 3-Methylpyridine (**4b**).* A solution of **1a** (1.50 g. 8.22 mmol) in 3-methylpyridine (10 ml) was refluxed for 3 h. After cooling, the resulting precipitate was collected by filtration. The recrystallization of the precipitate from *i*-PrOH gave a pure adduct (**5**): mp 161—162 °C; yield, 1.33 g (59%); PMR (DMSO-d_6), δ 2.52 (3H, s), 3.83 (3H, s), 4.37 (3H, s), 8.00—9.00 (4H, m). Found: C, 48.08; H, 4.82; N, 36.10%. Calcd for $C_{11}H_{13}N_7O_2$: C, 47.99; H, 4.76; N, 36.10%.

*Reaction of 2-Azido-4,6-dimethoxy-1,3,5-triazine (**1a**) with 2-Methylpyridine (**4a**), 4-Methylpyridine (**4c**), and 2,6-Dimethylpyridine (**4d**).* A typical example is shown in the case of 2-methylpyridine. A solution of **1a** (2.00 g, 11.0 mmol) in 2-methylpyridine (10 ml) was refluxed for 6 h. After the removal of the solvent, the residue was extracted with hot MeOH. The extract was purified by column chromatography on alumina (eluent: MeOH) to give 2-amino-4,6-dimethoxy-1,3,5-triazine (**6**) (0.575 g, 33.5%, mp 221—222

°C), which was identified by a mixed-melting-point test with an authentic sample.[10]

When the reaction was performed for 10 days at room temperature, **6** was obtained in a yield of 37.5%.

*Reaction of 2-Azido-4,6-dimethoxy-1,3,5-triazine (**1a**) with Triphenylphosphine.* To a stirred solution of triphenylphosphine (2.88 g, 11.0 mmol) in benzene (30 ml) we added, drop by drop, a solution of **1a** (2.00 g, 11.0 mmol) in benzene (50 ml) at 5 °C. After stirring for 1 h at room temperature, the resulting colorless precipitate was collected by filtration and recrystallized from benzene to afford *N*-(4,6-dimethoxy-1,3,5-triazin-2-yl)iminophosphorane (**7a**); mp 184—185 °C; yield, 3.30 g (72%); MS *m/e* 416 (M^+): PMR (DMSO-d_6), δ 3.68 (6H, s), 7.25—8.07 (15H, m). Found: C, 66.33; H, 5.13; N, 13.39%. Clacd for $C_{23}H_{21}N_4O_2P$: C, 66.34; H, 5.08; N, 13.45%.

The filtrate was concentrated and chromatographed on a silica gel column (eluent; benzene: MeOH=10: 1, v/v) to give the crude product of **8**, which was then recrystallized from benzene to give an analytical sample: mp 182—184 °C; yield, 0.074 g (1.6%); MS *m/e* 416 (M^+); IR (KBr), 1694 cm^{-1} (C=O); PMR ($CDCl_3$), δ 3.57 (1H, s), 3.67 (1H, s), 7.28—8.05 (5H, m). Found: C, 66.96; H, 5.05; N, 13.81%. Calcd for $C_{23}H_{21}N_4O_2P$: C, 66.34; H, 5.08; N, 13.54%.

*Reaction of 2-Azido-4,6-bis(dimethylamino)-1,3,5-triazine (**1b**) with Triphenylphosphine.* The reaction of **1b** (1.00 g, 4.81 mmol) with triphenylphosphine (1.27 g, 4.81 mmol) was carried out in a similar way. After stirring for 1 h, the solvent was removed *in vacuo*. The residue was recrystallized from a mixture of benzene and ligroin to give *N*-bis(dimethylamino)-1,3,5-triazinyliminophosphorane (**7b**): mp 207—209 °C; yield, 0.888 g (41.7%); PMR (DMSO-d_6), δ 2.83 (12H, s), 7.46—7.97 (15H, m). Found: C, 67.68; H, 6.11; N, 19.00%. Calcd for $C_{25}H_{27}N_6P$: C, 67.85; H, 6.15; N, 18.99%.

References

1) A. W. Johnson, "Ylide Chemistry," Academic Press, New York and London (1966), p. 217.

2) R. Kayama, H. Shizuka, S. Seikiguchi, and K. Matsui, *Bull. Chem. Soc. Jpn.*, **48**, 3309 (1975).

3) Structure **3a** can be written in terms of these five resonance structures:

(**3a**) ⟷ ⟷ ⟷ ⟷

On the other hand, in the cases of the **3b** and **3c** structures, four resonance forms can be written respectively; *e.g.*, for **3b**:

(**3b**) ⟷ ⟷ ⟷

4) For the same reason as has been presented above, the **5** adduct is considered to have a sturcture like **3a**.

5) R. Kayama, S. Hasunuma, S. Sekiguchi, and K. Matsui, *Bull. Chem. Soc. Jpn.*, **47**, 2825 (1974).

6) C. Suling, "Methoden zur Herstellung und Umwandlung von aromatischen Triazenen und hoheren Azahomologen," in Houben-Weyl "Methoden der Organischen Chemie," ed by E. Müller, Band 10/3 (1956), p. 731.

7) E. Bergmann and H. A. Wolff, *Chem. Ber.*, **63**. 1176 (1930).

8) J. E. Leffler, U. Honsberg, Y. Tsuno, and I. Forsblad, *J. Org. Chem.*, **26**, 4810 (1961).

9) J. S. Thayer and R. West, *Inorg. Chem.*, **3**, 406 (1964).

10) J. Thurston, J. Dudley, D. Kaiser, I. Hechenbleicker, F. Schaefer, and D. Holm-Hansen, *J. Am. Chem. Soc.*, **73**, 2981 (1951).

The Synthesis of Neobavaisoflavone and Related Compounds[1)]

Mitsuru NAKAYAMA,* Shizuko EGUCHI, Shûichi HAYASHI, Masao TSUKAYAMA,**
Tokunaru HORIE,** Toshihide YAMADA,** and Mitsuo MASUMURA**

Department of Chemistry, Faculty of Science, Hiroshima University, Higashisenda-machi, Hiroshima 730
***Department of Applied Chemistry, Faculty of Engineering, Tokushima University, Minami-Josanjima-cho, Tokushima 770*

(Received February 15, 1978)

The condensation of 7-benzoyloxy-4'-hydroxyisoflavone with 2-methyl-3-buten-2-ol gave 7-benzoyloxy-4'-hydroxy-3'-(3-methyl-2-butenyl)isoflavone. The hydrolysis of the alkylated isoflavone with dilute alkali afforded neobavaisoflavone [7,4'-dihydroxy-3'-(3-methyl-2-butenyl)isoflavone], which was then converted into isoneobavaisoflavone on heating with formic acid. 7-Benzyloxy-4'-hydroxyisoflavone was condensed with 2-methyl-3-buten-2-ol to give a chroman derivative, which was then converted into isoneobavaisoflavone by hydrolysis. 3'-(3-Methyl-2-butenyl)-5,7,4'-trihydroxyisoflavone was also synthesized from 7-benzoyloxy-5,4'-dihydroxyisoflavone in a similar manner.

Neobavaisoflavone has recently been isolated from *Psoralea corylifolia* seeds (fruits).[2,3)] Its structure has been shown to be 7,4'-dihydroxy-3'-(3-methyl-2-butenyl)-isoflavone (**1**) on the basis of spectral and degradative evidence.[2,3)] In this paper, the unambiguous synthesis of **1** will be reported to confirm the proposed structure of the natural isoflavone. Also, the synthesis of 3'-(3-methyl-2-butenyl)-5,7,4'-trihydroxyisoflavone (**2**) is attempted as an example for the introduction of the 3-methyl-2-butenyl group into the B ring in phloroglucinol-type isoflavone.

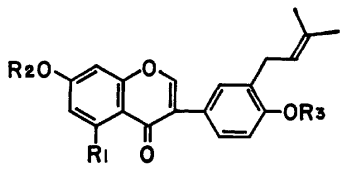

(**1**) $R_1=R_2=R_3=H$
(**2**) $R_1=OH$, $R_2=R_3=H$
(**5**) $R_1=R_3=H$, $R_2=C_6H_5CO$
(**6**) $R_1=H$, $R_2=R_3=CH_3CO$
(**12**) $R_1=OH$, $R_2=C_6H_5CO$, $R_3=H$

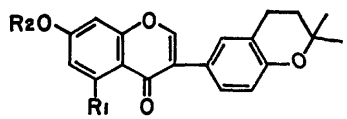

(**7**) $R_1=R_2=H$
(**9**) $R_1=H$, $R_2=C_6H_5CH_2$
(**13**) $R_1=OH$, $R_2=C_6H_5CO$
(**14**) $R_1=OH$, $R_2=H$

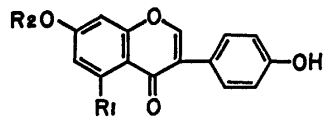

(**3**) $R_1=R_2=H$
(**4**) $R_1=H$, $R_2=C_6H_5CO$
(**8**) $R_1=H$, $R_2=C_6H_5CH_2$
(**10**) $R_1=OH$, $R_2=H$
(**11**) $R_1=OH$, $R_2=C_6H_5CO$

The partial benzoylation of daidzein (**3**) in pyridine gave 7-benzoyloxy-4'-hydroxyisoflavone (**4**). In the UV spectrum of **4**, the absorption maximum did not show a bathochromic shift in the presence of sodium acetate. The condensation of **4** with 2-methyl-3-buten-2-ol in the presence of boron trifluoride etherate[4)] afforded 7-benzoyloxy-4'-hydroxy-3'-(3-methyl-2-butenyl)isoflavone (**5**). The mass spectrum of **5** gave a molecular ion at *m/e* 426 and a fragment ion at *m/e* 371 $[M-C_4H_7]^+$. The NMR spectrum exhibited the presence of one methylene group as a doublet centering at δ 3.36 ppm and one vinyl proton as a triplet centering at δ 5.34 ppm. The compound **5** was hydrolyzed with dilute alkali to yield the desired neobavaisoflavone [7,4'-dihydroxy-3'-(3-methyl-2-butenyl)isoflavone] (**1**) (mp 191—192 °C).[2,3)] The acetylation of **1** by the acetic anhydride–pyridine method gave the diacetate (**6**). The isoflavone (**1**) was also heated with formic acid to be cyclized into the corresponding chroman derivative (isoneobavaisoflavone) (**7**) (mp 243—244 °C).[2,3)] The properties of this synthetic isoflavone (**1**) were fully consistent with those of the natural neobavaisoflavone.

The partial benzylation of **3** in acetone–*N*,*N*-dimethylformamide also gave 7-benzyloxy-4'-hydroxyisoflavone (**8**), the UV spectrum of which, like that of **4**, did not exhibit the bathochromic shift upon the addition of sodium acetate. The condensation of **8** with 2-methyl-3-buten-2-ol, in contrast with that of **4**, yielded a chroman derivative (**9**) [MS, *m/e* 412 (M^+)] alone. The hydrogenolysis of **9** with palladium on charcoal in ethyl acetate–methanol gave the chroman (**7**), which was identical with isoneobavaisoflavone.

Furthermore, this condensation was also found to be useful for the introduction of the 3-methyl-2-butenyl group into the B ring of phloroglucinol-type isoflavones such as **11**. 7-Benzoyloxy-5,4'-dihydroxyisoflavone (**11**), derived from genistein (**10**), was converted into 7-benzoyloxy-5,4'-dihydroxy-3'-(3-methyl-2-butenyl)isoflavone (**12**) with 2-methyl-3-buten-2-ol, along with the formation of a slight amount of a cyclization product, whose structure was identified as **13** on the basis of the NMR spectrum. In this condensation, neither 6- nor 8-(3-methyl-2-butenyl)-5,7,4'-trihydroxyisoflavone was obtained. The hydrolysis of **12** and **13** gave 3'-(3-methyl-2-butenyl)-5,7,4'-trihydroxyisoflavone (**2**) and the chroman derivative (**14**) respectively. The latter compound (**14**) was easily obtained from **2** by the

above method.

The condensation described above seems to be a general method which can be used for the introduction of the 3-methyl-2-butenyl group into the B ring of isoflavones.

Experimental

All the melting points are uncorrected. The IR spectra were taken on a Hitachi 215 spectrophotometer, and the UV spectra on a Hitachi 124 spectrophotometer. The NMR spectra were measured with a JEOL PS-100 spectrometer (100 MHz), using tetramethylsilane as an internal standard (δ, ppm). The mass spectra were taken on a Hitachi RMS-4 mass spectrometer with a direct inlet system operating at 70 eV. Column chromatography was carried out on Kieselgel 60 (70-230 mesh) (Merck).

7-Benzoyloxy-4'-hydroxyisoflavone (4). To a solution of daidzein (**3**)[5] (1.0 g) in pyridine (50 ml) was added, drop by drop, a mixture of benzoyl chloride (0.8 ml) and dry ether (5 ml) with stirring and cooling in an ice bath; the mixture was then stirred with cooling for 5 h. The reaction mixture was diluted with cold water and acidified with 2 M-hydrochloric acid to give light yellow precipitates, which were collected and recrystallized from ethyl methyl ketone as light yellow needles (**4**) (640 mg): mp 234—235 °C; UV λ_{max} nm (log ε) (EtOH) 258 (3.86), (EtOH+AcONa) 258 (4.04). Found: C, 73.71; H, 3.84%. Calcd for $C_{22}H_{14}O_5$: C, 73.74; H, 3.94%.

7-Benzoyloxy-4'-hydroxy-3'-(3-methyl-2-butenyl)isoflavone (5). To a solution of **4** (1.0 g) and boron trifluoride etherate (1 ml) in dry dioxane (50 ml) was gradually added a solution of 2-methyl-3-buten-2-ol (0.4 ml) in dry dioxane (10 ml); the mixture was then heated with stirring at 60 °C for 5 h. The reaction mixrure was poured into cold water and extracted with ether. The ethereal solution was washed with 3% aqueous solution of sodium carbonate and dried. After the removal of the solvent, the residue was chromatographed over a silica-gel column with chloroform to give isoflavone (**5**), which was subsequently recrystallized from benzene–ethyl acetate as colorless prisms (105 mg): mp 152—153 °C; UV λ_{max} nm (log ε) (EtOH) 258 (4.51), (EtOH+AcONa) 258 (4.55); NMR (DMSO) δ 1.78 (6H, s, $CH_3\times2$), 3.36 (2H, d, J=7 Hz, $C\underline{H}_2CH$=), 5.34 (1H, t, J=7 Hz, $CH_2C\underline{H}$=), 7.26—8.28 (9H, m, $C_6\underline{H}_5CO$, 6-, 8-, 2'-, 6'-H), 7.99 (1H, s, 2-H), 8.40 (1H, d, J=9 Hz, 5-H); MS *m/e* 426 (M^+), 371, 322. Found: C, 76.00; H, 5.35%. Calcd for $C_{27}H_{22}O_5$: C, 76.04; H, 5.20%.

Neobavaisoflavone [7,4'-Dihydroxy-3'-(3-methyl-2-butenyl)isoflavone] (1). Compound **5** (74 mg) was hydrolyzed with 5% aqueous solution of sodium hydroxide (3 ml) in methanol (7 ml) at 50 °C for 5 min. The reaction mixture was acidified with dilute hydrochloric acid and extracted with ether, and the ethereal solution was washed with water and dried. After the removal of the solvent, the residue was recrystallized from benzene–ethyl acetate to give the desired isoflavone (**1**) as colorless needles (33 mg): mp 191—192 °C (lit,[2,3] 195—196 °C); IR (KBr) 1625 cm^{-1}; UV λ_{max} nm (log ε) (MeOH) 248 (4.41), 258sh (4.37), 305sh (4.00), (MeOH+AcONa) 255 (4.55), 331 (4.11), (MeOH+NaOH) 255 (4.52), 331 (4.23); NMR (DMSO) δ 1.65 (6H, s, $CH_3\times2$), 3.20 (2H, d, J=7 Hz, $C\underline{H}_2CH$=), 5.25 (1H, t, J=7 Hz, $CH_2C\underline{H}$=), 6.78 (1H, d, J=9 Hz, 5'-H), 6.84 (1H, bs, 8-H), 6.90 (1H, q, J=9 and 2 Hz, 6-H), 7.16 (1H, q, J=9 and 2 Hz, 6'-H), 7.21 (1H, s, 2'-H), 7.95 (1H, d, J=9 Hz, 5-H), 8.23 (1H, s, 2-H), 9.48 (1H, s, 4'-OH), 10.84 (1H, s, 7-OH); MS *m/e* 322 (M^+, base), 307 (18), 293 (16), 267 (63), 237 (22), 137 (40), 131 (7). Found: C, 74.50; H, 5.70%. Calcd for $C_{20}H_{18}O_4$: C, 74.52; H, 5.63%.

Diacetate (6) of Neobavaisoflavone (1). After a mixture of **1** (20 mg), acetic anhydride (0.4 ml), and pyridine (0.2 ml) had been allowed to stand at room temperature for 24 h, cold water was added to the mixture. The resulting precipitates were recrystallized from benzene–ethyl acetate as colorless prisms (**6**) (20 mg): mp 115—116 °C (lit,[3] mp 120—121 °C); NMR ($CDCl_3$) δ 1.71 (6H, s, $CH_3\times2$), 2.32 and 2.36 (each 3H, s, CH_3CO), 3.28 (2H, d, J=7 Hz, $C\underline{H}_2CH$=), 5.23 (1H, t, J=7 Hz, $CH_2C\underline{H}$=), 7.06 (1H, d, J=9 Hz, 5'-H), 7.11—7.42 (4H, m, 6-, 8-, 2'-, 6'-H), 7.97 (1H, s, 2-H), 8.30 (1H, d, J=9 Hz, 5-H). Found: C, 71.04; H, 5.56%. Calcd for $C_{24}H_{22}O_6$: C, 70.92; H, 5.46%.

7-Benzyloxy-4'-hydroxyisoflavone (8). To a solution of daidzein (**3**) (800 mg) in acetone (10 ml) and *N,N*-dimethylformamide (10 ml) were addded benzyl chloride (0.5 ml), potassium iodide (600 mg), and 2% aqueous solution of potassium hydroxide (10.6 ml). The mixture was allowed to stand at room temperature for 24 h. The resulting precipitates were recrystallized from ethanol as colorless needles (**8**) (490 mg): mp 234.5—235.5 °C; UV λ_{max} nm (log ε) (EtOH) 262 (4.43), 306sh (4.01), (EtOH+AcONa) 262 (4.44), 306sh (4.02); NMR (DMSO) δ 5.22 (2H, s, $C_6H_5C\underline{H}_2$), 6.80 (2H, d, J=9 Hz, 3'-, 5'-H), 7.19 (1H, q, J=9 and 2 Hz, 6-H), 7.22 (1H, d, J=2 Hz, 8-H), 7.40 (2H, d, J=9 Hz, 2'-, 6'-H), 7.44 (5H, bs, $C_6\underline{H}_5CH_2$), 8.02 (1H, d, J=9 Hz, 5-H), 8.35 (1H, s, 2-H), 9.56 (1H, s, 4'-OH). Found: C, 76.52; H, 4.63%. Calcd for $C_{22}H_{16}O_4$: C, 76.73; H, 4.68%.

7-Benzyloxy-2',3'-dihydro-2',2'-dimethyl-3,6'-bi(4H-1-benzopyran)-4-one (9). To a solution of **8** (650 mg) and boron trifluoride etherate (0.6 ml) in dry dioxane (50 ml) was added a solution of 2-methyl-3-buten-2-ol (0.2 ml) in dioxane (10 ml), after which the mixture was heated with stirring at 60 °C for 5 h. The reaction mixture was then worked up in the same manner as in the preparation of **5**. The resulting product was chromatographed over a silica-gel column with benzene–ethyl acetate (10: 1) to give isoflavone (**9**), which was subsequently crystallized from carbon tetrachloride as colorless prisms (130 mg): mp 152—153 °C; NMR (DMSO) δ 1.28 (6H, s, $CH_3\times2$), 1.76 and 2.73 (each 2H, t, J=7 Hz, CH_2), 5.22 (2H, s, $C_6H_5C\underline{H}_2$), 6.72 (1H, d, J=9 Hz, 5'-H), 7.12 (1H, q, J=9 and 2 Hz, 6-H), 7.21 (1H, d, J=2 Hz, 8-H), 7.28 (1H, s, 2'-H), 7.32 (1H, d, J=9 Hz, 6'-H), 7.42 (5H, bs, $C_6\underline{H}_5CH_2$), 8.00 (1H, d, J=9 Hz, 5-H), 8.36 (1H, s, 2-H); MS m/*e* 412 (M^+), 397, 383, 357, 321. Found: C, 78.73; H, 6.02%. Calcd for $C_{27}H_{24}O_4$: C, 78.62; H, 5.86%.

Isoneobavaisoflavone [2'3'-Dihydro-2',2'-dimethyl-7-hydroxy-3,6'-bi(4H-1-benzopyran)-4-one] (7). Compound (**9**) (100 mg) was hydrogenated over palladium on charcoal (10%; 50 mg) in ethyl acetate–methanol (20 ml, 1: 3) until the uptake of hydrogen ceased. The solvent was then removed under reduced pressure, and the residue was recrystallized from benzene–ethyl acetate to give colorless prisms (**7**) (50 mg): mp 243—244 °C (lit,[2] 232—233 °C); NMR (DMSO) δ 1.29 (6H, s, $CH_3\times2$), 1.78 and 2.76 (each 2H, t, J=7 Hz, CH_2), 6.70 (1H, d, J=9 Hz, 5'-H), 6.85 (1H, bs, 8-H), 6.92 (1H, q, J=9 and 2 Hz, 6-H), 7.24 (1H, q, J=9 and 2 Hz, 6'-H), 7.28 (1H, d, J=2 Hz, 2'-H), 7.94 (1H, d, J=9 Hz, 5-H), 8.26 (1H, s, 2-H), 10.86 (1H, bs, 7-OH); MS *m/e* 322 (M^+), 307, 293, 267. Found: C, 74.30; H, 5.80%. Calcd for $C_{20}H_{18}O_4$: C, 74.52; H, 5.63%.

Isoneobavaisoflavone (**7**) was also prepared from neobavaisoflavone with formic acid according to the procedure of Bajwa *et al.*;[3] it had a melting-point of 243—244 °C (no

depression in a mixed-melting-point determination with the isoflavone synthesized above).

*7-Benzoyloxy-5,4'-dihydroxyisoflavone (**11**).* To a solution of genistein (**10**)[6] (3.0 g) in pyridine (100 ml) was added, drop by drop, a mixture of benzoyl chloride (1.9 g) and ether (20 ml) with stirring and cooling in an ice bath, after which the mixture was stirred with cooling for 6 h. The reaction mixture was then worked up in the same manner as in the case of **4** to give isoflavone (**11**), which was recrystallized from ethyl acetate as colorless needles (2.4 g): mp 245—246 °C; UV λ_{max} nm (log ε) (EtOH) 259 (4.67), 305 (3.81), 332 (3.73), (EtOH+AcONa) 259 (4.69), 305 (4.05), 336 (3.94). Found: C, 70.69; H, 3.90%. Calcd for $C_{22}H_{14}O_6$: C, 70.58; H, 3.77%.

*7-Benzoyloxy-5,4'-dihydroxy-3'-(3-methyl-2-butenyl)isoflavone (**12**) and 7-Benzoyloxy-2',3'-dihydro-2'2'-dimethyl-5-hydroxy-3,6'-bi(4H-1-benzopyran]-4-one (**13**).* To a solution of **11** (2.0 g) and boron trifluoride etherate (2.5 g) in dioxane (150 ml) was gradually added a solution of 2-methyl-3-buten-2-ol (0.72 g) in dioxane (20 ml), after which the mixture was heated with stirring at 50—55 °C for 6 h. The reaction mixture was then poured into cold water to give light yellow precipitates. After the starting material **11** (0.8 g) had been removed from the collected precipitates by recrystallization from methanol, the resulting compounds soluble in methanol were chromatographed over a silica-gel column with chloroform–ethyl acetate (30: 1), giving an oil and a colorless solid. The solid was recrystallized from methanol as colorless needles (**12**) (330 mg): mp 118—119 °C; UV λ_{max} nm (log ε) (EtOH) 262 (4.64), 334sh (3.91), (EtOH+AcONa) 262 (4.64), 334sh (3.92); NMR ($CDCl_3$) δ 1.81 (6H, s, $CH_3\times2$), 3.42 (2H, d, J=7 Hz, C$\underline{H}_2$CH=), 5.34 (1H, t, J= 7Hz, $CH_2C\underline{H}$=), 5.50 (1H, bs, 4'-OH), 6.65—6.9 (3H, m, 6-, 8-, 5'-H), 7.16—7.36 (2H, bs, 2'-, 6'-H), 7.4—7.8 and 8.1—8.3 (5H, m, $C_6\underline{H}_5CO$), 7.91 (1H, s, 2-H), 12.92 (1H, s, 5-OH). Found: C, 73.22; H, 4.92%. Calcd for $C_{27}H_{22}O_6$: C, 73.29; H, 5.01%.

The oil was rechromatographed over a silica-gel column with chloroform–carbon tetrachloride (30: 1) to give colorless needles (**13**) (80 mg): mp 164—165 °C; NMR ($CDCl_3$) δ 1.36 (6H, s, $CH_3\times2$), 1.83 (2H, t, J=7 Hz, CH_2), 2.84 (2H, t, J=7 Hz, CH_2), 6.65—6.92 (3H, m, 6-, 8-, 5'-H), 7.13—7.35 (2H, m, 2'-, 6'-H), 7.4—7.8 and 8.16—8.24 (5H, m, $C_6\underline{H}_5CO$), 7.94 (1H, s, 2-H), 12.95 (1H, s, 5-OH). Found: C, 73.04; H, 5.05%. Calcd for $C_{27}H_{22}O_6$: C, 73.29; H, 5.01%.

*3'-(3-Methyl-2-butenyl)-5,7,4'-trihydroxyisoflavone (**2**).* Isoflavone (**12**) (350 mg) was hydrolyzed with 5% aqueous solution of sodium hydroxide (20 ml) in methanol (30 ml) at 60 °C for 15 min. After the reaction mixture had then been worked up in the same manner as in the case of **1**, the resulting compound was chromatographed over a silica-gel column with chloroform–acetone (30: 1) to give colorless needles (**2**) (210 mg) which were subsequently recrystallized from 1,2-dichloroethane: mp 171—172 °C; UV λ_{max} nm (log ε) (EtOH) 263 (4.54), 295 (4.06), 330 (3.72), (EtOH+AcONa) 273 (3.55), 331 (4.01); NMR (DMSO) δ 1.68 (6H, s, $CH_3\times2$), 3.24 (2H, d, J=7 Hz, C$\underline{H}_2$CH=), 5.28 (1H, t, J=7 Hz, $CH_2C\underline{H}$=), 6.21 (1H, d, J=2 Hz, 6-H), 6.37 (1H, d, J=2 Hz, 8-H), 6.83 (1H, d, J=9 Hz, 5'-H), 7.19 (1H, q, J=9 and 2 Hz, 6'-H), 7.24 (1H, bs, 2'-H), 8.31 (1H, s, 2-H), 9.57 (1H, s, 4'-OH), 10.95 (1H, s, 7-OH), 13.11 (1H, s, 5-OH); MS *m/e* 338 (M^+, base), 323 (23), 309 (20), 283 (93), 253 (40), 153 (65), 131 (18). Found: C, 71.24; H, 5.45%. Calcd for $C_{20}H_{18}O_5$: C, 70.99; H, 5.36%.

*5,7-Dihydroxy-2'3'-dihydro-2'2'-dimethyl-3,6'-bi(4H-1-benzopyran)-4-one (**14**).* Compound (**13**) (60 mg) was hydrolyzed with 5% aqueous solution of sodium hydroxide (3 ml) in methanol (10 ml) under reflux for 15 min. The reaction mixture was then worked up in the same manner as in the case of **12** to give isoflavone (**14**), which was subsequently recrystallized from benzene–ethyl acetate as colorless needles (31 mg): mp 214—215 °C; NMR (DMSO) δ 1.30 (6H, s, $CH_3\times2$), 1.77 (2H, t, J=7 Hz, CH_2), 2.75 (2H, t, J=7 Hz, CH_2), 6.19 (1H, d, J=2 Hz, 6-H), 6.36 (1H, d, J=2 Hz, 8-H), 6.73 (1H, d, J=9 Hz, 5'-H), 7.13—7.40 (2H, m, 2'-, 6'-H), 8.32 (1H, d, 2-H), 10.90 (1H, s, 7-OH), 12.97 (1H, s, 5-OH); MS *m/e* 338 (M^+), 323, 309, 283. Found: C, 71.26; H, 5.43%. Calcd for $C_{20}H_{18}O_5$: C, 70.99; H, 5.36%.

Compound **14** was also obtained from **2** by the same method as in the case of **7**.

This work was partially supported by a Grant-in-Aid for Science Research from the Ministry of Education.

References

1) Part of this work was previously reported in a preliminary form: M. Nakayama, S. Hayashi, M. Masumura, T. Horie, M. Tsukayama, and T. Yamada, *Chem. Lett.*, **1975**, 281.

2) B. S. Bajwa, P. L. Khanna, and T. R. Seshadri, *Curr. Sci.*, **41**, 882 (1972); *Chem. Abstr.*, **78**, 97439w (1973).

3) B. S. Bajwa, P. L. Khanna, and T. R. Seshadri, *Indian J. Chem.*, **12**, 15 (1974).

4) F. Bohlmann and K. M. Kleine, *Chem. Ber.*, **99**, 885 (1966).

5) H. S. Mahal, H. S. Rai, and K. Venkataraman, *J. Chem. Soc.*, **1934**, 1769.

6) W. Baker, J. Chadderton, J. B. Harbone, and W. D. Ollis, *J. Chem. Soc.*, **1953**, 1852.

A Convenient Procedure for Esterification of Carboxylic Acids

Noboru ONO,* Takashi YAMADA,** Tadashi SAITO, Kazuhiko TANAKA, and Aritsune KAJI

Department of Chemistry, Faculty of Science, Kyōto University, Sakyo-ku, Kyoto 606

***Laboratory of Chemistry, Faculty of Science, Kōnan University, Okamoto, Higashinada-ku, Kobe 658*

(Received February 16, 1978)

A variety of carboxylic acids including simple acids, sterically hindered acids, thermally unstable acids and N-protected amino acids react with alkyl halides in the presence of 1,8-diazabicyclo[5.4.0]undec-7-ene (DBU) in benzene to give esters in good yields. The reaction is simple, affording a general method for esterification of carboxylic acids.

Esterification is an important reaction widely used in various fields of chemistry. Although a simple reaction, it often involves unexpected difficulties. For example, other functional groups in the molecule may be sensitive to the acidic or basic conditions, or the reaction may proceed very slowly as is frequently the case with sterically hindered acids. Many useful processes to avoid such difficulties have been reported. Boron trifluoride etherate–alcohol,[1] trialkyloxonium tetrafluoroborate,[2] dialkyl sulfate,[3] and 2-halopyridinum salt–alcohol[4] have been recommended as esterification reagents for a number of cases. Alkyl halides are also useful when the reaction is carried out with use of alkali metal salts of carboxylic acids in dipolar aprotic solvents.[5,6] Caesium salt as an alkali metal salt[5] and hexamethylphosphoric triamide (HMPA)[6] as a solvent are specially effective for esterification with alkyl halides. However, some of these methods are restricted by inconvenience in procedure or expense and inaccessibility of reagents or solvents.[6]

In this paper we wish to report an alternative simple procedure for esterification of carboxylic acids which is based on the reaction of carboxylic acids with alkyl halides in the presence of 1,8-diazabicyclo[5.4.0]-undec-7-ene (DBU). The reaction proceeds in a non-polar solvent such as benzene under mild conditions to give esters in good yields. Since alkyl halides are used as the esterification reagent, various esters are easily prepared. Thus, carboxylic acids including sterically hindered acids, thermally unstable acids, heterocyclic carboxylic acids and *N*-protected amino acids are readily converted into the corresponding esters. This new esterification process is noteworthy for converting *N*-protected amino acids into the corresponding esters without observable racemization.

Results and Discussion

Esterification was carried out as follows. A mixture of carboxylic acids, DBU and alkyl halides in benzene was refluxed or kept at room temperature for an appropriate period, after which the DBU-hydrohalides (DBU·HX) were either filtered off or washed out with water from the reaction mixture. The product was purified by distillation or recrystallization. The yields were excellent. Results obtained with various carboxylic acids and alkyl halides are given in Table 1. The esterification is shown by

$$R^1COOH + R^2X \xrightarrow[\text{benzene}]{\text{DBU}} R^1COOR^2 + DBU\cdot HX \quad (1)$$

No difficulties were encountered in the preparation of phenacyl esters,[7] methylthiomethyl esters,[8] esters of sterically hindered acids,[9] or esters of heterocyclic acids,[10] some of which are difficult to prepare by the usual esterification method.[7–10] Thermally unstable carboxylic acids such as malonic or cyanoacetic acid were also esterified by this procedure without decarboxylation. Active methylene compounds are carboxylated by using the reagent of DBU and carbon dioxide,[11] so the reagent system of DBU, carbon dioxide and alkyl halides may afford a new means for introduction of alkoxycarbonyl function to active methylene compounds.

Carboxylic acids having functional groups such as hydroxyl or amino group are esterified without protection of these groups. For example, *p*-aminobenzoic acid, *p*-hydroxybenzoic acid or *N*-benzyloxycarbonyl(*Z*)-threonine were converted into their esters in good yields with alkyl halides and DBU (Tables 1 and 2).

The new method has advantages over the conventional procedure. First, a wide variety of esters can be prepared under mild conditions. Secondly, the procedure is simple and easily scaled up. Thirdly, the reaction proceeds in benzene, making the work-up very simple; for instance, products can be obtained in sufficiently pure form only by removal of DBU·HX and benzene. Furthermore, DBU can be easily recovered by treatment of DBU·HX with a strong base such as sodium hydroxide. Thus, the troublesome preparation of anhydrous alkali metal salts of carboxylic acids or the use of expensive dipolar aprotic solvents becomes unnecessary. In general, it is difficult to carry out the alkylation reaction of carboxylate ions with alkyl halides in a non-polar solvent such as benzene, since few carboxylate ions are soluble in benzene. Recently, alkylation of carboxylate ions with alkyl halides in a non-polar solvent was reported, where the crown ether was used as a catalyst[12] or quarternary ammonium carboxylate was used instead of alkali metal salts.[13] The present method is superior to these methods in the following points. No prior preparation of carboxylate ions is necessary. No competing side reaction of dehydrohalogenation often encountered in the reaction of alkali metal salts of carboxylic acids with *s*-alkyl halides is observed. For example, the reaction of dry potassium acetate with 2-bromooctane in the presence of 18-

Table 1. Esterification of carboxylic acids using alkyl halides and DBU in benzene

$R^1COOH + R^2X \longrightarrow R^1COOR^2$

R^1	R^2X (eq)	Conditions		Yield (%)[a]	Bp or (Mp) °C
		Temp (°C)	Time (h)		
C_6H_5	C_2H_5I(1.0)	25 (room temp)	1.5	95	95/30 mmHg
C_6H_5	CH_3SCH_2Cl(1.2)	80 (refl.)	2.0	81	106—108/2 mmHg
Mesitoic[b]	C_2H_5I(1.0)	25	2.0	80	98/3 mmHg
Mesitoic	*p*-Br-$C_6H_4CCH_2Br$(1.0) (O)	80	2.0	70	(98—99)
Mesitoic	*s*-C_4H_9Br(1.5)	80	6.0	91	115/2 mmHg
p-Me_2N-C_6H_4	C_2H_5Br(1.5)	80	3.0	85	(60—62)
p-H_2N-C_6H_4	C_2H_5Br(1.5)	80	4.0	70	(86—88)
p-HO-C_6H_4	C_2H_5Br(2.0)	80	5.0	81	(114—116)
	C_2H_5Br(1.5)	80	3.0	90	(34)
CH_3	$C_6H_5CH_2CH_2Br$(0.67)	80	3.0	86[c]	120/20 mmHg
CH_3	$CH_3(CH_2)_5CHCH_3$(0.67) (Br)	80	10.0	91[c]	87/20 mmHg
CH_3	*p*-Br-$C_6H_4CCH_2Br$(1.0) (O)	80	1.0	89	(85—86)
$(CH_3)_3C$	*n*-C_4H_9Br(1.2)	80	2.0	81	67/20 mmHg
$(CH_3)_3C$	*s*-C_4H_9Br(1.2)	80	3.0	86	55/13 mmHg
$(CH_3)_3C$	$CH_3(CH_2)_5CHCH_3$(0.67) (Br)	80	3.0	80[c]	114/20 mmHg
$(CH_3)_3C$	$C_6H_5CH_2CH_2Br$(0.67)	80	3.0	90[c]	137/20 mmHg
$(CH_3)_2C=CH$	C_2H_5Br(1.5)	80	2.0	80	60/30 mmHg
$NC-CH_2$	*n*-C_4H_9Br(1.2)	80	2.0	91	110/20 mmHg
$HOOC-CH_2$	C_2H_5I(2.0)	25	10.0	84[d]	85/20 mmHg

a) Based on carboxylic acids unless otherwise mentioned. b) 2,4,6-Trimethylbenzoic acid. c) Based on alkyl halides. d) Diethyl malonate produced.

crown-6 in dry acetonitrile or benzene produces the corresponding acetate along with 10—15% yield of octenes in about 20 h at reflux temperature.[12] On the other hand, the reaction of acetic acid with 2-bromooctane in the presence of DBU in benzene gave 1-methylheptyl acetate in 91% yield without formation of octenes. No alkene products could also be detected by NMR or VPC technique from the reaction mixture of mesitoic acid or pivalic acid with 2-bromobutane, 2-bromooctane or phenethyl bromide in the presence of DBU. It should be noted that alkenes were produced in good yields in these reactions in the absence of carboxylic acids;[14] *e.g.*, the reaction of 2-bromooctane or phenethyl bromide with DBU gave octenes or styrene in 87 or 60% yield, respectively. The results clearly show that the carboxylate ions formed by the reaction of carboxylic acids with DBU in benzene are sufficiently reactive to alkyl halides to give esters in good yields, but they have not enough basicity to induce the elimination reaction from *s*-alkyl halides or phenethyl bromide. Namely, basicity of both DBU and carboxylate ions is greatly reduced by protonation.

The reaction of carboxylic acids with alkyl halides in the presence of usual amines such as triethylamine is too slow to be useful for the esterification reaction. For example, the reaction of benzoic acid with ethyl iodide in the presence of DBU at room temperature for one hour gave ethyl benzoate in 95% yield, but the same reaction using triethylamine as a base gave only 1% yield of ethyl benzoate under the same conditions. High temperature (*ca.* 150 °C) and long reaction time are usually required for esterification of carboxylic acids by means of alkyl halides and triethylamine.[15] The difference in reactivity between DBU salt and triethylamine salt of carboxylic acids can be attributed to the difference in dissociation of these salts in benzene. DBU or triethylamine reacts with carboxylic acids to form complex I or II, respectively. Complex I is more soluble in benzene than complex II, complex I having a larger and more delocalized cation than complex II.

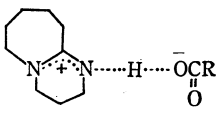

I

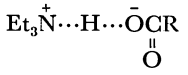

II

The principle of the present esterification reaction using DBU in benzene resembles that of the ion pair extractive alkylation or the method using crown ether. The biggest difference of the present reaction from the others is that the complex is not a free ion pair but is hydrogen-bonded between DBU and the carboxyl protons. The hydrogen bond plays an important role in the control of the reactivity of carboxylate ions. Namely, the free carboxylate ions can attack both the carbon and the hydrogen of alkyl halides, but the hydrogen-bonded complex I attacks carbon rather than hydrogen.

Table 2. Esterification of *N*-protected amino acids using alkyl haides and DBU in benzene

Z-AA-OH[a]	RX (eq)	Reflux time (h)	Yield (%)	Mp (°C)	$[\alpha]_D^{20}$	Lit Mp (°C)	Lit $[\alpha]_D^{20}$	Ref.
Z-Ala-OH	CH_3I(2)	2	92.0	45—46	−36.9° [b]	45—46	−36.0° [b]	19
Z-Pro-OH	CH_3I(2)	2	90.4	oil	−59.1° [b]		−57.3° [b]	20
Z-Val-OH	C_2H_5Br(2)	1	94.6	oil	−22.2° [b]		−19.6° [b]	21
Z-Val-OH	C_2H_5Br(2)	2	98.8	oil	−23.2° [b]			
Z-Val-OH	C_2H_5Br(2)	3	99.2	oil	−23.0° [b]			
Z-Phe-OH	C_2H_5Br(2)	2	99.0	oil	−12.1° [c]		−10.1° [c]	20
Z-Leu-OH	C_2H_5Br(2)	2	94.9	oil	−28.8° [b]		−27.5° [b]	20
Z-Ser-OH	BzlBr(1.2)[d]	2	92.9	83—84	+5.1° [e]	83.5—84.5	+6.1° [f]	22
Z-Thr-OH	BzlBr(1.2)	2	92.3	80—80.5	−13.8° [g]	80—81	−13.3° [g]	23
Z-Ser-OH	NBzlBr(1.2)[h]	2	95.7	116—117	−11.0° [b]	115.5—116.5	−11.87° [i]	24
Z-Thr-OH	NBzlBr(1.2)	2	100	114—115	−14.4° [j]	114—115	−14.01° [j]	24
Boc-Asn-OH	BzlBr(1.2)	2	81.4	120—121	−17.4° [k]	120—122	−17.29° [k]	5
Boc-Gln-OH	BzlBr(1.2)	2	80.1	109—110	−23.5° [k]	108—110	−22.67° [k]	5

a) Of the L-configuration. b) *c* 1, CH_3OH. c) *c* 1.4, C_2H_5OH. d) Benzyl bromide. e) *c* 2.95, $CHCl_3$, 24 °C. f) *c* 7, $CHCl_3$, 24 °C. g) *c* 2.5, $CHCl_3$. h) *p*-Nitrobenzyl bromide. i) *c* 0.9, CH_3OH. j) *c* 2, CH_3OH. k) *c* 1, DMF.

Recently, reports were given on the selective monoalkylation of methyl cyanoacetate[16] or tosylacetonitrile[17] using DBU in benzene as a base. The selectivity of monoalkylation in these reactions using DBU in benzene is much higher than that in the reaction using the ion pair extraction or phase transfer technique. In this case also the selectivity of monoalkylation is mainly controlled by the hydrogen bond between DBU and the active methylene compounds. Another good example of the importance of the hydrogen bonding in organic synthesis was recently demonstrated by Clark and Miller.[18] They showed that the hydrogen-bonded complex between a fluoride anion and carboxylic acids is a mild fluorinating agent but a strong acyloxylating agent.

Since the complex of DBU and carboxylic acids is a strong nucleophile but a weak base, it is expected that the optically active amino acids can be esterified without loss of the optical activities by the present procedure. Esterification of some *N*-*Z*-amino and *N*-*t*-butoxylcarbonyl(Boc)-amino acids was carried out by the use of DBU and alkyl halides in benzene in a similar way to that for the esterification of simple carboxylic acids. From the results of esterification of *N*-*Z*-valine, the standard reaction time, reflux for 2 h, was applied in all cases. The results are summarized in Table 2. Various *N*-protected amino acids were cleanly esterified in excellent yields without observable racemization. They have been esterified by other methods.[19-24] Recently, facile esterification of *N*-protected amino acids and peptides using their caesium salts and alkyl halides in *N*,*N*-dimethylformamide (DMF) was reported.[5] However, the present procedure for esterification of *N*-protected amino acids is superior to those methods as mentioned in esterification of simple carboxylic acids.

Experimental

Solvents and DBU were purified by distillation. Other commercial products were used without purification. Some typical examples of the procedure for esterification of carboxylic acids and the general procedure for esterification of *N*-protected amino acids are described below. The reaction conditions and the physical properties of esters are summarized in Tables 1 and 2.

Ethyl 2,4,6-Trimethylbenzoate. A solution of ethyl iodide (1.56 g, 0.01 mol) in 5 ml of benzene was added to a solution of 2,4,6-trimethylbenzoic acid (1.64 g, 0.01 mol) and DBU (1.52 g, 0.01 mol) in 15 ml of benzene and the mixture was stirred at room temperature for 2 h. The reaction mixture was then washed with water, dried over anhydrous magnesium sulfate, and distilled. Ethyl 2,4,6-trimethylbenzoate; bp 98 °C/3 mmHg, 1.53 g (80% yield) was obtained. NMR (CCl_4) δ=1.31 (t, 3), 2.21 (s, 6), 4.28 (q, 2), 6.72 (s, 2); IR (neat) 1710 cm^{-1} (C=O).

s-*Butyl 2,4,6-Trimethylbenzoate.* A mixture of *s*-buytlbromide (2.0 g, 0.15 mol), 2,4,6-trimethylbenzoic acid (1.64 g, 0.01 mol), DBU (1.52 g, 0.01 mol), and 20 ml of benzene was refluxed for 6 h. The reaction mixture was then washed with water, dried over anhydrous magensium sulfate, and distilled. *s*-Butyl 2,4,6-trimethylbenzoate, bp 115 °C/2 mmHg, 1.90 g (91% yield) was obtained. NMR (CCl_4) δ= 0.99 (t, 3), 1.30 (d, 3), 1.60 (m, 2), 2.22 (s, 9), 4.99 (m, 1), 6.70 (s, 2); IR (neat) 1710 cm^{-1} (C=O).

1-Methylheptyl Acetate. A mixture of 2-bromooctane (3.86 g, 0.02 mol), acetic acid (1.8 g, 0.03 mol), DBU (4.56 g, 0.03 mol), and 40 ml of benzene was refluxed for 10 h. The reaction mixture was then washed with water, dried over anhydrous magnesium sulfate, and distilled. 1-Methylheptyl acetate, bp 87 °C/20 mmHg, 3.1 g (91% yield), was obtained. NMR (CCl_4) δ=0.9—1.3 (m, 16), 1.98 (s, 3), 4.8 (m, 1); IR (neat) 1730 cm^{-1} (C=O).

Phenethyl Pivalate. A mixture of phenethyl bromide (1.9 g, 0.01 mol), pivalic acid (2.05 g, 0.02 mol), DBU (3.04 g, 0.02 mol), and 20 ml of benzene was refluxed for 3 h. The reaction mixture was then washed with water, dried over anhydrous magnesium sulfate, and distilled. Phenethyl pivalate, bp 137 °C/20 mmHg, 1.9 g (90% yield), was obtained. NMR (CCl_4) δ=1.12 (s, 9), 2.90 (t, 2), 4.20 (t, 2), 7.15 (s, 5); IR (neat) 1740 cm^{-1} (C=O).

n-*Butyl Cyanoacetate.* A mixture of *n*-butyl bromide (1.37 g, 0.01 mol), cyanoacetic acid (0.85 g, 0.01 mol), DBU (1.52 g, 0.01 mol), and 20 ml of benzene was refluxed. The reaction mixture was then washed with water, dried over an-

hydrous magnesium sulfate, and distilled. *n*-Butyl cyanoacetate, bp 110 °C/20 mmHg, 1.28 g (91% yield) was obtained. NMR (CCl_4) δ= 1.0(t, 3), 1.55 (m, 4), 3.52 (s, 2), 4.16 (t, 2); IR (neat) 1730 cm^{-1} (C=O).

Reaction of Phenethyl Bromide with DBU. A mixture of DBU (1.6 g, 0.11 mol), phenethyl bromide (1.9 g, 0.01 mol), and benzene (20 ml) was refluxed for 5 h. The reaction mixture was then washed with water, dried over anhydrous magnesium sulfate, and distilled. Styrene, bp 145 °C, 0.64 g (60% yield) was obtained.

General Procedure for Esterification of N-*Protected Amino Acids.* Alkyl halide (1.2 or 2 mmol) in benzene (1—2 ml) was added to a solution of *N*-protected amino acid (1 mmol) and DBU (152 mg, 1 mmol) in benzene (4 ml; 9 ml in the case of Z-Ser-OH, Boc-Asn-OH and Boc-Gln-OH), and the mixture was refluxed with stirring for 2 h. After cooling, the mixture was was diluted with diethyl ether (20 ml), and the precipitate (BDU·HX) was filtered and washed with diethyl ether or ethyl acetate. The filtrate and the washing were combined, washed with water, 1 M HCl (0.5 M citric acid in the case of N-Boc derivatives), 1 M $NaHCO_3$, and water again, and dried over sodium sulfate. The ester obtained after removal of solvent was treated as follows. In the case of ethyl ester, the product itself was satisfactorily pure, while methyl ester was treated with active carbon for removal of a trace of iodine. Benzyl ester and *p*-nitrobenzyl ester were recrystallized from ethyl acetate–petroleum ethrer or diethyl ether–petroreum ether. The results are summarized in Table 2.

The authors are grateful to the Sanyo Chemical Co. Ltd. (Kyoto) for the supply of DBU. The work was supported in part by a Grant-in-Aid from the Ministry of Education (No. 043017 1975—1976).

References

1) J. L. Marshall, K. C. Ericlson, and T. K. Folsoin, *Tetrahedron Lett.*, **1970**, 4011.

2) D. J. Raber and P. Gariano, *Tetrahedron Lett.*, **1971**, 4741.

3) a) J. Grundy, B. G. James, and G. Pattersom, *Tetrahedron Lett.*, **1972**, 757; b) J. Fairhyrst and D. C. Horwell, *Synth. Commun.*, **6**, 89 (1976).

4) K. Saigo, M. Usui, K. Kikuchi, E. Shimada, and T. Mukaiyama, *Bull. Chem. Soc. Jpn.*, **50**, 1863 (1977).

5) S. S. Wong, B. F. Gisin, D. P. Winter, R. Makofske, I. D. Kulesha, C. Tzougraki, and J. Meienhofer, *J. Org. Chem.*, **42**, 1286 (1977).

6) a) J. E. Shaw, D. C. Kunerth, and J. J. Shery, *Tetrahedron Lett.*, **1973**, 689; b) J. E. Shaw and D. C. Kunerth, *J. Org. Chem.*, **39**, 1968 (1974). The success of esterification is due to the use of HMPA as a solvent. However, HMPA has recently been found to cause cancer in laboratory animals [*Chem. Eng. News*, **17**, (Sept 29, 1975)]. Thus its use as a solvent should be restricted.

7) a) J. B. Hendrickson and C. Kandall, *Tetrahedron Lett.*, **1973**, 224; b) H. D. Durst, *Tetrahedron Lett.*, **1974**, 2421.

8) T. L. Ho and C. M. Wong, *J. Chem. Soc., Chem. Commun.*, **1973**, 224.

9) P. E. Pfeffer, T. A. Foglia, P. A. Barr, I. Schmeltz, and L. S. Sibert, *Tetrahedron Lett.*, **1972**, 4063; And Refs. 1—3.

10) R. K. Kadaba, *Synthesis*, **1972**, 628.

11) E. Haruki, M. Arakawa, N. Matsumura, Y. Otsuji, and E. Imoto, *Chem. Lett.*, **1974**, 427.

12) C. L. Liotta, H. P. Harris, M. McDermott, T. Gonzalez, and K. Smith, *Tetrahedron Lett.*, **1974**, 2417.

13) K. Holmberg and B. Hansen, *Tetrahedron Lett.*, **1975**, 3203.

14) The synthetic utility of DBU for dehydrohalogenation and other elimination reactions are reviewed. H. Oediger F. Moller, and K. Eiter, *Synthesis*, **1972**, 591.

15) R. L. Merker and M. J. Scott, *J. Org. Chem.*, **26**, 5190 (1961).

16) N. Ono, T. Yoshimura, R. Tanikaga, and A. Kaji, *Chem. Lett.*, **1977**, 871.

17) N. Ono, R. Tamura, R. Tanikaga, and A. Kaji., *Synthesis*, **1977**, 690.

18) J. H. Clark and J. M. Miller, *J. Am. Chem. Soc.*, **99**, 498 (1977).

19) D. Keglevic, A. Kornhauser, and S. Valentekovic, *Carbohydr. Res.*, **22**, 245 (1972).

20) A. Ito, R. Takahashi, and Y. Baba, *Chem. Pharm. Bull.*, **23**, 3081 (1975).

21) T. Yamada, N. Isono, A. Inui, T. Miyazawa, S. Kuwata, H. Watanabe, *Bull. Chem. Soc. Jpn.*, **51**, 1897 (1978).

22) E. Baer, D. Buchnea, and H. C. Stancer, *J. Am. Chem. Soc.*, **81**, 2166 (1959).

23) E. Baer and F. Eckstein, *J. Biol. Chem.*, **237**, 1449 (1962).

24) E. Wünsch, *Chem. Ber.*, **97**, 2490 (1964).

1,3-Dipolar Cycloadditions to Bicyclic Olefins. III. The Effects of Aromatic Solvents on the exo/endo Product Ratios for the 1,3-Dipolar Cycloadditions of Nitrile Oxides to Norbornadienes[1,2]

Hisaji TANIGUCHI* and Eiji IMOTO

Department of Applied Chemistry, College of Engineering, University of Osaka Prefecture, Mozu-umemachi, Sakai, Osaka 591

(Received March 16, 1978)

When no hydrogen-bonded complex is formed between the precursors (α-chloro-α-hydroxyiminoacetophenone (**5a**) and α-chloro-α-hydroxyiminoacetone (**5b**)) of nitrile oxides (phenylglyoxylonitrile oxide (**2a**) and methylglyoxylonitrile oxide (**2b**)) and norbornadienes(2,3-bis(methoxycarbonyl)norbornadiene (**1**) and norbornadiene (**6**)) in solvents, the exo/endo product ratios for the cycloadditions of **2a** and **2b** to **1** or **6** increase or decrease with increasing temperature. When the hydrogen-bonded complex between **5a** and **1** is formed in a solvent cage, however, the ratio keeps a constant value until the temperature is elevated up to a certain temperature, at which the ratio jumps up. After the jumping, the ratio has another constant value, regardless of the temperature. Similar results are obtained in the cycloaddition of **2b** to **1** in the aromatic solvents used.

The 1,3-dipolar cycloaddition of phenylglyoxylonitrile oxide (**2a**) to 2,3-bis(methoxycarbonyl)norbornadiene (**1**) gives both the exo and endo adducts (**3a** and **4a**).[3] When non-aromatic solvents are used, the exo/endo product ratio increases with an increase in the temperature (Fig. 1).[2] However, when aromatic solvents are used, strange phenomena are observed, as is shown in Fig. 2; that is, the plot of the exo/endo product ratio *vs.* the temperature gives horizontal lines, but jumps up at a certain temperature. After the jumping, the ratio takes another constant value, regardless of the temperature. In this paper, a tentative explanation for the phenomena will be given.

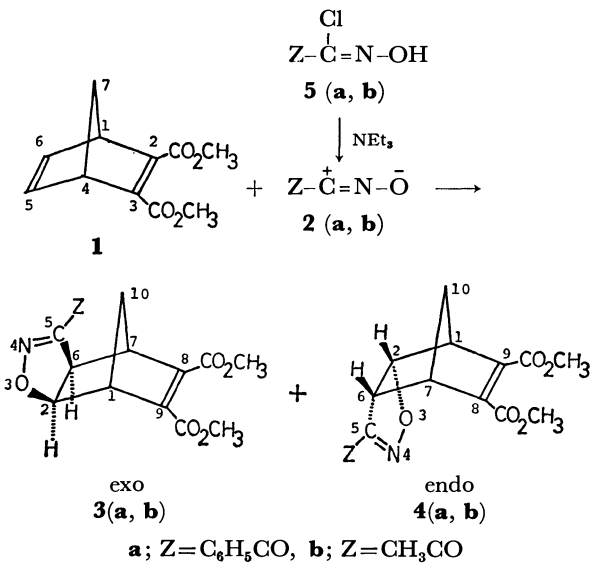

a; $Z=C_6H_5CO$, **b**; $Z=CH_3CO$

Results

The Relationship between the exo/endo Product Ratio and the Temperature. (i) The cycloaddition of **2a** to **1**: The results shown in Fig. 2 were obtained when the cycloaddition was carried out as follows: a dilute solution of triethylamine was slowly stirred into a solution of a mixture of **1** and α-chloro-α-hydroxyiminoacetophenone (**5a**), which is the precursor of **2a** (see

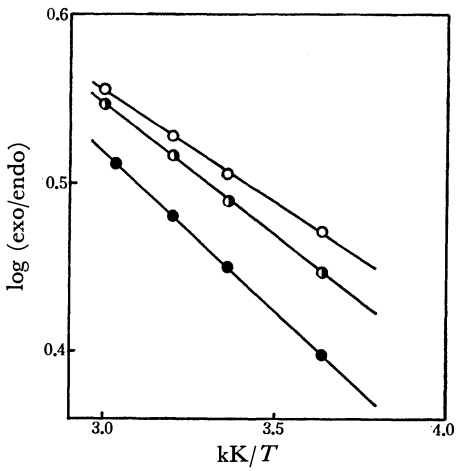

Fig. 1. The linear relationship between $1/T$ and the exo/endo product ratio for the cycloaddition of **2a** to **1** in non-aromatic solvents.
○: THF, ◑: $CHCl_3$, ●: acetone.

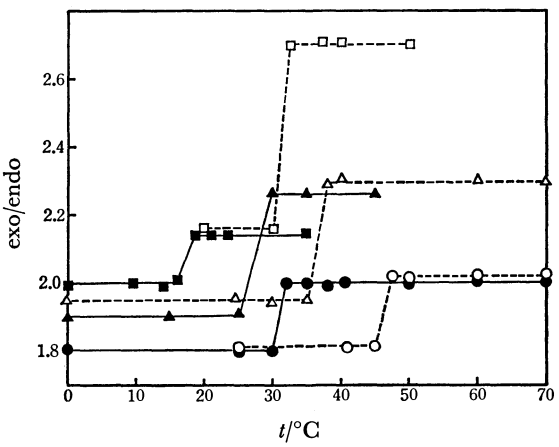

Fig. 2. Plots of exo/endo product ratio *vs.* temperature for the cycloaddition of **2a** to **1** in aromatic solvents.
●: Toluene, ○: benzene, ▲: anisole, △: chlorobenzene, □: nitrobenzene, ■: *o*-xylene.

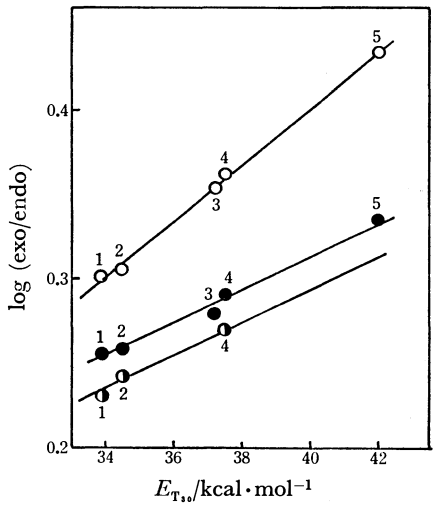

Fig. 3. Height of horizontal line *vs.* $E_{T,0}$ (25 °C) value. ○: exo/endo product ratio after the jumping for the cycloaddition of **2a** to **1**, ●: exo/endo product ratio before the jumping for the cycloaddition of **2a** to **1**, ◑: exo/endo product ratio for the cycloaddition of **2b** to **1**, 1: toluene 2: benzene, 3: anisole, 4: chlorobenzene, 5: nitrobenzene.

Method A in the Experimental section). The plots in Fig. 2 are characterized as follows.

a) The height of the horizontal lines in Fig. 2 can be linearly related to the E_T value[4] of the solvent, as is shown in Fig. 3.

b) The jumping temperature stands to the molar volume[5] of the solvent in a linear relation, as is shown in Fig. 4.

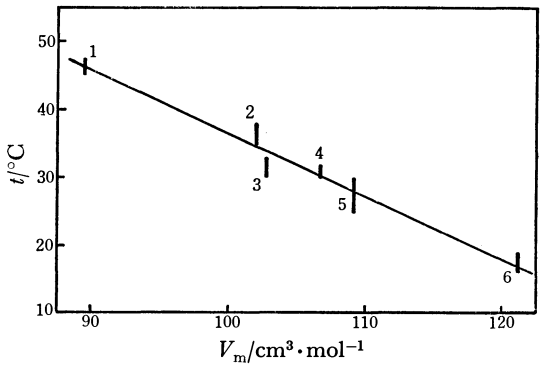

Fig. 4. Jumping temperatures *vs.* molar volumes of solvents (25 °C).
1: Benezene, 2: chlorobenzene, 3: nitrobenzene, 4: toluene, 5: anisole, 6: *o*-xylene.

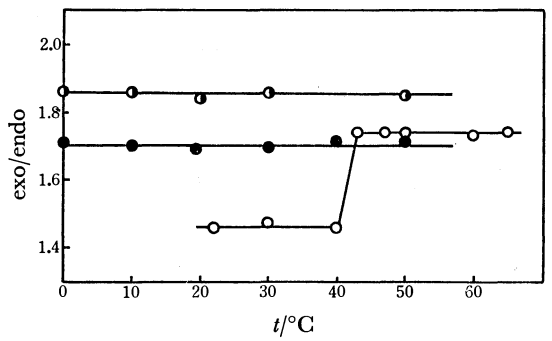

Fig. 5. Plots of exo/endo product ratio *vs.* temperature for the reaction of **2b** with **1**.
○: Benzene, ●: toluene, ◑: chlorobenzene.

(ii) The cycloaddition of **2b** to **1**: The cycloaddition was carried out in the manner described above. Figure 5 shows the results. When benzene was used, the exo/endo product ratio jumped up at about 40 °C. When toluene or chlorobenzene was used, however, the jumping did not occur. Also, in this case the height of the horizontal lines increased with an increase in the E_T value of the solvent (Fig. 3).[6]

(iii) The cycloaddition of **2a** to norbornadiene (**6**): The cycloaddition was carried out in benzene in a manner similar to that described above. The exo/endo product ratio decreased with an increase in the temperature (Fig. 6).

(iv) The cycloaddition of "free **2a**" to **1**: After having been generated in the reaction system, the dipole which we called "free **2a**" was allowed to react with **1** in toluene (Method B in the Experimental section). In this case, the exo/endo product ratio increased with an increase in the temperature (Fig. 7).

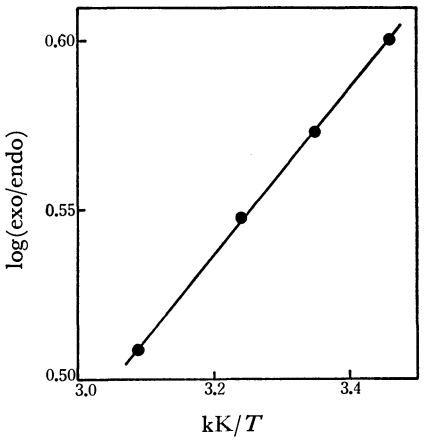

Fig. 6. Plots of exo/endo product ratio *vs.* temperature for the reaction of **2a** with **6**.

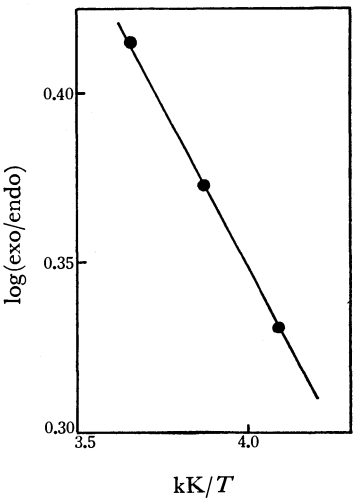

Fig. 7. Plots of exo/endo product ratio *vs.* temperature for the cycloaddition of "free **2a**" to **1** in toluene.

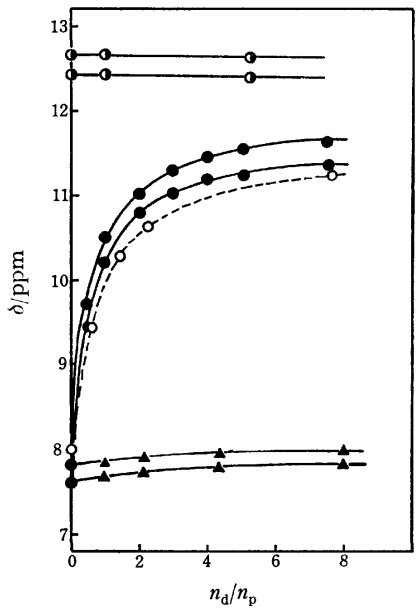

Fig. 8. Chemical sflifts of OH protons of **5a** and **5b** *vs.* n_d/n_p.
n_d=mole number of **1**(or **6**), n_p=mole number of **5a**(or **5b**), ◑: **1** to **5a**(in acetone), ●: **1** to **5a**(in benzene-d_6) ○: **1** to **5b**(in benzene-d_6), ▲: **6** to **5a** (in benzene-d_6).

Behavior of the Precursors of Nitrile Oxides in Solutions. (i) NMR chemical shifts of the precursors: When mixtures of **1** and **5a** in appropriate molar ratios were dissolved in acetone, the δ value[7] of the hydroxylic proton of **5a** did not change, regardless of the n_d/n_p ratio, as is shown in Fig. 8, where n_d is the number of moles of the dipolarophile and n_p is the number of moles of the precursor. In benzene-d_6, however, the δ value changed with the n_d/n_p ratio, as is shown in Fig. 8: The δ value increased rapidly as the value of n_d/n_p changed from 0 to 1. After n_d/n_p had reached 1, the δ value increased gradually with the increase in the n_d/n_p. For the precursor (α-chloro-α-hydroxyiminoacetone (**5b**)) of **2b** also, a similar phenomenon was observed (Fig. 8).[7] These results suggest that a 1:1 hydrogen-bonded complex is formed between **1** and **5a** (or **5b**) in benzene-d_6. When mixtures of **6** and **5a** in appropriate molar ratios were dissolved in benzene-d_6, the δ value of the hydroxylic proton of **5a** scarcely changed (Fig. 8). This result implies that no hydrogen-bonded complex is formed between **6** and **5a** in benzene-d_6.

Table 1. Solubilities of **5a** and **5b** (mg/cm³, 25 °C)

Solvent	**5a**	**5b**
Benzene	9.8	17
Toluene	7.7	15
Anisole	89	
Chlorobenzene	8.9	13
Nitrobenzene	80	
o-Xylene	7.3	
Norbornadiene	19	
BMCND[a)]	500	790
THF	1250	
Acetone	870	
Methyl acetate	620	
Ethanol	740	

a) 2,3-Bis(methoxycarbonyl)norbornadiene.

(ii) Solubility of the precursors: The precursors, **5a** and **5b**, are very soluble in non-aromatic solvents and in **1**, but they are only slightly soluble in aromatic solvents and in **1** (Table 1). Moreover, the following phenomena were observed: when 0.25 mmol of **5a** was added to 0.5 cm³ of benzene-d_6, a large portion of the **5a** remained insoluble. The addition of 0.25 mmol of **1** to this suspension gave a clear solution. Such a phenomenon was also observed for the other aromatic solvents used. For **5b** also, a similar phenomenon was observed. These results support the formation of the hydrogen-bonded complex of **1** with **5a** (or **5b**) in aromatic solvents.

Discussion

When no hydrogen-bonded complex is formed between the precursors of nitrile oxides and norbornadiene in solvents, the exo/endo product ratios for the reactions of the nitrile oxides and norbornadienes increase or decrease with an increase in the temperature. The reason for the increase or decrease of the ratios has been reported previously.[2] When the hydrogen-bonded complexes between the precursors of nitrile oxides and the norbornadiene, **1**, are formed in solvent cages, however, stepped lines are obtained, as is shown in Figs. 2 and 5. We will now give a tentative explanation for these phenomena.

At the moment the dipole is generated by the elimination of hydrogen chloride from the precursor, which is a component of the hydrogen-bonded complex in a solvent cage, it must be present near the polar ester groups. Then, it would be transferred to the exo or endo side of the C_5–C_6 double bond of **1**, taking some kind of rotation. The solvent cage can be divided into the exo and endo spaces by the plane containing the four carbon atoms (C_1, C_4, C_5, and C_6) (see the figure). Here, we assume that the exo/endo product ratio depends on the ease of approach of the dipole to the exo and endo sides and that the ease of approach depends on the size of the exo and endo spaces. If the exo and endo spaces are large enough for the dipole to take any pathway of transfer and any mode of rotation, the exo/endo product ratio will become the value obtained when the cycloaddition is carried out in a gas phase. If the solvent cage is small, however, the pathway of the transfer and the mode of rotation of the dipole may be limited. The endo space must be smaller than the exo space, because the ester groups in the endo space would attract the polar solvent. Hence, as the E_T value of the solvent becomes larger, the endo space may decrease more greatly than the exo space. This means that the exo/endo product ratio increases with an increase in the E_T value of the solvent (Fig. 3).

The sizes of the exo and endo spaces of the solvent cage would increase gradually with an increase in the temperature, and the former more rapidly than the

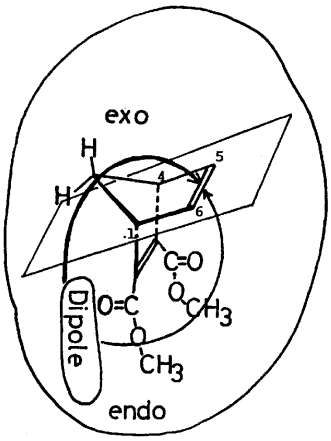

latter. Until the exo space reaches a certain size which is large enough for the dipole to take other pathways of translation and modes of rotation, the exo/endo product ratio keeps a constant value, and then it jumps up suddenly at this size. Since the size of the solvent cage increases with an increase in the molar volume of the solvent, the jumping temperatures will lower with an increase in the molar volume of the solvent, as is shown in Fig. 4.

Experimental

Solvents. Benzene was refluxed for 10 h over sodium and then carefully distilled; bp 80 °C. Toluene was refluxed for 10 h over sodium and distilled; bp 111 °C. Chlorobenzene was dried over $MgSO_4$ and distilled; bp 131—132 °C. Anisole was dried over sodium and then distilled; bp 155—156 °C. Nitrobenzene was dried over $MgSO_4$ and then distilled; bp 210—211 °C. *o*-Xylene was dried over sodium and then distilled; bp 144 °C.

Materials. The norbornadiene, **1**, was prepared by a method described in the literature.[9] Norbornadiene was purchased and distilled before use. The precursors of the nitrile oxides, **5a**[10] (mp, 131—132 °C) and **5b**[11] (mp, 104—105 °C), were also prepared by methods described in the literature.

Products. The cycloadducts obtained in the reaction of **2a** with **6** and the cycloadducts, **3a** and **4a**, have been characterized in a previous paper.[3]

The cycloadducts, 5-acetyl-8,9-bis(methoxycarbonyl)-2,6-exo-3-oxa-4-azatricyclo[5.2.1.$0^{2,6}$]deca-4,8-diene(**3b**), 5-acetyl-8,9-bis(methoxycarbonyl)-2,6-*endo*-3-oxa-4-azatricyclo-[5.2.1.$0^{2,6}$]deca-4,8-diene (**4b**), were isolated using column chromatography on silica gel and chracterized.

3b: Colorless viscous oil; IR (neat) 1720 (ester C=O), 1690 (C=O), and 1625 cm^{-1} (C=N); NMR ($CDCl_3$) δ=1.53 and 1.87 (2H, ABq, J=10.5 Hz, 10-CH_2), 2.44 (3H, s, $COCH_3$), 3.76 (3H, s), 3.79 (3H, s), 3.5—3.9 (3H, m, 1-H, 7-H, and 2-H_{endo}), 5.15 ppm (1H, d, J=8 Hz, 6-H_{endo}). 2,4-Dinitrophenylhydrazone of **3b**: mp 169—171 °C.

Found: C, 50.71; H, 3.78; N, 14.98%. Calcd for $C_{20}H_{19}N_5O_9$: C, 50.74; H, 4.05; N, 14.80%.

4b: Mp 128—130 °C (from MeOH–H_2O); IR(KBr) 1730 (ester C=O), 1690 (C=O), and 1620 cm^{-1} (C=N); NMR ($CDCl_3$) δ=1.50 and 1.90 (2H, ABq, J=10 Hz, 10-CH_2), 2.39 (3H, s, $COCH_3$), 3.5—4.0 (2H, m, 1-H and 7-H), 3.71 (3H, s), 3.75 (3H, s), 4.90 (1H, dd, J=10 and 4 Hz, 2-H_{exo}), 3.71 (3H, s), 3.75 (3H, s), 4.09 (1H, dd, J=10 and 4 Hz, 2-H_{exo}), and 5.56 ppm (1H, dd, J=10 and 4.5 Hz, 6-H_{exo}).

Found: C, 57.51; H, 5.03; N, 4.76%. Calcd for $C_{14}H_{15}NO_6$: C, 57.33; H, 5.16; N, 4.78%.

General Procedure for 1,3-Dipolar Cycloadditions. Method A (Cycloadditions Started from the Hydrogen-bonded Complex): A mixture of a norbornadiene (2.50 mmol) and a precursor of a nitrile oxide (2.50 mmol) was dissolved in an appropriate solvent (40 cm^3). Then, the temperature of the solution was maintained at a given temperature (which was controlled within±0.1 °C). A solution of triethylamine (TEA) (330 mg, 3.26) in the same solvent (10 cm^3) as that used above was added, drop by drop, over a period of 1 h. After an additional 1 h of stirring at the same temperature, the resulting triethylammonium chloride was removed by filtration. The filtrate was evaporated under reduced pressure to give a mixture of the exo and endo adducts. This mixture was then submited to a measurement of the exo/enso product ratio.

For the cycloaddition of **2a** to **6**, two molar equivalents of **6** with respect to **2a** were used.

Method B (Cycloadditions of "Free 2a" to 1): Compound **5a** (520 mg, 2.50 mmol) was dissolved in 40 cm^3 of toluene. The temperature of this solution was maintained at a given temperature by means of a thermostat (±0.1 °C). Into the solution, a solution of TEA (330 mg, 3.26 mmol) dissolved in 5 cm^3 of toluene was added all at once, after which the soultion was stirred for 4 min at the same temperature, A solution of **1** dissolved in 5 cm^3 of the same solvent as that used avobe was then added to the above reaction mixture all at once, after which the solution was stirred for 1 h at the same temperature. The resulting triethylammonium chloride was removed by filtration. The evaporation of the solvent left a mixture of the exo and endo adducts.

Measuerment of the exo/endo Product Ratios. The NMR technique employed for measuring the exo/endo product ratios is described in the literature.[2]

The measurement of each exo/endo product ratio for the cycloadditions of **2a** and **2b** to **1** or **6** at a given temperature was repeated twice using the NMR technique. The difference between the average and the experimental data was within±0.02. (Figs. 2, 5, 6, and 7.)

Measurement of Solubility of the Precursors, 5a and 5b. General procedure: An excess of the precursor of a nitrile oxide was added to an appropriate solvent of a constant volume. The solution was allowed to stand for about 12 h at 25 °C. Then, the insoluble material was removed by filtration. The filtrate was evporated to dryness under reduced pressure to give a residue. The weight of the residue was measured.

Measurement of the Chemical Shifts for OH Protons of 5a and 5b. General procedure: A mixture of a norbornadiene and **5a** (or **5b**) in an arbitary molar ratio was dissolved in a 0.5-cm^3 portion of benzene-d_6 (or acetone) containing a small amount of TMS in an NMR sample tube. Then, the chemical shift for the OH proton of the precusor of the nitrile oxide was measured. (The NMR spectra were recorded on a Hitachi NMR R-24A spectrometer at 60 MHz.)

The authors are indebted to Mr. Yoshimasa Kadoma for measuring the solubilities of **5a** and **5b**.

References

1) Presented at the 36th National Meeting of the Chemical Society of Japan, Higashi-Osaka, Japan, April 1977, Absrtacts II, 3S12 and presented at the 26th IUPAC Congress, Tokyo, Japan, September 1977, Abstracts Session I, 0F504.

2) Preceding paper: H. Taniguchi, Y. Yoshida, and E.

Imoto, *Bull. Chem. Soc. Jpn.*, **50**, 3335 (1977).

3) H. Taniguchi, T. Ikeda, Y. Yoshida, and E. Imoto, *Bull. Chem. Soc. Jpn.*, **50**, 2694 (1977).

4) K. Dimroth, C. Reichardt, T. Siepmann, and F. Bohlmann, *Justus Liebigs Ann. Chem.*, **661**, 1 (1963).

5) A. F. M. Barton, *Chem. Rev.*, **75**, 731 (1975).

6) For benzene, the exo/endo product ratio after the jumping was employed.

7) Both precursors, **5a** and **5b**, consist of two isomers, the *E*-form and the *Z*-form. Two sharp OH signals appear in the NMR spectrum of **5a**. This may be attibutable to a very slow chemical exchamge of the OH protons on the NMR time scale between the two isomers.[8] In the case of **5b**, only one broad singlet appears for the OH proton. This may be ascribed to a rapid chemical exchange of the OH protons between the two isomers.[8]

8) L. M. Jackman and S. Sternhell, "Application of Nuclear Magnetic Resonance Spectroscopy in Organic Chemistry," 2nd ed, Pergamon Press, London (1969), p. 17 and Chap. 2-1.

9) O. Diels and K. Alder, *Justus Liebigs Ann. Chem.*, **490** 236 (1931).

10) Y. Otsuji, Y. Tsuijii, A. Yoshidam, and E. Imoto, *Bull. Chem. Soc. Jpn.*, **44**, 223 (1971).

11) Y. Otsuji, J. Nishikawa, and E. Imoto, the 30th National Meeting of the Chemical Society of Japan, Higashi-Osaka, April 1974, Abstracts III, p. 1302.

Electrolytic Dissolution and Deposition of Overpotentials of Tantalum in KCl Melts

Ippei NAKAGAWA

Government Industrial Research Institute, Nagoya, Hirate-machi, Kita-ku, Nagoya 462

(Received February 24, 1978)

As part of electrochemical studies on tantalum, the electrolytic dissolution and deposition of solid tantalum in molten salt were studies by measuring its overpotentials in a steady state. The measurements were carried out using the dc current polarization technique in the concentration range of 2.00×10^{-4}—2.79×10^{-1} mole fraction at temperatures between 775 and 875 °C. The kinetic parameters (the exchange current densities, the transfer coefficients, the kinetic averaged valences, and the apparent activation energies) were determined for the anodic and the cathodic reactions in the Tafel region. The over-all reaction was indicated as:

$$(m_1+m_2)Ta^{2+} + (2m_1-2m_2)e \rightleftarrows m_1Ta^0 + m_2Ta^{4+}$$

The Ta^{2+} ion was previously supposed not to form a complex ion; the Ta^{4+}, however, was a complex ion which decomposed at above 850 °C.

Production of refractory metals by fused salt electrolysis has been intensively carried out. Much information on the chemical equilibria in the metal-molten systems has been accumulated in recent years. However, there have been only a few reports on the kinetic data for the refractory metals such as Zr, Hf, Nb, and Ta. Tanaka and Tamamushi[1] compiled the kinetic data in aqueous and in molten salt systems. However, the kinetic data available for the molten salt systems are skimpy by comparison those available for aqueous solutions.

Randles and White applied a relaxation method[2] to the electrode reactions in molten salts. About same time, Laitinen and Osteryoung used the same ac current technique with a platinum electrode in the LiCl–KCl system.[3] Hill *et al.* measured the impedance of tungsten in Ti(II)–Ti(III) couple in the LiCl–KCl eutectic.[4] Laitinen *et al.* measured the exchange current densities of solid metal electrodes (Cd, Zn, Pb, Bi, Ag, Ni, and Pt) and a redox system of V(II)–V(III) in the LiCl–KCl eutectic.[5] T. Kirihara *et al.* have measured the overpotentials of electrolytic dissolution and deposition of Ag,[6] Zr,[7] and Hf[8] in the NaCl–KCl (equiv mole) melts by a galvanostatic method and have evaluated the kinetic parameters (exchange current densities, transfer coefficients, and rate constents).

In the course of the electrochemical studies on Ta,[9-11] the present work was undertaken to determine the kinetic parameters. The electrode processes of dissolution and deposition of solid Ta in the NaCl–KCl (equiv mole) melts will be discussed along with the results of overpotential measurements in a steady state. The values of overpotentials for these processes are also very important in the electrorefining procedure.

Experimental

Chemicals and Procedures. Tantalum plate and wire (99.9%, Fansteel Co.), and tantalum pentachloride (99.9%, Mitsuwa Chemicals Co.) were used. Sodium and potassium chlorides of extra purity were melted under flowing chlorine and argon for further purification and then stored in a desiccator before use.

Electrodes. A working electrode was constructed by connecting a Ta plate with a surface area of 1 cm^2 with a Ta wire to a spectroscopic graphite rod 0.5 cm in diameter. A counter electrode with a surface area of 3 cm^2 and a reference electrode with a area of 1 cm^2 were made in a way similar to the working electrode.

All the electrodes were set in a quartz vessel ($4.5\phi\times45$ cm). An electrical resistance furnace was used to heat the vessel and the temperature was controlled by a current controller with a Pt–Pt·Rh thermocouple within ±2 °C between 775 and 875 °C.

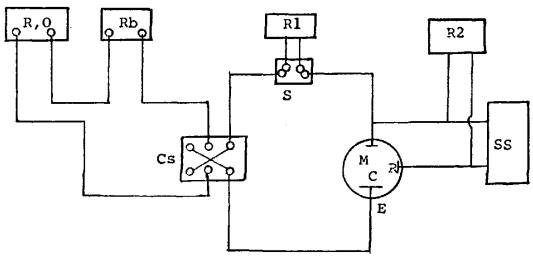

Fig. 1. Schematic diagram of apparatus for measurement of overpotential and resistance of melt.
B: Lead storage battery, O: frequency oscilator, Rb: resistance box, R1: recorder, R2: recorder, S: shunt, Cs: switch, E: cell, M: measuring electrode, R: reference electrode, C: counter electrode, SS: synchloscope.

Measurement of Ohmic Overpotential. A schematic diagram of the apparatus for measuerment of ohmic resistance of melt is shown in Fig. 1. A precise value of ohmic overpotential caused by ohmic resistance during polarization between the reference electrode and the working one is required to obtain an intrinsic overpotential. That is, $\eta_{total}=\eta_{MR}+\eta_{IR}$, where η_{MR} is the true overpotential and η_{IR} the ohmic one. Both voltage measurements alternating current (20—2000 Hz) and measurements of the initial jump in dc current were employed to determine the value of η_{IR}. The ohmic overpotentials obtained by those methods were in good agreement with each other. A typical example taken by the intial jump method is represented in Photo. 1. The ohmic drop was determined by the gap at the initial part of the curve, as has already been done by other workers.[12] The values of η_{IR} were 0.15—0.27 Ω at various concentrations and temperatures.

Measurement of Overpotential. A schmatic diagram of the apparatus for measurement of overpotemtial is shown in Fig. 1. A galvanostatic method was employed from a low current density to a higher one. The anodic polarization and the cathodic one were measured alternatively in the concentration range of 2.00×10^{-4}—2.79×10^{-1} mole fraction at

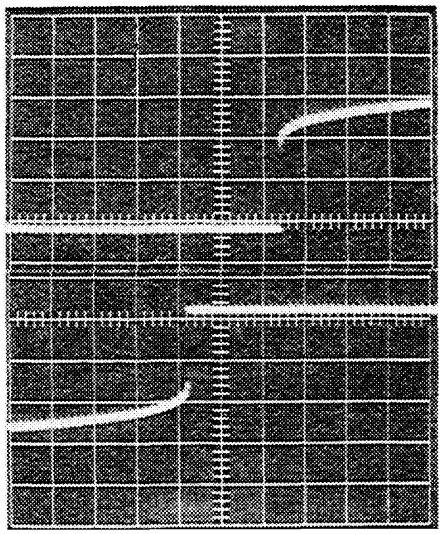

Photo. 1. Potential-time curve for measurement of resistance.
Upper part: dissolution curve, $IR+\eta_{MR}=2.0$ mV
$I=9.4$ mA
$R=0.21\ \Omega$
Lower part: deposition curve, $IR+\eta_{MR}=2.2$ mV
$I=9.4$ mA
$R=0.23\ \Omega$
Vert.: 1 mV/div, Hori.; 0.1 s/div,
Temp: 825 °C. Concn: 2.17×10^{-3} m.f.

temperatures between 775 and 875 °C. All measurements were carried out under an argon atmosphere.

Results and Discussion

Theoretical. The equilibrium reaction between Ta metal and tantalum chlorides has been found experimentally to be

$$Ta^{4+} + Ta = 2Ta^{2+},$$

in the KCl and in the NaCl–KCl (equiv mol) melts.[9-11] Two types of tantalum chlorides, $TaCl_2$ and $TaCl_4$, were found in the equilibrium state. Therefore, the electrode process can not be a simple process like an ordinary electrode reaction which concerns only a simple ion in the solution.

The theoretical treatment for a simultaneous electrode process has been studied by Gray and Cahill.[13] However, this theory is very complicated and it is difficult experimentally to determine the kinetic parameters. Thus we tried to treat the electrode processes for electrolytic dissolution and deposition of solid tantalum with the mobile equilibrium concept which has been explained for zirconium in the chloride system.[14] A more precise consideration will be given elsewhere for the tantalum–chloride system. In this paper, the author describes briefly the concept of mobile equilibrium for the tantalum electrode reactions.

According to emf measurements,[11] Ta^{2+} and Ta^{4+} ions were stable at the electrode surface. For tantalum electrolysis, the charge transfer reactions are usually expressed as

$$Ta^0 \underset{k_{c1}}{\overset{k_{a1}}{\rightleftarrows}} Ta^{2+} + 2e, \qquad \Delta G_1^\circ < 0 \qquad (1)$$

(ΔG°: free energy)

$$Ta^{2+} \underset{k_{c2}}{\overset{k_{a2}}{\rightleftarrows}} Ta^{4+} + 2e, \qquad \Delta G_2^\circ < 0 \qquad (2)$$

where k_a and k_c are the rate constants of each direction. The direction right to left means the cathodic reaction (deposition) and the opposite the anodic one (dissolution). The over-all reaction becomes

$$m_1Ta^0 \underset{k_c}{\overset{k_a}{\rightleftarrows}} (m_1-m_2)Ta^{2+} + m_1Ta^{4+} + 2(m_1-m_2)e, \qquad \Delta G_3^\circ < 0. \qquad (3)$$

When the Process 1 proceeds by m_1 mol, the Process 2 occurs for m_2 mol. If the electrode potentials are high enough,

$$\Delta G_3^\circ = m_1\Delta G_1^\circ + m_2\Delta G_2^\circ < 0,$$
$$-nFE_3^\circ = m_1\Delta G_1^\circ + m_2\Delta G_2^\circ. \qquad (4)$$

The electrode process will proceed according to Eq. 3.

The equilibrium reaction of tantalum is, however $Ta^{4+}+Ta=2\ Ta^{2+}$. So

$$m_1Ta^0 + m_2Ta^{4+} \underset{k_c}{\overset{k_a}{\rightleftarrows}} (m_1+m_2)Ta^{2+} + 2(m_1-m_2)e, \qquad (3')$$

and $\Delta G_{3'}^\circ = m_1\ \Delta G_1^\circ - m_2\ \Delta G_2^\circ = -nFE_{3'}^\circ$ will occur at lower overpotentials than Eq. 4, because

$$|\Delta G_3^\circ| > |\Delta G_{3'}^\circ|.$$

Accordingly, the charge transfer processes are described as

$$Ta^0 \underset{k_{c1}}{\overset{k_{a1}}{\rightleftarrows}} Ta^{2+} + 2e, \qquad (1')$$

$$Ta^{4+} + 2e \underset{k_{c2}}{\overset{k_{a2}}{\rightleftarrows}} Ta^{2+}. \qquad (2')$$

The mobile equilibrium concept for the electrode reaction means a quasi-equilibrium state which involves the electrical work applied to the solution. Therefore, the American convention was adopted to convenience. When mobile equilibrium was established for the Reaction 3′,

$$nFE + \Delta G = 0.$$

Thus, $nFE+\Delta G^\circ+RT\ln a_2^{m_1-m_1}+RT\ln a_4^{m_2}=0$. Accordingly, overpotentials of the cathodic or the anodic process for the Reaction 3′ can be expressed as

$$\eta = E - E_e = \frac{RT}{2(m_1-m_2)F}\{(\ln a_2^{\circ(m_1-m_1)} - RT\ln a_4^{\circ m_2}) - (\ln a_2^{(m_1-m_2)} - \ln a_4^{m_2})\},$$
$$= \frac{RT}{nF}\left\{\ln\left(\frac{a_2^\circ}{a_2}\right)^{(m_1-m_2)} + \ln\left(\frac{a_4}{a_4^\circ}\right)^{m_2}\right\}, \qquad (5)$$
$$= A\eta + (1-A)\eta,$$

where E_e means the equilibrium electrode potential, and a_2° and a_4° are the activities at the equilibrium state for Ta^{2+} and Ta^{4+}, respectively. A is the transfer coefficient and $n=2(m_1-m_2)$ the kinetic averaged valence.

When the diffusion process can be ignored, the relation between the current density and the overpotential can be expressed in wellknown equations for the deposition process:

$$I_c = I_{0c}\{\exp(-A_c n_c F\eta_c/RT) - \exp(A_a^c n_c F\eta_c/RT)\},$$
$$A_c + A_a^c = 1, \quad (6)$$

and for the dissolution process:

$$I_a = I_{0a}\{\exp(A_a n_a F\eta_a/RT) - \exp(-A_c^a n_a F\eta_a/RT)\},$$
$$A_a + A_c^a = 1, \quad (7)$$

Table 1. Exchange currents (I_{0a}, I_{0c})

Concn (mol fract.)	Temp (C°) 755	800	825	850	875
	I_{0a} (mA/cm)^2				
2.00×10^{-4}	0.42	0.48	0.50	0.76	1.00
2.17×10^{-3}	1.8	2.4	3.4	4.0	4.6
5.90×10^{-2}	9.0	10.5	12.0	15.0	20.0
1.91×10^{-1}	(31.1	25.0	28.0	21.0	30.0)
2.79×10^{-1}	27.0	30.0	32.0	35.0	42.0
	I_{0c} (mA/cm^2)				
2.00×10^{-4}	0.39	0.48	0.50	0.60	0.90
2.17×10^{-3}	1.8	2.4	2.8	3.7	4.0
5.90×10^{-2}	8.0	10.0	12.0	15.0	18.0
1.91×10^{-1}	(13.0	11.0	12.0	13.0	15.0)
2.79×10^{-1}	13.0	16.5	18.0	18.5	26.0

The values in parentheses are uncertain.

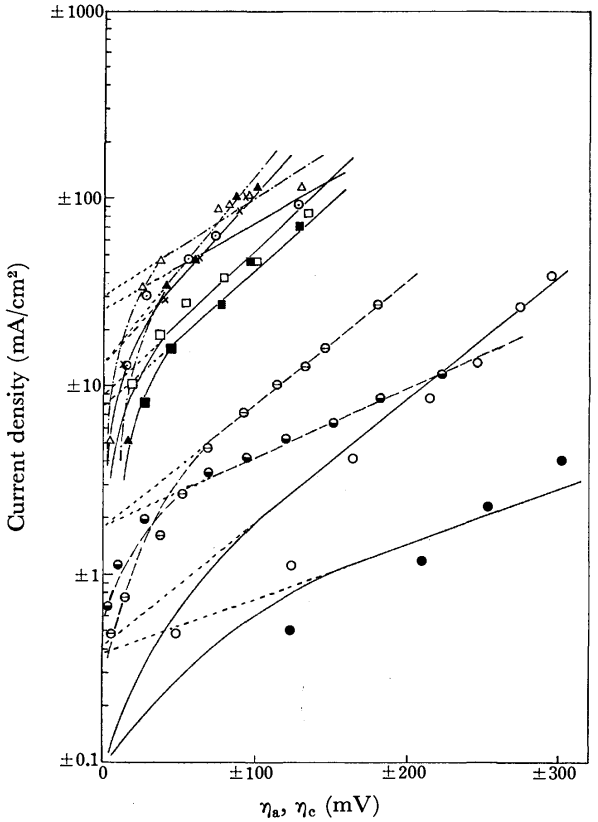

Fig. 2. Relationship between overpotentials and current densities of dissolution and deposition at 775 °C.
Concentration: mole fract.
○ (dissol.), ● (dep.) 2.00×10^{-4}
⊖ (dissol.), ◒ (dep.) 2.17×10^{-3}
□ (dissol.), ■ (dep.) 5.90×10^{-2}
△ (dissol.), ▲ (dep.) 1.91×10^{-1}
⊙ (dissol.), × (dep.) 2.79×10^{-1}

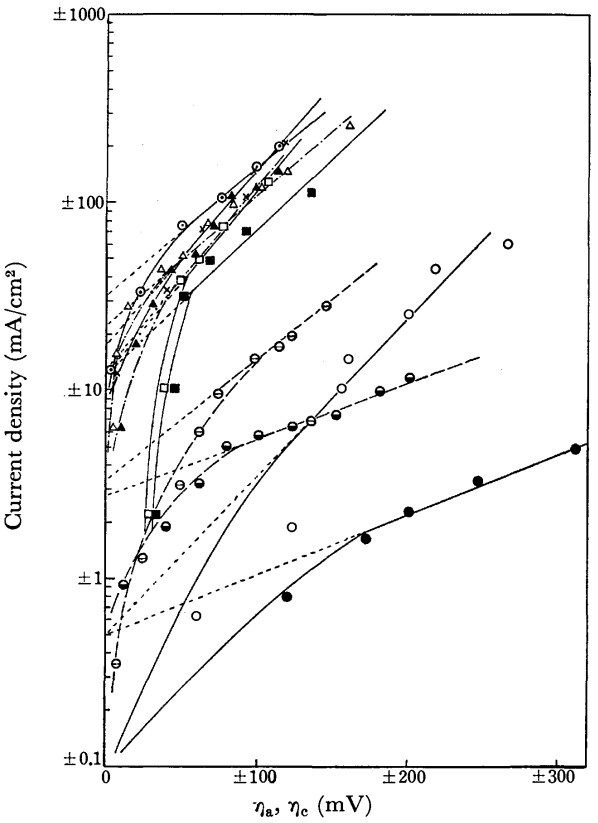

Fig. 3. Relationship between overpotentials and current densities of dissolution and deposition at 825 °C.
Marks are the same as those in Fig. 2.

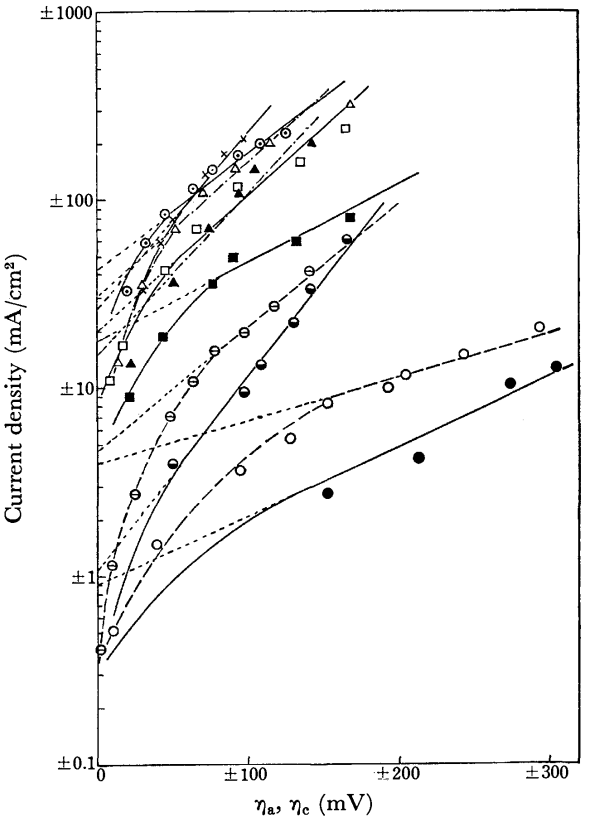

Fig. 4. Relationship between overpotentials and current densities of dissolution and deposition at 875 °C.
Marks are the same as those in Fig. 2.

where subscripts a and c represent the anodic and the cathodic reactions, respectively, I_0 is the exchange current density, I the current density, η the overpotential, A the apparent transfer coefficient, A^a and A^c are the apparent transfer coefficients of the opposing reactions, and F, R, and T have their usual meanings. At high overpotentials, the second terms in Eqs. 6 and 7 can be neglected in comparision with the large values of the first terms. Thus, Eqs. 6 and 7 can be simplified as follows:

$$I_c = I_{0c}\{\exp(-A_c n_c F\eta_c/RT)\}, \quad (6')$$

$$I_a = I_{0a}\{\exp(A_a n_a F\eta_a/RT)\}. \quad (7')$$

The logarithmic expression of Eqs. 6 and 7 gives a wellknown Tafel equation. When the overall faradaic current is equal to zero at $\eta=0$, $I_c=I_{0c}$, $I_a=I_{0a}$. If the electrode reactions are reversible on the Tafel line, $I_{0c}=I_{0a}$.

Exchange Current Densities (I_{0a}, I_{0c}). Plots of log I_a *vs.* η_a are shown in Figs. 2, 3, and 4 for the dissolution process at various temperatures and concentrations; similar relations, log I_c *vs.* η_c, are also represented in Figs. 2, 3, and 4 for the deposition process. The exchange current densities can be obtained from the figures stated above by extrapolation of I_a and I_c in the Tafel region to $\eta_a=0$ and $\eta_c=0$. The values of the exchange current densities thus obtained are tabulated in Table 1. It should be noted that $I_{0a}=I_{0c}$ in the concentration range of 2.00×10^{-4}—2.17×10^{-3} mole frac., and a slight difference between I_{0a} and I_{0c} was observed in the range of 5.90×10^{-2}—2.79×10^{-1} mole fraction. The accuracy of the exchange current densities was estimated to be ±0.2 mA/cm^2 at lower concentrations and ±2 mA/cm^2 at higher concentrations (5.90×10^{-2}—2.79×10^{-1} mole fraction).

The values of $A_a n_a$ and $A_c n_c$ were calculated from the slope of each straight line in Figs. 2, 3, and 4, and are given in Table 2. The n_a and n_c values can be calculated if the transfer coefficients A_a and A_c are determined.

Transfer Coefficients (A_a, A_c) and Kinetic Averaged Valences (n_a, n_c). If we can assume that the activity a^{4+} increases and the activity a^{2+} decreases as the anodic overpotentials for the anodic reaction rise, while for the cathodic reaction, the tendensy is reversed, these activities would vary proportionally to the total concentrations, C_o, which are expressed as mole fractions of the solute in the solution. The relation of log I_{0a} *vs.* log C_o, and that of log I_{0c} *vs.* log C_o gave two groups of straight lines, as shown in Figs. 5 and 6. Two values of the transfer coefficients were obtained, for the lower concentrations and for the higher one, respectively; these values are represented in Table 3. The values of n_a and n_c were calculated from the values in Tables 2 and 3, and given in Table 4.

Activation Energies (E_a, E_c). The apparent activation energies for the dissolution and deposition processes are calculated from the relationships between log I_{0a} and $1/T$ and that of log I_{0c} and $1/T$, according to the following equations:

$$I_{0a} = K\exp(-E_a/RT), \quad (8)$$

$$I_{0c} = K'\exp(-E_c/RT), \quad (9)$$

TABLE 2. $A_a n_a$ AND $A_c n_c$ VALUES

Concn (mole fract.)	Temp (C°) 775	800	825	850	875
	$A_a n_a$				
2.00×10^{-4}	1.87	1.88	1.84	1.84	2.21
2.17×10^{-3}	1.34	1.37	1.37	1.53	1.50
5.90×10^{-2}	1.62	1.64	(2.18)	1.62	1.75
1.91×10^{-1}	(1.14	1.45	1.65	2.18	1.87)
2.79×10^{-1}	1.41	1.28	1.25	1.10	1.03
	$A_c n_c$				
2.00×10^{-4}	0.63	0.66	0.76	0.85	0.87
2.17×10^{-3}	0.72	0.66	0.68	0.62	0.66
5.90×10^{-2}	1.52	1.37	1.72	1.33	1.18
1.91×10^{-1}	(1.62	2.75	2.25	2.19	1.97)
2.79×10^{-1}	2.32	2.20	1.94	1.81	1.63

The values in parentheses are uncertain.

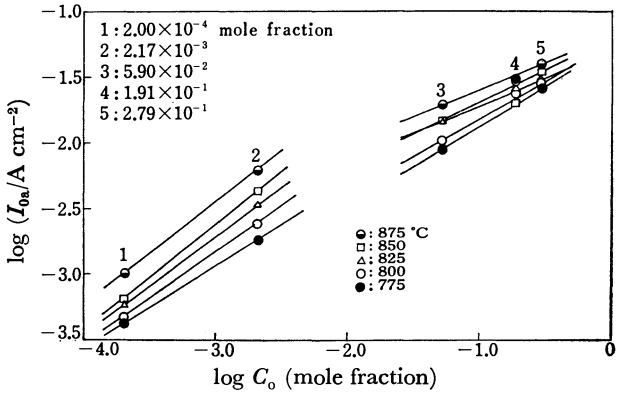

Fig. 5. Relationship between log I_{0a} and log C_o.

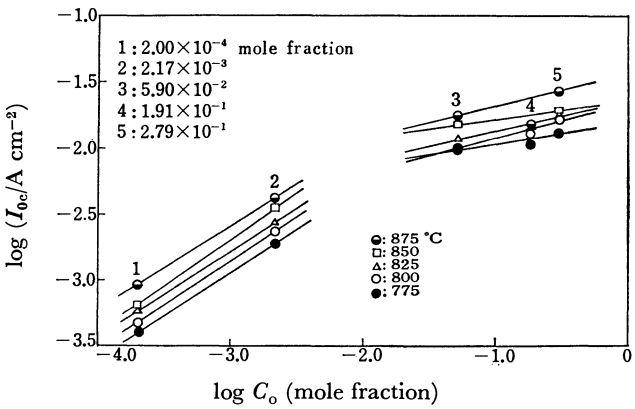

Fig. 6. Relationship between log I_{0c} and log C_o.

TABLE 3. TRANSFER COEFFICIENTS (A_a, A_c)

Temp (°C)	A_a a)	A_a b)	$1-A_c$ c)	$1-A_c$ d)
775	0.61	0.70	(0.56)	0.69
800	0.67	0.67	0.27	0.68
825	0.70	0.63	0.38	0.74
850	0.69	0.56	0.24	0.87
875	0.64	0.47	0.38	0.77

The value in parentheses is uncertain. a) Calculated from points 1 and 2 in Fig. 5. b) Calculated from points 3 and 5 in Fig. 5. c) Calculated from points 1 and 2 in Fig. 6. d) Calculated from points 3 and 5 in Fig. 6.

Table 4. Averaged valences (n_a, n_c)

Concn (mole fract.)	Temp (°C) 775	800	825	850	875
	n_a				
(A) 2.00×10^{-4}	3.0	2.8	2.6	2.7	3.4
2.17×10^{-3}	2.1	2.0	1.9	2.2	2.3
(B) 5.90×10^{-2}	2.3	2.4	3.4	3.0	3.7
2.79×10^{-2}	2.0	1.9	1.9	2.0	2.1
	n_c				
(A′) 2.00×10^{-4}	(1.1)	2.4	2.0	3.5	2.2
2.17×10^{-3}	(1.2)	2.4	(1.7)	2.5	1.7
(B′) 5.90×10^{-2}	2.2	2.0	2.3	1.5	1.5
2.79×10^{-1}	3.3	3.2	2.6	2.4	2.1

The values in parentheses are uncertain. (A) Calculated by using a) values in Table 3. (B) Calculated by using b) values in Table 3. (A′) Calculated by using c) values in Table 3. (B′) Calculated by using d) values in Table 3.

where K and K' are the frequency terms, $-E_a$ and $-E_c$ the apparent activation energies for the dissolution and the deposition processes, respectively, and T is the absolute temperature. If the electrode reactions do not change at the experimental temperatures, the relationship between the exchange current densities and the reciprocal temperatures should be linear. In almost all the cases, the values above 850 °C deviate from the straight lines (775—825 °C), as seen in Fig. 7. Thus the temperatures were divided into two regions, 775—825 and 850—875 °C. The activation energies obtained are given in Table 5. The values of E_a and E_c calculated from the straight lines (850—875 °C) were usually larger than those of E_a and E_c (775—825 °C). This fact may suggest that the complex ion[15,16] $[TaCl_6]^{2-}$ is stable at 775—825 °C and decomposes at above 850 °C.

Reaction Mechanism. The electrode reactions on the Tafel line were illustrated by Eq. 5. The stable ions related to the electrode reactions were Ta^{2+} and Ta^{4+} ions. According to Eq. 5, the activity of a_2 decreases and that of a_4 increases with rising overpotentials for the anodic process. For the cathodic process, the

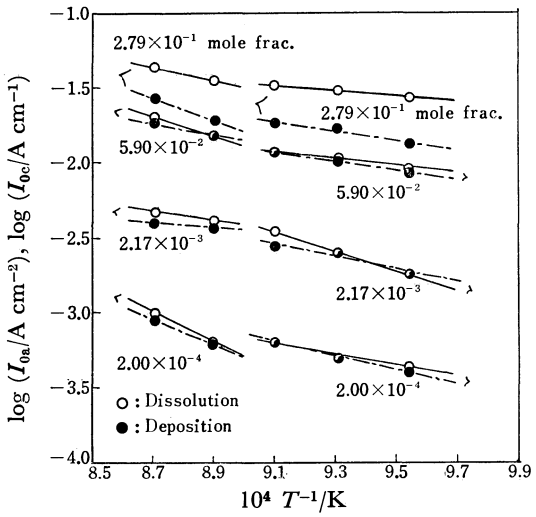

Fig. 7. Relationship between exchange current densities and $1/T^{-1}$/K.

Table 5. Activation energies (E_a, E_c)

Concn (mole fract.)	E_a a)	E_a b)	E_c a)	E_c b)
	(kcal/mol)			
2.00×10^{-4}	18.8	27.6	21.6	39.1
2.17×10^{-3}	26.7	(11.5)	19.2	(4.6)
5.90×10^{-2}	13.3	23.6	14.6	16.1
2.79×10^{-1}	(7.4)	18.4	14.2	(32.2)

The values in parentheses are uncertain. a) Calculated from the line (775—825°C). b) Calculated from the line (850—875°C).

opposite trend was observed. The transfer coefficients of $(1-A_c)$ values were chosen to calculate the n_a values, because the n_c values were greater than 5 when the A_c values were used. Therefore, the $(1-A_c)$ will be inserted into the first term and the A_c values into the second term in Eq. 7. The replacement of A_c by $(1-A_c)$ can be ascribed to the relation $(1-A)\eta+A\eta$ in Eq. 5. In other words, the $(1-A_c)\eta_c$ will be assigned to the Ta^{2+} ion and the $A_c\eta_c$ to the Ta^{4+} ion in the cathodic process.

At lower concentrations, 2.00×10^{-4}—2.17×10^{-3} mole frac., the Tafel relation was established at relatively high overpotentials as seen in Figs. 2, 3, and 4. At higher concentrations, 5.90×10^{-2}—2.79×10^{-1} mole frac., it was established at comparatively low overpotentials. Thus the electrode reactions at lower concentrations will correspond to Eq. 3′ and those at higher concentrations to Eq. 3.

The author wishes to express his thanks to Professor Tomoo Kirihara of Nagoya University for his helpful discussions.

References

1) N. Tanabe and R. Tamamushi, *Electrochim. Acta*, **9**, 963 (1964).
2) J. E. B. Randles and W. White, *Z. Electrochem.*, **56**, 666 (1955).
3) H. A. Laitinen and R. A. Ostertoung, *J. Electrochem. Soc.*, **102** 598 (1955).
4) D. L. Hills, G. J. Hills, L. Young, and J. O. Bockris, *J. Electrochem. Soc.*, **1**, 79 (1959).
5) H. A. Laitinen, R. P. Tisher, and D. K. Roe, *J. Electrochem. Soc.*, **107**, 546 (1960).
6) T. Kirihara, T. Sakakura, M. Iseki, and H. Oshima, Reports of the Faculty of Engineering, Nagoya University, **25**, 47 (1963).
7) T. Sakakura and T. Kirihara, *Electrochem, Soc. Jpn.*, **38**, 423 (1970).
8) T. Sakakura and T. Kirihara, *Electrochem. Soc. Jpn.*, **38**, 496 (1970).
9) I. Nakagawa and T. Kirihara, *Kogyo Kagaku Zashi*, **68**, 1854 (1965).
10) I. Nakagawa and T. Kirihara, *Nippon Kagaku Kaishi*, **1975**, 255.
11) I. Nakagawa, *Nippon Kagaku Kaishi*, **1975**, 958.
12) E. Matisson and J. O. M. Bockris, *Can. J. Chem.*, **37**, 190 (1959).
13) D. Gray and A. Cahill, *J. Electrochem. Soc.*, **116**, 198 (1969).
14) T. Kirihara, I. Nakagawa, and T. Sakakura, 11th Symposium on Chemistry of Molten Salts, 17 (**1977**), (Jpn. Electrochem. Soc.).
15) V. V. Safonov, *Zh. Neorg. Khim.*, **9**, 1406 (1946).
16) T. Suzuki, *Electrochim. Acta*, **15**, 20 (1970).

Synthesis of Merocyanine Dyes

Abdu E. ABDEL-RAHMAN* and Zarif H. KHALIL
Chemistry Department, Faculty of Science, Assiut University, Assiut, Egypt, A.R.E.
(Received July 25, 1977)

New 1-ethyl-2-[(2-substituted 3-oxoisoindolin-1-ylidene)methyl]-pyridinium or quinolinium iodide merocyanine dyes were obtained by the reaction of 2-methyl quaternary salts with *N*-substituted phthalimide in the presence of piperidine. 1-Ethyl-2-[(1-substituted 5-oxo-3-pyrrolin-2-ylidene)methyl] quinolinium iodide merocyanines were also prepared. Structural configuration of the synthesised compounds was confirmed by IR and UV spectral determination. 1-Ethyl-2-[[3-oxo-2-(4-phenylthiazol-2-yl)isoindolin-1-ylidene]methyl]-quinolinium iodide has high bactericidal activity againsist *E.Coli*, *Staphylococcus Aureus*, and *Staphylococcus Albas*.

Extensive studies have been made on the preparation and application of merocyanine dyes since their discovery in 1933.[1] In photography, they are widely used as photosensitisers,[2-8] in the production of direct positive photographic emulsions,[9,10] colour films[11-13] electron acceptors,[14] filter dyes,[14,15] and as sensitisers in photoconductive zinc oxide.[16] Phthalimidine dyes of good fastness were patented as dyestuffs for acrylonitrile fibers.[17]

New merocyanine dyes (III-1—22) were prepared. Interaction of 2-methyl quaternary salts with *N*-substituted imides in the presence of piperidine afforded the corresponding compounds (III-1—22) *via* the intermediate (II) which could be separated as colourless needles by the reaction of 1-ethyl-2-methylpyridinium-iodide with *N*-phenylphthalimide. The intermediate (II) is readily soluble in ethanol and in concentrated sulfuric acid from which iodine was liberated on heating. Its IR spectrum revealed an absorption band at 3450 cm^{-1} attributed to –OH group. Dehydration of II to 1-ethyl-2-[(3-oxo-2-phenylisoindolin-1-ylidene)methyl]pyridinium iodide (III-1) was carried out in several ways:

a) Thermal dehydration above melting point.

b) Acid treatment of its ethanolic solution using hydrochloric acid (1 : 1).

c) Prolonged reflux under the reaction conditions and leaving the reaction mixture at room temperature for several days.

The reaction is illustrated as follows:

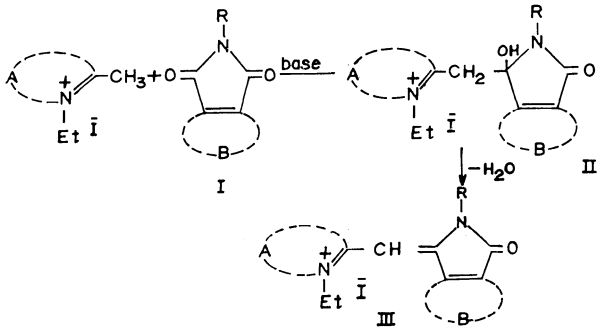

II. A=Pyridine, R=C_6H_5–, B=C_6H_4–.

III. A=Pyridine, B=C_6H_4–.
1: R=C_6H_5–, 2: R=*p*-CH_3-C_6H_4, 3: R=*p*-CH_3O-C_6H_4, 4: R=*p*-NO_2-C_6H_4, 5: R=*p*-Cl-C_6H_4, 6: R=α-$C_{10}H_7$.

III. A=Quinoline, B=C_6H_4–.
7: R=C_6H_5–, 8: R=*p*-CH_3-C_6H_4, 9: R=*p*-CH_3O-C_6H_4, 10: R=*p*-Cl-C_6H_4, 11: R=*p*-NO_2-C_6H_4, 12: R=*o*-CH_3-C_6H_4, 13: R=*o*-CH_3O-C_6H_4, 14: R=*o*-Cl-C_6H_4, 15: R=α-$C_{10}H_7$, 16: R=β-$C_{10}H_7$, 17: R=CH_2COOH, 18: R=4-phenylthiazol-2-yl.

III. A=Quinoline, B=H.
19: A=*p*-CH_3-C_6H_4, 20: R=*p*-CH_3O-C_6H_4, 21: R=*p*-NO_2-C_6H_4, 22: R=α-$C_{10}H_7$.

Infrared absorption spectra of the newly synthesized compounds showed an absorption band at 1740—1720 cm^{-1} attributed to the carbonyl group >C=O and

TABLE 1. 1-ETHYL-2-[(2-ARYL-3-OXOISOINDOLIN-1-YLIDENE)METHYL]PYRIDINIUM IODIDE MEROCYANINE DYES (III-1—III-6)

Compound No.	Mp °C	Solvent of crystallization	Yield %	Formula	Analysis % Calcd C	H	N	Found C	H	N	Absorption spectra λ_{max} nm(ε)
III-1	178	Dioxane	36	$C_{22}H_{19}N_2OI$	58.15	4.18	6.16	58.20	4.10	6.22	240(57100), 275(37000)
III-2	190—191	Ethanol/H_2O (1 : 1)	38	$C_{23}H_{21}N_2OI$	85.97	4.48	5.98	85.87	4.35	5.78	218(77000), 240(sh)(55200), 325(b.b)(11400)
III-3	145	Ethanol/H_2O (2 : 1)	45	$C_{23}H_{21}N_2O_2I$	57.02	4.34	5.78	57.10	4.38	5.65	215(67800), 245(sh)(35700), 270(28500), 330(25000)
III-4	245	Dioxane	40	$C_{22}H_{18}N_3O_3I$	52.90	3.60	8.41	52.82	3.55	8.25	218(37000), 240(sh)(26000), 310(sh)(17500), 320(20000)
III-5	175	Ethanol/H_2O	28	$C_{22}H_{18}N_2OClI$	54.04	3.68	5.73	54.12	3.70	5.65	220(37700), 240(13900)
III-6	190	Methanol/H_2O	32	$C_{26}H_{21}N_2OI$	61.90	4.16	5.55	62.00	4.12	5.43	215(103000), 285(23400)

(sh)=shoulder, (b.b)=broad band.

Table 2. 1-Ethyl-2-[(2-substituted 3-oxoisoindolin-1-ylidene)methyl]quinolinium iodide merocyanine dyes (III-7—III-18)

Compound	Mp °C	Solvent of crystallization	Yield %	Formula	Analysis % Calcd C	H	N	Found C	H	N	Absorption spectra λ_{max} nm(ε)
III-7	170	D	50	$C_{26}H_{21}N_2OI$	61.90	4.16	5.55	62.00	4.18	5.28	215(155300), 235(sh)(87000), 545(4000), 582(5000)
III-8	178	A	56	$C_{27}H_{23}N_2OI$	62.54	4.44	5.40	62.48	4.40	5.35	215(462000), 240(276000), 540(58000), 584(85000)
III-9	152	A	62	$C_{27}H_{23}N_2O_2I$	60.67	4.30	5.24	60.72	4.25	5.15	215(300000), 238(114000), 548(b.b)(1900), 590(b.b)(2400)
III-10	187	B	48	$C_{26}H_{20}N_2OClI$	57.93	3.71	5.19	57.85	3.80	5.20	213(294000), 243(94000), 520(5800), 557(8900)
III-11	249—250	C	65	$C_{26}H_{20}N_3O_3I$	56.83	3.64	7.65	56.90	3.70	7.58	215(252000), 236(84000), 530(sh)(11700), 556(15600)
III-12	176	A	42	$C_{27}H_{23}N_2OI$	62.54	4.44	5.40	62.60	4.38	5.25	215(133300), 245(45200), 520(sh)(11700), 554(20000)
III-13	141	D	38	$C_{27}H_{23}N_2O_2I$	60.67	4.30	5.24	60.58	4.35	5.19	215(792000), 238(189200), 540(10100), 582(20100)
III-14	128	C	40	$C_{26}H_{20}N_2OCl$	57.93	3.71	5.19	58.15	3.68	4.98	219(441700), 237(509200), 400(b.b)(5500), 490(b.b)(4200), 540(b.b)(4900)
III-15	152—153	B	58	$C_{30}H_{23}N_2OI$	64.98	4.15	5.05	65.10	4.20	5.15	223(64000), 238(b.b)(50000), 450(sh)(18900), 556(38800)
III-16	171	B	65	$C_{30}H_{23}N_2OI$	64.98	4.15	5.05	65.13	4.18	5.18	213(177000), 241(100700), 525(sh)(12500), 560(20830), 604(sh)(8600)
III-17	222—224	D	10	$C_{22}H_{19}N_2OI$	54.32	5.76	5.76	54.27	3.95	5.82	242(71400), 554(12800), 584(15200)
III-18	135	C	32	$C_{29}H_{22}N_3OSI$	59.28	3.74	7.15	59.32	3.70	3.70	242(160000), 540(10570, 586(10000)

A=Ethanol/H_2O(1 : 1), B=methanol, C=dioxane, D=ethanol/H_2O(3 : 1), (sh)=shoulder, (b.b)=broad band.

Table 3. 1-Ethyl-2-[(1-aryl-5-oxo-3-pyrrolin-2-ylidene)methyl]quinolinium iodide merocyanine dyes (III-19—III-22)

Compound No.	Mp °C	Solvent of crystallization	Yield %	Formula	Analysis % Calcd C	H	N	Found C	H	N	Absorption spectra λ_{max} nm(ε)
III-19	124	Ethanol/H_2O (2 : 1)	30	$C_{23}H_{21}N_2OI$	58.97	4.48	5.98	59.05	4.44	6.16	240(10400), 320(4100)
III-20	207	Ethanol/H_2O (1 : 1)	35	$C_{23}H_{21}N_2O_2I$	57.02	4.33	5.78	57.10	4.36	5.58	240(95800), 323(37500)
III-21	205	Dioxane	38	$C_{22}H_{18}N_3O_3I$	62.90	3.61	8.41	62.82	3.58	8.48	——
III-22	242	Methanol/H_2O (1 : 1)	28	$C_{26}H_{21}N_2OI$	61.90	4.16	5.55	62.03	4.20	5.48	221(92000), 238(31000), 280(15500), 320(13700)

another band at 875 cm^{-1} attributed to the terminal double bond on ring -CH=C<. Disappearance of the -NH absorption bands characteristic to the -NH group indicates the disrupture of the *N*-substituted imides.

Absorption spectra of III-1—III-22 showed mainly two or three absorption bands in the UV region; their positions and molar extinction coefficient are dependent on the type of *N*-substituted imides, as well as on that of the quaternary heterocyclic nuclei. The results are given in Tables 1, 2, and 3.

The merocyanine dyes, 1-ethyl-2-[(2-substituted 3-oxoisoindolin-1-ylidene) methyl] quinolinium iodides III-7—III-18 posses mainly two absorption bands in the visible region. Their position and molar extinction coefficient are influenced by the type of *N*-substituents on phthalimide moiety. Thus III-7 possesses two absorption bands at λ_{max} 545 nm, ε_{max} 4000 and another CT band at λ_{max} 582 nm, ε_{max} 5000. Introduction of an electron releasing group to the *p*-position of *N*-phenyl group, causes a red shift which is attributed to the increase of the coplanarity of the molecule (III-8 and III-9).

On the other hand, introduction of an electron withdrawing group to the same position causes a blue shift, (III-10 and III-11). Introduction of the same substituent to the *ortho*- position of *N*-phenyl group causes a blue shift as compared to its *para* isomer (III-8 and III-12; III-10 and III-14), probably due to a hindered rotation of the phenyl ring caused by the *ortho* substituent.

Substitution of the *N*-phenyl moiety with α-naphthyl group causes a blue shift by 26 nm (III-15), whereas the substitution with β-naphthyl group causes a red shift by 22 nm (III-16).

The spectrum of III-18 possesses only one absorption band in the ultraviolet region and two absorption bands in the visible region (Table 3).

Experimental

The IR spectra were determined with a Unicam SP 1200 spectrophotometer using KBr disk wafer technique; absorption spectra in the UV-visible region in ethanol 95% were recorded on a SP 8000 recording spectrophotometer. All melting points are uncorrected.

Preparation of N-*Substituted Phthalimide or Maleimide Derivatives.*[18] A mixture of equimolar proportions of phthalic anhydride (or maleic anhydride) and the amino compound was refluxed in the presence of glacial acetic acid for about 1 h. The product obtained was filtered off and washed with sodium hydrogencarbonate solution, except in the case of glycine when the product was washed with water, then with a few-ml ethanol. The compounds obtained were identical with that reported in litrature, except for the new molecules not reported *e.g. N*-(4-phenylthiazol-2-yl)phthalimide, mp 115—116 °C.

Synthesis of 1-Ethyl-2-[(1-hydroxy-3-oxo-2-phenylisoindolin-1-yl)methyl]pyridinium Iodide (II). Equimolar proportions (0.001 mol) of 1-ethyl-2-methylpyridinium iodide and *N*-phenylphthalimide were dissolved in ethanol (50 ml) to which piperidine (0.5 ml) was added. The mixture was refluxed for 1 h and concentrated to about 15 ml and allowed to cool. Colourless needles precipitated. The product (II) was filtered off, washed with ether and crystallized form aqueous ethanol (1:1) to give colourless needles, mp 156—157 °C. Found: C, 55.62; H, 4.39; N, 5.77, I, 26.5%. Calcd, for $C_{22}H_{21}N_2O_2I$: C, 55.58; H, 4.42; N, 5.89; I, 26.73%

Dehydration of the Intermediate (II). *Thermal Dehydration*: The intermediate was heated at 165—168 °C for 5 min. On colling, orange product was obtained. This was crystallized from dioxane to give orange needles (mp 178 °C).

Acid Treatment: A mixture of II, (0.5 g), ethanol (10 ml) and hydrochloric acid (1 : 1, 10 ml) was allowed to stand for 7 days. Fine orange needles were separated. The product was filtered off, washed with water and few ml of aqueous ethanol (1:1), then crystallized from dioxane to give orange needles, mp with an authentic sample 178 °C.

Prolonged Reflux. A mixture of II (0.5 g), ethanol (10 ml), and piperidine (0.5 ml) was refluxed for 18 h on a water bath. The reaction mixture was concentrated to about 5 ml and allowed to stand at room temperature for 8 days. Orange needles were precipitated. The product (III-1) was collected, washed with ethanol, and crystallized from dioxane to give orange needles, mp and mixed mp 178 °C.

Synthesis of 1-Ethyl-2-[(2-aryl-3-oxoisoindolin-1-ylidene)methyl]pyridinium Iodides, III-1—III-6. A mixture of 1-ethyl-2-methylpyridinium iodide (0.0015 mol), N-arylphthalimide (0.001 mol), ethanol (50 ml), and piperidine (1 ml) was refluxed on a water bath for 14 h. The reaction mixtures were left aside for several days (6—8 day). Coloured crystalline merocyanine dyes III-1—III-6 were deposited. They were filtered off, washed with ether and crystallized from the appropriate solvent. The results are given in Table 1.

Synthesis of 1-Ethyl-2-[(2-substituted 3-oxoisoindolin-1-ylidene)-methyl]quinolinium Iodide Merocyanine Dyes, III-7—III-18. A mixture of 1-ethyl-2-methylquinolinium iodide (0.0012 mol), *N*-substituted phthalimide (0.001 mol), ethanol (50 ml), and piperidine (0.5 ml) was refluxed for 1 h. The mixture was concentrated to about 20 ml and the products were precipitated by addition of water, filtered off, washed with water and then with ether, and crystallized from the appropriate solvent. The results are given in Table 2.

Synthesis of 1-Ethyl-2-[(1-aryl-5-oxo-3-pyrrolin-2-ylidene)-methyl]quinolinium Iodides, III-19—III-22. Equimolar proportions (0.005 mol) of 1-ethyl-2-methylquinolinium iodide, *N*-arylmaleimide, and piperidine (1 ml) in ethanol (50 ml) were refluxed on a water bath for 1 h. The products III-19—III-22 which were precipitated after concentration and dilution with water, were filtered off and crystallized from appropriate solvent. The results are given in Table 3.

Bactericidal Activity of 1-Ethyl-2-[[3-oxo-2-(4-phenylthiazol-2-yl)isoindolin-1-ylidene]methyl]quinolinium Iodide (III-18). The culture medium was normal nutrient agar (NA) medium[19] supplemented with one gram of yeast/litre. The bacterial suspension was prepared by adding one ml of sterile distilled water to a 24 h old culture of the test organism grown on NA slant. One ml aliquots of bacterial suspension were added to Erlenmeyer flasks containing 150 ml of NA and the flasks were incubated for 24 h.

Petri dishes containing sterile modified NA were flooded with the bacterial suspension of the test organisms (2 plates for each organism). Two filter paper discs (one cm diameter) containing merocyanine dye (III-18) dissolved in ethylene glycol (15 mg/l.) were placed on each plate. The plates were incubated at 37 °C for 24 h and the diameter of the inhibition zone was measured. The experiments were repeated 3 times and the results were averaged. Pathogenic bacterial strains *E. Coli*, *Staphylococcus Aureus*, and *Staphylococcus Albas* were supplied by Veterinary Hospital, Ministry of Agriculture, Assiut, Egypt and tested at the Botany Department, Faculty of Science, Assiut University. The results showed remarkable activity towards the tested organisms.

References

1) J. D. Kendal, Brit. Pat., 428222330, Oct. 1933.
2) F. G. Webster and L. G. S. Brooker (Eastman Kodak Co.), U. S. Pat. 3743638, 3 July 1973; Appl. 21210, 19 Mar. 1970.
3) O. Riester (Agfa-Gevaert A.-G.), Ger. Offen., 1916845 (Cl. C O9b. G O3c), 5 Nov. 1970, Appl. 2 Apr. 1969.
4) G. A. Rillaers and H. Depoorter (Agfa-Gevaert A.-G.), Ger. Offen. 1930224 (Cl. C O9b), 15 Jan. 1970. Brit. Appl. 5 July 1968).
5) P. W. Jenkins and L. G. S. Brooker (Eastman Kodak Co.), Fr. Pat. 1573591 (Cl. G O3c), 4 July 1969, U. S. Appl.
6) L. G. S. Brooker, A. Jr. Fumia (Eastman Kodak Co.), Fr. Pat. 1574253 (Cl. G O3c), 11 July 1969, U. S. Appl. 28 July 1967.
7) N. S. Kozlov, O. P. Zhikhareva, and S. A. Batishche, *Khim. Geterotsiki. Soedin.*, **1972**, 1619.
8) G. E. Ficken (Ilford Ltd.), Brit. Pat. 1253468 (Cl. C O9b, G O3c), 17 Nov. 1971, Appl. 3 July 1969.
9) L. L. Lincoln, D. W. Heseltine, (Eastman Kodak Co.) Ger. Offen. 2154124 (Cl. G O3c), 10 May 1972, U. S. Appl. 85707, 30 Oct. 1970.
10) O. Riester, H. Oehalschlanger, and H. Odenwaelder

(Agfa-Gevaert A.-G.), Ger. Offen. 2143967, 8 May 1973, Appl. P.21 42, 967.4, 27 Aug. 1971.

11) E. J. Poppe, Ger. Pat. (East) 71445 (Cl. G O3c), 20 Feb. 1970, Appl. 18 July 1968.

12) K. J. Bannert and D. J. Fry (Slford Ltd.), Brit. Pat. 181020 (Cl. G O3c), 11 Feb. 1970, 4 July 1967.

13) H. Depoorter, Th. H. Ghys (Agfa-Gevaert A.-G.), Ger. Offen., 2106517 (Cl. C O9b), 9 Sep. 1971, Brit Appl. 17 Feb. 1970.

14) E. J. Van Lare (Eastman Kodak Co.), U. S. Pat. 3615608 (Cl. 96/101; G O3c, C O9b), 26 Oct. 1971, Appl. 23 Dec. 1966.

15) F. J. Sauter (Eastman Kodak Co.), Fr. Demande 2190881 (Cl. C O9b. G O3c) 8 Mar. 1974, U. S. Appl. 266028, 26 June 1972.

16) F. G. Webster (Eastman Kodak Co.), Fr. Pat. 1597509 (C l. C O9b, G O3c), 7 Aug. 1970, U. S. Appl. 8 Sept. 1967.

17) H. R. Mueller and M. Seefolder (Badische Anilin-Und Soda-Fabrik A.-G.), Ger. Offen. 1812320 (Cl. C O9b, C O7d), 18 June 1970, Appl. Dec. 1968.

18) A. I. Vogel, "Practical Organic Chemistry," Longmans, Ltd., London (1956), p. 423.

19) E. T. Knudsen and G. N. Rolinson, 1959, Lancet 19/12/59, 1105.

NOTES

BULLETIN OF THE CHEMICAL SOCIETY OF JAPAN, VOL. 51 (8), 2419—2420 (1978)

The Ring Transformation of Tetrahydrofuran into 1-Propylpyrrolidine over Y-Zeolites

Kou HATADA, Katsuhiro FUJITA, and Yoshio ONO*

Department of Chemical Engineering, Tokyo Institute of Technology, Ookayama, Meguro-ku, Tokyo 152

(Received February 13, 1978)

Synopsis. The catalytic activities of Y-zeolites for the synthesis of 1-propylpyrrolidine from tetrahydrofuran and propylamine were examined. Aluminum cation exchanged zeolite was found most active, 65% yield of 1-propylpyrrolidine being attained at 360 °C. The kinetics of the reaction was examined and the reaction mechanism suggested.

The ring transformation of tetrahydrofuran (THF) into 1-alkylpyrrolidine proceeds over alumina.[1-2] Reppe and coworkers obtained 1-ethylpyrrolidine in 61% yield by the reaction of THF and ethylamine at 300 °C for 6 h over ThO_2-promoted alumina.[2] Synthetic zeolites are effective catalysts for the ring transformations of γ-butyrolactone into 1-alkyl-2-pyrrolidinones,[3] and THF into pyrrolidine.[4] This note reports that zeolites are effective also for the ring conversion of THF into 1-alkylpyrrolidine: Tetrahydrofuran is converted into 1-propylpyrrolidine by the reaction with propylamine over zeolites with a flow reactor under atmospheric pressure.

Experimental

THF and propylamine were distilled prior to each run. NaY zeolite (Linde Division of Union Carbide Corp.) was used. Various forms of Y-zeolites were prepared by the conventional cation exchange procedure using aqueous solution of the corresponding salt. The cation exchanged zeolites were pelleted without binder and crushed and sized into 9—16 mesh. A continuous flow reactor was used under atmospheric pressure. A silica tube (13 mm i.d.) placed in a vertical furnace was used as a reactor. The reactants were pumped into the preheating zone of the reactor containing 10 ml quarts powder. Nitrogen used as a diluent for regulating the initial pressure of the reactants was fed through a flow meter. Reaction products collected in the reciver were taken out at certain intervals during the course of run and analyzed by gas chromatography.

Results and Discussion

The reaction of THF and propylamine was carried out at 300 °C and at W/F=5.56 g h mol^{-1} (W is the weight of catalyst and F the molar flow rate), and the catalytic activities of the various cation forms of Y-zeolites for the ring conversion were examined. The results (Table 1) show that HY and zeolites with trivalent cations except CeY have high activity. Of the zeolites studied, the selectivity to 1-propylpyrrolidine was the highest with AlY, further study thus being made exclusively with AlY.

Figure 1 shows the temperature dependence of the

TABLE 1. ACTIVITY AND SELECTIVITY FOR THE REACTION OF THF AND PROPYLAMINE OVER VARIOUS Y-ZEOLITES

Catalyst	Conversion of THF %	Yield of 1-propylpyrrolidine %	Selectivity %
AlY	61	46	76
FeY	58	42	72
CrY	52	40	76
HY	41	21	50
MgY	33	16	50
CuY	24	10	42
CeY	12	6	50
NaY	10	1	10

Reaction temperature, 300 °C; W/F=5.56 g h mol^{-1}, W=1.0 g; reactant molar ratio, THF: propylamine: N_2=1: 5. 25: 2.

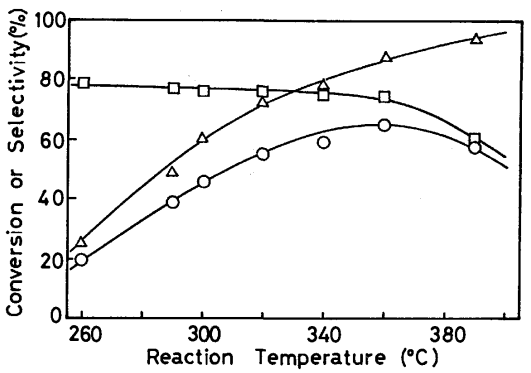

Fig. 1. Effect of reaction temperature on the catalytic behavior of AlY in the reaction of THF and propylamine (△): conversion of THF, (○): yield of 1-propylpyrrolidine, (□): selectivity to 1-propylpyrrolidine.

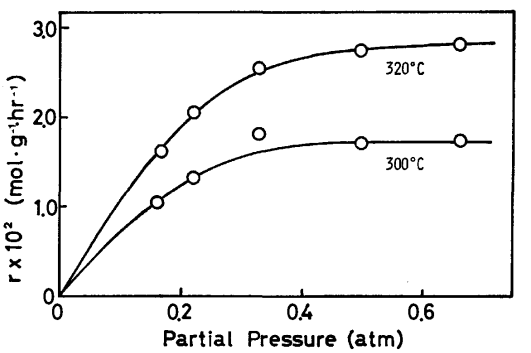

Fig. 2. Dependence of the reaction rate on the partial pressure of propylamine; W/F=2.78 g h mol^{-1}, P_{THF} =0.232 atm.

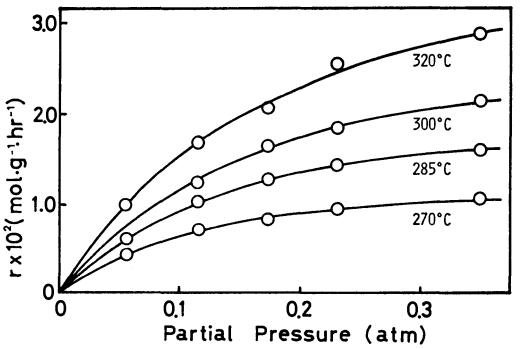

Fig. 3. Dependence of the reaction rate on the partial pressure of THF; $W/F=2.78$ g h mol^{-1}, $P_A=0.334$ atm.

THF conversion, the yield of and the selectivity to propylamine. The maximum yield of propylamine was obtained at 360 °C. A constant selectivity of 75% was obtained in the temperature range upto 360 °C, but the selectivity fell at 380 °C. No attempt was made to identify the byproducts.

The kinetics of the reaction was studied with AlY as a catalyst in the temperature range 270—320 °C under small contact time conditions. Figures 2 and 3 show the dependence of the reaction rate on the partial pressures of propylamine (P_A) and THF (P_{THF}), respectively. In both cases, the rate increases with an increase in the partial pressure of the reactants. The rate (r) is given by

$$r = k \cdot \frac{K_A P_A}{1+K_A P_A} \cdot \frac{K_{THF} P_{THF}}{1+K_{THF} P_{THF}}, \quad (1)$$

where k is the rate constant, and K_A and K_{THF} are the adsorption equilibrium constants of propylamine and THF, respectively. The plots of P_A/r against P_A and P_{THF}/r against P_{THF} give straight lines. The constants k, K_A, and K_{THF} are determined unequivocally. From the temperature dependence of the constants, the activation energy of the reaction, the heats of adsorption of propylamine and THF are determined to be 16 kcal mol^{-1} and 6 kcal mol^{-1}, respectively.

In a previous work,[3] a rate expression similar to Eq. 1 was obtained for the reaction of γ-butyrolactone and propylamine. A mechanism was proposed, in which the lactone and the amine are adsorbed on the metal cation (or proton) and zeolitic oxygen anion, respectively, the reaction of the adsorbed reactants being concluded as the rate determining step.

A similar mechanism may be applied to the reaction of THF and propylamine. Propylamine molecules are adsorbed and dissociated by oxygen anions, while THF molecules open the ring by the interaction with protonic sites, as has been assumed for the reaction of THF and ammonia.[4,5] The fact that the heat of adsorption of propylamine obtained from the kinetics of its reaction with THF (10 kcal mol^{-1}) agrees with that obtained from the kinetics of its reaction with γ-butyrolactone (9.9 kcal mol^{-1})[3] supports the essential similarity of the mechanism of the two reactions.

References

1) Yu. Yur'ev, V. I. Bazan, A. N. Esafova, S. M. Seliverstova, and S. I. Chernyakhover, *J. Gen. Chem. USSR*, **10**, 1839 (1940), *Chem. Abstr.*, **35**, 4377 (1941).

2) W. Reppe and co-workers, *Ann.*, **596**, 143 (1955).

3) K. Hatada and Y. Ono, *Bull. Chem. Soc. Jpn.*, **50**, 2517 (1977).

4) K. Fujita, K. Hatadas, Y. Ono, and T. Keii, *J. Catal.*, **35**, 325 (1974).

5) Y. Ono, K. Hatada, K. Fujita, A. Halgeri, and T. Keii, *J. Catal.*, **41**, 322 (1976).

BULLETIN OF THE CHEMICAL SOCIETY OF JAPAN, VOL. 51 (8), 2421—2422 (1978)

The Intrinsic Viscosity of Poly(4-vinylpyridine) of a Low Molecular Weight

Yoshiyuki HIRAI* and Taira YANAGIDA

Department of Chemistry, Faculty of Science, Science University of Tokyo, Kagurazaka, Shinjuku-ku, Tokyo 162

(Received February 13, 1978)

Synopsis. The intrinsic viscosities of poly(4-vinylpyridine) ($\bar{M}_n$: 1.37×10^3—9.67×10^4) were measured by use of various solvents. For every solvent, $\log[\eta]$-$\log\bar{M}_n$ plots gave lines with a slope of 1/2 in the region of low molecular weights ($\bar{M}_n\leq10^4$). These lines were parallel to one another. This viscosity behavior was interpreted in terms of the influence of solvents on short-range interactions in the polymer chains.

Many studies[1] of the intrinsic viscosities of polymers have shown that, in a region of low molecular weights, the equation $[\eta]=K_0M^{1/2}$ holds in spite of measurements made using good solvents. Here, the constant, K_0, appeared to be independent of the kind of solvent; its value was near that of K_θ, namely, $K_0M^{1/2}\approx K_\theta M^{1/2}$. These experimental facts suggested the possibility of the evaluation of characteristic dimensions from viscosity measurements of polymers of low molecular weights in good solvents. However, the polymer–good solvent systems so far examined have been mainly nonpolar polymer–nonpolar solvent systems, and so the investigation of other systems, such as polar polymer–polar solvent systems, and a better-defined interpretation of the viscosity behavior described above were desired.

On the other hand, a theoretical treatment of the viscosities of short chains (polymers of low molecular weights) was reported by Perico and Rossi.[2] They showed, for some polymer–good solvent systems, that the intrinsic viscosities of short chains could be evaluated from the model of independent hindered rotation by introducing "thickness b" by a parameter.

In the present study, the poly(4-vinylpyridine)–good solvent system is adopted as a specific polymer–solvent system, in which strong polymer-solvent interactions are presented; this polymer–solvent system is a polar polymer–polar solvent system. For such a system the relation of $[\eta]$-M is examined, and the origin of the viscosity behavior of $[\eta]=K_0M^{1/2}$ is investigated by using the theory by Perico and Rossi.[2]

Experimental

Samples of poly(4-vinylpyridine) of various molecular weights were prepared by radical polymerization (monomer: 10 ml, chloroform: 50 ml, α,α'-azobisisobutyronitrile, 60 °C); the polymers were recovered by precipitation in petroleum ether. The average molecular weights of these polymer samples ranges from 1.37×10^3 to 9.67×10^4 (average degrees of polymerization, $\overline{DP}$: 13.1—921). The moleculat weights were determined using a "KUNAUAR vapor-pressure osmometer and membrane osmometer" in chloroform solutions at 37 °C; the vapor-pressure osmometric method was applied to polymer samples of $\bar{M}_n\leq1.32\times10^4$, and the membrane osmometric method, to those of $\bar{M}_n\geq1.32\times10^4$. For these samples, no fractionations were carried out. However, it would have no significant influence on the present discussion because the present investigation is concerned only with the discussion of the dependence of curves of $[\eta]$ plotted against molecular weight on solvents.

The solvents used in the viscosity measurements were methyl alcohol, chloroform, and *t*-butyl alcohol. Ethyl methyl ketone/isopropyl alcohol (85/15 by wt) was also used as a relatively poor solvent (the expansion coefficient for the mixed solvent at 25 °C was evaluated as 1.06 in the viscosity study of poly(4-vinylpyridine) by Boyes and Strauss[3]). These solvent were purified by means of the usual method. The intrinsic viscosities were measured by use of the viscometers of the Ubbelohde type, the efflux times of which were 248.3, 214.1, 352.7, and 277.3 s for methyl alcohol, chloroform, *t*-butyl alcohol, and ethyl methyl ketone/isopropyl alcohol respectively. In the measurements, the temperature of water bath was maintained at 30±0.01 °C, and the efflux time was measured with a stopwatch reading to an accuracy of 0.1 s.

Results and Discussion

Plots of log $[\eta]$ *against log* M. Figure 1 shows the plots of log $[\eta]$ against log $\bar{M}_n$ for poly(4-vinylpyridine) in various solvents at 30 °C (the points for chloroform solutions fall on the line for methyl alcohol solutions; therefore, they are omitted in Fig. 1). In every case, the slope of the line decreases with a decrease in the molecular weight and becomes 1/2 in the region of molecular weights below 10^4.

For the poly(4-vinylpyridine)–good solvent system, as well as for the polymer–good solvent systems[1] examined previously, a slope of 1/2 is observed in the region of low molecular weights. However, the behavior of the lines with a slope of 1/2 is distinct from the previous observations[1] for various polymers; the lines with a slope of 1/2 for poly(4-vinylpyridine) are not concentrated on a line, but are parallel to one another.

The present data clearly indicate that the phenomenon of the slope of 1/2 is not associated with the θ state. The phenomenon should be attributed, rather, to the disappearance of long-range interactions resulting from the decrease in the molecular weights.

TABLE 1. INTRINSIC VISCOSITY FOR POLY(4-VINYLPYRIDINE) IN CH_3OH AT 30 °C

$\overline{DP}$[a]	N_c	R_s (Å)	$[\eta]$ (dl/g) calculated	$[\eta]$ (dl/g) measured
13.1	26	12.9	0.065	0.046
20.0	40	16.0	0.082	0.081
24.6	49	17.8	0.092	0.094
37.5	75	22.1	0.115	0.110
55.6	111	27.0	0.142	0.140
68.3	137	30.0	0.158	0.159
101	202	36.5	0.193	0.204

In calculations, $\Delta E=1.3$ kcal/mol, $b=4.8$ Å, and $\phi=2.87\times10^{21}$. a) Average degrees of polymerization.

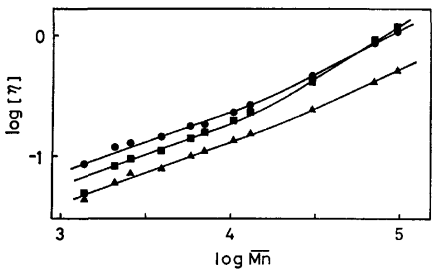

Fig. 1. Intrinsic viscosities of poly(4-vinylpyridine) in various solvents at 30 °C. ●: *t*-BuOH, ■: MeOH, ▲: EMK/*i*-PrOH (85/15 by wt).

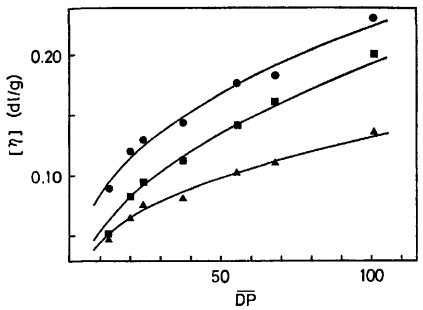

Fig. 2. Experimental viscosities and calculated curves by Eqs. 1 and 2. ●: *t*-BuOH, ■: MeOH, ▲: EMK/*i*-PrOH(85/15 by wt).

Table 2. The thickness (b) and energy (ΔE) for various solutions

Solvent	b (Å)	ΔE (kcal/mol)
MeOH	4.8	1.3
$CHCl_3$	4.8	1.3
t-BuOH	6.7	1.3
EMK/*i*-PrOH	4.5	1.1

Intrinsic Viscosity of Polymers of Low Molecular Weights. According to the theory of Perico and Rossi[2] for short chains,

$$[\eta] = \phi 6^{3/2}(R_s^3/M), \quad (1)$$

$$R_s = (\langle S_0^2 \rangle)^{1/2} + b, \quad (2)$$

where the constant, b, is the "thickness" of the polymer chains. ϕ is a hydrodynamic parameter, and it takes an almost constant value (2.87×10^{21}) for the carbon-number of the backbone (N_c)>20. $\langle S_0^2 \rangle$ is the mean-square radius of gyration.

Table 1 shows the results of applying Eqs. 1 and 2 to poly(4-vinylpyridine) ($\bar{M}_n \leq 10^4$) in methyl alcohol. In the calculation, 2.87×10^{21} was used as the value of ϕ. $\langle S_0^2 \rangle$ was calculated by assuming an independent hindered rotation in the rotational-isomeric model; in Table 1, ΔE represents the energy of the gauche state relative to the trans in the model of independent hindered rotation. Figure 2 shows the experimental viscosities and calculated curves for the methyl alcohol, *t*-butyl alcohol, and ethyl methyl ketone (EMK)/isopropyl alcohol solutions (the points for chloroform solutions are omitted). Figure 2 indicates that the viscosities for the region of low molecular weights can be calculated by choosing the appropriate values of b and ΔE. The b and ΔE values yielding the best-fit curves are summarized in Table 2. The values of b are quite great (the size of the pyridine ring: about 3 Å), while the magnitudes of ΔE are acceptable.

The pyridine ring of poly(4-vinylpyridine) behaves as an electron donor, while methyl alcohol and chloroform can behave as electron acceptors. These solvents could be solvated to the polymer. *t*-Butyl alcohol is known to form hydrogen bonds with poly(4-vinylpyridine)[3] (*t*-butyl alcohol is the most bulky among the solvents used in the present experiments). The solvation power for ethyl methyl ketone/isopropyl alcohol is weaker than that for the other solvents in the present experiments. The solvation and hydrogen bonding must result in the increase in the values of b, and may be effective in the increase of ΔE.

The values of b and ΔE in Table 2 can be well interpreted by considering the solvation and hydrogen bonding (polymer-solvent interaction) described above.

The viscosity data for any other polymer (low molecular weight)–good solvent system could also be explained in a similar manner.

On the basis of the above results and considerations, we can draw a conclusion regarding the polymers with low molecular weights (short chains) in solutions. The long-range interactions are ineffective in the polymers with low molecular weights. The conformations of the short chains are governed by the short-range interactions, in which polymer-solvent interactions are taken into account. The polymer-solvent interactions can be estimated in terms of b and ΔE. In the case of the systems in which the polymer-solvent interactions depend strongly on the solvents, parallel lines with a slope of 1/2 (this means $K_0 M^{1/2} \fallingdotseq K_\theta M^{1/2}$) are observed, and the dependence of b and ΔE on the solvents is detected.

The data for the poly(ethylene oxide) glycol-good solvent system[1,4] rather resemble the present observations. However, the polymer-solvent interaction in this system would be weak in comparison with that in the present system. As a result, the data were treated much like the data for various other polymer-good solvent systems.[1]

In the meantime, it has been pointed out, on the basis of various experiments[5] on polymers with low molecular weights, that the conformations and internal motion of short chains in solutions are somewhat different from those of polymers with high molecular weights. The conclusion derived in the present study would be useful for discussing such problems.

References

1) U. Bianchi and A. Peterlin, *J. Polym. Sci., A-2*, **6**, 1759 (1968).

2) A. Perico and C. Rossi, *J. Chem. Phys.*, **53**, 1217 (1970); C. Rossi and A. Perico, *ibid.*, **53**, 1223 (1970).

3) A. G Boyes and U. P. Strauss, *J. Polym. Sci.*, **XXII**, 463 (1956).

4) C. Rossi and C. Cuniberti, *Polym. Lett.*, **2**, 681 (1964).

5) For example, Y. Hirai, Y. Nunomura, and Y. Imamura, *Bull. Chem. Soc. Jpn.*, **49**, 2200 (1976); Y. Hirai, M. Yukawa, and Y. Imamura, *ibid.*, **50**, 1028 (1977), and the references cited therein.

BULLETIN OF THE CHEMICAL SOCIETY OF JAPAN, VOL. 51 (8), 2423—2424 (1978)

Pore Structure of Iron Oxides

Mahiko NAGAO,* Yasuhiro YOKOTA, and Tetsuo MORIMOTO

Department of Chemistry, Faculty of Science, Okayama University, Tsushima, Okayama 700

(Received February 20, 1978)

Synopsis. The pore structure of iron oxides, subjected to oxidation into α-Fe_2O_3 as well as reduction into Fe_3O_4, was investigated by means of the *t*-method. The results show that the reduction is accompanied by the formation of slit-shaped pores, width 14 Å, open at both ends.

The mechanism of solid reaction is one of the most incomprehensible problems. The surface chemistry of intermediate and final products will shed light on this problem. de Boer and Lippens[1] investigated the process of thermal decomposition of boehmite and bayerite. They developed the *t*-method and applied it to the N_2-adsorption data, and found the formation of slit-shaped pores during the course of decomposition reaction. The *t*-plots are constructed by plotting the amount of adsorbed nitrogen on a sample against the statistical thickness *t* of the adsorbed layer of nitrogen on a nonporous reference solid. The choice of reference *t*-curve, therefore, is important. Cranston and Inkley[2] and Lippens *et al.*[3] each used a definite standard *t*-curve. Other researchers selected the reference curve from the data on specimens of the same substance.[4,5]

It is known that α-Fe_2O_3 can be reduced to Fe_3O_4 in a mixed gas of H_2 and H_2O, the reverse reaction taking place in O_2 at high temperatures.[6] The purpose of the present work is to investigate the surface chemistry of iron oxides produced by oxidation and reduction, by measuring the N_2-adsorption isotherms and converting them into *t*-plots.

Experimental

The sample of iron oxide was prepared by oxidizing iron rods (purity 99.99%) at 600 °C in an electric furnace. It was ground, heated at 1400 °C for 2 h and evacuated at 1100 °C for 2 h in a vacuum of 1×10^{-3} Pa (sample S). From this sample, four kinds of iron oxides with different compositions were prepared in the following way. Sample H was obtained by oxidizing sample S in O_2 at 300 °C for 48 h, during which time the amount of O_2 taken up was measured. Sample S was reduced with a mixture of H_2 and H_2O (4: 1), the ratio being selected to be suitable for the formation of Fe_3O_4 on the equilibrium phase diagram,[6] at 400 °C for 48 h ,the H_2-uptake being measured (sample M). The other two samples were prepared by reducing sample H as well as by oxidizing sample M under the same conditions as described above. The reactions were continued until the composition of the products gave α-hematite and magnetite in a 1: 1 ratio, from measurement of the amount of absorbed H_2 or O_2 (samples Ih and Im). X-Ray analysis showed that samples H and M are α-hematite and magnetite, respectively, samples S, Ih, and Im being mixtures of them. From the amounts of absorbed O_2 and H_2 when samples H and M were produced, the composition of sample S was found to be 70% α-hematite and 30% magnetite. α-Fe_2O_3 prepared by the calcination of iron(II) sulfate was used as a nonporous reference material.[7]

Prior to the adsorption experiments, *ca.* 20 g of the sample was degassed at 600 °C for 4 h in a vacuum of 1×10^{-3} Pa in order to remove surface impurities such as chemisorbed water and carbon dioxide. Nitrogen adsorption isotherms were measured volumetrically at −196 °C.

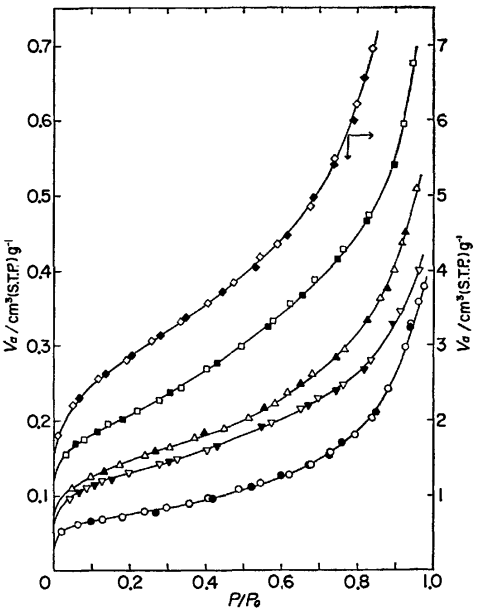

Fig. 1. N_2-adsorption isotherms on iron oxide samples. Sample S, ○; M, □; Ih, ▽; Im, △; preparation (II), ◇ (see the text). Filled points represent desorption.

Results and Discussion

Figure 1 shows the adsorption isotherms of N_2 on iron oxide samples. The isotherm for sample H was almost the same as that for sample S. Desorption isotherm was also measured, the result being consistent with the adsorption branch in the whole pressure range studied. The BET surface area (S_{BET}) is calculated as given in Table 1. It should be noted that oxidation and reduction treatment of iron oxide regularly alter the adsorbability of nitrogen molecules, *i.e.*, the specific surface area of the samples; the amount of adsorbed nitrogen increases in the course of the reduction of oxide, but decreases as the oxidation proceeds. This suggests that the reduction of iron oxide into Fe_3O_4 having the spinel structure is accompanied by the formation of pores in the products.

First, the *t*-plots were constructed on the basis of the standard *t*-curve of Lippens *et al.*[3] and that of Cranston and Inkley.[2] However, they did not give a straight line through the origin, showing disagreement with the BET area S_{BET}. The discrepancy between the *C*-value in the BET equation on a sample and that on the reference solid seriously affects the trend of

Table 1. BET C-VALUES AND SURFACE AREAS OF IRON OXIDE SAMPLES

Sample	C-value	Surface area ($m^2 g^{-1}$)		
		S_{BET}	S_t	S_{out}[a]
S	160	0.271	0.271	—
M	146	0.745	0.739	0.526
Ih	135	0.460	0.460	0.315
Im	140	0.518	0.518	0.397

a) S_{out} represents the outer surface area obtained from the t-plots ($t > 7$ Å).

t-plots.[8] In order to get an appropriate reference t-curve from the data on related substances, a nonporous α-Fe_2O_3 prepared by calcining iron(II) sulfate was treated as follows: evacuation at 600 °C for 4 h (I), followed by rehydration (II), calcination at 800 °C for 4 h and subsequent evacuation at 600 °C for 4 h (III), followed by rehydration (IV). The C-values in the N_2-adsorption isotherm on these preparations were found to be 124, 169, 243, and 253, respectively. We adopted the data on preparation (II) as the reference curve, because of the consistency of the C-value with that of the present samples (Table 1).

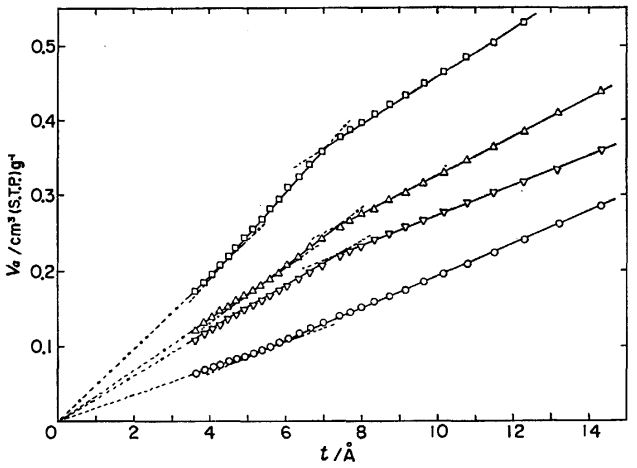

Fig. 2. t-Plots for N_2 adsorption on iron oxide samples. Sample S, ○; M, □; Ih, ▽; Im, △.

Figure 2 shows the t-plots for iron oxide samples subjected to oxidation or reduction treatment. In all cases the first part of the curves is in a straight line through the origin. The surface area S_t can be calculated from the slope of the straight line,[1] being in good agreement with S_{BET} (Table 1). Since S_t is a function of a particular t-curve employed, the agreement between S_t and S_{BET} is a good indicator for the validity of the reference t-curve.[8]

Sample S gives a straight line through the origin up to $t \approx 5$ Å, followed by a separate line with a greater slope. Although an upward deviation from the initial straight line represents a capillary condensation in pores,[1] no hysteresis appears in the isotherm of this sample. This might be due to reversible capillary condensation in wide and slit-shaped pores open at both ends.[9] A remarkable increase in surface area for sample M produced by reduction of sample S suggests the sample to be fairly porous. The t-plots for sample M consist of three straight lines: the first one up to $t \approx 4$ Å, the second one between 4 and 7 Å, and the last one beyond 7 Å. The former two of the three lines might correspond to the monolayer adsorption onto outer and inner surfaces, and the reversible capillary condensation in slit-shaped pores open at both ends, respectively, as on the sample S. Taking account of the density of liquid nitrogen at −196 °C, we obtain the monolayer thickness to be 3.54 Å.[3] Thus, since the pores would be filled when the thickness of the adsorbed layer is equal to half the width of pores, the width is found to be 14 Å. The last line indicates the adsorption in the wider pores as well as on the outer surface, the area calculated from this slope being 0.526 $m^2 g^{-1}$ (Table 1), which gives the inner surface area as 0.213 $m^2 g^{-1}$. The t-plots of sample Im obtained by partial oxidation of sample M have the same tendency as in the case of sample M. However, its surface area is less than the latter, because of partial closing of pores during the course of oxidation of Fe_3O_4. The inner surface of sample Im amounts to 0.121 $m^2 g^{-1}$, smaller than that of sample M. On the other hand, sample Ih shows a straight line with single break at $t \approx 7$ Å, indicating that the sample has pores accessible to nitrogen molecules in two statistical layers. This sample was obtained by partial reduction of sample H prepared by exhaustive oxidation of sample S having wide and slit-shaped pores. It appears evident that such pores were made in the course of reduction, since no change in S_{BET}-value was observed in the oxidizing process as stated above.

Thus, it is concluded that the reduction or oxidation of iron oxide is accompanied by the formation or closing of pores. The fact that the t-plots reveal distinct breaks at two definite t-values indicates the formation of pores of a regular size during the course of conversion into spinel structure. An increase either in the number or in the depth of such pores in the course of the reduction treatment will lead to an increase in surface area. The presence of pores might also lead to an elongation of the adsorption time of water.[10]

References

1) J. H. de Boer and B. C. Lippens, *J. Catal.*, **3**, 38, 44 (1964); **4**, 319 (1965).
2) R. W. Cranston and F. A. Inkley, *Adv. Catal.*, **9**, 143 (1957).
3) B. C. Lippens, B. G. Linsen, and J. H. de Boer, *J. Catal.*, **3**, 32 (1964).
4) R. F. Horlock and P. J. Anderson, *Trans. Faraday Soc.*, **63**, 717 (1967).
5) F. S. Baker, J. D. Carruthers, R. E. Day, K. S. W. Sing, and L. J. Stryker, *Discuss. Faraday Soc.*, **52**, 173 (1971).
6) K. Iwase, "Shinsei-Kinzoku-Koza, Tekko-Seiren II," Nippon Kinzoku Gakkai, Tokyo (1957), p. 206.
7) T. Morimoto, M. Nagao, and F. Tokuda, *J. Phys. Chem.*, **73**, 243 (1969).
8) K. M. Hanna, I. Odler, S. Brunauer, J. Haggymassy, Jr., and E. E. Bodor, *J. Colloid Interface Sci.*, **45**, 27 (1973).
9) J. H. de Boer, "The Structure and Properties of Porous Materials," Butterworth, London (1958), p. 68.
10) T. Morimoto, Y. Yokota, and M. Nagao, *J. Colloid Interface Sci.*, **64**, 188 (1978).

BULLETIN OF THE CHEMICAL SOCIETY OF JAPAN, VOL. 51 (8), 2425—2426 (1978)

Syntheses of 5-Hydroxyflavone-Transition Metal Complexes

Katsuma HIRAKI,* Masayoshi ONISHI,* Tsuyoshi IKEDA,
Kazuko TOMIOKA, and Yayoi OBAYASHI

Department of Industrial Chemistry, Faculty of Engineering, Nagasaki University, Bunkyo-machi, Nagasaki 852

(Received January 30, 1978)

Synopsis. New complexes $[M(hofl)_2(OH_2)_n]$ (Hhofl=5-hydroxyflavone; M=Co and Ni, $n=2$; M=Cu, $n=1$ and 0) and $[M(hofl)_3]$ (M=V and Fe) were synthesized and characterized by IR and electronic absorption spectroscopy. Polynuclear ethoxo(5-hydroxyflavonato)metal(II) complexes of cobalt and copper were also prepared.

Many hydroxyflavone derivatives are distributed widely in plants.[1,2] Morin and quercetin have been used as reagents for colorimetric and fluorescent analyses of metals.[3] The analyses are based on the chelating ability of the hydroxyflavones with metals.[4-7] However, hardly any work has been reported as regards isolation and characterization of the hydroxyflavone–metal complexes.

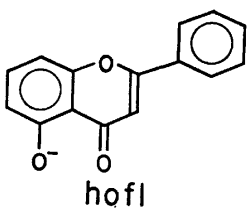

hofl

This note deals with the syntheses and properties of some new transition metal complexes with 5-hydroxyflavone (Hhofl), one of the simplest model compounds of hydroxyflavones.

Experimental

Materials. 5-Hydroxyflavone was synthesized from 2,6-dihydroxyacetophenone according to the method of Looker *et al.*,[8] and identified by elemental analysis, melting point and IR spectrum. Commercial metal chlorides were used without further purification. Solvents were dried by the usual methods and distilled.

General Procedure. IR and electronic spectra were measured on Hitachi 285 and 323 spectrometers, respectively. Melting points were determined on a Yanagimoto MP-S3 microstage apparatus in capillary tubes and are uncorrected.

Preparation of Bis- or Tris(5-hydroxyflavonato)metal Complexes. 5-Hydroxyflavone (8.0 mmol) and nickel(II) chloride (3.0 mmol) were mixed in ethanol. An ethanol solution of sodium acetate (10.0 mmol) was added to the mixture with stirring. After the reaction mixture had been refluxed for 4 h, the resulting precipitate was separated, recrystallized from benzene–hexane and dried *in vacuo* to give a yellow solid, $[Ni(hofl)_2(OH_2)_2]$ (yield 32%).

The complexes $[Co(hofl)_2(OH_2)_2]$, $[Cu(hofl)_2OH_2]$, and $[Cu(hofl)_2]$ were prepared similarly. Tris(5-hydroxyflavonato)metal(III) complexes of vanadium and iron were also prepared in a similar way except that anhydrous metal(III) chloride was used in place of divalent metal chloride.

Preparation of Ethoxo(5-hydroxyflavonato)metal(II) Complexes. An ethanol solution containing 5-hydroxyflavone (4.2 mmol) and sodium ethoxide (2.0 mmol) was added gradually to an ethanol solution of cobalt(II) chloride (2.0 mmol). The reaction mixture was refluxed for 3 h. The resulting precipitate was collected and washed with benzene and ethanol to afford a reddish brown solid, $[\{Co(OEt)(hofl)\}_n]$ (yield 63%). The complex, $[\{Cu(OEt)(hofl)\}_n]$ was prepared in a similar way.

Results and Discussion

The yields, properties, and the results of elemental analyses of the complexes are summarized in Table 1. Diaquabis(5-hydroxyflavonato)metal(II) and the tris(5-hydroxyflavonato)metal(III) complexes are soluble in usual organic solvents such as benzene and chloroform but not in hexane. The water content of the mononuclear copper(II) complexes changes with the heating temperature in the drying procedure. $[Cu(hofl)_2OH_2]$ and $[Cu(hofl)_2]$ were obtained by drying *in vacuo* at 125—135 °C for 2 h and at 150—160 °C for 5 h, respectively. No diaqua complex of copper(II) was obtained in a pure state.

The spectroscopic data are summarized in Table 2. IR spectra of the 5-hydroxyflavonato complexes show

Table 1. Yields and some properties of the 5-hydroxyflavone–transition metal complexes

Complex	Yield[a] (%)	Color	Mp (°C)	Elemental analyses[b] (%) C	H	M
$[Co(hofl)_2(OH_2)_2]$	14	Orange yellow	233—237(dec)	63.51(63.27)	3.39(3.90)	—
$[Ni(hofl)_2(OH_2)_2]$	32	Yellow	298—299(dec)	63.42(63.30)	3.23(3.90)	10.19(10.32)[c]
$[Cu(hofl)_2OH_2]$	28	Olive yellow	274—280(dec)	64.82(64.80)	3.12(3.63)	—
$[Cu(hofl)_2]$	65	Olive yellow	>300	66.97(66.71)	3.29(3.38)	—
$[V(hofl)_3]$	21	Dark green	166.5—171.5	70.63(70.87)	3.76(3.57)	—
$[Fe(hofl)_3]$	33	Reddish violet	>300	70.76(70.41)	3.45(3.55)	—
[Co(OEt)(hofl)]	63	Reddish brown	>300	59.42(59.84)	3.11(4.18)	—
[Cu(OEt)(hofl)]	22	Yellow brown	>300	58.22(59.04)	3.00(4.08)	—

a) Calculated on the basis of metal chloride. b) Calculated values in parentheses. c) By gravimetric analysis of bis(dimethylglyoximato)nickel(II) derived from the sample.

Table 2. Spectroscopic data of 5-hydroxyflavone and its transition metal complexes

Compound	IR spectrum[a] ν(C=O) (cm^{-1})	Electronic spectrum[b] ν_{max} (cm^{-1})	ε_{max}
Hhofl	1653	29800	4600
$[Co(hofl)_2(OH_2)_2]$	1639	24200	4400
$[Ni(hofl)_2(OH_2)_2]$	1639	24700	5800
$[Cu(hofl)_2OH_2]$	1627	—	—
$[Cu(hofl)_2]$	1618	24100	970
$[V(hofl)_3]$	1622	17800	1370
$[Fe(hofl)_3]$	1620	23500[c]	11600
[Co(OEt)(hofl)]	1635	—	—
[Cu(OEt)(hofl)]	1639	—	—

a) In KBr disk. b) In chloroform. c) Having a shoulder at 19230 cm^{-1}.

ν(CO) bands, shifting towards a frequency lower by 14—35 cm^{-1} from that observed for free 5-hydroxyflavone, indicating that the 5-hydroxyflavonato ligand is coordinated to the metal ion as a bidentate chelate. Both $[Co(hofl)_2(OH_2)_2]$ and $[Ni(hofl)_2(OH_2)_2]$ are assigned to a tetragonal bipyramid structure in consideration of its composition, by analogy with diaquabis(salicylaldehydato)nickel(II) complex.[9] $[V(hofl)_3]$ and $[Fe(hofl)_3]$ are ascribed to pseudo-octahedral structures.

The mononuclear complexes of iron(III), cobalt(II), nickel(II), and copper(II) exhibit a strong electronic absorption band near 24000 cm^{-1}, virtually independent of the metal ion. The intensity of this band is too strong to be assigned to a d-d transition. The band is located at a wave number lower by *ca.* 5800 cm^{-1} than the minimum energy absorption band of free 5-hydroxyflavone. Each of the iron(III), cobalt(II), nickel(II), and copper(II) ions in a ground state has one or more unoccupied d-orbitals. This indicates that the absorption band near 24000 cm^{-1} is ascribed to a charge transfer from the 5-hydroxyflavonato ligand to the metal d-orbital.

On the other hand, $[V(hofl)_3]$ shows a strong absorption band at 17800 cm^{-1}, besides a very strong band above 21000 cm^{-1}. The intensity of these bands is so strong that it is unlikely that they are associated with the d-d transitions. The vanadium(III) ion with a d^2 configuration has a vacant d-orbital located at a lower energy level than the unoccupied d-orbitals of the nickel(II) and copper(II) ions. The band at 17800 cm^{-1} is assigned to a charge transfer from the 5-hydroxyflavonato ligand to the vacant low-lying d-orbital of the vanadium(III) ion, probably obscuring a low intensity band expected to appear at a similar wave number, owing to the d-d transition.[10]

The electronic spectra and the molecular weights of the ethoxo(5-hydroxyflavonato)metal(II) complexes could not be measured, because of the high insolubility in the usual organic solvents. These complexes are supposed to have polymeric structures, by analogy with alkoxo(salicylaldehydato)copper(II) and its related complexes.[11] Attempts to prepare ethoxo(5-hydroxyflavonato)nickel(II) were unsuccessful.

References

1) T. A. Geissman, "The Chemistry of Flavonoid Compounds," Pergamon, Oxford (1962).
2) S. Fujise, S. Hishida, S. Sasaki, H. Obara, and H. Uda, "Dai-yuki Kagaku," Vol. 14, ed by M. Kotake, Asakura Shoten, Tokyo (1973), pp. 142—187 and references therein.
3) M. Katyal, *Talanta*, **15**, 95 (1968) and references therein.
5) a) H. Obara, N. Ishibashi, and Y. Ito, *Bunseki Kagaku*, **16**, 315 (1967); b) H. Obara and N. Ishibashi, *ibid.*, **16**, 470 (1967).
6) L. J. Porter and K. R. Markham, *J. Chem. Soc., C*, **1970**, 344.
7) A. Murata, M. Tominaga, H. Inoue, and T. Suzuki, *Bunseki Kagaku*, **22**, 179 (1972).
8) J. H. Looker, J. R. Edman, and J. I. Dappen, *J. Heterocycl. Chem.*, **1**, 141 (1964).
9) J. M. Stewart, E. C. Lingafelter, and J. D. Breazeale, *Acta Crystallogr.*, **14**, 888 (1961).
10) D. J. Machin and K. S. Murray, *J. Chem. Soc., A*, **1967**, 1498.
11) J. E. Andrew, A. B. Blake, and L. R. Fraser, *J. Chem. Soc., Dalton Trans.*, **1976**, 477.

BULLETIN OF THE CHEMICAL SOCIETY OF JAPAN, VOL. 51 (8), 2427—2428 (1978)

Syntheses and Properties of *gem*-Diolatotriarylantimony(V)

Akira OUCHI,* Fujio EBINA, Takashi UEHIRO, and Yukichi YOSHINO

Department of Chemistry, College of General Education, The University of Tokyo, Komaba, Meguro, Tokyo 153

(Received February 15, 1978)

Synopsis. Titled compounds of the general formula $R_3Sb(R'R''CO_2)$ have been prepared, where R=phenyl, *p*-tolyl or *p*-chlorophenyl, R',R''=CF_3,CF_3; CF_3,H; or CCl_3, H. From the infrared spectra and ^{1}H-NMR data, the *gem*-diolato group appears to bond to the antimony bidentately through two oxygen atoms, as in the 1,1,1-trifluoro-4-oxo-2,2-pentanediolato complex of triarylantimony(V).

Trifluoroacetylacetone reacted with dibromotriarylantimony(V), to give a new type complex, where the β-diketone hydrated and acted as a terdentate.[1,2] In that complex, the ligand bonds to the antimony through one keto oxygen near the methyl group, and two *gem*-diolato oxygens of the hydrated carbonyl group next to the trifluoromethyl one. From the X-ray structure analysis, the bond between antimony and the keto-oxygen is weaker than the other two.[1] Consequently *gem*-diols are also expected to form stable complexes with organoantimony(V), working as a bidentate ligands and making four membered ring chelates. This paper reports the reaction between dibromotriarylantimony(V) and some *gem*-diols, such as chloral hydrate.

Experimental

Synthesis of (2,2,2-Trichloroethane-1,1-diolato)triphenylantimony-(V). Two grams (4 mmol) of dibromotriphenylantimony(V), which was synthesized by the standard technique,[3] and 2,2,2-trichloro-1,1-ethanediol (Wako Pure Chemical Co., Ltd., G. R. grade) (0.83 g, 5 mmol) were dissolved in benzene (20 ml). To the solution, triethylamine (1.0 g, 10 mmol) was added as a deprotonation reagent. After stirring for 1 h at room temperature, the precipitated triethylammonium bromide was filtered off and the filtrate evaporated to dryness using a rotary evaporator (60 °C, water pump). The residue was recrystallized from acetonitrile, the yield being about 1.5 g (75%) on average after one recrystallization.

Seven other kinds of complex having the same formula, $R_3Sb(R'R''CO_2)$, where R=phenyl, *p*-tolyl, or *p*-chlorophenyl, R',R''=CF_3,CF_3; CF_3,H; CCl_3,H; were synthesized by the same technique from the reaction between the appropriate dibromotriarylantimony(V) and hydrated hexafluoroacetone, 2,2,2-trifluoro-1-ethoxyethanol, or chloral hydrate. The products thus obtained were very stable in air at room temperature, and kept for several months without any decomposition. Attempts to synthesize this type of compound using dihalogenotrialkyl antimony(V), or a ketone such as hexachloroacetone, acetophenone, benzophenone, or acetone were not successful.

Infrared spectra of the samples were obtained by a JASCO infrared spectrophotometer, type 403G, using Nujol and hexachloro-1,3-butadiene mull, and ^{1}H-NMR by a JEOL JNM-MH-100 (100 MHz) NMR spectrometer using a 20% $CDCl_3$ solution at 26 °C with TMS as the internal standard. The mp and decomposition points were obtained by the simultaneous TG-DTA technique using a Rigaku Denki M-8075 thermal analyser.

Results and Discussion

The analyses of the products, as well as their calculated values from the formula, $R_3Sb(R'R''CO_2)$, are shown as follows. R=C_6H_5, R'=CF_3, R''=CF_3; Found: C, 47.10; H, 2.84%. Calcd: C, 47.14; H, 2.82%. Mp 122 °C. R=C_6H_5, R'=CF_3, R''=H; Found: C, 51.36; H, 3.47%. Calcd: C, 51.43; H, 3.47%. Dec at 134 °C. R=C_6H_5, R'=CCl_3, R''=H; Found: C, 46.50; H, 3.10%. Calcd: C, 46.51; H, 3.21%. Dec. at 130 °C. R=*p*-tolyl, R'=CF_3, R''=CF_3; Found: C, 49.62; H, 3.42%. Calcd: C, 49.95; H, 3.62%. Dec at 132 °C. R=*p*-tolyl, R'=CF_3, R''=H; Found: C, 54.12, H, 4.46%. Calcd: C, 54.26; H, 4.36%. Dec at 115 °C. R=*p*-tolyl, R'=CCl_3, R''=H; Found: C, 49.46; H, 4.03%. Calcd: C, 49.46; H, 3.97%. Dec at 120 °C. R=*p*-chlorophenyl, R'=CF_3, R''=CF_3; Found: C, 39.22; H, 1.88%. Calcd: C, 39.51; H, 1.90%. Dec at 160 °C. R=*p*-chlorophenyl, R'=CCl_3, R''=H; Found: C, 39.54, H, 2.21%. Calcd: C, 38.76; H, 2.11%. Dec at 145 °C.

From the molecular weight measurement by the freezing point depression of the benzene solution, all of these compounds were shown to be monomers. All the products are white crystalline powders, stable at room temperature for several months, soluble in organic solvents such as benzene, acetone, chloroform, and insoluble in water.

The infrared spectra of these compounds were

TABLE 1. ν(C–O)[5] OF THE R_3Sb ($R'R''CO_2$), $R'R''C(OH)_2$, AND (1,1,1-TRIFLUORO-4-OXO-2,2-PENTANEDIOLATO)TRIPHENYLANTIMONY(V) (shown as Ph_3Sb(HtfacO) in the table) (cm^{-1})

R'	R''	$R_3Sb(R'R''CO_2)$ R=phenyl	$R_3Sb(R'R''CO_2)$ R=*p*-tolyl	$R_3Sb(R'R''CO_2)$ R=*p*-chlorophenyl	$R'R''C(OH)_2$
CF_3	CF_3	1092, 1063	1100, 1064	1090, 1063	1080,
CF_3	H	1110, 1050	1110, 1070		1100, 1075[a]
CCl_3	H	1105, 1065	1110, 1063	1110, 1063	1075
Ph_3Sb(HtfacO)		1019, 1089			

a) Ethyl hemiacetal.

Table 2. ^{1}H-NMR spectra (TMS=0, shown by δ ppm)
(J values of AB pattern quartets are shown in parentheses (Hz))

Compd	R								
	Phenyl		*p*-Tolyl			*p*-Chlorophenyl		CH
	Ar	CH	Ar	CH	Me	Ar	CH	
$R_3Sb(R'R''CO_2)$								
$R'=CF_3$, $R''=CF_3$	7.70, 7.60 m		7.67, 7.31 q(8)		2.43	7.64, 7.56 q(9)		
$R'=CF_3$, $R''=H$	7.74, 7.55 m	5.48	7.64, 7.35 q(8)	5.41	2.44			
$R'=CCl_3$, $R''=H$	7.75, 7.55 m	5.63	7.63, 7.34 q(7)	5.55	2.44	7.64, 7.48 q(8)	5.54	
$R_3Sb(HtfacO)$	7.65, 7.36 m					7.49, 7.33 q(8)		
R_3SbBr_2	8.17, 7.57 m		8.04, 7.37 q(8)		2.44	8.12, 7.58 q(8)		
R_3Sb	7.39 m		7.34 m		2.44	7.22 m		
$CCl_3CH(OH)_2$								5.38
$CF_3CH(OH)(OCH_3)$								4.85

m: multiplet, q: quartet.

examined. Almost all bands originated from the aryl groups, as well as those from the trihalogenomethyl groups which appeared in the same wave number region as those of the dibromotriarylantimonies, or the *gem*-diols, respectively. However, ν(OH) (about 3400 cm^{-1}),[4] as well as ν(C=O) (about 1700 cm^{-1})[4] were absent in the spectra of these compounds. The wave number of the ν(C=O) band[4,5] of the complexes as well as those of the corresponding *gem*-diols are shown in Table 1. As is evident this band splits into two peaks, likely *sym*- and *antisym*-stretching bands, which are also found in the spectra of the hydrated β-diketonato complex as shown in the Table. This strongly supports bonding between the diolato oxygens and the central metal.

The ^{1}H-NMR spectra of these complexes are shown in Table 2, together with those of related substances.[6] In general, the ^{1}H-NMR of the aryl group of Ar_3SbL_2 type organoantimony(V), shifts to the higher field, when the bonded HL is a weaker acid.[6,7] The lower field shifts of the phenyl peaks of these *gem*-diolato complexes were less than those of the carboxylato or halogeno derivatives.[6,7] Therefore, the *gem*-diolato ligands work as less negative ones than the carboxylato or phenolato derivatives. The hydrated β-diketone complex of triarylantimony(V) gives the same order shift for phenyl peaks. The splitting of each aryl proton peak due to the geometrical arrangement of the groups in the complex was not observed; in the case of the *p*-tolyl, or *p*-chlorophenyl derivatives, one sharp quartet of AB pattern was retained.

These results suggest that the *gem*-diolato ligand works bidentately in these complexes; and the central antimony is a penta coordinated one, probably in the trigonal bipyramidal configuration as in the cases of these type quinquevalent organoantimony compounds. From consideration of bond lengths,[2,8,9] the O–C–O bond of the ligand cannot span the central antimony from the equatorial direction, when there is serious deformation in the complex. Therefore, it may be assumed that the bidentate spans between apical and equatorial directions, although some deformation of the shape is inevitable in this case, too. Three aryl groups bonding to the antimony are thus in a facial array. As in the cases of other trigonal bipyramidal compounds,[10,11] Berry's rotation easily occurs, and the splitting of each aryl proton peak in the ^{1}H-NMR due to their situations was not observed, but only the average recognized.

References

1) F. Ebina, T. Uehiro, T. Iwamoto, A. Ouchi, and Y. Yoshino, *J. Chem. Soc., Chem. Commun.*, **1976**, 245.

2) F. Ebina, A. Ouchi, Y. Yoshino, S. Sato, and Y. Saito, *Acta Crystallogr., Sect. B*, **33**, 3252 (1977).

3) W. J. Dyke and W. J. Jones, *J. Chem. Soc.*, **1930**, I, 1921.

4) L. J. Bellamy, "The Infrared Spectra of Complex Molecules," Vol. 1, 3rd ed, Chapman and Hall London (1975), pp. 107, 149.

5) This band may be a coupled one with the other mode vibrations, such as (Sb–O). However, the shift by the coupling seems not be serious.

6) A. Ouchi, M. Nakatani, Y. Takahashi, S, Kitazima, T. Sugihara, M. Natsumoto, T. Uehiro, K. Kitano, K. Kawashima, and H. Honda, *Sci. Pap. Coll. Gen. Educ., Univ. Tokyo*, **25**, 73 (1975).

7) R. G. Goel and D. R. Ridley, *J. Organomet. Chem.*, **38**, 83 (1972).

8) A. Zalkin, D. H. Templeton, and T. Ueki, *Inorg. Chem.*, **7**, 1641 (1973).

9) M. C. Poore and D. R. Russell, *Chem. Commun.*, **1971**, 18.

10) J. R. Rhapley and J. A. Osborn, *Acc. Chem. Res.*, **6**, 305 (1973).

11) P. Meakin, E. L. Muetterties, and J. P. Jesson, *J. Am. Chem. Soc.*, **94**, 5271 (1972).

BULLETIN OF THE CHEMICAL SOCIETY OF JAPAN, VOL. 51 (8), 2429—2430 (1978)

Synthesis and Characterization of Copper Complexes with Schiff Bases Derived from 2-Thiophenealdehyde and Alkylamines

Hiro KUMA, Kyoji MOTOBE, and Shoichiro YAMADA*

Institute of Chemistry, College of General Education, Osaka University, Toyonaka, Osaka 560

(Received March 10, 1978)

Synopsis. Copper(I) and copper(II) complexes with Schiff bases derived from 2-thiophenealdehyde and alkylamines were prepared. Probable structures of these complexes are discussed mainly on the basis of electronic and infrared spectra and magnetism.

In a recent work,[1] the present authors have synthesized a number of cobalt(II), nickel(II), and copper(II) complexes with 2-thiophenealdehyde oxime and have concluded that the oxime is bound as a unidentate ligand through the nitrogen atom to the metal ions in these complexes, the sulfur atom not being involved in the bonding with the metal ion. As an extension to the previous study, the present paper describes synthesis and characterization of copper(I) and copper(II) complexes with Schiff bases (abbreviated as tal–R, I) obtained from 2-thiophenealdehyde and alkylamines. A single copper(II) complex of this series was reported in the literature.[2]

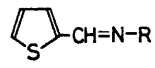

I

Experimental

Materials. *N*-(2-Thenylidene)alkylamines were prepared by methods similar to that described previously for the methyl-derivative.[2]

Copper(I) Complexes. Complexes of the type Cu(tal–R)X (R=CH_3, X=Cl, Br; R=*n*-C_3H_7, X=I; R=*i*-C_3H_7, X=Cl, Br, I) were obtained as yellow crystals by the following two methods A and B.

Method A (for R=CH_3, i-C_3H_7; X=Cl, Br). A mixture of $CuX_2 \cdot 2H_2O$ (0.01 mol) and 2,2-dimethoxypropane (25—30 ml) in ethanol (30 ml) was stirred at about 35 °C for 2 h. The solution was evaporated at about 40 °C nearly to dryness, and the residue was dissolved in ethanol (100 ml). To the resulting solution was added a Schiff base (0.02 mol) and heated at 70 °C for 2 h. A yellow precipitate was filtered and recrystallized from chloroform to yield pure crystals of the compound.

*Method B (for R=CH_3, X=Cl, Br; R=*i*-C_3H_7, X=Cl, Br, I; R=*n*-C_3H_7, X=I).* A mixture of CuX (0.01 mol) and a Schiff base (0.02 mol) in ethanol (100 ml) was heated at 50—60 °C for 1 h (R=CH_3, X=Cl, Br) or at 70—80 °C for 5—7 h (R=CH_3, X=I; R=*i*-C_3H_7, X=Cl, Br, I; R=*n*-C_3H_7, X=I). A yellow precipitate was filtered and recrystallized from chloroform or ethanol.

Cu(tal–CH_3)$_2$I was obtained by the method B.

The copper(I) complexes obtained are gradually decomposed in the atmosphere.

Copper(II) Complexes. Complexes of the type Cu(tal–R)$_2X_2$, (R=CH_3, X=Cl, Br; R=C_2H_5, X=Cl) were synthesized by heating a mixture of anhydrous CuX_2 (0.01 mol) and a Schiff base (0.02 mol) in ethanol (100 ml) at 60—70 °C for 2 h. A crystalline precipitate was washed with hot ethanol several times.

Table 1. Analytical data of copper(I) and copper(II) complexes with *N*-(2-thenylidene)alkylamines

Compound	Found, (Calcd) % C	H	N	Mp °C	μ
Cu(tal–CH_3)Cl	31.96 (32.14	3.33 3.15	6.08 6.25)	200—202	dia
Cu(tal–CH_3)Br	27.05 (26.90	2.96 2.64	5.38 5.23)	195—196	dia
Cu(tal–CH_3)$_2$I	32.52 (32.69	3.46 3.20	6.25 6.36)	125—126	dia
Cu(tal–*n*-C_3H_7)I	27.68 (27.96	3.42 3.23	4.16 4.08)	133—134	dia
Cu(tal–*i*-C_3H_7)Cl	37.87 (38.09	4.59 4.40	5.54 5.55)	141—142	dia
Cu(tal–*i*-C_3H_7)Br	32.20 (32.38	3.87 3.74	4.86 4.72)	193—194	dia
Cu(tal–*i*-C_3H_7)I	27.80 (27.96	3.38 3.23	4.23 4.08)	170—171	dia
Cu(tal–CH_3)$_2$Cl$_2$	37.44 (37.45	3.67 3.67	7.27 7.28)	187—188	1.98
Cu(tal–CH_3)$_2$Br$_2$	30.68 (30.42	3.18 2.98	5.85 5.91)	153—154	1.95
Cu(tal–C_2H_5)$_2$Cl$_2$	40.52 (40.23	4.39 4.45	6.79 6.85)	147—148	1.96

μ: BM at room temperature.

The copper(II) compounds obtained, which are brown-yellow (R=CH_3, X=Cl, Br) or grey-olive (R=C_2H_5, X=Cl), are soluble in pyridine but almost insoluble in other common organic solvents.

Analytical data of the complexes are shown in Table 1.

Measurements. Electronic absorption spectra of the complexes in Nujol were recorded on a Shimadzu MPS-50L spectrophotometer. Infrared spectra were measured as Nujol mulls on Hitachi EPI-S2, EPI-L, and FIS-3 infrared spectrophotometers.

Magnetic measurements at room temperature were carried out by the Gouy method using $CoHg(SCN)_4$ as a calibrant.

Results and Discussion

Copper(I) Complexes. The following two types of copper(I) complexes were isolated in the present work: (1) Cu(tal–R)X and (2) Cu(tal–CH_3)$_2$I. Some of the copper(I) complexes were obtained from copper(II) salts when the reactants containing 2,2-dimethoxypropane were refluxed (method B). Otherwise, copper(II) complexes were isolated instead of the copper(I) complexes. It is probable that 2,2-dimethoxypropane undergoes decomposition during the reactions to yield some reducing species in the solution.

These copper(I) complexes are diamagnetic and show

Table 2. Main infrared bands(cm^{-1}) of copper(I) complexes with *N*-(2-thenylidene)alkylamines

Compound	ν(C=N)	ν(Cu–X_{br})
Cu(tal–CH_3)Cl	1615	200
Cu(tal–CH_3)Br	1610	152
Cu(tal–CH_3)$_2$I	1605	135
Cu(tal–*i*-C_3H_7)Cl	1610	194
Cu(tal–*i*-C_3H_7)Br	1605	158
Cu(tal–*i*-C_3H_7)I	1605	130
Cu(tal–*n*-C_3H_7)I	1620	135

no d-d bands in the visible region. As seen in Table 2, ν(C=N) frequencies of the copper(I) complexes shift toward lower frequencies as compared with those (1640—1650 cm^{-1}) of the free ligands, suggesting that the ligands may be coordinated through the nitrogen atom to the copper(I) ion. Inspection of Table 2 also indicates that the halide ions function as bridging ligands, since the copper(I) complexes exhibit ν(Cu–X_{br}) frequencies in the region expected for the bridging Cu–X, and no infrared bands occur in the region (around 250 cm^{-1}) expected for the Cu–S frequencies.[3] All these results combined seem to show that in the copper(I) complexes the ligands tal–R are coordinated as unidentate ligands through the nitrogen atom, the halide ion acting as a bridging ligand. Binuclear, cyclic trinuclear, cubane or other multinuclear structures may be proposed for these copper(I) complexes.

A similar argument as to the infrared spectra applies to Cu(tal–CH_3)$_2$I (Table 2). Thus the ligand tal–CH_3 is coordinated as a unidentate ligand through the nitrogen atom, the iodide ion acting as a bridging ligand. The compound Cu(tal–CH_3)$_2$I may probably have a structure similar to that of Cu(tal–R)X, except that an additional ligand tal–CH_3 is placed on each copper(I) ion in Cu(tal–R)X.

Copper(II) Complexes. Copper(II) complexes of the type Cu(tal–R)$_2X_2$ were obtained in the present work. One of them, Cu(tal–CH_3)$_2Cl_2$, was reported previously.[2] A *trans*-planar configuration was predicted for this complex chiefly from formal analogy of this complex to bis[*N*-(2-pyrrolidene)methylaminato]copper(II). The compound of the same composition obtained in the present work is not soluble enough for the conductivity measurement in nitrobenzne.

The copper(II) complexes Cu(tal–R)$_2X_2$ are paramagnetic with moments corresponding to one spin-free electron (Table 1). They exhibit ν(C=N) bands at 1620—1625 cm^{-1}, which are significantly lower than those of the free ligands (1640—1650 cm^{-1}), showing that the ligands tal–R are coordinated through the nitrogen atom to the copper(II) ion.

The electronic absorption spectrum of Cu(tal–CH_3)$_2$-Br_2 is very similar to that of Cu(tal–C_2H_5)$_2Cl_2$, while the spectrum of Cu(tal–CH_3)$_2Cl_2$ differs from those of the other two complexes (Fig. 1). It is interesting to note that the spectra of Cu(tal–CH_3)$_2Br_2$ and Cu(tal–C_2H_5)$_2Cl_2$ are similar to those of Cu(tox)$_2Cl_2$ and Cu(py)$_2Cl_2$, which were previously concluded to have a multinuclear structure with six-coordinated copper(II)

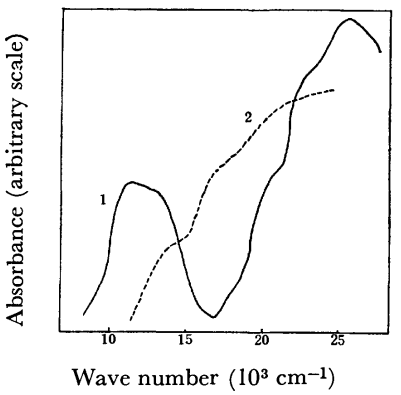

Fig. 1. Electronic absorption spectrum of copper(II) complexes in Nujol: 1, Cu(tal–CH_3)$_2Cl_2$; 2, Cu(tal–CH_3)$_2Br_2$.

ions and bridging chloride ions.[1,4] The notations tox and py represent 2-thiophenealdehyde oxime and pyridine, respectively. The maxima of their main d-d bands (14.6 and 14.7$\times 10^3$ cm^{-1}) are close to those of Cu(tox)$_2Cl_2$ and Cu(py)$_2Cl_2$ (14.3 and 14.5$\times 10^3$ cm^{-1}). It is, therefore, very likely that these two copper(II) complexes, may also have a structure similar to that of Cu(tox)$_2Cl_2$ and Cu(py)$_2Cl_2$.

The sulfur atom of the ligand is not bound with copper(II) ion in Cu(tal–CH_3)$_2Br_2$ and Cu(tal–C_2H_5)$_2$-Cl_2, since they show no charge transfer band characteristic of copper(II) complexes with sulfur-coordinating ligands. It has recently been reported that such copper(II) complexes show a characteristic band of considerably high intensity at about 23—31$\times 10^3$ cm^{-1}.[5] The very low frequency of the d-d band maximum for Cu(tal–CH_3)$_2Cl_2$ requires considerable distortion of the structure and seems to be consistent with a distorted tetrahedral or a trigonal bipyramidal structure.[6,7] A very intense charge transfer band, which is characteristic of the copper(II) complexes with sulfur-coordinating ligand, occurs at 25.7$\times 10^3$ cm^{-1} in the spectrum of Cu(tal–CH_3)$_2Cl_2$, suggesting that the sulfur atom as well as the nitrogen atom of the ligand tal–CH_3 is also bound with the copper(II) ion. A possibility of coordination of the chloride to copper ion or of a multinuclear structure may not be excluded.

References

1) H. Kuma, K. Motobe, and S. Yamada, *Bull. Chem. Soc. Jpn.*, **51**, 1101 (1978).
2) M. P. Coakley, L. H. Young, and R. A. Gallagher, *J. Inorg. Nucl. Chem.*, **31**, 1449 (1969).
3) R. Battistuzzi, G. Peyronel, and G. Debbi, *Z. Anorg. Allg. Chem.*, **427**, 274 (1976).
4) H. Tanaka and S. Yamada, *Bull. Chem. Soc. Jpn.*, **50**, 3259 (1977).
5) A. R. Amundsen, J. Whelan, and B. Bosnich, *J. Am. Chem. Soc.*, **99**, 6730 (1977).
6) D. E. Billing and A. E. Underhill, *J. Inorg. Nucl. Chem.*, **30**, 2147 (1968).
7) B. J. Hathaway and A. A. G. Tomlinson, *Coord. Chem. Rev.*, **5**, 1 (1970).

BULLETIN OF THE CHEMICAL SOCIETY OF JAPAN, VOL. 51 (8), 2431—2432 (1978)

The Reduction of Fluorenone Azine with Lithium Aluminum Hydride

Norio EDA,† Masahiro MINABE,* and Kazuo SUZUKI

Department of Industrial Chemistry, Faculty of Engineering, Utsunomiya University, Ishiicho, Utsunomiya 321-31

(Received November 28, 1977)

Synopsis. The title reaction yielded fluorenone 9-fluorenylhydrazone and 9,9′-azo(9,9′-bifluorenyl), accompanied by some fragmentary compounds.

The reaction of azine with phenylmagnesium bromide has been reported to give the corresponding hydrazone.[1] The reduction of fluorenone azine (**1**) has yielded 9,9′-hydrazofluorene,[2] which is of interest for its possible use in benzidine-type rearrangements. The present paper will deal with the reduction of **1**, for which some interesting findings will be reported.

The hydrogenation of **1** with hydrazine hydrate in the presence of Ru on C yielded fluorenone 9-fluorenylhydrazone (**2**) (mp 177—178 °C), but not 9,9′-hydrazofluorene (mp 174—175 °C).[2] The acetylation of **2** afforded the corresponding *N*-acetyl compound (**3**). The UV absorption maximum of **2** was observed at a longer wavelength than that of benzophenone benzhydrylhydrazone.[3]

The reduction of **1** with lithium aluminum hydride (LAH) unexpectedly gave 9,9′-azo(9,9′-bifluorenyl) (**4**) accompanied by **2**, fluorenone hydrazone (**5**),[4] 9′-fluorenimine (**6**),[2] 9-fluorenamine (**7**),[4] fluorene (**8**), and 9,9′-bifluorene (**9**). The individual reactions of these products showed that **2** cleaved into **5** and **8**, and that **5** was converted to **7** *via* **6** under similar conditions.

It can be explained that the reduction of **1** yielded **2** and 9,9′-azofluorene (**2a**) through 1,2- and 1,4-addition respectively. The hydrogen atom on the 9-carbon of **2a** is very labile; therefore, the equilibrium between **2** and **2a** lies in the direction of the **2**.[1] The formation of **4** and **9** may be assumed by the generation of the 9-fluorenyl radical from **2a**. The addition of 9-fluorenyl radicals to **1** might form **4** under mild conditions.

Experimental

All the melting points are uncorrected. The instruments used in this experiment have been described elsewhere.[5]

Hydrogenation of Azine 1. A solution of 3.56 g (10 mmol) of **1** and 12.8 ml of $H_2NNH_2 \cdot H_2O$ (80%) in 180 ml of pyridine was stirred in the presence of 520 mg of Ru on C (5%) at 70 °C for a period of 3.5 h. Upon filtration, the filtrate was concentrated to a small volume and poured into H_2O. The precipitates were separated by alumina-column chromatography (benzene) and purified by recrystallization from benzene–EtOH (1 : 1) to afford 2.86 g (80%) of **2** (mp 177—178 °C (dec)) and 0.16 g (4%) of **5** (mp 152—153 °C). UV_{max} of **2** (benzene), 350 nm (log ε 4.34); Raman spectrum, 2913 (CH), 3294 cm^{-1} (NH); NMR ($CDCl_3$) δ=5.86 (1H, d, J= 9.0 Hz), 6.67 (1H, d, disappeared by D_2O), 7.07—8.10 (16H, m); MS, *m/e*, 358 (M^+), 356, 193, 180, 165. Found: C, 86.88; H, 5.18; N, 7.96%. Calcd for $C_{26}H_{18}N_2$: C, 87.12; H, 5.06; N, 7.82%.

Acetylation of Hydrazone 2. A mixture of 3.00 g (8.4 mmol) of **2** and 2.64 g of AcCl in 40 ml of benzene was stirred at room temperature for 10 h and then refluxed for an additional 2 h to give 2.91 g (87%) of **3**: mp 173.5—174.5 °C (dec); UV_{max} (isooctane) 378 nm (log ε 3.55); IR 1642 cm^{-1} (C=O); NMR ($CDCl_3$) δ=1.91 (3H, s), 6.61—7.53 (16H, m), 7.97 (1H, s); MS, *m/e*, 400 (M^+), 358, 324, 222, 179, 165. Found: C, 83.82; H, 5.10; N, 6.82%. Calcd for $C_{28}H_{20}N_2O$: C, 83.97; H, 5.03; N, 7.00%.

A solution of **3** (0.40 g; 1 mmol) in EtOH (40 ml) was refluxed with Zn dust (1.0 g) and $CaCl_2$ (0.40 g) in H_2O (3 ml) for 3.5 h to yield 0.22 g (49%) of *N*-9-fluorenylacetamide (mp 260—262 °C (lit,[4] mp 260—261 °C)) and 0.05 g (14%) of **7** (mp 60.5—62.0 °C).

Reduction of Azine 1 with LAH. a): A suspension of 0.86 g (22.6 mmol) of LAH in 30 ml of THF was stirred, drop by drop, into a solution containing 5.00 g (14 mmol) of **1** in 200 ml of THF at room temperature for 10 min; the mixture

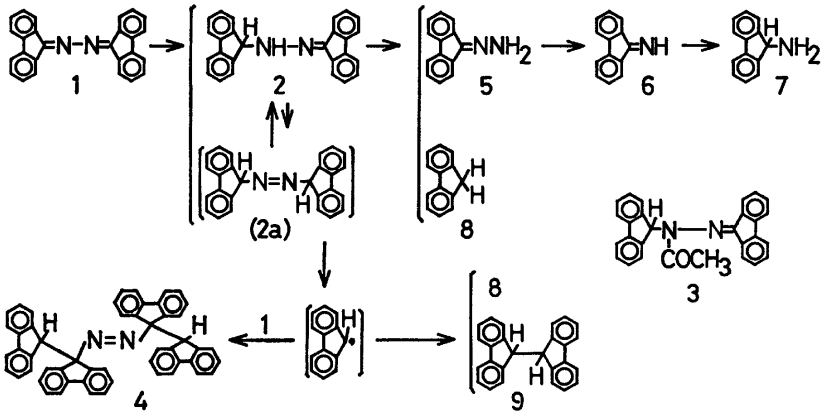

Scheme 1.

† Present address: Glaxo-Fuji Pharmaceutical Lab., Ltd., Imaichi 321-12.

was then refluxed for an additional 30 min. Upon cooling, the resulting mixture was decomposed with THF–H_2O and filtered. The filtrate was evaporated to dryness, and the residue was suspended in 50 ml of benzene and 50 ml of 4% hydrochloric acid.

The insoluble fraction was heated with the hydrochloric acid solution for 10 min and then collected. The precipitate was recrystallized from EtOH to give 0.05 g of fluorenone[6] (mp 83—84 °C). The filtrate was concentrated to a small volume to afford 0.96 g of hydrochloride of **7** (mp 220 °C (dec)).

The above-mentioned benzene solution was washed with H_2O, dried (Na_2SO_4), and chromatographed on alumina. The eluate yielded 0.86 g of **8** (mp 114—115 °C) and 0.18 g of **9** (mp 244—245 °C). Additionally, 1.40 g (28%) of **2** (mp 177—178 °C (dec)) and 0.08 g of **5** (mp 152—153 °C) were isolated from each band on the column.

b): A mixture of **1** (3.56 g; 10 mmol) and LAH (0.19 g; 5 mmol) in THF (280 ml) was stirred at room temperature for 4 h. By subsequent treatment similar to that described above, the resulting mixture afforded 0.47 g (14%) of **4**: mp 240—241 °C (dec); UV_{max} (benzene) 355 nm (log ε 4.22); IR 2923, 2852 cm^{-1} (CH); NMR ($CDCl_3$) δ=5.68 (1H, s), 6.89 (1H, s), 6.99—7.88 (32H, m). Found: C, 90.62; H, 4.92; N, 3.89%. Calcd for $C_{52}H_{34}N_2$: C, 90.93; H, 4.99; N, 4.08%.

Reduction of Azo Compound **4**. A solution of **4** (0.500 g; 0.7 mmol) in AcOH (50 ml) was refluxed with Zn dust (1.0 g) for 1 h.

When worked-up in a manner like that described above, the mixture yielded 9-amino-9,9′-bifluorene (0.169 g, mp 179—181.5 °C (dec), lit,[7] mp 181 °C (dec)), a hydrochloride of **7** (0.131 g, mp 218 °C (dec)), **8** (0.012 g, mp 112—114 °C), and **9** (0.007 g, mp 242—243 °C). IR of 9-amino-9,9′-bifluorene, 3350 (NH), 2889 cm^{-1} (CH); NMR ($CDCl_3$) δ=2.04 (2H, s), 4.74 (1H, s), 6.85—7.75 (16H, m); MS, *m/e*, 345 (M^+), 180, 165.

References

1) "The Chemistry of the Hydrazo, Azo and Azoxy Groups," ed by S. Patai, John Wiley and Sons, London (1975), Chaps. 4 and 18.

2) W. Schlenk and E. Bergmann, *Ann. Chem.*, **463**, 281 (1928).

3) S. G. Cohen and C. H. Wang, *J. Am. Chem. Soc.*, **77**, 2457 (1955).

4) T. Curtius and K. Kof, *J. Prakt. Chem.*, **86**, 113 (1912).

5) M. Minabe and K. Suzuki, *J. Org. Chem.*, **40**, 1298 (1975).

6) Imine **6** was converted quantitatively to fluorenone by hydrolyzing with dilute hydrochloric acid. The other compounds isolated by the same reaction were unchanged under these conditions.

7) L. A. Pinck and G. E. Hilbert, *J. Am. Chem. Soc.*, **68**, 377 (1946).

BULLETIN OF THE CHEMICAL SOCIETY OF JAPAN, VOL. 51 (8), 2433—2434 (1978)

Catalytic Activities of Salicylaldehyde Derivatives. V. Syntheses and Catalytic Activities of Some Trimethylammonio Derivatives of Salicylaldehyde in the Racemization of L-Glutamic Acid

Makoto ANDO* and Sakae EMOTO

The Institute of Physical and Chemical Research, Wako-shi, Saitama 351

(Received September 20, 1977)

Synopsis. (3-Formyl-2-hydroxyphenyl)trimethylammonium (**2**) and (3-formyl-4-hydroxyphenyl)trimethylammonium salts (**3**) have been prepared from the corresponding 3- and 5-nitrosalicylaldehydes *via* the 3- and 5-(dimethylamino)salicylaldehydes. The catalytic activities of **2**, **3**, and the (2-formyl-3-hydroxyphenyl)trimethylammonium salt have been studied at pH 10 and at 80 °C in the presence of copper(II) ion.

The rate constants, k_{obsd}, for the racemization of L-glutamic acid catalyzed by various 3-, 4-, and 5-substituted salicylaldehydes at pH 10 and at 80 °C in the presence of copper(II) ion have been examined. The plots of log k_{obsd} *versus* Hammett's constant, σ, for the corresponding substituent were on two straight lines: one corresponding to the 4- and 5-substituted salicylaldehydes and the other to the 3-isomers.[1] (4-Formyl-3-hydroxyphenyl)trimethylammonium bromide (**1**) was found to be the most active catalytically salicylaldehyde derivative.[1] Since the σ-value of the *m*-trimethylammonio group is larger than that of the *p*-group,[2] (3-formyl-2-hydroxyphenyl)trimethylammonium halide (**2**) and (3-formyl-4-hydroxyphenyl)trimethylammonium halide (**3**) may catalyze the racemization to a greater extent than **1**.

The syntheses of **2** and **3** and the catalytic activities of **2**, **3**, and (2-formyl-3-hydroxyphenyl)trimethylammonium salt (**4**)[3] in the racemization of L-glutamic acid under the conditions described above will be described.

Syntheses of 3- (**5**) and 5-(dimethylamino)salicylaldehydes (**6**) were carried out by the catalytic hydrogenation of the corresponding 3- (**7**)[4] and 5-nitrosalicylaldehydes (**8**)[5] over palladium on carbon in the presence of formaldehyde.[6]

For the *N*-methylation of 4-(dimethylamino)salicylaldehyde with methyl iodide to give **1**, it was necessary to add sodium hydroxide in methanol and to reflux the reaction mixture, the resulting products being a mixture of *N*-methylated and *N,O*-dimethylated compounds.[7] In the cases of **5** and **6**, however the corresponding iodides of **2** (**2a**) and **3** (**3a**) were synthesized in good yield at room temperature with neither solvent nor sodium hydroxide. Compounds **2a** and **3a** were converted into the corresponding bromides, **2b** and **3b**, in the usual way. Syntheses of the chloride of **4** (**4c**) and the fluorosulfate of **4** (**4d**) have been reported.[3]

The catalytic racemization of L-glutamic acid was carried out at pH 10 and at 80 °C in the presence of copper(II) ion.[1,7] Since the catalytic racemization follows first-order kinetics, the catalytic activity, (log α_0—log α_t)/t, should be a constant, where t is the time and α_0 and α_t are the observed optical rotations at the reaction time 0 and t min, respectively. The observed rate constant, k_{obsd}, was calculated by the following equation.

$$k_{obsd} = \frac{2.30 \times (\log \alpha_0 - \log \alpha_t)}{t}$$

TABLE 1. CATALYTIC ACTIVITY

Time min	(log α_0—log α_t) × $10^3/t$, (min^{-1})		
	2a	**3a**	**4c**
20	3.58	5.54	2.48
40	3.61	5.70	2.40
60	3.66	5.72	2.30
80	3.67	5.69	2.19
100	3.61	5.47	2.08
120	3.84	5.60	2.04
150	3.70	5.38	1.95
180	3.73	5.35	1.89
210	3.64	5.25	1.69
240	3.65	5.32	1.67
300	3.77	5.28	1.57
360	3.83	5.68	1.44

The catalytic activities of **2a** and **3a** were found to be almost constant, the catalytic activity of **4c** decreasing during the course of reaction, as shown in Table 1. The absorption peak of the reaction mixture at *ca.* 380 nm has been attributed to the chelation of the Schiff base of the catalyst and glutamic acid with copper(II) ion.[8] In the cases of **2a** and **3a**, the absorption peaks were nearly constant throughout the reaction, the absorption peak of **4c** decreasing gradually. Catalytic activity of **4c** also decreased, suggesting the decomposition of **4c**. Thus, the rate constant for the reaction catalyzed by **4c** could not be determined.

The observed rate constants for the racemization catalyzed by **2a** and **3a** were 8.5×10^{-3} and 12.7×10^{-3} min^{-1}, respectively, compared with 11.0×10^{-3} min^{-1} for **1**.[7] As expected from Hammett's constant, σ, the catalytic activity of **3a** was the largest among the salicylaldehyde derivatives examined. The catalytic activity of **2a**, having a bulky 3-substituent was considerably lower than that of **3a**, though both compounds had *m*-trimethylammonio groups with the same σ-value. Similar phenomena were also observed in various salicylaldehyde derivatives having a non-charged substituent at positions 3 and 5.[1] The catalytic activities of the 3-substituted salicylaldehydes were lowered since the phenol group's activity in the catalytic racemization was sterically hindered by the adjacent substituent at position 3.[1]

No conspicuous effect of the anion of the trimethylammonium salt was observed on the racemization yield

Table 2. Comparison of anions in the racemization yield of L-glutamic acid

	$100\times(\alpha_0-\alpha_t)/\alpha_0$, (%)	
	40 min	2 h
2a	40.8	78.7
2b	41.3	79.0
4c	18.3	42.9
4d	18.9	43.3

of L-glutamic acid (Table 2).

The plot of Hammett's constant, σ, versus log k_{obsd} for the racemization catalyzed by **3a** was on a straight line, on which the Hammett's plots for the racemization catalyzed by other 4- and 5- substituted salicylaldehydes were.[1] The Hammett's plot for **2a**, however deviates a great deal from the straight line of the Hammett's plots for the other 3-substituted salicylaldehydes.[1]

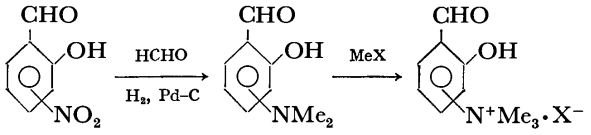

7: 3-
8: 5-

5: 3-
6: 5-

		X⁻
1	4-	Br^-
2a	3-	I^-
2b	3-	Br^-
3a	5-	I^-
3b	5-	Br^-
4c	6-	Cl^-
4d	6-	FSO_3^-

Experimental

Boiling points and melting points are uncorrected. Silica gel 60 (Merck No. 7734) was used for the column chromatography. IR spectra were measured with a Shimadzu IR-27G spectrometer.

3-(Dimethylamino)salicylaldehyde (5). A solution of 3-nitrosalicylaldehyde (**7**) (10.0 g) and a 37% formaldehyde solution (40 ml) in ethanol (250 ml) was catalytically hydrogenated over 10% Pd–C (5.0 g) at room temperature at atmospheric pressure. After 5 mol of hydrogen had been absorbed, the reaction mixture was filtered and the filtrate acidified with dilute hydrochloric acid and concentrated. The residue was dissolved in water, treated with charcoal, and neutralized with sodium hydroxide solution. The resulting mixture was extracted with ether, the extract dried ($MgSO_4$) and concentrated to give an oily residue. The residue was chromatographed on a silica-gel column (350 g). Elution with ethyl acetate–cyclohexane (1: 1 v/v) gave 6.8 g (69%) of **5**: bp 96—100 °C/3 mmHg; IR (neat) 1650 cm^{-1}. Found: C, 65.52; H, 6.54; N, 8.53%. Calcd for $C_9H_{11}NO_2$: C, 65.44; H, 6.71; N, 8.48%.

5-(Dimethylamino)salicylaldehyde (6). The compound was prepared from 5-nitrosalicylaldehyde (**8**) (10.0 g) in 71% yield following the method for the preparation of **5** except that 3.0 g of the catalyst was used: mp 33 °C; bp 123—126 °C/4 mmHg; IR (KBr) 3200 and 1660 cm^{-1}. Found: C, 65.70; H, 6.81; N, 8.60%. Calcd for $C_9H_{11}NO_2$: C, 65.44; H, 6.71; N, 8.48%.

(3-Formyl-2-hydroxyphenyl)trimethylammonium Iodide (2a). Methyl iodide (10 ml) was added immediately to **5** (2.5 g) at room temperature and the reaction mixture allowed to stand overnight at room temperature. Upon treatment with acetone, a crystalline product separated. This was recrystallized from water giving 4.1 g (90%) of **2a**: mp 198—199 °C dec; IR (KBr) 1650 cm^{-1}. Found: C, 39.07; H, 4.65; I, 41.16; N, 4.78%. Calcd for $C_{10}H_{14}INO_2$: C, 39.11; H, 4.60; I, 41.33; N, 4.56%.

(3-Formyl-4-hydroxyphenyl)trimethylammonium Iodide (3a). The compound was prepared from **6** in 88% yield following the method for the preparation of **2a**: mp 228—229 °C dec; IR (KBr) 1700 cm^{-1}. Found: C, 39.10; H, 4.63; I, 41.22; N, 4.33%. Calcd for $C_{10}H_{14}INO_2$: C, 39.11; H, 4.60; I, 41.33; N, 4.56%.

(3-Formyl-2-hydroxyphenyl)trimethylammonium Bromide (2b) and (3-Formyl-4-hydroxyphenyl)trimethylammonium Bromide (3b). Compounds **2a** and **3a** were converted in the usual way with silver bromide at room temperature into the corresponding **2b** and **3b** in 90% yields. **2b**: mp 199—200 °C dec. Found: C, 46.23; H, 5.47; Br, 30.58; N, 5.35%. Calcd for $C_{10}H_{14}BrNO_2$: C, 46.17; H, 5.43; Br, 30.72; N, 5.39%. **3b**: mp >300 °C. Found: C, 46.11: H, 5.47; Br, 30.73; N, 5.46%. Calcd for $C_{10}H_{14}BrNO_2$; C, 46.17; H, 5.43; Br, 30.72; N, 5.39%.

Procedure of Racemization. Racemization was carried out as described previously.[7]

The authors wish to thank Dr. Haruo Homma and his co-workers of this Institute for the elementary analyses. The work was partially supported by a Research Grant for Biosciences given by this Institute.

References

1) M. Ando and S. Emoto, *Bull. Chem. Soc. Jpn.*, **42**, 2628 (1969).
2) D. H. Mc Daniel and H. C. Brown, *J. Org. Chem.*, **23**, 420 (1958).
3) Part IV of this series: M. Ando and S. Emoto, *Bull. Chem. Soc. Jpn.*, **47**, 501 (1974).
4) H. Ichibagase and S. Terada, *Yakugaku Zasshi*, **72**, 878 (1952).
5) C. C. Hach, L. M. Liggett, and H. Diehl, *Iowa State Coll. J. Sci.*, **21**, 316 (1974); *Chem. Abstr.*, **42**, 1240 g (1948).
6) V. H. Ingram, *J. Chem. Soc.*, **1950**, 2247.
7) M. Ando and S. Emoto, *Bull. Chem. Soc. Jpn.*, **42**, 2624 (1969).
8) A. Nakahara, *Bull. Chem. Soc. Jpn.*, **32**, 1195 (1959).

BULLETIN OF THE CHEMICAL SOCIETY OF JAPAN, VOL. 51 (8), 2435—2436 (1978)

Catalytic Activities of Salicylaldehyde Derivatives. VI.[1] Syntheses of Some Dimethylsulfonio Derivatives of Salicylaldehyde

Makoto ANDO* and Sakae EMOTO

The Institute of Physical and Chemical Research, Wako-shi, Saitama 351

(Received September 20, 1977)

Synopsis. 3-, 4-, and 5-dimethylsulfonio derivatives of salicylaldehyde have been prepared from the corresponding 6-, 5-, and 4-bromo-2-methylanisoles *via* the bromo-2-methoxybenzylidene dibromides, bromo-*o*-anisaldehyde diethyl acetals, methylthio-*o*-anisaldehydes, and (methylthio)salicylaldehydes. 4-Methylthio-*o*-anisaldehyde has also been prepared from 2-bromo-5-(methylthio)anisole.

The racemization of L-glutamic acid catalyzed by various salicylaldehyde derivatives at pH 10 and at 80 °C in the presence of copper(II) ion has been examined. The Hammett's plots for the racemization catalyzed by 4- and 5-substituted salicylaldehydes *versus* the Hammett's constant, σ, were on a straight line.[2] Since the σ-values of the dimethylsulfonio groups are the largest among the σ-values obtained,[3] the dimethylsulfonio derivatives of salicylaldehyde appear to be more active catalysts than the known salicylaldehyde derivatives. Syntheses of 3- (**1**), 4- (**2**), and 5-dimethylsulfonio derivatives of salicylaldehyde (**3**) are described.

Treatment of 6- (**4**),[4] 5- (**5**),[5] and 4-bromo-2-methylanisoles (**6**)[6] with bromine gave the corresponding 3- (**7**), 4- (**8**), and 5-bromo-2-methoxybenzylidene dibromides (**9**), which were converted into the corresponding 3- (**10**), 4- (**11**), and 5-bromo-*o*-anisaldehyde diethyl acetals (**12**) with sodium ethoxide. The corresponding 3- (**13**), 4- (**14**), and 5-methylthio-*o*-anisaldehydes (**15**) were synthesized from **10**, **11**, and **12** by the Grignard reaction with dimethyl disulfide and subsequent hydrolysis. In the synthesis of **14**[7] the overall yield was remarkably improved by the Grignard reaction of 2-bromo-5-(methylthio)anisole (**16**)[8] with diethyl phenyl orthoformate.[9]

Demethylation of the methoxyl group in **13** and **15** with hydrogen bromide in acetic acid gave the corresponding 3- (**17**) and 5-(methylthio)salicylaldehydes (**19**). The reaction of **14** with the same reagents gave only a resinous product. Compound **14** was consequently treated with boron tribromide in dichloromethane in the usual way but no demethylation took place. The desired 4-(methylthio)salicylaldehyde (**18**) was obtained when the reaction was carried out in benzene under reflux. Compounds **18** and **19** were *S*-methylated with methyl *p*-toluenesulfonate to give the corresponding dimethylsulfonium *p*-toluenesulfonates, **2a** and **3a**. No *S*-methylation of **17** took place with the same reagent. The desired dimethylsulfonium fluorosulfate (**1b**) was obtained by treatment of **17** with methyl fluorosulfate.

Although these dimethylsulfonium salts are unstable at pH 10 and at 80 °C, the catalytic activities of the dimethylsulfonium salts in the racemization of L-glutamic acid are apparently larger than the salicylaldehyde derivatives examined in the initial stage of reaction.

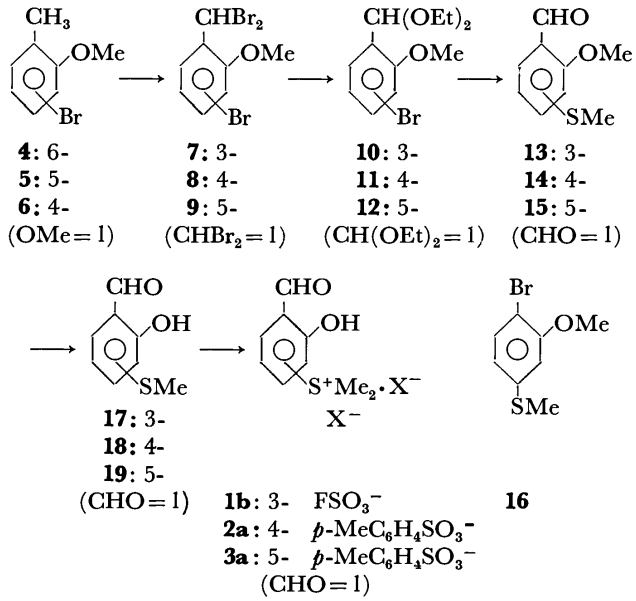

4: 6- **5**: 5- **6**: 4- (OMe=1)

7: 3- **8**: 4- **9**: 5- ($CHBr_2$=1)

10: 3- **11**: 4- **12**: 5- ($CH(OEt)_2$=1)

13: 3- **14**: 4- **15**: 5- (CHO=1)

17: 3- **18**: 4- **19**: 5- (CHO=1)

1b: 3- FSO_3^-
2a: 4- *p*-$MeC_6H_4SO_3^-$
3a: 5- *p*-$MeC_6H_4SO_3^-$
(CHO=1)

16

Experimental

Melting points and boiling points are uncorrected. IR spectra were recorded on a Shimadzu IR-27G instrument. Typical examples of syntheses of the intermediates are described. Reaction conditions, physical properties, and analytical data are given in Table 1.

3-Bromo-2-methoxybenzylidene Dibromide (7). Under illumination with a tungsten lamp, a solution of bromine (167 g) in carbon tetrachloride (100 ml) was added dropwise to a solution of 6-bromo-2-methylanisole (**4**) (99.3 g) in carbon tetrachloride (400 ml) with stirring over a period of 2 h under reflux. After a further 3 h reflux, the mixture was fractionally distilled.

3-Bromo-o-anisaldehyde Diethyl Acetal (10). To a solution of sodium (12.0 g) in absolute ethanol (350 ml) was added dropwise **7** (94.0 g) over a period of 30 min at room temperature with stirring. The mixture was refluxed and the solvent removed. The residue was extracted with water and ether and the ethereal extract dried ($MgSO_4$) and distilled.

3-Methylthio-o-anisaldehyde (13). Under a nitrogen atmosphere, a solution of dimethyl disulfide (20.8 g) in dry THF (100 ml) was added with stirring to a Grignard reagent prepared from a solution of **10** (63.8 g) in dry THF (500 ml) and magnesium (5.4 g), over a period of 20 min at room temperature and then refluxed for 2 h. The mixture was treated with a 20% NH_4Cl solution (1 l) below 20 °C and extracted with ether. The extract was dried ($MgSO_4$) and concentrated. To the residue was added 2 M sulfuric acid (500 ml) and the resulting mixture steam-distilled. The ethereal extract of the distillate was washed with aqueous NaOH and water successively and dried ($MgSO_4$). Re-

Table 1. Prepn and characteristics of the intermediates

Compd	Reaction time (h)	Yield (%)	Bp (°C/mmHg) (mp (°C))	IR (cm^{-1})	Found (%) C	H	Br or S	Calcd (%)
7	3	93	138—140/3		27.03	1.87	66.32	C, 26.77
8	2	74	144—148/4 (38—39)		27.04	1.98	66.37	H, 1.97
9	2	85[a]	(83—84)		26.94	1.98	66.74	Br, 66.80
10	48	71	119—122/2		49.56	5.56	27.95	C, 49.83
11	1	92	131—136/2		49.81	5.71	27.71	H, 5.93
12	4	95	131—133/3		49.75	6.02	27.85	Br, 27.63
13	2	68	(73—74)	1690[b]	59.36	5.37	17.50	C, 59.33
14	5	48[c,d]	(65)[e]	1670[b]	59.19	5.63	17.77	H, 5.53
15	2	70	136—138/3	1690[f]	58.71	5.34	16.99	S, 17.60
17	1	86	119—120/3	1670[f]	57.18	4.80	19.04	C, 57.12
18	—[g]	59[d]	(51)	1650[b]	57.35	4.68	19.04	H, 4.79
19	2	41	114—118/4	1660[f]	56.95	4.94	18.90	S, 19.06

a) Recrystd from *n*-BuOH. b) KBr disc. c) Prepd from **11**. d) Purified by a column of silica gel. e) Lit,[7] mp 63 °C; prepd by an alternative method. f) Neat. g) See Exptl.

moval of the solvent gave crude **13**, which was recrystallized from methanol.

3-(Methylthio)salicylaldehyde (17). A mixture of **13** (10.0 g), anhydrous hydrogen bromide (26.5 g) in acetic acid (100 ml), and a 48% hydrobromic acid (20 ml) was refluxed for 1 h, concentrated, and extracted with water and ether. The ethereal layer was extracted with NaOH solution and the aqueous layer acidified with hydrochloric acid. The resulting oily product was extracted with ether, dried ($MgSO_4$), and fractionally distilled.

(3-Formyl-2-hydroxyphenyl)dimethylsulfonium Fluorosulfate (1b). A solution of methyl fluorosulfate (6.7 g) in dry benzene (10 ml) was added with stirring to a solution of **17** (10.0 g) in dry benzene (50 ml) at room temperature over a period of 10 min. Stirring was continuted for another 1 h and the mixture allowed to stand overnight. The resulting precipitates were recrystallized from methanol giving 6.1 g (36%) of **1b**: mp 137—139 °C; IR (KBr) 3440 and 1650 cm^{-1}. Found: C, 38.22; H, 3.82; S, 22.37%. Calcd for $C_9H_{11}FO_5S_2$: C, 38.29; H, 3.93; S, 22.71%.

4-Methylthio-o-anisaldehyde (14) from 2-Bromo-5-(methylthio)-anisole (16). Under a nitrogen atmosphere, diethyl phenyl orthoformate (5.9 g) was added to a Grignard reagent prepared from a solution of **16** (7.0 g) in dry THF (100 ml) and magnesium (730 mg), over a period of 10 min at room temperature with stirring. The mixture was refluxed for 3 h and worked up in the usual way giving 4.2 g (77%) of **14**: mp 65 °C.

4-(Methylthio)salicylaldehyde (18). A solution of boron tribromide (15.1 g) in dry benzene (50 ml) was added to a stirred solution of **14** (11.0 g) in dry benzene (200 ml) over a period of 20 min in an ice bath. The mixture was stirred for 30 min at room temperature and then refluxed for 5 h. After removal of the solvent, ethanol (200 ml) and sodium acetate trihydrate (10.0 g) in water (30 ml) were added successively to the residue, refluxed for 2 h, and worked up in the usual way.

(4-Formyl-3-hydroxyphenyl)dimethylsulfonium p-*Toluenesulfonate (2a).* A mixture of methyl *p*-toluenesulfonate (2.0 ml) and **18** (1.0 g) was heated at 100 °C for 8 h and cooled. Ethyl acetate (5 ml) was added to the cold mixture. The resulting precipitates were recrystallized from methanol–acetone affording 0.7 g (33%) of **2a**: mp 146—147 °C; IR (KBr) 3450, 1660, 1210, and 1170 cm^{-1}. Found: C, 54.45; H, 5.04; S, 18.02%. Calcd for $C_{16}H_{18}O_5S_2$: C, 54.22; H, 5.12; S, 18.10%.

(3-Formyl-4-hydroxyphenyl)dimethylsulfonium p-*Toluenesulfonate (3a).* A mixture of **19** (5.0 g) and methyl *p*-toluenesulfonate (10 ml) was heated at 100 °C for 3 h and then cooled. Acetone (10 ml) was added to the mixture. The resulting precipitates were 9.6 g (91%) of **3a**: mp 178—179 °C; IR (KBr) 1670, 1200, and 1170 cm^{-1}. Found: C, 54.28; H, 5.20; S, 18.00%. Calcd for $C_{16}O_{18}O_5S_2$: C, 54.22; H, 5.12; S, 18.10%.

The authors wish to express their thanks to Dr. Haruo Homma and his staff of this Institute for the elementary analyses. The work was partially supported by a Research Grant for Biosciences given by this Institute.

References

1) Part V of this series: M. Ando and S. Emoto, *Bull. Chem. Soc. Jpn.*, **51**, 2433 (1978).
2) M. Ando and S. Emoto, *Bull. Chem. Soc. Jpn.*, **42**, 2628 (1969).
3) D. H. Mc Daniel and H. C. Brown, *J. Org. Chem.*, **23**, 420 (1958).
4) R. A. Benkeser and W. E. Buting, *J. Am. Chem. Soc.*, **74**, 3011 (1973).
5) J. J. Brown and G. T. Newbold, *J. Chem. Soc.*, **1953**, 1285.
6) M. Tomita, *Yakugaku Zasshi*, **57**, 689 (1937).
7) A. Martani and O. Roussel, *Ann. Chim. (Rome)*, **57**, 121 (1967); *Chem. Abstr.*, **67**, 43616f (1967).
8) A. Arcoria and G. Scarlata, *Ann. Chim. (Rome)*, **54**, 139 (1964); *Chem. Abstr.*, **61**, 11919h (1964).
9) H. Stetter and E. Reske, *Chem. Ber.*, **103**, 643 (1970).

BULLETIN OF THE CHEMICAL SOCIETY OF JAPAN, VOL. 51 (8), 2437—2438 (1978)

Catalytic Activities of Salicylaldehyde Derivatives. VII. Synthesis and Catalytic Activity of (2-Formyl-3-hydroxyphenyl)dimethylsulfonium Salt in the Racemization of L-Glutamic Acid

Makoto ANDO* and Sakae EMOTO

The Institute of Physical and Chemical Research, Wako-shi, Saitama 351

(Received January 10, 1978)

Synopsis. The title compound (**1**) was prepared from 6-nitro-*o*-anisidine *via* 2-bromo-*m*-anisidine, 2-bromo-3-(methylthio)anisole, 6-methylthio-*o*-anislaldehyde, and 6-(methylthio)salicylaldehyde. Compound **1** was found to be the most inactive catalyst among the dimethylsulfonio derivatives of salicylaldehyde, but the most active catalyst among the other salicylaldehyde derivatives examined in the racemization of L-glutamic acid at pH 10 and at 80 °C in the presence of copper(II) ion in the initial stage of the reaction.

Since salicylaldehyde derivatives having a dimethylsulfonio group at 3-, 4-, and 5-positions have been found to be active catalysts in the racemization of L-glutamic acid,[1] 6-isomer (**1**) may also actively catalyze the racemization.

Here we describe a synthesis of **1** from 6-nitro-*o*-anisidine (**2**)[2,3] and the catalytic activity of **1** in the racemization of L-glutamic acid. 2-Bromo-3-nitroanisole (**3**) was prepared from **2** in the usual way. Most of the reagents tested for the reduction of **3** to give 2-bromo-*m*-anisidine (**4**) brought about undesirable debromination. With hydrazine hydrate over Raney nickel W-2,[4] however hydrochloride of **4** (**4a**) was obtained in a good yield. In the usual way, **4a** was converted into 2-bromo-3-methoxybenzenethiol (**5**). *S*-Methylation of **5** afforded 2-bromo-3-(methylthio)anisole (**6**), which gave 6-methylthio-*o*-anisaldehyde (**7**) by the Grignard reaction with diethyl phenyl orthoformate. *O*-Demethylation of **7** to 6-(methylthio)salicylaldehyde (**8**) was successful with boron tribromide in dichloromethane, but not with hydrogen bromide in acetic acid. Although *S*-methylation of **8** was unsuccessful with methyl *p*-toluenesulfonate, methyl fluorosulfate gave the fluorosulfate of **1** (**1a**) which was converted into the chloride (**1b**) *via* the picrate (**1c**).

Following the earlier work,[5,6] the racemization of L-glutamic acid catalyzed by **1b** was carried out at 80 °C and at pH 10 in the presence of copper(II) ion.

As Table 1 shows, the catalytic activity of **1b** decreased gradually during the course of the reaction by its decomposition, similarly to the other dimethylsulfonio derivatives of salicylaldehyde.[1] At an early stage of the reaction, however **1b** was found to be a more active catalyst than the trimethylammonio derivatives of salicylaldehyde,[5,6] but a less active catalyst than the other dimethylsulfonio derivatives of salicylaldehyde.[1]

Table 1. Racemization yield and catalytic activity catalyzed by **1b**

Time min	Racemization yield $100\,(\alpha_0-\alpha_t)/\alpha_0$, (%)	Catalytic activity $(\log \alpha_0/\alpha_t)/t$, ($min^{-1}$)
20	22.6	5.57×10^{-3}
40	34.0	4.50
60	40.6	3.77
120	55.3	2.92
240	69.7	2.16
480	87.0	1.85

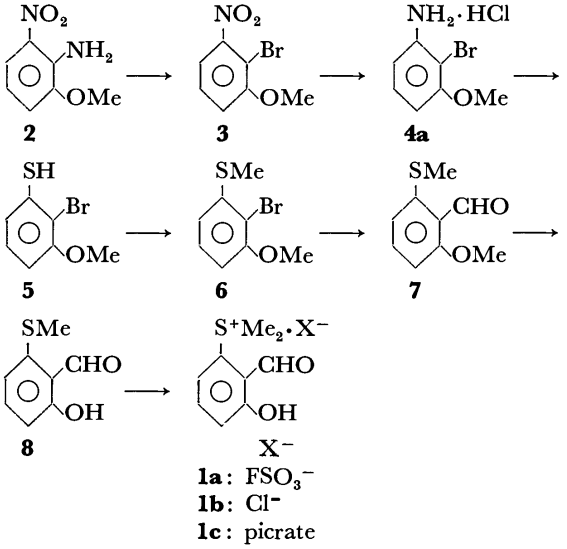

Experimental

All the melting points and boiling point are uncorrected. Silica gel 60 (Merck No. 7734) was used for column chromatography. UV, IR, and PMR spectra were recorded on a Hitachi 124, a Shimadzu IR-27G, and a Varian HA-100D spectrometer, respectively.

2-Bromo-3-nitroanisole (3). A solution of 6-nitro-*o*-anisidine (**2**) (56.0 g) in concentrated sulfuric acid (230 ml) was diluted with water (460 ml) and diazotized with $NaNO_2$ (25.0 g) in water (40 ml). The solution was added to a mixture of CuBr (27.0 g), 48% HBr (60 ml), and water (340 ml) with stirring at 60 °C over a period of 1 h and then refluxed for 1 h. The resulting precipitate was recrystallized from ethyl acetate, giving 66.7 g of **3**. Additional **3** in the filtrate was recovered by passing it through a column of silica gel (360 g). Elution with benzene gave 2.6 g of **3** (total yield, 90%): mp 93—94 °C; IR (KBr) 1530 and 1280 cm^{-1}. Found: C, 36.36; H, 2.69; Br, 34.34; N, 5.89%. Calcd for $C_7H_6BrNO_3$: C, 36.24; H, 2.61; Br, 34.44; N, 6.04%.

2-Bromo-m-anisidine Hydrochloride (4a). To a mixture of **3** (78.4 g), Raney Ni W-2 (6.0 ml), and methanol (1.5 l), a solution of 100% hydrazine hydrate (42.3 g) in methanol (50 ml) was added over a period of 90 min under reflux with stirring. After stirring for another 2 h, the cold mixture was filtered and the filtrate was concentrated to a syrup and extracted with benzene and NaOH solution. The concentrated benzene layer was extracted with hot 1 M HCl. The

extract was treated with charcoal and concentrated to give 74.1 g of **4a** (92%): mp 201—202 °C dec. Found: C, 35.37; H, 3.90; Br+Cl, 48.10; N, 5.86%. Calcd for $C_7H_9BrClNO$: C, 35.25; H, 3.80; Br+Cl, 48.36; N, 5.87%.

2-Bromo-3-methoxybenzenethiol (5). A solution of diazonium salt prepared from **4a** (56.4 g) in 2 M HCl (300 ml) with $NaNO_2$ (16.5 g) in water (30 ml) was adjusted to pH 5 by addition of crystalline sodium acetate (60 g) and then added to a solution of potassium *O*-ethyl dithiocarbonate (76.0 g) in water (80 ml) at 60 °C over a period of 30 min with stirring. After being kept at 80 °C for 2 h, the mixture was extracted with ethyl acetate and the ethyl acetate layer was evaporated to a syrup. A mixture of the syrup and NaOH (30.0 g) in 90% aqueous ethanol (300 ml) was refluxed for 6 h and then extracted with ethyl acetate and water. The aqueous layer was acidified with HCl and the resulting oily product was extracted with ethyl acetate. The extract was dried ($MgSO_4$) and distilled under nitrogen atmosphere to give 22.3 g of **5** (42%) and some polymerized residue: mp 36—37 °C; bp 113 °C/3 mmHg. Found: C, 38.28; H, 2.97; Br, 36.59; S, 14.75%. Calcd for C_7H_7BrOS: C, 38.73; H, 3.22; Br, 36.47; S, 14.64%.

2-Bromo-3-(methylthio)anisole (6). To a stirred solution of distilled **5** (22.1 g) and NaOH (20.0 g) in water (200 ml), dimethyl sulfate (25 ml) was added over a period of 20 min at 70 °C and the mixture was then refluxed for 2 h. The resulting precipitate was recrystallized from methanol to give 22.1 g of **6** (94%). The use of undistilled **5** was better in the overall yield (59% based on **4a**) than the use of purified **5**: mp 73 °C; IR (KBr) 1590 and 1270 cm^{-1}. Found: C, 41.49; H, 3.75; Br, 34.53; S, 13.74%. Calcd for C_8H_9BrOS: C, 41.22; H, 3.89; Br, 34.37; S, 13.75%.

6-Methylthio-o-anisaldehyde (7). To a Grignard reagent of **6** (16.3 g) in dry THF (160 ml) with magnesium (1.7 g), diethyl phenyl orthoformate (15.2 g) in dry THF (30 ml) was added at room temperature over a period of 10 min with stirring and refluxed for 20 h. The cooled mixture was treated with a 20% NH_4Cl solution (120 ml) and extracted with benzene. The extract was dried ($MgSO_4$), concentrated, and hydrolyzed in a hot ethanol (150 ml)–2.4 M HCl (100 ml). Recrystallization of the resulting precipitate from methanol gave 9.7 g of **7**. The mother liquor was concentrated and packed on a column of silica gel (75 g). Elution with benzene gave 0.5 g of **7** (total yield, 81%): mp 98 °C; UV_{max} (MeOH) 372 (ε 19000), 298 (ε 24900), and 236 nm (ε 74600); IR (KBr) 1660, 1590, and 1270 cm^{-1}; PMR ($CDCl_3$) δ=10.56 (1H, s, CHO), 3.92 (3H, s, OCH_3), and 2.42 (3H, s, SCH_3). Found: C, 59.42; H, 5.42; S, 17.53%. Calcd for $C_9H_{10}O_2S$: C, 59.33; H, 5.53; S, 17.60%.

6-(Methylthio)salicylaldehyde (8). A solution of boron tribromide (25.0 g) in dry dichloromethane (20 ml) was added with stirring to a solution of **7** (16.5 g) in the same solvent (330 ml) over a period of 20 min at −55—−65 °C. The mixture was kept for another 30 min at the same temperature and then at room temperature for 2 h and concentrated below 30 °C. To the residue ethanol (300 ml) and then sodium acetate trihydrate (16.5 g) in water (80 ml) were added. The mixture was refluxed for 2 h, concentrated, and extracted with benzene and water. From the benzene layer, which was washed with NaOH solution and then with water, 1.0 g of **7** was recovered. The aqueous layer was acidified with HCl and extracted with benzene. The extract was dried ($MgSO_4$) and concentrated, giving crude **8** which was recrystallized from methanol to give 8.7 g of **8**. The mother liquors of **8** were concentrated and chromatographed on a silica-gel column (250 g). Elution with benzene gave 2.6 g of **8** (total yield, 74%): mp 71—72 °C; UV_{max} (MeOH) 353 (ε 23800), 296 (ε 27000), and 237 nm (ε 99000); IR (KBr) 1650 and 1450 cm^{-1}; PMR ($CDCl_3$) δ=11.94 (1H, s, OH), 10.48 (1H, s, CHO), and 2.52 (3H, s, SCH_3). Found: C, 56.89; H, 4.56; S, 18.99%. Calcd for $C_8H_8O_2S$: C, 57.12; H, 4.79; S, 19.06%.

(2-Formyl-3-hydroxyphenyl)dimethylsulfonium Picrate (1c) and Chloride (1b). A solution of methyl fluorosulfate (5.7 g) and **8** (8.4 g) in dry dichloromethane (50 ml) was stirred for 1 h and allowed to stand for 4 days at room temperature. The resulting precipitate of crude fluorosulfate (**1a**) (mp 158—162 °C) was dissolved in methanol, treated with picric acid (11.0 g), and concentrated to give crude **1c**. Its recrystallization from methanol–acetone gave 9.7 g of **1c** (49%): mp 181—182 °C. Found: C, 43.67; H, 3.31; N, 10.00; S, 7.72%. Calcd for $C_{15}H_{13}N_3O_9S$: C, 43.80; H, 3.19; N, 10.22; S, 7.79%.

In the usual way, **1b** was prepared from **1c** in a 84% yield. It was slightly soluble in water and methanol: mp 173—174 °C dec; UV_{max} (H_2O) 380 (shoulder, ε 5500), 332 (ε 20900), and 255 nm (ε 21300); IR (KBr) 1670 cm^{-1}. Found: C, 49.25; H, 5.05; Cl, 15.98; S, 14.70%. Calcd for $C_9H_{11}ClO_2S$: C, 49.43; H, 5.07; Cl, 16.21; S, 14.66%.

Procedure of the Racemization. The racemization was carried out as described previously.[5]

The authors wish to thank Dr. Haruo Homma of this Institute and his staff for the elementary analyses and Mr. Jun Uzawa and Mrs. Tamiko Chijimatsu of this Institute for the measurements of PMR spectra. The work was partially supported by a Research Grant for Biosciences given by this Institute.

References

1) Part VI of this series: M. Ando and S. Emoto, *Bull. Chem. Soc. Jpn.*, **51**, 2435 (1978).
2) H. van Erp, *J. Prakt. Chem.*, [2] **127**, 20 (1930).
3) N. E. Sbarbati, *J. Org. Chem.*, **30**, 3365 (1965).
4) B. E. Leggetter and R. K. Brown, *Can. J. Chem.*, **38**, 2363 (1960).
5) M. Ando and S. Emoto, *Bull. Chem. Soc. Jpn.*, **42**, 2624 (1969).
6) M. Ando and S. Emoto, *Bull. Chem. Soc. Jpn.*, **51**, 2433 (1978).

BULLETIN OF THE CHEMICAL SOCIETY OF JAPAN, VOL. 51 (8), 2439—2440 (1978)

Oxidation of Thujopsene with Thallium Triacetate in Acetic Acid

Haruo SEKIZAKI,* Masaaki ITO, and Shoji INOUE**

Chemistry Laboratory, Department of General Education, Higashi Nippon Gakuen University, Onbetsu-cho, Hokkaido 088-01

***Faculty of Pharmacy, Meijo University, Tenpaku-ku, Nagoya 468*

(Received January 17, 1978)

Synopsis. Oxidation of thujopsene with thallium triacetate in acetic acid at room temperature gave a stereospecifically ring-contracted ketone (**3**) in 76% yield, whereas oxidation at 50 °C afforded an allylic oxidation product in 72% yield. The configuration of **3** was estimated by the NMR spectrum of a compound derived from it.

Oxidation of thujopsene (**1a**) with metal acetate was first described in 1959 by Nagahama *et al.*,[1] who used lead tetraacetate to try to determine the partial structure of **1a**. Recently, one of us[2] reported that oxidation of **1a** with mercury diacetate gave a mixture of allylic oxidation products, (**1b**) and (**1c**), and an acid-catalyzed isomerization-acetoxylation product (**2**).

This report describes some interesting results about the oxidation of thujopsene (**1a**) with thallium triacetate.[3] We have found that oxidation of **1a** with thallium triacetate in acetic acid at room temperature gave a stereospecifically ring-contracted product (**3**) and **1b** in 76 and 10% yield respectively, whereas, oxidation of **1a** at 50 °C gave mainly the product (**1b**) (72%), resulting from allylic oxidation of **1a**, together with the ketone **3** (8%). The product (**3**) was already reported by Nagahama *et al.*,[1] but the configuration of the acetyl group in **3** has not been reported.

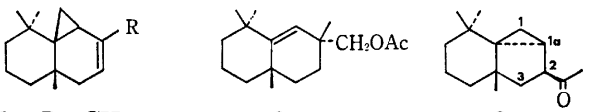

1a: R=CH_3
1b: R=CH_2OAc
1c: R=CHO

2 **3**

We estimated the relative configuration of the ketone **3** as follows. Alcohols, **5** (β-OH) and **7** (α-OH), were derived from **3** according to the method shown in Scheme 1. The structures of **1b**, **3**, **4**, **5**, and **6** were identical with authentic specimens (mp, IR).[1,2]

The NMR spectrum of C_2–H in the ketone **3** shows a doublet of doublets of doublets ($J_{C_2H-C_{1a}H}$=10.0, $J_{C_2H-C_{3\beta}H}$=10.0, and $J_{C_2H-C_{3\alpha}H}$=4.0 Hz) at 3.07 ppm. On the other hand, the spectrum of C_2–H in the β-hydroxy alcohol **5** shows a doublet of doublets of doublets ($J_{C_2H-C_{1a}H}$=8.0, $J_{C_2H-C_{3\beta}H}$=8.0, and $J_{C_2H-C_{3\beta}H}$=1.8 Hz) at 4.46 ppm, but that of C_2–H in the α-hydroxy alcohol **7** shows a doublet of doublets ($J_{C_2H-C_{3\beta}H}$=6.0, and $J_{C_2H-C_{3\beta}H}$=6.0 Hz) at 4.11 ppm. In these results, the spectrum of the C_2–H proton in **3** showed a pattern for the C_2–H which was in close agreement with the corresponding proton observed in β-hydroxy alcohol **5**, and therefore the acetyl group of **3** was assigned to be β.

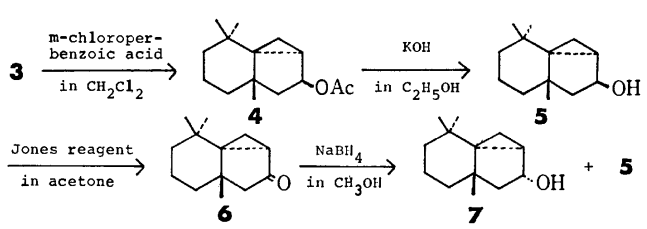

Scheme 1.

Oxidation of thujopsene (**1a**) with mercury diacetate[2] gave two allylic oxidation products, **1b** and **1c**, in 14.4 and 11.1% yield respectively, together with the other product **2** (5.4%). With lead tetraacetate,[1] **1a** was oxidized to the ring-contracted ketone **3** in 35% yield. However, with thallium triacetate, the ring-contracted ketone **3** was obtained in higher yield at room temperature and the acetate **1b** was obtained in higher yield at 50 °C on allylic oxidation. It is interesting that oxidation of thujopsene (**1a**) with thallium triacetate gives different products up to reaction temperature. The extention of oxythallation reaction to other compounds including allyl methyl moiety in their molecules would be valuable.

Experimental

The melting points were determined on a Yanagimoto micro melting point apparatus and uncorrected. The NMR spectra were recorded on a JEOL PMX-60 spectrometer at 60 MHz and on a JEOL PS-100 spectrometer at 100 MHz, using Me_4Si as an internal standard.

The IR spectra were determined on a Shimadzu IR-400 spectrometer.

Oxidation of Thujopsene (1a) at Room Temperature. To a stirred solution of thallium triacetate (1.19 g, 5 mmol) in acetic acid (10 ml) was added dropwise a solution of **1a** (1.02 g, 5 mmol) in acetic acid (20 ml) under nitrogen atmosphere at room temperature in 30 min. The mixture was stirred for 10 h, then poured into ice-water and extracted with ether. The extract was washed with aqueous $NaHCO_3$ solution, water, dried (Na_2SO_4), and evaporated to give an oily residue (1.32 g). The products were separated by column chromatography using silica gel. Elution with benzene gave **3** (791 mg) and **1b** (130 mg) as colorless liquids. The pure samples of **3** and **1b** were obtained by distillation under reduced pressure. **3**: bp 127—129 °C/7 mmHg. NMR ($CDCl_3$) 0.75 (s, 3, CH_3), 1.15 (s, 3, CH_3), 1.13 (s, 3, CH_3), 2.20 (s, 3, Ac), and 3.07 (ddd, 1, J=10.0, 10.0, and 4.0 Hz, C_2–H); 2,4-dinitrophenylhydrazone: mp 168—169 °C (lit,[1] mp 170—170.5 °C). Found: C, 62.11; H, 7.05; N, 13.99%. Calcd for $C_{19}H_{24}O_4N_4$: C, 62.98; H, 7.05; N, 13.99%. **1b**: bp 148—150 °C/6 mmHg.

Oxidation of Thujopsene (1a) at 50 °C. To a stirred solution of **1a** (1.02 g, 5 mmol) in acetic acid (30 ml), kept at 50 °C, was added thallium triacetate (1.91 g, 5 mmol) in portions under nitrogen atmosphere over 30 min. The mix-

ture was stirred for 7 h at the same temperature, then the same work up as that mentioned above gave **1b** (997 mg) and **3** (83 mg).

Oxidation of ***3***. To a stirred solution of **3** (2.20 g, 10 mmol) in dichloromethane (20 ml), kept at 7 °C, was added dropwise a solution of *m*-chloroperbenzoic acid (2.60 g, 11 mmol) in dichloromethane (20 ml) in 1 h. The mixture was stirred at room temperature overnight, then the usual work up gave crude **4** (2.61 g), which was chromatographed on a silica gel column. Elution with benzene gave **4** (2.28 g): colorless liquid; NMR ($CDCl_3$) 0.56 (s, 3, CH_3), 1.01 (s, 3, CH_3), 1.06 (s, 3, CH_3), 2.01 (s, 3, OAc), and 5.21 (m, 1, olefinic proton).

Hydrolysis of ***4***. The compound **4** (2.28 g) was hydrolyzed in alcohol (20 ml) with potassium hydroxide (860 mg) for 3 h. After the usual workup a crude product (2.23 g) was obtained. Sublimation under a reduced pressure gave **5** (1.91 g): mp 82—83 °C (lit,[1] mp 78 °C; NMR ($CDCl_3$) 0.51 (s, 3, CH_3), 1.01 (s, 3, CH_3), 1.05 (s, 3, CH_3), and 4.46 (ddd, 1, J=8.0, 8.0, and 1.8 Hz, C_2–H).

Oxidation of ***5***. The compound **5** (776.8 mg) was oxidized in acetone (10 ml) with the Jones reagent (8N, 1.1 ml) at room temperature for 2 h. The mixture was evaporated and ice-cooled water was poured into the resulting residue, which was then extracted with ether. The extract was washed with water, dried (Na_2SO_4), and evaporated to give crude crystals (778.2 mg). Recrystallization from hexane gave pure **6** (761.8 mg): mp 126—127 °C (lit,[1] mp 118—121 °C); NMR ($CDCl_3$) 0.66 (s, 3, CH_3), 1.13 (s, 3, CH_3), and 1.21 (s, 3, CH_3).

Reduction of ***6***. The compound **6** (407.8 mg) was reduced in methanol (10 ml) with sodium borohydride (200 mg) at 15 °C for 2 h. The usual workup gave a crude product (414.7 mg), which was chromatographed on a silica gel column. Elution with benzene gave α-hydroxy alcohol **7** (267.8 mg) and β-hydroxy alcohol **5** (100.7 mg). **7**: mp 107—108 °C (hexane); IR (KBr) 3350 (OH) and 3050 (cyclopropyl) cm^{-1}; NMR ($CDCl_3$) 0.60 (s, 3, CH_3), 1.05 (s, 6, CH_3), and 4.11 (dd, 1, J=6.0 and 6.0 Hz, C_2–H); Found: C, 79.17; H, 11.66%. Calcd for $C_{13}O_{20}O$: C, 80.35; H, 11.96%.

The authors are grateful to Takasago Perfumery Co. Ltd. for giving us the sample of crude thujopsene.

References

1) S. Nagahama, H. Kobayashi, and S. Akiyoshi, *Bull. Chem. Soc. Jpn.*, **32**, 366 (1959).

2) M. Ito. K. Abe, and H. Takeshita, *Bull. Chem. Soc., Jpn.*, **45**, 1913 (1972).

3) A. Mekillopand E. C. Taylor, *Chem. Brit.*, **9**, 4 (1973).

BULLETIN OF THE CHEMICAL SOCIETY OF JAPAN, VOL. 51 (8), 2441—2442 (1978)

Infrared Spectra of ^{13}C-Labelled Diphenylcyclopropenone and Related Derivatives

Yoshikazu TAKEHIRA and Fumio TODA*

Department of Industrial Chemistry, Faculty of Engineering, Ehime University, Matsuyama 790

(Received January 23, 1978)

Synopsis. The infrared spectra of diphenylcyclopropenone-1-^{13}C, its hydrate, 3-dicyanomethylene-1,2-diphenyl-1-cyclopropene-3-^{13}C, and 4-(2,3-diphenylcyclopropenylidene)-2-(diphenylmethylene)-1,3-cyclobutanedione-1'-^{13}C were studied.

Diphenylcyclopropenone (**3**) and related derivatives such as methylenecyclopropene (triafulvene) show complex IR bands. For example, **3** shows two strong bands at *ca.* 1850 and 1620 cm^{-1}, which were found to be mainly due to $\nu_{C=O}$ and $\nu_{C=C}$, respectively.[1] For the sake of confirmation and assignment of the IR bands of the hydrate of **3** (**4**),[2] 3-dicyanomethylene-1,2-diphenyl-1-cyclopropene (**5**),[3] and 4-(2,3-diphenylcyclopropenylidene)-2-(diphenylmethylene)-1,3-cyclobutanedione (**6**),[4] ^{13}C-labelled samples of these compounds were synthesized and their IR spectra were studied.

$$PhCH_2MgBr \xrightarrow{^{13}CO_2} PhCH_2{}^{13}COOH \xrightarrow{Ba(OH)_2}$$

$$(PhCH_2{}^{13}COO)_2Ba \xrightarrow{\Delta} PhCH_2{}^{13}COCH_2Ph \xrightarrow{Br_2}$$

1

$$PhCHBr{}^{13}COCHBrPh \xrightarrow{Et_3N}$$

2

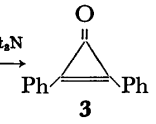

3

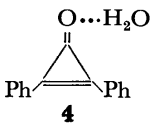

4

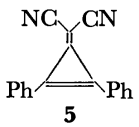

5

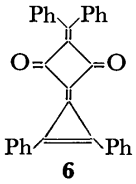

6

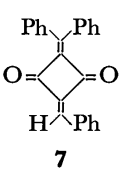

7

Experimental

^{13}C-Labelled Compounds. Phenylacetic acid-1-^{13}C (96.2 atom% ^{13}C) was prepared by carbonation of phenylmagnesium bromide with $^{13}CO_2$ evolved from $Ba^{13}CO_3$ (96.2 atom% ^{13}C), according to the standard procedure of isotope experiment.[5] From the phenylacetic acid-1-^{13}C, **3**-1-^{13}C was prepared successively *via* barium phenylacetate-1-^{13}C, 1,3-diphenyl-2-propanone-2-^{13}C (**1**-2-^{13}C), and 1,3-dibromo-1,3-diphenyl-2-propanone-2-^{13}C (**2**-2-^{13}C), according to the reported method[6] of preparation of non-labelled **3**. In ^{13}C-NMR spectrum, **3**-1-^{13}C showed a strong signal of the carbonyl carbon at 155.9 ppm (on $CDCl_3$, from TMS), which is comparable to that of **3**, 155.7 ppm (in $CDCl_3$, from TMS).[7]

Hydrate of **3**-1-^{13}C (**4**-1-^{13}C) was prepared according to the procedure of Toda and Akagi.[2] **5**-3-^{13}C and **6**-1-^{13}C were prepared by the condensation of **3**-1-^{13}C with dicyanomethane and 2-diphenylmethylene-1,3-cyclobutanedione,[4] respectively, following the preparation of non-labelled **5**[3] and **6**.[4]

IR Spectra. IR spectra were recorded with a Hitachi 285 grating spectrometer.

Results and Discussion

IR spectral data are summarized in Table 1. In the case of both **3** and **4**, the bands at *ca.* 1850 cm^{-1} shifts *ca.* 40 cm^{-1} towards lower frequencies when C-1 is labelled with ^{13}C, that at *ca.* 1620 cm^{-1} *ca.* 15 cm^{-1}. The results show that the bands are mainly due to their $\nu_{C=O}$ and $\nu_{C=C}$, respectively. The observed $\Delta\nu_{C=O}$ values agree with the calculated one, 41 cm^{-1}, for 1850 cm^{-1} band on the basis of $\nu^{12}{}_{C=O}/\nu^{13}{}_{C=O}=1.0227$.[8] Almost the same shift of $\nu_{C=O}$ by ^{13}C-labelling was observed for **1** and **2**.

Table 1. IR spectral data (cm^{-1})

Compound	State	ν(non-labelled)	ν(^{13}C-labelled)	$\Delta\nu$
1	Neat	1724[b]	1679	45
		1715[b]	1674	41
2	Nujol	1725[b]	1690	35
		1723[b]	1684	39
3	Nujol	1847[a]	1809	38
		1840[a]	1806	34
		1624[a]	1609	15
		1618[a]	1604	14
4	Nujol	1842[a]	1807	35
		1605[a]	1597	8
4	CCl_4	1861[a]	1817	44
		1640[a]	1626	14
5	Nujol	2206[b]	2207	1
		2197[b]	2198	1
		1872[c]	1854	18
		1867[c]	1849	18
6	Nujol	1888[d]	1888	0
		1847[c]	1828	19
		1843[c]	1821	22
		1756[d]	1757	1
		1659[a]	1659	0

a) Very strong. b) Strong. c) Medium. d) Weak.

Since the two bands of **5** at 1872 and 1867 cm^{-1} shift 18 cm^{-1} towards lower frequencies with ^{13}C-labelling, they seem to be mainly due to $\nu_{C=O}$ of *exo*-methylene moiety. However, a small shift of $\nu_{C\equiv N}$ of **5**, 2206 and 2197 cm^{-1}, was observed. No band of $\nu_{C=C}$ of cyclopropene moiety of **5** could be detected. The medium bands of **6** at 1847 and 1843 cm^{-1} would be mainly due to $\nu_{C=C}$ of *exo*-methylene of methylenecyclopropene moiety, since these bands of the ^{13}C-labelled sample appear at 19 and 22 cm^{-1} frequencies lower than those of the unlabelled compounds, respectively. The very

strong band of **6** at 1659 cm^{-1} not affected by ^{13}C-labelling could be assigned to $\nu_{C=O}$, since **7**[4] shows a similar $\nu_{C=O}$ band at 1680 cm^{-1}. However, neither 1888 nor 1756 cm^{-1} band could be assigned.

The authors wish to express their thanks to Professor Yoho Tsuno for his valuable suggestions on ^{13}C-labelling experiment.

References

1) A. Krebs, B. Schrader, and F. Höfler, *Tetrahedron Lett.*, **1968**, 5935.

2) F. Toda and K. Akagi, *Tetrahderon Lett.*, **1968**, 3735. Structural investigation of **4** by X-ray analysis has been reported; H. Tsukada, H. Shimanouchi, and Y. Sasada, *ibid.*, **1973**, 2455; H. L. Ammon, *J. Am. Chem. Soc.*, **95**, 7093 (1973).

3) Y. Kitahara and M. Funamizu, *Bull. Chem. Soc., Jpn.*, **37**, 1897 (1964).

4) F. Toda, *Chem. Lett.*, **1972**, 621.

5) A. Murray and B. L. Williams, "Organic Synthesis with Isotopes," Part I, Interscience, New York (1958).

6) R. Breslow, T. Eicher, A. Krebs, and R. A. Peterson, *J. Am. Chem. Soc.*, **87**, 1320 (1965).

7) M. T. W. Hearn and K. T. Potts, *J. Chem. Soc., Perkin Trans. 2*, **1974**, 1918.

8) M. Halmann and S. Pinchas, *J. Chem. Soc.*, **1958**, 1703.

BULLETIN OF THE CHEMICAL SOCIETY OF JAPAN, VOL. 51 (8), 2443—2444 (1978)

A New Route to *o*-Methylthiomethylated Phenols by Use of *S,S*-Dimethylsulfilimines

Tamotsu YAMAMOTO* and Makoto OKAWARA

Research Laboratory of Resources Utilization, Tokyo Institute of Technology, Nagatsuta-cho, Midori-ku, Yokohama 227

(Received February 4, 1978)

Synopsis. As convenient intermediates to introduce methyl groups into the *o*-positions of phenols, *o*-methylthiomethylphenols (*o*-MTM-phenols) were prepared in high selectivity and moderate yield by the reaction of phenols with sulfilimines such as *S,S*-dimethyl-*N*-(2,4-dinitrophenyl)- and *S,S*-dimethyl-*N*-tosylsulfilimines.

Phenols having methyl groups at the position ortho to the hydroxyl group are useful intermediates in organic synthesis.

The *o*-methylthiomethylation (*o*-MTM-ation) of phenol followed by reduction is known, as an indirect method to introduce methyl groups into the position ortho to hydroxyl group in phenols. For *o*-MTM-ation, methods using dimethyl sulfoxide together with dicyclohexylcarbodiimide,[1] acetic anhydride,[2] or pyridine–SO_3,[3] and dimethyl sulfide with *N*-chlorosuccinimide[4] have been reported. These methods have disadvantages such as low yield, minor selectivity, and trouble in handling.

We found that easily accessible sulfilimines, *S,S*-dimethyl-*N*-(2,4-dinitrophenyl)sulfilimine (**1a**) and *S,S*-dimethyl-*N*-tosylsulfilimine (**1b**), react with phenols to give the corresponding methylthiomethylated phenols, which are convertible into the corresponding methylated phenols,[1c,4] in good yield and with high selectivity.

2a **1** **3a** **4**

a: R=2,4-$(NO_2)_2C_6H_3$
b: R=Tos

A mixture of *o*-cresol (**2a**) and a half equivalent of **1a** was heated in bulk at 120—130 °C for 3 h. Work-up of the reaction mixture gave 6-MTM-2-methylphenol (**3a**) in 95% yield. The NMR data of **3a** were identical with those in literature.[1b] Similarly, from the reaction between **2a** and **1b** **3a** was obtained in 78% yield (based on reacted **1b**), which was found to be spectroscopically pure by NMR. In contrast with the former case, unreacted **1b** was conveniently recovered. The lower yield in the latter case might be caused by more difficult proton shift from **2a** to **1**.

A similar tendency was observed in the variation of methylthiomethylating agents, *N*-arylsulfonyl-*S,S*-dimethylsulfilimines (**1b**—**1e**) (Table 1): the sulfilimine having electron-donating group on benzene ring tends to give **3a** in a higher yield.

Although **1b** gives **3a** in a lower yield as compared with **1a**, the former is more accessible from dimethyl sulfide and chloramine T. The *o*-MTM-ation of other phenols with **1b** was examined. The corresponding *o*-MTM-phenols were obtained in a reasonable yield and with high selectivity at the position ortho to hydroxyl group (Table 2).

TABLE 1. EFFECT OF SUBSTITUTENT ON THE YIELD OF **3a**

	$Me_2S{=}NSO_2Ar$	Yield of **3a** (%)
1b	Ar=4-$CH_3C_6H_4$	50
1c	C_6H_5	39
1d	4-ClC_6H_4	35
1e	2,4,6-$(CH_3)_3C_6H_2$	62
1a	$Me_2S{=}NC_6H_3(NO_2)_2$(2, 4)	95[a]

a) Isolated yield.

TABLE 2. *o*-MTM-ATION OF PHENOLS USING **1b**[a]

$$\underset{\mathbf{2}}{HOAr} + \underset{\mathbf{1b}}{Me_2S{=}NTs} \longrightarrow \underset{\mathbf{3}}{HOAr'\text{-}MTM\text{-}(o)} + \underset{\mathbf{4b}}{H_2NTs}$$

2	**3** Y (%)	**3** Bp (°C/Torr)	**4b** Y (%)
a 2-$CH_3C_6H_4OH$	**a** 43 (73)	$73/3\times10^{-2}$ [$70/10^{-3}$][1b]	52 (≈100)
b 2-$CH_3OC_6H_4OH$	**b** 35 (78)	92—93/ 3×10^{-2}	45 (≈100)
c 2,5-$(CH_3)_2C_6H_3OH$	**c** 69 (96)	oil	72 (≈100)
d 3,5-$(CH_3)_2C_6H_3OH$	**d** 58 (58)[b]	oil	≈100
e 2,3,5-$(CH_3)_3CH_2OH$	**e** 37 (64)	oil	58 (≈100)

a) Data in parentheses show the yields based on the reacted **1b**. b) Bis-TMM-phenol was obtained in 35% yield.

The reaction scheme, in which *o*-MTM-phenols are formed from **2** and **1**, can be described partly from Moffatt's mechanism.[1] Especially in the first stage of the reaction, the proton shift (**2** to **1**), might play the most important role.

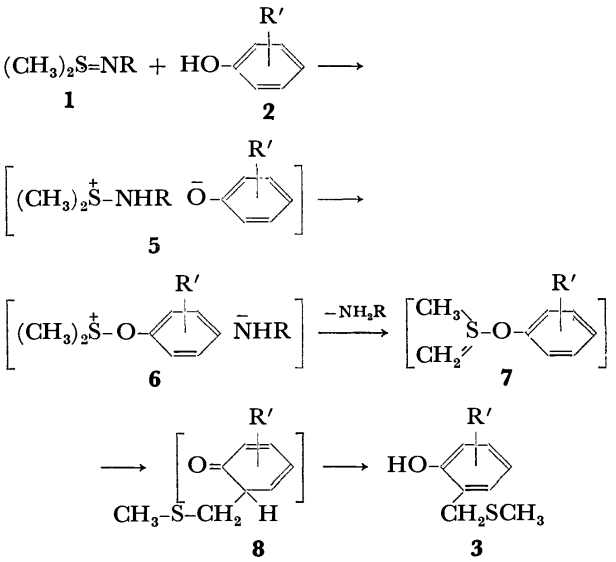

1 **2** **5** **6** **7** **8** **3**

Experimental

Materials. Chloramine T and chloramine B of reagent grade were used. Sodium salts of *N*-chloro-*p*-chlorobenzenesulfonamide and *N*-chloromesitylenesulfonamide were prepared by the treatment of corresponding sulfonamides with aq solution of sodium hypochlorite (7%).

Preparation of Sulfilimines. **1a** was prepared by the method described in a previous paper.[5] *N*-Arylsulfonyl-*S,S*-dimethylsulfilimines were prepared by the reaction of dimethyl sulfide with sodium salts of *N*-chloroarenesulfonamides.[6] **1b.** Yield: 92%; Mp: 154—155 °C (MeOH) (lit,[7] 154—155 °C). *N*-Phenylsulfonyl-*S,S*-dimethylsulfilimine (**1d**). Yield: 86%; Mp: 128—129 °C (MeOH) (lit,[8] 131 °C). *N*-(*p*-Chlorophenylsulfonyl)-*S,S*-dimethylsulfilimine (**1d**). Yield: 80%; Mp: 115—116 °C (MeOH); IR(KBr): 1273 ($\nu_{as}SO_2$), 1133 (ν_s SO_2), 958 (S=N), 820 cm^{-1} (*p*-C_6H_4). Found: C, 37.97; H, 3.97; N, 5.57% (Calcd for $C_8H_{10}ClNO_2S_2$: C, 38.16; H, 4.01; N, 5.56%). *S,S*-Dimethyl-*N*-(2,4,6-trimethylphenylsulfonyl)sulfilimine (**1e**). Yield: 83%; Mp: 167—168.5 °C (MeOH); IR(KBr): 1280 ($\nu_{as}SO_2$), 1134 (ν_sSO_2), 945 (S=N), 843 cm^{-1} (*p*-C_6H_4). Found: C, 50.84; H, 6.69; N, 5.49% (Calcd for $C_{11}H_7NO_2S_2$: C, 50.93; H, 6.62; N, 5.40%).

Reaction of 2 with 1. General Procedure: A mixture of 10—20 mmol of **2** and a half equivalent of **1** was heated at 120—130 °C for 3—7 h. After the reaction, excess **2** was removed by distillation under reduced pressure. The resulting residues were extracted with hexane. The combined extracts were evaporated to dryness to give very viscous oils, which were almost pure *o*-MTM-phenols (**3**) as confirmed by NMR. The oils were purified by distillation (for **3a** and **3b**) or column chromatography (silica gel–hexane, for **3c**, **3d** and **3e**) for confirmation of the structures. 2,4-Dinitroaniline (**4a**), *p*-toluenesulfonamide (**4b**) and unreacted **1b** were separated from insoluble parts in hexane by extraction with ether and identified by comparison with authentic samples.

Reaction of o-*Cresol (2a) with 1*: (A) 1.08 g (10 mmol) of **2a** was reacted with 1.12 g (5 mmol) of **1a** at 120—130 °C for 3 h to give 798 mg (95%, based on **1a**) of **3a** and 914 mg of **4a**. (B) 1.08 g of **2a** was reacted with 1.16 g (5 mmol) of **1b** at 120—130 °C for 5 h to give 361 mg of **3a** and 445 mg of **4b**. **3a**: Bp: 73 °C (3×10^{-2}) [lit,[1b] 70 (10^{-3})]. IR(neat): 3400—3300 and 1210—1190 cm^{-1} (OH). NMR ($CDCl_3$): δ 1.96 (s, 3H), 2.26 (s, 3H), 3.75 (s, 2H), 6.62 (s, 1H), 6.7—7.3 (m, 3H).[1b]

Reaction of Guaiacol (2b) with 1b: 2.48 g (20 mmol) of **2b** was reacted with 2.31 g (10 mmol) of **1b** at 120—130 °C for 5h to give 644 mg of 6-MTM-2-methoxyphenol (**3b**) and 770 mg of **4b**. **3b**; Bp: 92—93 °C (3×10^{-2}). IR (neat): 3500—3400 and 1220 (OH), 1260 and 1070 cm^{-1} (C–O–C). NMR ($CDCl_3$): δ 2.08 (s, 3H), 3.75 (s, 2H), 3.89 (s, 3H), 5.92 (s, 1H), 6.7—7.0 (m, 3H).[2a] (Found: C, 58.48; H, 6.73; S, 17.12%. Calcd for $C_9H_{12}O_2S$: C, 58.66; H, 6.58; S, 17.40%.)

Reaction of 2,5-Dimethylphenol (2c) with 1b: 2.44 g (20 mmol) of **2c** was reacted with 2.31 g of **1b** at 120—130 °C for 7 h to give 1.25 g of 6-MTM-2,5-dimethylphenol (**3c**) and 1.23 g of **4b**. **3c**: IR (neat): 3500—3400 and 1220 cm^{-1} (OH). NMR (CCl_4): δ 1.96 (s, 3H), 2.18 (s, 3H), 2.27 (s, 3H), 3.72 (s, 2H), 6.17 (s, 1H), 6.54 (d, 2 H), 6.86 (d, 2H).[1b] MS: *m/e* 182 (M^+).

Reaction of 3,5-Dimethylphenol (2d) with 1b: 2.44 g (20 mmol) of **2d** was reacted with 2.31 g of **1b** at 120—130 °C for 7 to give 1.06 g of 6-MTM-3,5-dimethylphenol (**3d**) and 1.70 g of **4b**. **3d**: IR (neat): 3400 and 1150 (OH), 830 cm^{-1} (C_6H_2). NMR (CCl_4): δ 1.99 (s, 3H), 2.22 (s, 3H), 2.29 (s, 3H), 3.72 (s, 2H), 6.17 (s, 1H), 6.33 (s, 1H), 6.54 (s, 1H). MS: *m/e* 182 (M^+).

Reaction of 2,3,5-Trimethylphenol (2e) with 1b: 2.72 g (20 mmol) of **2e** was reacted with 2.31 g of **1b** at 120—130 °C for 7 h to give 726 mg of 6-MTM-2,3,5-trimethylphenol (**3e**) and 991 mg of **4b**. **3e**: IR (neat): 3400—3350 and1140 cm^{-1} (OH). NMR (CCl_4): δ 1.97 (s, 3H), 2.12 (s, 3H), 2.25 (s, 3H), 3.75 (s, 2H), 6.22 (s, 1H), 6.47 (s, 1H). Found: C, 66.95; H, 8.08%. Calcd for $C_{11}H_{16}OS$: C, 67.29; H, 8.23%.

Effect of Substituents on the Yield of 3a: Reactions of 2 mmol of **2a** with 1 mmol of **1** (**b**—**c**) were carried out at 130 °C for 5 h without solvent. Excess **2a** was removed from the reaction mixtures by distillation *in vacuo*. The residues obtained were analyzed for **3a** by liquid chromatography (a Shimadzu High Speed Chromatograph 840, Permaphase ODS–50% MeOH–H_2O) after evaporation of hexane. The data obtained (yield of **3a**) are given in Table 1.

References

1) (a) M. G. Burdon and J. G. Moffatt, *J. Am. Chem. Soc.*, **87**, 4658 (1965); (b) *ibid.*, **88**, 5855 (1966); (c) *ibid.*, **89**, 4725 (1967).

2) (a) P. Claus, *Monatsh. Chem.*, **99**, 1034 (1968); (b) Y. Hayashi and R. Oda, *J. Org. Chem.*, **32**, 457 (1967); (c) For trifluoroacetic anhydride, Y. Hiraki, M. Kamiya, R. Tanikaga, N. Ono, and A. Kaji, *Bull. Chem. Soc. Jpn.*, **50**, 447 (1977).

3) P. Claus, *Monatsh. Chem.*, **102**, 913 (1971).

4) P. G. Gassman and D. R. Amik, *Tetrahedron Lett.*, **1974**, 889.

5) T. Yamamoto, Y. Harigaya, and M. Okawara, *Chem. Lett*, **1972**, 1009.

6) M. A. McCall, D. S. Tarbell, and M. A. Havill, *J. Am. Chem. Soc.*, **73**, 4476 (1951).

7) C. W. Todd, J. H. Fletcher, and D. S. Tarbell, *J. Am. Chem. Soc.*, **65**, 350 (1943).

8) M. V. Likhosherstov, *Zh. Obshch. Khim.*, **17**, 1478 (1947).

BULLETIN OF THE CHEMICAL SOCIETY OF JAPAN, VOL. 51 (8), 2445—2446 (1978)

Catalysis by Phosphine Complexes of Silylruthenium Hydrides of the Addition of Carbon Tetrachloride to 1-Octene[1)]

Hideyuki MATSUMOTO*, Taichi NAKANO, Yoichiro NAGAI, and Hiromichi KONO†

Department of Chemistry, Gunma University, Kiryu, Gunma 376

†*Sagami Central Research Center, Nishi-Ohnuma Sagamihara, Kanagawa 229*

(Received March 1, 1978)

Synopsis. Phosphine complexes of silylruthenium hydrides of types $[RuH_3(SiR_3)(PPh_3)_3]$ (where R_3Si= Et_3Si, Me_2PhSi, and $(MeO)_3Si$) and $[RuH(SiR_3)(PPh_3)_2]$ (where R_3Si=Cl_2MeSi and $(MeO)_3Si$) were found to be much more effective catalysts for the addition of carbon tetrachloride to 1-octene than $RuCl_2(PPh_3)_3$ or $RuH_2(PPh_3)_4$.

The addition reactions of carbon tetrachloride with olefins have been carried out with the aid of various catalysts (*e.g.*, peroxides, metal carbonyls and metal salts, *etc.*).[2)] We have recently found that the addition reactions were effectively catalyzed by a homogeneous ruthenium catalyst, dichlorotris(triphenylphosphine)-ruthenium(II).[3,4)] This catalyst was shown to have definite advantages (*e.g.*, high yields of 1: 1 adducts, unique selectivities and simplicity of the system, *etc.*)[3,4)] compared to usual free-radical addition reactions. Even more effective catalysts have now been found as described below.

We have prepared phosphine complexes of silylruthenium hydrides of types $[RuH_3(SiR_3)(PPh_3)_3]$ (where R_3Si=Et_3Si, Me_2PhSi, and $(MeO)_3Si$) and $[RuH(SiR_3)(PPh_3)_2]$ (where R_3Si=Cl_2MeSi and $(MeO)_3Si$) by the reactions of $RuH_2(PPh_3)_4$ or $RuCl_2(PPh_3)_3$ with hydrosilanes.[5)] and tested the catalytic efficiencies of these complexes for the reaction between carbon tetrachloride and 1-octene. All experiments were carried out in an argon atmosphere under reflux conditions using a 1: 3 mixture of the olefin and the chloride. The results are presented in Table 1 together with those for the reactions catalyzed by $RuCl_2(PPh_3)_3$ and $RuH_2(PPh_3)_4$. The Table also shows the turn-over number of these complexes.

$$n\text{-}C_6H_{13}CH{=}CH_2 + CCl_4 \xrightarrow{[Ru]} n\text{-}C_6H_{13}CHClCH_2CCl_3$$

$$[Ru] = RuH_3(SiR_3)(PPh_3)_3,\ RuH(SiR_3)(PPh_3)_2$$

An inspection of the Table clearly indicates that seven-coordinate ruthenium complexes, $RuH_3(SiR_3)$-$(PPh_3)_3$, are particularly excellent catalysts for the addition reaction. With these catalysts, the 1: 1 adduct was obtained in 57—85% yields with turn-over number 2650—4250 while the values for $RuCl_2(PPh_3)_3$ and $RuH_2(PPh_3)_4$ amounted to be 130 and 370, respectively. Therefore, it is apparent that these silylruthenium complexes are 20—32 times more active than the dichlororuthenium complex and 7—11 times more active than the dihydroruthenium complex.

Although the turn-over number of the complexes, $RuH(SiR_3)(PPh_3)_2$, were smaller than those of the trihydrido analogs, these four-coordinate complexes were also found to be 2—7 times effective than $RuCl_2$-$(PPh_3)_3$ and $RuH_2(PPh_3)_4$.

It has been known that phosphine complexes of ruthenium hydrides often catalyze double-bond migration in some unsaturated system.[6)] Such migration, however, was not found in the present system and only the terminal adduct, 1,1,1,3-tetrachlorononane, was obtained under the conditions employed.

Table 1. Reactions of carbon tetrachloride with 1-octene catalyzed by phosphine complexes of silylruthenium hydrides[a)]

Catalyst	Catalyst concentration, mol%[c)]	Yield of the 1: 1 adduct, %[d)]	Catalytic efficiency[e)]
$RuH_3(SiMe_2Ph)L_3$	0.02	57	2850
$RuH_3(SiMe_2Ph)L_3$	0.02	85	4250
$RuH_3(SiEt_3)L_3$	0.02	58	2900
$RuH_3[Si(OMe)_3]L_3$	0.02	53	2650
$RuH(SiCl_2Me)L_2$	0.05	44	880
$RuH[Si(OMe)_3]L_2$	0.05	46	920
RuH_2L_4	0.10	37	370
$RuCl_2L_3$ ($L=PPh_3$)	0.15	20	130

a) Reactions were carried out in an argon atmosphere under reflux conditions for 5 h using 50 mmol of the olefin and 150 mmol of the chloride. b) The system was carefully degassed by freeze-pump-thaw cycles and then flushed well with argon prior to the reaction. c) Based on the olefin charged. d) Yields (*via* GLC) of the adduct, 1,1,1,3-tetrachlorononane, are based on the olefin charged. e) The catalytic efficiency is meant by (moles of the adduct)/(moles of the catalyst).

Experimental

1-Octene and carbon tetrachloride were commercially available and purified by distillation prior to use. The complexes $RuCl_2(PPh_3)_3$,[7)] $RuH_2(PPh_3)_4$,[8)] $RuH_3(SiR_3)$-$(PPh_3)_3$,[5)] and $RuH(SiR_3)(PPh_3)_2$[5)] were prepared according to literature directions.

Procedure for Testing the Catalytic Efficiencies of Phosphine Complexes of Silylruthenium Hydrides. All runs were conducted in essentially the same manner; therefore, only the reacttion catalyzed by the $RuH_3(SiMe_2Ph)(PPh_3)_3$ complex is described in detail.

In a 50-ml round bottomed flask, equipped with a reflux condenser and a magnetic stirring bar were placed 5.61 g (50 mmol) of 1-octene, 23.05 g (150 mmol) of carbon tetrachloride and 0.11 g (0.010 mmol) of the complex. The system was flushed with argon and the solution was refluxed for 5 h with stirring. GLC analysis of the resulting mixture disclosed that the 1: 1 adduct, 1,1,1,3-tetrachlorononane, had been produced in 57% yield based on the olefin charged. Structural assignment for this adduct was performed by comparing their physical properties (IR and NMR spectra and

GLC retention times, *etc.*) with those of an authetic sample after isolation by GLC.

Another reaction was carried out with a slight modification in order to optimize the yield of the 1:1 adduct. Thus, the same mixture of the olefin, the chloride and the catalyst was cooled in liquid nitrogen, evacuated at 0.3 mm, flushed well with argon and then heated under reflux for 5 h. GLC analysis of the resulting mixture showed production of the 1:1 adduct in 85% yield.

References

1) Radical Reactions in the Coordination Sphere. VIII. Part VII: H. Matsumoto, T. Nakano, K. Ohkawa, and Y. Nagai, *Chem Lett.*, **1978**, 363.

2) For reviews, see (a) C. Walling, "Free Radicals in Solution," Wiley, New York (1957), p. 247; (b) C. Walling and E. S. Huyser, *Org. React.*, **13**, 51 (1963); (c) G. Sosnovsky, "Free Radical Reactions in Preparative Organic Chemistry," MacMillan, New York, N. Y. (1964), p. 19; (d) Y. Mori and J. Tsuji, *Kagaku No Ryoiki*, **27**, 197 (1973); (e) R. Kh. Freidlina and E. C. Chukovskaya, *Synthesis*, **1974**, 477; (f) F. Minisci, *Acc. Chem. Res.*, **8**, 165 (1975).

3) (a) H. Matsumoto, T. Nakano, and Y. Nagai, *Tetrahedron Lett.*, **1973**, 5147; (b) H. Matsumoto, T. Nikaido, and Y. Nagai, *ibid.*, **1975**, 899; (c) H. Matsumoto, T. Nakano, T. H. Nikaido, and Y. Nagai, *Chem. Lett.*, **1978**, 115; (d) H. Matsumoto, T. Nakano, K. Takasu, and Y. Nagai, *J. Org. Chem.*, in press; (e) T. Nakano, H. Arai, H. Matsumoto, and Y. Nagai, *Org. Prep. Proc. Int.*, in press.

4) Y. Sasson, and C. L. Rempel, *Synthesis*, **1975**, 448.

5) H. Kono, N. Wako, and Y. Nagai, *J. Organomet. Chem.*, **132**, 53 (1977).

6) (a) D. Bingham, D. E. Webster, and P. B. Wells, *J. Chem. Soc. Dalton Trans.*, **1972**, 1287; (b) D. Bingham, D. E. Webster, and P. B. Wells, *ibid.*, **1974**, 19; (c) F. Pennella and R. L. Banks, *J. Catal.*, **35**, 73 (1974); (c) F. Pennella and R. Rycheck, U. S. Patent 3793257 (1974); *Chem. Abstr.*, **81**, 63117 (1974).

7) T. A. Stephenson and G. Wilkinson, *J. Chem. Soc, A*, **1970**, 2497.

8) J. J. Levison and S. D. Robinson, *J. Chem. Soc., A*, **1970**, 2947.

BULLETIN OF THE CHEMICAL SOCIETY OF JAPAN, VOL. 51 (8), 2447—2448 (1978)

A Photoreaction of 4-Nitrophenylnitromethane in a Micellar System

Kazutoshi YAMADA,* Kiyoshi SHIGEHIRO, Toyohiko KIYOZUKA, and Hirotada IIDA

Department of Synthetic Chemistry, Faculty of Engineering, Chiba University, Yayoi-cho Chiba 280

(Received March 3, 1978)

Synopsis. The photoconversion of 4-nitrophenylnitormethane into 4-nitrobenzaldehyde in an ethanol–water system was found to proceed by an intramolecular rearrangement of oxygen of adjacent nitro group. Cationic surfactant increased the quantum yield of this photorearrangement by a factor of 20, but β-cyclodextrin decreased it.

4-Nitrophenylnitromethanide anion is formed in ethanol–water by removal of a proton from 4-nitrophenylnitromethane (**1**). The nitromethanide anion is thermally stable for at least 24 h. The present paper is concerned with its photorearrangement. The catalytic effect of a cationic surfactant and β-cyclodextrin (β-CDX) was also studied.

Photoreaction. Irradiation of a 20% (vol) ethanolic alkaline aqueous solution of **1** gave 4-nitrobenzaldehyde.

$$\text{Ar-CH}_2\text{-NO}_2 \rightleftharpoons \text{Ar-CH=NO}_2^- \rightleftharpoons \text{Ar-}\bar{\text{C}}\text{H-NO}_2$$

$$\downarrow h\nu$$

$$\left[\text{Ar-CH(O)-N-O}^-\right] \longrightarrow \text{Ar-CH=O}$$

The ionization, removal of a proton from **1**, and the decrease of the aci-nitroate anion of **1** during the course of irradiation followed the pseudo-first-order kinetics. The rate constant of the ionization was greater than that of the decrease under the present conditions.[1] The decrease of aci-nitroate anion is considered to be the rate-limiting step in the overall rate of photoreaction. The photoreaction was followed by ultraviolet spectroscopy. Isosbestic points were found at 312, 256, and 227 nm as the time of irradiation; the maximum absorbance of the aci-nitroate anion of **1** at 384 nm decreased, while a new maximum appeared at 268 nm, the position for λ_{max} of 4-nitrobenzaldehyde.

4-Nitrophenylacetonitrile which has a cyano group instead of a nitro group was photoconverted into 4-nitrobenzaldehyde by oxygen in an ethanol–aqueous alkali solution. It was not allowed to react under anaerobic conditions. The observed quantum yield for the photoconversion of **1**, however, did not change in the presence or absence of oxygen. From these results and the fact that the oxazirane ring decomposes by the action of alkali to the formation of carbonyl compounds[2] it is shown that the photoreaction of **1** proceeds by an intramolecular attack of oxygen on the adjacent nitro group to α-carbon.

In order to confirm the mechanism of this photorearrangement, the relation between the stability of the aci-nitroate anion and the photoreaction was studied. The presence of a cationic surfactant, hexadecyltrimethylammonium bromide (CTAB), and β-CDX caused a red shift in the λ_{max} for the aci-nitroate anion (Table 1). The λ_{max} for 8×10^{-5} M of **1** in 20% (vol) ethanolic aqueous buffer (pH 6.90) began to show the shift at a concentration of CTAB above 2.24×10^{-4} M, which indicates a critical micelle concentration (CMC) of CTAB for **1**.

The presence of CTAB and β-CDX in micellar concentration decreased the pK_a value of **1** (Table 1), indicating the stabilization of aci-nitroate anions This results from (a) electrostatic interaction with cationic head groups of CTAB and the anion form, and (b) electron delocalization by the hydrogen bond between an adjacent hydroxyl group of β-CDX and an oxygen atom of 4-nitro group of the substrate which forms a 1 : 1 inclusion complex with β-CDX.

The quantum yield for the photoreaction of **1** in 20% ethanolic aqueous buffer (pH 6.90) increased in the presence of micellar concentration of CTAB. The quantum yield started to increase above 1.78×10^{-4} M of CTAB in good agreement with CMC. Since the quantum yield reached saturation in high concentration

Table 1. The effect of CTAB and β-CDX on the visible spectra and the pK_a value of 4-nitrophenylnitromethane

	H_2O	CTAB[a]	β-CDX[b]
λ_{max}/nm[c]	384	404	390
pK_a[d]	6.00	4.92	4.84

a) In the presence of 10^{-2} M CTAB. b) In the presence of 4×10^{-3} M β-CDX. c) In 20% ethanolic aqueous buffer (pH 6.90). d) In 20% ethanolic water at room temperature. The pK_a values were measured according to the method of Wolff.[3]

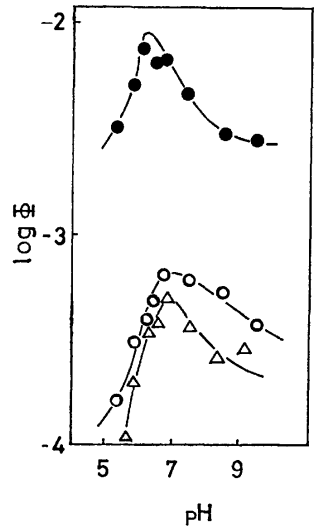

Fig. 1. A pH-quantum yield profile for the photorearrangement of 4-nitrophenylnitromethane. ○: In the absence of surfactants, ●: in the presence of 5×10^{-3} M CTAB, △: in the presence of 4×10^{-3} M β-CDX.

of CTAB, a general mechanism involving the micelle-substrate complex in a manner analogous to that for enzymatic catalysis[40] was applied. Micellar CTAB increased the quantum yield (Φ_{obsd}) for the photoreaction of **1** in 20% ethanolic aqueous buffer (pH 5.38) by a factor of 20, and increased the quantum yield for the formation of product from the micellar phase (Φ_2) by a factor of 12.

Variation of quantum yields over the pH range 5—10 was bell-shaped both in the absence and the presence of CTAB and β-CDX (Fig. 1). When CTAB was present, its maximum moved to a lower pH range. Stabilization of the aci-nitroate anion by CTAB micelle reflects directly on the quantum yield. The difference in OH^- concentration between micellar surface and bulk phase is an important factor. However, no such direct influence of stabilization appeared in the presence of β-CDX. The quantum yields decreased in the presence of β-CDX over all the pH range. Probably the dynamic equilibrium of micell micellar CTAB facilitates the rearrangement of oxygen of adjacent nitro group and the rigid cavity of β-CDX inhibits the rearrangement of substrate forming a complex with β-CDX.

Experimental

UV spectra were taken on a Hitachi ESR-3T or Shimadzu UV-200 spectrometer. The pH value was measured with a model HM-5A pH meter (TOA Electronics, Co., Ltd.). The following buffer solutions were used according to the required pH range: M/15 KH_2PO_4–Na_2HPO_4 (pH 5—9), M/20 H_3BO_3–KCL (pH 9—10), M/20 Na_2HPO_4–NaOH (pH 10—12). Commercial CTAB was recrystallized twice from methanol–ether.[5] Other materials were used without further purification. 4-Nitro-phenylnitromethane was prepared by the procedure of Hantzsch and Veit.[6]

Irradiation of 4-Nitrophenylnitromethane (1). A solution of 500 mg of **1** in 1 liter of ethanol-aqueous NaOH solution was as irradiated with an Ushio UM-452 450 W high pressure mercury lamp for 3 hs. After irradiation, the solvent was removed with a rotary evaporator and the oily residue was chromatographed on silica gel using hexane: benzene mixture as an eluent to give two products. The first product (90 mg) seemed a dimer-like compound, mp 286—290 °C, and MS, *m/e* 270 (M^+). No further effort has been made to determine the structure. The second product (20 mg) was identified as 4-nitrobenzaldehyde.

4-Nitrobenzoic acid analysis was carried out by high speed liquid chromatography with a Hitachi Liquid Chromatograph 634A equipped with a UV monitor. Hitachi gel #3020 was packed into the column (2.1ϕ × 500 mm) with a mobile phase of the mixture of methanol–water (8: 2) system. The flow rate of the phase 0.85 ml/min. with a column pressure of approximately 80 kg/cm². The column temperature was 50 °C. Under these conditions, the retention volume of 4-nitrobenzaldehyde and 4-nitrobenzoic acid was 3.06 ml and 1.79 ml, respectively. Variation of the concentration of 4-nitrobenzoic acid with the time of irradiation of **1** was obtained. The formation of 4-nitrobenzaldehyde was slow as compared with the photoreaction, giving no effect on the kinetics.

Kinetic Method. The kinetics was studied by following the reaction spectrophotometrically at the λ_{max} of the nitronate anion in each buffer solution at room temperature. All the data were treated as those of pseudo-first-order kinetics. The estimated rate constant values were converted into the the quantum yield.[7]

Effect of Dissolved Oxygen on the Reaction. After bubbling argon gas for a certain time in order to remove dissolved oxygen, the solution was irradiated and the rate was measured. The quantum yield obtained was compared with that in the pressure of dissolved oxygen.

References

1) For example, the k_{obsd} value for the ionization was 2.47×10^{-2} s^{-1} and that for the photoreaction was 5.41×10^{-5} s^{-1} in 20% (vol) ethanolic aqueous buffer (pH 6.90) at 15 °C. Avery and Bultler reported that the k_{obsd} for the ionization of **1** at zero buffer concentration is 5.75×10^{-3} s^{-1} in 1% dioxanborax buffer at pH 8.10 and 25 °C: S. P. Avery and A. R. Bultler, *J. Chem. Soc., Perkin Trans. 2*, **1973**, 1110.

2) W. D. Emmons, *J. Am. Chem. Soc.*, **79**, 5739 (1957).

3) M. J. Minch, M. Giaccio, and R. Wolff, *J. Am. Chem. Soc.*, **97**, 3766 (1975).

4) J. H. Fendler and E. J. Flendler, "Catalysis in Micellar and Macromolecular Systems," Academic Press, New York (1975).

5) E. F. J. Duynstee and E. Grunwald, *J. Am. Chem. Soc.*, **81**, 4540 (1959).

6) A. Hantzsch and A. Veit, *Ber.* **32**, 607 (1899).

7) K. Yamada, S. Kohmoto, and H. Iida, *Bull. Chem. Soc. Jpn.*, **49**, 1171 (1976).

BULLETIN OF THE CHEMICAL SOCIETY OF JAPAN, VOL. 51 (8), 2449—2450 (1978)

Studies on 5—8 Fused Ring Compounds. III. Hydrogenolysis of 4,4-Dimethyltricyclo[6.3.0.0^{1,7}]undecane-2,6-dione

Misao UMEHARA,* Shinzaburo HISHIDA,** Kunimi FUJIEDA,**
Haruo OGURA,*** and Hiroaki TAKAYANAGI***

Department of Chemistry, Keio University, Hiyoshi Kohoku-ku, Yokohama 223
***Naka Works, Hitachi Ltd., Ichige, Katsuta, Ibaraki 312*
****School of Pharmaceutical Sciences, Kitasato University, Shirokane, Minato-ku, Tokyo 108*

(Received March 30, 1978)

Synopsis. Hydrogenolysis of 4,4-dimethyltricyclo-[6.3.0.0^{1,7}]undecane-2,6-dione with a Pd-C catalyst gave *cis*-4,4-dimethylbicyclo[6.3.0]undecane-2,6-dione and 8,8-dimethylspiro[4.6]undecane-6,10-dione. The *cis* isomer has been shown to isomerize almost completely to the *trans* isomer under acidic and basic conditions.

Previously it has been reported that 4,4-dimethyltricyclo[6.3.0.0^{1,7}]undecane-2,6-dione (I) has been formed as the main product in the chlorination by sulfuryl chloride of 4,4-dimethylbicyclo[6.3.0]undecane(II).[1]

Hydrogenolysis of I in ethanol with a palladium-charcoal catalyst at ordinary room temperature and pressure cleaved the three-membered ring with ease to give *cis*-4,4-dimethylbicyclo[6.3.0]undecane-2,6-dione (III), mp 116—117 °C, as the main product together with a small amount of an isomer (IV), mp 62—63 °C. The ratio of III to IV was approximately 10: 1.

A molecular peak appeared at 208 in the mass spectrum of III as in the case of II.[2] The fragmentation of III was identical with that of II, differing only in relative intensity. Furthermore, III isomerized readily to II when left to stand at room temperature in acidic or alkaline methanol. This shows that II and III are the *cis* and *trans* isomers concerning the ring fusion of the 5—8 fused ring and that II is more stable than III. When a solution of either II or III in 0.4 mol/dm^3 KOH–methanol solution was left to stand at 25 °C, NMR and IR spectroscopy showed that only II was present; III was undetectable even after 45 h. It was not possible to separate II and III by gas chromatography, and hence the equilibrium constant for the reaction *cis*⇌*trans* could not determined.

X-Ray analysis of the 7-bromo derivative (V; mp 111—113 °C[1]†) of II showed that the 5—8 ring fusion of V was *trans*.[3] V was synthesised from II, the more stable isomer, by bromination with pyridinium bromide perbromide. The debromination of V by zinc dust[4] in acetic acid at room temperature yielded the starting dione (II). Hence the ring fusion of II was *trans*, the same as that of V. II resulted from the retro-aldol cleavage of a photoadduct VI,[2] and since the 5—4 ring fusion of VI was *cis*,[2] it is likely that the isomerization from an unstable *cis* configuration to a more stable *trans* configuration, occured in the retro-aldol cleavage to give II. The carbonyl group at position 2 in II and III undergoes enolization in an acidic or alkaline solution, facilitating the *cis-trans* isomerization.

IV arising from the hydrogenolysis of I over Pd–C showed the same molecular peak as that of II and III in its mass spectrum. However, the fragmentation of IV differs considerably from that of II or III. In the NMR spectrum of IV, hydrogen atoms other than those in the five-membered ring appear as singlets and there is an absence of coupling. The *gem*-dimethyl groups show a single peak at 1.05 δ(6H) and the three methylene groups at positions 7, 9, and 11 appear as singlets at 2.73 δ (2H), 2.69 δ(2H), and 2.42 δ(2H), respectively. These results suggest that the protons in the carbonyl-containing ring do not assume a fixed conformation and IV has been estimated to be a spiro compound, 8,8-dimethylspiro[4.6]undecane-6,10-dione. Consequently, in the hydrogenolysis of I over Pd–C, the C(1)–C(7) linkage is cleaved preferentially to give III, accompanied by a slight cleavage of the C(7)–C(8) linkage to give IV. However, the cleavage of the C(1)–C(8) linkage did not occur.

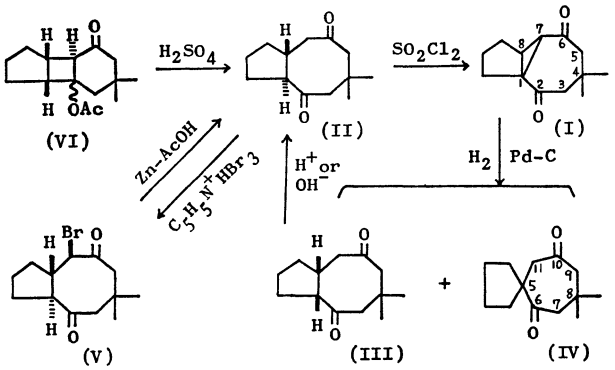

Experimental

Hydrogenolysis of I. A suspension of I (0.5 g) and 5% Pd–C (0.5 g) in a solution of ethanol (40 ml) was stirred at room temperature with hydrogen at 1 atm until absorption was complete (3 h). The filtered solution was concentrated under reduced pressure to give a crystalline residue. Crystallization from hexane gave III (0.24 g); mp 114—116 °C. Recrystallization from hexane gave pure III; mp 116—117 °C. IR (Nujol) 1700 cm^{-1}; (CCl_4) 1705 cm^{-1}. NMR ($CDCl_3$): δ 1.10 (3H, CH_3) and 1.20 (3H, CH_3). Found: C, 75.08; H, 9.55%. Calcd for $C_{13}H_{20}O_2$: C, 75.00; H, 9.62%. MS: *m/e* 208 (M^+, 7%), 193 (8), 190 (1), 180 (2), 152 (11), 141 (56), 124 (20), 112 (29), 95 (17), 83 (base, 100), 81 (5), 67 (32), 55 (23), and 41 (27).

The mother liquor afforded III (0.12 g), and IV (36 mg) as needles. IV; mp 60—62 °C, which was recrystallized from hexane; mp 62—63 °C. IR (Nujol) 1700 cm^{-1}; (CCl_4) 1700

† This compound was assumed to be the 5-bromo-derivative in a previous paper,[1] but X-ray analysis[3] showed it to be the 7-bromo derivative.

cm^{-1}. NMR ($CDCl_3$) δ 1.05 (s, 6H, *gem*-$(CH_3)_2$), 1.4—2.2 (broad, 8H, 5-membered ring H), 2.42 (s, 2H, CH_2), 2.69 (s, 2H, CH_2), and 2.73 (s, 2H, CH_2). Found: C, 75.12; H, 9.67%. Calcd for $C_{13}H_{20}O_2$: C, 75.00; H, 9.62%. MS: *m/e* 208 (M^+, 41%), 193 (2), 180 (2), 167 (5), 152 (6), 148 (5), 141 (13), 128 (16), 124 (15), 111 (23), 98 (6), 95 (8), 83 (base, 100), 81 (25), 70 (30), 67 (31), 56 (37), and 41 (39).

Epimerization of III to II. A solution of III (20 mg) in 5% H_2SO_4–methanol was left to stand at room temperature for 2 weeks, and extracted with ether. The extract was washed with aqueous sodium hydrogencarbonate and water, and then dried over sodium sulfate. After the removal of ether, a crystalline residue was obtained (mp 60—62 °C); the IR spectrum was identical with that of II.[2]

Equilibrium for the Reactions II⇌III. Equilibrium was approached from both sides by allowing each compound (II and III, 40 mg) to stand for 45 h in 0.4 mol/dm^3 KOH–methanol solution (5 ml) at 25 °C. The solution was extracted with ether and washed with water, dried and evaporated. In each case the products were identical to II on the basis of their IR and NMR spectra, and III was not detected. In GPC analysis II and III showed the same retention time.

Debromination of V. The bromination of II with pyridinium bromide perbromide in ethanol gave V.[1] To a solution of V (50 mg) in ether (4 ml) and acetic acid (1 ml), zinc dust (90 mg) was added. The reaction mixture was stirred at room temperature for 50 min and diluted with ether (10 ml). The ethereal solution was filtered and the zinc washed with ether. The combined ethereal solution was washed twice with aqueous sodium hydrogencarbonate and finally with water, and then dried over sodium sulfate. After the removal of ether, a crystalline residue was obtained (31 mg), mp 62—63 °C, and identified as II by IR spectroscopy. Recrystallization from hexane afforded pure II; mp 64—65 °C.

References

1) M. Umehara, S. Hishida, K. Fujieda, and H. Sasaki, *Bull. Chem. Soc. Jpn.*, **50**, 1074 (1977).

2) M. Umehara, T. Oda, Y. Ikebe, and S. Hisihda, *Bull. Chem. Soc. Jpn.*, **49**, 1075 (1976).

3) M. Umehara, H. Takayanagi, H. Ogura, and S. Hisida, *Bull. Chem. Soc. Jpn.*, in press.

4) E. J. Corey and R. A. Sneen, *J. Am. Chem. Soc.*, **78**, 6267 (1956).

ESR Study on Molecular Alignment of Various Nitroxides in a Nematic Liquid Crystal†

Hisao TANAKA*,†† and Keiji KUWATA

Department of Chemistry, Faculty of Science, Osaka University, Toyonaka, Osaka 560

(Received December 5, 1977)

Various nitroxides with characteristic molecular shapes were studied by ESR spectroscopy to determine the relation between the molecular shape and the ordering in the nematic phase. The hyperfine splitting shifts upon going from the nematic to the isotropic phase and the relative widths of the nitroxyl nitrogen hyperfine lines were examined. Together with an estimate of the molecular dimensions, these results revealed that the ordering properties in three types of nitroxides(each of which has its elongated molecular axis along one of the three principal axes of the nitroxyl nitrogen dipolar tensor) can all be understo od well in terms of the slender molecular shape. This led to the deduction that the Saupe-type anisotropic induced dipole-dipole interaction between the overall molecule of nitroxide and the nematic molecule is superior to the local interaction between the substituent moieties of nitroxide and nematic molecule. The dipolar anisotropy of the β-proton of nitroxide was evaluated to be 3 G.

In the nematic mesophase, the solvent molecules which arrange their elongated axes in parallel through the anisotropic potential presented by Maier and Saupe[1] align first in the direction of the external magnetic field; then the solute molecules dissolved in the mesophase are forced to align partially with the field due to the solute-solvent interaction.[2-4] In consequence of this partial orientation of the solute molecules, the anisotropic spin interactions cause characteristic changes of the spin coupling and relaxation in nuclear magnetic[5-8] and electron spin resonances.[9-12]

We have investigated the solute-solvent interaction in a nematic solution by an ESR technique, using nitroxides as solutes. In the course of these studies, nitroxides have shown some advantages: they are generally stable, have large anisotropies of the dipolar spin interaction of the nitroxyl nitrogen, give relatively simple ESR patterns, and also are rich in the variety of their compounds.

In present study we have examined the effect of the molecular shape of nitroxide on its ordering property in the nematic phase. Another approach to the problem has been made using the diamagnetic species as solutes.[13] We have synthesized many stable nitroxides with a variety of molecular shapes, *e.g.* small or large and spherical or slender, and have measured the hyperfine(hf) splittings in the nematic and isotropic phases together with the widths of the nitrogen hf lines. We wish to report here that a complete examination of the various nitroxides led to the idea that the molecular shape makes a major contribution to the ordering property.

Experimental

The nematic liquid crystal *N*-(4-methoxybenzylidene)-4-butylaniline(MBBA) purchased from Fuji Color Co. was purified by a zone refining method with *ca.* 30 repetitions using Dry Ice–methanol as cooling reagent. It was dried with a mixture of molecular sieves 3A and 5A, followed by distillation under vacuum. The melting point of the purified material and its nematic-isotropic transition point were 20 and 43 °C, respectively, as found from differential thermal analysis(DTA).

The nitroxides studied are shown in Fig. 1. 2,2,6,6-Tetramethyl-4-oxo-1-piperidinyloxyl (Tanone; **6**) and 4-hydroxy-2,2,6,6-tetramethyl-1-piperidinyloxyl (Tanol; **4**) were obtained from Frinton Laboratories Co. The hydrazone derivatives of Tanone,**1**, **2**, and **3**, were synthesized by condensation[14] of the corresponding hydrazine and Tanone in water–methanol solvent. The five-membered nitroxides **5** and **7** were produced[15] by the respective 1-pyrroline *N*-oxides and hydrogen atoms which were generated by a microwave discharge in hydrogen gas. The nitroxides **8** and **9** were synthesized through reactions[16] of *N*-*t*-butyl-α-phenylmethanimine *N*-oxide with phenyllithium and with butyllithium, respectively, followed by air oxidation.

The ESR samples were prepared as a nematic solution containing *ca.* 10^{-3} mol/dm^3 of nitroxide in MBBA and were degassed by several repetitions of a freezing and thawing cycle under vacuum. The ESR spectra were recorded using a home-made X-band spectrometer with a JEOL 30 cm magnet under 455 kHz field modulation at the low limits of microwave and modulation powers. The temperature of a given sample was regurated by controlling the flow rate and temperature of dry nitrogen gas which first passed over a heater and then went around a sample tube set in a double-walled quartz tube inside a cavity. The temperature was read from an Ohkura AM-1001 microvoltmeter by placing

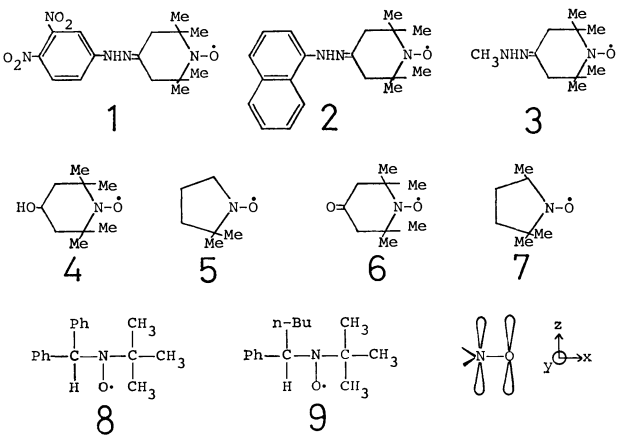

Fig. 1. The nitroxides in present study and the dipolar axes system of nitroxyl nitrogen.

† This work was presented at the 11th ESR symposium in Kanazawa, Oct. 1972.

†† Present address: Faculty of Pharmaceutical Sciences, Josai University, Sakado, Saitama 350-02.

a copper-constantan thermocouple near the sample tube and was constant to within ±1 °C.

Results

For the nitroxides **1**—**4** and **6**, the ESR spectrum consisted of only three hf absorptions due to the coupling of the nitroxyl nitrogen. For **5**, **7**, **8**, and **9** each of these three was further split into a doublet or triplet due to the couplings of one or two protons in β-position to the nitroxyl group. The nitrogen hf splitting a_N^{nem} and proton hf splitting a_H^{nem} measured in the nematic phase of MBBA at 25 °C, together with the a_N^{iso} and a_H^{iso} values in its isotropic phase at 50 °C, are given in Tables 1 and 2. For some nitroxides the temperature dependence of the nitrogen hf splitting in both nematic and isotropic phases is shown in Fig. 2.

The width of the low field nitrogen hf line, ΔH_1, was slightly but apparently different from the width of the central line, ΔH_0, although the linewidth on the high field side, ΔH_{-1}, was greatly broadened for all the nitroxides in the nematic phase. The relative widths $\Delta H_1/\Delta H_0$ and $\Delta H_{-1}/\Delta H_0$ which were estimated from the relation[17] $\Delta H_M/\Delta H_0=\sqrt{h_0/h_M}$ (h; peak to peak height) are listed in Table 3.

Table 1. Nitrogen hf splitting a_N^{nem} in the nematic phase of MBBA at 25 °C, a_N^{iso} in its isotropic phase at 50 °C, shift $a_N^{nem}-a_N^{iso}$, and ordering parameter θ_{zz} (1G=10^{-4} T)

Nitroxide	a_N^{nem}/G	a_N^{iso}/G	$(a_N^{nem}-a_N^{iso})$/G	θ_{zz}
1	12.35	14.56	−2.21	−0.135
2	12.98	14.69	−1.71	−0.104
3	13.74	14.64	−0.90	−0.055
4	15.49	15.51	−0.02[a]	—
5	13.55	13.55	0.00[a]	—
6	13.41	14.61	−1.20	−0.073
7	13.54	14.90	−1.36	−0.083
8	16.71	14.93	+1.78	+0.110
9	16.02	14.73	+1.26	+0.079

a) These are zero within an experimental error of ±0.05 G.

Table 2. Proton hf splitting a_H^{nem} in the nematic phase of MBBA at 25 °C, a_H^{iso} in its isotropic phase at 50 °C, and shift $a_H^{nem}-a_H^{iso}$ for the nitroxides with β-protons (1G=10^{-4} T)

Nitroxide	a_H^{nem}/G	a_H^{iso}/G	$(a_H^{nem}-a_H^{iso})$/G
5	19.17	19.18	−0.01
7	20.35	20.74	−0.39
8	3.16	3.36	−0.20
9	2.33	2.49	−0.16

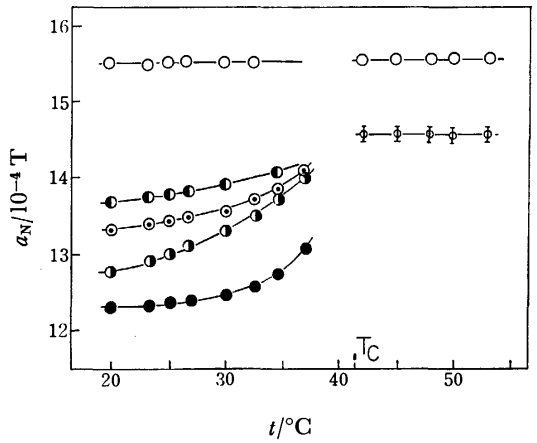

Fig. 2. Temperature dependence of the nitrogen hf splitting for some nitroxides measured above and below the nematic-isotropic transition point of MBBA (T_c): ●: **1**, ◑: **2**, ◐: **3**, ○: **4**, ⊙: **6**, and Φ; **1**—**3** and **6** in the isotropic range.

Table 3. Relative widths $\Delta H_1/\Delta H_0$ and $\Delta H_{-1}/\Delta H_0$ among three nitrogen hf lines, measured in the nematic phase of MBBA at 25 °C

Nitroxide	$\Delta H_1/\Delta H_0$	$\Delta H_{-1}/\Delta H_0$
1	0.94	1.83
2	0.96	1.62
3	0.96	1.55
6	1.04	1.45
7	1.03	1.42
8	1.04	1.85
9	1.04	1.75

As seen in Table 1, the coupling shift $a_N^{nem}-a_N^{iso}$ upon going from the nematic to the isotropic phase is a negative value for the nitroxides **1**—**3**, **6**, and **7**, is zero within experimental error for **4** and **5**, and is a positive value for **8** and **9**. The five nitroxieds with a negative shift are divided into two groups with respect to $\Delta H_1/\Delta H_0$: the three nitroxides **1**—**3** with $\Delta H_1/\Delta H_0$ less than 1.00 and the two **6** and **7** with $\Delta H_1/\Delta H_0$ more than 1.00. Thus, from the viewpoints of both splitting shift and relative width, the present nitroxides can be classified into four groups: **1**—**3**, **4** and **5**, **6** and **7**, and **8** and **9**.

Discussion

*Nitroxides **1**—**3**.* The principal axes system of the nitroxyl nitrogen dipolar tensor in nitroxides is shown in Fig. 1: here the z-axis is along the nitrogen π-orbital, the x-axis is extended along the N–O bond, and the y-axis is perpendicular to both the x- and the z-axes. We adopt the principal values[18] of the tensor of Tanone, *i.e.* $A_{Nzz}=16.4$ and $A_{Nxx}=A_{Nyy}=-8.2$ G for all the nitroxides studied here. Then, taking into account the axial symmetry of the dipolar tensor, the ordering element[19] about the z-axis, θ_{zz} can be simply related to the observed shift $a_N^{nem}-a_N^{iso}$, as in Eq. 1.[20]

$$a_N^{nem}-a_N^{iso}=\theta_{zz}A_{Nzz} \quad (1)$$

The parameter θ_{zz} takes a positive value between 0 and 1 when the z-axis is preferentially along the external magnetic field. It takes a negative value between 0 and −1/2 when the z-axis is preferentially across the field, in correspondence to a partial orien-

tation of the solute molecules in the nematic phase. In the extremes of alignment of the z-axis with respect to the field, the θ_{zz} value ideally reaches 1 or $-1/2$. Of course in the isotropic phase it is 0.

The θ_{zz} values at 25 °C are estimated from Eq. 1 and the $a_N^{nem}-a_N^{iso}$ values and are shown in Table 1. In this table we find that the θ_{zz} values in nitroxides **1**—**3** are all negative, while the absolute values are in the increasing order from **3** to **1**, indicating that the most preferential alignment of the z-axis across the field is in **1**. This order was conserved at all the other temperatures measured in the nematic phase, as shown in Fig. 3.

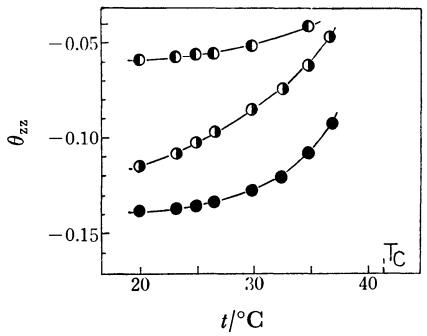

Fig. 3. Temperature dependence of the ordering parameter θ_{zz} for some nitroxides in the nematic phase of MBBA: ●: **1**, ◑: **2**, and ◐: **3**.

From the relative width $\Delta H_1/\Delta H_0$ we can determine the molecular axis directed preferentially to the field, according to the theoretical results[12,21-23] on the anisotropic spin relaxation in a low region of the solute alignment, such as present cases: the molecular axis with the maximum Brownian rotation is near the x-axis of nitroxide when $\Delta H_1/\Delta H_0<1$, while it is near the y- or z-axis when $\Delta H_1/\Delta H_0>1$. In addition, if the molecular shape of the present nitroxide is approximated as an ellipsoid,[13] the axis with the maximum Brownian rotation corresponds to the elongated molecular axis and hence the axis directed along the field.

Thus we can deduce that, for the nitroxides **1**—**3** with ΔH_1 smaller than ΔH_0, the x-axis represents the alignment axis along the field. Supporting this deduction, the Dreiding model for these radicals showed the elongated molecular axis closest to the x-axis. The alignment degrees of the x-axis, θ_{xx}, are calculated from the θ_{zz} values and the relation $\theta_{xx}=-2\theta_{zz}$, which is derived from the assumption of the traceless property of the ordering matrix ($\theta_{xx}+\theta_{yy}+\theta_{zz}=0$) and its axial symmetry in the ellipsoidal molecule ($\theta_{yy}=\theta_{zz}$); they are 0.27. 0.21, and 0.11 for the nitroxides **1**, **2**, and **3**, respectively. These values mean that the nitroxide **1** aligns along the field most preferentially, while **3** aligns the least.[24]

From a glance of Fig. 1, it can be seen that the above order in the alignment degrees is related to the difference in the molecular shapes. Indeed, the Dreiding model allows us to estimate rough molecular dimensions of the nitroxides and to give the $L_x/L_\perp$ values of 1.9, 1.5, and 1.2 for the nitroxides **1**, **2**, and **3**, respectively, where L_x is the molecular length along the x-axis and $L_\perp$ is the larger one of L_y and L_z.

A good agreement between the order of $L_x/L_\perp$ values and that of the θ_{xx} values indicates that the more slender the molecular shape of the nitroxide is, the higher its alignment degree becomes. The bulkiness of the molecule and the properties of the substituent moieties do not seem to exert a primary effect on the molecular ordering of the nitroxides.

*Nitroxides **4** and **5**.* These species showed no appreciable shift in the splitting constants (Table 1 and Fig. 2). An absence of the solute alignment can be explained in terms of the spherical property but not in terms of the smallness.

*Nitroxides **6** and **7**.* Interestingly, these small radicals can align in the nematic phase, giving negative splitting shifts, although the six-membered nitroxides **4** and **6**, as well as the five-membered nitroxides **5** and **7**, are similar to each other in molecular structure and in mass. In the latter two the introduction of the third methyl group into the β-position of the five-membered ring of **7** may lead to a slight extention of the molecular dimension along the y-axis of the dipolar principal axes in **7**. In fact, the $L_\perp/L_y$ value (where $L_\perp$ is the larger one of L_x and L_z) is 0.7 for **7** while it is 0.9 for **5**. This small difference in the molecular shape allows the y-axis of **7** to orient along the external field and prevents **5** from such an alignment. The observation of the relative width ($\Delta H_1/\Delta H_0>1$) could also support the alignment of the y-axis along the field in **7**, in contrast to the alignment of the x-axis along the field in **1**—**3**.

The nitroxide **6** has the carbonyl group in the γ-position of the six-membered ring and **4** has the hydroxyl group in the same position. In addition, as has been previously suggested,[25] **6** prefers a twisted form and **4** prefers a chair form in the ring conformation. Both these facts tend to shorten slightly the molecular dimension of the x-axis in **6**, while keeping the length of the y-axis in both nitroxides constant ($L_\perp/L_y$; 0.8 for **6** and 0.9 for **4**). This allows the y-axis of **6** to orient along the field as in the case of **7**. The relative width $\Delta H_1/\Delta H_0$ of 1.04 does not conflict with the above view.

From the results in the relatively small nitroxides **4**—**7** we recognize that the major factor in determining the solute alignment in the nematic phase is not the mass of the nitroxide but rather its slenderness. The effect of the local interaction between the polar group (hydroxyl in **4** or carbonyl in **6**) and the solvent molecule does not affect primarily the molecular ordering, as shown by the fact that the nitroxide **4** or **6** is analogous to **5** or **7**, respectively, in the ordering property.

*Nitroxides **8** and **9**.* These are unique nitroxides which provide positive splitting shifts and hence have their z-axes in the direction along the external field in the nematic phase. A possible explanation of the preferential alignment of the z-axis along the field is given on the basis of a special configuration: the elongated molecular axis linking the two phenyl moieties in **8** and that linking the phenyl and butyl moieties in **9** are nearly parallel to the respective z-axes; the free rotation around the bond between nitrogen and the carbon attached by those substituents is also restricted.

The above picture could be supported by estimating

the dihedral angle of the β-H–C bond to the π-orbital of the nitroxyl nitrogen in both nitroxides. The observed Fermi coupling of the β-proton, a_H^{iso}, is related to the dihedral angle ϕ_H in the McConnell Eq. 2,[26] where the negligible term independent of ϕ_H is excluded.

$$a_H^{iso} = B\rho_N \cos^2 \phi_H \quad (2)$$

The product $B\rho_N$, where B is a constant and ρ_N is the unpaired electron density on the nitrogen atom, is usually taken for nitroxide as 25 G ($B \simeq 50$G and $\rho_N \simeq 0.5$).[27] Then, from the a_H^{iso} values in Table 2, we can obtain *ca.* 70 ° for ϕ_H in both **8** and **9**. Hence, as seen in the Neumann projection (Fig. 4), the axis linking the two bulky groups which attach to the carbon which is bonded to the β-proton is approximately parallel to the z-axis.

Now we can conclude as follows, summarizing the results of the ordering preferences in all the nitroxides: with respect to the principal axes of the nitroxyl nitrogen dipolar tensor, the nitroxides **1**—**3** orient their elongated x-axes along the field, **6** and **7** orient their elongated y-axes along the field, and **8** and **9** orient their elongated z-axes along the field (Table 4). The nearly spherical nitroxides **4** and **5** do not show any appreciable orientation. The alignment degree becomes higher for the more slender ellipsoid in the molecular shape of the solute, as can be seen from the comparison among **1**—**3**. The substituent groups of the nitroxide mainly act on the ordering property through the effect of their shapes on the overall molecular shape. These results taken together lead us to consider that the major interaction between nitroxide and nematic molecules is the Saupe-typed anisotropic dispersion interaction[1-4] which is most stabilized when the long axes of both solute and solvent molecules, along which the induced dipoles are distributed uniformly over the molecules, are arranged in parallel to each other. Then the slender shape of the nitroxide molecule, corresponding to the high anisotropy of the induced dipole, causes its high ordering in the nematic phase through the effective solute-solvent interaction. These results correspond to the results[13] in the case of the use of diamagnetic species as solutes.

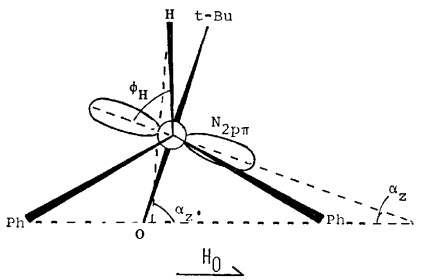

Fig. 4. Neumann projection of nitroxide **8** oriented to the external field in the nematic phase. In nitroxide **9** whether of the two phenyl moieties is only replaced by a butyl moiety. The ϕ_H, α_z, and $\alpha_{z'}$ are defined in the text.

TABLE 4. PREFERENTIAL ALIGNMENT TO THE EXTERNAL FIELD H_0 IN THE PRESENT NITROXIDES

H_0[a] ⟶	Sign of θ_{zz}	Relative width	Preferential axis along H_0[b]	Nitroxides
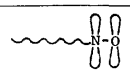	−	$\Delta H_0 > \Delta H_1$	x	1, 2, 3
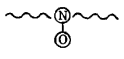	−	$\Delta H_0 < \Delta H_1$	y	6, 7
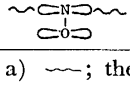	+	$\Delta H_0 < \Delta H_1$	z	8, 9

a) ⟶; the elongated molecular axis. b) x, y, and z; the principal axes of the nitrogen dipolar tensor.

Hf Anisotropy of β-Proton in Nitroxide. As shown in Table 2, the splitting shifts of the β-proton, $a_H^{nem} - a_H^{iso}$, in the nitroxides **7**—**9** are rather small compared with the respective splitting shifts of the nitroxyl nitrogen, indicating the small hf anisotropy of the β-proton. We can estimate the amount of the anisotropy from the example of nitroxide **8**: under a point dipole approximation[28] for the N–O group, the maximal principal value $A_{Hz'z'}(=-2A_{H\perp'})$ of the dipolar spin interaction is found along the axis directed from the β-proton towards the point dipole located in the center of the N–O bond. Then with respect to this axis(z') a relation similar to Eq. 1 exists also in the case of the β-proton ($a_H^{nem} - a_H^{iso} = \theta_{z'z'} A_{Hz'z'}$). From both equations the $A_{Hz'z'}$ is given by

$$A_{Hz'z'} = \frac{\theta_{zz} A_{Nzz} (a_H^{nem} - a_H^{iso})}{\theta_{z'z'} (a_N^{nem} - a_N^{iso})}. \quad (3)$$

The θ_{ii} is written as follows, assuming an ellipsoidal molecular shape:

$$\theta_{ii} = \theta_{mol}(3\cos^2\alpha_i - 1)/2, \quad (4)$$

where θ_{mol} is the alignment degree of the elongated molecular axis and α_i the angle which this makes with the i-axis.

We can take the elongated axis of the nitroxide **8** along the axis linking the centers of the phenyl groups, according to the previous result, and then find the α_z of 20° and $\alpha_{z'}$ of 86° by using the dihedral angle of 70° and the standard bond lengths and angles[29] (Fig. 4). Substituting the A_{Nzz} of Tanone and the $a_N^{nem} - a_N^{iso}$, $a_H^{nem} - a_H^{iso}$, θ_{zz}, and $\theta_{z'z'}$ of **8** into Eq. 3, we obtain 3.1 G for the $A_{Hz'z'}$. This value of the dipolar anisotropy is as small as expected and corresponds to the small splitting shifts in the nematic phase.

The authors wish to thank Professor E. G. Janzen of Georgia University for gifts of *N*-*t*-butyl-α-phenylmethanimine *N*-oxide and 1-pyrroline *N*-oxides and Professor Shyuzo Seki of Osaka University for zone refining and DTA measurements.

References

1) W. Maier and A. Saupe, *Z. Naturforsch., Teil A*, **14**, 1146 (1959); **15**, 287 (1960); **16**, 816 (1961).
2) A. Saupe, *Z. Naturforsch., Teil A*, **20**, 572 (1965).
3) D. H. Chen, P. G. James, and G. R. Luckhurst, *Mol. Phys.*, **11**, 205(1966).
4) P. G. James and G. R. Luckhurst, *Mol. Phys.*, **19**, 489 (1970).

5) L. C. Snyder and S. Meiboom, *J. Chem. Phys.*, **47**, 1480 (1967).
6) A. Saupe, *Angew. Chem. Int. Ed. Engl.*, **7**, 97 (1968).
7) J. Nehring and A. Saupe, *Mol. Cryst. Liq. Cryst.*, **8**, 403 (1969).
8) J. A. Murphy and J. W. Doane, *Mol. Cryst. Liq. Cryst.*, **13**, 93 (1971).
9) S. H. Glarum and J. H. Marshall, *J. Chem. Phys.*, **46**, 55 (1967).
10) R. Ferruti, G. Gill, M. A. Harpold, and M. P. Klein, *J. Chem. Phys.*, **50**, 4545 (1969).
11) C. Covaja, G. Giacometti, K. D. Kopple, and Ziauddin, *J. Am. Chem. Soc.*, **92**, 3919 (1970).
12) P. L. Nordio and P. Busolin, *J. Chem. Phys.*, **55**, 5485 (1970).
13) J. C. Robertson, C. T. Yim, and D. F. R. Gilson, *Can. J. Chem.*, **49**, 2345 (1971).
14) E. G. Rozantsev, "Free Nitroxyl Radicals," translated by B. J. Hazzard, Plenum Press, New York (1970).
15) E. G. Janzen, T. Kasai, and K. Kuwata, *Bull. Chem. Soc. Jpn.*, **46**, 2061(1973).
16) E. G. Janzen and B. J. Blackburn, *J. Am. Chem. Soc.*, **91**, 4481 (1969).
17) As is well known, the signal intensity(I) is related to the peak-to-peak height(h) and width(ΔH) as $I \propto h(\Delta H)^2$.
18) O. H. Griffith, D. W. Cornell, and H. M. McConnell, *J. Chem. Phys.*, **43**, 2809 (1965).
19) A. Saupe, *Z. Naturforsch., Teil A*, **19**, 161 (1964).
20) H. R. Falle and G. R. Luckhurst, *J. Magn. Reson.*, **3**, 161 (1970). Equation 1 is derived by setting $A_{Nxx}=A_{Nyy}$ in the general formula, $a_N^{nem}-a_N^{iso}=\theta_{zz}A_{Nzz}+(\theta_{xx}-\theta_{yy})(A_{Nxx}-A_{Nyy})/3$, where $\theta_{ii}=(3l_il_i-1)/2$. The l_i is the direction cosine between the principal i-axis of the tensor A_N and the external field.
21) J. H. Freed, *J. Chem. Phys.*, **41**, 2077 (1964).
22) P. L. Nordio, *Chem. Phys. Lett.*, **6**, 250 (1970).
23) P. L. Nordio, G. Rigatti, and U. Segre, *J. Chem. Phys.*, **56**, 2117 (1972).
24) Such a comparison among the radicals **1**—**3** is justified by the following reasoning: with an ellipsoidal approximation of molecular shape the alignment degree of the molecular i-axis, θ_{il}, can be written as $\theta_{il}=\theta_{mol}(3\cos^2\alpha-1)$, where θ_{mol} is the alignment degree of the elongated molecular axis and α the angle both axes make. The radicals **1**—**3**, all hydrazone derivatives of Tanone, have approximately the same angle of α. Then the structural difference in **1**—**3** changes the θ_{il} value only through the difference of θ_{mol}.
25) M. J. S. Dewar and P. J. Grisdale, *J. Am. Chem. Soc.*, **84**, 3539 (1962).
26) C. Heller and H. M. McConnell, *J. Chem. Phys.*, **32**, 1535 (1960).
27) J. C. Espie, H. Lemaire, and A. Rassat, *Bull. Soc. Chim. Fr.*, **1969**, 399.
28) Generally, this is recognized as a fairly good approximation for the β- or γ-proton.
29) J. A. Pople and D. L. Beveridge, "Approximete Molecular Orbital Theory," McGraw-Hill, New York (1970), p. 110. For the bond lengths and angles concerned here: N–O, 1.24; N–C, 1.47; C–C(phenyl), 1.52; C(phenyl)–C(phenyl), 1.39; and C–H, 1.09 Å; sp^2 angle, 120°, and sp^3 angle, 109.5°.

The Crystal Structure of the B-form of Stearic Acid

Midori GOTO* and Eiichi ASADA
National Chemical Laboratory for Industry, Hon-cho, Shibuya, Tokyo 151
(Received December 6, 1977)

The crystal structure of the B-form of stearic acid has been studied by X-ray diffraction. The structural parameters were refined by the block-diagonal least-squares method, and the final R value was 0.084. In this structure, the bond between the second and third carbon atoms was found to be the *gauche* conformation, although the other bonds were in the *trans* conformation usually seen in normal fatty acids.

The crystal structure of the B-form of stearic acid has been studied only by two-dimensional Fourier methods. von Sydow[1] determined the crystal structure in the a-axis projection, and subsequently Larsson and von Sydow[2] determined it in the b-axis projection. Larsson and von Sydow[2] mentioned, however, that an attempted three-dimensional refinement was not successful because of the disorder in the crystal.

The present authors could obtain fairly good single crystals of the B-form of stearic acid, and reinvestigated its crystal structure.

Experimental

Stearic acid was purified by recrystallization from a methanol solution. The B-form crystal was obtained by crystallization in a 2,2,4-trimethylpentane solution, kept for two weeks at room temperature.

The infrared absorption spectrum showed that the crystal was in the B-form, not in the E-form discovered by Holland and Nielsen.[3] Twinning was not observed for the crystal used.

The diffraction intensities were measured by means of a Rigaku-Denki four-circle diffractometer by using graphite monochromated Cu $K\alpha$ radiation.† The crystal data and experimental conditions are given in Table 1, compared with the corresponding data of other workers.[1,2]

Structure Determination

The $|F_c(hkl)|$ values calculated from (x,z) coordinates by Larsson *et al.*[2] and the (y,z) coordinates calculated by von Sydow,[1],†† did not agree with the $|F_o(hkl)|$ values obtained in this experiment; the disagreement of ($11l$) reflections was especially

Table 1. Crystal data, experimental conditions, and methods of analysis

	Present work (1977)	von Sydow[1] (1955)	Larsson and von Sydow[2],a) (1966)
Crystal system	Monoclinic	Monoclinic	Monoclinic
a	5.587(10) Å	5.591(11) Å	5.591(11) Å
b	7.386(6)	7.404(8)	7.404(8)
c	49.33(8)	49.38(10)	43.99(10)
β	117.24°(9)	117.22°(7)	94.60°(15)
Space group	$P2_1/a$	$P2_1/a$	$P2_1/a$
Total number of reflections	640($2\theta \leqq 120$)	158($\theta \leqq 60$)	100
Measurement of intensity	Four-circle diffractrometer with a scintillation counter	Weisenberg photograph by eye	Weisenberg photogradh by eye
$\frac{\sum\|k\|F_o^p\| - \|F_o^A\|\|}{\sum\|F_o^A\|}$ [b]	—	0.19(k=1.45)	0.21(k=1.00)
Analysis	Three-dimensional Least-squares method	$0kl$ projection Fourier and difference Fourier method	$h0l$ projection Full matrix least-squares method (Three-dimensional least-squares refinement was not successful.)
R	0.084	0.18	0.168

a) A transformed unit cell given by von Sydow (1955) was chosen for convenience of calculation. However, the c and β values given by Larsson *et al.* might be somewhat erroneously determined; more reasonable values would be c=43.84 Å and β=89.56°. If these corrective values are used, the unit cell given by Larsson *et al.* can be transformed by the following matrix to that of Sydow or the present authors.

$$\begin{vmatrix} -1 & 0 & 0 \\ 0 & -1 & 0 \\ 4 & 0 & 1 \end{vmatrix}$$

b) $|F_o^p|$: $|F_o|$ of the present work. $|F_o^A|$: $|F_o|$ by other authors.[1,2]

† The table of the observed and calculated structure factors has been deposited with the Office of the Chemical Society of Japan (Document No. 7828).

†† The z coordinates prepared by Larsson *et al.*[2] are almost identical with those prepared by von Sydow.[1]

noticeable. The least-squares method did not lead to further refinement at the R-value of 37% when their coordinates were used.

The present authors, therefore, reinvestigated the structure, determining the positions of carbon atoms from the Patterson map and the packing of the molecules.

The positions of oxygen atoms were obtained by means of difference synthesis. The hydrogen-atom positions, with the exception of that of the carboxyl hydrogen atom, were calculated by assuming C–H distances of 1.10 Å and a tetrahedral arrangement. The structure was refined by the block-diagonal least-squares method using the HBLS program (Ashida).[4] The R-value was reduced to 0.084. The final atomic parameters obtained are listed in Table 2.

The y and z coordinates obtained by the present authors do not significantly differ from those of von Sydow,[1] but the x coordinates of atoms, especially those near the carboxyl group, were not in agreement with those prepared by Larsson *et al.*[2]

Figure 1 illustrates the difference in the two structures by the projection along the b-axis. The two structures are different, especially near the carboxyl group. The atomic positions prepared by Larsson *et al.*[2] were too erroneous to be refined by the least-

Table 2(a). Fractional atomic coordinates ($\times 10^4$) and anisotropic temperature factors ($\times 10^4$) for C and O atoms

	X	Y	Z	B_{11}	B_{22}	B_{33}	B_{12}	B_{13}	B_{23}
C1	−1338(41)	278(29)	333(5)	391(103)	110(66)	8(2)	190(68)	60(11)	21(9)
C2	1564(30)	442(33)	578(5)	−189(74)	316(69)	8(2)	−136(69)	−16(8)	29(10)
C3	2181(31)	−458(30)	876(4)	170(85)	148(53)	3(1)	80(63)	−9(8)	8(7)
C4	910(38)	391(29)	1056(5)	356(105)	138(53)	8(2)	254(72)	57(11)	−16(9)
C5	2053(43)	−452(34)	1368(5)	710(151)	219(68)	5(2)	−205(89)	20(12)	13(9)
C6	803(41)	391(34)	1562(4)	535(124)	236(64)	2(1)	−132(83)	−7(10)	13(8)
C7	2045(32)	−328(31)	1881(5)	53(83)	177(59)	10(2)	−18(61)	46(10)	−17(9)
C8	753(35)	382(34)	2074(4)	210(98)	273(66)	5(2)	100(74)	5(9)	36(9)
C9	1945(46)	−367(32)	2399(5)	780(165)	134(55)	7(2)	4(82)	75(14)	−24(8)
C10	779(40)	413(32)	2595(5)	450(118)	152(54)	6(2)	23(80)	25(11)	−14(8)
C11	2004(37)	−356(30)	2920(5)	232(104)	126(51)	10(2)	104(70)	59(11)	−7(9)
C12	715(36)	373(33)	3106(5)	307(113)	206(65)	8(2)	225(74)	56(11)	6(9)
C13	2006(43)	−395(34)	3433(5)	748(157)	188(63)	5(2)	−51(89)	60(13)	−3(8)
C14	831(41)	388(34)	3629(5)	577(135)	229(70)	5(2)	−181(85)	44(11)	−3(9)
C15	2097(43)	−385(35)	3957(6)	546(141)	242(70)	11(2)	56(87)	101(14)	−33(10)
C16	876(37)	363(33)	4151(5)	261(108)	245(69)	7(2)	148(74)	27(10)	16(9)
C17	2224(54)	−419(39)	4476(6)	1104(200)	308(84)	7(2)	70(115)	97(16)	5(11)
C18	1155(49)	326(43)	4689(6)	445(139)	513(116)	13(3)	−235(113)	58(15)	−38(14)
O1	−2062(28)	1301(21)	94(3)	414(79)	216(39)	8(1)	102(49)	50(8)	35(7)
O1	−3041(25)	−764(21)	361(3)	356(75)	257(44)	7(1)	−101(57)	29(7)	12(6)

Table 2(b). Atom coordinates ($\times 10^3$) and isotropic temperature factors for H atoms (Å)

	X	Y	Z	B		X	Y	Z	B
H(C2)	167(88)	164(81)	63(9)	29(19)	H(C11)	427(40)	−19(32)	304(5)	10(7)
H(C2)	317(72)	−20(64)	48(8)	25(15)	H(C11)	175(40)	−175(35)	291(5)	10(7)
H(C3)	434(26)	−46(22)	103(3)	4(4)	H(C12)	−134(39)	17(34)	299(5)	10(7)
H(C3)	149(42)	−187(35)	86(5)	11(7)	H(C12)	78(38)	185(34)	311(4)	10(6)
H(C4)	−112(42)	8(33)	93(5)	11(7)	H(C13)	401(50)	−5(43)	355(6)	14(9)
H(C4)	126(44)	189(37)	109(5)	13(8)	H(C13)	180(42)	−191(36)	341(5)	11(8)
H(C5)	404(36)	−21(28)	148(4)	8(6)	H(C14)	−136(34)	10(28)	351(4)	7(5)
H(C5)	173(33)	−199(28)	134(4)	7(6)	H(C14)	112(34)	184(30)	365(4)	8(6)
H(C6)	−149(37)	5(28)	145(4)	8(6)	H(C15)	419(52)	−23(42)	404(6)	15(10)
H(C6)	114(34)	182(30)	158(4)	7(6)	H(C15)	177(39)	−182(32)	394(4)	9(6)
H(C7)	424(44)	−19(36)	199(5)	12(8)	H(C16)	−121(41)	22(33)	405(5)	10(7)
H(C7)	180(41)	−175(38)	188(5)	12(7)	H(C16)	111(33)	189(28)	415(4)	7(5)
H(C8)	−136(39)	16(32)	196(5)	10(7)	H(C17)	417(48)	−24(43)	458(6)	15(9)
H(C8)	80(40)	189(36)	209(5)	10(7)	H(C17)	193(31)	−182(26)	445(4)	6(5)
H(C9)	406(45)	−11(38)	251(6)	13(9)	H(C18)	−104(31)	6(25)	459(4)	5(5)
H(C9)	178(30)	−180(26)	238(3)	5(5)	H(C18)	234(51)	−25(30)	494(5)	10(6)
H(C10)	−142(33)	13(28)	247(4)	8(6)	H(C18)	134(47)	178(36)	470(5)	12(8)
H(C10)	97(36)	183(31)	261(4)	9(6)					

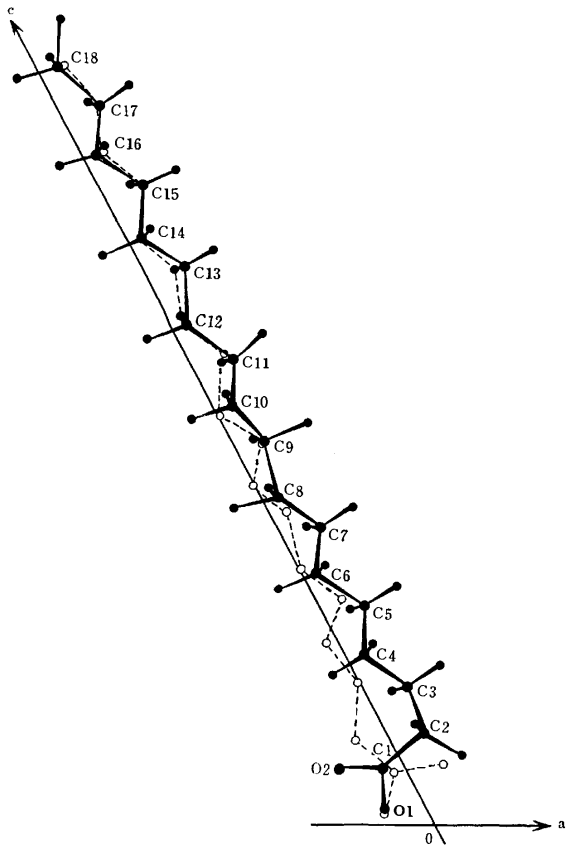

Fig. 1. The molecular structure projected along the b-axis. The structure obtained by Larsson *et al.* is shown by dotted lines (transformed into author's unit cell).

squares calculations.

Discussion

The bond lengths, bond angles, and internal rotation angles are shown in Table 3. An ORTEP[6] drawing is shown in Fig. 2.

It is evident from Fig. 1 or Fig. 2 that the molecules of the B-form of stearic acid do not form an all-*trans* zigzag chain, such as is usually found in fatty acids. The bond between the second and the third carbon atoms is in the gauche conformation. The internal rotation angle of this bond is calculated to be 68°, as is indicated in Table 3(c). von Sydow[1] suggested that the hydrocarbon chain was deformed near the carboxylic group, but he gave no details. Larsson *et al.*[2] did not mention this deformation; their structure was seen to be, rather, an all-*trans* zigzag chain.

The planarity of the chain is shown in Table 4. The dihedral angle between the plane of the carbon main chain and the plane containing the carboxyl group is 70°.

The subcell is orthorhombic, with dimentions of a_s=4.96 Å, b_s=7.39 Å, and c_s=2.50 Å. This is nearly the same as the C-form of lauric acid.[5]

The arrangement of the end group is shown in Fig. 3. As is commonly found in fatty acids, the molecules are bound together to form dimers through hydrogen bonds between the carboxyl groups. The hydrogen bond length is 2.65 Å, and the closest intermolecular

Table 3(a). Bond lengths (l/Å) and their estimated standard deviations

C1–O1	1.30(3)	C8–C9	1.53(3)
C1–O2	1.28(3)	C10–C11	1.54(4)
C1–C2	1.52(2)	C11–C12	1.50(4)
O2–O3	1.50(3)	C12–C13	1.54(3)
C3–C4	1.50(3)	C13–C14	1.51(4)
C4–C5	1.50(3)	C14–C15	1.55(3)
C5–C6	1.55(4)	C15–C16	1.51(4)
C6–C7	1.50(3)	C16–C17	1.54(3)
C7–C8	1.53(4)	C17–C18	1.53(5)

Table 3(b). Bond angles (φ/°) and their estimated standard deviations

C2–C1–O1	117(2)	C10–C9–C8	115(2)
C2–C1–O2	112(2)	C11–C10–C9	114(2)
C1–C1–O2	121(2)	C12–C11–C10	113(2)
C3–C2–C1	115(2)	C13–C12–C11	113(2)
C4–C3–C2	116(2)	C14–C13–C12	113(2)
C5–C4–C3	110(2)	C15–C14–C13	114(2)
C6–C5–C4	111(2)	C16–C15–C14	114(2)
C7–C6–C5	113(2)	C17–C16–C15	112(2)
C8–C7–C6	114(2)	C18–C17–C16	115(2)
C9–C8–C7	115(2)		

Table 3(c). Internal rotation angles (φ/°)

C3–C2–C1–O1	168	C11–C10–C9–C8	−180
C3–C2–C1–O2	−10	C12–C11–C10–C9	−177
C4–C3–C2–C1	−68	C13–C12–C11–C10	−179
C5–C4–C3–C2	−171	C14–C13–C12–C11	177
C6–C5–C4–C3	180	C15–C14–C13–C12	−180
C7–C6–C5–C4	−176	C16–C15–C14–C13	−179
C8–C7–C6–C5	−176	C17–C16–C15–C14	−179
C9–C8–C7–C6	178	C18–C17–C16–C15	178
C10–C9–C8–C7	176		

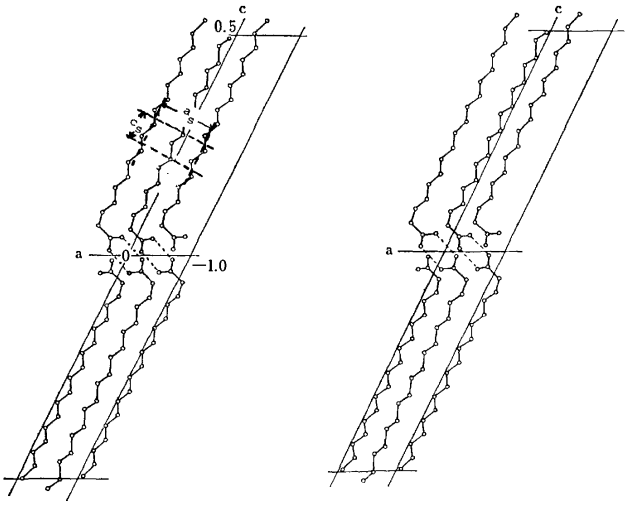

Fig. 2. A perspective view along the b direction drawn by ORTEP The a_sc_s plane of a subcell is shown by dotted lines.

Table 4. Least-squares planes and displacements of atoms from the planes

Carbon chain	Carboxyl group
$LX+MY+NZ=D$	$LX+MY+NZ=D$
$L=0.681$	$L=-0.256$
$M=0.732$	$M=0.731$
$N=-0.002$	$N=0.633$
$D=3.851$	$D=-1.302$

The equation expressed in the orthogonal Cartesian systm:
$Z//\mathbf{c}$ $X//\mathbf{a}^*$ $Y//\mathbf{c}\times\mathbf{a}^*$ in Å unit

Atom	Deviation	Atom	Deviation
C3	0.02	C1	−0.01
C4	0.05	C2	0.00
C5	−0.03	O1	0.00
C6	0.03	O2	0.00
C7	0.03		
C8	−0.02		
C9	−0.03		
C10	0.03		
C11	−0.01		
C12	−0.05		
C13	−0.03		
C14	−0.01		
C15	0.00		
C16	−0.01		
C17	0.02		
C18	0.06		
C1[a)]	−0.77		
C2[a)]	0.30		
O1[a)]	−0.46		
O2[a)]	−1.91		

a) These atoms are not included in the least-squares calculation.
The dihedral angle between the two planes=70°

distance of the end group (except the hydrogen bond) is 3.1 Å. This distance is nearly equal to that of the A-super form of lauric acid[7] and is shorter than that of the C-form of lauric acid,[5] in which the closest distance is 3.4 Å. This is because the C-form, the highest temperature form, is likely to have a looser structure than the B- and A- forms.

We wish to thank Professor Y. Iitaka of the University of Tokyo for his encouragement and helpful discussions. We are also grateful to Dr. J. Hiraishi and S. Tamura of this laboratory for performing the infrared absorption measurements.

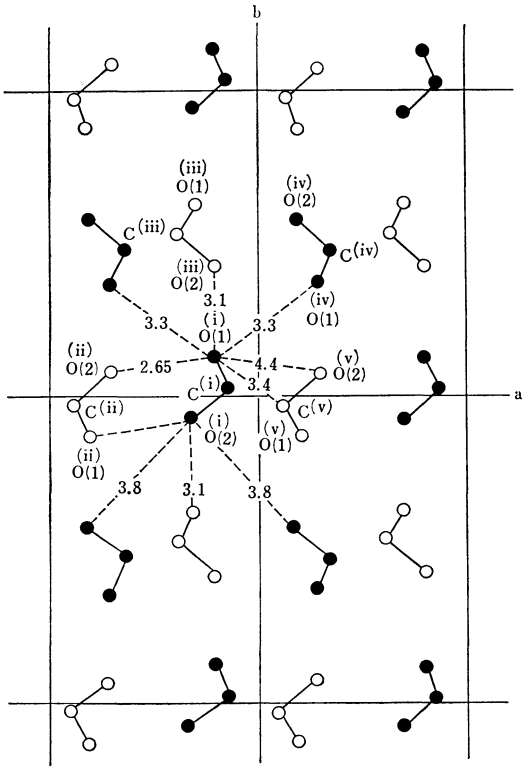

Fig. 3. Projection along the c axis.
Upper layer atoms ●,
lower layer atoms ○.
Symmetry operation code (i) x, y, z,
(ii) $-x, -y, -z$,
(iii) $1/2-x, 1/2+y, -z$,
(iv) $1/2+x, 1/2-y, z$,
(v) $1-x, 1-y, -z$.

References

1) E. von Sydow, *Acta Crystallogr.*, **8**, 557 (1955).
2) K. Larsson and E. von Sydow, *Acta Chem. Scand.*, **20**, 1203 (1966).
3) R. F. Holland and J. R. Nielsen, *J. Mol. Spectrosc.*, **9**, 436 (1962).
4) T. Ashida, HBLS(IV), The Universal Crystallographic Computing System (I), The Crystallographic Society of Japan, p. 65.
5) V. Vand, W. H. Morley, and T. R. Lomer, *Acta Crystallogr.*, **4**, 324 (1951).
6) C. K. Johnson, Oak Ridge National Laboratory ORNL-3794.
7) M. Goto and E. Asada, *Bull. Chem. Soc. Jpn.*, **51**, 70 (1978).

Absorption and Fluorescence Spectra of Anthracenecarboxylic Acids. I. 9-Anthroic Acid and Formation of Excimer

Satoshi SUZUKI,* Tsuneo FUJII, Nobuyuki YOSHIIKE,†
Shigeru KOMATSU,†† and Toshiko IIDA
Department of Industrial Chemistry, Faculty of Engineering, Shinshu University, Wakasato, Nagano 380

(Received December 8, 1977)

The absorption spectra of 9-anthroic acid (9-anthracenecarboxylic acid) in ethanol have been measured as a function of solute concentration. It was revealed that 9-anthroic acid forms a hydrogen-bonded dimer. The equilibrium constant for dimer formation was determined to be 6.6×10^4 mol^{-1} l in ethanol at 298 K. The fluorescence spectra of 9-anthroic acid have been investigated as a function of concentration and temperature in various solvents. An excimer mechanism was proposed for a broad fluorescence of 9-anthroic acid; the hydrogen-bonded dimer is excited and then associates with an unexcited hydrogen-bonded dimer to form an excited tetramer from which the broad fluorescence occurs.

The fluorescence spectrum of 9-anthroic acid (9-anthracenecarboxylic acid) in ethanol is strongly concentration-dependent. At a concentration below 10^{-5} mol/l the spectrum has an anthracene-like structure, while at a concentration above 10^{-3} mol/l it shifts to the red, turning into a broad structureless band. In order to elucidate this spectral change, Bazilevskaya and Cherkasov postulated that the linear-type dimers formed in the ground state rearrange themselves upon excitation into a characteristic excimer configuration, wherein the planes of anthracene rings are parallel.[1,2] On the other hand, Werner and Hercules explained the concentration dependence on the basis of an acid-base equilibrium, assigning the anthracene-like structured fluorescence to an ionized species.[3]

An excimer mechanism for the broad fluorescence of 9-anthroic acid is presented in this paper. In alcoholic solvents, 9-anthroic acid forms a hydrogen-bonded dimer in its ground state. The hydrogen-bonded dimer is excited and then associates with an unexcited hydrogen-bonded dimer to form an excited tetramer from which the broad fluorescence occurs. A discussion is given on an assumption of the excimer mechanism, validity of the assumption being made on the basis of experimental findings.

Experimental

9-Anthroic acid was purified by dissolution in base, precipitation with acid, and sublimation *in vacuo*. Ethanol (Wako Pure Chemical Industries, Inc., Super special grade) and propylene glycol (1,2-propanediol, Wako JIS S grade) were stored over molecular sieves 3A and then passed through a silica gel column. Toluene and methanol (Wako fluorometric grade) and acetonitrile (Wako spectrophotometric grade) were used. Hexane and isooctane (2,2,4-trimethylpentane) were purified in the usual way. The other solvents (JIS S grade) were used without further purification. The absorption spectra were recorded on a Hitachi EPS-3 recording spectrophotometer. The fluorescence and excitation spectra were obtained by means of a Hitachi MPF-2A fluorescence spectrophotometer and are given without corrections on quantum response of detecting and exciting systems and on reabsorption. The temperature was controlled with a metal cryostat (Torisha Laboratory, Ltd.).

Results and Discussion

Absorption Spectra and Dimer Formation. The absorption spectrum of 9-anthroic acid in ethanol closely resembles that of anthracene. The lowest frequency band with a fine structure may reasonably be assigned to the ^1L_a transition and the intense band at higher frequencies to the ^1B_b transition. Figure 1 shows the concentration dependence of absorption spectra of 9-anthroic acid in ethanol. As the concentration of 9-anthroic acid increases, the ^1L_a band shifts to the blue and the fine structure becomes less sharp. The ^1B_b band also shows a blue shift. Several isosbestic points appear in the spectra. These observations indicate that a certain equilibrium is involved in the ground state of this system.

The most probable origin of the appearance of the isosbestic points in the absorption spectra of 9-anthroic acid is monomer-dimer equilibrium or proton dissociation. In the following, discussion is made as to which

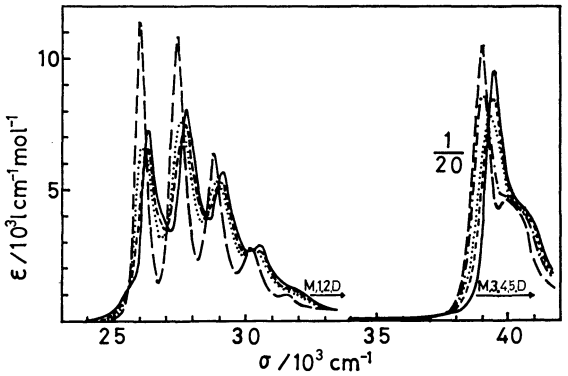

Fig. 1. The absorption spectra of 9-anthroic acid in ethanol at various concentrations and the estimated monomer and dimer absorption spectra. 1: 2.18×10^{-5} mol/l, 2: 1.09×10^{-4} mol/l, 3: 1.63×10^{-6} mol/l, 4: 1.63×10^{-5} mol/l, 5: 1.16×10^{-4} mol/l, M: the estimated monomer spectra, D: the estimated dimer spectra.

† Present address: Central Research Laboratory, Matsushita Electric Co., Ltd., Kadoma, Osaka.

†† Present address: Semiconductor Engineering Department, Semiconductor Division, Tokyo Shibaura Electric Co., Ltd., Kawasaki.

origin is valid on the basis of experimental evidence. Hereafter, the absorption band appearing at low concentrations in ethanol will be tentatively referred to as M absorption band, and the band at higher concentrations as D absorption band.

It has been well established that carboxylic acids have pK_a values in ethanol greater by about 5.8 than in water.[4,5] Since the reported pK_a value of 9-anthroic acid in water is 3.0[7] or 3.65,[6] it is estimated that that in ethanol is 8.8—9.4. If we assume that the concentration dependence of the absorption spectra in ethanol is attributed to proton dissociation, a pK_a value of 5.12 is obtained from the analysis of the observed concentration dependence of absorption spectra. This is too small to ascribe the concentration dependence of the absorption spectra to proton dissociation. From this point of view, proton dissociation is unfavorable as the origin of the spectral changes in this system.

When we ascribe the spectral changes to monomer-dimer equilibrium in this system, the equilibrium constant of dimer formation, K_D, can be determined by the usual procedure.[8] Thus, a K_D value of 6.6×10^4 mol^{-1} l was obtained for 9-anthroic acid in ethanol at 298 K. By using the observed spectral data at various concentrations and the K_D value, the monomer and dimer absorption spectra were determined. As shown in Fig. 1, the ^1L_a and ^1B_b bands become less sharp owing to dimer formation, which is consistent with general behavior of hydrogen bonding, but they show a blue shift. The origin of the unusual blue shift will be discussed later.

The formation of hydrogen-bonded dimers in aromatic carboxylic acids has been confirmed under various conditions for benzoic acid[8-11] and 1- and 2-naphthoic acids.[12] Besides the dimer formation, Kitamura and Baba reported that 1- and 2-naphthoic acid dimers further associate to give a higher-order complex which can be assumed to be a tetramer in a hydrocarbon rigid glass matrix at 77 K.[12] Similarly it is quite likely that 9-anthroic acid forms a hydrogen-bonded dimer under appropriate conditions. The monomer-dimer equilibrium constants for these acids are: 7.95×10^3 mol^{-1}. l for benzoic acid in hexane,[8] 7.6×10^4 mol^{-1} l for 1-naphthoic acid, and 3.4×10^4 mol^{-1} l for 2-naphthoic acid in a mixture of isopentane and methylcyclohexane (6:1 by volume).[12] It appears that the equilibrium constants increases with increase in the number of benzene rings and then decrease in solubility. Since 9-anthroic acid is hardly soluble in hydrocarbons, there is little possibility that monomer-dimer equilibrium is involved in hydrocarbon solvents. The monomer-dimer equilibrium of 9-anthroic acid might be observed only when a solvent of higher solubility such as ethanol is used. It thus seems that the K_D value we obtained is reasonable. In conclusion, 9-anthroic acid in ethanol forms a hydrogen-bonded dimer in its ground state.

9-Anthroic acid is hardly soluble in isooctane ($<10^{-5}$ mol/l). The absorption spectra of 9-anthroic acid in isooctane show no concentration dependence in the concentration range 10^{-5}—10^{-7} mol/l. The spectral shape in isooctane closely resembles D absorption band in ethanol. This indicates that 9-anthroic acid dissolves in isooctane in dimer form. The carboxyl group is a typical hydrophilic group, while the anthryl group is a hydrophobic group. The hydrophilic character of the carboxyl group will be masked by the dimer formation, so that the dimer form will be stable in aprotic solvents as compared with the monomer form.

Fluorescence Spectra. The fluorescence spectrum of 9-anthroic acid in ethanol has an anthracene-like structure at a concentration below 10^{-5} mol/l. With increase in concentration the fluorescence spectrum shifts to the red, turning into a broad structureless emission (Fig. 2). The structured fluorescence can tentatively be assigned to a monomer fluorescence and the broad fluorescence to an excimer fluorescence. Hereafter, the structured fluorescence band is referred to as M fluorescence band and the broad fluorescence band as E fluorescence band. The solvents in which 9-anthroic acid emits the structured M fluorescence are: *N*-methylformamide, formamide, ethylene glycol, propylene glycol, glycerol, methanol, ethanol, isobutyl alcohol, *s*-butyl alcohol, and water.

Figure 3 shows the concentration dependence of fluorescence spectra of 9-anthroic acid in toluene. 9-Anthroic acid emits a broad fluorescence which has a shoulder, lying at higher frequency than that of E fluorescence. The fluorescence of 9-anthroic acid in toluene shows no substantial concentration dependence

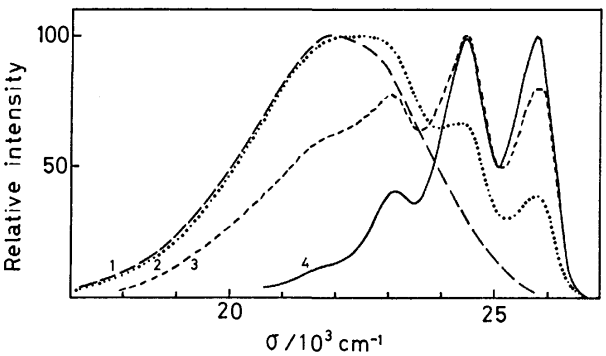

Fig. 2. The fluorescence spectra of 9-anthroic acid in ethanol at various concentrations. 1: 1.16×10^{-3} mol/l, 2: 1.29×10^{-4} mol/l, 3: 2.33×10^{-5} mol/l, 4: 1.16×10^{-6} mol/l. Methanol solution shows the analogous concentration dependence.

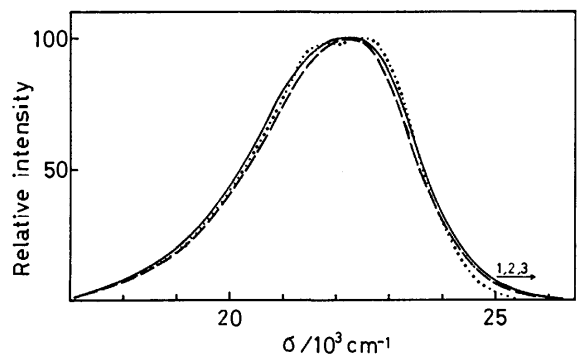

Fig. 3. The fluorescence spectra of 9-anthroic acid in toluene at various concentrations. 1: 1.2×10^{-3} mol/l, 2: 1.5×10^{-5} mol/l, 3: 3.0×10^{-7} mol/l.

down to 10^{-7} mol/l. These findings exclude the possibility of excimer emission for the broad fluorescence of 9-anthroic acid in toluene. The broad fluorescence band can be assigned to a dimer fluorescence and is hereafter referred to as D fluorescence band. The solvents in which 9-anthroic acid emits the broad D fluorescence only are: *N,N*-dimethylformamide, dimethyl sulfoxide, acetonitrile, acetone, 1,2-dichloroethane, tetrahydrofuran, methyl acetate, benzene, toluene, 1,4-dioxane, diethyl ether, hexane, isooctane, and *t*-butyl alcohol.

The spectral dependence of fluorescence spectra on the concentration of 9-anthroic acid in propylene glycol and isobutyl alcohol is given in Figs. 4 and 5. In propylene glycol, 9-anthroic acid emits M fluorescence only at lower concentrations. The fluorescence spectrum of 9-anthroic acid in isobutyl alcohol has M and D bands at 10^{-6} mol/l. The E band becomes obvious at concentration higher than 10^{-4} mol/l. Since 9-anthroic acid shows analogous spectral behavior both in ethanol and in propylene glycol, experimental studies on the temperature dependence of emission spectra were performed by using propylene glycol as a solvent instead of ethanol, because of experimental facility.

Figure 6 shows the excitation spectra of 9-anthroic acid at a concentration of 7.02×10^{-4} mol/l with observation at 410 and 540 nm. At this concentration,

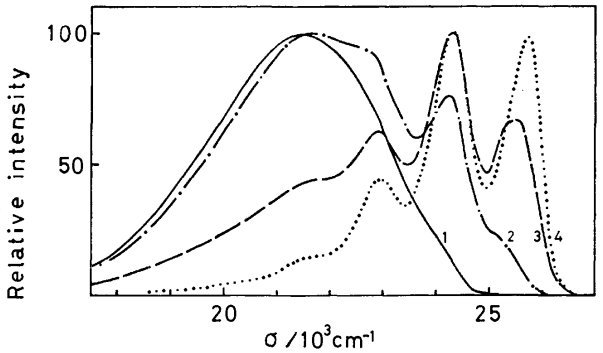

Fig. 4. The fluorescence spectra of 9-anthroic acid in propylene glycol at various concentrations. 1: 3.51×10^{-3} mol/l, 2: 7.02×10^{-4} mol/l, 3: 7.02×10^{-5} mol/l, 4: 1.01×10^{-5} mol/l.

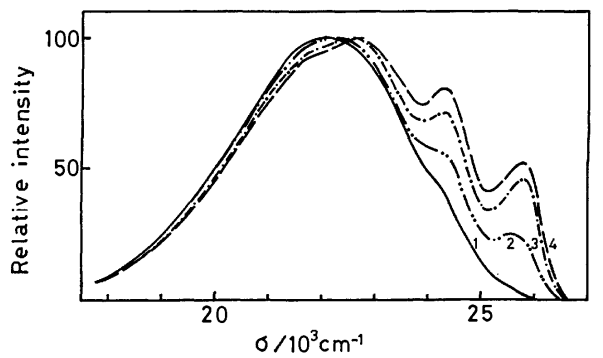

Fig. 5. The fluorescence spectra of 9-anthroic acid in isobutyl alcohol at various concentrations. 1: 10^{-3} mol/l, 2: 10^{-4} mol/l, 3: 10^{-5} mol/l, 4: 10^{-6} mol/l.

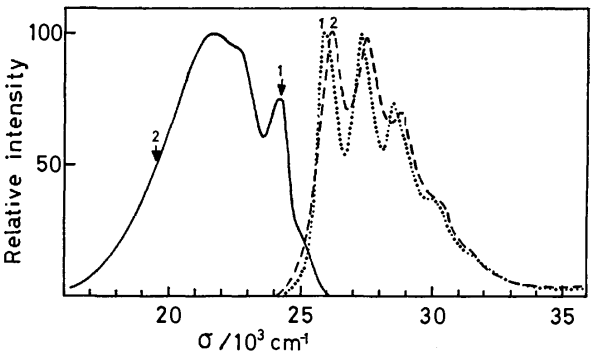

Fig. 6. The fluorescence and excitation spectra of 9-anthroic acid in propylene glycol at 299 K. Solute concentration: 7.02×10^{-4} mol/l. 1: observed at 410 nm, 2: observed at 540 nm.

the fluorescence has both structured and broad components. The excitation spectrum observed at the wavelength of the peak of M emission does not coincide with that observed at the wavelength of E emission. The former excitation spectrum corresponds to M absorption band, while the latter to D absorption band. It is therefore concluded that the broad E emission emerges only as a consequence of excitation of the species involved in solutions of higher concentrations.

As has been suggested by Werner and Hercules,[3] the most probable mechanism to account for a broad fluorescence is one involving rotation of the carboxyl group in the excited state into a position approaching coplanarity with the anthracene ring. A similar rotation may occur for the dimer molecules of 9-anthroic acid.

The results indicate that the use of a solvent having a hydroxyl or an imino group is essential for the appearance of M fluorescence, with exception of *t*-butyl alcohol. For instance, 9-anthroic acid emits M fluorescence in *N*-methylformamide, while it emits D fluorescence only in *N,N*-dimethylformamide. The solvents having a proton-accepting group only, such as acetone, 1,4-dioxane *etc.*, show no M fluorescence.

Werner and Hercules explained the concentration dependence of the fluorescence of 9-anthroic acid on the basis of an acid-base equilibrium.[3] For the molecular form of 9-anthroic acid a structureless fluorescence is observed. The large Stokes shift of the emission is a consequence of an excited state rotation of the carboxyl group into the plane of the anthracene ring. For the ionic form of 9-anthroic acid in protonic solvents, rotation is inhibited owing to strong ground-state solvation and an anthracene-like structured fluorescence is observed.

The simplest electrostatic theory based on Born's model predicts a linear relation between the medium effect on acid-base equilibria and the reciprocal of the dielectric constant of the solvents.[13] The experimental findings indicate that there is no correlation between the appearacne of the structured M fluorescence of 9-anthroic acid and the magnitude of dielectric constant of the solvent used. In view of the facts, we can rule out proton dissociation as the origin of M fluorescence for 9-anthroic acid.

Effect of Hydrogen Bonding. Figure 7 shows the effect of addition of acetic acid on absorption spectra of 9-anthroic acid in ethanol. Addition of acetic acid shifts the absorption spectra to the blue. As seen in Fig. 1, dimer formation also causes the blue shifts. These findings indicate that the blue shift caused by dimer formation is mainly attributed to hydrogen bonding between carboxyl groups rather than the exciton interaction between anthracene moieties.

A strong steric hindrance might exist between the carboxyl group and the peri-hydrogens, which would keep the carboxyl group from lying coplanar with the anthracene ring. It is likely that the hydrogen-bonded dimer in the ground state has a linear-type configuration in which two anthracene rings lie on the same plane and the plane of $-\overset{\diagup O\cdots HO\diagdown}{C\qquad\quad C}-$ bridge is almost $\diagdown OH\cdots O\diagup$ perpendicular to the plane of anthracene rings (Fig. 8). The anthracene-like structure of D absorption band supports this configuration for ground-state dimers, since the perpendicular configuration of the anthracene rings and $-\overset{\diagup O\cdots HO\diagdown}{C\qquad\quad C}-$ group minimizes resonance $\diagdown OH\cdots O\diagup$ interaction between these moieties.

Addition of a solvent having –OH or =NH group breaks the hydrogen bonds between a pair of 9-anthroic acid molecules and new hydrogen bonds are formed between "monomerized" acids and solvent molecules. The anthracene-like structure of M absorption band of 9-anthroic acid in ethanol supports the view that the hydrogen-bonded species with ethanol have a perpendicular configuration of the anthracene ring and the carboxyl group in the ground state.

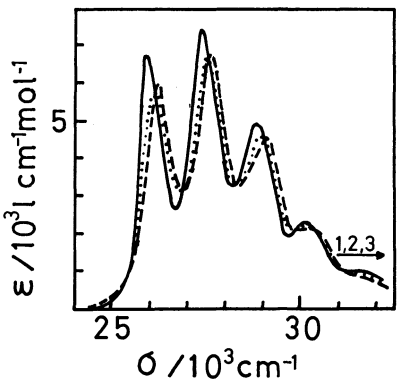

Fig. 7. The effect of addition of acetic acid on the absorption spectra of 9-anthroic acid in ethanol. Solute concentration: 8.05×10^{-6} mol/l. Acetic acid concentrations; 1: 0 mol/l, 2: 8.74×10^{-4} mol/l, 3: 8.74×10^{-2} mol/l.

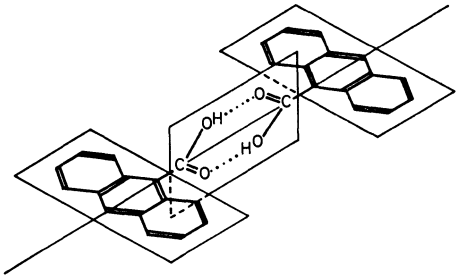

Fig. 8. The probable configuration of the hydrogen-bonded dimer of 9-anthroic acid.

9-Anthroic acid emits the structured fluorescence only when the solvent molecules have both proton-donating and accepting character such as –OH or =NH group. Such solvent molecules can self-associate through hydrogen bonding into a large variety of associated complex species (linear and cyclic polymers).[14,15] Fletcher studied the near-infrared absorption of decane solution of ethanol-*d* at 25 °C.[16] He found it to consist primarily of monomer, acyclic tetramer, and cyclic tetramer in ratios of 1:3.4:10.9, respectively. Kato and Fujiyama studied the local structures of a chloroform–ethanol system by light scattering.[17] They obtained the best fit between the calculated and observed concentration fluctuation by assuming that only an association of $(EtOH)_3CHCl_3$ can exist at 20 °C. The NMR study by Saunders and Hyne also confirmed that monomer-trimer and monomer-tetramer equilibria are dominant in ethanol–carbon tetrachloride system.[18] In the solvents in which 9-anthroic acid emits M fluorescence, the acid may associate with the solvent complex species through hydrogen bonding. This prevents the excited-state rotation of the carboxyl group, M fluorescence thus emerging. In *t*-butyl alcohol, 9-anthroic acid emits only a broad fluorescence. Probably, a bulky *t*-butyl group sterically hinders the formation of complex species, so that the excited-state rotation of a carboxyl group can not be prevented.

When a 9-anthroic acid molecule forms a dimer with another one in ethanol, the excited-state rotation of the carboxyl group will not be hindered because of the lack of the hydrogen-bonded linkages with solvent molecules. This leads to the excited-state rotation of $-\overset{\diagup O\cdots HO\diagdown}{C\qquad\quad C}-$ group into the plane of anthracene $\diagdown OH\cdots O\diagup$ rings, so that D fluorescence emerges. Thus, the appearance of the structured M fluorescence in ethanol may reasonably be interpreted within the framework of monomer-dimer equilibria.

The simplest exciton theory proposed by Kasha *et al.*[19,20] predicts the blue shift of the ^1B_b band and the red shift of the ^1L_a band, on the assumption that 9-anthroic acid dimer has the configuration shown in Fig. 8. Both the ^1B_b and ^1L_a bands of 9-anthroic acid show a blue shift (Fig. 1). The discrepancy on the shift of the ^1L_b band is due to the major contribution of the hydrogen-bonding effect on absorption spectra. This was confirmed experimentally as shown in Fig. 7. The hydrogen-bonded species with acetic acid show an absorption spectrum resembling D absorption band in ethanol. The contribution of exciton splitting is relatively small owing to the large distance of two anthracene rings separated by $-\overset{\diagup O\cdots HO\diagdown}{C\qquad\quad C}-$ linkage $\diagdown OH\cdots O\diagup$

and to small oscillator strength of the ^1L_a transition. The blue shift of the ^1L_a band is mainly attributed to hydrogen bonding.

Temperature Dependence of Fluorescence. Figure 9 shows the temperature dependence of fluorescence spectra of 9-anthroic acid in propylene glycol at higher concentration. Lowering the temperature largely displaces the fluorescence to the blue, but no structured fluorescence appears. The fluorescence observed at lower temperatures lies at a position between E and M fluorescence, having a spectral shape resembling D fluorescence. The excitation spectrum monitored at the maximum of this emission corresponds to D absorption band. The fluorescence observed at low temperature can be assigned to the fluorescence of 9-anthroic acid dimers on the assumption of monomer-dimer equilibrium. The fact that E fluorescence disappears at low temperature suggests an excimer-type mechanism as the origin of the broad E fluorescence.

The temperature dependence of the fluorescence spectra of 9-anthroic acid in propylene glycol at lower concentrations is given in Fig. 10. Lowering of temperature causes no substantial spectral changes except for sharpening of the spectrum. Figure 11 shows the temperature dependence of fluorescence in 1:3 methylcyclohexane and isopentane mixtures. Lowering of temperature shifts the fluorescence to the red, further

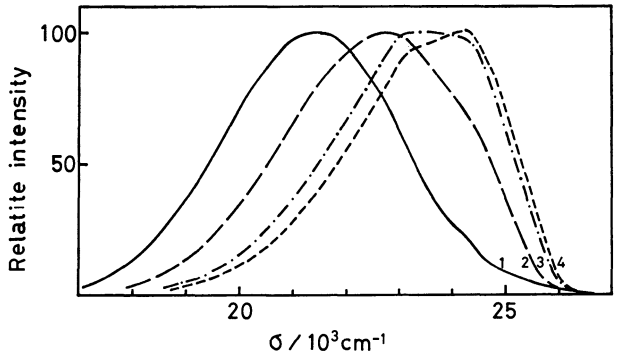

Fig. 9. The fluorescence spectra of 9-anthroic acid in propylene glycol at various temperatures. Solute concentration: 1.87×10^{-3} mol/l. Excitation wavelength: 362 nm. 1: 287 K, 2: 207 K, 3: 173 K, 4: 142 K.

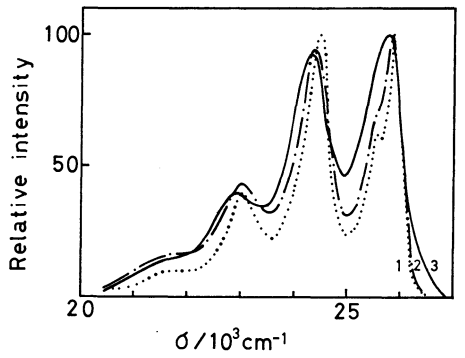

Fig. 10. The fluorescence spectra of 9-anthroic acid in propylene glycol at various temperatures. Solute concentration: 2.0×10^{-6} mol/l. Excitation wavelength: 362 nm. 1: 298 K, 2: 188 K, 3: 103 K.

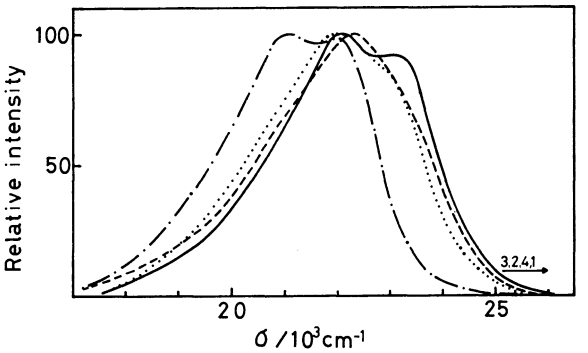

Fig. 11. The fluorescence spectra of 9-anthroic acid in 1:3 methylcyclohexane-isopentane mixture at various temperatures. Solute concentration: 9.6×10^{-6} mol/l. Excitation wavelength: 362 nm. 1: 286.5 K, 2: 260 K, 3: 140 K, 4: 77 K.

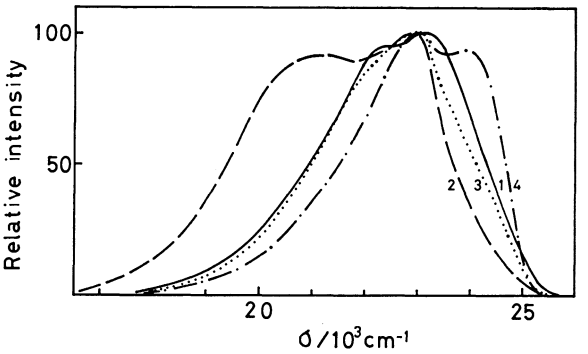

Fig. 12. The fluorescence spectra of 9-anthroic acid in diethyl ether at various temperatures. Solute concentration: 1.8×10^{-3} mol/l. Excitation wavelength: 362 nm. 1: 288 K, 2: 163 K, 3: 124 K, 4: 77 K.

lowering of temperature shifting the fluorescence to the blue, in line with the general behavior of the temperature dependence of fluorescence.[21]

The temperature dependence of fluorescence of 9-anthroic acid in diethyl ether at higher concentration is given in Fig. 12. At room temperature, 9-anthroic acid shows D fluorescence. On lowering the temperature, the component of E fluorescence appears in the spectrum. On further lowering of temperature, the emission shows blue shifts and E fluorescence disappears. Figure 13 gives the temperature dependence of 9-anthroic acid in diethyl ether at lower concentration. No component of E fluorescence appears in the whole temperature range at lower concentration. This indicates that excimer fluorescences can be observed in solvents other than alcohol, if appropriate conditions on concentration and temperature are fulfilled.

Figure 14 gives plots of $\log R$ *vs.* $1/T$ for 7.02×10^{-4} mol/l solution of 9-anthroic acid in propylene glycol. R is I_E/I_M, where I_E and I_M refer to the fluorescence intensity of E and M fluorescences, respectivley. The curve in Fig. 14 shows typical excimer behavior.[22,23] We can evaluate the binding energy of excimer, B, and the activation energy of excimer formation, W. On the assumption that the temperature dependence of the equilibrium constant is negligible within the limit-

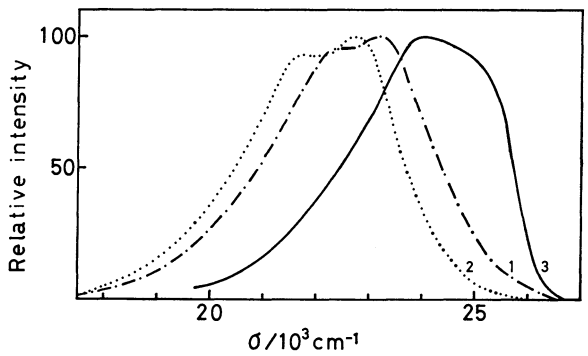

Fig. 13. The fluorescence spectra of 9-anthroic acid in diethyl ether at various temperatures. Solute concentration: 4.7×10^{-6} mol/l. Excitation wavelength: 362 nm. 1: 290 K, 2: 157 K, 3: 77 K.

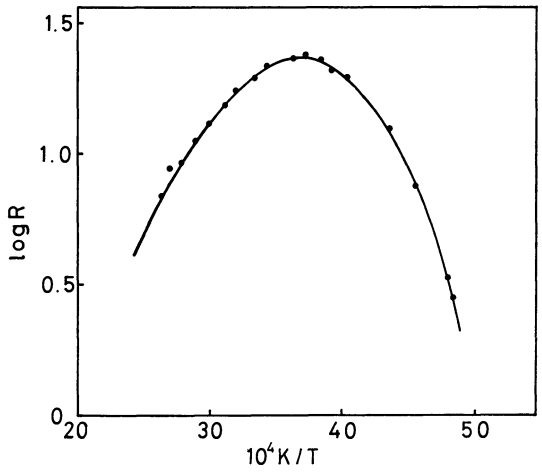

Fig. 14. The log R plot *vs.* $1/T$ for 7.02×10^{-4} mol/l solution of 9-anthroic acid in propylene glycol.

ed temperature range, $B=0.20$ eV was obtained from the slope at higher temperatures. The value of $W=0.36$ eV was also derived from the low-temperature slope of the curve. The values are in line with those obtained for other excimer-forming compounds. This indicates a "universal" type of excimer interaction on the dimer of 9-anthroic acid. Such behavior is unfavorable in the system involving proton dissociation. These findings support the excimer formation from the hydrogen-bonded dimers.

Kinetic Consideration. The ratio of the excimer fluorescence quantum yield to the monomer one is observed to be proportional to the monomer concentration in the case of usual excimer formation.[24] For 9-anthroic acid we propose the following scheme: A hydrogen-bonded dimer of 9-anthroic acid is excited and then associates with an unexcited dimer yielding an excited tetramer from which E emission occurs (Table 1). For steady excitation with light of intensity I_0, the rate equations for this scheme are

$$d[M^*]/dt = aI_0[M] - k_M[M^*],$$

$$d[D^*]/dt = bI_0[D] - (k_D + k_{ED}[D])[D^*] + k_{DE}[E^*],$$

$$d[E^*]/dt = k_{ED}[D][D^*] - (k_E + k_{DE})[E^*].$$

In the equations, the following supplementary parameters are defined:

Table 1. Reaction scheme

Process	Description	Rate parameter
$M^*\rightarrow M+h\nu_M$	fluorescence of M*	k_{FM}
$M^*\rightarrow M$	internal quenching of M*	k_{QM}
$D^*\rightarrow D+h\nu_D$	fluorescence of D*	k_{FD}
$D^*\rightarrow D$	internal quenching of D*	k_{QD}
$D^*+D\rightarrow E^*$	excimer formation	$k_{DE}[D]$
$E^*\rightarrow D^*+D$	regeneration of D* from dissociation of E*	k_{DE}
$E^*\rightarrow D+D+h\nu_E$	fluorescence of E*	k_{FE}
$E^*\rightarrow D+D$	internal quenching of E	k_{QE}

$$k_M = k_{FM} + k_{QM},$$

$$k_D = k_{FD} + k_{QD},$$

$$k_E = k_{FE} + k_{QE}.$$

M, D, and E refer to the monomer, hydrogen-bonded dimer, and excited tetramer, respectively. Under photostationary conditions $d[M^*]/dt=d[D^*]/dt=d[E^*]/dt=0$, and the following relations are obtained:

$$[D]/[M]^2 = K_D,$$

$$[E^*]/([D][D^*]) = K_E,$$

$$R = \frac{I_E}{I_M} = \frac{k_{FE}[E^*]}{k_{FM}[M^*]} \propto \frac{k_{FE}k_M K_E K_D^{1/2}}{k_{FM}} \frac{[D]^{3/2}}{k_D+(k_{ED}-k_{DE}K_E)[D]}.$$

The equation for R indicates that the ratio I_E/I_M is proportional to $[D]^{3/2}$ at low dimer concentrations.

The plot of log R *vs.* log [D] is given in Fig. 15. The I_M and I_E values are evaluated from the areas under the sharp and broad components, which are obtained by subtraction of the corrected M fluorescence spectrum, observed at the lowest concentration, from the corrected spectra observed at various concentrations. The broad component thus obtained closely resembles E fluorescence, indicating that the dimer fluorescence is not actually emitted in this system. It is seen from Fig. 15 that the slope of the plot for 9-anthroic acid

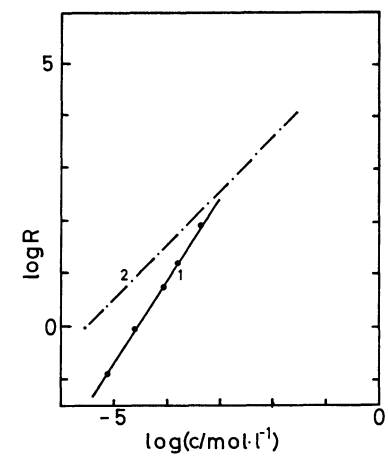

Fig. 15. The log R plot *vs.* log c. 1: The log R plot *vs.* log [D] for 9-anthroic acid in ethanol. 2: The log R plot *vs.* log [M] for 3-methylpyrene in cyclohexane.[23]

is 3/2. Figure 15 includes the plot of log R *vs.* log [M] for 3-methylpyrene, which forms a usual excimer. The slope of the plot is 1 as was expected. If we assume the reaction scheme according to Bazilevskaya and Cherkasov, the slope of the plot for log R *vs.* log [D] should be 1/2. On the other hand, the reaction scheme according to Werner and Hercules gives the slope of 1/2 *vs.* log [M]. We can therefore rule out the reaction scheme proposed by Bazilevskaya and Cherkasov and that by Werner and Hercules. If we assume that a hydrogen-bonded dimer molecule in the excited state associates with an unexcited monomer molecule, we can show that the slope of the plot for log R is 1 *vs.* log [D]. Kinetic consideration indicates the validity of the excited tetramer formed by the association of a hydrogen-bonded dimer in the excited state with a hydrogen-bonded dimer in the ground state.

Other Remarks and Conclusion. Cohen *et al.* gave a theoretical treatment on the general problem of the excimer emission from crystal, and applied it to the anthracene derivatives.[25] They suggested that 9-anthroic acid forms excimers in the head-to-head configurations in the crystal. Polarization study shows that the transition moment of the broad fluorescence has a component perpendicular to the dimer plane.[26] This observation also supports the conclusion stated above. The broad emission of 9-anthroic acid in alcoholic solvents originates from the excited tetramer formed by the association of an excited hydrogen-bonded dimer with an unexcited hydrogen-bonded dimer.

References

1) N. S. Bazilevskaya and A. S. Cherkasov, *Opt. Spectrosc.*, **18**, 30 (1965).
2) N. S. Bazilevskaya and A. S. Cherkasov, *Zh. Prikl. Spektroskopii, Akad. Nauk Berlorussk, SSR*, **3**, 548 (1965).
3) T. C. Werner and D. M. Hercules, *J. Phys. Chem.*, **73**, 2005 (1969).
4) G. Charlot and B. Trémillon, "Les réactions chimiques dans les solvants et les sels fondus," Gauthier-Villars and Cie, Paris (1963), Chap. 10; R. B. Heslop and P. L. Robinson, "Inorganic Chemistry," 3rd ed, Elsevier Publishing Co., Amsterdam (1967), p. 242.
5) E. W. Clare, D. Cook, E. C. F. Ko, Y. C. Mac, and A. J. Parker, *J. Am. Chem. Soc.*, **88**, 1911 (1966).
6) K. Lauer, *Chem. Ber.*, **70B**, 1288 (1937).
7) E. Vander Donckt and G. Porter, *Trans. Faraday Soc.*, **64**, 3218 (1968).
8) H. Hosoya, J. Tanaka, and S. Nagakura, *J. Mol. Spectrosc.*, **8**, 257 (1962).
9) M. Ito, *J. Mol. Spectrosc.*, **4**, 144 (1960).
10) M. Ito, H. Tsukioka, and S. Imanishi, *J. Am. Chem. Soc.*, **82**, 1559 (1962).
11) H. Baba and M. Kitamura, *J. Mol. Spectrosc.*, **41**, 302 (1972).
12) M. Kitamura and H. Baba, *Bull. Chem. Soc. Jpn.*, **46**, 3056 (1973).
13) E. J. King, "Acid-Base Equilibria," Pergamon Press, Oxford (1965), p. 256.
14) S. M. Vinogradov and R. H. Linnell, "Hydrogen Bonding," Van Nostrand Reinhold Co., New York (1971).
15) J. C. Davis, Jr. and K. K. Deb, *Adv. Magn. Reson.*, **4**, 201 (1970).
16) A. N. Fletcher, *J. Phys. Chem.*, **76**, 2562 (1972).
17) T. Kato and T. Fujiyama, *J. Phys. Chem.*, **80**, 2771 (1976).
18) M. Saunders and J. B. Hyne, *J. Chem. Phys.*, **29**, 1319 (1958).
19) M. Kasha, H. R. Rawls, and M. A. El-Bayoumi, *Pure Appl. Chem.*, **11**, 371 (1965).
20) E. G. McRae and M. Kasha, "Physical Processes in Radiation Biology," Academic Press Inc., New York (1964), p. 23.
21) H. Baba and C. Mugiya, *Bull. Chem. Soc. Jpn.*, **43**, 13 (1970).
22) J. B. Birks, *Prog. React. Kinet.*, **5**, 181 (1970).
23) J. B. Birks and L. G. Christophorou, *Spectrochim. Acta*, **19**, 401 (1963).
24) J. B. Birks, "Photophysics of Aromatic Molecules," Wiley-Interscience, London (1970), p.302.
25) M. D. Cohen, Z. Ludmer, and V. Yakhot, *Phys. Status Solidi, B*, **67**, 51 (1975).
26) S. Suzuki, T. Fujii, and N. Yoshiike, unpublished results.

Far-infrared Reflection Spectra, Raman Spectra and Lattice Vibrations of $CsMgCl_3$ and $CsCaCl_3$

Yoshiyuki MORIOKA* and Ichiro NAKAGAWA

Department of Chemistry, Faculty of Science, Tohoku University, Aoba, Aramaki, Sendai 980

(Received December 13, 1977)

Far-infrared reflection spectra of single crystals of $CsMgCl_3$ and $CsCaCl_3$ have been measured, and the frequencies of transverse and longitudinal modes of infrared active vibrations have been determined using Kramers-Kronig relation. For $CsMgCl_3$ a measurement of polarized Raman spectra has been made. A normal coordinate analysis of the optically active lattice vibrations has been performed, in which the rigid ion model for long range Coulomb interactions and the central force field including the 1st differential coefficients of the pair-wise potential functions have been used. The obtained short range force constants K(Mg–Cl) and K(Ca–Cl) are 0.715 and 0.63 mdyn/Å, respectively, which indicate that some amount of covalent character exists in the Mg–Cl and Ca–Cl bonds.

During the course of our studies on the lattice vibrations and interionic interations in the metal halide crystals of the type MX_2 and AMX_3 (M: divalent metal, A: alkali metal, and X: halogen), the rigid ion model for the Coulomb interaction and the central force field for the short range interaction have been used successfully for the normal coordinate analysis of the optically active vibration of crystals.[1,2] In order to establish the interionic potential in the metal halide crystals, further investigations for various types of crystals are needed.

In this paper we present the far-infrared reflection spectra and Raman spectra of $CsMgCl_3$ and $CsCaCl_3$ crystals and the results of the calculation for the interionic potential constants and effective ionic charges. There have been no data of the crystal spectra for these salts, although McPherson and Chang reported the infrared transmission spectra of the powder sample of $CsMgCl_3$.[3]

The crystal structure of $CsMgCl_3$ belongs to the space group D_{6h}^4-$P6_3/mmc$, and a primitive unit cell consists of 2 formula units (Fig. 1).[4] The crystal structure of $CsCaCl_3$ is the cubic perovskite structure with the space group O_h^1-Pm3m and a primitive unit cell consists of 1 formula unit (Fig. 2).[5] The numbers of optically active lattice vibrations in different species are determined by factor group analysis. The results are shown in Table 1.

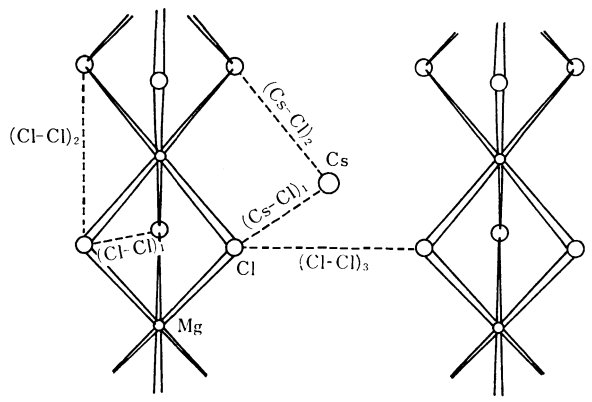

Fig. 1. Crystal structure of $CsMgCl_3$.

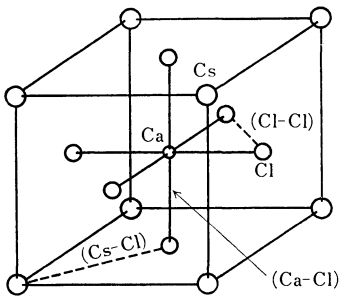

Fig. 2. Crystal structure of $CsCaCl_3$.

TABLE 1. RESULTS OF FACTOR GROUP ANALYSIS FOR OPTICALLY ACTIVE LATTICE VIBRATIONS OF $CsMgCl_3$ AND $CsCaCl_3$

Compound	Space group	Number of modes in each species
$CsMgCl_3$	D_{6h}^4-$P6_3/mmc$	$1a_{1g}+1a_{2g}+2b_{1g}+1e_{1g}+3e_{2g}+2a_{2u}+1b_{1u}+2b_{2u}+3e_{1u}+2e_{2u}$ (IR active: a_{2u}, e_{1u}; Raman active; a_{1g}, e_{1g}, e_{2g}[a])
$CsCaCl_3$	O_h^1-Pm3m	$3f_{1u}+f_{2u}$ (IR active: f_{1u})

a) Raman tensor; $\alpha_{xx}=\alpha_{yy}$, α_{zz}: a_{1g}, $\alpha_{xz}=\alpha_{yz}$: e_{1g}, α_{xy}, $\alpha_{xx}=-\alpha_{yy}$: e_{2g}.

Experimental

$CsMgCl_3$ was prepared from CsCl and $MgCl_2$. Equimolar amounts of CsCl and $MgCl_2$ were heated in the atmosphere of dry HCl gas for several hours, and then fused in vacuum. Polycrystalline samples of $CsMgCl_3$ were sealed into quartz ampoules, and single crystals were grown from the melt by Bridgman method. Obtained crystals cleave readily along the (110) plane. This cleavage plane includes the c axis of the hexagonal lattice, and was used for polarized infrared reflection measurements. Size of the reflecting plane was about 7×10 mm.

For polarized Raman measurements, a specimen of approximately $2\times2\times5$ mm, which was sealed into a glass tube to protect from hydration, was used.

$CsCaCl_3$ was prepared from CsCl and $CaCl_2$. A method of

preparation and a single crystal growth were the same as in the case of $CsMgCl_3$. Obtained crystals cleave along the (100) plane of the cubic lattice. This cleavage plane was used for infrared reflection measurements.

Spectrometers used for infrared reflection measurements were a Hitachi 285 infrared spectrometer for the range 4000—250 cm^{-1} and a Hitachi 070 far-infrared interferometer for the range 400—10 cm^{-1}, with wire-grid polarizers. A chromium mirror was used for the reference.

Polarized Raman spectra were recorded using a Narumi model 750Z-1200 double monochromator with a 514.5 nm line of an Ar^+ ion laser as a source.

Observed Spectra and Vibrational Frequencies

Observed reflection spectra of $CsMgCl_3$ by two types of linearly polarized light are shown in Figs. 3(a) and 3(b). When the polarization of the incident light is parallel to the c axis, the spectrum is related to the a_{2u} modes of lattice vibrations (Fig. 3(a)). When the polarization is perpendicular to the c axis, the spectrum is related to the e_{1u} modes (Fig. 3(b)).

The TO and LO frequencies were obtained by the procedure described in the previous paper,[2] among which one of the LO frequencies for the e_{1u} mode was determined from the maximum of $-\mathrm{Im}(1/\hat{\varepsilon}(\nu))$ as shown in Fig. 3(b).[6]

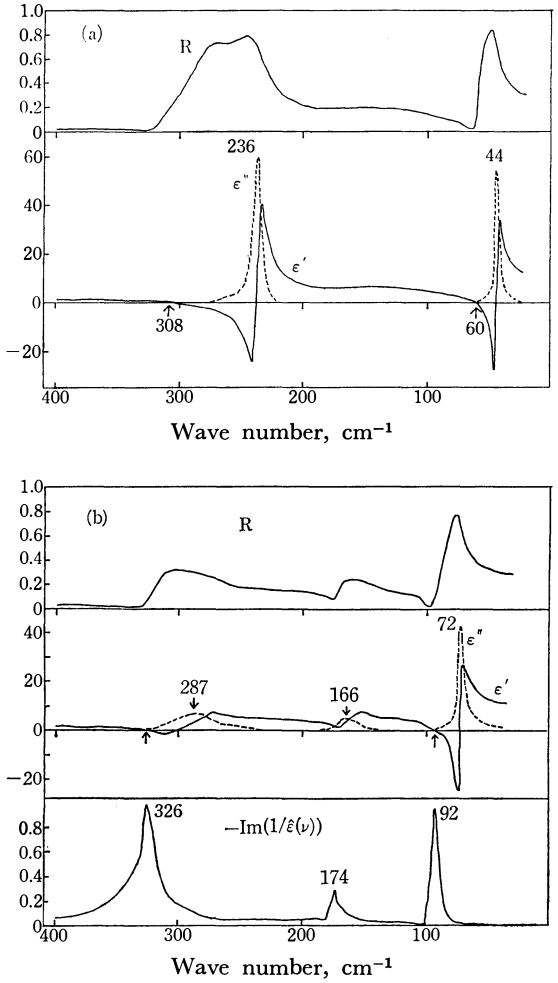

Fig. 3. Reflectivity and dielectric constants of $CsMgCl_3$. (a) The polarization of the light is parallel to the c axis, and (b) the polarization of the light is perpendicular to the c axis.

Figure 4 shows Raman spectra of $CsMgCl_3$, where the notations by Damen, Porto, and Tell are given.[7] A z-axis was taken to be parallel to the c axis of the crystal, and x,y-axes were taken to be perpendicular to the c axis.

The observed reflection spectrum and dielectric constants of $CsCaCl_3$ are shown in Fig. 5.

The observed frequencies of $CsMgCl_3$ and $CsCaCl_3$ are listed in Tables 3 and 5, respectively.

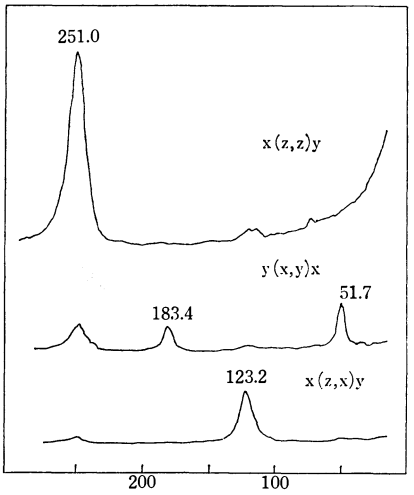

Fig. 4. Polarized Raman spectra of $CsMgCl_3$.

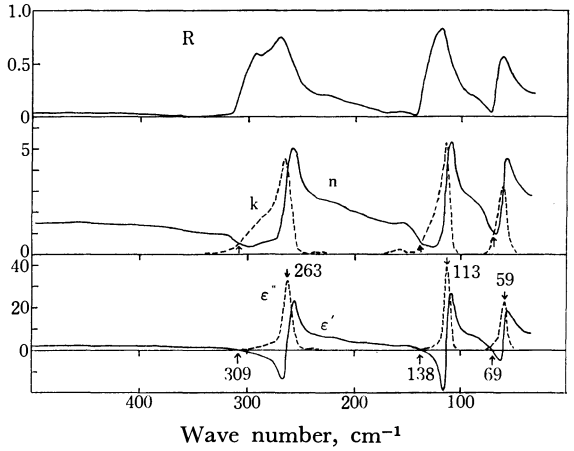

Fig. 5. Reflectivity, optical constants and dielectric constants of $CsCaCl_3$.

Normal Coordiante Analysis for the Optically Active Lattice Vibrations

The procedure of the normal coordinate analysis has been described in the previous paper.[2]

The relation between the effective ionic charges and the TO-LO splittings is expressed as:[8]

$$\frac{4\pi}{v_a}\left(2\frac{Z_{Cs}{}^2e^2}{m_{Cs}}+2\frac{Z_{Mg}{}^2e^2}{m_{Mg}}+6\frac{Z_{Cl}{}^2e^2}{m_{Cl}}\right) = \sum_i (\lambda_i(\mathrm{LO})-\lambda_i(\mathrm{TO})) \quad (1)$$

for $CsMgCl_3$,** and

$$\frac{4\pi}{v_a}\left(\frac{Z_{Cs}{}^2e^2}{m_{Cs}}+\frac{Z_{Ca}{}^2e^2}{m_{Ca}}+3\frac{Z_{Cl}{}^2e^2}{m_{Cl}}\right)=\sum_i(\lambda_i(LO)-\lambda_i(TO)), \quad (2)$$

for $CsCaCl_3$,** where v_a is the volume of the unit cell, Z_A and m_A are the effective ionic charge and mass of the A ion, and λ_i is the frequency parameter $4\pi^2\nu_i{}^2$ of the i-th mode of vibration. On considering a further condition on the electrical neutrality of a crystal as a whole ($\sum Z_i=0$), only one Z_i becomes independent in each crystal.

The short range interactions for the ion pairs within a distance of 4.0 Å were taken into account, which are shown in Figs. 1 and 2. The force constants are listed in the first column of Table 2 ($CsMgCl_3$) and Table 4 ($CsCaCl_3$). K(A–B) denotes $[\varphi''_{A-B}(r)]_{r=r_0(A-B)}$, and k(A–B) denote $[(1/r)\varphi'_{A-B}(r)]_{r=r_0(A-B)}$, where $\varphi_{A-B}(r)$ is the centrosymmetric potential function between A and B.

The equilibrium condition for the 1st differential coefficients of the pair-wise potential functions

$$\sum_{k,l'k'}\left[\frac{dr}{d\rho}\varphi'_{kk'}(r)\right]_{r=r_0(lk;\ l'k')}+\left[\alpha_M\frac{e^2}{\rho^2}\right]_{\rho=\rho_0}=0 \quad (3)$$

was taken into consideration, where α_M is the Madelung constant referred to ρ, and $r_0(lk;l'k')$ is an interionic distance between the k-th ion in the l-th unit cell and the k'-th ion in the l'-th unit cell. The Madelung constant of $CsMgCl_3$ referred to a_0, 34.03, was used. This value was calculated by Ewald's method. As for $CsCaCl_3$, the Madelung constant referred to a_0, 12.377, was used, which was calculated by Sherman for the cubic perovskite structure.[9]

Table 2. Short-range repulsive force constants and effective ionic charges of $CsMgCl_3$[a]

Short-rang repulsive force constants (mdyn/Å)		Corresponding interionic distances (Å)
K(Mg–Cl)	0.715 (0.029)	2.50
k(Mg–Cl)	−0.376 (0.037)	
K(Cs–Cl)$_1$	0.225 (0.028)	3.64
k(Cs–Cl)$_1$	0.109 (0.044)	
K(Cs–Cl)$_2$	−0.007 (0.016)	3.82
k(Cs–Cl)$_2$	0.001 (0.040)	
K(Cl–Cl)$_1$	0.0472[b]	3.39
k(Cl–Cl)$_1$	−0.0017[b]	
K(Cl–Cl)$_2$	0.0105[b]	3.66
k(Cl–Cl)$_2$	0.0002[b]	
K(Cl–Cl)$_3$	0.0019[b]	3.88
k(Cl–Cl)$_3$	0.0005[b]	
Effective ionic charges		
Z_{Cs}	0.604	
Z_{Mg}	1.376	
Z_{Cl}	−0.660	

a) Throughout this paper 1Å=0.1 nm, 1 mdyn/Å=10^2 N/m. The values in parenthesis denote standard deviations. b) Estimated from the nonbonded Cl···Cl interaction potential of Lennard-Jones 6-12 type.

** The relations of Eqs. 1 and 2 hold for each IR active species; *i.e.* for both a_{2u} and e_{1u} species of $CsMgCl_3$ and for f_{1u} species of $CsCaCl_3$. In $CsMgCl_3$, the relation for a_{2u} species was used to get Z_i's.

Table 3. Observed and calculated frequencies of $CsMgCl_3$ in cm^{-1}

	Obsd	Calcd
a_{1g}	251.0	219.6
e_{1g}	123.2	120.2
e_{2g}	183.4	177.9
e_{2g}	—	162.9
e_{2g}	51.7	50.9
a_{2u}(TO)	236	250.5
a_{2u}(TO)	44	50.3
a_{2u}(LO)	308	320.3
a_{2u}(LO)	60	59.8
e_{1u}(TO)	287	273.4
e_{1u}(TO)	166	161.3
e_{1u}(TO)	72	69.8
e_{1u}(LO)	326	327.6
e_{1u}(LO)	174	180.9
e_{1u}(LO)	92	80.0

The short range repulsive force constants between chlorine ions, $K(Cl–Cl)_i$ and $k(Cl–Cl)_i$, were estimated from the nonbonded chlorine-chlorine interaction potential of Lennard-Jones 6-12 type.[10] Other short range force constants were determined by the least squares method for several sets of effective ionic charges which satisfy Eqs. 1 and 2 and the condition of electrical neutrality for each crystal.

In the case of $CsMgCl_3$, the set of effective ionic charges corresponding to $Z_{Cl}=-0.66$ gives a most satisfactory result. (The sum of the squared deviations of the calculated frequencies from the observed ones becomes minimum for this set of Z_i's when Z_{Cl} is varied from −0.58 to −0.82). Obtained force constants and calculated frequencies are given in Tables 2 and 3.

In the case of $CsCaCl_3$, the sum of the squared deviations is more or less alike for the sets of Z_i's when Z_{Cl} is varied in the range $-0.78\leq Z_{Cl}\leq -0.58$. The converged sets of the short-range force constants and the calculated frequencies for three sets of effective ionic charges in the above range of Z_{Cl} are listed in Tables 4 and 5. Among these three sets of short range force constants and effective ionic charges, the set III may be most appropriate, on comparing the values of Z_{Cs} and Z_{Ca} in $CsCaCl_3$ with those of Z_{Cs} and Z_{Mg} in $CsMgCl_3$.

Discussion

The assumptions used in the calculation are the following:

(1) Ions are rigid and not deformable.

(2) Ions interact with neighbouring ions through central forces. Unlike valence force potential, angle bending forces are not taken into consideration.

(3) The interaction potential between the chlorine ions is the 6-12 Lennard-Jones type potential which

Table 4. Short-range repulsive force constants and effective ionic charges of $CsCaCl_3$

	Short-range repulsive force constants (mdyn/Å)			r_0[a] (Å)
	Set I	Set II	Set III	
K(Ca-Cl)	0.630(0.007)	0.635(0.012)	0.636(0.011)	2.70
k(Ca-Cl)	−0.186(0.012)	−0.183(0.016)	−0.199(0.012)	
K(Cs-Cl)	0.046(0.004)	0.036(0.005)	0.032(0.004)	3.82
k(Cs-Cl)	0.016(0.003)	0.015(0.004)	0.019(0.003)	
K(Cl-Cl)	0.0035[b]	0.0035[b]	0.0035[b]	3.82
k(Cl-Cl)	0.0005[b]	0.0005[b]	0.0005[b]	
Effective ionic charges				
	Set I	Set II	Set III	
Z_{Cs}	0.009	0.268	0.554	
Z_{Ca}	1.791	1.712	1.606	
Z_{Cl}	−0.600	−0.660	−0.720	

a) r_0: Corresponding interionic distances. b) See footnote b) of Table 2.

Table 5. Observed and calculated frequencies of $CsCaCl_3$ in cm^{-1}

	Obsd	Calcd		
		Set I	Set II	Set III
f_{1u}(TO)	263	263.5	263.4	264.3
f_{1u}(TO)	113	109.8	109.3	108.9
f_{1u}(TO)	59	61.5	63.4	59.7
f_{1u}(LO)	309	307.9	307.8	306.8
f_{1u}(LO)	138	143.1	145.7	146.4
f_{1u}(LO)	69	68.0	63.5	65.9

is applicable in the case of molecular force field. This model is simple but it explains quantitatively the TO-LO splittings, which are characteristic to ionic crystals.

The agreement between the observed and calculated frequencies is satisfactory as a whole . The metal-chlorine repulsive force constant K(Mg–Cl) 0.715 mdyn/Å in $CsMgCl_3$ is comparable with K(Ni–Cl) 0.764 mdyn/Å in $CsNiCl_3$.[2] This is quite reasonable, on comparing the interionic distance r_0(Mg–Cl)= 2.50 Å with r_0(Ni–Cl)=2.44 Å. K(Ca–Cl)=0.63 mdyn/Å in $CsCaCl_3$ is smaller than K(Mg–Cl), reflecting that r_0(Ca–Cl)=2.70 Å is longer than r_0-(Mg–Cl)=2.50 Å. It is to be noted that K(Ca–Cl) is larger than K(Cd–Cl)=0.540 mdyn/Å in $CdCl_2$, although r_0(Ca–Cl) is almost equal to r_0(Cd–Cl)= 2.69 Å in $CdCl_2$.[1] This is explained by the fact that the ionic radius of Cd^{2+} 0.95 Å is smaller than that of Ca^{2+} 1.00 Å and accordingly the contact of the metal ion with the chlorine ion is more tight in $CsCaCl_3$ than in $CdCl_2$.[11]

Since the metal-chlorine force constants K(Mg–Cl) and K(Ca–Cl) in $CsMgCl_3$ and $CsCaCl_3$ are rather larger than K(Na–Cl) or K(K–Cl) ≈0.2 mdyn/Å in NaCl or KCl crystals which are considered to be purely ionic crystals,[12] there may exist some amount of covalency in Mg–Cl and Ca–Cl bonds.

As for the potential constants corresponding to the $Cs^+\cdots Cl^-$ interaction, reasonable values of K(Cs–Cl) and k(Cs–Cl) were obtained with small standard deviations for $CsCaCl_3$. However, for $CsMgCl_3$ which has two kinds of $Cs^+\cdots Cl^-$ (3.64 and 3.82 Å), the converged force constants have rather large standard deviations as seen in Table 2. The values of $K(Cs–Cl)_1$ and $k(Cs–Cl)_1$ are too large while those of $K(Cs–Cl)_2$ and $k(Cs–Cl)_2$ are too small, on considering the corresponding interionic distances.***

Finally, the displacement of each ion for each vibration will be discussed for the AMX_3 crystal of cubic perovskite structure. This may be described on the basis of the eigenvectors $\boldsymbol{L}_x$ for $\boldsymbol{M}^{-1}(\boldsymbol{F}_x^R+\boldsymbol{F}_x^C)$, $\boldsymbol{X}=\boldsymbol{L}_x\boldsymbol{Q}$, where $\boldsymbol{F}_x^R$ and $\boldsymbol{F}_x^C$ are $\boldsymbol{F}$ matrices, in terms of Cartesian displacement coordinates, corre-

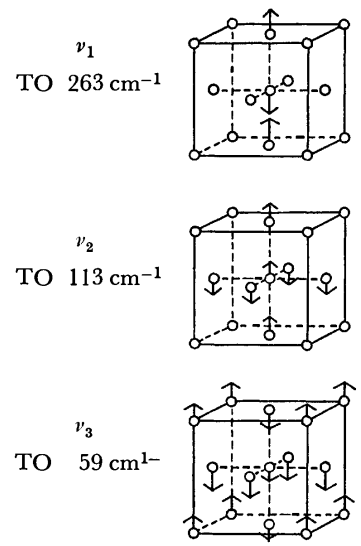

Fig. 6. Displacement of ions for three infrared active vibrations of $CsCaCl_3$.

*** The interionic distance $(Cs\cdots Cl)_2$ in $CsMgCl_3$ equals to that for (Cs···Cl) in $CsCaCl_3$. If we assume the values of $K(Cs–Cl)_2$ and $k(Cs–Cl)_2$ take the same values as those for $CsCaCl_3$ and perform the least squares calculation, the values of $K(Cs–Cl)_1$ and $k(Cs–Cl)_1$ would be converged to smaller values with less standard deviations.

sponding to the short-range repulsive and long-range Coulomb potentials. The result for $CsCaCl_3$ is given schematically in Fig. 6, which shows that the highest vibration ν_1 is a Ca–Cl stretching mode, ν_2 is a Ca–Cl bending mode and the lowest one ν_3 is a Cs– *vs.* $-CaCl_3$ type lattice mode. This result is in correspondence with that for BMO_3 studied by Last,[13] but in contrast with that for AMF_3 where the ν_1 mode is a M–F bending mode and the ν_2 mode is a M–F stretching mode.[14]

The authors wish to express their sincere thanks to Professor Ito Mitsuoof Tohoku University for permitting us to use a laser Raman spectrometer in his laboratory.

References

1) Y. Morioka and I. Nakagawa, *Spectrochim. Acta, Part A*, **34**, 5 (1978).
2) K. Akiyama, Y. Morioka, and I. Nakagawa, *Bull. Chem. Soc. Jpn.*, **51**, 103 (1978).
3) G. L. McPherson and J. R. Chang, *Inorg. Chem.*, **12**, 1196 (1973).
4) G. L. McPherson, T. J. Kistenmacher, and G. D. Stucky, *J. Chem. Phys.*, **52**, 815 (1970).
5) H. F. McMurdie, J. de Groot, M. Morris, and H. E. Swanson, *J. Res. Nat. Bur. Stand.*, **73A**, 621 (1969).
6) A. S. Barker, Jr., "Far-Infrared Properties of Solids," ed by S. S. Mitra and S. Nudelman, Plenum Press (1970).
7) T. C. Damen, S. P. S. Porto, and B. Tell, *Phys. Rev.*, **142**, 570 (1966).
8) J. Hiraishi, *Bull. Chem. Soc. Jpn.*, **46**, 1334 (1973).
9) J. Sherman, *Chem. Rev.*, **11**, 93 (1932).
10) T. Shimanouchi, I. Nakagawa, J. Hiraishi, and M. Ishii, *J. Mol. Spectrosc.*, **19**, 78 (1966).
11) R. D. Shannon and T. C. Prewitt, *Acta Crystallogr., Sect. B*, **25**, 925 (1969); **26**, 1046 (1970).
12) I. Nakagawa, *Appl. Spectrosc. Rev.*, **8**, 229 (1974).
13) J. T. Last, *Phys. Rev.*, **105**, 1740 (1957).
14) I. Nakagawa, *Spectrochim. Acta, Part A*, **29**, 1451 (1973).

The Application of Mathematical Programming in Theoretical Chemistry. I. Saddle-point-search Method Applied to a H_3 Molecule*

Yukio YONEDA

Department of Synthetic Chemistry, Faculty of Engineering, The University of Tokyo, Hongo, Bunkyo-ku, Tokyo 113

(Received December 23, 1977)

A new method to find the activated state of a reaction *without* preparing its potential energy surface was proposed and proved useful with the example of a H_3 molecule. The first and the second derivatives of the total energy, with respect to every cartesian coordinate of a H_3 molecule, were calculated by means of a perturbation method employing a modified EHMO. First, the bottom of the valley in the potential energy surface leading to the saddle point is sought with the aid of the quadratic approximation on the superplane on which the maximum curvature at the representative point lies. Second, the ascending path is determined to be the reverse of the steepest decending path according to the principle of microscopic reversibility. By repeating these procedures, the activated state was found without preparing the potential energy surface. The classical activation energy thus found was 8.8 kcal/mol, which is in good agreement with the experimental values.

The theoretical determination of activated state of a given reaction generally requires knowledge of the potential energy surface (PES) of the system. Quantum chemical calculations, non-empirical[1] and semi-empirical,[2] have been published on the gas-phase exchange reaction $H+H_2=H_2+H$ and its isotopic variants, which belong to the simplest class of chemical reactions. In these calculations, the activated state, or the saddle point, was pinpointed on a two-dimensional contour map, because the linear complex of a H_3 molecule is, fortunately, more stable than the non-linear one. The dimerization of two carbene molecules to produce an ethylene molecule[3] is a yet simpler reaction; the preparation of a complete PES of the system is, however, practically impossible because of its already large degree of freedom beyond two, *i.e.*, $6\times3-6=12$; hence, a fairly large number of calculations are necessary to obtain the total energies at the eighteen dimensional grid points. Thus, in the practical calculation, the bond distance, r_{CH}, was kept constant throughout the reaction and only a schematic diagram could be shown instead of a contour map.

Therefore, the development of a method which requires only a feasible number of calculations to obtain the reaction path is strongly desirable. By virtue of the method of optimization adopted, the method described in this paper does not require the preparation of the complete PES, and it is, therefore, particularly suitable when we need only information on the activated state and the reaction path.

Several methods of optimization, techniques in mathematical programming, have been widely employed, especially in engineering, to determine extreme value(s) without preparing a contour map of a given function; only the first derivatives (the first and second derivatives in some techniques) of the function at the successively proceeding representative point are required to arrive at the peak of the mountain.

A doctrinal formulation of reaction paths and activated states has been proposed by Fukui.[4] The purpose of the present work is to develop a new practical method for climbing up from the foot (the reactant) to the saddle point (the activated state) along the bottom of the valley connecting them, and then going down to another foot (the product). The simplest example, the H_3 system, will be presented to demonstrate the usefulness of this method.

The energy may be calculated by means of any method, including even the molecular force field, provided that the derivatives are calculable. In this paper, the energy was calculated quantum-chemically by means of a modified extended Hückel molecular orbital (EHMO) method.

This method can also be employed in larger systems with semi-empirical MO calculations; some results with MINDO/2 and 3 will be published later.

Theoretical

Saddle-point Search. The geometry of a reacting system such as H_3 is described by a representative point in a $3N_{at}$ dimensional space, where N_{at} is the number of atoms in the system. When $q_u(u=1$ to $3N_{at})$ represents every 3-dimensional cartesian coordinate of all the atoms, and E_b is the total bond energy of the system, the saddle point is defined by

$$\frac{\partial E_b}{\partial q_1}=\frac{\partial E_b}{\partial q_2}=\cdots\cdots=\frac{\partial E_b}{\partial q_{3N_{at}}}=0, \tag{1a}$$

$$\frac{\partial^2 E_b}{\partial b_r^2}<0 \text{ and } \frac{\partial^2 E_b}{\partial b_f^2}<0, \tag{1b}$$

$$\frac{\partial^2 E_b}{\partial b_1^2}>0,\ \frac{\partial^2 E_b}{\partial b_2^2}>0,\ \cdots, \tag{1c}$$

where $\partial^2 E_b/\partial b^2$ implies the second derivative of the total bond energy with respect to the bond length of a bond, b, while Eq. 1b represents the criteria of the curvatures of the PES along the rupturing bond, b_r, and the forming one, b_f, whereas Eq. 1c represents the criteria along the bonds which are not directly related to the activated state. On the other hand, the criteria of the most stable structure of a molecule, or the minimum energy geometry, are described by Eqs. 1a and 2:

$$\frac{\partial^2 E_b}{\partial q_1^2}>0,\ \frac{\partial^2 E_b}{\partial q_2^2}>0,\ \cdots,\ \frac{\partial^2 E_b}{\partial q_{3N_{at}}^2}>0 \tag{2}$$

* CHEMOGRAM, a Computer Program Package for Chemical Logic, Part I. A preliminary report of this work was presented at the 31st National Meeting of the Chemical Society of Japan, Sendai, October, 1974.

Thus, the criteria of the saddle point in cartesian coordinates becomes as follows where Eq. 1a holds, Eq. 1d is satisfied for a few coordinates which are directly related to the rupturing or forming bonds, and Eq. 1e holds for the remaining coordinates, a majority:

$$\frac{\partial^2 E_b}{\partial q^2} < 0 \text{ (for a few coordinates)}, \quad (1d)$$

$$\frac{\partial^2 E_b}{\partial q^2} > 0 \text{ (for the majority of coordinates)}. \quad (1e)$$

The mathematical definition of the bottom of the valley on the PES will be discussed below. Figure 1a shows a schematic diagram of a superplane or a PES around a valley, V. P is a representative point of the system which is not at the bottom, but fairly near it. S is a superplane *orthogonal* to V, on which the point P and a curve, PQ, which is a section of S and V and which has the maximum curvature at P, are laid. The minimum point, B, on the PQ curve is the bottom of the valley near P, as is shown in Fig. 1b. The PQ curve may have its maximum curvature even at B, because P is near B. In practical calculations, the PQ curve is determined by the second derivatives of the total bond energy at P, while the location of B is estimated by the quadratic approximation with the aid of the first and the second derivatives at P. If the B thus estimated is far from P, the same procedure may be repeated to assure that the true bottom of the valley is attained.

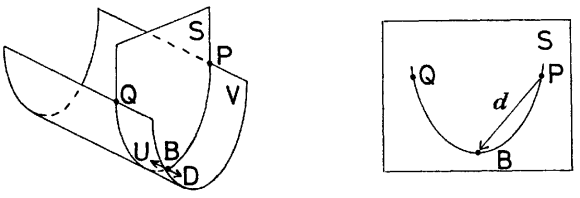

(a) (b)

Fig. 1. Schematic diagram for saddle point search method.
(a) Potential energy surface near a bottom of a valley.
(b) Bottom of a valley on a superplane S.

The reaction path along the bottom of the valley, V, is determined as follows. First, the direction of the steepest descent, BD, is decided with the aid of the first derivatives at the point B. This direction leads the system to the initial geometry; hence, the path to the saddle point, BU, will be the reverse direction to BD, by the principle of microscopic reversibility. The BU distance should be small enough, say 0.05 Å, so that the above principle can be applied . Even if the BU step is short, it can not be guaranteed that the U point is still at the bottom; hence, the same procedure employed with P is applied at U before ascending further toward the saddle point.

Modified EHMO and Its Perturbational Calculation of First and Second Derivatives. Generally, empirical or semi-empirical MO's, such as EHMO, CNDO, INDO, or MINDO, do not give correct values of the equilibrium distance or the energy profile of a hydrogen molecule. The total electronic energy calculated by EHMO implicitly involves the nuclear repulsion energy;[5] hence, the total electronic energy minus the sum of the Coulomb integrals, which are geometry-independent, gives the total bond energy. Salomon[6] calculated a semi-empirical PES by means of the Heitler-London method, employing modified overlap integrals to obtain a better fit of the calculated bond energy of H_2 to that of the Morse function.

By the same principle, we introduced a modified EHMO. We do not insist that this modification is a novel improvement of EHMO; we just used it as a less expensive MO, applicable only for hydrogen atoms with s orbitals alone, to demonstrate the validity of the present saddle-point-search method.

The resonance integrals were formulated, as is shown in Eq. 3b, to make the total bond energy as close as possible to the experimental value of a hydrogen molecule at various interatomic distances of interest:

$$\text{Coulomb integral: } H_{rr} = -13.60 \text{ eV}, \quad (3a)$$

$$\text{resonance integral: } H_{rs} = \frac{1}{2}\sum_k^w a_k |S_{rs}|^{k-1} \times S_{rs}(H_{rr}+H_{ss}), \quad (3b)$$

where r and s denote atomic orbitals. Thus, the resonance integral is expressed as a power series of an overlap integral, S_{rs}, which is calculated with the Slater orbitals by means of the Mulliken method. Then the coefficients, a_k, can be determined by the least-squares method so as to fit the Morse function.

The derivatives could be calculated by the method of finite differences from the eigenvalues of a slightly distorted system. The calculation, however, requires two extra geometries for each coordinate of an atom; thus, the number of calculations amounts to $2\times 3N_{at}$, which is 18 even for the smallest system, H_3. As the computation time of the diagonalization of a secular equation usually increases nearly propotionally to $N^{2.5-3}$, where N is the number of atomic orbitals, the method of finite differences may be inappropriate for a larger system.

In the case of EHMO, the total (electronic) energy of a system is calculated from the sum of the eigenvalues of a secular equation,

$$|H^{(0)}{}_{rs} - \varepsilon S^{(0)}{}_{rs}| = 0. \quad (4)$$

When a small change in one coordinate of an atom (Δq) is regarded as a perturbation, the perturbed matrices, H and S, may be described by

$$H = H^{(0)} + \lambda H^{(1)} + \lambda^2 H^{(2)}, \quad (5a)$$

$$= H^{(0)} + \left(\frac{\partial H^{(0)}{}_{rs}}{\partial q}\right)(\Delta q) + \frac{1}{2}\left(\frac{\partial^2 H^{(0)}{}_{rs}}{\partial q^2}\right)(\Delta q)^2, \quad (5b)$$

$$S = S^{(0)} + \lambda S^{(1)}, \quad (5c)$$

where $S^{(2)}$ was omitted for the sake of simplification and where parentheses denote a matrix. The total energy after perturbation, E, is given by

$$E = E^{(0)} + \lambda E^{(1)} + \lambda^2 E^{(2)} \quad (5d)$$

$$= E^{(0)} + (\partial E^{(0)}/\partial q)(\Delta q) + (1/2)(\partial^2 E^{(0)}/\partial q^2)(\Delta q)^2. \quad (5e)$$

Therefore, the first and the second derivatives of the total energy of the system with respect to the designated coordinate are given by

$$\frac{\partial E^{(0)}}{\partial q} = E^{(1)}, \tag{5f}$$

$$\frac{\partial^2 E^{(0)}}{\partial q^2} = 2E^{(2)}. \tag{5g}$$

Since the difference between the total bond energy, E_b, and the total energy, E, are constant, the derivatives of the former with respect to the coordinates are equal to those of the latter.

The non-zero elements of the first- and second-order perturbation matrices are given by the following equations:

First-order:

$$\frac{\partial H_{rs}}{\partial q_u} = \frac{\partial H_{rs}}{\partial S_{rs}} \cdot \frac{\partial S_{rs}}{\partial q_u} \quad \text{for off-diagonal,} \tag{6a}$$

$$\frac{\partial S_{rs}}{\partial q_u} \quad \text{for off-diagonal.} \tag{6b}$$

Second-order:

$$\frac{1}{2}\frac{\partial^2 H_{rs}}{\partial q_u^2} = \frac{1}{2}\left\{\frac{\partial^2 H_{rs}}{\partial S_{rs}^2}\left(\frac{\partial S_{rs}}{\partial q_u}\right)^2 + \frac{\partial H_{rs}}{\partial S_{rs}}\frac{\partial^2 S_{rs}}{\partial q_u^2}\right\} \quad \text{for off-diagonal.} \tag{7}$$

The first and the second derivatives of overlap integral can easily be calculated with the method of finite differences by shifting the coordinate in two directions for a small distance (usually 0.05 Å). Elements of Hamiltonian perturbation matrices can be analytically calculated with ease by the use of Eqs. 3, 6, and 7. Then the perturbation energies can be calculated by the method reported by Carbo.[7]

Calculation

Coefficients of the Modified Resonance Integral. The parameters for the Morse function, Eq. 8, are selected as follows:

$$V = D_e[1-\exp\{-a(r-r_e)\}^2]^2, \tag{8}$$

where $D_e = -4.76$eV, $a = 1.957$Å^{-1}, and $r = 0.7413$Å.

A seven-term polynomial for Eq. 3b was chosen ($w=7$), and the seven coeffieients were estimated as shown below at 15 interatomic distances from $r = 0.9r_e$ to $2.3r_e$:

$a_1 = 1.0405$, $a_2 = 0.4695$, $a_3 = 0.6302$, $a_4 = -1.3501$,

$a_5 = -0.6601$, $a_6 = 5.8697$, and $a_7 = -5.3563$.

The coincidence between these two sets of values at distances of interest is satisfactory, the standard deviation of differences between them being 0.009 eV, or 0.2 kcal/mol, for this range.

Flow Chart of Computer Program. The computation was carried out on a HITAC 8800/8700 system at the Computer Centre of the University of Tokyo. The block-flow chart of the main program, EHMP1, is shown in Fig. 2. The input data, essentially composed of coordinates of initial system, quantum chemical parameters, constraint parameters, and control variables, are analyzed. The eigenvalues and the eigenvectors are calculated in a subroutine, EHCAL. Second, the derivatives are calculated in another subroutine, MPEHPT, following the procedure described above. Thirdly, either the bottom of the valley or the ascending path, decided by a control variable,

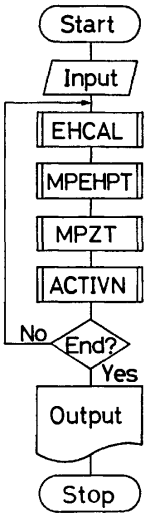

Fig. 2. Block flow chart of computer program EHMP1.

is searched with the above-mentioned algorithm stored in a third subroutine, MPZT. Finally, a fourth subroutine, ACTIVN, judges whether or not the saddle point is attained. If the system is still ascending, the procedures are repeated from EHCAL using renewed coordinates. During these iterations, the search of the bottom and that of the ascending path are repeated alternatively. If the representative point arrives at the saddle point, the coordinate is slightly changed so that the representative point is forced to move to the opposite side beyond the saddle point. Then repeated calculation from EHCAL searches the path down to the foot on the opposite side, that is, the product, by using the conventional optimization algorithm. The main program and subroutines are all written in FORTRAN IV. Some details of the procedures will now be explained.

Algorithm in Subroutines: The subtroutine EHCAL makes use of conventional quantum chemical calculations by using the EHMO, except that the modified resonance integrals shown in Eq. 3b are used.

The details of the processing in the subroutine MPEHPT are shown in Fig. 3. The input[1] consists of the eigenvalues and eigenvectors of the unperturbed system. The following processing is iterated[2] for x-, y-, and z- coordinates down to the decision box[9]. The overlap integral matrices of unperturbed($S^{(0)}$), and the first ($S^{(1)}$)- and the second ($S^{(2)}$)-order perturbation are calculated in the subroutine MPOVLP[3], Because the following relations hold throughout the system;

$$\partial S_{rs}/\partial q_v = -\partial S_{rs}/\partial q_w, \tag{9a}$$

$$\partial^2 S_{rs}/\partial q_v^2 = \partial^2 S_{rs}/\partial q_w^2, \tag{9b}$$

where the orbitals, r and s, belong to atoms whose coordinates along the same axis are q_v and q_w respectively, only one calculation in each iteration can give the derivatives for all atoms.

The perturbational calculation is iterated[4] for all the atoms from $u=1$ to $3N_{at}$ down to [8]. The perturbation matrices of the Hamiltonian of the first- and the second-order are prepared analytically. The

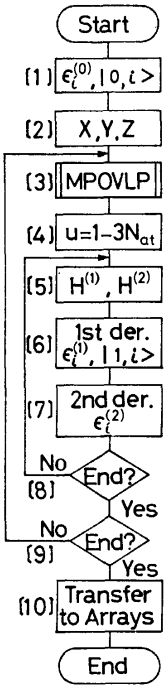

Fig. 3. Flow chart in a subroutine MPEHPT.

first-order perturbation eigenvalues and eigenvectors are calculated in [6] by following the algorithm of Carbo.[7] The second-order perturbation eigenvalues are calculated from them and $H^{(2)}$ by means of the above algorithm[7]. The derivatives of the total bond energy thus obtained are stored in arrays[10].

The algorithms in the subroutine MPZT are as follows. The vector, $\boldsymbol{d}$ in Fig. 1b that moves the representative point from P to B is given by the following equations (see Appendix):

$$d_i = -f_i'' \operatorname{sign}(f_i') \sum_i' \frac{|f_i'|f_i''}{\sum_i'(f_i'')^3} \quad \text{for } f_i'' \geqq 0, \tag{10a}$$

$$d_i = 0 \quad \text{for } f_i'' < 0, \tag{10b}$$

where

$$f_i' = \frac{\partial E^{(0)}}{\partial q_i}, \tag{10c}$$

$$f_i'' = \frac{\partial^2 E^{(0)}}{\partial q_i^2}, \tag{10d}$$

and

$$d = (d_1, d_2, \cdots\cdots d_i, \cdots\cdots d_{3N_{at}}) \tag{10e}$$

In this processing, the summation regarding a few coordinates which give negative second derivatives is excluded. If the bottom thus found is outside the designated restriction in distance from P, the same procedure is iterated using renewed coordinates.

The direction of the steepest decent, and hence that of the path to the saddle point, is then easily determined by using f_i' values.

The subroutine ACTIVN judges the arrival at the saddle point, and then moves the system beyond that point. The arrival at the saddle point is recognized when none of the absolute values of the first derivatives exceed the optioned threshold value, *EDRV1*. In spite of the criteria of the saddle point given in Eqs. 1d and 1e, judgement by Eq. 1a alone is sufficient because the system is ascending and no minimum can appear before any saddle point, even if a basin exists. Then the system is moved for twice the distance restricted by constraint parameters along the vector from the initial point to the saddle point. Thus, the system goes to the opposite side of the PES, sufficiently far from the saddle point for the system not to return to the original side, but close enough to it not to fall down beyond the ridges on the PES in another valley, which would guide the system to an unexpected product.

The path down to the product is determined by either linear or quadratic approximation methods in the subroutine MPZT.

Results and Discussion

The initial system is a linear molecule with interatomic distances of $r_{12}=1.600$ Å and $r_{23}=0.740$ Å, as

$$H^1 \cdots H^2 - H^3 \quad \text{(on X-axis)}. \tag{11}$$

The total bond energy of the molecule was −4.6437eV, with the parameters for the resonance integral given above. The first and the second derivatives with respect to the x-coordinate are compared in Table 1 with those obtained by the method of finite differences with a shift of the x-coordinates, δ, of ±0.025 Å. The agreement was proved excellent.

Table 1. Comparison of derivatives with respect to x values calculated by two methods

Method		Perturbation	Finite differences
First der. eV Å^{-1}	1[a]	0.404	0.402
	2	0.113	0.132
	3	−0.517	−0.538
Second der. eV Å^{-2}	1	0.90	0.84[b]
	2	37.0	36.8
	3	38.1	37.9

a) Atom ordinal. b) $\delta=\pm 0.05$ Å.

The parameters for processing were optioned as follows: the constraint parameters for atoms, which restrict their transfer distances in one step, were ±0.05 Å, and the threshold value, *EDRV1*, for the saddle point was 0.1 eV/Å.

At first, the bottom of a valley was searched for with derivatives of the initial system; it was found at the geometry of $r_{12}=1.592$ and $r_{23}=0.759$ Å with a total bond energy, *TBE*, of −4.6439 eV, which is 0.0002 eV lower than the initial one. Although we used no control to inhibit the change in coordinates along either the Y- or the Z-axis, the bond angle (123) was actually 180.0°, and this angle remained unchanged throughout the reaction.

Secondly, a control variable was changed in order to search for the ascending path, and the system was transferred to new coordinates, $r_{12}=1.540$ and $r_{23}=0.759$ Å, with $TBE=-4.6223$ eV. The above interim results and succeeding iterations are shown on a contour map, Fig. 4, which had been separately prepared by a conventional grid method for demonstration. Up to

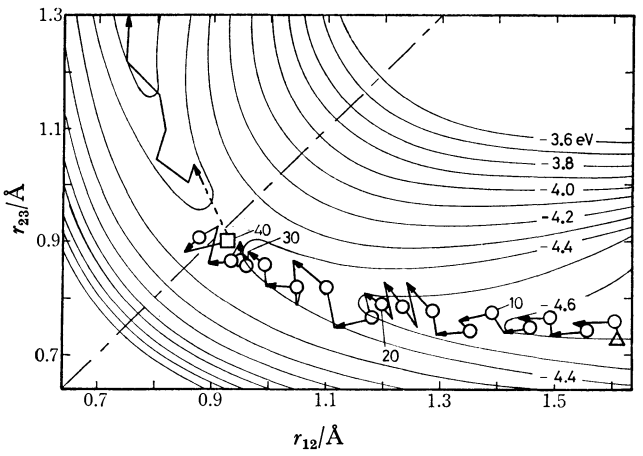

Fig. 4. Reaction path of H_3 system beyond activated state.
△: Initial system, ○: bottom of a valley.
←: Ascent during activation or decent during stabilization.
Numerals along the path indicate the iteration numbers, and those along the contour the *TBE*/eV.

TABLE 2. ATTRIBUTES OF ACTIVATED STATE SEARCHED FOR BY MATHEMATICAL PROGRAMMING

a. Activated state with restricted distance = 0.05 Å and *EDRV1* = 0.1 eV Å^{-1}.
1) Geometry: $r_{12}=0.9225$, $r_{23}=0.900$ Å, and angle(123) = 180.00°.
2) *TBE*: −4.3771 eV.
3) Derivatives along the X-axis:

Atom ordinal	1	2	3
First der./eV Å^{-1}	0.0459	−0.0207	−0.0252
Second der./eV Å^{-2}	7.75	−1.78	9.84

b. Symmetrical geometry.
1) Geometry: $r_{12}=r_{23}=0.91$ Å and angle(123) = 180.00°.
2) *TBE*: −4.3768 eV.
3) Derivatives along the X-axis:

Atom ordinal	1	2	3
First der./eV Å^{-1}	0.0530	0.0000	0.0530
Second der./eV Å^{-2}	8.88	−1.60	8.88

thirty iterations, the system, or the representative point, ascended nearly along the bottom of the valley leading to the saddle point. Meanwhile, two attempts to search for the bottom were carried out at the three iteration number of 16, 19, and 26. Beyond the iteration number of 30, the point began to wander on a fairly flat PES near the saddle point, designated by a square. At the iteration number of 40, all of the absolute values of the first derivatives became less than *EDRV1*, or 0.1 eV/Å in this case, and the system was judged to be at the saddle point. The system had the geometry, *TBE*, and derivatives shown in Table 2a. The first derivatives well satisfy one of the criteria, Eq. 1a, the second derivatives satisfy Eqs. 1d and 1e, and the H^2 atom is found to be related to the rupturing or forming bonds. The *TBE* of the reactant, that is, a hydrogen molecule with an equilibrium interatomic distance and a hydrogen atom which is sufficiently far from the former, is found to be −4.759eV by the present MO; thus, the classical activation energy, E_A(classical), is 0.382 eV = 8.8 kcal/mol, in good agreement with the experimental values.

No shallow basin seems to exist around the saddle point, judging from the wandering paths. Therefore, the true activated state is estimated to have a symmetric geometry of $r_{12}=r_{23}=0.91$Å. The attributes of the symmetric system are shown in Table 2b, where the first derivative of H^2 is naturally zero and where the second derivatives for H^1 and H^3 were identical, the value being negative for H^2. The *TBE* is −4.3768eV, only 0.0003 eV (7 cal/mol) higher than that in Table 2a. Hence, this symmetrical system can be regarded as the true activated state.

The coordinates of the system were changed by 0.1Å by means of the algorithm mentioned above along the arrow with a broken line. Then the system began to go down along the bottom of a new valley to the product, as the control variable changed the algorithm to stabilization.

The total CPU time on a HITAC 8800/8700 for 40 iterations up to the saddle point amounted to 10 s.

This simplest example may be judged to verify the validity and usefulness of the new method for searching for the reaction path beyond the saddle point. The path shown in Fig. 4 is not a trajectory of the reaction, but only records the intermediate walks following the algorithm, because this method employs a static model instead of a dynamic treatment. The smoothed locus of open circles in Fig. 4, however, may give a fairly good reaction trajectroy.

The author's thanks are due to Dr. Makoto Misono for his valuable discussion.

Appendix

Algorithm for Estimation of a Bottom of a Valley. The energy $E(\boldsymbol{d})$ at B in Fig. 1b, which was moved from P by a vector, $\boldsymbol{d}$, is expressed by the Taylor expansion by neglecting cross terms:

$$E(\boldsymbol{d}) \approx E(\boldsymbol{0}) + \sum_{i}^{3N_{at}} \left(f_i' d_i + \frac{1}{2} f_i'' d_i^2 \right), \tag{A1}$$

where $E(\boldsymbol{0})$ denotes the energy at P.

The $\boldsymbol{d}$ vector should be parallel to the $\boldsymbol{f}''$ vector, where its elements are f_i'', negative values being replaced with zero. The sign of d_i should be decided so as to decrease the energy from P to B; hence, the d_i component is given by Eq. A2, taking into account the fact that the effective f_i'' is non-negative:

$$d_i = \frac{k f_i'' \mathrm{sign}(-f_i')}{\{\sum_i{}' (f_i'')^2\}^{1/2}}, \tag{A2}$$

where Σ' denotes that the negative f_i'' is excluded from summation and where k is an undetermined multiplier.

Equation Al is converted to Eq. A3 by means of Eq. A2:

$$E(\boldsymbol{d}) = E(\boldsymbol{0}) + C\sum_i{}' \{ f_i' f_i'' \,\mathrm{sign}(-f_i') k + \frac{1}{2} C (f_i'')^3 k^2 \}, \tag{A3}$$

where $C=\{\sum_i{}'(f_i'')^2\}^{-1/2}$.

The energy at B should be at its minimum along the PQ curves; hence,

$$\frac{dE(\boldsymbol{d})}{dk} = C\sum_i{}'\{f_i'f_i'' \operatorname{sign}(-f_i') + C(f_i'')^3 k\} = 0. \quad \text{(A4)}$$

Thus,

$$k = -\frac{\sum_i{}' f_i'f_i'' \operatorname{sign}(-f_i')}{C\sum_i{}'(f_i'')^3}. \quad \text{(A5)}$$

Finally, the elements of $\boldsymbol{d}$—that is, the shifts in the coordinates—are derived as Eq. 10a from Eqs. A2 and A5, considering that $f_i' \operatorname{sign}(-f_i') = -|f_i'|$ and $\operatorname{sign}(-f_i') = -\operatorname{sign}(f_i')$.

References

1) *E.g.*, I, Shavitt, R. M. Stevens, F. L. Minn, and M. Karplus, *J. Chem. Phys.*, **48**, 2700 (1968); B. Liu, *ibid.*, **58**, 1925 (1973).

2) *E.g.*, S. Glasstone, K. J. Laidler, and H. Eyring, "The Theory of Rate Processes," McGraw-Hill, New York (1941); S. Sato, *Bull. Chem. Soc. Jpn.*, **28**, 450 (1955); I. Yasumori, *ibid.*, **32**, 1103, 1110 (1959); R. N. Porter and M. Karplus, *J. Chem. Phys.*, **40**, 1105 (1964).

3) R. Hoffmann, R. Gleiter, and F. B. Mallory, *J. Am. Chem. Soc.*, **92**, 1460 (1970); H. Fujimoto, S. Yamabe, and K. Fukui, *Bull. Chem. Soc. Jpn.*, **45**, 1566 (1972).

4) K. Fukui, *J. Phys. Chem.*, **74**, 4161(1970); "The World of Quantum Chemistry," ed by R. Daudel and B. Pullman, D. Reidel Publ. Co., Dordrecht, Holland (1974), p. 113.

5) R. Hoffmann, *J. Chem. Phys.*, **39**, 1397 (1963).

6) M. Salomon, *J. Chem. Phys.*, **51**, 2406 (1969).

7) R. Carbo, *Theor. Chim. Acta (Berl.)*, **17**, 74 (1970).

Absolute Intensity Measurement of Infrared Absorption by the Use of CO_2 Laser Source

Tetsuo SUZUKI and Tsunetake FUJIYAMA*

Department of Chemistry, Faculty of Science, Tokyo Metropolitan University, Setagaya-ku, Tokyo 158

(Received January 9, 1978)

The absolute infrared absorption intensities have been measured for the $^{Q}R_0(0)$ line (ν_3 fundamental) of methyl fluoride and the $^{R}R_8(9)$ line (ν_6 fundamental) of methyl iodide by the use of CO_2 laser lines of P(16) and P(8), respectively. The observed intensities, Γ, were: 12500 ± 4300 cm$^2\cdot$mol^{-1} for the ν_3 band of methyl fluoride and 1040 ± 40 cm$^2\cdot$mol^{-1} for the ν_6 band of methyl iodide.

The absorption intensity of vibration spectrum has been discussed as an intensity integrated over the whole absorption band.[1] This has been largely due to the limited resolution that the dispersion type spectrometers have which is insufficient to observe individual vibration-rotation lines. As the absorption intensities of vibration-rotation lines in the gas phase are often influenced by intramolecular interactions like Coriolis interaction, it is very important to observe intensities of individual vibration-rotation lines separately. Moreover, there are many problems to be examined in conventional intensity measurement of infrared absorptions, the most fundamental arising from the lack of resolution.[1]

From these respects, attention has been focussed on the highly monochromatic property of the laser radiation and an attempt has been made to measure the absorption intensity of a single vibration-rotation line by the use of a laser source. The CO_2 laser was used in this work, because of its ease of construction and handling. Although the output frequencies are not tunable, it is possible to measure absorption intensities by the use of pressure broadening of an absorption line at a relatively high sample gas pressure. The principles of the present work are based upon the ideas proposed by Shimizu *et al.*[2]

The ν_3 band of methyl fluoride and the ν_6 band of methyl iodide have been chosen because their vibration-rotation spectra have been fully analyzed[3–5] and their vibrational intensities have been reported by the use of conventional methods.[6,7]

Experimental

The experimental arrangement is shown in Fig. 1. The instrument was composed of an infrared laser source, a sample cell with Stark plates, and a detecting system. The CO_2 laser used in this experiment as an infrared radiation source was composed of a 2 m water-cooled discharge tube sealed with NaCl Brewster windows, a concave mirror (radius of 5 m), and a plane grating blazed at 10.6 μm (Photo Technical Research, Inc.). The concave mirror and the plane grating made up a laser cavity which was about 2.5 m in length. First order light of the grating was used for the resonant cavity and zero order light was obtained as the output power. The concave mirror was attached on a voice coil in order to finely adjust the cavity length by changing the direct electric current of the voice coil. The laser components were mounted on a steel H-beam.

The absorption cell was made of Pyrex galss 52.5 cm in length. Parallel aluminum electrodes were installed in the cell for observation of the Stark effect. The electrode glass spacers were 1.31 mm in thickness. In the case of a strong absorption intensity, an absorption cell 10 cm in length was used.

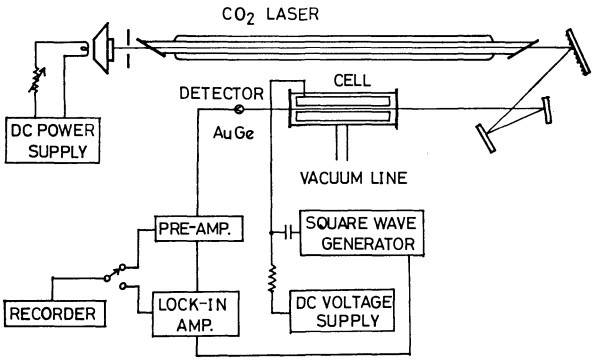

Fig. 1. Block diagram of the experimental arrangement.

The detecting system consisted of a gold doped germanium detector (Barnes Engineering, A-200), a hand-made preamplifier, a lock-in amplifier (NF Circuit Design Block, LI-573), and a pen recorder (Yokogawa Electric Works, Ltd., 3051). After passing through the absorption cell, the laser beam was detected by the gold doped germanium detector cooled by liquid nitrogen. The output signal from the detector was amplified and recorded by the pen recorder. In the case of the observation of Stark effect of an absorption line, the signal was detected by the standard phase sensitive detection method with square wave modulation of the Stark field. Potential across the electrodes was measured by a voltage divider and a potentiometer. The accuracy and the precision of the voltage measurement were 0.25 and 0.1%, respectively.

An absorption coefficient was determined by the intenstiy ratio of the light passing through an empty cell to that passing through a cell filled with sample gas. Pressure of the sample gas was measured by the use of an oil or mercury manometer, the precision of which was ascertained to be about 5%.

Results and Discussion

Generally, frequency of a laser line does not coincide with that of a molecular absorption line, so the absorption of laser radiation by molecules cannot usually be observed. In the case where the frequency difference between an absorption line and a laser line is small, however, we may observe the absorption of light by increasing the sample pressure and, therefore, by broadening the width of the absorption line. In the case where a line-width is mainly determined by collision broadening, the shape of a molecular absorption

line may be approximated by a Lorentzian function. Then, the absorption coefficient, $\alpha(\nu_l)$, of the molecular line at the frequency, ν_l, of laser light is given by the formula

$$\alpha(\nu_l) = \frac{\alpha_0(\gamma_p \cdot P)^2}{(\gamma_p \cdot P)^2 + (\nu_l - \nu_m)^2}, \quad (1)$$

where ν_m is the center frequency of the molecular absorption line, P the sample pressure, γ_p the pressure broadening parameter, and α_0 the constant independent of pressure. α_0 should be equal to the absorption coefficient at the center frequency of the absorption line. Equation 1 is reduced to a more convenient relation as[2]

$$\frac{1}{\alpha(\nu_l)} = \frac{1}{\alpha_0}\left(1 + \gamma^2 \frac{1}{P^2}\right), \quad (2)$$

where

$$\gamma = \frac{|\nu_l - \nu_m|}{\gamma_p}.$$

Equation 2 shows that the inverse of $\alpha(\nu_l)$ linearly depends on the inverse of P^2. If we measure the absorption coefficients at various pressures and plot $1/\alpha(\nu_l)$ against $1/P^2$, a straight line with a slope of γ^2/α_0 should be generated. The extrapolated $1/\alpha(\nu_l)$ value at $1/P^2 \to 0$ corresponds to the $1/\alpha_0$ value. If a $|\nu_l - \nu_m|$ value is known, the γ_p value may be determined and the value of the transition moment calcualted with α_0 and γ_p values. In the present work, the $|\nu_l - \nu_m|$ value was determined by observing the Stark effect.

ν_3 Band of CH_3F. It has been known that the vibration-rotation spectrum of methyl fluoride ν_3 band appears in the 9.4 μm region of the CO_2 laser.[3] This band has been previously studied by Stark spectroscopy using a CO_2 laser.[4] By the aid of these results, the absorption lines of $^qQ_1(1)$ and $^qR_0(0)$ were easily found near the CO_2 laser lines of P(18) and P(16), respectively. The absorption coefficients were measured

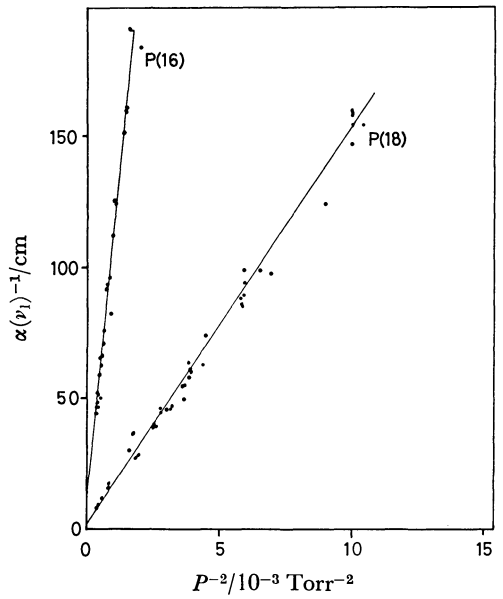

Fig. 2. Plots of measured $\alpha(\nu_l)^{-1}$ against P^{-2} for ν_3 band of CH_3F.

Table 1. Observed values of α_0, γ^2, $|\nu_l - \nu_m|$, γ_p, and $|\langle\partial\mu/\partial Q\rangle\langle 0|Q|1\rangle|$ for ν_3 band of CH_3F

	CH_3F ν_3	
	P(16)	P(18)
α_0/cm^{-1}	0.072(0.022)	0.47(0.18)
γ^2/Torr^2	7200(2500)	7200(2800)
$\lvert\nu_l - \nu_m\rvert$/MHz	4497	2133
γ_p/MHz Torr^{-1}	53(9)	25(5)
$\lvert\langle\partial\mu/\partial Q\rangle\langle 0\rvert Q\lvert 1\rangle\rvert$/Debye	0.224(0.038)	0.329(0.059)

Numbers in parenthesis indicate standard deviations.

at these two laser lines for various pressures. The measured $\alpha(\nu_l)^{-1}$ values were plotted againts P^{-2} values, the results of which are shown in Fig. 2. The values of α_0 and γ were determined by means of the least-squares method. The $|\nu_l - \nu_m|$ values obtained by Stark spectroscopy were used for the determination of the γ_p values. The resultant values of α_0, γ^2, $|\nu_l - \nu_m|$ and γ_p are shown in Table 1.

The transition dipole moment of ν_3 fundamental, $\langle\partial\mu/\partial Q\rangle\langle 0|Q|1\rangle$, was calculated from the observed α_0 and γ_p values for the convenience of comparing the present result with the integrated intensity previously observed by conventional infrared techniques. For a symmetric top molecule an absorption coefficient, α_0, is related to a transition dipole moment as[8]

$$\alpha_0 = \frac{8\pi^2 N_0 \nu_m d g_K g_I}{3ch\gamma_p Z_{R,V}} \exp\left(-\frac{E''}{kT}\right) \times \left\{1 - \exp\left(-\frac{h\nu_m}{kT}\right)\right\} |\Phi_{JK}^{J'K'}|^2 \left|\left\langle\frac{\partial\mu}{\partial Q}\right\rangle\langle 0|Q|1\rangle\right|^2, \quad (3)$$

where N_0 is the number density of molecules at unit pressure, d the degree of vibrational degeneracy, g_I the nuclear statistical weight, $Z_{R,V}$ the vibrational and rotational partition function, E'' the energy of the initial state, $\Phi_{JK}^{J'K'}$ a matrix element of a direction cosine, and $g_K = 1$ for $K = 0$ and $g_K = 2$ for $K > 0$. The value of the transition moment calculated from Eq. 3 is given in the last row of Table 1.

As seen from Table 1, the two values of the transition moments obtained at the laser lines, P(16) and P(18), do not agree with each other . The detailed spectral features of the ν_3 band in the neighborhood of two

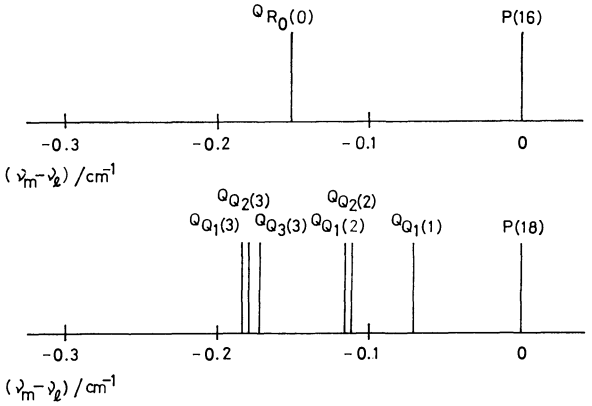

Fig. 3. Detailed spectral features of ν_3 band of CH_3F in the neighborhood of P(16) and P(18) laser lines.

laser lines are illustrated in Fig. 3. It is seen from the figure that there is only one absorption line, $^{Q}R_0(0)$, in the neighborhood of the P(16) line. In the neighborhood of the P(18) laser line, on the other hand, there are several Q-branch lines $^{Q}Q_2(2)$, $^{Q}Q_1(2)$, *etc.* in addition to the $^{Q}Q_1(1)$ line. Therefore the apparent value of the transition moment obtained from P(18) is expected to be larger than that from P(16), because of the contribution of the neighboring lines to the absorption of the P(18) laser radiation. In order to see the reliability of the observed transition moment value, the magnitude of the absorption of P(18) laser line due to these three absorption lines, $^{Q}Q_1(1)$, $^{Q}Q_2(2)$, and $^{Q}Q_1(2)$, was estimated by the use of the trasition dipole moment value of 0.224 Debye which was observed at the P(16) laser line. The $|\nu_1-\nu_m|$ values of these absorption lines were observed by Stark spectroscopy or calculated from the observed molecular constants.[4] The γ_p values of 25 MHz·Torr^{-1} were assumed for these absorption lines. The estimated pressure dependence of the absorption coefficient is shown in Fig. 4. The pressure dependence of the absorption estimated by taking into account only the $^{Q}Q_1(1)$ line is illustrated by the dash-dot line. This accounts for only half of the observed absorption. The absorption coefficient estimated by considering these three lines, $^{Q}Q_1(1)$, $^{Q}Q_2(2)$, and $^{Q}Q_1(2)$, is illustrated by the dashed line in Fig. 4. This explains the observed absorption coefficients very well. The solid line of Fig. 4 expresses the pressure dependence of the absorption coefficient calculated from the parameters given in Table 1. Thus it may be concluded that the transition moment value obtained at P(18) laser line is larger than that obtained at P(16) line because the absorption at P(18) laser line is not originating from a single absorption line, $^{Q}Q_1(1)$, but from a number of absorption lines. Consequently, the transition moment value obtained at the P(16) laser line has been adopted as the transition moment of the ν_3 fundamental of methyl fluoride.

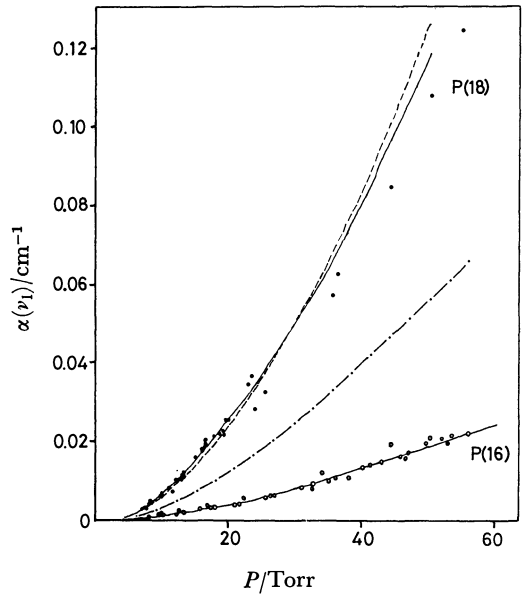

Fig. 4. Observed and estimated pressure dependence of absorption coeficients for CH_3F.

ν_6 Band of CH_3I. The band origin of the ν_6 band of methyl iodide is 882.7 cm^{-1} and a little far apart from the CO_2 laser region. However, the rotational structure spreads over a wide frequency range and, therefore, some of the absorption lines of this band may coincide with the 10.6 μm CO_2 laser lines. From the analysis of the conventional high resolution infrared spectrum[5] and the laser Stark spectroscopy, the $^{R}R_8(9)$ lines occurs near the P(8) line of the CO_2 laser. The observed values of $1/\alpha(\nu_1)$ at various pressures are shown in Fig. 5. The values of α_0, γ^2, $|\nu_1-\nu_m|$, and γ_p are calculated by the same way applied for the ν_3 band of methyl fluoride. The $1/\alpha(\nu_1)$ values observed at the pressure higher than 33 Torr were excluded from the least-squares fitting, because the $1/\alpha(\nu_1)$ values observed in this high pressure range were considered to be affected by the absorption of the neighboring lines. As the rotational energy levels of methyl iodide are expected to have hyperfine structures due to the nuclear quadrupole moment of the iodine atom, the ν_m value has been regarded as the center of the

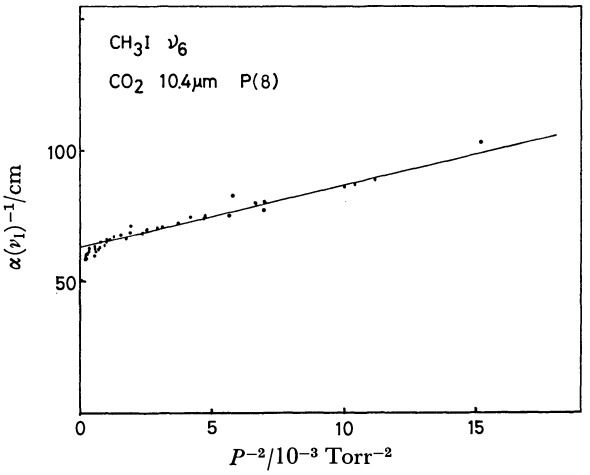

Fig. 5. Plots of measured $\alpha(\nu_1)^{-1}$ against P^{-2} for ν_6 band of CH_3I.

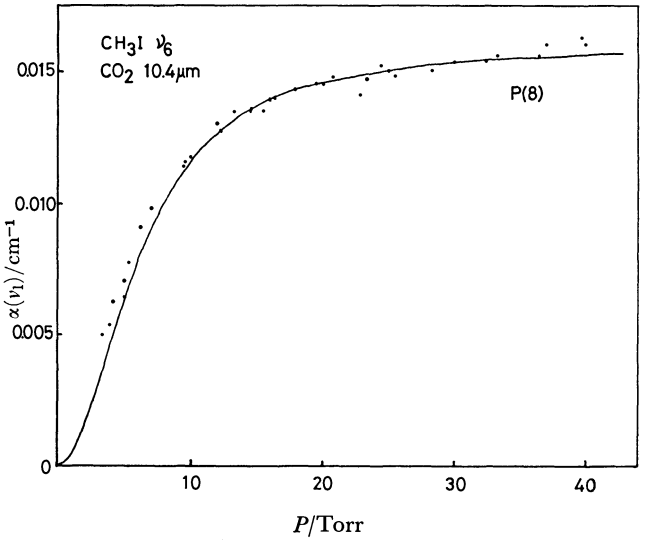

Fig. 6. Observed and estimated pressure dependence of absorption coefficient for CH_3I.

Table 2. Observed values of α_0, γ^2, $|\nu_1-\nu_m|$, γ_p, and $|(\partial\mu/\partial Q)\langle 0|Q|1\rangle|$ for ν_6 band of CH_3I

	CH_3I ν_6
α_0/cm^{-1}	0.0159(0.0002)
$\gamma^2/Torr^2$	37.1(2.1)
$\|\nu_1-\nu_m\|$/MHz	55
γ_p/MHz Torr^{-1}	9.03(0.25)
$\|(\partial\mu/\partial Q)\langle 0\|Q\|1\rangle\|$/Debye	0.0455(0.0005)

Numbers in parenthesis indicate standard deviations.

unresolved hyperfine structures. In Fig. 6 the pressure dependence of the absorption coefficient reproduced from the parameters of Table 2 is expressed by the solid line and the observed values by the closed circles.

The uncertainty expected for the observed $1/\alpha(\nu_1)$ value is samll relative to that for methyl fluoride. In the plot of $1/\alpha(\nu_1)$ against $1/P^2$, the slope of the straight line decreases in magnitude as the $|\nu_1-\nu_m|$ values decreases. On the other hand, the dispersion of the resultant $1/\alpha(\nu_1)$ value due to the uncertainty of the pressure measurement is smaller, if the slope of the straight line is small. Therefore, the standard deviation of the resultant $1/\alpha(\nu_1)$ for methyl iodide is much smaller than that for methyl fluoride, because the $|\nu_1-\nu_m|$ value for methyl fluoride is much larger than that for methyl iodide.

Comparison with the Result from Conventioanl Methods. The obtained transition moment value was converted into the absolute absorption intensity value in order to compare the present results with the absorption intensities obtained by conventional methods. The absolute absorption intensity, Γ, which is integrated over the whole absorption band, is defined as

$$\Gamma = \frac{1}{c_B l}\int_{\text{band}} \ln\left(\frac{I_0}{I}\right) d(\ln \nu), \qquad (\text{cm}^2\cdot\text{mol}^{-1}), \qquad (4)$$

where c_B is the molecular density in mol·cm^{-3}, l the path length in cm, and the integration covers the whole absorption band. The relation between the absolute absorption intensity, Γ, and the trnasition moment, $(\partial\mu/\partial Q)\langle 0|Q|1\rangle$, is expressed as[1)]

$$\Gamma = \frac{4\pi^2 N_A d}{3c\hbar}\left|\left(\frac{\partial\mu}{\partial Q}\right)\langle 0|Q|1\rangle\right|^2, \qquad (5)$$

where N_A is the Avogadro constant, and d the degree of vibrational degeneracy. In Table 3 the Γ values calculated from Eqs. 3 and 5, and the observed α_0 are compared with the Γ values obtained by conventional methods.

For the ν_3 band of methyl fluoride, the Γ value obtained in this work is somewhat larger than those obtained by conventional methods. This might be due to the weak Coriolis interaction between the ν_3 and ν_6 bands.[3)] However, since the standard error is considerably large this will not be explored further.

For the methyl iodide ν_6 band, the present result agrees well with that obtained by conventional methods. This indicates that there is no intramolecular perturbaion which influences the absorption intensity in the $|v_6=1>$ state.

Table 3. Absolute intensities Γ/cm^2·mol^{-1}

	CH_3F ν_3	CH_3I ν_6
This work	12500(4300)	1040(40)
References	9108(260)[6)]	1012(26)[7)]
	9056(906)[7)]	

Numbers in parenthesis indicate experimental errors.

Conclusive Discussion. This work has shown that the absorption intensity of a single vibration-rotation line of a molecule may be meaured by this method if the frequency of the laser line nearly coincides with that of the molecular absorption line, although the frequency of the laser radiation is not tunable. An accurate intensity value cannot be obtained, in the case that the absorption of the laser line due to plural number of lines occures simultaneously. The accuracy of the observed intenstiy value is governed mainly by the magnitude of the γ-value. For an absorption line with small γ, the intensity may be obtained with high accuracy. On the other hand, the γ-value is determined by the magnitudes of $|\nu_1-\nu_m|$ and γ_p. The γ_p-values are almost 10—50 MHz·Torr^{-1} for usual simple molecules, we can safely conclude that the experimental criterion for the accurate intensity measurement is $|\nu_1-\nu_m|\leq 4$ GHz. It is often difficult to observe the absorption intensities of a series of vibration-rotation lines in a certain vibration band by means of a frequency fixed laser. This method does not appear to be appropriate form obtaining detailed knowledge about the intensity distribution in a vibration band.

Incidentally, a rigorous assignment of rotation-vibration lines is required to apply the present technique to the observation of their intensities.

References

1) M. Davies, Ed, "Infrared Spectroscopy and Molecular Structure," Elsevier Publishing Co., New York (1963), Chap. X.

2) T. Shimizu, F. O. Shimizu, R. Turner, and T. Oka, *J. Chem. Phys.*, **55**, 2822 (1971).

3) W. L. Smith and I. M. Mills, *J. Mol. Spectrosc.*, **11**, 11 (1963).

4) S. M. Freund, G. Duxbury, M. Romheld, J. T. Tiedje, and T. Oka, *J. Mol. Spectrosc.*, **52**, 38 (1974).

5) H. Matsuura and J. Overend, *Spectrochim. Acta, Part A*, **27**, 2169 (1971).

6) S. Saeki, M. Mizuno, and S. Kondo, *Spectrochim. Acta, Part. A*, **32**, 403 (1976). In this report, the integrated intensity is expressed in the unit of A/cm^{-2}·mol^{-1} l. For convenience, we converted the value of A in the unit of Γ/cm^2 mol^{-1} by the use of the relation, $\Gamma=1000\nu_0^{-1}\cdot A$, where ν_0 is the wave number of the band origin.

7) J. W. Russell, C. D. Needham, and J. Overend, *J. Chem. Phys.*, **45**, 3383 (1966).

8) H. C. Allen, Jr., and P. C. Cross, "Molecular Vib-Rotors," John Wiley & Sons, Inc., New York (1963), Chap. 5.

Infrared Study of Surface Hydroxyl Groups on Zirconium Oxide

Tsutomu YAMAGUCHI,* Yasuko NAKANO, and Kozo TANABE
Department of Chemistry, Faculty of Science, Hokkaido University, Sapporo 060
(Received January 17, 1978)

Zirconium oxide has two absorption bands, at 3780 and 3680 cm^{-1}, after several hours' evacuation at 500 °C. The exchange of deuterium with the surface hydroxyl groups was studied by using D_2O, acetone-d_6, 2-propanol-d_8, and chloroform-d. D_2O, acetone-d_6, and 2-propanol-d_8 could completely exchange the hydrogens of the surface hydroxyl groups at room temperature, while chloroform-d could not exchange them even under saturated vapor pressure at room temperature. Hydroxyls showing 3780 cm^{-1} band were selectively and irreversibly chlorinated by chloroform-d. After deuteration, two deuteroxyl bands were observed, at 2780 and 2705 cm^{-1}; these were exchanged rapidly with ammonia and slowly with propylene. At room temperature propylene exchanged the hydrogen with the hydroxyls with a 2780 cm^{-1} band more rapidly than with the hydroxyls with a 2705 cm^{-1} band. In the adsorption and desorption of 2-propanol, the behavior of the 2780 cm^{-1} band was also found to be different from that of the 2705 cm^{-1} band. It was concluded that the 3780 and 3680 cm^{-1} bands could be assigned to surface hydroxyl groups, the nearest neighbors of which have different configurations, and the hydroxyl group of 3780 cm^{-1} is more reactive than the hydroxyl group of 3680 cm^{-1}.

Infrared spectroscopy is one of the most useful methods for the investigation of solid surfaces, and much work has been done on the nature of the hydroxyl groups on various oxides.[1] The presence of five types of hydroxyl groups on Al_2O_3 was reported by Peri.[2] The different natures of the five hydroxyl groups were suggested to arise from the difference in their nearest-neighbor configuration.[2] The two types of hydroxyl groups on SiO_2 were assigned to the surface and the bulk hydroxyls.[3] The MgO evacuated at 310 °C gave two types of hydroxyls, which were attributed to the surface and the second-layer hydroxyls.[4] Three types of hydroxyls were observed on CaO and attributed to groups with different circumstances.[5] Many reports have been reported on the hydroxyl groups on TiO_2, in which the presence of more than two groups has been reported.[6] The results were explained by Peri's model or a surface model on the (110) plane of rutile.[6c,d]

We have reported an interesting catalytic action of ZrO_2 toward the preferential production of 1-butene in the dehydration reaction of 2-butanol and the selective formation of *cis*-2-butene in the isomerization of 1-butene.[7] The results were explained in terms of the basic and acidic nature of this catalyst. The hydrogenation of olefins was also observed[8] on this oxide at a relatively low reaction temperature (0—50 °C), where hardly no deuterium-exchange reactions took place until the reaction temperature was raised above 200 °C.

In view of the interesting aspects of ZrO_2, we have investigated the nature of hydroxyl groups on the oxide. Tretyakov *et al.*[9] reported that two kinds of hydroxyls exist on ZrO_2. However, the relative reactivity of the two hydroxyls is not known. The purpose of the present paper is to report the relative reactivity of D_2O, acetone-d_6, 2-propanol-d_8, chloroform-d, ammonia, and propylene.

Experimental

The preparation of ZrO_2 has been described elsewhere.[7] The D_2O, acetone-d_6, 2-propanol-d_8, and chloroform-d, all supplied by Merck & Co., Inc., were degassed prior to use. The cylinder NH_3 was purified through molecular sieve 3A and sodium metal which was dispersed over quartz wool. Propylene obtained from Takachiho Chem. Ind., Ltd., was used without further purification.

ZrO_2 was ground and pressed into self-supported discs 20 mm in diam under 250 kg/cm^2. The disc was placed in an IR cell and evacuated at the desired temperatures for several hours. Oxygen treatment was applied to burn out organic contamination if necessary. Though it has been reported that oxygen treatment affects the behavior of the surface hydroxyl groups on TiO_2,[6b] no effect was observed in the case of ZrO_2.

All the spectroscopic measurements were carried out at room temperature by using a JASCO (Japan Spectroscopic Co., Ltd.) DS 701-G double-beam spectrometer. About 50 mg of typical sample discs transmitted about 10% of incident radiation at 4000 cm^{-1} after standard pre-treatment. Ordinate or abscissa scale expansion was applied if it was needed; the reference beam was attenuated for obtaining an appropriate transmittance.

Results

Exchange with D_2O. After several hours' evacuation at 500 °C, ZrO_2 showed two absorption bands, at 3780 and 3680 cm^{-1} (Fig. 1), in agreement with the spectra observed by Tretyakov *et al.*[9] These bands are characteristic in their narrow and symmetrical contours and have been assigned to hydroxyl groups which hereafter, for the sake of convenience, will be referred to as $(OH)_I$ and $(OH)_{II}$ respectively. It is not surprising that the half-width of the $(OH)_I$ band is narrow, but it is noteworthy that the other band of a low frequency also has a relatively narrow half-width.

Two or three treatments with 8 mmHg of D_2O at room temperature, followed by evacuation at 500 °C, lead to an almost complete replacement of the original hydroxyl bands with new deuteroxyl bands at 2780 and 2705 cm^{-1}. The former will be referred to as $(OD)_I$ and the latter, as $(OD)_{II}$, which correspond to $(OH)_I$ and $(OH)_{II}$ respectively. The process of the appearance of these bands is shown in Figs. 1c—1e. The $(OD)_I$ begins to appear on evacuation above 200 °C with a decrease in the lower-frequency band at 2705 cm^{-1}. After evacuation above 300 °C, the band at 2705 cm^{-1} decreases markedly in intensity, and two well-resolved bands are obtained at 2780 and 2705 cm^{-1}.

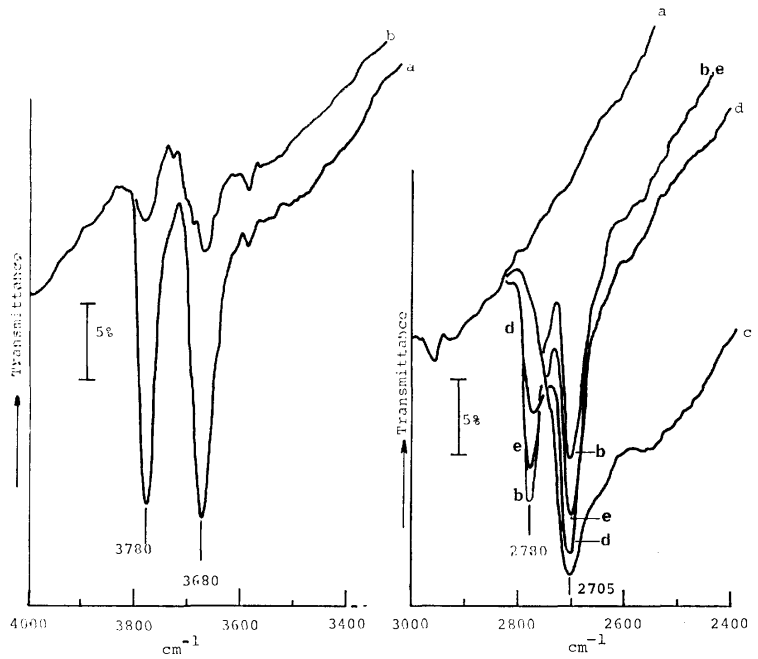

Fig. 1. Exchange of hydroxyl groups with D_2O.
(a) After evacuation at 500 °C for 5 h. (b) Adsorption of 8 mmHg of D_2O at room temperature followed by evacuation at 500 °C for 3 h. (c) Adsorption of 8 mmHg of D_2O at room temperature followed by evacuation at room temperature for 1 h. (d) Evacuation at 200 °C for 1 h. (e) Evacuation at 300 °C for 1 h.

Exchange with Deuterated Organic Compounds. The exchange between deuterated compounds and hydroxyl groups was also examined using acetone-d_6, 2-propanol-d_8, and chloroform-d.

a) Acetone-d_6. The results of the adsorption of acetone-d_6 are shown in Figs. 2 and 3. The adsorption of 1.35 mmHg of acetone-d_6 leads to the complete disappearance of the original OH bands and gives a broad band at 2655 cm^{-1}. The C–D stretching bands are also observed around 2225 cm^{-1}, and C–H bands which could originate from the partial exchange between C–D and hydroxyl groups, appear around 2935 cm^{-1}.

As is shown in Fig. 2, the two bands of $(OH)_I$ and $(OH)_{II}$ were reduced in intensity with an increase in the adsorption pressure of acetone-d_6, keeping their original shapes, while only a broad band appeared around 2700 cm^{-1}, no band of $(OD)_I$ being observed. This indicates that the deuteroxyl groups produced were hydrogen-bonded with each other or with acetone, and that no hydrogen bond was formed in the original hydroxyl groups in the course of adsorption.

During the course of desorption (Fig. 3), the behavior of the two deuteroxyl groups was nearly the same as in the case of D_2O. Evacuation at 200 °C resulted in the production of the $(OD)_I$ band at 2780 cm^{-1}, and above 300 °C two well-resolved bands were obtained, at 2780 and 2710 cm^{-1}.

The spectrum below 2000 cm^{-1} observed at temperatures lower than 200 °C indicates the presence of the formate and the acetate species, the former being assigned by means of the 1589 and 1350 cm^{-1} bands, and the latter, by means of the 1535 and 1440 cm^{-1} bands.[10] Formate species were removed by evacuation above 200 °C, while acetates could not be removed by evacuation up to 500 °C. The acetate species could only be removed by the admission of oxygen and by evacuation at 500 °C.

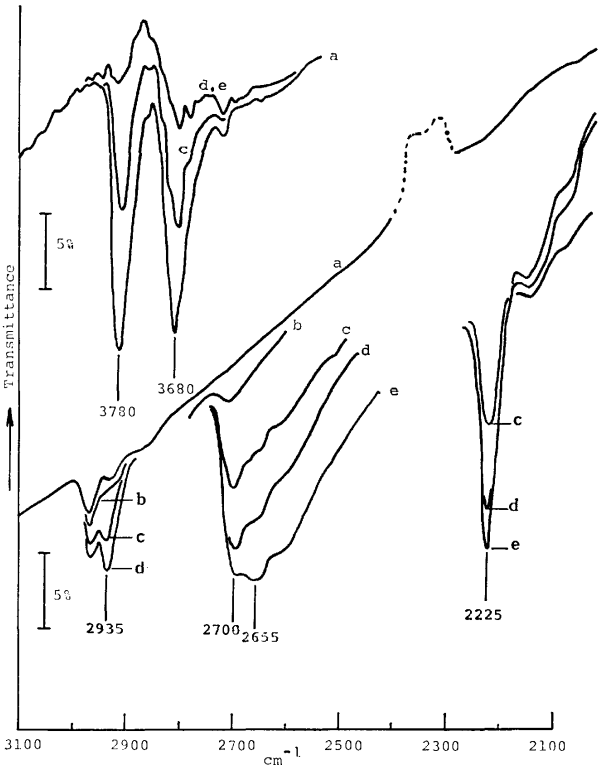

Fig. 2. Adsorption of acetone-d_6.
(a) Background, (b) 0.096 mmHg, (c) 0.23 mmHg, (d) 0.56 mmHg, (e) 1.35 mmHg. Each spectrum was obtained after evacuation at room temperature for 1 h.

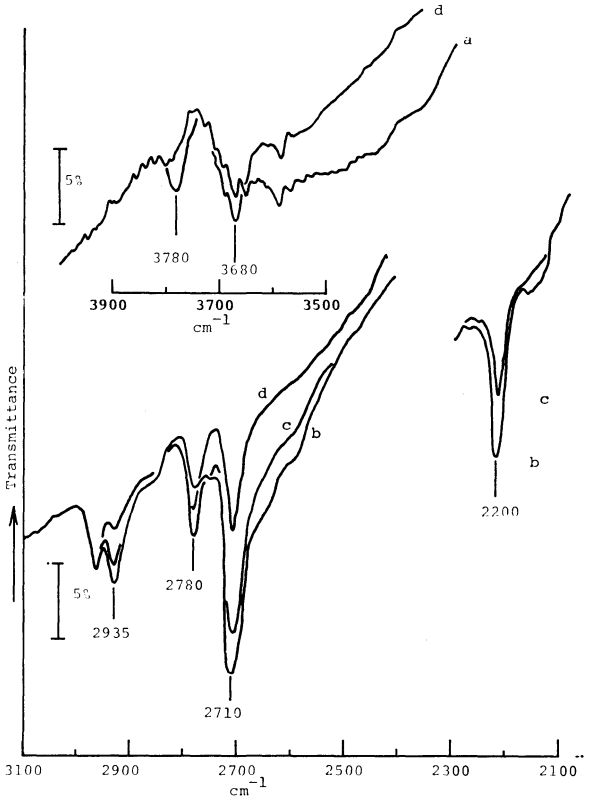

Fig. 3. Desorption of acetone-d_6.
(a) Adsorption of 1.35 mmHg of acetone-d_6 followed by evacuation at room temperature for 1 h. (b) Evacuation at 200 °C. (c) Evacuation at 300 °C. (d) Evacuation at 500 °C.

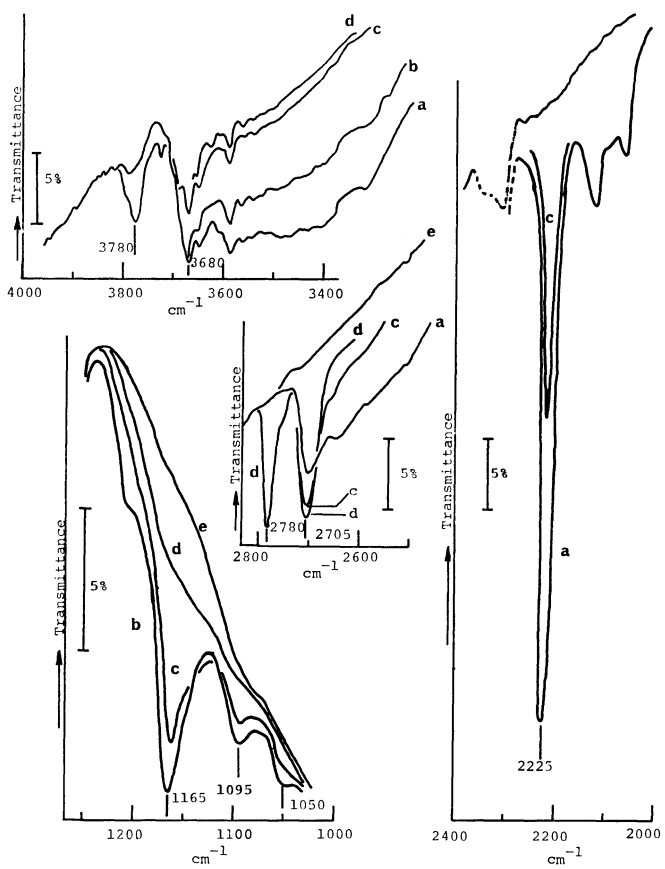

Fig. 4. Adsorption and desorption of 2-propanol-d_8.
(a) Adsorption of 1.32 mmHg of 2-propanol-d_8 followed by evacuation at room temperature for 1 h. (b) Evacuation at 200 °C. (c) Evacuation at 300 °C. (d) Evacuation at 400 °C. (e) Background.

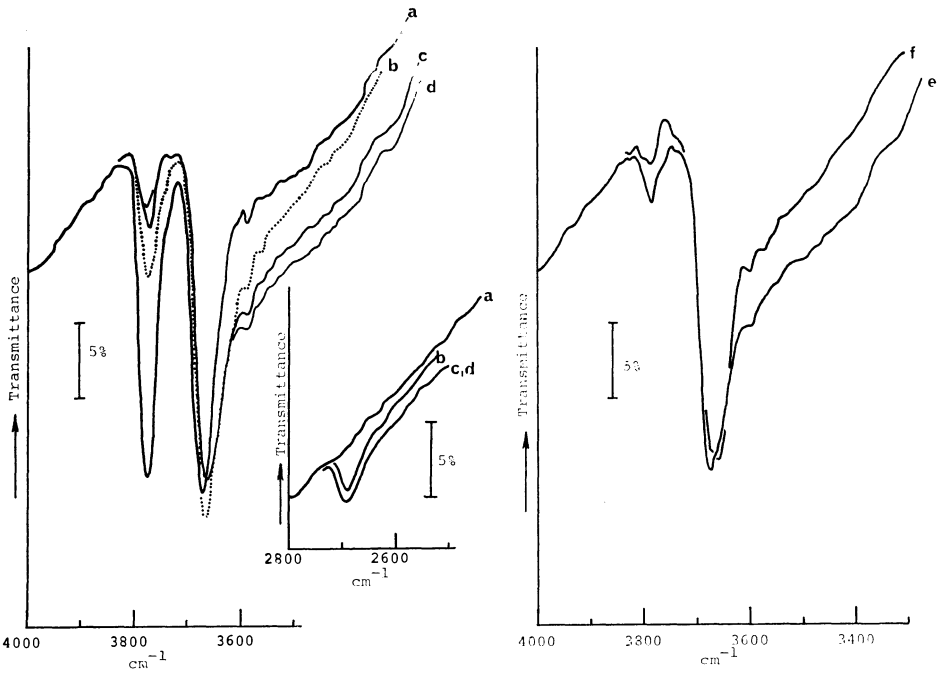

Fig. 5. Adsorption and desorption of chloroform-d.
(a) Background. (b) 0.23 mmHg. (c) 0.56 mmHg. (d) 1.32 mmHg. (e) 3.4 mmHg. Each spectrum was obtained after evacuation at room temperature for 1 h. (f) Evacuation at 400 °C.

b) 2-Propanol-d_8. The adsorption of 2-propanol-d_8 at room temperature resulted in the disappearance of two hydroxyl groups and the appearance of a broad band at 2705 cm^{-1}. No marked difference was observed in the behavior of the two hydroxyl bands at 3780 and 3680 cm^{-1} in the course of the adsorption. The observed bands at 2225, 1165, 1095, and 1050 cm^{-1} were assigned to ν_{C-D}, ν_{C-O}, δ_{as}, and δ_s respectively (Fig. 4). Adsorbed alcohol was stable up to 300 °C, and most of these species decomposed between 300 and 400 °C. The composition of the desorbed gas, which was collected and analyzed by means of gas chromatography, was as follows:

Propylene:Alcohol:Acetone=100:10:1.

No indication of the formation of carboxylate species on the surface was obtained.

A difficulty in restoring $(OD)_I$ was observed in the course of the desorption of alcohol. Below 300 °C, there is only one absorption maximum, at 2705 cm^{-1}. The restoration of $(OH)_I$ or $(OD)_I$ was observed above 200 °C in the case of acetone-d_6 or ammonia (which will be discussed later), even if these compounds remained on the surface. This discrepancy can be understood if one assumes that different sites are used for the adsorption of alcohol. 2-Propanol is supposed to adsorb on the sites which produce $(OH)_I$ or $(OD)_I$, when H_2O or D_2O is admitted.

*c) Chloroform-*d. Since chloroform has been used for characterizing strong and weak basic sites on CaO by comparing the results of benzaldehyde and 2-propanol in terms of the relative ease of the proton abstraction from these molecules,[11] we tried to examine the adsorption of chloroform-*d* on ZrO_2.

The results are shown in Fig. 5. Unlike the cases of D_2O and acetone-d_6 adsorption, the introduction of a small amount of chloroform-*d* leads preferentially to a marked decrease in the $(OH)_I$ band and has little effect on $(OH)_{II}$ except for causing a slight shift to lower frequencies. The $(OH)_I$ almost disappeared after the introduction of 0.56 mmHg of chloroform-*d*, while the 3680 cm^{-1} band kept its intensity. The band broadening at lower frequencies of 3680 cm^{-1} indicates the presence of a hydrogen bond. The formation of new OD bands was quite small compared with the cases of D_2O and acetone-d_6, and no $(OD)_I$ band was observed. Evacuation at elevated temperatures or even the introduction of water vapor do not cause any restoration of the $(OH)_I$ band. On the other hand, though the $(OH)_{II}$ band was extinguished by the adsorption of chloroform at 200 °C, complete restoration was attained by H_2O treatment and evacuation at elevated temperatures.

The production of only a small amount of OD band suggests that hydrogen-deuterium exchange or the abstraction of deuterium by the surface is difficult. Thus, the ZrO_2 surface seems to have only weak basic sites, and the irreversibility of $(OH)_I$ suggests the possible chlorination of $(OH)_I$ by chloroform, though the adsorbed species of chloroform have not been identified.

Exchange with Ammonia and Propylene. The exchange between deuterated surface and ammonia or propylene was also eaxmined. After the deuteration of ZrO_2, ammonia was admitted at room temperature and the changes in the OH and OD bands were recorded. As is shown in Fig. 6, the reduction of the peak intensities in the two OD bands and the formation of an OH band were observed. Again, as in the case of acetone-d_6, the OD bands keep their original shapes, while being reduced in intensity, while the OH band produced shows hydrogen bonding. This indicates a rapid exchange between deuteroxyl groups and ammonia.

Adsorbed ammonia gives absorption bands at 3400, 3350, 1600, and near 1160 cm^{-1}, as is shown in Fig. 7, those bands are assigned to asymmetric and symmetric stretching modes, and to asymmetric and symmetric bending modes, of ammonia respectively. Metal–ammine complexes, such as $[Ni(NH_3)_6]Cl_2$, $[Co(NH_3)_6]Cl_2$, or $[Fe(NH_3)_6]Cl_2$, show deformation bands at about 1600 and near 1160 cm^{-1}, the latter, δ_s, being sensitive to the metal and the environment.[12] The 3400 and 3355 cm^{-1} bands obtained on alumina were assigned to the symmetric and asymmetric stretching vibrations of coordinated ammonia,[12] and the deformation band

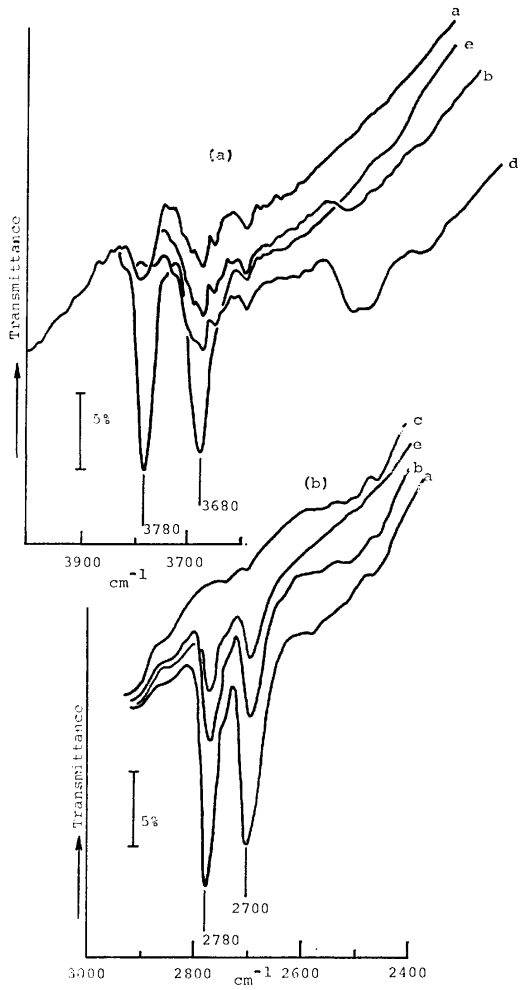

Fig. 6. Adsorption of ammonia on deuterated ZrO_2. (a) After exchange with D_2O. (b) 0.23 mmHg. (c) 0.56 mmHg. (d) 1.35 mmHg. Each spectrum was obtained after evacuation at room temperature for 1 h. (e) Evacuation at 500 °C.

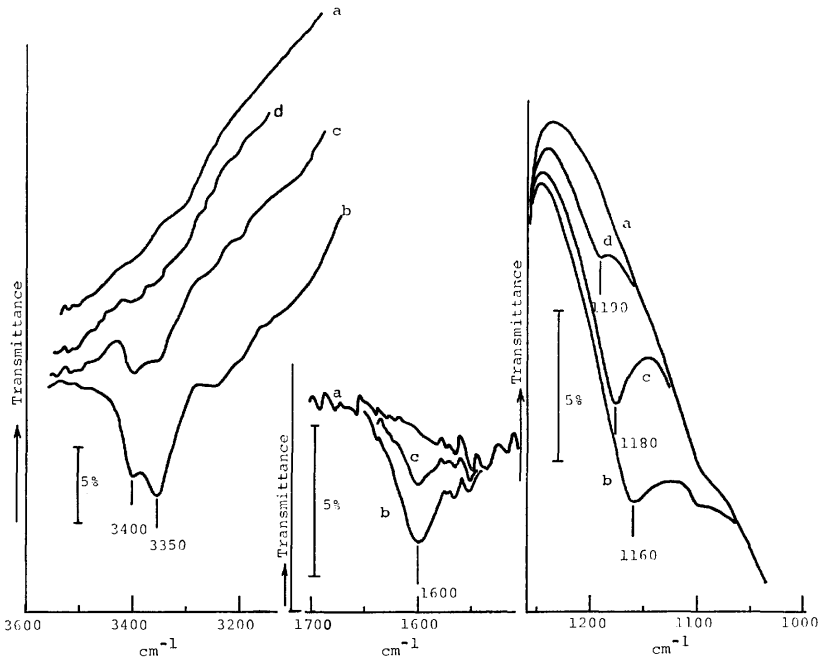

Fig. 7. Adsorption and desorption of ammonia.
(a) Background. (b) Adsorption of 1.35 mmHg of ammonia at room temperature followed by evacuation at room temperature for 1 h. (c) Evacuation at 200 °C. (d) Evacuation at 300 °C.

of coordinated ammonia appeared at 1620 cm^{-1}. Thus, on ZrO_2, the sets of the absorption bands obtained could be assigned to the ammonia coordinated to Lewis acid sites. The peak intensity of a 3350 cm^{-1} band was stronger than that of a 3400 cm^{-1} band when the adsorption pressure was high or the evacuation temperature was low. Thus, hydrogen-bonded species might be involved in the 3350 cm^{-1} band.

The isomerization of butenes took place at 80 °C, and *cis*-2-butene was the major product in the reaction from 1-butene.[7] In this connection, it is interesting to investigate the hydrogen exchanges between olefin molecules and surface hydroxyl groups. An exchange reaction was carried out, using propylene and deuterated ZrO_2, by following spectrometrically the intensity changes in deuteroxyl bands up to 300 °C. About half of the deuteroxyl groups were replaced by exchange in such a period as follows;

Temperature (°C)	r. t.	100	300
Time (h)	20	3	0.5

At higher temperatures, two deuteroxyl bands were reduced in intensity at the same rate, while the 2780 cm^{-1} band was reduced in intensity more rapidly than the 2705 cm^{-1} band at lower temperatures.

Discussion

More than two types of hydroxyl groups have been observed on various metal oxides, such as Al_2O_3,[2] SiO_2,[3] MgO,[4] CaO,[5] and TiO_2.[6] Typical hydroxyl groups on SiO_2[3] were assigned to the surface and the bulk hydroxyls, or to the isolated and the combined ones, on the basis of observations of the deuterium-exchange and particle-size dependencies. Peri has reported that the five types of hydroxyls which are present on the Al_2O_3 surface have different configurations in the nearest neighbors.[2] Because of the very high frequencies observed for the hydrogen–oxygen stretching vibrations of hydroxyl groups on Al_2O_3, Peri regarded them as ions rather than as groups covalently bonded to surface aluminum atoms. More than two kinds of hydroxyls have been observed on TiO_2 by many authors.[6] Parkyns[6d] found two main peaks, at 3728 and 3672 cm^{-1}, with reflections at 3707 and 3636 cm^{-1} on anatase evacuated at 400 °C; he also discussed the models, *i.e.*, the statistical, substitutional, and total hydration models, though he did not assign them individually. The presence of two kinds of hydroxyls (3780 and 3680 cm^{-1}) on rutile was reported by Parfitt,[6c] and these groups were attributed to bridged and terminal hydroxyls, assuming a model for the surface based on the (110) plane on rutile. From the different thermal stabilities of the two bands, the bridged type, $\overset{M}{M}\!>\!OH$, was thought to be more stable because of the bidentate configuration, while the terminal one, M–OH, was considered less stable.

The hydroxyl groups observed on ZrO_2 could be assigned to the surface hydroxyls by taking into consideration the peak shapes and exchange abilities observed in the present work. The assignment of $(OH)_{II}$ to the hydrogen-bonded ones seems to be unlikely because of its relatively narrow and symmetrical shape. We propose to assign two types of bands to the isolated surface hydroxyls which have different neighboring circumstances, *e.g.*, to the bridged and terminal groups, as has been postulated by Parfitt.[6c]

The characteristic behavior of the OH bands which were observed in the adsorption of the materials tested

here may be summarized as follows:

1. As is shown in Fig. 2 (acetone-d_6) and Fig. 6 (NH_3), the bands being reduced keep their original shapes, while the produced bands show a strongly hydrogen-bonded nature.
2. The $(OH)_I$ and $(OH)_{II}$ bands show different characters in the cases of alcohol and chloroform adsorption, in which the difficult restoration of $(OH)_I$ was observed during the desorption process.

The first phenomenon can be explained on the basis of a rapid hydrogen exchange between hydroxyls (or deuteroxyls) and adsorbates. When acetone-d_6 interacts with surface hydroxyls, rapid hydrogen-deuterium exchange may take place to form surface deuteroxyl groups, which are observed as a broad band at about 2655 cm^{-1} as a result of hydrogen bonding, while the OH groups which have not interacted with the adsorbate remain unchanged. The adsorption of 2-propanol may be supposed to cause an increase in the concentration of surface hydroxyl groups rather than an exclusive exchange of surface hydroxyl groups with 2-propanol. An increase in the surface hydroxyl groups causes an increase in hydrogen bonding in both the original and produced OH groups. The situation is the same in the case of NH_3, where the hydrogen bond was observed only in the produced hydroxyls, and not in the original deuteroxyls, as a result of the rapid exchange between the NH_3 and the surface OD groups.

The second phenomenon, in which the difficult restoration of the $(OH)_I$ group was observed, can be explained if we assume that alcohol and chloroform are adsorbed exclusively on $(OH)_I$ or $(OD)_I$ sites. As far as alcohol is concerned, the admission of alcohol to ZrO_2 may lead to an interaction only with the surface $(OH)_I$ and to the formation of alkoxyl groups on $(OH)_I$ sites. Such alkoxyl groups are stable up to 300 °C; they decompose to olefin above this temperature.

All the results obtained from the adsorption of chloroform or alcohol and the hydrogen-exchange reaction with propylene at lower temperatures reveal that $(OH)_I$ or $(OD)_I$ is more labile and reactive than $(OH)_{II}$ or $(OD)_{II}$.

References

1) L. H. Little, "Infrared Spectra of Adsorbed Species," Academic Press, New York and London (1966).
2) J. B. Peri, *J. Phys. Chem.*, **69**, 220 (1965).
3) R. S. McDonald, *J. Phys. Chem.*, **62**, 1168 (1958); V. Ya. Davydov, A. V. Kiselev, and L. T. Zhuravlev, *Trans. Faraday Soc.*, **60**, 2254 (1964).
4) N. Takezawa, K. Miyahara, and I. Toyoshima, *J. Res. Inst. Catal., Hokkaido Univ.*, **19**, 56 (1971).
5) M. J. D. Low, N. Takezawa, and A. J. Goodsel, *J. Colloid Interface Sci.*, **37**, 422 (1971).
6) a) D. J. C. Yates, *J. Phys. Chem.*, **65**, 746 (1961); b) K. E. Lewis and G. D. Parfitt, *Trans. Faraday Soc.*, **62**, 204 (1966); c) P. Jackson and G. D. Parfitt, *ibid.*, **67**, 2469 (1971); d) N. D. Parkyns, "Chemisorption and Catalysis," ed by P. Heppel, Elsevier Pub. Co., Amsterdam, p. 150.
7) T. Yamaguchi, H. Sasaki, and K. Tanabe, *Chem. Lett.*, **1973**, 1017.
8) T. Yamaguchi and J. W. Hightower, *J. Am. Chem. Soc.*, **99**, 4201 (1977).
9) N. E. Tretyakov, D. V. Dozdnyakov, O. M. Ornskaya, and V. N. Filimonov, *Zh. Fiz. Khim.*, **44**, 1077 (1970).
10) H. Miyata, M. Wakamiya, and Y. Kubokawa, *J. Catal.*, **34**, 117 (1974).
11) I. Iizuka, H. Hattori, Y. Ohno, J. Sohma, and K. Tanabe, *J. Catal.*, **22**, 130 (1971).
12) K. Nakamoto, "Infrared Spectra of Inorganic and Coordination Complexes," Wiley-Interscience, New York (1970).
13) J. B. Peri, *J. Phys. Chem.*, **69**, 231 (1965).

The Absolute Rate Constants of Reaction of Hydrogen Atoms with Several Olefins

Yo-ichi ISHIKAWA, Masaki YAMABE, Akihiko NODA, and Shin SATO*

Department of Applied Physics, Tokyo Institute of Technology, Ookayama, Meguro-ku, Tokyo 152

(Received February 3, 1978)

Using the techniques of pulse-radiolysis and of the absorption of Lyman-α radiation by hydrogen atoms, the absolute rate constants of reaction of hydrogen atoms with several olefins have been measured at room temperature.

Olefin	$k/10^{-12}$ cm^3 molecule^{-1} s^{-1}
Ethylene	1.1±0.1
Propylene	1.7±0.1
1-Butene	2.0±0.5
trans-2-Butene	1.1±0.2
cis-2-Butene	1.0±0.1
2-Methyl-1-propene	5.2±0.6
2-Methyl-2-butene	2.4±0.3

These rate constants were invariant over hydrogen pressures ranging from 200 to 1200 Torr.

When hydrogen gas at one atmosphere is irradiated with high energy electrons, many different active species are produced and react with each other as well as with hydrogen molecules; however, in a very short time (≈ 10 μs) after the irradiation, active species other than hydrogen atoms disappear in the reaction system. Since the recombination of hydrogen atoms and the diffusion to the wall of the reaction vessel are slow processes, the concentration of hydrogen atoms actually remains constant for a while. If a small amount of an olefin is present in this system, the decrease in the concentration of hydrogen atoms results from the reaction of hydrogen atoms with the olefin. The change of the concentration of hydrogen atoms can be pursued by the absorption of Lyman-α radiation. Hikida *et al.* used this technique for the measurement of the rate constants of reaction of hydrogen atoms with oxygen, carbon monoxide, nitric oxide, and ethylene.[1] Mihelcic *et al.* extended this technique to the reactions of H and D atoms with C_2H_4, C_2D_4, and C_3H_6.[2]

On the other hand, the relative rates of reaction of hydrogen atoms with various olefins have been measured by many investigators. Among them, Cvetanović and coworkers used three different photochemical techniques: the mercury-photosensitized decompositions of butane[3] and of hydrogen[4] and the photolysis of hydrogen sulfide,[5] as sources of hydrogen atoms, and measured the relative rates. These relative rate constants are one of the important sets for the reactions of hydrogen atoms.

Recently, we have constructed an apparatus similar to that used by Mihelcic *et al.* and measured the absolute rate constants of reaction of hydrogen atoms with several olefins.

Experimental

A schematic diagram of the set-up of instruments is shown in Fig. 1. As the source of Lyman-α, a water-cooled capillary discharge lamp with a flow of a gas mixture of 5% hydrogen and 95% helium was used. The highest ratio of signal/noise, about 10, was obtained at 600 V and 0.6 A. We could not find any strong lines other than Lyman-α between 104 and 200 nm.

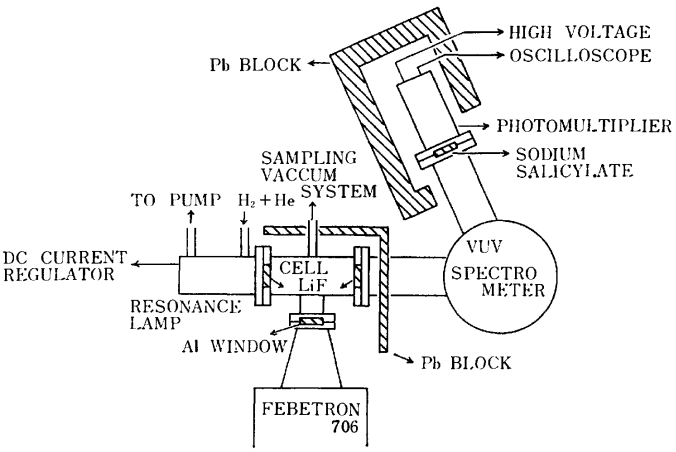

Fig. 1. The schematic diagram of the pulse radiolysis-resonance absorption apparatus.

The reaction vessel was made of stainless steel, 11 cm long and 5 cm in diameter. A pair of LiF windows was attached to the vessel perpendicularly to the path of the electron beam. At the entrance of the electron beam was framed another window covered with an aluminium foil, 80 μm in thickness. The LiF plates used were supplied by the Harshow Chem. Co., 2 mm thick, and can transmit over 70% of Lyman-α radiation.

The Lyman-α was isolated with the VUV monochromator (Shimadzu, Model SGV-50). The light signal was detected with a photomultiplier (Hamamatsu TV Co., R268) through the wave-shifter of sodium salicylate. The output of the photomultiplier was amplified and monitored with an oscilloscope (Tektronix 475). The risetime of the detection system was about 3 μs. The negative high voltage power sypply (Hamamatsu TV Co., Model HTV-C448) for the photomultiplier was operated at 700 V and the bleeder current was about 1 mA, which was about 10^3 times the signal current.

The pulsed electron beam— a few ns of the pulse-width and 600 keV of the upper-limit energy—was generated by a Febetron 706 (Hewlett Packard Co.). The total output energy was nominally 12 J pulse^{-1}. Only a small fraction of it was absorbed by the hydrogen gas because of the low electron density. The dose absorbed by hydrogen at 760 Torr

in the reaction vessel was estimated to be 10^{16} eV pulse^{-1} by using the dinitrogen oxide dosimeter. The *G*-value of nitrogen was assumed to be 12.4.[6]

The pressure of the gases introduced into the reaction vessel was measured with a Wallace and Tiernan type aneroid manometer (Nagano Keiki Co., Model GP 15-201). The high-purity dried hydrogen (Showa Denko Co.) was passed through a trap filled with molecular sieve 4A at the temperature of liquid nitrogen. The research grade olefins: ethylene, propylene, 1-butene, *cis*- and *trans*-2-butene, 2-methyl-1-propene, and 2-methyl-2-butene, were supplied by the Takachiho Shoji Co., and were used after thorough degassing.

Results

Pure Hydrogen. Figures 2a and 2b show the oscillograms for the time-dependence of hydrogen atom-concentration obtained with pure hydrogen at 1200 Torr. As Fig. 2a shows, the formation of hydrogen atoms is completed within 20 μs after the pulse irradiation. The signal shown before 20 μs does not correspond to the true change of the concentration of hydrogen atoms, because the recovery of the detection system from the large noise induced by the electron pulse is slow.

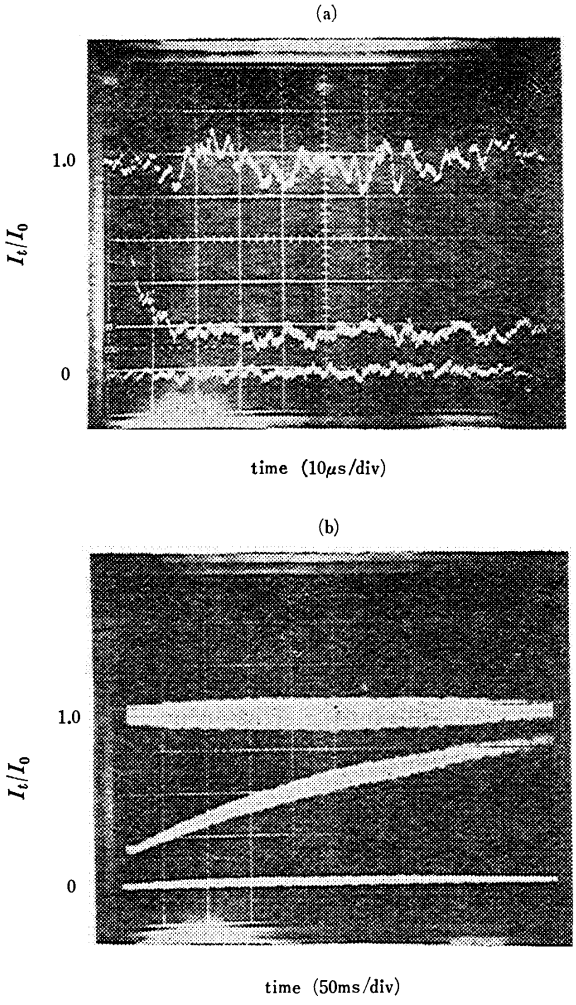

Fig. 2. Transmission of Lyman-α in the pulse irradiated pure hydrogen at 1200 Torr.

Figure 2b shows the gradual decrease of the concentration of hydrogen atoms. Most of the curves obtained with pure hydrogen at various pressures obeyed the first-order decay; for example, the lifetime obtained at 760 Torr was 0.18 s. As is shown later, this decay rate is two orders of magnitude slower than the slowest decay rate obtained in the presence of an olefin. The decrease in the concentration of hydrogen atoms observed with pure hydrogen is probably due to the diffusion of hydrogen atoms to the wall of the reaction vessel; however, the reaction with impurities eventually introduced cannot be ignored. Consequently, no further analysis has been attempted in the present experiment.

For the measurement of the concentration of hydrogen atoms, the present experiment uses the optical density for the Lyman-α radiation from the discharge lamp. However, since the profile of the Lyman-α cannot be the same as that of the absorption line of hydrogen atoms produced in the reaction vessel, the linearity between the concentration of hydrogen atoms and the optical density may not always hold.

Figure 3 shows the maximum optical density obtained with pure hydrogen after the pulse irradiation as a function of the hydrogen pressure. At low pressures, the energy transferred from high energy electrons to hydrogen gas may be regarded as proportional to the pressure; that is, the concentration of hydrogen atoms produced may be proportional to the pressure of hydrogen. As Fig. 3 shows, if the absorbance is lower than 60%, the linearity between the hydrogen atom-concentration and the optical density for Lyman-α may be used in the present experiment.

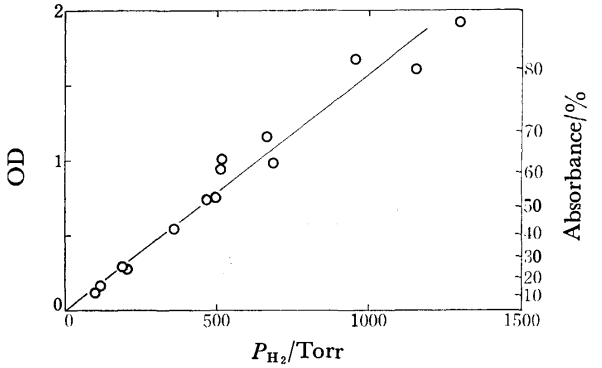

Fig. 3. The highest optical density after pulse irradiation as a function of the hydrogen pressure.

In the Presence of Olefin. Because of the high absorption coefficient of olefins at 121.6 nm, the pressure of olefins could not be raised above 0.15 Torr, which corresponds to 8.4×10^{-9} mol cm^{-3}.

One of the oscillograms for the decay of hydrogen atoms obtained in the presence of ethylene is shown in Fig. 4. From this oscillogram, we plotted the logarithm of the optical density as a function of time, as is shown in Fig. 5. The slope of this plot corresponds to the decay rate of hydrogen atoms. The rate constant of the reaction between hydrogen atoms and ethylene can be calculated by dividing this decay rate by the concentration of ethylene.

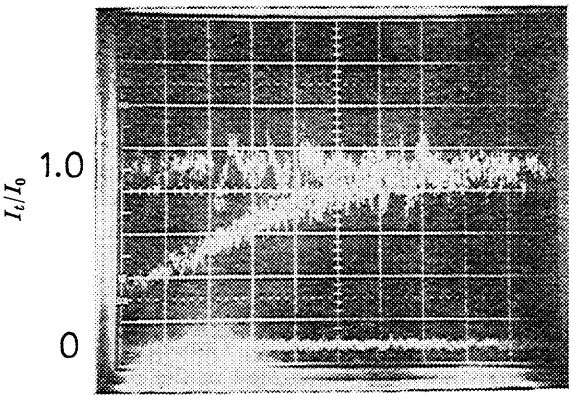

Fig. 4. Transmission of Lyman-α in the pulse irradiated hydrogen at 750 Torr containing 50 mTorr ethylene.

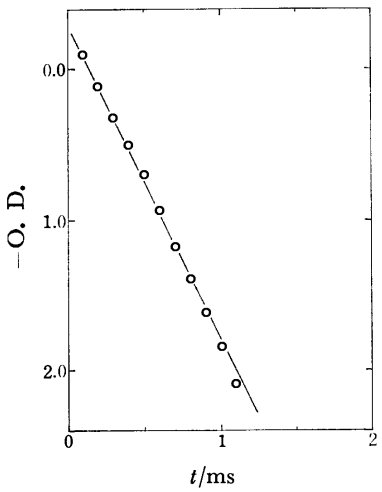

Fig. 5. The first order decay plot for the reaction of hydrogen atoms with ethylene.

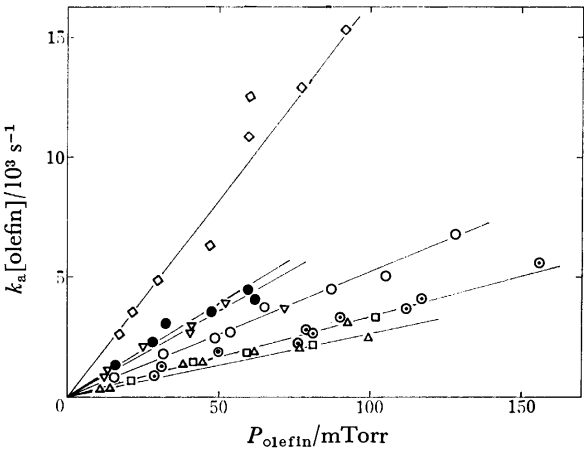

Fig. 6. Plots of the decay rates against the olefin pressures. The hydrogen pressure is around 750 Torr. ⊙: Ethylene, ○: propylene, ▽: 1-butene, □: *trans*-2-butene, △: *cis*-2-butene, ◇: 2-methyl-1-propene, ●: 2-methyl-2-butene.

All of the rate constants thus calculated are summarized in the last column of Table 1. The hydrogen pressure ranges from 200 to 1200 Torr and the olefin pressure from 0.02 to 0.15 Torr. The rate constant obtained with an olefin is independent of both the hydrogen and olefin pressures within the experimental errors. Figure 6 shows the decay rates obtained at around 750 Torr of hydrogen as functions of the pressures of olefins examined.

Discussion

The Initial Concentration of Hydrogen Atoms. Since no stable products can be obtained, the radiolysis of hydrogen has not been investigated except for that of the mixture of hydrogen and deuterium. For this mixture system, the famous chain reaction:

Table 1. Absolute rate constants of reaction of hydrogen atoms with olefins at room temperature

Author[a]	DLT	KD	DNW	BL	KPB	MSHP	This work
Method[b]	FD/MS	FD/CA	FD/MS	FP/RF	FP/RF	PR/RA	PR/RA
Pressure/Torr	2—25(∞)[c]	≃2	0.4—2.8	5—75(∞)[c]	5—500(∞)[c]	800—1650	200—1200
Third body	He	Ar	He	He, N_2	He	H_2	H_2
$[Olefin]_0/[H]_0$	1—100	≃3	0.01	>100	>100	>1000	>100
			$k_a/10^{-12}$ cm^3 molecule^{-1} s^{-1}				
Ethylene	2.0±0.7	0.18		1.00±0.15	1.36±0.19	1.25±0.09	1.1±0.1
Propylene	1.3±0.4		(0.76±0.04)[d]		1.61±0.04	1.68±0.04	1.7±0.1
1-Butene	1.5±0.45		1.38±0.08				2.0±0.5
trans-2-Butene			0.89±0.07	1.00±0.15			1.1±0.1
cis-2-Butene			0.79±0.06				1.0±0.1
2-Methyl-1-propene		5.3	(0.7)[d]	3.8±0.6			5.2±0.6
2-Methyl-2-butene			1.51±0.16				2.4±0.3

a) DLT: Dodonov, Lavrovskaya, and Tal'roze, Ref. 15; KD: Knox and Dalgleish, Ref. 16; DNW: Daby, Niki, and Weinstock, Ref. 17; BL: Braun and Lenzi, Ref. 18; KPB: Kurylo, Peterson, and Braun, Refs. 11 and 19; MSHP: Mihelcic, Schubert, Höfler, and Potzinger, Ref. 2. b) FD, flow discharge; MS, mass spectrometry; CA, calorimetry; FP, flash photolysis; RF, resonance fluorescence; PR, pulse radiolysis; RA, resonance absorption. c) The value in this column is the one extrapolated at infinite pressure. d) The values in parentheses are less reliable.

$$H_2^+ + H_2 \rightarrow H_3^+ + H,$$
$$H_3^+ + H_2 \rightarrow H_2 + H_3^+,$$

has been studied.[7] However, the G-value of hydrogen atoms has not been measured.

According to the theoretical calculation,[8] the G-values of initial active species in the radiolysis of hydrogen are as follows: $G(H_2^*, \text{excited state}) = 1.92$, $G(H^*, \text{hot atoms}) = 0.94$, $G(H) = 2.49$, $G(H^+) = 0.40$, and $G(H_2^+) = 2.43$. With these values, we can estimate the upper limit of the G-value of hydrogen atoms.

$$G(H) = 1.92 \times 2 + 0.94 + 2.49 + 0.40 + 2.43 \times 2$$
$$= 12.53$$

Using the absorbed dose of 10^{16} eV pulse^{-1}, the initial concentration of hydrogen atoms in the reaction system can be estimated to be 10^{-11} mol cm^{-3}.

An independent estimation can be made as follows. In the study of the reaction of hydrogen atoms, Michael and Weston measured the relationship between the optical density for Lyman-α and the concentration of hydrogen atoms.[9] The optical density of 0.5 was obtained at the hydrogen atom-concentration of 13.3×10^{12} atoms cm^{-3} with the optical path of 3.5 cm. Since their procedure is similar to the method in the present experiment, let us assume that the relation obtained by Michael and Weston holds for the present measurement, in which the optical path is 11 cm. Then, the concentration of hydrogen atoms at the optical density of 0.5 can be calculated to be 0.7×10^{-11} mol cm^{-3}.

The lowest olefin pressure used in the present experiment was 0.02 Torr, which corresponds to 1.0×10^{-9} mol cm^{-3}. The concentration ratio [H]/[olefin], therefore, is always smaller than 10^{-2}.

Active Species other than Hydrogen Atoms. The thermalization times of high energy electrons in various gases have been measured by Warman and Sauer.[10] In hydrogen gas, the product of the thermalization time and pressure, $\tau_{th} \times p$, was estimated to be 1.5×10^{-6} s Torr; *i.e.*, the thermalization time in hydrogen at 760 Torr is about 2 ns. Since the species heavier than electrons are thermalized more rapidly than electrons, all of the active species produced in hydrogen must be thermalized in a few ns after the electron pulse.

The neutralization time is one of the problems in radiation chemistry. In the study of the emission from the helium–mercury system irradiated by high energy electrons, we have recently measured the time-dependence of the emission and found that the slowest emission resulted from the neutralization reaction between mercury ions and thermalized electrons in helium at 760 Torr, which was completed within 10 μs.[11] Consequently, we can conclude that, at 20 μs after the pulse irradiation, no active species other than hydrogen atoms are present in the reaction system and that all hydrogen atoms are thermalized.

The Contribution of the Reaction of Alkyl Radicals. It is now well known that the reaction between hydrogen atoms and olefins is mainly the addition reaction forming alkyl radicals, and that the abstraction reactions of a hydrogen atom from an olefin make up less than 10% of the total reaction.[4]

$$\begin{aligned} H + \text{Olefin} &\rightarrow R && (1) \\ &\rightarrow H_2 + R' && (1') \end{aligned} \quad k_a$$

If the pressure in the reaction system is low, the radical produced in Reaction 1 may decompose before the thermalization. In the case of ethylene, this decomposition leads to the reformation of hydrogen atoms, so that the apparent decay rate of hydrogen atoms may be decreased with the decrease in the total pressure. However, as stated in the Results section, no such pressure dependence could be observed under the present experimental condition. Probably such a decomposition would occur at pressures lower than 200 Torr. In the present experiment, we could not make any measurements at pressures lower than 200 Torr, because the concentration of hydrogen atoms produced was too low for the measurement of decay rate.

The successive reactions of the radicals produced in Reaction 1 may be written as follows:

$$\begin{aligned} R + R &\rightarrow R_2 && (2) \\ &\rightarrow RH + \text{Olefin} && (2') \end{aligned} \quad k_b$$
$$\begin{aligned} R + H &\rightarrow RH && (3) \\ &\rightarrow H_2 + \text{Olefin} && (3') \end{aligned} \quad k_c$$

If Reactions 3 and 3′ are the only process for the disappearance of alkyl radicals, the decay rate of hydrogen atoms would become twice the value of k_a, the sum of the rate constants of Reactions 1 and 1′. However, Reactions 2 and 2′ are also fast processes and contribute to the disappearance of alkyl radicals. If the concentration ratio [H]/[olefin] is infinitely small, the apparent decay rate of hydrogen atoms is exactly equal to the sum of the rate of Reactions 1 and 1′.

In order to estimate the contribution of Reactions 3 and 3′, we defined the following correction factor:

$$\gamma = \frac{-\mathrm{d} \ln[H]/\mathrm{d}t}{k_a[\text{Olefin}]_0}.$$

Here $[\text{olefin}]_0$ stands for the initial concentration of olefins. On the basis of the reaction mechanism from (1) to (3′), we can construct simultaneous differential equations for [H], [olefin], and [R]. Using the Runge-Kutta numerical integration procedure, we calculated the value of γ as functions of the ratio of $[\text{olefin}]_0$ to $[H]_0$ and of the ratio of k_a/k_c. In this calculation, the following values were assumed: $k_b = 9.0 \times 10^{-12}$ cm^3 mol-

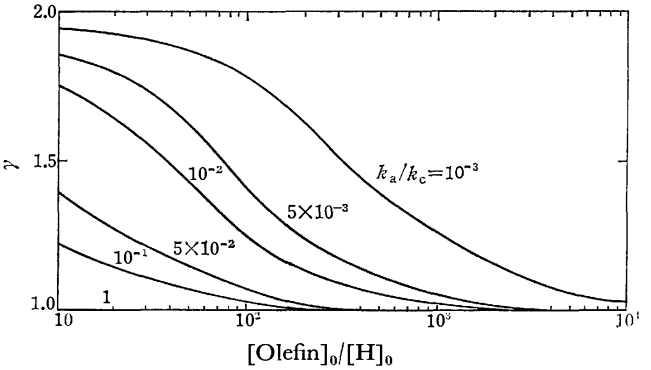

Fig. 7. The correction factor, γ, as functions of the ratios, $[\text{olefin}]_0/[H]_0$ and k_a/k_c.

Table 2. Relative rate constants of reaction of hydrogen atoms with olefins at room temperature

Author[a]	JC	WC	CD	CKMY	This work
Method[b]	Hg/PRA	PH/PRA	Hg/PRA	Hg/RA	PR/RA
Pressure/Torr	$\simeq$435	10—760	600—700	10—15	200—1200
Third body	n-C_4H_{10}	CO_2	H_2	He	H_2
$[Olefin]_0/[H]_0$	$\gg 1$	>100	$\gg 1$	>100	>100
	Relative rate constant				
Ethylene	(0.53)	0.62	0.60	0.41	0.63
Propylene	1.00	1.00	1.00	1.00	1.00
1-Butene	1.12	1.00		1.42	1.17
trans-2-Butene	0.63			0.57	0.63
cis-2-Butene	0.48			0.43	0.57
2-Methyl-1-propene	2.41	2.44	2.46	3.58	3.01
2-Methyl-2-butene			1.07		1.36

a) JC: Jennings and Cvetanović, Ref. 3; WC: Woolley and Cvetanović, Ref. 5; CD: Cvetanović and Doyle, Ref. 4; CKMY: Cowfer, Keil, Michael, and Yeh, Ref. 14. b) Hg, mercury photosensitization; PA, pulse radiolysis; PH, photolysis; PRA, product analysis; RA, resonance absorption. c) The value in parentheses is less reliable.

ecule^{-1} s^{-1},[12] $k_c=6.0\times10^{-11}$ cm^3 molecule^{-1} s^{-1},[13] and $[H]_0=6.0\times10^{12}$ molecule cm^{-3}. The result is shown in Fig. 7.

In the present experiment, $[olefin]_0/[H]_0>10^2$ and k_a/k_c is of the order of 10^{-2}. Therefore, the value of γ must be lower than 1.1. This means that no correction is needed for the present measurement of k_a.

Comparison with Other Measurements. Table 1 compares some of the measurements made for obtaining the absolute rate constants of reaction of hydrogen atoms with simple olefins.

As Mihelcic and coworkers summarized, numerous measurements have been reported for the reaction with ethylene.[2] The rate constants reported range from 0.15 to 1.5×10^{-12} cm^3 molecule^{-1} s^{-1}. The value obtained by Hikida *et al.* is $0.91\pm0.09\times10^{-12}$ cm^3 molecule^{-1} s^{-1}. The present result lies between the values obtained by two measurements in which the pulse radiolysis technique was used.

On the other hand, Table 2 compares our result with the relative rate constants obtained by Cvetanović and coworkers[3-5] and Cowfer *et al.*[14] Except for the values obtained with 2-methyl-1-propene and 2-methyl-2-butene, the present result is in good agreement with those reported by Cvetanović.

References

1) T. Hikida, J. A. Eyre, and L. M. Dorfman, *J. Chem. Phys.*, **54**, 3422 (1971).

2) D. Mihelcic, V. Schubert, F. Höfler, and P. Potzinger, *Ber. Bunsenges. Phys. Chem.*, **79**, 1230 (1975).

3) K. R. Jennings and R. J. Cvetanović, *J. Chem. Phys.*, **35**, 1233 (1961).

4) R. J. Cvetanović and L. C. Doyle, *J. Chem. Phys.*, **50**, 4705 (1969).

5) G. R. Woolley and R. J. Cvetanović, *J. Chem. Phys.*, **50**, 4697 (1969).

6) C. Willis, O. A. Miller, A. E. Rothwell, and A. W. Boyd, *Adv. Chem. Ser.*, **81**, 539 (1968).

7) T. Terao and R. A. Back, *J. Phys. Chem.*, **73**, 3884 (1969).

8) K. Okazaki and S. Sato, *Bull. Chem. Soc. Jpn.*, **48**, 3523 (1975).

9) J. V. Michael and R. E. Weston, Jr., *J. Chem. Phys.*, **45**, 3632 (1966).

10) J. M. Warman and M. C. Sauer, Jr., *J. Chem. Phys.*, **62**, 1971 (1975).

11) S. Sato, K. Okazaki, M. Yamabe, H. Umemoto, S. Tsunashima, T. Ueno, A. Yokoyama, and Y. Hatano, *Chem. Lett.*, **1976**, 385.

12) J. A. Kerr and A. F. P. Dickenson, *Prog. React. Kinet.*, **1**, 105 (1961).

13) M. J. Kurylo, N. C. Peterson, and W. Braun, *J. Chem. Phys.*, **53**, 2776 (1970).

14) J. A. Cowfer, D. G. Keil, J. V. Michael, and C. Yeh, *J. Phys. Chem.*, **75**, 1584 (1971).

15) A. F. Dodonov, G. K. Lavrovskaya, and V. L. Tal'roze, *Kinet. Katal.*, **10**, 22 (1969).

16) J. H. Knox and D. G. Dalgleish, *Int. J. Chem. Kinet.*, **1**, 69 (1969).

17) E. E. Daby, H. Niki, and B. Weinstock, *J. Phys. Chem.*, **75**, 1601 (1971).

18) W. Braun and M. Lenzi, *Discuss. Faraday Soc.*, **44**, 252 (1967).

19) M. J. Kurylo, N. C. Peterson, and W. Braun, *J. Chem. Phys.*, **54**, 4662 (1971).

Far-infrared Absorption Intensities and the Dipole Moments of Some Molecules in Solutions

Kimihiro SATO, Yusei OHKUBO, Tadaharu MORITSU, Shun-ichi IKAWA, and Masao KIMURA*

Department of Chemistry, Faculty of Science, Hokkaido University, Sapporo 060

(Received February 17, 1978)

The integrated intensities of the far-infrared absorptions of CH_3I, $CHCl_3$, CH_2Cl_2, CH_3CN, and their deuterated compounds in dilute solutions have been measured. They can be well explained by the rotational motion of the molecules with the dipole moments enlarged by Onsager's reaction field.

It is well known that the broad far-infrared absorption of a dipolar molecule in the liquid phase contains valuable information about the molecular rotational motion in the liquid. If the absorption is attributed solely to the rotational motion of the molecule, its band shape is reducible to the reorientational correlation function by the Fourier transformation[1] and its integrated intensity after correcting for the internal field effect[2-4] is related through Gordon's sum rule[5] to the dipole moment and the moments of inertia of the molecule. But all the integrated intensities so far observed,[6-15] except for the previous result for HCl dissolved in CCl_4,[16] are appreciably larger than the values estimated on the basis of the permanent dipole moments in the gas phase. Hitherto the excess absorptions have simply been ascribed to the temporary dipole moments induced by collision with neighboring molecules. However, even in the simple form of Gordon's sum rule, which was widely used,[6-16] the dipole moment involved is considered to be a gross dipole moment consisting of the permanent dipole moment in the free state and the statistical average of the induced dipole moment. In this case, the dipole moment may conveniently be interpreted in the macroscopic point of view. In the theory of dielectrics,[17,18] the actual dipole moment of a molecule in the liquid phase differs from the gas-phase value owing to the reaction field. Since the actual dipole moment which was referred to as the *internal moment* by Fröhlich,[17] simply follows the rotation of the molecular framework, it takes part in the far-infrared absorption. Then, the actual dipole moments estimated by the theory of dielectrics are worth comparing with the dipole moments obtained by Gordon's sum rule from the far-infrared absorption intensities.

In the present study, we have measured the far-infrared absorption intensities of CH_3I, $CHCl_3$, CH_2Cl_2, CH_3CN, and their deuterated compounds dissolved in non-polar solvents and adopted Onsager's reaction field for estimating the internal moments of the molecules.

Experimental

The far-infrared spectra were measured at room temperature on a HITACHI FIS-21 single beam spectrophotometer equipped with a germanium-bolometer detector which was operated at pumped liquid-helium temperature, 1.8 K. The resolution was higher than 2 cm^{-1} over the observed region, 10—360 cm^{-1}. Two cells of equal thickness with low-density polyethylene windows were set in a closed compartment placed between the monochromator and the detector. Atmospheric water vapor in the compartment was purged by a steady flow of dried nitrogen gas, while the monochromator was evacuated by a rotary pump. The two cells filled with the solution and the solvent were alternately introduced into the light path by manipulating from outside. The transmitted intensities were determined by observing for 5 min at every fixed wave number with intervals of 5—10 cm^{-1}. In this way, the S/N ratio was improved and the influences of the long-time fluctuations of the light source (high-pressure mercury lamp) and the bolometer sensitivity were effectively eliminated from the results. Spectroscopic grade reagents were used for C_6H_6, CCl_4, CS_2, n-C_6H_{14}, CH_2Cl_2, and CH_3CN. For CH_3I and $CHCl_3$, the commercially available samples were used after purification[19] to eliminate a slight amount of polar impurities, such as H_2O and C_2H_5OH. The deuterated compounds were purchased from CEA and used without further purification. The concentration ranges employed were 0.20—1.1 M, 0.25—1.1 M, 0.13—0.48 M, and 0.03—0.16 M for the solutions of CH_3I, $CHCl_3$, CH_2Cl_2, and CH_3CN respectively.

Results and Discussion

The observed absorption coefficients, $\sigma(\nu)$, of CH_3I dissolved in the non-polar solvents are shown in Fig. 1 as examples. The band shapes for all the solutions studied do not depend on concentration, but they depend appreciably on the solvents. By extrapolating the observed spectra to the origin, as shown by the fine broken lines in Fig. 1, the integrated intensities

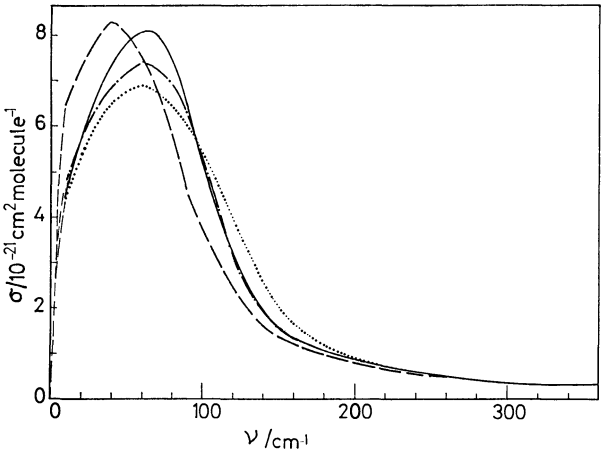

Fig. 1. Far-infrared absorption bands of CH_3I dissolved in C_6H_6(·····), CCl_4(——), CS_2(—·—), and n-C_6H_{14} (— — —).

were obtained by

$$A = \int_0^{360} \sigma(\nu)\mathrm{d}\nu, \tag{1}$$

where

$$\sigma(\nu) = \frac{1}{\rho l}\ln(T_0/T)_\nu ,$$

and ρ denotes the concentration of the dipolar molecule (molecules·cm^{-3}), l the sample thickness (cm), and T_0 and T the transmittance of the solvent and the solution, respectively. The most probable values of A were evaluated from the slopes of the Beer's law plots shown in Fig. 2, and are listed in Table 1. The internal-field correction was applied to A. The corrected intensities, A_c, were obtained by the equation[3,4]

$$A_c = n_s\left[\frac{(n/n_s)^2+2}{n^2+2}\right]^2 A, \tag{2}$$

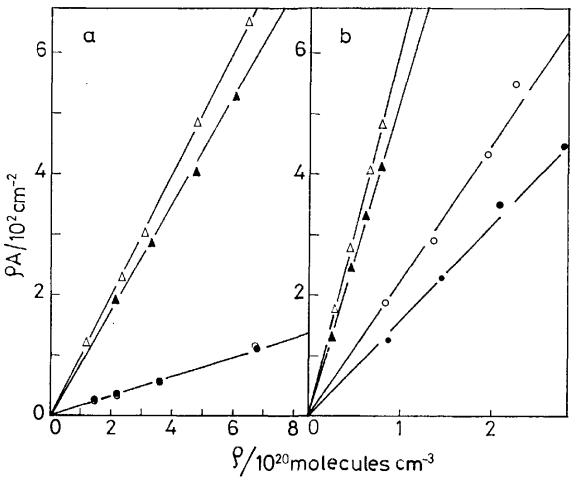

Fig. 2. Beer's law plots for CH_3I(a- △), CD_3I(a- ▲), $CHCl_3$(a- ○), $CDCl_3$(a- ●), CH_3CN(b- △), CD_3CN(b- ▲), CH_2Cl_2(b- ○), and CD_2Cl_2(b- ●) dissolved in CCl_4.

where n and n_s denote the refractive indices of the solute and the solvent respectively. In the present study, they were replaced by the values for the Na_D-line. This replacement introduces only a few percent uncertainty in the A_c values.

Since the dipole moment of the C_{2v} or C_{3v} symmetric molecule lies along one of the principal axes of the moment of inertia, say the z axis, Gordon's sum rule is reduced to[5]

$$A_c = \frac{\pi\mu^2}{3c^2}\left(\frac{1}{I_x}+\frac{1}{I_y}\right), \tag{3}$$

where c is the velocity of light, μ the dipole moment, and I_x and I_y the principal moments of inertia about the x and y axes. The μ values calculated from A_c by Eq. 3 are shown in Table 1, together with the values of the moments of inertia and the permanent dipole moments in the gas phase, μ_0, taken from the literature. The μ values are about 10—20% larger than the μ_0 values for all the compounds studied. Moreover, almost the same μ values were obtained for the H- and D- compounds, which have different moments of inertia. These facts can be explained by regarding μ as the internal moments in the solutions. According to the concept of the reaction field in the theory of the dielectrics,[17,18] the internal moment, μ^*, is larger than the dipole moment in vacuum or in the gas phase, μ_0.

In Onsager's model, the internal moment μ^* is expressed as[17,18]

$$\mu^* = \frac{1}{1-f\alpha}\mu_0, \tag{4}$$

where

$$f = \frac{1}{a^3}\cdot\frac{2\varepsilon-2}{2\varepsilon+1}, \tag{5}$$

and α is the average polarizability of the molecule, ε the dielectric constant of a continuous medium, and $a^3=3/4\pi N$ (N: the number of the molecules per cm^3). Introducing Eq. 5 into Eq. 4 and rewriting by the use

Table 1. Observed integrated intensities and dipole moments

Solute	Solvent	A	A_c	μ	μ^*	μ_0	I[a]
		10^{-20} cm·mol^{-1}		D			10^{-40} g·cm^2
CH_3I	C_6H_6	102	74.1	1.8_8	1.9_2	1.65[b]	$I_x=I_y=111.9$
	CCl_4	99.7	74.0	1.8_8	1.9_0		
	CS_2	99.4	71.2	1.8_4	1.9_7		
	n-C_6H_{14}	94.3	72.0	1.8_5	1.8_6		
CD_3I	CCl_4	86.2	64.0	1.9_4	1.9_0		$I_x=I_y=138.9$
$CHCl_3$	CCl_4	16.1	12.5	1.1_7	1.1_6	1.02[c]	$I_x=I_y=254.2$
$CDCl_3$	CCl_4	16.4	12.7	1.1_9	1.1_6		$I_x=I_y=258.3$
CH_2Cl_2	C_6H_6	230	179	1.9_1	1.8_3	1.62[b]	$I_x=26.22$, $I_y=273.8$
	CCl_4	227	178	1.9_0	1.8_2		
	n-C_6H_{14}	202	162	1.8_3	1.7_9		
CD_2Cl_2	CCl_4	157	123	1.8_2	1.8_2		$I_x=35.44$, $I_y=280.3$
CH_3CN	C_6H_6	662	538	4.6_1	4.3_4	3.92[b]	$I_x=I_y=91.22$
	CCl_4	615	502	4.4_0	4.3_2		
	CS_2	668	539	4.6_1	4.4_1		
	n-C_6H_{14}	569	473	4.3_2	4.2_5		
CD_3CN	CCl_4	535	437	4.4_7	4.3_2		$I_x=I_y=106.8$

a) Calculated from the rotational constants taken from Ref. 20. b) Ref. 20. c) Ref. 21.

of the Lorenz-Lorentz relation, $\alpha/a^3=(n^2-1)/(n^2+2)$, we have[17,18]

$$\boldsymbol{\mu}^* = \frac{(n^2+2)(2\varepsilon+1)}{3(2\varepsilon+n^2)}\boldsymbol{\mu}_0. \quad (6)$$

Since ε can be replaced by n_s^2 to a good approximation, Eq. 6 is also written as

$$\boldsymbol{\mu}^* = \frac{(n^2+2)(2n_s^2+1)}{3(2n_s^2+n^2)}\boldsymbol{\mu}_0. \quad (7)$$

Since $\boldsymbol{\mu}^*$ will always be in the same direction as $\boldsymbol{\mu}_0$, it follows the rotation of the molecular framework as $\boldsymbol{\mu}_0$ does. Then the molecule in the solution absorbs the far-infrared radiation through the dipole moment of μ^*.

The μ^* values calculated from μ_0 using Eq. 7 are listed in Table 1. They are in good agreement with the observed μ values. Thus, the far-infrared absorptions observed in the present study can be explained almost wholly by the rotational motion of the $\boldsymbol{\mu}^*$ vector. It follows that the observed band shape corresponds directly to the Fourier transform of the reorientational correlation function of the molecule.

The observed μ value of HCl dissolved in CCl_4 was nearly equal to the μ_0 value,[16] in contrast with the cases in the present study. Since the molar volume of CCl_4 is considerably larger than that of HCl, the cavity radius in Onsager's model must be larger than that estimated from the actual molar volume of HCl. In this case the $f\cdot\alpha$ value becomes small, or n^2 approaches to unity, so that the μ^* value may be nearly equal to the μ_0 value.

The authors wish to thank Prof. Tsunetake Fujiyama and Mr. Tetsuo Suzuki of Tokyo Metropolitan University for valuable discussions.

References

1) R. G. Gordon, *J. Chem. Phys.*, **43**, 1307 (1965).
2) S. R. Polo and M. K. Wilson, *J. Chem. Phys.*, **23**, 2376 (1955).
3) W. C. Mallard and J. W. Straley, *J. Chem. Phys.*, **27**, 877 (1957).
4) W. B. Person, *J. Chem. Phys.*, **28**, 319 (1958).
5) R. G. Gordon, *J. Chem. Phys.*, **38**, 1724 (1963).
6) S. G. Kroon and J. Van der Elsken, *Chem. Phys. Lett.*, **1**, 285 (1967).
7) M. Davies, G. W. F. Pardoe, J. Chamberlain, and H. A. Gebbie, *Trans. Faraday Soc.*, **66**, 273 (1970).
8) A. Mansingh, *J. Chem. Phys.*, **52**, 5896 (1970).
9) A. Gerschel, I. Darmon, and C. Brot, *Mol. Phys.*, **23**, 317 (1972).
10) A. I. Baise, *J. Chem. Soc., Faraday Trans. 2*, **68**, 1904 (1972).
11) M. W. Evans, *Spectrochim. Acta, Part A*, **30**, 79 (1974).
12) I. Larkin and M. Evans, *J. Chem. Soc., Faraday Trans. 2*, **70**, 477 (1974).
13) M. Evans, *Spectrochim. Acta, Part A*, **31**, 609 (1975).
14) G. J. Davies and M. Evans, *J. Chem. Soc., Faraday Trans. 2*, **72**, 40 (1976).
15) A. Gerschel, I. Dimicoli, J. Jaffre, and A. Riou, *Mol. Phys.*, **32**, 679 (1976).
16) Y. Ohkubo, S. Ikawa, and M. Kimura, *Chem. Phys. Lett.*, **43**, 138 (1976).
17) H. Fröhlich, "Theory of Dielectrics," 2nd ed, Oxford University Press, London (1960).
18) C. J. F. Böttcher, "Theory of Electric Polarization," 2nd ed, Elsevier, Amsterdam (1973).
19) A. Weissenberger, "Technique of Organic Chemistry, 7, Organic Solvents," Interscience, New York (1955).
20) Landort-Börnstein, "Numerical Data and Functional Relationships," New Series, II/4, Springer, Berlin (1967).
21) P. B. Reinhart, Q. William, and T. L. Weatherly, *J. Chem. Phys.*, **53**, 1418 (1970).

Reaction Mechanism of the Photooxidation of the Toluene–NO_2–O_2–N_2 System in the Gas Phase

Hajime Akimoto,* Mikio Hoshino, Gen Inoue, Michio Okuda, and Nobuaki Washida

The National Institute for Environmental Studies, P.O. Yatabe, Ibaraki 300-21

(Received February 15, 1978)

Photooxidation of the toluene (34 ppm)–NO_2(8—207 ppm)–N_2 and/or O_2(1 atm) system has been studied in a 67 dm^3 reaction chamber. The reaction was initiated by $O(^3P)$ atoms formed in the photolysis of NO_2. The main products were benzaldehyde, cresols, benzyl nitrate, *m*-nitrotoluene, 6-nitro-*o*-cresol, and 2-nitro-*p*-cresol. Their relative yields were studied as functions of reactant concentrations. The formation mechanisms of the products were proposed on the basis of the reactions of $O(^3P)$ and OH radicals with toluene in the presence of NO_2 and O_2.

Studies have been made on the photochemical oxidation of alkylbenzenes in the presence of nitrogen oxides (NO_x) and air in relation to photochemical air pollution. However, they deal mostly[1] with ozone formation and the so-called "photochemical reactivity."[2] A few reports[3-6] have been given on the reaction products and mechanisms of the gas phase photooxidation of alkylbenzenes–NO_x–air system.

Kopczynski[3] studied the photooxidation of alkylbenzenes–NO_2–air systems using a long-path infrared spectrometer and identified aldehydes, CO, CO_2, formic acid, and peroxyacetyl nitrate as reaction products. Nojima *et al.*[4a] studied the photooxidation of the benzene–NO_2–air system and identified nitrobenzene, nitrophenols, and dinitrophenols. They also reported[4b] the formation of glyoxal, methylglyoxal, and biacetyl which would have been produced by the cleaving of benzene rings in the photooxidation of benzene, toluene, and xylene. Ando *et al.*[5] studied the formation yield of nitrobenzenes in the benzene–NO_2–O_2–N_2 system as functions of O_2 and NO_2 concentrations.

Photooxidation of alkylbenzenes in the atmosphere is thought to be initiated by OH or O atoms. The photooxidation of alkylbenzene–HNO_2–air systems, in which OH radicals initiated the oxidation of benzene, toluene, and ethylbenzene, was studied and the reaction mechanisms were discussed in our previous study.[6] In this work,[7] photooxidation of the reaction systems of toluene (34 ppm), NO_2(8—207 ppm) in N_2 and/or O_2 at 1 atm was studied for the case in which O atoms from NO_2 initiate the oxidation, giving most of the oxidized products. The final reaction products and their relative yields as functions of reactant concentrations are reported and a discussion of the reaction mechanisms is presented.

Experimental

Figure 1 shows a schematic diagram of the apparatus. The reaction chamber is a Pyrex cylinder, 225 mm i.d., 1660 mm in length, 67 dm^3 in volume: evacuated to less than 1×10^{-6} Torr. Metal parts containing gas inlets and outlets are attached to both ends of the Pyrex cylinder with Viton O-rings, the inside walls of the metal parts being lined with Teflon in order to avoid any catalytic reactions on the metal surfaces. Each end of the reaction chamber is sealed with a Pyrex window 20 mm thick, through which a photolyzing light beam can be transmitted into the gas sample.

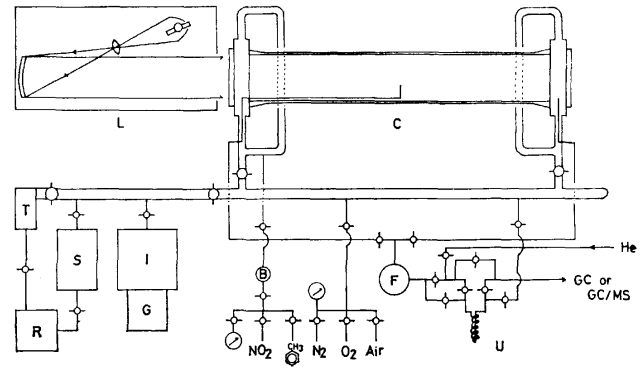

Fig. 1. Schematic diagram of the experimental apparatus. C: Reaction chamber; L: xenon arc lamp house; I: sputter ion pump; G: titanium getter pump; S: sorption pump; T: foreline trap; R: rotary pump; B: gas burette; F: sampling flask; U: low temperature spiral trap.

The light source was a 500 W xenon short arc lamp. A parallel light beam of *ca.* 200 mmϕ was obtained by using an elliptical mirror, lens, and an off-axis parabolic mirror. The effective light intensity as measured by the primary photodecomposition rate of NO_2 was 0.08 min^{-1}. The wavelengths of the irradiated light were greater than 320 nm. An oil free pumping system consisting of a sputter ion pump, titanium getter pump, cryo-sorption pump, and a rotary pump with a liquid nitrogen cooled foreline trap was used.

Toluene and NO_2 were first put into a 105-ml glass flask and then expanded into the reaction chamber. Air, O_2, or N_2 was then introduced through four gas inlets shown in Fig. 1. The pressure was measured with Capsulon gauges (Edward High Vacuum Co.), 50 and 760 Torr full scale which were calibrated by a mercury manometer. In order to confirm that the sample gases were mixed homogeneously, four sampling ports were attached to the chamber (only two of them are shown in Fig. 1), at the center, at one-fourth of the chamber length distance from one end, and at both ends. One hour after the gases had been introduced the concentration of the toluene taken from the four different ports was found to be the same, and irradiation was thus started. Sampling was repeatedly carried out through the center port at suitable time intervals. "Pure Air" (dew point lower than −70 °C), O_2 (>99.9%, graded as "Pure gas B") and N_2 (>99.995%, graded as "Pure gas B") were supplied from Nippon Sanso Co. NO_2 was obtained by mixing NO (research grade, Matheson) with excess O_2. Toluene (research grade, Wako Pure Chemical Ind.) was used without further pruification except

degassing. It contains *ca.* 0.01% xylenes, as impurity, which is negligible in the present study.

The reaction mixture was first introduced into a 700-ml constant volume glass flask and then concentrated in a GC sampling tube. The sampling tube, a Pyrex spiral of 2 mm i. d., about 4 m in extended length, was cooled to −60 °C. After the concentration, the sampling tube was heated with hot water and the sample was fed directly into a gas chromatograph. This procedure was found to minimize the yields of the products of thermal reactions of NO_2 with toluene and cresols in the smapling tube. Sampling for the GC analysis was made periodically every 45—60 min. GC analysis was carried out using a 3-m column of 5% SE-30 on Shimalite W. The GC oven temperature was raised from 80 to 200 °C at a rate of 4 °C/min. The concentration of NO_2 was monitored for several runs by the method of single beam photometry at a wavelength of 450 nm using the irradiation light as a light source. Identification of product was carried out by comparing the reference mass pattern and GC retention time using a GC-MS (JEOL, JMS-100) and a GC. In order to obtain the reference mass patterns and GC retention times, standard samples of benzaldehyde, *o*-, *m*-, *p*-cresols, benzyl nitrate, *o*-, *m*-, *p*-nitrotoluenes, *o*-nitrophenol, and 2- nitro-*p*-cresol were used. All chemicals except for benzyl nitrate were commercial products (Wako Pure Chemical Co.). Benzyl nitrate was prepared by fractional distillation of the reaction mixture of benzyl chloride and $AgNO_3$ in a dried acetonitrile solution. Identification of 6-nitro-*o*-cresol was performed by comparing the GC retention time with the reference sample obtained by the thermal reaction between *o*-cresol and NO_2. The mass pattern of 6-nitro-*o*-cresol was found to be nearly identical with that of 2-nitro-*p*-cresol.

For several experimental runs on the photooxidation of the HNO_2–NO_x–toluene–air system, known amounts of toluene and NO_2 were first introduced into the reaction chamber and then HNO_2–air mixture was introduced under a total pressure of 1 atm. The HNO_2–air mixture was produced by using 10 ml of 0.05 M $NaNO_2$ and 10 ml of 5% H_2SO_4.[6] The concentrations of HNO_2 and nitrogen oxides in the HNO_2–air mixture were determined[6] by the method of Cox[8] using a commercial chemiluminescence NO_x analyzer (Monitor Labs, Model 8440). The HNO_2–air mixture produced by the above method was found to contain *ca.* 12 ppm of HNO_2 and 2 ppm each of NO_2 and NO.

Results

The reaction products observed in the photooxidation of the toluene (34 ppm)–NO_2(8—207 ppm)–air(1 atm) system were benzaldehyde, cresols, benzyl nitrate, *m*-nitrotoluene, 6-nitro-*o*-cresol, and 2-nitro-*p*-cresol. Smaller amounts of *o*-nitrophenol and *o*- and *p*-nitrotoluene were also detected. The relative yield of *o*-cresol was about 80% of the total amout of cresols, the sum of *m*- and *p*-cresol being about 20% of the total. By means of the gas chromatograph column used in this work, *m*- and *p*-cresols could not be seperated. Figure 2 shows the relative product yields as functions of irradiation time for a typical run of toluene (34 ppm), NO_2 (7.7 ppm) and 1 atm air. In the present study product analysis was carried out at a low reactant conversion (<1%). Under these conditions amounts of all the products increased linearly with irradiation time and ratios of products could be calculated from

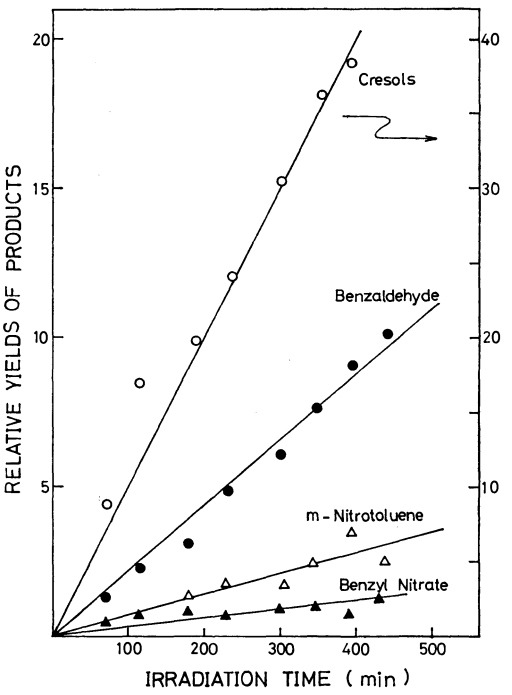

Fig. 2. Relative yields of the products *vs.* irradiation time in the photooxidation of NO_2 (7.7 ppm)–toluene (34 ppm)–air (1 atm) system. ○ Cresols; ● benzaldehyde; △ *m*-nitrotoluene and ▲ benzyl nitrate.

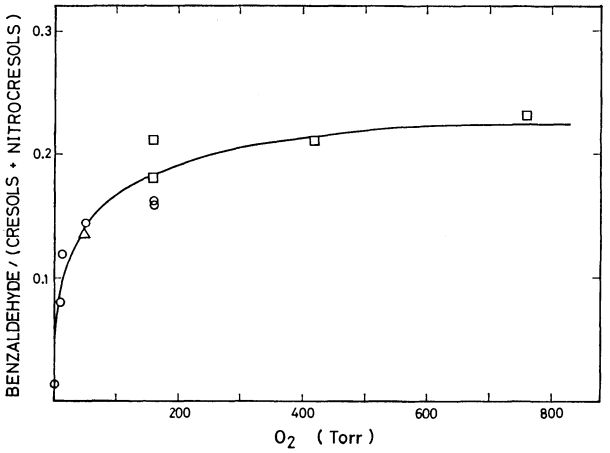

Fig. 3. The formation ratio of benzaldehyde to the sum of cresols and nitrocresols *vs.* partial pressure of O_2 in the photooxidation of NO_2–toluene (34 ppm)–O_2–N_2 (1 atm) system. Initial concentration of NO_2 are △ 6.4, ○ 24, and □ 30 ppm.

the slope ratio of the linear plots.

In order to clarify the formation mechanism of the products, experiments were carried out by varying the initial concentrations of O_2 and NO_2. Figure 3 shows the ratio of benzaldehyde to cresol as a function of O_2 partial pressure for several initial concentrations of NO_2. In these experiments, total pressure was kept at 760 Torr using N_2 as a buffer gas. It shoud be noted that in the absence of O_2 (NO_2–toluene–N_2 system) no benzaldehyde was formed, cresol being the major condensable product with trace amounts of

nitrocresols. The yields of nitrocresols were found to be much smaller than those in the NO_2–toluene–air system for the same initial concentration of NO_2. As shown in Fig. 3, the ratio of benzaldehyde to cresols increases with increase in the concentration of O_2, reaching a saturated value at an O_2 partial pressure higher than a few hundred Torr.

The ratio of nitrocresols (the sum of 6-nitro-*o*-cresol and 2-nitro-*p*-cresol) to cresols increases linearly with the concentration of NO_2 (Fig. 4), NO_2 being measured by UV absorption at 450 nm. Figure 5 shows the ratio of benzaldehyde to the sum of cresols and nitrocresols as a function of the photo-equilibrium concentration of NO_2. In the reaction system of air at 1 atm, the concentration of NO_2 reached the photoequilibrium level within 20 min after irradiation was started, remaining nearly constant during the course of irradiation time. The photo-equilibrium concentration of NO_2 was about 50% of the initial concentration of NO_2.

As shown in Fig. 5 the yield ratio of benzaldehyde to the sum of cresols and nitrocresols is independent of the concentration of NO_2. Thus, the yield of other products could be normalized by the sum of cresols and nitrocresols. Typical data for the product yields are given in Table 1.

The ratio of benzyl nitrate to benzaldehyde increased with an increase in the concentration ratio of NO_2 to O_2 (Fig. 6). Figure 7 shows the relative yield of *m*-nitrotoluene as a function of the initial concentration

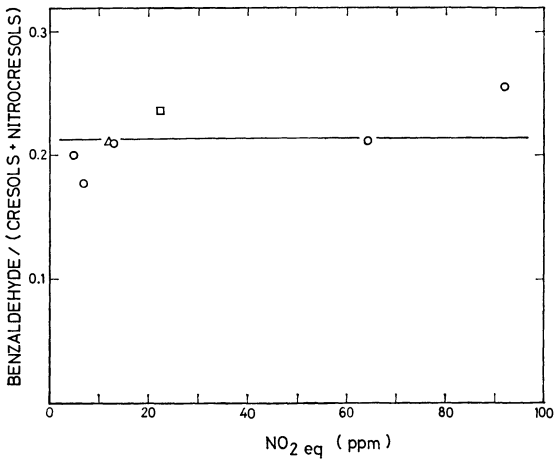

Fig. 5. The formation ratio of benzaldehyde to the sum of cresols and nitrocresols *vs.* equilibrium concentration of NO_2 for the NO_2–toluene (34 ppm)–O_2–N_2 (1 atm) system. Partial pressure of O_2 are ○ 160, △ 418, and □ 760 Torr.

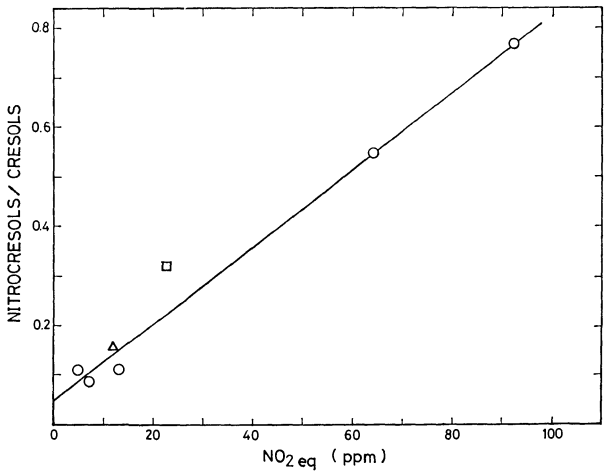

Fig. 4. The formation ratio of nitrocresols to cresols *vs.* equilibrium concentration of NO_2 for the NO_2–toluene (34 ppm)–O_2–N_2 (1 atm) system. Partial pressure of O_2 are ○ 160, △ 418, and □ 760 Torr.

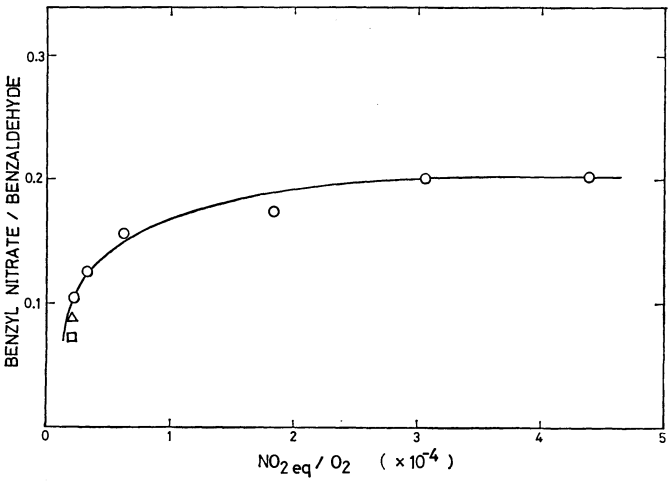

Fig. 6. The formation ratio of benzyl nitrate to benzaldehyde *vs.* the ratio of equilibrium concentration of NO_2 to O_2 for the NO_2–toluene (34 ppm)–O_2/N_2 system. Partial pressure of O_2 are △ 160, ○ 418, and □ 760 Torr.

Table 1. Relative product yield (cresols+nitrocresols=1.0) in the photooxidation of the NO_2–toluene–O_2/N_2 system (total pressure=760 Torr)

Initial NO_2 (ppm)	NO_{2eq} (ppm)	O_2 (Torr)	Benzaldehyde	Cresols	Benzylnitrate	*m*-Nitrotoluene	Nitrocresols
174	92	160	0.26	0.23	0.052	0.021	0.77
145	64	160	0.21	0.45	0.040	0.015	0.55
38	13	160	0.21	0.89	0.033	0.062	0.11
20	7	160	0.18	0.91	0.023	0.060	0.09
11	5	160	0.20	0.89	0.021	0.071	0.11
24	6	47	0.15	0.93	0.016	0.030	0.07
30	12	418	0.21	0.84	0.018	0.043	0.16
30	23	760	0.24	0.68	0.017	0.045	0.32

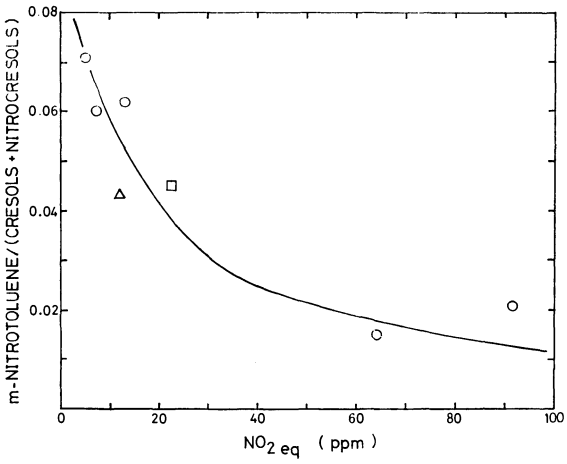

Fig. 7. The formation ratio of m-nitrotoluene to the sum of cresols and nitrocresols *vs.* equilibrium concentration of NO_2 for the NO_2–toluene (34 ppm)–O_2/N_2 system. Partial pressure of O_2 are ○ 160, △ 418, and □ 760 Torr.

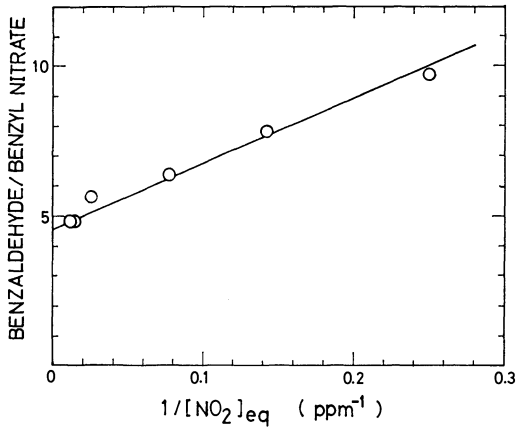

Fig. 8. The formation ratio of benzaldehyde to benzyl nitrate *vs.* the reciprocal of the equilibrium concentration of NO_2 for the NO_2–toluene (34 ppm)–air (1 atm) system.

of NO_2. It is remarkable that the relative yield of *m*-nitrotoluene, one of the nitrated products decreases with increase in NO_2 concentration. In order to compare the yield of *m*-nitrotoluene in the NO_2–toluene–air system with that in the HNO_2–NO_x–toluene–air system at a comparable initial concentrations of NO_2, two runs for the HNO_2 (12 ppm)–NO_2 (15 ppm and 25 ppm)–toluene(34 ppm)–air(1 atm) system were carried out. The result is shown in Fig. 9, where four data points for HNO_2 runs of lower NO_2 concentrations (less than 2 ppm) are taken from the work of Hoshino *et al.*[6]

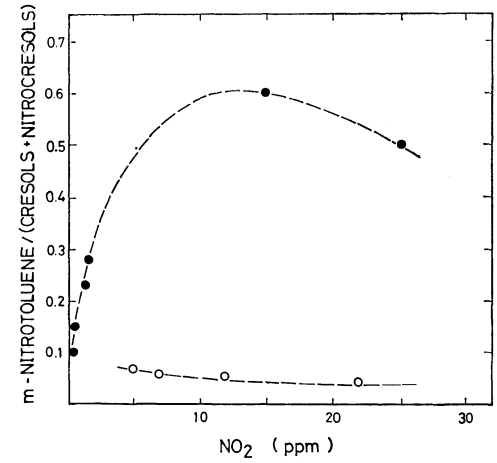

Fig. 9. The formation ratio of *m*-nitrotoluene to the sum of cresols and nitrocresols *vs.* initial concentration of NO_2 for the HNO_2–NO_2–toluene (34 ppm)–air (1 atm) system (●) and the NO_2–toluene (34 ppm)–air (1 atm) system (○).

Discussion

Formation Mechanisms of Cresol and Nitrocresol. Since in the present study the wavelength of the irradiated light is greater than 320 nm and toluene absorbs no light in this spectral region, the photooxidation is initiated by $O(^3P)$ atoms formed in the photolysis of NO_2:

$$NO_2 + h\nu(320\text{—}400\ \text{nm}) \longrightarrow NO + O(^3P). \quad (1)$$

The reaction of $O(^3P)$ atoms with toluene has been studied[9–11] in some detail by mercury photosensitization of the N_2O–toluene system. The main volatile products were cresols and CO. Small amounts of phenol, methane, and ethane, and predominant polymer formation were observed. There are differences in the relative yields of cresol isomers in these studies. The ratios of *o*-cresol to total cresols were reported to be 64% (Jones and Cvetanović[9]), 78% (Grovenstein and Mosher[10]), and 94% (Gaffney *et al.*[11]). Formation of *p*-cresol was noted only by Jones and Cvetanović.[9] In the present reaction system of NO_2–toluene–O_2–N_2, the cresols are the major condensable products in the absence of O_2, and also main products in the presence of O_2 (see Table 1). In both cases, more than 80% of total cresols was *o*-cresol. This is closer to the results of Gaffney *et al.*[11] From these data, the formation of *o*-cresols in the present reaction system is considered to be mainly due to the reaction of the $O(^3P)$ atom with toluene. This reaction would proceed *via* oxygen atom addition to the benzene ring followed by the intramolecular hydrogen atom transfer reaction.[9]

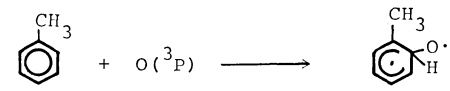

(2)

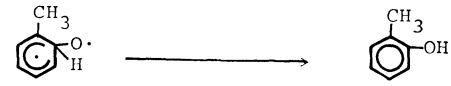

(3)

The existence of the long-lived biradical formed in Reaction 2 has been suggested in the work of Mani and Sauer.[12] However, it should be noted that the reaction of OH radicals with toluene also gives *o*-cresol.[6]

The ratio of nitrocresols to cresols increases linearly with the photo-equilibrium concentration of NO_2, while the ratio of the sum of cresols and nitrocresols to benzaldehyde remains constant (Figs. 4 and 5). The results suggest that nitrocresols should be formed in the competitive reaction of NO_2 with the same precursor as that giving cresols. The following reaction mechanism is proposed:

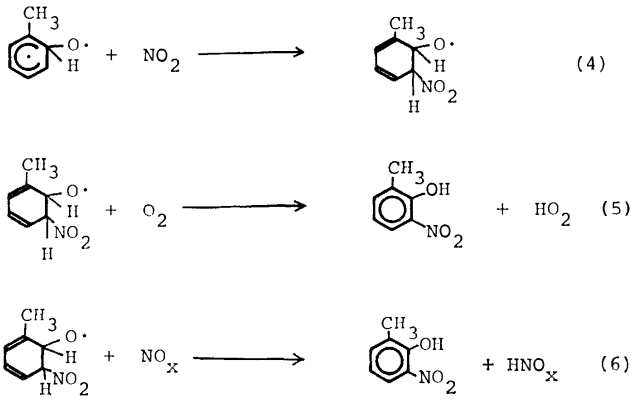

(4)

(5)

(6)

where NO_x denotes NO or NO_2. The result showing that the formation of nitrocresol is suppressed in the absence of O_2 can be explained by the absence of Reaction 5. According to Reactions 2—6, 6-nitro-*o*-cresol should be the major product among nitrocresol isomers if we assume that NO_2 combines with the biradical almost entirely at the carbon atom adjacent to the one to which the oxygen atom is attached (Reaction 4).

Formation Mechanisms of Benzaldehyde and Benzyl Nitrate. Benzaldehyde and benzyl nitrate were formed only in the presence of O_2. Formation of these products strongly suggests the presence of the benzyloxyl radical as their precursor in the reaction system. Competitive reactions

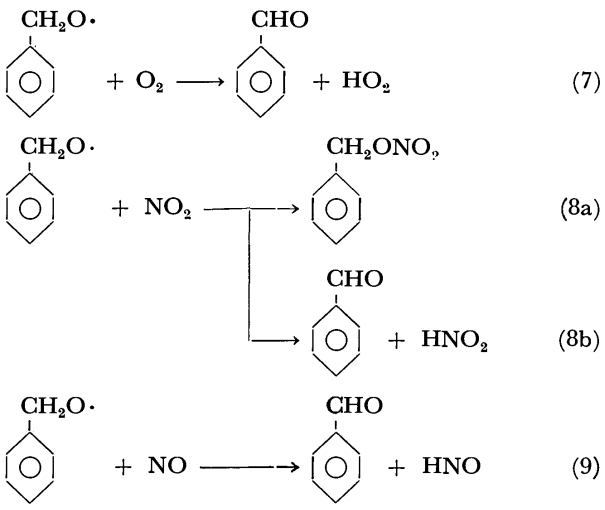

(7)

(8a)

(8b)

(9)

yield the relation

$$\frac{[\text{B.A.}]}{[\text{B.N.}]} = \frac{k_7}{k_{8a}}\frac{[O_2]}{[NO_2]_{eq}} + \frac{1}{k_{8a}}\left(k_{8b} + k_9\frac{[NO]_{eq}}{[NO_2]_{eq}}\right) \quad (10)$$

where B.A. and B.N. stand for benzaldehyde and benzyl nitrate, respectively, and $[NO]_{eq}$ and $[NO_2]_{eq}$ are the concentrations of NO and NO_2 under photoequilibrium. Under the conditions of 1 atm air, $[NO]_{eq}/[NO_2]_{eq}$ was nearly constant (≈ 1.0) irrespective of the initial NO_2 concentration. Thus, the plot of [B.A.]/[B.N.] *vs.* $[O_2]/[NO_2]_{eq}$ should give a straight line according to Eq. 10. The points (circular) in Fig. 6 are plotted again in Fig. 8 on the scale of [B.A.]/[B.N.] *vs.* $1/[NO_2]_{eq}$. From the slope of Fig. 8, the value of k_7/k_{8a} was deduced to be 1.4×10^{-4}. For similar reactions of methoxyl radicals

$$CH_3O + O_2 \longrightarrow CH_2O + HO_2 \quad (11)$$

$$CH_3O + NO_2 \longrightarrow CH_2ONO_2 \quad (12a)$$

$$\longrightarrow CH_2O + HNO_2 \quad (12b)$$

the value of $k_{11}/k_{12}=5.6\times10^{-5}$ was given by Wiebe *et al.*[13] Glasson[14] reported the value of $k_{11}/k_{12a}<(7.4\pm0.7)\times10^{-5}$. Our value for the benzyloxyl radical is nearly of the same order of magnitude, but slightly higher than the above values for the methoxyl radical.

Benzyloxyl radicals are thought to be formed *via* reactions

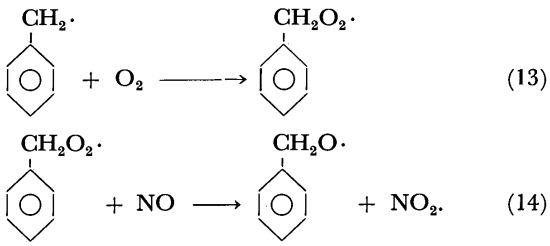

(13)

(14)

Analogous reactions for alkyl radicals have been proposed by Heicklen *et al.*[15] According to the above reaction scheme, no benzaldehyde and benzyl nitrate would be formed in the absence of O_2. Their yields would increase with the increase of the concentration of O_2 to the extent where all benzyl radicals are trapped by O_2. Our experimental result (Fig. 3) confirmed that this is the case for benzaldehyde. Our results that no benzaldehyde and benzyl nitrate could be detected in the O_2 free system also suggests the above reaction mechanism. Recently, Sloane[16] observed the product with an *m/e* of 106 in the reaction of $O(^3P)$ and toluene under molecular beam conditions and proposed a reaction

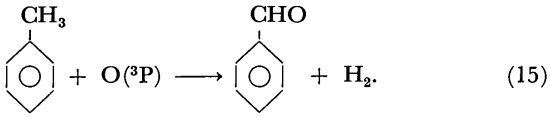

(15)

If this reaction had occurred in the present reaction system, benzaldehyde would have been formed even in the O_2 free system. Thus, Reaction 15 is not important under our experimental conditions.

Formation Mechanism of m-*Nitrotoluene.* The yield of *m*-nitrotoluene decreases with increase of NO_2. This unexpected behavior of *m*-nitrotoluene can be explained if we assume that it is formed by the reaction which is initiated by OH radicals rather than by $O(^3P)$ atoms. In our study of the photooxidation of toluene in the HNO_2–NO_x–toluene–air system, where the OH radical reaction predominates, the relative yield of *m*-nitro-

toluene to cresols is much higher than that in the present system. The yield of *m*-nitrotoluene in the HNO_2–NO_x–toluene–air system is compared with that in the NO_2–toluene–air system in Fig. 9. In the HNO_2 system, the relative yield of *m*-nitrotoluene to cresols+nitrocresols increases when the concentration of NO_2 increases in the region less than 10 ppm of NO_2. An opposite tendency is observed in the NO_2 system. The formation mechanism of *m*-nitrotoluene and cresols in the HNO_2–NO_x–toluene–air system, was proposed[6] to be as follows.

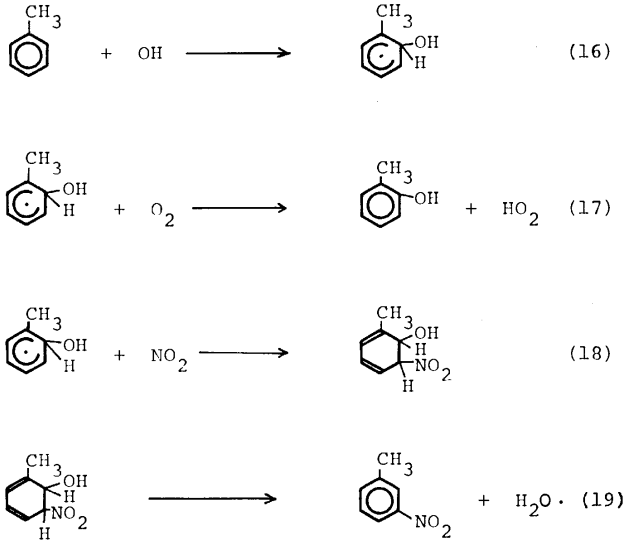

The increase in the ratio of *m*-nitrotoluene to cresols with increase in the concentration of NO_2 can be explained by the competition between Reactions 17 and 18. On the other hand, in the present reaction system of NO_2–toluene–air, most of the cresols are formed in the reaction of $O(^3P)$ with toluene, *m*-nitrotoluene being assumed to be formed in Reactions 16, 18, and 19. In this case, the competition between Reaction 16 and the following Reactions 20 and 21 would result in a decrease in the relative yield of *m*-nitrotoluene at higher NO_2 concentrations because of the quenching of OH radicals by NO_2 and NO.

$$OH + NO_2 \xrightarrow{M} HNO_3 \quad (20)$$

$$OH + NO \xrightarrow{M} HNO_2 \quad (21)$$

Although second order rate constants at 760 Torr for Reactions 20 and 21 are comparable,[17,18] Reaction 20 would be more effective sink of OH radicals since the photolysis of HNO_2 regenerates them.

Formation of Benzyl Radicals. According to the proposed reaction mechanism, side chain oxidation products, benzaldehyde and benzyl nitrate are formed *via* benzyloxyl radicals, which should be formed from benzyl radicals *via* Reactions 13 and 14. Benzyl radicals could be formed in the present reaction by the reaction of toluene with either $O(^3P)$ or OH radicals, *i.e.*,

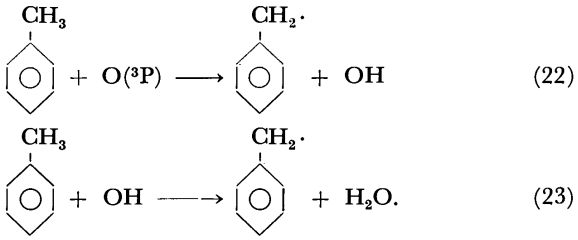

OH radicals are produced mainly by the reaction

$$HO_2 + NO \longrightarrow OH + NO_2 \quad (24)$$

where HO_2 radicals are formed in Reactions 5, 7, and 17. Reaction 22 and the photolysis of HNO_2 formed in Reactions 6, 8b, and 21 would also contribute to the production of OH radicals.

OH radicals abstract hydrogen atoms from the methyl group of toluene(Reaction 23) and also add to benzene ring (Reaction 16) at room temperature. From the pressure dependence of the rate constant of the reaction of OH radicals with toluene, Davis *et al.*[19] deduced that over half of the total reaction proceeds *via* addition reaction. Perry *et al.*[20] estimated the room temperature rate constant of the hydrogen abstraction reaction by extrapolation of the data above 380 K, where the reaction is assumed to proceed solely *via* abstraction, and obtained the fraction of the abstraction reaction of $16\pm^{0.07}_{0.05}\%$ at room temperature. In our product analysis study of OH radicals with toluene,[6] the fraction of abstraction reaction was estimated to be 25—35%.

The reaction of toluene with $O(^3P)$ has been thought to proceed only *via* ring addition since no dibenzyl formation takes place in the mercury photosensitization of the N_2O and toluene system. However, the NO_2 dependency on the formation of *m*-nitrotoluene (Fig. 9) shows that the contribution of OH radicals in the NO_2 system is not remarkable. Thus, the formation of benzaldehyde in the present study would be explained by Reaction 22. About 20% of the reaction of $O(^3P)$ with toluene should proceed *via* hydrogen abstraction from the methyl group of toluene.

The discrepancy might be caused by either of the following: (1) the contribution of OH radicals cannot be neglected in the present NO_2 system; the NO_2 dependency on the formation of *m*-nitrotoluene is a result of other unknown reactions or, (2) although benzyl radicals are formed in the mercury photosensitization of the N_2O and toluene system, they are quenched by the excess of oxygen atoms, turning polymers.

The authors wish to thank Dr. Matsui, the Hokuriku University, for his suggestion to synthesize benzyl nitrate.

References

1) (a) A. J. Haagen-Smit and M. M. Fox, *Ind. Eng. Chem.*, **48**, 1484 (1956); (b) A. P. Altshuller, I. R. Cohen, S. F. Slava, and S. L. Kopczyski, *Science*, **138**, 442 (1962); (c) J. M. Heuss and W. A. Glasson, *Environ. Sci. Technol.*, **2**, 1109 (1968); (d) W. A. Glasson and C. S. Tuesday, *Environ. Sci. Technol.*, **4**, 919 (1970); (e) G. J. Doyle, A. C. Lloyd, K. R. Darnall, A. M. Winer, and J. N. Pitts, *Environ. Sci. Technol.*, **9**, 237 (1975); (f) A. C. Lloyd, K. R. Darnall, A. M.

Winer, and J. N. Pitts, *J. Phys. Chem.*, **80**, 789 (1976).
2) A. P. Altschuller, *Int. J. Air. Wat. Poll.*, **10**, 713 (1966).
3) S. L. Kopczynski, *Int. J. Air. Wat. Poll.*, **8**, 107 (1964).
4) (a) K. Nojima, K. Fukaya, S. Fukui, and S. Kanno, *Chemosphere*, **6**, 77 (1975); (b) K. Nojima, K. Fukaya, S. Fukui, and S. Kanno, *Chemosphere*, **5**, 247 (1974).
5) W. Ando, K. Watanabe, and H. Ishikawa, private communication.
6) M. Hoshino, H. Akimoto, and M. Okuda, *Bull. Chem. Soc. Jpn.*, **51**, 718 (1978).
7) (a) H. Akimoto, G. Inoue, M. Okuda, M. Hoshino, and N. Washida, Photochemistry Symposium, Tokyo, November, 1975; (b) M. Hoshino, N. Washida, H. Akimoto, G. Inoue, and M. Okuda, Photochemistry Symposium, Fukuoka, October, 1976; (c) H. Akimoto, M. Hoshino, G. Inoue, M. Okuda, and N. Washida, Proceedings of International Conference on Photochemical Oxidant Pollution and Its Control., EPA-600/3-77-001a (1977).
8) R. A. Cox, *J. Photochem.*, **3**, 175 (1974).
9) G. R. H. Jones and R. J. Cvetanović, *Can. J. Chem.*, **39**, 2444 (1961).
10) E. Grovenstein, Jr., and A. J. Mosher. *J. Am. Chem. Soc.*, **92**, 3810 (1970).
11) J. S. Gaffney, R. Atkinson, and J. N. Pitts, Jr., *J. Am. Chem. Soc.*, **98**, 1828 (1976).
12) I. Mani and M. C. Sauer, Jr., *Adv. Chem. Ser.*, **82**, 142 (1968).
13) H. A. Wiebe, A. Villa, T. M. Hellman, and J. Heicklen, *J. Am. Chem. Soc.*, **95**, 7 (1973).
14) W. A. Glasson, *Environ. Sci. Technol.*, **9**, 1049 (1975).
15) J. Heicklen, K. Westberg, and N. Cohen, in "Chemical Reactions in Urban Atmosphere," ed by C. Tuesday, Elsevier, New York (1976), p. 55.
16) T. M. Sloane, *J. Chem. Phys.*, **67**, 2267 (1977).
17) R. Atkinson, R. A. Perry, and J. N. Pitts, Jr., *J. Phys. Chem.*, **65**, 306 (1976).
18) R. Atkinson, D. A. Hansen, and J. N. Pitts, Jr., *J. Phys. Chem.*, **62**, 3284 (1975).
19) D. D. Davis, W. Bollinger, and S. Fischer, *J. Phys. Chem.*, **79**, 293 (1975).
20) R. A. Perry, R. Atkinson, and J. N. Pitt, Jr., *J. Phys. Chem.*, **81**, 296 (1977).

Transient Absorption in the Sensitized Photoisomerization of Stilbene

Minoru SUMITANI,**,† Keitaro YOSHIHARA,***,† and Saburo NAGAKURA*,**,***

** *Institute for Solid State Physics, The University of Tokyo, Roppongi, Minato-ku, Tokyo 106*

*** *Institute of Physical and Chemical Research, Wako, Saitama 351*

(Received February 18, 1978)

The sensitized photoisomerization of stilbene was studied with nanosecond time-resolved absorption spectroscopy at room temperature. In non-viscous solvents (heptane, benzene, and ethanol), the transient spectrum does not depend upon a starting material being either *cis*- or *trans*-stilbene. The kinetic analysis of the transient spectrum due to stilbene shows that the observed spectrum consists of the T_n-T_1 absorption spectrum of *trans*-stilbene and that of twisted triplet (phantom triplet) stilbene. The lifetime of the twisted triplet stilbene is determined to be approximately 120 ns. In a viscous solvent (*t*-butyl alcohol), the transient behavior of triplet stilbene is dependent upon the starting materials being either *cis*- or *trans*-stilbene. The contribution of the twisted triplet stilbene to the transient spectrum is larger for the case starting from *cis*-stilbene than for the case starting from *trans*-stilbene.

In the reaction of *cis-trans* photoisomerization of stilbene, two possible mechanisms have been proposed mainly with the aid of the steady state method; (i) reaction occurs through the lowest triplet state (triplet mechanism), or (ii) through the lowest excited singlet state, S_1 (singlet mechanism). In both cases, the phantom singlet and triplet states with the twisted central double bond are possible intermediates in the course of the isomerization.[1-3] In searching these interesting species many attempts have been made without success by flash photolysis or laser photolysis.[4,5]

In the sensitized photoisomerization of stilbene, the reaction was found to occur through the triplet state of stilbene.[1] From the temperature dependence of quenching experiments, it was suggested that a small potential barrier existed between the triplet state of *trans*-stilbene and the phantom triplet state.[6,7] Very recently Benson and Williams[8] proposed a potential barrier from an experiment of the direct excitation to the triplet state by an argon-ion laser. The energy barriers obtained by direct and sensitized photoisomerization agree well with each other. From quenching experiments Saltiel *et al.*[9] estimated the effective lifetime of the triplet state of *trans*-stilbene to be of the order of 10^{-8} s in fluid solution.[10]

On the other hand, in the direct photoisomerization of stilbene, Saltiel and his coworkers[1,12] proposed the singlet mechanism on the basis of their quenching experiments. They further assumed that a phantom singlet state (^{1}p) is a possible intermediate of the reaction. Recently a decay of fluorescence consisting of two exponential decay components with the time constants of $\leq$0.2 and 1.4 ns at room temperature was reported by a photon-counting method.[13] The result was explained by a rapid equilibration of the population between S_1 and ^{1}p. Very recently, we investigated with a picosecond Nd^{3+}:YAG laser the temperature dependence of the fluorescence lifetime of *trans*-stilbene.[14] A smooth sigmoidal relation was obtained, quite similar to the temperature dependence of fluorescence quantum yields. Contrary to the photon-counting experiment the fluorescence had only one exponential decay component (0.11 ns) at room temperature and agreed with the S_1 lifetime estimated by a quenching experiment.[15] The results indicate that the back reaction to S_1 from the ^{1}p state does not contribute to the fluorescence decay, the ^{1}p state has a very short lifetime or the rate of back reaction is very slow.

In order to understand more clearly the *cis-trans* photoisomerization mechanism, it is necessary to elucidate the dynamical behavior of the reaction intermediate—^{1}p or ^{3}p. In the present work we examined the sensitized excitation of *cis*- and *trans*-stilbene to their triplet state and observed an absorption spectrum of a reaction intermediate by laser-flash time-resolved spectroscopy. The sensitized *cis-trans* isomerization mechanism and a role of the phantom triplet state were discussed on the basis of the observation of the transient absorption.

Experimental

The details of a N_2-laser photolysis system[6] and a dye laser photolysis system[7] were reported elsewhere. We used a coaxial type N_2-laser (peak power at 337 nm, 100 kW; pulse duration, 7 ns FWHM) as an actinic light for the photolysis with 2-acetonaphthone as a sensitizer. Stilbene is not excited efficiently by a N_2-laser. For the photolysis with biacetyl, we used a dye-laser with POPOP which was excited by a travelling-wave type N_2-laser (peak power, 1 MW; pulse duration, 6 ns FWHM).

An analyzing light was monitored by means of a Hamamatsu R666 photomultiplier and the signal was fed either to a Tektronix 465 oscilloscope or to a Tektronix 561B sampling oscilloscope combined with a 3S1 dual-trace sampling unit and a 3T77A sampling sweep unit.

The signal from the photomultiplier was monitored and amplified with a 465 oscilloscope. The amplified output signal from the oscilloscope was divided into two halves with a Tektronix 874-TPD divider. One of the signals was connected to the channel A of the 3S1 unit, and the other was passed through a delay cable and put into the channel B of the 3S1 unit. The sampling time of the channel A was fixed manually at a suitable delay position of the absorption with an intensity of $I(t)$, while the channel B was set before the pulse irradiation with an intensity of $I(0)$ (Fig. 1). The recorder output signals of the A and B channels were divided with an operational amplifier. A time-resolved absorption spectrum was obtained by scanning the wavelength and recording $I(t)/I(0)$. By sampling $I(t)$ and $I(0)$ form the same laser shot, we measured $I(t)/I(0)$ quite accurately ir-

† Present address: Institute for Molecular Science, Myodaiji, Okazaki, Aichi 444.

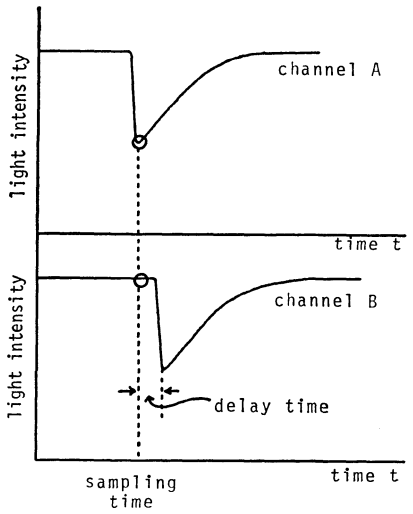

Fig. 1. The timing correlation of the absorption intensity at $t(I(t))$ and that at $t=0$ $(I(0))$. The former is fed into the channel A of the sampling oscilloscope and the latter into the channel B (see the text).

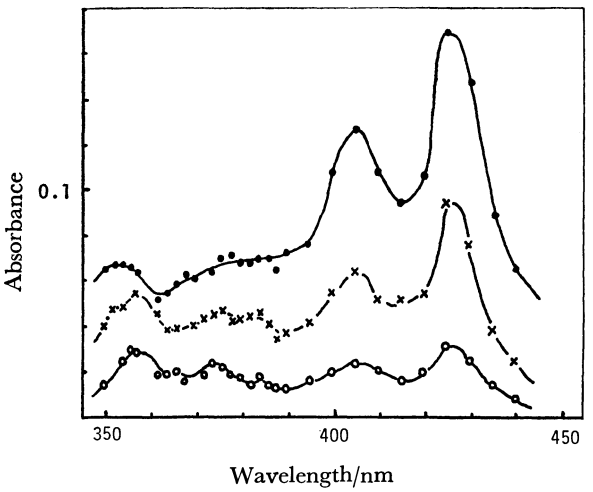

Fig. 2. Time-resolved absorption spectra of the 2-acetonaphthone-stilbene system in heptane: —●—, immediately after; —×—, 30 ns after; —○—, 70 ns after a laser pulse reached its maximum intensity.

respective of considerable amplitude variation of the laser pulse. The $I(t)/I(0)$ values were later converted to the absorbance scale.

trans-Stilbene and 2-acetonaphthone were purified with alumina column chromatography. *cis*-Stilbene and biacetyl were purified by distillation. The purity of all the samples was checked with gas chromatography to be more than 99%. The sample was deaerated with nitrogen flow and a fresh sample was supplied for each run.

Gas chromatographic analysis showed that the *cis-trans* isomerization reaction was straightforward and no other reaction took place during the laser irradiation.

Results

Transient Spectra. We chose 2-acetonaphthone as a sensitizer of the photoisomerization since the energy of the triplet state (E_T) is 59.3 kcal/mol (the lowest triplet state in $\pi\pi^*$,[18] just above the triplet state of *cis*-(E_T=56.7 kcal/mol) and *trans*-(E_T=49 kcal/mol) stilbenes. Figure 2 shows the time-resolved absorption spectra of *cis*-stilbene with 2-acetonaphthone in heptane at room temperature. We used heptane (η=0.418 cP; 20 °C) and benzene (η=0.649 cP; 20 °C) as nonpolar solvents and ethanol (η=1.08 cP; 25 °C) as a polar solvent. The absorption maxima, the shape of the absorption profile, and the time course of the absorption were found to be unaffected by the solvents so far as the viscosity is low. The "0 ns" spectrum (a spectrum observed just after the laser irradiation) has intense absorption bands at 424, 404, and 384 nm. These bands were assigned to the T_n-T_1 absorption of the sensitizer, 2-acetonaphthone, since the "0 ns" spectrum of 2-acetonaphthone in heptane gave the same spectrum. These bands decayed quickly and different absorption bands appeared about 70 ns after the laser pulse, irrespective of the starting materials being either *cis*- or *trans*-stilbene. The lifetime of this species was 110± 10 ns. This transient absorption spectrum was also observed in an additional experiment using biacetyl (the lowest triplet state is $n\pi^*$, E_T=56.3 kcal/mol[19]) as triplet sensitizer. We excited biacetyl with a dye-laser at 428 nm. Again the main spectral features in the region of 345—390 nm and the lifetimes were identical irrespective of the starting isomers. As described later, this transient absorption is due to a mixture of the triplet state of *trans*-stilbene and the phantom triplet.

The Rate of Triplet Energy Transfer from 2-Acetonaphthone to cis- *or* trans-*Stilbene.* In order to elucidate the mechanism of sensitization processes of the triplet state of *trans*-stilbene and twisted stilbene, we examined the first order decay rate of the 2-acetonaphthone triplet state as a function of the concentration of *cis*- or *trans*-stilbene. Figure 3 shows the Stern-Volmer relationship observed by the T_n-T_1 absorption at 430 nm in heptane. The plots give a straight line with a slope of 8.9×10^9 M^{-1} s^{-1} for *trans*-stilbene and 5.2×10^9 M^{-1} s^{-1} for *cis*-stilbene at room temperature.

*Transient Absorption in a Viscous Solvent (*t*-Butyl Alcohol).* The transient absorption of *cis*- or *trans*-stilbene in *t*-butyl alcohol with 2-acetonaphthone as a sensitizer has two components; the T_n-T_1 absorption of the sensitizer,

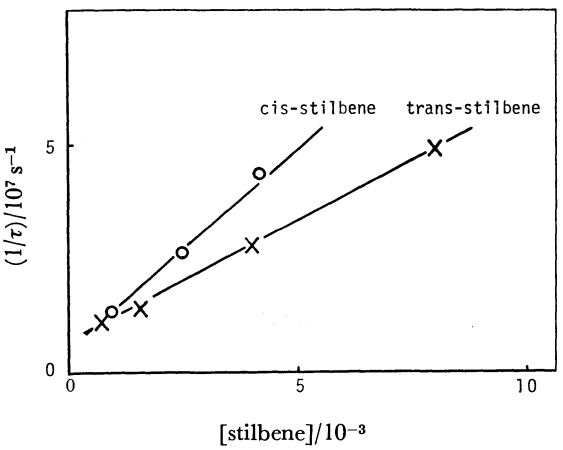

Fig. 3. The first-order decay rate of the 2-acetonaphthone triplet quenched by *cis*- and *trans*-stilbenes in heptane at room temperature.

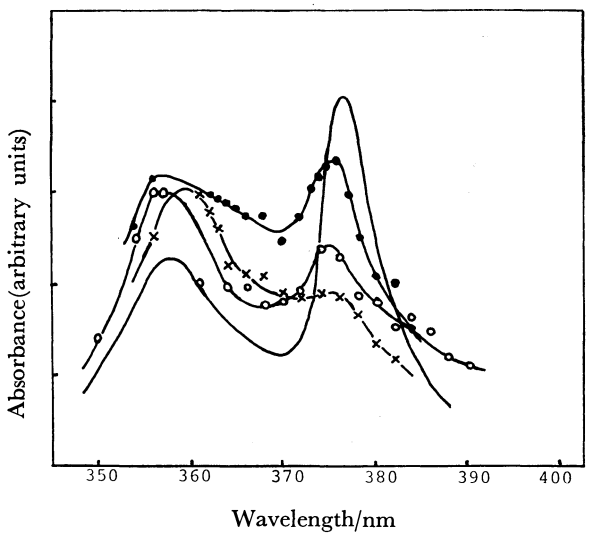

Fig. 4. Transient absorption of stilbene: —○—, *trans*-stilbene in non-viscous solvent; —●—, *trans*-stilbene in viscous solvent; —×—, *cis*-stilbene in viscous solvent; ——, the T_n-T_1 absorption spectrum of *trans*-stilbene at 77 K from Ref. 26.

2-acetonaphthone, which promptly decays, and the absorption due to the mixture of the triplet *trans*-stilbene and the phantom triplet. The time-resolved absorption spectrum of the long-lived species measured 60 ns after the laser irradiation is shown in Fig. 4. In a viscous solvent, contrary to the behavior in non-viscous solvents, the profiles of the transient absorption spectra were different for *cis*- and *trans*-stilbenes. The decay time of the long lived species was 120±10 ns and 80±10 ns for *cis*- and *trans*-stilbenes, respectively.

Discussion

Reaction Paths. The simplest mechanism which accounts for various observations of the sensitized photoisomerization of stilbene with a triplet donor (^{3}D) is shown as follows:[1,20]

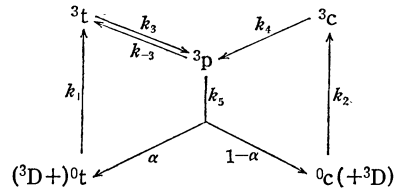

In the above diagram, t, c, and p stand for the *trans*-, *cis*-, and twisted stilbene, respectively. The superscripts 0 and 3 indicate the ground state and the lowest triplet state. The fraction of ^{3}p decaying to the transoid ground state is given by α. k's are the corresponding rate constants.

Recent theoretical studies show that the σ-π excited configuration mixing plays an important role in photochemical rearrengements involving rotation around double bonds. The results of an *ab initio* calculation for ethylene[21] show that the potential energy curve of the triplet state changes smoothly with an absolute minimum at $\theta=90°$, and stays always above the ground state potential. Thus there is no crossing. 1,3,5-Hexatriene, with the simplest π bond system in both sides of the central double bond, behaves in the same manner as ethylene for twisting the central double bond.[21] For styrene, Bruni *et al.*[22] discussed the predominant nature of the lowest triplet state was ethylenic, and showed a similar behavior as ethylene for twisting. In all cases, the main configuration of the lowest triplet state is the ethylenic π system, and becomes more and more localized in the ethylenic π bond during the internal rotation. We consider the same discussion is applicable to the potential surface of stilbene,[23–25] and a potential crossing between the ground and triplet state at $\theta=90°$ is not accounted.

Using 2-acetonaphthone as a sensitizer, the excitation rate constants k_1 and k_2 in heptane were obtained from the slope of the Stern-Volmer plots to be 8.9×10^9 and 5.2×10^9 M^{-1} s^{-1}, respectively. Considering the effect of the viscosity (η(benzene)/η(heptane) =1.5—1.6) on the bimolecular rate constants in benzene, these values become 5.6×10^9 and 3.2×10^9 M^{-1} s^{-1}, respectively. These are in good agreement with the values (5.0×10^9 M^{-1} s^{-1} for k_1, and 3.4×10^9 M^{-1} s^{-1} for k_2) obtained by Herkstroeter and Hammond[4] with conventional flash photolysis.

Kinetic Analysis of Observed Absorption. Let us analyze the observed absorption from the kinetic point of view based upon the reaction scheme in the previous section.

For the excitation of *trans*-stilbene,

$$d[^3t]/dt = k_1[^0t][^3D] + k_{-3}[^3p] - k_3[^3t], \quad (1)$$

$$d[^3p]/dt = k_3[^3t] - (k_{-3}+k_5)[^3p]. \quad (2)$$

For the excitation of *cis*-stilbene,

$$d[^3t]/dt = k_{-3}[^3p] - k_3[^3t], \quad (3)$$

$$d[^3p]/dt = k_4[^3c] + k_3[^3t] - (k_{-3}+k_5)[^3p]. \quad (4)$$

The differential equations are solved approximately as follows (see Appendix):

For the excitation of *trans*-stilbene,

$$[^3p]_t = k_3[^3D_0](e^{-\lambda_1 t}-e^{-\lambda_2 t})/a, \quad (5)$$

$$[^3t]_t = [^3D_0]\{(d-\lambda_1)e^{-\lambda_1 t}+(\lambda_2-d)e^{-\lambda_2 t}\}/a. \quad (6)$$

For the excitation of *cis*-stilbene,

$$[^3p]_c = [^3D_0]\{(k_3-\lambda_1)e^{-\lambda_1 t}+(\lambda_2-k_3)e^{-\lambda_2 t}\}/a, \quad (7)$$

$$[^3t]_c = k_{-3}[^3D_0](e^{-\lambda_1 t}-e^{-\lambda_2 t})/a. \quad (8)$$

Here

$$\lambda_{1,2} = \frac{1}{2}[(k_3+k_{-3}+k_5) \mp \{(k_3+k_{-3}+k_5)^2-4k_3k_5\}^{1/2}], \quad (9)$$

$$a = \lambda_2 - \lambda_1. \quad (9')$$

The ratio of $[^3t]$ to $[^3p]$ at time t is given as follows:

$$\left(\frac{[^3t]}{[^3p]}\right)_t = \frac{(d-\lambda_1)e^{-\lambda_1 t}+(\lambda_2-d)e^{-\lambda_2 t}}{k_3(e^{-\lambda_1 t}-e^{-\lambda_2 t})}, \quad (10)$$

$$\left(\frac{[^3t]}{[^3p]}\right)_c = \frac{k_{-3}(e^{-\lambda_1 t}-e^{-\lambda_2 t})}{(k_3-\lambda_1)e^{-\lambda_1 t}+(\lambda_2-k_3)e^{-\lambda_2 t}}. \quad (11)$$

Here $d=k_{-3}+k_5$.

In such non-viscous solvents as heptane, the observed

new transient species has a nearly single exponential decay. The decay rate of ^{3}p and ^{3}t are both approximated by the same λ_1. Therefore λ_1 should correspond to the observed long decay time ($\approx$110 ns). Since $\lambda_2 \gg \lambda_1$, the terms including $e^{-\lambda_2 t}$ can safely be disregarded in Eqs. 10 and 11.

$$\frac{([^3t]/[^3p])_t}{([^3t]/[^3p])_c} = \frac{(d-\lambda_1)(k_3-\lambda_1)}{k_3k_{-3}} = 1 \qquad (12)$$

This means that the transient absorption spectrum observed with the non-viscous solution is independent of the starting material being either *cis*- or *trans*-stilbene. The spectrum in the wavelength region, 345—390 nm, is quite similar to the T_n-T_1 absorption spectrum of *trans*-stilbene reported by Herkstroeter and McClure in solid solution at 77 K[26] (see Fig. 4). The spectrum is the absorption of ^{3}t, since the isomerization does not take place at 77 K. However, at shorter wavelengths, our spectrum has distinctly higher intensity. Subtracting the ^{3}t absorption from the transient absorption observed with the non-viscous solution, we have a new absorption band at $\approx$360 nm. The band is assigned to the intermediate between ^{3}t and the isomerization product, namely ^{3}p. The band at $\approx$360 nm becomes more predominant in the viscous solution.

The behavior of the transient species in a viscous solvent is dependent upon the starting materials as is shown in Fig. 4. The rotation is hindered in a viscous solvent. Since the forward rate constant k_3 is about nine times smaller in *t*-butyl alcohol than in benzene at room temperature[15], it is difficult to ignore the contribution of $e^{-\lambda_2 t}$ in the viscous solution. Thus we obtain much more complicated relation than Eq. 12,

$$\frac{([^3t]/[^3p])_t}{([^3t]/[^3p])_c} \approx \frac{e^{-2\lambda_1 t}+e^{-2\lambda_2 t}+e^{-(\lambda_1+\lambda_2)t}\{(k_3-\lambda_1)^2+(\lambda_2-k_3)^2\}/k_3k_{-3}}{e^{-2\lambda_1 t}+e^{-2\lambda_2 t}-2e^{-(\lambda_1+\lambda_2)t}} > 1. \qquad (13)$$

This relation shows that the concentration of ^{3}p relative to that of ^{3}t increases for the reaction from the *cis* isomer compared with the reaction from the *trans* isomer: in other words, the spectrum of the phantom triplet is more predominant in the transient spectrum from *cis*-stilbene than in that from *trans*-stilbene. This is consistent with the observation shown in Fig. 4 supporting the assignment of the 360 nm band to ^{3}p. We can see from Fig. 4 that the intensity ratio of the 360 nm band to the 376 nm band in the viscous solution is much larger in the transient spectrum from *cis*-stilbene than in that from the *trans*-stilbene.

In a viscous solvent the transient absorption decays differently depending upon the starting material. Exciting *trans*-stilbene, the lifetime is 80 ns at room temperature and this decay process (represented by λ_2) is considered to be from ^{3}t since the transient absorption spectrum mainly consists of the T_n-T_1 absorption spectrum. Exciting *cis*-stilbene, the transient absorption spectrum decays with the lifetime of 120 ns and is mainly due to ^{3}p, the decay process being controlled by λ_1.

The ratios of $[^3t]/[^3p]$ in heptane and *t*-butyl alcohol are estimated by taking the most reliable rate constants.[1,3] With the aid of Eqs. 10 and 11, these values *ca.* 50 ns after the laser irradiation are calculated and given in Table 1. We can see that in a viscous solvent $[^3t]/[^3p]$ is greatly different for *cis*- and *trans*-stilbenes.

Table 1. Viscosity dependence of $[^3t]/[^3p]$

Solvent		Heptane (non-viscous solv.)	*t*-Butyl alcohol (viscous solv.)
Viscosity(cP)	η	0.40	3.88
Rate constants (s^{-1})	k_3	10^8	1.3×10^7
	k_{-3}	10^7	1.3×10^6
	k_5	10^7	10^7
	λ_1	0.9×10^7	7.95×10^6
	λ_2	1.11×10^7	1.64×10^7
$([^3t]/[^3p])_t$		0.12	1.4
$([^3t]/[^3p])_c$		0.12	0.06

The initial concentrations of ^{0}t and ^{0}c are 0.1 M.

Appendix

The exact solution of linear differential equations 1, 2, 3, and 4 is as follows:
for the excitation of *trans*-stilbene,

$$[^3p]_t = k_3k_1[^0t][^3D_0]\left\{\frac{e^{-\lambda_1 t}}{ab}+\frac{e^{-\lambda_2 t}}{ac}+\frac{e^{-k_1[^0t]t}}{bc}\right\}, \qquad (A1)$$

$$[^3t]_t = k_1[^0t][^3D_0] \times \left\{\frac{d-\lambda_1}{ab}e^{-\lambda_1 t}-\frac{\lambda_2-d}{ac}e^{-\lambda_2 t}-\frac{k_1[^0t]-d}{bc}e^{-k_1[^0t]t}\right\}, \qquad (A2)$$

for the excitation of *cis*-stilbene,

$$[^3p]_c = k_2[^0c][^3D_0] \times \left\{\frac{k_3-\lambda_1}{ab'}e^{-\lambda_1 t}-\frac{\lambda_2-k_3}{ac'}e^{-\lambda_2 t}-\frac{k_3-k_2[^0c]}{b'c'}e^{-k_2[^0c]t}\right\}, \qquad (A3)$$

$$[^3t]_c = k_{-3}k_2[^0c][^3D_0]\left\{\frac{e^{-\lambda_1 t}}{ab'}+\frac{e^{-\lambda_2 t}}{ac'}+\frac{e^{-k_2[^0c]t}}{b'c'}\right\}, \qquad (A4)$$

where

$$\lambda_{1,2} = \frac{1}{2}[(k_3+k_{-3}+k_5) \mp \{(k_3+k_{-3}+k_5)^2-4k_3k_5\}^{1/2}],$$

$a = \lambda_2 - \lambda_1$,
$b = k_1[^0t] - \lambda_1$, $\quad b' = k_2[^0c] - \lambda_1$,
$c = \lambda_2 - k_1[^0t]$, $\quad c' = \lambda_2 - k_2[^0c]$,
$d = k_{-3} + k_5$.

$[^0c]$, $[^0t]$, and $[^3D_0]$ are the initial concentration of *cis*-stilbene, *trans*-stilbene, and sensitizer, respectively. Under our experimental conditions, we can make the concentrations of ^{0}t and ^{0}c high enough to have $k_1[^0t]$ and $k_2[^0c] \gg \lambda_1$, λ_2. The equations A1 to A4 are able to be approximated as Eqs. 5 to 8.

References

1) J. Saltiel, J. T. D'Agostino, E. D. Megarity, L. Metts, K. R. Neuberger, M. Wrighton, and O. C. Zafiriou, *Org. Photochem.*, **3**, 1 (1973).

2) J. Saltiel, J. T. D'Agostino, W. G. Herkstroeter, G. Saint-Ruf, and N. P. Buu-Hoï, *J. Am. Chem. Soc.*, **95**, 2543 (1973).

3) J. Saltiel and B. Thomas, *J. Am. Chem. Soc.*, **96**, 5660 (1974).
4) W. G. Herkstroeter and G. S. Hammond, *J. Am. Chem. Soc.*, **88**, 4769 (1966).
5) D. V. Bent and D. Schulte-Frohlinde, *J. Phys. Chem.*, **78**, 446 (1974).
6) J. Saltiel and J. T. D'Agostino, *J. Am. Chem. Soc.*, **94**, 6445 (1972).
7) J. Saltiel, D. W. L. Chang, E. D. Megarity, A. D. Rousseau, P. T. Shannon, B. Thomas, and A. K. Uriarte, *Pure Appl. Chem.*, **41**, 559 (1975).
8) R. Benson and D. F. Williams, *J. Phys. Chem.*, **81**, 215 (1977).
9) J. Saltiel, *J. Am. Chem. Soc.*, **90**, 6394 (1968).
10) Dainton *et al.*[11] measured the transient absorption in pulse radiolysis of *trans*-stilbene, its lifetime being about 110 ns at room temperature. Their assignment of this transient species is not clear.
11) F. S. Dainton, E. A. Robinson, and G. A. Salmon, *J. Phys. Chem.*, **76**, 3897 (1972).
12) J. Saltiel, *J. Am. Chem. Soc.*, **89**, 1036 (1967).
13) D. J. S. Birch and J. B. Birks, *Chem. Phys. Lett.*, **38**, 432 (1976).
14) M. Sumitani, N. Nakashima, K. Yoshihara, and S. Nagakura, *Chem. Phys. Lett.*, **51**, 183 (1977).
15) J. Saltiel and E. D. Megarity, *J. Am. Chem. Soc.*, **94**, 2742 (1972).
16) K. Yoshihara, M. Sumitani, K. Nishi, I. Yokoyama, and S. Nagakura, *Oyo Butsuri*, **43**, 335 (1974).
17) M. Sumitani, S. Nagakura, and K. Yoshihara, *Bull. Chem. Soc. Jpn.*, **49**, 2995 (1976).
18) G. F. Vesly and B. A. Prichard, *Mol. Photochem.*, **5**, 355 (1973).
19) M. Almgren, *Photochem. Photobiol.*, **6**, 829 (1967).
20) G. S. Hammond, J. Saltiel, A. A. Lamola, N. J. Turro, J. S. Bradshow, D. O. Cowan, R. C. Counsell, V. Vogt, and C. Dalton, *J. Am. Chem. Soc.*, **86**, 3197 (1964).
21) S. Iwata, private communication.
22) M. C. Bruni, F. Momicchioli, I. Baraldi, and J. Langlet, *Chem. Phys. Lett.*, **36**, 484 (1975).
23) Recently, Benson and Williams[8] proposed a potential curve of the triplet state which crosses that of the ground state and has an energy hump at about $\theta \approx 90°$. In order to account for their experimental results, it may be reasonable to adopt a potential curve proposed by Ting and McClure,[23,24] with two energy humps in both side of the potential minimum at $\theta \approx 90°$.
24) C. H. Ting and D. S. McClure, *J. Chinese Chem. Soc. (Taipei)*, **18**, 95 (1971).
25) We thank Dr. W. Siebrand, NRC Canada for pointing out this possibility.
26) W. G. Herkstroeter and D. S. McClure, *J. Am. Chem. Soc.*, **90**, 4522 (1968).

Studies on the Aqueous Solutions of Guanidinium Salts. VII. Activity Coefficients and Partial Molar Volumes for Guanidinium Salts with Hydrophobic Counter Anions in Aqueous Solutions

Koichiro MIYAJIMA,* Hiromitsu YOSHIDA, and Masayuki NAKAGAKI

Faculty of Pharmaceutical Sciences, Kyoto University, Yoshida-shimoadachi-cho, Sakyo-ku, Kyoto 606

(Received February 23, 1978)

Mean activity coefficients ($\gamma_\pm$) and partial molar volumes of guanidinium salts with hydrophobic counter anions were measured by isopiestic comparison method and densitometry, respectively. The values of $\gamma_\pm$ were low and the order of $\gamma_\pm$ values found to be acetate>propionate>benzoate. The b_v values from the Redlich-Rosenfeld's equation were slightly positive at 15 and 25 °C, and decreased with increased temperature. These results were interpreted in terms of the unique structure breaking action of guanidinium ions and the interionic interactions.

In a previous paper,[1] activity coefficients and partial molar volumes for guanidinium salts with hydrophilic counter anions in aqueous solutions were reported. The low mean activity coefficients ($\gamma_\pm$) of these salts were attributed to the structure breaking actions of these salts. The order of $\gamma_\pm$ values among these salts with different anions was interpreted as the interactions between the hydrated anions and cations. Among these salts, guanidinium acetate had the largest value of $\gamma_\pm$. The acetate ion has a methyl group which is different from other counter anions used in the previous studies.

To further investigate the properties of aqueous guanidinium ions and their interactions, mean activity coefficients and partial molar volumes of some guanidinium salts with hydrophobic counter anions were obtained by the isopiestic comparison method and densitometry, respectively. The results were interpreted in terms of the structure breaking action of the guanidinium ion and the interionic interactions.

Experimental

Materials. Guanidinium acetate, propionate, and benzoate were prepared by titrating aqueous guanidine solution with the corresponding carboxylic acid below 25 °C. These salts were recrystallized twice or more from an ethanol–ether mixture, and the elementary analyses are shown in Table 1. Reagent grade potassium chloride was used without further purification for the reference solute in the isopiestic measurements. These salts were dissolved in redistilled and deionized water.

Method. Osmotic coefficients were measured at 25±0.02 °C by the isopiestic method described elsewhere.[1] From the osmotic coefficient (ϕ), $\gamma_\pm$ was calculated from

$$\ln\gamma_\pm = (\phi-1)+2\int_0^{\sqrt{m}}\frac{\phi-1}{\sqrt{m}}\mathrm{d}\sqrt{m}, \quad (1)$$

where m is the molality. Density measurements were made at 15, 25, and 35±0.01 °C using a Seiko SDM-410 densimeter. Buoyancy corrections were made for guanidinium salts on the assumption that the densities of the solid states were all unity. From the densities of aqueous solutions, the apparent molar volume (ϕ_v) and the partial molar volume ($\overline{V}_2$) were calculated by

$$\phi_v = \frac{1000(d_0-d)}{Cd_0}+\frac{M}{d_0}, \quad (2)$$

$$\overline{V}_2 = \phi_v + \frac{1000-C\phi_v}{2000+C^{3/2}(\partial\phi_v/\partial\sqrt{C})}C^{1/2}\left(\frac{\partial\phi_v}{\partial\sqrt{C}}\right), \quad (3)$$

where d and d_0 are the densities of solution and solvent, respectively, and M and C are the molecular weight and molarity of the salt, respectively. The densities and the isopiestic molalities of aqueous solutions are shown in Tables 2 and 3. The reproducibility of the density measurements was found to be 5×10^{-5} g/cm^3 and the experimental determination of isopiestic concentrations was precise to 0.2%. Viscosities of aqueous BSA solutions were measured by using a Ubbelohde type viscometer at 25±0.01 °C. The reproducibility of flow time was found to be 5×10^{-2} s.

Table 1. Results of elementary analyses of guanidinium salts (%)

Compound		H	C	N	O
Guanidinium acetate	(Exp)	7.49	30.23	35.34	26.94
	(Calcd)	7.62	30.25	35.27	26.86
Guanidinium propionate	(Exp)	8.19	36.24	31.86	23.71
	(Calcd)	8.33	36.08	31.56	24.03
Guanidinium benzoate	(Exp)	6.23	52.78	23.03	17.96
	(Calcd)	6.12	53.03	23.09	17.56

Results and Discussion

Mean Activity Coefficients. The values of the mean activity coefficients and the osmotic coefficients are shown in Table 4. The plots of log $\gamma_\pm$ *vs.* concentration for guanidinium salts are shown in Fig. 1 together with those of the sodium salts of fatty acids.[3] Generally these curves reflect the ion-ion and ion-solvent interactions. All curves approach the Debye-Hückel limiting line (DH-L) from above at low concentrations, indicating the absense of ion pairs, as with cadmium sulfate. The relatively low values of log $\gamma_\pm$ for guanidinium salts compared with those of the sodium salts are attributed to the structure breaking action of the guanidinium ion. As seen in Fig. 1, the log $\gamma_\pm$ values of sodium acetate are lower than those of sodium propionate, while the log $\gamma_\pm$ values of guanidinium acetate are larger than those of guanidinium propionate. This may be explained as follows: The sodium ion is a hydrophilic structure maker in contrast with the guanidinium

Table 2. Densities of aqueous guanidinium salts at various temperatures

Guanidinium acetate		Guanidinium propionate		Guanidinium benzoate	
m	d(g/cm^3)	m	d(g/cm^3)	m	d(g/cm^3)
		at 15 °C			
0.05053	1.00063	0.05017	1.00064	0.05023	1.01539
0.07051	1.00123	0.07079	1.00124	0.06993	1.00238
0.09996	1.00211	0.10020	1.00207	0.10017	1.00375
0.15122	1.00355	0.15380	1.00364	0.15306	1.00614
0.19923	1.00492	0.20082	1.00496	0.20140	1.00827
0.29949	1.00782	0.30072	1.00770	0.50279	1.02072
0.49330	1.01302	0.40013	1.01036	0.70189	1.02830
0.70205	1.01833	0.50772	1.01311	0.98495	1.03751
1.00361	1.02554	0.70418	1.01797		
		1.00495	1.02491		
		at 25 °C			
0.05053	0.99855	0.06513	0.99886	0.05082	0.99931
0.07051	0.99910	0.07127	0.99900	0.06896	1.00009
0.09996	0.99991	0.09772	0.99970	0.10013	1.00143
0.15123	1.00133	0.19809	1.00240	0.20351	1.00578
0.19922	1.00266	0.26313	1.00384	0.29993	1.00971
0.29949	1.00534	0.27039	1.00402	0.48480	1.01693
0.49330	1.01033	0.29795	1.00502	0.68487	1.02426
0.70205	1.01543	0.48203	1.00967	0.96872	1.03378
1.00361	1.02232	0.65695	1.01388		
		0.82827	1.01778		
		at 35 °C			
0.04709	0.99544	0.05017	0.99548	0.05023	0.99548
0.09958	0.99683	0.07079	0.99603	0.06993	0.99603
0.18908	0.99902	0.10020	0.99747	0.10017	0.99830
0.29004	1.00188	0.15380	0.99835	0.15304	1.00047
0.36268	1.00450	0.20082	0.99955	0.20140	1.00250
0.50355	1.00737	0.30072	1.00210	0.29913	1.00636
0.60763	1.00992	0.40013	1.00464	0.50279	1.01401
0.71540	1.01258	0.50772	1.00721	0.70189	1.02108
0.89557	1.01682	0.70418	1.01174	0.98495	1.03066
1.00320	1.01893	1.00495	1.01823		

Table 3. Molalities of isopiestic solutions

Potassium chloride m	Guanidinium propionate m	Guanidinium benzoate m	Potassium chloride m	Guanidinium propionate m
0.1866	0.1968	0.2015	1.0558	1.1485
0.3299	0.3383	0.3736	1.7446	2.0086
0.3665	0.3787	0.4213	1.9271	2.2506
0.4235	0.4412	0.4960	2.5623	3.1653
0.4286	0.4437	0.4998	3.3918	4.4503
0.4828	0.5125	0.5791	3.7193	5.0231
0.5175	0.5352	0.6174	4.0070	5.5185
0.5341	0.5593	0.6556		
0.5899	0.6239	0.7392		
0.8179	0.8763	1.1204		
0.9087	0.9775	1.2569		

ion which is a structure breaker.[1,4-6] It is well known that a hydrophobic ion forms water structures around itself, which is so called "iceberg"[7] or "hydrophobic hydration."[8] The structure of the hydrated cosphere around the sodium ion and that of the hydrophobic ion are incompatible with each other and result in "structure salting out."[9] This explains why the $\gamma_{\pm}$ values of sodium propionate are larger than those of sodium acetate. The guanidinium ion is a large monovalent organic ion whose shape and size are quite similar to that of urea and its electric field to orient water molecules radially around itself is weaker than

Table 4. Osmotic and activity coefficients of Guanidinium salts at 25 °C

m	ϕ	$\gamma_\pm$	m	ϕ	$\gamma_\pm$	m	ϕ	$\gamma_\pm$
			Guanidinium propionate					
0.1	0.913	0.745	0.9	0.839	0.536	3.0	0.754	0.386
0.2	0.898	0.689	1.0	0.832	0.523	3.5	0.741	0.367
0.3	0.886	0.652	1.2	0.821	0.502	4.0	0.730	0.350
0.4	0.877	0.624	1.4	0.811	0.483	4.5	0.719	0.335
0.5	0.868	0.601	1.6	0.802	0.466	5.0	0.710	0.324
0.6	0.860	0.582	1.8	0.793	0.451	5.5	0.701	0.311
0.7	0.852	0.565	2.0	0.785	0.437			
0.8	0.845	0.550	2.5	0.768	0.409			
			Guanidinium benzoate					
0.1	0.891	0.713	0.5	0.767	0.485	0.9	0.691	0.383
0.2	0.845	0.624	0.6	0.746	0.454	1.0	0.675	0.365
0.3	0.817	0.567	0.7	0.726	0.427	1.2	0.645	0.333
0.4	0.790	0.521	0.8	0.708	0.404			

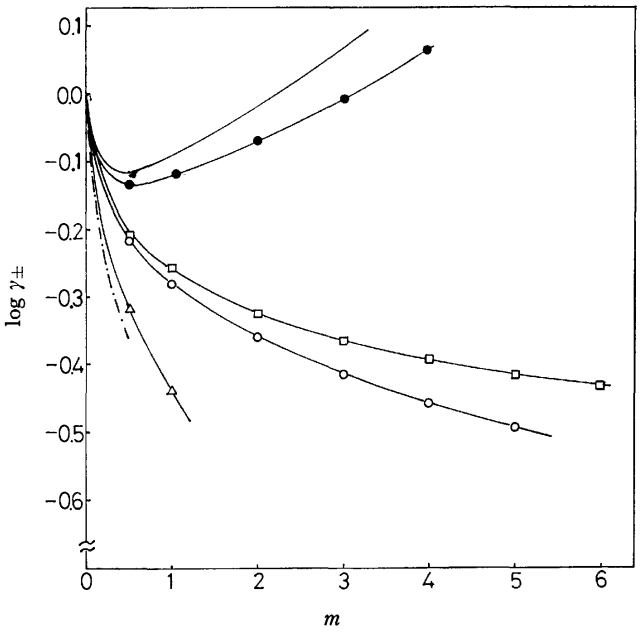

Fig. 1. Relations between log $\gamma_\pm$ and the molalities for various guanidinium salts and sodium salts at 25 °C. ——: Sodium propionate, —●—: sodium acetate, —□—: guanidinium acetate, —○—: guanidinium propionate, —△—: guanidinium benzoate, —·—: DH-L.

that of the alkali-metal ion. The guanidinium ion, however, has the ability to form hydrogen bonds with water molecules like urea, and the orientation of the hydrogen bonds with water does not fit the three dimensional network of ice-like structure. This leads to the conclusion that the structure breaking action of the guanidinium ion is different from that of the alkali-metal ions, such as Rb^+ and Cs^+. In fact, alkali halides and guanidinium halides behave in a different way when they are mixed with hydrocarbon gases[10] or symmetrical tetraalkylammonium halides[11] in aqueous solutions. Large alkali-metal halides produce salting out effects towards hydrophobic solutes,[11] while guanidinium halides produce salting in effects.[10,12]

The order of the $\gamma_\pm$ values among guanidinium salts with hydrophobic anions may be explained in two ways. As discussed above, the guanidinium ion breaks the structure of the bulk water which is in equilibrium with the structured water around the hydrophobic solute. This structure breaking action of the guanidinium ion is more pronounced in the highly structured solution containing the hydrophobic solute and results in the decrease of the $\gamma_\pm$ values of the salts. A second explanation is based on the more direct interaction between the guanidinium ion and the hydrophobic anion. Assuming that the hydrogen bond participates in the interaction between the guanidinium ion and the hydrated water molecules around it, may be possible to share the hydration cosphere with that of the hydrophobic anion. This interaction works as an attractive rather than a repulsive force and decreases the $\gamma_\pm$ values of the hydrophobic salts of guanidine. Although there is no evidence to support such an interaction, it cannot be neglected since the hydrophobic tetraalkylammonium halides form crystalline complexes with guanidinium halides and water,[13] and the $\gamma_\pm$ values of either salts in aqueous ternary solutions decrease each other as compared with those in each binary solution.[12] We cannot decide which of these mechanisms is really working at the present stage. Judging from the hydrophobicities of the counter anions, the $\gamma_\pm$ values of these salts should decrease in the order benzoate, propionate, and acetate in either mechanism.

Partial Molar Volumes of Guanidinium Salts. In general, the apparent molar volume (ϕ_v) of the salt may be expressed by Masson's equation (Eq. 4) or Redlich-Rosenfeld's equation (Eq. 5).[14]

$$\phi_v = \phi_v^0 + S_v^* \sqrt{C} \tag{4}$$

$$\phi_v = \phi_v^0 + S_v \sqrt{C} + b_v C \tag{5}$$

In these equations, ϕ_v is the apparent molar volume at infinite dilution and equal to $\overline{V}_2^0$, the partial molar volume at infinite dilution, C is the molarity and S_v^* is the experimental slope, and S_v is the constant obtained from the free energy change on pressure assuming that the $\gamma_\pm$ obeys the Debye-Hückel limiting law.[15] Therefore, b_v is the constant concerning the deviation of

TABLE 5. $\bar{V}_2^0$, S_v^*, AND b_v VALUES FOR GUANIDINIUM SALTS IN AQUEOUS SOLUTIONS AT VARIOUS TEMPERATURES

	Guanidinium acetate	Guanidinium propionate	Guanidinium benzoate	Temp (°C)
$\bar{V}_2^0$ (cm³/mol)	88.3	102.1	113.6	
S_v^* (cm³·l$^{1/2}$·mol^{-2})	2.0	2.2	2.4	15
b_v (cm³·l$^{1/2}$·mol$^{-3/2}$)	0.3	0.5	0.7	
$\bar{V}_2^0$ (cm³/mol)	90.0	103.6	136.4	
S_v^* (cm³·l$^{1/2}$·mol^{-2})	2.0	2.0	2.1	25
b_v (cm³·l$^{1/2}$·mol$^{-3/2}$)	0.1	0.2	0.2	
$\bar{V}_2^0$ (cm³/mol)	90.7	105.0	137.8	
S_v^* (cm³·l$^{1/2}$·mol^{-2})	1.7	2.0	2.1	35
b_v (cm³·l$^{1/2}$·mol$^{-3/2}$)	−0.4	−0.3	0.1	

volume from the predicted value by the Debye-Hückel theory and is regarded as a measure of the ion-solvent interactions. Negative b_v values have been reported on the aqueous solutions of various ammonium salts, such as tetraalkylammonium salts,[16] *n*-alkylamine hydrobromides,[17] and cyclic amine hydrochlorides.[18] These negative b_v values were attributed to the decrease in ice-likeness with increase of concentration by overlapping of the structural region around the hydrophobic solute,[17,18] or the increase of cage-like structure with increase of concentration.[19]

Concerning the sodium salts of fatty acids,[20] the values of b_v were slightly negative at 25 °C and these negative values increased with the carbon numbers of the chain as in the case of alkylamine hydrobromides. However, the temperature dependence of b_v values was negative in contrast with the case of the higher homolog of alkylamine salts. From the viscosity[21] and the NMR study,[5] the acetate ion was concluded to be a structure maker. Judging from the size of the ion and the delocalization of the charge,[22] the carboxylate ion may not have so much influence on the structure of water. If this is the case correct, then the structure making ability of the acetate ion originates from the methyl group of the acetate ion, that is, the acetate ion is a hydrophobic structure maker.

The formation of a cage-like structure around the hydrophobic solute makes a negative contribution to the partial molar volume of the solute.[23] If the guanidinium ion breaks the water structure around the hydrophobic ion in the unique way as discussed in the previous section, the guanidinium ion will increase the partial molar volume of the salt. Therefore the b_v values of the guanidinium salts will be positive if the structure breaking effect of the guanidinium ion dominates the structure making effect of the hydrophobic anions.

As seen in Table 5, the b_v values of three guanidinium salts were all positive at 25 °C and increased with the hydrophobicities of the counter anions. The negative b_v values of acetate and propionate at 35 °C and the negative temperature dependence of the b_v values for the each salt mean that the structure breaking ability of the guanidinium ion decreased with temperature increase, since the water structure was already broken to a considerable extent at high temperature.

Reduced Viscosity of BSA. The relation between the reduced viscosities of BSA (η_{sp}/C_2) and the concentration of guanidinium salts are shown in Fig. 2. The initial concentrations necessary to produce the denaturation are around 3 mol/l for these salts with hydrophobic anions and about 1 mol/l for chloride. The difference of the denaturation abilities of these two kinds of salts together cannot be compared, since the chloride ion is hydrophilic and the other two ions are hydrophobic. As discussed in the previous paper[1] and preceding sections of this paper, the modes of the interaction between the guanidinium ion and these two kinds of anions are different from each other. This suggests that the interactions of these two kinds of salts with proteins are also different. It does appear that the hydrophobic anions weaken the denaturating ability of the guanidinium ions. Assuming that the structure breaking actions of these salts play the most important role in the various interactions involved in the denaturation of BSA, the effective concentration of the

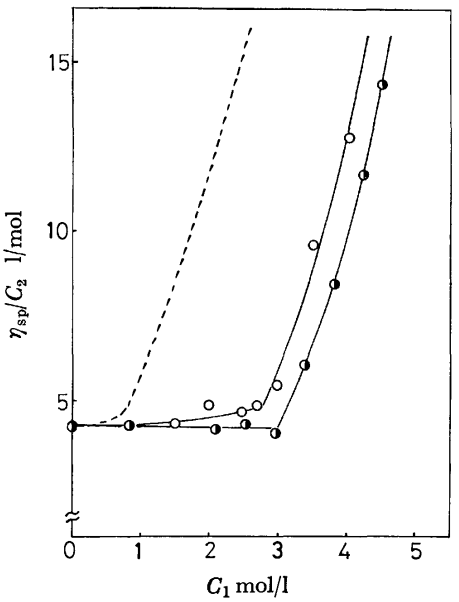

Fig. 2. Relation between the reduced viscosities of BSA and the concentrations of guanidinium salts.
----: Guanidinium chloride, —○—: guanidinium propionate, —◑—: guanidinium acetate.
C_1: Concentration of guanidinium salts (mol/l), C_2: concentration of BSA (7.6×10^{-2} g/ml aqueous salt solution).

propionate for the denaturation of BSA might be expected to be larger than that of acetate. In fact, the concentration of propionate was slightly smaller than that of acetate. This result is consistent with the denaturation of ribonuclease by tetraalkylammonium salts.[24] In the tetraalkylammonium salts, the homolog with larger alkyl chains promoted the denaturation more strongly than those with shorter alkyl chains.

In conclusion, it was difficult to explain the order of the denaturation abilities of the hydrophobic salts of guanidine only in terms of the $\gamma_{\pm}$ values and volume data of the aqueous binary solutions.

References

1) K. Miyajima, K. Inari, N. Hamaguchi, H. Yoshida, and M. Nakagaki, *Nippon Kagaku Kaishi*, **1975**, 1447.
2) H. S. Harned and B. B. Owen, "The Physical Chemistry of Electrolytic Solutions," Reinhold, New York (1950), p. 251.
3) R. A. Robinson and R. H. Stokes, "Electrolyte Solutions," Butterworths, London (1959), p. 492.
4) K. Miyajima, K. Inari, and M. Nakagaki, *Nippon Kagaku Kaishi*, **1974**, 2031.
5) K. Miyajima, K. Kitamura, K. Inari, and M. Nakagaki, *Nippon Kagaku Kaishi*, **1975**, 2060.
6) K. Miyajima, H. Yoshida, and M. Nakagaki, *Nippon Kagaku Kaishi*, **1976**, 366.
7) H. S. Frank and M. W. Evans, *J. Chem. Phys.*, **13**, 507 (1945).
8) F. Franks, *Ann. N. Y. Acad. Sci.*, **125**, 277 (1965).
9) J. E. Desnoyers, M. Arel, G. Perron, and C. Jolicoeur, *J. Phys. Chem.*, **73**, 3346 (1969).
10) D. B. Wetlaufer, S. M. Malik, L. Stoller, and R. F. Coffine, *J. Am. Chem. Soc.*, **76**, 508 (1964).
11) W-Y. Wen, K. Miyajima, and A. Ohtsuka, *J. Phys. Chem.*, **75**, 2148 (1971).
12) K. Miyajima, H. Yoshida, and M. Nakagaki, Abstr. No. 2M 11, 34th National Meeting of the Chemical Society of Japan, Hiratsuka, April 1976.
13) K. Miyajima, H. Yoshida, and M. Nakagaki, *Bull. Chem. Soc. Jpn.*, **50**, 2854 (1977).
14) O. Redlich and D. M. Meyer, *Chem. Rev.*, **64**, 221 (1964).
15) B. B. Owen and S. R. Brinkley, *Ann. N.Y. Acad. Sci.*, **51**, 753 (1949).
16) B. E. Conway, R. E. Verral, and J. E. Desnoyers, *Trans. Faraday Soc.*, **62**, 2738 (1964).
17) J. E. Desnoyers and M. Arel, *Can. J. Chem.*, **45**, 359 (1967).
18) S. Cabani, G. Conti, and L. Lepori, *J. Phys. Chem.*, **76**, 1338 (1972).
19) W-Y. Wen and S. Saito, *J. Phys. Chem.*, **68**, 2639 (1964).
20) M. Sakurai, *Bull. Chem. Soc. Jpn.*, **46**, 1596 (1974).
21) K. Tamaki, Y. Ohara, H. Kurachi, M. Akiyama, and H. Odaki, *Bull. Chem. Soc. Jpn.*, **47**, 384 (1974).
22) E. J. King, *J. Phys. Chem.*, **73**, 1220 (1969).
23) F. J. Millero, "Water and Aqueous Solutions," ed by R. A. Horne, Wiley Interscience, New York (1972), p. 558; W-Y. Wen, *ibid.*, p. 621.
24) P. H. von Hippel and T. Shleich, "Structure and Stability of Macromolecules," ed by Tismasheff and G. Fasman, Marcel Dekker, New York (1969), Vol. 2, p. 444.

Studies of Zone Melting. IV. The Equilibrium Distribution Coefficient of the Bibenzyl–Stilbene System†

Hidemoto NOJIMA

Department of Industrial Chemistry, Faculty of Engineering, Meiji University, Ikuta, Tama-ku, Kawasaki 214

(Received March 7, 1978)

Determinations of the equilibrium distribution coefficients of stilbene in bibenzyl by the zone-melting method were performed by using the theory proposed by Burton and his co-workers from the effective distribution coefficients, which were measured at various zone travel rates (0.73, 0.98, 1.16, and 1.47 cm/h) on five samples of bibenzyl containing 0.3, 0.5, 1.0, 2.0, and 4.0 wt % of stilbene. Also, the equilibrium distribution coefficient independent of the concentration was obtained as 5.08 by the extrapolation of the equilibrium distribution coefficient *vs.* the concentration plots to zero concentration. The validity of the obtained results is discussed by a comparison of the values estimated individually by two other methods: the equilibrium distribution coefficient (5.23) determined from the phase diagram of the bibenzyl–stilbene system, and that (5.08) calculated thermodynamically.

It is well known that the distribution of either a solute or an impurity between the solid and liquid phases in the fractional solidification process, in which the zone-melting method is included, is generally not in equilibrium because of the advance of the solid-liquid interface at a considerably rapid rate and the incomplete diffusion of the solute in the molten phase under ordinary experimental conditions.

If the argument is restricted to the binary systems, the distribution of the solute in both phases is represented by the effective distribution coefficient under the non-equilibrium conditions. On the other hand, if an equilibrium is established between the two phases, the distribution of the solute is indicated by the equilibrium distribution coefficient.

For the reasons described above, it is usually difficult for the equilibrium distribution coefficient to be determined directly from a zone-melting experiment. However, it can be estimated with the theory proposed by Burton and his co-workers[1] from the effective distribution coefficients obtained at various zone travel rates.

Determinations of the equilibrium distribution coefficients in this way have been achieved for a variety of binary systems, but the validity of the obtained results has been little discussed in terms of other methods, such as the phase diagram and thermodynamic theory.

In the previous paper,[2] the author attempted to estimate the equilibrium distribution coefficient of azobenzene in stilbene, which is less than unity, through the theory given by Burton and his co-workers[1] from zone-melting experiments, and also to compare it with the results obtained from the phase diagram of the system and from the thermodynamic theory of ideal solutions.

It will also be worth-while to study a system in which the distribution coefficient is greater than unity according to the above methods. Therefore, in this paper, similar discussions will be undertaken of the equilibrium distribution coefficient of *trans*-stilbene in bibenzyl, which is greater than unity. The obtained result was somewhat different from that found in the stilbene–azobenzene system.

No zone-melting experiments have previously been reported for the bibenzyl–stilbene system.

Experimental

Materials. The bibenzyl was purified once by recrystallization from ethanol, and the stilbene was zone-refined. The bibenzyl was mixed with stilbene in Pyrex beakers in the concentrations of 0.3, 0.5, 1.0, 2.0, and 4.0 wt %. After a small amount of acetone had been added to these mixtures, they were warmed and stirred gently until all of them were dissoved in acetone, and then the acetone was removed by evaporation in a vacuum desiccator. The samples were powdered in an agate mortar.

The bibenzyl was placed in a length of 27 cm in a Pyrex tube with an internal diameter of 0.7 cm and an outer diameter of 0.9 cm. In addition, the bibenzyl–stilbene mixture prepared by the procedures described above was placed on bibenzyl to a length of 3 cm. Then the tube was sealed off under a dry nitrogen atmosphere of about 0.9 atm.

Apparatus and Procedures. The zone-melting experiments were carried out with the apparatus described in a previous paper.[3]

The experiments of a single zone pass were carried out under the following conditions: the sample tube was moved upward at the different travel rates of 0.73, 0.98, 1.16, and 1.47 cm/h; the zone length was kept at 3 cm, and the zone temperature was set at 60 °C.

After a single passage of the molten zone, the sample was cut into 3-cm-long divisions. The concentration of stilbene in each portion was determined spectrophotometrically in an ethanol solution by means of a Hitachi 101 spectrophotometer at a wavelength of 295 nm.

Phase Diagram of the Bibenzyl–stilbene System. On the phase diagram of this system, several works have been reported.[4–6] Kolosov's work,[6] which is shown in Fig. 1, seems the most accurate among these works. Unfortunately, however, the accuracy in the range of low concentrations of stilbene, which is required for the determination of the equilibrium distribution coefficient from the phase diagram, is as poor in his diagram as in the others. For the purpose of correcting inaccuracies in Kolosov's data, the solidus and liquidus curves at low concentrations of stilbene were determined in detail with a Shimadzu differential scanning calorimeter, SC-20. The obtained results are presented in Fig. 2.

† A preliminary report of this work was presented at the 34th National Meeting of the Chemical Society of Japan, Hiratsuka, April 1976.

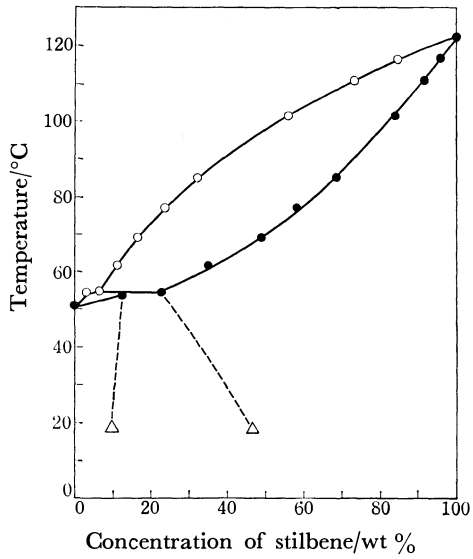

Fig. 1. Phase diagram of bibenzyl–stilbene system (after Kolosov[6]).

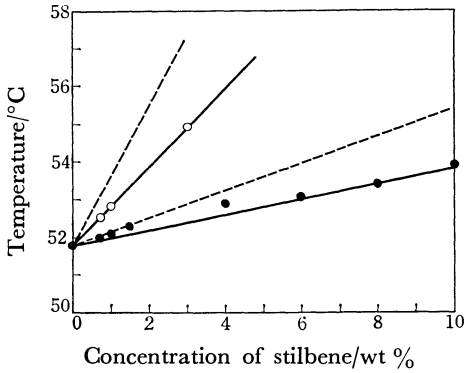

Fig. 2. Phase diagram of bibenzyl–stilbene system in the low concentration of stilbene.
○: Observed liquidus curve, ●: observed solidus curve, ----: ideal solidus and liquidus curves calculated thermodynamically.

Results and Discussion

Zone-melting Experiments. With the distributions of stilbene along the length of the samples after a single zone pass, the effective distribution coefficients were evaluated by the method of Sue and his co-workers.[7] In this method, the charge of the initial zone length consists of two components, that is, the solute whose distribution coefficient is to be measured and a solvent, while the remainder of the charge consists of a solvent only. The solute concentration, C, after a single zone passage is given at a distance, x, from the top of the sample by

$$\log\frac{C}{C_0} = -0.4343K_e\frac{x}{l} + \log K_e, \qquad (1)$$

where K_e is the effective distribution coefficient; C_0 is the initial concentration of the solute, and l is the zone length. Therefore, a plot of $\log(C/C_0)$ *vs.* x/l yields a straight line, and the slope and intercept of the line give the value of K_e. These relationships are shown in Fig. 3, in which, however, no whole data are represented in order to avoid complication; the values of K_e are shown in Table 1. The slope of Eq. 1 in the systems with distribution coefficients greater than unity is steeper than that in the systems with distribution coefficients less than unity, and the greater the coefficient, the steeper the slope. For this reason, the effective distribution coefficients were unavoidably estimated from only the three plots shown in Fig. 3.

Though the values of K_e estimated from both the slope and intercept in Eq. 1 should coincide with each other, the agreement is poor in the experimental results.[8,9] As one reason for this discrepancy, it may be considered that the assumptions used to derive Eq. 1 are not necessarily rigorously valid; the assumptions used are as follows: a constant distribution coefficient, no diffusion in the solid, a uniform concentration in

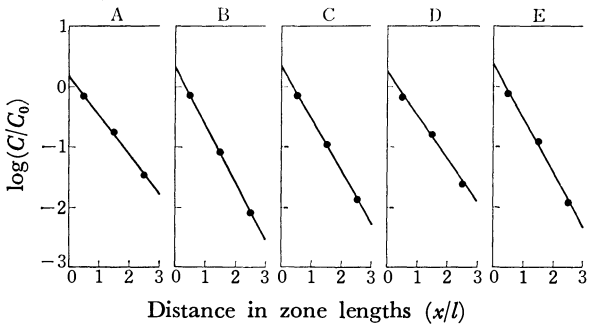

Fig. 3. $\log(C/C_0)$ *vs.* x/l.
A: 0.3% of stilbene; zone travel rate 0.73 cm/h, B: 0.5% of stilbene; zone travel rate 0.73 cm/h, C: 1.0% of stilbene; zone travel rate 0.73 cm/h, D: 2.0% of stilbene; zone travel rate 0.73 cm/h, E: 4.0% of stilbene; zone travel rate 0.73 cm/h.

Table 1. The effective distribution coefficient determined by the method of Sue and co-workers

Concentration of stilbene (wt %)	Zone travel rate (cm/h)	K_e from the intercept	K_e from the slope
0.3	0.73	1.57	1.52
	0.98	1.44	1.35
	1.16	1.32	1.25
	1.47	1.39	1.33
0.5	0.73	2.23	2.23
	0.98	2.01	1.89
	1.16	1.97	1.71
	1.47	1.80	1.80
1.0	0.73	2.04	2.00[a]
	0.98	1.85	2.08
	1.16	1.76	1.79
	1.47	1.65	1.76
2.0	0.73	1.72	1.67
	0.98	1.62	1.64
	1.16	1.66	1.68
	1.47	1.42	1.48
4.0	0.73	2.36	2.06
	0.98	2.50	2.16
	1.16	2.18	1.99
	1.47	2.06	1.86

a) The effective distribution coefficient obtained from the slope was adopted to calculate the equilibrium distribution coefficient.

the liquid, and no change in density on freezing.

The equilibrium distribution coefficient can be obtained from the effective distribution coefficients determined at various zone travel rates and expressed by the following equation by Burton *et al.*:[1]

$$\log\left(1-\frac{1}{K_e}\right)=\log\left(1-\frac{1}{K_0}\right)-0.4343\frac{\delta V}{D}, \qquad (2)$$

where K_e and K_0 are the effective and equilibrium distribution coefficients respectively; D, the diffusion coefficient of the solute in the melt; δ, the boundary layer thickness, and V, the freezing rate, which may be assumed to be identical with the zone travel rate in the zone-melting experiments. The value of K_0 can be estimated from the plot of $\log(1-1/K_e)$ *vs.* V by Eq. 2. In the estimation of K_0 from Eq. 2, for K_e we employed the values obtained from the intercepts in Fig. 3 except when the value of K_e was taken from the slope: the zone travel rate of 0.73 cm/h for 1.0% of stilbene.

The experimental results are represented in Fig. 4, while Table 2 and Fig. 5 show the relationship between the values of K_0 obtained from the intercepts of the lines in Fig. 4 and the concentrations of stilbene, C. This relationship can be expressed approximately by the following empirical equation:

$$K_0 = 2.50\exp(-3.11C) + 2.58. \qquad (3)$$

Then, the equilibrium distribution coefficient independent of the concentration is evaluated by substituting zero into the C in Eq. 3. Thus the value of 5.08 is obtained.

Here we found that, in contrast to finding for the stilbene–azobenzene system, the concentration dependence of the equilibrium distribution coefficient is fairly great.

Stilbene and azobenzene have the same crystal structure and almost the same molecular size, and form a complete series of solid solutions. On the other hand,

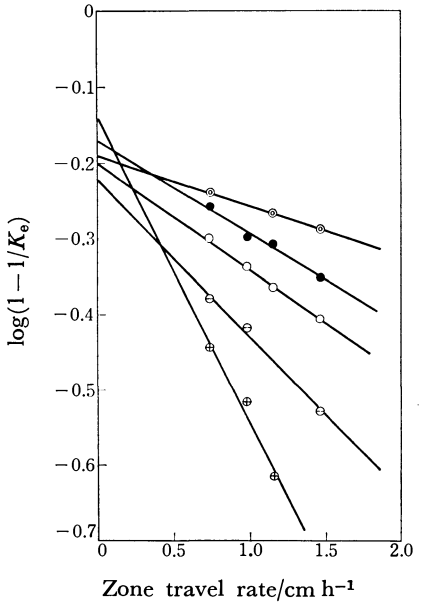

Fig. 4. $\log(1-1/K_e)$ *vs.* zone travel rate.
⊕: 0.3% of stilbene, ●: 0.5% of stilbene, ○: 1.0% of stilbene, ⊖: 2.0% of stilbene, ◎: 4.0% of stilbene.

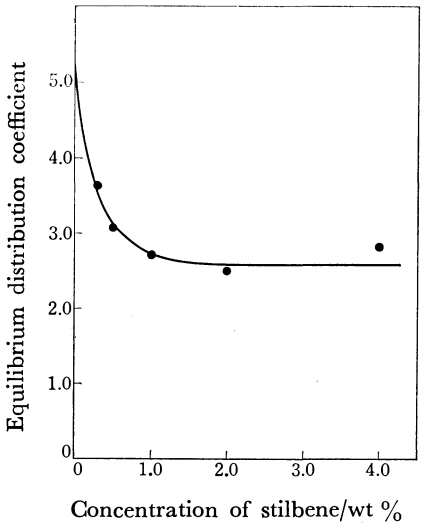

Fig. 5. The relation between equilibrium distribution coefficient and concentration of stilbene.
●: Observed values, ——: calculated curve by Eq. 3.

TABLE 2. THE RELATION BETWEEN THE CONCENTRAION OF STILBENE AND THE EQUILIBRIUM DISTRIBUTION COEFFICIENT

Concentration of stilbene (wt %)	Equilibrium distribution coefficient	
	Obsd	Calcd from Eq. 3
0.3	3.64	3.56
0.5	3.06	3.11
1.0	2.71	2.69
2.0	2.50	2.58
4.0	2.82	2.58

the similarities of the crystal structure and molecular size of bibenzyl and stilbene are less than those of stilbene and azobenzene;[10] hence, bibenzyl and stilbene form a peritectic system.

As one reason for such a difference between the concentration dependence of the equilibrium distribution coefficients found in the two systems, the fact described above may be considered.

In Fig. 4 straight lines for 0.5, 1.0, and 2.0% of stilbene are arranged in order of concentration. On the deviations from these arrangements of straight lines found in 0.3 and 4.0% of stilbene, it is considered that the effective distribution coefficient of 0.3% of stilbene might be smaller than the others because of the variation in the value of either D or δ for some reason. However the regularity, as shown in Table 2 and Fig. 5, might be restored in the equilibrium distribution coefficient, for it is independent of the above two factors. In the case of 4.0% of stilbene, the effective distribution coefficient becomes greater than those of 0.5—2.0% of stilbene. This result may be due to the transition at the peritectic point, at which a discontinuous change occurs in the distribution coefficient; this phenomenon is the so-called peritectic jump reported by Schildknecht.[11]

Determination by Phase Diagram. The solidus and liquidus curves shown in Fig. 2 are approximately

straight lines; their empirical equations are as follows:

$$t_s = 0.199C_s + 51.8, \quad (4)$$

$$t_l = 1.04C_l + 51.8, \quad (5)$$

where t_s and t_l are the solidus and liquidus temperatures in degrees of centigrade, and where C_s and C_l are the concentrations of stilbene in the solid and liquid phases respectively.

The equilibrium distribution coefficient independent of the concentration is given by Eq. 6 from the definition of distribution coefficient and Eqs. 4 and 5:

$$K_0 = \frac{C_s}{C_l} = \frac{1.04}{0.199} = 5.23. \quad (6)$$

Despite the fact that both solidus and liquidus curves are approximately straight, as shown in Fig. 2, the concentration dependence of the equilibrium distribution coefficient is fairly great in the results of the zone-melting experiments. This suggests that the equilibrium distribution coefficient estimated by the theory of Burton and his co-workers is the so-called interfacial distribution coefficient,[12] which seems to be not necessarily the same as the equilibrium distribution coefficient obtained by the phase diagram.

Determination by Thermodynamic Theory. In the binary systems, the relationship for the solid-liquid phase equilibrium is thermodynamically expressed by Eq. 7 at a constant pressure:

$$\ln\frac{a_s}{a_l} = \frac{\Delta H_0}{R}\left(\frac{1}{T} - \frac{1}{T_0}\right) + \frac{\Delta C_p}{R}\left(1 - \frac{T_0}{T} + \ln\frac{T_0}{T}\right), \quad (7)$$

where a_s and a_l are the activities of the solute in the solid and liquid phases respectively. ΔH_0 and T_0 are the heat of fusion and the melting point of the solute; T is the temperature at which the solid and liquid phases are in equilibrium with each other; ΔC_p is the difference between the heat capacities of the liquid and the solid solute at the melting point; R is the gas constant. The definition of the activity prescribes that, as the concentration of the solute tends to zero, the activity tends to be equal to the concentration. Therefore, for a dilute solution, the equilibrium distribution coefficient may be written as follows:

$$K_0 = \frac{a_s}{a_l} = \frac{C_s}{C_l}. \quad (8)$$

That is, the left-hand side of Eq. 7 can be rewritten as $\ln K_0$.

Since the tendency of the solute concentration to tend to zero is, in other words, for the composition to tend to that of a pure solvent, substituting the melting point of the solvent for T in Eq. 7 may yield an equilibrium distribution coefficient independent of the concentration.

In Fig. 2, the smaller the concentration of stilbene, the closer the gap between the observed lines, represented by the full lines, and those calculated by the thermodynamic theory of the ideal solution, represented by the dotted lines. Therefore, the equilibrium distribution coefficient independent of the concentration can be calculated by means of Eqs. 7 and 8. To calculate the value of K_0, the numerical values substituted in Eq. 7 are as fusion:

ΔH_0 is the heat of fusion of stilbene: 25800 J/mol,*

T_0 is the melting point of stilbene: 397.6 K,*

T is the melting point of bibenzyl: 325.0 K,*

ΔC_p is the difference between the heat capacities of liquid and solid stilbene at the melting point: 45.3 J/mol.**

Thus, the value of 5.08 was obtained.

Though the similarities in the crystal structure and in molecular size between stilbene and bibenzyl are less than those of stilbene and azobenzene, as has already been described, the assumption of an ideal solution also, in this system, holds in low concentrations of stilbene. Moreover, the equilibrium distribution coefficient calculated thermodynamically agrees with those obtained from the zone-melting experiments and phase diagram, as shown in Table 3.

Table 3. The equilibrium distribution coefficients determined by the three methods

Method employed for the determination of the equilibrium distribution coefficient	Equilibrium distribution coefficient
Zone melting	5.08
Phase diagram	5.23
Thermodynamic theory	5.08

Conclusion

In the zone-melting experiments, the equilibrium distribution coefficient extrapolated to zero concentration of stilbene agreed ultimately with the values determined from the phase diagram and thermodynamic theory. This fact differs considerably from that found in the stilbene–azobenzene system with regard to the concentration dependence of the equilibrium distribution coefficient. However, the determination of the equilibrium distribution coefficient through the theory of Burton and his co-workers, which is based on a dynamic process consisting of a heterogeneous reaction, was related to the methods taking account of the equilibrium conditions, that is, the phase diagram and the thermodynamic theory.

The author wishes to thank Professor Masaru Inagaki, of Meiji University, and Professor Sohachiro Hayakawa, of Tokyo Institute of Technology, for their valuable advice.

References

1) J. A. Burton, R. C. Prime, and W. P. Slichter, *J. Chem. Phys.*, **21**, 1987 (1953).
2) H. Nojima, M. Saito, and M. Inagaki, *Rev. Phys. Chem. Jpn.*, **46**, 76 (1976).
3) H. Nojima, *Nippon Kagaku Zasshi*, **91**, 810 (1970).
4) "International Critical Tables," McGraw-Hill Book Co., Vol. 4, New York (1928), p. 163.

* Measured on zone-refined specimens with a Shimadzu differential scanning calorimeter, SC-20.

** Estimated from the data cited in Timmermans' book.[13]

5) Landolt-Börnstein, "Zahlenwerte und Funktionen," 6th ed, Vol. 2, Part 2, Berlin (1956), p. 365.
6) A. I. Kitaigordsky, "Molecular Crystals and Molecules," Academic Press, New York (1973), p. 111.
7) P. Sue, J. Pauly, and A. Nouaille, *Bull. Soc. Chim. Fr.*, **5**, 593 (1958).
8) T. Hayakawa, and M. Matsuoka, "Kodo Bunri Gijutu," ed by The Society of the Chemical Engineering of Japan, Maruzen, Tokyo (1973), p. 115.
9) T. H. Gouw, "Progress in Separation and Purification," ed by E. S. Perry, Interscience Publishers, New York (1968), Vol. 1, p. 73.
10) A. I. Kitaigordsky, "Organic Chemical Crystallography," Consultants Bureau Enterprises, New York (1961), pp. 388—397.
11) H. Schildknecht, "Zone Melting," Academic Press, New York (1966), pp. 27—38.
12) J. S. Shah, "Crystal Growth," ed by B. P. Pamplin, Pergamon Press, Oxford (1975), p. 110.
13) J. Timmermans, "Physico-Chemical Constants of Pure Organic Compounds," Vol. 1, Elsevier Publishing Company, Amsterdam (1965), p. 176.

Hydrates of Organic Compounds. III. The Formation of Clathrate-like Hydrates of Tetrabutylammonium Dicarboxylates

Haruo NAKAYAMA* and Kazuichi WATANABE

Department of Chemistry, Faculty of Engineering, Yokohama National University, Ooka-machi, Minami-ku, Yokohama 232

(Received March 22, 1978)

The solid-liquid phase diagrams for the binary mixtures of water with 20 tetrabutylammonium dicarboxylates, $[(n\text{-}C_4H_9)_4N]_2OOC\text{–}R\text{–}COO$ (R = methylene chain ranging from 0 to 10 carbon atoms; methylene chain containing substituted groups such as $-CH_3$, $-C_2H_5$, $-NH_2$, and $-OH$; and $-C_6H_4-$ (three phthalate isomers)), have been investigated to see the effect of dicarboxylate anions on the formation of clathrate-like hydrates. It has been found that, with only the one exception of the dodecanedioate, all the other salts form hydrates which have large hydration numbers. Judging from these large hydration numbers, they are believed to be clathrate-like hydrates. From the relationship between the hydration numbers and the melting points, these hydrates can be classified into three groups at least. All the hydrates other than those of oxalate and of terephthalate are newly found in this study.

In 1959 McMullan and Jeffrey[1] pointed out that a series of hydrates formed by tetrabutyl(and tetraisopentyl)ammonium salts, which were originally found by Kraus and his co-workers,[2] were clathrate-like hydrates similar to the gas hydrates.[3] Later this reasoning was verified by detailed structural studies.[4–6]

In general, in these hydrates, each alkyl chain of the ammonium cation (and also each hydrophobic group of an anion, if such exists) is accommodated within a polyhedron (such as 14- or 15-hedron) which is constructed by hydrogen-bonded water molecules. Since most of these hydrates can easily be formed at moderate conditions, they provide us with a suitable model system for studying the nature of the interaction between water and hydrophobic molecules, especially in connection with the structural modification of water molecules in the vicinity of hydrophobic solutes in an aqueous solution.

The previous study[7] clearly showed that the most suitable alkyl chain of a tetraalkylammonium cation for the formation of stable clathrate-like hydrates was either butyl or isopentyl, and further that a shorter or longer chain than these groups drastically affected the stability of the hydrates. On the other hand, in the case of anions it is well known that many tetrabutyl(or isopentyl)ammonium salts with various anions (such as F^-, Cl^-, Br^-, CH_3COO^-, HCO_3^-, CrO_4^{2-}, WO_4^{2-}, $C_2O_4^{2-}$, and HPO_4^{2-}) can form clathrate hydrates,[1] and that the effect of an anion on the stability (*i.e.*, the melting points) of these hydrates is not so marked as that of the alkyl-chain length of the cation.

Of the anions which form clathrate-like hydrates, a carboxylate anion seems to be of special importance, since it may have an additional hydrophobic group. The formation of clathrate hydrates of tetrabutylammonium monocarboxylates have been reported for formate,[2] acetate,[1,2] propionate,[2] butyrate,[8] pentanoate,[8] benzoate,[2,5] and *m*-chlorobenzoate.[8] Such properties as hydration numbers and melting points for these hydrates have been either measured or estimated. The detailed crystal structure is known only for benzoate hydrate.[5] In this hydrate ($(n\text{-}C_4H_9)_4N\cdot OOCC_6H_5\cdot 39.5H_2O$), not only four butyl groups of the cation but also the benzyl group is enclathrated by the hydrogen-bonded water framework, and the oxygen atoms of the benzoate anion are hydrogen-bonded to the water framework and form part of the polyhedral structure. Essentially similar structures will be expected for the propionate, butyrate, and *m*-chlorobenzoate hydrates. The cases of the formate and the acetate are less simple to predict.[5]

On the other hand, for tetrabutylammonium dicarboxylates the formation of clathrate hydrate is known only for oxalate[1,2,8] and terephthalate,[8] for which hydration numbers have either been measured directly or estimated from the X-ray results (the Laue symmetry, unit-cell dimensions, and so forth). So far no other study has been reported about the formation of clathrate hydrates of a tetrabutylammonium dicarboxylate. In this paper, through the determination of the solid-liquid phase diagrams for the tetrabutylammonium dicarboxylate–water binary systems, an extensive study has been made in order to examine a variety of effects of dicarboxylate anions on the formation of clathrate hydrates: (1) the effect of the length of the methylene chain introduced between two carboxyl groups; (2) the effect of the type and the position of the substituted groups (such as $-CH_3$, $-C_2H_5$, $-NH_2$, and $-OH$); and (3) the effect of the geometrical relationship between the two carboxyl groups.

Experimental

Materials. The following tetrabutylammonium dicarboxylates $[(n\text{-}C_4H_9)_4N]_2OOC\text{–}R\text{–}COO$, were used, where R were: (1) $-(CH_2)_n-$ (n=0—8, and 10); (2) $-CH(C_2H_5)-$; (3) $-CH_2-CH(CH_3)-(CH_2)_m-$ (m=0—2); (4) $-CH(NH_2)-(CH_2)_l-$ (l=1,2); (5) $-CH_2-CH(OH)-$; and (6) $-C_6H_4-$ (*o*-, *m*-, and *p*-). All the salts were prepared by neutralizing tetrabutylammonium hydroxide solutions with the corresponding acids. The hydroxide was prepared from tetrabutylammonium iodide by means of silver oxide,[1,2] and purified by recrystallization from its dilute aqueous solution in the form of clathrate hydrate crystal.[2] The tetrabutylammonium iodide was prepared by the reaction between tributylamine and butyl iodide and was purified by repeated recrystallization from ethyl acetate.[7] All acids were reagent grade commercial materials and used without further purification except phthalic and isophthalic acids and four acids $HOOC(CH_2)_nCOOH$, whose n=3—8: phthalic and isophthalic acids were recrystallized from ethyl alcohol and

the latter acids from water. The salts which could form stable hydrates (whose melting points were higher than about 10 °C) were purified by recrystallization from water in the hydrate forms.

Procedures. For each salt, a sample (about 1—2 ml) of known composition was prepared by weighing its concentrated solution and water, and then was sealed in a small glass ampoule. No special care was taken to remove the air dissolved in the solution. The concentrated salt solution was prepared by dehydrating a relatively dilute solution over P_2O_5 in an desiccator; its concentration (water content) was determined by the Karl Fisher titration method on a MK-AII apparatus (Kyoto Electronics Manufacturing Co.). Each ampoule was gradually cooled until the solid phase appeared and was annealed for at least 24 h. After that, the ampoule was slowly warmed (at the rate about 0.3 °C per hour) with vigorous shaking in a constant temperature bath. The solid-liquid phase diagrams were determined by measuring the temperature at which the solid phase completely disappeared. When the temperature determination was somewhat ambiguous, especially at high mole fractions and at low temperatures, the differential scanning calorimeter (DSC) (Shimadzu Seisakusho, SC-20) was also employed.

Results

The solid-liquid phase diagrams for the salts of $[(n\text{-}C_4H_9)_4N]_2OOC\text{-}(CH_2)_n\text{-}COO$ with n=0—4 are shown in Fig. 1, and with n=5—8, and 10 in Fig. 2. With only one exception, the salt with n=10, all the other salts form hydrates with a large number of water molecules. All these hydrates melt congruently.

The oxalate (n=0) hydrate is quite stable. Its melting point is 16.6 °C and its hydration number is 58±1. This melting point is in good agreement with 16.8±0.1 reported by Jeffrey and co-workers[1] for the tetragonal structure. The hydration number, however, is greatly different from their values, 67 (by chemical analysis) and 64 (estimated from crystallographic data).[1] On the other hand, their other hydration number,

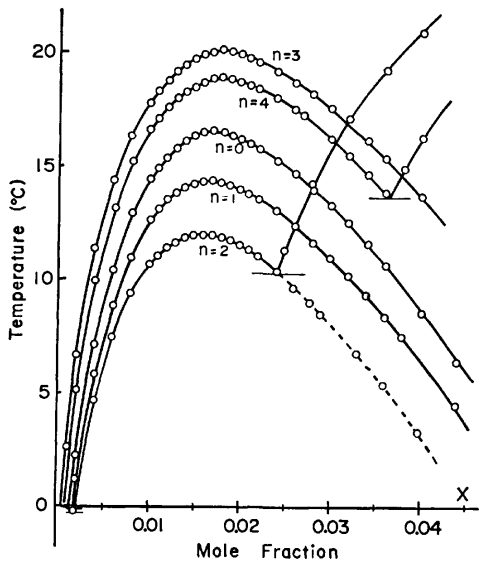

Fig. 1. The solid-liquid phase diagrams for the water-$[(n\text{-}C_4H_9)_4N]_2OOC(CH_2)_nCOO$ systems; n=0—4.

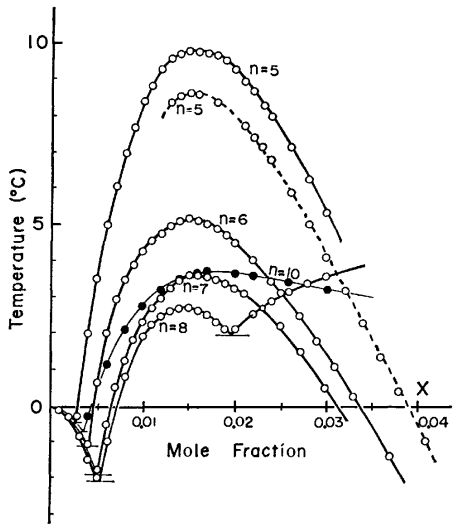

Fig. 2. The solid-liquid phase diagrams for the water-$[(n\text{-}C_4H_9)_4N]_2OOC(CH_2)_nCOO$ systems; n=5—8, and 10.

57.3±2,[8] which has been estimated for the cubic structure (a=24.58 Å) is in agreement with ours, though the melting point of this structure has not been reported.

As is seen from Figs. 1 and 2, the stabilities (*i.e.*, melting points) of these hydrates decrease, as a general trend, upon increasing the length of the methylene chain located between the two carboxyl groups. However, the hydrates of glutarate (n=3) and adipate (n=4) are exceptionally stable, indicating that $OOC\text{-}(CH_2)_3\text{-}COO$ and $OOC\text{-}(CH_2)_4\text{-}COO$ anions are most suitable for being accommodated within the hydrogen-bonded water framework. For the pimelic salt (n=5), another metastable phase appears when its aqueous solution is cooled rapidly. The stable phase appears only when the solution is maintained at temperatures around 0 °C for several days. The salt concentration of the hydrates (*i.e.*, the concentration of maximum temperature in each phase diagram) slightly decreases with increasing n from 0 to 2, shifts to a high (and almost the same) value for the salts with n=3 and 4, and again decreases and holds an approximately constant value for the salts with n=5—8 (Fig. 2).

In the case of the salts with n=2, 4, and 8, another solid phase appears at high mole fractions, around 0.02 for n=2 and 8 and 0.04 for n=4. It is not certain whether these phases are lower hydrates or anhydrous solids. For the salt with n=10, the phase diagram (Fig. 2) shows a very broad peak in the vicinity of X= 0.016—0.018. This solid phase, however, does not seem to be a hydrate similar to those of the other salts, judging from the fact that the shape of the phase diagram differs from the others and that it takes a long time to attain the dissolution equilibrium, as compared with other salts.

All the melting points and hydration numbers obtained in this paper are summarized in Table 1. The phase diagrams of such salts as ethylmalonate, methylsuccinate, aminosuccinate (L-asparate), hydroxysuccinate (L-malate), 3-methylglutarate, 2-aminoglutarate (L-glutamate), and 3-methyladipate have essentially

similar shapes to those of each parent salt, as shown in Fig. 1. Therefore, for the hydrates of these salts, only the melting points and hydration numbers which are read off each phase diagram are listed in Table 1.

Figure 3 gives the phase diagrams of three isomeric (*o*-, *m*-, and *p*-) phthalates. The phthalate gives the most stable hydrate among the salts studied in this paper. Although the water content of these hydrates is approximately identical, their melting points decrease in intervals of 4.0 degrees in the order of phthalate, isophthalate, and terephthalate. In the case of terephthalate, another solid phase appears at high mole fractions around 0.04; its composition is not known. The observed melting point and hydration number for the terephthalate hydrate, 12.3 °C and 62±2 (Table 1), are in disagreement with those reported by Jeffrey *et al.*,[8] 9.5 °C and 84±4. The latter hydration number has been deduced by inference from the structures already known.

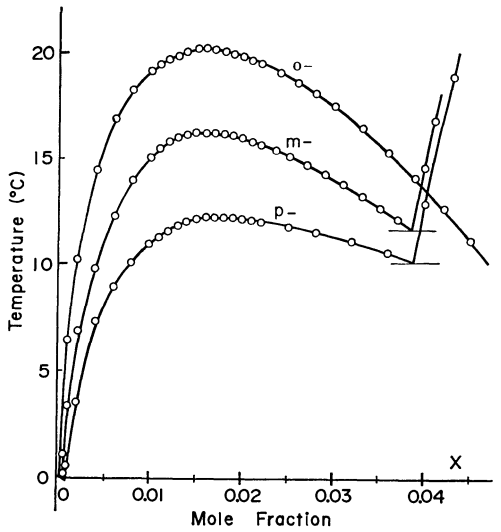

Fig. 3. The solid-liquid phase diagrams for the water-tetrabutylammonium phthalate systems.

TABLE 1. THE MELTING POINTS AND THE HYDRATION NUMBERS OF THE HYDRATES FORMED BY A SERIES OF TETRABUTYLAMMONIUM DICARBOXYLATES $[(n\text{-}C_4H_9)_4N]_2OOC\text{-}R\text{-}COO$

R	Melting point (°C)	Hydration number
None (oxalate)	16.6	58±1
$-CH_2-$	14.4	59±1
$-CH(C_2H_5)-$	15.9	62±1
$-CH_2-CH_2-$	12.1	61±1
$-CH_2-CH(CH_3)-$	14.9	63±1
$-CH_2-CH(NH_2)-$ (L)	9.8	63±2
$-CH_2-CH(OH)-$ (L)	11.1	63±1
$-CH_2-CH_2-CH_2-$	20.2	55±1
$-CH_2-CH(CH_3)-CH_2-$	16.2	55±1
$-CH(NH_2)-CH_2-CH_2-$ (L)	15.8	55±1
$-CH_2-CH_2-CH_2-CH_2-$	19.0	55±1
$-CH_2-CH(CH_3)-CH_2-CH_2-$	12.0	55±2
$-(CH_2)_5-$ (stable)	9.8	63±2
(metastable)	8.6	65±2
$-(CH_2)_6-$	5.2	65±3
$-(CH_2)_7-$	3.7	65±3
$-(CH_2)_8-$	2.7	65±3
$-C_6H_4-$ phthalate	20.3	62±1
isophthalate	16.3	62±1
terephthalate	12.3	62±2

Discussion

These results show that all the salts, except dodecanedioate, form hydrates which have large hydration numbers ranging from 55 to 65 and melt congruently. Although there is no evidence about the structure of these hydrates, they are believed to be clathrate-like hydrates for the following reasons. In general, arguing from the structure of several tetraalkylammonium salt hydrates,[1,4-7] 7—8 water molecules per one alkyl group, such as butyl and isopentyl, are needed in order to accommodate it by making a hydrogen-bonded water framework. Since the salts used in this study have 8 or 9 hydrophobic groups, the hydration numbers for these salt hydrates are expected to have values around 60 if they form similar types of hydrates, in good agreement with the values actually found.

As mentioned earlier, the detailed crystal structure of tetrabutylammonium carboxylate hydrates is known only for benzoate hydrate,[5] in which two oxygen atoms of the benzoate anion occupy two adjacent polyhedral sites. Thus it may be reasonably anticipated that, in the dicarboxylate hydrates found in this paper, four oxygen atoms of two terminal carboxyl groups will likewise occupy the appropriate hydrogen-bonded sites of the polyhedral vertices. This restriction will be one of the factors which will affect the stabilities of these hydrates. In addition, we may list other stability-controlling factors, such as (1) how well a hydrophobic group existing between two carboxyl groups is

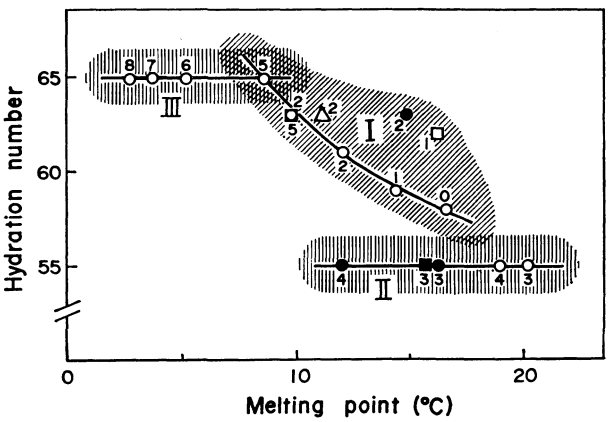

Fig. 4. The correlations between the hydration numbers and the melting points of the hydrates of tetrabutylammonium dicarboxylates. ○: Anions with no substituted group; ●: anions with methyl group; □: anions with ethyl group; ■: anions with $-NH_2$ group; △: anion with $-OH$ group. A numeral attached to each point indicates the number of carbon atoms in the methylene chain of the dicarboxylate anion.

accommodated within a hydrogen-bonded framework of waters and (2) the change in electrostatic potential due to the positional change of carboxyl anions with respect to a central $(n\text{-}C_4H_9)_4N^+$ cation.

Figure 4 gives the relationship between the hydration numbers and the melting points observed for our series of hydrates. The number attached to each point stands for the number of carbon atoms of the methylene chain in a dicarboxylate anion. From this figure we may tentatively classify these hydrates into three groups: I, II, and III.

Group I consists of the hydrates of the salts with $n=$ 0, 1, 2, and 5 and all their derivatives. In this group of hydrates the hydration number varies within the range of 58 and 63 depending upon the size and/or shape of the hydrophobic group of the anion and increases, in general, with decreasing the melting points. Of these hydrates, oxalate hydrate is the most stable and the stability gradually decreases upon increasing the length of the methylene chain. This fact will suggest that neither a small methylene chain as in the malonate ($n=1$) and the succinate ($n=2$) nor a large one as in the pimelic salt ($n=5$) is suitable in size to be encaged stably by a hydrogen-bonded water framework. The stabilities of these hydrates seem to be strongly influenced by the relative difficulty of fixing four oxygen atoms of two carboxyl groups into appropriate polyhedral sites. From the fact that oxalate (and also phthalate hydrate, Fig. 3 and Table 1) is fairly stable, it may be said that the existence of two carboxyl groups in the vicinity of one tetrabutylammonium cation is favorable for forming a stable hydrate. Thus in the oxalate hydrate, for example, the hydrate is made up by $[(n\text{-}C_4H_9)_4N\cdot OOC\text{–}COO]^-$ anions and $(n\text{-}C_4H_9)_4N^+$ cations, each surrounded by a hydrogen-bonded water framework.

It is interesting to note that the ethylmalonate hydrate is more stable than that of the malonate itself; the same relation is found between methylsuccinate and succinate hydrates. This indicates that the introduction of an ethyl or methyl group onto such small hydrophobic anions makes them more suitable in size to be surrounded by the hydrogen-bonded framework of water. The substitution of polar groups like $-NH_2$ and $-OH$ onto the succinic acid anion causes a slight decrease in the melting points of their hydrates. This presumably occurs as a result of the overlapping of two conflicting factors: a favorable factor of increasing the molecular volume of such a small anion; and a inconvenient factor of the disturbance in the stable formation of water polyhedra due to the occurrence of directional interaction (hydrogen-bonding) between these polar groups and water molecules which construct polyhedral cages. This effect of the introduction of a polar group into a guest molecule on the stability of its hydrate is, however, much less than expected; salts such as $(n\text{-}C_4H_9)_3(C_3H_6OH)NF$ and $(n\text{-}C_4H_9)_3(CH_3COOCH_2)NF$ cannot form stable hydrates at all,[9] in striking contrast to a very stable $(n\text{-}C_4H_9)_4NF$ hydrate.[7]

Group II consists of the hydrates of the salts having $n=3$ (glutarate) and $n=4$ (adipate) which are fairly stable and have the smallest hydration number of 55; these salts are favorable for water molecules to form the hydrogen-bonded framework most efficiently by sharing common faces of adjacent polyhedra as much as possible. The fact that the hydrates of these salts, including their methyl and amino derivatives, have almost the same hydration number will suggest that these hydrates have essentially the same structures, although their melting points are considerably changed by the type of anions. In contrast to the case of the malonate and succinate hydrates mentioned above, the introduction of a methyl group onto the methylene chain of a glutaric or adipic acid anion causes a decrease in the melting point of its hydrate. As pointed out above, since the dicarboxylate anion having three or four methylene groups with no substituted groups seems to be the optimum anion for the formation of a stable hydrate, the presence of the substituted group will either make the hydrophobic group unfavorably large or disturb the best fit of the methylene chain by reducing the degree of positional freedom of occupation. The effect of the substituted amino group on the stability of hydrate is relatively slight, just as in the case of the succinate.

The series of salts having $n=5$ (metastable phase), 6, 7, and 8 form fairly unstable hydrates whose hydration numbers lie about 65. These are classified as group III hydrates. From the fact that their hydration number is large and almost constant, and that the anions of these salts have rather long methylene chains which must be too large to be accommodated within a typical water polyhedron, and further that the salt with $n=5$ forms two kinds of hydrates (stable and metastable phases), this group of hydrates will presumably have a different crystal structure from the other two groups. Although there is no evidence about the crystal structure, we may imagine the following structure.

The principal constituents of these hydrates may be the tetrabutylammonium cations, each butyl group of which is encaged by a hydrogen-bonded water framework; an anion which has a long methylene chain is accommodated within a fairly distorted void made between the two adjacent cation sheaths. These hydrates will owe a considerable part of their stability to the closeness of fit in the cages of butyl groups of the cation. The long methylene chain of the anion will considerably distort the water framework in which it is accommodated, and therefore it will make the hydrates unstable rather than stabilize them, owing to its hydrophobic nature. These concepts are consistent with the experimental results that the melting points of these hydrates decrease with increasing the length of the methylene chain and that the salt with $n=10$ is no longer able to form a stable hydrate. It is uncertain whether this estimated structure has some correlation with the structure of fairly stable clathrate-like hydrates[10,11] made by a series of salts having the general formula $[(n\text{-}C_4H_9)_3N\text{–}(CH_2)_m\text{–}N(n\text{-}C_4H_9)_3]F_2$ ($m=5$, 6, and 8).

Three isomers of the phthalate also form hydrates which have almost the same hydration number of 62, indicating that they are isostructural. Although the benzene ring of the anion is large enough to be accom-

modated within a hydrogen-bonded framework, the distortion caused by the restriction that the four oxygen atoms of the two carboxyl groups, which are fixed at the specific position of the benzene ring, must be placed at one of the hydrogen-bonded sites of the polyhedral vertices seems to be the dominant factor which determines the stability of the hydrates. Because of this distortion effect, the water framework around the benzene ring could not be constructed as efficiently as in the group II hydrates, giving a fairly large hydration number as compared with 55 of the group II hydrates. It is not certain whether these hydrates should be included in group I or be classified as another group.

This work was partially supported by a Grant-in-Aid for Scientific Research from the Ministry of Education.

References

1) R. McMullan and G. A. Jeffrey, *J. Chem. Phys.*, **31**, 1231 (1959).
2) D. L. Fowler, W. V. Loebenstein, D. B. Pall, and C. A. Kraus, *J. Am. Chem. Soc.*, **62**, 1140 (1940).
3) M. von Stackelberg, *Z. Elektrochem.*, **58**, 24 (1954).
4) D. Feil and G. A. Jeffrey, *J. Chem. Phys.*, **35**, 1863 (1961).
5) M. Bonamico, G. A. Jeffrey, and R. K. McMullan, *J. Chem. Phys.*, **37**, 2219 (1962).
6) R. K. McMullan, M. Bonamico, and G. A. Jeffrey, *J. Chem. Phys.*, **39**, 3295 (1963).
7) H. Nakayama and K. Watanabe, *Bull. Chem. Soc. Jpn.*, **49**, 1254 (1976).
8) G. Beurskens, G. A. Jeffrey, and R. K. McMullan, *J. Chem. Phys.*, **39**, 3311 (1963).
9) Unpublished data.
10) H. Nakayama and K. Watanabe, to be published.
11) T. L. Broadwater and D. F. Evans, *J. Phys. Chem.*, **73**, 164 (1969).

Optical and Magnetic Properties of Solid Anion Radical Salts Derived from Halogen-Substituted *p*-Benzoquinones

Yôichi IIDA

Department of Chemistry, Faculty of Science, Hokkaido University, Sapporo 060

(Received March 22, 1978)

Crystalline anion radical salts derived from halogen-substituted *p*-benzoquinones are known to show charge-transfer transition between anion radicals in the low-energy region and to possess antiferromagnetic spin exchange interaction between the anion radicals. Using Hubbard Hamiltonian, the optical and magnetic properties of Na^+ *p*-Chloranil$^-$ were explained in terms of a dimer model, while those of K^+ *p*-Chloranil$^-$ and K^+ *p*-Bromanil$^-$, in terms of an infinite non-alternant linear chain model.

The prominent magnetic, electrical and optical properties of a number of solid ion radical salts have been the subject of many theoretical and experimental investigations over the past fifteen years.[1-5] In such ion radical salts, the planar ion radical molecules are known to form, in themselves, a segregated stacking into columns so as to make a large overlap between their half-occupied molecular orbitals.[5-8] In one case, ion radical molecules stack predominantly in a pair-by-pair manner, so that the crystal system can be practically confined to a dimer of ion radicals. Another case is that ion radical molecules stack into infinite non-alternant one-dimensional column. In both cases, since any individual radical molecule interacts through charge-transfer most strongly with other neighboring radicals, the electronic spectrum of the solid salt differs distinctly from the monomer spectrum of the radical ion in solution but shows a charge-transfer transition between ion radicals in the low-energy region.[3-5] In the present paper, we apply half-filled Hubbard Hamiltonian to the dimer and the non-alternant one-dimensional system of ion radical molecules and investigate the optical and magnetic properties of certain crystalline anion radical salts derived from *p*-chloranil, *p*-bromanil and 2,5-dibromo-3,6-dichloro-*p*-benzoquinone (*p*-QBr_2Cl_2).

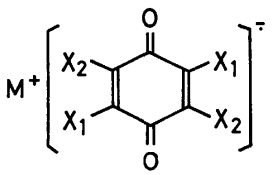

(a); $X_1 = X_2 = Cl$
(b): $X_1 = X_2 = Br$
(c): $X_1 = Br$, $X_2 = Cl$

Fig. 1. The anion radical salts derived from (a) *p*-chloranil, (b) *p*-bromanil, and (c) 2,5-dibromo-3,6-dichloro-*p*-benzoquinone (*p*-QBr_2Cl_2). M^+ represents an alkali metal cation such as sodium or potassium cation.

Na^+ *p*-Chloranil$^-$

Several years ago,[4] we measured the diffuse reflection spectrum of this solid salt, together with the absorption spectrum of the *p*-chloranil anion radical in acetone solution. The monomer spectrum of the *p*-chloranil anion radical consists of absorption bands at 22200 cm^{-1}, 26700, and 30300. These absorptions were assigned to the $^2B_{3g} \rightarrow {}^2B_{1u}$, $^2B_{3g} \rightarrow {}^2A_u$, and $^2B_{3g} \rightarrow {}^2B_{1u}$ transitions, respectively.[4] On the other hand, the solid-state spectrum of Na^+ *p*-Chloranil$^-$ salt shows a strong low-energy absorption at 11600 cm^{-1}, a high-energy band at 26500 and a shoulder beyond 30000. The high-energy band at 26500 cm^{-1} was assigned to the shifted band of the $^2B_{3g} \rightarrow {}^2B_{1u}$ transition at 22200 for the anion radical monomer, while the strong low-energy band at 11600 cm^{-1} characteristic of the solid salt, to the charge-transfer transition between *p*-chloranil anion radicals in the solid state.[4]

The magnetic property of solid Na^+ *p*-Chloranil$^-$ salt was examined by Sugano and Kuroda.[9] The temperature dependence of the observed static magnetic susceptibility could be well explained in terms of a dimer model of the *p*-chloranil anion radicals. The paramagnetism comes from triplet excited state lying $\delta = 1130$ cm^{-1} above the ground singlet state.

In order to understand the above experimental results in more detail, we consider the optical and magnetic properties of the dimer model of ion radicals in terms of Hubbard Hamiltonian, which is written by[10,11]

$$\mathscr{H} = \sum_{\sigma} T(C_{1\sigma}{}^{+}C_{2\sigma} + C_{2\sigma}{}^{+}C_{1\sigma}) + I(n_{1\uparrow}n_{1\downarrow} + n_{2\uparrow}n_{2\downarrow}), \qquad (1)$$

where $n_{i\sigma} = C_{i\sigma}{}^{+}C_{i\sigma}$, and $C_{i\sigma}{}^{+}$ and $C_{i\sigma}$, ($i=1$ or 2), are the creation and annihilation operators of an electron with σ-spin at the i-th site, respectively, and where T (<0) is the transfer matrix element between ion radicals in a dimer, and the repulsive potential, I, appears only when two electrons are at the same site. If we only take the half-occupied molecular orbital of ion radical for each site, there are six bases of the wave functions for the dimer. After solving the eigenvalue problem, we obtain, for the triplet state, $c = C_{1\uparrow}{}^{+}C_{2\uparrow}{}^{+}|0>$, $d = C_{1\downarrow}{}^{+}C_{2\downarrow}{}^{+}|0>$, and $a^+ = 2^{-1/2} \times \{C_{1\uparrow}{}^{+}C_{2\downarrow}{}^{+} + C_{1\downarrow}{}^{+}C_{2\uparrow}{}^{+}\}|0>$ with energy zero, while we obtain, for the singlet states, $(1+(E_{\pm}/2T)^2)^{-1/2} \times (a^- + (E_{\pm}/2T)b^+)$ with energy $E_{\pm} = I/2 \pm \{(I/2)^2 + (2T)^2\}^{1/2}$, and b^- with energy I. Here, $a^- = 2^{-1/2} \times \{C_{1\uparrow}{}^{+}C_{2\downarrow}{}^{+} - C_{1\downarrow}{}^{+}C_{2\uparrow}{}^{+}\}|0>$, $b^{\pm} = 2^{-1/2}\{C_{1\uparrow}{}^{+}C_{1\downarrow}{}^{+} \pm C_{2\uparrow}{}^{+}C_{2\downarrow}{}^{+}\}|0>$, and $|0>$ indicates the state of the dimer without any unpaired electron. The charge-transfer absorption of the dimer corresponds to the optical transition from the ground singlet state of $(1+(E_-/2T)^2)^{-1/2}(a^- + (E_-/2T)b^+)$ to the excited charge-transfer singlet state, b^-. Therefore, in the dimer model of ion radicals, the energy of the charge-

transfer absorption, $h\nu_{CT}$, and the singlet-triplet energy separation, δ, are given by[12]

$$h\nu_{CT} = \left\{\left(\frac{1}{2}I\right)^2 + (2T)^2\right\}^{1/2} + \frac{1}{2}I, \quad (2)$$

$$\delta = \left\{\left(\frac{1}{2}I\right)^2 + (2T)^2\right\}^{1/2} - \frac{1}{2}I. \quad (3)$$

This model was then applied to the above experimental results of the solid Na^+ p-Chloranil$^-$ anion radical salt. By putting the observed values of $h\nu_{CT}=11600\ cm^{-1}$ and $\delta=1130\ cm^{-1}$ into Eqs. 2 and 3, we obtain $I=h\nu_{CT}-\delta=10470\ cm^{-1}$ and $T=-1800\ cm^{-1}$, respectively. The $I=10470\ cm^{-1}$ value thus estimated for the Na^+ p-Chloranil$^-$ salt corresponds to the effective Coulomb repulsion energy in the solid salt. The repulsion energy is screened in the presence of neighboring sodium cations roughly by a factor of $(1-\alpha/r^3)$, where α is the polarizability of the cation and r is the effective distance between p-chloranil anion radical and neighboring cation.[13,14] In fact, in addition to the dimer formation in crystal, the p-chloranil anion radicals are known to dimerize even in ethanol solution,[15] where the screening appears to be less effective than in the solid state. The charge-transfer absorption of the dimer in ethanol solution is found at 14900 cm^{-1}, suggesting the I value much larger than the $I=10470$ cm^{-1} value of the dimer in the solid Na^+ p-Chloranil$^-$ salt.

Another interesting fact is that the charge-transfer band of solid Na^+ p-Chloranil$^-$ salt at 11600 cm^{-1} is much influenced by applying a pressure; the peak position exhibits a red-shift with 58 cm^{-1} per kbar.[15] As is shown in Eq. 2, if the applied pressure only causes an increase in the transfer matrix element, $|T|$, the charge-transfer band peak will show a blue-shift under high pressure. The main reason for the observed red-shift is then attributable to the decrease of the I value, because the factor $(1-\alpha/r^3)$ will be decreased with the decrease of the distance between p-chloranil anion radical and neighboring sodium cation by applying pressure.

K^+ p-Chloranil$^-$ and K^+ p-Bromanil$^-$

The crystal structure analysis of K^+ p-Chloranil$^-$ salt was made by Konno *et al.*[8] Although there are several polymorphs, in the structure of the orthorhombic α-form the p-chloranil anion radicals are stacked with equal intervals, forming non-alternant one-dimensional columns parallel to the c-axis, the interplanar spacing being 3.47 Å. The K^+ ion lies at the center of a rectangle formed by four oxygen atoms of the p-chloranil anion radicals related by c translation.

Earlier, we measured the solid-state spectrum of K^+ p-Chloranil$^-$ salt,[4] which shows a weak low-energy band at 11800 cm^{-1}, a strong high-energy band at 23300 and a shoulder around 30000. The latter two high-energy absorptions were assigned to the $^2B_{3g}\rightarrow{}^2B_{1u}$ transitions at 22200 cm^{-1} and at 30300, respectively, of the monomer spectrum, while the low-energy band at 11800 cm^{-1}, to the charge-transfer transition between the anion radicals along the one-dimensional column in the solid state. It was further noted that the spectroscopic features of the solid K^+ p-Chloranil$^-$ salt was rather similar to the monomer spectrum of the p-chloranil anion radical. On the other hand, although there is a phase transition around 210—260 K,[16] the temperature dependence of the observed magnetic susceptibility of the K^+ p-Chloranil$^-$ salt in the region above the transition temperature was well explained in terms of an antiferromagnetic linear Ising model with exchange interaction of 113 cm^{-1}.[9]

In previous papers,[17-20] we examined the optical and magnetic properties for a system of non-alternant one-dimensional stacks of ion radicals in terms of Hubbard Hamiltonian, which can be written by

$$\mathscr{H} = \sum_{i,j,\sigma} T_{ij}C_{i\sigma}^{+}C_{j\sigma} + I\sum_{i} n_{i\uparrow}n_{i\downarrow}, \quad (4)$$

where $T_{ij}(<0)$ is the transfer matrix element between the i-th and j-th sites. For non-alternant one-dimensional column of ion radicals, we consider the half-occupied molecular orbital of the unpaired electron as one site of ion radical molecule, and only take into account the transfer matrix element between the nearest neighbor sites. Hereafter, it is simply denoted by $T(<0)$. We consider a paramagnetic state for our system, and further assume a δ-function for each elementary transition in which the spin and the wave vector of an electron are conserved. The intermolecular charge-transfer absorption, $\sigma(\omega)$, is given by[17]

$$\sigma(\omega) \propto \frac{e^2}{4}\frac{I^2}{\omega^2\sqrt{\omega^2-I^2}}\sqrt{4T^2-\omega^2+I^2}. \quad (5)$$

A schematic representation of the absorption line shape has been given in Fig. 1 of Ref. 17. The theoretical charge-transfer absorption has a sharp divergent peak at $\omega=I$, and has a band width of $\sqrt{I^2+4T^2}-I$ in the region $\omega>I$. On the other hand, we examine the magnetic properties of the same system. In a region of small $|T|$ limit, the Hubbard model leads to a non-alternant one-dimensional antiferromagnet with an exchange interaction $J\approx 2T^2/I$ for our case.[14] Therefore, if we combine the experimental data on the peak energy of the observed charge-transfer absorption and the exchange interaction parameter derived from the magnetic susceptibility measurement, we can uniquely determine the magnitudes of I and T for our system.

We apply this approach to the system of non-alternant one-dimensional column of the K^+ p-Chloranil$^-$ salt. The observed peak energy of the charge-transfer absorption, 11800 cm^{-1}, thus corresponds to $I=11800\ cm^{-1}$. As for the antiferromagnetic exchange interaction, rigorously speaking, the J value of Heisenberg model should correspond to $2T^2/I$, but only the J value estimated with Ising model is available at the present time. Therefore, we approximately use the estimated $J=113\ cm^{-1}$ value as $J\approx 2T^2/I$. By putting the $I=11800\ cm^{-1}$ value into this relation, we obtain $T=-820\ cm^{-1}$ for the one-dimensional system of the potassium salt. The $|T|$ value thus estimated is found to be much smaller than the $|T|=1800\ cm^{-1}$ value of the Na^+ p-Chloranil$^-$ salt, indicating weak intermolecular interaction between the p-chloranil anion radicals in the potassium salt. This is sup-

ported by the fact that the intermolecular distance between the anion radicals in the potassium salt is as large as 3.47 Å and also by the spectroscopic features that the high-energy bands at 23300 cm^{-1} and 30000 of the potassium salt show no appreciable shifts in comparison with those of the monomer spectrum of the *p*-chloranil anion radical.

Next, we examine the case of solid K^+ *p*-Bromanil$^-$ salt, whose situation is found to be very similar to that of K^+ *p*-Chloranil$^-$. The solid-state spectrum of the K^+ *p*-Bromanil$^-$ salt shows a very weak charge-transfer band at 10900 cm^{-1}, a weak shoulder at 17500 and a strong high-energy band at 23000.[4] For this salt, the observed magnetic susceptibility data were analyzed with linear Ising model, and the antiferromagnetic spin exchange parameter, J, was estimated to be 97 cm^{-1}.[9] Therefore, in a way similar to that of K^+ *p*-Chloranil$^-$, the values of $I=10900$ cm^{-1} and $T=-730$ cm^{-1} were estimated for the one-dimensional system of the K^+ *p*-Bromanil$^-$ salt. Again, the $|T|$ value is found to be as small as that of the K^+ *p*-Chloranil$^-$ salt. Although there is no crystal structure data for purposes of reference, the intermolecular interaction between the *p*-bromanil anion radicals is certainly weak in the K^+ *p*-Bromanil$^-$ salt.

Na^+ *p*-$QBr_2Cl_2^-$ and K^+ *p*-$QBr_2Cl_2^-$

The solid-state spectrum of Na^+ *p*-$QBr_2Cl_2^-$ salt is quite different from the monomer spectrum of the *p*-QBr_2Cl_2 anion radical but shows a strong low-energy charge-transfer absorption at 12200 cm^{-1} and a high-energy band at 26300.[4] The latter band was assigned to the shifted band of the monomer absorption at 22100 cm^{-1}. Earlier, we measured the temperature dependence of the magnetic susceptibility of the Na^+ *p*-$QBr_2Cl_2^-$ salt.[21] Although no rigorous agreement between the observed and theoretical temperature dependences was obtained either by the singlet-triplet model or by the linear Ising model, the singlet-triplet energy separation, $\delta=970$ cm^{-1}, was estimated by the dimer model, while the antiferromagnetic exchange parameter, $J=810$ cm^{-1}, was estimated by the linear Ising model.[21] Although no crystal structure data are available at the present time, we may explain the electronic state of this solid salt in terms of either the dimer model or the non-alternant one-dimensional system of the anion radicals. In the case of the dimer model, we again took an approach similar to that of Na^+ *p*-Chloranil$^-$, and the values of $I=11200$ cm^{-1} and $T=-1730$ cm^{-1} were thus estimated for the Na^+ *p*-$QBr_2Cl_2^-$ salt. If the non-alternant one-dimensional model was applied, the values of I and T were found to be 12200 cm^{-1} and -2200 cm^{-1}, respectively.

On the other hand, the solid-state spectrum of K^+ *p*-$QBr_2Cl_2^-$ salt is rather similar to the monomer spectrum of the *p*-QBr_2Cl_2 anion radical and has a very weak charge-transfer absorption at 11500 cm^{-1}.[4] As for the magnetic properties, although no rigorous agreement between the observed and theoretical magnetic susceptibilities was again obtained, the singlet-triplet energy separation, $\delta=153$ cm^{-1}, was estimated by the dimer model, while $J=97$ cm^{-1} was estimated by the linear Ising model.[21] These optical and magnetic data lead to $I=11300$ cm^{-1} and $T=-710$ cm^{-1} for the dimer model or to $I=11500$ cm^{-1} and $T=-750$ cm^{-1} for the non-alternant one-dimensional model.

In either of the models, the magnitude of the transfer matrix element of the K^+ *p*-$QBr_2Cl_2^-$ salt was found to be much smaller than that of the Na^+ *p*-$QBr_2Cl_2^-$ salt. This means that the *p*-QBr_2Cl_2 anion radicals in the sodium salt stack, in themselves, very closely, while the intermolecular interaction between the anion radicals is very weak in the potassium salt. Detailed crystal structure analyses of the Na^+ *p*-$QBr_2Cl_2^-$ and K^+ *p*-$QBr_2Cl_2^-$ salts are now required to confirm the above situation and also to determine by which model (dimer model or non-alternant one-dimensional model) the *p*-QBr_2Cl_2 anion radicals are stacked in those solid salts.

References

1) L. R. Melby, R. J. Harder, W. R. Hertler, W. Mahler, R. E. Benson, and W. E. Mochel, *J. Am. Chem. Soc.*, **84**, 3374 (1962).

2) W. J. Siemons, P. E. Bierstedt, and R. G. Kepler, *J. Chem. Phys.*, **39**, 3523 (1963); R. G. Kepler, *ibid.*, **39**, 3528 (1963).

3) Y. Iida, *Bull. Chem. Soc. Jpn.*, **42**, 71, 637 (1969); **44**, 663, 1777 (1971); **45**, 105, 624 (1972).

4) Y. Iida, *Bull. Chem. Soc. Jpn.*, **43**, 2772 (1970).

5) J. Tanaka, M. Tanaka, T. Kawai, T. Takabe, and O. Maki, *Bull. Chem. Soc. Jpn.*, **49**, 2358 (1976), and the references cited therein.

6) G. R. Anderson and C. J. Fritchie, Jr., Second National Meeting, Society for Applied Spectroscopy, San Diego, Paper 111 (1963).

7) H. Kobayashi, Y. Ohashi, F. Marumo, and Y. Saito, *Acta Crystallogr., Sect B*, **26**, 459 (1970), and the references cited therein.

8) M. Konno, H. Kobayashi, F. Marumo, and Y. Saito, *Bull. Chem. Soc. Jpn.*, **46**, 1987 (1973).

9) T. Sugano and H. Kuroda, Paper presented at The Symposium on Molecular Structure, Osaka, Japan (1975), p. 321.

10) J. Hubbard, *Proc. R. Soc. London, Ser. A*, **276**, 238 (1963).

11) Y. Suezaki, *Phys. Lett.*, **38A**, 293 (1972).

12) As for the intensity of the charge-transfer absorption of the dimer, the transition dipole moment, μ_{EN}, is expressed by $(1+(E_-/2T)^2)^{-1/2}(\mu_0+(E_-/2T)\mu_1)$, where $\mu_0=-e\times\int b^-\sum_i \boldsymbol{r}_i a^- d\tau$ and $\mu_1=-e\int b^-\sum_i \boldsymbol{r}_i b^+ d\tau$. The μ_0 term will be proportional to the overlap integral between the half-occupied molecular orbitals of the dimer. In the weak interaction limit of $2|T|\ll I$, we have $E_-/2T\approx 2|T|/I$. In this case, the quantity involving the overlap integral will usually be rather small, and μ_{EN} may be approximated by $2|T|\mu_1/I$. The theoretical oscillator strength of the charge-transfer absorption, f, is proportional to $h\nu_{CT}\mu_{EN}^2\approx 4T^2\mu_1^2/I$, where we used the approximation $h\nu_{CT}\approx I$ in the limit of $2|T|\ll I$. Under the same condition, the singlet-triplet energy separation, δ, can be approximated by $\{(I/2)^2+(2T)^2\}^{1/2}-I/2\approx 4T^2/I$, so that we see that f is also proportional to δ.

13) O. H. LeBlanc, *J. Chem. Phys.*, **42**, 4307 (1965).
14) A. J. Epstein, S. Etemad, A. F. Garito, and A. J. Heeger, *Phys. Rev. B*, **5**, 952 (1972).
15) N. Sakai, I. Shirotani, and S. Minomura, *Bull. Chem. Soc. Jpn.*, **44**, 675 (1971).
16) J. J. Andre, J. Clementz, R. Jesser, and G. Weill, *C. R. Acad. Sc. Paris, Ser. B*, **266**, 1057 (1968).
17) Y. Iida, *Bull. Chem. Soc. Jpn.*, **50**, 1445 (1977).
18) Y. Iida, *Bull. Chem. Soc. Jpn.*, **50**, 2481 (1977).
19) Y. Iida, *Bull. Chem. Soc. Jpn.*, **51**, 434 (1978).
20) Y. Iida, *Bull. Chem. Soc. Jpn.*, **51**, 631 (1978).
21) T. Mizoguchi, Y. Iida, M. Kinoshita, and H. Akamatu, Paper presented at The 23rd National Meeting of the Chemical Society of Japan, Tokyo, Japan, Vol. I, p. 288 (1970).

^{1}H and ^{19}F NMR Study of *p*-Chlorobenzylidyne Trifluoride Partially Oriented in a Nematic Phase

Yuuji SUGINO and Kensuke TAKAHASHI*

Department of Industrial Chemistry, Nagoya Institute of Technology, Gokiso-cho, Showa-ku, Nagoya 466

(Received March 23, 1978)

The ^{1}H and ^{19}F NMR spectra of *p*-chlorobenzylidyne trifluoride dissolved in a nematic phase of EBBA have been analyzed, and the structure of the proton and fluorine skeleton has been determined. No presice information about the anisotropy of the indirect F-F coupling can be given.

Since Saupe and Englert first observed the NMR spectra in liquid crystals, many studies have been reported in this area.[1-4] The method has also been applied to the molecules with internal rotation.[5-10] There are few studies, however, about the molecules containing ^{19}F nuclei with internal rotation.[11] We have analyzed the ^{1}H and ^{19}F NMR spectra of *p*-chlorobenzylidyne trifluoride in a nematic phase of EBBA (*N*-(*p*-ethoxybenzylidene)-*p*-butylaniline), and obtained the relative internuclear distances and the orientation parameters of this molecule in EBBA.

Experimental

The sample studied consisted of a 14 mol% solution of commercially available *p*-chlorobenzylidyne trifluoride in EBBA. It was contained in a 5-mm NMR sample tube and degassed by repeated freeze-pump-thaw cycles and then sealed *in vacuo*. The ^{1}H NMR spectra were observed with a Hitachi R-20B spectrometer operated at 60 MHz in the field sweep mode without locking. The ^{19}F NMR spectra were observed with the same spectrometer equipped with a R-203F-B attachment at 56.45 MHz in the frequency sweep mode with an external lock. The ^{1}H and ^{19}F spectra extended over about 9.7 and 11.5 kHz, respectively, and contained 40 and 25 resolved lines; all resolvable lines were used for the determination of the spectral parameters. In both cases the spectra were obtained at 31.0±0.5 °C and accumulated on a Hitachi Al600-A signal averaging analyzer; the line width of each signal was about 20 Hz. The resonance position of the signal was determined on each recording chart by interpolation: the sweep width was calibrated by either the frequency counter or the side-band method; the error was about 5 Hz. The calculation of spectral and structural analyses was made by a HITAC-8450 computer system located in this Institute or a FACOM-230-75 system located in the Computer Center of Nagoya University.

Results and Discussion

Analyses of the Spectra. The ^{1}H and ^{19}F spectra of the sample are center-symmetric and divided into two and three parts, respectively. The observed upfield ^{1}H and ^{19}F spectra consisted of 20 and 10 resolved lines, and are shown in Figs. 1-a and 1-b. The central part of the observed ^{19}F spectrum consisted of 5 strong lines. Analyses of the spectra were followed by a program LAOCN3+D, which includes the direct coupling constants as the spectral parameters. This was slightly modified from the original LAOCN3,[12] described by Diehl *et al.*[13] The indirect coupling constants were kept constant in the iteration calculation and the values were estimated by means of an additivity.[14,15] The spectral parameters thus obtained are shown in Table 1. The numberings of the nuclei are shown in Fig. 2.

TABLE 1. SPECTRAL PARAMETERS FOR *p*-CHLOROBENZYLIDYNE TRIFLUORIDE IN Hz[a]

Direct coupling[b]		Indirect coupling[c]	
D_{23}	−2282.74±0.16	J_{23}	8.40
D_{25}	28.29±0.17	J_{25}	0.38
D_{26}	204.60±0.70	J_{26}	2.31
D_{35}	203.97±0.69	J_{35}	2.19
D_{27}	−494.63±0.34	J_{27}	−0.74
D_{37}	−169.00±0.34	J_{37}	0.82
D_{78}	1480.46±0.14		

a) The numberings of the nuclei are given in Fig. 2. b) The errors shown in the Table are the probable program output errors. The differences between the D_{26} and D_{35} and between W(2) and W(3) are small and within the experimental error; they are not important. c) The parameters are taken from Refs. 14 and 15.

Analyses of the Molecular Structure. The parameters obtained in Table 1 were used to obtain the geometrical information about the sample. The following assumptions were made: 1. The trifluoromethyl group rotates freely around the C_1–C_7 bond; 2. The benzene ring forms a hexagonal plane and the C–C and C–H bond lengths can be taken as 1.397 and 1.084 Å;[16] 3. The molecular vibrations need not be taken into consideration; 4. Anisotropies of the proton-fluorine and proton-proton indirect couplings are negligible. Relations between the ratios of the inter-proton distances and the direct couplings are given by the following equations:

$$r_{35}/r_{26} = (D_{26}/D_{35})^{1/3}, \tag{1}$$

$$D_{23}(r_{23}/r_{26}) - D_{25}\{(D_{26}/D_{35})^{1/3} + (r_{23}/r_{26})^2\}^{5/2} = -D_{26}(D_{26}/D_{35})^{1/3}, \tag{2}$$

$$(r_{25}/r_{26})^2 = (D_{26}/D_{35})^{1/3} + (r_{23}/r_{26})^2. \tag{3}$$

The orientation parameters S_{xx} and S_{zz} are related to the D's and r's by[3]

$$S_{xx} = -(4\pi^2/h\gamma_H^2)D_{26}r_{26}^3, \tag{4}$$

$$S_{zz} = -(4\pi^2/h\gamma_H^2)r_{23}^3[D_{23} - (D_{26}/4)(r_{23}/r_{26})^{-5} \times \{(D_{26}/D_{35})^{1/3} - 1\}^2]/[1 - (1/4)(r_{23}/r_{26})^{-2} \times \{(D_{26}/D_{35})^{1/3} - 1\}^2]. \tag{5}$$

By means of these equations, the inter-proton distances

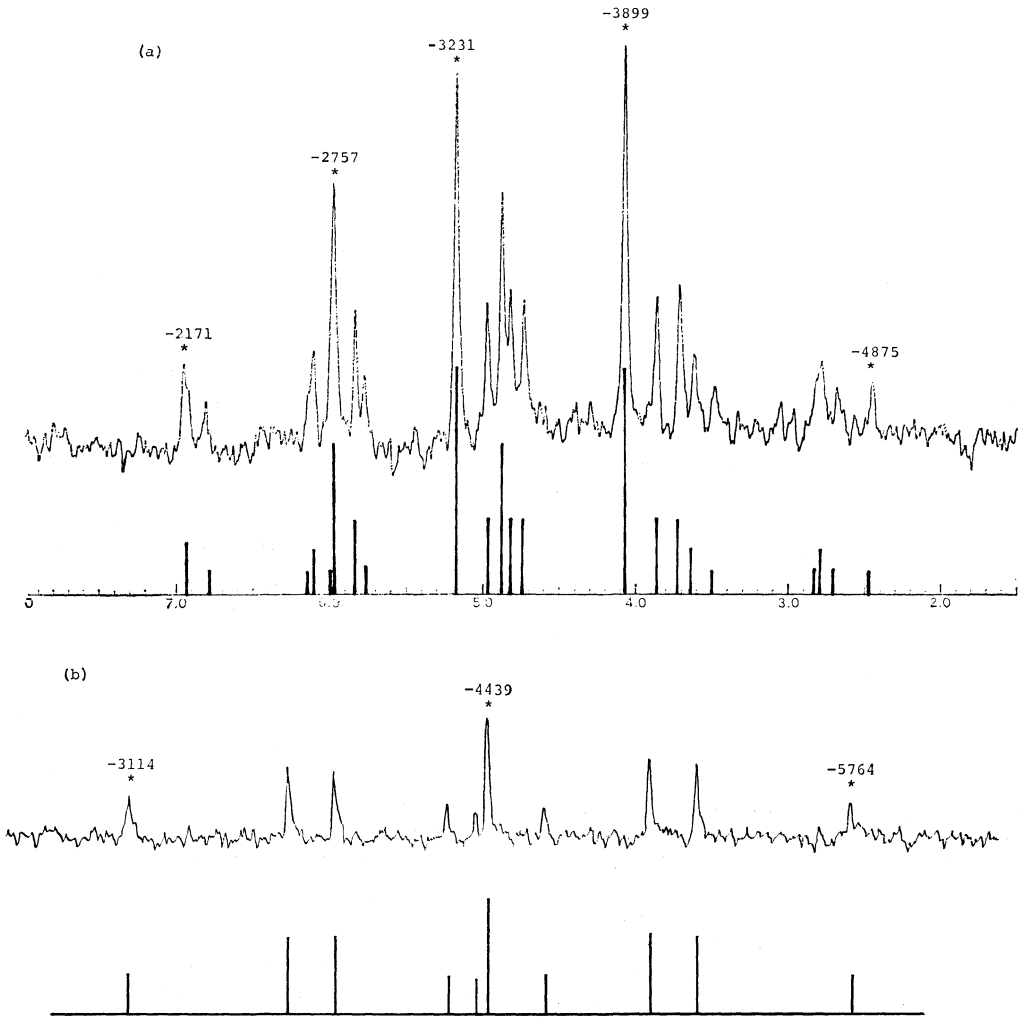

Fig. 1. Observed ^1H and ^{19}F NMR spectra of *p*-chlorobenzylidyne trifluoride dissolved in EBBA. Several peak positions are given in Hz with asterisk. Calculated stick spectra are also given under the observed one; (a) An upfield ^1H spectrum, accumulated 36 scans, (b) an upfield ^{19}F spectrum, accumulated 25 scans.

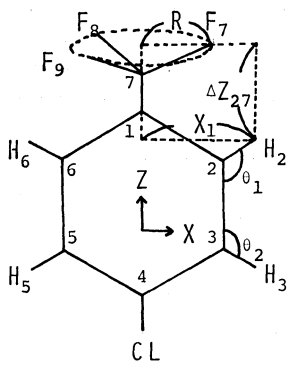

Fig. 2. Numbering system for *p*-chlorobenzylidyne trifluoride.

and the orientation parameters are determined as given in Table 2. The distances between the rotating trifluoromethyl fluorines and the protons are determined by the method used in Ref. 7. These values are also given in Table 2. The inter-proton distances obtained for the sample are similar to those obtained for benzene[16] (r_{23}=2.481, and r_{26}=4.297 Å)and a little different from those obtained for chlorobenzen[17] (r_{23}=2.509—2.465, r_{26}=4.297, and r_{35}=4.350—4.230) and benzylidyne trifluoride[11] (r_{23}=2.482, r_{26}=4.324, and r_{35}=4.298). The interfluorine distance obtained is smaller than that of benzylidyne trifluoride (r_{78}=2.165 Å).[11] Thus the radius of the circle formed by three fluorine nuclei is 1.228 Å, which is smaller than that of benzylidyne trifluoride (1.250 Å).[11]

TABLE 2. STRUCTURAL AND ORIENTATION PARAMETERS DERIVED FROM THE ^1H AND ^{19}F SPECTRA

r_{23}	2.481 ±0.003 Å
r_{26}	4.295 ±0.005 Å
r_{35}	4.300 ±0.005 Å
θ_1	120°06′±17′
θ_2	119°52′±17′
r_{78}	2.126 ±0.024 Å
R	1.228 ±0.014 Å
ΔZ_{27}	2.168 ±0.011 Å
S_{xx}	−0.1350 ±0.0004
S_{zz}	0.2902 ±0.0009

The Anisotropy of the Indirect Coupling. The D_{78} (or D_{FF}) coupling constant may contain a contribution from the anisotropy of the indirect coupling between the geminal fluorine nuclei. In the case of a trifluoromethyl group having a C_3 symmetry axis, the following relation has been reported:[3]

$$D_{78}^{exp} = D_{78}^{dir} + D_{78}^{ind}, \quad (6)$$

$$D_{78}^{ind} = S_{zz}\Delta J_{78}/3, \quad (7)$$

where

$$\Delta J_{78} = |J_{zz} - (J_{xx} + J_{yy})/2|_{78}.$$

J_{zz}, J_{xx}, and J_{yy} are the diagonal elements of the J-tensor. Due to the low accuracy of the determined r_{FF} distance in Table 2, the ΔJ_{FF} value can not be obtained uniquely. The anisotropy of J_{FF} is given as a function of r_{FF} in Table 3. The ΔJ_{FF} value shown in Table 3 is negative and this agrees with other reported values for CF_2 and CF_3 groups.[11,18,19]

Table 3. The anisotropy ΔJ_{FF} of the F-F indirect coupling as a function of the internuclear distance r_{FF}

r_{FF}, Å	D_{FF}^{dir}, Hz	D_{FF}^{ind}, Hz	ΔJ_{FF}, Hz
2.102	1660.2±5.2	−179.7±5.3	−1858±61
2.114	1632.1±5.1	−151.6±5.2	−1567±59
2.126	1604.6±5.0	−124.1±5.1	−1283±57
2.138	1577.7±4.9	−97.3±5.0	−1006±55
2.150	1551.5±4.8	−71.0±5.0	−734±53
2.167	1515.2±4.7	−34.8±4.8	−360±51

References

1) A. Saupe and G. Englert, *Phys. Rev. Lett.*, **11**, 462 (1963).
2) G. Englert and A. Saupe, *Z. Naturforsch.*, **19a**, 172 (1964).
3) P. Diehl and C. L. Khetrapal, "NMR Basic Principles and Progress," Vol. 1, Springer-Verlag, Berlin (1969).
4) L. Lunazzi, "Determination of Organic Structure by Physical Methods," Vol. 6, Academic Press, New York (1976).
5) G. Englert and A. Saupe, *Mol. Cryst.*, **1**, 503 (1966).
6) G. Englert, A. Saupe, and J. P. Weber, *Z. Naturforsch., Teil A*, **23**, 152 (1968).
7) P. Diehl, C. L. Khetrapal, W. Niederberger, and P. Partington, *J. Magn. Reson.*, **2**, 181 (1970).
8) P. Diehl, H. P. Kellerhals, and W. Niederberger, *J. Magn. Reson.*, **3**, 230 (1970).
9) P. Diehl, H. P. Kellerhals, and W. Niederberger, *J. Magn. Reson.*, **4**, 352 (1971).
10) P. Diehl, P. M. Henricks, and W. Niederberger, *Mol. Phys.*, **20**, 139 (1971).
11) J. Degelaen, P. Diehl, and W. Niederberger, *Org. Magn. Reson.*, **4**, 721 (1972).
12) A. A. Bothner-By and S. M. Castellano, "Computer Programs for Chemistry," Vol. 1, W. A. Benjamin, Inc., New York (1968).
13) P. Diehl, C. L. Khetrapal, and H. P. Kellerhals, *Mol. Phys.*, **15**, 333 (1968).
14) K. Hayamizu and O. Yamamoto, *J. Mol. Spectrosc.*, **25**, 422 (1968).
15) J. Kostelnik, M. P. Williamson, D. E. Wisnosky, and S. M. Castellano, *Can. J. Chem.*, **47**, 3313 (1969).
16) A. Langseth and B. P. Stoicheff, *Can. J. Phys.*, **34**, 350 (1956).
17) C. Canet, E. Haloui, and H. Nery, *J. Magn. Reson.*, **10**, 121 (1973).
18) A. D. Buckingham, E. E. Burnell, and C. E. deLange, *Mol. Phys.*, **15**, 285 (1968).
19) J. Gerritsen and C. MacLean, *J. Magn. Reson.*, **5**, 44 (1971).

The Crystal and Molecular Structures of (*SR*/*RS*)- and (*SS*/*RR*)-Dimethyl 2-(*p*-Tolylsulfinyl)-1,1-cyclopropanedicarboxylate

Fujiko Iwasaki,* Shuichi Mitamura,† and Gen-ichi Tsuchihashi†

Department of Materials Science, The University of Electro-Communications, Chofu-shi, Tokyo 182

† *Sagami Chemical Research Center, Nishi-Ohnuma, Sagamihara, Kanagawa 229*

(Received March 23, 1978)

The crystal structures of two diastereomers of dimethyl 2-(*p*-tolylsulfinyl)-1,1-cyclopropanedicarboxylate have been determined by the X-ray diffraction method. The configurations of these isomers have been elucidated to be (*SR*/*RS*) (**A**) and (*SS*/*RR*) (**B**). Crystals of **A** are monoclinic; the space group $P2_1/c$; $a=9.557$ (2), $b=18.400$ (5), $c=8.277$ (2) Å, $\beta=98.52$ (2)°, and $Z=4$. Those of **B** are triclinic; the space group $P\bar{1}$; $a=6.442$ (3), $b=18.243$ (8), $c=6.554$ (2) Å, $\alpha=90.59$ (4), $\beta=99.03$ (5), $\gamma=103.12$ (4)°, and $Z=2$. The structures were solved by the heavy-atom method and refined by the full-matrix least-squares method. The final R values were 0.063 for **A** and 0.050 for **B** respectively. Based on the established configurations and conformations of these isomers, a mechanism which involves the preferential formation of one of two diastereomers by the Michael addition of dimethyl malonate to 1-bromovinyl *p*-tolyl sulfoxide under specified reaction conditions is proposed.

The Michael addition of dimethyl malonate to 1-bromovinyl *p*-tolyl sulfoxide (**1**), with the concominant dehydrobromination, resulted in the formation of two diastereomers (isomer **A** and isomer **B**) of dimethyl 2-(*p*-tolylsulfinyl)-1,1-cyclopropanedicarboxylate (**2**). When the reaction was carried out in methanol in the presence of sodium methoxide, isomer **A** (mp 107—109 °C) was preferentially formed. On the other hand, the reaction in tetrahydrofuran (THF) in the presence of sodium hydride resulted in the exclusive formation of isomer **B** (mp 69—71 °C). Since the oxidation of these isomers gave the same sulfone, they should be diastereomers related to the chiral center of the sulfur atom.[1] An X-ray diffraction study was undertaken to establish the molecular conformations and configurations of these isomers in order to elucidate such a specific reaction mechanism.

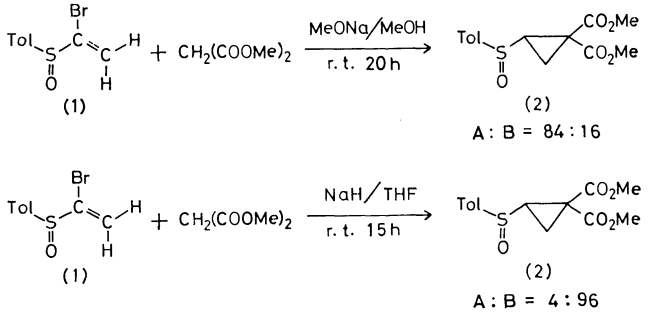

Scheme 1.

Experimental

Each of the isomers, **A** and **B**, was recrystallized from a hexane-ethanol solution. The crystals of **A** are colorless needles elongated along the b axis. The crystals of **B** are colorless flat plates with developed form {010}. They are both stable in air. The crystal data of both isomers are listed in Table 1.

Intensity data for both isomers were collected on a Rigaku automatic diffractometer, with Cu $K\alpha$ radiation monochromatized by a graphite monochromator. Reflections in the range $2\theta \leq 120°$ were measured by scanning in the ω-2θ mode with a scanning width of $\Delta\omega = 1.0° + 0.5° \tan\theta$ and a scanning speed of $4° \text{ min}^{-1}$ in 2θ. Background was counted for 10 s at both ends of the scan range for each reflection. For **A**, 1458 reflections had $|F_o| > 3\sigma(F_o)$ and were considered as observed. For **B**, 1893 reflections were obtained with $|F_o| > 3\sigma(F_o)$. No absorption corrections were applied.

Table 1. Crystal data

$C_{14}H_{16}O_5S$	$M.W.=296.34$	
	Isomer **A**	Isomer **B**
Crystal system	Monoclinic	Triclinic
Space group	$P2_1/c$	$P\bar{1}$
a	9.557 (2) Å	6.442 (3) Å
b	18.400 (5)	18.243 (8)
c	8.277 (2)	6.554 (2)
α	90.00°	90.59 (4)°
β	98.52 (2)	99.03 (5)
γ	90.00	103.12 (4)
U	1439.5 (7) Å^3	739.9 (5) Å^3
Z	4	2
D_x	1.367 g cm^{-3}	1.330 g cm^{-3}
D_m	1.37	1.33
$F(000)$	624	312
μ(Cu $K\alpha$)	20.3 cm^{-1}	19.8 cm^{-1}

Structure Determination

For each isomer, a sharpened three-dimensional Patterson synthesis was calculated from which the coordinates of the sulfur atom could be determined. A sulfur-phased Fourier synthesis then made it possible to locate all the carbon and oxygen atoms. The structure was refined using the block-diagonal least-squares method. When the R values were 0.085 and 0.080 for isomer **A** and isomer **B** respectively, difference syntheses were calculated which revealed the positions of all the hydrogen atoms. All the atoms were refined with three cycles of the block-diagonal least-squares method and one cycle of the full-matrix least-squares method, using anisotropic temperature factors for non-hydrogen atoms and isotropic ones for hydrogen atoms. The anomalous dispersion effect on the sulfur atoms was taken into consideration. The quantity minimized was $\Sigma w(|F_o| - k^{-1}|F_c|)^2$, where $w = 1/\sigma^2(F_o)$, as derived from the counting statistics. The final R values are 0.063 for **A** and 0.050 for **B**. The

Table 2. Atomic parameters with their estimated standard deviations of **A**

(a) Atomic coordinates and thermal parameters of non-hydrogen atoms. ($u_{ij} = 10^3 U_{ij}/\text{Å}^2$)
The anisotropic temperature factors are of the form:
$\exp\{-2\pi^2(U_{11}h^2a^{*2} + U_{22}k^2b^{*2} + U_{33}l^2c^{*2} + 2U_{12}hka^*b^* + 2U_{13}hla^*c^* + 2U_{23}klb^*c^*)\}$.
The B_{eq} values are the equivalent isotropic temperature factors.

	10^4x	10^4y	10^4z	u_{11}	u_{22}	u_{33}	u_{12}	u_{13}	u_{23}	$B_{eq}/\text{Å}^2$
S	8843(2)	1635(1)	201(2)	37(1)	41(1)	43(1)	−1(1)	18(1)	10(1)	3.1
O(1)	9211(5)	1157(3)	−1139(5)	66(3)	89(4)	42(3)	13(3)	28(2)	3(3)	5.0
O(2)	4095(5)	1367(3)	859(6)	50(3)	123(5)	60(3)	6(3)	31(3)	20(3)	5.9
O(3)	3857(4)	2040(3)	−1412(5)	40(3)	64(3)	60(3)	17(2)	18(2)	5(2)	4.2
O(4)	6673(6)	2114(3)	−2855(6)	86(4)	66(3)	62(3)	−20(3)	19(3)	23(3)	5.6
O(5)	5612(5)	1058(3)	−3597(5)	59(3)	68(3)	35(2)	0(2)	15(2)	−4(2)	4.2
C(1)	5912(6)	1342(3)	−832(7)	34(3)	41(3)	39(3)	0(3)	13(3)	7(3)	2.9
C(2)	7103(6)	1355(3)	554(7)	36(3)	40(3)	41(4)	1(3)	16(3)	2(3)	3.0
C(3)	6536(7)	653(3)	−59(9)	58(4)	37(4)	51(4)	−3(3)	12(3)	6(3)	3.8
C(4)	9736(6)	1284(3)	2069(7)	35(3)	37(3)	45(4)	−5(3)	16(3)	−1(3)	3.0
C(5)	9494(7)	1580(4)	3561(8)	45(4)	37(4)	54(4)	−3(3)	14(3)	−8(3)	3.5
C(6)	10193(6)	1307(4)	4998(8)	44(4)	53(4)	42(4)	−4(3)	12(3)	−7(3)	3.6
C(7)	11199(6)	761(3)	5021(7)	44(4)	43(4)	45(4)	−8(3)	15(3)	3(3)	3.4
C(8)	11437(7)	480(4)	3520(9)	50(4)	54(4)	61(5)	16(3)	13(4)	2(4)	4.3
C(9)	10736(7)	737(4)	2065(9)	45(4)	59(4)	49(4)	12(3)	19(3)	−2(4)	4.0
C(10)	11953(10)	473(5)	6593(11)	74(6)	61(6)	54(5)	0(5)	8(4)	11(4)	5.0
C(11)	4518(6)	1571(4)	−349(8)	39(4)	57(4)	49(4)	−10(3)	13(3)	−4(4)	3.7
C(12)	2537(9)	2338(6)	−1022(14)	44(5)	101(8)	88(8)	28(5)	17(5)	−2(7)	6.1
C(13)	6127(6)	1560(4)	−2531(7)	35(3)	56(4)	38(3)	6(3)	14(3)	6(3)	3.3
C(14)	5678(11)	1242(7)	−5307(10)	83(7)	125(9)	36(4)	14(6)	13(4)	−5(5)	6.4

(b) Atomic coordinates and thermal parameters of hydrogen atoms of **A**.

	10^3x	10^3y	10^3z	$B/\text{Å}^2$		10^3x	10^3y	10^3z	$B/\text{Å}^2$
H(2)	702(6)	157(3)	164(8)	4.7(15)	H(102)	1201(7)	0(4)	657(8)	5.2(19)
H(31)	599(7)	35(4)	63(8)	5.7(17)	H(103)	1302(8)	59(4)	671(8)	5.5(17)
H(32)	714(7)	35(4)	−73(8)	5.5(17)	H(121)	225(8)	268(4)	−183(9)	6.1(21)
H(5)	879(6)	200(3)	355(7)	4.3(14)	H(122)	191(8)	195(4)	−81(9)	6.8(23)
H(6)	1006(7)	151(4)	613(8)	5.9(17)	H(123)	276(7)	260(4)	1(9)	5.6(20)
H(8)	1217(6)	7(3)	350(7)	4.7(15)	H(141)	677(8)	128(4)	−536(8)	6.3(19)
H(9)	1083(7)	53(4)	92(8)	5.6(17)	H(142)	546(7)	82(4)	−579(9)	5.0(20)
H(101)	1171(8)	66(4)	752(9)	6.6(22)	H(143)	465(9)	142(4)	−577(9)	7.6(22)

atomic scattering factors were taken from "International Tables for X-Ray Crystallography."[2] The final atomic parameters and their estimated standard deviations are given in Tables 2 and 3. The observed and calculated structure factors are listed in Tables 4 and 5.[3]

Results and Discussion

Crystal Structures. The crystal structures of **A** and **B** are shown in Figs. 1 and 2 respectively. The distances of the molecular contacts are listed in Table 6.

The analyses established the configurations of the two diastereomers as (S_SR_C/R_SS_C) for **A** and (S_SS_C/R_SR_C) for **B**.

The packing arrangements of these two isomers are entirely different because of their different molecular geometries. These contacts are of the van der Waals type, but in each isomer relatively short contacts are observed between different groups. For **A**, the short contacts are found between the oxygen atom O(4) and the sulfur and C(2) atoms (C(2)···O(4^{v}), 3.162 Å; S···O(4^{v}), 3.631 Å). The short contacts of **B** are those between sulfinyl oxygen and carbon atoms of the tolyl group (O(1)···C(5^{ii}), 3.056 Å; O(1)···C(6^{ii}), 3.212 Å) and between methoxycarbonyl groups (O(2)···O(2^{vi}), 3.271 Å; O(2)···C(11^{vi}), 3.199 Å).

Molecular Structures. Figure 3 shows stereoscopic views of the **A** and **B** molecules. The bond lengths and angles, with their estimated standard deviations, are listed in Table 7. Deviations from the least-squares planes are listed in Table 8. The projections of the molecules onto the cyclopropane ring, with the numbering of atoms and some intramolecular nonbonding distances, are shown in Fig. 4.

The molecular dimensions of the two isomers almost agree with each other within the limits of experimental error, although the conformations and configurations of these molecules are quite different. The S–O distance of **B** (1.485 Å) is slightly shorter than that of **A** (1.497 Å), although these distances are close to those in other sulfoxides.[4–6] The S–C(2) distance

Table 3. Atomic parameters with their estimated standard deviations of **B**

(a) Atomic coordinates and thermal parameters of non-hydrogen atoms. ($u_{ij}=10^3U_{ij}/Å^2$)
The anisotropic temperature factors are of the form:
$\exp\{-2\pi^2(U_{11}h^2a^{*2}+U_{22}k^2b^{*2}+U_{33}l^2c^{*2}+2U_{12}hka^*b^*+2U_{13}hla^*c^*+2U_{23}klb^*c^*)\}$.
The B_{eq} values are the equivalent isotropic temperature factors.

	10^4x	10^4y	10^4z	u_{11}	u_{22}	u_{33}	u_{12}	u_{13}	u_{23}	$B_{eq}/Å^2$
S	4229(2)	2022(1)	3843(1)	66(1)	57(1)	43(1)	19(1)	0(0)	6(0)	4.4
O(1)	6316(5)	1883(2)	3438(5)	70(2)	109(3)	90(2)	49(2)	−7(2)	−11(2)	6.9
O(2)	7357(4)	4808(1)	5735(4)	58(2)	62(2)	47(1)	9(1)	−7(1)	0(1)	4.6
O(3)	6394(4)	4400(1)	2410(4)	61(2)	67(2)	38(1)	4(1)	2(1)	13(1)	4.6
O(4)	4808(5)	3150(2)	8304(4)	69(2)	135(3)	34(1)	18(2)	14(1)	21(2)	6.3
O(5)	8017(4)	3318(2)	7259(4)	53(2)	94(2)	43(1)	22(2)	−2(1)	24(1)	5.0
C(1)	5202(6)	3576(2)	4902(5)	44(2)	58(2)	31(2)	13(2)	0(2)	6(2)	3.5
C(2)	4234(6)	2963(2)	3229(5)	53(2)	56(2)	30(2)	10(2)	5(2)	5(2)	3.7
C(3)	2800(6)	3361(3)	4110(6)	45(2)	65(3)	48(2)	13(2)	1(2)	6(2)	4.2
C(4)	2189(6)	1574(2)	1757(5)	60(3)	50(2)	45(2)	12(2)	4(2)	4(2)	4.2
C(5)	80(7)	1348(3)	2093(7)	63(3)	75(3)	59(3)	21(2)	15(2)	7(2)	5.0
C(6)	−1471(8)	970(3)	527(8)	56(3)	75(3)	78(3)	12(2)	9(2)	11(3)	5.6
C(7)	−985(8)	804(2)	−1369(7)	74(3)	49(2)	64(3)	5(2)	−6(2)	7(2)	5.2
C(8)	1149(8)	1032(3)	−1672(7)	88(4)	72(3)	48(2)	7(3)	11(2)	−2(2)	5.6
C(9)	2727(8)	1415(3)	−127(6)	65(3)	71(3)	54(2)	5(2)	16(2)	1(2)	5.1
C(10)	−2704(13)	404(4)	−3119(11)	93(5)	77(4)	91(5)	−6(4)	−13(4)	−10(3)	7.4
C(11)	6453(6)	4322(2)	4446(5)	40(2)	62(2)	39(2)	18(2)	−1(2)	8(2)	3.7
C(12)	7488(9)	5122(3)	1782(8)	66(3)	71(3)	57(3)	−3(3)	1(3)	21(2)	5.4
C(13)	5942(6)	3328(2)	7038(5)	56(3)	61(2)	33(2)	9(2)	−1(2)	5(2)	4.1
C(14)	8926(10)	3059(4)	9229(9)	79(4)	114(5)	65(3)	28(4)	−13(3)	38(3)	6.9

(b) Atomic coordinates and thermal parameters of hydrogen atoms of **B**.

	10^3x	10^3y	10^3z	$B/Å^2$		10^3x	10^3y	10^3z	$B/Å^2$
H(2)	458(7)	307(2)	202(6)	5.6(11)	H(102)	−374(8)	37(3)	−268(8)	6.4(17)
H(31)	231(6)	375(2)	331(6)	5.5(10)	H(103)	−312(9)	−17(3)	−308(8)	9.0(15)
H(32)	191(6)	307(2)	503(6)	5.8(10)	H(121)	853(8)	533(3)	262(8)	7.2(14)
H(5)	−26(6)	152(2)	346(6)	5.9(10)	H(122)	669(7)	556(3)	207(7)	6.9(12)
H(6)	−295(8)	78(3)	77(7)	7.3(12)	H(123)	744(7)	503(2)	37(7)	6.6(12)
H(8)	148(7)	87(2)	−300(7)	6.9(11)	H(141)	1040(9)	304(3)	897(8)	8.8(16)
H(9)	421(7)	159(2)	−33(7)	7.0(12)	H(142)	814(8)	255(3)	938(8)	8.5(16)
H(101)	−210(9)	26(3)	−427(9)	8.8(17)	H(143)	874(8)	341(3)	1024(8)	8.3(17)

Table 6. Intermolecular distances (l)

(a) Isomer **A**

Symmetry code Superscript			
None	x	y	z
i	x	y	$z-1$
ii	$-x+1$	$-y$	$-z$
iii	$-x+2$	$-y$	$-z$
iv	$-x+2$	$-y$	$-z+1$
v	x	$-y+1/2$	$z+1/2$
vi	$x-1$	$-y+1/2$	$z-1/2$

	l/Å		l/Å
O(1)···C(6^{i})	3.474(9)	C(2)···O(4^{v})	3.162(8)
C(14)···O(2^{i})	3.315(14)	C(5)···S^{v}	3.642(7)
O(1)···C(9^{iii})	3.570(9)	C(12)···C(5^{vi})	3.449(14)
C(3)···C(10^{iv})	3.658(12)	C(12)···C(6^{vi})	3.536(14)
C(7)···C(7^{iv})	3.617(12)	O(1)···H(6^{i})	2.59(7)
C(8)···C(10^{iv})	3.673(12)	H(31)···H(31^{ii})	2.40(10)
C(9)···C(10^{iv})	3.693(12)	H(2)···O(4^{v})	2.49(6)
S···O(4^{v})	3.631(6)	H(5)···S^{v}	2.85(6)

(b) Isomer **B**

Symmetry code Superscript			
None	x	y	z
i	x	y	$z+1$
ii	$x+1$	y	z
iii	$x+1$	y	$z+1$
iv	$-x-1$	$-y$	$-z-1$
v	$-x+1$	$-y+1$	$-z$
vi	$-x+1$	$-z+1$	$-z+1$

	l/Å		l/Å
O(4)···O(3^{i})	3.382(4)	O(2)···O(3^{vi})	3.446(4)
O(4)···C(2^{i})	3.319(5)	O(2)···O(2^{vi})	3.271(4)
O(4)···C(9^{i})	3.384(6)	O(2)···C(3^{vi})	3.366(5)
O(1)···C(5^{ii})	3.056(6)	O(2)···C(11^{vi})	3.199(5)
O(1)···C(6^{ii})	3.212(6)	C(11)···C(11^{vi})	3.555(6)
O(14)···C(3^{iii})	3.687(9)	O(4)···H(2^{i})	2.47(4)
C(10)···C(10^{iv})	3.558(9)	O(1)···H(5^{ii})	2.44(4)
C(12)···C(12^{v})	3.593(8)		

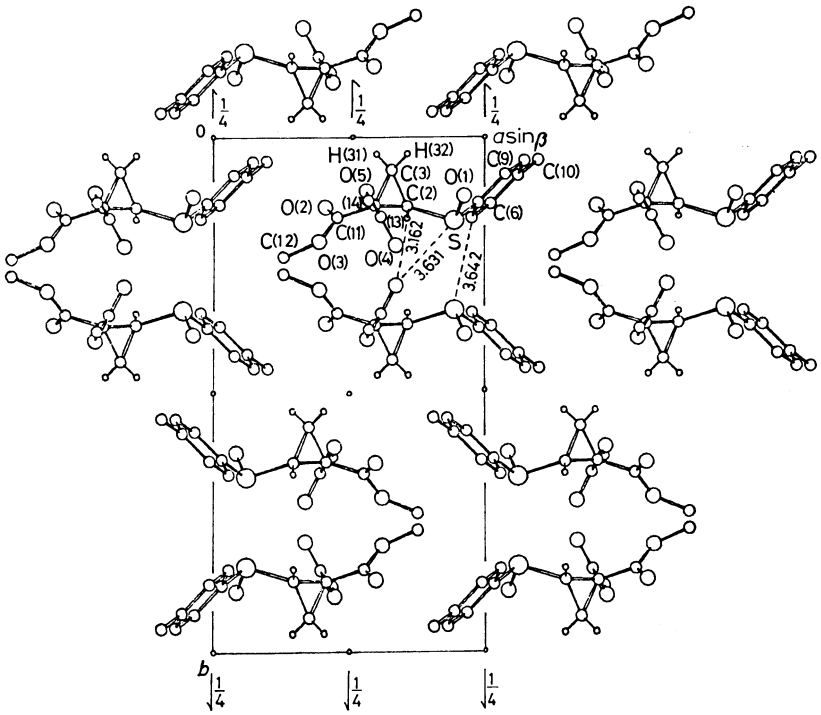

Fig. 1. Projection of the structure of **A** along the c axis.

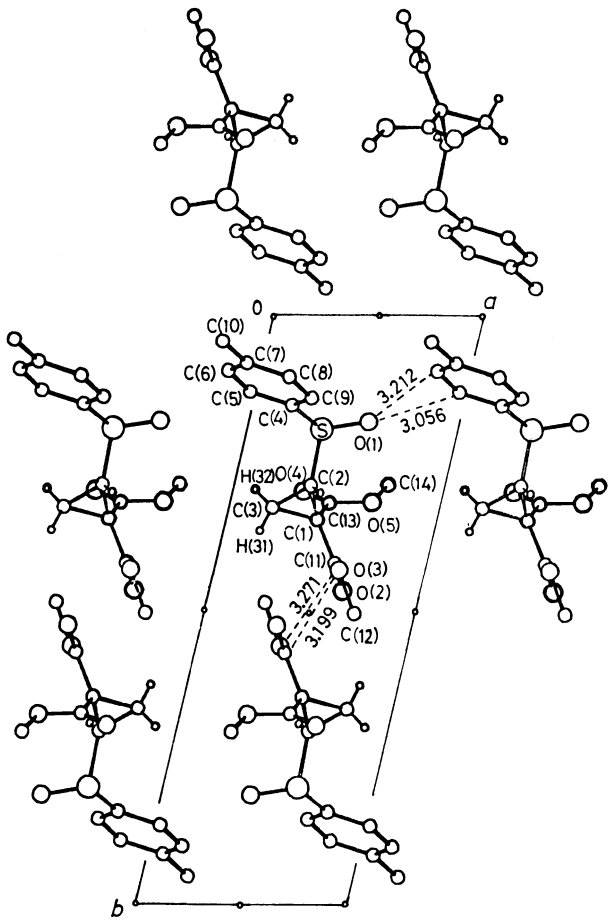

Fig. 2. Projection of the structure of **B** along the c* axis.

(1.806 Å) of **A** is significantly longer than that of **B** (1.767 Å). The former length agrees with the S–C length of (+)methyl *p*-tolyl sulfoxide.[5] The difference in S–C(2) between **A** and **B** is attributable to the conformational difference between **A** and **B**, the difference in non-bonding intramolecular contacts between sulfoxide and cyclopropane rings. The non-bonding distances, O(1)···C(3) are 2.979 and 3.960 Å for **A** and **B** respectively. The S–C(4) lengths (1.774 Å for **A**, 1.786 Å for **B**) are very close to those of other *p*-tolyl sulfoxides. The O(1)SC(2), O(1)SC(4), and C(2)SC(4) angles of both isomers have normal values of sulfoxides.

The average C–C distances in the cyclopropane rings are 1.486 and 1.500 Å for **A** and **B** respectively, virtually the same as those in cyclopropanecarbohydrazide (1.497 Å)[7] and cyclopropanecarboxamide (1.498 Å)[8] and slightly less than those in 1,1-cyclopropanedicarboxylic acid (1.510 Å).[9] The individual C–C lengths within the ring are remarkably different, however, the C–C lengths involving the carbon atom C(1), which connects the methoxycarbonyl groups, are longer than that of the 'back ring' bonds, C(2)–C(3) (1.462 Å for **A**, 1.475 Å for **B**). Such shortenings of the back-ring bonds with respect to the average ring-bond lengths have been found in 1,1-cyclopropanedicarboxylic acid (1.462 Å) and also cyclopropanecarboxamide (1.481 Å). The C(2)C(1)C(3) angles are slightly smaller than the other two intra-ring bond angles.

The SC(2)C(1) and SC(2)C(3) angles of both isomers are almost the same, but the angles related with the C(1) atoms and methoxycarbonyl groups, especially C(2)C(1)C(11), C(2)C(1)C(13), and C(3)C(1)C(13), are significantly different between **A** and **B**. Each

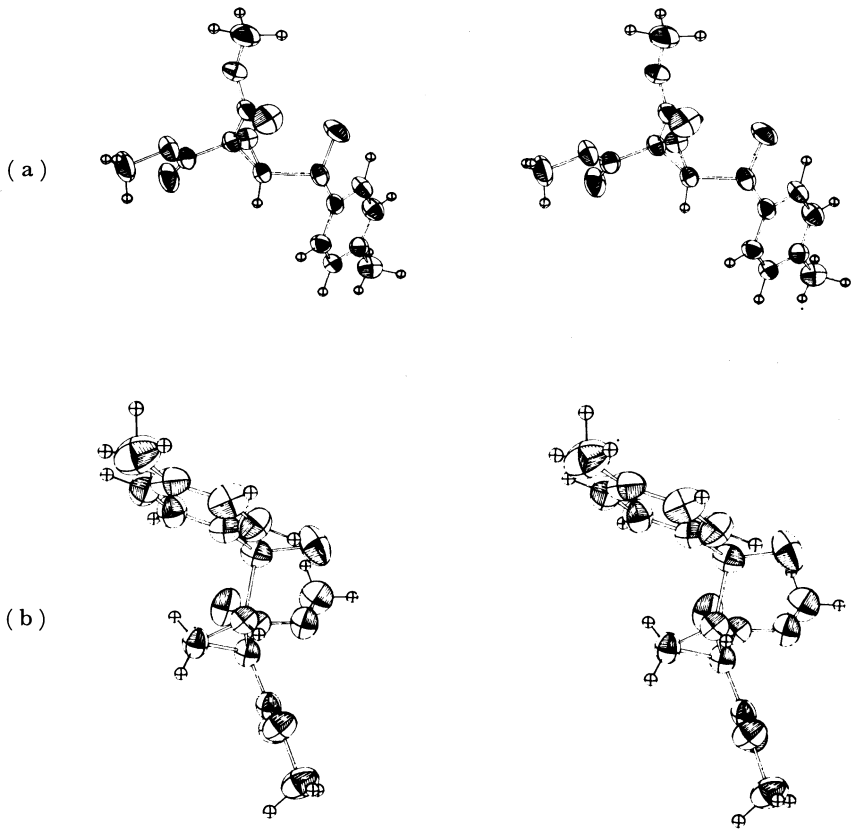

Fig. 3. Stereoscopic view of the molecules. (a) The isomer **A** (S_SR_C), (b) the isomer **B** (S_SS_C).

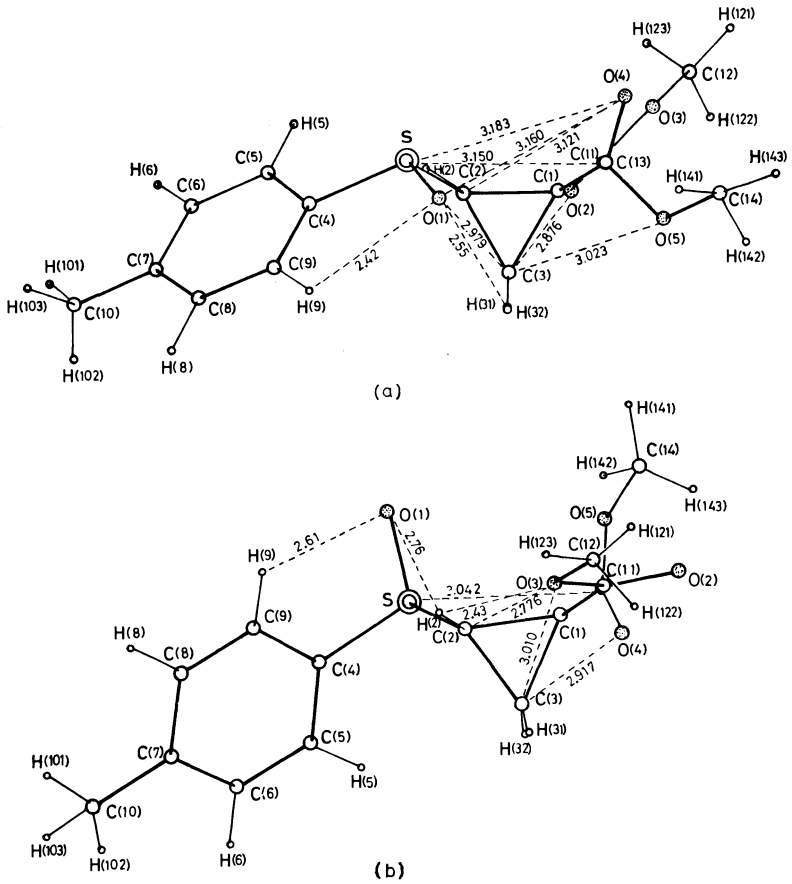

Fig. 4. Projections of the molecules onto the cyclopropane ring with the numbering of atoms and some intramolecular non-bonding distances. (a) The isomer **A**, (b) the isomer **B**.

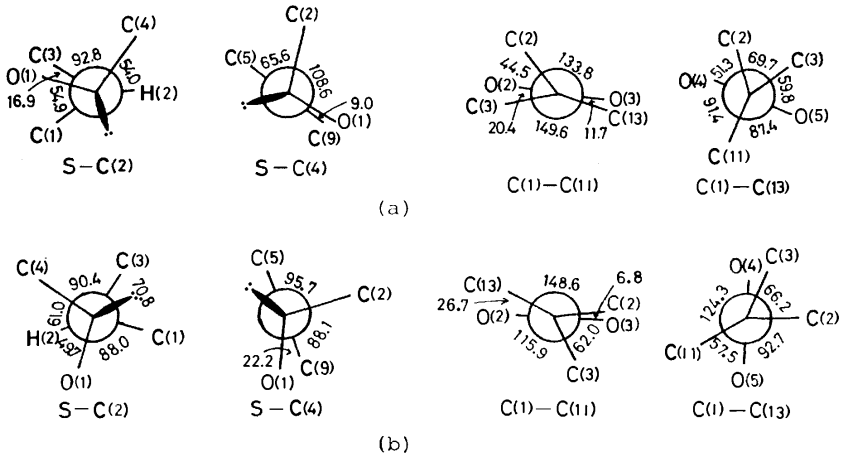

Fig. 5. Torsion angles in the molecules. (a) **A**, (b) **B**.

methoxycarbonyl group except the methyl group is planar. The angles between two planar C–C$\langle^{O}_{O}$ groups are 86.7° for **A** and 70.0° for **B**. For both isomers two methoxycarbonyl groups are non-equivalent to the cyclopropane ring. The dihedral angle between planes of the cyclopropane ring and the methoxycarbonyl group, being *trans* to the sulfinyl group about C(1)–C(2), is 93.4° for **A**. On the other hand, the angle between the cyclopropane ring and the *cis* methoxycarbonyl group is 53.3° for **A**. The corresponding values for **B** are 77.1 and 65.6° respectively. In the molecules of cyclopropanecarboxamide and 1,1-cyclopropane-dicarboxylic acid and other related compounds, the planes of the substituents are nearly perpendicular to the ring plane, and the oxygen atom lies over the three-membered ring. In the present case, the conformation of the *trans* methoxycarbonyl group for each isomer is similar to that in those compounds. The intramolecular O(2)···C(2) and O(2)···C(3) distances are 2.923 and 2.876 Å for **A** and O(3)···C(2) and O(3)···C(3) are 2.776 and 3.010 Å for **B**. The conformations of *cis* methoxycarbonyl groups are different from those of trans groups; the oxygen atoms are not pointed towards the cyclopropane ring, especially in the case of **A**. This may be due to the steric interaction between sulfinyl and methoxycarbonyl groups. The dimensions of the methoxycarbonyl groups are comparable with those of dimethyl α,α'-dimethyl-β,β'-dibromoadipate and the related compounds.[10]

Molecular Conformations. The torsion angles of the groups around the S–C(2), S–C(4), C(1)–C(11), and C(1)–C(13) bonds are shown in Fig. 5. The sulfinyl oxygen is *cis* to one of the carbon atoms, C(9), in the tolyl ring across the S–C(4) bond in each isomer. This conformation is similar to that of other *p*-tolyl sulfoxides.

For **A**, the hydrogen atom, H(2), is *trans* to the sulfinyl oxygen, O(1), and also *gauche* to the lone-pair orbital of the sulfur atom across the S–C(2) bond. On the other hand, H(2) is *gauche* to O(1) and *trans* to the lone-pair orbital of the sulfur in the case of **B**. The configuration of **A** is determined to be *S* at the sulfur atom and *R* at C(2), or *R* at sulfur and *S* at C(2). The configuration of **B** is S_SS_C or R_SR_C.

Since the configuration at the sulfur atom is considered to be retained during the course of the reaction,[1,4] an inspection of the molecular structures of these two isomers reveals the stereochemical pathway of the present reaction. The following reaction scheme will account for the formation of cyclopropane, **2**: the Michael addition of dimethyl malonate to **1** initially gives α-sulfinyl carbanion, **3**, which then turns into the more stable carbanion **4**. Then, the intramolecular S_N2 reaction of **4** proceeds, with the inversion of the configuration at C(2), to yield cyclopropane, **2**, as the final product. According to this reaction scheme, the crucial step in determining the stereochemistry of the whole reaction is the proton transfer, namely, the reaction from **3** to **4**. Thus, the dominant formation of isomer **A** in the sodium methoxide–methanol system is ascribed to the preferential formation of carbanion **4a**. The preference of **4a** is due to the conformational stability of the corresponding α-sulfinyl carbanion, **3a**, the electron lobe of which is located at the position *trans* to the sulfinyl oxygen. On the other hand, the exclusive formation of isomer **B** in the sodium hydride–THF system is attributed to the formation of **4b**, and

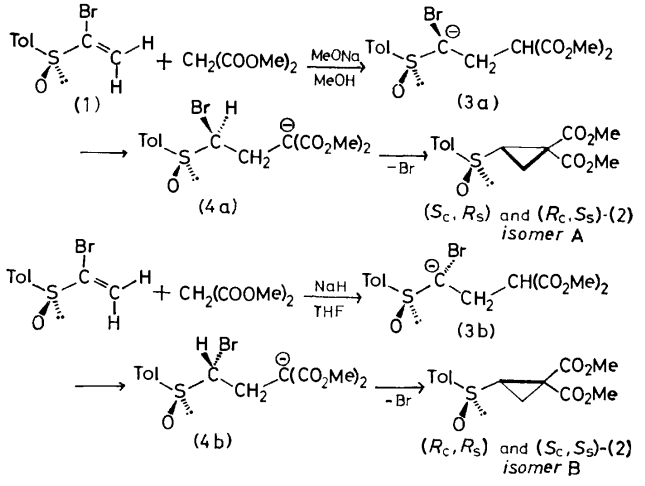

Scheme 2.

Table 7. Bond lengths (l) and angles (ϕ), with their estimated standard deviations

	A (l/Å)	**B** (l/Å)		**A** (ϕ/°)	**B** (ϕ/°)		**A** (l/Å)	**B** (l/Å)
S-O(1)	1.497(5)	1.485(4)	O(1)SC(2)	106.0(3)	106.8(2)	C(2)-H(2)	1.00(8)	0.87(4)
S-C(2)	1.806(6)	1.767(4)	O(1)SC(4)	107.3(3)	107.4(2)	C(3)-H(31)	1.00(7)	0.97(4)
S-C(4)	1.774(6)	1.786(4)	C(2)SC(4)	95.2(3)	97.4(2)	C(3)-H(32)	1.02(7)	0.97(4)
C(1)-C(2)	1.492(8)	1.512(5)	SC(2)C(1)	119.7(4)	118.2(3)	C(5)-H(5)	1.03(6)	1.02(4)
C(1)-C(3)	1.503(9)	1.512(6)	SC(2)C(3)	119.9(5)	120.0(3)	C(6)-H(6)	1.04(7)	0.98(5)
C(2)-C(3)	1.462(9)	1.475(6)	C(1)C(2)C(3)	61.2(4)	60.8(3)	C(8)-H(8)	1.04(6)	0.99(5)
C(1)-C(11)	1.508(9)	1.476(5)	C(1)C(3)C(2)	60.4(4)	60.8(3)	C(9)-H(9)	1.04(7)	0.97(5)
C(11)-O(2)	1.193(9)	1.197(5)	C(2)C(1)C(3)	58.4(4)	58.4(3)	C(10)-H(101)	0.91(8)	0.96(6)
C(11)-O(3)	1.324(8)	1.339(5)	C(2)C(1)C(11)	113.3(5)	121.9(3)	C(10)-H(102)	0.87(8)	0.76(6)
O(3)-C(12)	1.455(13)	1.442(6)	C(3)C(1)C(11)	115.7(5)	118.9(3)	C(10)-H(103)	1.04(7)	1.02(6)
C(1)-C(13)	1.506(9)	1.515(6)	C(2)C(1)C(13)	121.3(5)	117.0(3)	C(12)-H(121)	0.93(8)	0.81(5)
C(13)-O(4)	1.194(9)	1.189(5)	C(3)C(1)C(13)	121.4(5)	116.5(3)	C(12)-H(122)	0.96(8)	1.08(5)
C(13)-O(5)	1.321(8)	1.326(5)	C(11)C(1)C(13)	115.0(5)	113.5(3)	C(12)-H(123)	0.98(8)	0.94(5)
O(5)-C(14)	1.466(13)	1.461(8)	C(1)C(11)O(2)	123.8(6)	124.2(4)	C(14)-H(141)	1.05(8)	1.00(6)
C(4)-C(5)	1.400(9)	1.380(6)	C(1)C(11)O(3)	111.1(6)	111.8(3)	C(14)-H(142)	0.89(7)	0.97(6)
C(4)-C(9)	1.388(9)	1.379(6)	O(2)C(11)O(3)	125.1(7)	124.0(4)	C(14)-H(143)	1.05(8)	0·95(6)
C(5)-C(6)	1.370(9)	1.370(7)	C(11)O(3)C(12)	116.2(7)	116.5(3)			
C(6)-C(7)	1.389(9)	1.375(7)	C(1)C(13)O(4)	124.2(6)	124.8(4)		(ϕ/°)	(ϕ/°)
C(7)-C(8)	1.395(9)	1.390(7)	C(1)C(13)O(5)	110.4(6)	109.9(3)	SC(2)H(2)	104(4)	113(3)
C(8)-C(9)	1.372(10)	1.374(7)	O(4)C(13)O(5)	125.5(7)	125.3(4)	C(1)C(2)H(2)	123(4)	115(3)
C(7)-C(10)	1.488(11)	1.513(10)	C(13)O(5)C(14)	114.7(7)	115.7(4)	C(3)C(2)H(2)	126(4)	120(3)
			SC(4)C(5)	120.4(5)	119.0(3)	C(1)C(3)H(31)	120(4)	112(2)
			SC(4)C(9)	120.3(5)	120.6(3)	C(1)C(3)H(32)	117(4)	116(2)
			C(5)C(4)C(9)	119.3(6)	120.3(4)	C(2)C(3)H(31)	120(4)	117(2)
			C(4)C(5)C(6)	120.0(6)	119.2(4)	C(2)C(3)H(32)	118(4)	115(2)
			C(5)C(6)C(7)	121.6(6)	121.9(5)	H(31)C(3)H(32)	113(5)	121(3)
			C(6)C(7)C(8)	117.4(6)	118.1(5)			
			C(7)C(8)C(9)	122.1(7)	121.0(5)	Mean values		
			C(4)C(9)C(8)	119.4(6)	119.6(5)	CCH (benzene		
			C(6)C(7)C(10)	120.9(6)	122.0(5)	ring)	120(4)	120(3)
			C(8)C(7)C(10)	121.7(6)	119.9(5)	C(7)C(10)H	113(5)	110(4)
						HC(10)H	105(7)	101(6)
						O(3)C(12)H	108(5)	109(4)
						HC(12)H	111(7)	110(5)
						O(5)C(14)H	103(5)	105(3)
						HC(14)H	112(7)	114(5)

Table 8. Deviations (l) of atoms froms the least-squares planes and dihedral angles (ϕ) between planes

Planes. (1) C(1)—C(3) (2) C(4)—C(9) (3) C(1)-C(11)$\lessdot^{O(2)}_{O(3)}$ (4) C(1)-C(13)$\lessdot^{O(4)}_{O(5)}$

Deviations (l/Å)

Plane 1	**A**	**B**	Plane 2	**A**	**B**	Plane 3	**A**	**B**	Plane 4	**A**	**B**
C(1)	0.0	0.0	C(4)	0.010	−0.002	C(1)	−0.003	−0.003	C(1)	0.001	0.003
C(2)	0.0	0.0	C(5)	−0.014	0.003	C(11)	0.009	0.011	C(13)	−0.005	−0.009
C(3)	0.0	0.0	C(6)	0.011	−0.001	O(2)	−0.004	−0.005	O(4)	0.002	0.004
S*	−1.474	1.459	C(7)	−0.005	−0.001	O(3)	−0.003	−0.003	O(5)	0.001	0.003
O(1)*	−2.598	1.336	C(8)	0.002	0.002	C(12)*	−0.081	−0.050	C(14)*	0.092	0.047
C(11)*	1.325	−1.201	C(9)	−0.004	−0.001						
C(13)*	−1.208	1.298	S*	−0.029	0.094						
H(2)*	0.75	−0.73	O(1)*	0.152	0.694						
H(31)*	0.81	−0.84	C(10)*	0.017	−0.042						
H(32)*	−0.87	0.84									

* Atoms not used to define the least-squares plane.

Dihedral angles (ϕ/°)

Planes	(1) (2)	(1) (3)	(1) (4)	(2) (3)	(2) (4)	(3) (4)
A	55.6	93.4	53.3	38.5	70.9	86.7
B	33.5	77.1	65.6	50.0	44.0	70.0

therefore the stability of the α-sulfinyl carbanion, **3b**, the electron lobe of which is *gauche* to the sulfinyl oxygen. The conformational stability of the carbanion, **3b**, in the sodium hydride–THF system may be caused by the chelation between the counter cation, *i.e.*, Na^+, and the sulfinyl oxygen in a nonpolar solvent such as THF. The difference in these conformational stabilities of the carbanion adjacent to the chiral sulfinyl group under various reaction conditions accords with the Michael addition of diethyl malonate to (+)-(*R*)-*trans*-styryl *p*-tolyl sulfoxide[1] and the studies of the conformational stability of the carbanion adjacent to the chiral sulfinyl group.[11]

All the crystallographic computations were performed on a HITAC 8700/8800 computer of the Computer Center of the University of Tokyo, using the local version of the program system UNICS.[12] Figures 1, 2, and 3 were drawn by using the program ORTEP.[13]

The authors wish to express their thanks to Dr. Ei-ichi Asada and Mrs. Midori Goto, of the National Chemical Laboratory for Industry, for the use of the X-ray diffractometer.

References

1) G. Tsuchihashi, S. Mitamura, and K. Ogura, *Tetrahedron Lett.*, **1976**, 855.

2) "International Tables for X-Ray Crystallography," Vol. IV, Kynoch Press, Birmingham (1974), pp. 73, 102, 149.

3) Tables 4 and 5 have been submitted to, and are kept by, the Office of the Chemical Society of Japan, 1-5, Kanda-Surugadai, Chiyoda-ku, Tokyo 101, (Document No. 7830).

4) F. Iwasaki, S. Mitamura, and G. Tsuchihashi, *Bull. Chem. Soc. Jpn.*, **48**, 944 (1975); *ibid.*, **49**, 1676 (1976).

5) U. de la Camp and H. Hope, *Acta Crystallogr., Sect. B*, **26**, 846 (1970).

6) T. Svinning, F. Mo, and T. Bruun, *Acta Crystallogr., Sect. B*, **32**, 759 (1976).

7) D. B. Chesnut and R. E. Marsh, *Acta Crystallogr.* **11**, 413 (1958).

8) R. E. Long, H. Maddox, and K. N. Trueblood, *Acta Crystallogr., Sect. B*, **25**, 2083 (1969).

9) M. A. M. Meester, H. Schenk, and C. H. MacGillavry, *Acta Crystallogr., Sect. B*, **27**, 630 (1971).

10) D. Ravinovich and Z. Shakked, *Acta Crystallogr., Sect. B*, **33**, 809 (1977).

11) J. F. Biellmann and J. J. Vicens, *Tetrahedron Lett.*, **1974**, 2915; *ibid.*, **1978**, 467.

12) "The Universal Crystallographic Computation Program System," The Crystallographic Society of Japan (1967); T. Sakurai, T. Ito, H. Iwasaki, Y. Watanabe, and M. Fukuhara, *Rep. Inst. Phys. Chem. Res.*, **43**, 62 (1967).

13) C. K. Johnson, ORTEP, Report ORNL-3794, Oak Ridge National Laboratory, Oak Ridge, Tennessee (1965).

The Phosphate on the Iron Core of Horse Spleen Ferritin as Studied by a ^1H NMR Probe Method

Noboru IMAI,* Haruo TERADA, Yoji ARATA, and Shizuo FUJIWARA

Department of Chemistry, Faculty of Science, The University of Tokyo, Bunkyo-ku, Tokyo 113

(Received April 20, 1978)

Glycylglycylglycylglycine and tetramethylammonium chloride have been used as ^1H NMR probes to study the state and role of the phosphate on the surface of the iron core of ferritin. ^1H NMR signals of the probe molecules in a ferritin solution do not show any observable paramagnetic shift, and the linewidths are very small compared to an aqueous iron(III) solution which contains the same amount of iron. Iron of ferritin is markedly different from that of aqueous iron(III), but quite resembles that of synthetic iron polymer. It has been shown that the parameter k, which is the linewidth for the NMR probe divided by the concentration of iron, is dependent on the content of the phosphorus in ferritin. The k value for glycylglycylglycylglycine has a maximum in the physiological pH range 6—7, whereas that for tertramethylammonium chloride in which the charge does not change in the whole pH range gives a sigmoidal curve. From the pH dependence of the k values for tetramethylammonium chloride, the pK_a value of the phosphate group on the surface of the iron core has been estimated at 7.0 ± 0.2.

Ferritin, an iron storage protein distributed widely in both plant and animal kingdoms, consists of a shell of protein subunits surrounding the iron core which contains up to approximately 4000 iron atoms.[1,2] Several methods such as X-ray diffraction,[3] electron microscopy,[4,5] and neutron scattering[6] have so far been applied for the investigation of the structure of the iron core. The magnetic properties of the iron core have also been studied by the measurements of magnetic susceptibility[7,8] and Mössbauer effect.[9] It is well established that about 1 to 1.5% phosphate is contained in the iron core, and it has been suggested that the concentration of the phosphate group is higher on the surface than in the inner part of the iron core.[3,10] It has also been suggested that the negatively charged phosphate group is acting as a *go-between* for the binding of the iron core to the protein shell.[1]

Silk and Breslow[11] have carried out the potentiometric titration of apoferritin and ferritin, and observed that ferritin is more stable than apoferritin in the pH range 2.3—3.0, and above pH 8, there exists a large difference in the titration behavior between the two proteins. They have also shown that, compared to apoferritin, ferritin has two more groups per protein subunit which dissociate reversibly in the pH range 5.5—7.5, and concluded that these additional groups are the phosphate group on the iron core. In the present work, high resolution nuclear magnetic resonance (NMR) is used to investigate the structure and magnetic properties of the iron core of ferritin with emphasis on the phosphate group. Because of the large size of the molecule (molecular weight, 445000) and the existence of a large amount of paramagnetic iron, any NMR signal from the protein shell of the native ferritin cannot be detected; only ^1H signal observed is of the solvent water. ^{31}P NMR signal of the phosphate group was also not observable.

In a method presented in this paper, tetramethylammonium ion, glycylglycylglycylglycine, and water are used as the NMR probe to obtain information about the surface of ferritin. When the probe molecules are in close contact with the iron core of ferritin, the NMR signals of the probes are broadened as a result of the magnetic dipolar interactions. The dipolar interactions are strongly influenced by the electrostatic interactions between the probe molecules and the surface of ferritin. In view of this, we use tetramethylammonium ion with a positive charge throughout the pH range examined, and glycylglycylglycylglycine which has at the physiological pH a negative and positive charge at the N and C terminals of the peptide chain, respectively. The water molecule is also used as a neutral probe. On the basis of these experiments, the dissociation constant of the phosphate group on the surface of the iron core will be estimated.

Experimental

Materials. Horse spleen ferritin (crystallized twice, Cd free) was purchased from Nutritional Biochemicals Corporation (lot No. 4871 and 4493), and dialyzed against distilled water before use. Tetramethylammonium chloride, glycylglycylglycylglycine and other reagents used are of reagent grade. Polymeric iron hydrolysate (hereafter designated as iron polymer) was prepared by adding 0.5 M $NaHCO_3$ and 0.05 M NaOH to a 0.03 M ferric citrate solution; the iron polymer thus produced was isolated on a column of Bio-Gel P-30.[12] Iron polymer was also prepared by heating a 0.02 M solution of ferric nitrate at 80—85 °C for 10—20 h, followed by dialysis of the resultant solution.[13]

Analysis. The concentration of iron in ferritin preparations were determined by atomic absorption. No attempt was made to decompose the iron core before the samples were subject to atomic absorption. The iron content determined in this way is in excellent agreement with that obtained by atomic absorption with the iron core decomposed by reducing it with sodium sulfite. The result is also consistent with the value determined colorimetrically by using 2,2′-bipyridyl.[14] Protein concentrations were determined by the Lowry method,[15] and the concentration of the phosphate by a colorimetric method using ammonium molybdate and ascorbic acid.[16]

Instruments. ^1H NMR spectra were recorded using a JEOL PS-100 spectrometer operating at 100 MHz.

Methods. NMR spectra of glycylglycylglycylglycine (Gly_4) were measured in D_2O; in H_2O, due to the NH protons of the amino groups, the signals from the methylene protons of Gly_4 become complicated. The spectrum of tetramethylammonium chloride (TMA) was observed in H_2O. The concentrations of Gly_4 and TMA were constant throughout the experiments (10 mM). The concentration of ferritin in sample solutions was adjusted in either of the following two ways:

1) A small amount of a stock solution of ferritin at high concentrations (approximately 0.2—0.4 M as iron) was added to a Gly_4 or TMA solution. 2) Ferritin solutions were dialyzed against a glycine–HCl buffer solution which contains 10 mM TMA, and iron concentration of the solution was determined after dialysis. In all experiments described in the present work, the pH was changed by dialyzing a solution for 24 h against a 10 mM glycine–HCl buffer, and the dialyzed ferritin solution was added to a 10 mM Gly_4 or TMA solution where the pH was pre-adjusted to that of the ferritin solution added; before and after this treatment, very little change in pH is observed.

Results

^1H NMR Signals of the Solvent H_2O Containing Ferritin and Synthetic Iron Polymer. The H_2O proton signals of aqueous iron(III) solution, ferritin, and synthetic iron polymer solution are reproduced in Fig. 1. ^1H NMR signals of H_2O containing varying amounts of ferritin have the following common features. First, the signal is shifted to high field from that of pure H_2O. Presumably, this is because the bulk susceptibility of ferritin solutions is increased by the presence of a large quantity of paramagnetic iron. The observed difference in chemical shift between the ferritin solution and water would give the bulk magnetic susceptibility of the ferritin iron in water.[17] The result obtained was 3.8 μ_B. This value can be compared to that of Michaelis, 3.7—3.9 μ_B, which was obtained by using powder samples.[7] Second, the H_2O signal in ferritin solutions does not show any paramagnetic shift in the concentration range 0—0.4 M (as iron). This observation is in a marked contrast with a large paramagnetic shift which is observed in an aqueous iron(III) ion solution. Third, the linewidth of the H_2O signal of ferritin solutions is only about 2.5% of that for an aqueous iron(III) solution ($Fe(ClO_4)_3$/2 M $HClO_4$; solution 2, Fig. 1) which has the same iron concentration. Table 1 shows the paramagnetic shifts and linewidths of the H_2O signals of 0.05 M iron(III) and iron(II) solutions. The water signal of aqueous iron(III) solutions (d^5, high spin) always has very large linewidths (200—400 Hz); even a iron(III)–EDTA complex gives a linewidth of the water signal of larger than 100 Hz. It should also be noted that paramagnetic shifts are very small, if any, in the case of ferritin and synthetic iron polymers, whereas they are in the range of 100—200 Hz in the case of aqueous iron(III) and iron(II) solutions.

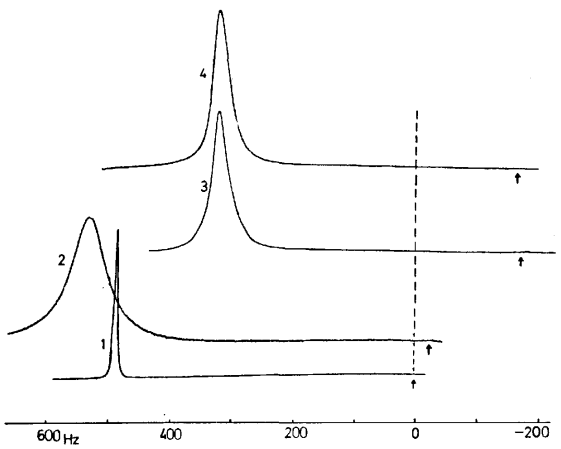

Fig. 1. ^1H NMR spectra of H_2O of 1: pure water, and aqueous solutions containing, 2: ferric ion (0.010 M $Fe(ClO_4)_3$/2 M $HClO_4$), 3: ferritin (0.11 M as iron, pH 7.4), and 4: iron polymer (0.13 M as iron pH 5.5). Arrows indicate the position of the peak of DSS used as internal reference. Locking on external H_2O was used in order to observe a relative shift of the DSS peak in spectra 2, 3, and 4 with respect to that for pure water. The observed shift presumably reflects a change in bulk magnetic susceptibility of the aqueous solutions.

Table 1. The paramagnetic shifts and the linewidths of H_2O solutions containing aqueous iron(III) and iron(II) ions, synthetic iron polymers and ferritin[a]

	Paramagetic shift (Hz)[b]	Linewidth (Hz)[b]
$Fe(ClO_4)_3$/2 M $HClO_4$	224	405
$FeCl_3$/2 M HCl	172	192
$Fe(NO_3)_3$/2 M HNO_3	194	385
$FeSO_4(NH_4)_2SO_4$/2M H_2SO_4	143	12
Fe(III)–EDTA	52	114
Ferritin	≈0	13
Iron polymer	≈0	11

a) The concentration of iron is 0.05 M in all cases.
b) Accurate to ±2 Hz.

As shown in Table 1, the iron polymer markedly resembles the iron core of ferritin; the H_2O signal of solutions of the iron polymer exhibits no paramagnetic shift and the linewidth is quite small. From the chemical shift of the H_2O signal, the magnetic susceptibility of the iron polymer of iron(III) citrate was estimated at 3.5 μ_B.

^1H NMR Spectra of Gly_4 and TMA in the Presence of Ferritin, Synthetic Iron Polymer, and Aqueous Iron(III) Ion. In order to compare more closely the different types of iron mentioned above, a small peptide Gly_4 was used as an NMR probe. Four peaks which correspond to the four kinds of the methylene protons (which from the N terminal will be designated as N, N2, N3, and C) can be observed separately in D_2O. The spectra of Gly_4 in the presence of either one of the three kinds of iron, *i.e.*, aqueous iron(III) ion ($Fe(ClO_4)_3$), ferritin, and synthetic iron polymer, are shown in Fig. 2. Upon adding an aqueous iron(III) solution, differential broadening of the four methylene peaks are clearly observed; the peak from the C terminal first becomes broad. Each of the four methylene peaks shows paramagnetic shift as shown in Fig. 2, A. In contrast to this, when ferritin is added, all four peaks become broader almost uniformly, without any paramagnetic shift. The dependence of the chemical shifts of the Gly_4 signals is plotted in Fig. 3 as a function of the iron concentration.

In the case of the ferritin solutions, although all lines are almost uniformly broadened, the peak from the N terminal broadens a little faster than the others

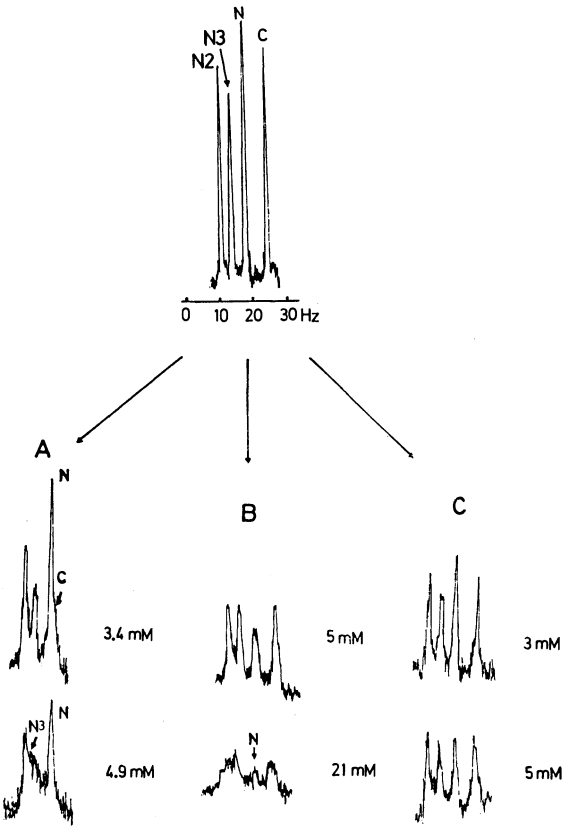

Fig. 2. ^1H NMR spectra of Gly_4 in D_2O in the presence of either one of the three kinds of iron. A, aqueous iron(III) ion ($Fe(ClO_4)_3$), pH 6.8; B, ferritin, pH 6.8; C, synthetic iron polymer, pH 6.8. The concentrations of iron added, and the assignment of the peaks are shown in the figure.

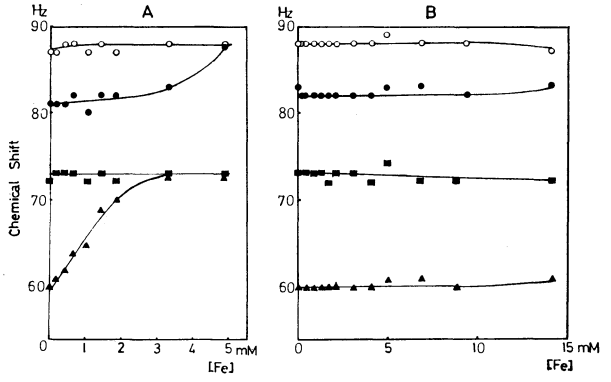

Fig. 3. The dependence of the chemical shifts of the Gly_4 signals as a function of the concentration of iron. (A) aqueous iron(III) ion, (B) ferritin. ▲, C terminal peak; ■, N terminal peak; ●, N3 peak; ○, N2 peak.

(Fig. 4, B). It has been confirmed that the linewidth of the NMR probes examined is not influenced by the presence of apoferritin. This means that the line broadening of the NMR probes is independent of the protein part, and therefore a contribution from the iron core can be observed separately by NMR. In view of this result, the paramagnetic contribution for each peak may be represented quantitatively by using the slope which is obtained from the relation between the

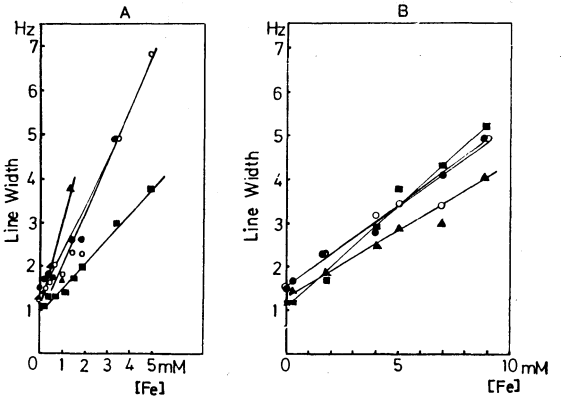

Fig. 4. The linewidths of the Gly_4 signals as a function of the concentration of iron. (A) aqueous iron(III) ion, (B) ferritin. ▲, C terminal peak; ■, N terminal peak; ●, N3 peak; ○, N2 peak.

iron added and the linewidths of the peaks. The observed linewidth ΔH_{obsd} may be written as follows:

$$\Delta H_{obsd} = \Delta H_0 + \Delta H_p, \quad (1)$$

where ΔH_0 is the intrinsic linewidth of each peak and ΔH_p represents the paramagnetic contribution. In the case of fast exchange where exchange between molecules which are under the influence of the iron core, and those which are free in solution is fast enough, the paramagnetic term (ΔH_p) should increase linearly with the iron concentration added. In this case, $k=\Delta H_p/C$ which represents a normalized paramagnetic contribution should be constant, and therefore Eq. 1 may be written as

$$\Delta H_{obsd} = \Delta H_0 + kC. \quad (2)$$

In Fig. 4 the observed linewidths are plotted as a function of the concentrations of iron added. The slopes k obtained from Fig. 4 may be considered as representing the binding ability of Gly_4 to ferritin, and therefore may be used to estimate the binding constant of Gly_4 with iron. The k values obtained are summarized in Table 2. In view of the fact that the k value for the C terminal protons is largest in an aqueous iron(III) solution and that the peak from the C terminal exhibits a largest paramagnetic shift, it is obvious that an aqueous iron(III) ion forms a complex with the carboxyl group of Gly_4. In the case of ferritin solutions, the slopes for the four peaks of Gly_4 are all small, and almost equal to each other. The slope for the N terminal protons are slightly larger than that of the C terminal

TABLE 2. THE OBSERVED k VALUES FOR Gly_4 IN H_2O SOLUTIONS OF AQUEOUS IRON(III) ION AND TWO DIFFERENT FERRITIN PREPARATIONS WHICH CONTAIN A DIFFERENT AMOUNT OF THE PHOSPHATE

	N2	N3	N	C
$Fe(ClO_4)_3$	1.2 Hz/mM	1.3	0.63	2.0
Ferritin[a)]	0.39	0.53	0.45	0.30
Ferritin[b)]	0.06	0.06	0.11	0.08

a) P/Fe=0.10. b) P/Fe=0.08.

protons. This result may be interpreted in terms of the existence of the negative charge of the phosphate group on the surface of the iron core.

For the sake of comparison, a synthetic iron polymer which does not contain any phosphate group, and also a different batch of ferritin which contains a less amount of the phosphate were examined. It has been confirmed that in the case of the iron polymer, the N-terminal peak is less broad than others as shown in Fig. 2, C. It is shown in Table 2 that the k values for the Gly_4 peaks in the presence of ferritin containing a less amount of phosphate are much smaller, and that the difference in k between the N and C terminal peaks becomes small. Furthermore, it was confirmed that the linewidth of the solvent H_2O signal is independent of the concentration of phosphate in the iron core. Therefore, it may be concluded that the broadening of the Gly_4 peaks is due to the existence of the negative charge of the phosphate on the surface of the iron core. The titration curve of k for Gly_4 shown in Fig. 5 indicates that the curve has a maximum and decrease above pH 7. Most probably, this is because the amino group of Gly_4 loses its charge at high pH and as a result of this, the interaction between Gly_4 and ferritin becomes weaker in this pH range. TMA in which the charge does not change in the whole pH range was used at the same time as a reference, and the results are given in Fig. 6.

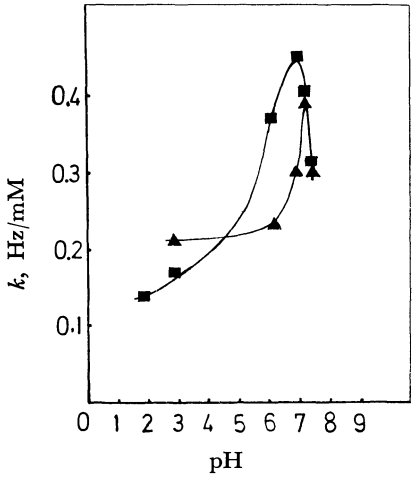

Fig. 5. The titration curve of the k values for Gly_4. ▲, C terminal peak; ■, N terminal peak.

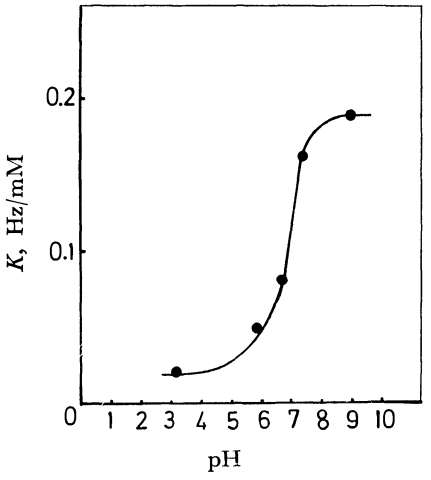

Fig. 6. The titration curve of the k values for tetramethylammonium ion.

The lienwidths of the peaks for Gly_4 are designated as ΔH_{mono} and ΔH_{di} when the phosphate group exists as mono- and di-anion, respectively. The fraction of the dianion is denoted by x. Then, the observed linewidth in the presence of ferritin may be given by

$$\Delta H_{obsd} = \Delta H_{mono} \cdot (1-x) + \Delta H_{di} \cdot x. \quad (3)$$

This equation is normalized by dividing it by C.

$$k_{obsd} = k_{mono} \cdot (1-x) + k_{di} \cdot x$$
$$= k_{mono} + (k_{di} - k_{mono}) \cdot x, \quad (4)$$

where C is the concentration of ferritin (as iron), $k_{obsd} = \Delta H_{obsd}/C$, $k_{mono} = \Delta H_{mono}/C$, $k_{di} = \Delta H_{di}/C$. A plot of k_{obsd} as a function of pH should represent the dissociation of the phosphate, and therefore give the pK_a of the phosphate group. From the plot in Fig. 6 obtained for TMA, a pK_a of 7.0 ± 0.2 for the phosphate is obtained. It is quite interesting that the value obtained is close to $pK_a = 7.2$ which has been reported for the second dissociation of an inorganic phosphate ion. In the case of Gly_4, the pH dependence of k is shown in Fig. 5. The curve for Gly_4 has a maximum in the pH range 6—7, suggesting that the interaction between Gly_4 and the phosphate becomes strongest in this pH range. In this narrow pH range, the slope for the C terminal methylene peak is much smaller than that for the N terminal. This suggests that in this pH range the positive charge of the amino group of Gly_4 is attracted to the negative charge of the phosphate group on the iron core.

Discussion

As mentioned previously, the linewidth of the H_2O signal in ferritin solution is quite small, and only about 2.5% of that for an aqueous iron(III) solution which contains the same amount of iron. The H_2O signal of ferritin solutions markedly resembles that for a solution containing synthetic iron polymer. This result suggests that the number of iron(III) ions which are in contact with water becomes very small when the ions polymerize, forming a large iron core. Therefore, a change in the surface area should greatly influence the linewidth. In the case of the ferritin preparation (lot No. 4871) used in most of the present experiment, the ratio of iron to protein is 0.20. The iron core is assumed to be spherical in shape; then in a close packing model[3], the radius of the sphere would be 24 Å and the core could contain 1600 iron atoms. This means that the average surface area per iorn atom of the iron core is about 1/16 of that for a free iron(III) ion. In addition to this, there is a difference in magnetic susceptibility between an aqueous iron(III) ion (5.9 μ_B) and ferritin iron (3.8 μ_B). Therefore, if the linewidth solely due to dipolar interactions between H_2O and the electron spin of iron, a factor of $(3.8/5.9)^2 = 0.41$ should also be considered for the linewidth of the NMR probes.[18] In the above simple model, a total reduction in linewidth becomes 2.4% ($1/16 \times 0.41 \times 100$) which

agrees well with the observed value. A quite similar result has been obtained in the case of a different batch of ferritin preparation (lot No. 4493). Although the quantitative agreement may be fortuitous, it appears that the observed linewidths may be accounted for by the above simple model.

It has been confirmed that the linewidth of the NMR probes examined is not influenced by the presence of apoferritin. This means that the line broadening of the NMR probes is independent of the protein part, and therefore a contribution from the iron core can be observed separately by NMR. In this respect, the present experiment using the NMR probes is essentially different from that by Silk and Breslow who using potentiometry attempted to acquire information concerning the phosphate on the iron core.[11] Since all dissociable groups are observed together in potentiometry, it is generally difficult to distinguish the dissociation in protein from that in the iron core. In fact, they assigned a group which dissociates in the pH range 5.5—7.5 to either histidine in the protein part, or the phosphate group on the iron core. Since the results obtained in potentiometry are based on the difference of the titration curves between ferritin and apoferritin, it is necessary to assume that in the whole pH range examined a difference in conformation between the two proteins, if any, does not influence the titration behavior. However, there is evidence on the basis of circular dichroism spectra that there is actually a difference in conformation in the two proteins.[19] These ambiguities do not occur in using the NMR probe method where information concerning the iron core can be obtained separately.

Evidences which support the role of the phosphate on the broadening of the NMR probes may be summarized as follows: 1) Broadening of the N terminal peak of Gly_4 occurs faster than that of the C terminal peak, indicating broadening of the Gly_4 signals is influenced by the negative charge. It should also be noted that the difference in broadening between the C and N terminal peaks becomes particularly larger in the pH range where the phosphate group dissociates. 2) In the case of the iron polymer which does not contain any phosphate group, the N terminal peak becomes equally broad as the C terminal peak. 3) In a ferritin preparation which contains less phosphate, the broadening of the Gly_4 peaks is less extensive. 4) The linewidth of the H_2O peaks remains constant in the pH range 2—10. From these results it is clear that the broadening of the Gly_4 peaks is primarily due to the phosphate group on the iron core. The protein part of ferritin also has the negative charge. However, the positive and negative charges are distributed over the surface of the protein, and effective negative net charge is -2——-6 in the pH range 5.5—7.5.[11] In contrast to this, the number of phosphate groups in one ferritin molecule is about 290 for the ferritin preparation (lot No. 4493) where the ratio iron/protein is 0.20 and phosphorus/iron is 0.10. If four fifth of these phosphate groups is assumed to exist on the surface of the core,[3] the number of charge on the core is more than two hundred, and becomes twice when the phosphate groups dissociate above pH 7. This result along with more extensive study using a variety of NMR probes now in progress in this laboratory further confirms that the NMR probe method presented here is quite useful in investigating in detail the surface of the iron core.

It should also be pointed out that when the pH of ferritin solutions is adjusted by adding acid or base directly to the solutions as performed in Silk and Breslow's experiments, it is quite likely that the quaternary structure of ferritin is perturbed, particularly in the high and low pH range.

It should be noted that Gly_4 interacts with ferritin most strongly at pH 6—7, and the interaction becomes weak with an increase or decrease in pH (see Fig. 5). In view of this result, it appears that the phosphate on the surface of the iron core interacts with the amino groups on the inner surface of the protein shell, playing a role to bind the iron core to the protein. It is quite interesting that the interaction between Gly_4 and ferritin becomes maximum at pH 6—7, the physiological pH which would be favorable for the binding of the iron core to the inner surface of the protein.

References

1) P. M. Harrison, R. J. Hoare, T. G. Hoy, and I. G. Macara, "Iron in Biochemistry and Medicine," ed by A. Jacobs and M. Worwood, Acadimic Press, London (1974), p. 73.
2) R. R. Crichton, *Struct. Bonding (Berlin)*, **17**, 67 (1973).
3) P. M. Harrison, F. A. Fishbach, T. G. Hoy, and G. H. Haggis, *Nature*, **216**, 1188 (1967).
4) G. H. Haggis, *J. Mol. Biol.*, **14**, 598 (1965).
5) W. H. Massover and J. M. Cowlew, *Proc. Nat. Acad. Sci. U.S.A.*, **70**, 3847 (1973).
6) H. B. Stuhrmann, J. Haas, K. Ibel, M. H. J. Koch, and R. R. Crichton, *J. Mol. Biol.*, **100**, 399 (1976).
7) L. Michaelis, C. D. Coryell, and S. Granick, *J. Biol. Chem.*, **148**, 463 (1943).
8) A. Blaise, J. Freon, J. L. Girardet, and J. J. Lawrence, *C. R. Acad. Sci.*, **265**, 1077 (1967).
9) G. W. Brady, C. R. Kurkjian, E. F. X. Lyden, M. B. Robin, P. Saltman, T. G. Spiro, and A. Terzis, *Biochemistry*, **7**, 2185 (1968).
10) S. Granick, *J. Biol. Chem.*, **146**, 451 (1942).
11) S. T. Silk and E. Breslow, *J. Biol. Chem.*, **251**, 6963 (1976).
12) T. G. Spiro, L. Pape and P. Saltman, *J. Am. Chem. Soc.*, **89**, 5555 (1967).
13) K. M. Towe and W. F. Bradley, *J. Colloid. Interface Sci.*, **24**, 384 (1967).
14) J. W. Drysdale and H. N. Munro, *Biochem. J.*, **95**, 851 (1965).
15) O. H. Lowry, N. J. Rosebrough, A. L. Farr, and R. J. Randall *J. Biol. Chem.*, **193**, 265 (1951).
16) P. S. Chen, Jr. T. Y. Toribara, and H. Warner, *Anal. Chem.*, **28**, 1756 (1956).
17) D. F. Evans, *J. Chem. Soc.*, **1959**, 2003.
18) A. Abragam, "The Principles of Nuclear Magnetism," Oxford, The Clarendon Press, p. 97.
19) G. C. Wood and R. R. Crichton, *Biochim. Biophys. Acta*, **229**, 83 (1971).

Application of Gel Chromatography to the Determination of the Stability Constants of a Magnesium Complex with Diphosphate

Tohru MIYAJIMA* and Shigeru OHASHI

Department of Chemistry, Faculty of Science, Kyushu University 33, Hakozaki, Higashiku, Fukuoka 812

(Received July 29, 1977)

Hummel-Dreyer's method was examined for its applicability to inorganic complexes, and a modified method was proposed. A sample solution containing magnesium and diphosphate was eluted with magnesium chloride solution on a gel column. The change of magnesium concentration in an effluent was measured with an atomic absorption detector. From the peak area of the eluted complex the stability constants ($\lg \beta_1$) at $I=0.1$ and 25 °C were evaluated to be 5.57 in tetramethylammonium chloride solution and 5.06 in sodium perchlorate solution. In the modified method the total magnesium concentration in a sample solution is made to be much higher than that in an eluent. This enables one to shorten the elution time.

Hummel and Dreyer first applied gel chromatography to the investigation of complex formation between biological macromolecules and low-molecular-weight substances.[1] Since then several workers have studied the complex formation of metal ions with biological macromolecules by this method.[2-6] However, no application has been reported to the complex formation of metal ions with relatively small ligands. In the present investigation, the fundamental problems of the gel chromatographic method for the determination of stability constants of such a metal complex were examined in detail, and the original Hummel-Dreyer's method was modified to overcome some difficulties encountered therein. As ligand, diphosphate ion was chosen, because it is fairly stable against hydrolytic degradation. As metal magnesium ion was chosen, because it was shown by our previous studies[7] that the elution behavior of magnesium on a gel column could be automatically recorded with an atomic absorption spectrophotometer. The stability constants of magnesium complexes with diphosphate were determined by this method, and the values obtained were compared with those obtained by other methods.

Theoretical

A reversible complex formation between a metal ion, M, and a ligand, L, is considered. L forms successively a series of complexes, ML, M_2L, ..., and M_nL. Charges are omitted for simplicity. The stability constant for the n-th complex is defined as follows:

$$\beta_n = \frac{[M_nL]}{[M]^n[L]}. \quad (1)$$

When the sample solution containing M, L, and the complexes is applied to a gel column conditioned with an eluent containing the same metal of a known concentration, $[M]_0$, and eluted with the same eluent, the elution pattern shown schematically in Fig. 1 is obtained. The initial free metal ion concentration in the sample solution, $[M]_s$, in general, differs from $[M]_0$. However, as the sample ligand zone (zone α) migrates through the column, the free metal ion concentration at zone α, $[M]_\alpha$, approaches $[M]_0$, and eventually becomes equal to $[M]_0$. After this time, the steady state at zone α is characterized by the specific condition that $[M]_\alpha=[M]_0$. A straightforward proof of the attainment of the above condition is the appearance of a horizontal line equal to $[M]_0$ at the right hand side of zone α, as shown in Fig. 1. Equation 1 can be rewritten as

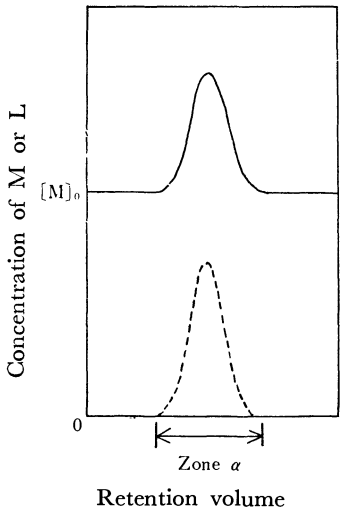

Fig. 1. Schematic elution pattern of zone α. The solid line refers to total metal ion concentration, and the broken line to total ligand concentration.

$$\beta_n = \frac{[M_nL]}{[M]_0^n[L]}. \quad (2)$$

The peak area of zone α represents the amount of bound metal which is present as complexes. The average number of bound metal ions per one ligand, $\bar{n}$, in zone α is obtained by dividing the amount of bound metal by the total amount of a ligand in zone α, which is equal to the total amount of the ligand applied to the column. $\bar{n}$ can be written as

$$\bar{n} = \frac{\sum_1^n i\beta_i[M]_0^i}{1+\sum_1^n \beta_i[M]_0^i}. \quad (3)$$

The following four prerequisites have to be fulfilled to use this method.

1. The size of the ligand should be much larger than that of the metal ion.
2. The peaks due to the ligand and the complexes should not be separated from one another. This can be achieved when the complex equilibria are established

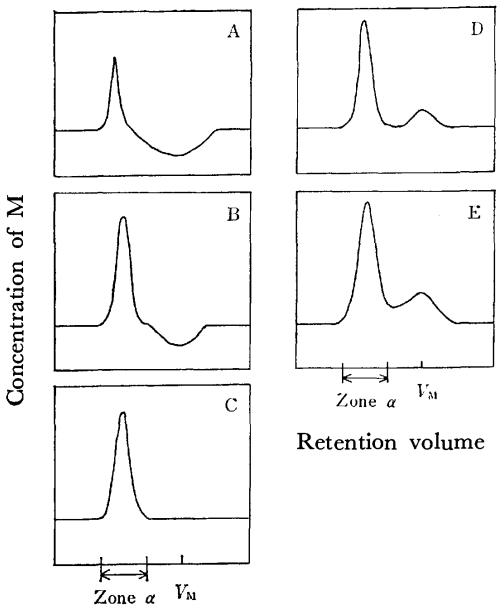

Fig. 2. Typical elution patterns of equilibrium systems of metal and ligand.

A ; $[M]_s \ll [M]_0$ $[M]_\alpha \fallingdotseq [M]_0$
B ; $[M]_s < [M]_0$
C ; $[M]_s = [M]_0$ $[M]_\alpha = [M]_0$
D ; $[M]_s > [M]_0$
E ; $[M]_s \gg [M]_0$ $[M]_\alpha \fallingdotseq [M]_0$

so fast that this separation is prevented.

3. The condition of the steady state, *i.e.*, $[M]_\alpha = [M]_0$, should be establsihed before zone α leaves the column.

4. The ionic strength of the eluent should be kept sufficiently high to prevent the Donnan redistribution. In other words $[M]_\alpha$ should be equal to $[M]_0$.

Figure 2 shows the schematic elution patterns of the metal ion on the assumption that the total ligand concentration in a sample solution, $[L]_t$, and $[M]_0$ are kept constant and that the total metal ion concentration in a sample, $[M]_t$, is varied. If, incidentally, $[M]_s$ is equal to $[M]_0$, an elution pattern such as that shown in Fig. 2C is obtained. Here, only the broadening of zone α occurs. When the difference between $[M]_s$ and $[M]_0$ is relatively small, a pattern like Figs. 2B or 2D is obtained. At the retention volume of the free metal ion, V_M, a negative or positive peak appears. In the three cases mentioned above, the peak areas of zone α are equal to one another. This indicates that the steady state mentioned above is established . However, when $[M]_s$ is much lower or higher than $[M]_0$, the steady state cannot be established until zone α leaves the column (Fig. 2A or 2E). The peak area of zone α in Fig. 2A is smaller than those in Figs. 2B, 2C, and 2D, and that in Fig. 2E is larger.

According to Hummel-Dreyer's method, a sample solution is prepared by dissolving the ligand in an eluent containing metal ions of $[M]_0$. The procedure is particular in that $[M]_t$ is equal to $[M]_0$. The expected elution pattern will be like that in Figs. 2A or 2B. Hummel-Dreyer's method has the disadvantage that, if the free metal ion is significantly depleted by the complex formation, there is no appearance of a horizontal line between a positive and a negative peak, as shown in Fig. 2A. In this case a longer column should be used to separate the two peaks completely. This requires a longer time for elution. In order to overcome this difficulty, a sample solution should be prepared so as to contain metal ions of $[M]_t$ much higher than $[M]_0$.

Experimental

Chemicals. A stock solution of magnesium chloride was standardized volumetrically with EDTA, using Eriochrome Black T as an indicator. A stock solution of sodium diphosphate prepared from analytical grade tetrasodium diphosphate decahydrate was standardized colorimetrically with a molybdenum(V)–molybdenum(VI) reagent.[8] Tetramethylammonium chloride obtained from Tokyo Kasei Kogyo Co. was used without further purification as a background electrolyte.

High Speed Gel Chromatographic Device with an Atomic Absorption Detector. A column of 8×700 mm Pyrex tubing was packed with Sephadex G-15 (Pharmacia). The temperature of the column was kept at 25.0 ± 0.1 °C. A JLC-P2 pumping system (JEOL) was used. A Model 403 atomic absorption spectrophotometer (Perkin Elmer) was used as a detector. The details of the present device were described elsewhere.[9-11]

Elution Experiments. The column was first conditioned with an eluent containing magnesium chloride of a desired concentration, 0.1 mol dm^{-3} tetramethylammonium chloride, and 5×10^{-3} mol dm^{-3} ammonia–10^{-3} mol dm^{-3} ammonium chloride as a buffer of pH 10. At this pH, the diphosphate ion is considered to be almost deprotonated. Sample solutions contained magnesium chloride and sodium diphosphate in varying concentrations, in addition to tetramethylammonium chloride, ammonia, and ammonium chloride of the same concentrations as those in the eluent. A 1.00 cm^3 portion of a sample solution was fed onto the column with an injection valve. The elution flow rate was kept at 1.71 cm^3 min^{-1}. The effluent was introduced into the detector for the automatic recording of the absorbance of magnesium at 285.2 nm. An effluent fraction of 2—6 min and that of 6—10 min were collected manually. The magnesium concentrations in these two fractions were determined by means of atomic absorption spectrophotometry.

Results and Discussion

The Effects of M and L Concentrations in a Sample Solution. The effects of $[M]_t$ and $[L]_t$ on the peak area of zone α were investigated for the complex formation of magnesium with diphosphate. The notations $[Mg]_0$, $[Mg]_t$, $[Mg]_s$, $[Mg]_\alpha$, and $[P]_t$ will be used hereafter. These correspond to $[M]_0$, $[M]_t$, $[M]_s$, $[M]_\alpha$, and $[L]_t$ which are defined in the "Theoretical" section. The elution patterns shown in Figs. 2A, 2B, *etc.*, will be called type A, type B, *etc.*

Figure 3 shows the peak areas of zone α for various $[Mg]_t$ and $[P]_t$. $[Mg]_0$ was fixed at 3.06×10^{-6} mol dm^{-3}. In the region on the left hand side of line X, the elution patterns of type A were obtained. This means that $[Mg]_s \ll [Mg]_0$. In the region on the right hand side of line Y, the elution patterns of type E were obtained. This means that $[Mg]_s \gg [Mg]_0$. In the

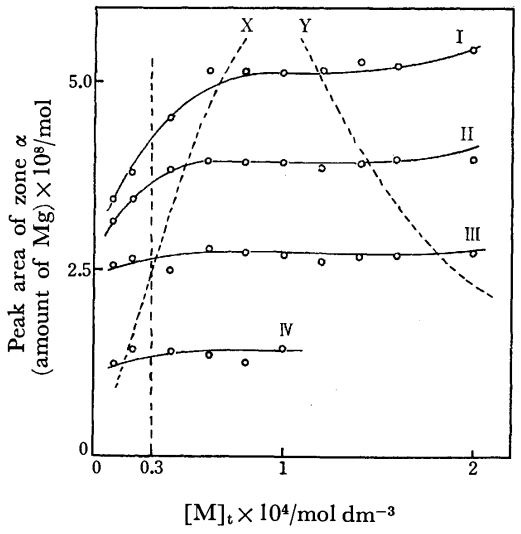

Fig. 3. Effects of $[Mg]_t$ and $[P]_t$ on the peak area of zone α.
$[Mg]_0=3.06\times10^{-6}$ mol dm^{-3}.
$[P]_t\times10^5$ /mol dm^{-3}; I: 9.90, II: 7.43, III: 4.95, IV: 2.48.

region between lines X and Y, the elution patterns of type B, C, or D were obtained. In these cases the steady state was established, *i.e.*, $[Mg]_\alpha=[Mg]_0$.

As shown in Fig. 3, for example, when $[Mg]_t=0.3\times10^{-4}$ mol dm^{-3}, the elution pattern of type B, C, or D will be obtained in case IV, but that of type A in cases I, II, and III. This indicates that, because $[P]_t$ is lower, the time for attainment of the condition that $[Mg]_\alpha=[Mg]_0$ is shorter. However, too low a value of $[P]_t$ leads to a small peak area of zone α, giving rise to a large error in the determination of $\bar{n}$. According to the original Hummel-Dreyer's method, $[Mg]_t$ is equal to $[Mg]_0$, *i.e.*, 3.06×10^{-6} mol dm^{-3}. In this case a much longer column should be used for the present purpose. Since in the modified method $[Mg]_t$ is made to be much higher than $[Mg]_0$, it is possible to use a shorter column.

The amount of bound magnesium thus obtained was plotted against the amount of total diphosphate. The resulting straight line is good evidence for the absence of an ML_2 type complex. The slope, $\bar{n}$, at $[Mg]_0=3.06\times10^{-6}$ mol dm^{-3} was 0.52.

The Effect of a Background Electrolyte. As mentioned above, it is important to confirm prerequisite 4. It should be noted that the anions of a background electrolyte in an eluent are excluded by the Donnan effect from zone α.[12] This in turn may result in the variation of magnesium ion concentration in zone α.

The magnitude of this effect was calculated according to the equation presented by Jordan *et al.*[13] in the case of the highest concentration of the fully deprotonated ligand used in this study, *i.e.*, 10^{-4} mol dm^{-3} of $P_2O_7^{4-}$. Even in this limiting case, the concentrations of free magnesium ions in the mobile and the stationary phases differ from each other by less than 0.5%.

A Source Material of Ligand. As a source material of diphosphate we used its sodium salt, but not its tetramethylammonium salt. The sodium ions in a sample solution are expected to be removed from zone α while this zone migrates through the column. In order to check this point, the sodium emission spectra of an effluent were examined. The peak of the sodium ions was found at 16 min and was completely separate from zone α (6—10 min, see Fig. 4). Therefore, it is concluded that we need not take into account the ion-pair formation of sodium ions with diphosphate ions. Consequently, we need not necessarily use a tetramethylammonium salt of diphosphate, which is usually employed for the determination of stability constants. This is the most remarkable characteristic of the gel chromatographic method.

Calculation of the Stability Constant. In Fig.4, the representative elution patterns for the magnesium–diphosphate system are shown. The positive peak at 7.7 min corresponds to the complexes formed (zone α), and the positive or the negative peak in the range of 12—17 min corresponds to free magnesium ions. When the negative peak appears, it is not clear whether zone α has reached the steady state or not, because of the overlapping of the positive peak at 7.7 min and the negative peak. On the contrary, zone α reaches the steady state when there appears a horizontal line between the rear edge of zone α and the front edge of a positive peak of free magnesium ions.

The amounts of bound magnesium can be calculated directly from the peak area of complexes.[11] In

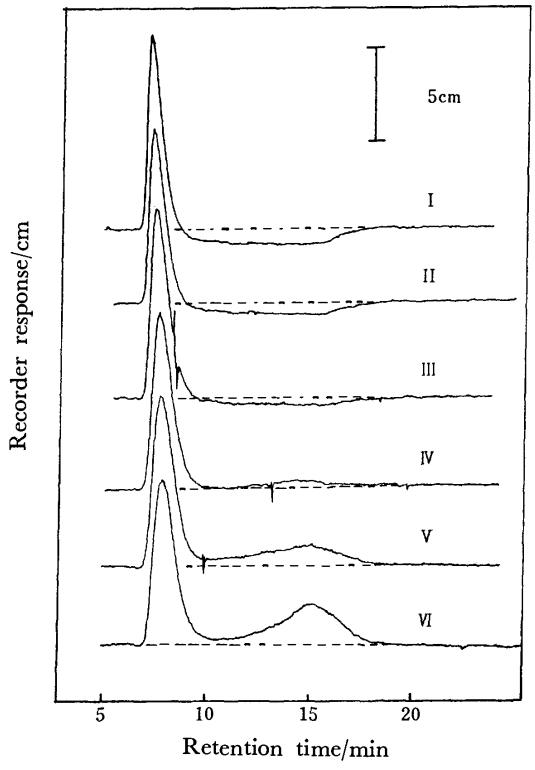

Fig. 4. Representative elution patterns of the Mg–P_2O_7 system.
$[Mg]_0=3.06\times10^{-6}$ mol dm^{-3}, $[P]_t=1.02\times10^{-4}$ mol·dm^{-3}.
$[Mg]_t\times10^5$ /mol dm^{-3}; I: 0.977, II: 1.95, III: 3.91, IV: 5.96, V: 7.92, VI: 9.77.

Table 1. The data of the gel chromatographic analysis for the $Mg-P_2O_7$ system
($[P]_t=0.828\times10^{-4}$ mol dm^{-3})

$[Mg]_0\times10^7$ / mol dm^{-3}	$[Mg]_t\times10^5$ / mol dm^{-3}	$\bar{n}$
3.21	0.988	0.11
3.93	0.988	0.12
4.94	0.988	0.14
6.22	0.988	0.18
7.88	0.988	0.22
9.88	1.98	0.28
12.5	1.98	0.32
15.6	1.98	0.37
19.8	1.98	0.42
24.7	1.98	0.50
31.2	3.95	0.54
39.3	5.93	0.61
49.5	5.93	0.66
62.3	5.93	0.70
78.4	5.93	0.75
98.8	5.93	0.77
125	7.90	0.83
156	7.90	0.86
198	7.90	0.88

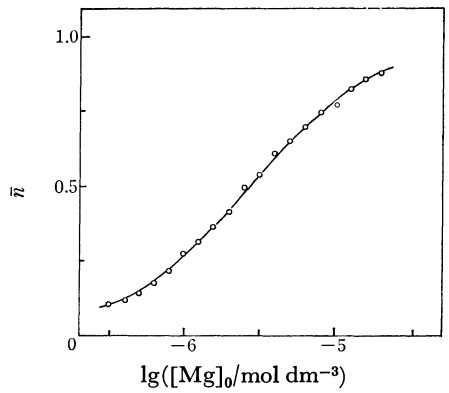

Fig. 5. Plots of $\bar{n}$ *vs.* lg $[Mg]_0$.
$[P]_t=0.828\times10^{-4}$ mol dm^{-3}.
The solid line is calculated from Eq. 3, when only the formation of an ML type complex is considered, and lg $\beta_1=5.57$.

this work, however, an effluent was fractionated as follows in order to determine $\bar{n}$ more precisely. The amount of bound magnesium was calculated from the difference between the total amount of magnesium in zone α (fraction of 6—10 min) and the amount of free magnesium ions in the preceding zone (fraction of 2—6 min). $\bar{n}$ obtained is tabulated in Table 1. The elution patterns obtained in these experiments were types B, C, and D. In Fig. 5 the plots of $\bar{n}$ *versus* lg $[Mg]_0$ are shown.

Since $\bar{n}$ is between 0.1 and 0.9, only the complexes of ML and M_2L type are taken into consideration. Equation 3 can be written as

$$\bar{n}=\frac{\beta_1[Mg]_0+2\beta_2[Mg]_0^2}{1+\beta_1[Mg]_0+\beta_2[Mg]_0^2}. \quad (4)$$

Equation 4 can be rearranged into

$$\frac{\bar{n}}{2-\bar{n}}\cdot\frac{1}{[Mg]_0^2}=\beta_2+\beta_1\frac{1-\bar{n}}{2-\bar{n}}\cdot\frac{1}{[Mg]_0}. \quad (5)$$

By plotting $\bar{n}/(2-\bar{n})[Mg]_0^2$ *versus* $(1-\bar{n})/(2-\bar{n})[Mg]_0$, we can obtain β_1 from the slope and β_2 from the intercept. By using the least squares method, β_1 was found to be 3.7×10^5 (lg $\beta_1=5.57$). Since the intercept was found to be nearly zero, it was concluded that the formation of the complex ML was predominant under these experimental conditions. The experimental plots in Fig. 5 lie close to the theoretical curve calculated from the value of lg β_1, 5.57.

The side reaction coefficient of ammonium ions for diphosphate ions is estimated to be nearly unity, because the stability constants of ion-pairs of ammonium ions are in general lower than those of potassium ions (lg β_1 for diphosphate, 0.80 at $I=1$ and at 25 °C),[14] and $[NH_4^+]=10^{-3}$ mol dm^{-3}.

The Stability Constants Obtained by Various Methods. For the purposes of comparison, the stability constant of an ML type complex of magnesium and diphosphate in sodium perchlorate solution was determined by both the gel chromatographic method and the ion-exchange method. For the latter, Schubert's method was employed.[15]

Table 2. Stability constants of MgP_2O_7 complex

lg (β_1/ mol^{-1} dm^3)	Method[a]	Ionic strength / mol dm^{-3}	Supporting electrolyte	Temp °C	Ref.
5.42	A	1	Me_4NBr	25	16
5.41	A	1	Me_4NCl	25	17
5.57	B	0.1	Me_4NCl	25	This work
4.7	A	0.1	$NaNO_3$	25	18
5.18	C	0.1	$NaClO_4$	21	This work
5.06	B	0.1	$NaClO_4$	25	This work

a) A: pH titration method; B: gel chromatographic method; C: cation-exchange method.

The stability constants of a magnesium–diphosphate complex thus obtained as well as those reported by other workers are listed in Table 2. The stability constants obtained by both the pH titration method and the gel chromatographic method agree fairly well with each other, even though the two methods are based on quite different principles. The stability constant obtained by the gel chromatographic method is somewhat larger than those obtained by the pH titration method. One of the possible reasons for this discrepancy may be due to the difference in the ionic strengths. The stability constants of the complex in sodium perchlorate solution obtained by both the ion-exchange method and the gel chromatographic method accord fairly well with each other. However, the stability constants of the complex in sodium nitrate solution obtained by the pH titration method is considered to be a little too low.

It has been shown by the present investigation that the gel chromatographic method is applicable even in the field of inorganic complex chemistry.

The authors wish to express their appreciation to Dr. Norimasa Yoza for his interest in this work and for many helpful suggestions.

References

1) J. P. Hummel and W. J. Dreyer, *Biochim. Biophys. Acta*, **63**, 532 (1962).
2) R. F. Colman, *Anal. Biochem*, **46**, 358 (1972).
3) R. F. Mantoura and J. P. Riley *Anal. Chim. Acta*, **78**, 193 (1975).
4) G. F. Fairclough, Jr., and J. S. Fruton, *Biochemistry*, **5**, 673 (1966).
5) E. Breslow and A. W. Girrotti, *J. Biol. Chem.*, **245**, 1527 (1970).
6) N. Yoza, *J. Chromatogr.*, **86**, 325 (1973).
7) N. Yoza, K. Kouchiyama, T. Miyajima, and S. Ohashi, *Anal. Lett.*, **8**, 641 (1975).
8) F. L. Conde and L. Prat, *Anal. Chim. Acta*, **16**, 473 (1957).
9) T. Miyajima, N. Yoza, and S. Ohashi, *Bunseki-kiki Zokan*, "Liquid Chromatography," 151 (1974).
10) N. Yoza and S. Ohashi, *Anal. Lett.*, **6**, 595 (1973).
11) T. Miyajima, Master's Thesis, Kyushu University, Fukuoka, Japan, 1975.
12) N. Yoza, T. Ogata, Y. Ueno, and S. Ohashi, *J. Chromatogr.*, **61**, 295 (1971).
13) D. O. Jordan, S. J. Lovell, D. R. Phillips, and D. J. Winzor, *Biochemistry*, **13**, 1832 (1974).
14) S. M. Lambert and J. I. Watters, *J. Am. Chem. Soc.*, **79**, 4262 (1957).
15) J. Schubert, *J. Phys. Chem.*, **52**, 340 (1948).
16) R. R. Irani, *J. Phys. Chem.*, **65**, 1463 (1961).
17) J. I. Watters and R. Machen, *J. Inorg. Nucl. Chem.*, **30**, 2163 (1968).
18) A. Johansson and E. Wänninen, *Talanta*, **10**, 769 (1963).

New Palladium(II) Carbene Complexes Containing a Cyclometallated Aryl Group†

Katsuma HIRAKI,* Masayoshi ONISHI,* Kiyoshi SEWAKI, and Keiichi SUGINO

Department of Industrial Chemistry, Faculty of Engineering, Nagasaki University, Bunkyo-machi, Nagasaki 852

(Received October 11, 1977)

New carbene complexes of (acetophenone oxime, 2-*C,N*)chloro(1,3-diphenylimidazolidin-2-ylidene)palladium(II) (**1**), (benzophenone oxime,2-*C,N*)chloro(1,3-diphenylimidazolidin-2-ylidene)palladium(II) (**2**), and chloro(*N,N*-dimethylbenzylamine,2-*C,N*)(1,3-diphenylimidazolidin-2-ylidene)palladium(II) (**3**) have been prepared by reactions between dimeric cyclopalladated complexes and 1,1′,3,3′-tetraphenyl-2,2′-biimidazolidinylidene. Chlorine atoms were shown to be situated at the *trans* position to the aryl-palladium σ bond on the basis of IR spectra. These carbene complexes underwent halogen metathesis with LiBr to yield the corresponding bromo derivatives. Triphenylphosphine displaced the chlorine atom in **1**, **2**, and **3**, converting each to a cationic carbene complex, in which the nitrogen donor of cyclopalladation moiety remained coordinated to palladium.

The electron rich olefin, 1,1′,3,3′-tetraphenyl-2,2′-biimidazolidinylidene,[1] has been used as an organic precursor for the syntheses of transition metal carbene complexes by Lappert *et al.*[2] Some palladium(II) carbene complexes have been prepared in reactions between di-μ-chloro-dichlorobis(trialkylphosphine)dipalladium(II) and the electron rich olefin.[2]

We have been interested in the halogen-bridge splitting reaction of cyclopalladated dimeric complexes and presented earlier a brief report on some palladium(II) complexes prepared with this method.[3] This paper will deal with several new palladium(II) complexes, which have been prepared by the halogen-bridge splitting reactions between the cyclopalladated dimeric complexes and the electron rich olefin. The product has been shown to contain both the carbene ligand and an aryl-palladium σ bond.

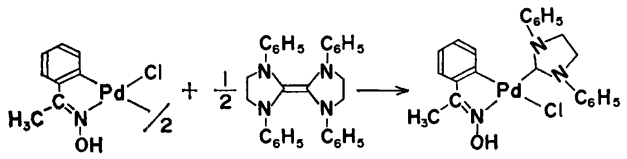

L_2 1

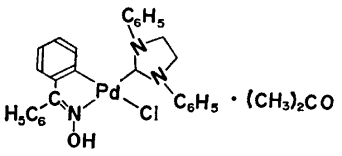

2

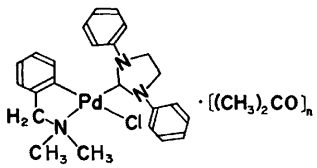

3a ; n = 1/2
3b ; n = 0

† A preliminary report of this work was presented at the 36th National Meeting of the Chemical Society of Japan, Higashi-Osaka, April 1977.

Experimental

General Procedures. Melting points were determined in capillary tubes on a Yanagimoto MP-S3 microstage apparatus and are uncorrected. IR spectra were recorded on a Hitachi model 285 spectrometer and a Shimadzu IR 450 spectrometer. ^{1}H-NMR spectra were run on a Japan Electron Optics Laboratory model JNM-MH-100 spectrometer (100 MHz), using tetramethylsilane as an internal standard. ^{13}C-NMR spectra were measured on a Bruker WH-90 spectrometer, operating the Fourier transform model at 22.63 MHz.[4] Molecular weights were determined using a JEOL model JMS-01SG double-focussing mass spectrometer referring to parent ion peaks. Molar conductivities were measured with a Toa Denpa CM-6A instrument.

Starting materials, [{PdCl(C_6H_4–C(=N–OH)R, 2-*C,N*)}$_2$],[5] [{PdCl($C_6H_4CH_2NMe_2$,2-*C,N*)}$_2$],[6] and 1,1′,3,3′-tetraphenyl-2,2′-biimidazolidinylidene (L_2)[7] were prepared and purified according to the methods described in the literature. Reactions were performed under dry nitrogen.

Reactions of the Electron Rich Olefin with the Dimeric Cyclopalladated Complexes. The olefin L_2 (0.45 g) and [{PdCl(C_6H_4–C(=N–OH)CH_3,2-*C,N*)}$_2$] (0.56 g) were heated under reflux in *m*-xylene for 10 min. The reaction mixture was allowed to cool and then filtered. The separated solid was recrystallized from dichloromethane and hexane to give a pale yellow crystalline powder, [PdCl(C_6H_4–C(=N–OH)CH_3, 2-*C,N*)L] (L = 1,3-diphenylimidazolidin-2-ylidene) (**1**), 0.58 g.

[PdCl(C_6H_4–C(=N–OH)C_6H_5,2-*C,N*)L]·$(CH_3)_2CO$ (**2**) and [PdCl($C_6H_4CH_2NMe_2$,2-*C,N*)L]·1/2$(CH_3)_2CO$ (**3a**) were prepared in a similar method as used for **1**, but acetone was used for the recrystallization. Complex **3a** was converted into a non-solvated complex (**3b**) by recrystallization from acetone and diethyl ether. The removal of acetone was confirmed by elemental analysis, IR, and ^{1}H-NMR spectrum of **3b**.

*Halogen Metathesis Reactions of **1**, **2**, and **3a**.* The chloro complex **1** (0.20 g) was treated with an excess of LiBr (0.1 g) in methanol under reflux for 4 h. The suspension was cooled and filtered. The separated solid was washed with methanol and diethyl ether to yield a pale yellow powder, [PdBr(C_6H_4–C(=N–OH)CH_3,2-*C,N*)L] (**4**), 0.14 g.

The complex **2** (0.15 g) and LiBr (0.05 g) were heated under reflux in acetone for 5 h. The solvent was evaporated, and the residue was washed with methanol and diethyl ether to give [PdBr(C_6H_4–C(=N–OH)C_6H_5,2-*C,N*)L] (**5**), 0.12 g.

[PdBr($C_6H_4CH_2NMe_2$,2-*C,N*)L] (**6**) was obtained similarly.

*Reactions of **1**, **2**, and **3a** with Triphenylphosphine.* The complex **1** (0.20 g) and PPh_3 (0.15 g) in acetone were heated

Table 1. Syntheses of new palladium(II) carbene complexes

	Color	Yield %	Mp[a] °C	Found (Calcd) % C	H	N	Λ_M[b]	M+ [c] (Calcd)
1	Pale yellow	57.6	230—268	55.44 (55.44	4.41 4.45	8.30 8.43)	2.15[d]	499 (498.3)
2	Cream	35.2	246—247	60.17 (60.21	4.76 4.89	6.97 6.79)	1.48[d]	560 (560.4)[f]
3a	White	55.8	215—272	58.11 (58.07	5.50 5.54	7.92 7.96)	7.18[d]	498 (498.3)[f]
3b	White		207—294	57.63 (57.85	5.29 5.26	8.52 8.43)		
4	Pale yellow	64.5	241—295	51.33 (50.90	4.07 4.09	7.77 7.74)		
5	Pale yellow	82.8	255—259	55.71 (55.61	4.02 4.00	7.03 6.95)		
6	White	65.8	227—235	53.29 (53.11	4.92 4.83	7.68 7.74)		
7	White	15.2	182—192	59.72 (59.72	4.58 4.52	5.13 5.00)	123[e]	
8	Cream	34.8	176—177	62.10 (62.31	4.43 4.43	4.65 4.74)	136[e]	
9	White	24.9	181—195	61.82 (61.17	5.15 5.01	5.13 5.10)	130[e]	

a) With decomposition. b) Molar conductivity, $\Omega^{-1}\,cm^2\,mol^{-1}$, at 25 °C, 10^{-3} mol/l. c) The strongest peak in the parent-ion isotope pattern of mass spectrum. d) In acetonitrile. e) In acetone. f) Calculated value for the non-solvated complex.

for 5 h with stirring. The reaction mixture was allowed to cool and filtered. Sodium perchlorate–water(1/1) (0.06 g) was added to the filtrate. After the suspension was stirred overnight, the solvent was removed *in vacuo*. The residue was recrystallized from dichloromethane and diethyl ether to afford a white crystalline product, [Pd(C_6H_4–C(=N–OH)CH_3, 2-*C*,*N*)L(PPh_3)]ClO_4 (**7**), 0.05 g.

[Pd(C_6H_4–C(=N–OH)C_6H_5,2-*C*,*N*)L(PPh_3)]ClO_4 (**8**) and [Pd($C_6H_4CH_2NMe_2$,2-*C*,*N*)L(PPh_3)]ClO_4 (**9**) were obtained similarly.

Results and Discussion

When the electron rich olefin and the cyclopalladated halogen-bridged dimeric complex were mixed in *m*-xylene under reflux, the reaction mixture immediately changed from pale yellow to pale orange or reddish violet and then to a black suspension owing to partial decomposition. A similarly highly colored state has also been observed in the reaction between the olefin and di-μ-chloro-dichlorobis(trialkylphosphine)dipalladium(II) or -diplatinum(II) by Lappert *et al.*[2] They assumed the formation of an intermediate π-complex, followed by cleavage of the double bond to yield a carbene complex.

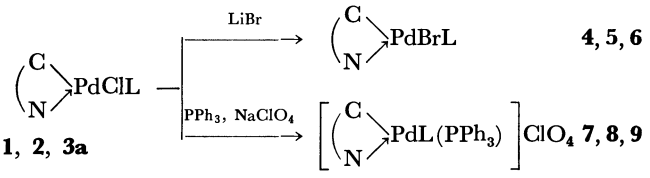

C,N acetophenone oxime, 2-*C*,*N*; **1**, **4**, and **7**
benzophenone oxime, 2-*C*,*N*; **2**, **5**, and **8**
N,*N*-dimethylbenzylamine, 2-*C*,*N*; **3a**, **6**, and **9**

Table 2. IR data of the Pd(II) carbene complexes[a]

	ν(O-H)[b]	ν(C_ϕ-N)[c,d]	Far-IR data[c,e]
1	3190	1270	431s, (315sh, 295s, 286sh, 277sh), 240w
2	3170	1275	429s, 315—303s, 240s
3b		1280	426m, 358w, (315sh, 289s), 253w
4	3225	1280	430s, 315w, 285—277w
5	3200	1272	428s, 311—295m, 245w
6		1275	421m, 357w, 314w, 264w
7	3480 / 3230	1274	423m, 275w
8	3470 / 3240	1270	426m
9		1275	429s, 251w

a) Values in cm^{-1}. b) In Nujol mull. c) In KBr disc. d) ν($C_{aromatic}$-N). e) Underlined numbers refer to ν(Pd-Cl).

The complexes, **1**, **2**, and **3a** underwent halogen metathesis with lithium bromide to yield the corresponding bromo-derivatives, and reacted with triphenylphosphine affording **7**, **8**, and **9**, respectively. Tables 1, 2, and 3 give the yields, analytical data, and physical and spectroscopic properties of the complexes obtained in this study.

Complexes **1**, **2**, and **3a** exhibited low conductivities, indicating non-ionic character[8] (Table 1). However, **7**, **8**, and **9** have been ascribed to the cationic complexes on the basis of high conductivities.[8] In the conversion of **1**, **2**, and **3a** to **7**, **8**, and **9**, respectively, triphenylphosphine displaced the chlorine atom of the initial complex and the nitrogen donor remained coordinated to the central metal.

TABLE 3. ^{1}H-NMR DATA OF THE CARBENE COMPLEXES

	NMR data[a,b], δ value, ppm				
	OH	Aromatic	NCH_2CH_2N	CH_2NMe_2	CH_3
1	9.85(s)	8.05—6.65(c)	4.34(c)		2.08(s)
2	10.07(s)	8.20—6.60(c)	4.45(c)		2.10(s, Me_2CO)
3b[c]		8.28—6.58(c)	4.33(c)	3.61(s)	2.59(s)
4	9.49(s)	8.14—6.72(c)	4.39(s)		2.12(s)
5	9.72(s)	8.33—6.77(c)	4.53(s)		
6[c]		8.28—6.66(c)	4.34(s)	3.66(s)	2.64(s)

a) δ value relative to TMS; in CD_2Cl_2, unless noted elsewhere. b) s=singlet, c=complex. c) In $CDCl_3$.

^{13}C-NMR spectrum of **3b** in $CDCl_3$ showed a resonance at δ 201.6 from TMS, assignable to a carbene carbon atom. As for the 1,3-diphenylimidazolidin-2-ylidene ligand, two methylene carbons showed a single resonance, indicating that the N–$C_{carbene}$–N plane was perpendicular to the coordination plane of the palladium atom and the *N*-substituted two phenyl carbons were spectroscopically equivalent. In the range of δ 137 to 160, the spectrum also gave resonances at δ 149.1, 147.8, and 141.8, which are assignable to three kinds of quarternary carbon atoms, methylene- and palladium-substituted phenylene carbons (1-C and 2-C) in the cyclopalladated moiety and *N*-substituted two phenyl carbons in the carbene ligand.[9]

On the basis of these facts, complex **3b** was ascribed to a new carbene complex which retained the cyclopalladated chelate structure of the starting compound. The complexes, **1** and **2** also exhibited chemical and spectroscopic properties similar to **3b**, and were assumed to have a structure similar to **3b**. These carbene complexes containing the cyclometallated aryl group are stable in air at room temperature.

Four methylene protons of the imidazolidin-2-ylidene group were represented by an A_2B_2 spin system in the ^{1}H-NMR spectra and showed a complex signal in chloro-type complexes, **1**, **2**, and **3b**, as shown in Table 3. Each of the bromo-type complexes, **4**, **5**, and **6**, gave virtually a singlet in the A_4 limit for the methylene protons.

The IR spectra of these nine carbene complexes showed a strong band near 1275 cm^{-1} for $\nu(C_{aromatic}–N)$ of the 1,3-diphenylimidazolidin-2-ylidene ligand. Two bands were observed in the range 3200—3500 cm^{-1} in **7** and **8**. The lower frequency band was tentatively assigned as a hydrogen-bonding ν(O–H) of an oxime group and the sharp higher frequency band as that of a non-hydrogen-bonding ν(O–H).[10]

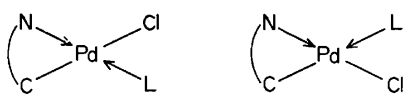

A B

Two structures are stereochemically possible for the carbene complexes, **1**, **2**, and **3b**. Crociani *et al.*[11] studied the ν(Pd–Cl) frequencies of mononuclear complexes derived from di-μ-chloro-bis(*N*,*N*-dimethylbenzylamine, 2-*C*,*N*)dipalladium(II) or related complexes and donor ligands. They reported that the ν(Pd–Cl) frequency *trans* to a tertiary amine-nitrogen donor fell in the range of 353—321 cm^{-1} and the ν(Pd–Cl) frequency *trans* to an aryl group in the range of 299—280 cm^{-1}, and correlated the differences of these frequencies to that of the *trans* influence of the respective ligands. In consideration of the data reported here and related ones,[12,13] structure A has been assigned for complexes **1** and **3b**. No evidence supporting the presence of the other geometrical isomer B for **1** and **3b** were found in the NMR and IR (450—200 cm^{-1}) spectra.

The ν(Pd–Cl) band for **2** could not be clearly assigned. However, **2** also appears to have structure A, since no band was observed in the range of 353—321 cm^{-1}. Obscurity of the ν(Pd–Cl) assignment of **2** may be accounted for either by overlapping of the weak ν(Pd–Cl) band with strong bands at 303—315 cm^{-1}, or by the large shift of the ν(Pd–Cl) frequency towards the lower wavenumber probably due to the intramolecular hydrogen-bonding of chlorine.

We are grateful to Professor Keinosuke Hamada and Mr. Hirofumi Morishita, Nagasaki University, for their help in the far IR measurements.

References

1) H. W. Wanzlick, *Angew. Chem.*, **80**, 809 (1968).
2) D. J. Cardin, B. Cetinkaya, E. Cetinkaya, and M. F. Lappert, *J. Chem. Soc., Dalton Trans.*, **1973**, 514.
3) M. Onishi, Y. Ohama, K. Sugimura, and K. Hiraki, *Chem. Lett.*, **1976**, 955.
4) The authors thank Dr. Makoto Takagi, Kyushu University for helpful discussions on ^{13}C-NMR spectra.
5) H. Onoue, K. Minami, and K. Nakagawa, *Bull. Chem. Soc. Jpn.*, **43**, 3480 (1970).
6) A. C. Cope and E. C. Friedrich, *J. Am. Chem. Soc.*, **90**, 909 (1968).
7) H. W. Wanzlick, *Org. Synth.*, **47**, 14 (1967).
8) W. J. Geary, *Coord. Chem. Rev.*, **7**, 81 (1971).
9) ^{13}C-NMR spectrum of di-μ-chloro-bis(*N*,*N*-dimethylbenzylamine, 2-*C*,*N*)dipalladium(II) in $CDCl_3$ showed two resonances at δ 147.1, and 143.1 for quarternary methylene- and palladium-substituted phenylene carbons in the range of δ 137 to 160.
10) Complexes, **7** and **8** are sparingly soluble in carbon tetrachloride and chloroform, and detailed examination of the hydrogen-bonding of these cationic complexes were not obtained.
11) B. Crociani, T. Boschi, R. Pietropaolo, and U. Belluco, *J. Chem. Soc., A*, **1970**, 531.
12) J. Dehand, M. Pfeffer, and M. Zinsius, *Inorg. Chim. Acta*, **13**, 229 (1975).
13) K. Suzuki and H. Yamamoto, *J. Organomet. Chem.*, **54**, 385 (1973).

ESR Study of ^{63}Cu(II) Doped in Single Crystals of Bis(methyl 3-alkylidenedithiocarbazato)nickel(II)

Takayuki ONIKI

Pre-dental Course of Kyushu Dental College, Manazuru, Kokurakita-ku, Kitakyushu 803

(Received December 16, 1977)

ESR spectra of ^{63}Cu(II) diluted by various single crystals of the title Ni(II) complexes are reported. The alkylidene groups denote 1-(2-naphthyl)ethylidene, 1-(*p*-tolyl)ethylidene, 1-phenylethylidene, benzylidene, 1-(*m*-nitrophenyl)ethylidene, and 1-(*p*-nitrophenyl)ethylidene, and the corresponding Ni(II) complexes are abbreviated as Ni(nedc)$_2$, Ni(tedc)$_2$, Ni(pedc)$_2$, Ni(bdc)$_2$, Ni(mndc)$_2$, and Ni(pndc)$_2$ respectively. Before the analyses of the ESR data, the crystal structures of Ni(nedc)$_2$ and Ni(tedc)$_2$ were determined. In both Ni(II) complexes, the molecules have been found to be of a C_2 symmetry, with a tetrahedrally distorted *cis*-NiN_2S_2 arrangement. The unpaired electrons of the Cu(II) complexes were thus described in terms of C_2 symmetry except for the case of Cu(bdc)$_2$. The d-orbital coefficients of the ground-state Kramers doublet were determined from the observed *g* values in such a way that the hyperfine parameters calculated from the coefficients closely reproduce the observed values. In ^{63}Cu(II)/Ni(bdc)$_2$, the *g* values are rhombic, and an additional hyperfine structure due to atoms which do not directly coordinate to Cu(II) ion was observed. The coordination of the Cu(II) ion in Ni(bdc)$_2$ was concluded from the ESR data to be a *trans* arrangement.

The complexes containing Cu–S bonds are interesting for their covalent character. The copper-ligand bindings have been studied by ESR, mainly in complexes with oxygen and nitrogen ligands, and there have been many studies of the square planar, CuS_4-type complexes, that is dithiocarbamates,[1,2] dithiophosphate,[3] bis(maleonitriledithiolato)copper(II),[4] and 1,4,8,11-tetrathiacyclotetradecane copper(II) tetrafluoroborate.[5] However relatively few studies have been reported of the CuN_2S_2-type complexes, that is *trans*-bis(thiosemicarbazide)copper(II) nitrate,[6] α-thiopicolinanilide copper(II),[7] and *N*,*N*′-ethylene bis(monothioacethylacetoniminato)copper(II).[8]

The evaluation of the bonding parameters from the ESR data requires a knowledge of the assignment of the d-d transition bands in the electronic spectra of Cu(II) complexes. In the electronic spectra of bis(methyl 3-alkylidenedithiocarbazato) copper(II), however, the intense charge-transfer bands mask the d-d transitions. The general method of calculating covalent parameters by the use of d-d energy could not be employed for these complexes.

In this study, the ESR spectra of ^{63}Cu(II) diluted by single crystals of six Ni(II) complexes and the crystal structures of Ni(nedc)$_2$ and Ni(tedc)$_2$ are reported (Fig. 1). The d-orbital coefficients of the ground state are determined from the *g* values with C_2 symmetry except for the case of Cu(bdc)$_2$, in which D_{2h} symmetry was used. The method of treating the ESR data follows the general scheme of Swalen *et al.*,[10] extended to C_2 symmetry.

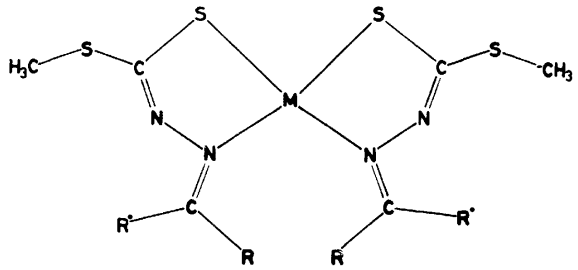

	R′	R	
a	$-CH_3$	2-naphthyl	Cu(nedc)$_2$
b	$-CH_3$	*p*-tolyl	Cu(tedc)$_2$
c	$-CH_3$	phenyl	Cu(pedc)$_2$
d	$-H$	phenyl	Cu(bdc)$_2$
e	$-CH_3$	*m*-nitrophenyl	Cu(mndc)$_2$
f	$-CH_3$	*p*-nitrophenyl	Cu(pndc)$_2$

Fig. 1. Assumed basic structure of bis(methyl 3-alkylidenedithiocarbazato)metal(II), and abbreviations of copper(II) complexes. The coordination around Cu(II) in Ni(bdc)$_2$ was concluded to be *trans* arrangement from ESR.

Experimental

The complexes were prepared according to a modification of the methods of Ref. 11. The single crystals were obtained by the slow evaporation of chloroform–ethanol solutions.

X-Ray Analyses. Three-dimensional intensity data were collected by the 2θ-θ scan technique on a Syntex $P\bar{1}$ four-circle diffractometer using Mo K_α radiation monochromated by a graphite plate. All the reflections with $2\theta \leqq 48°$ were collected. In this way, 3265 independent reflections were measured for Ni(tedc)$_2$, and 2100 for Ni(nedc)$_2$, of which 2642 and 1946 having $I \geqq 2\sigma$ (I) were used in the subsequent analyses. They were corrected for Lorentz and polarization effects, but corrections for absorption were not applied, as the samples were sufficiently small. The calculations were performed on the FACOM 230-75 computer of the Computer Center of Kyushu University, using the UNICS program system.[12] The scattering factors for all the atoms were taken from Ref. 13. The F_o-F_c table is kept at the office of This Bulletin as Document No. 7827.

ESR Measurements. The ESR spectra were recorded every 15° around three mutually perpendicular rotational axes. The most elongated axis was defined as the 2-axis, which is parallel to the crystal b-axis in the case of Ni(nedc)$_2$ or Ni(tedc)$_2$. The 1- and 3-axes were taken at will in the plane perpendicular to the 2-axis. The spectra were taken on a JEOL ME 3X spectrometer at the X band. Mn(II) diluted with MgO and DPPH were used as the *g* marker.

Results

Crystal Structures. The structures were solved by the heavy-atom technique. After block-diagonal least-squares refinement with anisotropic thermal

Table 1. Fractional atomic coordinates[a] and anisotropic temperature factors($\times 10^4$) for $Ni(nedc)_2$
The temperature factor is of this form: $\exp[-(B_{11}h^2+B_{22}k^2+B_{33}l^2+B_{12}hk+B_{13}hl+B_{23}kl)]$.

	x	y	z	B_{11}	B_{22}	B_{33}	B_{12}	B_{13}	B_{23}
Ni	0(0)	289(1)	2500(0)	8(0)	71(1)	52(1)	0(0)	14(1)	0(0)
S (1)	683(1)	2055(2)	3141(1)	12(0)	86(2)	89(1)	8(1)	19(1)	−11(3)
S (2)	1915(1)	1437(2)	4739(1)	12(0)	134(3)	66(1)	−20(1)	12(1)	−21(3)
N (1)	604(2)	−1187(5)	2701(3)	9(1)	83(6)	39(3)	−5(4)	13(3)	4(7)
N (2)	1188(2)	−841(5)	3535(3)	8(1)	105(7)	44(3)	−2(4)	11(3)	−1(7)
C (1)	1242(2)	650(7)	3761(4)	10(1)	108(9)	52(4)	−8(5)	19(3)	−5(9)
C (2)	2386(3)	−297(9)	5186(5)	13(1)	181(12)	79(7)	17(7)	13(4)	28(14)
C (3)	551(2)	−2454(6)	2171(4)	12(1)	84(8)	47(4)	2(5)	24(3)	6(9)
C (4)	1056(3)	−3572(8)	2480(5)	15(1)	129(10)	74(5)	25(6)	27(4)	−12(12)
C (5)	−24(2)	−2776(6)	1190(4)	12(1)	106(8)	42(4)	−2(5)	22(3)	−12(9)
C (6)	−258(3)	−4333(7)	986(5)	18(1)	117(9)	52(4)	−8(6)	29(4)	−27(10)
C (7)	−811(3)	−4609(8)	106(5)	18(1)	145(10)	59(4)	−13(6)	29(4)	−37(11)
C (8)	−1138(2)	−3368(8)	−612(4)	15(1)	157(10)	48(4)	−8(6)	23(4)	−39(11)
C (9)	−1712(3)	−3612(9)	−1524(5)	16(1)	230(14)	60(5)	−5(7)	24(4)	−66(14)
C (10)	−2004(3)	−2391(10)	−2200(5)	19(2)	267(16)	58(5)	19(8)	22(5)	−34(15)
C (11)	−1767(3)	−863(10)	−2031(5)	18(1)	261(15)	56(5)	25(8)	30(4)	26(14)
C (12)	−1208(3)	−570(8)	−1143(5)	17(1)	204(13)	51(4)	21(7)	29(4)	40(12)
C (13)	−891(2)	−1830(7)	−426(4)	13(1)	143(10)	45(4)	3(5)	26(4)	2(10)
C (14)	−325(2)	−1567(7)	497(4)	13(1)	120(9)	44(4)	−1(5)	24(3)	2(9)

a) The numbers in parentheses are the estimated standard deviations in units of the last significant digit.

Table 2. Fractional atomic coordinates and anisotropic temperature factors($\times 10^4$) for $Ni(tedc)_2$

	x	y	z	B_{11}	B_{22}	B_{33}	B_{12}	B_{13}	B_{23}
Ni	2374(1)	1495(1)	2752(0)	48(1)	84(1)	23(0)	2(1)	26(1)	−14(1)
S (1)	1699(2)	2557(2)	3406(1)	79(2)	124(3)	35(1)	0(3)	55(2)	−43(2)
S (1)'	2724(2)	3627(2)	2388(1)	77(2)	83(2)	37(1)	−1(3)	47(2)	−11(2)
S (2)	760(2)	1055(3)	4284(1)	86(2)	222(4)	29(1)	4(4)	60(2)	−43(3)
S (2)'	3161(2)	3962(2)	1096(1)	90(2)	120(3)	39(1)	12(4)	52(2)	41(2)
N (1)	1693(4)	−304(6)	2822(3)	39(4)	109(8)	20(2)	22(8)	24(4)	1(5)
N (1)'	3273(4)	630(6)	2368(3)	40(4)	88(7)	22(2)	3(8)	19(4)	0(5)
N (2)	1363(4)	−432(7)	3398(3)	52(4)	139(9)	22(2)	10(10)	31(4)	−7(6)
N (2)'	3378(4)	1381(6)	1783(3)	48(4)	101(8)	25(2)	−5(9)	25(4)	1(6)
C (1)	1314(5)	877(8)	3658(3)	44(5)	161(12)	23(2)	17(12)	22(5)	−21(8)
C (1)'	3123(5)	2759(7)	1774(3)	45(5)	109(10)	26(2)	−13(11)	15(5)	−4(7)
C (2)	16(5)	−644(9)	4133(4)	77(7)	177(14)	37(3)	0(15)	60(7)	19(10)
C (2)'	3470(6)	2661(9)	517(4)	85(7)	174(14)	36(3)	15(15)	55(7)	20(10)
C (3)	1445(4)	−1463(7)	2393(3)	35(4)	113(9)	19(2)	8(10)	17(4)	−17(7)
C (3)'	3803(5)	−563(7)	2567(3)	38(5)	92(9)	23(2)	−5(10)	10(5)	−20(7)
C (4)	1048(6)	−2888(8)	2575(4)	69(6)	121(11)	29(2)	−50(12)	39(6)	1(8)
C (4)'	4398(6)	−1225(9)	2160(4)	64(6)	168(13)	33(2)	71(14)	53(6)	9(9)
C (5)	1512(4)	−1286(7)	1688(3)	39(4)	93(9)	18(2)	−22(10)	13(4)	−9(6)
C (5)'	3835(5)	−1311(7)	3229(3)	38(4)	89(9)	25(2)	3(10)	18(5)	−2(7)
C (6)	1803(5)	−2484(7)	1362(3)	38(5)	112(9)	24(2)	−14(10)	23(4)	−17(7)
C (6)'	3933(5)	−412(8)	3827(3)	45(5)	142(11)	26(2)	18(12)	21(5)	−9(8)
C (7)	1817(5)	−2303(7)	682(3)	52(5)	117(10)	21(2)	−24(11)	22(5)	−8(7)
C (7)'	3998(5)	−1136(9)	4461(4)	51(5)	188(14)	28(2)	23(14)	19(5)	16(9)
C (8)	1514(5)	−971(8)	310(3)	45(5)	148(11)	19(2)	−33(12)	17(5)	−3(7)
C (8)'	3973(5)	−2676(9)	4508(4)	40(5)	190(14)	38(3)	20(13)	30(6)	53(10)
C (9)	1185(5)	224(8)	624(3)	46(5)	141(11)	24(2)	−23(12)	15(5)	4(8)
C (9)'	3856(5)	−3561(8)	3907(4)	52(5)	130(11)	37(3)	1(13)	23(6)	29(9)
C (10)	1183(5)	69(8)	1314(3)	38(5)	127(10)	23(2)	−20(11)	10(5)	−1(7)
C (10)'	3807(5)	−2872(8)	3274(4)	46(5)	110(10)	34(2)	7(11)	15(5)	12(8)
C (11)	1515(5)	−781(10)	−441(3)	79(6)	212(15)	19(2)	−35(15)	31(5)	16(9)
C (11)'	4097(5)	−3423(10)	5217(4)	94(7)	250(18)	26(3)	37(18)	38(6)	66(10)

Table 3. Important interatomic distances and angles for $Ni(nedc)_2$

Distances (Å)			
Ni-S (1)	2.147(2)	Ni-N (1)	1.926(5)
N (1)-N (2)	1.423(7)	S (1)-C (1)	1.741(7)
N (2)-C (1)	1.283(8)	C (1)-S (2)	1.740(7)
N (1)-C (3)	1.276(8)	C (3)-C (4)	1.502(10)
C (3)-C (5)	1.483(8)		
Angles (deg.)			
S (1)-Ni-S (1)	92.5(1)	N (1)-Ni-N (1)	99.4(3)
S (1)-Ni-N (1)	86.1(2)	Ni-S (1)-C (1)	93.2(3)
Ni-N (1)-N (2)	116.9(3)	N (1)-N (2)-C (1)	110.2(5)
N (2)-C (1)-S (1)	125.2(5)	N (2)-C (1)-S (2)	120.8(5)
S (1)-C (1)-S (2)	114.0(4)	Ni-N (1)-C (3)	128.5(4)
N (2)-N (1)-C (3)	114.6(5)		

Table 4. Important interatomic distances and angles for $Ni(tedc)_2$

Distances (Å)			
Ni-S (1)	2.142(3)	Ni-S (1)'	2.151(3)
Ni-N (1)	1.914(6)	Ni-N (1)'	1.921(6)
N (1)-N (2)	1.425(8)	N (1)'-N (2)'	1.418(8)
S (1)-C (1)	1.731(8)	S (1)'-C (1)'	1.736(8)
N (2)-C (1)	1.284(10)	N (2)'-C (1)'	1.273(9)
C (1)-S (2)	1.751(8)	C (1)'-S (2)'	1.757(8)
N (1)-C (3)	1.310(9)	N (1)'-C (3)'	1.291(9)
Angles (deg.)			
S (1)-Ni-S (1)'	93.0(2)	N (1)-Ni-N (1)'	99.1(2)
S (1)-Ni-N (1)	86.9(2)	S (1)'-Ni-N (1)'	85.7(2)
Ni-S (1)-C (1)	94.8(5)	Ni-S (1)'-C (1)'	92.5(5)
Ni-N (1)-N (2)	118.1(4)	Ni-N (1)'-N (2)'	116.8(4)
N (1)-N (2)-C (1)	110.6(6)	N (1)'-N (2)'-C (1)'	109.8(6)
N (2)-C (1)-S (1)	125.3(6)	N (2)'-C (1)'-S (1)'	126.0(6)
Ni-N (1)-C (3)	129.1(5)	Ni-N (1)'-C (3)'	129.0(5)
N (2)-N (1)-C (3)	112.8(5)	N (2)'-N (1)'-C (3)'	114.2(6)

parameters for non-hydrogen atoms, the final R values became 0.058 in both crystals. The parameters obtained are given in Tables 1—4.

Ni(nedc)$_2$: $NiS_4N_4C_{28}H_{26}$, formula weight 605.48, monoclinic, space group C2/c, a=26.518(8), b=8.399(1), c=14.546(3) Å, β=121.05(2)°, V=2775.6 Å^3, Z=4, D_m=1.423 g·cm^{-3} (by floatation), D_x=1.449 g·cm^{-3}.

The Ni atoms lie on the crystallographic two-fold axes. Each of the ligands is bonded to the Ni atom through the thiol S atom and one of the hydrazine N atoms, yielding a 5-membered chelate ring, and the Ni atom has a *cis*-planar coordination by two S and two N atoms. The molecule has a crystallographically imposed two-fold axis which bisects the S–Ni–S bond angle and which is parallel to the b-axis. The four ligator atoms are somewhat tetrahedrally disposed around the Ni atom. The interplanar angle between N–Ni–S planes is 22°. The packing of the complexes is illustrated in Fig. 2.

Ni(tedc)$_2$: $NiS_4N_4C_{22}H_{26}$, formula weight 533.41, monoclinic, space group $P2_1/c$, a=14.793(5), b=8.835(3), c=20.309(5) Å, β=110.77(2)°, V=2481.8 Å^3, Z=4, D_m=1.419 g·cm^{-3}, D_x=1.427 g·cm^{-3}.

The Ni atom has a coordination similar to that of $Ni(nedc)_2$. The molecule has a fictitious two-fold axis which is inclined from the b-axis. The interplanar angle between N–Ni–S planes is 24°. The packing is illustrated in Fig. 3.

ESR Spectra. *$^{63}Cu(II)/Ni(nedc)_2$*: There are four molecules in the unit cell. It was found, however, that there is only one copper quartet in all the crystal orientations. All the sites for copper ions were, therefore, magnetically indistinguishable. Figure 4 shows some representative spectra. The crystal b-axis is along the 2-axis. When the magnetic field($\boldsymbol{H}_0$) is in the 31-plane, the two Cu–N bondings are magnetically equivalent and the equally spaced nitrogen hyperfine structure(hfs) with an intensity ratio of 1:2:3:2:1 was well defined. The crystal c-axis is parallel to the 1-axis and nearly bisects the N–Cu–N angle, and the two Cu–N bondings are equivalent. The 23-plane is nearly parallel to the molecular plane. When the $\boldsymbol{H}_0$ is within 15° of one Cu–N bond direction, a nonequivalent nitrogen hfs is obtained (see b in Fig. 4). The g_z direction is parallel to the crystal b-axis, which is the molecular two-fold axis. The forbidden spectra corresponding to $\Delta m=\pm1$ and ±2 were not clearly

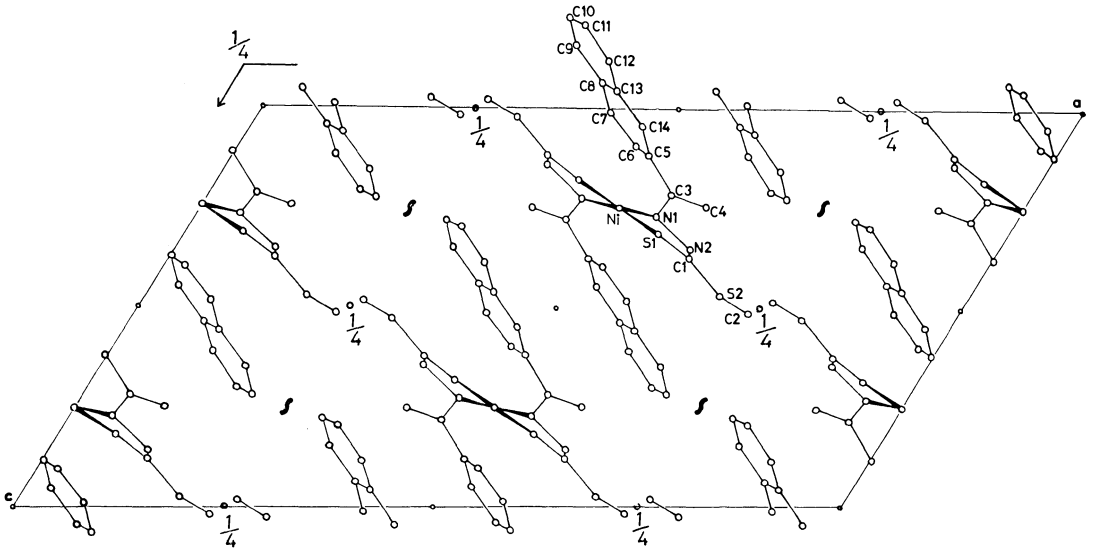

Fig. 2. Projection of the crystal structure along the b-axis of $Ni(nedc)_2$.

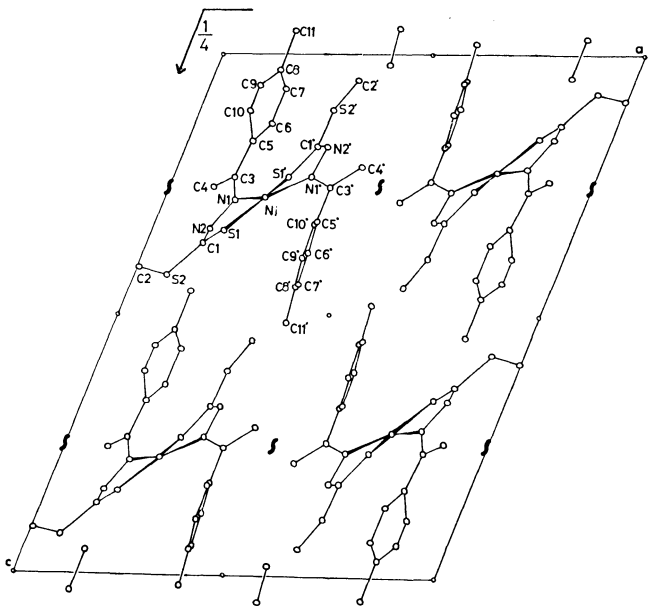

Fig. 3. Projection of the crystal structure along the b-axis of $Ni(tedc)_2$.

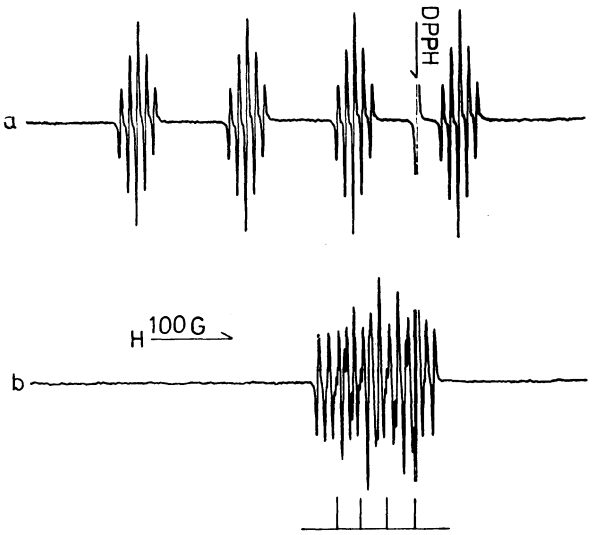

Fig. 4. Single crystal ESR spectra of $^{63}Cu(II)/Ni(nedc)_2$. a: $(\theta,\varphi)=(120°,0°)$, b: $(60°,90°)$.

identified, hence, no attempt was made to determine quadrupole coupling parameters. The g values and hf coupling constants were determined by a method similar to that of Fujimoto *et al.*[14]

$^{63}Cu(II)/Ni(mndc)_2$ and $Ni(pedc)_2$: The spectra in both complexes were very similar to those of $^{63}Cu(II)/Ni(nedc)_2$ except for the difference in the laboratory coordinate systems.

$^{63}Cu(II)/Ni(tedc)_2$: The crystal b- and a-axes are parallel to the 2- and 1-axes respectively. One set of absorption is obtained when $\boldsymbol{H}_0$ is in the 31-plane or along the 2-axis, while two sets are observed when $\boldsymbol{H}_0$ is in the 12- or 23-plane. The deviation of the g_z direction from the crystal b-axis is 24°.

$^{63}Cu(II)/Ni(pndc)_2$: Four sets of absorptions are observed when $\boldsymbol{H}_0$ is in the 31-plane. The four resonances merge into two more intense lines when $\boldsymbol{H}_0$

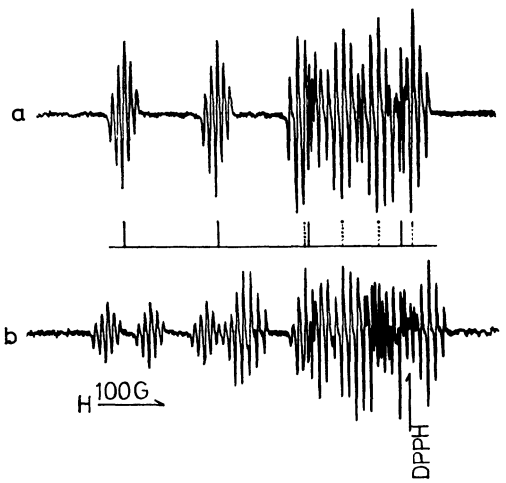

Fig. 5. Single crystal ESR spectra of $^{63}Cu(II)/Ni(pndc)_2$. a: (90°,15°), b: (165°,0°).

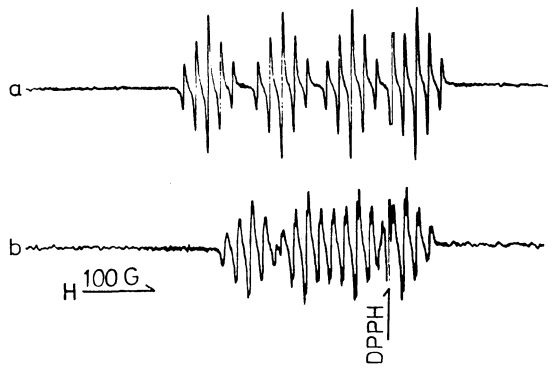

Fig. 6. Single crystal ESR spectra of ^{63}Cu(II)/Ni(bdc)$_2$.
a: (90°,0°), b: (15°,0°).

is along the 3- or 1-axis and when $\theta=45$ or 135°. When $\boldsymbol{H}_0$ is in the 12- or 23-plane, two sets are obtained, and these spectra are exactly identical in both planes.

^{63}Cu(II)/Ni(bdc)$_2$: When $\boldsymbol{H}_0$ is in the 31-plane or along the 2-axis, a single spectrum is observed, while two spectra are observed when $\boldsymbol{H}_0$ is in the 12- or 23-plane. The g and A^{Cu} values are rhombic. The nitrogen hfs is very large compared with those of the other samples, and the maximum direction of the nitrogen hfs agrees roughly with the g_x direction. The intensity ratio is 1:2:3:2:1 in all the crystal orientations. These results indicate that the Cu(II) ion in Ni(bdc)$_2$ is in a *trans* arrangement. The ESR parameters and the principal directions are very similar to those of *trans*-bis(thiosemicarbazide)copper(II) nitrate.[6]

When $\boldsymbol{H}_0$ is within 30° from the 3-axis, the additional hfs was observed (see b in Fig. 6). In the other orientations, the line width was very sharp but no additional hfs could be detected at room temperature. As far as the details of measurements around the 3-axis, it was found that the spectra consist of 3 lines with an intensity ratio of about 1:4:1. It is uncertain whether this hfs should be assigned to azomethine hydrogen or to two nitrogens in which one of the hfs is very small. The details are now under investigation.

Discussion

The molecule in Ni(nedc)$_2$ or Ni(tedc)$_2$ has the C_2 or the fictitious C_2 symmetry. The ESR results shall, therefore, be analyzed in terms of the C_2 symmetry except in the case of Cu(bdc)$_2$.

The ESR data of Cu(II) ions generally have been analyzed by the method of Abragam and Pryce,[15,16] which was adapted by Maki and McGarvey[17] to the ligand-field concept.[9,18] There is, however, difficulty caused by the increased number of parameters to be determined in the C_2 symmetry, since some coefficients in the linear combination of the Kramers doublet are complex.

Table 5. The g values and hyperfine coupling constants(10^{-4} cm^{-1}) for ^{63}Cu(II) in bis(methyl 3-alkylidenedithiocarbazato)nickel(II) at room temperature

Host	g	A(^{63}Cu)	A^N	Principal direction
Ni(nedc)$_2$	$g_x=2.032(1)$	$A_x=31(4)$		(0.25, 0, −0.97)
			$A_\perp=9.1(5)$	
	$g_y=2.130(1)$	$A_y=163(1)$		(0.97, 0, 0.25)
			$A_\parallel=12.1(5)$	
	$g_z=2.033(1)$	$A_z=33(4)$		(0, 1, 0)
Ni(mndc)$_2$	$g_x=2.032(1)$	$A_x=36(4)$		(0, 0.62, −0.78)
			$A_\perp=9.5(5)$	
	$g_y=2.129(1)$	$A_y=168(1)$		(0, 0.78, 0.62)
			$A_\parallel=13.2(5)$	
	$g_z=2.033(1)$	$A_z=33(5)$		(1, 0, 0)
Ni(pedc)$_2$	$g_x=2.032(1)$	$A_x=33(4)$		(0.76, 0, −0.65)
			$A_\perp=9.2(5)$	
	$g_y=2.132(1)$	$A_y=159(1)$		(0.65, 0, 0.76)
			$A_\parallel=11.0(5)$	
	$g_z=2.034(1)$	$A_z=34(4)$		(0, 1, 0)
Ni(tedc)$_2$	$g_x=2.031(1)$	$A_x=32(4)$		(0.82, ±0.38, 0.43)
			$A_\perp=8.5(5)$	
	$g_y=2.134(1)$	$A_y=155(1)$		(0.52, ∓0.15, −0.84)
			$A_\parallel=11.1(5)$	
	$g_z=2.034(1)$	$A_z=33(4)$		(0.25, ∓0.91, 0.32)
Ni(pndc)$_2$	$g_x=2.036(1)$	$A_x=31(4)$		(0.23, 0, ±0.97)
			$A_\perp=8.7(5)$	(0.97, 0, ∓0.23)
	$g_y=2.130(1)$	$A_y=155(1)$		(0.97, 0, ∓0.23)
			$A_\parallel=11.6(5)$	(0.23, 0, ±0.97)
	$g_z=2.038(1)$	$A_z=29(4)$		(0, 1, 0)
Ni(bdc)$_2$	$g_x=2.029(1)$	$A_x=30(4)$		(0.53, ∓0.05, −0.85)
			$A_\perp=15.0(5)$	
	$g_y=2.048(1)$	$A_y=41(4)$		(0.71, ∓0.51, 0.48)
			$A_\parallel=19.1(5)$	
	$g_z=2.138(1)$	$A_z=180(1)$		(0.46, ±0.86, 0.24)

The iteration method introduced by Swalen *et al.*[10] can determine the coefficients of the atomic d-orbitals from only the experimental g values and the normalization condition. The copper hfs is used only for a consistency check. The same procedure is followed in this work, and the hole description is adopted throughout in the formulation.

In the C_2 symmetry, $3d_{zx}$- and $3d_{yz}$-type orbitals belong to the same irreducible representation and form a linear combination:

$$\psi = a|zx> + ib|yz>. \tag{1}$$

In this case, the symmetry axis is parallel to the z-axis, and the $3d_{xy}$, $3d_{z^2}$, and $3d_{x^2-y^2}$ orbitals are then admixed *via* spinorbit coupling, $\xi \boldsymbol{l}\cdot\boldsymbol{s}$, to give the general expression for the Kramers doublet:

$$\psi^\alpha = a|zx>^\alpha + ib|yz>^\alpha + c|z^2>^\beta - d|x^2-y^2>^\beta - ie|xy>^\beta, \tag{2-1}$$

$$\psi^\beta = i\{a|zx>^\beta - ib|yz>^\beta - c|z^2>^\alpha + d|x^2-y^2>^\alpha - ie|xy>^\alpha\}, \tag{2-2}$$

where the superscripts α and β designate the spin functions.

The expressions for the g values are obtained as the matrix elements of the Zeeman term, $\boldsymbol{H}=\beta(\boldsymbol{l}+g_e\boldsymbol{s})\cdot\boldsymbol{H}_0$:[19]

$$g_x = (1-2b^2-2c^2-2d^2)g_e + 4ae - 4bd + 4\sqrt{3}\,bc, \tag{3-1}$$

$$g_y = (1-2b^2-2e^2)g_e - 4be + 4ad + 4\sqrt{3}\,ac, \tag{3-2}$$

$$g_z = (1-2c^2-2d^2-2e^2)g_e + 8de + 4ab, \tag{3-3}$$

where g_e represents the g value of the free electron.

The expressions for the hyperfine coupling constants are derived as follows:[20]

$$A_x = P[4ae-4bd+4\sqrt{3}\,bc-k(1-2b^2-2c^2-2d^2) + (2/7)(1+b^2-2d^2-3ab-\sqrt{3}\,ac+3ad-3be - 2\sqrt{3}\,cd-2\sqrt{3}\,ce)], \tag{4-1}$$

$$A_y = P[-4be+4ad+4\sqrt{3}\,ac-k(1-2b^2-2e^2) + (2/7)(-1-a^2+2d^2+3ab-\sqrt{3}\,bc-3bd + 3ae-2\sqrt{3}\,cd-2\sqrt{3}\,ce)], \tag{4-2}$$

$$A_z = P[8de+4ab-k(1-2c^2-2d^2-2e^2) + (2/7)(1-3c^2+d^2+e^2+\sqrt{3}\,ac-3ad - 3ae-\sqrt{3}\,bc-3bd-3be)], \tag{4-3}$$

where $P=g_e g_N \beta_e \beta_N \langle r^{-3}\rangle_{3d}$, and where k is the contact term.

The 3 equations and the normalization condition form a set of nonlinear simultaneous equations for a, b, c, d, and e, an iteration procedure similar to that of Swalen *et al.*[8] being used. The solutions were made with a value of $r(=c/d)$ between 0.5 and 2.0 by the use of an Olivetti P652 computer. The calculated values are given in Table 6.

Nitrogen hfs. From Table 6, the contributions of the upper states may be found to be very small. We shall thus ignore these admixtures in our calculation of the nitrogen hfs. We obtain the following antibonding molecular orbital of the unpaired electron:

$$|zx> = N^{1/2}[d_{zx} - (\alpha_1/\sqrt{2})(s^1-s^2) - (\alpha_2/2) \times (-p_x^1-p_z^2-p_x^1+p_z^2) - (\alpha_3/\sqrt{2}) \times (-s^3+s^4) - (\alpha_4/2)(p_x^3+p_x^4-p_z^3+p_z^4)], \tag{5}$$

where the z axis is along the two-fold axis, and 1,2 and 3,4 represent, respectively, the ligand nitrogen and sulfur atoms. The normalization of this orbital gives

$$N(1+\alpha_1^2+\alpha_2^2+\alpha_3^2+\alpha_4^2-2\sqrt{2}\,\alpha_1 S_1-4\alpha_2 S_2 - 2\sqrt{2}\,\alpha_3 S_3-4\alpha_4 S_4) = 1, \tag{6}$$

where $S_1=\langle d_{zx}|s^1\rangle$, $S_2=\langle d_{zx}|-p_x^1\rangle$, $S_3=\langle d_{zx}|-s^3\rangle$, and $S_4=\langle d_{zx}|p_x^3\rangle$.

The components of the nitrogen hfs are

$$A_\parallel^N = A_s + 2A_p, \tag{7-1}$$

$$A_\perp^N = A_s - A_p, \tag{7-2}$$

where the isotropic part, A_s, and anisotropic part, A_p, are

$$A_s = (8\pi/3)g_e g_N \beta_e \beta_N \times (1/2)N\alpha_1^2 \times |\psi_{2s}(0)|^2, \tag{8-1}$$

$$A_p = (4/5)g_e g_N \beta_e \beta_N \times (1/4)N\alpha_2^2 \times \langle r^{-3}\rangle_{2p}. \tag{8-2}$$

The values of $32.4\times10^{24}\,cm^{-3}$ for $|\psi_{2s}(0)|^2$ and $20.9\times10^{24}\,cm^{-3}$ for $\langle r^{-3}\rangle_{2p}$ of a nitrogen atom are obtained from the analytical SCF wave functions.[21] Table 7 gives the values of $N\alpha_1^2$, $N\alpha_2^2$, and $N\alpha_4^2$, the $N\alpha_4^2$ values have been calculated on the following bases: (1) the overlap integrals, $S_1=0.085$, $S_2=0.097$,

Table 6. The best values for the coefficients of Kramers doublet and calculated hyperfine coupling constants($10^{-4}\,cm^{-1}$)

Host	Ni(nedc)$_2$	Ni(mndc)$_2$	Ni(pedc)$_2$	Ni(tedc)$_2$	Ni(pndc)$_2$	Ni(bdc)$_2$[a]
r	0.60	1.50	0.60	0.60	1.30	0.688
a	0.9998	0.9998	0.9998	0.9997	0.9998	0.9990
b	0.0078	0.0079	0.0081	0.0081	0.0091	−0.0392
c	0.0094	0.0133	0.0096	0.0097	0.0129	0.0171
d	0.0157	0.0089	0.0160	0.0162	0.0099	0.0075
e	0.0078	0.0077	0.0078	0.0076	0.0086	0.0109
P	174	178	167	163	167	197
k	0.490	0.498	0.507	0.505	0.488	0.495
A_x	−31	−36	−33	−32	−31	−30
A_y	−163	−168	−159	−155	−155	−41
A_z	−33	−33	−34	−33	−29	−180

a) Calculated from Eqs. 10 and 11.

Table 7. Covalent parameters in bis(methyl 3-alkylidenedithiocarbazato)copper(II)

Host	$Ni(nedc)_2$	$Ni(mndc)_2$	$Ni(pedc)_2$	$Ni(tedc)_2$	$Ni(pndc)_2$	$Ni(bdc)_2$[a]
$N\alpha_1^2$	0.037	0.039	0.035	0.034	0.035	0.059
$N\alpha_2^2$	0.117	0.145	0.070	0.102	0.113	0.158
$N\alpha_4^2$ (N=0.70)	0.186	0.181	0.192	0.188	0.187	
(N=0.75)	0.222	0.216	0.231	0.226	0.224	

a) Calculated from Eq. 13.

and S_4=0.065, are assumed for the Cu–N and Cu–S distances of 1.92Å and 2.15Å; (2) α_3=0, and (3) the value of N is assumed to be 0.7 or 0.75, either of which is a reasonable value for CuN_2S_2 complexes.[6]

^{63}Cu(II)/Ni(bdc)$_2$. In a *trans* arrangement, $d_{x^2-y^2}$ and d_{z^2} belong to the same irreducible representation and the spin-orbitals of the ground state are

$$\psi^\alpha = a|x^2-y^2>^\alpha + b|z^2>^\alpha + ic|xy>^\alpha - id|yz>^\beta + e|zx>^\beta, \quad (9\text{-}1)$$

$$\psi^\beta = i\{a|x^2-y^2>^\beta + b|z^2>^\beta - ic|xy>^\beta - id|yz>^\alpha - e|zx>^\alpha\}, \quad (9\text{-}2)$$

x and y being the Cu–N and Cu–S bond directions respectively. By analogy with the case of C_2, the g and A^{Cu} values are calculated as follows:

$$g_x = (1-2c^2-2e^2)g_e + 4\sqrt{3}bd + 4ce + 4ad, \quad (10\text{-}1)$$

$$g_y = (1-2c^2-2d^2)g_e - 4\sqrt{3}be + 4ae + 4cd, \quad (10\text{-}2)$$

$$g_z = (1-2d^2-2e^2)g_e + 8ac - 4de, \quad (10\text{-}3)$$

$$A_x = P[4\sqrt{3}bd+4ce+4ad-k(1-2c^2-2e^2) + (2/7)\{-1+2a^2-d^2-2\sqrt{3}ab - \sqrt{3}b(e-2c)-3cd-3ae+3de\}], \quad (11\text{-}1)$$

$$A_y = P[-4\sqrt{3}be+4ae+4cd-k(1-2c^2-2d^2) + (2/7)\{-1+2a^2-e^2+2\sqrt{3}ab + \sqrt{3}b(d-2c)-3ce-3ad+3de\}], \quad (11\text{-}2)$$

$$A_z = P[8ac-4de-k(1-2d^2-2e^2) + (2/7)\{-1-a^2+3b^2-c^2-\sqrt{3}b(d-e) - 3(d+e)(c-a)\}]. \quad (11\text{-}3)$$

The molecular orbitals which contribute to the A^N values are

$$|A_{1g}> = N_1^{1/2}[d_{x^2-y^2} + (b/a)d_{z^2} - (\alpha_1/\sqrt{2})(s^1+s^2) - (\alpha_2/\sqrt{2})(-p_x^1+p_x^2) - (\alpha_3/\sqrt{2})(p_y^3-p_y^4)], \quad (12\text{-}1)$$

$$|zx> = N_2^{1/2}[d_{zx} - (\beta/\sqrt{2})(p_z^1-p_z^2)]. \quad (12\text{-}2)$$

The components of the A^N are

$$A_x^N = A_s + 2A_\sigma + A_\pi, \quad (13\text{-}1)$$

$$A_y^N = A_s - A_\sigma, \quad (13\text{-}2)$$

$$A_z^N = A_s - A_\sigma - A_\pi, \quad (13\text{-}3)$$

where A_s, A_σ, and A_π are

$$A_s = (8\pi/3)g_e g_N \beta_e \beta_N \times (1/2)a^2 N_1 \alpha_1^2 |\psi_{2s}(0)|^2, \quad (14\text{-}1)$$

$$A_\sigma = (4/5)g_e g_N \beta_e \beta_N \times (1/4)a^2 N_1 \alpha_2^2 \langle r^{-3}\rangle_{2p}, \quad (14\text{-}2)$$

$$A_\pi = (4/5)g_e g_N \beta_e \beta_N \times (3/4)ae(N_1N_2)^{1/2}\alpha_2\beta\langle r^{-3}\rangle_{2p}. \quad (14\text{-}3)$$

The calculation was performed with $r(=d/e)$ value from 0.5 to 1.0. The calculated values are given in Tables 6 and 7. The β value could not be determined because of the experimental error between A_z^N and A_y^N values.

In *cis*-planar copper(II) complexes, the g values have an axial symmetry. When tetrahedral distortion occurs, this is not true. The g_z and g_x values are no longer equal, as may be seen in Eq. 3. Even if the distortion occurs, the g values sometimes chance to have an axial symmetry. In *cis* bis(methyl 3-alkylidenedithiocarbazato)copper(II), however, the tetrahedral distortion of about 20° does not break the axial symmetry of the g values.

The values of g are rhombic in a *trans* arrangement.[6,14,22] It was concluded from this fact that Cu(II) in $Ni(bdc)_2$ is in a *trans* arrangement.

The ESR spectra in chloroform solutions of copper(II) complexes at room temperature have A^{Cu} values between 66 and 72×10^{-4} cm^{-1} for the *cis* complexes and of 82×10^{-4} cm^{-1} for $Cu(bdc)_2$. These values are in reasonable agreement with the attributions of negative signs to all the A^{Cu} components.

The A^N values are smaller in the *cis* complexes than in $Cu(bdc)_2$. It is expected that in the *cis* complexes, the Cu–N bond length is longer than in the *trans* arrangement because of steric repulsion by the large phenyl groups.

The author is grateful to Professor Tetsuya Komori of Kyushu University for his kind advice and for allowing him to use the Syntex P$\bar{1}$ automatic diffractometer, and to Professor Ikuhiko Ueda of Kyushu University for allowing him to take the Weissenberg photographs. Thanks are also due to Professor Sigeo Kida and Dr. Toshiyuki Isobe for allowing him to take ESR measurements. A part of this work has been carried out at the Coordination Chemistry Laboratory of Kyushu University.

References

1) H. R. Gersman and J. D. Swalen, *J. Chem. Phys.*, **36**, 3221 (1962).
2) R. Kirmse and B. V. Solovev, *J. Inorg. Nucl. Chem.*, **39**, 41 (1977).
3) R. K. Cowsik and R. Srinivasan, *J. Chem. Phys.*, **59**, 5517 (1973).
4) A. H. Maki, N. Edelstein, A. Davison, and R. H. Holm, *J. Am. Chem. Soc.*, **86**, 4580 (1964).
5) P. H. Davis, L. K. White, and R. L. Belford, *Inorg. Chem.*, **14**, 1753 (1975).
6) E, Buluggiu, A. Vera, and A. A. G. Tomlinson, *J. Chem. Phys.*, **56**, 5602(1972).
7) V. F. Anufrienko and A. P. Zeif, *Opt. Spectrosc.*, **20**, 365 (1966).
8) R. S. Giordano and R. D. Bereman, *Inorg. Nucl. Chem.*

Lett., **10**, 203 (1974).
9) D. Kivelson and R. Neiman, *J. Chem. Phys.*, **35**, 149 (1961).
10) J. D. Swalen, B. Johnson, and H. M. Gladney, *J. Chem. Phys.*, **52**, 4078 (1970).
11) M. A. Ali, S. E. Livingstone, and D. J. Phillips, *Inorg. Chem. Acta*, **5**, 493 (1971).
12) "The Universal Crystallographic Computation Program System," Crystallographic Society of Japan (1967).
13) "International Tables for X-Ray Crystallography," Vol. III, Kynoch Press, Birmingham (1962).
14) M. Fujimoto and J. Janecka, *J. Chem. Phys.*, **55**, 1152 (1971).
15) A. Abragam and M. H. L. Pryce, *Proc. R. Soc. London, Ser. A*, **205**, 135 (1951).
16) A. Abragam and M. H. L. Pryce, *Proc. R. Soc. London, Ser. A*, **206**, 164 (1951).
17) A. H. Maki and B. R. McGarvey, *J. Chem. Phys.*, **29**, 31 (1958).
18) T. R. Reddy and R. Srivasan, *J. Chem. Phys.*, **43**, 1404 (1965).
19) A. Abragam and B. Bleaney, "Electron Paramagnetic Resonance of Transition Ions," Oxford University Press (1970), p. 13.
20) B. R. McGarvey, *Transition Metal Chem.*, **3**, 89 (1966).
21) E. Clementi, C. C. J. Roothan, and Y. Yoshimine, *Phys. Rev.*, **127**, 1618 (1962).
22) E. Buluggiu, G. Dascola, D. C. Giori, and A. Vera, *J. Chem. Phys.*, **54**, 2191 (1971).

Glass Formation in the Li_2O-TiO_2-P_2O_5, MgO-TiO_2-P_2O_5, and CaO-TiO_2-P_2O_5 Systems

Akira KISHIOKA

Department of Chemistry, Faculty of Science and Technology, Sophia University, Kioicho, Chiyoda-ku, Tokyo 102

(Received December 20, 1977)

The glass-forming regions in the Li_2O–TiO_2–P_2O_5, MgO–TiO_2–P_2O_5, and CaO–TiO_2–P_2O_5 systems have been determined. Homogeneous glasses were formed with compositions of less than 50 mol% P_2O_5 in all three systems. The largest quantities of TiO_2 could be introduced into glass for compositions of 30 mol% P_2O_5. In compositions with more than 50 mol% P_2O_5 only a mixture of the glass and crystal was formed. With an increase in the TiO_2 content, the density of the glass increased and the volume per mole of oxygen decreased. These results indicate that the TiO_2 had been easily incorporated into the glass with compositions of lower P_2O_5 contents, contributing to the stabilization of the glass structure.

The role of intermediate ions such as Ti^{4+} and Al^{3+} in glass formation in ternary phosphate systems is interesting, since it reflects the glass structure. Reports concerning the glass-forming regions in ternary phosphate systems, however, are relatively few compared with those in ternary systems containing other glass-forming oxides. Recently, glass formation in the BeO–TiO_2–P_2O_5, CaO–TiO_2–P_2O_5, and K_2O–TiO_2–P_2O_5 systems and the electrical resistivity have been reported by Hayashi *et al.*[1] The present authors have reported glass formation in the Na_2O–BaO–TiO_2–P_2O_5 four-component system,[2] the ternary phosphate systems containing Al_2O_3,[3] and the role of the Al^{3+} ion in alkali aluminophosphate glasses.[4]

In this paper, glass-forming regions for the Li_2O–TiO_2–P_2O_5, MgO–TiO_2–P_2O_5, and CaO–TiO_2–P_2O_5 systems have been determined. The density of the glass has been determined and the volume per mole of oxygen calculated. On the basis of these results, the role of the titanium ion in the glass has been discussed.

Experimental

Determination of Glass-Forming Region. The materials used were reagent grade chemicals of titanium dioxide, orthophosphoric acid (85%), lithium hydroxide monohydrate, magnesium oxide, calcium hydrogenphosphate dihydrate, and calcium carbonate. A batch (15-g) obtained by mixing appropriate amounts of the above chemicals was placed in platinum dishes and heated in an electric furnace. After dehydration, the batch was kept at 1350 °C for 1 h. The melt was poured out and quenched by pressing with a copper plate cooled with water. The homogeneity of the glass was checked with a polarizing microscope and the naked eye.

Density of Glass. The density of the glass was determined pycnometrically using 1-butanol at 25.0 °C. For samples containing a small amount of crystal, only the glassy part was used for measurement.

Volume of Glass. The volume of the glass per mole of oxygen was calculated by the following equation:[5]

$$V_0 = (G.F.W./D) \times 1/N_0,$$

where V_0 is the volume of the glass per mole of oxygen, $G.F.W.$ is the gramme formula weight of the glass based on the batch composition, D is the density of the glass, and N_0 is the number of gramme molecular weights of oxygen (32 g units) in the glass.

Results and Discussion

Glass-Forming Tendency. The results are given in Figs. 1—3. The compositions whose batches melted completely at 1350 °C have been surrounded by dotted lines in the Figs. Homogeneous glasses were formed in compositions with less than 50 mol% P_2O_5. As shown by the arrows in Figs. 1—3, the content of TiO_2 in the glass was largest for compositions with 30 mol% P_2O_5 of each system; it was the largest for the MgO–TiO_2–P_2O_5 system. Considering that the phosphate species in the $47.5Na_2O \cdot 20Al_2O_3 \cdot 32.5P_2O_5$ glass were exclusively PO_4^{3-}-type ions,[4] those in the glasses with 30 mol% P_2O_5 containing more than 20 mol% TiO_2 are presumably also only PO_4^{3-} ions. Therefore, the above results indicate that the TiO_2 is incorporated easily into the glass with compositions of lower P_2O_5 content and the formation of the glass with higher TiO_2 contents is most favorable when there are no P–O–P chains.

All glasses were colored by the titanium ion of lower valency and the MgO–TiO_2–P_2O_5 glasses with higher TiO_2 content were brownish black. The Li_2O–TiO_2–

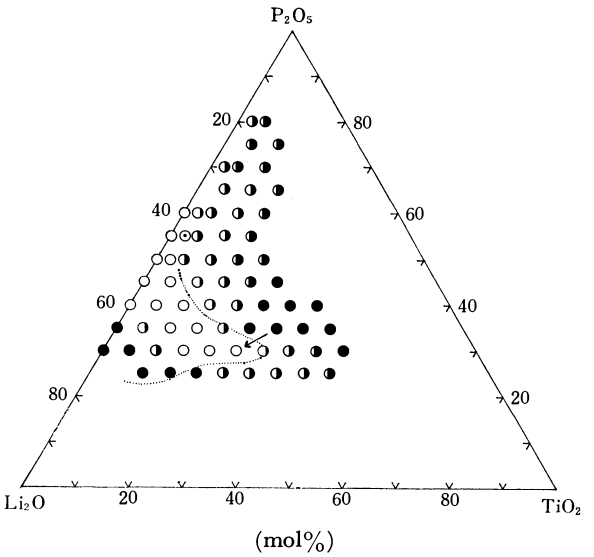

Fig. 1. Glass-forming region in Li_2O–TiO_2–P_2O_5 system. ○: Homogeneous glass, ⊙: trace amounts of crystal in glass, ◑: glass and crystal, ●: crystal.

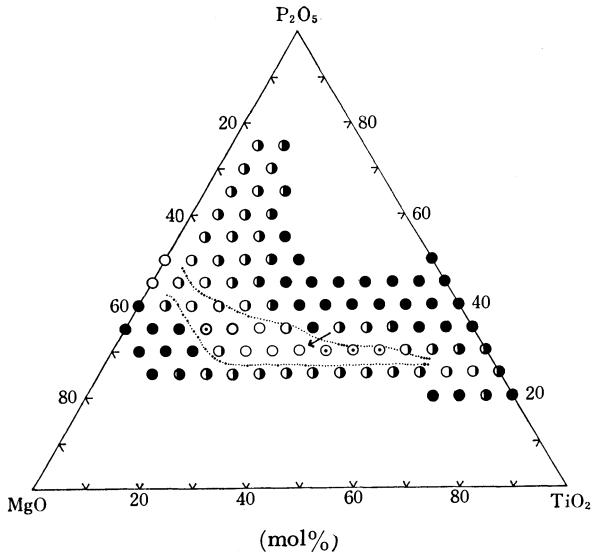

Fig. 2. Glass-forming region in MgO–TiO_2–P_2O_5 system.

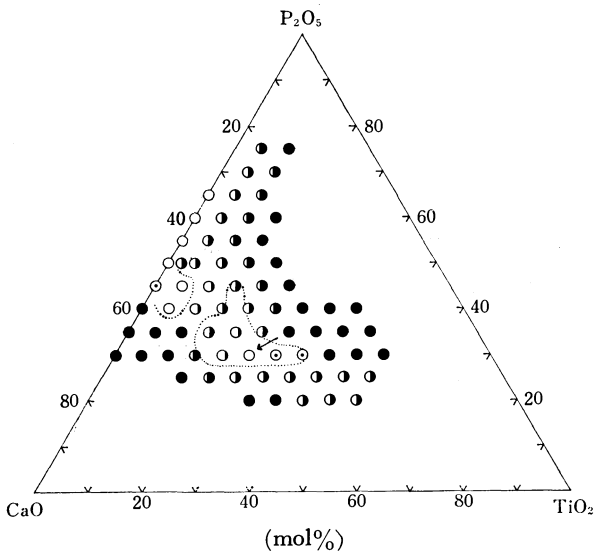

Fig. 3. Glass-forming region in CaO–TiO_2–P_2O_5 system.

P_2O_5 glasses were less colored than those containing MgO or CaO of the same molar composition.

In addition to the homogeneous glass, the following two types of products were formed; (a) a mixture of glass and crystal (produced by partial devitrification of the melt during quenching or separation of crystalline substance in the melt) and (b) a crystalline product formed as a result of devitrification during quenching or non-melting of the batch.

The glass-forming region in each system in the present work was smaller than those reported by Hayashi *et al.*[1] However, the observed tendency of glass formation in compositions with less than 50 mol% P_2O_5 agrees well with the results reported.[1]

In compositions with more than 50 mol% P_2O_5, only the mixture of the glass and the crystal was formed as the result of the separation of the crystalline substance in the melt. This makes a marked difference from the alkali (or alkaline earth) aluminophosphate system[3] where the homogeneous glasses were formed in the region with more than 50 mol% P_2O_5 in a three-component diagram. It can be considered that the action of the titanium ion in the glass formation is fairly different from that of the Al^{3+} ion in the same P_2O_5 content.

Density and Volume of Glass. The density and the volume per mole of oxygen of the glasses are given in Figs. 4—7. In Figs. 4 (a) and (b), the density and the volume in the Li_2O–TiO_2–P_2O_5 glasses with the same Li_2O contents are plotted *vs.* the TiO_2 content respectively. The plots of the density and the volume *vs.* the TiO_2 content in the glasses with the same P_2O_5 contents are given in Figs. 5—7. Except for Fig. 4 (b), these plots showed linear relationships. The density of the glass increased and the volume of the glass per mole of oxygen decreased with an increase in the TiO_2 content in all the systems. This indicates the

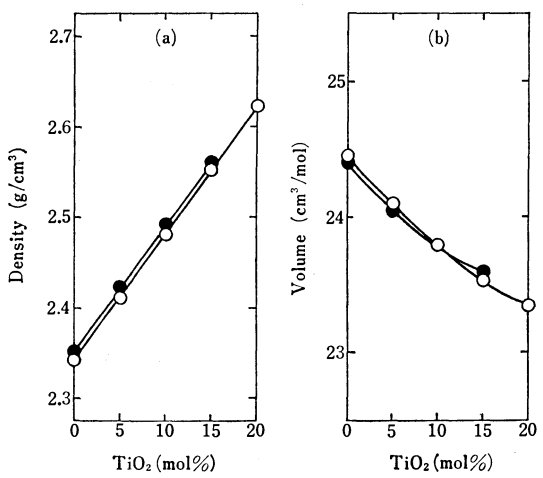

Fig. 4. Plots of (a) density *vs.* TiO_2 content, and (b) volume per mole of oxygen *vs.* TiO_2 content in the Li_2O–TiO_2–P_2O_5 glass with the same Li_2O contents. ○: 50 mol% Li_2O, ●: 55 mol% Li_2O.

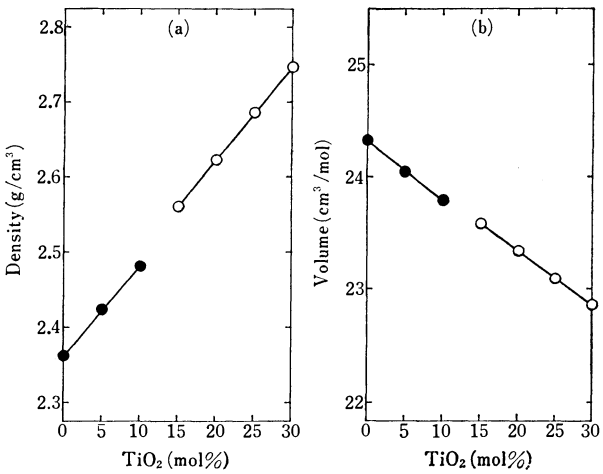

Fig. 5. Plots of (a) density *vs.* TiO_2 content, and (b) volume per mole of oxygen *vs.* TiO_2 content in the Li_2O–TiO_2–P_2O_5 glass with the same P_2O_5 contents. ○: 30 mol% P_2O_5, ●: 40 mol% P_2O_5.

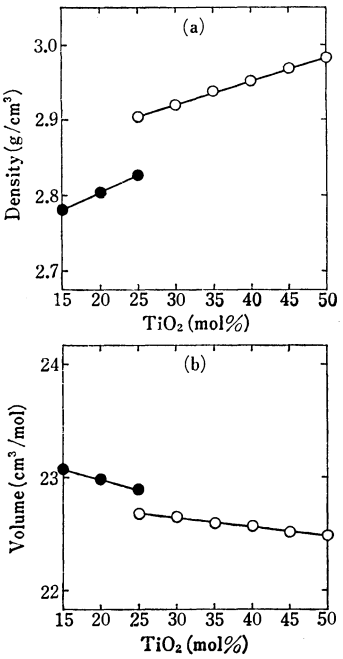

Fig. 6. Plots of (a) density *vs.* TiO_2 content, and (b) volume per mole of oxygen *vs.* TiO_2 content in the MgO–TiO_2–P_2O_5 glass with the same P_2O_5 contents. ○: 30 mol% P_2O_5, ●: 35 mol% P_2O_5.

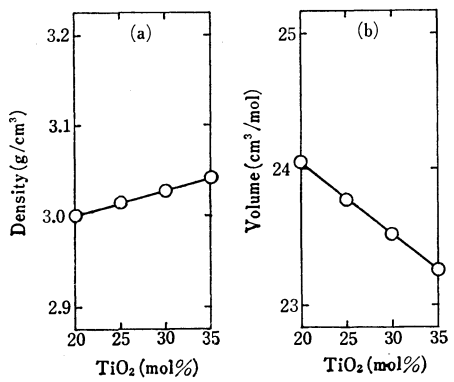

Fig. 7. Plot of (a) density *vs.* TiO_2 content, and (b) volume per mole of oxygen *vs.* TiO_2 content in the CaO–TiO_2–P_2O_5 glass with 30 mol% P_2O_5.

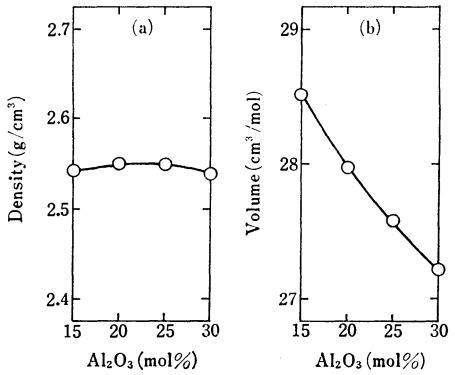

Fig. 8. Plot of (a) density *vs.* Al_2O_3 content, and (b) volume per mole of oxygen *vs.* Al_2O_3 content in the Na_2O–Al_2O_3–P_2O_5 glass with 32.5 mol% P_2O_5.

strength of the titanium ion contribution to the strengthening of the glass structure.

The contractions in the volume of the MgO–TiO_2–P_2O_5 glasses with an increase in the TiO_2 content (Fig. 6 (b)) are less than those of the glasses in the Li_2O- and CaO-systems (Figs. 5 (b) and 7 (b)). It can be said that the role of the titanium ion in the glass structure is similar to that of the Mg^{2+} ion and also that the titanium ion replaces the Mg^{2+} ion.

As shown in Fig. 8 (a), no increase was found in the density on an increase in the Al_2O_3 content for the Na_2O–Al_2O_3–P_2O_5 glass with 32.5 mol% P_2O_5. This suggests that the role of the titanium ion in the glass structure is different from that of the Al^{3+} ion in compositions with less than 50 mol% P_2O_5.

The author wishes to thank Associate Professor Makio Kinoshita of Sophia University for his interest and encouragement, and also Mr. Yuichi Yokoyama for his assistance in the experimental work.

References

1) T. Hayashi, K. Honda, and H. Saito, *Yogyo Kyokai Shi*, **84**, 403 (1976).
2) A. Kishioka, M. Haba, and M. Amagasa, *Bull. Chem. Soc. Jpn.*, **47**, 2493 (1974).
3) A. Kishioka, M. Hayashi, and M. Kinoshita, *Bull. Chem. Soc. Jpn.*, **49**, 3032 (1976).
4) A. Kishioka, *Bull. Chem. Soc., Jpn.*, **50**, 2088 (1977).
5) Bh. V. J. Rao, *Phys. Chem. Glasses*, **4**, 22 (1963).

Kinetics of the Oxidative Addition of Hydrogen to Chloro(acrylonitrile)-bis(triphenylphosphine)rhodium(I) in Benzene

Yoshimi OHTANI, Akihiko YAMAGISHI, and Masatoshi FUJIMOTO*

Department of Chemistry, Faculty of Science, Hokkaido University, Sapporo 060

(Received January 6, 1978)

The reaction between chloro(acrylonitrile)bis(triphenylphosphine)rhodium(I) and hydrogen was studied by the stopped-flow method under an anaerobic condition. A solution of $RhCl(CH_2{=}CHCN)(PPh_3)_2$ was mixed with a benzene solution containing hydrogen under the condition of $[Rh]<[H_2]_0<[CH_2{=}CHCN]$. A fast decrease in the absorbance was followed by a slow increase in the absorbance, until finally the absorbance returned to the initial value. It was proved that the faster reaction was the oxidative addition of hydrogen to $RhCl(CH_2{=}CHCN)(PPh_3)_2$; $RhCl(CH_2{=}CHCN)(PPh_3)_2+H_2 \underset{k_{43}}{\overset{k_{34}}{\rightleftharpoons}} RhClH_2(CH_2{=}CHCN)(PPh_3)_2$. The slower reaction was the process in which hydrogen was consumed in the course of the hydrogenation of acrylonitrile and $RhCl(CH_2{=}CHCN)(PPh_3)_2$ was reproduced. The values of the rate constants were evaluated to be $k_{34} \geq 7.8\times10^3$ mol^{-1} dm^3 s^{-1} and $k_{43} \leq 53$ s^{-1}.

Wilkinson's complex, $RhClL_3$ ($L=PPh_3$), is a useful catalyst for the hydrogenation of olefins.[1] Although many studies have been made to elucidate the reaction mechanism of the hydrogenation of olefins by means of Wilkinson's complex,[2-7] the mechanism has not yet been fully made clear. We previously proposed the following reaction mechanism, in which complex formation processes are assumed as a pre-equilibrium step,[7] though an intermediate species ($RhClH_2$(olefin)L_2) could not be detected spectrophotometrically:

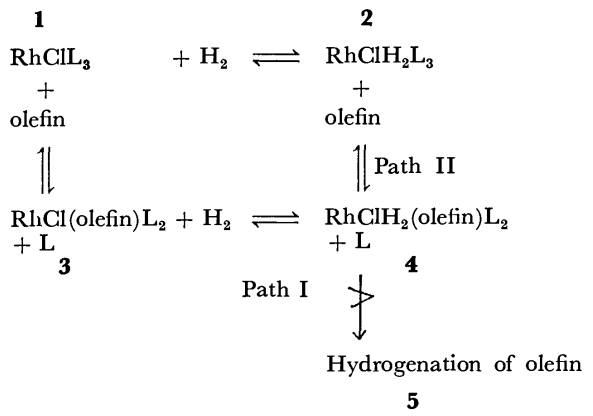

The predominant species of the Rh complex is considered to be $RhClH_2L_3$ (**2**) or $RhCl$(olefin)L_2 (**3**). Whether the $RhCl$(olefin)L_2 species becomes a predominant species or not depends on the coordinating ability of the olefin. Thus, the hydrogenation of olefins with a weakly coordinating power may proceed mainly through a so-called "hydride route" (Path II) as proposed by Halpern *et al.*[6] However, the hydrogenation of olefins with a strongly coordinating power is expected to proceed predominantly through an "unsaturate route" (Path I). However, the latter has not so far been observed with the use of Wilkinson's complex.

We intend in the present study to detect the intermediate species, $RhClH_2$(olefin)L_2 (**4**), and also to obtain the kinetic data of the reaction 3⇌4. Acrylonitrile was chosen as an olefin since it strongly coordinates to Wilkinson's complex and is rapidly hydrogenated.[3] The concentration of $RhClH_2(CH_2{=}CHCN)L_2$ increases as the concentration of free PPh_3 decreases. Thus, a solution of $RhCl(CH_2{=}CHCN)L_2$ containing no free PPh_3 was prepared by dissolving $RhCl(C_2H_4)L_2$ in a benzene solution containing acrylonitrile. The coordinated ethylene was then replaced by an acrylonitrile molecule[7] and $RhCl(CH_2{=}CHCN)L_2$ was produced in the solution. As there was no free PPh_3 in the solution, only olefin complexes **3** and **4** can exist. The oxidative addition of hydrogen to $RhCl(CH_2{=}CHCN)L_2$ was observed by the addition of a solution containing hydrogen to a solution of $RhCl(CH_2{=}CHCN)L_2$.

Experimental

A solution of $RhCl(CH_2{=}CHCN)(PPh_3)_2$ was prepared by dissolving $RhCl(C_2H_4)(PPh_3)_2$ in oxygen-free benzene containing acrylonitrile and by removing the dissociated ethylene. The coordinated ethylene was easily replaced by acrylonitrile,[7] and $RhCl(CH_2{=}CHCN)(PPh_3)_2$ was produced in benzene. The value of the equilibrium constant $K=[RhCl(CH_2{=}CHCN)(PPh_3)_2][C_2H_4]/[RhCl(C_2H_4)(PPh_3)_2][CH_2{=}CHCN]$ was calculated to be 0.5 from the values of $K'=[RhCl(C_2H_4)(PPh_3)_2][PPh_3]/[RhCl(PPh_3)_3][C_2H_4]=0.4$[5] and $K''=[RhCl(CH_2{=}CHCN)(PPh_3)_2][PPh_3]/[RhCl(PPh_3)_3]\cdot[CH_2{=}CHCN]=0.2$.

Chloro(ethylene)bis(triphenynylphosphine)rhodium(I), $RhCl(C_2H_4)(PPh_3)_2$ was prepared from $RhCl(PPh_3)_3$.[2] Benzene was distilled. Acrylonitrile was distilled under reduced pressure. Commercial hydrogen was used without purification; the concentration was determined by gas-chromatography using a Molecular sieve 5A.

Kinetic measurements were made at 20 °C using a Union Giken RA-1300 stopped-flow apparatus. A solution of $RhCl(CH_2{=}CHCN)(PPh_3)_2$ containing an appropriate concentration of acrylonitrile (0.004—0.228 mol dm^{-3}) was mixed with a solution of hydrogen containing the same concentration of acrylonitrile as in the solution of $RhCl(CH_2{=}CHCN)(PPh_3)_2$ ($[H_2]=(0.8—2.8)\times10^{-3}$ and $[CH_2{=}CHCN]=0.004—0.228$ mol dm^{-3}). The reaction was then carried out under a nitrogen or a hydrogen atmosphere. The change in the absorbance was observed at 458 nm (λ_{max} of $RhCl(CH_2{=}CHCN)(PPh_3)_2$).

The rate of hydrogen-gas uptake was measured as follows. A catalytic hydrogenation apparatus was evacuated and filled with 1 atm hydrogen. A benzene solution (10 ml) containing an appropriate concentration of acrylonitrile was introduced into the apparatus. The solution was vigorously stirred in order to saturate the apparatus with benzene vapor. The total pressure in the apparatus was 1 atm, and no attempt was made to compensate for the partial pressure of benzene. A

benzene solution of the Rh complex (10 ml; the Rh complex existed in the form of $H_2[RhCl(PPh_3)_2]_2$), saturated with 1 atm of hydrogen beforehand, was dropped into the vessel while the solution was being vigorously stirred. The dimeric form of the Rh complex was rapidly decomposed to a monomeric olefin complex by the reaction with acrylonitrile.[8] The absorption rate of hydrogen was measured by means of a 10 ml gas buret. The limitation of the uptake rate due to the ability of the apparatus was not less than 0.25 ml s^{-1}. In the kinetic runs, the fastest uptake rate was 0.02 ml s^{-1}, so there was no hydrogen starvation in the solution.

Results and Discussion

When a solution containing $RhCl(CH_2{=}CHCN)L_2$ was mixed with a solution containing hydrogen, stepwise reactions took place. Figure 1 shows a typical example of the absorbance changes.

The first decrease in the absorbance shows an exponential curve. It terminates within 0.1 s. The rate does not depend on $[CH_2{=}CHCN]$, but depends somewhat on $[H_2]$ (Fig. 2). The change in the absorbance

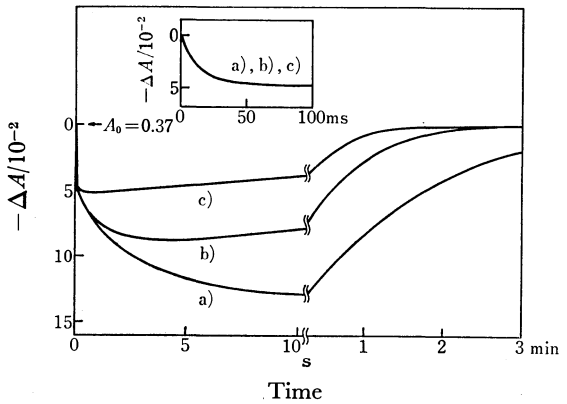

Fig. 1. Typical absorbance changes in the reaction between $RhCl(CH_2{=}CHCN)L_2$ and hydrogen in benzene. Inset shows an expanded signals for the first step of the reaction. $[RhCl(CH_2{=}CHCN)L_2]_0=3.2\times10^{-4}$ mol dm^{-3}, $[H_2]_0=1.4\times10^{-3}$ mol dm^{-3}, at 458 nm, and 20 °C. a) $[CH_2{=}CHCN]=0.004$, b) 0.076, and c) 0.228 mol dm^{-3}.

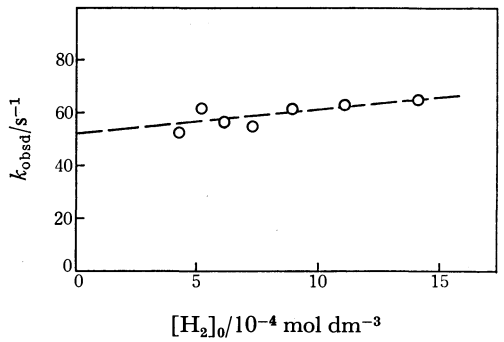

Fig. 2. Plot of k_{obsd} in the first step *vs.* $[H_2]_0$. $[Rh]=3.6\times10^{-4}$, $[CH_2{=}CHCN]=0.076$ mol dm^{-3}. Broken line is drawn assuming $K_{34}=k_{34}/k_{43}=1.5\times10^2$ $mol^{-1}\cdot dm^3$. As the concentration of $RhClH_2(CH_2{=}CHCN)L_2$ is small, the concentration of H_2, $[H_2]=[H_2]_0-[RhClH_2(CH_2{=}CHCN)L_2]$, is held nearly constant during the reaction.

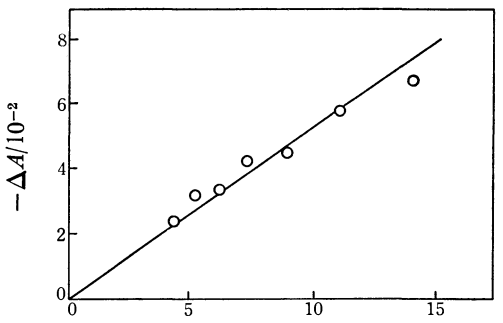

Fig. 3. Plot of the absorbance change, ΔA, in the first step *vs.* $[H_2]_0$. $[Rh]=3.6\times10^{-4}$, $[CH_2{=}CHCN]=0.076$ mol dm^{-3}.

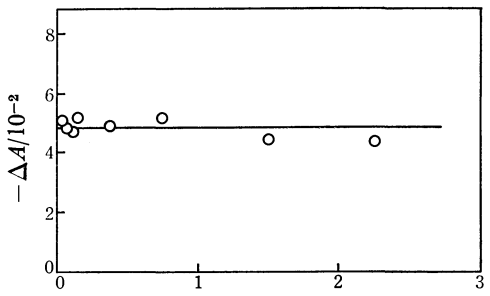

Fig. 4. Plot of the absorbance change, ΔA, in the first step *vs.* $[CH_2{=}CHCN]$. $[Rh]=3.2\times10^{-4}$ and $[H_2]_0=1.4\times10^{-3}$ mol dm^{-3}.

is nearly proportional to $[H_2]$ (Fig. 3), but does not depend on $[CH_2{=}CHCN]$ (Fig. 4). From these results it may be concluded that the coordination of hydrogen does not cause the dissociation of the previously coordinated acrylonitrile. The reaction in the first step is:

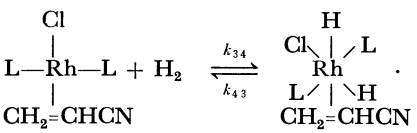

(1)

Figure 3 suggests that the equilibrium lies far to the reactant side even when $[H_2]=1.4\times10^{-3}$ mol dm^{-3}. If the molar absorption coefficient of the octahedral $RhClH_2(CH_2{=}CHCN)L_2$ at 458 nm is very small (as in the case of $RhClH_2L_3$) compared with that of the square-planar $RhCl(CH_2{=}CHCN)L_2$, the lower limit of the equilibrium constant of reaction (1) can be calculated by an equation: $K_{34}\geq(A_0-A)/A[H_2]$, where A_0 is the initial absorbance and A is the absorbance at the end of the first absorbance change. From Fig. 3, the value of K_{34} was evaluated to be $K_{34}\geq1.5\times10^2$ $mol^{-1}\cdot dm^3$. The broken line in Fig. 2 is drawn assuming that $K_{34}=k_{34}/k_{43}=1.5\times10^2$ mol^{-1} dm^3. The observed rate constant, $k_{obsd}=k_{34}[H_2]+k_{43}$, was mainly attributed to the rate constant of the reverse reaction. The rate constants were $k_{43}\leq53$ s^{-1} and $k_{34}\geq7.8\times10^3$ $mol^{-1}\cdot dm^3$ s^{-1}.

The addition and the dissociation rate constants, k_{34} and k_{43}, for several Rh(I) complexes are listed in

TABLE 1. ADDITION AND DISSOCIATION RATE CONSTANTS FOR THE HYDROGENATION OF SEVERAL Rh(I) COMPLEXES

Rh complex	k_1/mol^{-1} dm^3 s^{-1}	k_{-1}/s^{-1}	K_1/mol^{-1} dm^3
$RhCl(PPh_3)_3$ [a]	4.8	2.3×10^{-4} [d]	2.1×10^4
$RhCl(NCCH_3)(PPh_3)_2$ [b]	1.4×10^2	5.6×10^{-3} [d]	2.5×10^4
$RhCl(CH_2=CHCN)(PPh_3)_2$ [c]	$\geq7.8\times10^3$	≤53	$\geq1.5\times10^2$
$RhCl(PPh_3)_2$ [a]	$>7\times10^4$	—	

a) At 25 °C, from Ref. 4. b) At 20 °C, from Ref. 9. c) At 20 °C, the present study. d) Calculated from $k_{-1}=k_1/K_1$.

Table 1. The values of k_{34} increased in the sequence: $RhClL_3 < RhCl(NCCH_3)L_2 < RhCl(CH_2=CHCN)L_2 < RhClL_2$. The larger rate constant for $RhClL_2$ indicates that $RhClL_2$ has a labile site to which the benzene molecule coordinates. That the rate constant for $RhCl(CH_2=CHCN)L_2$ is larger than that for $RhClL_3$ suggests that $CH_2=CHCN$ is sterically less hindered than the PPh_3 attached to $RhClL_3$. A larger rate constant for $RhCl(CH_2=CHCN)L_2$ than that for $RhCl(NCCH_3)L_2$ may be predicted from the fact that the coordination of olefin stabilizes the lower valency state of the central metal more than the coordination of acetonitrile does.

The values of k_{43} increased in the sequence: $RhClL_3 < RhCl(NCCH_3)L_2 \ll RhCl(CH_2=CHCN)L_2$. $RhCl(CH_2=CHCN)L_2$ had an especially large rate constant. $CH_2=CHCN$ has the largest *trans*-effect among $CH_2=CHCN$, CH_3CN, and PPh_3. The Rh–H bond may be most weakened through the coordination of $CH_2=CHCN$. Thus, the dissociation of hydrogen from $RhClH_2(CH_2=CHCN)L_2$ is accelerated.

When $[CH_2=CHCN]$ is small, a second, slower decrease in the absorbance is observed (Fig. 1). The absorbance change gradually decreased with the increase in $[CH_2=CHCN]$ and finally disappeared. The accurate value of the rate constant cannot be obtained since the signal overlaps with that of the third step. The observed rate constant was about 0.35 ± 0.15 s^{-1} when $[H_2]_0=(1.41—0.56)\times10^{-3}$ and $[CH_2=CHCN]=7.6\times10^{-3}$ mol dm^{-3}.

Alternative explanations of the results will be presented below. One is an interpretation by the formation of a reaction intermediate alkyl complex (2), and another is an interpretation by the formation of a dimeric dihydrido species (3) which is inactive for the hydrogenation of olefin.

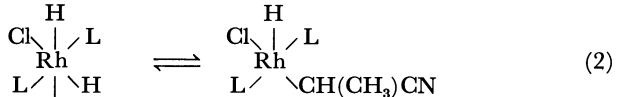

(2)

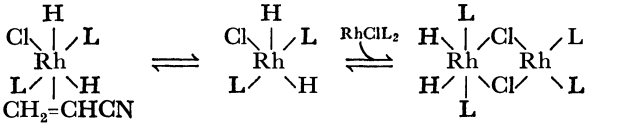

(3)

The less characteristic spectrum prevented us from distinguishing between $RhClH(-CH(CH_3)CN)L_2$ and $H_2(RhClL_2)_2$.

In the third step, the absorbance returned to that of the initial stage (Fig. 1). This step involves the consumption of hydrogen for the hydrogenation of acrylonitrile. The rate is dependent on $[CH_2=CHCN]$ when it is small, but gradually approaches the constant value as $[CH_2=CHCN]$ increases. The measurements of the hydrogen-gas uptake also showed that the hydrogenation rate depended on $[CH_2=CHCN]$ when it was small (Fig. 5). From Fig. 5, the value of k_{45}, the rate constant of the hydrogenation of $CH_2=CHCN$ in $RhClH_2(CH_2=CHCN)L_2$, can be estimated by means of the following equation

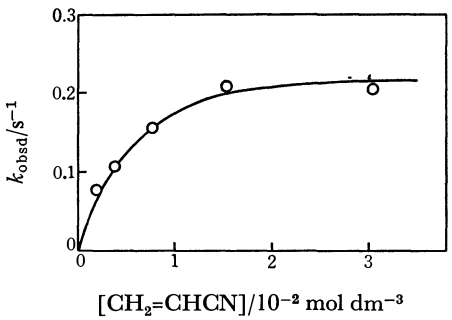

Fig. 5. Plot of the number of H_2 molecules taken up per Rh per s *vs.* $[CH_2=CHCN]$. $[Rh]=1.4\times10^{-4}$ mol dm^{-3} (2.8×10^{-6} mol), and $[H_2]=2.8\times10^{-3}$ mol dm^{-3} ($P(H_2)=1$ atm).

$$k_{45}=\frac{[RhCl(CH_2=CHCN)L_2]+[RhClH_2(CH_2=CHCN)L_2]}{[RhClH_2(CH_2=CHCN)L_2]}\times k_{obsd} \quad (4)$$
$$=\left(1+\frac{1}{K_{34}[H_2]}\right)\times0.22\ s^{-1}$$
$$\leq 0.74\ s^{-1}.$$

If an alkyl complex is formed in the second step, this result can be interpreted as follows: the addition of acrylonitrile to the vacant site of the alkyl complex weakens the *trans* Rh–H bond, and the insertion of the alkyl group to the second hydride is accelerated. At a high $[CH_2=CHCN]$ value, the formation of the alkyl complex becomes rate-determining for the hydrogenation of acrylonitrile.

If a dimeric dihydrido species is formed in the second step, the rate of hydrogenation depends on $[CH_2=CHCN]$ as the concentration of the active species decreases.

The total mechanism proposed is shown in Scheme 1. Because of the absence of the free PPh_3 molecule and the strong coordinating power of acrylonitrile, the hydrogenation of acrylonitrile proceeds through a so-called "unsaturate route." The existence of an intermediate species, $RhClH_2(CH_2=CHCN)L_2$, is indicated by the absorbance change, but no certain evidence of another reaction intermediate, $RhClH(-CH(CH_3)CN)L_2$, is

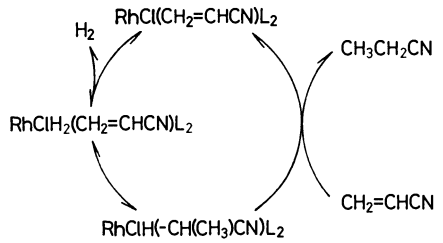

Scheme 1.

obtained in the present study.

Since the coordinating power of CH_3CH_2CN would be much smaller than that of $CH_2=CHCN$,[10] and since its concentration is small ($[CH_3CH_2CN] \leq [H_2]_0$), the formation of a propionitrile complex is very unlikely during the course of the hydrogenation.

References

1) B. R. James, "Homogeneous Hydrogenation," Wiley, New York, N. Y. (1973), pp. 204—250; G. N. Schrauzer, "Transition Metals in Homogeneous Catalysis," Marcel Dekker, New York, N. Y. (1971), pp. 31—36; M. M. T. Khan and A. E. Martell, "Homogeneous Catalysis by Metal Complexes," Vol. 1, Academic press, New York, N. Y. (1974), pp. 46—56.

2) J. A. Osborn, F. H. Jardine, J. F. Young, and G. Wilkinson, *J. Chem. Soc., A*, **1966**, 1711.

3) J. P. Candlin and A. R. Oldham, *Discuss. Faraday Soc.*, **46**, 60 (1968).

4) J. Halpern and C. S. Wong, *J. Chem. Soc., Chem. Commun.*, **1973**, 629.

5) C. A. Tolman, P. Z. Meakin, D. L. Lindner, and J. P. Jesson, *J. Am. Chem. Soc.*, **96**, 2762 (1974).

6) J. Halpern, T. Okamoto, and A. Zakhariev, *J. Mol. Catl.*, **2**, 65 (1977).

7) Y. Ohtani, M. Fujimoto, and A. Yamagishi, *Bull. Chem. Soc. Jpn.*, **50**, 1453 (1977).

8) Y. Ohtani, A. Yamagishi, and M. Fujimoto, *Chem. Lett.*, **1977**, 1187.

9) Y. Ohtani, A. Yamagishi, and M. Fujimoto, unpublished study.

10) The small value of $K=[RhCl(NCCH_3)L_2][L]/[RhClL_3][CH_3CN]=1.1\times10^{-3}$ suggests that CH_3CH_2CN may also have a low complexation constant.

Annihilation of Positron and Positronium in Benzene Solutions of Lanthanoid Dipivaloylmethanates

Kazutoyo ENDO,* Michiaki FURUKAWA,† Hideo YAMATERA,† and Hirotoshi SANO

Department of Chemistry, Faculty of Science, Tokyo Metropolitan University, Fukazawa, Setagaya, Tokyo 158

† *Department of Chemistry, Faculty of Science, Nagoya University, Chikusa, Nagoya 464*

(Received January 10, 1978)

The lifetime of *ortho*-positronium(*o*-Ps) was measured in benzene solutions of several lanthanoid dipivaloylmethanates. None of the paramagnetic lanthanoid dipivaloylmethanates, $Ln(dpm)_3$ (Ln=Eu, Gd, Tb, Dy, Ho, Er, and Yb), accelerated the *o*-Ps decay (τ_2=3.2 ns). On the other hand, diamagnetic tetrakis(dipivaloylmethanato)cerium(IV), $Ce(dpm)_4$, shortened the lifetime of *o*-Ps (τ_2=1.9 ns for a 0.02 mol dm^{-3} solution in benzene). These results clearly indicate that the acceleration of the *o*-Ps decay by lanthanoid complexes occurs through the oxidation mechanism, not through the spin-conversion mechanism. This confirms the previous conclusion from experiments with 3d transition-metal β-diketonates that the oxidation of *o*-Ps is mainly responsible for the rapid *o*-Ps decay caused by the Fe(III) and Mn(III) complexes. Factors which influence the intensity and decay rate of *o*-Ps are discussed in connection with the experimental results.

The reaction of *ortho*-positronium(*o*-Ps) with inorganic ions in aqueous solutions has been studied by many investigators. Jackson and McGervey[1] measured the lifetime of *o*-Ps in solutions of $KMnO_4$, $HgCl_2$, *etc.* and attributed the observed acceleration of *o*-Ps decay to the oxidation of *o*-Ps by the oxidizing ions. Ache and his coworkers[2-4] observed no significant changes in the lifetime of *o*-Ps in aqueous solutions containing Sn(II), Pb(II), Cd(II), *etc.* up to a concentration of about 2 M. On the other hand, the intensity (I_2) of *o*-Ps decreased with an increase in the solute concentration and approached a saturation value characteristic of each solute. The results were explained in terms of hot Ps reactions with solute species.

Previously,[5-6] we measured the lifetime of *o*-Ps in benzene solutions of 3d transition-metal acetylacetonates and dipivaloylmethanates, and showed that the decay rate of *o*-Ps was accelerated to a great extent by the Fe(III) and Mn(III) complexes and to a lesser extent by the Cu(II), Co(II), Co(III), and Cr(III) complexes, but that no acceleration was observed with the Al(III), Ni(II), and Zn(II) complexes. The complexes of the first group are oxidizing, those of the second group (except for the Co(III) complexes) are paramagnetic and poorly oxidizing, and the third-group complexes are non-oxidizing and diamagnetic. The conclusion was that, while the oxidation of *o*-Ps by oxidizing complexes proceeds very rapidly to result in a great acceleration of the *o*-Ps decay, the spin conversion of *o*-Ps through interaction with paramagnetic complexes proceeds slowly to result in a slight acceleration of the *o*-Ps decay.

The present study has been made with the intention of substantiating the previous conclusion and of determining the factors governing the rate of spin conversion. Lanthanoid dipivaloylmethanates were chosen for this purpose, since they show a series of different spin and total angular momenta (different quantum numbers, S and J) and since they include cerium(IV) dipivaloylmethanate, a unique compound which is diamagnetic and highly oxidizing.

Experimental

Lanthanoid tris(dipivaloylmethanato) complexes, $Ln(dpm)_3$, were prepared according to the procedure reported by Eisentraut and Sievers.[7] The compounds were purified by repeated sublimations and by recrystallization from mixed benzene-hexane. Tetrakis(dipivalolylmethanato)cerium(IV) was synthesized by a method analogous to that presented for tetrakis(acetylacetonato)cerium(IV), $Ce(acac)_4$.[8] The preparation of the dipivaloylmethanates of aluminium and 3d transition metals were described in a previous paper.[6] The compounds were identified by elemental analyses. A definite amount of each compound was dissolved in distilled benzene. The solution was then placed in a Pyrex tube and degassed repeatedly by a vacuum freeze-thaw technique. About 6 μCi of $^{22}Na(NaCl)$ of a high specific activity was used as the positron source. The lifetimes of the positron and positronium were measured with a fast-slow coincidence system, the details of which have been described elsewhere,[9] while the lifetime sepctrum was accumulated by means of a Hitachi 512-channel pulse-height analyzer. The time calibration was made by using coaxial cables of various lengths. The system as a whole gave a resolution (FWHM) of 750 ps for ^{60}Co prompt gamma rays and a 25 ns range of linear conversion.

Cyclic-voltammetric measurements were made of $Ce(dpm)_4$, $Eu(dpm)_3$, $Fe(dpm)_3$, $Co(dpm)_3$, $Co(acac)_2$, and $Cu(dpm)_2$ in dichloromethane(CH_2Cl_2) and partly in *N,N*-dimethylformamide(DMF), using 0.1 M tetrabutylammonium perchlorate(TBAP) as the supporting electrolyte. The measurement was carried out in a three-necked cell at room temperature. A platinum-inlay electrode (Beckman 32273) was used as the working electrode; the counter electrode was a piece of platinum wire. A saturated calomel electrode, used as a reference, was connected to the cell by two salt bridges: a saturated KCl solution in water and a 0.1 M TBAP solution in CH_2Cl_2 (or DMF). A Hokuto Denko Model HA-101 potentiostat and a Hokuto Denko Model HB-107 function generator were used. The scan rate was 0.50 and 1.00 V/s, and voltammograms were recorded by means of a Rikadenki X-Y recorder, Model BW 133.

Results and Discussion

The lifetimes of *o*-Ps, obtained from the measured lifetime spectra, are listed in Table 1, together with the I_2 values. The obtained decay constant, λ_2, of

o-Ps is plotted against the solute concentration in Fig. 1. None of the $Ln(dpm)_3$-type complexes (Ln=La, Gd, Tb, Ho, Dy, Er, and Yb) changed the lifetime of *o*-Ps in benzene, while $Ce(dpm)_4$ greatly accelerated the *o*-Ps decay. Since cerium(IV) has no unpaired electrons, the acceleration of the *o*-Ps decay by $Ce(dpm)_4$ can undoubtedly be attributed to its highly oxidizing nature, which was confirmed by cyclic voltammetry. The voltammograms of $Ce(dpm)_4$ and $Fe(dpm)_3$ in dichloromethane are compared in Fig. 2, while the E_{pc} values are listed in Table 2. It can be inferred from these results that $Ce(dpm)_4$ would be more oxidizing than $Fe(dpm)_3$ in benzene, too. Therefore,

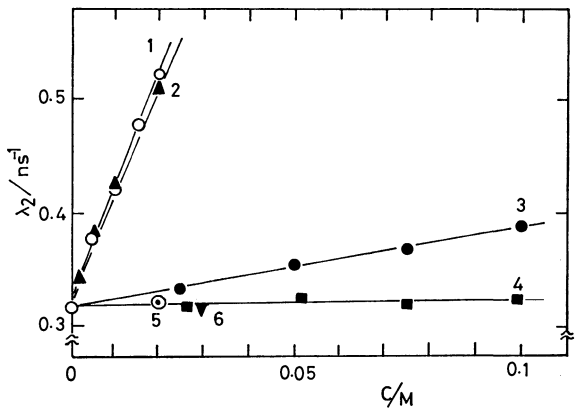

Fig. 1. Decay constant $\lambda_2(=\tau^{-1})$ *vs.* the solute concentration.
1: $Ce(dpm)_4$, 2: $Fe(dpm)_3$, 3: $Cr(dpm)_3$, 4: $Al(dpm)_3$, 5: $Gd(dpm)_3$, 6: $Yb(dpm)_3$.

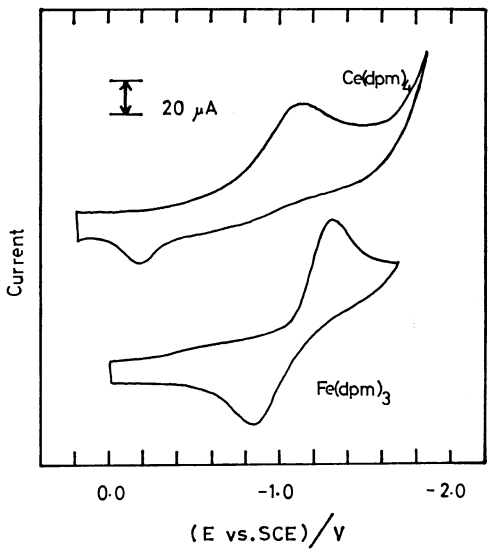

Fig. 2. Cyclic voltammograms for $Ce(dpm)_4$ and $Fe(dpm)_3$ in 0.1 M TEAP in CH_2Cl_2.

Table 1. The lifetimes and the intensities of *o*-Ps in 0.02 M benzene solutions of dipivaloylmethanates of lanthanoid and other metals

	λ_2/ns	$10^2 I_2$	Number of unpaired electrons[c]
Benzene	3.20±0.02	34.3	
$Al(dpm)_3$	3.03±0.02	31.9	0
$Cr(dpm)_3$	2.46±0.03[a]	32.0	3
$Fe(dpm)_3$	1.91±0.03	27.4	5
$La(dpm)_3$	3.23±0.03	31.3	0
$Ce(dpm)_4$	1.92±0.09	32.5	0
$Eu(dpm)_3$	3.21±0.03	32.0	6
$Gd(dpm)_3$	3.23±0.07	31.8	7
$Tb(dpm)_3$	3.16±0.02	32.8	6
$Dy(dpm)_3$	3.15±0.03	32.2	5
$Ho(dpm)_3$	3.16±0.03	32.2	4
$Er(dpm)_3$	3.22±0.03	31.5	3
$Yb(dpm)_3$	3.19±0.03[b]	32.6	1

a) A value for the 0.1 M solution. b) A value for the 0.03 M solution. c) Estimates from literature data on similar $[MO_6]$-type complexes.[14]

Table 2. Data of cyclic voltammetry and the rate constant for the reaction with *o*-Ps

	E_{pc}[a] V in CH_2Cl_2	E_{pc} V in DMF	$10^{-9}k$[c] $M^{-1}s^{-1}$
$Cr(dpm)_3$	−1.70[b]		0.66
$Fe(dpm)_3$	−1.32	−1.12	10.55
$Co(dpm)_3$	−1.70[b]	−1.32	0
$Co(acac)_3$	−1.28	−0.86	1.13
$Co(acac)_2$	−1.70[b]		0.99
$Cu(dpm)_2$	−1.70[b]		2.00
$Ce(dpm)_4$	−1.08		11.10
$Eu(dpm)_3$	−1.70[b]		0
$Gd(dpm)_3$			0
$Tb(dpm)_3$			0
$Dy(dpm)_3$			0
$Ho(dpm)_3$			0
$Er(dpm)_3$			0
$Yb(dpm)_3$			0

a) E_{pc}=Potential corresponding to the cathodic peak current (scan rate 0.5 and 1.0 V/s). b) The potential where the reduction of CH_2Cl_2 took place. c) k=rate constant for the reaction with *o*-Ps.

one might expect that *o*-Ps decay would be accelerated to a greater extent by the more oxidizing $Ce(dpm)_4$ than by the less oxidizing $Fe(dpm)_3$. However, experiments showed that the two complexes differed only slightly from each other in the rate constants for their reactions with *o*-Ps. This can be taken as demonstrating that the reaction is almost encounter-controlled in both cases.

Tripositive europium ions are known to be easily reduced to a dipositive state. However, the normal λ_2 value observed for a $Eu(dpm)_3$ solution shows that the complex is not oxidizing enough. Consistently, the E_{pc} value for $Eu(dpm)_3$ was found to be more negative than the potential where the reduction of the CH_2Cl_2 solvent took place.

Unlike 3d-transition-metal complexes, the paramagnetic lanthanoid complexes did not accelerate the *o*-Ps decay. In order to find the reason for this dissimilarity, the spin-conversion mechanism of *o*-Ps decay will now be examined. Whenever spin exchange occurs between

o-Ps and a metal complex with unpaired electrons, spin pairing will occur in the complex except when the partly filled shell has only one electron or hole. Thus, in order for spin exchange to occur, the kinetic energy of the *o*-Ps must at least counterbalance the spin-pairing energy. The latter is estimated to be about 2.5 eV for most lanthanoid complexes other than $Gd(dpm)_3$ ($\approx$3.9 eV), $Ho(dpm)_3$ ($\approx$3.5 eV), and $Yb(dpm)_3$ ($\approx$0).[10]

The Oré theory[11] shows that the most efficient formation of Ps occurs when the kinetic energy of a positron goes below the energy of the first excited level of the solvent (4.90 eV for benzene). Then, the kinetic energy of the positronium formed will be distributed mainly in the range below 2.46 eV; *i.e.*, (kinetic energy of positron) + (binding energy of positronium) − (ionization energy of benzene) = 4.90 + 6.80 − 9.24 = 2.46 (see Fig. 3).

Oré diagram for positronium formation in benzene (eV)			Kinetic energy of positronium (eV)
Ionization energy (E_I)	9.24	———	6.80
Energies of the excited levels	6.99	Excitation collisions and Ps formation	4.55
	6.19		3.75
	4.90	——— Ps formation	2.46
$E_I - E_b$*	2.44	———	0

*) E_b: Binding energy of positronium

Fig. 3. Oré diagram of positronium formation in benzene and the kinetic energy of positronium.

The foregoing argument raises an expectation that the *o*-Ps decay would be accelerated by $Yb(dpm)_3$, which requires no spin-pairing energy. The experimental results, however, failed to show this. This leads to the conclusion that the lanthanoid complexes (at least $Yb(dpm)_3$, but not $Ce(dpm)_4$) fail to accelerate the *o*-Ps decay, not because of a matter of energy balance, but because of the inertness of the 4f unpaired electrons. Abundant evidence shows that the 4f orbitals of the lanthanoid ions are well shielded from the surrounding ions by the 5s—5p closed shell. Thus, the overlap of the 4f orbital with the *o*-Ps orbital can be expected to be negligibly small. The present experimental findings not only conform with the negligible overlap, but also indicate that there exist no appreciable long-range interactions that would result in spin exchange between the 4f and *o*-Ps orbitals.

The effect of $Ce(dpm)_4$ on the I_2 value was not so great as that of $Fe(dpm)_3$, and it was similar to that of other lanthanoid complexes. With the Oré model of Ps formation, this can be attributed to the fact that, because of its closed-shell electron configuration, $Ce(dpm)_4$ has a relatively small number of excited states compared with the number for $Fe(dpm)_3$. When a molecule has thinly distributed excited states, it will have small chance of being excited on collision with a positron. Therefore, in a $Ce(dpm)_4$ solution, the *o*-Ps formation can be expected to compete favorably with the excitation of the complex, thus resulting in an unaffected I_2 value.

According to the spur model,[12,13] however, positrons combine with the electrons produced in the radiation spurs to form Ps. If an electron scavenger is present, the electron concentration in the spur will be reduced, and, therefore, a smaller amount of Ps will be formed. In the system investigated here, $Ce(dpm)_4$ is as strong an oxidizing agent or electron scavenger as $Fe(dpm)_3$, and should result in a reduced I_2. This is not consistent with the experimental results. If, however, the spur model is applicable to the present system, the observed inertness of $Ce(dpm)_4$ can be considered to show its slow rate of electron scavenging as compared with the rate of Ps formation.

References

1) J. E. Jackson and J. D. McGervey, *J. Chem. Phys.*, **38**, 300 (1963).
2) L. J. Bartal, J. B. Nicholas, and H. J. Ache, *J. Phys. Chem.*, **76**, 1124 (1972).
3) L. J. Bartal and H. J. Ache, *Radiochim. Acta*, **17**, 205 (1972).
4) J. B. Nicholas, R. E. Wild, L. J. Batal, and H. J. Ache, *J. Phys. Chem.*, **77**, 178 (1973).
5) K. Endo, M. Furukawa, and H. Yamatera, *Radiochem. Radioanal. Lett.*, **21**, 307 (1975).
6) K. Endo, M. Furukawa, and H. Yamatera, *J. Phys. Chem.*, **80**, 1540 (1976).
7) K. J. Eisentraut and R. E. Sievers, *J. Am. Chem. Soc.*, **87**, 5254 (1965).
8) B. W. Parry, *Inorg. Synth.*, **12**, 77 (1970).
9) K. Endo, K. Sasaki, M. Furukawa, and H. Yamatera, *Nucl. Instrum. Method*, **141**, 273 (1977).
10) The values are estimated to be 2.4 eV ($^5D_1 \leftarrow {}^7F_0$) for Eu^{3+}, 3.9 eV ($^6P_{7/2} \leftarrow {}^8S_{7/2}$) for Gd^{3+}, 2.6 eV ($^5D_4 \leftarrow {}^7F_6$) for Tb^{3+}, 2.6 eV ($^4F_{9/2} \leftarrow {}^6H_{15/2}$) for Dy^{3+}, 3.3 eV ($^3F_2 \leftarrow {}^5I_8$) for Ho^{3+}, and 2.4 eV ($^2H_{11/2} \leftarrow {}^4I_{15/2}$) for Er^{3+} (*cf.* W. T. Carnall, P. R. Fields, and K. Rajnak, *J. Chem. Phys.*, **49**, 4412 (1968)).
11) A. Oré, *Univ. Bergen Arbok Naturvitenskap. Rekke*, No. 9 (1949).
12) O. E. Mogensen *J. Chem. Phys.*, **60**, 998 (1974).
13) S. J. Tao, *Appl. Phys.*, **10**, 67 (1976).
14) S. Evans, A. Hamnett, A. F. Orchard, and D. R. Lloyd, *J. Chem. Soc., Faraday Discuss.* **54**, 227 (1972); W. E. Henry, *Phys. Rev.*, **88**, 559 (1952).

Syntheses and Thermal Properties of Some Bivalent Transition Metal Complexes with 1,4-Diazabicyclo[2.2.2]octane

Hiroko YOKOBAYASHI, Kenzo NAGASE,* and Kozo SONE†

College of General Education, Tohoku University, Kawauchi, Sendai 980

†*Department of Chemistry, Faculty of Science, Ochanomizu University, Otsuka, Bunkyo-ku, Tokyo 112*

(Received January 12, 1978)

New five-coordinate complexes $[MCl_3L(H^+L)]$, where M=Mn(II), Fe(II), Co(II), and Ni(II) and L=1,4-diazabicyclo[2.2.2]octane, were prepared in anhydrous ethanol. On being heated in the solid state, they begin to lose the non-charged ligand (L) in the order Co(147 °C)≪Fe(184 °C)<Ni(190 °C)<Mn(196 °C) and are transformed into the tetrahedral complexes $[MCl_3(H^+L)]$. The thermal stability of the five-coordinate complexes depends markedly on the nature of M(II). The octahedral complex $[NiCl_4(H_2O)_2]H_2L\cdot H_2O$ obtained from an aqueous solution shows a series of complicated color and structural changes on heating according to stepwise decomposition: $[NiCl_4(H_2O)_2]H_2L\cdot H_2O$ (greenish yellow, octahedral)→$[NiCl_4]H_2L$(light blue, tetrahedral)→$[NiCl_3(H^+L)]$(cobalt blue, tetrahedral)→$[NiCl_2L_{1/2}]$(reddish brown, probably square-pyramidal)→$NiCl_2$(yellow, octahedral).

Ouagliano and co-workers reported that the protonated and methylated cations of the cagelike ditertiary amine 1,4-diazabicyclo[2.2.2]octane(dabco; denoted in this paper by L) react with some bivalent transition metal halides to form four- and/or five-coordinate complexes.[1-3] The trigonal-bipyramidal complexes $[MX_3(H^+L)_2]X$ formed with Mn(II), Fe(II), Ni(II), and Cu(II) (X=halide anions) are generally insoluble and stable only in the crystalline state in the absence of moisture. Thus to study their relative stability, we considered that thermogravimetry would be a favorable technique.

We prepared the five-coordinate complexes according to the reported method,[2] but somewhat different results were obtained, *i.e.*, the formula of the complexes was $[MCl_3L(H^+L)]$ and not $[MCl_3(H^+L)_2]Cl$, except in the case of Cu(II), a five-coordinate complex of the same type being obtained with Co(II). The complexes $[MCl_3L(H^+L)]$ were found to be transformed into the tetrahedral complexes $[MCl_3(H^+L)]$ by heating with evolution of L. We could thus compare the thermal stability of the five-coordinate complexes of Mn(II), Fe(II), Co(II), and Ni(II) from their initial weight-loss temperatures determined by thermogravimetric analyses.

The cobalt(II) and nickel(II) complexes with the cagelike ditertiary amine 1,3,5,7-tetraazatricyclo[3.3.1.-$1^{3,7}$]decane (hmta), prepared from aqueous solutions, show striking color changes in the course of dehydration. With a proper combination of thermal analyses with visible and infrared spectroscopy, we have confirmed that these complexes can be formulated as $[M(H_2O)_6]X_2\cdot hmta\cdot nH_2O$ (X=Cl^-, Br^-, I^-), and the decrease in the number of coordinated water molecules brings about the coordination of halide ions first, and that of hmta only in the last stage of dehydration, with the decrease in coordination number from 6 to 4. This apparent reluctance of an amine, which usually shows a stronger coordination tendency than halide ions and water, is probably due to the bulkiness of hmta and its weak basicity(pK_b=8.87). In continuation of this study on the color and structural changes of the complexes containing water, anions and a cagelike amine by heating,[4] we undertook preparation of such a complex with L from an aqueous solution. Owing to the strong basicity of L(pK_b=5.40), hydroxide precipitates formed when cobalt and nickel salts were mixed with L in aqueous solutions. We therefore used the diprotonated species H_2LCl_2 and succeeded in the preparation of $[NiCl_4(H_2O)_2]H_2L\cdot H_2O$. As expected, the complex showed complicated color and structural changes involving dehydration and the elimination of HCl and L, which we could elucidate in some detail.

Experimental

Preparation of H_2LCl_2. A solution of 10 g of L in warm acetone was added with stirring to a warm solution prepared from 10 ml of concd HCl and 15 ml of 1,1-dimethoxypropane (dehydrating agent). The white crystals separated were recrystallized from anhydrous ethanol, and dried *in vacuo*. The analytical data are given in Table 1. Although the monoprotonated species HLCl has been reported,[1] only a diprotonated one was obtained in the present work, regardless of the L:HCl ratio.

General Preparation of $[MCl_3L(H^+L)]$(M=Mn(II), Fe(II), Co(II), and Ni(II)). A hot solution of anhydrous metal chloride (0.001 mol) in anhydrous ethanol was added with stirring to a hot solution of L(0.005 mol) and H_2LCl_2(0.005 mol) in the same solvent. In the case of Co(II), slight excess of L was necessary in order to avoid formation of the tetrahedral complex. The resulting solutions were allowed to stand at 60—70 °C for several hours under anhydrous conditions. The crystals formed were filtered in a stream of dry nitrogen, and dried *in vacuo* (Table 1). The iron complex is partially decomposed by air oxidation, turning yellowish, so that its data differ somethat from theoretical values. We tried to prepare the same complexes of Zn(II) and Cu(II), but the reactions of $CuCl_2$ and $ZnCl_2$ with a large excess of the ligands yielded only $[ZnCl_3(H^+L)]$ and $[CuCl_3(H^+L)_2]Cl$, respectively, which have already been prepared by Quagliano *et al.*[1,2]

Preparation of $[NiCl_4(H_2O)_2]H_2L\cdot H_2O$. An aqueous solution of H_2LCl_2(0.003 mol) with a few drops of concd, HCl was added to an aqueous solution of $NiCl_2\cdot 6H_2O$(0.001 mol). The resulting solution was allowed to stand in the open air at roon temperature until greenish yellow crystals appeared, which were filtered and dried in the open air (Table 1).

Measurements. The electronic spectra of the samples be-

Table 1. Elemental analyses of the complexes obtained in the present work

Compound	Color	Found (%)			Calcd (%)		
		C	H	N	C	H	N
H_2LCl_2	white	38.81	7.81	15.32	38.92	7.75	15.14
$[MnCl_3L(H^+L)]$	white	36.95	6.67	14.80	37.27	6.52	14.49
$[FeCl_3L(H^+L)]$	white	35.81	6.40	14.06	37.19	6.51	14.46
$[CoCl_3L(H^+L)]$	cobalt blue	36.55	6.58	14.49	36.89	6.45	14.34
$[NiCl_3L(H^+L)]$	deep pink	36.57	6.65	14.61	36.91	6.45	14.35
$[CuCl_3(H^+L)_2]Cl$	yellow	32.73	6.25	12.79	33.38	6.07	12.98
$[NiCl_4(H_2O)_2]H_2L\cdot H_2O$	greenish yellow	19.32	5.81	7.75	19.54	5.47	7.60

fore and after heating were obtained by the diffuse reflection method with a Hitachi EPS-3T spectrophotometer equipped with a standard integrating sphere attachment. All the measurements were carried out at room temperature using MgO as a reference material. Thermogravimetry(TG) and differential thermal analysis(DTA) were performed simultaneously with a Shinku Riko TGD-3000 differential thermal micro balance in a nitrogen atmosphere with a heating rate of 5 °C/min, 15—20 mg of sample being used for each measurement. The infrared absorption spectra(4000—250 cm^{-1}) were measured with a Hitachi 215 spectrophotometer by the Nujol mull method. X-Ray diffraction charts were obtained with a Toshiba ADG-101 diffractometer using manganese-filtered Fe $K\alpha$ radiation.

Results and Discussion

Spectral and Thermal Properties of the Five-Coordinate Complexes. The reflectance spectra of the colored five-coordinate complexes are shown in Fig. 1. The blue $[CoCl_3L(H^+L)]$ showed three absoptions at 15300, 16700, and 18300 cm^{-1} in the region 10000—30000 cm^{-1}. High spin trigonal-bipyramidal cobalt(II) complexes show at least four well-separated absorption bands in the region 5000—25000 cm^{-1}. Bertini *et al.*[5] showed that $[CoBr(Me_6tren)]Br$ gives well-separated absorptions at 5700, 12300, 16100, and 19600 cm^{-1} in its diffuse reflectance spectrum. They also presented the spectra of the tetrahedrally distorted trigonal-bipyramidal cobalt(II) complexes with similar ligands, and discussed spectral changes in going from an octahedral to a tetrahedral structure. A comparison with their results indicates that the outlook of the spectrum of $[CoCl_3L(H^+L)]$ is understandable if we assume that Co(II) is in a nearly undistorted trigonal-bipyramidal environment.

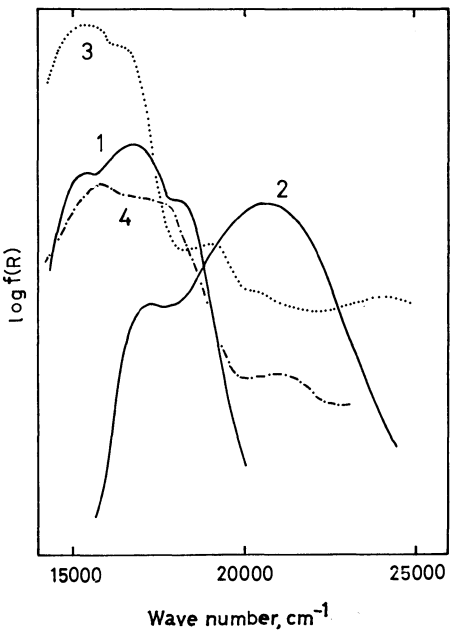

Fig. 1. Reflectance spectra of (1) $[CoCl_3L(H^+L)]$, (2) $[NiCl_3L(H^+L)]$, (3) $[CoCl_3(H^+L)]$, and (4) $[NiCl_3(H^+L)]$.

The deep pink $[NiCl_3L(H^+L)]$ shows two absorption bands at 17000 and 20600 cm^{-1}. This spectrum was quite similar to that of red $[NiCl_3(H_2O)(CH_3{}^+L)]$ which was found by X-ray analysis[6] to be in an almost undistorted trigonal-bipyramidal environment with three Cl atoms in the equatorial plane. Recently, similar structures were found for $[MCl_3(CH_3{}^+L)_2]ClO_4$ (M=Ni(II) and Cu(II)) by X-ray analyses.[7]

$[CoCl_3L(H^+L)]$ gives a very strong diffraction line at d=5.47 Å and some weak lines at 7.67, 4.22, 3.41, and 2.42 Å in its X-ray powder pattern. The corresponding Mn, Fe, and Ni complexes were found to be isomorphous with the cobalt complex. The infrared spectra of $[MCl_3L(H^+L)]$ were similar among the complexes of Mn, Fe, Co, and Ni. Thus, we conclude that the complexes of Mn and Fe have essentially the same trigonal-bipyramidal structure as that of Co and Ni. As an example, IR frequencies of the Co complex are given in Table 2, together with those of $[CuCl_3(H^+L)_2]Cl$ which shows a somewhat different spectrum.

The non-charged ligand L in $[MCl_3L(H^+L)]$ is expected to be released more easily than the protonated ligand H^+L on heating, a complex with a coordination number four being obtained. The TG-DTA curves of the complexes are shown in Fig. 2. A distinct break point is observed on each TG curve, the weight-loss values up to this point being 29.4(29.0), 21.3(28.9), 26.9(28.3), and 26.0(28.3)% for the Mn, Fe, Co, and Ni complexes respectively. The values in parentheses are the calculated ones for the evolution of L. The difference between the observed and calculated values for the Fe complex might be due to its partial decomposition owing to air oxidation before the TG measurement. The formation of the complex $[MCl_3(H^+L)]$ at this stage was also confirmed by IR and/or reflectance spectra of the products, together with their tetrahedral structure(*cf.* curves 3 and 4, Fig. 1).

Table 2. Comparison of IR frequencies (cm^{-1}) in the region 250—4000 cm^{-1} for $[CoCl_3L(H^+L)]$ and $[CuCl_3(H^+L)_2]Cl$[a]

$[CoCl_3L(H^+L)]$	$[CuCl_3(H^+L)_2]Cl$	Approximate description[b]
	2600 m 2525 m 2450 m	$\nu(N-H^+)$
1328 s	1327 s	ωCH_2
1293 mw	1282 w	τCH_2
	1248 mw	
1186 mw	1175 mw	
1058 vs	1052 vs	$\nu_{as}N-C-C$
1031 m 998 m	1030 m 1000 m	ν_sN-C-C
915 w	920 w	ν_sNC_3
847 s	850 s	$\nu_{as}NC_3$
808 sh 798 sh 783 s 756 w	802 sh 784 vs	ρCH_2
680 m	690 m	
	628 w	
	617 m	
421 m	423 m	$\delta_{as}NC_3$
282 s		$\nu(Co-Cl)$

a) Relative intensities: vs=very strong, s=strong, m=medium, mw=medium weak, w=weak, sh=shoulder. b) Based on the assignments made for the ligand molecule.[13]

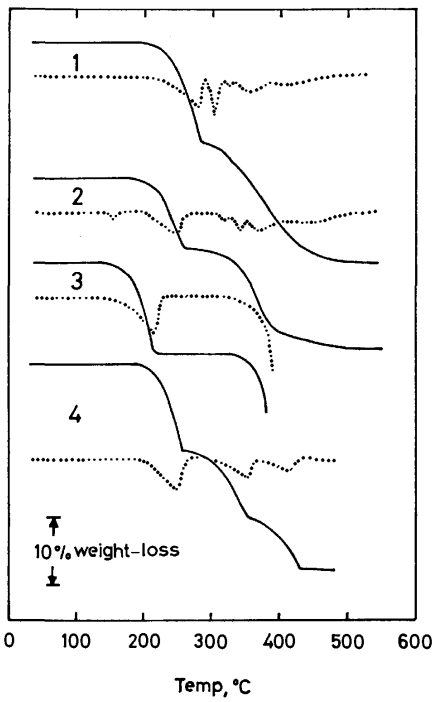

Fig. 2. TG(solid line) and DTA(dotted line) curves of $[MCl_3L(H^+L)]$. (1) Mn(II), (2) Fe(II), (3) Co(II), and (4) Ni(II).

From the spectral and thermal measurements, we can imagine the most probable structure of $[MCl_3L(H^+L)]$ to be as shown in Fig. 3. The unusual trigonal-bipyramidal coordination seems to be brought about chiefly by the steric requirements of the bulky and rigid cagelike ligands. The orientation of the ligands which favor the formation of the –N–H--N– hydrogen bonding might greatly contribute to the stabilization of the complex including both L and H^+L.[8]

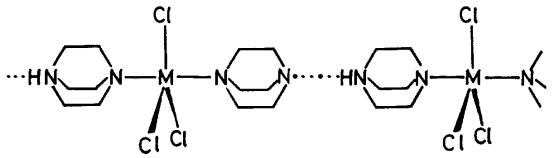

Fig. 3. Postulated structure of $[MCl_3L(H^+L)]$.

It seems to be of interest to examine the effect of the nature of metal ion on the trigonal-bipyramidal coordination. The initial weight-loss temperatures(t_i) on the TG curves can be considered as a measure of the relative stability of the complexes if the elimination reactions of L from them proceed with the same mechanism for all the complexes. The TG and DTA curves in the first step are similar among the four complexes of Mn to Ni (Fig. 2), supporting the assumption. The t_i values are summarized in Table 3, together with those of the tetrahedral complexes formed, which were observed on further heating. The order of corresponding DTA peak temperatures(t_m) was the same as that of t_i. We can conclude that the thermal stability of the trigonal-bipyramidal coordination depends strongly on the nature of the metal, increasing in the order Co≪Fe<Ni<Mn. In general, the trigonal-bipyramidal coordination seems to be favored with increase in the ionic radius of metal, except for the Ni complex which has the largest crystal field stabilization energy in the high-spin trigonal-bipyramidal environment.[9]

It is also of interest to compare the order of t_i of the trigonal-bipyramidal complexes with that of the tetrahedral complexes. As seen in Table 3, the stability of the latter complexes also depends on the nature of the metal. The TG and DTA curves in the second step are not similar in the complexes studied, no plateau being observed in the case of Mn between the two steps on its TG curve. In spite of this, however, we can safely say that the Co complex shows the largest thermal stability. This may also be the driving force for the thermal decomposition of $[CoCl_3L(H^+L)]$, which leads to its especially low thermal stability.

Thermal Decompositions of the Complex $[NiCl_4(H_2O)_2]$-$H_2L\cdot H_2O$. The reflectance spectrum of the greenish yellow $[NiCl_4(H_2O)_2]H_2L\cdot H_2O$ shows a pattern

Table 3. Comparison of initial weight-loss temperatures (t_i)

$[MCl_3L(H^+L)] \rightarrow [MCl_3(H^+L)]+L$		$[MCl_3(H^+L)] \rightarrow$ Decomposition	
M	t_i/°C	M	t_i/°C
Mn	196	Mn	<281
Fe	184	Fe	266
Co	147	Co	300
Ni	190	Ni	263

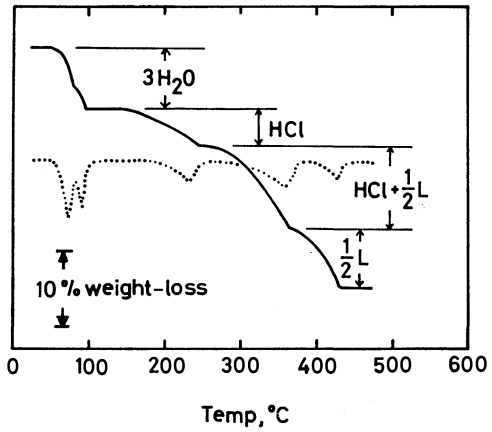

Fig. 4. TG(solid line) and DTA(dotted line) curves of $[NiCl_4(H_2O)]H_2L \cdot H_2O$.

characteristic of an octahedral coordination, and its ν_{max} (23000 cm^{-1}) lies between that of $NiCl_2 \cdot 2H_2O$ (22800 cm^{-1}) and $NiCl_2 \cdot 4H_2O$(23400 cm^{-1}), but is closer to the former, which is in fact a $NiCl_4O_2$-type complex with bridging Cl atoms. The IR spectrum indicates that L in this complex is not coordinated to the metal but is held in the crystal lattice as a counter cation(H_2L^{2+}). The formulation of this complex is based on these spectral data. Similar Ni(II) complexes with protonated *N*-methyl-dabco[1] and protonated piperazine[10] have been described.

The TG and DTA curves of $[NiCl_4(H_2O)_2]H_2L \cdot H_2O$ show that this complex decomposes in five steps up to 500 °C as shown in Fig. 4. In the first step, it loses $2H_2O$ and becomes yellow; in the second step, it loses the rest of water turning light blue. In the third step, HCl is evolved, and a cobalt blue substance of the composition $NiCl_3(H^+L)$ remains. In the fourth step, a reddish brown substance is obtained. Both TG and elemental analyses indicate that its composition is close to $NiCl_2L_{1/2}$. In the last step, yellow anhydrous $NiCl_2$ is obtained.

There were some difficulties in isolating these intermediate substances in pure form and/or in large quantities, except for the light blue one, since (i) there were no well-developed plateaus on the TG curve except for the second stage, (ii) the sample formed in the fourth step melted when it was kept in a crucible forming a thick layer, and (iii) the products formed in the last two stages contained a small amount of free carbon when the sample was heated in an inert gas atmosphere. We found that the melting can be avoided when the sample is heated very slowly in the form of a thin layer. No free carbon is formed when the sample is heated in the air, probably owing to the reaction $C+O_2 \rightarrow CO_2$, although $NiCl_2$ formed at the last stage is transformed gradually into NiO in the air. We could thus obtain only a mixture of $NiCl_2$ and NiO at the last stage.

We obtained each of the intermediates in an almost pure form by heating the complex at the desired temperatures in the air, and measured their reflectance and infrared spectra. The reflectance spectra of the light blue and reddish brown substances are shown in Fig. 5, together with that of the original complex.

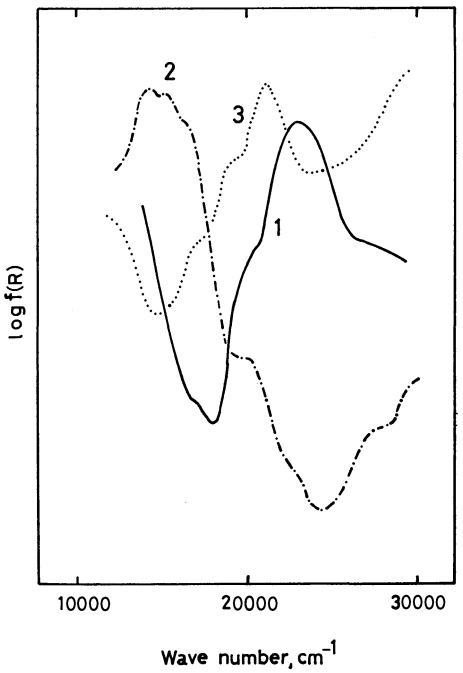

Fig. 5. Reflectance spectra of (1) $[NiCl_4(H_2O)_2]H_2L \cdot H_2O$, (2) $[NiCl_4]H_2L$, and (3) $[NiCl_2L_{1/2}]$.

The yellow substance of the composition $NiCl_4 \cdot H_2L \cdot H_2O$ shows the peak maximum at 22300 cm^{-1}, the frequency of which is still lower than that of the original complex. Thus the nickel atom in it seems to be surrounded by five or more chlorine atoms. The spectrum of the light blue substance of composition $NiCl_4 \cdot H_2L$ is very similar to that of $[NiCl_4]^{2-}$ in the literature[11] and therefore it should be formulated as $[NiCl_4]H_2L$. The spectrum of the cobalt blue substance of composition $NiCl_3(H^+L)$ is just the same as that of tetrahedral $[NiCl_3(H^+L)]$.

The reddish brown substance of composition $NiCl_2L_{1/2}$ shows three absorption bands at 17000, 19200, and 21000 cm^{-1}. The spectrum is somewhat similar to that of trigonal-bipyramidal $[NiCl_3L(H^+L)]$ except for a shoulder at 19200 cm^{-1} (*cf.* curve 2, Fig. 1). However, since the difference between the electronic spectrum of a trigonal-bipyramidal complex and that of a square-pyramidal one is not very large[12] in the region 15000—30000 cm^{-1}, this can not be taken as proof for its geometry. On the other hand, the infrared spectral pattern of $NiCl_2L_{1/2}$ in the region 650—1400 cm^{-1} was essentially similar to that of free L

Table 4. Comparison of IR frequencies (cm^{-1}) in the region 700—1400 cm^{-1} for $[NiCl_2L_{1/2}]$ and L

$[NiCl_2L_{1/2}]$	L[a]	Assignment
1321 m	1350 w	ωCH_2
1055 s	1057 vs	ν_{as}N-C-C
1013 m	986 m	ν_sN-C-C
928 m	897 m	$\nu_s NC_3$
844 m	830 m	$\nu_{as} NC_3$
812 s	755 m	ρCH_2

a) Values taken from Ref. 13.

molecule although there are considerable differences in the frequency values(Table 4). This indicates that the bands of L in the complex can be best assigned in terms of its D_{3h} symmetry.[13] This suggests that the complex consists of polymeric chains in which the nickels are surrounded by four bridging chlorines in a plane, and one bridging L perpendicular to the plane, forming a square-pyramidal coordination structure as shown in Fig. 6.

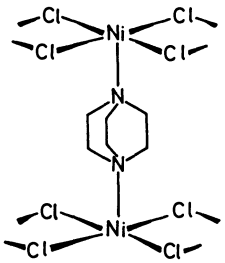

Fig. 6. Postulated structure of $[NiCl_2L_{1/2}]$.

The decomposition processes of $[NiCl_4(H_2O)_2]H_2L\cdot H_2O$ can be summarized as follows: $[NiCl_4(H_2O)_2]H_2L\cdot H_2O$(greensih yellow, octahedral) $\xrightarrow{-2H_2O}$ $NiCl_4H_2L\cdot H_2O$(yellow, octahedral) $\xrightarrow{-H_2O}$ $[NiCl_4]H_2L$(light blue, tetrahedral) $\xrightarrow{-HCl}$ $[NiCl_3(H^+L)]$ (cobalt blue, tetrahedral) $\xrightarrow{-(HCl+1/2L)}$ $[NiCl_2L_{1/2}]$(reddish brown, probably square-pyramidal) $\xrightarrow{-1/2L}$ $NiCl_2$(yellow, octahedral).

Comparing the results of the present study on the dabco complexes with those of our previous study on hmta complexes,[4] we find some differences between the two amines. (i) When hmta reacts with a heavy metal halide(MX_2) in aqueous solution, a complex containing $[M(H_2O)_6]^{2+}$ and uncoordinated hmta precipitates easily, whereas dabco precipitates only $M(OH)_2$ from aqueous solution (only when H_2L^{2+} is used instead of L, the complex $[NiCl_4(H_2O)_2]H_2L\cdot H_2O$ could be obtained). (ii) The complexes containing coordinated hmta, which are formed only at the last stage of dehydration of the complexes with $[M(H_2O)_6]^{2+}$, are mostly tetrahedral, but those of coordinated dabco obtained from ethanolic solutions are trigonal-bipyramidal. (iii) Heating of the anhydrous hmta complexes leads to decomposition, but heating of the anhydrous dabco complexes leads to the elimination of L and formation of new complexes with different geometries. These remarkable differences between the two amines are probably related to their difference in size, basicity, and the number and disposition of N atoms.

References

1) J. V. Quagliano, A. K. Banerjee, V. L. Goedken, and L. M. Vallarino, *J. Am. Chem. Soc.*, **92**, 482 (1970).
2) L. M. Vallarino, V. L. Goedken, and J. V. Quagliano, *Inorg. Chem.*, **11**, 1466 (1972).
3) V. L. Goedken, J. V. Quagliano, and L. M. Vallarino, *Inorg. Chem.*, **8**, 2331 (1969).
4) K. Nagase, H. Yokobayashi, and K. Sone, *Bull. Chem. Soc. Jpn.*, **49**, 1563 (1976).
5) I. Bertini, D. Gatteshi, and A. Scozzafava, *Inorg. Chem.*, **14**, 813 (1975).
6) F. K. Loss and G. D. Stucky, *Inorg. Chem.*, **8**, 2734 (1969).
7) W. J. Rozell and J. S. Wood, *Inorg. Chem.*, **16**, 1827 (1977).
8) However, we could not confirm the existence and strength of this hydrogen bond since the complexes showed no obvious band in the N–H stretching region of their infrared spectra.
9) For example, F. Basolo and R. G. Pearson, "Mechanisms of Inorganic Chemistry," 2nd ed, Wiley, N. Y. (1967), p. 69.
10) V. L. Goedken, L. M. Vallarino, and J. V. Quagliano, *J. Am. Chem. Soc.*, **92**, 303 (1970).
11) D. M. L. Goodgame, M. Goodgame, and F. A. Cotton, *J. Am. Chem. Soc.*, **83**, 4161 (1961).
12) J. S. Wood, *Prog. Inorg. Chem.*, **16**, 227 (1972).
13) J. R. McDivitt and G. L. Humphrey, *Spectrochim. Acta, Part A*, **30**, 1021 (1974).

Analytical Application of Oleophilic Quaternary Ammonium Salts. XV. Extraction of the Uranium(VI)–4-(2-Pyridylazo)resorcinol Complex with Tridodecylethylammonium Bromide

Yoshio SHIJO* and Kaoru SAKAI

Department of Environmental Chemistry, Faculty of Engineering, University of Utsunomiya, Ishii-machi, Utsunomiya 321-31

(Received January 14, 1978)

The uranium(VI)-4-(2-pyridylazo)resorcinol(PAR) chelate anion was extracted with tridodecylethylammonium bromide(TDEABr) into chloroform to form an ion associate. The ternary complex has an absorption maximum at 550 nm in the organic layer. The optimum pH range for the extraction is 6.8—10.7. The distribution ratio and the molar absorptivity are 1.34×10^{2} and 4.25×10^{4} cm^{-1} mol^{-1} l, respectively. The composition of the ternary complex is estimated to be $UO_2(X)(PAR)(R_3R'N)$. The equation representing the extraction equilibrium would be

$$UO_2(X)(PAR)^- + R_3R'NBr_{(o)} = UO_2(X)(PAR)(R_3R'N)_{(o)} + Br^-.$$

The extraction constant K_{ex} is given by $\log K_{ex}=3.07$.

4-(2-pyridylazo)resorcinol(PAR)[1] is a well-known chelating agent which is useful for the sensitive colorimetric determination of various metal ions. Recently, the ion-pairs of the metal–PAR chelate anions with bulky organic cations have been studied by several workers; the spectrophotometric determination of many metals was made by the extraction method. The PAR chelate anions of cobalt(III),[2,3] chromium,[4] copper,[5] iron(II),[2] iron(III),[6] gallium,[7] niobium,[8] nickel,[2,9] palladium,[10] vanadium(III),[11] vanadium(V),[2,12,13] and zinc[14] were extracted into an organic layer in the presence of zephiramine, tetraphenylarsonium, diphenylguanidine, or Crystal Violet. Uranium(VI) reacts with PAR to form a water-soluble red chelate. The chelate is slightly extractable into butanol, but not extractable into chloroform, carbon tetrachloride, and benzene. From the extraction experiments, it was found that the uranium(VI)–PAR chelate anion was extracted with tridodecylethylammonium bromide(TDEABr) in chloroform to form an ionic associate. The oleophilic quaternary ammonium salts such as TDEABr have been already used for the extraction of metal-Xylenol Oranges,[15]- Eriochrome Cyanine R,[16] and -Pyrocatechol Violet[17] chelate anions. In the present study, the fundamental conditions for the extraction of uranium(VI) as the uranium(VI)–PAR–TDEA ternary complex in chloroform and the composition of the ternary complex will be discussed.

Experimental

Reagent. About 2.5×10^{-3} M uranium(VI) solution was prepared by dissolving a definite amount of uranyl acetate in 0.05 M sulfuric acid. The resulting solution was standardized by the gravimetric method. The solution was diluted as required. A 5×10^{-4} M PAR solution was prepared by dissolving the Dotite PAR in a small amount of 0.2 M NaOH and diluted with deionized water. The TDEABr was prepared by refluxing an ethanolic solution of tridodecylamine and ethyl bromide for 4 h. After the evaporation of the solvent, the salt was recrystallized two times from butyl acetate. A 10^{-3} M TDEABr solution was prepared by dissolving the above TDEABr in the purified chloroform. A 0.05 M sodium borate solution was used as a buffer solution. All the other chemicals used were of guaranteed reagent quality.

Apparatus. A Hitachi 101 spectrophotometer, a Hitachi UV-vis. recording spectrophotometer, and a Hitachi-Horiba F-7 pH meter were employed.

Standard Procedure. Up to 30 μg of uranium(VI), a definite amount of 0.1 M sulfuric acid, and 2 ml of 5×10^{-4} M PAR solution were mixed in a 100 ml polypropylene beaker. The pH of the solution was adjusted to 9 by the addition of 5 ml of 0.05 M sodium borate solution and then the solution was diluted to 25 ml with deionized water. The solution was transferred into a 35 ml test tube and 5 ml of 5×10^{-3} M TDEABr in chloroform was added. The extraction was carried out for 5 min by turning the test tube upside down twice every 5 s. After the phase separation, the organic layer was taken out and centrifuged for 2 min at 3000 rpm.

The extract was transferred into an absorption cell and the absorbance at 550 nm was measured aginst the reagent blank obtained in the same way.

Results and Discussion

Absorption Spectra. The absorption spectra of the ternary complex extracted into chloroform and of

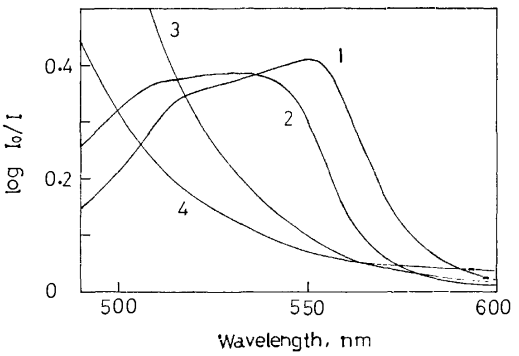

Fig. 1. Absorption spectra of the U–PAR–TDEA complex in chlorohorm and the U–PAR chelate in aqueous solution.
pH=9, V_{aq}=25 ml, V_o=5 ml, $[TDEABr]_o=5\times10^{-3}$ M.
(1): U-PAR-TDEA in chloroform, $[U]_{aq}=2\times10^{-6}$ M,
(2): U-PAR in aq soln, $[U]_{aq}=1\times10^{-5}$ M,
(3): PAR-TDEA in chloroform, $[PAR]_{aq}=4\times10^{-5}$ M,
(4): PAR in aq soln, $[PAR]_{aq}=2\times10^{-4}$M.

the uranium(VI)–PAR chelate anion in an aqueous solution, and also the absorption spectra of the respective blank solutions, are shown in Fig. 1. The ternary complex and the uranium(VI)–PAR chelate anion have an absorption maximum at 550 nm and 530 nm respectively. As compared with the corresponding absorption maximum of the chelate anion, that of the ternary complex is shifted toward the longer wavelengths by 20 nm.

Effect of pH. The aqueous solution containing uranium(VI) and PAR was adjusted to various pH values with the sodium acetate or sodiun borate buffer solution and the extraction was carried out by the above procedure. The results are shown in Fig. 2. The extraction of the ternary complex starts at pH>3, reaches a maximum at pH 6.8, and thereafter remains constant over a wide range (pH 7—10.7). The chloroform extract was stable for at least 1 h. PAR itself is readily extracted from aqueous solution.

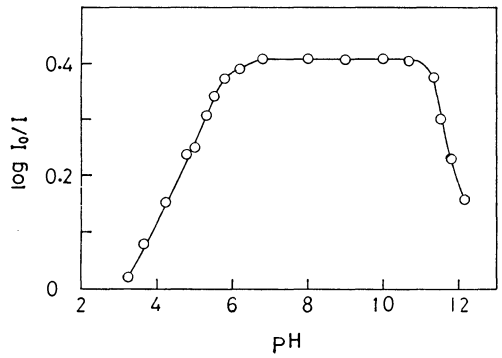

Fig. 2. Effect of pH on the extraction of the U-PAR-TDEA complex.
$[U]_{aq}=2\times10^{-6}$ M, $[PAR]_{aq}=4\times10^{-5}$ M, $[TDEABr]_o=5\times10^{-3}$ M, 550 nm.

Organic Solvents. Several kind of organic solvents which dissolved TDEABr were tested in order to achieve a quantitative extraction of the uranium(VI)–PAR chelate anion. The ternary complex is extracted in such solvents as chloroform, carbon tetrachloride, 1-butanol, butyl acetate, isobutyl methyl ketone, nitrobenzene, and benzene. Molar absorptivities of the ternary complex are much the same in these solvents. Chloroform was used throughout these experiments as the common solvent.

The Effect of the PAR Concentration. The extraction of uranium(VI) from an aqueous solution containing PAR of various concentrations was examined. The absorbance of the extract was found to be constant in the concentration range from 1×10^{-5} M to 1×10^{-4} M. The extraction of the ternary complex is depressed by use of a large excess of the PAR over the TDEABr.

The Effect of the TDEABr Concentration. The concentration of TDEABr in chloroform was varied. The absorbance of the extract was found to be constant in the concentration range from 1×10^{-3} to 5×10^{-3} M.

Effect of the Mixing Time. The mixing time was varied from 30 s to 10 min. The absorbance of the extract was constant for the mixing times from 3 to 10 min.

Extractability and Molar Absorptivity. An aqueous solution of 25 ml containing 29.8 μg of uranium(VI) and PAR was shaken with 5 ml of 5×10^{-3} M TDEABr in chloroform under the optimum conditions. Extraction was repeated for the remaining aqueous phase after the separation of the extract. The extractability of uranium was calculated from the absorbances of the extracts. It was found that 96.4% of uranium(VI) was extracted by one extraction. The distribution ratio and the molar absorptivity are 1.34×10^2 and 4.25×10^4 cm^{-1} mol^{-1} l respectively.

Calibration Curve. A calibration curve for the determination of uranium(VI) was made under the optimum conditions. A good linear relationship was obtained over the concentration range from 1 μg to 30 μg of uranium per 5 ml of chloroform.

The Composition of the Ternary Complex. Using the continuous variation method and the equilibrium-shift method, the mole ratio of uranium: PAR was found to be 1:1, as are shown in Figs. 3 and 4. The mole ratio of uranium: TDEA was found to be 1:1, as are shown in Figs. 5 and 6. The same resutls were obtained by applying the mole ratio method. Thus, the composition of the ternary complex was estimated to be $UO_2(X)(PAR)(R_3R'N)$.

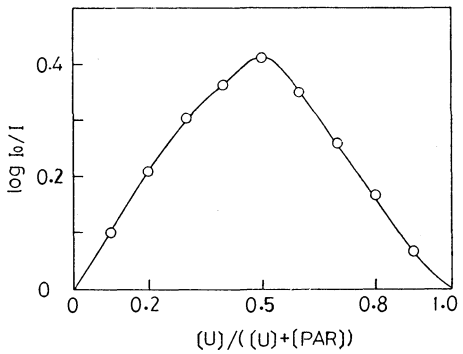

Fig. 3. Continuous variation method applied to the U-PAR-TDEA complex (U : PAR).
$[U]_{aq}+[PAR]_{aq}=2.5\times10^{-5}$ M, $[TDEABr]_o=5\times10^{-3}$ M, pH=9, 550 nm.

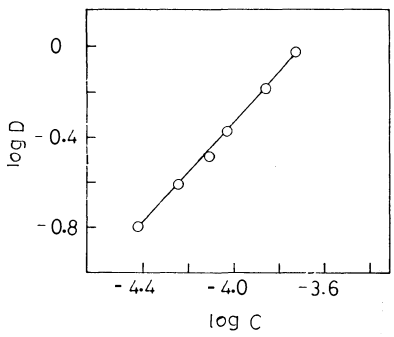

Fig. 4. Equilibrium-shift method applied to the U-PAR-TDEA complex (U:PAR).
$[U]_{aq}=1\times10^{-5}$ M, $[TDEABr]_o=5\times10^{-3}$ M, pH=3.6.
D: Distribution ratio of U-PAR-TDEA complex between chloroform and water, *C*: concentration of PAR in chloroform.

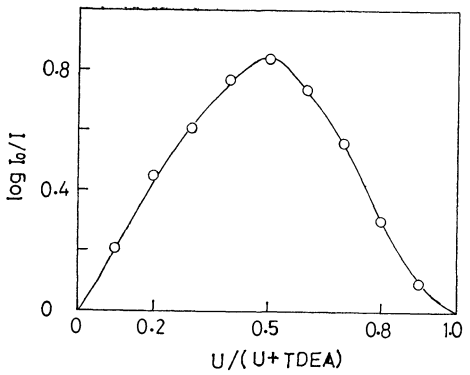

Fig. 5. Continuous variation method applied to the U-PAR-TDEA complex (U:TDEA).
U-PAR+TDEA=5×10^{-4} mmol, pH=9, 550 nm.

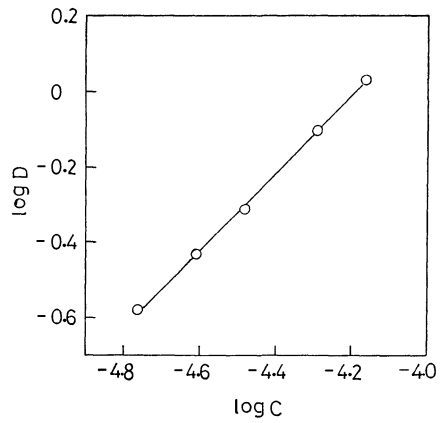

Fig. 6. Equilibrium shift method applied to the U-PAR-TDEA complex (U:TDEA).
$[U]_{aq}=2\times10^{-5}$ M, $[PAR]_{aq}=2\times10^{-5}$ M, pH=9.
D: Distribution ratio of U-PAR-TDEA complex between chloroform and water, C: concentration of TDEABr in chloroform.

Equilibrium Constant. When the uranium–PAR chelate anion is extracted with TDEABr into chloroform, the equation representing the extraction equilibrium would be

$$UO_2(X)(PAR)^- + R_3R'NBr_{(o)} = UO_2(X)(PAR)(R_3R'N)_{(o)} + Br^- \quad (1)$$

The extraction constant K_{ex} is given by

$$K_{ex} = \frac{[UO_2(X)(PAR)(R_3R'N)]_o[Br^-]}{[UO_2(X)(PAR)][R_3R'NBr]_o}, \quad (2)$$

where subscript o denotes the organic layer and X represents an unidentified univalent anion.

Determination of each of the component concentrations in Eq. 1 is a difficult problem, because the complete formation of the uranium–PAR chelate anion occurs in the presence of excess PAR. Under such conditions the equilibrium in Eq. 1 can be represented by the following two steps.

$$PAR^- + R_3R'NBr_{(o)} = R_3R'NPAR_{(o)} + Br^- \quad (3)$$

$$K_{ex1} = \frac{[R_3R'NPAR]_o[Br^-]}{[PAR^-][R_3R'NBr]_o} \quad (4)$$

$$UO_2(X)(PAR)^- + R_3R'NPAR_{(o)} = UO_2(X)(PAR)(R_3R'N)_{(o)} + PAR^- \quad (5)$$

$$K_{ex2} = \frac{[UO_2(X)(PAR)(R_3R'N)]_o[PAR^-]}{[UO_2(X)(PAR)^-][R_3R'NPAR]_o} \quad (6)$$

Thus K_{ex} is given by $K_{ex}=K_{ex1}K_{ex2}$. The concentrations of the $R_3R'NPAR_{(o)}$ species in Eq. 3 and the $UO_2(X)(PAR)(R_3R'N)_{(o)}$ species in Eq. 5 were determined spectrophotometrically as a function of $[Br^-]$ or $[PAR^-]$ respectively. The values of K_{ex1} and K_{ex2} were found to be 52.9 and 22.3 under the conditions shown in Table 1. The value of K_{ex} calculated from K_{ex1} and K_{ex2} is 1180, therefore log K_{ex}=3.07. The distribution ratio of the uranium complex between chloroform and water is described by

$$D = \frac{[UO_2(X)(PAR)(R_3R'N)]_o}{[UO_2(X)(PAR)]}. \quad (7)$$

Combining Eqs. 2 and 7, we have

$$D = K_{ex}\frac{[R_3R'NBr]_o}{[Br^-]}. \quad (8)$$

From Eq. 8, one can see that the value of D is a function of $[R_3R'NBr]_o$ and $[Br^-]$. That is, the value of D increases with the TDEABr concentration in chloroform. The larger solubility (about 0.1 M) of TDEABr in chloroform than in other solvents is favorable for the quantitative extraction of the uranium complex. The anions such as perchlorate, thiocyanate and io-

Table 1. Equilibrium extraction data for the PAR-$R_3R'NBr$, the $UO_2(X)(PAR)$-$R_3R'NPAR$, and the $UO_2(X)(PAR)$-$R_3R'NBr$ system at pH 9.0 in sodium borate buffer (10^{-4} M)

PAR-$R_3R'NBr$		$UO_2(X)(PAR)$-$R_3R'NPAR$		$UO_2(X)(PAR)$-$R_3R'NBr$
$[PAR^-]=5.0\times10^{-6}$ M		$[UO_2^{2+}]=4.0\times10^{-6}$ M		
$[R_3R'NBr]_o=5.0\times10^{-4}$ M		$[R_3R'NPAR]_o=5.0\times10^{-4}$ M		
$[Br^-]$ (M)	K_{ex1}	$[PAR^-]$ (M)	K_{ex2}	$K_{ex}=K_{ex1}K_{ex2}$
5.0×10^{-4}	52.1	2.0×10^{-4}	22.0	
1.0×10^{-3}	52.6	4.0×10^{-4}	21.1	
1.5×10^{-3}	53.7	8.0×10^{-4}	22.7	
2.0×10^{-3}	52.9	1.2×10^{-3}	23.1	
2.5×10^{-3}	53.2	1.6×10^{-3}	22.5	
Average value	52.9		22.3	1180 ($\log K_{ex}=3.07$)

All the concentrations in Table 1 are initial concentrations.

dide, which may have large extraction constants, would act as suppressing agents for the extraction.

References

1) S. Shibata, *Bunseki Kagaku*, **21**, 551 (1972).
2) T. Yotsuyanagi, R. Yamashita, and K. Aomura, *Bunseki Kagaku*, **19**, 981 (1970).
3) M. Siroki, Lj. Maric, and Z. Stefanac, *Anal. Chim. Acta*, **75**, 101 (1975).
4) T. Yotsuyanagi, Y. Takeda, R. Yamashita, and K. Aomura, *Anal. Chim. Acta*, **67**, 297 (1973).
5) M. Siroki and M. J. Herak, *J. Inorg. Nucl. Chem.*, **37**, 2309 (1975).
6) H. Hoshino, T. Yotsuyanagi, and K. Aomura, Abstr(1), p. 431, 35th National Meeting of the Chemical Society of Japan, Kanagawa, April, 1976.
7) Y. Harima, H. Oji, and K. Odajima, *Tekko*, **60**, 1869 (1974).
8) M. Siroki and C. Djordjevic, *Anal. Chem.*, **43**, 1375 (1971).
9) H. Hoshino, T. Yotsuyanagi, and K. Aomura, *Anal. Chim. Acta*, **83**, 317 (1976).
10) T. Yotsuyanagi, H. Hoshino, and, K. Aomura, *Anal. Chim. Acta*, **71**, 349 (1974).
11) H. Hoshino, R. Yamashita, T. Yotsuyanagi, and K. Aomura, *Nippon Kagaku Kaishi*, **1974**, 495.
12) M. Siroki and C. Djordjevic, *Anal. Chim. Acta*, **57**, 301 (1971).
13) M. Minczewski, J. Chwastowska, and P. T. Hong Mai, *Analyst*, **100**, 708 (1975).
14) D. Nonova, *Talanta*, **23**, 679 (1976).
15) Y. Shijo, *Bunseki Kagaku*, **23**, 884 (1974).
16) Y. Shijo, *Bull. Chem. Soc. Jpn.*, **48**, 2973 (1975).
17) Y. Shijo, *Bull. Chem. Soc., Jpn.*, **50**, 1013 (1977).

Derivatographic Studies on Transition Metal Complexes. XX.[1] Thermal Electron Transfer Reactions of Cobalt(III) Complexes Containing Phenylbiguanide in the Solid Phase[2]

Yoshinori IHARA, Akira UEHARA, Ryokichi TSUCHIYA,* and Eishin KYUNO**

Department of Chemistry, Faculty of Science, Kanazawa University, Kanazawa 920

***Department of Pharmaceutical Science, School of Pharmacy, Hokuriku University, Kanazawa 920*

(Received February 7, 1978)

The following six cobalt(III) complexes containing phenylbiguanide were prepared and the thermal reactions were followed both isothermally and non-isothermally (derivatographically) in the solid phase: *trans*-$[Co(A)_2(phbgH)_2]X_3 \cdot nH_2O$, where A denotes volatile ligands such as NH_3, CH_3NH_2 or C_5H_5N; phbgH denotes 1-phenylbiguanide, X chloride or bromide ion; and *n* is 2 or 3. From the electronic, IR and far-IR spectra and magnetic susceptibilities of these complexes before and after heating, the products obtained by evolving volatile ligands were found to be uniform bivalent cobalt complexes without rupture of the bonds of phbgH to cobalt in spite of the reduction of central cobalt(III) ion, except for the complexes containing ammonia. The reaction seems to be caused by the electron transfer from the coordinated phbgH to cobalt, not from the outer-sphere anions.

Werner found that the hydroxoaqua-cobalt(III) complexes *cis*-$[Co(OH)(NH_3)_4(H_2O)]X_2$ (X=Cl or Br) evolve water at *ca.* 100 °C to form the corresponding diol complexes in the solid phase.[3] Since then, thermal reactions of several cobalt(III) complexes have occasionally been investigated in the solid phase; *e.g.*, anation of $[Co(H_2O)(NH_3)_5]X_3$ (X=NO_3,[4a] Br,[4b] or ReO_4[4c]), *cis*↔*trans* isomerization of $[CoCl_2(NH_3)_4]IO_3$,[5] $[CoCl_2pn_2](H_5O_2)Cl_2$,[6] and $[CoCl_2(NH_3)_2en]SCN$,[7] and kinetics of the thermal decomposition of $[Co(NH_3)_6]X_3$ (X=Cl, Br, or I).[8]

Few systematic investigations have been carried out for cobalt(III) complexes to clarify their reactions in the solid phase. This is mainly due to the instability of cobalt(III) complexes upon heating. Most cobalt(III) complexes are apt to undergo a reduction of Co(III) to Co(II) ions followed by rapid and complicated decomposition. In fact, Tanaka and Nagase pointed out that the decomposition of the ammine complexes is initiated by the electron transfer from outer-sphere anions to central Co(III) ions.[8]

It was found that *trans*-$[Co(CH_3NH_2$ or $C_5H_5N)_2(bgH)_2]X_3$ (bgH=biguanide and X=Cl or Br) lose two moles of methylamine or pyridine to yield uniform bivalent cobalt(II) complexes without destruction of the bond of the bgH with cobalt ion upon heating.[9] The stiffness of the complexes was thought to be due to the inherent characteristics of biguanide; namely biguanide can form extremely stable planar complexes[10] containing pseudoaromaticity.[11]

The present study was undertaken (1) to prepare such instructive model complexes in which the skeletons are indestructible even at the end of the reduction of Co(III) to Co(II) ions, (2) to investigate isothermally and non-isothermally overall reaction processes of the complexes obtained, and (3) to confirm the origin of the electron transfer; *i.e.*, whether it is promoted from counter anion or ligand to Co(III) ion.

As compounds suitable for our purposes, *trans*-$[Co(A)_2(phbgH)_2]X_3 \cdot nH_2O$ were selected. PhbgH has the following characteristics: two molecules of each bidentate ligand can occupy the opposite four coordination sites of octahedral cobalt(III) ion with planar geometry; pseudoaromaticity can be induced by coordination to Co(III) ion. PhbgH has the following constitutional formula:

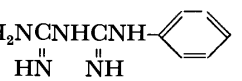

phbgH .

It is π-electron-rich as compared with bgH by virtue of the electron-donating effect of an introduced $-C_6H_5$ group.

Experimental

Preparation of Ligand. 1-Phenylbiguanide ($C_6H_5NHC(=NH)NHC(=NH)NH_2 \cdot HCl$) was prepared by the method reported.[12]

Preparation of Complexes. trans-$[Co(A)_2(phbgH)_2]X_3 \cdot nH_2O$ *(A=NH_3, CH_3NH_2 or C_5H_5N; X=Cl or Br).* These complexes were prepated by the method of Rây[13] modified as follows: 6.5 g of phbgH·HCl was dissolved in 150 ml of 10% sodium hydroxide solution. To this was added drop by drop with stirring a solution of $CoCl_2 \cdot 6H_2O$ (3.5 g) in 10 ml of water. When the solution turned yellow from brown, yellow precipitates (probably $[Co(phbg)_2]$) were obtained. After filtration, the precipitates were suspended in appropriate bases and oxidized by addition of a few deops of 35% hydrogen peroxide solution. As the bases, 120 ml of 28% aqueous ammonia, 120 ml of 40% methylamine solution and 120 ml of 60% pyridine solution were used to prepare *trans*-diammine, *trans*-bis(methylamine) and *trans*-bis(pyridine) complexes, respectively. After a small portion of cobalt(II) hydroxide deposited had been filtered off, the filtrate was neutralized by using concentrated hydrochloric acid. The use of concentrated hydrobromic acid instead of concd HCl gave the corresponding bromide complexes. As soon as neutralization was complete, pink crystals were obtained. They were recrystallized from water, and then washed with cold ethanol and ether. Yield about 2 g for each complex.

The analytical data of the six complexes are summarized in Table 1, together with deamination temperatures and isothermal conditions which were determined from the respective derivatograms (Figs. 1 to 3).

Derivatographic Measurements. The derivatograms for the above complexes were recorded with a MOM Derivatograph Typ-OD-102. All the measurements were carried out

Table 1. Analytical data, deamination temperatures, and isothermal conditions of the starting complexes

Complex	Analytical data C% Found	C% Calcd	H% Found	H% Calcd	N% Found	N% Calcd	Deamination Temp (°C)	Isothermal conditions Temp (°C)	Isothermal conditions Time (h)
trans-$[Co(NH_3)_2(phbgH)_2]Cl_3 \cdot 2H_2O$ (I)	32.62	32.58	5.40	5.47	28.53	28.50	—	—	—
trans-$[Co(NH_3)_2(phbgH)_2]Br_3 \cdot 3H_2O$ (II)	25.77	25.93	4.40	4.35	22.76	22.68	—	—	—
trans-$[Co(CH_3NH_2)_2(phbgH)_2]Cl_3 \cdot 2H_2O$ (III)	34.89	34.99	5.75	5.87	26.88	27.20	148	160	13
trans-$[Co(CH_3NH_2)_2(phbgH)_2]Br_3 \cdot 2H_2O$ (IV)	28.72	28.78	4.63	4.83	22.42	22.37	172	175	7
trans-$[Co(py)_2(phbgH)_2]Cl_3 \cdot 2H_2O$ (V)	43.34	43.74	4.74	5.08	23.29	23.54	86	160	10
trans-$[Co(py)_2(phbgH)_2]Br_3 \cdot 2H_2O$ (VI)	36.86	36.86	4.62	4.28	19.32	19.84	106	165	7

under a constant flow of nitrogen at a heating rate 1.0—1.5 °C $min.^{-1}$.

Isothermal Measurements. The products from which methylamine or pyridine was eliminated were obtained by an isothermal method using Cho 100-L thermobalance in static air. The isothermal conditions for obtaining uniform products are given in Table 1.

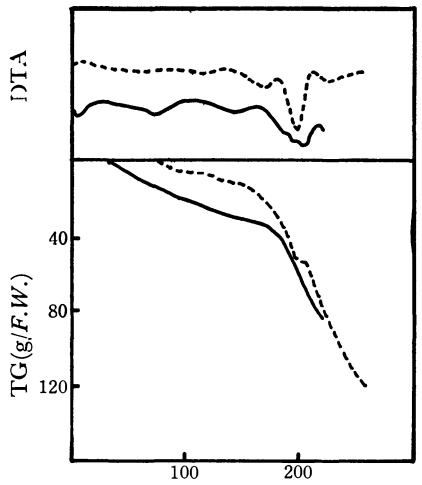

Fig. 1. Derivatograms of complexes I (——) and II (----).

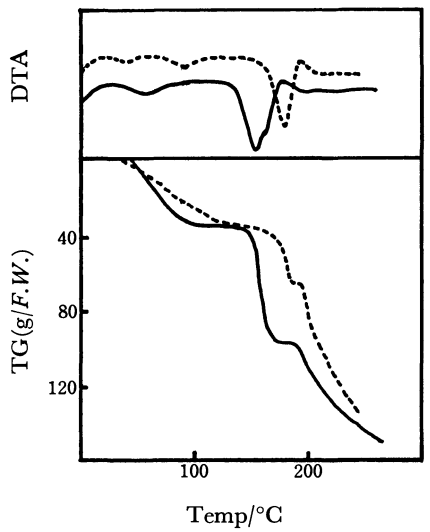

Fig. 2. Derivatograms of complexes III (——) and IV (---).

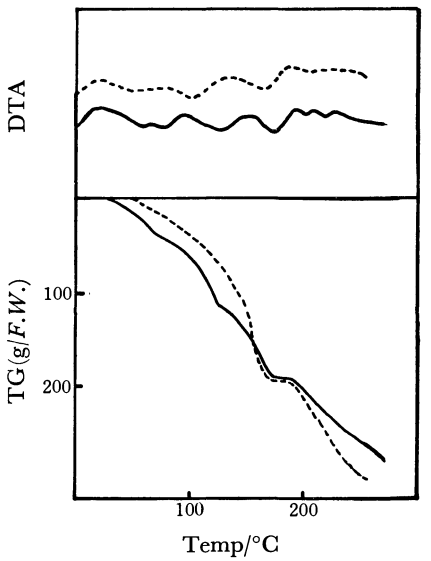

Fig. 3. Derivatograms of complexes V (——) and VI (----).

Spectral Measurements. The electronic spectra in the solid state were measured by a diffuse reflectance method with a Hitachi EPU-2A spectrophotometer equipped with a standard Hitachi reflection attachment (Type R-3). The IR and far-IR specta were measured by the KBr disk method with a JASCO-A-3 infrated spectrophotometer and by the Nujol method with a JASCO IR-F far-infrared spectrophotometer.

Measurements of Magnetic Susceptibilities. The effective magnetic moments were evaluated from the magnetic susceptibilities measured by the Gouy method at room temperature. $Hg[Co(NCS)_4]$ was employed as a reference material. The susceptibitities of the complexes were corrected by using Pascal's constants for each element or atomic group contained.

Results and Discussion

Derivatography. The derivatograms of a series of *trans*-$[Co(A)_2(phbgH)_2]X_3 \cdot nH_2O$ are shown in Figs. 1—3, the complexes being numbered according to Table 1. The TG and DTA curves in complex IV exhibit two distinct thermal steps, the first corresponding to the evolution of water and the second to the liberation of one mole of methylamine coordinated. Two thermal steps are also observed in complexes III, V, and VI, the second step corresponding to the liberation of

two moles of amines. On the other hand, no such distinct steps accompanied by the liberation of ammonia could be observed in complexes I and II owing to rapid decomposition. The liberation of amines in each complex was confirmed.

Thermal Two-mol-deamination Reaction ($[Co(A)_2(phbgH)_2]X_3 \cdot nH_2O \rightarrow Co(II)\text{-}product + 2A + nH_2O$). Complexes III, V, and VI fall in this category; complex III is discussed in detail. The gas evolved from complex III by isothermal heating at 160 °C in a silicon bath was dissolved in water. The resulting solution turned violet by addition of an ethanol containing chloranil ($C_6Cl_4O_2$). The solution was neutralized with dilute hydrochloric acid and concentrated to obtain white precipitates. The IR spectrum of the precipitates resembles that of methylamine hydrochloride prepared as a reference material. The results support the view that the evolved gas is not ammonia formed by the decomposition of phbgH, but methylamine itself.

Figure 4 shows the IR spectra of complex III before and after heating together with the spectrum of complex IV. By comparing their IR spectra with that of methylamine hydrochloride, the peaks at 1419, 1293, and 817 cm^{-1} before heating are considered to be characteristic bands with respect to methylamine. They disappeared completely after heating. Thus, the liberated molecule was found to be two moles of the coordinated methylamine in *trans* position.

Figure 5 shows the far-IR spectra of complex III before and after heating. The peak at 498 cm^{-1}, which is due to the Co–N(CH_3NH_2) stretching vibration, disappears upon heating. On the other hand, the peak at 510 cm^{-1} assignable to the Co–N(phbgH) stretching vibration remains even after heating. The assignments of these peaks were made by a comparison of the two peaks appearing in the other *trans*-diamine-bis(phbgH) complexes.

The analytical data, absorption maxima and magnetic moments for all the complexes obtained upon heating are summarized in Table 2. The electronic spectrum of complex III in the solid state changes remarkably upon heating (Fig. 6). The distinct feature of the spectra commonly found in these complexes before heating lies in the strong charge trnasfer band, which covers the second absorption band, suggesting the presence of the strong π-bond character

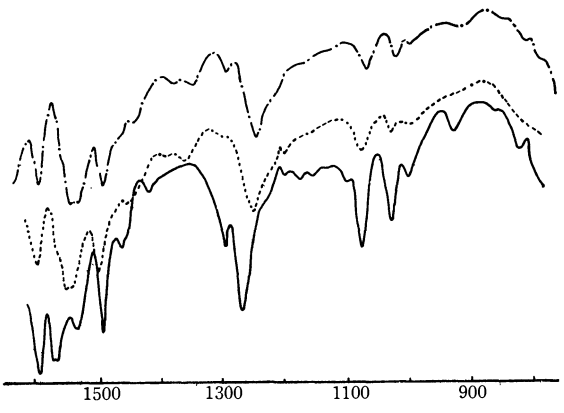

Fig. 4. IR spectra of complex III before heating (——) and after heating (----), and complex IV after heating (—·—).

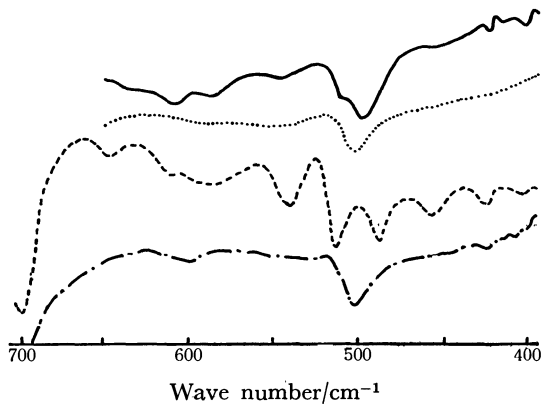

Fig. 5. Far-IR spectra of complex III before heating (——) and after heating (·····), and complex VI before heating (----) and after heating (—·—).

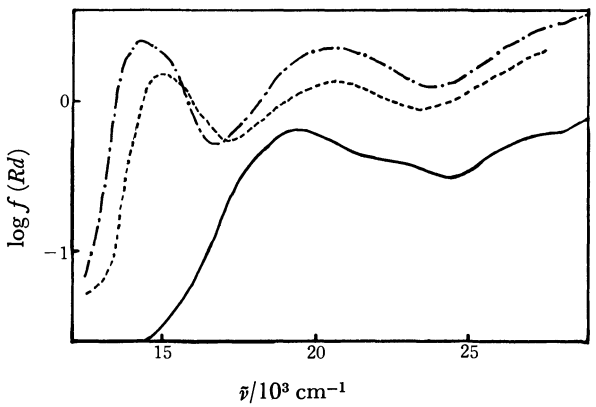

Fig. 6. Electronic spectra of complex III before heating (——) and after heating (----), and complex IV after heating (—·—).

Table 2. Analytical data, absorption maxima, and magnetic moments of the products obtained

Starting complex	Product	Analytical data C% Found	C% Calcd	H% Found	H% Calcd	N% Found	N% Calcd	Absorption maxima ($\bar{\nu}/10^3$ cm^{-1})		μ_{eff} (B.M.)
III	$[CoCl(phbgHCl)_2]$	36.57	36.98	4.40	4.27	26.85	26.95	14.8	20.7	2.40
IV	$[Co(CH_3NH_2)(phbgHBr)_2]Br$	30.08	29.85	3.98	3.98	22.18	22.52	14.3	20.7	2.57
V	$[CoCl(phbgHCl)_2]$	37.19	36.98	4.35	4.27	25.23	26.95	14.9	20.7	2.74
VI	$[CoBr(phbgHBr)_2]\cdot 2H_2O$	29.25	29.42	3.95	3.40	21.09	21.45	14.7	20.5	2.96

of the phbgH to the metal. On the other hand, three bands including charge transfer band are observed after heating at 160 °C. The obvious difference in the spectra before and after heating is the appearance of the peak at 14.8×10^3 cm^{-1} after heating. The peak has a narrow half-width characteristic of bivalent cobalt complexes.[14] In studies on the low spin five-coordinated cobalt(II) complexes, three peaks are often detected at 6—9, 14—17, and 19—25×10^3 cm^{-1}.[15] The spectral pattern of the product resembles them, especially those of the five-coordinated complexes, $[CoCl(dpe)_2]ClO_4$[15d] and β-$Co(paphy)Cl_2$,[15e] where dpe and paphy are 1,2-bis-(diphenylphosphino)ethane and 1,3-bis(2′-pyridyl)-2,3-diaza-1-propene, respectively.

The value of 2.4 B. M. for the heated product of complex III suggests it to be the low spin cobalt(II) complexes.[16] Since the coordination structure of the C_{4v} symmetry mode is considered to require low spin state from the ligand field splitting pattern[17] and two molecules of biguanides coordinated have a tendency to occupy the plane containing a metal ion in the bis-type complexes,[10,11] the product is presumed to be the low spin, square pyramidal five-coordinated cobalt-(II) complex.

The evolved gas analyses for chlorine were carried out to confirm whether or not the reduction by halide ions takes place. However, neither the color reaction by *o*-tolidine (3,3′-dimethylbenzidine) nor KI-starch method denied the evolution of gaseous chlorine. In order to detect chlorine, the solution containing the evolved gas was acidified with sodium hydrogensulfite which can convert chlorine into chloride ion. However, addition of silver nitrate to the solution produced no precipitates of silver chloride. Futhermore, no mass losses corresponding to the evolution of gaseous chlorine were observed in the TG curve. Thus, it is conceivable that the reduction is not due to the chloride ions in outer-sphere. The coordinated methylamines are also not responsible for the reaction since they were liberated without any change in structure.

The cause might be attributed to the ligand (phbgH), which forms a six-membered chelate ring with π-electron delocalization with a metal ion. The reduction of Co(III) to Co(II) ion can be understood to be due to the electron transfer from the two π-electron-rich phbgH's to the central cobalt ion. This is supported by the IR and far-IR data. As is shown in Fig. 4, both bands at 1572 and 1267 cm^{-1} in complex III which are assigned to the stretching vibrations of C=N and C–N bonds, respectively, shift to lower wavenumber regions by about 20 cm^{-1}. The shifts may arise from the decrease of π-electron delocalization in the phbgH due to the electron transfer from the phbgH to the cobalt(III) ion.

The decrease in the stretching vibration of Co–N (phbgH) is also observed in far-IR region upon heating (510 sh→502 cm^{-1}, Fig. 5). The decrease may result from the difference in the force constants of Co(III)–N and Co(II)–N bonds. Actually, the values of the force constants in the hexaammine complexes are reported to be 1.05 and 0.33 mdyn/A(UBF) for Co(III)–N and Co(II)–N, respectively,[18] the energy difference in the stretching vibrations being beyond 100 cm^{-1}. Taking the above value into account, the energy difference observed in the stretching vibrations of Co(III)–N (phbgH) and Co(II)–N(phbgH) is considerably smaller. Such difference between the known and the observed values may be ascribed to the increasing character of the covalent bond between cobalt and phbgH in the bivalent cobalt complex, which supports the occurrence of the inner-sphere electron transfer reaction.

The final problem is to determine the outcome of the chloride ions upon heating, which are generally known to enter into the coordination sphere through anation. A key to this lies in the appearance of a peak at 1355 cm^{-1} in the IR region which is newly observed after heating (Fig. 4), PhbgH is thought to have the coordination mode with a positive charge at N(4) site due to the six membered ring aromaticity.[11] The positive charge will increase owing to the electron transfer. It is reasonable to consider that the band is attributable to the vibration of the NH^+–Cl^- which seems to be formed after heating. Thus, of the three chloride ions, two are added to the phbgH, and the remaining one enters into the coordination sphere.

The following reaction scheme can be represented for the thermal electron trnasfer reaction of complex III.

$$\textit{trans}\text{-}[Co(CH_3NH_2)_2(phbgH)_2]Cl_3\cdot2H_2O \xrightarrow[\Delta]{-(2H_2O+2CH_3NH_2)} [Co^{II}Cl(phbgHCl)_2]$$

The product is stable in the solid state, but unstable in various solvents; it decomposes even by the addition of ethanol separating white crystals. The IR spectrum of the crystals shows the structure of the phbgH to remain even after the electron transfer reaction.

The patterns of the thermal reactions of complexes V and VI can be understood in a similar way. As an example, the far-IR spectra of complex VI are shown in Fig. 5. The three peaks at 645, 487, and 455 cm^{-1} which are specified to be in-plane ring deformation of pyridine molecule, Co–N(py) stretching vibration and out of plane ring deformation of pyridine molecule, respectively, are entirely quenched by the thermal treatment. This indicates the liberation of two moles of the coordinated pyridine.

The band shifts and the appearance of the peak near 1350 cm^{-1} upon heating of complexes V and VI are summarized in Table 3. The bands of the Co–N (phbgH) stretching vibration are also shifted to lower

Table 3. IR data of complexes V and VI before and after heating

	Complex V		Complex VI	
	Before heating	After heating	Before heating	After heating
	(cm^{-1})		(cm^{-1})	
$\nu_{C=N}$	1550	1540	1550	1538
ν_{C-N}	1270	1247	1273	1248
δ_{NH_2}	1674	1685	1668	1679
$\delta_{NH^+-X^-}$	—	1354	—	1356

wavenumber regions in the far-IR spectra (510→504 cm^{-1}, and 513→502 cm^{-1} for complexes V and VI, respectively).

The electronic spectral pattern of both products obtained upon heating are identical with the pattern of complex III. The absorption maxima and the values of magnetic mometns are given in Table 2 for the products of complexes V and VI.

The following thermal electron transfer reactions are considered to proceed during the course of thermal treatment in complexes V and VI:

$$trans\text{-}[Co(py)_2(phbgH)_2]X_3\cdot 2H_2O \xrightarrow[\Delta]{-(2H_2O+2py)} [Co^{II}X(phbgHX)_2] \quad (X=Cl \text{ or } Br).$$

Thermal One-mol-deamination Reaction ($[Co(A)_2(phbgH)_2]X_3\cdot nH_2O \rightarrow Co(II)\text{-}product + A + nH_2O$). The IR spectrum of complex IV after heating is shown in Fig. 4. The peaks at 1292, 1000, and 820 cm^{-1}, characteristic of methylamine, remain even in the heated product. Shifts similar to those of complexes III, V, and VI are observed in the IR region upon heating ($\nu_{C=N}$, 1561→1545 cm^{-1}; ν_{C-N}, 1258→1243 cm^{-1}), suggesting the occurrence of electron transfer from the phbgH to the cobalt(III) ion. A new peak assignable to the vibration of the NH^+–Br^- bond appears at 1350 cm^{-1}.

The electronic spectral pattern of the product was analogous to those of complexes III, V, and VI. However, the absorption maximum of the product from complex IV (14.3×10^3 cm^{-1}) appears in a lower wavenumber region to some extent as compared with those ($14.7—14.9\times10^3$ cm^{-1}) of complexes III, V, and VI (Table 2). The shift is attributable to the coordination of the remaining one mole of methylamine.

The following equation might hold for the thermal reaction of complex IV:

$$trans\text{-}[Co(CH_3NH_2)_2(phbgH)_2]Br_3\cdot 2H_2O \xrightarrow[\Delta]{-(2H_2O+CH_3NH_2)} [Co^{II}(CH_3NH_2)(phbgHBr)_2]Br.$$

Difference in the Ease of Electron Transfer. A comparison of the liberation temperatures of amines is suitable for estimating the reactivity in the thermal reaction. The temperatures observed in the derivatograms are summarized as deamination temperatures in Table 1. We see the following order of reactivity depending upon the kind of the coordinated amine and counter ion.

i) $NH_3 < CH_3NH_2 <$ py

ii) $Br^- < Cl^-$

Order i), the reverse of that in the strength of the ligand field, is the order of the ease of the liberation of the coordinated amine. This is understandable if the liberation of the coordianted amines is considered to be a trigger of the reactions. The fact that ammine complexes I and II decomposed without a distict liberation step of ammonia upon heating can be explained by the fact that the temperatures of complexes I and II reached the decomposition points prior to the liberation of the coordinated ammonia. The liberation temperatures of ammonia in these complexes might be higher than those of the methylamine or pyridine complexes.

Order ii) is related to the order of the ease of anation and addition of the halide ions to phbgH.

Refernces

1) Part XIX: T. Yoshikuni, R. Tsuchiya, A. Uehara, and E. Kyuno, *Bull. Chem. Soc. Jpn.*, **51**, 113 (1978).

2) Presented in part at the 36th National Meeting of the Chemical Society of Japan, Osaka, April, 1977.

3) A. Werner, *Chem. Ber.*, **40**, 4437 (1907).

4) a) M. Mori, *Inorg. Synth.*, **5**, 131; b) F. Basolo and R. K. Murmann, *Inorg. Synth.*, **4**, 171; c) H. Diehl, H. Clark, and H. H. Willard, *Inorg. Synth.*, **1**, 186.

5) H. E. LeMay, Jr. and J. C. Bailar, Jr., *J. Am. Chem. Soc.*, **89**, 5577 (1967).

6) a) N. Serpone and D. G. Bickley, Prograess in Inorganic Chemistry, Vol. 17, ed by J. O. Edwards, John Wiley & Sons, Inc. (1972), p. 391; b) H. E. LeMay, Jr., *Inorg. Chem.*, **7**, 2531 (1968); c) R. Tsuchiya, K. Murai, A. Uehara, and E. Kyuno, *Bull. Chem. Soc. Jpn.*, **43**, 1383 (1970).

7) R. Tsuchiya, M. Suzuki, and E. Kyuno, *Bull. Chem. Soc. Jpn.*, **44**, 709 (1971).

8) N. Tanaka and K. Nagase, *Bull. Chem. Soc. Jpn.*, **40**, 546 (1967).

9) R. Tsuchiya, A. Uehara, K. Otsuka, and E. Kyuno, *Chem. Lett.*, **1974**, 833.

10) P. Rây, *Chem. Rev.*, **61**, 313 (1961).

11) Sen employed the term "ring aromaticity": see D. Sen, *J. Chem. Soc., A*, **1969**, 2900.

12) P. Rây and H. P. Bhattachaya, *J. Indian Chem. Soc.*, **16**, 629 (1939).

13) a) P. Rây and A. N. Majumdar, *J. Indian Chem. Soc.*, **23**, 73 (1946); b) S. P. Ghosh and J. N. Gupta, *J. Indian Chem. Soc.*, **33**, 193 (1956).

14) R. L. Carlin, Transition Metal Chemistry, Vol. 1, ed by R. L. Carlin, Marcel Dekker, Inc. (1965), p. 1.

15) a) W. Dew. Horrocks, Jr., G. R. Van Hecke, and D. Dew. Hall, *Inorg. Chem.*, **6**, 694 (1967); b) J. G. Hartley, D. G. E. Kerfoot, and L. M. Venanzi, *Inorg. Chim. Acta*, **1**, 145 (1967); c) W. E. Hill, *J. Chem. Soc., Dalton Trans.*, **1973**, 143; d) Y. Nishida and H. Shimohori, *Bull. Chem. Soc. Jpn.*, **46**, 2406 (1973); e) I. G. Dance, M. Gerloch, J. Lewis, F. S. Stephens, and F. Lions, *Nature*, **210**, 298 (1966).

16) a) B. N. Figgs and R. S. Nyholm, *J. Chem. Soc.*, **1954**, 12; b) Y. Nishida and S. Kida, *Bull. Chem. Soc. Jpn.*, **45**, 461 (1972).

17) U. Murakami and K. Sakata, "Chelate Kagaku," Vol. 1, ed by K. Ueno, Nankodo, Co., Tokyo (1976), p. 91.

18) T. Shimanouchi and I. Nakagawa, *Inorg. Chem.*, **3**, 1805 (1964).

Studies of the Yields of ^{57}Fe(II)-species Produced after the EC-decay and of ^{60}Co(II)-species Produced in the (n, γ) Reaction in Cobalt(III) Coordination Compounds

Hirotoshi SANO,* Masayuki HARADA, and Kazutoyo ENDO

Department of Chemistry, Faculty of Science, Tokyo Metropolitan University, Fukasawa, Setagaya, Tokyo 158

(Received February 13, 1978)

The yields of ^{57}Fe(II)-species produced after EC-decay were compared with those of ^{60}Co(II)-species produced in the ^{59}Co(n,γ)^{60}Co reaction for twelve cobalt(III) coordination compounds. The results indicate that the radiochemical yield of ^{60}Co(II)-species correlates with the yield of ^{57}Fe(II)-species except in the case of $[Co(NH_3)_6]_2(CrO_4)_3$. The anomalously low yield of ^{57}Fe(II)-species in $[Co(NH_3)_6]_2(CrO_4)_3$ is ascribed to the reaction of chromate anions with ammine ligands initiated by the nuclear transformation in a solid.

A number of studies of the chemical effects of ^{59}Co(n,γ)^{60}Co nuclear reactions in cobalt(III) coordination compounds have thus far been reported. Although several working hypotheses have been proposed in hot-atom chemistry concerning the initial distribution of the transformed nuclides into different chemical states,[1] these hypotheses have all been made on the assumption that radiochemical separation processes have little influence on the analytical results of the transformed nuclides. It is well-known, however, that the results depend on the experimental conditions, such as the time and the temperature both of irradiation and storage, and the chemical and physical state of the sample used for irradiation.[1,2]

Mössbauer emission spectroscopy provides a unique way of studying *in situ* the chemical state of atoms produced as a result of nuclear decay in a solid. The technique has been extensively used in investigations of ^{57}Fe-species produced after the EC-decay of ^{57}Co, but few studies of the Mössbauer emission spectroscopy of cobalt(III) compounds have been concerned with the results of ^{59}Co(n,γ)^{60}Co hot-atom chemistry. We have reported previously that the chemical states of ^{57}Fe produced after the EC-decay of ^{57}Co depend upon the radiolytic character of the ligands or anions surrounding the decaying atoms.[3,4] In the present work, the radiochemical yield of ^{60}Co(II)-species found in the (n,γ) reaction was compared with the yield of ^{57}Fe(II)-species produced after the EC-decay for twelve cobalt(III) coordination compounds, including three compounds reported previously.[4]

Experimental

Target and ^{57}Co-labelled Compounds. $[Co(NH_3)_6]CO_3Cl$,[5] $[Co(NH_3)_6]SO_3Cl$,[6] $[Co(NH_3)_6]_2(CO_3)_3\cdot 3H_2O$,[7] $[Co(NH_3)_6]_2(SO_4)_3\cdot 5H_2O$,[8] $[Co(NH_3)_6]_2(CrO_4)_3$,[9] $[Co(NH_3)_6](NO_3)_3$,[8] $[Co(NH_3)_6]Cl_3$,[8] $[Co(NH_3)_5(OH_2)](NO_3)_3$,[10] and $[Co(NH_3)_5(OH_2)]_2(C_2O_4)_3\cdot 4H_2O$[10] were prepared from soltuions, each containing 50 mg of cobalt(II), by following the methods described in Refs. 5 to 10. The ^{57}Co-labelled compounds were prepared from solutions containing about 1 mCi ^{57}Co, but otherwise in the same way as described above. The purity was checked by elemental analysis and X-ray diffraction and found to be at least 97%.

Neutron Irradiation and Chemical Separation. The samples were irradiated for 10 min at the reactor temperature in a thermal column in a TRIGA Mark II reactor at the Institute for Atomic Energy of Rikkyo University. After being allowed to stand for half an hour, the irradiated sample was dissolved into an aqueous solution containing 10 mg cobalt(II) chloride as a carrier, after which a small amount of diluted hydrochloric acid was added to keep the acidity at pH 3—4. The cobalt(II) species were separated by solvent extraction after adding 1-nitroso-2-naphthol, hydrogen peroxide, and chloroform to the solution. The radiochemical yield of ^{60}Co(II) was determined by counting 1.17 and 1.33 MeV γ-rays with a Ge(Li) semiconductor detector and a multichannel analyser, CANBERRA Model 8100.

Mössbauer Emission Spectroscopic Measurements. The ^{57}Co-labelled compounds were kept in a crysotat, and the Mössbauer spectra were measured against an ^{57}Fe-enriched stainless-steel absorber moving in a constant-acceleration mode at room temperature. The velocity calibrartions were carried out by using an ^{57}Fe-enriched iron foil absorber moving against a stationary ^{57}Co(Pt) source at room temperature.

Results and Discussion

Some typical Mössbauer emission spectra of the source compounds measured at 78 K are shown in Figs. 1 and 2. The peak component ascribed to ^{57}Fe(II)-species was estimated from the isomer-shift and quadrupole-splitting values. The yield of ^{57}Fe(II)-species was evaluated from the area under the component and the total area of the spectrum by assuming that the recoil-free fraction of each ^{57}Fe-species was nearly the same at 78 K, as has previously been described in Ref. 4.

Table 1 summarizes the results concerning the radiochemical yield of ^{60}Co(II), together with the yield of ^{57}Fe(II) evaluated from the Mössbauer emission spectroscopy. It has already been reported that practically the same yield of ^{60}Co(II) is obtained by using either solvent extraction or paper electrophoresis for neutron-irradiated tris(dimethylglyoximato)cobalt(III).[11] Our previous result concerning the radiochemical yield of ^{60}Co(II) obtained for the neutron-irradiated $[Co(NH_3)_6](NO_3)_3$ by means of paper electrophoresis is shown in Table 1 for the sake of comparison.

We have demonstrated repeatedly that the distribution of the decayed atom into the different chemical states depends on the radiolytical property of the species surrounding the decayed atom.[17-19] It was also reported that not only the nearest neighbors of the decayed atom, but also the next nearest neighbors,

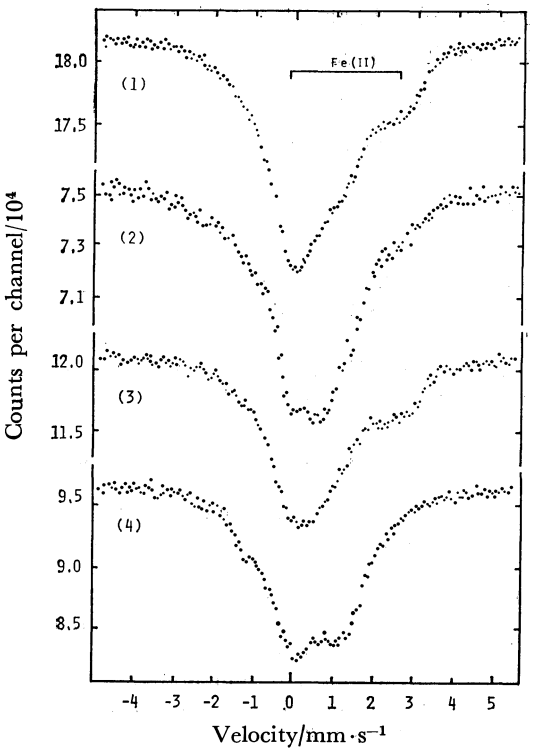

Fig. 1. Mössbauer spectra at 78 K of ^{57}Co-labelled (1) $[Co(NH_3)_6]Cl_3$, (2) $[Co(NH_3)_6]_2(CO_3)_3\cdot 3H_2O$, (3) $[Co(NH_3)_6]_2(SO_4)_3\cdot 5H_2O$, and (4) $[Co(NH_3)_6]_2(CrO_4)_3$ sources.
All the velocity scales were normalized with respect to metallic iron.

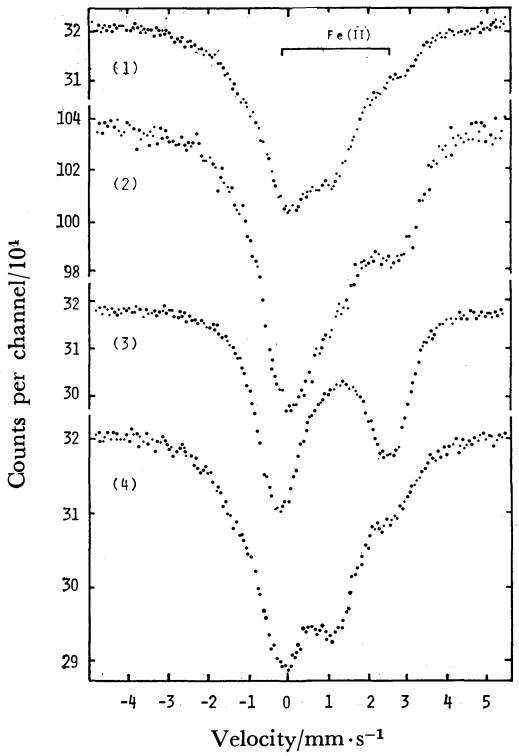

Fig. 2. Mössbauer spectra at 78 K of ^{57}Co-labelled (1) $[Co(NH_3)_6]CO_3Cl$, (2) $[Co(NH_3)_6]SO_3Cl$, (3) $[Co(NH_3)_5OH_2]_2(C_2O_4)\cdot 4H_2O$, and (4) $[Co(NH_3)_5OH_2](NO_3)_3$ sources.
All the velocity scales were normalized with respect to metallic iron.

TABLE 1. SUMMARY OF THE YIELDS OF ^{57}Fe(II)-SPECIES PRODUCED AFTER EC-DECAY AND THE RADIOCHEMICAL YIELDS OF THE ^{60}Co(II)-SPECIES IN THE HOT-ATOM CHEMISTRY OF THE ^{59}Co(n, γ)^{60}Co REACTION

Compound	Yield of ^{57}Fe(II) in EC-decay, %	Yield of ^{60}Co(II) in ^{59}Co(n γ)^{60}Co, %
$[Co(NH_3)_6]Cl_3$	42±1	57.5
$[Co(NH_3)_6]_2(CO_3)_3\cdot 3H_2O$	34±1	45.1
$[Co(NH_3)_6]_2(SO_4)_3\cdot 5H_2O$	54±1	96.0[12]
$[Co(NH_3)_6]_2(CrO_4)_3$	1±1	63.2[12]
$[Co(NH_3)_6]CO_3Cl$	41±1	61.0
$[Co(NH_3)_6]SO_3Cl$	52±1	67.8
$[Co(NH_3)_6](NO_3)_3$	38±1; 40±1[14]	66.9; 66.7[12]
$[Co(NH_3)_6]_2(C_2O_4)_3\cdot 4H_2O$	72±1[14]	91.0[14]
$[Co(NH_3)_5OH_2](NO_3)_3$	34±1	51.3[13]
$[Co(NH_3)_5OH_2]_2(C_2O_4)\cdot 4H_2O$	68±1	82.9[13]
$[Co(NH_2CH_2CH_2NH_2)_3](NO_3)_3$	53±1[14]	69.4[15]
$K_3[Co(C_2O_4)_3]\cdot 3H_2O$	85[16]	98.6[14]

are involved in determining the oxidation state of the decayed atom in the local radiolytic processes initiated by the EC-decay.[3,4] A large amount of ^{57}Fe(II)-species found in the spectrum of $[Co(NH_3)_5(OH_2)]_2(C_2O_4)_3\cdot 4H_2O$ can be ascribed to the effect of oxalate anions in the second coordination sphere, as was mentioned in the case of $[Co(NH_3)_6]_2(C_2O_4)_3\cdot 4H_2O$.[4] Electrons produced in the process:

$$C_2O_4^{2-} \longrightarrow 2CO_2 + 2e^-$$

may be involved in enhancing the yield of ^{57}Fe(II)-species.

Including our previous data on $[Co(NH_3)_6](NO_3)_3$, $[Co(NH_3)_6]_2(C_2O_4)_3\cdot 4H_2O$, and $K_3[Co(C_2O_4)_3]\cdot 3H_2O$, Fig. 3 compares the yield of ^{60}Co(II) after the (n,γ) reaction with the yield of ^{57}Fe(II) after the EC-decay. A fairly good correlation may be found between them except for $[Co(NH_3)_6]_2(CrO_4)_3$ which shows a very low yield in the ^{57}Fe(II) state, whereas there is quite large yield in the ^{60}Co(II) state. The correlation between the yield of ^{57}Fe(II) and that of ^{60}Co(II) for the other compounds can be understood by assuming that there should be little irregular influence on the trend of distribution of ^{60}Co atoms produced in the (n,γ) hot-atom reaction through traditional chemical separation.

The results suggest that the fate of the ^{60}Co atoms produced in the (n,γ) reaction is similar, after their slow-down, to that of the ^{57}Fe atoms produced in the EC-decay except for the difference between the chemical behavior of cobalt and iron. The similarlity may be partly explained by the fact that ^{60}Co-species are also produced through the ^{59}Co(n,γ)^{60m}Co reaction and the I. T. (I. C.) process. The large cross-section of the ^{59}Co(n,γ)^{60m}Co reaction (σ : 18 barn), the short ir-

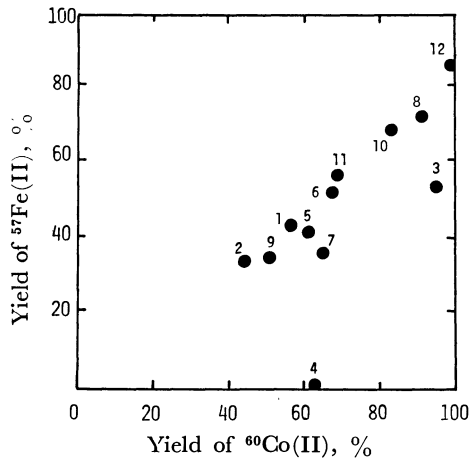

Fig. 3. Comparison of the radiochmiecal yield of $^{60}Co(II)$-species in the $^{59}Co(n,\gamma)^{60}Co$ hot-atom chemistry with the yield of $^{57}Fe(II)$-species produced after EC-decay.
1: $[Co(NH_3)_6]Cl_3$, 2: $[Co(NH_3)_6]_2(CO_3)_3 \cdot 3H_2O$, 3: $[Co(NH_3)_6]_2(SO_4)_3 \cdot 5H_2O$, 4: $[Co(NH_3)_6]_2(CrO_4)_3$, 5: $[Co(NH_3)_6]CO_3Cl$, 6: $[Co(NH_3)_6]SO_3Cl$, 7: $[Co(NH_3)_6](NO_3)_3$, 8: $[Co(NH_3)_6]_2(C_2O_4) \cdot 4H_2O$, 9: $[Co(NH_3)_5OH_2](NO_3)_3$, 10: $[Co(NH_3)_5OH_2]_2(C_2O_4)_3 \cdot 4H_2O$, 11: $[Co(NH_2CH_2CH_2NH_2)_3](NO_3)_3$, and 12: $K_3[Co(C_2O_4)_3] \cdot 3H_2O$.

radiation time, and the large internal conversion coefficient (α_k : 41) provide the conditions necessary to produce multi-charge decayed atoms just like those provided by the EC-decay process.[21] The fate of the so-called hot-atoms may be determined through the chemical interaction with the host material—local radiolytic process—either after the (n,γ) reaction or after the EC-decay. The distribution of ^{60}Co atoms in the reduced state, Co(II), may depend upon the local radiolytic property of the host cobalt(III) coordination compound, which determines the yield of the ^{57}Fe atoms produced in the EC-decay into the reduced ferrous state as well.

The anomalous results found in the case of $[Co(NH_3)_6]_2(CrO_4)_3$ indicate that the decayed ^{57}Fe atoms remain in the ligand-deficient Fe(III) state after the EC-decay process. It seems reasonable to assume that the following process:

$$CrO_4^{2-} + 2e^- \longrightarrow CrO_4^{4-}$$

consumes electrons and keeps the decaying atoms in a higher oxidation state, since chromate(IV) anions are known to be stable in Ba_2CrO_4 and Ca_2CrO_4.[20] Chromate(VI) anions may also be supposed to react with ammine lignads in the following processes:

$$CrO_4^{2-} + NH_3 \rightarrow \frac{1}{2}Cr_2O_3 + \frac{1}{2}N_2 + \frac{1}{2}H_2O + OH^-$$

$$Cr_4O^{2-} + \frac{2}{3}NH_3 \rightarrow CrO_2 + \frac{1}{3}N_2 + 2OH^-$$

through the local radiolytic process triggered by the nuclear transformation, giving reduced Cr(IV) or Cr(III) species, nitrogen, and hydroxide ions. The ligand-deficient species produced through the nuclear transformation may decompose into a reduced species, giving a large radiochemical yield of the reduced species—the $^{60}Co(II)$-species in the present case—after the sample has been dissolved for the traditional radiochemical analysis, whereas the ligand-deficient ^{57}Fe-species remaining in the original oxidation state can be observed as $^{57}Fe(III)$-species by the Mössbauer emission spectroscopy. A similar trend is also found slightly in the case of $[Co(NH_3)_6]_2(SO_4)_3$, although here the effect of sulfate anions seems not so remarkable as that of chromate(VI) anions.

The present results indicate that the trends observed in the traditional hot-atom chemistry correlate with those observed in the Mössbauer emission experiments, if there are no or few addtional effects through the chemical analyses, and that the comparison of the results obtained for the hot-atom chemistry of the (n,γ) process in cobalt compounds with those of the Mössbauer emission spectroscopic studies of the same compounds can provide clues for use in clarifying the reaction mechanism which may occur around the "hot-atoms" in a solid.

References

1) H. Müller, *Angew. Chem., Int. Ed. Engl.*, **6**, 133 (1967).
2) G. L. Stucky and R. W. Kiser, *Radiochim. Acta*, **11**, 5 (1967).
3) H. Sano and H. Iwagami, *Chem. Commun.*, **1971**, 1637; H. Sano, K. Sato, and H. Iwagami, *Bull. Chem. Soc. Jpn.*, **44**, 726 (1971).
4) H. Sano and T. Ohnuma, *Chem. Phys. Lett.*, **26**, 348 (1974); *Chem. Lett.*, **1974**, 589; *Bull. Chem. Soc. Jpn.*, **48**, 258 (1975).
5) L. Jacobson, *Overs. Danske Sedsk. Fork*, **1899**, 595.
6) G. Vortmann and G. Magdeburg, *Ber.*, **22**, 2636 (1889).
7) W. Gibbs and F. A. Genth, *Am. J. Sci.*, **23**, 339 (1857).
8) S. M. Jörgensen, *Z. Anorg. Chem.*, **17**, 457 (1898).
9) W. Gibbs and F. A. Genth, *Am. J. Sci.*, **23**, 337 (1857); *Lieb. Ann.*, **104**, 305 (1857).
10) S. M. Jörgensen, *Z. Anorg. Chem.*, **17**, 461 (1898).
11) N. Saito, T. Tominaga, and H. Sano, *Bull. Chem. Soc. Jpn.*, **35**, 1739 (1962).
12) N. Saito, T. Tominaga, and H. Sano, *Bull. Chem. Soc. Jpn.*, **35**, 365 (1962).
13) N. Saito, T. Tominaga, and H. Sano, *Bull. Chem. Soc. Jpn.*, **36**, 232 (1963).
14) N. Saito, H. Sano, and T. Tominaga, *Chem. Ind. (London)*, **1964**, 1622.
15) N. Saito, T. Tominaga, and H. Sano, *Bull. Chem. Soc. Jpn.*, **38**, 1407 (1965).
16) J. M. Friedt and L. Asch, *Radiochim. Acta*, **12**, 208 (1968).
17) H. Sano, N. Matsubara, and N. Saito, *Bull. Chem. Soc. Jpn.*, **38**, 333 (1965).
18) H. Sano and F. Hashimoto, *Bull. Chem. Soc. Jpn.*, **38**, 684 (1965).
19) H. Sano and M. Kanno, *Chem. Commun.*, **1969**, 601.
20) K. A. Wilhelmi and O. Jenssen, *Acta Chem. Scand.*, **15**, 1415 (1961).
21) N. Ikeda, H. Shoji, Y. Sakai, and S. Nakajima, *Research Report of Lab. Nucl. Sci., Tohoku Univ.*, **9**, 253 (1976); N. Ikeda, Y. Sakai, and H. Shoji, *ibid.*, **10**, 111 (1977).

Absorption and Circular Dichroism Spectra of Cobalt(III) Complexes Containing *N,N*-Dimethylethylenediamine

Keiji AKAMATSU* and Yoichi SHIMURA

Department of Chemistry, Faculty of Science, Osaka University, Toyonaka, Osaka 560

(Received March 3, 1978)

Nine new cobalt(III) complexes containing *N,N*-dimethylethylenediamine are prepared. The geometrical configurations of isomers are assigned on the basis of their visible and ultraviolet absorption spectra, proton magnetic resonance spectra, and the optical resolution of the chiral isomers. The absorption and circular dichroism spectra are discussed in comparison with those of the corresponding complexes containing ethylenediamine, *N*-methylethylenediamine, *N,N'*-dimethylethylenediamine, or tris-2-(aminoethyl)amine.

There have been several investigations concerning the Co(III) complexes of *N*-methylethylnediamine (*N*-Me-en)[1-3] and *N,N'*-dimethylethylenediamine (*N,N'*-Me_2-en).[3,4] No Co(III) complexes have ever been reported for *N,N*-dimethylethylenediamine (*N,N*-Me_2-en), though some Cu(II),[5] Ni(II),[6] and Rh(III)[7] complexes have been prepared for this tertiary amine ligand. In this paper the preparation and the properties of the Co(III) complexes containing *N,N*-dimethylethylenediamine are reported.

Experimental

Preparations. *(1)* trans(*NO_2*)-[*Co(*NO_2*)*$_2$(N,N-*Me_2*-en)*$_2$]-*ClO_4*: This complex was prepared by the same method as that of Buckingham *et al.*[2] for *trans*, *trans*-[$Co(NO_2)_2$-(*N*-Me-en)$_2$]ClO_4. To an ice-cold solution of $CoCl_2 \cdot 6H_2O$(4.76 g, 2.0×10^{-2} mol) in 10 cm^3 of water was added a cold solusion of *N,N*-dimethylethylenediamine(3.52 g, 4.0×10^{-2} mol) in 1.7 cm^3 of 12 M HCl, and then $NaNO_2$(2.8 g, 4.2×10^{-2} mol) was added. A vigorous stream of air was introduced to this red bown solution for 5 h at room temperature. The resulting solution was evaporated to dryness by a rotary evaporator below 40 °C. To the residue was added 50 cm^3 of methanol and the resulting NaCl precipitated was filtered off. Ten grams of $NaClO_4$ was added to precipitate a crystalline powder by scratching the flask. This was filtered and recrystallized from warm water. Found: C, 22.28; H, 5.75; N, 19.66%. Calcd for [$Co(NO_2)_2$(*N,N*-Me_2-en)$_2$]-ClO_4: C, 22.51; H, 5.68; N, 19.69%.

(2) cis*(Cl)*-[*CoCl*$_2$*(*N,N-*Me*$_2$*-en)*$_2$]*Cl*O_4: Three grams of *trans*(NO_2)-[$Co(NO_2)_2$(*N,N*-Me_2-en)$_2$]ClO_4 was suspended in 50 cm^3 of alcoholic hydrogen chloride(saturated at ice-bath temperature) and stirred overnight at room temperature. The blue green powder deposited was filtered, washed with ethanol and ether, and dried in air. Found: C, 23.87; H, 6.15; N, 14.10%. Calcd for [$CoCl_2$(*N,N*-Me_2-en)$_2$]-ClO_4: C, 23.68; H, 5.97; N, 13.81%.

(3) trans*(*N_3*)-* *and* cis*(*N_3*)*-[*Co(*N_3*)*$_2$*(*N,N-*Me*$_2$*-en)*$_2$]X; *X*=*ClO*$_4$*(*trans*)* *and* *Cl*·H_2O*(*cis*)*: One gram of *cis*(Cl)-[$CoCl_2$(*N,N*-Me_2-en)$_2$]ClO_4 was dissolved in 5 cm^3 of water, and to this blue solution was added 0.6 g of NaN_3 and stirred at 40 °C for 1 h. On cooling to room temperature, dark brown-violet crystals were deposited. The crystals were separated by filtration from the dark green solution and recrystallized from water at 50 °C. From the measurement of absorption spectrum it was found that this brown-violet isomer has a *trans*(N_3) structure. Found: C, 22.69; H, 5.81; N, 33.67%. Calcd for *trans*(N_3)-[$Co(N_3)_2$(*N,N*-Me_2-en)$_2$]-ClO_4: C, 22.94; H, 5.78; N, 33.45%.

The corresponding *cis* isomer was isolated from the same reaction mixture by column chromatographic method. The reaction mixture was completely dissolved with water and poured into a cation exchanger column(SP-Sephadex C-25, Na^+ form) and eluted with a 0.05 M NaCl aqueous solution. Two bands appeared; dark brown-violet one(*trans* isomer) and dark green one(*cis* isomer), in this order. The dark green band was eluted and evaporated to dryness below 30 °C by a rotary evaporator. From the residue the complex was extracted into methanol and NaCl precipitated was filtered off. The dark green filtrate was evaporated to dryness and the resulting powder was recrystallized from the minimum amount of water and dried in air. This was proved to be a *cis*(N_3) isomer through the optical resolution. Found: C, 25.34; H, 6.94; N, 36.88%. Calcd for *cis*(N_3)-[$Co(N_3)_2$(*N,N*-Me_2-en)$_2$]Cl·H_2O: C, 25.77; H, 7.04; N, 37.58%.

(4) *Optical Resolution of* cis*(*N_3*)*-[*Co(*N_3*)*$_2$*(*N,N-*Me*$_2$*-en)*$_2$]-*Cl*·H_2O: The racemic chloride monohydrate, *cis*(N_3)-[$Co(N_3)_2$(*N,N*-Me_2-en)$_2$]Cl·H_2O (0.2 g, 5.6×10^{-4} mol) was dissolved in 2 cm^3 of water and to this dark green solution was added ammonium $(+)_{589}$-(1*R*, 3*S*, 4*S*, 7*R*)-3-bromocamphor-9-sulfonate(0.17 g, 5.0×10^{-4} mol). On stirring, a crystalline powder was deposited, filtered, and washed with a small amount of water. This diastereoisomer was sparingly soluble in water at room temperature but soluble in methanol, ethanol, or acetone. The less soluble diastereoisomer was recrystallized from water at 30 °C, washed with water and dried in air. Found: C, 32.40; H, 6.33; N, 20.83%. Calcd for [$Co(N_3)_2$(*N,N*-Me_2-en)$_2$]$C_{10}H_{14}O_4SBr\cdot2H_2O$: C, 32.48; H, 6.37; N, 21.10%.

The less soluble diastereoisomer was converted into $(+)_{589}$-perchlorate by use of a column chromatographic method. Found: C, 22.61; H, 5.85; N, 33.45%. Calcd for $(+)_{589}$-[$Co(N_3)_2$(*N,N*-Me_2-en)$_2$]ClO_4: C, 22.94; H, 5.79; N, 33.45%.

(5) trans*(NCS)-* *and* cis*(NCS)*-[*Co(NCS)*$_2$*(*N,N-*Me*$_2$*-en)*$_2$]-*Cl*·H_2O: One and three tenths grams of *cis*(Cl)-[$CoCl_2$(*N,N*-Me_2-en)$_2$]ClO_4 and four tenths grams of KSCN were dissolved in 50 cm^3 of water and stirred at 40 °C for thirty min to obtain a red violet solution. The resulting solution was poured into a cation exchanger column(SP-Sephadex C-25, Na^+ form) and the adsorbed complex was eluted with a 0.05 M NaCl aqueous solution. Four bands appeared; dark reddish purple, deep purple, light purple, and dark purple ones in this order. The fractions of each the first and the second band were collected and evaporated to dryness below 30 °C by a rotary evaporator. From the residue the complex was extracted into methanol and the solution was evaporated to dryness. The crystalline powder was recrystallized from water and dried in air. The first dark purple band was proved to be a *trans*(NCS) isomer from the measurement of absorption spectrum. Found: C, 29.14; H, 6.34; N, 21.00%. Calcd for *trans*(NCS)-[$Co(NCS)_2$(*N,N*-Me_2-en)$_2$]Cl·H_2O: C, 29.66; H, 6.48; N, 20.76%. The second deep purple band was proved to be a *cis*(NCS) isomer from the successful optical resolution. Found: C, 29.17; H, 6.46; N, 20.62%. Calcd

for *cis*(NCS)-[$Co(NCS)_2$(*N,N*-Me_2-en)$_2$]Cl·H_2O: C, 29.66; H, 6.48; N, 20.76%. The third and fourth bands turned out to be monoisothiocyanato complexes from their elemental analyses.

(6) Optical Resolution of cis*(NCS)*-[*Co(NCS)*$_2$(N,N-*Me*$_2$-*en*)$_2$]*Cl·H*$_2$*O*: The racemic chloride monohydrate, *cis*(NCS)-[$Co(NCS)_2$(*N,N*-Me_2-en)$_2$]Cl·H_2O (0.23 g, 5.7×10^{-4} mol) and ammonium $(+)_{589}$-(1*R*, 3*S*, 4*S*, 7*R*)-3-bromocamphor-9-sulfonate(0.19 g, 5.8×10^{-4} mol) were dissolved in 30 cm^3 of water at 40 °C. The reddish purple solution was evaporated to half the initial volume and cooled in a refrigerator overnight. Reddish purple crystals deposited were filtered and washed with a small amount of water and dried in air. This diastereoisomer was rather soluble in methanol, ethanol, or acetone than in water. Found: C, 35.55; H, 5.75; N, 12.54%. Calcd for [$Co(NCS)_2$(*N,N*-Me_2-en)$_2$]$C_{10}H_{14}O_4$-SBr·0.5H_2O: C, 35.82; H, 5.87; N, 12.53%.

The less soluble diastereoisomer was converted into $(+)_{589}$-perchlorate by a column chromatographic method: C, 25.78; H, 5.47; N, 18.13%. Calcd for $(+)_{589}$-[$Co(NCS)_2$(*N,N*-Me_2-en)$_2$]ClO_4·0.5H_2O: C, 26.11; H, 5.49; N, 18.28%.

(7) [*Co(CO*$_3$*)*(N,N-*Me*$_2$-*en*)$_2$]*ClO*$_4$: The dichloro complex, *cis*(Cl)-[$CoCl_2$(*N,N*-Me_2-en)$_2$]ClO_4(0.4 g, 1.0×10^{-3} mol) was ground with Ag_2CO_3(0.3 g, 1.1×10^{-3} mol). Five cm^3 of water was added and the grinding was continued for half an hour. The color of the solution changed from blue green to violet. The solid AgCl deposited was filtered off and washed with a small amount of water. The filtrate and washing were evaporated almost to dryness and 10 cm^3 of ethanol was added. The blue-violet crystalline solid precipitated was filtered, washed with ethanol and ether and dried in a desiccator. Found: C, 26.29; H, 6.58; N, 13.99%. Calcd for [$Co(CO_3)$(*N,N*-Me_2-en)$_2$]ClO_4·0.5H_2O: C, 26.77: H, 6.25; N, 13.88%.

(8) [*Co(ox)*(N,N-*Me*$_2$-*en*)$_2$]*ClO*$_4$: To a solution of *cis*(Cl)-[$CoCl_2$(*N,N*-Me_2-en)$_2$]ClO_4(1.0 g, 2.5×10^{-3} mol) in 10 cm^3 of water was added five tenths grams of oxalic acid dihydrate, and this mixture was heated to 90 °C in a water bath, concentrated to half the initial volume, and cooled to room temperature. The red-purple crystalline powder precipitated was filtered, washed with ethanol and ether, and dried in air. Found: C, 27.11; H, 6.87; N, 12.75%. Calcd for [Co(ox)(*N,N*-Me_2-en)$_2$]ClO_4·H_2O: C, 27.27; H, 5.96; N, 12.71%.

(9) [*Co(NH*$_3$*)*$_4$(N,N-*Me*$_2$-*en*)]*Cl*$_3$: Two grams of *cis*(Cl)-[$CoCl_2$(*N,N*-Me_2-en)$_2$]ClO_4 was treated with 30 cm^3 of liquid ammonia in a pressure bottle. The blue green complex dissolved in liquid ammonia to give a pale orange solution. After removal of ammonia by introducing dry air, the pink-orange powder was suspended in methanol, and filtered, washed with ethanol and ether, and recrystallized from the minimum amount of water by adding ethanol. Found: C, 13.38; H, 7.72; N, 24.18%. Calcd for [$Co(NH_3)_4$(*N,N*-Me_2-en)]Cl_3·1.5H_2O: C, 13.78; H, 7.82; N, 24.11%.

(10) Other Complexes: Other complexes were prepared by the same methods as seen in the literature: en,[8-12] *N*-Me-en,[2] *N,N'*-Me_2-en,[4] and tris(aminoethyl)amine (tren)[13] complexes. The diazido- and diisothiocyanato-complexes containing *N*-Me-en or tren were prepared by the ligand substitution of *trans*(Cl)-[$CoCl_2$(*N*-Me-en)$_2$]$^{+}$[2] or [$CoCl_2$-(tren)]$^{+}$[14] with KSCN or NaN_3.

Measurements. The visible and ultraviolet absorption measurements were made by a Shimadzu UV-200 spectrophotometer in aqueous solutions, except for the dichloro complex, which was measured in methanol to prevent the aquation. The CD spectra were recorded on a JASCO MOE-1 spectropolarimeter and the PMR spectra were obtained in dimethyl-d_6 sulfoxide on a Varian XL-100-15 spectrometer using tetramethylsilane(TMS) as an internal standard.

Results and Discussion

Preparation and Isomerization. Three methods were tried for the preparation of the dinitro complex, [$Co(NO_2)_2$(*N,N*-Me_2-en)$_2$]$^{+}$; by use of atmospheric oxidation of a mixture of Co^{2+}, *N,N*-Me_2-en, $NaNO_2$, and HCl, and by use of ligand-substitution of either [$Co(CO_3)_3$]$^{3-}$ or [$Co(NO_2)_6$]$^{3-}$. The air-oxidation method only was successful. The product of this reaction was proved to be a *trans*(NO_2) isomer from the parallel relationship between the absorption spectra of this and the corresponding *trans*(NO_2)-[$Co(NO_2)_2$-(en)$_2$]$^{+}$ complex. The *cis*-dinitro complex was not obtaned, although the *cis* isomers of diazido-, diisothiocyanato-, and dichloro-complexes were prepared. The diammine complex, [$Co(NH_3)_2$(*N,N*-Me_2-en)$_2$]$^{3+}$ was not yielded on the tretment of the dichloro complex, *cis*(Cl)-[$CoCl_2$(*N,N*-Me_2-en)$_2$]$^{+}$ with liquid ammonia; the reaction gave only tetraammine complex, [$Co(NH_3)_4$(*N,N*-Me_2-en)]$^{3+}$. When the *trans*-dinitro complex was treated with either alcoholic hydrogen chloride at room temperature of concentrated aqueous hydrogen chloride at 70 °C, only a *cis* isomer of the dichloro complex was obtained, and the reaction of the dichloro complex with $NaNO_2$ yielded only one dinitro complex which was identical with the starting material, *trans*(NO_2)-[$Co(NO_2)_2$(*N,N*-Me_2-en)$_2$]$^{+}$. The dichloro complex was decomposed in the presence of moisture to give a brown insoluble mud. The substitution reaction of *cis*(Cl)-[$CoCl_2$(*N,N*-Me_2-en)$_2$]$^{+}$ with NaN_3 or KSCN resulted in the production of both *trans* and *cis* isomers of diazido or diisothiocyanato complex. The correseponding substitution reaction of *trans*(Cl)-[$CoCl_2$(*N*-Me-en)$_2$]$^{+}$ with either NaN_3 or KSCN gave only the *trans* isomer, and *trans*(Cl)-[$CoCl_2$(*N,N'*-Me_2-en)$_2$]$^{+}$ did not react with these reagents.

Structural Assignments. Figure 1 shows five possible geometrical isomers of a [CoX_2(A-B)$_2$] type complex and their symmetries. In this paper X stands for anions (Cl^-, NO_2^-, N_3^-, or NCS^-) and A-B for *N,N*-dimethylethylenediamine; where A and B signify a

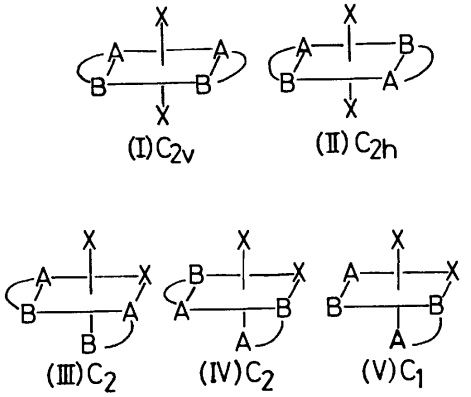

Fig. 1. Possible configurations of [CoX_2(A-B)$_2$]$^{+}$ type complex.

Table 1. Assignment of chemical shifts for PMR of $[CoX_2(N,N\text{-}Me_2\text{-}en)_2]^+$ ($X=N_3^-$, NCS^-, and NO_2^-)
(All frequencies in ppm on low-field side of TMS)

Complex	N-CH_3	-CH_2-CH_2-	N-H	Structure
trans(NO_2)-	2.07	≈2.40, 3.11	5.68	II
trans(N_3)-	2.09	2.29, 2.82	5.60	II
trans(NCS)-	2.21	≈2.46, 2.91	6.43	II
cis(N_3)-	2.10, 2.14	≈2.40, ≈3.2[a]	4.72, 5.56	III
cis(NCS)-	2.25, 2.37	≈2.5,[b] ≈2.95	5.70, 6.00	III

a) Overlapped with -OH signal. b) Overlapped with dimethyl sulfoxide signal.

tertiary and a primary amine, respectively. The upper two complexes I and II in Fig. 1 are *trans*(X) isomers and the lower three III-V *cis*(X) ones. All the three *cis*(X) isomers are chiral and therefore the isomer which can be resolved turns out to be one of the *cis*(X) isomers. PMR spectra can also distinguish among the isomers (I, II), (III, IV), and (V).

Table 1 shows the chemical shifts(in ppm) for PMR spectra of $[CoX_2(N,N\text{-}Me_2\text{-}en)_2]^+$($X=NO_2^-$, NCS^-, and N_3^-). From the PMR data it is confirmed that the *trans* isomers of dinitro-, diisothiocyanato-, and diazido-complexes have I or II structure and that the *cis* isomers of diazido- and diisothiocyanato-complexes III or IV structure. No well-defined PMR spectrum was obtained for the dichloro complex, because of the unstable nature of this complex. It is impossible to distinguish between isomers I and II or between isomers III and IV solely on the basis of the PMR splitting patterns. However a consideration of molecular models provides the following answers for this problem.

The structure I has bulky *N,N*-dimethyl-substituted amines(A) in *cis* positions, which produce rather large repulsion between them and make the structure unstable. A similar consideration is true for the *cis*(X) isomers, that is, the structure IV and V are less stable than the structure III. Accordingly, it is concluded that the *trans*(X) isomers have the structure II and the *cis*(X) isomers the structure III. This conclusion is well supported by the consideration of the absorption spectra mentioned below.

Absorption and Circular Dichroism Spectra. Figure 2 shows the electronic absorption spectra of *trans*-(NO_2)-complexes of en, *N*-Me-en, *N,N'*-Me_2-en, and *N,N*-Me_2-en. It is found that the increase in the number of the *N*-methyl-groups induces the shift of the spectra to lower side, and that the *N,N*-Me_2-en complex has its absorption at lower energy than the *N,N'*-Me_2-en complex. The trough at *ca.* 25000 cm^{-1} disappears in the *N,N*-Me_2-en complex owing to the overlap of the first charge transfer band at *ca.* 27000 cm^{-1}.

Figures 3 and 4 show the absorption spectra of *trans*-(NCS)- and *trans*(N_3)-complexes, respectively. Besides the shift of each band to longer wavelength region with an increase in the degree of *N*-methyl-substitution, two more features are found. The first is the splitting of the first d-d absorption band; there is a broad peak at 19300 cm^{-1} with a shoulder at about 16500 cm^{-1} for the diisothiocyanato *N,N*-Me_2-en complex, and two distinct peaks at 14300 and 18200 cm^{-1} for the diazido

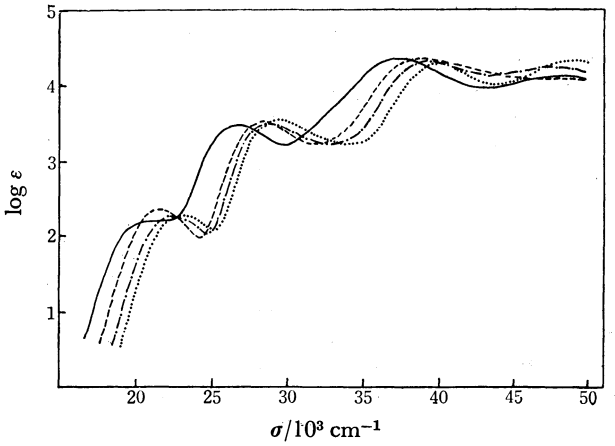

Fig. 2. Absorption spectra of *trans*(NO_2)-[$Co(NO_2)_2$-(diamine)$_2$]$^+$: *N,N*-Me_2-en (——); *N,N'*-Me_2-en (----); *N*-Me-en (—·—); and en (·····).

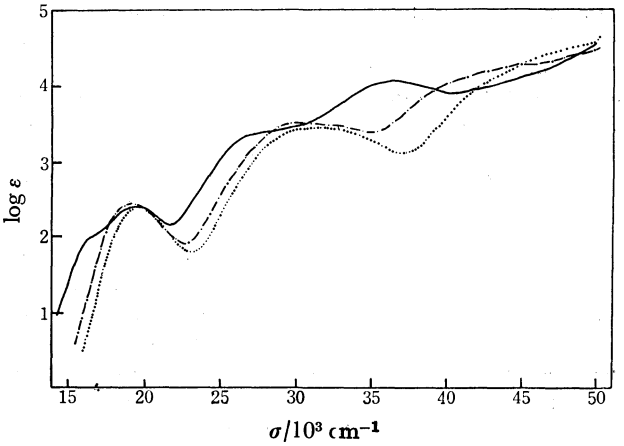

Fig. 3. Absorption spectra of *trans*(NCS)-[$Co(NCS)_2$-(diamine)$_2$]$^+$: *N,N*-Me_2-en (——); *N*-Me-en (—·—); and en (·····).

N,N-Me_2-en complex. The second is a new peak (log $\varepsilon \approx 4$) in the ultraviolet region 35000—40000 cm^{-1} for both NCS- and N_3-complexes; the band is not found for the corresponding ethylenediamine and *N*-methylethylenediamine complexes. The new ultraviolet absorption band also appears for *cis* isomers of the *N,N*-Me_2-en complex at about the same position with the same intensity as those for the *trans* isomers (see Figs. 5 and 6, and Table 2).

Figures 5 and 6 show the absorption and the CD spectra of *cis*(NCS)- and *cis*(N_3)-complexes of en,

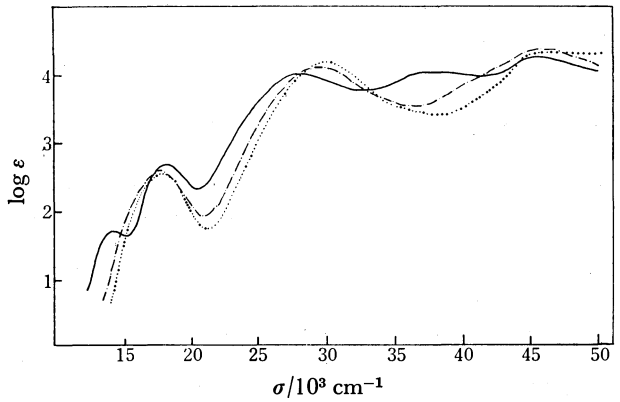

Fig. 4. Absorption spectra of *trans*(N_3)-[$Co(N_3)_2$-(diamine)$_2$]$^+$: *N,N*-Me_2-en (——); *N*-Me-en (—·—); and en (·····).

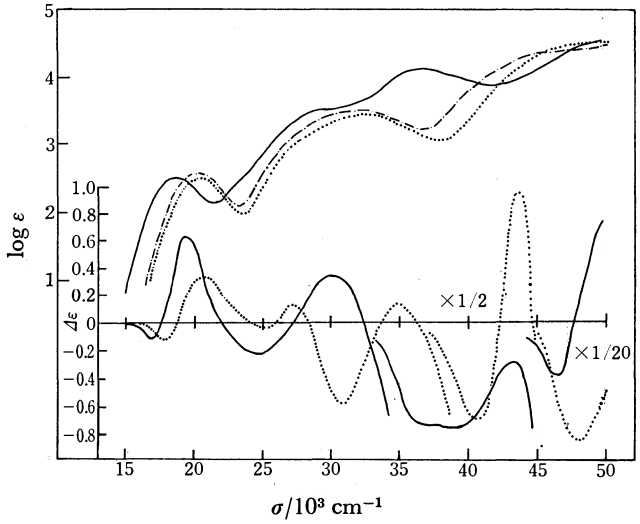

Fig. 5. Absorption and CD spectra of *cis*(NCS)-[Co-(NCS)$_2$(amine)]$^+$: $(+)_{589}$-(*N,N*-Me_2-en)$_2$ (——); tren (—·—); and $(-)_{589}$-$(en)_2$ (·····).

tren, and *N,N*-Me_2-en. Tren is a tripod tetradentate amine and the *cis*-[CoX_2(tren)]$^+$ complexes (X=NCS$^-$ and N_3^-) have a plane of symmetry and are achiral. Both absorption and CD spectra of *N,N*-Me_2-en complexes shift to longer wavelength region than those of the en complexes. The CD spectrum of $(+)_{589}$-[$Co(N_3)_2$(*N,N*-Me_2-en)$_2$]$^+$ correlates to that of $(-)_{589}$-[$Co(N_3)_2(en)_2$]$^+$ on the whole, except a small negative band at 38000 cm^{-1} related to the new absorption peak (Fig. 6). On the other hand, the CD spectrum of $(+)_{589}$-[$Co(NCS)_2$(*N,N*-Me_2-en)$_2$]$^+$ may not correlate at a glance, to that of $(-)_{589}$[$Co(NCS)_2(en)_2$]$^+$ in the ultraviolet region (Fig. 5). This is because the intensity ratio of the CD peaks at 25000—35000 cm^{-1} is reversed between *N,N*-Me_2-en and en complexes; the intensity is weak at 24600 cm^{-1} and strong at 30000 cm^{-1} in the *N,N*-Me_2-en complex(solid line), but strong at 31000 cm^{-1} and weak at 35000 cm^{-1} in the en complex(broken line). At the new absorption peak of 36600 cm^{-1} one or two negative CD bands appear.

Table 2. The absorption data of Co(III) complexes containing *N,N*-Me_2-en and related amines
(Wave numbers and log ε values (in parentheses) are given in 10^3 cm^{-1} and mol^{-1} dm^3 cm^{-1}, respectively.)

Complex	d-d transition region		Charge transfer region		
trans-[$Co(NO_2)_2(en)_2$]$ClO_4\cdot 0.5H_2O$	23.20(2.29)		29.41(3.56)	40.16(4.31)	49.38(4.36)
trans-[$Co(NO_2)_2$(*N*-Me-en)$_2$]ClO_4	22.57(2.28)		28.90(3.51)	39.53(4.35)	48.08(4.27)
trans-[$Co(NO_2)_2$(*N,N'*-Me_2-en)$_2$]ClO_4	21.69(2.37)		28.65(3.53)	39.22(4.37)	48.54(4.13)
trans-[$Co(NO_2)_2$(*N,N*-Me_2-en)$_2$]ClO_4	21.32(2.24)		26.81(3.49)	37.45(4.39)	48.08(4.15)
trans-[$Co(NCS)_2(en)_2$]$Cl\cdot 0.5H_2O$	19.53(2.39)		31.15(3.45)		
trans-[$Co(NCS)_2$(*N*-Me-en)$_2$]$Cl\cdot H_2O$	19.21(2.44)		31.10(3.51)		
trans-[$Co(NCS)_2$(*N,N*-Me_2-en)$_2$]$Cl\cdot H_2O$	≈16.5 (sh) 19.34(2.39)		≈27.5(≈3.37)	36.50(4.06)	≈44.5(≈4.07)
trans-[$Co(N_3)_2(en)_2$]$Cl\cdot H_2O$	17.79(2.53)	≈25.7 (sh)	29.85(4.15)	≈35 (sh≈3.4)	46.62(4.29)
trans-[$Co(N_3)_2$(*N*-Me-en)$_2$]ClO_4	17.66(2.56)		29.41(4.09)		45.87(4.33)
trans-[$Co(N_3)_2$(*N,N*-Me_2-en)$_2$]ClO_4	14.29(1.68) 19.34(2.39)		28.01(3.98)	38.02(4.00)	45.46(4.22)
cis-[$Co(NCS)_2(en)_2$]Cl	20.37(2.51)		32.15(3.43)		
cis-[$Co(NCS)_2$(*N,N*-Me_2-en)$_2$]$Cl\cdot H_2O$	18.62(2.52)		≈29.5(≈3.48)	36.63(4.10)	
cis-[$Co(NCS)_2$(tren)]Cl	20.12(2.59)		31.85(3.48)		
cis-[$Co(N_3)_2(en)_2$]$Cl\cdot H_2O$	19.27(2.52)	≈27.4 (sh)	33.11(4.07)		46.73(4.30)
cis-[$Co(N_3)_2$(*N,N*-Me_2-en)$_2$]$Cl\cdot H_2O$	17.61(2.45)	≈22 (sh)	32.26(3.95)	38.02(4.07)	46.08(4.13)
cis-[$Co(N_3)_2$(tren)]$ClO_4\cdot H_2O$	19.12(2.57)		33.00(4.14)		46.06(4.29)
cis-[$CoCl_2(en)_2$]Cl[23]	18.87(1.88)	25.64(1.87)		41.67(4.28)	
cis-[$CoCl_2$(*N,N*-Me_2-en)$_2$]$ClO_4\cdot 0.5H_2O$	16.31(2.05)	≈24 (≈2.0)		39.06(4.25)	
[$Co(CO_3)(en)_2$]ClO_4	19.53(2.16)	27.78(2.12)			42.19(4.14)
[$Co(CO_3)$(*N,N*-Me_2-en)$_2$]$ClO_4\cdot 0.5H_2O$	17.92(2.09)	25.58(2.10)		39.06(4.22)	45.87(≈4.0)
[$Co(CO_3)$(tren)]$ClO_4\cdot 1.5H_2O$	19.76(2.13)	≈25.5(≈1.9) 28.05(2.06)			41.24(4.16)
[$Co(CO_3)$(*N,N*-Me_2-en)$_2$]$ClO_4\cdot 0.5H_2O$	18.28(2.12)	25.64(2.17)		38.16(4.18)	42.37(4.22)
[$Co(NH_3)_4$(*N,N*-Me_2-en)]$Cl_3\cdot 1.5H_2O$	20.37(1.88)	28.99(1.84)		≈42.37(≈4.1)	47.85(4.23)

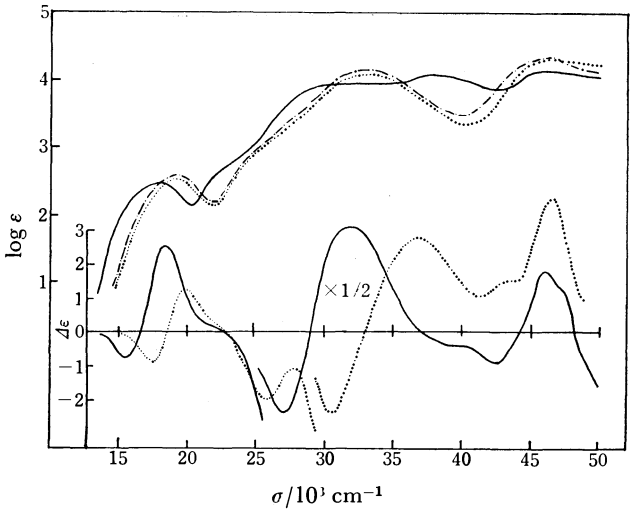

Fig. 6. Absorption and CD spectra of *cis*(N_3)-[Co(N_3)$_2$(amine)]$^+$: $(+)_{589}$-(*N*,*N*-Me_2-en)$_2$ (——); tren (—·—); and $(-)_{589}$-(en)$_2$ (·····).

The feature of the absorption spectra of the Co(III) complexes containing *N*,*N*-Me_2-en is well explained with an assumption that the diamine(A-B) has different ligand-field strengths at each end; the tertiary amine end(A) has very weak ligand-field and the primary amine end(B) the same as ethylenediamine. Yamatera's parameter[15] of the tertiary amine end, δ(A), can be calculated from the absorption data of the *trans*(N_3) isomer which shows a large splitting in the first absorption band region. Such a large splitting can be explained well by the structure II and not by I. Thus the peak situated at lower energy is thought to be shifted by $1/2\delta(N_3)+1/2\delta(A)$ from the peak of the parent complex, $[Co(en)_3]^{3+}$(21400 cm^{-1}). That is, $1/2\delta(N_3)+1/2\delta(A)=14300-21400=-7100\ cm^{-1}$, and with an assumption that $\delta(N_3)=-7900\ cm^{-1}$ (from the first absorption band position 17250 cm^{-1} of *mer*-$[Co(N_3)_3(NH_3)_3]$,[16] we obtain $\delta(A)=-6300\ cm^{-1}$, which is weaker than those of the oxalato and carbonato ligands, $\delta(ox)=-4800$ cm^{-1} and $\delta(CO_3)=-5900\ cm^{-1}$ obtained from the reported absorption spectral data.[17,18] Therefore, on the whole, *N*,*N*-dimethylethylenediamine has somewhat weak strength in the ligand-field as compared with amino acids. From this and the other values, $\delta(NO_2)=+4000\ cm^{-1}$ and $\delta(NCS)=-4300\ cm^{-1}$ (from the first absorption band position 23210 cm^{-1} and 19050 cm^{-1} of *mer*-$[Co(NO_2)_3(NH_3)_3]$[19] and *mer*-$[Co(NCS)_3(NH_3)_3]$[20], respectively), the first absorption bands of all the *trans* isomers of *N*,*N*-Me_2-en complexes can be well explained. Yamatera's rule predicts that the *cis*(N_3) complex of structure III has the split components of the first absorption band at 16300 and 17500 cm^{-1}, while that of the structure IV at 14300 and 17900 cm^{-1}. The observed first absorption band of the *cis*(N_3) complex is located at 17610 cm^{-1}. The absence of the band of 14300 cm^{-1} supports strongly the structure III for this complex. Similarly the *cis*(NCS) complex is assigned to have the strucutre III, which is parallel to the conclusion from pmr and molecular model considerations. The dichloro complex cannot be assigned on the basis of PMR spectra. However, if it is the *trans*(Cl) isomer II, it should have a split component at *ca.* 12900 cm^{-1} (from $\delta(Cl)=-10700$ cm^{-1} [21]). Because the complex shows no component there, it is assigned to the *cis*(Cl) isomer.

In a previous paper we reported that the near ultraviolet charge-transfer band (so-called specific band) of a *trans* isomer of bis(aniono) Co(III) complexes is more bathochromic than that of the corresponding *cis* isomer.[22] This is also the case of the present *N*,*N*-Me_2-en complexes; for example, the band of the *trans*-(N_3) complex is at 28010 cm^{-1}, while that of *cis*(N_3) at 32260 cm^{-1}. All the present dianiono complexes of *N*,*N*-Me_2-en show a broad absorption band in the region of 35000—39000 cm^{-1} (Table 2). The tetraamine complex, $[Co(NH_3)_4(N,N\text{-}Me_2\text{-}en)]^{3+}$ also shows this kind of band at *ca.* 42000 cm^{-1}. This new band of charge-transfer character is attributed to the coordinated tertiary amine; the observed peak or so-called end absorption at *ca.* 50000 cm^{-1} may be attributed to the coordinated primary amine. In this connection it is worthwhile to point out that none of the tren complexes show the peak attributed to the tertiary amine, which may reflects that the tertiary amine of the tren ligand has a nature different from that of *N*,*N*-Me_2-en.

Absolute Configuration. From the parallel relationship between the CD spectra of $(+)_{589}$-$[CoX_2(N,N\text{-}Me_2\text{-}en)_2]^+$ and $(-)_{589}$-$[CoX_2(en)_2]^+$ (X=N_3^- and NCS^-), it is concluded that the $(+)_{589}$ -isomers of *cis* dianiono complexes of *N*,*N*-Me_2-en have the absolute configuration same as that of the $(-)_{589}$-isomers of the corresponding en complexes (see Table 3). Because the latter complexes have been assigned to *Λ* configuration,[12] the present $(+)_{589}$-*N*,*N*-Me_2-en complexes

Table 3. The CD data of *cis*(X)-$[CoX_2(diamine)_2]^+$ (diamine=en, *N*,*N*-Me_2-en) complexes

(Wave numbers and $\Delta\varepsilon$ values (in parentheses) are given in $10^3\ cm^{-1}$ and $mol^{-1}\ dm^3\ cm^{-1}$, respectively.)

$(-)_{589}$-$[Co(NCS)_2(en)_2]Cl$	$(+)_{589}$-$[Co(NCS)_2(N,N\text{-}Me_2\text{-}en)_2]ClO_4$
17.73(−0.130)	16.89(−0.133)
20.60(+0.340)	19.31(+0.642)
25.13(−0.04)	
27.17(+0.13)	
30.77(−0.60)	24.39(−0.233)
34.72(+0.15)	29.85(+0.35)
40.65(−1.42)	36.76(−1.52)
43.48(+1.96)	38.17(−1.55)
47.85(−17.5)	46.30(−3.73)
$(-)_{589}$-$[Co(N_3)_2(en)_2]ClO_4$	$(+)_{589}$-$[Co(N_3)_2(N,N\text{-}Me_2\text{-}en)_2]ClO_4$
17.45(−0.871)	15.24(−0.826)
19.72(+1.286)	18.02(+2.558)
25.77(−1.97)	
30.67(−4.76)	26.81(−4.79)
37.04(+5.47)	31.75(+6.32)
43.48(+2.91)	≈40 (≈−0.8)
	42.37(−1.84)
46.73(+7.93)	45.87(+3.69)

are also assigned to *Λ*.

In a previous paper[12] it was reported that the *Λ* isomers of diazido- and diisothiocyanatobis(ethylenediamine)cobalt(III) complexes show a CD pattern of negative and then positive signs in the order of increasing energy in the longest wavelength charge-transfer band region, so-called specific band region. As is seen in Figs. 5 and 6, and in Table 3, this is also valid for the *N,N*-Me_2-en complexes. The CD sign in the region of tertiary amine band is negative for the *Λ* isomers.

References

1) D. A. Buckingham, L. G. Marzilli, and A. M. Sargeson, *J. Am. Chem. Soc.*, **89**, 825 (1967).

2) D. A. Buckingham, L. G. Marzilli, and A. M. Sargeson, *Inorg. Chem.*, **7**, 915 (1968).

3) J. I. Legg and B. E. Douglas, *Inorg. Chem.*, **7**, 1452 (1968).

4) J. A. Tiethof and W. Cooke, *Inorg. Chem.*, **11**, 315 (1972).

5) R. Nasanen, M. Koskinen, and R. Penttonen, *Suom. Kemistil. B*, **40**, 25 (1967).

6) D. M. L. Goodgame and H. A. Hitchman, *Inorg. Chem.*, **5**, 1303 (1965); M. G. B. Drew, D. M. L. Goodgame, M. A. Hitchman, and D. Rogers, *Proc. Chem. Soc.*, **1964**, 363.

7) M. P. Hancock, B. T. Heaton, and D. H. Vaughan, *J. Chem. Soc., Dalton Trans.*, **1976**, 931.

8) H, F. Holtzclaw, D. P. Sheetz, and B. D. McCarty, *Inorg. Synth.*, **4**, 176 (1953).

9) P. J. Staples and M. L. Tobe, *J. Chem. Soc.*, **1960**, 482.

10) A. Werner and F. Braunlich, *Z. Anorg. Allg. Chem.*, **22**, 147 (1900).

11) P. Pfeiffer and O. Angern, *Ber.*, **66**, 308 (1927).

12) K. Yamasaki, J. Hidaka, and Y. Shimura, *Bull. Chem. Soc. Jpn.*, **49**, 3060 (1976).

13) King-Wen Kuo and S. K. Madan, *Inorg. Chem.*, **8**, 1580 (1969).

14) E. Kimura, S. Young, and J. P. Collman, *Inorg. Chem.*, **9**, 1183 (1970).

15) H. Yamatera, *Bull. Chem. Soc. Jpn.*, **31**, 95 (1958).

16) M. Linhard and M. Weigel, *Z. Anorg. Allg. Chem.*, **267**, 113 (1951).

17) N. Matsuoka, J. Hidaka, and Y. Shimura, *Bull. Chem. Soc. Jpn.*, **40**, 1868 (1967).

18) M. Mori, M. Shibata, E. Kyuno, and T. Adachi, *Bull. Chem. Soc. Jpn.*, **29**, 883 (1956).

19) M. Linhard and M. Weigel, *Z. Anorg. Allg. Chem.*, **267**, 113 (1951).

20) H. Siebert, *Z. Anorg. Allg. Chem.*, **389**, 22 (1972).

21) K. Ohkawa, J. Hidaka, and Y. Shimura, *Bull. Chem. Soc. Jpn.*, **39**, 1715 (1966).

22) K. Akamatsu, J. Hidaka, and Y. Shimura, *Bull. Chem. Soc. Jpn.*, **50**, 533 (1977).

23) F. Basolo, *J. Am. Chem. Soc.*, **72**, 4393 (1950).

Preparation and Properties of Cu(II) Complexes of *N*-Picolinoyl-*S,S*-tetramethylenesulfilimine, *N*-(Trimethylammonio)-picolinamidate, and Related Ylides

Hideo KISE* and Manabu SENŌ

Institute of Industrial Science, The University of Tokyo, Roppongi, Minato-ku, Tokyo 106

(Received April 8, 1978)

The reactions of *N*-picolinoyl-*S,S*-tetramethylenesulfilimine (PS) and *N*-(trimethylammonio)picolinamidate (PA) with copper(II) chloride dihydrate in ethanol afforded complexes of the formula $CuCl_2(Y)$ and $CuCl_2(Y)_2$ (Y=PA or PS). The structures of these complexes were examined by spectroscopic and magnetic methods, and it was found that all of them have mononuclear chelate structures. It was concluded that in $CuCl_2(PS)$, the ligand is coordinated through two nitrogen atoms, whereas in $CuCl_2(PS)_2$, the ligands are coordinated through carbonyl oxygens and nitrogens in pyridine rings. The structures of $CuCl_2(PA)$, $CuCl_2(PA)_2$, and CuCl(PA) are closely similar to each other and the possibility of coordination through ylidic nitrogens with large ionic contributions to the structures was strongly suggested. Several Cu(II) complexes with monodentate sulfilimines and aminimides were also prepared, and the structural analyses revealed that the nature of the coordination depends largely on the structure of the ylides.

It has been reported that *N*-picolinoyl-*S,S*-tetramethylenesulfilimine (PS) and *N*-(trimethylammonio)-picolinamidate (PA) are bidentate and ambident ligands and form 1:1 chelate complexes with $PdCl_2$ and $PtCl_2$ in which the ligands are coordinated through two nitrogen atoms.[1] In this paper the formation of Cu(II) and Cu(I) complexes of these ylides and the determination of their structure by magnetic and spectroscopic methods are reported. An interesting feature of the chemistry is the nature of the metal-ligand coordination bonds which has not been investigated in detail.

Although numerous reports have been published on the transition metal–ylide complexes, only a limited number of them describe copper complexes. Chia *et al.*[2] claim that *N*-(1-pyridinio)benzenesulfonamidate forms complexes with Cu(II) perchlorate and halides *via* ylidic nitrogen atoms. Measurements of magnetic moments suggested a dimeric structure for the $CuCl_2$ complex, whereas *N*-(1-pyridinio)benzamidate gave a monomeric complex with $CuCl_2$ by coordination *via* ylidic nitrogen. Another Cu(II)–ylide complex reported is the reaction product of triphenylphosphonium phenacylide with $CuCl_2$,[3] which is diamagnetic and likely to have a dimeric or polymeric structure.

Results and Discussion

Complexes of N-*Picolinoyl*-S,S-*tetramethylenesulfilimine (PS) with* $CuCl_2$. By addition of an ethanol solution of PS to an ethanol solution of $CuCl_2 \cdot 2H_2O$ in an equimolar ratio, a 1:1 complex was obtained as a precipitate. The magnetic moment of the complex (Table 1) is normal for an isolated Cu(II) metal and rules out dimeric or polymeric structures. The ylide PS has resonance structures shown below, and the anionic charge is considered to be delocalized over the N–C–O atoms. The large contribution of the enolate ion structure is confirmed by the low C=O stretching band (1547 cm^{-1}), which is comparable to that of carboxylate ions. The IR spectrum of the 1:1 complex exhibits a C=O stretching band at 1655 cm^{-1}, which is 108 cm^{-1} higher than that of the free ligand (Table 2) and close to the bands of carboxamides, clearly indicating coordination through ylidic nitrogen. The proposed square plannar structure in Fig. 1 (**1**) requires coordination through another nitrogen in the pyridine ring, and this is supported by the observed higher frequency shift of the pyridine deformation band from 615 cm^{-1} in the free ligand to 647 cm^{-1} in the complex.[4] These results are quite similar to those of the complexes of PS with $PdCl_2$ and $PtCl_2$, and it may be concluded that the complex has a structure shown in Fig. 1 (**1**) in which the Cu(II)–ylidic nitrogen coordination is essentially covalent (σ) bonding. Although an alternative dimeric square plannar structure like that of dihalo(2-methylpyridine)copper(II) may be possible, in which the two planes interact through Cu–Cl–Cu bond,[5] the inter-

TABLE 1. ANALYSES AND PROPERTIES OF COMPLEXES

Complex	Yield (%)	Mp (°C)[a]	Color	Found, %			Calcd, %			μ_{eff}[b] (B.M.)
				C	H	N	C	H	N	
$CuCl_2(PS)$	84	>198	blue-green	34.25	3.40	8.70	35.04	3.54	8.18	1.96
$CuCl_2(PS)_2$	90	126—128	blue-green	43.98	4.97	9.96	43.59	4.40	10.17	1.86
$CuCl_2(FS)_2$	77	152—154	green-yellow	20.65	4.03	7.82	20.90	4.10	8.13	1.90
$CuCl_2(AS)$	43	127—128	red-brown	26.66	4.25	5.38	25.76	3.97	5.01	1.97
$CuCl_2(PA)$	79	215—216	blue	33.84	4.24	13.04	34.46	4.18	13.40	1.94
$CuCl_2(PA)_2$	96	192—193	blue	42.00	5.87	16.61	42.31	5.53	16.45	1.88
CuCl(PA)	75	195—196	blue-green	39.40	5.34	15.46	38.85	4.72	15.11	—
$CuCl_2(AA)$	87	190—191	yellow-brown	24.50	4.92	10.98	23.96	4.84	11.18	1.94
$CuCl_2(BA)$	75	122—125	red-brown	37.73	5.22	8.43	38.41	4.52	8.96	1.68

a) The complexes melt with decomposition. b) At room temperature.

Table 2. IR data of ylides and their complexes (cm^{-1})

Compound	C=O st.	Aromatic ring st.	C–N st.	Aromatic C–H def.	Pyridine def.
$(CH_2)_4S{=}NCOC_5H_4N$ (PS)	1547	1587	1330	750, 703	615
$CuCl_2$ (PS)	1655	1600	1320	760, 689	647
$CuCl_2(PS)_2$	1530	1606	1375	767, 691	656
$(CH_3)_2S{=}NCOH$ (FS)	1574	—	1233	—	—
$CuCl_2(FS)_2$	1600	—	1200	—	—
$(CH_2)_4S{=}NCOCH_3$ (AS)	1540	—	1290	—	—
$CuCl_2$(AS)	1502	—	1390	—	—
$(CH_3)_3\overset{+}{N}\text{-}\overset{-}{N}COC_5H_4N$ (PA)	1560	1605	1350	750, 705	623
$CuCl_2$(PA)	1585	1615	1360	758, 690	648
$CuCl_2(PA)_2$	1582	1610	1355	755, 690	655
CuCl(PA)	1582	1610	1355	755, 690	654
$(CH_3)_3\overset{+}{N}\text{-}\overset{-}{N}COCH_3$(AA)	1575	—	1335	—	—
$CuCl_2$(AA)	1570	—	1345	—	—
$(CH_3)_3\overset{+}{N}\text{-}\overset{-}{N}COC_6H_5$ (BA)	1560	1600	1334	726	—
$CuCl_2$(BA)	1690, 1545	1592	1352, 1275	710	—

action would be very weak considering the large magnetic moment of $CuCl_2$(PS).

The electronic spectral data are summarized in Table 3. The ligand PS and PA have structural similarity to picolinamides which liberate a hydrogen atom in alkaline media to form neutral complexes with Cu(II). An example is shown in Fig. 1 (**7**) which was reported to be reddish violet and to have λ_{max} at 530 and 585 nm in chloroform and water, respectively.[6] It is interesting to note that in the case of $CuCl_2$(PS), only a small difference in the absorption maximum was observed in chloroform and water, in contrast to complex **7** which shows a red shift in water due to the coordination of water to form an octahedral structure. The electric conductivity of $CuCl_2$(PS) in chloroform is low and indicates no dissociation, but in water the complex is a strong electrolyte (Table 3). Therefore, the chloride ions are considered to be fully replaced by water, and this might compensate for the red shift which is expected in the change to the octahedral structure in water.

From the reaction of $CuCl_2\cdot 2H_2O$ with two equivalents of PS, a complex was obtained which was formulated as $CuCl_2(PS)_2$ and has the normal paramagnetic character of a monomeric structure. However, the C=O stretching absorption band appears at 1530 cm^{-1}, 17 cm^{-1} lower than that of the free ligand, in contrast to the higher frequency shift of $CuCl_2$(PS) described above. In addition, the C–N stretching band shifts from 1330 to 1375 cm^{-1} indicating an increase in double bond character in the complex, and it is very likely that the ligands are coordinated through carbonyl oxygens.

Table 3. Electronic spectral data and molar conductivity of complexes

Complex	$\lambda_{max}(\varepsilon)$		Λ[a]	
	in H_2O	in $CHCl_3$	in H_2O	in $CHCl_3$
$CuCl_2$(PS)	715(27)	720(70)	267	1.03
$CuCl_2(PS)_2$	670(39)	820(106)	221	1.89
$CuCl_2(FS)_2$	815(15)	—[b]	274	—[b]
$CuCl_2$(AS)	800(13)	—[b]	202	—[b]
$CuCl_2$(PA)	710(24)	730(99)	250	1.04
$CuCl_2(PA)_2$	660(44)	850(155)	227	2.99
CuCl(PA)	660(41)	840(82)	117	1.72
$CuCl_2$(AA)	830(3.4)	—[b]	184	—[b]
$CuCl_2$(BA)	820(9.7)	—[b]	265	—[b]

a) Measured at 10^{-3} M, $\mho\,cm^2\,mol^{-1}$. b) Insoluble in $CHCl_3$.

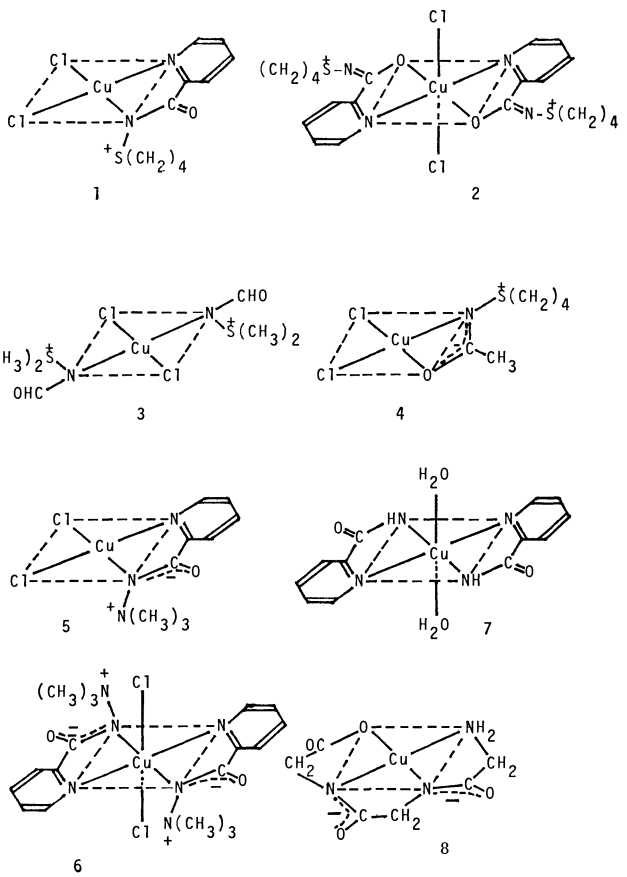

Fig. 1. Structure of Cu(II) complexes.

Although a large number of metal complexes of carbonyl-stabilized ylides have been reported, very few have coordination *via* carbonyl oxygens.[7] The change of the coordination site from the ylidic nitrogen to the carbonyl oxygen in going from 1:1 to 1:2 complexes may be the consequence of the steric hindrance around Cu(II). A close interaction observed in a structural model between a pyridine ring of a ligand and a tetramethylenesulfonium group in another one supports this consideration. The 1:2 complex is also a nonelectrolyte and has absorption maximum at 820 nm in chloroform, and an octahedral structure was proposed as shown in Fig. 1 (**2**). In water this complex is a strong electrolyte and the absorption band falls to 670 nm, probably because of the lowering of the microsymmetry to a more distorted octahedral or square plannar structure due to the weaker metal–chloride bonding by strong hydration of the chloride ions.

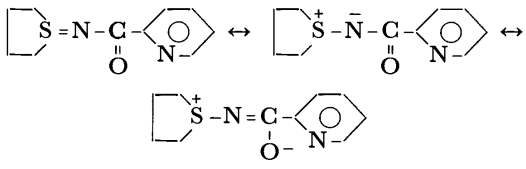

PS

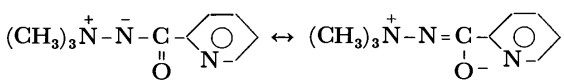

PA

Complexes of N-*Formyl*-S,S-*dimethylsulfilimine (FS) and* N-*Acetyl*-S,S-*tetramethylenesulfilimine (AS) with* $CuCl_2$. These ligands behave quite differently in the complex formation. Elemental analyses reveal that the ylide FS forms a 1:2 complex, while AS forms a 1:1 complex. Furthermore, the former exhibits a C=O stretching band at 1600 cm^{-1}, 26 cm^{-1} higher than in the free ligand, whereas the latter exhibits the C=O band at 1502 cm^{-1}, 38 cm^{-1} lower than in the free ligand. Thus, metal–ylidic nitrogen and metal–carbonyl oxygen coordinations are implied for $CuCl_2(FS)_2$ and $CuCl_2(AS)$, respectively, and supported also by each observed shift of the C–N stretching band in going from the free ligands to the complexes. The complexes show normal paramagnetism (Table 1), and the most probable structures are indicated in Fig. 1 (**3**) and (**4**). Taking into consideration the small shift of the carbonyl band in $CuCl_2(FS)_2$, the Cu(II)–ylide bond is likely to have ionic character; that is, the ligand has appreciable ylidic nature retained in the complex. The structure in Fig. 1 (**4**) is similar to those of π-allyl complexes, but only few ylides have been reported to form complexes of this η^3 structure.[7] Electronic spectra were not obtained in nonpolar solvents because of the low solubility of the complexes, and the data available do not allow more positive conclusions on the structure of these complexes.

Complexes of N-*(Trimethylammonio)picolinamidate (PA) with* $CuCl_2$ *and* $CuCl$. Both 1:1 and 1:2 complexes of PA with $CuCl_2$ were prepared in similar ways to those of the PS complexes. In addition, the reaction of PA with two equivalents of CuCl afforded a 1:1 complex, CuCl(PA). A characteristic feature for these PA complexes is that they give almost identical IR spectra (Table 2), implying an identical coordination mode of the ligand in these complexes. The C=O bands appear near 1580 cm^{-1}, about 20 cm^{-1} higher than that of the free PA suggesting coordination *via* ylidic nitrogen. However, the shifts are relatively small compared to that observed in $CuCl_2(PS)$ and the complexes of PA with Pd(II) and Pt(II),[1] and the frequencies are much lower than that of picolinamide. The C=O band frequency of Pd(II) and Pt(II) complexes is sensitive to the structure of the ylide and has been discussed in terms of the covalent and ionic character of the metal–ylide bond.[1] Since the basicity of aminimides is higher than that of the sulfilimines,[8] the small frequency shifts of PA complexes are more likely to be a consequence of the large ionic character of the coordination than that of the weak covalent bond between Cu(II) and the ylides. The situation may be analogous to the Cu(II) complexes of oligopeptides, one of which is shown in Fig. 1 (**8**).[9]

The d-d transition spectra of $CuCl_2(PA)$ and $CuCl_2(PA)_2$ and their solvent effects are quite similar to those of $CuCl_2(PS)$ and $CuCl_2(PS)_2$ (Table 3), and analogous discussion may be made for the PA complexes and the proposed structures are shown in Fig. 1 (**5**) and (**6**).

The electronic spectrum and electric conductivity of CuCl(PA) as well as IR spectrum are close to those of $CuCl_2(PA)_2$. Therefore, the nature of the ligand coordination is considered to be similar to the Cu(II) complex, though it is difficult to draw any definite structure.

Complexes of N-*(Trimethylammonio)acetamidate (AA) and* N-*(Trimethylammonio)benzamidate (BA) with* $CuCl_2$. Both AA and BA afforded 1:1 complexes with $CuCl_2$, but the magnetic moment of the latter is lower than the supposed value for a monomeric structure, whereas the former gave a normal value for paramagnetism. In the case of $CuCl_2(AA)$, spectroscopic data are in accord with the structure analogous to **4** in Fig. 1, in which the ligand is coordinated through N and O atoms. On the other hand, the IR spectrum of BA complex exhibits two carbonyl absorption bands at 1545 and 1690 cm^{-1}. Considering also a low magnetic moment, the complex is considered to be a mixture of N- and O- bonded monomeric or polymeric structures.

Experimental

Melting points, uncorrected, were determined on a Yamato model MP-21 apparatus using open capillaries. Infrared spectra were taken on a JASCO IRA-2 spectrometer using KBr disks, and electronic spectra were recorded on a Union 401 spectrometer. Elemental analyses were performed on a Perkin Elmer 240 analyzer, and magnetic susceptibility was measured by the Faraday method at room temperature with a Shimadzu magnetic balance. Electric conductivity was determined with a Toa CM-2A conductometer at 25±0.2 °C.

The syntheses of the sulfilimines and aminimides which were used as ligands have been described in previous papers.[1,8]

Preparation of Complexes. The preparation of dichloro(*N*-picolinoyl-*S*,*S*-tetramethylenesulfilimine)copper(II), $CuCl_2(PS)$, is described as a standard method for the preparation of the complexes. A solution of *N*-picolinoyl-*S*,*S*-tetramethylenesulfilimine (PS) (0.456 g, 2.19 mmol) in

ethanol (5 ml) was added with stirring to a solution of copper dichloride dihydtate (0.364 g, 2.14 mmol) in ethanol (5 ml) at room temperature. The mixture was stirred overnight, and the blue-green precipitate was separated by filtration, washed with small portions of ethanol and dried *in vacuo*. The product is soluble in water and methanol, slightly soluble in ethanol and chloroform, and insoluble in hydrocarbons. It gradually decomposes above 198 °C changing to a brown color. Reprecipitation from methanol–ether afforded the compound with almost the same spectroscopic properties and thermal stability as the crude product.

From the reaction of $CuCl_2 \cdot 2H_2O$ with two equivalents of the sulfilimine, a clear blue solution with a small amount of precipitate was obtained under the same conditions as described above. After the removal of the precipitates by filtration, ether was added to the filtrate and the precipitates formed were separated, washed with ether, and dried *in vacuo*. The product has the formula of $CuCl_2(PS)_2$ and is soluble in water and ethanol, partly soluble in chloroform, and insoluble in hydrocarbons.

Other complexes were prepared under essentially the same conditions as shown above, and the complexes $CuCl_2(FS)_2$, $CuCl_2$(AS), $CuCl_2$(PA), and $CuCl_2$(AA) were obtained simply from the reaction mixture as precipitates, while $CuCl_2(PA)_2$, CuCl(PA), and $CuCl_2$(BA) were obtained by the addition of ether to the reaction mixtures. The reactions of PS and AA with CuCl gave crude products which were not analytically pure and the purification was unsuccessful. The reaction of *N*-benzoyl-*S*,*S*-tetramethylenesulfilimine with $CuCl_2 \cdot 2H_2O$, and those of FS, AS, and BA with CuCl were also attempted, but no solid products were isolated by the above described methods.

References

1) H. Kise, H. Endō, and M. Senō, *Bull. Chem. Soc. Jpn.*, **50**, 3245 (1977).

2) L. Y. Chia, S. A. Dias, and W. R. McWhinnie, *J. Inorg. Nucl. Chem.*, **38**, 1263 (1976).

3) P. A. Arnup and M. C. Baird, *Inorg. Nucl. Chem. Lett.*, **5**, 65 (1969).

4) M. Nonoyama and K. Yamasaki, *Inorg. Chim. Acta*, **3**, 585 (1969).

5) P. Singh, D. Y. Jeter, W. E. Hatfield, and D. J. Hodgson, *Inorg. Chem.*, **11**, 1657 (1972).

6) a) K. Yamasaki and M. Sekizaki, *Bull. Chem. Soc. Jpn.*, **38**, 2206 (1965); b) M. Sekizaki and K. Yamasaki, *Nippon Kagaku Zasshi*, **87**, 1053 (1966).

7) a) K. Itoh, S. Kato, and Y. Ishii, *J. Organomet. Chem.*, **34**, 293 (1972); b) S. Kato, T. Kato, M. Mizuta, K. Itoh, and Y. Ishii, *J. Organomet. Chem.*, **51**, 167 (1973). In these papers, the formation of tetramethylene[α-(trimethylstannyl)phenacyl]sulfonium salt was reported by the reaction of trimethyltin chloride with tetramethylenesulfonium phenacylide. The proposed structure of the sulfonium salt has coordination through ylidic carbon and carbonyl oxygen resulting in a four membered chelate ring, though the nature of the bonding is not discussed in detail.

8) H. Kise, Y. Sugiyama, and M. Senō, *J. Chem. Soc. Perkin Trans. 2*, **1976**, 1869.

9) "Coordination Chemistry," ed by A. E. Martell Van Nostrand Reinhold Co., New York (1971), Vol. 1, p. 182.

Ultrasonic Absorption Studies of the Nickel(II) Amino Acid Complexes in Aqueous Solutions

Shoji HARADA, Kazumi HIGASHI, Kiyoshi TAMURA, Michinori HIRAISHI, and Tatsuya YASUNAGA*

Department of Chemistry, Faculty of Science, Hiroshima University, Higashisenda-machi, Hiroshima 730

(Received April 17, 1978)

The ultrasonic absorption has been measured in aqueous solutions of Ni(II) complexes of glycine, β-alanine, 4-aminobutyric acid, and 6-aminohexanoic acid. The relaxation absorption could not be ascribed to one of the steps of the ordinary step-by-step complex formation mechanism. Kinetic data were obtained as functions of the initial concentrations of Ni(II) and amino acids, the pH, and the temperature. The relaxation absorption was attributed to the formation-breaking equilibrium of an intramolecular hydrogen bond due to the carboxylato group of amino acid coordinated to the Ni(II) ion. The rate constant of the hydrogen bond-breaking process has been obtained. The relationship between the relaxation parameters and the acid dissociation constant of the carboxyl group of the amino acid ligands is discussed with reference to the analogous result for the carboxylato ligands reported previously. Supplementary work is also carried out for Ni(II)–aspartato and glutamato complexes.

With the help of the relaxation techniques, the kinetics of the metal complex formation has been widely studied, and a step-by-step complex formation mechanism involving the rate-determining release of the solvent molecule from the inner-sphere of the metal ion has been proposed.[1] Most of the ultrasonic relaxation absorptions in the metal complex solutions have been interpreted in terms of the above mechanism.[2–4] In a previous paper,[5] the present authors have reported that the ultrasonic relaxation absorption in the Ni(II)–carboxylato solutions can be ascribed to a reaction different from one of the steps of the above mechanism. Recently, the same kind of relaxation absorption has also been found in the Ni(II)–amino acid complex solutions.

The metal–amino acid complexation is not only interesting in itself, but is also important as the model system for the metal–protein interaction, and so it has been extensively studied from the static[6] and the kinetic[7–11] points of view. The purposes of the present investigation are to assign the relaxation absorption in the MHz frequency range, to obtain the kinetic parameters of the very fast reaction related to this absorption, and, moreover, to obtain information concerning the details of the Ni(II)–amino acid complex formation reaction. Studies were carried out for the Ni(II) complexes of glycine(gly), β-alanine(β-ala), 4-aminobutyric acid(ABA), and 6-aminohexanoic acid(AHA). Supplementary work was also performed for the complexes of aspartic acid(asp) and glutamic acid(glu).

Experimental

All the chemicals used were of a reagent grade and were used without further purification. Deionized and distilled water was used for the preparation of all solutions. Sample solutions were freshly prepared by dissolving $Ni(NO_3)_2$ and amino acid in water and by adjusting the pH by the drop-by-drop of dilute NaOH and/or HNO_3. The pH was adjusted to an appropriate value by taking into account the dissociation constant, K_a, of carboxyl group of amino acid and the hydrolysis of the Ni(II) ion. The ionic strength was kept constant at 2, with some exceptions, by addition of $NaNO_3$.

The ultrasonic absorption was measured by the pulse method[12] in the frequency range from 3.5 to 95 MHz. The sound velocity was measured at 1.92 MHz by the sing-around method. All the measurements were carried out at 25.0± 0.05 °C. All of the absorptions were expressed by the following single-relaxation equation for the excess absorption per wavelength $(\alpha'\lambda)$:[13]

$$(\alpha'\lambda) = 2(\alpha'\lambda)_{max} \cdot \frac{(f/f_r)}{1+(f/f_r)^2} \quad (1)$$

were α' is the excess absorption coefficient;[14] λ, the wavelength; f, the frequency, and f_r, the relaxation frequency; the subscript, max, indicates the maximum value.

A blank solution of either $Ni(NO_3)_2$ or amino acid showed no discernible relaxation absorption. These results suggest that the present relaxation absorption is ascribed to the Ni(II)–amino acid complex formation reaction, but to neither the hydrolysis of the Ni(II) ion nor to the protonation of amino acid.[15,16]

Results and Discussion

The relaxation absorption was studied as functions of Ni(II) and amino acid concentrations by keeping one constant and varying the other. The results are summarized in Table 1, where three features may be noted. The first is the independence of the relaxation frequency of both the Ni(II) and amino acid concent-

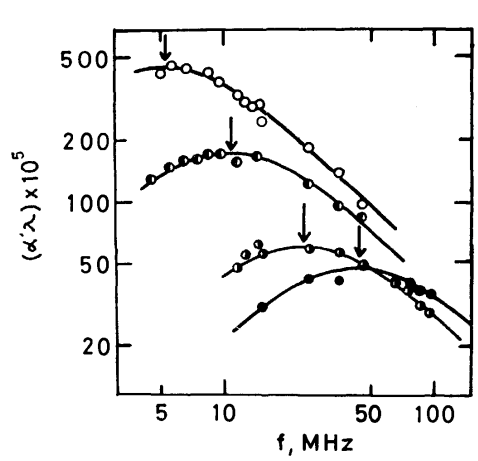

Fig. 1. Ultrasonic absorptions of the Ni(II)–amino acid complex solutions at 25 °C: ΣNi=1.0 M, Σamino acid=2.0 M.
(●): Ni(II)-gly, (◑): Ni(II)-β-ala,
(◐): Ni(II)-ABA, (○): Ni(II)-AHA.

Table 1. Ultrasonic parameters for the Ni(II)–amino acid complex solutions at 25 °C

ΣNi (M)	ΣL (M)	pH	f_r (MHz)	$(\alpha'\lambda)_{max} \times 10^5$
		Glycine		
0.5	2.0	5.4	45	39
1.0	2.0	5.1	44	48
		β-Alanine		
1.0	1.0	5.3	25	40
1.0	1.5	5.3	23	53
1.0	2.0	5.3	25	61
1.0	2.5	5.3	23	70
		4-Aminobutyric acid		
0.5	0.5	5.3	11	17
0.5	1.0	5.9	12	55
1.0	0.5	5.5	12	40
1.0	2.0	6.4	11	173
1.5	0.5	5.2	11	53
		6-Aminohexanoic acid		
0.2	1.0	6.4	4.5	140
0.4	1.0	6.4	5.0	152
1.0	0.5	5.8	4.8	163
1.0	2.0	6.4	5.2	461
		Aspartic acid		
0.5	1.0	5.2	22	20
		Glutamic acid		
0.5	0.5	5.2	18	60
0.5	1.0	5.3	19	150

rations. The second is the increase in the absorption with the increases in both the Ni(II) and amino acid concentrations. The third is the specificity of the ligand effect on the relaxation frequency and the excess absorption. Some representative absorptions of the Ni(II)–amino acid solutions are shown in Fig. 1.

The effect of the pH on the relaxation absorption was studied for the Ni(II)–glu system. As may be seen in Table 2, a decrease in pH causes an increase in f_r and a decrease in the excess absorption. The temperature dependence of the relaxation absorption was studied for the Ni(II)–ABA system; the results are shown in Table 3. In order to obtain the value of pK_a of amino acids, an experiment of pH titration was carried out at 25 °C. The results are listed in Table 4.

The complex formation reactions of Ni(II) with amino acids (*e.g.*, gly[7] or β-ala[8]) have been expressed as follows:

$$\underset{①}{NiL_{n-1} + L} \underset{k_{21}}{\overset{k_{12}}{\rightleftharpoons}} \underset{②}{NiL_{n-1}O\overset{H}{\underset{H}{<}} L} \underset{k_{32}}{\overset{k_{23}}{\rightleftharpoons}} \underset{③}{NiL_n} \quad (n=1,\ 2,\ \text{or}\ 3) \qquad (2)$$

Here ① is the free ions, ② the outer-sphere complex, and ③ the inner-sphere complex; L is the ligand complexing with the metal (the charges have been neglected in this paper). To begin with, the present relaxation absorption was investigated by assigning it to one of these steps.

The outer-sphere complex formation process, ①⇌②, is considered to be very rapid, and the relaxation frequency of this process would lie, if observed, in a frequency range not lower than 200 MHz. Moreover, the ligand specificity should not be reflected in this process.[1,13] These characteristics were not, however, observed.

Table 2. pH dependence of the ultrasonic parameters for the Ni(II)–glutamic acid complex solutions at 25 °C

ΣNi (M)	ΣGlu (M)	pH	f_r (MHz)	$(\alpha'\lambda)_{max} \times 10^5$
1.0	0.5	3.7	16	73
1.0	0.5	3.5	23	66
1.0	0.5	3.3	28	64
1.0	0.5	3.0	32	51

Table 3. Temperature dependence of the ultrasonic parameters for the Ni(II)–4-aminobutyric acid complex solutions

ΣNi (M)	ΣABA (M)	pH	t (°C)	f_r (MHz)	$(\alpha'\lambda)_{max} \times 10^5$
1.0	2.0	5.9	10	8.0	139
1.0	2.0	5.9	20	10.8	162
1.0	2.0	5.9	25	11.5	173
1.0	2.0	5.9	30	13.5	196

The inner-sphere complex formation, ②⇌③, is the rate-determining process, and the relaxation time $\tau(=(2\pi f_r)^{-1})$ is expressed by the following equation:

$$\tau^{-1} = 2\pi f_r = k_{23} \cdot \frac{K_{12}\{[NiL_{n-1}]+[L]\}}{1+K_{12}\{[NiL_{n-1}]+[L]\}} + k_{32}, \qquad (3)$$

where $K_{12}=k_{12}/k_{21}$.

When the following relations are introduced,

$$0 < \frac{K_{12}\{[NiL_{n-1}]+[L]\}}{1+K_{12}\{[NiL_{n-1}]+[L]\}} < 1, \qquad (4)$$

Eq. 3 gives

$$\tau^{-1} < k_{23} + k_{32}. \qquad (5)$$

The k_{23} values for the water release from NiL_{n-1} are: $3\times10^4\ s^{-1}$ for $n=1$ (*i.e.*, Ni^{2+} ion), $1.2\times10^5\ s^{-1}$ for $n=2$, and $4.0\times10^5\ s^{-1}$ for $n=3$ when L=gly.[7] In the Ni(II)–amino acid system, $k_{32} \ll k_{23}$ is generally established. Then, the τ^{-1} value due to the ②⇌③ process cannot exceed $10^6\ s^{-1}$ (or $f_r<0.2$ MHz), no matter how increased the ionic concentration is. When L=β-ala,[8] the chelate-ring closure step is known to be rate-determining. The rate constant of this process is smaller than that for the first coordination to the metal. The above discussion shows that the present relaxation absorption of $\tau^{-1}>3\times10^7\ s^{-1}$ can not be ascribed to one of the steps of the inner-sphere complex-formation reaction where the release of the coordinated water molecule from Ni(II) is connected and rate-determining.

It is generally believed that the zwitterionic form of amino acid is unreactive and that only the anionic form is reactive for the complex formation.[7-11,17,18] Cassatt and Wilkins[10] discussed the unreactivity of the zwitterionic form of the amino acid and argued that even if the coordination is initiated by the carboxylato

group, the bond breaks much faster than the deprotonation of the $-NH_3^+$ group, followed by a chelate formation. On the other hand, the results of the present relaxation absorption studies definitely show that relatively stable complexes are formed even in the case of the ABA and AHA systems, where the chelate complex is not conceivable. This implies that the zwitterionic form of amino acid can form a complex by the coordination of its carboxylato group to Ni(II), by analogy with the corresponding carboxylato ion. Some of the experimental evidence of the complex formation of the zwitterionic form has also been given by pH titration,[19] solubility,[20] and Raman spectral[21] investigations.

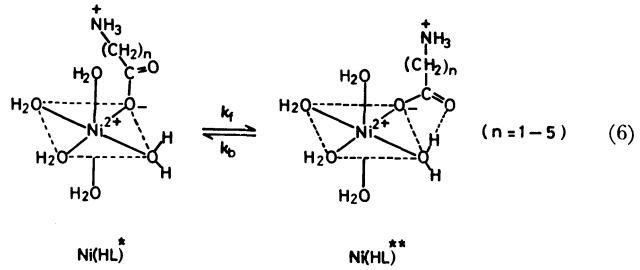

$(n=1-5)$ (6)

Fig. 2. Appropriate model of the intramolecular hydrogen bond equilibrium of the Ni(II)–amino acid complex.

The reaction associated with the relaxation absorption has the following features: (1) it involves the Ni(II) complex of the zwitterionic form of amino acid unidentated by its carboxylato group; (2) it is not concerned with the water release from Ni(II), and (3) it occurs very rapidly and has a time constant of the order of 10^{-7}—10^{-8} s. An appropriate mechanism is Reaction 6 in Fig. 2. This is similar to that earlier proposed by the present authors for the interpretation of the relaxation absorption of the Ni(II)–carboxylato solutions.[5] Further support for the assignment is as follows: (1) For Reaction 6, the relaxation frequency is related to the rate constants by this equation:[22]

$$2\pi f_r = k_f + k_b. \tag{7}$$

As the concentration term is not involved in this equation, the independence of f_r of the ionic concentrations can be approved.

(2) The maximum excess absorption per wavelength, $(\alpha'\lambda)_{max}$, for Reaction 6 is given by[13]

$$(\alpha'\lambda)_{max} = \frac{\pi(\Delta V)^2}{2\beta_0 RT}\cdot\left\{\frac{1}{[Ni(HL)^*]}+\frac{1}{[Ni(HL)^{**}]}\right\}^{-1} = \frac{\pi(\Delta V)^2}{2\beta_0 RT}\cdot[Ni(HL)]\cdot\frac{K}{(1+K)^2}, \tag{8}$$

where $[Ni(HL)]=[Ni(HL)^*]+[Ni(HL)^{**}]$, $K=k_f/k_b$, ΔV is the reaction volume change, and β_0 is the adiabatic compressibility. This equation shows that $(\alpha'\lambda)_{max}$ is proportional to the Ni(HL) complex concentration. Since the stability constant for the complex of the zwitterionic form of amino acid, K_{HL},

$$K_{HL} = \frac{[Ni(HL)]}{[Ni]\cdot[HL]} \tag{9}$$

has not been reported for Ni(II), the absolute value

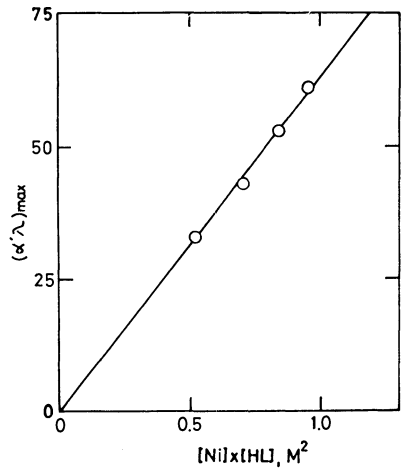

Fig. 3. $(\alpha'\lambda)_{max}$ *vs.* [Ni]·[HL] plot for the Ni(II)–β-ala system.

of the Ni(HL) complex concentration cannot be known. However, the relative change can be assumed by replacing with $K_{HL}\cdot[Ni]\cdot[HL]$ (see Eq. 9). Figure 3 shows the $(\alpha'\lambda)_{max}$ *vs.* [Ni]·[HL] plot for the Ni(II)–β-ala system, for which the literature values of the stability constants[23] enabled us to calculate the ionic concentrations. The plot gives a straight line which cuts through the origin of the coordinates. This result conforms to Eq. 8.

(3) As may be seen in the data of the Ni(II)–glu system in Table 2, the relaxation absorption decreases with the decrease in the pH. This result can be easily understood from the fact that the complex concentration decreases with the decrease in the concentration of the unprotonated ligand. On the other hand, however, the increase in f_r with the decrease in the pH cannot be easily understood because the decrease in the concentration of the unprotonated ligand generally induces a decrease in f_r. The conflict has now been resolved by considering the catalyzing effect of the hydrogen ion on the hydrogen-bond formation and breaking.[24] According to this idea, the increase in f_r can be considered to be due to that of the rate constant, k_b and/or k_f, induced by the increase in the proton concentration.

(4) The apparent activation energy can be obtained from the temperature dependence of f_r. For the Ni(II)–ABA system, $\Delta H^*=4$ kcal mol^{-1} was obtained. This value is relatively small compared to those of the ordinary complex formations, but it is appropriate for the formation of a hydrogen bond.[25] The same value was also obtained in the case of the Ni(II)–carboxylato system.[5]

(5) One of the features of the relaxation absorption of the amino acid complexes is the intimate correlation between the pK_a value of the carboxyl group and the relaxation parameters, f_r and $(\alpha'\lambda)_{max}$. As is shown in Table 1 and Fig. 1, f_r increases and $(\alpha'\lambda)_{max}$ decreases with the decrease in the pK_a of the amino acid ligand. The same tendency was observed in the case of the Ni(II)–carboxylato complexes.[5] Moreover, as is shown in Fig. 4, the overlapping of the f_r *vs.* pK_a plots for the two groups suggests that the present absorption is caused

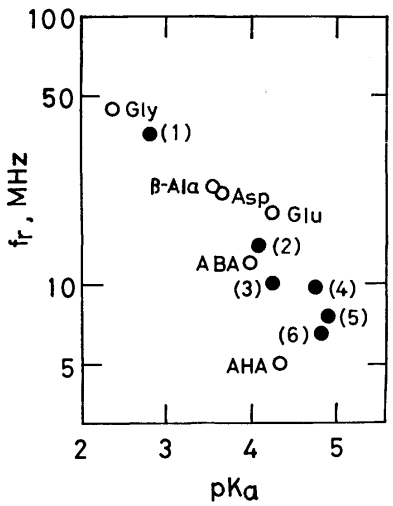

Fig. 4. f_r *vs.* pK_a plot for a series of Ni(II)–amino acid complexes(○) and Ni(II)–carboxylato complexes(●) at 25 °C: (1) chloroacetate, (2) 3-chloropropionate, (3) acrylate, (4) acetate, (5) propionate, (6) butyrate.

by the interactions between Ni(II) and the carboxylato group. If one assumes the $k_f \ll k_b$ relation, Eq. 7 can be reduced to

$$2\pi f_r = k_b. \tag{10}$$

The lower the value of pK_a of the carboxyl group is, the more labile the complex becomes. Analogously, the decrease of the pK_a value labilizes the hydrogen bond[26] in Ni(HL)**, which will induce the increase of the k_b value. Therefore the values of pK_a may be inversely proportional to f_r, as is shown in Fig. 4. The k_b values for the series of Ni(II)–amino acid complexes were obtained by means of Eq. 10: they are listed in Table 4. The magnitude of $(\alpha'\lambda)_{max}$ was in the order of the AHA>ABA>β-ala>gly systems under the same metal-ligand concentration, as is shown in Fig. 1. For a series of complexes, the ΔV value can be assumed to be the same. Therefore, from Eq. 8, the factors which contribute mainly to the value of $(\alpha'\lambda)_{max}$ seem to be the concentration and the K terms. Since the stability constant K_{HL} of Eq. 9 depends on the pK_a of the carboxyl group[26] and the electrostatic repulsion between the metal and the $-NH_3^+$ group,[27] the magnitude of the concentrations of Ni(HL) would seem to be in the order of: AHA>ABA>β-ala>gly. On the other hand, the larger the pK_a of a ligand is, the stronger will the intramolecular interaction between the carboxylato ion and the water molecule become. Therefore, the values of K in Eq. 8 would be in the order of: AHA>ABA>β-ala>gly. Whether the contribution of the concentration of Ni(HL) is predominant or that of the value of K, the ligand specificity observed in $(\alpha'\lambda)_{max}$ may, then, be well interpreted by the present mechanism.

Table 4. Rate constants of the intramolecular hydrogen bond-breaking process for the Ni(II)–amino acid complexes and the pK_a values of the carboxyl group of the amino acids

Ligand	pK_a	$k_b \times 10^{-7}$ (s^{-1})
Glycine	2.45[a]	28
β-Alanine	3.70[a]	15
4-Aminobutyric acid	3.94[b]	7.5
6-Aminohexanoic acid	4.34[b]	3.1
Aspartic acid	3.78[a]	14
Glutamic acid	4.25[a]	11

a) R. C. Weast, "Handbook of Chemistry and Physics," ed by J. Lewis and R. G. Wilkins, Interscience, New York, N. Y. (1960). b) This work.

The kinetic information obtained in this study of the Ni(II)–amino acid complexes, together with that reported previously on the Ni(II)–carboxylato complexes, provides a new type of equilibrium involving the coordination of the carboxylato group to the metal, as is shown in Reaction 6. As the relaxation effect is due to the motion of the carboxylato groups, the same kind of absorption can be expected to be observed in other divalent metal complexes of carboxylic acids and amino acids. Unfortunately, however, in other divalent metal systems, the relaxation effect based on the inner-sphere complex formation reaction falls into nearly the same time range as that of the present relaxation effect, and so it becomes rather difficult to study the latter effect separately. Studies of some of these systems are now in progess, however, and will be reported on it due course.

References

1) M. Eigen and L. Demaeyer, "Technique of Organic Chemistry," Vol. VIII, 2nd ed, ed by S. L. Friess, Interscience Publishers, New York, N. Y. (1963).
2) L. G. Jackopin and E. Yeager, *J. Phys. Chem.*, **74**, 3766 (1970).
3) N. Purdie and M. M. Farrow, *Coord. Chem. Rev.*, **11**, 189 (1973).
4) A. Bechtler, K. G. Bretischwerdt, and K. Tamm, *J. Chem. Phys.*, **52**, 2975 (1970).
5) S. Harada, T. Yasunaga, K. Tamura, and N. Tatsumoto, *J. Phys. Chem.*, **80**, 313 (1976).
6) L. G. Sillen and A. E. Martell, "Stability Constants of Metal-Ion Complexes," Special Publication No. 17, The Chemical Society, London (1964).
7) G. G. Hammes and J. I. Steinfeld, *J. Am. Chem. Soc.*, **84**, 4639 (1962).
8) K. Kustin, R. F. Pasternack, and E. M. Weinstock, *J. Am. Chem. Soc.*, **88**, 4610 (1966).
9) R. E. Pasternack, E. Gibbs, and J. C. Cassatt, *J. Phys. Chem.*, **73**, 3814 (1969).
10) J. C. Cassatt and R. G. Wilkins, *J. Am. Chem. Soc.*, **90**, 6045 (1968).
11) R. G. Wilkins, *Acc. Chem. Rev.*, **3**, 408 (1970).
12) N. Tatsumoto, *J. Chem. Phys.*, **47**, 4561 (1967).
13) J. Stuehr and E. Yeager, "Physical Acoustics," Vol. IIB, ed by W. P. Mason, Academic Press, New York, N. Y. (1965).
14) The absorption coefficient of the solution minus that of the non-relaxational part.
15) H. Inoue, *J. Sci. Hiroshima Univ., Ser. AII*, **34**, 17 (1970).
16) K. Applegate, L. J. Slutsky, and R. C. Parker, *J. Am. Chem. Soc.*, **90**, 6909 (1968).
17) W. Makinen, A. Pearlmutter, and J. Stuehr, *J. Am. Chem. Soc.*, **91**, 4083 (1969).

18) J. A. Miceli and J. E. Stuehr, *Inorg. Chem.*, **11**, 2763 (1972).
19) C. W. Childs and D. D. Perrin, *J. Chem. Soc., A*, **1969**, 1039.
20) R. M. Keefer, *J. Am. Chem. Soc.*, **70**, 476 (1948).
21) K. Krishnan and R. A. Plane, *Inorg. Chem.*, **6**, 55 (1967).
22) In case the reaction is coupled with other fast reactions, the relaxation equation becomes rather complicated. In the present case, however, Reaction 6 is a few orders faster than the neighboring coupled reactions, and so the coupling effect on the present relaxation equation can be ignored.
23) H. Irving, R. J. P. Williams, D. J. Ferrett, and A, E. Williams, *J. Chem. Soc.*, **1954**, 3494.
24) R. D. Corsaro and G. Atkinson, *J. Chem. Phys.*, **55**, 1971 (1971).
25) G. C. Pimentel and A. L. McClellan, "The Hydrogen Bond," ed by W. H. Freeman, San Francisco, California (1960).
26) G. Kohnstam and D. L. H. Williams, "The Chemistry of Carboxylic Acids and Esters," ed by S. Patai, Interscience Publishers, (1969), Chap. 16.
27) C. T. Lin and D. B. Rorabacher, *Inorg. Chem.*, **12**, 2402 (1973).

Aromatic Nucleophilic Substitution. X.[1] Confirmation of the Anionic σ Complex in the Base-catalyzed Smiles Rearrangement of 2-(Acetylamino)ethyl 2,4-Dinitrophenyl Ether in Dimethyl Sulfoxide

Keiji OKADA, Kohji MATSUI, and Shizen SEKIGUCHI*

Department of Synthetic Chemistry, Gunma University, Tenjincho, Kiryu, Gunma 376

(Received July 27, 1977)

2,4-Dinitrofluorobenzene reacts with 2-(acetylamino)ethanol in dioxane in the presence of sodium to give 2-(acetylamino)ethanol 2,4-dinitrophenyl ether (**7**), *N*-(2-acetoxyethyl)-2,4-dinitroaniline (**8**), which is considered to be a Smiles rearranged product of **7**, and *N*-(2-hydroxyethyl)-2,4-dinitroaniline (**9**), a hydrolysis product of **8**. Furthermore, **7** undergoes a Smiles rearrangement in DMSO in the presence of $NaOCH_3$ or $KOC(CH_3)_3$, giving **8** and **9**. Spiro Janovsky complex was spectrometrically confirmed to exist during the course of rearrangement.

The Smiles rearrangement is known as a typical intramolecular aromatic nucleophilic substitution reaction:

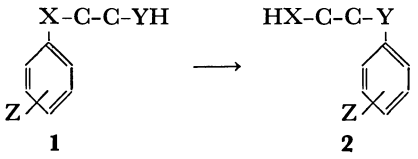

1 **2**

Z: activating group

It is well established that aromatic nucleophilic substitution reactions proceed *via* Bunnett's intermediate mechanism.[2] The Smiles rearrangement is considered to be a good model for studying the mechanism of aromatic nucleophilic substitution reactions.

Although several pathways are possible for the conversion of **1** into **2**, the intermediate (**3**) (spiro Meisenheimer or Janovsky complex, hereinafter referred to as σ complex) might be confirmed spectrometrically or

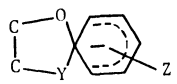

3

isolated in certain systems in which an aromatic ring is much activated by nitro, cyano, or other electron-attracting group. This has been recently reviewed in detail.[3] Kleb[4] reported the rearrangement of 2-(methylamino)ethyl 4-nitrophenyl ether to *N*-(2-hydroxyethyl)-*N*-methyl-4-nitroaniline, in which the reaction proceeds very rapidly, no cyclic intermediate being detected.

Bernasconi *et al.*[5] reported the base-catalyzed reverse Smiles rearrangement of *N*-methyl-*N*-(2-hydroxyethyl)-2,4-dinitroaniline (**4**), in which the formation of the spiro σ complex (**5**) was confirmed by absorption and NMR spectra. Skarzewski and Skrowaczeska[6] recently carried out the Smiles rearrangement of 2,4-dinitrofluorobenzene (**6**) with 2-(acetylamino)ethoxides and

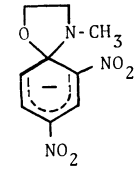

5

2-aminoethoxides, but they did not confirm the intervention of σ complexes such as **5**.

In order to study the reaction of 2-(acetylamino)ethyl 2,4-dinitrophenyl ether (**7**) with bases, we attempted to synthesize **7**

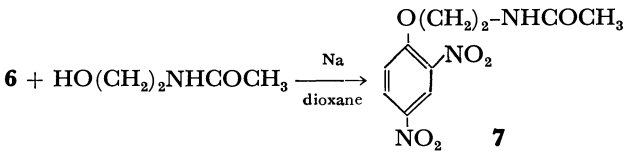

7

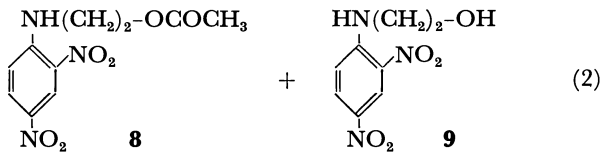

8 **9** (2)

by the following reaction. However, a mixture of **8** and **9** was obtained in a larger amount than **7**. **8** and **9** were formed from the base-catalyzed Smiles rearrangement of **7**.

We wish to report the reaction path of the base-catalyzed Smiles rearrangement of **7** and the spectrometrical confirmation of an anionic σ complex during the course of rearrangement.

Results and Discussion

Reaction of 2,4-Dinitrofluorobenzene (6) with 2-(Acetylamino)ethanol (AAE). Treatment of **6** with AAE in the presence of metallic sodium (equivalent to **6**) in dioxane gave **7**, *N*-(2-acetoxyethyl)-2,4-dinitroaniline (**8**), and *N*-(2-hydroxyethyl)-2,4-dinitroaniline (**9**) in 14, 9, and 37% yields, respectively (see Experimental). **6** has a tendency to react with an oxide ion rather than an acetamido group.[7] The hydroxyl hydrogen of AAE is more acidic than the amide hydrogen.[8]

Thus AAE is expected to react with metallic sodium to give 2-(acetylamino)ethoxide ion, **7** being the main product. Compounds **8** and **9** can be considered to be formed *via* the Smiles rearrangement of **7**. The results prompted us to carry out the Smiles rearrangement of **7** under alkaline conditions.

Reaction of 2-(Acetylamino)ethyl 2,4-Dinitrophenyl Ether (7) with $NaOCH_3$ or $KOC(CH_3)_3$. Treatment of a solution of **7** in DMSO with an equimolar amount of $NaOCH_3$ at room temperature for 1 h gave **8** and **9** in 54 and 23% yields, respectively, and a small amount of **10** as shown in the following. No reaction took

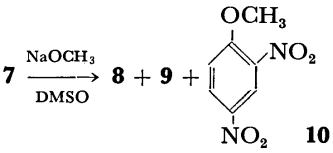

(3)

place in the absence of $NaOCH_3$. This indicates that **8** in Eq. 2 is formed from **7** *via* the Smiles rearrangement and **8** partly decomposes into **9** with $NaOCH_3$.[9]

In order to obtain closer insight into the decomposition of **8** to **9**, **8** was treated under similar alkaline conditions. Treatment of **8** in DMSO with an equimolar amount of $NaOCH_3$ followed by neutralization with an aqueous HCl solution gave **9** in 89% yield. On the other hand, treatment of **7** in DMSO with an equimolar amount of $KOC(CH_3)_3$ followed by neutralization with an aqueous HCl solution gave **8** in 78% yield and a trace amount of **9**. Thus the formation of a larger amount of **9** in the case of $NaOCH_3$ than in the case of $KOC(CH_3)_3$ indicates that methoxide ion attacks **8** at the acetyl group more easily than *t*-butoxide ion due to the former being less bulky.

Visible and NMR Spectra Relevant to the Reactions of 2-(Acetoxylamino)ethyl 2,4-Dinitrophenyl Ether (7) and N-(2-Acetoxyethyl)-2,4-dinitroaniline (8) with $NaOCH_3$ or $KOC(CH_3)_3$. In order to study the detailed reaction path of the Smiles rearrangement of **7**, the absorption and NMR spectra relevant to the reactions of **7** and **8** with $NaOCH_3$ or $KOC(CH_3)_3$ in DMSO were measured.

Immediately after the addition of 50 equivalents of $NaOCH_3$, a solution of **7** (9.15×10^{-8} mol) in 3 ml of DMSO turned red [λ_{max} 346 (ε 14300), 359 (ε 13800), and 506 nm (ε 28000), Fig. 1b], indicating the formation of a complex. Curve b (Fig. 1) is similar in shape to that of **5** [λ_{max} 347 (ε 12400), 358 (sh), and 501 nm (ε 22800), aqueous 80% DMSO].[10] It turned into curve d [λ_{max} 432 and 490 nm (sh)] after 8 h. Similar

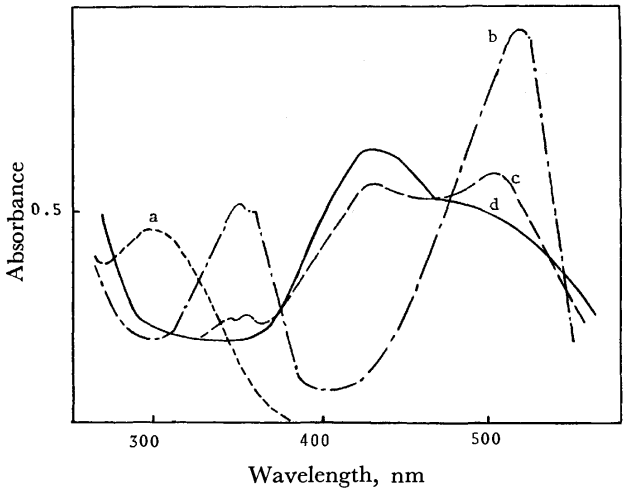

Fig. 1. Visible spectra relevent to the reaction of **7** (9.15×10^{-8} mol) with $NaOCH_3$ (molar ratio 1 : 50) in DMSO at 25 °C; curve a (----), **7** before the addition of $NaOCH_3$; curves b (——), c (——), and d (——) *ca.* 0, 4, 8 h after the addition of $NaOCH_3$, respectively.

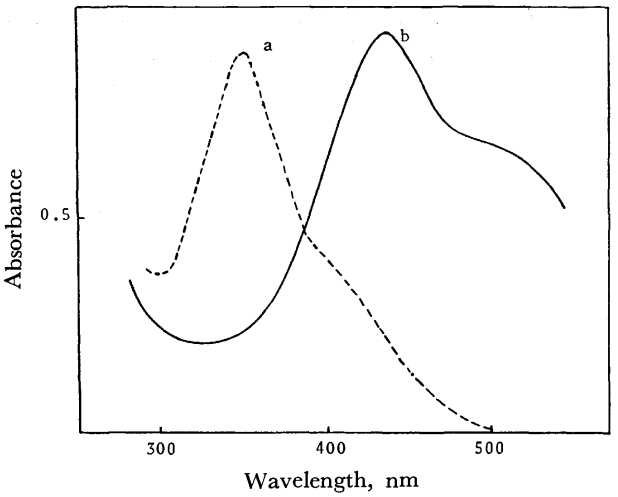

Fig. 2. Visible spectra relevant to the reaction of **8** (1.26×10^{-7} mol) with $NaOCH_3$ (molar ratio 1 : 50) in DMSO at 25 °C; curve a (----) **8** before addition of $NaOCH_3$; curve b (——) immediately after the addition of $NaOCH_3$.

spectral changes were obtained for the molar ratios 100 and 1000.

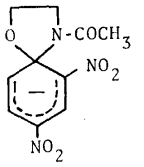

11

A solution of **8** (1.26×10^{-7} mol, Fig. 2a) in 3 ml of DMSO immediately turned red [λ_{max} 432 (ε 21000) and 490 nm (sh, ε 15700), Fig. 2b] after the addition of 50 equivalents of $NaOCH_3$. Curve b (Fig. 2) is similar in shape to curve d (Fig. 1). Thus, curve d can be attributed to the anilide ion of **8**. Hosoya *et al.*[11] concluded by MO calculation that curve b is attributable to the σ complex (**11**).

In order to examine the reversible conversion between **7** and **11**, the visible spectral changes were measured when $NaOCH_3$ and HCl (aqueous solution) were successively added. On addition of 50 equivalents of $NaOCH_3$ (0.165 M, 27.8 μl), a solution of **7** (9.15×10^{-8} mol) in 3 ml of DMSO immediately turned red to give the same spectrum as that of curve b in Fig. 1. On subsequent addition of 100 equivalents of HCl (1.00 M, 9.2 μl), the solution immediately turned yellow to give the same spectrum as that of curve a (Fig. 1). When 150 equivalents of $NaOCH_3$ (1.65 M, 8.2 μl) were added thereto, **11** was immediately formed again. The results indicate that a reversible conversion between **7** and **11** exists and the life of **11** is relatively long.

The NMR spectra of the reaction system of **7** or **8** with $KOC(CH_3)_3$ were measured, since NMR measurements are known to be useful for the confirmation of anionic σ complexes.[12] Immediately after the addition of an equimolar amount of $KOC(CH_3)_3$, the red solution gave the spectrum (b) (sweep time 500 Hz/50 s), H^A resonance peak disappearing and H_3, H_5, and H_6

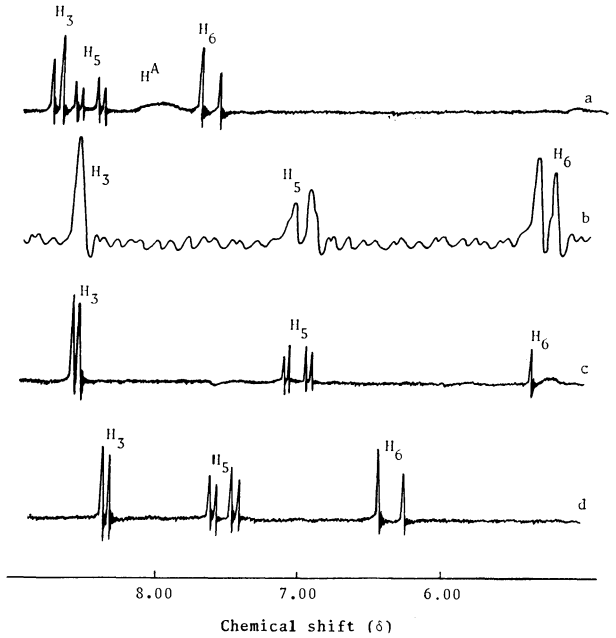

Fig. 3. NMR spectra of the reaction of **7** with $KOC(CH_3)_3$ in DMSO-d_6: a **7** before addition of $KOC(CH_3)_3$; b and c immediately after the addition of $KOC(CH_3)_3$, measured at the faster and normal sweep velocity; d several min after additon of $KOC(CH_3)_3$.

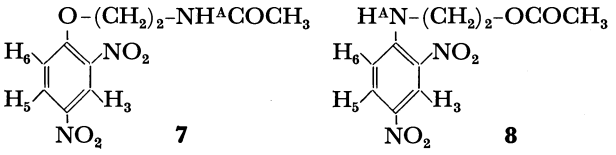

resonance peaks shifting upfield. The upfield shifts are typical of a negatively charged 2,4-dinitrobenzene or 1,1-disubstituted 2,4-dinitrophenyl anionic σ complex such as **5**, **11**, **12**, **16**, or **17**.[13] The chemical shifts of aromatic protons of other similar stable σ complexes are given in Table 1 for comparison. The results show that spectrum (b), where poor resolution is due to the fast sweep time (Fig. 3b), is attributable to **11**. Spectrum (c) measured at the normal sweep time immediately after the addition of $KOC(CH_3)_3$, is similar to spectrum (b), although the H_6 resonance peak collapsed a little in shape owing to the proceeding reaction. A few minutes after addition of $KOC(CH_3)_3$, spectrum (c) turned into spectrum (d) attributable to

Table 1. Chemical shifts of anionic σ complexes

	5	12[a)]	11
H_3	8.50(d)	8.52(d)	8.57(d)
H_5	6.88(dd)	6.90(dd)	7.00(dd)
H_6	5.13(d)	5.36(d)	5.33(dd)

a) **12**: [13]

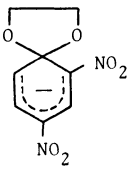

the anilide ion of **8** formed by the abstraction of H^A, since the same spectrum was obtained when **8** was treated with an equimolar amount of $KOC(CH_3)_3$ in DMSO.

All the results are in line with the following scheme:[12] **7** functions as an acid in strongly basic media[14] to produce the amide ion (**13**) and then **11**. In **11** the C_1–O bond is more easily cleaved than the C_1–N bond as seen in ordinary aromatic nucleophilic substitution.[15] The intramolecular attack of the oxide ion (**14**) on the carbonyl carbon gives **15** and then **16**. A less bulkier alkoxide ion such as CH_3O^- reacts with **16** at the carbonyl carbon to give **17**.

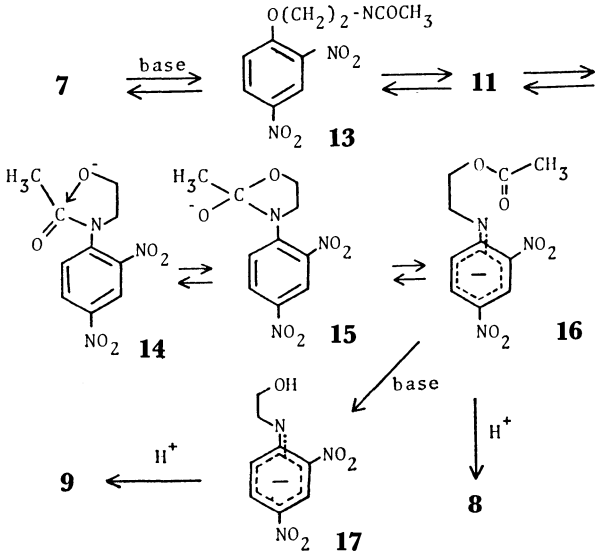

Scheme.

In the normal Smiles rearrangement our case is the first example in which the anionic σ complex was detected.

Experimental

Melting points were uncorrected. NMR spectra were recorded with a Varian A-60D spectrometer. Elemental analyses were performed at the Microanalytical Center of Gunma University. Visible spectra were measured with a Hitachi-124 UV-VIS spectrophotometer. All the reagents were purified by recrystallization or by ditillation.

2-(Acetylamino)ethyl 2,4-Dinitrophenyl Ether (7). After 0.60 g (0.030 mol) of metallic sodium had been added to a stirred solution of 4.64 g (0.045 mol) of 2-(acetylamino)-ethanol (AAE) in 50 ml of dioxane, the mixture was refluxed for 5 h so that sodium was completely dissolved. After a solution of 5.6 g (0.030 mol) of 2,4-dinitrofluorobenzene (**6**) in 30 ml of dioxane had been added dropwise under stirring, the mixture was stirred at 30 °C for 4 h. The mixture was then poured into 200 ml of ice–water and extracted with chloroform. After the organic layer had been dried over anhydrous Na_2SO_4, the solvent was evaporated to give crude products, which were separated by column chromatography (silica gel, benzene–acetone) and recrystallized from benzene or benzene–ligroin, mp 105—105.5 °C, λ_{max} 298 nm (ε 11300) (**7**), 131—132 °C, λ_{max} 358 (ε 17400) and 410 nm (sh) (**8**), and 91—92 °C, λ_{max} 362 (ε 17700) and 390 nm (sh) (**9**). Yield 14% (**7**), 9% (**8**), and 37% (**9**). Found: C, 44.33; H, 4.04%

for **7**; C, 44.42; H, 4.02% for **8**. Calcd for $C_{10}H_{11}N_3O_6$ (**7** and **8**): C, 44.61; H, 4.12%. Found: C, 44.01; H, 3.89%. Calcd for $C_8H_9N_3O_5$ (**9**): C, 44.29; H, 3.99%.

Reaction of **7** *with Sodium Methoxide.* (a) To a solution of 0.692 g (2.57×10^{-3} mol) of **7** in 10 ml of DMSO was added 0.68 ml (2.57×10^{-3} mol) of methanolic $NaOCH_3$ (3.78 M) at room temperature under stirring, and the mixture was stirred for 1 h. After 2.57 ml of 2.00 M HCl solution had been added under stirring, the mixture was poured into 100 ml of water, extracted with chloroform, and dried over anhydrous Na_2SO_4. The solvent was evaporated to give crude products, which were separated by column chromatography (silica gel, benzene) and recrystallized from benzene or benzene-ligroin. **8** and **9** were obtained in 82% yield and in a small amount, respectively. (b) To a stirred solution of 0.708 g (2.63×10^{-3} mol) of **7** in 3 ml of DMSO was added at room temperature 2.44 ml (2.64×10^{-3} mol) of methanolic $NaOCH_3$ (1.08 M). After the mixture had been stirred for 1 h, 5.26 ml of 1.00 M HCl aqueous solution was added. The mixture was treated according to procedure (a). **8**, **9**, and **10** were obtained in 54 and 23% yields and in a small amount, respectively.

Reaction of **7** *with Potassium* t-*Butoxide.* To a stirred solution of 0.778 g (2.89×10^{-3} mol) of **7** in 10 ml of DMSO was added at room temperature 2.37 ml (2.89×10^{-3} mol) of *t*-butyl alcoholic $KOC(CH_3)_3$ (1.22 M). After the mixture had been stirred for 1 h, 2.89 ml of 2.00 M HCl solution was added. The mixture was then treated according to procedure (a). **8** and **9** were obtained in 78% yield and in a small amount, respectively.

Reaction of **8** *with Sodium Methoxide.* To a stirred solution of 0.341 g (1.27×10^{-3} mol) of **8** in 10 ml of DMSO was added at room temperature 0.62 ml (1.27×10^{-3} mol) of methanolic $NaOCH_3$ (2.05 M). After the mixture had been stirred for 30 min and 2.53 ml of 1.00 M HCl solution added, the mixture was treated according to procedure (a). **9** was obtained in 89% yield.

Reaction of **8** *with Hydrochloric Acid.* To a stirred solution of 0.309 g (1.15×10^{-3} mol) of **8** in 10 ml of DMSO was added 2.30 ml (2.30×10^{-3} mol) of 1.00 M HCl aqueous solution at room temperature. After stirring for 30 min at room temperature, the mixture was poured into 100 ml of water, filtered, dried, and purified. **8** was quantitatively recovered.

NMR Measurement. About 35 mg of a sample was dissolved in *ca.* 0.25 ml of DMSO in NMR tube. After an equimolar amount of alkoxide had been added to the solution through a microsyringe and shaken vigorously, the mixture was subjected to measurement.

The present work was partially supported by a Grant-in-Aid for Scientific Research from the Ministry of Education.

References

1) Part IX, K. Okada and S. Sekiguchi, *J. Org. Chem.*, in press.
2) (a) J. F. Bunnett and J. J. Randall, *J. Am. Chem. Soc.*, **80**, 6020 (1958); (b) J. F. Bunnett and R. H. Grast, *ibid.*, **87**, 3875 (1965); (c) J. F. Bunnett and R. E. Zahler, *Chem. Rev.*, **49**, 275 (1951).
3) (a) W. E. Truce, E. H. Kreider, and W. W. Brand, *Org. React.*, **18**, 99 (1970); (b) H. J. Shine, "Aromatic Rearrangements," Elsevier, New York, N. Y. (1967), p. 307.
4) K. G. Kleb, *Angew. Chem., Int. Ed. Engl.*, **7**, 291 (1968).
5) C. F. Bernasconi, R. H. deRossi, and C. L. Gehringer, *J. Org. Chem.*, **38**, 2838 (1973).
6) J. Skarzweski and Z. Skrowaczewska, *Tetrahedron*, **32**, 1221 (1976).
7) S. Uno, K. Nakamura, Y. Inoue, S. Sekiguchi, and K. Matsui, *Bull. Chem. Soc. Jpn.*, **46**, 2257 (1973).
8) J. Hine and M. Hine, *J. Am. Chem. Soc.*, **74**, 5266 (1952).
9) The possibility that **9** is formed by acidification with HCl in the post-treatment can be excluded because the ester group of **8** undergoes no acid catalysis (see Experimental).
10) C. F. Bernasconi and R. H. deRossi, *J. Org. Chem.*, **38**, 500 (1973).
11) H. Hosoya, S. Hosoya, and S. Nagakura, *Theor. Chim. Acta (Berl.)*, **12**, 117 (1968).
12) (a) M. J. Strauss, *Chem. Rev.*, **70**, 667 (1970). (b) M. R. Crampton, *Adv. Phys. Org. Chem.*, **7**, 211 (1969).
13) R. Foster, C. A. Fyfe, P. H. Emsilei, M. I. Foremen, *Tetrahedron*, **23**, 227 (1967).
14) R. B. Homer and C. D. Johnson, "The Chemistry of Amides," ed by J. Zabicky, Interscience, New York, N. Y. (1970), p.187, and reference cited therein.
15) J. March, "Advanced Organic Chemistry: Reactions, Mechanisms, and Structure," McGraw-Hill, New York, N. Y. (1968), p. 488.

Syntheses of Cyano Derivatives of Triphenylphosphoniocyclopentadienide

Shigeo YONEDA, Masatake WATANABE, and Zen-ichi YOSHIDA*

Department of Synthetic Chemistry, Kyoto University, Yoshida, Kyoto 606

(Received October 4, 1977)

Bromo derivatives of triphenylphosphoniocyclopentadienide were found to react with copper cyanide in *N,N*-dimethylformamide to give the corresponding nitriles without decomposition. The mono- and dicyano derivatives were prepared under relatively mild reaction conditions, but no tricyano derivatives were obtained from the cyclopentadienide having more than three bromine atoms in the cyclopentadienyl ring.

Preceding papers contain reports on the electronic structures[1-3] and the syntheses[4-7] of various derivatives of triphenylphosphoniocyclopentadienide (**1**)[8] by the reactions of **1** with electrophiles and electron-deficient unsaturated compounds such as dialkyl acetylenedicarboxylate, tetracyanoethylene and maleimide. In the present research, the syntheses of the cyano derivatives of **1** have been attempted. Introduction of cyano groups into the five-membered ring might result in the stabilization of **1**, since cyano-substituted cyclopentadienide anions are known to be remarkably stable. Webster[9] synthesized tetra- and pentacyanocyclopentadienide salts from diazotetracyanocyclopentadiene prepared with use of 1,1,-2,3,4,4-hexacyano-2-butene dianion and observed that these highly cyano-substituted cyclopentadienides are very stable. For example, the potassium salt of pentacyanocyclopentadienide is so stable that it can be heated at 400 °C in the air without decomposition. The pK_a values of polycyanocyclopentadienes are extremely small as compared with those of 14—15 for cyclopentadiene,[10] indicating that the cyano group effectively stabilizes the cyclopentadienide anion. We have succeeded in introducing cyano groups into the cyclopentadienyl ring of **1** by cyano-debromination at the cyclopentadienyl ring (a different method from that of Webster). The reactions of the bromo derivatives of **1** with cuprous cyanide have been attempted in *N,N*-dimethylformamide(DMF). The cyanation products were obtained in good yields, when the derivatives substituted by two or three bromine atoms together with other substituents such as nitro, phenylazo, formyl, methoxycarbonyl and cyano groups in the cyclopentadienyl ring were employed as the bromo derivatives. The substitution reaction of bormine atom(s) in cyclopentadienyl ring with cyano group is a convenient method to introduce cyano group into cyclopentadienyl ring.

Results and Discussion

The bromo derivatives of **1** employed in the reaction were synthesized by the reactions of **1** and its derivatives with *N*-bromosuccinimide. The yields, melting points and analytical data are given in Table 1. The starting materials **2**, **3**, **4**, and **5** were prepared by nitration, diazo coupling and Vilsmeier reaction of **1**.[4,7] The substitution at 2-position was indicated by the reaction indices calculated from HMO treatment[7] and confirmed experimentally in the diazo coupling[11] and nitrosation reactions.[7] Triphenylphosphonio-2,5-bis(methoxycarbonyl)cyclopentadienide (**6**) was prepared by the oxidation of **5** and subsequent treatment with diazomethane. Refluxing of the oxime of **5** in acetic anhydride afforded triphenylphosphonio-2,5-dicyanocyclopentadienide (**7**). The remaining hydrogens in the cyclopentadienyl ring of these derivatives (**2**, **3**, **4**, **5**, **6**, and **7**) were easily bromainted by *N*-bromosuccinimide.

Triphenylphosphonio-2,5-dibromocyclopentadienide (**8**) was prepared by treatment of **1** with cyanogen bromide. Cyanogen bromide is known as a reagent for direct cyanation of aromatic compounds in the presence of Lewis acid.[12] However, the reaction of **1** with cyanogen bromide in the presence of aluminum trichloride gave the 2,5-dibrominated one(**8'**) but no cyanation product. Compound **8'** is not as stable as the other bromo drivatives, but diazo coupling reaction of **8'** led to the formation of a stable compound, **9'**. All the bromo derivatives (**2'**, **3'**, **4'**, **5'**, **6'**, **7'**, **8'**, and **9'**) are new compounds.

The reactions of these bromo derivatives with cuprous cyanide (Rosenmund-von Braun type reaction) were examined. The preparative method of aryl cyanides from aryl halides and cuprous cyanide was established,[13] its improvement[14,15] and mechanism[16,17] also being reported. Reactions of the bromo derivatives, **2'**, **3'**, **4'**, **5'**, and **6'** with cuprous cyanide in DMF under reflux resulted in the formation of the cyanation products, which showed the characteristic absorption due to the cyano groups in the IR spectrum. Elemental analyses indicated the products to be dicyano-substituted one, **2''**, **3''**, **4''**, **5''**, and **6''**. No tricyanation compounds were obtained even under reflux for a week. This can be attributed to the steric hindrance in the formation of the intermediate complex [RBr–CuCN], through which the reaction might proceed.

The chlorinated derivatives of **1** did not undergo Rosenmund-von Braun type reaction. For example, triphenylphosphonio-2,5-diformyl-3,4-dichlorocyclopentadienide with cuprous cyanide in DMF did not take place under reflux for several days.

The bromine atoms of 2,5-dicyano-3,4-dibromocyclopentadienide (**7'**) were not replaced with cyano groups. The result can be accounted for by the poor interaction between the copper metal and the bromine atom, presumably because of the dominant interaction of copper with the cyano groups attached to the 2,5-positions.

In the reaction of triphenylphosphonio-2,5-dibromocyclopentadienide (**8'**) with cuprous cyanide, decomposition immediately occurs to afford a tarry substance. The inherently unstable derivative **8'** was

TABLE 1. BROMO-SUBSTITUTED DERIVATIVES OF TRIPHENYLPHOSPHONIOCYCLOPENTADIENIDE

Starting material	Reagent	Bromo-derivative	Yield (%)	Mp (°C)	Formula	Elemental analysis (%)		
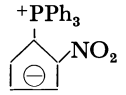 **2**	NBS	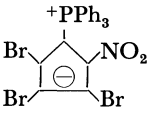 **2′**	81	190 (dec)	$C_{23}H_{15}Br_3NO_2P$	C	H	Br
						Calcd 45.43	2.49	39.43
						Found 45.34	2.54	39.52
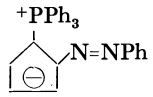 **3**	NBS	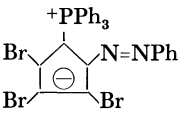 **3′**	83	191 (dec)	$C_{29}H_{20}Br_3N_2P$	C	H	Br
						Calcd 52.21	3.02	35.93
						Found 52.10	3.25	36.01
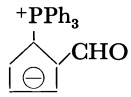 **4**	NBS	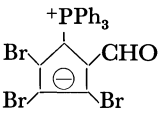 **4′**	72	208 (dec)	$C_{24}H_{16}Br_3OP$	C	H	Br
						Calcd 48.76	2.72	40.55
						Found 48.65	3.02	40.31
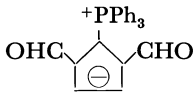 **5**	NBS or Br_2	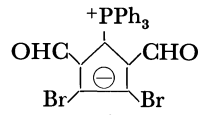 **5′**	89	186 (dec)	$C_{25}H_{17}Br_2O_2P$	C	H	Br
						Calcd 55.58	3.17	29.58
						Found 55.14	3.30	28.30
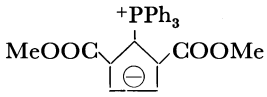 **6**	NBS	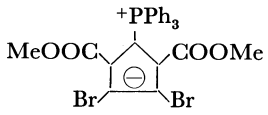 **6′**	90	232 (dec)	$C_{27}H_{21}Br_2O_4P$	C	H	Br
						Calcd 54.03	3.53	5.16
						Found 53.72	3.55	5.10
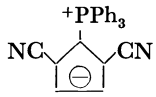 **7**	NBS	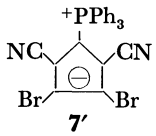 **7′**	92	258 (dec)	$C_{25}H_{15}Br_2N_2P$	C	H	P
						Calcd 56.21	2.83	29.91
						Found 56.20	3.07	31.56
1	$BrCN/AlCl_3$	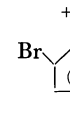 **8′**	68	122 (dec)	$C_{23}H_{17}Br_2P$	C	H	P
						Calcd 57.05	3.53	6.40
						Found 57.15	3.72	6.66
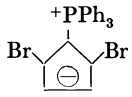 **8′**	PhN_2Cl	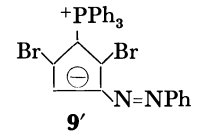 **9′**	83	228 (dec)	$C_{29}H_{21}Br_2N_2P$	C	H	Br
						Calcd 59.21	3.60	27.16
						Found 58.89	3.72	27.92

not recovered. More stable derivative **9′** reacts with cuprous cyanide to give the monocyano-substituted product, **9″**. The results are summarized in Table 2. Although the positions of the cyano-debromination in the five-membered ring were not experimentally determined for **2″**, **3″**, **4″**, and **9″**, most probable structures were deduced from examination of the intermediate complex in the reaction by the use of CPK atomic models.

Attempt to replace the bromine atoms in the five-membered ring of **2′**—**9′** with cyano groups using sodium cyanide was unsuccessful, but treatment of the bromo derivatives with sodium cyanide in the presence of cuprous bromide gave the cyano-substituted derivatives. The reaction of the bromo derivatives with cupric cyanide also afforded the cyanated products. Thus, it is obvious that copper is important as a catalyst in the substitution of the bromine by cyano group on the five-membered ring of triphenylphosphoniocyclopentadienide. The reaction is considered to proceed *via* a complex of copper with bromine atom and cyanide ion.

All the cyano-substituted products synthesized are stable in the air as well as in acidic and basic media.

Experimental

Spectra. Ultraviolet spectra were taken on a Hitachi EPS-3T recording photometer. Infrared spectra were recorded on a Hitachi grating infrared spectrophotometer, Model 215, and NMR spectra on a JNM C-60H NMR spectrometer with tetramethylsilane as an internal standard.

*Preparation of Triphenylphosphoniocyclopentadienide and Its Derivatives, **1**—**7** (Starting Materials in Table 1).* Triphenylphosphoniocyclopentadienide (**1**) and the derivatives (**2**, **3**, **4**, and **5**) were prepared according to the methods reported.[4-8] The derivative **6** was prepared by the oxidation of **5** and subsequent treatment with diazomethane. Mp 244 °C; IR(KBr) 1695 cm^{-1} (C=O); NMR ($CDCl_3$), δ=7.5—8.0 (15H, m, phenyl), 6.85 (2H, d, J_{P-H}=5.0 Hz, cyclopentadienyl), 3.80 (6H, s, methyl).

TABLE 2. REACTIONS OF BROMO DERIVATIVES (**2′**—**9′**) WITH CUPROUS CYANIDE IN *N,N*-DIMETHYLFORMAMIDE

Bromo derivatives	Reaction temperature	Reaction time (h)	Cyanation product.	Yield (%)	Mp (°C)
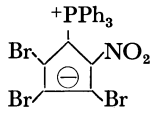 **2′**	Reflux	2	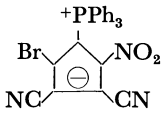 **2″**	47	259 (dec)
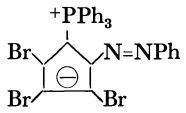 **3′**	130—135 °C	0.5	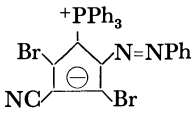 **3″**	68	266 (dec)
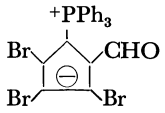 **4′**	Reflux	2	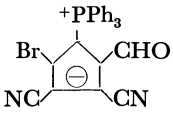 **4″**	32	257 (dec)
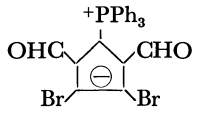 **5′**	Reflux	2	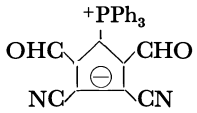 **5″**	75	263 (dec)
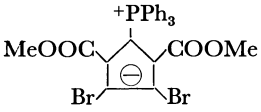 **6′**	Reflux	2	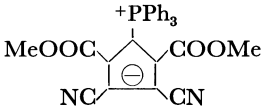 **6″**	74	273—274 (dec)
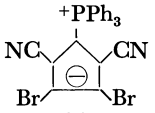 **7′**	Reflux	12	No reaction	—	
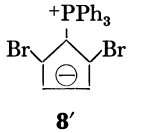 **8′**	110—115 °C	1	Decomposition	—	—
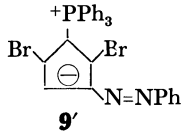 **9′**	130—135 °C	4	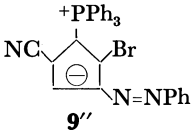 **9″**	84	191 (dec)

Found: C, 73.21; H, 5.20; P, 6.85%. Calcd for $C_{27}H_{23}O_4P$: C, 73.29; H, 5.23; P, 7.00%.

The 2,5-dicyano derivative **7** was prepared by the reaction of acetic anhydride with the dialdehyde oxime derived from **5** under reflux for 1 h. The IR spectrum showed and absorption band at 2250 cm^{-1} due to the cyano group; NMR ($CDCl_3$) δ=7.4—7.9 (15H, m, phenyl), 3.45 (2H, d, J_{P-H}=5.5 Hz, cyclopentadienyl).

Found: C, 72.83; H, 5.09; N, 6.79%. Calcd for $C_{25}H_{17}N_2P$: C, 72.54; H, 5.37; N, 6.86%.

Bromination of Triphenylphosphoniocyclopentadienide Derivatives. A solution of *N*-bromosuccinimide was added to a solution of triphenylphosphonio-2-nitro, 2-phenylazo, 2-formyl, 2,5-diformyl, 2,5-bis(methoxycarbonyl), and 2,5-dicyano-substituted cyclopentadienides (**2**—**7**). Stirring was continued for 30 min at room temperature and the precipitate was collected and recrystallized from dichloromethane–methanol.

Triphenylphosphonio-2,5-dibromocyclopentadienide (**8′**) was prepared by the following procedure. 0.750 g (0.70 mol) of cyanogen bromide in 20 ml of dichloromethane was added at 0—5 °C for 10 min to a solution of 1.141g (0.035 mol) of **1** in 100 ml of dichloromethane. After being stirred for 1 h at 110—115 °C the solvent was evaporated and the residue was chromatographed on alumina using dichloromethane as an eluent. A solid product precipitated when hexane was added to the dichloromethane solution. The precipitate was collected and purified by recrystallization from dichloromethane–methanol. The product **8′** is unstable, and accordingly the successive reaction should be carried out in mild conditions. However, triphenylphosphonio-2,5-dibromo-3-phenylazocyclopentadienide (**9′**) prepared by the diazo coupling reaction of **8′** is stable.

The yields, melting points and analytical data of **2′**—**9′** are summarized in Table 1.

Reaction of Bromo-substituted Phosphoniocyclopentadienide (2′—9′) with Cuprous Cyanide. The reactions of the bromo derivatives with cuprous cyanide in DMF were carried out under the reaction conditions given in Table 2. The reaction mixture was poured into water and the procut precipitated was collected, washed with water and purified by column chromatography on alumina using dichloromethane–methanol as eluents. The yields and the melting points are summarized

in Table 2. The spectral and analytical data of each product are as follows.

Triphenylphosphonio(2-nitro-3,4-dicyano-5-bromo)cyclopentadienide (**2''**): mp 295 °C (dec); IR (KBr) 2220 cm^{-1} (C≡N); NMR ($CDCl_3$) δ=7.4—8.0 (m, phenyl); UV_{max} (CH_3CN) 222 nm (log ε 4.54), 393 (4.08).

Found: C, 60.29; H, 3.25; N, 8.28: P, 5.88%. Calcd for $C_{25}H_{15}N_3O_2Br$: C, 60.01; H, 3.03; N, 8.48; P, 6.11%.

Triphenylphosphonio(2-phenylazo-3,5-dibromo-4-cyano)-cyclopentadienide (**3''**): mp 266 °C (dec); IR (KBr) 2210 cm^{-1} (C≡N); NMR ($CDCl_3$) δ=6.6—7.2 (5H, m, phenylazo), 7.4—8.0 (15H, m, P-phenyl); UV_{max} (CH_3CN) 223 nm (log ε 4.64), 432 (4.32).

Found: C, 58.96; H, 3.23; N, 6.97%. Calcd for $C_{30}H_{20}N_3PBr_2$: C, 58.75; H, 3.29; N, 6.85%.

Triphenylphosphonio(2-formyl-3,4-dicyano-5-bromo)cyclopentadienide (**4''**): mp 257 °C (dec); IR (KBr) 2210 (C≡N) 1665 cm^{-1} (C=O): NMR ($CDCl_3$) δ=7.3—8.0 (15H, m, phenyl), 9.81 (1H, formyl); UV_{max} (CH_3CN) 232 nm (log ε 4.61), 254 (4.57), 316 (4.18).

Found: C, 64.63; H, 3.49; N, 5.67%. Calcd for $C_{26}H_{16}N_2OPBr$: C, 64.41; H, 3.34; N, 5.80%.

Triphenylphosphonio(2,5-diformyl-3,4-dicyano)cyclopentadienide (**5''**): mp 263 °C (dec); IR (KBr) 2210 (C≡N), 1670 cm^{-1} (C=O); NMR ($CDCl_3$) δ=7.4—8.1 (15H, m, phenyl), 10.39 (2H, s, formyl): UV_{max} (CH_3CN) 269 nm (log ε 4.61), 278 (4.69), 327 (3.92).

Found: C, 74.64; H, 4.11; N, 6.47%. Calcd for $C_{27}H_{17}N_2O_2P$: C, 74.99; H, 3.97; N, 6.48%.

Triphenylphosphonio-2,5-bis(methoxycarbonyl)-3,4-dicyanocyclopentadienide (**6''**): mp 273.5—274.0 °C; IR (KBr) 2200 (C≡N), 1710 cm^{-1} (C=O); NMR ($CDCl_3$) δ=7.6—8.0 (15H, m, phenyl), 3.90 (6H, s, methyl); UV_{max}(CH_3CN) 233 nm (log ε 4.63), 253 (4.65), 276 (4.15), 292 (4.11).

Found: C, 70.45; H, 4.45; N, 5.76; P, 6.21%. Calcd for $C_{29}H_{21}N_2O_4P$: C, 70.73; H, 4.30; N, 5.69; P, 6.29%.

Triphenylphosphonio(2-bromo-3-phenylazo-5-cyanocyclopentadienide (**9''**); mp 191 °C (dec); IR (KBr) 2210 cm^{-1} (C≡N); NMR ($CDCl_3$) δ=5.80 (1H, d, J_{P-H}=6.0 Hz, cyclopentadienyl), 6.7—7.3 (5H, m, phenylazo), 7.3—8.0 (15H, m, phenyl); UV_{max} (CH_3CN) 220 nm (log ε 4.53), 4.28 (4.08).

Found: C, 67.15; H, 3.87; N, 7.56%. Calcd for $C_{30}H_{21}N_3PBr$: C, 67.42; H, 3.97; N, 7.86%.

References

1) Z. Yoshida, K. Iwata, and S. Yoneda, *Tetrahedron Lett.*, **1976**, 1519.
2) K. Iwata, S. Yoneda, and Z. Yoshida, *J. Am. Chem. Soc.*, **93**, 6745 (1971).
3) Z. Yoshida, S. Yoneda, and M. Hazama, *J. Chem. Soc., C*, **1971**, 716.
4) Z. Yoshida, S. Yoneda, Y. Murata, and H. Hashimoto, *Tetrahedron Lett.*, **1971**, 1523.
5) Z. Yohsida, S. Yoneda, H. Hashimoto, and Y. Murata, *Tetrahedron Lett.*, **1971**, 1527.
6) Z. Yoshida, S. Yoneda, and T. Yato, *Tetrahedron Lett.*, **1971**, 2973.
7) Z. Yoshida, S. Yoneda, and Y. Murata, *J. Org. Chem.*, **38**, 3537 (1973).
8) F. Ramirez and S. Levy, *J. Org. Chem.*, **21**, 488 (1956).
9) O. W. Webster, *J. Am. Chem. Soc.*, **87**, 1820 (1965).
10) R. E. Dessy, Y. Okuzumi, and A. Chen, *J. Am. Chem. Soc.*, **84**, 2899 (1962).
11) F. Ramirez and S. Levy, *J. Am. Chem. Soc.*, **79**, 6167 (1957).
12) P. Karrer and E. Zeller, Helv. Chim. Acta, **2**, 482 (1919); P. Karrer, A. Rebmann, and E. Zeller, *ibid.*, **3**, 261 (1920).
13) D. T. Mowry, *Chem. Rev.*, **42**, 207 (1948).
14) L. Friedman and H. Schechter, *J. Org. Chem.*, **26**, 2525 (1961).
15) M. S. Newman and H. Boden, *J. Org. Chem.*, **26**, 2525 (1961).
16) R. G. R. Bacon and H. A. O. Hill, *J. Chem. Soc.*, **1964** 1097.
17) T. Ito and K. Watanabe, *Bull. Chem. Soc. Jpn.*, **41**, 419 (1968).

Thermolysis of Bis(diarylmethylenecarbamoyl) Peroxides

Tadashi SUEHIRO,* Yukio MATSUI, and Yoshio INOGUCHI

Department of Chemistry, Faculty of Sciences, Gakushuin University, Mejiro, Toshima-ku, Tokyo 171

(Received October 24, 1977)

Diacyl peroxides of structure $(XC_6H_4)_2C{=}N{-}C(=O)OOC(=O){-}R$ ($R=(XC_6H_4)_2C{=}N$, X=H (**1**), X=2-CH_3 (**3**), X=4-CH_3; R=4-ClC_6H_4, X=H (**2**) have been prepared by the reaction between the corresponding carbamoyl chloride and hydrogen peroxide–urea complex in the presence of pyridine or between the carbamoyl chloride and 4-chloroperbenzoate in anhydrous ether at low temperature. Thermolysis of **1**—**3** follows first order kinetics. The large rates of thermolysis of **1** and **3** relative to those of bis(diphenylmethyleneacetyl) peroxide have been ascribed to steric compressions of **1** and **3** in the ground state and to the concerted cleavage of three bonds. Stable diphenylmethyleneamino radicals do not substitute in toluene by themselves but they do with the aid of aroyloxy radicals. The iminyl radicals abstract hydrogen from the methyl group of toluene, and the rate constant has been estimated to be 5×10^2—2×10^3 $M^{-1}s^{-1}$ at 50 °C.

The rates of the addition reactions of acyloxy radicals to benzene relative to those of their decomposition reactions to give carbon dioxide and aryl or alkyl radicals have been studied.[1] During the course of the studies it has been found that some of the ortho substituents in aroyloxy radicals such as methoxyl and bromo groups exhibited an increase in the activation energies for the decomposition of aroyloxy radicals.[2] The activation energy of the decomposition of cinnamoyloxy radicals was also higher than that of benzoyloxy radicals.[2] Studies on these phenomena could disclose the exact manner of the carbon dioxide cleavage of acyloxy radicals. Investigation of methylenecarbamoyloxy radicals would enable clarification of the nature of the $=N{-}CO_2$ bond in comparison with the $=CH{-}CO_2$ bond. Since the bond dissociation energies of C–N are 2—9 kcal/mol smaller than those of C–C bonds,[3] some amount of concerted multibond fission in the thermolysis of the peroxides having a $=N{-}CO_2$ structure is expected. This work also aimed to confirm the reactivity of N-centered radicals, of which increasing interest has been recently shown in reviews on aminyl radicals,[4] hydrazynyl radicals,[5] and aminium radicals.[6]

Results and Discussion

Preparation of Bis(diarylmethylenecarbamoyl) Peroxides. The preparations of bis(diarylmethylenecarbamoyl) peroxides were difficult due to the hydrolysis of carbamoyl chloride. Carbamoyl chlorides, when treated with a hydrogen peroxide–urea complex[7] and pyridine in anhydrous ether under cooling at −20 °C were however successful in the preparation of the peroxides.

Bis(di-2-methylphenylmethylenecarbamoyl) peroxide (**3**) is very labile and on standing at room temperatures turns yellow in a few minutes. The CH-analysis of the peroxide agrees fairly well with the calculated values, but the active oxygen determinations gave values below 100%: the di-2-methylphenyl compound **3** gave 67%, the di-4-methylphenyl peroxide **5** 85%, and the diphenyl peroxide **1** 86%, in comparison with bis(diphenylmethyleneacetyl) peroxide (**4**) 97%. The low values of active oxygen suggest a fast breakdown of the $=N{-}CO_2$ bond, yielding imniyl radicals, which are reduced slowly.

Product Studies. Products formed in the thermolysis of **1** and **2** in toluene at 50 and 100 °C, respectively, are given in Table 1.

During the thermolysis of **2** the absorption bands at 1740, 1700, and 1280 cm^{-1}, presumably the 4-chlorobenzoate of benzophenone oxime and 4-chlorobenzoic acid appear, and increase in intensities. The same appearance of absorption bands, however, was not found in the case of **1**.

Diphenylmethyleneamino radicals abstract hydrogen from the methyl group of toluene. Diphenylmethylenecarbamoyloxy radicals, if formed, loose carbon dioxide very rapidly, so that the carbamoyloxy radicals hardly add to the solvent toluene. The fast cleavage of carbon dioxide from diphenylmethylenecarbamoyloxy radicals was partly suggested by the iodometric determination of active oxygen, giving 67—86% of the theoretical value, and partly by the experiments, attempting to prepare methyltetraphenylmethanes by the reaction between **1** and triphenylmethyl radicals in toluene. This reaction is applicable to benzoyl peroxide,[1a] but it was not successful in the case of **1**.

TABLE 1. PRODUCTS FORMED IN THE THERMOLYSIS OF BIS(DIPHENYLMETHYLENECARBAMOYL) PEROXIDE AND OF 4-CHLOROBENZOYL DIPHENYLMETHYLENECARBOMOYL PEROXIDE IN TOLUENE[a]

Product	Peroxide	
	$(Ph_2C{=}NCOO)_2$ at 50 °C	$ClC_6H_4COOOCON{=}CPh_2$ at 100 °C
$Ph_2C{=}NH$	71.5	26.3
$Ph_2C{=}N{-}CH_2Ph$	14.7	0.8
$(Ph_2C{=}N{-})_2$	35.2	3.2
$PhCH_2C_6H_4CH_3$-(3)	1.2	—
$PhCH_2CH_2Ph$	0	5.0
$Ph_2C{=}N{-}C_6H_4CH_3$-(2)	0	1.8
-(3)	0	2.5
-(4)	0	1.4

a) Yield in mol % per mole peroxide, determined by GLPC.

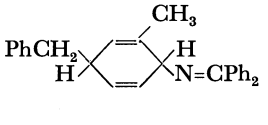

A

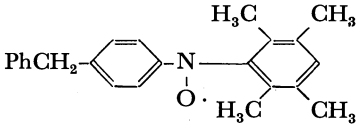

B

Although benzoyloxy radicals add to the solvent toluene under these reaction conditions, they do not appreciably abstract hydrogen from toluene. In the thermolysis of **1** therefore it is expected that the hydrogen abstraction by diphenylmethylenecarbamoyloxy radicals does not occur and diphenylmethyleneamine would be formed solely by the reaction of the iminyl radicals.

Hydrogen sources responsible for the high yield of diphenylmethyleneamine from **1** and **2** have not been explained well: some of the diphenylmethyleneamine could be formed in secondary reactions. In the thermolysis of **1** a small amount of *m*-tolylphenylmethane was found (1.2%). Its precurcer would be an adduct of the benzyl radical to toluene trapped by the diphenylmethyleneamino radicals, **A**, which on heating will give diphenylmethyleneamine and *m*-tolylphenylmethane. A similar addition of benzyl radicals to benzene has been observed in spin trapping experiments of the thermolysis of azobisphenylmethane in benzene in the presence of 2,3,5,6-tetramethylnitrosobenzene (nitrosodurene), yielding nitroxide **B**.[8]

Bis(diphenylmethylene)hydrazine has been reported to give diphenylmethyleneamine and other compounds on heating at 375—500 °C.[9] During the GLPC determination of bis(diphenylmethylene)hydrazine at 220 °C, however, no formation of the imine was observed. In the thermolysis of **2** the presense of the ester of benzophenone oxime was suggested by IR spectra, and the suggestion was that the ester might give diphenylmethyleneamine in the GLPC determination.

In the thermolysis of **1**, 3,3′-dimethylbiphenyl was not detected. If the iminyl radicals can add to toluene to give (diphenylmethyleneamino)methylcyclohexadienyl radicals, the cyclohexadienyl radicals could subsquently dimerize and decompose yielding dimethylbiphenyl and diphenylmethyleneamine. The formation of biphenyl and ammonia by the reaction mechanism between amino radicals and benzene has been suggested.[10]

Further marked differences between the products from **1** and **2** are that no bibenzyl and no (diphenylmethyleneamino)toluenes were formed from **1**, but were produced from **2**. The (dipheynylmethyleneamino)toluenes from **2** were composed of more meta isomer than ortho and para derivatives. The substitution at the meta position of toluene by diphenylmethyleneamino radicals agrees with the findings of Ishikawa *et al.*[11] in the photolysis of the benzoate and the 4-chlorobenzoate of benzophenone oxime in toluene. The subsititution of diphenylmethyleneamino radicals proceeds probably *via* the intermediate aroyloxycyclohexadienyl radicals as in the case of the homolytic triphenylmethylation of toluene in the reaction between triphenylmethyl radicals and benzoyl peroxide in toluene.[1a] Diphenylmethyleneamino radicals do not subsitute in toluene by themselves but they do with the aid of aroyloxy radicals.

During the thermolysis of **2** the concentration ratio $(PhCH_2\cdot)/(Ph_2C{=}N\cdot)$ will be larger than that in the case of **1**, sicne the half moiety of the peroxide molecule **2** is chlorobenzoyloxyl and 4-chlorophenyl radicals derived from the aroyloxy radicals are effective in abstracting hydrogen. Two benzyl radicals more frequently combine together in the thermolysis of **2** than in the case of **1**.

For the thermolysis of **1** and **2** the following scheme can be formulated.

For **1**

$$Ph_2C{=}N\underset{\underset{O}{\|}}{C}O\underset{\underset{O}{\|}}{C}N{=}CPh_2 \longrightarrow 2Ph_2C{=}N\cdot + 2CO_2 \quad (1)$$

$$Ph_2C{=}N\cdot + PhCH_3 \longrightarrow Ph_2C{=}NH + PhCH_2\cdot \quad (2)$$

$$Ph_2C{=}N\cdot + PhCH_2\cdot \longrightarrow Ph_2C{=}N{-}CH_2Ph \quad (3)$$

$$2Ph_2C{=}N\cdot \longrightarrow Ph_2C{=}N{-}N{=}CPh_2 \quad (4)$$

$$PhCH_2\cdot + PhCH_3 \longrightarrow PhCH_2\dot{C}_6H_5CH_3 \quad (I)$$

$$(I) + Ph_2C{=}N\cdot \longrightarrow Ph_2C{=}N(CH_3)C_6H_5CH_2Ph \quad (II)$$

$$(II) \longrightarrow Ph_2C{=}NH + PhCH_2C_6H_4CH_3 \quad (5)$$

For **2**

$$Ph_2C{=}N\underset{\underset{O}{\|}}{C}O\underset{\underset{O}{\|}}{C}C_6H_4Cl \longrightarrow Ph_2C{=}N\cdot + CO_2 + ClC_6H_4COO\cdot \quad (6)$$

$$ClC_6H_4COO\cdot \longrightarrow ClC_6H_4\cdot + CO_2 \quad (7)$$

$$Ph_2C{=}N\cdot \text{ or } ClC_6H_4\cdot + PhCH_3 \longrightarrow Ph_2C{=}NH \text{ or } ClC_6H_5 + PhCH_2\cdot \quad (8)$$

$$2PhCH_2\cdot \longrightarrow PhCH_2{-}CH_2Ph \quad (9)$$

$$ClC_6H_4COO\cdot + PhCH_3 \longrightarrow ClC_6H_4COO\dot{C}_6H_5CH_3 \quad (III)$$

$$(III) + Ph_2C{=}N\cdot \longrightarrow ClC_6H_4COOC_6H_5(CH_3)N{=}CPh_2 \quad (IV)$$

$$(IV) \longrightarrow CH_3C_6H_4N{=}CPh_2 + ClC_6H_4COOH \quad (10)$$

$$Ph_2C{=}N\cdot + ClC_6H_4COO\cdot \longrightarrow Ph_2C{=}N{-}OCOC_6H_4Cl \quad (11)$$

Reactions (3) and (4).

Kinetic Studies. Peroxides **1**—**4** were decomposed in benzene and in toluene under nitrogen. The rate of decompostion was followed by observing the decrease in absorption bands $\nu_{C=O}$ (1775 cm^{-1}), ν_{O-O}(1095 cm^{-1} for **1** and **3**, 1065 cm^{-1} for **4**), and ν_{C-O}(1195 and 1120 cm^{-1} for **2**). The change of toluene for benzene caused no effect in the rates. The decompositions followed first order kinetics and the activation parameters are given in Table 2. The extent of the free radical decomposition of **1** was 99% (DPPH) and 90% (Galvinoxyl) at 50 °C. The value for **2** was 81% (DPPH). These results indicate homolytic reactions for **1** and **2**, accompanied by a small degree of cage reaction for **2** (about 20%). Reaction 11 in the Scheme is a cage reaction.

The very fast and nearly complete homolyses of **1** and **2** are characterized by small activation parameters, ΔH^* and ΔS^*. *t*-Butyl peroxycarbamate were reported to decompose *via* a homolytic pathway to the extent of 73—95%,[12] although the ESR studies on the

Table 2. Rate constants and activation parameters for thermolysis of **1**, **2**, **3**, and **4** together with those of benzoyl peroxide and *t*-butyl diphenylmethyleneperoxycaramate

Peroxide	k[a] min^{-1}	Temp °C	ΔH^*[b] kcal/mol	ΔS^*[c] cal/mol, deg
1	$1.06\cdot10^{-2}$	40	24.2	+ 1
2	$1.91\cdot10^{-3}$	50	27.7	+ 6
3	$3.87\cdot10^{-2}$	40	21.9	+ 5
4	$2.24\cdot10^{-2}$	50	25.4	+ 12
$(C_6H_4COO)_2$	$1.16\cdot10^{-4}$	60	32.7	+13.3[d]
	$7.02\cdot10^{-4}$	78[e]		
$Ph_2C{=}NCOOBu^t$ (O)	$1.09\cdot10^{-5}$ [f]	50	29.8	+ 7

a) Error ±3% for **1**—**4**. b) Error ±0.8 kcal/mol. c) Error ±2 eu. d) P. D. Bartlett and R. R. Hiatt. *J. Am. Chem. Soc.*, **80**, 1398 (1958). e) G. B. Gill and G. H. Williams, *J. Chem. Soc.*, **1965**, 995. f) Calculated using the rate constant $22.1\times10^{-4}\,s^{-1}$ at 130 °C and the ΔH^*. (*cf.* Rüchardt and R. Pantke, *Ann.*, **762**, **88** (1971)).

photochemical decomposition of *t*-butyl *N*-alkylperoxycarbamates showed the presence of the alkylbutyloxyamino radicals instead of the alkylamino radicals.[13] Examination of the decomposition of **1** in toluene at 50 °C by the ESR technique showed formation of diphenylmethyleneamino radicals in about 10^{-5} M from the peroxide in 3×10^{-2} molar concentration. The spectrum of the iminyl radical (triplet of septets, a_N 10.20 G and a_H 0.34 G) agrees exactly with those reported by Hudson *et al.*,[14] in the study of thiocarbamate of benzophenone oxime.

The activation enthalpies and enthropies of **1** and **3** are smaller than those of benzoyl peroxide, and the situation is the same for **2** but to a smaller extent. These results suggest a concerted cleavage of three bonds in a manner similar to those of peresters investigated by Bartlett and Hiatt.[15] The activation enthalpy for peroxide **4** is about 5 kcal/mol smaller than that of benzoyl peroxide, contrary to almost the same value of activation entropy for both peroxides. This indicates an appreciable assistance in thermolysis caused by the phenyl groups, resulting in an elevation of the energy of the ground state due to steric compression. Steric compression by phenyl groups is also expected in the peroxides **1**—**3**. In **1**—**3** some reorganization of bonds is operating in the transition state, leading to a decrease in the activation entropy: partial formation of stable free radicals $Ph_2C{=}N\cdot$ and carbon dioxide will be the cause of the reorganization of the bonds.

The methyl substituents in the peroxide **3** make the steric compression more serious and the conformations of tolyl groups in the ground state resembles those of ditolylmethyleneamino radicals as suggested by Symons.[16] A much smaller ΔH^* and a moderate decrease in ΔS^* arises from these situations.

The smaller rate constant for **2** than that for **1** implies a marked contribution of the diphenylmethyleneamino group to the thermolysis rate. In general the rates of decomposition of asymmetric diacyl peroxides are larger than the symmetric ones, owing to the polar effect of asymmetric structure in the transition state. Walling *et al.*[17] and Leffler and More[18] have discussed the effect of the polar nature in the transition state. The effect of the asymmetric structure of **2** on the rate of decomposition is probably a minor one in the presence of the diphenylmethyleneamino group.

Promotion of the decomposition by non-bonding electrons on nitrogen atoms through donation to the O–O bond will be of minor importance because the conformation **C** is more hindered than that of **D** owing to the bulkiness of the diphenylmethyleneamino groups. In the confornation **C** the phenyl groups P_1, P_2, P_1', and P_2' come near to each other more seriously than the phenyl groups P_2 and P_1' do in the conformation **D**. Consequently the former conformation will be destabilized more than the latter. The participation of the non-bonding electrons on nitrogen in electron donation to the O–O bond would be facilitated if the σ^* orbital of the O–O bond overlaps strongly with the non-bonding orbital of nitrogen. The favorite conditions for overlapping can be expected more in conformation **C** than in **D**. (Fig. 1).

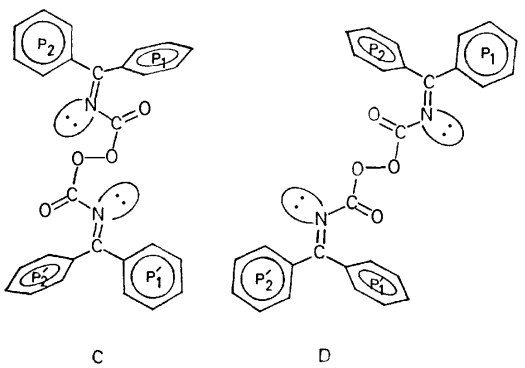

Fig. 1.

Estimation of Rate Constant of Hydrogen Abstraction Reaction of Diphenylmethyleneamino Radical from Methyl Group of Toluene. The main products of the thermolysis of **1** in toluene at 50 °C were diphenylmethyleneamine, 71.5%, *N*-(diphenylmethylene)benzylamine, 14.7%, and bis(diphenylmethylene)hydrazine, 35.2%. Although the yield of diphenylmethyleneamine was as high as 71.5%, the formation of the methyleneamine was not solely confined to Reaction 2. If all diphenylmethyleneamine were produced by the process, Reaction

2, then the termination reaction products of benzyl radicals, which were formed in the Raction 2, should be detected in an equal amount as diphenylmethyleneamine. *N*-(Diphenylmethylene)benzylamine and *m*-tolylphenylmethane have been determined together in 15.9% and a large amount of benzyl radicals (about 55%) could not be explained. For simplification it has been assumed that diphenylmethyleneamino radicals abstract hydrogen from toluene to an extent to yield benzyl radicals in *ca.* 15% per mole peroxide and that diphenylmethyleneamine was also produced *via* an unknown parallel process, 55%. Based on these assumptions the rate constant k_2 of the reaction sequences of Eqs. 2—4 can be estimated assuming a steady state in benzyl radicals, if k_4 and the stationary concentration of the diphenylmethyleneamino radicals (N) were known. Thus the Relation 12 is obtained:

$$\frac{\mathrm{d(ketazine)}/dt}{\mathrm{d(diphenylmethylenebenzylamine)}/dt} = \frac{k_4(\mathrm{N})^2}{k_3(\mathrm{N})(\mathrm{benzyl_radical})} = \frac{k_4(\mathrm{N})^2}{k_2(\mathrm{N})(\mathrm{toluene})}. \quad (12)$$

The value of k_4 was reported to be 2×10^8 M^{-1} s^{-1} at -35 °C.[19] At 50 °C k_4 will be 10^9 M^{-1} s^{-1}. The stationary concentration of the iminyl radicals was assumed by ESR technique to be 10^{-5} M at 50 °C in toluene when a solution of **1** in 3×10^{-2} M was used. Setting (toluene) = 10 M, gives

$$k_2 = 5\times10^2\ M^{-1}\ s^{-1}.$$

This is the lower limiting value of k_2. Another estimation will give maximum of k_2, if we assume that Reaction 2 is the sole process for the formation of diphenylmethyleneamine and that benzyl radicals in 55% per mole are ignored in the determination. From Relation 13,

$$\frac{\mathrm{d(ketazine)}/dt}{\mathrm{d(diphenylmethyleneamine)}/dt} = \frac{k_4(\mathrm{N})^2}{k_2(\mathrm{N})(\mathrm{toluene})}, \quad (13)$$

$$k_2 = 2\times10^3\ M^{-1}\ s^{-1}.$$

The rate constant 5×10^2 M^{-1} s^{-1} of diphenylmethyleneamino radicals for the hydrogen abstraction reaction from toluene at 50 °C is larger than the value 23 M^{-1} s^{-1} of trichloromethyl radicals from cyclohexane at 40 °C,[20] and 2.7×10^{-2} M^{-1} s^{-1} of *t*-butylperoxy radicals from toluene at 30 °C.[21] These can be explained in terms of heats of reaction using bond dissociation energies,[22] =N–H, $PhCH_2$–H, Cl_3C–H, C_6H_{11}–H, and *t*-BuOO–H of ⩾95, 85, 96, 94, and 90 kcal/mol, respectively.

Experimental

Peroxides. Diarylmethylenecarbamoyl chlorides were prepared by the reaction between diarylmethyleneamine and phosgen or oxalyl chloride by the method of Samaraj and others.[23] To a mixture of diarylmethlylenecarbamoyl chloride and a 20% excess of hydrogen peroxide–urea complex[7] in dry ether was added at -20 °C a 20% excess of pyridine in ether under stirring. Stirring was continued for 5 h and the mixture treated to the usual work up. Recrystallization of peroxide was effected from dichloromethane–methanol.

*$(Ph_2C{=}NCOO)_2$ (**1**).* Yield 18%. Mp 108—108.5 °C, dec. Active oxygen determined by iodometry was 86% of the theoretical value. Found: C, 74.71; H, 4.52; N, 6.21%. Calcd for $C_{28}H_{20}N_2O_4$: C, 74.99; H, 4.50; N, 6.25%.

*4-$ClC_6H_4COOOCON{=}CPh_2$ (**2**).* Sodium 4-chloroperbenzoate, prepared from peracid and sodium hydride, was set in dry ether at -15 °C and to this was added diphenylmethylenecarbamoyl chloride. Yield 66%. Mp 98.5—99 °C, dec. Found: C, 66.34; H, 3.54; N, 3.70%. Calcd for $C_{21}H_{14}NO_4Cl$: C, 66.41; H, 3.72; N, 3.68%.

*$((2\text{-}CH_3C_6H_4)_2C{=}NCOO)_2$ (**3**).* Yield 16%. Mp 78—80 °C, dec. Active oxygen by iodometry 67%. Found: C, 75.77; H, 5.50; N, 5.40%. Calcd for $C_{30}H_{24}N_2O_4$: C, 76.18; H, 5.59; N, 5.55%.

*$(Ph_2C{=}CHCOO)_2$ (**4**).* Diphenylmethyleneacetyl chloride, prepared from 1,1-diphenylethylene and oxalyl chloride,[24] was transformed to peroxide. Mp 98—99 °C, dec. Yield 23%. Active oxygen 97.1%. Found: C, 80.60; H, 4.85%. Calcd for $C_{30}H_{22}O_4$: C, 80.70; H, 4.97%.

*$((4\text{-}CH_3C_6H_4)_2C{=}NCOO)_2$ (**5**).* Yield 3%. Mp 103—105 °C, dec. Active oxygen 85%. Found: C, 75.75; H, 5.90; N, 5.42%. Calcd for $C_{30}H_{24}N_2O_4$: C, 76.18; H, 5.59; N, 5.55%.

Authentic Compounds for GLPC. Diphenylmethyleneamine: Prepared from diphenylmethyleneamine hydrochloride and sodium methylate. Bp 121—122 °C/0.5 Torr. Mp 59—63 °C.[25]

Diphenylmethylenebenzylamine: Obtained from benzophenone and benzylamine, Mp 60—61 °C.[26]

Bis(diphenylmethylnene)hydrazine: Prepared from benzophenone and hydrazine. Mp 164—165 °C.[27]

N-*(o-, m-, and p-Diphenylmethyleneamino)toluenes*: Toluidine and benzophenone were heated in the presence of fused zinc chloride for 2 h at 150 °C. Mp 48.5—50 °C (*o*-),[28] 77—78 °C (*m*-),[28] and 45—46 °C (*p*-).[28]

m-*Tolylphenylmethane*: Obtained by the method of Lamneck, Jr., and Wise.[29] Bp 86—86.5 °C/0.5 Torr.

GLPC Measurements. The products of thermolysis of peroxides were determined by GLPC using a JGC-1100 (JEOL) type apparatus, 3-m column of Apiezon L (5% on Chromosorb W(AW)) at 220 °C, and 3-m column of Apiezon L (1.5% on Cohrmosorb W(AW)) at 154 °C. Helium as carrier gas.

For the elemental analyses of the peroxides we are grateful to Dr. Shozo Masuda of the University of Tokyo.

References

1) a) T. Suehiro, S. Igeta, O. Kuwabara, and M. Hirai, *Tetrahedron*, **26**, 963 (1970); b) T. Suehiro and M. Ishida, *Bull. Chem. Soc. Jpn.*, **44**, 1692 (1971).
2) To be published. Read before the 28th National Meeting of the Chemical Society Japan (1973), No. 2G25.
3) S. W. Benson, *J. Chem. Educ.*, **42**, 502 (1965).
4) W. G. Danen and F. A. Neugebauer, *Angew. Chem. Int. Ed. Engl.*, **14**, 783 (1975).
5) F. A. Neugebauer, *Angew. Chem.*, **85**, 485 (1975).
6) Y. L. Chow, *Acc. Chem. Res.*, **6**, 354 (1973).
7) H. Stolzenberg, *Ber.*, **49**, 1545 (1916).
8) Unpublished work.
9) S. S. Hirsch, *J. Org. Chem.*, **32**, 2433 (1967).
10) P. Davis, M. G. Evans, and W. C. E. Higginson, *J. Chem. Soc.*, **1951**, 2563.
11) S. Ishikawa, H. Sakuragi, M. Yoshida, N. Inamoto, and K. Tokumaru, *Chem. Lett.*, **1975**, 819.

12) E. L. O'Brien, F. M. Beringer, and R. B. Mesrobian, *J. Am. Chem. Soc.*, **79**, 6238 (1957); **81**, 1506 (1959); E. Hedaya, R. L. Hinman, V. Schomaker, S. Theodoropulos, and L. M. Kyle, *ibid.*, **89**, 4875 (1967).
13) W. C. Danen, C. T. West, and R. T. Kenslar, *J. Am. Chem. Soc.*, **95**, 5716 (1973).
14) R. F. Hudson, A. J. Lawson, and E. A. C. Lucken, *Chem. Commun.*, **1971**, 807.
15) Ref. d) in Table 2.
16) M. C. R. Symons, *Tetrahedron*, **29**, 615 (1973); R. F. Hudson, A. J. Lawson, and K. A. F. Record, *J. Chem. Soc., Chem. Commun.*, **1974**, 488.
17) C. Walling, H. P. Waits, J. Milovanovic, anc C. G. Pappiaonnou, *J. Am. Chem. Soc.*, **92**, 4927 (1970).
18) J. E. Leffler and A. A. More, *J. Am. Chem. Soc.*, **94**, 2483 (1972).
19) D. Griller, G. D. Mendenhall, W. Van Hoof, and K. U. Ingold, *J. Am. Chem. Soc.*, **96**, 6068 (1974).
20) M. L. White and R. R. Kuntz, *Int. J. Chem. Kinet.*, **3**, 127 (1971).
21) J. A. Howard and S. Korcek, *Can. J. Chem.*, **48**, 2165 (1970).
22) S. W. Benson, *J. Am. Chem. Soc.*, **87**, 972 (1965); J. A. Kerr, *Chem. Rev.*, **66**, 465 (1966). D(=N–H) will be larger than 95 kcal/mol of $D(Me_2N–H)$.
23) L. I. Samaraj, O. W. Wischnewskij, and G. I. Derkatsch, *Chem. Ber.*, **102**, 2972 (1969).
24) F. Bergmann, M. Weizmann, E. Dimant, J. Patai, and J. Szmuskowicz, *J. Am. Chem. Soc.*, **70**, 1612 (1948).
25) G. Reddelien, *Ber.*, **54**, 3129 (1926).
26) G. Reddeline, *Ber.*, **53**, 337 (1925).
27) E. R. Blout, V. W. Eager, and R. M. Gofstein, *J. Am. Chem. Soc.*, **68**, 1983 (1946).
28) G. Reddelien, *Ber.*, **42**, 4760 (1914); **46**, 2718 (1918).
29) J. E. Lamneck, Jr., and P. H. Wise, *J. Am. Chem. Soc.*, **76**, 1104 (1954).

α,β-Unsaturated Carboxylic Acid Derivatives. XV. The Reaction of Ethyl 3-Nitro-2-alkenoate with Bromine Azide or Bromine, and Transformations of the Products[1)]

Chung-gi SHIN,* Yasuchika YONEZAWA, Kaoru SUZUKI, and Juji YOSHIMURA**

Laboratory of Organic Chemistry, Faculty of Technology, Kanagawa University, Rokkakubashi, Kanagawa-ku, Yokohama 221

***Laboratory of Chemistry for Natural Products, Faculty of Science, Tokyo Institute of Technology, Nagatsuta, Midori-ku, Yokohama 227*

(Received November 4, 1977)

The reaction of ethyl (*Z*)-3-nitro-2-alkenoate (**1**) with one or two equivalents of bromine azide gave a one-to-one mixture of ethyl (*E*)-2-azido-3-nitro-2-alkenoate (**3**) and 4-ethoxycarbonyl-1,2,5-oxadiazole 2-oxide (**5**), or ethyl 3-bromo-2,2-diazido-3-nitroalkanoate (**6**), respectively, and the subsequent thermal and photochemical reactions of (*E*)-**3** gave 2-ethoxycarbonyl-3-nitro-1-azirine, together with a small amount of **5**. The addition of bromine to **1**, and the subsequent elimination of hydrogen bromide from the product, gave exclusively, the (*Z*)-2-bromo derivative (**9**). The reduction of **6** and **9** with diethyl phosphonate was examined, and the reaction mechanisms were discussed.

Although a few articles have been published on the properties of vicinal azido nitro olefins as intermediates, their isolation and their conversion into the corresponding nitroazirines have never been reported, except for the formation of 1,2,5-oxadiazole 2-oxides.[2–4)] Previously, however, we have ourselves reported the synthesis of stable α- and β-azido olefins[5,6)] and their conversion into the corresponding azirines[6)] and enamines.[7)]

In this paper, the reaction of bromine azide or bromine with ethyl 3-nitro-2-alkenoate[8)] and the subsequent elimination, substitution, and thermal and photochemical reactions of the products were examined, in order to isolate stably and convert the azido nitro olefins into the nitroazirine derivatives. Consequently, the expected several kinds of new vicinal azido nitro and bromo nitro compounds, nitroazirine, and 1,2,5-oxadiazole 2-oxide derivatives were obtained, as is shown in Scheme 1.

Results and Discussion

When an equimolar amount of ethyl (*E*)- or (*Z*)-3-nitro-2-alkenoate (**1**; **a**; R=CH_3, **b**; R=C_2H_5, **e**; R=C_6H_5) was treated with halo azide [formed from *N*-bromo- or *N*-chlorosuccinimide (NBS and NCS) and sodium azide in water][9)] in *N*,*N*-dimethylformamide (DMF), a syrup composed of two chemical species was obtained. In order to separate the mixture, it was carefully subjected to chromatography on a silica gel column, using benzene–petroleum ether (1:1 v/v), to give a pale yellow syrup (**3**) (1st fraction) and a colorless syrup (**5**) (2nd fraction) in a ratio of *ca.* 1:1. On the other hand, when the reaction was carried out in benzene under refluxing, **5** and a colorless syrup (**4**) were obtained in a ratio of *ca.* 1:1.

The structures of **3**, **4**, and **5** were assigned to ethyl 2-azido-3-nitro-2-alkenoate, 3-substituted 2-ethoxycarbonyl-3-nitro-1-azirine and 3-substituted 4-ethoxycarbonyl-1,2,5-oxadiazole 2-oxide respectively on the basis of their spectroscopic data as well as the results

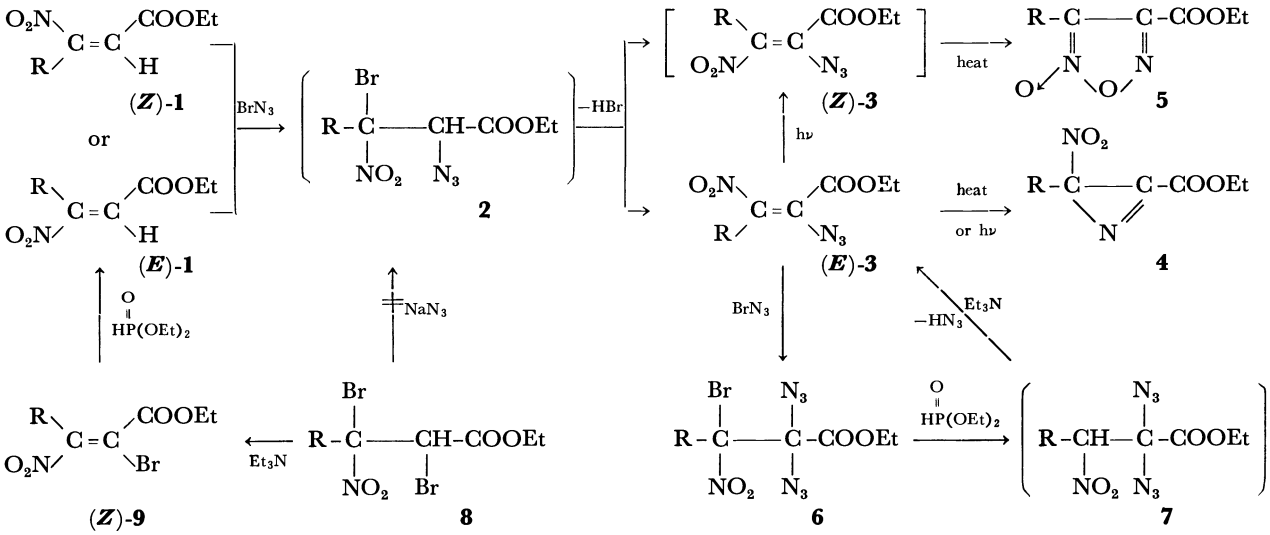

a; R=CH_3, **b**; R=C_2H_5, **c**; R=*n*-C_3H_7, **d**; R=*i*-C_3H_7, **e**; R=C_6H_5

Scheme 1.

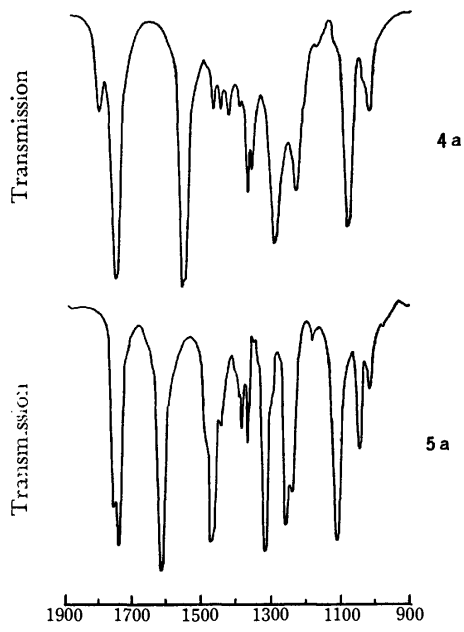

Fig. 1. IR spectrum of **4a** and **5a**.

of their elemental analyses. The difference between **4** and **5** can be characterized unambiguously by a comparison of their IR spectral data, shown in Fig. 1. The absorption bands at 1555—1560 and 1370 cm^{-1} assigned to the nitro group and the carbon-nitrogen double bond[6] of the azirine ring at 1790—1800 cm^{-1} indicate the formation of nitroazirine (**4**), whereas the disappearance of the nitro group in **5** supports the idea of ring formation between the oxygen in the nitro group and the nitrogen atom caused by the azido group.[2-4]

The configuration of a separated isomer of **3** could be determined as (*E*)-geometry by the formation of **4**, since the (*Z*)-isomer of vicinal azido nitro olefins is known to convert immediately at a higher temperature into the corresponding 1,2,5-oxadiazole 2-oxide.[2-4] It is noteworthy that (***E***)-**3** is the first example of an isolated azido nitro olefin.

Next, the thermal isomerization from (***E***)-**3** to (***Z***)-**3** was performed in benzene under reflux; however, only **4** was obtained in *ca.* a 60% yield. The irradiation of (***E***)-**3** in carbon tetrachloride externally with a high-pressure mercury lamp under a stream of nitrogen gas at room temperature also gave **4** in *ca.* a 35% yield, together with a small amount of **5**. This shows that (***E***)-**3** is slightly isomerized to (***Z***)-**3**, which is then immediately cyclized to **5**.

Moreover, the similar treatment of (***E***)-**1** or (***Z***)-**1** with two molar bromine azide gave the same compound as a colorless syrup in *ca.* a 70% yield. It was identified, by means of spectroscopic analyses, as ethyl 3-bromo-2,2-diazido-3-nitro-alkanoate (**6**). It is known that diethyl phosphonate does not react with both nitro[10] and azido[11] groups in the carboxylic acid ester and that it reduces the halogen atom.[12] Accordingly, when **6** was treated with diethyl phosphonate in benzene in the presence of triethylamine, (***E***)-**3** was obtained in a fairly good yield, along with **5** in a low ylied. This fact indicates that the bromide atom of **6** is reduced with phosphonate to form an unstable intermediate, ethyl 2,2-diazido-3-nitroalkanoate (**7**); the subsequent rapid elimination of hydrazoic acid[13] in the presence of the base from **7** gives (***E***)-**3** snd (***Z***)-**3**, the latter of which is further transformed into **5**.

From the above facts, the formation of **3** and **6** from **1** seems to be through successive the addition reaction of bromine azide to **1** and the elimination of hydrogen bromide to give (***E***)-**3** and (***Z***)-**3**, formed as a labile intermediate, which in turn reacts further with excess bromine azide to give **6**, as is shown in Scheme 1. The latter addition was substantiated unambiguously by the reaction of the isolated (***E***)-**3** with bromide azide.

The yields, physical constants, and spectral data of **3**—**6** are summarized in Tables 1 and 2.

On the other hand, the dehydrobromination of ethyl 2,3-dibromo-3-nitroalkanoate (**8**), prepared in a good yield from the reaction of (***E***)-**1** or (***Z***)-**1** with bromine in chloroform, with triethylamine gave 2-bromo-3-nitro-2-alkenoate (**9**) in *ca.* a 90% yield. Although the compound, **8**, derived from individual (***E***)-**1** and (***Z***)-**1** consisted of two stereoisomers in various ratios, listed in Table 3, according to the reaction, a single product, **9**, was formed stereospecifically. The configuration of **9** could be determined as the (*Z*)-geometry by conversion into (***E***)-**1** in *ca.* a 50% yield by reduction with diethyl phosphonate. From the above results, it was deduced that the base-catalyzed β-elimination of **8** composed of erythro- and threo-stereoisomers (see Table 3) proceeded by means of ElcB mechanism *via* the corresponding nitronate carbanion.[8] Attempts at the substitution of the bromo atom at the 2-position with the azido group in **8** and **9** by treatment with sodium azide was unsuccessful, forming an ambiguous mixture.

Table 1. The yields and spectral data of **3** and **6**

Compound[a] R	Yield[b] (%)	Yield[c] (%)	IR spectrum in KBr (cm^{-1}) N_3	ester	C=C	NO_2	NMR spectrum[d] 3-alkyl (J_{Hz}) (3-phenyl)
(***E***)-**3a** CH_3	41.9	85.1	2100,	1730,	1640,	1515, 1320	2.20 s
(***E***)-**3b** C_2H_5	38.8	81.2	2100,	1732,	1635,	1520, 1330	2.61 q (7.2 Hz)
(***E***)-**3e** C_6H_5	36.5	75.8	2110,	1735,	1622,	1532, 1335	(7.30 s)
6a CH_3	70.3		2100,	1750,		1562, 1332	2.48 s
6b C_2H_5	74.2		2100,	1750,		1565, 1320	2.28—3.08m
6e C_6H_5	75.2		2120,	1760,		1570, 1340	(7.45—7.76m)

a) **3**; pale yellow syrup, **6**; colorless syrup. b) From **1**. c) From **6**. d) δ value, measured in $CDCl_3$.

Table 2. The yields, physical constants, and spectral data of **4** and **5**

Compound	R	Yield (%)[a]	Yield (%)[b]	Yield (%)[c]	Yield (%)[d]	(Mp °C) Bp °C/mmHg	Formula	Found (Calcd), % C	H	N	IR spectrum[f] (cm^{-1}) N→O C=N	Ester	NO_2	NMR spectrum[g] 3-alkyl (J_{Hz}) (3-phenyl)
4a	CH_3	32.5	62.5	36.7	—	69—72/0.5	$C_6H_8N_2O_4$	41.90 (41.86	4.70 4.68	16.19 16.28)	1800,	1750,	1555 1370	2.70 s
4b	C_2H_5	40.1	55.7	35.5	—	71—77/0.5	$C_7H_{10}N_2O_4$	45.12 (45.16	5.44 5.41	15.15 15.05)	1790,	1750,	1558 1370	3.06 q (7.6 Hz)
4e	C_6H_5	29.1	61.2	38.5	—	syrup	$C_{11}H_{10}N_2O_4$	56.40 (56.41	4.22 4.30	11.89 11.96)	1795,	1750,	1560 1370	(7.38—8.00m)
5a	CH_3	2.5	—	32.5	10.5	67—71/0.5	$C_6H_8N_2O_4$	41.91 (41.86	4.72 4.68	16.25 16.28)	1615,	1745		2.46 s
5b	C_2H_5	3.1	—	40.2	12.5	70—75/0.5	$C_7H_{10}N_2O_4$	45.11 (45.16	5.43 5.41	15.08 15.05)	1610,	1742		2.86 q (7.5 Hz)
5e	C_6H_5	3.2	—	35.6	17.2	(51—52)[e]	$C_{11}H_{10}N_2O_4$	56.44 (56.41	4.39 4.30	11.88 11.96)	1585,	1745		(7.48—7.77m)

a) From the photochemical reaction of **3**. b) From the thermal reaction of **3**. c) From **1**. d) From **6**. e) Colorless needles from ethanol. f) Recorded in KBr. g) δ value, measured in $CDCl_3$.

Table 3. The yields, physical constants, and spectral data of **8** and **9**

Compound	R	Yield (%)	Bp °C/mmHg (Mp °C)	Formula	Found (Calcd), % C	H	N	IR spectrum in KBr (cm^{-1}) Ester	C=C	NO_2	MNR spectrum[a] 2-H	E[d] : T[e] ratio[c]
8a	CH_3	95.0	67—68/0.33	$C_6H_9NO_4Br_2$	22.52 (22.57	2.80 2.82	4.81 4.89)	1752,		1570, 1330	5.05 s, 5.03 s	6 : 1
8b	C_2H_5	92.3	88—90/0.13	$C_7H_{11}NO_4Br_2$	25.26 (25.22	3.34 3.30	4.25 4.20)	1745,		1560, 1325	5.29 s, 5.19 s	4 : 1
8c	*n*-C_3H_7	93.5	93—95/0.13	$C_8H_{13}NO_4Br_2$	27.39 (27.66	3.75 3.75	4.06 4.03)	1745,		1560, 1330	5.27 s, 5.14 s	3 : 1
8d	*i*-C_3H_7	61.5	84—85/0.18	$C_8H_{13}NO_4Br_2$	27.60 (27.66	3.72 3.75	4.05 4.03)	1760,		1580, 1325	5.28 s, 5.15 s	6 : 1
8e	C_6H_5	60.5	colorless syrup	$C_{11}H_{11}NO_4Br_2$	34.55 (34.65	2.97 2.87	3.62 3.67)	1750,		1570, 1330	5.72 s, 5.61 s	1 : 5
9b	C_2H_5	85.5	64—70/0.2	$C_7H_{10}NO_4Br$	33.40 (33.33	3.97 3.96	5.49 5.55)	1735,	1640,	1545, 1337		
9c	*n*-C_3H_7	87.7	75—79/0.4	$C_8H_{12}NO_4Br$	36.37 (36.09	4.35 4.51	5.33 5.26)	1730,	1635,	1535, 1330		
9d	*i*-C_3H_7	91.1	65—66/0.3	$C_8H_{12}NO_4Br$	36.12 (36.09	4.45 4.51	5.30 5.26)	1735,	1620,	1545, 1338		
9e	C_6H_5	90.2	(96.5—97.5)[b]	$C_{11}H_{10}NO_4Br$	44.05 (44.00	3.35 3.33	4.62 4.67)	1740,	1650,	1527, 1328		

a) δ value, measured in $CDCl_3$. b) Colorless needles crystallized from benzene-petroleum ether. c) Evaluated from the intensity of the methine proton in the 2-position. d) Erythro. e) Threo.

The yields, physical constants, and spectral data of **8** and **9** are listed in Table 3.

Experimental

All the boiling and melting points are uncorrected. The IR spectra were recorded with a Hitachi EPI-G3 Spectrometer. The NMR spectra were measured with a JNM-PS-100 Spectrometer (Japan Electron Optics Laboratory Co., Ltd.), using tetramethylsilane as the internal standard.

*Preparation of **3**, **4**, and **5**.* Into a solution of NBS or NCS (0.06 mol) in DMF (100 ml) we stirred, drop by drop, a solution of sodium azide (0.06 mol) in water (18 ml) at −20 °C for 15 min. The resulting solution was added, drop by drop, to a solution of (***E***)-**1** or (***Z***)-**1** (0.06 mol) in DMF (20 ml) at −40——45 °C. After stirring at −30 °C for 45 min, the mixture was poured into ice-water (350 ml). After continuous stirring for 1 h, the aqueous solution was extracted three times with dichloromethane (130 ml). The extracts were collected, washed twice with water, and then dried over anhydrous magnesium sulfate. The dichloromethane layer was evaporated to give a residual syrup, which was chromatographed on a silica gel column, using benzene–petroleum ether (1:1 v/v) as an eluent below 5 °C. Mainly two fractions were obtained. After concentrating each fraction, the (***E***)-**3** compound as a pale yellow syrup from the first eluted fraction and **5** as a colorless syrup from the second eluted one were obtained.

On the other hand, the syrup obtained from the above dichloromethane solution was directly dissolved in dry benzene (60 ml), and then the benzene solution was refluxed for 1 h. The resulting solution was evaporated to give a residual syrup, which was distilled under reduced pressure to give a colorless syrup composed of a mixture of **4** and **5**. A similar separation gave **4** and **5** in *ca.* a 1:1 ratio.

*Preparation of **6**.* *Procedure A*: Into a solution of (***E***)-**1** or (***Z***)-**1** (0.05 mol) and NBS (0.11 mol) in DMF (100 ml) we stirred drop by drop, a solution of sodium azide (0.11 mol) in DMF–water (1:1 v/v) (30 ml) below −10 °C. After continuous stirring for 40 min, the mixture was poured into ice water (400 ml). After stirring for 1 h, the aqueous solution was extracted three times with hexane (100 ml). The extracts were collected, washed twice with water, dried over sodium sulfate, and finally evaporated under reduced pressure to dryness. The residual syrup was placed in a silica gel column using benzene as the eluent. The fractions were collected and evaporated under reduced pressure to give **6** as a colorless syrup.

Procedure B: Into a solution of (***E***)-**3** (0.01 mol) in DMF (30 ml) we stirred drop by drop, a solution of NBS (0.01 mol) and sodium azide (0.01 mol) in water (10 ml) below −10 °C. After continuous stirring for 30 min, the mixture was worked up such as has been described in Procedure A.

*Thermal Reaction of (**E**)-**3**.* A solution of (***E***)-**3** (0.03 mol) in dry benzene (20 ml) was refluxed for 1 h. After the removal of the solvent under reduced pressure, the residual syrup was purified on a silica gel column, using benzene–ethyl acetate (20:1 v/v) as the eluent. The fraction was then collected and concentrated. The residue was distilled under reduced pressure to give **4**.

*Photochemical Reaction of (**E**)-**3**.* A solution of (***E***)-**3** (0.03 mol) in dry carbon tetrachloride (80 ml) was irradiated with a high-pressure mercury lamp (450 W) in a stream of nitrogen gas at 10 °C for *ca.* 7 h, at which time the azido group band at *ca.* 2100 cm^{-1} disappeared. The resultant solution was evaporated; the purification of the residual syrup thus obtained was worked up such as above to give **4** and **5** in *ca.* a 10:1 ratio.

*Reaction of **6** with Diethyl Phosphonate.* Into a mixture of **6** (0.01 mol) and diethyl phosphonate (0.01 mol) in dry benzene (30 ml) we stirred, drop by drop, triethylamine (0.01 mol) below 10 °C. After continuous stirring for 30 min, triethylammonium bromide was filtered off, and then the benzene layer was concentrated under reduced pressure. The residual syrup was chromatographed on a silica gel column, using benzene as the eluent; two fractions were thus obtained. After each fraction had been concentrated under reduced pressure, the first fraction gave (***E***)-**3** in *ca.* an 80% yield, while the second one gave **5** in *ca.* a 13% yield.

*Preparation of **8**.* To a solution of (***E***)-**1** or (***Z***)-**1** (0.1 mol) in chloroform (70 ml) we added, drop by drop, a solution of bromine (0.1 mol) in chloroform (30 ml) with occasional shaking. The mixture was allowed to stand at room temperature for 24 h and then concentrated to dryness. The residual oil was distilled under reduced pressure to give **8** as a colorless oil.

*Preparation of **9**.* Into a solution of **8** (0.1 mol) in dry benzene (80 ml) we stirred, drop by drop, triethylamine (0.12 mol) under cooling. After continuous stirring overnight at room temperature, triethylammonium bromide was precipitated. It was filtered off, and the filtrate was washed sucessively with 3 M-hydrochloric acid and water. The resulting benzene layer was dried over anhydrous magnesium sulfate and concentrated under reduced pressure to give a residual syrup. The residue was distilled under reduced pressure to give (***Z***)-**9** as a colorless oil.

*Reaction of (**Z**)-**9** with Diethyl Phosphonate.* Into a solution of (***Z***)-**9** (0.1 mol) and diethyl phosphonate (0.1 mol) in dry benzene (70 ml) we stirred, drop by drop, triethylamine (0.12 mol) under cooling. After continuous stirring for 1 h at room temperature, triethylammonium bromide was filtered off and the filtrate was washed successively with 3 M-hydrochloric acid and water. The benzene layer was dried over anhydrous magnesium sulfate and concentrated under reduced pressure to give (***E***)-**1** as a colorless oil.

References

1) Part XIV: C. Shin, Y. Kosuge, M. Yamaura, and J. Yoshimura, *Bull. Chem. Soc. Jpn.*, **51**, 1134 (1978).
2) W. D. Emmons and J. P. Freeman, *J. Org. Chem.*, **40**, 456 (1975).
3) T. E. Stevens and W. D. Emmons, *J. Am. Chem. Soc.*, **80**, 338 (1958).
4) A. N. Thakeore, J. Buchshriber, and A. C. Oehleschlager, *Can. J. Chem.*, **51**, 2406 (1973).
5) C. Shin, Y. Yonezawa, and J. Yoshimura, *Tetrahedron Lett.*, **1974**, 7.
6) C. Shin, Y. Yonezawa, and J. Yoshimura, *Chem. Lett.*, **1976**, 1063.
7) C. Shin, Y. Yonezawa, and J. Yoshimura, *Chem. Lett.*, **1976**, 1095.
8) C. Shin, Y. Yonezawa, H. Narukawa, K. Nanjo, and J. Yoshimura, *Bull. Chem. Soc. Jpn.*, **45**, 3595 (1972); C. Shin, Y. Yonezawa, and J. Yoshimura, *Nippon Kagaku Kaishi*, **1974**, 718.
9) D. V. Ende and A. Krief, *Angew. Chem. Int. Ed. Engl.*, **13**, 279 (1974).
10) C. Shin, Y. Yonezawa, K. Katayama, and J. Yoshimura, *Bull. Chem. Soc. Jpn.*, **46**, 1727 (1973).
11) Unpublished data.
12) S. Dershowitz and S. Proskauer, *J. Org. Chem.*, **26**, 3595 (1961); A. J. Speziale and C. C. Tung, *ibid.*, **28**, 1353 (1963).
13) A. Hassner and F. W. Fowler, *J. Am. Chem. Soc.*, **90**, 2869 (1968).

α,β-Unsaturated Carboxylic Acid Derivatives. XVI. Synthesis and Configuration of Diels-Alder Adducts from Ethyl 3-Nitro-2-alkenoate and 1,3-Butadiene[1]

Chung-gi SHIN,* Masanori YAMAURA, Eiji INUI, Yuzuru ISHIDA, and Juji YOSHIMURA**

Laboratory of Organic Chemistry, Faculty of Technology, Kanagawa University, Rokkakubashi, Kanagawa-ku, Yokohama 221

*** Laboratory of Chemistry for Natural Products, Faculty of Science, Tokyo Institute of Technology, Nagatsuta, Midori-ku, Yokohama 227*

(Received November 2, 1977)

The Diels-Alder reaction of individual (*E*)- and (*Z*)-isomers of ethyl 3-nitroacrylate and 3-nitrocrotonate with 1,3-butadiene, 1-acetoxy- or 1,4-diacetoxy-1,3-butadiene was conducted to give ethyl 6-nitro-3-cyclohexene-, 5-acetoxy-, and 2,5-diacetoxy-6-nitro-3-cyclohexene-carboxylates, respectively. The stereochemistry of the cycloaddition products has been elucidated by analysis of the NMR spectrum.

In previous papers, the Diels-Alder reaction of cyclopentadiene with ethyl (*E*)- and (*Z*)-3-nitrocrotonate (**6**) or ethyl (*Z*)-3-nitrocinnamate and subsequent reduction of the resulting (2+2)- and (2+4)-nitro adducts with aluminum–amalgam (Al–Hg) were carried out to give unique tricyclic isoxazolidione derivatives.[1,2]

In order to synthesize desirable starting materials for antibiotics oryzoxymycin[3] and related compounds[4,5] having a 6-amino-5-hydroxy-1,3-cyclohexadiene-1-carboxylate structure, here, the cycloaddition reaction of ethyl (*E*)-3-nitroacrylate (**1**) or **6** has been extended to 1,3-butadiene, 1-acetoxy- and 1,4-diacetoxy-1,3-butadienes. The conformational determination of all the new (2+4)-nitro adducts has been established on the basis of the spectral data.

Results and Discussion

*Reaction of **1** with 1,3-Butadiene.* According to the method of Shechter[6] and Shin,[7,8] compound **1** was prepared stereoselectively from the reaction of ethyl 2-chloro-3-nitropropanoate with sodium acetate. Thermal and photochemical isomerization of **1** to its (*Z*)-isomer failed. However, the structure of **1** was determined to be the (*E*)-isomer from the coupling constant between C-1 and C-6 protons and the spectral properties of the cycloaddition products.

Heating a solution of (***E***)**-1** and 1,3-butadiene in chloroform in an autoclave at 80—100 °C under 2—3 atmospheres for *ca.* 40 h gave a cycloaddition product of a colorless oil (**2**) in *ca.* 80% yield. The reaction of **1** with 1-acetoxy-1,3-butadiene in benzene at room temperature for 72 h afforded an analogous nitro adduct (**3**) as colorless crystals in a 57.4% yield. Similarly, the reaction of **1** with 1,4-diacetoxy-1,3-butadiene[9] under reflux for 5.5 h gave only the nitro adduct (**5**) quantitatively as colorless crystals. The reaction conditions and yields for **2** and **3** are listed in Tables 1 and 2.

Table 1. Cycloaddition of **1** with 1,3-butadiene

Reaction condition[a]				
Temp (°C)	Pressure (atm)	Time (h)	Molar ratio diene/**1**	Yield of **2** (%)
80	2—3	40	1.5	80.8
r. t[b]	1	100[c]	1.5	0
100	2—3	37	1.5	80.1
80	2—3	40	1.2	59.7
150	2—3	35	1.5	61.2
120	12—15	35	1.5	63.4

a) In chloroform. b) Room temperature. c) With stirring.

Table 2. Cycloaddition of **1** with 1-acetoxy-1,3-butadiene

Reaction conditions					
Temp (°C)	Pressure (atm)	Time (h)	Solvent	Molar ratio diene/**1**	Yield of **3** (%)
r. t[a]	1	72[b]	benzene	1.2	57.4
90—100	2—3	7	chloroform	1.2	47.3
reflux	1	6	toluene	1.2	21.2

a) Room temperature. b) With stirring.

From the NMR spectral and TLC analyses, it was found that each reaction proceeded stereospecifically to give a homogeneous product. The structural assignment of **2**, **3**, and **5** was based on their NMR spectral data as well as the satisfactory elemental analysis. The chemical shifts and the coupling constants are given in Table 4. The structure of **3**, being either (A) or (B) as illustrated in Fig. 1, was confirmed chemically to be (A) as shown in Scheme 1. The reduction

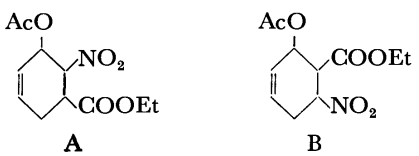

Fig. 1.

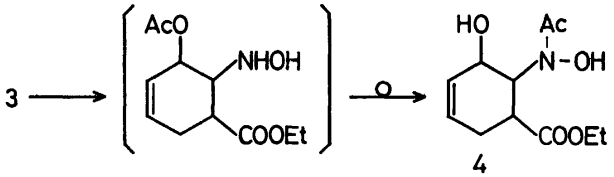

Scheme 1.

of **3** with Al–Hg gave the corresponding hydroxyamino derivative, in which *O*-acetyl 1,4-shift to nitrogen occurred to give ethyl 6-*N*-acetylhydroxyamino-5-hydroxy-3-cyclohexene-1-carboxylate (**4**). The migration product gave satisfactory elemental analysis and turned deep violet with ferric chloride in methanol, indicating the presence of a hydroxamic acid structure.

Furthermore, the conformational assignment of **2**, **3**, and **5** was studied. In the spectrum of **2**, the signals at δ 3.24 ($J_{1,6}=J_{1,2a}=11.0$ Hz, $J_{1,2e}=6.0$ Hz) and 4.88 ($J_{5a,6}=10.0$ Hz, $J_{5e,6}=6.0$ Hz) appearing as two sextets are attributable to the two protons at C-1 and C-6 positions, respectively. The similar signals at δ 3.43 and 4.90 in the spectrum of **3** exhibit a sextet ($J_{1,6}=J_{1,2a}=11.8$ Hz) and a quartet ($J_{5e,6}=3.9$ Hz), respectively, which have been assigned as axial hydrogens. From the relatively large J value (11.8 Hz), the dihedral angle between C-1 and C-6 or C-2a protons has been deduced to be near to 180°. The orientation of C-5 (δ 5.76, $J_{5e,6}=7.0$ Hz) and C-6 positions of **3** have been established by a spin-spin decoupling method, since the irradiation of C-6 proton collapsed C-5 proton at δ 5.76 to a doublet ($J_{4,5}=4.0$ Hz). The large J value of C-2 ($J_{2a,2e}=18.0$ Hz) is in agreement with the quasi-axial and quasi-equatorial protons at allyl positions on shikimic acid ($J_{2a,2e}=18.5$ Hz).[10] The signals of **5** at δ 3.49 and 5.04 and the coupling constant ($J_{1,6}=12.0$ Hz) between C-1 and C-6 protons are remarkably identical with those of **3**, but the J value between C-1 and C-2 protons exhibits 9.2 Hz as a broad doublet. Moreover, the chemical shift and coupling constant of the C-5 proton (δ 5.86, $J_{5e,6}=6.0$ Hz) of **5** was also remarkably similar to that of C-5 proton of **3**. Accordingly, the orientation of the C-2 proton has been assigned as quasi-axial and, therefore, that of the C-2 acetoxyl group as quasi-equatorial. The above results are further confirmed by the irradiation of the signal at δ 5.64 due to the C-2 proton collapsing to a quartet ($J_{1,2e}=9.2$ Hz) of methine proton to a doublet ($J_{1,6}=12.0$ Hz).

From the above facts, the structures of the three (2+4)-nitro adducts have been unambiguously assigned to be ethyl *t*-6-nitro-3-cyclohexene-*r*-1-carboxylate (**2**), ethyl *t*-5-acetoxy-*t*-6-nitro- (**3**) and *t*-2, *t*-5-diacetoxy-*t*-6-nitro-3-cyclohexene-*r*-1-carboxylates (**5**), respectively, all of which have half-chair conformations. The physical constants and IR spectral data of **2**, **3**, and **5** are summarized in Table 3.

*Reaction of **6** with 1,3-Butadienes.* The reaction of (***E***)-**6** with 1,3-butadiene in chloroform in a sealed tube at 100 °C for 35 h gave only a kind of syrup (**7**) in 66.6% yield. Similarly, the reaction of (***E***)-**6** with 1-acetoxy-1,3-butadiene for 25 h gave a syrup, containing two diastereomers (**8** and **9**) in poor yield. Similarly, the reaction of (***Z***)-**6**[8] with 1,3-butadiene gave a syrup (**10**) in 20.0% yield together with **7** in 22.9% yield, whereas the reaction of (***Z***)-**6** with 1-acetoxy-1,3-butadiene gave crystals (**11**) in poor yield along with a mixture of **8** and **9**. This indicates that (***Z***)-**6** is partially isomerized by heating[8] to (***E***)-**6**, which undergoes the cycloaddition to give **8** and **9**.

The structures and conformations of **7**—**10** and **11** have also been elucidated from their spectroscopic data and elemental analyses (see Tables 3 and 4).

The NMR spectra of **7** and **10** showed the C-1 proton signals at δ 3.49 ($J_{1,2a}=10.0$ Hz, $J_{1,2e}=7.0$ Hz) and 3.40 ($J_{1,2a}=5.5$ Hz, $J_{1,2e}=2.5$ Hz) as a quartet. Furthermore, from the comparison of the NMR spectral data of **7** and **10** with that of **2** and **3**, the conformations of **7** and **10** were inferred to be ethyl *c*-6-methyl-*t*-6-nitro- and *t*-6-methyl-*c*-6-nitro-3-cyclohexene-*r*-1-carboxylates. Although the mixture of **8** and **9** could not be separated, both signals at δ 3.57 ($J_{1,2a}=11.5$ Hz,) $J_{1,2e}=6.3$ Hz) and 3.26 ($J_{1,2a}=11.3$ Hz, $J_{1,2e}=6.3$ Hz) as a quartet have been clearly assigned to be an axial protons of C-1 position. However, the coupling constant ($J_{4,5}=10.0$ Hz) of **8** was remarkably different from that of **9** ($J_{4,5}=4.8$ Hz), suggesting that the orientation of the 3-acetoxyl group of **8** was quasi-axial whereas that of **9** was quasi-equatorial. The different NMR spectral pattern of **11** ($J_{1,2e}=6.3$ Hz, $J_{1,2a}=8.8$ Hz) contrasted to that of **8** and **9** and of the

Table 3. Physical data and IR spectra of ethyl 6-nitro-3-cyclohexene-1-carboxylates

Compound No.	Yield (%)	Bp °C/mmHg (Mp °C)	Formula	Found, %			Calcd, %			IR spectrum, cm^{-1} in KBr		
				C	H	N	C	H	N	COOEt	C=C	NO_2
2	80.8	86—88/0.5	$C_9H_{13}NO_4$	54.77	6.72	6.92	54.26	6.58	7.03	1740,	1660,	1555, 1380
3	57.4	(75—76)	$C_{11}H_{15}NO_6$	51.65	5.92	5.44	51.36	5.88	5.45	1755, 1735[a]	1660,	1565, 1380
5	91.3	(119—120)	$C_{13}H_{17}NO_8$	49.76	5.50	4.47	49.52	5.44	4.44	1745, 1740, 1735[b]	1650,	1560, 1380
7	66.6 (22.9)[c]	85—88/0.55	$C_{10}H_{15}NO_4$	55.94	7.23	6.86	56.32	7.09	6.57	1740,	1660,	1550, 1390
8	10.0	125—129/0.5[e]	$C_{12}H_{17}NO_6$	53.01	6.28	5.30	53.13	6.32	5.16	1760,	1660,	1550, 1370
9	6.2 (8.3)[d]											
10	20.0	93—95/0.7	$C_{10}H_{15}NO_4$	56.03	7.01	6.80	56.32	7.09	6.57	1740,	1660,	1550, 1390
11	6.2	(85—86)	$C_{12}H_{17}NO_6$	53.77	6.51	5.23	53.13	6.32	5.16	1760, 1740[a]	1660,	1550, 1380

a) Band of 5-acetoxyl group. b) Bands of 2,5-diacetoxyl groups. c) By-products from (***Z***)-**6** and 1,3-butadiene. d) By-products from (***Z***)-**6** and 1-acetoxy-1,3-butadiene. e) Boiling point of a mixture of **8** and **9**.

Table 4. Chemical shifts (δ) and coupling constants (Hz) of the Diels-Alder adducts

Compound No.	H^1	H^{2a}	H^{2e}	H^3	H^4	H^{5a}	H^{5e}	H^6	6-CH_3	$OCOCH_3$
2	3.24(dt) $J_{1,2a}=11.0$ $J_{1,6}=11.0$	4.2—6.0(m) $J_{1,2e}=6.0$		5.70(m)		4.2—6.0(m)		4.88(dt) $J_{5a,6}=10.0$ $J_{5e,6}=6.0$	—	—
3	3.43(dt) $J_{1,2a}=11.8$ $J_{1,6}=11.8$	2.24(dd) $J_{2a,2e}=18.0$ $J_{1,2a}=11.8$	2.76(bd)	5.94(m) $J_{2e,3}=3.0$		—	5.76(dd) $J_{4,5e}=7.0$ $J_{5e,6}=3.9$	4.90(dd) $J_{5e,6}=3.9$ $J_{1,6}=11.8$	—	2.00(s)
5	3.49(dd) $J_{1,2a}=9.2$ $J_{1,6}=12.0$	5.64(d) $J_{1,2a}=9.2$	—	6.13(m)		—	5.86(m) $J_{4,5e}=6.0$	5.04(dd) $J_{5e,6}=4.2$ $J_{1,6}=12.0$	—	2.04(s) 2.14(s)
7	3.47(dd) $J_{1,2a}=10.0$ $J_{1,2e}=7.0$	2.22(d) $J_{2a,2e}=19.5$	2.61(m) $J_{1,2e}=7.0$	5.68(m)		2.46(d) $J_{5a,5e}=14.8$	2.80(m)	—	1.69(s)	—
8	3.57(dd) $J_{1,2a}=11.5$ $J_{1,2e}=6.3$	2.25(d) $J_{2a,2e}=18.8$	2.76(m) $J_{1,2e}=6.3$	5.98(m)		—	5.52(d) $J_{4,5e}=10.0$	—	1.84(s)	1.95(s)
9	3.26(dd) $J_{1,2a}=11.3$ $J_{1,2e}=6.3$	2.25(d) $J_{2a,2e}=18.8$	2.76(m) $J_{1,2e}=6.3$	5.85(m)		5.35(d) $J_{4,5a}=4.8$	—	—	1.68(s)	2.05(s)
10	3.40(dd) $J_{1,2a}=5.5$ $J_{1,2e}=2.5$	2.0—3.4(m) $J_{1,2e}=2.5$		5.67(m)		2.0—3.4(m)		—	1.65(s)	—
11	3.17(dd) $J_{1,2a}=8.1$ $J_{1,2e}=6.3$	2.44(bd) $J_{2a,2e}=18.0$	2.85(bd) $J_{1,2e}=6.3$	5.54(m)	6.00(m)	5.58(m)	—	—	1.65(s)	2.08(s)

Measured in $CDCl_3$.

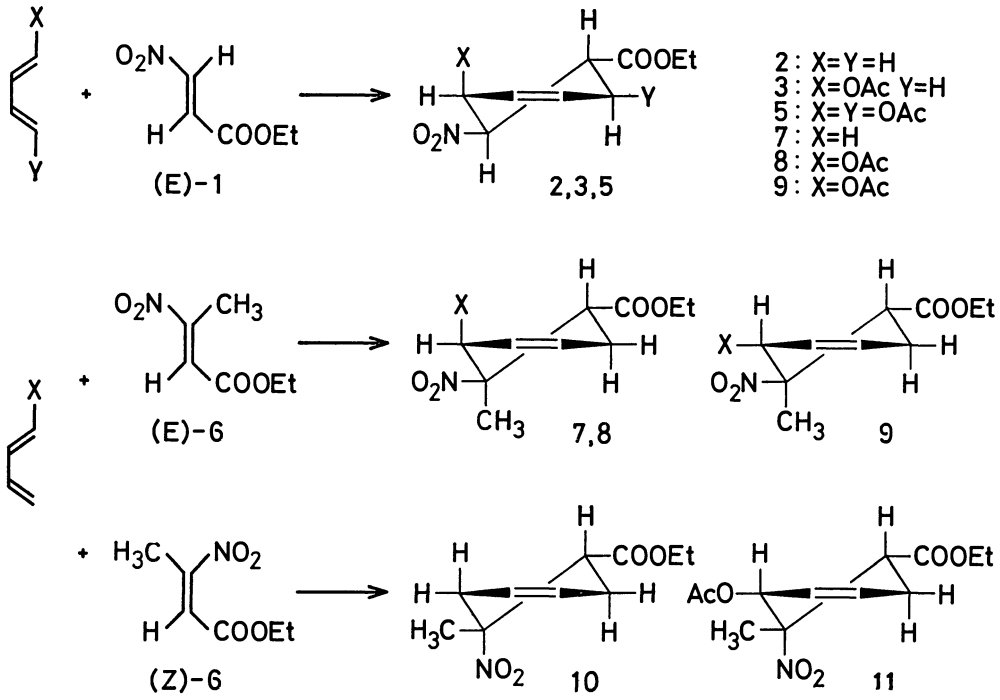

Scheme 2.

cis-addition principle, indicates the structure of **11** to be ethyl *t*-5-acetoxy-*t*-6-methyl-*c*-6-nitro-3-cyclohexene-*r*-1-carboxylate.

Experimental

All boiling and melting points are uncorrected. The IR spectra were recorded with a Hitachi EPI-G3 Spectrometer. The NMR spectra were measured with a JNM-PS-100 Spectrometer (Japan Electron Optics Laboratory Co., Ltd), using tetramethylsilane as an internal standard.

Preparation of ***1*** *and* ***6***. A solution of ethyl acrylate (70 g, 0.7 mol) and nitrosyl chloride (90 g, 1.36 mol) in $CHCl_3$ (500 ml) was allowed to stand at room temperature for 2 weeks. After the usual work up, 63.4 g (50.1%) of ethyl 2-chloro-3-nitropropionate, bp 64—68 °C/1 mmHg was ob-

tained. Subsequently, to a mixture of AcONa (100 g, 1.2 mol) in ether (300 ml) was added the prepared propionate (100 g, 0.55 mol) at room temperature. After stirring for 24 h, the excess AcONa and the precipitated NaCl were filtered off and the ether filtrate concentrated. The residue was distilled under reduced pressure to give **1** as a pale yellow oil, bp 95—98 °C/21 mmHg, yield 71.3 g (89.5%). IR (KBr): 1740 (ester), 1650 (C=C), 1555 and 1360 (NO_2) cm^{-1}. NMR ($CDCl_3$): δ 7.09 and 7.73 (2H, d, $J_{2,3}$=13.5 Hz, 2, 3-H).

The (*E*)- and (*Z*)-isomer of **6** were prepared by the method previously reported.[7,8]

Preparation of ***2***. *Typical Procedure*: To a solution of 1,3-butadiene (22.7 g, 0.42 mol) in dry $CHCl_3$ (50 ml) was added **1** (40 g, 10.2 mol) at room temperature. The resulting solution was heated in an autoclave at 80 °C under 2—3 atmospheres for 40 h. After removal of $CHCl_3$, the residue was distilled under reduced pressure to give **2** as a colorless oil.

Preparation of ***3***. *Typical Procedure*: To a solution of 1-acetoxy-1,3-butadiene (34 g, 0.34 mol) in dry benzene (200 ml) was added **1** (40 g, 0.28 mol), with stirring, at room temperature. After stirring for 72 h, the mixture was evaporated under reduced pressure to give a syrup. The syrup was dissolved in a solution of EtOH (50 ml) and petroleum ether (20 ml). After standing in the refrigerator for 1—2 days, the crystals separated out, were collected and washed once with petroleum ether. Recrystallization from EtOH gave **3** as colorless needles.

Reduction of ***3***. A solution of **3** (7 g, 27.2 mmol) in ether (20 ml) was added dropwise to a suspension of Al-Hg (made from Al (5 g) and $HgCl_2$ (5 g)) in ether (200 ml) with vigorous stirring at room temperature. After a few minutes, the ether began to reflux, the state being maintained by addition of a few drops of water at 20-min intervals. After addition was complete, stirring was continued for 6 h. The mixture was extracted several times with ether and the combined extracts evaporated to a crude syrup (4.8 g) which gradually solidified to give crystals. Recrystallization from $CHCl_3$ gave colorless needles to be ethyl *t*-6-*N*-acetyl-hydroxyamino-*t*-5-hydroxy-3-cyclohexene-*r*-1-carboxylate (**4**), yield 2.1 g (32%) mp 148—150 °C. IR (KBr): 3220 (OH), 1740 (ester), 1655 (C=C), 1630 (amide) cm^{-1}. NMR (DMSO-d_6): δ 1.97 (3H, s, CH_3), 2.31 (1H, dd, $J_{2a,2e}$=15.5 Hz, 2a-H), 2.49 (1H, dq, 2e-H), 3.13 (1H, dt, $J_{1,6}$=12.0 Hz, $J_{1,2e}$=5.5 Hz, $J_{1,2a}$=12.0 Hz, 1-H), 4.09 (1H, m, 5-H), 4.44 (1H, dd, $J_{5,6}$=8.0 Hz, $J_{1,6}$=12.0 Hz, 6-H), 5.73 (2H, d, 3, 4-H), 4.93 and 8.96 (2H, s and bs, OH).

Found: C, 54.38; H, 7.03; N, 5.87%. Calcd for $C_{11}H_{17}NO_5$: C, 54.31; H, 7.04; N, 5.76%.

Preparation of ***5***. A solution of 1,4-diacetoxy-1,3-butadiene (1.0 g, 5.9 mmol) and **1** (1.0 g, 6.9 mmol) in dry benzene (30 ml) was refluxed for 5.5 h and then evaporated under reduced pressure to give **5** as colorless prisms after recrystallization from EtOH.

Preparation of ***7***. A solution of (***E***)-**6** (5.0 g, 31 mmol) and 1,3-butadiene (2.0 g, 37 mmol) in dry $CHCl_3$ (30 ml) was heated in a sealed tube at 100 °C for 35 h. After removal of $CHCl_3$, the syrup was distilled under reduced pressure to give **7** as a colorless oil.

Preparation of ***8*** *and* ***9***. In the same manner, the reaction of (***E***)-**6** (4.0 g, 25 mmol) with 1-acetoxy-1,3-butadiene (3.4 g, 30 mmol) in $CHCl_3$ (30 ml) for 25 h gave a mixture of **8** and **9** as a colorless oil.

Preparation of ***10***. Similarly, the reaction of (***Z***)-**6** (5.0 g, 25 mmol) with 1-acetoxy-1,3-butadiene (2.0 g, 37 mmol in $CHCl_3$ (80 ml) for 35 h gave a mixture of **7** and **10** (6:5), which on distillation afforded **10** (20.0%).

Preparation of ***11***. A solution of (***Z***)-**6** (4.0 g, 25 mmol) and 1-acetoxy-1,3-butadiene (3.4 g, 30 mmol) in dry $CHCl_3$ (50 ml) was stirred overnight at room temperature. After removal of $CHCl_3$, the residual syrup was chromatographed on a silica gel column (benzene) to give two fractions. After removal of benzene under reduced pressure, the first fraction gave **11** as colorless crystals and the second one gave a mixture of **8** and **9** as a colorless oil.

References

1) Part XV: C. Shin, Y. Yonezawa, K. Suzuki, and J. Yoshimura, *Bull. Chem. Soc. Jpn.*, **51**, 2614 (1978).

2) C. Shin, H. Narukawa, Y. Yamaura, and J. Yoshimura, *Tetrahedron Lett.*, **1977**, 2147.

3) T. Hashimoto, S. Kondo, T. Takita, M. Hamada, T. Takeuchi, Y. Okami, and H. Umezawa, *J. Antibiot.*, **21**, 653 (1968); T. Hashimoto, S. Takahashi, H. Naganawa, T. Takita, K. Maeda, and H. Umezawa, *ibid.*, **25**, 350 (1972); T. Hashimoto, S. Kondo, H. Naganawa, T. Takita, K. Maeda, and H. Umezawa, *ibid.*, **27**, 86 (1974).

4) J. R. D. McCormik, J. Reichenthal, U. Hirsch, and N. O. Sjolander, *J. Am. Chem. Soc.*, **84**, 3711 (1962).

5) Y. Sumino, S. Akiyama, K. Haibara, M. Asai, and K. Mizuno, *J. Antibiot.*, **29**, 476 (1976).

6) H. Shechter, F. Conrad, A. L. Daulton, and R. B. Kaplan, *J. Am. Chem. Soc.*, **74**, 3052 (1952); T. E. Stevens and W. D. Emmons, *ibid.*, **80**, 338 (1957).

7) C. Shin, Y. Yonezawa, H. Narukawa, K. Nanjo, and J. Yoshimura, *Bull. Chem. Soc. Jpn.*, **45**, 3595 (1972).

8) C. Shin, Y. Yonezawa, and J. Yoshimura, *Nippon Kagaku Kaishi*, **1974**, 718.

9) R. K. Hill and M. Carlson, *Tetrahedron Lett.*, **1964**, 1157.

10) L. D. Hall, *J. Org. Chem.*, **29**, 297 (1964).

Reduced Copper Catalyzed Conversion of Primary Alcohols into Esters and Ketones

Kenji TAKESHITA,* Shigeaki NAKAMURA,** and Kazuaki KAWAMOTO
Institute of Commodities, Faculty of Economics, Kagawa University, Saiwaimachi, Takamatsu, Kagawa 760

(Received November 17, 1977)

Vapor phase reactions of a mixture of two types of primary alcohols to esters and ketones over a reduced copper catalyst have been investigated. The reactions between primary alcohols and propionaldehyde have also been investigated. The effects of the molar ratio of the reactants and the reaction temperature on the yields of esters, ketones, and aldehydes have been examined. A mixture of ethyl alcohol and propyl alcohol when passed over the catalyst, the main products have been found to be propyl acetate, ethyl acetate, propyl propionate, ethyl propionate, ethyl methyl ketone, diethyl ketone, acetone, acetaldehyde, and propionaldehyde. The formation of the ester and the ketone may be presented as follows:

$$RCHO + R'CH_2OH \rightarrow \left[\begin{array}{c} OH \\ | \\ R-C-O-CH_2R' \\ | \\ H \end{array}\right] \rightarrow RCOOCH_2R' + H_2,$$

$$RCHO + R'CH_2OH \rightarrow RCOR' + CO + 2H_2.$$

Many investigators[1] have shown that the esters and the ketones were obtained, upon passing primary alcohols, aldehydes, and mixtures of them over catalysts such as copper chromite, zinc oxide, copper, metallic palladium, magnesia, and alkalized zinc chromium oxide. These papers have shown that primary alcohols with n carbon atoms are readily converted to symmetrical ketones with $2n-1$ carbon atoms and esters with $2n$ carbon atoms. The mechanism has been described in these papers for ester formation as the Tischenko Reaction mechanism. Recently, another mechanism for ester formation has been proposed by Kunugi *et al.*[2] and one of the present authors.[3] The former investigators found that the ester was formed by the reaction between an aldehyde and an alcohol. In a study of the action of the reduced copper catalyst on alcohols, one of the present authors reported that the ester was formed by a hemiacetal mechanism.

In the formation of ketones, Komarewsky *et al.*[4] found that, in the presence of a chromium oxide catalyst, primary alcohols were converted to ketones by the following mechanism: (1) the dehydrogenation of the alcohol to the aldehyde, (2) the aldol condensation of the aldehyde, (3) the removal of carbon monoxide from the CHO group of the aldol, leaving a secondary alcohol, and (4) the dehydrogenation of this alcohol to the ketone. Kagan *et al.*[5] found that ethyl acetate was an important intermediate when ethyl alcohol was converted to acetone. Matsota *et al.*[6] reported that aliphatic ketones were prepared by heating esters in the presence of manganese oxide at 400—500 °C. Bolotov *et al.*,[7] however, reported that ethyl acetate was not an intermediate in the formation of acetone. Geisler *et al.*[8] examined the catalytic ketonization of ethyl alcohol in the presence of water vapor, and found that the formation of the ketone was presented by the reaction equation as follows:

$$2C_2H_5OH + H_2O \rightarrow CH_3COCH_3 + CO_2 + 4H_2.$$

The present investigation has been undertaken in order to clarify the mechanism of the formation of the ester and the ketone.

Experimental

Reactants. The aliphatic alcohols such as ethyl alcohol, propyl alcohol, butyl alcohol, and isobutyl alcohol were purified, after being dried with calcium oxide or potassium carbonate, by distillation through a fractionating column. Propionaldehyde, ethyl acetate, propyl propionate, ethyl propionate, propyl acetate, isobutyl acetate, and ethyl isobutyrate were purified by drying with anhydrous sodium sulfate, followed by fractional distillation under atmospheric pressure. The purity of the reactants was confirmed by gas chromatographic analysis. (PEG-6000, DEGS, and PEG-1000 F columns.)

Catalyst. The catalyst was prepared by the same method as described in a previous paper.[9]

Apparatus and Procedure. The apparatus and the procedure employed were similar to those used in a previous investigation.[9] Experiments were performed at 250 and 300 °C under atmospheric pressure.

Identification and Analysis of the Reaction Products. The reaction products were separated by gas chromatography (PEG-6000, DEGS, and Tween-80 columns. For the determination of water, a 3 m column packed with Shimalite F impregnated with PEG-1000 was used.), and each constituent was identified by NMR and IR spectra. The gaseous products were analyzed by gas chromatography. (activated charcoal and silica-gel columns.) The quantitative analysis of liquid and gaseous products was performed by gas chromatography.

Results

Table 1 shows the influences of the molar ratio of the reactants and the reaction temperature on the yields of the products. The results obtained by passing a mixture of butyl alcohol and propyl alcohol or propionaldehyde over the catalyst are summarized in Table 2. Further, the results obtained by the reaction of isobutyl alcohol and propyl alcohol or propional-

** Present address: Department of Chemistry, Takamatsu Technical College, Takamatsu, Kagawa 760.

Table 1. The Cu-catalyzed reaction of the mixture of ethyl alcohol and propyl alcohol or propionaldehyde

Experiment No.	1	2	3	4	5	6	7	8	9	10	11	12	13	14
Reaction temp (°C)	250	250	250	250	250	250	250	250	250	250	250	250	300	300
Reactant charged (g)														
Ethyl alcohol	20.10	14.13	11.64	7.91	5.92	4.06	—	15.54	11.79	9.59	5.55	—	7.76	7.62
Propyl alcohol	—	6.21	7.72	10.31	15.36	15.13	19.96	—	—	—	—	—	10.11	—
Propionaldehyde	—	—	—	—	—	—	—	6.69	7.49	11.97	15.47	16.19	—	9.85
Velocity (g/h)	7.2	6.5	6.6	6.1	6.8	6.5	7.2	7.0	6.5	6.9	6.9	7.1	6.5	6.7
Liquid products (g)	19.02	18.89	18.15	17.35	20.13	17.99	19.00	20.68	18.29	20.06	19.22	15.15	16.40	16.02
Composition of liquid products[a] (%)														
Acetaldehyde	18.1	13.8	9.9	6.9	6.1	3.4	—	12.4	9.9	8.3	4.1	—	12.4	12.9
Ethyl alcohol	61.7	31.6	24.0	16.2	14.6	10.8	0.5	34.0	25.3	21.9	12.2	—	7.3	16.9
Propyl alcohol	—	13.4	20.2	24.8	30.6	37.5	62.7	6.4	6.3	5.3	4.4	2.6	11.5	5.3
Propionaldehyde	—	5.5	6.4	8.4	12.7	13.1	15.4	15.4	21.2	38.7	57.7	95.0	18.0	35.0
Ethyl acetate	16.8	14.0	13.0	8.4	2.5	0.9	—	16.2	12.5	6.6	3.0	—	8.5	6.2
Propyl acetate	—	5.9	7.1	9.0	7.1	5.9	—	1.6	1.2	0.8	0.5	—	9.4	T
Propyl propionate	—	2.3	3.8	8.3	10.5	13.1	13.7	1.9	1.7	1.5	1.2	0	8.4	1.4
Ethyl propionate	—	3.5	4.6	5.2	3.9	2.9	—	5.9	12.7	10.4	10.0	—	5.2	6.6
Acetone	1.6	1.5	1.2	0.8	0.5	0.2	—	1.6	1.2	0.6	0.5	—	1.4	1.0
Ethyl methyl ketone	—	5.7	6.0	6.7	5.9	4.3	—	3.0	6.4	5.1	4.7	—	9.7	8.9
Diethyl ketone	—	1.2	1.6	3.4	4.0	6.1	6.4	T	T	T	T	—	5.5	0.2
Acetic acid	T	T	T	T	T	T	—	T	T	T	T	—	0.6	0.4
Propionic acid	—	0.2	0.2	0.3	0.4	0.4	0.5	0.4	0.4	0.5	0.8	2.4	0.3	0.9
Aldol	0.3	T	T	T	T	T	—	T	T	T	T	—	T	T
Crotonaldehyde	0.2	T	T	T	T	T	—	T	T	T	T	—	T	T
Butyraldehyde	0.2	T	T	T	T	T	—	T	T	T	T	—	T	T
2-Buten-1-ol	0.2	T	T	T	T	T	—	T	T	T	T	—	T	T
Butyl alcohol	0.4	T	T	T	T	T	—	T	T	T	T	—	T	T
Methyl alcohol	0.1	T	T	T	T	T	0.2	T	T	T	T	—	1.3	1.2
Water	T	T	T	T	T	T	T	T	T	T	T	T	T	T
Unidentified products	0.4	1.4	2.0	1.6	1.2	1.4	0.6	1.2	1.2	0.3	0.9	T	0.5	3.1

a) The yields of each compound produced were given by (grams of each compound per grams of total reaction product) × 100(%). T=Trace.

Table 2. Cu-catalyzed reaction of the mixture of propyl alcohol or propionaldehyde and butyl alcohol (Reaction temp: 250 °C)

Experiment No.	15	16	17
Reactant charged (g)			
Propyl alcohol	8.36	—	—
Propionaldehyde	—	9.43	—
Butyl alcohol	10.21	12.12	19.98
Velocity (g/h)	6.4	6.8	7.2
Liquid products (g)	17.94	19.95	18.84
Composition of liquid products (%)			
Propionaldehyde	5.8	21.4	—
Propyl alcohol	29.3	14.7	0.2
Butyraldehyde	7.0	7.2	18.9
Butyl alcohol	31.7	39.9	64.0
Propyl propionate	3.5	0.2	—
Butyl propionate	4.1	3.7	—
Butyl butyrate	4.7	2.5	15.7
Propyl butyrate	4.4	0.4	—
Diethyl ketone	0.1	T	—
Ethyl propyl ketone	0.4	0.2	—
Dipropyl ketone	0.2	0.1	0.5
Propionic acid	0.2	0.6	—
Butyric acid	T	T	T
Ethyl alcohol	0.3	0.3	0.2
Methyl alcohol	T	0.1	0.1
Water	T	T	T
Unidentified products	8.3	8.7	0.4

T=Trace.

Table 3. Cu-catalyzed reaction of the mixture of propyl alcohol or propionaldehyde and isobutyl alcohol (Reaction temp: 250 °C)

Experiment No.	18	19
Reactant charged (g)		
Propyl alcohol	8.41	—
Propionaldehyde	—	9.47
Isobutyl alcohol	10.36	12.44
Velocity (g/h)	6.6	6.5
Liquid products (%)	17.71	20.75
Composition of liquid products (%)		
Propionaldehyde	6.1	23.1
Propyl alcohol	29.4	13.7
Isobutyraldehyde	6.3	6.0
Isobutyl alcohol	32.3	43.1
Propyl propionate	3.2	0.2
Isobutyl propionate	4.1	2.9
Isobutyl isobutyrate	4.6	2.2
Propyl isobutyrate	4.9	0.4
Diethyl ketone	0.1	T
Ethyl isopropyl ketone	0.6	0.2
Diisopropyl ketone	0.3	0.2
Propionic acid	0.3	0.7
Isobutyric acid	T	T
Ethyl alcohol	0.2	0.2
Methyl alcohol	T	T
Water	T	T
Unidentified products	7.6	7.1

T=Trace.

dehyde are summarized in Table 3. Tables 4 and 5 show the results of the catalytic decomposition of the esters. The yields of each compound shown in these tables are an average of two and three experiments under constant operating conditions.

Influence of the Molar Ratio of the Reactants on the Yields of Esters and Ketones. *a) Reaction between Ethyl Alcohol and Propyl Alcohol*: As may be seen from Table 1, the yields of esters and ketones depended on the molar ratio of the reactants as follows: 1) The yield of ethyl acetate increased with an increase in the molar ratio of ethyl alcohol to propyl alcohol. 2) The yield of propyl propionate decreased with an increase in the molar ratio of ethyl alcohol to propyl alcohol. 3) The maximum yields of propyl acetate and ethyl propionate were obtained when ethyl and propyl alcohols were mixed in the ratio of approximately 1:1. 4) Further, the yield of each ester was in the following order: propyl acetate>ethyl acetate, propyl propionate>ethyl propionate. 5) The yield of acetone increased with an increase in the molar ratio of ethyl alcohol to propyl alcohol, but the yield of diethyl ketone decreased. When the molar ratio of the reactants was about 1:1, the maximum yield of ethyl methyl ketone was obtained. As may be seen from Table 1, the yield of the unsymmetrical ketone was larger than that of the symmetrical ketone except in the case of a large excess of propyl alcohol.

From these results, it is considered that ethyl acetate and acetone may be formed from ethyl alcohol, that propyl propionate and diethyl ketone may be formed from propyl alcohol, and that propyl acetate, ethyl propionate, and ethyl methyl ketone may be formed by the reaction between ethyl alcohol and propyl alcohol.

When the mixture of two alcohols or an alcohol and propionaldehyde was passed over the catalyst, carbon monoxide, carbon dioxide, and hydrocarbon were detected as gaseous products, and it was found that the molar ratio of carbon monoxide to carbon dioxide was 3 : 1—2 in the cases of Experiment Nos. 2—6 in Table 1.

b) Reaction between Ethyl Alcohol and Propionaldehyde: As may be seen from Table 1, when propionaldehyde was used in place of propyl alcohol, the kinds of reaction products were the same as those obtained by passing the mixture of ethyl and propyl alcohols over the catalyst, but there were distinct differences in the yields of the ester and the ketone in the products. It was found that, when propionaldehyde was used in place of propyl alcohol, the yield of ethyl propionate increased remarkably, but the yield of propyl esters decreased, and little diethyl ketone was obtained. As is shown in Experiment No. 12 of Table 1, propionaldehyde did not condense to give the ester and ketone.

c) Reaction between Secondary Alcohol and Primary Alcohol or Propionaldehyde: When the mixture of a secondary alcohol and a primary alcohol or propionaldehyde was passed over the catalyst, the esters and the ketones were obtained. For example, when

Table 4. Cu-catalyzed decomposition of various esters

Experiment No.	20	21	22	23	24
Reaction temp (°C)	250	250	300	300	250
Reactant charged (g)					
Ethyl acetate	18.24	—	—	—	10.22
Propyl acetate	—	—	13.47	—	—
Ethyl propionate	—	—	—	12.57	—
Propyl propionate	—	18.08	—	—	—
Propyl alcohol	—	—	—	—	6.08
Hydrogen (l)	—	—	2.85	2.61	—
Velocity					
Liquid reactant (g/h)	6.6	7.0	7.1	7.1	6.5
Hydrogen (l/h)	—	—	2.85	2.61	—
Liquid products (g)	17.31	17.02	12.06	11.73	14.98
Composition of liquid products (%)					
Acetaldehyde	0.3	—	2.8	1.9	1.5
Ethyl alcohol	0.5	—	2.0	2.5	2.2
Propionaldehyde	—	0.3	4.4	3.5	6.0
Propyl alcohol	—	0.3	4.8	2.7	20.7
Ethyl acetate	97.9	—	1.1	0.3	50.7
Propyl acetate	—	—	79.3	0.3	6.4
Ethyl propionate	—	—	0.5	84.7	0.4
Propyl propionate	—	98.5	0.9	0.5	3.9
Acetone	0.5	—	0.2	0.1	1.9
Ethyl methyl ketone	—	—	3.7	3.1	4.1
Diethyl ketone	—	0.3	T	T	1.5
Acetic acid	0.4	—	T	T	T
Propionic acid	—	0.4	T	T	0.3
Water	T	T	T	T	T
Unidentified products	0.4	0.2	0.3	0.4	0.4

T=Trace.

propyl alcohol and isopropyl alcohol were used as the reactants, propyl propionate, isopropyl propionate, diethyl ketone, and acetone were obtained.

Influence of the Reaction Temperature on the Yields of Ester and Ketone. As may be seen in Experiment Nos. 4 and 13 of Table 1, the conversion of primary alcohols depended upon the reaction temperature, and the yields of aldehydes and ketones increased with a rise in the reaction temperature, but the yield of the ester was little affected.

Decomposition of Ester. When ethyl acetate was passed over the catalyst, acetone was obtained, and in the case of propyl propionate, diethyl ketone. Experiment Nos. 22 and 23 of Table 4 showed that the kinds of the reaction products obtained by using propyl acetate as the reactant were the same as those obtained by using ethyl propionate. Further, Table 5 showed that the kinds of the products obtained from isobutyl acetate were the same as those obtained from ethyl isobutyrate, when isobutyl acetate and ethyl isobutyrate were passed over the catalyst in the presence of hydrogen.

Experiment Nos. 20 and 21 of Table 4 showed that, when the ester type $C_nH_{2n+1}COOC_{n+1}H_{2n+3}$ such as $CH_3COOC_2H_5$, $C_2H_5COOC_3H_7$, and $C_3H_7COOC_4H_9$ was passed over the catalyst, a symmetrical ketone was produced. However, Experiment Nos. 22, 23, 25, and 26 of Tables 4 and 5 showed that, when the other esters were passed over the catalyst, the results were as follows: (1) most of the ketones formed were unsymmetrical ketones. (2) the yield of the ketone increased in the presence of hydrogen. (3) the yield of carbon monoxide was larger than that of carbon dioxide.

Discussion

The Formation Mechanism of Ester and Ketone Obtained by the Catalytic Reaction of Primary Alcohols. a) Formation Mechanism of Ester: Eto[10] reported that the copper catalyst strongly accelerated the ester formation by the Tischenko Reaction. Saito and Tanabe[11] also reported that the formation of the ester was similar to the Tischenko Reaction mechanism, when benzyl benzoate was formed from benzaldehyde in the presence of magnesium oxide or calcium oxide.

However, in the present research, propionaldehyde did not condense to give the ester. This indicates that the Tischenko Reaction type esterification does not take place under the present reaction conditions. Kunugi *et al.*[12] reported that the ester was not formed by the Tischenko Reaction mechanism, but by the reaction between an alcohol and an aldehyde. Dolgow[13] found that, when the mixture of alcohol or aldehyde and hydrogen was passed over the copper catalyst, an ester was obtained. He proposed a hemiacetal intermediate mechanism as the scheme of the

TABLE 5. THE Cu-CATALYZED DECOMPOSITION OF ISOBUTYL ACETATE AND ETHYL ISOBUTYRATE
(Reaction temp: 300 °C)

Experiment No.	25	26
Reactant charged (g)		
Isobutyl acetate	13.00	—
Ethyl isobutyrate	—	12.59
Hydrogen (l)	2.75	2.05
Velocity		
Liquid reactant (g/h)	7.1	7.1
Hydrogen (l/h)	1.5	1.1
Liquid products (g)	11.98	11.49
Composition of liquid products (%)		
Acetaldehyde	2.3	1.8
Ethyl alcohol	2.0	2.4
Isobutyraldehyde	3.6	1.7
Isobutyl alcohol	4.6	1.4
Isobutyl acetate	83.0	0.2
Ethyl acetate	1.0	0.2
Ethyl isobutyrate	0.4	86.1
Isobutyl isobutyrate	0.8	0.4
Isopropyl methyl ketone	2.2	1.7
Acetone	T	T
Diisopropyl ketone	T	T
Acetic acid	T	T
Isobutyric acid	T	T
Water	T	T
Unidentified products	0.1	4.1

T=Trace.

formation of the ester. It was reported by Tarama[14] that, when the hydrogenolysis of an ester was carried out, the ester was converted to two alcohols *via* a hemiacetal. Covert *et al.*[15] reported that a cyclic acetal was converted to ether, alcohol, and hydrocarbon *via* a hemiacetal.

As reported above, when propionaldehyde was used in place of propyl alcohol, the yield of propyl esters which appear to be produced by the participation of propyl alcohol was very small, suggesting that the ester is produced by the reaction between the aldehyde and the alcohol.

From these results, the formation mechanism of esters may be explained by the hemiacetal intermediate mechanism as follows:

$$CH_3CH_2CH_2OH \rightarrow CH_3CH_2CHO + H_2$$

$$CH_3CH_2CHO + CH_3CH_2CH_2OH \rightarrow \left[\begin{array}{c} OH \\ | \\ CH_3CH_2-C-O-CH_2CH_2CH_3 \\ | \\ H \end{array}\right]$$

$$\left[\begin{array}{c} OH \\ | \\ CH_3CH_2-C-O-CH_2CH_2CH_3 \\ | \\ H \end{array}\right] \rightarrow CH_3CH_2-\overset{O}{\overset{\|}{C}}-O-CH_2CH_2CH_3 + H_2$$

b) Formation Mechanism of Ketone: Komarewsky *et al.*[16] reported that aldehydes and aldols seemed to be logical intermediates when the ketone was formed from primary alcohols, and that the order of the conversion of the reactants to the ketones was aldol> aldehyde>alcohol. Bolotov *et al.*[7] reported that the acetone was formed by the aldol condensation of acetaldehyde. Geisler and Danneberg[8] reported that ethyl alcohol was converted to acetone *via* the aldehyde and acid. Further, Kagan *et al.*[5] reported that, when ethyl alcohol was converted to acetone, ethyl acetate was an important intermediate in the chain of reactions involved. Dolgow and Golodnikow[17] showed that the ketone was obtained by the catalytic reaction of primary alcohol, and that the reaction was proceeded by an ester intermediate mechanism.

In the present research, however, as may be seen in Experiment No. 12 of Table 1, no ketone and aldol were produced from propionaldehyde. Aldol condensation products were not obtained by the catalytic reactions of the alcohols except ethyl alcohol. Therefore, aldol appears not to be an intermediate of the ketone formation from primary alcohol with the reduced copper catalyst.

From the experimental results obtained in the reaction between ethyl alcohol and propyl alcohol or propionaldehyde and by the decomposition of esters, the formation of ketones with the reduced copper catalyst may proceed along two paths.

I) One appears to be formed by the following scheme.

$$\left.\begin{array}{l} CH_3CH_2CH_2OH + CH_3CHO \\ CH_3CH_2OH + CH_3CH_2CHO \end{array}\right\} \longrightarrow CH_3CH_2-\overset{O}{\overset{\|}{C}}-CH_3 + CO + 2H_2$$

II) Another may be accounted for by Kagan's Process[5] as follows:

$$2C_2H_5COOC_3H_7 \rightarrow C_2H_5COC_2H_5 + C_3H_7OH + C_3H_6 + CO_2 .$$

From the molar ratio of carbon monoxide to carbon dioxide, it is considered that, when the primary alcohol is converted to the ketone, the ketone may be produced by either Process I or II, but that Process I predominates. In the case of the decomposition of the esters, most of the ketone may be formed by Process I.

References

1) (a) R. E. Dunbar, *J. Org. Chem.*, **3**, 242 (1938); R. E. Dunbar and M. R. Arnold, *ibid.*, **10**, 501 (1945); (b) V. N. Ipatieff and V. Haensel, *J. Org. Chem.*, **7**, 189 (1942); (c) V. I. Komarewsky, C. F. Price, and J. R. Coley, *J. Am. Chem. Soc.*, **69**, 238 (1947); V. I. Komarewsky and J. T. Stringer, *ibid.*, **63**, 921 (1941); J. R. Coley and V. I. Komarewsky, *ibid.*, **74**, 4448 (1952); (d) M. Takayasu, *Nippon Kagaku Zasshi*, **64**, 457, 461, 676, 684 (1943); (e) K. Hoshiai, *Kogyo Kagaku Zasshi*, **54**, 238 (1951); **56**, 381 (1953); **57**, 76 (1954); (f) S. Kudo, *Kogyo Kagaku Zasshi*, **58**, 719 (1955); (g) T. Ishiguro and Otsuka, *Yakugaku Zasshi*, **78**, 454 (1958); (h) B. N. Dolgov, B. A. Bolotov, and L. A. Komissarova, *J. Appl. Chem. USSR*, **28**, 61 (1955); B. A. Bolotov, and P. M. Adrov, *ibid.*, **28**, 271 (1955); B. A. Bolotov, P. M. Adrov, and L. K. Prokhorova, *ibid.*, **28**, 489 (1955); B. A. Bolotov and N. A. R. Marshova, *Zh. Prikl. Khim.*, **30**, 286 (1957); B. A. Bolotov and L. K. Smirnova, *Zh. Obshch. Khim.*, **25**, 1987 (1955); (i) Kh. M. Minachev, G. A. Loginov, and

M. A. Markov, *Kinet. Katal.*, **7**, 904 (1966); (j) U. R. Rao, R. Kumar, and N. R. Kuloor, *I&EC Process Design and Development*, **8**, 9 (1969); (k) K. Tanabe, K. Saito, T. Iizuka, H. Hattori, T. Yamaguchi, M. Sakashita, and I. Matsuzaki, *Asahigarasu Kogyo Gijyutsu Shoreikai Kenkyu Hokoku*, **15**, 303 (1969); (l) E. Donath, *Chem.-Ztg.*, **12**, 1191 (1889).

2) T. Kunugi, T. Matsuura, and T. Kono, *Kogyo Kagaku Zasshi*, **71**, 1517 (1968).

3) K. Kawamoto and Y. Nishimura, *Bull. Chem. Soc. Jpn.*, **44**, 819 (1971).

4) V. I. Komarewsky and J. R. Coley, *J. Am. Chem. Soc.*, **63**, 700, 3269 (1941).

5) M. J. Kagan, I. A. Sobolew, and G. D. Lubarsky, *Chem. Ber.*, **68**, 1140 (1935).

6) N. P. Matsota and V. D. Mezhov, *Chem. Abstr.*, **75**, 88114x (1971).

7) B. A. Bolotov and S. N. Borisov, *Zh. Obshch. Khim.*, **27**, 1237 (1957); B. A. Bolotov and B. N. Dologov, *Chem. Abstr.*, **59**, 8579a (1963).

8) G. Geisler and R. Danneberg, *J. Prakt. Chem.*, **26**, 296 (1964); M. Raetzch and G. Geisler, *Z. Chem.*, **5**, 229 (1965).

9) S. Nakamura and K. Kawamoto, *Bull. Chem. Soc. Jpn.*, **44**, 1072 (1971).

10) K. Eto, *Yuki Gosei Kagaku Kyokai Shi*, **21**, 61 (1963).

11) K. Saito and K. Tanabe, *Nippon Kagaku Kaishi*, **1973**, 1845.

12) T. Kunugi, T. Kono, H. Yoshino, and Y. Shinohara, *Kogyo Kagaku Zasshi*, **71**, 1638 (1968); T. Kunugi and T. Kono, *ibid.*, **72**, 1282 (1969); T. Kunugi, T. Kono, and H. Yoshino, *Nippon Kagaku Kaishi*, **1972**, 2265; T. Kunugi, T. Kono, M. Yanagisawa, and H. Arai, *ibid.*, **1972**, 2271; T. Kunugi, T. Kono, and Y. Shinohara, *ibid.*, **1973**, 454.

13) B. N. Dolgow "Die Katalyse in der Organishen Chemie," Veb Deutscher Verlag der Wissenschaften, Berlin (1963), pp. 275—277.

14) K. Tarama "Hannobetsu Jitsuyoshokubai," Kagaku Kogyo Sha, Tokyo (1970), p. 293.

15) L. W. Covert, R. Connor, and H. Adkins, *J. Am. Chem. Soc.*, **54**, 1651 (1932).

16) V. I. Komarewsky, "Advanced in Catalyst and Related Subjects," Vol. VIII, ed by W. G. Frankenburg, V. I. Komarewsky, and E. K. Rideal, Academic Press, New York, N. Y. (1956), pp. 207—217.

17) B. N. Dolgow and G. V. Golodnikow, *Zh. Obshch. Khim.*, **24**, 987, 1167, 1364 (1954).

Photo-induced Oxidation of Diethylene Glycol Dimethyl Ether and Analogues with Aqueous Hydrogen Peroxide[1a)]

Yoshiro OGATA,* Kohtaro TOMIZAWA, and Kohzo FUJII

Department of Applied Chemistry, Faculty of Engineering, Nagoya University, Chikusa-ku, Nagoya 464

(Received December 19, 1977)

Photo-oxidation of diethylene glycol dimethyl ether(DEDE), ethylene glycol dimethyl ether(EDE) and ethylene glycol monomethyl ether(EME) in the presence of aqueous H_2O_2 has been studied. DEDE and EDE give photo-oxidation products containing methanol, EME, methoxyacetaldehyde, methoxyacetic acid and methyl formate. EME gives products containing methanol, methoxyacetaldehyde and methyl formate. The oxidation is started by hydrogen atom abstraction by HO· radicals formed by the photolysis of H_2O_2. A reaction mechanism leading to the products(derived by initial C–O and C–C fissions) is postulated.

The photolysis of ethylene glycol monomethyl ether (EME) alone gives formaldehyde, methane, methanol, hydrogen *etc.*,[1b)] while that of EME and ethylene glycol dimethyl ether(EDE) under oxygen atmosphere gives formaldehyde, methanol, methyl formate.[2)]

However, no data are available on the photo-oxidation of glycols and their ethers in the presence of hydrogen peroxide. We are interested in this photo-oxidation as a model reaction for the photo-oxidative removal of nonionic surfactants in waste water which are difficult to remove biologically.

Here we wish to present data on the products and probable schemes for the photo-oxidation of diethylene glycol dimethyl ether(DEDE), EDE and EME in the presence of aqueous H_2O_2. Most of the experiments were carried out with DEDE, since it is the most suitable model compound for polyethylene glycols.

Results

A. Diethylene Glycol Dimethyl Ether(DEDE). Products: The photo-oxidation products of 0.25 M DEDE in the presence of 0.48 M H_2O_2 in water at pH 3.9 in a quartz tube with a high-pressure Hg lamp for 1 h gave the following products after vacuum distillation: CH_4, C_2H_6, CH_3OH, CH_3CHO, HCO_2CH_3, HCO_2H, $HOCH_2CH_2OH$, CH_3OCH_2CHO, $CH_3OCH_2CH_2OH$-(EME), $CH_3OCH_2CO_2H$, $HCO_2CH_2CH_2O_2CH$ and $CH_3OCH_2CH_2OCH_2CH_2OH$. The products were identified by GC-MS analysis and also by GLC analysis in comparison with GLC peaks of authentic samples using two kinds of columns.

Photolysis of H_2O_2. The rate of photo-oxidation of 0.184 M DEDE with 0.937 M H_2O_2 in water at pH 3.7 was measured at 20 °C by iodometry of H_2O_2 and GLC analysis of substrate (Table 1A). With the progress of reaction, the yields of the products changed (Table 1B).

$$\text{Yield (\%)} = \frac{\text{[produced product] (M)}}{\text{[decomposed substrate] (M)}} \times \frac{\text{carbon number of product}}{\text{carbon number of substrate}} \times 100$$

The decomposition of H_2O_2 is of zeroth-order within 60 min, and over two equivalents of H_2O_2 are necessary in order to decompose DEDE(Table 1A).

The yields changed only in a small range after 20 min irradiation(Table 1B). This suggests fast attainment of steady state in which the formation and consumption of the intermediates are fairly balanced.

Table 1A. Photo-decomposition of 0.937 M H_2O_2 and 0.184 M DEDE in aqueous solution at 20 °C

Irrad. time min	$[H_2O_2]$ M	Dec $[H_2O_2]$ %	[DEDE] M	Dec [DEDE] %
0	0.937	—	0.184	—
10	0.888	5.2	0.168	8.7
20	0.833	11.1	0.141	23.4
30	0.766	18.2	0.103	44.0
40	0.700	25.3	0.072	61.0
60	0.598	36.2	0.060	67.2

Table 1B. Yields of products with the progress of photolysis of DEDE-H_2O_2 at 20 °C

Irrad. time min	CH_3OH %	HCO_2H %	HCO_2CH_3 %	CH_3OCH_2CHO %	$CH_3OCH_2CH_2OH$ (EME) %	$CH_3OCH_2CO_2H$ %
10	15.8	—	3.4	8.4	39.1	8.6
20	10.5	—	3.0	6.0	18.8	4.4
30	8.1	—	1.6	4.6	17.9	3.0
40	5.6	trace	1.9	5.1	17.1	2.6
60	10.2	1.0	1.6	5.3	16.9	2.0

TABLE 2A. EFFECT OF INITIAL CONCENTRATION OF H_2O_2 ON PHOTO-OXIDATION OF DEDE[a)]

Run	$[H_2O_2]_0$ M	Dec $[H_2O_2]$ M	$[DEDE]_0$ M	Dec [DEDE] M	Dec [DEDE] %
1	2.85	0.239	0.194	0.114	58.8
2	1.90	0.359	0.191	0.129	67.7
3	0.927	0.391	0.200	0.146	73.2
4	0.208	0.174	0.186	0.086	46.0
5	0.095	0.085	0.183	0.048	26.0

a) Irradiated for 1 h in H_2O at 20 °C.

TABLE 2B. EFFECT OF INITIAL CONCENTRATION OF H_2O_2 ON THE PRODUCTS YIELDS IN PHOTO-OXIDATION OF DEDE[a)]

Run	$[H_2O_2]_0$ M	CH_3OH %	HCO_2H %	HCO_2CH_3 %	CH_3OCH_2CHO %	$CH_3OCH_2CH_2OH$ (EME) %	$CH_3OCH_2CO_2H$ %
1	2.85	7.2	0.8	4.8	1.1	10.2	3.6
2	1.90	7.9	1.6	3.4	3.1	11.4	2.8
3	0.927	7.2	0.8	1.6	3.8	12.5	1.5
4	0.208	8.1	trace	trace	6.3	17.7	0.9
5	0.095	7.9	—	trace	6.6	20.7	0.9

a) Irradiated for 1 h in H_2O at 20 °C.

Effect of Initial Concentration of H_2O_2. In order to examine the contribution of H_2O_2 to the oxidation of DEDE, the effects of initial concentration of H_2O_2 ($[H_2O_2]_0$) on the oxidation rate of DEDE(Table 2A) and on product distribution(Table 2B) were studied with a nearly constant initial concentration of DEDE.

The decomposition of DEDE is proportional to that of H_2O_2, indicating the efficient oxidation of the substrate by H_2O_2. The decomposition rates of H_2O_2 in runs 1—3(Table 2A) are greater than those in runs 4 and 5. The number of absorbed photon per unit time is almost constant regardless of the initial concentration of H_2O_2 and substrate. Thus the observed variation of decomposition rates of H_2O_2 with change of $[H_2O_2]_0$ indicates the presence of a scheme for the decomposition of H_2O_2 induced by HO· radicals and/or other radicals generated by substrate decomposition.

The product distribution depends considerably on $[H_2O_2]_0$. The yields of methoxyacetic acid, methyl formate and formic acid increase with increasing $[H_2O_2]_0$. The effect of $[H_2O_2]_0$ on the yields of methoxyacetaldehyde and ethylene glycol monomethyl ether (EME) is reversed, these products being more susceptible to further oxidation as compared with other products.

Effect of Pyrex-filtered Light. Photo-oxidation with light through a Pyrex-filter was examined with an aqueous mixture of 0.060 M DEDE and 1.18 M H_2O_2 at pH 3.6 for 5 h. The conversion of substrate was 28% after 1 h; 39% after 2 h; 47% after 3 h; 63% after 5 h. Photo-oxidation in a Pyrex vessel is slower than that in a quartz vessel, since Pyrex absorbs 250 nm light which is much more effective for decomposition of H_2O_2 than above 300 nm light.

Formation of CO_2. To test the possibility of complete oxidation of DEDE, an aqueous mixture of

TABLE 3. YIELDS OF PRODUCTS IN PHOTO-OXIDATION OF 0.223 M EDE WITH 0.909 M H_2O_2 AT 20 °C

Irrad. time min	Dec $[H_2O_2]$ %	Dec [EDE] %	CH_3OH %	HCO_2CH_3 %	CH_3OCH_2CHO %	EME %	$CH_3OCH_2CO_2H$ %
5	2.8	11.2	19.4	8.5	trace	25.8	2.9
10	7.4	24.3	15.7	6.9	2.5	22.9	3.1
15	11.6	35.8	14.5	7.8	2.1	19.6	2.0
20	16.5	42.3	14.6	7.3	3.7	16.2	1.8
30	27.3	57.1	14.3	6.0	4.1	16.2	1.3

TABLE 4. YIELDS OF PRODUDTS IN PHOTO-OXIDATION OF 0.167 M EME WITH 0.919 M H_2O_2 AT 20 °C

Irrad. time min	Dec $[H_2O_2]$ %	Dec [EME] %	CH_3OH %	HCO_2H %	HCO_2CH_3 %	CH_3CO_2H %	CH_3OCH_2CHO %
5	2.9	5.4	30.2	—	trace	—	11.8
10	4.6	13.6	18.8	trace	3.1	—	8.0
15	7.3	13.8	24.5	0.1	4.5	trace	9.2
20	7.8	20.6	19.5	0.1	3.2	0.1	8.0
30	13.8	40.1	16.1	0.2	2.4	0.2	6.6

0.0711 M DEDE and 1.16 M H_2O_2 was irradiated for 29 h. The CO_2 gas evolved, which was absorbed in aqueous $Ba(OH)_2$, was 77.5% of calculated value from the substrate. Taking into account the probable loss of CO_2, polyglycols may be completely converted to CO_2 and water after long irradiation.

B. Ethylene Glycol Dimethyl Ether (EDE). Photo-oxidation of 0.233 M EDE with 0.909 M H_2O_2 in water at pH 3.7 afforded the same products as those from DEDE, but with different composition (Table 3).

C. Ethylene Glycol Monomethyl Ether (EME). Photo-oxidation of 0.167 M EME with 0.919 M H_2O_2 in water gave the same products as those from EDE along with acetic acid (Table 4).

Discussion

The absorption coefficients(ε) for H_2O_2 and DEDE in an aqueous solution were measured at 250 nm, which is the principal wavelength of the high-pressure Hg lamp employed. The values of ε were: 26.4(250 nm) for H_2O_2, 0.437(250 nm) for DEDE, 0.94(300 nm) for H_2O_2, 0.36(315 nm) for H_2O_2 and 0(over 300 nm) for DEDE. Thus the photolysis of DEDE itself should be negligible in comparison with that of H_2O_2. The same is true with other substrates(EDE and EME). The initial step for the photo-oxidation should be the excitation and photo-decomposition of H_2O_2 as[3,4]

$$H_2O_2 \xrightarrow{h\nu} [H_2O_2]^* \longrightarrow 2\cdot OH. \quad (1)$$

The hydroxyl radicals formed are known to react, abstracting H-atom from both substrate and another molecule of H_2O_2.[4,5]

$$HO\cdot + H_2O_2 \longrightarrow H_2O + HOO\cdot \quad (2)$$

The HOO· radicals may abstract H-atom from substrate and add to substrate radicals. Otherwise, HOO·radicals disappear by reacting with each other ($2\,HOO\cdot \rightarrow H_2O_2 + O_2$) or with H_2O_2 ($HOO\cdot + H_2O_2 \rightarrow H_2O + O_2 + \cdot OH$).[4,5]

The products observed from DEDE can be explained by the following:

$CH_3OCH_2CH_2OCH_2CH_2OCH_3$—
1 (DEDE)

$$\xrightarrow[-H_2O]{\cdot OH} \begin{cases} \rightarrow \dot{C}H_2OCH_2CH_2OCH_2CH_2OCH_3 \ (\mathbf{2}) & (3) \\ \rightarrow CH_3O\dot{C}HCH_2OCH_2CH_2OCH_3 \ (\mathbf{3}) & (4) \\ \rightarrow CH_3OCH_2\dot{C}HOCH_2CH_2OCH_3 \ (\mathbf{4}) & (5) \end{cases}$$

The H-atom may be abstracted from 3-positions of DEDE as shown by Eqs. 3, 4, and 5. Their rates of abstraction were calculated to be *ca.* $3.6\times10^8\ M^{-1}\,s^{-1}$ for Eq. 3 and $5.6\times10^8\ M^{-1}\,s^{-1}$ for Eqs. 4 and 5 on the basis of the reported abstraction rates for CH_3OH ($0.6\times10^8\ M^{-1}\,s^{-1}$) and RCH_2OR ($1.4\times10^8\ M^{-1}\,s^{-1}$).[6]

Three radicals (**2**, **3**, and **4**) formed from DEDE by H-atom abstraction may undergo β-fission and/or HOO·radical addition to give products and/or other radicals(Eqs. 6—15). The products and radicals produced by Eqs. 6—15 may undergo secondary reaction to give fairly stable products (Eqs. 16—38), all of which were identified.

$\cdot CH_2OCH_2CH_2OCH_2CH_2OCH_3$ (**2**)

$$\xrightarrow{\beta\text{-fis.}} HCHO + \cdot CH_2CH_2OCH_2CH_2OCH_3\ (\mathbf{5}) \quad (6)^{8a,8b}$$

$$\xrightarrow{HO\cdot\ (\text{or } H_2O_2)} HOCH_2OCH_2CH_2OCH_2CH_2OCH_3\ (\mathbf{6}) \quad (7)$$

$CH_3O\dot{C}HCH_2OCH_2CH_2OCH_3$ (**3**)

$$\xrightarrow{\beta\text{-fis.}} CH_3\cdot\ (\mathbf{7}) + OHCCH_2OCH_2CH_2OCH_3\ (\mathbf{8}) \quad (8)$$

$$\xrightarrow{\beta\text{-fis.}} CH_3OCH{=}CH_2\ (\mathbf{9}) + \cdot OCH_2CH_2OCH_3\ (\mathbf{10}) \quad (9)$$

$$\xrightarrow{HOO\cdot} CH_3OCH(OOH)CH_2OCH_2CH_2OCH_3\ (\mathbf{11}) \quad (10)^{2)}$$

$$\xrightarrow{H^+} CH_3\overset{+}{O}{=}CH\text{-}CH_2\cdot\ (\mathbf{12}) + HOCH_2CH_2OCH_3\ (\text{EME}) \quad (11)^{7,8a)}$$

$CH_3OCH_2\dot{C}HOCH_2CH_2OCH_3$ (**4**)

$$\xrightarrow{\beta\text{-fis.}} CH_3O\cdot\ (\mathbf{13}) + CH_2{=}CHOCH_2CH_2OCH_3\ (\mathbf{14}) \quad (12)$$

$$\xrightarrow{\beta\text{-fis.}} CH_3OCH_2CHO + \cdot CH_2CH_2OCH_3\ (\mathbf{15}) \quad (13)$$

$$\xrightarrow{HOO\cdot} CH_3OCH_2CH(OOH)OCH_2CH_2OCH_3\ (\mathbf{16}) \quad (14)^{2)}$$

$$\xrightarrow{H^+} CH_3OH + \cdot CH_2\text{-}CH{=}\overset{+}{O}CH_2CH_2OCH_3\ (\mathbf{17}) \quad (15)^{7,8a)}$$

$\cdot CH_2CH_2OCH_2CH_2OCH_3$ (**5**)

$$\xrightarrow{HO\cdot\ (\text{or } H_2O_2)} HOCH_2CH_2OCH_2CH_2OCH_3\ (\text{DEME}) \quad (16)^{8a,8b}$$

$$HOCH_2OCH_2CH_2OCH_2CH_2OCH_3 \xrightarrow[\text{solvolysis}]{H_2O} HCHO + HOCH_2CH_2OCH_2CH_2OCH_3 \quad (17)$$
6 (DEME)

$$CH_3\cdot \xrightarrow{\text{H-abstr.}} CH_4 \quad (18)$$
7

$$CH_3\cdot \xrightarrow{CH_3\cdot} C_2H_6 \quad (19)$$

$$CH_2{=}CHOCH_3 \xrightarrow[\text{solvolysis}]{H_2O} CH_3CHO + CH_3OH \quad (20)^{9)}$$
9

$$CH_2{=}CHOCH_3 \xrightarrow{HO\cdot} CH_3O\dot{C}HCH_2OH \quad (21)^{10)}$$
18

$$\cdot OCH_2CH_2OCH_3 \xrightarrow{\text{H-abstr.}} HOCH_2CH_2OCH_3 \quad (22)$$
10 (EME)

$$\cdot OCH_2CH_2OCH_3 \xrightarrow{HO\cdot\ (\text{or } H_2O_2)} OHCCH_2OCH_3 + H_2O \quad (23)^{8a,8b)}$$

$$CH_3OCH(OOH)CH_2OCH_2CH_2OCH_3 \longrightarrow HCO_2CH_3 + HOCH_2OCH_2CH_2OCH_3 \quad (24)^{2)}$$
11 **19**

$$CH_3\overset{+}{O}{=}CHCH_2\cdot \xrightarrow[\text{solvolysis}]{H_2O} CH_3OH + CH_3CHO \quad (25)$$
12

$$CH_3\overset{+}{O}{=}CHCH_2\cdot \xrightarrow{H_2O,\ HO\cdot,\ -H^+} CH_3OCH_2OH + HCHO \quad (26)^{7)}$$
20

$$CH_3O\cdot \xrightarrow{\text{H-abstr.}} CH_3OH \quad (27)$$
13

$$CH_3O\cdot \xrightarrow[\text{disprop.}]{CH_3O\cdot} HCHO + CH_3OH \quad (28)^{11)}$$

$$CH_2{=}CHOCH_2CH_2OCH_3 \xrightarrow[\text{solvolysis}]{H_2O} CH_3CHO + HOCH_2CH_2OCH_3 \quad (29)^{9)}$$
14 (EME)

$$CH_2{=}CHOCH_2CH_2OCH_3 \xrightarrow{HO\cdot} HOCH_2\dot{C}HOCH_2CH_2OCH_3 \quad (30)^{10)}$$
21

$$CH_2CH_2OCH_3 \xrightarrow{HO\cdot\ (\text{or } H_2O_2)} HOCH_2CH_2OCH_3 \quad (31)$$
15 (EME)

$$CH_3OCH_2CH(OOH)OCH_2CH_2OCH_3 \longrightarrow CH_3OCH_2OH + HCO_2CH_2CH_2OCH_3 \quad (32)^{2)}$$
16 **20** **22**

$$\cdot CH_2CH{=}\overset{+}{O}CH_2CH_2OCH_3 \xrightarrow[\text{solvolysis}]{H_2O} CH_3CHO + HOCH_2CH_2OCH_3 \quad (33)$$
17 (EME)

$$\cdot CH_2CH{=}\overset{+}{O}CH_2CH_2OCH_3 \xrightarrow{H_2O,\ HO\cdot,\ -H^+} HOCH_2OCH_2CH_2OCH_3 + HCHO \quad (34)$$
19

$$CH_3O\dot{C}HCH_2OH \xrightarrow{H^+} CH_3\overset{+}{O}{=}CHCH_2\cdot + H_2O \quad (35)^{7,8a)}$$
18 **12**

$$HOCH_2OCH_2CH_2OCH_3 \xrightarrow[\text{solvolysis}]{H_2O} HCHO + HOCH_2CH_2OCH_3 \quad (36)$$
19 (EME)

$$CH_3OCH_2OH \xrightarrow[\text{solvolysis}]{H_2O} HCHO + CH_3OH \quad (37)$$
20

$$CH_3OCH_2CH_2O\dot{C}HCH_2OH \xrightarrow{H^+} CH_3OCH_2CH_2\overset{+}{O}{=}CHCH_2\cdot + H_2O \quad (38)^{7,8a)}$$
21 **17**

Table 5. GC-MS analysis of photolysis of DEDE

Compound	M^+	*m/e* (main value)								
CH_3OH	32	32	31	30	29					
CH_3CHO	44	44	43	31	29					
HCO_2H	46	46	45	44	29	28	18			
HCO_2CH_3	60	60	44	32	31	29	15			
$HOCH_2CH_2OH$	62	62	61	46	45	44	33	31	29	15
CH_3OCH_2CHO	(74) [a]	73	60	46	45	44	43	31	29	15
$CH_3OCH_2CH_2OH$	76	76	58	47	46	45	44	43	31	29
$CH_3OCH_2CO_2H$	(90) [a]	74	60	58	45	43	33	31	29	15
$HCO_2CH_2CH_2O_2CH$	(118) [a]	72	60	45	44	43	33	29		

a) No M^+ was detected.

Acid-catalyzed decomposition of radicals in Eqs. 11 and 15 were postulated for the oxidation of 1,2-diols with Ti(III) peroxide system in acidic media at lower pH (≤ 2).[7,8a] The acidity was in pH range 3.5—4.0. With the progress of oxidation the acidity increased gradually to pH$\approx$3. Therefore, the contribution of Eqs. 11 and 15 to the reaction of radicals would be less than that of the reaction with H_2O_2 in higher concentration. The observed increase of acidity may be due to the formation of acidic products.

The processes for the formation of alkyl radicals (Eqs. 6, 8, and 13) are less probable than those for the formation of alkoxyl radicals(Eqs. 9 and 12) because of the stability of alkoxyl radicals as compared with alkyl radicals.

The presence of peroxides such as **11** and **16** is suggested from the reported photochemical autoxidation of EDE and EME.[2] These peroxides afford C–C fission products, methyl formate and formadlehyde hemiacetal, respectively(Eqs. 24 and 32). Disproportionation of methoxyl radical to formaldehyde and methanol (Eq. 28) was reported.[11]

Equations 20 and 29 are those of well-known acid-catalyzed solvolysis of vinyl ethers.[9] The reactions between vinyl ethers and HO·radical (Eqs. 21 and 30) were studied by ESR spectroscopy.[10] Equations 36 and 37 are also those of well-known acid-catalyzed hydrolysis of hemiacetal.

The unexpectedly low yields of formic acid and formaldehyde are ascribed to their facile oxidation to CO_2 in the presence of H_2O_2. Only trace of products **8** and **22** was detected by GC-MS and GLC analyses.

In the photo-oxidation of EME, the yield of MeOH is larger than that of methoxyacetaldehyde, hence the C–O fission appears to occur preferentially at the ether linkage rather than at the hydroxyl linkage. As shown in Table 4, the conversion of EME and H_2O_2 is generally low. Thus further oxidation product (*e.g.*, methoxyacetic acid) from methoxyacetaldehyde is smaller than that shown in Tables 2B and 3.

The formation of acetic acid in photo-oxidation of EME may be due to the preferential C–O fission of **23** at the ether linkage (Eq. 39) and/or due to acid-catalyzed reaction of **18** (Eqs. 35 and 26) and **23** (Eq. 41). The acetaldehyde formed should undergo the further oxidation by H_2O_2 or O_2 (Eq. 42).

CH_3OCH_2CHOH **23**

$\xrightarrow{\beta\text{-fis.}}$ $CH_3O\cdot + CH_2{=}CHOH(\text{or } CH_3CHO)$ (39)

$\xrightarrow{HO\cdot \text{ or } H_2O_2}$ CH_3OCH_2CHO (40)

$\xrightarrow{H^+}$ $CH_3OH + \cdot CH_2CH{=}\overset{+}{O}H$ (41)[7,8a]

$CH_3CHO \xrightarrow{O} CH_3CO_2H$ (42)

Experimental

Materials. Commercial diethylene glycol dimethyl ether(DEDE), bp 160—161 °C, ethylene glycol dimethyl ether(EDE), bp 82—83 °C and ethylene glycol monomethyl ether(EME), bp 123—124 °C of first grade materials were used after distillation. Their GLC analyses showed single peaks. Hydrogen peroxide (90%, Mitsubishi Gas Chem. Co.) was used.

Photo-oxidation. An ice-cooled aqueous solution of DEDE was mixed with ice-cooled 90% H_2O_2 with stirring. The mixture was introduced into a quartz cell and warmed to room temperature. The cell was irradiated at 20 °C with a 300 W high-pressure Hg lamp through a water filter or a Pyrex filter. After completion of reaction, the mixture was cooled with ice.

Analyses. The ice-cooled mixture was analyzed by iodometry in order to determine the content of H_2O_2. The organic products were analyzed by GLC. After being condensed by evaporation, the products were analyzed by GC-MS. GLC analysis was carried out with a Yanagimoto GCG 550F gas chromatograph with a hydrogen flame ionization detector employing two kinds of columns, Porapak QS and PEG 20M. The products were identified by comparison of GLC peaks with those of authentic samples in two columns. Estimation of yield was carried out by GLC with a Porapak QS using 2-propanol as an internal standard.

The GC-MS analysis of the products was carried out with a Shimadzu GCMS-7000 mass spectrometer with a column of Porapak QS. The main *m/e* values of products are given in Table 5.

The CO_2 evolved was absorbed in saturated aqueous $Ba(OH)_2$ and titrated with HCl. The organic gaseous products were collected in a gas burette and analyzed by GLC (TCD and FID) using columns of Porapak QS and Porapak T. The acidity was measured with a Hitachi-Horiba M-7 type pH meter.

References

1) (a) Contribution No. 240; (b) R. Ford, H-P. Schuchmann, and C. von Sonntag, *J. Chem. Soc., Perkin Trans. 2*, **1975**, 1338.
2) H. Inoue, K. Tamaki, and E. Imoto, *Kogyo Kagaku Zasshi*, **66**, 645 (1966).
3) D. H. Volman and J. C. Chen, *J. Am. Chem. Soc.*, **81**, 4141 (1959).
4) T. Foster and P. R. West, *Can. J. Chem.*, **52**, 3589 (1974).
5) K. Omura and T. Matsuura, *Tetrahedron*, **24**, 3475 (1968).
6) M. Anbar, D. Meyerstein, and D. Neta, *J. Chem. Soc., B*, **1966**, 742.
7) B. C. Gilbert, J. P. Larkin, and R. O. C. Norman, *J. Chem. Soc., Perkin Trans. 2*, **1972**, 794.
8) (a) B. C. Gilbert, R. O. C. Norman, and R. C. Sealy, *J. Chem. Soc., Perkin Trans. 2*, **1974**, 824; (b) Y. Ogata and K. Tomizawa, *J. Org. Chem.*, **43**, 261 (1978).
9) T. Okuyama, T. Fueno, H. Nakatsuji, and J. Furukawa, *J. Am. Chem. Soc.*, **89**, 5826 (1967).
10) D. J. Edge, B. C. Gilbert, R. O. C. Norman, and P. R. West, *J. Chem. Soc., B*, **1971**, 189.
11) H. C. McBay and O. Tucker, *J. Org. Chem.*, **19**, 869 (1954).

Solvolysis in Carboxamides. IV.[9] Solvolytic Elimination of *exo*-2-Norbornyl Arenesulfonates in Carboxamides. Kinetic, Product, and Deuterium Tracer Studies

Seiki SAITO,* Toshio MORIWAKE, Ken'ichi TAKEUCHI,** and Kunio OKAMOTO**

Department of Synthetics Chemistry, School of Engineering, Okayama University, Tsushima, Okayama 700

** *Department of Hydrocarbon Chemistry, Faculty of Engineering, Kyoto University, Sakyo-ku, Kyoto 606*

(Received January 17, 1978)

Solvolysis of *exo*-2-norbornyl arenesulfonates (RX: X=OTs (**1a**), $-OSO_2C_6H_4$-*p*-OCH_3, $-OSO_2C_6H_5$, and OBs) and the deuterium labeled tosylates (**1a**-3-*endo-d*, **1a**-3-*exo-d*, and **1a**-3,3-d_2) has been carried out in four carboxamides (*N*-methylformamide, *N*-methylacetamide, *N,N*-dimethylformamide, and *N,N*-dimethylacetamide (DMA) at 25—100 °C. The solvolysis has also been conducted in the solvents containing 0.01—0.2 mol/dm^3 water. On the basis of kinetic measurements, product analyses, and the examination of isotopic distribution in the reclaimed substrate and the products (nortricyclene, norbornene, and *exo*-norbornyl carboxylates) it has been suggested that the reaction proceeds by *syn*-*E*l and S_Nl mechanisms, and that the carboxylates which are produced in the presence of water are derived from an imidatonium ion [R-Amide]$^+$, which is formed by the attack of carboxamide on the intimate ion-pair [R$^+$X$^-$]. It has been observed that the isotopic scrambling occurs only between C(3) and C(7) positions of both norbornene and the reclaimed **1a**-3-*endo-d* in DMA solvolysis at 75 °C, and that the isotopic distribution to these positions in norbornene is 57:43 at 10% completion and reaches 50:50 at half-life, indicating that only Wagner-Meerwein rearrangement is predominant in the course of norbornene formation, and also that the intimate ion-pair, from which norbornene is formed, is unsymmetrical and most probably with "classical" norbornyl-cation structure.

In the previous paper,[1] it was demonstrated that 7β-methylbicyclo[3.3.1]non-3β-yl tosylate undergoes S_N1 and *E*1 type reactions in the carboxamide solvents such as *N*-methylformamide (NMF), *N*-methylacetamide (NMA), *N,N*-dimethylformamide (DMF), and *N,N*-dimethylacetamide (DMA), to give the unrearranged olefin as a major product. The 5,1-hydride shift, which is a major course in acetic acid[2] and in 80% ethanol,[3] was markedly suppressed in the carboxamide solvents. The following scheme has been presented to account for the main course of the solvolytic elimination.

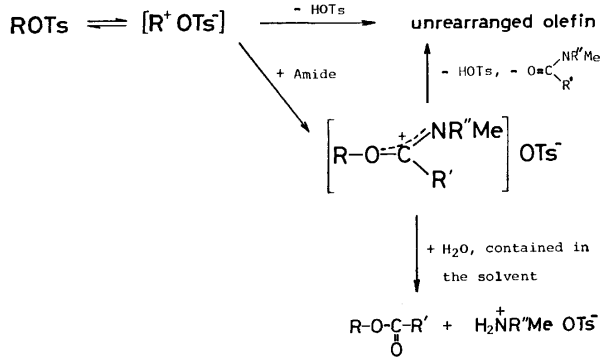

Scheme 1.

The predominant formation of the unrearranged olefin in the carboxamide solvolysis, as compared with other solvolyses,[2,3] was reasonably ascribed to the acceleration of *syn*-*E*l process by the leaving tosylate anion, because the basicity of the tosylate anion is expected to increase in such non-hydroxylic solvents owing to very weak hydrogen-bonding ability of these carboxamides.[1]

Thus, one of the principal characteristics of the carboxamide solvolysis of secondary cycloalkyl tosylates is that the carboxamides suppress the formation of rearranged products even when the substrate has a structure prone to rearrangement. Therefore, it is of interest to explore the generality of this phenomenon by the use of the *exo*-2-norbornyl system, because the 2-norbornyl cation, generated both in solvolytic conditions[4] and in stable ion conditions,[5] easily undergoes three types of rearrangement, *i.e.*, Wagner-Meerwein, 6,2-hydride, and 3,2-hydride shifts.

These processes take place, however, to regenerate the identical structure with that of the starting ion (automerization[6] or degenerated rearrangement[7]). Consequently, we selected *exo*-2-norbornyl tosylate labeled at the 3-position (**1a**-3-*endo-d*, **1a**-3-*exo-d*, and **1a**-3,3-d_2) to follow automerization.

In this paper, we report on a) the rates and products of the solvolysis of several *exo*-2-norbornyl *p*-substituted arenesulfonates (**1a**—**d**) in NMF, NMA, DMF, and DMA, b) effects of added water on the product distributions, and c) deuterium distributions of the products in the solvolyses of the tosylate labeled at C(3). We also discuss the generality of the mechanism (Scheme 1) and the structural problem of the norbornyl ion intermediate, since it remains as a controversial problem

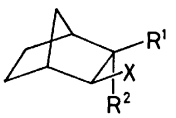

1a $R^1=R^2=H$, X=OTs
1a-3-*endo-d* $R^1=H$, $R^2=D$, X=OTs
1a-3-*exo-d* $R^1=D$, $R^2=H$, X=OTs
1a-3,3-d_2 $R^1=R^2=D$, X=OTs
1b $R^1=R^2=H$, X=*p*-MeO-$C_6H_4SO_3$
1c $R^1=R^2=H$, X=$C_6H_5SO_3$
1d $R^1=R^2=H$, X=OBs

Table 1. Kinetic data for the solvolysis of *exo*-2-norbornyl tosylate **1a** in various carboxamides[a]

	Amide			
	DMA	DMF	NMA	NMF
$k_1/(10^{-5}\ s^{-1})$:				
Temp/°C				
100	21.6±0.4			
75	1.99±0.01	7.34±0.10	83.1±0.5	
50		0.493±0.005	5.15±0.01	30.6±0.1
33.3				3.79±0.04
25[b]	0.00494	0.0201	0.197	1.21
$\Delta H^*/(4.184\ kJ/mol)$:[c]				
	24.1±0.3	23.7±0.2	24.3±0.1	24.1±0.2
$\Delta S^*/(4.184\ J/(K\ mol))$:[c]				
	−11.1±0.7	−9.8±0.4	−3.0±0.2	−0.1±0.4

a) [**1a**]=0.075 mol/dm³; [C_5H_5N]=0.077 mol/dm³; [H_2O]=0.003 (for DMA or DMF), 0.01 (for NMA), or 0.02−0.03 (for NMF) mol/dm³. b) Extrapolated from data at other temperatures. c) At 25 °C.

and still is a basic problem of organic chemistry toward which active effort continues both experimentally and theoretically.[8]

Results and Discussion

Solvolysis Rates of exo-*2-Norbornyl Arenesulfonates in Carboxamides.* The rates of solvolysis of **1a**—**d** in the carboxamides were determined titrimetrically by the use of the same method as described in the previous paper.[1] A good first-order behavior was observed for all the kinetic runs over two to three half-lives. The results, along with the thermodynamic parameters, are tabulated in Table 1 for **1a** and in Table 2 for **1b**—**d**.

The following findings present unambiguous evidence which demonstrates that the solvolysis proceeds *via* a typical S_N1 or *E*1 mechanism. First, pyridine, added to neutralize the liberated arenesulfonic acids, did not alter the rates. Secondly, a satisfactory linear free-energy relationship was observed when log k_1 values of **1a** were plotted against those for 2-adamantyl tosylate in carboxamides[9] and a number of other solvents (Fig. 1). Since 2-adamantyl tosylate has a mechanistic feature of S_N1 substrate,[10] it is a suitable model substrate for the examination of the S_N1 character of other secondary substrates. The slope (0.864) of the least-squares line is larger than those (0.55—0.78)[11] for other secondary systems. Furthermore, the magnitude (0.83)[12] of the Grunwald-Winstein *m* value is also larger than those (0.4—0.7) for the solvolysis of usual secondary substrates[13] and is comparable to that (0.87)[14] for 2-adamantyl tosylate. Thirdly, at 5% completion of the solvolysis of **1a**-3-*endo*-*d* in DMA the recovered tosylate was incorporated with *exo*-2-norbornyl-7-*anti*-*d* tosylate (25%), which must be formed *via* an ionization and a subsequent return step (*vide infra*).

Products of the Solvolysis of ***1a—d*** *in the Carboxamides.* As expected from the Scheme 1, the products in the solvolysis of **1a**—**d** in the carboxamides were elimination products, nortricyclene and norbornene. If water is contained in the amides, the substitution products, *exo*- and *endo*-norbornyl carboxylates were found as the additional products (Scheme 2).

Table 2. Products and rates for the solvolysis of *exo*-2-norbornyl *p*-X-benzenesulfonates in the carboxamides at 75 °C[a]

Amide	X	k_1	Yield/%[b]			
		$10^{-5}\ s^{-1}$	**2**	**3**	**4**[c]	**5**[c]
DMA	OCH_3	1.04	85.7	13.2	0.8	0.3
	CH_3	1.99	87.0	12.2	0.6	0.2
	H	4.78	89.5	10.0	0.3	0.2
	Br	31.2	91.6	7.5	0.6	0.3
DMF	OCH_3	4.73	86.6	9.5	3.0	0.9
	CH_3	7.34	89.1	7.8	2.1	1.0
	H	17.7	89.7	5.5	3.3	1.1
	Br	88.4[d]	92.2	3.7	3.0	1.1
NMA	OCH_3	51.8	92.1	3.6	4.1	0.2
	CH_3	83.1[d]	93.2	3.0	3.5	0.3
	H	203[d]	92.8	1.9	4.4	0.2
	Br	378[d]	92.0	1.4	6.2	0.4
NMF[e]	OCH_3	237[d]	94.3	1.7	3.9	0.1
	CH_3	499[d]	91.3	1.1	7.3	0.3
	H	971[d]	88.5	0.7	10.3	0.3
	Br	1830[d]	90.4	0.4	9.0	0.2

a) [$ROSO_2C_6H_4$-*p*-X]=0.075 mol/dm³; [C_5H_5N]=0.077 mol/dm³; [H_2O]=0.003 (for DMA or DMF), 0.01 (for NMA), or 0.02—0.03 (for NMF) mol/dm³. b) The averages of two or three determinations, with reproducibility of ±3%, relatively. c) Acetate for DMA and NMA, and formate for DMF and NMF. d) Extrapolated from data at other temperatures. e) The amounts of the substrates were three times as much as those for other amides.

The compositions of the products were determined by the use of GLC and ^1H NMR spectroscopy. The yield of a mixture of *exo*- and *endo*-norbornyl esters was assayed by means of GLC. The epimeric ratio was determined also by means of GLC analysis after conversion of the ester mixture to corresponding norbornanol mixture by lithium aluminum hydride. The

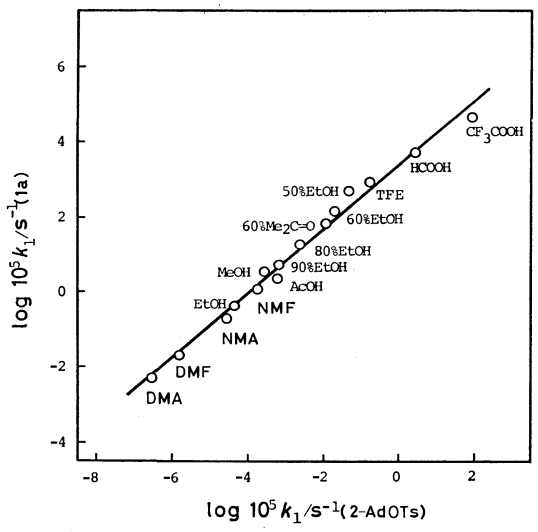

Fig. 1. A linear free-energy relationship between log k_1(**1a**) and log k_1(2-adamantyl tosylate) in various solvents at 25 °C: slope: 0.864, correlation coefficient: 0.994, and standard deviation: 0.22. For the rate constants of 2-adamantyl tosylate in representative solvents other than the amides, see (a) F. L. Schadt, T. W. Bentley, and P. v. R. Schleyer, *J. Am. Chem. Soc.*, **98**, 7667 (1976). (b) H. C. Brown, "The Nonclassical Ion Problem," Plenum Press, New York, N. Y. (1977), p. 193, and Ref. 10. For the rate constants of **1a** in representative solvents other than the amides, 90, 60, and 50% aqueous ethanols, and 60% aqueous acetone, see reference (b).

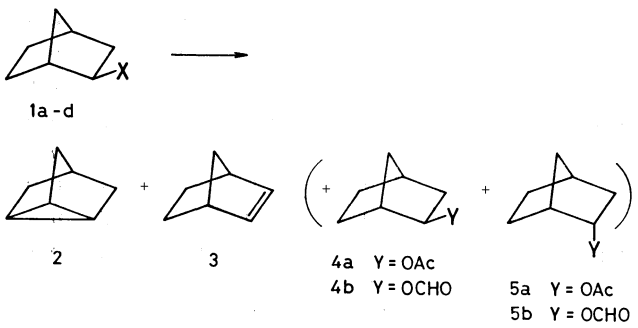

Scheme 2.

yield of norbornene was determined by measuring the integrated intensity of NMR signals of olefinic protons relative to that of the methyl protons of anisole (internal marker). The results of the product analysis are summarized in Table 2.

As illustrated in Scheme 1, the esters may be formed by the reaction of an imidatonium ion[15] with water, which is contained in the carboxamides. In this connection, the effect of water content on the product distribution was examined for the solvolysis of **1a** in DMA and in DMF in the presence of various amounts of water. The results are tabulated in Table 3 and illustrated in Figs. 2-1 and 2-2.

In completely dry DMA or DMF nortricyclene and norbornene were sole products, and there was no longer obtained any esters (Fig. 2), indicating that the esters are not a primary solvolysis product in DMA or in DMF.

Table 3. Effects of added H_2O on product distribution for *exo*-2-norbornyl tosylate **1a** in DMA and DMF at 75 °C[a]

Amide	$[H_2O]$ mol/dm³	Yield/%[b] 2	3	4[d]	5[d]
DMA	0.0030[c]	87.1	12.1	0.6	0.2
	0.0074	83.1	12.6	2.7	0.6
	0.0163	80.1	11.6	7.4	0.9
	0.0252	76.1	11.6	11.8	0.5
	0.0474	68.5	11.0	20.0	0.5
	0.0918	59.3	9.8	30.4	0.5
	0.120	55.3	9.9	34.3	0.5
	0.181	49.4	9.4	40.8	0.3
DMF	0.0030[c]	89.2	7.7	2.1	1.0
	0.040	47.8	6.4	45.3	0.5
	0.077	28.8	4.7	66.2	0.3
	0.185	11.8	4.0	84.0	0.2

a) [**1a**] = 0.075 mol/dm³; [C_5H_5N] = 0.077 mol/dm³. b) Trace amounts of 2-norbornanol was detected on GLC (≤0.1%). c) Remaining water in the amides after purification. d) See footnote (c) in Table 2.

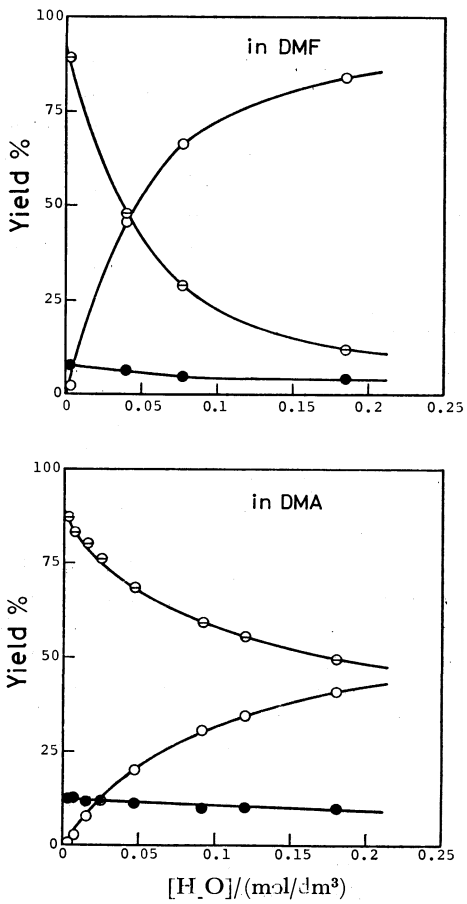

Fig. 2. Effect of water content of DMA(bottom) and of DMF(upper) on the formation of norbornene **3** (●), *exo*-ester **4** (○), and nortricyclene **2** (⊖).

The yield of norbornene was not much affected by the water content of DMA or of DMF (*vide infra*). The yield of nortricyclene, however, decreased with an

increase in water content of DMA and of DMF, and the yield of *exo*-norbornyl acetate or formate increased complementing the decrease in the yield of nortricyclene (Figs. 2-1 and 2-2). Therefore, these results indicate that the direct products from the intimate ion-pair [R^+X^-] are norbornene and an imidatonium ion [R-Amide]$^+$. The latter is so unstable that it would be rapidly converted to nortricyclene, otherwise it would be hydrolyzed by the water in the amide solvent; this is illustrated in Scheme 3.

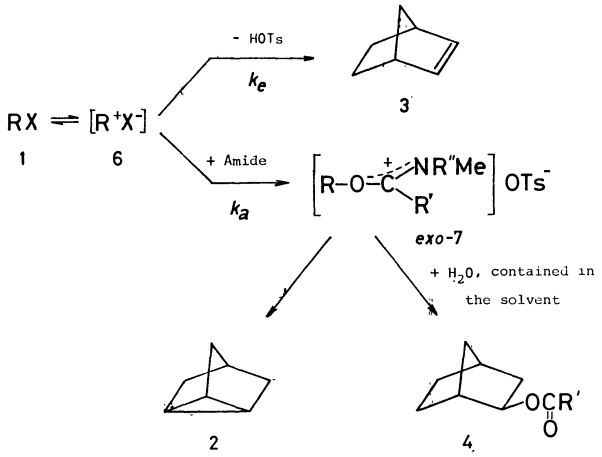

Scheme 3.

When log k_1 values were plotted against the logarithms of the ratio (%**2**+%**4**): %**3**, a reactivity-selectivity linear relation[16] was observed; this linear relation was established for each carboxamide solvent (Fig. 3). This also indicates that norbornene and the imidatonium ion stem from a single intermediate, *i.e.*, an intimate ion-pair [R^+X^-].

This mechanism is essentially the same as that depicted in Scheme 1 for the carboxamide solvolysis of bicyclo[3.3.1]nonyl system.

syn-*El Mechanism for the Formation of Norbornene.* The formation of norbornene depends on the nature of both the leaving group and the solvent. Thus, the norbornene yield increases in the order **1b** (MeO)> **1a** (Me)>**1c**(H)>**1d** (Br) in any carboxamide solvent (Table 2), the sequence fitting in with the order of the increase in the electron-releasing nature of the *para*-substituent in the respective leaving groups. Furthermore, the yield of norbornene also increased in the solvent sequence DMA>DMF>NMA>NMF for each substrate (Table 2), similarly to the order observed in the yield of unrearranged olefin in the case of bicyclo-[3.3.1]nonyl system.[1] This sequence may be explained in terms of the change in the basicity of the leaving group anion which is affected by the hydrogen-bonding ability (NMF>NMA>DMF>DMA)[1] of the respective carboxamides. These trends in the yield of norbornene suggest that a *syn-El* reaction occurs in the norbornene forming step, and that the leaving group anion acts as a base.

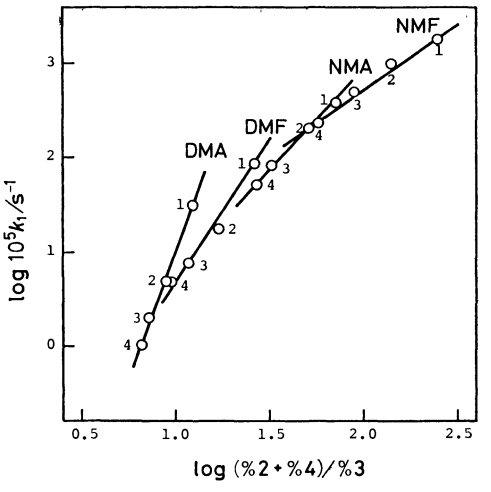

Fig. 3. Linear reactivity-selectivity relationships between log k_1 and log (%**2**+%**4**)/%**3** for the solvolysis of **1a—d** in the carboxamide solvents at 75 °C: 1= **1d** (Br); 2=**1c** (H); 3=**1a** (CH_3); 4=**1b** (OCH_3).

In order to confirm this, the stereochemistry of the *El* reaction was examined on the solvolysis of **1a**-3-*exo-d* and **1a**-3-*endo-d* in DMA at 75 °C. The norbornene was converted into norbornene–phenyl azide adduct (**8**) by 1,3-dipolar cycloaddition reaction of phenyl azide to norbornene,[17] because of the ease in separation and purification of small amounts of norbornene (Scheme 4).

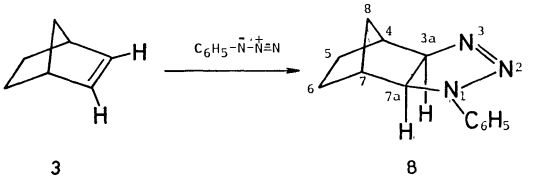

Scheme 4.

The adduct **8** was analyzed by ^{13}C NMR spectroscopy in order to obtain the information on the rearrangements during solvolysis by determining the carbon bearing a deuterium atom which shows –CD– triplet (see Experimental). ^{13}C chemical shifts for the adduct **8** were assigned from the multiplicities of the individual nuclei in the off-resonance decoupled spectra and from comparison with the spectra of other substituted norbornanes.[18] Spectral assignments of the ^{13}C NMR are given in Table 4, together with those for the other norbornane derivatives.

In the case of **1a**-3-*exo-d*, the spectrum of **8** derived from norbornene exhibited –CD– triplet only at 31.9 ppm, indicating the presence of deuterium at C(8) of the adduct **8**. On the other hand, the spectrum of **8** obtained in the case of **1a**-3-*endo-d* showed three triplets (–CD–) at 0.3 ppm upfield from C(3a), C(7a), and C(8) signals. These results clearly indicate that the leaving anion abstracts exclusively *syn*-β-hydrogen atom (or deuterium atom) of the intimate ion-pair intermediate **6**; they also demonstrate that the formation of the ion-pair is attended by the Wagner-Meerwein rearrangement (Table 5, *vide infra*).

Cram and Sahyun,[19a] Cocivera and Winstein,[19b] Skell and Hall,[19c] and Kim and Brown[19d] have emphasized the importance of the nature of the counter ion and its possible assistance to the proton abstraction in the intimate ion-pair.

In order to know a quantitative relationship between the rate, k_e, of norbornene forming step and the leaving

Table 4. ^{13}C chemical shifts of nortricyclene, *exo*-2-substituted norbornyl derivatives, and adduct **8**

Compound	Chemical shift[a,b]								
	C-1	C-2	C-3	C-4	C-5	C-6	C-7	CH_3	C=O
Nortricyclene[c]	9.7	9.7	32.9	29.3	32.9	9.7	32.9		
Acetate	41.4	77.6	39.6	35.4	28.2	24.4	35.3	21.3	170.6
Formate[d]	41.6	77.2	39.6	35.5	28.2	24.3	35.3		160.6
Tosylate	42.0	85.3	39.5	35.1	27.7	23.8	34.9	21.5	
	C-7	C-7a	C-3a	C-4	C-5	C-6	C-8		
Adduct **8**[e]	40.2*	60.3	86.4	41.5*	25.7†	25.0†	32.2		

a) Chemical shifts are expressed in ppm downfield from Me_4Si (in $CDCl_3$ except for the adduct **8** (CD_2Cl_2)). b) Signals marked *, †, may be interchangeable in the column where they appear. c) See Ref. 18a. d) See Ref. 18c. e) The numbering is shown in Scheme 4.

group structure, a linear relationship between log k_e and the Hammett σ value of the *para*-substituent in the leaving group was examined. The log k_e values were estimated from the product distribution (Table 2) using Eqs. 1 and 2, where the magnitude of k_a[Amide] is a constant in the respective carboxamide solvents. The plot of log %**3**/(%**2**+%**4**) against the σ value is illustrated in Fig. 4.

$$\%\mathbf{3}/\%\mathbf{7} = \%\mathbf{3}/(\%\mathbf{2}+\%\mathbf{4}) = k_e/k_a[\text{Amide}] \quad (1)$$

$$\log k_e = \log \%\mathbf{3}/(\%\mathbf{2}+\%\mathbf{4}) + \log k_a[\text{Amide}] \quad (2)$$

Good linear relations, with negative ρ values, -0.54——-1.2, were observed for the series of carboxamides. These linear relations also suggest that in the *E*1 process the leaving group anion intramolecularly abstracts the C(3) proton at the stage of the intimate ion-pair intermediate **6**.

Wagner-Meerwein Rearrangement in the Intimate Ion-Pair and 6,2-Hydride Shift in the Imidatonium Ion. The solvolyses of **1a**-3-*endo-d* in DMA, DMF, and NMF were carried out at 75 °C and the deuterium distribution of *exo*-norbornyl carboxylate, norbornene, and nortricyclene were determined by means of ^{13}C and, in some cases, ^1H NMR spectroscopies in the Fourier transform mode (see Experimental). The results of the deuterium analyses of the products are tabulated in Table 5 and also illustrated in Scheme 5.

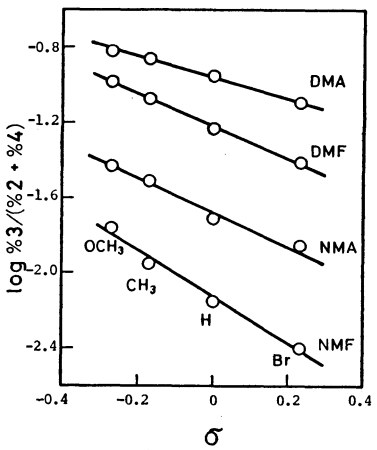

Fig. 4. Linear free-energy relationships between log %**3**/(%**2**+%**4**) and σ for the solvolysis of **1a**—**d** in the carboxamide solvents at 75 °C: $\rho = -0.54$, -0.86, -0.86, and -1.2, respectively for DMA, DMF, NMA, and NMF.

In norbornene the deuterium at *endo*-position of C(3) of **1a**-3-*endo-d* scrambled at the C(3) and C(7) positions, whereas in the *exo*-norbornyl ester (acetate or formate) the deuterium scrambled to C(5) position besides C(3) and C(7) positions.

In addition, when the deuterium distribution in the

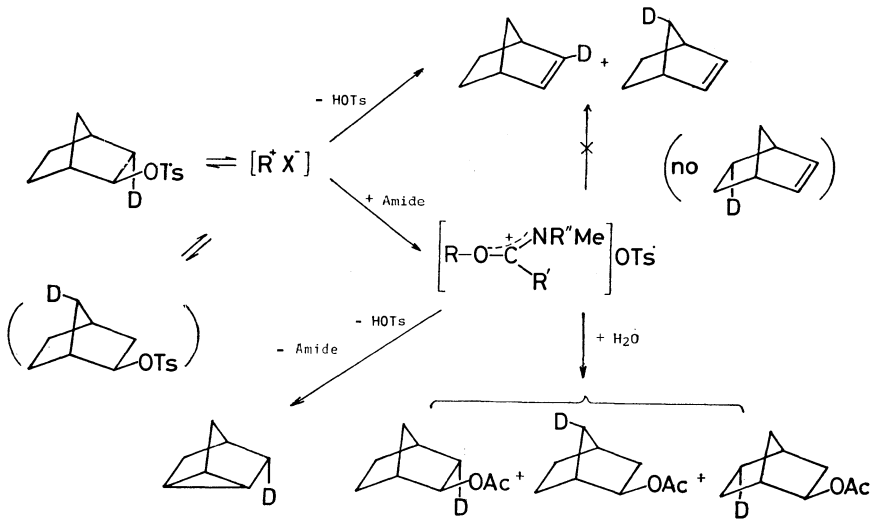

Scheme 5.

Table 5. Isotope distributions of the products in DMA, DMF, or NMF solvolysis of **1a**-3-*endo*-*d*, **1a**-3-*exo*-*d*, and **1a**-3,3-d_2, at 75 °C[a]

Compound	Amide	$[H_2O]$ mol/dm³	Product	Yield %	Deuterium, %[b] C-3	C-5	C-7
1a-3-*endo*-*d*	DMA	0.04	**2**	70.3		100	
			3[c]	11.3	44	0	56
			4a[d,h]	18.0	41	23	39
	DMA	0.20	**4a**[e,h]	42.0	43	12	43
	DMF	0.04	**4b**[f,h]	45.0	46	5	47
	NMF	0.15	**2**	20.3		100	
			3[c,i]	0.7	48	0	52
			4b[g,h]	79.0	49	0	49
1a-3-*exo*-*d*	DMA	0.003	**3**[c]	11.6	0	0	63
1a-3,3-d_2	DMA	0.003	**2**	87.0		100	

a) [ROTs]=0.075 mol/dm³; [C_5H_5N]=0.077 mol/dm³. b) The percentages of deuterium at the carbons other than C(3), C(5), and C(7) are below the limit of the accuracy (<1%); reproducibility=±3%. c) Calculated from data of the adduct **8**. d) Contaminated with 2.7% of *endo*-isomer. e) Contaminated with 0.9% of *endo*-isomer. f) Contaminated with 0.4% of *endo*-isomer. g) Contaminated with 0.2% of *endo*-isomer. h) ^{13}C signals of *endo*-isomer do not overlap with those of *exo*-isomer. i) Determined by means of ^1H NMR; the spectrum of the corresponding adduct **8** is identical with that obtained from DMA solvolysis.

Table 6. Change in deuterium distributions of the tosylate in the course of the solvolysis of **1a**-3-*endo*-*d* in DMA at 75 °C[a]

%Reaction[b]	Deuterium, %[c] C-3	C-5	C-7
5	75	0	25
10	66	0	34
25	50	0	50
50	51	0	49
90	53	0	47

a) [ROTs]=0.075 mol/dm³; [C_5H_5N]=0.077 mol/dm³; $[H_2O]$=0.003 mol/dm³. b) Calculated from the reaction time by the use of the rate constant $k_1=1.69\times10^{-5}$ s^{-1}. c) The percentages of deuterium at the carbons other than C(3), C(5), and C(7) are below the limit of the accuracy (< 1%); reproducibility=±3%.

unchanged tosylate was examined in the course of the solvolysis of **1a**-3-*endo*-*d* in DMA, the deuterium was detected at C(3) and C(7) positions, but no deuterium was found at C(5) position. This is summarized in Table 6.

Since the scrambling of the C(3) deuterium to C(7) position must be caused by the Wagner-Meerwein rearrangement and the appearance of deuterium at C(5) position must be caused by 6,2-hydride shift, it is concluded that only the Wagner-Meerwein rearrangement attends the formation of the intimate ion-pair intermediate (Scheme 5) and that 6,2-hydride shift takes place at the stage of the subsequent reaction of the imidatonium ion (Scheme 5). Furthermore, it is deduced that the imidatonium ion can not return to the intimate ion-pair. If such a return course is probable, the deuterium should be located at C(5) positions of norbornene and of the unchanged tosylate. This, however, is not the case (Tables 5 and 6). Similarly, since no deuterium was found at C(5) of norbornene, it is deduced that the imidatonium ion can not give rise to norbornene.

This absence of the 6,2-hydride shift at the stage of the intimate ion-pair may be ascribed to an increase in the solvent capture caused by the relatively high nucleophilicity of carboxamides, and also to acceleration in *syn*-*E*1 as mentioned above. Such accelerations of both of the subsequent reactions are expected to decrease the life-time of the intimate ion-pair, thereby suppressing the 6,2-hydride shift.

The 6,2-hydride shift, when it occurs in the imidatonium ion, is suppressed in the order of DMF>DMA (Table 5). In addition the increase in the water content of NMF and DMA also suppresses the 6,2-hydride shift in the ester product. Especially, in NMF no 6,2-hydride shift was found in **4b**[20] when the solvolysis was carried out in the presence of 0.15 mol/dm³ of water. These are summarized in Table 7. These trends clearly indicate that the 6,2-hydride shift competes with the hydrolysis of the imidatonium ion [R-Amide]$^+$, which is originally formed without any 6,2-hydride shift.

Table 7. Distribution % of deuterium for esters as a function of water content in the carboxamide solvolysis of **1a**-3-*endo*-*d* at 75 °C[a]

Amide	$[H_2O]$ mol/dm³	Product[b]	Deuterium, %[c] C-3	C-5	C-7
DMA	0.04	**4a**	41	23	39
	0.20	**4a**	43	12	43
NMF	0.15	**4b**	49	0	49

a) See footnote (a) in Table 5. b) See footnote (d), (e), (g), and (h) in Table 5. c) The percentages of deuterium at the carbons other than C(3), C(5), and C(7) are below the limit of the accuracy (< 1%); reproducibility=±3%.

Examination of 3,2-Hydride Shift in the Intimate Ion-Pair and in the Imidatonium Ion Intermediate. Roberts and his collaborators[21] have demonstrated that the 6,2-hydride shift is highly competitive with solvent capture of the 2-norbornyl cation and that the intrusion of the 3,2-hydride shift is much more pronounced in the less nucleophilic solvent such as formic acid. Lee and Lam[22] have suggested that even in acetic acid the 3,2-hydride shift occurs to a significant extent prior to the attack by solvent on the cation. Under the stable ion conditions, it has also been demonstrated that both 3,2- and 6,2-hydride shifts attend the formation of the 2-norbornyl cation.[23]

Thus, we examined by the use of **1a**-3,3-d_2 whether the 3,2-hydride shift actually occurs in this solvolysis or not. When the solvolysis was carried out in DMA solvent at 75 °C, and then isolated nortricyclene was subjected to ^{13}C NMR analysis, the spectrum showed a single $-CD_2-$ signal (quintet) centered at 32.3 ppm, 0.6 ppm upfield from C(3), C(5), or C(7) signal of nortricyclene (Table 4), but no sign of another quintet or triplet. This result unequivocally indicates that neither 3-*exo*- nor 3-*endo*-deuterium has migrated from C(3) to C(2) position and that the 3,2-hydride shift never attends the formation of nortricyclene. This means that no 3,2-hydride shift occurs in the stage of the intimate ion-pair.

The absence of deuterium at the C(2) position in the *exo*-norbornyl ester (acetate or formate) (Table 5) also shows that the 3,2-hydride shift does not occur in the course of the formation of these esters in DMA or in DMF.

Structure of the Ion-Pair Intermediate and the Reaction Pathway for the Formation of Deuterium Labeled Norbornene. The deuterium distributions in the norbornene and in the unchanged tosylate were determined at intervals in the course of the solvolysis of **1a**-3-*endo*-*d* in DMA at 75 °C; the results are tabulated in Tables 8 and 6, respectively. Since no deuterium was detected at C(5) positions of norbornene and of the unchanged tosylate, it is obvious, as mentioned above, that merely the Wagner-Meerwein rearrangement competes with the *syn*-*E*1 elimination and with the solvent capture.

Table 8. Change in deuterium distributions of norbornene in the course of solvolysis of **1a**-3-*endo*-*d* in DMA at 75 °C[a]

%Reaction[b]	Deuterium, %[c,d]		
	C-3	C-5	C-7
10	57	0	43
25	54	0	46
50	50	0	50
100	44	0	56

a) $[ROTs]=0.075$ mol/dm^3; $[C_5H_5N]=0.077$ mol/dm^3; $[H_2O]=0.003$ mol/dm^3. b) Calculated from the reaction time by use of the rate constant: $k_1=1.69\times10^{-5}$ s^{-1}. c) The percentages of deuterium at the carbons other than C(3), C(5), and C(7) are below the limit of the accuracy (< 1%); reproducibility = ±3%. d) Calculated from data of the adduct **8**.

The structural problem of this intimate ion-pair has been long debated[8] and it is pertinent to discuss it in the light of the change of the deuterium distribution in norbornene in the progress of the solvolysis.

When the intimate ion-pair has a non-classical structure (**10**) depicted in Scheme 6, it would give rise to **1a**-7-*anti*-*d* and norbornene, **3**-2-*d* and **3**-7-*d*, by an internal return and by *syn*-*E*1 pathway, respectively. In addition, the tosylate **1a**-7-*anti*-*d* can also afford the intimate ion-pair which has the structure identical with that from the starting tosylate **1a**-3-*endo*-*d*. In other words, there is a single structure (non-classical) **10** in the course of the norbornene formation from both **1a**-3-*endo*-*d* and **1a**-7-*anti*-*d*. Consequently, the ratio of norbornene **3**-2-*d* and **3**-7-*anti*-*d* should be invariant regardless the degree of conversion of the tosylate, even if the ratio of the tosylate **1a**-3-*endo*-*d* and **1a**-7-*anti*-*d* varies as the solvolysis proceeds (see Scheme 6).

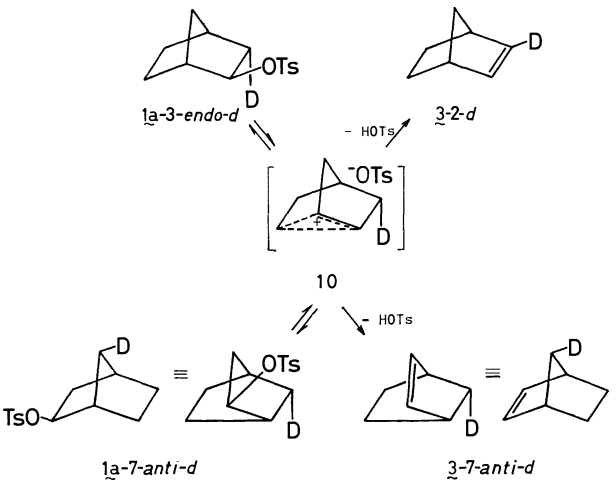

Scheme 6.

On the other hand, if the intermediate exists as an equilibrium mixture of the classical ions **6**-3-*endo*-*d* and **6**-7-*anti*-*d*, and in addition, if the *syn*-*E*1 elimination can compete with the Wagner-Meerwein rearrangement between these ions, the ratio of norbornene **3**-2-*d* and **3**-7-*anti*-*d* would vary as the elimination progresses (Scheme 7).

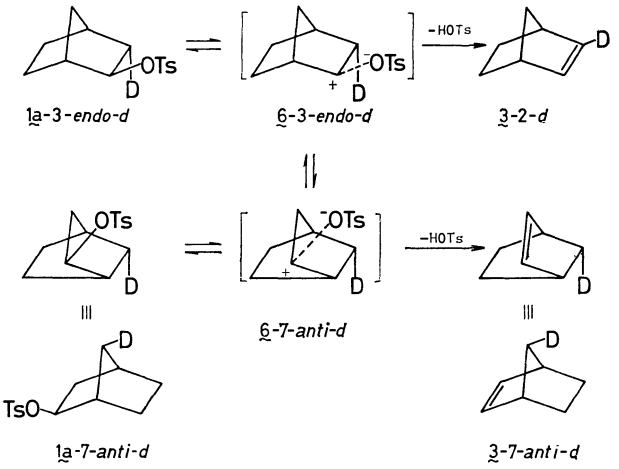

Scheme 7.

Since the deuterium distribution in the norbornene varies as the reaction proceeds in DMA, as is shown in Table 8, it is clear that the structure of the intimate ion-pair can not be expressed by the non-classical ion **10**, but by the classical ion **6**, in so far as the norbornene is produced strictly from the intimate ion-pair.

The deuterium content at C(3) of the tosylate decreases from 100 to 50% at 25% completion of the solvolysis, and then increases to 53% at 90% completion (Table 6). Meanwhile, the deuterium content at C(7) of norbornene increases from 50 to 56% as the reaction proceeds from 50 to 100% completion. The slight accumulation of deuterium at C(3) of **1a**-3-*endo-d* and that at C(7) of **3**-7-*anti-d* may be ascribed to the possible slight sluggishness in the rate of solvolysis of **1a**-3-*endo-d* as compared with **1a**-7-*anti-d*. In fact the secondary isotope effect of **1a**-3-*endo-d* amounts to 1.18± 0.02 in DMA at 75 °C.[24] However, the accumulation of deuterium at C(7) of norbornene at 100% reaction appears to be too high to be ascribed to the possible secondary isotope effect, even if the experimental error (±3%) is taken into account. This point will be subjected to a more detailed study with precision.

The Formation of exo-*2-Norbornyl-5-*d *Carboxylates and Nortricyclene.* The C(5) positions of *exo*-2-norbornyl esters contain appreciable amounts of deuterium, as it is shown in Table 5. This indicates that the *exo*-imidatonium ion **7**-3-*endo-d* easily rearranges to the **7**-5-*endo-d* ion by the 6,2-hydride shift. Since the classical intermediates **11**-3-*endo-d* and **11**-5-*endo-d* (Scheme 8) give rise to the identical nortricyclene, **2**-3-*d*, we can not obtain more detailed information about the mechanistic insights. Therefore, the possibility of 6,2-hydride shift *via* non-classical structure, **12**-3-*endo-d*,[25] can not be ruled out in the γ-elimination of the *exo*-imidatonium ion **7**.

It is not clear at the present stage of our knowledge why the *exo*-imidatonium ion can easily afford nortricyclene, and why the *exo*-imidatonium ion easily undergoes 6,2-hydride shift.

The Formation of endo-*2-Norbornyl Carboxylates.* Small amounts of *endo*-norbornyl acetate or formate, **5a** (≤0.9%) or **5b** (≤1.1%), were produced in the solvolysis of **1a**—**d** in the carboxamide solvents as it is shown in Tables 2 and 3. However, these are in substantial amounts as compared with the result of acetolysis of *exo*-norbornyl brosylate **1d** (0.02%),[26] and also in comparison with the amounts of *exo*-2-norbornyl carboxylates (Table 2). The formation of *endo*-norbornyl esters obviously indicates that the *endo*-imidatonium ion is actually formed in the course of solvolysis. This *endo*-imidatonium ion most probably is formed from the intimate ion-pair with a classical norbornyl ion structure, since it is rather difficult that the *endo* product is formed from a non-classical norbornyl ion.

The C(6) hydrogen of the *endo*-imidatonium ion **13** may be easily abstracted in a cyclic fashion, as depicted in Scheme 9, to give rise to nortricyclene. Peeters and Anteunis[27] have proposed similar cyclic mechanism for solvolytic dehydrobromination of 2-methyl-2-pentyl bromide in DMF at the imidatonium ion stage.

A Possible Norbornene Formation from exo-*Imidatonium Ion.* The possibility that norbornene is formed through the *exo*-imidatonium ion **7**, as depicted in Scheme 10, may not be ruled out. Thus the slight decrease in the yield of norbornene with an increase in water content (Fig. 2) might be attributable to the intrusion of this process. However, as mentioned above, it is clear that at the stage of the imidatonium ion the deuterium scrambles to C(5) position as the result of the 6,2-hydride shift. Therefore, if the elimination occurs by the pathway depicted in Scheme

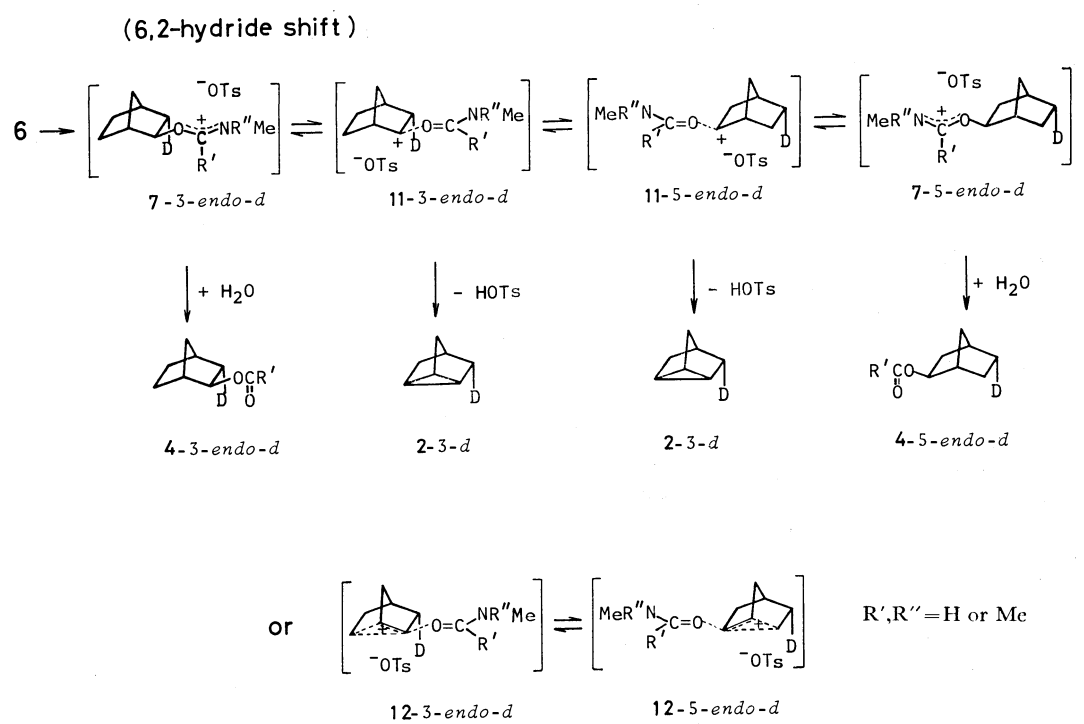

Scheme 8.

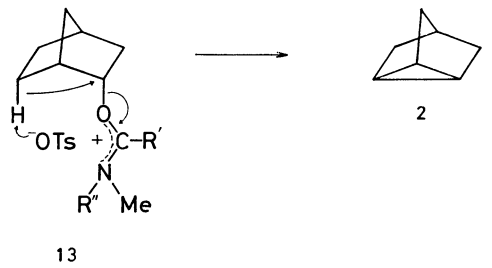

Scheme 9.

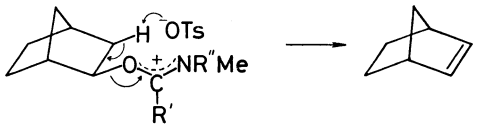

Scheme 10.

10, norbornene labeled at C(5) position would be formed; however, this is not the case (Table 5 and Scheme 5). Thus, only the decrease in the basicity of the tosylate anion, due to the increase in the water content, can explain the decrease in the yield of norbornene (Fig. 2).

Experimental

All the melting points are uncorrected. NMR spectra were measured with a Hitachi R-24 (60 MHz) or JEOL JMN MH-100 (100 MHz) instruments. Tetramethylsilane was used as an internal standard in $CDCl_3$ unless otherwise noted. IR spectra were obtained with Hitachi EPI-S2 spectrometer, only the major absorptions being cited. GLC analysis was performed with a Hitachi K-53 gas chromatograph fitted with TCD and a 3 m column (i.d.=3 mm) packed with PEG 6000 on Chromosorb W.

Materials. The four carboxamides were purified by the same method described in the previous paper.[1] Norbornene oxide,[28] *exo*-2-norbornanol,[29] norcamphor,[29] phenyl azide,[30] $(n\text{-Bu})_4NOAc$,[31] trifluoroacetic acid-*d*,[32] *p*-methoxybenzenesulfonyl chloride,[33] and 1-adamantyl bromide[34] were prepared following the published methods. Reagent grade chemicals were used without further purification unless otherwise mentioned. Norbornene was commercial product purified by sublimation.

exo-*2-Norbornyl Arenesulfonates* ***1a—d.*** The *exo*-alcohol was converted into the corresponding sulfonates in the usual manner.[35] Tosylate **1a**: mp 54.5—55.5 °C (lit, mp 53—54 °C,[4] 53.7—54.6 °C[36]). Brosylate **1d**: mp 55.5—57 °C (lit,[4] mp 55.3—57 °C). Benzenesulfonate **1c** could not be crystallized and was purified by being settled as an oil repeatedly from pentane solution at −30 °C: IR (neat); 1360 (SO_2), 1190 (SO_2), 1100 (Ar–S), and 875—960 cm^{-1} (five max, S–O–C): NMR (60 MHz) δ=0.8—1.75 (m, 8H), 2.3 (broad s, 2H, bridge head CH), 4.36 (t, 1H, $CHOSO_2$), and 7.25—8.0 ppm (m, 5H, Ar–H).

Found: C, 61.93; H, 6.28%. Calcd for $C_{13}H_{16}O_3S$: C, 61.88; H, 6.39%.

p-Methoxybenzenesulfonate **1b**: mp 47.5—49 °C; IR (KBr); 1356 (SO_2), 1263 (Ar–O–C), 1190 (SO_2), 1170, 1100 (Ar–S), and 875—960 cm^{-1} (five max, S–O–C); NMR (60 MHz) δ=0.8—1.8 (m, 8H), 2.30 (broad s, 2H, bridge head CH), 3.88 (s, 3H, OCH_3), 4.41 (t, 1H, $CHOSO_2$), 6.98 (d, 2H, Ar–H), and 7.81 ppm (d, 2H, Ar–H).

Found: C, 59.65; H, 6.38%. Calcd for $C_{14}H_{18}O_4S$: C, 59.55; H, 6.43%.

exo-*2-Norbornanol-3*-endo-d *and Its Tosylate* ***1a****-3*-endo-d. *endo*-3-Deuterium was introduced by the $LiAlD_4$ reduction of norbornene oxide.[37,38] A solution of $LiAlD_4$ (99.5% D, 3.0 g) and norbornene oxide[28] (7.3 g) in DME (distilled from Na–benzophenone ketyl, 250 cm^3) was heated at 100—105 °C for 28 h. After the mixture had been cooled in an ice bath, a mixture of THF–H_2O (1:1, v/v, 200 cm^3) was added slowly, and then K_2CO_3 was added to separate water layer. An organic layer was dried ($MgSO_4$), concentrated (Vigreux column), and the residual oil was distilled to give *endo*-3-*d* alcohol (6.0 g, 80% yield): bp 178—179 °C. Sublimed sample of the alcohol was subjected to ^1H NMR (100 MHz) spectroscopic analysis to show an isotopic purity of 99%. The alcohol was converted into the tosylate in the usual manner.[35] **1a**-3-*endo-d*: mp 54—55 °C; NMR (60 MHz) δ=0.85—1.75 (m, 7H), 2.3 (broad s, 2H, bridge head CH), 2.43 (s, 3H, Ar–CH_3), 4.34 (s, 1H, CHOTs), 7.34 (d, 2H, Ar–H), and 7.78 ppm (d, 2H, Ar–H). ^{13}C NMR spectrum of the tosylate indicated the absence of deuterium scrambling during its preparation.

exo-*2-Norbornanol-3*-exo-d *and Its Tosylate* ***1a****-3*-exo-d. *exo*-3-Deuterium was introduced by deuterioboration of norbornene.[37,39] Deuterioboration–oxidation was carried out according to the standard procedure including external generation of diborane-d_6.[39] The 3-*exo-d* alcohol was obtained in 80% yield. ^1H NMR (100 MHz) analysis showed an isotopic purity of 97%. Tosylate **1a**-3-*exo-d* was synthesized from this alcohol in the usual manner.[35] **1a**-3-*exo-d*: mp 54—55 °C; NMR (60 MHz) δ=0.85—1.75 (m, 7H), 2.27 (broad s, 2H, bridge head CH), 2.43 (s, 3H, Ar–CH_3), 4.45 (d, 1H, J=6.2 Hz, CHOTs), 7.32 (d, 2H, Ar–H), and 7.79 ppm (d, 2H, Ar–H). ^{13}C NMR spectrum of the tosylate showed the absence of deuterium scrambling throughout its synthesis.

exo-*2-Norbornanol-3,3*-d_2 *and Its Tosylate* ***1a****-3,3*-d_2. Norcamphor-3,3-d_2 was prepared by the method of Schaefer *et al.*[40] in 70% yield: bp 168—169 °C. ^1H NMR (100 MHz) analysis showed an isotopic purity of 97.7%. Reduction of the ketone with $LiAl(OCH_3)_3H$ in THF afforded the *endo*-alcohol stereoselectively[41] (98%) in 94% yield. Then, the alcohol was converted into the brosylate in the usual manner,[35] which was then partially solvolyzed in AcOH–NaOAc for 2 h at 45 °C. The usual work-up and recrystallization from pentane at −30 °C gave *endo*-2-norbornyl-3,3-d_2 brosylate in 70% yield based on the *endo*-alcohol. The brosylate was subjected to S_N2 reaction with $(n\text{-Bu})_4NOAc$[31] in benzene (reflux, 3 h),[37] furnishing *exo*-2-acetate-3,3-d_2 in 98% yield after Kugelrohr distillation. Reduction of the acetate with $LiAlH_4$ gave *exo*-2-norbornanol-3,3-d_2 in 90% yield. ^{13}C NMR analysis showed the absence of deuterium scrambling during the procedures. Tosylate **1a**-3,3-d_2 was prepared in the usual manner:[35] mp 53.5—54.5 °C; NMR (60 MHz) δ=0.87—1.75 (m, 6H), 2.30 (broad s, 2H, bridge head CH), 2.43 (s, 3H, Ar–CH_3), 4.44 (s, 1H, CHOTs), 7.32 (d, 2H, Ar–H), and 7.78 ppm (d, 2H, Ar–H).

Product Analysis. Arenesulfonate (2—3 mmol) was weighed into an ampoule (dried in an oven), which was then repeatedly evacuated and filled with dry nitrogen. A desired amount of solvent was introduced to attain the concentration of the substrate to be 0.075 mol/dm^3 with a syringe through a septum and then pyridine (3% excess) was added in the same manner as above. The ampoule was then sealed under nitrogen and kept at 75 °C for ten half-lives. The ampoule was opened and weighed amounts of anisole was added to the mixture. The resulting solution was poured

into ice–water and extracted with pentane. The pentane solution was washed several times with water, dried ($MgSO_4$), and concentrated carefully by the use of 30-cm column packed with glass helices to *ca.* 1 cm^3. A part of the condensed pentane solution was transferred into an NMR tube with a syringe and the sample was repeatedly scanned over the respective regions for olefinic protons of norbornene **3** and O–CH_3 protons of anisole ten times at 30 s intervals. The ratio of the peak area of CH=CH to O–CH_3 was calculated as an average of these scans. The yield calculated from the ratio was reproducible relatively to $\pm 3\%$ or less on repeated runs.

Another part of the pentane solution was analyzed for nortricyclene **2**, norbornene **3**, and esters **4** and **5** by means of GLC.

The remaining pentane solution was combined with that used for NMR assay, concentrated, and the residue was chromatographed over SiO_2, being eluted successively with pentane, pentane–CH_2Cl_2 (8 : 2, v/v), and CH_2Cl_2. The CH_2Cl_2 fractions afforded the ester (**4**+**5**) which was reduced with $LiAlH_4$ in ether to give norbornanol, epimeric composition of which was analyzed by means of GLC (80 °C).

Preparation of Norbornene–Phenyl Azide Adduct. Norbornene **3** obtained from partial or complete solvolysis of **1a**-3-*endo-d* or **1a**-3-*exo-d* was converted into the adduct with phenyl azide[30] (1-phenyl-4,7-methano-3a,4,5,6,7,7a-hexahydrobenzotriazole, **8**) by the method described by Huisgen *et al.*[17] for the sake of easy separation and purification of small amounts (~mg) of norbornene **3** from the solvolysis products without loss and scrambling of deuterium.[42] A typical run is described in the followings.

Tosylate **1a**-3-*endo-d* (2 g) was solvolyzed in DMA for 0.5 half-lives in the same manner as described above. A mixture of nortricyclene **2**, norbornene **3**, the acetates **4** and **5**, and unchanged tosylates was obtained as a pentane solution after the usual work-up. The mixture was passed through an SiO_2 column and the column was eluted with additional pentane. To the combined pentane solution was added dry benzene (0.25 cm^3) and the mixture was concentrated carefully through a column packed with glass helices to *ca.* 1 cm^3. Then, phenyl azide[30] (0.02 cm^3) was added to the condensate and the resulting solution was allowed to stand at room temperature for three days. The volatile components were removed under reduced pressure to give yellow crystalline residue which was recrystallized from hexane to furnish the adduct as fine needles (0.02 g), mp 100—101 °C (lit,[17] mp 100—101 °C, unlabeled adduct **8**).

Separation of Nortricyclene. Tosylate **1a**-3,3-d_2 (0.5 g) was solvolyzed in DMA at 75 °C for ten half-lives. A condensed pentane solution was obtained in the same manner as described above. The solution was then treated with *m*-chloroperbenzoic acid in CH_2Cl_2 (slight excess to norbornene **3**) at 0 °C for 1 h. The mixture was washed with 10% Na_2CO_3, dried ($MgSO_4$), and concentrated by use of 30-cm column packed with glass helices. The residue was chromatographed over SiO_2 (5 g), being eluted with pentane (30 cm^3). The pentane solution was again concentrated through the column and the residue was allowed to stand open to the atmosphere at room temperature for 30 min to give crystalline nortricyclene **2**, which was then separated and purified by sublimation.

Separation of Unchanged Tosylate. The tosylate recovered from partial solvolysis was separated from pentane solution by repeated recrystallization at −30 °C. Colorless crystalline tosylate was obtained, which was kept under high vacuum at room temperature overnight.

^{13}C NMR Spectra. Chemical Shift Determinations. ^{13}C spectra were determined on a JEOL JMN FX-100 spectrometer operated at 25.05 MHz and equipped with JEOL JEC 980B computer (8K) in the Fourier transform mode. All ^{13}C chemical shifts are reported relative to tetramethylsilane in $CDCl_3$ or in CD_2Cl_2.

Spectral assignments were made easily from the multiplicities of the individual nuclei in the off-resonance decoupled spectra and from comparisons with the chemical shifts reported for other substituted norbornanes.[18] The chemical shifts of nortricyclene[18a] and the formate[18c] were available in the literature and our data were satisfactorily consistent with those reported.

Quantitative Intensity Measurements. For the deuterium distribution analysis, the proton-decoupled spectra of nortricyclene **2**, the esters **4a** and **4b**, the adduct **8**, and recovered tosylate were recorded at spectral widths of 2000, 2500, 3000, and 1000 Hz, respectively, by use of a 90° pulse and a pulse repetition of 30 s. A 180°-τ-90° pulse sequence[43] was used to demonstrate that 30 s delay was comparable to $5T_1$ for each of the observed nuclei. A pulse repetition of 60 s was also used to determine more definitely the nuclei labeled by deuterium atom. To circumvent the potential source of error on quantitative analysis,[44] the NOE suppressed gated decoupling technique[45] was used and each spectrum was compared with calibration spectra taken for unlabeled sample, employing unaffected carbon signals such as $\underline{C}H_3$-COO, –$\underline{C}(6)H_2$–, and Ar–$\underline{C}H_3$, respectively for **4a**, **4b** and **8**, and **1a**, as an internal calibration.

For the acetate **4a** deuterium distribution analysis was carried out as follows. The spectrum of an unlabeled sample in $CDCl_3$ was recorded by use of the operating parameters as indicated above. The ratio of the peak area of each observed nuclei to that of $\underline{C}H_3COO$ was directly computed on a JEOL 980B computer with SYSTEM Q/D PROGRAM FAFT08/11. The spectrum of a deuterated sample was then recorded in the identical manner as used in the case of the unlabeled sample. The ratio of the peak area of each observed nuclei so that of $\underline{C}H_3COO$ was measured in the same method as described above. A decrease in the intensity of –CH_2– signals was calculated from the each ratio obtained.

The deuterium distribution analysis of the adduct **8** obtained from the partial solyolysis of low %reaction ($\leq 50\%$) was carried out by means of ^1H NMR spectroscopy in the Fourier transform mode. Since the ^{13}C spectrum of the adduct **8**, obtained from the solvolysis of **1a**-3-*endo-d* in DMA (100% reaction), has indicated that the deuterium is located at C(3) and C(7) positions of norbornene skeleton, a decrease in the peak area of well-resolved C(3a)- and C(7a)-proton signals was measured. The ratio of the peak area of the concerned protons to that of the bridge head protons was directly obtained by the same method as described for the ^{13}C intensity measurement, which was compared with the corresponding ratio for the unlabeled sample. The operating parameters employed were a spectral width of 1000 Hz, a 45° pulse, pulse repetition of 10 s, and 10—200 pulses, to provide almost same S/N ratio for each sample.

Kinetic Measurements. Solvolysis rates for **1a—d** and specifically-labeled tosylates in the carboxmaides were determined in the same manner as described in the previous paper,[1] by the use of KOH (in EtOH) titrant and Thymol Blue–phenolphthalein indicator.

Except for the case of NMA, an experimental infinity titer was in excess of the theoretical one, in proportion to the amounts of the carboxylic acid which was produced by an acid-catalyzed hydrolysis of the amide solvent. The solvent hydrolysis is caused by contaminated water even after rigorous

purification of the amide. In all cases, however, $\log a/(a-x)$ $-t$ plots gave straight lines with intercept at an origin even when the excessive infinity titer was employed to calculate $a/(a-x)$ values. In fact, there have been obtained essentially the same rate constants for the solvolysis of **1a—d** in the amides containing various amounts of water, although the infinity titers were in the range of 1.1—1.65 times the theoretical titer.

Another control experiment was carried out; the rate constant obtained by the acid-base titration method, infinity titer being in excess, was the same as that obtained by the Volhard method within an experimental error for the solvolysis of 1-adamantyl bromide in the amides.

Rate constants listed in Tables 1 and 2 are the data calculated from experimental infinity titers without correction for the excess because the above-mentioned findings do not require the correction for the excess.

The rates of solvolysis of **1a** in aqueous ethanol and in aqueous acetone were determined titrimetrically in a usual manner.

Control Experiments. All the products were stable under the conditions employed in the present study. It was found that the presence of pyridinium tosylate, acetic acid, formic acid, or pyridine in equimolar amounts to the substrates did not alter the respective yields of the solvolysis products.

References

1) S. Saito, T. Yabuki, T. Moriwake, and K. Okamoto, *Bull. Chem. Soc. Jpn.*, **51**, 529 (1978).

2) M. A. Eakin, J. Martin, W. Parker, S. C. Egan (D. H. G.), and S. H. Graham, *Chem. Commun.*, **1968**, 337.

3) L. Stéhelin, L. Kanellias, and G. Ourisson, *J. Org. Chem.*, **38**, 847 (1973).

4) S. Winstein and D. Trifan, *J. Am. Chem. Soc.*, **74**, 1154 (1952); for a leading review, see D. G. Sargent in "Carbonium Ions," Vol. 3, ed by G. A. Olah and P. v. R. Schleyer, Wiley-Interscience, New York, N. Y. (1972), Chap. 24.

5) For representative reviews, see a) G. A. Olah, *J. Am. Chem. Soc.*, **94**, 808 (1972); b) G. A. Olah, *Acc. Chem. Res.*, **9**, 41 (1976).

6) A. T. Balaban and D. Fărcasiu, *J. Am. Chem. Soc.*, **89**, 1958 (1967).

7) R. E. Leone and P. v. R. Schleyer, *Angew. Chem.*, **82**, 889 (1970).

8) For examples, see a) H. C. Brown, *Tetrahedron*, **32**, 179 (1976) and the references cited therein; b) H. Maskill, *J. Am. Chem. Soc.*, **98**, 8482 (1976); c) H. C. Brown and M. Ravindranathan, *ibid.*, **99**, 299 (1977); d) M. J. S. Dewar, R. C. Haddon, A. Komornicki, and H. Rzepa, *ibid.*, **99**, 377 (1977); e) H. C. Brown, K. Takeuchi, and M. Ravindranathan, *ibid.*, **99**, 2684 (1977); f) G. A. Olah, G. K. S. Prakash, and G. Liang, *ibid.*, **99**, 5683 (1977); see also Ref. 5b.

9) S. Saito, K. Doihara, T. Moriwake, and K. Okamoto, *Bull. Chem. Soc. Jpn.*, **51**, 1565 (1978); Part III.

10) T. W. Bentley and P. v. R. Schleyer, *J. Am. Chem. Soc.*, **98**, 7658 (1976) and the references cited therein.

11) Calculated from the data in Ref. 10 based on m_{EW} for 2-adamantyl tosylate.

12) E. Grunwald and S. Winstein, *J. Am. Chem. Soc.*, **70**, 846 (1948): calculated from the data for the carboxamides and other solvent families (7 points).

13) A. Streitwieser, Jr., *Chem. Rev.*, **56**, 571 (1956).

14) Calculated from data for the carboxamides and other solvent families (8 points; available from literatures cited in footnote in Fig. 1).

15) See Ref. 17 cited in Ref. 1: see also a) R. A. McClelland, *J. Am. Chem. Soc.*, **97**, 3177 (1975) and b) R. A. McClelland and M. Ahmad, *ibid.*, **99**, 5356 (1977).

16) R. A. Sneen, J. V. Carter, and P. S. Kay, *J. Am. Chem. Soc.*, **88**, 2594 (1966): see also Ref. 16 cited in Ref. 1.

17) R. Huisgen, L. Möbius, G. Müller, H. Stangl, G. Szeimies, and J. M. Vernon, *Chem. Ber.*, **98**, 3992 (1965).

18) a) J. B. Grutzner, M. Jautelat, J. B. Dence, R. A. Smith, and J. D. Roberts, *J. Am. Chem. Soc.*, **92**, 7107 (1970); b) J. B. Stothers, C. T. Tan, A. Nickon, F. Huang, R. Sridhar, and R. Weglein, *ibid.*, **94**, 8581 (1972); c) R. S. Bly, R. K. Bly, J. B. Hamilton, J. N. C. Hsu, and P. K. Lillis, *ibid.*, **99**, 216 (1977).

19) a) D. J. Cram and M. R. V. Sahyun, *J. Am. Chem. Soc.*, **85**, 1257 (1963); b) M. Cocivera and S. Winstein, *ibid.*, **85**, 1702 (1963); c) P. S. Skell and W. L. Hall, *ibid.*, **85**, 2851 (1963); d) C. J. Kim and H. C. Brown, *ibid.*, **94**, 5051 (1972).

20) The amount at C(5) position would be below the limit of the accuracy (*ca.* 1%).

21) a) J. D. Roberts and C. C. Lee, *J. Am. Chem. Soc.*, **73**, 5009 (1951); b) J. D. Roberts, C. C. Lee, and W. H. Saunders, Jr., *ibid.*, **76**, 4501 (1954).

22) C. C. Lee and L. K. M. Lam, *J. Am. Chem. Soc.*, **88**, 2831, 5355 (1966).

23) a) P. v. R. Schleyer, W. E. Watts, R. C. Fort, Jr., M. B. Comisarow, and G. A. Olah, *J. Am. Chem. Soc.*, **86**, 5679 (1964); b) M. Saunders, P. v. R. Schleyer, and G. A. Olah, *ibid.*, **86**, 5680 (1964); c) F. R. Jensen and B. H. Beck, *Tetrahedron Lett.*, **1966**, 4287.

24) S. Saito and T. Moriwake, unpublished data.

25) See Ref. 5b: see also a) G. A. Olah and A. M. White, *J. Am. Chem. Soc.*, **91**, 3956 (1969) and b) G. A. Olah, A. M. White, J. R. DeMember, A. Commeyras, and C. Y. Lui, *ibid.*, **92**, 4627 (1970).

26) H. L. Goering and C. B. Schewene, *J. Am. Chem. Soc.*, **87**, 3516 (1965).

27) H. L. Peeters and M. Anteunis, *J. Org. Chem.*, **40**, 312 (1975).

28) H. C. Brown, J. H. Kawakami, and S. Ikegami, *J. Am. Chem. Soc.*, **92**, 6914 (1970).

29) D. C. Kleinfelter and P. v. R. Schleyer, *Org. Synth.*, **42**, 79 (1962).

30) a) R. O. Lindsay and C. F. H. Allen, *Org. Synth.*, Coll. Vol., 3, 710 (1955); b) W. v. E. Doering and R. A. Odum, *Tetrahedron*, **22**, 81 (1966).

31) R. Baker, J. Hudec, and K. L. Rabone, *J. Chem. Soc., C*, **1966**, 1605.

32) H. C. Brown and K.-T. Liu, *J. Am. Chem. Soc.*, **97**, 2469 (1975).

33) M. S. Morgan and L. H. Cretcher, *J. Am. Chem. Soc.*, **70**, 375 (1948).

34) St. Landa, S. Kriebel, and E. Knobloch, *Chem. Listy*, **48**, 61 (1954).

35) R. S. Tipson, *J. Org. Chem.*, **9**, 235 (1944): see also H. C. Brown and G. Ham, *J. Am. Chem. Soc.*, **78**, 2735 (1956).

36) P. v. R. Schleyer, M. M. Donaldson, and W. E. Watts, *J. Am. Chem. Soc.*, **87**, 375 (1965).

37) B. L. Murr and J. A. Conkling, *J. Am. Chem. Soc.*, **92**, 3462 (1970).

38) N. M. Yoon and H. C. Brown, *J. Am. Chem. Soc.*, **90**, 2927 (1968): although Yoon and Brown used diglyme as a solvent, we employed 1,2-dimethoxyethane instead for the sake of easy separation and purification of the alcohol without the drop in a yield and also without the formation of 7-hydroxy

derivative.
39) G. Zweifel and H. C. Brown, *Org. React.*, **13**, 1 (1963).
40) J. P. Schaefer, M. J. Dagani, D. S. Weinberg, *J. Am. Chem. Soc.*, **89**, 6938 (1967).
41) H. C. Brown and H. R. Deck, *J. Am. Chem. Soc.*, **87**, 5620 (1965).
42) The mechanism by which norbornene and phenyl azide react is concerted in nature: for a leading reference, see R. Huisgen, *J. Org. Chem.*, **41**, 403 (1976).
43) T. C. Farrar and E. D. Becker, "Pulse and Fourier Transform NMR," Academic Press, New York, N. Y. (1971), Chap. 2.
44) J. B. Stothers in "Topics in Carbon-13 NMR Spectroscopy," Vol. 1, ed by G. C. Levy Wiley-Interscience, New York, N. Y. (1974), pp. 231—237.
45) R. Freeman, H. D. W. Hill, and R. Kaptein, *J. Mag. Reson.*, **7**, 327 (1972).

Preparation and Properties of Nickel–Phosphine Complexes Coordinated with α,β-Unsaturated Ester

Junichi Ishizu, Takakazu Yamamoto,* and Akio Yamamoto
Research Laboratory of Resources Utilization, Tokyo Institute of Technology, Nagatsuta-cho, Midori-ku, Yokohama 227
(Received January 24, 1978)

Reactions of bis(1,5-cyclooctadiene)nickel, $Ni(cod)_2$, with α,β-unsaturated esters in the presence of tertiary phosphine give a series of nickel–phosphine complexes formulated as Ni(tertiary phosphine)$_n$L (L=alkyl methacrylates, methyl acrylate, or methyl cinnamate; n=2 for $P(C_6H_5)_3$, $P(C_2H_5)(C_6H_5)_2$, $P(CH_3)_2(C_6H_5)$, $P(C_2H_5)_3$, n=1 for P(cyclo-$C_6H_{11})_3$). Elemental analyses, IR and NMR spectra, and chemical properties of the complexes confirm the molecular formula. The olefinic proton signals of methyl acrylate and alkyl methacrylates coordinated to nickel shift to upfield by 2.6—4.9 ppm from those of free olefins in the ^{1}H-NMR spectra, indicating that the α,β-unsaturated esters coordinate to nickel through the double bond. The IR spectra show only small low frequency shifts of the ν(C=O) bands of the α,β-unsaturated esters on complex formation. The reactions of Ni(P-$(C_6H_5)_3)_2$ (ethyl methacrylate) and Ni(P(cyclo-$C_6H_{11})_3$) (ethyl methacrylate) with vinyl acetate at room temperature cause the scission of the C–O bond in vinyl acetate to yield ethylene and nickel acetate.

Although a number of nickel–olefin complexes are known,[1] only a few reports have appeared on the isolation of nickel complexes coordinated with α,β-unsaturated esters.[2] No studies seem to have been carried out on the isolation of a series of α,β-unsaturated ester–nickel complexes with stabilizing ligands such as tertiary phosphines or on the effects of the stabilizing ligands on the properties of the isolated complexes. In the course of our study on the C–O bond activation of esters in contact with some zero-valent nickel complexes,[3] we found that the reactions of bis(1,5-cyclooctadiene)nickel $Ni(cod)_2$ with α,β-unsaturated esters in the presence of tertiary phosphine ligands serve as a convenient and versatile synthetic route to α,β-unsaturated ester–coordinated nickel complexes having various tertiary phosphine ligands, although the reactions of $Ni(cod)_2$ with other types of esters (alkenyl acetates, phenyl carboxylates, *etc.*) in the presence of tertiary phosphine ligands often lead to the scission of the C–O bonds in the esters.[3]

In this paper we report the isolation of α,β-unsaturated ester–nickel complexes having tertiary phosphine ligands from the reaction mixtures of $Ni(cod)_2$, α,β-unsaturated esters (methyl acrylate, alkyl methacrylate, and methyl cinnamate), and tertiary phosphine ligands and some chemical properties of the isolated complexes.

Results and Discussion

Reactions of $Ni(cod)_2$ with methyl acrylate (mac), methyl methacrylate (mma), ethyl methacrylate (ema), and methyl cinnamate (mci) in the presence of tertiary phosphines at room temperature give orange or red nickel–phosphine complexes formulated as Ni(tertiary phosphine)$_n$(α,β-unsaturated ester) in high yields (62—92%):

$$Ni(cod)_2 + \text{tertiary phosphine} + CH(R_1)=C(R_2)COOR_3 \longrightarrow (PR_3)_nNi\text{---}\underset{R_2}{\overset{R_1}{C=C}}\overset{H}{}\overset{}{}COOR_3 \quad (1)$$

where PR_3 represents the tertiary phosphine ligand,

	Tertiary phosphine	R_1	R_2	R_3	n
1a	PPh_3	H	CH_3	C_2H_5	2
1b	$PEtPh_2$	H	CH_3	C_2H_5	2
1c	PMe_2Ph	H	CH_3	C_2H_5	2
1d	PEt_3	H	CH_3	C_2H_5	2
1e	PCy_3	H	CH_3	C_2H_5	1
1f	PPh_3	H	CH_3	CH_3	2
1g	PPh_3	H	H	CH_3	2
1h	PPh_3	C_6H_5	H	CH_3	2

PCy_3: tricyclohexylphosphine.

Table 1 summarizes the analytical data of the isolated complexes. Complex **1a** was also obtained by the ligand exchange reaction of $Ni(cod)(PPh_3)_2$ with ema. When the cone angle θ[4] of the phosphine ligand is large as in the case of tricyclohexylphosphine PCy_3 (θ=179°) a complex with one phosphine ligand (**1e**) is obtained. Similar acrylonitrile–nickel[5] and acrylaldehyde–nickel[6] complexes with one PCy_3 ligand are known. On the contrary, in other cases when the cone angle of the phosphine ligand is smaller as given in Table 1, complexes with two phosphine ligands are obtained. Since triethylphosphine and tricyclohexylphosphine have similar basicities, the difference in the number of the coordinated ligands can be ascribed mainly to the steric rather than electronic effect. Attempts to prepare an ema–nickel complex by use of bidentate phosphine ligands, 1,2-bis(diphenylphosphino)ethane(dpe), gave only $Ni(dpe)_2$, no ema-coordinated dpe complex being isolated. Among the ema complexes with two phosphine ligands (**1a**—**1d**) the sensitivity of the complex to oxygen increases with the increase in the basicity of the phosphine ligand in the order **1a**<**1b**<**1c**<**1d**. Complex **1a** is moderately stable in air. However, complex **1d** is highly air-sensitive.

NMR and IR Spectra of the Complexes. Table 2 summarizes the IR and ^{1}H-NMR data of the complexes. Figure 1 shows the ^{1}H-NMR spectrum of complex **1a** in benzene at room temperature with and without ^{31}P-decoupling. The signals of olefinic protons of ema shift on complex formation to the upfield region where the signals of olefinic protons in the usual

Table 1. Analytical data of Ni(tertiary phosphine)$_n$(α,β-unsaturated ester)

Complex[a]		Yield (%)	Color	Mp (°C)	Cone angle[b] (°)	Analytical data[c] C	H	Ni
$Ni(PPh_3)_2$ (ema)	**1a**	90	red	141—143	145	72.5 (72.3)	6.0 (5.8)	8.4 (8.4)
$Ni(PEtPh_2)_2$ (ema)	**1b**	67	orange	75— 80	141	68.1 (67.9)	6.9 (6.7)	9.3 (9.8)
$Ni(PMe_2Ph)_2$ (ema)	**1c**	79	orange	46— 48	127	58.7 (58.8)	7.5 (7.2)	13.2 (13.1)
$Ni(PEt_3)_2$ (ema)	**1d**	62	orange	−15	132	d)		21.6 (21.9)
$Ni(PCy_3)_2$ (ema)	**1e**	75	orange	134—136	179	63.7 (63.6)	10.1 (9.6)	
$Ni(PPh_3)_2$ (mma)	**1f**	85	red	137—138	145	72.0 (72.1)	5.7 (5.6)	8.5 (8.6)
$Ni(PPh_3)_2$ (mac)	**1g**	65	red	133—136	145	71.7 (71.8)	5.5 (5.4)	10.4 (10.5)
$Ni(PPh_3)_2$ (mci)	**1h**	65	red	155—156	145	74.5 (74.1)	5.5 (5.4)	

a) $PPh_3=P(C_6H_5)_3$, $PEtPh_2=P(C_2H_5)(C_6H_5)_2$, $PMe_2Ph=P(CH_3)_2(C_6H_5)$, $PEt_3=P(C_2H_5)_3$, $PCy_3=P(\text{cyclo-}C_6H_{11})_3$, ema=ethyl methacrylate, mma=methyl methacrylate, mac=methyl acrylate, mci=methyl cinnamate. b) See Ref. 4. The cone angles of $PEtPh_2$ and PMe_2Ph are not given in the reference but calculated by using the equation given in Ref. 4b). c) Calculated values are in parentheses. d) Microanalyses of C and H were not obtained due to the low melting point and high air-sensitivity of complex **1d**.

Table 2. IR and NMR data of the α,β-unsaturated ester–nickel complexes

Complex		ν(C=O)[a] (cm^{-1})	Δν[b] (cm^{-1})	NMR signals of the α,β-unsaturated ester ligand[c] (δ, ppm from TMS) $-CH_2(COOR)$	H–C=(*cis*)	H–C=(*trans*)	H–C=(α)	α-CH_3	$CH_3(COOR)$
$Ni(PPh_3)_2$(ema)	**1a**	1685	43	3.87(m)	3.21(m)	2.28(m)		1.69 (d, 6 Hz)	1.05 (t, 7 Hz)
$Ni(PEtPh)_2$(ema)	**1b**	1664	64	4.02 (q, 7 Hz)	2.90(m)	2.15(m)[d]		1.87 (d, 6 Hz)	1.07 (t, 7 Hz)
$Ni(PMe_2Ph)_2$(ema)	**1c**	1662	66	4.10 (q, 7 Hz)	2.80(br)	2.20(br)		1.97(s)	1.12 (t, 7 Hz)
$Ni(PEt_3)_2$(ema)	**1d**	1672[e]	56	4.10(m)	2.31(m)	1.71(m)		1.73 (d, 6 Hz)	1.11 (t, 8 Hz)[d]
$Ni(PCy_3)$(ema)	**1e**	1707	21	4.06 (q, 7 Hz)	3.34(m)	2.70(m)		1.87 (d, 4 Hz)	1.12 (t, 7 Hz)[d]
$Ni(PPh_3)_2$(mma)	**1f**	1688	44		1.24(m)	0.92(m)		1.66 (d, 6 Hz)	3.28(s)
$Ni(PPh_3)_2$(mac)	**1g**	1675	64		3.00(m)	2.10(m)	3.50(m)		3.06(s)
$Ni(PPh_3)_2$(mci)	**1h**	1681	43		4.46(m)		3.72(m)		3.25(s)

a) In KBr disk except for **1d**. b) $\nu(C=O)_{free}-\nu(C=O)_{complex}$. c) In C_6D_6 at room temperature; s=singlet, d=doublet, t=triplet, q=quartet, m=multiplet; br=broad; *cis*- and *trans*-CH are referred to the ester groups. The tertiary phosphine signals are omitted from the table. d) This signal is partly overlapped with the tertiary phosphine signals. e) In benzene.

π-type transition metal–olefin complexes are observed.[1] Without ^{31}P-decoupling the two olefinic protons of ema in **1a** give rise to complex multiplet signals due to the geminal coupling and the coupling with one or two ^{31}P's (Fig. 1a). The ^{31}P-decoupled ^1H-NMR spectrum of **1a** gives an AB quartet pattern typical of the geminal olefinic protons coupled with each other (Fig. 1b). The α-CH_3 protons are coupled with one of the ^{31}P nuclei of the two PPh_3 ligands. The existence of the coupling between ^{31}P of PPh_3 ligand and ^1H's of ema indicates that these ligands are bonded to nickel on NMR time scale.

The appearance of PPh_3 signal as a sharp quartet in $^{31}P\{H\}$-NMR spectrum of **1a** (Fig. 2a) reveals that two PPh_3 ligands occupy magnetically non-equivalent positions to each other in the square planar complex, there being neither rapid dissociation of ligands nor rotation of the ema ligand around the Ni–ema bond axis.

The CH_2 protons of OC_2H_5 group of ema in **1a** give rise to a complex pattern (probably a double quartet) in the ^1H-NMR spectrum. The pattern is not simplified by the ^{31}P-decoupling, indicating that the two protons in the OCH_2 group are magnetically non-equivalent. The non-equivalence of the two protons most probably arises from the prevention of free rotation about the O–CH_2 bond axis due to steric hindrance.

The IR spectrum of **1a** shows a shift of ν(C=O) band

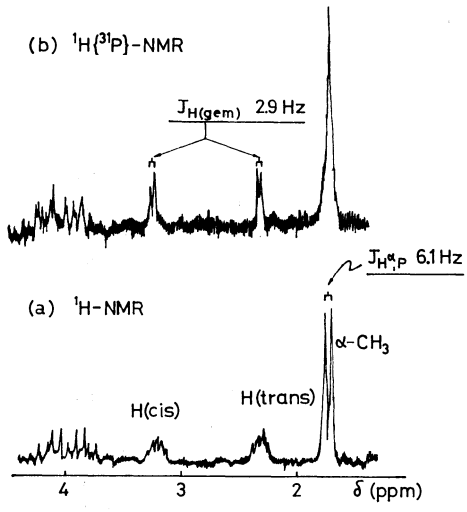

Fig. 1. (a) ^1H-NMR spectrum of complex **1a**, (b) ^{31}P-decoupled ^1H-NMR spectrum of **1a**; in benzene-d_6 at room temperature. *cis*-H and *trans*-H are referred to the ester group.

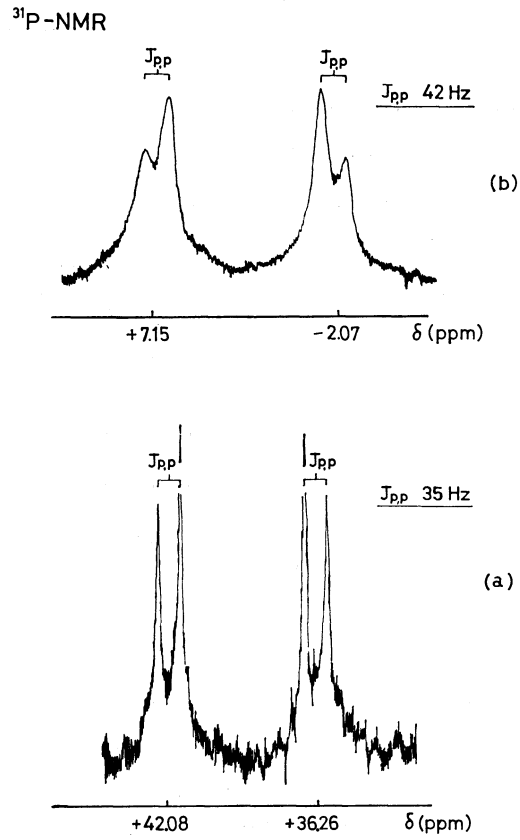

Fig. 2. ^{31}P-NMR spectra of (a) **1a** and (b) **1c** in toluene at room temperature. δ value is referred to external PPh_3 (downfield positive).

of ema to a lower frequency by 43 cm^{-1}, suggesting that there is no direct end-on type interaction between the C=O group and the nickel atom. When a carbonyl group of an ester has direct end-on type interaction with a metal, the ν(C=O) band usually shifts to lower frequency by more than 100 cm^{-1}.[7]

These NMR and IR data indicate that the ema ligand in **1a** is coordinated to nickel predominantly through the C=C double bond. It has recently been established by X-ray structural analysis that methyl acrylate (mac) in solid Ni(2,2′-bipyridine)$(mac)_2$ is coordinated to nickel through the C=C double bond the carbonyl group not participating in the direct bonding.[8] In this complex the ν(C=O) of mac shifts to lower frequency by 50 cm^{-1} on coordination.[2a]

The ^1H-NMR spectrum of **1d** is similar to that of **1a**, showing coupling of olefinic and α-CH_3 protons with ^{31}P of PEt_3 and non-equivalence of the two protons in the OCH_2 group. The ^1H-NMR spectrum of **1b** is also similar to that of **1a** showing the coupling of ^{31}P of $PEtPh_2$ with olefinic and α-CH_3 ^1H's of ema, but in this spectrum the OCH_2 signal appears as a simple quartet indicating that free rotation around the O–CH_2 bond occurs.

In contrast to **1a**, **1b**, and **1d**, the ^1H-NMR spectrum of **1c** shows that the α-CH_3 protons of ema are not coupled with ^{31}P of PMe_2Ph and the signals of the olefinic protons of ema are somewhat broadened at room temperature. The ^{31}P-NMR spectrum of **1c** also shows broadening of the AB quartet (Fig. 2b). On cooling a toluene solution of **1c** to −70 °C the coupling between α-CH_3 protons and ^{31}P of PMe_2Ph becomes observable in the ^1H-NMR spectrum and the AB quartet in the ^{31}P-NMR spectrum becomes sharp. These results indicate that coordinated ema in **1c** is rapidly exchanged at room temperature with a trace amount of free ema liberated from the complex:

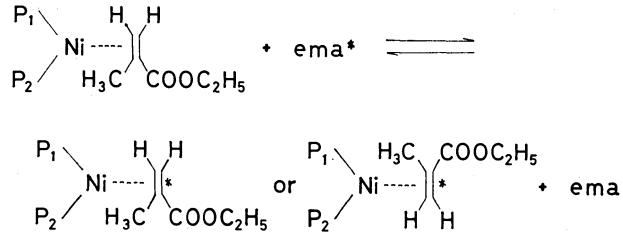

Peaks assignable to free ema are not observable in the ^1H-NMR of **1c** both at room temperature and at −70 °C presumably because of minor dissociation of ema from the complex.

In the Ni–ema complexes having two phosphine ligands there is a tendency that the upfield shift of the olefinic protons of ema on coordination increases with increase in the basicity of the phosphine ligand. The trend is more obvious with *cis*-olefinic proton than with *trans*-olefinic proton. Figure 3 shows plots of the chemical shifts of the olefinic protons against the pK_a value of the conjugate acid of the phosphine ligand. The relation shown indicates that the coordination of a basic phosphine ligand enhances the migration of electrons from nickel to ema to increases the shielding of the olefinic protons. The shift of ν(C=O) to lower frequency also supports this view. When the IR spectrum is taken in a KBr disc the coordination of a more basic phosphine ($PEtPh_2$($pK_a^{9)}$=4.9) or PMe_2Ph($pK_a^{9)}$=6.2)) to nickel causes a larger shift of ν(C=O) than the coordination of the less basic phosphine (PPh_3-($pK_a^{9)}$=3.0)), suggesting that the coordination of a more basic phosphine causes a greater Ni→ema back-

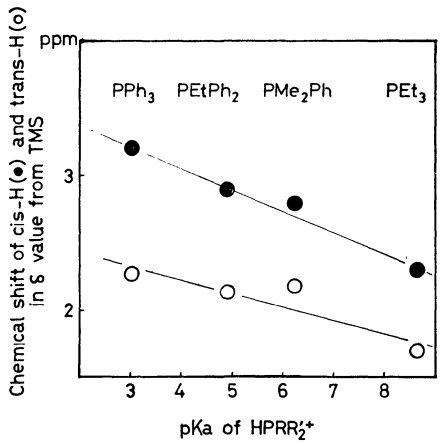

Fig. 3. Polts of the chemical shifts of *cis*-H(●) and *trans*-H(○) of Ni(ema)(tretiary phosphine)$_2$ against the pK_a[9] value of conjugate acids of the tertiary phosphines.

donation decreasing the bond order of the C=O group.

The olefinic protons of mma, mac, and mci are also shifted upfield in the ^{1}H-NMR spectra on complex formation, the coupling between ^{31}P of PPh_3 and α-CH_3 protons of mma being observable in the ^{1}H-NMR spectrum of **1f**.

Reactions of the Complexes. The α,β-unsaturated esters are readily liberated from the complex on addition of excess amounts of tertiary phosphines or pyridine:

$$\mathbf{1a} + PPh_3 \text{ (excess)} \xrightarrow{\text{r. t.}} \text{ema (100\%)} + Ni(PPh_3)_4. \quad (2)$$

The α,β-unsaturated esters in the complexes are hydrogenated by dry HCl in diethyl ether to yield the corresponding saturated esters (*e.g.*, ethyl isobutyrate from ema).

Reactions of the α,β-unsaturated ester–nickel complexes with vinyl acetate give no nickel-vinyl acetate adduct expected as a product of a simple ligand exchange reaction. However, they lead to the scission of the C–O bond in vinyl acetate to yield ethylene and nickel acetate in high yields (Eq. 3), a result similar to our findings on the C–O bond activation of vinyl acetate by $RuH_2(PPh_3)_4$[10] and by bis(1,5-cyclooctadiene)nickel Ni(cod)$_2$ in the presence of phosphine ligands (Eq. 4):[3]

$$\mathbf{1} + CH_2{=}CHOCOCH_3 \longrightarrow Ni(CH_3COO)_2(PR_3)_n + CH_2{=}CH_2, \quad (3)$$

$$Ni(cod)_2 + CH_2{=}CHOCOCH_3 + PR_3 \longrightarrow Ni(CH_3COO)_2(PR_3)_n + CH_2{=}CH_2. \quad (4)$$

Reaction 3 presumably proceeds through the olefin exchange reaction and the activation of the C–O bond of vinyl acetate on the nickel atom:

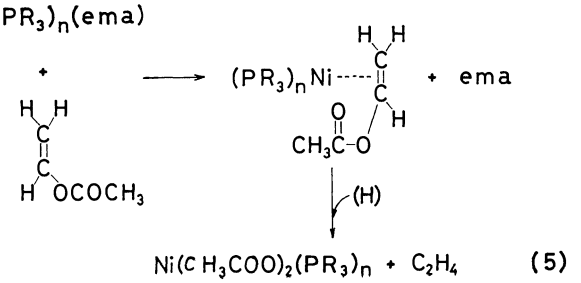

Ease of the cleavage of the C–O bond in vinyl acetate promoted by **1** depends on the coordinated phosphine ligand. Thus, the PCy_3-coordinated complex **1e** promotes cleavage of the C–O bond even at 10 °C, whereas the PPh_3-coordinated complex **1a** causes it only at 50 °C or above. A similar effect of the coordinated phosphine ligand on the activation of the C–O bond in phenyl carboxylate by Ni has been found.[3] The sources of hydrogen to yield ethylene from the vinyl moiety (Eq. 5) have not been clarified yet.

The interaction of some transition metal complexes with olefic esters such as alkyl methacrylates and vinyl acetate causes the activation of the olefinic C–H bond to form σ-alkenyl-transition metal complexes.[11] However, no C–H bond activation of such a type has been observed for the nickel complexes we prepared.

Experimental

General Procedures and Materials. Preparation and recrystallization of complexes **1a**—**1h** were carried out under deoxygenated nitrogen or argon. Melting points were determined in sealed tubes in a vacuum. Bis(1,5-cyclooctadiene)nickel, Ni(cod)$_2$ was purchased from Merck Co., Ltd. and recrystallized. α,β-Unsaturated esters were purified by distillation. Tertiary phosphine ligands were used as purchased or synthesized by the methods given in literature.[12] Solvents were dried by the usual procedures, distilled, and stored under argon or nitrogen. Yields and melting points of the complexes are given in Table 1.

Preparation of α,β-Unsaturated Ester–Nickel Complexes.. *Ni(PPh$_3$)$_2$(ema)* ***1a***: ema (0.55 g, 4.8 mmol) was added to a mixture of Ni(cod)$_2$ (0.92 g, 3.4 mmol) and PPh_3 (1.76 g, 6.8 mmol) dispersed in 2 ml of hexane. Stirring of the mixture for 5 h at room temperature afforded an orange solution, which was condensed to give a light orange precipitate. The precipitate was collected by filtration and recrystallized from diethyl ether–hexane at −30 °C.

Ni(PEtPh$_2$)$_2$(ema) ***1b***: $PEtPh_2$ (0.95 g, 5.8 mmol) was added to a mixture of Ni(cod)$_2$ (0.80 g, 2.9 mmol) and ema (1.0 g, 8.0 mmol) dispersed in 3 ml of diethyl ether. Stirring of the solution for 6 h at 10 °C gave an orange solution which was condensed to give an orange oil. The oil was dissolved in a mixture of ether and hexane and standing of the solution at −30 °C for 2 days yielded orange crystals.

Ni(PMe$_2$Ph)$_2$(ema) ***1c***: PMe_2Ph (0.74 g, 5.4 mmol) was added to a mixture of Ni(cod)$_2$ (0.74 g, 2.7 mmol) and ema (0.46 g, 4.0 mmol) dispersed in 2 ml of diethyl ether. Stirring of the mixture at 10 °C for 6 h gave a homogeneous red solution. This was condensed to afford a black oil, which was crystallized from diethyl ether–hexane.

Ni(PEt$_3$)$_2$(ema) ***1d***: PEt_3 (0.46 g, 3.9 mmol) was added to a mixture of Ni(cod)$_2$ (0.54 g, 2.0 mmol) and ema (1 g, 0.88 mmol) dispersed in 3 ml of diethyl ether. After stirring the mixture at 10 °C overnight the orange solution obtained was condensed to give an orange oil. The oil was crystallized from hexane at −78 °C. The orange crystals obtained were washed several times with ether at −78 °C and dried in a vacuum.

Ni(PCy$_3$)(ema) ***1e***: ema (2.7 g, 24 mmol) was added to a mixture of Ni(cod)$_2$ (0.73 g, 2.7 mmol) and PCy_3 (1.9 g, 6.8 mmol) dispersed in a mixture of 2 ml of hexane. Stirring of the mixture for 1 h at −15—10 °C gave a homogeneous solution. After further stirring for 5 h at room temperature the yellow precipitate formed was collected by filtration and

recrystallized from tetrahydrofuran or toluene at −20 °C.

Ni(PPh$_3$)$_2$(mma) **1f**: mma (0.47 g, 4.7 mmol) was added to a mixture of Ni(cod)$_2$ (0.56 g, 2.0 mmol) and PPh$_3$ (1.1 g, 4.2 mmol) dispersed in a mixture of 2 ml of diethyl ether and 1 ml of hexane. The mixture was stirred at 0 °C for 6 h to give a homogeneous solution. This was cooled to −30 °C to yield a yellow precipitate, which was collected by filtration and recrystallized from toluene containing mma. When the solvent contained no excess mma, no analytically pure compound was obtained.

Ni(PPh$_3$)$_2$(mac) **1g**: mac (0.90 g, 10.6 mmol) was added to a mixture of Ni(cod)$_2$ (0.50 g, 1.8 mmol) and PPh$_3$ (0.96 g, 3.7 mmol) dispersed in 3 ml of diethyl ether. The solution was stirred at room temperature for 8 h to give a homogeneous orange solution, which was condensed to give an orange oil. The oil was dissolved in a mixture of tetrahydrofuran and hexane. Cooling of the solution to −20 °C gave red crystals.

Ni(PPh$_3$)$_2$(mci) **1h**: A toluene (2 ml) solution containing mci (0.68 g, 4.2 mmol), Ni(cod)$_2$ (1.13 g, 4.1 mmol), and PPh$_3$ (2.2 g, 8.4 mmol) was stirred at room temperature for 6 h to give a red precipitate, which was collected by filtration, washed with diethyl ether, and recrystallized from acetone.

Spectral Measurements and Analysis. IR spectra were recorded on a Hitachi Model 295 infrared spectrophotometer, ^{1}H-NMR spectra on a Japan Electron Optics Laboratory (JEOL) Mode JNM-PS-100 spectrometer, and ^{31}P-NMR spectra on a JEOL Model JNM-PFT-PS-100 Fourier transform spectrometer. PPh$_3$ was used as an external standard. Microanalyses of C and H were performed by Mr. T. Saito in our laboratory with a Yanagimoto CHN Autocorder Type MT-2. Macroanalyses of nickel were carried out by volumetric titration.[13] The analyses of gaseous and liquid products obtained by the reactions of complexes were carried out with a Shimadzu GC-3BT gas chromatograph.

References

1) Review articles: (a) M. Herberhold, "Metal π-Complexes," Vol. II, Elsevier, Amsterdam (1972); (b) P. W. Jolly and G. Wilke "The Organic Chemistry of Nickel," Vol. I, Academic Press, New York (1974).

2) (a) T. Yamamoto, A. Yamamoto, and S. Ikeda, *J. Am. Chem. Soc.*, **93**, 3350 (1971); (b) S. Otsuka, T. Yoshida, and Y. Tatsuno, *ibid.*, **93**, 6462 (1971); (c) S. Otsuka, T. Yoshida, and Y. Tatsuno, *Chem. Commun.*, **1971**, 67; (d) M. Dubini and F. Montino, *ibid.*, **1966**, 749.

3) J. Ishizu, T. Yamamoto, and A. Yamamoto, *Chem. Lett.*, **1976**, 1091.

4) (a) C. A. Tolman, *J. Am. Chem. Soc.*, **92**, 2056 (1970); (b) C. A. Tolman, W. C. Seidel, and L. W. Gosser, *ibid.*, **96**, 53 (1974).

5) M. Pfajfer, Ph. D. Dissertation, University of Bochum (1971).

6) R. van der Linde and B. Bogdanovic, Proc. Int. Conf. Organometal. Chem., 4th, 1969 U8 (1969).

7) M. F. Lappert, *J. Chem. Soc.*, **1961**, 817.

8) P. Binger and C. Krüger, private communication.

9) W. A. Henderson and S. A. Buckler, *J. Am. Chem. Soc.*, **82**, 5794 (1960).

10) S. Komiya and A. Yamamoto, *J. Organomet. Chem.*, **87**, 333 (1975).

11) (a) S. Komiya and A. Yamamoto, *Chem. Lett.*, **1975**, 475; (b) S. Komiya, T. Ito, M. Cowie, A. Yamamoto, and J. A. Ibers, *J. Am. Chem. Soc.*, **98**, 3874 (1976); (c) M. Kubota, A. Miyashita, S. Komiya and A. Yamamoto, *J. Organomet. Chem.*, **139**, 111 (1977); (d) T. Ito, F. Ozawa, K. Mita, and A. Yamamoto, 8th International Conf. Organometal. Chem., 1A28, Kyoto (1977).

12) (a) H. Goetz and S. Domin, *Ann. Chem.*, **704**, 1 (1967); (b) G. M. Kosolapoff and L. Maier, "Organic Phosphorus Compounds," Vol. 1, John Wiley, New York (1972), p. 156 and references cited therein.

13) K. Ueno "Chelate Titration," Nankodo, Tokyo (1960), p. 238.

Kinetic and Stereochemical Studies of the Reaction of Trialkyl-(alkylthio and arylthio)stannanes with Haloalkanes

Seizi KOZUKA* and Sadamu OHYA

Department of Applied Chemistry, Faculty of Engineering, Osaka City University, Sugimoto-cho, Sumiyoshi-ku, Osaka 558

(Received January 28, 1978)

A kinetic study has been conducted on the reaction of arylthio(trimethyl)stannane with haloalkanes giving halotrimethylstannane and alkyl aryl sulfide. The reaction has been found to obey second order kinetics. Substituent effects of the arylthio group, solvent effects, relative reactivities of the leaving halogens and steric effects of the haloalkanes have been investigated. Optically active (+)-1-methylheptyl bromide gives an inverted product *i.e.*, (−)-methyl 1-methylheptyl sulfide by the reaction with trimethyl(methylthio)stannane. A mechanism involving bimolecular nucleophilic attack of the sulfur atom on the haloalkane has been confirmed for the reaction.

The reactions of methylthiostannanes with iodomethane have been known to give iodostannane and

$$R_2Sn(SMe)_2 \xrightarrow{MeI} R_2SnI_2 + 2Me_3S^+I^-$$

$$R_3SnSMe \xrightarrow{MeI} R_3SnI + Me_3S^+I^-$$

R=Me, Et, and *n*-Bu

trimethylsulfonium iodide.[1] Recently, the reactions of trialkyl(arylthio)stannanes with various haloalkanes have been examined and it has been found that the reactions proceed in a way similar to those of methylthiostannanes but give alkyl aryl sulfides, instead of sulfonium salts.[2]

$$R_3SnSAr \xrightarrow{R'X} R_3SnX + R'SAr$$

R=Me, *n*-Bu, R'=Me, Et, 2-Pr, and benzyl.

Several different mechanisms have been forwarded for the reaction: Five-coordination of the tin atom to iodine (I) has been suggested by Balcombe *et al.*[1] Four-centered reaction (II) is another plassible process in view of the analogous reaction of stannanes.[3] Contrary to these mechanisms, formation of a transient sulfonium salt (III) by a nucleophilic attack of the sulfur atom has been suggested based on the observations that the reaction of trimethyl(phenylthio)stannane with iodomethane proceeds much slower than that of trimethyl(methylthio)stannane.[2] The salt III

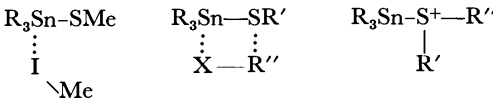

(I) (II) (III)

had been accepted as the final product of the reaction of trimethyl(methylthio)stannane with iodomethane[4] but recently it has been shown to be a non-isolable intermediate.[2] In this paper, the kinetic and stereochemical studies of the reaction are reported and the reaction mechanism discussed.

Results and Discussion

Kinetics. The rate of the reaction of trimethyl(*p*-tolylthio)stannane with a 10-fold excess of iodomethane in chloroform solution at 100 °C was measured by following the decrease and rise of the ^1H NMR of the starting trimethyl signal and product. A pseudo-first-order kinetic plot was obtained up to nearly completion of the reaction. First order dependency of the rate was observed on the concentration of iodomethane. Thus, the reaction was found to be second order, first order with respective to thiostannane and haloalkane.

Activation parameters were observed for the reactions of the tolylthiostannane and trimethyl(phenylthio)stannane with iodomethane. Remarkably large negative entropy values were obtained for the reactions in non-polar solvents. These results indicate tight transition states for the reactions but do not suggest a 4-centered reaction since the rate is markedly accelerated in better solvents for ionic reaction (PhCN). Also the entropy vales appeares to be reasonable in magnitude for a bimolecular reaction. The tight transition state may be rationalized in terms of an ionic reaction which is forced to proceed in non-polar solvents.

Clear evidence was obtained in the present study supporting nucleophilic attack as the mechanism. Hammett plots of the rates of reactions for *p*-substituted phenylthiostannanes gave a significant negative ρ values (−1.4) against σ parameters. This result does not support the mechanism involving 5-coordination of the tin atom to the halogen since the mechanism would result in a positive ρ value of moderate magnitude. The reactions of more efficient nucleophiles, such as trimethyl(methylthio)stannane and other alkylthiostannanes with haloalkanes would proceed by the same mechanism to that of arylthio(trimethyl)stannane, since the nucleophilic reaction has been confirmed for the reaction of a less efficient nucleophile *i.e.*, arylthiostannane.

The kinetics of the reactions with various haloalkanes were also performed to elucidate steric and electronic effects on the rate of reaction. The steric effect observed for the reactions with iodomethane, iodoethane and 2-iodopropane (k_{rel} : 1.00, 0.125, and 0.014, respectively) appears smaller than that for standard S_N2 reactions[5] but consistent with that observed with the benzenethiolate ion as the nucleophile.[6] The small steric retardation is undoubtedly due to the longer length of the forming carbon–sulfur bond. Relative reactivity of benzyl chloride, bromide and iodide (k_{rel}: 0.023, 1.2, and 5.9, respectively) was observed in the present study and is in good agreement with that of S_N2 reactions.[5,7] These results obtained by the kinetic studies are shown in the Table 1.

Table 1. Rate constants for the reactions of arylthio(trimethyl)stannanes with haloalkanes

Me_3SnS-C_6H_4Y-p[a] Y	RX	Mole ratio RX/SnS	Solvent	Temp °C	$k_{obsd} \times 10^4$	Remark
CH_3	CH_3I	10.0	$CHCl_3$	115	2.24	1.00[b]
CH_3	CH_3I	10.0	$CHCl_3$	100	1.03	13.4, −41.2[c]
CH_3	CH_3I	10.0	$CHCl_3$	85	0.480	
CH_3	CH_3I	15.1	$CHCl_3$	100	1.67	
CH_3	CH_3I	20.3	$CHCl_3$	100	2.04	
H	CH_3I	10.0	$CHCl_3$	115	1.45	
H	CH_3I	10.0	$CHCl_3$	100	0.637	13.4, −42.0[c]
H	CH_3I	10.0	$CHCl_3$	90	0.413	
H	CH_3I	10.0	PhCN	100	10.3[d]	16.8, −27.6[c]
H	CH_3I	10.0	PhCN	75	1.85	
H	CH_3I	10.0	PhCN	60	0.513	
H	CH_3I	10.0	PhCN	50	0.263	
CH_3	CH_3I	10.0	C_6H_6	130	0.734	
CH_3	CH_3I	10.0	C_6H_6	120	0.397	
CH_3	CH_3I	10.0	C_6H_6	100	0.154	14.5, −42.1[c]
OCH_3	CH_3I	10.0	$CHCl_3$	100	1.16	
Cl	CH_3I	10.0	$CHCl_3$	100	0.204	
NO_2	CH_3I	10.0	$CHCl_3$	100	0.0457	−1.40[e]
CH_3	C_2H_5I	10.0	$CHCl_3$	115	0.281	0.125[b]
CH_3	2-C_3H_7I	10.0	$CHCl_3$	115	0.0321	0.014[b]
CH_3	$C_6H_5CH_2I$	10.0	$CHCl_3$	115	13.3	5.9[b]
CH_3	$C_6H_5CH_2Br$	10.0	$CHCl_3$	115	2.65	1.2[b]
CH_3	$C_6H_5CH_2Cl$	10.0	$CHCl_3$	115	0.0515	0.023[b]

a) 6.0×10^{-2} mol/l as the initial concentration. b) Relative rate. c) Activation parameters, ΔH^*(kcal/mol) and ΔS^*(e. u.), respectively. d) Estimated value. e) ρ value against σ constants.

Stereochemistry. Inversion of configuration of the alkyl group of the haloalkane would be expected by the bimolecular nucleophilic attack of the sulfur atom on the haloalkane. Retention or partial racemization, on the other hand, may result if the reaction proceeded by 5-coordination of the tin atom or by a 4-centered process.

Optically active (+)-1-methylheptyl bromide was allowed to react with the thiostannane in order to confirm the mechanism. Trimethyl(methylthio)stannane, instead of arylthio(trimethyl)stannane, was employed for the reaction with the optically active bromide since the sterically hindered secondary bromide is less reactive. The reaction was stopped at about half completion. The product, methyl 1-methylheptyl sulfide did not undergo sulfonium salt formation with the remaining bromide probably due to steric hindrance of the bulky 1-methylheptyl groups. The stereochemical result is shown below. This result indicates inversion of configuration of the alkyl carbon atom during the reaction since S_N2 reaction of optically active 1-methylheptyl bromide with sodium methanethiolate in ethanol has been shown to give optically active methyl 1-methylheptyl sulfide of opposite sign.[8] The starting bromide underwent partial racemization during the reaction and consequently, the stereospecificity of the reaction could not be determined. However, high stereospecific inversion may be assumed for the present reaction in comparison with the optical activities of the bromide and sulfide with stereochemical results obtained by the S_N2 reaction.[8]

$$(CH_3)_3SnSCH_3 + (+)\text{-}n\text{-}C_6H_{13}CH(CH_3)Br \xrightarrow{120\,^\circ C,\ 115\,h} (CH_3)_3SnBr + (-)\text{-}n\text{-}C_6H_{13}CH(CH_3)\text{-}S\text{-}CH_3 + \text{recov. } (+)\text{-}n\text{-}C_6H_{13}CH(CH_3)Br$$

$[\alpha]_D^{30}$ $+36.4^\circ$ → $[\alpha]_D^{30}$ -9.7° + $[\alpha]_D^{30}$ $+24.3^\circ$

Mechanism. All the results are consistent with a mechanism involving bimolecular nucleophilic attack of the sulfur atom on the haloalkane to form the sulfonium salt III as a transient intermediate. No evidence was found to support the 5-coordination or 4-centered mechanism for the reaction.

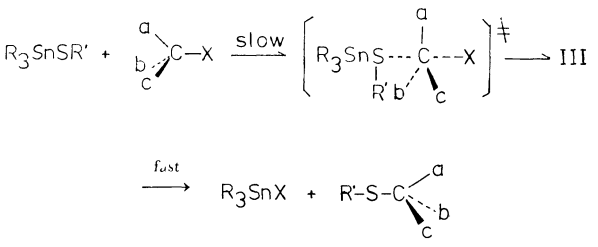

Experimental

Materials. Preparation of the thiostannanes have previously been reported.[2,9] Solvents for the kinetic studies were dried and distilled before use. Commercial haloalkanes except for benzyl iodide were used for the kinetic studies

after distillation. Benzyl iodide was prepared from benzyl bromide by the halogen exchange reaction with sodium iodide.

Kinetic Procedure. The general procedure was as follows: arylthio(trimethyl)stannane (3×10^{-4} mol) and haloalkane (3×10^{-3} mol) were dissolved in the solvent using a 5 ml volumetric flask. The solution was divided into 10 portions and sealed in glass tubes of *ca.* 0.7 ml volume. The tubes were heated in a constant temperature bath (100 °C) and samples taken at appropriate intervals. Each sample of the solution was analyzed by ^1H NMR with 5-repeated integrations of the starting trimethyl signal (δ 0.38 ppm, Me_3SnSPh) and that of the product (δ 0.88 ppm, Me_3SnI). Pseudo-first-order rate constant was obtained by a least square calculation of the relative intensities of the signals at the time intervals.

Preparation of (+)-1-Methylheptyl Bromide. The bromide was prepared from L-(−)-2-octanol and phosphorus tribromide by the usual procedure,[10] bp 82 °C/16 mmHg, $[\alpha]_D^{30}$ +36.4° (c=2.00, acetone).

Reaction of (+)-1-Methylheptyl Bromide with Trimethyl(methylthio)stannane. The stannane (300 mg, 1.42 mmol) and the bromide (277 mg, 1.42 mmol) were mixed and heated at 120 °C for 115 h in a sealed tube. Bromotrimethylstannane, methyl 1-methylheptyl sulfide and the remaining 1-methylheptyl bromide were identified in the reaction mixture by GLC analysis (Silicon SE-30, 2 m, 70 °C). Among these, methyl 1-methylheptyl sulfide, $[\alpha]_D^{30}$ −9.7° (c=0.65, acetone), and 1-methylheptyl bromide, $[\alpha]_D^{30}$ +24.3° (c=0.07, acetone), were isolated by GLC and the rotations measured. No appreciable racemization of 1-methylheptyl bromide was found when the bromide was heated alone or with bromotrimethylstannane in chloroform under the reaction conditions (120 °C, 115 h).

References

1) C. I. Balcombe, E. C. Macullin, and M. E. Peach, *J. Inorg. Nucl. Chem.*, **37**, 1353 (1975).
2) S. Kozuka and S. Ohya, *J. Organomet. Chem.*, **149**, 161 (1978).
3) For example, R. C. Paul, K. K. Soni, and S. P. Narula, *J. Organomet. Chem.*, **40**, 355 (1972).
4) E. W. Abel and D. B. Brady, *J. Chem. Soc.*, **1965**, 1192.
5) T. H. Lowry and K. S. Richardson, "Mechanism and Theory in Organic Chemistry," Harper & Row, New York (1976), p. 179.
6) H. M. R. Hoffmann, *J. Chem. Soc.*, **1965**, 6753.
7) E. M. Kosower, "An Introduction to Physical Organic Chemistry," John Wiley & Sons, Inc., New York (1968), p. 81.
8) H. Matsuyama, H. Minato, and M. Kobayashi, *Bull. Chem. Soc. Jpn.*, **48**, 3287 (1975).
9) J. L. Wardell and D. W. Grant, *J. Organomet. Chem.*, **20**, 91 (1969).
10) R. L. Shriner and J. H. Young, *J. Am. Chem. Soc.*, **52**, 3337 (1930).

Molecular Conformations of γ-Aminobutyric Acid and γ-Amino-β-hydroxybutyric Acid in Aqueous Solution†

Kaori TANAKA, Hideo AKUTSU,** Yukihiro OZAKI,** Yoshimasa KYOGOKU,*,** and Ken-ichi TOMITA

Faculty of Pharmaceutical Sciences, Osaka University, Suita, Osaka 565

*** Institute for Protein Research, Osaka University, Suita, Osaka 565*

(Received February 8, 1978)

Proton magnetic resonance and Raman spectra indicate that the backbone of γ-aminobutyric acid is fairly flexible and rotational isomers are almost equally populated in aqueous solution. The population is not much affected by change of pH. On the other hand, in γ-amino-β-hydroxybutyric acid the *trans*†† -*trans* and *gauche-trans* conformations of the backbone are equally populated in neutral solution, *trans-trans* conformation being predominant in non-zwitterionic forms. The conformation in solution is discussed in relation to the structure of these molecules in crystal.

γ-Aminobutyric acid (GABA) has been found in mammalian brain,[1] where it is enzymatically produced from glutamic acid.[2] By virtue of its potent synaptic effect and other evidences, GABA seems to play the physiological role as "inhibitory transmitter" in mammalian central nervous system.[3–6] γ-Amino-β-hydroxybutyric acid (GABOB) is also a central inhibitory transmitter like GABA.[7] Their chemical structures are shown in Fig. 1. The crystal structures of GABA, GABOB, and their analogues have been reported.[8–13]

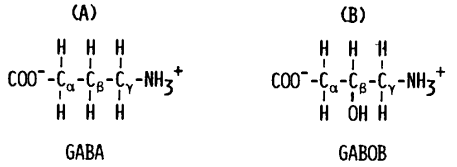

Fig. 1. Chemical structures of (A) γ-aminobutyric acid (GABA) and (B) γ-amino-β-hydroxybutyric acid (GABOB).

It is remarkable that a difference in the conformation of GABA molecule was found for crystal structures of GABA[9] and its hydrochloride:[10] the conformation of C_α–C_β–C_γ–N skeleton of GABA hydrochloride is all *trans*, but that of GABA in its free form is *gauche* (73.6°) about the C_α–C_β bond and *trans* about the C_β–C_γ bond, while GABOB takes the all *trans* conformation as GABA hydrochloride.[11]

The preferred conformation of GABA is theoretically predicted by molecular orbital calculations.[14–16] Pullman and Berthod[16] predicted that the intrinsically preferred conformation of the isolated GABA molecule is a highly holded one, but the hydrated zwitterionic GABA molecule might exist as a mixture of a number of conformers having different degrees of folding.

In the present study, we aimed to elucidate the molecular conformations of GABA and GABOB in aqueous solution by means of proton magnetic resonance (PMR), attempting to correlate the conformations in solution with those in crystal by measuring laser Raman spectra.

† This paper is Part VIII of "Crystal and Molecular Structure of ω-Amino Acids, ω-Amino Sulfonic Acids, and Their Derivatives."

†† The term *trans* used in the present paper denoted *s-trans* or *anti* in the nomenclature of stereochemistry.

Materials and Procedures

GABA and racemic GABOB (Nakarai Chemical Co., Kyoto) were used without further purification. GABA hydrochloride was prepared from GABA and crystallized.

Proton magnetic resonance spectra were recorded on a JEOL-PFT-100 pulse Fourier transform NMR spectrometer equipped with temperature control apparatus. The probe temperature was kept at 45 °C unless otherwise stated. The resolution due to digitalization by computer is 0.04 Hz. The sample solutions were prepared in D_2O with concentration of 100 mg/ml. The pD value was adjusted with DCl and NaOD. Sodium 3-(trimethylsilyl)propionate-2,2,3,3-d_4 (TMSP-d_4) was used as an internal reference. The assignments of resonance signal were made by comparison with those of GABA and GABOB analogues, 3-aminopropanesulfonic acid, 3-amino-2-hydroxypropanesulfonic acid and γ-guanidinobutyric acid. The spin analysis of the spectra was accomplished by computer with an iterative program based on the least-squares method. The spectra were analyzed as six spin system for GABA and five spin system for GABOB. Raman spectra were taken with a JEOL-JRS-02AS and JEOL-JRS-400D Raman spectrometer by excitation with argon ion laser (wavelength, 488.0 nm).

Results and Discussion

PMR Spectra of γ-Amino-β-hydroxybutyric Acid (GABOB). The 100-MHz proton magnetic resonance spectra of GABOB in solution at pD 1.7 and 7.2 are shown in

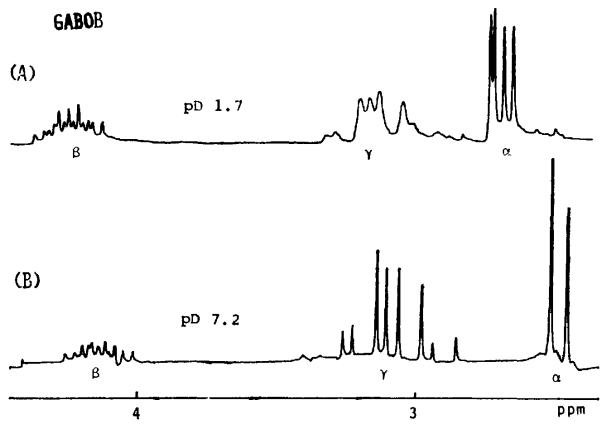

Fig. 2. The 100 MHz PMR spectra of γ-amino-β-hydroxybutyric acid in D_2O (A) at pD 1.7 and (B) at pD 7.2. Assignment are shown in the spectra.

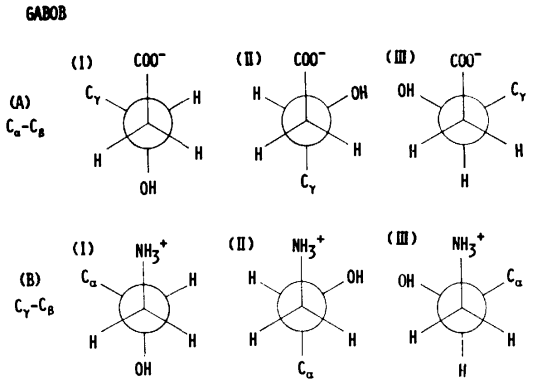

Fig. 3. The possible rotational isomers of γ-amino-β-hydroxybutyric acid (A) about the C_α–C_β bond and (B) about the C_β–C_γ bond.

Fig. 2. GABOB is considered to exist as a mixture of three possible rotational isomers both about the C_α–C_β bond and about the C_β–C_γ bond. The Newman projections of the possible rotamers of zwitterionic GABOB molecule which has the ABX spin system are shown in Fig. 3. The rotamers are thought to interconvert rapidly to each other. The observed coupling constants are weighted mean values of those for the distinct rotamers.

The vicinal coupling constants are assumed to satisfy the Karplus equation[17] and the coupling constants of either *gauche* or *trans* conformer are assumed to have the same value regardless of the particular conformation. The vicinal coupling constants, J_{ax} and J_{bx}, are then given by

$$J_{ax} = P_I J_t + P_{II} J_g + P_{III} J_g, \quad (1)$$

$$J_{bx} = P_I J_g + P_{II} J_t + P_{III} J_g, \quad (2)$$

where P_I, P_{II}, and P_{III} are the populations of the rotamers I, II, and III, respectively, and J_g and J_t are the coupling constants for the *gauche* and *trans* conformations with respect to the two C–H bonds.

In this case, J_g was determined by application of the Karplus type equation to hydroxyproline,[18] since the C_α–C_β part of GABOB corresponds to the C_3–C_4 part of hydroxyproline and the C_β–C_γ of GABOB to the C_4–C_5 of hydroxyproline. Thus J_g of GABOB was assumed to be 2.73 Hz with respect to the C_α–C_β and 2.53 Hz for the C_β–C_γ bond, respectively. J_t was determined as follows according to the method reported by Abraham and Pachler.[19] The average coupling constant is defined by

$$J_{av} = 1/3(J_t + 2J_g). \quad (3)$$

On the other hand, J_{av} was found to be proportional to the total electronegativities as follows.

$$J_{av} = 17.97 - 0.796 \sum_{n=1}^{6} E_n \quad (4)$$

With use of Huggins' electronegativities,[20] J_t was calculated to be 11.92 Hz for C_α–C_β part and 11.24 Hz for the C_β–C_γ part.

Figure 4 shows the populations of GABOB conformers calculated from the coupling constants obtained at various pD values. In the case of GABOB, it is impossible to assign J_{ax} and J_{bx}, namely, P_I and P_{II} only from the spin analyses. The rotamer populations mainly depend on steric and ionic interactions. It seems that rotamer II is more favorable and more stable than rotamers I and III for non-zwitterionic structure as considered from the attractive interactions between the hydroxyl and the polar groups. Thus we assigned the predominant conformer to rotamer II. The assumption is supported by the unambiguously determined population for some β-monodeuterated amino acid.[21] Thus about the C_α–C_β bond in the zwitterionic form, rotamers I and II equally exist with a population of about 40% as shown in Fig. 4 mainly due to the ionic interactions of the ionized amino and carboxyl groups. The effect of intermolecular interaction on population can be neglected since the vicinal coupling constants do not change in any of the concentrations 10, 1, and 0.1%.

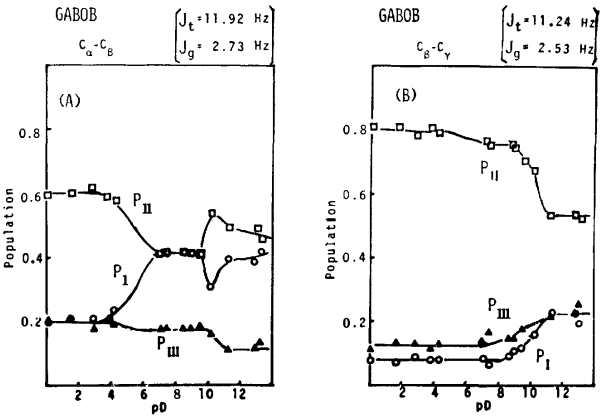

Fig. 4. The effect of pD on the populations of γ-amino-β-hydroxybutyric acid (A) about the C_α–C_β bond and (B) about the C_β–C_γ bond.

It appears anomalous with increase in pD from neutral to alkaline, that the vicinal coupling constants of rotamers I and II about the C_α–C_β bond once diverge and converge again to a common value; the vicinal coupling constants diverge at pD 10 by deprotonation of the amino group whose pK_a is about 9.5 obtained from the PMR chemical shift. However, it seems impossible to explain the convergence of the constants at about pD 10 only by the change in intramolecular interactions. Figure 5 shows the temperature dependence of the coupling constants of the GABOB molecule

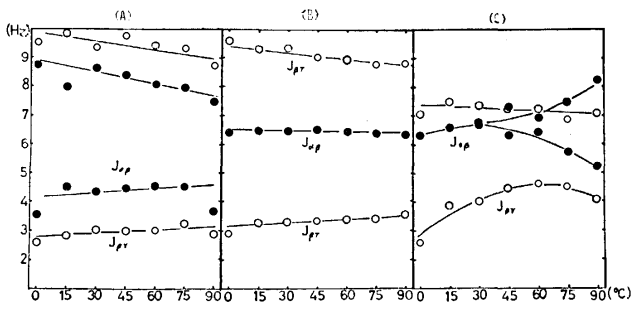

Fig. 5. The observed vicinal coupling constants at various temperatures for γ-amino-β-hydroxybutyric acid: (A) cationic form, (B) zwitterionic form and (C) anionic form.

at anionic, zwitterionic and cationic states, respectively. It is intuitively expected that when the temperature increases, the rotamer populations would tend to become equal according to the Boltzmann distribution; the coupling constants, therefore, would converge to a common value. At either zwitterionic or cationic state, the constants actually converged with increasing temperature, but they diverged at anionic state in alkaline solution. Another effect of intramolecular interaction accessible only in the anionic state should be considered. From the NMR studies of ^{23}Na ion in aqueous solution,[22] it was suggested that the sodium ion forms weak complex with several anions, notably with hydroxy and keto acids such as α- and β-hydroxybutyric acid.

As regards the C_β–C_γ bond, rotamer II is the most stable at any pD value. This is similar to the case of acetylcholine[23] and phosphatidyl choline and phosphatidyl ethanolamine[24] in which the O–C–C–N system is in the *gauche* conformation in aqueous solution. If there is no correlation between the population about the C_α–C_β bond and that about the C_β–C_γ bond in neutral solution, about 30% of GABOB molecules have the *trans*(about the C_α–C_β bond)-*trans*(about the C_β–C_γ bond) conformation as well as the *gauche-trans* conformation. Thus the *trans-trans* conformation of GABOB found in the crystal structure may correspond to one of the stable conformations in aqueous solution as anticipated from the PMR studies. In acidic solution, on the other hand, about 50% of GABOB molecules are in the *trans-trans* conformation and about 15% of GABOB in the *gauche-trans*.

PMR Spectra of γ-Aminobutyric Acid (GABA). Figure 6 shows the 100 MHz proton magnetic resonance spectra of GABA at pD 13.3, where the upper is the magnified spectrum of lower one. GABA is considered to exist as a mixture of three rotational isomers in regard to both the C_α–C_β bond and the C_β–C_γ bond. The Newman projections of the rotamers of the zwitterionic GABA molecule are shown in Fig. 7. In this case, it was considered that GABA has the A_2B_2 spin system both about the C_α–C_β and the C_β–C_γ bonds. The A_2B_2 type spectra are described in terms of four coupling constants, J, J', J_t, and J_g, defined by

$$J = P_t J_g + 1/2 P_g (J_t + J_g), \quad (5)$$

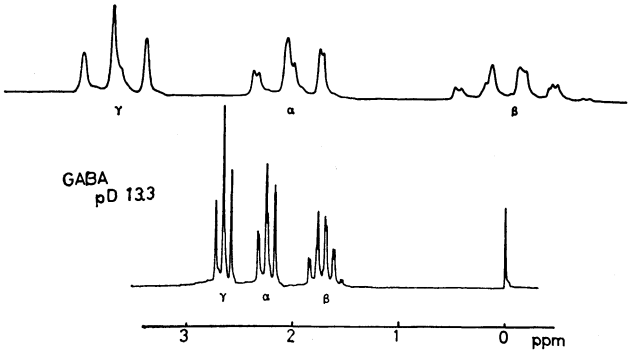

Fig. 6. The 100 MHz PMR spectra of γ-aminobutyric acid in D_2O at pD 13.3. The upper is the magnified spectrum of the lower one in the region between 1.4 and 2.8 ppm.

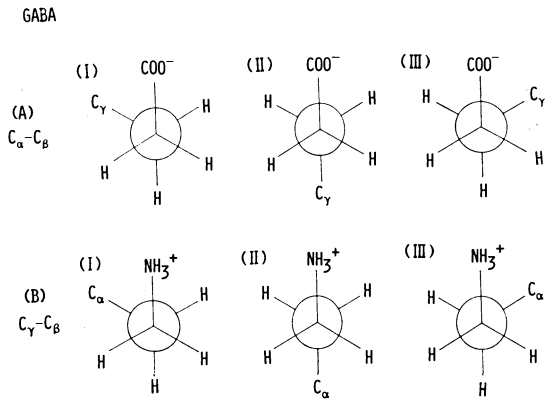

Fig. 7. The possible rotational isomers of γ-aminobutyric acid (A) about the C_α–C_β bond and (B) about the C_β–C_γ bond.

$$J' = P_t J_t + P_g J_g, \quad (6)$$

where P_t and P_g are the populations of the *trans* and *gauche* rotamers, respectively, and

$$L = J - J' = (1/2 - 3/2P_t)(J_t - J_g), \quad (7)$$

$$P_t = 1/3 - 2L/3(J_t - J_g). \quad (8)$$

Eq. 8 indicates that if L is positive, P_t is smaller than 1/3 and; if negative, P_t is larger than 1/3, since $(J_t - J_g)$ is positive in general. In this analysis, the sign of L, namely, J and J', could not be assigned to each of the coupling constants obtained from the spin analysis. The average coupling constant is defined by

$$J_{av} = 1/3(2J + J'). \quad (9)$$

As regards Eq. 4 Abraham and Pachler[19] found the relation between the average coupling constants J_{av} and the electronegativity of attached atoms. In the case of pD 13.3, the $3J_{av}$ value about the C_α–C_β bond is 22.9 Hz by virtue of Eq. 9, if L is assumed to be positive, and $3J_{av}$ becomes 21.8 Hz if L is negative, while Eq. 4 gives 20.49 Hz for $3J_{av}$. By comparison of the three values, it seems likely that the sign of L is negative. Likewise, if L is positive, $3J_{av}$ about the C_β–C_γ bond should be 22.3 Hz. If L is negative, it becomes 21.2 Hz, whereas it is calculated to be 19.41 Hz from Eq. 4. Thus the sign of L is also considered to be negative.

The value obtained for L and calculated populations of the rotamers from the spin analyses at pD 13.3 and 7.6 are given in Table 1. The coupling constant at pD 0.9 could not be obtained, because of the broadening of the C_γ-proton signals. Only the data at pD 7.6 about the C_α–C_β bond are given in the Table, since L for C_β–C_γ is too small (<0.2 Hz) to be determined

Table 1. Populations of *trans* and *gauche* forms in GABA

Torsional axis	pD	J(Hz)	J'(Hz)	L(Hz)	P_t	P_g
C_α–C_β	13.3	6.9	8.0	−1.1	0.40	0.60
	7.6	7.0	7.6	−0.6	0.37	0.63
C_β–C_γ	13.3	6.7	7.8	−1.1	0.40	0.60

by the least squares method.

It is of interest to compare the conformation of the GABA molecule in solution at various pD with the crystal structure and the predicted conformations from theoretical calculations. Five possible conformations of GABA molecule are *trans-trans gauche-trans*, *trans-gauche*, *gauche-gauche*(A) and *gauche-gauche*(B) as the rotational isomers about the C_α–C_β bond and the C_β–C_γ bond. If the population of trans isomer is 1/3 about both the C_α–C_β bond and the C_β–C_γ bond, the estimated populations of the five conformations are 1/9, 2/9, 2/9, 2/9, and 2/9, respectively. As the result of PMR studies of GABA, the population of each isomer in alkaline solution is 0.16(*trans-trans*), 0.24(*gauche-trans*), 0.24(*trans-gauche*), 0.18(*gauche-gauche*(A)), and 0.18 (*gauche-gauche*(B)). The *trans-trans* conformation is a little more predominant than the case of freely rotating molecule. Although the spectrum of GABA in acidic solution is too broad to be used for spin analysis, its pattern does not differ a great deal from that of alkaline solution. Thus the conformation of GABA in acidic solution might be similar to that in alkaline solution. The crystal structure of GABA hydrochloride shows the GABA molecule to be *trans-trans*, while the molecular conformation of neutral GABA in the crystal is *gauche-trans*. The present PMR data and the crystal data both imply that the energy difference between the two conformers is small. The GABA molecule in aqueous solution can take many conformations, and the change in population by pH is estimated within 10%. The extended Hückel MO calculation predicted that the *trans-trans* conformation is most stable for the zwitterionic GABA molecule,[14] not agreeing with our PMR result. The CNDO/2 calculations also predicted that for non-zwitterionic form six stable conformations involving all *trans* and for zwitterionic form some folded conformations are preferable.[15] The result is not in line with ours. The PCILO and SCF *ab initio* calculations by Pullman and Berthod[16] showing GABA to be a mixture of a number of conformers agree with our PMR result.

Raman Spectra of γ-Aminobutyric Acid and γ-Amino-β-hydroxybutyric Acid. The Raman spectra of GABOB in solid state, neutral solution and acidic solution are given in Fig. 8. Because of the complex spectra, it is hard to assign each band to the definite vibrational mode. From X-ray diffraction studies, the conformation of GABOB was found to be *trans-trans* in the solid state. From PMR studies the *trans-trans* conformation is thought to exist *ca.* 30% in neutral solution and *ca.* 50% in acidic solution. As a whole the Raman spectrum in solid and that in neutral solution is similar to each other. But no Raman line corresponding to the line at 830 cm^{-1} either in neutral or in acidic solution was observed in solid. Therefore, the Raman line at 830 cm^{-1} is thought to be due to the *gauche-trans* conformation, differing from the *trans-trans* conformation found in crystal.

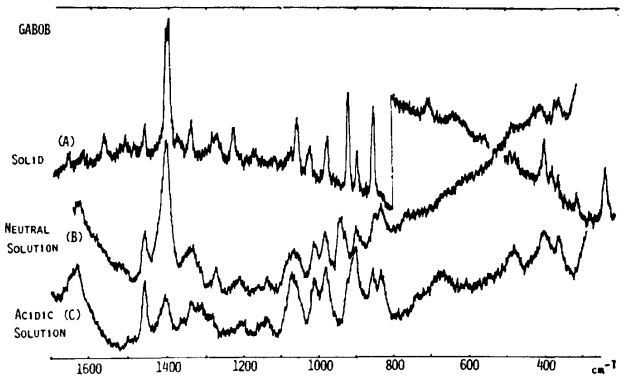

Fig. 8. The Raman spectra of γ-amino-β-hydroxybutyric acid (A) in solid, (B) in neutral solution and (C) in acidic solution.

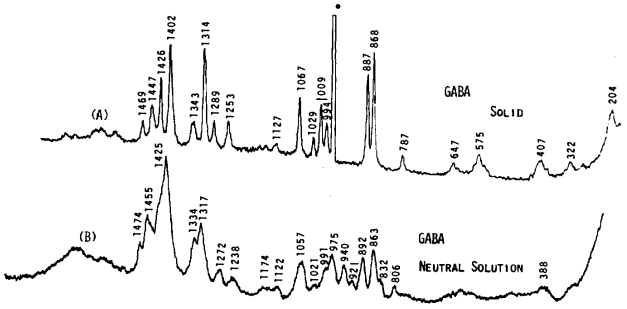

Fig. 9. The Raman spectra of γ-aminobutyric acid (A) in solid and (B) in neutral solution. The Raman line with asterisk is due to the ghost of spectrometer.

The Raman spectra of GABA in solid state and in neutral solution are given in Fig. 9. The spectral features differ from each other: the Raman lines are observed at 921 and 940 cm^{-1} in neutral solution, but there is no line in the range 887—994 cm^{-1} in solid state. These lines which are sensitive to the conformational change should be mainly due to the stretching modes of the C–C skeletal bonds or the rocking modes of the CH_2 group. The Raman spectra of GABA hydrochloride either in solid or solution are also not very similar to each other, especially in the region 800—1100 cm^{-1}. It is apparent that the molecular conformation of GABA found in crystal is not retained in solution.

Conclusion

Proton magnetic resonance and Raman spectra indicate that the backbone of the GABA molecules is fairly flexible and probable rotational isomers are almost equally populated in aqueous solution. The population is not much affected by changing pH. On the other hand, the GABOB molecule tends to take *trans* conformation about each backbone bond. The *trans-trans* and *gauche-trans* are equally populated in neutral solution, the *trans-trans* conformation being predominant in the non-zwitterionic forms. In the crystal, zwitterionic GABA molecule is in the *gauche-trans* form and its hydrochloride takes the *trans-trans* form, while the neutral GABOB is in the *trans-trans* form. It is interesting to note that the molecular structure of GABA in the crystal is restricted to the *trans-trans* and *gauche-trans* forms, and the GABOB molecules take mainly the *trans-*

trans and *gauche-trans* conformations in solution. It seems that GABA and GABOB are apt to take either of the two forms under certain circumstances, the forms being important for the exhibition of their biological activities.

The authors wish to express their thanks to Dr. M. Abe, Shoin Women's College, for her invaluable discussion on the vibrational spectra.

References

1) J. Awapara, A. J. Landua, R. Fuerst, and Seale, *J. Biol. Chem.*, **187**, 35 (1950).
2) E. Roberts and S. Frankel, *J. Biol. Chem.*, **187**, 55 (1950).
3) D. P. Purpura, M. Girado, and H. Grundfest, *Science*, **125**, 1200 (1957).
4) J. F. Mitchell and V. Sprinivasan, *Nature*, **224**, 663 (1969).
5) D. R. Curtis, A. W. Duggan, D. Felex, and G. A. R. Johnsten, *Nature*, **226**, 1222 (1970).
6) K. Krnjević, *Nature*, **228** 119 (1970).
7) T. Hayashi and K. Nagai, Proc. 20th Internatl. Physio. Cong., 410 (1956).
8) K. Tomita, *Tetrahedron Lett.*, **1971**, 2587.
9) K. Tomita, H. Higashi and T. Fujiwara, *Bull. Chem. Soc. Jpn.*, **46**, 2199 (1973); E. G. Steward, R. Player, J. P. Quilliam, D. A. Brown, and M. J. Pringle, *Nature, New Biol.*, **233**, 87 (1971).
10) K. Tomita, *Jpn. J. Brain Physiol.*, **61**, 1 (1965); E. G. Steward, R. B. Player, and D. Warner, *Acta Crystallogr., Sect. B*, **29**, 2825 (1973).
11) K. Tomita, M. Harada, and T. Fujiwara, *Bull. Chem. Soc. Jpn.*, **46**, 2854 (1973).
12) T. Maeda, T. Fujiwara, and K. Tomita, *Bull. Chem. Soc. Jpn.*, **45**, 3628 (1972).
13) K. Tomita, K. Urabe, Y. B. Kim, and T. Fujiwara, *Bull. Chem. Soc. Jpn.*, **47**, 1988 (1974).
14) L. B. Kier and E. B. Truitt, Jr., *Experimentia*, **26**, 988 (1970).
15) D. Warner and E. G. Steward, *J. Mol. Struct.*, **25**, 403 (1975).
16) B. Pullman and H. Berthod, *Theor. Chim. Acta (Berl.)*, **36**, 317 (1975).
17) M. Karplus, *J. Chem. Phys.*, **30**, 11 (1959).
18) R. J. Abraham and K. A. McLauchlan, *Mol. Phys.*, **5**, 513 (1962).
19) R. J. Abraham and K. G. R. Pachler, *Mol. Phys.*, **7**, 165 (1963).
20) M. L. Huggins, *J. Am. Chem. Soc.*, **75**, 4123 (1953).
21) M. Kainosho and K. Ajisaka, *J. Am. Chem. Soc.*, **97**, 5630 (1975).
22) O. Jarjetzly and J. E. Wertz, *J. Am. Chem. Soc.* **82**, 318 (1960).
23) C. C. J. Culvenor and N. S. Ham, *Chem. Commun.*, **1966**, 537.
24) H. Akutsu and Y. Kyogoku, *Chem. Phys. Lipids*, **18**, 285 (1977).

Chlorination of Phenylsulfinylcyclopropanes and Phenylthiocyclopropanes

Toshiaki MASUDA, Naomichi FURUKAWA, and Shigeru OAE*

Department of Chemistry, University of Tsukuba, Sakura-mura, Niihari-gun, Ibaraki 300-31

(Received February 17, 1978)

Chlorination of phenylsulfinylcyclopropanes or phenylthiocyclopropanes with various chlorinating agents provides the corresponding 1-chloro-1-(phenylthio)cyclopropanes but not any ring opening product. Kinetic isotope effects, (k_H/k_D), for the chlorination were measured with 1-deuterated cyclopropane derivatives and found to be small, *i.e.*, 1.6—2.8. The chlorination is considered to be a kind of the Pummerer reaction of the chlorosulfonium salt formed as the initial intermediate in the reaction of sulfides or sulfoxides with such chlorinating agents as *N*-chlorosuccinimide (NCS) or thionyl chloride and proceeds *via* the ylide-ylene intermediate.

Earlier, the formation of α-chloro sulfides from the reaction of sulfides with chlorinating agents was suggested to go through an ylide-ylene type intermediate (B) after the initial formation of the chlorosulfonium salt, as shown below,[2] as in the ordinary Pummerer reaction.

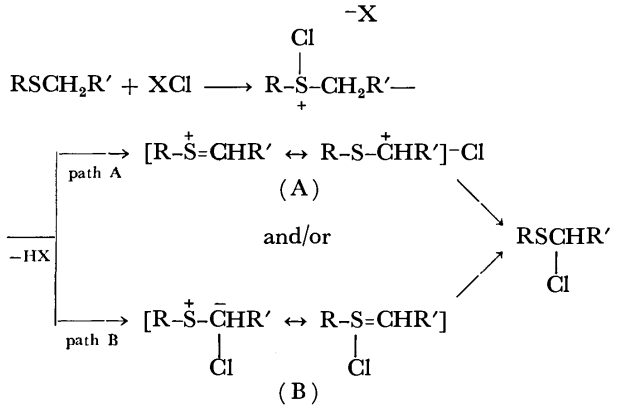

Scheme 1.

As to the subsequent S–Cl bond cleavage and the α-C–Cl bond formation, both an E2 like process forming an incipient carbonium ion (A)[3] and an ElcB type mechanism through an ylide-ylene (B)[4] have been proposed. The former involves a free carbonium ion (A) stabilized by the sulfur's lone pair electron while the latter implies a chloro-migration in the ylide-ylene intermediate (B). Thus the whole process is considered to be a kind of the Pummerer reaction. Meanwhile our recent work[5] revealed that the Pummerer reaction of phenylsulfinylcyclopropanes with acetic anhydride afforded the corresponding 1-acetoxy-1-(phenylthio)cyclopropanes nearly quantitatively without any ring opening, whereas the solvolysis of 1-chloro-1-(phenylthio)cyclopropanes gave a concomitant mixture of both the unrearranged solvolysis products and some ring opening allylic products. Accordingly, the Pummerer reaction of this system is considered to proceed *via* an ylide-ion pair but not a free carbonium ion.

As an extension of our studies on the Pummerer reaction, we have carried out the reaction of phenylsulfinylcyclopropanes (**1a**—**c**) and phenylthiocyclopropanes (**2a**—**c**) with various chlorinating agents, in order to examine the formation of any ring opening product, since the cyclopropyl cation once formed will definitely give the ring opening products. However, the chlorination afforded nothing but the corresponding 1-chloro-1-(phenylthio)cyclopropanes in good yields.

This paper describes the reaction of phenylsulfinylcyclopropanes (**1a**—**c**) and phenylthiocyclopropanes (**2a**—**c**) with various chlorinating agents and the hydrogen–deuterium kinetic isotope effects estimated by the competitive reaction between the 1-deuterated and undeuterated cyclopropane derivatives in the chlorinations.

Results

*Chlorination of Phenylsulfinylcyclopropanes (**1a**—**c**) and Phenylthiocyclopropanes (**2a**—**c**).* Chlorination of **1** with thionyl chloride or propionyl chloride under reflux for 1 h in methylene chloride afforded 1-chloro-1-(phenylthio)cyclopropanes (**3**) in good yields without any ring opening (Table 1). The products (**3a**—**c**) obtained were purified further by distillation *in vacuo* (by bulb to bulb distillation) and identified by their IR and NMR spectra (Table 2) and by conversion to the corresponding sulfoxides (**4a**—**c**) upon treatment with *m*-chloroperbenzoic acid in dichloromethane (Scheme 2 and Table 2).

Meanwhile, chlorination of **2** with NCS at room temperature for overnight in benzene also afforded **3** in high yields without any ring opening (Scheme 3 and Table 3).

The Hydrogen-Deuterium Kinetic Isotope Effects for the Chlorination. The hydrogen-deuterium kinetic isotope effects were estimated by the competitive reaction of both 1-deuterated phenylsulfinylcyclopropane (**5**) and undeuterated compound (**1a**) with thionyl

Table 1. The reaction of phenylsulfinylcyclopropanes (**1a**—**c**) with chlorinating agents in dichloromethane at reflux for 1 h

Starting sulfoxide (**1a**—**c**)	R_1	R_2	R_3	R_4	Chlorinating agent XCl	Products (**3a**—**c**)	and their yields (%)
1a	H	H	H	H	$SOCl_2$	**3a**	Quant.
1a	H	H	H	H	EtCOCl	**3a**	Quant.
1b	Me	H	H	Me	$SOCl_2$	**3b**	85
1c	Me	Me	H	H	$SOCl_2$	**3c**	71[a]

a) 1-(Phenylthio)-2,2-dimethylcyclopropane (**2c**) was obtained in 14% yield.

Table 2. IR and NMR spectrum data of 1-chloro-1-(phenylthio)cyclopropanes (**3a—c**) and 1-chloro-1-(phenylsulfinyl)cyclopropanes (**4a—c**)

3a—c	Bp(bath tempt) (°C/mmHg) (lit)	NMR Spectra ($CDCl_2$) (δ-ppm)	**4a—c**	Mp (°C)	IR Spectra (cm^{-1}) (S=O)	NMR Spectra ($CDCl_3$) (δ-ppm)	Analysis Found (Calcd)
3a	84/3	1.3—1.6(m, 4H,) 7.0—7.6(m, 5H, PhS-)	**4a**	50—51	1060	1.1—1.8(m, 4H,) 7.2—7.8(m, 5H, PhS(O)-)	C, 54.10 (53.86) H, 4.57 (4.52) S, 15.76 (15.98)
3b	115/1	1.0—1.5(m, 8H,) 7.0—7.6(m, 5H, PhS-)	**4b**	76—77	1050	1.0—1.8(m, 8H,) 7.3—7.8(m, 5H, PhS(O)-)	C, 58.00 (57.76) H, 5.77 (5.73) S, 14.22 (14.02)
3c	115/1 (85—7/0.2)[13]	1.2(q, 2H,) 1.33 and 1.44 (s, 3H and s, 3H, and) 7.0—7.5(m, 5H, PhS-)	**4c**	76—77	1050	1.13 and 1.52(d, 1H and d, 1H, and) 1.40 and 1.63 (s, 3H and s, 3H, and) 7.3—7.8(m, 5H, PhS(O)-)	C, 58.00 (57.76) H, 5,73 (5.73) S, 13,78 (14.02)

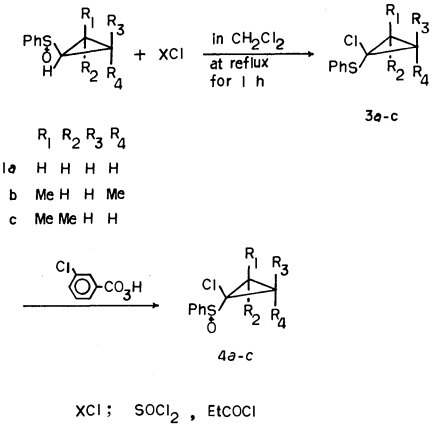

Scheme 2.

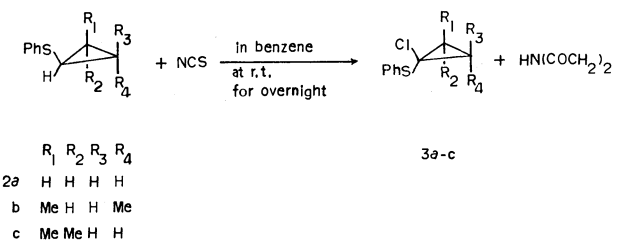

Scheme 3.

Table 3. Chlorination of phenylthiocyclopropanes (**2a—c**) with NCS in benzene at room temperature for overnight

Starting sulfide (**2a—c**)	R_1	R_2	R_3	R_4	Products (**3a—c**) and their yields (%)	
2a	H	H	H	H	**3a**	90
2b	Me	H	H	Me	**3b**	81
2c	Me	Me	H	H	**3c**	82

Table 4. The hydrogen-deuterium kinetic isotope effects in competitive reaction of undeuterated phenylsulfinylcyclopropane (**1a**) and 1-deuterated compound (**5**) with thionyl chloride or acetyl chloride

Chlorinating agent XCl	Conversion (%)	[H]/[D] (mmol l^{-1})	k_H/k_D	
$SOCl_2$	0.0	45.31/48.15	—	
	22.8	31.74/40.42	2.0	
	47.1	18.96/30.50	1.9	2.1±0.3
	67.4	7.52/22.97	2.4	
MeCOCl	0.0	45.66/45.78	—	
	16.2	35.58/41.09	2.3	
	32.6	26.17/35.50	2.2	2.1±0.3
	50.8	17.99/27.02	1.8	

chloride and acetyl chloride by means of quantitative GLC and GLC-mass spectrometry (Table 4). The kinetic isotope effects of these competitive chlorinations were calculated by the following equation:

$$\frac{k_H}{k_D} = \frac{\ln([H]_f/[H]_0)}{\ln([D]_f/[D]_0)}. \quad (1)$$

The extent of conversion of the reaction was estimated by comparing the relative peak areas of phenylsulfinylcyclopropane for each reacting sample with that without thionyl chloride, respectively, in GLC. Ratios of [H]/[D] were determined from the relative intensities of the sulfoxides in the respective molecular peaks in GLC-mass spectrometry.

Meanwhile, the hydrogen-deuterium kinetic isotope effects in the competitive chlorination of 1-deuterated phenylthiocyclopropane (**6**) and undeuterated compound (**2a**) with NCS and sulfuryl chloride were also determined by quantitative GLC and GLC-mass spectrometry (Table 5).

Table 5. The hydrogen-deuterium kinetic isotope effects in competitive chlorination of undeuterated phenylthiocyclopropane (**2a**) and 1-deuterated compound (**6**) with NCS or sulfuryl chloride

Chlorinating agent XCl	Conversion (%)	[H]/[D] (mmol l^{-1})	k_H/k_D	
SO_2Cl_2	0.0	73.94/59.62	—	
	22.8	53.95/49.19	1.6	
	48.7	32.56/35.98	1.6	1.8±0.3
	64.6	15.77/29.61	2.2	
NCS	0.0	73.94/59.62	—	
	18.5	55.94/52.96	2.4	
	38.0	36.48/46.31	2.8	2.3±0.5
	59.3	22.76/31.60	1.9	

Discussion

The Pummerer reaction of sulfoxides with thionyl chloride or acyl chloride has been shown by Bordwell *et al.*[2c,d] to yield α-chlorosulfides. However, the reaction of sulfoxides with such chlorinating agents as acetyl chloride afforded the reduced sulfide though the reaction also involves the initial formation of the chlorosulfonium salt intermediate.[6]

The Pummerer reaction of **1** with thionyl chloride or propionyl chloride in methylene chloride afforded readily the corresponding α-chlorosulfides (**2**) in a good yield without any ring opening, though, in the case of 2,2-dimethyl-1-(phenylsulfinyl)cyclopropane (**1c**), 2,2-dimethyl-1-(phenylthio)cyclopropane (**2c**) was obtained only in 14% yield (Table 1).

Meanwhile, the reaction of sulfides with such chlorinating agents as NCS is generally considered to proceed *via* the initial formation of the chlorosulfonium salt which then decomposes to afford the α-chlorosulfides. Mechanism of the chlorination of sulfides has previously been proposed by Wilson, Jr. *et al.*[3] to involve a free carbonium ion intermediate. Tuleen *et al.*,[4] however, suggested the reaction to proceed *via* an ylide-ylene intermediate. The chlorination of **2** with NCS was also carried out and was found to afford the corresponding (**3**) in a high yield without any ring opening (Table 3). The lack of any ring opening product both in the Pummerer reaction of **1** with thionyl chloride and acyl chlorides and in the chlorination of **2** with NCS suggests that these chlorinations do not proceed *via* the mechanistic route which involves a free carbonium ion intermediate, since the methanolysis[7] and acetolysis[5a] of 1-chloro-1-(phenylthio)cyclopropanes gave the ring opening products which undoutedly arise from the cyclopropyl carbonium ion as the intermediate.

In the reaction of **1a/5** with thionyl chloride to yield **2a**, the kinetic isotope effect, (k_H/k_D), determined by the competitive chlorinations, was found to be 2.1 (Table 4), while, in chlorination of **2a/6** with sulfuryl chloride the value was 1.8 (Table 5). Thus, the kinetic isotope effects obtained in these chlorinations are quite small in comparison with those of chlorinations of tetrahydrothiophene with chlorine[3b] and of benzyl phenyl sulfide with NCS;[4a] namely 5.1 and 5.7, respectively. These observed values of the kinetic isotope effects are smaller than even those of the general Pummerer reaction (2.9 for the reaction methyl *p*-tolyl sulfoxide with acetic anhydride).[8] The kinetic isotope effects of the chlorination of **1a/5** with thionyl chloride or **2a/6** with sulfuryl chloride are of nearly the same order of magnitude with that of the Pummerer reaction of methylphenylsulfonium methylide with acetic anhydride, *i.e.*, 1.57. Incidentally the Pummerer reaction of methylphenylsulfonium methylide is believed to proceed *via* an ElcB path.[9]

Tuleen[4a] proposed that both the acidity of α-proton of sulfides and the basicity of the counter anion ($^-$X) of the chlorosulfonium salt are two important factors in the chlorination of sulfides.

In Tables 4 and 5 are presented the kinetic isotope effects of chlorination of the sulfoxides (**1a/5**) and the sulfides (**2a/6**) with various chlorinating agents. The basicities of the counter anion ($^-$X) fall in the following order; $^-N(COCH_2)_2 > ^-O_2CMe > ^-Cl$. However, the results obtained cannot be correlated with the order of the basicities; these observed values of kinetic isotope effects are nearly identical. Thus, the results revealed that the basicity of the counter anion ($^-$X) does not significantly affect on the process.

The product distribution, *i.e.*, lack of any ring opening product, the small size of the kinetic isotope effect

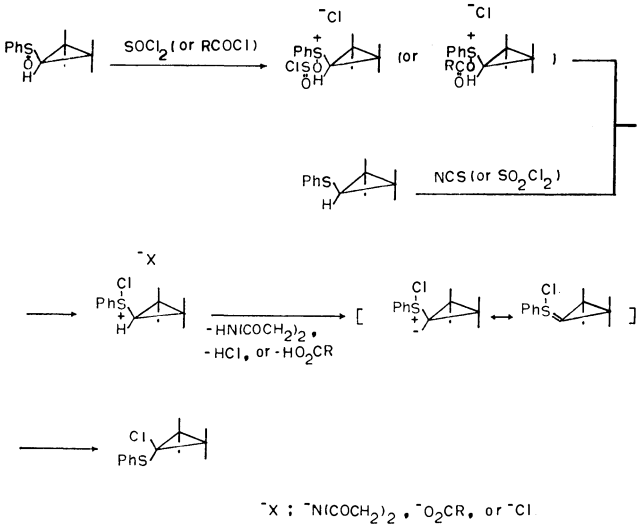

Scheme 4.

and the insensitivity of the reaction toward basicity of the counter anion, all seems to suggest that both the Pummerer reaction of **1** and the chlorination of **2** with chlorinating agents such as thionyl chloride or NCS proceed *via* an ylide-ylene intermediate.

Experimental

Material. Spectroscopic grade dichloromethane and benzene and acetic acid-*d*, which were obtained from E. Merck, were used without further purification. All the chlorinating agents, *i.e.*, NCS, thionyl chloride, sulfuryl chloride, acetyl chloride and propionyl chloride were purified by recrystallization or distillation.

*Phenylthiocyclopropanes (**2a—c**).* Phenylthiocyclopropane (**2a**) was prepared by the reaction of 3-chloropropylphenyl sulfide with sodium amide in liquid ammonia.[10] Other phenylthiocyclopropanes (**2b, c**) were prepared by the reaction of chloromethyl phenyl sulfide and potassium *t*-butoxide in 2-methylpropene or *trans*-2-butene.[11]

*Phenylsulfinylcyclopropanes (**1a—c**).* Phenylsulfinylcyclopropanes (**1a—c**) were prepared by the usual oxidation (H_2O_2–AcOH) of the corresponding sulfides (**2a—c**) by the method described in our previous paper.[5c]

*The Reaction of Phenylsulfinylcyclopropanes (**1a—c**) with Chlorinating Agents.* The reaction was carried out as follows. To a solution of 3 mmol of phenylsulfinylcyclopropane (**1**) in 10 ml of dichloromethane was added a 1.2 mol excess of thionyl chloride (or propionyl chloride) in 10 ml of dichloromethane. The mixture was kept refluxing for 1 h and then at room temperature for 2 h. Then, the solution was poured into 50 ml of 5% aqueous sodium carbonate and washed with water. The dichloromethane layer was dried over magnesium sulfate. After removal of dichloromethane, the product (**3**) was purified by distillation *in vacuo* (by bulb to bulb distillation). The products obtained (**3a—c**) were identified by their IR and NMR spectra (see Table 2) and by conversion on treatment with *m*-chloroperbenzoic acid in dichloromethane to the corresponding sulfoxides **4a—c**) (see Table 2).

*Chlorination of Phenylthiocyclopropanes (**2a—c**) with NCS.* The reaction was carried out as follows. A 1.2 mol excess of NCS was added to a solution of 2 mmol of phenylthiocyclopropane (**2**) in 20 ml of benzene in the presence of a 1.5 mol excess of pyridine at room temperature. After keeping the mixture for overnight at room temperature, the solution was poured into cold water and washed with 5% aqueous sodium thiosulfate, water, 5% aqueous hydrochloric acid, and again water. The product (**3**) was purified further by distillation *in vacuo* (by bulb to bulb distillation).

*Preparation of 1-Chloro-1-(phenylsulfinyl)cyclopropanes (**4a—c**).* A 1.2 mol excess of (dichloroiodo)benzene was added to a solution of 3 mmol of phenylsulfinylcyclopropane (**1**) in 10 ml of dichloromethane in the presence of a 1.5 mol excess of pyridine at 0 °C. After keeping the mixture for 3 h at room temperature, the reaction mixture was poured into cold water and washed with 5% aqueous sodium thiosulfate and water. After removal of dichloromethane, the residue was subjected to the column chromatography packed with silica gel using dichloromethane as eluent. The product (**4**) was purified further by recrystallization from ether–hexane. The structures of these products (**4a—c**) were determined from their IR and NMR spectra (see Table 2). Yields of the products were 92, 87, and 86% for **4a**, **b**, and **c**, respectively.

1-Chloro-1-(phenylsulfinyl) cyclopropanes (**4a—c**) were also prepared in yields of 78, 72, and 73% for **4a**, **b**, and **c**, respectively, by the reaction of **3a—c** with an equimolar amount of *m*-chloroperbenzoic acid in dichloromethane at 0 °C for 5 h. These compounds obtained (**4a—c**) were identified by comparing their IR and NMR spectra with those of the samples obtained by the reaction of **1a—c** with (dichloroiodo)benzene.

*Preparation of 1-Deuterated Phenylsulfinylcyclopropane (**5**).* 1-Deuterated phenylsulfinylcyclopropane (**5**) was prepared by treating the corresponding sulfoxide (**1a**) in NaOD/D_2O-MeOD at reflux for 12 h.[5c]

*Preparation of 1-Deuterated Phenylthiocyclopropane (**6**).* 1-Deuterated phenylthiocyclopropane (**6**) was prepared by treating the corresponding sulfide (**2a**) with butyllithium it tetrahydrofuran at 0 °C for 2 h and then quenching with acetic acid-*d*.[12]

Determination of the Hydrogen-Deuterium Kinetic Isotope Effects in Competitive Chlorination. The kinetic isotope effect in the competitive reaction of phenylsulfinylcyclopropane (**1a**/**5**) was carried out as follows. Three samples, which were dissolved 0.5, 1.0, or 1.5 ml of the dichloromethane solution of thionyl chloride (about 172.8 mmol l^{-1}) in 5 ml of dichloromethane containing known amount of the mixture of **1a** and **5**, respectively, and one sample without thionyl chloride were prepared. These four samples were allowed to react for 24 h at 20±1 °C until the reaction was complete. Then from each sample an aliquot portion (5 μl) of the content was directly injected into the GLC column (1% OV-1; 1 m; 3 mm i.d.; glass column; temperature 100 °C; He flow 40 ml min^{-1}) and the extent of conversion for each sample was calculated from the relative peak areas of phenylsulfinylcyclopropane for each sample and one sample without thionyl chloride, respectively. Meanwhile, ratio of [H]/[D] for each compound was calculated from the intensities of the molecular peaks for undeuterated phenylsulfinylcyclopropane (**5**), respectively, by GLC-mass spectrometry. The hydrogen-deuterium kinetic isotope effects in this competitive reaction were calculated by the Eq. 1. The result was summarized in Table 4.

The kinetic isotope effects in other chlorinations were also estimated similarly in the competitive reactions as described above. These results were summarized in Tables 4 and 5.

References

1) Preliminary report; T. Masuda, N. Furukawa, and S. Oae, *Chem. Lett.*, **1977**, 1103.

2) a) C. C. Price and S. Oae, "Sulfur Bonding," The Ronald Press Co., New York, N. Y. (1962), p. 59; b) W. E. Truce, G. H. Birum, and E. T. McBee, *J. Am. Chem. Soc.*, **74**, 3594 (1952); c) F. G. Bordwell and B. M. Pitt, *ibid.*, **77**, 572 (1955); d) F. G. Bordwell, G. D. Cooper, and H. Morita, *ibid.*, **79**, 376 (1957); e) L. A. Paquette, *ibid.*, **86**, 4085 (1964).

3) a) G. E. Wilson, Jr., and R. Albert, *J. Org. Chem.*, **38**, 2156 (1973); b) G. E. Wilson, Jr., and R. Albert, *ibid.*, **38**, 2160 (1973).

4) a) D. L. Tuleen and V. C. Marcum, *J. Org. Chem.*, **32**, 204 (1967); b) D. L. Tuleen, *ibid.*, **32**, 4006 (1967); c) D. L. Tuleen and T. B. Stephens, *ibid.*, **34**, 31 (1969).

5) a) T. Masuda, T. Numata, N. Furukawa, and S. Oae, *Chem. Lett.*, **1977**, 745; b) T. Masuda, T. Numata, N. Furukawa, and S. Oae, *ibid.*, **1977**, 903; c) T. Masuda, T. Numata, N. Furukawa, and S. Oae, *J. Chem. Soc., Perkin Trans. 2*, **1978**, in press.

6) a) S. Allenmark, *Acta Chem. Scand.*, **20**, 910 (1966); b) T. Numata and S. Oae, *Chem. Ind. (London)*, **1973**, 277; c) J. S. Grossert, W. R. Hardstaff, and R. F. Langler, *Can.*

J. Chem., **55**, 421 (1977).
7) U. Schöllkopf, E. Ruban, P. Tonne, and K. Riedel, *Tetrahedron Lett.*, **1970**, 5077.
8) a) S. Oae and M. Kise, *Tetrahedron Lett.*, **1968**, 2261; b) S. Oae and M. Kise, *Bull. Chem. Soc. Jpn.*, **43**, 1426 (1970).
9) T. Yagihara and S. Oae, *Tetrahedron*, **28**, 2759 (1972).
10) W. E. Truce, K. R. Hollister, L. B. Lindy, and J. E. Parr, *J. Org. Chem.*, **33**, 43 (1968).
11) U. Schöllkopf, G. J. Lehmann, J. Paust, and H. D. Härtl, *Chem. Ber.*, **97**, 1527 (1964).
12) B. M. Trost, D. Keeley, and M. J. Bogdanowicz, *J. Am. Chem. Soc.*, **95**, 3068 (1973).
13) U. Schöllkopf, F. P. Woerner, and E. Wiskott, *Chem. Ber.*, **99**, 806 (1966).

A Highly Stereoselective Reduction of Substituted Cyclohexanones Using Triisobutylaluminum–Amine Complexes

Toshimitsu SUZUKI, Maki ITOH,* Shigeyuki OGAWA, and Yoshinobu TAKEGAMI

Department of Hydrocarbon Chemistry, Faculty of Engineering, Kyoto University, Kyoto 606

(Received February 23, 1978)

The stereochemistry of the reduction of substituted cyclohexanones with a triisobutylaluminum(TIBA)–amine complex has been investigated, and the origin of the stereoselectivity has been discussed. Although a reduction of 4-*t*-butylcyclohexanone with free TIBA at 60 °C gave 83% *trans* alcohol, with a high stereoselectivity, 91—98% *trans* alcohol was obtained in this study. In order to discuss the reactivity of the reagent, the mode of the complexing of an amine to TIBA was investigated by infrared and NMR spectroscopy.

The stereochemistry of the reduction of substituted cyclohexanones has been investigated by many workers, and there have been a large number of discussions about factors controlling stereoselectivity.[1] Eliel *et al.*[2] reported the reduction of 4-*t*-butylcyclohexanone with $LiAlH_4$ to give 91—93% *trans*(OH equatorial) alcohol. Recently Ashby[3] reexamined the reduction of the same ketone with several metal hydrides and demonstrated it to give 86—92% *trans* alcohol in THF. Eliel *et al.*[2] reported the epimerization equilibrium of 4-*t*-butylcyclohexanol with aluminum isopropoxide in 2-propanol, resulting in 79% *trans* and 21% *cis* isomers.

The origin of stereochemical controls was first reported by Dauben *et al.*,[4] who suggested two concepts, *i.e.*, "product development control" and "steric approach control." On the other hand, Chérest and Felkin[5] considered "steric strain" and "torsional strain" as alternatives to these concepts. Richer[6] proposed that steric interactions take place between the entering group and 3,5-axial hydrogens.

The reduction of substituted cyclohexanones with triisobutylaluminum (TIBA) was studied by Haubenstock[7] and Ashby,[8] who reported interesting stereochemical results. In this experiment, the reduction of 4-*t*-butylcyclohexanone and other substituted cyclohexanones with a TIBA–amine complex was investigated, and the changes in the stereoselectivity were discussed. A remarkable change in the product distribution was observed. Recently Mukaiyama *et al.*[9] reported a selective reduction of carboxamides to aldehydes with aluminum diamide hydrides.

Experimental

Materials. The toluene was distilled over calcium hydride and stored under an argon atmosphere.

4-*t*-Butylcyclohexanone prepared by the oxidation of 4-*t*-butylcyclohexanol[10] was purified by vacuum distillation (93 °C/10 Torr).

The pyrrole, piperidine, and aniline were purified by vacuum distillation.

The triisobutylaluminum(TIBA) and triethylaluminum (TEA) were purified by vacuum distillation and prepared as about a 1 M toluene solution. The concentration of the solution was determined by titration using EDTA·2Na.

The 3,3,5-trimethylcyclohexanone, 2,2,6-trimethylcyclohexanone, camphor, norcamphor, diphenylamine, dicyclohexylamine, diethylamine, pyrrolidine, benzylamine, octylamine, triethylamine, triphenylamine, and *N*,*N*-dimethylaniline were commercially available reagents and were used without further purification.

Ketones and amines were used as 1 M toluene solutions, which were stored over "Drierite"(calcium sulfate) or calcium hydride.

Procedure. The following procedure for the reduction of a ketone is representative. A three-necked flask equipped with a magnetic stirrer, a gas inlet, a self-sealing rubber cap, and a gas outlet connected to a bubbler was flushed with argon. Eight ml of toluene and 1 ml (1 mmol) of an amine solution were then introduced into the flask at 0 °C, after which 1 ml(1 mmol) of a TIBA solution was stirred in. After a three-hours' reaction, 1 ml (1 mmol) of a ketone solution was added, and then the reaction was carried out at 60 °C. After a certain reaction time, the reaction mixture was hydrolyzed with a small piece of ice and the aluminum hydroxide was removed. Then the solution was extracted with ether, and the ether solution was dried over "Drierite". GLC(Hitachi model F6-D with a Golay R45 column) was employed for the qualitative and quantitative analyses.

Results and Discussion

Various amines were selected for use in the modification of TIBA, and the reductions of 4-*t*-butylcyclohexanone(4*t*BC) and several substituted cyclohexanones were investigated. The results of the reductions of ketones with amine-modified TIBA and free TIBA at 60 °C in toluene are shown in Table 1.

In the case of 4*t*BC, as the conformation of the cyclohexane ring is fixed by the bulky 4-*t*-butyl group, the stereochemistry of the reduction will be discussed only in terms of the steric requirement of the reducing agent. When 4*t*BC was reduced with free TIBA at 60 °C, 83% *trans* alcohol was obtained. This is almost an equilibrium composition of two isomeric alcohols. When diphenylamine, dicyclohexylamine, pyrrole, triethylamine, or *N*,*N*-dimethylaniline was used as an amine, the reduction of 4*t*BC proceeded quantitatively, and 91—98% *trans* alcohol was obtained. In contrast to this, the reaction hardly proceeded at all with TIBA–piperidine, pyrrolidine, benzylamine, or octylamine system.

3,3,5-Trimethylcyclohexanone(335TMC) introduces a methyl group in the 3-axial position which hinders axial attack strongly. An equatorial attack of $LiAlH_4$ predominates to give 75—80% OH axial alcohol.[3] However, in the reduction of 335TMC with TIBA, the diisobutylaluminum 3,3,5-trimethylcyclohexyl oxide undergoes epimerization to give 99.7% OH equato-

Table 1. Reduction of Substituted cyclohexanones with a TIBA–amine system[a]

Run	Amine	Time (h)	Unreac. ketone (%)	Products (%)[b] OH ax.	OH eq.
4-*t*-Butylcyclohexanone					
1	——	3.0	2	17	83
2	——	3.0	64.5	29.8	70.2[c]
3	Diphenylamine	0.5	14	15	85
		2.0	1	4.5	95.5
4	Dicyclohexylamine	2.0	0	2	98
5	Pyrrole	2.0	0.5	4.5	95.5
6	Diethylamine	2.0	13	30	70
7	Piperidine	2.0	100	0	0
8	Pyrrolidine	2.0	100	0	0
9	Aniline	3.0	79	39	61
10	Benzylamine	3.0	100	0	0
11	Octylamine	3.0	≃100	0	trace
12	Triethylamine	3.0	6	6	94
13	Triphenylamine	3.0	9	18	82
14	*N,N*-Dimethylaniline	3.0	15	9	91
3,3,5-Trimethylcyclohexanone					
15	——	2.0	32.5	82.7	17.3[d]
		31.0	30.7	0.3	99.7[d]
16	Diphenylamine	2.0	31	40	60
		24.0	26	0	100
17	Pyrrole	2.0	15	30	70
		24.0	6	0	100
18	Diethylamine	2.0	20	67	33
		24.0	15	7	93
2,2,6-Trimethylcyclohexanone					
19	——	3.0	52	61	39[c]
20	Diphenylamine	24.0	22	56	44
		48.0	22	50	50
Camphor				(OH exo)	(OH endo)
21	——	3.0	11	87	13
22	Dicyclohexylamine	3.0	≃0	87	13
23	Aniline	3.0	41	90	10
Norcamphor					
24	——	3.0	50	7	93
25	Dicyclohexylamine	3.0	≃0	7	93

a) The reaction was carried out in a 1:1:1 ratio of an amine, TIBA, and a ketone at 60 °C in toluene. b) The isomeric alcohols produced are standardized at 100%. c) Reaction at 0 °C. d) Ref. 7. Reaction at 41 °C in benzene.

rial alcohol during the prolonged reaction time.[8] In this study, at an early stage of the reaction 30—70% OH axial alcohol was obtained, depending on the amine employed. Also, during the course of a prolonged reaction, isomeric aluminum alkoxide underwent epimerization to give OH equatorial alcohol almost entirely.

As 2,6-methyl groups(axial and equatorial) hinder the reaction at the carbonyl group in the reduction of 2,2,6-trimethylcyclohexanone (226TMC), the rate of reduction was very slow and the stereoselectivity was not seen; that is, a 1:1 mixture of isomeric alcohols was obtained after 48 h reaction. 61% OH axial alcohol was obtained in the reduction with TIBA itself at 0 °C.

An attack from the less hindered side was seen in the reduction of camphor and norcamphor, and the reaction proceeded almost 100% with the dicyclohexylamine–TIBA system. The stereoselectivity was the same as in the reduction with free TIBA.

As has been shown above, an improvement in the stereoselectivity using amine-modified TIBA compared with the case of the reduction with free TIBA was observed in the reduction of 4*t*BC, which has not so severe a steric hindrance as the other ketones used in this study.

The results of the reductions of 4*t*BC and 335TMC using an excess of TIBA–amine reagent are shown in Table 2. The reduction of 4*t*BC with a threefold quantity of TIBA–diphenylamine gave 55% *cis* alcohol. Reduction with excess TIBA did not change the products distribution compared with the 1:1 reaction of TIBA and 4*t*BC at 0 °C. The reduction of 335TMC with a threefold quantity of TIBA and diphenylamine gave 93% OH axial alcohol even after 24 h reaction.

Table 2. Reduction of 4*t*BC and 335TMC with different TIBA–amine–ketone ratios[a]

Run	Amine	Time (h)	Unreac. ketone (%)	Products (%)[b] OH ax.	OH eq.
4-*t*-Butylcyclohexanone					
26	——	3.0	24.4	28	72[c]
27	Diphenylamine	2.0	26	55	45
28	Dicyclohexylamine	3.0	5	36	64
29	Piperidine	3.0	≃100	0	trace
30	Aniline	3.0	80	46	54
3,3,5-Trimethylcyclohexanone					
31	Diphenylamine	2.0	45	93	7
		24.0	27	93	7

a) The reaction was carried out in a 3:3:1 ratio of an amine, TIBA, and a ketone at 60 °C in toluene. b) The isomeric alcohols produced are standardized at 100%. c) Reaction in a 2:1 ratio of TIBA and a ketone at 0 °C. Ashby reported 60% *trans* alcohol in 1:1, 2:1, and 5:1 ratios of TIBA and 4*t*BC, and 70% *trans* alcohol in a 1 : 2 ratio at 22 °C in benzene.

IR Spectroscopy of the TIBA–Amine–4tBC System. With respect to TIBA and diphenylamine, Neumann[11] reported that an aluminum amide was not produced at room temperature, but was produced slowly at 50 °C and rapidly at 80 °C. In this study, the reaction of TIBA with an amine was carried out at 0 °C; an aluminum amide was not formed, however.

The infrared spectral data of TIBA–amine–4*t*BC systems are given in Table 3. When diphenylamine was added to TIBA in toluene at room temperature, the ν_{NH} of the amine shifted to a lower frequency, *i.e.*, from 3430 to 3200 cm^{-1}. This indicates that a TIBA–amine complex is formed. When 4*t*BC was added to this complex, ν_{NH} appeared at 3430 cm^{-1} and $\nu_{C=O}$ was not observed. When the reaction of TIBA

Table 3. IR characteristic absorptions of TIBA-amine-ketone systems in toluene[a)]

Sample	ν_{NH} (cm^{-1})	$\nu_{C=O}$ (cm^{-1})
Free 4*t*BC	—	1720, sharp
Free diphenylamine	3430, sharp	—
Diphenylamine + TIBA	3200, broad	—
Diphenylamine + TIBA + 4*t*BC	3430, sharp	not observed
Free piperidine	3310, broad	—
Piperidine + TIBA	3230, sharp	—
Piperidine + TIBA + 4*t*BC	3230, broad	1640, broad

a) Reaction carried out at room temperature. $[TIBA]_0 = 1.0$ M.

and diphenylamine was carried out at 60 °C for 4 h, the ν_{NH} disappeared, thus indicating the formation of aluminum amide.

The reduction of 4*t*BC with the TIBA–piperidine system was completely interupted. The IR data of this system exhibits a red shift of ν_{NH} from 3310 cm^{-1} to 3230 cm^{-1}, indicating the formation of a complex. The addition of 4*t*BC to this complex, however, did not change the ν_{NH} frequency. In addition, a broad absorption at 1640 cm^{-1} due to $\nu_{C=O}$, which was at a frequency 80 cm^{-1} lower than that of free 4*t*BC in toluene was observed. These findings indicate that the amine and the ketone are complexed to TIBA at the same time; that is, the ketone added to the TIBA–amine complex coordinates to TIBA, but the amine was not liberated from the complex as in the case of the results described above.

^1H NMR Spectroscopy of TEA–Amine Systems. In order to discuss the difference in the reactivity of TIBA–amine complexes, ^1H NMR studies were carried out. Triethylaluminum(TEA)–amine systems were employed instead of TIBA–amine systems. The internal shifts of the CH_3–CH_2 group in various TEA–amine systems are given in Table 4. In general, the internal shift($\Delta\delta$) of the ethyl derivative, CH_3–CH_2–X, is proportional to the electronegativity of the substituent, X.[12)] A larger value of $|\Delta\delta|$ means a stronger coordination of an amine to TEA. The internal shift, τ_{CH_3}-τ_{CH_2}, of free TEA was −0.80 ppm, while

Table 4. Internal shifts of the ethyl group in various TEA-amine systems[a)]

Amine	τ_{CH_3}-τ_{CH_2}	Difference from free TEA	pK_b of Amine
——	−0.80	0	
Piperidine	−1.33	−0.53	2.80 (in water)
Pyrrolidine	−1.33	−0.53	2.7[b)]
Diphenylamine	−0.93	−0.13	13.2
Pyrrole	−0.83	−0.03	13.6
Aniline	−0.80	0	9.40 (in water)[c)]
Triphenylamine	−0.80	0	

a) 60 MHz ^1H NMR in C_6D_6; shifts in ppm. b) Ref. 13. c) Ref. 14.

those of the piperidine and pyrrolidine complexes were −1.33 ppm. Those of the diphenylamine and pyrrole complexes were −0.93 and −0.83 ppm respectively. In the case of the aniline complex, a sharp peak appeared at δ 0.97, indicating the formation of ethane and an aluminum amide. Triphenylamine seems to be difficult to coordinate to TEA because of its bulkiness, so the value of the internal shift was not changed. The reduction of 4*t*BC with the TIBA–triphenylamine system gave 82% *trans* alcohol, similar to the result of the reduction with free TIBA.

Meanwhile, the pK_b values of amines are correlated with the internal shrfts; *i.e.*, the basicity is not so strong in diphenylamine and pyrrole, but is very strong in piperidine and pyrrolidine.

The coordination between Al and N being strong for an amine such as piperidine, the amine cannot be liberated from the TIBA–amine complex upon the addition of a ketone. Thus, the ketone cannot coordinate to TIBA enough to undergo subsequent reduction. When the Al–N coordination is moderately strong, the amine is liberated from the TIBA–amine complex upon the addition of a ketone; then a high selectivity is obtained. Moreover, triphenylamine showed no effect in selectivity because of the difficulty of complexing; this result is the same as in the reduction with free TIBA.

In the reduction of 4*t*BC with TIBA–diphenylamine, in which the reaction of TIBA and the amine was carried out at 60 and 80 °C, about 50% 4*t*BC was reduced to give 74 and 83% *trans* alcohol respectively. Thus, the formation of an aluminum amide decreases the reactivity and the stereoselectivity. The addition of diphenylamine to the reaction mixture of 4*t*BC and TIBA did not change the composition of isomeric alcohols. The high selectivity to *trans* alcohol was caused by the complexation of an amine to TIBA and the liberation of the amine from the complex upon the addition of a ketone, and not by the formation of an aluminum amide.

As is shown in Table 2, when excess TIBA–amine was allowed to reduce 4*t*BC or 335TMC, a larger amount of OH axial alcohol was produced compared with the case of the equimolar reaction of TIBA–amine to a ketone. In these ketones, OH axial alcohol is produced by the attack from the less hindered side; *i.e.*, the equatorial attack that was seen in the reduction of camphor and norcamphor. Especially in the reduction of 335TMC, 93% OH axial alcohol was produced, irrespective of the reaction time, with a three-fold quantity of TIBA–diphenylamine. On the other hand, 100% OH equatorial alcohol was produced after 24 h with equimolar TIBA–diphenylamine. As is shown in the reduction of 335TMC with TIBA at 41 °C in benzene, 82.7% OH axial alcohol was obtained after 2 h, while 99.7% OH equatorial alcohol was obtained in 31 h(Table 1, Run 15). Thus, diisobutylaluminum 3,3,5-trimethylcyclohexyloxide undergoes epimerization to a more stable isomer remarkably well. This epimerization was scarcely observed in an excess of TIBA–amine to the 335TMC system. The results of the reduction of 335TMC with excess TIBA–

amine show the net steric course of the reducing agent to this ketone; the subsequent epimerization is almost suppressed. The result, 93% OH axial alcohol, is highly stereoselective compared with that in the reduction with $LiAlH_4$ in THF, which gives 75—80% OH axial alcohol.[2)]

Considering the suppression of epimerization using an excess of a TIBA–amine reagent, the 55% OH axial alcohol obtained in the reduction of 4*t*BC with a threefold quantity of TIBA–diphenylamine shows stereoselectivity at the point of the attacking of the reducing agent. When one-to-one TIBA–amine to 4*t*BC was used, however, a great amount of OH equatorial alcohol was obtained.

It is also noteworthy that the reaction was almost completed in 2 or 3 h when an equimolar amount of TIBA–amine to a ketone was used, while a large quantity of unreacted ketone existed in the presence of an excess of the TIBA–amine complex. Therefore, the completion of the reaction seems to be one of the factors in the epimerization to a more stable isomer.[15)] In the reduction of 4*t*BC with free TIBA, however, the reaction also proceeded almost quantitatively to give only 83% *trans* alcohol.

When the reaction time was 0.5 h in the reduction of 4*t*BC with an equivalent amount of TIBA–diphenylamine, unreacted 4*t*BC remained and the *trans* alcohol was 85%. Even if the remaining 14% of 4*t*BC is allowed to be reduced only by axial attack, the amount of *trans* alcohol cannot reach 95.5%, the result after a reaction time of 2 h. The high selectivity to *trans* alcohol may be interpreted not only by the steric requirement of the transition state, but also by the enhancement of the reaction rate and epimerization. This is more marked in the reduction of 335TMC.

As has been mentioned above, when a TIBA–amine reagent was used in an amount equimolar to a ketone, epimerization between diisobutylaluminum alkoxide of *cis*- and *trans*-4-*t*-butylcyclohexanol occurred; it was promoted further in the presence of an amine (Eqs. 1 and 2). Consequently, 95—98% *trans* alcohol was obtained after hydrolysis.

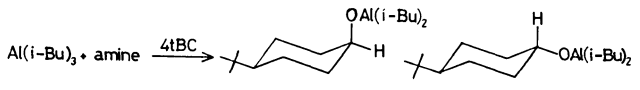

(1)

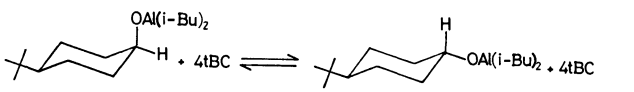

(2)

When a large excess of a TIBA–amine reagent was used, the amount of the least stable axial alcohol increased and a large amount of unreacted ketone was found. This means that the reduction of the ketone and the epimerization of the diisobutylaluminum alkoxide that produced are suppressed by an excess of a TIBA–amine complex. This unusual behavior of the reagent cannot be interpreted at present, indicating that the characteristics of the reagent are more complicated than those of a usual reducing agent such as $LiAlH_4$.

References

1) J. D. Morrison and H. S. Mosher, "Asymmetric Organic Reactions," Prentice-Hall, New Jersey (1971).
2) E. L. Eliel and R. S. Ro, *J. Am. Chem. Soc.*, **79**, 5992 (1957).
3) E. C. Ashby and J. R. Boone, *J. Org. Chem.*, **41**, 2890 (1976).
4) W. G. Dauben, G. J. Fonken, and D. S. Noyce, *J. Am. Chem. Soc.*, **78**, 2579 (1956).
5) M. Chérest and H. Felkin, *Tetrahedron Lett.*, **1968**, 2205.
6) J. C. Richer, *J. Org. Chem.*, **30**, 324 (1965).
7) H. Haubenstock and E. B. Davidson, *J. Org. Chem.*, **28**, 2772 (1963).
8) G. E. Heinsohn and E. C. Ashby, *J. Org. Chem.*, **38**, 4232 (1973).
9) M. Muraki and T. Mukaiyama, *Chem. Lett.*, **1975**, 875.
10) E. J. Eisenbraun, *Org. Synth.* Coll. Vol. V, 310 (1973).
11) W. P. Neumann, *Ann. Chem.*, **667**, 1 (1963).
12) a) B. P. Dailey and J. N. Shoolery, *J. Am. Chem. Soc.*, **77**, 3977 (1955); b) B. Brownstein, B. C. Smith, G. Ehrlich, and A. E. Laubengayer, *ibid.*, **81**, 3826 (1959); c) J. R. Cavanaugh and B. P. Dailey, *J. Chem. Phys.*, **34**, 1099 (1961).
13) H. B. Hetzer, R. G. Bates, and R. A. Robinson, *J. Phys. Chem.*, **67**, 1124 (1963).
14) H. H. Stroh und G. Westphal, *Chem. Ber.*, **96**, 184 (1963).
15) In most cases when more than 20% of *cis* alcohol was produced in the reaction of 4*t*BC with the TIBA–amine system, 10—80% of the unreacted 4*t*BC remained: reaction at a low temperature, result at an early stage of the reaction, reduction with TIBA–diethylamine or TIBA–aniline, and so on.

Layered Compounds. LIII.[1] Unique Skeletal Rearrangement of Multilayered [2.2]Paracyclophanes

Hisanori HORITA, Yosuke KOIZUMI, Tetsuo OTSUBO, Yoshiteru SAKATA, and Soichi MISUMI*

The Institute of Scientific and Industrial Research, Osaka University, Suita, Osaka 565

(Received March 10, 1978)

Skeletal rearrangements of multilayered [2.2]paracyclophanes to [2.2]metaparacyclophanes with several Friedel-Crafts acids have been studied. Two types of rearrangements depending on the catalyst were observed. Treatment of triple-layered paracyclophane(**8**) with $AlCl_3$–HCl gave mainly triple-layered metaparacyclophane(**9**), which was derived by migration of one of the ethylene bridges attached to the outer benzene rings. Treatment of **8** with mild protonic acids such as $SnCl_4$–HCl, $TiCl_4$–HCl, *etc.* afforded two kinds of metaparacyclophanes **10** and **11** in high yields, which arose from double migration of the two ethylene bridges attached to the inner benzene ring. Such a double migration of substitutents was also observed in the case of tertamethyl[2.2]paracyclophane and quadruple-layered one. The structures of products were determined by means of NMR spectra, alternative syntheses, and X-ray analyses. The mechanism of the rearrangements is discussed in view of protonation experiment.

[2.2]Paracyclophane(**1**), a typical layered compound, has been extensively investigated from the viewpoint of transannular π-electronic interaction. A number of anomalous physical and chemical behaviors have been reported.[2] Cram and his coworkers observed an interesting skeletal rearrangement of **1** to [2.2]metaparacyclophane(**2**) in the presence of aluminium chloride–hydrogen chloride.[3] This reaction is known to be the most practical and convenient method for the preparation of **2** since the starting material **1** is commercially available.

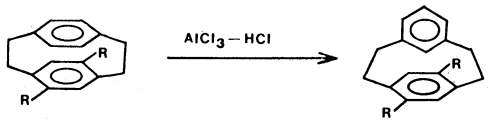

1: R=H 2: R=H

3: R=CH_3 4: R=CH_3

Multilayered [2.2]paracyclophane,[4] in which stronger electronic interaction[4a] and severer strain[5] than in **1** were observed, are expected to be highly reactive with Friedel-Crafts acid. In this paper, we report two types of skeletal rearrangement of double-, triple-, and quadruple-layered [2.2]paracyclophanes with several Friedel-Crafts acids to give unique multilayered metaparacyclophanes, and discuss their mechanisms.

Results and Discussion

Rearrangement and Structure. Before starting with multilayered cyclophanes, methyl-substituted [2.2]paracyclophanes were examined according to Cram's procedure.[3] Treatment of 4,7-dimethyl[2.2]paracyclophane(**3**) with $AlCl_3$–HCl at 0 °C for 30 min gave a 38% yield of 12,15-dimethyl[2.2]metaparacyclophane (**4**), which was formed by 1,2-migration of an ethylene bridge attached to the non-substituted benzene ring. Product **4** was identified by comparison of its melting point and NMR data with those of an authentic sample.[6a,b] Under the same conditions, D_2-symmetric 4,7,12,15-tetramethyl[2.2]paracyclophane(**5**) afforded 4,6,12,15-tetramethyl[2.2]metaparacyclophane(**6**) in 15% yield, which was derived by positional exchange

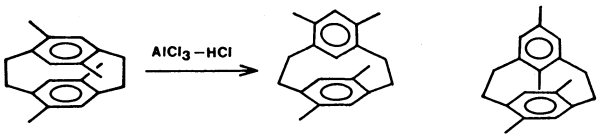

5 6 7

of a methyl group and an ethylene bridge attached to a benzene ring. The structure of **6** was easily assigned by comparing its NMR data with those of 4,6- and 12,15-dimethyl[2.2]metaparacyclophanes.[6b] Another isomer **7** expected to be formed by single 1,2-migration of an ethylene bridge was not obtained, probably because of severe steric repulsion between the inner methyl group and the faced para-bridging benzene ring.

Treatment of more highly strained triple-layered [2.2]paracyclophane(**8**)[5b] under the same conditions as in the case of double-layered ones gave only polymeric material. However, when the reaction was

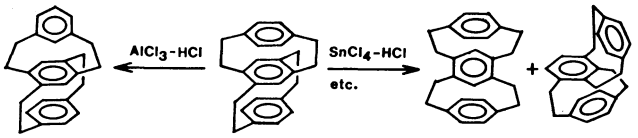

9 8 10 11

carried out at a lower temperature (−17 °C) in a shorter time, triple-layered metaparacyclophane **9** was obtained in 39% yield, together with a small amount of two isomeric cyclophanes **10** and **11**. Compound **9** was identified with the authentic sample synthesized by an alternative, stepwise method.[6a,b]

On the other hand, when **8** was treated with a large excess of weak Friedel-Crafts acid $SnCl_4$–HCl at room temperature, a mixture of **10** and **11** in a 56:46 ratio was obtained in 80% yield along with a very small amount of polymeric substance, no detectable amount of isomer **9** being observed. Use of $TiCl_4$–HCl, BF_3–HCl, or $ZnCl_2$–HCl as a catalyst gave results similar to the case of $SnCl_4$–HCl as shown in Table 1. It is of great interest that the formation of **10** and **11** is achieved by double migration of the two ethylene bridges attached to the inner benzene ring and that a molar ratio of 1.2:1 of the two isomers remains unaltered even by

Table 1. Rearrangement conditions of cyclophane **8** in dry dichloromethane

Friedel-Crafts Acid	Temp (°C)	Time (min)	Yield (%)	Product ratios (%)[a]					
				8	**9**	**10**	**11**	**10** :	**11**
$AlCl_3$-HCl	−17	15	51	3	76	11	10	52	48
$SnCl_4$-HCl	29	30	80	—	—	54	46	54	46
	30	180	64	—	—	55	45	55	45
$TiCl_4$-HCl	29	30	72	—	—	54	46	54	46
	29—31	180	69	—	—	48	52	48	52
$BF_3 \cdot Et_2O$-HCl	−17	60	Recovery of starting material						
	29—31	30	74	15	—	47	38	55	45
	29—31	180	79	—	—	53	47	53	47
$ZnCl_2$-HCl	Reflux	180	80	1	—	56	43	56	44
HF	0	20	20	13	—	11	76	—	—

a) Determined by the intensities in NMR spectra (100 MHz).

elongation of the reaction time and by the use of different kinds of catalyst. Application of $GaCl_3$–HCl, $SbCl_5$–HCl, or $FeCl_3$–HCl as a catalyst gave rise to only the formation of polymeric material and/or the recovery of the starting cyclophane **8**. Hydrogen fluoride was found to catalyze the reaction to give a mixture of **10** and **11** in a low yield (Table 1), while no rearrangement takes place in the presence of hydrogen chloride or hydrogen bromide alone. Treatment of double-layered cyclophanes **3** and **5** with weak protonic acid $SnCl_4$–HCl caused no formation of migration products, indicating that triple-layered paracyclophane is much more reactive than a double-layered one.

Isomers **10** and **11** were separated by fractional crystallization from benzene. Gel permeation liquid chromatography was also useful for separating them. Cyclophane **10** is identical with an authentic sample.[6a,b] The structure of new cyclophane **11** having a prehnitene (1,2,3,4-tetramethylbenzene) framework as the inner benzene ring was assigned by its spectral data and elemental analysis. Its NMR signals are explained in terms of the anisotropic effect of benzene rings (Fig. 1). The molecular structure of **11** was confirmed by X-ray crystallographic analysis of its bromoderivative **12** which was derived by bromination of **11** almost quantitatively (Figs. 2 and 3).[7a] Analysis showed no appreciable nonbonding interaction between bromine and its neighboring atoms, *viz.*, a structural resemblance

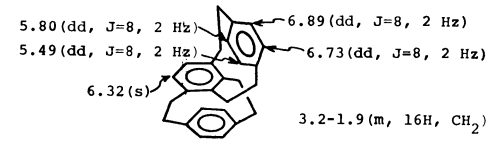

11

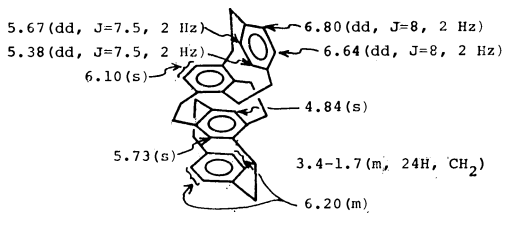

14

Fig. 1. NMR data of triple- and quadruple-layered [2.2]metaparacyclophanes **11** and **14** (δ values in $CDCl_3$, 60 MHz).

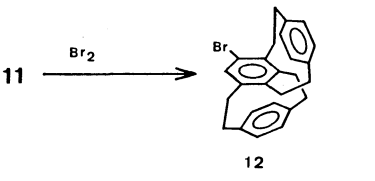

12

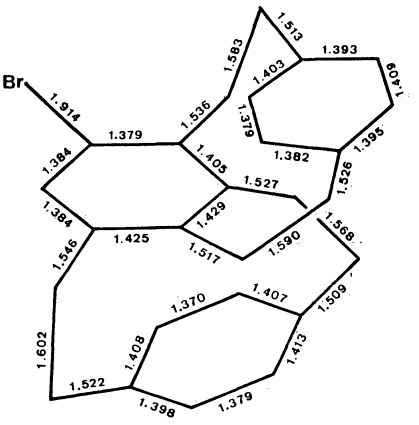

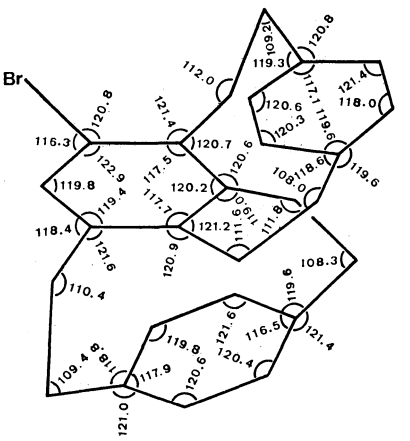

Fig. 2. Profile of the compound **12** together with bond lengths (Å) and angles (°).

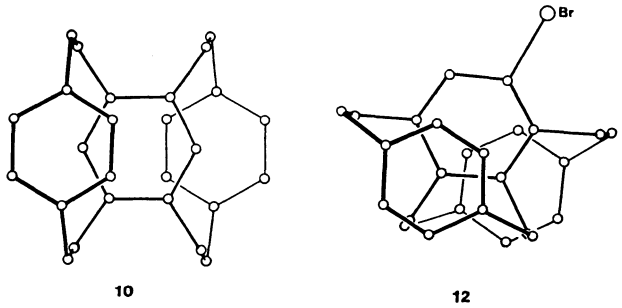

Fig. 3. Projection of the compounds **10** and **12** along the normal to the plane defined with the inner benzene ring.

of **12** to the parent hydrocarbon **11** is seen.

A similar rearrangement was observed in the treatment of quadruple-layered [2.2]paracyclophane(**13**) with boron trifluoride etherate–hydrochloric acid at 0 °C for 30 min. Compound **14** was isolated by column chromatography on silica gel from the reaction mixture.

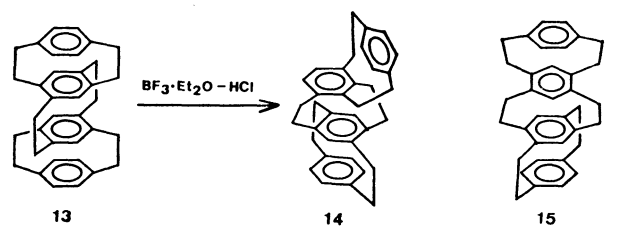

However, there was no detectable isomer **15**, corresponding to **10** in the case of triple-layered series.[6c] No rearranged product was obtained from **13** by treatment with mild reagent $ZnCl_2$–HCl. The results indicate relatively low stability of **13** as compared with **1** and **8**. The structure of **14**, determined on the basis of its elemental analysis and NMR data (Fig. 1), can be assigned by considering the data of **11** and the anisotropic effect of an additional benzene ring.

In previous papers,[6b,c] the electronic spectra of multilayered metaparacyclophanes except for cyclophanes **11** and **14** having a prehnitene framework were reported and a discussion on the relationship between structure and spectrum was given. The spectra of compounds **10**, **11**, and **14**, derived from skeletal rearrangement on the inner benzene ring, are shown in Fig. 4 together with the spectrum of compound **15**. The spectral resemblance between **10** and **11** can be attributed to the same extent of overlapping between the inner and the two outer benzene rings (Fig. 3), although their modes of overlapping differ to some extent. A similarity was observed in the spectra of quadruple-layered metaparacyclophanes **14** and **15**.

Mechanism. Cram *et al.* reported the NMR spectral measurement of protonated compound **16** formed by dissolving **1** in fluorosulfuric acid–sulfuryl chloride fluoride–dichloromethane at −98 °C, and proposed a mechanism of the rearrangement of **1** to **2**, the first step of which is the protonation at a bridgehead carbon, followed by 1,2-migration of the ethylene bridge attached to the protonated carbon and finally by deprotonation.[3b]

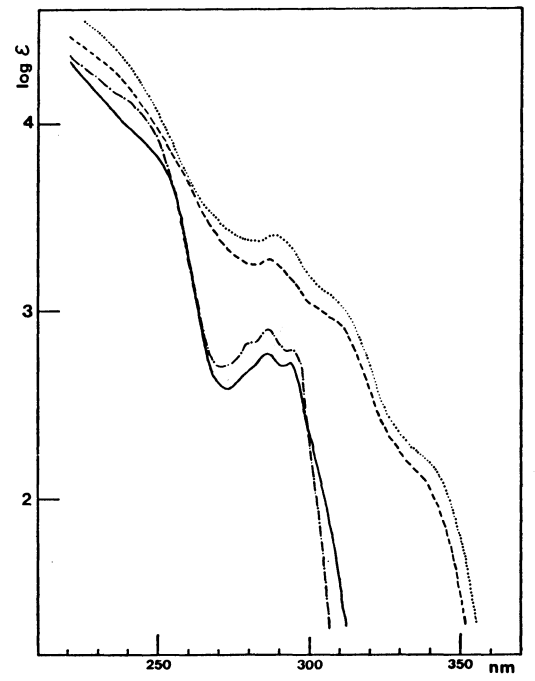

Fig. 4. Electronic spectra of cyclophanes **10** (—·—), **11** (——), **14** (----), and **15** (·····) in tetrahydrofuran.

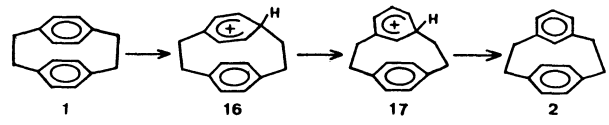

A similar treatment of cyclophane **8** in the same reagent at −78 °C gave a deep red solution, in which a single protonated species **18** was confirmed as the main product by NMR analysis. As seen in Fig. 5, the aromatic protons of the inner benzene ring appear at δ 7.21 and 6.11 ppm as singlets showing downfield shifts by 1.81 and 0.71 ppm, respectively, as compared to the corresponding protons of **8**. Such downfield shifts are comparable to the values (1.80 and 1.12 ppm)[3b] observed in protonation of [2.2]para-

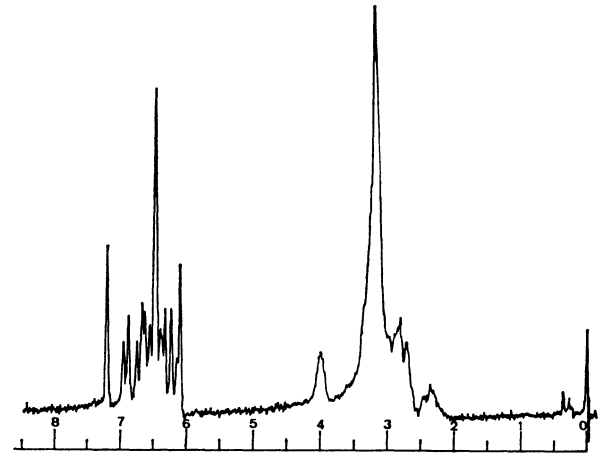

Fig. 5. NMR spectrum (100 MHz) of protonated triple-layered [2.2]paracyclophane **18** in FSO_3H-SO_2ClF-CD_2Cl_2 at −100 °C.

cyclophane. The fact that protonation occurred preferentially at a bridgehead carbon of the inner benzene is ascribed to a stronger basicity than that of the outer benzene ring due to the difference in the number of alkyl substituent and to considerable relief of bond angle strain, *viz.*, π-π repulsive strain between two benzene rings. On the other hand, the protonation of **10** occurred at bridgehead carbons of the two outer benzenes in preference to more basic inner one to give diprotonated species under marked strain release. The results of protonation demonstrate the strain relief to be a more important factor than π-basicity.

We propose a mechanism of the rearrangement of **8** to **10** and **11** as follows. At the initial stage, a proton would add to a bridgehead carbon (C_3) in the inner

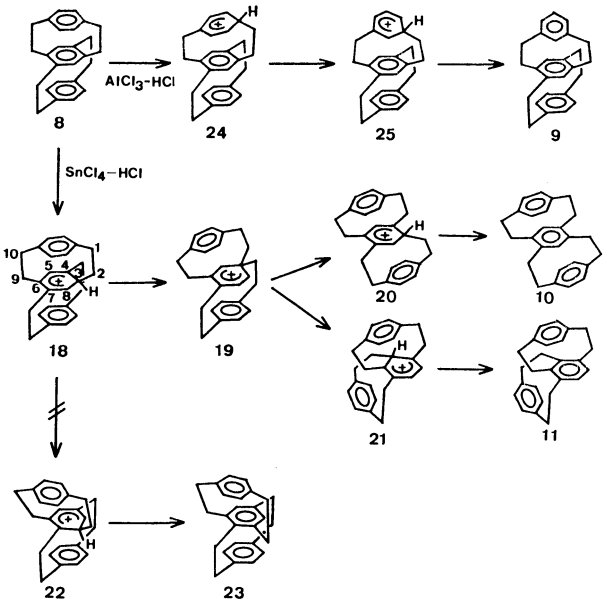

benzene ring of **8** to form a cation (**18**), releasing bond angle strain of **8**. Although the same extent of strain relief is considered for another possible protonated species **24**, the difference in π-basicity of the inner and the outer benzene rings and the difference in relative stability of the two cations **18** and **24** due to transannular π-electronic delocalization are probably responsible for the predominance of **18**. The ethylene bridge attached to the protonated carbon would migrate intramolecularly to the adjacent bridgehead carbon C_4 to yield cation **19**, in which considerable strain reduction might result between the inner ring and both outer rings. Cation **19** is probably a common intermediate for the two rearranged products **10** and **11**, since a constant ratio was obtained for these products in the reaction mixtures regardless of the kind of weak protonic acid, reaction time, and temperature (Table 1), no interconversion between **10** and **11** being found under the same conditions. Finally, another ethylene bridge attached to the carbon C_4 would migrate in two ways, *viz.*, to C_3 and C_5 to give cations **20** and **21**, respectively, from which products **10** and **11** would be formed by deprotonation. No other possible migration of **18** to cation **22** was realized due to severe strain in the structure **23** as expected from the examination with molecular models.

In the rearrangement with aluminium chloride–hydrogen chloride, the initial protonation might take place at a bridgehead carbon of the outer benzene rings under strain relief, followed by bridge migration to cation **25** and deprotonation to **9**. Predominance of such a different type of initial protonation may be associated with the strong acidity and/or the bulkiness of this protonic acid.

The results suggested that the relief in molecular strain functions as a driving force in both the rearrangements **8**→**9** and **8**→**10**+**11**, and the relative π-basicity serves as an additional factor in the case of the latter rearrangement.

Experimental

Melting points are uncorrected. All the solvents are of reagent grade unless otherwise stated. Commercial Lewis acids were used. Chromatography was carried out on silica gel (Merck, activity II) or neutral alumina (Woelm, activity I). PMR spectra were taken with Hitachi-Perkin-Elmer R-20 (60 MHz) and Nihon Denshi JNM-TS-100 (100 MHz) spectrometers using TMS as an internal standard, MS with Hitachi RMU-7 spectrometer at 70 eV using a direct insertion technique, IR with Jasco DS-402 and UV with Hitachi EPS-3T spectrophotometers. Multilayered [2.2]paracyclophanes were synthesized according to the 1,6-Hofmann elimination method.[4a,c]

Rearrangemnet of 4,7-Dimethyl[2.2]paracyclophane ***3*** *to 12,15-Dimethyl[2.2]metaparacyclophane* ***4***. After dry hydrogen chloride gas had been bubbled into a stirred solution of anhyd aluminium chloride (1.694 g, 12.7 mmol) in dry dichloromethane (50 ml) for 30 min, 4,7-dimethyl[2.2]paracyclophane **3** (500 mg, 2.12 mmol) was added at once to the solution. The resulting blood red complex solution was vigorously stirred at 4—6 °C for 180 min, cooled to −15 °C, and decomposed with 6*N*-hydrochloric acid. The aqueous layer was extracted with dichloromethane and the combined organic layer was successively washed with water, saturated aq sodium hydrogencarbonate and water. After drying and evaporation of the solvent, the residual oil was filtered through neutral alumina (6 g) with hexane. The crystals obtained from the filtrate were recrystallized from pentane to give 192 mg (38%) of **4**, colorless plates, mp 66.5—67.5 °C (lit, 65—66 °C).[6a]

Rearrangement of D_2*-symmetric 4,7,12,15-Tetramethyl[2.2]paracyclophane* ***5*** *to 4,6,12,15-Tetramethyl[2.2]metaparacyclophane* ***6***. A suspension of anhyd aluminium chloride (2.28 g, 17.1 mmol) in dry dichloromethane (150 ml) was saturated with dry hydrogen chloride and cooled to −15 °C. Compound **5** (750 mg, 2.84 mmol) was added in one portion to the solution and the resulting deep red solution was stirred at −9—−10 °C for 100 min under slow bubbling of dry hydrogen chloride. The reaction mixture was worked up in the same way as in the case of **4**. Chromatography on silica gel (80 g) with hexane gave, after elution of unidentified oily products, 112 mg (15%) of 4,6,12,15,-tetra methyl[2.2]metaparacyclophane **6**, white columns from hexane, mp 78—81 °C. Further recrystallization from the same solvent gave pure **6**, mp 81—82 °C.

Found: C, 90.60; H, 9.18%. Calcd for $C_{20}H_{24}$: C, 90.85; H, 9.15%. NMR($CDCl_3$, δ ppm): 6.88(s, 1H, ArH), 6.62 (s, 1H, ArH), 5.69(s, 1H, ArH), 5.34(s, 1H, ArH), 3.4—1.9 (m, 8H, CH_2), 2.45(s, 3H, CH_3), 2.22(s, 6H, CH_3), 1.65 (s, 3H, CH_3): MS (rel intensity): 264(M^+, 52), 249(57),

133(63), 132(100), 117(30), 91(18); UV λ_{max} in THF, nm(ε): 279(520), 287.5(540).

When the above reaction was carried out at −20——21 °C for 15 min, the starting material was recovered, a tarry material only being produced at 0 °C for 1 h.

Rearrangement of Triple-layered [2.2]Paracyclophane ***8***.

a) With Aluminium Chloride–Hydrogen Chloride: A suspension of powdered anhyd $AlCl_3$ (472 mg, 3.54 mmol) in dry dichloromethane (40 ml) was saturated with dry HCl and cooled to −20 °C. Triple-layered [2.2]paracyclophane **8** (200 mg, 0.59 mmol) was added to the solution at once and the resulting deep red solution was stirred at −17 °C for 15 min. After cold 6M-HCl had been added, the separated aqueous layer was extracted with dichloromethane. The combined organic solution was washed with water, dried over anhyd magnesium sulfate, and evaporated to dryness. The residual oil was chromatographed on silica gel (30 g) with hexane. From the first eluate, triple-layered [2.2]metaparacyclophane **9** was obtained and recrystallized from benzene–ethanol to give 60 mg of colorless plates, mp 141—142 °C (lit, 144—145 °C).[6a]

The mother liquor and the following eluates gave a mixture of cyclophane (42 mg) consisting of **8**:**9**:**10**:**11**=3:76:11:10 on the basis of NMR analysis (100 MHz).

b) With Stannic Chloride–Hydrogen Chloride: To a stirred solution of anhyd $SnCl_4$ (460 mg, 1.75 mmol) in dry dichloromethane (20 ml) saturated with hydrogen chloride was added **8** (100 mg, 0.30 mmol). The resulting purple red solution was stirred at 29 °C for 30 min and quenched with cold dil hydrochloric acid. The reaction mixture was worked up as above and the product was purified by filtration through alumina (7 g) with 10% benzene–hexane to give a mixture of **10** and **11** (79.7 mg, 80% yield). Repeated recrystallization of the mixture from benzene gave two forms of crystal, colorless plates **10** and colorless prisms **11**, which were separated with tweezers and purified by recrystallization. The mixture was also separated into **10** and **11** by gel permeation chromatography (Nihon Bunsekikogyo LC-08). Cyclophane **10** gave spectral data and melting point (259—260 °C) identical with those of an authentific sample.[6a] Data of the new cyclophane **11** are as follows: mp 209—210 °C (partly sublime).

Found: C, 92.42; H, 7.63%. Calcd for $C_{26}H_{26}$: C, 92.26; H, 7.74%. The NMR datum is given in Fig. 1. MS (rel intensity): 338(M^+, 100), 233(38), 219(47), 104(92). UV λ_{max} in THF, nm(ε): 285(590), 293(530).

The rearrangement of **8** was carried out with the other protonic acids, $TiCl_4$–HCl, BF_3–HCl, and $ZnCl_2$–HCl in the same way as in the case of $SnCl_4$–HCl. The results are given in Table 1. A similar treatment with $GaCl_3$–HCl (at 28 °C, 30 min), $SbCl_5$–HCl (−5——2 °C, 60 min), and $FeCl_3$–HCl (29 °C, 10 min) gave only polymeric substances; with $SbCl_5$–HCl (−40——30 °C, 60 min) and HCl (reflux, 180 min) or HBr alone (22 °C, 60 min) the starting cyclophane **8** was recovered .

c) With Hydrogen Fluoride: Hydrogen fluoride (5 ml) was distilled in a solution of **8** (100 mg, 0.30 mmol) in dichloromethane (20 ml) which had been cooled in a Dry Ice–acetone bath. The resulting purplish red solution was gradually warmed up to 0 °C under stirring over a period of 20 min, stirring being continued at the temperature for 20 min. After HF had been removed, the reaction mixture was poured into a saturated aq. sodium hydrogencarbonate solution and worked up as described above. A mixture (20 mg, 20%) of **8**, **10**, and **11** was obtained in the ratio given in Table 1.

6-Bromo[2.2]paracyclo(4,8)[2.2]metaparacyclophane ***12***.

To a stirred solution of bromine (14.2 mg, 0.11 mmol) in carbon tetrachloride (0.3 ml) was added triple-layered metaparacyclophane **11** (37.2 mg, 0.11 mmol) in dry dichloromethane (1.5 ml) at 0 °C. The mixture was slowly warmed up to room temperature and then stirred for 15 min. After filtration through neutral alumina (1 g) and removal of the solvent, the residue was chromatographed on silica gel (10 g) with 10% benzene–hexane to give 45.1 mg (98%) of the desired bromoderivative **12**, colorless prisms from benzene –ethyl acetate, mp 242—243 °C with decompn. (in a sealed tube).

Found: C, 74.70; H, 5.96; Br, 18.82%. Calcd for $C_{26}H_{25}Br$: C, 74.82; H, 6.04; Br, 19.14%. NMR($CDCl_3$, δ ppm): 6.91 (dd, J=8, 2 Hz, 2H, ArH), 6.75(dd, J=8, 2 Hz, 1H, ArH), 6.62(s, 1H, ArH), 6.05(dd, J=8, 2 Hz, 1H, ArH), 5.92(dd, J=8, 2 Hz, 1H, ArH), 5.63 (dd, J=8, 2 Hz, 1H, ArH), 5.62(dd, J=8, 2Hz, 1H, ArH), 3.3—1.7 (m, 16H, CH_2). MS (rel intensity): 416(M^+, 32), 418(M^++2, 33), 337(37), 314(6), 312(6), 233(15), 104(100), 91(10). UV λ_{max} in THF, nm(ε): 285(620), 294(280), 305(210)(sh).

Rearrangement of Quadruple-layered [2.2]Paracyclophane ***13*** *with Boron Trifluoride Etherate–Hydrogen Chloride.* To a solution of boron trifluoride etherate (0.49 ml, 3.82 mmol) in dry dichloromethane (60 ml) saturated with dry HCl was added quadruple-layered [2.2]paracyclophane **13** (300 mg, 0.64 mmol) at once under stirring. The purplish blue solution was stirred at 0 °C for 30 min and then decomposed with dil hydrochloric acid. The mixture was worked up as usual. Chromatography of the product on silica gel (20 g) with 2% benzene–hexane gave quadruple-layered metaparacyclophane **14**, colorless prisms from benzene–hexane, mp 336.5—337.5 °C, yield 25 mg (8%).

Found: C, 92.53; H, 7.60%. Calcd for $C_{36}H_{36}$: C, 92.26; H, 7.74%. The NMR datum is given in Fig. 1. MS (rel intensity): 468(M^+, 100), 363(44), 349(34), 245(32), 104(44). UV λ_{max} in THF, nm(ε): 286(1790).

Protonation of Triple-layered [2.2]Para- and Metapara-cyclophanes ***8***, ***10***, *and* ***11***. Protonation was carried out according to the general procedure for **8** described below.

Sulfuryl chloride fluoride (0.6 ml) and fluorosulfuric acid (0.2 ml, freshly distilled) were carefully added successively at −78 °C to a solid of **8** (40 mg) placed in an NMR tube. When the tube was shaken, the solution turned clear deep red. After the NMR spectrum of protonated species **19** was measured, the solution was poured into water, compound **8** being recovered quantitatively. Cyclophane **10** was also protonated in a similar manner to yield diprotonated species, which was analyzed by NMR spectrum.

Diprotonated species of **10**, NMR(SO_2ClF–FSO_3H–CD_2Cl_2, δ ppm): 8.70(br d, J=8 Hz, 2H), 7.91(br d, J=8 Hz, 2H), 7.48(br d, J=8 Hz, 2H), 6.51(br d, J=8 Hz, 2H), 5.98(br s, 2H), 4.16(br s, 2H), 4.0—2.0(m, 16H).

The present work was partly supported by a Grant-in-Aid for Scientific Research from the Ministry of Education.

References

1) Part LII: A. Iwama, T. Toyoda, M. Yoshida, T. Otsubo, Y. Sakata, and S. Misumi, *Bull. Chem. Soc. Jpn.*, in press.

2) B. H. Smith, "Bridged Aromatic Compounds," Academic Press, New York, N. Y. (1964); D. J. Cram and J. M. Cram, *Acc. Chem. Res.*, **4**, 204 (1971); F. Vögtle and P. Neumann, *Angew. Chem.*, **84**, 75 (1972); *Synthesis*, **1973**, 85; S. Misumi, *Kagaku No Ryoiki*, **28**, 927 (1974); Y. Sakata,

ibid., **28**, 947 (1974); S. Misumi, *Mem. Inst. Sci. Ind. Res., Osaka Univ.*, **33**, 53 (1976); S. Misumi and T. Otsubo, *Acc. Chem. Res.*, **11**, 251 (1978).

3) a) D. J. Cram, R. C. Helgeson, D. Lock, and L. A. Singer, *J. Am. Chem. Soc.*, **88**, 1324 (1966); b) D. T. Hefelfinger and D. J. Cram, *ibid.*, **93**, 4754 (1971).

4) a) T. Otsubo, S. Mizogami, I. Otsubo, Z. Tozuka, A. Sakagami, Y. Sakata, and S. Misumi, *Bull. Chem. Soc. Jpn.*, **46**, 3519 (1973); b) T. Otsubo, S. Mizogami, Y. Sakata, and S. Misumi, *ibid.*, **46**, 3831 (1973); c) T. Otsubo, H. Horita, and S. Misumi, *Synth. Commun.*, **6**, 591 (1976).

5) a) H. Mizuno, K. Nishiguchi, T. Otsubo, S. Misumi, and N. Morimoto, *Tetrahedron Lett.*, **1972**, 4981; H. Mizuno, K. Nishiguchi, T. Toyoda, T. Otsubo, S. Misumi, and N. Morimoto, *Acta Crystallogr., Sect. B*, **33**, 329 (1977); b) K. Nishiyama, M. Sakiyama, S. Seki, H. Horita, T. Otsubo, and S. Misumi, *Tetrahedron Lett.*, **1977**, 3739.

6) a) N. Kannen, T. Umemoto, T. Otsubo, and S. Misumi, *Tetrahedron Lett.*, **1973**, 4537; b) N. Kannen, T. Otsubo, Y. Sakata, and S. Misumi, *Bull. Chem. Soc. Jpn.*, **49**, 3203, 3307 (1976); c) N. Kannen, T. Otsubo, and S. Misumi, *ibid.*, **49**, 3208 (1976).

7) a) T. Toyoda, Y. Koizumi, H. Horita, and S. Misumi, 32nd National Meeting of the Chemical Society of Japan, Tokyo, April 1975, Abstr. Vol. I, p. 184; b) Y. Koizumi, T. Toyoda, N. Kannen, H. Horita, and S. Misumi, The Symposium on Molecular Structure, Osaka, November 1975, Abstr. p. 455.

Synthesis of 1,4-Dithiafulvenes and 1,4-Dithiafulvalenes by Carbonyl Olefination Using 2-Dimethoxyphosphinyl-1,3-benzodithiole

Kin-ya AKIBA,* Kiyofumi ISHIKAWA, and Naoki INAMOTO

Department of Chemistry, Faculty of Science,
The University of Tokyo, Hongo, Tokyo 113

(Received April 11, 1978)

The reactions of 1,3-dithiolylium salts with tertiary phosphines and trialkyl phosphites in dry acetonitrile gave the corresponding phosphonium salts and the phosphonates respectively in high yields. Both 2-triphenylphosphonio-1,3-benzodithiole tetrafluoroborate and 2-dimethoxyphosphinyl-1,3-benzodithiole were deprotonated with butyllithium in THF at −78 °C and the resulting phosphorane (*A*) and the phosphonate carbanion (*B*) reacted with a variety of carbonyl compounds to give 1,4-benzodithiafulvenes in 74—98% yields. Moreover, *B* reacted with conjugated cyclic ketones (**5**) such as dibenzo[a,d]cyclohepten-5-one, 10*H*-9-thiaanthracen-10-one, 9-alkyl-9,10-dihydro-9-azaanthracen-10-one, 9-fluorenone, and so on to give 1,4-benzodithiafulvalenes (**6**) in 73—96% yields. The UV spectral data of **6** were discussed in comparison with those of **5**.

Heteroaromatic cations such as pyrylium, thiopyrylium, pyridinium, thiazolium, and dithiolylium have been attractive target of research both for physical organic and synthetic chemists. Preparation and use of dithiolylium salts have acquired renewed interest in connection with the synthesis of tetrathiafulvalene derivatives, one component of organic metals. Our interest to develop new utility of heteroaromatic cations in organic synthesis has led us to general preparation of 1,4-dithiafulvenes and fulvalenes, starting from 1,3-dithiolylium salts.

On the other hand, fulvenes and fulvalenes have been investigated from the standpoint of both synthetic and theoretical aspects and dithia analogues have also been investigated as their iso-π-electronic systems.

However, there has been no general synthetic method of 1,4-dithiafulvenes (2-alkylidene-1,3-dithioles), although those with electron-withdrawing groups on the exo-methylene can be prepared by condensation of 2-methylthio-1,3-dithiolylium salts with acitve methylene compounds in 34—77% yields.[1] Some of them were obtained among photolysis products of 1,2,3-thiadiazoles in 45—50% yields.[2] It was also reported that 2-benzylidene-4-phenyl-1,3-dithole was prepared by the reaction of 2-methylthio-4-phenyl-1,3-dithiolylium iodide with benzylmagnesium chloride, but this method required long reaction time and the yield was low.[3]

On the other hand, there are a couple of recent reports on the preparation of 2-alkylidene-1,3-dithioles when electron-withdrawing groups are on the ring. 1,3-Dithiol-2-ylidene-tributylphosphoranes were prepared *in situ* by addition of activated acetylenes to a mixture of tributylphosphine and carbon disulfide and used for subsequent Wittig reaction.[4] Intermediate phosphorane can be trapped as a phosphonium salt when the active acetylene has at least one carboxylic acid group.[5] The intermediacy of the same kind of phosphorane during desulfurization of 4,5-dicyano-1,3-dithiole-2-thione with tertiary phosphines was recently reported,[6] however, Scherowsky and Weiland could not detect the same kind of phosphorane in desulfurization of 1,3-benzodithiole-2-thione with triethyl phosphite.[7] To our knowledge, only these three special cases have been reported to date on this type of phosphorane and their Wittig reaction.

1,4-Dithiafulvalenes have been prepared by condensation of 1,3-dithiolylium salts with cyclopentadienide anions[8] and active methylenes contained in heterocycles,[9] and their properties were compared with sesquifulvalenes which are iso-π-electronic each other.

Now, it is expected that 1,4-dithiafulvenes can generally be prepared by a single method, *i.e.*, Wittig-Horner reaction with acyclic and cyclic carbonyl compounds, if phosphonium salts or phosphonates are prepared from 1,3-dithiolylium salts. This paper offers a new synthetic method for such type of compounds.

Results and Discussion

Synthesis of 2-Phosphonio- and 2-Dialkoxyphosphinyl-1,3-dithioles. Slightly exothermic reaction took place immediately on addition of tertiary phosphine to 1,3-dithiolylium tetrafluoroborate (**1**) in dry acetonitrile solution and stirring was continued for 2 h at room temperature. After evaporation of the solvent under reduced pressure, addition of dry ether to the residue gave the precipitates, 2-phosphonio-1,3-dithiole tetrafluoroborate (**2**) in high yields.

1,3-Dithiolylium salt (**1**) reacted also with trialkyl phosphite in the presence of an equimolar amount of sodium iodide in dry acetonitrile under nitrogen at room temperature. Michaelis-Arbuzov reaction took place very rapidly to give 2-dialkoxyphosphinyl-1,3-dithioles (**3**) in high yields while the reaction did not take place in the absence of sodium iodide under otherwise the same conditions. Yields and mp of **2** and **3** are shown in Table 1.

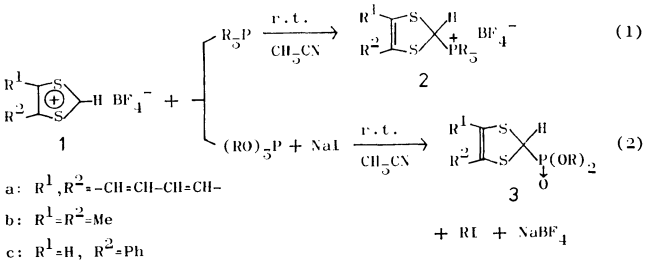

Scheme 1.

The structures of these products (**2** and **3**) were confirmed by means of elemental analyses, IR, and NMR spectra. The IR spectra of **2** showed very strong absorption bands at about 1100 and 520 cm^{-1}

Table 1. Yields and mp of phosphonium salts (**2**) and phosphonates (**3**)

Compound	R^1	R^2	R	Yield (%)	Mp (°C)
2a	-CH=CH-CH=CH-		Ph	87	211.5—212.5 (dec)
2b	-CH=CH-CH=CH-		*n*-Bu	90	166.5—167.0
2c	Me	Me	Ph	84	175.0—177.0 (dec)
3a	-CH=CH-CH=CH-		Me	93	122.0—123.0
3b	-CH=CH-CH=CH-		Et	90	115.5—116.5
3c	Me	Me	Me	83	—
3d	H	Ph	Me	90	87.0— 88.0

(BF_4^-). The NMR spectrum of each of **2** showed a broad singlet signal assignable to 2-CH (*i.e.*, $J_{PCH} \fallingdotseq 0$). The NMR spectrum of **2c** showed a singlet signal at an extraordinarily high field as a vinylic methyl ($\delta = 1.30$) assignable to two methyl groups at 4 and 5 positions. IR spectra of all the phosphonates (**3**) showed strong absorption bands characteristic of P=O (1250—1260) and P-O-C (1050—1065 and 1030—1040 cm^{-1}), respectively.

Each NMR spectrum of **3** showed a doublet signal at δ 4.75—5.06 ($J_{PCH} = 4.4$—5.8 Hz) assignable to 2-CH and also a doublet signal at δ 3.63—3.85 ($J_{POCH} =$ 10.4—10.8 Hz) assignable to POMe except for **3b**. The compounds (**3a**, **b**, and **d**) showed the parent peak (4—9%) and the base peak assignable to $M^+ - P(O)(OR)_2$ in MS.

The ^{31}P-NMR spectrum of **3a** exhibited a signal at δ −19 ppm.

Gross *et al.*[10] reported that the ^{31}P-NMR spectrum of 5,6-dichloro-2-diethoxyphosphinyl-1,3-benzodioxole exhibited a signal at δ −7.3 ppm, and that this value was compared with those of diethyl methylphosphonate and its monochloro-, dichloro-, and trichloromethyl compounds (δ_P −30, −18.1, −9.3, and −6.5 ppm, respectively)[11] in relation to the electronegativity of the substitutent. The effect of the substitution of a catechol ring for two hydrogen atoms of the methyl group nearly corresponded to that of three chlorine atoms for three hydrogen atoms of the methyl group. In the present case, the effect of the substitution of a thiocatechol ring for two hydrogen atoms of the methyl group is smaller than that of a catechol ring and corresponds approximately to that of one chlorine atom for the methyl group.

The compound (**3c**) has low melting point (−20 °C), and was purified by dry column chromatography over neutral alumina. However, this compound is so hygroscopic and sensitive to air as an oil or in solution that it could not be purified enough for elemental analysis.

*Wittig-Horner Reaction of 2-Triphenylphosphonio-1,3-benzodithiole Tetrafluoroborate (**2a**) and 2-Dimethoxyphosphinyl-1,3-benzodithiole (**3a**): Synthesis of 1,4-Benzodithiafulvenes (**4**).*[12] Both 2-triphenylphosphonio-1,3-benzodithiole tetrafluoroborate (**2a**) and 2-dimethoxyphosphinyl-1,3-benzodithiole (**3a**) were deprotonated with butyllithium in THF at −78 °C and the resulting phosphorane (*A*) and phosphonate carbanion (*B*) were allowed to react with a wide variety of carbonyl compounds to give the expected products, *i.e.*, 1,4-benzodithiafulvene (**4**) at low temperatures in very good yields. The reaction scheme is shown below.

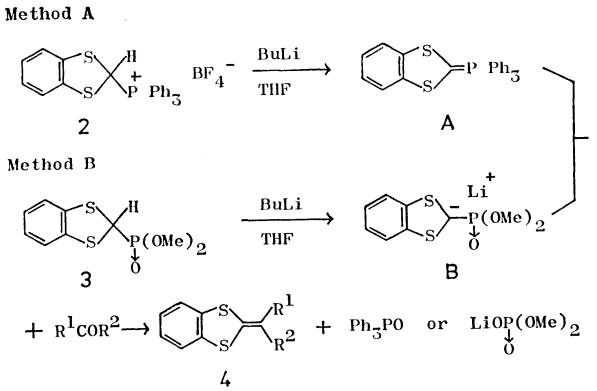

Scheme 2.

Comparison of two methods recommends Method B for synthetic purpose by the following reasons: i) shorter reaction time of Method B than Method A, because the former can be carried out in homogeneous solution but the deprotonation of **2a** is a heterogeneous reaction, ii) no need of chromatographic separation of the product, the resulting phosphoric acid being soluble in water, iii) higher reactivity of *B* than *A*, hence the former can be carried out at lower temperatures than the latter, and *B* reacted smoothly with *p*-dimethylaminobenzaldehyde at low temperature to give **4a** in high yield, but *A* did not react with the same aldehyde even under reflux of THF, iv) higher yield in every case, and v) no by-production of dibenzotetrathiafulvalene, which is the case in method A when the reaction is carried out at higher temperatures (room temperature).

Yields and mp of **4** are shown in Table 2.

All the products (**4a**—**g**) showed correct elemental analysis and reasonable IR, ^1H-NMR, and MS spectra. All **4** showed the parent peak as the base peak in MS, with the exception of **4b** and **4f**. This fact shows large stability of the parent radical cations which are contained in 1,4-benzodithiafulvene ring. The parent peak of **4b** appeared at *m/e* 272 (88%) and the base peak at *m/e* 257 assignable to $M^+ - Me$. The parent peak of **4f** appeared at *m/e* 268 (94%) and the base peak at *m/e* 128 assignable to $M^+ - C_6H_4S_2$.

The phosphonate carbanion (*B*) reacted also with 3-buten-2-one (methyl vinyl ketone) to give crude 2-(1-methyl-2-propenylidene)-1,3-benzodithiole (**4r**) in 53% yield. But this compound could not be purified

Table 2. Yields and mp of 1,4-benzodithiafulvenes (**4**)

	R^1	R^2	Method	Yield (%)	Mp (°C)
4a	*p*-$Me_2NC_6H_4$	H	A	No reaction	
			B	95	145—146
b	*p*-$MeOC_6H_4$	H	A	77 [75][a)]	155—156
c	*p*-MeC_6H_4	H	A	75 [74]	149.5—151
			B	94	
d	Ph	H	A	74 [72]	133—134.5
e	*p*-ClC_6H_4	H	A	82 [79]	190—190.8
f	PhCH=CH	H	A	78 [80]	148—149
g	MeCH=CH	H	B	95	72— 73
h	$-(CH_2)_4-$		B	96	105.5—107
i	$-(CH_2)_5-$		B	98	96— 97.5
j	$-CH=CMeCH_2CMe_2CH_2-$		B	87	99—100
k	PhCH=CH	Me	B	96	170—171
l	*p*-MeC_6H_4	Me	B	92	80— 81
m	Ph	Me	B	94	oil
n	*p*-ClC_6H_4	Me	B	91	97— 98
o	*p*-$MeOC_6H_4$	*p*-$MeOC_6H_4$	B	96	105—106
p	Ph	Ph	B	80	96— 97
q	*p*-ClC_6H_4	*p*-ClC_6H_4	B	95	113—114

a) Numerical values in parentheses show yields of triphenylphosphine oxide.

enough for elemental analysis because of its instability.

The reaction of *B* with acetaldehyde was also carried out under the genreal procedure. Purification of the product by preparative thin-layer chromatography (SiO_2/CCl_4) afforded, however, only a trace amount of a product. The structure of the compound was proposed to be the dimer of the expected one from its ^{1}H-NMR spectral data; δ (CCl_4) 1.07 (t, 3H), 1.99 (s, 3H), 2.42 (q, 2H), and 6.7—7.6 (m, 8H).

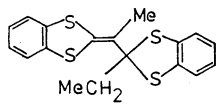

The same type of dimerization accompanied by prototropy is known for active methylene contained in benzothiazoline.[13]

The reaction of *B* with 9(10*H*)-anthracenone resulted in proton abstraction to give an oxidized product, *i.e.*, 9,10-anthracenedione, whereas *B* did not react with 10,10-dibenzyl-10*H*-anthracen-9-one at all, probably because of steric hindrance.[14]

Moreover, the phosphonate carbanion derived from **3d** reacted with 4,4'-dichlorobenzophenone to give 2-[bis(*p*-chlorophenyl)methylene]-4-phenyl-1,3-dithiole in 83% yield.

It should be noted that extraordinarily rapid Wittig-type reaction was observed in both methods A and B as compared with usual reaction conditions.[15] Furthermore, *B* reacted with cycloalkanones, acetophenones, and even benzophenones at low temperatures in contrast to 1,3-dithiacyclohexylidenetrimethoxyphosphorane which did not react with those ketones mentioned above even by heating at 60 °C for 24 h.[16] It seems that the high reactivity of phosphorane (*A*) and phosphonate carbanion (*B*) can be attributed to the following reasons. These intermediates, especially *B*, can be classified as antiaromatic anions and hence high reactivity is expected toward carbonyl compounds, moreover, it is also probable in our case that some contribution of pseudoaromaticity (dithiolylium) to the product lowered the energy of the transition state, because that of Wittig reaction has been shown to lie at the decomposition of the betaine.[17]

In fact, Mikolajczyk *et al.*[18] and Kruse *et al.*[19] recently reported the preparation of di(thioalkyl)methylphosphonates and their use in Wittig-Horner reaction to give ketone dithioacetals in high yields at low temperatures. However, comparison of reactivity of carbanions of these phosphonates and *B* has not yet been done.

As described above, Wittig-Horner reaction of 2-dimethoxyphosphinyl-1,3-dithioles has been shown to be very useful for the synthesis of 1,4-dithiafulvenes which could not be synthesized by conventional methods or were obtained only in low yields. At the same time, some limitations (steric hindrance, *etc.*) of this new method were revealed.

*Wittig-Horner Reaction of 2-Dimethoxyphosphinyl-1,3-benzodithiole (**3a**) with Conjugated Cyclic Ketones: Synthesis of 1,4-Benzodithiafulvalenes (**6**).*[20] A new synthetic method for the preparation of **4** by Wittig-

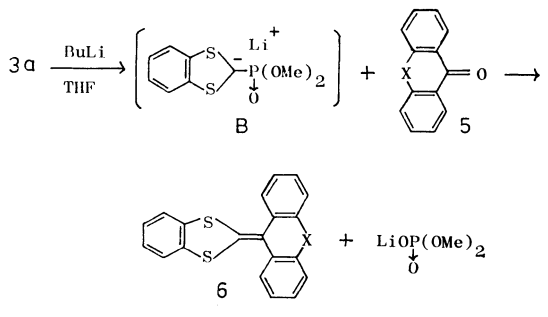

Scheme 3.

Horner reaction of **3a** was extended successfully to the preparation of 1,4-benzodithiafulvalenes (**6**). The phosphonate carbanion (*B*) derived from **3a** reacted with conjugated cyclic ketones (**5**) such as dibenzo-[a,d]cyclohepten-5-one, 9-thiaanthracen-10-one, 9-alkyl-9*H*-9-azaanthracen-10-one, 9-oxaanthracen-10-one (xanthone), 9-fluorenone, tetraphenylcyclopentadienone (tetracyclone), and so on, to afford 1,4-dithia-analogs of heptafulvalene or sesquifulvalene (**6**) in good yields. Yields and mp of **6** and UV spectral data of **6** and **5** are shown in Table 3.

It is noteworthy that all **6** were obtained by the same procedure irrespective of the nature of the carbonyl compounds (**5**), *i.e.*, group I (**5a**, **b**, **c**, **d**, and **e**) which

Table 3. Yields and mp of 1,4-benzodithiafulvalenes (**6**) and fulvenes (**4o**, **4p**) and UV spectral data of them and the corresponding ketones (**5**)

		Mp (°C)	**6** Y: 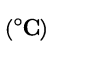		**5** Y: =O		
		Yield (%)	$\lambda_{max}^{CH_2Cl_2}$ a) (nm)	log ε	$\lambda_{max}^{CH_2Cl_2}$ a) (nm)	log ε	$\Delta\lambda$ b) (nm)
6a	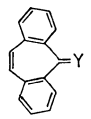	179.0—180.0 83	340 sh	4.15	361	3.89	−21
6b	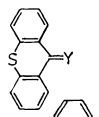	219.0—220.0 88	363	4.36	382	3.98	−19
6c	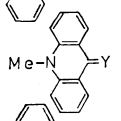	210.0—211.0 62	395	4.28	400	4.13	−5
6d	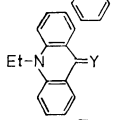	205.0—206.0 56	399	4.28	401	4.26	−2
6e	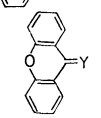	202.0—203.0 84	370	4.42	341.5	3.89	+28.5
6f	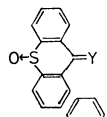	246.0—247.5 75	370	4.37	340	3.67	+30
6g	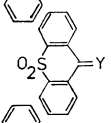	315.0—316.0 92	402	4.24	286	3.96	+116
6h	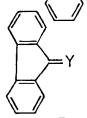	205.0—206.0 96	402 sh	4.66	327.5 sh	3.57	+74.5
6i	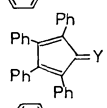	383.0—385.0 75	435	4.60	340	3.88	+95
6j	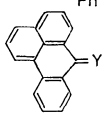	256.0—257.0 80	424	4.49	407 sh	4.06	+17
4o	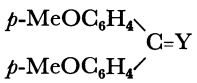	105.0—106.0 96	326	4.35	292	4.48	+34
4p	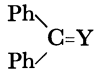	96.0— 97.0 80	329	4.34	252.5	4.34	+76.5
Cf.	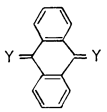	262.0—263.0 73	416	3.97	—	—	—

a) Only the longest absorption maximum, whose log ε are greater than 3.5 (probably ascribed to π-π^* excitation with CT character), is shown. See experimental section for other data. b) The difference of λ_{max} of the product (**6**) and the ketone (**5**) is shown, *i. e.*, $\Delta\lambda=\lambda_{max}(\mathbf{6})-\lambda_{max}(\mathbf{5})$

can be classified as π-excessive carbonyl compounds, group II (**5h**, **i**, and **j**) which can be classified as π-deficient carbonyl compounds, group III (**5o** and **p**) which are benzophenones.

The structures of these 1,4-benzodithiafulvalenes (**6**) were confirmed by means of the elemental analyses, IR, ^{1}H-NMR, UV, and mass spectra. All **6** showed reasonable IR and ^{1}H-NMR spectra without any significant characteristic features. The molecular ion peak in MS was the base peak in all **6** except for **6d** and **6f**. This fact shows large stability of the parent radical cations which are conjugated through the ring system. The parent peak of **6d** appeared at *m/e* 359 (72%) and the M^+-Et peak as the base peak. The parent peak of **6f** appeared at *m/e* 364 (48%) and the $M^+-C_7H_4OS_2$ ($C_{13}H_8S$) peak as the base peak.

A comparison of absorption maxima of the longest wave length in the UV spectra of compounds **5** and **6** with log $\varepsilon>3.5$ (probably to be ascribed to π-π^* excitation with CT character) reveals the following facts:

—In group I, the longest absorption of **6** is observed at a shorter wavelength than that of **5**, except for the case of **6e**.

—In groups II and III, the longest absorption of **6** and **4** is observed at a longer wavelength than that of **5**.

—In comparison of the data of the sulfides (**5b**/**6b**), the sulfoxides (**5f**/**6f**), and the sulfones (**5g**/**6g**), the distinct change is observed from the blue shift (−19 nm) to the red shifts (+30 and +116 nm) according to the increase of electron-withdrawing ability of the sulfur group.

—In the case of xanthone (**5e**/**6e**), the red shift which is almost equal to that of the sulfoxide is observed in spite of the presence of a lone pair of electrons on the oxygen atom.

These facts may be explained as follows, although assignment of each absorption has not been made. The facts obtained in group I may be understood by assuming that the resonance contribution of a polar structure to π^* state in **5a**—**d** is significant and thus the excitation energy is reduced, whereas the contribution of a polar structure to π^* state in **6a**—**d** is less significant due to the competition between the electron-donating power of the 1,3-benzodithiol-2-ylidene moiety and that of the other part of the molecule, *i.e.*, the π-excessive cyclic system containing vinyl, sulfur, or nitrogen group, and hence the excitation energy is enhanced relatively. This enhancement of the excitation energy due to the electron-donating power of the 1,3-benzodithiol-2-ylidene moiety appears to be stronger than the lowering of the excitation energy by the extenstion of the conjugated system in **6** by the inclusion of the 1,3-benzodithiol-2-ylidene group instead of the carbonyl oxygen atom. The latter effect should be common to groups I, II, and III.

The stretching frequency of a carbonyl group in IR is affected by the contribution of a polar structure to the ground state in a carbonyl compound, *i.e.*, the lower the frequency, the larger the polar character. Indeed, the carbonyl frequencies of group I compounds are lower compared with those of group II compounds

Table 4. The IR spectral data of some of the carbonyl compounds

Compounds	IR (KBr), $\nu_{C=O}$ (cm^{-1})	Group
5a	1630	I
5b	1630	I
5c	1625	I
5d	1625	I
5e	1670	I
5f	1675	—
5g	1680	—
5h	1700	II
5p	1660	III

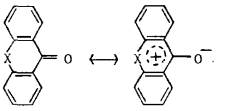

5a—e

due to the π-excessive character of the ring as shown in Table 4.

Carbonyl frequency of **5e** is very close to that of **5f**. This may be the reason for the exception of **5e**/**6e** (+28.5 nm shift) as a member of group I, that is, the contribution of the polar structure in **5e** is smaller than those in **5a**—**d** due to the large electronegativity of the ring oxygen and is almost the same as that by sulfoxide group of **5f** (+30 nm shift). The fact in the case of **5f,g**/**6f,g** can similarly be understood.

However, it has been shown that even tropone is a highly polyenic compound in the ground state with some contribution of a polar structure.[21] Hence, the degree of the contribution of the polar structure to the ground state in all these carbonyl compounds may not be so significant.

The findings obtained in groups II and III may be understood by assuming that the contribution of a polar structure to π^* state in **6h**—**j** is significant due to the electron-donating property of the 1,3-benzodithiolylidene moiety in concurrence with the electron-withdrawing property of the other part of the molecule, whereas the contribution of a polar structure to π^* in **5h**—**j** is less significant. The decrease in the excitation energy of **4o,p** as compared with **5o,p** may chiefly be ascribed to the extension of the conjugated system in **4o,p** by the inclusion of the 1,3-benzodithiolylidene group instead of the carbonyl oxygen atom.

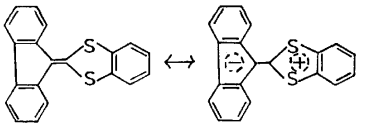

The assumption that the contribution of a polar structure to the ground state in **6** is not so significant was supported by the observed ESCA spectral data of **6a**, **b**, **c**, **e**, and **h** ($S_{2P\ 3/2}=163.1\pm0.3$ eV, respectively), which showed almost equal binding energy for all the sulfur atoms contained in a number of molecules.[22]

Neuenschwander *et al.*[23] reported also that the resonance contribution of a dipolar form is not significant in sesquifulvalene, fulvene, and heptafulvene,

which were shown to have a largely olefinic character from their ^{13}C-NMR spectral data and relatively small dipole moments.

Experimental

All the melting points are not corrected. IR spectra were measured with a Hitachi EPI-G2 spectrometer, ^1H-NMR spectra with Hitachi R-20B and Hitachi R-24 spectrometers (60 MHz, TMS as an internal standard), MS with a Hitachi RMU-6L mass spectrometer at 70 eV, and UV spectra with a Hitachi EPS-3 spectrophotometer. ^{31}P-NMR spectra were measured with a Hitachi R-20B-R-204-PB (24.3 MHz) spectrometer using 85% phosphoric acid as an external standard. ESCA spectra were recorded on a McPherson ESCA 36 electron spectrometer. The Al $K_{\alpha 1,2}$ line (1486.6 eV) provided the activation energy. The instrument was adjusted so that the Au-$4f_{7/2}$ line fell at 84.0 eV. Accuracy: $\pm$0.15 eV.

Materials. 1,3-Benzodithiolylium tetrafluoroborate (**1a**) was prepared according to the literature, mp 149—150 °C (dec) (lit,[24] mp 149—150 °C). 4,5-Dimethyl-1,3-dithiolylium tetrafluoroborate (**1b**), mp 123—125 °C (lit,[25,26] mp is not described), was prepared from 4,5-dimethyl-1,3-dithiole-2-thione[27] and 4-phenyl-1,3-dithiolylium tetrafluoroborate (**1c**), mp 143.5—145.5 °C (dec) (lit,[28] mp 161 °C for ClO_4^- and 180 °C for HSO_4^- salts), was prepared from 4-phenyl-1,3-dithiole-2-thione.[3]

Dibenzo[a,d]cyclohepten-5-one (**5a**) was a commercial material from Sakai Rikagaku Kenkyujyo, mp 88.0—89.0 °C; IR (KBr): 1630 cm^{-1} (C=O); UV (CH_2Cl_2): λ_{max}= 257 (log ε=4.92), 309.5 (4.47), and 361 nm (3.89).

10*H*-9-thiaanthracen-10-one (thioxanthone) (**5b**) was prepared from *o*-mercaptobenzoic acid and benzene by treatment with concentrated sulfuric acid, mp 214—215 °C (from EtOH) (lit,[29] mp 209 °C); IR (KBr): 1630 cm^{-1} (C=O); UV (CH_2Cl_2): λ_{max}=257.5 (log ε=4.74), 289 sh (3.89), 301 (3.86), 364 (3.90), and 382 nm (3.98).

9-Methyl-9,10-dihydro-9-azaanthracen-10-one (*N*-methylacridone) (**5c**) was prepared by the oxidation of *N*-methylacridinium salt with potassium hexacyanoferrate (III) in aqueous alkaline solution, mp 208—209 °C (lit, 199 °C[30] and 203 °C[31]); IR (KBr): 1625 cm^{-1} (C=O); UV (CH_2Cl_2): λ_{max}=258 (log ε=4.75), 268 sh (4.50), 277 (4.41), 293.7 (3.98), 306 (3.77), 361 sh (3.70), 380 (4.01), and 400 nm (4.13).

9-Ethyl-9,10-dihydro-9-azaanthracen-10-one (*N*-ethylacridone) (**5d**) was also prepared from *N*-ethylacridinium salt, mp 162.5—163.0 °C (lit,[31] 159 °C); IR (KBr): 1625 cm^{-1} (C=O); UV (CH_2Cl_2): 258 (log ε=4.84), 268 sh (4.54), 277 (4.45), 294 (3.87), 306 (3.76), 363 sh (3.81), 381 sh (4.12), and 401 nm (4.26).

10*H*-9-oxaanthracen-10-one (xanthone) (**5e**) was a commercial material, mp 173.0—174.0 °C (from EtOH); IR (KBr): 1670 cm^{-1} (C=O); UV (CH_2Cl_2): λ_{max}=239 (log ε= 4.70), 261.5 (4.15), 277 sh (3.68), 286.5 sh (3.69), 327 sh (3.81), and 341.5 nm (3.89).

10*H*-9-thiaanthracen-10-one 9-oxide (**5f**) was prepared by the oxidation of **5b** with *m*-chloroperbezoic acid (1.33 eq.) in dichloromethane at room temperature and separated from **5b** and its sulfone by dry column chromatography (SiO_2/CH_2Cl_2), yield 50% together with 30% of sulfone, mp 205—206 °C (lit,[32] 199—201 °C); IR (KBr): 1675 (C=O), 1040, and 1095 cm^{-1} (SO); UV(CH_2Cl_2): λ_{max}=284 sh (log ε= 4.17) and 340 nm (3.67).

10*H*-9-thiaanthracen-10-one 9,9-dioxide (**5g**) was prepared by the oxidation of **5b** with *m*-chloroperbenzoic acid (2 eq.) in dichloromethane at room temperature, yield 90%; mp 190.0—191.0 °C (lit,[33] 185.5—186 °C); IR (KBr): 1680, 1310, 1300, 1170, and 1145 cm^{-1} (SO_2); UV (CH_2Cl_2): λ_{max}=286 sh (log ε=3.96); (CH_3CN): λ_{max}=229.5 (log ε= 4.32), 237 sh (4.23), 254 sh (3.88), 263 (3.89), and 283 nm (3.89).

9-Fluorenone (**5h**) was a commercial material, mp 83.0—84.0 °C (from PhH-EtOH); IR (KBr): 1700 cm^{-1} (C=O); UV (CH_2Cl_2): λ_{max}=250.5 (log ε=4.91), 259 (5.15), 284.5 sh (3.84), 296 (3.90), 311.5 sh (3.72), 327.5 sh (3.57), 358 sh (2.43), 378 (2.50), and 398 sh nm (2.46).

Tetraphenylcyclopentadienone (**5i**) was prepared by the reported method, mp 218—220 °C (lit,[34] mp 218—220 °C); UV (CH_2Cl_2): λ_{max}=262 (log ε=4.46), 340 (3.88), and 510 nm (3.03); (CH_3CN): λ_{max}=260 (log ε=4.40) and 338 nm (3.79); (CH_3CN with HBF_4): λ_{max}=258.5 (log ε= 4.40), 337 (3.81), and 502 nm (3.09).

7*H*-benz[d,e]anthracen-7-one (**5j**) was a commercial material, mp 169.0—170.0 °C (from PhH-EtOH); UV (CH_2Cl_2): λ_{max}=231.5 (log ε=4.60), 237 (4.56), 242 (4.51), 254 (4.46), 276 sh (4.06), 285 (4.07), 310 (4.03), 338 sh (3.66), 355 sh (3.86), 389 (4.13), and 407 sh (4.06).

10,10-Dibenzyl-9(10*H*)-anthracenone was prepared by refluxing 9(10*H*)-anthracenone and benzyl chloride with aq. sodium hydroxyde in THF, mp 232.0—233.0 °C. IR (KBr): 1650 cm^{-1} (C=O).

*Preparation of 2-Phosphonio-1,3-dithiole Salts (**2**). General Procedure*: Tertiary phosphine (10 mmol) was added to a stirred solution of 1,3-dithiolylium tetrafluoroborate (**1**: 10 mmol) in dry acetonitrile (50 ml) at room temperature. After stirring for 2 h, the solvent was evaporated to about 10 ml under reduced pressure. Dry ether (50 ml) was added to the residue and the precipitates were collected, washed with ether, and recrystallized from ethanol.

2-Triphenylphosphonio-1,3-benzodithiole tetrafluoroborate (**2a**), yield 87%; mp 211.5—212.5 °C (dec); IR (KBr): 1140—1020 and 520 (BF_4^-), 1430, 770, 760, 750, 740, 730, 720, 700, and 690 cm^{-1}; ^1H-NMR (DMSO-d_6): δ 6.7—7.3 (m, 5H, aromatic and 2-CH), and 7.3—8.2 (m, 15H, aromatic).

Found: C, 59.94; H, 4.05%. Calcd for $C_{25}H_{20}BF_4PS_2$: C, 59.78; H, 4.01%.

2-Tributylphosphonio-1,3-benzodithiole tetrafluoroborate (**2b**), yield 90%; mp 166.5—168.0 °C; IR (KBr): 1140—1020 and 520 (BF_4^-), 1440, and 760 cm^{-1}; ^1H-NMR (DMSO-d_6): δ 0.5—2.5 (m, 27H, *n*-Bu), 6.42 (bs, 1H, PCH), and 7.0—7.6 (m, 4H, aromatic).

Found: C, 51.30; H, 7.52%. Calcd for $C_{19}H_{32}BF_4PS_2$: C, 51.59; H, 7.29%.

4,5-Dimethyl-2-triphenylphosphonio-1,3-dithiole tetrafluoroborate (**2c**), yield 84%; mp 175.0—177.0 °C (dec); IR (KBr): 1120—1140 and 520 (BF_4^-), 1430, 750, 730, 720, and 690 cm^{-1}; ^1H-NMR (DMSO-d_6): δ 1.30 (s, 6H, 4- and 5-Me), 7.35 (bs, 1H, 2-CH), and 7.2—8.4 (m, 15H, aromatic).

Found: C, 57.29; H, 4.65%. Calcd for $C_{23}H_{22}BF_4PS_2$: C, 57.51; H, 4.62%.

*Preparation of 2-Dialkoxyphosphinyl-1,3-dithiole (**3**). General Procedure*: Trialkyl phosphite (10 mmol) and sodium iodide (1.5 g, 10 mmol) were added successively to a stirred solution of 1,3-dithiolylium tetrafluoroborate (10 mmol) in dry acetonitrile (50 ml) under a nitrogen atmosphere at room temperature . The reaction took place rapidly and was slightly exothermic. Stirring was continued for about 30 min, and the solvent was evaporated *in vacuo*. The residue was extracted with dichloromethane (30 ml×3) after addition of water (50 ml). The combined extracts were

dried over anhydrous magnesium sulfate and dichloromethane was removed under reduced pressure. The residue was recrystallized from ethyl acetate or ethanol to give 2-dialkoxyphosphinyl-1,3-dithiole.

2-Dimethoxyphosphinyl-1,3-benzodithiole (**3a**), yield 80%; mp 122.0—123.0 °C (from EtOH); IR (KBr): 1260 (P=O), 1050, and 1035 cm^{-1} (P-O-C): ^{1}H-NMR ($CDCl_3$): δ 3.63 (d, J_{POCH}=10.4 Hz, 6H, $POCH_3$), 4.75 (d, J_{PCH}=5.8 Hz, 1H, PCH), and 6.7—7.3 (m, 4H, aromatic); ^{31}P-NMR ($CDCl_3$): δ_P −19 ppm; MS: *m/e* 262 (M^+, 8%), 153 ($M^+-P(O)(OMe)_2$, 100), and 77 (Ph^+, 21).

Found: C, 41.01; H, 4.14; S, 24.40%. Calcd for $C_9H_{11}O_3PS_2$: C, 41.21; H, 4.23; S, 24.45%.

2-Diethoxyphosphinyl-1,3-benzodithiole (**3b**), yield 95%; mp 115.5—116.5 °C (from EtOH); IR (KBr): 1250 (P=O), 1050, and 1030 cm^{-1} (P-O-C); ^{1}H-NMR ($CDCl_3$): δ 1.22 (t, J_{HCCH}=6.8 Hz, 6H, $POCCH_3$), 4.15 (dq, J_{POCH}=7.7, J_{HCCH}=6.8 Hz, 4H, $POCH_2$), 4.89 (d, J_{PCH}=5.2 Hz, 1H, PCH), and 6.9—7.3 (m, 4H, aromatic). The triplet signal at δ 1.22 of $POCCH_3$ was irradiated to give a doublet signal at δ 4.15 for $POCH_2$ with a coupling constant of 7.7 Hz. MS: *m/e* 290 (M^+, 4.4%), 153 ($M^+-P(O)(OEt)_2$, 100), and 77 (Ph^+, 23).

Found: C, 45.43; H, 5.25; S, 22.21%. Calcd for $C_{11}H_{15}O_3PS_2$: C, 45.51; H, 5.21; S, 22.09%.

4,5-Dimethyl-2-dimethoxyphosphinyl-1,3-dithiole (**3c**); After usual work-up, the product was submitted to dry column chromatography over neutral alumina (activity III) with dichloromethane. The fraction (R_f 0.2—0.4) was eluted with ethyl acetate to give 83% yield of **3c**. This compound has low melting point (<20 °C), and is so hygroscopic and sensitive to air in an oily state or in solution that it could not be purified enough for elemental analysis. IR (neat): 1255 (P=O), 1180, 1055, and 1030 cm^{-1}; ^{1}H-NMR (CCl_4): δ 1.83 (s, 6H, 4,5-dimethyl), 3.80 (d, J_{POCH}=10.4 Hz, 6H, $POCH_3$), and 4.73 (d, J_{PCH}=4.5 Hz, 1H, PCH).

Found: C, 33.52; H, 5.23%. Calcd for $C_7H_{13}O_3PS_2$: C, 34.99, H, 5.45%.

2-Dimethoxyphoshinyl-4-phenyl-1,3-dithiole (**3d**), yield 90%; mp 87.0—88.0 °C (from AcOEt); IR (KBr): 1255 (P=O), 1180, 1065, and 1040 cm^{-1}; ^{1}H-NMR ($CDCl_3$): δ 3.89 (d, J_{POCH}=10.5 Hz, 6H, $POCH_3$), 5.06 (d, J_{PCH}=4.5 Hz, 1H, PCH), 6.24 (s, 1H, 5-CH), and 7.2—7.5 (m, 5H, aromatic); MS: *m/e* 288 (M^+, 9.4%), 179 ($M^+-P(O)(OMe)_2$, 100); metastable ion, found: 111.3, calcd for 288→179: 111.25.

Found: C, 45.82; H, 4.55; S, 21.91%. Calcd for $C_{11}H_{13}O_3PS_2$: C, 45.82; H, 4.54; S, 22.24%.

Wittig Reaction of (1,3-Benzodithiol-2-ylidene)triphenylphosphorane (Method A). General Procedure: To a suspension of 2-triphenylphosphonio-1,3-benzodithiole tetrafluoroborate (**2a**) (1.005 g, 2.0 mmol) in THF (50 ml) was added butyllithium in hexane (1.5 ml, 2.3 mmol) at −78 °C under a nitrogen atmosphere with stirring. Stirring was continued for 2.0—2.5 h to give a dark red solution of (1,3-benzodithiol-2-ylidene)triphenylphosphorane (*A*). A carbonyl compound (2.0 mmol) was added at −78 °C. Immediately the dark red color of the solution turned yellow. The mixture was allowed to get warm to room temperature and the solvent was evaporated under reduced pressure. The residue was extracted with dichloromethane (30 ml×3) after addition of water (50 ml). The combined extracts were dried over anhydrous magnesium sulfate, dichloromethane was removed under reduced pressure, and the residue was submitted to dry column chromatography over silica gel (activity III) with carbon tetrachloride as a developing solvent. The fraction of R_f value 0.7—0.9 was eluted with dichloromethane or ether to give 2-alkylidene-1,3-benzodithiole (**4**) and the fraction of R_f value 0.1—0.2 was eluted with ethyl acetate to give triphenylphosphine oxide.

Reaction of **2a** with *p*-anisaldehyde gave triphenylphosphine oxide, yield 75%, mp 155.0—156.0 °C (from AcOEt), and 2-(*p*-methoxyphenylmethylene)-1,3-benzodithiole (**4b**), yield 77%; mp 144.5—145.5 °C (from ErOH-Et_2O); IR (KBr): 1250, 1180, and 1040 cm^{-1}; ^{1}H-NMR ($CDCl_3$): δ 3.83 (s, 3H, OCH_3), 6.51 (s, 1H, olefinic), and 6.8—7.6 (m, 8H, aromatic); MS: *m/e* 272 (M^+, 88%), 257 (M^+-Me, 100), and 229 (257−CO, 26).

Found: C, 66.17; H, 4.38; S, 23.36%. Calcd for $C_{15}H_{12}OS_2$: C, 66.14; H, 4.44; S, 23.54%.

Reaction of **2a** with *p*-tolualdehyde gave triphenylphosphine oxide (74%) and 2-(*p*-tolylmethylene)-1,3-benzodithiole (**4c**), yield 75%; mp 149.5—151.0 °C (from EtOH); IR (KBr): 1580, 1550, 1445, 1430, 1130 and 930 cm^{-1}; ^{1}H-NMR ($CDCl_3$): δ 2.33 (s, 3H, Me), 6.51 (s, 1H, olefinic), and 6.9—7.5 (m, 8H, aromatic); MS: *m/e* 256 (M^+, 100%), 140 ($C_6H_4S_2^{+\cdot}$, 14), 128 (M^{2+}, 14), and 115 ($M^+-C_6H_5S_2$, 20).

Found: C, 70.52; H, 4.58; S, 24.88%. Calcd for $C_{15}H_{12}S_2$: C, 70.27; H, 4.72; S, 25.01%.

Reaction of **2a** with benzaldehyde gave triphenylphosphine oxide (72%) and 2-benzylidene-1,3-benzodithiole (**4d**), yield 74%; mp 133.0—134.5 °C (from EtOH); IR (KBr): 1580, 1470, and 1430 cm^{-1}; ^{1}H-NMR ($CDCl_3$): δ 6.60 (s, 1H, olefinic) and 7.0—7.6 (m, 9H, aromatic); MS: *m/e* 242 (M^+, 100%), 165 (M^+-Ph, 18), 140 ($C_6H_4S_2^{+\cdot}$, 39), 121 (M^{2+}, 37), and 108 (140−S, 18).

Found: C, 69.25; H, 4.10; S, 26.33%. Calcd for $C_{14}H_{10}S_2$: C, 69.38; H, 4.16; S, 26.46%.

Reaction of **2a** with *p*-chlorobenzaldehyde gave triphenylphosphine oxide (79%) and 2-(*p*-chlorophenylmethylene)-1,3-benzodithiole (**4e**), yield 82%; mp 190.0—190.8 °C (from EtOH); IR (KBr): 1580, 1540, and 1100 cm^{-1}; ^{1}H-NMR ($CDCl_3$ with CF_3CO_2H[35]): δ 5.05 (s, 2H, benzyl proton), 7.1—7.7 (m, 4H, aromatic), and 7.8—8.7 (m, 4H, aromatic); MS: *m/e* 278 (M^+ for ^{37}Cl, 47%), 277 (M^+-1, 24), 276 (M^+, for ^{35}Cl, 100), 240 (M^+-HCl, 24), and 140 ($C_6H_4S_2^{+\cdot}$, 47).

Found: C, 60.52; H, 3.21; S, 22.89; Cl, 12.99%. Calcd for $C_{14}H_9S_2Cl$: C, 60.75; H, 3.28; S, 23.17; Cl, 12.81%.

Reaction of **2a** with cinnamaldehyde gave triphenylphosphine oxide (80%) and 2-(3-phenyl-2-propenylidene)-1,3-benzodithiole (**4f**), yield 78%; mp 148.0—149.0 °C (from EtOH-Et_2O); IR (KBr): 1570, 1540, 960, and 950 cm^{-1}; ^{1}H-NMR ($CDCl_3$): δ 5.9—6.8 (m, 3H, olefinic) and 6.8—7.5 (m, 9H, aromatic); MS: *m/e* 268 (M^+, 94%), 140 ($C_6H_4S_2^{+\cdot}$, 23), 134 (M^{2+}, 20), and 128 ($M^+-C_6H_4S_2^{+\cdot}$, 100).

Found: C, 71.60; H, 4.39; S, 24.02%. Calcd for $C_{16}H_{12}S_2$: C, 71.60; H, 4.51; S, 23.89%.

Reaction of **2a** with *p*-dimethylaminobenzaldehyde did not proceed and a red color of the phosphorane did not disappear up to room temperature. Therefore, the solution was refluxed for 30 min, when the solution slightly darkend. Many products were observed by TLC, however, the expected product (**4a**) could not be isolated.

Wittig-Horner Reaction of 2-Dimethoxyphosphinyl-1,3-benzodithiole (3a) (Method B). General Procedure: Butyllithium in hexane (1.5 ml, 2.3 mmol) was added to a stirred solution of 2-dimethoxyphosphinyl-1,3-benzodithiole (**3a**) (524.6 mg, 2.0 mmol) in THF (20 ml) at −78 °C under a nitrogen atmosphere. After 10 min, a carbonyl compound (2.0 mmol) was added to the yellow solution of the resulting phosphonate carbanion (*B*). The mixture was stirred for 10 min at −78 °C, allowed to get warm to room temperature,

and THF was evaporated under reduced pressure. The residue was extracted with dichloromethane (30 ml×3) after addition of water (50 ml). The combined extracts were dried over anhydrous magnesium sulfate, dichloromethane removed under reduced pressure, and the residue was recrystallized from an appropriate solvent to give the corresponding 2-alkylidene-1,3-benzodithiole (1,4-benzodithiafulvene) (**4**).

Reaction of **3a** with *p*-dimethylaminobenzaldehyde gave 2-(*p*-dimethylaminophenylmethylene)-1,3-benzodithiole (**4a**), yield 95%; mp 145.0—146.0 °C (from EtOH); IR (KBr): 1600, 1510, 1440, and 1360 cm^{-1}; ^{1}H-NMR ($CDCl_3$): δ 2.97 (s, 6H, N-CH_3), 6.47 (s, 1H, olefinic), and 6.6—7.4 (m, 8H, aromatic); MS: *m/e* 285 (M^+, 100%), 270 (M^+ —Me, 28), 240 (M^+ —Me_2NH, 10), and 142.5 (M^{2+}, 26): metastable ion, found: 255.5, calcd for 285→270: 255.7.

Found: C, 66.81; H, 5.21; N, 4.82: S, 22.60%. Calcd for $C_{16}H_{15}NS_2$: C, 67.33; H, 5.30; N, 4.91; S, 22.47%.

Reaction of **3a** with *p*-tolualdehyde gave 2-(*p*-tolylmethylene)-1,3-benzodithiole (**4c**), yield 94%; mp 150.0—151.0 °C (from EtOH).

Reaction of **3a** with *trans*-2-butenal gave 2-(2-butenylidene)-1,3-benzodithiole (**4g**), yield 95%; mp 72.0—73.0 °C (from ethanol–hexane); IR (KBr): 1540, 1440, 1430, and 960 cm^{-1}; ^{1}H-NMR ($CDCl_3$): δ 1.79 (d, J_{HCCH}=6.0 Hz, 3H, CH_3), 5.2—6.3 (m, 3H, olefinic), and 6.9—7.4 (m, 4H, aromatic); MS: *m/e* 206 (M^+, 100%), 205 (M^+—H, 31), 179 (205—C_2H_2, 39), and 140 ($C_6H_4S_2^{+\cdot}$, 39).

Found: C, 63.53; H, 4.83; S, 31.00%. Calcd for $C_{11}H_{10}S_2$: C, 64.03; H, 4.89; S, 31.08%.

Reaction of **3a** with cyclopentanone gave 2-cyclopentylidene-1,3-benzodithiole (**4h**), yield 96%; mp 105.5—107.0 °C (from EtOH); IR (KBr): 1440, 1420, and 1120 cm^{-1}; ^{1}H-NMR ($CDCl_3$): δ 1.4—2.6 (m, 8H, aliphatic)and 6.7—7.4 (m, 4H, aromatic); MS: *m/e* 220 (M^+, 100%), 219 (M^+—H, 31), 192 (M^+—C_2H_4, 97), 179 (M^+—C_3H_5, 14), 166 (M^+—C_4H_6, 23), and 153 (M^+—C_5H_7, 29).

Found: C, 65.43; H, 5.44; S, 29.04%. Calcd for $C_{12}H_{12}S_2$: C, 65.41; H, 5.49; S, 29.10%.

Reaction of **3a** with cyclohexanone gave 2-cyclohexylidene-1,3-benzodithiole (**4i**), yield 98%; mp 96.0—97.5 °C (from EtOH); IR (KBr): 1420, 1120, and 740 cm^{-1}; ^{1}H-NMR ($CDCl_3$): δ 1.2—1.8 (m, 6H, 3′-CH_2, 4′-CH_2 and 5′-CH_2), 1.8—2.2 (m, 4H, 2′-CH_2 and 6′-CH_2), and 6.7—7.3 (m, 4H, aromatic); MS: *m/e* 234 (M^+, 100%), 233 (M^+—H, 21), 205 (233—C_2H_4, 39), 179 (M^+—C_4H_7, 31), 166 (M^+—C_5H_8, 31), and 153 (M^+—C_6H_9, 53).

Found: C, 66.37; H, 6.28; S, 27.24%. Calcd for $C_{13}H_{14}S_2$: C, 66.62; H, 6.02; S, 27.36%.

Reaction of **3a** with 3,5,5-trimethyl-2-cyclohexen-1-one gave 2-(3,5,5-trimethyl-2-cyclohexenylidene)-1,3-benzodithiole (**4j**), yield 87%; mp 99.0—100.0 °C (from EtOH); IR (KBr): 1560, 1540, 1440, 1420, and 1120 cm^{-1}; ^{1}H-NMR ($CDCl_3$): δ 0.95 (s, 6H, 5′,5′-dimethyl), 1.7—1.95 (m, 5H, 3′-CH_3 and 4′-CH_2), 1.97 (s, 2H, 6′-CH_2), 5.85—5.95 (m, 1H, 2′-CH), and 6.9—7.4 (m, 4H, aromatic). The multiplet signal at δ 1.7—1.95 was irradiated to give a singlet signal at δ 5.9 for 2′-CH. Protonation occurred at 3′-position, giving a conjugated cation; ^{1}H-NMR ($CDCl_3$ with CF_3CO_2H): δ 1.02 (s, 3H, 5′-CH_3), 1.20 (s, 3H, 5′-CH_3), 1.29 (d, J_{HCCH}=6.8 Hz, 3H, 3′-CH_3), 1.5—1.75 (m, 2H, 4′-CH_2), 2.47 (br s, 2H, 6′-CH_2), 2.6—2.9 (m, 1H, 3′-CH), 7.58 (br s, 1H, 2′-H), and 7.8—8.5 (m, 4H, aromatic). MS: *m/e* 274 (M^+, 100%), 259 (M^+—Me, 36), 231 (259—C_2H_4, 13), 153 (M^+—C_9H_{13}, 44), and 121 (C_9H_{13}, 23); metastable ion, found, 244.9, calcd for 274→259: 244.8.

Found: C, 69.95; H, 6.61; S, 23.05%. Calcd for $C_{16}H_{18}S_2$: C, 70.02; H, 6.61; S, 23.37%.

Reaction of **3a** with benzylideneacetone gave 2-(1-methyl-3-phenyl-2-propenylidene)-1,3-benzodithiole (**4k**), yield 96%; mp 170.0—171.0 °C (from EtOH); IR (KBr): 955, 750, and 695 cm^{-1}; ^{1}H-NMR ($CDCl_3$): δ 1.99 (s, 3H, 1′-CH_3), 6.44 (d, J_{HCCH}=16 Hz, 1H, olefinic), 7.03 (d, J_{HCCH}=16 Hz, 1H olefinic), and 7.0—7.7 (m, 9H, aromatic); MS: *m/e* 282 (M^+, 100%), 153 (M^+—PhC_4H_4, 30), 142 (M^+—$C_6H_4S_2$, 71), and 141 (142—H, 44); metastable ion, found: 71.6, calcd for 282→142: 71.5.

Found: C, 72.14; H, 4.89; S, 22.39%. Calcd for $C_{17}H_{14}S_2$: C, 72.30; H, 5.00; S, 22.71%.

Reaction of **3a** with *p*-methylacetophenone gave 2-(1-*p*-tolylethylidene)-1,3-benzodithiole (**4l**), yield 92%; mp 80.0—81.0 °C (from EtOH); ^{1}H-NMR ($CDCl_3$): δ 2.15 (s, 3H, 2′-CH_3), 2.38 (s, 3H, ArMe), and 6.8—7.5 (m, 8H, aromatic); MS: *m/e* 270 (M^+, 100%), 269 (M^+—H, 31), 255 (M^+—Me, 8), 179 (M^+—tolyl, 17), and 153 (M^+—C_9H_9, 33); metastable ion, found: 240.9, calcd for 270→255: 240.8.

Found: C, 70.96; H, 5.18; S, 23.86%. Calcd for $C_{16}H_{14}S_2$: C, 71.07; H, 5.22; S, 23.71%.

Reaction of **3a** with acetophenone gave the crude product which was submitted to dry column chromatography over silica gel with carbon tetrachloride as an eluent to afford oily 2-(1-phenylethylidene)-1,3-benzodithiole (**4m**), yield 94%; IR (neat): 3050, 1590, 1435, 1130, and 1035 cm^{-1}; ^{1}H-NMR (CCl_4): δ 2.09 (s, 3H, CH_3) and 6.7—7.5 (m, 9H, aromatic); MS: *m/e* 256 (M^+, 100%), 255 (M^+—H, 17), 179 (M^+—Ph, 12), and 153 (M^+—C_8H_7, 11); metastable ion, found: 125.1, calcd for 256→179: 125.16.

Found: C, 70.12; H, 4.67; S, 24.88%. Calcd for $C_{15}H_{12}S_2$: C, 70.27; H, 4.72; S, 25.01%.

Reaction of **3a** with *p*-chloroacetophenone gave 2-(1-*p*-chlorophenylethylidene)-1,3-benzodithiole (**4n**), 91%; mp 97.0—98.0 °C (from hexane); IR (KBr): 1580, 1480, 1425, 1095, and 1015 cm^{-1}; ^{1}H-NMR (CCl_4): δ 2.10 (s, 3H, CH_3) and 6.7—7.4 (m, 8H, aromatic); MS: *m/e* 292 (M^+, for ^{37}Cl, 39%), 291 (M^+—H, 30), 290 (M^+, for ^{35}Cl, 100), 289 (M^+—H, 30), 255 (M^+—Cl, 12), and 153 (M^+—C_8H_6Cl, 31); metastable ion, found 224.2, calcd for 290→255: 224.2.

Found: C, 62.25; H, 3.72; S, 22.07%. Calcd for $C_{15}H_{11}S_2Cl$: C, 61.95; H, 3.81; S, 22.05%.

Reaction of **3a** with 4,4′-dimethoxybenzophenone gave 2-[bis(*p*-methoxyphenyl)methylene]-1,3-benzodithiole (**4o**), yield 96%; mp 105.0—106.0 °C (from ethyl acetate and hexane); IR (KBr): 1600, 1495, 1240, 1170, 1030 cm^{-1}; UV (CH_2Cl_2): λ_{max}=247 (logε=4.55), 256 sh (4.49), 326 nm (4.35); ^{1}H-NMR (CCl_4): δ 3.78 (s, 6H, OCH_3), 6.78 (d, J=8.6 Hz, 4H, aromatic), 7.00 (br s, 4H, aromatic), and 7.20 (d, J=8.6 Hz, 4H, aromatic); MS: *m/e* 378 (M^+, 100%) and 363 (M^+—Me, 43); metastable ion, found: 349.0, calcd for 378→363: 348.6.

Found: C, 69.76; H, 4.60; S, 17.21%. Calcd for $C_{22}H_{18}O_2S_2$: C, 69.81; H, 4.79; S, 16.94%.

Reaction of **3a** with benzophenone gave 2-(diphenylmethylene)-1,3-benzodithiole (**4p**), yield 80%; mp 96.0—97.0 °C (from ethyl acetate and hexane); IR (KBr): 1570, 1535, 1435, and 1130 cm^{-1}; UV (CH_2Cl_2): λ_{max}=244 (log ε=4.51), 252 sh (4.43), and 329 nm (4.34); MS: *m/e* 318 (M^+, 100%) and 178 (M^+—$C_6H_4S_2$, 36).

Found: C, 75.15; H, 4.29; S, 20.09%. Calcd for $C_{20}H_{14}S_2$: C, 75.43; H, 4.43; S, 20.14%.

Reaction of **3a** with 4,4′-dichlorobenzophenone gave 2-[bis(*p*-chlorophenyl)methylene]-1,3-benzodithiole (**4p**), yield 95%; mp 113.0—114.0 °C (from EtOH); IR (KBr): 1480, 1100, and 1020 cm^{-1}; ^{1}H-NMR ($CDCl_3$): δ 7.1 (br s, 4H, aromatic) and 7.3 (br s, 8H, aromatic); MS: *m/e* 390 (M^+,

for two ^{37}Cl, 18%), 389 (17), 388 (M^+, for one ^{37}Cl and one ^{35}Cl, 68), 387 (23), and 386 (M^+ for two ^{35}Cl, 100); ESCA: $S_{2P\,3/2}=163.1\pm0.15$ eV.

Found: C, 61.98; H, 3.42; S, 16.70; Cl, 18.50%. Calcd for $C_{20}H_{12}S_2Cl_2$: C, 62.02; H, 3.12; S, 16.56; Cl, 18.31%.

Reaction of **3a** with 3-buten-2-one gave crude 2-(1-methyl-2-propenylidene-1,3-benzodithiole (**4r**), yield 53%; mp 87.0—89.0 °C (from ethanol and hexane); IR (KBr): 1595, 1440, and 1425 cm^{-1}; ^1H-NMR ($CDCl_3$): δ 1.86 (s, 3H, CH_3), 4.8—5.3 (m, 2H, olefinic CH), 6.2—6.8 (m, 1H, olefinic CH), and 6.8—7.4 (m, 4H, aromatic); MS: *m/e* 206 (M^+, 100%), 205 (M^+-H, 31), 179 ($M^+-C_2H_3$, 26), 166 ($M^+-C_3H_4$, 91), and 153 ($M^+-C_4H_5$, 21); metastable ion, found: 133.9, calcd for 206→166: 133.8. This compound was not so stable as to give an analytically pure sample.

Reaction of **3a** with acetaldehyde in 1.0 mmol scale gave a crude product (170 mg). However, purification by preparative thin-layer chromatography (SiO_2/CCl_4) afforded only a trace amount of a dimeric compound. The structure of the compound was proposed to be shown below from its ^1H-NMR spectral data. ^1H-NMR (CCl_4): δ 1.07 (t, J= 7 Hz, 3H, $-C-CH_3$), 1.99 (s, 3H, CH_3), 2.42 (q, J=7 Hz, 2H, CH_2-C), and 6.7—7.6 (m, 8H, aromatic).

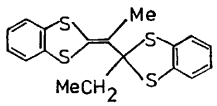

Reaction of **3a** with 9(10*H*)-anthracenone gave a reaction mixture which was submitted to dry column chromatography over neutral alumina with dichloromethane to give 9,10-anthracenedione (73%, mp 285 °C) together with recovered **3a** (41%).

Reaction of **3a** with 10,10-dibenzyl-9(10*H*)-anthracenone did not take place even under reflux for 30 min. A large amount of the ketone was recovered (70—80%).

Reaction of 2-dimethoxyphosphinyl-4-phenyl-1,3-dithiole (**3d**) with 4,4'-dichlorobenzophenone in 1.0 mmol scale gave 4-phenyl-2-[bis(*p*-chlorophenyl)methylene]-1,3-dithiole, yield 83%; mp 183.5—185.0 °C (from methanol and hexane); IR (KBr): 1480, 1100, 1090, and 1020 cm^{-1}; ^1H-NMR ($CDCl_3$): δ 6.40 (s, 1H, olefinic) and 7.2—7.5 (m, 13H, aromatic); MS: *m/e* 416 (M^+ for two ^{37}Cl, 15%), 415 (16), 414 (M^+, for one ^{37}Cl and one ^{35}Cl, 74), 413 (22), and 412 (M^+ for two ^{35}Cl, 100).

Found: C, 64.07; H, 3.20; Cl, 16.65%. Calcd for $C_{22}H_{14}S_2Cl_2$: C, 63.92; H, 3.41; Cl, 17.15%.

Reaction of **3a** with dibenzo[a,d]cyclohepten-5-one (**5a**) gave 2-(dibenzo[a,d]cyclohepten-5-ylidene)-1,3-benzodithiole (**6a**), yield 83%; mp 179.0—180.0 °C (from EtOH); IR (KBr): 1570, 1440, 1425, and 1125 cm^{-1}; UV (CH_2Cl_2): λ_{max}=232 (log ε=4.73), 273 (4.39), 299 (4.37), and 340 sh nm (4.15); ^1H-NMR ($CDCl_3$): δ 6.83 (s, 2H, olefinic), 7.00 (s, 4H, aromatic), 7.2—7.7 (m, 8H, aromatic); MS: *m/e* 342 (M^+, 100%), 308 (M^+-H_2S, 16), 234 ($M^+-C_6H_4S$, 13), 202 ($M^+-C_6H_4S_2$, 35), and 189 ($M^+-C_7H_5S_2$, 35); ESCA: $S_{2P\,3/2}=163.3\pm0.15$ eV.

Found: C, 77.38; H, 3.93; S, 18.54%. Calcd for $C_{22}H_{14}S_2$: C, 77.16; H, 4.12; S, 18.72%.

Reaction of **3a** with 10*H*-9-thiaanthracen-10-one (**5b**) gave 10-(1,3-benzodithiol-2-ylidene)-10*H*-9-thiaanthracene (**6b**), yield 88%; mp 219.0—220.0 °C (from EtOH); IR (KBr): 1525, 1445, 1425, and 1125 cm^{-1}; UV (CH_2Cl_2): λ_{max}=243.5 (logε=4.69), 270.5 sh (4.16), 312 sh (4.05), and 363 nm (4.36); MS: *m/e* (M^+, 100%); ESCA: $S_{2P\,3/2}=162.9\pm0.15$ eV.

Found: C, 68.73; H, 3.54%. Calcd for $C_{20}H_{12}S_3$: C, 68.93; H, 3.47%.

Reaction of **3a** with 9-methyl-9,10-dihydro-9-azaanthracen-10-one (**5c**) in 1.0 mmol scale gave 9-methyl-10-(1,3-benzodithiol-2-ylidene)-9,10-dihydro-9-azaanthracene (**6c**) yield 62%; mp 210.0—211.0 °C (from EtOH). Refluxing of the mixture (30 min) was necessary to effect the reaction. IR (KBr): 1455, 750, and 740 cm^{-1}; UV (CH_2Cl_2): λ_{max}=238 (logε=4.77), 262.5 sh (4.26), 314 (4.18), 395 nm (4.30); ^1H-NMR ($CDCl_3$): δ 3.39 (s, 3H, $N-CH_3$) and 6.8—7.7 (m, 12H, aromatic); MS: *m/e* 345 (M^+, 100%), 330 (M^+-Me, 77), 222 ($330-C_6H_4S$, 10), and 172.5 (M^{2+}, 12); ESCA: $S_{2P\,3/2}=162.9\pm0.15$ eV.

Found: C, 72.90; H, 4.38; N, 4.31; S, 18.68%. Calcd for $C_{21}H_{15}NS_2$: C, 73.01; H, 4.38; N, 4.05; S, 18.56%.

Reaction of **3a** with 9-ethyl-9,10-dihydro-9-azaanthracen-10-one (**5d**) in 1.0 mmol scale gave 9-ethyl-10-(1,3-benzodithiol-2-ylidene)-9,10-dihydro-9-azaanthracene (**6d**), yield 56%; mp 205.0—206.0 °C (from EtOH). Refluxing of the mixture was necessary to effect the reaction. IR (KBr): 1455, 1445, and 1260 cm^{-1}; UV (CH_2Cl_2): λ_{max}=238 (logε= 4.73), 263 sh (4.26), 314 (4.18), and 399 nm (4.28); ^1H-NMR ($CDCl_3$): δ 1.43 (t, J=6.8 Hz, 3H, $N-C-CH_3$), 4.03 (q, J= 6.8 Hz, 2H, $N-CH_2-C$), and 6.9—7.7 (m, 12H, aromatic); MS: *m/e* 359 (M^+, 72%), 330 (M^+-Et, 100), and 296 ($330-H_2S$, 9); metastable ion, found: 303.3, calcd for 359→330: 303.3.

Found: C, 73.60; H, 4.78; N, 3.84; S, 17.50%. Calcd for $C_{22}H_{17}NS_2$: C, 73.50; H, 4.77; N, 3.90; S, 17.84%.

Reaction of **3a** with 10*H*-9-oxaanthracen-10-one (**5e**) gave 10-(1,3-benzodithiol-2-ylidene)-10*H*-9-oxaanthracene (**6e**), yield 84%; mp 202.0—203.0 °C (from EtOH); IR (KBr): 1440, and 1265 cm^{-1}; UV (CH_2Cl_2): λ_{max}=255 sh (log ε= 4.44), 300 (4.01), and 370 nm (4.42); MS: *m/e* 332 (M^+, 100%) and 166 (M^{2+}, 29); ESCA: $S_{2P\,3/2}=163.2\pm0.15$ eV.

Found: C, 72.50; H, 3.48; S, 19.36%. Calcd for $C_{20}H_{12}OS_2$: C, 72.26; H, 3.64; S, 19.29%.

Reaction of **3a** with 10*H*-9-thiaanthracen-10-one 9-oxide (**5f**) in 1.0 mmol scale gave 10-(1,3-benzodithiol-2-ylidene)-10*H*-9-thiaanthracene 9-oxide (**6f**), yield 75%; mp 246.0—247.5 °C (from EtOH); IR (KBr): 1090 and 1040 (S=O) cm^{-1}; MS: *m/e* 364 (M^+, 48%), 348 (M^+-O, 76), 316 (M^+-SO, 39), 212 ($M^+-C_7H_4S_2$, 85), and 196 ($M^+-C_7H_4OS_2$, 100).

Found: C, 65.05; H, 3.05%. Calcd for $C_{20}H_{12}OS_3$: C, 65.90; H, 3.32%.

Reaction of **3a** with 10*H*-9-thiaanthracen-10-one 9,9-dioxide (**5g**) in 1.0 mmol scale gave 10-(1,3-benzodithiol-2-ylidene)-10*H*-9-thiaanthracene 9,9-dioxide (**6g**), yield 92%; mp 315.0—316.0 °C (from EtOH); IR (KBr): 1570, 1520, 1300 (SO_2, asym.), 1170, and 1165 (SO_2, sym) cm^{-1}; UV (CH_2Cl_2): λ_{max}=402 nm (logε=4.24); (MeCN): λ_{max}=265 (logε=4.06), 295.5 (3.72), 318.5 (3.76), and 396 nm (4.32); MS: *m/e* 380 (M^+, 100%) and 316 (M^+-SO_2, 7).

Found: C, 62.57; H, 2.99%. Calcd for $C_{20}H_{12}O_2S_3$: C, 63.13; H, 3.18%.

Reaction of **3a** with 9-fluorenone (**5h**) gave 2-(9-fluorenylidene)-1,3-benzodithiole (**6h**), yield 96%; mp 205.0—206.0 °C (from EtOH and $CHCl_3$). This compound was only slightly soluble in usual solvents such as benzene, chloroform, ethanol, and dimethyl sulfoxide. IR (KBr): 1540, 1440, and 775 cm^{-1}; UV (CH_2Cl_2): λ_{max}=251 (logε=4.98), 298 (4.00), 309 (4.02), 329 sh (4.07), 388 (4.68), 402 sh nm (4.66); (MeCN): λ_{max}=248.5 (log ε=4.83), 273 sh (3.88), 296.5 sh (3.66), 307.5 sh (3.71), 326 sh (3.79), 385 (4.52), and 400 sh nm (4.49); ESCA: $S_{2P\,3/2}=163.4\pm0.15$ eV; MS: *m/e* 316 (M^+, 100%) and 158 (M^{2+}, 29).

Found: C, 75.76; H, 4.12; S, 20.30%. Calcd for $C_{20}H_{12}S_2$: C, 75.91; H, 3.82; S, 20.27%.

Reaction of **3a** with tetraphenylcyclopentadienone (**5i**) gave 2-(tetraphenylcyclopentadienylidene)-1,3-benzodithiole (**6i**), yield 75%; mp 383—385 °C (from $CHCl_3$ and EtOH). This compound was only slightly soluble in usual solvents. IR (KBr): 1475, 1460, and 885 cm^{-1}; UV (CH_2Cl_2): λ_{max}= 247 sh (logε=4.45), 255.5 (4.50), 274 sh (4.39), and 435 nm (4.60); (MeCN): λ_{max}=244.5 sh (logε=4.33), 253 (4.38), 272 sh (4.24), and 430 nm (4.45); (MeCN with HBF_4): λ_{max}=232 sh (logε=4.43), 314 sh (3.75), and 532 nm (4.44); MS: *m/e* 520 (M^+, 100%).

Found: C, 82.70; H, 4.86; S, 11.71%. Calcd for $C_{36}H_{24}S_2$: C, 83.04; H, 4.65; S, 12.32%.

Reaction of **3a** with 7*H*-benz[d,e]anthracen-7-one (**5j**) gave 2-(7*H*-benz[d,e]anthracen-7-ylidene)-1,3-benzodithiole (**6j**), yield 80%; mp 256.0—257.0 °C (from $CHCl_3$ and EtOH); IR (KBr): 830, 770, and 735 cm^{-1}; UV (CH_2Cl_2): λ_{max}= 247.5 sh (logε=4.66), 272 sh (4.38), 318 (4.40), and 424 nm (4.49); MS: *m/e* 366 (M^+, 100%), 332 (M^+-H_2S, 14), and 183 (M^{2+}, 47).

Found: 78.37; H, 3.58; S, 17.36%. Calcd for $C_{24}H_{14}S_2$: C, 78.65; H, 3.85; S, 17.50%.

Reaction of **3a** with 9,10-anthracenedione in 1.0 mmol scale gave yellow crystals of 9,10-bis(1,3-benzodithiol-2-ylidene)-9,10-dihydroanthracene, yield 73%; mp 262.0—263.0 °C (from EtOH); UV (CH_2Cl_2): λ_{max}=237 (log ε= 4.34), 273 sh (3.77), 352 sh (3.78), 395 sh (3.89), and 416 nm (3.97); ESCA: $S_{2P\ 3/2}$=162.9±0.15 eV; MS: *m/e* 480 (M^+, 100%) and 240 (M^{2+}, 51).

Found: C, 69.70; H, 3.16; S, 26.28%. Calcd for $C_{28}H_{16}S_4$: C, 69.96; H, 3.36; S, 26.68%.

Authars are grateful to Itoh Science Foundation for partial support of this work.

References

1) E. Campaigne and R. D. Hamilton, *J. Org. Chem.*, **29**, 1711 (1964).
2) K.-P. Zeller, H. Meier, and E. Mueller, *Ann. Chem.*, **766**, 32 (1972); W. Kirmse and L. Horner, *ibid.*, **614**, 4 (1958).
3) R. Mayer, B. Hunger, R. Prousa, and A.-K. Mueller, *J. Prakt. Chem.*, **35** (**4R**), 294 (1967).
4) H. D. Hartzler, *J. Am. Chem. Soc.*, **93**, 4961 (1971).
5) C. U. Pittman, Jr., and M. Narita, *J. Chem. Soc., Chem. Commun.*, **1975**, 960; *Bull. Chem. Soc. Jpn.*, **49**, 1996 (1976).
6) M. G. Miles, J. S. Wagner, J. D. Wilson, and A. R. Siedle, *J. Org. Chem.*, **40**, 2577 (1975).
7) G. Scherowsky and J. Weiland, *Chem. Ber.*, **107**, 3155 (1974).
8) A. Luettringhaus, H. Berger, and H. Prinzbach, *Tetrahedron Lett.*, **1965**, 2121; R. Gompper and E. Kutter, *Chem. Ber.*, **98**, 2825 (1965).
9) R. Gompper and R. Weiss, *Angew. Chem.*, **80**, 277 (1968).
10) H. Gross, G. Engelhardt, J. Freiberg, W. Bürger, and B. Costisella, *Ann. Chem.*, **707**, 35 (1967).
11) V. Mark, C. H. Dungan, M. M. Crutchfield, and J. R. Van Wazer, "Topics in Phosphorus Chemistry," Vol. 5, John Wiley & Sons, Inc., New York (1967).
12) Preliminary report: K. Ishikawa, K. Akiba, and N. Inamoto, *Tetrahedron Lett.*, **1976**, 3695.
13) J. Metzger, H. Larive', E. J. Vincent, and R. Dennilauler, *J. Chim. Phys.*, **60**, 944 (1963).
14) Molecular model shows that one of the phenyl group of two benzyl groups comes over the molecule.
15) A. Maercker, *Org. React.*, **14**, 270 (1965).
16) E. J. Corey and G. Maerkl, *Tetrahedron Lett.*, **1967**, 3201; F. A. Carey and J. R. Neergaard, *J. Org. Chem.*, **36**, 2731 (1971).
17) D. E. Bissing and A. J. Speziale, *J. Am. Chem. Soc.*, **87**, 2683 (1965).
18) M. Mikolajczyk, S. Grzejszczak, A. Zatorski, and B. Mlotkowska, *Tetrahedron Lett.*, **1976**, 2731.
19) C. G. Kruse, N. L. J. M. Broekhof, A. Wijisman, and A. van der Gen, *Tetrahedron Lett.*, **1977**, 885.
20) Preliminary report: K. Akiba, K. Ishikawa, and N. Inamoto, *Synthesis*, **1977**, 861.
21) D. J. Bertelli and T. G. Andrews, Jr., *J. Am. Chem. Soc.*, **91**, 5280 (1969); D. J. Bertelli, T. G. Andrews, Jr., and P. O. Crews, *ibid.*, **91**, 5286 (1969).
22) Even the three sulfur atoms of **6b** were not discriminated.
23) M. Neuenschwander and W. K. Schenk, *Chimia*, **26**, 194 (1972); M. Neuenschwander, R. Hollenstein, A. Mooser, and W. von Philipsborn, *Angew. Chem. Int. Ed. Engl.*, **13**, 551 (1974).
24) J. Nakayama, K. Fujiwara, and M. Hoshino, *Chem. Lett.*, **1975**, 1099.
25) E. M. Engler and V. V. Patel, *Tetrahedron Lett.*, **1975**, 1259.
26) F. Wudl, A. A. Kruger, M. L. Kaplan, and R. S. Hutton, *J. Org. Chem.*, **42**, 768 (1977).
27) J. P. Ferraris, T. O. Poehler, A. N. Bloch, and D. O. Cowan, *Tetrahedron Lett.*, **1973**, 2553.
28) D. Leaver, W. A. Robertson, and D. M. Mikinnon, *J. Chem. Soc.*, **1962**, 5104.
29) E. G. Davis and S. Smiles, *J. Chem. Soc.*, **97**, 1296 (1910).
30) H. Decker and W. Petsch, *J. Prakt. Chem.*, **143**, 211 (1935).
31) C. Graebe and K. Lagodzinski, *Ann. Chem.*, **276**, 35 (1893); B. I. Mikhantev and V. A. Sklyarov, *Zh. Obshch. Khim.*, **26**, 784 (1956); *Chem. Abstr.*, **50**, 14760h (1956).
32) J. P. A. Castrillón and H. H. Szmant, *J. Org. Chem.*, **32**, 976 (1967); A. L. Ternay, Jr., and D. W. Chasar, *ibid.*, **32**, 3814 (1967).
33) B. Mayer, *Ber.*, **42**, 1132, 3046 (1909).
34) J. R. Johnson and O. Grummitt, *Org. Synth.*, Coll. Vol. 3, 806 (1955).
35) The compound (**4e**) was slightly soluble in chloroform and was protonated in this solution.

General Synthesis of Phosphonates from Heteroniaanthracene Cations and Their Use in Wittig-Horner Reaction

Kiyofumi ISHIKAWA, Kin-ya AKIBA,* and Naoki INAMOTO

Department of Chemistry, Faculty of Science, The University of Tokyo, Hongo, Tokyo 113

(Received April 11, 1978)

Heteroaromatic cations such as 9-heteroniaanthracene (acridinium, xanthylium, and thioxanthylium) and 1-thionianaphthalene (thiochromenylium) ions reacted with trimethyl phosphite in the presence of sodium iodide in acetonitrile at room temperature to give the corresponding phosphonates (**2** and **4**) respectively in 76—92% yields. The phosphonates were deprotonated with butyllithium in THF at −78 °C, and the resulting carbanions reacted with *p*-tolualdehyde, cinnamaldehyde, and 4,4′-dichlorobenzophenone to afford the corresponding exomethylene containing heterocyclic compounds, respectively, in 52—96% yields. However, the phosphonate carbanions derived from **2** did not react with cycloalkanones and butanal.

The reactions of heteroaromatic cations with a wide variety of nucleophiles have been investigated extensively. However, there are only a few reports on the reactions with phosphorus nucleophiles such as phosphines and phosphites.[1] Evenmore, the utilization of the expected reaction products (*e.g.*, phosphonium salts or phosphonates) as reagents for carbonyl olefination has been described only by two reports, one on the use of the phosphonium salt obtained from pyrylium perchlorate[1a], and the other on that of phosphonates obtained from acridinium salts.[1f]

The preceding paper and its preliminary reports showed that 1,3-dithiolylium salts reacted with phosphines or phosphites to give the corresponding phosphonium salts or phosphonates in high yields and that they, especially the latter, could be used in Wittig-Horner reaction to give various derivatives of 1,4-dithiafulvenes and fulvalenes in high yields.[2] Consequently, versatile utility in the synthesis of heterocyclic compounds was expected for analogous phosphonates, if they could be prepared from heteroaromatic cations and trialkyl phosphite.

We report here a general synthesis of the phosphonates[3] from heteroaromatic cations such as acridinium, xanthylium, thioxanthylium, and thiochromenylium ions, and their use in Wittig-Horner reaction.

Results and Discussion

Preparation of Phosphonates from Heteroaromatic Cations. Under a nitrogen atmosphere at room temperature, trimethyl phosphite was added at once to a stirred solution of 9-heteroniaanthracene salt (acridinium, xanthylium, or thioxanthylium salts) (**1a**—**f**) in dry acetonitrile, then immediately sodium iodide was added,

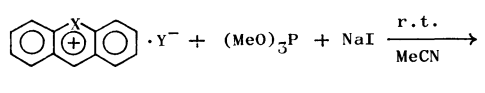

1 a: X=NH, Y=Cl
b: X=NMe, Y=$MeSO_4$
c: X=NEt, Y=$EtSO_4$
d: X=NCH_2Ph, Y=Br
e: X=O, Y=ClO_4
f: X=S, Y=ClO_4

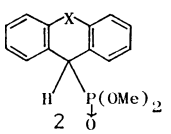

+ MeI + NaI

Scheme 1.

TABLE 1. YIELDS, MP, AND IR SPECTRAL DATA OF THE PHOSPHONATES (**2**)

Compound	Yield (%)	Mp (°C)	IR (KBr) (cm^{-1}) $\nu_{P=O}$	ν_{P-O-C}	
2a	85	170.0—171.0	1225	1055(as)	1030(s)
2b	85	98.0—99.0	1270 or 1240	1045(as)	1020(s)
2c	92	100.0—100.5	1260 or 1250	1060(as)	1020(s)
2d	76	147.0—148.0	1240	1060(as)	1030(s)
2e	90	132.0—133.0	1255	1050(as)	1020(s)
2f	87	194.0—195.0	1245	1055(as)	1025(s)

and the solution was stirred for 1 h. Usual treatment of the mixture gave the corresponding phosphonate (**2a**—**f**) in high yields. The results are shown in Table 1.

The structure of **2a**—**f** was confirmed by means of elemental analyses, IR, ^{1}H-NMR, and mass spectra.

As shown in Table 1, the IR spectra of **2a**—**f** showed strong absorption bands at 1225—1270 (P=O), 1045—1060, and 1020—1030 cm^{-1} (P-O-C). The IR spectrum of **2a** showed also a sharp absroption band at 3270 cm^{-1} (NH).

All **2a**—**f** gave reasonable ^{1}H-NMR spectra, each of which showed a doublet signal at δ 3.46—3.53 due to $POCH_3$ (J_{POCH}=10.5 Hz), and a doublet signal at δ 4.49—4.69 with a relatively large value of coupling constnat (J=24.8—28.7 Hz) assignable to PCH. This fact will be discussed later.

The ^{31}P-NMR spectrum of **2e** exhibited a signal at δ_P −24 ppm supporting the phosphonate structure.[4]

The mass spectra of the phosphonates (**2a**—**f**) showed the parent peak (3—6%), the base peak assignable to $M^+-P(O)(OMe)_2$, and the metastable peak due to the direct fragmentation of the parent ion to the $M^+-P(O)(OMe)_2$ ion.

As described above, it was ascertained first that the Michaelis-Arbuzov reaction of 9-heteroniaanthracene salt (**1a**—**f**) with trimethyl phosphite proceeded easily even at room temperature in the presence of sodium iodide in acetonitrile, similarly to the case of 1,3-dithiolylium salt.[2]

Furthermore, 2-methyl-1-thionianaphthalene perchlorate [(2-methyl)thiochromenylium perchlorate] (**3**) was also allowed to react with trimethyl phosphite under the same conditions to give 4-dimethoxyphosphinyl-2-methyl-4*H*-1-thianaphthalene (**4**; yield 91%) exclusively.

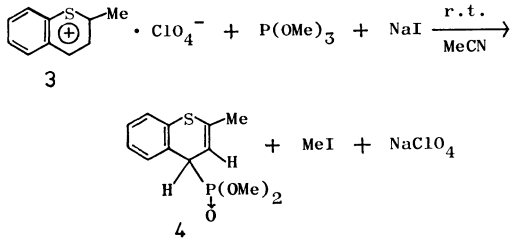

Scheme 2.

The structure of **4** was confirmed by means of elemental analysis, IR, ^{1}H-NMR, and mass spectra, and was also supported by the result of its reaction with 4,4'-dichlorobenzophenone described later. The isomeric structure, 2-dimethoxyphosphinyl-2-methyl-2*H*-1-thianaphthalene was ruled out based on the ^{1}H-NMR spectral data.

The IR spectrum of **4** showed strong absorptions at 1240 (P=O), 1055, and 1025 cm^{-1} (P–O–C).

The phosphonate (**4**) exhibits a rather complex ^{1}H-NMR spectrum compared with those of **2** due to the presence of an asymmetric carbon atom at the 4-position, however, it is fully assigned as shown in Table 2.

Table 2. ^{1}H-NMR spectral data of the phosphonate (**4**) (in $CDCl_3$)

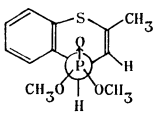

δ 2.06 (3H, ddd, J_{PCCCCH}=6.0, J_{HCCCH}=1.4, J_{HCCCCH}=0.9 Hz, 2-C-CH_3);
3.61 (3H, d, J_{POCH}=10.4 Hz, $POCH_3$);
3.72 (3H, d, J_{POCH}=10.4 Hz, $POCH_3$);
4.18 (1H, qdd, J_{PCH}=28.5, J_{HCCH}=6.8, J_{HCCCCH}=0.9 Hz, 4-CH);
5.62 (1H, qdd, J_{HCCH}=6.8, J_{PCCH}=4.2, J_{HCCCH}=1.4 Hz, 3-CH);
7.18 (4H, br s, aromatic H)

There are two significant features in relation to the coupling constants between phosphorus and hydrogen: (a) the J_{PCH} value (28.5 Hz) is one of the largest ones ever known and is much larger than J_{PCCH} (4.2 Hz), usually the reverse should be the case,[5] and (b) the long range coupling between phosphorus and 2-C–CH_3 (J_{PCCCH}=6.0 Hz) is exceptionally large. These facts were confirmed by comparison of the spectra obtained at 60 MHz and at 100 MHz. Moreover, the 2-C–CH_3 signal was irradiated to give double doublet signals for 3-CH and 4-CH with the coupling constants shown above.

The mass spectrum of **4** showed the parent peak at *m/e* 270 (5%), the base peak at *m/e* 161 assignable to $M^+-P(O)(OMe)_2$, and the metastable peak at *m/e* 96.0 due to the direct fragmentation of the parent ion to the $M^+-P(O)(OMe)_2$ ion.

Chemical shifts and coupling constants of PCH of related phosphonates are shown in Table 3. These facts can be summarized as follows: i) coupling constants (J_{PCH}) of phosphonates of 1,3-dithioles lie around 5 Hz, these of 1,3-oxathioles around 8 Hz, those of 1,3-dioxoles around 30 Hz, and those of 1-hetera-2,5-cyclohexadienes around 27 Hz and ii) an electronegative group increases the coupling constants.

Table 3. Chemical shifts and coupling constants of PCH of related phosphonates (in $CDCl_3$)

Compound		PCH (δ)	J_{PCH} (Hz)
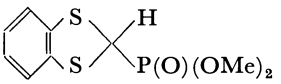		4.75	5.8
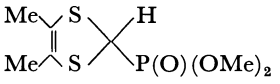		4.73	4.5
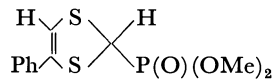		5.06	4.5
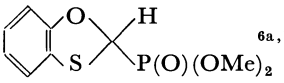 [6a,b]		6.08	8.2
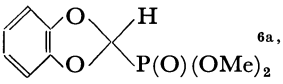 [6a,b]		6.22	29.8
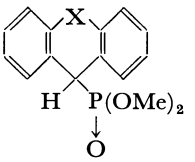	X=NH	4.58	24.9
	X=NMe	4.55	26.1
	X=O	4.49	24.8
	X=S	4.69	28.7
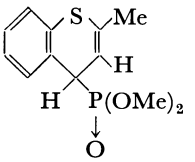		4.18	28.5
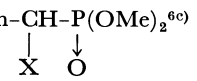 [6c]	X=Cl	4.97	14.0
	X=OAc	6.13	13.5
	X=OTs	5.62	15.5

a) In CCl_4.

Costisella and Gross suggested recently that there is a relationship similar to Karplus equation between the value of J_{PCH} and the dihedral angle (β) for phosphinyl-containing compounds.[6b] However, bond lengths (C–H and C–P) and bond angle ($\angle$HCP) should also be important factors and detailed discussion cannot be given here.

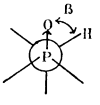

Wittig-Horner Reaction of the Phosphonates. Under a nitrogen atmosphere at −78 °C, butyllithium in hexane was added to stirred solution of the phosphonate (**2a**, **b**, **e**, or **f**) in tetrahydrofuran (THF). The resulting carbanion was allowed to react with a carbonyl compound to give the exo-methylene-containing compound (**5**) in a high yield. The reaction with *p*-tolu-

Table 4. Yields and mp of 5 and 6

Product	X	R^1	R^2	Yield (%)	Mp (°C)
5a[a]	NH	*p*-$CH_3C_6H_4$	H	53	164.0—166.0 (dec)
5b	NMe	*p*-$CH_3C_6H_4$	H	93	127.5—128.5
5c	O	*p*-$CH_3C_6H_4$	H	84	112.0—113.0
5d	S	*p*-$CH_3C_6H_4$	H	93	128.0—129.0
5e	NMe	PhCH=CH	H	96	112.5—113.5
5f	O	PhCH=CH	H	91	91.0— 92.0
5g	S	PhCH=CH	H	92	165.0—166.0
5h	NMe	*p*-ClC_6H_4	*p*-ClC_6H_4	52	257.0—258.0
5i	O	*p*-ClC_6H_4	*p*-ClC_6H_4	95	209.0—210.0
5j	S	*p*-ClC_6H_4	*p*-ClC_6H_4	—	—
6		*p*-ClC_6H_4	*p*-ClC_6H_4	78	158.5—159.5

a) See the text.

aldehyde and cinnamaldehyde took place rapidly at low temperature (—78 °C to room temperature) but that with 4,4′-dichlorobenzophenone was effected in refluxing THF. The phosphonate (**4**) was also deprotonated and the resulting carbanion reacted with 4,4′-dichlorobenzophenone to give 4-[bis(*p*-chlorophenyl)methylene]-2-methyl(thiochromene) (**6**). The reaction of **2f** and 4,4′-dichlorobenzophenone did not proceed even under reflux, and the starting materials were recovered (**2f**; 58%; ketone, 73%).[7] The results are shown in Table 4.

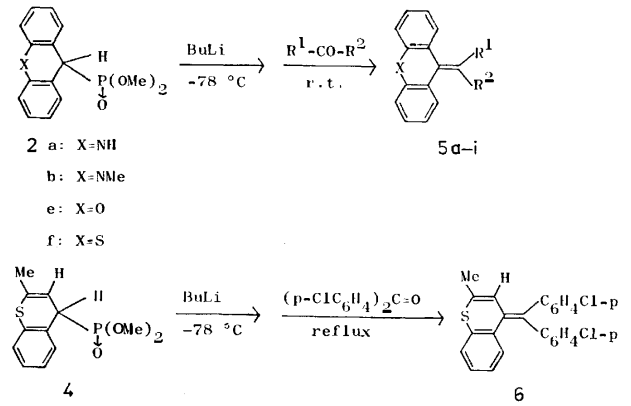

Scheme 3.

The structures of **5** and **6** were confirmed by means of elemental analyses, IR, ^{1}H-NMR, and MS. The molecular ion peak is in each case the most intense peak in the mass spectra except for **5e** (M^+, 63%; M^+—Ph, 100%). The structure of **5a** was confirmed to be 9-(*p*-methylbenzyl)acridine formed by prototropy of the initially produced benzylidene type compound (absence of NH in IR and presence of a methylene group in NMR).

Furthermore, the reaction of the phosphonate carbanion derived from **2b** or **2e** with cycloalkanones (*e.g.*, cyclohexanone or cyclopentanone) and butanal was tried, however, the expected product could not be obtained even under reflux and the starting material (**2b** or **2e**) was recovered exclusively. The inertness of the reaction seems to be attributable chiefly to steric hindrance between the peri-hydrogens of the phosphonate (**2**) and the α-methylene hydrogens of a carbonyl compound.

Experimental

All the melting points are not corrected. IR spectra were measured with a Hitachi EPI-G2 spectrometer, ^{1}H-NMR spectra with Hitachi R-20B, Hitachi R-24 (60 MHz), and JEOL JNM-4H-100 (100 MHz) spectrometers (TMS as an internal standard), and MS with a Hitachi RMU-6L mass spectrometer at 70 eV. ^{31}P-NMR spectra were measured with a Hitachi R-20B-R-204-PB (24.3 MHz) spectrometer using 85% phosphoric acid as an external standard.

*Materials: 9-Azoniaanthracene Salts (Acridinium Salts) (**1a—d**).* Each 9-azoniaanthracene salt was prepared by the reaction of 9-azaanthracene (aciridine) with RX in good yields.

Compound	R	X	Mp (°C)
1a	H	Cl	220.5—222 (dec)[1c),a)]
1b	Me	$MeSO_4$	207—208 (dec)[8),a)]
1c	Et	$EtSO_4$	275—277 (dec)[8),a)]
1d	$PhCH_2$	Br	225—227 (dec) [lit,[9] 209 (dec)]

a) Melting points were not indicated for **1a**, **1b**, and **1c** in the literatures.

9-Oxoniaanthracene perchlorate (xanthylium perchlorate) (**1e**) was prepared by the treatment of 10*H*-9-oxaanthracen-10-ol (mp 125—126 °C, lit,[10] 124—126 °C), which was obtained by the reduction of xanthone (5.89 g, 0.03 mol) with sodium borohydride (2.3 g) in refluxing absolute methanol (150 ml), with 70% perchloric acid (20 ml) in dry ether (200 ml) at —78 °C, mp 237 °C (dec) (lit,[11] mp 225—226 °C), total yield 7.40 g (88%).

9-Thioniaanthracene perchlorate (thioxanthylium perchlorate) (**1f**) was prepared from thioxanthone (6.4 g, 0.03 mol) by the same procedure as **1e** in total ylied of 6.14 g (69%), mp 229—230 °C (dec) (lit, mp 217—219 °C[12], 229 °C[13]).

2-Methyl-1-thionianaphthalene perchlorate (**3**) was prepared from 2-methyl-4*H*-1-thianaphthalen-4-one[14] (5.28 g, 0.03 mol) by the same procedure as **1e** in total yield of 5.70 g (73%), mp 143—145 °C. This compound was colored blue due to the presence of a small amount of impurity (*e.g.*, cyanine dye) but was used for the next step without further

purification because of its instability.

Michaelis-Arbuzov Reaction of Heteroaromatic Cations with Trimethyl Phosphite. General Procedure: Trimethyl phosphite (1.2 ml, 10 mmol) was added to a stirred solution of heteroaromatic cation (10 mmol) in dry acetonitrile (50 ml) at room temperature under nitrogen and then followed with dry sodium iodide (1.5 g, 10 mmol). After the mixture had been stirred for 1 h, the solvent was evaporated under reduced pressure. Water (50 ml) was added to the residue and the product was extracted with dichloromethane (30 ml×3). The combined extracts were dried over anhydrous magnesium sulfate and the solvent was removed under reduced pressure. Recrystallization of the residue from ethyl acetate and ether gave the corresponding phosphonate. Dry column chromatography (neutral alumina) was often used for purification.

Reaction of 9-azoniaanthracene chloride (**1a**) with trimethyl phosphite gave 10-dimethoxyphosphinyl-9,10-dihydro-9-azaanthracene (**2a**), yield 85%, mp 170.0—171.0 °C (from AcOEt); IR (KBr): 3270 (NH), 1480, 1225 (P=O), 1055, and 1030 cm^{-1} (P–O–C); ^{1}H-NMR ($CDCl_3$): δ 3.53 (d, J_{POCH}=10.5 Hz, 6H, $POCH_3$), 4.58 (d, J_{PCH}=24.9 Hz, 1H, PCH), and 6.5—7.4 (m, 9H, aromatic and NH); MS: *m/e* 289 (M^+, 4%), 180 ($M^+-P(O)(OMe)_2$, 100), 179 (180 −H, 15), and 152 (180−CH_2N, 5); metastable ion, found: 112.1 calcd for 289→180: 112.1; found: 128.4, calcd for 180→152: 128.36.

Found: C, 62.19; H, 5.66; N, 4.62%. Calcd for $C_{15}H_{16}NO_3P$: C, 62.28; H, 5.58; N, 4.84%.

Reaction of 9-methyl-9-azoniaanthracene methyl sulfate (**1b**) with trimethyl phosphite gave 10-dimethoxyphosphinyl-9-methyl-9,10-dihydro-9-azaanthracene (**2b**), yield 85%, mp 98.0—99.0 °C (from AcOEt and Et_2O); IR (KBr): 1580, 1470, 1240 (P=O), 1045, and 1020 cm^{-1} (P–O–C); ^{1}H-NMR ($CDCl_3$): δ 3.39 (s, 3H, NCH_3), 3.49 (d, J_{POCH}=10.5 Hz, 6H, $POCH_3$), 4.55 (d, J_{PCH}=26.1 Hz, 1H, PCH), and 6.7—7.5 (m, 8H, aromatic); MS: *m/e* 303 (M^+, 6%), 194 ($M^+-P(O)(OMe)_2$, 100), and 179 (194−Me, 17); metastable ion, found: 124.2, calcd for 303→194: 124.21; found: 165.2, calcd for 194→179: 165.16.

Found: C, 63.11; H, 6.05; N, 4.53%. Calcd for $C_{16}H_{18}NO_3P$: C, 63.36; H, 5.98; N, 4.62%.

Reaction of 9-ethyl-9-azoniaanthracene ethyl sulfate (**1c**) with trimethyl phosphite gave 10-dimethoxyphosphinyl-9-ethyl-9,10-dihydro-9-azaanthracene (**2c**), yield 92%, mp 100.0—100.5 °C (from PhH and CH_2Cl_2); IR (KBr): 1590, 1260 or 1250 (P=O), 1060, and 1020 cm^{-1} (P–O–C); ^{1}H-NMR ($CDCl_3$): δ 1.38 (t, J=6.8 Hz, 3H, N-C-CH_3), 3.46 (d, J_{POCH}=10.5 Hz, 6H, $POCH_3$), 3.99 (q, J=6.8 Hz, 2H, N-CH_2-C), 4.52 (d, J_{PCH}=25.5 Hz, 1H, PCH), and 6.7—7.5 (m, 8H, aromatic); MS: *m/e* 317 (M^+, 6%), 208 ($M^+-P(O)(OMe)_2$, 100), 180 (208−C_2H_4, 22), and 152 (180−CH_2N, 4); metastable ion, found: 136.5, calcd for 317→208: 136.48; found 155.8, calcd for 208→180: 155.77; found 128.4, calcd for 180→152: 128.36.

Found: C, 64.16; H, 6.44; N, 4.57%. Calcd for $C_{17}H_{20}NO_3P$: C, 64.35; H, 6.35; N, 4.41%.

Reaction of 9-benzyl-9-azoniaanthracene bromide (**1d**) with trimethyl phosphite gave 9-benzyl-10-dimethoxyphosphinyl-9,10-dihydro-9-azaanthracene (**2d**), yield 76%, mp 147.0—148.0 °C (from AcOEt); IR (KBr): 1470, 1240 (P=O), 1060, and 1030 cm^{-1} (P–O–C); ^{1}H-NMR ($CDCl_3$): δ 3.52 (d, J_{POCH}=10.5 Hz, 6H, $POCH_3$), 4.62 (d, J_{PCH}=25.7 Hz, 1H, PCH), 5.18 (s, 2H, N–CH_2–Ph), and 6.5—7.5 (m, 13H, aromatic); MS: *m/e* 379 (M^+, 6%), 270 ($M^+-P(O)(OMe)_2$, 100), and 179 (270−$PhCH_2$, 19); metastable ion, found: 192.4, calcd for 379→270: 192.35.

Found: C, 69.58; H, 5.98; N, 3.51%. Calcd for $C_{22}H_{22}NO_3P$: C, 69.65; H, 5.85; N, 3.69%.

Reaction of 9-oxoniaanthracene perchlorate (**1e**) with trimethyl phosphite gave 10-dimethoxyphosphinyl-10*H*-9-oxaanthracene(**2e**), yield 90%, mp 132.0—133.0 °C (from AcOEt and Et_2O) (lit,[15] 128—129 °C); IR (KBr): 1475, 1255 (P=O), 1050, and 1020 cm^{-1} (P–O–C); ^{1}H-NMR ($CDCl_3$): δ 3.53 (d, J_{POCH}=10.5 Hz, 6H, $POCH_3$), 4.49 (d, J_{PCH}=24.8 Hz, 1H, PCH), and 6.9—7.5 (m, 8H, aromatic): ^{31}PNMR ($CDCl_3$): δ_P−24 ppm; MS: *m/e* 290 (M^+, 3%), and 181 ($M^+-P(O)(OMe)_2$, 100).

Reaction of 9-thioniaanthracene perchlorate (**1f**) with trimethyl phosphite gave 10-dimethoxyphosphinyl-10*H*-9-thiaanthracene (**2f**), yield 87%, mp 194.0—195.0 °C (from AcOEt and Et_2O); IR (KBr): 1245 (P=O), 1055 and 1025 cm^{-1} (P–O–C); ^{1}H-NMR ($CDCl_3$): δ 3.52 (d, J_{POCH}=10.5 Hz, 6H, $POCH_3$), 4.69 (d, J_{PCH}=28.7 Hz, 1H, PCH), and 7.1—7.5 (m, 8H, aromatic); MS: *m/e* 306 (M^+, 5%) and 197 ($M^+-P(O)(OMe)_2$, 100).

Found: C, 58.63; H, 5.06; S, 10.55%. Calcd for $C_{15}H_{15}O_3PS$: C, 58.82; H, 4.94; S, 10.47%.

Reaction of 2-methyl-1-thioniaanaphthalene perchlorate (**3**) with trimethyl phosphite gave 4-dimethoxyphosphinyl-2-methyl-4*H*-1-thianaphthalene (**4**), yield 91%, mp 99.0—100.0 °C (from AcOEt); IR (KBr): 1240 (P=O), 1055, and 1025 cm^{-1} (P–O–C); ^{1}H-NMR ($CDCl_3$): δ 2.06 (ddd, J_{PCCCCH}=6, J_{HCCCH}=1.4, J_{HCCCCH}=0.9 Hz, 3H, 2-C-CH_3), 3.61 (d, J_{POCH}=10.4 Hz, 3H, $POCH_3$), 3.72 (d, J_{POCH}=10.4 Hz, 3H, $POCH_3$), 4.18 (qdd, J_{PCH}=28.5, J_{HCCH}=6.8, J_{HCCCH}=0.9 Hz, 1H, 4-CH), 5.62 (qdd, J_{HCCH}=6.8, J_{PCCH}=4.2, J_{HCCCH}=1.4 Hz, 1H, 3-CH), and 7.18 (br s, 4H, aromatic); (100 MHz, in $CDCl_3$): δ 2.06 (ddd, 3H, 2-C-CH_3), 3.61 (d, 3H, $POCH_3$), 3.72 (d, 3H, $POCH_3$), 4.18 (qdd, 1H, 4-CH), 5.62 (qdd, 1H, 3-CH), and 7.18 (br s, 4H, aromatic). The 2-C-CH_3 signal at δ 2.06 was irradiated to give double doublet signals for 3-CH (δ 5.62) and 4-CH (δ 4.18) with the coupling constants shown above.

MS: *m/e* 270 (M^+, 5%), 161 ($M^+-P(O)(OMe)_2$, 100), 128 (161−SH, 10), and 155 (161−CH_2S, 6); metastable ion, found: 96.0, calcd for 270→161: 96.0; found 101.8, calcd for 161→128: 101.76.

Found: C, 53.17; H, 5.84; S, 11.37%. Calcd for $C_{12}H_{15}O_3PS$: C, 53.33; H, 5.59; S, 11.86%.

Witting-Horner Reaction of the Phosphonates Derived from Heteroaromatic Cations. General Procedure: To a stirred solution of a phosphonate (1.0 mmol) in THF (10 ml), butyllithium in hexane (0.75 ml, 1.15 mmol) was added at −78 °C under nitrogen. The solution colored yellow or yellowish brown due to the resulting carbanion. After 10 min, a solution of a carbonyl compound (1.0 mmol) in THF (5—10 ml) was added. Stirring was continued for 10 min at −78 °C and the mixture was then allowed to get warm to room temperature. When the carbonyl compound was not an aldehyde but a ketone, the reaction mixture was heated under reflux for 30 min. The solvent was evaporated under reduced pressure and the mixture was extracted with dichloromethane (20 ml×3) after addition of water (50 ml). The combined extracts were dried over anhydrous magnesium sulfate, the solvent was evaporated, and the residue was recrystallized to give the corresponding product.

Reaction of **2a** with *p*-tolualdehyde gave 9-(*p*-methylbenzyl) acridine (**5a**), yield 53%, mp 164.0—166.0 °C (dec) (from MeOH); IR (KBr): 1510, 770, 760, and 740 cm^{-1}; ^{1}H-NMR (CCl_4): δ 2.24 (s, 3H, CH_3), 4.89 (s, 2H, CH_2), 6.95 (s, 4H, aromatic), and 7.1—8.4 (m, 8H, aromatic); MS: *m/e* 283 (M^+, 100%), 282 (M^+−H, 49), 268 (M^+−Me, 50), 267 (268−H, 38), 141 (282^{2+}, 15), and 134 (268^{2+}, 31).

Found: C, 89.02; H, 5.85; N, 5.09%. Calcd for $C_{21}H_{17}N$: C, 89.01; H, 6.05; N, 4.94%.

Reaction of **2b** with *p*-tolualdehyde gave 10-methyl-9-(*p*-tolylmethylene)-9,10-dihydroacridine (**5b**), yield 93%, mp 127.5—128.5 °C (from MeOH); IR (KBr): 1580, 1445, 860, 815, and 755 cm^{-1}; ^1H-NMR (CCl_4): δ 2.32 (s, 3H, Ar-CH_3), 3.48 (s, 3H, N-CH_3), and 6.4—7.7 (m, 13H, aromatic and olefinic); MS: *m/e* 297 (M^+, 100%), 296 (M^+-H, 51), 282 (M^+-Me, 16), 281 (296—Me, 25), 267 (282—Me, 19), 266 (281—Me, 23), 148.5 (M^{2+}, 11), 141 (282^{2+}, 22), and 140.5 (281^{2+}, 35).

Found: C, 88.60; H, 6.29; N, 5.00%. Calcd for $C_{22}H_{19}N$: C, 88.85; H, 6.44; N, 4.71%.

Reaction of **2e** with *p*-tolualdehyde gave 9-(*p*-tolylmethylene) xanthene (**5c**), yield 84%, mp 112.0—113.0 °C (from MeOH); IR (KBr): 1440, 1250, 805, 760, and 745 cm^{-1}; ^1H-NMR (CCl_4): δ 2.33 (s, 3H, CH_3) and 6.5—7.8 (m, 13H, aromatic and olefinic); MS: *m/e* 284 (M^+, 100%), 283 (M^+-H, 24), 269 (M^+-Me, 36), 268 (283—Me, 56), 142 (M^{2+}, 8), 134.5 (269^{2+}, 13), and 134 (268^{2+}, 30).

Found: C, 88.44; H, 5.54%. Calcd for $C_{21}H_{16}O$: C, 88.70; H, 5.67%.

Reaction of **2f** with *p*-tolualdehyde gave 9-(*p*-tolylmethylene) thioxanthene (**5d**), yield 93%, mp 128.0—129.0 °C (from MeOH); IR (KBr): 1430, 815, 770, 760, and 740 cm^{-1}; ^1H-NMR (CCl_4): δ 2.30 (s, 3H, CH_3) and 6.5—7.8 (m, 13H, aromatic and olefinic); MS: *m/e* 300 (M^+, 100%), 285 (M^+-Me, 46), 284 (285—H, 49), 252 (285—SH, 22) and 142 (284^{2+}, 38).

Found: C, 84.20; H, 5.20; S, 10.68%. Calcd for $C_{21}H_{16}S$: C, 83.96; H, 5.37; S, 10.67%.

Reaction of **2b** with *trans*-3-phenyl-2-propenal gave 10-methyl-9-(3-phenyl-2-propenylidene)-9,10-dihydroacridine (**5e**), yield 96%, mp 112.5—113.5 °C (from EtOH); IR (KBr): 1580, 1450, 760, and 745 cm^{-1}; ^1H-NMR (CCl_4): δ 3.37 (s, 3H, N-CH_3) and 6.2—7.7 (m, 16H, aromatic and olefinic); MS: *m/e* 309 (M^+, 63%), 308 (M^+-H, 46), 232 (M^+-Ph, 100).

Found: C, 89.24; H, 6.09; N, 4.42%. Calcd for $C_{23}H_{19}N$: C, 89.28; H, 6.19; N, 4.53%.

Reaction of **2e** with *trans*-3-phenyl-2-propenal gave 9-(3-phenyl-2-propenylidene)xanthene (**5f**), yield 91%, mp 91.0—92.0 °C (from EtOH); IR (KBr): 1595, 1450, 1310, 1270, 945, 770, 765, 750, and 695 cm^{-1}; ^1H-NMR (CCl_4): δ 6.4—7.8 (m, aromatic and olefinic); MS: *m/e* 296 (M^+, 100%), 295 (M^+-H, 86), 219 (M^+-Ph, 97), and 218 (296—Ph, 46).

Found: C, 89.02; H, 5.21%. Calcd for $C_{22}H_{16}O$: C, 89.16; H, 5.44%.

Reaction of **2f** with *trans*-3-phenyl-2-propenal gave 9-(3-phenyl-2-propenylidene)thioxanthene (**5g**), yield 92%, mp 165.0—166.0 °C (from EtOH); IR (KBr): 1455, 1430, 970, 765, 740, and 690 cm^{-1}; ^1H-NMR (CCl_4): δ 6.4—7.8 (m, aromatic and olefinic); MS: *m/e* 312 (M^+, 100%), 311 (M^+-H, 68), 235 (M^+-Ph, 78), 234 (311—Ph, 40), 221 (235—CH_2, 26), and 202 (235—SH, 11).

Found: C, 84.85; H, 5.00; S, 10.22%. Calcd for $C_{22}H_{16}S$: C, 84.58; H, 5.16; S, 10.26%.

Reaction of **2b** with 4,4′-dichlorobenzophenone gave 10-methyl-9-[bis(*p*-chlorophenyl)methylene]-9,10-dihydroacridine (**5h**), yield 52%, mp 257.0—258.0 °C (from EtOH); IR (KBr): 1590, 1455, 1350, 1095, 820, 810, and 755 cm^{-1}; ^1H-NMR (CCl_4 and $CDCl_3$, 1:1): δ 3.50 (s, 3H, N-CH_3) and 6.4—7.5 (m, 16H, aromatic); MS: *m/e* 431 (M^+ for two ^{37}Cl, 12%), 430 (25), 429 (M^+ for one ^{37}Cl and one ^{35}Cl, 80), 428 (44), and 427 (M^+ for two ^{35}Cl, 100).

Found: C, 75.95; H, 4.48; N, 3.32; Cl, 16.98%. Calcd for $C_{27}H_{19}NCl_2$: C, 75.71; H, 4.47; N, 3.27; Cl, 16.55%.

Reaction of **2e** with 4,4′-dichlorobenzophenone gave 9-[bis(*p*-chlorophenyl)methylene]xanthene (**5i**), yield 95%, mp 209.0—210.0 °C (from MeOH); IR (KBr): 1440, 1250, 1090, 1015, 825, 760, and 755 cm^{-1}; MS: *m/e* 418 (M^+ for two ^{37}Cl, 14%), 417 (20), 416 (M^+ for one ^{37}Cl and one ^{35}Cl, 68), 415 (32), 414 (M^+ for two ^{35}Cl, 100), 378 (M^+-HCl, 28), and 342 (378—HCl, 17).

Found: C, 75.49; H, 3.63; Cl, 16.95%. Calcd for $C_{26}H_{16}OCl_2$: C, 75.19; H, 3.88; Cl, 17.07%.

Reaction of **2f** with 4,4′-dichlorobenzophenone gave no expected product and the starting materials (4,4′-dichlorobenzophenone, 73%, and **2f**, 58%) were recovered. Moreover, 10*H*-9-thiaanthracen-10-one was detected by thin-layer chromatography (SiO_2/CH_2Cl_2).

Reaction of **2b** or **2e** with cycloalkanones (*e.g.*, cyclohexanone and cyclopentanone) did not take place under general procedure and the color of the carbanion (**2b**, brown; **2e**, orange) disappeared, when the solution was refluxed. However, the expected product could not be obtained and the starting material (**2b** or **2e**) was recovered.

Reaction of **4** with 4,4′-dichlorobenzophenone in refluxing THF for 30 min gave 2-methyl-4-[bis(4-chlorophenyl)methylene]-4*H*-1-thianaphthalene (**6**), yield 78%, mp 158.5—159.5 °C (from MeOH); IR (KBr): 1480, 1095, 825, 760, and 750 cm^{-1}; ^1H-NMR ($CDCl_3$): δ 1.99 (br s, 3H, 2-C-CH_3), 6.52 (br s, 1H, 3-CH), and 6.7—7.9 (m, 12H, aromatic); MS: *m/e* 398 (M^+ for two ^{37}Cl, 18%), 397 (20), 396 (M^+ for one ^{37}Cl and one ^{35}Cl, 72), 395 (31), 394 (M^+ for two ^{35}Cl, 100), 358 (M^+-HCl, 20), and 344 (358—CH_2, 17).

Found: C, 69.58; H, 3.84%. Calcd for $C_{23}H_{16}SCl_2$: C, 69.88; H, 4.08%.

We are grateful to Itoh Science Foundation for partial support of this work.

References

1) a) S. V. Krivun, O. F. Voziyanova, and S. N. Baranov, *Zh. Obshch. Khim.*, **42**, 298 (1972); *Chem. Abstr.*, **77**, 34224f (1972); b) S. V. Kriunn, O. F. Voziyanova, and S. N. Baranov, *Dopov. Akad. Nauk. Ukr. RER, Ser. B*, **34**, 529 (1972); *Chem. Abstr.*, **77**, 101765y (1972); c) A. K. Sheinkman, G. V. Samoilenko, and S. N. Baranov, *Dokl. Akad. Nauk. SSSR*, **196**, 1377 (1971); *Chem. Abstr.*, **75**, 20514x (1971); d) D. Redmore, US Patent, 3694144 (1972); *Chem. Abstr.*, **78**, P 29998c (1972); e) U. Berg, R. Gallo and J. Metzger, *J. Org. Chem.*, **41**, 2621 (1976); f) D. Redmore, *J. Org. Chem.*, **34**, 1420 (1969): We noticed this paper after we submitted this manuscript and added here during retyping.

2) a) K. Akiba, K. Ishikawa, and N. Inamoto, *Bull. Chem. Soc. Jpn.*, **51**, 2674 (1978); b) K. Ishikawa, K. Akiba, and N. Inamoto, *Tetrahedron Lett.*, **1976**, 3695; c) K. Akiba, K. Ishikawa, and N. Inamoto, *Synthesis*, **1977**, 861.

3) Preliminary report: K. Akiba, K. Ishikawa, and N. Inamoto, *Synthesis*, **1977**, 862.

4) R. Richards, A. Y. Jones, and A. R. Katritzky, *Angew. Chem.*, **74**, 60 (1962).

5) a) M. J. Gallagher, *Aust. J. Chem.*, **21**, 1197 (1968); b) D. J. Peterson, *J. Org. Chem.*, **31**, 960 (1966); c) M. Yoshifuji, *Yuki Gosei Kagaku Kyokai Shi*, **28**, 191, 192 (1970).

6) a) H. Gross and B. Costisella, *Synthesis*, **1977**, 622; b) B. Costisella and H. Gross, *J. Prakt. Chem.*, **319**, 8 (1977); c) D. Seyferth, R. S. Marmor, and P. Hilbert, *J. Org. Chem.*, **36**, 1379 (1971).

7) The distance between two peri hydrogens at 4 and 5 positions is 5.1 Å for **5** with X=NMe and is 4.6 Å for **5** with X=S, which was measured by CPK model. Therefore,

steric hindrance may certainly be the reason for failure of synthesis of **5j**.

8) a) H. Decker and W. Petsch, *J. Prakt. Chem.*, **143**, 211 (1935) b) H. Decker and G. Dunant, *Ber.*, **39**, 2722 (1906).
9) F. Krohnke and H. L. Honig, *Chem. Ber.*, **90**, 2226 (1957).
10) A. A. Goldberg and A. H. Wragg, *J. Chem. Soc.*, **1957**, 4823.
11) W. Bonthrone and D. H. Reid, *J. Chem. Soc.*, **1959**, 2773.
12) W. Bonthrone and D. H. Reid., *Chem. Ind. (London)*, **1960**, 1192.
13) C. C. Price, M. Hori, T. Parasaran, and M. Polk, *J. Am. Chem. Soc.*, **85**, 2278 (1963).
14) F. Bossert, *Ann. Chem.*, **680**, 40 (1964).
15) A. Mustafa, M. M. Sidky, and F. M. Soliman, *Ann. Chem.*, **698**, 109 (1966).

Macrocyclic Enzyme Model Systems. Catalytic Activity of Cyclic Peptides Involving Hydrophobic Segments†

Yukito MURAKAMI,* Akio NAKANO, Kiyoshi MATSUMOTO, and Kiyoshi IWAMOTO

Department of Organic Synthesis, Faculty of Engineering, Kyushu University, Hakozaki, Higashi-ku, Fukuoka 812

(Received April 13, 1978)

In order to develop an effective hydrolase model, BCP-1 was synthesized and its kinetic behavior investigated. The corresponding linear hexapeptide was prepared by the solid phase method and subjected to cyclization by the azide method. BCP-1 enhanced the hydrolysis of *p*-nitrophenyl carboxylates bearing a long alkyl chain. The pH-rate profile for the hydrolysis of *p*-nitrophenyl hexadecanoate (PNPP) as effected by BCP-1 was not of a bell-shaped type but a sigmoid, from which the kinetic pK_a value was estimated as 12.3. The initial reaction rate was found to level off beyond a certain range of substrate concentration (saturation-type kinetics), the kinetic data being analyzed on the basis of Michaelis-Menten scheme. The large hydrophobic binding ability of BCP-1 toward PNPP (K_m(app) $\simeq 10^{-6}$ M) was attributed to its double-layered bicyclic structure. The Hammett plot for the hydrolysis of substituted phenyl hexadecanoates gave a satisfactory linear correlation. Consequently, the acyl transfer from the bound substrate to the imidazole anion of the histidyl residue of BCP-1 was referred to the rate-determining step. The large negative entropy change for the acyl transfer step seems to indicate that the Michaelis complex does not have a conformation favorable for such acyl transfer process. The catalytic effectiveness (k_{cat}/K_m(app)) for the BCP-1 catalysis in PNPP hydrolysis is comparable to that for enzymatic hydrolysis.

Catalytic functions of macrocyclic compounds such as cycloamyloses,[1] cyclophanes,[2] and cyclic peptides[3] have been investigated in order to explore the possibility of developing novel and efficient enzyme models. Cyclic peptides would simulate enzyme functions in a more favorable manner among these model systems since all enzymes are polypeptides. A few cyclic peptides so far synthesized were constructed only with α-amino acids, their hydrolase-like functions being much lower than those of real enzymes. The low efficiency may be primarily attributed to the network formation in their interior cavity by intramolecular hydrogen bonding, so that the hydrophobic binding ability can not be exercised. Such extensive intramolecular hydrogen bonding has been observed for cyclic hexapeptides by means of NMR[4] and CD[5] measurements.

In the present study, we designed cyclic peptides which bear long-chain alkyl segments in their skeleton to reduce the extent of intramolecular hydrogen bonding interaction, providing an efficient hydrophobic cavity for binding substrates. CP-1 was designed as a papain model with the aid of a space-filling molecular model (CPK model) so that the cyclic peptide has both an imidazole group of L-His and a thiol group of L-Cys at the juxtaposition within hydrogen bonding distance. In spite of this interesting aspect, CP-1 was not obtained but its dimeric form with a disulfide bond (BCP-1) was isolated. BCP-1 has only imidazole moieties as active functional groups and is considered to exist as a double-layered structure in aqueous media due to strong hydrophobic interaction between the two cyclic skeletons. We have investigated the esterase-like activity of BCP-1 in the ester hydrolysis for which the model compound would show a profound binding ability toward the substrates. In order to clarify the catalytic mechanism involved in the ester hydrolysis effected by BCP-1, other related compounds BCP-2 and CP-3 were also prepared and their kinetic effects studied.

† Contribution No. 483 from this Department.

Chart 1:

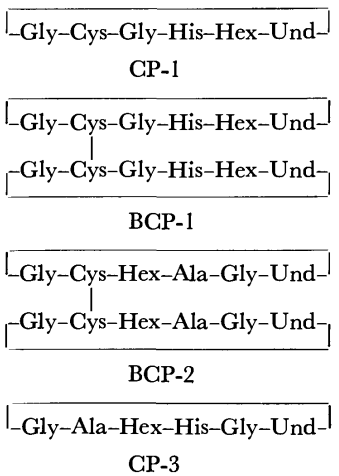

(Hex, 6-aminohexanoyl; Und, ω-aminoundecanoyl)

CP-1, *cyclo*-glycyl-L-cysteinylglycyl-L-histidyl-6-aminohexanoyl-ω-aminoundecanoyl; BCP-1, *S,S'*-bis(*cyclo*-glycyl-L-hemicystylglycyl-L-histidyl-6-aminohexanoyl-ω-aminoundecanoyl); BCP-2, *S,S'*-bis(*cyclo*-glycyl-L-hemicystyl-6-aminohexanoyl-L-alanylglycyl-ω-aminoundecanoyl); CP-3, *cyclo*-glycyl-L-alanyl-6-aminohexanoyl-L-histidylglycyl-ω-aminoundecanoyl.

Experimental

The synthetic procedures for the protected CP-1 (PCP-1) and BCP-1 are outlined in Scheme. 1. The linear hexapeptide hydrazide (**4**) was prepared by the solid phase method[6] and subjected to cyclization by the azide method.

Chloromethylated Styrene-2% Divinylbenzene Copolymer[7] (**1**). Copolystyrene-2%divinylbenzene (Protein Research Foundation, 100—200 mesh; 48 g) was made to swell in chloroform (300 ml) by stirring at room temperature for 2.5 h and was then cooled down to 0 °C. A solution of anhydrous stannic chloride (7.5 ml) in chloromethyl methyl ether (50 ml) was added to this mixture at 0 °C in 30 min, and stirred for 1 h at the same temperature. The mixture was filtered and the solid recovered was washed with dioxane-water (3 : 1 by volume, 1 litre) and subsequently with dioxane-3M HCl

Boc-Und-OCH_2-P (**2**; 4.0 g, 3.2 mmol)

↓ 1. CF_3CO_2H/CH_2Cl_2 (2 : 3)
↓ 2. $(C_2H_5)_3N/CH_2Cl_2$ (1 : 10)
↓ 3. Boc-Hex-OH (2.22 g, 9.6 mmol), DCC/CH_2Cl_2

Boc-Hex-Und-OCH_2P

↓ 1. CF_3CO_2H/CH_2Cl_2 (2 : 3)
↓ 2. $(C_2H_5)_3N$/DMF (1 : 10)
↓ 3. Boc-His(Bzl)-OH (3.31 g, 9.6 mmol), DCC/DMF

Boc-His(Bzl)-Hex-Und-OCH_2-P

↓ 1. 1 M-HCl (in CH_3CO_2H)
↓ 2. $(C_2H_5)_3N/CH_2Cl_2$ (1 : 10)
↓ 3. Boc-Gly-OH (1.68 g, 9.6 mmol)/[CH_2Cl_2/DMF], DCC/CH_2Cl_2

Boc-Gly-His(Bzl)-Hex-Und-OCH_2-P

↓ 1. 1 M-HCl (in CH_3CO_2H)
↓ 2. $(C_2H_5)_3N/CH_2Cl_2$ (1 : 10)
↓ 3. Boc-Cys(Bzl)-OH (2.99 g, 9.6 mmol), DCC/CH_2Cl_2

Boc-Cys(Bzl)-Gly-His(Bzl)-Hex-Und-OCH_2-P

↓ 1. 1 M-HCl (in CH_3CO_2H)
↓ 2. $(C_2H_5)_3N/CH_2Cl_2$ (1 : 10)
↓ 3. Boc-Gly-OH (1.68 g, 9.6 mmol)/[CH_2Cl_2/DMF], DCC/CH_2Cl_2

Boc-Gly-Cys(Bzl)-Gly-His(Bzl)-Hex-Und-OCH_2-P (**3**)

↓ NH_2NH_2/DMF

Boc-Gly-Cys(Bzl)-Gly-His(Bzl)-Hex-Und-$NHNH_2$ (**4**)

↓ 1. 2 M-HCl (in CH_3OH)
↓ 2. 2 M-HCl (in THF), $(CH_3)_2CHCH_2CH_2NO_2$/DMF
↓ 3. $(C_2H_5)_3N$/DMF

cyclo-Gly-Cys(Bzl)-Gly-His(Bzl)-Hex-Und (**5**, PCP-1)

↓ Na/liq. NH_3

cyclo-Gly-Cys-Gly-His-Hex-Und
|
cyclo-Gly-Cys-Gly-His-Hex-Uud (BCP-1)

Scheme 1. Synthetic procedures for BCP-1: Hex, 6-aminohexanoyl: Und, ω-aminoundecanoyl; Boc, *t*-butoxycarbonyl; Bzl, benzyl; P, styrene-2%divinylbenzene copolymer.

(3 : 1 by volume, 1 litre). The cream-colored beads were washed further with water first and then with aqueous dioxane, the dioxane content of which was increased gradually up to 100%. After the beads had been washed with pure dioxane, they were washed with dioxane-methanol with gradual increase in methanol content and finally with pure methanol. No abrupt change in solvent composition was made during the course of washing. The product was dried *in vacuo* at 100 °C: yield 53.2 g; 1.98 mmol Cl/g.

N-t-*Butoxycarbonyl-ω-aminoundecanoyl Resin (2)*. A solution of *N-t*-butoxycarbonyl-ω-aminoundecanoic acid[8] (8.94 g, 29.7 mmol) and triethylamine (3.3 ml, 24.0 mmol) in 40 ml of dry ethanol was mixed with **1** (100—200 mesh, 10.0 g). The mixture was stirred under reflux for 144.5 h and filtered to recover the resin, which was subsequently washed thoroughly with ethanol, hot ethanol, aqueous ethanol, water, aqueous methanol, and methanol, and then dried *in vacuo*; the content of ω-aminoundecanoic acid by nitrogen analysis, 0.80 mmol/g (conversion 40.4%).

N-t-*Butoxycarbonylglycyl*-S-*benzyl*-L-*cysteinylglycyl*-N^{Im}-*benzyl*-L-*histidyl-6-aminohexanoyl-ω-aminoundecanoyl Resin (3)*. A portion of **2** (4.0 g, 3.2 mmol) was coupled first with *N-t*-butoxycarbonyl-6-aminohexanoic acid[8] (Table 1) with a Shimadzu peptide synthesizer APS-80. The subsequent coupling reactions were carried out in a similar manner; modifications with regard to solvents and reagents are shown in Scheme 1. Additional washing with a solvent for the corresponding coupling reaction was carried out for the subsequent coupling steps between treatment Nos. 10 and 11 in Table 1. *N-t*-Butoxycarbonyl-N^{Im}-benzyl-L-histidine[9] and *N-t*-butoxycarbonyl-*S*-benzyl-L-cysteine[10] were prepared according to the procedures reported.

N-t-*Butoxycarbonylglycyl*-S-*benzyl*-L-*cysteinylglycyl*-N^{Im}-*benzyl*-L-*histidyl-6-aminohexanoyl-ω-aminoundecanoic Acid Hydrazide (4)*. To a suspension of protected linear hexapeptide resin **3** (4.85 g) in *N,N*-dimethylformamide (30 ml) was added freshly prepared anhydrous hydrazine (bp 113.5 °C; 5.0 ml, 157 mmol). The mixture was stirred at room temperature for 48 h, and filtered to separate the resin which was subsequently washed with *N,N*-dimethylformamide (100 ml). The filtrate and washings were combined and evaporated *in vacuo*, and the residue was treated with water (200 ml) in order to isolate the insoluble product (610 mg). The crude material was purified on a column (2.5 × 81.0 cm) of Sephadex LH-20 with methanol as an eluent: yield 560 mg (18.2% based on *N-t*-butoxycarbonyl-ω-aminoundecanoyl resin); ninhydrin test, positive; hydrazide test, positive; R_f with 1-butanol–water–acetic acid (4:2:1), 0.89; mp 144—147 °C. IR (KBr disc): 3280 (NH str.); 2910 and 2840 (CH str.); 1635 (C=O str.); 770, 730, and 700 cm^{-1} (CH bend. of benzene). NMR (DMSO-d_6, TMS): δ 1.23 (22H, s, $-NHCH_2-(CH_2)_{n-2}CH_2CO-$), 1.38 (9H, s, $(CH_3)_3CO-$), 2.02 (4H, broad, $-NHCH_2(CH_2)_{n-2}CH_2CO-$), 2.85 (2H, broad,

Table 1. Operational sequence for coupling reaction of Boc-Hex-OH with **2** programmed on a Shimadzu peptide synthesizer (ASP-80)

Treatment No.	Reagent	Shaking period	Repeating frequency	Each amount
1	CH_2Cl_2	4 min	3	40 ml
2	CF_3CO_2H-CH_2Cl_2 (2 : 3 v/v)	60 min	1	40 ml
3	CH_2Cl_2	4 min	3	40 ml
4	C_2H_5OH	4 min	3	40 ml
5	CH_2Cl_2	4 min	3	40 ml
6	$(C_2H_5)_3N$-CH_2Cl_2 (1 : 10 v/v)	10 min	1	50.4 ml
7	CH_2Cl_2	4 min	5	40 ml
8	Charge: Boc-Hex-OH/CH_2Cl_2	10 min	1	2.22 g/29 ml
9	Charge: DCC/CH_2Cl_2	19 h	1	1.98 g/20.5 ml
10	CH_2Cl_2	4 min	4	40 ml
11	C_2H_5OH	20 min	2	40 ml

–NHCH(CH$_2$SCH$_2$Ph)CO–), 3.00 (4H, broad, –NHCH$_2$–(CH$_2$)$_{n-2}$CH$_2$CO–), 3.50 (4H, s, –NHCH$_2$CO–), 3.68 (2H, broad, –NHCH(CH$_2$ImCH$_2$Ph)CO–), 3.75 (2H, s, –SCH$_2$–Ph), 4.50 (2H, broad, –CH–), 5.12 (2H, s, N^{Im}-CH$_2$Ph), 6.85 (1H, s, imidazolyl H), 7.30 (10 H, s, phenyl H's), 7.62 (1H, s, imidazolyl H), 7.83—8.60 (6H, broad, –NH–), and 9.00 (2H, broad, –NHNH$_2$). Found: C, 60.83; H, 7.76; N, 14.20%. Calcd for $C_{49}H_{74}N_{10}O_8S$: C, 61.10; H, 7.74; N, 14.54%.

cyclo-*Glycyl*-S-*benzyl*-L-*cysteinylglycyl*-N^{Im}-*benzyl*-L-*histidyl*-6-*aminohexanoyl*-ω-*aminoundecanoyl* (**5**, *PCP-1*). Linear hexapeptide hydrazide **4** (884 mg, 0.98 mmol) was dissolved in freshly prepared 2M hydrogen chloride in dry methanol (60 ml), and the mixture was stirred at room temperature for 3 h and then evaporated *in vacuo*. The residue was triturated in anhydrous ether, washed with the same solvent, and dried *in vacuo* at 40 °C to give pale yellow crystals. To the product dissolved in dry *N,N*-dimethylformamide (70 ml) was added freshly prepared 1.85 M hydrogen chloride in dry tetrahydrofuran (35 ml) and isopentyl nitrite (0.5 ml, 3.69 mmol) at −30 °C. After the reaction mixture being allowed to stand at −30 °C for 90 min, the absence of residual hydrazide in it was confirmed. A mixture of 0.3 M iron(III) chloride in 0.1 M acetic acid and 0.2 M potassium hexacyanoferrate(III) in 0.1 M acetic acid was used for detection. The mixture was diluted with dry *N,N*-dimethylformamide (540 ml) at −60 °C, followed by addition of dry triethylamine (21.7 ml, 155.4 mmol). The reaction mixture was allowed to stand at −10 °C for 48 h with stirring, and evaporated *in vacuo*. The residue was treated with water (200 ml) in order to recover the insoluble product. The crude product was purified by chromatography on columns of Amberlite IR-45 (1.5×27 cm) and Amberlite IRC-50 (1.5×27 cm) with dichloromethane–methanol–*N,N*-dimethylformamide–water (32:17:5:6 by volume), and then on a column of Sephadex LH-20 (2.5×81.0 cm) with methanol to give a white solid: yield 165.2 mg; mp(dec) 207—210 °C; ninhydrin test, negative; hydrazide test, negative. IR (KBr disc): 3300 (NH str.); 2920 and 2860 (CH str.); 1640 (C=O str.); and 770, 730, and 700 cm^{-1} (CH bend. of benzene). NMR (DMSO-d_6, TMS): δ 1.25 (22H, s, –NHCH$_2$(CH$_2$)$_{n-2}$CH$_2$CO–), 2.08 (4H, broad, –NHCH$_2$–(CH$_2$)$_{n-2}$CH$_2$CO–), 2.85 (2H, broad, –NHCH(CH$_2$SCH$_2$–Ph)CO–), 3.07 (4H, broad, –NHCH$_2$(CH$_2$)$_{n-2}$CH$_2$CO–), 3.42 (4H, s, –NHCH$_2$CO–), 3.65(2H, broad, –NHCH–(CH$_2$ImCH$_2$Ph)CO–), 3.80 (2H, s, –SCH$_2$Ph), 4.50 (2H, broad, –CH–), 5.22 (2H, s, N^{Im}-CH$_2$Ph), 7.00 (1H, s, imidazolyl H), 7.38 (10H, s, phenyl H's), 7.85 (1H, s, imidazolyl H), and 7.96—8.58 (7H, broad, –NH–). Mol wt: osmometry (methanol), 830; calcd for $C_{44}H_{62}N_8O_6S$, 831.1. Found: C, 62.16; H, 7.61; N, 12.82%. Calcd for $C_{44}H_{62}N_8O_6S\cdot H_2O$: C, 62.24; H, 7.63; N, 13.20%.

S,S′-*Bis*(cyclo-*glycyl*-L-*hemicystylglycyl*-L-*histidyl*-6-*aminohexanoyl*-ω-*aminoundecanoyl*) (*BCP-1*). To a solution of the protected cyclic peptide (**5**) (100 mg, 0.12 mmol) in liquid ammonia (100 ml, distilled in the presence of sodium metal) was added a small amount of sodium metal with stirring until the blue color of the solution remained for at least 2 min. In order to quench the excess sodium metal, a small amount of ammonium chloride was added to the solution which was subsequently evaporated to dryness *in vacuo* at room temperature. The residue was then treated with water (100 ml). The insoluble product was recovered by filtration, washed thoroughly with water, and dried *in vacuo* to give a white solid: yield 52.5 mg (67%); ninhydrin test, negative; Pauly test, positive; nitroprusside test, negative; Ellman test, negative. IR (KBr disc): 3300 (NH str.); 2920 and 2860 (CH str.); 1645 cm^{-1} (C=O str.). NMR (DMSO-d_6, TMS): δ 1.23 (22H, s, –NHCH$_2$(CH$_2$)$_{n-2}$CH$_2$–CO–), 2.10 (4H, broad, –NHCH$_2$(CH$_2$)$_{n-2}$CH$_2$CO–), 2.80 (2H, broad, –NHCH(CH$_2$S–)CO–), 3.13 (4H, s, –NHCH$_2$(CH$_2$)$_{n-2}$CH$_2$CO–), 3.38 (4H, s, –NHCH$_2$CO–), 3.65 (2H, s, –NHCH(CH$_2$Im)CO–), 4.46 (2H, broad, –CH–), 6.80 (1H, s, imidazolyl H), and 7.54 (1H, s, imidazolyl H). Amino acid analysis: Hex, 0.9 (1); His, 1.0 (1); Gly, 1.9 (2); Cys, 0.8 (1). The product showed very limited solubility in water and in most organic solvents; molecular weight determination by vapor pressure osmometry was not possible. Found: C, 54.21; H, 7.77; N, 16.09%. Calcd for $C_{60}H_{98}N_{14}O_{12}S_2\cdot 2H_2O$: C, 53.87; H, 7.84; N, 16.75%.

Other Cyclic Peptides. *cyclo*-Glycyl-L-cysteinyl-6-aminohexanoyl-L-alanylglycyl-ω-aminoundecanoyl (CP-2) and CP-3 were prepared in a manner similar to that described for BCP-1. Elimination of the protecting group in the last step of the CP-2 synthesis was performed with anhydrous hydrofluoric acid.

CP-2: white powder; ninhydrin negative, nitroprusside positive, and Ellman positive at pH 8. IR (KBr disc): 3295 (NH str.); 2920 and 2850 (CH str.); 1625 and 1540 cm^{-1} (C=O str.). NMR (DMSO-d_6, TMS): δ 1.22 (22H, s, –NHCH$_2$(CH$_2$)$_{n-2}$CH$_2$CO–), 2.15 (4H, broad, –NHCH$_2$(CH$_2$)$_{n-2}$CH$_2$CO–), 2.77 (2H, broad, –CH$_2$SH), 3.04 (4H broad, –NHCH$_2$(CH$_2$)$_{n-2}$CH$_2$CO–), 3.63 (4H, s, –NHCH$_2$CO–), and 4.58 (2H, broad, –CH–). Amino acid analysis: Gly, 2.2 (2); Ala, 1.1 (1); Cys, 1.0 (1); Hex, 1.1 (1). BCP-2 was prepared by air-oxidation of CP-2 before use until nitroprusside test turned out to be completely negative.

CP-3: white powder; ninhydrin negative, and Pauly positive; R_f with 1-butanol–water–acetic acid (4 : 2 : 1 by volume), 0.53. IR (KBr disc): 3280 (NH str.); 2920 and 2850 (CH str.); 1640 and 1550 cm^{-1} (C=O str.). NMR (methanol-d_4, TMS): δ 1.32 (22H, s, –NHCH$_2$(CH$_2$)$_{n-2}$–CH$_2$CO–), 2.26 (4H, broad, –NHCH$_2$(CH$_2$)$_{n-2}$CH$_2$CO–), 3.79 (4H, s, –NHCH$_2$CO–), 4.26 (2H, broad, –CH–), 6.91 (1H, s, imidazolyl H), and 7.67 (1H, s, imidazolyl H). Amino acid analysis: Gly, 2.2 (2); Ala, 1.1 (1); His, 1.0 (1); Hex, 0.7 (1). Found: C, 56.79; H, 8.22; N, 17.02%; M^+, 619. Calcd for $C_{30}H_{50}N_8O_6\cdot H_2O$: C,56.58; H, 8.23; N, 17.59%; mol wt ($C_{30}H_{50}N_8O_6$), 618.81.

Substrates. Substituted phenyl esters were prepared by the general method[11] from acid chlorides and substituted phenols in the presence of a trace amount of magnesium and confirmed by IR and NMR spectroscopy. Analytical and physical data for the esters are given in Table 2.

Kinetic Measurements. Rates of phenol liberation from a substituted phenyl ester were measured either with a Union Giken high sensitive spectrophotometer SM-401 or with a Hitachi 124 spectrophotometer at the following wavelengths: *p*-cyanophenyl hexadecanoate, 275 nm; *p*-acetylphenyl hexadecanoate, 330 nm; *m*-nitrophenyl and *p*-nitrophenyl hexadecanoate, and other *p*-nitrophenyl esters, 400 nm. Each run was initiated by adding a dioxane solution(30 μl) of a substrate ester to a mixture of a reaction medium (3.0 ml) and a *N,N*-dimethylformamide solution (30 μl) of a catalyst, which was pre-equilibrated at an appropriate temperature in a thermostatted cell set in the spectrophotometer. The reaction temperature was maintained constant within an accuracy of ±0.1 °C. The reaction medium was prepared as follows: 10.0 ml of 1.0 M aqueous potassium chloride, 10.0 ml of an appropriate aqueous buffer, and 10.0 ml of dry dioxane were placed in a 100-ml volumetric flask; and subsequently the flask was filled with deionized and distilled water. Aqueous buffer solutions used are as follows:

1/10 M potassium dihydrogenphosphate-1/20 M sodium borate for pH 6—9, 1/20 M sodium borate-1/20 M sodium carbonate for pH 10—11, and 1/10 M sodium hydroxide —1/10 M sodium hydrogenphosphate for pH 11—12. pH Measurements were carried out with a TOA HM-9A pH meter equipped with a TOA GC-125 combined electrode after calibration with a combination of appropriate aqueous standard buffers.

Results and Discussion

Catalytic Effects and Substrate Specificity. The catalytic efficiency of BCP-1 in the hydrolysis of *p*-nitrophenyl esters of some carboxylic acids has been investigated by the kinetic method in 10.0%(v/v) dioxane–1.0%(v/v) *N*,*N*-dimethylformamide–water at μ 0.10 (KCl). Apparent pseudo-first-order rate constants were obtained from the initial stage of the reaction by measuring the amount of liberated *p*-nitrophenol. The first-order kinetics was found to hold at least up to 65% conversion of the substrate under the conditions [S]>[E]; S and E stand for substrate and catalyst species, respectively. The kinetic data are summarized in Table 3. The result shows BCP-1 only catalyzes the hydrolysis of *p*-nitrophenyl esters bearing a long alkyl chain such as *p*-nitrophenyl hexadecanoate (PNPP) and dodecanoate (PNPL). In order to observe the catalytic effect by BCP-1, the substrate is required to involve a bulky group of suf-

Table 2. Analytical and physical data for substrates

Substrate[a]	Formula	Found (%)			Calcd (%)			Mp/Bp
		C	H	N	C	H	N	
PNPP	$C_{22}H_{35}NO_4$	70.06	9.08	3.90	69.99	9.34	3.71	62—64 °C
MNPP	$C_{22}H_{35}NO_4$	70.07	9.41	3.63	69.99	9.34	3.71	61—62 °C
PAPP	$C_{24}H_{38}O_3$	76.84	10.84		76.96	10.23		62—63 °C
PCPP	$C_{23}H_{35}NO_2$	77.21	9.94	3.84	77.26	9.87	3.92	75—76 °C
PNPCHC	$C_{13}H_{15}NO_4$	62.75	6.16	5.40	62.64	6.06	5.61	154—174 °C/0.7 mmHg
PNPG	$C_{16}H_{14}N_2O_6$	58.17	4.29	8.53	58.18	4.27	8.48	130—132 °C

a) Abbreviations: PNPP, *p*-nitrophenyl hexadecanoate; MNPP, *m*-nitrophenyl hexadecanoate; PAPP, *p*-acetylphenyl hexadecanoate; PCPP, *p*-cyanophenyl hexadecanoate; PNPCHC, *p*-nitrophenyl cyclohexanecarboxylate; PNPG, *p*-nitrophenyl *N*-benzyloxycarbonylglycinate.

Table 3. Apparent first-order rate constants for the BCP-1 catalyzed hydrolysis of *p*-nitrophenyl carboxylates at 40.0±0.1 °C and μ 0.10 (KCl) in 10.0%(v/v) dioxane–1.0%(v/v) *N*,*N*-dimethylformamide–water[a]

Substrate, R[b]	$k_{hyd}\times10^5$ (s^{-1})	$k_{obsd}\times10^5$ (s^{-1})	$k_c\times10^5$ [c] (s^{-1})	pH
$CH_3(CH_2)_{14}$-	2.78	4.77	1.99	11.45
$CH_3(CH_2)_{10}$-	30.7	34.5	3.80	10.91
$CH_3(CH_2)_8$-	300	300	—	10.91
CH_3-	1625	1625	—	10.91
	400	400	—	10.91
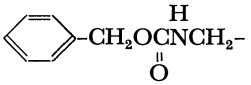	1385	1385	—	9.72

a) Initial concentrations: substrates, 0.984—0.989$\times10^{-5}$ M; BCP-1, 0.49$\times10^{-6}$ M. b) R for *p*-NO_2-C_6H_4-OC(O)R. c) $k_c=k_{obsd}-k_{hyd}$; k_{obsd}, observed first-order rate constants; k_{hyd}, hydrolysis rate constant in the absence of the catalyst.

Table 4. Apparent first- and second-order rate constants for the catalyzed hydrolysis of *p*-nitrophenyl hexadecanoate at 40.0±0.1 °C and μ 0.10 (KCl) in 10.0%(v/v) dioxane–1.0%(v/v) *N*,*N*-dimethylformamide–water[a]

Catalyst species[b] (E)	$k_{obsd}\times10^4$ (s^{-1})	$k_c\times10^4$ [c] (s^{-1})	k_c/[E] ($s^{-1}M^{-1}$)	pH
BCP-1 (0.49$\times10^{-6}$ M)	3.13	1.03	210	12.30
CP-3 (7.63$\times10^{-6}$ M)[d]	2.10	0	—	12.28
PCP-1 (2.55$\times10^{-5}$ M)	1.39	inhibition	—	12.30
BCP-2 (0.51$\times10^{-5}$ M)	1.12	inhibition	—	12.26
Imidazole (0.987$\times10^{-2}$ M)	2.60	0.50	5.07×10^{-3}	12.30
OH^- [e]	2.10	—	1.05×10^{-2}	12.30

a) Initial concentration of PNPP, 0.985$\times10^{-5}$ M. b) The concentration of each catalyst (E) is indicated in the parentheses right after its name. c) $k_c=k_{obsd}-k_{hyd}$. d) The maximum attainable concentration under the present conditions. e) Alkaline hydrolysis.

ficient hydrophobicity as observed for the paracyclophane catalysis.[2] The rate constants for the hydrolysis of PNPP in the presence of various synthetic catalysts are summarized in Table 4. Among the synthetic cyclic peptides employed, only BCP-1 showed a significant catalytic activity toward PNPP. On the other hand, PCP-1 and BCP-2 inhibited the alkaline hydrolysis of PNPP. This indicates that both cyclic compounds can incorporate PNPP into their cyclic skeletons, preventing the hydroxide attack on the bound substrate. It seems that hydrophobicity provided by the single layered structure of CP-3 in aqueous media is not sufficient to incorporate PNPP. The apparent second-order rate constant (k_c/[E]) for the hydrolysis catalyzed by BCP-1 is larger than that for imidazole catalysis by 4.2×10^4 fold. The high catalytic efficiency of BCP-1 is attributed to the binding capability of its hydrophobic cavity toward the substrate of hydrophobic character.

pH-Dependence of Kinetic Behavior. The pH-rate profile is not the bell-shaped type observed in enzymatic reactions,[12] but a sigmoid as shown in Fig. 1. This indicates that BCP-1 has a functional group or groups which can be activated by deprotonation above pH 12. The active functional group is referred to the anionic imidazole group of the histidyl residue: pK_a (graphically estimated), 12.3. Relative to the corresponding pK_a value for imidazole (14.5 at 25 °C and μ 0.5 in aqueous medium),[13] the pK_a value obtained for BCP-1 is somewhat lower. The intramolecular hydrogen bonding between two imidazole groups in the single molecule may act to reduce the pK_a value since these two imidazole groups in BCP-1 can be placed at the juxtaposition within their hydrogen bonding distance according to the CPK model. The access of these groups would be enhanced by the intramolecular hydrophobic interaction between the two cyclic skeletons. Our attempt to determine the pK_a of the imidazole group of L-His residue of BCP-1 by spectrophotometric or potentiometric titration was not successful due to its limited solubility. Overberger *et al.* observed that the solvolysis rate of *p*-nitrophenyl acetate is enhanced by homopolymers of 4-vinylimidazole and 5-vinylbenzimidazole. They attributed the rate enhancement to the reduction of pK_a of the polymers brought about by internal hydrogen bonding interaction.[14]

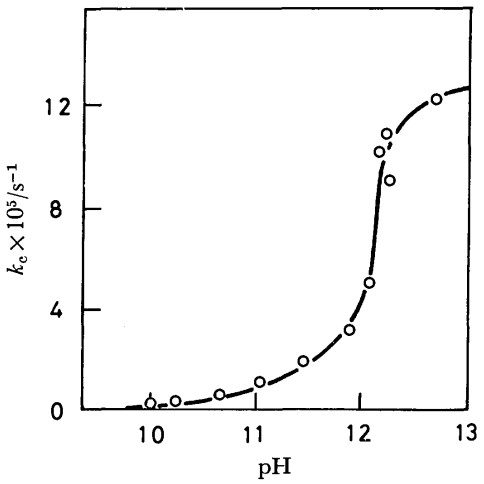

Fig. 1. pH-Rate profile for the BCP-1 catalyzed hydrolysis of *p*-nitrophenyl hexadecanoate (PNPP) in 10.0% (v/v) dioxane–1.0% (v/v) *N*,*N*-dimethylformamide–water at 40.0±0.1 °C and μ 0.10 (KCl); $k_c=k_{obsd}-k_{hyd}$. Initial concentrations: PNPP, 0.985×10^{-5} M; BCP-1, 0.49×10^{-6} M.

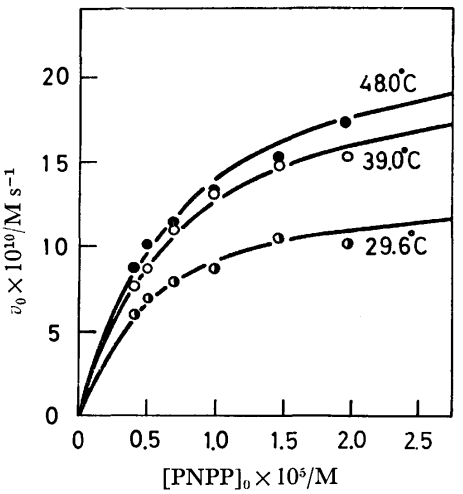

Fig. 2. Saturation-type kinetics for the hydrolysis of *p*-nitrophenyl hexadecanoate as catalyzed by BCP-1 in 10.0% (v/v) dioxane–1.0% (v/v) *N*,*N*-dimethylformamide–water at pH 12.35 and μ 0.10 (KCl): initial concentration of BCP-1, 0.49×10^{-6} M; v_0, initial reaction velocity; $[PNPP]_0$, initial concentration of PNPP.

Michaelis-Menten Analysis. The initial hydrolysis rate (v_0) as catalyzed by BCP-1 was determined at various concentrations of PNPP. The initial rate was found to level off beyond a certain range of substrate concentration (saturation-type kinetics) as seen in Fig. 2. The kinetic data were analyzed in terms of the Michaelis-Menten kinetics based on the overall reaction pathway given by the following:

$$\begin{array}{ccccccc} E + S & \overset{K_S}{\rightleftharpoons} & (ES) & \xrightarrow{k_2} & (ES)' & \xrightarrow{k_3} & E + P_2 \\ & & \downarrow{\scriptstyle k_{hyd}} & & + & & \\ & & P_1 + P_2 & & P_1 & & \end{array} \quad (1)$$

where P_1 and P_2 stand for the alcohol and the acid moiety, respectively, formed in the hydrolysis of ester substrate S; (ES) and (ES)′ are the Michaelis-type complex and the acylated catalyst, respectively; k_2 and k_3 refer to the rate constants for acylation and deacylation steps performed on the catalyst, respectively. For the three-step kinetic model, apparent Michaelis constant K_m(app) and catalytic coefficient k_{cat} are defined by Eqs. 2 and 3, respectively, on the basis of the steady-state approximation, where $K_s=[E][S]/[ES]$.

$$K_m(\text{app}) = \frac{k_3}{k_2+k_3}K_S \quad (2)$$

$$k_{cat} = \frac{k_2k_3}{k_2+k_3} \quad (3)$$

The rate of *p*-nitrophenolate (P_1) liberation was found

to follow the apparent first-order kinetics for at least 65% conversion of PNPP when [S]>[E], no detectable induction period being observed for all runs of the present study. The observations are consistent with a reaction mechanism which involves complex formation between the substrate and the catalyst followed by the rate-determining acyl-transfer step (k_2) to form acylated catalyst (ES)'. The catalyst species was regenerated through the final fast deacylation step (k_3); so-called turnover behavior was observed. In order to confirm that the acylation step is rate determining, the kinetic data obtained under [S]>[E] for the hydrolysis of substituted phenyl esters of hexadecanoic acid were treated in terms of Hammett equation. A good linear correlation (Fig. 3) indicates that the acylation step is rate determining: Eqs. 2 and 3 can be simplified as $K_m(\text{app})=K_s$ and $k_{cat}=k_2$, respectively. The evaluated ρ-value (3.5) is quite large for the ordinary nucleophilic displacement reaction at the substituted phenyl ester bond. This high sensitivity may result from a tight interaction of the ester bond with the anionic nucleophile in the desolvated cage. It seems that the reaction center is located in the hydrophobic cavity of BCP-1. The Michaelis-Menten parameters obtained by the Lineweaver-Burk plots are given in Table 5.

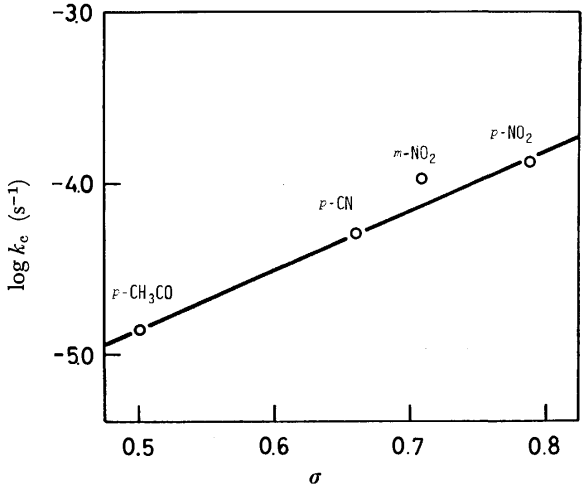

Fig. 3. Correlation of apparent catalytic rate constant k_c with Hammett σ. All runs were carried out in 10.0%(v/v) dioxane-1.0%(v/v) *N,N*-dimethylformamide-water at pH 12.30, 40.0±0.1 °C, and μ 0.10 (KCl). Initial concentrations: BCP-1, 0.49×10^{-6} M; PNPP, 0.985×10^{-5} M; MNPP, 0.984×10^{-5} M; PCPP, 0.984×10^{-5} M; PAPP, 0.981×10^{-5} M.

Nakajima and Okawa investigated the catalytic behavior of *cyclo*(His-Gly-Cys-D-Phe-Gly)$_2$ in the hydrolysis of *p*-nitrophenyl acetate:[3e] $k_{cat}=2.8\times10^{-3}$ s^{-1}, $K_m(\text{app})=2.7\times10^{-3}$ M, $k_{cat}/K_m(\text{app})=1.04$ M^{-1} s^{-1} at pH 7.73 and 24.0 °C. The k_{cat} value for their cyclic peptide is comparable to that for BCP-1 of the present study. However, the $k_{cat}/K_m(\text{app})$ value of the cyclic decapeptide is much smaller than that of BCP-1 by an order of 5×10^2, most likely due to the lower hydrophobic effect of the former. The importance of the hydrophobic effect for incorporation of the bulky substrate was further confirmed by a solvent effect study on the BCP-1 catalyzed hydrolysis. The catalytic ability of BCP-1 completely disappeared when the content of dioxane was raised to 20% (v/v) in reaction media.

The thermodynamic parameters for the substrate-binding process (Table 6) indicate that the formation of a substrate-catalyst complex is primarily controlled by the entropy effect for which the hydrophobic interaction between BCP-1 and PNPP is responsible. In reference to the activation parameters for both BCP-1 catalyzed and alkaline hydrolyses of PNPP, the rate enhancement by BCP-1 (k_{cat}) over the corresponding alkaline hydrolysis (k_{hyd}) is attributed to the enthalpy effect. The unfavorable entropy change is more than compensated by the enthalpy change. The unfavorable entropy effect in the pseudo-intramolecular acyl-transfer was unexpected and might be due to particular steric conformation in the Michaelis-type complex not favorable for the subsequent acylation reaction.

Effect of Mercury(II) Ion. An appropriate metal ion is expected to show a unique effect on the reactivity of BCP-1 since the catalyst has several donor atoms. The mercuric ion gave no effect in the hydro-

Table 6. Thermodynamic parameters for the hydrolysis of *p*-nitrophenyl hexadecanoate as catalyzed by BCP-1[a]

Quantity	ΔG_{312K} (kcal/mol)	ΔH (kcal/mol)	ΔS (e. u.)
$K_m(\text{app})$[b]	7.33	0±2	−23.5±0.1
k_{cat}[c]	21.6	5.32	−52.7
k_{hyd}[c]	23.5	12.9	−33.9

a) Based on the data given in Table 5. b) $\Delta G^0=-RT\ln K_m(\text{app})=\Delta H^0-T\Delta S^0$. c) $\Delta G^*=RT\ln(\kappa T/h k_r)=\Delta H^*-T\Delta S^*$; κ, Boltzmann's constant; h, Plank's constant; k_r, rate constant (k_{cat} or k_{hyd}).

Table 5. Kinetic parameters for the BCP-1 catalyzed hydrolysis of *p*-nitrophenyl hexadecanoate at pH 12.32 and μ 0.10 (KCl)[a]

Temp (°C)	v_{max}[b] $\times10^9$ ($M\,s^{-1}$)	$K_m(\text{app})$[b] $\times10^6$ (M)	k_{cat}[c] $\times10^3$ (s^{-1})	$[k_{cat}/K_m(\text{app})]\times10^{-2}$ ($M^{-1}s^{-1}$)
29.6	1.39	5.20	2.84	5.46
39.0	2.20	7.39	4.50	6.08
48.0	2.38	7.01	4.86	6.94

a) In 10.0%(v/v) dioxane-1.0%(v/v) *N,N*-dimethylformamide-water with the initial BCP-1 concentration ($[E]_0$) of 0.49×10^{-6} M. b) Kinetic parameters, v_{max} and $K_m(\text{app})$, were evaluated from the initial rates measured at various substrate concentrations ($0.394-1.97\times10^{-5}$ M). c) $k_{cat}=v_{max}/[E]_0$.

Table 7. First-order rate constants for the hydrolysis of *p*-nitrophenyl hexadecanoate in the presence and absence of mercury(II) ion[a]

$HgCl_2$ (M)	k_{hyd}[b] $\times 10^3$ (s^{-1})	k_{obsd}[c] $\times 10^3$ (s^{-1})
None	2.50	3.65
0.988×10^{-6}	2.50	1.96
0.988×10^{-5}	2.50	1.83

a) In 10.0% (v/v)dioxane-1.0% (v/v) *N*,*N*-dimethylformamide-water; pH, 12.45; μ, 0.10 (KCl); temp, 40.0±0.1 °C. b) Apparent first-order rate constant for the alkaline hydrolysis of PNPP. c) Apparent first-order rate constant for the hydrolysis of PNPP in the presence of BCP-1; initial concentration of BCP-1, 0.49×10^{-6} M.

lysis of PNPP without BCP-1, but considerably retarded the reaction with cooperation of the cyclic peptide (Table 7). The reaction rate was reduced below the catalyst-absence level (k_{hyd}). The result suggests that BCP-1 deactivated by the coordination of the mercuric ion at its imidazole group still holds a significant ability to bind the substrate.

Substrate-Binding Ability of BCP-1 and PCP-1. PCP-1 retarded the alkaline hydrolysis of PNPP by incorporating the substrate into its cavity in line with the kinetic pathway expressed by the following:

$$\begin{array}{ccccc} S + C & \overset{K_b}{\rightleftharpoons} & (SC) & \xrightarrow{k_{in}} & P \\ & & \downarrow{\scriptstyle k_{hyd}} & & \\ & & P & & \end{array} \qquad (4)$$

where cyclic peptide C and substrate S yield association complex (SC) with binding constant K_b, and the free and bound substrates undergo hydrolysis with rate constants k_{hyd} and k_{in}, respectively. The observed pseudo-first-order rate constant (k_{obsd}) is given by

$$k_{obsd} = \frac{k_{hyd} + k_{in}K_b[C]_0}{1 + K_b[C]_0}, \qquad (5)$$

where $[C]_0$ stands for the initial concentration of PCP-1. Equation 5 can be rearranged to give

$$\frac{1}{k_{hyd} - k_{obsd}} = \frac{1}{k_{hyd} - k_{in}} + \frac{1}{(k_{hyd} - k_{in})K_b[C]_0}. \qquad (6)$$

A good linear relationship has been obtained by plotting $1/(k_{hyd} - k_{obsd})$ against $1/[C]_0$. The values of k_{in} and K_b obtained are 1.68×10^{-4} s^{-1} and 8.47×10^4 M^{-1}, respectively, at pH 12.3, 40.0±0.1 °C, and μ 0.10. The hydrolysis constant for the bound PNPP is smaller than that for the free ($k_{hyd}=2.91\times10^{-4}$ s^{-1}) by 1.7-fold. The binding constant for the complex of PCP-1 and PNPP is smaller than that for the complex of BCP-1 and PNPP by 1.6-fold. BCP-2 also retarded the alkaline hydrolysis of PNPP to a similar extent to that observed for PCP-1 (Table 4). CP-3 did not give out any meaningful effect on the alkaline hydrolysis of PNPP. The result indicates that the hydrophobic effect provided by the CP-3 cavity is not enough to incorporate PNPP.

Conclusion. Since CP-3 has no catalytic activity in the hydrolysis of PNPP, depth of the single-layered cyclic peptide does not seem to provide sufficient hydrophobic effect to incorporate a hydrophobic substrate. On the other hand, BCP-1, being a double-layered bicyclic species, provides a strong hydrophobic cavity. The efficient hydrophobic nature of the double-layered cyclic peptide was further substantiated by investigation on the substrate-binding property of BCP-2. Although we were not successful in developing an efficient papain model, the thiol group of L-Cys residue not being left active upon disulfide-bond formation during the course of CP-1 synthesis, the apparent second-order rate constant (k_{cat}/K_m(app)) for the PNPP hydrolysis effected by BCP-1 is comparable to those for the papain-catalyzed hydrolysis of esters and amides.[15] The overall rate enhancement by BCP-1 is apparently provided by a much stronger hydrophobic binding ability than that of papain and chymotrypsin toward the present particular substrate. In order to develop a more effective hydrolase model, the steric control needs to be exercised toward a bound substrate, so that the unfavorable entropy effect observed in the acylation step of the present study would be markedly improved.

This work was partially supported by the Kurata Foundation. The authors are indebted to Drs. Motosuke Kikutani and Masatsune Ishiguro, Faculty of Pharmaceutical Sciences, Nagasaki University, for the amino acid analysis.

References

1) For example: R. Breslow and L. E. Overman, *J. Am. Chem. Soc.*, **92**, 1075 (1977).
2) (a) Y. Murakami, J. Sunamoto, and K. Kano, *Bull. Chem. Soc. Jpn.*, **47**, 1238 (1974); (b) Y. Murakami, J. Sunamoto, H. Okamoto, and K. Kawanami, *Bull. Chem. Soc. Jpn.*, **48**, 1537 (1975); (c) Y. Murakami, Y. Aoyama, K. Dobashi, and M. Kida, *Bull. Chem. Soc. Jpn.*, **49**, 3633 (1976); (d) Y. Murakami, Y. Aoyama, and K. Dobashi, *J. Chem. Soc., Perkin Trans. 2*, **1977**, 24; (e) Y. Murakami, Y. Aoyama, and K. Dobashi, *J. Chem. Soc., Perkin Trans. 2*, **1977**, 32; (f) Y. Murakami, Y. Aoyama, M. Kida, and A. Nakano, *Bull. Chem. Soc. Jpn.*, **50**, 3365 (1977).
3) (a) K. D. Kopple and D. E. Nitecki, *J. Am. Chem. Soc.*, **84**, 4457 (1962); (b) K. D. Kopple, R. R. Jarabak, and P. L. Bhatia, *Biochemistry*, **2**, 958 (1963); (c) J. C. Sheehan, G. B. Bennett, and J. A. Schneider, *J. Am. Chem. Soc.*, **88**, 3455 (1966); (d) A. R. Mitchell, S. K. Gupta, and R. W. Roeske, *J. Org. Chem.*, **35**, 2877 (1970); (e) K. Nakajima and K. Okawa, *Bull. Chem. Soc. Jpn.*, **46**, 1811 (1973); (f) Y. Imanishi, T. Sugihara, M. Tanihara, and T. Higashimura, *Chem. Lett.*, **1975**, 261.
4) K. D. Kopple, M. Ohnishi, and A. Go, *Biochemistry*, **8**, 4087 (1969).
5) S. M. Ziegler and C. A. Bush, *Biochemistry*, **10**, 1330 (1971).
6) J. M. Stewart and J. D. Young, "Solid Phase Peptide Synthesis," W. H. Freeman & Co., San Francisco, Calif. (1969).
7) R. B. Merrifield, *J. Am. Chem. Soc.*, **85**, 2149 (1964).
8) P. Kusch, *Kolloid-Z. Z. Polym.*, **208**, 138 (1966).
9) E. Schnabel, *Justus Liebigs Ann. Chem.*, **702**, 188 (1967).

10) J. L. Wood and V. de Vigneaud, *J. Biol. Chem.*, **130**, 109 (1939).
11) S. Kreisky, *Acta Chem. Scand.*, **11**, 913 (1957).
12) For example: M. L. Bender and L. T. Brubacher, *J. Am. Chem. Soc.*, **88**, 5880 (1966).
13) H. Walba and R. W. Isensee, *J. Org. Chem.*, **21**, 702 (1956).
14) C. G. Overberger, T. St. Pierre, N. Vorchheimer, J. Lee, and S. Yaroslavsky, *J. Am. Chem. Soc.*, **87**, 296 (1965).
15) (a) A. L. Lehninger, "Biochemistry," Worth Publishers, Inc., New York, N. Y. (1970), Chap. 4; (b) A. Williams, E. C. Lucas, and A. R. Rimmer, *J. Chem. Soc., Perkin Trans. 2*, **1972**, 627; (c) J. E. Mole and H. R. Horton, *Biochemistry*, **12**, 816 (1973).

Photoreduction of 1-Benzyl-3-carbamoylpyridinium Chloride in Aqueous Ammonia[1)]

Teruo MATSUURA,* Toshio ITAHARA, Toshiaki OTSUKI, and Isao SAITO
Department of Synthetic Chemistry, Faculty of Engineering, Kyoto University, Kyoto 606
(Received April, 18 1978)

Irradiation of 1-benzyl-3-carbamoylpyridinium chloride (BNA$^+$Cl$^-$) in the presence of ascorbic acid in 28% aqueous ammonia gives the corresponding 1,4-dihydronicotinamide as the major product. The spectroscopic behavior of BNA$^+$ in aqueous ammonia and the adduct formation between BNA$^+$ and chloroform are also described.

Among various reactions of *N*-alkylpyridinium salts containing electronwithdrawing groups as models for the biological oxido-reductions involving nicotinamide coenzymes, NAD(P)$^+$, the chemical or electrochemical reduction of 1-alkyl-3-carbamoylpyridinium salts has received considerable attention, where 1,2-,[2)] 1,4-,[3,4)] and 1,6-dihydronicotinamides[5)] are formed two-electron transfer and a 6,6'-dihydro dimer[3)] by one-electron transfer. Relatively few attention has been drawn to

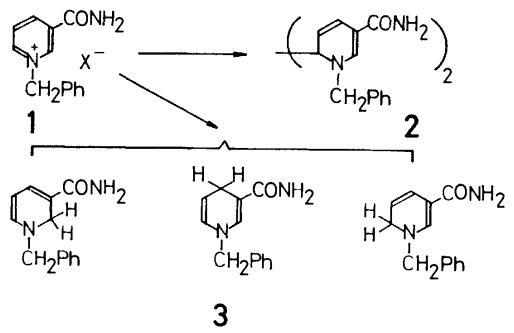

the photochemical reduction of NAD$^+$ or its analogs, which may serve as a model for the electron transport in photosynthetic system. Earlier workers have shown that photolysis of NAD$^+$ or its analog, 1-benzyl-3-carbamoylpyridinium chloride (**1**; BNA$^+$Cl$^-$), in the presence of ascorbic acid appreciably gives a reduced nicotinamide detected by its absorption spectrum, only in aqueous pyridine containing ammonia[6,7)] or in the presence of NADP reductase in aqueous solution.[8,9)] Kano and Matsuo have recently found that BNA$^+$Cl$^-$ (**1**) is photoreduced in the presence of diethylamine and/or ethylenediaminetetraacetic acid in aqueous solution to give 6,6'-dihydrodimer **2** as the main product(15—19%).[10,11)] We now report that the photoreduction of **1** in the presence of ascorbic acid in aqueous ammonia gives 1-benzyl-3-carbamoyl-1,4-dihydropyridine (**3**).

Results and Discussion

Irradiation of a 2×10^{-2} M solution of BNA$^+$Cl$^-$ (**1**) in 28% aqueous ammonia in the presence of an excess of ascorbic acid with a high-pressure mercury lamp (Pyrex) under nitrogen for 12 h gave the known 1,4-dihydro compound **3**[12)] in 22% yield, as the major component of the chloroform extract of the reaction mixture. TLC analysis of the chloroform extract revealed the presence of a trace of nicotinamide (**4**), but no other dihydronicotinamides and dihydrodimers. The aqueous layer contained a complex mixture of products from which no pure compound could be isolated. The photoreaction of **1** under various conditions was examined (Table 1). The characteristic features of the photoreduction are as follows. (1); Catechol could be used as a reducing agent instead of ascorbic acid, although the yield of **3** was lower. (2); The kind of the counter anion of BNA$^+$ appears to give no effect; the photolysis of BNA$^+$Br$^-$ under the same conditions gave virtually the same result. (3); When various amines were used instead of ammonia, only a trace of **3** was detected and the yield of **4** somewhat increased. Upon irradiation in 30% aqueous trimethylamine under similar conditions, **3** was found to be recovered almost unchanged. This result indicates that **3**

TABLE 1. PHOTOREACTION OF 1-BENZYL-3-CARBAMOYLPYRIDINIUM SALTS
(Irradiated with a high pressure mercury lamp (Pyrex) for 12 h.)

Pyridinium salt	Solvent	Reducing agent	Yield of products (%)[a)]	
			3	Nicotinamide (**4**)
BNA$^+$Cl$^-$	28% aq NH_3	ascorbic acid	22	trace[b)]
BNA$^+$Br$^-$	28% aq NH_3	ascorbic acid	20	trace
BNA$^+$Cl$^-$	28% aq NH_3	pyrocatechol	9	4
BNA$^+$Cl$^-$	30% aq $MeNH_2$	ascorbic acid	trace	3
BNA$^+$Cl$^-$	30% aq Me_2NH	ascorbic acid	trace	5
BNA$^+$Cl$^-$	30% aq Me_3N	ascorbic acid	trace	5
BNA$^+$Cl$^-$	30% aq $EtNH_2$	ascorbic acid	trace	4
BNA$^+$Cl$^-$	30% aq Et_2NH	ascorbic acid	trace	5
BNA$^+$Cl$^-$	H_2O[c)]	ascorbic acid	—	—
BNA$^+$Cl$^-$	5.7 M NaOH[d)]	ascorbic acid	trace	—

a) Based on the starting BNA$^+$ salt. b) Detected on TLC. c) Almost no reaction was observed. d) A complex mixture of products was obtained.

might not be formed in the photolysis of **1** in the presence of trimethylamine. (4); Replacemnet of ammonia by sodium hydroxide gave a complex mixture of products including a trace of **3**. These results indicate that the presence of ammonia are essential for the photochemical formation of the 1,4-dihydronicotinamide **3**.

Recently, Ohnishi has reported that treatment of **1** with aqueous ammonia in the dark gives **3** in small yield.[13] This finding prompted us to carry out a control experiment under similar conditions. Thus, when **1** was treated with 28% aqueous ammonia for 12 h in the dark, **3** was found to form in 7% yield in a complex mixture of products. This result indicates that the major portion of the compound **3** formed under the irradiation is resulted from a photochemical process.

In order to gain informations on the role of ammonia in the photochemical formation of **3**, the spectroscopic and chemical behaviors of BNA$^+$Cl$^-$ (**1**) in aqueous ammonia were examined. At a low concentration (4×10^{-5} M), **1** apparently undergoes chemical transformation at least with three steps. The ultraviolet absorption spectra of **1** with or without ammonia in aqueous solution are shown in Fig. 1. The absorption maximum at 258 nm of **1** in aqueous solution increased with increased amount of added ammonia and a new maximum appeared at 323 nm (stage I). The intensity of the latter absorption strongly depends upon ammonia concentration, as shown by the fact that the 323 nm maximum does not appear at ammonia concentrations of below 15% w/v. Acidification of the strong ammonia solution of **1** with hydrochloric acid gave rise to a spectrum identical with that of **1** in aqueous solution, indicating that the change into stage I is reversible.

When the ammonia solution at stage I was kept on standing at room temperature for several hours, a spectral change occurred gradually to reach a new spectrum having a maximum at 345 nm (stage II) with three isosbestic points at 273, 294, and 334 nm (Fig. 2). The spectral change of stage I to stage II

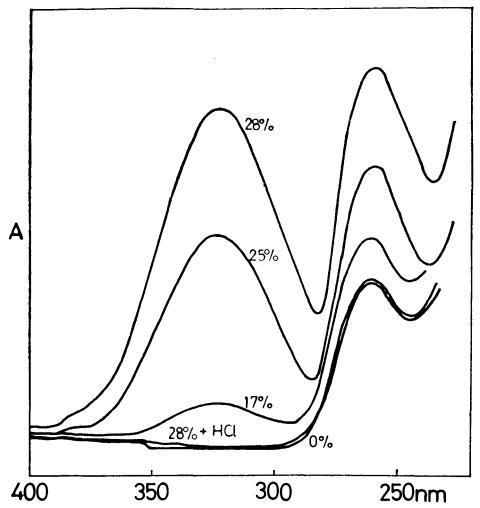

Fig. 1. UV spectra of BNA$^+$Cl$^-$ (**1**) in aqueous solution and in aqueous ammonia solution with different concentrations. BNA$^+$Cl$^-$: 4.0×10^{-5} M. Ammonia concentrations are shown by w/v %.

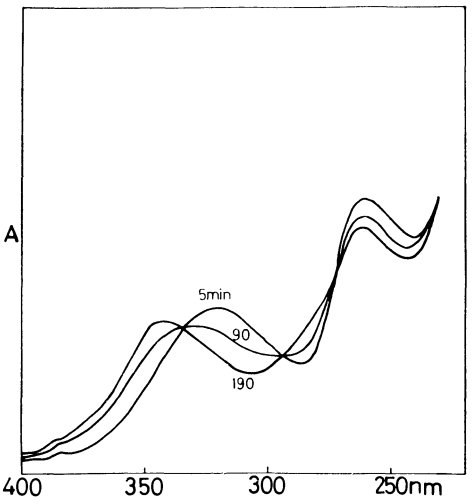

Fig. 2. UV spectral change of a solution of BNA$^+$Cl$^-$ (**1**) in 23% aqueous ammonia at 5, 90, and 190 min after dissolution. BNA$^+$Cl$^-$: 4.0×10^{-5} M.

was highly sensitive to the concentration of **1**. Thus, at higher concentrations of **1** the change became obscure, suggesting the occurrence of bimolecular reactions of the transient species having the 345 nm maximum. In fact, a 0.16 M solution of **1** in 28% aqueous ammonia became turbid and deposited an yellowish brown precipitate in a few hours (stage III). Figure 3 shows the spectra of the freshly prepared precipitate and the aqueous filtrate, suggesting a complex nature of stage III. These results may be simply summarized as the following scheme:

$$\text{NBA}^+\text{Cl}^- + \text{NH}_3\ \text{aq} \rightleftharpoons \text{stage I} \rightarrow \text{stage II} \rightarrow \text{stage III}$$

Since the photolysis of **1** in aqueous ammonia was done at a relatively high concentration (2×10^{-2} M), the reduction product **3** seems to originate from some of the intermediate species corresponding to these three stages.

Various attempts were made to isolate the species formed in the stages I, II, and III, but were unsuccessful because of their instability. During these attempts, it was found that when a 0.27 M solution of **1** in 28%

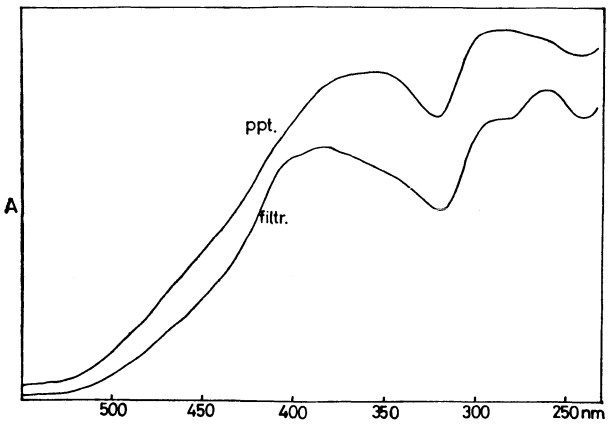

Fig. 3. UV spectra of the precipitate and the filtrate obtained from a solution of BNA$^+$Cl$^-$ (**1**) in 28% aqueous ammonia after standing for 12 hr. BNA$^+$Cl$^-$ (2.0 g) in 28% aqueous ammonia (50 ml).

aqueous ammonia is stirred with chloroform for 3 h, two adducts between BNA^+ and the trichloromethanide anion, **5** (19%) and **6** (15%) are obtained from the chloroform layer. The structure of the latter product was assigned as **6** which had already been reported by Gündel.[14] The structure **5** was assigned by comparing its spectral data with those of the known 2,6-dichlorobenzyl analog.[14] Similar adduct formation between pyridinium salts and the trihalomethanide anions has been reported.[14-16]

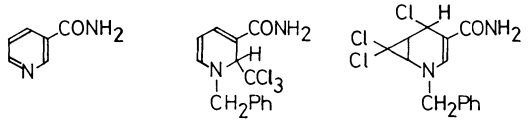

4 **5** **6**

Because of the failure to identify any of the intermediate species in stages I, II, and III, the nature of the present photoreduction remains unknown. However, on the basis of the probable equilibrium of ammonia in water, $NH_3+H_2O \rightleftharpoons NH_4^+ + OH^-$ ($K_B=[NH_4^+][OH^-]/[NH_3]_t=1.75\times10^{-5}$ (25°)), where $[NH_3]_t$ denotes the total concentration of ammonia,[17] NH_3 would be able to act as a nucleophile rather than OH^-. Therefore, it seems reasonable to assume that adducts, **7a**, **8a**, and **9a**, which are formed between **1** and ammonia, play a role in the formation of the 1,4-dihydronicotinamide **3**. Comparing the absorption maxima at stages I (323 nm), II (345 nm), and III (350—400 nm) in Figs. 2 and 3 with those of *N*-(2,6-dichlorobenzyl)dihydronicotinamides, **7b** (ca. 420 nm), **8b** (350 nm), and **9b** (355 nm),[2,5] *N*-(2,6-dichlorobenzyl)-2-trichloromethyl-1,2-dihydronicotinamide (**7c**) (364 nm),[14] *N*-benzyl-4-trichloromethyl-1,4-dihydronicotinamide (**8d**) (365 nm),[14] and **5** (360 nm), there appeared rather difficult to assign the structures of the adducts in stages I, II, and III. However, considering from the difference between stages I and II in their absorption maxima, the adducts in stage I and II may be assigned as **8a** and **7a** (or **9a**) respectively. The precipitates of stage III may be very likely to consist of a mixture of the adducts and/or their decomposition products. The relatively low yield of the 1,4-dihydronicotinamide **3** may have resulted from the simultaneous occurence of side reactions of the adducts. A similar formation of the unstable adducts from **1** or its analogs by the action of a nucleophile such as the hydroxide anion,[18,19] amines,[13] and formate,[20] has been claimed. Such adducts are considered to be interconvertible, although the nature of the reaction is usually complex.

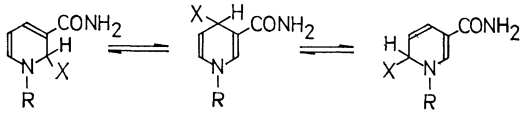

7 **8** **9**

a: X=NH_2 R=$PhCH_2$
b: X=H; R=2,6-$Cl_2C_6H_3CH_2$
c: X=CCl_3; R=2,6-$Cl_2C_6H_3CH_2$
d: X=CCl_3; R=$PhCH_2$

Experimental

All the melting points are uncorrected. UV, IR, NMR, and mass spectra were measured on a Shimadzu UV-200, a JASCO IRA-1, an NEVA T-60 (TMS, internal standard), and a Hitachi RMS-4 spectrometers, respectively. BNA^+ (**1**) was prepared by the known method.[21]

Photoreduction of 1-Benzyl-3-carbamoylpyridinium Chloride (1). A solution of **1** (1.0 g) and ascorbic acid (1.0 g) in 28% aqueous ammonia (180 ml) was irradiated internally with a 100 W high-pressure mercury lamp (Pyrex housing) under nitrogen for 12 h. The photolysate was extracted with chloroform. Evaporation of the chloroform extracts gave a solid (0.19 g) which on TLC (silica gel; chloroform) showed a major spot of *N*-benzyl-1,4-dihydronicotinamide (**3**) and a minute spot of nicotinamide (**4**). Recrystallization of the solid from aqueous ethanol gave crystals which were identical with an authentic sample of **3**[12] (NMR, IR, and TLC). Attempts to isolate pure products from the aqueous layer were unsuccessful.

Photolysis of **1** and the corresponding bromide (BNA^+Br^-) was carried out (Table 1). A solution of the pyridinium salts (1.0 g) and ascorbic acid or pyrocatechol (1.0 g) in a given solvent (180 ml) was irradiated under similar conditions. The photolysate was worked up as above.

Dark Reaction of 1 with Aqueous Ammonia. A solution of **1** (1.0 g) in 28% aqueous ammonia (180 ml) was kept on standing at room temperature under nitrogen for 12 h. After evaporating ammonia *in vacuo*, the mixture was extracted with chloroform. The chloroform layer was dried (Na_2SO_4) and evaporated to give a reddish brown solid (419 mg), which was found to contain **3** by TLC (silica gel; EtOAc–MeOH (10:1)). The NMR analysis of the solid with *t*-butyl alcohol as an internal standard showed that the yield of **3** was less than 7%.

Reaction of 1 with Chloroform in Aqueous Ammonia. A solution of **1** (2.0 g) in 28% aqueous ammonia (30 ml) was stirred with chloroform (60 ml) at room temperature for 3 h. The chloroform layer was dried (Na_2SO_4) and evaporated to give an yellowish brown solid (1.65 g), which was chromatographed on a silica gel column (Wakogel C-200). Elution with chloroform–ethyl acetate (2:3) yielded *N*-benzyl-2-trichloromethyl-1,2-dihydronicotinamide (**5**) as a pale yellow solid (0.50 g; 19%), which was recrystallized from benzene–cyclohexane as pale yellow crystals; mp 118—123 °C; λ_{max}^{EtOH} 360 nm (ε 5500); MS, *m/e* (rel int.) 213 (41) (M^+-CCl_3), 91 (65) ($PhCH_2^+$), 85 (100), 83 (65); NMR ($CDCl_3$), δ 4.80 (s, 2H, benzyl protons), 5.27 (dd, 1H, 5-H, J=6.6, 6.6 Hz), 5.70 (broad, 2H, NH_2, D_2O-exchangeable), 5.73 (d, 1H, 2-H, J=1.8 Hz), 6.58 (dd, 1H, 6-H, J=6.6, 1.8 Hz), 7.03 (d, 1H, 4-H, J=6.6 Hz), 7.32 (m, 5H, phenyl protons).

Found: C, 51.28; H, 4.05; Cl, 30.83; N, 8.27%. Calcd for $C_{14}H_{13}Cl_3N_2O$: C, 50.70; H, 3.95; Cl, 32.08; N, 8.45%.

Further elution with the same solvent yielded 5,7,7-trichloro-4-carbamoyl-2-benzyl-2-azabicyclo[4.1.0]hept-3-ene (**6**) as a pale yellow solid (0.41 g; 15%), which was recrystallized from ether–petroleum ether as colorless needles; mp 55—60 °C (containing 1 equivalent mole of ether of crystallization) (lit,[14] mp 130—131 °C, from dichloromethane); λ_{max}^{EtOH} 263 nm (ε 4400), 313 (4400); MS, *m/e* (rel int.) 213 (54) (M^+-CCl_3), 91 (100) ($PhCH_2^+$), 85 (23), 83 (35); NMR ($CDCl_3$), δ 1.20 (t, 6H, CH_2-CH_3, J=6 Hz), 3.49 (q, 4H, -O-CH_2-CH_3, J=6 Hz), 4.53 (s, 2H, benzyl protons), 4.55 (d, 1H, 5-H, J=6 Hz), 5.21 (dd, 1H, 6-H, J=6, 7.2 Hz), 5.60 (broad, 2H, NH_2, D_2O-exchangeable), 6.38 (dd, 1H, 1-H, J=7.2, 1.2 Hz), 7.24 (m, 5H, phenyl protons), 7.33 (d, 1H, 3-H,

J=1.8 Hz). (Found: C, 53.03; H, 5.65; N, 7.04; O, 8.19%. Calcd for $C_{14}H_{13}Cl_3N_2O \cdot C_2H_5OC_2H_5$: C, 53.28; H, 5.71; N, 6.90; O, 7.89%.)

This work was supported by a Grant-in-Aid for Scientific Research from the Ministry of Education.

References

1) Photoinduced Reactions, Part 105.
2) K. Wallenfels and M. Gellrich, *Chem. Ber.*, **92**, 1406 (1959).
3) D. Mauzerall and F. H. Westheimer, *J. Am. Chem. Soc.*, **77**, 77 (1955).
4) J. N. Burnett and A. L. Underwood, *J. Org. Chem.*, **30**, 1154 (1965); A. J. Cunningham and A. L. Underwood, *Biochemistry*, **6**, 266 (1967).
5) K. Wallenfels and H. Schultz, *Angew. Chem.*, **67**, 517 (1955); **69**, 505 (1957); *Justus Liebigs Ann. Chem.*, **621**, 106 (1959).
6) A. A. Krasnovskii and G. P. Brin, *Dokl. Acad. Nauk. SSSR*, **67**, 325 (1949); A. A. Krasnovskii, G. P. Brin, and N. N. Drozdova, *ibid.*, **150**, 1157 (1963); G. P. Brin and A. A. Krasnovskii, *Biokhimiya*, **24**, 1085 (1959).
7) G. R. Seely, *J. Phys. Chem.*, **69**, 2779 (1965).
8) T. T. Bannister and J. E. Bernardini, *Biochem. Biophys. Acta*, **59**, 188 (1962).
9) L. P. Vernon, A. S. Pietro, and D. A. Limbach, *Arch. Biochem. Biophys.*, **109**, 92 (1965).
10) K. Kano and T. Matsuo, *Tetrahedron Lett.*, **1975**, 1389.
11) K. Kano and T. Matsuo, *Bull. Chem. Soc. Jpn.*, **49**, 3269 (1976).
12) D. Mauzerall and F. H. Westheimer, *J. Am. Chem. Soc.*, **77**, 2261 (1955).
13) Y. Ohnishi, *Tetrahedron Lett.*, **1977**, 2109.
14) W.-H. Gündel, *Z. Naturforsch.*, **30b**, 616 (1975).
15) A. Lambardo and D. C. Dittmer, *Bioorganic Chemistry*, **1**, 400 (1971).
16) V. Mann, G. Schneider, and F. Kröhnke, *Tetrahedron Lett.*, **1973**, 683.
17) Kagaku Daijiten (Encyclopedia Chimica), Kyoritsu Publ. Co. (1960), Vol. 1, p. 532.
18) F. M. Maracci, A. Casini, F. Liberatore, and V. Carelli, *Tetrahedron Lett.*, **1976**, 3723.
19) H. Minato, E. Yamazaki, and M. Kobayashi, *Chem. Lett.*, **1976**, 525.
20) Y. Onishi and S. Tanimoto, *Tetrahedron Lett.*, **1977**, 1909.
21) P. Karrer and F. J. Stare, *Helv. Chim. Acta*, **20**, 418 (1937).

Preparation of D:B-Friedoolean-5(10)-en-1-one and Related Compounds. A Comment on the Structure of "Glut-5(10)-en-1-one" from *Euphorbia Nerifolia*[1]

Eri AKIYAMA, Yoshihiko MORIYAMA, Tatsushi MURAE, Takahiko TSUYUKI, and Takeyoshi TAKAHASHI*

Department of Chemistry, Faculty of Science, The University of Tokyo, Hongo, Bunkyo-ku, Tokyo 113

(Received April 19, 1978)

In order to examine the structure, "glut-5(10)-en-1-one", proposed for a new triterpene from *Euphorbia nerifolia*, this ketone (≡D : B-friedoolean-5(10)en-1-one) was prepared. Oxidation of D : B-friedoolean-5(10)-ene with chromium trioxide-pyridine complex gave the allylic oxidation products, D : B-friedoolean-5(10)-en-1-one, D : B-friedoolean-5(10)-en-6-one, and D : B-friedoolean-5(10)-ene-1,6-dione. The spectral data and physical constants of the synthetic ketone (D : B-friedoolean-5(10)-en-1-one) were not identical with those of the new triterpene; this requires revision of the structure of this natural triterpene. Oxidation of D : B-friedoolean-5(10)-en-3-one enol acetate under the same conditions to give D : B-friedooleane-1,5(10)-dien-3-one is also described.

From the stems and leaves of *Euphorbia nerifolia* Linn. (Euphorbiaceae), a new triterpene, $C_{30}H_{48}O$, mp 312—314 °C, $[\alpha]_D$ +50°, was isolated together with 3α- and 3β-hydroxyfriedelanes and taraxerol by Row *et al.*[2] Based on the spectral data, this new compound was inferred to be a pentacyclic triterpene ketone conjugated with a tetrasubstituted double bond. Catalytic reduction of the ketone into glut-5(10)-ene (**1**≡D : B-friedoolean-5(10)-ene**) and investigation on the UV spectra of both the ketone and its 2,4-dinitrophenylhydrazone led to the conclusion that the new triterpene is glut-5(10)-en-1-one (**2**≡alnus-5(10)-en-1-one≡D : B-friedoolean-5(10)-en-1-one**).[2]

However, the proposed structure for this triterpene is very questionable, because the UV absorption at 218 nm (log ε 3.87) and three weak bands at 880, 840, and 810 cm^{-1} in the IR spectrum described for this compound,[2] could not be compatible with the proposed structure. In this paper, we describe an unambiguous synthesis of D:B-friedoolean-5(10)-en-1-one (**2**) by oxidation of D:B-friedoolean-5(10)-ene (**1**)[3] with chromium trioxide–pyridine complex[4] and that the synthetic triterpene (**2**) is different from the natural one, indicating that the structure for the natural triterpene from *Euphorbia nerifolia* should be revised.

D:B-Friedoolean-5(10)-ene (**1**), prepared by the Huang-Minlon reduction of D:B-friedoolean-5(10)-en-3-one (**3**),[3,5] was subjected to oxidation with chromium trioxide–pyridine complex[4a] according to Ratcliffe's modified procedure[4b] to give a complex mixture, from which two ketones (**2** and **4**) and a diketone (**5**), together with the unchanged starting material (**1**) were isolated by column chromatography on alumina and subsequent separation by preparative TLC on silica gel.

Since the carbonyl moiety in these ketones (**2** and **4**) was shown to be conjugated with a tetrasubstituted double bond from the spectral measurement (*vide infra*), these ketones were inferred to be the allylic oxidation products at C-1 and C-6, respectively. The Huang-Minlon reduction of both **2** and **4** gave the same hydrocarbon as the starting D:B-friedoolean-5(10)-ene (**1**). Thus the position of the tetrasubstituted double bond in both **2** and **4** was determined to be between C-5 and C-10.

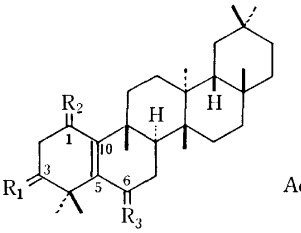

1 $R_1=R_2=R_3=H_2$
2 $R_1=R_3=H_2$, $R_2=O$
3 $R_1=O$, $R_2=R_3=H_2$
4 $R_1=R_2=H_2$, $R_3=O$
5 $R_1=H_2$, $R_2=R_3=O$

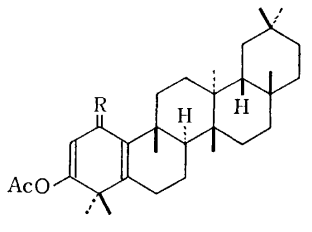

6 $R=H_2$
7 $R=O$

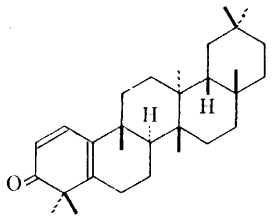

8

The more polar ketone (**2**), $C_{30}H_{48}O$, mp 257.5—259 °C, $[\alpha]_D$ −53°, showed the UV absorption at 249 nm (ε 19100), IR absorption band at 1660 cm^{-1}, and complex signals (4H) due to $-CO-CH_2-$ and $-\overset{|}{C}=\overset{|}{C}-CH_2-$ groupings at δ 2.0—2.7 in the PMR spectrum, while the other (**4**), $C_{30}H_{48}O$, mp 243—245 °C, $[\alpha]_D$ −11°, the UV absorption at 250 nm (ε 10800), IR absorption band at 1655 cm^{-1}, and complex signals (4H) due to $-CO-CH_2-$ and $-\overset{|}{C}=\overset{|}{C}-CH_2-$ groupings at δ 2.0—2.5 in the PMR spectrum. In the PMR measurement using Eu(fod)$_3$-d_{27} for a 7% (w/v) solution of **4** in $CDCl_3$ in a molar ratio (**4**/the shift reagent) of 1:1, two of the four protons which had given the complex signals at δ 2.0—2.5, appeared at δ_A 12.40 and δ_B 11.92 as an AB part of an ABX-type signal, respectively, and *one* proton corresponding to the X-part was also observed at δ_X 6.42. On irradiation at δ_A 12.40 and δ_B 11.92, the signals due to H_X changed into a singlet like and a doublet, respectively. Irradiation at δ_X 6.42 changed the signal due to the AB-part into an AB quartet. These observations confirmed the presence of the grouping $-CO-CH_AH_B-\overset{|}{C}H_X-$ (J_{AB}=18, J_{AX}=12, and J_{BX}=6 Hz) and therefore the less polar

** In this paper, friedooleanane nomenclature was used.

Table 1. The CD spectral data for the enones (**2** and **4**)

Compound	Observed cotton effect			Predicted sign		
	R-Band	K-Band		Enone helicity	Allylic axial chirality contribution	α'-Axial chirality contribution
2	$[\theta]_{330}+2000$	$[\theta]_{242}-34500$	$[\theta]_{213}+14300$	+	4α-CH_3 (+) 6α-H (−)[a] 9β-CH_3 (−)[a]	2α-H (+)
4	$[\theta]_{350}-3300$	$[\theta]_{268}+1900$	$[\theta]_{225}-15700$	−	1β-H (+)[b] 4α-CH_3 (+)[b] 9β-CH_3 (−)	7β-H (−)

a) Contribution of 9β-CH_3 and 6α-H may be greater than that of 4α-CH_3.
b) Contribution of 4α-CH_3 and 1β-H may overcome that of 9β-CH_3.

ketone (**4**) could be formulated as D : B-friedoolean-5(10)-en-6-one. Thus the structure of the polar ketone (**2**) was concluded to be D : B-friedoolean-5(10)-en-1-one.

The diketone (**5**), $C_{30}H_{46}O_2$, was identified to be D : B-friedoolean-5(10)-ene-1,6-dione based on the spectral data. This received support by the fact that each of the ketones **2** and **4** gave the same diketone (**5**) on oxidation under the same conditions as above.

The circular dichroism data (Table 1) for the enones (**2** and **4**) could be interpreted by the enone helicity rule[6] for the R-band Cotton effect, and by the allylic axial chirality contribution rule[7] and the α'-axial chirality contribution rule[7] for the K-band Cotton effect.

If an additional double bond is introduced between C-2 and C-3 in the D:B-friedoolean-5(10)-ene framework, it would be expected that the C-1 methylene group might be more susceptible to the allylic oxidation than the C-6 methylene group. D : B-Friedoolean-5-(10)-en-3-one (**3**) was converted into the corresponding enol acetate (**6**), which was subjected to the oxidation under the same conditions as above. However, the expected allylic oxidation product (**7**) could not be obtained, but only a dienone (**8**) was isolated in about 50% yield. The dienone (**8**), mp 217—219 °C, was shown to be identical with D:B-friedooleane-1,5(10)-dien-3-one.[3,8] Goldblum and Mechoulam[9] reported a novel oxidative rearrangement leading to α-benzoyloxy ketones in allylic oxidation of various enol benzoates with sodium chromate in acetic acid. The formation of the 1,5(10)-dien-3-one (**8**) could be explained by the same mechanism as described by Mechoulam.[9]

In conclusion, the spectral data and physical constants of the synthetic ketone, D:B-friedoolean-5(10)-en-1-one (**2**) are clearly shown to be different from those of the natural triterpene*** described by Row *et al.*[2] Therefore the structure proposed for the natural triterpene should be revised.

Experimental

IR spectra were measured using a Hitachi EPI-G2 spectrometer. UV spectra were determined on a Hitachi EPS-3 spectrometer. CD measurements were carried out on a JASCO Model J-20 spectrometer. Optical rotations were measured on a JASCO DIP-SL polarimeter. Mass spectra were taken on a Hitachi RMU-6 Tokugata mass spectrometer with a direct inlet system operating at 70 eV. PMR spectra were measured using a JEOL 4H-100 (100 MHz) or a Hitachi R-20 (60 MHz) spectrometer. Chemical shifts were expressed in δ downfield from TMS as an internal standard, and coupling constants in Hz. HPLC analyses were carried out at room temperature using a Liquid Chromatograph Model ALC/GPC 202/401 (Waters Assoc.) with a UV detector (column: μ-Porasil 1/8 (inch) × 1 (foot); solvent system: 25% CH_2Cl_2-hexane; flow rate: 0.4 ml/min; pressure: *ca.* 500 psi). TLC was carried out on Kieselgel G nach Stahl, Kieselgel GF_{254} nach Stahl, and Kieselgel 60 PF_{254} (E. Merck, Darmstadt). For column chromatography, Wakogel C-200 (Wako Pure Chem. Ind.) and Activated Alumina (Showa Chem.) were used. Melting points were measured on a Mel-temp capillary melting point apparatus (Laboratory Devices) and were uncorrected.

*Oxidation of D:B-Friedoolean-5(10)-ene (**1**).* Chromium trioxide (2.5 g) was added to a mixture of pyridine (4 ml) and dichloromethane (70 ml) with stirring for 15 min.[4b] To the solution, D:B-friedoolean-5(10)-ene[3,5] [**1**; 1.04 g, prepared from D:B-friedoolean-5(10)-en-3-one (**3**)] in dichloromethane (100 ml) was added. The reaction mixture was stirred at room temperature for 21 h. Ether (*ca.* 300 ml) was added and the ethereal layer was washed with 5% aqueous sodium hydroxide solution, 5% hydrochloric acid, and then with saturated aqueous sodium hydrogencarbonate solution, and dried over sodium sulfate. Evaporation of the solvent gave a residue (1.3 g) which was dissolved in petroleum ether, passed through a column of alumina (100 g), and eluted with the following solvents (each 100 ml). Petroleum ether, frs 1—3; benzene, frs 7—15. On evaporation, fractions 1—3 gave the starting material (**1**; 64 mg), fractions 7 and 8 gave a mixture of 1,6-dione (**5**) and 6-one (**4**), and fractions 11—15 gave a mixture of 6-one (**4**) and 1-one (**2**). These mixtures were subjected to separation by preparative TLC (developed with benzene-hexane, 1 : 1) giving rise to **2** (85 mg), **4** (195 mg), and **5** (98 mg).

*D : B-Friedoolean-5(10)-en-1-one (**2**).* Mp 257.5—259 °C (recrystallized from ethyl acetate), $[\alpha]_D$ −53° (*c* 0.73, $CHCl_3$); IR (KBr) 1660 cm^{-1}; UV (EtOH) λ_{max} 249 nm (ε 19100); PMR ($CDCl_3$) δ 0.97, 1.05, 1.10, 1.14 (each s, 3H, *t*-Me), 1.00, 1.20 (each s, 6H, 2×*t*-Me), and 2.0—2.7 (4H, complex); CD (*c* 0.094, dioxane): Table 1; MS *m/e* (%) 424 (M^+; 100), 409 (37), 245 (41), 205 (62), 191 (85), 177 (78), and 163 (57); MW Found: *m/e* 424.3756. Calcd for $C_{30}H_{48}O$: 424.3703; Found: C, 85.12; H, 11.24%. Calcd for $C_{30}H_{48}O$: C, 84.84; H, 11.39%.

*D : B-Friedoolean-5(10)-en-6-one (**4**).* Mp 243—245 °C (recrystallized from ethyl acetate); $[\alpha]_D$ −11° (*c* 0.83, $CHCl_3$); IR (KBr) 1655 cm^{-1}; UV (EtOH) λ_{max} 250 nm (ε 10800); PMR ($CDCl_3$) δ 0.97, 1.06, 1.10, 1.25 (each s, 3H, *t*-Me),

***An authentic sample was not available.

1.03, 1.20 (each s, 6H, 2×*t*-Me), and 2.0—2.5 (4H, complex); CD (*c* 0.102, dioxane): Table 1; MS *m/e* (%) 424 (M^+; 75), 409 (9), 205 (46), and 151 (100); *MW* Found: *m/e* 424.3788. Calcd for $C_{30}H_{48}O$: 424.3703; Found: C, 84.66; H, 11.54%. Calcd for $C_{30}H_{48}O$: C, 84.84; H, 11.39%.

D : B-Friedoolean-5(10)-ene-1,6-dione (5). Mp 236—237 °C (recrystallized from chloroform-methanol); $[\alpha]_D$ −8° (*c* 1.07, $CHCl_3$); IR (KBr) 1680 cm^{-1}; UV (EtOH) λ_{max} 264 nm (ε 9800); PMR ($CDCl_3$) δ 0.98, 1.02, 1.04, 1.13, 1.20, 1.26, 1.28, 1.33 (each s, *t*-Me), and 2.1—2.65 (4H, complex); MS *m/e* (%) 438 (M^+; 100), 314 (39), 205 (50), 123 (74), and 109 (70); *MW* Found: *m/e* 438.3626. Calcd for $C_{30}H_{46}O_2$: 438.3496; Found: C, 82.15; H, 10.87%. Calcd for $C_{30}H_{46}O_2$: C, 82.14; H, 10.57%.

Conversion of D : B-Friedoolean-5(10)-en-1-one (2) and -6-one (4) into D : B-Friedoolean-5(10)-ene-1,6-dione (5). D : B-Friedoolean-5(10)-en-1-one (**2**; 14 mg) in dichloromethane (3 ml) was oxidized with chromium trioxide-pyridine complex[4b] (chromium trioxide 100 mg, pyridine 0.2 ml, and dichloromethane 2.4 ml) at 30 °C for 5 days. The reaction mixture was worked up as before and a mixture of D : B-friedoolean-5(10)-ene-1,6-dione (**5**) and the unchanged starting material (**2**) was obtained. Although separation of the mixture was not attempetd, HPLC examination showed that the mixture consisted of **5** and **2** (their retention times 24 min and 30 min, respectively) in a ratio of 5 : 1. And the mixture gave an overlapped mass spectrum of **5** and **2** in the same ratio.

D : B-Friedoolean-5(10)-en-6-one (**4**; 18.7 mg) in dichloromethane (3 ml) was treated with the same reagent[4b] (chromium trioxide 50 mg, pyridine 0.1 ml, and dichloromethane 1.2 ml) under the same conditions as above. After usual treatment, separation by preparative TLC gave D:B-friedoolean-5(10)-ene-1,6-dione (**5**; *ca.* 2 mg) and a minute quantity of the starting 6-one (**4**). The IR spectrum of the former product (**5**) was shown to be identical with that of D:B-friedoolean-5(10)-ene-1,6-dione (**5**).

Wolff-Kishner Reduction of D : B-Friedoolean-5(10)-en-1-one (2) and -6-one (4) under Forced Conditions. D : B-Friedoolean-5(10)-en-1-one (**2**; 15 mg) was treated with diethylene glycol (5 ml), sodium (100 mg), and anhydrous hydrazine[10] (1 ml) under a nitrogen atmosphere according to the Barton's procedure.[11] The reaction product was subjected to separation by column chromatography of silica gel (5 g) impregnated with silver nitrate (1.25 g) using petroleum ether as eluent. D : B-Friedoolean-5(10)-ene (**1**; 4 mg) was obtained as the major reduction product and the mp, IR, and MS were all in accord with those of an authentic specimen.

The Wolff-Kishner reduction of D : B-friedoolean-5(10)-en-6-one (**4**; 45.4 mg) was effected under the same conditions as above to give D : B-friedoolean-5(10)-ene (**1**; 10 mg), whose IR spectrum was identical with that of an antheutic sample.

D : B-Friedoolean-5(10)-en-3-one Enol Acetate (6). A mixture of D:B-friedoolean-5(10)-en-3-one (**3**; 170 mg), isopropenyl acetate (12 ml), and *p*-toluenesulfonic acid (40 mg) was heated and distilled slowly. After 2 ml of the solvent was distilled off, the reaction mixture was refluxed for 17 h. Usual treatment gave a residue, which was dissolved in benzene-ether (10 : 1), passed through a column of alumina (5 g), and eluted with the same solvents. Recrystallization from ethyl acetate afforded the enol acetate (**6**; 168 mg), mp 241—243 °C; IR (KBr) 1760, 1210, and 905 cm^{-1}; PMR ($CDCl_3$) δ 2.15 (3H, s; -OAc), 2.76 (2H, d, J=4 Hz; $C_{(1)}$-H_2), and 5.31 (1H, t, J=4 Hz; C=C-H); MS *m/e* (%) 466 (M^+; 8), 451 (35), 424 (41), 409 (11), 406 (13), 205 (91), 136 (100), 121 (91), and 109 (91); Found: C, 82.39; H, 10.61%. Calcd for $C_{32}H_{50}O_2$: C, 82.35; H, 10.80%.

Oxidation of Enol Acetate (6). D : B-Friedoolean-5(10)-en-3-one enol acetate (**6**; 100 mg) in dichloromethane (12 ml) was treated with the chromium trioxide-pyridine complex[4b] (chromium trioxide 235 mg, pyridine 0.8 ml, and dichloromethane 12 ml) at room temperature for 1.25 h with stirring. Usual workup and recrystallization from chroloform-methanol afforded D:B-friedooleane-1,5(10)-dien-3-one (**8**; 45 mg), mp 217—219 °C (lit,[3] 216—217 °C; lit,[8] 212.5—215 °C); IR (KBr) 1675, 1620, and 812 cm^{-1}; UV (EtOH) λ_{max} 323 nm (ε 5470) [lit,[3] 322 nm (ε 5500); lit,[8] 320 (ε 5000)]; PMR ($CDCl_3$) δ 2.3 (2H, m; $C_{(6)}$-H_2), 6.0 and 7.1 (2H, ABq, J=10 Hz; CH=CH-C=O); MS *m/e* (%) 422 (M^+; 23), 407 (13), 205 (52), and 109 (100).

References

1) This work was reported in a preliminary form: E. Akiyama, K. Ogawa, Y. Moriyama, T. Tsuyuki, and T. Takahashi, *Chem. Lett.*, **1977**, 1059.

2) A. S. R. Anjeneyulu, L. R. Row, C. Subrahmanyam, and K. S. Murty, *Tetrahedron*, **29**, 3909 (1973).

3) J. M. Beaton, F. S. Spring, R. Stevenson, and J. L. Stewart, *Tetrahedron*, **2**, 246 (1958).

4) a) W. G. Dauben, M. Lorber, and D. S. Fullerton, *J. Org. Chem.*, **34**, 3587 (1969); b) R. Ratcliffe and R. Rodehorst, *ibid.*, **35**, 4000 (1970).

5) S. Chapon, *Bull. Soc. Chim. Fr.*, **1955**, 1076 and 1630.

6) G. Snatzke, *Tetrahedron*, **21**, 413, 421, and 439 (1965).

7) A. W. Burgstahler and R. C. Barkhurst, *J. Am. Chem. Soc.*, **92**, 7601 (1970).

8) J. W. ApSimon, R. R. King, and J. J. Rosenfeld, *Can. J. Chem.*, **47**, 1989 (1969).

9) A. Goldblum and R. Mechoulam, *J. Chem. Soc., Perkin Trans. 1*, **1977**, 1889.

10) K. Kusama, *J. Biochem.*, **44**, 375 (1957).

11) D. H. R. Barton, D. A. J. Ives, and B. R. Thomas, *J. Chem. Soc.*, **1955**, 2056.

The Removal of Heavy Metal, Phosphate, and COD Substances from Wastewater by the Lime Sulfurated Solution (Calcium Polysulfide) Process

Toshiro ARATANI,* Yasuyuki NAKATA,† Hitoshi MATOBA,† Shigeki YASUHARA, and Takeo YANO

Department of Chemical Engineering, College of Engineering, University of Osaka Prefecture, Mozu-Ume, Sakai, Osaka 591

(Received October 26, 1977)

A new chemical precipitation process that had been developed for the removal of heavy metals was extended to the removal of phosphate and COD substances. For simulated wastewater contaminated with heavy metal, phosphate, and COD substances, removal experiments were undertaken in a batch, stirred vessel by using the lime sulfurated solution as a single coagulant. The coagulant, the main component of which is CaS_x, decomposes in water on contact with air or CO_2 gas, and liberates H_2S, CaS_2O_3, $CaCO_3$, $CaSO_4$, and solid sulfur particles. While heavy metals are precipitated as metal sulfides or hydroxides, phosphate is precipitated as calcium phosphate and COD substances are sorbed on the surfaces of the precipitates and they removed. The experimental findings are as follows: (1) The simulated wastewater contaminated simultaneously with phosphate and cadmium ions can be treated better than that contaminated only with the phosphate ion. Also, the CaS_x process is found to be more effective than the $Ca(OH)_2$ process for the removal of phosphate. (2) The removal percentages of COD substances ranged from 40% to 90% according to the sort of substance. The COD removal can be attained by the sorption of the substances mainly on the liberated solid sulfur particles, and partly on the calcium salts.

Wastewater issuing from communities and various industries is often contaminated simultaneously with many sorts of chemical species. Therefore, it is advantageous to develop a wastewater treatment process that can treat these contaminants by a single procedure. As the contaminants, phosphate and nitrogen compounds as well as heavy metals and COD substances have occasioned much public discussion. For the removal of nitrogen compounds, biological denitrification processes have recently been developed and have been playing very important role in the protection of the environment. As for the phosphate removal, however, there are only a few processes that can be practically applied. They are the precipitation processes of phosphate by injecting calcium hydroxide, aluminum sulfate, or iron salts into the wastewater.

In this paper, a new precipitation process is proposed for the removal of phosphate together with heavy metal and COD substances. This process has already been tested for the removal of heavy metals from simulated wastewater.[1,2] By utilizing the lime sulfurated solution as a single coagulant, the apparent reaction kinetics for the removal of heavy metals (Hg^{2+}, Cd^{2+}, Pb^{2+}, Cu^{2+}, Zn^{2+}, Cr^{3+}, and Cr(VI)) has been studied by us.[1] We have also discussed the conditions necessary for the precipitation of heavy metals at various initial concentrations from various examples of simulated wastewater with a variety of pH's and temperatures by injecting different amounts of the coagulant at several agitating speeds.[2] Sufficient removal below the water quality standards in our country has been ascertained for the heavy metals, which are precipitated as metal sulfides by the H_2S and CaS_2O_3 that are liberated on the decomposition of CaS_x by air or CO_2 gas, or as metal hydroxides by the strong alkaline base of the CaS_x solution. Accompanied by the decomposition of CaS_x in water, calcium ion and solid sulfur particles are also liberated. The phosphate ion in the wastewater can be expected to be precipitated as calcium phosphate by the calcium ion. Good removal may also be anticipated for the COD substances that may be sorbed on the solid sulfur particles and the other precipitates.

In the present study, experiments were carried out for the removal of phosphate, heavy metal, and some COD substances from the simulated wastewater. Discussion was also made for their removal percentages.

† Present address: Ataka Kogyo Co., Ltd., Sueyoshibashi, Minami-ku, Osaka 542.

Experimental

Apparatus. The batch stirred vessel utilized in this experiment was the same as that used in the previous works.[1,2] The agitating speed of the impeller was fixed at 10 Hz. The vessel was immersed in a constant-temperature bath at 25 °C. Gas (air or CO_2) was blown into the vessel at a rate of 500 cm^3/min.

Method. For the phosphate contamination, distilled water containing potassium dihydrogenphosphate was used as simulated wastewater. As examples of COD contamination, water solutions of acetone, CMC (carboxymethylcellulose), and Methyl Violet were provided. After the start of a run by blowing in air or CO_2 gas, sample liquors were taken at predetermined time intervals. For the concentration determination with heavy metal, phosphate, and acetone, the liquors were filtered by means of No. 5C filter paper. The heavy metal concentration was determined by means of an atomic absorption spectrophotometer. The phosphate was detected according to JIS-K0102. The acetone was developed by a gas chromatograph (F. I. D.). For the measurement of the CMC concentration, a Stokes viscometer was applied to the liquor filtered by membranes of various pore sizes after the viscosity had been calibrated against the CMC concentration. In the case of Methyl Violet, the centrifugal separation of the precipitates in the liquor was executed at 4,000 G for 10 min, because Methyl Violet is a kind of dye and so, if filtered, it might be sorbed on the filter paper. The supernatant liquors were examined by means of a spectrophotometer in order to determine their concentrations of residual Methyl Violet.

Results and Discussion

Removal of Phosphate. Figure 1 shows the removal of the phosphate ion, PO_4^{3-}, by means of the CaS_x process and the $Ca(OH)_2$ process. The ordinate indicates the residual PO_4^{3-} concentration after aeration for 180 min in order to decompose CaS_x in the case of the CaS_x process. The $Ca(OH)_2$ process does not need aeration. The abscissa implies the mole ratio of Ca^{2+} in the CaS_x or in the $Ca(OH)_2$ added per PO_4^{3-}.

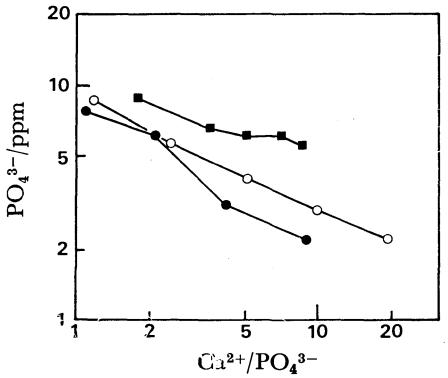

Fig. 1. Residua PO_4^{3-} concn against mole ratio of Ca^{2+} in CaS_x or in $Ca(OH)_2$. Initial concn of PO_4^{3-}=25 ppm, initial pH=6 and final pH=6.2. ■: PO_4^{3-} by $Ca(OH)_2$ process, ○: PO_4^{3-} by CaS_x process with aeration, ●: $PO_4^{3-}+Cd^{2+}$ by CaS_x process with aeration, initial concns are 25 ppm.

The initial concentrations of PO_4^{3-} and Cd^{2+} are both 25 ppm. For the simulated wastewater contaminated only with phosphate, the CaS_x process can treat PO_4^{3-} more effectively than the $Ca(OH)_2$ process for the same ratio of Ca^{2+}/PO_4^{3-}. This better removal of the CaS_x process can be thought to be due to the coprecipitation of calcium phosphate with the solid sulfur particles and calcium salts ($CaCO_3$ and $CaSO_4$) which are liberated from CaS_x. When the wastewater is contaminated simultaneously with PO_4^{3-} and Cd^{2+}, the removal is more effective. As a reason for this effective removal, the precipitation of PO_4^{3-} by Cd^{2+} may be considered. The residual Cd^{2+} concentration was determined to be 0.01 ppm, *i.e.*, far below the effluent standard of 0.1 ppm, for the treatment by the CaS_x process of the simulated wastewater contaminated simultaneously with Cd^{2+} and PO_4^{3-}.

Removal of COD Substances. The percentage of the removal of acetone whose initial cencentration was 1500 ppm was measured for the CaS_x process. The resulting removal percentage of the acetone is shown in Fig. 2 against the mass ratio of sulfur in the CaS_x added per acetone. A removal of more than 40% can be realized by the use of the CaS_x process. The peak of the removal percentage at a mass ratio of about 0.8 may be explained as follows. With the decrease in the quantity of the coagulant, the particle size of the solid sulfur liberated from CaS_x is reduced, as was found in a previous work.[2] The finer particles have a larger surface area in sum total, and so they can sorb more acetone. The removal percentages of acetone by

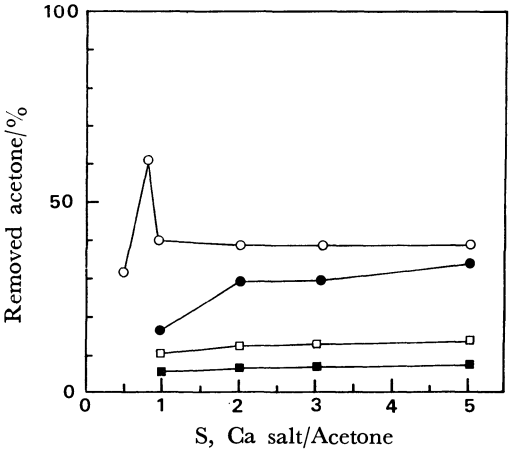

Fig. 2. Removal percentage of acetone against mass ratio of sulfur in CaS_x or of precipitated sulfur and of calcium salts, per acetone. Initial concn of acetone=1500 ppm.
○: By CaS_x process with aeration, ●: by precipitated sulfur, □: by precipitated $CaCO_3$, ■: by $CaSO_4$.

the precipitated sulfur particles and calcium salts ($CaCO_3$(precipitated), $CaSO_4$) are also shown in Fig. 2, since the sulfur particles and the salts are components of the precipitates of the CaS_x process.[1,2] The precipitated sulfur particles used in the experiment of Fig. 2 were prepared by the decomposition of a CaS_x solution (1,000 ppm) with 0.1 M-HCl. The precipitates were filtered by No. 5C and washed with distilled water in order to dissolve the $CaCl_2$. The dried cake of the sulfur particles was assured to have a purity of more than 99.5% of sulfur. Figure 2 shows that the precipitated sulfur particles can sorb about 30% of acetone, while the removal percentages with $CaCO_3$ and $CaSO_4$ are, respectively, 10 and 5%. The CaS_x process can remove about 40% of the acetone, while the precipitated sulfur sorbs 30%. The colloidal sulfur particles generated by the CaS_x process may sorb more acetone by means of some force such as the attractive force by the surface charge,[7] though the mechanism is not evident at present.

In Fig. 3, the residual concentrations of CMC are plotted against the pore size of the membrane filters used for the filtration of sample liquors. R is defined as the mass ratio of S in CaS_x per CMC. Without CaS_x injection, a part of the CMC, with so long a molecular length, was removed only by filtration with the membrane whose pore size was less than 0.5 μm. The initial concentration of CMC was 60 ppm. The residual concentration of CMC was about 12 ppm for the case of R=25 by aeration with a 0.45 μm membrane, as is shown in Fig. 3. The removal percentage for this case is about 75%. The apparent particle size of the precipitates (S, $CaCO_3$, and $CaSO_4$ with CMC) for the removal of CMC by the CaS_x process was measured by using membranes with various pore sizes like a standard sieve mesh. The apparent particle size distributions are shown in Fig. 4. These distributions are obtained by weighing the masses of the membranes and the cakes, after a processing time of 60 min using the CaS_x process. Aeration gives a little larger

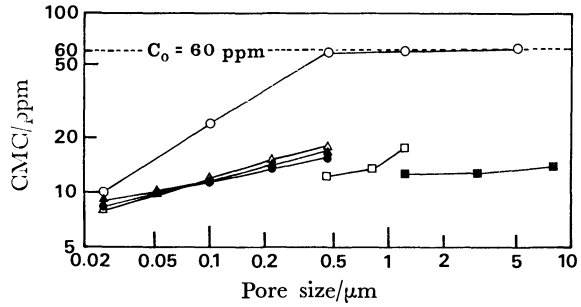

Fig. 3. Residual CMC concn against pore size of membrane. Initial concn of CMC=60 ppm.
○: Only by membrane filtration, ▲: R(mass ratio of S in CaS_x per CMC)=6.25 with aeration, ●: R=12.5 with aeration, □: R=25 with aeration, ■: R=50 with aeration, △: R=25 with CO_2 blowing.

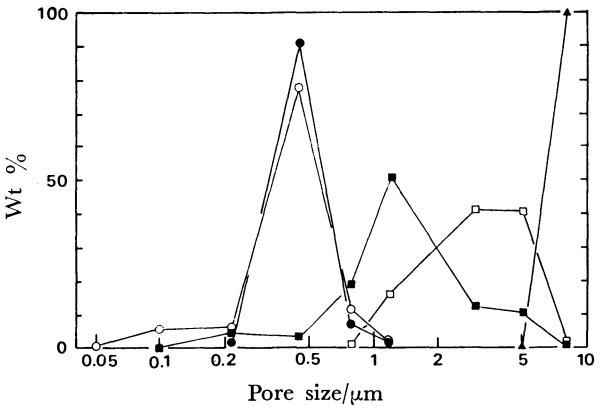

Fig. 4. Apparent particle size distributon of the precipitates formed on the removeal of CMC by CaS_x process.
○: R=6.25 with aeration, ●: R=12.5 with aeration, □: R=25 with aeration, ▲: R=50 with aeration, ■: R=25 with CO_2 blowing.

particle size than CO_2 blowing for the same R value of 25. The R value of more than 50 gives a particle size sufficient for the easy separation of the precipitates in the case of CMC processing by the CaS_x process. The particle size shown in Fig. 4 is rather finer than that observed for heavy-metal removal by the CaS_x process, as was reported in a previous paper.[2] This finer particle size may be due to the emulsifying characteristics of the CMC.

Figure 5 shows the removal of Methyl Violet. The initial concentration of 5 ppm was reduced within 0.1 ppm. The removal percentage is about 80% to 90%. The precipitates separated centrifugally were as violet in their color as if they had been dyed. On the other hand, a tentative experiment was carried out for the removal of Methyl Violet by the iron(III) hydroxide process. The removal percentage was only about 1%.

Figures 6 and 7 show photographs of the precipitates taken by means of an electron microscope when CaS_x decomposes in contact with air. Figure 6 shows the precipitates as cake caught on the fibril of No. 5C filter paper. A magnified photograph of the precipitates is shown in Fig. 7. Figures 8 and 9 (magnified) show precipitates obtained by the decomposition of CaS_x with CO_2 gas blowing. Figures 6 to 9 are cases when the substance is precipitated from the water which does not contain any contaminants but 1 cm^3 of the CaS_x solution per dm^3 of distilled water. Photographs of the precipitates when the water is contaminated with 25 ppm of Cd^{2+} and when the mole ratio of S in the CaS_x added per Cd^{2+} is equal to 25 are shown in Figs. 10 to 11 (magnified). While iron(III) hydroxide precipitates are known to be amorphous, the precipitates of the CaS_x process are found to be spheres, and so they have the advantage of easy filtration. Particle properties of the CdS precipitated from aqueous solution

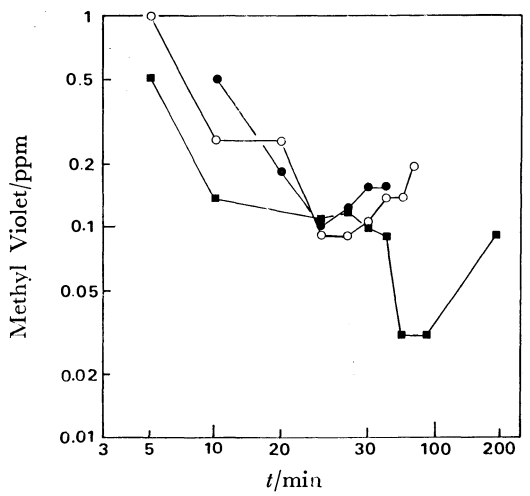

Fig. 5. Residual Methyl Violet concn against aeration time.
●: R(mass ratio of S in CaS_x per Methyl Violet)=25, ○: R=50, ■: R=125.

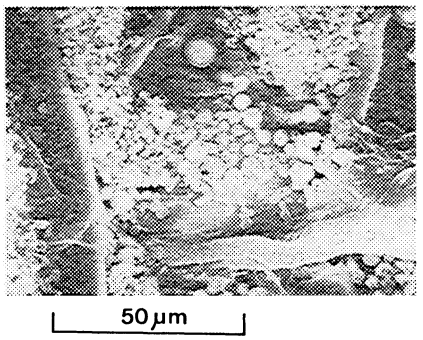

Fig. 6. Precipitates by decomposition of CaS_x with aeration.

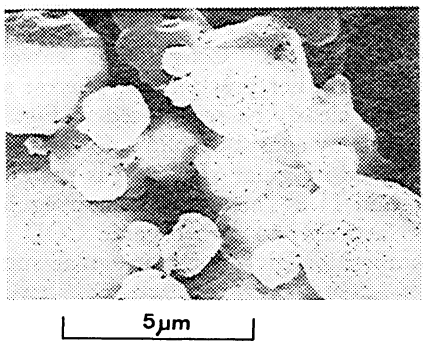

Fig. 7. Magnification of a part of Fig. 6.

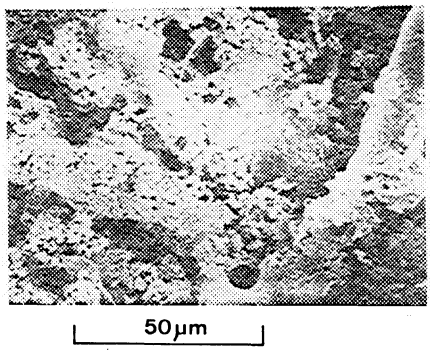

Fig. 8. Precipitates by decomposition of CaS_x with CO_2 blowing.

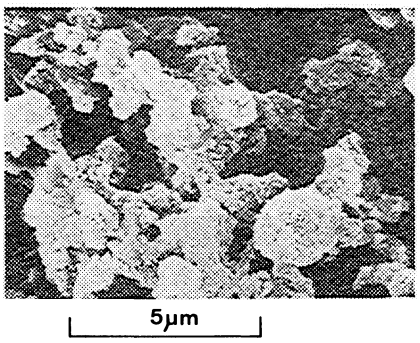

Fig. 9. Magnification of a part of Fig. 8.

of $Cd(NO_3)_2$ or $CdSO_4$ by adding $Na_2S_2O_3$ or H_2S have been studied recently by Hashimoto *et al.*[5] They have shown that the CdS particles are spherical in shape and that the diameter becomes the bigger for the higher concentration of Cd^{2+}. Since the solid sulfur particles formed in the CaS_x process are also spherical in shape as may be seen in Figs. 6 and 7, it is scarcely possible to distinguish CdS from solid sulfur in Figs. 10 and 11. The cubes in Fig. 10 are probably $CaCO_3$ as is shown in Ref. 6. Coagulation between $CaCO_3$ (cubes) and the other precipitates(spheres: solid sulfur and CdS) can clearly be recognized in Fig. 10. Most of the spheres may consist of solid sulfur particles, which have porous or irregular surfaces, as may be seen in Figs. 7, 9, and 11. These porous or irregular surfaces may work favorably to sorb organic COD substances. CO_2 decomposition gives more irregular surfaces than

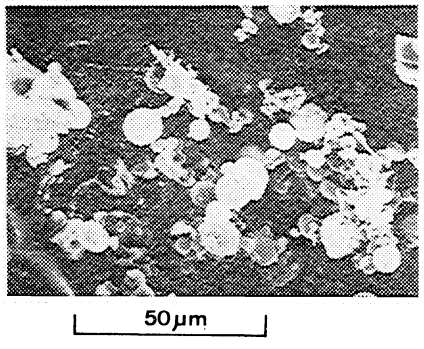

Fig. 10 Precipitates of Cd^{2+} processing by CaS_x process with blowing a gas which contains 97% of air and 3% of CO_2 gas. Initial concn of Cd^{2+}=25 ppm and mole ratio of S in CaS_x per Cd^{2+}=25.

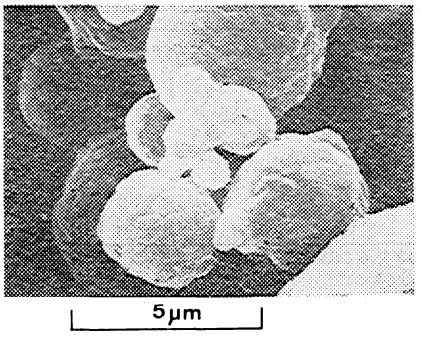

Fig. 11. Magnification of a part of Fig. 10.

that by aeration. The reason for this is not evident, but the fact that the CO_2 blowing gives rise to the rapid decomposition of CaS_x[1] may be connected with this irregularity.

The removal of heavy metals when the target material was simultaneously contaminated with COD substances was experimented within several cases. However, heavy-metal removal is not so severely affected by the simultaneous contamination with the COD substances used in the present experiments. This tendency may be explained by the fact that the COD substances were removed by the sorption on the solid sulfur particles and other precipitates, while the heavy metals were precipitated by reacting with H_2S and CaS_2O_3. The CMC might give finer particle sizes of the precipitates and so a lower removal percentage of heavy metals. However, so long as the No. 5C filter paper was employed for the separation of the precipitates, the heavy-metal removal was not affected by the COD contamination in the CaS_x process. It was shown by an auxiliary experiment that No. 5C filter paper had apparent pore sizes equivalent to membranes of between about 0.1 and 0.2 μm, and that the precipitates of the heavy metal sulfides or hydroxides were larger than these pore sizes. COD substances that form soluble-metal compounds, such as EDTA (ethylenediamine tetraacetic acid), citric acid, and tartaric acid, may affect the removal of heavy metals.[3]

An experiment was made at removing NH_3 in water by means of the CaS_x process. The initial NH_3 concentration of 25 ppm was reduced to 1 ppm after 60 min of aeration by the injection of CaS_x at an amount 25 times that of NH_3 in mole ratio. If the nitrogen compounds in the sewage are reduced as far as to free NH_3, a good removal can be realized by means of the CaS_x process. This good removal may be attributed mainly to the stripping of NH_3 from water to the exhaust-gas phase, as in the NH_3 stripping process,[4] or partly to the sorption of NH_3, though the reason for this is not evident, on the surfaces of the precipitates, for the odors of the exhaust gas and the sludge are that of NH_3 and the exhaust gas has a stronger odor than the sludge.

Conclusion

The CaS_x process is simple in its operation and makes it possible to remove various contaminants simultaneously. Thus, a good effect can be expected in water-

pollution control. The CaS_x process can also be applied to the advanced treatment of sewage which usually contains COD/BOD substances, phosphate, ammonia, and a trace of heavy metals.

The authors wish to express their appreciation of their useful discussions with Mr. Kiyochika Yahikozawa of Shinshu University, Prof. Dr. Ryuzo Ito of Osaka University, Profs. Drs. Takataro Suda and Yoshiki Sanoh of Shinshu University, and Assoc. Prof. Dr. Kei Miyanami of the University of Osaka Prefecture.

The present work was partially supported by a Grant-in-Aid for Developmental Scientific Research from the Ministry of Education.

References

1) K. Yahikozawa, T. Aratani, R. Ito, T. Suda, and T. Yano, *Bull. Chem. Soc. Jpn.*, **51**, 613 (1978).
2) T. Aratani, K. Yahikozawa, H. Matoba, S. Yasuhara, and T. Yano, *Bull. Chem. Soc. Jpn.*, **51**, 1755 (1978).
3) M. Munemori, T. Aoki, Y. Inoue, and T. Hata, The 26th IUPAC Congress (Tokyo), No. 7A501 (1977).
4) M. Sittig, "How to Remove Pollutants and Toxic Materials from Air and Water A Practical Guide," Noyes Data Corporation, Park Ridge, New Jersey (1977), p. 35.
5) K. Hashimoto, Y. Toda, and M. Kobayashi, *Nippon Kagaku Kaishi*, **1977**, 330, 656.
6) "Funtai-Bussei Zukan," Funtai-Kohgaku Kenkyukai and Nihon Funtai-Kogyo Kyokai, Sangyo Gijitsu Center, Tokyo (1975), p. 286.
7) W. Pauli, *J. Colloid Sci.*, **2**, 333 (1947).

Studies in Isodielectric Media. The Standard Potentials of Ag–AgCl and Ag–AgBr Electrodes in 1,2-Ethanediol–2,2′-Oxydiethanol Mixtures at 25 °C

P. SIVAPRASAD and C. KALIDAS*

Department of Chemistry, Indian Institute of Technology, Madras 600036, India

(Received September 16, 1977)

Standard potentials of Ag–AgCl and Ag–AgBr electrodes in various compositions of 1,2-ethanediol–2,2′-oxydiethanol (ethylene glycol–diethylene glycol) mixtures at 25 °C are reported. The free energies of transfer of the hydrogen halides from ethylene glycol to the mixtures were evaluated on mole fraction scale. The transfer free energies of H^+ and the halide ions were determined employing the ferrocene reference method. The results suggest that the basicity of the mixtures increases with the addition of diethylene glycol and that it is more basic than ethylene glycol.

Studies in isodielectric solvent mixtures have provided valuable information[1,2] on solute-solvent interactions in mixed solvents in recent years. In particular, such investigations enable one to study the influence of the chemical effect of the solvents on the thermodynamics of transfer between different solvents, for the electrostatic effects arising out of the difference in the dielectric constants of the solvent components are expected to be small in these media. Although a few emf studies in isodielectric media have been made,[3,4] no measurements have been reported in the binary mixtures of glycols. Since the dielectric constants of ethylene glycol (EG) and diethylene glycol (DEG) at 25 °C are 41.20 and 31.20 respectively and those of their mixtures are expected to be between these limits, all these solvents should serve approximately as isodielectric media. In continuation of our earlier work on the thermodynamic behaviour of electrolytes and ions in glycolic solvents,[5,6,7] the present work therefore deals with the determination of standard potentials of the silver–silver chloride and silver–silver bromide electrodes in 20 to 80 wt % EG–DEG mixtures at 25 °C. The cell (1) was used for the determination of the standard potential of the Ag–AgCl electrodes.

$$\text{Pt, } H_2\text{(g, 1 atm)/HCl(m) solvent/AgCl, Ag} \qquad (1)$$

and the buffered cell (2)

$$\text{Pt, } H_2\text{(g, 1 atm)/HOAc(m1), NaOAc(m2), KX(m3) solvent/AgX, Ag} \qquad (2)$$

containing acetic acid (HOAc), sodium acetate (NaOAc) and potassium bromide (KBr) with X=Br was used for determining the standard potentials of Ag–AgBr electrode. The dissociation constant of acetic acid required in the evaluation of the standard potentials of Ag–AgBr electrode in these solvents was determined as described later.

Experimental

EG (LR, BDH) and DEG (LR, BDH) were purified by the methods described earlier.[5,8] The preparation of the stock acid solutions was as described elsewhere.[8]

Ag–AgCl and Ag–AgBr electrodes were of the thermal electrolytic type and were prepared according to the method of Janz and Ives.[9] The preparation of the hydrogen electrode and the experimental set up employed in EMF measurements are similar to those described in detail in earlier work.[5] The cells were thermostated with an accuracy of ±0.05 °C during equilibration. The cells normally attained equilibrium 5—6 h after the start of hydrogen bubbling in all the mixtures and constancy of emf values to ±0.1 mV over a period of half an hour was considered as an adequate criterion of equilibrium. The vapour pressures of the solvents being very small, no vapour pressure correction was applied to the emf data. The transfer free energy of proton in these mixtures was determined by employing the ferrocene reference method according to the procedure described earlier.[10]

Results and Discussion

The standard molal potentials ${}_sE^\circ_m$ of the cell (1) in different solvent mixtures were obtained by extrapolation of the function

$$E^{\circ\prime} = E + 2k\log m - 2kA'm^{1/2}/(1+aB'm^{1/2}) - 2k\log(1+0.002\,mM_{xy}) = {}_sE^\circ_m - 2k\,b\,m \qquad (3)$$

to zero molality. In the above equation,

$$k = 2.303\,RT/F, \qquad (4)$$

m is the molality of HCl, A' and B' are the Debye-Hückel constants on the molality scale, a is the ion size parameter, b is the coefficient occurring in the activity coefficient expression as a function of molality and M_{xy} is the mean molar mass of the mixed solvent as defined earlier.[5] In determining ${}_sE^\circ_m$, a=5 Å was used as this was found to give good linear plots with the least slope. The standard potentials of the Ag–AgCl electrode on molar (${}_sE^\circ_c$) and mole fraction scales (${}_sE^\circ_N$) were calculated from (${}_sE^\circ_m$) with the help of usual relationships given earlier.[5] All these values at 25 °C are given in Table 1.

The standard potentials (${}_sE^\circ_m$) of the Ag–AgBr electrode at 25 °C in different solvent mixtures were obtained from a plot of the function $E^{\circ\prime}$ defined by

$$E^{\circ\prime} = E - 2.303\frac{RT}{F}\mathrm{p}K_{(\mathrm{HOAC})} + 2.303\frac{RT}{F}\log\frac{m\,\mathrm{HOAC}\;m\,\mathrm{Br}^-}{m\,\mathrm{OAC}^-} = {}_sE^\circ_m - 2.303\frac{RT}{F}\log\frac{\gamma\mathrm{HOAC}\;\gamma\mathrm{Br}^-}{\gamma\mathrm{OAC}^-} = {}_sE^\circ_m + f(\mu) \qquad (5)$$

against μ, the ionic strength, by extrapolating to μ=0. $E^{\circ\prime}$ values were computed by using the values of $\mathrm{p}K_{(\mathrm{HOAC})}$ and the measured EMF values of cell (2) with X=Br for various buffer compositions. $\mathrm{p}K_{(\mathrm{HOAC})}$ values required in Eq. 5 were obtained from measurements

Table 1. Standard potentials of the Ag–AgCl and Ag–AgBr electrodes (V) in ethylene glycol–diethylene glycol mixtures at 25 °C

DEG wt %	Ag-AgCl electrode			Ag-AgBr electrode		
	E°_m	E°_c	E°_N	E°_m	E°_c	E°_N
0	0.0240[a]	0.0294	−0.1188	−0.0991[b]	−0.0938	−0.2419
20	0.0242	0.0298	−0.1142	−0.0932	−0.0876	−0.2316
40	0.0190	0.0246	−0.1145	−0.0987	−0.0931	−0.2322
60	−0.0034	0.0022	−0.1247	−0.1091	−0.1035	−0.2372
80	−0.0191	−0.0135	−0.1412	−0.1257	−0.1200	−0.2478
100[c]	−0.0308	−0.0251	−0.1461	−0.1451	−0.1395	−0.2604

a) *J. Chem. Soc., Faraday Trans. 1*, **73**, 284 (1977). b) *J. Chem. Eng. Data*, **15**, 209 (1970). c) Our unpublished work.

Table 2. Standard free energies of transfer of HCl, HBr, H^+ and halide ions from ethylene glycol to ethylene glycol–diethylene glycol mixtures (mole fraction scale) at 25 °C (J mol^{-1})

DEG wt %	$\Delta G^\circ_{t(HCl)}$	$\Delta G^\circ_{t(HBr)}$	$\Delta G^\circ_{t(H^+)}$	$\Delta G^\circ_{t(Cl^-)}$	$\Delta G^\circ_{t(Br^-)}$
0	0	0	0	0	0
20	−444	−994	25	−469	−1019
40	−415	−936	−39	−376	−897
60	569	−454	−268	837	−186
80	2162	569	−922	3084	1491
100	2635	1785	−1267	3902	3052

on cell 2 with X=Cl and utilizing the ${}_sE^\circ_m$ values of Ag–AgCl electrode in these solvents obtained with cell (1). In calculating $E^{\circ\prime}$, it was assumed that KBr and NaOAc are completely dissociated in all the solvents, and that the dissociation of HOAc is so small that it does not affect the effective concentration of HOAc and OAc^-. The ${}_sE^\circ$ values on different scales are also presented in Table 1.

The transfer free energy of proton, $\Delta G^\circ_{H^+}$ in these mixtures was determined as described earlier from the relation

$$\Delta G^\circ_{cell} = F({}_sE^\circ_N - {}_{EG}E^\circ_N) = \Delta G^\circ_{FIC^+(el)} - \Delta G^\circ_{H^+}, \quad (6)$$

where ${}_sE^\circ_N$ and ${}_{EG}E^\circ_N$ represent the standard potentials of the cell

$$\frac{\text{Pt, } H_2\text{(g, 1 atm)}}{H^+ \text{ in the solvent}} \;\Big|\; \frac{FiC^+, FOC\ 1:1 \text{ in the solvent}}{\text{Pt}} \quad (7)$$

in the solvent and EG respectively on the mole fraction scale.

$\Delta G^\circ_{FIC^+(el)}$ which represents the electrostatic transfer free energy of the ferricinium ion from EG to the solvent was determined from the Born equation using the dielectric constants of the solvent mixtures (our unpublished results) determined by us.

The standard free energy change, ΔG°_t, for the transfer of one mole of HX from the standard state in one reference solvent to the standard state in another can be calculated from the standard potential data of the Ag–AgX electrodes in different solvents. Considering EG as the reference solvent, $\Delta G^\circ_{t(HX)}$ for HCl and HBr were computed by

$$\Delta G^\circ_t = F({}_{EG}E^\circ_N - {}_sE^\circ_N), \quad (8)$$

where ${}_{EG}E^\circ_N$ and ${}_sE^\circ_N$ are the standard potentials in EG and the solvent mixtures respectively. They are recorded in Table 2 and are accurate to ±90 J. The free energies of transfer of H^+, and the halide ions are also given in Table 2. The ΔG°_t values for both acids are found to have small negative values initially, pass through a minimum at about 20 wt % DEG and then increase (become positive) with the further addition of DEG. Thus while the transfer of HCl and HBr from EG to the mixed solvents is thermodynamically favourable upto about 40 wt % DEG, the transfer process is not favoured at higher compositions of DEG. For any solvent the values for HBr are more negative than for HCl indicating that the transfer is relatively easier for HBr than for HCl. The nature of the variation of ΔG°_t with solvent composition suggests that two opposing factors must operate so as to give the observed minimum in the EG rich region. The transfer free energies of the proton together with the data for the halide ions (Table 2) in these solvent mixtures lend support to the above conclusion because $\Delta G^\circ_{t(H^+)}$ and $\Delta G^\circ_{t(Cl^-)}$ clearly vary in opposite directions. However, it is seen that the changes in $\Delta G^\circ_{t(X^-)}$ predominate over that of $\Delta G^\circ_{t(H^+)}$ and thus govern the overall variation of $\Delta G^\circ_{t(HX)}$ with the solvent composition.

In general, the basicity of the solvent mixtures increases with increasing proportion of DEG and also DEG is more basic than EG. These results are in agreement[10] with the conclusions arrived on the basis of proton medium effects determined by the ferrocene reference method in DEG–water and EG–water mixtures earlier.

References

1) K. K. Kundu, A. L. De, and M. N. Das, *J. Chem. Soc., Dalton Trans.*, **1972**, 373.
2) H. P. Bennetto and J. J. Spitzer., *J. Chem. Soc., Faraday Trans.*, **69**, 1491 (1973).
3) K. K. Kundu and A. K. Das, *Indian J. Chem.*, **11**, 952 (1973).
4) C. Kalidas, P. Sivaprasad, and U. V. Venkatram, *Z. Naturforsch.*, **32a**, 791 (1977).
5) C. Kalidas and V. Srinivas Rao, *J. Chem. Eng. Data*, **19**, 201 (1974).
6) V. Srinivas Rao and C. Kalidas, *J. Chem. Eng. Data*, **21**, 314 (1976).
7) V. Srinivas Rao and C. Kalidas, *Bull. Chem. Soc. Jpn.*, **48**, 2957 (1975).
8) C. Kalidas and S. R. Palit, *J. Chem. Soc.*, **1961**, 3998.
9) G. J. Hills and D. J. G. Ives, "Reference Electrodes," D. J. G. Ives and G. J. Janz, Es., Academic Press, New York, N. Y. (1961), p. 190.
10) V. Srinivas Rao and C. Kalidas, *Indian J. Chem.*, **13**, 1303 (1975).

Variation of Transport Properties as Functions of Temperature and Composition in Glass-forming Melts — An Isoenergic Equation

Nurul ISLAM,* Satendra KUMAR, and Kunwar Pal SINGH
Department of Chemistry, Aligarh Muslim University, Aligarh 202001, India
(Received November 24, 1977)

Measurements of density, ρ, viscosity, η, and electrical conductance, Λ, in glass-forming molten mixtures of manganese(II) chloride–tetrabutylammonium bromide were made as functions of temperature and composition. The non-Arrhenius temperature dependence of transport properties has been discussed in terms of equations based on the free-volume model. Composition dependence of viscosities has been explained satisfactorily through a parabolic equation, $\eta=p+qN+rN^2+sN^3$, where p, q, r, and s are the empirical parameters and N is the mole fraction of the solute. The minimum in the viscosity isotherms has been observed at $N=-q/2r$. A better applicability of isoenergic equation, $Y(=\phi$ or $\Lambda)=(A_{0Y}-Q_{1Y}N)c^{-1/2}(T_{0(0)}+Q_2N)^{-1/2}\exp[-k_{1Y}/(T_{0(0)}+Q_2N)\text{-}(c-1)]$ over an isothermal equation (both based upon free volume model) in explaining the transport process in all the glass-forming melts has been emphasized.

Temperature dependence of transport properties starting from very high temperatures where it is of Arrhenius' type passes through the middle region from T_g to $2T_g$ where it becomes of non-Arrhenius' type, and once again it is of Arrhenius' type at low temperatures. Such dependence in the middle region has been studied by several workers in terms of equations based upon free-volume and configurational entropy models; of these based upon the former are

$$Y = A_{1Y}T^{-1/2}\exp[-k_{1Y}/(T-T_0)], \quad (1)$$

$$Y = A_{2Y}\exp[-k_{2Y}/(V-V_0)], \quad (2)$$

where symbols have their usual significances. Equally important composition dependence has been described by considering the variation of the empirical parameters, A_Y and T_Y with concentration of these equations. Angell[1,2] proposed an isothermal equation by assuming A_Y and k_Y as composition independent and only T_0 varying linearly with concentration, which is of the form

$$Y = A_{1Y}T^{-1/2}\exp[-k_{1Y}/Q_2(N_0\delta-N)], \quad (3)$$

where N is the concentration in mol%, Q_2 is the slope of T_0 *versus* N plots, and N_0, the characteristic composition at which the isothermal temperature, T becomes the glass transition temperature, T_g of the system. Recently, a linear decrease of A_{1Y} terms[3,4] with composition has been observed and Eq. 3 was modified[5] accordingly in order to account for that, and is of the form

$$Y = (A_{0Y}-Q_{1Y}N)T^{-1/2}\exp[-k_{1Y}/Q_2(N_0-N)]. \quad (4)$$

Q_{1Y} is the negative slope of A_Y *versus* N plots and A_{0Y} the preexponential term for the pure solvent. This equation was satisfactorily employed to explain the composition dependence of transport properties of several molten salt mixtures.[5,6] However, such an isothermal equation may only be employed within the temperature limits ranging between the T_0's of the solvent and the solute. Beyond this range N_0 will have values which are either less than zero or more than 100 mol% and such values may not have any physical meaning whatsoever. To overcome these difficulties an expression based upon configurational entropy model was suggested in an earlier paper,[7] in which the use of isentropic condition, $c=T/T_0$ was made based upon the definition of configurational entropy[8] as $S_c=\Delta C_p \ln(T/T_0)$ where ΔC_p is the difference in heat capacities of liquid and glassy state. Assuming ΔC_p as almost composition invariant at equal values of T/T_0, the entropy may also be considered as constant. However, we remain unable to give sufficient support to this assumption that ΔC_p is compostiion independent. Therefore, another modified expression based upon free volume model has been suggested here to explain more satisfactorily the composition dependence of transport properties of glass-forming melts. Tetrabutylammonium bromide–$MnCl_2$ system has been selected here for further studies of such behavior. The system under consideration is of importance, as its viscosities show an abnormal composition dependence. Such behavior of viscosity has been explained through a parabolic equation as well as modified free-volume expression.

Experimental

Tetrabutylammonium bromide (Fluka) was used as solvent in molten state and anhydrous $MnCl_2$[9] as solute. The experimental techniques used and the precision of measurements are similar to those reported earlier.[7,10] Also the ranges of composition and temperature measurements are the same as reported in a previous paper.[7]

Results and Discussion

The measured densities of the system under investigation have been least-squares fitted to a linear function of the form $\rho=a-bT$ (K) and the values of computed parameters are given in Table 1.

TABLE 1. COMPUTED PARAMETERS FOR DENSITY EQUATION, $\rho(\text{gm/cm}^3)=a-bT(\text{K})$ OF TBAB[a]-$MnCl_2$ MELTS

Mn^{2+} mol %	a (gm/cm^3)	$b\times10^3$	Std dev in ρ
5.00	1.2650	0.6420	0.54×10^{-3}
10.07	1.2611	0.5841	0.31×10^{-3}
15.09	1.3057	0.6331	0.67×10^{-3}
19.66	1.3250	0.6275	0.22×10^{-3}
25.04	1.3398	0.6099	0.19×10^{-3}
30.14	1.3806	0.6558	0.39×10^{-3}

a) TBAB=tetrabutylammonium bromide.

TABLE 2. EQUIVALENT CONDUCTANCE ($cm^2\ equiv^{-1}\ ohm^{-1}$) AND FLUIDITY ($P^{-1}$)[a] DATA OF TBAB-$MnCl_2$ MELTS

T (K)	mol % of Mn^{2+}					
	5.00	10.07	15.09	19.66	25.04	30.14
373.0	0.3399 (0.8624)	0.3287 (1.0279)	0.2056 (0.8672)	0.1641 (0.8171)	0.1267 (0.5994)	0.1060 (0.5326)
378.0	0.4181 (1.0778)	0.4022 (1.1640)	0.2486 (1.0784)	0.2083 (1.0009)	0.1587 (0.7960)	0.1256 (0.6482)
383.0	0.5052 (1.3150)	0.4690 (1.4277)	0.2936 (1.3184)	0.2488 (1.2146)	0.1910 (0.9775)	0.1539 (0.7897)
388.0	0.5947 (1.5966)	0.5579 (1.7244)	0.3445 (1.5834)	0.3003 (1.4699)	0.2322 (1.1713)	0.1853 (0.9426)
393.0	0.7159 (1.9524)	0.6490 (2.1064)	0.3981 (1.9056)	0.3545 (1.7677)	0.2744 (1.3995)	0.2212 (1.1318)
398.0	0.8469 (2.4006)	0.7532 (2.5231)	0.4592 (2.2662)	0.4163 (2.1494)	0.3177 (1.6724)	0.2588 (1.3485)
403.0	1.0006 (3.0020)	0.8499 (3.0357)	0.5264 (2.7310)	0.4822 (2.5394)	0.3746 (2.0083)	0.3014 (1.6138)
408.0	1.1582 (3.7455)	0.9740 (3.6777)	0.6160 (3.2888)	0.5629 (2.9780)	0.4427 (2.3519)	0.3450 (1.9017)
413.0	1.3327 (4.6168)	1.1395 (4.4609)	0.6994 (3.9097)	0.6497 (3.4781)	0.5095 (2.6634)	0.4028 (2.2045)

a) Fluidity data are within parentheses.

Temperature Dependence of Fluidities and Conductances. The conductance and fluidity data (Table 2) show non-Arrhenius temperature dependence and therefore least-squares fitted to Eqs. 1 and 2. The empirical parameters of these Eqs. along with standard deviations in $\ln \phi$ and $\ln \lambda$ are given in Table 3. Linear plots (Fig. 1) of $\log(\phi T^{1/2})$ and $\log(\lambda T^{1/2})$ *versus* $1/(T-T_0)$ show the applicability of Eq. 1 to explain the temperature dependence. Further, the plots of ϕ and λ *versus* $(V-V_0)$ were found to be non-linear signifying the inability of the Hildebrand equation,[11] $Y(=\phi$ or $\lambda)=B(V-V_0)/V_0$, to explain the transport behavior in the present system. However, linear plots (Fig. 2) of $\log \phi$ and $\log \lambda$ *versus* $1/(V-V_0)$ demonstrate a better fit of these data to Doolittle Eq. 2. Empirical parameters of this equation are given in Table 3 along with standard deviations in $\ln \phi$ and $\ln \lambda$.

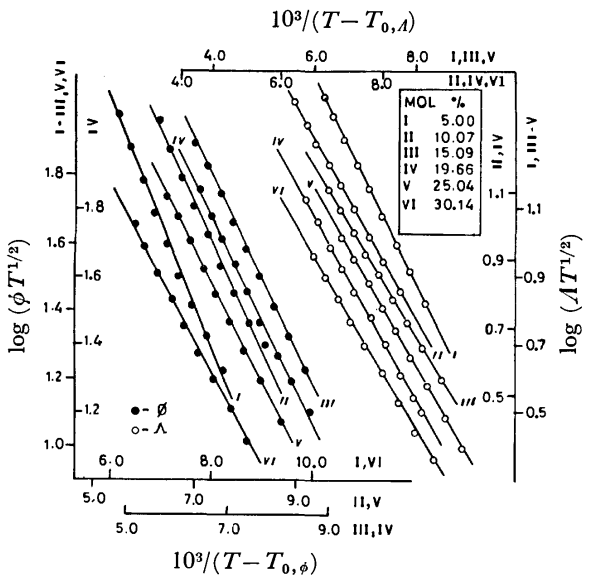

Fig. 1. Plots of $\log(YT^{1/2})$ *vs.* $1/(T-T_0)$ for TBAB-$MnCl_2$ melts.

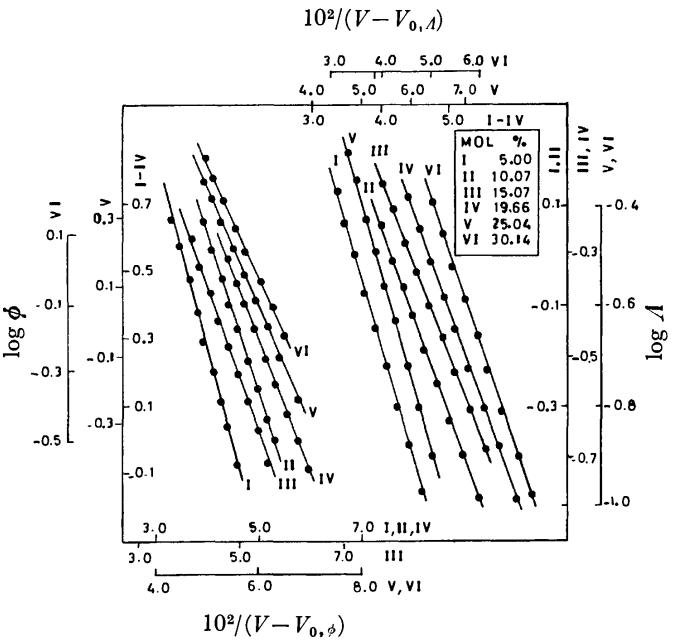

Fig. 2. Plots of $\log Y$ *vs.* $1/(V-V_0)$ for TBAB-$MnCl_2$ melts.

Both Eqs. 1[12] and 2[13] based upon the free volume approach are similar to one another. The parameter A_{2Y} of Doolittle Eq. is expected to depend on composition as in the case of A_{1Y} of free-volume model. Similarly k_{2Y} in the exponential term is related to k_{1Y} as being composition independent. Moreover, values of $T_{0,\phi}$ and $T_{0,\Lambda}$ and $V_{0,\phi}$ and $V_{0,\Lambda}$ obtained from Eqs. 1 and 2, respectively, are very close to one another thereby indicating the thermodynamic nature of glass transition temperature, T_0 and intrinsic volume, V_0 rather than kinetic. $k_\phi \approx 700$ K and $k_\Lambda \approx 600$ K seem

Table 3. Computed parameters for Eqs. 1 and 2 for the fluidity[a] and equivalent conductance data of TBAB-$MnCl_2$ melts

Mn^{2+} mol %	A_{1Y}	k_{1Y} (K)	$T_{0,Y}$ (K)	Std dev in ln Y	A_{2Y}	k_{2Y}	$V_{0,Y}$ (cm^3/mol)	Std dev in ln Y
5.00	1121.40 (7658.50)	605.20 (712.00)	253.54 (253.24)	0.054 (0.095)	57.66 (436.29)	111.59 (136.13)	283.10 (283.14)	0.017 (0.056)
10.07	1000.80 (7252.40)	596.20 (702.69)	255.62 (255.68)	0.018 (0.054)	33.37 (250.50)	84.97 (102.80)	271.70 (271.62)	0.016 (0.053)
15.09	748.60 (6802.70)	606.80 (697.60)	257.64 (257.75)	0.036 (0.032)	18.34 (212.21)	81.00 (99.04)	255.69 (255.78)	0.017 (0.030)
19.66	651.40 (6300.60)	602.25 (687.21)	259.67 (259.73)	0.014 (0.035)	25.80 (176.98)	83.87 (89.25)	243.50 (243.60)	0.011 (0.022)
25.04	522.60 (5505.70)	604.08 (699.50)	260.38 (260.34)	0.018 (0.037)	26.21 (137.58)	83.76 (79.49)	229.89 (230.90)	0.014 (0.017)
30.14	414.40 (4812.30)	590.00 (695.80)	262.64 (262.34)	0.020 (0.070)	13.39 (96.14)	69.66 (76.17)	217.34 (217.08)	0.017 (0.024)

a) Fluidity data are within parentheses.

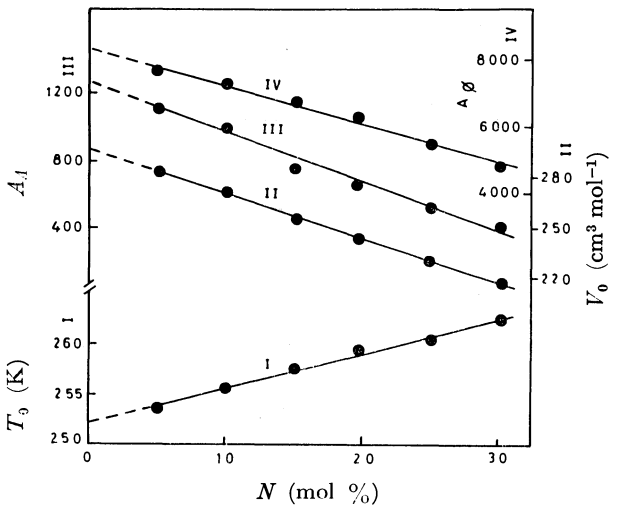

Fig. 3. Variation of T_{0Y}, $V_{0,\phi,A}$, and A_{1Y} with composition for TBAB-$MnCl_2$ melts.

to be very close to the values assigned to them as being universal constants.

The values of the preexponential factors of both Eqs. 1 and 2 decrease linearly with concentration (Fig. 3). Although there is a marked difference in the magnitude of A_Y terms of these equations which may be due to the absence of $T^{-1/2}$ in the preexponential term in Eq. 2. According to Cohen and Turnbull,[14] the A_Y terms may be expected to show direct dependence on $r/m^{1/2}$, where r and m are the effective radius and mass, respectively of the component particles of the system. In the present system there is a decrease in average molar mass by the addition of $MnCl_2$ to the molten TBAB, hence one can predict an increase in A_Y terms with increase in [$MnCl_2$]. However, an opposite trend has been obtained in the variation of A_Y with composition and may be represented as

$$A_Y = A_{0Y} - Q_{1Y}N, \tag{5}$$

where A_{0Y} is the value of the preexponential term for the pure solvent and Q_{1Y} gives the negative slopes of A_Y *versus* N plots.

An alternative explanation may be accorded for such a change in A_Y terms. According to Maxwell

$$Y = \frac{1}{\tau G}, \tag{5}$$

where τ is the relaxation time of the flowing entities and G is the rigidity modulus of the system. Using Eyring's expression, Eq. 6 may be written as

$$Y = \frac{1}{G\tau_0} \exp\left[-E_Y/RT\right], \tag{7}$$

in which τ_0 is the period of vibration of the flowing entity in its equilibrium position and E_Y is the activation energy for the transport process. R and T have their usual significances. Comparing Eqs. 1 and 7 we may obtain

$$A_{1Y} = \frac{T^{1/2}}{\tau_0 G}. \tag{8}$$

The above expression implies that A_Y is a function of rigidity of the system and as the concentration increases the rigidity of the system may increase. Moreover, the transition probability decreases with increasing concentration, in other words, the relaxing species will vibrate for a longer time in its equilibrium position with an increase in concentration. Accordingly, this may account for the linear decrease of A_Y terms with increasing [$MnCl_2$]. Further, the larger value for the slope of the linear plot of A_ϕ *versus* N than that of A_A *versus* N implies that A_ϕ decreases more rapidly than A_A with increase in concentration. Therefore, conductance appears to be less prone to the change in rigidity of the system than the fluidity.

In the system under investigation as well as in a variety of other[3,5,12,15] systems T_0 shows a linear relationship with mol % of solute (Fig. 3) which may be expressed as

$$T_0 = T_{0(0)} + Q_2N, \tag{9}$$

where $T_{0(0)}$ is the glass transition temperature for the pure solvent and Q_2 is the slope of T_0 *versus* N plot. This linear increase of T_0 with composition can be explained by considering that T_0 depends upon coulombic interactions or cohesive energy of the system.[12] The interactions increase with increase in [Mn^{2+}] thereby increasing T_0 values. In other words, an increase in T_0 with an increase in [$MnCl_2$] may be

Table 4. Computed parameters for Eqs. 10 and 11 for Walden product of TBAB–$MnCl_2$ melts

Mn^{2+} mol %	A_3	k_3 (K)	$T_{0,\Lambda\eta}$ (K)	Std dev in $\Lambda\eta$	A_4	k_4	$V_{0,\Lambda\eta}$ (cm^3/mol)	Std dev in $\Lambda\eta$
5.00	0.1679	102.85	253.21	0.049	0.1559	20.59	283.20	0.043
10.07	0.1410	103.45	255.57	0.047	0.1269	18.50	271.70	0.035
15.09	0.0947	105.64	257.43	0.021	0.0852	18.87	255.58	0.023
19.66	0.0887	105.74	259.54	0.052	0.1436	6.15	243.60	0.011
25.04	0.0854	108.37	260.42	0.056	0.1438	5.28	230.80	0.011
30.14	0.0837	106.74	262.54	0.061	0.1473	4.46	217.10	0.009

attributed to an increase in net cohesion in the system due to complex formation which leads to an eventual supercooling to glassy state. Therefore, it appears that in the absence of crystallization, addition of an excess amount of solute to any ionic solution results in glass formation and a sharp increase in viscosity may result, and such a concentration will be the glass transition composition, N_0. Also the linear increase in $T_{0,\gamma}$ with increase in [$MnCl_2$] may be due to the decrease in average mass of the system with the addition of $MnCl_2$ to TBAB melts.[7] Moreover, the values of $V_{0,\phi}$ and $V_{0,\Lambda}$ (Fig. 3) appear to decrease with increase in [$MnCl_2$] which may be due to the close packing of the system.

Temperature Dependence of Walden's Product. The temperature dependence of Walden's product, $\Lambda\eta$ may be represented through expressions[5] essentially based upon Eqs. 1 and 2 of the form

$$\Lambda\eta = A_3 \exp\left[k_3/(T-T_0)\right], \tag{10}$$

and

$$\Lambda\eta = A_4 \exp\left[k_4/(V-V_0)\right], \tag{11}$$

where A_3, k_3, A_4 and k_4 are empirical constants. The best fit values of these parameters are given in Table 4. The simultaneous representation of the temperature dependences of Λ and η appears to be more sound due to their interdependent nature.

The temperature dependence of $\Lambda\eta$ product may also be expressed satisfactorily by Frenkel's equation[16]

$$\Lambda^n\eta = \text{constant}, K. \tag{12}$$

This is apparent from its recent application to the $\Lambda\eta$ products of $CoCl_2$–$Ca(NO_3)_2.3.91H_2O$ molten mixtures.[5] Computed parameters for Eq. 12 are given in Table 5 for the present system. Here n is the ratio of E_ϕ/E_Λ, which is found to be greater than one. It may be further emphasized that failure of Walden's rule in molten salts may be due to the higher activation energies for viscous flow than ionic and is likely due to the difference in the availability of the species for relaxation in the two processes.

Table 5. Computed parameters for Eq. 12 for the products of Λ and η of TBAB–$MnCl_2$ melts

Mn^{2+} mol %	n	ln K	Std dev in ln η
5.00	1.2223	1.1219	0.031
10.07	1.2328	1.3068	0.035
15.09	1.2319	1.7886	0.009
19.66	1.0764	1.7041	0.018
25.04	1.0713	1.7292	0.017
30.14	1.0635	1.7522	0.015

Composition Dependence of Fluidities and Conductances. A regular decrease in electrical conductance with increase in composition is observed (Table 2) which may be attributed to the removal of more mobile anions as a result of complex formation and simultaneous decrease in free volume. While an increase in fluidity is observed as the concentration of $MnCl_2$ increases from ≈5 to ≈10 mol % and then decreases with further increase in concentration. The minimum at ≈10 mol % of Mn^{2+} appears to flatten as the temperature increases (Fig. 4). Such an unexpected trend in the viscosity isotherms has earlier[3] been observed in the molten TBAI+$CoCl_2$ systems. Similar abnormal behavior of viscosity as well as conductance isotherms has also been reported in several other binary molten mixtures.[15,17,18]

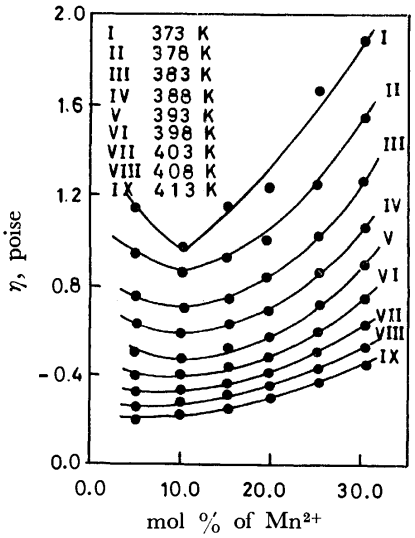

Fig. 4. Viscosity, η isotherms for TBAB–$MnCl_2$ melts.

The decrease in the viscosity in concentration range up to ≈10 mol % of $MnCl_2$ may be attributed to the decrease in electrostatic force holding a solvent ion-pair together due to the presence of free metal ions in its neighborhood. Such a dissociation with increase in concentration of solute at constant temperature depends upon the number of free metal ions and the thermal energy of the solvent.[19] The minimum in the viscosity isotherms corresponds to a point where dissociation is maximum. Furthermore, when the dissociation of solvent molecules (TBAB) increases

with increase in [$MnCl_2$], the solvent anions, *i.e.*, Br^- ion formed in this way form a complex species with the free metal ion as $MnBr_4^{2-}$, the presence of which has been supported by its ligand-field bands.[10] The complex species formed associates with the solvent cation, Bu_4N^+. Such a simultaneous complexation and association at higher concentrations may increase the viscosity of the system from ≈ 0.1 to ≈ 0.30 mole fraction of $MnCl_2$. This abnormal nature of viscosity isotherms has been empirically described by least-squares fitting the data to a polynomial equation of the form

$$\eta = p + qN + rN^2 + sN^3, \quad (13)$$

where p, q, r, and s are empirical constants, using POLRG computer program. This computer program is similar to that reported by Easteal and Hodge[17] and can fit the data to polynomials up to seventh degree. The computed values of the empirical constants are presented in Table 6 along with the standard deviation from the observed η. It is apparent from the table that in most of the cases the polynomial is quadratic and the expected minimum at the mole fraction, $N=-q/2r$ fairly coincides with those of the viscosity isotherms, *viz.* ≈ 0.1 (Fig. 4).

The conventional activation eneriges, E_ϕ and E_Λ were computed from the corresponding derivatives of Eq. 1. A regular decrease in activation energies, E_ϕ and E_Λ with temperature was obtained which may be due to the thermal expansion of the system thereby decreasing the interionic forces or, in other words, lowering the height of the potential energy barrier for the flow processes.

Table 6. Computed parameters for Eq. 13 for the viscosity of TBAB-$MnCl_2$ melts

T (K)	p	q	r	s	Std dev in η
373.0	1.6613	−14.160	87.76	−127.01	0.047
378.0	1.0632	−3.666	17.49	—	0.014
383.0	0.8673	−2.928	14.11	—	0.012
388.0	0.7199	−2.521	12.13	—	0.009
393.0	0.5859	−2.009	9.93	—	0.008
398.0	0.4592	−1.164	5.53	4.85	0.010
403.0	0.3486	−0.454	2.26	7.44	0.006
408.0	0.2970	−0.731	3.56	4.75	0.009
413.0	0.2282	−0.434	3.95	—	0.005

On the other hand, an abnormal behavior in the composition dependence of E_ϕ has been observed. E_ϕ decreases initially with an increase in the concentration of $MnCl_2$ and passes through a minimum at ≈ 10 mol % of $MnCl_2$ and then increases with further increase in [$MnCl_2$] as observed in the case of Bu_4NI–$CoCl_2$ melts.[3] The decrease in activation energy for viscous flow up to ≈ 10 mol % may be due to the dissociation of solvent molecules which results in an ease to viscous flow. Furthermore, the increase in E_ϕ following minimum may be due to the complexation and association as discussed above. However, at equal values of T/T_0 the corrected activation energies ($E_Y + 1/2RT$) of the molten salt systems may be considered as constant,[2,20] which may be termed as an isoenergic condition. Therefore, the fluidities and conductances may be plotted *versus* composition at constant T/T_0 values. The significance of such plots is that a better quantitative illustration of the composition dependence of transport properties may be made at equal T/T_0 values by accounting for the composition dependence of individual parameters in Eq. 1. At T/T_0=constant, c, Eq. 1 becomes

$$Y = A_{1Y}(cT_0)^{-1/2} \exp\left[-k_{1Y}/T_0(c-1)\right]. \quad (14)$$

The values of fluidities and equivalent conductances at constant T/T_0 ratios ranging from 1.4 to 2.1 were calculated from Eq. 14 and are in turn least-squares fitted to the equation obtained by substituting the linear variations of A_Y and T_0 with composition, in Eq. 14 as

$$Y = (A_{0Y} - Q_{1Y}N)c^{-1/2}(T_{0(0)} + Q_2N)^{-1/2} \exp\left[-k_{1Y}/(T_{0(0)} + Q_2N)(c-1)\right]. \quad (15)$$

Table 7. Computed parameters for Eq. 15 (c=1.4 to 2.1) for the fluidities[a] and equivalent conductances of TBAB-$MnCl_2$ melts

Volues of c	A_{0Y}	Q_{1Y}	k_{1Y} (K)	$T_{0(0)}$ (K)	Q_2	Std dev in ln Y
1.4	1278.0	27.52	607.8	251.5	0.368	0.098
	(8229.0)	(103.20)	(703.8)	(251.2)	(0.375)	(0.097)
1.5	1282.0	28.08	607.7	251.6	0.365	0.089
	(8241.0)	(103.70)	(703.4)	(251.3)	(0.374)	(0.081)
1.6	1285.0	28.44	608.2	251.6	0.366	0.084
	(8244.0)	(104.50)	(704.6)	(251.4)	(0.373)	(0.070)
1.7	1272.0	28.07	608.5	251.4	0.364	0.079
	(8246.0)	(104.80)	(703.6)	(251.2)	(0.374)	(0.062)
1.8	1275.0	28.36	608.7	251.6	0.362	0.076
	(8248.0)	(104.60)	(704.6)	(251.3)	(0.375)	(0.057)
1.9	1270.0	28.20	608.5	251.7	0.363	0.073
	(8243.0)	(105.20)	(700.0)	(251.4)	(0.370)	(0.053)
2.0	1268.0	28.20	608.2	251.6	0.367	0.071
	(8245.0)	(106.60)	(702.8)	(251.4)	(0.374)	(0.049)
2.1	1272.0	28.40	609.6	251.5	0.364	0.070
	(8243.0)	(106.20)	(703.8)	(251.3)	(0.373)	(0.047)

a) Parameters for fluidity are within paratheses.

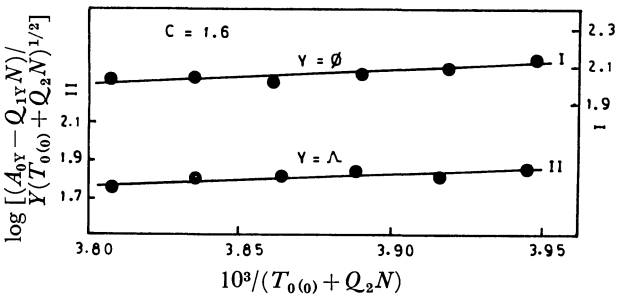

Fig. 5. Plots of $\log[(A_{0Y}-Q_{1Y}N)/Y(T_{0(0)}+Q_2N)^{1/2}]$ *vs.* $1/(T_{0(0)}+Q_2N)$ for TBAB-$MnCl_2$ melts.

Reasonably good fits were obtained at different c values and the computed values of the parameters are given in Table 7. The successful applicability of Eq. 15 to explain composition dependence of transport properties in the system under investigation may be emphasized by linear plots (Fig. 5) of $\log[(A_{0Y}-Q_{1Y}N)/Y(T_{0(0)}+Q_2N)^{1/2}]$ *versus* $1/(T_{0(0)}+Q_2N)$ which pass through the origin. The computer fitted values of the parameters A_{0Y}, Q_{1Y}, k_{1Y}, Q_2, and $T_{0(0)}$ were found to be very close to those obtained from the corresponding plots (Fig. 3). Thus the value of $T_{0(0)}$ obtained from Eq. 15 is in good resemblance with that obtained by extrapolating the plot of T_0 *versus* N to zero mol% of $MnCl_2$.

It may be concluded that the isoentropic conditions used in the earlier paper[7] [TBAX (X=Cl, I)-$MnCl_2$ systems] and the isoenergic conditions used in the present system, satisfactorily represent the composition dependence of viscosities and conductances in the glass-forming melts irrespective of the geometry of the complex species present. However, the latter conditions seem to be more satisfactory because of having sound experimental base and may be employed over wide range of temperature without depending on the T_0's of the solvent and solute.

The authors are thankful to Professor W. Rahman, Head of the Department of Chemistry, for providing necessary facilities. Financial assistance of CSIR (India) to two of us (S. K. and K. P. S.) is gratefully acknowledged.

References

1) C. A. Angell, *J. Phys. Chem.*, **70**, 3988 (1966).
2) C. A. Angell, *Aust. J. Chem.*, **23**, 929 (1970).
3) N. Islam, M. R. Islam, B. Waris, and Ismail K, *J. Phys. Chem.*, **80**, 291 (1976).
4) C. T. Moynihan, C. R. Smalley, C. A. Angell, and E. J. Sare, *J. Phys. Chem.*, **73**, 2287 (1969).
5) N. Islam and Ismail K, *J. Phys. Chem.*, **80**, 1929 (1976).
6) N. Islam, S. Kumar, and K. P. Singh, *Can. J. Chem.* in press.
7) N. Islam, K. P. Singh, and S. Kumar, communicated for publication.
8) G. Adam and J. H. Gibbs, *J. Chem. Phys.*, **43**, 139 (1965).
9) J. H. Kleinheksel and H. C. Kremers, *J. Am. Chem. Soc.*, **50**, 959 (1928).
10) N. Islam, M. R. Islam, S. Ahmad, and B. Waris, *J. Am. Chem. Soc.*, **97**, 3026 (1975).
11) J. H. Hildebrand and R. H. Lamoreux, *J. Phys. Chem.*, **77**, 1471 (1973).
12) C. A. Angell, *J. Phys. Chem.*, **68**, 218 (1964); *ibid.*, **68**, 1917 (1964); *ibid.*, **69**, 2137 (1965).
13) A. K. Doolittle, *J. Appl. Phys.*, **22**, 1471 (1951).
14) M. H. Cohen and D. Turnbull, *J. Chem. Phys.*, **31**, 1164 (1959).
15) N. Islam and Ismail K, *J. Phys. Chem.*, **79**, 2180 (1975).
16) J. Frenkel, "Kinetic Theory of Liquids," Dover Publications, New York, N. Y. (1955), p. 441.
17) A. J. Easteal and I. M. Hodge, *J. Phys. Chem.*, **74**, 730 (1970).
18) H. Bloom, "The Chemistry of Molten Salts," Benjamine New York (1967), p. 87—94; 105.
19) N. P. Yao and D. N. Bennian, *J. Phys. Chem.*, **75**, 3586 (1971).
20) The corrected activation energies, E_{corr}, for conductance and viscous flows were obtained as $E_{corr}/Rk_{1Y}=[T/(T-T_0)]^2$ from the derivatives of Eq. 1, where R is the gas constant and k_{1Y} is the empirical constant in Eq. 1. If we take T_0 as the corresponding temperature scale instead of absolute temperature, T then at the constant value of T/T_0 we have $E_{corr}/Rk_{1Y}=[(T/T_0/(T/T_0-1)]^2$. Therefore, E_{corr}/Rk_{1Y} may have a constant value at equal T/T_0 values.

A Molecular Orbital Treatment of the Electronic Spectra of Linear and Cross Conjugated Systems. Thienyl Phenyl Ketones and *N*-Thenylideneanilines

R. Abu-Eittah* and R. Hilal

Department of Chemistry, Faculty of Science, University of Cairo, Giza, Cairo, Egypt

(Received July 25, 1977)

The electronic absorption spectral measurements as well as MO calculations have been conducted on representatives of a cross conjugated system, thienyl phenyl ketones, and a linear conjugated system, *N*-thenylideneanilines. Results have proved that, although the two systems may be "π"-isoelectronic yet, their electronic spectra differ substantially. The nodal properties of the molecular orbitals of the two systems explain nicely their differences in conjugation. Steric factors play no roll concerning the differences in the spectra of the two systems.

The conformational analysis of composite molecules is a subject of increasing importance yet, the difficulties encountered in the experimental determination of their structure[1-3] turn the attention to the theoretical procedures. Most composite molecules possess a "complex-type" of orbital interactions[4] which are not treated explicity in most theoretical treatments; one such complicated interaction is the cross-conjugation[5] in these molecules.

The aim of the present investigation is to examine the effect of cross and linear conjugation on the electronic spectra of a series of typical composite molecules, namely, 2-thienyl phenyl ketones and *N*-thenylideneanilines.

Qualitative interpretation of the spectra of 2-thienyl phenyl ketone was reported by Koper and Boer[6,7] whereas the spectra of *N*-thenylideneanilines have not been investigated before, although they were synthesized and showed wide applicability.[8]

Experimental

Solvents and apparatus used are described before.[9] 2-Thienyl phenyl ketones were prepared by stirring thiophene and the appropiate aroyl chloride in the presence of anhydrous aluminum chloride at low temperature.[10] The mixture is then refluxed, cooled and poured on ice and extracted with ether. Vacuum distillation and crytallization from petroleum ether gave pure products with melting points identical to those reported.[10]

N-(2-Thenylidene)anilines were prepared by azeotropic condensation of thiophene-2-aldehyde with the corresponding aniline. The products were purified by vacuum distillation.

Results and Discussion

I. Electronic Absorption Spectra. (A) 2-Thienyl Phenyl Ketones: In the composite molecule 2-thienyl phenyl ketone, a competition is assumed to exist between the thienyl and phenyl moieties for conjugation with the carbonyl group. If the two moieties interact equally with the carbonyl group *e.g. via* both the resonance and electron repulsion integrals, then Conformer I will predominate and the electronic spectrum of the composite molecule should differ substantially from that of its subsystems. On the other hand, if one moiety enjoys greater overlap with the $2p_z$ orbital of the carbonyl carbon atom then conformers II or III will predominate. In the latter case the interaction of the phenyl ring with

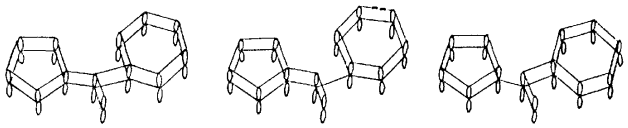

I II III

the thienyl ketone (II) or the thienyl ring with the phenyl ketone (III) will be *via* electron repulsion terms only. Rotation about the sigma bond joining the two subsystems (in Conformers II and III) could lead to a nonplanar conformation for the composite molecule.

Figure 1 shows the electronic absorption spectra of 2-thienyl phenyl ketone, which consists mainly of two overlapping transitions. This spectrum is very much similar to that of 2-acetylthiophene indicating that the interaction of the phenyl group with the thienyl ketone group is not substantial. Consequently, Conformer II is a predominant one. If the phenyl ring aquires a plane perpendicular to the plane of the rest of the molecule, the n_0 electrons would be conjugated with the "π"

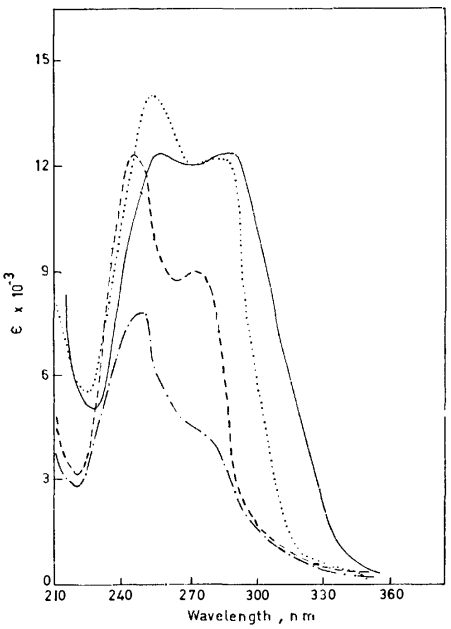

Fig. 1. Electronic absorption spectra.
——: 2-Thienyl phenyl ketone in ethanol, ·····: 2-thienyl phenyl ketone in cyclohexane, ----: 2-acetylthiophene in ethanol, -·-·-: 3-acetylthiophene in ethanol.

system of the benzene nucleus. This explains the absence of an n-π^* transition in the spectra of such a molecule.

To confirm the above results, the spectra of *p*-methoxyphenyl 2-thienyl ketone and *p*-nitrophenyl 2-thienyl ketone were investigated (Fig. 2). The spectrum of the *p*-methoxy derivative is slightly different from that of 2-thienyl phenyl ketone; bands are slightly red shifted and intensified. This effect is expected only if the phenyl ring is not planar with the rest of the molecule. The band at 220 nm most probably corresponds to the ^1L_a of the *p*-methoxyphenyl moiety.[11] Although the ionization potential of anisole[12] (8.4 eV) is less than that of thiophene (9.1 eV) yet, conjugation is still between the carbonyl group and the thiophene nucleus.

The spectrum of *p*-nitrophenyl 2-thienyl ketone (Fig. 2) is different in many respects from that of the parent compound. The first band appears at ≈294 nm (3000) and the second band at 252 nm (21000). These bands compare very well with the corresponding transitions of *p*-nitroacetophenone (297 nm (2300) and 258 nm (16000)). This leads one to suggest that in *p*-nitrophenyl 2-thienyl ketone conjugation extends on the nitro group, the benzene nucleus, and the carbonyl group. It is interesting to remember that this was not the case in either the unsubstituted ketone or in the *p*-methoxy derivative. Rationalization of these results is easily found when considering the symmetry properties of the molecular orbitals of the subsystems, which will be discussed in the next section.

In the case of 2-acetylthiophene, 2-thienyl phenyl ketone and *p*-methoxyphenyl 2-thienyl ketone, the band at 280 nm has a pronounced "charge-transfer" character indicating that in all of them the donor site is the same, *i.e.* the thienyl moiety. For the *p*-nitro derivative this band has a λ_{max} at 294 nm in cyclohexane and 303 nm in methanol indicating that the donor and acceptor sites are different.

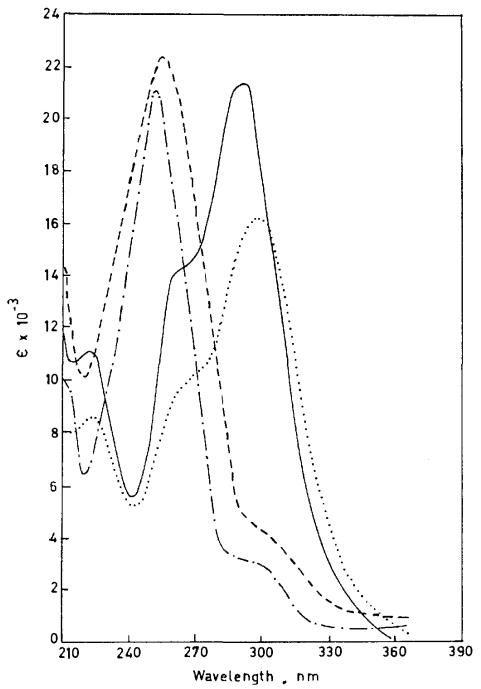

Fig. 2. Electronic absorption spectra.
——: *p*-Methoxyphenyl 2-thienyl ketone in methanol, ……: *p*-methoxyphenyl 2-thienyl ketone in cyclohexane, ----: *p*-nitrophenyl 2-thienyl ketone in methanol, -·-·: *p*-nitrophenyl 2-thienyl ketone in cyclohexane.

Table 1. Band maxima and intensities of the studied thienyl phenyl ketones and thenylideneanilines in cyclohexane

Compound	λ_{max}, nm	ε, $m^{-1}cm^{-1}$	f
2-Thienyl phenyl ketone	279	12604	0.40
	252	14164	0.42
p-Methoxyphenyl 2-thienyl ketone	288	21452	0.58
	264	14133	0.36
	220	11104	0.39
p-Nitrophenyl 2-thienyl ketone	294	3000	0.05
	252	21170	0.55
N-(2-Thenylidene)-methylamine	273	6266	0.11
	255	9558	0.27
N-(2-Thenylidene)aniline	320	8489	0.22
	288	10033	0.32
	264	8682	0.23
	225	8872	0.28
o-Methoxy-*N*-(2-thenylidene)aniline	340	5829	0.15
	285	11830	0.30
	255	11629	0.39
p-Methoxy-*N*-(2-thenylidene)aniline	336	17018	0.47
	282	17673	0.52
	255	17345	0.52
o-Chloro-*N*-(2-thenylidene)aniline	324	7559	0.19
	288	13837	0.42
	266	13069	0.31
p-Chloro-*N*-(2-thenylidene)aniliee	330	12665	0.31
	294	12892	0.41
	264	11257	0.33
	226	9856	0.32
o-Nitro-*N*-(2-thenylidene)aniline	366	3977	0.09
	270	12263	0.23
	252	16240	0.45
	228	16240	0.57
p-Nitro-*N*-(2-thenylidene)aniline	320	10633	0.25
	282	7733	0.18
	256	6766	0.18

Table 1 gives the values of the molar extinction coefficients, band maxima and oscillator strengths of the observed transitions for the studied thienyl phenyl ketones in cyclohexane as a solvent.

(B) N-*(2-Thenylidene)anilines*: Thenylideneaniline is "π"-isoelectronic with 2-thienyl phenyl ketone. If the two compounds possess the same type of "π" conjugation their spectra would be similar. Comparison of Figs. 1 and 3 shows that this is not entirely the case, though the spectra of 2-acetylthiophene and *N*-(2-thenylidene)methylamine (Fig. 4) are very much similar. Consequently, there must be a substential difference in the degree of interaction of the phenyl group with the rest of the molecule in the two systems, 2-thienyl phenyl ketone and *N*-(2-thenylidene)aniline.

The features of the spectra of *N*-(2-thenylidene)aniline and *N*-(2-thenylidene)methylamine are completely different contrary to the case of 2-thienyl phenyl ketone

and 2-acetylthiophene. The spectrum of *N*-(2-thenylidene)aniline (Fig. 3) is characterized by the presence of overlapping transitions and consists mainly of two band systems whose intensities and positions vary in different ways as one goes from polar to nonpolar solvents. This suggests that they correspond to different electronic transitions. These results confirm a near planar structure for the thenylideneaniline.

The complications of the spectrum of *N*-(2-thenylidene)aniline makes it necessary to examine the spectra of some of its derivatives before any conclusion can be made. The spectra of *o*- and *p*-chloro, methoxy and nitro derivatives of *N*-(2-thenylidene)aniline are examined (Figs. 5—7). The general features of the spectra are similar to those of the parent compound. Substitution has perturbed all the observed transitions. Since the planar conformer is an adequate description of

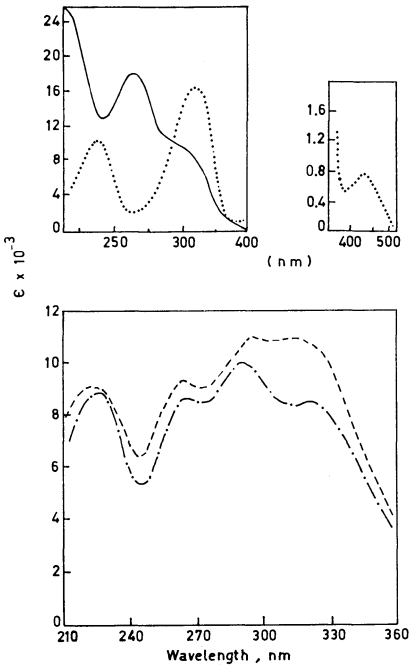

Fig. 3. Electronic absorption spectra of *N*-(2-thenylidene)aniline in methanol (----), cyclohexane (-·-·), and of *N*-benzylideneaniline in ethanol (——), azobenzene in 15% ethanol (·····).

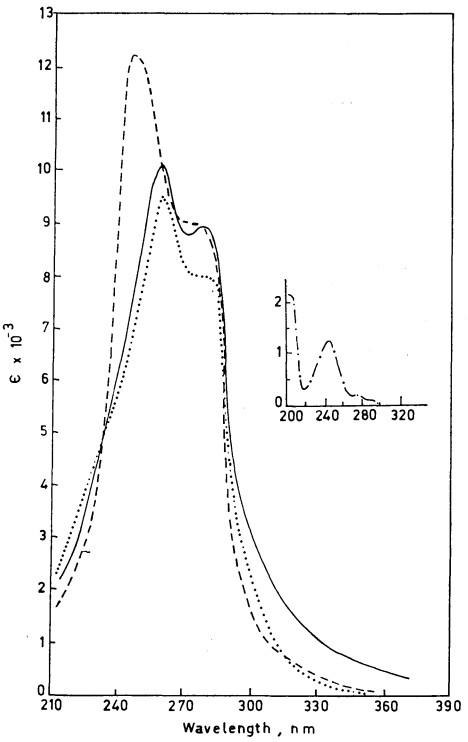

Fig. 4. Electronic absorption spectra of *N*-(2-thenylidene)methylamine in methanol (——) in cyclohexane (·····), and of 2-acetylthiophene in ethanol (----), benzylideneamine in ethanol (-·-·).

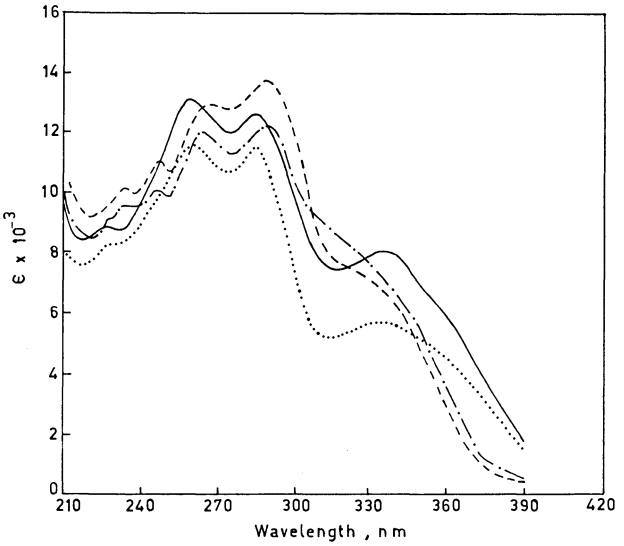

Fig. 5. Electronic absorption spectra of *o*-methoxy-*N*-(2-thenylidene)aniline in methanol (——), cyclohexane (·····), and of *o*-chloro-*N*-(2-thenylidene)-aniline in methanol (----), cyclohexane (-·-·).

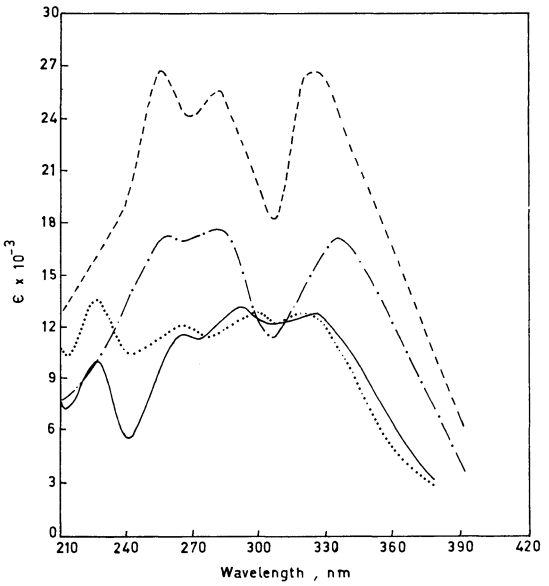

Fig. 6. Electronic absorption spectra of *p*-methoxy-*N*-(2-thenylidene)aniline in methanol (----), cyclohexane (-·-·), and of *p*-chloro-*N*-(2-thenylidene)-aniline in methanol (——), cyclohexane (·····).

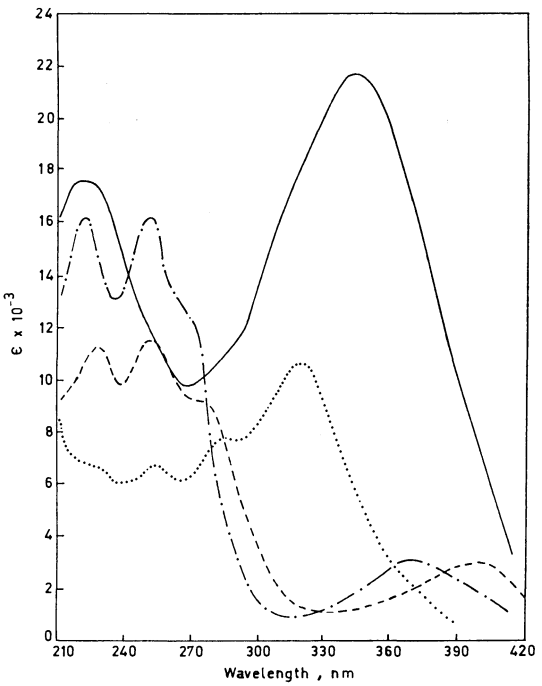

Fig. 7. Electronic absorption spectra of *o*-nitro-*N*-(2-thenylidene)aniline in methanol (----), cyclohexane (-·-·), and of *p*-nitro-*N*-(2-thenylidene)aniline in methanol (——), cyclohexane (·····).

thenylideneanilines; the observed bands correspond to transitions to "mixed-states" of the subsystems as well as a significant contribution of "charge-transfer" configurations.

II. Molecular Orbital Calculations. (A) 2-Thienyl Phenyl Ketone: The SCF wave functions of the molecule are determined assuming that the participation of the sulfur atom d-orbitals is trivial. The resonance integral terms are calculated using the relation[13]

$$\beta_{uv} = [S_{uv}/(1+S_{uv})][(I_u+I_v)/2]. \quad (1)$$

The electron repulsion terms are calculated using Nishimoto-Mataga[14] equation.

The self-consistent molecular orbitals of the composite molecule A-B are those of the separate constituents A and B. The extent of interaction between the two subsystems is determined by the value of the resonance integral β_{uv} and repulsion integrals γ_{uv} (atom u on A and atom v on B). The general expression for the interaction between two different singly excited configurations $^1\psi_{a-b}$ and $^1\psi_{c-d}$ is given by[15]

$$\langle {}^1\psi_{a-b}|\hat{H}|{}^1\psi_{c-d}\rangle = 2(cd|ab)-(ca|bd),$$

where $\hat{H}$ is the total Hamiltonian for the system.

Application to the Planar Conformer: The SCMO's of benzene are symbolized by the lower case letters (θ's), those of thienyl ketone by (y's). The corresponding states are symbolized by upper case letters (θ, Y). The singly excited states of benzene are

$$\Theta_\beta = (1/2)^{1/2}(\theta_3^{-1}\theta_4-\theta_2^{-1}\theta_5);\ \Theta_\beta = (1/2)^{1/2}(\theta_3^{-1}\theta_5+\theta_2^{-1}\theta_4),$$
$$\Theta_p = (1/2)^{1/2}(\theta_3^{-1}\theta_4-\theta_2^{-1}\theta_5);\ \Theta_\alpha = (1/2)^{1/2}(\theta_3^{-1}\theta_5+\theta_2^{-1}\theta_4).$$

For the 2-thienyl ketone the energies of the different configurations, $y_4^{-1}y_5$, $y_4^{-1}y_6$, $y_4^{-1}y_7$, $y_3^{-1}y_5$, $y_3^{-1}y_6$, $y_3^{-1}y_7$, are computed by the usual procedure[18] and the configuration interaction matrix of 2-thienyl ketone is solved. The form of the wave functions corresponding to the singly excited states of 2-thienyl ketone are available on request.

In the planar conformer the resonance integral β_{uv} is not zero and will mix together configurations which differ by the position of just one electron. The integrals to be evaluated are

$$\int \psi_o \hat{H}_{core} \psi_a^{-1} \psi_b \quad d\tau = (2)^{1/2} \int \psi_a(i) \hat{H}_i^{core} \psi_b(i) d\tau_i,$$
$$\int \psi_c^{-1} \psi_a \hat{H}_{core} \psi_c^{-1} \psi_b \quad d\tau = \int \psi_a(i) \hat{H}_i^{core} \psi_b(i) d\tau_i,$$
$$\int \psi_a^{-1} \psi_c \hat{H}_{core} \psi_b^{-1} \psi_c \quad d\tau = -\int \psi_a(i) \hat{H}_i^{core} \psi_b(i) d\tau_i.$$

The above integrals will be zero unless ψ_a belongs to one subsystem and ψ_b to the other. To calculate the electronic states of 2-thienyl phenyl ketone one has to consider the interaction between (1) ground state and "charge-transfer" states, (2) "charge-transfer" states to produce "charge-resonance" wave functions, (3) locally excited configurations and charge-resonance, and (4) locally excited configurations of the two subsystems.

To begin with, the charge-transfer (CT) configurations, $y_4^{-1}\theta_4$, $\theta_3^{-1}y_5$, $y_4^{-1}\theta_5$, $\theta_2^{-1}y_5$, are combined to produce the charge-resonance wave functions (CR's)

$$CR_I = (1/2)^{1/2}(\theta_3^{-1}y_5+y_4^{-1}\theta_4),$$
$$CR_{II} = (1/2)^{1/2}(\theta_3^{-1}y_5-y_4^{-1}\theta_4),$$
$$CR_{III} = (1/2)^{1/2}(\theta_2^{-1}y_5+y_4^{-1}\theta_5),$$
$$CR_{IV} = (1/2)^{1/2}(\theta_2^{-1}y_5-y_4^{-1}\theta_5).$$

The interaction terms between the fifteen different states, namely, the ground state, the four CR's, and the ten singly excited states localized on the two subsystems (Θ's and Y's) are computed (mathematical procedure is given before[16]). The interaction matrix is solved and the resultant energies and state wave functions of the ground and first three excited states are

		eV
(1)	$0.9855\psi_o-0.06226CR_I+0.05667CR_{II}$ $+0.1003CR_{III}$,	−0.137
(2)	$0.4948Y_1-0.5946Y_2+0.1434Y_3$ $+0.1958\Theta_\alpha+0.0480\Theta_P+0.0828CR_I$ $-0.4239CR_{II}+0.2136CR_{III}-0.3014CR_{IV}$,	3.375
(3)	$-0.7051Y_1-0.4095Y_2-0.3853\Theta_\alpha$ $-0.1499\Theta_\beta-0.1411\Theta_\beta-0.2313CR_I$ $-0.2094CR_{II}-0.3035CR_{III}-0.2796CR_{IV}$,	3.998
(4)	$0.1232Y_1-0.2018Y_2+0.0887Y_3$ $+0.6519\Theta_\alpha+0.1610\Theta_p+0.4835CR_I$ $+0.3205CR_{II}-0.1500CR_{III}-0.4319CR_{IV}$.	4.050

The calculated value 3.5 eV for the transition energy of the planar conformer of 2-thienyl phenyl ketone is significantly lower than the experimental one (4.4 eV). This is a strong evidence that either the planar conformer is a poor description of the molecule, or the molecule is planar but conjugation is not extending over the entire molecule. The spectrum of the molecule indi-

cates that conjugation extends only on the thienyl and carbonyl groups *i.e.* not including the benzene nucleus.

Application to the Perpendicular Conformer: The interaction between locally excited states Y's and Θ's is computed adopting the ZDO approximation. The matrix elements are computed for the ten states (six Y's and four Θ's) of 2-thienyl phenyl ketone. Solving this matrix, the energies and state wave functions are obtained. The first three are

	eV
(1) $-0.9985Y_1-0.0893\Theta_\alpha-0.0883\Theta_p$,	4.29
(2) $-0.9960Y_2+0.0862\Theta_\alpha+0.0127\Theta_\beta$,	4.59
(3) $0.0870Y_1+0.0870Y_2-0.1325Y_3$ $+0.9829\Theta_\alpha+0.0129\Theta_p$.	4.90

Comparison with experiment is postponed till we consider the "π"-isoelectronic *N*-(2-thenylidene)aniline.

(B) N-*(2-Thenylidene)aniline.* Computations are carried out in a similar way to that followed in the case of 2-thienyl phenyl ketone. Two conformers were considered, the *cis-* and the *trans-* planar ones. The numerical values of the parameters used are[17] (eV)

$$\alpha_C = -11.16;\ \alpha_N = -14.12;\ \alpha_S = -23.12,$$
$$\gamma_{CC} = 11.13;\ \gamma_{NN} = 12.34;\ \gamma_{SS} = 11.19.$$

The wave functions and the corresponding energies are given in Tables 2 and 3.

Comparison with Experiment: Table 4 compares the experimental and theoretically computed transition energies. For the 2-thienyl phenyl ketone values obtained for the perpendicular conformer agree satisfactorily with the experimental ones. On the other hand, planar conformers are good description for the *N*-(2-thenylidene)anilines with the *trans*-configuration nearer to reality than the *cis*-one.

Table 2. State function and energy of the ground and first four excited states for the *cis*-conformer of *N*-(2-thenylidene)aniline

	eV
(1) $0.9901\phi_0+0.0212CR_I-0.0672CR_{II}$ $-0.0702CR_{III}-0.0958CR_{IV}$	−0.112
(2) $-0.8659Y_1+0.1290Y_2-0.2432\Theta_\alpha$ $+0.1950\Theta_\beta+0.1433\Theta_\beta-0.1736CR_I$ $+0.1383CR_{II}+0.2249CR_{III}$	3.835
(3) $0.2761Y_1+0.1697Y_2-0.1203Y_3$ $-0.0138Y_6-0.8735\Theta_\alpha-0.3172CR_I$ $+0.0780CR_{III}+0.0878CR_{IV}$	4.814
(4) $-0.1450Y_1-0.7916Y_2-0.1443Y_3$ $-0.1580\Theta_\alpha-0.3897\Theta_\beta-0.1788\Theta_\beta$ $+0.1360\Theta_p+0.2567CR_{II}-0.1518CR_{III}$ $+0.1450CR_{IV}$	4.90
(5) $0.2037Y_2-0.7386Y_3+0.1011Y_4$ $+0.2305\Theta_\alpha+0.1477\Theta_p-0.2922CR_I$ $+0.1169CR_{II}-0.4364CR_{III}+0.1902CR_{IV}$	5.15

Table 3. State function and energy of the ground and first four excited states of the *trans*-conformer of *N*-(2-thenylidene)aniline

	eV
(1) $0.9902\phi_0+0.0199CR_I-0.0672CR_{II}$ $-0.0702CR_{III}-0.0960CR_{IV}$	−0.112
(2) $-0.8848Y_1+0.0656Y_2-0.1602\Theta_\alpha$ $+0.2161\Theta_\beta+0.1696\Theta_\beta+0.1103CR_I$ $+0.1614CR_{II}+0.1387CR_{III}+0.2239CR_{IV}$	3.811
(3) $0.1786Y_1+0.1815Y_2-0.1165Y_3$ $-0.9015\Theta_\alpha-0.2863CR_I+0.1165CR_{II}$	4.782
(4) $-0.1093Y_1-0.4472Y_2-0.6044Y_3$ $+0.0710Y_4-0.2660\Theta_\beta-0.0897\Theta_\beta$ $-0.2360CR_I+0.3119CR_{II}-0.3950CR_{III}$ $+0.1583CR_{IV}$	5.049
(5) $-0.7605Y_2+0.4093Y_3-0.2441\Theta_\alpha$ $-0.2451\Theta_\beta+0.1913CR_I+0.0865CR_{II}$ $+0.2790CR_{III}$	5.267

Table 4. Calculated and experimental transition energies of 2-thienyl phenyl ketone and *N*-(2-thenylidene)aniline

Compound	Transition energy, eV		*f*	
	Calcd	Obsd	Calcd	Obsd
2-Thienyl phenyl ketone				
perpendicular	4.29	4.42	0.31	0.40
	4.59	4.91	0.22	0.42
planar	3.51		0.06	
	4.13		0.11	
N-(2-Thenylidene)aniline				
cis-	3.95		0.04	
	4.92		0.33	
	5.01		0.65	
	6.26		0.09	
trans-	3.92	3.87	0.33	0.22
	4.87	4.30	0.29	0.32
	5.16	4.70	0.14	0.23
	5.38	5.51	0.07	0.28

Discussion and Conclusions

The spectra shown in Figs. 1 to 7 and the results of molecular orbital calculations (Table 4) indicate that, in 2-thienyl phenyl ketone, "π" conjugation does not extend over the entire molecule. This happens in two situations, (i) the phenyl ring lies in a plane perpendicular to that of the rest of the molecule, or (ii) the whole molecule is planar but the "cross-conjugation" behavior is pronounced; the net result would be the same. Drawing the molecules using Pauling atomic radii shows no sign of steric hinderance. Results at hand can not firmly differentiate between a perpendicular conformer and a planar "cross-conjugated" one. Also computations with a more sophisticated method would not be able to do so. Results of the theoretical treatment of 2-thienyl phenyl ketone shows a good agreement between the perpendicular conformer and the spectra. The wave functions of the excited states are merely those of either the thienyl ketone or the phenyl moieties of the molecule and mixing of states can be considered negligible.

Extensive interaction exists between the thienyl and phenyl groups with the azomethine group in the case

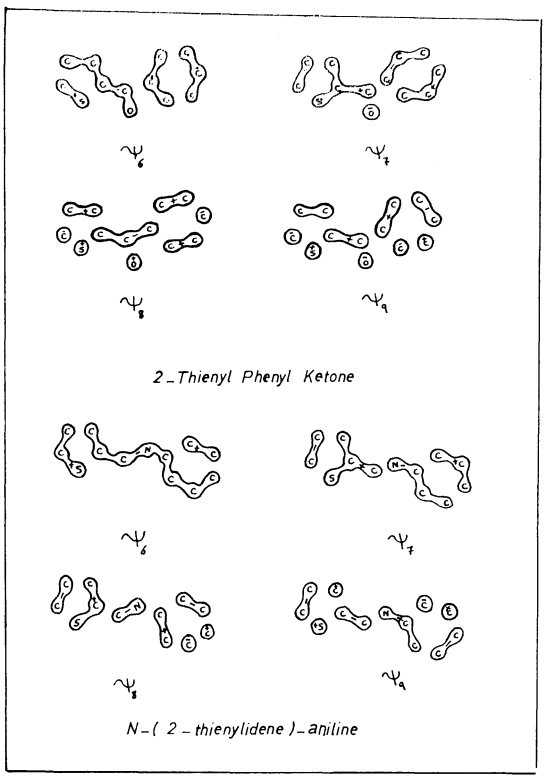

Fig. 8. The nodal properties of the highest two occupied and lowest two vacant MO's of 2-thienyl phenyl ketone and *N*-(2-thenylidene)aniline.

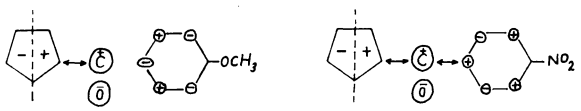

Fig. 9. The nodel properties of the highest two occupied and lowest two vacant MO's of 2-thienyl phenyl ketone.

of *N*-(2-thenylidene)anilines. Examination of Tables 2 and 3 indicates clearly that the wave functions of the excited states of the composite molecule represent mixed-states resulting from extensive interaction between the states of the two subsystems. As a result, the observed transitions can not be assigned to localized ones.

The cross-conjugation behavior is very nicely seen when considering the nodal properties of the molecular orbitals. Figure 8 represents the hieghest two occupied and lowest two vacant SCFMO's of 2-thienyl phenyl ketone and *N*-(2-thenylidene)aniline. Although a planar conformer is considered for both compounds with comparable resonance integrals yet, the antibonding character between the phenyl and carbonyl groups is pronounced in the molecular orbitals of 2-thienyl phenyl ketone as reflected in the values of the mobile "π"-bond order between the carbonyl carbon and the two competing moieties *i.e.* 2-thienyl and phenyl, which are 0.4100 and 0.1964 respectively. On the other hand, bonding character between the azomethine group and both the 2-thienyl and phenyl nuclei is pronounced ("π"-bond orders are 0.3324 and 0.2980 respectively). Hence, classification of the two compounds as cross and linear conjugated ones is reflected quite well in their electronic properties.

References

1) G. E. Eaten and W. N. Lipscomb, "NMR Studies of Boron Hydrides and Related Compounds," W. A. Benjamin, N. Y. (1969).
2) J. T. J. Johansen and B. L. Valles, *Proc. Nat. Acad. Acta Berl.*, **26**, 157 (1971).
3) A. Golebiwski and A. Parczewski, *Chem. Revs.*, **74**, 519 (1974).
4) M. Orchin and H. H. Jaffé, "Summetry, Orbitals and Spectra," John Wiley & Sons, Inc., (1971), p. 55.
5) N. Phelan and M. Orchin, *J. Chem. Educ.*, **45**, 6 (1968).
6) L. Koper, J. U. Veenland, and Th. J. De Boer, *Spectrochim. Acta, Part A*, **23**, 2605 (1967).
7) L. Koper, J. U. Veenland, and Th. J. De. Boer, *Spectrochim. Acta, Part A*, **24**, 1971 (1968).
8) R. J. Head and R. Alan, *Aust. J. Chem.*, **19**, 1747 (1968).
9) R. Abu-Eittah and M. Hammed, *Bull. Chem. Soc. Jpn.*, **47**, 2576 (1974).
10) W. Minis, *Org. Synth.*, XII, 62 (1932).
11) H. H. Jaffé and M. Orchin, "Theory and Application of Ultraviolet Spectroscopy," John Wiley & Sons, Inc., N. Y. (1962).
12) D. W. Turner, C. Baker, A. D. Baker, and C. R. Brundle, "Molecular Photoelectron Spectroscopy," Wiley-Interscience, London (1971).
13) G. Rasch, *Z. Chem.*, **2**, 347 (1962).
14) K. Nishimoto and M. Mataga, *Z. Phys. Chem. (Frankfurt)*, **12**, 225 (1957).
15) J. A. Pople, *Proc. Phys. Soc., Ser. A*, **68**, 329 (1955).
16) R. Abu-Eittah and R. Hilal, *Bull. Chem. Soc. Jpn.*, **49**, 2158 (1976).
17) R. L. Flurry, Jr., "Molecular Orbital Theories of Bonding in Organic Molecules," Marcel Dekker, Inc., N.Y. (1968).
18) S. P. McGlynn, L. Vanquicken, M. Kinoshita, and D. Carrol, "Introduction to Applied Quantum Chemistry," Holt, Reinhart and Winston, N. Y. (1972).

Complexing Behaviour of 2*H*-1,2,4-Triazole-3-thiol Complexes of Co(II), Ni(II), Cu(II), Ru(II), Rh(III), Pd(II), Pt(II), and Au(I)

Birendra Kumar GUPTA,† D. S. GUPTA,† and U. C. AGARWALA*

Indian Institute of Technology, Kanpur 208016, India

†*Department of Chemistry, V.S.S.D. College, Kanpur 208016, India*

(Received April 26, 1977)

Complexes of Co(II), Ni(II), Cu(II), Ru(II), Rh(III), Pd(II), Pt(II), and Au(I) with 2*H*-1,2,4-triazole-3-thiol have been prepared. Probable structures have been proposed for the complexes on the basis of visible and infrared spectra, magnetic susceptibility, and chemical analysis. Crystal field parameters have been calculated wherever possible.

In the course of studies on metal complexes derived from the ligands having the skeletal unit NH–C(=S)–, the ligand 2*H*-1,2,4-triazole-3-thiol, whose *N*-substituted derivatives are of great biochemical interest,[1-3] has been found to be a good complexing agent. The isolation and characterization of complexes with the metal having d^{10} configuration have been described.[4] In this paper, the synthesis and structural studies of the complexes of Co(II), Ni(II), Cu(I/II), Ru(II), Rh(III), Pd(II), Pt(II), and Au(I) are reported.

Experimental

All the chemicals were or Analar or chemically pure grade.

Preparation of the Ligand. *(a) 2H-1,2,4-Triazole-3-thiol (I)*: The ligand in the H form and its sodium salt were prepared by the method given in literature.[4,5]

(b) Deuterated form of 2H-1,2,4-Triazole-3-thiol: About 0.1 g of the ligand was dissolved in 25 ml D_2O. The resulting solution was refluxed for *ca.* 4 h, heated to dryness, and kept overnight in a desiccator.

General Method of Preparation of Complexes. Conditions for preparation and analytical data of the complexex are given in Table 1. All the complexes were prepared by mixing an aqueous solution of an appropriate metal salt (sulfate or chloride) with an alcoholic solution of the ligand. The mixed solutions were heated on a water bath or refluxed, whereby the complexes of all the metal ions were precipitated out. The complexes were separated by centrifuging the slurry and were washed with methanol or ethanol and ether, and dried in a vaccum desiccator.

Analyses. Sulfur, chloride (wherever present), and metal ions were analysed by the standard methods[6-8] after fusion in a Parr-bomb by Na_2O_2 and KNO_3. Analyses of carbon, hydrogen, and nitrogen were carried out in the Microanalytical Section of the Indian Institute of Technology, Kanpur, India.

Magnetic Susceptibility. Magnetic susceptibility was determined at room temperature with a Gouy balance. Mercurytetrathiocyanatocobaltate(II) was used as a magnetic

TABLE 1. CONDITIONS FOR PREPARATION AND ANALYTICAL DATA OF THE COMPLEXES

Complex[a]	Reaction[b] condition (M : L)	Heating[c] time (h)		Analysis (%) C	H	N	S	M	Colour[d]
$CoL_2(H_2O)_3$	A (1 : 2)	5 (R)	Calcd	15.3	3.2	26.8	20.4	18.8	g
			Found	15.5	3.0	26.3	20.3	18.6	
$CoL'(H_2O)_3$	B (1 : 2)	5 (R)		11.2	3.7	19.7	15.0	27.7	p
				11.1	3.5	19.5	14.9	27.5	
$NiL_2(H_2O)_3$	A + 1 ml of pyridine (1 : 2)	2 Room temp		15.3	3.2	26.8	20.5	18.8	g
				15.2	3.0	26.6	20.3	18.5	
$Cu_2L_x(LH)_y(H_2O)_4$ $(x+y=2)$	C (1 : 2)	No heating		12.0	3.0	21.0	16.0	31.8	bl
				12.2	3.0	21.3	16.2	31.5	
$RhL_2(LH)$	B (1 : 3)	2 (W)		18.0	1.5	31.4	23.9	25.2	bl
				18.2	1.7	31.7	23.7	—	
$RhL_2(H_2O)_2$	C (1 : 1)	2 (W)		16.4	2.3	28.6	21.8	23.4	bl
				16.7	2.6	28.7	21.6	—	
PdL_2	D (1 : 2)	2 (W)		15.7	1.5	27.4	20.9	34.7	o
				15.6	1.2	27.8	20.9	34.5	
$Pt(LH)_4Cl_2$[e]	E (1 : 5)	2 (R)		14.5	1.9	25.0	19.0	29.2	y
				14.0	1.6	24.7	18.8	—	
AuL	C (1 : 2)	3 (W)		8.1	0.7	14.1	10.8	66.3	y
				8.6	0.9	14.4	10.5	—	

a) L, $(C_2H_2N_3S)$; (LH), $(C_2H_3N_3S)$; L′, (C_2HN_3S). b) Number in parentheses indicates the molar ratio (metal : ligand) in 25 ml of solvents; A, metal salt dissolved in water and ligand in ethanol; B, both metal and ligand dissolved in ethanol; C, metal salt and sodium salt of ligand dissolved in water; D, metal salt in water and ligand in ethanol; E, H_2PtCl_6 in 5 ml ethanol and ligand in 10 ml ethanol. c) R, refluxed; W, water bath. d) g, green; p, pink; bl, black; o, orange; y, yellow. e) In $Pt(LH)_4Cl_2$ the chloride was found to be 10.4% (Calcd value, 10.6%).

Table 2. Electronic spectral bands and their assignments

Complex	Band position (nm)	Assignment	Magnetic moment (BM)	Solubility
$NiL_2(H_2O)_3$	950	$^3A_{2g}\rightarrow{}^3T_{1g}(F)$	3.2	I
	640	$^3A_{2g}\rightarrow{}^3T_{2g}$		
	380	$^3A_{2g}\rightarrow{}^3T_{1g}(P)$		
$CoL_2(H_2O)_3$	585	$^4T_{2g}\rightarrow{}^4A_{2g}$	4.5	s
	540	$^4T_{2g}\rightarrow{}^2T_{1g}(P)$		
PdL_2	735	$^1A_{1g}\rightarrow{}^3A_{2g}$	D	I
	530	$^1A_{1g}\rightarrow{}^3E_g$		
	490	$^1A_{1g}\rightarrow{}^1A_{2g}$		
	370	$^1A_{1g}\rightarrow{}^3B_{1g}$		
	330	$^1A_{1g}\rightarrow{}^1E_g$		
PtL_4Cl_2	650	$^1A_{1g}\rightarrow{}^3A_{2g}$	D	S
	480	$^1A_{1g}\rightarrow{}^3E_g$		
	455	$^1A_{1g}\rightarrow{}^1A_{2g}$		
	435	$^1A_{1g}\rightarrow{}^3B_{1g}$		
$Cu_2L_x(LH)_y(H_2O)_4$ $(x+y=2)$	800—450(br)	—	0.9	I
	440(sh)	Cu(I)-Cu(II) charge transfer		

Abbreviations: br, broad band; D, diamagnetic; I, insoluble; S, soluble in water and alcohol; s, slightly soluble in water; sh, shoulder.

susceptibility standard. Diamagnetic corrections were made by the method given in literature.[9] Electronic spectral bands and their assignments are given in Table 2.

Spectra. Visible and ultraviolet spectra were recorded in Nujol mulls with a Cary-14 spectrophotometer in the range 1600—300 nm. Infrared spectra were taken with a Perkin-Elmer 521 Grating Spectrophotometer in the range 4000—250 cm^{-1}, using Nujol mulls and KBr pellets. The major infrared bands are given in Table 3.

Results and Discussion

The ligand in solution exists in either thiol or thioxo form, behaving as a weak dibasic acid. In either form it has four bonding sites (three N's and one S). It can thus behave as a mono, bi, tri, or tetradentate towards one or more metal ions. However, a chelate ion is difficult to envisage, because of a four membered

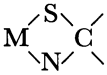

ring, where C and N belong to a five membered heterocycles. We, thus, expect bridge configurations through the ligands which are bonded to two or more metal atoms. The formation of polymeric complexes is more likely to occur. This is also suggested by poor solubility of the complexes (except that of Pt(II)) in water or in organic solvents. Methods like NMR, molecular weight or conductivity measurements could not be used for their structural studies.

Magnetic Moments. The magnetic moments of Ni(II) and Co(II) (green) complexes (Table 2) are close to those of other octahedral complexes.[10] The value of Co(II) (pink) complex was slightly lower than the normal octahedral complexes but somewhat higher than the distorted tetrahedral complexes.[10,11] The distortion in the octahedral arrangement in the latter may thus be comparable to that of green complex.[11]

The complexes of Au(I), Rh(III), and Pd(II) are dia-

Table 3. Assignments of the major infrared bands of the ligand and complexes (cm^{-1})

Ligand		Complexes[a]			
Hydrogen form	Deuterated from	Ni(II), Co(II), Cu(II), Pd(II), Rh(III), Au(I)	Pt(II)	Cu(II)/(I) and Co(II) (pink)*	Assignment
3050(s)		3000	3160, 3140		νNH
—	2180, 2250(s)	—	—	—	νND
1580(s)	1550, 1530(w)	1570	1575, 1550	—	Thioamide band I[b]
1480(s)	1470(s)	1500(s)	1500, 1495	1475	νCN+δNH+νNN
1320(ms)	1310(ms)	1335(m)	1365	1330	
1275(m)	—	1290(m)	1270, 1280	1280	Thioamide band II[c]
1200(s)	1200(s)	1200	1220, 1210	1200	δCH
	1160	—	—	—	Mainly due to δND
1080(s)	1085(ms)	1075	1085, 1065 (1015)	1070	Due to νCN+νC=S
—	965	—	—	—	Mainly due to δND
960	960(m)	980	965, 975	970	νCN+νCS
690(m)	—	695	680, 685	—	τNH
650(m)	680(m)	640	650, 635	635, 540	Thioamide band IV
550(m)	550(m)	530	500(br)		
—	520(mw)	—	—	—	τND
—	—	300—400	280—325	300—400	May be due to νMS and/or νMN

a) All those having water have bands due to νOH and δOH around 3300 and 1650 cm^{-1}. b) Mainly due to δNH+νCN. c) Due to δNH+νCN+δOH+νCN; * broad bands.

magnetic. This is what would be expected if they assume linear, octahedral, and square planar configurations, respectively.

The diamagnetism of the ruthenium complex is rather unexpected since $RuCl_3 \cdot xH_2O$ was used as the starting material for its synthesis. This could be due to either the presence of ruthenium in +2 oxidation state or spin pairing through NCS group. The former seems to be more probable since Ru(III) is a relatively powerful oxidizing agent and might be reduced to Ru(II) by the ligand during the course of the reaction.

Platinum complex was also found to be diamagnetic indicating the presence of platinum of +2 or +4 state. It is probable that platinum(IV) is reduced by the ligand to +2 state during the course of preparation.[12]

The magnetic moment of copper complex (0.9 B.M.) was found to be lower than that expected for one electron. Possibly Cu(II) ions were partially reduced to +1 state during the course of preparation, so that the complex obtained contains copper both in +2 and +1 states. This is also suggested by the black coloration of the complex where the charge transfer between Cu(I) and Cu(II) may be taking place through NCS group of the ligand. When the complex was decomposed in pyridine in N_2 atmosphere, the pyridine complex of Cu(II) of the type $Cu(py)_xL_y$ where $x<4$ was formed in solution, indicating at least a part of copper to be present in +2 state in the complex. Although a similar anomalous magnetic moment of Cu(II) in some copper complexes was interpreted in terms of antiferromagnetic interactions, either by forming σ or δ bond between two copper ions or by superexchange phenomenon through NCS group, a consideration of the reducing power of the ligand and the oxidizing power of the Cu^{2+} suggest that the partical quenching of paramagnetism in the complex is not due to such effects.

Visible Spectra. The visible spectra of all the complexes showed bands around 410 and 390 nm. The bands were also observed, slightly on the higher wave number side, in the spectrum of the ligand. They are thus due to ligand molecule (possibly arising from transition $n \rightarrow \pi^*$ or $\pi \rightarrow \pi^*$ of NCS group).

The positions of the bands in the spectrum of $NiL_2 \cdot 3H_2O$ (Table 2) are characteristic of those found for octahedral complexes of Ni(II)[11] which supports the octahedral structure of the complex. The bands at 950 and 640 nm are unsymmetrical, possibly owing to a slight distortion[12] from the O_h symmetry towards a rhombic or tetragonal one. From the positions of these bands the values of $10Dq$, B, β, and the position of the band due to $^3A_{2g} \rightarrow {}^3T_{1g}$ were calculated[13] to be 10160 cm^{-1}, 870 cm^{-1}, 0.85, and 10160 cm^{-1}, respectively, assuming O_h symmetry (approximately). The calculated value (10160 cm^{-1}) is quite close to that found experimentally (10530 cm^{-1}) which supports assignments. The value of β (0.85) indicates that the bonds between the ligand and the metal ion are essentially ionic having a small degree of covalence.[14]

In the assignment of the bands of $CoL_2 \cdot 3H_2O$ (assuming approximately octahedral symmetry) (Table 2), fitting the positions of the bonds give Dq, B and β as 860, 750 cm^{-1}, and 0.74 and places the $^4T_{2g}(F) \rightarrow {}^4T_{1g}(F)$ absorption band at 6480 cm^{-1} (near IR region) which could not be observed in our spectrum. Some splitting was found in the bands at 540 and 585 nm. This indicates that the orbital degenerate terms T_{1g} and T_{2g} are split because of the lowering of the symmetry of the complex from O_h.

The spectrum of $CoL \cdot 3H_2O$ showed a very broad weak band at 500 nm with shoulders at 530, 490, 470. The intensities of these shoulder bands were found to be nearly equal to each other as indicated by their respective optical densities. Apparently there is practically no symmetry in the complex, the degenerate terms *e.g.*, T_{1g} and T_{2g}, being split completely into non-degenerate ones. The evidence in support of the lowering of symmetry also comes from the magnetic moment values (4.5 B.M.), which is too low for an octahedral Co(II) ion.

The spectrum of copper complex showed a continuous absorption from 800 nm down to 450 nm followed by three, bands at 440, 410, and 395 nm. If copper in the complex is present in +2 state, we should expect one, three, and four bands in O_h, D_{4h}, and D_{2h} symmetry respectively. The continuous absorption and the presence of 440 nm band together with the magnetic evidence supports the view that copper in the complex exists in two mixed valence states. The band at 440 nm may then be assigned to mixed valence state band similar to that present in other mixed valence state copper complex.[15] It is the origin of the very dark coloration of this complex (dark brown to black) which is also characteristic of a mixed valence complex.

The spectrum of gold complex showed no band except the ligand bands at 410 and 395 nm. This suggests the oxidation state of gold as +1, which is also indicated by the formulla AuL where one of the two protons of NH groups is deprotonated.

The spectrum of ruthenium complex is similar to that of copper with ligand bands at 410 and 390 nm, no d-d band appearing in the visible region owing to intense absorption.

The bands at 650 and 480 nm in the spectrum of PtL_4Cl_2, and at 735 and 530 nm in the PdL_2 spectra were found to be much weaker than the other bands. In a d^8 system, we expect six transitions in D_{4h} symmetry (three spin allowed and three weak spin forbidden bands)[16] (Table 2). The values of parameters calculated from the positions of these bands are as follows: PdL_2: $\Delta_1=23800$ cm^{-1}, $\Delta_2=7200$ cm^{-1}, $\Delta_3=2900$ cm^{-1}, $B=200$ cm^{-1}, $C=3300$ cm^{-1}; PtL_4Cl_2: $\Delta_1=25300$ cm^{-1}, $C=3300$ cm^{-1}. In the case of Pd, the calculated frequency for the band due to $^1A_{1g} \rightarrow {}^1B_{1g}$ was found to be 29700 cm^{-1} which is close to the value found experimentally (30000 cm^{-1}), supporting our assignments. In case of Pt, owing to the lack of data, some of the parameters have not been calculated.

The spectrum of Rh complex showed no band except at 410 and 395 nm. However, there was a continuous strong absorption whose intensity decreased gradually from 650 to 400 nm. The weak d-d bands are possibly obscured by the intense charge transfer band (L→M) present in the visible region. No information regarding the structure of the complex has been obtained from

the visible spectral studies.

Infrared Spectra. The ligand is best described as a resonance hydrid of the structures:

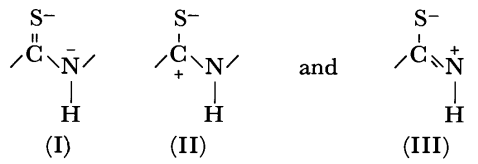

(I) (II) (III)

Metal coordination through sulfur will lead to a decrease in the thiocarbonyl stretching force constant and an increase in CN force constant. Coordination to nitrogen, on the other hand, would increase the contribution of structure I to the ground state of the complexes and cause an increase in the thiocarbonyl frequencies and decrease in CN and NH stretching frequencies.[17,18]

In order to determine the coordination sites in the complexes, we have classified the spectra of the complexes into the following four groups (A to D):

(A) Spectra of Ni(II), Co(II), Cu(II), Pd(II), Rh-(III), and Au(I).

(1) The positions of those bands having contributions from νCN (1480, 1320, 1275 cm^{-1}) shifted towards higher wave number (+20 cm^{-1}) suggesting the increase in CN bond order.

(2) The shifts in the positions of bands at 1080 and 960 cm^{-1} were small (±10 cm^{-1}). There also appeared a band around 1020 cm^{-1} which may be due to two different types of νCN.

(3) The positions of the bands arising mainly from νCS, *viz.*, 650 and 550 cm^{-1} shifted to lower wave numbers (−20 cm^{-1}).

(4) The positions of the bands arising from νNH, δNH and τNH remained practically constant, their relative intensities decreasing.

(5) In the spectra of Ni(II), Co(II), Cu(II), and Rh(II) the characteristic bands due to νOH and δOH were present around 3400 cm^{-1} (broad) and 1650 cm^{-1} (medium) respectively.

All the above shifts can be explained by the assumption that the metal ion is coordinated to one of the NH groups after deprotonation and the thiocarbonyl sulfur with relatively strong interaction.

(B) Spectra of Pt(II).

(1) All the bands having contributions from νNH, δ NH and τNH were split with the separation ±10 cm^{-1} around the positions found in the spectrum of the ligand.

(2) The positions of νCN bands shifted to higher wave numbers and were split (10—20 cm^{-1}).

(3) The positions of the νCS bands shifted to lower wave number. The band at 500 cm^{-1} was broad while that of 525 cm^{-1} was split.

These observations can be explained if the platinum ion in the complex is assumed to be bonded separately with four thiocarbonyl sulfur atoms of the four ligand molecule arranged in a square planar arrangement to form an ionic complex $[PtL_4]Cl_2$.

In such a bonding scheme we should expect the interaction between νCN bands and δNH bands in one ligand molecule to give asymmetric and symmetric modes of vibration.

(C) Spectrum of Ru(II). The spectrum of ruthenium is quite complicated, but the positions and shifts of the bands appear to be similar to those of the combined spectra of Group A (*e.g.*, Ni(II) or Co(II)) and Group B (Pt(II)) complexes, with the bands at 3000, 3150, 1570, 1550, 1500, 1335, 1360, 1290(br), 1200(br), 1075, 1060, 980, 970, 695, and 680 cm^{-1}). It is therefore assumed that two of the three ligand molecules are linked with thiocarbonyl sulfur and nitrogen after deprotonation, while the third ligand molecule is linked with thiocarbonyl sulfur strongly and nitrogen without deprotonation weakly. This is in line with the charge balance in the complex where ruthenium atom is assumed to be in +2 oxidation state.

(D) Spectra of Cu(II/I) and Co(II) (pink). Since it is improbable for cobalt to be reduced in +1 state by the ligand, the formula indicates that both the NH groups of the ligand are deprotonated. Owing to the presence of broad bands due to water molecule around 3300 and 1600 cm^{-1}, the band due to νNH could not be confirmed. However, no band at 690 cm^{-1} assigned to τNH appeared in the spectrum of the complex, suggesting the possibility of complete deprotonation. Further in the finger print region bands were rather broad and no definite conclusion regarding their structure could be drawn. The general pattern in the shifts of the band positions are similar to those of Group A, suggesting at least a linkage of the ligand through nitrogen and thiocarbonyl sulfur.

On the basis of these data the following structures were assigned:

(i) $NiL_2(H_2O)_3$, $CoL_2(H_2O)_3$, $CoL(H_2O)_3$, $RhL_3(H_2O)_2$, RuL_3, $CuL(H_2O)_2$: Octahedron with bonding through thiocarbonyl sulfur and –NH nitrogen, the latter after deprotonation. Except for Rh and Ru complexes water molecules are also coordinated.

(ii) PdL_2: Square planar with bonding through thiocarbonyl sulfur and –NH nitrogen, the latter after deprotonation.

(iii) PtL_4Cl_2: Square planar with bonding through thiocarbonyl sulfur.

(iv) AuL: Linear with bonding through thiocarbonyl sulfur and –NH nitrogen, the latter after deprotonation.

References

1) A. S. Greenfield, C. M. Seidel, and C. W. Von Meyer, *Ger. Offen.* **1**, 966, 806 (1974).

2) E. E. Schweizer and B. J. Pogers, *Weeds*, **12**, 7 (1964).

3) M. Posson, *Laboratire Roger Bellon, Fr.*, **1**, 273, 881 (1962).

4) B. K. Gupta, D. S. Gupta, S. K. Dikshit, and U. Agarwala, *Indian J. Chem.*, in press.

5) C. Ainsworth, *Org. Synth.*, **40**, 99 (1960).

6) F. P. Treadwell and W. T. Hall, "Analytical Chemistry," Vol. II, John Wiley & Sons Inc., New York, N. Y. (1958), pp. 77, 199.

7) A. I. Vogel, "A Text Book of Quantitative Inorganic Analysis," 3rd ed, Longmans Green & Co. Ltd., (1961), pp. 460, 462, 480, 497, 509, 511, 513, 575.

8) F. E. Beamish, "The Analytical Chemistry of the

Noble Metals," Vol. 24, Pergamon Press, Oxford (1966), pp. 273, 286, 308, 314.
9) A. Earnshan, "Magnetochemistry," Academic Press, New York (1968), pp. 6—7.
10) C. Stoufer, D. W. Smith, E. A. Clevenger, and T. E. Norris, *Inorg. Chem.*, **5**, 1167 (1966).
11) B. N. Figgis, "Introduction to Ligand Field Theory," Interscience Publishers, Inc., New York, N. Y. (1966).
12) A. V. Radushev, A. N. Checkneva, and I. I. Mudretsova, *Zh. Anal. Khim.*, **26**, 796 (1971).
13) O. Bostrup and C. K. Jørgensen, *Acta Chem. Scand.*, **11**, 1223 (1957).
14) C. E. Schaffer, Abstracts, 140th National Meeting of the American Chemical Society, Chicago. Ill., Sept. 1961, p. 24N.
15) M. B. Robin and Peter Day, Mixed Valence Chemistry in "Advances in Inorganic Chemistry," 1st ed, ed by H. J. Emelius and A. G. Sharp, Vol. 10, Academic Press, New York, (1967), pp. 312.
16) C. J. Ballhausen and H. B. Cray, "Coordination Chemistry," Vol. I, ed by A. E. Martel, Von Nostrand Reinhold Co., New York (1971), p. 66.
17) C. F. Svatos, C. Curran, and J. V. Quagliano, *J. Am. Chem. Soc.*, **77**, 6159 (1955).
18) R. B. Penland, S. Muzushima, C. Curran, and J. V. Quagliano, *J. Am. Chem. Soc.*, **79**, 1575 (1957).

Topological Properties of Benzenoid Systems. IV.[1] On Aihara's Resonance Energy

Ivan GUTMAN

Department of Chemistry, Faculty of Sciences, University of Kragujevac, 34000 Kragujevac, R. Domanovića 12, Yugoslavia

(Received December 22, 1977)

Different mathematical properties of a resonance energy, recently defined by Aihara (This Bulletin, **50**, 2010 (1977)), are presented.

In a recent paper[2] Aihara defined a new resonance energy, *RE**, by

$$RE^* = K\sum_{k=1}^{m} X_k, \tag{1}$$

where X_k denotes the roots of the equation $A(X)=0$, arranged in descending order. The polynominal $A(X)$ is defined by

$$A(X) = \sum_{k=0}^{m} (-1)^k r(k) X^{2m-2k},$$

where $r(k)$ denotes the resonant sextet numbers.[3] The main properties of *RE** and its relation to the resonance energy of Dewar and that of Herndon were determined.[2] The present paper reports an attempt to establish further relations for this new concept, in order to clarify its mathematical meaning; Aihara's notations have been used. Sometimes notations $RE^*=RE^*(G)$, $A(X)=A(G, X)$ and $r(k)=r(G,k)$ are used to indicate quantities corresponding to a particular benzenoid molecule G.

Aihara noted[2] that in certain cases the X_k values become complex numbers. Equation 1 should thus be modified as

$$RE^* = K\sum_{k=1}^{m} x_k, \tag{1'}$$

where x_k is the real part of X_k. In the following this generalized definition of *RE** is considered. Equation 1′ is reduced to Eq. 1 when all X_k values are real.

*Identities, Bounds and Approximate Topological Formulas for RE**. There is a formal analogy between Eqs. 1 and 1′ and the definition of the total π-electron energy (E) in Hückel molecular orbital (HMO) theory. A number of known results for E can thus be applied and changed into relations valid for *RE**. For this it is important to recognize the analogy between $A(X)$ and the HMO characteristic polynominal.[2]

Let us denote the first derivative of the polynomial $A(X)$ by $A'(X)$ and a complex variable by z. Then according to Coulson,[4] the sum of the form (Eq. 1′) fulfills the equations

$$RE^* = \frac{K}{2\pi i}\int_C \left[2m - \frac{z\,A'(z)}{A(z)}\right] dz \tag{2}$$

and

$$RE^* = \frac{K}{2\pi}\int_{-\infty}^{+\infty} \left[2m - \frac{iX\,A'(iX)}{A(iX)}\right] dX, \tag{3}$$

where i is the imaginary unit, the contour C in Eq. 2 being chosen to encircle the non-negative part ($Re\ z \geqslant 0$) of the complex plain. Note that the polynominal $A(X)$ is constructed in such a manner that all its roots differ from zero.

Equation 3 is further transformed into[5]

$$RE^* = \frac{K}{2\pi}\int_{-\infty}^{+\infty} f(X)dX, \tag{4}$$

where

$$f(X) = X^{-2}\ln\sum_{k=0}^{m} r(k)X^{2k} = X^{-2}\ln B(X^2)$$

and $B(X)$ is the sextet polynomial of Hosoya and Yamaguchi.[2,3]

Let G_1 and G_2 be two benzenoid systems and let their A-polynomials be of the order $2m_1$ and $2m_2$, respectively. Then another result of Coulson[6] gives the identity

$$RE^*(G_1) - RE^*(G_2) = \frac{K}{2\pi}\int_{-\infty}^{+\infty} \ln\left[(-X^2)^{m_2-m_1}\frac{A(G_1, iX)}{A(G_2, iX)}\right] dX. \tag{5}$$

Three topological parameters of benzenoid systems are of importance in the following discussion. They are $r(G, 1)$—the number of resonant sextets in G, m—the maximal number of mutually resonant sextets in G and $r(G, m)$—the number of ways in which m resonant sextets are selected in G. Although no simple and general procedure exists for calculating these quantities, it is not difficult to determine them from an inspection of the molecular network of a benzenoid system.[7]

The significance of m, $r(1)$ and $r(m)$ becomes evident if one remembers that they play formally the same role in $A(X)$, as the number of carbon atoms, the number of carbon-carbon bonds and the algebraic structure count in the HMO characteristic polynomial.[8] Thus it is easy to transform the known[9] lower and upper bounds for E into bounds for *RE**. Hence we get

$$\begin{aligned} &r(1) - mr(m)^{1/m} \leq mr(1) - (RE^*/K)^2 \leq \\ &\leq (m-1)[r(1) - mr(m)^{1/m}]. \end{aligned} \tag{6}$$

A special case of the relation (Eq. 6) is the simple formula

$$m \leq RE^*/K \leq \sqrt{mr(1)}\ .$$

A class of approximate topological formulas for *RE** is obtained using a general method[10] which we will apply to Eq. 4. Similar conclusions can be reached from Eqs. 3 and 5.

The integrand $f(X)$ in Eq. 4 is a bell-shaped function, showing the following asymptotic behavior.

$$f(X) \approx \begin{cases} r(1) & \text{for } |X| \to 0 \\ 2m\, X^{-2} \ln X & \text{for } |X| \to \infty \end{cases} \quad (7)$$

Moreover, we have

$$f(1) = \ln SC, \quad (7')$$

since $B(1) = r(0) + r(1) + \cdots\cdots + r(m)$ is equal to the structure count (SC) of the benzenoid system under consideration.[3]

If another function $g(X)$ fulfills the relations (Eqs. 7 and 7'), then the expression $\frac{K}{2\pi}\int_{-\infty}^{+\infty} g(X)\, dX$ is expected[10] to give a good estimate of RE^*. A suitable function of this type is

$$g(X) = \frac{T^2 r(1) + m \ln(1+X^2)}{T^2 + X^2},$$

with

$$T^2 = (\ln SC - m \ln 2)/(r(1) - \ln SC).$$

Straightforward integration yields

$$RE^*/K \approx \frac{1}{2} T\, r(1) + m \frac{\ln(1+T)}{T}. \quad (8)$$

It can be shown that the above relation is suitable for numerical calculations. However, we are herewith mainly interested in the topological properties of Eq. 8, namely in the finding of the main structural factors which contribute to RE^*. We see that RE^* is grossly determined by three structural parameters $r(1)$, m, and SC. Since Eq. 8 does not depend explicitly on $r(m)$, we conclude that this quantity has only a second order influence on the value of RE^*. The functional dependence of RE^* on $r(1)$, m, and SC is rather complicated. In order to get a qualitative insight into this dependence, one can use the fact that T is small, which results in an essential simplification of Eq. 8.

$$RE^*/K \approx m + \frac{1}{2} T\, r(1) \quad (9)$$

Hence the main contribution to RE^* comes from the maximal number of mutually resonant sextets (m), while the number of simply resonant sextets ($r(1)$) has a smaller effect. An inspection of both Eqs. 8 and 9 suggests that RE^* is proportional to ln SC, but the functional dependence between RE^* and ln SC does not seem to be linear.

RE^*'s of Non-Branched Cata-Condensed Benzenoid Systems. For every non-branched cata-condensed benzenoid (NBCCB) system[11] G with n hexagons, an acyclic graph T with $n+1$ vertices can be constructed, such that its characteristic polynominal $P(T, X)$ fulfills the relation[12]

$$X^{n+1-2m} A(G, X) = P(T, X). \quad (10)$$

It follows from this relation that $RE^*(G)/K = E(T)/2$. Hence Aihara's resonance energy (in terms of K) of a NBCCB molecule is equal to half of the Hückel energy (in terms of β) of a particular acyclic graph. This simple result enables us to apply the numerous relations known for acyclic graphs and their Hückel energy[13] to the theory of RE^*. A few selected examples are given.

The way in which an "L, A-sequence" is associated with a NBCCB system and the procedure of the construction of the graph T have been reported.[12] As an example, in the case of a linear polyacene with n hexagons (an L^n-system), the corresponding T-graph is the star S_{n+1} with $n+1$ vertices. The characteristic polynomial of the star reads[13]: $P(S_{n+1}, X) = X^{n+1} - nX^{n-1}$. Consequently, it is $E(S_{n+1}) = 2\sqrt{n}$ and $RE^*(L^n) = \sqrt{n}K$. This latter result is equivalent to Aihara's Eq. 15.[2]

By a similar argument we obtain general formulas for the RE's of further classes of NBCCB molecules given below, where n denotes the total number of hexagons. RE^* is expressed in terms of K.

$$RE^*(L^n) = \sqrt{n}$$

$$RE^*(L^a A L^b) = \sqrt{n + 2\sqrt{ab}} \qquad (a+b+1=n)$$

$$RE^*(L^a A^2 L^b) = \sqrt{n + 2\sqrt{ab} + n - 2} \qquad (a+b+2=n)$$

$$RE^*(L^a (AL^a)^b) = \sum_{j=1}^{b+1} \sqrt{a + \cos^2 \frac{\pi j}{b+2}} \qquad (a+b+ab=n)$$

$$RE^*(LA^{n-2}L) = \begin{cases} \operatorname{cosec} \frac{\pi}{2n+4} - 1 & \text{if } n \text{ is odd} \\ \operatorname{cotg} \frac{\pi}{2n+4} - 1 & \text{if } n \text{ is even} \end{cases}$$

$$RE^*(L^2A^{n-3}L) = \begin{cases} \operatorname{cotg} \frac{\pi}{2n+4} & \text{if } n \text{ is odd} \\ \operatorname{cosec} \frac{\pi}{2n+4} & \text{if } n \text{ is even} \end{cases}$$

$$RE^*(L^2A^{n-4}L^2) = \begin{cases} \operatorname{cosec} \frac{\pi}{2n+4} + 1 & \text{if } n \text{ is odd} \\ \operatorname{cotg} \frac{\pi}{2n+4} + 1 & \text{if } n \text{ is even} \end{cases}$$

The T-graph associated with a NBCCB system of the type L^n and $LA^{n-2}L$ is the star S_{n+1} and the path P_{n+1}, respectively, with $n+1$ vertices.[12] It has been proved[13] that for all acyclic graphs T with $n+1$ vertices, $E(S_{n+1}) \leq E(T) \leq E(P_{n+1})$. This implies that among NBCCB systems with n hexagons, the linear polyacene (L^n) has minimal and the angular polyacenes ($LA^{n-2}L$) have maximal values of RE^*.

References

1) Part III of this series see: I. Gutman, H. Hosoya, T. Yamaguchi, A. Motoyama, and N. Kuboi, *Bull. Soc. Chim. Beograd*, **42**, 503 (1977).
2) J. Aihara, *Bull. Chem. Soc. Jpn.*, **50**, 2010 (1977).
3) H. Hosoya and T. Yamaguchi, *Tetrahedron Lett.*, **1975**, 4659.
4) C. A. Coulson, *Proc. Cambridge Phill. Soc.*, **36**, 201 (1940).
5) I. Gutman and N. Trinajstić, *J. Chem. Phys.*, **64**, 4921 (1976).

6) C. A. Coulson, *J. Chem. Soc.*, **1954**, 3111.
7) For additional work on $r(1)$ and $r(m)$ see: T. Yamaguchi, M. Suzuki and H. Hosoya, *Nat. Sci. Rept. Ochanomizu Univ.*, **26**, 39 (1975); O. E. Polansky and D. H. Rouvray, *Match*, **2**, 91 (1976); J. Aihara, *Bull. Chem. Soc. Jpn.*, **49**, 1429 (1976).
8) A. Graovac, I. Gutman, N. Trinajstić, and T. Živković, *Theoret. Chim. Acta*, **26**, 67 (1972).
9) I. Gutman, *Chem. Phys. Lett.*, **24**, 283 (1974).
10) I. Gutman, *J. Chem. Phys.*, **66**, 1652 (1977).
11) Part I: I. Gutman, *Croat. Chem. Acta*, **46**, 209 (1974).
12) Part II: I. Gutman, *Theoret. Chim. Acta*, **45**, 309 (1977).
13) I. Gutman, *Theoret. Chim. Acta*, **45**, 79 (1977) and references therein.

Kinetics and Mechanism of the Oxidation of Alcohols by Pyridinium Chlorochromate

Kalyan K. BANERJI
Department of Chemistry, University of Jodhpur, Jodhpur 342001, India
(Received January 9, 1978)

The kinetics of the oxidation of ten primary alcohols by pyridinium chlorochromate has been studied. The main product of the oxidation is the corresponding aldehyde. The reaction is of first order with respect to the concentration of the alcohol and oxidant. The reaction is catalysed by acid, the catalysed reaction being nearly first order in acidity. The kinetic isotope effect, k_H/k_D is 5.71 at 303 K for ethanol. The reaction does not induce polymerisation of acrylonitrile. The reaction constant ρ^* for the uncatalysed and acid-catalysed oxidations have the values −1.93 and −1.75 at 303 K respectively. Probable mechanisms are discussed.

Pyridinium chlorochromate (PCC) is a complex of chromium trioxide, pyridine and hydrochloric acid.[1] Corey and Suggs[1] reported that this complex converts alcohols to carbonyl products in yields over 80%. There seems to be no previous report on the mechanism of this useful reaction. The present paper deals with the oxidation of some primary alcohols in 1 : 1 (v/v) dichloromethane–nitrobenzene solution and evaluates the reaction constant.

Results

The rate laws and other experimental data were obtained for all the alcohols investigated. Since results are similar, only those of ethanol are reproduced.

The oxidation of ethanol by PCC results in the formation of acetaldehyde as the main product, which is isolable in 75±5% yield as its 2,4-dinitrophenylhydrazone.

Stoichiometry. Excess of PCC was allowed to react with 0.08 M of ethanol at various acidities and the unreacted oxidant estimated. For some runs the carbonyl product was estimated, using an excess of the alcohol. The overall reaction corresponds to

$$3RCH_2OH + 2Cr(VI) \longrightarrow 3RCHO + H^+ + 2Cr(III). \quad (1)$$

Rate Laws. When the alcohol is in excess, the rate of disappearence of PCC follows first rate laws. The rate constant is independent of the initial concentration of PCC (Table 1). The reaction is of first order with respect to the alcohol concentration also (Table 2). The reaction is catalysed by acid. The catalysed reaction being nearly first order in acidity. The actual order is 0.88±0.02 (Table 3). Because of the non-aqueous nature of the solvent, constant ionic strength could not be maintained.

TABLE 1. OXIDANT DEPENDENCE OF THE REACTION RATE

[EtOH] 0.10 M	Temp 303 K				
10^3 [PCC] M	2.0	4.0	6.0	8.0	10.0
$10^6 k_1$ s^{-1}	10.0	9.73	10.6	10.0	9.84

TABLE 2. SUBSTRATE DEPENDENCE OF THE REACTION RATE

[PCC] 0.002 M	Temp 303 K				
[EtOH] M	0.05	0.10	0.20	0.40	0.80
$10^6 k_1$ s^{-1}	5.13	10.0	20.7	41.0	78.3

TABLE 3. ACIDITY DEPENDENCE OF THE REACTION RATE

[EtOH] 0.10 M	[PCC] 0.002 M		Temp 303 K		
[TsOH] M	0.05	0.10	0.20	0.30	0.40
$10^6 k_1$ s^{-1}	14.4	18.9	27.0	38.1	44.9

TABLE 4. DEPENDENCE OF THE REACTION RATE ON SOLVENT COMPOSITION

[EtOH] 0.10 M	[PCC] 0.002 M		[TsOH] 0.10 M		Temp 303 K
Percentage of nitrobenzene	30	40	50	60	70
Dielectric constant	16.8	19.4	22.0	24.5	27.1
$10^6 k_1$ s^{-1}	50.1	28.2	18.9	13.5	10.6

The rate of the oxidation of ethan-1,1-d_2-ol and ethanol at 303 K are 10^5k=1.75 and 10.0 l mol^{-1} s^{-1} respectively. The kinetic isotope effect, k_H/k_D is 5.72 at 303 K.

Effect of Solvent Composition. The acid-catalysed oxidation of ethanol was studied in solutions containing varying proportion of dichloromethane and nitrobenzene (Table 4). Increasing proportion of nitrobenzene in the solution reduces the rate.

The oxidation of ethanol, in an atmosphere of nitrogen, failed to induce polymerisation of acrylonitrile. In control experimetns, with the alcohol absent, the concentration of PCC does not change.

TABLE 5. RATE CONSTANTS FOR THE UNCATALYSED OXIDATION OF PRIMARY ALCOHOLS, RCH_2OH, BY PYRIDINIUM CHLOROCHROMATE

Substituent (R)	$10^6 k$ l mol^{-1} s^{-1}			
	303	308	313	318K
Me	100	140	193	263
Et	155	210	282	375
n-Pr	166	224	300	400
i-Pr	240	320	417	550
t-Bu	400	507	646	832
Cyclohexy.	182	246	327	432
H	11.5	18.2	28.2	43.1
$MeOCH_2$	10.2	16.2	25.7	39.9
$BrCH_2$	1.10	1.91	3.28	5.50
$ClCH_2$	1.00	1.76	3.06	5.20

Table 6. Rate constants for the acid-catalysed oxidation of primary alcohols, RCH_2OH, by pyridinium chlorochromate

Substituent (R)	$10^5 k$ l² mol⁻² s⁻¹			
	303	308	313	318K
Me	189	251	336	443
Et	282	363	490	630
n-Pr	295	389	513	676
i-Pr	417	543	708	910
t-Bu	675	850	1070	1380
Cyclohexyl	330	427	550	725
H	27.0	38.9	56.2	79.5
$MeOCH_2$	24.0	34.7	50.1	72.5
$BrCH_2$	3.16	5.07	7.76	12.3
$CClCH_2$	2.95	4.68	7.24	11.5

The uncatalysed and acid-catalysed oxidation of the primary alcohols were studied at different temperatures (Tables 5 and 6) and the activation parameters evaluated (Table 7). The average error limits in the values of ΔH^*, ΔS^*, and ΔF^* (at 303 K) are ± 6 kJ mol^{-1}, ± 10 J mol^{-1} K^{-1}, and ± 7 kJ mol^{-1} respectively.

Discussion

A near constancy of the free energy of activation shows that the same mechanism is operative in all the alcohols. The free energy of activation of the acid-catalysed oxidation is consistently lower than that of the uncatalysed reaction but are of the same order indicating that the mechanisms of the two reactions are essentially similar.

The linear increase in the oxidation rate with acidity suggests involvement of a protonated Cr(VI) species in the rate-determining step. Involvement of such species are well known in chromic acid oxidation.[2] The kinetic isotope effect suggests that the rate-determining step involves a C–H bond rupture.

The activation enthalpies and entropies of both the uncatalysed and acid-catalysed reactions are linearly related (r=0.9993 and 0.9991 respectively). The correlations were tested and found genuine by applying Exner's criterion.[3] The isokinetic temperatures computed from these polts are 436 and 502 K respectively. Current views do not attach much physical significance to isokinetic temperature,[4] though a linear correlation is usually a necessary condition for the validity of linear free energy relationships.

Dielectric constants for dichloromethane–nitrobenzene mixtures are not available, but can be estimated approximately from the dielectric constants of the pure solvents.[5] The estimated dieletctric constants of the solvent mixtures are recorded in Table 4. A plot of $\log k_1$ against the inverse of dielectric constant is a straight line with a positive slope. This indicates an interaction between a dipole and a positive ion.[6] This accords with the observation regarding involvement of a protonated Cr(VI) species in the rate-determining step.

The oxidation rates of the primary alcohols correlate well with Taft's σ^* values with negative reaction constants (Table 8).

A hydrogen abstraction mechanism may be discounted in view of the failure to induce polymerisation of acrylonitrile and the magnitude of the reaction constant. In most hydrogen abstraction reactions the reaction constants have small magnitude.[7] The large negative reaction constant together with the substantial deuterium isotope effect indicate a considerable carbonium ion character in the transition state. The above results points to a hydride-ion transfer in the rate-determining step. The hydride transfer may take place directly (Scheme 1) or may involve the prior formation of a chromate ester (Scheme 2). The similarity in the rate laws with chromic acid oxidations[2] suggests a chromate ester formation. However, the observed kinetic isotope effect is rather

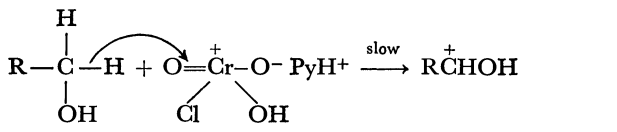

$$+ (HO)_2CrClO^- PyH^+ \quad (2)$$

$$RCHOH \xrightarrow{fast} RCHO + H^+ \quad (3)$$

Scheme 1.

Table 7. Activation parameters for the oxidation of alcohols, RCH_2OH, by pyridinium chlorochromate

Substituent (R)	Uncatalysed			Acid-catalysed		
	ΔH^* kJ mol⁻¹	$-\Delta S^*$ J mol⁻¹ K⁻¹	ΔF^* kJ mol⁻¹	ΔH^* kJ mol⁻¹	$-\Delta S^*$ J mol⁻¹ K⁻¹	ΔF^* kJ mol⁻¹
Me	51.8	153	98.2	45.9	148	90.7
Et	47.3	164	97.0	43.6	153	90.0
n-Pr	47.2	164	96.9	43.4	153	89.8
i-Pr	44.1	171	95.9	41.9	155	88.9
t-Bu	39.3	183	94.7	38.0	164	87.7
Cyclohexyl	46.5	166	96.8	41.9	157	89.5
H	70.7	109	104	58.9	125	96.8
$MeOCH_2$	73.2	101	104	59.1	122	96.1
$BrCH_2$	86.1	77	109	72.1	95	101
$ClCH_2$	88.2	71	110	72.3	96	101

Table 8. Temperature dependence of the reaction constant and regression coefficient

Temp K	Uncatalysed		Acid-catalysed	
	$-\rho^*$	r	$-\rho^*$	r
303	1.93	0.9998	1.75	0.9997
308	1.83	0.9998	1.67	0.9998
313	1.73	0.9997	1.61	0.9997
318	1.64	0.9996	1.54	0.9998

large for the non-linear transition state implied in Scheme 2. The present data, thus do not enable one to distinguish between the two mechanisms. Chromate ester formation is not likely to be very much susceptible to structural influence.[8,9] The large negative reaction constant can thus arise only out of the differential effects of the substituents on the rate-determining step.

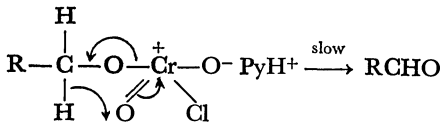

$$+ \overset{+}{\mathrm{HOCr}}\mathrm{ClO}^- \ \mathrm{PyH}^+ \qquad (4)$$

Scheme 2.

Experimental

Materials. The preparation and specification of the alcohols used have been described earlier.[10] Isotopic purity of ethan-1,1-d_2-ol, as determined by NMR, was 89±5%. The oxidant was prepared by the method of Corey and Suggs.[1] *p*-Toluenesulfonic acid (TsOH) was used as a source of hydrogen ions. The solvents were purified and dried in the usual manner.[11] All reagents were of analytical grade.

Product Analysis. Acetaldehyde was characterised and estimated by the isolation of its 2,4-dinitrophenylhydrazone.

Kinetic Measurements. The reactions were carried out under pesudo-first-order conditions by keeping a large excess of the alcohol over PCC. The temperature was kept constant to ±0.1 K. The reactions were followed iodometrically. The rate constant were computed from the plots of log [oxidant] against time and were reproducible within ±4%. The solvent was dichloromethane–nitrobenzene —1:1 (v/v)—, unless otherwise stated. The reaction mixtures were homogenous in the solvent systems used. The rate for the deuterated alcohol was corrected for the ordinary alcohol present.

References

1) E. J. Corey and W. J. Suggs, *Tetrahedron Lett.*, **1975**, 2647.
2) K. B. Wiberg, "Oxidation in Organic Chemistry," Part A, Academic Press, New York (1965), p. 69.
3) O. Exner, *Coll. Czeck. Chem. Commun.*, **29**, 1094 (1964).
4) J. E. Leffler, *J. Org. Chem.*, **31**, 533 (1966).
5) C. N. R. Rao, "A Hand Book of Physics and Chemistry," Affiliated Press, New Delhi (1967), p. 169.
6) E. S. Amis, "Solvent Effects on Reaction Rates and Mechanisms," Academic Press, New York (1967), p. 42.
7) K. B. Wiberg, "Physical Organic Chemistry," Academic Press, New York (1963), pp. 406, 410.
8) N. C. Deno and M. S. Newman, *J. Am. Chem. Soc.*, **72**, 3852 (1950).
9) U. Klanning and M. C. R. Symons, *J. Chem. Soc.*, **1961**, 3204 and references therein.
10) K. K. Banerji, *Bull. Chem. Soc. Jpn.*, **46**, 3623 (1973).
11) D. D. Perrin, W. L. Armarego and D. R. Perrin, "Purification of Organic Compounds," Pergamon Press, Oxford (1966).

NOTES

BULLETIN OF THE CHEMICAL SOCIETY OF JAPAN, VOL. 51 (9), 2735—2736 (1978)

Polarization Dispersion in the Resonance Raman Spectra of EDA Complexes with TCNE and TCNB

Masao TAHARA,* Susumu MATSUZAKI,† and Shiro MAEDA

Research Laboratory of Resources Utilization, Tokyo Institute of Technology, Midori-ku, Yokohama 227

† *Department of Chemistry, Faculty of Science, Kumamoto University, Kumamoto 860*

(Received February 6, 1978)

Synopsis. Polarization dispersion of the $\nu_{C\equiv N}$ Raman line of the *N,N*-dimethylaniline–TCNB complex indicated that the two CT absorption bands are assignable to different acceptor orbitals, in contrast with those of TCNE complexes.

The resonance Raman effect (RRE) can be used to probe the nature of electronic excited states, and its faculty is fully exhibited by investigating the excitation profile and polarization dispersion. Charge transfer (CT) excited states of electron-donor-acceptor (EDA) complexes can suitably be investigated by RRE, as was demonstrated by Kaya *et al.*[1] for the complexes of tetracyanoethylene (TCNE) with benzene homologues. They observed the RRE of $\nu_{C=C}$ and $\nu_{C\equiv N}$ of complexed TCNE by exciting radiations within the first CT absorption band, and concluded that some increase of equilibrium C=C and C≡N distances from the ground to CT excited states was responsible for the resonant intensity of those lines.

It has been known that two CT absorption bands appear in the complexes with strong electron acceptors such as chloranil and TCNE.[2] Those CT bands have been explained by the two CT configurations (illustrated in Fig. 1a) distinguished by the difference in electron-donating orbitals. On the other hand, Iwata *et al.*[3] showed that the two CT absorption bands observed for some complexes of 1,2,4,5-tetracyanobenzene (TCNB), though quite similar to the TCNE case, were more reasonably interpreted by another multi-CT scheme (shown in Fig. 1b) in which two CT configurations are distinct in the electron-accepting orbitals of TCNB. In order to investigate the validity of these multi-CT schemes further, the RRE has been measured for the *N,N*-dimethylaniline–TCNB complex and some TCNE complexes.

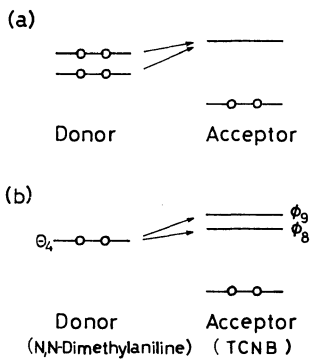

Fig. 1. Schematic diagram of CT excited states a) naphthalene–TCNE, and b) *N,N*-Dimethylaniline–TCNB complexes.

Experimental

Commercially obtained samples were used after appropriate purification, with the exception of TCNB, which was synthesized from pyromellitic acid and purified by sublimation. Raman spectra were recorded on JRS-S1 and JRS-400D spectrometers using exciting radiations from Ar^+ (457.9…514.5 nm), Kr^+(530.9, 568.2, 647.1 nm), and He–Ne (632.8 nm) lasers. The measurement was carried out on donor-excess solutions by using a rotating cell. The intensity and depolarization ratio were determined by checking with appropriate internal standards; these were solvent CH_2Cl_2 for TCNE and purposely added CCl_4 for TCNB.

Results and Discussion

Figure 2 shows the excitation profiles and polarization dispersions measured on $\nu_{C=C}$ (1560 cm^{-1}) and $\nu_{C\equiv N}$ (2230 cm^{-1}) of TCNE in the solution of naphthalene–TCNE complex. About 80% of TCNE is bound to form the complex[2] in the present donor-excess condition, so that the non-resonant intensity from free TCNE may be unimportant. The $\nu_{C\equiv N}$ Raman band

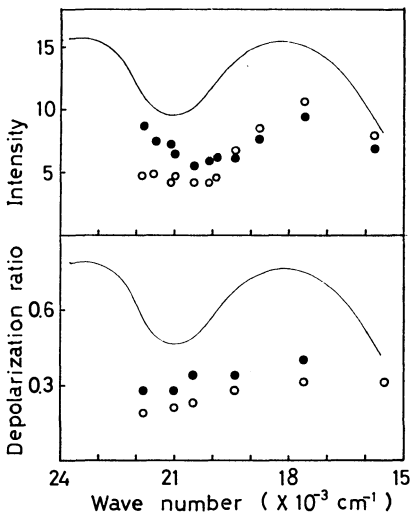

Fig. 2. Excitation profile and polarization dispersion of naphthalene–TCNE complex, naphthalene=0.1 mol/l, TCNE=0.005 mol/l in CH_2Cl_2 solution. (○): $\nu_{C=C}$(1560 cm^{-1}), (●): $\nu_{C\equiv N}$(2230 cm^{-1}), (——); absorption.

includes both A_g and B_{1g}** C≡N stretching modes. Since the ρ value is rather close to 1/3, which is the value expected for a Franck-Condon type resonance enhancement of the A_g mode, the depolarized B_{1g} intensity does not seem to be appreciably resonant in the CT band region. If the B_{1g} mode were resonant due to a vibronic coupling of the CT levels, the ρ plot should have shown generally higher values than that observed and tended upward at the high frequency side as in observed for the intensity plot. The slight dispersive trend of ρ observed for both $\nu_{C=C}$ and $\nu_{C\equiv N}$ may possible be caused by the interference of contributions from the first and second CT levels. Such an interference can take place because those CT transition moments may not be exactly parallel to each other on account of the mixing with locally excited states. Similar measurements have been carried out for the TCNE complexes of durene and pyrene, which also have two CT absorption bands in the visible; similar features of the depolarization ratio were found.

Figure 3 shows the results of the corresponding observations on *N,N*-dimethylaniline–TCNB complex.*** It is remarkable that the ρ ($\nu_{C\equiv N}$) increases towards the CT absorption maximum up to about 0.7 at a 514.5 nm excitation, while ρ ($\nu_{C=C}$) is kept nearly constant at about 1/3. This indicates that the depolarized $\nu_{C\equiv N}$ (B_{1g}) line is quite resonant in this system. The RRE intensity of a non-totally symmetric mode normally originates from vibronic coupling; thus,

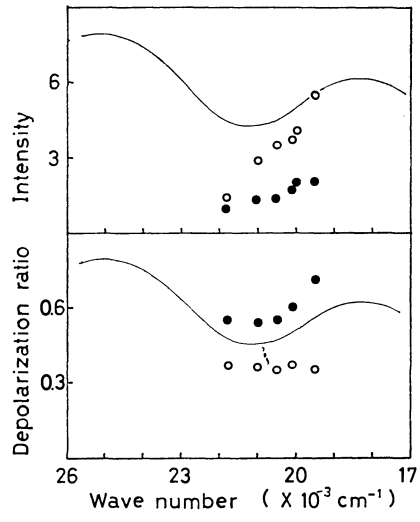

Fig. 3. Excitation profile and polarization dispersion of *N,N*-dimethylaniline–TCNB complex, TCNB= 0.007 mol/l in *N,N*-dimethylaniline solution. (○): $\nu_{C=C}$(1542 cm^{-1}), (●): $\nu_{C\equiv N}$(2240 cm^{-1}), (——): absorption.

** Representation of the D_{2h} group of TCNE.

*** Several other donors tried at the same time were not suitable enough to allow significant observation, because of insufficient solubility, CT band locations remote from available laser lines, apparent interference from intense locally excited absorptions, *etc.*

the above case may be most reasonably understood by the coupling of the first and second CT states illustrated in Fig. 1b, as will be descrived below. The contribution to a Raman tensor from a vibronic coupling of ψ_e and ψ_s states is proportional to the integral $\int \psi_e^*(\partial H/\partial Q_a)_0\ \psi_s d\tau$,[5] where Q_a is a normal coordinate. The integral can be reduced to a single electon one such as

$$\int \psi_e^*(H\partial/\partial Q_a)_0 \psi_s d\tau_1 \cdots d\tau_N = \int v^a(1)\rho_{es}(1)d\tau_1, \qquad (1)$$

where v^a is the potential from a set of point dipoles produced by the nuclear displacement of mode a and ρ_{es} is the transition density defined by

$$\rho_{es}(1) = N\int \psi_e^*(1, \cdots, N)\psi_s(1, \cdots, N)d\tau_2 \cdots d\tau_N. \qquad (2)$$

Now, let us assume that the CT states of *N,N*-dimethylaniline–TCNB complex can be represented by

$$\psi_{CT1} = \Phi(\theta_4^{-1}\phi_8), \qquad \psi_{CT2} = \Phi(\theta_4^{-1}\phi_9), \qquad (3)$$

$$\Phi(\theta_4^{-1}\phi_k) = (1/\sqrt{2})[|\theta_1 \cdots \phi_4\bar{\phi}_k \cdots \bar{\phi}_7| + |\theta_1 \cdots \phi_k\bar{\theta}_4 \cdots \bar{\phi}_7|], \qquad (4)$$

where θ and ϕ represent the MO's of *N,N*-dimethylaniline and TCNB respectively, as shown in Fig. 1b. It is readily shown that

$$\rho_{CT1,CT2} = \phi_8\phi_9, \qquad (5)$$

which signifies that the transition density is spacially localized on the TCNB moiety. Then the significant coupling of the CT states (3) can take place only by the vibrational modes of the TCNB moiety, as is obvious from Eq. 1, providing that the mode a belongs to the same representation of TCNB symmetry (D_{2h}) as $\rho_{CT1,\ CT2}$ does. Since

$$\Gamma(\phi_8) \times \Gamma(\phi_9) = A_u \times B_{1u} = B_{1g},$$

the $\nu_{C\equiv N}$ (B_{1g}) mode meets the above requirement. On the other hand, it is obvious by a similar consideration that the transition density between the two CT configurations of Fig. 1a is one-sided on the donor molecule, so that the vibronic coupling by acceptor modes may be quite unlikely.

On the basis of above discussion, the present RRE result may be thought of as further evidence for the multi-CT schemes of Figs. 1a and b proposed for TCNE and TCNB complexes.

References

1) K. Kaya, A. Nakatsuka, N. Kubota, and M. Ito, *J. Raman Spectroscopy*, **1**, 595 (1973).

2) G.Briegleb, "Electronen-Donator-Acceptor Komplexe," Springer-Verlag, Berlin, (1961).

3) S. Iwata, J. Tanaka, and S. Nagakura, *J. Am. Chem. Soc.*, **88**, 894 (1966).

4) E. A. Lawdon and D. D. Mcritchie, *J. Org. Chem.*, **24**, 26 (1959).

5) A. C. Albrecht, *J. Chem. Phys.*, **34**, 1476 (1961).

6) J. N. Murrell and J. A. Pople, *Proc. Phys. Soc.*, **A69**, 245 (1956).

BULLETIN OF THE CHEMICAL SOCIETY OF JAPAN, VOL. 51 (9), 2737—2738 (1978)

Temperature Effects on CD Spectra of α-Cyclodextrin Complexes with *m*- and *p*-Nitrophenol

Kazuaki HARATA

Research Institute for Polymers and Textiles, Sawatari 4, Kanagawa-ku, Yokohama 221

(Received March 17, 1977)

Synopsis. The CD spectra of α-cyclodextrin complexes with *m*- and *p*-nitrophenol were measured at 10, 30, 50, and 70 °C in aqueous solutions of various α-cyclodextrin concentrations. The CD intensity of both complexes was decreased to 14—61% of the intensity measured at 10 °C with the increase of temperature to 70 °C, but no significant change was observed in the spectral shape. The thermodynamic parameters for the complex formation were determined.

α-Cyclodextrin (α-CDx) forms inclusion complexes with *m*-nitrophenol (*m*-NP) and *p*-nitrophenol (*p*-NP). The structure of the *p*-nitrophenol complex in aqueous solutions has been investigated by CD[1,2] and NMR[3,4] spectra. Recent X-ray analyses revealed the detailed structure of the *m*-nitrophenol and *p*-nitrophenol complexes.[5,6] In the crystalline states, the *m*-nitrophenol molecule has been suggested to be more loosely bound to the α-cyclodextrin ring than the *p*-nitrophenol molecule. In the presnet study, the CD spectra of these complexes were meausred at various temperatures in order to investigate the α-cyclodextrin interaction with *m*- and *p*-nitrophenol in aqueous solutions.

Experimental

α-Cyclodextrin (G.R., Tokyo Kasei Co.) was crystallized from water and dried *in vacuo* over phosphorus pentaoxide at room temperature. *m*- and *p*-nitrophenol (G.R., Tokyo kasei Co.) were used without further purification. Solutions were prepared with deionized water, and the concentrations of *m*- and *p*-nitrophenol were adjusted to 9.66 and 8.81×10^{-4} mol, respectively. The concentration of α-cyclodextrin was varied from 0.001 to 0.054 mol. The CD spectra were recorded at 10, 30, 50, and 70 °C on a JASCO J-40A circular dichrograph with a J-DPZ data-processor by use of a 1 mm quartz cell. The temperature was regulated by using a Tokyo Rico TC-100 thermo-controller with an accuracy of ±0.5 °C inside the cell.

Results and Discussion

The CD spectra of α-cyclodextrin complexes with *m*- and *p*- nitrophenol are shown in Figs. 1 and 2. The CD intensity in these spectra decreased gradually with the increase of the temperature, although no significant change is observed in the spectral shape. The intensity changes for various molar ratios of [α-CDx]/[guest] ([C]/[G]) were measured at 280 nm for the *m*-nitrophenol complex and at 340 nm for the *p*-nitrophenol complex, as shown in Figs. 3 and 4. At 10 °C, the intensity of both complexes increased rapidly with the increase of the concentration of α-cyclodextrin up to the [C]/[G] value of 10, but only a small intensity enhancement was observed at the

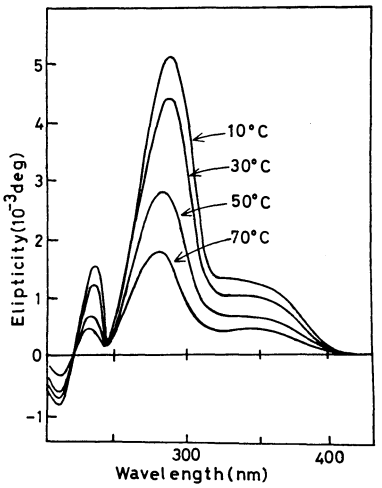

Fig. 1. The CD spectra of α-cyclodextrin–*m*-nitrophenol complex at 10, 30, 50, and 70 °C. The concentrations of α-cyclodextrin and *m*-nitrophenol are 1.8×10^{-2} and 9.66×10^{-4} mol, respectively, and a 1 mm cell was used.

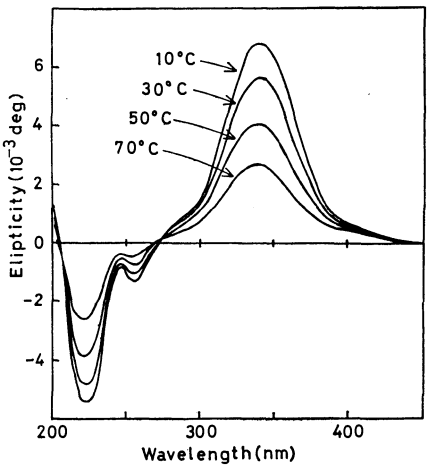

Fig. 2. The CD spectra of α-cyclodextrin–*p*-nitrophenol complex at 10, 30, 50, and 70 °C. The concentrations of α-cyclodextrin and *p*-nitrophenol are 1.8×10^{-2} and 8.81×10^{-4} mol, respectively, and a 1 mm cell was used.

[C]/[G] values greater than 20. On the other hand, at 70 °C, the CD intensity changes more slowly, and showed a gradual increase. When the temperature was raised from 10 to 70 °C, the CD intensity of the *m*-nitrophenol complex fell to 54% at the highest [C]/[G] value, while the intensity decreased to 14% at the lowest [C]/[G] value. A similar intensity change was observed in the *p*-nitrophenol complex. The in-

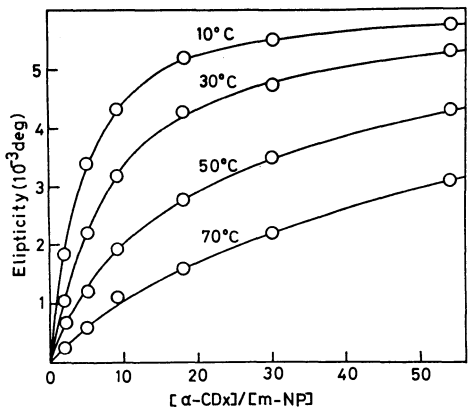

Fig. 3. Plot of the CD intensity measured at 280 nm against the [α-CDx]/[*m*-NP] ratio. The concentration of *m*-nitrophenol is 9.66×10^{-4} mol.

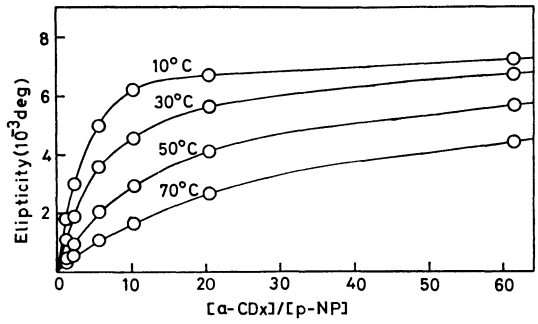

Fig. 4. Plot of the CD intensity measured at 340 nm against the [α-CDx]/[*p*-NP] ratio. The concentration of *p*-nitrophenol is 8.81×10^{-4} mol.

tensity at 340 nm fell to 61% in the solution with a [C]/[G] value of 61 and to 19% in that with a value of 1.

The dissociation constants of the complexes were determined by the Rose-Drago method,[7] on the assumption that α-cyclodextrin forms only a 1:1 complex. This assumption may be supported by the fact that no significant spectral shift or change of the spectral shape, but only an intensity decrease was found with increasing temperature or with decreasing [C]/[G] value. The observed intensity change gave a good fit to the equilibrium equation for the 1:1 stoichiometry. The results are shown in Table 1. The dissociation constants of the *m*-nitrophenol complex were 1.6—2.0 times greater than the corresponding values of the *p*-nitrophenol complex. In both complexes, about a ten-fold increase of the dissociation constants was observed when the temperature was raised from 10 to 70 °C. The enthalpy and entropy changes (ΔH and ΔS) for the complex formation were estimated: −33(1) kJ mol^{-1} and −70(4) J K^{-1} mol^{-1} for the *m*-nitrophenol complex and −30(1) kJ mol^{-1} and −56(3) J K^{-1} mol^{-1} for the *p*-nitrophenol complex, where values in parentheses are standard deviations. The ΔH and ΔS values of the *p*-nitrophenol complex are in good agreement with the values of −31 kJ mol^{-1} and −63 J·K^{-1} mol^{-1} determined by Lewis and Hansen.[8] These thermodynamic parameters indicate that *m*-nitrophenol is bound to α-cyclodextrin as strongly as *p*-nitrophenol. X-ray studies,[5,6] however, indicated that *m*-nitrophenol is more loosely bound to α-cyclodextrin than *p*-nitrophenol. In the crystalline complexes, the *p*-nitrophenol molecule deeply penetrates into the α-cyclodextrin ring and is rigidly fixed, while only a partial inclusion of the guest molecule is observed in the *m*-nitrophenol complex. On the other hand, NMR studies[2,3] have suggested that *p*-nitrophenol molecule is not deeply inserted into the α-cyclodextrin ring. In the *m*-nitrophenol complex, the deep penetration of the guest molecule is impossible because of the steric hindrance. If *m*- and *p*-nitrophenol form complexes in aqueous solutions in the same manner as found in the crystalline complexes, it seems likely that the structural difference between the two complexes will affect the enthalpy of the complex formation.[6] A possible explanation for the observed thermodynamic parameters may be that the *p*-nitrophenol molecule is only partially and loosely included in the α-cyclodextrin ring in aqueous solutions, as suggested from the NMR studies.

Table 1. Dissociation constants and free energies for the complex formation

Values in parentheses are standard deviations.

	p-NP complex		*m*-NP complex	
t °C	K_d 10^{-3} mol^{-1}	ΔG kJ mol^{-1}	K_d 10^{-3} mol^{-1}	ΔG kJ mol^{-1}
10	2.4(0.6)	−14.2(0.6)	3.5(0.4)	−13.4(0.3)
30	5.0(0.5)	−13.4(0.3)	8.1(0.7)	−12.1(0.2)
50	11.7(0.6)	−11.7(0.2)	18(3)	−10.9(0.4)
70	22(6)	−10.9(0.7)	41(9)	−9.2(0.6)

The author wishes to thank Dr. Hisashi Uedaira for supporting this study and for his helpful discussions.

References

1) K. Takeo and T. Kuge, *Staerke*, **24**, 281 (1972).
2) K. Harata and H. Uedaira, *Sen'i Kobunshi Zairyo Kenkyusho Kenkyu Hokoku*, **112**, 1 (1976).
3) R. Bergeron and R. Rowan, III, *Bioorg. Chem.*, **5**, 425 (1976).
4) D. J. Wood, F. E. Hruska, and W. Saenger, *J. Am. Chem. Soc.*, **99**, 1735 (1977).
5) K. Harata, *Bull. Chem. Soc. Jpn.*, **50**, 1416 (1977).
6) K. Harata, H. Uedaira, and J. Tanaka, *Bull. Chem. Soc. Jpn.*, **51**, 1627 (1978).
7) N. J. Rose and R. S. Drago, *J. Am. Chem. Soc.*, **81**, 6138 (1959).
8) E. A. Lewis and L. H. Hansen, *J. Chem. Soc., Perkin Trans. 2*, **1973**, 2081.

BULLETIN OF THE CHEMICAL SOCIETY OF JAPAN, VOL. 51 (9), 2739—2740 (1978)

The Polarographic Behavior of 6-Mercaptopurine in Aqueous Solutions

Toshio YAO,* Junji UDA, Tamotsu WASA, and Soichiro MUSHA

Department of Applied Chemistry, College of Engineering, University of Osaka Prefecture, Mozuumemachi, Sakai 591

(Received February 16, 1978)

Synopsis. The polarographic reduction of 6-mercaptopurine at the dropping mercury electrode took place in two steps; they were a two-electron process producing the 1,6-dihydro derivative, followed by a further two-electron process producing the 1,2,3,6-tetrahydro derivative. An anodic wave corresponding to the reaction with the mercury of the electrode material was observed at a relatively low potential, and its analytical utility for the determination of 6-mercaptopurine is suggested.

The electrochemical reduction of purines and pyrimidines, which are important components of nucleic acids, have been investigated in aqueous[1-3] and nonaqueous solutions.[4-6]

Mercaptopurines containing exocyclic sulfur are often anticarcinogens. In particular, 6-mercaptopurine is being used as an anti-leukemia agent. The present work was carried out in order to study the polarographic behavior of 6-mercaptopurine and its applicability to the polarographic determination of this compound.

Experimental

Chemicals. The 6-mercaptopurine(6-MP) was obtained from the Sigma Chemical Company and was recrystallized from water. The other chemicals were of a reagent grade and were used without further purification.

Apparatus. The polarograms were recorded using a Yanagimoto P-8 type Polarograph. The dropping mercury electrode (DME) had the following characteristics: mercury flow rate, m, 2.30 mg/s, and drop time, t, 3.25 s, with an open circuit under the mercury head of 70 cm, in 1 mol/dm^3 $HClO_4$. A saturated calomel electrode was employed as a reference electrode, and a platinum wire, as a counter electrode, A mercury pool electrode was also used for the controlled potential electrolysis and the coulometric measurements.

Results and Discussion

Polarography and Controlled Potential Electrolysis.

Cathodic Waves: It is known[1] that purine, which is the model compound of 6-MP, exhibits two pH-dependent waves when in an acidic solution, but none when in a neutral or alkaline solution. Similarly, 6-MP exhibits two cathodic waves at fairly negative potentials. The diffusion-current constant (I_d) and the half-wave potential of 6-MP as a function of the pH values are shown in Fig. 1.

At pH values below 4.5, two relatively close polarographic waves(wave I and II) were observed. The half-wave potentials of the two waves shifted linearly towards a negative potential with an increase in the pH; $E_{1/2}$(*vs.* SCE)/V$=-0.680-0.120$ pH for the I wave and $E_{1/2}$ (*vs.* SCE)/V$=-1.016-0.061$ pH for the II wave. The I_d values for both the waves, particularly

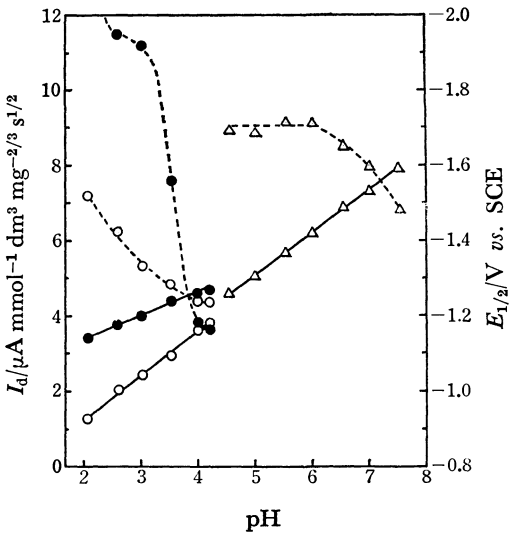

Fig. 1. Effect of pH on the diffusion-current constant (I_d) and half-wave potential of the reduction waves of 0.2×10^{-3} mol/dm^3 6-MP.
○: Wave I, ●: wave II, △: wave III.
(——: $E_{1/2}$, ----: I_d)

that for the II wave, were very large in highly acidic solutions (pH 0—3), but were kept constant at pH values around 4. It is known that the first wave of purine is attributable to a two-electron diffusion-controlled process. The I_d value for this wave was 3.60 μA mmol^{-1} dm^3 mg$^{-2/3}$ s$^{1/2}$. At pH 4.02, the I_d values for the I and II waves of 6-MP were *ca.* 4.4 and 3.8 μA mmol^{-1} dm^3 mg$^{-2/3}$ s$^{1/2}$, corresponding to a two-electron reduction process.

At pH values above 4.5 these two waves merged, and the resulting composite wave(wave III) had a pH dependence of $E_{1/2}$(*vs.* SCE)/V$=-0.746-0.113$ pH. The I_d value of the III wave remained almost constant up to pH *ca.* 6; its value corresponded to a four-electron reduction step. At pH values above 6.0, however, the height of the III wave decreased gradually with an increase in the pH. Since the pK_a of 6-MP was determined to be 7.6 by utilizing the UV absorption method of Shugar and Fox,[7,8] this decrease in the wave-height seems to imply that 6-MP dissociates into an electroinactive ion in solutions above pH *ca.* 7.

The coulometric measurements at the controlled potentials were performed in order to determine the number of electrons involved in the overall electron-transfer reactions. The controlled potential electrolysis at a potential on the crest of the I wave in the Britton-Robinson buffer (pH 4.02) indicated that 2.1 ± 0.2 electrons were transferred per molecule of 6-MP. A coulometric n value for the II wave gave an unusually high value. Also, the electrolytic current remained at a high value throughout the electrolysis

and the pH of the solution increased. This behavior indicates that a major part of the current is a catalytic reduction of hydrogen ions, rather than being due to the reduction of 6-MP itself. Also, the electrolysis at a potential on the crest of the II wave resulted in the liberation of H_2S (detected by lead acetate paper), but no such liberation was detected in the case of the electrolysis at a potential on the crest of the I wave. At pH 6.00 the coulometric n value of the III wave was 5.8±0.4, and the liberation of H_2S was detected just as in the case of the electrolysis at a potential on the crest of the II wave. This discrepancy between the polarographic and coulometric n values may be explained by a ECE mechanism comprised of a slow chemical reaction (liberation of H_2S) which does not occur during the lifetime of a mercury drop, but which becomes important under conditions of prolonged electrolysis.

It is known[1] that purine is reduced in two steps at the DME; the first step is a two-electron reduction to 1,6-dihydropurine, while the second is a further two-electron reduction to 1,2,3,6-tetrahydropurine, which is then hydrolyzed by water to [(5-aminoimidazol-4-ylmethyl)amino]methanol. The mechanisms for the reduction of 6-MP were also proposed. The values of αn_a and of P(the number of hydrogen ions involved in the rate-determining step) were calcualted for the I wave on the basis of the wave-slope($E_{1/4}$-$E_{3/4}$) and the slope of the $E_{1/2}$-pH plots.[9] An average αn_a value of 1.05 and an average P value of 2.13 were determined. Also, the I wave was a two-electron process judging from its I_d values. These facts suggest the hydrogenation of a double bond. Thus by analogy with the first step of purine, the I wave of 6-MP is probably a two-electron process, producing the 1,6-dihydro derivative(**1**). The II wave would then seem to result from a further two-electron reduction to the 1,2,3,6-tetrahydro derivative(**2**) of 6-MP. The UV absorption spectrum of a solution obtained by controlled-potential electrolysis on the crest of the II wave is essentially superimposed on that of the product of the complete electrolysis at a potential on the crest of the second wave of purine, indicating the identity of the two products. The formation of identical products in the reduction processes of 6-MP and purine requires the elimination of the 6-mercapto group from the **2** of 6-MP; this can be explained from the facts that the n values obtained coulometrically at a potential on the crests of the II and III waves were both *ca.* 6 and the liberation of H_2S was detected during the electrolysis. These experimental results seem to indicate that the **2** produced by a four-electron reduction of 6-MP evolves H_2S by means of a relatively slow chemical reaction to produce 2,3-dihydropurine(**3**), which then undergoes a further two-electron reduction to produce 1,2,3,6-tetrahydropurine(**4**), which is probably hydrolyzed to [(5-aminoimidazol-4-ylmethyl)-amino]methanol (**5**) as an end product.

Anodic Waves: An anodic wave of 6-MP was also observed at the DME over the pH range of 2—12. The relationship between the half-wave potentials and the pH was composed of two straight lines. At pH values below 7.6, the anodic wave shifted linearly towards negative potentials with an increase in the pH; $E_{1/2}$(*vs.* SCE)/V=0.140—0.060 pH. At pH values above 7.6, however, the half-wave potential of the anodic wave was independent of the pH; $E_{1/2}$= −0.324 V *vs.* SCE. The pH values at the intersection of these two lines was 7.66, which agreed very closely with the pK_a value (7.60) determined by the UV absorption method,

The height of the anodic wave remained almost constant at the I_d value corresponding to a one-electron faradaic process. The anodic current was proportional to the square root of the height of the mercury head, and the temperature coefficient was 1.3% per degree, indicating that the anodic current was controlled by diffusion.

However, this anodic wave was not observed in this potential range when a platinum electrode was used as the working electrode.

From these experimental results, it seems that the anodic wave of 6-MP does not correspond to the oxidation of 6-MP itself, but to the following reaction of 6-MP with the DME:

$$\mathrm{pH}<\mathrm{p}K_a \quad \mathrm{RSH} + \mathrm{Hg} \longrightarrow \mathrm{RSHg} + \mathrm{H^+} + \mathrm{e},$$

$$\mathrm{pH}>\mathrm{p}K_a \quad \mathrm{RS^-} + \mathrm{Hg} \longrightarrow \mathrm{RSHg} + \mathrm{e}$$

(RSH : 6-MP).

Analytical Application. Compared with the cathodic waves of 6-MP, the anodic wave of this compound was observed at a relatively low potential and was well-defined over the wide pH range of 2—12. The height of this wave in the Britton-Robinson buffer was proportional to the concentrations ranging (5×10^{-5}—10^{-3})mol/dm^3. The satisfactorily wide range of this linear relation suggests that the polarographic method may have analytical utility for the determination of 6-MP, which is being used as an anti-leukemia agent.

References

1) D. L. Smith and P. J. Elving, *J. Am. Chem. Soc.*, **84**, 1412 (1962).
2) G. Dryhurst and P J. Elving, *Talanta*, **16**, 855 (1969).
3) B. Janik and P. J. Elving, *J. Electrochem. Soc.*, **116** 1087 (1969).
4) J. E. O'Reilly and P. J. Elving, *J. Am. Chem. Soc.*, **93**, 1871 (1971).
5) T. Yao and S. Musha, *Bull. Chem. Soc. Jpn.*, **47**, 2650 (1974).
6) T. Yao, T. Wasa, and S. Musha, *Nippon Kagaku Kaishi*, **1976**, 704.
7) D. Shugar and J. J. Fox, *Biochim. Biophys. Acta*, **9**, 199 (1952).
8) J. J. Fox and D. Shugar, *Bull. Soc. Chim. Belg.*, **61**, 44 (1952).
9) T. Yao and S. Musha, *Bull. Chem. Soc. Jpn.*, **48**, 435 (1975).

BULLETIN OF THE CHEMICAL SOCIETY OF JAPAN, VOL. 51 (9), 2741—2742 (1978)

The Preparation of 2,2′-Bipyridinedicarbonato and Dicarbonato-1,10-phenanthroline Complexes of Cobalt(III)

Yayoi IDA, Kiyoyuki IMAI, and Muraji SHIBATA*

Department of Chemistry, Faculty of Science, Kanazawa University, Kanazawa 920

(Received April 26, 1978)

Synopsis. Two new dicarbonato complexes, K[Co$(CO_3)_2$(bpy)]·$2H_2O$ and K[Co$(CO_3)_2$(phen)]·H_2O, have been prepared by the method starting from the $[Co(CO_3)_3]^{3-}$ complex and resolved by means of diastereoisomer formation.

The preparative method starting from a green solution of potassium tricarbonatocobaltate(III) has been characterized by the successive replacement of the CO_3^{2-} ion in the starting material with other ligands, and various dicarbonato complexes which are products of the first-step replacement have been reported; such complexes as *cis*-$[Co(CO_3)_2(NH_3)_2]^-$, $[Co(CO_3)_2(en)]^-$, *cis*-$[Co(CO_3)_2(NO_2)_2]^{3-}$, *cis*-$[Co(CO_3)_2(CN)_2]^{3-}$, and *cis*- and *trans*-$[Co(CO_3)_2(py)_2]^-$ are those examples,[1] and have been used as convenient intermediates for further synthesis.[1,2] The present work was undertaken in order to prepare dicarbonato complexes of 2,2′-bipyridine (bpy) and 1,10-phenanthroline (phen) by reactions of the green solution with these ligands. By the way, the preparation of (mono)carbonato complexes from the green solution has been reported by Kashiwabara *et al.*[3]

Experimental

To a cold, green solution of tricarbonatocobaltate(III) ($Co(NO_3)_2·6H_2O$, 5.8 g, 0.02 mol scale), we added 2,2′-bipyridine (3.1 g, 0.02 mol) dissolved in 50 cm^3 of methanol, after which the mixture was stirred at room temperature for 1 h. To the resulting violet solution we added 100 cm^3 of ethanol, and the whole was cooled in an ice bath for 2 h. The solution was then filtered to remove the by-products, which contained a small amount of the bis(bipyridine)-carbonato complex. To the filtrate we added ether, and then the green, oily portion produced was removed by decantation. The supernatant was kept in a refrigerator overnight to deposit the crude product. Recrystallization of the product was performed from warm water (*ca.* 35 °C) by the addition of a small amount of ethanol. The yield was *ca.* 1.5 g. Found: C, 35.14; H, 2.96; N, 6.71%. Calcd for K[Co$(CO_3)_2(C_{10}H_8N_2)$]·$2H_2O$: C, 35.13; H, 2.95; N, 6.83%.

The corresponding dicarbonatophenanthroline complex was prepared in the manner described above except for the use of 1,10-phenanthroline instead of 2,2′-bipyridine. The yield was *ca.* 1.5 g. Found: C, 39.47; H, 2.30; N, 6.49%. Calcd for K[Co$(CO_3)_2(C_{12}H_8N_2)$]·H_2O: C, 39.54; H, 2.61; N, 6.59%.

The K[Co$(CO_3)_2$bpy]·$2H_2O$ compound (4.1 g, 0.01 mol) was dissolved in a warm solution of $(-)_{589}$[Co$(NO_2)_2(en)_2$]-$(C_2H_3O_2)$[4] (0.005 mol in 20 cm^3 H_2O, *ca.* 40 °C), and then the mixture was cooled in an ice bath. After the side of the vessel had been scratched for a while, the whole was kept in an ice bath for 1 h. The crystals thus obtained were recrystallized from warm water (*ca.* 35 °C). The less soluble diastereoisomer was found to be $(-)_{589}$[Co$(NO_2)_2$-$(en)_2$]·$(+)_{589}$[Co$(CO_3)_2$(bpy)]. The yield was *ca.* 1 g. Found: C, 28.87; H, 4.60; N, 17.43%. Calcd for [Co$(NO_2)_2(C_2H_8N_2)_2$]·[Co$(CO_3)_2(C_{10}H_8N_2)$]·$3H_2O$: C, 29.10; H, 4.58; N, 16.97%.

The resolution of the $[Co(CO_3)_2(phen)]^-$ complex was achieved with $(-)_{589}$[Co(ox)$(en)_2$]$(C_2H_3O_2)$[5] in a manner similar to that used for the bipyridine complex. The less soluble diastereoisomer contained the $(-)_{589}$ form of the complex. The yield was *ca.* 1 g. Found: C, 38.12; H, 3.73; N, 13.22%. Calcd for [Co$(C_2O_4)(C_2H_8N_2)_2$]·[Co$(CO_3)_2$-$(C_{12}H_8N_2)$]: C, 38.35; H, 3.86; N, 13.42%.

By the way, two known carbonato complexes, $[CoCO_3(bpy)_2]^+$ and $[CoCO_3(phen)_2]^+$, as well as two known tris complexes, $[Co(bpy)_3]^{3+}$ and $[Co(phen)_3]^{3+}$, could be prepared by the reactions of the $[Co(CO_3)_3]^{3+}$ complex and the ligands in stoichiometric amounts; in the case of the latter complexes, activated charcoal was used.

The absorption spectra were measured with a Hitachi 323 recording spectrophotometer. The CD spectra were recorded with a JASCO J-40CS automatic recording spectropolarimeter equipped with a JASCO Model J-DPZ data processor for CD, and with the samples converted into potassium salts by means of the ion-exchange technique. For the measurement of the optical rotation, a JASCO Model DIP-SL automatic polarimeter was used.

Results and Discussion

The absorption and CD spectra are shown in Fig. 1. The maximum of the first absorption band is observed

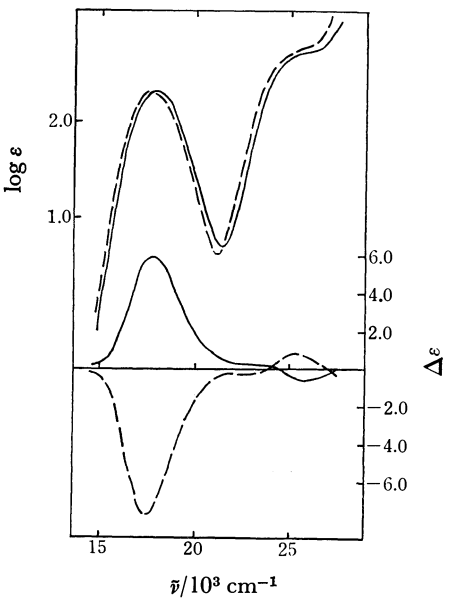

Fig. 1. Absorption and CD spectra of
—— $(+)_{589}$[Co$(CO_3)_2$(bpy)]$^-$ and
—— $(-)_{589}$[Co$(CO_3)_2$(phen)]$^-$.

at 17800 cm^{-1} ($\log\varepsilon=2.18$) for the bpy complex and at 17600 cm^{-1} ($\log\varepsilon=2.18$) for the phen complex. The second absorption band is observed as a shoulder at *ca.* 25600 cm^{-1} (log ε, *ca.* 2.38) for the bpy complex and as one at *ca.* 25400 cm^{-1} (log ε, *ca.* 2.40) for the phen complex.

Recently, we studied the CD spectra of the $[Co(O,O)_2(N)_2]^-$-type complexes ($O,O=CO_3^{2-}$, ox^{2-} and mal^{2-}; $(N)_2$=en, $2NH_3$ and 2py) and found that the related $(+)_{589}[Co(CO_3)_2(en)]^-$, $(-)_{589}[Co(CO_3)_2(NH_3)_2]^-$ and $(+)_{589}[Co(CO_3)_2(py)_2]^-$ complexes exhibit only one CD peak in the first absorption band region; 17600 cm^{-1} ($\Delta\varepsilon=-1.91$) for the en complex, 17800 cm^{-1} ($\Delta\varepsilon=-2.32$) for the NH_3 complex, and 18400 cm^{-1} ($\Delta\varepsilon=+2.94$) for the py complex.[6] The absolute configurations of these complexes were assigned on the basis of the (+) sign of the CD peak referring to Λ, and the (−) sign, to Δ.[6] The CD spectra of the present dicarbonato complexes also exhibit only one CD peak in the first band region; 17700 cm^{-1} ($\Delta\varepsilon=+5.93$) for the bpy complex and 17500 cm^{-1} ($\Delta\varepsilon=-7.72$) for the phen complex. From these CD signs, the Λ configuration is given to the $(+)_{589}[Co(CO_3)_2(bpy)]^-$ complex and the Δ configuration to the $(-)_{589}[Co(CO_3)_2(phen)]^-$ complex. The large $\Delta\varepsilon$ values observed for the present complexes may be attributed to the chelating bpy or phenligand. In an aqueous solution, the $(-)_{589}[Co(CO_3)_2(phen)]^-$ complex racemized with a half-life of *ca.* 7 h at room temperature. In this connection, the $(-)_{589}[Co(CO_3)_2(NH_3)_2]^-$ complex racemized with a half-life of *ca.* 3 min.[7]

References

1) M. Shibata, *Proc. Jpn. Acad.*, **50**, 779 (1974), and the references cited therein.
2) T. Ito and M. Shibata, *Inorg. Chem.*, **16**, 108 (1977).
3) K. Kashiwabara, K. Igi, and B. E. Douglas, *Bull. Chem. Soc. Jpn.*, **49**, 1573 (1976).
4) *Inorg. Synth.*, Vol. 4, 195 (1953).
5) F. P. Dwyer, A. M. Sargeson, and I. K. Reid, *J. Am. Chem. Soc.*, **83**, 1285 (1961).
6) S. Muramoto, K. Kawase, and M. Shibata, *Bull. Chem. Soc. Jpn.*, submitted for publication.
7) S. Muramoto and M. Shibata, *Chem. Lett.*, **1977**, 1499.

BULLETIN OF THE CHEMICAL SOCIETY OF JAPAN, VOL. 51 (9), 2743—2744 (1978)

Cyclopentadienyl- and Pentamethylcyclopentadienylbis(isocyanide)cobalt(I)[1]

Yasuhiro YAMAMOTO,* Takaya MISE, and Hiroshi YAMAZAKI
The Institute of Physical and Chemical Research, Wako-shi, Saitama 351

(Received February 28, 1978)

Synopsis. Compounds, η-$C_5H_5Co(RNC)_2$ and η-$Me_5C_5Co(RNC)_2$ were prepared from $Co_2(RNC)_8$ and C_5R_5H (R=H, CH_3), and from η-$C_5H_5Co(CO)_2$ and isocyanide.

The cobalt complexes having cyclopentadienyl or pentamethylcyclopentadienyl group as a ligand, η-$C_5H_5CoL_2$ (L=CO,[2] phosphorus ligands[3]) η-$Me_5C_5Co(CO)_2$[4] and η-$C_5H_5Co(CO)L$ (L=PPh_3,[5] RNC[6]) have been known. The chemical reactions of these complexes have been widely provided. However, analogous η-$R_5C_5Co(RNC)_2$ has not been known yet. We here report the preparation and reactions of this type of complexes.

The two methods for the preparation are; (1) the reaction of octakis(isocyanide)dicobalt(0) with cyclopentadiene or pentamethylcyclopentadiene, and (2) the reactions of η-$C_5H_5Co(CO)_2$ with isocyanide. The reaction of $Co_2(2,6\text{-}Me_2C_6H_3NC)_8$ with cyclopentadiene in toluene at 120 °C gave two products, dark brown complex **1a** formulated as η-$C_5H_5Co(2,6\text{-}Me_2C_6H_3NC)_2$ and unknown brown organic compound **2**[7] formulated as $(C_5H_6)(C_9H_9N)_4$.

$$Co_2(RNC)_8 + C_5H_6 \rightarrow \eta\text{-}C_5H_5Co(RNC)_2 + (C_5H_6)(RNC)_4. \quad (1)$$

The chemical shifts of the *ortho*-methyl resonances of coordinated isocyanides were independent of the concentration of free $2,6\text{-}Me_2C_6H_3NC$ added in the NMR spectra of η-$C_5H_5Co(2,6\text{-}Me_2C_6H_3NC)_2$, suggesting the absence of dissociation. When $Co_2(2,6\text{-}Me_2C_6H_3NC)_8$ was treated with pentamethylcyclopentadiene, only η-$Me_5C_5Co(2,6\text{-}Me_2C_6H_3NC)_2$ **1b** was formed.

The reaction of η-$C_5H_5Co(CO)_2$ or η-$Me_5C_5Co(CO)_2$ with excess 2,6-xylyl isocyanide proceeded with substitution of a carbon monoxide at room temperature to give η-$R_5C_5Co(CO)$ $(2,6\text{-}Me_2C_6H_3NC)$ (**3a**: R=H, **3b**: R=CH_3) (Eq. 2). Upon heating at 120 °C, the further displacement of CO took place to afford **1a**, although no displacement of CO occurred in the case of pentamethylcyclopentadienyl analog. This is due to the results that back-bonding Co(3d)→C≡O(π^*) in **3b** is more extensive than that in **3a**, as shown in the C≡O stretching frequencies of **3a** (1956 cm^{-1}) and **3b** (1924 cm^{-1}) (Table 1).

Compounds **3a** and **3b** were regenerated together with a small amount of η-$R_5C_5Co(CO)_2$, when **1a** and **1b** were treated with CO (Eq. 3). These reactions were formally reversible.

$$\eta\text{-}C_5H_5Co(CO)_2 + RNC \rightarrow \eta\text{-}C_5R_5(CO)(RNC) + CO \quad (2)$$

$$\eta\text{-}C_5H_5Co(CO)(RNC) + RNC \rightleftharpoons \eta\text{-}C_5H_5Co(RNC)_2 + CO \quad (3)$$

Compound **1c** was also prepared from η-$C_5H_5Co(CO)_2$ and mesityl isocyanide. However, when η-$C_5H_5Co(CO)_2$ was treated with aliphatic isocyanides such as *t*-butyl or cyclohexyl isocyanide under similar conditions, one mole of CO was substituted to produce η-$C_5H_5Co(CO)(RNC)$,[6] without producing bis(isocyanide) derivative.

Table 1. Infrared spectra of **1** and **3**

	Compound	IR (cm^{-1})[a] ν(N≡C)	ν(C≡O)
1a	η-$C_5H_5Co(2,6\text{-}Me_2C_6H_3NC)_2$	2068 1990	
1b	η-$C_5Me_5Co(2,6\text{-}Me_2C_6H_3NC)_2$	2052 1942	
1c	η-$C_5H_5Co(2,4,6\text{-}Me_3C_6H_2NC)_2$	2053 1989	
3a	η-$C_5H_5Co(CO)(2,6\text{-}Me_2C_6H_3NC)$	2075	1956
3b	η-$C_5Me_5Co(CO)(2,6\text{-}Me_2C_6H_3NC)$	2038	1924

a) Measured in benzene.

The reaction of **1a** with iodine in a 1:1 molar ratio took place readily to give $[\eta\text{-}C_5H_5Co(2,6\text{-}Me_2C_6H_3NC)I]I$, and that with an excess of iodine gave $[\eta\text{-}C_5H_5Co(2,6\text{-}Me_2C_6H_3NC)_2I]I_3$. The similar type of complex, $[\eta\text{-}Me_5C_5Co(2,6\text{-}Me_2C_6H_3NC)_2I]I_3$, was also obtained from **1b** and iodine.

Compound **1a** reacted readily with TCNE to give the olefin complex η-$C_5H_5Co(2,6\text{-}Me_2C_6H_3NC)$(TCNE), whereas no reaction occurred on treatment with dialkyl maleate. When **1a** was treated with azobenzene at 120 °C, the reaction led to recovery of **1a**, contrasted with the reaction leading to the formation of η-$C_5H_5Co(o\text{-}N(Ph)NHC_6H_4)$ from η-$C_5H_5Co(CO)_2$[8] or η-$C_5H_5Co(CO)$(*t*-BuNC) and azobenzene.

The relatively low reactivity of η-$C_5H_5Co(RNC)_2$ may be due to the steric hindrance and no dissociation of ligands.

Experimental

*Preparation of η-$Me_5C_5Co(2,6\text{-}Me_2C_6H_3NC)_2$ **1b** from $Co_2(2,6\text{-}Me_2C_6H_3NC)_8$[9] and Me_5C_5H.* A mixture of pentamethylcyclopentadiene (0.45 ml, 2.65 mmol) and $Co_2(2,6\text{-}Me_2C_6H_3NC)_8$, prepared from $Co_2(CO)_8$ (0.18 g, 0.53 mmol) and $2,6\text{-}Me_2C_6H_4NC$ (0.69 g, 5.3 mmol), *in situ* was heated in toluene at 120 °C. After 4 h, the solvent was removed in vacuo and the residue was chromatographed on alumina. Eluting with hexane–benzene (1:1) gave dark red crystals of η-$Me_5C_5Co(2,6\text{-}Me_2C_6H_3NC)_2$ **1b** (0.175 g, 36%, mp (N_2) ≈108 °C(dec)), which was crystallized from hexane at −30 °C. NMR(C_6H_5Cl): δ 1.95 (bs, Me_5C_5) and 2.25 (bs, 12H, CH_3). Found: C, 73.13; H, 7.34; N, 6.05%. Calcd for $C_{28}H_{33}N_2Co$: C, 73.67; H, 7.29; N, 6.14%.

*Preparation of η-$C_5H_5Co(2,6\text{-}Me_2C_6H_3NC)_2$ **1a** from η-$C_5H_5Co(CO)_2$ and 2,6-Xylyl Isocyanide.* A mixture of η-$C_5H_5Co(CO)_2$ (0.90 g, 5.0 mmol) and 2,6-xylyl isocyanide (2.0 g, 1.53 mmol) in toluene (15 ml) was heated at 120 °C. After

6 h, the solvent was removed in vacuo and the residue was chromatographed on alumina, using hexane-benzene (1:1). The solvent was removed in vacuo, and the brown residue was crystallized from hexane at −30 °C to afford the title complex (1.7 g, 88%, mp(N_2) 94—97 °C(dec)). Mass spectrum M^+ 386 (386.39) Found: C, 71.49; H, 6.01; N, 7.26%. Calcd for $C_{23}H_{23}N_2Co$: C, 71.50; H, 6.00; N, 7.25%. Compound **1c** (72%; mp 72—74 °C(dec)) was prepared from η-$C_5H_5Co(CO)_2$ and mesityl isocyanide by the procedure similar to the method (2). Found: C, 72.41; H, 6.58; N, 6.81%. Calcd for $C_{25}H_{27}N_2Co$: C, 72.45; H, 6.57; N, 6.76%.

Preparation of η-$C_5H_5Co(CO)$ *(2,6-*$Me_2C_6H_3NC$*).* A mixture of η-$C_5H_5Co(CO)_2$ (0.18 g, 1.0 mmol) and 2,6-xylyl isocyanide (0.30 g, 2.3 mmol) in toluene (15 ml) was kept at room temperature for 5 h. The work-up of the reaction mixture gave the title compound (0.25 g, 92%, mp 70—71 °C(dec)). Mass M^+ 283(283.22). Found: C, 63.52; H, 4.89; N, 5.03%. Calcd for $C_{15}H_{14}OCo$: C, 63.61; H, 4.92; N, 4.95%.

Reaction of η-$R_5C_5Co(2,6$-$Me_2C_6H_3NC)_2$. *a) With Iodine*: To a solution of η-$C_5H_5Co(2,6$-$Me_2C_6H_3NC)_2$ (0.09 g, 0.23 mmol) in benzene (5 ml) was added iodine (0.09 g, 0.35 mmol) in benzene (5 ml) at room temperature. After 45 min, the resulting black brown crystals (0.065 g, 44%; mp 143—145 °C (dec)) were filtered off, which were crystallized from CH_2Cl_2-hexane. The complex contains one molecule of CH_2Cl_2 in crystallization. IR(KBr): 2189 (N≡C) cm^{-1}. NMR($CDCl_3$): δ 2.54 (s, CH_3) 6.27 (bs, C_5H_5), and 7.16 (bs, C_6H_3) ppm. Found: C, 40.19; H, 3.33; N, 3.97%. Calcd for $C_{24}H_{25}N_2Cl_2I_2Co$: C, 39.75; H, 3.48; N, 3.86%.

[η-$C_5H_5Co(2,4,6$-$Me_3C_6H_2NC)_2I$]I (83%, mp ≈160 °C (dec)) was prepared by the procedure similar to that mentioned above. IR(KBr): 2178 (N≡C) cm^{-1}. NMR($CDCl_3$): δ 2.33 (s, *p*-Me), 2.51 (s, *o*-Me) 6.30 (bs, C_5H_5) and 6.92 (s, C_6H_2) ppm. Found: C, 44.70; H, 4.02; N, 4.26%. Calcd for $C_{25}H_{27}N_2I_2Co$: C, 44.94; H, 4.07; N, 4.19%.

[η-$Me_5C_5Co(2,6$-$Me_2C_6H_3NC)_2I$]I_3 (mp 166—168 °C(dec)) was obtained from **1b** and an excess of I_2 in hexane. IR(KBr): 2151 and 2165 (N≡C) cm^{-1}. NMR($CDCl_3$): δ 2.21 (s, Me_5C_5), 2.47 (s, *o*-Me), and *ca.* 7.18 (m, C_6H_3). Found: C, 34.85; H, 3.46; N, 2.67; I, 51.40%. Calcd for $C_{28}H_{33}N_2I_4Co$: C, 34.88; H, 3.45; N, 2.91; I, 52.62%.

[η-$C_5H_5Co(2,6$-$Me_2C_6H_3NC)_2I$]I_3 (mp 105 °C (dec)). IR(KBr): 2185 (N≡C) cm^{-1}. Found: C, 30.14; H, 2.54; N, 3.01%. Calcd for $C_{23}H_{23}N_2I_4Co$: C, 30.90; H, 2.59; N, 3.13%.

b) With Tetracyanoethylene (TCNE): A solution of TCNE (0.04 g, 0.31 mmol) in benzene (3 ml) was added to a solution of **1a** (0.12 g, 0.31 mmol) in benzene (5 ml) at room temperature and stirred for 1 h. The mixture was chromatographed on alumina. Eluting with CH_2Cl_2 gave brown crystals of η-$C_5H_5Co(2,6$-$Me_2C_6H_3NC)$(TCNE) (0.46 g, 39%, mp >300 °C). IR(benzene): 2220 (C≡N) and 2152 (N≡C) cm^{-1}. Found: C, 62.43; H, 3.69; N, 18.35%. Calcd for $C_{20}H_{14}N_5Co$: C, 62.67; H, 3.68; N, 18.27%.

The work was partially supported by the Ministry of Education of Japan (Grant No. 264162) (Y.Y.).

References

1) Studies on interactions of isocyanide with transition metal complexes 17. For preceding paper in this series, see Y. Yamamoto and H. Yamazaki, *J. Org. Chem.*, **42**, 4136 (1977).

2) (a) T. S. Piper, F. A. Cotton, and G. Wilkinson, *J. Inorg. Nucl. Chem.*, **1**, 165 (1955); (b) A. Nakamura and N. Hagihara, *Nippon Kagaku Zasshi*, **82**, 1392 (1961).

3) (a) H. Yamazaki and N. Hagihara, *Bull. Chem. Soc. Jpn.*, **44**, 2260 (1971); (b) H. Yamazaki and Y. Wakatsuki, *J. Organomet. Chem.*, **139**, 157 (1977); (c) V. Harder, J. Müller and H. Werner, *Helv. Chim. Acta*, **54**, 1 (1971).

4) R. B. King and M. B. Bisnette, *J. Organomet. Chem.*, **8**, 287 (1967).

5) A. J. Hart-Davis and W. A. G. Graham, *Inorg. Chem.*, **9**, 2658 (1970).

6) Y. Yamamoto and N. Hagihara, *Mem. Inst. Sci. Ind. Res., Osaka Univ.*, **27**, 109 (1970).

7) The structure is unknown.

8) T. Joh, N. Hagihara, and S. Murahashi, *Bull. Chem. Soc. Jpn.*, **40**, 661 (1967).

9) Y. Yamamoto and H. Yamazaki, *J. Organomet. Chem.*, **137**, C31 (1977).

BULLETIN OF THE CHEMICAL SOCIETY OF JAPAN, VOL. 51 (9), 2745—2746 (1978)

The Use of Zinc/Silver Couple in the Cyclocoupling Reaction of Polybromo Ketones and Furan

Tsuneo SATO and Ryoji NOYORI*

Department of Chemistry, Nagoya University, Chikusa, Nagoya 464

(Received May 18, 1978)

Synopsis. The title 3+4→7 reaction, followed by Zn/Cu couple reduction in methanol, affords 8-oxabicyclo-[3.2.1]oct-6-en-3-ones in satisfactory yields.

During the course of our recent project on *C*-nucleoside synthesis,[1] the need arose for the large-scale preparation of the oxabicyclic product **5** by the reductive cyclocoupling reaction of $\alpha,\alpha,\alpha',\alpha'$-tetrabromoacetone (**1**) and furan.[2] Among various reducing agents, Zn/Ag couple[3] was found to be an effective reagent for such purpose. Thus reaction of **1** and furan in THF with the aid of Zn/Ag couple and subsequent treatment of the product with Zn/Cu couple[5] in methanol gave rise to **5** in 55% yield. The yield of the present 3+4 cyclocoupling reaction was not as high as that of the iron carbonyl promoted reaction[4] but these reaction conditions may be suitable for the medium- to large-scale synthesis of **5** because of the operational simplicity and from economical point of view. Use of Zn/Cu couple[5] or activated Zn[6] in place of Zn/Ag couple resulted in decrease in product yield.[7] THF was the best among solvents so far examined. Zn/Ag couple could be employed also in the reaction of the polybromo ketones **2**—**4** and furan.

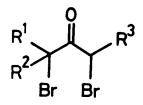

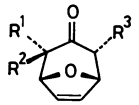

1, $R^1=R^3=Br$; $R^2=H$ **5**, $R^1=R^2=R^3=H$
2, $R^1=R^3=Br$; $R^2=CH_3$ **6**, $R^1=CH_3$; $R^2=R^3=H$
3, $R^1=R^2=CH_3$; $R^3=Br$ **7**, $R^1=R^2=CH_3$; $R^3=H$
4, $R^1=R^3=CH_3$; $R^2=H$ **8**, $R^1=R^3=CH_3$; $R^2=H$

Experimental

The brominated ketones **1**—**4**[8] and Zn/Cu couple[5] were made by the known methods. Zn/Ag couple was prepared by the Heathcock's procedure using 65 mg of $AgOCOCH_3$ per g of Zn.[3a] Solvent THF was freshly distilled from sodium/benzophenone in a recycling still. All reactions were carried out under argon atmosphere. Filtration was carried out using a Celite 545 pad. Unless otherwise stated, concentration of solutions containing nonvolatile materials was achieved on a rotary evaporator (30—40 mmHg) at room temperature. Drying of organic solutions was performed over anhydrous Na_2SO_4. All melting and boiling points are uncorrected.

8-Oxabicyclo[3.2.1]oct-5-en-3-one (5). A mixture of Zn/Ag couple (29.3 g, 0.450 g-atom) and furan (210 ml, 3.00 mol) in dry THF (450 ml) was placed in a 2-litre three-necked flask and cooled at −10 °C. A solution of **1** (112 g, 0.300 mol) in dry THF (200 ml) was added dropwise over a period of 2 h with stirring and then the resulting mixture was allowed to warm up to room temperature and stirred for 12 h. The insoluble materials were removed by filtration and the filtrate was concentrated. The tarry brown residue was chromatographed on a silica gel column (E. Merck, 700 g, 1:20 to 1:5 hexane/ethyl acetate mixture as eluent) to give crude 2α,4α-dibromo-8-oxabicyclo[3.2.1] oct-6-en-3-one[4] as yellowish crystals (55 g). Recrystallization from hexane gave a pure sample melting at 126.5—127 °C. The dibromo adduct was dissolved in saturated NH_4Cl solution in CH_3OH (1.3 litre) and to this was added portionwise Zn/Cu couple (120 g, 1.85 g-atom) over 10 min at room temperature. The suspension was stirred for an additional 1 hr and filtered. The filtrate was divided into four portions and each portion was diluted with water (200 ml) and saturated Na_2H_2edta solution (300 ml). Extraction was then performed with CH_2Cl_2 successively (300 ml and then 200 ml×2). The combined extracts were dried and CH_2Cl_2 was removed by distillation at atmospheric pressure through a 40-cm Vigreux column. Finally the residue was subjected to light suction by an aspirator at room temperature to leave the bicyclic compound **5**, contaminated with a small amount of CH_2Cl_2, as a pale yellow liquid (20.4 g, 95% pure by NMR analysis[4]). Overall yield based on **1** was 55%. Pure crystalline sample of **5**, mp 37—39 °C, was obtained by bulb-to-bulb distillation (50—80 °C/0.01 mmHg).

2α-Methyl-8-oxabicyclo[3.2.1]oct-6-en-3-one (6). A mixture of Zn/Ag couple (29.3 g, 0.450 g-atom) and furan (210 ml, 3.00 mol) in THF (450 ml) was cooled at −10 °C and to this was added a solution of **2** (116 g, 0.300 mol) in THF (200 ml) in a dropwise manner over 1.5 h. The reaction mixture was stirred at the same temperature for 1 h and then at room temperature for 17 h, and filtered. The filtrate was concentrated and chromatographed on a column of silica gel (700 g, 1:20 to 1:5 hexane/ethyl acetate) to give 2,4-dibromo-2-methyl-8-oxabicyclo[3.2.1] oct-6-en-3-one as a pale yellow solid (54 g). Mp 78—79 °C (from hexane). This adduct, dissolved in saturated NH_4Cl solution in CH_3OH (1.2 litre), was treated with Zn/Cu couple (120 g, 1.85 g-atom) with stirring at room temperature for 1 h and filtered. The resulting solution was worked up with aqueous Na_2H_2edta and CH_2Cl_2 in the same fashion as described in the preparation of **5**. The combined CH_2Cl_2 solutions were dried and concentrated with a Vigreux column at atmospheric pressure and then with an aspirator (30—40 mmHg, room temperature) to afford **6** (21.9 g, contaminated with 7% of CH_2Cl_2 as determined by NMR[4]). The overall yield was 53% based on **2**. Pure sample of **6** was obtained by bulb-to-bulb distillation (70—100 °C/0.02 mmHg).

2,2-Dimethyl-8-oxabicyclo[3.2.1]oct-6-en-3-one (7). To a cooled (−10 °C) mixture of Zn/Ag couple (29.3 g, 0.450 g-atom), furan (210 ml, 3.00 mol), and THF (450 ml) was added a solution of **3** (96.6 g, 0.300 mol) in THF (200 ml) over a period of 1.5 h. The mixture was then stirred at room temperature for 19 h, filtered, and concentrated. The resulting tarry residue was chromatographed (silica gel 700 g, 1 : 20 to 1 : 5 hexane/ethyl acetate) to give 2,2-dimethyl-4α-bromo-8-oxabicyclo[3.2.1]oct-6-en-3-one as crystalline solid (38 g). Mp 95—96 °C (from hexane). The

bromide was dissolved in CH_3OH saturated with NH_4Cl (1.4 litre) and treated with Zn/Cu couple (100 g, 1.54 g-atom) at room temperature for 1 h. The reaction mixture was filtered and the filtrate was worked up with aqueous Na_2H_2-edta and CH_2Cl_2 as described above. The combined organic layers were dried and concentrated using a Vigreux column. Subsequent light suction by an aspirator (30—40 mmHg, at room temperature) left **7** of 93% purity (NMR analysis,[4] 22.5 g, 50% overall yield based on **3**), the only impurity being CH_2Cl_2. Its bulb-to-bulb distillation (80—110 °C/0.05 mmHg) afforded pure sample of **7**, mp 46—47 °C.

2α,4α-Dimethyl-8-oxabicyclo[3.2.1]oct-6-en-3-one (8). A mixture of Zn/Ag couple (19.6 g, 0.300 g-atom), furan (140 ml, 2.00 mol) and THF (300 ml) was stirred at −10 °C, to which a solution of **4** (48.8 g, 0.200 mol) in THF (150 ml) was added dropwise over a period of 1 h. Then the mixture was allowed to warm up to room temperature and stirred for an additional 12 h. The insoluble precipitate was removed by filtration and the filtrate was concentrated. Chromatography of the residue on a silica gel column (500 g, 1:20 to 1:5 hexane/ethyl acetate) afforded **8** as a colorless liquid (24.2 g, 80% yield), identical with authentic sample.[4] No other stereoisomers were formed.

References

1) R. Noyori, T. Sato, and Y. Hayakawa, *J. Am. Chem. Soc.*, **100**, 2561 (1978); T. Sato, R. Ito, Y. Hayakawa, and R. Noyori, *Tetrahedron Lett.*, **1978**, 1829.

2) Review: R. Noyori, *Ann. New York Acad. Sci.*, **295**, 225 (1977).

3) a) R. D. Clark and C. H. Heathcock, *J. Org. Chem.*, **41**, 636 (1976); b) J. M. Denis, C. Girard, and J. M. Conia, *Synthesis*, **1972**, 549.

4) R. Noyori, S. Makino, T. Okita, and Y. Hayakawa, *J. Org. Chem.*, **40**, 806 (1975); H. Takaya, S. Makino, Y. Hayakawa, and R. Noyori, *J. Am. Chem. Soc.*, **100**, 1765 (1978).

5) E. LeGoff, *J. Org. Chem.*, **29**, 2048 (1964).

6) S. Yamamura, M. Toda, and Y. Hirata, *Org. Synth.*, **53**, 86 (1973).

7) For a modified procedure using Zn and triethyl borate as reducing agent, see H. M. R. Hoffmann and M. N. Iqbal, *Tetrahedron Lett.*, **1975**, 4487.

8) C. Rappe, *Acta Chem. Scand.*, **16**, 2467 (1962).

BULLETIN OF THE CHEMICAL SOCIETY OF JAPAN, VOL. 51 (9), 2747—2748 (1978)

Synthesis of 5-(Substituted methyl)-6,8-dimethyl-4-chromanones[1)]

Akira NINAGAWA* and Haruo MATSUDA

Department of Petroleum Chemistry, Faculty of Engineering, Osaka University, Yamadakami, Suita, Osaka 565

(Received February 17, 1978)

Synopsis. 5-(Substituted methyl)-6,8-dimethyl-4-chromanones were synthesized from the reactions of 5-hydroxymethyl-6,8-dimethyl-4-chromanone with nucleophilic reagents in acid media, and the reactions of its 5-halomethyl derivatives with ethoxide or phenoxide nucleophiles.

In previous papers,[2)] polymers having 4-chromanones have been synthesized since 4-chromanones are useful ultraviolet absorbers.

In this paper, the syntheses of 5-(substituted methyl)-6,8-dimethyl-4-chromanones from the reactions of 5-hydroxymethyl-6,8-dimethyl-4-chromanone(**1**) with nucleophilic reagents in the presence of acid catalysts are presented. In addition, 5-(substituted methyl)-6,8-dimethyl-4-chromanones have been prepared from 5-halomethyl derivatives of **1**.

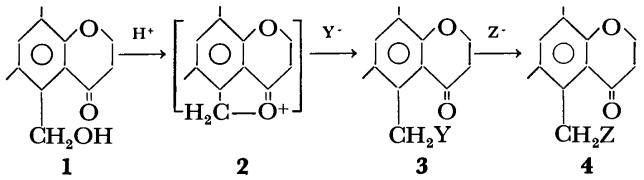

1 **2** **3** **4**

3a Y=Cl–
3b Y=Br–
3c Y=CH_3O–
3d Y=C_2H_5O–
3e Y=HO–C6H4–
3f Y=(OH, H_3C)–C6H3–
3g Y=(OH, ×)–C6H3–
3h Y=HO–(×,×)–C6H2–
3i Y=–C6H4–S–
3j Y=H_3C–C6H4–S–
4d Z=C_2H_5O– (from **3b**)
4k Z=–C6H4–O– (from **3a**)
4m Z=H_3C–C6H4–O– (from **3a**)

×=*t*-Bu–

Results and Discussion

*Reactions of **1** with Nucleophilic Reagents.* The reactions of **1** with nucleophilic reagents in acidic media were carried out and reaction conditions are shown in Table 1.

The chlorination of **1** in dioxane solution in the presence of hydrochloric acid as the catalyst and nucleophilic reagent gave 5-chloromethyl-6,8-dimethyl-4-chromanone(**3a**). Similarly, the bromination of **1** in dioxane in the presence of hydrobromic acid afforded 5-bromomethyl-6,8-dimethyl-4-chromanone(**3b**). The methanolysis of **1** in a mixture of methanol and dioxane with perchloric acid as the catalyst gave 5-methoxymethyl-6,8-dimethyl-4-chromanone(**3c**). The ethanolysis of **1** in ethanol in the presence of perchloric acid gave 5-ethoxymethyl-6,8-dimethyl-4-chromanone(**3d**).

The reactions of **1** with phenol and *p*-cresol in ethanol gave 5-(4-hydroxybenzyl and 2-hydroxy-5-methylbenzyl)-6,8-dimethyl-4-chromanones(**3e** and **3f**), respectively. The reaction of **1** with *p*-cresol gave a mixture of **3f** and **3d** in the mole ratio of 8:9, which was measured by the peak area in the ^{1}H-NMR spectrum. The low yield of **3f** is due to the lower fractionation of **3f** from the reaction mixture. When a mixed solution of dioxane and ethanol was used, the reaction gave **3f** along with a small amount of resinous product. No formation of **3d** was detected. With increasing ratio of dioxane to ethanol, the resinous product increased. When dioxane solvent was used solely in the reaction of **1** with *p*-cresol, phenol, and *p*-*t*-butylphenol, 5-substituted methyl compounds were not isolated from the reaction mixtures. It was found that the reaction was affected markedly by the character of the solvents, dioxane causing a remarkable effect in the yield of products.

The reaction of **1** with excess 2,6-di-*t*-butylphenol in dioxane gave 5-(4-hydroxy-3,5-di-*t*-butylbenzyl)-6,8-dimethyl-4-chromanone(**3h**).

Thiophenol and *p*-thiocresol gave 5-phenylthiomethyl and 5-(*p*-tolylthiomethyl) compounds(**3i** and **3j**), respectively, in larger yields than in the cases of phenol and *p*-cresol.

The results shown in Table 1 indicate that the yield of the products are largely dependent on the nucleophilicity[3)] of reagents and the stability of the oxonium ion(**2**)[1)] in acidic solvents.

*Synthesis of **4d**, **4k**, and **4m** from 5-Halomethyl Derivatives (**3a** and **3b**).* The reaction of **3b** with sodium ethoxide gave **4d** quantitatively, but the use of **3a** under similar conditions gave the starting material. The reactions of **3a** with phenol and *p*-cresol gave 5-phenoxymethyl and 5-(*p*-tolyloxymethyl) derivatives (**4k** and **4m**), respectively.

Experimental

Melting points are uncorrected. IR spectra were obtained using KBr pellets in a Hitachi EPI-G2 spectrophotometer. ^{1}H-NMR spectra were recorded on a JEOR Model PS-100 spectrometer with tetramethylsilane as the internal standard. Mass spectra were obtained on a Hitachi RUM-6 mass spectrometer operating at 70 eV.

Materials. **1** was prepared by the reported method,[1)] mp 95—97 °C [lit,[1)] mp 95—97 °C].

*Reactions of **1** with Nucleophilic Reagents.* The following procedure for the preparation of 5-(substituted methyl)-6,8-dimethyl-4-chromanone is representative.

A mixture of **1** and hydrochloric acid in dioxane was stirred at 80 °C for 6 h. After completion of the reaction, the reaction mixture was poured into water, and then extracted with chloroform. The chloroform layer was washed

Table 1. Reactions of 5-hydroxymethyl-6,8-dimethyl-4-chromanone with nucleophilic reagents

Reaction conditions: temp; 80 °C, time; 6 h, catalysts; HCl=hydrochloric acid(36%), HBr=hydrobromic acid(47%), $HClO_4$=perchloric acid(70%)

Reactant (mmol) 1	Phenols		Catalyst (ml)		Solvent (ml)		Product	Yield (%)
5.0			HCl	10.0	Dioxane	35.0	**3a**	83.2
5.0			HBr	10.0	Dioxane	35.0	**3b**	81.4
5.0[a]			$HClO_4$	10.0	MeOH Dioxane	10.0 35.0	**3c**	70.0
5.0			$HClO_4$	10.0	EtOH	35.0	**3d**	57.2
5.0	Phenol	10.0	$HClO_4$	10.0	EtOH	35.0	**3e**	5.0
5.0	*p*-Cresol	10.0	$HClO_4$	10.0	EtOH	35.0	**3f**	5.4
1.0	*p*-Cresol	2.0	$HClO_4$	2.0	EtOH Dioxane	5.0 2.0	**3f**	27.0
1.0	*p*-Cresol	2.0	$HClO_4$	2.0	EtOH Dioxane	1.0 6.0	**3f**	20.3
5.0	*p*-Cresol	10.0	$HClO_4$	10.0	Dioxane	35.0	—	—
5.0	*p*-*t*-Butylphenol	10.0	$HClO_4$	10.0	EtOH	35.0	**3g**	11.8
5.0[b]	2,6-di-*t*-Butylphenol	25.0	$HClO_4$	0.5	Dioxane	6.0	**3h**	22.4
5.0	Thiophenol	10.0	$HClO_4$	10.0	EtOH	35.0	**3i**	24.2
2.5	*p*-Thiocresol	5.0	$HClO_4$	5.0	EtOH	17.5	**3j**	28.2

a) Temp: 60 °C, Time: 4 h. b) Time: 4 h.

with aqueous sodium hydroxide and water, successively. After removal of the solvent, the residue was recrystallized to give the 5-chloromethyl derivative.

3a: Mp 102—104 °C (from ligroin). IR: 1665(C=O), 690 cm^{-1} (C–Cl). NMR($CDCl_3$): δ=2.14(3H, s), 2.30(3H. s), 2.79(2H, t), 4.45(2H, t), 5.11(2H, s), 7.12(1H, s). MS: *m/e* 226(M^+), 189(M^+—Cl). Found: C, 64.19; H, 5.86%. Calcd for $C_{12}H_{13}O_2Cl$: C, 64.15; H, 5.83%.

3b: Mp 118—120 °C (from ligroin). IR: 1670(C=O), 542 cm^{-1} (C–Br). NMR(CCl_4): δ=2.14(3H, s), 2.28(3H, s), 2.73(2H, t), 4.46(2H, t), 5.03(2H, t), 7.05(1H, s). MS: *m/e* 270(M^+), 189(M^+—Br). Found: C, 53.56; H, 4.88%. Calcd for $C_{12}H_{13}O_2Br$: C, 53.55; H, 4.87%.

3c: Mp 47 °C (from petroleum ether). IR: 2810(O–CH_3), 1680 cm^{-1} (C=O). NMR(CCl_4): δ=2.11(3H, s), 2.23 (3H, s), 2.65(2H, t), 5.27(3H, s), 4.38(2H, t), 4.72(2H, s), 6.98 (1H, s). MS: *m/e* 220(M^+), 205(M^+—CH_3). Found: C, 70.91; H, 7.19%. Calcd for $C_{13}H_{16}O_3$: C, 70.89; H, 7.32%.

3d: Mp 70 °C (from petroleum ether). IR: 2800(O–C_2H_5), 1678 cm^{-1} (C=O). NMR(CCl_4): δ=1.14(3H, t), 2.13(3H, s), 2.27(3H, s), 2.71(2H, t), 3.48(2H, q), 4.44 (2H, t), 4.78(2H, s), 7.00(1H, s) MS: *m/e* 234(M^+), 205 (M^+—C_2H_5). Found: C, 71.78; H, 7.76%. Calcd for $C_{14}H_{18}O_3$: C, 71.77; H, 7.74%.

3e: Mp 215—216 °C (from benzene). IR: 3275(OH), 1658 cm^{-1} (C=O). NMR(DMSO-d_6): δ=2.05(3H, s), 2.13 (3H, s), 2.72(2H, t), 4.31(2H, s), 4.45(2H, t), 6.64(4H, q), 7.12(1H, s), 9.02(1H, s). MS: *m/e* 282(M^+), 266(M^+—H_2O), 189(M^+—PhOH). Found: C, 76,48; H, 6.14%. Calcd for $C_{18}H_{18}O_3$: C, 76.57; H, 6.42%.

3f: Mp 164—166 °C (from ligroin). IR: 3275(OH), 1660 cm^{-1} (C=O). NMR(CCl_4): δ=2.11(3H, s), 2.15(3H, s), 2.20(3H, s), 2.73(2H, t), 4.18(2H, s), 2.42(2H, t), 6.34 (1H, s), 6.47(1H, d), 6.59(1H, d), 6.67(1H, dd), 7.08(1H, s). MS: *m/e* 296 (M^+), 281(M^+—CH_3), 278(M^+—H_2O), 189(M^+—MePhOH). Found: C, 76.89; H, 6.83%. Calcd for $C_{19}H_{20}O_3$: C, 77.00; H, 6.80%.

3g: Mp 135—136 °C (from ligroin). IR: 3250(OH), 1660 cm^{-1} (C=O). NMR(CCl_4): δ=1.18(9H, s), 2.15(3H, s), 2.20(3H, s), 2.77(2H, t), 4.20(2H, s), 4.40(2H, t), 6.60(1H, d), 6.75(1H, s), 6.77(1H, d), 6.93(1H, dd), 7.08 (1H, s). MS: *m/e* 338(M^+), 323(M^+—CH_3), 189(M^+—*t*-BuPhOH). Found: C, 78.99; H, 7.75%. Calcd for $C_{22}H_{26}O_3$: C, 78.07; H, 7.75%.

3h: Mp 200—203 °C (from ligroin). IR: 3620(OH), 1670 cm^{-1} (C=O). NMR($CDCl_3$): δ=1.35(18H, s), 2.17 (3H, s), 2.19(3H, s), 2.74(2H, t), 4.41(2H, t), 4.41(2H, s), 4.88(1H, s), 6.82(2H, s), 7.11(1H, s). MS: *m/e* 394(M^+), 379(M^+—CH_3), 337(M^+—*t*-Bu), 189(M^+—*t*-Bu_2PhOH). Found: C, 78.94; H, 8.79%. Calcd for $C_{26}H_{34}O_3$: C, 79.15; H, 8.69%.

3i: Mp 98—99 °C (from ligroin). IR: 1650 cm^{-1} (C=O). NMR(CCl_4): δ=2.12(3H, s), 2.16(3H, s), 2.60(2H, t), 4.35(2H, t), 4.61(2H, s), 6.98—7.36(6H, m). MS: *m/e* 298(M^+), 189(M^+—PhS). Found: C, 72.90; H, 6.17%. Calcd for $C_{18}H_{18}O_2S$: C, 72.45; H, 6.08%.

3j: Mp 93—95 °C (from ligroin). IR: 1670 cm^{-1} (C=O). NMR(CCl_4): δ=2.13(6H, s), 2.30(3H, s), 2.60(2H, t), 4.35(2H, t), 4.55(2H, s), 6.98(1H, s), 7.06(4H, q). MS: *m/e* 312(M^+), 189(M^+—MePhS). Found: C, 73.51; H, 6.31%. Calcd for $C_{19}H_{20}O_2S$: C, 73.04; H, 6.45%.

4k: A mixture of phenol (0.26 g, 2.8 mmol) and sodium (0.07 g, 3.0 mmol) in ethanol (20 ml) was stirred for 2 h at 80 °C. **3a**(0.56 g, 2.5 mmol) was then added to the solution and refluxed for 4 h. The resulting sodium chloride was removed by filtration, filtrate condensed and recrystsallized from ligroin to give **4k**; yield 0.11 g, mp 152—154 °C. IR: 1670 cm^{-1} (C=O). NMR(CCl_4): δ= 2.17(3H, s), 2.29(3H, s), 2.70(2H, t), 4.43(2H, t), 5.41(2H, s), 6.72—7.23(6H, m). MS: *m/e* 282(M^+), 189(M^+—PhO). Found: C, 76.33; H, 6.58%. Calcd for $C_{18}H_{18}O_3$: C, 76.57; H, 6.42%.

4m: *p*-Cresol (0.30 g, 2.8 mmol) was treated with sodium (0.07 g, 3.0 mmol), **3a** (0.56 g, 2.5 mmol), and ethanol (20 ml) essentially as described in the preparation of **4k**. The product was recrystallized from ligroin to give **4m**; yield 0.10 g, mp 164—166 °C. IR: 1675 cm^{-1} (C=O). NMR(CCl_4): δ=2.16(3H, s), 2.25(3H, s), 2.28 (3H, s), 2.69(2H, t), 4.42(2H, t), 5.36(2H, s), 6.40—7.24(4H, m), 7.06(1H, s), MS: *m/e* 296(M^+), 189(M^+—MePhO). Found: C, 76.68; H, 6.98%. Calcd for $C_{19}H_{20}O_3$: C, 77.00; H, 6.80%.

Synthesis of ***4d*** *from* ***3b***. **3b**(0.28 g, 1.0 mmol) was added slowly to ethanol (10 ml) containing sodium ethoxide (0.078 g, 1.5 mmol). The solution was stirred at 80 °C for 2 h, and the solvent removed under reduced pressure. The residue was dissolved in ligroin and filtered off. The filtrate was evaporated to dryness under reduced pressure to give **4d**; yield 0.22 g, mp 70 °C, after recrystallization from ligroin.

References

1) Part 22: A. Ninagawa and H. Matsuda, *Bull. Chem. Soc. Jpn.*, **51**, 1874 (1978).

2) A. Ninagawa, K. Oohashi, and H. Matsuda, *Makromol. Chem.*, **177**, 2553 (1976); A. Ninagawa, Y. Oomi, and H. Matsuda, *Nippon Kagaku Kaishi*, **1976**, 1926.

3) J. B. Hendrickson, D. J. Cram, and G. S. Hammond, "Organic Chemistry," 3rd ed, McGraw-Hill Inc., New York (1970), p. 416.

BULLETIN OF THE CHEMICAL SOCIETY OF JAPAN, VOL. 51 (9), 2749—2750 (1978)

Hetero-atom Effect on the Benzene-Prismane and Related Reactions Perturbation Density Matrix of Intramolecular Cycloadditions

Sherif EL-BASIL* and Rifaat HILAL†

Organic Chemistry Department, Faculty of Pharmacy, Cairo University, Kasr El-Aini St., Cairo, Egypt

† *Chemistry Department, Faculty of Science, Cairo University, Cairo, Egypt*

(Received December 14, 1977)

Synopsis. A formalism is presented for studying intramolecular cycloadditions in terms of their corresponding perturbation density matrices. The effect of hetero-atom on a particular intramolecular cycloaddition is discussed.

Although the conversion of benzene into prismance (I) might formally be considered as a ($\pi 2_s + \pi 2_a + \pi 2_a$) intramolecular cycloaddition, and inspite of the fact that such a process is thermally "allowed," Reaction 1[1] and the related ones, Reaction 2 and 3, as well as the corresponding cycloreversions are not observed in the ground state.[2] On the other hand, derivatives of the oxa analogue (IV) of quadricyclene (III) are smoothly transformed into the corresponding oxepines when heated[3] (backward of Reaction 4 in Fig. 1). Conservations of orbital symmetry do not provide a clear explanation of such intramolecular cycloadditions. In this note a formalism is given in which such reactions are quantitatively described.

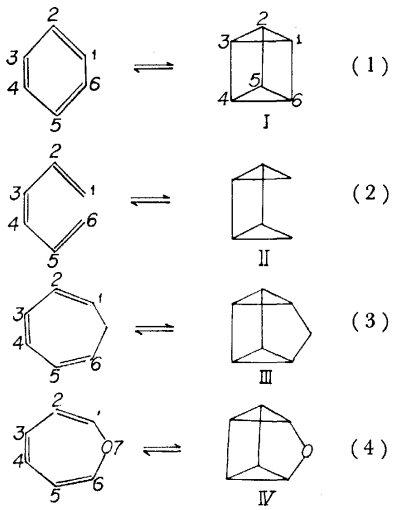

Fig. 1.

For a particular intramolecular cycloaddition reaction, calculations proceed as follows:

(1) An $n \times n$ perturbation matrix, P, is written to describe the particular intramolecular process, where n is the number of p-orbitals in conjugation in the starting polyene. The elements of such a matrix will vanish except those at positions where sigma resonance integrals change from a value of zero to some finite value as a result of overlap during the process.

(2) The initial perturbation ΔE which is a measure of the feasibility of a particular cycloaddition is given by

$$\Delta E = 1/2 \sum_{i=1}^{n/2} e_i \langle \phi_i | P | \phi_i \rangle = \sum_{r>s} \sum C_{ir} C_{is} \gamma_{rs}, \quad (1)$$

where

$$\gamma_{rs} = \langle \chi_r | P | \chi_s \rangle = \begin{cases} -|\gamma| & \text{(r, s; interacting)} \\ 0 & \text{(otherwise).} \end{cases}$$

In Eq. 1, e_i is the number of electrons in the ith MO. The eigenvectors $|\phi_i\rangle$ and $\langle \phi_i|$ are the SCF column and row vectors of the ith MO. The factor of 1/2 avoids counting a particular interaction twice. Matrix elements such as $\langle \phi_i | P | \phi_i \rangle$ form the main diagonal in the corresponding "perturbation density matrix."

TABLE 1. INITIAL PERTURBATIONS[a] ΔE FOR STUDIED INTRAMOLECULAR CYCLOADDITION REACTIONS (Fig. 1)

Reaction	Contribution to ΔE from	ΔE_{total}	Exptl.
1	ϕ_1, $\Delta E_1 = -1.000$		
	ϕ_2, $\Delta E_2 = 1.000$		
	ϕ_3, $\Delta E_3 = 0.6667$	0.6667	Not observed
2, 3	ϕ_1, $\Delta E_1 = -3.6370$		
	ϕ_2, $\Delta E_2 = -0.7282$		
	ϕ_3, $\Delta E_3 = 4.3880$	0.0228	Not observed
4	ϕ_1, $\Delta E_1 = -0.1654$		
	ϕ_2, $\Delta E_2 = -2.0588$		
	ϕ_3, $\Delta E_3 = -0.6988$		
	ϕ_4, $\Delta E_4 = 2.7304$	−0.1926	Observed

a) All values are divided by $|\gamma|$. A negative ΔE implies stabilization of the system and *vice-versa*.

Table 1 outlines the results of calculations using a previously described version of the SCF-PPP method.[4] The following points are worth observing:

(1) While the dominating interactions are always contributed by HOMO, one should not draw a conclusion based upon such an interaction alone. Rather, all interactions must be considered. Reaction 4 is particularly illustrative of this point.

(2) Examination of Reactions 2 and 3 on one hand and Reaction 4, on the other, makes it clear that the HOMO provides the most destabilizing component to the cycloaddition process and that such destabilization is decreased upon introduction of the hetero-atom in the molecule. In simple terms one might say that the introduction of an oxygen atom in quadricyclene (III), "buffers" an "energy-raising" component into the transition state of its cycloreversion.

References

1) J. F. M. Oth, *Angew. Chem.*, **80**, 633 (1968); *Angew. Chem. Int. Ed. Engl.*, **7**, 646 (1968); *Rec. Trav. Chim. Pays-Bas*, **87**, 1185 (1968).

2) H. Prinzbach and J. River, *Tetrahedron Lett.*, **1967**, 3713.

3) H. Prinzbach, M. Argüelles, and E. Druckrey, *Angew. Chem.*, **78**, 1057 (1966); *Angew. Chem. Int. Ed. Engl.*, **5**, 1039 (1966); H. Prinzbach, P. Vogel, and W. Auge, *Chimia*, **21**, 469 (1967).

4) R. Abu-Eittah and R. Hilal, *Bull. Chem. Soc. Jpn.*, **49**, 2158 (1976).

Interaction of Synthetic Polypeptides with Lipids in Monolayers

Takuya YAMASHITA, Akira SHIBATA, and Shinsuke YAMASHITA*

Faculty of Pharmaceutical Sciences, Tokushima University, Shomachi, Tokushima 770

(Received October 3, 1977)

The interaction of polypeptide (benzyloxycarbonyl derivatives of basic poly(α-amino acid), benzyl esters of acidic poly(α-amino acid), and poly(L-leucine)) and lipid (fatty acids, fatty alcohols and cholesterol) at the air–water interface was investigated. From the additivity rule of mean molecular areas and the work of collapse of the monolayers, it was found that the characteristic interaction occurs in the polymer rich region (less than 0.2 lipid mol fraction), and that the interaction is stronger for the polymer with higher helical content. The interaction was found to take place between side chains of polypeptides and lipids, and to be mainly of hydrophobic nature. The components in mixed polypeptide–cholesterol monolayers exhibit characteristic miscibilities depending upon the chemical composition of polymer side chains. The polarized infrared spectra of collapsed films consisting of single or mixed components indicate that the polymer component is aligned in a direction parallel to the compressing barrier.

Lipid-protein interactions are of great interest for understanding the structure and function of biological membranes. Spread monolayers provide one of the most promising means for studying molecules in fixed orientations, constituting an important model system for many naturally-occurring phenomena which involve surfaces or oriented arrays of molecules. The monolayer approach has been found very useful for understanding molecular aspects of lipid-protein interactions presumably occurring in biomembranes.[1–3] Synthetic polypeptides are useful as a simple model of proteins. A number of investigations on the physicochemical and biological properties have been carried out.[4]

Recently, the interactions of lipid monolayers spread at the air–water interface with synthetic polypeptides dissolved in the subsolution have been investigated.[5–8] For poly(L-lysine) and stearic acid system, the maximum interaction occurs at a pH value where polypeptide is in the helical conformation, and the helical conformation of the poly(L-lysine) molecule can be stabilized by electrostatic interaction with the ionized stearic acid monolayer.[7] On the other hand, from studies on various combinations of lipid monolayers (phosphatidyl serine, DL-α-dipalmitoyllecithin) and synthetic polypeptides-(poly(L-aspartic acid), poly(L-glutamic acid), poly(L-lysine)), in the subsolution, it has been found that the interaction between lipids and polypeptides at the interface is essentially hydrophobic.[8] The interactions have also been studied by using mixed monolayers of synthetic polypeptides and lipids. The mixed monolayer approach is particularly useful for studying the surface compatibility of polypeptides and lipids.[9–11] No interactions are detected probably owing to the quite different steric arrangement of the two components at the interface.[9,10] On the other hand, the formation of 5:1 and 1:1 (residue: molecule) complexes for poly-(DL-leucine) and sodium octadecyl sulfate system and 1:1 complex for poly(DL-phenylalanine) and sodium octadecyl sulfate system has been also reported.[11]

The purpose of this investigation is to establish the existence or nonexistence of interactions between synthetic polypeptides and lipids, and to clarify the nature of the interaction at the interface.

Experimental

Poly(δ-benzyloxycarbonyl-L-ornithine) (PLO(Z)), poly-(ε-benzyloxycarbonyl-L-lysine) (PLL(Z)), poly(L-leucine) (PLLeu), poly(β-benzyl-L-aspartate) (PBLA), poly(γ-benzyl-L-glutamate) (PBLG), and poly(γ-benzyl-DL-glutamate) (PBDLG-1, PBDLG-2) were prepared by the polymerization of the *N*-carboxy anhydrides of respective amino acids. The molecular weights determined from the viscosities at 25 °C in *N*,*N*-dimethyl-formamide (DMF)[12] or dichloroacetic acid (DCA)[13] are given in Table 1. Infrared spectra indicate that, with the exception of PBDLG-1 and PBDLG-2, these polymers are in the α-helical conformation in the solid state. The helical content of poly(γ-benzyl-DL-glutamates) was more than 90% regular α-helix for PBDLG-1, and 13% regular α-helix and 60% perturbed α-helix for PBDLG-2. No β-conformation was found for PBDLG-1 and PBDLG-2. The regular α-helix and perturbed α-helix have been designated by Tsuboi *et al.*[14] The perturbed α-helix portion in a polypeptide molecule contains an antipode residue, the sequence length being relatively short.

Table 1. Molecular weights of polypeptide samples

Polymer	[η]	*MW*
PLO(Z)	2.17(DMF)	3.5×10^5
PLL(Z)	2.40(DMF)	3.8×10^5
PBLA	0.28(DCA)	4.0×10^4
PBLG	1.67(DCA)	3.1×10^5
PBDLG-1	0.34(DCA)	5.0×10^4
PBDLG-2	0.40(DCA)	6.0×10^4
PLLeu: $\eta_{sp}/c=4.56$ ($c=0.2\%$ TFA)		

Lipids employed were myristic acid (C_{14} acid), stearic acid (C_{18} acid), 1-tetradecanol (C_{14} alcohol), 1-octadecanol (C_{18} alcohol), and cholesterol. These materials were purified either by fractional distillation or by recrystallization, and were chromatographycally pure.

The spreading solvents (DMF, dichloromethane (DCM) and trifluoroacetic acid (TFA)) were distilled under nitrogen atmosphere. The subsolution, 0.01 M HCl, was made up from twice distilled water and distilled 6 M HCl.

The spreading solvents were DCM for PBLA- and PBG (PBLG, PBDLG-1 and PBDLG-2)-lipid systems, a 9:1 (v/v) mixture of DCM and DMF for PLO(Z)- and PLL(Z)-lipid

systems, and a 9: 1 (v/v) mixture of DCM and TFA for PLLeu. When a 0.3 cm^3 solvent was deposited on water surface, a 10 to 1 compression of the surface produced less than 0.1 dyn/cm film pressure. The solutions of polypeptide and lipid were prepared separately, and mixed in the desired ratio immediately before spreading. The spreading solution was deposited from a micrometer syringe onto the surface of subsolution, and left to stand for 15 min. Polypeptide or lipid concentration in the spreading solution was 4—6 mg/10 cm^3. Unless otherwise stated, the initial spreading-area was 50 $Å^2$ (0.5 nm^2)/residue or molecule. The trough (65×15×1 cm) and compressing barriers were made of Teflon. The film was compressed at a rate of 10 mm/min (1 $Å^2$/residue or molecule/min). The surface pressure was measured by the Wilhelmy method. Measurements were carried out at 25 °C.

The polarized infrared spectra of collapsed films were measured by a JASCO DS-701G spectrometer. The monolayer was spread and compressed until collapse under the same conditions as in the case of surface pressure measurement. In order to remove the monolayer, it was compressed between two Teflon barriers, until the separation was about 1.5 cm. The polymer was then removed by drawing a stainless steel net across the trough between the barriers. The transferred collapsed film was dried at room temperature.

Results

Figure 1 shows the surface pressure-area (π-A) curves for PLO(Z), PLL(Z), PLLeu, PBLA, and PBG's. Plateaux or inflections are seen in the curves. The plateau or inflection which is characteristic of a number of synthetic polypeptide monolayers is associated with the collapse or transition of the monolayer in the α-helical conformation from a two-dimensional oriented state to a three-dimensional disoriented state.[4,15] The limiting areas extrapolated to zero surface pressure for the steep region are 22.5 $Å^2$/residue for PLO(Z), 23.8 $Å^2$/residue for PLL(Z) and 20.7 $Å^2$/residue for PBLA. When the monolayers were formed at the various spreading areas (40—60 $Å^2$/residue), the π-A curves were reproducible to ±0.2 $Å^2$/residue in repeated experiments. The areas are in good agreement with those reported by other workers.[4,16-19] The limiting area for PLLeu is 17.4±0.3 $Å^2$/residue which is smaller than that reported by Yamashita (19 $Å^2$/residue).[20] According to Malcolm,[21] the result may be associated with the difficult spreading of PLLeu.

The π-A curves of PBLG, PBDLG-1 and PBDLG-2 are shown in Fig. 1-b. The limiting area and monolayer transition pressure are 21.6 $Å^2$/residue and about 5.3 dyn/cm for PBLG, 21.0 $Å^2$/residue and 7.8 dyn/cm for PBDLG-1, and 20.8 $Å^2$/residue and 8.1 dyn/cm for PBDLG-2. The transition pressure of PBLG is much lower than that of PBDLG-1 and PBDLG-2. This might be related to the conformational difference between monolayers of PBLG and PBDLG's at the air–water interface. The difference in transition pressures of PBDLG-1 and PBDLG-2 is quite small. For PBG's, it has been reported that the temperature coefficient of transition pressure is dependent upon the regular α-helix content: the negative value of temperature coefficient is smaller for PBDLG-1 than for PBDLG-2 (regular α-helix content; PBDLG-1>PBDLG-2).[22] The height of transition pressure may be reversed at higher temperature. The monolayer of PBLG is more expanded than that of PBDLG-1 and PBDLG-2 (Fig. 1-b). The compressibility at close packed area is 0.027 for PBLG, 0.014 for PBDLG-1, and 0.015 for PBDLG-2.

The π-A curves of various lipids are shown in Fig. 2. C_{14} acid gives an expanded monolayer. On the other hand, the monolayers of C_{18} acid, C_{14} alcohol, C_{18} alcohol, and cholesterol are of condensed type. The film of cholesterol is highly incompressible.

As typical examples, the π-A curves of mixed PLO(Z)–C_{14} acid and mixed PLO(Z)–cholesterol monolayers are shown in Fig. 3. Two transition points are shown to

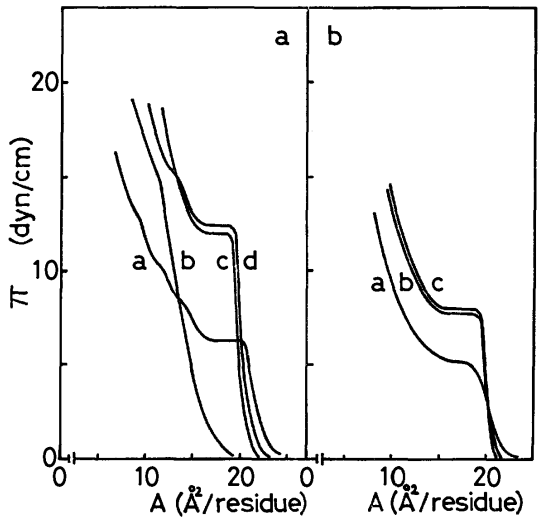

Fig. 1. Surface pressure-area curves of polypeptide monolayers on 0.01 M HCl at 25 °C. 1 dyn=10^{-5} N, 1 Å=0.1 nm. a) a: PLL(Z), b: PLLeu, c: PBLA, d: PLO(Z). b) a: PBLG, b: PBDLG-1, c: PBDLG-2.

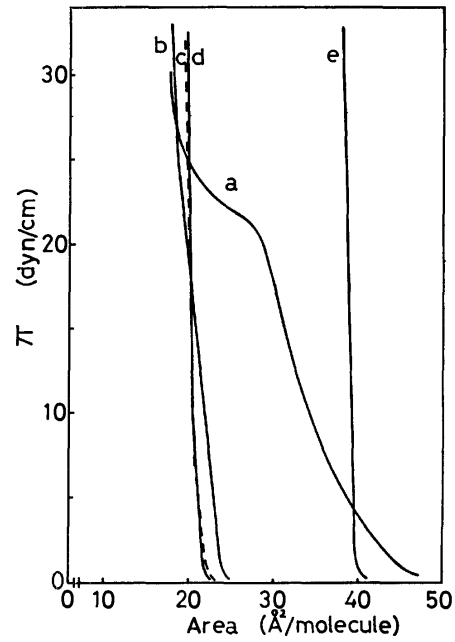

Fig. 2. Surface pressure-area curves of lipid monolayers on 0.01 M HCl at 25 °C. a: C_{14} acid, b: C_{18} acid, c: C_{14} alcohol, d: C_{18} alcohol, e: cholesterol.

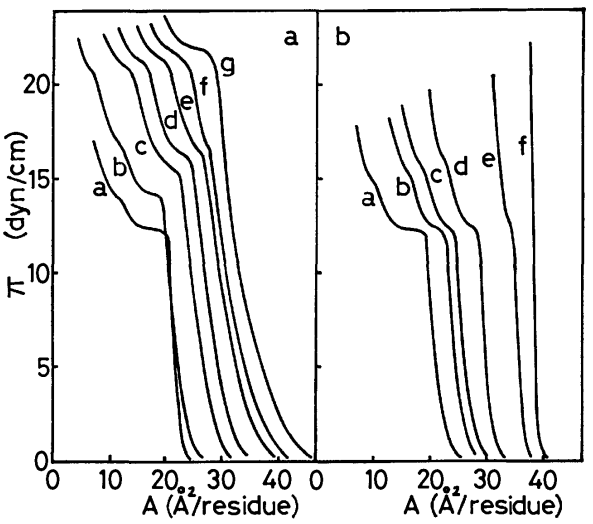

Fig. 3. Surface pressure-area curves of mixed monolyers on 0.01 M HCl at 25 °C. a) PLO(Z)–C_{14} acid, a: 1: 0, b: 4: 1, c: 7: 3, d: 1: 1, e: 3: 7, f: 1: 4, g: 0: 1, b) PLO(Z)-cholesterol, a: 1: 0, b: 4: 1, c: 7: 3, d: 1: 1, d: 1: 1, e: 1: 4, f: 0.: 1 (residue mol: mol).

exist (Fig. 3-a). The surface pressure at the lower point increases with increase in C_{14} acid mol fraction, while the higher point (about 22 dyn/cm) is independent of the mol fraction of C_{14} acid. The lower transition point is evidently caused by the polymer component. Discussion will be limited to this lower transition point or pressure. For mixed PLO(Z)–C_{14} acid system, up to C_{14} acid mole fraction of 0.5, the transition pressure caused by the polymer component increases steeply, the increase becoming gradual beyond this mole fraction. No significant change in transition pressure is observed for the mixed PLO(Z)–cholesterol system (Fig. 3-b).

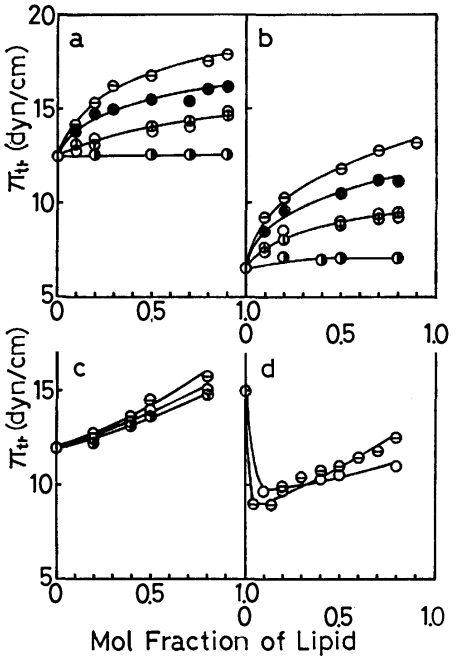

Fig. 4. Transition pressure of mixed monolayers as a function of lipid mole fraction at 25 °C.
a) PLO(Z)-lipid, b) PLL(Z)-lipid, c) PBLA-lipid, d) PLLeu-lipid, ⊖: polypeptide–C_{14} acid. ○: polypeptide–C_{18} acid, ●: polypeptide–C_{14} alcohol, ⓘ: polypeptide–C_{18} alcohol, ◑: polypeptide–cholesterol.

Figure 4 shows the relationship between the transition pressure and the composition of lipid in mixed monolayers for PLO(Z)–lipid, PLL(Z)–lipid, PBLA–lipid and PLLeu–lipid systems. From Figs. 4-a and 4-b, we see that no difference in transition pressures between PLO(Z)–C_{18} acid and PLO(Z)–C_{18} alcohol molayers and between PLL(Z)–C_{18} acid and PLL(Z)–C_{18} alcohol monolayers. In addition, the transition pressures for mixed PLL(Z)–lipid systems are larger than those for mixed PLO(Z)–lipid systems. PLO(Z) has less methylene group as compared with PLL(Z).

The transition pressure for PBLA–lipid systems (Fig. 4-c) differs remarkably from PLO(Z)–lipid and PLL(Z)–lipid systems. The difference in transition pressure among PBLA–C_{14} acid, PBLA–C_{18} acid and PBLA–cholesterol is small. There is an inflection point at about 15 dyn/cm for a monolayer of PLLeu (Fig. 1). For mixed monolayers of PLLeu and either C_{14} acid or C_{18} acid (Fig. 4-d), we see that the transition pressure decreases remarkably with the addition of a small amount of lipid, becoming minimum at about 0.2 lipid mole fraction.

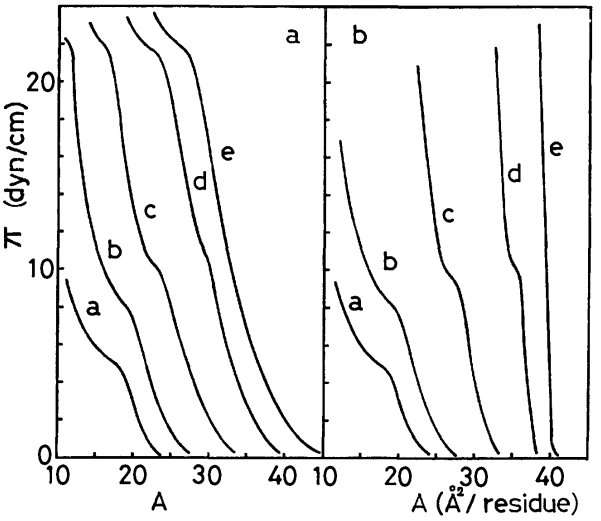

Fig. 5. Surface pressure-area curves of mixed monolayers on 0.01 M HCl at 25 °C. a) PBLG–C_{14} acid, b) PBLG–cholesterol. a: 1: 0, b: 4: 1, c: 1: 1, d: 1: 4, e: 0: 1 (residue mol: mol).

Figure 5 shows the π-A curves of mixed PBLG–C_{14} acid and mixed PBLG–cholesterol monolayers. It was found that the π-A curves for mixed monolayers of C_{14} acid, and either PBDLG-1 or PBDLG-2 also shows a similar tendency to that for mixed PBLG–C_{14} acid monolayers.

Figure 6 shows the relationship between the transition pressure and the composition of lipid for mixed monolayer of PBG with C_{14} acid, C_{18} acid or cholesterol. The increment of the transition pressure is in the order of α-helical content of polymers in solid state. With exception of mixed PBLG–cholesterol monolayers, the change in transition pressure is considerably small

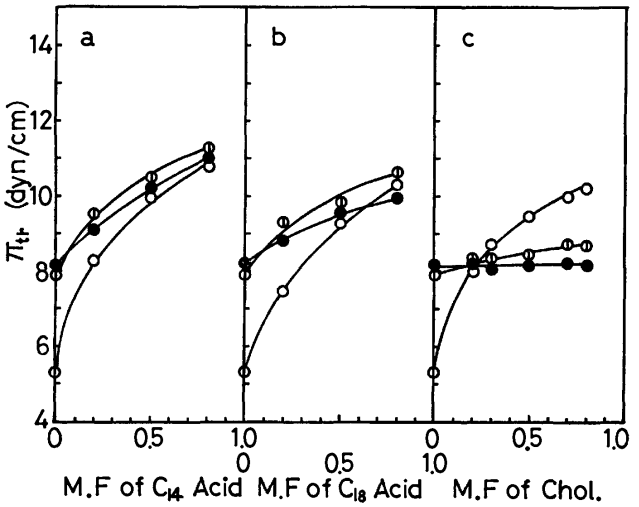

Fig. 6. Transition pressure of mixed monolayers as a function of lipid mole fraction at 25 °C.
a) PBG–C_{14} acid, b) PBG–C_{18} acid, c) PBG–cholesterol. ○: PBLG–lipid, ⓘ: PBDLG-1–lipid, ●: PBDLG-2–lipid.

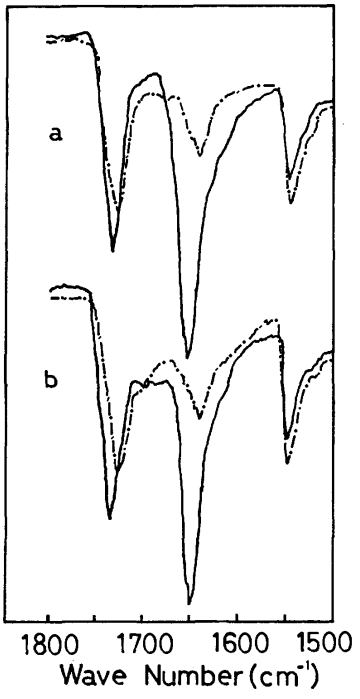

Fig. 7. Polarized IR spectra of collapsed films transferred onto a stainless steel net. a) PBLG, b) PBLG–C_{14} acid mixture (4: 1(residue mol: mol)). ——: Electric vector parallel to the barrier used to collapes the film, –•–•: electric vector perpendicular.

(PBDLG-1) or practically absent (PBDLG-2).

As a typical example, the polarized infrared spectra for collapsed films of PBLG and a 4: 1 (residue mol: mol) mixture of PBLG and C_{14} acid are shown in Fig. 7. The amide I and amide II bands (about 1650 cm^{-1} and about 1550 cm^{-1}) suggest that the polymer is in α-helical conformation. Dichroism is also observed at about 1730 cm^{-1} (assignable to stretching of the ester C=O bond of the side chain). A similar tendency was observed for other single and mixed films.

Discussion

Polypeptide–Lipid Interaction. One way to explain the interaction occurring in mixed monolayers is the application of the surface phase rule.[23,24] If a polypeptide and a lipid are completely miscible in the monolayer and the new three-dimensional phase begins to appear at the transition point, the transition pressure should vary with composition. If, on the other hand, the monolayer components are immiscible, the transition pressure is independent of composition. As can be seen in Figs. 4 and 6, the mixed systems of cholesterol with PLO(Z), PLL(Z), PBDLG-1 or PBDLG-2 are immiscible, other systems forming homogeneous miscible monolayers.

In general, the interaction between two different lipid components results in a deviation from the additivity rule of molecular areas only if one or both components form expanded monolayer. The additivity rule is also satisfied if two components are completely immiscible.

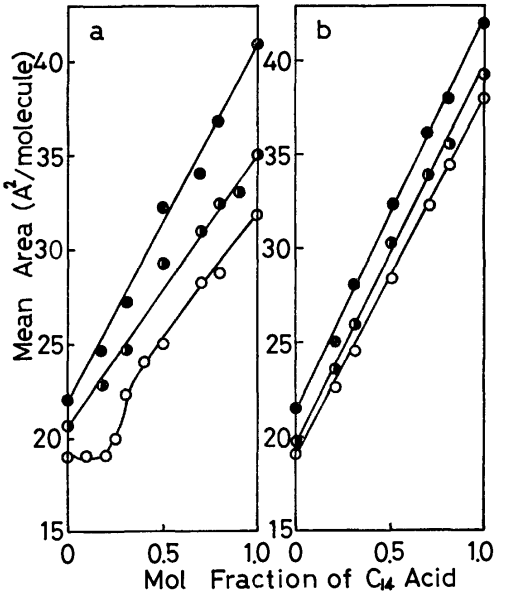

Fig. 8. Mean molecular areas of mixed monolayers as a function of lipid mole fraction at 25 °C.
a) PLO(Z)–C_{14} acid (●: 3 dyn/cm, ◑: 7 dyn/cm, ○: 10 dyn/cm), b) PBLG–C_{14} acid (●: 2 dyn/cm, ◑: 4 dyn/cm, ○: 5 dyn/cm).

Figure 8 shows the plots of mean molecular (residual) areas of mixed PLO(Z)–C_{14} acid and PBLG–C_{14} acid monolayers as a function of the composition under constant pressure. The maximum deviation can be seen at about 0.2 mole fraction of C_{14} acid at the pressure near the transition point of PLO(Z) (Fig. 8-a). A similar maximum deviation was observed for mixed PLL(Z)–C_{14} acid monolayer. No deviation can be seen for mixed PBLG–C_{14} acid monolayer (Fig. 8-b). No deviation was found for other mixed polypeptide–lipid systems (PLO-(Z)– and PLL(Z)–C_{18} acid, PLO(Z)– and PLL(Z)–cholesterol, PBDLG-1– and PBDLG-2–C_{14} acid, PBDLG-1– and PBDLG-2–cholesterol). From the results of two-

dimentional phase rule and additivity rule, it was found that for the miscibility between two component the side chain composition of polypeptide is important.

The results given in Fig. 4 indicate that the hydrophobic portion of lipid and polypeptide side chains is much more important for the interaction than the hydrophilic portion. The transition pressures of mixed PLO(Z)–C_{14} acid and PLL(Z)–C_{14} acid monolayers are higher than those of PLO(Z)–C_4 alcohol and PLL(Z)–C_{14} alcohol monolayers, respectively. This suggests that the state of monolayers of lipid is also important; C_{14} acid and C_{14} alcohol form a expanded monolayer and a condensed monolayer, respectively, at 25 °C. There is a considerable difference in the transition pressure between PBLA–lipid and PLO(Z)–lipid (or PLL(Z)–lipid) systems. It is of interest that in mixed PBLA–cholesterol system the transition pressure increase with lipid composition. On the contrary, in the case of mixed PLO(Z)–cholesterol and PLL(Z)–cholesterol systems, the change in transition pressure is practically absent. This suggests that for interaction the size and shape of lipid molecules (fatty acids, fatty alcohols and cholesterol) are important.

The work of collapse of mixed monolayers may provide a further information concerning the polypeptide-lipid interaction. The work of collapse, W, is given by

$$W = \pi_{tr} \cdot \Delta A,$$

where π_{tr} is the transition pressure, and ΔA is the difference between initial and final areas of collapse.

Figure 9 shows the work of collapse as a function of lipid mole fraction. Corresponding to the results shown in Fig. 4-c, the PBLA–lipid systems differ a great deal from other mixed systems. The work of collapse decreases with lipid mole fraction. As shown in Fig. 9-b, there is a remarkable difference in W values between PBLA and PBLG. The difference in side chain length would mainly affect the work of adhesion to water.[19] A significant difference in solution and solid properties has been reported between PBLA and PBLG.[25] It can be seen that with exception of PBLA–lipid systems, the maximum work of collapse is found at about 0.2 lipid mol fraction in agreement with the maximum deviation from the additivity rule of molecular areas for PLO(Z) (or PLL(Z))–C_{14} acid system at the pressure near the transition point of polypeptides. At about 0.2 lipid mole fraction, the cohesive force might be reinforced as a result of the formation of the 4: 1 complex (residue: molecule) of polypeptide and lipid in monolayers. Although no deviation from the molecular areas is found for PLLeu–C_{14} acid and PLLeu–C_{18} acid systems, the relationship between the transition pressure and the mol fraction of lipid suggests that the 4: 1 complex is also formed in these systems.

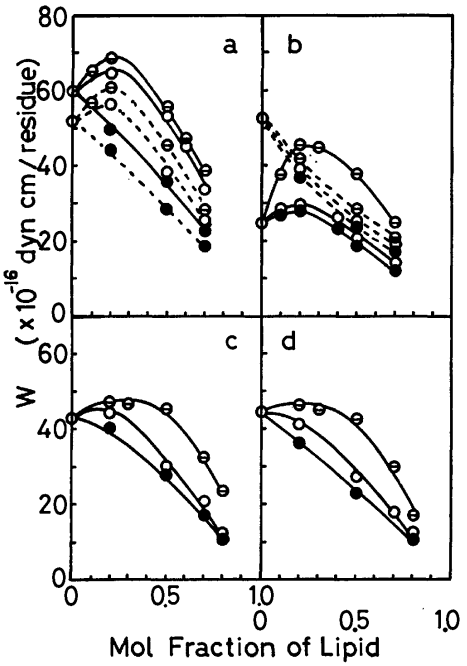

Fig. 9. Work of collapse for mixed monolayers as a function of lipid mole fraction at 25 °C.
a) PLO(Z)-lipid(——), PLL(Z)-lipid(——-), b) PBLG-lipid(——), PBLA-lipid(----), c) PBDLG-1-lipid, d) PBDLG-2-lipid. ⊖: polypeptide–C_{14} acid, ○: polypeptide–C_{18} acid, ●: polypeptide–cholesterol.

The drastic decrease in transition pressure of PLLeu with the incorporation of small amounts of C_{14} acid and C_{18} acid also suggests that the hydrophobic interaction is important (Fig. 4-d). As a result of hydrophobic interaction between polypeptide side chains and lipids, the adhesive force of PLLeu decreases remarkably, the film collapsing more easily than in the case of PLLeu alone.

The dichroism (amide I band) shown in Fig. 7 indicates that the horizontally oriented polypeptide molecules at the interface are aligned in a direction parallel to the compressing barrier. The dichroism at about 1730 cm^{-1} suggests that the side chain is considerably ordered at the interface. This might favor the polypeptide–lipid interaction at close packed state in the monolayer.

The discussion given above is summarized as follows: 1) the interaction between polypeptide and lipid is mainly of hydrophobic nature, 2) the interaction is considered to depend on the orientation and the chemical composition of polypeptide side chains and on the size, shape and state of lipid molecules in the monolayer.[26] In connection with the number of residue in a turn of the α-helix (3.6 residues), the intermolecular complex between polypeptide and lipid is formed at a molar ratio of 4: 1 (0.2 lipid mole fraction).

Effect of Conformation on Interactions. The effect of polypeptide conformation on the polypeptide–lipid interaction was investigated by using PBG's of different α-helical content in solid state.

As shown in Fig. 6, the change in transition pressure of mixed PBG–fatty acid monolayer is in order PBLG> PBDLG-1>PBDLG-2. Thus, it is assumed that PBLG interacts most strongly with the lipids. The interaction is the weakest for PBLG-2. It is of interest that this order corresponds to the helical content in the solid state. The maximum interaction of lipid monolayers with polypeptides occurs when the polypeptides dissolved in the subsolution in the α-helical conformation.[5,6,8]

If we assume that a PBLG monolayer is in the α-helical

conformation[15,27] and a perturbed helix portion of PBDLG is unfolded at the interface owing to relatively weak stability of the helix.[22,28] PBLG might become more hydrophobic than PBDLG's, since the polypeptide main chain is considerably shielded from the interaction with water molecules. This can be seen from the fact that the transition pressure of a monolayer of PBLG is much lower than that of PBDLG (Fig. 1-b).

The PBLG monolayer is more compressible than the PBDLG monolayers. Because of a highly rigid nature of the polypeptide main chain of the α-helix compared with other conformations. The high compressibility of a PBLG monolayer can be ascribed to the flexibility of side chains. The flexible side chains of PBLG might undergo rearrangement more easily into position favorable to the interaction with normal alkyl chain of a fatty acid. The state of a lipid monolayer and the flexibility of side chains of a polypeptide seem to affect the degree of interaction. C_{14} acid interacts more strongly than C_{18} acid with PBG.

The influence of cholesterol on the PBG monolayers is much more pronounced than that of fatty acids. PBLG interacts characteristically with cholesterol. However, PBDLG-1 and PBDLG-2 interact with considerable difficulty. Cholesterol does not interact with benzyloxycarbonyl derivatives of basic poly(α-amino acid). The interaction of cholesterol with synthetic polypeptides in monolayers depends upon the chemical composition of side chains of a polymer. The present study indicates that the conformation of a polymer is also important for the interaction. The change in transition pressure is in the order PBLG–cholesterol > PBDLG-1–cholesterol > PBDLG-2–cholesterol. This corresponds to the helical content of respective polymers.

From the work of collapse shown in Figs. 9-b, -c, and -d, it can be seen that the strong interaction between two components takes place at about 0.2 lipid mole fraction for PBLG–fatty acid and PBLG–cholesterol systems. For PBDLG–lipid systems except PBDLG–cholesterol systems, a specific interaction is found in a polymer rich region (less than 0.2 mole fraction of a lipid). This might indicate that side chains in the helical region in a polymer molecule is an interacting site.

The above arguments are summerized as follows: 1) the flexibility of polypeptide side chains is related to the conformation of a polypeptide at the interface, 2) the hydrophobic interaction of PBG's and lipids in monolayers is considerably affected by the conformation of a polymer, and the interaction is stronger when the α-helical content in the film is higher. This seems to be important in relation to the nature of lipid-protein interactions in biomembranes.

This research was supported by a Scientific Research Grant from the Ministry of Education.

References

1) I. R. Miller, *Prog. Surface Membrane Sci.*, **4**, 299 (1971).
2) I. R. Miller and D. Bach., "Surface and Colloid Science," ed by E. Matijević, John Wiley and Sons Inc., New York (1973), Vol. 6, p. 185.
3) "Biological Horizons in Surface Science," ed by L. M. Prince and D. F. Sears, Academic Press Inc., New York (1973).
4) B. R. Malcolm, *Prog. Surface Membrane Sci.*, **7**, 183 (1973).
5) D. O. Shah, *Biochim. Biophys. Acta*, **193**, 217 (1969).
6) D. Hammermeister and G. Barnett, *Biochim. Biophys. Acta*, **332**, 125 (1974).
7) P. T. Shafer, *Biochim. Biophys. Acta*, **373**, 425 (1974).
8) P. Chatelain, C. Berliner, J. -M. Ruysschaert, and J. Jaffe, *J. Colloid Interface Sci.*, **51**, 239 (1975).
9) D. E. Hookes, Ph. D. Thesis, University of London (1971).
10) G. Gabrielli, *J. Colloid Interface Sci.*, **53**, 148 (1975).
11) G. Kretzschmar, *Kolloid Z. Z. Polym.*, **234**, 1030 (1969).
12) E. Daniel and E. Katchalsky, "Polyamino Acids, Polypeptides and Proteins," ed by M. A. Stahmann, The University of Wisconsin Press, Madison (1962), p. 188.
13) P. Doty, J. H. Bradbury, and A. M. Holtzer, *J. Am. Chem. Soc.*, **78**, 947 (1956).
14) M. Tsuboi, Y. Mitsui, A. Wada, T. Miyazawa, and N. Nagashima, *Biopolymers*, **1**, 297 (1963).
15) B. R. Malcolm, *Proc. R. Soc. London, Ser. A*, **305**, 363 (1968).
16) B. R. Malcolm, *Biochem. J.*, **110**, 733 (1968).
17) G. I. Loeb and R. E. Baier, *J. Colloid Interface Sci.*, **27**, 38 (1968).
18) B. R. Malcolm, *Biopolymers*, **9**, 911 (1970).
19) B. R. Malcolm, *J. Polym. Sci., Part C*, **34**, 87 (1971).
20) T. Yamashita, *Nature*, **231**, 445 (1971).
21) B. R. Malcolm, *Adv. Chem. Ser.*, **145**, 338 (1975).
22) T. Yamashita and S. Yamashita, *Bull. Chem. Soc. Jpn.*, **43**, 3969 (1970).
23) "Insoluble Monolayers at Liquid-Gas Interfaces," ed by G. L. Gaines, Jr., Interscience, New York (1966), p. 208.
24) D. J. Crisp, "Surface Chemistry Suppl. Research," London (1949), p. 17.
25) "Poly-α-Amino Acids," ed by G. D. Fasman, Marcel Dekker, New York (1967).
26) D. O. Shah and J. H. Schulman, *J. Lipid Res.*, **8**, 215 (1967).
27) G. I. Loeb, *J. Colloid Interface Sci.*, **26**, 236 (1968).
28) T. Yamashita and S. Yamashita, *Maku (Membrane, in Japanese)*, **2**, 291 (1977).

Effect of Water Structure on Mixed Synthetic Polypeptide-Lipid Monolayers

Akira SHIBATA, Shinsuke YAMASHITA, and Takuya YAMASHITA*

Faculty of Pharmaceutical Sciences, Tokushima University, Shomachi, Tokushima 770

(Received October 3, 1977)

The effect of water structure on the interaction of synthetic polypeptides with fatty acids in monolayers at the air-water interface was investigated. It was found that SCN^-, F^-, and urea exert a remarkable effect upon the hydrophobic interaction in monolayers. SCN^- and urea disrupt the hydrated structure biult up around the hydrocarbon moieties of polypeptides and lipids at the interface. On the other hand, the presence of F^- as a structure maker tends to stabilize the hydrophobic bonding. The infrared spectra of polymer components were practically identical for the collapsed films in the absence and presence of SCN^-, F^-, and urea.

The hydrophobic bonding is important in stabilizing macromolecular structures such as proteins and biological membranes.[1] Water is considered to affect the properties and structure of biopolymers at the interface. Recent evidence suggests that the water adjacent to interfaces significantly differs from bulk water.[2]

In relation to the structure of water at the interfacial region, we have reported the effects of monovalent anions on the surface pressure-area (π-A) curves of poly(ε-benzyloxycarbonyl-L-lysine).[3] The effects of anions on increasing the surface pressure were in the order $SCN^->Br^->Cl^->F^-$ in line with that of these anions as breakers of water structure.[4]

The action of urea on macromolecular structures closely resembles that of chaotropic ions in which both unfolding and denaturation are strongly favored. It is not clear if the action of urea is similarly mediated by a modification in the structure of water. However, there is widespread belief that in the presence of urea, hydrophobic bonding is weakened.[5]

The purpose of this work is to clarify the effect of SCN^-, F^-, and urea on the interaction of polypeptides and lipids in relation to the structure of water at the interfacial region.

Experimental

Synthetic polypeptides used in the present study were poly(δ-benzyloxycarbonyl-L-ornithine) (PLO(Z)), poly(ε-benzyloxylcarbonyl-L-lysine) (PLL(Z)), poly(γ-benzyl-L-glutamate) (PBLG), and poly(γ-benzyl-DL-glutamate) (PBDLG) (13% regular α-helix and 60% perturbed α-helix). Lipids used were myristic acid (C_{14} acid) and stearic acid (C_{18} acid). Polypeptides, lipids, and spreading solvents were the same as those used in the preceding work.[6] Salts and urea solutions were treated with activated charcoal in order to remove surface-active contaminants, and were used as a subsolution after being adjusted to contain 0.01 M HCl. A 10 to 1 compression of the surface of the salt or urea subsolutions, after being left to stand for 10 min, produced less than 0.1 dyn/cm film pressure.

The surface pressure was measured by the Wilhelmy method at 25±0.5 °C. The films were compressed at a rate of 1 Å²/residue/min.

The polarized infrared spectra of collapsed films were measured with a JASCO DS-701G instrument.[6]

Results

Figure 1 shows the π-A curves for PBLG, PBDLG, PBLG–C_{14} acid and PBDLG–C_{14} acid mixtures (1: 1 (residue mol: mol)) spread on 0.01 M HCl, and on 2 M KSCN and 2 M KF subsolutions containing 0.01 M HCl. The transition pressures for PBLG and PBDLG monolayers are much higher on the subsolution containing KSCN than on 0.01 M HCl. On the other hand, in the presence of KF, the film transition pressure becomes slightly lower. In the presence of KSCN, film expansion is observed for PBLG and PBDLG. The effect of KF on exapansion is quite small. Similar tendencies were observed for the mixed monolayers.

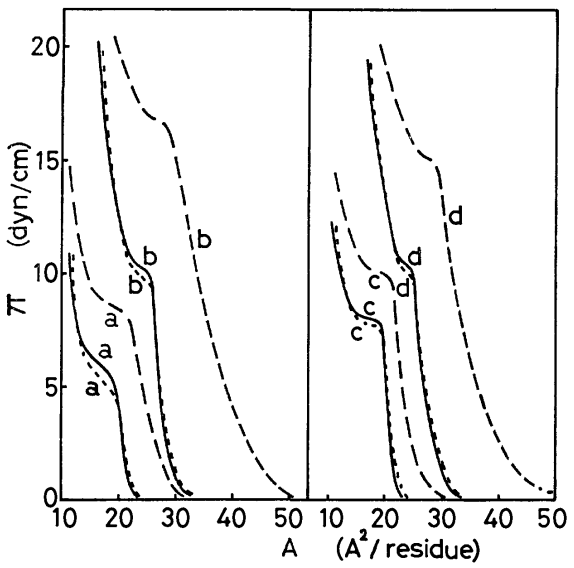

Fig. 1. Surface pressure-area curves of single and mixed monolayers on 0.01 M HCl(——), 2 M KSCN(— —) and 2 M KF(----) at 25 °C. 1 dyn=10^{-5} N, 1 Å=0.1 nm. a: PBLG, b: PBLG–C_{14} acid (1: 1(residue mol: mol)), c: PBDLG, d: PBDLG–C_{14} acid (1: 1(residue mol: mol)).

Figure 2 shows the π-A curves for PLO(Z), PLL(Z), PBLG and PBDLG spread on 0.01 M HCl and 2 M urea subsolutions together with those for C_{14} acid and C_{18} acid monolayers. The transition pressure of polypeptide monolayers increases in the presence of urea. Expansion of polypeptide and lipid monolayers is also observed. The monolayer behavior in the presence of urea is similar to that of KSCN.

Figure 3 shows the film transition pressure, π_{tr}, and the limiting area extrapolated to zero surface pressure for the steep region, A_0, against urea and KSCN concentrations. Up to the concentration of 6 M urea

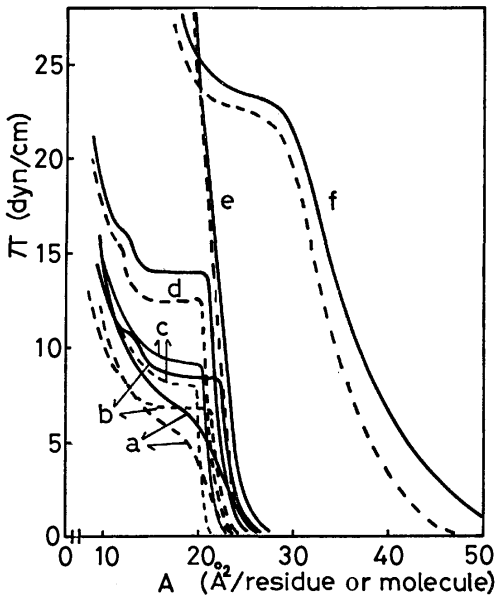

Fig. 2. Surface pressure-area curves of polypeptide and lipid monolayers on 0.01 M HCl(-----) and 2 M urea (——) at 25 °C. a: PBLG, b: PLL(Z), c: PBDLG, d: PLO(Z), e: C_{18} acid, f: C_{14} acid.

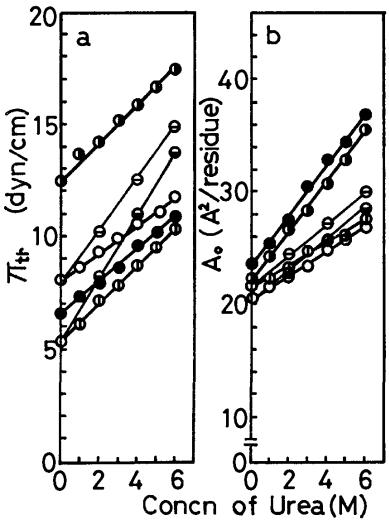

Fig. 3. Transition pressure, a, and limiting area, b, of polypeptide monolayers as a function of urea and KSCN concentration at 25 °C. Urea; ◑: PLO(Z), ●: PLL(Z), ⓘ: PBLG, ○: PBDLG. KSCN; ◒: PBLG, ⊖: PBDLG.

and KSCN, π_{tr} and A_0 increase linearly. The effect of KSCN on π_{tr} and A_0 is much larger than that of urea.

As a typical example of mixed monolayers, Fig. 4 shows the π-A curves for mixed PLO(Z)-C_{14} acid monolayer on 0.01 M HCl and 2 M urea subsolutions. The transition pressures caused by the polymer components increase with increase in lipid mol fraction irrespective of the absence and presence of urea.

Figure 5 shows the polarized infrared spectra of collapsed films of PBLG formed on the subsolutions in the absence and presence of urea, KSCN and KF. In the α-helical amide I (about 1650 cm^{-1}) and amide

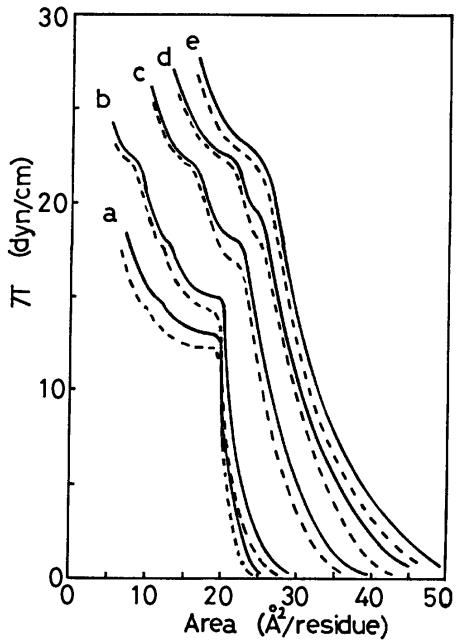

Fig. 4. Surface pressure-area curves of mixed monolayers of PLO(Z) with C_{14} acid on 0.01 M HCl(——) and 2 M urea(——) at 25 °C. a: 1: 0, b: 4: 1, c: 1: 1, d: 1: 4, e: 0: 1 (residue mol: mol).

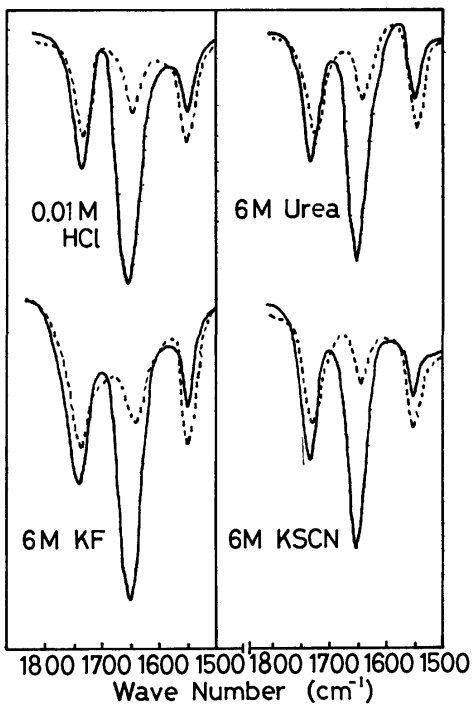

Fig. 5. Polarized IR spectra of collapsed films of PBLG formed on 0.01 M HCl, 6 M urea, 6 M KF and 6 M KSCN subsolutions. ——: Electric vector parallel to the barrier used to collapse the film, -----: electric vector perpendicular.

II (about 1550 cm^{-1}) regions, the spectra are practically identical with each other. Dichromism is also observed at about 1730 cm^{-1} (assignable to stretching of the ester C=O bond of the side chain). Similar results were

obtained for the other single and mixed monolayers. This suggests that polypeptide molecules are aligned in a parallel direction to the compressing barrier, irrespective of the kind of subsolution. The highly ordered alignment of polypeptide molecules may be favorable for the interaction between polypeptide and lipid.

Discussion

Effect of Salts. The order of film expansion is KSCN>KF≥0.01 M HCl (Fig. 1). This suggests that salts are transferred into the interface relative to the surface without monolayer. Fatty acid and fatty alcohol monolayers expand in the presence of salts[7] and urea.[8] Ralston and Healy gave an expansion for fatty alcohol monolayer in terms of interfacial water structure.[7] The film transition pressure is related to the collapse of monolayers from a two-dimensional oriented state to a three-dimensional disoriented state.[9,10]

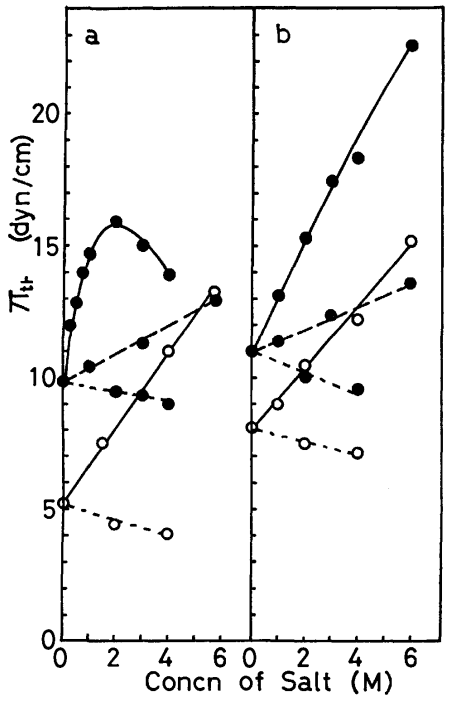

Fig. 6. Transition pressure of single and mixed monolayers as a function of concentration of KSCN(——), KF(----) and urea(——) at 25 °C. a) ○: PBLG, ●: PBLG–C_{14} acid (1: 1 (residue mol: mol)). b) ○: PBDLG, ●: PBDLG–C_{14} acid(1: 1(residue mol: mol)).

Figure 6 shows the transition pressure as a function of salts and urea concentrations for PBLG, PBDLG together with PBLG– and PBDLG–C_{14} acid mixtures (1: 1 (residue mol: mol)) spread on KSCN or KF subsolution. The transition pressures of PBLG and PBDLG increase linearly with increase in KSCN concentration. The hydrated structure around the hydrocarbon moieties of the side chains of polypeptides disrupted by SCN^- ion preferentially accumulated on the surface. As a result of the disruption, the affinity of the hydrocarbon moieties to water might increase.[1,11,12] The increment of transition pressure appears to be caused by destabilized hydrophobic bonding as a result of breakdown of the water structure. From the relationship between the transition pressure and the KSCN concentration in Fig. 3, the value of $d\pi_{tr}/dC$ for PBLG is larger than that of PBDLG. This can be attributed to the difference in the conformation in monolayer states between PBLG and PBDLG. In the conformation of synthetic polypeptides in monolayers, the α-helical conformation is reported to be one of the stable conformations.[9] Other conformations can also exist depending upon conformation in the solid state[13] or solution[14] and stability of the helix.[15,16] In the presence of KF, contrary to the case of KSCN, the transition pressure decreases linearly with the concentration for polypeptide monolayers. The decrease of transition pressure (Fig. 6) indicates that the adhesive force of polypeptide to water becomes weak with the formation of hydrated structure at the interface by the action of F^- as a maker of water structure.[4]

For mixed PBLG–C_{14} acid monolayer, there is a maximum value in transition pressure at 2 M KSCN. On the other hand, for mixed PBDLG–C_{14} acid monolayer, the transition pressure increases linearly. This can be associated with the difference in the stability of the hydrophobic bonding between two mixed systems. In analogy with SCN^-, the presence of urea also gives rise to the increase of transition pressure and the expansion in single and mixed monolayers. For PBLG– and PBDLG–C_{14} acid mixtures (1: 1 (residue mol: mol)), the effect of SCN^- on transition pressure is more remarkable than that of urea (Fig. 6). For PBLG–C_{14} acid mixture in particular, the transition pressure gives a maximum value at 2 M KSCN, while in the presence of urea, the pressure increases linearly with concentration. A remarkable difference in the increment of transition pressure is also observed for PBDLG–C_{14} acid mixture, suggesting that the effect of SCN^- on the hydrophobic interaction is much larger than that of urea. In the presence of KF, the decrease in transition pressure is small (about 1 dyn/cm at 4 M KF), little difference between PBLG and PBDLG monolayers, and between mixed PBLG–C_{14} acid and mixed PBDLG–C_{14} acid monolayers being observed. This suggests that the hydrophobic bonding tends to be stabilized by the action of F^-.

The results suggest that the action of ions (SCN^- and F^-) takes place on water and not primarily on the monolayer components itself. The monolayer behavior on salt subsolutions is closely related to the interfacial water structure.

Effect of Urea. It would be enlightening to elucidate the effect of urea in the polypeptide monolayers.

Film characteristics of synthetic polypeptides are given in Table 1. Film compressibility extrapolated to zero surface pressure, δ, is shown in the absence and presence of urea, together with the increment of limiting area and transition pressure against the urea concentration (dA_0/dC and $d\pi_{tr}/dC$). The change in limiting area of polypeptide with increase in the concentration of urea can be attributed to the penetration of a polypeptide monolayer by urea in the subsolution. The

TABLE 1. FILM CHARACTERISTICS OF SYNTHETIC POLYPEPTIDES

Polypeptide	dA_0/dC (Å²/residue/M)	$d\pi_{tr}/dC$ (dyn/cm/M)	δ ((dyn/cm)$^{-1}$) 0.01 M HCl	δ ((dyn/cm)$^{-1}$) 6 M urea
PLO(Z)	2.47	0.83	0.0131	0.0202
PLL(Z)	2.42	0.72	0.0144	0.0205
PBLG	1.12	0.81	0.0270	0.0333
PBDLG-2	1.18	0.60	0.0151	0.0284

increments of the limiting areas of PBLG and PBDLG against urea concentration differ a great deal from those of PLO(Z) and PLL(Z). This suggests that the surface activity of urea depends on the difference in the composition and geometrical arrangement of side chains between benzyloxycarbonyl derivatives of basic poly(amino acid) and benzyl esters of acidic poly(amino acid).

In the presence of 6 M urea, the film compressibility of a polypeptide increases considerably. The film transition pressure increases with urea concentration. This indicates that the affinity of hydrophobic moieties of polypeptide side chains to water and the side chain flexibility increase with the penetration by urea as a breaker of water structure.[4,17,18] The value of $d\pi_{tr}/dC$ for PBLG (0.81) is larger than that for PBDLG (0.60). This suggests that urea molecules mainly affect the side chains in the α-helical region of a polypeptide molecule.

Any deviation of mixed monolayer behavior from the additivity rule of molecular area might give useful information as regards the miscibility and interaction in the film. Figure 7 shows the mean molecular areas of mixed PLL(Z)–C_{14} acid and mixed PLL(Z)–C_{18} acid monolayers as a function of lipid mole fraction in the

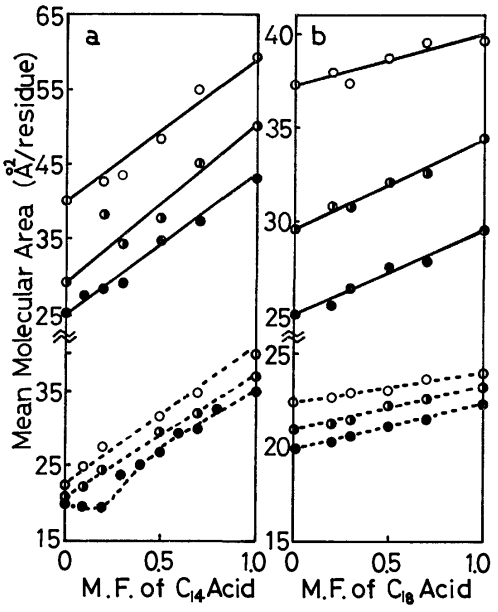

Fig. 7. Mean molecular area of mixed monolayers as a function of lipid mole fraction at 25 °C. ----: 0.01 M HCl, ——: 6 M urea. a) PLL(Z)–C_{14} acid (○: 2 dyn/cm, ◑: 4 dyn/cm, ●: 6 dyn/cm). b) PLL(Z)–C_{18} acid(○: 2 dyn/cm, ◑: 4 dyn/cm, ●: 6 dyn/cm).

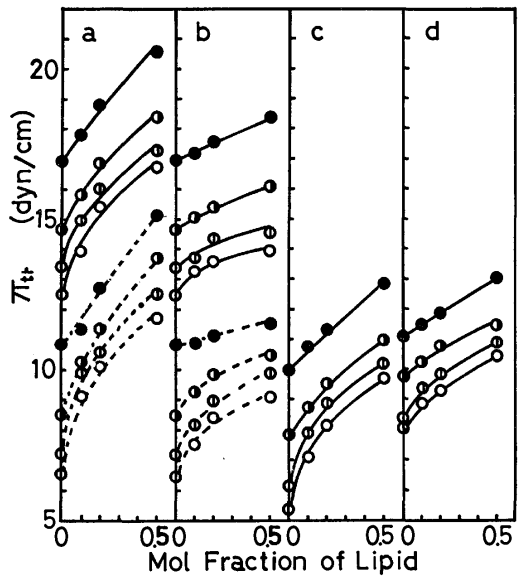

Fig. 8. Transition pressure of mixed monolayers as a function of lipid mole fraction in various concentration of urea at 25 °C. a) PLO(Z)–C_{14} acid (——), PLL(Z)–C_{14} acid(----). b) PLO(Z)–C_{18} acid (——), PLL(Z)–C_{18} acid(----). c) PBLG–C_{14} acid. d) PBDLG–C_{14} acid. ●: 6 M urea, ◑: 3 M urea, ⓘ: 1 M urea, ○: 0.01 M HCl.

absence and presence of 6 M urea. When PLL(Z) is mixed with C_{14} acid which forms an expanded monolayer, the maximum negative deviation is observed at about 0.2 mole fraction of the acid in the absence of urea. However, no deviation from the additivity rule takes place in the presence of 6 M urea. A similar tendency was observed for mixed PLO(Z)–C_{14} acid monolayers.

When there is no deviation from the additivity rule of mean molecular areas, it is difficult to determine the miscibility in the film. Figure 8 shows the transition pressure as a function of lipid mole fraction for mixed monolayers of fatty acid with PLO(Z), PLL(Z), PBLG or PBDLG for various concentrations of urea. The film transition pressure caused by the polymer component increases with C_{14} acid mole fraction (Fig. 8-a). The surface phase rule[19,20] predicts that two film components are miscible in the presence and absence of urea in the subsolutions. In the presence of 6 M urea, the transition pressure increases linearly with lipid mole fraction. This suggests that an ideal surface mixture of PLO(Z) (or PLL(Z)) and C_{14} acid is formed in the film at high concentration of urea.

The molecular area additivity rule[6] holds in other mixed monolayers such as PLO(Z) with C_{18} acid, PLL(Z) with C_{18} acid, PBLG with C_{14} acid, and PBDLG with C_{14} acid. On the other hand, the film transition pressure against lipid mole fraction for these mixed monolayers indicates that the film components are miscible, irrespective of urea concentration (Figs. 8-b, -c, and -d).

The formation of an ideal surface mixture can be ascribed to the breaking of hydrated structure around the hydrophobic moieties of polypeptide and lipid by the action of urea. As a result, the affinity of polypeptide

side chains and a nonpolar portion of the lipid to water[21] and the flexibility of polypeptide side chains increase. This might be supported by the film expansion (Figs. 2 and 4) and the increased compressibility of polypeptide monolayers in the presence of urea (Table 1).

From the conformational aspects of polypeptide monolayers, the action of urea on the interactions of PBLG–lipid and of PBDLG–lipid in monolayers are of interest. The perturbed α-helix portion of PBDLG molecule might be unfolded in the monolayer state owing to the relatively weak stability of the helix.[15,16] The interaction of PBDLG and lipid is weak as compared with that of PBLG and lipid.[5] The results shown in Figs. 8-c and -d indicate that the change in transition pressure against C_{14} acid mole fraction is smaller for PBDLG than for PBLG. This supports the view that the perturbed helix is unstable in monolayers. Urea molecules predominantly attack the hydrophobic moieties around the regular helix.

This research was supported by a Scientific Research Grant from the Ministry of Education.

References

1) W. B. Dandliker and V. A. de Saussure, "The Chemistry of Biosurface," ed by M. L. Hair, Marcel Dekker, New York (1971), Vol. 1, p. 1.
2) W. Drost-Hansen, "Chemistry of the Cell Interface," ed by H. D. Brown, Academic Press, New York (1971), Part B, p. 1.
3) T. Yamashita, A. Shibata and S. Yamashita, *Chem. Lett.*, **1978**, 11.
4) R. W. Gurney, "Ionic Processes in Solution," McGraw-Hill, New York (1953), Chap. 9.
5) S. Subramanian, D. Balasubramaniam, and J. C. Ahluwalia, *J. Phys. Chem.*, **73**, 266 (1969).
6) T. Yamashita, A. Shibata, and S. Yamashita, *Bull. Chem. Soc. Jpn.*, **51**, 2751 (1978).
7) J. Ralston and T. W. Healy, *J. Colloid Interface Sci.*, **42**, 629 (1973).
8) D. F. Sears, *J. Colloid Interface Sci.*, **29**, 288 (1969).
9) B. R. Malcolm, *Proc. R. Soc. London, Ser. A*, **305**, 363 (1968).
10) B. R. Malcolm, *Prog. Surface Membrane Sci.*, **7**, 183 (1973).
11) Y. Hatefi and W. G. Hanstein, *Proc. Natl. Acad. Sci. U.S.A.*, **62**, 1129 (1969).
12) S. B. Schryver, *Proc. R. Soc. London, Ser. B*, **83**, 96 (1910).
13) T. Yamashita, *Nature*, **231**, 445 (1971).
14) G. I. Loeb and R. E. Baier, *J. Colloid Interface Sci.*, **27**, 38 (1968).
15) T. Yamashita and S. Yamashita, *Maku (Membrane, in Japanese)*, **2**, 291 (1977).
16) T. Yamashita and S. Yamashita, *Bull. Chem. Soc. Jpn.*, **43**, 3969 (1970).
17) E. G. Finer, F. Franks, and M. J. Tait, *J. Am. Chem. Soc.*, **94**, 4424 (1972).
18) H. D. Ellerton and P. J. Dunlop, *J. Phys. Chem.*, **70**, 1831 (1966).
19) D. J. Crisp, "Surface Chemistry Suppl. Research," London (1949), p. 17.
20) G. L. Gaines, Jr., "Insoluble Monolayers at Liquid-Gas Interfaces," Interscience, New York (1966), p. 281.
21) J. A. Rupley, *J. Phys. Chem.*, **68**, 2002 (1964).
22) G. I. Loeb, *J. Polym. Sci., Part C*, **34**, 63 (1971).

An Upper Limit to the Excited Electron-Cation Recombination Lifetimes of Trapped Electrons in Ethanol and 2-Methyltetrahydrofuran Glasses at 4 and 77 K

Masaaki OGASAWARA*,† and Larry KEVAN

Department of Chemistry, Wayne State University, Detroit, Michigan 48202, USA

(Received October 19, 1977)

N,N,N',N'-Tetramethyl-*p*-phenylenediamine (TMPD) fluorescence lifetimes in 2-methyltetrahydrofuran (MTHF) glass at 77 K (13.5 ns) and in ethanol glass at 77 K (12.3 ns) and 4 K (11.5 ns) were measured using 347 nm excitation from a frequency doubled ruby laser. Trapped electrons and $TMPD^+$ were generated in these matrices by photoionization and the recombination fluorescence stimulated by 694 nm laser light was found, within an experimental limit of 1 ns, to occur with the same lifetime as the directly excited fluorescence. A convolution analysis indicates that the electron-cation recombination lifetimes are ≤ 1 ns in all these matrices at the temperatures given. It is also suggested that a lower limit for the electron mobility of 0.005 $cm^2\ V^{-1}\ s^{-1}$ is implied by these data.

Electrons have been trapped in a variety of organic glasses and their electronic and geometric structures have been extensively studied.[1] Both bound-bound and bound-continuum transitions seem to occur depending on the matrix and on the exciting light energy. However, little is known about the excited state lifetimes because no luminescence is observed. Indirect laser photobleaching methods suggest that the excited state lifetime is ≤ 6 ps in liquid water[2] and <10 ps in aqueous glass at 77 K.[3]

Another approach to obtain the excited state lifetime of trapped electrons is to measure the recombination lifetime of laser stimulated recombination luminescence. In this method the trapped electrons are produced by photoionization of an aromatic solute whose excited states luminesce.[4,5] The closest localized electrons to the solute cations recombine with them isothermally by tunneling[6] to produce isothermal recombination luminescence. More distant localized electrons can be optically stimulated to recombine with the solute cation. If the optical excitation of the trapped electron is energetic enough to excite the electron to the conduction state of the matrix, the total recombination lifetime will consist of four parts: (a) the lifetime of the localized continuum or quasi-continuum state of the electron, (b) the electron lifetime in the conduction state, (c) the lifetime of the localized continuum state of the excited solute, and (d) the lifetime of the fluorescent state of the solute. Contribution (b) can be estimated from electron mobility data if known. We expect (c) to be short compared to (d) because lifetimes are generally shorter for more highly excited states. Thus a delay of the recombination fluorescence lifetime beyond the directly excited fluorescence lifetime of the solute (contribution d) may yield information about the excited electron state lifetime.

This type of experiment was initially tried for *N,N,N',N'*-tetramethyl-*p*-phenylenediamine (TMPD) in 3-methylpentane (3 MP) glass at 77 K, although the focus was on an estimate of lifetime (c) and contributions (a) and (b) were not considered.[7] The recombination fluorescent lifetime and an upper limit of 1 ns on the electron-cation recombination step was deduced.

In the present work we have extended this type of experiment to polar matrices, 2-methyltetrahydrofuran (MTHF) and especially ethanol, and have made measurements at both 4 and 77 K in ethanol. New information is obtained on the natural fluorescent lifetimes of TMPD under these various conditions, but even in these polar matrices only upper limit for the electron-cation recombination step can be deduced.

Experimental

Chemicals were purified as described previously.[5,6] A Korad Pockel cell switched ruby laser was used for excitation. The 694 nm output energy was about 1 J per pulse of half-width 15—25 ns. For fluorescence lifetime measurements the laser output frequency was doubled to 347 nm. For recombination fluorescence, trapped electrons were first generated by photoionizing TMPD (7×10^{-4} mol/dm^3) with 320 ± 20 nm light from a filtered mercury lamp; then within 3—10 min fluorescence was stimulated with a 694 nm laser pulse. Laser induced emission was detected through a Bausch and Lomb monochromator at 400 ± 10 nm with a 1P28 photomultiplier for nanosecond response[8] and photographed on a 7904 Tektronix scope. Temperature at 77 K was controlled by cold helium gas in a Dewar. At 4 K the sample was in a Dewar for liquid helium in which the sample position was not shielded by liquid nitrogen. Samples were prepared in 3 mm i.d. pyrex tubes.

Results and Discussion

The directly excited TMPD fluorescence intensity *vs.* time is similar to the laser pulse profile but its peak is typically shifted by 7—10 ns from the laser pulse peak. Accurate fluorescence lifetimes thus required a deconvolution procedure. For greater accuracy a Laplace transform method was used.[9] The fluorescence lifetime τ_f was determined from

$$\bar{L}(p)/\bar{G}(p) = (p/I_0) + (I_0\tau_f)^{-1}, \quad (1)$$

where I_0 is the initial fluorescence intensity after instantaneous excitation, p is the Laplace transform parameter $\bar{G}(p)$ is the Laplace transform of the observed fluorescence curve, $\bar{L}(p)$ is the Laplace transform of the 347 nm laser pulse and exponential decay for the fluorescence

† Present address: Faculty of Engineering, Hokkaido University, Kita-ku, Sapporo 060.

was assumed. The left side of Eq. 1 was calculated by a computer program and plotted *vs.* p to give a linear plot from which τ_f was obtained. The τ_f values obtained in this way are estimated to be accurate to $\pm 10\%$ which is thus the effective time resolution of the apparatus with the deconvolution procedure (*i.e.* $\approx$1 ns). The values of τ_f were checked by convoluting the exponential fluorescence decay with laser pulse to simulate the observed fluorescence curves; agreement was excellent in all cases. The fluorescence lifetimes are summarized in Table 1.

Table 1. Fluorescence decay times of TMPD in various matrices

Matrix	T/K	Decay time[a]/ns
Ethanol	Room	9.3, 7.1[b]
Ethanol	77	12.3
Ethanol	4	11.5
MTHF	77	13.5
Cyclohexane	Room	4.3[b]
3-Methylpentane	77	7.4$\pm$1.1[c]

a) Estimated error $\pm 10\%$ except where noted. b) I. B. Berlman, "Handbook of Fluorescence Spectra of Aromatic Molecules," 2nd ed, Academic Press, New York (1971), pp. 168—169. c) Ref. 7.

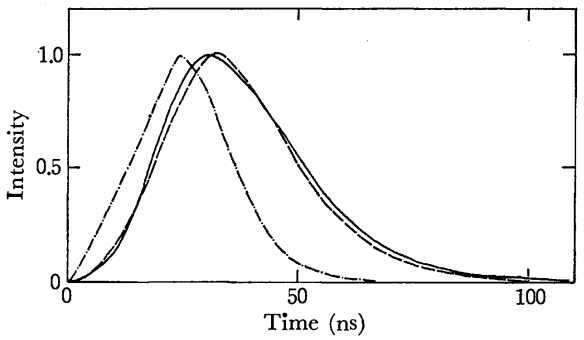

Fig. 1. Intensity *vs.* time profile of the 694 nm laser pulse (-·-) and the recombination fluorescence (——) in ethanol glass at 77 K containing 7×10^{-4} mol/dm^3 TMPD which was previously photoionized by UV light. The dashed curve is calculated TMPD fluorescence convoluted from the 694-nm laser pulse and an exponential fluorescence decay with a liferime of 12.3 ns.

The same deconvolution analysis gives recombination fluorescence lifetime within 10% of the direct fluorescence lifetimes. This is shown pictorially in Fig. 1. The laser stimulated recombination fluorescence for TMPD in ethanol at 77 K is shown in Fig. 1 as is the 694 nm laser pulse profile. The fluorescence calculated from the 694 nm laser pulse and the fluorescence lifetime is seen to coincide, within experimental uncertainty, with the recombination fluorescence. Similar results are obtained for TMPD in ethanol at 4 K and in MTHF at 77 K.

Excited TMPD$^+$ is not expected to contribute to the recombination fluorescence at 400 nm. This was verified by observing no emission from ethanol glass containing 4×10^{-5} to 2×10^{-4} mol/dm^3 TMPD$^+$ ClO_4^- and excited by 694 nm light. Direct excitation of TMPD by 694 nm laser light *via.* double quantum absorption was negligible, since no emission was observed when ethanol glass containing 7×10^{-4} mol/dm^3 TMPD was irradiated by 694 nm laser pulse.

The coincidence of the directly excited and the recombination fluorescence lifetimes indicated that the electron-cation recombination process occurs within $\approx$1 ns which is our estimated time resolution with the deconvolution procedure. Thus the more polar matrices (MTHF and ethanol) show the same upper limit as the nonpolar 3-methylpentane (3MP) matrix.[7]

The upper limit of $\approx$1 ns corresponds to the upper limits for each of the three possible contributions: lifetime of localized continuum states of excited electron (a) and of excited solute (c) and lifetime of the electron in the conduction state (b). From the upper limit of the conduction state lifetime, cation field and recombination distance one can estimate the lower limit of the electron mobility. Assuming the average recombination distance of 10 nm the field independent electron mobilities in MTHF and ethanol matrices are $\mu>0.005$ cm^2 V^{-1} s^{-1} based on the 1 ns upper limit and the increase in cation field as the recombination distance decreases.** This limit is consistent with the reported drift mobility of 0.055 cm^2 V^{-1} s^{-1} for MTHF glass at 77 K.[10]

The same lower limit on electron mobility is implied for ethanol glass at both 77 and 4 K unless tunneling recombination dominates (see below). This implication is particularly interesting at 4 K since it indicates that the electron mobility remains relatively high to quite low temperature.

In 3MP and MTHF the 694 nm light is energetic enough to excite the trapped electron to the conduction state as indicated by photoconductivity data.[1] However in ethanol the 694 nm (1.8 eV) light appears insufficient to excite the trapped electron to the conduction state since the photoionization threshold is 2.3$\pm$0.1 eV.[11] If the trapped electron is sufficiently close to the cation the Coulomb potential can distort the electron potential well and cause the recombination threshould to be less than the photoionization threshould. However, at separation distances of $\approx$3.0 nm this difference should be within the experimental uncertainty of $\pm$0.1 eV. In fact, the same threshold for electron loss is observed from photoconductivity, photobleaching and stimulated luminescence methods.[1]

Let us see whether tunneling recombination from an

** The average recombination distance can be estimated from a tunneling model for the recombination process[6] prior to laser stimulation. The tunneling rate constant k is given by the equation, $\log k = 15 - 0.44 d V_b^{1/2}$, assuming a simple one dimentional tunneling model with a square barrier of height V_b and width d. The V_b values can be taken as the electron trap depth in MTHF (1.6 eV) and in ethanol (2.3 eV).[1] Then at 200 s which is the average time between photoionization and laser excitation, one finds distances of 3.1 nm (MTHF) and 2.6 nm (ethanol). The average recombination distance will be several times greater than the minimum recombination distance thus estimated and we assume 10 nm. Assuming a dielectric constant of 2 the cation field at 10 nm is 7.2×10^4 V cm^{-1}.

excited state of the electron in ethanol can account for the observed recombination time. With a barrier height of 2.3 −1.8=0.5 eV, the simple tunneling model[6] predicts tunneling from 1.9 nm or less within 1 ns. However, the same tunneling model predicts that all electrons within 2.6 nm will have tunneled through the full 2.3 eV barrier in ethanol during the ≈200 s between photoionization and laser excitation. Thus there will not be any electron left within 1.9 nm of the cation at the time of laser excitation and the tunneling mechanism seems improbable. It is necessary to reduce the barrier height to 0.25 eV or less for the tunneling distance in 1 ns to be >2.7 nm and to make the tunneling mechanism a possible alternative.

A second possibility is that a few of the electrons constituting the 1 eV wide absorption band in ethanol are in shallow enough traps to be excited to the conduction state by 694 nm light. Since fluorescence is a more sensitive detection technique than photoconductivity it may be possible to observed such a small population of electrons if they exist. The observation that the stimulated fluorescence in ethanol glass is 1—2 orders of magnitude weaker than that in MTHF glass may support this suggestion.

We conclude that the localized continuum state lifetimes of trapped electrons and excited TMPD in 3MP and MTHF glasses are ≤1 ns at 77 K and in ethanol glass are ≤1 ns between 4 and 77 K. Likewise the electron conduction state lifetime is ≤1 ns which suggests a lower limit to the electron mobility of 0.005 $cm^2 V^{-1} s^{-1}$ in these matrices.

This work was supported by the U. S. Energy Research and Development Administration through contract number E(11-1)-2086. We thank Dr. S. A. Rice for comments on the Laplace transform analysis. One of the authers, LK thanks Prof. H. Yoshida of Hokkaido University for his cooperation and support while this work was completed.

References

1) L. Kevan, *Adv. Radiat. Chem.*, **4**, 181 (1974).
2) G. A. Kenney-Wallace and D. C. Walker, *J. Chem. Phys.*, **55**, 447 (1971).
3) D. C. Walker and R. May, *Int. J. Radiat. Phys. Chem.*, **6**, 345 (1974).
4) A. C. Albrecht, *Acc. Chem. Res.* **3**, 328 (1970).
5) H. Mockel, J. Yuen and L. Kevan, *Int. J. Radiat. Phys. Chem.*, **7**, 251 (1975).
6) K. K. Ho and L. Kevan, *J. Phys. Chem.*, **81**, 1865 (1977).
7) D. S. Kliger, J. D. Laposa and A. C. Albrecht, *J. Chem. Phys.*, **48**, 4326 (1968).
8) J. W. Hunt and J. K. Thomas, *Radiat. Res.* **32**, 149 (1967).
9) W. P. Helman, *Int. J. Radiat. Phys. Chem.*, **3**, 283, (1971).
10) T. Huang and L. Kevan, *J. Chem. Phys.*, **61**, 4660 (1974).
11) A. Bernas, D. Grand and C. Chachaty, *Chem. Commun. (J. Chem. Soc., D)*, **1970**, 1667.

Study of Metal Oxide Catalysts by Temperature Programmed Desorption. 3. Formation and Reactivity of Adsorbed Oxygen over α-Ferric Oxide

Masakazu IWAMOTO,** Yukihiro YODA, Noboru YAMAZOE, and Tetsuro SEIYAMA*

Department of Materials Science and Technology, Faculty of Engineering, Kyushu University, Hakozaki, Higashi-ku, Fukuoka 812

(Received November 17, 1977)

Formation and reactivity of oxygen adsorbates on the surface of α-Fe_2O_3 were investigated in the temperature range 0—600 °C by means of a temperature programmed desorption (TPD) technique. At least four different states of adsorbed oxygen were indicated by four TPD peaks, the maxima of which appeared at 50—300 (α), 350—360 (β), 480—490 (γ), and >600 °C (δ), respectively. Mode of preparation hardly affected the essential nature of oxygen adsorption (or desorption) except the relative amounts of respective desorptions. Of these adsorbates, α, whose desorption peak shifts over a wide temperature range depending upon adsorption conditions, was interpreted to be molecular oxygen (O_2 or O_2^-) bonded to the oxide surface with an extraordinarily broad heterogeneity, while β and γ species were tentatively assigned to O_2^- and O^-, respectively, adsorbed on different sites. The activation energies of desorption were 23.8 and 54.6 kcal/mol for β and γ, respectively. On exposure to gaseous hydrogen, β species as well as α turned more reactive than γ, though γ was also reactive at higher temperatures. The reaction of β and α species with hydrogen at lower temperatures gave rise to an increase in γ adsorption. This is accounted for by assuming a reaction in which the molecular adsorbates (α and β) react with hydrogen to leave the atomic adsorbates (γ) behind.

For an understanding of catalytic oxidation of reactants over metal oxide catalysts, it is important to know the kinds of oxygen adsorbates present on the oxide surface, their binding energies and populations, and how the structure or the preparation method of oxide catalysts affects the oxygen adsorption.

The problems might be best examined by use of a temperature programmed desorption (TPD) technique,[1] which adopts programmed heating of a catalyst surface covered with adsorbates. If all the adsorbates are in a given energy state, the increasing desorption probability with a rise in temperature results in a peak in the desorption flux; otherwise more than one peak are expected. The desorption temperature, peak shape and the variation of desorption temperature with the initial surface coverage are all related to the properties of adsorbates so that we can determine several adsorption (desorption) characteristics from the TPD chromatograms.[2] By this technique we studied oxygen adsorption on nickel oxide[3] and Cu(II) ion exchanged Y-type zeolite,[4] and revealed the existence of several modes of oxygen adsorbates on these adsorbents. We have applied the same technique to the investigation of oxygen adsorption on α-Fe_2O_3.

Ferric oxide, with the standard heat of formation ($-\Delta H_f^\circ$) of a moderate magnitude, exhibits high catalytic activity and selectivity for the oxidative dehydrogenation of butene to butadiene.[5] The correlation of the oxidation state of iron oxide with their catalytic activity has been discussed.[6,7] Fe_2O_3 is a n-type semiconductor in contrast to the p-type of NiO. It is of interest to compare the behavior of the two oxides. Recently, Halpern and Germain[8] examined the desorption of oxygen from powdered oxides of first transition metals by means of flash desorption. For Fe_2O_3 they obtained a spectrum with three desorption peaks at *ca.* 60, 250, and 550 °C. However, the limination of the method, *i.e.*, very rapid and non-linear heating (*ca.* 30 °C/s in average), prevented them from investigating the phenomenon in sufficient detail. The purpose of the present study is to clarify the formation, nature and reactivity of several modes of oxygen adsorbates on the surface of α-Fe_2O_3.

** Present Address: Department of Industrial Chemistry, Faculty of Engineering, Nagasaki University, Nagasaki 852.

Experimental

Apparatus. The TPD apparatus is essentially the same as that used previously.[3] It consists of two parts; one in which sample conditioning and oxygen adsorption under specified conditions are carried out in the conventional manner, the other in which adsorbates on the sample undergo thermal desorption into a helium carrier under programmed heating. The concentration of the desorbed gas was monitored and recorded with a thermal conductivity detector.

Materials. Helium gas of ultra-high-purity grade (> 99.995%) was supplied from Air Products and Chemicals. Before use, helium was passed through a liquid nitrogen cold trap in order to remove a trace amount of moisture. Oxygen gas was also dried before use by liquefaction and vaporization in a cold trap.

Ferric oxide samples were prepared by calcining ferric hydroxide, ferric nitrate or ferric oxalate, the corresponding sample being denoted by Fe_2O_3-I, II, or III, respectively. The calcination conditions and BET surface areas are summarized in Table 1. All the samples were identified to be α-Fe_2O_3 by X-ray powder diffraction. They were sieved to 20—60 mesh for TPD experiments.

Methods and Procedures. Ferric oxide, 1 g, was put into the TPD cell. Each fresh sample was evacuated for more than 2 h at 600 °C untill no more water was condensed in a liquid

Table 1. Ferric oxide samples

Catalyst	Starting materials	Calcination conditions	Surface area (m^2/g)
Fe_2O_3-I	$Fe(OH)_3$	600 °C, 5 h	5.5
Fe_2O_3-II	$Fe(NO_3)_3 \cdot 9H_2O$	600 °C, 5 h	6.6
Fe_2O_3-III	$FeC_2O_4 \cdot 2H_2O$	600 °C, 5 h	1.9

nitrogen trap connected to the cell. The sample was then repeatedly subjected to a series of routine TPD procedures consisting of sample pretreatment, oxygen adsorption and temperature programmed desorption. As pretreatment, the sample was exposed to 100 Torr of oxygen for 1 h followed by evacuation ($<10^{-5}$ Torr) at 600 °C for 1 h. Oxygen was usually adsorbed according to one of the following ways.

Procedure I: After being cooled to the desired temperature, the sample was exposed to an oxygen atmosphere (100 Torr) for 1 h and then evacuated for 15 min before further cooling down to 10 °C within 30 min *in vacuo*.

Procedure II: On the introduction of 100 Torr of oxygen at 600 °C, the sample was made to cool at a rate of *ca.* 10 °C/min down to 10 °C, at which the system was evacuated for 15 min.

After these manipulations, a carrier gas (helium) was diverted to flow through the reactor at a rate of 30 cm³/min and the programmed heating was started. The heating rate was 21±1 °C/min unless specified otherwise. The thermally desorbed oxygen was recorded as a TPD chromatogram, its amount being evaluated from the peak area of the chromatogram.

In order to examine the reactivity of adsorbed oxygen toward hydrogen, various amounts of hydrogen were injected in a pulse at specified temperatures, with a helium carrier (30 cm³/min). After ten min from the hydrogen pulse, the sample was cooled to 10 °C and heated up to take a TPD chromatogram. In all these runs, a liquid nitrogen trap was equipped between the TPD cell and the detector in order to separate off water vapor desorbed from the reacted surface. The monitored gas was identified to be oxygen alone throughout the experiments by gas chromatography and mass spectroscopy.

Results and Discussion

Desorption Chromatograms of Oxygen from Fe_2O_3. Desorption chromatograms of oxygen from Fe_2O_3 were found to vary with the sample preparation and conditions of oxygen adsorption. Figures 1 and 2 show typical examples obtained for Fe_2O_3-I and II, respectively, after oxygen adsorption was performed at various temperatures by Procedure I (all runs except 1 and 6) or II (runs 1 and 6) as indicated. Although the amounts

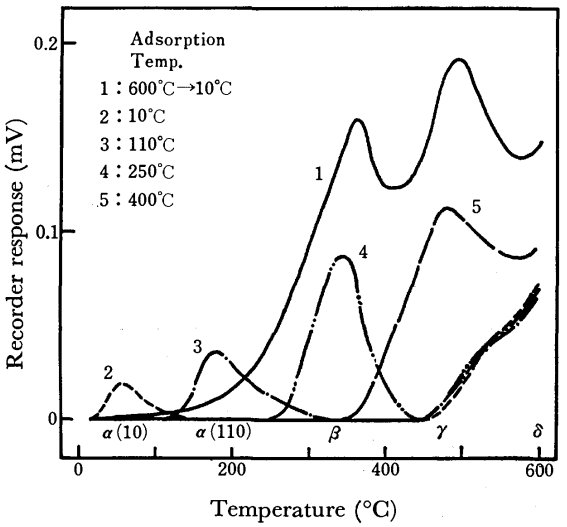

Fig. 1. TPD chromatograms of oxygen adsorbed on Fe_2O_3-I.

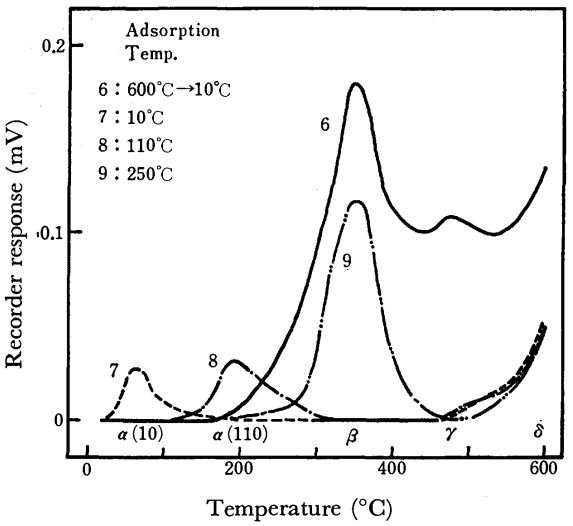

Fig. 2. TPD chromatograms of oxygen adsorbed on Fe_2O_3-II.

of oxygen desorption are dependent upon sample preparation to some extent, oxygen desorption is reproducible in the same temperature range irrespective of the sample preparation if oxygen has been adsorbed under the same conditions. The change in adsorption temperature T_{ad}, however, cause pronounced effects on TPD chromatograms, since it affects the states and concentrations of adsorbed oxygen. Thus, for various T_{ad} values five desorption peaks appear whose maxima appear respectively at 50—70 (α_{10}), 180—200 (α_{110}), 350—380 (β), 480—490 (γ), and >600 °C (δ). The subscripts attached to α for the first two peaks denote T_{ad}. The peaks are assigned to the same kind of oxygen species adsorbed on a heterogeneous surface. The desorption peak δ appears invariably in all the chromatograms with similar shapes and magnitudes, suggesting that it is a sort of desorption of lattice oxygen from Fe_2O_3 toward a non-stoichiometric oxide. In contrast, the other peaks change in magnitude markedly with the conditions of oxygen adsorption and can be attributed to adsorbed oxygen species. β and γ peaks, which also appear in chromatograms 1 and 6, can be assigned to respective kinds of oxygen adsorbates. On the other hand, a marked feature of the α species is the desorption temperature shifts over a wide range from room temperature to *ca.* 300 °C, depending on T_{ad}.

The amounts of desorbed (or adsorbed) oxygen per unit surface area (V_d) were determined from the

Table 2. Amounts of desorbed oxygen from the ferric oxides

Adsorption temp (°C)	Desorption peak	Amount of desorbed oxygen (cm³/m²)		
		Fe_2O_3-I	Fe_2O_3-II	Fe_2O_3-III
10	α(10)	1.88×10^{-4}	2.19×10^{-4}	4.86×10^{-4}
110	α(110)	4.34×10^{-4}	3.00×10^{-4}	3.96×10^{-4}
250	β	9.22×10^{-4}	1.07×10^{-3}	1.80×10^{-3}
400	γ	1.73×10^{-3}		3.81×10^{-3}
600→10	β+γ+δ[a]	4.39×10^{-3}	3.15×10^{-3}	1.18×10^{-2}

a) Total oxygen desorbed below 600 °C.

desorption peak areas, data for the three samples being summarized in Table 2. For runs in which Procedure II was used for oxygen adsorption, only the total amounts of oxygen desorbed below 600 °C ($\beta+\gamma+\delta$) are given. The amounts are in the order $\alpha_{10} \lesssim \alpha_{110} < \beta < \gamma$, differing somewhat with sample. We can estimate the surface coverage from these values. The amount of $\beta+\gamma+\delta$, for example, is 4.39×10^{-3} cm^3/m^2 or 1.18×10^{13} oxygen molecules/cm^2 for Fe_2O_3-I. If we assume that the adsorbent surface is (0001) or (11$\bar{2}$0) plane of α-Fe_2O_3 which contains 4.55×10^{14} or 2.92×10^{14} surface iron atoms/cm^2, respectively, the above value corresponds to only *ca.* 0.02 or 0.04 O_2 molecules per surface iron atom, respectively. This suggests that some sort of surface defect is responsible for the oxygen adsorption. There is little possibility that oxygen adsorbs on a surface impurity, since the desorption of oxygen is inherent for each oxide and the amount of desorbed oxygen seems to be related with the heat of oxide formation ($-\Delta H_f^\circ$).[9]

It is interesting to compare the adsorptive properties of Fe_2O_3 (a n-type semiconductor) and NiO (a p-type semiconductor). The TPD experiments show that the surface coverage of adsorbed oxygen is nearly the same for both oxides. This suggests that, contrary to the accepted view, the type of semiconductor has little effect on the amount of adsorbed oxygen.

Sample preparation affects only the relative amounts of desorption peaks, the essential nature of the oxygen desorption (or adsorption) remaining unaffected. Thus the experiments were performed only with Fe_2O_3-I. Interconversion between the oxygen adsorbates is negligible during the course of evacuation, cooling, and heating applied. For instance, chromatogram 4 which shows a single desorption peak, β, indicates that none of β adsorbates were converted into γ, α_{110}, or α_{10} during the TPD experiments. Similar conclusions can be drawn from the other runs.

Characterization of Desorption Peaks. Oxygen desorption below 350 °C was investigated in detail. Figure 3 shows the effect of oxygen adsorption temperature (T_{da}) on the TPD chromatogram. In each case

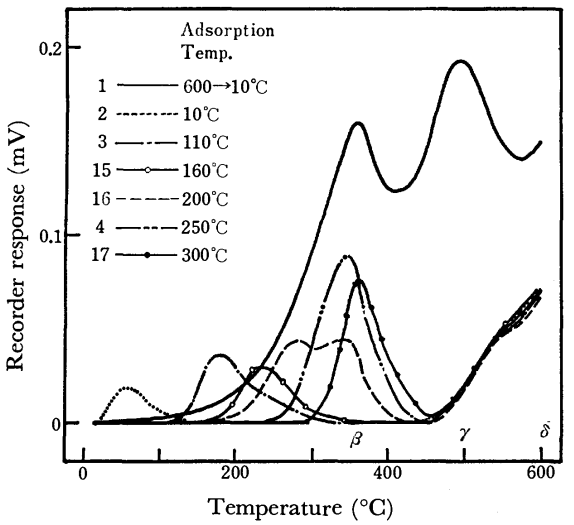

Fig. 3. Effect of the adsorption temperature on TPD chromatograms of oxygen.

of T_{ad}=10, 110, and 160 °C, a single desorption peak appears below 400 °C; oxygen desorption starts at a temperature near T_{ad}, reaches a maximum around a temperature 40—80 °C higher than T_{ad} and then decreases with a very long tailing. With T_{ad}=200 °C, however, there appear two desorption peaks with maxima at 280 and 350 °C, the former apparently being of the same feature as the above and the latter assignable to β desorption. Further increase in T_{ad} to 250 °C again gives rise to a single desorption peak (β) at 350 °C. This indicates that the desorption peak at the lower temperature region shifts continuously with T_{ad}. Such a phenomenon can not be explained in terms of the change in the kind of adsorbed species, but is best understood in terms of a single kind of adsorbate (α) desorbing from the oxide surface with a broad heterogeneity, though the actual nature of the adsorption sites is not clear. It is assumed that, while α adsorbates can take continuous adsorption states with broadly dispersing bonding energies, at a given T_{ad} only α species with a certain range of bonding energies are formed. In connection with such behavior of α desorption, it is noted that remarkable leadings are seen, prior to the β peak (Figs. 1 and 2, runs 1 and 6). These are considered to be partly contributed by the broadly dispersed α desorption. The β peak maxima (350—360 °C) are scarcely affected at all by adsorption conditions, showing little heterogeneity associated with it.

Interactions between oxygen adsorbates were studied as follows.

(1) The sample on which oxygen had been adsorbed at 110 °C was further exposed to an oxygen atmosphere (100 Torr) at 10 °C for 1 h. The results coincided with these in chromatogram 3, indicating that the presence of α_{110} inhibits adsorption in α_{10}. Probably the oxide surface had been saturated with α_{110}, no more room being left for α_{10}.

(2) After β species was adsorbed in the same way as for chromatogram 4, the sample was further exposed to 100 Torr of oxygen at 110 °C for 1 h. The chromatogram obtained showed two desorption peaks of α_{110} and β. The amount of α_{110}, 2.1×10^{-4} cm^3/m^2, was about a half of that for chromatogram 3, whereas that of β, 9.1×10^{-4} cm^3/m^2, was almost the same as for chromatogram 4. Suppression of α_{110} as compared with chromatogram 3 suggests a steric or electrostatic hindrance by β species.

(3) A sample, exposed to 100 Torr of oxygen at 600 °C for 1 h in advance, was cooled down to 10 °C at a rate of *ca.* 10 °C/min in the same atmosphere, with pause at 400 °C for 1 h. The resulting chromatogram was in precise agreement with chromatogram 1. This shows that all the adsorption sites for β and γ are fully occupied in chromatogram 1 (Procedure II), and that β and γ do not interact with each other, or in other words, they adsorb on independent adsorption sites.

For β and γ species, the activation energies of desorption were measured on the basis of the equations derived by Cvetanovic and Amenomiya.[1] When the sample temperature increases linearly with time at a heating rate b and desorption takes place from a homogeneous surface without appreciable readsorption,

we obtain Eqs. 1 and 2, for the first order and second order desorptions, respectively.[2,10,11]

$$2\ln T_M - \ln b = \frac{E_d}{RT_M} + \ln\frac{E_d v_m}{Rk_0} \quad (1)$$

$$2\ln T_M - \ln b = \frac{E_d}{RT_M} + \ln\frac{E_d v_m^2}{2Rk_0} - \ln v_m\theta_M \quad (2)$$

Here T_M is the temperature of the desorption peak maximum, v_m the amount of adsorbate at the full surface coverage, θ_M the surface coverage at the peak maximum, and k_0 and R are constants. In the first order desorption, when T_M is measured as a function of b, E_d can be obtained from the plots of $(2\ln T_M - \ln b)$ *vs.* $1/T_M$. For the second order desorption, the computer simulation analyses of TPD chromatograms[12] show that θ_M is little affected by b if the initial surface coverage is kept constant. Based on Eq. 2, the conditions allow us to evaluate E_d of the second order desorption also from the same plots as above. This means that we can estimate E_d, at least as an approximation, from the same plots without knowing exact desorption orders. Recently Konvalinka *et al.* reached the same conclusion by computer simulation analyses.[13] Such an approximation is permissible only for the homogeneous surface.[14]

Table 3. Temperature programmed desorption of β and γ oxygen

β oxygen			γ oxygen		
b °C/min	T_M K	V_d cm³/m²	b °C/min	T_M K	V_d cm³/m²
10.0	609	2.44×10^{-3}	9.1	745	1.27×10^{-3}
			9.5	745	1.31
15.0	616	2.46	14.5	755	1.34
20.0	624	2.48	18.5	759	1.24
25.0	632	2.46	22.3	761	1.16
30.0	641	2.42	29.0	766	1.42

b heating rate, T_M peak temperature, and V_d desorbed amount.

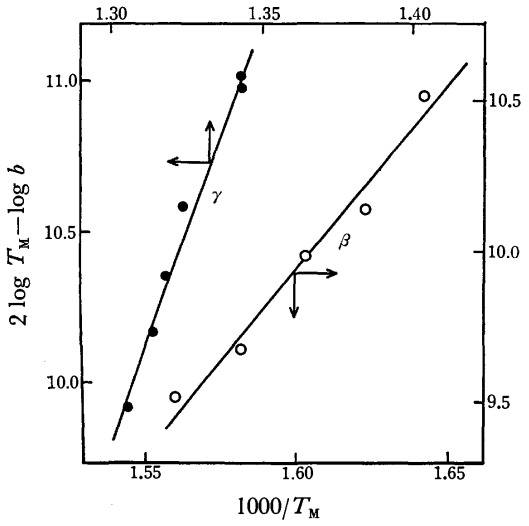

Fig. 4. Activation energy of desorption for β and γ adsorbates.

The analyses were applied to β and γ desorption. In order to obtain respective desorption peaks in adequate magnitudes, oxygen adsorption was performed by Procedure II for β, and by Procedure I for γ at 410 °C. In the analyses of β, the contribution of α adsorbates to the leading part was disregarded. The results are summarized in Table 3. For both cases of β and γ, T_M increases with increase in b. The plot of $(2\ln T_M - \ln b)$ *vs.* $1/T_M$ gave straight lines in agreement with the above equations (Fig. 4). From the slopes, the activation energies for β and γ were determined to be $E_d(\beta)=23.8$ and $E_d(\gamma)=54.6$ kcal/mol, respectively.

The desorption orders for β and γ remain undetermined. Phenomenologically, differentiation of the desorption order can be made according to whether or not T_M is independent of the amount of adsorbates (V_d) at a constant heating rate. No experiments were carried out for the sake of confirmation. However, there is some evidence that β and γ desorption are of the first and second order, respectively. Figure 3 shows that T_M of β desorption is almost unchanged with a change in magnitude of the desorption peak (runs 1, 4, 16, and 17), suggesting the first order desorption. On the other hand, T_M of γ desorption shifts to the higher side with a decrease in V_d (Figs. 6 and 7), indicating the second order desorption.

Winter[15] has studied the isotopic exchange reaction of oxygen over α-Fe_2O_3 pretreated in various ways, and found that the activation energy of the reaction is 19—27 kcal/mol at 260—400 °C. The value is in good agreement with $E_d(\beta)$. It appears that the rate determining step of the reaction is the desorption of molecular oxygen from the surface, in line with Winter's suggestion.

Reaction of Adsorbed Oxygen with Hydrogen. The oxygen adsorbates were found to react easily with hydrogen. After oxygen adsorption by Procedure II, the sample was brought in contact with a hydrogen pulse (0.025—0.200 cm³ (STP)) at selected temperature.

The effect of the pulse (reaction) temperature on the TPD chromatogram is shown in Fig. 5. The hydrogen pulse, 0.05 cm³, is twice the amount necessary to convert all the adsorbed oxygen into H_2O. The left part of the peak β disappears at 80 °C or below. α adsorbates are consumed simultaneously under these conditions, since this part is partly contributed by the α desorption as mentioned above. With an increase in temperature up to 188 °C, increasing amounts of β are consumed. Such consumption of β adsorbates (and α in part) is coupled with a roughly proportional increase in γ desorption. Thus the γ desorption becomes the largest after the hydrogen pulse at 188 °C. It was cinfirmed that the γ species also reacts with hydrogen above 300 °C.

The effect of the amount of hydrogen pulse at 125 °C on TPD chromatogram is shown in Fig. 6. Increase in pulse amount up to 0.2 cm³ causes γ desorption to increase at the expense of β (and α), in a similar manner to that above. Since the injection of 1.0 cm³ of hydrogen gave a chromatogram almost the same as chromatogram 30, it is concluded that γ adsorbates are inactive to hydrogen at 125 °C. Whilst all the adsorbates are

able to react with hydrogen under adequate conditions, α and β adsorbates are much more reactive than γ.

Why does the γ adsorbates increase coupled with the consumption of β (and α)? For each run in Figs. 5 and 6, the amounts of decrease in $\beta(V_{dec})$ and increase in $\gamma(V_{inc})$ were determined from the respective peak areas. It was found that the relation $V_{inc}/V_{dec} \simeq 1/2$ holds in all runs (Table 4). To account for this relation, we assume that α and β adsorbates are molecular while γ is atomic, and that the molecular species reacts with hydrogen at 50—188 °C to leave the atomic species (γ) behind. The reaction may be represented as follows, if the electronic states of adsorbates are disregarded.

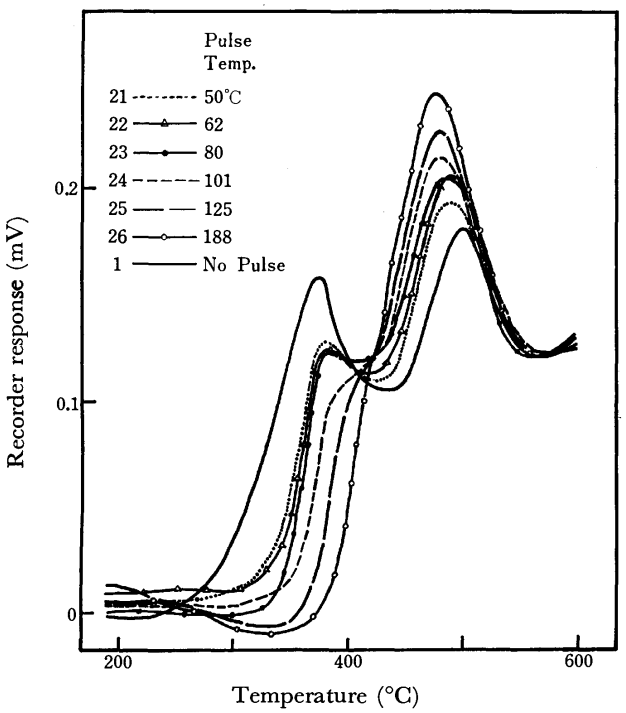

Fig. 5. TPD chromatograms of oxygen adsorbed on Fe_2O_3-I after the reaction with hydrogen pulsed at various temperature.

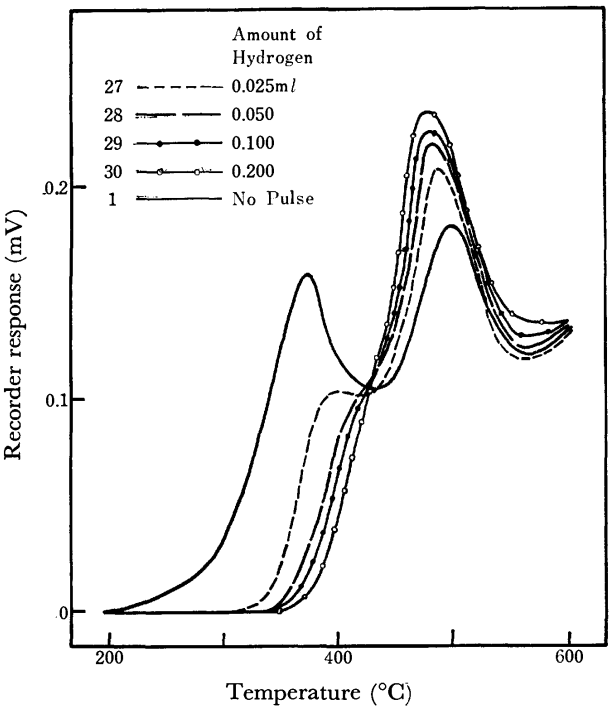

Fig. 6. Influence of the pulse amounts of hydrogen on TPD chromatograms of oxygen adsorbed on Fe_2O_3-I.

Table 4. Reaction of oxygen adsorbed on Fe_2O_3-I with hydrogen

Run No.	Reaction temp (°C)	Amount of hydrogen pulse (cm^3)	Decrease in β, V_{dec} (cm^3/m^2)	Increase in γ V_{inc} (cm^3/m^2)	$\frac{V_{inc}}{V_{dec}}$
21	50	0.05	0.65×10^{-3}	0.22×10^{-3}	0.34
22	62	0.05	0.70	0.38	0.54
23	80	0.05	0.95	0.44	0.46
24	101	0.05	1.10	0.59	0.53
25	125	0.05	1.52	0.69	0.45
26	188	0.05	1.79	0.91	0.51
27	125	0.025	1.31	0.53	0.40
28	125	0.050	1.52	0.69	0.45
29	125	0.100	1.77	0.95	0.54
30	125	0.200	1.79	1.14	0.64

$$O_2(ad) + H_2 \longrightarrow O(ad) + H_2O$$

Since adsorption in γ must have been saturated after the oxygen adsorption by Procedure II, the increase of adsorbates indicates that additional sites for γ adsorption are created by the above reaction. It was confirmed that oxygen adsorption by Procedure II after the pulse reaction gave precisely the same TPD chromatogram as in run 1. This indicates that the surface can be brought back reversibly to the original state during the course of adsorption. It seems that the hydrogen pulse creates additional γ sites to accommodate atomic oxygens. It is possible that β sites are made to turn into γ sites tempolarily due to the chemical reaction involved.

The assumption that α and β adsorbates are molecular is not unreasonable, considering that they form or desorb at relatively low temperatures. β desorption shows a feature of the first order desorption in which the desorption temperature is little affected by the surface coverage. In contrast, the desorption temperature for γ is dependent on the surface coverage as exemplified by chromatograms in Figs. 5 and 6, a feature of the second order desorption or the dissociative adsorption. The plots of log V_{dec} *vs.* inverse of the pulse temperature give a straight line. From the slope, the activation energy for the above reaction was obtained as 4.5 kcal/mol, which may correspond to the energy of rupturing O–O bond in the molecular adsorbates.

There is no definite evidence to indicate the electronic states of α, β, and γ adsorbates. However, many metal oxides have been known to adsorb oxygen as O_2 or O_2^- at relatively low temperatures, while adsorption as O^- or O^{2-} is favored at higher temperatures. At present, we assume tentatively that α, β, and γ adsorbates are O_2 or O_2^-, O_2^-, and O^-, respectively.

The reactivity of adsorbed oxygen exhibits very interesting features not so far foreseen, though the assumption used to interpret them needs further verifica-

tion. This kind of information would be important for the understanding of catalytic oxidations.

References

1) R. J. Cvetanović and Y. Amenomiya, *Adv. Catal.*, **17**, 103 (1967).
2) M. Smutek, S. Cerny, and F. Buzek, *Adv. Catal.*, **25**, 343 (1975).
3) M. Iwamoto, Y. Yoda, M. Egashira, and T. Seiyama, *J. Phys. Chem.*, **80**, 1989 (1976).
4) M. Iwamoto, K. Maruyama, N. Yamazoe, and T. Seiyama, *J. Phys. Chem.*, **81**, 622 (1977).
5) G. C. A. Shuit, *ACS Adv. Chem. Ser.*, **76**, 261 (1968).
6) G. K. Boreskov, V. V. Popovskii, and V. A. Sazonov, *Proc. 4th Intern. Congr. Catalysis, Moscow*, 1968, Vol. 1, p. 439.
7) M. Misono, Y. Nozawa, and Y. Yoneda, *Proc. 6th Intern. Congr. Catalysis, London*, 1976, Vol. 1. p. 386.
8) B. Halpern and J. E. Germain, *J. Catal.*, **37**, 44 (1975),
9) M. Iwamoto, Y. Yoda, N. Yamazoe, and T. Seiyama, *J. Phys. Chem.*, in press.
10) Y. Amenomiya and R. J. Cvetanović, *J. Phys. Chem.*, **67**, 144, 2046, 2705 (1963).
11) J. L. Stakebake, *J. Phys. Chem.*, **77**, 581 (1973).
12) M. Iwamoto and T. Seiyama, unpublished results.
13) J. A. Konvalinka, J. J. F. Sholten, and J. C. Rasser, *J. Catal.*, **48**, 365 (1977).
14) The method of determining E_d over the heterogeneous surface has been investigated: Y. Tokoro, M. Misono, T. Uchijima, and Y. Yoneda, *Bull. Chem. Soc. Jpn.*, **51**, 85 (1978).
15) E. R. S. Winter, *J. Chem. Soc., A*, **1968**, 2889.

The Phosphorescence Spectra of 1,4-Naphthoquinone and Its Alkyl Derivatives in Solutions at 77 K

Akira KUBOYAMA

National Chemical Laboratory for Industry, Shibuya-ku, Tokyo 151

(Received November 28, 1977)

The phosphorescence spectra of 1,4-naphthoquinone (NQ), 2-methyl-, 2,6-dimethyl-, 2,6-diisopropyl-, and 2,6-di-*t*-butyl-NQ's in various kinds of solutions at 77 K were studied. The phosphorescence bands of NQ and 2,6-di-*t*-butyl-NQ in all the solutions and those of the other NQ's in saturated hydrocarbon solutions are assigned to the n,π^* band. In the ethanol solution, 2-methyl-NQ shows a dual phosphorescence, the lifetimes of which are different and which depends on the excitation wavelength. In the Daifloil solutions, 2-methyl- and 2,6-dimethyl-NQ's also show a dual phosphorescence. In the toluene solutions, these two NQ's show remarkably broad phosphorescence bands. These facts are discussed on the basis of the electronic structures at the excited states of these NQ's.

Heretofore, we have studied the n,π^* phosphorescence spectra of various kinds of quinones in solutions at 77 K.[1-3] In many organic solvents, 1,4-naphthoquinone (NQ) shows n,π^* phosphorescence at 77 K, while 2,3-dimethyl-NQ shows no n,π^* phosphorescence. In this connection, it is interesting to study the phosphorescence spectra of other NQ alkyl derivatives. However, few studies of the phosphorescence spectra of NQ alkyl derivatives have been reported.[4] In this work, we have studied the phosphorescence spectra of NQ, 2-methyl-, 2,6-dimethyl-, 2,6-diisopropyl-, and 2,6-di-*t*-butyl-NQ's in various kinds of solutions at 77 K.

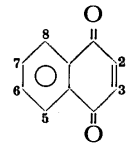

(NQ)

Experimental

Measurements. The phosphorescence spectra and their lifetimes in solutions at 77 K have been measured using an Aminco-Bowman spectrofluorophotometer in the manner described in previous papers.[1-3] Hg 313 and 365 nm lines of a Hanovia 150W xenon-mercury lamp were used as the exciting light. Two photomultipliers, HTV R106 and R105UH, were used for the measurements of phosphorescence spectra and their lifetimes respectively. The spectral response of the photomultiplier tube and the spectral transmittance of the monochromator have not been taken into account. The concentrations of sample solutions ranged from 10^{-3} to 10^{-5} mol/dm^3. The solvents used were normal paraffins (hexane, heptane, and octane), methylcyclohexane, ethanol, Daifloil (polymers of trifluorochloroethylene), and toluene. Except for the case of normal paraffins, all the solutions formed the glass state at 77K.

Materials. Commercially-available NQ was purified by active-carbon treatment in cyclohexane (mp 124.3—125.3 °C). Commercially-available 2-methyl-NQ was purified by the zone-melting method (mp 106.8—107.4 °C). 2,6-Dimethyl-, 2,6-diisopropyl-, and 2,6-di-*t*-butyl-NQ's[5,6] were synthesized from 2,6-dimethyl, 2,6-diisopropyl, and 2,6-di-*t*-butylnaphthalenes respectively. 2,6-Dimethyl-NQ was purified by vacuum sublimation, and the others, by recrystal lization from ethanol (mp 138.0—139.0 °C, 62.5—63.5 °C, and 84.0—85.0 °C respectively). Spectro-grade hexane, heptane, methylcyclohexane, and toluene of the Dozin Yakukagaku Co., spectro-grade octane of the Tokyo Kasei Kogyo Co., analytical-grade ethanol of the Wako Junyaku Kogyo Co., and Daifloil #1 (mean molecular weight 500) of the Daikin Kogyo Co. were used without further purification.

Results

The phosphorescence spectra of all the NQ's in the saturated hydrocarbon solutions slowly cooled were too weak to be observed, while those in other solutions slowly cooled were almost the same in all respects as those in these solutions rapidly cooled. Therefore, in this paper the phosphorescence spectra of the sample solutions rapidly cooled are reported. The main phosphorescence spectra obtained are shown in Figs. 1—7. The wavelengths of the main peaks and the observed lifetimes of the phosphorescence spectra are shown in Tables 1 and 2 respectively. No phosphorescence spectrum can be observed for 2,6-di-*t*-butyl-NQ in the normal paraffin solutions. The spectrum of 2,6-dimethyl-NQ in the toluene solution is similar to that of 2-methyl-NQ in Fig. 7.

Discussion

First, the phosphorescence spectra of the saturated hydrocarbon solutions of the NQ's will be discussed. They may be assigned to the n,π^* phosphorescence

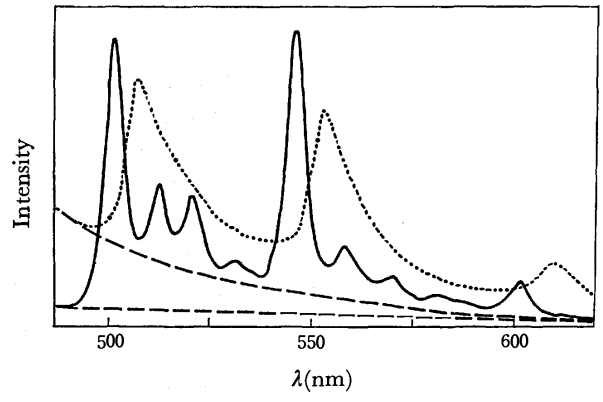

Fig. 1. Phosphorescence spectra of NQ and 2,6-(t-Bu)$_2$-NQ in solutions, 77 K.
——: NQ, hexane, ——: 2,6-(t-Bu)$_2$-NQ, methylcyclohexane.

TABLE 1. MAIN PEAK WAVELENGTHS IN THE PHOSPHORESCENCE SPECTRA (nm)

	Methyl-cyclohexane	Hexane	Heptane	Octane	Ethanol	Daifloil	Toluene
NQ	501.5	501.5			498.5	495	493
	547	546.5			541.5	538	539
2-Me-NQ	497	496	496		498.5	497.5	≈521
	541.5	541	498.5		510.5	540.5	≈544.5
			540		541.5		
			544.5				
2,6-Me_2-NQ	496.5		498.5	493.5	513.5	498	≈521
	541		543.5	538	545.5	510	≈547.5
						540	
2,6-(i-Pr)$_2$-NQ	501	501	501		502	500	515
	546.5	545.5	545		546.5	543	547.5
2,6-(t-Bu)$_2$-NQ	507.5				506	504.5	509
	554				550.5	550	553

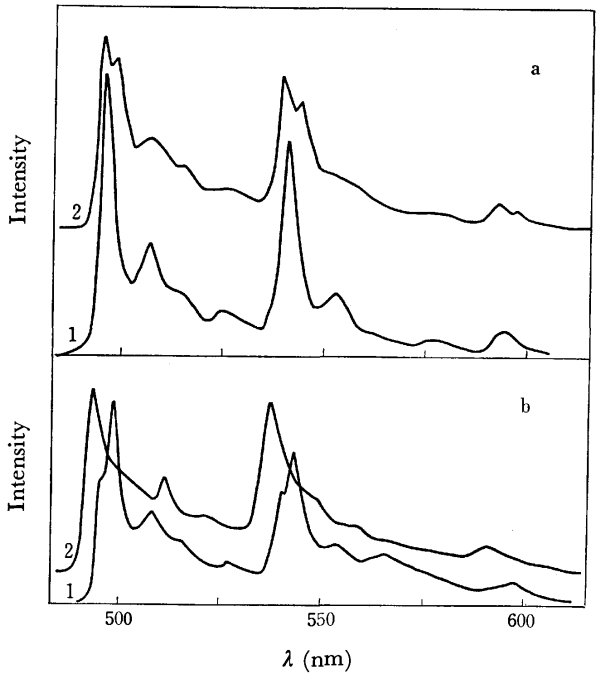

Fig. 2. Phosphorescence spectra of 2-Me- and 2,6-Me_2-NQ's in solutions, 77 K.
a: 2-Me-NQ, 1. hexane, 2. heptane, b: 2,6-Me_2-NQ, 1. heptane, 2. octane.

band, based on their main progressions of the C-O stretching vibration and their short lifetimes, as may be seen in Figs. 1—3 and Tables 1 and 2.[7] In the methylcyclohexane solutions, as may be seen in Table 1, the phosphorescence bands of 2-methyl- and 2,6-dimethyl-NQ's show a blue shift, in comparison with that of NQ, while that of 2,6-diisopropyl-NQ shows no shift and that of 2,6-di-t-butyl-NQ shows a considerable red shift. The blue shift in the cases of 2-methyl- and 2,6-dimethyl-NQ's is characteristic of the n,π^* transition.[8] The red shift in the case of 2,6-di-t-butyl-NQ may be due to the interaction between the t-butyl group and the lone-electron-pair of the carbonyl group located close to it. The shorter lifetime of the phosphorescence band of 2,6-di-t-butyl-NQ than those of the other NQ's, as may be seen in Table 2, may also be due to the same reason.

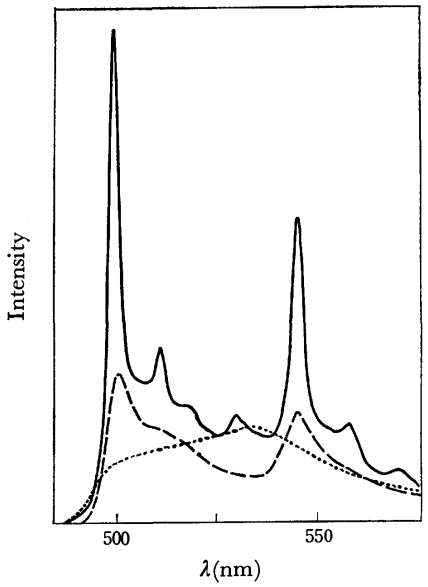

Fig. 3. Phosphorescence spectra of 2,6-(i-Pr)$_2$-NQ in solutions, 77 K.
——: Hexane, ——: heptane, ·····: octane.

As for the Shpol'skii effect,[9] sharp spectra are observed in the normal paraffin solutions, as may be seen in Figs. 1—3. In the heptane solutions of 2-methyl- and 2,6-dimethyl-NQ's, two closely located phosphorescence bands are observed, as in the case of anthraquinone[2] previously reported. It is noticeable that, in 2,6-diisopropyl-NQ, the heptane solution alone shows a sharp band.

Let us turn to the phosphorescence spectra of the

TABLE 2. OBSERVED LIFETIMES OF THE PHOSPHORESCENCE BANDS (ms)

	Heptane	Ethanol	Daifloil	Toluene
NQ	$\lesssim$0.5	$\lesssim$0.5	1.2	1.3
2-Me-NQ	0.65	1.5	1.6	2.0
2,6-Me_2-NQ	0.75	1.6	1.8	2.1
2,6-(i-pr)$_2$-NQ	0.9	1.6	1.8	2.1
2,6-(t-Bu)$_2$-NQ	$\ll$0.5[a]	$\ll$0.5	$\ll$0.5	$\ll$0.5

a) The datum in the methylcyclohexane solution.

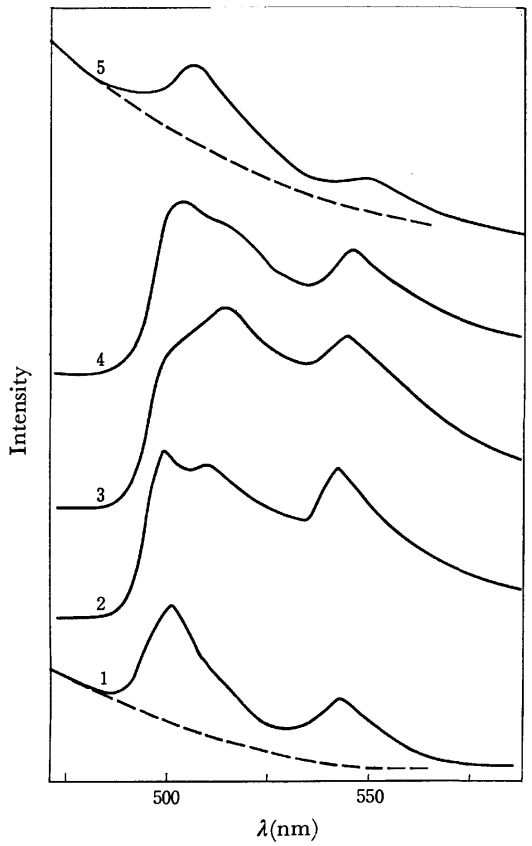

Fig. 4. Phosphorescence spectra of the NQ's in the ethanol solutions, 77 K.
1: NQ, 2: 2-Me-NQ, 3: 2,6-Me_2-NQ, 4: 2,6-(i-Pr)$_2$-NQ, 5: 2,6-(t-Bu)$_2$-NQ.

NQ's in the ethanol solutions. The phosphorescence bands of the NQ's except for 2,6-dimethyl-NQ are assigned to the n,π^* band in the ethanol solutions, since they show clear vibrational structures of the C–O stretching mode and have short lifetimes (Fig. 4 and Tables 1 and 2). The phosphorescence spectrum of 2,6-dimethyl-NQ shows no vibrational structure of the C–O stretching mode and may be assigned to the π,π^* band. From the comparison between Curves 2 and 3 in Fig. 5, we can see that the intensity of the shortest wavelength peak decreases for 2-methyl-NQ with a decrease in the turning-rate of the sector. This means that 2-methyl-NQ shows two closely located phosphorescence bands (the so-called dual phosphorescence[10]) with different lifetimes. The one containing the shortest wavelength sharp peak has a shorter lifetime than the other and may be assigned to the n,π^* band. The other band, which is broad and which shows no C–O stretching vibrational structure, may be assigned to the π,π^* band. In Table 2, the lifetime for 2-methyl-NQ in the ethanol solution is that of the broad band.

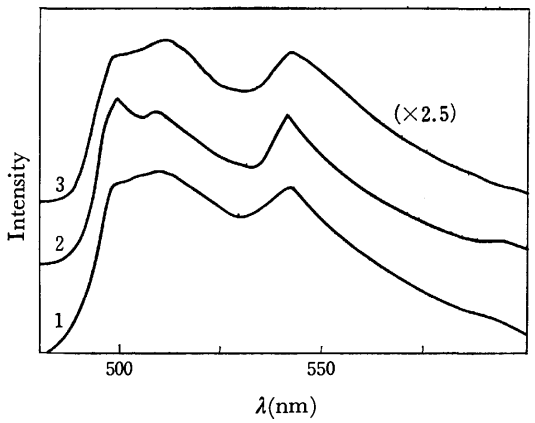

Fig. 5. Phosphorescence spectra of 2-Me-NQ in the ethanol solution, 77 K.
1: 313 nm line ex., sector fast, 2: 365 nm line ex., sector fast, 3: 365 nm line ex., sector slow.

It is considered that the lowest ^{3}(n,π^*) and $^3(\pi,\pi^*)$ levels are higher and lower respectively for 2-methyl-NQ than for NQ[11] as a result of the methyl-group substitution, and that in each quinone these levels are higher and lower respectively in the ethanol solution than in the saturated hydrocarbon solutions, as a result of the hydrogen-bond formation[1] between ethanol and the quinone. Consequently, in the ethanol solution of 2-methyl-NQ, the lowest ^{3}(n,π^*) and $^3(\pi,\pi^*)$ levels may reasonably be assumed to be very close. The above-mentioned dual phosphorescence may result from this closeness of the lowest ^{3}(n,π^*) and $^3(\pi,\pi^*)$ levels of 2-methyl-NQ in the ethanol solution. It is uncertain at this stage whether the two phosphorescences have their origin in like molecules or in differently solvated species. In 2,6-dimethyl-NQ, considering the case of 2-methyl-NQ, the lowest $^3(\pi,\pi^*)$ level may be somewhat lower than the lowest ^{3}(n,π^*) level in the ethanol solution because of the two methyl-group substitution, so only the π,π^* phosphorescence band is observed. The short lifetimes of the phosphorescence bands assigned to the π,π^* band in Table 2 may result from the mixing of the phosphorescent $^3(\pi,\pi^*)$ states with the nearby ^{3}(n,π^*) states.

In 2-methyl-NQ, as may be seen from a comparison between Curves 1 and 2 in Fig. 5, the phosphorescence spectra observed by the two kinds of excitations, the 313 and 365 nm line excitations, where the former corresponds to the excitation to the $^3(\pi,\pi^*)$ state, and the latter to the excitations to both the ^{3}(n,π^*) and $^3(\pi,\pi^*)$ states,[16,17] are different. From this fact it may be concluded that a part of the quinone molecules excited to the $^3(\pi,\pi^*)$ state at the 313 nm line excitation directly transfer to a high-energy triplet state through the intersystem crossing.

Since all the phosphoresence bands of the NQ's in the Daifloil solutions show clear progressions of the C–O stretching vibration and short lifetimes (Tables 1 and 2), these bands may be assigned to the n,π^* band. The phosphorescence band of NQ in the Daifloil solution shows a more considerable blue shift than do those in the saturated hydrocarbon solutions (Table 1). This blue shift may be mainly due to the n-σ type charge-transfer interaction between the lone-pair orbitals of the carbonyl groups of NQ and the σ^*-orbitals of the C–Cl bonds of Daifloil.[3]

The phosphorescence spectrum of 2,6-dimethyl-NQ in the Daifloil solution depends on the turning-rate of the sector (Fig. 6). A similar situation is also observed

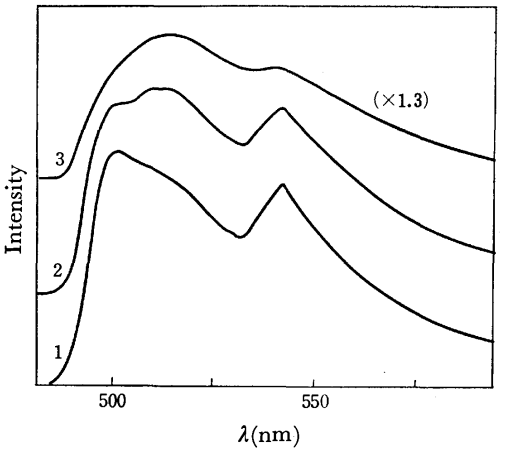

Fig. 6. Phosphorescence spectra of 2,6-Me_2-NQ in the Daifloil solution, 77 K.
1: No sector, 2: sector fast, 3: sector slow.

for 2-methyl-NQ. Therefore, as may be seen in Fig. 6, a dual phosphorescence which consists of a sharp band and a broad band appears in these two NQ's in the Daifloil solutions, as in the case of 2-methyl-NQ in the ethanol solution. The lifetimes for these two NQ's in the Daifloil solutions in Table 2 are those of the broad bands. In this case, the phosphorescence spectra do not depend on the exciting wavelength.

As for the phosphorescence spectra of the NQ's in the toluene solutions, as may be seen in Fig. 7 and Tables 1 and 2, their lifetimes are all short; those of NQ and 2,6-di-*t*-butyl-NQ show a clear vibrational structure

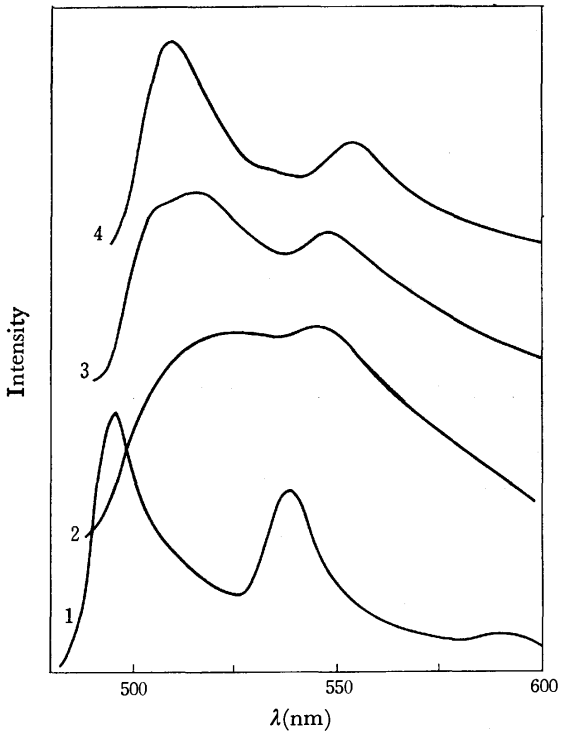

Fig. 7. Phosphorescence spectra of the NQ's in the toluene solutions, 77 K.
1: NQ, 2: 2-Me-NQ, 3: 2,6-(i-Pr)$_2$-NQ, 4: 2,6-(t-Bu)$_2$-NQ.

of the C–O stretching mode, while those of the other NQ's do not show it. Especially those of 2-methyl- and 2,6-dimethyl-NQ's show almost no structure. The former may reasonably be assigned to the n,π^* band, but the latter may be assigned to the π,π^* band, which has the n,π^* character to some extent, in view of their short lifetimes.

The phosphorescence band of NQ in the toluene solution shows a larger blue shift than those in the ethanol and Daifloil solutions (Table 1) as a result of the π-π type charge-transfer interaction between toluene and NQ.[1] As for the above-mentioned phosphorescence bands of 2-methyl- and 2,6-dimethyl-NQ's in the toluene solutions, the phosphorescent π,π^* states may mix with the triplet charge-transfer states also, for they are remarkably broad. On the other hand, the phosphorescence band of NQ in the toluene solution does not show such a broadening. The reason for this may be that, in NQ, it is difficult for the phosphorescent n,π^* state to mix with the triplet charge-transfer state because of the small overlapping between the donor π-orbital of toluene and the n-orbital of the carbonyl oxygen atoms of NQ.

As for the observed lifetimes of the phosphorescence bands of the NQ's in Table 2, those for all the NQ alkyl derivatives except for 2,6-di-*t*-butyl-NQ are, in each kind of solution, a little longer than that for NQ. The short lifetimes in the case of 2,6-di-*t*-butyl-NQ have been discussed before. It is noticeable that the observed lifetimes are, in each quinone, regularly in the following order of solvents: toluene>Daifloil>ethanol>heptane.

References

1) A. Kuboyama and S. Matsuzaki, *Bull. Chem. Soc. Jpn.*, **40**, 2475 (1967); *Rep. Gov. Chem. Ind. Res. Inst., Tokyo*, **64**, 105 (1969).
2) A. Kuboyama, *Bull. Chem. Soc. Jpn.*, **43**, 3373 (1970); *Rep. Gov. Chem. Ind. Res. Inst., Tokyo*, **66**, 176 (1971).
3) A. Kuboyama and M. Anze, *Nippon Kagaku Kaishi*, **1972**, 229; *J. Nat. Chem. Lab. Ind.*, **67**, 165 (1972); A. Kuboyama and S. Matsuzaki, *Nippon Kagaku Kaishi*, **1973**, 2248; *J. Nat. Chem. Lab. Ind.*, **69**, 69 (1974).
4) N. A. Shcheglova and D. N. Shigorin, *Russ. J. Phys. Chem.*, **38**, 684 (1964); G. D. Baruah, S. N. Singh, and R. S. Singh, *Bull. Chem. Soc. Jpn.*, **42**, 3572 (1969); T. Vo Dinh and U. P. Wild, *Z. Phys. Chem. (Leipzig)*, **251**, 395 (1972); J. J. Aaron and J. D. Winefordner, *Anal. Chem.*, **44**, 2122 (1972).
5) R. Weissberger and O. Kruber, *Ber.* **52**, 356 (1919); L. F. Fieser and A. M. Seligmann, *J. Am. Chem. Soc.*, **56**, 2690 (1934).
6) H. M. Crawford and M. C. Glesmann, *J. Am. Chem. Soc.*, **76**, 1108 (1954).
7) In the heptane solution of NQ, a broad n,π^*-type phosphorescence band is observed besides a sharp n,π^*-type band; the former is far stronger and at wavelengths longer by *ca.* 750 cm^{-1} than the latter. Since the relative intensity of the former to the latter decreases with the lowering of concentration of the sample solutions, the former may be due to the aggregates.
8) A. Kuboyama, *Bull. Chem. Soc. Jpn.*, **35**, 295 (1962); *Rep. Gov. Chem. Ind. Res. Inst., Tokyo*, **59**, 347 (1964).
9) E. V. Shpol'skii, *Sov. Phys. Usp.*, **3**, 372 (1960); *ibid.*, **5**, 552 (1962); *ibid.*, **6**, 411 (1963).

10) For example, S. -Y. Chu and L. Goodman, *Chem. Phys. Lett*, **34**, 232 (1975); W. Amrein, I. -M. Larsson, and K. Schaffner, *Helv. Chim. Acta*, **57**, 2519 (1974).

11) NQ is thought to have two low-energy $^3(n, \pi^*)$ levels, the energy difference between which is several hundreds cm^{-1}, as in the case of *p*-benzoquinone.[2] In the text, the $^3(n, \pi^*)$ level corresponds to the lower one of them, while the higher one is neglected in order to simplify the discussion. According to the CNDO/S+CI calculations,[13,14] the lowest $^1(n, \pi^*)$ state of NQ is the $^1A_2$ state, so the lowest $^3(n, \pi^*)$ state may also be the $^3A_2$ state, considering the case of *p*-benzoquinone.[12] On the other hand, the lowest $^3(\pi, \pi^*)$ state is the $^3B_2$ state, according to both the CNDO/S+CI[13,14] and P-P-P[15,16] calculations.

12) H. P. Trommsdorff, *J. Chem. Phys.*, **50**, 5358 (1972); H. Veenvliet and D. A. Wiersma, *Chem. Phys.*, **8**, 432 (1975); Y. Miyagi, M. Koyanagi, and Y. Kanda, *Chem. Phys. Lett.*, **40**, 98 (1976).

13) J. DelBene and H. H. Jaffe, *J. Chem. Phys.*, **48**, 1807 (1968); R. L. Ellis, G. Kuehnlenz, and H. H. Jaffe, *Theoret. Chim. Acta*, **26**, 131 (1972).

14) Y. Sato and A. Kuboyama, to be published.

15) R. Pariser and R. G. Parr, *J. Chem. Phys.*, **21**, 466, 767 (1953); J. A. Pople, *Trans. Faraday Soc.*, **49**, 1375 (1953).

16) A. Kuboyama, S. Matsuzaki, M. Takagi, and H. Arano, *Bull. Chem. Soc. Jpn.*, **47**, 1604 (1974); *J. Nat. Chem. Lab. Ind.*, **69**, 492 (1974).

17) S. Nagakura and A. Kuboyama, *Nippon Kagaku Zasshi*, **74**, 499 (1953); S. Nagakura and A. Kuboyama, *J. Am. Chem. Soc.*, **76**, 1003 (1954).

Relaxation Phenomena after an Area Strain on the Adsorbed Surfaces of Aqueous Solutions of Poly(oxyethylene) Dodecyl Ethers

Masao NAKAMURA* and Shinichi TAKEUCHI

Department of Chemistry, Faculty of Science, Tokai University, Kitakaname, Hiratsuka 259-12

(Received December 10, 1977)

The relaxations were observed after suddenly dilating or compressing the equilibrium surfaces of aqueous solutions of poly(oxyethylene) dodecyl ethers, $C_{12}H_{25}(OC_2H_4)_nOH$ ($n=5$ and 7), at 303 K. The relaxation is expressed as the Maxwell model, with a Hookean surface-area modulus and a Newtonian surface-area viscosity, if the absolute value of an area strain is less than 0.3. The surface-area modulus is dependent upon the amount of surfactant molecules adsorbed in the surface, Γ, regardless of the sign of the area strain. The relaxation time, τ_c, in the case of compression is dependent on Γ, and τ_d in the case of dilation depends on the monodispersed concentration of the surfactant in the bulk solution, C. The surface dilational viscosity, η_0^A, has a maximum around the concentration at which the surface reaches the saturated adsorption. The rate constants for the adsorption and desorption were estimated by determining empirically the functions of $1/\tau_d$ and $1/\tau_c$ with respect to C and Γ respectively.

The rheological properties, especially the resistances against an area strain, of an interface containing adsorbed surfactants have been pointed out as important factors in stabilizing some dispersions through the resistance against the rupture of the interface.[1,2] In a previous paper[3] there has been proposed a concept that a liquid surface with adsorbed surfactant molecules behaves as a two-dimensional open system, in which the number of surfactant molecules changes during the processes, involving some area strains. Thus, when the surface is dilated, an adsorption of surfactant molecules proceeds from the bulk solution to cover the lack in the surface. On the other hand, when the surface is compressed, an excess of surfactant molecules desorbs into the bulk solution. It is the purpose of the present paper to determine quantitatively both the surface-area modulus and the surface-area viscosity of the surface adsorbed with surfactants and, further, relate them to the molecular behavior characterized by the two-dimensional open system. For this purpose, measurements were made of the stress relaxation, with the area strain kept constant, either positive or negative, after suddenly dilating or compressing the surface in equilibrium with the bulk solution at a constant temperature of some nonionic surfactants. That is, the system was simple as possible.

Experimental

The nonionic surfactants, poly(oxyethylene) dodecyl ethers $C_{12}H_{25}(OC_2H_4)_nOH$ ($n=5$ and 7), were kindly provided by Nihon Surfactant Kogyo K.K.; they had a purity above 99% and no distribution of polymerization in the hydrophilic part, as verified by gas chromatography.[4] The solvent was obtained by distilling the alkaline permanganate solution in ion-exchanged water after refluxing for 15 h.

An equilibrium surface was obtained by filling a Langmuir-type trough with a solution, maintaining the temperature constant at 303 K, after sweeping the surface 6 times in 1 h with three glass barriers coated with paraffin; the trough was then allowed to stand for *ca.* 15 h. The area, A_0, of the equilibrium surface was changed suddenly to another area, A, by moving one of the two barriers which had confined the area. As the result, the surface underwent an area strain, $\Delta A/A$ ($\Delta A=A-A_0$). According to the direction of the movement of the barrier, the surface was either dilated or compressed, the sign of area strain being positive or negative. When the area strain was maintained constant, the surface pressure, π, which had deviated as a result of the sudden change in the area, converged gradually to the equilibrium value, π_e. Such phenomena were measured by the Wilhelmy method using a torsion balance with a glass plate.[5] The surface pressure was determined at a precision within ± 0.05 mN m^{-1}, particularly by controlling the level of the surface to avoid any changes in the position of the plate due to the change in the surface level which accompanies the movement of the barrier.

Results and Discussion

The relations of the surface pressure, π, with the time, t, after sudden area strains are shown in Fig. 1 when, for example, the surface of a solution of 3.56×10^{-2} mol m^{-3} of $n=5$ is dilated with various proportions. As may be seen in the figure, π converges to an equal value if the area strain does not exceed 0.67. The converged value was regarded as the equilibrium surface pressure, π_e, of the surface at that temperature. The stress corresponding to the area strain at time t is the

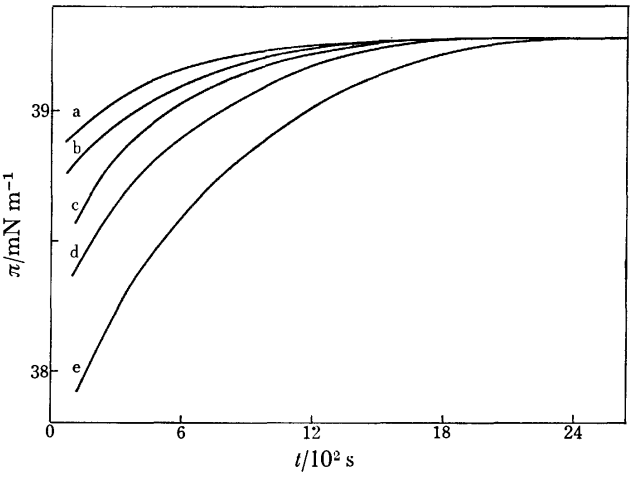

Fig. 1. Surface pressure change with time after sudden area strain for the equilibrium surface of aq $C_{12}H_{25}(OC_2H_4)_5OH$ soln of 3.56×10^{-2} mol m^{-3} at 303 K. Area strain: a 0.15, b 0.2, c 0.3, d 0.44, e 0.67.

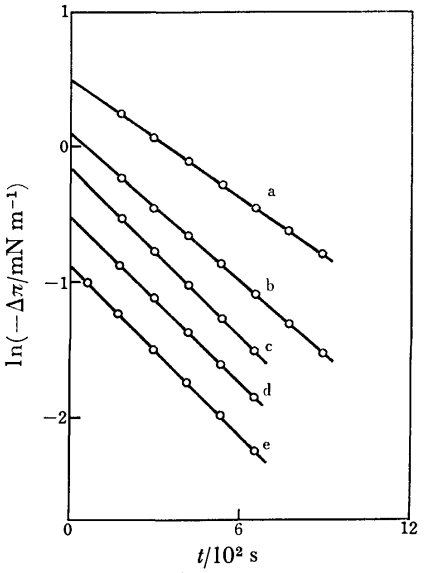

Fig. 2. Stress relaxation plots for the curves in Fig. 1.

difference in the surface pressure from the equilibrium value, $\Delta\pi=\pi-\pi_e$, which has the sign opposite to the strain; it is negative in the case of the dilation and positive in the compression.

The curves in Fig. 1 show the stress relaxation when the area strain is kept constant. The natural logatithm of the absolute value of the stress, which is estimated from the curves in Fig. 1, decreases linearly with time t, as is shown in Fig. 2. The relations between $\Delta\pi$ and t can be expressed by

$$\Delta\pi = K\exp(-t/\tau) \quad (1)$$

for each area stress, where K is the initial stress and τ is the relaxation time; these values are obtained from the value extrapolated to $t=0$ and the slope of the straight line in Fig. 2 respectively.

Equation 1 corresponds correctly to the relaxation of the Maxwell model with the surface-area modulus, ε^A, and the surface-area viscosity, η^A, when the model undergoes a constant area strain, $\Delta A/A$.[6] Accordingly, K, τ, ε^A, and η^A are connected with each other by

$$K = -\varepsilon^A(\Delta A/A), \quad (2)$$

and

$$\tau = \eta^A/\varepsilon^A. \quad (3)$$

Since K has the sign opposite to $\Delta A/A$, as has been mentioned above, ε^A is always positive. Both ε^A and η^A can be obtained from the measured K and τ by applying Eqs. 2 and 3. As a result of repeated measurements of the surfaces with an equal bulk concentration, as is shown in Fig. 3, it may be concluded that both ε^A and η^A are independent of the area strain, $\Delta A/A$; they are, therefore, Hookean and Newtonian respectively if the area strain is less than 0.3. Only if the absolute value of the area strain does not exceed 0.3 were ε^A and η^A confirmed to be Hookean and Newtonian for any surface under investigation, with either the dilation or compression of the surface.

The equilibrium surface tension, σ_e, which was estimated by subtracting the converged surface pressure, π_e, in the relaxation curve from the surface tension of pure water at 303 K, 71.15 mN m^{-1}, [7] is plotted against

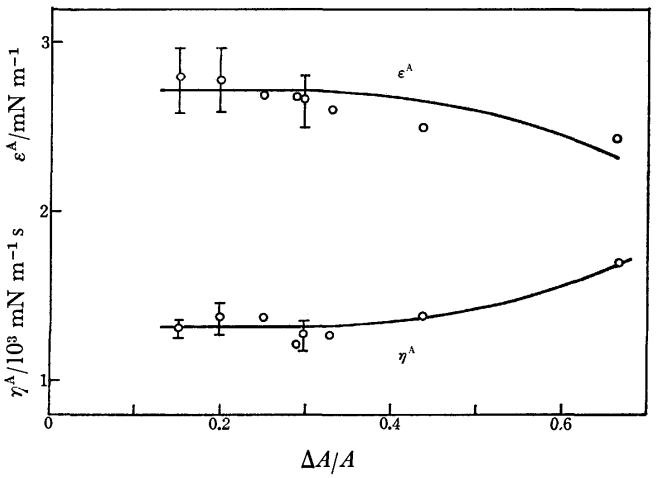

Fig. 3. Surface-area modulus ε^A and surface-area viscosity η^A *vs.* area strain plots for $C_{12}H_{25}(OC_2H_4)_5OH$ soln of 3.56×10^{-2} mol m^{-3}.

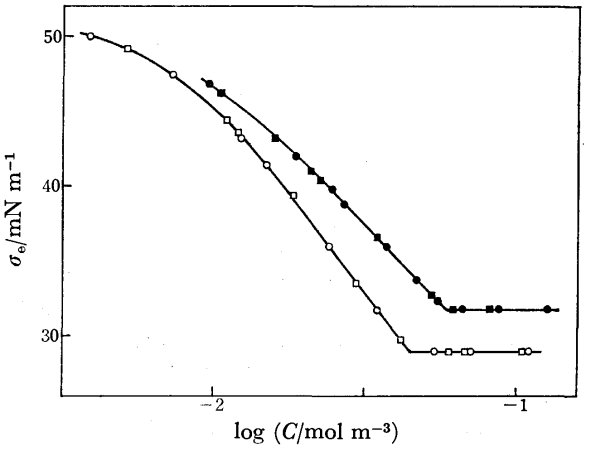

Fig. 4. Equilibrium surface tension *vs.* log concn plots for aq $C_{12}H_{25}(OC_2H_4)_nOH$ soln.
n: 5 7
○ ●: dilation
□ ■: compression

the logarithm of concentration, C, in Fig. 4. All the plots fall on a single curve for $n=5$ and 7, whether π_e is measured by means of the dilation or the compression of the surface. This means that the measured relaxation process is a process approaching a final state, irrespective of the dilation or compression, *i.e.*, it is approaching a true equilibrium state. The concentrations at the break points, corresponding to the critical micelle concentration, CMC, are 4.5 and 5.9×10^{-2} mol m^{-3} for $n=5$ and 7, smaller than the values at 6.8 and 6.9×10^{-2} mol m^{-3} at 278 K measured by Ohba and Takahashi for the same substances,[4] but the differences are not so great in the surface tension. The CMC value for $n=5$ determined by van Voorst Vader *et al.*[8] is 12×10^{-2} mol m^{-3}, far larger and rather close to the value found by our preliminary experiments using the drop-weight method. These facts indicate that the break point on the surface tension *vs.* log C curve, corresponding to the CMC, has a tendency to be smaller in concentration as the surface tension approaches the equilibrium value.

The surface-area modulus, ε^A, increases with an

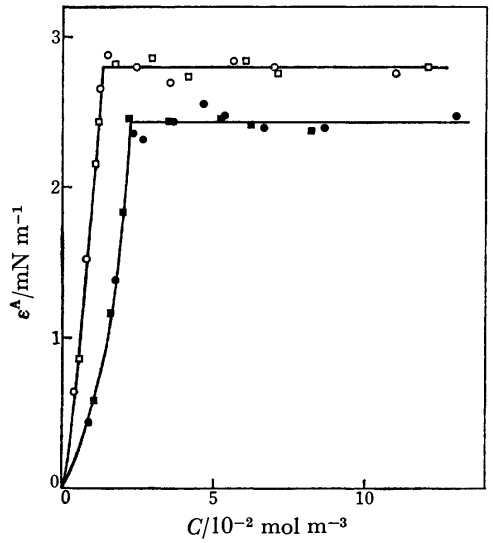

Fig. 5. Surface-area modulus *vs.* bulk concn plots. Marks are the same as in Fig. 4.

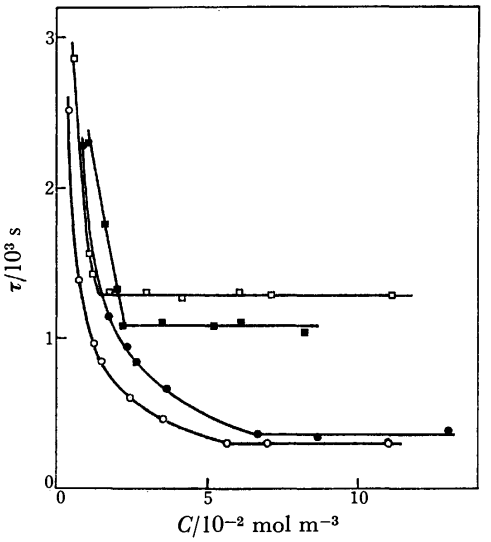

Fig. 6. Relaxation time *vs.* bulk concn plots. Marks are the same as in Fig. 4.

increase in the bulk concentration, C, and reaches a constant value at a concentration, shown in Fig. 5, in which the values do not differ between the cases of dilation and compression. The concentration at which ε^A becomes constant corresponds exactly to the concentration at which σ_e changes into the linear region in Fig. 4, for both $n=5$ and 7. When the Gibbs adsorption equation is applied to the curves in Fig. 4, such concentrations are found to be equal to those at which the surface is saturated with the surfactant molecules, because the amount of adsorption or surface excess is proportional to the tangent of the σ_e *vs.* log C curve. These facts reveal that ε^A increases with an increase in the amount of adsorption on the surface, Γ, and becomes constant when the surface is saturated, even if the concentration increases as the micelles appear in the bulk solution. ε^A can, therefore, be determined only by the state of the surface. The independence of ε^A of the dilation or compression indicates that the initial state of the surface immediately after the area strain applied is the same for both directions of the strain. Taking into account, in addition, the fact that the process converges to the same state, irrespective of the sign of the area strain, it may be concluded that the initial state corresponds to a state of the surface in the lack of surfactant molecules when dilated and to a state with an excess of them in the case of compression, and that ε^A is, therefore, equal to the reciprocal of the compressibility of the adsorbed film when it is assumed to be insoluble.[9] Thus, ε^A reflects the properties characterized by the two-dimensional closed system.

On the other hand, the relaxation time when the surface is dilated, τ_d, is significantly different from the relaxation time when it is compressed, τ_c. Both of them tend to decrease with an increase in the bulk concentration, C, and to attain a constant value. However, the constant value and the concentration of its attainment are quite different between τ_d and τ_c, as is shown in Fig. 6. Thus, the concentration needed for τ_c to become constant is equal to that for ε^A, at which concentration the surface is saturated. The decrease in τ_c in the lower-concentration region may, then, be attributed to the increase in the amount of adsorption on the surface with an increase in the concentration. On the other hand, the concentration at which τ_d is unchanged is in good agreement with the break point in Fig. 4, *i.e.*, the CMC, at which the monodispersed molecules are saturated in the bulk solution. τ_d is affected not by the saturation of the surface with surfactant molecules, but by the monodispersed concentration in the bulk solution.

Since τ_c and τ_d depend only upon the amount of adsorption of the surfactant molecules on the surface, Γ, and only upon the monodispersed concentration of surfactant molecules in the bulk solution, C, respectively, it may be concluded that the measured relaxation processes are the desorption process of the surfactant molecules in excess in the surface due to a negative area strain in the case of compression, and the adsorption process of the surfactant molecules to supply the lack in the surface due to a positive area strain in the case of dilation. Thus, the characteristics of the adsorbed film as an open system appear specifically in the relaxation time against the area strain.

The surface dilational viscosity, η_d^A, and the surface compressional viscosity, η_c^A, which were estimated from ε^A and either τ_d or τ_c according to Eq. 3, are plotted against the bulk concentration, C, in Fig. 7. η_c^A increases with C and has a constant value in the saturated adsorption region. On the other hand, η_d^A increases with C in the dilute region, but decreases in the saturated adsorption region up to the CMC. As a consequence, there appears a maximum in η_d^A around the concentration at which the surface becomes saturated. An adsorbed film, and thus some dispersions stabilized by such a film may be expected to become most stable against the surface-area changes around such a concentration. When a periodical area strain is given to a surface by repeating the dilation and compression in turn, an equal area viscosity has often been assumed for both processes symmetrically.[10] Such an assumption is not consistent with the present results.

If both the adsorption and desorption processes of

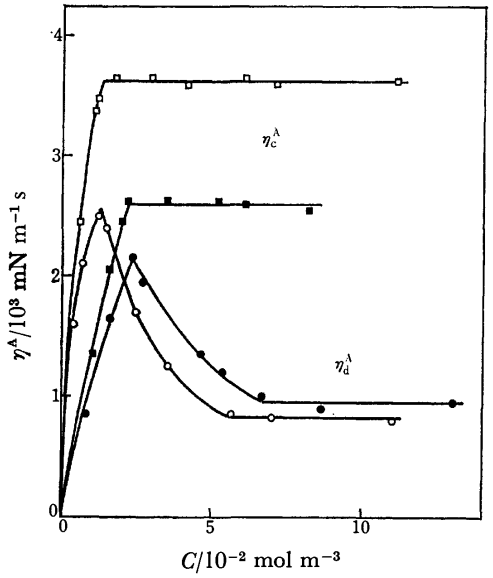

Fig. 7. Surface-area viscosity *vs.* bulk concn plots. Marks are the same as in Fig. 4.
η_d^A: Surface dilational viscosity, η_c^A: surface compressional viscosity.

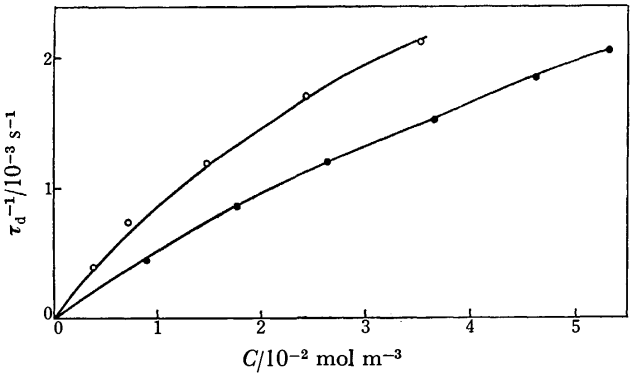

Fig. 8. Reciprocal of relaxation time when dilated *vs.* monodispersed concn plots.
○: $n=5$, ●: $n=7$.

surfactant molecules are represented by a single relaxation process, as in the present results, the activated adsorption mechanism[11] would be more fitting than the diffusion-controlled mechanism,[12] which has been assumed by most authors since Ward and Tordai,[13] because the former mechanism needs a single exponential term with respect to time, while the latter needs plural such terms, according to Sutherland.[14] The reciprocal of the relaxation time would correspond to the rate for the process. When the reciprocal of τ_d is plotted against the bulk concentration below the CMC, curves are obtained for $n=5$ and 7, as is shown in Fig. 8. These curves may be approximated by

$$1/\tau_d = k_d \cdot C^{0.8}, \quad (4)$$

by expressing both axes with the logarithmic scale and by drawing two straight lines for $n=5$ and 7 parallel to each other; here k_d may be regarded as the rate

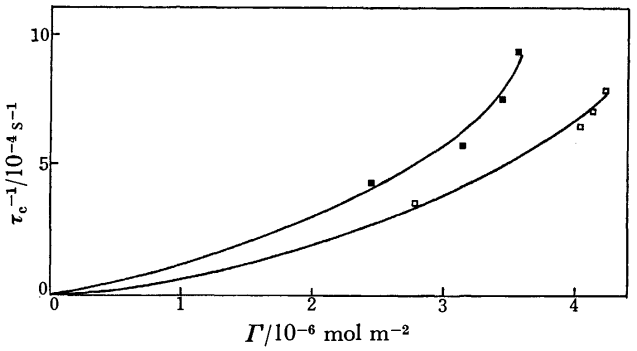

Fig. 9. Reciprocal of relaxation time when compressed *vs.* adsorption amount in the surface plots.
□: $n=5$, ■: $n=7$.

Table 1. Rate constants for the adsorption, k_d, and desorption, k_c, of $C_{12}H_{25}(OC_2H_4)_nOH$ at 303 K

n	$k_d \times 10^2$	$k_c \times 10^{-7}$
5	3.5	4.2
7	2.0	6.5

constant for the adsorption process. On the other hand, if the reciprocal of τ_c is plotted against the amount of adsorption of the surfactant molecules, Γ, evaluated by applying the Gibbs adsorption equation to the curves in Fig. 4, then the curves shown in Fig. 9 are obtained for $n=5$ and 7. The curves may be approximated by

$$1/\tau_c = k_c \cdot \Gamma^2, \quad (5)$$

by treating them similarly to the relation between τ_d and C, where k_c is the rate constant for the desorption process. As is shown in Table 1, the degree of polymerization of poly(oxyethylene) chain, n, has a reverse effect on k_d and k_c. This reveals that the rate-determinig steps can be different for the adsorption and desorption processes.

The authors wish to express their heartly thanks to Professor Mitsuo Muramatsu of Tokyo Metropolitan University for his helpful advice in the preparation of the paper.

References

1) J. K. Kitchener, "Recent Progress in Surface Science," ed by J. F. Danielli, K. G. A. Pankhurst, and A. C. Riddiford, Academic Press, New York (1964), Vol. 1, p. 51.
2) M. van den Tempel, "Surface Chemistry," ed by P. Ekwell, K. Groth, and V. Runnström-Reio, Munksgaad, Copenhagen (1965), p. 306.
3) M. Nakamura, *Bull. Chem. Soc. Jpn.*, **48**, 3013 (1975).
4) N. Ohba and A. Takahashi, *Proc. 5th Intern. Congr. Surface Active Substances*, **2**, 481 (1968).
5) M. Nakamura and T. Sasaki, *J. Sci. Instrum.*, **44**, 855 (1967).
6) T. Alfrey, Jr., and E. F. Gurnee, "Rheology, Theory and Applications," ed by F. R. Eirich, Academic Press, New York (1956), Vol. 1, p. 387.
7) "Landolt-Börstein Tabellen," Springer Verlag (1956), 6 Aufl., II Band, 3 Teil, p. 421.

8) F. van Voorst Vader, Th. F. Erkens, and M. van den Tempel, *Trans. Faraday Soc.*, **60**, 1170 (1964).
9) G. L. Gains, Jr., "Insoluble Monolayers at Liquid-Gas Interface," Interscience Publishers, New York (1966), p. 23.
10) J. Lucassen and M. van den Tempel, *Chem. Eng. Sci.*, **27**, 1283 (1972).
11) M. C. R. Johnson and L. Saunder, *Chem. Phys. Lipids*, **10**, 318 (1973).
12) J. Lucassen and D. Giles, *J. Chem. Soc., Faraday Trans. 1*, **71**, 217 (1975).
13) A. F. H. Ward and L. Tordai, *J. Chem. Phys.*, **14**, 453 (1946).
14) K. L. Sutherland, *Aust. J. Sci. Res., Ser. A*, **5**, 683 (1952).

Hydrogen Bond of 4-Amino-5*H*-[1]benzopyrano[3,4-*c*]pyridin-5-one Derivatives with Alcohols. I. Experimental Considerations

Akira FUJIMOTO and Kozo INUZUKA*

Department of Applied Science, Faculty of Technology, Tokyo Denki University, Kanda, Chiyoda-ku, Tokyo 101

(Received December 21, 1977)

The hydrogen bond between 4-amino-5*H*-[1]benzopyrano[3,4-*c*]-pyridin-5-one (benzopyranopyridine) derivatives including their related compounds (pyridine, aniline, and coumarin) and alcohols (methanol and ethanol) is discussed experimentally in detail. The formation of a hydrogen bond between the nitrogen atom of the benzopyranopyridine ring and the hydroxyl group of methanol was investigated by IR spectral measurements. The equilibrium constants for the formation of hydrogen-bonded 1:1 complexes were determined from the UV spectral data. The enthalpy changes accompanying complex formation were obtained from a knowledge of the temperature dependence of the equilibrium constants. The values of the enthalpy changes range approximately from 4.5 to 5.2 kcal/mol in the benzopyranopyridine–ethanol systems. It may be concluded that the hydrogen bond of the benzopyranopyridine–ethanol system occurs mainly at the nitrogen atom of benzopyranopyridine ring, because the thermodynamic properties for hydrogen bond formation between benzopyranopyridine and ethanol showed a striking resemblance to those of the pyridine–ethanol system. In addition, the presence of an intramolecular hydrogen bond between the amino and carbonyl groups of benzopyranopyridine derivatives was confirmed by means of IR spectra.

The hydrogen bond of organic compounds has been studied by many workers in recent years.[1] However, the hydrogen bond of 4-amino-5*H*-[1]benzopyrano-[3,4-*c*]pyridin-5-one (benzopyranopyridine) derivatives has not been investigated except in the benzopyranopyridine derivative–acetic acid systems.[2] In this paper the hydrogen bond between the benzopyranopyridine derivatives and alcohols was investigated in detail by means of IR and UV spectra. The spectra for the systems of the related compounds of benzopyranopyridine derivatives (pyridine, aniline, and coumarin) and alcohols were also measured. Some discussions were made of the hydrogen bond by comparing the IR and UV spectra of the benzopyranopyridine–alcohol systems with those of the related compound–alcohol systems.

Experimental

Six benzopyranopyridine derivatives **1**—**6** (Fig. 1) were prepared by the methods described by Sakurai *et al.*[3]

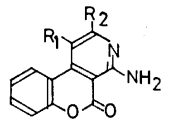

1	R_1= CH_3	R_2=H
2	R_1= n-C_5H_{11}	R_2=H
3	R_1= n-C_9H_{19}	R_2=H
4	R_1= H	R_2=CH_3
5	R_1= H	R_2=n-C_5H_{11}
6	R_1= H	R_2=n-C_9H_{19}

Fig. 1. Benzopyranopyridine derivatives; 4-amino-1-methyl-5*H*-[1]benzopyrano[3,4-*c*]pyridin-5-one (**1**), 4-amino-1-*n*-pentyl-5*H*-[1]benzopyrano[3,4-*c*]pyridin-5-one (**2**), 4-amino-1-*n*-nonyl-5*H*-[1]benzopyrano[3,4-*c*]pyridin-5-one (**3**), 4-amino-2-methyl-5*H*-[1]benzopyrano[3,4-*c*]pyridin-5-one (**4**), 4-amino-2-*n*-pentyl-5*H*-[1]benzopyrano[3,4-*c*]pyridin-5-one (**5**), and 4-amino-2-*n*-nonyl-5*H*-[1]benzopyrano[3,4-*c*]pyridin-5-one (**6**).

These compounds were purified by recrystallization from ethanol several times and then by sublimation *in vacuo* at *ca.* 230 °C. Pyridine was refluxed over barium oxide and distilled. Aniline was dried over potassium hydroxide for a long time, and then fractionated under reduced pressure. Coumarin was recrystallized from ethanol and ligroin several times. The purifications of methanol, ethanol, carbon tetrachloride, and isooctane (2,2,4-trimethylpentane) were done in the usual ways.[4]

The IR and UV spectra were measured using the Hitachi Model 215 infrared spectrophotometer and Hitachi Model 323 spectrophotometer, respectively. All the infrared absorption measurements were carried out at room temperature in carbon tetrachloride solution. All the UV absorption spectra were measured in isooctane solution. The temperature of the UV absorption cells was regulated by use of the Komatsu-Yamato Model CTR-120 electronic cooling circulator within the temperature range between 10 and 50 °C.

Results and Discussion

The compounds **1** and **4** which have the simplest structure among the benzopyranopyridine derivatives synthesized by Sakurai *et al.*[3] are soluble only in carbon tetrachloride (6×10^{-3} mol/l) and isooctane (4×10^{-5} mol/l) at room temperature. However, **2**, **3**, **5**, and **6** have higher solubility in these solvents than **1** and **4** at room temperature. Consequently, the IR and UV spectra of these compounds were measured more easily than those of **1** and **4**. On the basis of these data of **1**—**6** the intermolecular interaction between the benzopyranopyridine derivatives and alcohols was investigated in the non-polar solvents.

First, the formation of an intramolecular hydrogen bond by the benzopyranopyridine derivative was studied by the IR spectral measurement in CCl_4 solution. The asymmetric (ν_{as}) and symmetric (ν_s) stretching frequencies for the NH_2 group of a primary amine can be expressed by the following empirical equation:[5]

$$\nu_s = 345.5 + 0.876\nu_{as}, \quad (1)$$

where ν_s is attributed to the lower frequency and ν_{as}

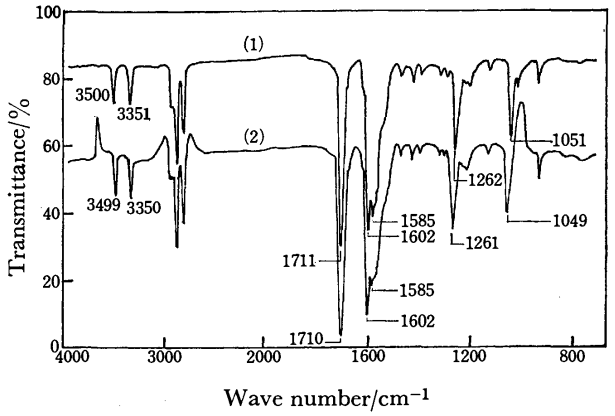

Fig. 2. IR spectra of **6** (1) and the **6**–methanol system (2) in carbon tetrachloride solution. Concentration of **6**: 1.2×10^{-2} mol/l. Concentration of methanol: 9.9×10^{-2} mol/l.

to the higher one. As is shown in Fig. 2, the two bands of the amino group of **6** appear at 3500 and 3351 cm^{-1}. The value of ν_s calculated using Eq. 1 with the value of ν_{as} (3500 cm^{-1}) became 3412 cm^{-1}. This value is higher than the observed value (3351 cm^{-1}). A similar example has been seen for the NH_2 group of *o*-nitroaniline[6] in chloroform. In the case of the *o*-nitroaniline, the corresponding bands appear at 3510 and 3380 cm^{-1}. The observed value (3380 cm^{-1}) for the symmetric frequency is lower than the calculated value (3420 cm^{-1}). This discrepancy in the two values of *o*-nitroaniline may be attributed to an intramolecular hydrogen bond between the NH_2 and NO_2 groups. On the analogy of *o*-nitroaniline, the discrepancy between the calculated and observed frequency values of **6** would be due to the formation of an intramolecular hydrogen bond between the NH_2 and C=O groups. The formation of the intramolecular hydrogen bond of benzopyranopyridine derivative is further confirmed by the following experimental results:

(1) The IR absorption bands of the NH_2 and C=O groups of **6** were measured in concentration from 2.1×10^{-3} to 4.3×10^{-1} mol/l, but there was no variation in the frequencies of these bands.

(2) The C=O stretching vibration of **6** appeared at 1711 cm^{-1} (Fig. 2), while the C=O bands of coumarin appeared at 1757 and 1742 cm^{-1} (Fig. 5). The decrease in the C=O frequency of **6** may be attributed to an intramolecular hydrogen bond.

Another consideration of this intramolecular hydrogen bond will be given in a subsequent paper[7] in further detail.

Benzopyranopyridine has four positions (the ring nitrogen atom, the oxygen atoms of carbonyl group and coumarin ring, and the hydrogen atom of amino group) for the hydrogen bond formation with alcohol. Therefore, there are four kinds of 1 : 1 hydrogen-bonded complexes in the benzopyranopyridine–methanol system. The IR spectral techniques were employed to determin which hydrogen-bonded complex is predominant among the four complexes. The IR spectrum of the **6**–methanol system is presented in Fig. 2. The position of the IR absorption bands corresponding to the NH_2 and C=O groups, and that of the absorption bands of each type (1262, 1051 cm^{-1}) shifted to the lower frequency side by about 1—2 cm^{-1}, and the intensity of these absorption bands did not change, compared with the IR spectrum of **6**. Nevertheless, the absorption band at 1585 cm^{-1} corresponding to the stretching vibration of the benzopyranopyridine ring disappeared, while a new shoulder was observed at 1590 cm^{-1} (Fig. 3)

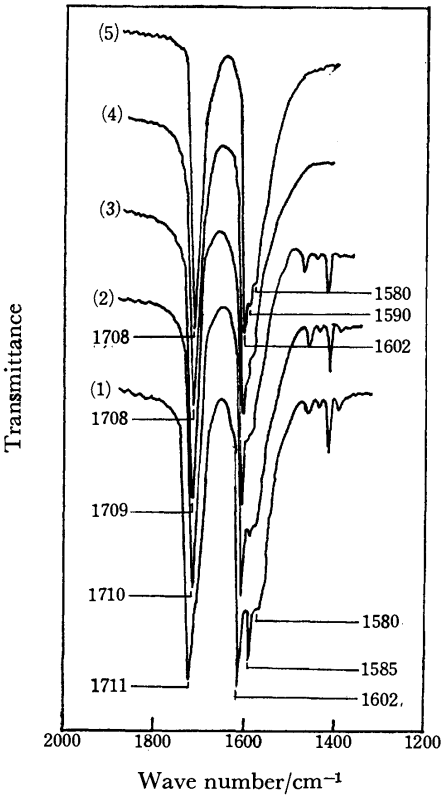

Fig. 3. IR spectra of **6** in carbon tetrachloride solution at room temparature in the presence of methanol of various concentrations. Concentration of **6**: 1.2×10^{-2} mol/l. Concentrations of methanol (mol/l): (1) 0, (2) 9.9×10^{-2}, (3) 4.0×10^{-1}, (4) 2.5, (5) 5.0.

after an addition of methanol. In the IR spectra of the systems of each compound from **1** to **5** and of methanol a similar new shoulder was observed near 1590 cm^{-1}. Furthermore, when ethanol was used in the place of methanol, the new shoulder band was observed near 1590 cm^{-1}. This result indicates that there is no difference between the two alcohols with respect to the hydrogen bond with benzopyranopyridine.

The IR spectra of the pyridine–methanol system were measured and compared with those of the benzopyranopyridine–methanol system. The spectra of this system are shown in Fig. 4. The two absorption peaks corresponding to the stretching vibration of the pyridine ring at 1597 and 1577 cm^{-1} disappeared with an increase of methanol concentration, while a new peaks appeared at 1590 cm^{-1}. The present results of the pyridine–methanol system are compatible with those reported by Takahashi *et al.*[8] (Fig. 4). In high concentrations of methanol, the two absorption bands of the NH_2 group of **6** could not be observed owing to the

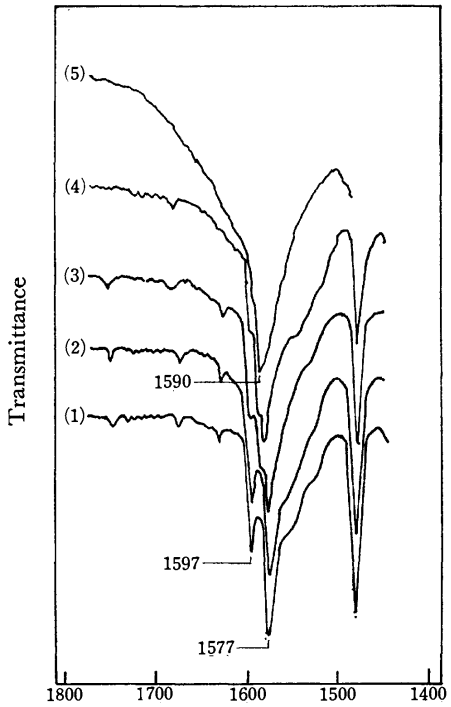

Fig. 4. IR spectra of pyridine in carbon tetrachloride solution at room temperature in the presence of methanol of various concentrations. Concentration of pyridine: 1.3×10^{-1} mol/l. Concentrations of methanol (mol/l): (1) 0, (2) 9.9×10^{-2}, (3) 2.5×10^{-1}, (4) 4.5×10^{-1}, (5) 5.0.

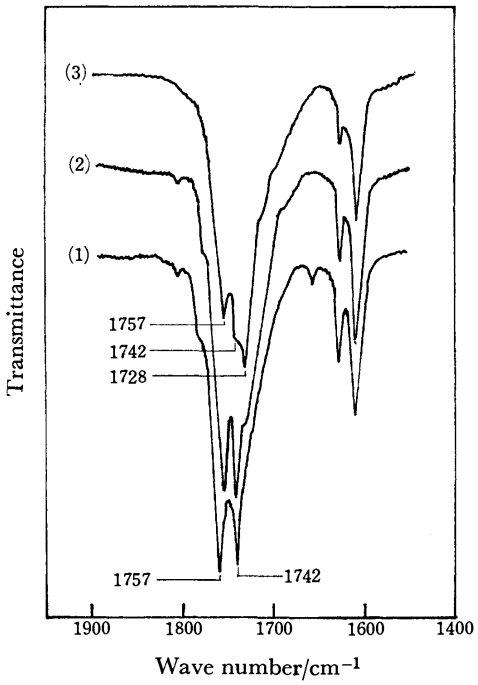

Fig. 5. IR spectra of coumarin in carbon tetrachloride solution at room temperaure in the presence of methanol of various concentrations. Concentration of coumarin: 2.0×10^{-2} mol/l. Concentrations of methanol (mol/l): (1) 0, (2) 8.7×10^{-1}, (3) 3.5.

overlap of an intense absorption band of the OH group of the alcohol. However, the absorption bands of this amino group were observed in the concentration range of 0 to 3×10^{-1} mol/l. The corresponding bands of the amino group shifted to the lower frequency side with increasing methanol concentration. But this spectral shift was smaller than that of the amino group for the aniline–methanol system. It is thought that the hydrogen-bonded species formed between the amino group of benzopyranopyridine and the hydroxyl group of alcohol is negligibly small in concentration.

The C=O absorption bands of coumarin were observed at 1757 and 1742 cm^{-1}, as shown in Fig. 5. When methanol was added to the coumarin system, a new band appeared at 1728 cm^{-1}. This band may be due to the formation of a hydrogen bond between the C=O group of coumarin and the OH group of methanol. However, in the case of the benzopyranopyridine derivative–methanol system the C=O absorption band of **6** at 1711 cm^{-1} shifts by 3 cm^{-1} (Fig. 3). This spectral shift is very small compared with that of the coumarin–methanol system. Therefore, the C=O group of benzopyranopyridine is weaker than that of coumarin in hydrogen bonding ability. Another example is found in the salicylaldehyde–*n*-butyl alcohol system. The C=O stretching vibration of salicylaldehyde appears at 1668 cm^{-1} in CCl_4 solution and 1667 cm^{-1} in *n*-butyl alcohol solution.[9] Its C=O stretching frequency changes only by 1 cm^{-1} in *n*-butyl alcohol solution. The reason may be attributed to the intramolecular hydrogen bond of the C=O group. With increasing concentration of methanol, the absorption band at 1051 cm^{-1} of **6**, which may be assigned to the ether type absorption, was hidden by the intense absorption band of the OH group of alcohol, while the absorption band at 1261 cm^{-1} corresponding to the ether type of **6** was not so effected by an addition of methanol. This result suggests that the hydrogen-bonded complex formed at the oxygen atom of the coumarin ring may be negligible. From the above experimental results, it may be concluded that the hydrogen-bonded species formed at the nitrogen atom of the benzopyranopyridine ring is the most predominant among the four hydrogen-bonded ones.

The equilibrium constant (K), enthalpy changes ($-\Delta H$), and entropy changes ($-\Delta S$) were obtained by means of the UV spectroscopic method, as given below. As is partly shown in Figs. 6 and 7, remarkable changes are produced in the UV spectra of **3** and **6** by the addition of ethanol to the isooctane solution. It may safely be assumed that these spectral changes are due to the formation of a hydrogen-bonded species between the benzopyranopyridine derivatives and alcohols. In this case the hydrogen bond is represented by the following equilibrium:

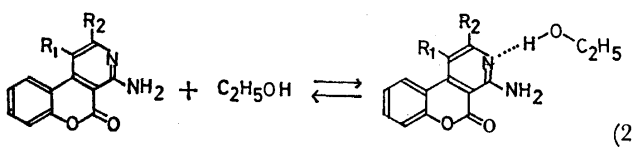

(2)

where benzopyranopyridine derivative acts as a proton acceptor and ethanol as a proton donor. No considera-

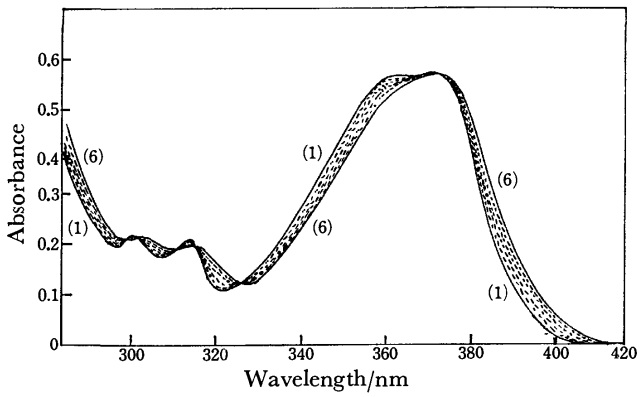

Fig. 6. UV spectra of **3** in isooctane solution at 25.0 °C in the presence of ethanol of various concentrations. Concentration of **3**: 6×10^{-5} mol/l. Concentrations of ethanol (mol/l): (1) 0, (2) 7.0×10^{-2}, (3) 1.0×10^{-1}, (4) 5.0×10^{-1}, (5) 1.0, (6) 2.0.

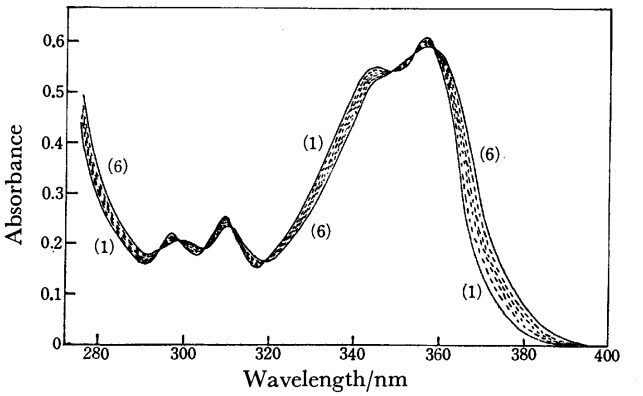

Fig. 7. UV spectra of **6** in isooctane solution at 27.0 °C in the presence of ethanol of various concentrations. Concentration of **6**: 5.3×10^{-5} mol/l. Concentrations of ethanol (mol/l): (1) 0, (2) 7.0×10^{-2}, (3) 1.0×10^{-1}, (4) 5.0×10^{-1}, (5) 1.0, (6) 2.0.

tion is given here to the hydrogen-bonded form in which one benzopyranopyridine is associated with two or more ethanols, because several clear isosbestic points are observed from the UV spectra. The **1**–ethanol and **2**–ethanol systems showed a remarkable resemblance to the **3**–ethanol system in spectral behavior. However, the spectral changes of the **4**–ethanol and **5**–ethanol systems were similar to that of the **6**–ethanol system.

The equilibrium constants K of the hydrogen bonding reactions were obtained by the use of

$$1/(\varepsilon-\varepsilon_f) = [1/\{K(\varepsilon_b-\varepsilon_f)\}](1/C) + [1/(\varepsilon_b-\varepsilon_f)],^{10)} \quad (3)$$

where ε_f is the molar absorption coefficient of the non-hydrogen-bonded or free solute species, and ε_b is that of the hydrogen-bonded species. ε is the molar absorption coefficient observed for a solution in which the initial concentration of ethanol is C. All these absorption coefficients refer to a given wavelength.

The enthalpy changes $(-\Delta H)$ accompanying hydrogen-bond formation can be obtained from a knowledge of the variation of K with temperature, according to the well known-equation,

$$-\Delta H = R[\mathrm{d}\ln K/\mathrm{d}(1/T)]. \quad (4)$$

In the present experiment the values of K were determined for each system at five points of temperature within the range from 10 to 50 °C. The free energy changes ΔG were calculated by

$$\Delta G = -RT\ln K. \quad (5)$$

The entropy changes were obtained from

$$\Delta G = \Delta H - T\Delta S. \quad (6)$$

Table 1. Thermodynamic properties of hydrogen-bond formation in benzopyranopyridine derivative–ethanol systems (1 cal=4.184 J)

Compd	K[a]	$-\Delta H$	$-\Delta S$
	l mol^{-1}	kcal mol^{-1}	cal K^{-1} mol^{-1}
1	2.90	4.6	13.3
2	3.05	4.5	12.9
3	3.00	4.7	13.6
4	3.35	5.0	14.4
5	4.05	5.2	14.7
6	3.25	5.0	14.4
Pyridine	1.60	4.2	13.2
Aniline	0.35	2.1	9.2
Coumarin	1.01	3.8	12.7

a) The values were interpolated at 25.0 °C.

The values of K, $-\Delta H$, and $-\Delta S$ for the systems of benzopyranopyridine derivatives, pyridine, aniline, and coumarin with ethanol are given in Table 1. From Table 1 it is found that the $-\Delta H$ values are *ca.* 4.6 kcal/mol for the 1-alkyl derivative–ethanol systems, and *ca.* 5.1 kcal/mol for the 2-alkyl derivative–ethanol systems. The values of K, $-\Delta H$, and $-\Delta S$ of 2-alkyl derivative–ethanol systems are slightly larger than those of 1-alkyl derivative–ethanol systems. The nitrogen atom of 2-alkyl derivatives is activated by the nearest-neighbour alkyl group which is situated at the

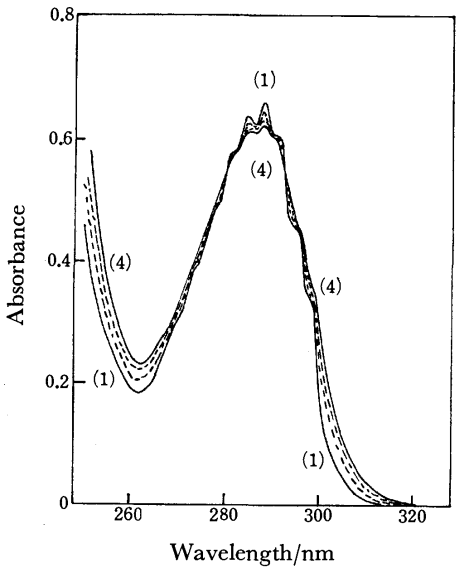

Fig. 8. UV spectra of aniline in isooctane solution at 24.8 °C in the presence of ethanol of various concentrations Concentration of aniline: 2.3×10^{-4} mol/l. Concentrations of ethanol (mol/l): (1) 0, (2) 1.0×10^{-1}, (3) 5.0×10^{-1}, (4) 2.0.

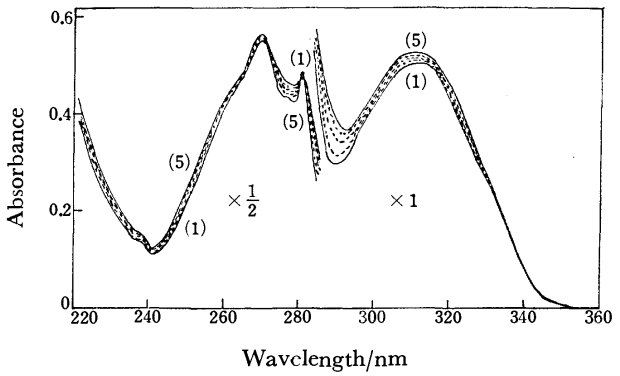

Fig. 9. UV spectra of coumarin in isooctane solution at 28.0 °C in the presence of ethanol of various concentrations. Concentration of coumarin: 2.3×10^{-4} mol/l. Concentrations of ethanol (mol/l): (1) 0, (2) 1.0×10^{-1}, (3) 3.0×10^{-1}, (4) 5.0×10^{-1}, (5) 1.0.

α-position with respect to the ring nitrogen atom, but the 1-alkyl group which is substituted at the β-position cannot activate the ring nitrogen atom.

The UV spectral change of the aniline–ethanol system was not so large when ethanol was added in a fairly large amount (Fig. 8). The $-\Delta H$ of this system is smaller than that of benzopyranopyridine derivative–ethanol system. This result indicates that the hydrogen-bonded complex formed between the amino group of benzopyranopyridine and ethanol is not so important. The UV spectra for the coumarin–ethanol system is shown in Fig. 9. The value of $-\Delta H$ for the coumarin–ethanol system is 3.8 kcal/mol. This value indicates that the carbonyl group of coumarin has a fairly strong hydrogen bonding ability. However, in the case of benzopyranopyridine the hydrogen bonding ability of its carbonyl group is not so strong as that of the carbonyl group of coumarin, because the carbonyl group of benzopyranopyridine is already occupied by an intramolecular hydrogen bond.

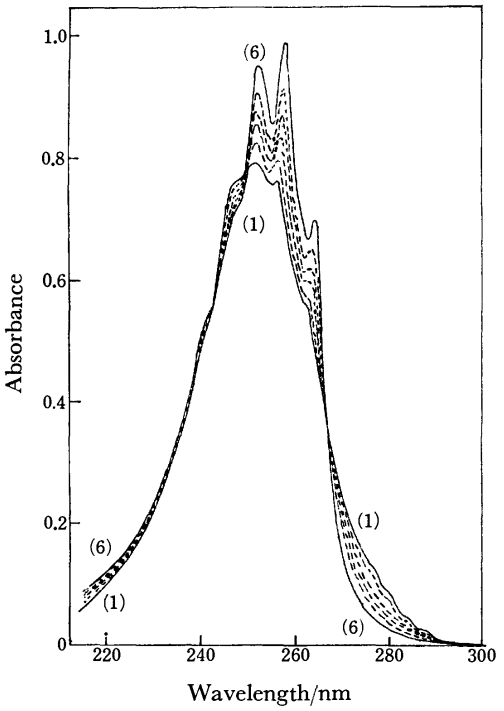

Fig. 10. UV spectra of pyridine in isooctane solution at 19.2 °C in the presence of ethanol of various concentrations. Concentration of pyridine: 4.4×10^{-4} mol/l. Concentrations of ethanol (mol/l): (1) 0, (2) 7.0×10^{-2}, (3) 2.0×10^{-1}, (4) 5.0×10^{-1}, (5) 1.0, (6) 2.0.

The UV spectral data of the pyridine–ethanol system is presented in Fig. 10. As is listed in Table 1, the values of K, $-\Delta H$, and $-\Delta S$ for the pyridine–ethanol system obtained by this study are 1.60 l/mol, 4.2 kcal/mol, and 13.2 kcal/(K mol), respectively. These values are in fair agreement with the K (2.31 l/mol), $-\Delta H$ (4.4 kcal/mol), and $-\Delta S$ (11.7 cal/(K mol))[11] for the pyridine–methanol system obtained by the IR spectral experiment. It is to be noted that these values of the pyridine–ethanol system are approximately equal to those of the benzopyranopyridine–ethanol system, although the values of K and $-\Delta H$ for the benzopyranopyridine–ethanol system are slightly larger than those of the pyridine–ethanol system. This is because the nitrogen atom of the benzopyranopyridine ring is activated by the adjacent alkyl and amino groups. In addition, as the π-conjugation of the benzopyranopyridine molecule is larger than that of the pyridine molecule, the hydrogen bond makes the benzopyranopyridine–ethanol system more stable than the pyridine–ethanol system.

This work was supported by grants from the Tokyo Denki University Research Fund. The authors would like to express their sincere thanks to Drs. Takeshi Oishi and Akio Sakurai of the Institute of Physical and Chemical Research for their kindness concerning the IR spectroscopic measurements.

References

1) R. S. Drago, N. O'Bryan, and G. C. Vogel, *J. Am. Chem. Soc.*, **92**, 3924 (1970); T. Bercovici, J. King, and R. S. Becker, *J. Chem. Phys.*, **56**, 3956 (1972).

2) A. Fujimoto, A. Sakurai, H. Midorikawa, and E. Iwase, *Nippon Kagaku Kaishi*, **1974**, 1.

3) A. Sakurai, H. Midorikawa, and Y. Hashimoto, *Bull. Chem. Soc. Jpn.*, **43**, 2925 (1970); A. Sakurai, H. Midorikawa, and Y. Hashimoto, *ibid*, **44**, 1677 (1971).

4) J. A. Riddick and E. E. Toops,"Organic Solvents, Physical Properties and Methods of Purification," Interscience Publishers, Inc., New York (1955).

5) L. J. Bellamy and R. L. Williams, *Spectrochim. Acta*, **9**, 341 (1957).

6) K. Semba, *Bull. Chem. Soc. Jpn.*, **33**, 1640 (1960).

7) K. Inuzuka and A. Fujimoto, *Bull. Chem. Soc. Jpn.*, **51**, 2786 (1978).

8) H. Takahashi, K. Mamola, and E. K. Plyler, *J. Mol. Spectrosc.*, **21**, 217 (1966).

9) H. Yamada, *Bull. Chem. Soc. Jpn.*, **32**, 1051 (1959).

10) H. Baba and S. Suzuki, *J. Chem. Phys.*, **35**, 1118 (1961); S. Suzuki and H. Baba, *ibid*, **38**, 349 (1963).

11) T. Kitao and C. H. Jarboe, *J. Org. Chem.*, **32**, 407 (1967).

Hydrogen Bond of 4-Amino-5*H*-[1]benzopyrano[3,4-*c*]pyridin-5-one Derivatives with Alcohols. II. Theoretical Considerations

Kozo INUZUKA* and Akira FUJIMOTO

Department of Applied Science, Faculty of Technology, Tokyo Denki University, Kanda, Chiyoda-ku, Tokyo 101

(Received December 21, 1977)

In a previous paper the experimental considerations on the hydrogen bonding between benzopyranopyridine derivatives including related compounds (pyridine, coumarin, and aniline) and alcohols were made, and the thermodynamic constants for the formation of the hydrogen-bonded complexes were obtained from UV spectroscopic studies. In this paper the molecular orbital calculation by the CNDO/2 method was conducted to further clarify the experimental results. Several conclusions were drawn from the present calculation: (1) Benzopyranopyridine has an intramolecular hydrogen bond between its amino and carbonyl groups. (2) The hydrogen bond energy of 2-alkyl benzopyranopyridines with alcohol is larger than that of the 1-alkyl compounds. (3) Benzopyranopyridine has four positions for hydrogen bond formation with alcohol, that is, the ring nitrogen atom, the carbonyl group, the ring oxygen atom, and the amino group. The ring nitrogen atom gave rise to the largest hydrogen bond energy among the four positions. Therefore, the corresponding hydrogen-bonded complex plays an important role in the benzopyranopyridine–alcohol system. (4) The hydrogen bond energy depended on the charge density of the atom which gave rise to the hydrogen bond with alcohol. Especially, substitution of the electron donating group such as amino and methyl groups at the position which increases the charge density of the atom giving rise to a hydrogen bond with alcohol increases the hydrogen bond energy.

Recently, the CNDO/2 method developed by Pople *et al.*[1] has been applied to elucidate the enthalpy and equilibrium distance of hydrogen bond formation. These studies[2–6] look successful and are encouraging. In a previous paper[7] the hydrogen bond between 4-amino-5*H*-[1]benzopyrano[3,4-*c*]pyridin-5-one (abbreviated to benzopyranopyridine) derivatives including related compounds (pyridine, coumarin, and aniline) and alcohols (methanol and ethanol) was discussed experimentally using the IR and UV spectral data.

In this paper the molecular orbital calculation by the CNDO/2 method was carried out to further clarify the experimental results and to compare the calculated results with the experimental ones.

Methods of Calculation and Molecular Models

The CNDO/2 method developed by Pople *et al.*[1] was used. The method has been described in detail in the literature.[1]

The molecule of benzopyranopyridine was assumed to be planar and the model substituted by a methyl group is shown in Fig. 1. The bond distance and bond angle of the molecular model used for the present calculation is as follows:

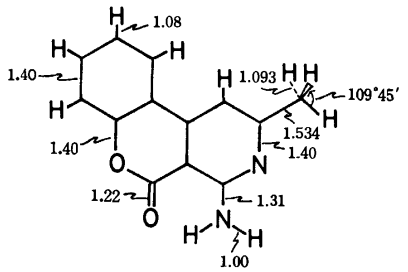

Fig. 1. A molecular model of methyl-substituted 4-amino-5*H*-[1]benzopyrano-[3,4-*c*]pyridin-5-one used for the present calculation.

Water:[8] O–H 0.9572 Å, ∠HOH 104.52°

Results and Discussion

Electronic Properties of Benzopyranopyridine Derivatives in the Ground State. The CNDO/2 method was applied to compounds **1** and **4** which correspond to the 1- and 2-methyl benzopyranopyridines and compound **7** which corresponds to the unsubstituted benzopyranopyridine in order to elucidate the total energies, dipole moments, π-bond orders of carbonyl groups, total charge densities, and π-charge densities. The calculated results are shown in Table 1 and Fig. 2. Methyl-substitution makes

Table 1. Total energies, dipole moments and π-bond orders of carbonyl group of 4-amino-1-methyl-5*H*-[1]benzopyrano[3,4-*c*]pyridin-5-one (**1**), 4-amino-2-methyl-5*H*-[1]benzopyrano[3,4-*c*]pyridin-5-one (**4**), and 4-amino-5*H*-[1]benzopyrano[3,4-*c*]pyridin-5-one (**7**)

Compound	Total energy (a. u.) E_T	Dipole moment (D) μ	π-Bond order $P_{C=O}$
1	−160.1193	3.643	0.822
4	−160.1734	3.995	0.819
7	−151.4720	3.735	0.821

compound **4** more stable than compound **1** by 34 kcal/mol. The π-bond order of the carbonyl group of compound **1** is a little larger than that of compound **4**, but it is almost equal to that of compound **7**. These results suggest that the carbonyl stretching frequency of compound **1** may be a little higher than that of compound **4**, but it may be equal to that of compound **7**. The observed carbonyl stretching vibration of compound **1** appears at 1708 cm^{-1} in CCl_4 solution, but the corresponding one of compound **4** at 1706 cm^{-1}. The IR spectrum of compound **7**, however, is unavailable for comparison because the synthesis has not been successful. There is no difference in the carbonyl stretching

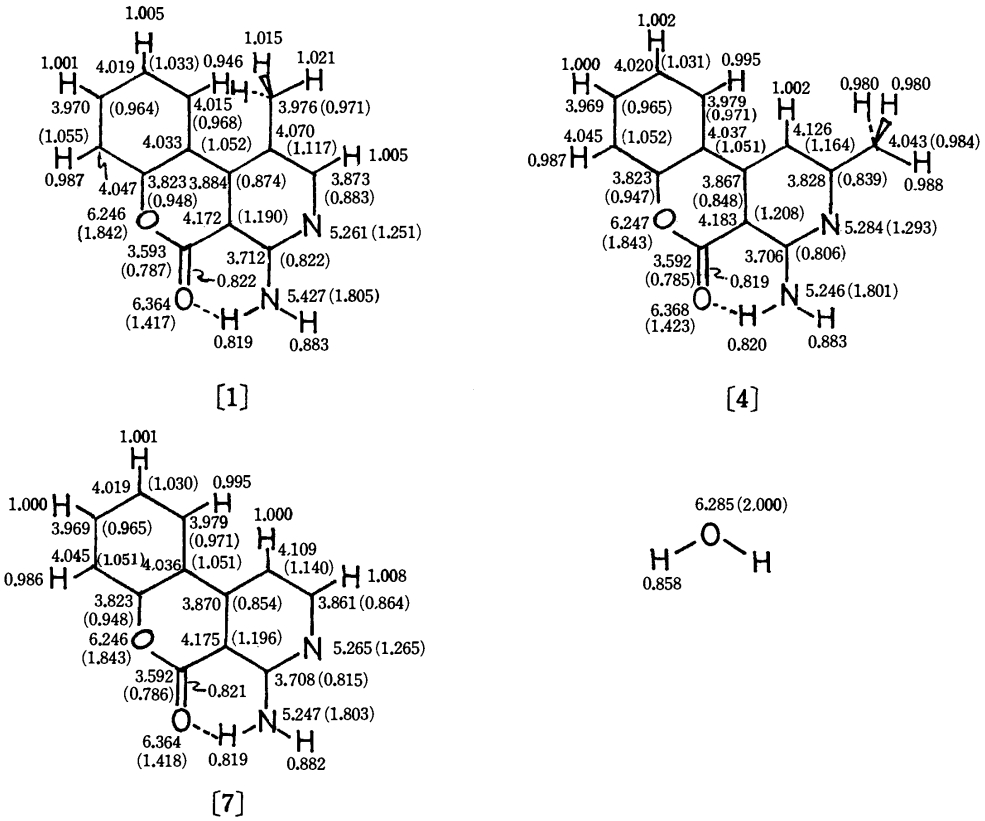

Fig. 2. Total charge densities and π-charge densities of **1**, **4**, **7**, and water.

frequency of compounds **2**, **3**, **5**, and **6**[7] which have an alkyl group longer than the methyl group.

The calculated dipole moment of **1** is smaller than that of **4** but it is approximately equal to that of compound **7**. In Fig. 2 the effect of methyl substitution on the charge density of **7** is mainly limited to that of the pyridine ring. It is significant that the 2-methyl-substitution increases the charge density of the ring nitrogen atom while the 1-methyl-substitution decreases the charge density compared with that of **7**.

Intramolecular Hydrogen Bond. (i) The charge density on the two hydrogen atoms of the amino group of compounds **1**, **4**, and **7** are 0.882—0.883 and 0.819—0.820, respectively. The former values correspond to the charge density of the hydrogen atom adjacent to the ring nitrogen atom and the latter values to the hydrogen atom of the opposite side (Fig. 2). The charge densities of the hydrogen atoms of the amino group of 2-aminopyridine are 0.883 and 0.882, the former value corresponding to the values 0.882—0.883 of compounds **1**, **4**, and **7**, and the latter values to the values 0.819—0.820. The charge densities of the hydrogen atom near the ring nitrogen atom is almost equal in the four compounds, even if they are different in molecular structure. However, the charge density of the hydrogen atom of the opposite side is different in 2-aminopyridine and benzopyranopyridine derivatives. The large decrease in charge density from 0.882—0.883 to 0.819—0.820 may be attributed to the intramolecular hydrogen bonding between the carbonyl and amino groups, because the charge density of the hydrogen atom concerned with hydrogen bond formation decreases to a large extent due to the charge migration.

(ii) The carbonyl stretching vibration of the six benzopyranopyridine derivatives in a previous paper[7] appeared in the range of 1706 to 1711 cm^{-1}. The corresponding one of coumarin, which is split into two peaks shows a large difference appearing at 1757 and 1742 cm^{-1}. The large decreases in the carbonyl stretching frequencies of benzopyranopyridine derivatives may be largely attributed to intramolecular hydrogen bonding.

(iii) The two models **8** and **9** were used to investigate the effect of intramolecular hydrogen bonding in the charge densities of the oxygen atom of the carbonyl group and the hydrogen atoms of the amino group and on the π-bond order of the carbonyl group. Model **8** has a non-planar amino group with three valence angles of 112° with respect to the nitrogen atom. Model **9** has a planar amino group twisted by 90° about the C–N bond. If an intramolecular hydrogen bond exists between the oxygen atom of the carbonyl group and the hydrogen atom of the amino group, it may be weaker in **8** than in **7** but it may be broken in **9**. The values of the charge densities and π-bond order of the carbonyl group and the charge densities of the hydrogen atoms of the amino group are shown in the models **8** and **9** with the total energies. The model **8** is higher in energy than **7** with a planar amino group by 1.52 kcal/mol. The 2-aminopyridine with a non-planar amino group and three valence angles of 112° is more stable than that with a planar amino group by 4.22

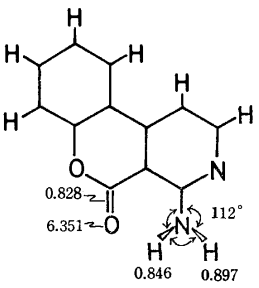

−151.4718a.u.

[8]

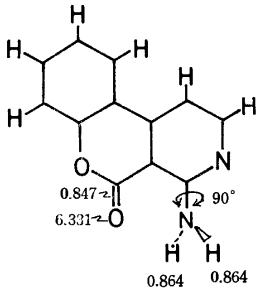

−151.4369a.u.

[9]

kcal/mol. The charge density of the oxygen atom of the carbonyl group of **8** decreases more than that of **7**. At the same time the charge density of the hydrogen atom of the amino group of the **8** increases more than that of the **7**. These trends are more conspicuous in **9** than in **8**. Added to this the π-bond order of carbonyl groups increases in the order from **7** to **9**. These results suggest that an intramolecular hydrogen bond exists between the carbonyl and amino groups.

Intermolecular Hydrogen Bond. Benzopyranopyridine has four positions which give rise to the hydrogen bond with alcohol, that is, the ring nitrogen atom, the carbonyl group, the ring oxygen atom, and the amino group. Each of these charge densities of the atom in the four positions shown in Fig. 2 are almost equal to each other except for the ring nitrogen atom among the three compounds. The charge density on the ring nitrogen atom of compound **4** is larger than that of compounds **1** and **7**, but the charge densities of the ring nitrogen of the latter two compounds are approximately equal. From this result it may be expected that the hydrogen bond energy of compound **4** may be larger than that of compounds **1** and **7**, but approximately equal in **1** and **7**, if there is hydrogen bond formation between the ring nitrogen atom and alcohol. However, if hydrogen bonding between the remaining three positions and alcohol occurs, it is expected that there will be no interpretable differences in energy of the corresponding hydrogen bonds among the three compounds.

In order to calculate the four kinds of hydrogen bond energies for the benzopyranopyridine–alcohol system the following models were used as shown in Fig. 3. In order to simplify the present calculation a water molecule was used in place of alcohol, and the unsubstituted benzopyranopyridine used.

Model A: The equilibrium distance between the ring nitrogen atom and the hydrogen atom of water, 1.6 Å of model A corresponds to the value determined for the pyridine–water system. The two molecules lie in the same plane and the O–H bond of water lies along the n-orbital of the ring nitrogen atom.

Model B: The equilibrium distance between the oxygen atom of the carbonyl group and the hydrogen atom of water, 1.6 Å and bond angle between the carbonyl axis and hydroxyl bond, 60° were used for model B refering to the values determined for the *s-trans*-acrylaldehyde–water system. The equilibrium distance 1.6 Å and bond angle 60° correspond to the conformation with the maximum hydrogen bond energy.

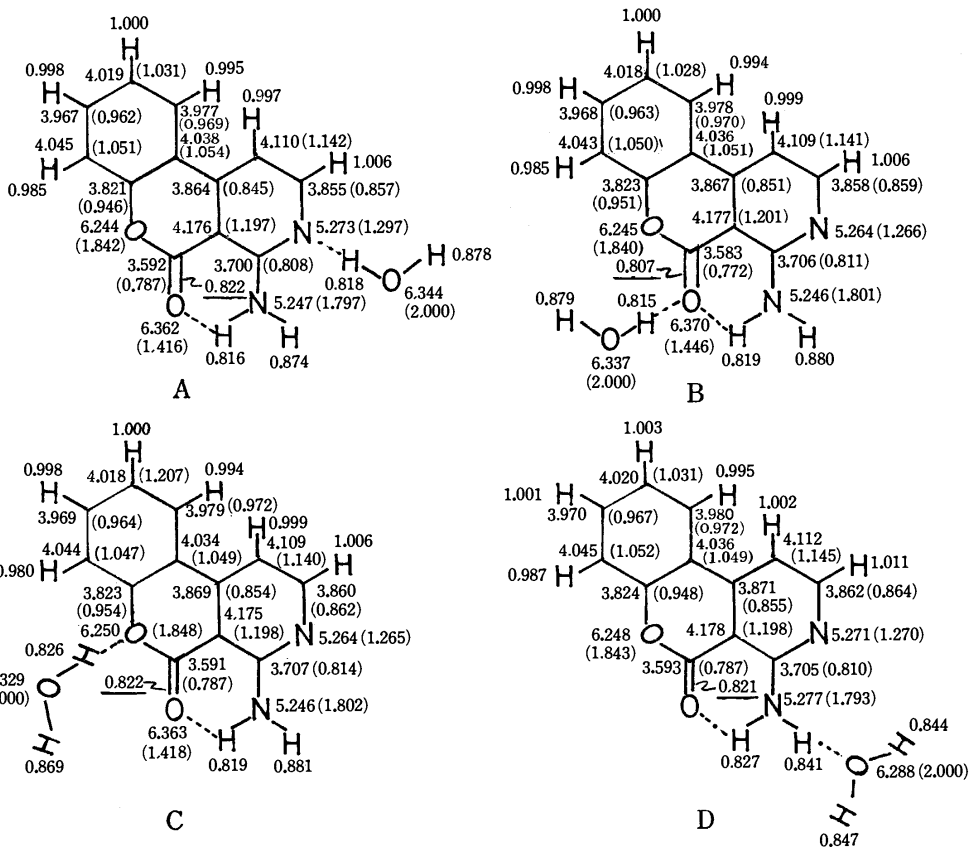

Fig. 3. Hydrogen-bonded complex models between **7** and water.

Model C: The two molecules were assumed to lie in the same plane refering to the calculated results of conformation of the hydrogen-bonded complex for the tetrahydrofuran (THF)–water and THF–methanol systems.[9] The equilibrium distance between the ring oxygen atom and the hydrogen atom of water, 1.6 Å which was determined for the coumarin–water system was used.

Model D: The equilibrium distance between the hydrogen atom of the amino group and the oxygen atom of water, 1.6 Å which was determined for the 2-aminopyridine–water system was used.

Table 2. Hydrogen bond energies, dipole moments and π-bond orders of carbonyl group of the hydrogen-bonded 1:1 complexes formed between 4-amino-5*H*-[1]benzopyrano[3,4-*c*]pyridin-5-one and water

Hydrogen-bonded complex	Hydrogen bond energy $-\Delta H$ (kcal/mol)	Hydrogen bond energy $-\Delta H_c$ (kcal/mol)	Dipole moment μ (D)	π-Bond order $P_{C=O}$
A	9.41	4.99	6.291	0.822
B	7.96	4.22	6.432	0.807
C	6.61	3.51	3.828	0.822
D	5.04	2.69	2.883	0.821

The calculated hydrogen bond energy, dipole moment, and π-bond order of the carbonyl group for the four models are listed in Table 2. The calculated hydrogen bond energies are larger than the observed energies in a previous paper.[7] The same methods was applied to the pyridine–methanol system to compare the calculated hydrogen bond energy with the observed value. The calculated value was 8.29 kcal/mol while the observed value was 4.4 kcal/mol.[10] The values $-\Delta H_c$ in Table 2 were corrected by multiplying by the factor 4.4/8.29 to the values $-\Delta H$ on the assumption that the same ratio applies to the present calculated and observed values. The corrected value $-\Delta H_c$ is better than the uncorrected value for a comparison with the observed value.

The calculated hydrogen bond energy of model A is the largest among the four models. The order of hydrogen bond energy from model A to D seems reasonable. The ratio of the models from A to D in equilibrium concentration at 300 K was evaluated by use of the values $-\Delta H_c$ assuming the Boltzmann distribution. The calculated ratio, A: B: C: D became 0.72: 0.20: 0.06: 0.02. These values suggest that the hydrogen bond such as model A is the most important one. The numerical values of the Boltzmann distribution ratio indicate the possibility of model B, however it is not significant. The hydrogen-bonded complexes such as models C and D may be negligible.

The observed average hydrogen bond energy for 1-alkyl benzopyranopyridines was about 4.6 kcal/mol, while that of 2-alkyl ones was about 5.1 kcal/mol. This indicates that the 2-alkyl substituted benzopyranopyridines are larger in hydrogen bond energy than the 1-alkyl compounds. The calculated value 4.99 kcal/mol may correspond to the observed value 4.6 kcal/mol for 1-alkyl benzopyranopyridines as discussed in the previous section. The hydrogen bond energy 3.8 kcal/mol, observed for the coumarin–ethanol system[7] was assigned to the energy of the hydrogen bond formation between the carbonyl group and alcohol from the IR spectrum, since coumarin showed a sharp carbonyl band split into two peaks located at 1757 and 1742 cm^{-1} in CCl_4 solution while a new band appeared at 1728 cm^{-1} by an addition of methanol to coumarin.[7] The observed value 3.8 kcal/mol corresponds well to the calculated value 4.22 kcal/mol for model B.

Experimentally, the presence of the hydrogen bond such as model A was confirmed by IR spectrum but the remaining species, like the models B, C, and D were not clearly determined.[7]

The calculation of π-bond order indicates that the hydrogen bond formation between carbonyl and hydroxyl groups gives rise to large decreases in the π-bond order of the carbonyl group in model B as shown in Table 2. This suggests that a large carbonyl frequency shift due to hydrogen bond formation may be expected. However, experimentally a small frequency shift (1—2 cm^{-1}) was observed in addition of methanol in large amounts. The small shift suggests that the intramolecular hydrogen bond disturbs the hydrogen bond formation. The formation of the hydrogen-bonded complex such as model B may be difficult because model B may correspond to the 1: 2 complex with respect to the carbonyl group. The entropy change $|-\Delta S|$ for the formation of the 1: 2 complex may become larger than that for the 1: 1 complex.

The calculated energy $-\Delta H_c$ for the coumarin–water hydrogen-bonded complex between the ring oxygen atom and hydroxyl group such as model C became 3.44 kcal/mol. If the observed value 3.8 kcal/mol for the coumarin–ethanol system is assigned to the energy value for the formation between the ring oxygen atom and alcohol, it is difficult to explain the large frequency shift in the carbonyl vibration, because the above coumarin-water model makes no change in the π-bond order of the carbonyl group.

The calculated hydrogen bond energy 2.69 kcal/mol for model D shows a good correspondence to the observed value 2.1 kcal/mol for the aniline–alcohol system where it is expected a hydrogen bond is formed between the amino group of aniline and ethanol.[7]

Charge Density Distribution in Hydrogen-Bonded Complex. In model A there are variations of the charge densities in the pyridine ring and water, in which the charge densities of the α- and γ-carbon atoms of the pyridine ring decrease but the charge density of the nitrogen atom increases. The charge density of water increases by 0.039. This increase denotes that the charge migration occurs from the proton acceptor to the donor. Locally, the charge variation occurs such as $\overset{-}{N}\cdots\overset{+}{H}\text{–}\overset{-}{O}$ on the atoms of the hydrogen bridge. In model B the large charge density variation occurs mainly in the carbonyl group and in water. In model B also the charge density increases in water by 0.031 the same as in model A. In model C the charge density increases in water by 0.023 and in model D it decreases by 0.021 and the charge migration occurs from water to benzo-

pyranopyridine. In models A to C the amount of the charge migration is proportional to the hydrogen bond energy, while in model D the direction of the charge migration is reverse to that of the other three models.

This work was supported by grants from the Tokyo Denki University (T. D. U.) Research Fund. The authors especially wish to acknowledge the assistance of the staffs of the T. D. U. Computing Center in the present work.

References

1) J. A. Pople, D. P. Santry, and G. A. Segal, *J. Chem. Phys.*, **43**, 129 (1965); J. A. Pople and G. A. Segal, *ibid.*, **43**, 136 (1965); J. A. Pople and G. A. Segal, *ibid.*, **44**, 3289 (1966).
2) A. Pullman and H. Berthod, *Theor. Chim. Acta*, **10**, 461 (1968).
3) J. R. Holyand and L. B. Kier, *Theor. Chim. Acta*, **15**, 1 (1969).
4) C. N. R. Rao, A. Goel, K. G. Rao, and A. S. N. Murthy, *J. Phys. Chem.*, **75**, 1744 (1971).
5) A. Goel, A. S. N. Murthy, and C. N. R. Rao, *J. Chem. Soc., A*, **1971**, 190.
6) A. S. N. Murthy, S. N. Bhat, and C. N. R. Rao, *J. Chem. Soc.*, **1970**, 1251.
7) A. Fujimoto and K. Inuzuka, *Bull. Chem. Soc. Jpn.*, **51**, 2781 (1978).
8) W. S. Benedict, N. Gailar, and E. K. Plyler, *J. Chem. Phys.*, **24**, 1139 (1956).
9) K. Inuzuka, to be published.
10) T. Kitao and C. H. Jarboe, *J. Org. Chem.*, **32**, 407 (1967).

A Study of Surfactant Solutions Using the Liquid Membrane Electrode Selective to Alkyl Sulfate Ions

Akira YAMAUCHI,* Takuma KUNISAKI, Toshiaki MINEMATSU, Yukiko TOMOKIYO, Takeo YAMAGUCHI, and Hideo KIMIZUKA

Department of Chemistry, Faculty of Science, Kyushu University 33, Fukuoka 812

(Received January 27, 1978)

Liquid membrane electrodes selective to alkyl sulfate ions were devised for octyl, decyl, and dodecyl sulfate ions, and employed in the study of micellar solutions. A nitrobenzene solution of hexadecyltrimethylammonium–alkyl sulfate complex was used as the liquid membrane. The membrane potential-logarithmic concentration showed a maximum at the critical micelle concentration (CMC), an increase with the Nernstian slope at the lower concentrations and a decrease at the higher concentrations. Below CMC, the presence of excess inorganic salt did not alter the Nernstian slope, *i.e.*, the liquid membrane was more highly permselective to alkyl sulfate ions than to inorganic anions. From a simple thermodynamic consideration of a micellar solution based on the pseudo phase model of the micelle, the change in the activity of alkyl sulfate ions and the dissociation of the micelle were discussed. It has been deduced that the concentration of the singly dispersed surfactant ions above CMC is reduced with concentration, except for the presence of a large excess of added electrolyte, and that the degree of dissociation of the micelle is unaltered even when the excess electrolyte is added.

The surfactant ion activity in surfactant solutions has been studied by using solid exchange membranes, including the cation-selective glass electrode.[1–6] Botré *et al.*[1] used the solid ion exchange membranes of both negative and positive types and evaluated the degree of association of the counterions with micelles in aqueous solutions of sodium laurate and dodecylamine hydrochloride. Satake *et al.*[2] used the sodium glass electrode for estimating the degree of association of Na ions in the micelles of sodium alkyl sulfates. Further, Sasaki *et al.*[3] determined the mean activity of sodium dodecyl sulfate in aqueous solutions by using both the sodium ion response glass electrode and the solid anion exchange membrane.

On the other hand, only a few studies[7–9] have been performed with a liquid membrane electrode with a response only for surfactant ions, although various ion-selective electrodes using liquid membranes have recently been devised.[10–13] By virtue of the response only for a particular ion, the use of the liquid membrane would be superior to the solid ion exchange membrane in the study of surfactant solutions. In this respect, new information can be obtained by applying the surfactant ion selective liquid membrane to the study of micellar solutions.

This paper is concerned with the study of the selective permeability coefficient of various surfactant ions as well as the states of surfactant ions in the solution.

Experimental

Materials. The surfactants used were sodium alkyl sulfate (SAS) with chain length C_8 to C_{12}, *i.e.*, sodium octyl sulfate (SOS), sodium decyl sulfate (SDeS), and sodium dodecyl sulfate (SDS). The purified alcohol was obtained by fractional distillation and sulfated with chlorosulfuric acid, then neutralized with sodium hydroxide solution and recrystallized from ethanol. The crystalline sodium alkyl sulfate was finally purified by the solvent extraction with diethyl ether for 48 h. The purity of specimen was confirmed by the absence of a minimum in the surface tension *vs.* concentration curve. Hexadecyltrimethylammonium bromide (HTAB) of guaranteed grade was used after recrystallization from redistilled water. The membrane material, hexadecyltrimethylammonium–alkyl sulfate complex (HTA–AS), was prepared by mixing HTAB solution with SAS solution and washing the precipitate with distilled water. The nitrobenzene solution of HTA–AS was used as the liquid membrane which is denoted as the AS membrane. All the other reagents were of guaranteed grade and used without further purification.

Membrane Potential Measurement. An Orion model 801A digital ion analyzer was used for measuring the membrane potential of the following concentration cell:

$$\begin{array}{l}\text{Calomel}\,\|\,\text{Satd } NH_4Cl\text{ Agar}\,\|\,10^{-3}\text{ mol dm}^{-3}\text{ SAS Ref. Soln}\,\|\\ 10^{-4}\text{ mol dm}^{-3}\text{ HTA–AS in Nitrobenzene}\,\|\,\text{SAS Soln with varying Concn}\,\|\\ \text{Satd } NH_4Cl\text{ Agar}\,\|\,\text{Calomel}\end{array} \quad \text{(A)}$$

where the left half cell including the AS membrane may be termed the AS ion selective electrode. For the study of the selectivity of some inorganic and alkyl sulfates (AS) ions to the dodecyl sulfate (DS) ion electrode, the following cell was used:

$$\begin{array}{l}10^{-3}\text{ mol dm}^{-3}\text{ SDS Ref. Soln}\,\|\,10^{-4}\text{ mol dm}^{-3}\text{ HTA–DS in Nitrobenzene}\,\|\\ 10^{-3}\text{ mol dm}^{-3}\text{ SAS or}\\ 10^{-3}\text{ mol dm}^{-3}\text{ Inorganic Anion}\end{array} \quad \text{(B)}$$

For the study of the effect of electrolyte, a constant concentration of NaCl was added to the test solution with varying concentrations of surfactant. The potential reached a steady value (± 0.2 mV) within 10 min. The measurements were carried out at 25.0 ± 0.1 °C.

Results and Discussion

In Fig. 1, typical response curves for the AS electrodes are shown for SOS, SDeS, and SDS. The kink point in the response curve agreed with the values of CMC in the literature.[14] The values of CMC observed were: SDS, 8.0×10^{-3} mol dm^{-3}; SDeS, 3.3×10^{-2} mol dm^{-3}; SOS, 1.2×10^{-1} mol dm^{-3}. Below CMC, the membrane potential V obeyed the Nernst equation,

$$V = \frac{RT}{F} \ln \frac{C_{AS}}{C_{AS}^{\circ}}, \quad (1)$$

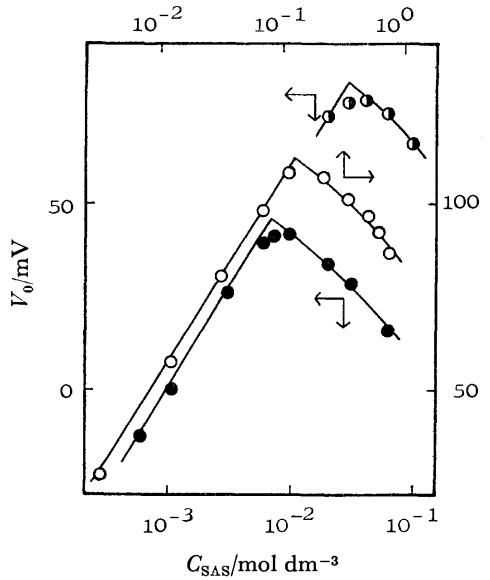

Fig. 1. Response curves of HTA–DS and HTA–DeS and HTA–OS liquid membrane for SDS, SDeS, and SOS solutions with 10^{-3} mol dm^{-3} SDS, SDeS, and SOS reference solutions, respectively.
●: SDS, ◑: SDeS, ○: SOS.

where $C_{AS}°$ and C_{AS} denote the concentration of AS ion in the reference solution and the test solution, respectively. This indicates that the AS electrode is ideally permselective to AS ions and the change in the activity coefficient of AS ions as well as the interference by Na ions may be ignored. Above CMC, the decrease in the potential with increasing SAS concentration, an indicative of the decrease in the apparent surfactant ion activity, was observed.

The selectivities of some inorganic and alkyl sulfate ions to the DS electrode were examined by using the cell systems (B). The selectivity was calculated according to the following equation for the membrane potential V:

$$V = \frac{RT}{F} \ln K^{pot.}_{DS,X} \frac{a_X}{a_{DS}}, \qquad (2)$$

where a_X and a_{DS} denote the activity of X ion and that of DS ion, respectively, and $K^{pot.}_{DS,X}$, the selectivity of X ion to DS ion. In estimating the selectivities, the activity coefficients were assumed to be unity, since the concentrations of sodium alkyl sulfates and inorganic salts were low. The selectivities are summarized in Table 1. It is seen in Table 1 that chloride and bromide ions hardly interfere with the response of the DS electrode to DS ions. On the other hand, the responses of the DS electrode to perchlorate and thiocyanate ions are more or less greater than those to halide anions. Thus, these inorganic anions may interfere with DS ions in the response to the DS electrode. It is known that the perchlorate and thiocyanate ions dissolve considerably in the organic solvent.[15] This may be responsible for the higher selectivities of these inorganic ions, since the selectivity is given by the product of the ratio of transport coefficients and that of partition coefficients. The selective permeability coefficients of the homologous alkyl sulfate ions increased by a factor of about 10 with the increase in alkyl chain length by two methylene groups.

Table 1. Selective permeability coefficients

Examined salt	$K^{pot.}_{DS,J}$
STS(C_{14})	10
SDS(C_{12})	1
SDeS(C_{10})	2.8×10^{-1}
SOS(C_8)	1.2×10^{-2}
$NaClO_4$	4.4×10^{-2}
KSCN	2.8×10^{-2}
KBr	1.1×10^{-3}
NaCl	6.0×10^{-4}

This agrees with the Traube rule and reflects the greater partition coefficient of a surfactant of longer chain length in the organic solvent. The longer the chain length, the greater the selectivity; thus tetradecyl sulfate (TS) ion, which has more carbon atoms than DS ion, exhibited greater response to the DS electrode, as shown in Table 1.

The selective permeability coefficient of Cl ion is of the order of 10^{-4}. This implies that even though Cl ions coexist in the test solutions of cell system (B), there would be little influence on the response of the AS electrode to AS ions. Thus, using the cell system (B), the study of the effect of added electrolytes in aqueous SAS solutions was performed. In Figs. 2 to 4, the response curves for SAS solutions in the presence of 0.1 and 0.01 mol dm^{-3} NaCl are shown together with those for the salt-free systems. For all the cases of the surfactants with alkyl chain length from C_8 to C_{12}, CMC of each surfactant solution in the presence of NaCl agreed well with that in the literature.[14] It is also shown in these figures that the presence of inorganic salt more or less decreased the membrane potential below CMC. Furthermore, the longer the chain length, the greater the decrease in the potential. This tendency was also enhanced as the added amount of electrolytes increased. This may reflect a decrease in the activity

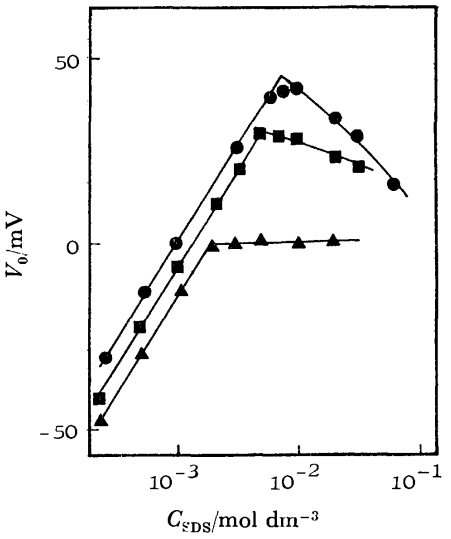

Fig. 2. Membrane potential as a function of concentration of SDS in test solution in the presence of added electrolytes.
●: No NaCl, ■: 0.01 mol dm^{-3} NaCl, ▲: 0.1 mol dm^{-3} NaCl.

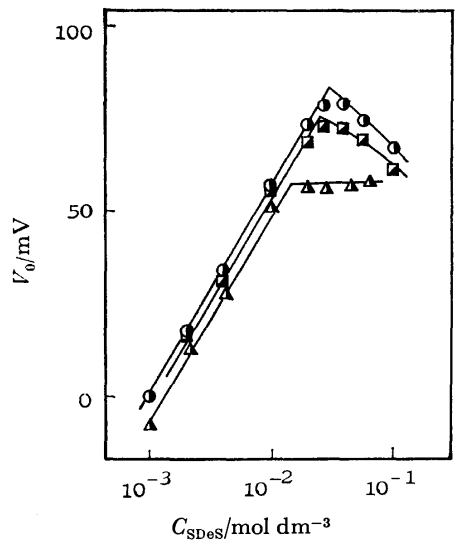

Fig. 3. Membrane potential as a function of concentration of SDeS in test solution in the presence of added electrolytes.
◐: No NaCl, ◪: 0.01 mol dm^{-3} NaCl, ▲: 0.1 mol dm^{-3} NaCl.

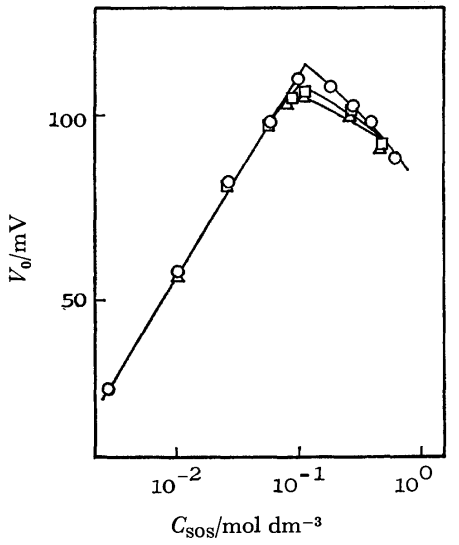

Fig. 4. Membrane potential as a function of concentration of SOS in test solution in the presence of added electrolytes.
○: No NaCl, □: 0.01 mol dm^{-3} NaCl, △: 0.1 mol dm^{-3} NaCl.

of surfactant ion caused by the added electrolyte. Mukerjee *et al.*[16,17] suggested the existence of a detergent dimer below CMC, on the basis of conductivity measurements of the SDS solution. In the present study, however, there was no sign of the dimerization of surfactant ions, because the concentration dependence of the membrane potential possessed the Nernstian slopes. The potential equation may be given by

$$V = \frac{RT}{F} \ln \frac{a_{AS}}{a_{AS}^{\circ}}, \quad (3)$$

where a_{AS} denotes the activity of AS ions in the presence of NaCl, and a_{AS}°, the activity of AS ions in the 10^{-3} mol dm^{-3} SAS solution without added electrolyte. Equation 3 becomes

$$V = \frac{RT}{F} \ln \frac{C_{AS}}{C_{AS}^{\circ}} + \frac{RT}{F} \ln \frac{\gamma_{AS}}{\gamma_{AS}^{\circ}}, \quad (4)$$

where γ_{AS} and γ_{AS}° denote the activity coefficients of AS ions in the presence and the absence of NaCl, respectively. Thus, the decrement due to the added electrolyte may be ascribed to the decrease in the activity coefficient of AS ions caused by the added electrolyte. Since the Nernstian slope was unaltered even in the presence of the added electrolyte, the AS electrode may be regarded as ideally permselective to singly dispersed AS ions. In the absence of electrolyte, Eq. 4 is reduced to Eq. 1.

Above CMC, a decrease of the membrane potential was observed; this tendency was accelerated by increasing the amount of the added electrolyte or the chain length. These phenomena may be attributed to the change in the activity of surfactant ions.

The chemical potential of the surfactants in the bulk phase μ_b and that, μ_m, in the micellar phase are described as follows:

$$\mu_b = \mu_b^{\circ} + RT \ln a_{Na} a_{AS}, \quad \mu_m = \mu_m^{\circ} + RT \ln a_m, \quad (5)$$

where a_{AS}, a_{Na}, and a_m denote the activity of the surfactant ion, Na ion, and NaAS in the micelle, respectively; μ_b° and μ_m° are the standard chemical potential for the dissociated surfactant and the micelle. Taking the micelle as a pseudo phase, the activity of the micelle may be set at unity. Since the singly dispersed surfactants are equilibrated with the micelles, we have from Eq. 5,[18,19]

$$a_{Na} a_{AS} = \text{const.} \quad (6)$$

We may conclude that the response of the AS electrode to the micellar AS ions can be ignored, since the potentials never increase with surfactant concentrations. The potential should increase if the AS electrode responds to the micellar AS ions. The fact that the potential is kept constant in the large excess of added electrolyte, as shown in Figs. 2 and 3, supports this view.

Below CMC, the activity coefficient of AS ions may be regarded as a constant. Thus, the potential decrease above CMC implies the decrease in the concentration of singly dispersed surfactant ion providing that the activity coefficient does not change appreciably above CMC. On the other hand, since the potential remains constant in the presence of a large excess of electrolyte, a_{AS} as well as C_{AS} remains constant in this region. This can be deduced from Eq. 6, *i.e.*, in the presence of a large excess of electrolyte, a_{Na} may be regarded as a constant and hence a_{AS} becomes constant. Furthermore the activity coefficient of singly dispersed surfactant ions may be regarded as a constant due to the large excess of inorganic electrolyte, and thus C_{AS} might be constant. These conclusions agree with those obtained by Sasaki *et al.*[3,4] from the gel filtration data.

It is usually assumed that above CMC the concentration of singly dispersed surfactant ions is kept constant even though the total analytical concentration of surfactant increases. This hypothesis should be true only in the presence of a large excess of added electrolyte.

On the other hand, the activity of Na ions in the bulk phase may be expressed by

$$a_{Na} = \gamma_{Na}[C_S + C_{AS} + \alpha(C - C_{AS})], \quad (7)$$

where C_S, C_{AS}, and C denote the concentration of the added NaCl, that of the singly dispersed surfactant ions, and the total analytical concentration of surfactant, respectively; γ_{Na} is the activity coefficient of Na ions, and α, the degree of dissociation of the micelle. A similar relation is proposed by Botré *et al.*,[1] for a system with no added salt. Subtracting the potential at CMC, V^*, from V by the use of Eq. 3, we have

$$V - V^* = \frac{RT}{F} \ln \frac{a_{AS}}{a_{AS}^*}, \quad (8)$$

where the asterisk refers to CMC.

Comparing this with Eq. 6, we obtain

$$V - V^* = \frac{RT}{F} \ln \frac{a_{Na}^*}{a_{Na}}. \quad (9)$$

Assuming that γ_{Na} does not change appreciably above CMC, we have, from Eqs. 7 and 9,

$$V - V^* = \frac{RT}{F} \ln \frac{C_S + C_{AS}^*}{C_S + C_{AS} + \alpha(C - C_{AS})}, \quad (10)$$

where C_{AS}^* denotes CMC.

In the presence of a large excess of added salt, C_{AS}^*, C_{AS}, and $(C - C_{AS})$ can be ignored as compared with C_S, and thus $V = V^*$, which agrees with the experimental results.

TABLE 2. DEGREE OF DISSOCIATION OF MICELLE CALCULATED ACCORDING TO Eqs. 8 AND 10

SAS	SDS	SDeS	SOS
α	0.20	0.23	0.27

For other cases, the potential decreases with concentration above CMC. As pointed out previously, C_{AS} can be evaluated according to Eq. 8, if γ_{AS} is assumed to be constant. Table 2 shows the values of α calculated according to Eqs. 8 and 10 by assuming a constant activity coefficient of AS ions. This table indicates that the value of α is approximately constant for a given surfactant. This coincides with the additivity rule for the counterions of the polyelectrolyte in the presence of added electrolyte.[20]

The present work was partially supported by a Grant-in-Aid for Scientific Research from the Ministry of Education. Project number, 247009.

References

1) C. Botré, V. L. Crescezi, and A. Mele, *J. Phys. Chem.*, **63**, 650 (1959).
2) I. Satake, T. Tahara, and R. Matuura, *Bull. Chem. Soc. Jpn.*, **42**, 319 (1969).
3) T. Sasaki, M. Hattori, J. Sasaki, and K. Nukina, *Bull. Chem. Soc. Jpn.*, **48**, 1397 (1975).
4) T. Sasaki, *Yukagaku*, **24**, 207 (1975).
5) K. Shirahama, *Kolloid Z. Z. Polym.*, **250**, 620 (1972).
6) K. Kaibara, T. Nakahara, I. Satake, and R. Matuura, *Mem. Fac. Sci., Kyushu Univ., Ser. C*, **7**, 1 (1970).
7) C. Gavach and P. Seta, *Anal. Chim. Acta*, **50**, 407 (1970).
8) B. J. Birch and D. E. Clarke, *Anal. Chim. Acta*, **61**, 159 (1972).
9) A. Matsubara and K. Nomura, *Mem. Fac. Sci., Kyushu Univ., Ser. C*, **10**, 37 (1976).
10) J. Sandblom, G. Eisenman, and J. L. Walker, Jr., *J. Phys. Chem.*, **71**, 3862 (1967).
11) G. Scibona, L. Mantall, and P. R. Danesi, *Anal. Chem.*, **42**, 844 (1970).
12) G. Shean and K. Sollner, *J. Membrane Biol.*, **9**, 297 (1972).
13) A. Yamauchi, T. Minematsu, and H. Kimizuka, *Maku (Membrane, in Japanese)*, **2**, 69 (1977).
14) P. Mukerjee and K. J. Mysels, *Nat. Stand. Ref. Data Ser. Nat. Bur. Stand.*, **36**, 51 (1971).
15) R. A. Robinson and R. H. Stokes, "Electrolyte Solutions," Butterworths, London (1959), p. 63.
16) P. Mukerjee, K. J. Mysels, and C. I. Dulin, *J. Phys. Chem.*, **62**, 1390 (1958).
17) P. Mukerjee, *J. Phys. Chem.*, **62**, 1397 (1958).
18) K. Shinoda, T. Nakagawa, B. Tamamushi, and T. Isemura, "Colloidal Surfactants," Academic Press, New York (1963), p. 6.
19) P. H. Elworthy and K. J. Mysels, *J. Colloid Interface Sci.*, **21**, 331 (1966).
20) B. E. Conway and R. G. Barradas, "Chemical Physics of Ionic Solutions," John Wiley & Sons, New York (1966).

Theoretical Studies on the Electronic Structure of the H_2S Anion Radical

Shinichi NAGATA,*,† Tokio YAMABE, and Kenichi FUKUI

Department of Hydrocarbon Chemistry, Faculty of Engineering, Kyoto University, Sakyo-ku, Kyoto 604

(Received February 23, 1978)

The electronic structure of the H_2S anion radical has been investigated by means of the non-empirical unrestricted Hartree-Fock method. The most stable conformation of this radical has been obtained at bond length R(S–H) = 1.550 Å and bond angle θ (<HSH) = 160°. These values are relatively larger in comparison with observed values of the neutral molecule (R = 1.335 Å and θ = 92.2°). ESR hyperfine coupling constants and excitation energies have also been examined through analyses of the electronic structure of the most stable conformation of this radical. Furthermore, the dissociation process, $H_2S \rightarrow H_2 + S^-$ or $HS^- + H$, has been discussed.

There have been a number of studies on the electronic structure of sulfur compounds from both theoretical and experimental aspects.[1] Most of the theoretical investigations on simple molecules such as H_2S have been done employing the *ab initio* SCF method and discussed the role of the vacant 3d-orbitals of sulfur.[2] Previous studies[2] seem to have led to the conclusion that the 3d-orbitals of sulfur with normal valences do not greatly contribute to the molecular properties in the ground state. This has, however, led to an improvement in the quality of the calculation. Recently, Schwenzer and Schaefer[3] also came to similar conclusions for the ground electronic state of the hypervalent molecules, SH_4 and SH_6, although they pointed out that the contribution of the 3d-orbitals is larger for SH_6 and SH_4 than SH_2. However, the contribution of the 3d-orbitals cannot be neglected in the ground state as well as the excited one as indicated from the theoretical studies of Hillier *et al.*[2b] and Bendazzoli *et al.*[2c]

Experimental studies on the H_2S anion radical have been few compared to H_2S or H_2S^+,[4] since it is difficult to produce the H_2S anion radical. For example, the radiation method[5] showed that H_2S reacts with an e^- at a higher rate ($k = 1.35 \times 10^{10}\ M^{-1}\ s^{-1}$) and produces predominantly H and HS^- with minor fractions H_2 and S^-. In 1966, Bennett *et al.*[6] reported the ESR spectrum of the H_2S anion radical in the reaction between an alkali-metal atom and H_2S or D_2S at 77 K. Theoretical studies on the H_2S anion radical followed: Cook *et al.*[7] performed the non-empirical calculation using the mixed basis method with d-orbitals and found poor agreement between the theoretical and experimental values of ESR hyperfine coupling constants of sulfur nuclei. Claxton *et al.*[8] carried out the *ab initio* UHF calculation on the same molecule with minimal Gaussian basis set and expressed considerable doubt on the interpretation of the ESR spectrum assigned to the H_2S anion radical by Bennett *et al.*[6] An inexplicable discrepancy between their calculation[8] and Cook's result[7] was reported.

In the present paper, the *ab initio* UHF calculation on the H_2S anion radical has been performed in the LCAO MO approximation with spin annihilation to obtain the pure doublet spin state. SCF atomic orbitals used for this calculation are the minimal basis set of Csizmadia *et al.*,[9] minimal STO-3G basis,[10] and larger basis of "double ζ" quality (4-31 G).[11] The primary purposes of this work are (1) to determine the stable conformation of the H_2S anion radical in both the $^2B_2$ and the $^2A_1$ states, taking the correlation of the Walsh diagram into consideration; (2) to calculate and examine the molecular properties of ESR hyperfine coupling constants and excitation energies; (3) to investigate the formation of solvated electrons in the system of H_2S and electrons as experimentally observed in H_2O, or the dissociation towards $H + HS^-$ or $H_2 + S^-$ of the H_2S anion radical.

Method of Calculation

The UHF calculations have been performed based on the minimal Gaussian-type orbitals (MGTO) by Csizmadia *et al.*,[9] STO-3G,[10] and 4-31 G[11] basis sets. The exponent values of the STO's, ζ, are the same as reported previously.[9,10] In the STO-3G expansion, the values of the exponents (α_m) and coefficients (d_m) of the GTO's were taken from Stewart[12] ($\chi_r = \mathrm{STO}(\zeta) = \sum_{m=1} d_m\ \mathrm{GTO}(\alpha_m)$). For the 4-31 G basis set the bases for the valence shells were split into inner and outer parts over the smaller minimal set, and the standard scale factors presented by Hehre *et al.*[11] were used. Consideration of the total energies, orbital energies, charge densities, and spin densities was made with the results obtained after the single annihilation.[13]

Excitation energies of the H_2S anion radical were calculated from the following equations[14] using values of ε, J, and K obtained from the calculation of H_2S equivalent with the geometry of the H_2S anion radical:

$$\Delta E_{p\to k} = \varepsilon_k - \varepsilon_p,$$

$$\Delta E_{i\to p} = \varepsilon_p - \varepsilon_i - 2J_{pi} + K_{pi} + J_{pp},$$

$$\Delta E_{i\to k}(1) = \varepsilon_k - \varepsilon_i - (J_{pi} - K_{pi}/2) - (J_{ki} - 2K_{ki}) + (J_{pk} - K_{pk}/2),$$

$$\Delta E_{i\to k}(2) = \varepsilon_k - \varepsilon_i - (J_{pi} - K_{pi}/2) - J_{ki} + (J_{kp} + K_{kp}/2),$$

where, i, p, and k denote the doubly occupied, singly occupied, and virtual orbitals, respectively.

Results and Discussion

(1) The calculations of the H_2S anion radical were performed with MGTO,[9] STO-3G,[10] and 4-31 G[11] basis sets, varying the angle θ (<HSH) from 92.2

† Present address: Research Institute of Marine Cargo Transportation, Kobe University of Mercantile Marine, Higashinada-ku, Kobe 658.

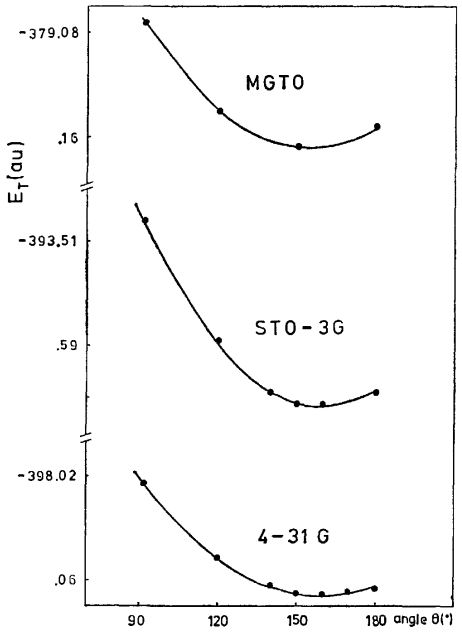

Fig. 1. Total energies of H_2S anion radical, with the angle variation, calculated by MGTO, STO-3G, and 4-31 G basis.

(experimentally determined for H_2S)[15] to 180°, fixing the bond distance at 1.335 Å.[15] The results obtained are shown in Fig. 1, and demonstrate the superiority of the STO-3G and 4-31 G basis sets in comparison with the MGTO basis. Consequently the results obtained from the STO-3G and 4-31G basis will be discussed later. It is worth noting that the H_2S anion radical is most stable at $\theta=160°$ in these basis sets. Here, it should be remembered that the calculations of this anion radical reported previously[7,8] were conducted using the same geometry as H_2S (92.2°).

The ground and lowest excited states of the H_2S anion radical are the $^2B_2$ and $^2A_1$ states, respectively. The $^2B_2$ and $^2A_1$ states are equivalent with the entrance of one electron into the $3b_2$ orbital (lowest unoccupied

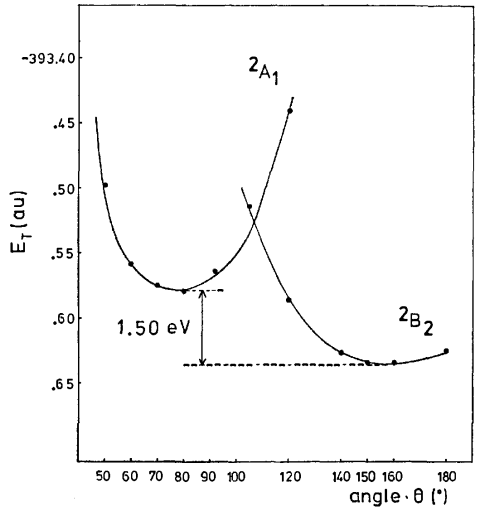

Fig. 2. Total energies of $^2B_2$ and $^2A_1$ states with the variation of angle θ.

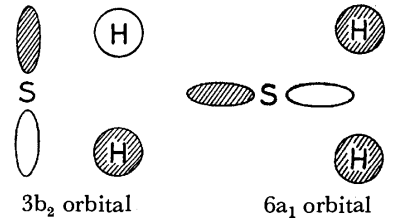

Fig. 3. Orbital shapes of $3b_2$ and $6a_1$ orbitals of H_2S molecule (angle θ(<HSH)=92.2°).

molecular orbital (LUMO)) and the $6a_1$ orbital (LUMO +1), respectively. Energy changes for both states as a function of the angle θ are shown in Fig. 2, which were obtained from the calculation of STO-3G basis. The $^2B_2$ state is energetically more stable compared to the $^2A_1$ state by 1.50 eV. Interestingly, the angle θ has become larger for the former and smaller for the latter than that of the H_2S molecule (92.2°). Examination of the extension of $3b_2$ and $6a_1$ orbitals and the relationship of the chemical bonds of H_2S (see Fig. 3) showed that the $3b_2$ and $6a_1$ orbitals are antisymmetric and symmetric on the lane bisecting the angle θ (<HSH), respectively. Accordingly excess electrons of H_2S^- entering into the $3b_2$ and $6a_1$ orbitals may decrease the electronic repulsion between the hydrogen atoms and form a bond between them, respectively. Such considerations are consistent with the calculated results of the most stable conformation of $^2B_2$ and $^2A_1$ states of the H_2S anion radical.

It is interesting and important to consider the correlation between the total energies and orbital energies from the Walsh diagram[16] of both states. Figure 4 shows the one-electron orbital energy changes of H_2S as a function of the angle θ. This figure demonstrates that the electron occupancy into the $3b_2$ orbital makes the angle θ larger, while in the case of the $6a_1$ orbital the reverse is indicated, *i.e.*, the angle θ becomes smaller. The present qualitative consideration is in good agree-

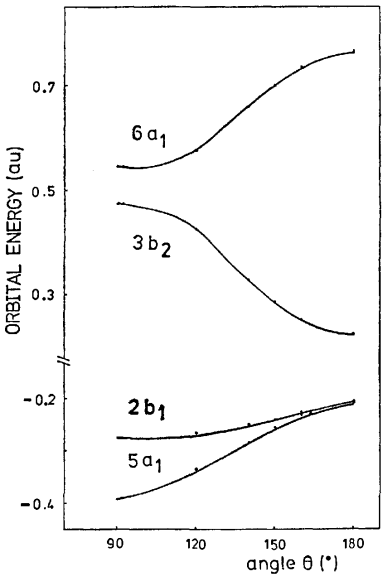

Fig. 4. Orbital energy diagram of H_2S from 90 to 180° calculated by STO-3G basis set.

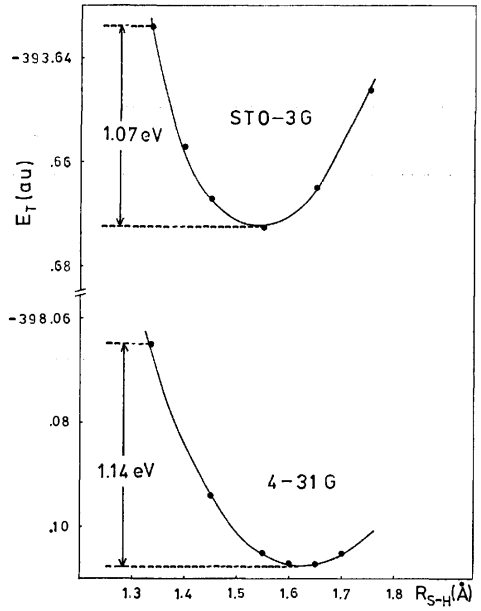

Fig. 5. Total energies of H_2S anion radical (angle θ(<HSH)=160°) with the variation of R(S–H).

ment with the changes of total energies (Fig. 2) and also appears to be interpretable for the H_2S cation radical which has been treated in a previous paper,[4] that is, the $^2B_1$ and $^2A_1$ states of the H_2S cation radical are most stable for θ=92.9 and 127° in accord with the observed values obtained from the emission spectra,[17] respectively.

Subsequently the changes in the total energy of the H_2S anion radical for the variation of R(S–H) were examined, since the excess electron on H_2S may lead to molecular deformation caused by decreasing the electronic repulsion between hydrogen and hydrogen or sulfur atoms. As expected, Fig. 5 clearly shows the minimum energy of the anion radical at R(S–H)=1.650 Å from the calculation of 4-31 G basis and 1.550 Å from STO-3G basis, respectively. Namely, the total energy decreases *ca.* 1.14 and 1.07 eV by the lengthening of the S–H bond, 0.315 and 0.215 Å, in comparison with R(S–H)=1.335 Å of H_2S, respectively.

Table 1. Calculated hyperfine coupling constants (G) of H_2S anion radical (angle (<HSH)=160°) by STO-3G and 4-31 G basis

	STO-3G	4-31 G	Exptl[a]
a_H	187.27	327.60	±7.7±0.3
a_S	159.35	−207.24	±60.0±2.0

a) Ref. 6.

(II) The molecular properties of ESR hyperfine coupling constants (a_H and a_S) of the H_2S anion radical are given in Table 1 which represents the calculated hyperfine coupling constants by both basis sets, where the following results for both a_H and a_S are indicated, *i.e.*, the calculated values are far larger than observed ones. This discrepancy between theory and experiment may be the same as that pointed out in the previous studies.[7,8] The authors obtained good agreement with the experimental values (a_H) for the H_2S cation radical[4] by the use of the same basis set as the present one. Furthermore, Claxton *et al.*[8] were also successful in the calculation of hyperfine coupling constants on many kinds of radicals except for the H_2S anion radical. Taking these results into consideration, the authors have joined Symons[18] and Claxton *et al.* in entertaining considerable doubt on the interpretation of the ESR spectrum assigned to the H_2S anion radical. This discussion will be made in a later section.

Table 2. Calculated excitation enegies (eV) of H_2S anion radical (angle θ (<HSH)=160°) by STO-3G and 4-31 G basis sets

	STO-3G	4-31 G	Exptl[a]
$\Delta E(9\rightarrow10)$[b]	6.28	1.79	1.22—1.77
$\Delta E(8\rightarrow10)$	7.81	2.81	3.10
$\Delta E(10\rightarrow11)$	11.24	9.14	
$\Delta E(9\rightarrow11)^{(1)}$	14.69	8.05	
$\Delta E(9\rightarrow11)^{(2)}$	17.68	10.52	

a) Ref. 6. b) 9, 10, and 11 denote the highest occupied, singly occupied, and lowest unoccupied molecular orbitals of H_2S anion radical, respectively.

An attempt was made to calculate the excitation energies of the H_2S anion radical, with reference to the experiments of Bennett *et al.*,[6] the details of which are given in the preceding section. The results calculated by using both basis sets are tabulated in Table 2. The absorption band found experimentally[6] at 1.22—1.77 eV may be assigned to the $2b_1\rightarrow3b_2$ transition, *i.e.*, from the lone pair electrons of sulfur to the anti-bonding orbital of the S–H bond. Such a large red shift of this band compared to H_2S is due to the fact that the σ^*_{S-H} orbital lowers, to a large extent, by the presence of an excess electron. The next band at 3.10 eV may be assigned to the $5a_1\rightarrow3b_2$ transition, that is, from the σ_{S-H} orbital to the σ^*_{S-H} one. Similarly, the red shift of this band compared to that of H_2S may be ascribed to the lowering of the σ^*_{S-H} orbital as mentioned above. Since the intensity of these absorption bands has not been experimentally determined as yet, there is no alternative except to discuss in terms of the excitation energy. In the present calculation, the $2b_1\rightarrow3b_2$ transition is theoretically forbidden (f=0.0). On the contrary, the intensity of the $5a_1\rightarrow3b_2$ band is considerably large (f=0.117, calculated) because of the symmetry allowance between both states. The excitation energies calculated by the 4-31 G basis were in good accordance with the experimental ones,[6] but those of STO-3G basis are somewhat larger, which is mainly due to the higher-energy location of virtual orbitals obtained from this basis.

(III) In the preceding section, the electronic structures and molecular properties of the H_2S anion radical were discussed. It is interesting to consider this anion radical as a reaction product of H_2S+e^- and the starting molecule for dissociation into $H+HS^-$. At the outset, it is supposed that the electron outside H_2S is describable by placing the diffuse s-type orbital outside

TABLE 3. CALCULATED HYPERFINE COUPLING CONSTANTS (G) AND CHARGE DENSITIES OF H_2S ANION RADICAL (angle θ ($<$HSH)=160 AND 92.2°) WITH OUTER 2s-TYPE ORBITAL ($\xi_{2s}=0.1$)[a]

Distance (Å)[b]	H_2S^- (160°)				H_2S^- (92.2°)			
	E_T(au)	a_H	a_S	ρ (outer orbital)	E_T(au)	a_H	a_S	ρ (outer orbital)
0.5	−393.6641	189.18	165.37	0.273				
1.0	−393.7134	229.07	82.44	0.349				
1.5	−393.7349	192.34	50.00	0.780	−393.8049	−18.86	16.54	0.942
2.5	−393.7653	52.32	8.83	0.931	−393.8744	−6.95	1.94	0.982
3.5	−393.7790	5.37	0.42	1.001	−393.8957	−0.48	0.35	0.992
5.0	−393.7747	1.51	−0.01	1.000	−393.8935	0.58	−0.07	0.999

a) Calculations were carried out using STO-3G basis set. b) Between sulfur atom of H_2S and diffuse 2s-type orbital on the line bisecting the angle θ($<$HSH).

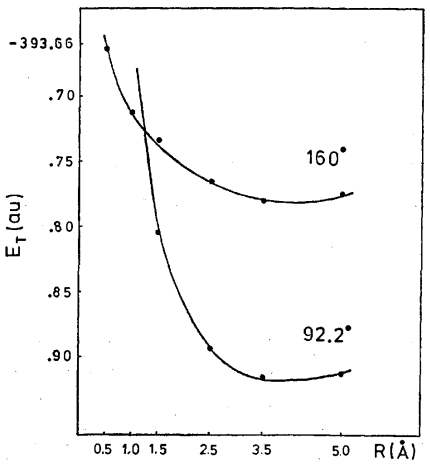

Fig. 6. Total energies of H_2S anion radical (angle θ($<$HSH)=92.2 and 160°) in the condition of locating the diffuse 2s-type orbital.

t, that is, on the bisector of the angle θ and the opposite side of the pσ orbital of sulfur on the H_2S plane. The calculated results for two kinds of angle ($<$HSH), 92.2 and 160°, are shown in Fig. 6 and Table 3, which were obtained from the calculation consisting of both STO-3G basis and diffuse 2s type orbital. From these, it can be rationalized that the H_2S+e^- system is impelled to destabilize as the e^- approaches H_2S. At the same time, one can easily recognize that in the distant region (>1.5 Å) between H_2S and e^- this system retains the original form of H_2S (92.2°) and separated electron, but that the approach of the e^- to H_2S in the region less than 1.5 Å tends to make the angle θ open (see the point of intersection of Fig. 6). As a consequence, the H_2S+e^- system is inclined to form the H_2S anion radical in the region less than 1.5 Å. Such a tendency may also be explained from the change of charge densities on the outer orbital (Table 3), *i.e.*, the excess electron of the H_2S anion radical may be regarded as flowing into the diffuse orbital placed outside the region over 1.5 Å, and delocalizing by the orbital hybridization in the region less than 1.5 Å, respectively.

Here, it should be remembered that the minimum energy was found at *ca.* 4 Å in both cases of 92.2 and 160°, implying that the H_2S anion radical is highly reactive and that H_2S forms a kind of solvated electron in this region as observed in the case of H_2O.[5] Hyperfine coupling constants and charge densities calculated by the addition of outer orbitals are given in Table 3, from which the remarkable decrement of a_H and a_S values with the separation of e^- are seen. The hyperfine coupling constants of H_2S anion radical are far larger than the experimental ones[6] and hence the possibility of the formation of a solvated electron or trapped electron for the H_2S+e^- system cannot be neglected.

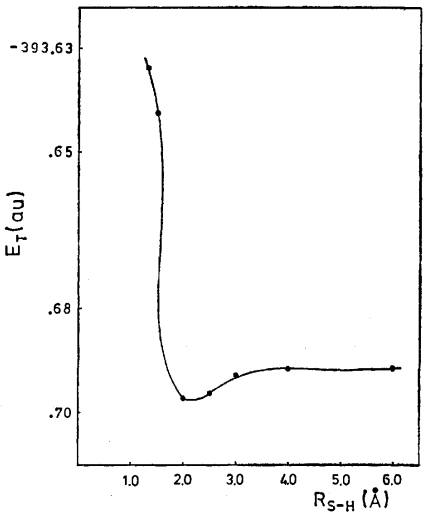

Fig. 7. Total energies accompanied with the dissociation reaction of $H_2S^- \rightarrow HS^- + H$.

Finally the dissociation process of the H_2S anion radical to HS^-+H will be discussed. Figure 7 suggests that the H_2S anion radical tends to separate such as HS^-+H through weak bonding at R(S–H)=2.2 Å.[20] Taking these results into account, the process may be as follows; the separated system of H_2S+e^-, which is originally stable, begins to interact to form a quasi-stable anion radical which dissociates into $H+HS^-$, probably because of an excess electron entered into the antibonding orbital of the S–H bond of the b_2 symmetry. The process leading to the formation of H_2+S^- may be explained in terms of the dissociation through the $^2A_1$ state due to an excess electron in the $6a_1$ orbital, since the bonding nature between the hydrogen atoms is indicated from the analysis of the charge density contour maps.

Conclusion

The present calculation on the H_2S anion radical indicates that the most stable conformation is the $^2B_2$ state with $\theta=160°$ and that the bond length of R(S–H) increases a little compared with that of H_2S. These results on the bond angle and bond length seem to be reasonable from the Walsh diagram and chemical reasoning. The H_2S anion radical itself, however, is very unstable and tends to dissociate as discussed. Consequently, more accurate experiments will make more detailed discussion on the H_2S anion radical possible, as Bennett *et al.*[6] obtained the ESR spectrum assigned to this anion radical. Moreover, the possibility of the formation of a solvated electron for the H_2S+e^- system should be examined from both theoretical and experimental aspects.

This work was supported by a Grant-in-Aid for Scientific Research from the Ministry of Education of Japan (No. 047068).

References

1) A. Senning, "Sulfur in Organic and Inorganic Chemistry," Marcel Dekker, Inc. (1972), Vols. 1—3.

2) (a) F. P. Boer and W. N. Lipscomb, *J. Chem. Phys.*, **50**, 989 (1969); (b) I. H. Hillier and V. R. Saunders, *Chem. Phys. Lett.*, **5**, 384 (1970); (c) S. Rothenberg, R. H. Young, and H. F. Schaefer, *J. Am. Chem. Soc.*, **92**, 3243 (1970); (d) J. R. Sabin, *ibid.*, **93**, 3613 (1971); (e) G. L. Bendazzoli, G. Gottarelli, and P. Palmieri, *ibid.*, **96**, 11 (1974).

3) G. M. Schwenzer and H. F. Schaefer, *J. Am. Chem. Soc.*, **97**, 1393 (1975). See also, for comparison, V. B. Koutecky and J. I. Musher, *Theor. Chim. Acta (Berl.)*, **33**, 227 (1974).

4) H. Sakai, S. Yamabe, T. Yamabe, K. Fukui, and H. Kato, *Chem. Phys. Lett.*, **25**, 541 (1974) and references cited therein.

5) E. J. Hart and M. Anbar, "The Hydrated Electron," Wiley-Interscience, New York (1970), p. 113.

6) J. E. Bennett, B. Mili, and A. Thomas, *Chem. Commun.*, **1966**, 182.

7) D. B. Cook, A. Hinchliffe, and P. Palmieri, *Chem. Phys. Lett.*, **3**, 223 (1969).

8) T. A. Claxton, D. McWilliams, and N. A. Smith, *Chem. Phys. Lett.*, **4**, 505 (1970).

9) I. G. Csizmadia, M. C. Harrison, J. W. Moskowitz, and B. T. Sutcliffe, *Theor. Chim. Acta (Berl.)*, **6**, 191 (1966); A. Rauk and I. G. Csizmadia, *Can. J. Chem.*, **46**, 1205 (1966).

10) W. J. Hehre, R. F. Stewart, and J. A. Pople, *J. Chem. Phys.*, **51**, 2657 (1969).

11) R. Ditchfield, W. J. Hehre, and J. A. Pople, *J. Chem. Phys.*, **54**, 724 (1971); W. J. Hehre and W. A. Lathan, *ibid.*, **56**, 5255 (1972).

12) R. F. Stewart, *J. Chem. Phys.*, **52**, 431 (1970).

13) T. Amos and L. C. Snyder, *J. Chem. Phys.*, **41**, 1773 (1964).

14) A. Ishitani and S. Nagakura, *Theor. Chim. Acta (Berl.)*, **4**, 236 (1956).

15) H. C. Allen, Jr., and E. K. Plyer, *J. Chem. Phys.*, **25**, 1132 (1956).

16) A. D. Walsh, *J. Chem. Soc.*, **1953**, 2260.

17) G. Duxbury, M. Horani, and J. Rostas, *Proc. R. Soc. London, Ser. A*, **331**, 109 (1972).

18) M. C. R. Symons, *Adv. Chem. Ser.*, **82**, 1 (1968).

19) D. G. Carroll, A. T. Armstrong, and S. P. McGlynn, *J. Chem. Phys.*, **44**, 1865 (1966).

20) R(S–H) indicates the distance between sulfur of HS^- and hydrogen atoms separated accompanied with the progress of reaction.

Thermodynamic Study on the Adsorption of 1-Octadecanol at Hexane/Water Interface

Norihiro MATUBAYASI,*,† Kinsi MOTOMURA, Makoto ARATONO, and Ryohei MATUURA

Department of Chemistry, Faculty of Science, Kyushu University, Fukuoka 812

(Received March 8, 1978)

The interfacial tension γ between water and hexane solution of 1-octadecanol has been measured as functions of temperature T, pressure p, and mole fraction of 1-octadecanol in hexane x_1^0 by the pendant drop method. The curves of γ *vs.* T, γ *vs.* p, and γ *vs.* x_1^0 show noticeable break points. Calculated thermodynamic quantities such as energy changes, entropy changes, and volume changes associated with the adsorption show the points of discontinuity at a certain temperature, pressure, and composition, corresponding to the above breaking points. It has been clarified that the first order phase transition between the expanded and condensed states takes place at the interface like that of monomolecular films spread on water surfaces. The expanded state is characterized by a relatively high energy, high entropy, and large volume, while the condensed state by low energy, low entropy, and small volume.

In a previous paper, the structure and properties of adsorbed films of 1-tetradecanol at the hexane/water interface were clarified by applying the thermodynamic treatment developed previously.[1,2] As an extension of the work, the adsorbed films of 1-octadecanol at the same interface was studied, and it was expected that a longer chain alcohol exhibits a phase transition from an analogy with the insoluble monolayer spread on water surface. There has been little data to suggest the phase transition at the liquid/liquid interface, and, in particular, the analysis appears to be insufficiently rigorous thermodynamically.[4-10] The major purpose of this work was to confirm that the phase transition really takes place in the adsorbed film and to clarify the type of the phase transition thermodynamically.

Experimental

1-Octadecanol used was purified by distillation and the purity checked by gas-liquid chromatography; only one peak was obtained. Water distilled three times from $KMnO_4$ solution was used as the aqueous phase. Hexane was dehydrated and the impurities removed by passing hexane through an activated alumina column. Interfacial tension measurements were performed by the pendant drop method, the detailed descriptions of which have been previously reported.[2,3]

Results

To calculate the entropy change Δs, the volume change Δv of the interface formation, and the interfacial density of 1-octadecanol Γ_1^{II}, data of the variations of interfacial tension with temperature T, pressure p, and mole fraction of 1-octadecanol in hexane x_1^0 are required. The interfacial tension was measured at 293.15, 295.65, 298.15, 300.65, and 303.15 K over the pressure range from 0.1 to 150 MPa, and concentration up to 2.3×10^{-3} mol fraction. In Figs. 1 and 2 the interfacial tension is plotted against the pressure at constant concentration and at constant temperature, 303.15 and 298.15 K. It is seen that the interfacial tension increases linearly with increasing pressure at low concentration, like the case of the 1-tetradecanol solution.[2] At an intermediate concentration, however, it decreases abruptly at a certain pressure which is dependent on the concentration of 1-octadecanol in hexane. The broken lines in Figs. 1 and 2 are obtained by connecting these break points. This behavior was not observed for 1-tetradecanol over the same range of temperature, pressure, and concentration.[2] At a high concentration, the interfacial tension decreases with the increase in pressure up to a point at which the crystallization of 1-octadecanol solution starts. It is clearly demonstrated in the Figures that the break point is affected by temperature. Figure 3 showes the variation of interfacial tension γ with temperature T at constant concentration, and pressure of 0.1 MPa. At low concentration a linear relation is obtained between γ and T and the slope varies from negative to positive with the increase in concentration in a similar manner to that of 1-tetradecanol. At high concentration, however, the γ *vs.* T curve has a break point. It is found that the decrease in

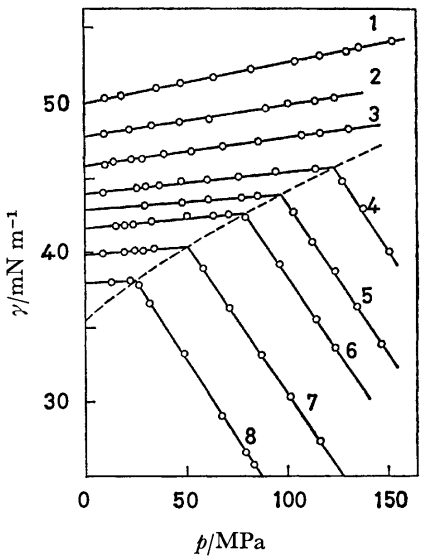

Fig. 1. Interfacial tension *vs.* pressure curves at constant mole fraction of octadecanol in hexane at 303.15 K. 1: $x_1^0=0$, 2: 1.04×10^{-4}, 3: 3.08×10^{-4}, 4: 6.31×10^{-4}, 5: 8.82×10^{-4}, 6: 1.08×10^{-3}, 7: 1.60×10^{-3}, 8: 2.38×10^{-3}.

† Present address: Faculty of Fisheries, Nagasaki University, Bunkyo-cho Nagasaki 852.

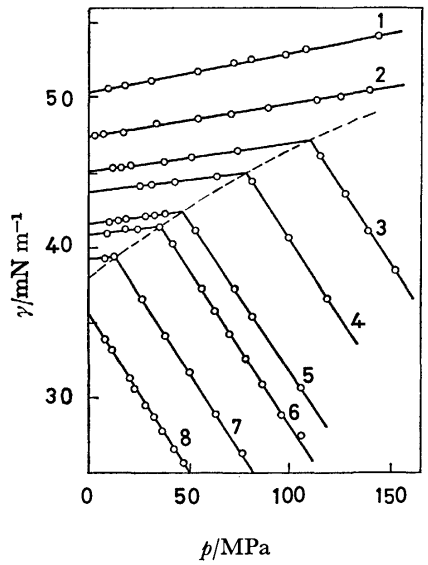

Fig. 2. Interfacial tension *vs.* pressure curves at constant concentration at 298.15 K. 1: $x_1^0=0$, 2: 1.46×10^{-4}, 3: 4.16×10^{-4}, 4: 6.18×10^{-4}, 5: 9.49×10^{-4}, 6: 1.13×10^{-3}, 7: 1.58×10^{-3}, 8: 2.21×10^{-3}.

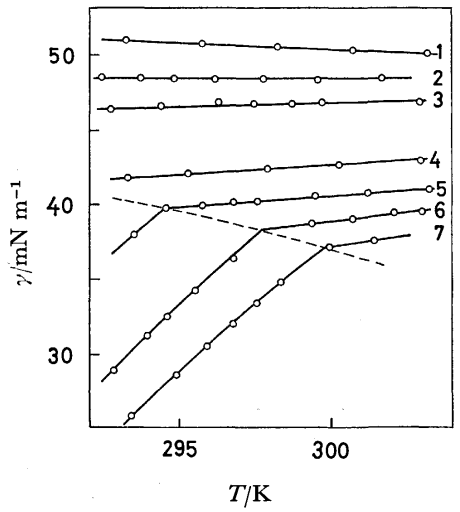

Fig. 3. Interfacial tension *vs.* temperature curves at constant concentration under 0.1 MPa. 1: $x_1^0=0$; 2: 1.33×10^{-4}, 3: 2.55×10^{-4}, 4: 8.05×10^{-4}, 5: 1.26×10^{-3}, 6: 1.68×10^{-3}, 7: 2.32×10^{-3}.

temperature and increase in concentration gives rise to the break in the curve. At any pressure similar figures as that in Fig. 3 can be drawn with the aid of the above γ *vs.* p curves. No striking difference was observed, but the temperature of the break point increase with the increase in pressure.

The interfacial tension γ can be plotted as a function of the concentration x_1^0 of 1-octadecanol in hexane at any temperature and pressure. In order to show that the break points in the γ *vs.* p curves clearly reflect those in the γ *vs.* x_1^0 curves, the behavior is illustrated in Fig. 4 at the temperatures of 293.15, 298.15, and 303.15 K at a constant pressure of 80 MPa.

At 0.1 MPa, the γ *vs.* x_1^0 curve breaks only at low temperature, and at 150 MPa, it breaks in a lower

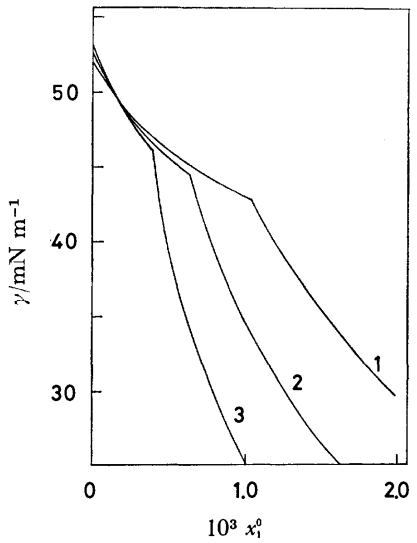

Fig. 4. Interfacial tension *vs.* concentration curves at constant temperature under 80 MPa. 1: 303.15 K, 2: 298.15 K, 3: 293.15 K.

concentration range. It seems appropriate to show the behavior of the break point in figures at 80 MPa, and in the following section the data at 80 MPa will be used for the thermodynamic discussion.

Discussion

Over the range of experimental conditions, the interfacial tension varies almost linearly with temperature and pressure, apart from the characteristic break points observed. It is conceivable that the phase transition in the interfacial film causes an abrupt change in the curves. Lutton *et al.*[8] also observed that the γ *vs.* T curve exhibits a break point for the system of triglyceride oil solutions of propylene glycol monoester and monoglyceride and water. They suggested that the behavior observed could be accounted for in terms of a melting of the surfactant monolayer adsorbed at the interface. Hutchinson[4-6] studied the adsorption of myristic acid at the cyclohexane/water interface and observed that the interfacial pressure *vs.* area per molecule curve displayed a transition. He assumed that the transition takes place between the liquid expanded and the liquid condensed films. A similar observation for 1-octadecanol in the cyclohexane/mercury system was made by Ambawani *et al.*[9] In order to understand the mechanism, it is necessary to analyze the experimental results thermodynamically.

For the system under consideration, it may be assumed that the mutual solubility of hexane and water is in fact negligible and 1-octadecanol is soluble only in hexane. In comformity with this view, the thermodynamic treatment applied to the adsorption of 1-tetradecanol at the hexane/water interface is applied in this study.[2] Since the measurements were made on the solution of solute mole fraction below 2.3×10^{-3}, the solution was regarded as an ideal one. The interfacial density of 1-octadecanol is given by the equation

$$\Gamma_1^{\mathrm{H}} = -(x_1^0/RT)(\partial\gamma/\partial x_1^0)_{T,p}. \quad (1)$$

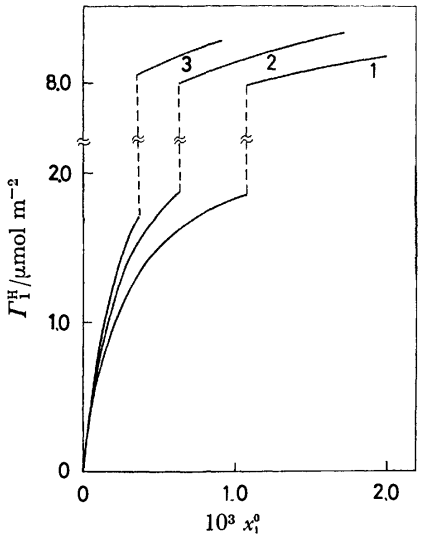

Fig. 5. Interfacial density *vs.* concentration curves at constant temperature under 80 MPa. 1: 303.15 K, 2: 298.15 K, 3: 293.15 K.

Figure 5 shows Γ_1^H as a function of x_1^0 at various temperatures and at 80 MPa. The discontinuous change on the Γ_1^H *vs.* x_1^0 curve indicate a phase transition in the adsorbed film of 1-octadecanol.

To further elucidate the adsorption, the relationships between the interfacial pressure π and the area per molecule A are given in Fig. 6 at three temperatures at 80 MPa, and in Fig. 7 at four pressures at 303.15 K. The isothermal and isobaric π *vs.* A curves show typical phase transition between the expanded and condensed films. Further, the intermediate region between both states become narrow with increasing temperature at constant pressure or with decreasing pressure at constant temperature. This behavior is comparable with that of the myristic acid monomolecular film spread at the air/water interface.[11]

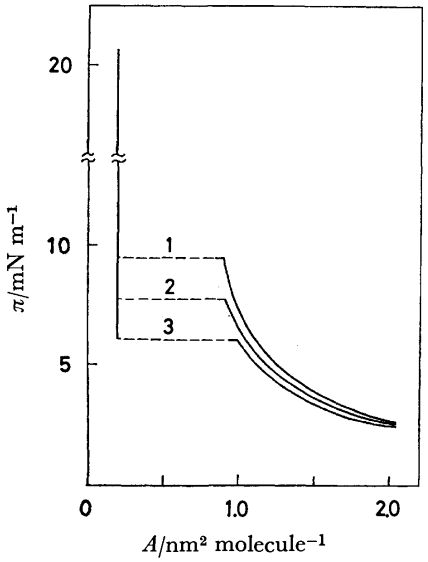

Fig. 6. Interfacial pressure *vs.* area curves at constant temperature under 80 MPa. 1: 303.15 K, 2: 298.15 K, 3: 293.15 K.

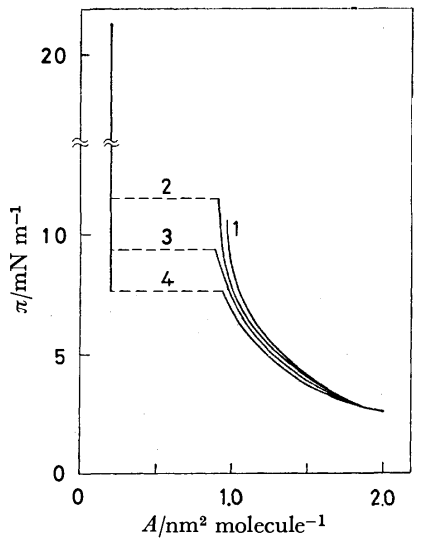

Fig. 7. Interfacial pressure *vs.* area curves at constant pressure at 303.15 K. 1: 0.1 MPa, 2: 40 MPa, 3: 80 MPa, 4: 120 MPa.

Entropy and volume changes of interface formation are given by the equations

$$\Delta s = -(\partial\gamma/\partial T)_{p,x_i'} \tag{2}$$

and

$$\Delta v = (\partial\gamma/\partial p)_{T,x_i'}. \tag{3}$$

In Figs. 8 and 9, the values of Δs and Δv are plotted as functions of concentration at 293.15, 298.15, and 303.15 K and at a constant pressure 80 MPa. In the expanded state, Δs and Δv are independent of temperature and pressure within the precision of the observations. Both the positive values of Δs and Δv for the system of pure hexane and water indicate that the contact between hexane and water causes increases in entropy and volume. With increasing concentration both values decreases gradually. This means that the adsorption of 1-octadecanol at the interface makes a negative contribution to Δs and Δv and that the partial molar entropy and volume of the adsorption are negative, as in the case of

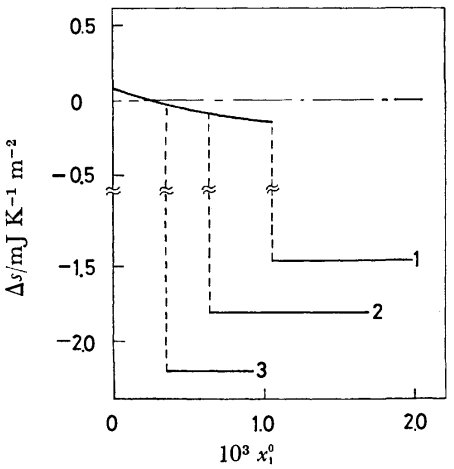

Fig. 8. Entropy change *vs.* concentration curves at constant temperature under 80 MPa. 1: 303.15 K, 2: 298.15 K, 3: 293.15 K.

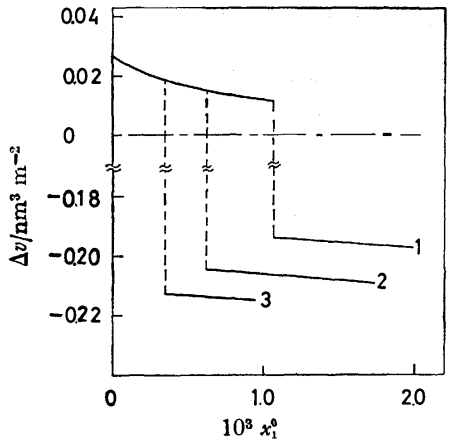

Fig. 9. Volume change *vs.* concentration curves at constant temperature under 80 MPa. 1: 303.15 K, 2: 298.15 K, 3: 293.15 K.

1-tetradecanol. In the condensed state, on the other hand, it is apparent that both Δs and Δv are dependent on temperature and are characterized by remarkably negative values.

The striking discontinuities in the Δs *vs.* x_1^0 and Δv *vs.* x_1^0 curves indicate that the break points in the γ *vs.* T and γ *vs.* p curves are the first order phase transition points, and at these points the expanded and condensed films coexist. With reference then to the gas-liquid equilibrium, the expanded state is favored by relatively high entropy and large volume and the condensed state by low entropy and small volume. Thus the increase in pressure and the decrease in temperature favor the condensed state.

It has been known that the differentials of interfacial tension in the condensed and expanded phases are expressed respectively as

$$d\gamma = -\Delta s^c dT + \Delta v^c dp - \Gamma_1^{H\cdot c}(\partial\mu/\partial x_1^0)dx_1^0 \quad (4)$$

and

$$d\gamma = -\Delta s^e dT + \Delta v^e dp - \Gamma_1^{H\cdot e}(\partial\mu/\partial x_1^0)dx_1^0, \quad (5)$$

where the condensed and expanded states are denoted by the superscript c and e, respectively. From these equations, it may be seen that

$$(\partial\gamma^{eq}/\partial T)_p = -(\Delta s^c/\Gamma_1^{H\cdot c} - \Delta s^e/\Gamma_1^{H\cdot e})/(1/\Gamma_1^{H\cdot c} - 1/\Gamma_1^{H\cdot e}) \quad (6)$$

and

$$(\partial\gamma^{eq}/\partial p)_T = (\Delta v^c/\Gamma_1^{H\cdot c} - \Delta v^e/\Gamma_1^{H\cdot e})/(1/\Gamma_1^{H\cdot c} - 1/\Gamma_1^{H\cdot e}). \quad (7)$$

The left-hand sides of these equations can be easily obtained as the slopes of the broken lines of Figs. 2 and 3, and the right-hand side may be calculated by the quantities derived above. The values of both sides of Eq. 6 at 298.15 K and at 80 MPa are 0.37 and 0.45 mJ K^{-1} m^{-2}, and those of Eq. 7 are 0.71 and 0.81 mm^3 m^{-2}, respectively. Taking into account the precision of the right hand sides of equations, the agreement is not unsatisfactory. Then this fact supports that the phase transition in the adsorbed film of 1-octadecanol is the first order phase transition.

The energy change associated with the adsorption

Table 1. Comparison of thermodynamic quantities at 303.15 K and 80 MPa

$10^3 x_1^0$	State of film	γ / mJ m^{-2}	$T\Delta s$ / mJ m^{-2}	$p\Delta v$ / mJ m^{-2}	Δu / mJ m^{-2}
0.0	*e*	52.02	27.3	2.10	77.2
0.2	*e*	48.74	6.6	1.66	53.8
0.4	*e*	46.63	−9.1	1.40	36.1
0.6	*e*	45.15	−21.2	1.22	22.7
0.8	*e*	43.96	−30.9	1.08	12.0
1.0	*e*	42.95	−39.1	0.97	2.9
1.2	*c*	39.92	−452	−15.7	−395
1.4	*c*	36.88	−455	−15.8	−402
1.6	*c*	34.18	−455	−15.8	−405
1.8	*c*	31.87	−455	−15.9	−407
2.0	*c*	29.81	−457	−16.0	−411

may be obtained at any temperature, pressure, and composition with the aid of the relation

$$\Delta u = \gamma + T\Delta s - p\Delta v. \quad (8)$$

In Table 1, values of Δu, γ, $T\Delta s$, and $p\Delta v$ at 303.15 K and at 80 MPa are given. It is seen that in the expanded state the values of Δu decrease with increase in concentration in a similar way as in the case of 1-tetradecanol.[2] In the condensed state the adsorption of 1-octadecanol remarkably lowers the hexane/water interface energy.

All work prior to this has been carried out without taking into account the effect of pressure on interfacial tension provided that it has no pronounced effect on the properties of the condensed phase. For the system investigated in this study, the term $p\Delta v$ makes a relatively smaller contribution to Δu than $T\Delta s$ as shown in Table 1, and in fact has only a negligible contribution at atmospheric pressure. But it is important to investigate the effect of pressure on interfacial tension which will provide important data concerning the volumetric properties of the interface as discussed above.

This work was supported in part by a Scientific Research Grant from the Ministry of Education, Japan (No. 147010).

References

1) K. Motomura, *J. Colloid Interface Sci.*, **64**, 348 (1978).
2) K. Motomura, N. Matubayasi, M. Aratono, and R. Matuura, *J. Colloid Interface Sci.*, **64**, 356 (1978).
3) N. Matubayasi, K. Motomura, S. Kaneshina, M. Nakamura, and R. Matuura, *Bull. Chem. Soc. Jpn.*, **50**, 523 (1977).
4) E. Hutchinson, *J. Colloid Interface Sci.*, **3**, 219 (1948).
5) E. Hutchinson, *J. Colloid Interface Sci.*, **3**, 235 (1948).
6) E. Hutchinson and D. Randall, *J. Colloid Interface Sci.*, **7**, 151 (1952).
7) C. E. Stauffer, *J. Colloid Interface Sci.*, **27**, 625 (1968).
8) E. S. Lutton, C. E. Stauffer, J. B. Martin, and A. J. Fehl, *J. Colloid Interface Sci.*, **30**, 283 (1969).
9) D. S. Ambawani, R. A. Jao, and T. Fort, Jr., *J. Colloid Interface Sci.*, **42**, 8 (1973).
10) M. Lin, *C. R. Acad. Sci. Ser. B*, **281**, 619 (1975).
11) N. K. Adam, "The Physics and Chemistry of Surface," Oxford University Press, (1938).

Nuclear Quadrupole Resonance Study of β-Chloroisocrotonic Acid

Kiyoshi ICHIMURA,* Nobuo NAKAMURA, and Hideaki CHIHARA
Department of Chemistry, Faculty of Science, Osaka University, Toyonaka 560
(Received March 9, 1978)

^{35}Cl nuclear quadrupole resonance frequencies have been measured in powders of β-chlorocrotonic acid and β-chloroisocrotonic acid to be 34.966 and 34.261 MHz, respectively, at 78 K. Zeeman effect experiments were conducted on a single crystal of β-chloroisocrotonic acid and the asymmetry parameter of the electric field gradient has been determined to be 0.174±0.016 at 78 K. The π-electron density on the chlorine site has been estimated from the asymmetry parameter according to Bersohn and discussed on the basis of the semi-empirical Pariser-Parr-Pople molecular orbital treatment.

The electronic structure of organic compounds has been examined extensively by electronic spectra, photoelectron spectroscopy and other experimental techniques and the results of these experiments have been used to check the theoretically elucidated atomic and molecular wave functions and *vice versa*. It is still difficult to obtain good wave functions for such heavy atoms as chlorine, bromine, *etc.* which may play very important roles in determining the molecular and crystal structure as well as the reactivity of simple organic compounds.

Pure nuclear quadrupole resonance (NQR) is a powerful tool to examine the electronic structure of the ground state of molecules in crystals and has been applied to numerous organic compounds which contain quadrupole nuclei such as nitrogen, chlorine, bromine, and iodine. This method can be more effective to determine the molecular wave functions if the nuclear quadrupole coupling constant e^2Qq and the asymmetry parameter η of the electric field gradient (EFG) at the resonating nucleus can be measured, but it is necessary to do Zeeman effect experiments on single crystals to obtain η in the case of chlorine and bromine. Although the electronic structure of the chemical bonds between halogens and the carbon atoms in simple halogen-substituted ethylenes has been studied by the NQR method,[1] only semi-quantitative discussions have been possible because of the lack of precise e^2Qq and η in these compounds. The difficulty in obtaining e^2Qq and η stems mainly from the difficulty in growing large single crystals of halogen-substituted olefinic compounds.

The purpose of the present paper is to measure e^2Qq and η of ^{35}Cl precisely in a single crystal of β-chloroisocrotonic acid which contains a typical olefinic C–Cl bond and to discuss the electronic structure of this substance in detail. The bond parameters of the olefinic system elucidated by a semi-empirical molecular orbital method based on the Pariser-Parr-Pople theory are also evaluated.

Experimental

A mixture of ethyl β-chloroisocrotonate and ethyl β-chlorocrotonate was prepared from ethyl acetoacetate and PCl_5 in benzene solution according to methods in the literature.[2,3] The esters were separated by fractionation, and hydrolyzed with hydrochloric acid to give the free acids. The crystals of the acids thus precipitated were collected, and purified by sublimation *in vacuo*. β-chloroisocrotonic acid (hereafter abbreviated as CICA) and β-chlorocrotonic acid (CCA) were identified by high resolution NMR, the melting points being 56 and 90 °C, respectively. A single crystal of the CICA (approximately $1\times2\times3.5$ cm^3) was grown from a solution of water–methanol system.

The ^{35}Cl NQR frequencies were measured between 20 and 80 K, and at 196 and 291 K by using a Dean-type super-regenerative spectrometer on a powdered specimen. The uncertainty in the frequency measurement was within ±1 kHz. Single crystal Zeeman effect experiments were conducted at the liquid nitrogen and at the room temperatures. The zero-splitting loci of the ^{35}Cl resonance line were determined on an oscilloscope by rotating the magnetic field about two mutually orthogonal axes. Details of the apparatus and the method of the frequency determination and the Zeeman measurements have been previously described.[4]

The analysis of the data of the Zeeman effect measurement was performed by using a high-speed electronic computer (NEAC-2200) which has been programmed by Mano.[5]

Results and Discussion

Description of the Crystal Structure. CICA crystallizes in a monoclinic system with the space group $P2_1/c$ and contains four molecules in the unit cell. Two molecules in the unit cell are connected to each other by hydrogen bonds and form a plane dimer.[6] The center of symmetry lies at the center of the dimer, therefore all the chlorines are at equivalent sites in the crystal. The crystal structure of CCA has not been determined.

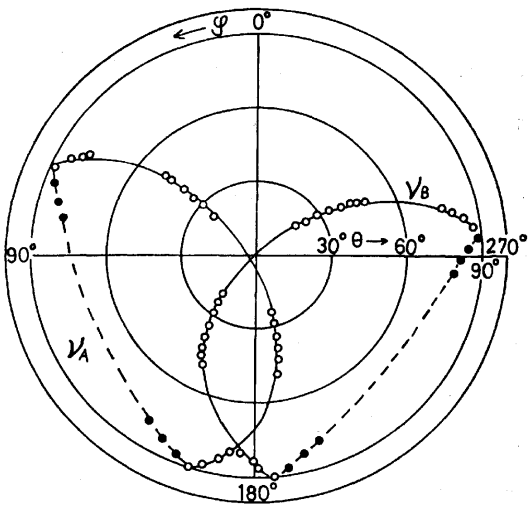

Fig. 1. Zero-splitting loci due to two C–Cl bonds at room temperature. The zero-splitting loci above and below the plane of the paper are distinguished by open and closed circles.

Table 1. Nuclear quadrupole resonance frequencies, quadrupole coupling constants, asymmetry parameters and the direction cosines of principal Z-axis of electric field gradient tensors in a laboratory-fixed coordinate system

The standard deviations are given in parentheses.

Resonance line	Temperature/K	Frequency/MHz	e^2Qqh^{-1}/MHz	η	Direction cosines		
					X_L	Y_L	Z_L
ν_A	291	33.605	66.88 (0.34)	0.172 (0.005)	−0.5397	−0.6151	0.5748
ν_B	291	33.605	66.86 (0.27)	0.177 (0.004)	−0.3822	0.7451	0.5466
ν_A	78	34.261	68.23 (1.10)	0.160 (0.016)	−0.5339	−0.6042	0.5916
ν_B	78	34.261	68.11 (1.10)	0.190 (0.016)	−0.3728	0.7576	0.5358

^{35}Cl Nuclear Quadrupole Resonance. ^{35}Cl NQR frequencies in CICA were 34.372±0.001 MHz at 20 K and 33.605±0.001 MHz at 291 K. The resonance frequency of CICA decreases monotonously with increasing temperature as expected by the Bayer-Kushida theory[7,8] and no phase transition was found over the whole temperature range of the measurement. The temperature coefficient $d\nu/dT$ was 2.00±0.25 (Hz K^{-1}) at 50 K which is comparable to that in *trans*-$C_2H_2Cl_2$.[9] The result of the Zeeman effect study on CICA crystal is shown in Fig. 1. In this figure one may see the location of the two zero-splitting cones in the laboratory-fixed coordinate system. These cones are related to each other by the two-fold screw axis. From these experimental results the nuclear quadrupole coupling constants, the asymmetry parameters and the direction cosines of the principal axes of the electric field gradient tensors were calculated by fitting these zero-splitting data to the relation[10]

$$\sin^2\theta = \frac{2}{3-\eta\cos 2\varphi}, \tag{1}$$

where θ and φ are the polar and the azimuthal angles of the direction of the Zeeman field with respect to the principal coordinate system of the EFG tensors. The number of data collected were 92 for Cl_1 and 99 for Cl_2 at room temperature. The results of the analysis are recorded in Table 1.

The angle between the two principal Z-axes of EFG with different orientations was calculated to be 93.3° which agrees well with 93.1° obtained by the X-ray analysis.[6] It can be seen from Table 1 that the η and the direction cosines of the principal axes X, Y, and Z at 78 K and room temperature were nearly the same.

Semi-empirical Molecular Orbital Treatment of the NQR Parameters. According to the Townes-Dailey theory the electric field gradient *eq* and the asymmetry parameter η of a free molecule may be expressed in terms of the population difference of the outer p-electron orbitals. If we assume that the population difference of the p_x, p_y, and p_z orbitals are U_x, U_y, and U_z, then

$$q = q_p\left(U_z - \frac{U_x+U_y}{2}\right), \tag{2}$$

and

$$\eta = \frac{3(U_y-U_x)}{U_x+U_y-2U_z} = \frac{3q_p}{2q}(U_y-U_x) = \frac{3e^2Qq_p(U_y-U_x)}{2e^2Qq}, \tag{3}$$

where eq_p is the field gradient due to one p-electron in the valence shell and the Z-axis is assumed to coincide with the C–Cl bond. By putting e^2Qq_p/h=109.6 MHz,[11] e^2Qq/h=68.18 MHz, η=0.174, and U_y=2 (the population in the chlorine p_y orbital perpendicular to the π-bond between two carbons), U_x was calculated to be 1.93 for the partially π-bonded chlorine orbital p_x in CICA. Here we have neglected the intermolecular contribution to η.

Grabe[12] calculated the values of U_x for several chlorine-substituted ethylenes by means of a semi-empirical molecular orbital theory proposed by Pariser, Parr, and Pople.[13] In order to examine the reliability of the parameters presented by Grabe we applied the Pariser-Parr-Pople method to CICA. In the calculation the usual assumptions have been adopted as follows:

$$S_{\mu\nu} = \langle\mu|S|\nu\rangle = \delta_{\mu\nu}$$

$$\alpha_\mu = \langle\mu|H^{core}|\mu\rangle \neq 0$$

$$\beta_{\mu\nu} = \langle\mu|H^{core}|\nu\rangle \begin{cases} \neq 0 \text{ when } \mu \text{ and } \nu \text{ are the neighbors} \\ = 0 \text{ when } \mu \text{ and } \nu \text{ are not the neighbors} \end{cases}$$

$$\langle\alpha\beta|r_{ab}^{-1}|\mu\nu\rangle = \delta_{\alpha\mu}\delta_{\beta\nu}\gamma_\mu$$

The same notations as in Ref. 12 were used here. The core integral was assumed to be

$$\alpha_\mu = W_\mu - (n_\mu-1)\gamma_{\mu\mu} - \sum_{\mu\neq\nu} n_\nu\gamma_{\mu\nu}.$$

The other parameters were taken as

$$\beta_{\mu\nu} = \beta_0 + \delta_{\mu\nu}{}^\beta(R_{\mu\nu}-R_0),$$

$$W_\mu = W_0 + \sum_\nu \Delta W_\mu(\nu),$$

$$\gamma_{\mu\nu} = \gamma_0 + \delta_{\mu\nu}{}^\gamma(R_{\mu\nu}-R_0),$$

$$\Delta W_\mu(\nu) = \Delta W_\mu{}^0(\nu) + \delta_{\mu\nu}{}^W(R_{\mu\nu}-R_0),$$

where R_0 is the reference distance and $R_{\mu\nu}$ is the real distance between atoms μ and ν. These parameters were determined according to Refs. 12, 14—16 by using the crystal structure data. The ionization potential

Table 2. Ionization potential and π-orbital population in β-chloroisocrotonic acid

I_p/eV (calcd)	π-electron density	
9.62	C_{methyl}	1.961
10.19	C_β	0.946
11.75	C_α	1.049
12.68	$C_{carboxyl}$	0.606
13.55	Cl	1.964
	$O_{carbonyl}$	1.587
	$O_{hydroxyl}$	1.885

and the orbital populations calculated by using these parameters are given in Table 2. As there are no available experimental data on the ionization potential of CICA, the values in Table 2 cannot be evaluated at the present stage.

We now compare the π-electron density in CICA with those in other olefinic compounds. The π-electron densities on the chlorines in vinyl chloride and *cis*-dichloroethylene in the gaseous state have been deduced to be 1.94[17] and 1.95,[18] respectively, from microwave measurements. These values agree fairly well with 1.97 calculated for these compounds by the Pariser-Parr-Pople method.[12] In the case of CICA the agreement between the experimental π-electron density 1.93 and the calculated one, 1.96, is comparable to the cases of vinyl chloride and *cis*-dichloroethylene. The experimental π-electron density in CICA is the smallest of these three olefinic compounds, suggesting that the conjugation of the π-orbitals extends over the whole molecule and makes it easy to form strong π-bonding between the C_β and the terminal chlorine atom. There may be some contribution to η at the chlorine site from the intermolecular interactions which cannot be estimated at the present stage.

The authors wish to thank Dr. Koichi Mano for the computer program for the analysis of the Zeeman data. They are also grateful to Mr. Tokutsuka Kiichi for his help in programming the molecular orbital calculation.

References

1) D. E. Koltenbah and A. A. Siluidi, *J. Chem. Phys.*, **52**, 1270 (1970).
2) E. L. Skau and B. Saxton, *J. Am. Chem. Soc.*, **50**, 2693 (1928).
3) L. F. Hatch and R. H. Perry, Jr., *J. Am. Chem. Soc.*, **77**, 1137 (1955).
4) T. Kiichi, N. Nakamura, and H. Chihara, *J. Magn. Reson.*, **6**, 516 (1972).
5) K. Mano, *J. Magn. Reson.*, **26**, 393 (1977).
6) C. Garbuglio, M. Mammi and V. Busetti, *Z. Kristallogr.*, **127**, 45 (1968).
7) H. Bayer, *Z. Phys.*, **130**, 227 (1951).
8) T. Kushida, *J. Sci. Hiroshima Univ.*, **A19**, 327 (1955).
9) H. Okuma, Ph. D. Thesis, Osaka University, 1971, unpublished.
10) C. Dean, *Phys. Rev.*, **96**, 1053 (1954).
11) V. Jaccarino and J. G. King, *Phys. Rev.*, **83**, 471 (1951).
12) B. Grabe, *Acta Chem. Scand.*, **22**, 2237 (1968).
13) R. Pariser and R. G. Parr, *J. Chem. Phys.*, **21**, 466, 767 (1953); J. A. Pople, *Proc. Phys. Soc. (London)*, *Ser. A*, **68**, 81 (1955).
14) H. Jensen and P. N. Skancke, *Acta Chem. Scand.*, **22**, 2899 (1968).
15) B. Roos, *Acta Chem. Scand.*, **21**, 2318 (1967).
16) G. Hojer, *Acta Chem. Scand.*, **23**, 2589 (1969).
17) D. Kivelson, E. B. Wilson, and D. R. Lide, *J. Chem. Phys.*, **32**, 205 (1960).
18) W. H. Flygare and J. A. Howe, *J. Chem. Phys.*, **36**, 440 (1962).

The Enantioselective Dehydrogenation of Racemic Secondary Alcohols Catalyzed by Dimeric Ruthenium(II) Chiral Diphosphine Complexes

Katsutoshi OHKUBO,* Ikuhiro TERADA, and Kohji YOSHINAGA

Department of Synthetic Chemistry, Faculty of Engineering, Kumamoto University, Kurokami, Kumamoto 860

(Received March 13, 1978)

The asymmetric dehydrogenation of racemic alcohols by an effective $Ru_2Cl_4((-)\text{-diop})_3$ (diop=2,3-*O*-isopropylidene-1,4-bis(diphenylphosphino)butane) was investigated with and without unsaturated hydrogen acceptors at 120—195 °C, with particular reference to the enantioselective factors and the reaction mechanism. The magnitude of enantioselectivity was substantially affected by the structures of the alcohols and of the hydrogen acceptors and by the reaction temperature; the hydrogen acceptors ($R^1CH=CHR^2$: $R^1 \neq H$ and $R^2 \neq H$) contributed to the enhancement of the selectivity through the newly formed asymmetric centers which result from their coordination to the chiral Ru(II) complex. The activation parameters (ΔH^* and ΔS^*) obtained from the linear Arrhenius dependence of the rate constants of each enantiomer (*R*- or *S*-alcohol) established an isokinetic relationship, and the defference in the parameters of the each enantiomer ($\Delta\Delta H^*$ and $\Delta\Delta S^*$) also showed a satisfactorily linear correlationship between them. It is deduced from the present study that the enantioselection of *R*- and *S*-alcohols occurs at different coordination distances toward the chiral Ru(II) complex between the enantiomers under asymmetric circumstances.

Enantio-differentiating reactions with chiral transition-metal complexes have currently received considerable attention in the asymmetric hydrogenation (of prochiral olefins) which was originally developed in 1968.[1,2] Asymmetric induction by chiral metal complexes, especially by rhodium(I) chiral phosphine complexes, in the hydrogenation of prochiral olefins has been extensively investigated by taking notice of the structural effects of chiral ligands or of prochiral olefins on the optical yields of chiral products;[3-13] enantiomeric excesses of 95—96% are now possible in the asymmetric hydrogenation of α-(acylamino)acrylic acids by [Rh(1,5-cyclooctadiene)biphosphine]$^+BF_4^-$ (biphosphine=1,2-bis[(*o*-methoxyphenyl)phenylphosphino]ethane).[7,12]

On the other hand, the catalytic enantioselection of racemates with chiral metal complexes is also of interest and significant in connection with the asymmetric synthesis of chiral compounds with metal complexes. In our laboratory, Ru(II) chiral phosphine complexes were found catalytically effective for the enantioselective dehydrogenation of racemic alcohols with or without hydrogen acceptors.[14] Ru(II) chiral phosphine complexes have hitherto been the objects of only a limited investigation in terms of an examination of their asymmetric catalyses. In regard to chiral phosphine ligands, a diphosphine of (+)- or (−)-2,3-*O*-isopropylidene-1,4-bis(diphenylphosphino)butane (diop) has recently been accepted as an efficient chiral ligand when used in the rhodium-[5,8,15-24] and ruthenium-[25,26] catalyzed asymmetric hydrogenation of prochiral olefins, and it is also extensively used as a polymer-attached active phosphine ligand.[27-30] Therefore, we examined the efficiency of the diphosphine (diop) as a chiral ligand of ruthenium in the enantioselective dehydrogenation of racemic secondary alcohols (RR'CHOH) by $Ru_2Cl_4((-)\text{-diop})_3$[5] with and without unsaturated hydrogen acceptors ($R^1CH=CHR^2$):

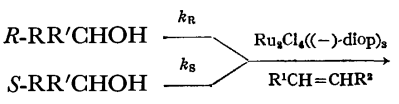

$$RR'C{=}O + R^1CH_2CH_2R^2 \quad (1)$$

where k_R and k_S denote, respectively, the pseudo-first-order rate constants for *R* and *S* enantiomers.

In the present work, some isolated crystalline complexes, such as $RuCl_2((+)\text{-bmpp})_3$ (bmpp=benzylmethylphenylphosphine) and an *in situ* prepared complex of $RuCl_2((+)\text{-nmdp})_3$ (nmdp=neomenthyldiphenylphosphine), were also used in Reaction 1 instead of the dimeric $Ru_2Cl_4((-)\text{-diop})_3$ complex for the sake of comparison.

Experimental

Materials. (−)-*O*-2,3-Isopropylidene-1,4-bis(diphenylphosphino)butane (diop) was prepared by Kagan's method,[5] and the chiral phosphines of (−)-*o*-methoxyphenylmethylphenylphosphine (*o*-ampp), (−)-propylmethylphenylphosphine (pmpp), and (+)-benzylmethylphenylphosphine (bmpp) were prepared according to Mislow *et al.*[31] (+)-Neomenthyldiphenylphosphine (nmdp) was made by means of Morrison's method.[32] $Ru_2Cl_4((-)\text{-diop})_3$ was supplied by James *et al.*,[25] and $RuCl_2$ $((+)\text{-nmdp})_3$ was prepared *in situ* from $[(+)\text{-nmdp}]_0/[RuCl_2(PPh_3)_3]_0=6$. The other complexes, $RuCl_2((-)\text{-ampp})_2(PPh_3)$, $RuCl_2((-)\text{-pmpp})_3$, and $RuCl_2((+)\text{-bmpp})_3$, were made according to the phosphine-exchange method;[33] $RuCl_2\text{-}(PPh_3)_4$ and the chiral phosphine (in their molar ratio of 1:4) were refluxed in hexane for 1—10 h in a nitrogen atmosphere until a change in the solution color was observed, and satisfactory elementary analyses were obtained for the isolated crystalline complexes, as is shown below: $Ru_2Cl_4((-)\text{-diop})_3$: ^1H NMR ($CDCl_3$) δ 0.86 (s, 6H), 1.57 (broad, 12H), 3.02 (broad, 6H), 6.98 (m, 2OH), 7.18 (m, 40H). Found: C, 60.78; H, 5.73; Cl, 7.58%. Calcd for: C, 60.72; H, 5.22; Cl, 7.72%. $RuCl_2((-)\text{-ampp})_2(PPh_3)$: ^1H NMR ($CDCl_3$) δ 1.54 (d, 6H, J=4 Hz), 3.75 (s, 6H), 7.25 (m, 33H). Found: C, 61.80; H, 5.14; Cl, 7.82%. Calcd for: C, 61.74; H, 5.03; Cl, 7.94%. $RuCl_2((-)\text{-pmpp})_3$: ^1H NMR ($CDCl_3$) δ 0.80 (broad, 3H), 1.77 (broad, 7H), 7.23 (m, 5H). Found: C, 53.82; H, 6.57; Cl, 10.35%. Calcd for: C, 53.74; H, 6.77; Cl, 10.58%. $RuCl_2((+)\text{-bmpp})_3$: ^1H NMR ($CDCl_3$) δ 1.60 (broad, 3H), 3.45 (broad, 2H), 7.02 (m, 5H), 7.32 (m, 5H). Found: C, 62.01; H, 5.64; Cl, 8.61%. Calcd for: C, 61.92; H, 5.57; Cl, 8.70%.

Reaction Procedure and Optical Analysis. The dehydrogenation of freshly distilled secondary alcohols (1-phenyl-

ethanol and 1-phenyl-1-propanol) by the Ru(II) chiral phosphine complex was carried out without solvents at 120—195 °C in a N_2 atmosphere in the absence or in the presence of unsaturated hydrogen acceptors such as benzylideneacetone. After a desired conversion of the reaction was obtained, the unreacted alcohol was fractionally distilled under reduced pressure and then subjected to optical-rotation measurements. In the dehydrogenation of achiral alcohols such as benzyl alcohol with the Ru(II) chiral phosphine complexes at 120—195 °C, it was confirmed that the distilled alcohols include no optically active contaminants, such as the chiral Ru(II) complex, chiral ligands, and their decomposed products. To determine the optical purity of the alcohol enriched in one of the enantiomers, the average value of the optical rotations measured four times with a highly sensitive UNION PM-101 polarimeter was used as the observed one. The distribution of reaction products was followed by gas-chromatographic analyses, and some side reaction products, such as the racemic or meso bis(α-methylbenzyl) ether obtained from the dehydrogenation of 1-phenylethanol, were identified by means of 60 MHz ^{1}H NMR after their fractional collection by gas chromatography.

Results and Discussion

Pseudo-first-order Enantioselective Reaction. When the asymmetric dehydrogenation of the alcohol (8.34×10^{-2} mol) by using $Ru_2Cl_4((-)\text{-diop})_3$ (2 mM) or $RuCl_2L^*_3$ (L*=chiral ligand) (4 mM) was carried out with a hydrogen acceptor (6.84×10^{-2} mol) at 120—195 °C, the optical purity (O.P.) of the unreacted alcohol (RR'CHOH), obtained by fractional distillation without any optically active contaminants, increased with an increase in the conversion (Conv.), obeying pseudo-first-order rate law up to Conv. $\simeq$65% with a constant k_R/k_S ratio, which reflects the enantioselectivity (Table 1).

$$k_R = (\ln [R]_0/[R])/t$$
$$= \ln (10^4/(100-\text{Conv.})(100-\text{O.P.}))/t \quad (2a)$$
$$k_S = (\ln [S]_0/[S])/t$$
$$= \ln (10^4/(100-\text{Conv.})(100+\text{O.P.}))/t \quad (2b)$$

where $[R]_0$ and $[S]_0$ mean, respectively, the initial concentrations of the *R* and *S* enantiomers, and where *t* is the reaction time. As is indicated in Table 1, the present chiral Ru(II) catalyst produced acetophenone as the main dehydrogenation product of 1-phenylethanol, with a quantitative saturation of the unsaturated hydrogen acceptor, but small amounts of racemic and meso bis(α-methylbenzyl) ether (^{1}H NMR($CDCl_3$) δ 1.46 (d, 6H, J=6.4 Hz), 4.53 (q, 2H, J=6.4 Hz), 7.29 (s, 10H) and δ 1.40 (d, 6H, J=6.4 Hz), 4.25 (q, 2H, J=6.4 Hz), 7.31 (s, 10H)) were also detected, together with negligible amounts of styrene and ethylbenzene. The formation of such a side product of the ether was remarkably accelerated by RhCl((−)-diop) (prepared *in situ* from $[\text{diop}]_0/[(RhCl(C_2H_4)_2)_2]_0=3$); hence, the ruthenium–diop complex is superior to the rhodium–diop complex in terms of the promotion of the hydrogen transfer from the racemic alcohols to hydrogen acceptors, with a higher enantioselection of the former.

Efficiency of diop as a Chiral Ligand. In order to confirm the actual efficiency of diop as a chiral ligand of the Ru(II) complex in comparison with other chiral phosphine ligands, we examined the asymmetric dehydrogenation of 1-phenyl-1-propanol in the presence of benzylideneacetophenone at 165 °C with $Ru_2Cl_4((-)\text{-diop})_3$, $RuCl_2((-)\text{-ampp})_2(PPh_3)$, $RuCl_2((-)\text{-pmpp})_3$, $RuCl_2((+)\text{-bmpp})_3$, and $RuCl_2((+)\text{-nmdp})_3$. Although the enantioselective ability of the dimeric $Ru_2Cl_4((-)\text{-diop})_3$ complex is not directly comparable with those of the other monomeric derivatives ($RuCl_2L^*_3$ or $RuCl_2L^*_2(PPh_3)$: L*=chiral ligand), among the complexes tested, the diop ligand substantially brought about the highest activity for the binuclear $Ru_2Cl_4((-)\text{-diop})_3$ complex in the dehydrogenation and enantioselection of racemic 1-phenyl-1-propanol (Table 2). One could suppose, here, that the low enantioselective ability of $RuCl_2L^*_3$ (or $RuCl_2L^*_2(PPh_3)$), including the Mislow phosphine ligand (L*), was the result of the incomplete racemization of L* at 165 °C, even as the metal complexes. However, this is not true, because the $RuCl_2L^*_3$ (or $RuCl_2L^*_2(PPh_3)$) complex appreciably increased its dehydrolyzing and enantioselective ability even at temperatures higher than 165 °C; for example, $RuCl_2((-)\text{-ampp})_2(PPh_3)$ resulted in O.P.(Conv.)=0.80% (50.5%), $k_R=6.59\times10^{-6}$ s^{-1}, $k_S=8.33\times10^{-6}$ s^{-1}, and $k_R/k_S=1.023$ at 185 °C in the same reactions in Table 2. Presumably, the slightly higher temperature promotes the dissociation of the chlorine atom from the Ru(II) complex so as to make active sites and that of

Table 1. Enantioselective dehydrogenation of 1-phenylethanol (8.34×10^{-2} mol) by $Ru_2Cl_4((-)\text{-diop})_3$ (2 mM) with benzylideneacetone (6.84×10^{-2} mol) at 165 °C

Time (h)	Conv. (%)	$-[\alpha]_D^{23}$ a) (deg)	O.P. (%)	10^6k_R (s^{-1})	10^6k_S (s^{-1})	k_R/k_S	Products (mol %) b) AP	PEE	Others
2	23.0	0.46	0.88	37.5	35.1	1.07	98.89	trace	—
3	32.7	0.65	1.24	37.8	35.5	1.06	83.56	15.51	0.93
4	41.0	0.92	1.75	37.9	35.4	1.07	87.01	12.33	0.66
6	54.9	1.28	2.44	38.0	35.7	1.06	88.00	11.38	0.62
8	65.3	1.49	2.84	37.8	35.8	1.06	88.37	11.17	0.46
48 c)	39.2	0.046	0.088	2.88	2.87	1.00_3	13.85	85.07	1.08
74 c)	53.7	0.084	0.16	2.89	2.88	1.00_3	28.80	70.67	0.53

a) $[\alpha]_D^{23}$ −52.5° (*c* 2.27, CH_2Cl_2).[41] b) AP=acetophenone; PEE=racemic or meso bis(α-methylbenzyl) ether; others=styrene and ethylbenzene. c) *in situ* prepared RhCl((−)-diop) (2 mM) formed from $[\text{diop}]_0/[(RhCl(C_2H_4)_2)_2]_0=3$ was used instead of $Ru_2Cl_4((-)\text{-diop})_3$.

Table 2. Enantioselective dehydrogenation of 1-phenyl-1-propanol (8.34×10^{-2} mol) by chiral ruthenium(II) complexes with benzylideneacetophenone ($6.84\times10^{-}$ mol) at 165 °C

Complex	Concn (mM)	Time (h)	Conv. (%)	$-[\alpha]_D^{20}$ a) (deg.)	O.P. (%)	10^6k_R (s^{-1})	10^6k_S (s^{-1})	k_R/k_S
$Ru_2Cl_4((-)\text{-diop})_3$	2.0	24	56.8	4.41	11.0	11.1	8.51	1.30
$RuCl_2((-)\text{-ampp})_2(PPh_3)$	4.0	78	51.8	0.04	0.09	2.60_2	2.596	1.00_2
$RuCl_2((-)\text{-pmpp})_3$	4.0	3	40.5	0.12	0.24	48.3	47.6	1.01
$RuCl_2((+)\text{-bmpp})_3$	4.0	70	26.3	0.54	1.36	1.27	1.16	1.09
$RuCl_2((+)\text{-nmdp})_3$	4.0	72	59.1	0.21	0.51	3.47	3.43	1.01

a) $[\alpha]_D^{17-20}$ +40.0° (*c* 5, C_6H_6).[42]

the hydrogen attached to the α-carbon in the alcohol.

Structural Effect of Hydrogen Acceptors. The addition of hydrogen acceptors to the reaction system substantially enhanced the enantioselection of the racemic alcohol by the chiral Ru(II) complex in comparison with that in the same reaction without hydrogen acceptors, and a structural effect of hydrogen acceptors on the enantioselectivity defined by k_R/k_S was observed (Table 3). Such a structural effect of hydrogen acceptors has also been reported in the enantioselective dehydrogenation of 1-phenylethanol by $RhCl((+)\text{-nmdp})_3$ prepared *in situ*[34] or by $RuCl_2((+)\text{-nmdp})_3$.[35] There are two possible explanations of such a structural effect of the hydrogen acceptors on the selectivity: (a) the change in the type of hydrogen acceptor affects the equilibrium of the $Ru_2Cl_4((-)\text{-diop})_3$ complex in the solution, if there is an equilibrium of the complex, and (b) the coordination of the unsaturated hydrogen acceptor ($R^1CH{=}CHR^2$) to the chiral Ru(II) complex gives rise to newly formed asymmetric centers, as is shown below:

$$R^1CH{=}CHR^2\ (R^1{\neq}H \text{ and } R^2{\neq}H) + (Ru) \rightleftharpoons \underset{R^1\overset{*}{C}H\text{——}\overset{*}{C}HR^2}{\overset{(Ru)}{\diagup\ \diagdown}}\ (I) \qquad (3)$$

where (Ru) denotes a catalytically active species supplied from $Ru_2Cl_4((-)\text{-diop})_3$.

The equilibrium of the bridged dimer complex of $(diop)Cl_2Ru\text{-}P\text{-}P\text{-}RuCl_2(diop)$ (P-P=diop) in solutions has not yet been established, but one species which can be obtained from the dimeric complex is $(diop)Cl_2RuP$ (P=ligand produced by the dissociation of P-P). Even though an equilibrium between $(diop)Cl_2Ru\text{-}P\text{-}P\text{-}RuCl_2\text{-}(diop)$ and $(diop)Cl_2RuP$ could be expected in solutions, it seems unreasonable to explain the effect of $R^1CH{=}CHR^2$ on the selectivity only on the basis of the (a) explanation. On the other hand, the (b) explanation seems plausible because such newly formed asymmetric centers induced by the coordination of olefins to chiral metal complexes (*viz.*, platinum amine one) have

Table 3. Structural effect of hydrogen acceptors on the enantioselectivity in the dehydrogenation of 1-phenylethanol (8.34×10^{-2} mol) by $Ru_2Cl_4((-)\text{-diop})_3$ (2 mM) with hydrogen acceptors (6.84×10^{-2} mol)

Hydrogen acceptor	Temp (°C)	Time (h)	Conv. (%)	$-[\alpha]_D^{23}$ (deg.)	O.P. (%)	10^5k_R (s^{-1})	10^5k_S (s^{-1})	k_R/k_S
Benzylideneacetophenone	150	22.0	33.5	0.183	0.34	0.520	0.511	1.02
	170	14.0	23.9	0.175	0.34	0.548	0.535	1.02
	180	8.0	37.9	0.543	1.03	1.69	1.62	1.04
	190	5.0	48.4	1.77	3.37	3.87	3.49	1.11
Benzylideneacetone	120	34.0	18.5	0.152	0.29	0.234	0.228	1.03
	130	24.0	35.9	0.324	0.62	0.522	0.509	1.03
	150	6.0	27.1	0.303	0.58	1.49	1.44	1.03
trans-Stilbene	170	10.0	12.9	0.372	0.71	0.395	0.374	1.08
	180	10.0	20.3	0.620	1.18	0.665	0.600	1.10
	190	10.0	28.3	1.45	2.76	1.25	1.06	1.18
Ethyl cinnamate	170	5.0	22.8	0.599	1.14	1.50	1.38	1.09
	180	5.0	28.8	0.674	1.28	1.96	1.82	1.08
	190	4.0	37.9	1.44	2.74	3.51	3.13	1.13
2-Ethylhexyl methacrylate	170	5.0	37.4	2.98	5.68	2.93	2.29	1.28
	180	5.0	53.4	3.23	6.15	4.59	3.91	1.17
	190	4.0	72.4	2.24	4.27	9.25	8.66	1.07
(*E*)-α-Methylcrotonic acid[a]	165	8.0	65.4	2.55	4.85	4.17	3.84	1.09
None	170	8.0	11.6	0.063	0.120	0.431	0.422	1.02
	180	7.0	15.7	0.127	0.243	0.690	0.688	1.02
	190	6.0	21.1	0.154	0.294	1.11	1.08	1.03

a) e.c. of *R*-(−)-$MeCH_2CH(Me)CO_2H$ formed=21.0%.

already been confirmed.[36-38] Although, in the case of the platinum amine complexes, Reaction 3 has been established only at temperatures much lower than 120—195 °C,[36-38] the newly formed asymmetric centers in the (I) intermediate might not be completely diminished *via* the epimerization,[36-37] even in the present temperature range. The possibility of Reaction 3 is also supported by the fact that the prochiral (*E*)-α-methylcrotonic acid used as a hydrogen acceptor instead of achiral olefins was converted into a chiral species (*R*-(−)-$MeCH_2CH(Me)CO_2H$) in an enantiomeric excess of 21.0% in the dehydrogenation of 1-phenylethanol by $Ru_2Cl_4((-)\text{-diop})_3$ at 165 °C with O.P.= 4.85%(Conv.=68.4%) of *S*-(−)-1-phenylethanol (Table 3). This double asymmetric-transfer hydrogenation with Ru(II) chiral phosphine complexes seems promising; the details of an investigation which is now in progress will be presented in a succeeding paper.

In connection with the above structural effect of hydrogen acceptors on the enantioselectivity, the change in the type of hydrogen donor(RR'CHOH) also affected the magnitude of the selection by $Ru_2Cl_4((-)\text{-diop})_3$ (Table 4); the change from 1-phenylethanol to 1-phenyl-1-propanol affected the selectivity substantially.

Reaction Mechanism. If the induced asymmetry in the (I) intermediate plays an important role in the enhancement of the enantioselectivity, the coordination of the hydrogen acceptor to the chiral metal complex is required before the coordination of the alcohol to the complex can proceed; that is, the reaction between the alcohol and the (I) intermediate should be realized. In this regard, the increase in the concentration of the hydrogen acceptor with respect to that of the alcohol resulted in a monotonous acceleration of the reaction rate up to $[R^1CH{=}CHR^2]_0/[RR'CHOH]_0 \simeq 1$, but the excess concentration of $R^1CH{=}CHR^2$ ($[R^1CH{=}CHR^2]_0/[RR'CHOH]_0 > 1$) retarded the reaction (Fig. 1). This probably implies that the increase in the $R^1CH{=}CHR^2$ concentration raises the concentration of the (I) intermediate, which reacts with the alcohol in the following way:

$$\text{(I)} + RR'CHOH \xrightarrow{-H^+} \left[RR'CHO\text{—}(Ru)\begin{matrix}{}^{*}CHR^1\\ |\\ {}^{*}CHR^2\end{matrix}\right]$$

$$\longrightarrow \left[RR'C{=}O\text{—}(Ru)\begin{matrix}H\\ {}^{*}CHR^1\\ |\\ {}^{*}CHR^2\end{matrix}\right]^{+}$$

$$\longrightarrow \left[RR'C{=}O\text{—}(Ru\text{-}H)\begin{matrix}{}^{*}CHR^1\\ |\\ {}^{*}CHR^2\end{matrix}\right]$$

$$\longrightarrow [RR'C{=}O\text{—}(Ru)\text{-}{}^{*}CHR^1CH_2R^2]$$

$$\xrightarrow{H^+} RR'C{=}O + R^1CH_2CH_2R^2 + (Ru) \qquad (4)$$

In the case of the excess concentration of $R^1CH{=}CHR^2$, the shielding of active sites of the (I) intermediate by $R^1CH{=}CHR^2$ depresses the reaction between the (I) intermediate and RR'CHOH in Reaction 4. The reaction between the (I) intermediate and RR'CHOH starts *via* the deprotonation of RR'CHOH. The deprotonation process, which corresponds to the rate-determing step, can be explained by the basicity effect on the rate enhancement in the dehydrogenation of alcohols; the dehydrogenation of ethanol by $[Ru_2Cl_3(PEt_2Ph)_6]Cl$ is enhanced by potassium hydroxide,[39] and the transfer hydrogenation of benzylideneacetophenone by $PhCH(Me)O^-Na^+$ with $RuCl_2(PPh_3)_3$ is markedly accelerated as compared with the same reaction including PhCH(Me)OH instead of $PhCH(Me)O^-Na^+$.[40]

Activation-Parameter Relationships. The rate of the dehydrogenation of RR'CHOH by the (I) intermediate is dependent on the reaction temperature between the enantiomers; hence, the enantioselectivity defined by k_R/k_S comes to be affected by the temperature (Table 3). The temperature dependence of the rate constant for each enantiomer can be expressed by the linear Arrhenius relationship (Fig. 2); the activation param-

TABLE 4. ENANTIOSELECTIVE DEHYDROGENATION OF 1-PHENYL-1-PROPANOL BY $Ru_2Cl_4((-)\text{-diop})_3$ WITH PhCH=CHCOR (R = Ph AND Me)[a]

	Hydrogen acceptor		
	PhCH=CHCOPh		PhCH=CHCOMe
Temp/°C	165	175	165
Time/h	24	11	8
Conv./%	56.8	75.7	5.63
$-[\alpha]_D^{20}$/deg.	4.41	5.63	1.01
O.P./%	11.0	14.1	2.52
$10^6 k_R/s^{-1}$	11.1	39.6	33.1
$10^6 k_S/s^{-1}$	8.51	32.4	31.3
k_R/k_S	1.30	1.22	1.03

a) The reaction conditions are the same as in Table 1.

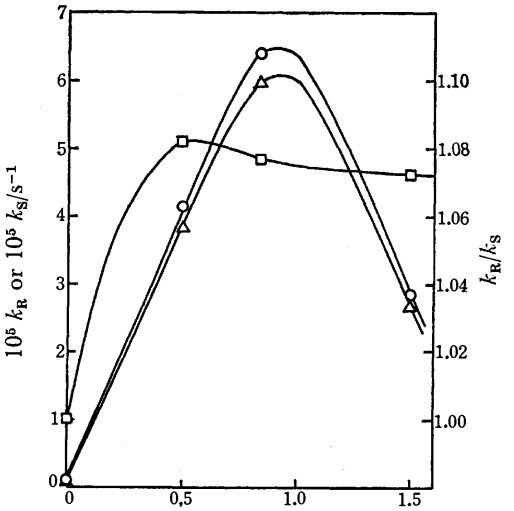

Fig. 1. Concentration effect of the hydrogen acceptor on the enantioselectivity in the dehydrogenation of 1-phenylethanol (8.34×10^{-2} mol) by $Ru_2Cl_4((-)\text{-diop})_3$ (2 mM) with benzylideneacetone at 165 °C. ((Conv. (%), AP(mol %), PEE (mol %) =A(45.7, 35.2, 64.4); B(25.0, 97.4, trace); C(28.4, 98.8, trace); D(18.2, 98.3, trace).) ○: k_R, △: k_S, □: k_R/k_S.

Table 5. Activation parameters obtained from the dehydrogenation of 1-phenyl-1-propanol by $Ru_2Cl_4((-)\text{-diop})_3$ with hydrogen acceptors[a)]

No.	Hydrogen acceptor	$\Delta H^{\ddagger}_R$	$\Delta H^{\ddagger}_S$ (kcal/mol)	$\Delta\Delta H^{\ddagger}$	$-\Delta S^{\ddagger}_R$	$-\Delta S^{\ddagger}_S$ (e.u.)	$\Delta\Delta S^{\ddagger}$
1	Benzylideneacetone	20.36±0.11	20.30±0.15	0.06	33.11±0.26	33.31±0.36	0.20
2	Benzylideneacetophenone	38.89±0.03	37.27±0.05	1.62	−4.39±0.06	−0.72±0.06	3.67
3	*trans*-Stilbene	22.65±0.01	20.34±0.01	2.31	33.00±0.01	38.31±0.02	5.31
4	Ethyl cinnamate	16.41±0.02	15.86±0.02	0.55	44.51±0.02	45.91±0.02	1.40
5	2-Ethylhexyl methacrylate	22.64±0.03	26.26±0.03	3.62	29.10±0.02	21.41±0.02	7.69
6	None	18.42±0.00	18.32±0.00	0.10	42.33±0.00	42.61±0.00	0.28

a) The reaction conditions are the same as in Table 3, in which, also, the rate constants are specified.

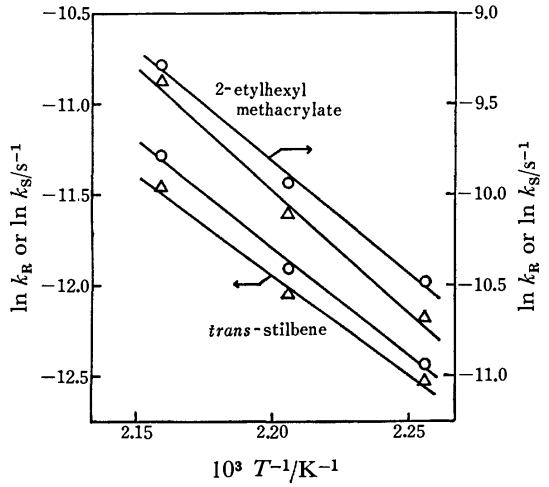

Fig. 2. Typical Arrhenius relationships of the present reaction. ○: R, △: S.

eters ($\Delta H^{\ddagger}$ and $\Delta S^{\ddagger}$) obtained for the series of experiments shown in Table 3 are summarized in Table 5. The activation parameters which reflect those for the rate-determining hydrogen-abstraction process in Reaction 4 established an isokinetic relationship well; that is, the smaller $\Delta H^{\ddagger}$ values for one of the enantiomers always require negatively larger $\Delta S^{\ddagger}$ values (Fig. 3). Such an isokinetic relationship is also obtained from the

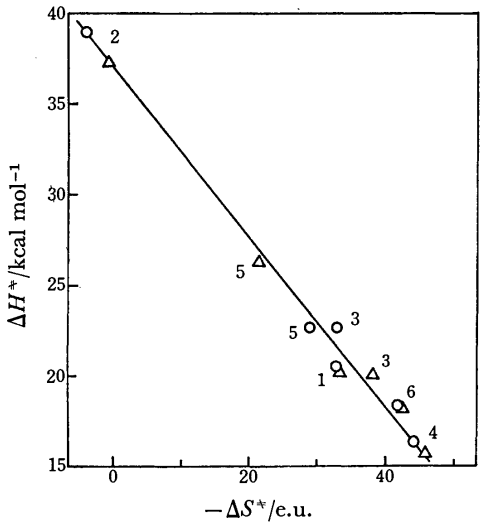

Fig. 3. An isokinetic relationship of the present reaction (numbers are the same as in Table 5). ○: R, △: S.

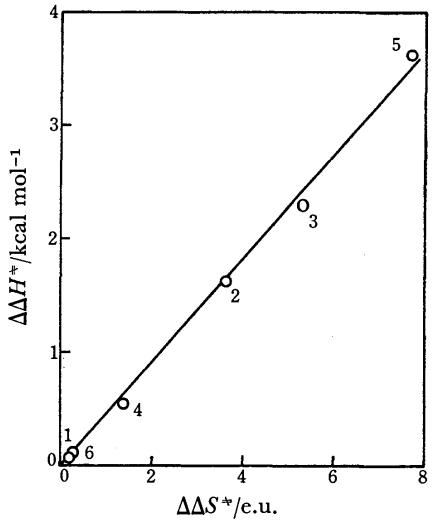

Fig. 4. Correlation between the $\Delta\Delta H^{\ddagger}$ and $\Delta\Delta S^{\ddagger}$ values (numbers are the same as in Fig. 3).

reaction steps common to the present reaction, especially from the transition state shown in Reaction 4. The difference in the electronic factors reflected in $\Delta H^{\ddagger}$ between the *R* and *S* enantiomers ($\Delta H^{\ddagger}_R$ and $\Delta H^{\ddagger}_S$ respectively) leads to the idea that the coordination distance between the oxygen atom and the Ru metal in the transition state might be different between the enantiomers; the shorter coordination distance makes the $\Delta H^{\ddagger}$ value smaller, while requiring a negatively larger $\Delta S^{\ddagger}$ one. If this is true, the difference between the $\Delta H^{\ddagger}_R$ and $\Delta H^{\ddagger}_S$ values, $\Delta\Delta H^{\ddagger}$, will be correlated with that between the $\Delta S^{\ddagger}_R$ (for *R* enantiomer) and $\Delta S^{\ddagger}_S$ (for *S* one) values, $\Delta\Delta S^{\ddagger}$. In this respect, there is a linear correlationship between the $\Delta\Delta H^{\ddagger}$ and $\Delta\Delta S^{\ddagger}$ values with the intersect of zero (Fig. 4). It may be deduced, therefore, that the enantioselective coordination of *R*- and *S*-RR'CHOH to the chiral complex occurs at a different coordination distance between the enantiomers under asymmetric circumstances (*viz.*, stereochemical influences of chiral ligands).

References

1) W. S. Knowles and M. J. Sabacky, *Chem. Commun.*, **1968**, 1445.
2) L. Horner, H. Siegel, and H. Büthe, *Angew. Chem., Int. Ed. Engl.*, **7**, 942 (1968).
3) W. S. Knowles, M. J. Sabacky, and B. D. Vineyard, *Chem. Commun.*, **1972**, 10.

4) L. Horner and H. Siegel, *Phosphorus*, **1**, 209 (1972).
5) H. B. Kagan and T-P. Dang, *J. Am. Chem. Soc.*, **94**, 6429 (1972).
6) R. E. Harman, S. K. Gupta, and J. Brown, *Chem. Rev.*, **73**, 21 (1973).
7) W. S. Knowles, M. J. Sabacky, B. D. Vineyard, and D. J. Weinkauff, *J. Am. Chem. Soc.*, **97**, 2567 (1975).
8) H. B. Kagan, N. Langlois, and T-P. Dang, *J. Organomet. Chem.*, **90**, 353 (1975).
9) M. Tanaka and I. Ogata, *Chem. Commun.*, **1975**, 735.
10) T. Hayashi, T. Mise, S. Mitachi, K. Yamamoto, and M. Kumada, *Tetrahedron Lett.*, **1976**, 1133.
11) J. D. Morrison, *Adv. Catal.*, **26**, 81 (1976), and the references cited therein.
12) B. D. Vineyard, W. S. Knowles, M. J. Sabacky, B. L. Bachman, and D. J. Weinkauff, *J. Am. Chem. Soc.*, **99**, 5946 (1977).
13) M. D. Fryzuk and B. Bosnich, *J. Am. Chem. Soc.*, **99**, 6262 (1977).
14) K. Ohkubo, K. Hirata, K. Yoshinaga, and M. Okada, *Chem. Lett.*, **1976**, 183; K. Ohkubo, T. Aoji, K. Hirata, and K. Yoshinaga, *Inorg. Nucl. Chem. Lett.*, **12**, 837 (1976); K. Ohkubo, I. Terada, and K. Yoshinaga, *Chem. Lett.*, **1977**, 1467.
15) T-P. Dang and H. B. Kagan, *Chem. Commun.*, **1971**, 481.
16) W. R. Cullen, A. Fenster, and B. R. James, *Inorg. Nucl. Chem. Lett.*, **10**, 167 (1974).
17) A. Levi, G. Modena, and G. Scorrano, *Chem. Commun.*, **1975**, 6.
18) T-P. Dang, J. C. Poulin, and H. B. Kagan, *J. Organomet. Chem.*, **91**, 105 (1975).
19) G. Gelbard, H. B. Kagan, and R. Stern, *Tetrahedron*, **32**, 233 (1976).
20) R. Glaser, *Tetrahedron Lett.*, **1975**, 2127; R. Glaser and M. Twaik, *Tetrahedron Lett.*, **1976**, 1219.
21) R. Glaser, S. Geresh, and J. Blumenfeld, *J. Organomet. Chem.*, **112**, 255 (1976).
22) R. Glaser and B. Vainas, *J. Organomet. Chem.*, **121**, 249 (1976).
23) R. Glaser, S. Geresh, J. Blumenfels, B. Vainas, and M. Twaik, *Isr. J. Chem.*, **15**, 17 (1977); R. Glaser and S. Geresh, *Tetrahedron Lett.*, **1977**, 2527.
24) I. Ojima, T. Kogure, and M. Kumagai, *J. Org. Chem.*, **42**, 1671 (1977).
25) B. R. James, D. K. W. Wang, and R. F. Voigt, *J. Chem. Soc., Chem. Commun.*, **1975**, 574.
26) C. Botteghi, M. Bianchi, E. Benedetti, and U. Matteoli, *Chimia*, **29**, 256 (1975).
27) W. Dumont, J-C. Poulin, T-P. Dang, and H. B. Kagan, *J. Am. Chem. Soc.*, **95**, 8295 (1973).
28) E. Bayer and V. Schurig, *Chem. Tech.*, **1976**, 212.
29) N. Takaishi, H. Imai, C. A. Bertelo, and J. K. Stille, *J. Am. Chem. Soc.*, **100**, 264 (1978).
30) T. Masuda and J. K. Stille, *J. Am. Chem. Soc.*, **100**, 268 (1978).
31) K. Naumann, G. Zon, and K. Mislow, *J. Am. Chem. Soc.*, **91**, 7012 (1969).
32) J. D. Morrison and W. F. Masler, *J. Org. Chem.*, **39**, 271 (1974).
33) P. W. Armit and T. A. Stephenson, *J. Organomet. Chem.*, **57**, C80 (1973).
34) K. Ohkubo, T. Ohgushi, and K. Yoshinaga, *Chem. Lett.*, **1976**, 775.
35) K. Ohkubo, K. Hirata, and K. Yoshinaga, *Chem. Lett.*, **1976**, 577.
36) G. Paiaro and A. Pannunzi, *J. Am. Chem. Soc.*, **86**, 5148 (1964); A. Pannunzi and G. Paiaro, *J. Am. Chem. Soc.*, **88**, 4843 (1966).
37) P. Corradini, G. Paiaro, A. Pannunzi, and S. F. Mason, *J. Am. Chem. Soc.*, **88**, 2563 (1966).
38) R. Lazzaroni, P. Salvadori, and C. Bertucci, *J. Organomet. Chem.*, **99**, 475 (1975).
39) J. Chatt, B. L. Shaw, and A. E. Field, *J. Chem. Soc.*, **1964**, 3466.
40) Y. Sasson and J. Blum, *J. Org. Chem.*, **40**, 1887 (1975).
41) U. Nagai, T. Shishido, R. Chiba, and H. Mitsuhashi, *Tetrahedron*, **21**, 1701 (1965).
42) J. Kenyon, S. M. Partridge, and H. Phillips, *J. Chem. Soc.*, **1937**, 207.

Physical Properties and Constitution of the 5,6: 11,12-Bis(epidithio)-naphthacene-Iodine Complexes (TTT-I_n)

Tamotsu INABE and Yoshio MATSUNAGA*

Department of Chemistry, Faculty of Science, Hokkaido University, Sapporo 060

(Received March 16, 1978)

The electrical resistivity of the 5,6: 11,12-bis(epidithio)naphthacene(TTT)–iodine system was examined using polycrystalline compactions. The room-temperature resistivity reaches a minimum of 0.3 ohm cm at the composition of the well-studied metallic phase, TTT–$I_{1.5}$, and a shoulder as large as 200 ohm cm occurs at the composition of the other metallic phase, TTT–$I_{2.7}$. The apparent activation energy for semiconduction at the latter composition is as much as 0.13 eV, indicating some semiconductor behavior in directions other than the needle axis. The appearance of the latter phase is also manifested by a drastic increase in the Seebeck coefficient near this composition, which corresponds to a change in the amount of charge per TTT molecule from 0.68 to 0.85. The diffuse reflection spectra were recorded for TTT–$I_{1.53}$ and TTT–$I_{2.79}$. The resemblance between the spectrum of the iodine-rich complex and that of TTT–Br is noted.

It has been known for some time that 5,6: 11,12-bis(epidithio)naphthacene(TTT[1]) can produce highly

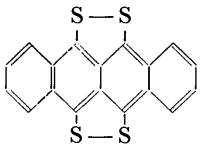

conducting ionic molecular complexes and also cation radical salts. The former group consists of the complexes with *o*-haloanils,[2-4] tetracyanoethylene,[2,3] tetracyanoquinodimethane,[5-8] and bis(1,2-ethylenedithiolato)nickel(II),[9] while the latter includes halides and thiocyanate.[10] Recently, there has been a great deal of interest in TTT–$I_{1.5}$, which is among the most conducting organic compounds so far developed.[11-14] Here, we wish to report the electrical properties of TTT–I_n as functions of the composition. Earlier, similar studies were made on the four semiconducting thiazine–iodine systems.[15] The location of electrical singularities was shown to be a powerful tool for elucidating the constitution of organic compound-iodine systems. For instance, we demonstrated that a shoulder in the resistivity-composition isotherm, a decrease in the activation energy for semiconduction by a factor of two, and a change in the sign of the Seebeck coefficient from negative to positive can be observed at a composition of two molecules of phenothiazine to five atoms of iodine and that the incorporation of a half mole of iodine to this compound gives rise to a resistivity minimum.

Experimental

Materials. TTT was synthesized following the method reported by Marschalk and Stumm and recrystallized three times from trichlorobenzene.[16] Samples were prepared by grinding the weighed TTT and iodine or the weighed sample of a less iodine content and iodine in an agate mortar in the presence of a small amount of benzene. The iodine contents were determined by microanalysis. Two additional samples were prepared by the reaction between TTT and iodine in boiling nitrobenzene and benzene respectively. Their compositions were TTT–$I_{1.53}$ and TTT–$I_{2.79}$.

Measurements. The electrical resistivities and Seebeck coefficients of polycrystalline compactions were recorded as functions of the temperature from −120 to 20 °C by the procedures described in our previous paper.[17] The diffuse reflectance of samples diluted with sodium chloride was measured by means of a Beckman DK 2A spectroreflectometer in the range from 325 to 2500 nm. The reference was pure sodium chloride. The spectrum was then plotted using the Kubelka-Munk function.

Results and Discussion

Electrical Properties. In Fig. 1, the logarithm of electrical resistivity at 20 °C is plotted against the number of iodine atoms per TTT molecule, *n*. Two shaded circles indicate that these samples were made by the reaction in boiling nitrobenzene or benzene; therefore, they were supposed to be more homogeneous than the others. It must be emphasized that the shaded circles fit in well to the resistivity-composition isotherm made with open circles. A minimum resistivity of about 0.3 ohm cm is found at $n=1.5$. Then the resistivity reaches a shoulder at $n=2.7$, the value being about 200 ohm cm. Although Buravov *et al.* have reported a phase corresponding to $n\simeq 1$,[11] no singularity due to this phase could be detected in our isotherm. Kamaras

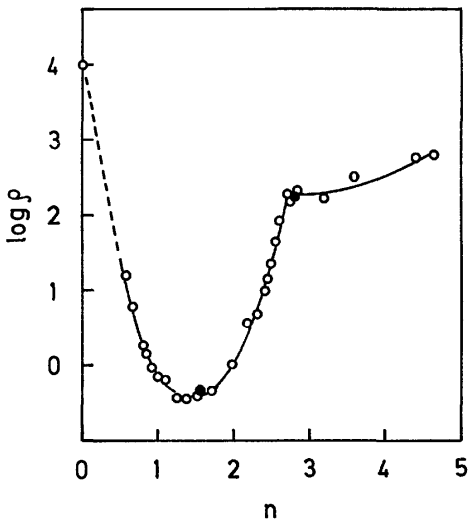

Fig. 1. Electrical resistivity at 20 °C plotted against the iodine content (*n* I atoms/TTT molecule).

et al. have noted that the phase can be obtained only occasionally, together with TTT and TTT–$I_{1.5}$;[13] therefore, the amount of TTT–I in our samples may be too small to show any singularity.

Now we wish to summarize briefly the electrical behavior of mixtures. If two coexisting phases are strictly stoichiometric and mechanically mixed without interaction, Lichtenecker's logarithmic mixing rule may apply for the resistivity.[18,19] The composition of a distinct compound may correspond to a minimum in the resistivity-composition isotherm when its resistivity is the lowest in the system or to an abrupt change in the slope when its resistivity is not the lowest. If the incorporation of a marked stoichiometric imbalance is conceivable for a phase, the electrical behavior may depend quite differently upon the composition. When additional carriers are introduced by the imbalance, the stoichiometric composition may be indicated by a maximum in the resistivity-composition isotherm. When the effect of an excess of one of the components on the resistivity is small or when the stoichiometric phase is incapable of existence, a shoulder may be observed instead of a maximum.

The composition of the well-studied TTT–$I_{1.5}$ phase has been reported to vary within narrow limits, from $n=$ 1.50 to 1.56;[14,20] therefore, the appearance of a resistivity minimum at this composition seems to be more likely than that of a maximum. Even if a maximum exists, the presently-observed resistivity values around $n=1.5$ arise essentially from contact between the crystals and are probably much larger than the maximum value. All the reported resistivity values along the needle axis are of the order of 0.001 ohm cm.[11–13] The electrical behavior found for the phase around $n=2.7$ is clearly of a nonstoichiometric type, and is in agreement with the observation made by Kamaras *et al.*, namely, the composition of their recrystallized samples ranges from $n=2.6$ to 2.9.[13] The sharp edge appearing in Fig. 1 shows that the ideal composition of this phase is $n=2.7$ and also that the incorporation of an excess of TTT considerably lowers the resistivity. This large effect seems to agree qualitatively with the observation by Kamaras *et al.* again. They have examined about twenty crystals in this phase and have found resistivity values along the needle axis scattered by a factor of 16. However, it must be added that the values in Fig. 1 are three orders of magnitude greater than the reported values, namely, from 0.01 to 0.2 ohm cm. This disagreement suggests that the anisotropy in the TTT–$I_{2.7}$ phase is anomalously large and is much larger than that in the TTT–$I_{1.5}$ phase.

The temperature dependence of the resistivity, ρ, follows the typical semiconductor behavior: $\rho=\rho_0 \exp(E_a/kT)$. The activation energy for semiconduction, E_a, thus obtained is plotted against n in Fig. 2. As the single crystal resistivities measured along the needle axes in both the TTT–$I_{1.5}$ and TTT–$I_{2.7}$ phases are known to be metallic in the temperature range from 200 to 300 K, the activation energy observed with the polycrystalline compactions must be attributed to the activation energy for semiconduction in the directions other than the needle axis and, at least in part, to contact between the crystals. The small activation energy found near $n=1.5$ may be mostly due to the latter; however, the value as large as 0.13 eV found for the TTT–$I_{2.7}$ phase arises undoubtedly from the semiconductor behavior along the axes other than the needle axis.

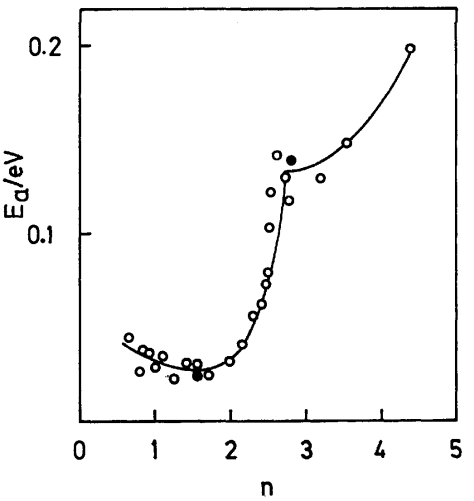

Fig. 2. Activation energy for semiconduction plotted against the iodine content.

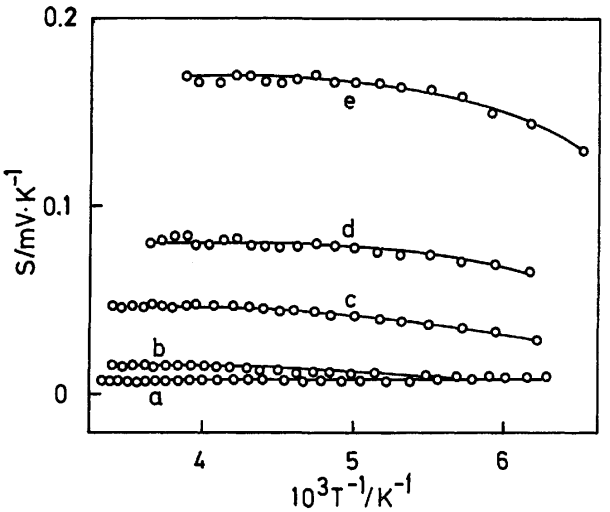

Fig. 3. Seebeck coefficient of the TTT–iodine complexes; a) $n=1.71$, b) 2.59, c) 2.84, d) 3.20, and e) 3.58.

The Seebeck coefficients of all the samples are positive throughout the examined temperature range, and tend to saturate at high temperatures (see Fig. 3). Similar behavior, but with the opposite sign, has been known to be characteristic of TCNQ salts with metallic conductivity.[21] According to the theory of Beni,[22] their Seebeck coefficients in the high temperature limit, $S(T\to\infty)$, are given by the equation,

$$S(T\to\infty) = -\frac{k}{|e|}\ln 2(1-\gamma)/\gamma,$$

where γ is the carrier concentration defined by the ratio of the number of carriers to the number of sites, in other words, the amount of negative charge per TCNQ molecule. Following the proposal by Beni *et al.* that the above equation is the most direct way of

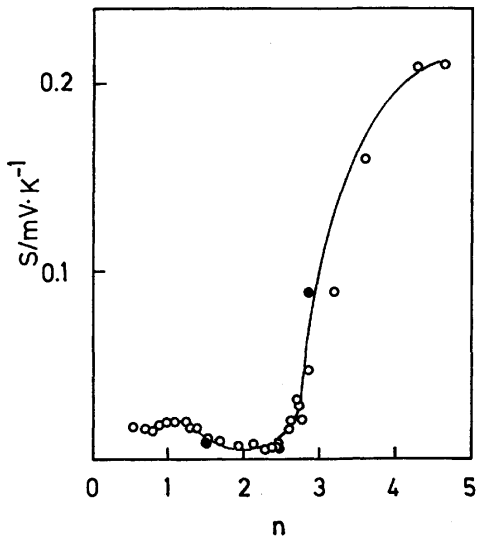

Fig. 4. Seebeck coefficient at −20 °C plotted against the iodine content.

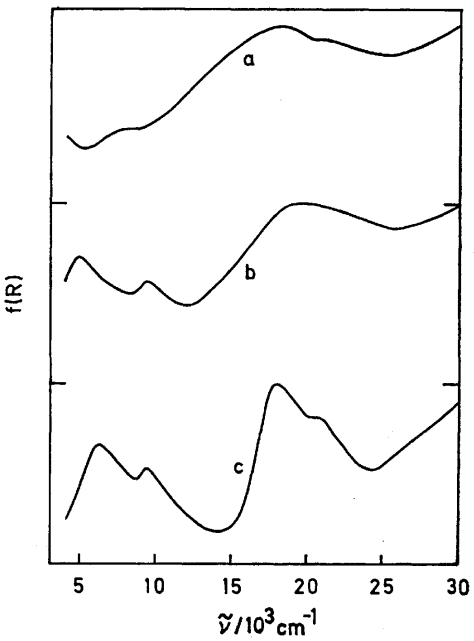

Fig. 5. Diffuse reflection spectra of a) TTT-$I_{1.53}$, b) TTT-$I_{2.79}$, and c) TTT-Br.

determining the value of γ,[23] we earlier found 0.52—0.55 for the high-conductivity 1:2 salts and 0.60—0.62 for the 2:3 salts by measurements on the polycrystalline compactions.[24] These values agree reasonably well with the expected ones, namely, 1/2 and 2/3. The high-temperature limit for the Seebeck coefficient is governed entirely by the entropy change per added carrier and is expected to be independent of the charge sign.[25] Consequently, the Beni equation may be employed for the estimation of the amount of positive charge per TTT molecule, because both TTT-$I_{1.5}$ and TTT-$I_{2.7}$ phases are known to be metallic. The positive coefficients are indicative of the γ values larger than 2/3. The value estimated for the TTT-$I_{1.5}$ phase is 0.68 and that for the TTT-$I_{2.7}$ phase, 0.80—0.85. If all the iodine atoms in these phases exist as triiodide ions, the expected γ values are 1/2 and 9/10 respectively. The $S(T\rightarrow\infty)$ value for the former γ is $-60\ \mu V\ K^{-1}$ and that for the latter is $+130\ \mu V\ K^{-1}$. Thus, the estimated amount of charge per TTT molecule in the TTT-$I_{1.5}$ phase is significantly larger than the expected one. If one assumes that a part of the iodine is in the form of iodide ions, I^-, and that $\gamma=2/3$ for the sake of simplicity, the constitution at $n=1.5$ may be expressed by the formula: $(TTT^+)_{2/3}(TTT^0)_{1/3}(I_3^-)_{5/12}(I^-)_{1/4}$. The abrupt increase of the Seebeck coefficient in a narrow range of $n=2.6$ to 3.0 shown in Fig. 4 corresponds to the change of γ from 0.68 to 0.85. The temperature-dependence of the Seebeck coefficient in the range above $n=3$ is similar to that below $n=3$. Tentatively applying the Beni equation to the range near $n=3$, it is concluded that the TTT molecule does not attain a unit positive charge even at the highest iodine content. Therefore, the TTT-$I_{2.7}$ phase may contain a higher polyiodide ion, possibly a pentaiodide ion, or an iodine molecule in addition to the triiodide ion.

Electronic Spectra. In Fig. 5, the Kubelka-Munk plots of diffuse reflectance are presented for samples TTT-$I_{1.53}$ and TTT-$I_{2.79}$. Each spectrum in the region below $10\times10^3\ cm^{-1}$ consists of two peaks; however, their locations are markedly dependent on the composition. The TTT-$I_{1.5}$ phase shows one peak below $4\times10^3\ cm^{-1}$, the limit of the spectroreflectometer employed, and the other at about $7.5\times10^3\ cm^{-1}$, while the TTT-$I_{2.7}$ phase shows peaks at 4.8×10^3 and $9.4\times10^3\ cm^{-1}$. The presence of two peaks in the infrared region is characteristic of solid TTT cation radical salts.[26] For comparison, the spectrum of TTT-Br taken from our previous work is added to Fig. 5. This bromide has been reported to exhibit a resistivity of 50 ohm cm at 25 °C by Perez-Albuerne *et al.*[10] Here, the peaks are located at 6.2×10^3, 9.5×10^3, and $18.0\times10^3\ cm^{-1}$, with a shoulder at $20\times10^3\ cm^{-1}$. As the appearance of such low-energy absorption bands attributable to electronic transitions are common to low-resistivity organic compounds, it is strange that no absorption has been noted below $10\times10^3\ cm^{-1}$ in the spectra of samples TTT-$I_{1.6}$ and TTT-$I_{2.8}$ presented by Kamaras *et al.*[13] Although the lowest energy band in the TTT-$I_{2.7}$ phase is shifted a little to the lower-energy side compared with that in the TTT-Br, the close resemblance in the spectral features of these two may be noted. In agreement with the high γ value estimated on the basis of the Seebeck coefficient, this resemblance suggests that the major fraction of TTT molecules is in the form of monopositive ions. The strong peak with a shoulder in the visible region shown by the solid TTT-Br is the cause of the dark red color and characterizes the TTT^+ ion. However, this peak cannot be identified in the spectra of black-colored TTT-$I_{1.53}$ and TTT-$I_{2.79}$ because of overlap with strong absorption bands due to triiodide and/or polyiodide ion.

The present work was partially supported by a Grant-in-Aid for Scientific Research from the Ministry of Education (No. 234028).

References

1) As the trivial name, tetrathiotetracene given by C. Marschalk and C. Stumm (Ref. 16) has been widely used; TTT is the abbreviation in accord with those in the references.
2) Y. Matsunaga, *J. Chem. Phys.*, **42**, 2248 (1965).
3) Y. Okamoto, S. Shah, and Y. Matsunaga, *J. Chem. Phys.*, **43**, 1904 (1965).
4) E. Krikorian and R. J. Sneed, *J. Appl. Phys.*, **40**, 2306 (1969).
5) J. H. Perlstein, J. P. Ferraris, V. V. Walatka, Jr., D. O. Cowan, and G. A. Candela, *A. I. P. Conf. Proc. Magnetism Magenetic Materials*, **10**, 1494 (1972).
6) O. N. Eremenko, M. L. Khidekel, D. N. Fedutin, and E. B. Yagubskii, *Izv. Akad. Nauk, Ser. Khim.*, **1972**, 984.
7) P. Delhaès, S. Flandrois, G. Keryer, and P. Dupuis, *Mat. Res. Bull.*, **10**, 825 (1975).
8) R. C. Wheland and J. L. Gilson, *J. Am. Chem. Soc.*, **98**, 3916 (1976).
9) L. V. Interrante, J. W. Bray, H. R. Hart, Jr., J. S. Kasper, P. A. Piacente, and G. D. Watkins, *J. Am. Chem. Soc.*, **99**, 3523 (1977).
10) E. A. Perez-Albuerne, H. Johnson, Jr., and D. J. Trevoy, *J. Chem. Phys.*, **55**, 1547 (1971).
11) L. I. Buravov, G. I. Zvereva, V. F. Kaminskii, L. P. Rosenberg, M. L. Khidekel, R. P. Shibaeva, I. F. Shchegolev, and E. B. Yagubskii, *J. Chem. Soc., Chem. Commun.*, **1976**, 720.
12) L. C. Isett and E. A. Perez-Albuerne, *Solid State Commun.*, **21**, 433 (1977).
13) K. Kamaras, K. Ritvay-Emandity, G. Mihaly, and G. Grüner, *Solid State Commun.*, **24**, 93 (1977).
14) V. F. Kaminskii, M. L. Khidekel, R. B. Lyubovskii, I. F. Shchegolev, R. P. Shibaeva, E. B. Yagubskii, A. V. Zvarykina, and G. L. Zvereva, *Phys. Status Solidi (A)*, **44**, 77 (1977).
15) S. Doi, T. Inabe, and Y. Matsunaga, *Bull. Chem. Soc. Jpn.*, **50**, 837 (1977).
16) C. Marschalk and C. Stumm, *Bull. Soc. Chim. Fr.*, **1948**, 418.
17) K. Kan and Y. Matsunaga, *Bull. Chem. Soc. Jpn.*, **45**, 2096 (1972).
18) K. Lichtenecker, *Z. Elektrochem.*, **40**, 11 (1934).
19) K. Ulbert, *Aust. J. Chem.*, **23**, 1347 (1970).
20) D. L. Smith and H. R. Luss, *Acta Crystallogr., Sect. B*, **33**, 1744 (1977).
21) L. I. Buravov, D. N. Fedutin, and I. F. Shchegolev, *Soviet Phys. JETP*, **32**, 612 (1971).
22) G. Beni, *Phys. Rev. B*, **10**, 2186 (1974).
23) G. Beni, J. F. Kwak, and P. M. Chaikin, *Solid State Commun.*, **17**, 1549 (1975).
24) Y. Matsunaga and T. Tanaka, *Bull. Chem. Soc. Jpn.*, **49**, 2713 (1976).
25) P. M. Chaikin and G. Beni, *Phys. Rev. B*, **13**, 647 (1976).
26) Y. Matsunaga, *Bull. Chem. Soc. Jpn.*, **45**, 770 (1972).

Intramolecular Charge Transfer in the Polar Fluorescent State of 1- and 2-Acylanthracenes

Takashi TAMAKI

Research Institute for Polymers and Textiles, Sawatari, Kanagawa-ku, Yokohama 221

(Received March 22, 1978)

The absorption and emission spectra of 1- and 2-aroyl- and acetylanthracenes were measured in various solvents. The emission spectra moved to longer wavelengths and their forms changed from the structured ones to the structureless ones with increasing solvent polarity, while the absorption spectra showed no appreciable changes under the same conditions. These emissive features became more distinguished with increasing electron-withdrawing ability of the aroyl group. The dipole moments of the fluorescent state as estimated from the Lippert-Mataga formula were 7—16 D for these compounds. The assignments of the low-lying excited states are described in terms of the electronic transitions of the parent anthracene, ^1L_a and ^1L_b, which undergo perturbation by the substitution.

In a recent study on the photoaroylation of anthracene (**1**) with benzoyl chloride, and its *p*- or *m*-substituted compounds, the ketone products formed were found to be positionally selective, the product distribution being different from that of the thermal Friedel-Crafts benzoylation.[1] This positional selectivity has attracted our continuing attention. Since the product distribution obtained is inconsistent with that theoretically expected from the reactivity calculated, which is acceptable for a non-interacting aromatic molecule, we tentatively postulate a specific intermolecular interaction between the reactants to ensure the positional selectivity. In fact, a strong interaction was evidenced by the efficient quenching of the fluorescence of **1** by these aroyl chlorides. Furthermore, the Hammett treatment of the quenching rate constant was indicative of an exciplex formation.

To further elucidate the electronic interaction of **1** with the aroyl system, we planned to study the spectral and emissive behaviors of aroylanthracenes, in which the constituents are intimately combined. The information about the intramolecular interaction may be helpful to account for the mechanisms of the intermolecular interaction concerned.

The introduction of a substituent group into an aromatic ring, in general, leads to a spectral deformation due to degradation of the molecular symmetry and due to effective electronic conjugation with the group.[2] It is well known that the absorption spectra of the anthracene derivatives, except for the meso substitution, are quite different from that of the parent (**1**).[3-5] The factors influencing the spectra are also discussed.

Experimental

Aroylanthracenes (**2c** and **3b—f**) were prepared in similar ways to those described in a preceding paper.[1b] The preparation of acetylanthracenes (**2a** and **3a**) was carried out after Luttinghaus and Kacer.[6] The emission spectra were measured in an air atmosphere, using a Hitachi MPA-2A spectrophotofluorometer. The sample absorbance in a 1-cm square quartz cell was made to be 0.1 at the exciting wavelength (390 nm), so that the reabsorption was negligible and that the relative emission intensities were comparable with each other.

Solvents used were spectro- or G.R. grade reagents (the numbers in parentheses refer to those presented in the figures): hexane (1), cyclohexane (2), carbon tetrachloride (4), dioxane (5), dibutyl ether (6), dipropyl ether (7), chloroform (8), butyl acetate (10), ethyl acetate (11), dichloromethane (13), 1,2-dichloroethane (14), pyridine (15), *t*-butyl alcohol (16), and 2-propanol (17) were used as commercially available; benzene (3), diethyl ether (9), tetrahydrofuran (12), acetone (18), *N,N*-dimethylformamide (19), ethanol (20), acetonitrile (21), and methanol (22) were dried by standard procedures and purified by fractional distillation.

The measurements of the fluorescence polarization spectra were made in a glycerol solution in order to minimize the rotational relaxation. The monitoring wavelength was 520 nm.

Results and Discussion

Absorption Spectra. The absorption spectra of 1- (**2c**) and 2-benzoylanthracene (**3c**) in hexane are shown in Fig. 1. The intense absorption bands in the short wavelength region (<300 nm) may consist of the transition bands which originate from the constituent aromatic moieties. In this region, the anthryl and the phenyl rings give intense progressions, which are assigned to the ^1B_b and the ^1L_a band, respectively.[2] The assignment of the short wavelength bands was not undertaken in this study.

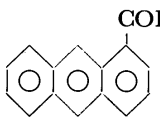

2

a, R=CH_3
c, R=Ph

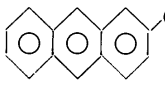

3

a, R=CH_3
b, R=*p*-$C_6H_4OCH_3$
c, R=Ph
d, R=*m*-C_6H_4Cl
e, R=*m*-C_6H_4CN
f, R=*p*-C_6H_4CN

In the longer wavelength region, above 300 nm, the absorption spectra are quite different from that of the parent anthracene (**1**), in which a progression of the ^1L_a transition alone is prominent. As is shown in Fig. 1, the compounds (**2c** and **3c**) give two electronic transition bands, which are closely overlapping each other in the former spectrum and clearly separate in the latter spectrum. These bands are conveniently named as I and II, according to the sequence of their peak energy

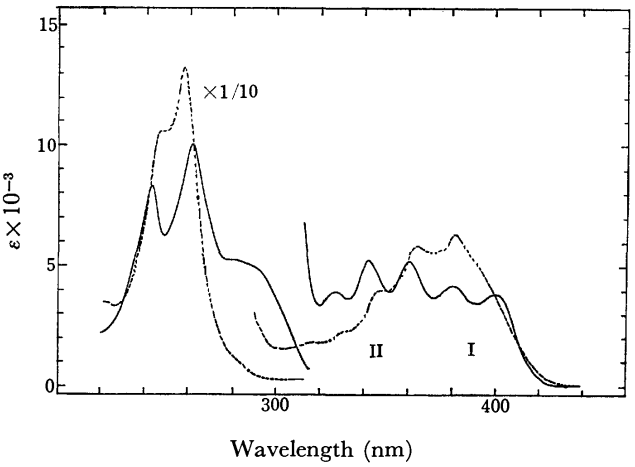

Fig. 1. Absorption spectra of 1-benzoylanthracene (——) and 2-benzoylanthracene (——) in hexane.

(see Fig. 1). The absorption spectra of acetylanthracenes (**2a** and **3a**) are the same as those of the corresponding benzoylanthracenes. Such spectral deformation is rather common to the anthracene to which a powerful substituent group attaches.[2,4,5] Thus, the general form of the absorption spectrum is fundamentally dependent on the aromatic C-position at which the substitution occurs.

It is of special interest to clarify the roots of the I and II transition bands. Although a few papers have discussed the problem, the arguments among articles are confused because the fundamental dissimilarity to the parent spectrum prevents one from deducing conclusive assignments of the transition bands with certainty.[2,4,5] So far, the most plausible assignment arises from the resonance theory,[3,4] which claims that a substituent group largely affects the aromatic transition band lying in the same direction as that of the extending conjugation. Since an 1-substituent group lies nearly along the short axis of an aromatic molecule, it primarily influences the transverse-polarized ^1L_a band. Likewise, since a 2-substituent group lies nearly along the long axis, the longitudinally polarized ^1L_b band is mainly subjected to its influence. These substituent effects are well accepted for naphthalene derivatives: the 1-substitution gives rise to large bathochromic and hyperchromic shifts of the ^1L_a band, and the 2-substitution causes the similar shifts of the ^1L_b band.[2]

Suzuki and Baba have discussed the assignment of the electronic transition bands of anthrol and anthrylamine in terms of such substitution perturbation.[4] On the assumption that the degradation of the molecular symmetry due to substitution would lead to the emergence of the ^1L_b transition, which is forbidden in the parent spectrum, they ascribed the lowest (I) and the second (II) bands of the 1-derivatives to the perturbed ^1L_a and ^1L_b bands, respectively, and those of the 2-derivatives to the perturbed ^1L_b and ^1L_a bands, respectively. These assignments are also favored in the cases of the acylanthracenes studied here, because their absorption spectra have close resemblances to those of the corresponding anthrols or anthrylamines.

Judging from the MO treatments of the parent

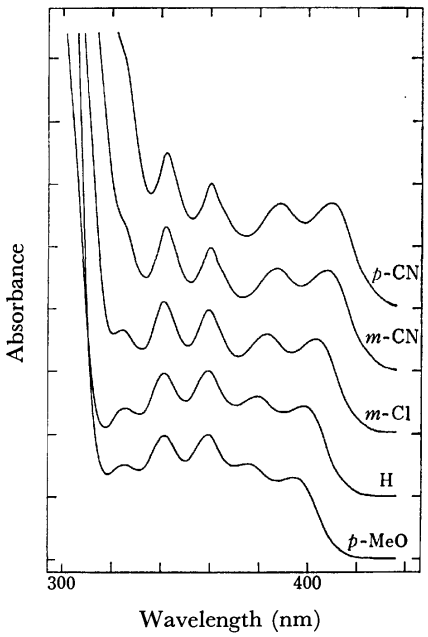

Fig. 2. Absorption spectra of 2-(substituted benzoyl)-anthracene in hexane.

spectrum, which suggest that the transition energy of the forbidden band (^1L_b) is slightly higher than that of the predominant band (^1L_a),[7] it appears striking that the former band extensively emerges on the lower frequency side of the latter band, when the substituent group is introduced at the 2-position of **1**. To examine this for the cases of the compounds concerned, we measured the absorption spectra of the series of 2-aroylanthracenes, which have a *p*- or *m*-substituent group on the benzoyl ring. As is shown in Fig. 2, the I band is apparently dependent on the substituent group, whereas the II band is little affected, its peak positions lying at the same wavelengths (325, 342, and 360 nm) for these compounds. The peak positions of their longest wavelength bands and their peak height ratio are listed in Table 1. The results indicate that the bathochromic and presumably hyperchromic effects on the I band become larger with increasing electron-withdrawing ability of the substituent group. The peak energy of the I band is well correlated with the Hammett substituent constant, σ. The ρ value obtained is 2.3, a value close to that derived from the inductive effect on the electron-abstracting process of the benzoyl system.[8]

These spectral features are quite consistent with the transition-band assignments in view of the resonance theory. It appears likely that the substituent perturba-

Table 1. Peak position and peak height ratio of absorption bands of 2-aroylanthracenes

Compound	λ_{II} (nm)	λ_I (nm)	$\varepsilon_I/\varepsilon_{II}$
3b	360	394	0.65
3c	360	399	0.72
3d	360	404	0.77
3e	361	408	0.77
3f	362	410	0.83

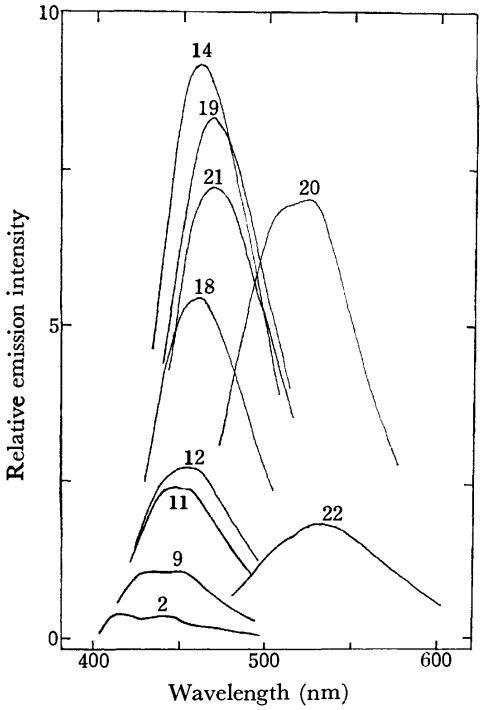

Fig. 3. Emission spectra of 2-benzoylanthracene in various solvents.

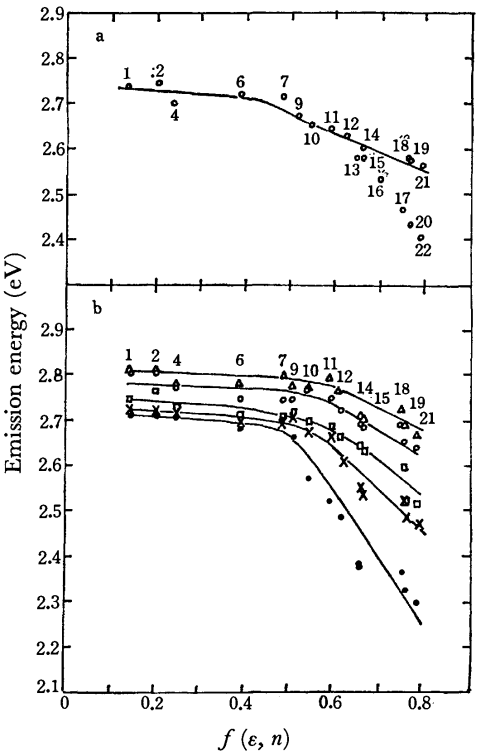

Fig. 4. Solvent effects on the emission peak maxima of 1-benzoylanthracene (a) and 2-(substituted benzoyl)-anthracene (b): *p*-MeO (△), H (○), *m*-Cl (□), *m*-CN (×), *p*-CN (●).

tion extends the spectral deformation, which was first generated from the degradation of the aromatic symmetry.

Solvent Effects on the Emission Spectra. The increase of the solvent polarity degradates the vibrational structure of the I band, with a slight broadening of the band, while the II band undergoes only a slight red-shift without changing its fundamental form. In contrast with these small changes of the absorption spectra, the emission spectra are greatly dependent on the solvent properties, as is shown in Fig. 3. The emission spectra in non-polar solvents are equal to the mirror image of the I band. When the solvent is changed from non-polar to polar, they are converted into structureless bands with large Stokes' shifts. Neverthless, their excitation spectra in all cases are in good agreement with the absorption spectra.

Lippert and Mataga have independently developed the theoretical treatments for solvent-induced changes of the excited electronic structure.[9] In the theory, the emission energy is to a good approximation correlated with the quasimacroscopic parameter for solvent polarity, $f(\varepsilon, n)=2(\varepsilon-1)/(2\varepsilon+1)-(n^2-1)/(2n^2+1)$, in which ε and n are the dielectric constant and refractive index of the continuum medium, respectively. As is shown in Fig. 4, the peak energy in most solvents used is in good correlation with the parameter, $f(\varepsilon, n)$, although the deviation from the plots is observed for some solvents, which specifically interact with the solute. The protic solvents in particular induce anomolous red-shifts, presumably due to formation of the hydrogen bond. The excess of stabilization energy for the hydrogen bond is of the order of 1500 cm^{-1}, as estimated from the difference between the frequencies of the peak maxima in acetonitrile and in methanol, which are of the same polarity. Further discussions for the cases of the protic solvents will not be made.

The emission energy plots obtained for all compounds examined give curvatures which have at least two slopes, as is shown in Fig. 4. The slope in the non-polar region is nearly horizontal and that in the polar region is definitely negative. The inflection appears at the intermediate-polarity solvent, ethyl ether. This solvent dependence indicates that the fluorescent state of **2** and **3** becomes highly polar with increasing the solvation, while the ground state is little affected. In Table 2 are liested the values of the dipole moment in the fluorescent state, as calculated from the Lippert-Mataga formula on the assumption that the radius of the solvent cavity is 5 Å, approximately what would be expected from the molecular model. The values of the dipole moment are 7 D for **2**, 9 D for **3a**, and 10 D for **3c**.

As is shown in Fig. 4b, the peak shift in the polar region is very sensitive to the substituent group of the benzoyl phenyl ring. The greater the electron-withdrawing ability of the substituent group, the more the peak moves to the longer wavelengths and the greater the value of the dipole moment calculated (Table 2).

Table 2. Dipole moments in polar fluorescent states

Compound	Dipole moment (debye)	Compound	Dipole moment (debye)
2a	7	**3c**	10
2c	7	**3d**	12
3a	9	**3e**	13
3b	9.5	**3f**	16

From these results, it appears probable that the charge transfer occurs from the anthryl ring to the acetyl or benzoyl moiety in the excited equilibrium state.

In this connection, it was observed that *N,N*-dimethylaniline, which is an electron donor, strongly quencehd the fluorescence of the compounds (**2** and **3**) to give an exciplex emission in non-polar solvents. On the other hand, an electron acceptor such as dicyanobenzene had no such quenching ability. These facts support the assertion that the anthryl ring is greatly electron-deficient in the excited state owing to the charge transfer to the substituent group.

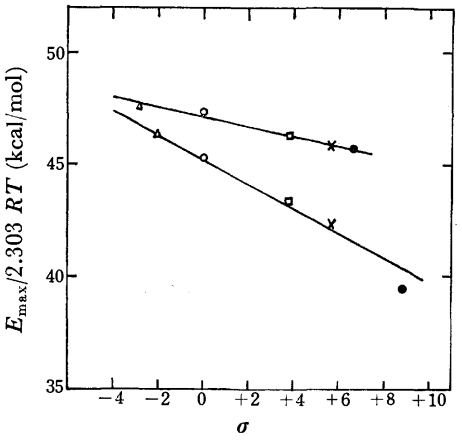

Fig. 5. Hammett correlation of the emission peak maxima of 2-(substituted benzoyl)anthracene in hexane (upper plots) and in acetonitrile (lower plots).

The Hammett plots for the emission energy of **3b—f** are shown in Fig. 5. The emission energy in hexane shows a linear Hammett correlation, with ρ equal to that obtained from the similar plots of the absorption energy. While the inductive contribution is importtant for the electronic transition processes in the non-polar solvents, the emission energy in acetonitrile requires an exalted substituent constant, σ^-, to give a linear Hammett correlation, which suggests the validity of the resonance contribution for the stabilization of the polar fluorescent state. The ρ value obtained for the acetonitrile solution is 5.5, a value so high as to be consistent with the charge transfer required in a large electron-demand process.

The solvent dependence of the emission intensity is complicated, as is shown in Fig. 6. Generally speaking, the emission intensity increases with increasing the solvent polarity, and then decreases in a highly polar region. Very weak emission in non-polar solvents may correspond to the case of 9-benzoylanthracene, which is non-fluorescent because of rapid radiationless decay through a thermally activated intersystem crosssing to the upper triplet state in a slightly higher energy level than that of the lowest excited singlet state.[10] It appears likely that the energy gaps between the relevant electronic levels of the compounds (**2** and **3**) are so large that the radiative transition rate is comparable to the radiationless decay rate. If this energy gap is more enlarged when the fluorescent state moves

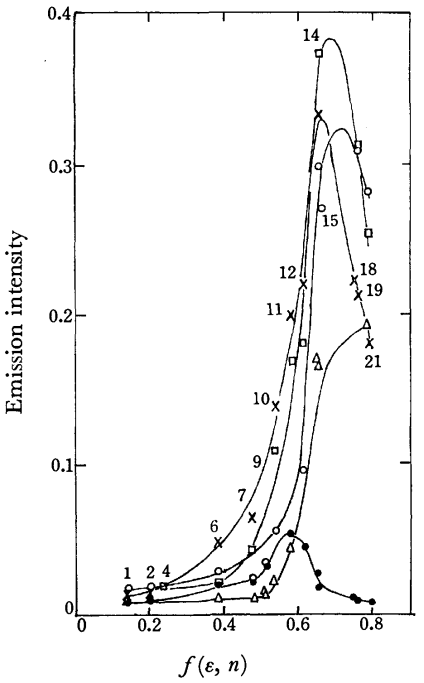

Fig. 6. Solvent effects on the emission intensity of 2-(substituted benzoyl)anthracene: *p*-MeO (△), H (○), *m*-Cl (□), *m*-CN (×), *p*-CN (●).

to the lower frequency region with increasing the solvation, the radiative probability would increase at the expense of the intersystem-crossing probability. The decrease of the emission intensity in highly polar solvents is remarkable for the compounds (**3**), which have a powerful substituent group such as a cyanobenzoyl group. This suggests that a complete charge separation would be accomplished for these highly solvated compounds, resulting in the decrease of the radiative transition probability.

The excitation-polarization spectra of **2a** and **3a** in glycerol are shown in Fig. 7. When the I band is excited, the degree of the polarization obtained is *ca.* 0.3 suggesting that this band corresponds to the emitting band. If the rotational relaxation is severly inhibited, the polarization degree would become close to the maximum value, 0.5.[11] The excitation of the II band leads to the decrease of the polarization, which supports

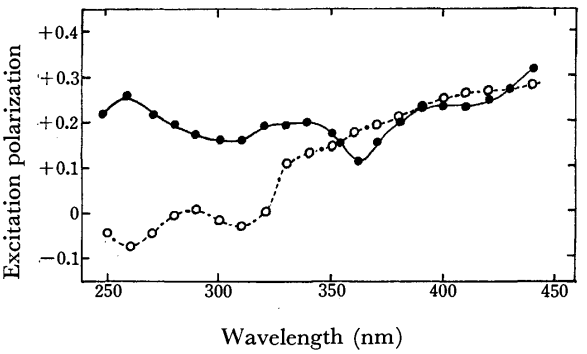

Fig. 7. Excitation polarization spectra of 1-acetylanthracene (-----) and 2-acetylanthracene (——) in glycerol. Monitoring wavelength, λ 520 nm.

the idea that the transition moments of the I and II bands are oriented at large angles to each other. While the polarization behaviors of these long wavelengths bands are similar for all compounds examined, the situation of the short wavelengths bands is quite different for the polarization spectra of **2** and of **3**: the former shows a negative polarization (*ca.* −0.1), but the latte shows a large positive polarization (*ca.* 0.25). The dissimilarity in the polarization spectra may reflect the difference in the mutual orientation of the exciting and emitting transition moments of these compounds. The exciting band of acetylanthracene (**2a** and **3a**) in this short wavelength region is ascribed to the anthryl ^1B_b band, although the contribution of the phenyl ^1L_a transition to excitation is unclear in the cases of benzoylanthracene (**2c** and **3c**). Since the ^1B_b band lies along the long axis,[7] the results for the polarization provide a possible orientation of the I band of **2** and **3**, which is approximately in line with the consequences of the transition-band assignments based on the absorption spectra.

The emissive features of aroylanthracenes are informative to account for the mechanisms of the intermolecular interaction between **1** and the aroyl chlorides:[1] 1) the charge transfer in the polar fluorescent state is related to an intermolecular exciplex formation; and 2), the inversion of the excited states in 2-benzoylanthracene is indicative of the validity of the ^1L_b state in determining the positional selectivity in the photoaroylation.

References

1) a) T. Tamaki, *J. Chem. Soc., Chem. Commun.*, **1976**, 335; b) T. Tamaki, *Bull. Chem. Soc. Jpn.*, **51**, 1145 (1978).
2) H. H. Jaffe and M. Orchin, "Theory and Applications of Ultraviolet Spectroscopy," John Wiley and Sons, Inc., (1962), pp. 242—344.
3) R. N. Jones, *J. Am. Chem. Soc.*, **67**, 2127 (1945).
4) a) H. Baba and S. Suzuki, *Bull. Chem. Soc. Jpn.*, **35**, 683 (1962); b) S. Suzuki and H. Baba, *ibid.*, **37**, 519 (1963).
5) K. Rotkiewicz and Z. R. Grabowski, *Trans. Faraday Soc.*, **65**, 3263 (1969).
6) P. H. Gore, *Chem. Rev.*, **55**, 229 (1955).
7) K. Nishimoto and R. Fujishiro, *Bull. Chem. Soc. Jpn.*, **37**, 1660 (1964).
8) H. H. Jaffe, *Chem. Rev.*, **53**, 191 (1953).
9) a) N. Mataga, Y. Kaifu, and M. Koizumi, *Bull. Chem. Soc. Jpn.*, **28**, 690 (1955); b) E. Lippert, *Z. Naturforsch.*, **10a**, 541 (1955); c) H. Beens, H. Knibbe, and A. Weller, *J. Chem. Phys.*, **47**, 1183 (1967).
10) a) D. J. Mitchell, G. B. Schuster, and H. G. Drickamer, *J. Am. Chem. Soc.*, **99**, 1145 (1977); b) S. Hirayama, *Bull. Chem. Soc. Jpn.*, **48**, 2653 (1975).
11) A. Jablonski, *Z. Phys.*, **96**, 236 (1935).

A Study on the Anode Effect in KF-2HF System. III. Influence of Bath Temperature and Surface Tension and Addition of Fluoride Particles on the Occurrence of the Anode Effect

Hiroki IMOTO, Kazuo UENO, and Nobuatsu WATANABE*

Department of Industrial Chemistry, Faculty of Engineering, Kyoto University, Yoshida, Sakyo-ku, Kyoto 606

(Received March 24, 1978)

The decomposition reaction of the graphite fluoride film formed on the edge plane of pyrolytic graphite, carbon, and graphite electrodes was faster in a KF·HF bath (250 °C) than in a KF·2HF bath (100 °C) due to the higher temperature of KF·HF bath. The critical current densities (CCD's)[1] were about 0.1 A/cm² for the layer and edge planes of pyrolytic graphite, carbon, and graphite electrodes in the KF·HF bath, and the CCD for each electrode was larger in the KF·HF bath than in the KF·2HF bath. The anode effect took place easily on the glassy carbon electrode in the KF·2HF bath. However, the anode effect did not take place in liquid hydrogen fluoride due to its very low surface tension, although the graphite fluoride film was formed on the electrode surface. The zeta-potential of aluminum fluoride particles in liquid hydrogen fluoride containing 0—20 mol of potassium fluoride/l and that of magnesium fluoride particles in liquid hydrogen fluoride were almost zero at 0 °C. From the results it is not proper that the effect of the addition of dispersed particles upon the anode effect is explained by the view of electrostatic force of the particles proposed so far.[2]

The anodic behavior of four kinds of electrodes (graphite, carbon, pyrolytic graphite, and glassy carbon) have been investigated in KF·2HF bath.[2-4] It has been suggested that the occurrence of the anode effect is influenced by the wettability of the anode surface with the bath and the kinetic balance of the rates of the formation and decomposition reaction of the graphite fluoride, $(CF)_n$,[5] film on the anode. The wettability and the kinetic balance vary with the surface tension and the operating temperature of the bath, respectively. Table 1 shows the surface tensions of the KF–HF system. The surface tension of liquid hydrogen fluoride (LHF, 0 °C) is much lower than that of KF·2HF melt (100 °C). The surface tension of KF·HF melt (250 °C) is almost the same as that of KF·2HF melt. Therefore, in the present study, LHF and KF·HF melt were used as baths for investigating the influence of the surface tension and the temperature of the baths on the occurrence of the anode effect.

TABLE 1. SURFACE TENSION OF KF–HF SYSTEM

	LHF[a]	KF·2HF[b]	KF·HF[c]
Temperature (°C)	0	100	245
Surface tension (dyn/cm)	10	95	118
Temperature coefficient of surface tension (dyn/cm °C)	−0.08	−0.1	

a) H. H. Hyman, and J. J. Katz, "Non-Aqueous Solvent Systems," ed by T. C. Waddington, Academic Press, London and New York (1965), p. 53. b) N. Watanabe, M. Ishii, and S. Yoshizawa, *Denki Kagaku*, **29**, 492 (1961). c) A. J. Rudge, "Industrial Electrochemical Processes," ed by A. T. Kuhn, Elsevier Publishing Company, Amsterdam-London-New York (1971), p. 12.

The addition of lithium fluoride, nickel fluoride, aluminum fluoride, calcium fluoride,[6] magnesium fluoride[7] particles to the KF·2HF bath is effective for preventing the anode effect. This effect has been explained on the basis of the zeta-potential of the fluoride particles.[2] In order to confirm the explanation proposed, the zeta-potentials of aluminum fluoride (AlF_3) and magnesium fluoride (MgF_2) particles dispersed in KF–HF system were measured at 0 °C.

Experimental

The cell was kept at 100 and 250 °C for KF·2HF and KF·HF baths, respectively. A platinum rod was used as a reference electrode in both baths. Further detailed descriptions of the apparatus and the procedure for the measurement in the KF·2HF bath have been given in previous papers.[4,8] The measurement in the KF·HF bath was the same as that in the KF·2HF bath. The electrolytic cell for LHF was identical to that reported before[9] and cooled at 0 °C in ice bath. The Cu/CuF_2 electrode was used as a reference electrode, and a nickel plate as a counter electrode. Small amounts of potassium fluoride were added to LHF as a supporting electrolyte. LHF in the cell was dehydrated by pre-electrolysis with nickel electrodes for 2 days. The glassy carbon electrode was connected with a nickel lead by winding fine copper wires. The nickel lead and all parts of the glassy carbon except for the working electrode surface were protected with perflon paint[10] and Teflon (poly(tetrafluoro-

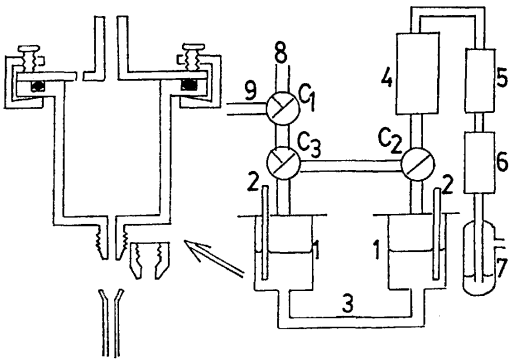

Fig. 1. Apparatus for the measurement of zeta-potential (microelectrophoresis cell).
1: Electrolytic cell, 2: electrode (nickel), 3: transparent pipe (Kel-F), 4: reflux condenser (methanol at −20 °C), 5: HF absorber (NaF pellets), 6: silica gel, 7: atmospheric seal, 8: HF inlet, 9: N_2 inlet, C_1, C_2, and C_3: Teflon stopcocks.

ethylene)) tape. Before ESCA measurement, the electrode of pyrolytic graphite was washed with LHF in order to remove the KF·HF remaining on the electrode. The ESCA spectrum of C 1s electron for the electrode has two peaks at 284 and 288.5 eV.[8] The former peak corresponds to the binding energy of the C 1s electron for the carbon atom which has only the C–C bond, and the latter peak corresponds to the one for the carbon atom with C–F bond. The height of the peaks at 284 and 288.5 eV were represented by h_0 and h_1, respectively and the value of $h_1/(h_0+h_1)$ was adopted as the relative amount of $(CF)_n$ on the electrode surface. The zeta-potential of particles dispersed in the KF–HF system was measured using a microelectrophoresis apparatus as shown in Fig. 1. The cell was specially designed for the corrosive hydrogen flouride, that is, the microscopic observation tube (3) was made of transparaent poly(trifluorochloroethylene) and the other parts were made of Teflon. The parts (1), (2), and (3) in Fig. 1 were kept at 0 °C in a cold air bath. The potential gradient between the nickel electrodes (2) was varied from 0 to 2.7 V/cm.

Results and Discussion

Effect of the Temperature of Bath. Figure 2 shows the *I-V* curves obtained by the linear potential sweep method for the layer plane (G_L) and edge plane (G_E) of the pyrolytic graphite electrodes in the KF·HF bath at 250 °C. The potential of the electrode G_L or G_E was swept from 0 to 7.0 V *vs.* Pt (forward sweep) and subsequently from 7 to 3.5 V (backward sweep). Two peaks were observed on both curves (a) and (b) on the forward sweep. This may be explained in terms of formation of two kinds of $(CF)_n$ films on the anode surface,[3] that is, the $(CF)_n$ film which has extremely low surface energy is formed at the second peak, and the current decreases rapidly with increasing potential. But the current restored on the backward sweep only on the electrode G_E, indicating that decomposition took place easily on the electrode. The peak current densities on the forward (second peak) and the backward sweeps were represented by P_f and P_b, respectively. The value of P_b/P_f for the electrode G_E was about twice as large in the KF·HF bath as in the KF·2HF bath, because the former cell temperature was about 150 °C higher than the latter one and therefore the $(CF)_n$ film easily decomposed in the KF·HF bath.[11] On the other hand, the current was hardly restored on the backward sweep on the electrode G_L, which means that the $(CF)_n$ film on the electrode G_L was hardly decomposed.

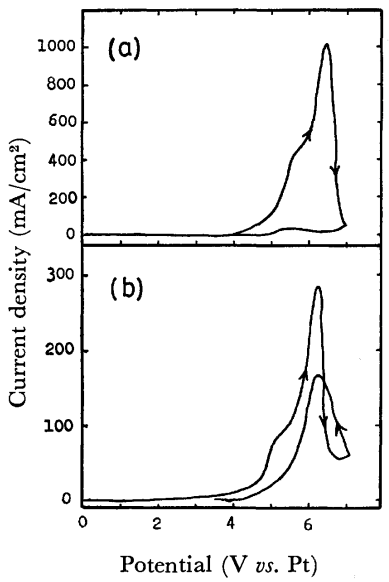

Fig. 2. *I-V* curves (potential sweep) in KF·HF bath at 250 °C.
Anode: (a) electrode G_L, (b) electrode G_E, potential sweep rate: 50 mV/s.

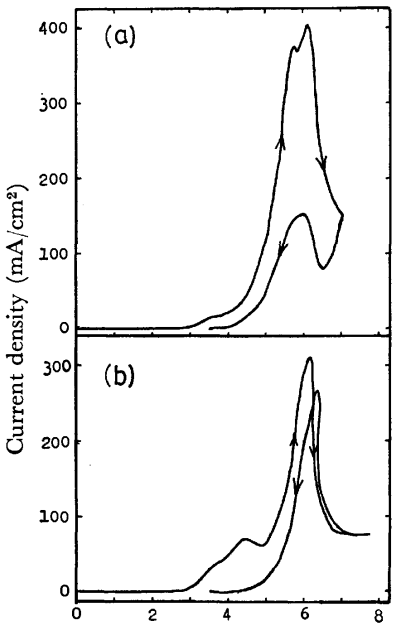

Fig. 3. *I-V* curves (potential sweep) in KF·HF bath at 250 °C.
Anode: (a) graphite, (b) carbon, potential sweep rate: 50 mV/s.

Figure 3 shows the *I-V* curves for the commercial carbon and graphite electrode. The values of P_b/P_f for the graphite and carbon electrodes were two and three times larger in the KF·HF bath than in KF·2HF bath, respectively. Consequently, the rate of decomposition of the $(CF)_n$ film on the anode surface is faster in KF·HF bath than in the KF·2HF bath when the electrode G_E and the carbon and graphite electrodes are used as anodes.

Figure 4 shows the potential sweep rate dependence of the P_f value for the four kinds of electrodes mentioned above. The dependence of the P_f values for these electrodes on the potential sweep rate showed the same tendency in both the KF·2HF and the KF·HF baths. Only the peak current density for the electrode G_L increased with the potential sweep rate much more than those for the other electrodes. From previous discussion,[4] this indicates that the covering rate of the electrode surface with the $(CF)_n$ was slower on the electrode G_L than on the other electrodes. Furthermore, the peak current densities for the four kinds of electrodes were independent of potential sweep rate within the

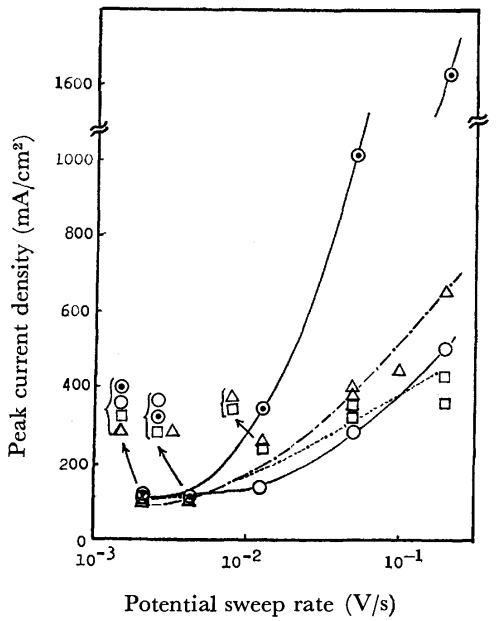

Fig. 4. Dependence of peak current densities on potential sweep rate in KF·HF bath (250 °C).
⊙ Electrode G_L, ○ electrode G_E, △ graphite, □ carbon.

region of low sweep rate. As the steady state condition was established within the region, the critical current densities (CCD's)[1] were found to be about 0.1 A/cm² for all electrodes from the peak current densities. The CCD's for the carbon, graphite, G_L, and G_E electrodes in the KF·2HF bath were 80, 25, 20, and 55 mA/cm², respectively. From the results, the KF·HF bath has advantages for operating the fluorine cell at higher current density compared with the KF·2HF bath.

When the electrode G_L or G_E was potentiostatically polarized in the KF·HF bath, the current reached a stationary value within 10 min. The ESCA spectra of C 1s electron for these electrodes were obtained after the polarization. The potential dependence of the values of $h_1/(h_0+h_1)$ is shown in Fig. 5. The potential

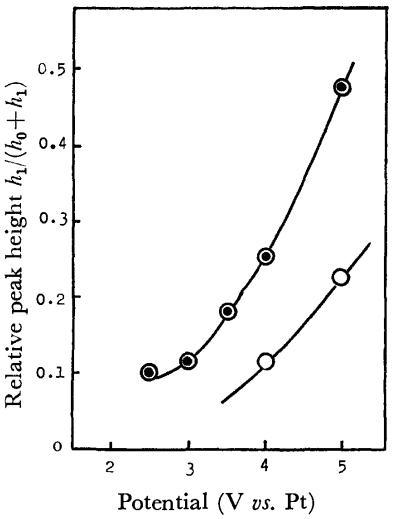

Fig. 5. Potential dependence of ESCA spectra of C 1s electron for pyrolytic graphite anode surface.
⊙ Electrode G_L, ○ electrode G_E.

dependence of the amount of the $(CF)_n$ film formed on the electrode G_L in the KF·HF bath was similar to that in the KF·2HF bath. However the $(CF)_n$ film was hardly observed on the electrode G_L polarized at lower potential than 3.5 V, although the $(CF)_n$ film was formed on the electrode polarized at 2 V in the KF·2HF bath. These facts suggest that the $(CF)_n$ formed on the electrode G_E at lower potential was easily decomposed due to the higher temperature of the KF·HF bath and the film on the electrode G_L was thermally more stable than that on the electrode G_E. These results may support the interpretation of the *I-V* curves described above.

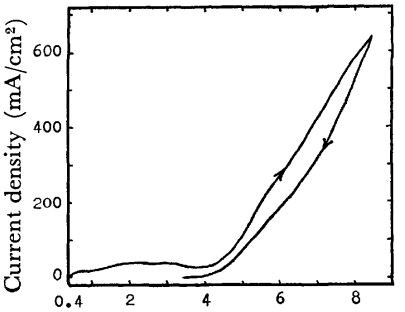

Fig. 6. *I-V* curve (potential sweep) in liquid hydrogen fluoride at 0 °C.
Electrode: glassy carbon, potential sweep rate: 12.5 mV/s.

Effect of Surface Tension of Bath. Only the polarization curve of the glassy carbon electrode could be obtained even in the LHF bath.[12] Figure 6 shows *I-V* curve for the glassy carbon electrode obtained by the linear potential sweep method at the potential between 0.4—8.4 V (the potential is converted into the potential *vs.* hydrogen electrode only in this section). The *I-V* curve obtained in the LHF bath was significantly different from that obtained in the KF·2HF bath, since the current increased with increasing potential without the anode effect becoming apparent. On the other hand, the current decreased rapidly at about 5.5 V with increasing potential due to the anode effect in the KF·2HF bath. The ESCA spectrum of C 1s electron for the surface of the glassy carbon electrode polarized at 4.9 V for 10 min in the LHF bath indicated the existence of the $(CF)_n$ film on the electrode surface. When the $(CF)_n$ film is formed on the glassy carbon electrode by the anodic polarization in the KF·2HF bath, the anode effect takes place, because the elctrode does not come into direct contact with the bath due to the high surface tension of the bath. However, the anode effect does not take place in the LHF bath in spite of the formation of the $(CF)_n$ film on the electrode, because the electrode surface comes into contact with the bath due to the very low surface tension of the LHF bath. The results verify the mechanism of the occurrence of the anode effect proposed,[2,13,14] and agree with the fact that when the carbon anode is used, the CCD's are 50—60 and 60—80 mA/cm² in KF·2HF (100 dyn/cm, 90 °C) and KF·3HF (75 dyn/cm, 80 °C) baths, respectively.[2]

Effect of Addition of Fluoride Particles. The following explanation was proposed[15,16] to account for the suppressive effect of fluoride particles on the anode effect. If the fluorine gas bubbles generated on the anode have negative charges, it is difficult for the bubbles to be separated from the anode because of the electrostatic attractive forces. If the colloidal fluoride particles have positive charges, they would be absorbed on the fluorine bubbles to neutralize the negative charges of the bubbles. Consequently the electrostatic force between the fluorine gas bubbles and the anode becomes remarkably weak and the fluorine gas bubbles can be readily separated from the anode surface. The zeta-potential of AlF_3 and MgF_2 particles dispersed in the KF–HF system were measured. The zeta-potentials of AlF_3 in LHF containing 0—20 mol of potassium fluoride/l and of MgF_2 in LHF were almost zero at 0 °C. Therefore, the zeta-potentials of AlF_3 and MgF_2 particles are thought to be almost zero in the KF·2HF bath of which the ionic strength is very high. From the results, it was found that the suppressive effect of the dispersed fluoride particles upon the anode effect cannot be accounted for in terms of the electrostatic interaction proposed so far.

Conclusion

1) The rate of decomposition of the graphite fluoride film formed on the edge plane of pyrolytic graphite, carbon, and graphite anodes was faster in the KF·HF bath than in the KF·2HF bath, and each critical current density for the pyrolytic graphite, carbon, and graphite electrodes was higher in the KF·HF bath than in the KF·2HF bath.

2) The anode effect did not take place in liquid hydrogen fluoride due to the very low surface tension of liquid hydrogen fluoride, which verifies the mechanism of the anode effect in KF·2HF bath proposed so far.

3) It was found that the suppressive effect of the dispersed fluoride particles upon the anode effect cannot be explained from the view of electrostatic force proposed so far.

References

1) An value of current density for the tendency to the occurrence of the anode effect. Anode effect takes place inevitably above the current density.

2) N. Watanabe, M. Ishii, and S. Yoshizawa, *Denki Kagaku*, **29**, 497 (1961).

3) M. Nishimura, A. Tasaka, K. Nakanishi, and N. Watanabe, *Denki Kagaku*, **38**, 294 (1970).

4) H. Imoto and N. Watanabe, *Bull. Chem. Soc. Jpn.*, **49**, 1736 (1976).

5) $(CF)_n$ has very low surface energy. See N. Watanabe, H. Takenaka, and S. Kimura, *Nippon Kagaku Kaishi*, **1975**, 1655.

6) N. Watanabe, M. Ishii, and S. Yoshizawa, *Denki Kagaku*, **29**, 492 (1961).

7) A. J. Rudge, "Industrial Electrochemical Processes," ed by A. T. Kuhn, Elsvier publishing Co., Amsterdam-London-New York (1971), p. 25.

8) H. Imoto and N. Watanabe, *Bull. Chem. Soc. Jpn.*, **48**, 1633 (1975).

9) M. Haruta and N. Watanabe, *J. Fluorine Chem.*, **7**, 159 (1976).

10) The fluorine-contained rubber dissolved in 2-butanone.

11) H. Imoto and N. Watanabe, *Denki Kagaku*, being submitted.

12) A. G. Doughty, M. Fleishmann, and D. Pletcher, *Electroanal. Chem. Interf. Electrochem.*, **51**, 456 (1974).

13) N. Watanabe, Y. Fujii, and S. Yoshizawa, *Denki Kagaku*, **31**, 611 (1963).

14) N. Watanabe, F. Kato, and K. Omura, *Denki Kagaku*, **37**, 274 (1969).

15) N. Watanabe, M. Inoue, and S. Yoshizawa, *Denki Kagaku*, **31**, 698 (1963).

16) N. Watanabe and N. Ooba, *Denki Kagaku*, **35**, 178 (1967).

Studies on Aqueous Solutions of Guanidinium Salts. VIII. Free Energy of Mixing of Guanidinium Bromide and Tetrabutylammonium Bromide in Aqueous Solution at 25 °C

Koichiro MIYAJIMA, Hiromitsu YOSHIDA, and Masayuki NAKAGAKI*

Faculty of Pharmaceutical Sciences, Kyoto University Yoshida-Shimoadachi-cho, Sakyo-ku, Kyoto 606

(Received March 18, 1978)

Osmotic and activity coefficients have been determined by the isopiestic comparison method on the water–guanidinium bromide–tetrabutylammonium bromide system at 25 °C. The values of the excess free energy change of mixing and the interaction parameter g_0 on Friedman's formalism were large and negative in magnitude. These results have been discussed in terms of the mixed ion pairing and structural change of water.

Guanidinium salts and their related compounds are well known as protein denaturants, but the mechanism of the denaturation remains ambiguous. Two types of mechanism have so far been postulated, one is the direct interaction between the acid amide groups of proteins and denaturants leading to the destruction of the hydrogen bond between the acid amide groups and the other is the indirect interaction between proteins and denaturants through the change of water structure which stabilizes the natural conformation of protein in the aqueous solution. Robinson and Jencks[1] investigated the former mechanism by examining the effect of several perturbants on the activity coefficient of acetyltetraglycine ethyl ester. By measuring the solubility they concluded that the non-hydrophobic interaction made a major contribution to the effectiveness of perturbants in protein denaturation in aqueous solution. Kauzmann[2] and Tanford[3] suggested that the hydrophobic bond played an important role in the stability of tertiary or higher structures of proteins. In the aqueous ternary systems containing urea and hydrocarbons, urea increased the solubility of the latter.[4] Similarly the decrease in the activity coefficient of tetrabutylammonium bromide (Bu_4NBr) and a positive enthalpy of transfer were obtained for the water–urea–tetraalkylammonium salt system.[5,6] Potassium bromide, on the other hand, increased the activity coefficient of tetrapropylammonium bromide in the aqueous ternary system.[7] These results were discussed in terms of the changes of the hydrophobic interactions by the structure breaking of potassium bromide and urea.[5–7] Based on the similartities of molecular shape, size and functional groups between urea and the guanidinium ion (Gu^+), the authors postulated[8] that the mechanism of the structure breaking by the guanidinium ion was similar to that by urea rather than by large alkali metal ions such as potassium and caesium ions. The differences would be more pronounced in aqueous solutions containing structure making solutes such as tetraalkylammonium salts than in pure water. The excess thermodynamic function of mixing in aqueous electrolyte solutions has been studied mainly on inorganic salt mixtures, several cases containing tetraalkylammonium salt as a component. The free energy change of mixing of Bu_4NBr and guanidinium bromide (GuBr) has been studied by the isopiestic comparison method and the results discussed in terms of the interionic interaction and the hydrophobic hydration.

Experimental

Materials. Guanidinium bromide was obtained by concentrating the aqueous solution of guanidine neutralized with hydrobromic acid. The crystal obtained was recrystallized twice or more from acetone and dried *in vacuo* before use. Tetrabutylammonium bromide was purchased from Wako Junyaku Co., Ltd. and recrystallized twice or more from the mixed solvent (ethyl acetate: diethyl ether=3: 1).

Method. Measurements of osmotic coefficients were carried out by the isopiestic comparison method at 25±0.02 °C using the same apparatus as reported previously.[9] In order to calculate the molality of each ternary solution, buoyancy corrections were made adopting the densities of the solid as 1.894 for GuBr, 1.152 for Bu_4NBr, and unity for the aqueous solutions. Both GuBr and Bu_4NBr were used as reference solutes. The experimental determination of the isopiestic concentration were precise to within 0.5%.

Theory

Activity Coefficient. Mckay and Perring's method[10] was used to evaluate the activity coefficients of each component in the ternary solution which was prepared by mixing two kinds of 1 : 1 electrolyte solutions. Under the conditions of equal vapour pressure among the three solutions, *i.e.* of GuBr (solute B), Bu_4NBr (solute C) and a mixture of both of them, the relation of Eq. 1 holds.

$$\nu_B M_B \phi_B = \nu_C M_C \phi_C = \nu m \phi, \quad (1)$$

where ν_B and ν_C are the number of moles of ions formed from 1 mol of solute B and C, M_B and M_C are the molality of solute B and C in the binary solutions which have the corresponding osmotic coefficients ϕ_B and ϕ_C, respectively. ν is the number of ions formed from 1 mol of pseudo-binary salt $(1-x)Gu^+xBu_4N^+Br^-$ and m is the total molality of the ternary solution which has the corresponding osmotic coefficient ϕ. x is the ionic mole fraction of electrolyte C in the mixture defined as

$$x = m_C/m = I_C/I, \quad (2)$$

where I_C and I are the ionic strengths of electrolyte C and the total one of the mixed electrolyte, respectively. The activity coefficient of solute B (γ_B) in the ternary solution may be obtained from the following equations:

$$\ln \gamma_B = \ln \Gamma_B + \ln R_B + \int_0^{M_B\phi_B} f(m, M_B, x)\, d(M_B\phi_B) \quad (3)$$

and

$$f(m, M_B, x) = \left(\frac{\partial m}{\partial \ln x}\right) \Big/ m^2 + 1/m - 1/M_B, \quad (4)$$

where Γ_B is the activity coefficient of solute B in the binary solution in equilibrium with the ternary solution, R_B is the isopiestic ratio (M_B/m). Approximating R_B to[10]

$$R_B = 1 - a_B x - b_B x^2, \quad (5)$$

Eq. 3 reduces to

$$\ln \gamma_B = \ln \Gamma_B + \ln R_B + x^2 \int_0^{M_B\phi_B} \frac{b_B}{M_B} d(M_B\phi_B). \quad (6)$$

The activity coefficient of solute C can also be obtained from the same procedure.

Free Energy of Transfer ΔG^{tr} at Constant Mole Fraction (N). Using the activity coefficient of each solute in a ternary solution calculated by the above method, the free energy of transfer of one component from the binary to the ternary solution at constant mole fraction (N) can be obtained[11] as follows. In the case of solute C being transferred from water to a solution containing solute B, the free energy of transfer is defined as

$$\Delta G_C^{tr} = \nu_C RT \ln (f_C^*/f_C^0), \quad (7)$$

where f_C^* and f_C^0 are the activity coefficients of solute C in mole fraction scale in the ternary and the binary solutions, respectively. They are defined by

$$f_C^0 = \gamma_C^0(1+0.001 M_A \nu_C m_C^0), \quad (8)$$

$$f_C^* = \gamma_C(1+0.001(\nu_C m_C' + \nu_B m_B)), \quad (9)$$

and

$$m_C' = (1+0.001 M_A \nu_B m_B) m_C^0, \quad (10)$$

where m_C^0 and γ_C^0 are the molality and the molal activity coefficient of solute C in the binary solution, while m_C' and γ_C are the corresponding quantities in the ternary solution, having the same mole fraction (N_C) as the binary solution. M_A is the molecular weight of water. Free energy of transfer of solute B was also obtained from the same method.

Excess Free Energy Change on Mixing Solution at Constant Ionic Strength $\Delta_m G^{ex}$. $\Delta_m G^{ex}$ is defined by[12]

$$\Delta_m G^{ex}(x, I) = G^{ex}(x, I) - xG^{ex}(1, I) - (1-x)G^{ex}(0, I), \quad (11)$$

where $G^{ex}(1, I)$ and $G^{ex}(0, I)$ are the excess free energies of binary solutions of solute C and B, respectively. $G^{ex}(x, I)$ is the corresponding quantity in the ternary solution of which the total ionic strength equals I and the fraction of ionic strength is x. The excess free energy of pseudo-binary salt solutions is defined by

$$G^{ex}(x, I) = \nu RTI(\ln \gamma_\pm + (1-\phi)), \quad (12)$$

where $\gamma_\pm$ and ϕ are the mean activity coefficient and osmotic coefficient of the solute, respectively, R being the gas constant and T the absolute temperature. By applying the Gibbs-Duhem relation to Eq. 12, one obtains

$$G^{ex}(x, I) = -2\nu IRT \int_0^{\sqrt{I}} \frac{1-\phi}{\sqrt{I}} d\sqrt{I}. \quad (13)$$

The integration of Eq. 13 was carried out by computer program assuming Relation 14 between ϕ and I at the same fraction x.

$$\phi = 1 - \sum_{i=1}^{5} q_i I^{i/2} \quad (q_1 = 0.3902). \quad (14)$$

Theoretically, $\Delta_m G^{ex}(x, I)$ would be expressed as a power series of the ionic strengths of each component in the mixed solution and those coefficients of the power series are related to the magnitudes of various interactions of ions. Friedman's extention based on Mayer's ionic cluster expansion theory has been adopted which yields the following expression:

$$\Delta_m G^{ex}(x, I) = I^2 RTx(1-x)(g_0 + g_1(1-2x) + \cdots), \quad (15)$$

where g_i is the interaction parameter. The first two interaction parameters of Eq. 15 were determined graphically by plotting $\Delta_m G^{ex}(x, I)/I^2 RTx(1-x)$ against x.

Results

Isopiestic Solutions. The isopiestic and related data are shown in Table 1. The second column gives the molalities of the reference GuBr solutions (M_B) having the osmotic coefficients ϕ_B. The next two columns show the molalities of GuBr (m_B) and those of Bu_4NBr (m_C), respectively, in the ternary solutions being isopiestic with the reference solution. The fifth shows the ionic mole fraction of solute C (x), the sixth

Table 1. Isopiestic data

Set	M_B	m_B	m_C	x	R_B
1.	0.12221	0.12221	0.0	0.0	1.0
		0.10464	0.01867	0.15141	0.99106
		0.08355	0.04107	0.32955	0.98076
		0.06425	0.06152	0.48914	0.97170
		0.04203	0.08507	0.66930	0.96167
		0.02060	0.10772	0.83944	0.95239
		0.0	0.12949	1.0	0.94380
2.	0.26367	0.26367	0.0	0.0	1.0
		0.23063	0.04062	0.14976	0.98263
		0.19278	0.08249	0.29966	0.96550
		0.17921	0.09930	0.35654	0.95906
		0.11978	0.16115	0.57367	0.93484
		0.08428	0.20066	0.70423	0.92054
		0.04607	0.25108	0.84496	0.90535
		0.0	0.29738	1.0	0.88889
3.	0.31266	0.31266	0.0	0.0	1.0
		0.28110	0.03505	0.11087	0.98894
		0.23878	0.08203	0.25569	0.97459
		0.19178	0.13415	0.41160	0.95927
		0.16472	0.16414	0.49912	0.95074
		0.07706	0.26115	0.77214	0.92444
		0.05007	0.29099	0.85319	0.91673
		0.0	0.34629	1.0	0.90289
4.	0.39966	0.39966	0.0	0.0	1.0
		0.35325	0.05422	0.13307	0.98083
		0.30481	0.11040	0.26589	0.96254
		0.23660	0.18833	0.44321	0.94053
		0.17369	0.25978	0.59931	0.92200
		0.11716	0.32431	0.73461	0.90528
		0.07196	0.37236	0.83804	0.89947
		0.0	0.44790	1.0	0.89228

TABLE 1. (Continued)

Set	M_B	m_B	m_C	x	R_B	Set	M_B	m_B	m_C	x	R_B
5.	0.53096	0.53096	0.0	0.0	1.0	12.	1.67762	1.67762	0.0	0.0	1.0
		0.44768	0.10839	0.19492	0.95484			1.57633	0.25937	0.14129	0.91389
		0.37483	0.19676	0.34424	0.92892			1.44222	0.56080	0.27998	0.83755
		0.92851	0.29312	0.49545	0.89744			1.22701	0.99595	0.44803	0.75468
		0.22420	0.37511	0.62591	0.88595			0.94534	1.41250	0.59906	0.71151
		0.15374	0.45871	0.74898	0.86694			0.57339	1.73649	0.75177	0.72628
		0.06859	0.54761	0.88868	0.86166			0.23091	1.93762	0.89352	0.77362
		0.0	0.61004	1.0	0.87030			0.0	2.03654	1.0	0.82376
6.	0.53388	0.53388	0.0	0.0	1.0	13.	1.80300	1.80300	0.0	0.0	1.0
		0.47321	0.07729	0.14040	0.96982			1.70207	0.28006	0.14129	0.90963
		0.40394	0.16405	0.28883	0.93995			1.57316	0.61171	0.27998	0.82522
		0.33408	0.25099	0.42899	0.91250			1.35551	1.10026	0.44803	0.73419
		0.26119	0.33923	0.56499	0.88917			1.04272	1.55799	0.59906	0.69327
		0.17900	0.43384	0.70792	0.87116			0.63404	1.92017	0.75177	0.70589
		0.09331	0.52753	0.84971	0.85994			0.25284	2.12126	0.89352	0.75932
		0.0	0.62391	1.0	0.85571			0.0	2.21554	1.0	0.81380
7.	0.58144	0.58144	0.0	0.0	1.0	14.	1.87978	1.87978	0.0	0.0	1.0
		0.48203	0.08059	0.14324	0.96763			1.75358	0.33271	0.15947	0.90101
		0.43461	0.18851	0.30253	0.93312			1.63252	0.66385	0.28909	0.81859
		0.36542	0.27270	0.42735	0.91119			1.42272	1.16103	0.44936	0.72754
		0.27883	0.37751	0.57515	0.88588			1.12686	1.64062	0.59282	0.67923
		0.18736	0.48208	0.72012	0.86855			0.69197	2.07502	0.74992	0.67936
		0.08706	0.59004	0.87142	0.85872			0.25058	2.34963	0.90363	0.72293
		0.0	0.67562	1.0	0.86060			0.0	2.44853	1.0	0.76772
8.	0.71676	0.71676	0.0	0.0	1.0	15.	2.39195	2.39195	0.0	0.0	1.0
		0.64232	0.10545	0.14102	0.95854			2.27552	0.49227	0.17786	0.86420
		0.56157	0.21199	0.27404	0.92658			2.16287	1.16538	0.35018	0.71868
		0.46199	0.34391	0.42674	0.88940			2.07564	1.93970	0.48307	0.59570
		0.36959	0.46041	0.55471	0.86348			1.65860	2.39766	0.59110	0.58969
		0.26635	0.57942	0.68508	0.84746			1.11530	2.92231	0.72377	0.59242
		0.11646	0.57347	0.86362	0.83937			0.57681	3.21014	0.84768	0.63163
		0.0	0.84834	1.0	0.84490			0.0	3.33282	1.0	0.71770
9.	0.87984	0.87984	0.0	0.0	1.0	16.	2.41652	2.41652	0.0	0.0	1.0
		0.80209	0.10375	0.11453	0.97130			2.30000	0.49756	0.17785	0.86363
		0.71083	0.24181	0.25383	0.92358			2.18895	1.17943	0.35015	0.71728
		0.61126	0.37979	0.38322	0.88779			2.05673	1.92202	0.48307	0.60724
		0.51319	0.50646	0.49670	0.86288			1.68454	2.43516	0.59110	0.58647
		0.25506	0.77737	0.75295	0.85220			1.13067	2.96258	0.72377	0.59025
		0.14756	0.87550	0.85576	0.86000			0.58417	3.25110	0.84768	0.62996
		0.0	1.00303	1.0	0.87718			0.0	3.37008	1.0	0.71674
10.	0.86845	0.86845	0.0	0.0	1.0	17.	2.78046	2.78046	0.0	0.0	1.0
		0.78189	0.12837	0.14102	0.95407			2.74880	0.44417	0.13911	0.87081
		0.68938	0.26023	0.27404	0.91453			2.74060	1.06264	0.27940	0.73108
		0.57048	0.42467	0.42674	0.87268			2.67769	1.97325	0.42427	0.59783
		0.45760	0.57005	0.55471	0.84509			2.37537	2.91612	0.55110	0.52546
		0.32938	0.71653	0.68508	0.83033			1.56784	3.61773	0.69765	0.53619
		0.14289	0.90486	0.86362	0.82887			0.67519	3.88295	0.85187	0.61000
		0.0	1.03178	1.0	0.84170			0.0	3.78731	1.0	0.73415
11.	1.27620	1.27620	0.0	0.0	1.0	18.	2.91109	2.91109	0.0	0.0	1.0
		1.13238	0.25725	0.18512	0.91838			2.88161	0.46563	0.13911	0.86970
		0.98478	0.52191	0.44639	0.84702			2.90398	1.12599	0.27940	0.72236
		0.80164	0.79482	0.49786	0.79940			2.88040	2.12264	0.42427	0.58187
		0.61840	1.02140	0.62288	0.77828			2.55490	3.13652	0.55110	0.51149
		0.44449	1.20608	0.73071	0.77319			1.67344	3.86139	0.69765	0.52596
		0.24695	1.37809	0.84804	0.78534			0.72096	4.14620	0.85187	0.59811
		0.0	1.55424	1.0	0.82111			0.0	3.98861	1.0	0.72985

TABLE 2. OSMOTIC COEFFICIENTS OF PSEUDO-BINARY SALT WITH VARIOUS IONIC MOLE FRACTION x

m	x=0.1	x=0.2	x=0.3	x=0.4	x=0.5	x=0.6	x=0.7	x=0.8	x=0.9
0.1	0.9064	0.9022	0.8980	0.8941	0.8901	0.8860	0.8819	0.8779	0.8738
0.2	0.8783	0.8713	0.8644	0.8576	0.8511	0.8446	0.8383	0.8321	0.8261
0.3	0.8588	0.8494	0.8402	0.8312	0.8228	0.8147	0.8071	0.7998	0.7933
0.4	0.8434	0.8317	0.8204	0.8095	0.7997	0.7904	0.7822	0.7746	0.7683
0.5	0.8302	0.8163	0.8031	0.7907	0.7796	0.7696	0.7611	0.7538	0.4784
0.6	0.8186	0.8024	0.7874	0.7736	0.7616	0.7511	0.7425	0.7359	0.7319
0.7	0.8080	0.7897	0.7729	0.7579	0.7450	0.7342	0.7259	0.7203	0.7179
0.8	0.7983	0.7779	0.7593	0.7432	0.7295	0.7186	0.7109	0.7062	0.7057
0.9	0.7891	0.7665	0.7464	0.7992	0.7149	0.7039	0.6964	0.6934	0.6948
1.0	0.7804	0.7559	0.7342	0.7160	0.7011	0.6901	0.6830	0.6816	0.6849
1.2	0.7640	0.7358	0.7112	0.6911	0.6751	0.6643	0.6583	0.6599	0.6670
1.4	0.7487	0.7173	0.6900	0.6681	0.6511	0.6405	0.6356	0.6402	0.6505
1.6	0.7341	0.7001	0.6703	0.6467	0.6287	0.6183	0.6144	0.6216	0.6346
1.8	0.7201	0.6839	0.6521	0.6267	0.6077	0.5975	0.5945	0.6039	0.6187
2.0	0.7068	0.6687	0.6351	0.6079	0.5882	0.5780	0.5757	0.5867	0.6027
2.5	0.6765	0.6345	0.5975	0.5662	0.5447	0.5341	0.5328	0.5455	0.5615
3.0	0.6524	0.6044	0.5652	0.5307	0.5081	0.4966	0.4954	0.5067	0.5207
3.5	0.6380	0.5770	0.5357	0.4999	0.4773	0.4646	0.4630	0.4715	0.4849
4.0	0.6377	0.5508	0.5060	0.4719	0.4505	0.4371	0.4353	0.4416	0.4606

the isopiestic ratio (R_B).

Activity Coefficients. The activity coefficients of guanidinium bromide (γ_B) and tetrabutylammonium bromide (γ_C) for various ionic mole fractions obtained from Mckay and Perring's method are shown in Figs. 1 and 2, respectively. Each activity coefficient decreased as the total molality increased. In the system of the common ion mixing, the log γ curves for each electrolyte in aqueous ternary solutions with constant ionic mole fraction plotted against the total molality are usually located between those curves for the two binary systems. Put another way, the higher log γ values of the two electrolytes decreases on moving from the binary system to the ternary one, and *vice versa*. As shown in Fig. 1, the log γ values of guanidinium bromide in the H_2O–GuBr–Bu_4NBr system obeyed this rule in the concentration range studied, since the log γ values of GuBr

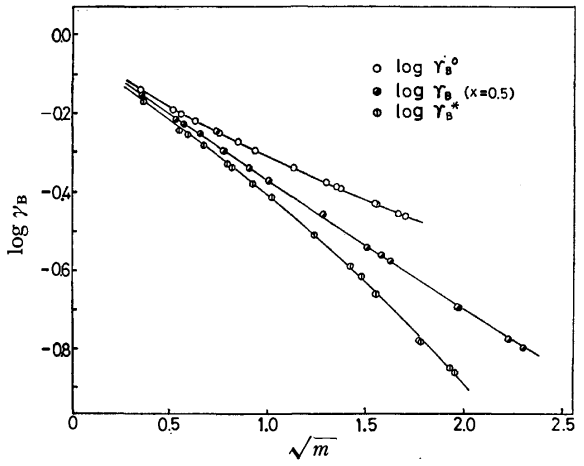

Fig. 1. Activity coefficient of GuBr (solute B) γ_B, plotted against $\sqrt{m}$. γ_B^0 is the activity coefficient in binary solution of solute B. γ_B^* is the activity coefficient of solute B in the solution containing only solute C (trace activity coefficient of B).

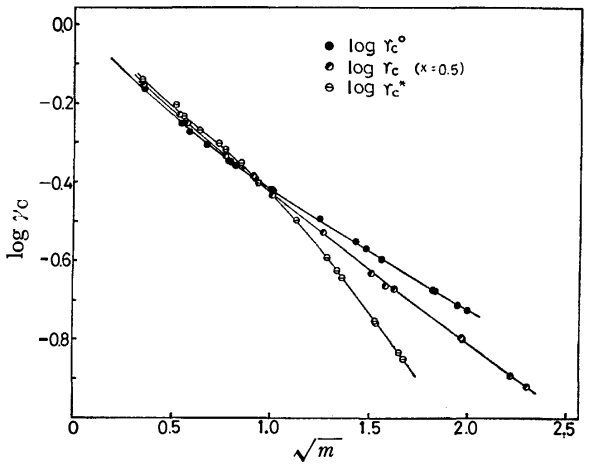

Fig. 2. Activity coefficient of Bu_4NBr (solute C) γ_C, plotted against $\sqrt{m}$. γ_C^0 is the activity coefficient in binary solution of solute C. γ_C^* is the activity coefficient of solute C in the solution containing only solute B (trace activity coefficient of C).

(log γ_B^0) were higher than those of Bu_4NBr (log γ_C^0) in each binary solution at the same molalities. As seen in Fig. 2, the activity coefficients of Bu_4NBr (log γ_C) in this ternary system were higher than those in the binary solution (log γ_C^0) below 1 molal, while the log γ_C values were lower than log γ_C^0 above 1 molal. Therefore the two curves cross each other around 1 molal. In order to express more clearly the influence of one electrolyte on the activity coefficient of the other in the ternary system, extended Harned's equation have been proposed as follows:[13,14]

$$\log \gamma_B = \log \gamma_B^0 - \alpha_B m_C - \beta_B m_C^2 = \log \gamma_B^0 - \alpha_B mx - \beta_B m^2 x^2 \quad (16)$$

and

$$\log \gamma_C = \log \gamma_C^0 - \alpha_C m_B - \beta_C m_B^2 = \log \gamma_C^0 - \alpha_C m(1-x) - \beta_C m^2(1-x)^2, \quad (17)$$

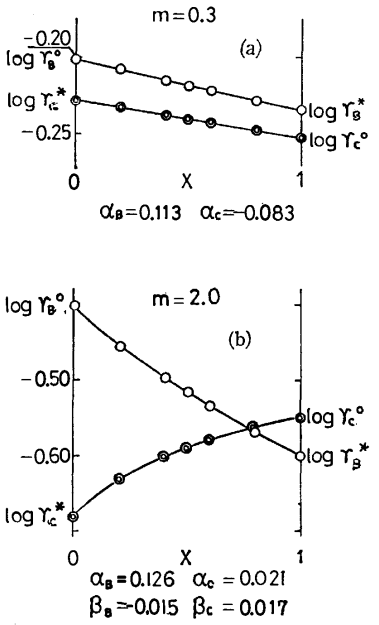

Fig. 3. (a) The variation of two activity coefficients against x at the total molality of 0.3. (b) The variation of two activity coefficients against x at the total molality of 2.0.

where α and β are the empirical constants which represent the type and magnitude of interionic interactions. In Figs. 3-a and 3-b, the relation between the activity coefficient of each salt and the mole fraction of Bu_4NBr (x) are shown at total molality $0.3m$ and $2.0m$, respectively. In Fig. 3-a, log γ_B decreases almost linearly with the increase of x, log γ_C increases from log γ_C^0 to log γ_C^* (trace activity coefficient of Bu_4NBr) linearly as x decreases from 1 to 0. The values of α_B and α_C were 0.113 and -0.083, respectively, and the values of β were nearly zero. As seen in Fig. 3-b, however, an abnormal change appeared when the total molality was at $2.0m$. The values of log γ_B decreased with the increase of value of x, while log γ_C decreased with the decrease of x. Therefore, the two curves were non-linear and the values of α_B and α_C were 0.126 and 0.021, respectively, while β_B and β_C were -0.015 and 0.017, respectively. Curves of this type which cross have so far been rarely reported in aqueous ternary solutions containing two kinds of inorganic electrolytes.

Free Energy of Transfer ΔG^{tr}. It is difficult to distinguish whether the change of the activity coefficient are based on salting-out, salting-in or "mutual" effect by plotting the activity coefficients at constant x against total molality. In the case of ΔG^{tr}, it is distinguishable because the free energy of transfer can be calculated from Eqs. 7—10, converting the activity coefficients to those in the mole fraction scale. They are shown in Tables 3-a and 3-b. Negative values of ΔG^{tr} were obtained for each electrolyte and the absolute value of ΔG^{tr} for each electrolyte increased with the molality of the other.

Excess Free Energy Change of Mixing $\Delta_m G^{ex}$. The osmotic coefficients of pseudo-binary salts (ϕ) for various ionic mole fraction x are shown in Table 2. These

Table 3-a. Free energy of transfer of tetrabutylammonium bromide from water to guanidinium bromide solution at constant mole fraction N_C

m_C	N_C	m_B 0.5	1.0	2.0	3.0
0.0	0.0000	−776	−1116	−1994	−2304
0.5	0.0089	−278	−475	−932	−1357
1.0	0.0174	−181	−386	−768	−1090

Table 3-b. Free energy of transfer of guanidinium bromide from water to tetrabutylammonium bromide solution at constant mole fraction N_B

m_B	N_B	m_C 0.5	1.0	2.0	3.0
0.0	0.0000	−790	−1076	−1530	−1924
0.5	0.0089	−200	−548	−956	−1302
1.0	0.0174	−141	−508	−871	−1168

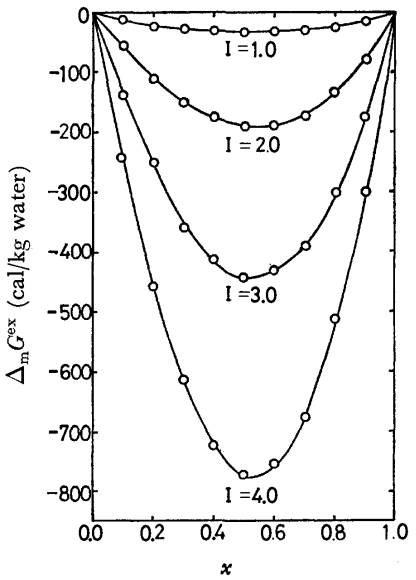

Fig. 4. Excess free energy change of mixing $\Delta_m G^{ex}$ against x at the constant total ionic strength I.

Table 4. Interaction parameters, g_0 and g_1

I	g_0(mol^{-1})	g_1 (mol^{-1})
0.5	−0.1362	0.0148
1.0	−0.2382	0.0298
1.5	−0.2965	0.0530
2.0	−0.3228	0.0581
2.5	−0.3298	0.0539
3.0	−0.3273	0.0466
3.5	−0.3221	0.0386
4.0	−0.3219	0.0386

values were read from the ϕ-I curves obtained by a least squares fit to Eq. 14. $\Delta_m G^{ex}$ at constant ionic strength was obtained from Eqs. 13 and 11 as shown in Fig. 4. The curves are nearly parabolic but the minimum point is slightly displaced towards the right from the

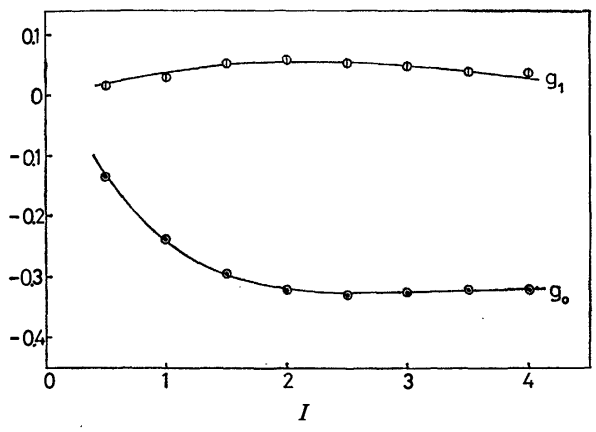

Fig. 5. Interaction parameters g_0 and g_1 plotted against I.

vertical line of $x=0.5$. The value of $\Delta_m G^{ex}$ at the minimum decreases as the total ionic strength increases. The interaction parameters g_0 and g_1 obtained from Eq. 15 are shown in Fig. 5 and Table 4. The negative values of g_1 slightly increased up to about $I=2.0$ and decreased with the increase of I.

Discussion

In most aqueous ternary systems containing two kinds of inorganic electrolytes with a common anion, the relation between log γ and the concentration of each electrolyte obeys "Harned's rule" for a wide range of concentration.[14] This means that the values the interaction parameter for a mixed cation pair corresponds almost to the arithmetic mean value of those for like cation pairs.[15] As shown in Fig. 3-a, the system of H_2O–GuBr–Bu_4NBr showed a similar behavior at low concentration to the aqueous ternary systems with two kinds of inorganic electrolytes, although the slopes of the log γ *vs.* x curves were considerably larger. However, as seen in Fig. 3-b, when the total molality increased, the log γ *vs.* x curves were quite different from those of Fig. 3-a. This implies that Harned's rule does not hold at high concentration, that is, the attractive interaction between Bu_4N^+ and Gu^+ increases and dominates the other pair interactions. This salting-in effect is expressed in terms of the free energy of transfer ΔG^{tr} similar to that of the H_2O–urea–Bu_4NBr system. The values of ΔG^{tr} for Bu_4NBr in the H_2O–GuBr–Bu_4NBr system are almost twice as large as those in the H_2O–urea–Bu_4NBr system.[5] This result is closely related to the effective concentration of these solutes in the denaturation of proteins in aqueous solutions. As seen in Fig. 4, the values of $\Delta_m G^{ex}$ are all negative and depend parabolically on x at all ionic strengths, suggesting that the g_0 terms are more important than the g_1 terms in the concentration region studied.[7] However the skewness of the curves at high ionic strength shows that the g_1 terms cannot be ignored. As shown in Fig. 5 and Table 4, the positive g_1 values increased as the concentration increased up to around 2.0*m* and decreased above this concentration. However the magnitudes of g_0 are 6 or 10 times larger than those of g_1. In the symmetrical mixture of electrolyte, g_0 and g_1 are expressed as[16]

$$g_0 = (g^{B^+C^+} - g^{B^+B^+} - g^{C^+C^+}) + I(g^{B^+C^+Br^-} - g^{B^+B^+Br^-} - g^{C^+C^+Br^-}) + \text{triplet type of same cations} \quad (18)$$

and

$$g_1 = I(g^{B^+C^+C^+} - g^{B^+B^+C^+} + g^{B^+B^+B^+} - g^{C^+C^+C^+}), \quad (19)$$

where B^+ and C^+ are Gu^+ and Bu_4N^+, respectively, and g^{ij} is the interaction parameter of free energy of ions i and j, g^{ijk} is the same quantity of three ions i, j, and k. Though it will be of great interest to find the values of g^{ij} and g^{ijk}, it is quite impossible using this experimental approach. The g_0 coefficients listed in Table 4 are related to the coefficient of Harned's equation[12] as

$$g_0 = -2.303((\alpha_B+\alpha_C) + I(\beta_B+\beta_C)) + \cdots. \quad (20)$$

The pairwise interaction parameter in Eq. 18, $(g^{B^+C^+} - g^{B^+B^+} - g^{C^+C^+})$ corresponds to $-2.303\ (\alpha_B+\alpha_C)$. The values of this ion pair term at 0.3*m* and 2.0*m* are -0.069 and -0.339, respectively. The sign and magnitude of the values at 2.0*m* are almost the same as those of g_0 in Table 4 suggesting that the pairwise interaction is quite important at this concentration. The negative sign of the pairwise interaction term implies that the mixed cation pair Gu^+–Bu_4N^+ is more favored over the like ion pairs Gu^+–Gu^+ and Bu_4N^+–Bu_4N^+. In a previous paper,[17] it was reported that guanidinium bromide formed a crystalline complex with tetrabutylammonium bromide at high concentrations in aqueous solutions. From this fact and the large negative values of the pairwise interaction term in Eq. 18 at moderate concentrations, it seems plausible that the formation of mixed cation pair, Gu^+–Bu_4N^+ makes an important contribution to the mutual salting-in. However, Friedman's treatment is not sufficiently rigorous in which water is regarded as a continuum solvent with the dielectric constant of 80. Therefore the interionic interaction through the change of water structure caused by the addition of ions has to be considered. This effect may work as an attractive or repulsive force between ions. Previously,[9] the guanidinium ion was reported to be a structure breaker ion, while Bu_4N^+ was regarded as a hydrophobic structure maker which formed the clathrate hydrate in aqueous solution. As pointed out in a previous paper,[8] the interaction between Gu^+ and Bu_4N^+ decreases the water structure around Bu_4N^+. This effect also makes a negative contribution to g_0 values even if these two kinds of cations do not form a mixed ion pair.

It is interesting to compare $\Delta_m G^{ex}$ and ΔG^{tr} of this system and those of the H_2O–KBr–Pr_4NBr[7] and H_2O–urea–Bu_4NBr[5] systems. In the H_2O–KBr–Pr_4NBr system, $\Delta_m G^{ex}$ *vs.* x curves are usually parabolic as in the case of this system, but the sign of $\Delta_m G^{ex}$ is opposite. Wen[6] and Wood[18] concluded from the measurements of free energy and heats of mixing that Pr_4N^+–Pr_4N^+ was favored over the mixed ion pair in that system. Both the potassium[20] and guanidinium ions are classified as structure breakers but the mechanism of the breaking of the water structure should be quite different from each other,[7,8] since the effects of those ions toward hydrophobic hydration are quite different. On the other hand, ΔG^{tr} of Bu_4NBr from water to the aqueous solutions of urea and GuBr are both negative and the magnitudes of ΔG^{tr} are comparable to each other.

These results suggest that the shape, size, and functional groups play important roles in the effect of organic solutions on hydrophobic hydration at high concentration. The next stage, in progress now, is to measure the heat of mixing of these salts in aqueous solution.

References

1) D. R. Robinson and W. P. Jencks, *J. Am. Chem. Soc.*, **87**, 2462, 2470 (1965).
2) W. Kauzmann, *Adv. Protein Chem.*, **14**, 1 (1959).
3) C. Tanford, *Adv. Protein Chem.*, **23**, 121 (1968).
4) D. B. Wetlaufer, S. K. Malik, L. Stoller, and R. L. Coffin, *J. Am. Chem. Soc.*, **86**, 508 (1966).
5) W-Y. Wen and C. L. Chen, *J. Phys. Chem.*, **73**, 2895 (1969).
6) T. S. Salma and J. C. Ahluwalia, *J. Phys. Chem.*, **76**, 1366 (1972): R. B. Cassel and W-Y. Wen, *ibid.*, **76**, 1370 (1972).
7) W-Y. Wen, K. Miyajima, and A. Otsuka, *J. Phys. Chem.*, **75**, 2148 (1971).
8) K. Miyajima, H. Yoshida, and M. Nakagaki, *Bull. Chem Soc. Jpn.*, **51**, 2508 (1978).
9) K. Miyajima, K. Inari, S. Hamaguchi, H. Yoshida, and M. Nakagaki, *Nippon Kagaku Kaishi*, **1976**, 366.
10) H. A. C. Mckay and J. K. Perring, *Trans. Faraday Soc.*, **49**, 163 (1953); R. A. Robinson, *J. Am. Chem. Soc.*, **65**, 662 (1961).
11) H. Uedaira, *Bull. Chem. Soc. Jpn.*, **48**, 2006 (1975).
12) H. L. Friedman, *J. Chem. Phys.*, **32**, 1351 (1960); H. L. Friedman, "Ionic Solution Theory," Interscience Pub. New York, London (1962), Vol. 3.
13) R. A. Robinson and R. H. Stokes, "Electrolyte Solutions," 2nd ed, Butterworth London (1970).
14) H. S. Harned and B. B. Owen, "Physical Chemistry of Electrolytic Solutions," 3rd ed, Reinhold (1958).
15) E. A. Guggenheim, *Trans. Faraday Soc.*, **62**, 3446 (1966).
16) R. H. Wood and H. L. Anderson, *J. Phys. Chem.*, **70**, 992 (1966).
17) K. Miyajima, H. Yoshida, and M. Nakagaki, *Bull. Chem. Soc. Jpn.* **50**, 2854 (1977).
18) R. H. Wood and H. L. Anderson, *J. Phys. Chem.*, **71**, 1871, (1967).
19) K. Miyajima, K. Inari, and M. Nakagaki, *Nippon Kagaku Kaishi*, **1974**, 2031.
20) E. R. Nitingale, Jr., "Chemical Physics of Ionic Solutions," ed by B. E. Conway and R. G. Barradas, John Wiley & Sons Inc., New York (1966).

Multiple Transmission Method of Time Domain Spectroscopy

Hiroshi SATO,* Koichi ITOH, and Hiroaki TAKAHASHI

Department of Chemistry, School of Science and Engineering, Waseda University, Shinjuku, Tokyo 160

(Received March 27, 1978)

A new multiple transmission method of time domain spectroscopy was developed. A small amount of the sample (0.6 cm^3) is needed in this measurement. The dielectric dispersion and absorption curves of 1-propanol, 1-butanol, and 1-pentanol have been obtained as recorder traces of the spectra stored in the minicomputer. Three dielectric parameters, ε_∞, ε_0, and τ, are estimated for these alcohols.

Time domain spectroscopy (the TDS method), which was initially proposed by Fellner-Feldegg in 1969,[1] has a great advantage over the usual frequency domain method; it can considerably reduce the time needed in obtaining continuous spectra of the dielectric constant and loss. Recently several other groups have developed various ways of measurement and analysis for the TDS method, *viz.*, the thin sample method[2,3] and the methods of lumped capacitance,[4-6] multiple reflection,[7,8] and multiple transmission.[9]

In this report, we shall describe a new measurement system for the multiple transmission method, which requires only a small amount of the sample (0.6 cm^3). The results of the measurements, using this system, of the dielectric dispersion and absorption were found to be in fair agreement with those of the preceding works.

Experimental

Principle. When an annular disk of the dielectric sample is inserted in the coaxial lines, the characteristic impedance of the line changes at Point A (Fig. 1). After having been propagated through the coaxial lines, the electromagnetic waves reach the sample, where these waves are partially reflected and partially transmitted. Suppose that the input voltage is represented by a function of the time $v(t)$, and the transmitted voltage from the disk by $r(t)$. The total transmission coefficient $S(\omega)$ at a given angular frequency, ω, will be expressed in terms of Fourier transforms of $v(t)$ and $r(t)$ as follows:

$$S(\omega) = \frac{\int_0^\infty r(t) \exp(-j\omega t)\,dt}{\int_0^\infty v(t) \exp(-j\omega t)\,dt}. \quad (1)$$

On the other hand, $S(\omega)$ is related to the dielectric constant of the sample, $\varepsilon(\omega)$, by the following formula:[10]

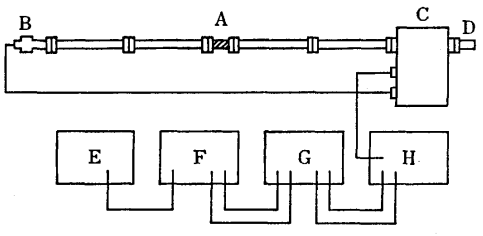

Fig. 1. Block diagram of the measurement system.
A: Sample cell, B: pulse generator, C: sampler, D: 50Ω termination, E: recorder, F: minicomputer, G: interface, H: sampling oscilloscope.

$$S(\omega) = \frac{(1-\rho^2(\omega)) \exp(-(\omega l/c) j\sqrt{\varepsilon(\omega)})}{1-\rho^2(\omega) \exp(-(2\omega l/c) j\sqrt{\varepsilon(\omega)})}, \quad (2)$$

where $\rho(\omega)$ is the reflection coefficient of the air-dielectric interface and is given by $(1-\sqrt{\varepsilon(\omega)})/(1+\sqrt{\varepsilon(\omega)})$, and where l is the thickness of the sample, and c, the velocity of light.

Apparatus. The main instruments for measurements and analyses are: (a) the Hewlett-Packard 180 TDR system with a 28 ps pulse generator, (b) GR 900-L30 precision air lines, and (c) the Melcom 70 minicomputer. The sampling oscilloscope in the system was modified in such a way as the time base could be swept externally. The measurement system used in the present work is shown schematically in Fig. 1.

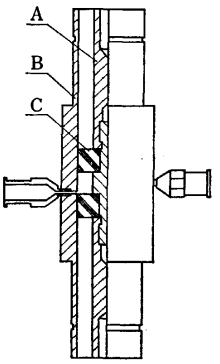

Fig. 2. Cross section of a dielectric specimen-holder.
A: Inner conductor (outer diam. 0.6204 cm), B: outer conductor (inner diam. 1.4288 cm), C: Teflon window (outer diam. 1.43 cm, inner diam. 0.43 cm, thickness 0.50 cm).

Details of Part A in Fig. 1 are shown in Fig. 2. The inner and outer conductors are the precision inner conductor rod (GR 900-9508) and the outer conductor tube (GR 900-9509), respectively. The thickness of the sample cell is 5.00 mm, and its volume is about 0.6 cm^3. The inner conductor is undercut to minimize the reflection at the surface of the Teflon. The cell is connected with the measurement system by means of two GR 900 BT precision connectors.

Measurements and Analyses. The two wave forms, $v(t)$ and $r(t)$, recorded by the oscilloscope are sampled at equal intervals along the time axis, and stored in the core memory of the minicomputer. The two signals relating to $v(t)$ and $r(t)$ are obtained when the cell is empty and when it is filled with the sample, respectively. The number of sampling points is about 1024, and the sampling interval, about 5 ps.

In order to analyze the data, the transmitted signal, $r(t)$, should have the same time origin as the input signal, $v(t)$. A set of five data-points is chosen for this reason from the steepest part of the transient, either $v(t)$ or $r(t)$, and a least-

squares approximation is applied to fit the set of data to a straight line. The point at which this straight line intersects the voltage base-line is assumed to be the time reference point.

The Fourier transforms of $v(t)$ and $r(t)$ were obtained by the Samulon method.[11] The results of calculation, however, sometimes become unsatisfactory when the iteration procedure is employed in solving a complicated function such as Eq. 2. In such a case, different damping factors were used for the real and imaginary part — for example, 1.0 for the real part and 0.3 for the imaginary part; then consistent and converged values were obtained for all calculations.

To determine the limiting high- and low-frequency dielectric constants ε_∞, ε_0, and the relaxation time τ, the Debye equation,

$$\varepsilon(\omega) = \varepsilon_\infty + \frac{\varepsilon_0 - \varepsilon_\infty}{1 + j\omega\tau} \tag{3}$$

was fitted to the data by the least-squares method.

All the calculations were carried out by using a Melcom 70 minicomputer and programs written in an assembler language.

Results and Discussion

Figure 3 shows an example of the input and transmitted signals observed for 1-propanol at room temperature. Each signal was an average of thirty-two scans. This average procedure reduced the jitter noise generated by the measurement system.

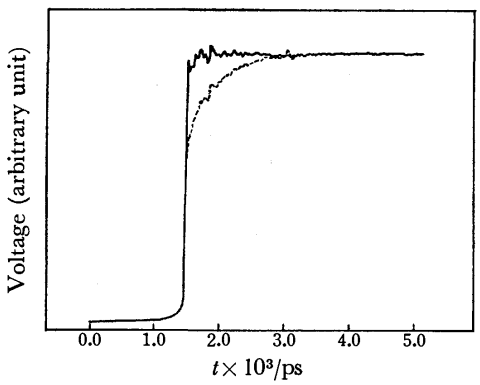

Fig. 3. Changes of the input (——) and transmitted voltages (– – –) with time, t.

From Fig. 3, the dielectric dispersion and absorption spectra are obtained (see the upper curves in Fig. 4). All the curves shown in Fig. 4 are direct recorder traces of the spectra stored in a minicomputer.

It has been reported that aliphatic normal alcohols show the second and third dielectric dispersions in the high frequency region.[12] The single Debye equation, however, was fitted to our data in the 0.1—2.5 GHz frequency region to obtain the limiting high- and low-frequency dielectric constants, ε_∞, ε_0, and the relaxation time, τ, because our measurement values were not so accurate as to give many parameters in the Budo equation.[13] The ε_∞, ε_0, and τ values for 1-propanol obtained are summarized in Table 1, together with the literature values. The dielectric measurements were also carried out on 1-butanol and 1-pentanol. The ε_∞, ε_0, and τ values obtained for these alcohols are recorded in Table 2.

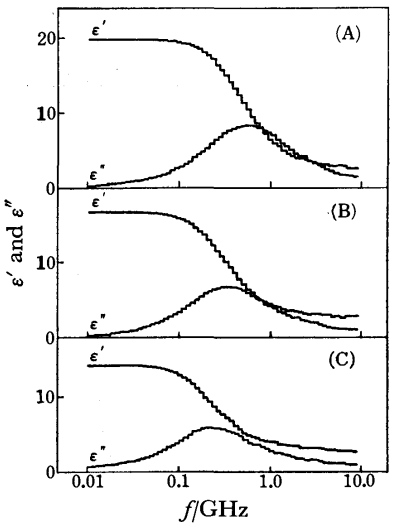

Fig. 4. Recorder traces of dielectric dispersion, ε' and absorption, ε'' spectra *vs.* frequency, f.
(A) 1-Propanol, (B) 1-butanol, (C) 1-pentanol.

TABLE 1. THE LIMITING HIGH- AND LOW-FREQUENCY DIELECTRIC CONSTANTS, ε_∞ AND ε_0, AND RELAXATION TIME, τ, FOR 1-PROPANOL

	This work	Literature
ε_0	20.3	20.6,[a,b,c,e] 20.5[d]
ε_∞	2.9	4.3,[a] 3.9,[f] 3.7,[c] 3.6,[d] 3.4,[e] 3.0[b]
τ/ps	317	360,[d] 340,[f] 332,[c] 330,[b] 325[a]

a) M. J. C. Gemert, Ref. 10. b) A. Suggett *et al.*, *Nature*, **228**, 456 (1970). c) T. S. Clarkson *et al.*, Ref. 8. d) H. Fellner-Feldegg, Ref. 2. e) S. S. Stuchly *et al.*, Ref. 5. f) T. Koshii *et al.*, *Bull. Chem. Soc. Jpn.*, **47**, 618 (1974).

TABLE 2. THE LIMITING HIGH- AND LOW-FREQUENCY DIELECTRIC CONSTANTS, ε_∞ AND ε_0, AND RELAXATION TIME, τ

	Substance	
	1-Butanol	1-Pentanol
ε_0	17.4	14.9
ε_∞	3.0	3.2
τ/ps	429	665

The authors wish to express their sincere gratitude to Professor Keniti Higasi for his encouragement and discussions during this work.

References

1) H. Fellner-Feldegg, *J. Phys. Chem.*, **73**, 616 (1969).
2) H. Fellner-Feldegg, *J. Phys. Chem.*, **76**, 2116 (1972).
3) A. H. Clark, F. A. Quickenden, and A. Suggett, *Trans. Faraday Soc.*, **11**, 1847 (1974).
4) M. F. Iskander and S. S. Stuchly, *IEEE Trans. Instrum. Meas.*, IM-**21**, 425 (1972).

5) S. S. Stuchly, M. A. Rzepecka, and M. F. Iskander, *IEEE Trans. Instrum. Meas.*, IM-**23**, 56 (1974).
6) M. A. Rzepecka and S. S. Stuchly, *IEEE Trans. Instrum. Meas.*, IM-**24**, 27 (1975).
7) A. M. Nicolson and G. F. Loss, *IEEE Trans. Instrum. Meas.*, IM-**19**, 377 (1970).
8) T. S. Clarkson and G. Williams, *Chem. Phys. Lett.*, **34**, 461 (1975).
9) B. Gestblom and E. Noreland, *J. Phys. Chem.*, **81**, 782 (1977).
10) M. J. C. Gemert, *Philips Res. Repts.*, **28**, 530 (1973).
11) H. A. Samulon, *Proc. I.R.E.*, **37**, 10 (1949).
12) S. K. Garg and C. P. Smyth, *J. Phys. Chem.*, **69**, 1294 (1965).
13) A. Budo, *Phys. Z.*, **39**, 706 (1938).

Proton Diffusion in the Premelted State of 1-Hexadecanol

Norio MURASE,*,† Teruyuki FUJITA, Naotake MORIKAWA,** and Shozo KOGA

The Institute of Applied Microbiology, The University of Tokyo, Bunkyo-ku, Tokyo 113

***Radioisotope Centre, The University of Tokyo, Bunkyo-ku, Tokyo 113*

(Received March 27, 1978)

Proton diffusion in the α-phase of polycrystalline 1-hexadecanol was studied using $C_{16}H_{33}O^3H$ and $C_{15}H_{31}$-$^{14}CH_2OH$. It was found that hydroxyl proton diffuses translationally more easily than the whole molecule. A value of $(7\pm5)\times10^{-7}$ cm²/s was obtained for the diffusion coefficient of the hydroxyl proton in the α-phase. This fast diffusion is ascribed to the presence of molecular rotation involving hydrogen-bond networks in the α-phase of the crystal. Since the mechanism for the proton diffusion seems to be the same as that for the protonic conduction in this α-phase, proton mobility can be calculated from the diffusion coefficient, assuming that molecular rotation makes the rate determining step in both processes.

It has been shown in the literatures that proton conduction takes place in the premelted state (α-phase) of 1-hexadecanol (cetyl alcohol) through hydrogen bridges by way of the Grotthus mechanism.[1-3] Proton conduction is observed neither in the liquid state nor in the lower temperature solid phase of the alcohol. For the proton conduction to occur in solid, the presence of hydrogen-bond networks and their reorientation ability along the applied electric field are needed.[1,4-7] In the α-phase of 1-hexadecanol the molecules are known to be rotating around their hydrocarbon chains.[1,8] For further analysis of the mechanism of the proton conduction, it is necessary to know about the value of the proton mobility. There have been few data obtained about it so far on account of the small mobility and the occurence of electrode polarization, *etc.*[9-12] This study was made to obtain the diffusion coefficient of proton in the α-phase of 1-hexadecanol and also to calculate from it the value of the proton mobility.[13-16]

Experimental

1-Hexadecanol(guaranteed grade) used was obtained from Tokyo Kasei Co., Ltd. (Tokyo), and was used without further purification in this experiment. Two types of radioactive tracer were used in this experiment; tritiated 1-hexadecanol ($C_{16}H_{33}O^3H$), in which hydroxyl protons were tritium-labeled, and [1-^{14}C]-labled 1-hexadecanol ($C_{15}H_{31}$-$^{14}CH_2OH$).

Tritiated 1-hexadecanol was prepared by mixing 2 grams of melted 1-hexadecanol with 2 ml of tritiated water (100 mCi/ml) in an evacuated vessel (10^{-4} mmHg), followed by repeated annealing. The labeled alcohol was separated from the water and kept sealed in an evacuated flask until it was used for the experiment. The activity, obtained by this preparation, was about 3 μCi/mg and was ascertained before each experiment.

[1-^{14}C]1-Hexadecanol was obtained from the Radiochemical Centre(Amersham) as benzene solution whose radioactivity was 55.4 μCi/mg.

In order to distinguish the diffusion of the hydroxyl protons from that of the whole molecules, ^{14}C, ^3H-double labeled 1-hexadecanol was used. This double-labeled specimen was prepared in an evacuated vessel by mixing tritiated 1-hexadecanol with ^{14}C-labeled one in the liquid state and also sealed in the evacuated vessel. Its activity was 1.7 μCi/mg for ^3H and 2.4×10^{-1} μCi/mg for ^{14}C in the mixed state, respectively. During the measurement of diffusion coefficient, all handlings were carried out in a glove box where the atmosphere was replaced by nitrogen gas dried with P_2O_5. This is to prevent the tritium of 1-hexadecanol from being exchanged with protons of water molecules in the atmosphere followed by being re-exchanged with hydroxyl protons of other alcohol molecules at a distance.

A cyclinder-form cell made of polyethylene, the size of which was 1 cm in diameter and about 4 cm in height, was closed at one end and filled with melted 1-hexadecanol. The cell was put in an aluminium box and the temperature of the total system was controlled using thermister at 47 ± 0.5 °C where 1-hexadecanol takes α-phase. Two or three drops of melted double-labeled 1-hexadecanol were dropped on the flat surface of the alcohol kept in the α-phase using a warmed glass syringe. The whole cell was immediately covered with the lid of acrylic resins and separated completely from the surroundings. After keeping the sample in this state for 2 weeks, it was sectioned, weighed and assayed for radioactivity using a liquid scintillation counter. The composition of the scintillation solution used in this experiment was dioxane 1 dm³, naphthalene 100 g, 2,5-diphenyloxazole 1 g, *p*-bis(4-methyl-5-phenyl-2-oxazolyl)benzene 0.25 g.

Results and Discussion

The equation which described the tracer diffusion from an infinitely thin surface layer into a semi-infinitely thick solid is given by

$$C(x,t)=\frac{C_0}{\sqrt{\pi Dt}}\exp\left(-\frac{x^2}{4Dt}\right), \quad (1)$$

where $C(x,t)$ is the concentration of the tracer at a distance of x into the solid at time t, C_0 is the initial concentration of the tracer present and D is the diffusion coefficient. The diffusion coefficient can, therefore, be obtained from a plot of $\ln C$ *vs.* x^2. From the measurement of the ^3H-diffusion rate, it was found that $\ln C$-x^2 plots were almost linear except for their initial part where possible existence of micro-cracks through the thin specimens gave larger values. Carbon-14-labeled molecules did not diffuse at all during the same period of experiments. These results are shown in Fig. 1 and Table 1.

Since a cold sample used as a blank test in parallel run showed no radioactivity, the water vapor in the environment seemed to have been almost perfectly removed. The proton diffusion observed in this experi-

† Present address: Laboratory of Chemistry, Faculty of Science and Engineering, Tokyo Denki University, Hatoyama-mura, Hiki-gun, Saitama-ken 350-03.

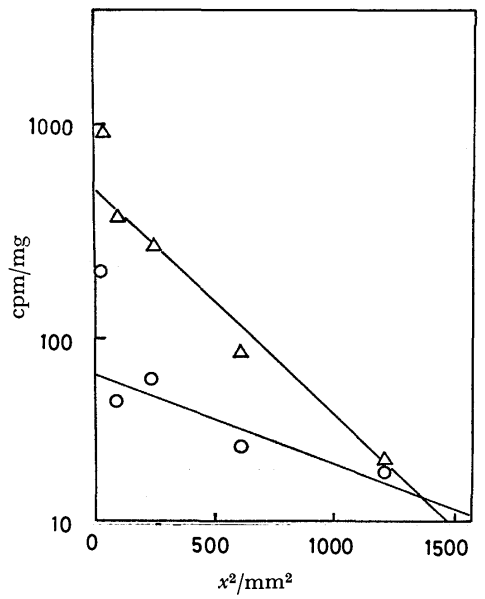

Fig. 1. Profile of the diffusion of ^{3}H in the α-phase of 1-hexadecanol.
○: After 14 days, △: after 12 days.

Table 1. Diffusion of ^{3}H, ^{14}C in the α-phase of 1-hexadecanol

Distance mm	^{3}H [a] cpm·mg^{-1}	^{14}C [a] cpm·mg^{-1}
5	198.3	<0.1
10	46.4	<0.1
15	60.1	<0.1
25	28.4	<0.1
35	20.8	<0.1

a) Initial activity was 1.7 μCi/mg for ^3H and 2.4×10^{-1} μCi/mg for ^{14}C, respectively.

ment is considered to have taken place through the bulk without involving proton exchanges with water vapor in the atmosphere. Moreover, tritium diffusion through the partially molten spots in the sample can be ignored, because the ^{14}C-labeled molecules had scarcely diffused despite the temperature was kept just below the melting point. It was concluded, therefore, that hydroxyl protons diffuse rather fast and independently of the whole molecule in the α-phase of the alcohol, presumably *via* the hydrogen-bond networks extending through the crystals.

The diffusion coefficient, D, was calculated in accordance with Eq. 1 as

$$D = (7\pm5)\times10^{-7}\ \mathrm{cm^2/s}. \quad (1)$$

Measurements of the diffusion coefficient for proton using radioisotope as a tracer have been reported with other crystals such as ice,[14,15] imidazole,[16] and pivalic acid.[13] In the plastic phase of pivalic acid, it was reported that the diffusion coefficient of carboxyl protons is about 10^{-7} cm^2/s at 25 °C, which is approximately 10^2 times faster than that of the whole molecules. The diffusion coefficient is related to the mobility of charge carrier by Einstein's equation

$$\mu kT = qD, \quad (2)$$

where μ is the mobility, k is the Boltzmann constant, and q is the charge of the ion. Using this equation, the proton mobility in the α-phase of 1-hexadecanol is calculated as follows from the value of the diffusion coefficient obtained in this experiment.

$$\mu = (3\pm2)\times10^{-5}\ \mathrm{cm^2\ V^{-1}\ s^{-1}}.$$

It seems that Eq. 2 can only be applied when the independent charged-particles diffuse through the material. Charge transfer is not necessarily involved in the present diffusion process because diffusion can also be effected by some non-ionic exchange mechanism. However, if the rate-determining step in both the electric conduction and the concentration diffusion through the hydrogen-bond networks is not in the proton transfer process, but in the process of molecular rotation or reorientation of the hydrogen-bonded portion,[5] then Eq. 2 can be used to evaluate the effective mobility for the electric conduction of 1-hexadecanol in the α-phase.

References

1) Y. Kakiuchi, H. Komatsu, and S. Kyoya, *J. Phys. Soc. Jpn.*, **6**, 321 (1951).
2) N. Murase, K. Gonda, I. Kagami, and S. Koga, *Chem. Lett.*, **1974**, 333.
3) J. M. Thomas, J. R. N. Evans and T. J. Lewis, *Discuss. Farad. Soc.*, **51**, 73 (1971).
4) D. D. Eley and D. I. Spivey, *Trans. Farad. Soc.*, **57**, 2280 (1961).
5) A. Kawada, A. R. McGhie, and M. M. Labes, *J. Chem. Phys.*, **52**, 3121 (1970).
6) L. Glasser, *Chem. Rev.*, **75**, 21 (1975).
7) N. Murase, K. Gonda, I. Kagami, and S. Koga, *Chem. Phys. Lipids*, **19**, 339 (1977).
8) W. O. Baker and C. P. Smyth, *J. Am. Chem. Soc.*, **60**, 1229 (1938).
9) M. Eigen, L. DeMaeyer, and M-Ch Spatz, *Ber. Bunsenges. Phys. Chem.*, **68**, 19 (1964).
10) B. Bullemer and N. Riehl, *Phys. Kondens. Materie*, **7**, 248 (1968).
11) J. S. Ham and D. N. Rose, *J. Chem. Phys.*, **60**, 4778 (1974).
12) M. A. Maldique, A. von Hippel, and W. B. Westphal, *J. Chem. Phys.*, **54**, 150 (1971).
13) G. M. Hood, N. C. Lockhardt, and J. N. Sherwood, *J. Chem. Soc., Faraday Trans. 1*, **68**, 736 (1972).
14) O. Dengel and N. Riehl, *Phys. Kondens. Materie*, **1**, 191 (1963).
15) L. Onsager and L. K. Runnels, *J. Chem. Phys.*, **50**, 1089 (1969).
16) A. R. McGhie, H. Blum, and M. M. Labes, *J. Chem. Phys.*, **52**, 6141 (1970).

The G-value of Nitrogen Atoms Produced in the γ-Radiolysis of Liquid Nitrogen and the Ozone Formation in the γ-Irradiated Liquid Nitrogen Solution of Oxygen

Akihiko MATSUMOTO, Rei YUGETA, Hidetoshi KARASAWA, and Shin SATO*

Department of Applied Physics, Tokyo Institute of Technology, Ookayama, Meguro-ku, Tokyo 152

(Received April 7, 1978)

The γ-radiolyses of liquid nitrogen solutions of nitrogen oxide and of oxygen gave nitrogen dioxide and ozone, respectively, as the main products. Over the solute concentrations from 0.01 to 0.1 mol l^{-1}, the G-values of both products were constants: $G(NO_2)=3.3$ and $G(O_3)\approx 7$. The G-value of nitrogen dioxide in the former solution probably corresponds to the G-value of nitrogen atoms from liquid nitrogen. For the formation of ozone in the latter solution, a possible reaction mechanism is discussed. Dinitrogen oxide was found as a minor product, the G-value being about 0.1 for both solutions.

The γ-radiolysis of liquid nitrogen containing a certain solute is one useful method for the investigation of the reactions of nitrogen atoms with the solute molecule or the radicals eventually produced from the solute in the solution, although this method is restricted by the solubility of the solute in liquid nitrogen. In previous papers,[1] we used several hydrocarbons as the solute and observed various nitrogen-containing compounds as the products; however, because of the complexity of the reactions occurring in the solution, we could not precisely determine the G-values of active species produced in the γ-irradiated liquid nitrogen.

In the study of active nitrogen in the gas phase, it is now well known that the titration using nitrogen oxide is one of the best methods for determining the concentration of nitrogen atoms.[2] We, therefore, attempted to study the γ-radiolysis of liquid nitrogen containing nitrogen oxide in the hope that the G-value of nitrogen atoms could be determined.

The formation of ozone in the γ-irradiated liquid nitrogen containing oxygen has long been known; however, the G-value of ozone did not seem to be measured. Since the technique used for the determination of the G-value of nitrogen dioxide can be applied for the estimation of ozone yield, the G-value of ozone from the liquid nitrogen solution of oxygen has also been measured.

Experimental

The dried high-purity nitrogen supplied by the Nihon Sanso Co. was used after having been passed through sulfuric acid. The research grade nitrogen oxide and oxygen were purchased from the Takachiho Shoji Co.

The procedures of preparation and of γ-irradiation at 77 K of the samples were the same as those previously reported.[1] The dose rate was 1.06×10^6 R h^{-1} and the irradiation time ranged from 20 min to 2 h. The absorbed dose was estimated by the Fricke dosimetry.

After the γ-irradiation, the inside of the sampling tube was slowly pumped out at 77 K. Usually two hours were taken for complete evacuation. When nitrogen oxide was used as the solute, the pumping was stopped at the pressure of 0.1 Torr, in order to prevent the pumping-out of nitrogen oxide. The products thus obtained were subjected to analysis.

In the case of the solution of nitrogen oxide, the observed products were nitrogen dioxide and a small amount of dinitrogen oxide. The amount of nitrogen dioxide was estimated by the optical density at 450 nm using a Hitachi Model 200-20 spectrophotometer. Since an excess amount of nitrogen oxide was present in the analyzing vessel, the following two equilibrium reactions had to be taken into account:

$$NO + NO_2 \rightleftarrows N_2O_3,$$

$$2NO_2 \rightleftarrows N_2O_4.$$

The equilibrium constants were taken from the literature.[3,4]

The analysis of dinitrogen oxide was made by a gaschromatograph equipped with a 5 m dimethyl sulfolane column of 20% w/w on celite. Before introducing the products into the gaschromatograph, nitrogen dioxide was separated by the distillation at -120 °C.

When oxygen was used as the solute, the formation of nitrogen dioxide could not be observed. The observed products were ozone and a small amount of dinitrogen oxide. Since ozone is easily decomposed at room temperature, the following procedure was used for the measurement. After the evacuation of the γ-irradiated solution at 77 K, a known amount of nitrogen oxide was introduced into the sampling tube. Then the liquid nitrogen Dewar flask was removed, so that all molecules of ozone should have been converted into nitrogen dioxide according to the stoichiometric reaction:

$$O_3 + 3NO = 3NO_2.$$

Then the amount of nitrogen dioxide was measured as stated above.

Results

Figure 1 shows the G-value of nitrogen dioxide as a function of the amount of nitrogen oxide introduced

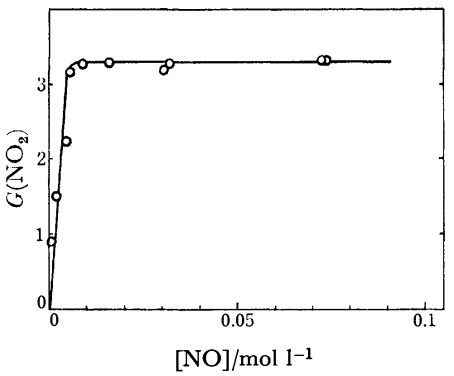

Fig. 1. The G-value of nitrogen dioxide as a function of the concentration of nitrogen oxide.

Table 1. The measurement of dinitrogen oxide

	Liquid N_2/cm³	Solute/ 10^{-3} M	Irradiation time/min	$G(N_2O)$
Nitrogen oxide	30	6.6	60	0.10
	30	6.2	30	0.13
Oxygen	10	6.7	20	0.09
	20	11.4	20	0.08
	10	33.0	30	0.10

in liquid nitrogen. Below 0.01 mol l^{-1}, the yield of nitrogen dioxide was about equal to a half of the amount of nitrogen oxide introduced. At the concentrations higher than 0.01 mol l^{-1}, the following G-values were obtained: $G(NO_2)=3.3$ and $G(N_2O)=0.1$. Table 1 summarizes the results of the measurement of dinitrogen oxide.

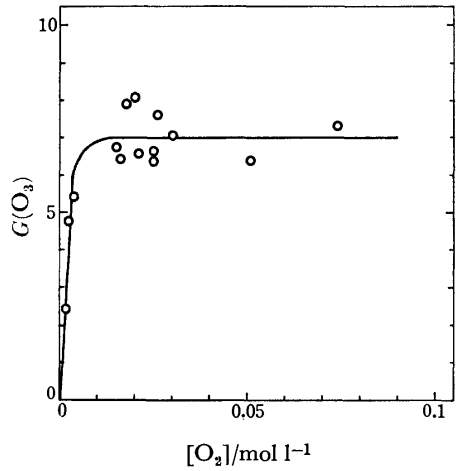

Fig. 2. The G-value of ozone as a function of the concentration of oxygen.

Figure 2 shows the G-value of ozone as a function of the amount of oxygen introduced in liquid nitrogen. Although the data are a little scattered, the following G-values were obtained at the concentrations higher than 0.01 mol l^{-1} of oxygen: $G(O_3)=7.0\pm0.5$ and $G(N_2O)=0.1$.

Discussion

The formation of nitrogen dioxide in the γ-irradiated liquid nitrogen containing nitrogen oxide can be simply explained by the following reactions:

$$N + NO \longrightarrow N_2 + O, \quad (1)$$

$$O + NO \longrightarrow NO_2. \quad (2)$$

This reaction mechanism is consistent with the fact that at the concentrations lower than 0.01 mol l^{-1}, the yield of nitrogen dioxide is equal to a half of the amount of nitrogen oxide introduced in liquid nitrogen. If the above mechanism is the only process for the formation of nitrogen dioxide, the value of 3.3 is the G-value of nitrogen atoms from liquid nitrogen.

Since the ionization potential of nitrogen oxide is lower than that of nitrogen, a charge transfer from nitrogen molecule ion to nitrogen oxide is possible; the neutralization reaction of the nitrogen oxide ion thus produced may form nitrogen and oxygen atoms. These atoms will produce nitrogen dioxide through Reactions 1 and 2. However, if the neutralization of nitrogen molecule ions and the charge transfer from nitrogen molecule ion to nitrogen oxide are in competition, a very high concentration of the positive ion interceptor, nitrogen oxide in the present case, must be necessary to suppress the neutralization completely.[5] According to Fig. 1, only 0.01 mol l^{-1} is enough to saturate the G-value of nitrogen dioxide. This is incompatible with the formation of nitrogen dioxide through the charge transfer from nitrogen molecule ion to nitrogen oxide.

Another possible mechanism is the energy transfer reaction from excited nitrogen molecules to nitrogen oxide. However, this reaction is believed not to occur even in the gas phase reaction of active nitrogen at room temperature.[2]

Consequently it may be concluded that the G-value of nitrogen atoms from liquid nitrogen is 3.3.

In the γ-radiolyses of liquid nitrogen solutions of hydrogen and of various hydrocarbons,[1] the sum of the G-values of nitrogen containing products we could observe did not exceed 1.5, while the present experiment suggested $G(N)=3.3$. This difference may be due to the fact that back reactions, such as

$$NH + NH \longrightarrow N_2 + H_2, \quad (3)$$

$$RN + NH \longrightarrow N_2 + RH, \quad (4)$$

$$RN + RN \longrightarrow N_2 + R_2, \quad (5)$$

are important processes when hydrogen and hydrocarbons are used as solutes. Here, R stands for hydrocarbon radicals.

For the formation of ozone in the γ-irradiated liquid nitrogen containing oxygen, we tentatively considered the following reaction mechanism:

$$N_2 \rightsquigarrow N_2^+ + e^-, N_2^*, \quad (6)$$

$$N_2^* + O_2 \longrightarrow N_2 + 2O, \quad (7)$$

$$e^- + O_2 \longrightarrow O_2^-, \quad (8)$$

$$N_2^+ + O_2^- \longrightarrow N_2 + 2O, \quad (9)$$

$$O + O_2 \longrightarrow O_3. \quad (10)$$

Here, N_2^* is the excited state of nitrogen molecule, probably $^3\Sigma_u^+$ state.[1] The direct participation of nitrogen atoms was ignored because the reaction between nitrogen atoms with oxygen molecule to form nitrogen oxide is known to be a slow reaction.[6] This is consistent with the experimental result that no nitrogen dioxide formation could be observed in this solution.

It may be worthwhile to mention here that the bond dissociation energy of O_2 (5.15 eV) is much smaller than that of NO (6.54 eV) and also smaller than the excitation energy of the lowest excited state $^3\Sigma_u^+$ of nitrogen (6.17 eV).

Although an oxygen molecule is a good electron scavenger, 0.01 mol l^{-1} of oxygen concentration is not high enough to scavenge all the electrons ejected into the solution.[7] Consequently, the main process of the ozone formation probably consists of Reactions 7 and

10 at low concentrations of oxygen. If so, the G-value of N_2^* becomes 3.5. As possible origins of N_2^*, the following three processes have to be considered: the direct formation due to the γ-irradiation, the neutralization reaction of nitrogen molecule ions, and the recombination reaction of nitrogen atoms. The specific allotment of each contribution is beyond our present knowledge.

References

1) K. Horigome, S. Hirokami, and S. Sato, *Bull. Chem. Soc. Jpn.*, **51**, 725 (1978), and references cited therein.

2) B. Brocklehurst and K. R. Jennings, "Progress in Reaction Kinetics," ed by G. Porter, Pergamon Press, Oxford (1967), Vol. 4, p. 1.

3) I. C. Hisatsune, *J. Phys. Chem.*, **65**, 2249 (1961).

4) "C. R. C. Handbook of Chemistry and Physics," **50**, D67 (1969—1970).

5) For example, S. Sato, *Bull. Chem. Soc. Jpn.*, **41**, 304 (1968).

6) M. A. A. Clyne and B. A. Thrush, *Proc. R. Soc. London, Ser. A*, **261**, 259 (1961).

7) S. Sato and S. Satoh, "Organic Scintillators and Liquid Scintillation Counting," ed by D. L. Horrocks and C.-T. Peng, Academic Press, Inc., New York and London (1971), p. 371.

Phosphorescence Emissions and Nonradiative Properties of Vapors of Aromatic Carbonyl Compounds at Low Pressure

Takao ITOH, Hiroaki BABA,* and Takeshi TAKEMURA

Division of Chemistry, Research Institute of Applied Electricity, Hokkaido University, Sapporo 060

(Received April 17, 1978)

The phosphorescence quantum yields of benzaldehyde, acetophenone, *p*-fluorobenzaldehyde, *p*-chlorobenzaldehyde, and benzophenone vapors, measured at low pressure down to the order of 10^{-3} Torr as a function of excitation wavelength, are essentially constant in the region of excitation energy corresponding to the $S_1(n, \pi^*)$ state, whereas the yields decrease very sharply as the excitation energy is raised to the value corresponding to the S_2 (π, π^*) state. This indicates that the nonradiative pathway in the carbonyl compound varies according to the type of the singlet state to which the molecule is initially excited. When excited to the S_1 and S_2 states, the molecule passes to the phosphorescent triplet state and a decomposing state, respectively. Two mechanisms are suggested and examined for understanding the nonradiative properties of the carbonyl compound vapors: (I) The internal conversion $S_2 \rightarrow S_1$ is slow compared with the conversion from S_2 to the decomposing state; (II) the vibrational energy redistribution in S_1 between the vibrational mode populated through $S_2 \rightarrow S_1$ and the mode to be populated optically is slow compared with the conversion from the former mode to the decomposing state.

In the vapor phase at low pressure, organic molecules often show photochemical or photophysical properties that cannot be observed in the condensed phase.[1,2] The photochemical reactivity of benzaldehyde and acetophenone in the vapor phase is known to be very sensitive to the excitation energy or to the nature of the electronic state excited.[3,4] The vapor-phase phosphorescence yields of benzaldehyde and benzophenone also are known to be sensitive to the excitation energy.[5,6]

In a previous paper,[7] it was reported preliminarily that the phosphorescence quantum yield of benzaldehyde vapor varies, depending on the type of singlet state to which the benzaldehyde molecule is initially excited. That is, the quantum yield is essentially constant in the region of excitation energy corresponding to the $S_1(n,\pi^*)$ state, but it decreases very sharply as the energy is raised to the value corresponding to the $S_2(\pi,\pi^*)$. Since the excited-electronic-state dependence of the molecular emission property is of prime importance in connection with the mechanism of radiationless transition, we have extended this sort of study to various derivatives of benzaldehyde. The present paper reports the emission and excitation spectra of acetophenone, *p*-fluorobenzaldehyde, *p*-chlorobenzaldehyde, and benzophenone vapors at low pressure, down to the order of 10^{-3} Torr, in comparison with the corresponding spectral data on benzaldehyde. It is shown that, in all the molecules studied, the phosphorescence quantum yields decrease greatly on changing the excitation from $S_0 \rightarrow S_1$ to $S_0 \rightarrow S_2$.

Experimental

Benzaldehyde and acetophenone obtained from Nakarai Chemicals, Kyoto and *p*-fluorobenzaldehyde from Aldrich Chemical Company were purified by means of repeated vacuum distillations. *p*-Chlorobenzaldehyde obtained from Tokyo Chemical Industry was purified by repeated vacuum sublimations. Benzophenone from Nakarai Chemicals was vacuum sublimated and zone-refined. Carbon tetrachloride from Merck was used as a foreign gas without further purification. All the sample vapors were degassed in a mercury-free vacuum system, and their pressures were determined from the intensities of the $S_0 \rightarrow S_3$ absorption spectra. It was confirmed that no impurity emission was detected from the sample vapors.

Emission and excitation spectra were measured with a high-sensitivity spectrophotometer[8] equipped with a Hamamatsu TV R-585 photomultiplier, using the photon-counting method. Absorption spectra were measured with a Hitachi EPS-3, a Shimadzu MPS-5000, or a Cary-15 spectrophotometer. For most of the emission measurements, square 10-mm path length quartz cells were used. A spherical 160-mm path length cell with quartz windows was also used for benzaldehyde and *p*-fluorobenzaldehyde at very low pressure ($<$7 mTorr).

The excitation spectra were obtained with a 1- or 2-nm bandwidth for the excitation monochromator and a 19-nm bandwidth for the emission monochromator, and were corrected for the spectral intensity distribution of the exciting light by the use of an aqueous solution of rhodamine B as a quantum counter. The spectral measurements were conducted at 85 °C for benzophenone and at room temperature for the other compounds.

Results

The vapor-phase emission spectra of the carbonyl compounds studied are shown in Figs. 1 and 2. These

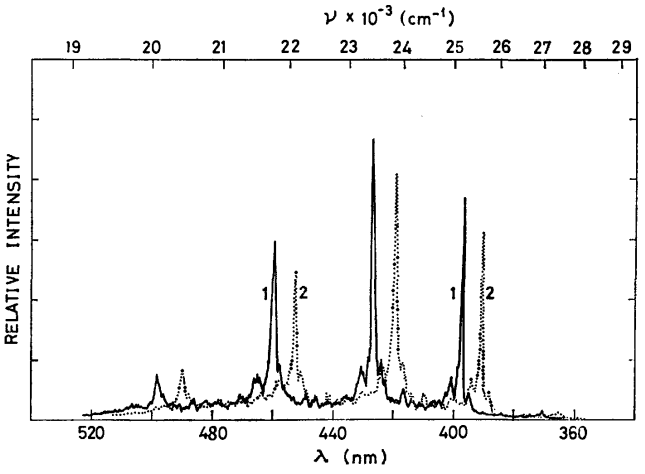

Fig. 1. Vapor-phase emission spectra of (1) benzaldehyde (bandwidth, 0.3 nm) and (2) *p*-fluorobenzaldehyde (bandwidth, 0.4 nm). The spectra are not corrected for the spectral response of the monochromator-photomultiplier system.

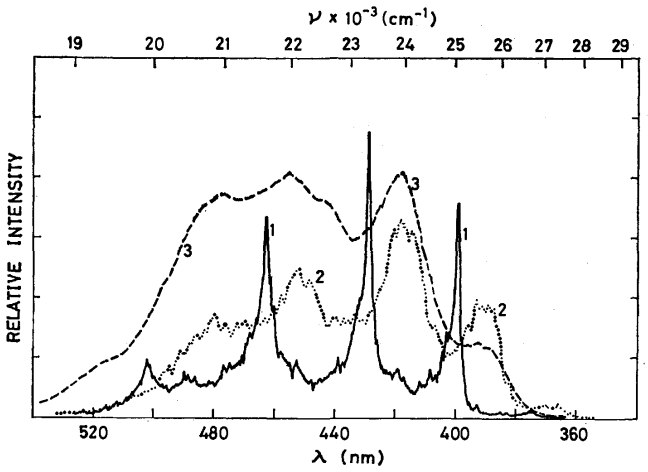

Fig. 2. Vapor-phase emission spectra of (1) *p*-chlorobenzaldehyde (bandwidth, 0.9 nm), (2) acetophenone (bandwidth, 1.2 nm), and (3) benzophenone (bandwidth, 1.0 nm). The spectra are not corrected for the spectral response of the monochromator-photomultiplier system.

spectra consist mainly of phosphorescence, accompanied by very weak E-type delayed fluorescence at shorter wavelengths. The spectral shapes were found to be independent of the pressure and excitation energy within the limit of experimental error.

Figures 3(a)—7(a) show corrected phosphorescence excitation spectra at different pressures of the vapors of the carbonyl compounds, together with the vapor-phase absorption spectra. In the presence of high-pressure carbon tetrachloride as a foreign gas, the excitation spectrum agrees well with the corresponding absorption spectrum for all the carbonyl compounds, except for benzophenone. The absorption spectrum of benzophenone in the long wavelength region is not known because of its low vapor pressure. However, its corrected excitation spectrum in the presence of high-pressure carbon tetrachloride resembles the absorption spectrum in isopentane solution. It is assumed, therefore, that the former excitation spectrum can be used as a substitute for the vapor-phase absorption spectrum. In the case of pure carbonyl compound vapors at low pressure, the intensities of the corrected excitation spectra are markedly low in the S_2 region, as compared with the absorption spectra.

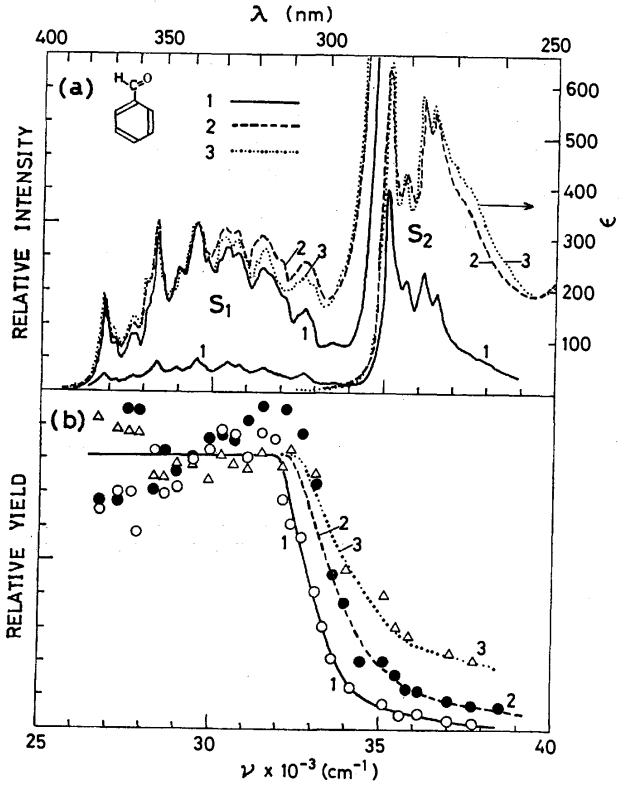

Fig. 3. (a) Phosphorescence excitation spectra at different pressures (1 and 2) and absorption spectrum (3) of benzaldehyde vapor. (1) 3 mTorr; (2) 500 mTorr of benzaldehyde in the presence of added CCl_4 (≈100 Torr). Higher-intensity spectra are obtained by multiplying the ordinate values of the corresponding lower-intensity spectra by factors of 5 and 20, respectively, for curve 1 and for curves 2 and 3. (b) Plots of phosphorescence quantum yields of benzaldehyde vapor *vs.* excitation energy at different pressures. (1) 2 mTorr; (2) 4 mTorr; (3) 10 mTorr.

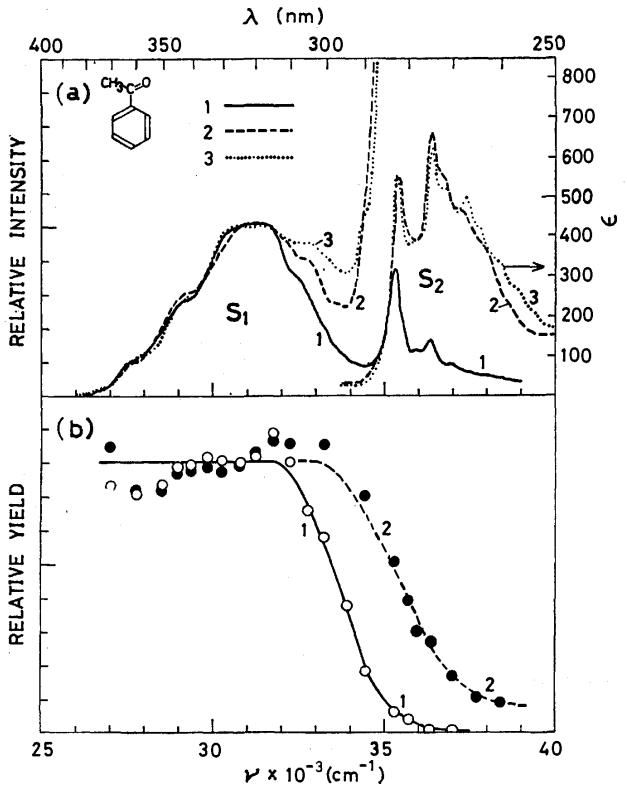

Fig. 4. (a) Phosphorescence excitation spectra at different pressures (1 and 2) and absorption spectrum (3) of acetophenone vapor. (1) 20 mTorr; (2) 30 mTorr of acetophenone in the presence of added CCl_4 (≈200 Torr). Higher-intensity spectra are obtained by multiplying the ordinate values of the corresponding lower-intensity spectra by a factor of 10 for curves 2 and 3. (b) Plots of phosphorescence quantum yields of acetophenone vapor *vs.* excitation energy at different pressures. (1) 20 mTorr; (2) 220 mTorr.

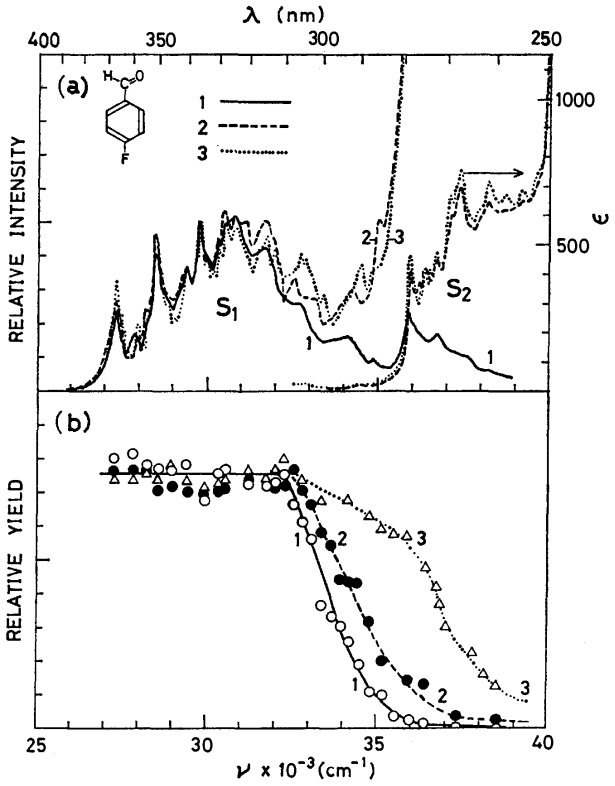

Fig. 5. (a) Phosphorescence excitation spectra at different pressures (1 and 2) and absorption spectrum (3) of *p*-fluorobenzaldehyde vapor. (1) 7 mTorr; (2) 300 mTorr of *p*-fluorobenzaldehyde in the presence of added CCl_4 (≈100 Torr). Higher-intensity spectra are obtained by multiplying the ordinate values of the corresponding lower-intensity spectra by a factor of 20 for curves 2 and 3. (b) Plots of phosphorescence quantum yields of *p*-fluorobenzaldehyde vapor *vs.* excitation energy at different pressures. (1) 7 mTorr; (2) 30 mTorr; (3) 100 mTorr.

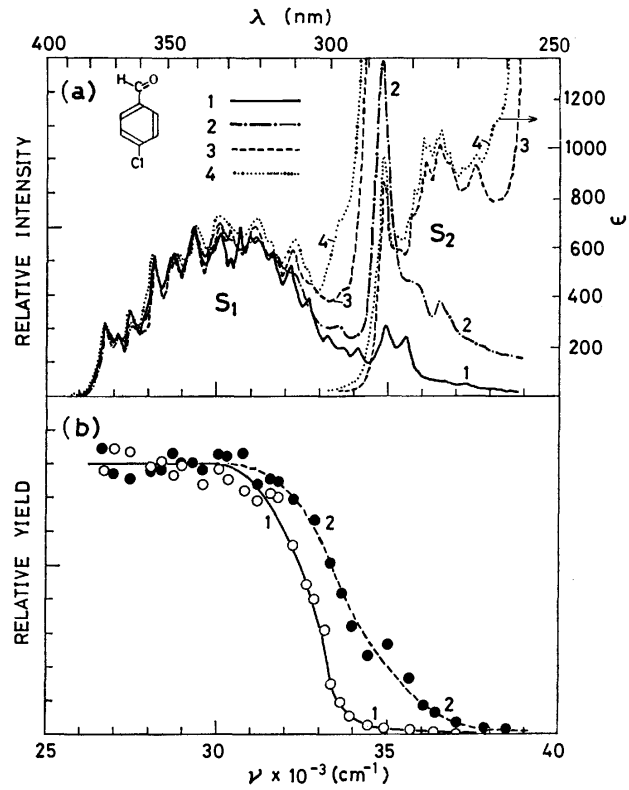

Fig. 6. (a) Phosphorescence excitation spectra at different pressures (1, 2, and 3) and absorption spectrum (4) of *p*-chlorobenzaldehyde vapor. (1) 9 mTorr; (2) 40 mTorr; (3) 50 mTorr of *p*-chlorobenzaldehyde in the presence of added CCl_4 (≈400 Torr). Higher-intensity spectra are obtained by multiplying the ordinate values of the corresponding lower-intensity spectra by a factor of 20 for curves 3 and 4. Since the molar extinction coefficients (ε) of this compound could not be determined directly because of its low vapor pressure, the ε values in the vapor phase were estimated from those in isopentane solution. (b) Plots of phosphorescence quantum yields of *p*-chlorobenzaldehyde vapor *vs.* excitation energy at different pressures. (1) 9 mTorr; (2) 60 mTorr.

Relative phosphorescence quantum yields are plotted against the excitation energy in Figs. 3(b)—7(b) for different pressures of the carbonyl compound vapors; in each of the figures the average values of the yields in the S_1 region are normalized to a common magnitude. These plots were obtained from comparison of the intensities of absorption and corrected excitation spectra. It should be emphasized that although the phosphorescence quantum yields, Φ_P, are essentially constant in the whole range of excitation energy corresponding to the S_1 state, they undergo an abrupt, step-like change when the excitation energy is raised to the value corresponding to S_2.

Figure 8 shows plots of $\Phi_P(S_2^0)/\Phi_P(S_1)$ against the pressure, p, for benzaldehyde, acetophenone, and *p*-fluorobenzaldehyde. Here, the Φ_P values obtained by excitation into the S_1 state and into the zero-point vibrational level of the S_2 state are denoted by $\Phi_P(S_1)$ and $\Phi_P(S_2^0)$, respectively; since in each of the carbonyl compounds $\Phi_P(S_1)$ is approximately constant regardless of the magnitude of the excess vibrational energy, the vibrational level excited is not specified in the case of $\Phi_P(S_1)$. As p is reduced to zero, the ratios $\Phi_P(S_2^0)/\Phi_P(S_1)$ appear to approach zero. This pressure dependence of the quantum yield ratios is consistent with the observation that the step-like changes of Φ_P, caused by changing the excitation from $S_0 \rightarrow S_1$ to $S_0 \rightarrow S_2$, become more pronounced as p is lowered (see Figs. 3(b)—7(b)).

The pressure dependence of $\Phi_P(S_1)$ and $\Phi_P(S_2^0)$ was already shown in the previous paper[7] for benzaldehyde; both $\Phi_P(S_1)$ and $\Phi_P(S_2^0)$ have a value of about 0.02 at 0.8 Torr. It was found that the phosphorescence quantum yields of other carbonyl compounds are comparable to that of benzaldehyde, when p is relatively large.

Discussion

We have measured the phosphorescence excitation spectra of carbonyl compounds at pressures lower than previous authors employed. The results show that Φ_P decreases very sharply as the excitation energy is raised

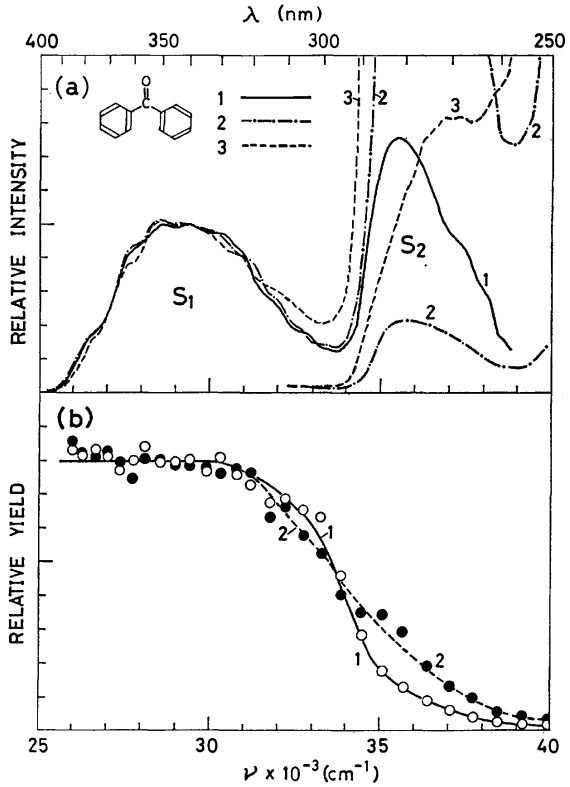

Fig. 7. (a) Phosphorescence excitation spectra at different pressures of benzophenone vapor. (1) 1 mTorr; (2) 110 mTorr; (3) 20 mTorr of benzophenone in the presence of added CCl_4 (≈400 Torr). Higher-intensity spectra are obtained by multiplying the ordinate values of the corresponding lower-intensity spectra by a factor of 10 for curves 2 and 3. (b) Plots of phosphorescence quantum yields of benzophenone vapor *vs.* excitation energy at different pressures. (1) 1 mTorr; (2) 110 mTorr.

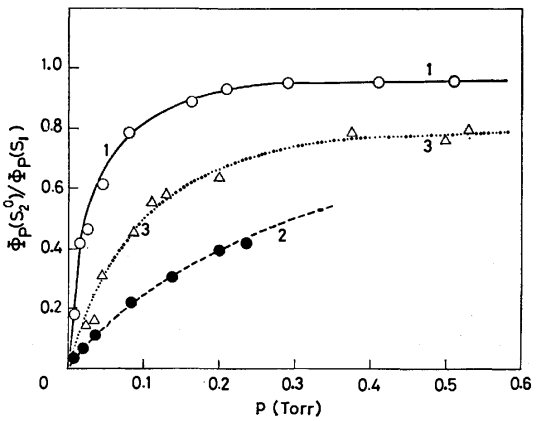

Fig. 8. Plots of $\Phi_P(S_2^0)/\Phi_P(S_1)$ *vs.* p for (1) benzaldehyde, (2) acetophenone, and (3) *p*-fluorobenzaldehyde.

to the value corresponding to the S_2^0 level, and that $\Phi_P(S_2^0)$ appears to approach zero as p is reduced to zero.

Berger *et al.*[3,4] studied the photochemistry of benzaldehyde and acetophenone vapors by determining the quantum yields of photoproducts as well as the lifetimes and quantum yields of phosphorescence emissions over a range of pressures and of excitation wavelengths. They reported that the molecules excited to the S_2 state decompose with unit probability at low pressure to produce carbon monoxide and benzene from benzaldehyde, and methyl and benzoyl radicals from acetophenone, but that excitation to the S_1 state does not result in such decomposition. They concluded also that the decomposition occurs from the excited vibrational levels of triplet states of these molecules.

It is possible that a decomposing level which leads to the step-like change of Φ_P may be situated accidentally near the S_2^0 level. For all the carbonyl compounds studied, however, Φ_P shows a sharp decrease when the excitation energy approaches the value corresponding to the S_2^0 level. This can be most clearly seen by comparing the excitation energy dependence of Φ_P of *p*-fluorobenzaldehyde (S_2^0, 35970 cm^{-1}) with that of *p*-chlorobenzaldehyde (S_2^0, 34970 cm^{-1}). In fact, on going from the former to the latter molecule, the starting point of the sharp decrease of Φ_P is red-shifted by about 1000 cm^{-1} (Figs. 5 and 6). It is, therefore, reasonable to consider that Φ_P varies according to the nature of the singlet electronic state to which the molecule is initially excited.

The pressure dependence of Φ_P suggests that the decomposition process occurs *via* a long-lived state such as a triplet, as will be explained in detail later. This decomposing state will hereafter be named an intermediate state, and will be denoted by Im. It is inferred that the state Im is relaxed to the phosphorescent state by collision.

Kinetic Considerations. The radiative and nonradiative properties of the vapors of the carbonyl compounds can be explained by the kinetic scheme illustrated in Fig. 9. For S_1 excitation,

$$S_1^v \xrightarrow{k_1} T_1^v, \tag{1}$$

$$T_1^v + S_0 \xrightarrow{k_2} T_1^0 + S_0, \tag{2}$$

and for S_2 excitation,

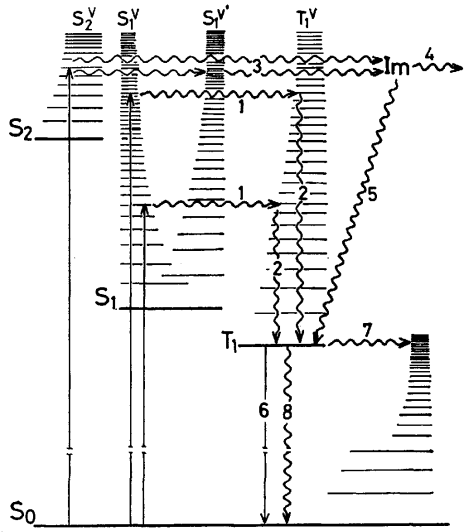

Fig. 9. A schematic diagram showing photophysical and photochemical processes in the carbonyl compound vapors.

$$S_2^v \xrightarrow{k_3} \text{Im}, \quad (3)$$

$$\text{Im} \xrightarrow{k_4} \text{Products}, \quad (4)$$

$$\text{Im} + S_0 \xrightarrow{k_5} T_1^0 + S_0. \quad (5)$$

Processes 1 and 3 represent intersystem crossing from S_1^v to T_1^v and overall conversion from S_2^v to Im, respectively. Here, S_1^v and S_2^v mean the optically populated vibrational levels in S_1 and S_2, respectively, and T_1^v is the vibrational level in T_1 populated as a result of the crossing from S_1^v; $v=0$ corresponds to the zero-point vibrational level for each of the electronic states. Process 4 is the decomposition of the carbonyl compounds in the Im state. The resulting products in benzaldehyde and acetophenone have already been mentioned. No information is available as to the decomposition products in *p*-fluorobenzaldehyde, *p*-chlorobenzaldehyde, and benzophenone, but similar cleavage is expected to occur also in these compounds. Processes 2 and 5 represent, respectively, collisional deactivation of T_1^v and Im to T_1^0; here, T_1^0 means lower vibrational levels of T_1, including the zero-point level. Since the shapes of the observed phosphorescence spectra are independent of the pressure, the emission originates only from the T_1^0 state.

The molecule in the T_1^0 state resulting from process 2 or 5 is deactivated in the following ways:

$$T_1^0 \xrightarrow{k_6} S_0 + h\nu, \quad (6)$$

$$T_1^0 \xrightarrow{k_7} S_0, \quad (7)$$

$$T_1^0 + S_0 \xrightarrow{k_8} 2S_0. \quad (8)$$

Process 7 represents the pressure-independent intersystem crossing from T_1^0 to the ground state, and process 8 the self-quenching. In this model, the quenching of the excited molecule by the cell wall is not taken into account for the sake of simplicity, although such a wall effect cannot be neglected in the measurement at very low pressure.

In the case of S_2 excitation, process 3 is followed exclusively by the decomposition process 4 when p is very small, but at large p values process 5 competes favorably with the decomposition. On the other hand, optical excitation to the S_1 state, *i.e.* excitation to S_1^v, does not lead to the decomposition.[3,4] These observations account for the fact that the quantum yield ratios $\Phi_P(S_2^0)/\Phi_P(S_1)$, which are zero at $p\simeq 0$, increase with increasing pressure (see Fig. 8).

In terms of the kinetic scheme mentioned above, $\Phi_P(S_1^v)$ and $\Phi_P(S_2^v)$ as functions of p are given by

$$\Phi_P(S_1^v) = \Phi_{ISC}(S_1^v \rightarrow T_1^v)\kappa, \quad (9)$$

$$\Phi_P(S_2^v) = \Phi(S_2^v \rightarrow \text{Im})\frac{k_5 p}{k_4 + k_5 p}\kappa, \quad (10)$$

where

$$\kappa = \frac{k_6}{k_6 + k_7 + k_8 p},$$

and $\Phi_{ISC}(S_1^v \rightarrow T_1^v)$ and $\Phi(S_2^v \rightarrow \text{Im})$ are the quantum yields of the intersystem crossing $S_1^v \rightarrow T_1^v$ and the overall conversion $S_2^v \rightarrow$ Im, respectively. It follows from Eqs. 9 and 10 that

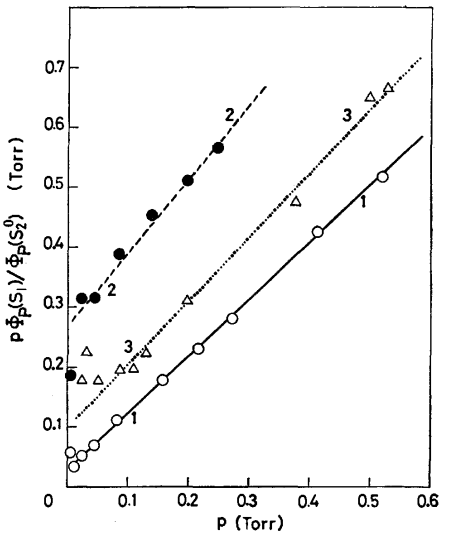

Fig. 10. Plots of $p\Phi_P(S_1)/\Phi_P(S_2^0)$ *vs.* p for (1) benzaldehyde, (2) acetophenone, and (3) *p*-fluorobenzaldehyde.

$$p\frac{\Phi_P(S_1^v)}{\Phi_P(S_2^v)} = \frac{\Phi_{ISC}(S_1^v \rightarrow T_1^v)}{\Phi(S_2^v \rightarrow \text{Im})}\left(\frac{k_4}{k_5} + p\right). \quad (11)$$

The experimental data given in Fig. 8 are analyzed on the basis of Eq. 11 for benzaldehyde, acetophenone, and *p*-fluorobenzaldehyde, with the results shown in Fig. 10. Thus, the plots of $p\Phi_P(S_1)/\Phi_P(S_2^0)$ against p give straight lines, as may be expected from Eq. 11. From the intercepts and slopes of the straight lines, the values of k_4/k_5 and $\Phi_{ISC}(S_1 \rightarrow T_1^v)/\Phi(S_2^0 \rightarrow \text{Im})$ are evaluated, respectively, to be 0.03 Torr and 0.95 for benzaldehyde, 0.23 Torr and 1.20 for acetophenone, and 0.10 Torr and 1.06 for *p*-fluorobenzaldehyde.

Berger *et al.*[3] pointed out that the decomposition of benzaldehyde occurs in two states with different lifetimes, but the linear plot in Fig. 10 appears to indicate that only a single state participates in the decomposition so far as the pressure region employed in Fig. 10 is concerned.

The Intermediate State and Nonradiative Processes. In terms of the kinetic model, the lifetime of the intermediate state is given by

$$\tau_{Im} = \frac{1}{k_4 + k_5 p}. \quad (12)$$

The value of the collisional deactivation rate constant, k_5, may be assumed to be equal to or less than that of the bimolecular rate constant for collision, k_c. On the basis of the hard sphere model, the k_c values are estimated to be 1.07×10^7, 1.13×10^7, and 1.02×10^7 Torr^{-1} s^{-1}, respectively, for benzaldehyde (5.5 Å), acetophenone (5.8 Å), and *p*-fluorobenzaldehyde (5.6 Å), with the molecular diameters given in parentheses. If k_5 is assumed to be equal to k_c, the value of k_4 can immediately be obtained by using the k_4/k_5 values which have already been determined. In this way the lifetimes at zero pressure, $\tau_{Im}(=1/k_4)$, are found to be 3.1×10^{-6}, 3.8×10^{-7}, and 9.8×10^{-7} s for benzaldehyde, acetophenone, and *p*-fluorobenzaldehyde, respectively.

The fact that fluorescence is not observed from S_1 and S_2 means that the lifetimes of these singlet states

are very short ($<1\times10^{-9}$ s), and therefore Im cannot be the S_1 nor S_2 state. Taking this into account, Im should be one of the following states: (1) a dissociative vibrational mode in T_1, denoted by $T_1^{v'}$, which is different from T_1^v in nature; (2) a higher triplet state, $T_j(j>1)$; (3) a reaction intermediate which cannot be identified as any of the excited states of the initial carbonyl compound.

As has been shown, the phosphorescence quantum yield of the carbonyl compound vapor varies according to the nature of the singlet state (S_1 or S_2) to which the molecule is initially excited. This indicates that the molecule excited to S_2 takes a nonradiative pathway different from the one taken by the molecule excited to S_1. According to the kinetic scheme already mentioned, the excitation to S_2^v is followed by the overall $S_2^v\rightarrow$Im conversion, whereas the molecule excited to S_1^v converts to T_1^v.

Two mechanisms, (I) and (II), are conceivable for the overall $S_2^v\rightarrow$Im conversion. (I) S_2^v converts to Im without passing through S_1, *i.e.* $S_2^v\rightarrow$Im. (II) S_2^v converts to Im *via* $S_1^{v'}$, *i.e.* $S_2^v\rightarrow S_1^{v'}\rightarrow$Im, where $S_1^{v'}$ represents the vibrational mode in S_1 populated as a result of the $S_2\rightarrow S_1$ internal conversion; $S_1^{v'}$ is in general different from S_1^v in nature (see Fig. 9). In the former mechanism the $S_2^v\rightarrow S_1^{v'}$ conversion should be slow compared with the $S_2^v\rightarrow$Im conversion, while in the latter the vibrational energy redistribution between $S_1^{v'}$ and S_1^v should be slow compared with the $S_1^{v'}\rightarrow$Im conversion.

We have mentioned three possible states (1)—(3) for Im and two mechanisms (I) and (II) for $S_2^v\rightarrow$Im. It is at present difficult to know which state is most probable and which mechanism is more important. If Im is $T_j(j>1)$ or a reaction intermediate, the mechanism (I) will be more important, because the $S_2\rightarrow S_1$ internal conversion in the carbonyl compounds studied is expected to be relatively slow owing to the large energy separation ($\approx$8000 cm^{-1}) between S_2^0 and S_1^0. When Im is $T_1^{v'}$, the mechanism (I) corresponds to the process $S_2^v\rightarrow T_1^{v'}$. If this process occurs directly, its rate must be slow because of the large energy gap between S_2^0 and T_1^0, so that the mechanism (II) will become favorable compared with (I). It is possible, however, that the process $S_2^v\rightarrow T_1^{v'}$ may occur *via* a higher-energy triplet state. In any case, in order that $T_1^{v'}$ may be a candidate for Im, both the intersystem crossing $S_1^v\rightarrow T_1^{v'}$ and the vibrational energy redistribution between T_1^v and $T_1^{v'}$ should occur only slowly; otherwise the optical excitation to S_1^v would lead to the decomposition reaction.

References

1) "Organic Molecular Photophysics," ed by J. B. Birks, Wiley, New York (1975), Vol. 2, pp. 457—465.
2) C. S. Parmenter, *Adv. Chem. Phys.*, **22**, 365 (1972).
3) M. Berger, I. L. Goldblatt, and C. Steel, *J. Am. Chem. Soc.*, **95**, 1717 (1973).
4) M. Berger and C. Steel, *J. Am. Chem. Soc.*, **97**, 4817 (1975).
5) J. Metcalfe, R. G. Brown, and D. Phillips, *J. Chem. Soc., Faraday Trans. 2*, **71**, 409 (1975).
6) N. A. Borisevich, A. A. Kotov, and G. B. Tolstorozhez, *Izv. Akad. Nauk SSSR, Ser. Fiz.*, **36**, 935 (1972).
7) T. Itoh, T. Takemura, and H. Baba, *Chem. Phys. Lett.*, **40**, 481 (1976).
8) K. Chihara and H. Baba, *Bull. Chem. Soc. Jpn.*, **48**, 3093 (1975).

Standard Redox Potentials of R^-/R^+ Reference Redox Couples and Solvent Activity Coefficients

Tadaaki KAKUTANI, Yoshikazu MORIHIRO, Mitsugi SENDA,* Reiji TAKAHASHI,** and Koichi MATSUMOTO**

Department of Agricultural Chemistry, Kyoto University, Kyoto 606
***Department of Chemistry, Ritsumeikan University, Kyoto 603*

(Received April 20, 1978)

The standard redox potentials of five R^-/R^+ redox couples that can be considered as candidates for the reference redox couple, *i.e.*, the anion/cation couples of tris(2,2′-bipyridine)iron(II), tris(2,2′-bipyridine)ruthenium(II), cobaltocene, perylene, and 9,10-diphenylanthracene, have been determined in acetonitrile, dimethyl sulfoxide, *N,N*-dimethylformamide and propylene carbonate by means of polarography and voltammetry. The results confirmed that the standard potentials of these redox couples are independent of the solvents studied so that they can be used as solvent-independent reference points for potential comparisons. The solvent activity coefficients of the silver ion have been estimated on the basis of these reference redox couples.

The evaluation of single-ion solvent activity coefficients, ${}^{o}\gamma^{s}_{ion}$, for the transfer of ions from a reference solvent (superscript o) to another solvent (superscript s) is one of the most interesting problems of solution chemistry. Since the problem is not accessible to exact thermodynamics, extrathermodynamic procedures must be followed. Thus various extrathermodynamic procedures have been proposed by several authors for the estimation of the solvent activity coefficients of single ions. The current status of this field has been comprehensively reviewed in several recent papers.[1-6]

In a previous paper,[7] two of the authors (M.S. and R.T.) proposed that the standard redox potential, $E^{\circ}_{R^-/R^+}$, of the R^-/R^+ redox couple may work as a solvent-independent reference point in various solvents if the R^-/R^+ redox couples, being named the reference redox couples, have the following chemical features: a) the R^+ and R^- ions are very large in size with the charge shielded by large organic groups, and b) the charge distribution in the R^+ ion is the same or very nearly the same as that in the R^- ion. It was also pointed out that the standard redox potentials can be estimated from polarographic reversible half-wave potentials of R/R^+ and R^-/R couples and that this approach should give an accurate and convenient estimation of single-ion solvent activity coefficients.

In this study the standard redox potentials of several R^-/R^+ redox couples that can be considered as candidates[7] for the reference redox couple (*i.e.*, the anion/cation couples of tris(2,2′-bipyridine)iron(II), tris(2,2′-bipyridine)ruthenium(II), cobaltocene, perylene and 9,10-diphenylanthracene) have been determined in acetonitrile (AN), dimethyl sulfoxide (DMSO), *N,N*-dimethylformamide (DMF), and propylene carbonate (PC) by means of polarography and voltammetry. Furthermore the solvent activity coefficients of the silver ion have been estimated on the basis of these R^-/R^+ reference redox couples. An estimation of the absolute electrode potentials of the silver/silver ion electrodes in nonaqueous solvents has been attempted.

Experimental

Chemicals. Commercial PC(a Merk product for synthesis) was dried over molecular sieves 5A for several days and fractionally distilled twice under vacuum. The central 70% fraction of the distillate was collected from each distillation and stored under a nitrogen atmosphere after dry nitrogen gas had been passed through the distillate for several hours. Spectro grade DMF was stirred with molecular sieves 4A overnight and distilled under vacuum. The central 60% fraction was collected and stored under a nitrogen atmosphere after dry nitrogen gas had been passed though the distillate for one hour. Spectro grade DMSO was dried over molecular sieves 5A for two days and twice distilled under vacuum. The central 70% fraction was collected in each distillate and stored under a nitrogen atmosphere. Analytical grade AN was refluxed over phosphorus pentaoxide (5 g/l) for 15 min and distilled at the rate of 100 ml/h. The central 80% fraction of the distillate was refluxed over CaH_2(2 g/l) for half an hour and fractionally distilled through Widmer's fractional distillation column at the rate of 100 ml/h. The central 80% fraction was collected and dried over anhydrous sodium carbonate. Just before use the dried AN was fractionally distilled through a 1 m column packed with stainless steel helices.

Tetraethylammonium perchlorate (TEAP) was prepared and purified by the method previously described.[8] The salt was vacuum-dried at 100 °C for 24 h and stored in a desiccator. Just before use the salt was again vacuum-dried at 100 °C for two hours. Commercial silver perchlorate was purified by repeated recrystallization with dried thiophene-free benzene[9] and vacuum-dried at 60 °C, both processes being carried out in the dark. Silver nitrate of analytical grade (a product of Wako Pure Chemicals) was used without further purification. Rubidium perchlorate was prepared by the equimolar addition of perchloric acid to an aqueous solution of rubidium bromide, which was then purified by repeated recrystallization with twice distilled water and vacuum-dried at 100 °C for 24 h. Tris(2,2′-bipyridine)iron(II) perchlorate ($Fe(bpy)_3(ClO_4)_2$) and tris(2,2′-bipyridine)ruthenium(II) bromide ($Ru(bpy)_3Br_2$) were kindly supplied by Dr. T. Matsumura-Inoue of Nara University of Education. Reagent grade perylene was purified by repeated recrystallization with toluene. Analytical grade 9,10-diphenylanthracene (DPA) (a product of Nakarai Chemicals for scintillation use) was used without further purification. Cobalticenium hexafluorophosphate (Cp_2CoPF_6) was prepared according to Wilkinson's procedure[10] with a slight modification,[11] and purified by repeated recrystallization from a 2:1 methanol–acetone mixture.

Electrochemical Measurements. Dc polarograms and cyclic voltammograms were measured with a potentiostat, Yanaco

Model PE-21-TB2S, equipped with a function generator, YHP 3310B. Ac polarographic measurements were performed with a lock-in amplifier, NF LI-572B, equipped with the above potentiostat system. Double potential-step measurements[12] for chemical kinetics following charge transfer were carried out with the same system as the dc polarograph. The data were recorded using both a transient memory, Union Giken System 71-02, and an X-Y recorder, Yokogawa 3077.

All voltammetric measurements were performed in Cell A under potentiostatic conditions. A three electrode system consisting of a working electrode (dropping mercury, platinum plane button, or hanging mercury drop electrode), a coiled platinum wire auxiliary electrode, and a nonaqueous silver/silver ion reference electrode, at room temperature (25±1 °C) under a dry nitrogen atmosphere was used.

Cell A: Hg (or Pt) | 0.5—1 mM depolarizer; 0.2 M TEAP; solvent s || 1 mM $AgNO_3$ or $AgClO_4$; (10 mM $AgNO_3$ in DMF); 0.2 M TEAP; solvent s | Ag

The half cells in Cell A were interconnected through sintered glass. The platinum working electrode (area 7.9×10^{-3} cm^2), sealed in glass, was polished with emery paper (#3000) and then immersed in an aqueous iron(II) sulfate solution for approximately half an hour. It was then washed in distilled water, dried, and pre-immersed in the solution to be studied. Good experimental reproducibility was obtained by using this procedure. The hanging mercury drop electrode was a Metrohm mercury drop electrode E 410. As the reference electrode an Ag/1 mM $AgNO_3$(or $AgClO_4$), 0.2 M TEAP, s, electrode was used for the measurements in s=PC, DMSO or AN. The potential of the reference electrode was found to be stable and reproducible for at least 2 h after the electrode's preparation. However, the Ag/1 mM $AgNO_3$ electrode was unstable in DMF and this was most likely due to the reduction of the silver ion by the solvent[13] (the potential of the electrode which was left standing for 4 hours was about 20 mV more negative compared to that of the freshly prepared electrode). Therefore an Ag/10 mM $AgNO_3$, 0.2 M TEAP, DMF electrode was used for the measurements in DMF. This electrode was found to be satisfactorily stable and gave reproducible results for at least 2 h after the preparation. For these reasons the reference electrodes were freshly prepared for each measurement, and the measurements were finished within 2 h after the preparation. The data in DMF obtained with the above reference electrode were converted to those referred to the Ag/1 mM $AgNO_3$, 0.2 M TEAP, DMF electrode by using the emf value of the following freshly prepared cell:

Ag | 1 mM $AgNO_3$; 0.2 M TEAP; DMF || 10 mM $AgNO_3$; 0.2 M TEAP; DMF | Ag

Results

Nonaqueous electrochemistry of $Fe(bpy)_3^{2+}$,[14,15] $Ru(bpy)_3^{2+}$,[15] Cp_2Co^+,[11,16,17] DPA,[18] and perylene[18] has been studied by many authors. These studies have revealed that in aprotic dipolar media these compounds give one-electron reversible reduction or oxidation steps, involving redox couples R/R^+ and R^-/R, defined by the equations: $R^+ + e = R$ and $R + e = R^-$. These compounds are also of relatively large size. For these reasons the above compounds were selected as the candidates for the R^-/R^+ reference redox couple.

Electrochemical Reduction of $Fe(bpy)_3^{2+}$ and $Ru(bpy)_3^{2+}$. These complexes[14,15] gave four reduction waves in aprotic media. The second and third reduction steps were assigned to the redox reactions of $M(bpy)_3^{2+} + e = M(bpy)_3$ and $M(bpy)_3 + e = M(bpy)_3^-$, respectively. In general the behavior of these complexes in the four solvents as investigated in this study was found to agree with data obtained by previous authors. The dc half-wave potentials, $E_{1/2}$, of these reduction steps conformed, within experimental error, to the corresponding ac peak

Table 1. Electrochemical data of the second and third reduction steps of $Fe(bpy)_3^{2+}$ and $Ru(bpy)_3^{2+}$ in nonaqueous solvents containing 0.2 M TEAP at 25 °C

Complex	Step	$-E_{1/2}$/V	ΔE/mV	$-E_{1/2}^{CV}$/V	ΔE_p^{CV}/mV	$-E_p^{AC}$/V	ΔE_p^{AC}/mV
		(a) Propylene carbonate					
$Fe(bpy)_3^{2+}$	2nd	2.21	55	2.22	60	2.21	90
	3rd	2.44	55	2.45	69	2.45	93
$Ru(bpy)_3^{2+}$	2nd	2.19	56	2.20	59	2.20	95
	3rd	2.42	55	2.43	66	2.43	90
		(b) DMF					
$Fe(bpy)_3^{2+}$	2nd	1.85	55	1.85	62	1.85	97
	3rd	2.10	55	2.11	74	2.11	95
$Ru(bpy)_3^{2+}$	2nd	1.84	55	1.84	60	1.84	92
	3rd	2.09	55	2.09	70	2.09	89
		(c) Acetonitrile					
$Fe(bpy)_3^{2+}$	2nd	1.79	50	1.79	62	1.79	90
	3rd	2.03	50	2.03	64	2.03	100
$Ru(bpy)_3^{2+}$	2nd	1.78	50	1.77	60	1.77	90
	3rd	2.02	50	2.01	60	2.01	88
		(d) DMSO					
$Fe(bpy)_3^{2+}$	2nd	1.68	58	1.68	61	1.68	90
	3rd	1.92	55	1.92	63	1.92	95
$Ru(bpy)_3^{2+}$	2nd	1.66	55	1.66	60	1.66	90
	3rd	1.90	55	1.90	60	1.90	90

potentials, E_p^{AC}, and the half-wave potentials, $E_{1/2}^{CV}$, calculated from the cyclic voltammetric (CV) peak potentials. The conventional criteria of the reversibility, such as the dc polarographic slope, $\Delta E(\equiv E_{1/4}-E_{3/4})$, CV anodic-cathodic peak separation, ΔE_p^{CV}, ac polarographic half-width, ΔE_p^{AC}, *etc.*, showed that the second and third reduction steps are a reversible one-electron process in all the solvents studied. Some experimental results are shown in Table 1.

Electrochemical Reduction of Cp_2Co^+. Previous work[16,17] has revealed that this compound gives two reduction waves in AN and that the first reduction step corresponds to a simple reversible one-electron reduction from the cobaltocene cation to neutral cobaltocene:

$$Cp_2Co^+ + e \rightleftarrows Cp_2Co \qquad E_1 \qquad (a)$$

Regarding the reduction mechanisms of the second step, there are several points of disagreement between the two previous papers.[16,17] In contrast to the earlier report by Gubin *et al.*[17] that the second reduction step is a one-electron irreversible process, Geiger[16] has recently reported that in AN the neutral cobaltocene formed at the first reduction step is reduced by an ECE mechanism;

$$Cp_2Co + e \rightleftarrows Cp_2Co^- \qquad E_2 \qquad (b)$$

$$Cp_2Co^- \longrightarrow Z \qquad (c)$$

$$Z + e = Z^- \qquad E_3 \qquad (d)$$

where the intermediate Z is more reducible than the cobaltocene. He also showed that the rate of the chemical reaction (c) was relatively slow ($k\approx 0.1$ s^{-1} in AN). In addition the redox reaction (b) was shown to be highly reversible in AN.[11] The polarographic data on this compound in AN, DMF, and PC found here were consistent with the reduction mechanism proposed by Geiger.[16] The polarographic limiting current of the second reduction step, $i_l^{(2)}$, was slightly larger than that of the first reduction step, $i_l^{(1)}$, and the ratio, $i_l^{(2)}/i_l^{(1)}$, when corrected for drop time, decreased and approached unity with increasing mercury column height, as shown in Table 2. A plot of log $[i/(i_l-i)]$ *vs.* E for the second wave gave a straight line with a slope of 59 mV. On CV, the cathodic peak height of the second reduction step, $i_{cp}^{(2)}$, was not proportional to the square root of the scan rate, in contrast to the behavior of the first reduction step. As the scan rate increased the ratio $i_{cp}^{(2)}/i_{cp}^{(1)}$, $i_{cp}^{(1)}$ being the cathodic peak height of the first step, decreased and approached unity ($i_{cp}^{(2)}/i_{cp}^{(1)}\approx 1$ at $v\geq 0.5$ V/s). The peak potential of the second cathodic peak was practically invariant with the change in the scan rate. These results can be interpreted by assuming the ECE mechanism[19-22] with a slow chemical reaction (c). The rate constant of the chemical reaction (c) was estimated from the polarographic limiting currents[20,22] as given in Table 2. Analysis of the CV data yielded a rate constant of the same order of magnitude; $k=0.1$ to 0.2 s^{-1} in these solvents. The dc polarographic theory[22] for the ECE mechanism predicts that, for $k=0.2$ s^{-1} or less, the observed half-wave potential of the second step will agree with the reversible half-wave potential of the Cp_2Co/Cp_2Co^- couple within a few millivolts when $E_3\geq E_2$. Thus it can be concluded that the deviation of the observed half-wave potential from the true reversible half-wave potential of this redox couple (b) will be negligibly small in AN, DMF, and PC. It was also found that the ac peak potential of the second step agreed with the corresponding dc half-wave potential. On the other hand, this compound gave three reduction waves in DMSO. The first reduction step was found to represent a one-electron reversible reduction from the cobaltocene cation to cobaltocene. The second and third reduction steps appeared irreversible, showing no corresponding anodic peaks on the CV curves at $v=1$ V/s. Thus, the reversible half-wave potential of the Cp_2Co/Cp_2Co^- couple in DMSO could not be determined.

Table 2. Polarographic results of cobalticenium hexafluorophosphate in aprotic media containing 0.2 M TEAP at 25 °C

h/cm[a]	τ/s[b]	$i_l^{(2)}/i_l^{(1)}$ [c]	k/s^{-1} [d]
	(a) AN		
40	2.47	1.199	0.19
50	1.96	1.169	0.20
60	1.66	1.125	0.17
70	1.40	1.117	0.18
	(b) DMF		
40	2.71	1.124	0.10
50	2.19	1.100	0.10
60	1.82	1.063	0.07
70	1.56	1.038	0.05
	(c) PC		
40	2.56	1.124	0.11
50	2.05	1.075	0.08
60	1.70	1.108	0.14
70	1.45	1.092	0.14

a) Mercury column height. b) Drop time at the potential where $i_l^{(2)}$ was measured. c) Instantaneous current ratio, corrected for drop time. d) Calculated by the table in Ref. 20.

Electrochemical Oxidation and Reduction of DPA and Perylene. It has been reported that DPA and perylene undergo reversible one-electron oxidations and reductions to produce reasonably stable cation and anion radicals,[18] respectively. For this reason these compounds were also selected as candidates for the R⁻/R⁺ reference redox couple. All polarographic and voltammetric data obtained in this study indicated that the first reduction steps of these compounds are reversible one-electron reductions to anion radicals, which are highly stable in all four solvents studied. On the other hand, these compounds were found to undergo reversible one-electron oxidations to produce stable cation radicals in AN and PC only. In DMSO, DPA gave no oxidation wave within the limits of anodic potential range, whereas perylene gave an irreversible oxidation wave in this solvent, showing no corresponding cathodic peak on the CV curves at $v=1$ V/s. In DMF, DPA gave an oxidation wave, which was most likely complicated by a succeeding chemical reaction of the cation radical. Thus in CV, the ratio of cathodic to anodic peak current, i_{cp}/i_{ap}, increased with the increasing voltage scan rate. Also the anodic to cathodic peak

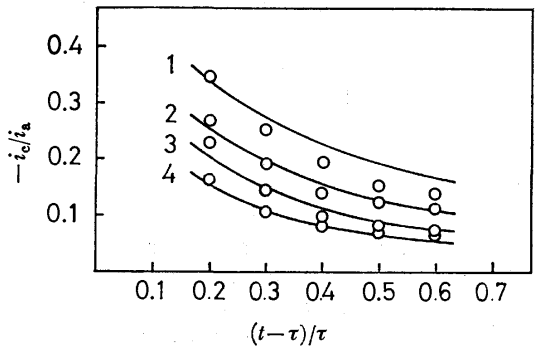

Fig. 1. Plots of $-i_c/i_a$ *vs.* $(t-\tau)/\tau$ for the oxidation step of DPA in DMF containing 0.2 M TEAP at 25 °C. Solid lines represent theoretical curves for $k=3.7\ s^{-1}$ and points are experimental results; (1) $\tau=0.192$ s; (2) $\tau=0.295$ s; (3) $\tau=0.384$ s; (4) $\tau=0.491$ s.

separation increased as the voltage scan rate was increased. These results indicate that this oxidation step is a quasi-reversible one-electron oxidation succeeded by a chemical reaction. To estimate the reversible half-wave potential of the DPA/DPA$^+$ couple in this solvent, an attempt was made to determine the rate constant of the succeeding chemical reaction, using the double potential step method developed by Shwarz and Shain.[12] The initial dc potential was set at 0.49 V *vs.* the Ag/10 mM $AgNO_3$ electrode, and the anodic polarization step of 0.99 V was applied for a given interval, τ, followed by the cathodic polarization at 0.49 V. Typical results, corrected for the base current, for different intervals are shown in Fig. 1. The points represent the experimental results and the solid lines represent the theoretical curves for $k=3.7\ s^{-1}$. Therefore, based on the theory,[23] in CV the deviation of the observed anodic peak potential of this compound from the supposed anodic peak potential of a hypothetical redox couple, either reversible or quasi-reversible, without succeeding chemical reaction should be less than 1 mV at $v=1$ V/s. Thus the reversible half-wave potential was estimated from the CV data at $v\geq 1$ V/s, as follows. According to Matsuda and Ayabe,[24] the anodic peak potential, E_p(quasi), of a quasi-reversible oxidation step can be written as

$$E_p(\text{quasi}) = E^r_{1/2} + (RT/nF)\Xi(\Lambda),$$

where $E^r_{1/2}$ is the reversible half-wave potential and Λ is a function of the electrochemical kinetic parameters, k_s and α, and the voltage scan rate, v. The parameter Λ can be estimated from the CV peak separation, ΔE_p, by using a working curve of $\Psi(\equiv\Lambda/\sqrt{\pi})$ *vs.* ΔE_p calculated by Nicholson.[25] Using this Λ value, the $\Xi(\Lambda)$ value can be obtained and consequently the $E^r_{1/2}$ value.[24] The results are summarized in Table 3, assuming $\alpha=0.5$. The values of $E^r_{1/2}$ estimated at various scan rates were constant, indicating that the value of $E^r_{1/2}$ estimated by this method is reliable. In DMF, perylene gave an oxidation wave, however the oxidation appeared irreversible and showed no corresponding cathodic peak on the CV curves.

Table 3. Cyclic voltammetric results of DPA in DMF containing 0.2 M TEAP at 25 °C

v/V s^{-1}	1	4.7	9.7
E_p/V	0.96	0.98	1.00
ΔE_p/mV	115	150	199
$\Lambda/\sqrt{\pi}$	0.39	0.20	0.12
$\Xi(\Lambda)$	2.33	3.21	4.05
$E^r_{1/2}$/V	0.90	0.90	0.90

Table 4. Polarographic reversible half-wave potential of R/R$^+$, R$^-$/R, and R$^-$/R$^+$ redox couples measured against Ag/1 mM Ag$^+$, 0.2 M TEAP electrode in various solvents at 25 °C

	$-E^r_{1/2}$·(R/R$^+$)/V	$-E^r_{1/2}$·(R$^-$/R)/V	$-E^r_{1/2}$·(R$^-$/R$^+$)/V
(a) Propylene carbonate			
DPA	−0.51	2.56	1.03
Perylene	−0.30	2.37	1.04
Cobaltocene	1.63	2.55	2.09
Fe(bpy)$_3$	2.21	2.45	2.33
Ru(bpy)$_3$	2.20	2.43	2.32
Rb$^+$	2.63	—	—
(b) DMF			
DPA	−0.90	2.23	0.67
Perylene	irr	2.03	irr
Cobaltocene	1.27	2.21	1.74
Fe(bpy)$_3$	1.85	2.11	1.98
Ru(bpy)$_3$	1.84	2.09	1.97
Rb$^+$	2.42	—	—
(c) Acetonitrile			
DPA	−0.96	2.16	0.60
Perylene	−0.75	1.96	0.61
Cobaltocene	1.19	2.12	1.66
Fe(bpy)$_3$	1.79	2.03	1.91
Ru(bpy)$_3$	1.77	2.01	1.89
Rb$^+$	2.21	—	—
(d) DMSO			
DPA	n.w.	2.01	—
Perylene	irr	1.82	irr
Cobaltocene	1.11	irr	irr
Fe(bpy)$_3$	1.68	1.92	1.80
Ru(bpy)$_3$	1.66	1.90	1.78
Rb$^+$	2.26	—	—

Table 4 summarizes the reversible half-wave potentials of R/R$^+$ and R$^-$/R redox couples of the five compounds studied and of the rubidium ions in PC, DMF, AN and DMSO. In addition the corresponding reversible half-wave potentials of the five R$^-$/R$^+$ redox couples, $E^r_{1/2}$(R$^-$/R$^+$), which were calculated by

$$E^r_{1/2}(R^-/R^+) = (E^r_{1/2}(R/R^+) + E^r_{1/2}(R^-/R))/2,$$

are illustrated.

Discussion

As described previously,[7] the standard redox potential of the R$^-$/R$^+$ redox couple, $E^\circ_{R^-/R^+}$, measured against a silver/silver ion reference electrode can be expressed by

$$E^\circ_{R^-/R^+}: R^+ + 2e = R^-, \quad (1)$$

$$E^\circ_{R^-/R^+} = (E^\circ_{R/R^+}+E^\circ_{R^-/R})/2 = (A+I)/2F-(G^s(R^-)-G^s(R^+))/2F + \Delta G^s(Ag/Ag^+)/F, \quad (2)$$

where E°_{R/R^+} and $E^\circ_{R^-/R}$ are the standard redox potentials of the redox couples, R/R^+ and R^-/R, respectively, as defined by

$$E^\circ_{R/R^+}: R^+ + e = R, \quad (3a)$$

$$E^\circ_{R^-/R}: R + e = R^-. \quad (3b)$$

In Eq. 2, A and I respectively represent the electron affinity and ionization potential of the neutral molecule R derived from R^+ or R^- by the above redox reaction (3a) or (3b), $G^s(R^i)$ $(i=+, -)$ is the solvation energy of the ion R^i, and $\Delta G^s(Ag/Ag^+)$ is the free energy change of the reference electrode reaction,

$$Ag^+ + e = Ag \quad (3c)$$

in solvent, s. When R^+ and R^- are very large in size with the charge shielded by large organic groups and the charge distribution in the R^+ ion is the same or nearly the same as that in the R^- ion, it can be assumed that

$$\Delta G^s_{R^-/R^+} = G^s(R^-) - G^s(R^+) = 0. \quad (4)$$

Then $E^\circ_{R^-/R^+}$ should be solvent-independent;

$$E^\circ_{R^-/R^+} = (A+I)/2F + \Delta G^s(Ag/Ag^+)/F. \quad (5)$$

The half-wave potential $E^r_{1/2}(R^-/R^+)$ is related to the standard potential $E^\circ_{R^-/R^+}$ by

$$E^r_{1/2}(R^-/R^+) = E^\circ_{R^-/R^+} + (RT/2F)\ln(f_+\sqrt{D_-}/f_-\sqrt{D_+}),$$

where f_+ and f_- are the activity coefficients and D_+ and D_- the diffusion coefficients of R^+ and R^-, respectively. It is quite reasonable to assume $f_+=f_-$ and $D_+=D_-$ for the R^-/R^+ couple, so that $E^r_{1/2}(R^-/R^+)$ equated to $E^\circ_{R^-/R^+}$ is a very good approximation (see Table 4).

According to the molecular orbital theory the sum of A and I should be constant for alternant aromatic hydrocarbons. Thus Eq. 5 predicts that for a given solvent $E^\circ_{R^-/R^+}$ of alternant aromatic hydrocarbons should be constant independent of the species of alternant aromatic hydrocarbon. Results in Table 4 show this is the case with perylene and DPA in PC and AN, indicating the validity of Eq. 4 for alternant aromatic hydrocarbons in nonaqueous solvents.[49]

From Eq. 2 the difference $\Delta^I E^{II}(s)$ between the $E^\circ_{R^-/R^+}$'s of two couples, I and II, in a solvent, s, is given by

$$\Delta^I E^{II}(s) = E^\circ_{R^-/R^+}(I, s) - E^\circ_{R^-/R^+}(II, s) = (A_I+I_I)/2F - (A_{II}+I_{II})/2F - (\Delta G^s_{R^-/R^+}(I)-\Delta G^s_{R^-/R^+}(II))/2F. \quad (6a)$$

Accordingly, if $\Delta^I E^{II}(s)$ were found to be independent of the solvent s for any pair of redox couples, I and II, it must hold that $\Delta\Delta^I G^{II}(s)=\Delta G^{s'}_{R^-/R^+}(I)-\Delta G^s_{R^-/R^+}(II) \approx 0$, because $\Delta\Delta^I G^{II}(s)$, if appreciable, should be dependent on the solvent s. The last condition means that $\Delta G^s_{R^-/R^+}(I)\approx\Delta G^s_{R^-/R^+}(II)\approx\Delta G^s_{R^-/R^+}(III)\approx\cdots$, which in turn implies that all these $\Delta G^s_{R^-/R^+}$'s are negligibly small or that Eq. 4 is valid, because $\Delta G^s_{R^-/R^+}(I)$, $\Delta G^s_{R^-/R^+}(II)$, $\Delta G^s_{R^-/R^+}(III)$,$\cdots$, if appreciable, should be dependent on the redox couples I, II, III, $\cdots$, respectively. In conclusion, if $\Delta^I E^{II}(s)$ is independent of the solvent s, Eq. 4 is valid, so that

$$\Delta^I E^{II}(s) = (A_I+I_I)/2F - (A_{II}+I_{II})/2F. \quad (6b)$$

A similar argument leads to the conclusion that if the difference $\Delta^{s'}E^{s''}(I)$ between the $E^\circ_{R^-/R^+}(I)$'s of a redox couple, I, in any two solvents, s' and s'', is independent of the redox couple I, Eq. 4 is valid, so that $\Delta^{s'}E^{s''}(I)$ should indicate the solvent activity coefficient, ${}^{s'}\gamma^{s''}$, of the ion involved in the reference electrode reaction, as shown by

$$\Delta^{s'}E^{s''}(I) = E^\circ_{R^-/R^+}(I, s') - E^\circ_{R^-/R^+}(I, s'') = (\Delta G^{s'}(Ag/Ag^+) - \Delta G^{s''}(Ag/Ag^+))/F = (RT/F)\ln {}^{s'}\gamma^{s''}_{Ag^+}. \quad (7)$$

Thus the validity of the five R^-/R^+ redox couples employed here as the reference R^-/R^+ redox couple can be checked. Table 5 shows the values of $\Delta^I E^{II}(s)$ obtained with pairs of the five redox couples in the solvents studied. Table 6 summarizes the $\Delta^{s'}E^{s''}(I)$ values for various solvent pairs measured against the silver/silver ion electrode. These results show that the theoretical predictions (6b) and (7) are satisfied within experimental error by all the five R^-/R^+ redox couples. In particular, it is noteworthy that the hydrocarbon and metal complex systems give practically the same

Table 5. $\Delta^I E^{II}(s)$ in various solvents at 25 °C

I	II	$\Delta^I E^{II}(s)$/V			
		PC	DMF	AN	DMSO
DPA	$Fe(bpy)_3$	1.30	1.31	1.31	
DPA	$Ru(bpy)_3$	1.29	1.30	1.29	
DPA	Perylene	0.01		0.01	
DPA	Cobaltocene	1.06	1.07	1.06	
Perylene	Cobaltocene	1.05		1.05	
Perylene	$Fe(bpy)_3$	1.29		1.30	
Perylene	$Ru(bpy)_3$	1.28		1.28	
$Ru(bpy)_3$	Cobaltocene	−0.23	−0.23	−0.23	
$Ru(bpy)_3$	$Fe(bpy)_3$	0.01	0.01	0.02	0.02
$Fe(bpy)_3$	Cobaltocene	−0.24	−0.24	−0.25	

Table 6. $\Delta^{s'}E^{s''}$ (I) for various redox couples at 25 °C

s'	s''	$\Delta^{s'}E^{s''}(I)$/V					
		DPA	Perylene	$Fe(bpy)_3$	$Ru(bpy)_3$	Cobaltocene	Average
DMF	PC	0.36		0.35	0.35	0.35	0.35
AN	PC	0.43	0.43	0.42	0.43	0.43	0.43
DMSO	PC			0.53	0.54		0.54
AN	DMF	0.07		0.07	0.08	0.08	0.08
DMSO	DMF			0.18	0.19		0.19
DMSO	AN			0.11	0.11		0.11

results although they are quite different in their chemical structures.

Regarding the charge distribution in the hydrocarbon ions, it can be confidently assumed that the π-electron spin-density distributions are the same for the monocation and monoanion of an alternant aromatic hydrocarbon. The pairing theorem[26,27] predicts that the π-electron spin-density distributions should be the same for the cation and anion of an alternant aromatic hydrocarbon. Some experimental results[28,29] seem to show that this theorem holds to a high degree of approximation for alternant hydrocarbon ions. Significant differences observed between the ESR spectra of the positive and negative hydrocarbon ions have been interpreted[30,31] in terms of the variation of the σ-π parameter, Q^{H}_{CH}, in McConnell's relation. Therefore it is quite reasonable to assume that[7] the charge distributions in the cation and anion radicals of perylene and DPA are very nearly the same. In fact, this assumption has been adopted by Case and his coworkers[32] in their estimation of the surface potential of acetonitrile. Parker,[33] in his studies on the energetics of electrode reactions of aromatic hydrocarbons, has also proceeded on this assumption. On the other hand the charge distributions in the cations of the bipyridine complexes seem somewhat different from those in the corresponding anions, since in the first three one-electron reduction steps of the bipyridine complexes each added electron may occupy one of the three vacant π^*-orbitals localized mainly in the ligand molecules.[15] This difference in charge distribution between the R^+ and R^- ions fortunately seems to result in a small effect (probably less than 0.01 eV)[7] on the difference of solvation energy, as indicated by the above $\Delta^{I}E^{II}$(s)- and $\Delta^{s'}E^{s''}$(I)-tests. Recently Ogata, Fujisawa, and Tanaka[50] have proposed a $Co(bipy)_3^{3+}/Co(bipy)_3^{2+}$ couple as a candidate for the reference redox couple.

The Born equation for the free energy of ion solvation was first modified by Latimer, Pitzer, and Slansky[34] and later by numerous other authors.[3,6] This was done by introducing the empirical radius corrections specific to the solvent s, R_+(s) and R_-(s) for cations and anions, respectively. This correction should imply supplemental energies of ion solvation which are not involved in the simple Born equation. These supplemental energies may consist of a part of electrostatic energy of solvation due to ion-multipole interactions, as discussed by Buckingham,[35] and a part of non-electrostatic (or van der Waals') interaction energy of solvation. The latter is dependent on the orientation of solvent molecules in the first solvation sheath. Thus, in the modified Born equation the difference in the solvation free energy between two oppositely charged ions having the same radius should be reflected in the difference between R_+(s) and R_-(s). According to Strehlow,[6] $R_+(AN)=0.072$ and $R_-(AN)=0.061$ nm, which will result, for example, in $\Delta G^{AN}_{R^-/R^+}=0.02$ eV for the metal bipyridine complex redox couples.[7] Although Tanaka and Ogata[51] and Nedermeijer-Denessen, de Ligny, and Remijnse[36] have recently shown that the existence of R_+(s) and R_-(s) which are valid for *all* kinds of ions in a specified solvent, s, is questionable, this estimation of $\Delta G^{S}_{R^-/R^+}$ based on the empirical radius corrections as well as the discussion on the $\Delta^{I}E^{II}$(s)- and $\Delta^{s'}E^{s''}$(I)-test described above shows that the error, introduced by assuming $\Delta G^{S}_{R^-/R^+}=0$ (Eq. 4) for the redox couples investigated here, is probably not larger than ± 0.01 eV. Thus it may be concluded that the standard potentials of the R^-/R^+ redox couples studied here are solvent-independent within an error of ± 0.01 V.

To estimate the solvent activity coefficient of an ion at $\mu=0$, μ being the ionic strength, it is necessary to know the dependence of the activity coefficient on the ionic strength in each solvent. Table 7 shows $\Delta E^{r}_{1/2}$(exptl) as the difference of two experimental values of $E^{r}_{1/2}(R^-/R^+)$ at two different concentrations of the supporting electrolyte, *i.e.*, 0.05 and 0.2 M TEAP, referred to Ag/1 mM Ag^+ in 0.05 and 0.2 M TEAP, s, electrodes, respectively. Since $E^{r}_{1/2}(R^-/R^+)\approx E^{\circ}_{R^-/R^+}$ the difference $\Delta E^{r}_{1/2}$(exptl) should be equated to the difference of the two reference electrodes, which is expressed by $\Delta E^{r}_{1/2}=(RT/F)\ln[f^{+}_{Ag}(0.05\ M)/f^{+}_{Ag}(0.2M)]$. Table 7 shows $\Delta E^{r}_{1/2}$(calcd) as the difference calculated by this equation with the Davies equation, $\log f=-A[\sqrt{\mu}/(1+\sqrt{\mu})-0.3\ \mu]$.[37] Good agreement between $\Delta E^{r}_{1/2}$(exptl) and $\Delta E^{r}_{1/2}$(calcd) indicates that the Davies equation is applicable to estimate the ionic activity coefficients of the silver ion in the solvents studied. Thus the solvent activity coefficients of the silver ion were corrected for $\mu=0$ using the Davies equation. Table 8 gives the solvent activity coefficients of the silver ion at $\mu=0$, $(RT/F)\ln {}^{S'}\gamma^{S''}_{Ag^+(\mu=0)}$, in molality scale, as obtained by this procedure. Table 8 also gives for comparison the solvent activity coefficients estimated on the basis of other extrathermodynamic assumptions by other authors.[41,46-48] The $(RT/F)\ln {}^{S'}\gamma^{S''}_{Ag^+(\mu=0)}$ values in molarity scale[47,48] were conventionally converted to the values in molality scale by

TABLE 7. REVERSIBLE HALF-WAVE POTENTIALS OF R^-/R^+ REDOX COUPLES AT DIFFERENT CONCENTRATIONS OF SUPPORTING ELECTROLYTE IN AN AND PC

Solvent	R^-/R^+ couple	$-E^{r}_{1/2}(R^-/R^+)$/V		$\Delta E^{r}_{1/2}$(exptl)/mV	$\Delta E^{r}_{1/2}$(calcd)/mV[c]
		0.2 M TEAP[a]	0.05 M TEAP[b]		
AN	DPA	0.603	0.607	4±2	7
	Cobaltocene	1.658	1.663	5±2	7
	$Fe(bpy)_3$	1.911	1.918	7±2	7
PC	DPA	1.025	1.028	3±2	3

a) V *vs.* Ag/1 mM Ag^+, 0.2 M TEAP. b) V *vs.* Ag/1 mM Ag^+, 0.05 M TEAP.
c) Calculated by Davies equation.

Table 8. Solvent activity coefficients of silver ion at zero ionic strength, $(RT/F)\ \ln {}^{PC}\gamma^{s}_{Ag^+(\mu=0)}$, in molality scale estimated on various assumptions at 25 °C

The assumptions, as numbered in the table, are (1) $\ln {}^{o}\gamma^{s}_{Ph_4As^+} = \ln {}^{o}\gamma^{s}_{Ph_4B^-}$;[48] (2) ferrocene scale;[47] (3) negligible liquid junction;[47] (4) modified Born equation.[41,46]

s	$-(RT/F)\ \ln {}^{PC}\gamma^{s}_{Ag^+(\mu=0)}$/V				
	This work	(1)	(2)	(3)	(4)
AN	0.43	0.40	0.47	0.43	0.39
DMF	0.35	0.35	0.40	0.38	0.36
DMSO	0.53	0.51	0.56	0.57	0.53
Water	(0.23)[a]	0.17	0.09	0.24	0.23

a) Calculated by Eq. 8 (see text).

$$\ln {}^{s'}\gamma^{s''}_{Ag^+(\mu=0)}(\text{molal}) + \ln (d^{s'}_{o}/d^{s''}_{o}) = \ln {}^{s'}\gamma^{s''}_{Ag^+(\mu=0)}(\text{molar}),$$

where $d^{s'}_{o}$ and $d^{s''}_{o}$ are the densities of pure solvents, s′ and s″, respectively. Assumption 1, the reference electrolyte method,[38] equates the solvent activity coefficients of tetraphenylarsonium cation and tetraphenylboride anion, $\log {}^{o}\gamma^{s}_{Ph_4As^+} = \log {}^{o}\gamma^{s}_{Ph_4B^-}$. Assumption 2, based on Strehlow's ferrocene scale, equates the solvent activity coefficients of ferrocene and ferricinium cation.[39] Assumption 3 neglects the liquid junction potential in a cell composed of a nonaqueous salt bridge of tetraethylammonium picrate.[40] Assumption 4 is based on the solvent activity coefficient of rubidium ion calculated by a modified Born equation.[41] The internal coherency of the solvent activity coefficient of the silver ion estimated by these assumptions seems generally satisfactory in these four solvents. In particular, good agreement is seen between the results reported here and those based on assumptions 1 or 4. Such a correspondence, considering the similarities between assumption 1 and ours, would be expected. The modified Born equation with appropriate empirical parameters seems to give a reasonable estimation to the differences in the solvation free energies of large alkali ions between two solvents.

When electron affinity and ionization potential data are available for the neutral compounds R, the free energy change of the reference electrode reaction, $\Delta G^{s}(Ag/Ag^+)$, by Eq. 5 can be calculated. At present the experimental data are not available, but theoretical values of the electron affinity and ionization potential for perylene are available: $(A+I)_{perylene} = 8.23$ eV[42] or 8.68 eV.[43] Alternatively, for the $(A+I)$ value of perylene, the average value of the experimental data of $(A+I)$ for several other alternant aromatic hydrocarbons can be used, since the molecular orbital theory[44] predicts that the $(A+I)$ for alternant aromatic hydrocarbons should be constant, and available experimental results support this relationship: $(A+I)^{ex}_{av} = 8.22$ eV.[32] Assuming 8.22 eV for the $(A+I)$ of perylene, $\Delta G^{s}(Ag/Ag^+)$ by Eq. 5 was calculated and the results are summarized in Table 9. Table 9 also gives the values of the standard free energy change (in molality scale) of the reference electrode reaction, $\Delta G^{os}(Ag/Ag^+)$, conventionally calculated by

$$\Delta G^{os}(Ag/Ag^+) = \Delta G^{s}(Ag/Ag^+) + RT \ln [f_{Ag^+} C_{Ag^+}/d_o],$$

where d_o is the density of the pure solvent and C_{Ag^+} the molar concentration of the silver ion involved in the reference electrode. In the calculations it was also assumed that 1 mM silver salt contained in the reference electrode solution was perfectly dissociated in all the solvents studied. Table 10 shows the values of $(A+I)$ of the compounds used here as the R^-/R^+ reference redox couple which were calculated from Eq. 5 by taking 8.22 eV for the $(A+I)$ of perylene.

Table 9. Standard free energy changes of reference electrode reactions (Ag/Ag^+, s) and solvent activity coefficients of silver ion at 25 °C

s	$(1/F)\Delta G^{s}$. (Ag/Ag^+)/V	$(1/F)\Delta G^{os}$. (Ag/Ag^+)/V	$(RT/F)\cdot \ln {}^{w}\gamma^{s}_{Ag^+(\mu=0)}$/V
PC	−5.15	−5.34	0.23
AN	−4.72	−4.92	−0.19
DMF	−4.79	−4.99	−0.12
DMSO	−4.62	−4.82	−0.29

Table 10. Sum of electron affinity and ionization potential for five reference redox couples studied

	$(A+I)$/eV
Perylene	8.22[a]
DPA	8.24
Cobaltocene	6.12
$Fe(bpy)_3$	5.64
$Ru(bpy)_3$	5.66

a) Reference value.

Recently Trasatti[45] has recalculated the absolute potential of the standard hydrogen electrode using the more reliable value of the hydration free energy of protons; $\varepsilon^{\circ}_{abs} = 4.31 \pm 0.04$ V. This value agreed well with those estimated from the calculated absolute potentials of several alkali metal/alkali metal ion electrodes in water. Thus the absolute electrode potential of an Ag/Ag^+ half-cell in water can be calculated; $\Delta G^{ow}(Ag/Ag^+) = -5.11$ eV. From this the solvent activity coefficients for the transfer of the silver ion from water to nonaqueous solvent can be calculated by

$$(RT) \ln {}^{w}\gamma^{s}_{Ag^+(\mu=0)} = \Delta G^{ow}(Ag/Ag^+) - \Delta G^{os}(Ag/Ag^+). \quad (8)$$

The results are given in Tables 8 and 9. These values agree well with those estimated on the basis of the modified Born equation,[41,46] but deviate by about −0.05 V from those estimated by the reference electrolyte method.[48] Note that the determination of solubilities of the reference electrolyte in water is sometimes associated with inaccuracy.[47]

Addendum. After completion of this work,[52] a paper was published by C. Madec and J. Courtot-Coupez,[53] which contains experimental results that confirm that the R^-/R^+ system of alternant aromatic hydrocarbons can be used as a solvent-independent reference for potential comparisons.[7]

We are grateful to Dr. Takeko Matsumura-Inoue of Nara University of Education for her kind gift of bipyridine complexes used in this work. This work was supported by a grant from the Japanese Ministry of Education.

References

1) D. Bauer and M. Breant, "Electroanalytical Chemistry," ed by A. J. Bard, Marcel Dekker, New York (1975), Vol. 8, p. 281.
2) R. G. Bates, "Solute-Solvent Interactions," ed by J. F. Coetzee and C. D. Ritchie, Marcel Dekker, New York (1969), p. 46.
3) O. Popovych, *Crit. Rev. Anal. Chem.*, **1**, 73 (1970).
4) A. J. Parker, *Electrochim. Acta*, **21**, 671 (1976).
5) I. M. Kolthoff, *Pure Appl. Chem.*, **25**, 305 (1971).
6) H. Strehlow, "The Chemistry of Non-Aqueous Solvents," ed by J. J. Lagowski, Academic Press, New York (1966), p. 129.
7) M. Senda and R. Takahashi, *Rev. Polarogr. (Kyoto)*, **20**, 56 (1974).
8) T. Kakutani, S. Totsuka, and M. Senda, *Bull. Chem. Soc. Jpn.*, **46**, 3652 (1973).
9) S. R. Brinkley, Jr. *J. Am. Chem. Soc.*, **62**, 3524 (1940).
10) G. Wilkinson, *J. Am. Chem. Soc.*, **74**, 6148 (1952).
11) W. E. Geiger, Jr., and D. E. Smith, *J. Electroanal. Chem. Interfacial Electrochem.*, **50**, 31 (1974).
12) W. M. Schwarz and I. Shain, *J. Phys. Chem.*, **69**, 30 (1965).
13) C. K. Mann, "Electroanalytical Chemistry," ed by A. J. Bard, Marcel Dekker, Vol. 3, New York (1969), p. 57.
14) N. Tanaka and Y. Sato, *Electrochim. Acta*, **13**, 335 (1968).
15) T. Saji and S. Aoyagui, *J. Electroanal. Chem. Interfacial Electrochem.*, **58**, 401 (1975).
16) W. E. Geiger, Jr., *J. Am. Chem. Soc.*, **96**, 2632 (1974).
17) S. P. Gubin, S. A. Smirnova, and L. I. Denisovich, *J. Organomet. Chem.*, **30**, 257 (1971).
18) C. K. Mann and K. K. Barnes, "Electrochemical Reactions in Nonaqueous Systems," Marcel Dekker, New York (1970).
19) I. Tachi and M. Senda, "Advances in Polarography," ed by I. S. Longmuir, Pergamon Press, London (1960), Vol. 2, p. 454.
20) R. S. Nicholson, J. M. Wilson, and M. L. Olmstead, *Anal. Chem.*, **38**, 542 (1966).
21) R. S. Nicholson and I. Shain, *Anal. Chem.*, **37**, 178 (1965); *ibid.*, **37**, 190 (1965).
22) H. Matsuda, *J. Electroanal. Chem. Interfacial Electrochem.*, **56**, 165 (1974).
23) R. S. Nicholson and I. Shain, *Anal. Chem.*, **36**, 706 (1964).
24) H. Matsuda and Y. Ayabe, *Z. Elektrochem.*, **59**, 494 (1955).
25) R. S. Nicholson, *Anal. Chem.*, **37**, 1351 (1965).
26) A. D. MacLachlan, *Mol. Phys.*, **2**, 271 (1959).
27) H. M. MacConnell and R. E. Robertson, *J. Chem. Phys.*, **28**, 991 (1958).
28) J. R. Bolton and G. K. Fraenkel, *J. Chem. Phys.*, **40**, 3307 (1964).
29) G. J. Hoijtink and W. P. Weijland, *Recl. Trav. Chim. Pays-Bas*, **76**, 836 (1957).
30) J. R. Bolton, "Radical Ions," ed by E. T. Kaiser and L. Kevan, Interscience Publishers, New York (1968), p. 1.
31) G. Vincow, Ref. 30, p. 151.
32) B. Case, N. S. Hush, R. Parsons, and M. E. Peover, *J. Electroanal. Chem. Interfacial Electrochem.*, **10**, 360 (1965).
33) V. D. Parker, *J. Am. Chem. Soc.*, **98**, 98 (1976).
34) W. M. Latimer, K. S. Pitzer, and C. M. Slansky, *J. Chem. Phys.*, **7**, 108 (1939).
35) A. D. Buckingham, *Discuss. Faraday Soc.*, **24**, 151 (1957).
36) H. J. M. Nedermeijer-Denessen, C. L. de Ligny, and A. G. Remijnse, *J. Electroanal. Chem. Interfacial Electrochem.*, **77**, 153 (1977).
37) C. W. Davies, "Ion Association," Butterworths, London (1962).
38) E. Grunwald, G. Baughman, and G. Kohnstam, *J. Am. Chem. Soc.*, **82**, 5801 (1960).
39) H. M. Koepp, H. Wendt, and H. Strehlow, *Z. Elektrochem.*, **64**, 483 (1960).
40) A. J. Parker and R. Alexander, *J. Am. Chem. Soc.*, **90**, 3313 (1968).
41) J. F. Coetzee and J. J. Campion, *J. Am. Chem. Soc.*, **89**, 2513 (1967).
42) T. Kunii and H. Kuroda, *Theor. Chim. Acta*, **11**, 97 (1968).
43) M. J. S. Dewar, J. A. Hashmall, and N. Trinajstic, *J. Am. Chem. Soc.*, **92**, 5555 (1970).
44) N. S. Hush and J. A. Pople, *Trans. Faraday Soc.*, **51**, 600 (1955).
45) S. Trasatti, *J. Chem. Soc., Faraday Trans. 1*, **70**, 1752 (1974); *J. Electroanal. Chem. Interfacial Electrochem.*, **52**, 313 (1974).
46) N. Matsuura and K. Umemoto, *Bull. Chem. Soc. Jpn.*, **47**, 1334 (1974).
47) R. Alexander, A. J. Parker, J. H. Sharp, and W. E. Waghorne, *J. Am. Chem. Soc.*, **94**, 1148 (1972).
48) B. G. Cox, G. R. Hedwig, A. J. Paker, and D. W. Watts, *Aust. J. Chem.*, **27**, 477 (1974).
49) D. Bauer and J-P. Beck, *Bull. Soc. Chim. Fr.*, **1973**, 1252.
50) T. Ogata, T. Fujisawa, and N. Tanaka, Paper Presented at the Polarographic Meeting, Oct. 7—8, 1976, Nagano; abstract, *Rev. Polarogr. (Kyoto)*, **22**, 124 (1976).
51) N. Tanaka and T. Ogata, *Sci. Rep. Tohoku Univ., Ser. 1*, **57**, 57 (1974).
52) T. Kakutani, Y. Morihiro, M. Senda, R. Takahashi, and K. Matsumoto, Paper presented at the Polarographic Meeting, Nov. 4—5, 1977, Osaka; abstract, *Rev. Polarogr. (Kyoto)*, **23**, 45 (1977).
53) C. Madec and J. Courtot-Coupez, *J. Electroanal. Chem. Interfacial Electrochem.*, **84**, 177 (1977).

Crystal Structures of *N*-(Benzyloxycarbonyl)prolylleucine Ethyl Ester and *N*-(*t*-Butoxycarbonyl)prolylleucine Benzyl Ester

Harumasa SUGINO, Isao TANAKA,* and Tamaichi ASHIDA

Department of Applied Chemistry, Nagoya University, Chikusa-ku, Nagoya 464

(Received April 24, 1978)

The molecular structures of *N*-(benzyloxycarbonyl)prolylleucine ethyl ester and *N*-(*t*-butoxycarbonyl)-prolylleucine benzyl ester, were determined by the X-ray method. The former belongs to the orthorhombic system $P2_12_12_1$ with $Z=4$, $a=9.917(3)$, $b=21.960(3)$, and $c=9.956(1)$ Å; the latter belongs to the monoclinic system $P2_1$ with $Z=2$, $a=10.475(1)$, $b=17.910(1)$, $c=6.303(1)$ Å, and $\beta=90.213(7)°$. Both structures were determined by the direct method; the final R indexes are 0.062 for the former and 0.072 for the latter. An extended conformation found in both dipeptides shows that in terms of the Pro–Leu unit alone this conformation is preferable to the folded β-turn conformation such as is found in longer peptides. The leucyl side chain conformations found in peptides or amino acids were also studied. For the residues occurring in the peptides the $C'-C^{\alpha}-C^{\beta}-C^{\gamma}-C^{\delta 1}$ trans-zigzag conformation was found overwhelmingly, without any obvious relationships to the main chain torsion angles. On the other hand, for the C-termini leucyl residues and leucines the $N-C^{\alpha}-C^{\beta}-C^{\gamma}-C^{\delta 2}$ trans-zigzag conformation was rather preferred and the ϕ values were restricted to a narrow range.

Several linear oligopeptides containing the Pro–Leu sequence have been studied by the X-ray method. They are benzyloxycarbonyl(Z)–Gly–Pro–Leu–Gly–Pro,[1] Z(*o*-Br)–Gly–Pro–Leu–Gly–Pro,[2] Z(*p*-Br)–Gly–Pro–Leu–Gly,[3] *t*-butoxycarbonyl(Boc)–Pro–Leu–Gly,[4] *S*-benzyl–Cys–Pro–Leu–Gly–NH_2,[5] Pro–Leu–Gly–NH_2,[6] and Z–Gly–Pro–Leu.[7] All the oligopeptides but the last two have the β-turn of type I[8] with a 4→1 hydrogen bond, in which Pro and Leu residues are located at the second and third sites of the β-turn. On the other hand, the Pro–Leu parts in Pro–Leu–Gly–NH_2 and Z–Gly–Pro–Leu take more extended forms, somewhat similar to the poly(L-proline) II.

In this study, Z–Pro–Leu–OEt(ethyl ester) and Boc–Pro–Leu–OBzl(benzyl ester), which cannot have an intramolecular hydrogen bond of the β-turn, were prepared and their crystal structures were worked out by the X-ray method.

Experimental

Z–Pro–Leu–OEt and Boc–Pro–Leu–OBzl were prepared from the corresponding N-protected proline and the C-protected leucine.

The X-ray diffraction data were collected on a Hilger and

TABLE 1. CRYSTAL AND EXPERIMENTAL DATA

		Z–Pro–Leu–OEt	Boc–Pro–Leu–OBzl
Molecular formula		$C_{21}H_{30}N_2O_5$	$C_{23}H_{34}N_2O_5$
Molecular weight		390.48	418.53
Crystal system		Orthorhombic	Monoclinic
Space group		$P2_12_12_1$	$P2_1$
Z		4	2
Cell dimensions	$a=$	9.917(3) Å	10.475(1) Å
	$b=$	21.960(3)	17.910(1)
	$c=$	9.956(1)	6.303(1)
	$\beta=$	—	90.213(7)°
	$U=$	2168.2 Å^3	1182.9 Å
D_m, floatation(NaI_{aq})		1.178 g/cm	1.165 g/cm
D_x		1.197	1.175
Number of reflections		2104	1266
(Non-zero reflections)		(1963)	(1182)
$2\theta_{max}$		130°	100°
Crystal size		0.3×0.15×0.07 mm	0.3×0.2×0.02 mm
μ(Cu $K\alpha$)		6.51 cm^{-1}	6.30 cm^{-1}

TABLE 2. Z–Pro–Leu–OEt. FINAL PARAMETERS

(e.s.d.'s in parentheses)

(a) Fractional co-ordinates (×10^4).

	x	y	z		x	y	z
O(1)	5253(2)	1872(1)	3777(2)	C(8)	6030(3)	1840(1)	4894(3)
O(2)	6893(2)	1454(1)	5061(2)	C(9)	4800(3)	2787(1)	5435(2)
O(3)	6609(2)	3131(1)	3969(2)	C(10)	4761(3)	3150(1)	6760(3)
O(4)	6242(2)	4514(1)	4932(2)	C(11)	6141(3)	3027(1)	7372(3)
O(5)	7213(2)	4611(1)	2914(2)	C(12)	6433(3)	2374(1)	7026(3)
N(1)	5693(2)	2278(1)	5768(2)	C(13)	5420(3)	3178(1)	4324(2)
N(2)	4603(2)	3606(1)	3816(2)	C(14)	5166(3)	4086(1)	2987(3)
C(1)	4571(4)	2191(1)	1089(3)	C(15)	4091(3)	4561(1)	2576(3)
C(2)	3790(4)	2297(1)	−60(3)	C(16)	2920(4)	4338(1)	1760(3)
C(3)	3289(4)	1812(1)	−784(3)	C(17)	1976(4)	4870(2)	1458(4)
C(4)	3536(3)	1237(1)	−361(3)	C(18)	3347(5)	4044(2)	463(4)
C(5)	4283(4)	1131(1)	779(3)	C(19)	6263(3)	4417(1)	3751(3)
C(6)	4807(3)	1608(1)	1504(3)	C(20)	8410(3)	4904(1)	3503(4)
C(7)	5661(3)	1474(1)	2696(3)	C(21)	9329(4)	4422(2)	3996(4)

(b) Anisotropic thermal parameters ($\times 10^4$) expressed in the form: $\exp\{-(\beta_{11}h^2+\beta_{22}k^2+\beta_{33}l^2+\beta_{12}hk+\beta_{13}hl+\beta_{23}kl)\}$.

	β_{11}	β_{22}	β_{33}	β_{12}	β_{13}	β_{23}
O(1)	114(2)	23(1)	108(2)	17(2)	−56(4)	−11(2)
O(2)	103(2)	26(1)	145(3)	23(2)	−52(5)	8(2)
O(3)	92(2)	33(1)	126(2)	15(2)	38(4)	15(2)
O(4)	164(3)	38(1)	121(2)	−21(3)	9(5)	−25(2)
O(5)	101(2)	32(1)	155(3)	−18(2)	22(5)	6(2)
N(1)	107(3)	24(1)	88(2)	13(2)	−33(5)	9(2)
N(2)	81(2)	23(1)	92(2)	−1(2)	6(4)	13(2)
C(1)	202(5)	25(1)	103(3)	−15(4)	−3(8)	−11(3)
C(2)	270(6)	29(1)	103(3)	1(4)	−20(9)	14(4)
C(3)	189(5)	46(1)	91(3)	−21(4)	−41(7)	−11(4)
C(4)	166(5)	31(1)	134(4)	−31(3)	−52(8)	−26(3)
C(5)	181(5)	26(1)	139(4)	−4(3)	−68(8)	−33(3)
C(6)	108(4)	27(1)	110(3)	4(3)	0(6)	−25(2)
C(7)	151(4)	35(1)	154(4)	41(4)	−91(8)	−61(4)
C(8)	91(3)	24(1)	105(3)	−7(3)	−34(6)	14(3)
C(9)	100(3)	24(1)	80(3)	9(3)	−8(5)	11(2)
C(10)	164(4)	35(1)	91(3)	34(4)	40(7)	−2(3)
C(11)	175(5)	39(1)	104(4)	16(4)	−49(8)	−28(3)
C(12)	125(4)	39(1)	100(3)	29(3)	−48(7)	−2(3)
C(13)	100(3)	20(1)	79(3)	5(3)	−16(5)	−4(2)
C(14)	99(3)	20(1)	93(3)	−2(2)	3(6)	9(2)
C(15)	123(4)	24(1)	107(3)	1(3)	−6(6)	17(3)
C(16)	150(4)	30(1)	167(4)	−27(3)	−83(8)	35(4)
C(17)	163(5)	42(1)	216(6)	3(4)	−113(10)	52(4)
C(18)	287(7)	46(1)	250(7)	47(6)	−266(14)	−71(5)
C(19)	96(3)	21(1)	120(3)	8(3)	23(6)	−3(3)
C(20)	112(4)	33(1)	260(6)	−22(4)	−42(10)	−3(4)
C(21)	145(5)	50(1)	278(7)	14(5)	−89(10)	1(5)

(c) Hydrogen positional ($\times 10^3$) and isotropic thermal ($\times 10$) parameters.

	x	y	z	B	Bonded to		x	y	z	B	Bonded to
H(1)	491(3)	253(1)	156(3)	50(8)	C(1)	H(16)	563(3)	390(1)	218(3)	27(6)	C(14)
H(2)	352(3)	272(1)	−28(3)	59(9)	C(2)	H(17)	385(3)	479(1)	343(3)	34(6)	C(15)
H(3)	272(3)	191(1)	−167(3)	56(8)	C(3)	H(18)	473(2)	492(1)	197(3)	29(6)	C(15)
H(4)	318(3)	86(1)	−78(3)	60(8)	C(4)	H(19)	243(3)	404(1)	225(3)	52(8)	C(16)
H(5)	448(3)	65(1)	111(3)	59(8)	C(5)	H(20)	111(3)	469(1)	89(3)	62(8)	C(17)
H(6)	556(4)	98(1)	305(3)	74(9)	C(7)	H(21)	173(4)	512(1)	225(4)	98(11)	C(17)
H(7)	672(3)	153(1)	262(3)	53(8)	C(7)	H(22)	231(3)	521(1)	89(3)	47(8)	C(17)
H(8)	388(2)	263(1)	509(2)	5(4)	C(9)	H(23)	241(4)	386(1)	4(3)	88(11)	C(18)
H(9)	457(3)	365(1)	661(3)	31(6)	C(10)	H(24)	424(5)	428(1)	−17(4)	111(12)	C(18)
H(10)	409(3)	295(1)	728(3)	40(7)	C(10)	H(25)	383(3)	373(1)	62(4)	76(10)	C(18)
H(11)	685(3)	328(1)	700(3)	49(8)	C(11)	H(26)	811(3)	523(1)	431(3)	48(7)	C(20)
H(12)	616(3)	313(1)	836(3)	38(7)	C(11)	H(27)	888(4)	524(1)	287(3)	70(9)	C(20)
H(13)	745(2)	225(1)	693(3)	32(6)	C(12)	H(28)	991(3)	464(1)	453(4)	75(10)	C(21)
H(14)	617(3)	202(1)	771(3)	43(7)	C(12)	H(29)	879(3)	420(1)	492(3)	71(9)	C(21)
H(15)	373(2)	365(1)	418(2)	11(5)	N(2)	H(30)	967(4)	411(1)	312(4)	104(12)	C(21)

Watts four circle diffractometer with Ni-filtered Cu $K\alpha$ radiation and ω-2θ step scan. Lorentz and polarization factors were applied, but no absorption corrections were made. The crystal and experimental data are listed in Table 1.

Structure Determination and Refinement

Both structures were determined by the direct method using the program *MULTAN*[9] and refined by the block-diagonal least-sequares method with the program *HBLS* V.[10] Since the ($\bar{2}01$) reflection of Boc–Pro–Leu–OBzl suffered much from extinction, it was omitted from the refinement. The final R values were 0.062 for Z–Pro–Leu–OEt and 0.072 for Boc–Pro–Leu–OBzl. The minimized function was $\sum\omega(\Delta F)^2$, with $\omega=0.0$ for $|F_o|=0$, and $\omega=(\sigma^2(F)+a|F_o|+b|F_o|^2)^{-1}$ for $|F_o|>0$, where $\sigma(F)$ was the standard deviation based on the counting statistics. The parameters were: $a=-0.157$ and $b=0.008$ for Z–Pro–Leu–

OEt, and $a=-0.073$ and $b=0.004$ for Boc–Pro–Leu–OBzl.

All the atomic scattering factors were taken from International Tables for X-Ray Crystallography.[11] The calculations were made on FACOM 230-60 and 75 of Nagoya University. The final positional and thermal parameters are also listed in Tables 2 and 3.[12]

Results and Discussion

Bond Lengths and Angles. The bond lengths and angles of the two molecules (Figs. 1 and 2) are in

Table 3. Boc–Pro–Leu–OBzl. Final parameters
(e.s.d.'s in parentheses)

(a) Fractional co-ordinates ($\times 10^4$).

	x	y	z		x	y	z
O(1)	6298(4)	4822(2)	12019(6)	C(9)	5949(7)	2890(4)	13517(10)
O(2)	6389(4)	4294(2)	15378(6)	C(10)	4231(6)	3789(4)	9867(10)
O(3)	3438(4)	3742(3)	11328(6)	C(11)	2590(6)	3983(3)	7162(10)
O(4)	2993(5)	2732(2)	6075(8)	C(12)	2191(7)	4705(3)	5952(10)
O(5)	1413(4)	3346(2)	4566(6)	C(13)	2336(8)	5402(4)	7255(13)
N(1)	5996(5)	3607(2)	12426(6)	C(14)	1849(8)	6073(4)	5813(15)
N(2)	3903(5)	4004(2)	7942(7)	C(15)	1680(10)	5399(5)	9392(16)
C(1)	7881(8)	5595(4)	13865(15)	C(16)	2399(6)	3298(3)	5844(11)
C(2)	5532(10)	5865(4)	14102(16)	C(17)	1200(7)	2721(4)	3169(12)
C(3)	6661(9)	6014(4)	10720(12)	C(18)	338(6)	2963(4)	1407(10)
C(4)	6595(8)	5591(3)	12780(12)	C(19)	−220(7)	3656(4)	1308(11)
C(5)	6206(6)	4251(4)	13416(11)	C(20)	−1010(7)	3859(5)	−475(12)
C(6)	5619(6)	3547(3)	10226(8)	C(21)	−1176(7)	3350(5)	−2008(12)
C(7)	5739(7)	2697(3)	9801(10)	C(22)	−686(8)	2650(5)	−1950(12)
C(8)	5401(8)	2354(4)	11915(11)	C(23)	68(9)	2456(4)	−265(13)

(b) Anisotropic thermal parameters ($\times 10^4$) expressed in the form:
$\exp\{-(\beta_{11}h^2+\beta_{22}k^2+\beta_{33}l^2+\beta_{12}hk+\beta_{13}hl+\beta_{23}kl)\}$.

	β_{11}	β_{22}	β_{33}	β_{12}	β_{13}	β_{23}
O(1)	154(6)	24(1)	191(14)	−9(6)	−32(15)	6(8)
O(2)	181(7)	34(1)	180(13)	−28(6)	−82(16)	6(9)
O(3)	113(6)	60(2)	280(15)	5(7)	34(15)	51(11)
O(4)	140(7)	28(1)	587(22)	16(6)	−210(20)	14(12)
O(5)	89(5)	34(2)	305(15)	7(5)	−26(15)	15(9)
N(1)	117(7)	23(2)	111(13)	2(6)	−102(16)	−22(10)
N(2)	95(6)	32(2)	186(16)	4(6)	−96(16)	73(10)
C(1)	173(14)	50(4)	600(44)	−93(13)	−180(39)	7(22)
C(2)	235(15)	33(3)	620(43)	34(13)	355(41)	−60(19)
C(3)	219(13)	30(3)	300(28)	−8(10)	−72(32)	36(15)
C(4)	158(11)	21(2)	353(29)	−35(9)	−3(29)	−28(15)
C(5)	118(9)	29(2)	302(24)	−3(9)	12(24)	32(15)
C(6)	84(7)	27(2)	168(17)	0(8)	83(19)	−20(13)
C(7)	131(9)	18(2)	310(24)	1(9)	73(24)	−22(15)
C(8)	193(13)	21(2)	321(26)	−23(9)	−154(30)	9(15)
C(9)	159(11)	24(3)	286(24)	−14(9)	−30(27)	86(14)
C(10)	79(7)	24(2)	334(23)	−4(8)	55(22)	−19(14)
C(11)	79(8)	26(2)	342(25)	14(8)	−79(22)	9(14)
C(12)	142(10)	16(2)	246(23)	0(8)	−88(24)	38(13)
C(13)	135(11)	35(3)	506(36)	8(11)	0(31)	70(18)
C(14)	158(12)	42(3)	572(41)	17(11)	−133(35)	53(20)
C(15)	279(18)	39(4)	614(44)	25(14)	76(45)	−57(22)
C(16)	81(9)	32(3)	410(29)	13(9)	−159(26)	45(15)
C(17)	132(10)	28(3)	436(29)	−28(10)	−75(28)	−57(17)
C(18)	70(8)	41(3)	257(23)	−10(8)	−39(22)	−34(14)
C(19)	110(9)	31(3)	414(27)	25(9)	−53(26)	−28(17)
C(20)	111(10)	45(3)	453(31)	−8(10)	−100(28)	−33(17)
C(21)	97(10)	70(4)	344(27)	−31(11)	−93(26)	−27(19)
C(22)	162(12)	71(4)	274(26)	−32(13)	−110(28)	−97(20)
C(23)	131(10)	54(4)	447(33)	−38(11)	92(29)	−59(20)

(c) Hydrogen positional ($\times 10^3$) and isotropic thermal ($\times 10$) parameters.

	x	y	z	B	Bonded to		x	y	z	B	Bonded to
H(1)	813(6)	618(4)	1412(10)	46(18)	C(1)	H(18)	218(6)	394(3)	885(9)	46(19)	C(11)
H(2)	871(6)	539(3)	1311(10)	43(18)	C(1)	H(19)	131(5)	459(3)	582(9)	34(17)	C(12)
H(3)	780(7)	530(4)	1502(11)	52(19)	C(1)	H(20)	286(6)	471(3)	463(9)	38(17)	C(12)
H(4)	583(7)	645(4)	1489(11)	57(20)	C(2)	H(21)	343(6)	549(3)	776(9)	36(17)	C(13)
H(5)	558(6)	551(3)	1586(9)	34(17)	C(2)	H(22)	187(6)	650(3)	655(10)	43(18)	C(14)
H(6)	438(6)	587(3)	1304(10)	36(17)	C(2)	H(23)	93(5)	609(3)	569(9)	30(16)	C(14)
H(7)	670(6)	659(3)	1108(9)	39(17)	C(3)	H(24)	263(6)	610(3)	483(10)	37(17)	C(14)
H(8)	579(6)	598(3)	1040(10)	44(19)	C(3)	H(25)	175(6)	581(3)	1023(11)	45(19)	C(15)
H(9)	737(6)	574(3)	980(11)	43(18)	C(3)	H(26)	190(6)	489(3)	1070(10)	50(20)	C(15)
H(10)	623(5)	385(3)	927(8)	24(15)	C(6)	H(27)	55(6)	531(4)	872(10)	43(18)	C(15)
H(11)	681(6)	262(3)	938(9)	39(17)	C(7)	H(28)	79(6)	233(4)	407(10)	44(18)	C(17)
H(12)	510(6)	258(3)	833(9)	35(17)	C(7)	H(29)	207(6)	259(3)	228(10)	45(18)	C(17)
H(13)	568(5)	180(3)	1191(8)	29(15)	C(8)	H(30)	−7(5)	410(3)	243(8)	23(15)	C(19)
H(14)	446(6)	226(3)	1251(9)	41(18)	C(8)	H(31)	−157(5)	443(3)	−53(8)	22(15)	C(20)
H(15)	687(6)	269(3)	1444(9)	38(17)	C(9)	H(32)	−175(6)	339(3)	−321(9)	42(18)	C(21)
H(16)	547(5)	292(3)	1489(8)	34(16)	C(9)	H(33)	−74(6)	232(3)	−258(9)	44(19)	C(22)
H(17)	470(6)	413(3)	726(9)	44(18)	N(2)	H(34)	52(6)	204(3)	−19(10)	49(19)	C(23)

TABLE 4. TORSION ANGLES (ϕ, ψ) AND SIDE CHAIN CONFORMATION OF LEUCINE[a]

	ϕ/°	ψ/°	Type[b]	Ref.
N-Acetyl-Leu-isopropylamide	−90	158	I	15
Leu-Pro-Gly	—	153.4	I	16
Benzoyl-DL-Leu-Gly-OEt (A)	−94.2	151.4	I	17
Z-Pro-Leu-OEt	−56.2	147.7	I	
N-Acetyl-DL-Leu-ethylamide	−91	144	I	18
Benzoyl-DL-Leu-Gly-OEt (B)	−64.8	142.6	I	17
N-Acetyl-DL-Leu-*N*-methylamide	−93.8	140.4	I	19
Pro-Leu-Gly-NH_2	−61.2	127.8	I	6
Z-Leu-*p*-nitrophenyl ester	−93.5	48.8	I	20
Boc-Pro-Leu-Gly	−110.8	26.7	I	4
Z-Gly-Pro-Leu-Gly	−115.8	15.4	I	21
Z-Gly-Pro-Leu-Gly-Pro	−107.3	12.0	I	1
Z(*o*-Br)-Gly-Pro-Leu-Gly-Pro	−104.7	8.4	I	2
Z(*p*-Br)-Gly-Pro-Leu-Gly	−104.0	8.0	I	3
S-Benzyl-Cys-Pro-Leu-Gly-NH_2 (A)	−74.1	−8.5	III	5
S-Benzyl-Cys-Pro-Leu-Gly-NH_2 (B)	−71.6	−11.9	II	5
Leu-Tyr Cu(II)	—	−14.7	I	22
D-Leu-Gly	—	−145.4	I	23
Boc-Pro-Leu-OBzl	−99.1	−159.9	I	
Cyclic peptides				
cyclo-(Pro-Leu)	−41.5	33.8	I	24
Ilamycin B_1 (1)	−123	2	I	25
cyclo-(His-Leu)	20.2	−10.4	I	26
C termini residues				
Z-Gly-Pro-Leu	−89.4	(38.1)[c]	I	7
Pro-Leu	−74.8	(−18.9)	I	27
Gly-Leu	−54.9	(−30.2)	II	28
Amino acids				
2Leucine·HCl (A)	—	(−13.1)	II	29
Leucine·HI	—	(−13.3)	II	30
Leucine·HBr	—	(−15.2)	II	31
2Leucine·HCl (B)	—	(−17.7)	II	29
DL-Leucine	—	(−37.1)	II	32
N-methyl-leucines				
N-methyl-DL-Leu-Gly	−57.9	118.3	II	33
Ilamycin B_1 (2)	−128	99	II	25
Ilamycin B_1 (3)	−121	38	I	25
┌-D-HyIv-L-MeIleu-D-HyIv-L-MeLeu-┐	77.9	−33.7	I	34

a) All the torsion angles for the L-isomers are listed. b) Type I, II, and III have the trans-zigzag chains of C'–C^α–C^β–C^γ–$C^{\delta 1}$, N–C^α–C^β–C^γ–$C^{\delta 2}$, and C'–C^α–C^β–C^γ–$C^{\delta 2}$, respectively. c) In cases of C termini leucyl residue and leucine amino acid, ψ means the torsion angle N–C^α–C'–O.

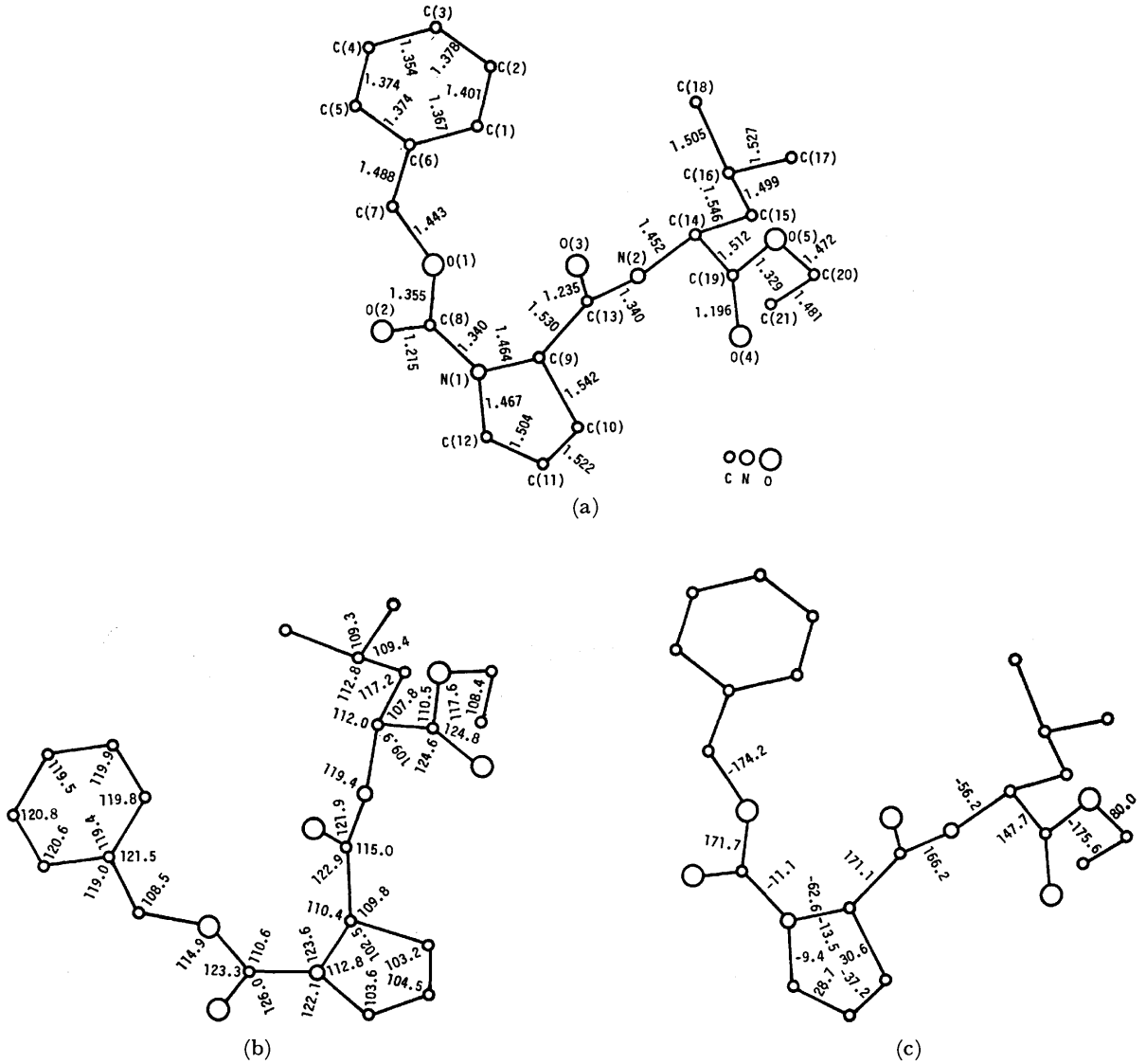

Fig. 1. (a) Bond lengths (Å), (b) angles (°), and (c) torsion angles (°) for Z–Pro–Leu–OEt.

accordance with the average values of the peptides, within the experimental error. Seemingly abnormal large values observed at the C^{β} atoms of the leucyl residues (117.2° in Z–Pro–Leu–OEt and 113.3° in Boc–Pro–Leu–OBzl) are common to all the leucines so far studied. They are attributed to the steric repulsion between the peptide plane and the bulky leucyl side chain.[3]

Prolyl Side Chain. Both pyrrolidine rings are designated as C^{γ}-*endo*, conformation B by the definition of Balasubramanian *et al.*[13] But following the more detailed classification by Ashida and Kakudo,[14] they can be distinguished as C_2–C^{γ}-*endo* for Z–Pro–Leu–OEt and an intermediate state between C_2–C^{γ}-*endo* and C_s–C^{γ}-*endo* for Boc–Pro–Leu–OBzl.

Leucyl Side Chain. Most of the side chain conformations of the leucyl residues so far analyzed can be classified into three trans-zigzag conformations, *i.e.* C′ to $C^{\delta 1}$(type I), N to $C^{\delta 2}$(type II), and C′ to $C^{\delta 2}$(type III).[4] (see Table 4 footnote) The two molecules in this study take a type I conformation.

The main chain torsion angles (ϕ,ψ) and the leucyl side chain conformations are presented in Table 4. For the leucyl residues occurring in the peptides, type I is found overwhelmingly, without any obvious relationships to the main chain torsion angles. On the other hand, for the C termini leucyl residues and leucines, type II is rather preferred and the ψ values seem to be restricted to a narrow range.

Peptide Chain. The main chain torsion angles are shown in Figs. 1 and 2. Both of the peptides analyzed in this study, Z–Pro–Leu–OEt and Boc–Pro–Leu–OBzl, take an extended conformation, in contrast to the folded β-turn conformation of the longer peptides so far analyzed. This observation suggests that an extended conformation is preferable to the folded conformation for the simple Pro–Leu unit. The folded conformation has only been found with the 4⟶1 hydrogen bond. The conformational difference between the dipeptides and the longer peptides suggests an important role for the semi-local interactions, such as the 4⟶1 hydrogen bond, in the folding of peptide chains.

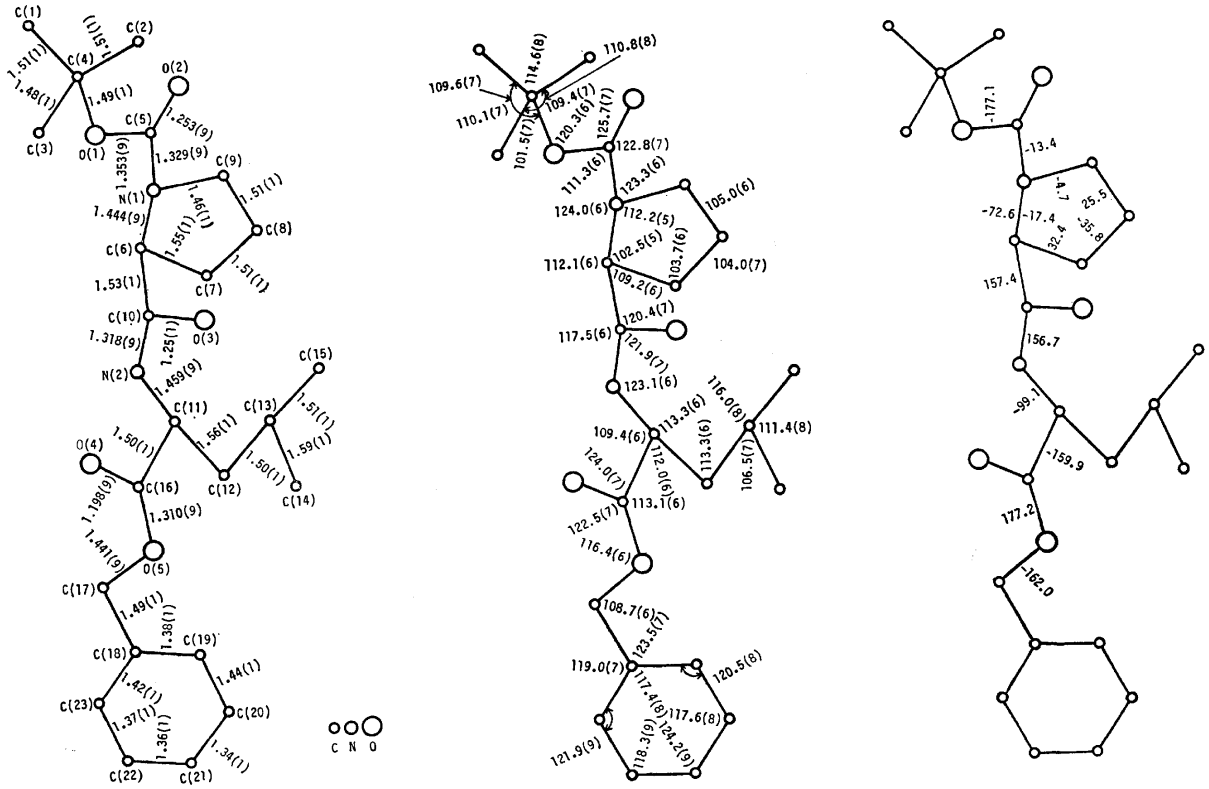

(a) (b) (c)

Fig. 2. (a) Bond lengths (Å), (b) angles (°), and (c) torsion angles (°) for Boc–Pro–Leu–OBzl.

Crystral Structure. The crystal structures of the two compounds are shown in Figs. 3 and 4. Although there is no close relationship between the two structures, the hydrogen bonds between the carbonyl oxygen atom of the oxycarbonyl group and the nitrogen atom of the leucyl residue are commonly observed. This fact, together with the clustering of the Boc or Z group and the other hydrophobic groups in each crystal, suggests that the two N-protecting groups, Boc and Z, play a similar role in crystal packing.

The authors would like to express their sincere thanks to Prof. J. Tanaka of Nagoya University for his very kind permission to use the diffractometer. A part of the cost of this research was covered by a Scientific Research Grant from the Ministry of Education, to which the authors' thanks are due.

References

1) S. Bando, N. Tanaka, T. Ashida, and M. Kakudo, Ann. Meet. Crystallogr. Soc. Japan, Osaka (1973).
2) T. Ueki, S. Bando, T. Ashida, and M. Kakudo, *Acta Crystallogr., Sect. B*, **27**, 2219 (1971).
3) T. Ueki, T. Ashida, M. Kakudo, Y. Sasada, and Y. Katsube, *Acta Crystallogr., Sect. B*, **25**, 1840 (1969).
4) T. Ashida, I. Tanaka, Y. Shimonishi, and M. Kakudo, *Acta Crystallogr., Sect. B*, **33**, 3054 (1977).
5) A. D. Rudko and B. W. Low, *Acta Crystallogr., Sect. B*, **31**, 713 (1975).
6) L. L. Reed and P. L. Johnson, *J. Am. Chem. Soc.*, **95**, 7523 (1973).
7) T. Yamane, T. Ashida, Y. Shimonishi, M. Kakudo, and Y. Sasada, *Acta Crystallogr., Sect. B*, **32**, 2071 (1976).
8) C. M. Venkatachalam, *Biopolymers*, **6**, 1425 (1968).
9) G. Germain, P. Main, and M. M. Woolfson, *Acta Crystallogr., Sect. A*, **27**, 368 (1971).
10) T. Ashida, The Universal Crystallographic Computing System-Osaka, The Computation Center, Osaka Univ. (1973), p. 55.
11) "International Tables for X-Ray Crystallography," The Kynoch Press, Birmingham (1974), Vol. IV, p. 149.
12) The F_o and F_c tables are kept as Document No. 7832a for Z–Pro–Leu–OEt and No. 7832b for Boc–Pro–Leu–OBzl at the Chemical Society of Japan.
13) R. Balasubramanian, A. V. Lakshminarayanan, M. N. Sabesan, G. Tegoni, K. Venkatesan, and G. N. Ramachandran, *Int. J. Protein Res.*, **3**, 25 (1971).
14) T. Ashida and M. Kakudo, *Bull. Chem. Soc. Jpn.*, **47**, 1129 (1974).
15) A. Aubry, Ph. D. Thesis, University of Nancy, Nancy, France, 1976.
16) Y. C. Leung and R. E. Marsh, *Acta Crystallogr.*, **11**, 17 (1958).
17) P. A. Timmins, *Acta Crystallogr., Sect. B*, **31**, 2240 (1975).
18) A. Aubry, M. Marraud, J. Protas, and J. Neel, *C. R. Acad. Sci., Ser. C*, **278**, 697 (1974).
19) T. Ichikawa and Y. Iitaka, *Acta Crystallogr., Sect. B*, **25**, 1824 (1969).
20) V. M. Coiro, F. Mazza, and G. Mignucci, *Acta Crystallogr., Sect. B*, **30**, 2607 (1974).
21) Y. Matsuura, private communication (1977).
22) D. van der Helm, S. E. Ealick, and J. E. Burks, *Acta Crystallogr., Sect. B*, **31**, 1013 (1975).

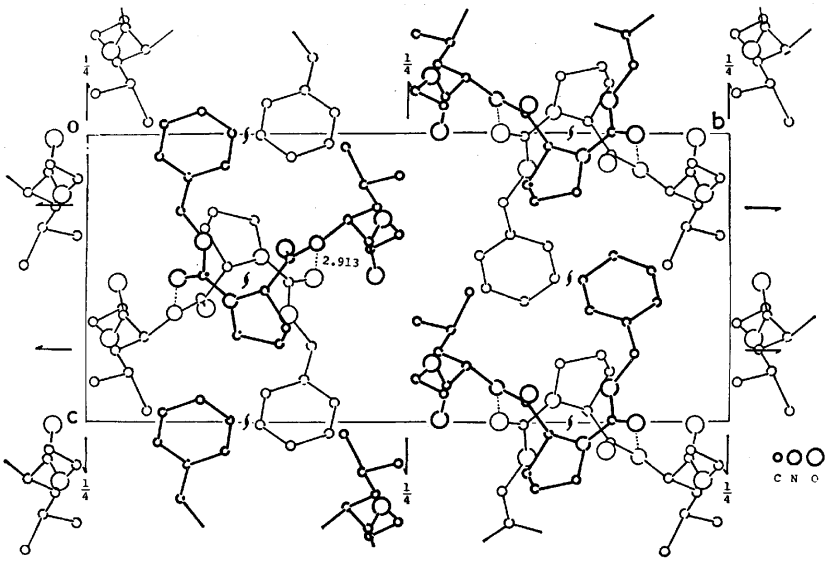

Fig. 3. Crystal structure of Z–Pro–Leu–OEt. Hydrogen bonds are shown with dashed lines.

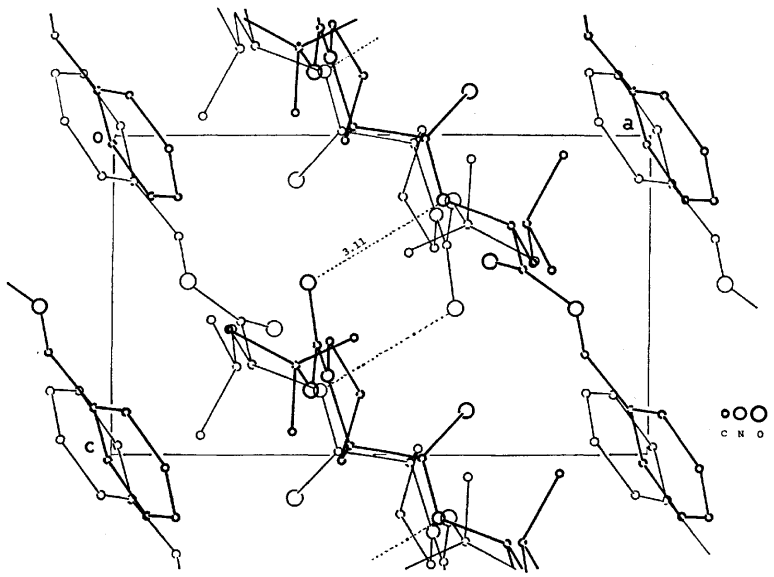

Fig. 4. Crystal structure of Boc–Pro–Leu–OBzl. Hydrogen bonds are shown with dashed lines.

23) S. T. Rao, *Z. Kristallogr.*, **129**, 50 (1969).
24) I. L. Karle, *J. Am. Chem. Soc.*, **94**, 81 (1972).
25) Y. Iitaka, H. Nakamura, K. Takada, and T. Takita, *Acta Crystallogr., Sect. B*, **30**, 2817 (1974).
26) I. Tanaka, T. Iwata, N. Takahashi, T. Ashida, and M. Tanihara, *Acta Crystallogr., Sect. B*, **33**, 3902 (1977).
27) I. Tanaka, Y. Asada, H. Sugino, and T. Ashida, unpublished data.
28) V. Pattabhi, K. Venkatesan, and S. R. Hall, *J. Chem. Soc., Perkin Trans. 2*, **1974**, 1722.
29) L. Golic and W. C. Hamilton, *Acta Crystallogr., Sect. B*, **28**, 1265 (1972).
30) M. O. Chaney, O. Seely, and L. K. Steinrauf, *Acta Crystallogr., Sect. B*, **27**, 544 (1971).
31) E. Subramanian, *Acta Crystallogr.*, **22**, 910 (1967).
32) B. D. Blasio, C. Pedone, and A. Sirigu, *Acta Crystallogr., Sect. B*, **31**, 601 (1975).
33) R. Chandrasekaran and E. Subramanian, *Acta Crystallogr., Sect. B*, **25**, 2599 (1969).
34) J. Konnert and I. L. Karle, *J. Am. Chem. Soc.*, **91**, 4888 (1969).

The Theoretical Study of External Magnetic Field Effect on Chemical Reactions in Solution

Hisaharu HAYASHI and Saburo NAGAKURA*

The Institute of Physical and Chemical Research, Wako, Saitama, 351

(Received April 8, 1978)

External magnetic field effects on chemical reactions in solution are studied theoretically and consequently reactions through radical pairs are shown to be controlled by a magnetic field. Some conditions necessary for the occurrence of the magnetic field effects are discussed, the effects being classified into three types: (1) the electronic Zeeman effect ($\Delta g\beta H$), (2) the hyperfine interaction effect, and (3) the mixed effect.

Recently, magnetic field effects on dynamical processes of excited states have been extensively studied. The phenomena can be divided into two classes; intramolecular and intermolecular cases. The intramolecular phenomena include magnetic field effects on radiative[1] and nonradiative[2] decay processes, predissociation,[3] and reactivity of triplet sublevels.[4] The intermolecular phenomena are related with the selection rule of reactions induced by the collision of excited molecules or radicals with some spin multiplicities (*i.e.* triplet+triplet, triplet+doublet, doublet+doublet *etc.*). In actuality, the intermolecular magnetic field effect has been observed with delayed fluorescence,[5] photoconductivity,[6] chemiluminescence,[7] chemically induced dynamic electron and nuclear polarization (CIDEP and CIDNP).[8]

Concerning external magnetic field effects upon chemical reactions through excited states, reliable studies have scarcely been done. A magnetic field effect upon photo-decomposition has been observed with iodine molecules in gas phase.[3] Gupta and Hammond[9] reported magnetic field effects on some photoisomerization reactions through exciplexes in solution.[10]

Recently, the yields of some excited states produced by pulse radiolysis[11] and laser photolysis[12,13] have been found to be affected by a magnetic field. The Novosibirsk group[14,15] found an external magnetic field effect on the yield ratio of a cage product to a free radical product in some thermal reactions between alkyl lithium and alkyl halide. We also found an external magnetic field effect on the reaction yields of both the cage product and the free radical products in the singlet sensitized photolysis of dibenzoyl peroxide in solution.[16]

In this paper, we have developed a theory for the external magnetic field effect on chemical reactions through radical pairs in solution on the basis of the general formula for the spin hamiltonian of a weakly coupled radical pair which was developed in a previous paper[17] and was used as one of the basic theories for CIDNP.[8] The purpose of the present study is to clarify the conditions necessary for the magnetic field control of chemical reactions.

Theory

It has already been shown that the singlet-triplet conversion in a radical pair in solution is affected by an external magnetic field when the energy separation between the singlet and triplet ground states, $|2J|$, is comparable to or smaller than the difference between the Zeeman energies of the component radicals or their hyperfine energies.[8] Therefore in this paper, we consider only a separated radical pair in solution. In the previous paper,[17] we obtained the matrix elements between the singlet $|S_0; M\rangle$ and triplet $|T_m; M'\rangle$ ($m=0, \pm1$) ground states of a radical pair. It can be expressed in general as follows:

$$v^m_{M',M} = \langle T_m; M'|H_{st}|S_0; M\rangle, \tag{1}$$

where H_{st} in the second-order matrix element representing the interaction between the orbitally degenerate singlet and triplet states,[17] and M and M' stand for the sets of the nuclear states of the singlet and triplet ground states, respectively. The non-vanishing elements for the separated radical pair in solution are given as follows:

$$\langle T_m; M_i^a, M_j^b|H_{st}|S_0; M_i^a, M_j^b\rangle = v_N + (1-m^2)[(g^a-g^b)\beta H+\sum A_i^a M_i^a-\sum A_j^b M_j^b]/2, \tag{2}$$

$$\langle T_{\pm1}; M_i^a \mp 1, M_j^b|H_{st}|S_0; M_i^a, M_j^b\rangle = \mp A_i^a[I_i^a(I_i^a+1)-M_i^a(M_i^a\mp1)]^{1/2}/(8)^{1/2}, \tag{3}$$

$$\langle T_{\pm1}; M_i^a, M_j^b \mp 1|H_{st}|S_0; M_i^a, M_j^b\rangle = \pm A_j^b[I_j^b(I_j^b+1)-M_j^b(M_j^b\mp1)]^{1/2}/(8)^{1/2}. \tag{4}$$

Here g^ν (ν=a or b) is the average value of the three principal values of the g^ν tensor, A_k^ν is the Fermi contact term of the k-th nucleus, and H is the strength of the external magnetic field. As is shown in Appendix, v_N is the usual matrix element for radiationless transition between the singlet and triplet ground states of the radical pair. This corresponds to the radiationless transition rate constant for a large molecule and may safely be assumed to be much samller than the second term on the right-hand side of Eq. 2 for the separated radical pair in solution as is shown in Appendix. Thus, we disregard v_N hereafter in the present paper.

According to the radical pair theory of CIDNP derived by Kaptein,[18] the yield, $P^\Gamma(H)$ (Γ=S(singlet), T(triplet), or F(free radical)) of the cage product through the singlet ground state[19] of a radical pair formed from a Γ-precursor is given for the case where the singlet-triplet transition rate, $k^m_{M',M}$ is small ($k^m_{M',M}=(1/\hbar)\ |v^m_{M',M}| \ll 1/t_d$):

$$P^S(H) = (\lambda/N)\sum_m\sum_M\sum_{M'}(p-x^m_{M',M}), \tag{5}$$

$$P^T(H) = (\lambda/3N(1-p))\sum_m\sum_M\sum_{M'}x^m_{M',M}, \tag{6}$$

$$P^F(H) = (\lambda/4N)\sum_m\sum_M\sum_{M'}[1+\{p(1-\lambda)+\lambda x^m_{M',M}\}/(1-p\{1-\lambda(1-\lambda)/2\})]. \tag{7}$$

Here $k^m_{M',M}$ is the transition rate between $|S_0; M\rangle$ and

$|T_m; M'>$, t_d is the lifetime of the radical pair, λ is the probability for recombination during a singlet encounter, p is the total probability of at least one reencounter appearing in Noyes' reencounter function, $f(t)=m_0t^{-3/2}\exp(-m_0p^2/t)$[20] where m_0 is a constant with the dimension of $s^{1/2}$. N is the number of the nuclear states, $|S_0; M>$, and $x^m_{M'.M}$ is given as follows:[18]

$$x^m_{M'.M} = m_0\pi^{1/2}(v^m_{M'.M})^2(\omega^m_{M'.M})^{-3/2}, \quad (8)$$

where

$$\omega^m_{M'.M} = [\{J+m(g^a+g^b)\beta H/2\}^2+(v^m_{M'.M})^2]^{1/2}. \quad (9)$$

For the case of large $k^m_{M'.M}$ we need a numerical calculation[11-13] for evaluation $P^T(H)$. But for the extreme case where $k^m_{M'.M}$ is very large ($k^m_{M'.M}\gg t_d^{-1}$, $(1/\hbar|J|)$, the singlet–triplet conversion rate is so fast that $|S_0; M>$ and $|T_m; M'>$($m=0$, ±1 for the zero field and $m=0$ for high field) are assumed to exist in equilibrium with each other. Therefore, we can derive the following equations for $P^T(0)$ and $P^T(H_\infty)$:

$$P^S(0) = p\lambda(1+p(1-\lambda/4)+\cdots)/4$$
$$= p\lambda/[4(1-p(1-\lambda/4))], \quad (10)$$
$$P^S(H_\infty) = p\lambda(1+p(1-\lambda/2)+\cdots)/2$$
$$= p\lambda/[2(1-p(1-\lambda/2))], \quad (11)$$
$$P^T(0) = P^S(0), \quad (12)$$
$$P^T(H_\infty) = p(1+p(1-\lambda/2)+\cdots)/6$$
$$= p\lambda/[6(1-p(1-\lambda/2))]. \quad (13)$$

Here $H_\infty\gg 2v^m_{M'.M}/(g^a+g^b)\beta$. In the above evaluation, we assumed, for simplicity, that the radicals escaped from the cage disappear so fast that no cage product is formed through the free radicals.

In order to compare the theory with experiments, we define the relative change in the yield for the cage product, $R^T(H)$, and that for the i-th free radical product, $Q^T_i(H)$, as follows:

$$R^T(H) = [P^T(H)-P^T(0)]/P^T(0), \quad (14)$$
$$Q^T_i(H) = [F^T_i(H)-F^T_i(0)]/F^T_i(0). \quad (15)$$

Here $F^T_i(H)$ is the yield of the i-th free radical product and can be expressed with the fraction, f_i, for giving the product from the escaped radical:

$$F^T_i(H) = f_i[1-P^T(H)]. \quad (16)$$

Therefore, $Q^T_i(H)$ can be rewritten as

$$Q^T_i(H) = -R^T(H)P^T(0)/(1-P^T(0)). \quad (17)$$

This equation means that $Q^T_i(H)$ is independent of f_i and has the opposite sign to $R^T(H)$.

Types of External Magnetic Field Effects on Chemical Reactions

As mentioned above, the matrix elements between the singlet and triplet states of a separated radical pair are expressed by the difference between the g factors and hyperfine interactions of the component radicals. Here we classify the external magnetic field effects on chemical reactions into the following three types: (1) effect of $\Delta g\beta H$ ($\Delta g=g^a-g^b\neq0$ and $A_i^a=A_j^b=0.$), (2) effect of hyperfine interactions ($\Delta g=0$, $A_i^a\neq0$, and $A_j^b\neq0.$), and (3) mixed effect of $\Delta g\beta H$ and hyperfine interactions.

Effect of Electronic Zeeman Interaction ($\Delta g\beta H$). In this case, the following equations hold:

$$v^0_{M'.M} = \Delta g\beta H/2\delta_{M'.M} = v\delta_{M'.M}, \quad (18)$$
$$v^{\pm1}_{M'.M} = 0. \quad (19)$$

These equations show that the conversion occurs only between $|S_0; M>$ and $|T_0; M>$. At first, we consider a reaction through a singlet precursor. For a small v ($(1/\hbar)v\gg t_d^{-1}$), $R^S(H)$ can be given as follows:

$$R^S(H) = -fx/p. \quad (20)$$

Here f is the fraction with which a cage product is given through separated pairs,[21] $x=m_0\pi^{1/2}v^2\omega^{-3/2}$, and $\omega^2=J^2+v^2$. For $v\ll|J|$ (case a) and $v\gg|J|$ (case b), x can be approximated to be $m_0\pi^{1/2}v^2|J|^{-3/2}$ and $m_0\pi^{1/2}v^{1/2}$, respectively. Thus we can derive the following equations:

$$\text{(case a)} \quad R^S(H) = -fm_0\pi^{1/2}(\Delta g\beta H)^2/(p|J|^{3/2}), \quad (21)$$
$$\text{(case b)} \quad R^S(H) = -fm_0\pi^{1/2}(\Delta g\beta H)^{1/2}/p. \quad (22)$$

For the extreme case where H is very large (case c), $R^S(H)$ can be given with the aid of Eqs. 5 and 11 as follows:

$$\text{(case c)} \quad R^S(H) = 1/[2(1-p(1-\lambda/2))]-1. \quad (23)$$

Equations 21—23, clearly show that $R^S(H)$ is proportional to H^2 at low fields and $H^{1/2}$ at higher field, but it saturates at much higher fields. This is shown in Fig. 1.

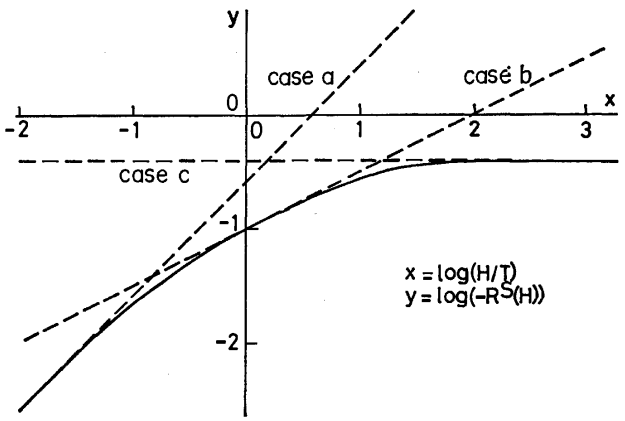

Fig. 1. The calculated contribution of the electronic Zeeman effect to the magnetic field dependence of $R^S(H)$: ——, plot of $\log(-R^S(H))$ *versus* $\log H$ for the whole magnetic field region; ——, plots of $\log(-R^S(H))$ *versus* $\log H$ for cases a, b, and c.

An example of this type of the magnetic field effect is the singlet sensitized photo-decomposition reaction of dibenzoyl peroxide in toluene.[16] It was observed that the yield of phenyl benzoate, the cage product of the reaction, decreased proportionaly to the square root of the applied field strength. This means that the reaction shows a case b type magnetic field effect. From the slope of the observed $R^S(H)$ for phenyl benzoate, *versus* $H^{1/2}$, fm_0/p was determined to be 1.08×10^{-6} $s^{1/2}$ with the aid of Eq. 22. Since $f\lesssim1$, $0.5<p<1$, and $m_0\approx10^{-6}$ $s^{1/2}$,[18] the theoretical value of fm_0/p agrees well with the experimental value.

As for the free radical products (2-methylbiphenyl, 4-methylbiphenyl, and 1,2-diphenylethane) in the

reaction, their $Q_i^S(H)$ values were observed to be independent of f_i and increased by 2% in the presence of 4.3 T field.[16] Since $R^S(4.3\ T)$ and $P^S(0)$ were observed to be -0.08 and 0.12, respectively, for phenyl benzoate,[16,25] $Q_i^S(4.3\ T)$ was calculated to be 0.01 with the aid of Eq. 17. This value also agrees with the observed one (0.02)[16] within the limitations of experimental error.

Next, let us consider reactions through a triplet precursor. For a small v, $P^T(H)$ can be evaluated as follows:

$$P^T(H) = fx/[3(1-p)]. \quad (24)$$

This shows that $P^T(H)$ has the opposite sign to $R^S(H)$ (see Eq. 20). In the extreme case where v is very large, $P^T(H)$ is given by Eq. 13. The reaction showing an external magnetic field effect of this type has not yet been observed. We are now studying the triplet sensitized photo-decomposition reaction of dibenzoyl peroxide. This reaction may be the example of this type.

Effect of Hyperfine Interactions. The effects of hyperfine interactions on some reaction intermediates have been studied by Brocklehurst,[11] Michel-Beyerle *et al.*,[12] and Schulten *et al.*.[13] They evaluated numerically the effects for some ideal cases. Although it is impossible to derive a simple analytical expression for the effect, its qualitative features correspond fairly well to the extreme case where $k^m_{M',M}$ is very large. For this case, the singlet-triplet conversion occurs between $|S_0; M>$ and $|T_m; M'>$ ($m=0, \pm1$ for zero field and $m=0$ for high field, H_∞). Thus $P^\Gamma(H_\infty)$ for this case are given by Eqs. 10—13. According to these equations, the yield of the cage product from the singlet (triplet) precursor increases (decrease) on the application of a strong external magnetic field. Actually, H_∞ is less than 0.1 T for many cases.[11-13] On the other hand, the yield of each free radical product from the singlet (triplet) precursor is proved to decrease (increase) on the application of the field.

For a smaller $k^m_{M',M}$, the change in the yield of each product on the application of a strong field shows the same tendency as that for the strong limit case. But the degree of the change may be smaller than that of the strong limit case because of the diffusion of the radical pair to free radicals. An example of this type of the effect is the thermal reaction of benzylic chloride with butyllithium studied by Sagdeev *et al.*[14]

Mixed Effect of $\Delta g\beta H$ and Hyperfine Interactions. Although it is also difficult to obtain a simple analytical form for this case, qualitative analysis can be done for small $|J|$ ($|J| \ll v^m_{M',M}$) as follow. (1) At zero field, the conversion between $|S_0; M>$ and $|T_m; M'>$ ($m=0, \pm1$) occurs through hyperfine interactions. (2) At a higher field, H_1, where $A/g\beta \ll H_1 \ll A/\Delta g\beta$, and A and g are the orders of hyperfine interactions and g factors of the component radicals, respectively, only the conversion between $|S_0; M>$ and $|T_0; M>$ occurs through hyperfine interactions. Therefore, the yield of the cage product from the singlet (triplet) precursor is shown to increase (decrease) on the application of the field, H_1. (3) at a much higher magnetic field, H_2 (where $A/\Delta g\beta \ll H_2$), the conversion between $|S_0; M>$ and $|T_0; M>$ occurs through $\Delta g\beta H_2$ and hyperfine interactions as shown by Eq. 2. Thus the yield of the cage product at H_2 through the singlet (triplet) precursor is concluded to be smaller (larger) than that at H_1. From Eq. 16, the magnetic field dependence of $F^\Gamma_i(H)$ is also shown to be inverse to that of $P^\Gamma(H)$.

This type of the effect has been observed for the cage and free radical products in the thermal reaction of decafluorodiphenylchloromethane with butyllithium[15] and some free radical products (dimethylbiphenyls and tolyl benzoates) in the photo-decomposition reaction of dibenzoyl peroxide.[26]

The mixed effect at a high field, H ($H>H_1$) can easily be evaluated by taking the matrix element, $v^0_{M,M}$, between $|S_0; M>$ and $|T_0; M>$ as follows:

$$v^0_{M,M} = [(g^a - g^b)\beta H + \sum A_i^a M_i^a - \sum A_j^b M_j^b]/2. \quad (25)$$

In this case, with a method similar to that used for the electronic Zeeman effect, $P^S(H)$ can be given for small $v^0_{M,M}$ as follows:

$$P^S(H) = (\lambda/N)\sum_M (p - fx^0_{M,M}), \quad (26)$$

where

$$x^0_{M,M} = m_0\pi^{1/2}(v^0_{M,M})^2(\omega^0_{M,M})^{-3/2}$$

and

$$(\omega^0_{M,M})^2 = J^2 + (v^0_{M,M})^2.$$

In order to compare the theory with experiments, we define $R^S_{H_1}(H)$ as follow:

$$R^S_{H_1}(H) = [P^S(H_2) - P^S(H)]/[P^S(H_2) - P^S(0)]. \quad (27)$$

When H and H_2 are large enough, $P^S(H)$ and $P^S(H_2)$ can be evaluated by Eq. 26, and $P^S(0)$ can be assumed to be equal to λp. In actuality the $R^S_{4.3T}(H)$ values were calculated for phenyl benzoate in the photo-decomposition reaction of dibenzoyl peroxide, the high magnetic field approximation being adopted and the observed hyperfine coupling constants for *ortho*-(1.74 mT), *meta*-(0.59 mT), and *para*-(0.19 mT) protons of the phenyl radical[24] being used. Since no hyperfine structure was observed for the benzoxyl radical,[22] we did not consider its hyperfine interaction. The calculated $R^S_{4.3T}(H)$ values for various J values are plotted

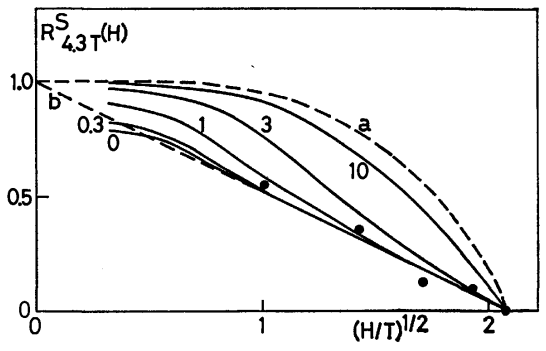

Fig. 2. The dependence of $R^S_{4.3T}(H)$ *versus* $H^{1/2}$ for phenyl benzoate as the photo-decomposition product of dibenzoyl peroxide: ——, the calculated dependence considering both the electronic Zeeman effect and the hyperfine interaction effect; $|J|=0$, 0.3, 1, 3, and 10 mT, for curves 0, 0.3, 1, 3, and 10 respectively; ----, the calculated dependence for case a (curve a) and for case b (curve b) considering only the electronic Zeeman effect: ●, the observed $R^S_{4.3T}(H)$ values for phenyl benzoate.[16]

as the function of $(H)^{1/2}$ in Fig. 2 (solid lines). In this figure are also shown the experimental results of phenyl benzoate (filled circle) and the $R^{S}(H)$-$H^{1/2}$ relationship corresponding to cases a and b of the electronic Zeeman effect (broken lines).

The $R^{S}_{4.3T}(H)$-$H^{1/2}$ plots for $|J|=0$ and $|J|=0.3$ mT agree well with curve b corresponding to case b. This means that in the small $|J|$ region the effect of the hyperfine interactions can safely be disregarded for this reaction compared with that of $\Delta g\beta H$. With increasing $|J|$, the $R^{S}_{4.3T}(H)$ dependence against H gradually deviates from curve b and approaches curve a corresponding to case a. The observed data fit to the curves for $|J|=0$ and $|J|=0.3$ mT (0.281×10^{-3} cm^{-1}). This shows that the magnetic field effect upon formation of phenyl benzoate is mainly due to the electronic Zeeman ($\Delta g\beta H$) effect.

Discussion

The magnetic field effect upon intramolecular processes of an excited state observed for small molecules in gas phase[2,3] is interpreted in terms of the enhancement of the non-radiative decay from the state into a quasi-continuum by the Zeeman interaction and also by the energy shift and broadening of rovibronic levels due to the Zeeman effect.[27,28]

A magnetic field effect on the dynamical process of an exciplex itself has been observed in solid phase[29] or in polymer.[30] This is the case where the acceptor and donor stay separately for a considerable time. In non-viscous solution, it seems difficult to observe any magnetic field effect on the dynamical process of an exciplex itself. The magnetic field effect in non-viscous solution, however, has been observed for reactions through the ion pair after exciplex formation.[12,13] This effect can be explained in terms of the radical pair theory treated in this paper. Recently, Hata observed a magnetic field effect on the photo-isomerization of isoquinoline *N*-oxide.[31] This might be due to a level-crossing[26] in an intermediate radical pair.

We summarize the conditions necessary for the magnetic field control of chemical reactions through raidcal pairs. (1) The magnetic field effect can be observed for reactions which proceed mainly through separated pairs, where $v^{m}_{M'.M}\gg v_{N}$. It is believed that the reaction through close pairs shows no magnetic field effect.[18] (2) The conversion rate $k^{m}_{M'.M}$ between $|S_0; M\rangle$ and $|T_m; M'\rangle$ should not be much smaller than the separation rate of radical pair to free radicals. As is shown in Eqs. 2—4, $k^{m}_{M'.M}$ is large when Δg, hyperfine constants, and the number of the nuclei giving the hyperfine interactions are large. The second condition is the same as that necessary for CIDNP.[8,18] On the other hand, the first condition is not necessary for CIDNP because even a small amount of the product through a separated pair can give the strong CIDNP signal. The magnetic field effect on chemical reactions is useful not only for the determination of the reaction mechanism but also for the control of the product yields. This paper will give a theoretical guidance to the future investigation of the magnetic field effect upon chemical reactions.

We wish to thank Professor K. Tokumaru and Dr. H. Sakuragi, The University of Tsukuba and Dr. Y. Tanimoto, Kanazawa University for their stimulating discussions. We are also indebted to Dr. N. Kanamaru, The Nagoya University and Dr. N. Nishi, The University of Tokyo for valuable comments on radiationless transitions.

Appendix

Since we use a pure-spin BO representation[32] in this paper, the matrix elements between the singlet and triplet states for the usual radiationless transition ($H'_{mr,nt}$) and the hyperfine and electronic Zeeman interactions ($H^{s}_{mr,nt}$) can be written as follows:

$$\begin{aligned}H'_{mr,nt} &= \langle{}^1\psi_{mr}|H_{LS}|{}^3\psi_{nt}\rangle \\ &+ \sum\langle{}^1\psi_{mr}|T_N|{}^1\psi_{ts}\rangle\langle{}^1\psi_{ts}|H_{LS}|{}^3\psi_{nt}\rangle/(E_n-E_t) \\ &+ \sum\langle{}^1\psi_{mr}|H_{LS}|{}^3\psi_{ts}\rangle\langle{}^3\psi_{ts}|T_N|{}^3\psi_{nt}\rangle/(E_n-E_t),\end{aligned} \tag{A-1}$$

$$\begin{aligned}H^{s}_{mr.nt} &= \langle{}^1\psi_{mr}|H_{SI}|{}^3\psi_{nt}\rangle \\ &+ \sum\langle{}^1\psi_{mr}|H_{LZ}|{}^1\psi_{ts}\rangle\langle{}^1\psi_{ts}|H_{LS}|{}^3\psi_{nt}\rangle/(E_n-E_t) \\ &+ \sum\langle{}^1\psi_{mr}|H_{LS}|{}^3\psi_{ts}\rangle\langle{}^3\psi_{ts}|H_{LZ}|{}^3\psi_{nt}\rangle/(E_n-E_t),\end{aligned} \tag{A-2}$$

with

$${}^1\psi_{mr}(q, Q) = {}^1\phi_m(q, Q)\Lambda_{mr}(Q), \tag{A-3}$$

$${}^3\psi_{nt}(q, Q) = {}^3\phi_n(q, Q)\Lambda_{nt}(Q), \tag{A-4}$$

$${}^{\mu}\psi_{ts}(q, Q) = {}^{\mu}\phi_t(q, Q)\Lambda_{ts}(Q), \quad (\mu=1 \text{ or } 3), \tag{A-5}$$

where q and Q denote the sets of electronic, $\phi(q,Q)$, and vibrational, $\Lambda(Q)$, states, respectively. Here H_{LS}, H_{SI}, and H_{LZ} are the spin-orbit, hyperfine, and electronic Zeeman interaction terms, respectively, and T_N is the nuclear kinetic-energy term. Matrix elements v_P and v_F corresponding to the radiationless transitions $S_0\leftarrow T_1$ and $T_1\leftarrow S_1$, respectively, and the matrix element v_R corresponding to the singlet-triplet conversion of a separated radical pair can be given for a large molecule:

$$v_P = \sum_r\sum_t\sum_s(H'_{mr,n0}+H^{s}_{mr,n0}), \tag{A-6}$$

$$v_F = \sum_t\sum_t\sum_s(H'_{m0,nt}+H^{s}_{m0,nt}), \tag{A-7}$$

$$v_R = \sum_t\sum_s(H'_{m0,n0}+H^{s}_{m0,n0}). \tag{A-8}$$

Here we used a low-temperature approximation.

Concerning evaluation of v_P, $H'_{mr,n0}$ is usually approximated to be propotional to its Franck-Condon facter, $\langle\Lambda_{mr}|\Lambda_{n0}\rangle$[32], and $H^{s}_{mr.n0}$ can also be shown to be propotional to it. Thus v_P can be approximated as follows:

$$v_P = \sum_r(h'_{mn}+h^{s}_{mn})\langle\Lambda_{mr}|\Lambda_{n0}\rangle, \tag{A-9}$$

where $h'_{m,n}$ and h^{s}_{mn} are the propotional coefficients of $H'_{mr,n0}$ and $H^{s}_{mr.n0}$ respectively. They can be determined by the electronic wave functions at the equilibrium position for Q. Since βH is 0.467 cm^{-1} for $H=1$ T, and vibronic couplings are usually estimated larger than 100 cm^{-1}, h^{s}_{mn} can safely be ignored in the evaluation of v_P for usual experimental conditions. In a similar way, $H^{s}_{m0.nt}$ can also be shown to be disregarded for estimating v_F.

Concerning evaluation of v_R, $H^{s}_{m0.n0}$ is shown to be proportional to its Franck-Codon factor which may be assumed to be equal to unity for a separated raidcal pair. Therefore, $H^{s}_{m0.n0}$ in Eq. A-8 can be replaced by h^{s}_{mn} as are shown in Eqs. 2—4. On the other hand, $H'_{m0,n0}$, can be assumed to be much

smaller than $H^{S}_{m0,n0}$ as is shown below. The first order term in $H'_{m0,n0}$ vanishes since the singlet and triplet ground states have the same electronic structure. The second order terms are shown to be proportional to the following integral according to the promoting mode, Q_k:

$$\langle\chi_n^{k0}(0)|\mathbf{O}^1(Q_k)|\chi_i^{ks}(v_i^{ks})\rangle\langle\chi_i^{ks}(v_i^{ks})|\chi_m^{k0}(0)\rangle.$$

Here $\chi_p^{kq}(v_p^{kq})$ is the q-th vibrational wave function of the k-th promoting mode in the p-th electronic state with the vibrational quantum number, v_p^{ks}, and $\mathbf{O}^1(Q_k)$ is a linear operator according to Q_k Since $|\chi_n^{k0}(0)\rangle$ is nearly the same as $|\chi_m^{k0}(0)\rangle$ for the radical pair, the above integral vanishes for a harmonic oscillator. Thus this integral can safely be assumed to be much smaller than h^{S}_{mn}/h'_{mn}. Therefore, $H'_{m0,n0}$ in Eq. A-8 can safely be disregarded in estimating v_R, as is assumed in this paper. Of course there may be the case where it can not be disregarded.

References

1) W. B. Fowler, M. J. Marrone, and M. N. Kabler, *Phys. Rev. B*, **3**, 5909 (1973).

2) A. Matsuzaki and S. Nagakura, *Bull. Chem. Soc. Jpn.*, **49**, 359 (1976); A. Matsuzaki and S. Nagakura, *Z. Phys. Chem.*, **101**, S283 (1976).

3) L. A. Turner, *Z. Phys.*, **65**, 464 (1930); E. O. Debenkolb, J. I. Steinfeld, E. Wasserman, and W. Klemperer, *J. Chem. Phys.*, **51**, 615 (1969).

4) M. Leung, and M. A. El-Sayed, *J. Am. Chem. Soc.*, **97**, 669 (1975).

5) R. C. Johnson and R. E. Merrifield, *Phys. Rev. B*, **1**, 896 (1970).

6) N. E. Geacintov, M. Pope, and S. Fox, *J. Phys. Chem. Solids*, **31**, 1375 (1970).

7) L. R. Faulkner and A. J. Bard, *J. Am. Chem. Soc.*, **91**, 209 (1969).

8) "Chemically Induced Magnetic Polarization," ed by A. R. Lepley and G. L. Closs, Wiley & Sons, New York (1973).

9) A. Gupta and G. S. Hammond, *J. Chem. Phys.*, **57**, 1789 (1972).

10) We reexamined their experiments with no effect to be observed; H. Hayashi, Y. Sakaguchi, and S. Nagakura, presented at the 26th International Congress of Pure and Applied Chemistry, Tokyo, Spetember 1977.

11) B. Brocklehurst, *J. Chem. Soc. Faraday Trans. 2*, **70**, 769 (1976).

12) M. E. Michel-Beyerle, R. Haberkorn, W. Bube, E. Bube, E. Steffens, H. Schroder, H. J. Neusser, and E. W. Schlang, *Chem. Phys.*, **17**, 139 (1976); R. Haberkorn, *ibid.*, **19**, 165 (1977).

13) K. Schulten, H. Staerk, A. Weller, H.-J. Werner, and B. Nicker, *Z. Phys. Chem.* **101**, S371 (1976).

14) R. Z. Sagdeev, T. V. Leshina, M. A. Mamkha, S. M. Shein, and Yu. N. Molin, *Org. Magn. Res.*, **5**, 603 (1973).

15) A. V. Podoplelov, R. Z. Sagdeev, T. V. Leshina, Yu. A. Grishin, and Yu. N. Molin, *Dokl. Akad, Nauk USSR*, **221**, 866 (1975).

16) Y. Tanimoto, H. Hayashi, S. Nagakura, H. Sakuragi, and K. Tokumaru, *Chem. Phys. Lett.*, **41**, 267 (1976).

17) K. Itoh, H. Hayashi, and S. Nagakura, *Mol. Phys.*, **17**, 561 (1969).

18) R. Kaptein, *J. Am. Chem. Soc.*, **94**, 6251 (1972).

19) In this paper, the products are assumed to be derived only from singlet states. The cases where some products are given through triplet states can be treated in a similar way.[11–13]

20) R. M. Noyes, *J. Am. Chem. Soc.*, **78**, 5486 (1956).

21) In the actual reaction, a cage product is considered to be given through not only separated pairs but also close pairs. For the latter case, x can safely be assumed to be zero because its $|J|$ value may be much large than v.

22) In the calculation, Δg was given by the difference between the g factors of the benzoxyl (2.0117)[23] and phenyl (2.0024)[24] radicals determined by ESR experiments.

23) N. J. Karck, E. T. Koh, B. L. Whitsel, and J. M. Mcbride, *J. Am. Chem. Soc.*, **97**, 6729 (1975).

24) P. H. Kasai, P. A. Clarke, and E. B. Whipple, *J. Am. Chem. Soc.*, **92**, 2640 (1970).

25) K. Tokumaru, A. Oshima, T. Nakata, H. Sakurai, and T. Mishima, *Chem. Lett.*, **1974**, 571; T. Nakata, and K. Tokumaru, *Bull. Chem. Soc. Jpn.*, **43**, 3315 (1970).

26) Y. Sakaguchi, H. Hayashi, and S. Nagakura, *Chem. Phys. Lett.*, to be published.

27) A. Matsuzaki, and S. Nagakura, *Helv. Chim. Acta*, **61**, 675 (1978).

28) P. W. Atkins, and P. R. Stannard, *Chem. Phys. Lett.*, **47**, 113 (1977).

29) R. P. Groff, A. Suna, P. Avakian, and R. E. Merrified, *Phys. Rev. B*, **9**, 2655 (1974).

30) K. Okamoto, A. Itaya, and S. Kusabayashi, *Chem. Lett.*, **1976**, 99.

31) N. Hata, *Chem. Lett.*, **1976**, 547.

32) B. R. Henry and W. Siebrand, "Organic Molecular Photophysics," ed by J. B. Birds, Wiley & Sons, New York (1975), Vol. 1, p. 153.

Electronic Structures and Spectra of Aminoacetophenones and Related Compounds

Ryoichi NAKAGAKI,† Saburo NAGAKURA,*,†,†† Takayoshi KOBAYASHI,†† and Suehiro IWATA††

†*The Institute for Solid State Physics, The University of Tokyo, Minato, Tokyo 106*

††*The Institute of Physical and Chemical Research, Wako, Saitama 351*

(Received June 10, 1978)

The $S_n \leftarrow S_0$ and $S_n \leftarrow S_1$ transition bands were measured with *m*- and *p*-dimethylaminoacetophenones and related compounds in order to clarify the characters of the excited singlet states. The observed spectra were reasonably interpreted by the use of the theoretical results based on the composite molecule method. The longest wavelength band ($S_1 \leftarrow S_0$) of the meta isomer has mainly the local excitation (LE) character of aniline ($^1B_2 \leftarrow {}^1A_1$), while that of the para isomer is ragarded as the intramolecular charge-transfer band. In the para isomer the LE transition corresponding to $^1B_2 \leftarrow {}^1A_1$ is covered by the intense CT band. The $S_n \leftarrow S_1$ transitions of the meta isomer are almost of LE character, whereas those of the para isomer are of back CT nature. This is mainly attributed to the difference in the character of S_1.

The π-electron systems of organic compounds containing electron donor and electron acceptor group have been extensively studied from the standpoint of intramolecular charge-transfer interaction.[1-13] Disubstituted benzene molecules, D–C_6H_4–A, where D and A represent an electron donor and an electron acceptor, respectively, are typical intramolecular donor-acceptor systems and exhibit characteristic absorption spectra. The spectra have been interpreted by the composite molecule method (the molecules in molecule method) for nitroanilines, nitrophenols, cyanophenols, and other compounds.[4,7,14,15] More recently, McGlynn and coworkers studied the luminescence spectra and kinetic parameters of cyanoanisoles, fluorobenzonitriles, cyanoanilines, and nitroanilines.[16-18] The $T_n \leftarrow T_1$ transitions of aminobenzenes and cyanobenzenes were measured and discussed in terms of intramolecular charge-transfer interaction.[19,20]

In the present work, the $S_n \leftarrow S_0$ and $S_n \leftarrow S_1$ (transient) absorption spectra of aminoacetophenones and related compounds have been measured in order to clarify the characters of the excited states. The $S_n \leftarrow S_0$ and $S_n \leftarrow S_1$ transitions of aminoacetophenones were analyzed with the aid of the theoretical results based on the composite molecule method, in which the intramolecular charge-transfer interaction of the aminophenyl group with the carbonyl group was considered.

Experimental

Materials. Commercially available *m*- and *p*-aminoacetophenones (*m*- and *p*-AAP), *p*-dimethylaminobenzaldehyde (*p*-DMABA), *N*,*N*-dimethyl-*p*-nitroaniline (*p*-DMNA) were chromatographed from benzene on activated alumina and recrystallized from the same solvent. The meta and para isomers of dimethylaminoacetophenone (*m*- and *p*-DMAAP) and *p*-dimethylaminobenzonitrile (*p*-DMABN) were synthesized according to the methods described in literature,[21-23] and purified in the same manner as mentioned above.

Measurements. Visible and ultraviolet absorption spectra were measured on a Cary 14 recording spectrophotometer. Emission spectra were measured with a Spex 1700-II grating monochromator equipped with an EMI 6256S photomultiplier and a PAR 128 lock-in amplifier. The fluorescence quantum yield was determined by the use of a Shimadzu RF-502 spectrofluorometer, 2,5-diphenyloxazole with the quantum yield of 1.00 in cyclohexane[24] being used as the standard. A method for the determination of fluorescence lifetimes was the same as described previously.[25]

For the measurement of transient absorption spectra two methods were employed; the one is an ordinary N_2 laser photolysis method (method I), the details of which were already reported,[25] and the other is a method using superradiant fluorescence from solution as an analyzing light source (method II).[26] The transient absorption spectra obtained by the latter method were superposition of the $S_n \leftarrow S_1$ and $T_n \leftarrow T_1$ transitions. Even for fluorescent compounds method II is applicable to the measurement of the $S_n \leftarrow S_1$ transition bands. In method II, dyes used were as follows: 3-cyano-7-hydroxy-4-methylcoumarin, coumarin 1 (7-dimethylamino-4-methylcoumarin), coumarin 30 (3-(2′-methyl-1-benzimidazolyl)-7-diethylaminocoumarin), 7-diethylamino-4-(trifluoromethyl)-coumarin, Brilliant Sulfaflavine, Uranine, Rhodamine 6G, Rhodamine B, Cresyl Violet perchlorate–Rhodamine 6G mixture, and Cresyl Violet perchlorate–Rhodamine B mixture.

For the measurement of the transient absorption spectra the concentration of the solution was adjusted so that the absorbance at 337.1 nm was $\approx$1.0 in 1 mm light-path.

Theoretical

Molecular Geometry of Aminoacetophenones. In carrying out the MO calculations on aminoacetophenones the following assumptions were made concerning the molecular geometry; the molecules are planar, the phenyl rings are equilateral hexagonals with the C–C distance of 1.397 Å,[27] and the angle between the double bond of the carbonyl group and the single bond linked to the phenyl ring is 120°. Other atomic distances were taken from the data on *p*-aminoacetophenone determined by X-ray crystal analysis:[28] namely, the C–C distance in the single bond between the carbonyl and the phenyl group is 1.468 Å, the C–O distance in the carbonyl double bond is 1.215 Å, and the C–N distance is 1.376 Å.

Configuration Interaction Calculation. In the present treatment aminoacetophenones are considered to be composite molecules consisting of an electron donor, aminophenyl group, and an electron acceptor, carbonyl group. The π-electron energy and wave functions of several electron configurations; the ground (G) configuration, the locally excited (LE) configura-

tions within the aminophenyl group, and the charge-transfer (CT) configurations in which an electron in the occupied orbital of the donor is transferred into the anti-bonding orbital of the acceptor. The diagonal energies corresponding to the local excitations of aminophenyl group were taken from the spectroscopic data on anilines and *N*-alkylated derivatives in the previous paper.[9]

To evaluate the off-diagonal elements between LE and CT configurations, the accurate wave functions for the LE's of aminophenyl groups were required. At first, the LCAO SCF MO's of the π-electron systems of aniline and *N*,*N*-dimethylaniline, $\phi_i (i=1\text{—}7)$, were calculated by the aid of the Pariser-Parr-Pople method.[29] The wave functions for the ground and excited states of aniline and *N*,*N*-dimethylaniline were obtained by considering CI among electron configurations constructed from the SCF MO's. The configurations considered in the CI calculation are given below: for A_1 symmetry, 28 configurations, that is, the ground, 5 singly excited, 14 doubly excited, and 8 triply excited configurations, and for B_2 symmetry, 25 configurations, that is, 5 singly excited, 12 doubly excited, and 8 triply excited configurations. From the resultant excited wave functions the lowest 3 wave functions with A type symmetry and the lowest 3 wave functions with B type symmetry were picked up as LE configurations for the further CI calculations of energy levels and wave functions of aminoacetophenones.

The molecular orbitals of the carbonyl group obtained by Tanaka were used in the present calculation.[30]

The CT configurations taken in the CI calculation for aminoacetophenones were given below:

$$\text{CT(4-A)} = (\phi_4^{-1}\text{A}),\ \text{CT(3-A)} = (\phi_3^{-1}\text{A}),\ \text{and}$$
$$\text{CT(2-A)} = (\phi_2^{-1}\text{A}).$$

Here, A denotes the anti-bonding orbital of the acceptor, carbonyl group, and ϕ_i the *i*-th occupied orbital of aniline, the highest occupied orbital being ϕ_4. The energies of the CT configurations were evaluated by the equation,

$$E(\text{CT}) = I_P(\phi_i) - E_A(\text{C=O}) - C,$$

where $I_P(\phi_i)$ is the ionization potential of the donor, E_A(C=O) is the electron affinity of the acceptor, and C is the coulombic interaction energy between the donor and acceptor groups. The values of I_P were taken from the photoelectron spectroscopic data,[31,32] the affinity E_A was assumed as -1.2 eV,[5] and C values were calculated by using the values of two center Coulomb repulsion integrals (rr|ss), which were evaluated according to the Pariser-Parr method.[29]

The off-diagonal matrix elements of the total electronic Hamiltonian were evaluated by the aid of the formulations by Pople[33] and by Longuet-Higgins and Murrell.[3] They were given in terms of $\beta_{C\text{-}C=O}$, the core resonance integral between the ring carbon and the carbonyl carbon. Actual calculations were made by changing $\beta_{C\text{-}C=O}$ as a parameter from -1.50 eV to -1.90 eV by a step of 0.10 eV. Consequently, the results were found to be insensitive to the parameter. The energies and wave functions for $\beta_{C\text{-}C=O}$ of -1.90 eV are shown in Table 1.

Table 1. The energy levels and wave functions of *m*- and *p*-dimethylaminoacetophenone

(*m*-DMAAP)

$W_0 = -0.23$ eV

$\Psi_0 = -0.9815\Psi_G + 0.1398\Psi_{CT(4-A)} + 0.1129\Psi_{CT(2-A)} + \cdots$

$W_1 = 3.87$ eV

$\Psi_1 = -0.7615\Psi_{1B_2} + 0.6044\Psi_{CT(4-A)} + 0.1960\Psi_{2A_1} + \cdots$

$W_2 = 4.77$ eV

$\Psi_2 = 0.5965\Psi_{1B_2} + 0.5783\Psi_{2A_1} + 0.5427\Psi_{CT(4-A)} + \cdots$

$W_3 = 5.34$ eV

$\Psi_3 = 0.6924\Psi_{2A_1} - 0.5306\Psi_{CT(4-A)} + 0.4145\Psi_{CT(3-A)} - 0.2017\Psi_{1B_2} + \cdots$

$W_4 = 5.63$ eV

$\Psi_4 = 0.7203\Psi_{CT(3-A)} - 0.4098\Psi_{2B_2} - 0.3706\Psi_{2A_1} + 0.3133\Psi_{3A_1} + \cdots$

(*p*-DMAAP)

$W_0 = -0.28$ eV

$\Psi_0 = -0.9747\Psi_G - 0.1821\Psi_{CT(4-A)} - 0.1278\Psi_{CT(2-A)} + \cdots$

$W_1 = 4.17$ eV

$\Psi_1 = 0.8049\Psi_{CT(4-A)} - 0.5635\Psi_{2A_1} - 0.1514\Psi_G + \cdots$

$W_2 = 4.25$ eV

$\Psi_2 = -0.9822\Psi_{1B_2} + 0.1799\Psi_{CT(3-A)} + \cdots$

$W_3 = 5.57$ eV

$\Psi_3 = 0.7403\Psi_{CT(3-A} + 0.6463\Psi_{2B_2} + 0.1712\Psi_{1B_2} + \cdots$

$W_4 = 5.61$ eV

$\Psi_4 = 0.8250\Psi_{2A_1} + 0.5531\Psi_{CT(4-A)} + \cdots$

G, the ground configuration; nA$_1$, the n-th LE of aniline with A_1 symmetry ($n \geq 2$); mB$_2$, the m-th LE of aniline with B_2 symmetry ($m \geq 1$); CT(i-A), CT from the i-th MO of aniline to acceptor.

The oscillator strengths were calculated by the use of the equation,

$$f = 8.753 \times 10^{-2} Q^2 \Delta E,$$

where $Q = (\Psi_0 | er | \Psi_1)$, and ΔE is the transition energy in eV. The theoretical results of the transition energies and oscillator strengths are shown in Table 2, together with the observed values.

Table 2. Transition energies (ΔE (eV)) and oscillator strengths (f) observed and calculated for the meta and para isomers of dimethylamino-acetophenone

Transition	Calcd		Obsd		
	ΔE	f	ΔE[a]	f[a]	ΔE[b]
(*m*-DMAAP)					
$\Psi_1 \leftarrow \Psi_0$	4.10	0.028	3.51	0.046	
$\Psi_2 \leftarrow \Psi_0$	5.00	0.099	4.79	0.13	
$\Psi_3 \leftarrow \Psi_0$	5.57	0.186	5.18	0.49	
$\Psi_4 \leftarrow \Psi_0$	5.86	0.018	>5.58		
(*p*-DMAAP)					
$\Psi_1 \leftarrow \Psi_0$	4.45	0.076	3.97	(0.46)	3.49
$\Psi_2 \leftarrow \Psi_0$	4.53	0.028			≈4.1
$\Psi_3 \leftarrow \Psi_0$	5.85	0.225	5.33	(0.13)	≈5.0
$\Psi_4 \leftarrow \Psi_0$	5.88	0.682			≈5.4

a) In cyclohexane. b) In 1,1,1,3,3,3-hexafluoro-2-propanol (HFP).

Results and Discussion

The $S_n \leftarrow S_0$ Transition Bands of m- *and* p-*Dimethylaminoacetophenones.* In cyclohexane, the $n\pi^*$ band of *m*-DMAAP or *p*-DMAAP was observed as a weak tail (log $\varepsilon \leq 2$) at the longer wavelength side of the lowest $\pi\pi^*$ or CT band. In polar solvents, however, it was found to be covered by the intense $\pi\pi^*$ or CT band.

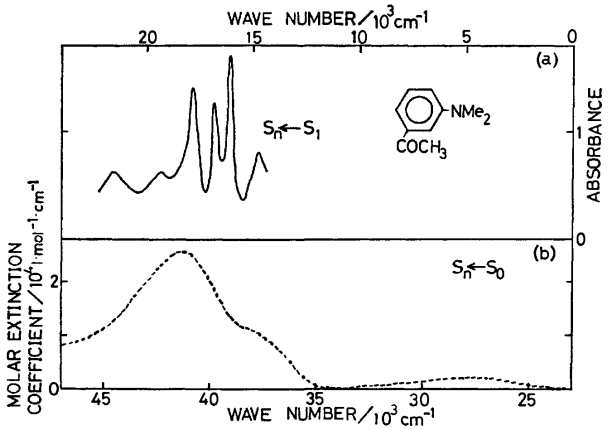

Fig. 1. (a) Upper: the transient absorption spectrum of *m*-DMAAP in ethanol at room temperature obtained by method II. The transition energy is indicated on the upper abscissa in the units of 1000 cm^{-1}. (b) Lower: the absorption spectrum of *m*-DMAAP in ethanol at room temperature. The transition energy is indicated on the lower abscissa in the units of 1000 cm^{-1}.

In the absorption spectrum of ethanolic solution of *m*-DMAAP (Fig. 1-b), we can see four $\pi\pi^*$ transition bands: three bands at 27600, 37800, and 41300 cm^{-1} and an additional tail at higher energy side (45000 cm^{-1}). In cyclohexane solution of *p*-DMABA or *p*-DMAAP (Fig. 3 or 4), two bands were observed in the region, 28000—47000 cm^{-1}.

The intense long wavelength band of *p*-DMAAP or *p*-DMABA shows the increasing red-shift on going from the nonpolar solvent, cyclohexane, to the polar ones: cyclohexane<acetonitrile<ethanol<water<1,1,1,3,3,3-hexafluoro-2-propanol (HFP) (see Figs. 2-b, 4, and 5). The largest red-shift was observed in HFP solution, in spite of the rather low dielectric constant and refractive index of this solvent (16.62 at 25 °C and 1.2750 at Na D line) compared with those of ethanol (24.3 and 1.3618), acetonitrile (37.5 and 1.3437), and water (78.54 and 1.3330). This fact indicated that the red-shift observed in HFP is mainly due to hydrogen bonding.[34] In the HFP solution of *p*-DMAAP or *p*-DMABA, four $\pi\pi^*$ or CT bands were observed: *e.g.* for *p*-DMABA, one strong band at 27400, and three bands at $\approx$33000, $\approx$39800, and $\approx$43500 cm^{-1} (Fig. 3). Formation of strong hydrogen bonds between the solute, *p*-DMAAP or *p*-DMABA, and the solvent, HFP, causes the large red-shift of some of the absorption bands. On the other hand, the bands less sensitive to the hydrogen bonding show small solvent shift. As the result the two bands observed in cyclohexane split into four components in strongly hydrogen bonding HFP.

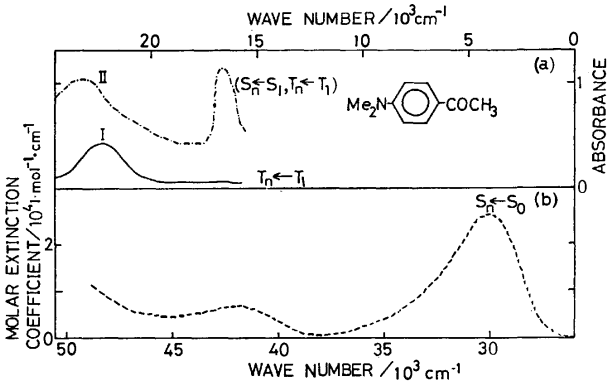

Fig. 2. (a) Upper: I, the $T_n \leftarrow T_1$ transition spectrum of *p*-DMAAP in ethanol at room temperature obtained by method I. II, the transient absorption spectrum of *p*-DMAAP in ethanol at room temperature obtained by method II. The transition energy is indicated on the upper abscissa in the units of 1000 cm^{-1}. (b) Lower: the absorption spectrum of *p*-DMAAP in ethanol at room temperature. The transition energy is indicated on the lower abscissa in the units of 1000 cm^{-1}.

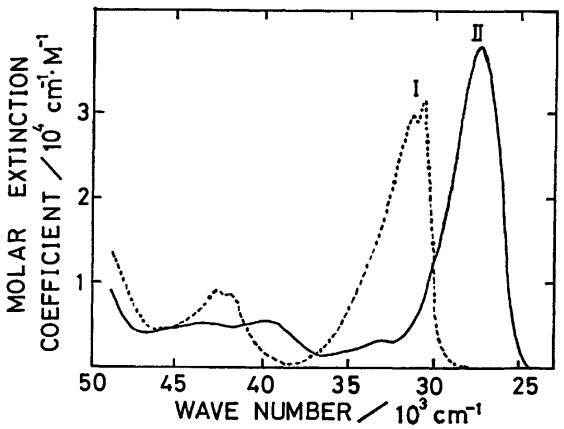

Fig. 3. The absorption spectrum of *p*-DMABA at room temperature. I: in cyclohexane, II: in HFP.

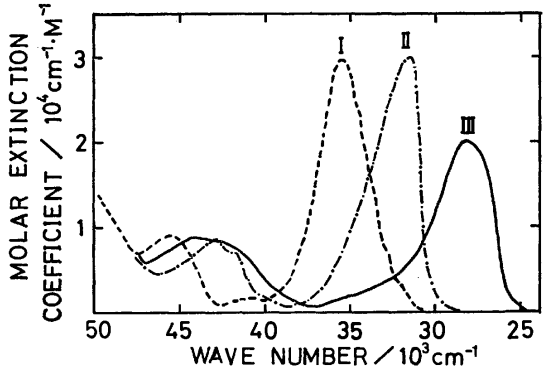

Fig. 4. The absorption spectra in cyclohexane at room temperature.
I: *p*-DMABN, II: *p*-DMAAP, and III: *p*-DMNA.

The energy levels calculated for *m*- and *p*-DMAAP with and without CI are shown in Fig. 6. The calculations predict four transitions for *m*-DMAAP and *p*-DMAAP below 6 eV and can explain the observed

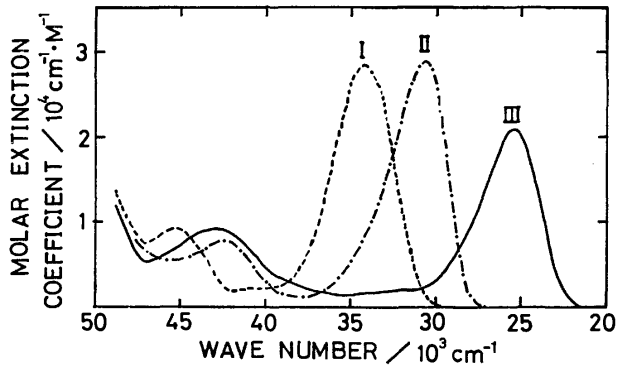

Fig. 5. The absorption spectra in acetonitrile at room temperature.
I: *p*-DMABN, II: *p*-DMAAP, and III: *p*-DMNA.

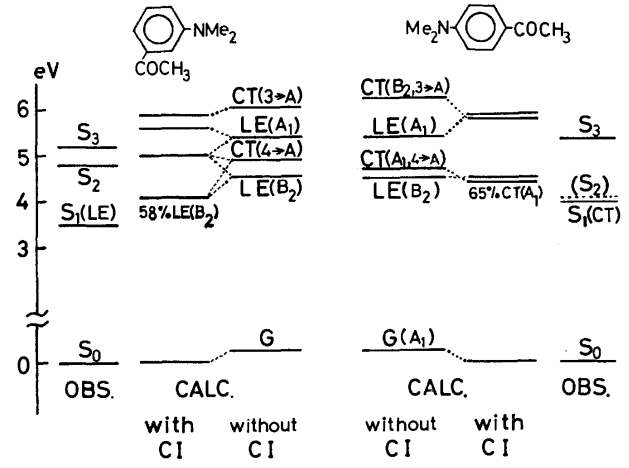

Fig. 6. Energy levels of *m*-DMAAP and *p*-DMAAP with and without CI.

results at least semi-quantitatively (see Table 2).

The S_n←S_1 Transitions of m- *and* p-*Dimethylaminoacetophenones.* The transient absorption spectrum of *m*-DMAAP is given in Fig. 1, together with the S_n←S_0 spectrum. The T_n←T_1 transition of *m*-DMAAP was not detected by method I in the region, 14300—27800 cm^{-1}. Therefore, the transient absorption spectrum obtained by method II is purely attributed to the S_n←S_1 transitions. From the consideration of the observed frequencies of the S_n←S_0 transition bands, the S_n←S_1 band at 17000 cm^{-1} is safely assigned to the S_3←S_1 transition. This band shows vibrational structures, suggesting that this transition is largely of forbidden character. The oscillator strength of the S_3←S_1 transition was calculated to be 0.07, by assuming that the molecular geometry in the excited state is the same as that in the ground state. This theoretical prediction is consistent with the observed result.

The transient spectra of *p*-DMAAP are given in Fig. 2-a. Very similar transient spectra are also obtained for *p*-DMABA. The T_n←T_1 spectrum of *p*-DMAAP was observed by method I, and the transient spectrum measured by method II was found to be composed of the S_n←S_1 and the T_n←T_1 transition bands. The S_n←S_1 transition band appears at 16700 cm^{-1} for *p*-DMAAP and may be assigned to the S_3←S_1 or S_4←S_1 transitions from the consideration of the observed frequencies of the S_n←S_0 transition bands of *p*-DMAAP (Table 2). The oscillator strength was evaluated to be 0.03 and 0.50 for the S_3←S_1 and S_4←S_1 transitions, respectively, in the same assumption as mentioned above. Hence, the S_4←S_1 assignment was preferred.

The Characters of the Lowest Excited Singlet States of m- *and* p-*Dimethylaminoacetophenones.* The kinetic parameters for the lowest excited singlet states were determined in EPA (5:5:2) at 77 K. The results are as follows: for *m*-DMAAP, τ_f(fluorescence lifetime)=54 ns and ϕ_f(fluorescence quantum yield)=0.85, and for *p*-DMAAP, τ_f=3.5 ns and ϕ_f=0.64. From these values the fluorescence radiative rate constants are calculated to be 1.7×10^7 s^{-1} for *m*-DMAAP, and 1.8×10^8 s^{-1} for *p*-DMAAP. This fact, together with the spectral difference between the absorptions of *m*-DMAAP and *p*-DMAAP (lower figures of Figs. 1 and 2) shows that the lowest excited states of both isomers have different electronic structures. According to the present theoretical consideration, the longest wavelength band of *m*-DMAAP originates mainly from the local excitation of aniline ($^1B_2$←$^1A_1$), while that of *p*-DMAAP or *p*-DMABA is assigned as the CT band which is associated with the charge-transfer configuration (ϕ_4←^{1}A). The theoretical result is supported by the fact that the longest wavelength band of *p*-DMAAP or *p*-DMABA has the transition moment nearly parallel to the molecular long axis.[35] Thus it is concluded that the S_1 state of the meta-isomer has the LE character within *N,N*-dimethylaniline, while that of the para-isomer the CT character.

Let us consider the spectral difference in the S_n←S_1 transitions between the meta- and para-isomers on the basis of the above-mentioned nature of the S_1 states. The final states of the S_n←S_1 transition bands, S_3 of the meta-isomer and S_4 of the para-isomer are nearly of the same nature: LE of *N,N*-dimethylaniline ($^1A_1$←$^1A_1$) perturbed by CT(4-A). Hence, the S_n←S_1 transition band can be interpreted as the LE band for the meta-isomer and as the back CT band for the para-isomer.

The Characters of Lower-lying Excited States of Several Related Aniline Derivatives. The spectra of dimethylaminoacetophenones are correlated with those of aminoacetophenones and other aniline derivatives containing various acceptor groups.

The two isomers of aminoacetophenone, *m*-AAP and *p*-AAP exhibit absorption spectra similar to those of the corresponding *N,N*-dimethylated compounds, *m*-DMAAP and *p*-DMAAP. Concerning the S_1←S_0 transition, the decrease of the transition energy and the increase of the oscillator strength were observed alkylation of the amino group. This observation is reasonably interpreted in terms of the CT interaction. The red-shift and intensification of the longest wavelength band due to alkylation can be interpreted in terms of the lowering of the ionization potential of the electron donor.

In the region, 24000—47000 cm^{-1}, the para-substituted *N,N*-dimethylanilines show four bands of CT or LE character (Figs. 4 and 5). The two lower-lying states are closely located and characterized by CT from *N,N*-

Table 3. Absorption maxima (in cm^{-1}) of some *p*-substituted *N,N*-dimethylanilines, *p*-$(H_3C)_2N$–C_6H_4–X in cyclohexane

X	CT band	LE band
CN	35710	31000—35000[a]
$COCH_3$	31750	
CHO	31250	
NO_2	28170	31000—34000[b]

a) A weak structured band overlapped by the CT band. b) A broad shoulder at the shorter wavelength side of the CT band.

dimethylaniline to the acceptor substituent and also by LE corresponding to $^1B_2 \leftarrow {}^1A_1$ of *N,N*-dimethylaniline. From the absorption maxima of the para-substituted *N,N*-dimethylanilines (Table 3), we can see that the red-shift of the intense CT band is associated with the increase in the electron affinity of the acceptor substituent and the resultant increase in the CT character in S_1. The transition energies of the LE bands seem to remain unchanged by replacing the substituent on the para position. Thus we can expect that the reversal occurs in the order of the two lower-lying states by changing the acceptor substituent group: in cyclohexane, the S_1 state of the cyanoaniline is of LE, while the S_1 state of the nitroaniline is of CT. The reversal is also observed by changing solvents. In nonpolar solvents, the lowest excited singlet state of the cyano-substituted aniline is mainly of LE character, and a reversal of the order of the two lower-lying states occurs by replacing a nonpolar solvent, cyclohexane by polar solvents, such as acetonitrile, ethanol, water, and HFP. Concerning carbonyl-substituted *N,N*-dimethylanilines in the nonpolar solvents the weak LE band is located slightly above the strong CT band and cannot be discernible, while it can be observed separately in HFP.

Table 4. Wave numbers of $T_n \leftarrow T_1$ transitions, ν_{max}, S-T separations, $\Delta\nu_{ST}$, and phosphorescence lifetimes, τ_p for *p*-substituted *N,N*-dimethylanilines, *p*-$(H_3C)_2N$–C_6H_4–X

X	$\nu_{max}(cm^{-1})$	$\Delta\nu(cm^{-1})$	$\tau_p(s)$
CN	25000[a]	6450[c]	2.16 ± 0.02[c]
$COOCH_3$	24300[d] 23000		
$COCH_3$	22300[a]	4800[b]	0.62 ± 0.02[b]
CHO	22600[a]	4600[b]	0.25 ± 0.01[b]
NO_2	19400[a]	3750[c]	0.22 ± 0.02[c]

a) This work, in ethanol at room temperature. b) This work, in EPA (5:5:2) at 77 K. c) Ref. 36, in EPA (5:5:2) at 77 K. d) Ref. 37, in ethanol at 93 K. e) Ref. 38, in EPA (5:5:2) at 77 K.

The wave numbers of the $T_n \leftarrow T_1$ transitions, the values of S-T separation, and the phosphorescence lifetimes are given in Table 4 for various para-substituted *N,N*-dimethylanilines. The lifetime data indicate that the lowest excited triplet states are of $\pi\pi^*$ character. Since each CT triplet state has the same energy as the corresponding CT singlet state in the zero differential overlap approximation, the decrease of S-T splitting values shows clearly the increase of the CT character in T_1. The increasing CT character in T_1, reflecting the order of the electron affinity of the acceptor substituent, is parallel to the red-shift of the $T_n \leftarrow T_1$ transitions. The decrease of the phosphorescence lifetimes can be qualitatively interpreted in terms of the enhancement of spin-orbit coupling by the intramolecular CT interaction in the same manner as in anilines.[39-41]

We wish to thank Dr. Kazuo Shibata and Dr. Yorinao Inoue, The Institute of Physical and Chemical Research, for their kindness in putting the spectrofluorometer (Shimadzu RF-502) at our disposal.

References

1) S. Nagakura and J. Tanaka, *J. Chem. Phys.*, **22**, 236 (1954).
2) S. Nagakura, *J. Chem. Phys.*, **23**, 1441, (1955).
3) H. C. Longuet-Higgins and J. N. Murrell, *Proc. Phys. Soc.*, **A68**, 601 (1955); J. N. Murrell, *Proc. Phys. Soc.*, *A*, **68**, 969 (1955).
4) J. Tanaka and S. Nagakura, *J. Chem. Phys.*, **24**, 1274, (1956).
5) S. Nagakura, *Mol. Phys.*, **3**, 105, 152 (1960).
6) S. Nagakura, *Pure Appl. Chem.*, **7**, 79 (1960).
7) J. Tanaka, *Bull. Chem. Soc. Jpn.*, **36**, 833 (1963).
8) S. Nagakura, M. Kojima, and Y. Maruyama, *J. Mol. Spectrosc.*, **13**, 174 (1964); K. Tabei, and S. Nagakura, *Bull. Chem. Soc. Jpn.*, **38**, 965 (1965).
9) K. Kimura and S. Nagakura, *Mol. Phys.*, **9**, 117 (1965).
10) H. H. Jaffé and M. Orchin, "Theory and Applications of Ultraviolet Spectroscopy," John Wiley & Sons, Inc., New York (1962) p. 256.
11) J. N. Murrell, "The Theory of the Electronic Spectra of Organic Molecules," Methuen, London (1963).
12) H. Suzuki, "Electronic Absorption Spectra and Geometry of Organic Molecules," Academic Press, New York (1967).
13) C. J. Seliskar, O. S. Khalil, and S. P. McGlynn, "Excited States" ed by E. C. Lim., Academic Press, New York (1974), Vol. 1, p. 231.
14) J. N. Murrell, *Tetrahedron*, **19**, Suppl. 2, 277 (1963); M. Godfrey and J. N. Murrell, *Proc. R. Soc.* London, *Ser. A*, **278**, 69 (1964).
15) R. Grinter and E. Heilbronner, *Helv. Chim. Acta*, **45**, 2496 (1962).
16) Y. H. Lui and S. P. McGlynn, *J. Mol. Spectrosc.*, **55**, 163 (1975).
17) Y. H. Lui and S. P. McGlynn, *J. Lumin.*, **9**, 449 (1975); *ibid.*, **10**, 113 (1975).
18) O. S. Khalil and S. P. McGlynn, *J. Lumin.*, **11**. 185 (1975/76).
19) K. Kimura, *Mol. Phys.*, **15**, 109 (1968).
20) H. Morita, S. Matsumoto, and S. Nagakura, *Bull. Chem. Soc. Jpn.*, **48**, 420 (1975).
21) H. Rupe, A. Braun, and K. von Zembrzuski, *Ber.*, **34**, 3522 (1901).
22) D. E. Pearson and J. D. Burton, *J. Am. Chem. Soc.*, **73**, 864 (1951).
23) H. W. Bresler, W. H. Friedemann, and J. Mai, *Ber.*, **39**, 876 (1906).
24) I. B. Berlman, "Handbook of Fluorescence Spectra of Aromatic Molecules," 2nd ed, Academic Press, New York (1971), p. 291.

25) R, Nakagaki, T. Kobayashi, J. Nakamura, and S. Nagakura, *Bull. Chem. Soc. Jpn.*, **50**, 1909 (1977).
26) T. Kobayashi, S. Matsumoto, and S. Nagakura, *Chem. Lett.*, **1975**, 235.
27) K. Kimura and M. Kubo, *J. Chem. Phys.*, **32**, 1776 (1960).
28) M. Haisa, S. Kishino, T. Yuasa, and K. Akigawa, *Acta Crystallogr., Sect B*, **32**, 1326 (1976).
29) R. Parieser and R. G. Parr, *J. Chem. Phys.*, **21**, 466, 767 (1953).
30) J. Tanaka, *Nippon Kagaku Zasshi*, **78**, 1636 (1957).
31) J. P. Maier and D. W. Turner, *J. Chem. Soc., Faraday Trans. 2*, **1973**, 521.
32) T. Kobayashi and S. Nagakura, *Bull. Chem. Soc. Jpn.*, **47**, 2563 (1974).
33) J. A. Pople, *Proc. Phys. Soc., A*, **68**, 81 (1955).
34) A. Kuboyama, Y. Sato, and H. Arano, *Bull. Chem. Soc. Jpn.*, **49**, 3685 (1976).
35) H. Labhart and G. Wagniere, *Helv. Chim. Acta*, **46**, 1314 (1963).
36) O. S. Khalil, R. H. Hofeldt, and S. P. McGlynn, *Spectrosc. Lett.*, **6**, 147 (1973).
37) I. A. Zhmyreva, V. P. Kolobkov, and S. V. Volkov, *Opt. Spectrosc.*, **20**, 162 (1966).
38) O. S. Khalil, C. J. Seliskar, and S. P. McGlynn, *J. Chem. Phys.*, **58**, 1607 (1973).
39) E. C. Lim and S. K. Chakrabarti, *Chem. Phys. Lett.*, **1**, 28 (1967).
40) E. C. Lim and S. K. Chakrabarti, *J. Chem. Phys.*, **47**, 4726 (1967).
41) M. Kasha and H. R. Rawls, *Photochem. Photobiol.*, **7**, 561 (1968).

Reduction of Calcium Interference on Barium Using the Nitrogen-Shielded Nitrous Oxide-Acetylene Flame in Atomic Absorption Spectroscopy†

Hisao KAWAMURA

Division of Radioecology, National Institute of Radiological Sciences, Isozaki, Nakaminato, Ibaraki 311-12

(Received November 15, 1977)

The interference effects of calcium on barium in atomic absorption spectroscopy, *i.e.*, background absorption and noise effect having been attributed to the CaOH green band were further studied. The behavior of the interfering calcium hydroxide radical and the barium atom itself was studied in relation to the distribution of natural species, OH and CN, using conventional and nitrogen-shielded nitrous oxide–acetylene flames. A remarkable reduction in the calcium interference was demonstrated using a nitrogen-shielded version of moderately fuel-rich flames. This effect was attributed to the suppression of CaOH formation which was brought about by an improvement in the reducing nature of the flame with shielding.

The calcium interference effects on barium, *i.e.*, background absorption and noise effect have been attributed to the molecular absorption and emission spectra of CaOH, and remain as major obstacles in the determination of this element in biological and geological materials, necessitating the removal of calcium in atomic absorption spectroscopy using nitrous oxide–acetylene flames.[1-3] Correcting for background absorption using a continuum source[4] appears impracticable due to the noisy signal of barium in the presence of calcium.[1] Gas-shielded burners have been used but with only limited information available on the behavior of the interferent.[5] It is difficult to meet the conditions for maximum barium absorbance and minimum calcium interference. The behavior of the barium atom in relation to the interfering CaOH radical in the nitrous oxide–acetylene flames does not appear to have been studied although the atomization of elements has often been discussed.[6-9]

Assuming that the oxides and hydroxides of alkaline earth elements in flames are in equilibrium with the oxidizing natural species,[10] making the flames more reducing may result in a reduction of the calcium hydroxide formation. In this paper, the distribution of barium atoms and CaOH radicals in the nitrous oxide–acetylene flames, as influenced by flame stoichiometry and inert gas shielding, has been studied as well as the distribution of OH and CN radicals. The CaOH population in a moderately fuel-rich nitrous oxide–acetylene flame has been clearly shown to be further suppressed by nitrogen shielding which results in a reduction in the calcium interference effects under optimum conditions for atomizing barium.

Experimental

A Perkin-Elmer Model 403 atomic absorption spectrophotometer was used. A barium hollow cathode lamp of maximum current 30 mA d.c. was operated at 26 mA as in previous work.[1] An Osram 64633 iodine-filled tungsten lamp was used at approximately 10 V a.c. with air cooling. A Perkin-Elmer nitrous oxide burner head was used with two types of laboratory-made gas shielding apparatuses, shown in Fig. 1. The first type (a) was fitted to the burner tightly covering the cooling fin and, in this way, the vertical holes encircling the head formed in the cooling block ensured laminar flow of the shielding gas. When the second type (b) was used, the burner head was removed from the cooling fin and fitted to this apparatus. Pure nitrogen or argon (99.9995% purity) was used as the shielding gas.

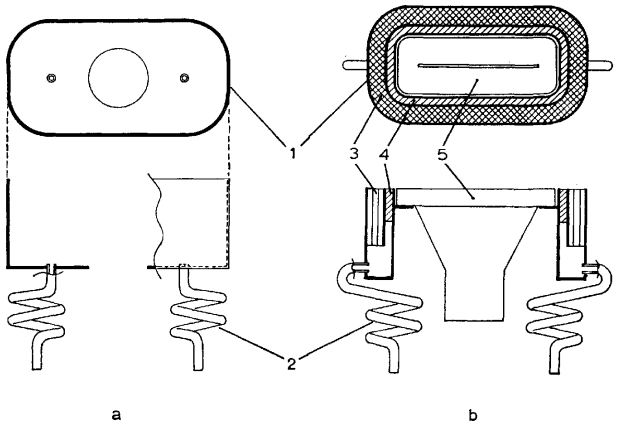

Fig. 1. Schematic diagram of burner with nitrogen shielding apparatus.
1: 1-mm thick brass box, 2: inert gas inlet, 4-mm diam. copper tube, 3: array of 2-mm diam. aluminum tubes 25 mm in length, 4: asbestos packing, 5: nitrous oxide burner head removed of cooling fin.

The position of the burner assembly was displaced manually by adjusting the installed racking mechanism stepwise by 2.5 and 0.43 mm in the vertical and horizontal directions, respectively. The flow rate of nitrous oxide was kept constant throughout the experiments, 13.2 dm^3/min (40.0 divisions of the flow meter reading at 30.0 psi). The acetylene flow rate was changed in seven steps from 7.36 to 8.33 dm^3/min (58.5 to 65.5 divisions at 8.0 psi). Thus, the nitrous oxide-to-acetylene flow ratio or molar ratio of the mixed gases as denoted by ρ[6] was lowered stepwise from 1.79 to 1.58. The setting of the flow meters was periodically checked during the course of measurements. Flow rates were read on the calibration graph revised by the manufacturer[11] neglecting possible small variations among flow meters of the same specification.

† This work was announced in part at the 22nd Annual Meeting of the Japan Society for Analytical Chemistry, November 23—26, 1973, Fukuoka, and at the 26th International Congress of Pure and Applied Chemistry, September 4—10, 1977, Tokyo.

The mask for the transmitting window on the right-hand side of the burner housing[1] was replaced with one having a 12-mm diam. circular aperture. When observing the spatial distribution of emission signal, another mask with a 4.5-mm diam. circular hole was attached to the window. Spatial resolution in the barium atom absorbance measurement was estimated as approximately 1.4 and 3.0 mm in the horizontal and vertical directions, respectively, measured at the focal plane close to the center of the burner slot. Spatial resolution in the emission study was estimated by viewing the filament of a small tungsten valve at the end of the slot nearer to the monochromator at 554 nm, as 1.3 and 4.7 mm in the horizontal and vertical directions, respectively.

The emission and absorption of CaOH was measured at 554 nm with a spectral band width of 0.4 nm, while 0.14 nm was used in recording the spectral profile. Flame background emission on aspirating distilled water at 554 nm, consisting of a C_2 band and continuum, was substracted.

The emission intensity of OH was measured using the 306.4 nm head with a spectral band width of 0.2 nm. The net intensity was obtained by substracting the contribution of the continuum, measured at 305 nm.

The OH and CN absorbances were measured using the Osram lamp by scanning each band with the head at 306.4 and 388.3 nm, respectively, employing a 0.07 nm spectral band width.

All emission and absorption measurements were carried out on aspirating either distilled water or salt solutions containing hydrochloric acid (0.1 mol dm^{-3}). Reagents used were of analytical grade, except for the Johnson Matthey "Specpure" barium carbonate and calcium carbonate.

Results and Discussion

Practically no difference was found between the two types of shielding apparatuses and between nitrogen and argon, with respect to the shielding effects on the CaOH emission intensity and flame stability. At a nitrogen flow rate of 13.5 dm^3/min, virtual suppression of the CaOH emission was achieved. Noise in emission and absorption measurements was found to increase above this flow rate.

Distribution of OH and CN in the Nitrous Oxide–Acetylene Flames as Influenced by Nitrogen Shielding. Spatial Distribution of the OH Emission Band: The distribution of the OH emission band in conventional and nitrogen-shielded flames of approximately optimum stoichiometry for barium atom absorbance ($\rho=1.67$) is shown in Fig. 2. The emission intensity in the central part of the flame, corresponding to the interconal zone, was remarkably depressed with nitrogen shielding (Fig. 2b) while the red feather, about 15 mm in height in the conventional flame, was elongated to about 30 mm in the nitrogen-shielded version. In the outer zone, the OH emission grew more intense up the flame to form broad maxima on both sides of the flame at about 15 mm from the burner top in the non-shielded flame. The emission in this region was strongly suppressed with nitrogen shielding. The observed large reduction in the OH emission band intensity with nitrogen shielding in the interconal and outer zones, shows that the suppressed formation of OH at the boundary of the interconal zone and the suppressed diffusion of OH to the center of the flame[12] are caused by the depression in secondary combustion reactions due to the lack of entrained air. The persisting OH band emission in the primary reaction zone may be explained by the formation of the species and its strong chemiluminescence in

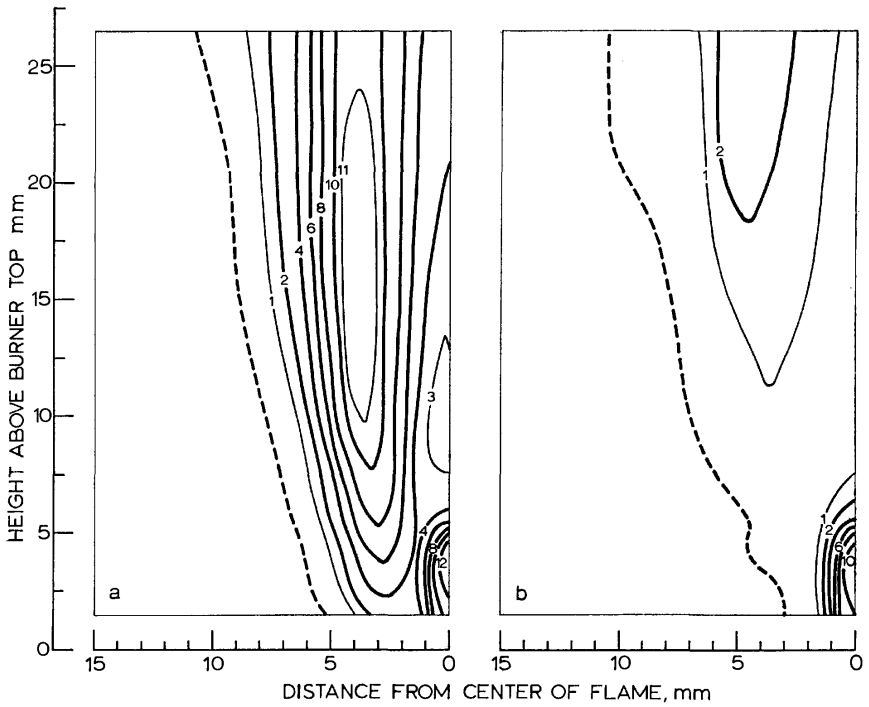

Fig. 2. Spatial distribution of OH emission intensity in the N_2O–C_2H_2 flames, of ρ 1.67.
a: Conventional flame, b: nitrogen-shielded flame.
——Flame envelope.
Figures on contour lines represent intensity in arbirary unit.

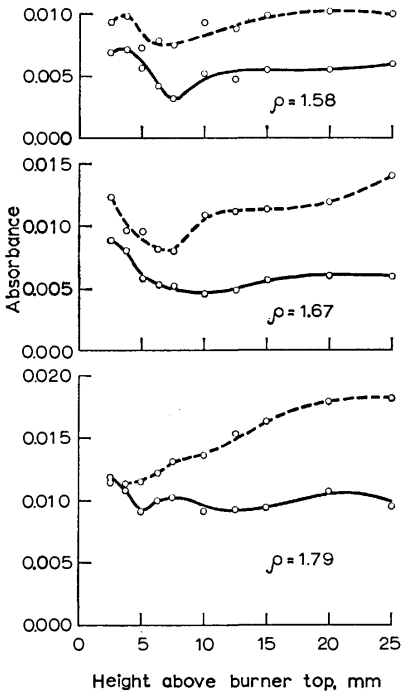

Fig. 3. Vertical distribution of OH absorbance in the N_2O–C_2H_2 flames.
——Conventional flame, ——nitrogen-shielded flame.

this region.[10]

Vertical Distribution of the OH Absorption Band: The vertical absorbance profile of OH was studied. The results shown in Fig. 3 show the less pronounced effect of nitrogen shielding than that on OH emission. The absorbance was reduced by 57% at 10 mm when $\rho=1.67$. A dip in absorbance just above the primary reaction zone was observed suggesting the presence of OH scavenging reactions involving carbon-containing species, 2C or C_2,[13] and C_2 and CH.[14]

Vertical Distribution of CN Absorption Band: The front of the CN absorbance profile moved up the flame along with decreasing ρ in the conventional and nitrogen-shielded flames as shown in Fig. 4. This approximately corresponded to the elongation of the red zone. A remarkable enhancement effect due to nitrogen shielding was observed above 5 mm, but hardly observable at 2.5 mm. The enhancement factor was 3 at 12.5 mm when $\rho=1.67$. The enhancement mechanism for CN absorbance is thought to be depression on shielding in the partial pressure of oxidizing species, O, OH, and H_2O[15] which rapidly consume CN.

From the results of the distribution of OH and CN, it was confirmed that the reducing nature of the interconal region of fuel-rich nitrous oxide–acetylene flames could be further enhanced by nitrogen shielding.

Absorbance Profile of Barium Atom in the Nitrous Oxide–Acetylene Flames as Influenced by Nitrogen Shielding. The barium absorbance in the fuel-rich nitrous oxide-acetylene flames in the presence and absence of an ionization suppressor as influenced by ρ and nitrogen shielding was studied. The results at typical ρ values are shown in Figs. 5 and 6. The addition of potassium at a concentration of 1000 μg cm^{-3} caused a shift in optimum height due to build-up of neutral atoms which were otherwise depleted through ionization. The optimum ρ value in the conventional flames was

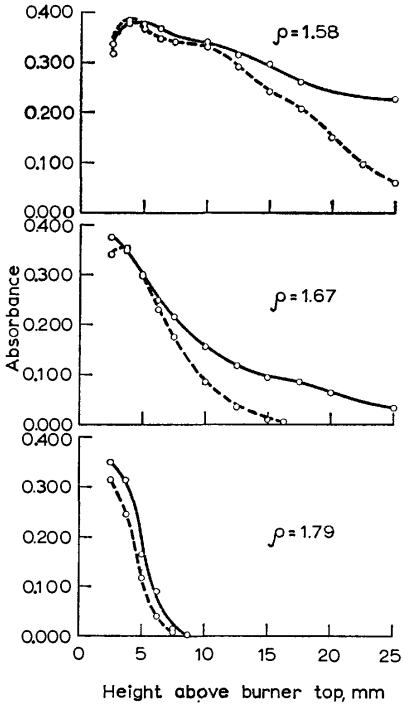

Fig. 4. Vertical distribution of CN absorbance in the N_2O–C_2H_2 flames.
——Conventional flame, ——nitrogen-shielded flame.

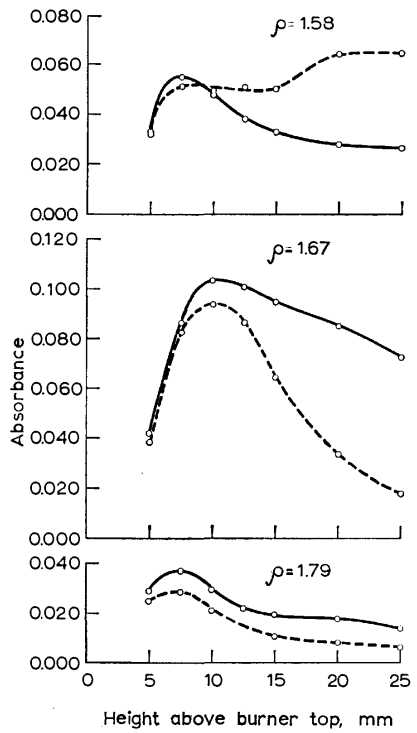

Fig. 5. Vertical absorbance profile of barium atom in the presence of an ionization suppressor in the N_2O–C_2H_2 flames.
5 μg cm^{-3} Ba+1000 μg cm^{-3} K.
——Conventional flame, ——nitrogen-shielded flame.

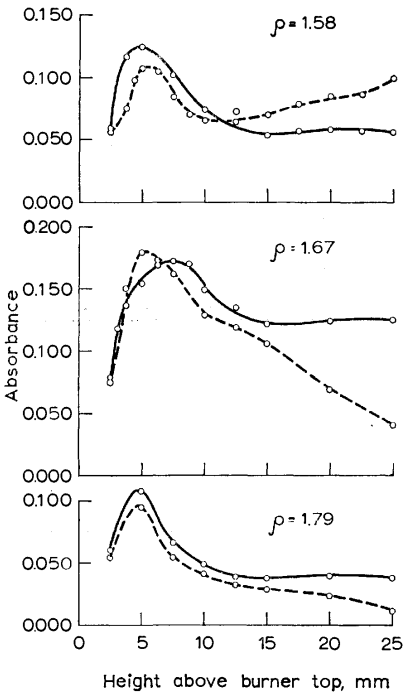

Fig. 6. Vertical absorbance profile of barium in the N_2O-C_2H_2 flames.
50 μg cm^{-3} Ba.
——Conventional flame, ——nitrogen-shielded flame.

1.66—1.67 on the ionization suppression. These results seem to differ from the published data.[6]

With the nitrogen-shielded flame of ρ 1.67, the rapid decrease of barium atom absorbance up the flame changed to show enhanced and markedly broader profiles. The optimum ρ was found to be slightly shifed to the lean side. These results suggest that free barium atoms are protected by the enhanced reducing atmosphere of the interconal zone of the shielded flames, in spite of a decrease in flame temperature on shielding reported in the literature.[16]

When the flame became extremely fuel-rich and slightly luminous with excessive carbon ($\rho=1.58$), the absorbance decreased and the vertical profile was found to be quite different from those at higher ρs. The absorbance increased again at higher positions above 12.5 mm in the conventional flame and this was found to disappear when the flame was shielded. In these flames, it was inferred that the flame temperature was too low to sufficiently atomize barium, due to deficiency of oxidant. Barium, mostly in the bound state under these conditions, may respond to changes in flame temperature rather than to the reducing nature of flames. A certain increase in temperature above the primary reaction zone between 15 and 25 mm has been reported in an unshielded fuel-rich nitrous oxide-acetylene flame while in the nitrogen-shielded counterpart, a sharp drop in temperature has been observed in the same region.[16] It is interesting to consider possible bound forms of barium in these conditions. Oxide and hydroxide cannot account for this since CaOH, having a similar energy of dissociation, 4.0±0.4 eV, to that of BaOH, 4.64±0.09 eV,[10] was suppressed according to the molecular absorption study described later. A possibility of incomplete solute vaporization due to the added potassium chloride was rejected since essentially the same phenomenon was observed in the absence of the potassium salt (Fig. 6, $\rho=1.58$). It may

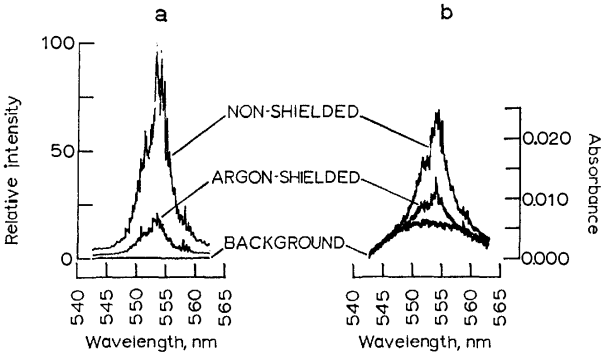

Fig. 7. Spectral profiles for CaOH emission and absorption bands in the N_2O-C_2H_2 flame as influenced by argon shielding.
a: Emission spectra, 1000 μg cm^{-3} Ca, b: absorption spectra, 4000 μg cm^{-3} Ca, C_2H_2 flow rate 7.90 dm^3/min, Observation height 20 mm.

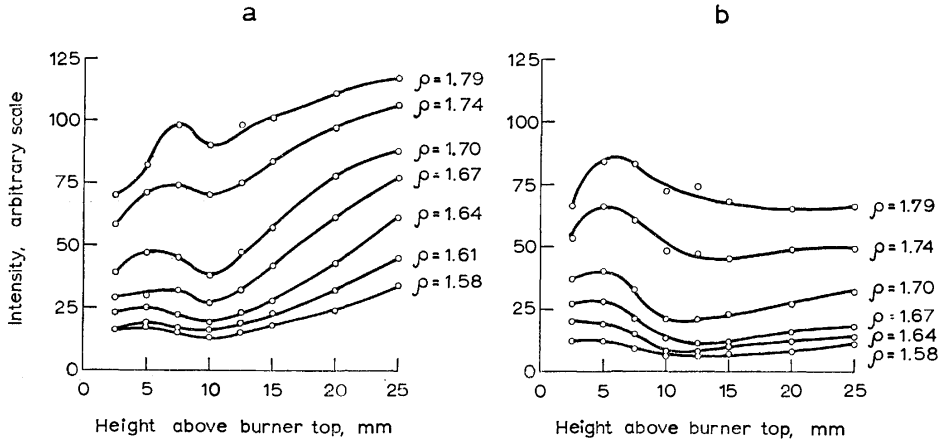

Fig. 8. Vertical distribution of CaOH emission intensity in the N_2O-C_2H_2 flames.
1000 μg cm^{-3} Ca.
a: Conventional flame, b: nitrogen-shielded flame.

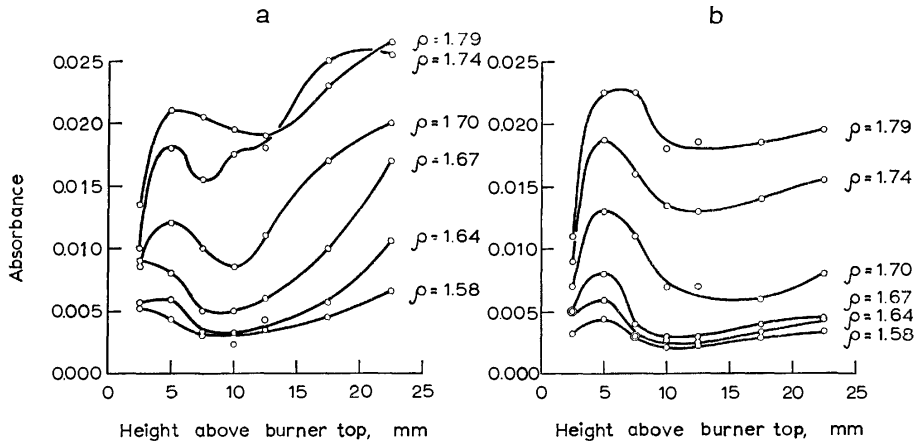

Fig. 9. Vertical distribution of CaOH absorbance in the N_2O–C_2H_2 flames.
4000 μg cm^{-3} Ca.
a: Conventional flame, b: nitrogen-shielded flame.

be inferred that carbon-containing barium compounds[6] are responsible for this phenomenon.

Distribution of CaOH in the Nitrous Oxide–Acetylene Flames as Influenced by Nitrogen Shielding. Vertical Profile of CaOH Emission Band: The emission band spectra of the CaOH green band in the fuel-rich nitrous oxide–acetylene flames as influenced by argon shielding are shown in Fig. 7a. The emission lines near 560 nm having been observed[1] were identified as the seven calcium atom lines lying between 558.2 and 560.3 nm the occurrence of which has been described in arc and spark;[18] this was proved by their distribution in flames and response to flame conditions.

As shown in Fig. 8a, the emission intensity of CaOH in the flames was gradually decreased when ρ was lowered. A small maximum between 5 and 7.5 mm and a minimum around 10 mm above the burner top was observed and the intensity was observed to remarkably increase further up the non-shielded flame. By shielding the flame with nitrogen, the CaOH emission was generally reduced, especially beyond 10 mm in height (Fig. 8b).

CaOH Absorbance Profile as Influenced by Flame Shielding: The suppressing effect of argon shielding on the CaOH absorption band in the flame is shown in Fig. 7b.

As shown in Fig. 9, the absorbance signal decreased as ρ was lowered. However, on shielding the flames, the absorbance was remarkably reduced further beyond 10 mm while being unchanged at 5 mm.

It may be concluded that the background absorption and noise effect due to calcium may be minimized by employing a moderate ρ value, *i.e.*, 1.67 required for maximum barium atom absorbance in the nitrogen-shielded flame.

Spatial Distribution of CaOH Emission Intensity: The distribution of CaOH emission intensity in the transverse section of the flames of ρ 1.67 was studied to investigate the occurrence of CaOH with respect to flame structure. The results are shown in Fig. 10. In the outer mantle of the conventional flame, a large build-up of the CaOH emission intensity was found up the flame (Fig. 10a). The central part of the flame up to 15 mm of weaker intensity was observed to correspond to a space inside

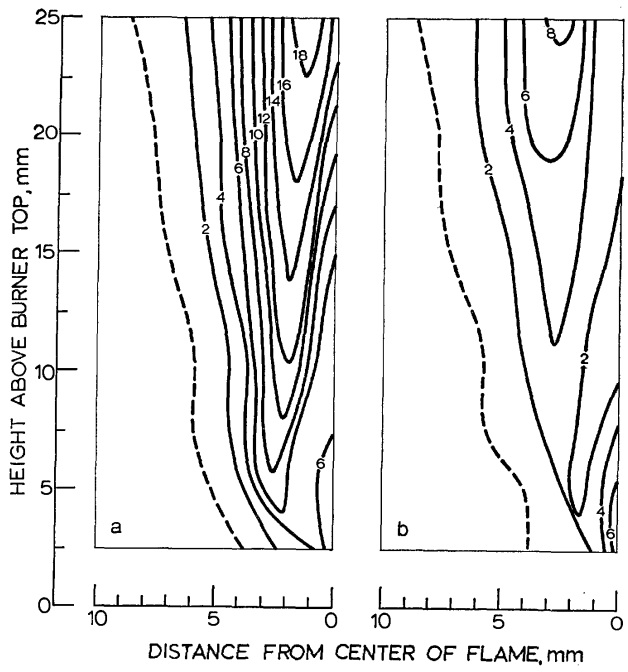

Fig. 10. Spatial distribution of CaOH emission intensity in the N_2O–C_2H_2 flames of ρ 1.67.
a: Conventional flame, b: nitrogen-shielded flame.
----Boundary of CaOH emission.
Figures on contour lines represent intensity in arbitrary unit.

the red feather, or the interconal zone. A small island-like region of strong CaOH emission was observed near the primary reaction zone. In the shielded flame, the emission band was suppressed throughout the flame, with the central part of weaker intensity being enlarged (Fig. 10b). The whole pattern of spatial distribution of the CaOH emission band may be compared with that of OH (Fig. 2).

These results suggest that CaOH, produced in the primary reaction zone, is markedly subjected to depopulation in the interconal zone of the nitrogen-shielded nitrous oxide-acetylene flames. This may be due to reactions with carbon-containing species, *i.e.*, C_2, CH,

etc., as well as the suppression of oxidizing species, *i.e.*, O, OH, and H_2O.

Effect of Nitrogen Shielding on the Background Absorption and Signal-to-Noise Ratio in the Barium Absorbance Signal in the Presence of Calcium. For the purpose of determining barium in the absence of calcium, an accord in conditions of the flame stoichiometry and height for maximum barium atom absorbance and those for minimum CaOH absorbance and emission intensity, is favorable. This may be due to the similarity in dissociation energies of the monoxide and hydroxide of barium and calcium.

TABLE 1. THE EFFECT OF NITROGEN SHIELDING ON BARIUM ATOM ABSORBANCE AT 553.6 nm IN THE PRESENCE OF CALCIUM OF VARIOUS CONCENTRATIONS IN THE NITROUS OXIDE–ACETYLENE FLAME

Calcium concn (μg/ml)	Conventional flame		N_2-shielded flame	
	Absorbance	Rel. S/N	Absorbance	Rel. S/N
0	0.073	1.00	0.147	1.00
500	0.079	0.84	0.132	0.90
1000	0.091	0.66	0.126	0.83
5000	0.102	0.30	0.143	0.82

10 μg cm^{-3} Ba+1000 μg cm^{-3} K. Observation height 17 mm.

The background absorption and relative S/N ratio in the presence of different concentrations of calcium were measured employing optimum flame stoichiometry, ρ 1.67, and the results are shown in Table 1. A height of 17 mm above the burner top was adopted for the purpose of comparison with previous work.[1] Using the nitrogen-shielded flame, the background absorbance due to calcium was substantially eliminated and the relative S/N ratio was found to be little affected by calcium in various concentration levels. This effect was also proved at an optimum height for the practical determination. As shown in Fig. 11, the interfering effects of calcium at concentrations of 2000 μg cm^{-3} were essentially eliminated.

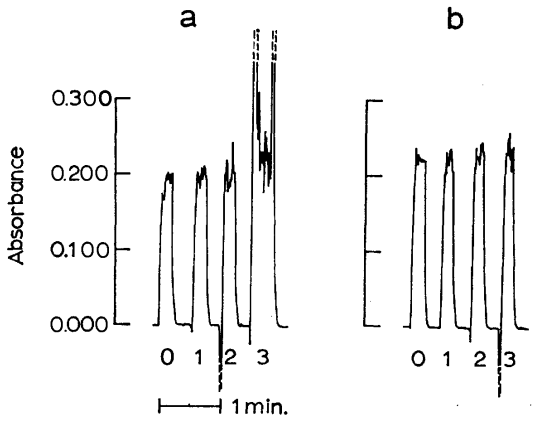

Fig. 11. Effect of nitrogen shielding on barium atom absorbance in the presence of calcium.
a: Conventional flame, b: nitrogen-shielded flame. Ca concn 0: None, 1: 500, 2: 1000, 3: 2000 μg cm^{-3}. 10 μg cm^{-3} Ba+1000 μg cm^{-3} K. Observation height 10 mm.

Conclusion

The nitrogen shielding of a fuel-rich nitrous oxide–acetylene flame remarkably reduced the spectral interference and the noise effect of calcium on the barium determination by atomic absorption spectroscopy. Spectroscopically, this was shown to be due to the suppression of CaOH radical formation by the enhanced reducing nature of the flame of an optimum oxidant-to-fuel flow ratio for maximum barium atom absorbance. By using this technique, the chemical separation of barium from calcium will be unnecessary or, at least, the time and tedious labor for perfect removal of calcium will be saved in the analysis of biological and geological materials of high calcium contents.

The author would like to thank Dr. Gi-ichiro Tanaka for his interest and support in this study and to Mrs. Yoshie Matsumoto *nee* Kanno for technical assistance. The courtesy of Dr. Yoshihiko Ohyagi, Chiba University, Chiba, for criticizing the manuscript is gratefully acknowledged. The author is also indebted to Dr. G. F. Kirkbright, Imperial College, London, for reading the manuscript.

References

1) H. Kawamura, G. Tanaka, and Y. Ohyagi, *Spectrochim. Acta, Part B*, **28**, 309 (1973).
2) F. J. Bano, *Analyst*, **98**, 655 (1973).
3) D. J. David, in "Flame Emission and Atomic Absorption Spectrometry," ed by J. A. Dean and T. C. Rains, Marcel Dekker, New York (1975), Vol. 3, pp. 33—64.
4) S. R. Koirtyohann and E. E. Pickett, *Anal. Chem.*, **38**, 585 (1966).
5) I. Rubeška, *At. Absorption Newslett.*, **12**, 33 (1973).
6) V. A. Fassel, J. O. Rasmuson, R. N. Kniseley, and T. G. Cowley, *Spectrochim. Acta, Part B*, **25**, 559 (1970).
7) K. Fujiwara, H. Haraguchi, and K. Fuwa, *Bull. Chem. Soc. Jpn.*, **48**, 857 (1975).
8) J. O. Rasmuson, V. A. Fassel, and R. N. Kniseley, *Spectrochim. Acta, Part B*, **28**, 365 (1973).
9) G. F. Kirkbright, M. Sargent, and T. S. West, *Talanta*, **16**, 1467 (1969).
10) R. Mavrodineanu and H. Boiteux, "Flame Spectroscopy," John Wiley, New York (1965), Chap. 19 and 22.
11) "Analytical Methods for Atomic Absorption Spectrophotometry," supplement to March 1971 ed, Perkin-Elmer Corp., Norwalk, Connecticut, USA (1973), p. 12.
12) D. R. Jenkins and T. M. Sugden, in "Flame Emission and Atomic Absorption Spectrometry," ed by J. A. Dean and T. C. Rains, Marcel Dekker, New York (1969), Vol. 1, Chap. 5.
13) T. G. Cowley, V. A. Fassel, and R. N. Kniseley, *Spectrochim. Acta, Part B*, **23**, 771 (1968).
14) G. F. Kirkbright, M. K. Peters, and T. S. West, *Talanta*, **14**, 789 (1967).
15) G. F. Kirkbright, M. K. Peters, M. Sargent, and T. S. West, *Talanta*, **15**, 663 (1968).
16) G. F. Kirkbright, and S. Vetter, *Spectrochim. Acta, Part B*, **26**, 505 (1971).
17) R. W. B. Pearse, and A. G. Gaydon, "The Identification of Molecular Spectra," 4th ed, Chapman and Hall, New York (1976), p. 131.
18) "M. I. T. Wavelength Tables," John Wiley, New York, p. 71.

The Synthesis of Hydrated Rare Earth Carbonate Single Crystals in Gels

Hisanobu WAKITA

Department of Chemistry, Faculty of Science, Fukuoka University, Nanakuma, Nishi-ku, Fukuoka 814

(Received July 29, 1977)

Hydrated rare earth carbonate single crystals were obtained in metasilicate gels. The formulas of the crystals were determined to be $(RE)_2(CO_3)_3 \cdot 8H_2O$ (RE=La, Pr) and $(RE)_2(CO_3)_3 \cdot 4.54H_2O$ (RE=Nd), and the crystal structures were determined to be of the lanthanit type.

Rare earth elements, having ionic radii larger than neodymium, were crystallized in lanthanite-type hydrated normal carbonates, $(RE)_2(CO_3)_3 \cdot 8H_2O$, whereas, rare earth elements with ionic radii smaller than neodymium were crystallized in tengerite-type hydrated normal carbonates, $(RE)_2(CO_3)_3 \cdot 2—3H_2O$.[1] The differences in the hydration numbers of, and in the ionic radii of rare earth elements in the lanthanite and tengerite type structures, seem to characterize differences in their structures and properties. Since these carbonates have been prepared as powders, accurate structural and chemico-physical data have not been obtained.[2] Shinn and Eick[3] obtained a single crystal of hydrated lanthanum carbonate, $La_2(CO_3)_3 \cdot 8H_2O$, by slow hydrolysis of lanthanum trichloroacetate. They determined the crystal structure of this crystal and found that it contains 4 formula units in an orthorhombic cell of space group Pccn with lattice parameters of $a=8.984\pm0.004$, $b=9.580\pm0.004$, and $c=17.00\pm0.01$ Å, and has a density, $\rho_{obsd}=2.72\pm0.02$ g cm^{-3}, which is very similar to the calculated value, $\rho_{calcd}=2.732$ g cm^{-3}.

Crystalline rare earth carbonates are generally obtained by the hydrolysis of trichloroacetates of rare earth elements, but they usually precipitate as a powder.[2] Henisch *et al.*[4] synthesized single crystals of various slightly soluble materials by means of a silica gel technique. Their results indicated that this technique could be adapted to the crystal growth of rare earth carbonates.

In this study, the crystal growth of hydrated normal rare earth carbonates by the gel method was attempted at various temperatures and with various ratios of rare earth ions and precipitant.

Experimental

Synthesis of the hydrated normal rare earth carbonates was carried out by the reaction between carbonates and rare earth salts in sodium metasilicate gels. Two methods have been examined for this purpose.[5] In the first the gel containing the carbonate was used. Aqueous mixtures of sodium metasilicate and various kinds of carbonates were prepared and the pH was adjusted. As carbonates, 0.008—0.2 M aqueous solutions of Na_2CO_3, $(NH_4)_2CO_3$, $NaHCO_3$, and NH_4HCO_3 were used. After the gel had set, rare earth salt solution was placed on top of the gel and allowed to diffuse. An aqueous solution of 0.008—0.2 M rare earth was prepared from $RECl_3$(RE= La, Ce, Nd, Sm, Gd, Dy, Ho, Yb, Sc). The gels were made from analytical grade $Na_2SiO_3 \cdot 9H_2O$. A 0.23 M Na_2SiO_3 aqueous solution, adjusted to a pH between 7 and 8 with dilute hydrochloric acid, was set in reaction tube and left overnight at room temperature. A simple test tube (25×200 mm) was used as the reaction tube. In the second method, each reagent, rare earth salt solution and carbonate solution, was diffused into the gel from each side of a U-tube (25×200 mm) or double tube. It appears that neither method has any significant advantage. Well-shaped crystals up to 2 mm in size were grown in 12 to 16 weeks. Well-shaped crystals were taken out of the tube and, after dissolving the gel with concentrated alkali solution, were washed with water, air-dried, and subjected to chemical, X-ray diffractometric, and thermal analyses.

Results and Discussion

In the test tube, milky precipitates appeared at the upper growth front and with time penetrated down into the gel. In the cases of lanthanum, praseodymium, and neodymium, well-shaped crystals separated from these milky precipitates after several weeks. Figure 1 shows a micrograph of a praseodymium carbonate crystal. The green, clear-cut crystals cleaved parallel to (001). In the cases of lanthanoids heavier than neodymium, well-shaped crystals did not appear even after several months. Sometimes, spherulites of the carbonates (RE=Nd) were obtained.

Factors Which Influence Crystal Growth. The following experiments were carried out in order to investigate the various factors which influence the growth behavior of neodymium carbonate: the temperature, the concentration of rare earth (in this case of neodymium) and carbonate ions, and the growth period of the crystals. In Fig. 2-a, r, the penetration depth[7,8] of the crystal-growth front is plotted against the square root of the diffusion time. It is observed in Fig. 2-a that r increases linearly with the increase of the square root of t until the diffusion time reaches 49 h. Over 49 h the slope

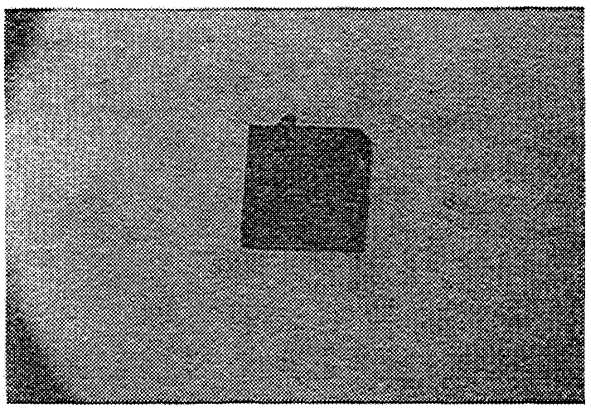

Fig. 1. Micrograph of praseodymium carbonate. Edge lengths of this plane: 2.5 mm.

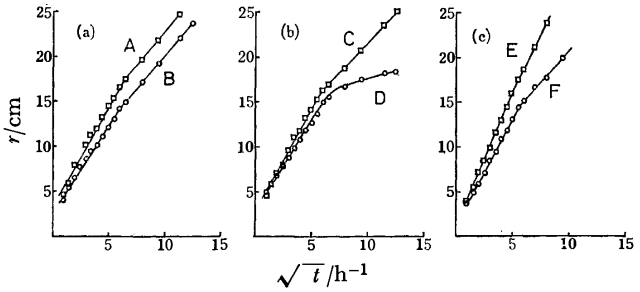

Fig. 2. Penetration rates of neodymium ions in gels.

	Concentration of neodymium mol/l	System's temepratures °C	Molar ratios of Na_2SiO_3: $(NH_4)_2CO_3$
A	0.1	35	3 : 1
B	0.1	25	3 : 1
C	0.1	30	3 : 1
D	0.1	30	2 : 1
E	0.2	25	3 : 1
F	0.1	25	3 : 1

Added volumes of neodymium ion are 0.5 ml. The pH of the gels is 7.4.

changed with time. During the period in which the linear relationship is maintained, the penetration rates obey a first order kinetic relationship. Beyond 49 h, because masses of the precipitate interfere with the diffusion of neodymium ions, this linear relationship breaks down. In Figs. 2-a, 2-b, and 2-c, the penetration rates were plotted against changes in temperature, concentration of the precipitant, and concentration of neodymium salt, respectively. As for sparingly soluble salts such as the rare earth carbonates, the penetration rates are primarily criteria of the diffusion rates. In the synthesis of single crystals of slightly soluble salts, it is important to have a controlled supply of the reactant; that is, the diffusion rates are to be controlled. Well-shaped and large crystals were produced under the following conditions: the temperature was at 25 °C, Na_2SiO_3: $(NH_4)_2CO_3$ was 3: 1 and the concentration of neodymium ion was 0.2 M.

TABLE 1. CHEMICAL ANALYSIS OF SYNTHESIZED RARE EARTH CARBONATES
(Quantities are molar ratios.)

RE	RE_2O_3 :	CO_2 :	H_2O
La	1.00	3.00	8.04
Pr	1.00	2.99	7.90
Nd	1.00	2.99	4.54
Sm	1.00	2.85	2.85
Gd	1.00	2.76	2.59

Chemical Analysis. Carbon, hydrogen, and rare earth elements of the crystals obtained were analysed using elemental analytical techniques. The carbonates obtained from this method are liable to be contaminated by sodium and silicon because sodium metasilicate gel were used. However, no sodium and silicon were detected from these carbonates by either flame analysis or EPMA. The results of the chemical analyses of air-dried carbonates are given in Table 1; the molar ratios of the first two correspond to $RE_2(CO_3)_3 \cdot 8H_2O$ (RE= La, Pr), the next to $RE_2(CO_3)_3 \cdot 4.54H_2O$ (RE=Nd), and last two to $RE_2(CO_3)_3 \cdot 2—3H_2O$ (RE=Sm, Gd), respectively. The absence of OH^- ions was demonstrated by infrared spectroscopy. Molar ratios are not whole numbers, this anomaly was described in a previous paper.[1] Carbonates of holmium, ytterbium, and scandium could not be analysed, because they were very fine powdered samples and they could not be separated from the gels. Cerium carbonate was not analysed because it was amorphous and contaminated.

X-Ray Diffraction Analyses. The X-ray powder diffraction data of these carbonates are shown in Table

TABLE 2. X-RAY POWDER DATA FOR SYNTHESIZED RARE EARTH CARBONATES

La		Pr		Nd			Sm		Gd	
d/Å	I	d/Å	I	d/Å	I	hkl	d/Å	I	d/Å	I
8.61	100	8.47	100	8.59	100	002	7.70	100	7.65	60
4.79	15	4.71	10	4.75	10	020	5.74	20	5.69	15
4.50	10	4.45	10	4.48	10	200	3.95	70	3.92	100
4.27	50	4.23	30	4.25	40	113 004	3.86	75	3.82	60
4.18	15	4.12	10	4.13	10	022	3.09	5		
3.98	10	3.93	10	3.95	10	202	3.02	5		
3.89	10	3.85	15	3.88	10	014	2.76	5		
3.85	10	3.82	15	3.83	10	104	2.57	40	2.55	35
3.58	5	3.55	5			114	2.41	5		
3.29	15	3.24	15	3.24	15	213 220	2.25	5		
3.19	10	3.15	10	3.16	5	221 024	2.07	30	2.06	50
3.07	20	3.06	10	3.07	10	204 222	1.97	10	1.96	15
3.02	10	3.02	15	3.02	15	115			1.81	10
a= 9.00 Å		a= 8.90 Å		a= 8.96 Å (calculated from 200)						
b= 9.58 Å		b= 9.42 Å		b= 9.50 Å (calculated from 020)						
c=17.22 Å		c=16.94 Å		c=17.18 Å (calculated from 002)						

2. This table indicates that the X-ray powder data of lanthanum, praseodymium, and neodymium are almost identical to that of lanthanite, while the data for samarium and gadolinium are almost identical to that of tengerite. A single crystal of the neodymium carbonate was employed in taking Weisenberg and precession photographs in order to determine the cell parameters and the space group. Systematic absence occured for $h00$, $0k0$, and $00l$ when h, k, or $l=2n+1$, for $0kl$ and $h0l$ when $l=2n+1$ and for $hk0$ when $h+k=2n+1$. Therefore, Pccn is a possible space group. The lattice parameters obtained from powder diffractometric data are: $a=8.97$ (calculated from 200), $b=9.49$ (calculated from 020), and $c=17.18$ (calculated from 002) Å. The density (2.76 g cm^{-3}) calculated for four formula units was in agreement with the density obtained by the heavy liquid method (2.75 g cm^{-3}). The crystalline carbonate of cerium was not obtained by this method. Perhaps cerium(III) in the starting solution had been oxidized in cerium(IV) during the diffusion. No report of a carbonate of cerium(IV) was found in the literature surveyed. Because the carbonates were not separated from the gels, no X-ray powder diffraction peaks of the carbonates of holmium, ytterbium, and scandium were obtained. This is the first report of samarium and gadolinium carbonates crystallizing with the tengerite type structure at such low temperatures (≈25 °C) and that neodymium carbonate crystallizes with a lanthanite type structure.

Thermal Analyses. The thermal analysis of the carbonates of lanthanite type was carried out with a heating rate of 10 °C/min in air. The results of the thermogravimetric analysis, TGA, and differential scanning calorimetry, DSC, of the carbonates of lanthanum and neodymium are shown in Fig. 3. The decomposition processes of neodymium and lanthanum carbonate were similar. On the TGA curve for the neodymium carbonate, there is initially a loss of water, which corresponds to the formation of anhydrous carbonate. This step is also prominent for the lanthanum compound. The DSC curve in Fig. 3 shows that the endothermic effects in the 100—200 °C range corresponds to the formation of the anhydrous carbonate. The continuous raising of the temperature leads to the formation of some intermediate phases, shown in the following schemes:

$$Nd_2(CO_3)_3\cdot 8H_2O \xrightarrow{ca.\,150\,^\circ C} Nd_2(CO_3)_3 \xrightarrow{ca.\,450\,^\circ C} Nd_2O(CO_3)_2 \xrightarrow{ca.\,750\,^\circ C} Nd_2O_3 \quad (1)$$

$$La_2(CO_3)_3\cdot 8H_2O \xrightarrow{ca.\,150\,^\circ C} La_2(CO_3)_3 \xrightarrow{ca.\,450\,^\circ C} La_2O_2(CO_3) \xrightarrow{ca.\,700\,^\circ C} La_2O_3 \quad (2)$$

The intermediate phases appearing at *ca.* 450 °C were different with each carbonate sample, despite the fact that the initial compositions of these compounds were identical. The results of the thermal analysis of samarium and gadolinium carbonates obtained were similar to that of tengerite.[6]

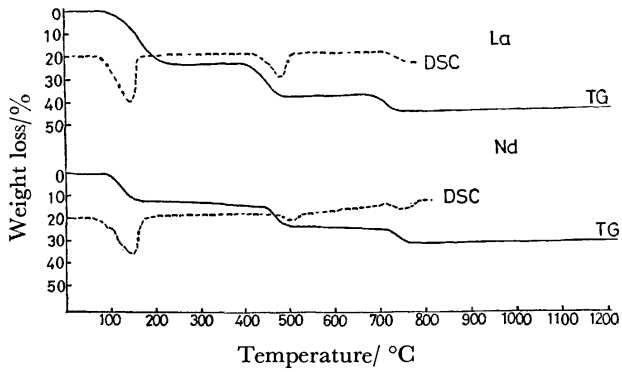

Fig. 3. Thermal analyses of lanthanum and neodymium carbonates.

I wish to express my deep gratitude to Professor Isao Masuda, Fukuoka University and Professor Kozo Nagashima, The University of Tsukuba, for their encouragement through the course of this work.

References

1) H. Wakita and K. Nagashima, *Bull. Chem. Soc. Jpn.*, **45**, 2476 (1972).
2) K. Nagashima, H. Wakita, and A. Mochizuki, *Bull. Chem. Soc. Jpn.*, **46**, 152 (1973).
3) D. B. Shinn and H. A. Eick, *Inorg. Chem.*, **7**, 1340 (1968).
4) H. K. Henisch, J. I. Hanoka, and J. Dennis, *J. Electrochem. Soc.*, **112**, 627 (1965).
5) H. J. Nickl and H. K. Henisch, *J. Electrochem. Soc.*, **116**, 1258 (1969).
6) K. Nagashima and H. Wakita, *Nippon Kagaku Zasshi*, **89**, 856 (1968).
7) A. R. Patel and S. K. Arora, *J. Mater. Sci.*, **11**, 843 (1976).
8) S. A. Cho, J. A. Gomez, R. Camisotti, and J. C. Ohep, *J. Mater. Sci.*, **12**, 816 (1977).

The Formation of Trapped Electrons upon the Thermal Dehydration-condensation of Hydrated Hydrogenorthophosphates

Hiroshi KAWAZOE,* Masaru NISHINO, Hideo HOSONO, Kei ISOZAKI, Kazuo AMETANI,† Masahiko IMAI,† and Takafumi KANAZAWA

Department of Industrial Chemistry, Faculty of Technology, Tokyo Metropolitan University, Fukazawa, Setagaya-ku, Tokyo 158

†*Tokyo Metropolitan Isotope Research Center, Fukazawa, Setagaya-ku, Tokyo 158*

(Received September 19, 1977)

Radical formation was found in the thermal dehydration-condensation process of hydrated hydrogenorthophosphates (HHP). It was considered that the intermediate radical reacted with lattice defects, thus resulting in the generation of trapped electrons. The gray coloration and the ESR sensitivity of the heated HHP were assigned to the formation of the trapped electron.

Some hydrated hydrogenorthophosphates (HHP), such as $MgHPO_4 \cdot 3H_2O$ (DMP3) and $Mg(H_2PO_4)_2 \cdot 2H_2O$, turn gray in the course of the thermal dehydration-condensation (D-C) reaction, resulting in a pyro- or meta-phosphate formation. These colored materials are bleached before the completion of the reaction; they change into white polycrystalline powders of pyro- or meta-phosphate. These facts suggest that a color center forms in the reaction process. In the present work, the nature of the color center was studied by means of ESR- and electronic-spectroscopies. The change in the concentration of the center with the reaction time was determined. The role of the center in the reaction was then discussed on the basis of these measurements.

Experimental

All the chemicals used here were guaranteed-grade reagents produced by Kanto Chemicals, Ltd. These reagents, *i.e.*, $MgHPO_4 \cdot 3H_2O$, $NaH_2PO_4 \cdot 2H_2O$, $Na_2HPO_4 \cdot 12H_2O$, $CaHPO_4 \cdot 2H_2O$, $Ca(H_2PO_4)_2 \cdot H_2O$, $KH_2PO_4 \cdot nH_2O$, and K_2HPO_4, were used as the starting samples without further purification. The $Mg(H_2PO_4)_2 \cdot 2H_2O$ sample was synthesized from MgO and H_3PO_4.[1)]

Thermogravimetric and differential thermal analyses were made to determine the temperatures of dehydration and crystallization of their dehydrated phosphate samples.

Electron spin resonance measurements were carried out for the materials obtained by thermal treatment with varying temperatures and times for HHP. The spectra were recorded on a JEOL JES-PE spectrometer at an X band microwave frequency. The concentrations of an unpaired spin in the heated samples were measured by using a double-mode cavity, with a known amount of polycrystalline DPPH as a reference.

A visible-UV spectrum was taken on a Shimadzu UV-200 spectrometer for the colored HHP dissolved in a sodium metaphosphate glass matrix.

The crystallinities of heat-treated DMP3, *i.e.*, a fraction of the $Mg_2P_2O_7$ crystal, at 700 °C at various times were determined by comparing the X-ray diffraction intensity for the (022) of $Mg_2P_2O_7$ in the sample with that in the calibration curve. This curve was obtained from mixtures of crystalline $Mg_2P_2O_7$ and amorphous $MgHPO_4$ in various mixing ratios.

Results and Discussion

Nature of the ESR Center. The electron spin resonance spectra for the samples obtained by the thermal treatment of several HHP are shown in Fig. 1. The heating temperatures and times noted in the figure were the conditions under which the most intense absorptions were observed for the respective HHP. All HHP excepting for K_2HPO_4 showed ESR absorptions of a singlet type, no other signals were recognized. The features of the singlets were regarded as the same for all the samples, even though the absorption intensities for the respective phosphates were different from one another. Three common natures of the absorptions were recognized: the first, no hyperfine structure; the second, a line width of 1—2 G measured at a peak-to-peak width in the derivative curve, and the last, a nearly isotropic spectroscopic splitting tensor with a value equivalent to that of a free electron (g=2.002). In the

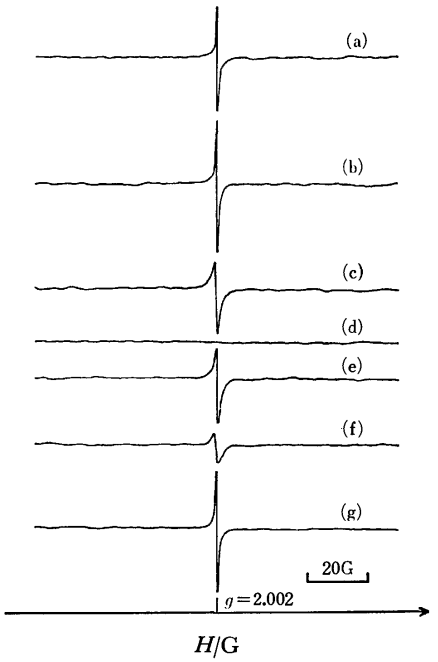

Fig. 1. ESR spectra for hydrated hydrogenorthophosphates heat-treated under the conditions shown below, a: $NaH_2PO_4 \cdot 2H_2O$, at 500 °C for 1 h, b: $Na_2HPO_4 \cdot 12H_2O$, at 500 °C for 1 h, c: $KH_2PO_4 \cdot nH_2O$, at 500 °C for 1 h, d: K_2HPO_4, at 200—800 °C for 0.5—10 h, e: $Ca(H_2PO_4)_2 \cdot H_2O$, at 400 °C for 1 h, f: $CaHPO_4 \cdot 2H_2O$, at 300 °C for 1 h, g: $Mg(H_2PO_4)_2 \cdot 2H_2O$, at 700 °C for 1 h. The spectra were recorded at 25 °C.

cases of $CaHPO_4 \cdot 2H_2O$, $KH_2PO_4 \cdot nH_2O$, and $Ca(H_2PO_4)_2 \cdot H_2O$, the g tensor was slightly anisotropic; *i.e.*, $g_{\parallel}=2.0025$ and $g_{\perp}=2.0023$. It should be noticed that K_2HPO_4 contains no water of crystallization. It may be expected, therefore, that lattice defects formed by the dehydration of HHP contribute to trapping the unpaired electron. Similar ESR centers were found in SiO_2, MgO, and CaS, all subjected to an explosive shock.[2] The color of these powdered materials was also gray.

We found that metaphosphate glasses are good trappers of these electrons. Sodium metaphosphate containing a small amount of HHP (1% in wt) was fused at 700 °C for 10 min and then quenched by using two plates of stainless steel. The glasses thus obtained were gray in color, but transparent to visible light. These glasses are suitable for the photo-bleaching and the measurement of an electronic spectrum. An electron spin resonance spectrum measured on the glass is shown in Fig. 2(b). The same singlet as that obtained by heating HHP (Fig. 1) reappeared. A unique difference between the spectrum of heated HHP (a) and that of HHP-doped metaphosphate glass (b) was a remarkable increase in the absorption intensity (in the order of 10^1—10^3) for the glass.

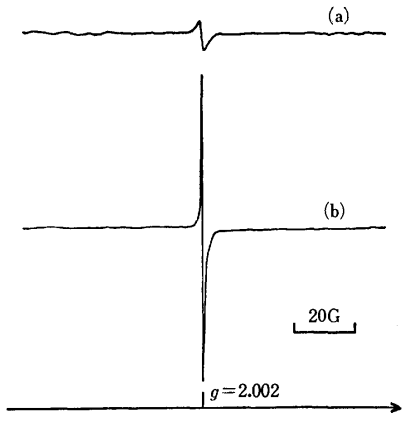

Fig. 2. ESR spectra of $CaHPO_4 \cdot 2H_2O$. a: Heated at 300 °C for 1 h in air and b: dissolved in sodium metaphosphate melt at 700 °C and quenched to form glass. The spectra were obtained at 25 °C. The concn of $CaHPO_4 \cdot 2H_2O$ was 1 wt %.

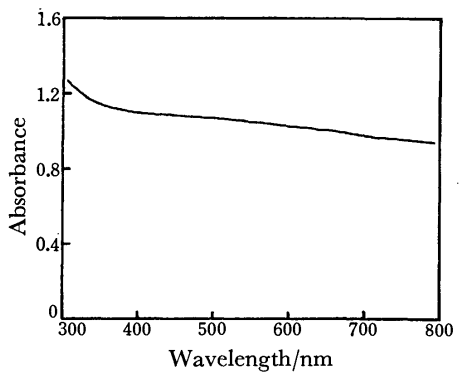

Fig. 3. Visible-UV spectrum of ESR center dissolved in sodium metaphosphate glass matrix.

Figure 3 shows the UV-visible spectrum for the glass containing DMP3. There was no characteristic peak, but a considerably intense absorption was seen over the range of wavelengths measured. If the lattice defect which is trapping an electron is assumed to make a three-dimensional, square-well potential, the difference between the energy levels for a trapped electron depends on the linear dimensions of the well. The size of the defects may be expected to be distributed in these amorphous matrices, and the absorption frequency may also be anticipated to have a wide distribution.

It is well known that DMP3 releases three water molecules at 180 °C and changes into $Mg_2P_2O_7$ gradually liberating one more water molecule by a condensation reaction between two $HOPO_3^{2-}$ ions at temperatures above 300 °C.[3] The process of the reaction should not, however, be viewed as so simple as is illustrated by the above scheme. In solid matrices the reaction does not always take place homogeneously; the extent of the reaction and the kind of the reaction products may be different for local sites and for sites in bulk specimens. For example, the condensation process of two $HOPO_3^{2-}$ ions is accompanied by the formation of the isolated amorphous MgO and "overcondensed" magnesium tetrametaphosphate.[4] The ESR spectrum obtained at 25 °C is displayed in Fig. 4 for the DMP3 sample,

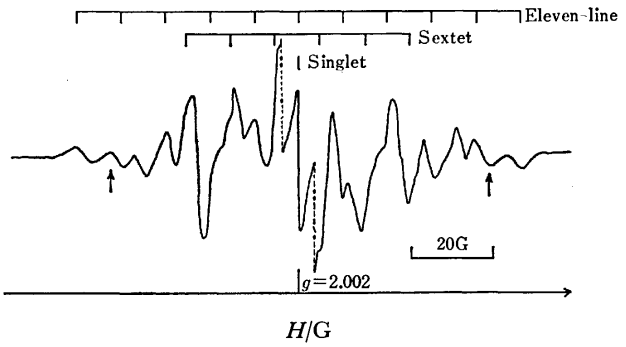

Fig. 4. ESR spectrum of DMP3 heated at gradually increasing temperatures up to 700 °C. Measurement was conducted at 25 °C. Signal gain for the central part is 1/10 of that for the outer parts. The expected locations of the singlet, sextet and eleven-line are also shown.

heated at gradually increasing temperatures with a small rate up to 700 °C. This spectrum was assigned to an F center in MgO.[5] It is expected that 53% of all magnesium-oxygen octahedra should have ^{24}Mg and ^{26}Mg ($I=0$), since the only abundant (10.05%) isotope with a nonzero nuclear spin is ^{25}Mg ($I=5/2$). One should see a single narrow line for an electron in a negative-ion vacancy with such an environment. There are also centers with one or two ^{25}Mg ions around one electron, and these should give a six- or an eleven-line hyperfine pattern centered upon the strong component. Such centers constitute 36 and 10% of the total number respectively. The contributions of those centers with 3, 4, and 5 ^{25}Mg neighbors can be neglected because of their small populations. For the unit intensity of the central line, one should have an intensity of 0.11 for the

sextet and $0.0052n$ for the group of eleven lines, where $n=1, 2, 3, 4, 5, 6, 5, \cdots, 1$. In the figure, the absorptions responsible for the F center with 0, 1, and 2 ^{25}Mg are classified. A nerly isotropic hyperfine coupling tensor was assumed. The locations and intensities of the members of the sextet were in satisfactory agreement with the expection. However, the fourth and eighth members of the eleven lines diminished. This might be due to the interference of the two adjacent members of the more intense sextet. Furthermore, the locations of the second and tenth members were shifted, because the absorptions which are marked by arrows and which are not assignable overlapped with the member lines. The locations and intensities of the other members of the eleven lines were in fair agreement with the expectation. The hyperfine coupling constant was found to be 11 ± 1 G, which is larger than those ($A=5$ G and $A=3.5$ G) found in the single crystal of MgO.[5]

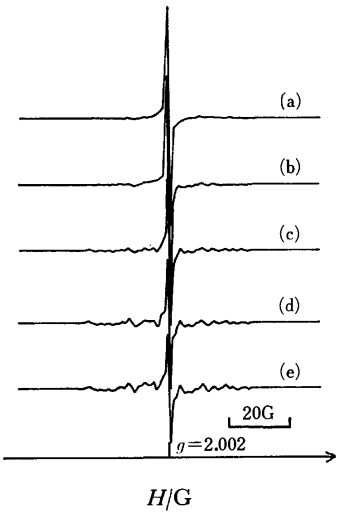

Fig. 5. ESR spectra for $MgHPO_4 \cdot 3H_2O$ heated at 700 °C for 1 h. The spectra were measured at a: −100 °C, b: −30 °C, c: 50 °C, d: 150 °C, and e: 245 °C.

The absorption profile shown in Fig. 4 changed gradually when the measuring temperature was varied. The spectra measured at different temperatures are illustrated in Fig. 5. The increase in the intensities of the sextet and eleven lines with an increase in the temperature was clearly recognized, whereas an inverse change was seen in the intensity of the central line. The change was found to be reversible. This fact suggests that an electron transfered from an F center in MgO to a lattice defect at lower temperatures, since the strong central line contains the contributions of the trapped electron in a lattice defect, besides that of the F center with no ^{25}Mg ion.

We may conclude here that a lattice defect formed in the reaction process acts as an electron-trapping site. The energy levels for the trapped electrons differ from site to site, corresponding to the distribution of the linear dimensions of the electron-trapping defects. Thus, the electronic spectrum for the electron has no peaks centered on a specific wavelength, but shows a rather wide absorption over the range of visible light.

Mechanism of Formation of Trapped Electrons. A major problem remaining is the mechanism of the dehydration-condensation reaction of HHP. In this article we wish to discuss the process by which an ESR center forms.

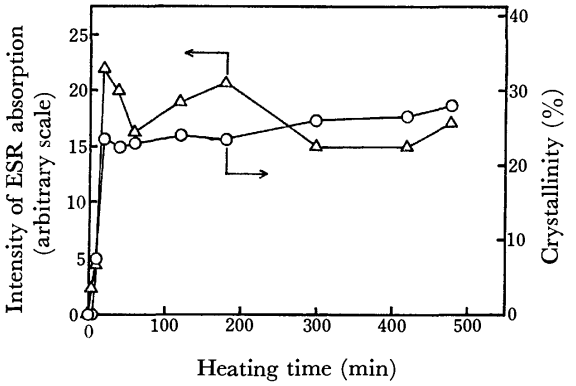

Fig. 6. Changes in ESR absorption intensity and crystallinity of $Mg_2P_2O_7$ with heating time. Specimens were $MgHPO_4 \cdot 3H_2O$ heated at 700 °C. The maximum concn of the trapped electron was ≈100 ppm.

This center emerged during the decomposition of $HOPO_3^{2-}$ ions. The intensities of ESR absorption and the crystallinities of magnesium pyrophosphate for DMP3 heated at 700 °C for various times are given in Fig. 6. The two properties changed similarly in the initial stage (≲20 min), but they varied inversely afterwords. The initial variations in the two features are considered to be due to the release of water of crystallization and the successive decomposition of $HOPO_3^{2-}$ ions. The latter stage of the changes in the crystallinity is viewed as a rearrangement of the resultant amorphous magnesium pyrophosphate to form a crystalline lattice. The slow extinction of the trapped electron (20 min≲) is probably due to the reaction of the electron with fragment ions. The value of the initial crystallinity (≈25%) depends on the experimental conditions. In this experiment, the samples initially equilibrated at room temperature were placed in an electric furnace maintained at 700 °C. The lattice structure of the HHP subjected to an abrupt temperature rise was destroyed by the vaporization of the water of crystallization. The resulting amorphous hydrogen-orthophosphate, containing many cavities or voids among its constituent ions, was suitable for trapping an electron, but unsuitable for forming crystalline pyrophosphate. In the initial heating times, parallel changes in the two properties were recognized. The minimum temperature of heat-treatment generating the detectable ESR absorption for the respective HHP were also the lowest temperatures for the formation of the condensed phosphates. These two facts indicate that the trapped electron emerges during the decomposition of the $HOPO_3^{2-}$ ions.

It can be supposed that the D-C reaction between two $HOPO_3^{2-}$ ions proceeds at least partly through the formation of radicals at elevated temperatures, and that the trapped electron results from the reaction between the radical and the lattice defect. Distinct mechanisms

have been proposed for the D-C reaction of $CaHPO_4 \cdot 2H_2O$ at higher temperatures and at lower temperatures.[6] No intermediate radical expected to be generated during the reaction, such as $H^\bullet$, $^\circ_\bullet OH$, $^\circ_\bullet OPO_3^{2-}$, and $^\circ_\bullet PO_3^{2-}$, was detected directly by the ESR method, but one of the derivatives of phosphine was found.[7] It may, therefore, be inferred that atomic hydrogen, $H^\bullet$, forms upon the reaction. One possible mechanism of forming a trapped electron is the process shown below:

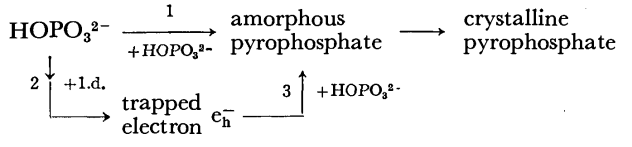

Here, l.d. expresses a lattice defect. The 1 process was regarded as the direct radical condensation corresponding to the initial crystallinity shown in Fig. 6:

$$HOPO_3^{2-} \longrightarrow H^\bullet + {}^\circ_\bullet OPO_3^{2-}$$

$$H^\bullet + HOPO_3^{2-} + {}^\circ_\bullet OPO_3^{2-} \longrightarrow H_2O + P_2O_7^{4-}.$$

The 2 stage was viewed as the formation of the trapped electron:

$$H^\bullet + \text{l.d.} \longrightarrow e_h^- + H^+ \quad \text{or}$$

$$H^\bullet + HOPO_3^{2-} \longrightarrow H_2O + {}^\circ_\bullet PO_3^{2-}$$

$${}^\circ_\bullet PO_3^{2-} + \text{l.d.} \longrightarrow PO_3^- + e_h^-.$$

The 3 reaction was considered to be the extinction of the e_h^- of forming the $P_2O_7^{4-}$ ions:

$${}^\circ_\bullet OPO_3^{2-} + e_h^- + PO_3^- \longrightarrow P_2O_7^{4-}.$$

Other side reactions, such as the formation of a hydrogen molecule ($H^\bullet + H^\bullet \rightarrow H_2$) and the substitution of a hydrogen for an oxygen in a PO_4 tetrahedron, may be possible.

References

1) Gmelins, "Handb. d. Anorg. Chem. 27(B)," 397 (1937).
2) M. C. R. Symons, *J. Chem. Soc., A*, **1971**, 1648.
3) T. Kanazawa, *Kagaku No Ryoiki*, **24**, 222 (1970).
4) H. Kawazoe, K. Ametani, M. Imai, and T. Kanazawa, *Bull. Chem. Soc. Jpn.*, **51**, 2886 (1978).
5) J. E. Wertz, P. Auzins, R. A. Weeks, and R. H. Silsbee, *Phys. Rev.*, **107**, 1535 (1957).
6) S. Matsuno and K. Takai, *Kogyo Kagaku Zasshi*, **74**, 624 (1971).
7) H. Kawazoe, Y. Tokunaga, K. Ametani, M. Imai, and T. Kanazawa, 36th National Meeting of the Chemical Society of Japan, Osaka, April 1977, Abstr. No. 1N14.

The "Overcondensation" of Phosphate Ions and the Formation of Conjugate Metal Oxide upon the Thermal Dehydration-condensation of Hydrogenorthophosphates

Hiroshi KAWAZOE,* Kazuo AMETANI,† Masahiko IMAI,† and Takafumi KANAZAWA

Department of Industrial Chemistry, Faculty of Technology, Tokyo Metropolitan University, Fukazawa, Setagaya-ku, Tokyo 158

†*Tokyo Metropolitan Isotope Research Center, Fukazawa, Setagaya-ku, Tokyo 158*

(Received September 19, 1977)

On the thermal reaction of H_3PO_4 or $NH_4H_2PO_4$ with metal salts, such as Na_2CO_3 or $Mg(OH)_2$, the "overcondensation" of the phosphate anions and the conjugate formation of metal oxide were observed. The "overcondensation" was defined as a formation reaction of the phosphate with a larger polymerization degree than that of the product to be expected from the [MO or M_2O]/[P_2O_5] mole ratio of the starting mixtures. The "overcondensed" tetrametaphosphate and the conjugate oxide, magnesium oxide, were detected on the thermal condensation of $MgHPO_4 \cdot 3H_2O$ and of a mixture of $NH_4H_2PO_4$ or H_3PO_4 and $Mg(OH)_2$. The "overcondensed" tripoly- and trimeta-phosphate were found in the course of the formation reaction of Na pyrophosphate from a mixture of Na_2CO_3 and $NH_4H_2PO_4$.

A free electron was found to be trapped in a lattice defect formed during the dehydration-condensation (abbreviated as D-C) reaction of hydrated hydrogen-orthophosphates.[1] Especially, on the thermal condensation of $MgHPO_4 \cdot 3H_2O$ (DMP3), an ESR center which may be assigned to the trapped electron at an oxygen vacancy in MgO (the so-called F center) was detected. The magnesium oxide was considered to arise upon the reaction. The formation of MgO must be accompanied by the formation of the condensed phosphate, which has a greater polymerization degree than that of pyrophosphate. Therefore, it may be supposed that the thermal condensation reaction progresses through the separation of metal oxide and the "overcondensation" of phosphates. This "overcondensation" is defined as the formation reaction of the condensed phosphates with a larger polymerization degree than that of the product to be expected from the mole ratio of the starting sample, [MO or M_2O]/[P_2O_5].

It is the purpose of the present paper to examine whether or not a pair of conjugate reactions, the "overcondensation" of phosphates and the isolation of metal oxide, generally occurs on the D-C of orthophosphates. The condensation reactions of some sodium- and magnesium-orthophosphates to the respective pyrophosphates were done, and the "overcondensed" phosphates were identified by means of X-ray diffraction or ESR spectroscopy for irradiated samples. The formation of amorphous magnesium oxide was verified by using the ESR technique for the Mn(II)-doped samples.

Experimental

In order to obtain the intermediates in the reaction, a mixture of metal salt and phosphate or phosphoric acid was placed in a high-alumina crucible and heated in an electric furnace at several fixed temperatures. The thermal reactions for preparing the respective pyrophosphates were as follows:

$$2Na_2CO_3 + 2NH_4H_2PO_4 \longrightarrow Na_4P_2O_7 + 2NH_3 + 2CO_2 + 3H_2O$$

$$2Mg(OH)_2 + 2NH_4H_2PO_4 \longrightarrow Mg_2P_2O_7 + 2NH_3 + 5H_2O$$

$$2Mg(OH)_2 + 2H_3PO_4 \longrightarrow Mg_2P_2O_7 + 5H_2O$$

$$2MgHPO_4 \cdot 3H_2O \longrightarrow Mg_2P_2O_7 + 7H_2O.$$

All the chemicals used except DMP3 were guaranteed-grade reagents (Kanto Chemicals, Ltd.). The magnesium hydrogenphosphate trihydrate was produced by the reaction of $Mg(OH)_2$ with H_3PO_4 and was used as one of the starting samples for magnesium pyrophosphate (MP) preparation. The magnesium salts doped with Mn(II) were also prepared in order to examine whether or not the isolated MgO deposits in the course of the reaction. The manganese carbonate was dissolved in phosphoric acid or added to a mixture of powdered $Mg(OH)_2$ and $NH_4H_2PO_4$. The mole ratio of Mn/Mg was 1×10^{-4}.

The measurement of the X-ray diffraction were made for the powdered samples to check changes in the structure of the phosphates during the thermal reaction.

The measurements of the ESR absorption were carried out for the γ-irradiated specimens (^{60}Co source, for two hours at a dose rate of 0.5 Mrad/h) and Mn(II)-doped samples on a JEOL JES-PE-3X ESR spectrometer, mainly at room temperature.

Results and Discussion

"Overcondensed" Phosphates Detected by the X-Ray Powder Diffraction Method. Figure 1 shows the X-ray diffraction patterns of the specimens obtained by a thermal treatment of a mixture of Na_2CO_3 and $NH_4H_2PO_4$. The pattern for the material heated at 300 °C (d) was attributed to that of sodium tripolyphosphate (Form II).[2] A successive heating up to 520 °C (b) resulted in the crystallization of sodium trimetaphosphate[3] in addition to tripolyphosphate. The degradation of the "overcondensed" phosphates, *i.e.*, tripoly- and trimeta-phosphates, into sodium pyrophosphate occurred above 620 °C (a).[4]

The X-ray diffraction patterns for the heat-treated magnesium salts are shown in Fig. 2. As may be seen in the figure, the diffraction patterns were identical for the two cases starting from different phosphates, *i.e.*, ammonium dihydrogenphosphate and phosphoric acid. The crystalline material formed by heating at 730 °C (b, e) was identified as not magnesium pyrophosphate, but magnesium tetrametaphosphate.[5,6] In this stage

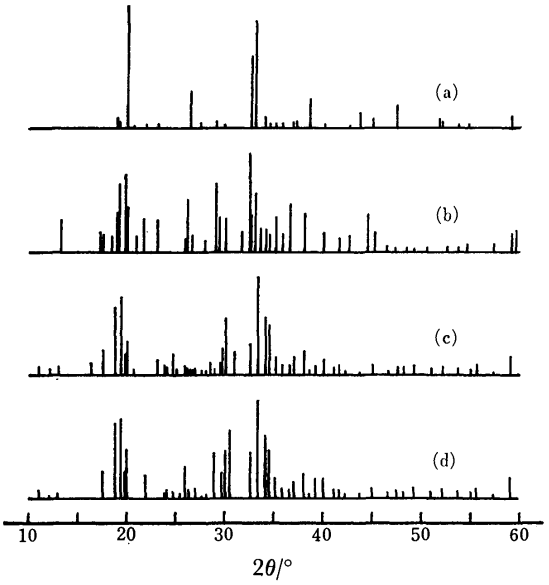

Fig. 1. X-Ray diffraction patterns of the mixture of Na_2CO_3 and $NH_4H_2PO_4$ (1: 1 in mole ratio) heated at a: 620, b: 520, c: 400, and d: 300 °C.

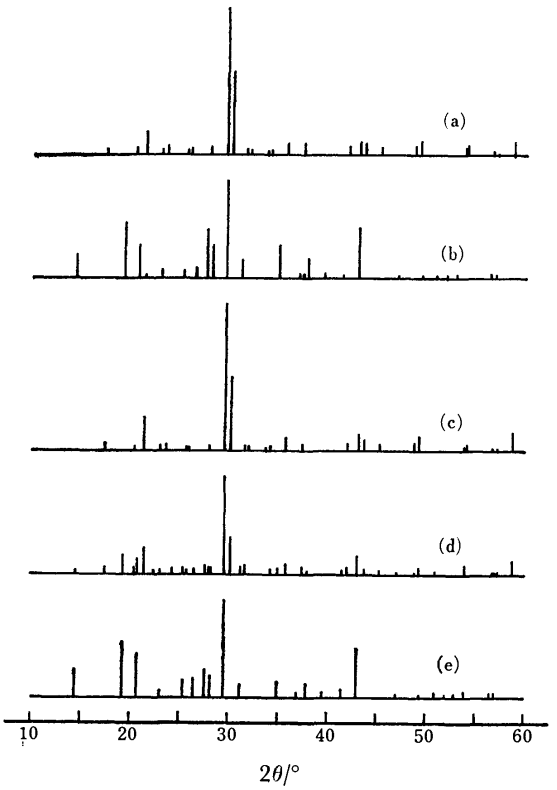

Fig. 2. X-Ray diffraction patterns of the mixtures of $Mg(OH)_2$ and a phosphate (MgO/P_2O_5 mole ratio=2) heated at a: 1075 °C for 2 h, b: 730 °C for 15 h, c: 1075 °C for 2 h, d: 920 °C for 2 h, and e: 730 °C for 15 h. Orthophosphoric acid was used as a starting reagent for a and b, whereas $NH_4H_2PO_4$ was utilized for c, d, and e.

of the reaction, no other crystalline phosphates were found. The tetrametaphosphate changed into MP at higher temperatures (a, c, d).[7] The results are summarized in Table 1. It may be inferred from these results that the formation of "overcondensed" phosphates with a larger polymerization degree than that of pyrophosphate takes place in the course of the condensation of orthophosphates. The condensation through the formation of the "overcondensed" phosphates must be the predominant path, since the crystallinity of the samples obtained by heating at lower temperatures was quite high (in the order of 10%) and no detectable signal of pyrophosphate formation was seen in the diffraction patterns. It may be noted that the formation of the oxides in the heated samples was not detected by the X-ray method because of the relatively low crystallinity of MgO and the unstability of Na_2O.

Detection of the Amorphous "Overcondensed" Phosphates and Amorphous Magnesium Oxide by the ESR of Mn(II). We made a prediction that the "overcondensation" is accompanied by the isolation of metal oxide. The utilization of ESR of incorporated Mn(II) made it possible to examine the formation of amorphous magnesium oxide. The ESR spectra for Mn(II)-doped samples are shown in Fig. 3. Only the fine-structure component responsible for the $M=1/2\leftrightarrow-1/2$ transition with six hyperfine structure lines produced by ^{55}Mn ($I=5/2$) had a detectable strength of the signals. The (a) and (c) spectra were taken as the references; (a) was the well-known pattern of Mn(II) in the MgO host crystal,[8] while (c) was the absorption due to Mn(II) in polycrystalline magnesium tetrametaphosphate.[9] The (b) pattern, taken from the specimen heated at 730 °C, may be regarded as a close superposition of the other two spectra, (a) and (c). An extra peak found near $g=2.002$ is attributable to the electron trapped in a lattice defect.[1] It may, therefore, be

Table 1. Crystalline phases identified in samples heat-treated under various conditions

$2Na_2CO_3+2NH_4H_2PO_4$[a]		$2Mg(OH)_2+2NH_4H_2PO_4$ or $2H_3PO_4$[a]		$MgHPO_4\cdot3H_2O$
Heating condition	Identified crystal	Heating condition	Identified crystal	Identified crystal
300 °C 15 h	$Na_5P_3O_{10}$	730 °C 15 h	$Mg_2P_4O_{12}$	$Mg_2P_2O_7$
400 °C 2 h	$Na_5P_3O_{10}$	920 °C 2 h	$Mg_2P_2O_7$	$Mg_2P_2O_7$
520 °C 2 h	$Na_5P_3O_{10}$ $(NaPO_3)_3$	1075 °C 2 h	$Mg_2P_2O_7$	$Mg_2P_2O_7$
620 °C 2 h	$Na_4P_2O_7$			

a) Samples obtained by mixing the reagents shown in this table.

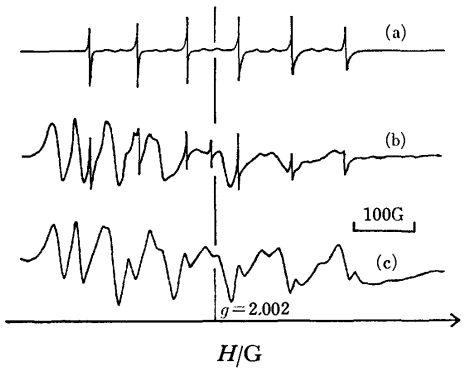

Fig. 3. ESR spectra of Mn(II) in various host crystals. a: In MgO, b: in the specimen obtained by heating 1:1 mixture of $Mg(OH)_2$ and $NH_4H_2PO_4$ at 730 °C and c: in $Mg_2P_4O_{12}$.

concluded that the "overcondensation" of phosphate ions and the isolation of magnesium oxide proceed simultaneously in the course of the D-C reactions of orthophosphate with magnesium salt.

No trace of the "overcondensation" of phosphates or of the isolation of MgO crystals was seen by X-ray diffraction when DMP3 was used as the starting sample. The process of the D-C reaction of DMP3 to MP is well established:[10]

$$MgHPO_4 \cdot 3H_2O \xrightarrow[-3H_2O]{1\ 180\,^\circ C} \text{amorph. } MgHPO_4 \xrightarrow[-H_2O]{2\ \text{above } 300\,^\circ C}$$

$$\text{amorph. } Mg_2P_2O_7 \xrightarrow{3\ \text{above } 450\,^\circ C} \text{cryst. } Mg_2P_2O_7.$$[11]

In the above reaction, the conversion to crystalline MP is slow at temperatures lower than about 900 °C. If amorphous "overcondensed" phosphate forms competitively with amorphous MP in Stage 2, it is undetectable by X-ray diffraction. In order to confirm the formations of the "overcondensed" phosphate and its conjugate oxide, ESR measurements were carried out on Mn(II)-doped DMP3 heated at 700 °C for several hours, which was still gray-colored and which exhibited the weak X-ray diffraction characteristic of crystalline MP. The results are shown in Fig. 4(a). The signals represented as F may be attributable to the F center in magnesium oxide.[12] The peaks labelled by M may be interpreted as resulting from the Mn(II) in the MgO host lattice. This fact strongly supports the formation of the isolated magnesium oxide. The manganese ions, of course, occupy also the sites of Mg ions in the condensed phosphates. Thus, the absorption responsible for these Mn(II) ions would be expected to appear. However, the environment of Mn(II) ions was considered to be distorted or to be widely distributed in these amorphous phosphates, and the resultant absorption was too broad to be shown in the figure. The underlying vague absorption (not shown in the figure) was assigned to these manganese ions.

In order to detect the counterpart of the isolated MgO, that is, the "overcondensed" phosphates, the measurements of ESR absorption were made on γ-irradiated samples which had been obtained by heating DMP3 doped with Mn(II) at 730 °C for 15 h in order to bleach out the trapped electron. The representative

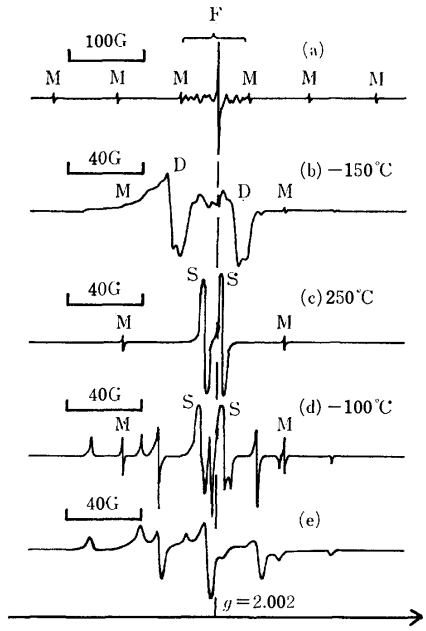

Fig. 4. ESR spectra for $MgHPO_4 \cdot 3H_2O$. a: Mn(II)-doped sample heated at 700 °C. b, c, d: Specimens obtained by heating DMP3 doped with Mn(II) at 730 °C for 15 h and by irradiating with γ-ray at a liquid nitrogen temperature. The spectrum b was recorded without intervening warming up to room temperature and c was measured at 250 °C. The spectrum d was obtained at −100 °C after bleaching out (at 300 °C) the intense signals arising from PO_4^{2-} radicals. e: γ-irradiated $Mg_2P_4O_{12}$ obtained by heating 1:1 mixture of $NH_4H_2PO_4$ and $Mg(OH)_2$ at 1100 °C. Signal gain for c and d is ten times larger than that for b.

spectra are shown in Fig. 4 (b, c, d). The (b) spectrum was recorded without intervening warming up to room temperature after irradiation at the temperature of liquid nitrogen and (c) was measured at 250 °C. The (d) spectrum was obtained at −100 °C after bleaching out (at 300 °C) the intense signals arising from PO_4^{2-} radicals. The intense doublet seen in the (b) pattern (labelled by D) is identified as the PO_4^{2-} radical.[13] At present, the nature of the radical responsible for the doublet, S, in the (c) pattern is not clear, but a little should be mentioned about this center. This absorption was found to arise generally by the irradiation to pyrophosphates and to be stable up to 300 °C. The remarkable peak of the trapped electron was also visible near the g value of a free electron. The (e) spectrum was recorded on the γ-irradiated specimen obtained by heating a 1:1 mixture of $NH_4H_2PO_4$ and $Mg(OH)_2$ at 1100 °C. The crystalline component in this sample was magnesium tetrametaphosphate. This spectrum was attributed to the radical (U) formed by the irradiation to the tetrametaphosphate crystal or its glass.[14] The center was formed only in the irradiated tetrametaphosphate and was not detected in other related, irradiated magnesium phosphates. The spectrum broadened beyond detection at above 200 °C because of the relatively short relaxation time. Three types of

ESR centers are recognized in the (d) pattern. The first is the unknown center (the doublet, S), the second, the radical (U) in the tetrametaphosphate host lattice, and the last, Mn(II) in the MgO host matrix.

It may, therefore, be concluded that the "overcondensation" of phosphates and the counterpart isolation of MgO occur also in the course of the D-C reaction of DMP 3.

References

1) H. Kawazoe, M. Nishino, H. Hosono, K. Isozaki, K. Ametani, M. Imai, and T. Kanazawa, *Bull. Chem. Soc. Jpn.*, **51**, 2882 (1978).
2) ASTM X-Ray Powder Data File 11-652.
3) ASTM X-Ray Powder Data File 11-648.
4) ASTM X-Ray Powder Data File 10-187.
5) ASTM X-Ray Powder Data File 11-41.
6) A. G. Nord and K. B. Lindberg, *Acta Chem. Scand.*, **A29**, 1 (1975).
7) ASTM X-Ray Powder Data File 8-38.
8) W. Low, *Phys. Rev.*, **105**, 793 (1957).
9) H. Kawazoe, M. Nishino, M. Chikazawa, T. Umegaki, and T. Kanazawa, 36th National Meeting of the Chemical Society of Japan, Osaka, April 1977, Abstr. No. 2J25.
10) T. Kanazawa, *Kagaku No Ryoiki*, **24**, 222 (1970).
11) The second stage of the reaction could not be viewed as dehydration from the viewpoint of the microscopic mechanism of the reaction. This stage was found to proceed through the detachment of atomic hydrogen. This has been discussed in Ref. 1.
12) J. E. Wertz, P. Auzins, R. A. Weeks, and R. H. Silsbee, *Phys. Rev.*, **107**, 1535 (1957).
13) M. Miura and A. Hasegawa, *Bull. Chem. Soc. Jpn.*, **39**, 1432 (1966); S. Sabramanian, M. C. R. Symons, and H. W. Wardale, *J. Chem. Soc., A*, **1970**, 1239.
14) D. M. Yudin, A. V. Shendrik, M. L. Petrovskaya, and G. P. Nikolina, *Soviet Phys. Solid State*, **15**, 1754 (1974); *Fiz. Tverd. Tela.*, **15** 2636 (1973).

Extraction of Lanthanoids from Hydrochloric and Nitric Acid Solutions by Di(2-ethylhexyl)phosphoric Acid†

Yoshiyuki HIRASHIMA,* Yasuhiro YAMAMOTO, Shigeru TAKAGI, Taisuke AMANO, and Jiro SHIOKAWA

Department of Applied Chemistry, Faculty of Engineering, Osaka University, Yamada-kami, Suita, Osaka 565

(Received December 24, 1977)

Di(2-ethylhexyl)phosphoric acid† (D2EHPA or HX) extracts lanthanoids (Ln) from a moderately acidic solution by cation exchange reaction: $Ln^{3+}+m(HX)_n \rightleftarrows LnX_3 \cdot 3HX+3H^+$. From the mode of extraction m is estimated to be 3 in benzene diluent, and smaller than 3 in heptane diluent. The change of the relative extractability with the atomic number of lanthanoids is in line with what is expected from the concept of the tetrad effect proposed by Peppard *et al.* When the hydrogen ion concentration is very high, the main reaction is solvation: $Ln^{3+}+3A^-+q(HX)_n \rightleftarrows LnA_3 \cdot 4HX$. In benzene diluent q is 2 and n is 2, while q is 1.6—1.7 in heptane diluent. It can be attributed to the difference in the association degree of D2EHPA that m or q is smaller in heptane than in benzene.

Di(2-ethylhexyl)phosphoric acid† (D2EHPA or HX) extracts a lanthanoid by a cation exchange reaction expressed by

$$Ln^{3+}_{(aq)} + 3(HX)_{2(org)} \rightleftarrows LnX_3 \cdot 3HX_{(org)} + 3H^+_{(aq)}, \quad (1)$$

where the subscripts (aq) and (org) represent the aqueous and organic phase, respectively.[1,2] In a saturated aliphatic hydrocarbon, however, the extraction behavior of the lanthanoids differs slightly from what is expected from Eq. 1.[3,4] The association degree of D2EHPA is higher than 2 in such a solvent.[5] Sato and Ueda assumed that the extracted species is different from that described in Eq. 1.[4] Assuming that a lanthanoid is extracted only by a cation exchange reaction, the distribution ratio of the lanthanoid is expected to decrease with the increase in acid concentration in aqueous phase. However, in the extraction of metals by a dialkyl phosphoric acid the distribution ratio increases with the acid concentration in the region in which acid concentration is very high.[6-8] This suggests that some other reactions occur. We have studied the distribution equilibria of some lanthanoids with D2EHPA.

Experimental

Materials. D2EHPA (Union Carbide Corporation) was purified[9] and then diluted with heptane or benzene to the desired concentration. The lanthanoid salt solutions were prepared as described for chloride solutions.[3]

Procedure. Equal volumes of organic D2EHPA solution and the aqueous lanthanoid solution were placed in an Erlenmeyer flask with a glass stopper. The flask was shaken vigorously for 15 min, allowed to stand for 30 min, and again shaken for 10 min. After the flask had been allowed to stand for 30 min or longer, the glass stopper was replaced by the glass stopcock used for separation of the two liquids, and the two phases were separated. All the equilibration procedures were carried out at 20.0±0.2 °C.

Determination of Equilibrium Data. The lanthanoids and yttrium extracted into the organic phase were recovered by back-extracting four times with equal volumes of 6M hydrochloric or nitric acid solution. The concentrations of lanthanoids and yttrium were determined by EDTA titration with Xylenol Orange as an indicator. The concentration of hydrogen ion in the aqueous solution was determined by titration with a standard solution of sodium hydroxide with Bromophenol Blue as an indicator. The concentration of D2EHPA in organic solution was determined by titration with a standard sodium hydroxide solution in an ethanol–water (4: 1 volume ratio) solvent with a pH meter. The concentration of D2EHPA was determined as the monomer unit. The distribution ratio of a lanthanoid is defined to be the ratio of the concentration of the lanthanoid in the organic phase to that in the aqueous phase.

† Bis(2-ethylhexyl) hydrogenphosphate in IUPAC notation.

Results and Discussion

Figure 1 shows the variation of the distribution ratios of dysprosium and europium with the concentration of

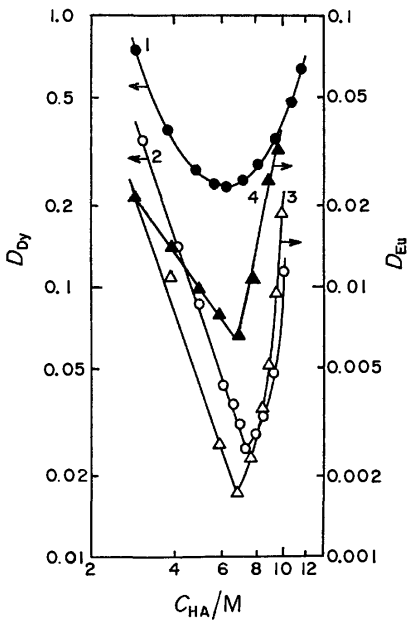

Fig. 1. Relationship between the distribution ratio, D, and the concn of the acid or the anion in the aq phase in the extraction of Eu or Dy by 1 M D2EHPA in heptane.
1: 0.05 M $Dy(NO_3)_3$–HNO_3 system, HA: HNO_3, 2: 0.05 M $DyCl_3$–HCl system, HA: HCl, 3: 0.05 M $EuCl_3$–HCl system, HA: HCl, 4: 0.05 M $EuCl_3$–HCl–LiCl system, C_{HCl}=2.88 M, $C_{HA}=C_{HCl}+C_{LiCl}$. 1M= 1 mol/dm³.

hydrochloric or nitric acid in aqueous phase. With the increase in the concentration of acid the distribution ratio decreases in the lower acid concentration region and increases in the higher concentration ragion, exhibiting a minimum at acid concentration 6—8 M. Similar data were obtained in other systems. From the extraction behavior we see that D2EHPA extracts a lanthanoid mainly by a cation exchange reaction in the low acid concentration region and by some other reactions in the high acid concentration region.[6]

Low Acid Concentration Region. The cation exchange reaction for the extraction of a trivalent lanthanoid by D2EHPA can be expressed as follows, taking into account the association degree of D2EHPA, n.

$$Ln^{3+}_{(aq)} + m(HX)_{n(org)} \rightleftarrows LnX_3 \cdot xHX_{(org)} + 3H^+_{(aq)}, \quad (2)$$

where the ratio of D2EHPA to the lanthanoid in the extracted species is $(3+x)$, and $m \times n$ is equal to $(3+x)$. Three hydrogen ions are transferred into the aqueous phase per each lanthanoid extracted.[3]

It was confirmed that Eq. 1 is valid in benzene diluent. The association degree of D2EHPA was found cryoscopically to be nearly equal to 2. The plot of log D *vs.* log C_{HX} shows that the distribution ratio of the lanthanoid is of third power with respect to D2EHPA concentration.

Table 1. Extractant dependency of the extraction of Eu by D2EHPA in heptane

Series	$C_{HA,I}$[a] / M[f]	$C_{Eu,I}$[b] / M[f]	Extractant dependency[c] estimated for $x=3$	$x=2$
1[d]	0.50	0.05	2.16	2.17
2[d]	0.40	0.05	2.12	2.20
3[d]	0.40	0.14	2.25	2.25
4[d]	0.076	0.208	2.28	2.73
5[e]	0.194	0.05	2.23	2.38

a) The initial concentration of hydrochloric or nitric acid in aq phase. b) The initial concentration of Eu in aq phase. c) Estimated from the slope of the plot of $\lg D_{Eu}$ *vs.* $\lg C_{HX}$ (C_{HX}: 0.1—1.0 M). d) $EuCl_3$–HCl system. e) $Eu(NO_3)_3$–HNO_3 system. f) 1 M=1 mol/dm^3.

The extractant dependency estimated for the extraction of europium with D2EHPA in heptane is given in Table 1. The equilibrium concentration, C_{HX}, was estimated by the equation $C_{HX}=C_{HX,I}-(3+x)C_{Eu(org)}$, derived from Eq. 2, where $C_{HX,I}$ and $C_{Eu(org)}$ are the initial concentration of D2EHPA and the equilibrium concentration of europium in the organic phase, respectively. In the estimation the cases $x=3$ and $x=2$ were assumed.[3,10] Mason *et al.* proposed an equation in which x is 2 and m is 2.5 regarding D2EHPA as dimeric in heptane. When x is 3, the estimated dependency is nearly equal for all the series. On the other hand, when x is 2 the dependency differs a great deal for series 4 from those for the others. Thus it is reasonable to assume x to be 3 rather than 2. Eq. 2 can be rewritten as

$$Ln^{3+}_{(aq)} + m(HX)_{n(org)} \rightleftarrows LnX_3 \cdot 3HX_{(org)} + 3H^+_{(aq)}. \quad (3)$$

The extractant dependency for the nitrate system (series 5) is nearly equal to that for chloride systems (Table 1) suggesting that there is no serious difference in the extraction reaction between the two systems. The values of the extractant dependency are considerably smaller than 3, the value obtained for the benzene system. The difference in value of the two systems may be explained in terms of the difference of the association degree of D2EHPA, since the ratio of D2EHPA to a lanthanoid in the extracted species is 6 in both systems, though the effect of the activity coefficient should be taken into account for discussion. The extractant dependency for several lanthanoids and yttrium is given in Table 2.

Table 2. Extractant dependency of the extraction of lanthanoids (Ln) and yttrium

	Extractant dependency
La	2.40
Pr	2.26
Nd	2.22
Sm	2.15
Eu	2.16
Gd	2.18
Tb	2.12
Dy	2.06
Er	2.05
Yb	2.11
Y	2.11

Extraction conditions: C_{HX}=0.1—1.0 M, $C_{Ln,I}$=0.02—0.05 M, C_{HCl}=0.15—2 M. 1 M=1 mol/dm^3.

Figure 2 shows the relative extractability of several lanthanoids and yttrium. The relative extractability was estimated from the difference of the distribution ratios normalized to an identical condition. The average separation factor for the adjacent lanthanoids is evaluated to be 2.28, which is in rough accord with that reported by Pierce *et al.*[11] The relative extractability is not a smooth function of the atomic number, Z, of the lanthanoid. The shape of the curve is in fair agreement with that expected from the concept of the tetrad effect proposed by Peppard *et al.*[12] A tendency similar to the concept was also reported by Siekierski.[13] The relative extractability of yttrium seems to be between holmium and erbium; that of holmium was not determined in this study.

In order to check the validity of the relations stated above with regard to the distribution equilibrium, the equilibrium values calculated by the use of the following equations were compared with the actual extraction isotherms.[3]

$$D = K' \times \frac{C^a_{HX}}{C^3_{H^+}}, \quad C_{HX} = C_{HX,I} - 6C_{Ln(org)}, \text{ and}$$

$$C_{H^+} = C_{H^+,I} + 3C_{Ln(org)}$$

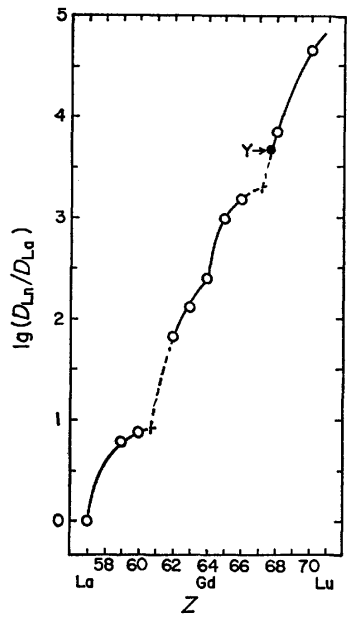

Fig. 2. Variation of the distribution ratio, D, with the atomic number, Z, of lanthanoids in the extraction from the chloride solutions by 1M D2EHPA in heptane. $C_{LnCl_3,i}=0.02$—0.05M, $C_{HCl}=1$M, $C_{HX}=0.5$ M. 1M=1 mol/dm³.

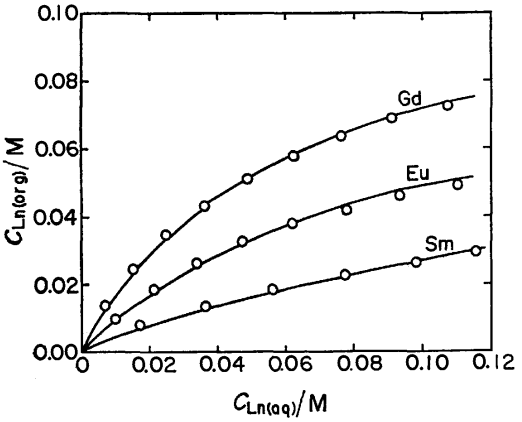

Fig. 3. Distribution equilibria for $SmCl_3$–HCl–, $EuCl_3$–HCl–, and $GdCl_3$–HCl–1M D2EHPA in heptane systems.
$[H^+]=1$M. The solid curves represent the calculated values. 1M=1 mol/dm³.

In the calculation the constant K' was evaluated from the equilibrium data observed for the system where $C_{Ln,i}=0.1$ M†† and $C_{H^+}=1$ M.†† $C_{H^+,i}$ represents the initial concentration of hydrogen ion. For the value of a, the extractant dependency given in Table 2 was used. Figure 3 shows the extraction isotherms for the $SmCl_3$–HCl–, $EuCl_3$–HCl–, and $GdCl_3$–HCl–D2EHPA in heptane systems. The calculated values are denoted by three curves and the experimental values by open circles. The validity of the relations is demonstrated by the agreement between the calculated and observed values.

†† Throughout this paper, 1M=1 mol/dm³.

High Acid Concentration Region. Solvation is a predominant reaction at high acidity, which is expressed by

$$Ln^{3+} + 3A^- + q(HX)_n \rightleftarrows LnA_3 \cdot qnHX, \quad (4)$$

where A^- represents an anion.[4,7] This indicates that the effect of the concentration of a mineral acid on the extraction by solvation is essentially attributed to the corresponding anion. It is demonstrated by the similarity in shape of curves 3 and 4 (Fig. 1), though a little difference can be attributed to the difference in HCl concentration. The shapes of the curves can be explained as follows. (i) Increase in HCl concentration causes decrease in the amount of the extraction of europium by the cation exchange reaction, since the extraction reaction is of inverse third power dependence on the hydrogen ion concentration. (ii) Increase in chloride concentration depresses the extraction of a lanthanoid by the cation exchange reaction, since the concentration of the trivalent lanthanoid ion, one reactant in Eq. 2, decreases by complexing between the lanthanoid and chloride. (iii) Increase in chloride concentration increases the amount of the extraction of the lanthanoid by the solvation expressed by Eq. 4. The extractant dependency of the extraction of lanthanoids from highly acidic solutions where the lanthanoids are extracted almost only by solvation is given in Table 3. The

Table 3. Extractant dependency of the extraction of lanthanoids

Ln	HA	$C_{HA,i}$ a) / M b)	Diluent	Extractant dependency c)
Er	HNO_3	12.0	Benzene	2.15
Er	HCl	10.5	Benzene	2.10
Eu	HCl	10.0	Benzene	2.08
Er	HNO_3	12.0	Heptane	1.60
Er	HCl	10.5	Heptane	1.68
Dy	HNO_3	12.0	Heptane	1.63
Dy	HCl	10.5	Heptane	1.73
Eu	HCl	10.0	Heptane	1.70

a) The initial concentration of the acid in aq phase. b) 1 M=1 mol/dm³. c) Estimated from the slope of the plot of lg D_{Ln} *vs.* lg C_{HX} ($C_{Ln,i}=0.05$ M, $C_{HX}=0.1$—1.0 M).

extractant dependency is about 2.0 both for the nitrate and the chloride systems when benzene is a diluent, and Eq. 4 can be rewritten for such systems as follows since D2EHPA is practically dimeric in benzene.

$$LnA_3 + 2(HX)_2 \rightleftarrows LnA_3 \cdot 4HX \quad (5)$$

On the other hand the dependency is smaller in heptane diluent as in the case of the cation exchange reaction.

References

1) D. F. Peppard, J. R. Ferraro, and G. W. Mason, *J. Inorg. Nucl. Chem.*, **7**, 231 (1958).
2) T. G. Lentz and M. Smutz, *J. Inorg. Nucl. Chem.*, **30**, 621 (1968).
3) Y. Hirashima, M. Mugita, and J. Shiokawa, *J. Inorg. Nucl. Chem.*, **37**, 1249 (1975).

4) T. Sato and M. Ueda, *J. Inorg. Nucl. Chem.*, **35**, 1003 (1973).
5) J. R. Ferraro, G. W. Mason, and D. F. Peppard, *J. Inorg. Nucl. Chem.*, **22**, 285 (1961).
6) A. M. Kiwan and R. S. Amin, *J. Inorg. Nucl. Chem.*, **33**, 2221 (1971).
7) O. Navratil and L. Dubinin, *J. Inorg. Nucl. Chem.*, **31**, 2927 (1969).
8) C. J. Hardy, *Nucl. Sci. Eng.*, **16**, 401 (1963).
9) T. Goto and M. Smutz, *J. Inorg. Nucl. Chem.*, **27**, 1369 (1965).
10) G. W. Mason, D. N. Metta, and D. F. Peppard, *J. Inorg. Nucl. Chem.*, **38**, 2077 (1976).
11) T. B. Pierce, P. F. Peck, and R. S. Hobbs, *J. Chromatogr.*, **12**, 81 (1963).
12) D. F. Peppard, G. W. Mason, and S. Lewey, *J. Inorg. Nucl. Chem.*, **31**, 2271 (1969); D. F. Peppard, C. A. A. Bloomquist, E. P. Horwitz, S. Lewey, and G. W. Mason, *ibid.*, **32**, 330 (1970).
13) S. Siekierski, *J. Inorg. Nucl. Chem.*, **32**, 519 (1970); *ibid.*, **33**, 337 (1971).

Cobalt(IV) Ammine Complexes with 5-Nitrosalicylato or Similar Ligands. IV.[1] Preparation, ^{1}H-NMR, ^{13}C-NMR, and IR Spectra

Yoshihisa YAMAMOTO

Faculty of Pharmaceutical Science, Higashi Nippon Gakuen University, Ishikari-Tobetsu, Hokkaido 061-02

(Received January 5, 1978)

The ^{1}H-NMR spectrum of the 5-nitrosalicylatotetraamminecobalt(IV) complex did not show the signals of phenyl protons of the salicylato ligand, but did show those of ammine protons at 3.7 (s, 6H) and 3.3 ppm (s, 6H). The ^{13}C-NMR peaks could not be observed because of the paramagnetism. The ^{1}H-NMR spectra of the salicylatotetraamminecobalt(III) complexes showed peaks at 3.96 (s, 6H), 3.65 (s, 3H), and 3.38 ppm (s, 3H) for the ammine protons and at 6.7—8.1 ppm (m, 4H) for the phenyl protons of the salicylato ligand. Their ^{13}C-NMR spectra showed seven signals for the salicylato ligand. The IR peaks assignable to the rocking deformation vibration were observed at 830—855 cm^{-1} for the ammine ligands of 5-nitrosalicylatotetraamminecobalt(IV) complexes and at 820—840 cm^{-1} for those of salicylatotetraamminecobalt(III) complexes, in conformity with the view that the former complexes are actually cobalt(III) complexes of a free radical nature.

The previous papers have been concerned with the preparation[2,3] and some physical properties[4] of cobalt(IV) ammine complexes with 5-nitrosalicylato and similar ligands. The delocalization of an electron hole over the cobalt and 5-nitrosalicylato ligand system of the "cobalt(IV)" ammine complex ion with 5-nitrosalicylato or similar ligands was inferred from the magnetic susceptibility[4] and the electrical resistivity.[4] The present paper will deal with the results of measurements of the ^{1}H-NMR, ^{13}C-NMR, IR-spectra and the isolation of 5-nitrosalicylatotetraamminecobalt(IV) dinitrates and 5-nitrosalicylatotetraamminecobalt(III) nitrate.

Results and Discussion

Formation of the Complexes. The salicylatotetraammine cobalt complexes studied in this research, together with the abbriviations adopted in this paper, are listed in Table 1. The **2a**—**2c** complexes are oxidized and changed to the **1a**—**1c** complexes respectively, but the **2d** complex is not oxidized with 60% nitric acid. The **1g** and **1h** complexes have been synthesized for the first time. The **1h** complex has been prepared only from the **1g** complex by metathesis. The **1g** and **1h** complexes are green and paramagnetic. Their absorption spectra show a characteristic peak at 660 nm (log $\varepsilon \approx 4$) as do other cobalt(IV) ammine complexes with 5-nitrosalicylato or similar ligands. The **1g** complex has the electrical resistivity of 10^{11} Ω cm.

The **3a** and **3b** complexes are orange and are insoluble in most organic solvents, but are soluble in water and dimethyl sulfoxide. Neither the **3a** complex nor the **3b** complex changes to a green, paramagnetic complex, **1h** and **1a** with 60% nitric acid respectively. The **3a** and **3b** complexes were characterized by the measurement of the magnetic susceptibility (diamag.), the absorption spectra (510 nm, $\varepsilon \approx 190$), the ^{1}H-NMR spectra [ammine protons (12H), and the 5-nitrosalicylato ligand protons (3H)] and equivalent conductance (114 S cm^2 for the **3a** complex). These data show that the **3a** and **3b** complexes are cobalt(III) complexes of the low-spin type.

NMR Spectra. The ^{1}H-NMR spectrum of the **1d** complex was measured in 1.8 M deuteriosulfuric acid at room temperature. The spectrum, as is shown in Fig. 1, did not show peaks of the phenyl protons of the salicylato ligand, but did show those of the ammine protons, the chemical shifts of which are close to those of the **2a** complex. The chemical shift of the methyl

Table 1. List of salicylatotetraammine cobalt complexes

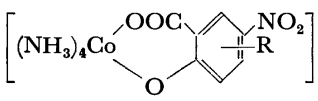

1 $X \cdot Y \cdot nH_2O$

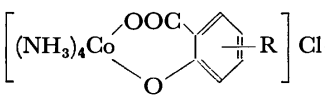

2 $Cl \cdot H_2O$

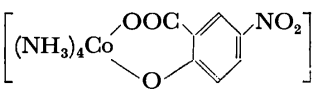

3 $X \cdot nH_2O$

	1a	**1b**	**1c**	**1d**	**1e**	**1f**	**1g**	**1h**	**2a**	**2b**	**2c**	**2d**	**3a**	**3b**
R	H	3-CH_3	4-CH_3	H	3-CH_3	4-CH_3	H	H	H	3-CH_3	4-CH_3	5-CH_3		
X	Cl	Cl	Cl	Cl	Cl	Cl	pic[a]	NO_3					NO_3	Cl
Y	NO_3	NO_3	NO_3	Cl	Cl	Cl	pic[a]	NO_3						
n	1	1	1	3	3	3	2	1/2					1	2

a) pic:

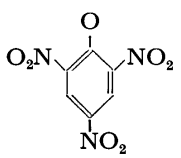

Table 2. The ^{1}H-NMR and IR spectra of cobaltammine complexes

No.	Ammine $\delta(^1NH_3\text{-Co-}^4NH_3)$	Ammine $[\delta(^2NH_3\text{-Co-}^3NH_3)]$ $\delta(^2NH_3\text{-Co})$	Ammine $[\delta(^2NH_3\text{-Co-}^3NH_3)]$ $\delta(^3NH_3\text{-Co})$	(CH_3)-salicylato $\delta(CH_3\text{-Sal})$	(CH_3)-salicylato $\delta(C_6H_{3-4})$	Solvents	IR spectra $\rho_r(NH_3)_r$ cm^{-1}
1a	3.73, s, 6H	[3.23, s, 6H]		—		1	835
1d	3.76, s, 6H	[3.30, s, 6H]		—		1	840
1e	3.53, s, 6H	[3.20, s, 6H]		1.73, s, 3H		2	840
1f	3.75, s, 6H	[3.20, s, 6H]		2.0, s, 3H		2	855
2a	3.96, s, 6H	3.65, s, 3H	3.38, s, 3H	—	6.7—8.1, m, 4H	1	
2a	3.63, s, 6H	3.40, s, 3H	3.07, s, 3H	—	6.4—7.7, m, 4H	2	840
2b	3.63, s, 6H	3.44, s, 3H	3.18, s, 3H	2.02, s, 3H	6.4—7.7, m, 3H	2	830
2c	3.68, s, 6H	3.43, s, 3H	3.13, s, 3H	2.16, s, 3H	6.4—7.7, m, 3H	2	820
2d	3.60, s, 6H	3.33, s, 3H	3.0, s, 3H	2.03, s, 3H	6.9—7.4, m, 3H	2	820
3a	3.63, s, 6H	[3.16, s, 6H]		—	6.7—8.3, m, 3H	3	828
3b	3.87, s, 6H	3.47, s, 3H	3.30, s, 3H	—	7.0—8.9, m, 3H	1	840
L[a]				—	6.8—8.0, m, 4H	4	
L[b]				2.26, s, 3H	6.9—7.8, m, 3H	4	

Abbreviations: **L**[a]: salicylic acid, **L**[b]: 3-methylsalicylic acid. Standards: **L**[a] and **L**[b] were used with the internal TMS in the $CDCl_3$ and the other complexes were used with the external TMS in the $CDCl_3$. Solvents: 1: 1.8 M D_2SO_4, 2: D_2O and CF_3COOH, 3: 0.2 M DCl, 4: $CDCl_3$. ρ_r $(NH_3)_r$: 855 for the **1b** complex, 830 for the **1g** complex, and 835 cm^{-1} for the **1h** complex.

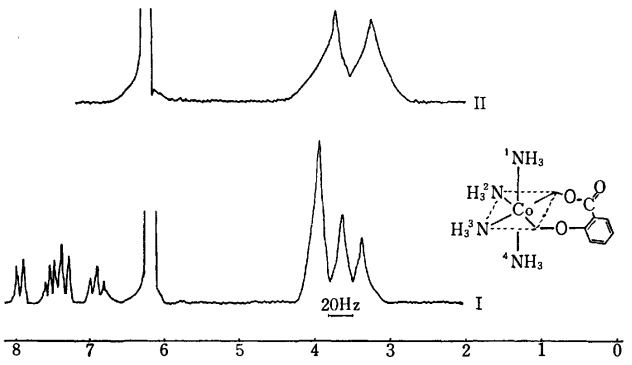

Fig. 1. The ^{1}H-NMR spectra of complexes **2a** and **1d**.

I; $[(NH_3)_4Co(OOC)(O)C_6H_3]Cl\cdot H_2O$ in 1.8M D_2SO_4.

II; $[(NH_3)_4Co(OOC)(O)C_6H_3(NO_2)]Cl_2\cdot 3H_2O$ in 1.8M D_2SO_4.

Standard: External TMS in $CDCl_3$.

protons of the salicylato ligand in the **1e**, **1f**, and **2b—2d** complexes did not show any appreciable change, either, as is shown in Table 2. The measurements of the ^{13}C-NMR spectra of the **1a**, **1c**, and **1d** complexes were attempted in several solvents, at varying concentrations at low and at room temperature. The spectra did not show the expected signals because of the paramagnetism of those complexes. These results lead to the conclusion that, in the **1a—1h** complexes, the electron hole is not distributed over the ammine ligands and the methyl group of substituted 5-nitrosalicylato ligand, though it seems to be delocalized over the chelate ring containing the cobalt atom and the benzene ring of the 5-nitrosalicylato ligand.

^{1}H-NMR spectrum of the **2a** complex showed three singlets of ammine groups and a multiplet of the salicylato ligand in the expected integral ratio (3:3:6:4) at room temperature, as is shown in Fig. 1. The singlet (3.38 ppm) at the highest field was assigned to the protons of the ammine ligand in a position *trans* to the carboxyl oxygen of the salicylato ligand in the **2a** complex. The singlet at 3.65 ppm is assigned to the protons of the ammine ligand in a position *trans* to the phenolic oxygen, which is less electronegative than the carboxyl oxygen, while that at 3.96 ppm is assigned to the protons of two ammine ligands in positions *cis* to the salicylato ligand. The multiplet (6.7—8.1 ppm) at the lowest field was assigned to the protons of the salicylato ligand. The above assignment was made in view of the following: studies of pentaammineaniono-cobalt(III) ions, $[Co(NH_3)_5X]^{n+}$ (X: Cl, Br, OH ···), have been reported by Buckingham,[5] Jolly,[6] and Clifton,[7] who described that the chemical shift of the NH_3 group in a position *trans* to the electronegative atom (X) is at higher fields than those of NH_3 groups in a position *cis* to the electronegative atom. The chemical shift of the NH_3 group in a position *trans* to the electronegative atom (HSO_4^-) is at higher field than that of the NH_3 group in a position *trans* to other electronegative atoms (H_2O, Cl, ···).[6] Marzilli[8] and Hawkins[9] also reported the case of sarcosinatotriethylenetetraminecobalt(III) ions in which the proton signals of the NH_2 group in a position *trans* to the coordinated carboxyl oxygen of sarcosinato ligand appeared at higher fields than those of the NH_2 group in a position *cis* to the coordinated carboxyl oxygen.

The ^{13}C-NMR spectra of the **2a** complex were measured in heavy water at room temperature. The assignment of the salicylato ligand of the complex was attempted by means of a consideration of the assignment of salicylaldehyde[10] and methylsalicylate.[10] Two signals, C-1 and C-3, of the salicylato ligand overlapped, as is shown in Table 3, but they split when the pH was

TABLE 3. $^{13}C\{^1H\}$-NMR OF THE COMPLEXES, $[(NH_3)_4Co(OOC\text{-}C_6H_3(R)\text{-}O)]Cl\cdot H_2O$, AND LIGANDS

No.	δ (R)	δ (salicylato ligand)							—	Solvents and standards
	(H), CH_3	C-1	C-2	C-3	C-4	C-5	C-6	C-7		
2a	(—)	117.5	167.5	117.5	134.6	124.1	132.7	174.1		D_2O[a]
2b	17.5	116.8	166.7	133.2	134.6	116.4	130.2	174.7		D_2O[a]
2c	21.2	114.6	167.4	118.9	145.8	123.8	132.5	174.0		D_2O[a]
2d	20.3	117.2	165.3	124.0	135.8	126.9	130.0	174.1		D_2O[a]
3a	(—)	118.0	166.5	123.4	134.9	125.4	129.9	175.5		DMSO-d_6[b]
3b	(—)	114.6	169.8	124.2	135.0	126.8	129.6	175.8		DMSO-d_6[b]
L^a	(—)	113.8	162.7	118.0	136.6	120.2	131.5	173.6		MeOH[c]
L^b	15.6	112.9	161.0	127.2	137.2	119.7	129.0	174.3		MeOH[c]
L^c	21.8	111.1	162.7	118.1	148.3	121.5	131.4	173.6		MeOH[c]
L^d	20.4	113.3	160.2	117.9	137.6	129.7	131.1	173.6		MeOH[c]
L^e	(—)	121.0	161.4	117.4	136.6	119.6	133.6	196.7		—
L^f	(—)	114.6	168.5	119.9	141.7	128.4	131.9	172.5		MeOH-d_4[d]

Standards: a) MeOH (δ=49.8 ppm), b) DMSO-d_6 (δ=39.5 ppm), c) Internal TMS (δ=0ppm), measured in methanol and heavy water. d) MeOH-d_4 (δ=49.8 ppm). Abbreviations: L^a: salicylic acid, L^b: 3-methylsalicylic acid, L^c; 4-methylsalicylic acid, L^d: 5-Methylsalicylic acid, L^e: salicylaldehyde,[10] and L^f: 5-nitrosalicylic acid.

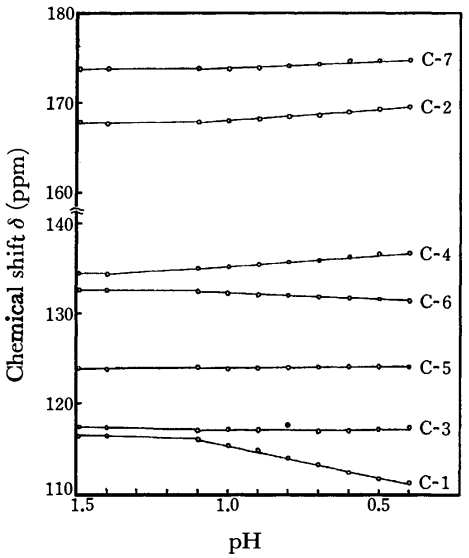

Fig. 2. ^{13}C-NMR chemical shift *vs.* pH of the complex **2a**.

$[(NH_3)_4Co(OOC\text{-}C_6H_4\text{-}O)]Cl\cdot H_2O$ in D_2O and HCl.

Standard: MeOH (δ=49.8 ppm).

lowered below 1.1 by the addition of hydrochloric acid. In hydrochloric acid, the carbon signal of C-5 did not shift, that of C-3 shifted slightly to a higher field, C-6 shifted to a higher field, and those of C-2, C-4, and C-7 shifted to a lower filed, as is shown in Fig. 2. This observation seems to be due to the hydrogen bonding[11,12] between the lone pairs of the carbonyl oxygen atom of the salicylato ligand and proton of hydrochloric acid.

The ^1H-NMR spectra of the **3a**—**3b** complexes are similar to those of the **2a**—**2d** complexes. The ^{13}C-NMR spectra of the **3a**—**3b** complexes in DMSO-d_6 are shown in Table 3. The chemical shifts of the substituted carbon atom of the salicylato ligand both in the **2b**—**2c** complexes and in the free ligands, L^b-L^d, L^f, move to a lower field upon the substitution of methyl and nitro groups. These shifts are coincident with the data reported by Levy and Nelson.[13,14] The exceptions are the carbon signals of the C-5 position of the 5-methyl- or 5-nitrosalicylato ligands in the **2d** and **3a**—**3b** complexes which do not shift to a lower field.

IR Spectra. It was reported by Nakamoto,[15] Wilmshuist[16] and Svatos[17] that the rocking deformation vibration of metal ammine complexes, which appears as a broad band, is influenced by the oxidation state of the metal in the ammine complex. Thus, it appears at 650 cm^{-1} in hexaamminecobalt(II) chloride[17-19] and at 827 cm^{-1} in hexaamminecobalt(III) chloride.[17-19] The rocking deformation vibration was observed as a broad band at 830—855 cm^{-1} for the **1a**—**1f** complexes, at 820—840 cm^{-1} for the **2a**—**2d** complexes, and at 828—840 cm^{-1} for the **3a**—**3b** complexes, showing little difference among these complexes. From the above facts, the most reasonable conclusion seems that the ammine ligands in the **1a**—**1f** complexes are similar to those of the **2a**—**2d** complexes and that the **1a**—**1f** complexes have a free radical nature in which the electron hole is delocalized over the 5-nitrosalicylato ligand and the cobalt ion in agreement with magnetic susceptibility,[4] the electrical resistivity[4] and the NMR spectra of the **1a** and **1d**—**1f** complexes. The situation might be similar to the cases of μ-peroxo and μ-hyperoxo dicobalt complexes, both of which have the rocking deformation band of ammine at around 800 cm^{-1} and are considered to contain trivalent cobalt.[20,21]

Experimental

Measurements. The NMR spectra were measured with a FX-60 (JEOL) for ^{13}C-NMR and JNM-PMX-60 (JEOL), R-40 (Hitachi) for ^{1}H-NMR. The IR spectra were measured with a JASCO spectrophotometer, DS 402-G, and an EPI 238 Hitachi apparatus in potassium bromide disks for the **1a—1h** and **2a—2d** complexes and in Nujol mulls for the **3a—3b** complexes. The visible absorption spectra were recorded with Shimadzu MPS-5000 recording spectrophotometer. The electrical resistivity was measured with a Toa Denpa Kogyo Microvolt ammeter. The magnetic susceptibilities were measured by the Gouy method with a magnetic balance (Shimadzu) at room temperature. The pH was measured with a Toa Electronics pH-meter, HM-5B.

Preparation of Complexes. *The **1a**, **1b**, **1c**, **1d**, **1e**, and **1f** complexes* were prepared as has been described in previous papers.[2,3] *The **2a**, **2b**, **2c**, and **2d** complexes* were prepared by Morgan and Smith's method.[22]

*5-Nitrosalicylatotetraamminecobalt(IV) Picrate Dihydrate (**1g**).* An aqueous solution of 0.8 g (1.89 mmol) of the **1a** complex was slowly added to an aqueous solution of 0.87 g (3.79 mmol) of picric acid, and mixture was stirred. The precipitated green complex was filtered off, washed with water, and dried. Yield: 0.94 g (62.3%), Found: C, 28.49; H, 2.87; N, 19.41%. Calcd for $CoC_{19}H_{23}N_{11}O_{21}$ (*MW*: 800.39) C, 28.51; H, 2.90; N, 19.25%. The absorption maximum in the visible spectrum was at 660 nm ($\varepsilon=12700$) in water.

*5-Nitrosalicylatotetraamminecobalt(IV) Nitrate Hemihydrate(**1h**).* 0.5 g (0.62 mmol) of the **1g** complex was dissolved in 60% nitric acid, and some picric acid was precipitated. The solution was then filtered with a glass filter (G4), and the filtrate was added to acetone. The precipitated green complex was filtered off, washed and dried. Yield: 0.20 g (72.7 %), Found: C, 19.47; H, 3.80; N, 21.66%. Calcd for $CoC_7H_{16}N_7O_{11.5}$: (*MW*: 441.18) C, 19.06; H, 3.65; N, 22.22%. Visible absorption peaks: 450 nm ($\varepsilon=3700$) and 660 nm ($\varepsilon=14100$) in 60% nitric acid.

*5-Nitrosalicylatotetraamminecobalt(III) Nitrate Monohydrate(**3a**).* The **1a** complex was precipitated by the addition of acetone to a 60% nitric acid solution of 3.0 g (9.5 mmol) of the **2a** complex according to the method presented in a previous paper.[2] The **3a** complex was isolated from this orange-colored acetone solution, recrystallized from water, and dried. Yield: 0.96 g (18.5%), Found: C, 21.82; H. 4.53; N, 21.90%. Calcd for $CoC_7H_{17}N_6O_9$: (*MW*: 387.52) C, 21.70; H, 4.42; N, 21.69 %. The visible absorption peak was 510 nm ($\varepsilon=196$) in water.

*5-Nitrosalicylatotetraamminecobalt(III) Chloride Dihydrate Hydrochloric Acid (**3b**).* 0.4 g (1.03 mmol) of the **3a** complex was dissolved in 30% hydrochloric acid. The precipitate formed by the addition of acetone was filtered off, washed, and dried. Yield: 0.26 g (58.2%), Found: C, 20.34; H, 4.85; N, 16.27; Cl, 17.62%. Calcd for $CoC_7H_{20}N_5O_7Cl_2$: (*MW*; 416.12) C, 20.21; H, 4.84; N, 16.83; Cl, 17.04%. The visible absorption peak was 512 nm ($\varepsilon=185$) in 35% hydrochloric acid.

The author wishes to express his gratitude to Professor Masayasu Mori of Osaka City University for his discussion and to Dr. Genetsu Matsubayashi of Osaka University for the NMR spectra.

References

1) Paramagnetic Cobalt Complexes with Organo Ligands. IV. Presented at the 27th Symposium on Coordination Chemistry of the Chemical Society of Japan, Matsumoto, 1977.
2) Y. Yamamoto, K. Ito, H. Yoneda, and M. Mori, *Bull. Chem. Soc. Jpn.*, **40**, 2580 (1967).
3) Y. Yamamoto, M. Mori, H. Yoneda, S. Misumi, and K. Ito, *Bull. Chem. Soc. Jpn.*, **42**, 984 (1969).
4) Y. Yamamoto, *Bull. Chem. Soc. Jpn.*, **42**, 999 (1969).
5) D. A. Buckingham, I. Olsen, and A. M. Sargeson, *Aust. J. Chem.*, **20**, 597 (1967).
6) W. L. Jolly, A. D. Jarris, and T. S. Briggs, *Inorg. Chem.*, **4**, 1064 (1965).
7) P. Clifton and L. Pratt, *Proc. Chem. Soc.*, **1963**, 339.
8) L. G. Marzilli and D. A. Buckingham, *Inorg. Chem.*, **6**, 1042 (1967).
9) C. J. Hawkins, "Absolute Configuration of Metal Complexes," Wiley-Interscience, New York (1971), p. 268.
10) L. F. Johnson and W. C. Jankowski, "Carbon-13 NMR Spectra, A Collection of Assigned, Coded, and Indexed Spectra," Wiley-Interscience, New York (1972), No. 231, 293.
11) G. E. Maciel and G. C. Ruben, *J. Am. Chem. Soc.*, **85**, 3903 (1963).
12) G. E. Maciel and J. J. Natterstad, *J. Chem. Phys.*, **42**, 2752 (1965).
13) G. C. Levy, G. L. Nelson, and J. D. Cargioli, *J. Am. Chem. Soc.*, **94**, 3089 (1972); *Chem. Commun.*, **1971**, 506.
14) G. C. Levy and G. L. Nelson, "Carbon-13 NMR for Organic Chemist," Wiley-Interscience, New York (1972), p. 81.
15) K. Nakamoto, "Infrared Spectra of Inorganic and Coordination Compounds," Wiley-Interscience, New York (1970), p. 150.
16) J. K. Wilmshurst, *Can. J. Chem.*, **38**, 467 (1960).
17) G. F. Svatos, D. M. Sweeny, S. Mizushima, C. Curran, and J. V. Qvagloano, *J. Am. Chem. Soc.*, **79**, 3313 (1957).
18) L. Sacconi, A. Sabatini, and P. Gans, *Inorg. Chem.*, **3**, 1772 (1964).
19) D. B. Powell and N. Sheppard, *J. Chem. Soc.*, **1956**, 3108.
20) M. Mori, J. A. Weil, and M. Ishiguro, *J. Am. Chem. Soc.*, **90**, 615 (1968).
21) J. A. Weil and J. K. Kinnaird, *J. Phys. Chem.*, **71**, 3341 (1967).
22) G. T. Morgan and J. D. M. Smith, *J. Chem. Soc.*, **1922** 1956.

Trimethylenediamine Complexes. VI.[1] Kinetic and Equilibrium Studies of Ligand Substitution Reactions of the *trans*-Aquabis(diamine)sulfito- and *trans*-Bis(diamine)-hydroxosulfitocobalt(III) Complexes

Yoshiaki Ito, Akira Terada, and Shinichi Kawaguchi*

Department of Chemistry, Faculty of Science, Osaka City University, Sumiyoshi-ku, Osaka 558

(Received January 20, 1978)

Substitution reactions of the *trans*-$CoSO_3$ (H_2O or OH) (en or tn)$_2$ complex with Cl^-, Br^-, CH_3COO^-, N_3^-, NO_2^-, NCS^-, CN^-, and SO_3^{2-} have been studied by the spectrophotometric method. The equilibrium constant of anation $K^X_{H_2O}$ spans many orders of magnitude, *e.g.* from 1.24 for bromide to 1.23×10^7 M^{-1} for cyanide in the case of the en complex, and is correlated to the electron donor constant E_n which was defined by Edwards. The kinetics of the substitution reactions is adequately interpreted by virtue of the reversible **D** mechanism *via* a five-coordinate intermediate $CoSO_3(AA)_2^+$. Release of the ligand X^{n-} from *trans*-$CoSO_3(X)(tn)_2^{(1-n)+}$ proceeds 10—25 times faster than from the corresponding bis(ethylenediamine) complex, and the kinetic ring-size effect is attributed to the larger stability of the en complex as compared with the tn complex at the ground state.

Although cobalt(III) complexes are usually inert,[2] two groups of complexes are known to perform rapid ligand substitution. One is those containing unsaturated macrocyclic(N_4) ligands, which have been shown to enhance the rate of ligand substitution at the metal center by many orders of magnitude.[3] The increasing degree of unsaturation in the encircling macrocycle is considered to enhance softness of the central metal ion, thus stabilizing five-coordinate intermediates and increasing the rates of ligand displacement.[4]

The other group of rather labile cobalt(III) complexes contain S-bonded ligands such as sulfite[5] and sulfinate,[6] σ-bonded organo ligands,[7] and P-bonded phosphonate ligands[8] which exert a significant labilizing effect on the trans ligand. By comparing activation enthalpies, Stranks and Yandell[9] concluded that the labilizing effect of the sulfite ligand in the *trans*-aqua(or hydroxo)-bis(ethylenediamine)sulfitocobalt(III) complex arises from stabilization of the five-coordinate intermediate in the dissociative (**D**) reaction pathway. On the other hand Palmer and Deutsch attributed the trans labilizing effect of the sulfinate ligand in *trans*-bis(dimethylglyoximato)methanol(*p*-toluenesulfinato)cobalt(III) to its trans influence, that is a ground-state weakening of the trans bond.[6]

The present paper is concerned with the reactions of *trans*-$CoSO_3(Y)(AA)_2^{(1-m)+}$ with various nucleophiles X^{n-}, where AA=ethylenediamine(en) or trimethylenediamine(tn), Y^{m-}=OH^- or H_2O, and X^{n-}=Cl^-, Br^-, CH_3COO^-, NO_2^-, N_3^-, NCS^-, SO_3^{2-}, or CN^-. The equilibrium and kinetic studies of these reactions have revealed that they proceed *via* the **D** mechanism, and afforded a quantitative relationship between the electron-donating properties of X^{n-} and the formation constants of *trans*-$CoSO_3(X)(AA)_2^{(1-n)+}$.

Experimental

Preparation of Complexes. trans-*Aquabis(ethylenediamine)-sulfitocobalt(III) Perchlorate Monohydrate,* $[CoSO_3(H_2O)(en)_2]ClO_4\cdot H_2O$, was prepared by the method of Baldwin[10] and recrystallized twice from water containing sodium perchlorate and a trace amount of perchloric acid. It contained one molecule of crystalline water contrary to Baldwin's anhydrous compound. Found: C, 12.17; H, 5.10; N, 14.55%. Calcd for $C_4H_{20}N_4O_9SClCo$: C, 12.17; H, 5.11; N, 14.20%.

trans-*Aquasulfitobis(trimethylenediamine)cobalt(III) Perchlorate Monohydrate,* $[CoSO_3(H_2O)(tn)_2]ClO_4\cdot H_2O$, was prepared by a similar method. The compound $CoCl(SO_3)(tn)_2\cdot H_2O$[11] (14 g) was dissolved in a dilute perchloric acid solution (pH=4) and a trace amount of insoluble material was filtered off. About three times molar amount of sodium perchlorate was added to this solution and the mixture was kept standing at 0 °C in the dark to give light brown thin crystals. The precipitate was filtered off, washed with ethanol and acetone successively, and dried over silica gel. The yield was 43% (7.4 g), and the compound was recrystallized twice from water containing sodium perchlorate and a trace amount of perchloric acid. Found: C, 16.91; H, 5.65; N, 13.22%. Calcd for $C_6H_{24}N_4O_9SClCo$: C, 17.05; H, 5.72; N, 13.25%.

trans-*Aquasulfitobis(trimethylenediamine)cobalt(III) Nitrate Hemihydrate,* $[CoSO_3(H_2O)(tn)_2]NO_3\cdot 1/2H_2O$, was derived from the perchlorate. The perchlorate (1 g) was dissolved in cold water (7 ml), and treated with a slightly excess amount of pulverized silver nitrate. After filtration of silver chloride, two drops of concentrated nitric acid, 0.3 g of ammonium nitrate and 50 ml of ethanol were added to the solution and the mixture was kept in a refrigerator. A light brown precipitate was recrystallized twice from ethanol–water (5:1 by volume), washed with ethanol and acetone successively, and then air-dried. The yield was 18% (0.2 g). Found: C, 19.06; H, 6.27; N, 18.62%. Calcd for $C_6H_{23}N_5O_{7.5}SCo$: C, 19.15; H, 6.16; N, 18.61%.

Sodium Disulfitobis(trimethylenediamine)cobaltate(III) Trihydrate, $Na[Co(SO_3)_2(tn)_2]\cdot 3H_2O$, was prepared by a previous method.[11] Found: C, 16.06; H, 6.09; N, 12.48%. Calcd for $C_6H_{26}N_4O_9S_2CoNa$: C, 16.22; H, 5.90; N, 12.61%.

All the nucleophilic reagents are sodium salts of A. R. grade.

Measurements. The ionic strength was adjusted with sodium perchlorate to 1.00 M. The hydrogen ion concentration was determined by means of a Beckman "Century" SS-1 pH meter with a Beckman 39301 glass electrode and a Beckman 39402 B-4U calomel electrode. A saturated solution of sodium chloride was employed in place of potassium chloride for the calomel electrode in order to prevent precipitation of potassium perchlorate, and a 4.302×10^{-3} M solution of perchloric acid (μ=1.00 M) was used as a reference solution.

Absorption spectra were recorded on a Hitachi EPS-3T spectrophotometer and NMR spectra on a JOEL C-60 HL

spectrometer. IR spectra were measured in Nujol with JASCO IR-E (4000—600 cm^{-1}) and Hitachi EPI-L (700—200 cm^{-1}) Infrared Spectrophotometers. Reactions were followed by the stopped-flow method with a Union Stopped-Flow, Rapid-Scan Spectrophotometer RA-1300.

Results

Characterization of the Aqua Sulfitobis(trimethylenediamine)-cobalt(III) Complex. The IR spectrum of $[CoSO_3(H_2O)(tn)_2]ClO_4\cdot H_2O$ in Nujol shows a single sharp band at 899 cm^{-1} which is assigned to the CH_2 rocking vibration, suggesting a trans structure.[12] The proton NMR spectrum in a 0.3 M D_2SO_4–D_2O solution at 25 °C displays three signals at 1.73 (4H), 2.59 (8H), and 3.67 (8H) ppm from DSS (sodium 2,2-dimethyl-2-silapentane-5-sulfonate). They are assigned to the β-CH_2, α-CH_2, and NH_2 protons, respectively, of the trimethylenediamine ligands $NH_2CH_2(\alpha)CH_2(\beta)CH_2(\alpha)NH_2$. Usually the amine protons in a *trans*-bis(diamine)cobalt(III) complex resonate as a single peak, whereas those in a *cis* isomer exhibit two bands.[13,14] The trans structure of $CoSO_3(H_2O)(tn)_2^+$ is thus supported by the NMR data, too.

In order to inspect IR spectra in the 1200—1000 cm^{-1} region, the perchlorate anion in the outer sphere, which has absorption in this region, was replaced by the nitrate ion. $[CoSO_3(H_2O)(tn)_2]NO_3\cdot 1/2H_2O$ shows absorption bands assignable to the sulfite ligand at 1120(s), 1092(s, br), 980(vs), 628(vs, br), and 524(sh) cm^{-1}. The frequencies are higher as compared with those of free sulfite ion, suggesting S-bonding to the cobalt atom.[15] The S-bonding of the sulfite ligands has been ascertained by X-ray analysis for $[CoSO_3(NH_3)_5]Cl\cdot H_2O$,[16] *trans*-$[CoSO_3(H_2O)(en)_2]ClO_4\cdot H_2O$,[17] *trans*-$[CoSO_3(H_2O)$(quarterpyridine)$]NO_3\cdot H_2O$,[18] and *trans*-$[CoSO_3(NCS)(en)_2]\cdot 2H_2O$.[19]

Equilibrium Studies. The pK_a value of *trans*-$CoSO_3(H_2O)(en)_2^+$ was reported by Stranks and Yandell to be 9.45 at 25 °C.[9] Now pK_a of *trans*-$CoSO_3(H_2O)(tn)_2^+$ was determined to be 9.10 ± 0.05 at 25.0 °C and $\mu=$ 1.00 M from the customary acid-base titration curve using 0.05 M NaOH as the base titrant.

$$trans\text{-}CoSO_3(H_2O)(AA)_2^+ \rightleftharpoons trans\text{-}CoSO_3(OH)(AA)_2 + H^+ \quad (1)$$

Equilibrium constants of the anation reactions of $CoSO_3(H_2O)(AA)_2^+$ with various ligands (X^{n-}) spanned many orders of magnitude, and were measured by the following three methods at 25.0 °C and $\mu=1.00$ M. The complex concentration was kept much smaller as compared with $[X^{n-}]$ in the case of (i) and (ii), and with $[OH^-]$ in (ii) and (iii).

(i) Substitution with Chloride, Bromide and Acetate Ions: Anation reactions of *trans*-$CoSO_3(H_2O)(en)_2^+$ with chloride at pH 3.46, bromide at pH 3.45 and acetate ions at pH 3.19—5.01,[20] and of *trans*-$CoSO_3(H_2O)(tn)_2^+$ with these anions at pH 3.40, 4.45, and 3.84—4.90,[20] respectively, proceed to attain equilibria

$$trans\text{-}CoSO_3(H_2O)(AA)_2^+ + X^{n-} \rightleftharpoons trans\text{-}CoSO_3(X)(AA)_2^{(1-n)+} + H_2O. \quad (2)$$

The spectral change in either case exhibits isosbestic points at 223, 247, and 276 nm (Cl^-); 255 and 286 nm (Br^-); 241 and 269 nm (CH_3COO^-) in the case of the en complex, and at 236, 257, and 283 nm (Cl^-); 265 and 290 nm (Br^-); 242, 254, and 274 nm (CH_3COO^-) for the tn complex.

The equilibrium constant of each reaction is expressed by

$$K^X_{H_2O} = \frac{[RX]}{[ROH_2][X^{n-}]} = \left(\frac{A-A_{ROH_2}}{A_{RX}-A}\right)\frac{1}{[X^{n-}]}, \quad (3)$$

where RX and ROH_2 denote *trans*-$CoSO_3(X)(AA)_2^{(1-n)+}$ and *trans*-$CoSO_3(H_2O)(AA)_2^+$, respectively, and A is the absorbance of a solution equilibrated at given concentrations of the complex (c_M) and X^{n-}(c_X), and $A_{ROH_2}=\varepsilon_{ROH_2}c_M$, $A_{RX}=\varepsilon_{RX}c_M$. All quantities except $K^X_{H_2O}$ and ε_{RX} are observable, since $[X^{n-}]=c_X$ when $c_X \gg c_M$. Eq. 3 is transformed into

$$\frac{1}{A-A_{ROH_2}} = \frac{1}{A_{RX}-A_{ROH_2}} + \frac{1}{(A_{RX}-A_{ROH_2})K^X_{H_2O}}\cdot\frac{1}{[X^{n-}]}. \quad (4)$$

By plotting the left side tem against $[X^{n-}]^{-1}$, a straight line is obtained for each reaction (Eq. 2), and values of the equilibrium constant $K^X_{H_2O}$ and the molar extinction coefficient ε_{RX} of the anation product are calculated from the slope and intercept of the straight line. The results are included in Table 1.

(ii) Substitution with Azide, Nitrite, Thiocyanate, and Sulfite Ions: Basic solutions are suitable for investigation of these reactions, which are reversible and exhibit the following isosbestic points: 455 nm(NO_2^-), 486 and 556 nm (NCS^-) for AA=en and 474 nm (NO_2^-), 391, 402, and 507 nm (NCS^-), 498 nm(SO_3^{2-}) for AA=tn. In the reactions with azide ions no isosbestic points were observed in the 340—700 nm region.

$$trans\text{-}CoSO_3(OH)(AA)_2 + X^{n-} \rightleftharpoons trans\text{-}CoSO_3(X)(AA)_2^{(1-n)+} + OH^- \quad (5)$$

The equilibrium constant K^X_{OH} of Reaction 5 is defined by

$$K^X_{OH} = [RX][OH^-]/[ROH][X^{n-}], \quad (6)$$

where ROH stands for *trans*-$CoSO_3(OH)(AA)_2$. In a similar manner to Eq. 4, the spectral data are related to K^X_{OH} and ε_{RX} by Eq. 7, of which values are included in Table 1.

$$\frac{1}{A-A_{ROH}} = \frac{1}{A_{RX}-A_{ROH}} + \frac{1}{(A_{RX}-A_{ROH})K^X_{OH}}\cdot\frac{[OH^-]}{[X^{n-}]} \quad (7)$$

(iii) Substitution with Cyanide Ion: In a basic solution, the reversible replacement by the cyanide ion also proceeds according to Eq. 5, and the spectral change displays isosbestic points at 364, 380 and 440 nm in the case of the en complex and at 366, 396 and 456 nm for the tn complex. Since the values of K^{CN}_{OH} are large enough to complete reactions in the presence of excessive cyanide, the molar extinction coefficients ε_{RX} of *trans*-$CoSO_3(CN)(AA)_2$ were determined under these conditions. Then the equilibrium constant K^X_{OH} was calculated by Eq. 6 using

$$[RX] = (A-\varepsilon_{ROH}c_M)/(\varepsilon_{RX}-\varepsilon_{ROH}),$$
$$[ROH] = (\varepsilon_{RX}c_M-A)/(\varepsilon_{RX}-\varepsilon_{ROH}),$$
$$[X^{n-}] = c_X - [RX],$$

Table 1. Equilibrium constants for the substitution reactions of *trans*-$CoSO_3(H_2O)(AA)_2^+$ and *trans*-$CoSO_3(OH)(AA)_2$ with nucleophiles X^{n-} at 25.0 °C and μ=1.00 M ($NaClO_4$)

X^{n-}	E_n [a] / V	log $K^X_{H_2O}$	log K^X_{OH}	ε [b] / $cm^{-1}\cdot M^{-1}$	Wavelength / nm
			AA = en		
Cl^-	1.24	0.171±0.034	−4.18±0.09	(9.64±0.40)×10^3	300
Br^-	1.51	0.093±0.040	−4.26±0.10	(4.36±0.75)×10^3	310
CH_3COO^-	0.95	1.65 ±0.01	−2.70±0.07	(1.50±0.01)×10^4	290
N_3^-	1.58	2.56 ±0.09	−1.79±0.03	(3.98±0.13)×10^2	470
NO_2^-	1.73	3.59 ±0.07	−0.758±0.007	(2.15±0.01)×10^2	430
NCS^-	1.83	3.38 ±0.07	−0.975±0.012	(2.37±0.02)×10^2	458
CN^-	2.79	7.09 ±0.09	2.74 ±0.03	(5.26±0.05)×10	470
SO_3^{2-}	2.57	3.92[c]	−0.434[c]	(3.88±0.09)×10^2[c]	432[c]
OH^-	1.65	4.35 ±0.06	0	—	—
			AA = tn		
Cl^-	1.24	−0.044±0.019	−4.74 ±0.08	(9.19±0.47)×10^3	310
Br^-	1.51	1.18 ±0.09	−3.53 ±0.15	(1.55±0.01)×10^4	280
CH_3COO^-	0.95	1.58 ±0.01	−3.12 ±0.07	(1.88±0.01)×10^4	290
N_3^-	1.58	3.26 ±0.09	−1.44 ±0.03	(5.42±0.17)×10^2	490
NO_2^-	1.73	4.29 ±0.06	−0.409±0.003	(2.32±0.01)×10^2	450
NCS^-	1.83	4.39 ±0.065	−0.313±0.005	(2.72±0.01)×10^2	474
CN^-	2.79	6.75 ±0.07	2.05 ±0.01	(5.14±0.05)×10	490
SO_3^{2-}	2.57	3.76 ±0.07	−0.939±0.006	(4.04±0.06)×10^2	430
OH^-	1.65	4.70 ±0.06	0	—	—

a) J. O. Edwards, *J. Am. Chem. Soc.*, **76**, 1540 (1954); S. Yamada and M. Tanaka, *J. Inorg. Nucl. Chem.*, **37**, 587 (1975). b) Molar extinction coefficient of *trans*-$CoSO_3(X)(AA)_2^{(1-n)+}$ at the indicated wavelength. c) Ref. 9.

where c_X is the total concentration of cyanide ions.

The equilibrium constants $K^X_{H_2O}$ and K^X_{OH} can be converted into each other by virtue of the interrelation

$$\log K^X_{H_2O} = \log K^X_{OH} - pK_a - \log K_w, \quad (8)$$

and are collected in Table 1. Here, log K_w=−13.80 at 25.0 °C and μ=1.00 M($NaClO_4$).[21]

Kinetic Studies. The substitution Reaction 5 was followed spectrophotometrically by the stopped-flow method. Azide, nitrite, thiocyanate, sulfite and cyanide ions were used as the nucleophile X^{n-}, and the reaction with sulfite ion was studied only with the trimethylenediamine complex, since the corresponding reaction with the ethylenediamine complex was previously reported by Stranks and Yandell.[9]

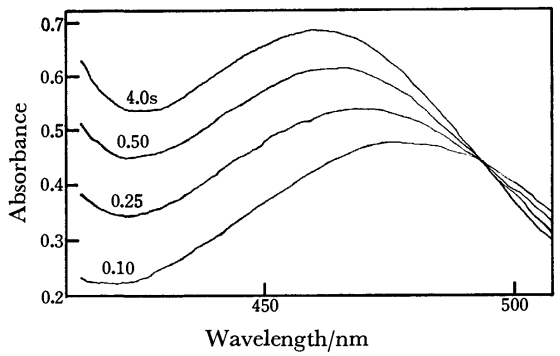

Fig. 1. The spectral change in the course of reaction between *trans*-$CoSO_3(OH)(tn)_2$ and SO_3^{2-} at 23.0 °C and μ=1.00 M ($NaClO_4$) with c_M=2.990×10^{-3} M, $c_{Na_2SO_3}$=0.116 M and c_{OH}=33.59×10^{-3} M. The reaction is in equilibrium after 4 s.

As an example of the results, the spectral change during the reaction of *trans*-$CoSO_3(OH)(tn)_2$ with sulfite is displayed in Fig. 1. The reaction attains an equilibrium 4 s after the commencement and an isosbestic point is observed at 494 nm which nearly coincides with that observed in the equilibrium study (498 nm). Concentrations of sulfite and hydroxide ions were both varied in the region of large excess over the complex. In the case of other nucleophiles, on the other hand, [OH^-] was kept constant and only [X^{n-}] was changed. In either case the plot of log $|A_\infty - A_t|$ against time gave a straight line over about 90% conversion.

Figures 2 and 3 show that the pseudo first order rate constant k_{obsd} increases linearly with [X^{n-}]/[OH^-] in conformity with the equation

$$k_{obsd} = k_f([X^{n-}]/[OH^-]) + k_r. \quad (9)$$

Ligand substitution reactions of several cobalt(III) sulfite complexes have been reported to proceed *via* the **D** mechanism,[5,9] and the present rate Eq. 9 is also compatible with the following reversible **D** mechanism.

$$\textit{trans}\text{-}CoSO_3(OH)(AA)_2 \underset{k_{OH}}{\overset{k_{-OH}}{\rightleftharpoons}} CoSO_3(AA)_2^+ + OH^- \quad (10)$$

$$CoSO_3(AA)_2^+ + X^{n-} \underset{k_{-X}}{\overset{k_X}{\rightleftharpoons}} \textit{trans}\text{-}CoSO_3(X)(AA)_2^{(1-n)+} \quad (11)$$

Assuming that the stationary state approximation is applicable to the five-coordinate intermediate $CoSO_3(AA)_2^+$, then

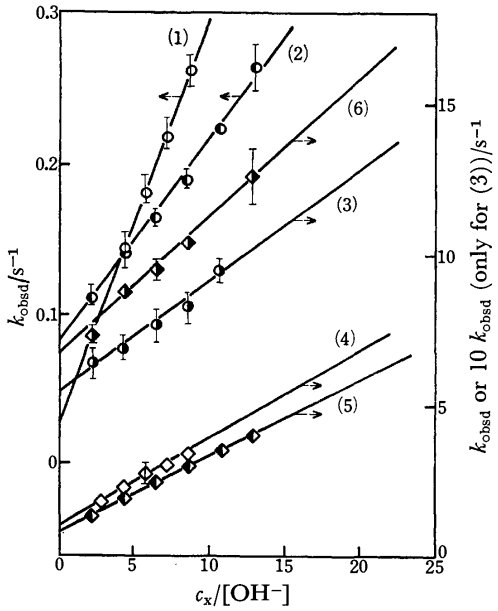

Fig. 2. Linear plots of the pseudo first order rate constants k_{obsd} for attaining the equilibrium, *trans*-$CoSO_3(OH)(AA)_2+X^{n-}\rightleftharpoons$*trans*-$CoSO_3(X)(AA)_2^{(1-n)+}+OH^-$ at 25.0 °C and $\mu=1.00$ M ($NaClO_4$) against $c_X/[OH^-]$. Lines 1 (NCS^-), 2 (NO_2^-) and 3 (N_3^-) are for the en complex, and 4 (NCS^-), 5 (NO_2^-) and 6 (N_3^-) are for the tn complex. $[OH^-]=0.0353$ M and $c_M=(1.500—1.657)\times10^{-3}$ M.

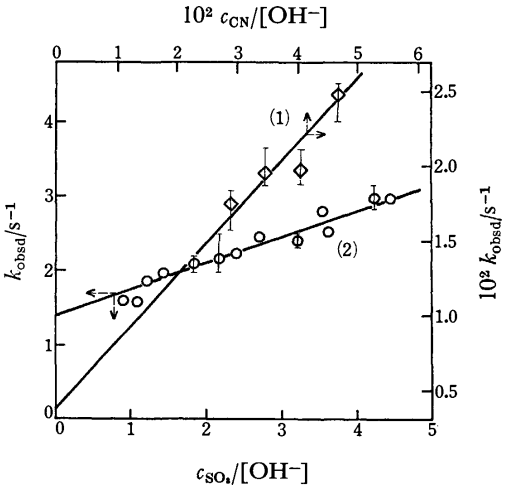

Fig. 3. Linear plots of the pseudo first order rate constants k_{obsd} for attaining the equilibrium, *trans*-$CoSO_3(OH)(tn)_2+X^{n-}\rightleftharpoons$*trans*-$CoSO_3(X)(tn)_2^{(1-n)+}+OH^-$ at 25.0 °C and $\mu=1.00$ M ($NaClO_4$) against $c_X/[OH^-]$, 1: $X^{n-}=CN^-$, $[OH^-]=0.03530$ M and $c_M=2.08\times10^{-5}$ M; 2: $X^{n-}=SO_3^{2-}$, $[OH^-]=0.02203$—0.08089 M, and $c_M=1.500\times10^{-3}$ M. Each point represents an average of at least five measurements.

$$k_{obsd}=\frac{k_Xk_{-OH}[X^{n-}]+k_{OH}k_{-X}[OH^-]}{k_{OH}[OH^-]+k_X[X^{n-}]}. \quad (12)$$

If $k_{OH}[OH^-]\gg k_X[X^{n-}]$ over the concentration range employed, Eq. 12 is reduced to

$$k_{obsd}=\frac{k_Xk_{-OH}}{k_{OH}}\frac{[X^{n-}]}{[OH^-]}+k_{-X}, \quad (13)$$

which is of the same form as Eq. 9, leading to

$$k_f=k_Xk_{-OH}/k_{OH},\quad k_r=k_{-X}. \quad (14)$$

In Table 2 are listed values of k_f, k_r, and the equilibrium constant for Reaction 5 which is calculated by

$$(K_{OH}^X)_{kin}=k_f/k_r,$$

and is to be compared with K_{OH}^X determined at the equilibrium state.

The reaction of *trans*-$CoSO_3(OH)(tn)_2$ with sulfite was studied at several temperatures other than 25.0 °C to obtain the rate data listed in Table 3. Eyring plots of k_f and k_r afforded good straight lines leading to $\Delta H^*=16.7\pm0.4$ kcal·mol^{-1} and $\Delta S^*=-2.1\pm1.2$ cal·K^{-1}·mol^{-1} for the dissociation of a sulfite ion from *trans*-$Co(SO_3)_2(tn)_2^-$.

For the reaction of *trans*-$CoSO_3(OH)(en)_2$ with cyanide, the equilibrium constant is so large and the rate is so small that determination of the forward and

Table 2. Rate and equilibrium data for the reactions *trans*-$CoSO_3(OH)(AA)_2+X^{n-}\rightleftharpoons$ *trans*-$CoSO_3(X)(AA)_2^{(1-n)+}+OH^-$ at 25.0 °C and $\mu=1.00$ M ($NaClO_4$)

X^{n-}	Wavelength[a] / nm	k_f/s^{-1}	k_r/s^{-1}	$(K_{OH}^X)_{kin}$	K_{OH}^X
			AA = en		
N_3^-	470	$(3.62\pm0.23)\times10^{-2}$	$(5.56\pm0.16)\times10^{-1}$	$(6.51\pm0.60)\times10^{-2}$	$(1.61\pm0.09)\times10^{-2}$
NO_2^-	430	$(1.34\pm0.05)\times10^{-2}$	$(8.21\pm0.41)\times10^{-2}$	$(1.63\pm0.14)\times10^{-1}$	$(1.75\pm0.03)\times10^{-1}$
NCS^-	458	$(2.53\pm0.14)\times10^{-2}$	$(4.00\pm0.89)\times10^{-2}$	$(6.3\pm1.8)\times10^{-1}$	$(1.06\pm0.03)\times10^{-1}$
CN^-	470	$(1.33\pm0.05)\times10^{-2}$ [b]	$(2.41\pm0.23)\times10^{-5}$	—	552 ± 29
SO_3^{2-}	432	$(4.09\pm0.05)\times10^{-2}$ [c]	$(1.11\pm0.05)\times10^{-1}$ [c]	$(3.68\pm0.21)\times10^{-1}$ [c]	$3.6_8\times10^{-1}$ [c]
			AA = tn		
N_3^-	490	$(4.55\pm0.20)\times10^{-1}$	6.75 ± 0.15	$(6.74\pm0.45)\times10^{-2}$	$(3.63\pm0.19)\times10^{-2}$
NO_2^-	450	$(2.51\pm0.03)\times10^{-1}$	$(8.10\pm0.20)\times10^{-1}$	$(3.10\pm0.11)\times10^{-1}$	$(3.90\pm0.03)\times10^{-1}$
NCS^-	474	$(2.89\pm0.12)\times10^{-1}$	1.00 ± 0.07	$(2.89\pm0.32)\times10^{-1}$	$(4.86\pm0.05)\times10^{-1}$
CN^-	290	$(4.48\pm0.44)\times10^{-1}$	$(3.6\pm1.6)\times10^{-3}$	124 ± 67	112 ± 2
SO_3^{2-}	430	$(3.31\pm0.20)\times10^{-1}$	1.41 ± 0.05	$(2.35\pm0.23)\times10^{-1}$	$(1.15\pm0.06)\times10^{-1}$

a) Wavelength utilized for the kinetic measurement. b) Determined at the irreversible condition (see text).
c) Ref. 9.

Table 3. Rate data for the reaction *trans*-$CoSO_3(OH)(tn)_2+SO_3^{2-}\rightleftharpoons$*trans*-$Co(SO_3)_2(tn)_2^-+OH^-$ at various temperatures and $\mu=1.00$ M ($NaClO_4$)

Temp/°C	k_f/s^{-1}	k_r/s^{-1}
10.0	0.083±0.009	0.275±0.015
15.0	0.123±0.003	0.490±0.018
20.0	0.216±0.013	0.780±0.043
25.0	0.331±0.020	1.41 ±0.05
29.9	0.533±0.034	2.02 ±0.13
35.0	0.790±0.091	3.42 ±0.29

backward rates in the above manner was difficult. Alternatively the cyanide concentration was kept in large excess to render the reaction irreversible. In this case the pseudo first order rate constant is expressed by

$$k_{obsd} = k_{CN}k_{-OH}[CN^-]/(k_{OH}[OH^-]+k_{CN}[CN^-]), \quad (15)$$

which is transformed into

$$\frac{1}{k_{obsd}} = \frac{1}{k_{-OH}} + \frac{k_{OH}}{k_{CN}k_{-OH}}\left(\frac{[OH^-]}{[CN^-]}\right). \quad (16)$$

A plot of the observed rate data according to Eq. 16

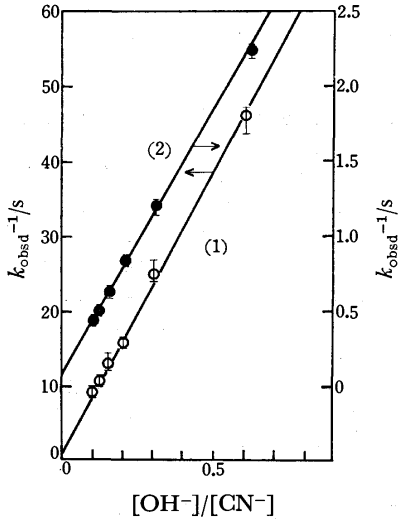

Fig. 4. The plot of $1/k_{obsd}$ *vs.* $[OH^-]/[CN^-]$ for the reaction *trans*-$CoSO_3(OH)(AA)_2+CN^-\rightarrow$*trans*-$CoSO_3(CN)(AA)_2+OH^-$ at 25.0 °C and $\mu=1.00$ M ($NaClO_4$). 1: AA=en, $[OH^-]=0.03656$ M and $c_M=4.485\times10^{-4}$ M. 2: AA=tn, $[OH^-]=0.03657$ M and $c_M=4.400\times10^{-4}$ M.

gave a straight line displayed in Fig. 4, which also contains another plot for the reaction of *trans*-$CoSO_3(OH)(tn)_2$ performed in a similar condition for the sake of comparison. The intercepts and slopes of these straight lines gave the following constants: $k_{-OH}=1.19\pm0.81$ s^{-1}(AA=en) and 13.9 ± 2.7 s^{-1}(AA=tn), $k_{CN}/k_{OH}=(1.12\pm0.80)\times10^{-2}$(AA=en) and $(2.02\pm0.42)\times10^{-2}$(AA=tn) at 25.0 °C and $\mu=1.00$ M. Furthermore, by combining the value of slope $k_{OH}/k_{CN}k_{-OH}$ with that of the equilibrium constant K_{OH}^{CN} listed in Table 1, k_{-CN} was calculated to be $(2.41\pm0.23)\times10^{-5}$ s^{-1} for the en complex. The value of $k_f=k_{CN}k_{-OH}/k_{OH}=0.280\pm0.004$ s^{-1} for the tn complex, which was calculated from the slope of the straight line (2) in Fig. 4, nearly coincides with that obtained in the reversible condition (Table 2).

Division of the k_f value in Table 2 by $k_{-OH}=1.19\pm0.81$ (AA=en) or 13.9 ± 2.7 (AA=tn) s^{-1} affords k_X/k_{OH} (*cf.* Eq. 14) which is shown in Table 4. The ratio indicates that the nucleophilic reactivity of hydroxide ion toward $CoSO_3(AA)_2^+$ is 30—90 times larger than that of other nucleophiles examined. The hydroxide ion was also reported to be at least 4×10^5 times more reactive than H_2O toward $CoSO_3(en)_2^+$,[9] and 8×10^3 times more reactive than NH_3 toward $CoSO_3(NH_3)_4^+$.[22] It was suggested[5a] that the high reactivity of OH^- might reflect a Grotthus-type mechanism.

Discussion

Linear Free Energy Relations (LFER) have been widely used to sort out the various factors that contribute to the rate and equilibrium of organic[23] and inorganic[24] reactions. On the supposition that nucleophilic character of a reagent is a combination of several factors, Edwards proposed an equation

$$\log(K/K_0) = \alpha E_n + \beta H, \quad (17)$$

where K and K_0 are the rates or equilibrium constants of reactions of a particular substrate with a nucleophile and water, respectively, α and β are two substrate constants, and E_n and H are electron donor constant and basicity constant, respectively.[25] Recently Tanaka related the formation constant K_{ML}^L of a complex ML with the Edwards' parameters by

$$\log K_{ML}^L = \log K_{os(M,L)} + \alpha E(L) + \beta H(L), \quad (18)$$

where $K_{os(M,L)}$ denotes the formation constant of an outer-sphere complex [M, L].[26]

Equation 18 was derived on the basis of the Eigen

Table 4. The rate of X^{n-} release (k_{-X}) from *trans*-$CoSO_3(X)(AA)_2^{(1-n)+}$ and the reactivity ratio of X^{n-} and OH^- (k_X/k_{OH}) toward $CoSO_3(AA)_2^+$ at 25.0 °C and $\mu=1.00$ M ($NaClO_4$)

X^{n-}	AA = en		AA = tn		$\frac{k_{-X}(tn)}{k_{-X}(en)}$
	k_{-X}/s^{-1}	k_X/k_{OH}	k_X/s^{-1}	k_X/k_{OH}	
N_3^-	$(5.56\pm0.16)\times10^{-1}$	$(3.0\pm2.3)\times10^{-2}$	6.75±0.15	$(3.28\pm0.78)\times10^{-2}$	12.1 ±0.6
NO_2^-	$(8.21\pm0.41)\times10^{-2}$	$(1.1\pm1.5)\times10^{-2}$	$(8.1\pm0.2)\times10^{-1}$	$(1.81\pm0.37)\times10^{-2}$	9.87±0.74
NCS^-	$(4.00\pm0.89)\times10^{-2}$	$(2.1\pm1.6)\times10^{-2}$	1.00±0.07	$(2.08\pm0.49)\times10^{-2}$	25.0 ±7.3
CN^-	$(2.41\pm0.23)\times10^{-5}$	$(1.1\pm0.8)\times10^{-2}$	$(3.6\pm1.6)\times10^{-3}$	$(3.23\pm0.94)\times10^{-2}$	149±80
SO_3^{2-}	$(1.11\pm0.05)\times10^{-1}$ [a]	$(3.4\pm2.4)\times10^{-2}$ [a]	1.41±0.05	$(2.38\pm0.61)\times10^{-2}$	12.7 ±1.0
OH^-	1.19±0.81	1	13.9 ±2.7	1	12±10

a) Ref. 9.

($\mathbf{I_d}$) mechanism, the rate of dissociation of the ligand L from the complex ML being assumed to be inversely proportional to both the electron donating property and the Brønsted basicity of the leaving group L. The present reactions, on the other hand, are presumed to proceed *via* the **D** mechanism and contribution of the outer-sphere complex as in Eq. 18 need not be considered.

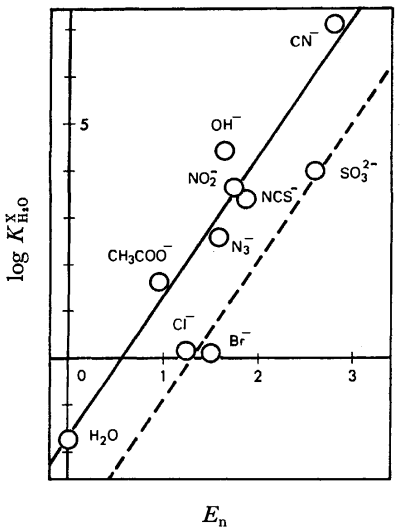

Fig. 5. A plot of log $K^X_{H_2O}$ for Reaction 2 (AA=en) against the electron donor constant E_n of X^{n-}.

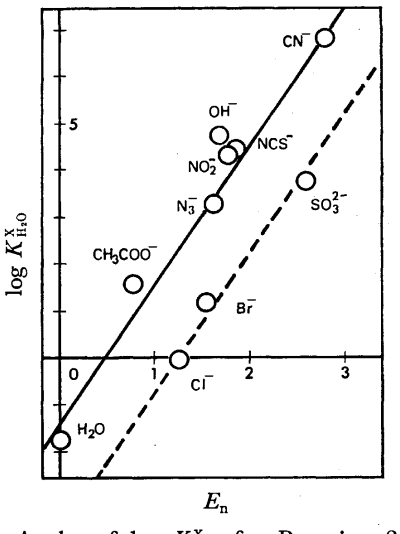

Fig. 6. A plot of log $K^X_{H_2O}$ for Reaction 2 (AA=tn) against the electron donor constant E_n of X^{n-}.

In Figs. 5 and 6 are plotted log $K^X_{H_2O}$ (Eq. 3) against E_n of a nucleophile X^{n-}. For both the en and tn complexes LFER holds and data for the ligands containing O, N, or C as donor atom lie on a straight line in conformity with

$$\log K^X_{H_2O} = \alpha E_n + \gamma. \quad (19)$$

The value of substrate constant α is nearly the same for the en(3.0) and tn(2.9) complexes, indicating the similarity of the two complexes in the electron-donor discrimination. The value of intercept γ is -1.6 for the en complex and -1.4 for the tn complex, both being near to $\log K^{H_2O}_{H_2O} = -\log [H_2O] = -1.74$ which is obtained by merely substituting X^{n-} in Eq. 3 with H_2O. Thus Eq. 19 coincides with Eq. 17 under the conditions of $\beta=0$, indicating that the $CoSO_3(AA)_2^+$ moiety is soft enough to render the stability constant of *trans*-$CoSO_3(X)(AA)_2^{(1-n)+}$ depend not on the Brønsted basicity but on the electron donating property of X^{n-}. In fact the set of values of α and β for $CoSO_3(AA)_2^+$ (3.0, 0) is comparable with those for Ag^+ (3.60, -0.09), Cu^+ (3.92, 0.18), and CH_3Hg^+ (4.21, 0.11)[27] which are typically soft according to Pearson's classification.[28] Usually Co(III) is hard, but in the present compounds the sulfite ion is soft and makes Co(III) prefer a soft ligand at the sixth coordination site trans to SO_3^{2-}. This may be an example of chemical symbiosis proposed by Jørgensen.[29]

In Figs. 5 and 6 Cl^-, Br^-, and SO_3^{2-} remarkably deviate from the straight line established by the other ligands, and lie on another straight line (dotted) paralleling the former. Such a behavior can not be rationalized at the present stage of investigation. Tanaka[26,30] succeeded in estimating the formation constant of a mixed ligand complex MAL and a $1:n$ complex ML_n by introducing additional terms $\sum_i\sum_j \delta_{ij}X_i(A)Y_j(L)$ into Eq. 18 in order to take into account the effect of interaction between donor atoms X_i and Y_j in the coexisting ligand and entering one. In the present case effect of the nitrogen atoms in en and tn on the O, N, or C atom in the entering ligand might be similar, but that on the Cl, Br, or S atom might be much larger in the repulsive sense partly because of the larger size of the latter donor atoms (the atomic radius: N=0.74, C=0.772, O=0.74, S=1.04, Cl=0.99, Br=1.14 Å[31]). A similar situation is also noticed when we correlate the equilibrium constants for the substitution of H_2O

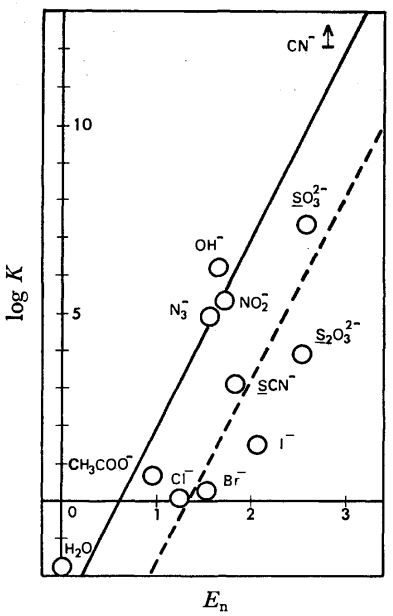

Fig. 7. Relation of the equilibrium constant K for anation of aquacobalamin with the electron donor constant E_n of a nucleophile. Data from Ref. 32 are plotted.

in aquacobalamin which were determined by Pratt and his collaborators[32] with the E_n value of each nucleophile (Fig. 7).

In a previous paper[33] it was reported that the rate of nitrite release from $Co(NO_2)_4(tn)^-$ is 4.5 times and the rate of aqua ligand release from $Co(NO_2)_3(H_2O)(tn)$ is 7.2 times larger than those of the corresponding en complexes. Now Table 4 indicates that the ratio $(k_{-X})_{tn}/(k_{-X})_{en}$ for *trans*-$CoSO_3(X)(AA)_2^{(1-n)+}$ amounts to 10—25 except for the cyano complex. The larger kinetic ring-size effect in the present case may be due to the increase in number of the chelate ring. The enthalpy of activation for the sulfite release from *trans*-$Co(SO_3)_2(en)_2^-$ was reported[9] to be 20.5 ± 0.6 kcal·mol^{-1} and that for the corresponding reaction of *trans*-$Co(SO_3)_2(tn)_2^-$ was now obtained as 16.7 ± 0.4 kcal·mol^{-1}. Holmes and Williams determined the thermodynamic functions of the copper(II) and nickel(II) complexes of en and tn.[34] In either case the en complex is more stable than the tn complex, and the difference in the enthalpy of formation of $M(en)_2(H_2O)_2^{2+}$ and $M(tn)_2(H_2O)_2^{2+}$ amounts to 2.69 kcal·mol^{-1} in the case of the Cu(II) complex and 3.85 kcal·mol^{-1} for Ni(II). A similar amount of excess ground-state stabilization may be offered to *trans*-$Co(SO_3)_2(en)_2^-$ as compared with *trans*-$Co(SO_3)_2(tn)_2^-$ and may be responsible for the excess $\Delta H^{\neq}$ of 3.8 kcal·mol^{-1}. Thus the kinetic ring-size effect seems to stem from the energy difference at the ground state. This is the same conclusion as that drawn in a previous paper.[33]

The cyanide release from *trans*-$CoSO_3(CN)(tn)_2$ is 149 ± 80 times faster than from the corresponding en complex (Table 4). An enormous difference in the aquation rate of the en and tn complexes of the type *trans*-$CoBr_2(AA)_2^+$ and *trans*-$CoCl_2(AA)_2^+$ has previously been reported, $k(tn)/k(en)$ being 680[35] and 1666[36] at 25 °C, respectively. The $k(tn)/k(en)$ for the *trans*→*cis* isomerization of $Co(H_2O)_2(AA)_2^{3+}$ was also recorded as 1450, while the rate ratio for the similar isomerization of $Co(OH)_2(AA)_2^+$ was only 13.[35] Reasonable explanation for these abnormal kinetic ring-size effect is quite difficult.

The authors wish to thank Mr. Junichi Gohda for the elemental analysis and are also grateful to the Ministry of Education for Grant-in-Aid.

References

1) Part V: Y. Ito and S. Kawaguchi, *Bull. Chem. Soc. Jpn.*, **51**, 2321 (1978).
2) F. Basolo and R. G. Pearson, "Mechanisms of Inorganic Reactions," 2nd ed, Wiley, New York (1967), p. 158.
3) C. K. Poon, *Coord. Chem. Rev.*, **10**, 1 (1973).
4) C. K. Poon, W. K. Wan, and S. S. T. Liao, *J. Chem. Soc., Dalton Trans.*, **1977**, 1247.
5) (a) J. E. Byrd and W. K. Wilmarth, *Inorg. Chim. Acta Rev.*, **5**, 7 (1971); (b) L. Richards and J. Halpern, *Inorg. Chem.*, **15**, 2571 (1976).
6) J. M. Palmer and E. Deutsch, *Inorg. Chem.*, **14**, 17 (1975).
7) J. H. Espenson and R. Russell, *Inorg. Chem.*, **13**, 7 (1974) and references cited therein.
8) W. C. Trogler, R. C. Stewart, and L. G. Marzilli, *J. Am. Chem. Soc.*, **96**, 3697 (1974).
9) D. R. Stranks and J. K. Yandell, *Inorg. Chem.*, **9**, 751 (1970).
10) M. E. Baldwin, *J. Chem. Soc.*, **1961**, 3123.
11) H. Kawaguchi and S. Kawaguchi, *Bull. Chem. Soc. Jpn.*, **43**, 2103 (1970).
12) M. E. Baldwin, *J. Chem. Soc.*, **1960**, 4369.
13) C. J. Hawkins, "Absolute Configuration of Metal Complexes," Wiley, New York (1971), Chap. 6.
14) H. Kawaguchi and S. Kawaguchi, *Bull. Chem. Soc. Jpn.*, **46**, 3453 (1973).
15) K. Nakamoto, "Infrared Spectra of Inorganic and Coordination Compounds," 2nd ed, Wiley-Interscience, New York (1970), p. 177.
16) R. C. Elder and M. Trkula, *J. Am. Chem. Soc.*, **96**, 2635 (1974).
17) E. N. Maslen, C. L. Raston, A. H. White, and J. K. Yandell, *J. Chem. Soc., Dalton Trans.*, **1975**, 327.
18) E. N. Maslen, C. L. Raston, and A. H. White, *J. Chem. Soc., Dalton Trans.*, **1975**, 323.
19) S. Baggio and L. N. Becka, *Acta Crystallogr., Sect. B*, **25**, 946 (1969).
20) A constant concentration of acetic acid was used and $[CH_3COO^-]$ at various pH was calculated by virtue of $pK_a=4.50$ at 25.0 °C and $\mu=1.01$ M (NaCl) [H. S. Harned and B. B. Owen, "The Physical Chemistry of Electrolytic Solutions," 3rd ed, Reinhold, New York (1958), p. 676].
21) L. G. Sillén and A. E. Martell, "Stability Constants of Metal-Ion Complexes," Special Publication No. 25, The Chemical Society, London (1971), p. 14.
22) J. Halpern, R. A. Palmer, and L. M. Blakely, *J. Am. Chem. Soc.*, **88**, 2877 (1966).
23) J. E. Leffler and E. Grunwald, "Rates and Equilibria of Organic Reactions," Wiley, New York (1963).
24) J. O. Edwards, "Inorganic Reaction Mechanisms," Benjamin, New York (1964).
25) J. O. Edwards, *J. Am. Chem. Soc.*, **76**, 1540 (1954).
26) M. Tanaka, *J. Inorg. Nucl. Chem.*, **35**, 965 (1973).
27) S. Yamada and M. Tanaka, *J. Inorg. Nucl. Chem.*, **37**, 587 (1975).
28) R. G. Pearson, *J. Am. Chem. Soc.*, **85**, 3533 (1963).
29) C. K. Jørgensen, *Inorg. Chem.*, **3**, 1201 (1964); R. G. Pearson, *Inorg. Chem.*, **12**, 712 (1973).
30) M. Tanaka, *J. Inorg. Nucl. Chem.*, **36**, 151 (1974).
31) L. Pauling, "The Nature of the Chemical Bond," 3rd ed, Cornell Univ. Press (1960).
32) R. A. Firth, H. A. O. Hill, J. M. Pratt, R. G. Thorp, and R. J. P. Williams, *J. Chem. Soc., A*, **1969**, 381.
33) Y. Ito and S. Kawaguchi, *Bull. Chem. Soc. Jpn.*, **51**, 1083 (1978).
34) F. Holmes and D. R. Williams, *J. Chem. Soc., A*, **1967**, 1702.
35) I. R. Jonasson, R. S. Murray, D. R. Stranks, and Y. K. Yandell, *Proc. Int. Conf. Coord. Chem.*, **12**, 32 (1969).
36) M. C. Couldwell, D. A. House, and H. K. J. Powell, *Inorg. Chem.*, **12**, 627 (1973).

The Complexing of the Ammonium Ion in Acetonitrile with Other Solvents. Investigation Using a Cation-sensitive Glass Electrode

Kosuke IZUTSU, Toshio NAKAMURA,* Taiji MURAYAMA, and Taitiro FUJINAGA†

Chemistry Department, Faculty of Science, Shinshu University, Asahi, Matsumoto 390

†*Chemistry Department, Faculty of Science, Kyoto University, Sakyo-ku, Kyoto 606*

(Received January 23, 1978)

As a part of potentiometric studies of the complexing of univalent cations in acetonitrile with other solvents by the use of a cation-sensitive glass electrode, investigations were carried out of the complexing of the ammonium ion in acetonitrile with such solvents as water, methanol, *N*-methylformamide, *N,N*-dimethylformamide, *N,N*-dimethylacetamide, dimethyl sulfoxide, 1-methyl-2-pyrrolidone, and hexamethylphosphoric triamide, and also with dibenzo-18-crown-6. Prior to the study of the complexing, the cation-sensitive glass electrode was confirmed to respond in a Nernstian way to the change in the ammonium-ion activity which occurs due to the change of the solvent (solvent effect). The ammonium ion in acetonitrile formed complexes of mono- and di-solvated species with methanol and water. Formations of up to tri-solvated species were formed with DMF, DMA, and DMSO, and up to tetra-solvated species with 1-methyl-2-pyrrolidone and NMF. With HMPA, even penta-solvated species were formed. The complex formation constants of the mono-solvated ammonium ion, β_1 (mol^{-1} dm^3), were 1.$_7$ with methanol, 5.6 with DMF, 14 with DMSO, 17 with DMA, 31 with 1-methyl-2-pyrrolidone, 3.0×10^2 with NMF, and 1.2×10^3 with HMPA. The association constant of ammonium perchlorate in acetonitrile was determined conductometrically to be 25 mol^{-1} dm^3.

Recently, the complexing of univalent cations with other solvents has been investigated in acetonitrile (AN) by using such techniques as nuclear magnetic resonance,[1] infrared spectroscopy,[2] conductometry,[3] and potentiometry,[4-6] but few reports have appeared concerning the complexing of the ammonium ion in acetonitrile. In the present paper, we have studied the complexing of the ammonium ion in acetonitrile with other dipolar solvents, such as water, methanol, *N*-methylformamide (NMF), *N,N*-dimethylformamide (DMF), *N,N*-dimethylacetamide (DMA), dimethyl sulfoxide (DMSO), 1-methyl-2-pyrrolidone, and hexamethylphosphoric triamide (HMPA), and with dibenzo-18-crown-6, by using a potentiometric method similar to that used in the previous reports.[4-6] The emf of the following cell was measured:

Ag|0.005 M $AgNO_3$, 0.01 M Et_4NClO_4(AN)‖
0.1 M Et_4NClO_4(AN)‖10^{-3} M NH_4ClO_4,
0.01 M Et_4NClO_4(AN+D)|Cation-sensitive
Glass Electrode ··· Cell I

where D denotes the solvents added and where M=mol dm^{-3}. The formation constants, β_x in $(mol^{-1}\ dm^3)^x$, for Reaction 1 were obtained by analyzing the emf data under assumptions similar to those in the previous reports.[4-6]

$$NH_4^+{}_s + xD = NH_4^+{}_{xD} \quad (1)$$

$$\beta_x = \frac{(NH_4^+{}_{xD})}{(NH_4^+{}_s)[D]^x} \quad (2)$$

In Eq. 1, $NH_4^+{}_s$ shows ammonium ions solvated only with acetonitrile and $NH_4^+{}_{xD}$ those complexed by molecules of D in AN+D. In Eq. 2, $(NH_4^+{}_s)$ and $(NH_4^+{}_{xD})$ are the activities, and [D], the concentration, of the respective species in the molar scale.

Experimental

Apparatus. Most of the apparatus and experimental techniques used for the potentiometric determination of the complex formation constants were the same as those in the previous reports.[4-6] A Horiba No. 1826A-05T glass electrode was used to determine the acid dissociation constant of the pyridinium ion in acetonitrile. The conductance was measured with a universal bridge model 4255A of the Yokogawa-Hewlett-Packard Co., Ltd. Polarograms were measured with a three-electrode polarograph, Yanagimoto P8-PS. All these measurements were carried out at 25 °C.

Reagents. The ammonium perchlorate was prepared by introducing ammonia into a solution of perchloric acid, purified by recrystallizing from water, and dried *in vacuo* at 110 °C. The pyridinium perchlorate was prepared by passing evaporated pyridine into an aqueous solution of perchloric acid and purified by recrystallizing it from ethanol. It was dried at room temperature under a high vacuum with P_2O_5. The dibenzo-18-crown-6, which has been prepared by the method of Pedersen,[7] was recrystallized from chloroform. The 1-methyl-2-pyrrolidone was a product of Wako Chemicals Co., Ltd., and was purified according to the method of Sears *et al.*[8] The DMA[9] was purified by distillation, first from BaO, next from CaH_2, and finally without any additives. The other solvents and reagents used in this experiment were the same as those described in the previous reports.[4-6]

Results

Response of the Cation-sensitive Glass Electrode to the Activity of the Ammonium Ion. The cation-sensitive glass electrode used in this study showed a response of a slope of 56 mV for the ammonium-ion concentration between 10^{-2} and 10^{-4} M in acetonitrile − 0.01 M Et_4NClO_4. If correction is made for the change in the salt-effect activity coefficient, which is calculated by using the Debye-Hückel equation: $\log f = -AI^{1/2}/[1+BaI^{1/2}]$, assuming $A=1.64$ $mol^{-1/2}$ $dm^{3/2}$, $B=4.86\times10^8$ $mol^{-1/2}$ $dm^{1/2}$, and $a=5\times10^{-8}$ cm, the slope of the response to $pa_{NH_4^+}$ becomes 58.5 mV, which is very near to the Nernstian slope of 59.16 mV.

In order to confirm that the glass electrode also

responds to the change in the activity of the ammonium ion due to the solvent effect, the emfs of Cell II were measured in various solvents, D, and were compared with the polarographic half-wave potentials of the ammonium ion, which were measured in 10^{-3} M NH_4ClO_4–0.01 M Et_4NClO_4(D) by using a salt bridge and a reference electrode similar to those in Cell II.

Ag|0.005 M $AgNO_3$, 0.01 M Et_4NClO_4(AN)‖
0.1 M Et_4NClO_4(AN)‖10^{-3} M NH_4ClO_4,
0.01 M Et_4NClO_4(D)|Cation-sensitive Glass Electrode ··· Cell II

(D denotes AN, DMF, DMA, and DMSO)

The results are shown in Fig. 1. For D solvents such as acetonitrile, DMF, DMA, and DMSO, the values on the abscissa agree fairly well with the values on the coordinate. Because the polarographic behavior of the ammonium ion is nearly reversible in these solvents, these results can be considered to confirm the Nernstian response of the glass electrode to the effect of the solvent on the activity of the ammonium ions. For other solvents, the polarographic behavior of the ammonium ion was not reversible or did not give a well-defined wave, and so a comparison as in Fig. 1 was impossible. However, it would be reasonable to assume that even in these solvents the glass electrode can respond in a Nernstian way to the effect of the solvent on the ammonium-ion activity.

Complexing of the Ammonium Ion in Acetonitrile with Other Solvents. From the emf measurement of Cell I, the values of the complex formation constants of the ammonium ion in acetonitrile with other solvents, such as water, methanol, NMF, DMF, DMA, DMSO, 1-methyl-2-pyrrolidone, and HMPA, were obtained by the method used in the previous papers.[4-6] The results are summarized in Table 1. The values of β_1 in Table 1 seem to be reliable within $\pm 10\%$ for aprotic solvents. However, for β_1 in the cases in which D was a protic solvent and for β_2 to β_5, the reliability seems to be somewhat less because of the deviations from the ideal conditions assumed in calculating these values.[4] The formation constants with water are shown in parentheses

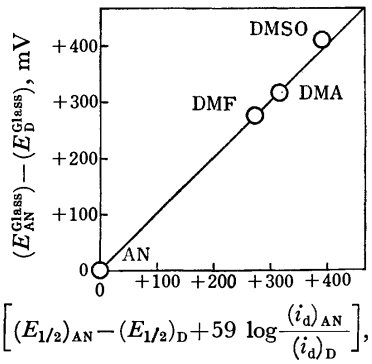

Fig. 1. Relation between the emf of Cell II and the half-wave potential of the ammonium ion in different solvents. Both referred to the values in acetonitrile.

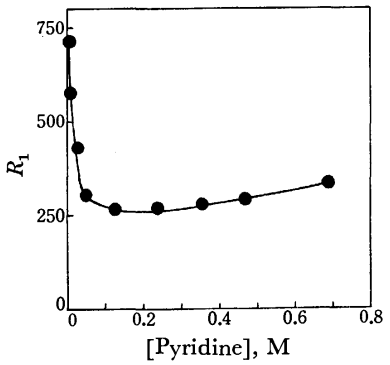

Fig. 2. The exceptional relation of R_1-[D] for the case in which D=pyridine (see text).

Table 1. Complex formation constants, β_x in $(mol^{-1}\ dm^3)^x$, of the ammonium ion in acetonitrile with other solvents and a crown ether (at 25 °C)

Ligand	Max. concn of ligand added (M)	β_1	β_2	β_3	β_4	β_5
Methanol	0.7	1.$_7$	0.$_4$			
	0.7	1.$_8$	0.$_3$			
DMF	0.7	5.3	6.8	8.$_7$		
	0.7	5.9	6.9	7.$_6$		
H_2O	1.1	(5.$_5$)[a]	(4.$_2\times 10$)[a]			
	0.5	(5.$_6$)[a]	(4.$_6\times 10$)[a]			
DMSO	0.7	14	31	$7._1\times 10$		
	0.7	14	30	$8._4\times 10$		
DMA	0.7	16	41	$5._7\times 10$		
	0.7	17	40	$5._1\times 10$		
1-Methyl-2-pyrrolidone	0.5	30	1.7×10^2	$2._8\times 10^2$	7×10^2	
	0.6	31	1.7×10^2	$3._0\times 10^2$	6×10^2	
NMF	0.7	2.9×10^2	1.7×10^3	$3._6\times 10^3$	9×10^3	
	0.5	3.0×10^2	1.9×10^3	$3._3\times 10^3$	8×10^3	
HMPA	0.2	1.2×10^3	2.1×10^5	3.5×10^6	$5._8\times 10^7$	2×10^8
	0.2	1.2×10^3	2.0×10^5	3.9×10^6	$4._7\times 10^7$	2×10^8
Dibenzo-18-crown-6	0.03	4.9×10^3	1.1×10^5			
	0.03	5.0×10^3	8.7×10^4			

a) See text for the values in parentheses.

in Table 1. This is because the potential of the glass electrode was not stable enough when water was titrated in Cell I. When pyridine was used as the D solvent, the relation between R_1** and the concentration of pyridine added to Cell I (Fig. 2) was peculiar and an extremely big R_1 value was obtained at a small concentration of pyridine. The complex formation constants of the ammonium ion in acetonitrile with dibenzo-18-crown-6 were determined by adding a solution of 6.25×10^{-2} M crown ether to a solution of 5×10^{-3} M NH_4ClO_4 in acetonitrile–5×10^{-2} M Et_4NClO_4. These results are also shown in Table 1.

The Acid Dissociation Constant of the Pyridinium Ion. The acid dissociation constant of the pyridinium ion (pyH^+) in acetonitrile was determined by measuring the emf of Cell III:

Ag|0.005 M $AgNO_3$, 0.01 M Et_4NClO_4(AN)‖
0.1 M Et_4NClO_4(AN)‖4×10^{-3} M $pyHClO_4$,
x M pyridine(AN)|Glass Electrode ··· Cell III

The Horiba 1826A-05T glass electrode in Cell III was calibrated in a 5×10^{-3} M picric acid–5×10^{-3} M tetraethylammonium picrate buffer solution in acetonitrile by using the pK_a value of 11.0[10] for picric acid. The pyridine concentration added to Cell III was varied from 2.00×10^{-4} to 2.74×10^{-2} M. The pa_{H^+} value was calculated by assuming a response of 59.16 mV/pa_{H^+} and the pK_a value (K_a in mol dm^{-3}) was obtained from the simple Henderson equation by making a correction for the change in the activity coefficient according to the Debye-Hückel limiting law, $-\log f=1.64\{I/(\text{mol dm}^{-3})\}^{1/2}$. As is shown in Table 2, a pK_a value of 12.60 ± 0.01 was obtained. The pK_a value was also determined in the presence of an indifferent electrolyte of 1.0×10^{-2} M Et_4NClO_4 in Cell III, a pK_a value of 12.53 was thus obtained, which is in fairly good agreement with the literature data of 12.33.[11]

Table 2. The dissociation constants of the pyridinium ion from the glass electrode measurements

[pyH^+] M×10³	[Pyridine] M×10³	E mV	log f	pa_{H^+}	$pK_a^{pyH^+}$
4.00	0.200	17.5	-0.10_4	11.40	12.60
4.00	0.500	−5.9	-0.10_4	11.80	12.60
4.00	0.959	−22.0	-0.10_4	12.07	12.59
3.99	1.92	−39.7	-0.10_4	12.37	12.59
3.99	2.87	−50.7	-0.10_4	12.56	12.60
3.99	3.83	−57.5	-0.10_4	12.67	12.59
3.98	4.78	−63.2	-0.10_4	12.77	12.59
3.98	5.73	−68.5	-0.10_3	12.86	12.60
3.97	6.68	−73.2	-0.10_3	12.94	12.61
3.97	7.65	−76.4	-0.10_3	12.99	12.60
3.95	11.5	−87.1	-0.10_3	13.17	12.61
3.92	19.2	−101.2	-0.10_3	13.41	12.62
3.89	27.4	−110.8	-0.10_2	13.57	12.62

** R_1 is obtained by the use of the relation $R_1=\{10^{(E_{AN}-E_{AN-D})/59.16}-1\}/[D]$, where E_{AN} and E_{AN-D} are the emfs of Cell I in the absence and in the presence respectively of the D solvent. In ordinary cases, the following relation holds: $R_1=\beta_1+\beta_2[D]+\beta_3[D]^2+\cdots$.[4]

Determination of the Association Constant of the Ammonium Perchlorate. The conductometric measurements of the ammonium perchlorate in acetonitrile were carried out at (25±0.01) °C at ammonium-perchlorate concentrations from 4.20×10^{-4} to 3.33×10^{-2} M. The association constant and the molar conductivity of ammonium perchlorate, obtained with the Schedolovsky equation, were 25 mol^{-1} dm^3 and 200.$_6$ S cm^2 mol^{-1} respectively. By using the molar ionic conductivity, $\lambda_0(ClO_4^-)$, of 103.7 S cm^2 mol^{-1} [12] in acetonitrile, $\lambda_0(NH_4^+)$ can be calculated to be 96.$_9$ S cm^2 mol^{-1}, which is between the λ_0 (H^+) value of 99 S cm^2 mol^{-1} [13] and the $\lambda_0(Me_4N^+)$ value of 94.5 S cm^2 mol^{-1}. [12]

Discussion

From the results in Fig. 1, it may be considered that the cation-sensitive glass electrode can respond well to the activity of the ammonium ion in solvents of different species or compositions.

The ammonium ion in acetonitrile behaves as a Lewis acid, and the complex formation constant, β_1, increases with the solvent basicity. The values in Table 1 show that the complexing of the ammonium ion in acetonitrile with other solvents is generally more extensive than in the cases of the sodium and thallium(I) ions and that it is roughly comparable to the case of the lithium ion[5]. Kolthoff and Coetzee[14] indicated, as the results of their polarographic measurements, that the free energy of the solvation of the ammonium ion is considerably larger in water than in acetonitrile. Coetzee and Padmanabhan reported similar results.[11] The complex formation constants of the ammonium ion with water are, as is shown in Table 1, fairly large and are comparable to the complex formation constants with DMF. For sodium and thallium(I) ions, on the other hand, the formation constants with water are smaller than those with DMF.[4,6]

The formation constants of the ammonium ion with dibenzo-18-crown-6 (Table 1) are considerably larger than the polarographic results of Angelis *et al.*[15] They obtained the formation constant of 3.1×10^2 in a 0.1 M tetrabutylammonium perchlorate–acetonitrile solution, but they mentioned that the validity of their value may be somewhat in doubt since the electrode-reaction kinetics of the ammonium ion may be influenced by the adsorption of the polyether complex. The existence of the 2:1 crown ether–NH_4^+ complex seems to be reasonable if we consider the fact that the Pauling crystal diameter of the ammonium ion (2.96 Å) and the diameter of the cavity of dibenzo-18-crown-6 (2.6 Å according to Corey-Pauling-Koltun atomic models and 3.2 Å according to Fisher-Hirschfelder-Taylor atomic models).[16]

When pyridine was used as the D solvent in Cell I, a peculiar change in the glass electrode potential was observed, as is shown by the R_1 value in Fig. 2. Because the acid dissociation constants of the ammonium and pyridinium ions in acetonitrile are, as pK_a values, 16.5[11] and 12.6 respectively, the NH_4^++py→NH_3+pyH^+ reaction should occur to some extent. However our attempt to explain the behavior of the glass-electrode potential in terms of the above reaction was unsuccessful.

More complicated phenomena, including homo- and hetero-conjugations between ammonium ions and pyridine, may be occurring.[11]

The association of the univalent cation under investigation with the perchlorate ion may affect, at least theoretically, the complex formation constants of the cation with other solvents.[4-6] The association constant of the ammonium perchlorate in acetnitrile, which was determined conductometrically, was *ca.* 25 mol^{-1} dm^3, somewhat smaller than that of the thallium(I) perchlorate.[17] We determined the complex formation constant of the ammonium ion in acetonitrile with DMSO in the presence of varing concentrations of Et_4NClO_4 from 0 to 0.1 M. However no appreciable change in the formation constant was observed with the change in the concentration of Et_4NClO_4. These results suggest that the association of the ammonium ion with the perchlorate ion, which was detected by conductometric measurement, does not significantly affect the potentiometric results of the formation constants of complexes between the ammonium ion and solvent molecules.

The authors wish to thank Mr. Eiji Kubota of Shinshu University for his kindness in analyzing the conductivity data with a computer. They also wish to thank the staff of the Tokyo University Computation Center and the Shinshu University Remote Batch Computation Center for the use of their computers.

The present work was partially supported by a Grant-in-Aid for Scientific Research from the Ministry of Education (No. 247031).

References

1) G. W. Stockton and J. S. Martin, *J. Am. Chem. Soc.*, **94**, 6921 (1972).
2) I. D. Kuntz, Jr., and C. J. Cheng, *J. Am. Chem. Soc.*, **97**, 4852 (1975).
3) M. K. Chantooni, Jr., and I. M. Kolthoff, *J. Am. Chem, Soc.*, **89**, 1582 (1967).
4) K. Izutsu, T. Nomura, T. Nakamura, H. Kazama, and S. Nakajima, *Bull. Chem. Soc. Jpn.*, **47**, 1657 (1974).
5) T. Nakamura, *Bull. Chem. Soc. Jpn.*, **48**, 1447 (1975).
6) T. Nakamura, *Bull. Chem. Soc. Jpn.*, **49**, 1304 (1976).
7) C. J. Pedersen, *J. Am. Chem. Soc.*, **89**, 7017 (1967).
8) P. G. Sears, W. H. Fortune, and R. L. Blumenshine, *J. Chem. Eng. Data*, **11**, 406 (1966).
9) R. S. Drago, R. L. Carlson, and K. F. Purcell, *Inorg. Chem.*, **4**, 15 (1965).
10) I. M. Kolthoff and M. K. Chantooni, Jr., *J. Am. Chem. Soc.*, **87**, 4428 (1965).
11) J. F. Coetzee and G. R. Padmanabhan, *J. Am. Chem. Soc.*, **87**, 5005 (1965).
12) C. H. Springer, J. F. Coetzee, and R. L. Kay, *J. Phys. Chem.*, **73**, 471 (1969).
13) J. F. Coetzee and D. K. McGuire, *J. Phys. Chem.*, **67**, 1810 (1963).
14) I. M. Kolthoff and J. F. Coetzee, *J. Am. Chem. Soc.*, **79**, 870 (1957).
15) K. Angelis, M. Brězina, and J. Koryta, *J. Electroanal. Chem.*, **45**, 504 (1973).
16) H. K. Frensdorff, *J. Am. Chem. Soc.*, **93**, 600 (1971).
17) H. L. Yeager and B. Kratochvil, *J. Phys. Chem.*, **74**, 963 (1970).

Synthesis, Reactions and Catalytic Properties of Stable Alkoxocopper, Phenoxocopper and Related Copper Complexes Containing Triphenylphosphine Ligands

Minoru KUBOTA and Akio YAMAMOTO

Research Laboratory of Resources Utilization, Tokyo Institute of Technology, Nagatsuta, Midori-ku, Yokohama 227

(Received February 14, 1978)

A variety of new alkoxocopper and phenoxocopper(I) complexes containing triphenylphosphine ligands have been prepared by the reactions of methylbis(triphenylphosphine)copper(I) etherate (I) with the corresponding alcohols and phenols. The isolated complexes were characterized by elemental analysis, IR and NMR spectroscopy and chemical reactions. The reactions of the alkoxocopper and phenoxocopper complexes with alkyl halides and acyl halides or carboxylic anhydrides yield ethers and carboxylic esters, respectively. The stoichiometric exchange reactions of the alkoxo group in the alkoxocopper complexes with carboxylic esters proceed smoothly and the alkoxocopper complexes were found to act as excellent catalysts for the transesterifications between carboxylic esters and alcohols. The exchange reactions take place also between the alkoxocopper complexes and phenols or thiols producing phenoxocopper or alkylthiocopper complexes with the liberation of alcohols. Amides and nitromethane react with the alkoxocopper complexes releasing alcohols to give *N*-bonded amidocopper and *O*-bonded acinitrocopper complexes, respectively. The thermolysis of the alkoxocopper complexes in various solvents were studied and the mechanism and the factors influencing the course of thermolysis discussed.

The versatility of alkyl- and arylcopper(I) reagents in organic syntheses has been well established[1] but the utility of alkoxo- and phenoxocopper(I) complexes has been less explored.[2] There are only a few reported examples of well characterized alkoxocopper compounds. Poorly characterized copper methoxide has been reported to be thermally unstable and explosive.[3] *t*-Butoxocopper provides the most stable example amongst the known alkoxocopper compounds without ligands and the reactions of copper *t*-butoxide have been studied.[5-7] Other primary and secondary alkoxides are less stable and they have been prepared by heterogeneous reactions *in situ* and characterized only through indirect means.[8] Copper phenoxide is more stable than the alkoxide and substituted and unsubstituted phenoxocopper compounds have been prepared and utilized for ether and ester syntheses.[9] Copper(II) alkoxides, copper(II) methoxides[3a,10] and copper(II) acetylacetonate methoxide[11] are known.

The remarkable stabilizing effect of tertiary phosphines on the thermal stability of alkylcopper compounds has been reported before.[12,13] The reactions of alcohols with the alkylcopper(I) complexes having tertiary phosphine ligands led to the preparation of a variety of stable alkoxocopper(I) complexes having tertiary phosphine ligands. The stabilizing effect of the tertiary phosphine ligands was also evident in the alkoxocopper complexes which provide convenient materials for studying the properties of the synthetically useful alkoxocopper complexes and allow examination of the mechanism of thermolysis of the alkoxocopper complexes and to compare the results with the thermolysis behavior of the alkylcopper complexes. This paper describes the synthesis and properties of the alkoxocopper complexes containing triphenylphosphine.

Results and Discussion

Synthesis of Alkoxocopper(I) Complexes with Triphenylphosphine Ligands. Methylbis(triphenylphosphine)-copper etherate, $CH_3Cu(PPh_3)_2 \cdot 0.5Et_2O$ (I)[12] reacts with alcohols and phenols to give alkoxo- and phenoxocopper complexes (II—XI) containing triphenylphosphine ligands. Some complexes include diethyl ether as the solvent of crystallization.

$$CH_3Cu(PPh_3)_2 \cdot 0.5Et_2O + ROH \xrightarrow{Et_2O} ROCu(PPh_3)_m(Et_2O)_n + CH_4 \quad (1)$$

R = Me (II), Et (III), Pr^n (IV), CH_2=CH-CH_2- (V), Pr^i (VI), $PhCH_2$- (VII)

Ethylene glycol reacts at one of the hydroxyl groups producing hydroxyethoxocopper complex (VIII):

$$CH_3Cu(PPh_3)_2 \cdot 0.5Et_2O + HOCH_2CH_2OH \xrightarrow{Et_2O} HOCH_2CH_2OCu(PPh_3)_2 + CH_4 \quad (2)$$

(VIII)

Phenol reacts similarly with I to give the known phenoxocopper complex prepared by different route.[9]

$$CH_3Cu(PPh_3)_2 \cdot 0.5Et_2O + PhOH \xrightarrow{Et_2O} PhOCu(PPh_3)_2 + CH_4 \quad (3)$$

(IX)

o-Formyl- and *o*-acetyl-substituted phenols afford six-membered chelates:

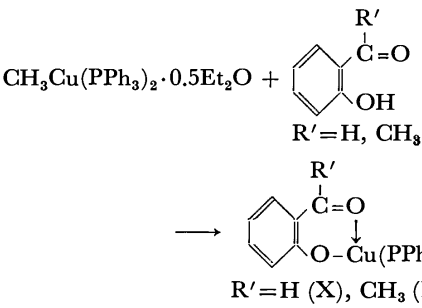

$R' = H, CH_3$

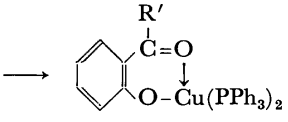

$R' = H$ (X), CH_3 (XI)

These reactions, 1—4, proceed smoothly at −10 to 0 °C evolving 1 mol equiv. of methane per mol of I to give white or yellow precipitate of II—XI in high yields.

Table 1 summarizes the yields, melting points, analytical results and molecular weights of the isolated copper complexes and Table 2 shows the relevant NMR and IR data. The alkoxocopper complexes are sensitive to oxygen and water but their thermal stabilities are substantially enhanced in comparison with the alkoxocopper compounds without triphenylphosphine as exemplified by the high melting point (dec) 65 °C of $CH_3OCu(PPh_3)_2 \cdot 0.5Et_2O$ compared with CH_3OCu which explodes on heating. The decomposition temperature of the series of alkoxocopper complexes rises with increasing alkyl chain length, a similar trend being observed in the thermal stabilities of alkylcopper complexes.[12] Albeit the alkoxocopper complexes have high decomposition temperatures in the solid state, they are less stable in solution and decompose in benzene at about 0 °C preventing the cryoscopic determination of the molecular weight in benzene. The reaction of I with ethylene glycol was expected to yield a bridged ethylene glycol derivative of copper. The molecular weight and analytical data of VIII together with the presence of the free ν(OH) band at 3300 cm^{-1} in the IR spectrum indicated that one of the two OH groups of ethylene glycol remains intact after reaction with I.

The phenoxocopper complexes showed much higher decomposition temperatures than the alkoxocopper complexes. The formation of the six-membered chelates in X and XI was deduced on the basis of the shifts of the ν(C=O) bands to lower frequencies (35 and 40 cm^{-1}) from those of the free salicylaldehyde and *o*-hydroxyacetophenone. These alkoxocopper complexes containing triphenylphosphine may also be obtained by the reaction of lithium or sodium alkoxide with bromobis(triphenylphosphine)copper, but the yield was poor and the purification of the product was more difficult than that of the complexes prepared by Eq. 1.

The phenoxocopper complex was prepared by the reaction of cuprous oxide with phenol in the presence of triphenylphosphine giving a yield of 59% based on copper.

$$Cu_2O + 2PhOH + 4PPh_3 \xrightarrow{75\,^\circ C \text{ in toluene}} 2PhOCu(PPh_3)_2 + H_2O$$
IX

The reaction required a higher temperature and a longer reaction period than the preparation starting from I.

The preparation of alkoxocopper complexes higher than butoxocopper was also attempted using I but the reaction was too slow to give the corresponding alkoxocopper complexes without the decomposition of the alkoxocopper complexes formed.

Reactions of Alkoxocopper Complexes. One of the features of the alkoxocopper complexes is the ability to exchange the alkoxo group. The alkoxo group bound to copper can be readily displaced by other components to give new organic copper complexes. The reactions appear to proceed smoothly, particularly when the product is more stable than the starting alkoxocopper complex. Thus, ethoxocopper complex III reacts with 1.5 equivalents of phenol in diethyl ether at 0 °C to

Table 1. Analytical data of alkoxocopper complexes

Complex		Yield (%)	Mp[a] (°C)	Analysis Found (Calcd) (%) C	H	*M.W.*[b] (Calcd)
$CH_3OCu(PPh_3)_2 \cdot 0.5Et_2O$	(II)	59	65 (dec)	71.2 (71.4	5.16 5.79)	
$CH_3CH_2OCu(PPh_3)_2$	(III)	72	88 (dec)	71.5 (72.1	5.51 5.53)	
$CH_3CH_2CH_2OCuPPh_3 \cdot 0.5Et_2O$	(IV)	77	89 (dec)	65.2 (65.5	6.26 6.41)	
$CH_2=CHCH_2OCu(PPh_3)_2$	(V)	66	98 (dec)	72.9 (72.6	5.47 5.43)	
$(CH_3)_2CHOCuPPh_3$	(VI)	79	118 (dec)	65.3 (65.5	5.45 5.72)	
$PhCH_2OCu(PPh_3)_2 \cdot Et_2O$	(VII)	72	145 (dec)	73.3 (73.4	5.68 6.18)	712±10 (768.5)
$HOCH_2CH_2OCu(PPh_3)_2$	(VIII)	76	123 (dec)	70.5 (70.3	5.20 5.40)	601±10 (648.5)
$PhOCu(PPh_3)_2$	(IX)	48	218	73.5 (74.0	5.04 5.14)	635±10 (680.5)
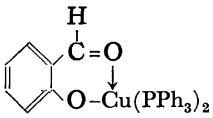	(X)	86	207—208 (dec)	73.2 (72.8	5.29 4.94)	659±10 (708.5)
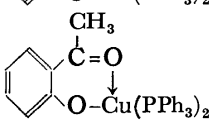	(XI)	76	179—180 (dec)	72.8 (73.1	5.19 5.12)	674±10 (722.5)

a) Measured in vacuum-sealed capillaries. b) Cryoscopic in benzene.

Table 2. ^{1}H-NMR and IR data of alkoxocopper complexes

Complex	^{1}H-NMR (solvents)		IR[a] (KBr disk) (cm^{-1})
II	δ 1.1 (t, 3H in Et_2O) δ 3.2(q, 2H in Et_2O) δ 3.4 (s, 3H in OCH_3) δ 7.0 (m, 18H in PPh_3)	δ 7.6 (m, 12H in PPh_3) (toluene-d_8, −20 °C)	ν (C–O) 1050 (m) and 985 (m)
III	δ 1.2 (t, 3H) δ 3.9 (q, 2H) δ 7.0 (m, 18H) δ 7.5 (m, 12H)	(toluene-d_8, −20 °C)	ν (C–O) 1105 (s) and 1045 (m)
IV	δ 0.85 (t, 3H) δ 1.1 (t, 3H in Et_2O) δ 1.6 (m, 2H) δ 3.2 (q, 2H in Et_2O)	δ 4.2 (q, 2H) δ 7.0 (m, 9H in PPh_3) δ 7.6 (m, 6H in PPh_3) (toluene-d_8, −32 °C)	ν (C–O) 1060 and 1020
V	δ 3.8 (m, 2H) δ 5.0 (m, 1H) δ 5.3 (m, 1H) δ 5.8 (m, 1H)	δ 7.0 (m, 18H in PPh_3) δ 7.4 (m, 12H in PPh_3) (toluene-d_8, −20 °C)	ν (C–O) 1140 (w), 1120 (w) or 1010 (w)
VI	δ 1.3 (d, 6H) δ 4.5 (m, 1H) δ 7.0 (m, 9H in PPh_3) δ 7.7 (m, 6H in PPh_3)	(toluene-d_8, −30 °C)	ν (C–O) 1125 (s)
VII	δ 1.1 (t, 6H in Et_2O) δ 3.2 (q, 4H in Et_2O) δ 5.0 (s, 2H) δ 7.0 (m, 18H in PPh_3 and 5H in Ph)	δ 7.4 (m, 12H in PPh_3) (toluene-d_8, −32 °C)	ν (C–O) 1100 (m)
VIII	δ 4.1 (m, 4H) δ 5.7 (s, 1H broad) δ 7.1 (m, 18H in PPh_3) δ 7.5 (m, 12H in PPh_3)	(benzene-d_6, r.t.)	ν (O–H) 3300 (s, broad) ν (C–O) 1070 (vs)
IX	δ 6.5—6.9 (m, 4H in PhO group) δ 7.0 (m, 18H in PPh_3 and 1H in PhO group) δ 7.6 (m, 12H in PPh_3)	(benzene-d_6, r.t.)	ν (C=C) 1580 (s) ν (C–O) 1270 (s), 1150 (m)
X	δ 7.0 (m, 18H in PPh_3 and 2H in phenoxo group) δ 7.6 (m, 12H in PPh_3 and 2H in phenoxo group) δ 9.26 (s, 1H)	(benzene-d_6, r.t.)	ν (C=O) 1630 (vs) ν (C–O) 1230 (w), 1140 (s) or 1015 (m)
XI	δ 2.12 (s, 3H) δ 7.0 (m, 18H in PPh_3 and 2H in phenoxo group) δ 7.6 (m, 12H in PPh_3 and 2H in phenoxo group)	(benzene-d_6, r.t.)	ν (C=O) 1603 (vs) ν (C–O) 1245 (m), 1205 (s) or 1025 (w)

a) vs=very strong, s=strong, m=medium, w=weak.

produce the more thermally stable phenoxocopper complex IX in high yield:

$$\underset{\text{III}}{EtOCu(PPh_3)_2} + PhOH \longrightarrow \underset{\text{IX (78\%)}}{PhOCu(PPh_3)_2} + \underset{\text{(85\%)}}{EtOH}$$

Such alcohol exchange reactions have been extensively utilized in the preparation of new alkoxides of Al, Ge, Sn, Ti, Zr, Hf, Nb, Ta, Fe, La, Th, U, and Pu.[14]

Similarly thiols react smoothly with the ethoxocopper complex with the liberation of ethanol:

$$EtOCu(PPh_3)_2 + EtSH \longrightarrow \underset{\text{XII (82\%)}}{EtSCu(PPh_3)_2} + \underset{\text{(89\%)}}{EtOH}$$

An amide also is exchanged with the alkoxocopper complex quite readily. Complex III reacts with an equivalent amount of acetanilide in diethyl ether at 0 °C to produce the thermally stable (acetanilido-*N*)-bis(triphenylphosphine)copper (XIII) and ethanol:

$$EtOCu(PPh_3)_2 + PhNHCOCH_3 \longrightarrow \underset{\text{XIII (65\%)}}{\begin{matrix}Ph\\ \diagdown\\ \quad N\text{–}Cu(PPh_3)_2\\ \diagup\\ CH_3CO\end{matrix}} + \underset{\text{(72\%)}}{EtOH}$$

The ν(C=O) band in XIII was observed at 1685 cm^{-1}

with scarcely any shift from that of the free acetanilide suggesting the *N*-bonded structure.

Furthermore, the alkoxocopper complex reacts with active methylene compounds such as nitromethane and acetylacetone to afford the known complexes XIV and XV:[15,16]

$$\underset{\text{III}}{EtOCu(PPh_3)_2} + CH_3NO_2 \longrightarrow (CH_2NO_2)Cu(PPh_3)_2 + EtOH$$
$$\text{XIV (82\%)} \qquad (87\%)$$

$$EtOCu(PPh_3)_2 + Hacac \longrightarrow (acac)Cu(PPh_3)_2 + EtOH$$
$$\text{XV (74\%)} \qquad (80\%)$$

The reactive alkoxocopper complexes function as a transesterification reagent for various carboxylic esters. The reaction of the ethoxocopper complex III with methyl methacrylate, for example proceeds smoothly below room temperature to yield ethyl methacrylate and the methoxocopper complex II in high yields:

$$EtOCu(PPh_3)_2 + CH_2{=}C(CH_3)COOMe \longrightarrow CH_2{=}C(CH_3)COOEt + MeOCu(PPh_3)_2\cdot 0.5Et_2O$$
$$(89\%) \qquad\qquad \text{II (78\%)}$$

Related transesterification reactions between carboxylic esters and metal alkoxides such as tin,[17] aluminium,[18] zirconium, hafnium,[19] and titanium[19,20] are known.

In the transesterification reaction of carboxylic esters with alkoxocopper and phenoxocopper complexes it has been noted that reactive alkoxocopper complexes such as methoxo- and ethoxocopper complexes undergo transesterification with a variety of carboxylic esters but the more stable complexes are less reactive. Thus, the phenoxocopper complex failed to react with ethyl acetate, benzyl acetate, allyl acetate, and vinyl acetate, whereas the ethoxocopper complex III underwent the transesterification with all of these esters to give excellent to moderate yields. The reactions of III with vinyl and isopropenyl acetates proceed beyond the simple transesterification and give the known C-bonded 1-acetoxyvinyl and 1-acetoxy-1-methylvinylcopper complexes[21] together with by-product acetatocopper complex in high yields:

$$EtOCu(PPh_3)_2 + CH_2{=}C(R)OCOCH_3 \quad (R=H,\ CH_3)$$
$$\xrightarrow{CH_3COOEt} [CH_2{=}CROCu(PPh_3)_2] \xrightarrow{CH_2=C(R)OCOCH_3}$$

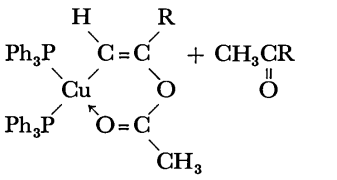

$$R=H\ (XVI),\ CH_3\ (XVII)$$

Furthermore, the alkoxocopper complexes serve as excellent catalysts for transesterification between various esters and alcohols. The transesterification reactions of alkyl methacrylates, alkenyl acetates, alkyl acetates, alkyl benzoates, aryl acetates, alkyl carbonates, and alkyl phosphites with alcohols are catalyzed by small amounts of the alkoxocopper complexes under very mild conditions.

$$CH_2{=}C(CH_3)COOMe + EtOH \xrightarrow[-5\,^\circ C]{EtOCu(PPh_3)_2} CH_2{=}C(CH_3)COOEt + MeOH$$
$$\text{conversion} = 73\%$$

Since the catalytic reactions proceed cleanly under mild and neutral conditions, the alkoxocopper complexes provide some synthetic utility.

Reactions of organic halides with copper alkoxides without the tertiary phosphine ligands have been examined by Whitesides[8] and Hashimoto,[9] and the formation of various ethers has been reported. The alkoxo- and phenoxocopper complexes prepared in the present study react readily with organic halides producing ethers.

$$\underset{\text{III}}{EtOCu(PPh_3)_2} + Bu^nCl \xrightarrow{-5\,^\circ C,\ Et_2O} CH_3OBu^n \quad (36\%)$$

$$\underset{\text{VIII}}{HOCH_2CH_2OCu(PPh_3)_2} + MeI \xrightarrow{-30\text{--}10\,^\circ C} HOCH_2CH_2OMe \quad (76\%)$$

$$\underset{\text{IX}}{PhOCu(PPh_3)_2} + MeI \xrightarrow{\text{room temp}} PhOMe \quad (99\%)$$

The reactions of the alkoxocopper complexes with acyl chloride have been further examined. Complex III reacts readily with propionyl chloride to produce ethyl propionate in good yield:

$$EtOCu(PPh_3)_2 + CH_3CH_2COCl \longrightarrow CH_3CH_2COOEt \quad (82\%)$$

Reaction of the ethoxocopper complex III with acetic anhydride also produces ethyl acetate and the known acetatocopper complex XVI in good yields.

$$EtOCu(PPh_3)_2 + (CH_3CO)_2O \longrightarrow CH_3COOEt + CH_3COOCu(PPh_3)_2$$
$$76\% \qquad\qquad \text{XVIII (72\%)}$$

Similar reactions of metal alkoxides with acyl halides and acid anhydrides have been reported.[22,23]

Thermal Decomposition of Alkoxocopper Complexes. In contrast to the copper alkoxides without tertiary phosphine the thermal stabilities of the present alkoxocopper complexes with triphenylphosphine ligands are considerably enhanced. For a comparison of the thermolysis behavior of simple copper alkoxides with that of phosphine-stabilized alkoxocopper complexes the thermolysis products in various media were examined and compared with those reported by Whitesides (Table 3).

Table 3. Thermal decomposition of alkoxocopper complexes[a)]

Complex	Solvent (H donor ability)[b)]	Alcohol/[c)] Carbonyl	Product balance, %
$CH_3CH_2OCu(PPh_3)_2$ (III)	benzene (0.0004)	9.4	92
	toluene (1.0)	16.8	89
	THF (23)	22.3	95
$CH_3CH_2CH_2OCuPPh_3 \cdot 0.5Et_2O$ (IV)	benzene (0.0004)	11.7	89
	THF (23)	18.2	92
$CH_2=CHCH_2OCu(PPh_3)_2$ (V)	benzene (0.0004)	5.2	95
	THF (23)	13.2	99
$(CH_3)_2CHOCuPPh_3$ (VI)	benzene (0.0004)	4.7	86
	toluene (1.0)	4.3	90
	THF (23)	20.5	93
$PhCH_2OCu(PPh_3)_2 \cdot Et_2O$ (VII)	benzene (0.0004)	1.0	96
	toluene (1.0)	1.2	85
	THF (23)	3.0	93
	toluene and styrene[d)] (1:1)	3.2	87
$PhOCu(PPh_3)_2$ (IX)	in the solid state[e)]	only PhOH	89

a) Alkoxocopper complexes (0.20 g) in 2 ml of various solvents were heated at the boiling points or at 100 °C for 30 min in a closed system. b) The method used to estimate these numbers is described in Ref. 8. c) "Alcohol/carbonyl" in the ratio of the alcohol- and carbonyl-containing products derived from the alkoxo moiety of the alkoxocopper complexes. d) Ethyl benzene (10% per Cu) was detected. e) The phenoxocopper complex was heated above decomposition point in a closed system for 30 min.

The alkoxocopper complexes liberate alcohols, aldehydes or ketones on thermolysis, the former being produced in higher yields relative to those of the carbonyl-containing products. Two principal pathways are possible in the thermolysis of the secondary and primary alkoxocopper complexes. One involves the β-elimination mechanism forming aldehyde and copper hydride which may further react with another alkoxocopper complex to produce an alcohol. The other involves the homolytic splitting of the Cu–O bond producing alkoxy radicals which either disproportionate to the alcohol and aldehyde or abstract hydrogen from the solvent to generate the alcohol. Table 3 indicates the effects of solvents with different hydrogen atom donating abilities on the alcohol/carbonyl ratio. It can be seen that an effective hydrogen donor such as tetrahydrofuran significantly increased the ratio. The result as a whole agrees with the result of Whitesides who used copper alkoxide without the tertiary phosphine ligands and is compatible with the homolytic cleavage of the RO–Cu bond, although the formation of a "free radical" in the homolysis remains to be established. In the benzyloxocopper complex VII the decomposition behavior seems to be somewhat different from that of the rest of the complexes. Furthermore, when the thermolysis was carried out in the presence of styrene, a significant amount of ethylbenzene was produced. The result may be taken as an indication of the presence of β-hydrogen elimination in thermolysis of VII.

Experimental

All preparations, recrystallizations and reactions of copper complexes were carried out under deoxygenated nitrogen, argon, or in a vacuum. Solvents were dried by the usual procedures, distilled and stored under argon or nitrogen. IR spectra were recorded on a Hitachi Model 295 spectrometer using KBr discs under nitrogen. ^{1}H-NMR spectra were recorded with a Japan Electron Optics Lab. JNM-PS 100 spectrometer (TMS as internal standard). Evolved gas was analyzed with a Hitachi RMU 5B mass-spectrometer and a Shimadzu GC-5B gas chromatograph, and the volume measured with a Toepler pump. The microanalysis of carbon, hydrogen and nitrogen was performed by Mr. T. Saito in this laboratory with a Yanagimoto CHN Autocorder Type MT-2.

Preparation of Methoxobis(triphenylphosphine)copper(I) Etherate (II) and Related Alkoxocopper Complexes III, IV, V, VI, and VII. Methanol (109 μl, 3.2 mmol) was added to the methylcopper complex, $CH_3Cu(PPh_3)_2 \cdot 0.5Et_2O$ (I) (1.732 g, 2.706 mmol) suspended in diethyl ether (5 ml). After stirring the yellow suspension at -10 to 0 °C for a day a white precipitate was produced with the evolution of methane (0.92 mol per mol of Cu). The white precipitate was recrystallized from a mixture of diethyl ether and methanol to give II (1.047 g).

Other alkoxocopper complexes: III, IV, V, VI, and VII were prepared by the reaction of I with the corresponding alcohols in a similar way to that for II.

Preparation of (2-Hydroxyethoxo)bis(triphenylphosphine)copper (VIII). Ethylene glycol (16 mmol) was added to I(1.682 g, 2.63 mmol) suspended in diethyl ether (5 ml). After stirring the yellow suspension at -10 °C for 0.5 h a white precipitate was produced with the evolution of methane (0.92 mol per mol of Cu). The white precipitate was recrystallized from a mixture of toluene and ethylene glycol to give VIII (1.279 g).

Preparation of Phenoxobis(triphenylphosphine)copper (IX). Phenol (0.188 g, 2 mmol) was added to I (1.280 g, 2 mmol) suspended in diethyl ether (10 ml). The yellow suspension was stirred at 0 °C for 20 min to produce a white precipitate with the evolution of 1.0 mol of methane per Cu. Recrystal-

lization of the precipitate from toluene afforded white crystals of IX (0.653 g).

Preparation of IX from Cu_2O, PhOH, and PPh_3. A mixture of Cu_2O (0.143 g, 1 mmol), PhOH (0.190 g, 2 mmol), and PPh_3 (1.05 g, 4 mmol) in toluene (10 ml) was heated at 75 °C for 10 h. The gray precipitate produced was recrystallized from toluene to give $PhOCu(PPh_3)_2$ (IX) (0.803 g, yield 59% based on Cu_2O).

Preparation of (o-Formylphenoxo)bis(triphenylphosphine)copper (X) and (o-Acetylphenoxo)bis(triphenylphosphine)copper (XI). Salicylaldehyde (1.5 mmol) was added to I (0.944 g, 1.475 mmol) suspended in diethyl ether (10 ml). On stirring the yellow emulsion at −10—0 °C for 1 h an orange precipitate was produced with the evolution of methane (0.86 mol per mol of Cu). The precipitate was recrystallized from toluene to give orange crystals of X (0.899 g).

Complex XI (0.549 g) was prepared by the reaction of I (0.64 g, 1 mmol) with *o*-hydroxyacetophenone (1 mmol) in a similar way to the preparation of complex X.

Reaction of III with Phenol. Phenol (0.48 mmol) was added to III (0.20 g, 0.32 mmol) suspended in diethyl ether (2 ml). After stirring the white suspension at −5 to 0 °C for 10 h a clear supernatant and precipitate were produced. The formation of ethanol (yield 85% per Cu) was confirmed in the supernatant by GLC analysis. The precipitate was recrystallized from toluene to give white crystals of IX (0.168 g, yield 78%) which was identified on the basis of its IR spectrum.

Reaction of III with Ethanethiol. The reaction of III (0.20 g, 0.32 mmol) with ethanethiol (0.48 mmol) in diethyl ether (2 ml) at −5 to 0 °C for 10 h produced a white precipitate and released ethanol (yield 89% based on Cu). The precipitate was crystallized from toluene to give white crystals of XII (0.168 g, yield 82%); mp 139 °C (dec). Found: C, 70.4; H, 5.3; S, 5.1%. Calcd for $C_{38}H_{35}P_2SCu$: C, 70.4; H, 5.4; S, 4.9%. IR(KBr): 2950 w, 2900 w, 2850 w, 1235 m cm^{-1} and other absorptions due to PPh_3 ligands. ^{1}H-NMR (C_6D_6, r.t.): δ 1.2 (t, 3H), 2.8 (q, 2H), 7.1 (m, 18H, *m,p*-phenyl), 7.5 (m, 12H, *o*-phenyl).

Reaction of III with Acetanilide. The reaction of III (0.100 g, 0.158 mmol) with acetanilide (0.158 mmol) in diethyl ether (2 ml) at 0 °C for 24 h liberated ethanol (yield 72% based on Cu) to give a precipitate which on recrystallization from a mixture of diethyl ether and toluene afforded white crystals of XIII (0.074 g, yield 65%). Complex XIII, mp 151 °C (dec). Found: C, 72.7; H, 5.5; N, 2.4%. $C_{34}H_{38}ONP_2Cu$ calcd for: C, 73.2; H, 5.3; N, 1.9%. IR(KBr): 1680 m, 1585 m, 1510 s, 1490 s, 1450 w, 1240 m, 940 m, 800 m, 580 w, cm^{-1} and other absorptions to PPh_3. ^{1}H-NMR (C_6D_6, r. t.): δ 2.16 (s, 3H), 7.0 (m, 23H, 18H of *m,p*-phenyl of PPh_3 and 5H of phenyl), 7.6 (m, 12H, *o*-phenyl of PPh_3).

Reaction of III with Nitromethane and Acetylacetone. Nitromethane (1 ml) was introduced into a Schlenk type flask containing III (0.100 g, 0.158 mmol) in diethyl ether (1 ml) by a trap-to-trap distillation in a vacuum. After stirring the white emulsion at −20 to 0 °C for 24 h a white precipitate was produced with liberation of ethanol (yield 87% per Cu). The precipitate was repeatedly washed with THF and dried in a vacuum to give the white complex XIV (0.084 g, yield 82%) which was characterized as nitromethanidobis(triphenylphosphine)copper(I) on the basis of its IR and ^{1}H-NMR spectra. $(CH_2NO_2)Cu(PPh_3)_2$ (XIV), IR(KBr): ν(C=N), 1562 s, 1550 m; $\nu(NO_2$, asym), 1250 s; $\nu(NO_2$, sym), 952 s cm^{-1}. ^{1}H-NMR (CD_2Cl_2): δ 5.76 (s, 2H, CH_2), 7.1 (m, 30H, $2PPh_3$).

The reaction of III (0.20 g, 0.32 mmol) with acetylacetone (1 ml) was carried out in a similar way to give a white precipitate with the liberation of ethanol (80% per Cu). Recrystallization from diethyl ether gave acetylacetonatobis(triphenylphosphine)copper(I) (0.163 g, yield 74%).[16] (acac)Cu$(PPh_3)_2$ (XV), IR(KBr): ν(C=O), 1598 vs cm^{-1}. ^{1}H-NMR (C_6D_6): δ 2.04 (s, 6H, $2CH_3$), 5.56 (s, 1H), 7.1 (m, 18H, *m,p*-phenyl), 7.7 (m, 12H, *o*-phenyl).

Exchange Reaction of III with Methyl Methacrylate. A suspension of III (0.20 g, 0.32 mmol) in diethyl ether (2 ml) was treated with methyl methacrylate (0.32 mmol) at −5 °C for 12 h. Formation of ethyl methacrylate (yield 89% based on Cu) was confirmed by gas chromatographic analysis. The precipitate formed after the reaction was characterized as II (yield 78%) on the basis of its IR spectrum.

Reaction of III with Vinyl Acetate and Isopropenyl Acetate. Vinyl acetate (2 ml) was introduced into a Schlenk type flask containing III (0.20 g, 0.32 mmol) by a trap-to-trap distillation in a vacuum. After stirring the white emulsion at −5 to 0 °C for 12 h, ethyl acetate (yield 97% based on Cu), acetaldehyde (yield 15% based on Cu) and a small amount of polyvinyl acetate were produced besides a white precipitate. The precipitate was recrystallized from THF to give white crystals (174 mg, yield 81% based on Cu) of 1-acetoxyvinylbis(triphenylphosphine)copper[21](XVI) which was identified by IR and ^{1}H-NMR spectroscopy. Complex XVI, IR(KBr): ν(C=O) 1605 cm^{-1}. ^{1}H-NMR (C_6D_6): δ 1.92 (s, 3H, CH_3); 5.23 (d, 1H, J=7 Hz, =CH); δ 7.0 (m, 18H, *m,p*-phenyl); 7.6 (m, 12H, *o*-phenyl); 8.62 (d, 1H, J=7 Hz, =CH).

The reaction of III (0.20 g, 0.32 mmol) with isopropenyl acetate (2 ml) was carried out in a similar way to that of vinyl acetate to produce ethyl acetate, acetone and a precipitate (180 mg) containing 1-acetoxy-1-methylvinylbis(triphenylphosphine)copper[21](XVII) and acetatobis(triphenylphosphine)copper[21] (XVIII) which were identified by IR and ^{1}H-NMR spectroscopy. Complex XVII, IR(KBr): ν(C=O) 1595 cm^{-1}. ^{1}H-NMR (C_6D_6): δ 2.0 (s, 6H, $OCOCH_3$ and CH_3); 5.42 (s, 1H); 7.0 (m, 18H, *m,p*-phenyl); 7.6 (m, 12H, *o*-phenyl). Complex XVIII, IR(KBr): ν(OCO, asym), 1550; ν(OCO, sym), 1413; δ(OCO, sym), 667 cm^{-1}. ^{1}H-NMR (C_6D_6): δ 2.36 (s, 3H, CH_3); 7.0 (m, 18H, *m,p*-phenyl); 7.6 (m, 12H, *o*-phenyl).

Catalytic Transesterification Reaction Using III. Complex III (0.100 g, 1.06 mmol) was dissolved in a mixture of methyl methacrylate (0.73 ml, 6.77 mmol) and ethanol (5 ml) and the solution stirred at −5 °C for 24 h. Ethyl methacrylate was identified by gas chromatographic analysis of the reaction mixture (yield 73%).

Reaction of Alkoxocopper Complexes with Alkyl Halides. A measured amount of an alkyl halide was introduced into a Schlenk type flask containing the alkoxocopper complex by a trap-to-trap distillation in a vacuum or by means of a syringe at −30 °C. The reaction mixture was stirred for 12 to 24 h below 0 °C. The amount of ether formed in the reaction was determined by means of gas chromatography.

Reaction of III with Propionyl Chloride. Propionyl chloride (0.458 mmol) was added to III (0.20 g, 0.32 mmol) suspended in diethyl ether (2 ml). After stirring the white suspension at −5 °C for 2 h ethyl propionate (yield 82% per Cu) was produced.

Reaction of III with Acetic Anhydride. Acetic anhydride (0.458 mmol) was added to III (0.20 g, 0.32 mmol) suspended in diethyl ether (2 ml). After stirring the white suspension at −5 °C to r.t. for 24 h a white precipitate and ethyl acetate (yield 76% per Cu) were produced. The precipitate was crystallized from THF to give white crystals which were characterized as $CH_3COOCu(PPh_3)_2$ (XVIII) (yield 72%) on the basis of its IR and ^{1}H-NMR spectra.

References

1) (a) P. E. Fanta, *Chem. Rev.*, **64**, 613 (1964); (b) R. G. R. Bacon and H. A. O. Hill, *Quart. Rev., Chem. Soc.*, **19**, 95 (1965); (c) R. G. Bacon and O. J. Stewart, *J. Chem. Soc., C*, **1969**, 301; (d) J. F. Normant, *Synthesis*, **1972**, 63.

2) (a) H. Weingarten, *J. Org. Chem.*, **29**, 977 (1964); (b) H. Weingarten, *ibid.*, **29**, 3624 (1964).

3) (a) G. Costa, A. Camus, and N. Marsich, *J. Inorg. Nucl. Chem.*, **27**, 281 (1965); (b) The presence of copper(I) methoxide is implicated in methanolysis of methyl copper. C. E. H. Bawn and F. J. Whitby, *J. Chem. Soc.*, **1960**, 3926.

4) T. Tsuda, T. Hashimoto, and T. Saegusa, *J. Am. Chem. Soc.*, **94**, 658 (1972).

5) (a) T. Tsuda, T. Nakatsuka, T. Hirayama, and T. Saegusa, *J. Chem. Soc., Chem. Commun.*, **1974**, 557; (b) T. Tsuda, T. Nakatsuka, and T. Saegusa, The Twenty Second Symposium on Organometallic Chemistry Japan, Kyoto, 1974, Abstr. 211A.

6) T. Tsuda, H. Habu, S. Horiguchi, and T. Saegusa, *J. Am. Chem. Soc.*, **96**, 5930 (1974).

7) T. Tsuda, S. Sanada, and T. Saegusa, *J. Organomet. Chem.*, **116**, C10 (1976).

8) G. M. Whitesides, J. S. Sadowski, and J. Liburn, *J. Am. Chem. Soc.*, **96**, 2829 (1974).

9) (a) T. Kawaki and H. Hashimoto, *Bull. Chem. Soc. Jpn.*, **45**, 1499 (1972); (b) W. T. Reichle, *Inorg. Chim. Acta*, **5**, 325 (1971).

10) C. H. Brubaker, Jr., and M. Wicholas, *J. Inorg. Nucl. Chem.*, **27**, 59 (1965).

11) J. A. Bertrand and R. I. Kaplan, *Inorg. Chem.*, **4**, 1657 (1965).

12) (a) A. Yamamoto, A. Miyashita, T. Yamamoto, and S. Ikeda, *Bull. Chem. Soc. Jpn.*, **45**, 1583 (1972); (b) A. Miyashita and A. Yamamoto, *Bull. Chem. Soc. Jpn.*, **50**, 1102 (1977); (c) A. Miyashita, T. Yamamoto, and A. Yamamoto, *Bull. Chem. Soc. Jpn.*, **50**, 1109 (1977).

13) T. Ikariya and A. Yamamoto, *J. Organomet. Chem.*, **72**, 145 (1975).

14) D. C. Bradley, "Progress in Inorganic Chemistry," ed by F. A. Cotton, Interscience Publishers New York (1960), Vol. 2, p. 303 and references therein.

15) (a) A. Camus, N. Marsich, G. Nardine, and L. Landaccio, *Inorg. Chim. Acta*, **17**, L33 (1976); (b) N. Marsich and A. Camus, *J. Inorg. Nucl. Chem.*, **39**, 275 (1977).

16) (a) N. Marsich and A. Camus, *J. Organomet. Chem.*, **81**, 87 (1974); (b) F. Cariati, and L. Nardini, *Gazz. Chim. Ital.*, **95**, 3 (1965); (c) D. Gibson, B. F. G. Johnson, and J. Lewis, *J. Chem. Soc., A*, **1970**, 367; (d) T. Yamamoto, M. Kubota, A. Miyashita, and A. Yamamoto, *Bull. Chem. Soc. Jpn.*, **51**, 1835 (1978).

17) (a) B. Delmond, J. C. Pommier, and J. Valade, *Tetrahedron Lett.*, **1969**, 2089; (b) A. J. Bloodworth and A. G. Davies, *Chem. Ind. (London)*, **1972**, 490.

18) (a) R. H. Baker, *J. Am. Chem. Soc.*, **60**, 2673 (1938); (b) C. Barkenbus, M. B. Naff, and K. E. Rapp, *J. Org. Chem.*, **19**, 1316 (1954).

19) R. C. Mehrotra, *J. Am. Chem. Soc.*, **76**, 2266 (1954).

20) D. C. Bradley and I. M. Thomas, *Chem. Ind. (London)*, **1958**, 1231.

21) M. Kubota, A. Miyashita, S. Komiya, and A. Yamamoto, *J. Organomet. Chem.*, **139**, 111 (1977).

22) (a) J. S. Jennings, W. Wardlaw, and W. J. R. Way, *J. Chem. Soc. (London)*, **1936**, 637; (b) D. C. Bradley, D. C. Hancock, and W. Wardlaw, *J. Chem. Soc. (London)*, **1952**, 2773.

23) (a) R. C. Mehrotra and K. C. Pande, *Z. Anorg. Allg. Chem.*, **286**, 291 (1956); (b) *ibid.*, **290**, 95 (1957).

Mixed Ligand Complexes of Copper(II)-1-(2-Pyridylazo)-2-naphthol with Bidentate Ligands

Hiroko WADA,* Kazuyoshi IKUTA, and Genkichi NAKAGAWA*

Laboratory of Analytical Chemistry, Nagoya Institute of Technology, Gokiso-cho, Showa-ku, Nagoya 466

(Received February 23, 1978)

Formation constants of mixed ligand complexes of copper(II)–1-(2-pyridylazo)-2-naphthol chelate (Cu(pan)) with bidentate ligands, which accelerate the rate of color change of 1-(2-pyridylazo)-2-naphthol (PAN) indicator in copper(II)–EDTA titrations, were determined by the spectrophotometric method in 5 or 10% v/v dioxane–H_2O at μ=0.1 (KNO_3) and at 25 °C. The overall formation constants ($\log K^{\text{pan.L}}_{\text{Cu(pan)L}}$=log ([Cu(pan)L]/[Cu][L][pan]) are 21.26 (5% dioxane) for 2,2′-bipyridine, 21.64 (10% dioxane) for ethylenediamine, 22.80 (5% dioxane) for 8-hydroxy-5-quinolinesulfonic acid, 19.39 (10% dioxane) for glycine, and 20.68 (10% dioxane) for iminodiacetic acid. These ligands coordinate with Cu(pan) chelate as bidentate ligands, and the mixed ligand complexes may have a distorted octahedron structure. Thus the Cu–pan bond in the mixed ligand complex is weakened.

In the EDTA-titration of copper(II), 1,10-phenanthroline, 2,2′-bipyridine, ethylenediamine, 8-quinolinol, glycine, and iminodiacetic acid accelerate the rate of the color change of 1-(2-pyridylazo)-2-naphthol (PAN) indicator.[1] In a previous work[2] the mechanism of the acceleration by 1,10-phenanthroline was elucidated: *i.e.* the mixed ligand complex of Cu(pan) chelate with 1,10-phenanthroline is formed and undergoes a faster substitution with EDTA than does Cu(pan) chelate. In the present paper the composition and the formation constants of the mixed ligand complexes of Cu(pan) chelate with 2,2′-bipyridine(bpy), ethylenediamine-(en), 8-hydroxy-5-quinolinesulfonic acid(Hoxs), glycine (Hgly), and iminodiacetic acid (H_2ida) are reported.

Experimental

Reagents. The copper(II) solution and the Hpan solution were the same as those used in previous work.[2] Reagent grade chemicals were purified by recrystallization. A 2,2′-bipyridine dioxane solution, and ethylenediamine aqueous solution, a glycine aqueous solution, a 8-hydroxy-5-quinolinesulfonic acid alkaline aqueous solution, and an iminodiacetic acid aqueous solution were used. The ionic strength was maintained constant with potassium nitrate. Dioxane was purified as described in the previous paper.[2] Buffer solutions: 0.02 M 2-morpholino-1-ethanesulfonic acid (MES)–NaOH buffer for pH 4—7, and 0.01 M disodium tetraborate–HNO_3 or NaOH buffer for pH 7.5—11 were used.

Apparatus. A Hitachi 124 Spectrophotometer, a Hitachi 356 Two-wavelength Spectrophotometer, a Radiometer PHM 26 pH meter equipped with a Radiometer G202B glass electrode and a K401 calomel electrode (saturated KCl), and a Hitachi-Horiba F-5 pH meter equipped with an Orion 94-29A copper(II) ion-selective electrode or a Hitachi-Horiba 1026-05T glass electrode and a Hitachi-Horiba 2080-05T calomel electrode (3.3 M KCl) were used. These glass electrodes were calibrated with the two standard buffers: 0.025 M KH_2PO_4 +0.025 M Na_2HPO_4 and 0.05 M $KH_3(C_2O_4)_2\cdot 2H_2O$, 0.05 M $KHC_6H_4(COO)_2$, 0.05 M $Na_2B_4O_7\cdot 10H_2O$ or saturated (25 °C) $Ca(OH)_2$.

Procedure. All measurements were carried out in 5 or 10% v/v dioxane–water media, depending upon the solubility of mixed ligand complexes, at an ionic strength of 0.1 M (KNO_3) and at 25±1 °C. The acid dissociation constants and the formation constants of copper(II) complexes of the ligands (bpy, en, Hoxs, Hgly, H_2ida) were determined under the same conditions as those employed for the determination of the formation constants of mixed ligand complexes. All constants determined are written in the form of mixed constants involving hydrogen ion activity.

Determination of the Acid Dissociation Constants of the Ligands and the Formation Constants of the Cu(II) Complexes. The acid dissociation constant of protonated 2,2′-bipyridine (Hbpy) was determined by a spectrophotometric method. The acid dissociation constants of protonated ethylenediamine (H_2en), 8-hydroxy-5-quinolinesulfonic acid (H_2oxs), glycine (H_2gly), and iminodiacetic acid (H_2ida), and the formation constants of Cu–ida complexes were determined by the pH-tritration with a NaOH standard solution. The formation constants of Cu–bpy, Cu–en, Cu–oxs, and Cu–gly complexes were determined by the potentiometric method with a copper(II) ion-selective electrode.[3] The acid dissociation constants of the ligands and the formation constants of the copper(II) complexes are summarized in Table 1.

Determination of the Formation Constants of the Mixed Ligand Complexes. The formation constant of a mixed ligand complex is defined by Eq. 1. Charges are omitted for simplicity.

TABLE 1. EQUILIBRIUM CONSTANTS OF LIGANDS (L)
25 °C, μ=0.1 (KNO_3)

Ligand (L)	pk_1	pk_2	Method[a]	$\log\beta_{\text{CuL}}$	$\log\beta_{\text{CuL}_2}$	$\log\beta_{\text{CuL}_3}$	Method[a]	Dioxane (%)
bpy	4.37		3	8.59	14.09	17.84	2	5
en	7.14	9.98	1	10.56	19.55		2	10
Hoxs	3.90	8.82	1, 3	11.86	21.87		2	5
Hgly	2.52	9.40	1	8.12	14.71		2	10
H_2ida	2.86	9.51	1	10.93	16.67		1	10

a) Method 1: pH titration, Method 2: potentiometry with Cu(II) ion-selective electrode, Method 3: spectrophotometry.

$$\beta_{Cu(pan)L_n} = \frac{[Cu(pan)L_n]}{[Cu(pan)][L]^n}, \quad (1)$$

where L represents the free ligand. The conditional formation constant of Cu–pan complexes, taking into account the formation of mixed ligand complexes, is given by

$$K_{(Cupan)'} = \frac{[(Cupan)']}{[Cu'][pan']} = \frac{K_{Cupan}\alpha_{Cupan(L)}}{\alpha_{Cu(L)}\alpha_{pan(H)}}, \quad (2)$$

where

$$[(Cupan)'] = [Cu(pan)] + [Cu(pan)L] + [Cu(pan)L_2] + \cdots + [Cu(pan)L_n], \quad (3)$$

$$K_{Cupan} = \frac{[Cu(pan)]}{[Cu][pan]}, \quad (4)$$

$$\alpha_{Cupan(L)} = 1 + \sum_{n=1}^{n} \beta_{Cu(pan)L_n}[L]^n, \quad (5)$$

$$\alpha_{Cu(L)} = 1 + \sum_{m=1}^{m} \beta_{CuL_m}[L]^m, \quad (6)$$

$$\alpha_{pan(H)} = 1 + \frac{[H]}{k_2} + \frac{[H]^2}{k_1 k_2}. \quad (7)$$

β_{CuL_m} is the overall formation constant of CuL_m, and k_1 and k_2 are the acid dissociation constants of H_2pan.

The total concentration of Cu–pan complexes [(Cupan)'] can be obtained from the absorbance at the wavelength where the absorbance of the mixed ligand complex is equal to that of Cu(pan) chelate. [Cu'] and [pan'] are calculated by means of the following equations:

$$[Cu'] = C_{Cu} - [(Cupan)'], \quad (8)$$

$$[pan'] = C_{Hpan} - [(Cupan)'], \quad (9)$$

where C_{Cu} and C_{Hpan} represent the analytical concentrations of Cu and Hpan, respectively. Thus the values of $K_{(Cupan)'}$ are obtained at the various concentrations of the ligand and the various pHs of the solutions.

On the other hand the concentration of free ligand L is calculated by

$$[L] = \frac{[L']}{\alpha_{L(H)}}, \quad (10)$$

where

$$\alpha_{L(H)} = 1 + \frac{[H]}{k_p} + \frac{[H]^2}{k_p k_{p-1}} + \cdots + \frac{[H]^p}{k_p \cdots k_2 k_1},$$

and [L'] represents the total concentration of the ligand not combined with copper, and $k_1, k_2, \cdots k_p$ are the acid dissociation constants of the ligand. In this work a large excess of the ligand compared with copper and Hpan was used; thus [L'] is approximately equal to the initial concentration of the ligand C_L. $\alpha_{Cu(L)}$ and $\alpha_{pan(H)}$ are calculated from the concentration of L and the pH of the solution by means of Eqs. 6 and 7, respectively.

Thus $K_{Cupan}\alpha_{Cupan(L)}$ can be written as Eq. 11 and evaluated from $K_{(Cupan)'}$ by the use of Eq. 2.

$$K_{Cupan}\alpha_{Cupan(L)} = K_{Cupan}(1 + \sum_{n=1}^{n} \beta_{Cu(pan)L_n}[L]^n) \quad (11)$$

From the plots of $\log K_{Cupan}\alpha_{Cupan(L)}$ *vs.* log [L] the formation constants of Cu(pan) and $Cu(pan)L_n$ complexes were obtained by the curve fitting method.

Results

2,2'-Bipyridine. Under the conditions: C_{Cu}= 0.223—11.1×10^{-5} M, C_{Hpan}=1.01—20.2×10^{-6} M, C_L=3.00—500×10^{-4} M, pH 8.18—9.07, dioxane 5% v/v, the absorption spectra were measured. Some of them are shown in Fig. 1. By the addition of 2,2'-bipyridine the absorption maximum of Cu(pan) chelate shifted from 550 to 540 nm, and the absorbance at λ_{max} decreased with increasing the concentration of 2,2'-bipyridine, because the replacement of Cu(pan) chelate by 2,2'-bipyridine proceeds together with the formation of the mixed ligand complex. The isosbestic point of the curves 2—8 at 502 nm indicates the existence of the mixed ligand complex and Hpan in the presence of 2,2'-bipyridine. From the absorbances at 545 nm the total concentration of Cu–pan complexes and then the values of $K_{(Cupan)'}$ were calculated. A plot of $\log K_{Cupan}\alpha_{Cupan(L)}$ *vs.* the logarithm of free 2,2'-bipyridine concentration log [bpy] yielded a straight line with a slope of 1.0 (Fig. 2). Thus, over the concentration range of 2,2'-bipyridine from 10^{-4} to 10^{-1} M a mixed ligand complex

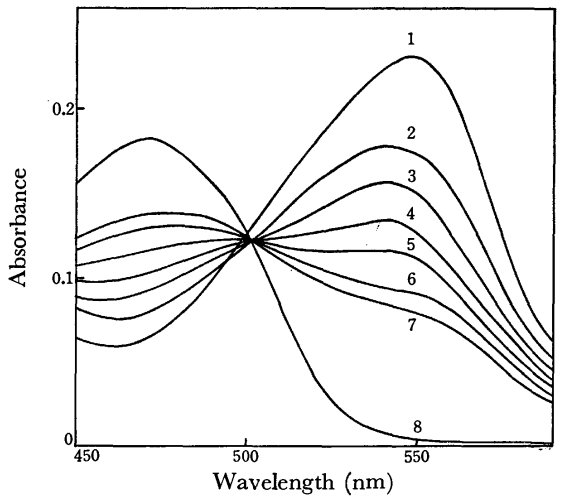

Fig. 1. Absorption spectra of Cu(pan)(bpy). C_{Cu}=1.11×10^{-4} M, C_{Hpan}=1.01×10^{-5} M, pH 9.05, C_{bpy}=: (1) 0 (pH 5.78), (2) 1.50×10^{-2} M, (3) 2.00×10^{-2} M, (4) 2.50×10^{-2} M, (5) 3.00×10^{-2} M, (6) 3.50×10^{-2} M, (7) 4.00×10^{-2} M, (8) only Hpan.

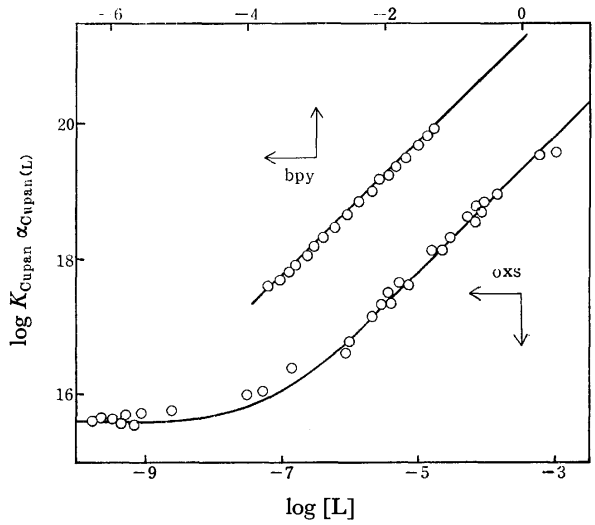

Fig. 2. Plots of log $K_{Cupan}\alpha_{Cupan(L)}$ *vs.* log [L]. Solid lines are the theoretical curves calculated with the values obtained by curve fitting.

Table 2. Formation constants of the mixed ligand complexes of Cu(pan)
25 °C, μ=0.1 (KNO_3)

Ligand (L)	λ_{max} (nm)	log $K^{pan.L}_{Cu(pan)L}$	log $K^{pan}_{Cu(pan)L}$	log $K^{L}_{Cu(pan)L}$	Δlog K	dioxane (%)
phen	540	21.18	12.20	5.60	−3.38	5
bpy	540	21.26	12.67	5.68	−2.91	5
en	548	21.64	11.08	5.65	−4.91	10
Hoxs	550	22.80	10.94	7.22	−4.64	5
Hgly	545	19.39	11.27	3.40	−4.72	10
H_2ida	550	20.68	9.75	4.69	−6.24	10
H_2O	550	15.60[a]				5
		16.00[b]				10
		15.58[c]				5
		15.99[c]				10

Hpan: pk_1=2.87, pk_2=11.55 (dioxane 5%) pk_1=2.90, pk_2=11.68 (dioxane 10%). a) In the presence of Hoxs. b) In the presence of en, H_2ida, or Hgly. c) In the absence of auxiliary complexing agents.

Cu(pan)(bpy) is formed, as in the case of 1,10-phenanthroline. The value of log $K^{pan.bpy}_{Cu(pan)bpy}$ was obtained from the value of log $K_{Cupan\alpha Cupan(L)}$ at log[bpy]=0 (Table 2).

Ethylenediamine. By the addition of ethylenediamine the absorption maximum of Cu(pan) chelate shifted to 548 nm. Increasing the concentration of free ethylenediamine caused the formation of the mixed complex and the substitution with ethylenediamine to proceed. Under the conditions: $C_{Cu}=2.14—12.9\times10^{-4}$ M, $C_{Hpan}=9.97—10.2\times10^{-6}$ M, $C_L=1.57—12.1\times10^{-2}$ M, pH 6.08—10.22, dioxane 10% v/v, the absorbances at 549 nm were measured. As shown in Fig. 3, the values of log $K_{Cupan\alpha Cupan(L)}$ became higher than that of log K_{Cupan} when the concentration of free ethylenediamine exceeded 10^{-6} M, and a straight line with a slope of 1.0 was obtained at concentrations higher than 10^{-4} M. Thus a mixed ligand complex Cu(pan)(en) is formed.

8-Hydroxy-5-quinolinesulfonic Acid. In this case Cu-oxs chelate is extremely stable, so the substitution of Cu(pan) chelate with oxs proceeded even at a low concentration of oxs. Hence the following experimental conditions were employed: $C_{Cu}=1.6—488\times10^{-5}$ M, $C_{Hpan}=2.94—32.2\times10^{-6}$ M, $C_L=0.378—113\times10^{-4}$ M, pH 3.58—11.00, dioxane 5% v/v. A plot of log $K_{Cupan\alpha Cupan(L)}$ *vs.* log [oxs] is shown in Fig. 2. The formation of a mixed ligand complex Cu(pan)(oxs) was observed.

Glycine. In this case the absorption maximum of Cu(pan) chelate shifted to the shorter wavelength (545 nm) with increase in the concentration of free glycine. The absorbances at 547.5 nm were measured under the conditions: $C_{Cu}=4.29\times10^{-6}—1.07\times10^{-3}$ M, $C_{Hpan}=3.00—9.01\times10^{-6}$ M, $C_L=1.62—19.8\times10^{-2}$ M, pH 5.84—9.28, dioxane 10% v/v. The results are shown in Fig. 3 and Table 2.

Iminodiacetic Acid. The absorption spectrum was slightly shifted to the shorter wavelengths compared with that of Cu(pan) chelate. The experiments were carried out under the conditions: $C_{Cu}=8.00—80.0\times10^{-5}$ M, $C_{Hpan}=0.923—1.18\times10^{-5}$ M, $C_L=3.62—45.3\times10^{-3}$ M, pH 5.14—9.66, dioxane 10% v/v. The results are shown in Fig. 3 and Table 2.

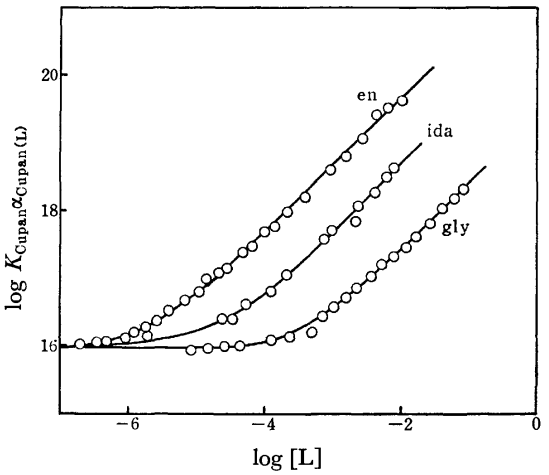

Fig. 3. Plots of log $K_{Cupan\alpha Cupan(L)}$ *vs.* log [L]. Solid lines are the theoretical curves calculated with the values obtained by curve fitting.

Discussion

In all cases, the replacement of Cu(pan) chelate by auxiliary complexing agents takes place before the complete formation of the mixed ligand complex. Thus, it was assumed that the molar absorptivity of the mixed ligand complex is the same as that of Cu(pan) chelate at the middle wavelength of these two absorption maxima, as observed in the case of 1,10-phenanthroline.[2] Since the plots of log $K_{Cupan\alpha Cupan(L)}$ *vs.* log [L] fitted well with a normalized curve plotting y *vs.* log x for $y=\log(1+x)$, and since in the case of 8-hydroxy-5-quinolinesulfonic acid, ethylenediamine, iminodiacetic acid, and glycine the formation constants of Cu(pan) chelate obtained from the horizontal parts of the curves were in good agreement with the values obtained in the absence of auxiliary complexing agents[4] (Table 2), the above assumption should be correct. In each case at higher concentrations of free ligand a straight line with a slope of 1.0 was obtained; hence one molecule of ligand coordinates with one molecule of Cu(pan) chelate.

To compare the formation constants of Cu(pan) and Cu(pan)L, $K^{pan}_{Cu(pan)L}$ was calculated from $K^{pan.L}_{Cu(pan)L}$, as

$$K^{pan}_{Cu(pan)L}=\frac{[Cu(pan)L]}{[CuL][pan]},$$

and values of Δlog K defined by Sigel[5] were calculated:

$$\Delta\log K=\log K^{pan}_{Cu(pan)L}-\log K_{Cupan}.$$

In all cases Δlog K are negative (Table 2). Therefore, by the formation of the mixed ligand complex the bonds between copper and pan may be weakened.

Tabata and Tanaka determined the formation constants of mixed ligand complexes of copper(II)-4-(2-pyridylazo)resorcinol (Cu(par)) chelate with unidentate ligands(L) such as SCN^-, Cl^-, Br^-, I^-, NH_3, pyridine, CH_3COO^- and N_3^-.[6] Comparing the values of $K^L_{Cu(pan)L}$ obtained in this work with those of $K^L_{Cu(par)L}$ by Tabata and Tanaka, $K^L_{Cu(pan)L}$ for 1,10-phenanthroline, 2,2'-bipyridine, and 8-hydroxy-5-quinolinesulfonic acid are much larger than $K^L_{Cu(par)L}$ for pyridine. $K^L_{Cu(pan)L}$ for

ethylenediamine, and iminodiacitic acid are also greater than $K^{L}_{Cu(par)L}$ for NH_3, while in the case of glycine $K^{L}_{Cu(pan)L}(=10^{3.40})$ is of the same order as $K^{L}_{Cu(par)L}$ $(=10^{3.51})$ for NH_3. On the other hand, in the EDTA titration of copper(II) with PAN indicator the rate of the color change is accelerated with glycine,[1] but glycine methyl ester slows down the rate of color change, as does pyridine.** Thus glycine may coordinate with Cu(pan) chelate as a bidentate ligand. The calculated $\Delta\log K$ value for iminodiacetic acid was small, if iminodiacetic acid were to act as a terdentate ligand; thus iminodiacetic acid may coordinate as a bidentate ligand with the amine nitrogen and one of the carboxyl oxygen atoms.

All ligands examined in this study coordinate with Cu(pan) chelate as bidentate ligands and the mixed ligand complexes may have a distorted octahedron structure. This is the reason why 1,10-phenanthroline, 2,2′-bipyridine, ethylenediamine, 8-hydroxy-5-quinolinesulfonic acid, glycine, or iminodiacetic acid accelerates the rate of color change of PAN indicator in copper(II)-EDTA titrations.

** The formation constant of the mixed ligand complex of Cu(pan) with glycine methyl ester could not be determined, because of the small solubility in H_2O–dioxane.

References

1) G. Nakagawa and H. Wada, *Talanta*, **20**, 829 (1973).
2) G. Nakagawa and H. Wada, *Talanta*, **22**, 563 (1975).
3) G. Nakagawa, H. Wada, and T. Hayakawa, *Bull. Chem. Soc. Jpn.*, **48**, 424 (1975).
4) G. Nakagawa and H. Wada, *Nippon Kagaku Zasshi*, **84**, 639 (1963).
5) H. Sigel, *Chimia*, **21**, 489 (1967). R. Griesser and H. Sigel, *Inorg. Chem.*, **9**, 1238 (1970).
6) M. Tabata and M. Tanaka, *J. Inorg. Nucl. Chem.*, **38**, 1529 (1976).

Binuclear Metal Complexes. XXIII.[1] Molecular Structure of a Hetero-metal Binuclear Complex, CuCo(fsaen)·3H$_2$O($C_{18}H_{18}N_2O_9CoCu$)

Masahiro MIKURIYA, Hisashi OKAWA, Siego KIDA,* and Ikuhiko UEDA†

Department of Chemistry, Faculty of Science, Kyushu University 33, Hakozaki, Higashi-ku, Fukuoka 812

†*Colledge of General Education, Kyushu University 01, Ropponmatsu, Fukuoka 810*

(Received April 13, 1978)

The crystal structure of hetero-metal binuclear complex, CuCo(fsaen)·3H$_2$O, with *N,N'*-bis(3-carboxysalicylidene)ethylenediamine (H_4fsaen) was determined by the single-crystal X-ray diffraction method. The crystals are trigonal, space group $P3_221$, $a=b=12.845(2)$, $c=9.962(1)$ Å, $V=1423.5(4)$ Å^3, and $Z=3$. The structure was solved by the heavy atom method and refined by the block-diagonal least-squares method to an *R* factor of 0.028. The copper atom is coordinated by two nitrogen atoms and two phenolic oxygen atoms in a square-planar manner. The cobalt atom is coordinated by two equatorial carboxyl oxygen atoms, two equatorial phenolic oxygen atoms and two axial water oxygen atoms in a distorted octahedral geometry. The detailed structure determined is in conformity with the magnetic and spectral properties previously reported.

In the previous papers of this series,[2,5] it was shown that the Schiff bases derived from 3-formylsalicylic acid and diamines are binucleating ligands with coordinative selectivity. By use of these ligands, many hetero-metal binuclear complexes have been synthesized and characterized on the basis of elemental analyses, IR, electronic spectra, and magnetic measurements over the temperature range.[1-4] However, no direct proof of the structure has been given yet. Therefore, it is desired to establish the basic structure of these hetero-metal binuclear complexes. In this study, the crystal structure of CuCo(fsaen)·3H$_2$O which is one of those hetero-metal binuclear complexes was analyzed by the single-crystal X-ray diffraction method, where H_4fsaen represents *N,N'*-bis(3-carboxysalicylidene)ethylenediamine.

According to the previous paper,[3] the electronic spectrum of CuCo(fsaen)·3H$_2$O was interpreted in terms of the planar copper(II) in the "inside" coordination site and the octahedral cobalt(II) in the "outside" coordination site. On the basis of the magnetic property, it was assumed that the ground state of the cobalt(II) is orbitally singlet and, hence, the geometry around the cobalt atom is slightly distorted from the regular octahedron. Hence, in view of this assumption, it is interesting to provide the detailed structural data of this complex obtained by the X-ray analysis.

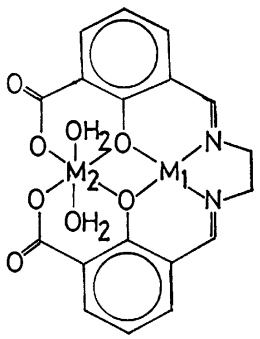

Experimental

CuCo(fsaen)·3H$_2$O was prepared by the method previously reported.[3] Crystals suitable for an X-ray study were obtained as red-purple prisms by crystallization from a dilute aqueous solution.

Preliminary Weissenberg photographs showed that the complex crystallizes in a trigonal system. The cell parameters and intensities were measured on a Syntex P$\bar{1}$ automated four-circle diffractometer with monochromated Mo $K\alpha$ radiation ($\lambda=0.71073$ Å). The crystal was ground to a sphere (radius 0.152 mm). The cell parameters were determined by the least-squares refinement based on the 15 reflections in the range of $17<2\theta<38°$. The values are $a=b=12.845$ (2), $c=9.962$ (1) Å, and $V=1423.5$ (4) Å^3. The density $D_m=1.84$ g/cm^3 obtained by floatation in hexane–1,2-dibromoethane solution agrees well with the density $D_C=1.85$ g/cm^3 calculated for three molecules per unit cell. The crystallographic data are given in Table 1.

Table 1. Crystal data

Molecular formula	CuCo($C_{18}H_{12}N_2O_6$)·3H$_2$O
Molecular weight	528.8
Crystal system	Trigonal
Space group	$P3_121$ or $P3_221$
$a=b=12.845(2)$, $c=9.962(1)$ Å	
$V=1423.5(4)$ Å^3	
$Z=3$	
$D_m=1.84$ g/cm^3	
$D_c=1.85$ g/cm^3	
$\mu=21.1$ cm^{-1} (for Mo $K\alpha$)	

Intensity data were collected by the θ-2θ scan technique with a variable scan rate of 4.0 to 24.0°/min. Three standard reflections were monitored every 50 reflections, and their intensities showed a good stability. A total of 4493 reflections with $2\theta<48°$ were collected. The intensities were corrected for the Lorentz and the polarization effects, but corrections for absorption were not applied on account of $\mu r=0.32$. 839 independent reflections with $|F_o|\geq 2.5\sigma(F_o)$ were considered as "observed" and were used for the structure analysis.

Solution and Refinement of the Structure

The observed Laue symmetry of the reflections is $\bar{3}$ml. The observed setting of the symmetry, $I(hkl)=I(khl)$, and the systematic absences of $00l$ for $l\neq 3n$ indicate that either of the two enantiomorphous space groups $P3_121$ or $P3_221$ is possible.

The structure was solved by the heavy atom method. The positions of the copper and cobalt atoms were

determined by a three-dimensional Patterson synthesis. The copper and cobalt atoms were located on the twofold axes in the special positions. The successive Fourier syntheses and the difference Fourier syntheses revealed all the nonhydrogen atoms. Refinement was carried out by the block-diagonal least-squares method. One of the water oxygens, O(5) was found to be positionally disordered, with a half-occupancy of the two positions related by the twofold axis. Being introduced anisotropic thermal parameters, the block-diagonal least-squares refinement yielded a discrepancy factor $R_1=\sum||F_o|-|F_c||/\sum|F_o|=0.046$. At this stage, a difference Fourier map revealed all the hydrogen atoms. The refinement was performed for both the enantiomorphous space groups $P3_121$ and $P3_221$. The final discrepancy factors were : $R_1=0.038$ and $R_2=[\sum w(|F_o|-|F_c|)^2/\sum w|F_o|^2]^{1/2}=0.059$ for space group $P3_121$; $R_1=0.028$ and $R_2=0.045$ for space group $P3_221$. As has been pointed out,[6,7] the best refinement should correspond to the correct configuration. Accordingly, the hypothesis of space group $P3_121$ can be rejected at a confidence level higher than 99.5%.[9] A further check on the $P3_221$ configuration was carried out in comparing the intensities of Friedel pairs. Table 2 lists observed and calculated intensity relations between some *hkl* and $\bar{h}\bar{k}l$ reflections. Inspecting these relations, one can confirm that $P3_221$ is the correct space group for the crystal studied here.

In the least-squares refinement the function minimized was $\sum w(|F_o|-k|F_c|)^2$, and the weighting scheme was $w=(10+|F_o|+0.01|F_o|^2)^{-1}$.[8] The final shift in the atomic parameters of the nonhydrogen atoms averaged 0.05σ with the maximum of 0.26σ. Atomic scattering factors for Cu, Co, O, N, C_{val}, and H, and the anomalous dispersion corrections, $\Delta f'$ and $\Delta f''$ for Cu

Table 2. Observed and calculated intensity relations between some *hkl* and $\bar{h}\bar{k}l$ reflections

h	k	l	$F_c(hkl)$	Obsd	$F_c(\bar{h}\bar{k}l)$	$\bar{h}$	$\bar{k}$	l
4	7	1	20.2	>	16.2	$\bar{4}$	11	1
6	4	1	12.9	<	16.6	$\bar{6}$	10	1
6	5	1	15.3	>	10.7	$\bar{6}$	11	1
1	3	2	15.0	<	17.9	$\bar{1}$	4	2
1	10	2	9.3	<	11.9	$\bar{1}$	11	2
2	2	2	19.8	<	24.3	$\bar{2}$	4	2
2	8	2	13.9	<	15.4	$\bar{2}$	10	2
3	1	2	15.2	<	18.0	$\bar{3}$	4	2
3	2	2	17.8	<	20.9	$\bar{3}$	5	2
4	6	2	6.1	<	10.2	$\bar{4}$	10	2
7	4	2	21.0	>	17.1	$\bar{7}$	11	2
9	2	2	13.5	<	16.2	$\bar{9}$	11	2
1	1	3	29.8	<	36.2	$\bar{1}$	2	3
5	5	3	19.7	<	23.6	$\bar{5}$	10	3
4	7	4	10.3	>	6.5	$\bar{4}$	11	4
6	4	4	13.3	<	16.5	$\bar{6}$	10	4
6	5	4	16.8	>	12.8	$\bar{6}$	11	4
4	6	5	6.9	<	10.2	$\bar{4}$	10	5
5	6	5	11.8	>	8.9	$\bar{5}$	11	5
7	4	5	13.0	>	9.6	$\bar{7}$	11	5

Table 4. Fractional positional parameters ($\times 10^3$) and isotropic temperature factors of hydrogen atoms (The average of estimated standard deviations of the isotropic temperature factors is 1.4.)

Atom	X	Y	Z	B
H(O4)	169(7)	245(7)	−252(7)	4.5
H(O4)′	182(7)	157(7)	−243(7)	4.4
H(O5)	−58(11)	−17(17)	165(30)	3.1
H(O5)′	−143(10)	−63(11)	59(10)	1.9
H(C3)	−20(8)	460(8)	−32(7)	5.3
H(C4)	75(6)	656(6)	0(6)	2.8
H(C5)	276(5)	745(5)	−1(5)	1.3
H(C8)	461(6)	736(6)	2(5)	2.7
H(C9)	639(6)	730(6)	108(5)	3.1
H(C9)′	667(8)	766(8)	−54(7)	5.9

Table 3. Fractional positional parameters and anisotropic temperature factors ($\times 10^4$) of non-hydrogen atoms with their estimated standard deviations in parentheses

Temperature factors are of the form: $\exp[-(h^2B_{11}+k^2B_{22}+l^2B_{33}+2hkB_{12}+2hlB_{13}+2klB_{23})]$.

Atom	X	Y	Z	B_{11}	B_{22}	B_{33}	B_{12}	B_{13}	B_{23}
Cu	4520(1)	4520(1)	0	32(1)	32(1)	83(1)	5(1)	−2(1)	2(1)
Co	2165(2)	2165(2)	0	32(1)	32(1)	83(1)	17(1)	−1(1)	1(1)
O(1)	2844(3)	4000(3)	41(4)	36(3)	25(3)	113(5)	13(3)	13(3)	14(3)
O(2)	550(3)	2014(4)	211(4)	30(3)	32(3)	112(5)	10(3)	−1(3)	7(3)
O(3)	−891(4)	2403(4)	−240(4)	36(3)	51(4)	107(4)	20(3)	−8(3)	−4(4)
O(4)	2066(5)	2199(5)	−2139(5)	76(4)	79(5)	103(5)	50(4)	−17(4)	−1(4)
O(5)	−943(9)	−482(9)	807(9)	60(9)	78(10)	106(10)	20(8)	−18(8)	7(8)
N	5026(5)	6196(4)	77(4)	55(5)	36(4)	61(4)	11(3)	−5(4)	−3(3)
C(1)	174(5)	2747(5)	−36(5)	38(4)	46(5)	71(6)	29(4)	−4(4)	−4(4)
C(2)	1034(5)	4087(6)	−28(5)	63(6)	51(5)	56(5)	36(5)	1(5)	−13(4)
C(3)	521(7)	4807(6)	−58(6)	75(6)	63(6)	78(6)	49(5)	0(5)	−1(5)
C(4)	1169(6)	6045(6)	−38(7)	83(7)	41(5)	97(6)	34(5)	−8(5)	−10(5)
C(5)	2408(8)	6608(6)	16(6)	122(8)	34(5)	85(6)	42(5)	−15(6)	−11(5)
C(6)	2999(6)	5927(5)	29(5)	82(6)	42(5)	57(5)	34(5)	12(5)	11(4)
C(7)	2310(5)	4639(5)	−4(5)	43(5)	28(4)	62(5)	17(4)	−1(4)	−4(4)
C(8)	4262(6)	6585(5)	62(5)	60(5)	34(4)	59(6)	13(4)	5(5)	−1(4)
C(9)	6323(6)	7001(6)	171(7)	48(6)	54(6)	103(7)	5(5)	−9(5)	−2(5)

and Co, were taken from International Tables for X-Ray Crystallography.[9] The final difference Fourier map showed no important features, the highest peak being 0.3 e/Å^3.

The final positional and thermal parameters with their estimated standard deviations are given in Tables 3 and 4.***

The calculations were carried out at the Computer Center of Kyushu University, by the use of the UNICS-II program system.

Description of the Structure and Discussion

The molecular structure obtained is shown in Fig. 1. As has been expected, the molecule is a binuclear complex in which two metal atoms (M_1 and M_2) are coordinated by fsaen^{4-}. Metal atoms, M_1 and M_2, lie on the twofold axis. The molecule has the C_2 symmetry on this twofold axis. The "inside" metal atom, M_1, is coordinated by two nitrogen atoms of the ethylenediamine and two phenolic oxygen atoms in the typical square-planar manner. The "outside" metal atom, M_2, is octahedrally coordinated by two equatorial carboxyl oxygen atoms, two equatorial phenolic oxygen atoms, and two axial water oxygen atoms. Therefore, we can conclude that M_1=Cu and M_2=Co, since no alternative assignment is compatible with the magnetic and spectral properties as were already discussed in the previous paper.[3] The bond distances and angles with their estimated standard deviations are listed in Tables 5 and 6, respectively. Some least-squares planes with the deviations of atoms from the planes are given in Table 7. The Cu–O distance (1.909(5) Å) and the Cu–N distance (1.915(6) Å) are of the normal in-plane coordination. The Co–O distance (2.065(4) Å) of the bridging oxygen atom is slightly longer than that (1.995(5) Å) of the terminal oxygen atom. This relation had also been observed in the structures of some other binuclear complexes with Schiff bases.[10-12] As seen in Table 5, the Co–O(1) distance is considerably longer than the Cu–O(1) distance. This is consistent with a fact that Co–O distances are generally longer than Cu–O ones.[13] The axial Co–O distance (2.137(5) Å) is somewhat longer than that of the in-plane coordination. As seen in Table 6, the in-plane O–Co–O angles considerably deviate from right angle (77.1(2), 86.2(2), and 110.7(2)°), whereas the apical O–Co–basal O angles are 86.6(2), 89.5(2), and 92.2(2)°. As seen in Table 7, four coordinating atoms around the copper atom are almost coplanar with the deviations within ±0.02 Å. On the other hand, four equatorial atoms around the cobalt atom deviate from the mean plane by ±*ca.* 0.07 Å and show a slight distortion toward the tetrahedron. Accordingly the coordination geometry about

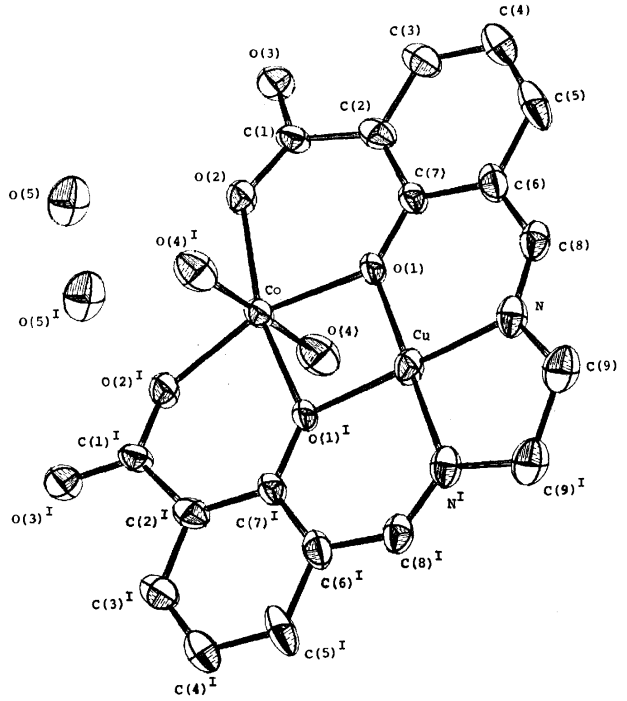

Fig. 1. Molecular structure of CuCO(fsaen)·3H$_2$O with thermal ellipsoids.

*** A list of structure factors has been deposited with the Chemical Society of Japan as a Document No. 7836.

Table 5. Interatomic distances (l/Å) in the molecule of CuCo(fsaen)·3H$_2$O

The standard deviations are given in parentheses.

Cu–Co	3.025(2)	N–C(9)	1.460(8)
Cu–O(1)	1.909(5)	C(1)–C(2)	1.511(8)
Cu–N	1.915(6)	C(2)–C(3)	1.378(13)
Co–O(1)	2.065(4)	C(3)–C(4)	1.378(10)
Co–O(2)	1.995(5)	C(4)–C(5)	1.381(11)
Co–O(4)	2.137(5)	C(5)–C(6)	1.414(14)
O(1)–C(7)	1.307(9)	C(6)–C(7)	1.435(8)
O(2)–C(1)	1.279(10)	C(2)–C(7)	1.424(9)
O(3)–C(1)	1.226(8)	C(6)–C(8)	1.406(10)
N–C(8)	1.305(11)	C(9)–C(9)^{I}	1.548(14)

I) y, x, −z.

Table 6. Bond angles (ϕ/°) with their estimated standard deviations in parentheses

O(1)–Cu–O(1)^{I}	84.7(2)	O(2)–C(1)–O(3)	122.1(5)
O(1)–Cu–N	94.7(2)	O(2)–C(1)–C(2)	120.5(5)
N–Cu–N^{I}	85.9(3)	O(3)–C(1)–C(2)	117.4(7)
O(1)–Co–O(1)^{I}	77.1(2)	C(1)–C(2)–C(3)	116.2(6)
O(1)–Co–O(2)	86.2(2)	C(1)–C(2)–C(7)	124.8(7)
O(2)–Co–O(2)^{I}	110.7(2)	C(3)–C(2)–C(7)	119.0(6)
O(1)–Co–O(4)	89.5(2)	C(2)–C(3)–C(4)	123.9(7)
O(1)^{I}–Co–O(4)	92.2(2)	C(3)–C(4)–C(5)	118.5(9)
O(2)–Co–O(4)	92.2(2)	C(4)–C(5)–C(6)	120.7(6)
O(2)^{I}–Co–O(4)	86.6(2)	C(5)–C(6)–C(7)	120.0(6)
O(4)–Co–O(4)^{I}	177.8(2)	C(5)–C(6)–C(8)	116.3(6)
Cu–O(1)–Co	99.1(2)	C(7)–C(6)–C(8)	123.7(8)
Cu–O(1)–C(7)	129.3(3)	O(1)–C(7)–C(2)	121.5(5)
Co–O(1)–C(7)	131.4(3)	O(1)–C(7)–C(6)	120.6(6)
Co–O(2)–C(1)	131.7(3)	C(2)–C(7)–C(6)	117.8(7)
Cu–N–C(8)	122.2(4)	C(6)–C(8)–N	129.3(6)
Cu–N–C(9)	115.1(6)	N–C(9)–C(9)^{I}	110.6(6)
C(8)–N–(C(9)	122.7(6)		

I) y, x, −z.

Table 7. Analysis of mean planes
(Daviations from planes (l/Å))

I. Plane through O(1), N, O(1)^{I}, and N^{I}
(Copper coordination sphere)
$0.0228X-0.0395Y+0.9990Z=0.0000$[a]

Cu	0.000	O(1)^{I}	0.018
O(1)	−0.018	N^{I}	−0.017
N	0.017		

II. Plane through O(1), O(2), O(1)^{I}, and O(2)^{I}
(Cobalt coordination sphere)
$0.0459X-0.0795Y+0.9958Z=0.0000$[a]

Co	0.000	O(1)^{I}	0.077
O(1)	−0.077	O(2)^{I}	−0.060
O(2)	0.060		

III. Plane through C(2), C(3), C(4), C(5), C(6), and C(7)
(Benzene ring)
$-0.0302X-0.0005Y+0.9995Z=-0.0755$[a]

C(2)	0.010	C(5)	0.007
C(3)	−0.003	C(6)	0.000
C(4)	−0.005	C(7)	−0.009

IV. Plane through Cu, Co, O(1), O(2), O(3), N, C(1), C(2), C(3), C(4), C(5), C(6), C(7), C(8), C(9), O(1)^{I}, O(2)^{I}, O(3)^{I}, N^{I}, C(1)^{I}, C(2)^{I}, C(3)^{I}, C(4)^{I}, C(5)^{I}, C(6)^{I}, C(7)^{I}, C(8)^{I}, and C(9)^{I}
(CuCo(fsaen) moiety)
$-0.0022X+0.0039Y+1.0000Z=0.0000$[a]

Cu	0.000		
Co	0.000		
O(1)	0.047	O(1)^{I}	−0.047
O(2)	0.218	O(2)^{I}	−0.218
O(3)	−0.223	O(3)^{I}	0.223
N	0.083	N^{I}	−0.083
C(1)	−0.023	C(1)^{I}	0.023
C(2)	−0.013	C(2)^{I}	0.013
C(3)	−0.037	C(3)^{I}	0.037
C(4)	−0.014	C(4)^{I}	0.014
C(5)	0.037	C(5)^{I}	−0.037
C(6)	0.043	C(6)^{I}	−0.043
C(7)	0.008	C(7)^{I}	−0.008
C(8)	0.073	C(8)^{I}	−0.073
C(9)	0.174	C(9)^{I}	−0.174
O(4)	−2.130	O(4)^{I}	2.130
O(5)	0.807	O(5)^{I}	−0.807

I) y, x, −z. a) Equations have the form $AX+BY+CZ=D$ where X, Y, and Z are Cartersian axes lying along $\boldsymbol{a}\times\boldsymbol{c}^*$, $\boldsymbol{b}$, and $\boldsymbol{c}^*$, respectively.

the cobalt atom evidently deviates from a regular octahedron, so that the orbital degeneracy of the ground state ($^4T_{1g}$) in O_h symmetry is removed. The first excited state may possibly be thermally nonaccessible, thereby the cryomagnetic behavior of CuCo(fsaen)·3H$_2$O being expressed by the Van Vleck equation based on the Heisenberg model with $S_1=1/2$ and $S_2=3/2$.

The unit cell contains three binuclear molecules and three uncoordinated crystal water molecules. The carboxyl oxygen O(3) and the water oxygen O(4) coordinated to the cobalt atom of the adjacent molecule are hydrogen-bonded and the O(3)···O(4) distance is 2.699(8) Å. The crystal water is in the vicinity of the carboxyl oxygen O(2) by hydrogen bonding with the O(5)···O(2) distance of 2.86(1) Å. The absolute configuration of the packing is that of a left-handed helical sequence of molecules, the axis of the helix being the c axis. Each binuclear molecule points its "outside" moiety toward the inside of the helix in which the crystal water molecules are housed.

The authors wish to express sincere thanks to Dr. Yoshihiko Kushi of Hiroshima University for his helpful advice and discussion. They are also grateful to Dr. Shigeaki Kawano of Kyushu University for use of the UNICS-II program. Thanks are also due to Dr. Yuzo Nishida of Kyushu University for the help in data collection, and to Mr. Naoyuki Torihara for helping us in the preparation of the complex.

References

1) N. Torihara, H. Okawa, and S. Kida, *Chem. Lett.*, **1978**, 185.
2) H. Okawa, M. Tanaka, and S. Kida, *Chem. Lett.*, **1974**, 987.
3) H. Okawa, Y. Nishida, M. Tanaka, and S. Kida, *Bull. Chem. Soc. Jpn.*, **50**, 127 (1977).
4) N. Torihara, H. Okawa, and S. Kida, *Inorg. Chim. Acta*, **26**, 97 (1978).
5) M. Tanaka, M. Kitaoka, H. Okawa, and S. Kida, *Bull. Chem. Soc. Jpn.*, **49**, 2469 (1976).
6) W. C. Hamilton, *Acta Crystallogr.*, **18**, 502 (1965).
7) J. A. Ibers and W. C. Hamilton, *Acta Crystallogr.*, **17**, 781 (1964).
8) "Computing Methods in Crystallography," ed by J. S. Rollett, Pergamon Press, Oxford (1965), p. 114.
9) "International Tables for X-Ray Crystallography," Kynoch Press, Birmingham (1974), Vol. IV.
10) M. D. Glick and R. L. Lintvedt, *Prog. Inorg. Chem.*, **21**, 233 (1976).
11) B. Tomlonovic, R. L. Hough, M. D. Glick, and R. L. Lintvedt, *J. Am. Chem. Soc.*, **97**, 2925 (1975).
12) M. D. Glick, R. L. Lintvedt, D. P. Gavel, and B. Tomlonovic, *Inorg. Chem.*, **15**, 1654 (1976).
13) "International Tables for X-Ray Crystallography," Kynoch Press, Birmingham (1962), Vol. III.

A Dimeric Structure of Dimethyllead(IV) Complexes with ONO Tridentate Schiff-base Ligands and the Interaction of These Complexes with Donor Solvents

Tetsuro MAJIMA and Yoshikane KAWASAKI*

Department of Petroleum Chemistry, Osaka University, Yamadakami, Suita, Osaka 565

(Received April 14, 1978)

From measurements of the molecular weights, dimethyllead(IV) complexes with ONO tridentate Schiff-base ligands, 2-(2-oxidobenzylideneamino)phenolatos, were found to have dimeric six-coordinate structure in $CHCl_3$, in which either one of the two oxygen atoms in the ligands bridges the lead atoms. The $^2J(^{207}Pb\text{–}CH_3)$ values increase and the $\delta(Pb\text{–}CH_3)$ values shift to a higher magnetic field with an increase in the donor strength of the solvents. Linear relationships between the $^2J(^{207}Pb\text{–}CH_3)$ and $\delta(Pb\text{–}CH_3)$ values and Hammett's σ values of the substituents on the Schiff-base ligands were obtained. These results suggest that the complexes form monomerically as a result of coordination with one and/or two solvent molecules in such donor solvents as DMSO and HMPA, and that the $^2J(^{207}Pb\text{–}CH_3)$ values is dependent mainly on the change in the positive charge on the lead atom: the change in the mean excitation energy, ΔE, in the Fermi contact term.

In a series of spectroscopic studies of several dimethyllead(IV) complexes of 8-quinolinols,[1] β-diketones,[2] benzoates,[3] and quadridentate Schiff bases,[4] we have found that these dimethyllead(IV) complexes are monomeric and take a six-coordinate configuration in non-coordinating solvents, $CHCl_3$ and CH_2Cl_2, and that in such donor solvents as DMSO and HMPA, the lead atom is coordinated with a solvent molecule as the seventh ligand. In both types of solvents, the C–Pb–C skeleton is always linear. On the other hand, Bosco and Cefalù[5] have prepared a dimethyllead(IV) complex with a ONO tridentate Schiff-base ligand and claimed that the complex has a five-coordinate configuration. The C–Pb–C skeleton of the complex is not linear, judging from the following observations: 1) the molecular weight in acetone shows a monomeric value, and 2) the spin-spin coupling constant, $^2J(^{207}Pb\text{–}CH_3)$, in $CDCl_3$ is very small (132 Hz) as compared with those of usual six-coordinate dimethyllead(IV) complexes (*ca.* 150 Hz) with the linear C–Pb–C skeleton.[1–4,6] However, a possibility that the coordination of an acetone molecule to the lead atom gives the monomeric value can not be disregarded, since we have elucidated from spectroscopic studies[3] that acetone interacts more or less strongly with dimethyllead(IV) complexes. Moreover, the configuration of the C–Pb–C skeleton in dimethyllead(IV) complexes, as ascertained in a series of our studies,[1–4,7,8] is not correlated directly with the $^2J(^{207}Pb\text{–}CH_3)$ values. Therefore, we have reinvestigated the molecular weights of the some dimethyllead(IV) complexes with ONO tridentate Schiff-base ligands in $CHCl_3$, in which the possibility of the coordination of solvent molecules to the lead atom seems negligibly small.

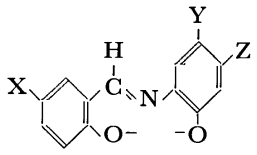

	complex; $(CH_3)_2PbL$
L=**1**: X=Z=H, Y=NO_2	(complex I)
L=**2**: X=Y=H, Z=NO_2	(complex II)
L=**3**: X=Y=Z=H	(complex III)
L=**4**: X=Z=H, Y=CH_3	(complex IV)
L=**5**: X=OCH_3, Y=Z=H	(complex V)
L=**6**: X=OCH_3, Y=CH_3, Z=H	(complex VI)

We also wish to report on the effects of the substituents on the Schiff-base ligands and of the donor strength of solvents upon the $^2J(^{207}Pb\text{–}CH_3)$ and the $\delta(Pb\text{–}CH_3)$ values.

As the planar ONO tridentate Schiff-base ligands, 2-(2-oxidobenzylideneamino)phenolates, L=**1**—**6**, were used.

Experimental

Materials. The dimethyllead dichloride was prepared by the chlorination of tetramethyllead in ethyl acetate at −10 °C.[9] The Schiff bases, 2-(2-hydroxybenzylideneamino)phenols (H_2L), were prepared by dehydration reactions between the corresponding *o*-aminophenols and salicylaldehydes by refluxing in alcoholic solutions. The solvents were reagent grade and were purified according to the standard method except for $CDCl_3$, which was used as supplied.

Preparation of the Complexes, I—VI. The dimethyllead complexes, $(CH_3)_2PbL$, I—VI, with the corresponding ligands, **1**—**6** respectively, were prepared according to the following procedures. A dry methanol solution (20 dm) of sodium salts of an appropriate Schiff base (Na_2L), prepared from sodium methoxide in methanol (Na; 0.5 g, 20 mmol) and H_2L (10 mmol), was added, drop by drop, into dimethyllead dichloride (2.5 g, 10 mmol) in dry methanol (30 dm). The mixture was then stirred for a few hours. The precipitates were filtered, washed by benzene and methanol, and recrystallized from methanol (I and IV), *N*,*N*-dimethylformamide/methanol(II), or dichloromethane/hexane (III, V, and VI). Elemental analyses of the lead of all the complexes were carried out by decomposition with concentrated sulfuric and nitric acids.[10]

Molecular-weight and Conductivity Measurements. The molecular weights in $CHCl_3$ (0.5 wt %) were measured by means of a Mechrolab vapor pressure osmometer at 25 °C. The molar conductances in DMSO were measured by means of a Yokogawa F-225A Universal bridge and a cell with the cell constant of 0.377 cm^{-1} at 25±0.1 °C. The specific conductance of DMSO used was $\kappa=4.2\times10^{-7}$ Ω^{-1} cm^{-1}. The molar conductances (Λ_m) of IV—I in DMSO (10^{-3} mol·dm^{-3}) were 1.1—1.9 Ω^{-1} cm^2 mol^{-1} (Table 1). All the complexes were found to be non-electrolytes.

Table 1. Analytical data, physical properties, and IR spectral data of $(CH_3)_2PbL$

Complex	Color	Mp (°C)	Found (Calcd) (%) C	H	N	Pb	Λ_m[a] (Ω^{-1} cm^2 mol^{-1})	mol wt[b] Found (Calcd)	ν(C=N) (cm^{-1}) in CH_2Cl_2 (in DMSO)
I	yellow-brown	230[c]	36.61 (36.51)	3.11 (2.86)	5.34 (5.68)	41.72 (41.99)	1.21	949 (493)	1606 (1595)
II	red	264[c]	36.30 (36.51)	2.81 (2.86)	5.83 (5.68)	42.11 (41.99)	1.17	977 (493)	1605 (1598)
III	yellow-red	252[d]	39.97 (40.17)	3.43 (3.37)	3.11 (3.12)	46.27 (46.20)	1.85	902 (449)	1600[e] (1597)
IV	yellow	190[c]	41.50 (41.55)	3.72 (3.70)	3.30 (3.03)	45.19 (44.80)	1.73	976 (463)	1602 (1597)
V	brown	223[c]	39.93 (40.16)	3.50 (3.58)	2.95 (2.93)	43.02 (43.30)	1.62	987 (479)	1603 (1595)
VI	red-brown	215[c]	41.44 (41.46)	3.59 (3.89)	2.71 (2.84)	41.78 (42.07)	1.96	962 (493)	1600 (1595)

a) In DMSO. b) In $CHCl_3$. c) Decomposed. d) Sublime. e) 1605 cm^{-1} in the solid state, reported by Bosco and Cefalù.[5]

IR and ^1H NMR Spectra. The IR Spectra were recorded on a Hitachi 225 spectrophotometer. ^1H NMR studies were carried out on a JEOL-PS-100 spectrometer operating at 100 MHz. All the data were obtained in 4 wt % or in saturated solutions. The chemical shifts were measured relative to TMS as the internal standard at the ambient temperature.

The analytical data, physical properties, and IR and ^1H NMR spectral data for the complexes, I—VI, are given in Tables 1 and 2.

Results and Discussion

The color, melting point, ν(C=N), and δ(Pb–CH_3) and $^2J(^{207}Pb–CH_3)$ values of III obtained by us (Tables 1 and 2) are in good agreement with those reported by Bosco and Cefalù.[5] As can be seen from Table 1, the molecular weights of I—VI were twice the values produces by the use of the $(CH_3)_2PbL$ formula. These results indicate that either one of the two oxygen atoms of the ligand bridges the lead atoms, resulting in the formation of a six-coordinate configuration (**A**), in which the C–Pb–C skeleton may be linear, although a distorted octahedral structure with a slightly bent C–Pb–C skeleton is possible. A similar dimeric structure is found in the case of $[(CH_3)_2Pb(ox)X]_2$ (ox=8-quinolinolato, X=Cl and Br), in which the halogen atoms bridge two lead atoms.[11] These results are in marked contrast to those for dimethyltin(IV) complexes; *i.e.*, the dimethyltin complexes of **1**, **3**, and **4**[12] and $(CH_3)_2Sn(ox)X$ (X=Cl and Br)[13] have the five-coordinate and distorted trigonal bipyramidal structures, with a bent C–Sn–C skeleton.

The bridging of the oxygen atom in Complex I—VI is weak and is easily severed by a solvent molecule, forming a six-coordinate configuration (**B**) in donor solvents, since a monomeric value was observed for III in such weak donor solvent as acetone.[5] The dimethyllead species may have a six-coordinate configuration with an acetone molecule as the sixth ligand (**B**). The existence of seven-coordinate ones (**C**) can not be excluded, especially in such strong donor solvents as DMSO and HMPA. The $^2J(^{207}Pb–CH_3)$ values of V and VI in DMSO and HMPA are comparable to those of $(CH_3)_2Pb(ox)_2$ in DMSO (176.4 Hz),[1] in which the seven-coordinate configuration was assumed, and of an isolated seven-coordinate complex, $(CH_3)_2Pb(gbha)(H_2O)$ (gbha=2,2′-(ethanediylidenediimino)diphenolato) (176—178 Hz).[8]

The $^2J(^{207}Pb–CH_3)$ values of III and IV in $CDCl_3$ (133.6 and 135.0 Hz respectively) are smaller than those of many other six-coordinate complexes (*ca.* 150 Hz).[1-4,6] Those of I and II with an electron-withdrawing nitro group on the ligands are much smaller: 120.7 and 123.1 Hz respectively. On the other hand, those of V and VI with an electron-releasing methoxyl group (155.0 and 156.7 Hz respectively) are larger than those of I—IV, and have values similar to that of $(CH_3)_2Pb(acac)_2$ (acac=acetylacetonato) (154.7 Hz), having a six-coordinate configuration with a linear C–Pb–C skeleton.[14] The independence of the $^2J(^{207}Pb–CH_3)$ values on the configuration of the C–Pb–C skeleton may better be understood by the linear relationship between these values and Hammett's σ values of the substituents on the phenyl ring of the ligands for I—IV (Fig. 1).

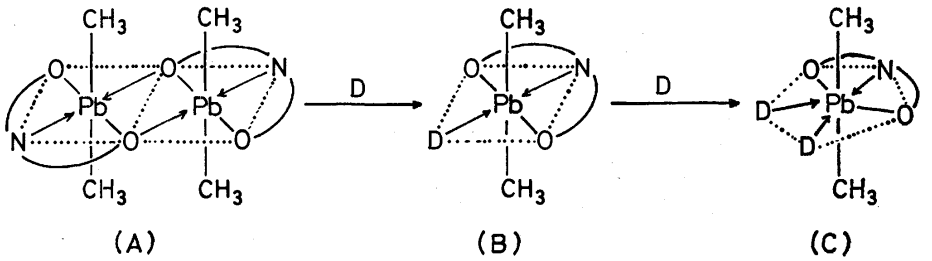

D=HMPA, DMSO, Pyridine, $(CH_3O)_3PO$, CH_3OH, $(CH_3)_2CO$

TABLE 2. THE ^{1}H NMR

Solvent	I				II				III		
	δ_1	δ_2	^2J	^3J	δ_1	δ_2	^2J	^3J	δ_1	δ_2	^2J
$CDCl_3$	2.13	8.12	120.7	5.0	2.10	—[b]	123.1	—[b]	2.07 2.05[c]	8.32 8.20[c]	133.6 132[c]
CH_2Cl_2	2.12	8.59	120.8	5.2	—[b]	—[b]	—[b]	—[b]	2.05	8.39	135.9
CH_3OH	2.00	8.48	138.0	5.6	2.02	—[b]	140.0	—[b]	1.91	8.41	138.6
$(CH_3O)_3PO$	1.98	8.66	150.9	10.8	1.94	8.56	154.8	—[b]	1.81	8.47	141.2
Pyridine	2.18	—[d]	151.8	—[d]	—[b]	—[b]	—[b]	—[b]	2.04	—[d]	144.5
DMSO	1.81	8.60	160.5	14.7	1.84	8.64	164.7	13.1	1.74	8.56	152.4
HMPA	1.77	8.95	166.6	15.5	1.82	9.19	165.6	15.2	1.70	8.75	158.0

a) δ_1, δ_2, ^2J, and ^3J are δ(Pb–CH_3) (ppm), δ(Pb–N=CH) (ppm), $^2J(^{207}Pb–CH_3)$ (Hz), and $^3J(^{207}Pb–N=CH)$
d) Obscured by the solvent peaks.

This relationship indicates that the $^2J(^{207}Pb–CH_3)$ values decrease with an increase in the electron-withdrawing character of the substituent on the ligand. The electron-withdrawing group leads to an increase in the polarization in $Pb^{\delta+}–O^{\delta-}$ bonds, resulting in an increase in the positive charge on the lead atom. Indeed, the δ(Pb–CH_3) values are found to shift to a lower magnetic field in this order: IV, III, II, and I (Fig. 1). Similarly, an increase in the $^2J(^{207}Pb–CH_3)$ values and a higher magnetic-field shift of the δ(Pb–CH_3) values with an increase in the donor strength of the solvents (Table 2) can also be explained by the decrease in the positive charge on the lead atom with the increase in the donor strength of the solvents. These results are consistent with our previous assumption[1,3,4,7,15] that the change in the mean excitation energy, ΔE, in the Fermi contact term plays a dominant role in determining the $^2J(^{207}Pb–CH_3)$ value for dimethyllead(IV) complexes. Therefore, the small $^2J(^{207}Pb–CH_3)$ value can not be connected directly with the conclusion that the C–Pb–C skeleton is bent in the dimethyllead(IV) complexes. This is substantiated by the observation that the $^2J(^{207}Pb–CH_3)$ values of the dimethyllead(IV) cation, $(CH_3)_2Pb^{2+}$, with a linear C–Pb–C skeleton, are very smaller, ranging from 101 to 132 Hz in several strong acids.[7]

It should also be noted that the amount of variation in the $^2J(^{207}Pb–CH_3)$ values upon a change in the solvent from $CDCl_3$ to HMPA are in this order: I, II (*ca.* 50 Hz)>III, IV (*ca.* 30 Hz)>V, VI (*ca.* 20 Hz). These values are attributable to the fact that the strength of coordination of the solvent molecule to the lead atom differs from complex to complex, probably increasing with an increase in the positive charge on the lead atom.

As in the case of $(CH_3)_2Pb(saln)\cdot CH_3OH$,[4] we have also obtained the spin-spin coupling constants between the lead nucleus and the azomethine proton, $^3J(^{207}Pb–N=CH)$, in the case of I and II, although Bosco and Cefalù did not report these values.[5] The couplings were not detected in the other complexes, since the azomethine proton signals of the complexes are broad (with a half-height width of 4—8 Hz). The broadenings are presumed to be due to the coupling with the lead nucleus. By comparison with the values of $(CH_3)_2Pb(saln)\cdot CH_3OH$ (23.4—29.3 Hz),[4] those of I and II (5.0—15.5 Hz) are quite small and change remarkably along with the coordinating ability of the solvents. Therefore, the above results suggest that the coordination of the nitrogen atom to the lead atom in I—VI is weaker than in $(CH_3)_2Pb(saln)\cdot CH_3OH$. On the other hand, the $^3J(^{119}Sn–N=CH)$ values of $(CH_3)_2SnL$ (L=**3**) decrease with an increase in the donor strength of the solvents, although the $^2J(^{119}Sn–CH_3)$ values increase.[11]

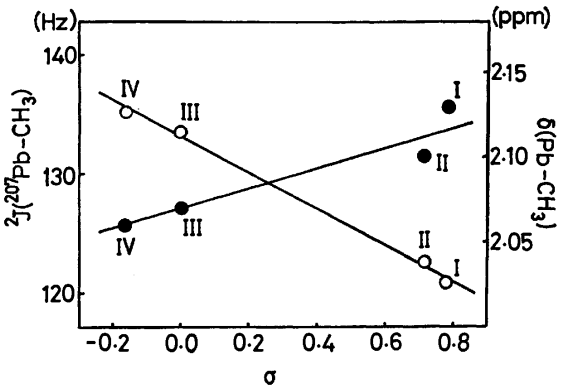

Fig. 1. Plots of the $^2J(^{207}Pb–CH_3)$ (—○—) and the δ(Pb–CH_3) values (—●—) in $CDCl_3$ *vs.* Hammett's σ for $(CH_3)_2PbL$, I—IV.

In conclusion, Complexes I—VI have a dimeric six-coordinate structure (**A**) in such non-coordinating solvents as $CHCl_3$ and CH_2Cl_2. On the other hand, in such donor solvents as DMSO and HMPA the complexes form a monomeric six- and/or seven-coordinate structure, (**B**) and/or (**C**), with one or two donor solvent molecules. In either solvent, the C–Pb–C skeleton is linear and is perpendicular to the coordination plane. Therefore, the results are fundamentally different from those for the dimethyltin(IV) complexes, in which the C–Sn–C skeleton is quite flexible.

References

1) M. Aritomi and Y. Kawasaki, *J. Organomet. Chem.*, **81**, 363 (1974).
2) M. Aritomi, Y. Kawasaki, and R. Okawara, *Inorg. Nucl. Chem. Lett.*, **8**, 69 (1972).
3) M. Aritomi and Y. Kawasaki, *J. Organomet. Chem.*, **90**,

DATA OF $(CH_3)_2PbL$[a)]

Complex								
IV			V			VI		
δ_1	δ_2	^2J	δ_1	δ_2	^2J	δ_1	δ_2	^2J
2.06	8.32	135.0	2.05	8.35	155.0	2.04	8.34	156.7
2.01	8.32	138.5	2.01	8.38	157.5	2.00	8.36	159.7
1.94	8.48	145.2	1.96	8.48	158.7	1.93	—[b)]	166.4
1.83	8.50	149.6	—[b)]	—[b)]	—[b)]	1.89	8.47	167.1
2.11	—[d)]	155.4	2.00	—[d)]	157.6	2.02	—[d)]	159.0
1.75	8.43	156.1	1.87	8.47	167.4	1.87	8.46	168.8
1.70	8.72	166.8	1.83	8.84	172.8	1.83	8.78	178.3

(Hz) respectively. b) The solubility is insufficient for measurements. c) Reported by Bosco and Cefalù.[5)]

185 (1975).
4) Y. Kawasaki and T. Majima, *Inorg. Nucl. Chem. Lett.*, **11**, 779 (1975); T. Majima and Y. Kawasaki, *Bull. Chem. Soc. Jpn.*, in press.
5) R. Bosco and R. Cefalù, *J. Organomet. Chem.*, **26**, 225 (1971).
6) V. G. Kumar Das and W. Kitching, *J. Organomet. Chem.*, **13**, 523 (1968).
7) Y. Kawasaki and M. Aritomi, *J. Organomet. Chem.*, **104**, 39 (1976).
8) T. Majima and Y. Kawasaki, *Bull. Chem. Soc. Jpn.*, **51**, 1893 (1978).
9) G. Grüttner and E. Krause, *Chem. Ber.*, **49**, 1419 (1916).
10) H. Gilman and J. Robinson, *J. Am. Chem. Soc.*, **50**, 1714 (1928).
11) $[(CH_3)_2Pb(ox)X]_2$ (X=Cl and Br) were prepared by a photoreaction of $(CH_3)_2Pb(ox)_2$ in CHX_3 or CH_2X_2. The $^2J(^{207}Pb-CH_3)$ values are 148—152 Hz in $CDCl_3$ or CH_2Cl_2: Y. Kawasaki, to be published.
12) K. Kawakami and T. Tanaka, *J. Organomet. Chem.*, **49**, 409 (1973).
13) K. Kawakami and R. Okawara, *J. Organomet. Chem.*, **6**, 249 (1965).
14) Y. Kawasaki, *J. Organomet. Chem.*, **9**, 549 (1967).
15) M. Aritomi, K. Hashimoto, and Y. Kawasaki, *J. Organomet. Chem.*, **93**, 181 (1975).

Kinetic and Equilibrium Studies of the Complex Formation of Mercury(II) Acetate in Aqueous Solutions

Kiyoshi TAMURA, Shoji HARADA,† Michinori HIRAISSH,† and Tatsuya YASUNAGA†,*

Department of Chemistry, National Defense Academy, Hashirimizu, Yokosuka 239

†Department of Chemistry, Faculty of Science, Hiroshima University, Higashisenda-machi, Hiroshima 730

(Received April 17, 1978)

An ultrasonic absorption study has been carried out on aqueous acidic solutions of mercury(II) acetate. The absorption data shows a single-relaxation phenomenon in the frequency range of 15—95 MHz. On the other hand, the results of the pH measurement indicate that the only mecury(II) acetate complexes conceivable in solution are of the HgL^+ and HgL_2 forms (L^- denotes the acetate ion); the succesive formation constants of these complexes, together with the mercury(II) hydrolysis constants, are also determined. The equilibrium constants reported are: 2.1×10^3 for K_1, 4.9×10^3 for K_2, 6×10^{-4} for K_{h1}, and 1.0×10^{-3} for K_{h2}, at 30 °C and $I=1$. On the basis of the above results, the ultrasonic relaxation absorption is ascribed to the complex formation reaction: $HgL^+ + L^- \rightleftarrows HgL_2$. The rate constants and the volume change of this reaction are determined to be: $k_f^\circ = 7.8\times10^9$ M^{-1} s^{-1}, $k_b^\circ = 1.6\times10^6$ s^{-1}, and $\Delta V = 18$ cm^3 mol^{-1}, at 30 °C.

It is well known[1] that the rate of a metal-complex formation reaction in an aqueous solution is controlled by the water release from the metal and that the rate constant of this step depends strongly on the nature of the metal ion, *e.g.*, on the charge, the electronic configuration, the ionic radius, and the coordination number. Although many studies[2] have provided us with much information about the complexation kinetics for most "labile" metals, few kinetic studies about mercury(II) complexes[2,3] have been made up to the present. This is because some experimental difficulties exist in the studies; *e.g.*, mercury(II) exhibits a considerable hydrolysis-tendency, and it is one of the most labile of metals.

The purpose of the present study is to obtain kinetic information on mercury(II) acetate complexes through an elucidation of ultrasonic absorption in aqueous mercury(II) acetate solutions. The kinetic analysis of the absorption data requires an exact knowledge about the nature of complexes in solution and about the formation constants. The literature[4-6] gives little information on these constants, and so the present study included a determination of them by means of a pH measurement method.

Experimental

Equilibrium Measurements. The formation constants of the mercury(II) acetate complexes were obtained from the pH measurements. A Hitachi-Horiba Expandomatic pH meter, Model F-7SS, with general-purpose glass and calomel electrodes was used and calibrated with standard buffer solutions. The pH values were determined to an accuracy of ±0.005 unit. Sample solutions were prepared from mercury(II) acetate and stock solutions of nitric acid and/or acetic acid; the ionic strength was kept constant at $I=1$ by the addition of $NaNO_3$. The concentrations of the acid solutions were determined by titrating with standard NaOH.

The experiments were carried out for three kinds of systems. The first contains 0.001—0.4 M mercury(II) acetate and 0.01—0.4 M nitric acid; pH=1.0—3.1. The second contains 0.15—0.5 M mercury(II) acetate, 0.02—0.1 M nitric acid, and 0.25 M acetic acid; pH=2.0—2.6. The third contains 0.005—0.4 M mercury(II) acetate and 0.07—0.25 M acetic acid; pH =2.7—3.3. The dissociation constant of acetic acid was also obtained from the pH measurement of solutions containing 0.025—0.9 M acetic acid and 0.01—0.2 M sodium acetate ($I=1$ with $NaNO_3$); the pH value lay in the 3.3—4.5 range.

The concentrations of hydrogen ions in the solutions were calculated from the measured pH values by using an apparent activity coefficient, γ_H, which was determined by the pH measurement of solutions containing nitric acid at various concentrations and sufficient amounts of $NaNO_3$ to maintain the ionic strength at unity. All the pH measurements were carried out at 30.0 ± 0.5 °C.

Kinetic Measurement. Sample solutions were prepared from mercury(II) acetate and sodium acetate. The pH values of the solutions were adjusted by the addition of perchloric acid; no supporting electrolytes were added. The ultrasonic absorption was measured in the frequency range of 5—95 MHz by the pulse technique[7] at 30.00 ± 0.05 °C.

The relaxation absorption spectra were represented by the single-relaxation equation:

$$\frac{\alpha}{f^2} = \frac{A}{1+(f/f_r)^2} + B, \tag{1}$$

or:

$$(\alpha'\lambda) = \left(\frac{\alpha}{f^2} - B\right)cf = \frac{2\mu_m(f/f_r)}{1+(f/f_r)^2}, \tag{2}$$

where α is the ultrasonic absorption coefficient; f, the frequency of the sound; f_r and A, the relaxation frequency and amplitude, respectively; B, the high-frequency value of α/f^2; $(\alpha'\lambda)$, the excess absorption per wavelength; c, the velocity of sound, and μ_m $(=cAf_r/2)$, the maximum excess absorption per wavelength.

The values of f_r, A, and B were determined by fitting the data to Eq. 1. A least-squares fit was obtained by using a routine in which the root-mean-square percentage deviation between the experimental and calculated α/f^2 values was minimized.

Results and Discussion

The Formation Constants of Mercury(II) Acetate Complexes. In the mercury(II) acetate systems studied, the following equilibria may exist:

$$HL \overset{K_H}{\rightleftarrows} H^+ + L^-, \tag{3}$$

$$Hg(OH)_{m-1}^{3-m} \overset{K_{hm}}{\rightleftarrows} Hg(OH)_m^{2-m} + H^+, \quad m=1, 2, \tag{4}$$

$$HgL_{n-1}^{3-n} + L^- \overset{K_n}{\rightleftarrows} HgL_n^{2-n}, \quad n=1, 2, \cdots N, \tag{5}$$

where L^- denotes the acetate ion and where K_H is the dissociation constant of acetic acid; the K_{hm}'s are the mercury(II) hydrolysis constants, and the K_n's, the formation constants of the complexes. Then, the average number, $\bar{n}$, of acetate ions bound to the central metal may be defined by[8]

$$\bar{n} = \frac{\sum_n n\beta_n[L^-]^n}{1+\sum_n \beta_n[L^-]^n}, \quad \beta_n = K_1K_2 \cdots K_n, \tag{6}$$

where the brackets indicate the molar concentration at equilibrium and where the summation is to be carried out for all the whole values of n from 1 to N.

In the first place, the data analysis was tried by ignoring the hydrolysis Reactions 4 from the above equilibria. Then, we could evaluate $[L^-]$ and $\bar{n}$ by means of the following relations:[6]

$$[L^-] = K_H(\sum \text{acid} - [H^+])/[H^+], \tag{7}$$

$$\bar{n} = \{\sum L - (1+[H^+]/K_H)[L^-]\}/\sum Hg, \tag{8}$$

where $\sum Hg$ and $\sum L$ are the total stoichiometric concentrations of mercury(II) and acetate ions, respectively, and where $\sum$acid is the sum of those of nitric and acetic acids. The dissociation constant, K_H, was determined from the measured hydrogen-ion concentrations of the acetic acid–sodium acetate system by means of the relation: $pK_H = p[H^+] + \log\{(C_1 - [H^+])/(C_2 + [H^+])\}$, were C_1 and C_2 are the stoichiometric concentrations of acetic acid and sodium acetate, respectively. The K_H value obtained is shown in Table 1; it was used for the evaluation of $[L^-]$ and $\bar{n}$ (Eqs. 7 and 8).

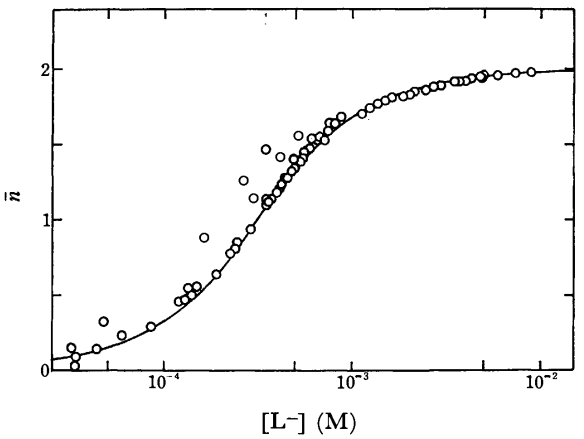

Fig. 1. Graph of $\bar{n}$ *vs.* $[L^-]$ for the mercury(II) acetate system at 30 °C and $I=1$. Open circle refers to the $\bar{n}$ and $[L^-]$ values determined approximately by Eqs. 7 and 8. The solid curve expresses the $\bar{n}$ value calculated by Eq. 6 using the K_1 and K_2 values in Table 1.

As is shown in Fig. 1, a graph of the $\bar{n}$ *vs.* $[L^-]$ plot thus obtained forms almost a single curve except for some data in the low $[L^-]$ region which exhibit somewhat large deviations from the curve. Probably these deviations reflect the fact that the effect of the hydrolysis reactions cannot be ruled out in this region. Furthermore, the fact that the $\bar{n}$ value increases as a whole with an increase in $[L^-]$ and tends to an asymptotic value of 2 in the high $[L^-]$ region indicates that the only mercury(II) acetate complexes conceivable in solution are of the HgL^+ and HgL_2 forms.

Since graphical methods for determining equilibrium constants[9] may not be simply applied to the present systems, the data analysis was carried out as follows. From the equilibria (3—5) with $m=1, 2$ and $n=1, 2$, we obtain the following conservation relations:

$$\sum Hg = [Hg^{2+}]\left(1+\frac{K_{h1}}{[H^+]}+\frac{K_{h1}K_{h2}}{[H^+]^2}+K_1[L^-]+K_1K_2[L^-]^2\right), \tag{9}$$

$$\sum L = [L^-]\left(1+\frac{[H^+]}{K_H}\right)+[Hg^{2+}](K_1[L^-]+2K_1K_2[L^-]^2), \tag{10}$$

$$\sum \text{acid} = [H^+]\left(1+\frac{[L^-]}{K_H}\right)-[Hg^{2+}]\left(\frac{K_{h1}}{[H^+]}+\frac{2K_{h1}K_{h2}}{[H^+]^2}\right). \tag{11}$$

If a set of values is given to the four parameters, K_{h1}, K_{h2}, K_1, and K_2, the values of $[Hg^{2+}]$ and $[L^-]$ may be evaluated from the known values of $\sum Hg$, $\sum L$, and $[H^+]$ by using Eqs. 9 and 10. Then, Eq. 11 enables us to calculate $\sum$acid. Therefore, the values of the equilibrium constants were determined by repeating a number of similar calculations, in which the values of the parameters were varied independently, and finally by obtaining a set of values which minimize the root-mean-square percentage deviation between the experimental and calculated $\sum$acid values. The calculations were carried out by using a computer program. The values of the equilibrium constants obtained are shown in Table 1. The calculated $\sum$acid values agree with the experimental values within $\pm 3\%$. The $\bar{n}$ value was recalculated by means of Eq. 6 using the K_1 and K_2 values in Table 1; it is shown by a solid line in Fig. 1. The calculated curve is consistent with the $\bar{n}$ *vs.* $[L^-]$ plot which was obtained approximately by means of Eqs. 7 and 8.

Table 1. Equilibrium constants for the aqueous mercury(II) acetate system at 30 °C and $I=1$

Dissociation constant of acetic acid	$K_H = (3.19\pm0.07)\times10^{-5}$
Mercury(II) hydrolysis constants	$K_{h1} = (6\pm2)\times10^{-4}$ $K_{h2} = (1.0\pm0.4)\times10^{-3}$
Formation constants of mercury(II) acetate complexes	$K_1 = (2.1\pm0.1)\times10^3$ $K_2 = (4.9\pm0.3)\times10^3$

The K_{h1} and K_{h2} values in Table 1 are within the ranges of those reported by the earlier workers.[4] On the other hand, the results obtained for mercury(II) acetate complexes are very different from those reported by Banerjea and Singh.[6] They reported the presence of four kinds of complexes (*i.e.*, $n=1$—4) in solution and obtained these values: 3.59×10^5, 5.54×10^3, 9.6×10^3, and 6.1×10^3 for K_1, K_2, K_3, and K_4, respectively, at 30 °C and $I=1$. Their K_1 value is larger by almost two orders of magnitude than the corresponding one in Table 1, though their K_2 value is close to that obtained here. For comparison, the $\bar{n}$ value was calculated by means of Eq. 6 using their four equilibrium constants; it ranges from 1.1 to 4 in the $[L^-]$ range in Fig. 1,

TABLE 2. EXPERIMENTAL CONDITIONS AND ULTRASONIC RELAXATION PARAMETERS FOR THE AQUEOUS MERCURY(II) ACETATE SYSTEM[a] AT 30 °C

Sample No.	∑L (M)	pH	Equilibrium concentrations of species (10^{-2} M)[b]							f_r (MHz)	A	B
			HL	L^-	Hg^{2+}	$HgOH^+$	$Hg(OH)_2$	HgL^+	HgL_2		10^{-17} cm^{-1} s^2	
1	1.08	2.28	23.5	0.17	4.4	0.25	0.04	6.8	38.5	54±13	21±2	22±2
2	1.10	2.51	20.1	0.25	2.3	0.22	0.06	5.2	42.2	38±5	30±2	24±1
3	1.13	2.83	17.2	0.46	0.8	0.15	0.09	3.1	45.8	35±3	48±2	23±1
4	1.15	3.28	15.7	1.17	0.1	0.07	0.11	1.3	48.4	21±2	113±9	24±2
5	1.18	3.56	16.2	2.30	—	0.03	0.10	0.7	49.2	19±1	146±7	23±1
6	1.10	2.46	21.0	0.24	2.6	0.22	0.05	5.5	41.6	43±12	45±4	21±5
7	1.30	2.46	35.2	0.39	0.9	0.08	0.02	3.5	45.4	37±8	71±7	19±4
8	1.50	2.46	52.6	0.56	0.4	0.04	0.01	2.3	47.2	33±3	95±5	18±2
9	1.70	2.46	71.3	0.72	0.2	0.02	0.01	1.7	48.1	27±2	114±8	22±2
10	2.00	2.46	100	0.91	0.1	0.01	—	1.1	48.8	27±5	109±14	22±3
11	2.25	2.46	125	1.03	—	0.01	—	0.8	49.2	27±7	93±18	22±4

a) Each solution contains 0.500 M ∑Hg. b) I=0.2—1.3.

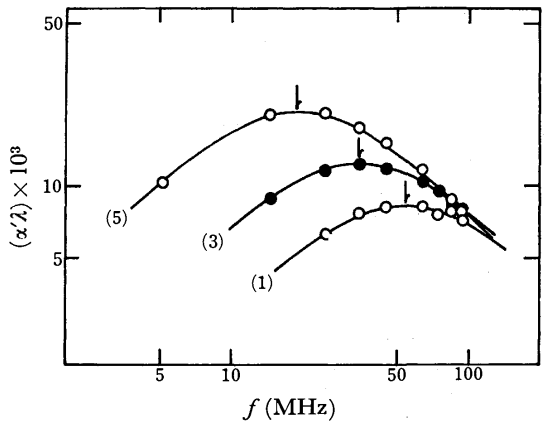

Fig. 2. Graph of $(\alpha'\lambda)$ *vs.* f for the mercury(II) acetate system containing $HClO_4$ in a definite concentration (*ca.* 0.2 M), at 30 °C. The arrow indicates the relaxation frequency. The number in parentheses refers to the sample number in Table 2.

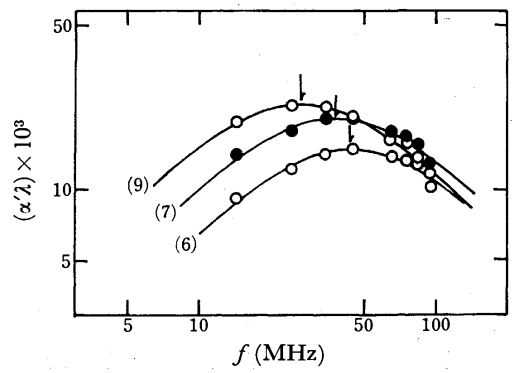

Fig. 3. Graph of $(\alpha'\lambda)$ *vs.* f for the mercury(II) acetate system in a definite pH (2.46), at 30 °C. The arrow indicates the relaxation frequency. The number in parentheses refers to the sample number in Table 2.

being too large to be consistent with the present results.

Ultrasonic Absorption of Mercury(II) Acetate Solutions. The experimental conditions and the adsorption parameters obtained are summarized in Table 2. The data consist of those from two kinds of systems. One contains $HClO_4$ in a definite concentration of *ca.* 0.2 M (sample No. 1—5), while the other has been adjusted to a definite pH of 2.46 (sample No. 6—11). Representative absorption curves for these systems are shown in Figs. 2 and 3, where the excess absorption per wavelength $(\alpha'\lambda)$ is plotted against f.

The equilibrium concentrations of species in solution were evaluated from the ∑Hg, ∑L, and pH values in Table 2, together with the values of the equilibrium constants which were calculated from those in Table 1 by using Meites' equation[10] for the activity coefficients of ions. Calculations by a recurrence method resulted in self-consistent values for the equilibrium concentrations, the ionic strength, the activity coefficients, and the corrected equilibrium constants. The results are also shown in Table 2.

The kinetic analysis of the absorption data was carried out by associating the relaxation process with one of the equilibria (3—5). An examination of the concentration dependence of the observed relaxation frequency showed that only the following reaction is consistent with the experimental data (furthermore, all the species in this reaction are considered to be of a reasonable order of magnitude over the whole concentration range studied):

$$HgL^+ + L^- \underset{k_b}{\overset{k_f}{\rightleftarrows}} HgL_2. \qquad (12)$$

The relaxation frequency associated with this reaction is expressed by

$$2\pi f_r = k_f^\circ\{\gamma_\pm^2([HgL^+]+[L^-])+1/K_2^\circ\}, \qquad (13)$$

where $\gamma_\pm$ is the mean activity coefficient of HgL^+ and L^-, and where the superscript (o) indicates the quantities at I=0. In the above expression, the equilibrium relation of $K_2^\circ=k_f^\circ/k_b^\circ$ is employed. As is shown in Fig. 4, a graph of the f_r *vs.* $\{\gamma_\pm^2([HgL^+]+[L^-])+1/K_2^\circ\}$ plot gives a straight line passing through the point of origin, and the rate constant, k_f°, was obtained from the slope of this line. The values of k_f° and k_b° $(=k_f^\circ/K_2^\circ)$ are shown in Table 3. The maximum excess absorption per wavelength corresponding to Eq. 13 is given by

$$\mu_m = \frac{(\pi\Delta V)^2}{2RT\beta_s}\left\{\frac{1}{[HgL^+]}+\frac{1}{[L^-]}+\frac{1}{[HgL_2]}\right\}^{-1}, \qquad (14)$$

where R is the gas constant; T, the absolute temperature

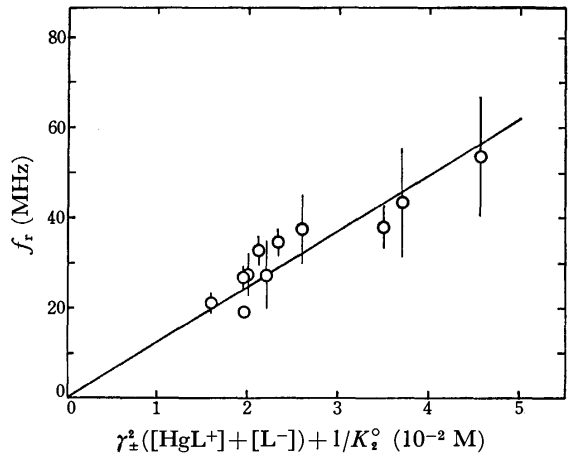

Fig. 4. Graph of f_r *vs.* $\{\gamma_\pm^2([HgL^+]+[L^-])+1/K_2^\circ\}$ for the mercury(II) acetate system at 30 °C. The vertical lines indicates the uncertainty intervals given in Table 2.

Table 3. Kinetic results for the formation of $Hg(CH_3CO_2)_2$ at 30 °C

Rate constants	$k_f^\circ=(7.8\pm0.9)\times10^9$ $M^{-1}s^{-1}$
	$k_b^\circ=(1.6\pm0.2)\times10^6$ s^{-1}
Volume change	$\Delta V=18\pm2$ cm^3 mol^{-1} [a]

a) Effective value in the I range of 0.2—1.3.

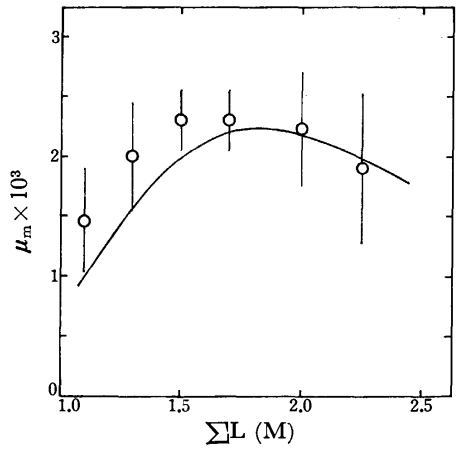

Fig. 5. Graph of μ_m *vs.* $\sum L$ for the mercury(II) acetate system under the conditions of $\sum Hg=0.500$ M, pH=2.46, and 30 °C. The vertical lines indicate the uncertainty intervals obtained from the data in Table 2. The solid curve expresses the μ_m value calculated by Eq. 14 using the ΔV value in Table 3.

and β_s, the adiabatic compressibility of the solution; ΔV is the volume change of the complex formation reaction 12. The ΔV value was determined by Eq. 14; it is also shown in Table 3. Figure 5 shows the observed μ_m values plotted against $\sum L$ for the solutions of $\sum Hg=0.5$ M and pH=2.46, while the calculated μ_m value is also shown by the solid line. The calculated curve expresses fairly well the concentration dependence of the observed μ_m value. These results indicate that the observed relaxation absorption is associated with Reaction 12.

By an electric-field-dispersion method, Eigen and Eyring[3] obtained the rate constant, $(5—10)\times10^9$ M^{-1} s^{-1} (at 24—25 °C and $I\approx0$), for the $HgCl_2$ formation reaction. The similarity of the k_f° value in Table 3 to the above value indicates that the formation reactions of the mercury(II) complexes proceed *via* the Eigen mechanism,[11,12] which involves the loss of a water molecule in the rate-determining step. By assuming that the outer-sphere association process reaches equilibrium much faster than the ligand substitution, the complex formation rate constant, k_f, may be expressed in terms of the association constant, K_o, of the outersphere complex and the rate constant, k_o, of ligand substitution; *i.e.*, $k_f=K_ok_o$. For Reaction 12, the K_o value was estimated to be 1.3 (at $I=0$) by means of the Fuoss equation,[13] in which the center-to-center distance between the reaction partners was assumed to be 5 Å. Then, the k_f° value in Table 3 gives $k_o=6\times10^9$ s^{-1}, which is in line with the corresponding values reported for the d^{10} cations:[1] *i.e.*, $(2.5—3)\times10^7$ s^{-1} for Zn^{2+}, $(2.5—4)\times10^8$ s^{-1} for Cd^{2+}, and 2×10^9 s^{-1} for Hg^{2+}, at 20 °C.

References

1) M. Eigen, *Pure Appl. Chem.*, **6**, 97 (1963).
2) M. Eigen and R. G. Wilkins, *Adv. Chem. Ser.*, **49**, 55 (1964).
3) M. Eigen and E. M. Eyring, *Inorg. Chem.*, **2**, 636 (1963).
4) "Stability Constants of Metal-Ion Complexes," 2nd ed, ed by L. G. Sillen and A. E. Martell, Chemical Society, London (1964).
5) P. Mahapatra, S. Aditya, and B. Prasad, *J. Indian Chem. Soc.*, **30**, 509 (1953).
6) D. Banerjea and I. P. Singh, *Z. Anorg. Allg. Chem.*, **331**, 225 (1964).
7) N. Tatsumoto, *J. Chem. Phys.*, **47**, 4561 (1967).
8) J. Bjerrum, "Metal Ammine Formation in Aqueous Solution," P. Haase and Son, Copenhagen (1957).
9) F. J. C. Rossotti and H. S. Rossotti, *Acta Chem. Scand.*, **9**, 1166 (1955).
10) L. Meites, "Handbook of Analytical Chemistry," 1st ed, ed by L. Meites, McGraw-Hill Book Co., London (1963), pp. 1—8.
11) M. Eigen and K. Tamm, *Z, Elektrochem. (Ber. Bunsenges. Phys. Chem.)*, **66**, 93, 107 (1962).
12) M. Eigen, *Ber. Bunsenges. Phys. Chem.*, **67**, 753 (1963).
13) R. M. Fuoss, *J. Am. Chem. Soc.*, **80**, 5059 (1958).

The Solution Behavior of Thenoyltrifluoroacetone in Alcoholic Solvents

Hidenori SHIBUYA, Hitoshi WATARAI, and Nobuo SUZUKI*

Department of Chemistry, Faculty of Science, Tohoku University, Sendai 980

(Received April 17, 1978)

The solution behavior of thenoyltrifluoroacetone (TTA) has been investigated in a series of higher alcohols which are often used in solvent extraction by means of UV and NMR spectrometries. It was experimentally confirmed that TTA exists in the enol and hemiacetal forms in dehydrated alcohol, while in wet alcohol we should also take a hydrate form into consideration. The fractions of the species at equilibrium were determined, and their dependencies on the water concentration and on the solvent properties, *i.e.*, the dielectric constant and the solubility parameter, were examined. The interconversion rate between the enol and hemiacetal forms were also observed as a function of the water concentration.

The identification of the chemical form of a partitioning species is one of the most important problems in fundamental research into solvent extraction. TTA (4,4,4-trifluoro-1-(2-thienyl)-1,3-butanedione) has been extensively used as a powerful extractant for metal ions, especially for heavy metals.[1] The predominant form of TTA in the inert solvents commonly used in solvent extraction is known to be the enol form, and in aqueous solvents, the hydrate form.[2-4] In addition, it has been reported that TTA reacts with methanol.[5] However, there is no information on whether TTA reacts with the higher alcohols used in solvent extraction. Recently, Suzuki *et al.*[6] observed that the partition rate of TTA between higher alcohol and water is very slow compared to that between an inert solvent and water. This fact seems to suggest a specific interaction between TTA and higher alcohol.

In the present study, a quantitative investigation has been carried out on the chemical equilibrium and the kinetic behavior of TTA in eleven higher alcohols by means of UV and ^{19}F and ^{1}H NMR spectrometries.

Experimental

Materials. The TTA (Dojindo G. R.) was purified by vacuum sublimation. The purity was checked by mp measurement (43.2—43.8 °C, lit, 42.5—43.2 °C[1]). Commercially purchased alcohols were fractionally distilled over calcium oxide or calcium sulfate. The purified TTA and alcohols were stored in a silica-gel desiccator. The dioxane was purified by the ordinary method.[7] The deuterated methanol (CD_3OD, 99%), dehydrated methanol, and perchloric acid were all reagent-grade. Redistilled water was used throughout.

Determination of Water Concentration. The concentration of water in alcohol was determined by the Karl-Fischer method. Water-saturated alcohol was prepared by placing a diluted aqueous solution (pH=3.5) of perchloric acid in contact with purified alcohol for several days in a thermostated room at 25 °C. The determination was repeated three times for each sample.

NMR Measurement. A deuterated methanol solution of TTA (1M) was prepared one day before measurement. The ^{1}H NMR spectra of the solution were taken on a Varian A-60 NMR apparatus. An alcohol solution of TTA (0.3M) was prepared for each alcohol at 25±0.5 °C. In order to establish the equilibration, the solutions were allowed to stand for four days in the case of dehydrated solutions and for two or three days in the case of water-containing solutions. The ^{19}F NMR spectra of the solutions were taken on a JEOL-PS-100 NMR apparatus at 94 MHz and 25±2 °C. The signal integration of a resonance peak was repeated at least four times. As an internal standard of the chemical shift, tetramethylsilane was used for the ^{1}H NMR and fluorotrichloromethane for the ^{19}F NMR.

Kinetic Measurements. The interconversion rate among the species of TTA was measured by observing the decrease in the enol concentration photometrically; 50 μl of a dioxane solution of TTA (0.003 M) was spiked into 5 ml of alcohol in a quartz cell, and the subsequent decrease in the transmittance at 340 nm (absorption maximum of enol form) was recorded on a Hitachi 356 UV-VIS spectrophotometer at 25±0.2 °C.

Results and Discussion

Chemical Species of TTA in Alcoholic Solvents. The ^{1}H NMR spectra of the deuterated methanol solution of TTA are shown in Fig. 1. The two multiplets at 7.76 and 7.10 ppm are assigned to the thienyl group, and the singlet at 6.48 ppm, to the α-proton of the enol form. The quartet at 3.34 ppm with a coupling constant of

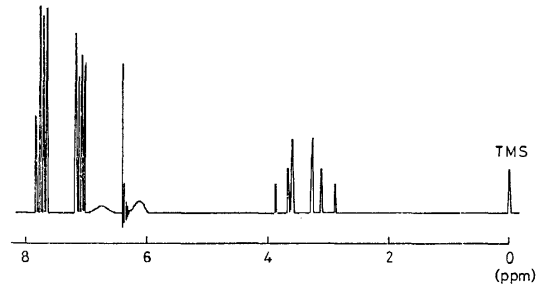

Fig. 1. ^{1}H NMR spectrum of the deuterated methanol solution of TTA.

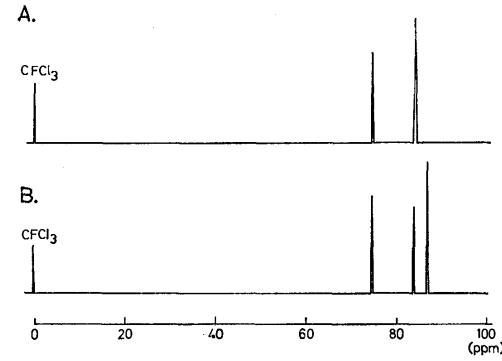

Fig. 2. ^{19}F NMR spectra of the alcoholic solution of TTA.
A: Dehydrated methanol solution,
B: water-saturated 1-hexanol solution.

J=15.7 cps and the doublet at 3.52 and 3.12 ppm are thought to be assignable to species other than the enol form. The ^{19}F NMR spectra of a dehydrated methanol solution of TTA is shown in Fig. 2(A). Two singlet signals were observed at 77.2 and 83.6 ppm. In the other dehydrated alcohols also, similar spectra were observed except for the cases of 2-octanol and 3-methyl-1-butanol. These results show that TTA is in two forms in dehydrated alcohols, *viz.*, enol and hemiacetal produced by a reaction with alcohol:

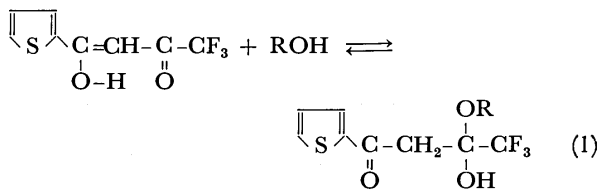

(1)

The hemiacetal form has two α-protons which are not equivalent because of the effect of the asymmetric carbon atom at the adjacent position. Since the α-protons belong to the AB-type group, they may be expected to show a quartet. Consequently, the quartet at 3.34 ppm can be assigned to the α-protons of the hemiacetal form. The doublet in Fig. 1 can be explained by considering a proton-deuteron exchange in one of the α-protons as follows:

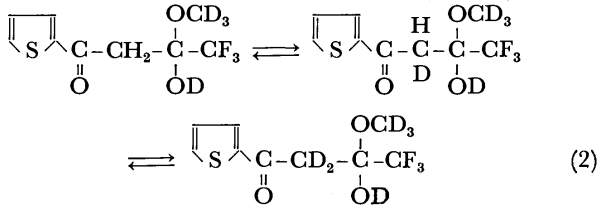

(2)

In this way, the NMR spectra of methanol solution of TTA can be thoroughly interpreted by considering the enol and the hemiacetal forms.

The ^{19}F NMR spectra of a water-saturated 1-hexanol solution of TTA are shown in Fig. 2(B). Three singlet signals, at 77.6, 84.1, and 88.2 ppm, were observed. In the other water-saturated alcohols, similar spectra were obtained except for the cases of 2-octanol and 3-methyl-1-butanol. The signal of 88.2 ppm, which appears only in wet alcohol, is assigned to the hydrate form, because the signal becomes progressively larger as the water concentration increases. The other two signals are consistent with the signals assigned to the enol and hemiacetal forms in dehydrated alcohol.

The equilibrium fraction of each species was determined from the integrated intensity of the corresponding signal of the ^{19}F spectra. In Table 1, the fractions of the TTA species in hydrated and water-saturated alcohols are listed, together with the solubility of water, the dielectric constant, and the solubility parameter.

Solvent Effect on the Equilibria among the Three Species.

From the NMR spectra, it was found that TTA in dehydrated alcohol exists as an equilibrium mixture of the enol (E) and hemiacetal (A) forms. Furthermore, Table 1 shows that the ratio of E% to A% is not greatly affected by the solvent employed, while in water-saturated alcohols the fraction of the hydrate form (H) depends on the solvent. Since the hydration reaction is expressed by the following equation:

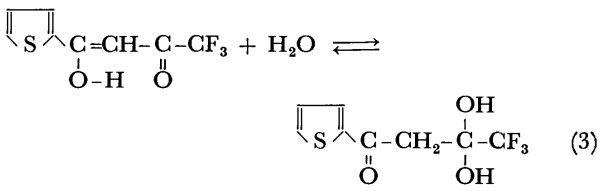

(3)

the fraction of the hydrate form can be expected to depend on the water concentration. In Table 2, the fractions of the three forms in 1-butanol containing water in various concentrations are listed. A linear correlation between ln [H]/[E] and ln X_W (mole fraction of water) was obtained in the mole-fraction range from 0.136 to 0.514, as is shown in Fig. 3. However, the plots for water-saturated alcohols are appreciably scattered from the line obtained for aqueous 1-butanol, hence, it is found that the water concentration is the primary, but not the only, factor governing the fraction of the hydrate form. It is considered that

Table 1. Fractions (%) of TTA species in dehydrated and water-saturated alcohols[a)]

No.	Solvent	Dehydrated		Water-saturated			Solubility[c)] of water (mole fraction)	ε[c)]	δ[f)]
		Enol (%)	Hemiacetal (%)	Enol (%)	Hydrate (%)	Hemiacetal (%)			
1	1-Butanol	29.2	71.8	13.6	62.7	23.7	0.514	17.5	11.4
2	1-Pentanol	32.0	68.0	18.2	54.9	26.9	0.283	13.9	10.9
3	1-Hexanol	34.2	65.8	20.9	49.1	30.0	0.313	13.3	10.7
4	1-Heptanol	33.6	66.4	21.9	46.6	31.5	0.267[d)]	11.5	10.9
5	1-Octanol	33.9	66.1	24.9	40.5	34.6	0.237[d)]	10.3	10.3
6	2-Ethyl-1-hexanol	—	—	21.1	28.7	50.2	0.162	4.4	9.5
7	2-Octanol	93.4	3.5, 3.1[b)]	34.1	59.4	3.6, 2.9[b)]	0.228[d)]	7.9	8.5
8	3-Methyl-1-butanol	30.3	19.4, 50.3[b)]	17.0	51.9	8.3, 22.7[b)]	0.343	14.7	11.0
9	Cyclohexanol	—	—	15.0	80.8	4.2	0.426[e)]	15.0	11.4
10	2-Methyl-1-propanol	26.8	73.2	13.2	60.7	26.0	0.456	17.7	10.8
11	Benzyl alcohol	36.5	63.5	15.2	64.6	20.2	0.354[e)]	13.1	11.1

a) Determined from the ^{19}F NMR spectra at 25±2 °C. b) The fraction for each of the two signals which appear at the chemical shift corresponds to the hemiacetal form. c) Data quoted from Ref. 7 (25 °C). d) This work (25 °C). e) At 20 °C. f) G. H. Morrison and H. Freiser, "Solvent Extraction in Analytical Chemistry," John Wiley & Sons, New York (1957), p. 249.

TABLE 2. FRACTIONS (%) OF THE THREE SPECIES OF TTA IN AQUEOUS BUTANOL SOLUTIONS

Mole fraction of water	Enol (%)	Hydrate (%)	Hemiacetal (%)
0.000	29.2	—	71.8
0.070	25.0	19.2	55.8
0.136	20.9	34.0	45.1
0.222	18.1	45.8	36.1
0.343	16.9	55.5	27.6
0.423	15.2	60.6	24.2
0.514	13.6	62.7	23.7

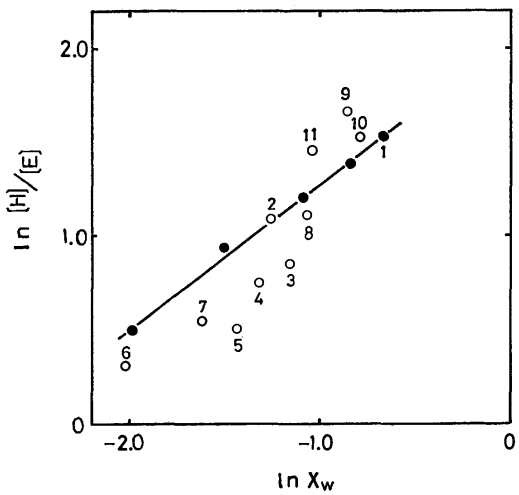

Fig. 3. Dependence of the enol-hydrate equilibrium constant on water mole fraction in alcohol; ●, aqueous 1-butanol, ○, water-saturated alcohols. The numbers in this figure correspond to those in Table 1.

alcohols affect the solubilities of both water and the hydrate form. Therefore, we also examined the influence of the physical properties of alcohols on the fraction ratio of [H]/[E].

Bernstein and Powling[8] have accounted for the influence of the solvent on the keto-enol tautomerism of β-diketones in terms of Onsager's model, which consideres the different energies of the electrostatic interaction of each tautomer with its surroundings. According to the relationship established in their work, the enthalpy of hydration, ΔH, may be represented as follows:

$$\Delta H_{\text{gas}} = \Delta H_{\text{solution}} + \left(\frac{\varepsilon-1}{2\varepsilon+1}\frac{1}{V_0}\right)_{\text{solvent}}(\mu_H^2-\mu_E^2), \quad (4)$$

where μ_H and μ_E are the dipole moments of the hydrate form and the enol form respectively, and where V_0 and ε are the molar volume and the dielectric constant of alcohol respectively. Equation 4 suggests the correlation between the free energy of the hydration, which is equal to $-RT$ ln [H]/[E], and $(\varepsilon-1)/V_0(2\varepsilon+1)$. In Fig. 4, ln [H]/[E] is plotted against the solvent quantity $(\varepsilon-1)/V_0(2\varepsilon+1)$. The plots almost follow a straight line, and the positive sign of the slope means that $\mu_H > \mu_E$.

Recently, the solubility parameter concept has been applied to the interpretation of the solvent effect of alcohols on the partition equilibrium of TTA.[6] Accord-

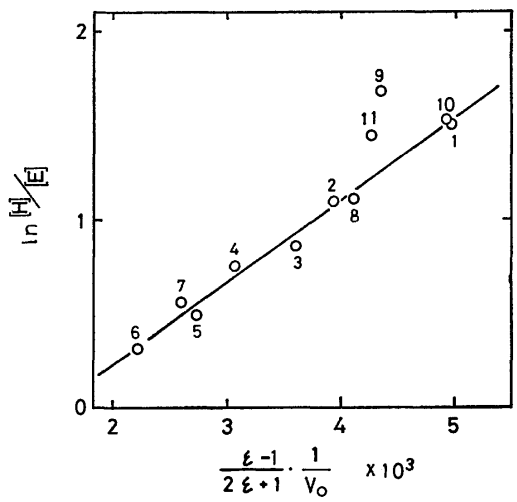

Fig. 4. Correlation between the enol-hydrate equilibrium constant and the solvent quantity $(\varepsilon-1)/V_0(2\varepsilon+1)$. The numbers in this figure correspond to those in Table 1.

ing to the solubility parameter theory, the equilibrium constant of the hydration reaction can be represented approximately by

$$\ln [H]/[E] = \frac{V_E}{RT}(\delta_H-\delta_E)(2\delta_0-\delta_E-\delta_H) + \text{const}, \quad (5)$$

where V_E is the molar volume of the enol form and where δ_H, δ_E, and δ_0 are the respective solubility parameters of the hydrate form, the enol form, and the water-saturated alcohol. The influence of water on the solubility parameter of the water-saturated alcohols is not serious in most alcohols, except for the cases of 1-butanol and 2-methyl-1-propanol, in which the next equation can be used for correction:

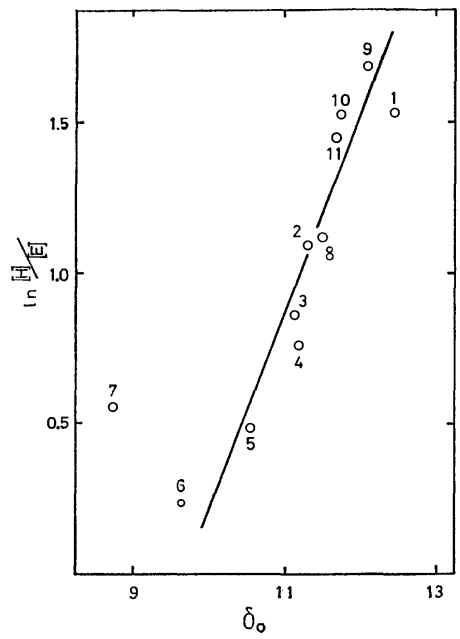

Fig. 5. Correlation between the enol-hydrate equilibrium constant and the solubility parameter of alcohol. The numbers correspond to those in Table 1.

$$\delta_0 = \phi_s\delta_s + \phi_a\delta_a, \quad (6)$$

where ϕ_a and ϕ_s are the respective volume fractions of water and alcohol and where δ_a and δ_s are the respective solubility parameters of water (23.4 $cal^{1/2}$ $cm^{-3/2}$) and alcohol. In Fig. 5, ln [H]/[E] is plotted against the solubility parameter of the alcohol. In most alcohols, the plots follow a straight line. The positive sign of the slope means that $\delta_H > {}_E\delta$, which corresponds to the result of $\mu_H > \mu_E$. From above results, we can state that the fraction of the hydrate form increases with the solvent quantity, ε or δ.

Inversion Rate of the Hemiacetal Form. The observed first-order rate constant (k) in dehydrated alcohol is the sum of the forward rate constant (k_a) and the reverse rate constant (k_e) in Eq. 2, *i.e.*, $k=k_a+k_e$. The enolization rate constant is calculated by means of the following relation:

$$k_e = fk, \quad (7)$$

where f is the enol fraction. The observed rate constant and the calculated enolization rate constant are listed in Table 3 for several alcoholic systems. The rate constant in 2-methyl-1-propanol is smaller than the others. This may be the result of the steric effect in the transition state.

Table 3. Observed interconversion rate constant (k) between the enol and hemiacetal forms and the estimated enolization rate constant (k_e) of TTA in alcoholic solutions

Solvent	Mole fraction of water	$k\times10^3$ (min^{-1})	$k_e\times10^3$ (min^{-1})
1-Butanol	0.000	2.39	0.70
	0.025		2.31
	0.049		3.72
	0.133		8.96
	0.234		20.7
1-Pentanol	0.000	3.48	1.11
1-Hexanol	0.000	11.7	4.00
1-Octanol	0.000	3.96	1.34
2-Methyl-1-propanol	0.000	1.07	0.29

In the case of a water-containing alcoholic solution, the following reaction can be expected to occur:

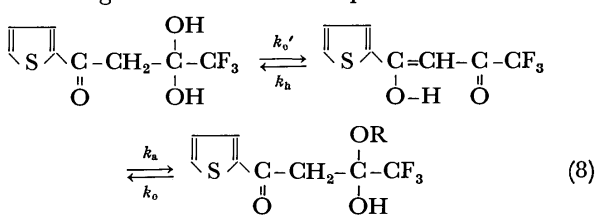

(8)

The rate equation for the above reaction may be described as

$$-\frac{d}{dt}[E] = (k_h+k_a)[E]-k_e'[H]-k_e[A]. \quad (9)$$

When the hydration rate is fast and the equilibrium between the enol form and the hydrate form is instantly established, Eq. 9 becomes

$$-\frac{d}{dt}[E] = \left(\frac{k_a}{1+K}+k_e\right)([E]-[E]_{eq}), \quad (10)$$

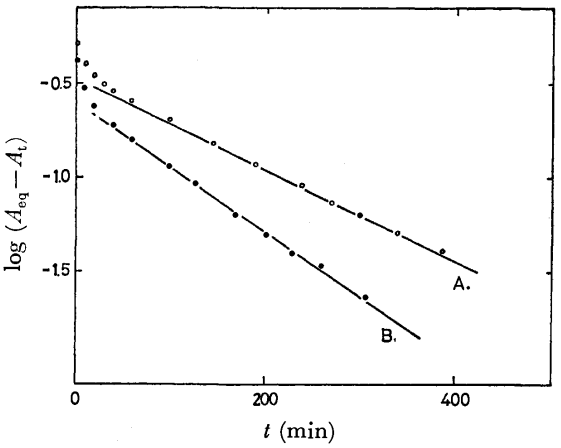

Fig. 6. Absorbance change of the enol form in aqueous 1-butanol solution; A, $X_w=0.025$, B, $X_w=0.049$.

where K is the equilibrium constant, $K=[H]_{eq}/[E]_{eq}$. The integration of Eq. 10 gives the final equation:

$$\log([E]_{eq}-[E]) = -\frac{k_a+(1+K)k_e}{2.30(1+K)}t + \text{const.} \quad (11)$$

Typical absorbance changes of the enol form observed in the aqueous 1-butanol solutions are shown in Fig. 6. The fast-reaction part and the subsequent slow-reaction part are clearly seen. The fast-reaction is connected with the hydration reaction. From the slope of the slow-reaction part, the rate constant of the enol-hemiacetal reaction was obtained. The rate constant for the process from the hemiacetal form to the enol form was calculated from the following reaction:

$$k_e = (1+K)fk. \quad (12)$$

The obtained values for k and k_e are listed in Table 3. The value of k_e increases with the water concentration. In Fig. 7, log ($k_e-k_e^\circ$) is plotted against the molar concentration of water, where k_e° denotes the enolization rate constant in dehydrated 1-butanol. A linear correlation with a slope of 0.92 was obtained. The result suggests that one water molecule participates in the

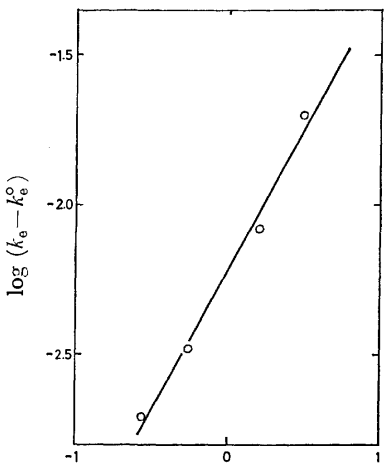

Fig. 7. Water concentration dependence of the enolization rate constant of the hemiacetal form in aqueous 1-butanol.

transformation from the hemiacetal form to the enol form. Takada *et al.*[9] examined the water-concentration dependence of the hydration rate of TTA in both dioxane and acetonitrile and suggested the third order in water. Bell *et al.*[10] have reported that three water molecules participate in the hydration of 1,3-dichloroacetone and that the water can be replaced by either carboxylic acid or 2,6-dichlorophenol. In the present system also, it can reasonably be expected that one water and some alcohol molecules participate cooperatively in the enolization process of the hemiacetal form.

From the results that the fraction of the hemiacetal forms is 20—30% for most water-saturated alcohols and that the inversion rate to the enol form is very slow, it can be expected that the hemiacetal form plays an important role in the kinetics and mechanism of metal extraction with TTA in an alcohol/water system.

References

1) A. K. De, S. M. Khopkar, and R. A. Chalmers, "Solvent Extraction of Metals," Van Nostrand Reinhold, London (1970), p. 56.

2) M. Yamazaki and T. Takeuchi, *Kogyo Kagaku Zasshi*, **72**, 2223 (1969).

3) J. C. Reid and M. Calvin, *J. Am. Chem. Soc.*, **72**, 2948 (1950).

4) M. R. Jaffe, D. P. Fay, M. Cefola, and Sutin, *J. Am. Chem. Soc.*, **93**, 2878 (1971).

5) Y. Kodama, K. Sato, and K. Arakawa, *Nippon Kagaku Zasshi*, **87**, 1092 (1966).

6) N. Suzuki, K. Akiba, T. Kanno, and T. Wakahayashi, *J. Inorg. Nucl. Chem.*, **26**, 2521 (1964).

7) A. Weissberger, E. S. Proskauer, J. A. Riddick, and E. E. Troops, Jr., "Technique of Organic Chemistry," Interscience, New York (1955), Vol. 7..

8) J. Powling and H. J. Bernstein, *J. Am. Chem. Soc.*, **73**, 4353 (1951).

9) H. Watarai, Y. Takada, and N. Suzuki, unpublished result.

10) R. P. Bell and J. E. Critchlow, *Proc. R. Soc. London, Ser. A*, **325**, 35 (1971).

Anodic Voltammetry and Its Analytical Application to the Detection and Simultaneous Determination of Hypoxanthine, Xanthine, and Uric Acid

Toshio YAO,* Yoichi TANIGUCHI, Tamotsu WASA, and Soichiro MUSHA

Department of Applied Chemistry, College of Engineering, University of Osaka Prefecture, Mozuumemachi, Sakai 591

(Received April 21, 1978)

The voltammetric oxidation of hypoxanthine, xanthine, and uric acid was investigated by means of linear-sweep voltammetry, cyclic voltammetry, and controlled-potential coulometry. Hypoxanthine, xanthine, and uric acid each gave a single oxidation peak at a different potential, with a stationary glassy carbon electrode, over the wide pH range of 0—13. Hypoxanthine was initially oxidized in a two-electron step to xanthine, which was then further oxidized in a two-electron step to uric acid, as well as the enzymatic oxidation. All three substances were strongly adsorbed on the surface of the glassy carbon electrode, so that the concentration *vs.* anodic peak current curves were not linear. The adsorption on the electrode was very dependent on the pH, and especially at pH values around neutrality the anodic peaks were ill-defined. However, in such acid solutions as H_3PO_4 and H_2SO_4, the voltammetric oxidation was a diffusion-controlled process and the differences between the peak potentials were most pronounced (*ca.* 400 mV). Consequently, it was possible to determine simultaneously three hydroxypurine bases by using 1 M H_2SO_4 or 1 M H_3PO_4 as a supporting electrolyte, without prior treatment or separation procedures.

The electrochemical oxidation and reduction of biologically important compounds have been investigated with much interest. It is important to understand fully their redox behavior in considering the methabolism and analytical determination of biologically important compounds. Several works[1-3] have suggested a possible parallelism between the modes of electrochemical behavior and the biological transformation, *e.g.*, the enzymatic oxidation.

The electrochemical reduction of purine bases, which are important components of nucleic acids, has been investigated in both aqueous[4-6] and nonaqueous solutions[7,8] at the dropping mercury electrode (DME). However, in aqueous solutions none of the purine bases except adenine were easily reduced at the DME.

A few studies of the electrochemical oxidation of purine bases have been done at the pyrolytic graphite electrode (PGE)[9-11] and the glassy carbon electrode (GCE).[12] Both adenine and guanine gave a anodic peak at different potentials over a wide pH range. Our own previous paper[12] described a method whereby adenine, guanine, and their nucleosides could be determined simultaneously by linear-sweep voltammetry using a stationary planar GCE.

In the present work, the oxidation behavior of three hydroxypurine bases (hypoxanthine, xanthine, and uric acid) was investigated by means of linear-sweep voltammetry, cyclic voltammetry, and controlled-potential coulometry. The mutual relation of the primary oxidation process of each of these hydroxypurine bases was investigated. Also, in order to develop a satisfactory analytical method of the three hydroxypurine bases it was found necessary to investigate in some detail the adsorption behavior on the GCE. This paper will describe the oxidation behavior and a method for the simultaneous determination of hypoxanthine, xanthine, and uric acid.

Experimental

Chemicals. The hypoxanthine, xanthine, and uric acid were all obtained from the Wako Pure Chemical Co. The other chemicals were of a reagent grade and were used without further purification.

Apparatus. The anodic voltammograms were recorded using a Yanagimoto P-8 type Polarograph. Cyclic voltammograms were obtained with a versatile solid-state instrument constructed in this laboratory following the design of Goolsby and Sawyer,[13] with the triangular voltage sweeps supplied by a NF circuit design block Co. Model FG-104T function generator. The current-voltage curves were recorded on a IWATSU Model DS-5016 dual-beam oscilloscope equipped with a camera. Controlled-potential coulometry was done with a NICHIA NP-1 type potentiostat, and a glassy carbon beaker (40 ml in volume, Tokai Electrode Co.) was used as the working electrode.

A three-electrode voltammetric cell maintained at (25±0.1) °C was used for all the experiments. A saturated calomel electrode (SCE) was employed as a reference electrode, while a platinum wire was employed as a counter electrode. A working electrode was constructed from a 3-mm glassy carbon rod (Grade GC-20, Tokai Electrode Co.). The rod was cut into a length of 10 mm and was sealed in one end of a glass tube (3 mm in diameter) with epoxy cement. The end of the glass tube-carbon rod assembly was polished with 400-grade emery paper until it was quite smooth. Then, by polishing with 1500-grade emery paper and then with a paste of CeO_2 on asphalt pitch, the surface of the electrode was brought to a mirror finish.

Voltammetric Procedure. In order to obtain reproducible results, a standard pretreatment procedure was applied before recording each voltammogram. The GCE was polished for 30 s with 1500-grade emery paper and then with a paste of CeO_2 on asphalt pitch until the surface of the electrode was brought to a mirror finish. The surface of the electrode was then washed with a fine spray of distilled water. Any water remaining on the electrode surface and the shaft of the electrode was removed by touching the surface very gently with a piece of soft absorbent paper. The test solutions were not deaerated. The voltage scan was commenced after quiescency

for about 20 s at the starting potential (usually 0.0 V *vs.* SCE).

At least three replicate voltammograms were recorded for each test solution. A current-voltage curve of the background solution was recorded in the same way, while the peak current was obtained by arithmetrically subtracting the observed background current at the peak potential from that of the test solution.

Results and Discussion

Linear-Sweep Voltammetry. *Effect of pH*: Hypoxanthine, xanthine, uric acid each gave an oxidation peak at a stationary GCE over the wide pH range of 0—13. The anodic voltammograms recorded at various pH values are shown in Fig. 1 for uric acid and in Fig. 2

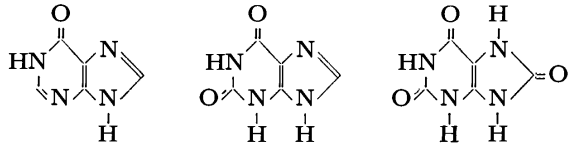

Hypoxanthine Xanthine Uric acid

for xanthine. The oxidation peaks of uric acid and xanthine tended to become ill-defined with the increase in pH, and their peak currents decreased gradually. Similar behavior was also observed for hypoxanthine.

The half-peak potentials ($E_{p/2}$) of the oxidation peaks of the three hydroxypurine bases (uric acid, xanthine, and hypoxanthine), as is shown in Fig. 3, shifted linearly towards negative potentials with the increase in pH; $E_{p/2}$ (*vs.* SCE)/V=0.69—0.050 pH for uric acid, $E_{p/2}$ (*vs.* SCE)/V=1.08—0.059 pH for xanthine, and $E_{p/2}$(*vs.* SCE)/V=1.50—0.068 pH for hypoxanthine. The analytical significance of these experimental results lies in the fact that the voltammetric oxidation peak-potential for each of the three hydroxypurine bases is quite different at each of the pH values studied.

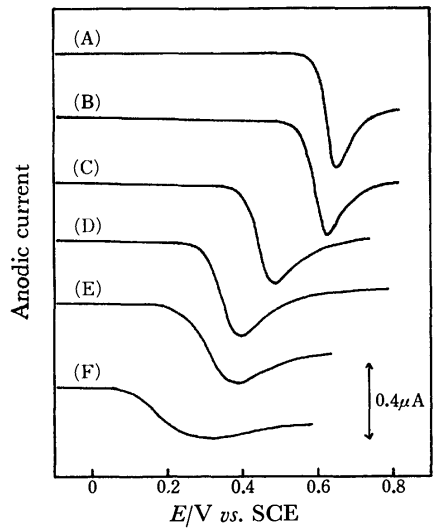

Fig. 1. Anodic voltammograms of 0.1 mM uric acid recorded at different pH values.
Supporting electrolytes: (A) 1M H_3PO_4; Britton-Robinson buffer (B) pH 2.03, (C) pH 4.39, (D) pH 6.36, (E) pH 8.20, (F) pH 10.04.
GCE geometric area: 7.1 mm², scan rate: 3.3 mV/s.

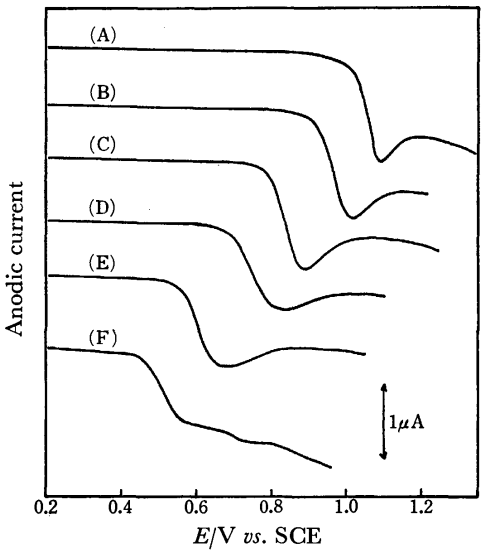

Fig. 2. Anodic voltammograms of 0.1 mM xanthine recorded at different pH values.
Supporting electrolytes: (A) 1M H_3PO_4; Britton-Robinson buffer (B) pH 2.08, (C) pH 4.05, (D) pH 6.07, (E) pH 8.02, (F) pH 9.92.
GCE geometric area: 7.1 mm², scan rate: 3.3 mV/s.

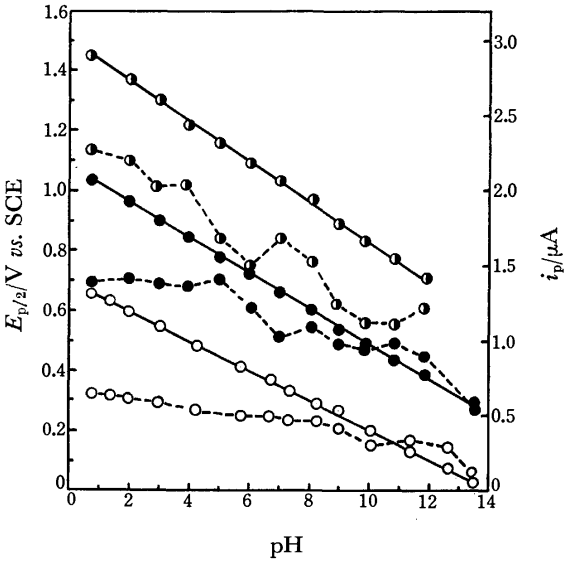

Fig. 3. The effect of pH on the peak current and the half-peak potential of the voltammetric oxidation peaks of 0.1 mM uric acid (○), xanthine (●), and hypoxanthine (◑).
GCE geometric area: 7.1 mm², scan rate: 3.3 mV/s.
----: i_p, —— : $E_{p/2}$.

The peak current of the oxidation peaks gradually decreased with the increase in pH, as is shown in Fig. 3, particularly in the case of hypoxanthine. This experiment was undertaken at a relatively low concentration (0.1 mM) of the hydroxypurine bases. When the depolarizer concentration was fairly high (1.0 mM), the pH values were found to have a pronounced effect on the peak current of the hydroxypurine bases. That is, the peak current decreased extremely at the pH values

around neutrality, as is shown in Fig. 4 for hypoxanthine. However, the peak current was relatively constant in the Britton-Robinson buffer at pH 2.1 and in acid solutions (1 M H_2SO_4, $HClO_4$, and H_3PO_4) as supporting electrolytes. Also, in electrolytes containing chloride ions such as HCl, the oxidation peak of hypoxanthine was masked by the facile oxidation of the chloride ion in the background electrolyte. Similar relationships between the peak current and the pH values were also obtained for the oxidation peaks of xanthine and uric acid.

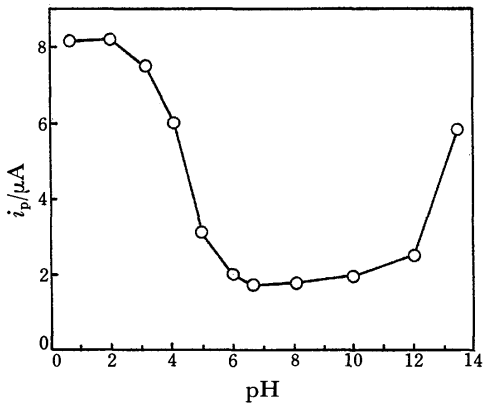

Fig. 4. The effect of pH on the peak current of 1.0 mM hypoxanthine.
GCE geometric area: 7.1 mm², scan rate: 3.3 mV/s.

Effect of the Scan Rate: In order to study the adsorption of the hydroxypurine bases on the stationary GCE, the effect of the voltage scan rate on the peak current of each hydroxypurine base was examined.

For a linear diffusion-controlled peak, the peak current function, $i_p/ACV^{1/2}$, should be a constant[14] in spite of the variation in the scan rate, where A is the area of the electrode surface; C, the bulk concentration of depolarizer; and V, the scan rate. In 1 M H_2SO_4 or H_3PO_4, the peak current function for each of the three hydroxypurine bases was almost independent of the scan rate. In the electrolyte solution with pH values around neutrality, however, the peak current functions increased with the increase in the scan rate, especially in the case of hypoxanthine. This behavior is typical of an electrode process where the reactant is adsorbed on the electrode,[15] but in 1 M H_2SO_4 or H_3PO_4 the voltammetric oxidation is a diffusion-controlled process.

Effect of the Concentration: In the 0.5 M phosphate buffer (pH 6.6), the relationship between the peak current and the concentration were nearly linear for both xanthine and uric acid, but non-linear for hypoxanthine, as is shown in Fig. 5. The peak potential was also dependent on the concentration and slightly shifted to more positive values with the increase in the concentration. Over the concentration range of 0.02—0.2 mM, this shift was about 14 mV for uric acid, 29 mV for xanthine, and 55 mV for hypoxanthine. In the Britton-Robinson buffer with pH values of 8—10, hypoxanthine showed a post-peak at a more positive potential than the main peak at concentrations above *ca.* 1 mM. This post-peak appeared at rather variable potentials.

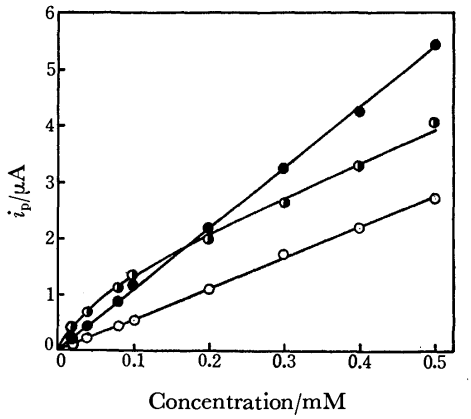

Fig. 5. The relationships between the peak current and the concentration in 0.5 M phosphate buffer (pH 6.6).
○: Uric acid, ●: xanthine, ◑: hypoxanthine.

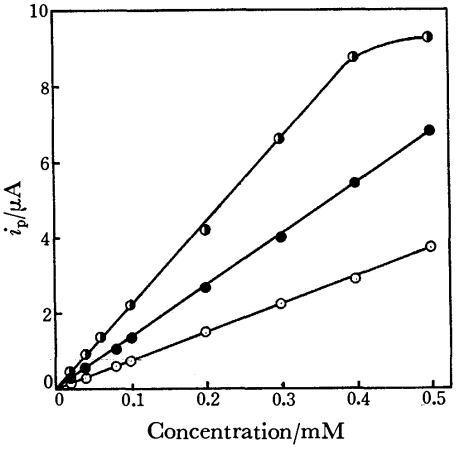

Fig. 6. The relationships between the peak current and the concentration in 1 M H_3PO_4.
○: Uric acid, ●: xanthine, ◑: hypoxanthine.

However, in such acid solutions as 1 M H_3PO_4 and H_2SO_4, each of these hydroxypurine bases showed a good linear relationship between the peak current and the concentrations ranging from 0.02 to 0.4 mM, as is shown in Fig. 6. Also, the peak potential was independent of the concentration.

These effects of the concentration and the pH on the peak current imply that the adsorption of the depolarizer on the GCE is very dependent on the pH, but in 1 M H_3PO_4 or H_2SO_4 solutions the voltammetric oxidation is a diffusion-controlled process.

Mutual Relation of Primary Oxidation Processes. Cyclic voltammograms at fast scan rates were recorded for each of the three hydroxypurine bases. The results are shown in Fig. 7. Scanning from 0.0 V at a clean electrode toward a positive potential, only a single anodic peak was observed for hypoxanthine. The principle point of interest in this voltammogram is that two new and small anodic peaks (Peaks I and II) were observed on the second sweep toward the positive potential, Peak I at 0.65 V and Peak II at 0.99 V (*vs.* SCE) in the Britton-Robinson buffer at pH 2.1. However, the peak potentials of these new peaks were

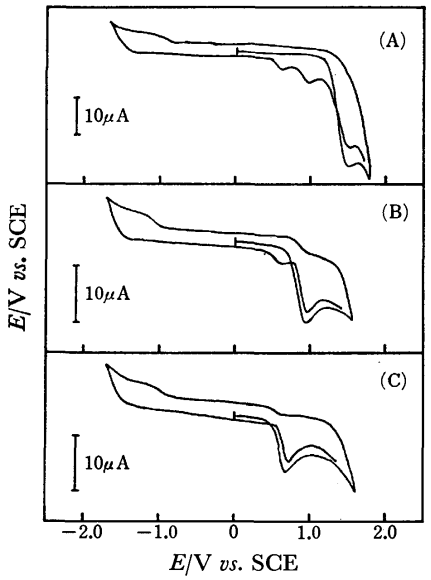

Fig. 7. Cyclic voltammograms of hypoxanthine (A), xanthine (B), and uric acid (C) in the Britton-Robinson buffer at pH 2.1.
Scan rate; (A): 10.3 V/s, (B): 6.4 V/s, (C): 6.6 V/s.

TABLE 1. COULOMETRIC *n* VALUES FOR THE CONTROLLED-POTENTIAL ELECTROLYSIS OF OXYPURINE BASES IN 1 M H_3PO_4

Oxypurine bases	Applied potential (V *vs.* SCE)	$n^{a)}$
Uric acid	0.80	2.21
Xanthine	1.20	4.16
Hypoxanthine	1.60	5.88

a) Average value of triplicate determinations.

dependent on the pH of electrolyte solutions. At various pH values, the peak potentials for these two anodic peaks, I and II, were the same as those of the anodic peaks for the oxidation of uric acid and xanthine respectively. Similarly, xanthine showed a new anodic peak on the second sweep toward the positive potential. This peak appeared at almost the same peak potential as the anodic peak of uric acid.

Controlled-potential coulometry for each of three hydroxypurine bases was carried out in 1 M H_3PO_4. The electrolysis was continued until all of the depolarizers were completely oxidized. Typical coulometric data are presented in Table 1; the *n* value for uric acid was about two, for xanthine it was four, and for hypoxanthine it was six.

In summary, the cyclic voltammetric and coulometric data suggest that hypoxanthine is initially oxidized in a two-electron step to produce xanthine, which is then further oxidized in a two-electron step to produce uric acid. It is also known[16] that uric acid is oxidized in a two-electron process to produce 4,5-dihydroxy-4,5-dihydrouric acid, which is unstable and which fragments predominantly to allantoin, but a very small fraction is further oxidized to parabanic acid. Hypoxanthine is also enzymatically oxidized to uric acid *via* xanthine by the action of the xanthine oxidase. Thus, it is interesting that the electrochemical oxidation is very similar to the enzymatic oxidation.

Analytical Application. The anodic voltammograms for the mixtures of uric acid, xanthine, and hypoxanthine were recorded in three electrolyte solutions (Fig. 8). In 1 M H_2SO_4 three successive well-defined oxidation peaks were observed, but in the 0.5 M phosphate buffer and 1 M NaOH solutions the three peaks were ill-defined, as a result that the increase in the pH of the electrolyte solutions made the voltammetric peaks sensitive to the adsorption of depolarizers on the GCE. Accordingly, for the detection and quantitative determination of the three hydroxypurine bases, the use of a 1 M H_2SO_4 or H_3PO_4 solution as the supporting electrolyte was suitable. In order to test the quantitative method developed here, the voltammograms for some mixtures of three hydroxypurine bases were recorded in 1 M H_2SO_4 at a stationary GCE. The concentration of each hydroxypurine base was determined by the calibration-curve method from the respective heights of the resulting voltammetric oxida-

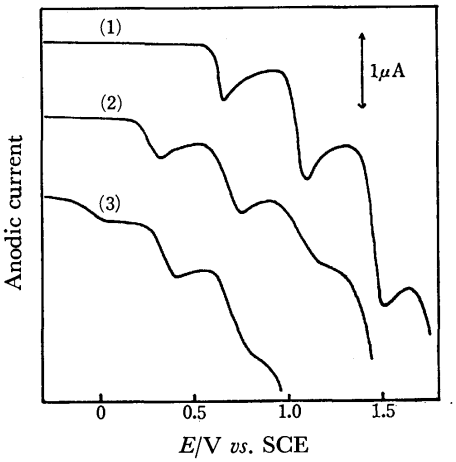

Fig. 8. Anodic voltammograms for the mixtures of uric acid, xanthine, and hypoxanthine.
Concentration of each of uric acid, xanthine, and hypoxanthine: 0.1 mM. Supporting electrolyte; (1): 1 M H_2SO_4, (2): 0.5 M phosphate buffer (pH 6.6), (3): 1 M NaOH.

TABLE 2. VOLTAMMETRIC RESULTS FOR THE DETERMINATION OF EACH COMPONENT IN MIXTURES OF URIC ACID, XANTHINE, AND HYPOXANTHINE

Taken (mM)			Found (mM)		
A	B	C	A	B	C
0.05	0.05	0.05	0.04	0.05	0.05
0.10	0.10	0.10	0.10	0.10	0.09
0.10	0.10	0.30	0.10	0.09	0.32
0.20	0.20	0.20	0.19	0.21	0.20
0.40	0.40	0.20	0.41	0.38	0.18
0.20	0.20	0.30	0.20	0.20	0.29

A, Uric acid; B, xanthine; C, hypoxanthine. Supporting electrolyte, 1 M H_2SO_4; GCE geometric area, 7.1 mm^2; scan rate, 3.1 mV/s.

tion peaks. Some typical analytical results are shown in Table 2. Clearly this method is readily capable of determining simultaneously each component in mixtures of the three hydroxypurine bases.

The principal advantage of the proposed method is the rapidity of analysis. The speed of analysis is aided by the fact that no prior treatment or separation procedure is needed. Furthermore, as dissolved oxygen does not interfere with the anodic voltammetry, no deaeration is required.

References

1) W. A. Struck and P. J. Elving, *Biochem.*, **4**, 1343 (1965).
2) G. Dryhurst and P. J. Elving, *J. Electrochem. Soc.*, **115**, 1014 (1968).
3) G. Dryhurst, *J. Electrochem. Soc.*, **116**, 1097 (1969).
4) D. L. Smith and P. J. Elving, *J. Am. Chem. Soc.*, **84**, 1412 (1962).
5) G. Dryhurst and P. J. Elving, *Talanta*, **16**, 855 (1969).
6) P. J. Elving, S. J. Pace, and J. E. O'Reilly, *J. Am. Chem. Soc.*, **95**, 647 (1973).
7) T. Yao and S. Musha, *Bull. Chem. Soc. Jpn.*, **47**, 2650 (1974).
8) T. Yao, T. Wasa, and S. Musha, *Nippon Kagaku Kaishi*, **1976**, 704.
9) G. Dryhurst and P. J. Elving, *J. Electrochem. Soc.*, **115**, 1014 (1968).
10) G. Dryhurst and G. F. Pace, *J. Electrochem. Soc.*, **117**, 1259 (1970).
11) G. Dryhurst, *Talanta*, **19**, 769 (1972).
12) T. Yao, T. Wasa, and S. Musha, *Bull. Chem. Soc. Jpn.*, **50**, 2917 (1977).
13) A. D. Goolsby and D. T. Sawyer, *Anal. Chem.*, **39**, 411 (1967).
14) R. S. Nicholson and I. Shain, *Anal. Chem.*, **36**, 706 (1964).
15) R. H. Wopschall and I. Shain, *Anal. Chem.*, **39**, 1514 (1967).
16) G. Dryhurst, *J. Electrochem. Soc.*, **118**, 699 (1971).

Preparation and Solid-phase Thermal *cis-α* ⟷ *cis-β* Isomerization of the Chromium(III) Triethylenetetramine Complexes[1)]

Ryokichi TSUCHIYA,* Akira UEHARA, Kazuhiko NOJI, and Hitoshi YAMAMURA

Department of Chemistry, Faculty of Science, Kanazawa University, Kanazawa 920

(Received April 24, 1978)

Heating of a mixture of $CrCl_3 \cdot 6H_2O$ and triethylenetetramine (trien) produced violet products which gave *cis*-α-$[Cr_2(OH)_2trien_2]X_4 \cdot 2H_2O$ and *cis*-α-$[Cr(OH)(H_2O)trien]X_2 \cdot H_2O$ (X=Cl, Br or I) on treatment with aqueous NaX solutions. *cis*-α-$[CrCl_2trien]Cl \cdot 2H_2O$ were obtained in the presence of a trace amount of water. Absolutely dry conditions are necessary for the preparation of *cis*-β-$[CrCl_2trien]Cl$. The thermally induced reversible *cis*-α↔*cis*-β isomerization was detected in the complexes *cis*-α-$[Cr(OH)(H_2O)trien]Cl_2 \cdot H_2O$ and *cis*-β-$[CrCl_2trien]Cl$ by means of derivatography and high-temperature IR spectroscopy. The former *cis*-α-hydroxoaqua complex was found to be converted irreversibly into *cis*-β-form above 225 °C in the solid-phase. The *cis*-β-form obtained readily isomerized to *cis*-α-form in aqueous media. The dimeric *cis*-α-$[Cr_2(OH)_2trien_2]^{4+}$ was converted gradually into the monomeric *cis*-α-$[Cr(OH)(H_2O)trien]^{2+}$ in water.

Three geometrically possible isomers are expected for the chromium(III)–triethylenetetramine (trien) complexes: *cis*-α, *cis*-β, and *trans*-forms (Fig. 1). In the case of the cobalt(III)[2-8] and rhodium(III)[9,10] complexes, the three geometrical isomers as well as other conformational isomers, especially of the dihalogeno complexes [Co or Rh Cl_2 trien]$^+$ have been reported. As regards the chromium(III) complexes, however, only *cis*-α-form is known[11,12] except for the recent report by Fordyce *et al.*[13] on *cis*-β-$[CrCl_2trien]Cl$. This is partly because the *cis*-β complexes are apt to undergo rapid aquation and isomerization in aqueous media. Special care is thus necessary for preparation of the *cis*-β complexes. Difficulties might be overcome if hydrous chromium(III) salts could be used in the preparation of the desired complexes.

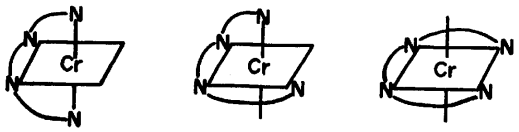

cis-α *cis*-β *trans*

Fig. 1. Geometrically possible isomers of the Cr(III)–trien complexes.

We have attempted to prepare the Cr(III)–trien complexes by the reaction of $CrCl_3 \cdot 6H_2O$ and trien in a matrix state in order to clarify the solid-phase *cis*-α↔*cis*-β thermal isomerization of the complexes obtained. The survey of the isomerization in the solid-phase enables us to predict the possibility of the formation of *cis*-β complexes hardly obtainable in the presence of water.

Experimental

Preparation of Complexes. cis-α-*Di-μ-hydroxo-bis(triethylenetetraminechromium(III)) Iodide Dihydrate,* cis-α-$[Cr_2(OH)_2trien_2]I_4 \cdot 2H_2O$ *(bluish violet).* 30 g (0.11 mol) of chromium(III) chloride hexahydrate and 18 g (0.12 mol) of trien were triturated in a mortar of 12 cm diameter and heated at 180 °C for 6 h in an air-bath. The resulting violet masses were crushed. Excess ethanol was added to extract unreacted trien. After the extraction had been repeated 2 or 3 times, the bluish violet products were dissolved in 200 ml of hot water. Greenish residues were then removed by filtration. To the violet filtrate, 30 g (0.2 mol) of sodium iodide was added. Bluish violet crystals were soon separated out. The crystals had to be quickly recrystallized from water, otherwise the following hydroxoaqua complex was obtained. Yield about 20 g.

Found: C, 14.62; H, 4.15; N, 11.76%. Calcd for $C_{12}H_{42}O_4N_8I_4Cr_2$: C, 14.79; H, 4.08; N, 11.95%.

cis-α-*Hydroxoaquatriethylenetetraminechromium(III) Chloride Monohydrate,* cis-α-*[Cr(OH)(H$_2$O)trien]Cl$_2$·H$_2$O (pink).* The violet filtrate was allowed to stand in a refrigerator overnight without addition of NaI, pink products being obtained. Recrystallization was carried out from water. Yield 3 g.

The complex was also obtained when the aqueous solution of the di-μ-hydroxo complex was allowed to stand overnight.

The corresponding bromide and iodide were obtained as monohydrates by addition of NaBr and NaI, respectively, to the aqueous solution of *cis*-α-$[Cr(OH)(H_2O)trien]Cl_2 \cdot H_2O$.

The *cis*-α complex was converted irreversibly into *cis*-β-form above 225 °C in the solid-phase. Isomerization makes it possible to prepare the *cis*-β complex. However, we could not purify the product because of the absence of a suitable solvent. Recrystallization from water always gave *cis*-α-form.

cis-α-*Dichlorotriethylenetetraminechromium(III) Chloride Dihydrate,* cis-α-*[CrCl$_2$trien]Cl·2H$_2$O (violet) and* cis-β-*Dichlorotriethylenetetramine Chloride,* cis-β-*[CrCl$_2$trien]Cl (violet).* These

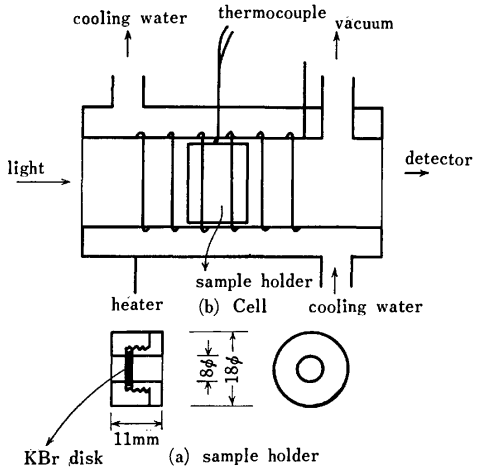

Fig. 2. Devices for measuring IR spectra at elevated temepartures.
(a) Sample holder, (b) cell.

were prepared from *cis*-α-[Cr(ox)trien]Br·nH$_2$O (n=3 or 0 respectively) according to the method of Fordyce *et al.*[13] slightly modified and identified by means of elemental analysis and IR spectroscopy. The striking difference in preparation between the *cis*-α and *cis*-β complexes is that the former can be obtained even in the presence of a trace amount of water, while water should be absolutely avoided in the preparation of the latter.

Instruments. Derivatograms, IR and UV spectra, and molar conductivities were measured by the same apparatus as reported.[14] The IR spectra at elevated temperatures were monitored with a temperature-controlled cell (Fig. 2). The cell was then set up on a JASCO A-3 IR spectrophotometer. The 9 mm diam KBr disk prepared in the usual way was loaded in the steel holder (Fig. 2-(a)), which was then put in a cell regulated at the desired constant temperatures (Fig. 2-(b)). The sample (KBr disk) temperature was measured and controlled with a SINYO RIKA DIGICON-1200 equipped with an alumel-chromel thermocouple.

Results and Discussion

IR Spectra. The band due to the NH asymmetric bending vibration in the region 1550—1600 cm^{-1} is diagnostically useful for distinguishing *cis*-α from *cis*-β complexes: *cis*-α has one band, *cis*-β 2 or 3 bands in this region.[2,12,13] Figure 3 shows the IR spectra of *cis*-α-[CrCl$_2$trien]Cl·2H$_2$O, *cis*-α-[Cr(ox)trien]Br·3H$_2$O, *cis*-α-[Cr(OH)(H$_2$O)trien]Cl$_2$·H$_2$O and *cis*-β-[CrCl$_2$trien]Cl. The spectrum of *cis*-α-[Cr$_2$(OH)$_2$trien$_2$]I$_4$·2H$_2$O is omitted since it is essentially the same as that of *cis*-α-[Cr(OH)(H$_2$O)trien]Cl$_2$·H$_2$O. The numerical data for the samples before, during and after heating at appropriate temperatures are summarized in Table 1. All the *cis*-α complexes have a sharp band, while the *cis*-β complex has three distinctive peaks. Noticeable changes could be detected in the IR spectra of *cis*-α-[Cr(OH)(H$_2$O)trien]Cl$_2$·H$_2$O and *cis*-β-[CrCl$_2$trien]Cl at elevated temperatures. The changes thermally reversible may come from the reversible *cis*-α↔*cis*-β isomerization of these complexes.

Electronic Spectra. *Hydroxo Complexes*: The absorption maxima due to d-d transition of each complex are summarized in Table 2. The dimeric structure for *cis*-α-[Cr$_2$(OH)$_2$trien$_2$]I$_4$·2H$_2$O is supported by the appearance of the band at about 36.6×10^3 cm^{-1} (log

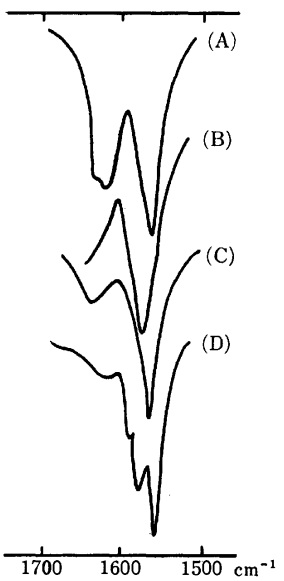

Fig. 3. IR spectra.
(A) *cis*-α-[CrCl$_2$trien]Cl·2H$_2$O, (B) *cis*-α-[Cr(ox)trien]Br·3H$_2$O, (C) *cis*-α-[Cr(OH)(H$_2$O)trien]Cl$_2$·H$_2$O, (D) *cis*-β-[CrCl$_2$trien]Cl.

$\varepsilon\approx4.1$) assignable to the bridging OH groups.[15] The absorption maxima of the complex in water shift gradually to higher wavenumber regions. After being left to stand they became similar to those of *cis*-α-[Cr(OH)(H$_2$O)trien]Cl$_2$·H$_2$O, suggesting that the dimeric di-μ-hydroxo complex is gradually converted into the monomeric complex in water.

Dichloro Complexes: The electronic spectra of *cis*-α-[CrCl$_2$trien]Cl·2H$_2$O and *cis*-β-[CrCl$_2$trien]Cl were measured both in dry methanol and in 0.1 mol dm^{-3} hydrochloric acid. The resemblance in color between the *cis*-α and *cis*-β complexes is recognizable from the similarity of their electronic spectral data in dry methanol used for preventing aquation of the complexes. However, both the complexes differ remarkably from each other in hydrochloric acid solution. As seen in Table 2, the first band (18.3×10^3 cm^{-1}) of the *cis*-β complex shifts to higher wavenumber regions (19.2×10^3 cm^{-1}) within only 3 minutes after the complex was dissolved in 0.1 mol dm^{-3} hydrochloric acid, the

Table 1. IR data for NH asymmetric bending vibration

Complex	Temp	Wave number (cm^{-1})[a]
cia-α-[CrCl$_2$trien]Cl·2H$_2$O	Room temp	1567 (vs)
cis-α-[Cr(ox)trien]Br·3H$_2$O	Room temp	1576 (vs)
cis-α-[Cr(OH)(H$_2$O)trien]Cl$_2$·H$_2$O	Room temp	1570 (vs)
	160 and 230 °C	1592 (w), 1575 (s), 1556 (vs)
	Cooled to room temp after heating at 160 °C	1570 (vs)
	Cooled to room temp after heating at 230 °C	1592 (w), 1575 (s), 1558 (vs)
cis-α-[Cr$_2$(OH)$_2$trien$_2$]I$_4$·2H$_2$O	Room temp	1568 (vs)
cis-β-[CrCl$_2$trien]Cl	Room temp	1591 (w), 1578 (s), 1561 (vs)
	70 °C—decomp temp (285 °C)	1581 (vs)
	Cooled to room temp after heating at 70—285 °C	1592 (w), 1579 (s), 1558 (vs)

a) The terms w, s, and vs denote weak, strong and very strong, respectively.

Table 2. Absorption maxima due to d-d transition ($\bar{\nu} \times 10^3$ cm^{-1})

Complexes	$\bar{\nu}_I$(log ε)	$\bar{\nu}_{II}$(log ε)
cis-α-[$Cr_2(OH)_2trien_2$]$I_4 \cdot 2H_2O$		
in DMSO	18.4(2.11)	25.2(2.09)[a]
in water	19.2(1.96)	25.9(1.85)
cis-α-[Cr(OH)(H_2O)trien]$Cl_2 \cdot H_2O$		
in water	19.2(1.96)	25.9(1.85)
cis-α-[$CrCl_2$trien]$Cl \cdot 2H_2O$		
in dry methanol	18.5(2.00)	24.6(2.01)
in 0.1 mol dm^{-3} HCl[b]	18.6(2.01)	25.1(1.98)
cis-β-[$CrCl_2$trien]Cl		
in dry methanol	18.3(2.01)	24.6(1.95)
in 0.1 mol dm^{-3} HCl[b]	19.2(2.05)	25.3(1.89)[c]

a) The complex gave the specific band at about 36.6×10^3 cm^{-1} (log $\varepsilon \approx 4.1$) due to the di-μ-hydroxo group. b) Measured 3 min after the complex was dissolved. c) The data are closely similar to those of *cis*-α-[CrCl(H_2O)trien]$^{2+}$ reported previously.[13]

spectrum being quite similar to those of *cis*-α-[CrCl(H_2O)trien]$^{2+}$.[13] On the other hand, only a slight shift was observed in the case of the *cis*-α complex ($18.5 \times 10^3 \rightarrow 18.6 \times 10^3$ cm^{-1}). The *cis*-α complex was also found to be finally aquated to form *cis*-α-[CrCl(H_2O)trien]$^{2+}$. These results indicate that the *cis*-β complex aquates and isomerizes quite rapidly as compared with the *cis*-α complex.

Thermally Induced cis-α↔cis-β *Isomerization in the Solid-phase.* Reversible *cis*-α↔*cis*-β isomerization was found to be thermally induced in the complexes *cis*-α-[Cr(OH)(H_2O)trien]$Cl_2 \cdot H_2O$ and *cis*-β-[$CrCl_2$trien]Cl. Figure 4 shows the derivatograms of both the complexes measured in a nitrogen stream at a heating rate of 1 °C min^{-1}.

As seen from the TG curve of *cis*-α-[Cr(OH)(H_2O)trien]$Cl_2 \cdot H_2O$, the complex evolves 1 mol of water at 50—135 °C, remaining unchanged up to 295 °C, and then decomposes in a complicated way. Two small but distinct endothermic peaks are observed in the DTA curve after the dehydration step. The original pink color of the complex becomes slightly violet at the first endothermic peak (*ca.* 160 °C), the violet tone returning to the original pink color upon cooling at room temperature. The reversibility was repeatedly found in each step between the first (160 °C) and the second (225 °C) DTA peaks. However, thermochromism becomes irreversible above the temperature of the second DTA peak.

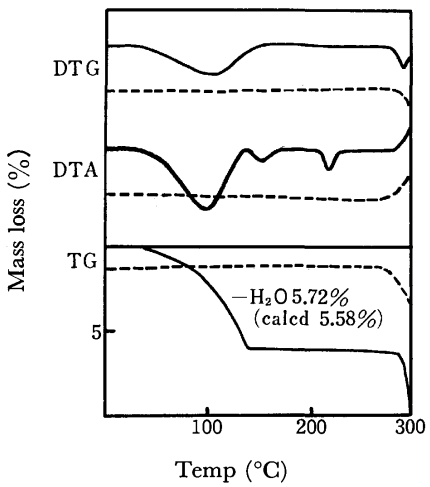

Fig. 4. Derivatograms of *cis*-α-[Cr(OH)(H_2O)trien]$Cl_2 \cdot H_2O$ (——) and *cis*-β-[$CrCl_2$trien]Cl (----).

The thermochromic behavior was monitored by measuring IR spectra below and above respective DTA peaks. As seen from Table 1, the complex exhibits one sharp band at room temperature, and three bands (1592, 1575, and 1556 cm^{-1}) at 160 °C. The three bands were quenched when the complex was cooled to room temperature, its original one band being recovered. Such IR spectral changes were reversible between the first (160 °C) and the second (225 °C) DTA peaks. The changes became irreversible above 230 °C (Table 1). The results suggest that the complex undergoes reversible *cis*-α↔*cis*-β isomerization at 160—225 °C, being converted into *cis*-β-form irreversibly above 225 °C. This implies that the heating of the *cis*-α complex above 225 °C furnishes a useful method for preparing *cis*-β complex which is hardly obtained in solution. However, the *cis*-β complex thus obtained could not be purified.

cis-α-[Cr(OH)(H_2O)trien]$Cl_2 \cdot H_2O$ underwent no olation upon heating, although hydroxoaqua Co(III) and Cr(III) complexes usually evolve the coordinated water to form the corresponding di-μ-hydroxo complexes.[16]

On the other hand, the violet color of *cis*-β-[$CrCl_2$trien]Cl became faintly bluish above 70 °C, and the bluish tone returned to the initial violet when the complex was cooled to room temperature. The change was also reversible. No change was found in both the TG and DTA curves up to 285 °C, above which the complex began to decompose (Fig. 4).

Monitoring of the IR spectra revealed that the band due to the NH asymmetric bending vibration appears as three peaks (1591, 1578, and 1561 cm^{-1}) and as one sharp peak (1581 cm^{-1}) at room temperature and at a temperature above 70 °C, respectively. The one sharp peak, however, returned to three peaks when the complex was allowed to stand at room temperature. Such a spectral change was also reversible, suggesting the occurrence of the reversible *cis*-β↔*cis*-α isomerization. Fordyce *et al.*[13] reported that the *cis*-β complex does not isomerize to *cis*-α-form even after the complex was held at 120 °C for 24 h. Their results are understandable in view of our finding that the isomerization is reversible in the temperature region from 70 °C to the decomposition temperature (285 °C). In contrast to *cis*-α-[Cr(OH)(H_2O)trien]$Cl_2 \cdot H_2O$, no clear isomerization temperature was observed in the DTA curve of *cis*-β-[$CrCl_2$trien]Cl. This might be due to a small difference in their relative enthalpies between *cis*-β and *cis*-α complexes.

The isomerization of *cis*-α-[Cr(OH)(H_2O)trien]$Cl_2 \cdot H_2O$ is completed at about 225 °C to give the *cis*-β complex, whereas the isomerization of *cis*-β-[$CrCl_2$trien]Cl remains to be reversible until the complex begins to decompose. This might be interpreted as follows: two

adjacent coordination sites in octahedral environment are occupied by OH and H_2O in *cis*-α-[Cr(OH)(H_2O)-trien]$Cl_2 \cdot H_2O$, and two chloride ions in *cis*-β-[$CrCl_2$-trien]Cl. The size of Cl ion is considerably greater than that of OH or H_2O. If isomerization takes place through twist-mechanism, the size of Cl ion hinders the completion of isomerization. Thus the *cis*-β dichloro complex might decompose prior to reaching the completion-temperature of isomerization. On the contrary, the completion-temperature (about 225 °C) of the isomerization of *cis*-α-[Cr(OH)(H_2O)trien]$Cl_2 \cdot H_2O$ is far lower than the decomposition temperature (295 °C).

References

1) Presented at the 37th National Meeting of the Chemical Society of Japan, Yokohama, April 1978.

2) D. A. Buckingham and D. Jones, *Inorg. Chem.*, **4**, 1387 (1965).

3) A. M. Sargeson and G. H. Searle, *Inorg. Chem.*, **4**, 45 (1965).

4) E. Kyuno, L. J. Boucher, and J. C. Bailar, Jr., *J. Am. Chem. Soc.*, **87**, 4458 (1965).

5) D. A. Buckingham, P. A. Marzilli, and A. M. Sargeson, *Inorg. Chem.*, **6**, 1032 (1967).

6) A. M. Sargeson and G. H. Searle, *Inorg. Chem.*, **6**, 787 (1967).

7) G. H. Searle and A. M. Sargeson, *Inorg. Chem.*, **12**, 1014 (1973).

8) P. S. Sheridan and A. W. Adamson, *Inorg. Chem.*, **13**, 2482 (1974).

9) P. M. Gidney, R. D. Gillard, B. T. Heaton, P. S. Sheridan, and D. H. Vaughan, *J. Chem. Soc., Dalton Trans.*, **1973**, 1462.

10) B. Bosnich, R. D. Gillard, E. D. McKenzie, and G. A, Webb, *J. Chem. Soc., A*, **1966**, 1331.

11) O. King and H. L. Schläfer, *Z. Anorg. Allg. Chem.*, **313**, 187 (1961).

12) D. A. House and C. S. Garner, *J. Am. Chem. Soc.*, **88**, 2156 (1966).

13) W. A. Fordyce, P. S. Sheridan, E. Zinato, P. Riccieri, and A. W. Adamson, *Inorg. Chem.*, **16**, 1154 (1977).

14) M. Kimura, A, Uehara, E. Kyuno, and R. Tsuchiya, *Bull. Chem. Soc. Jpn.*, **51**, 466 (1978).

15) Y. Inamura and Y. Kondo, *Nippon Kagaku Zasshi*, **74**, 627 (1953).

16) a) P. Pfeiffer, *Z. Anorg. Allg. Chem.*, **56**, 261 (1907); b) A. Werner, *Ber.*, **40**, 4434 (1907); c) R. Tsuchiya, A. Uehara, and E. Kyuno, *Bull. Chem. Soc. Jpn.*, **46**, 3737 (1973).

Induced Circular Dichroism Spectra of Some Achiral and Racemic Cobalt(III)-Amine Complexes in Aqueous (*R,R*)-Tartrate and (*R,R*)-Tartratoantimonate(III) Solutions

Katsuhiko MIYOSHI, Chang Eon OH, Hiroshi NAKAZAWA, and Hayami YONEDA*

Department of Chemistry, Faculty of Science, Hiroshima University, Hiroshima 730

(Received May 1, 1978)

The induced circular dichroism (ICD) spectra were measured in the first d-d transition region for the following cobalt(III)-amine complexes in aqueous solutions of (*R,R*)-tartrate and (*R,R*)-tartratoantimonate(III) anions; $[Co(en)_n(NH_3)_{6-2n}]^{3+}$ (n=0—3) and *cis*-$[Co(en)_2(RNH_2)_2]^{3+}$ (R=methyl and ethyl). It was found that a single negative CD band was induced for all the complexes in (*R,R*)-tartrate solution, while a single positive one was induced for most of them in (*R,R*)-tartratoantimonate(III) solution; the ICD developed in it was composed of a single negative band for $[Co(en)_3]^{3+}$ and of two bands with opposite sign for *trans*-$[Co(en)_2(NH_3)_2]^{3+}$ and *cis*-$[Co(en)_2(EtNH_2)_2]^{3+}$. The ICD spectra obtained for racemic complexes were interpreted in terms of differential interactions of Λ- and Δ-enantiomers with (*R,R*)-tartrate or (*R,R*)-tartratoantimonate(III), and an attempt was made to correlate the sign of their ICD spectra with their chromatographic behavior on an SP-Sephadex ion-exchanger with these chiral anions as an eluent.

When a racemic or achiral metal complex is mixed with a chiral substance in solution, relatively weak circular dichroism (CD) is induced in the d-d transition region of the complex. If the racemic complex is optically labile, this phenomenon is referred to as the Pfeiffer effect and has been ascribed to a displacement of the chiral equilibrium between the enantiomers of the complex. On the other hand, CD is similarly induced even if the complex is optically stable or inherently achiral, and it is called induced circular dichroism (ICD).

Mason and Norman[1] were the first to report this phenomenon for a transition metal complex in aqueous diethyl (*R,R*)-tartrate. Since then, special attention has been paid to $[Co(NH_3)_6]^{3+}$ and $[Co(en)_3]^{3+}$ to elucidate the mechanism leading to the ICD in achiral and racemic metal complexes.[2-4] In the present paper, an attempt is made to correlate the sign of the ICD spectra developed for a series of racemic cobalt(III)-amine complexes in aqueous (*R,R*)-tartrate and (*R,R*)-tartratoantimonate(III) solutions with their chromatographic behavior on an SP-Sephadex ion-exchanger with these chiral anions as an eluent.

Experimental

Preparation of the Complexes. *(1)* cis-$[Co(en)_2(NH_3)_2]Br_3\cdot H_2O$ *and* trans-$[Co(en)_2(NH_3)_2](NO_3)_3$: $[Co(CO_3)(en)_2]NO_3$[5] was added to concentrated nitric acid, which was then evaporated to dryness on a water bath. The resulting nitrato complex was dissolved in dimethylsulfoxide (DMSO), through which NH_3 gas was bubbled until the color of the DMSO solution changed to orange yellow. The precipitate formed by the addition of ethanol was dissolved in hot water. Less soluble *trans*-$[Co(en)_2(NH_3)_2](NO_3)_3$ was precipitated on cooling and was collected by filtration. The filtrate was loaded on an SP-Sephadex C-25 ion-exchanger and was eluted with sodium phosphate (0.05 M) to remove the *trans*-isomer completely. The addition of sodium bromide to the effluent led to the precipitation of the desired *cis*-isomer as bromide salt. Found: C; 12.05, H; 5.61, N; 32.13%. Calcd for *trans*-$[Co(en)_2(NH_3)_2](NO_3)_3$: C; 12.03, H; 5.51, N; 31.58%. Found: C; 10.32, H; 5.17, N; 17.54%. Calcd for *cis*-$[Co(en)_2(NH_3)_2]Br_3\cdot H_2O$: C; 10.20, H; 5.10, N; 17.83%. Optical resolution of the *cis*-isomer was performed after the method described in the literature.[6] The value of $\Delta\varepsilon$ at 492 nm was +0.575 and −0.561 for the Λ- and Δ-enantiomers, respectively (*cf.* 0.42 reported by McCaffery *et al.*[7]).

(2) cis-$[Co(en)_2(RNH_2)_2](NO_3)_3$ ($R=CH_3$ *and* C_2H_5): These were prepared from $[Co(CO_3)(en)_2]NO_3$ and the corresponding amines by the same method as described above. The yield of *trans*-isomers was so low that only *cis*-isomers were collected. *cis*-$[Co(en)_2(CH_3NH_2)_2]^{3+}$ was partially resolved *via* diastereomeric salt formation with *d*-α-nitrocamphoronate. Found: C, 16.78; H, 6.20; N, 29.82%. Calcd for *cis*-$[Co(en)_2(CH_3NH_2)_2](NO_3)_3$: C, 16.86; H, 6.09; N, 29.51%. Found: C, 20.25; H, 6.92; N, 26.75%. Calcd for *cis*-$[Co(en)_2(C_2H_5NH_2)_2](NO_3)_3\cdot H_2O$: C, 20.29; H, 6.77; N, 26.64%.

(3) $[Co(en)(NH_3)_4]I_3$: *trans*(*Cl*),*cis*(*N*)-$[Co(Cl)_2(en)(NH_3)_2]Cl$[8] was dissolved in DMSO, through which NH_3 gas was bubbled. The orange yellow crystal precipitated by the addition of ethanol was dissolved in a minimum amount of water. The iodide salt was obtained upon the addition of sodium iodide to the solution. Found: C, 4.50; H, 3.66; N, 14.84%. Calcd for $[Co(en)(NH_3)_4]I_3$: C, 4.23; H, 3.52; N, 14.79%.

(4) $[Co(NH_3)_6]Cl_3$ *and* $[Co(en)_3]Cl_3\cdot 3H_2O$: These were prepared by well-established methods.

Chromatographic Resolution and Measurements. Chromatographic resolution of racemic complexes was carried out in the same manner as described by Kojima *et al.*[9] CD spectra were recorded on a JASCO J-40CS spectropolarimeter and ICD spectra were measured for aqueous sodium (*R,R*)-tartrate (0.1 M) or sodium (*R,R*)-tartratoantimonate(III) (0.1 M) solution containing 0.01 M of each complex. When the association constant was obtained by recording the CD intensities, the cell compartment was temperature-controlled at 25±0.2 °C.

Results and Discussion

In Figs. 1 and 2 are shown the ICD spectra obtained in the first d-d transition region for all the complexes examined in aqueous (*R,R*)-tartrate ((*R,R*)-tart^{2-}) and (*R,R*)-tartratoantimonate(III) (Sb_2(*R,R*)-tart$_2^{2-}$) solutions, respectively.

Achiral Complexes. The ICD spectra for achiral

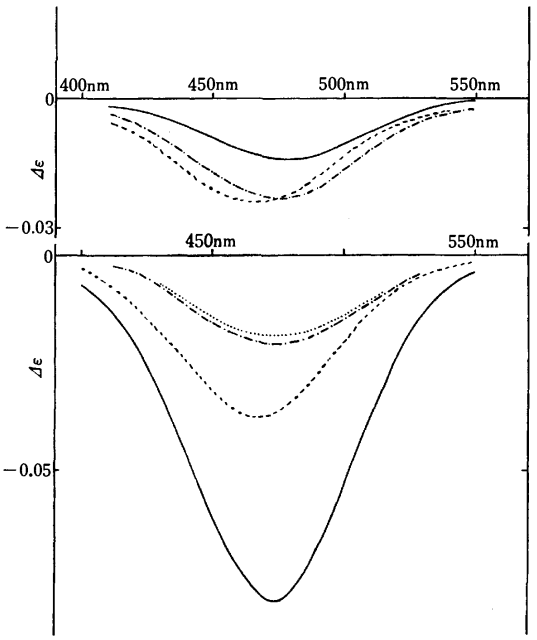

Fig. 1. ICD spectra in aqueous (*R,R*)-tart^{2-} solution. Upper curves; $[Co(NH_3)_6]^{3+}$(——), $[Co(en)(NH_3)_4]^{3+}$ (-•••-), *trans*-$[Co(en)_2(NH_3)_2]^{3+}$(– – –). Lower curves; *rac*-$[Co(en)_3]^{3+}$(——), *rac-cis*-$[Co(en)_2(NH_3)_2]^{3+}$(– – –), *rac-cis*-$[Co(en)_2(MeNH_2)_2]^{3+}$ (-•••-), *rac-cis*-$[Co(en)_2(EtNH_2)_2]^{3+}$ (……).

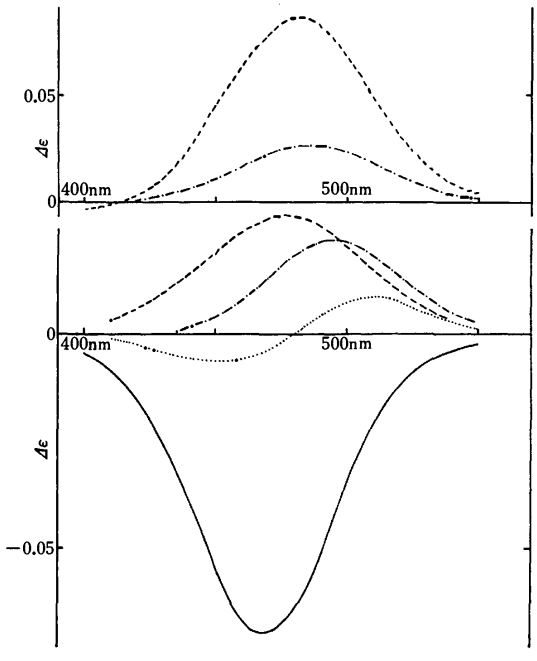

Fig. 2. ICD spectra in aqueous $Sb_2(R,R)$-$tart_2^{2-}$ solution. Upper curves; $[Co(en)(NH_3)_4]^{3+}$(-•••-), *trans*-$[Co(en)_2(NH_3)_2]^{3+}$(——). Lower curves; *rac*-$[Co(en)_3]^{3+}$(——), *rac-cis*-$[Co(en)_2(NH_3)_2]^{3+}$(– – –), *rac-cis*-$[Co(en)_2(MeNH_2)_2]^{3+}$(-•••-),*rac-cis*-$[Co(en)_2(EtNH_2)_2]^{3+}$ (……).

complexes are shown in the upper parts of Figs. 1 and 2. It is seen that, in (*R,R*)-tart^{2-} solution, a single negative CD band is induced, and its intensity decreases in the following order; *trans*-$[Co(en)_2(NH_3)_2]^{3+}$ $\gtrsim [Co(en)(NH_3)_4]^{3+} \gg [Co(NH_3)_6]^{3+}$. This order is tentatively ascribed to the difference in the degree of hydration of these complexes, because hydration of these amine complexes *via* their N–H groups are known to have a profound influence on their association behavior with various anions.[10] In contrast, Taniguchi *et al.*[11] reported the reversed order in acetone containing diethyl (*R,R*)-tartrate and interpreted it in terms of the number of N–H groups on the complexes available for hydrogen bonding with diethyl (*R,R*)-tartrate.

In $Sb_2(R,R)$-$tart_2^{2-}$ solution, on the other hand, $[Co(en)(NH_3)_4]^{3+}$ has a single positive ICD band, but *trans*-$[Co(en)_2(NH_3)_2]^{3+}$ has an additional small, negative band at the higher energy side of a dominant positive band. Since $[Co(NH_3)_6]^{3+}$ forms sparingly soluble precipitate with $Sb_2(R,R)$-$tart_2^{2-}$, the ICD measurement is impossible for this complex. A noteworthy fact is that the magnitude of the ICD is much greater for *trans*-$[Co(en)_2(NH_3)_2]^{3+}$ than for $[Co(en)(NH_3)_4]^{3+}$. This fact may be also interpreted in terms of the degree of hydration of these complexes and suggest some contribution to the ICD from a conformational change of en chelate rings caused by the association with $Sb_2(R,R)$-$tart_2^{2-}$, as Bonsnich pointed out.[12] However, it is difficult at this stage to offer precise explanation to the mechanism of the ICD developed in these achiral complexes.

Racemic Complexes. The ICD spectra for racemic complexes are shown in the lower parts of Figs. 1 and 2. In (*R,R*)-tart^{2-} solution, a single negative CD band is induced for all the racemic complexes just like for achiral complexes. On the other hand, different ICD patterns are developed in $Sb_2(R,R)$-$tart_2^{2-}$ solution; a single positive band is induced for *cis*-$[Co(en)_2(NH_3)_2]^{3+}$ and *cis*-$[Co(en)_2(MeNH_2)_2]^{3+}$, and two bands with opposite sign for *cis*-$[Co(en)_2(EtNH_2)_2]^{3+}$, but the ICD for $[Co(en)_3]^{3+}$ is composed of only a single negative band like in (*R,R*)-tart^{2-} solution.

It is now well known that the CD spectrum of $[Co(en)_3]^{3+}$ is appreciably affected by the addition of (*R,R*)-tart^{2-} [2,13] or $Sb_2(R,R)$-$tart_2^{2-}$;[14] the absolute intensity is decreased and increased for the E and A_2 components, respectively. Since *Λ*-$[Co(en)_3]^{3+}$ has positive E and negative A_2 components in the first d-d transition region, and the sign of the ICD for racemic $[Co(en)_3]^{3+}$ is negative in both (*R,R*)-tart^{2-} and Sb_2-(*R,R*)-$tart_2^{2-}$ solutions, the CD change caused by the addition of these chiral anions must be greater for the *Λ*-enantiomer than for the *Δ*-enantiomer. This is easily confirmed experimentally.[14,15] If it is assumed that a greater CD change is brought about by the stronger association with (*R,R*)-tart^{2-} or $Sb_2(R,R)$-$tart_2^{2-}$, these anions are expected to have a greater affinity for *Λ*-$[Co(en)_3]^{3+}$. This has been actually verified by some workers.[2,14,16]

Recently a number of cationic metal complexes have been resolved on an SP-Sephadex ion-exchanger with (*R,R*)-tart^{2-} or $Sb_2(R,R)$-$tart_2^{2-}$ as an eluent. Present authors[14] and Searle[17] have explicitly evoked that the strength of ion association of metal complexes with the chiral eluent is the most important factor determining the elution order in ion exchange chromatography.

Table 1. Elution order and sign of induced CD

	Chromatography	Induced CD (affinity)
$Na_2(R,R)$-tart		
$[Co(en)_3]^{3+}$	Λ	negative (Λ)
cis-$[Co(en)_2(NH_3)_2]^{3+}$	(Λ)	negative (Λ)
cis-$[Co(en)_2(MeNH_2)_2]^{3+}$	(Λ)	negative (Λ)
cis-$[Co(en)_2(EtNH_2)_2]^{3+}$	(Λ)	negative (Λ)
$Na_2Sb_2(R,R)$-$tart_2$		
$[Co(en)_3]^{3+}$	Λ	negative (Λ)
cis-$[Co(en)_2(NH_3)_2]^{3+}$	Λ	positive (Δ)
cis-$[Co(en)_2(MeNH_2)_2]^{3+}$	(Δ)	positive (Δ)
cis-$[Co(en)_2(EtNH_2)_2]^{3+}$	(Δ)	positive (Δ) [a]

a) See the text.

Then, it is in principle possible to predict the elution order from the sign of the ICD spectra if the above-mentioned assumption is generally valid.

In Table 1 is summarized the sign of the ICD developed for a series of racemic complexes in (R,R)-$tart^{2-}$ and $Sb_2(R,R)$-$tart_2^{2-}$ solutions. From the discussion presented above, negative and positive ICD corresponds to a greater affinity for the Λ- and Δ-enantiomer, respectively, as shown in the parentheses, since the Λ-enantiomers of these complexes have in common a dominant positive CD band (E component) at the longer wavelength region and its intensity is all diminished by the addition of (R,R)-$tart^{2-}$ or $Sb_2(R,R)$-$tart_2^{2-}$. Also listed under the heading of "chromatography" in Table 1 is the absolute configuration of the enantiomer eluted first by (R,R)-$tart^{2-}$ or $Sb_2(R,R)$-$tart_2^{2-}$ on an SP-Sephadex. The symbol Λ or Δ is parenthesized when the chromatographic resolution is incomplete under our experimental conditions. It is seen in Table 1 that, when (R,R)-$tart^{2-}$ is used, the resulting elution order is in complete agreement with the prediction from the sign of the ICD spectra for all the complexes.

When $Sb_2(R,R)$-$tart_2^{2-}$ is used, the Λ-enantiomer is eluted first for $[Co(en)_3]^{3+}$, in accord with the prediction from its ICD spectrum. Similarly the elution order for *cis*-$[Co(en)_2(MeNH_2)_2]^{3+}$ and *cis*-$[Co(en)_2(EtNH_2)_2]^{3+}$ is in agreement with the order expected from their ICD spectra, though the Δ-enantiomers are eluted first, as seen in Table 1. However, the ICD spectrum exceptionally fails to predict the elution order for *cis*-$[Co(en)_2(NH_3)_2]^{3+}$; its ICD is positive, suggesting a greater affinity of $Sb_2(R,R)$-$tart_2^{2-}$ for the Δ-enantiomer, but actually the Λ-enantiomer is eluted first. In order to solve this apparent discrepancy, the CD spectra of Λ- and Δ-*cis*-$[Co(en)_2(NH_3)_2]^{3+}$ were measured in water as well as in aqueous (R,R)-$tart^{2-}$ and $Sb_2(R,R)$-$tart_2^{2-}$ solutions, and they are shown in Figs. 3 and 4, where dotted curves correspond to the CD spectra in the presence of (R,R)-$tart^{2-}$ or $Sb_2(R,R)$-$tart_2^{2-}$. It is clearly seen that the CD change is greater for the Λ-enantiomer in (R,R)-$tart^{2-}$ solution, while it is greater for the Δ-enantiomer in $Sb_2(R,R)$-$tart_2^{2-}$ solution. Since the ICD spectrum is a simple sum of the two dotted curves, the ICD spectra of *cis*-$[Co(en)_2(NH_3)_2]^{3+}$ shown in Figs. 1 and 2 are completely reproduced here. That is to say, it is explicitly demonstrated in Figs. 3 and 4 that differential CD changes between the Λ- and Δ-enantiomers upon the addition of (R,R)-$tart^{2-}$ or $Sb_2(R,R)$-$tart_2^{2-}$ are responsible for the appearance of

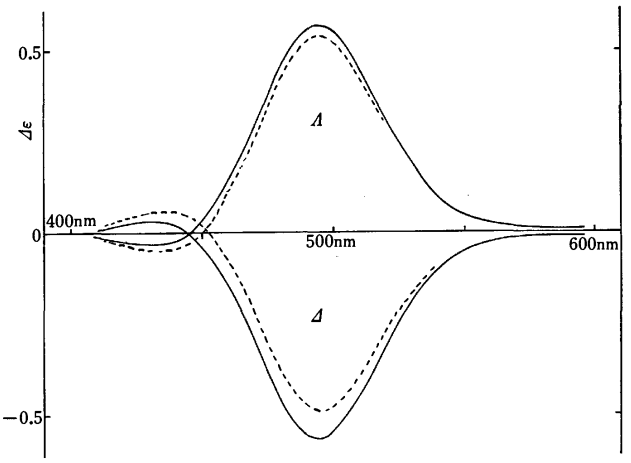

Fig. 4. CD spectra of Λ- and Δ-*cis*-$[Co(en)_2(NH_3)_2]^{3+}$ (4×10^{-3} M) in water (solid curves) and in 0.04 M aqueous $Sb_2(R,R)$-$tart_2^{2-}$ solution (dotted curves).

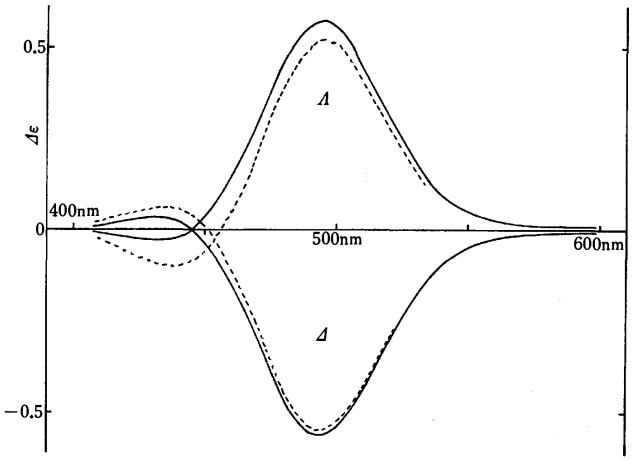

Fig. 3. CD spectra of Λ- and Δ-*cis*-$[Co(en)_2(NH_3)_2]^{3+}$(4×10^{-3} M) in water (solid curves) and in 0.04 M aqueous (R,R)-$tart^{2-}$ solution (dotted curves).

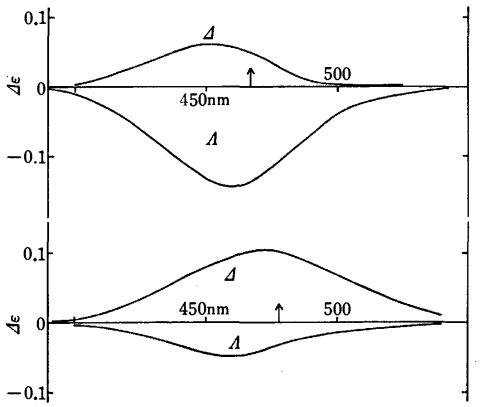

Fig. 5. Differential CD spectra of Λ- and Δ-*cis*-$[Co(en)_2(NH_3)_2]^{3+}$ (4×10^{-3} M) in 0.1 M aqueous (R,R)-$tart^{2-}$ solution (upper curves) and in 0.1 M aqueous $Sb_2(R,R)$-$tart_2^{2-}$ solution (lower curves).

the ICD for *cis*-$[Co(en)_2(NH_3)_2]^{3+}$. The same should hold for other racemic complexes.

This is more clearly confirmed in Fig. 5, where the difference CD spectra (the difference between the dotted and solid curves in Fig. 3 or 4) are depicted for *cis*-$[Co(en)_2(NH_3)_2]^{3+}$ both in (*R*,*R*)-tart^{2-} and Sb_2(*R*,*R*)-$tart_2^{2-}$ solutions, and the position of a small arrow corresponds to the wavelength at which the ICD has a maximum intensity. It should be noted here that the difference CD spectrum of the *Λ*-enantiomer differs from that of the *Δ*-enantiomer not only in magnitude but also in pattern in both (*R*,*R*)-tart^{2-} and Sb_2(*R*,*R*)-$tart_2^{2-}$ solutions. Therefore, it is concluded that both (*R*,*R*)-tart^{2-} and Sb_2(*R*,*R*)-$tart_2^{2-}$ interact with one enantiomer of the complex in a different fashion from the other. The same is found true for $[Co(en)_3]^{3+}$. If the peak positions of difference CD spectra for *Λ*- and *Δ*-enantiomers differ greatly from each other, the resulting ICD spectrum is expected to have two components with opposite sign. This is probably the case with *cis*-$[Co(en)_2(EtNH_2)_2]^{3+}$ in Sb_2(*R*,*R*)-$tart_2^{2-}$ solution. Judging from the relative intensities of the two ICD components of this complex (Fig. 2), it is supposed the *Δ*-enantiomer is subject to a greater CD change in Sb_2(*R*,*R*)-$tart_2^{2-}$ solution, so that "positive (*Δ*)" is inserted in the last column of Table 1 for this complex.

Now, we have to solve one important problem why *Λ*-*cis*-$[Co(en)_2(NH_3)_2]^{3+}$ is eluted first by Sb_2(*R*,*R*)-$tart_2^{2-}$ on an SP-Sephadex, despite the fact that it gives rise to a greater CD change for the *Δ*-enantiomer, as shown in Fig. 5. For this purpose, the association constants of *Λ*- and *Δ*-*cis*-$[Co(en)_2(NH_3)_2]^{3+}$ with (*R*,*R*)-tart^{2-} and Sb_2(*R*,*R*)-$tart_2^{2-}$ were obtained by measuring their CD intensities in aqueous solutions. Experimental details have been described earlier.[14] Since the CD change of *cis*-$[Co(en)_2(NH_3)_2]^{3+}$ was small as compared with that of $[Co(en)_3]^{3+}$, somewhat higher concentrations of *Λ*- or *Δ*-*cis*-$[Co(en)_2(NH_3)_2]Cl_3$ and Na_2(*R*,*R*)-tart or K_2Sb_2(*R*,*R*)-$tart_2$ had to be employed, so that sodium perchlorate was not added to adjust the ionic strength. Instead, the amounts of the complex and the chiral anion were appropriately varied to maintain a constant ionic strength. The final plots of $C_M(C_A-x)/(\Delta CD/2)$ *vs.* (C_A-x) obtained by a successive approximation[14] are shown in Fig. 6, and the derived association constant K_A and the value of molar CD change $(\Delta\varepsilon_{MA}-\Delta\varepsilon_M)$ are listed in Table 2. For comparison, the corresponding values for $[Co(en)_3]^{3+}$ obtained previously[14,16] are also given here.

It is seen in Table 2 that the association constant K_A of *cis*-$[Co(en)_2(NH_3)_2]^{3+}$ with (*R*,*R*)-tart^{2-} is slightly greater for the *Λ*-enantiomer, in accord with the result of present chromatography that the *Λ*-enantiomer is eluted first by (*R*,*R*)-tart^{2-}, but only incomplete resolution is attained. On the other hand, the K_A value of the *Λ*-enantiomer with Sb_2(*R*,*R*)-$tart_2^{2-}$ is almost twice as great as that of the *Λ*-enantiomer. Then, it is natural that complete chromatographic resolution is effected with the *Λ*-enantiomer eluted first by Sb_2(*R*,*R*)-$tart_2^{2-}$. As a result, it follows that the *Λ*-enantiomer associates favorably with Sb_2(*R*,*R*)-$tart_2^{2-}$ in such a fashion that its CD spectrum is not appreciably affected in comparison with the *Δ*-enantiomer, as is indicated by the values of their molar CD change $(\Delta\varepsilon_{MA}-\Delta\varepsilon_M)$. In contrast, for $[Co(en)_3]^{3+}$, both the K_A and $(\Delta\varepsilon_{MA}-\Delta\varepsilon_M)$ values are greater for the *Λ*-enantiomer, so that the ICD spectra provide a correct prediction of the elution order

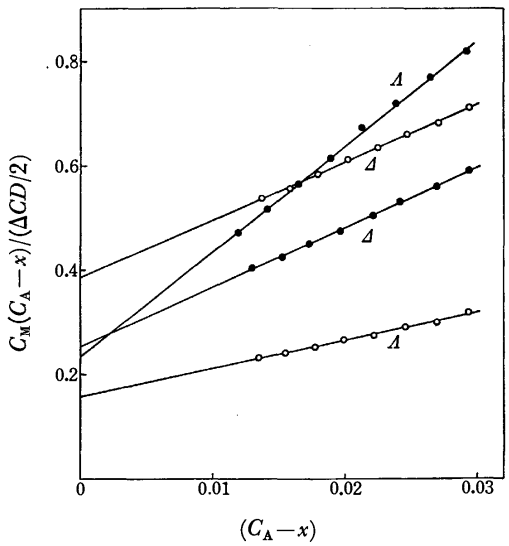

Fig. 6. Final plots of $C_M(C_A-x)/(\Delta CD/2)$ *vs.* (C_A-x) for *cis*-$[Co(en)_2(NH_3)_2]^{3+}$-(*R*,*R*)-tart^{2-}(○) and -Sb_2-(*R*,*R*)-$tart_2^{2-}$(●) system in water.

Table 2. Association constant K_A and molar CD change at 25 °C[a]

	nm[b]		K_A	$(\Delta\varepsilon_{MA}-\Delta\varepsilon_M)$
(*R*,*R*)-tart^{2-}				
cis-$[Co(en)_2(NH_3)_2]^{3+}$	446	*Λ*	32±1	0.192±0.005
		Δ	28±1	0.092±0.002
$[Co(en)_3]^{3+}$	430	*Λ*	13.0±0.1	0.85±0.01
		Δ	10.5±0.4	0.66±0.03
Sb_2(*R*,*R*)-$tart_2^{2-}$				
cis-$[Co(en)_2(NH_3)_2]^{3+}$	446	*Λ*	85±3	0.050±0.001
		Δ	45±1	0.088±0.001
$[Co(en)_3]^{3+}$	430	*Λ*	46.6±0.7	0.251±0.003
		Δ	25.6±0.9	0.197±0.006

a) Ionic strength is 0.1 adjusted by sodium perchlorate for $[Co(en)_3]^{3+}$ and is 0.08 without sodium perchlorate for *cis*-$[Co(en)_2(NH_3)_2]^{3+}$, so that the direct comparison of the two systems is almost meaningless. b) Wavelength at which CD changes were measured.

in both (*R*,*R*)-tart^{2-} and Sb_2(*R*,*R*)-$tart_2^{2-}$ solutions.

In this way, the ICD spectra are found useful to predict the elution order of several racemic complexes on an SP-Sephadex ion-exchanger with (*R*,*R*)-tart^{2-} or Sb_2(*R*,*R*)-$tart_2^{2-}$ as an eluent. Similar experiments on other metal complexes are now under way to extend the applicability of the ICD spectra to ion exchange chromatography.

References

1) S. F. Mason and B. J. Norman, *Chem. Commun.*, **1965**, 335.
2) B. Norden, *Acta Chem. Scand.*, **26**, 111 (1972); *Chem. Ser.*, **7**, 14 (1975).
3) I. Jonas and B. Norden, *Acta Chem. Scand.*, **A28**, 289 (1974).
4) P. E. Schipper, *J. Am. Chem. Soc.*, **98**, 7938 (1976); *ibid.*, **100**, 1433 (1978).
5) J. Springbørg and C. E. Schäffer, *Inorg. Synth.*, **14**, 64 (1973).
6) K. Garbett and R. D. Gillard, *J. Chem. Soc., A*, **1966**, 802.
7) A. J. McCaffery, S. F. Mason, and B. J. Norman, *J. Chem. Soc.*, **1965**, 5094.
8) A. V. Ablov and T. A. Malkova, *Zh. Neorg. Khim.*, **5**, 2704 (1960).
9) M. Kojima, H. Takayanagi, and J. Fujita, *Bull. Chem. Soc. Jpn.*, **50**, 1891 (1977).
10) H. Yoneda, M. Muto, T. Baba, and T. Miura, *Bull. Chem. Soc. Jpn.*, **44**, 689 (1971); M. Muto, A. Takada, T. Baba, and H. Yoneda, *J. Chromatogr.*, **154**, 244 (1978).
11) Y. Taniguchi, J. Hidaka, and Y. Shimura, *Bull. Chem. Soc. Jpn.*, **50**, 2093 (1977).
12) B. Bosnich, *J. Am. Chem. Soc.*, **89**, 6143 (1967).
13) S. F. Mason and B. J. Norman, *J. Chem. Soc., A*, **1966**, 307.
14) T. Taura, H. Nakazawa, and H. Yoneda, *Inorg. Nucl. Chem. Lett.*, **13**, 603 (1977).
15) M. Fujita and H. Yamatera, *Bull. Chem. Soc. Jpn.*, **49**, 1301 (1976).
16) H. Yoneda and T. Taura, *Chem. Lett.*, **1977**, 63.
17) G. H. Searle, *Aust. J. Chem.*, **30**, 2625 (1977).

Pyrolytic Sulfurization Gas Chromatography. III. Simultaneous Determination of the Atomic Ratio between C, H, O, and N in a Metallo-organic Compound

Tadashi HARA,* Kaoru FUJINAGA, and KATSUYA TSUJI

Department of Applied Chemistry, Faculty of Engineering, Doshisha University, Karasuma Imadegawa, Kamigyo-ku, Kyoto 602

(Received May 12, 1978)

Simultaneous determination of the atomic ratio between C, H, O, and N in a metallo-organic compound containing transition element is possible by the pyrolytic sulfurization gas chromatographic method, addition of reducing agent being unnecessary. Analytical results of metallo-organic compounds depend on the characteristics of their metal oxides. A few organophosphorus compounds were analyzed. The formation of water could be predicted from the atomic ratio of carbon to oxygen in a compound.

Simultaneous determination of the atomic ratio between C, H, O, and N in a sample can be achieved with the usual organic compounds[1] by pyrolytic sulfurization gas chromatography (PSGC).[2] The present study has been carried out to confirm whether PSGC can be applied to the analysis of various metallo-organic compounds containing transition elements. The affinity of metallic elements for oxygen is so strong that quantitative release of oxygen from their oxides is difficult. Simultaneous determination of oxygen with C, H, and N is impossible by the conventional methods. The oxygen in the metallo-organic compound has been determined either by subtracting the total amount of C, H, N, and metal oxide from the weight of a smple or by estimating the oxygen separately from the determination of C, H, and N. The former method is apt to introduce a relatively large error and is not applicable to samples containing molybdenum, cadmium, and so on, the oxides of which are volatile under the analytical conditions. The latter method has a disadvantage in that some reducing agent must be added to the sample in order to liberate oxygen from the combustion residues.

However, the present PSGC method based on a sulfur combustion technique, is characterized by converting the metal in a compound into sulfide, even in the case where the metal oxide is more stable than the corresponding sulfide since carbon atoms in the compound act as the reducing agent, releasing the whole oxygen in the sample. It is possible to determine the atomic ratio without a special procedure such as addition of reducing agent.

Experimental

Apparatus and Reagents. The reagents and apparatus used were the same as those reported[1] except that peak areas of the gas chromatogram were read out by use of a Shimadzu digital integrator ElA. A definite amount of sample was taken with a Shimadzu microbalance MDP-5.

Procedure. The preparation and reaction conditions of sample as well as conditions of gas chromatographic analysis are similar to those reported.[1]

Samples. The following samples were prepared by the methods found in literature for their gravimetric analyses: magnesium oxalate, $MgC_2O_4 \cdot 2H_2O$;[3] cobalt(II) oxalate, $CoC_2O_4 \cdot 2H_2O$;[3] copper(II) oxalate, CuC_2O_4;[4] cadmium oxalate, CdC_2O_4;[5] bis(8-quinolinolato)magnesium, $Mg(C_9H_6ON)_2$;[6] oxobis(8-quinolinolato)titanium(IV), $TiO(C_9H_6ON)_2$;[6] dioxobis(8-quinolinolato)molybdenum(VI), $MoO_2(C_9H_6ON)_2$;[6] dioxobis(8-quinolinolato)tungsten(VI), $WO_2(C_9H_6ON)_2$;[6] bis(8-quinolinolato)copper(II), $Cu(C_9H_6ON)_2$;[6] dioxo(8-quinolinol)bis(8-quinolinolato)uranium(VI), $UO_2(C_9H_6ON)_2(C_9H_7ON)$;[6] bis(8-quinolinolato)zinc(II), $Zn(C_9H_6ON)_2$;[6] bis(8-quinolinolato)manganese(II), $Mn(C_9H_6ON)_2 \cdot 2H_2O$;[6] tris(8-quinolinolato)iron(III), $Fe(C_9H_6ON)_3$;[6] bis(8-quinolinolato)cobalt(II), $Co(C_9H_6ON)_2 \cdot 2H_2O$;[6] bis(8-quinolinolato)nickel(II), $Ni(C_9H_6ON)_2$;[6] tris(8-quinolinolato)aluminium, $Al(C_9H_6ON)_3$;[6] tris(8-quinolinolato)lanthanum(III), $La(C_9H_6ON)_3$;[6] bis(8-quinolinolato)cadmium(II), $Cd(C_9H_6ON)_2 \cdot 2H_2O$;[6] tris(8-quinolionlato)chromium(III), $Cr(C_9H_6ON)_3$;[7] bis(2,3-butanedione dioximato)palladium(II), $Pd(C_4H_7O_2N_2)_2$;[8] bis(2,3-butanedione dioximato)nickel(II), $Ni(C_4H_7O_2N_2)_2$;[8] (benzoin oximato)copper(II), $Cu(C_{14}H_{11}O_2N)$;[8] bis(anthranilato)copper(II), $Cu(C_7H_6O_2N)_2$;[8] bis(anthranilato)zinc(II), $Zn(C_7H_6O_2N)_2$;[8] bis(anthranilato)nickel(II), $Ni(C_7H_6O_2N)_2$;[8] bis(anthranilato)manganese(II), $Mn(C_7H_6O_2N)_2$;[8] bis(anthranilato)cobalt(II), $Co(C_7H_6O_2N)_2$;[8] bis(anthranilato)cadmium(II), $Cd(C_7H_6O_2N)_2$;[8] bis(salicylaldehyde oximato)copper(II), $Cu(C_7H_6O_2N)_2$.[8] The composition and purity of samples were confirmed by the C and H analysis carried out in the Elemental Analysis Center of Pharmaceutical Department for Kyoto University (Table 1). The experimental results were in fair agreement with the theoretical values. Naphthalene, thiourea, sucrose, cyanoguanidine, bis(2,4-pentanedionato)magnesium, and tris(2,4-pentanedionato)iron(III) for elemental analysis were of reagent grade, the other reagents being commercial products. The metal oxides were of analytical grade and treated at 950 °C before use.

Results and Discussion

Reactivity of Metal Oxide. The reactivity between metal oxide and sulfur was investigated prior to the analysis of metallo-organic compounds. The reaction of silver nitrate ($AgNO_3$) as a reference substance seems to proceed completely in accordance with Eq. 1, since 1) a large, positive value of ΔG°_{1200K} in Eq. 1, 642.6 kJ·mol^{-1} was obtained from the thermodynamic data[9] by means of Ulich's approximate equation, 2) $AgNO_3$ produced only nitrogen molecule (N_2) and sulfur dioxide (SO_2) as reaction products, and 3) proportionality holds between the amount of $AgNO_3$ and the peak area of SO_2. The reactivity of metal oxide is expressed in terms of α, which refers to the mole ratio of SO_2 from the metal oxide, M_mO_n against that from

TABLE 1. ANALYTICAL RESULTS OF CARBON AND HYDROGEN IN METALLO-ORGANIC COMPOUNDS

Sample	Carbon wt %			Hydrogen wt %		
	Calcd	Found	Error	Calcd	Found	Error
Magnesium oxalate $MgC_2O_4 \cdot 2H_2O$	16.19	16.31	0.12	2.72	2.84	0.12
Bis(8-quinolinolato)magnesium $Mg(C_9H_6ON)_2$	69.15	68.94	−0.21	3.87	4.11	0.24
Tris(8-quinolinolato)lanthanum(III) $La(C_9H_6ON)_3$	56.76	56.06	−0.70	3.18	3.41	0.23
Dioxo(8-quinolinol)bis(8-quinolinolato)-uranium(VI) $UO_2(C_9H_6ON)_2(C_9H_7ON)$	46.10	45.87	−0.23	2.72	2.84	0.12
Oxobis(8-quinolinolato)titanium(IV) $TiO(C_9H_6ON)_2$	61.38	60.34	−1.04	3.43	3.36	−0.07
Tris(8-quinolinolato)chromium(III) $Cr(C_9H_6ON)_3$	66.94	67.14	0.20	3.75	3.98	0.23
Dioxobis(8-quinolinolato)molybdenum(VI) $MoO_2(C_9H_6ON)_2$	51.94	51.74	−0.19	2.91	3.09	0.18
Dioxobis(8-quinolinolato)tungsten(VI) $WO_2(C_9H_6ON)_2$	42.88	43.13	0.25	2.40	2.62	0.22
Bis(anthranilato)manganese(II) $Mn(C_7H_6O_2N)_2$	51.39	51.41	0.02	3.70	3.81	0.11
Tris(8-quinolinolato)iron(III) $Fe(C_9H_6ON)_3$	66.41	66.58	0.17	3.72	3.48	−0.24
Bis(anthranilato)cobalt(II) $Co(C_7H_6O_2N)_2$	50.77	49.81	−0.96	3.65	3.64	−0.01
Bis(2,3-butanedione dioximato)nickel(II) $Ni(C_4H_7O_2N_2)_2$	33.26	33.45	0.19	4.88	4.96	0.08
Bis(anthranilato)nickel(II) $Ni(C_7H_6O_2N)_2$	50.81	49.92	−0.89	3.65	4.07	0.42
Bis(8-quinolinolato)nickel(II) $Ni(C_9H_6ON)_2$	62.30	62.29	−0.01	3.49	3.23	−0.26
Bis(anthranilato)copper(II) $Cu(C_7H_6O_2N)_2$	50.07	50.18	0.11	3.60	3.74	0.14
Bis(salicylaldehyde oximato)copper(II) $Cu(C_7H_6O_2N)_2$	50.07	50.04	−0.03	3.48	3.61	0.13
(Benzoin oximato)copper(II) $Cu(C_{14}H_{11}O_2N)$	58.23	57.71	−0.52	3.84	4.21	0.37
Bis(8-quinolinolato)zinc $Zn(C_9H_6ON)_2$	61.13	60.95	−0.18	3.42	3.68	0.26
Bis(anthranilato)zinc $Zn(C_7H_6O_2N)_2$	49.80	49.70	−0.10	3.58	3.82	0.24
Bis(anthranilato)cadmium $Cd(C_7H_6O_2N)_2$	43.71	43.45	−0.26	3.14	3.29	0.15
Bis(8-quinolinolato)cadmium $Cd(C_9H_6ON)_2$	49.50	49.53	0.03	3.69	3.96	0.27
Tris(8-quinolinolato)alminium $Al(C_9H_6ON)_3$	70.59	70.39	−0.20	3.95	4.22	0.27

$AgNO_3$. Thus, the reactivity of metal oxide in Eq. 2 is approximately estimated by Eq. 3, where $A°(SO_2)$ and $A(SO_2)$ refer to the peak areas of SO_2 obtained with a mol of $AgNO_3$ and b mol of M_mO_n, respectively. The oxides of molybdeneum(VI),

$$AgNO_3 + S_2 = \frac{1}{2}Ag_2S + \frac{1}{2}N_2 + \frac{3}{2}SO_2 \quad (1)$$

$$\frac{3}{2}a = A°(SO_2),$$

$$M_mO_n + xS_2 = M_mS_n + \frac{n}{2}SO_2 \quad (2)$$

$$\frac{n}{2}b\alpha = A(SO_2),$$

TABLE 2. RELATIVE CONVERSIONS OF METAL OXIDES

Metal oxide	Relative conversion[a] α	Metal oxide	Relative conversion α
MgO	0	Fe_2O_3	1.1
CaO	0.67	NiO	0.33
TiO_2	0	CuO	0.94
U_3O_8	0.13	ZnO	1.1
V_2O_5	0.40	Al_2O_3	0
MoO_3	1.0	SiO_2	0
WO_3	0.88	Bi_2O_3	1.0
Cr_2O_3	0.70	Mn_3O_4	0.96

a) Estimated by Eq. 3.

$$\alpha = \frac{A(SO_2)3a}{A^\circ(SO_2)nb}, \quad (3)$$

manganese(II, III), iron(III), copper(II), zinc(II), and bismuth(III) react quantitatively with sulfur (Table 2). The oxides of calcium(II), uranium(VI), vanadium(V), tungsten(VI), and nickel(II) react with sulfur to some extent, oxygen being liberated as SO_2. However, the oxides of magnesium(II), titanium(IV), aluminium-(III), and silicon(III) are barely reduced by sulfur under the experimental conditions.

The value of ΔG°_{1200K} for Eq. 2 gives a measure of the reactivity of metal oxide with sulfur. The results shown

Table 3. Equilibrium between the oxide and sulfide of each metal

Metal oxide	Reaction[a]	ΔG°_{1200K} / kJ mol^{-1}
Na_2O	$Na_2O(s)+3/4S_2(g)\rightarrow Na_2S(s)+1/2SO_2(g)$	−169.12
MgO	$MgO(s)+3/4S_2(g)\rightarrow MgS(s)+1/2SO_2(g)$	49.16
CaO	$CaO(s)+3/4S_2(g)\rightarrow CaS(s)+1/2SO_2(g)$	−56.32[d]
TiO_2[b]	$TiO_2(s)+3/2S_2(g)\rightarrow TiS_2(s)+SO_2(g)$	182.84[d]
MoO_3	$MoO_3(s)+9/4S_2(g)\rightarrow MoS_3(s)+3/2SO_2(g)$	−88.99[d]
Mn_3O_4	$Mn_3O_4(s)+5/2S_2(g)\rightarrow 3MnS(s)+2SO_2(g)$	−177.49
Fe_2O_3	$Fe_2O_3(s)+7/4S_2(g)\rightarrow 2FeS(s)+3/2SO_2(g)$	−75.14
CuO	$CuO(s)+3/4S_2(g)\rightarrow CuS(s)+1/2SO_2(g)$	−108.20
ZnO	$ZnO(s)+3/4S_2(g)\rightarrow ZnS(s)+1/2SO_2(g)$	−59.91
CdO	$CdO(s)+3/4S_2(g)\rightarrow CdS(s)+1/2SO_2(g)$	−105.73
SiO_2	$SiO_2(s)+3/2S_2(g)\rightarrow SiS_2(s)+SO_2(g)$	287.19
Bi_2O_3	$Bi_2O_3(s)+9/4S_2(g)\rightarrow Bi_2S_3(s)+3/2SO_2(g)$	−202.09[d]

a) (s): Solid phase, (g): gaseous phase. b) TiO_2: Rutile. c) SiO_2: Quartz.
d) ΔG° at 1000K.

Table 4. Analytical results of metallo-organic compounds

Sample[a]	Group	C wt %			H wt %			O wt %			N wt %		
		Theor	Exptl	Error	Theor	Exptl	Error	Theor	Exptl	Error	Theor	Exptl	Error
Tris(8-quinolinolato)-lanthanum(III) $La(C_9H_6ON)_3$	III A	74.99	74.77	−0.22	4.19	4.13	−0.06	11.10	10.85	−0.25	9.72	10.25	0.53
Uranyl(VI) acetate $UO_2(CH_3COO)_2\cdot 2H_2O$	III A	25.81	30.83	5.02	5.41	6.20	0.79	68.77	62.96	−5.81			
Dioxo(8-quinolinol)-bis(8-quinolinolato)-uranium(VI) $UO_2(C_9H_6ON)_2\cdot(C_9H_7ON)$	III A	69.67	71.60	1.93	4.11	4.32	0.21	17.19	15.13	−2.06	9.03	8.95	−0.08
Oxobis(8-quinolinolato)-titanium(IV) $TiO(C_9H_6ON)_2$	IV A	71.05	74.71	3.66	3.97	4.21	0.24	15.77	11.71	−4.06	9.21	9.36	0.15
Tris(8-quinolinolato)-chromium(III) $Cr(C_9H_6ON)_3$	VI A	74.99	74.48	−0.51	4.19	4.15	−0.04	11.10	11.34	0.24	9.72	10.02	0.30
Dioxobis(8-quinolinolato)-molybdenum(VI) $MoO_2(C_9H_6ON)_2$	VI A	67.50	66.85	−0.65	3.78	3.88	0.10	19.98	19.95	−0.03	8.75	9.32	0.57
Dioxobis(8-quinolinolato)-tungsten(VI) $WO_2(C_9H_6ON)_2$	VI A	67.50	67.34	−0.16	3.78	3.31	−0.47	19.98	20.08	0.10	8.75	9.26	0.51
Bis(8-quinolinolato)-manganese(II) $Mn(C_9H_6ON)_2\cdot 2H_2O$	VII A	66.66	65.95	−0.71	4.97	4.92	−0.05	19.73	20.30	0.57	8.64	8.82	0.18
Bis(anthranilato)-manganese(II) $Mn(C_7H_6O_2N_2)$	VII A	61.76	62.16	0.40	4.44	4.15	−0.29	23.51	23.74	0.23	10.29	9.95	−0.34
Tris(2,4-pentane-dionato)iron(III) $Fe(C_5H_7O_2)_3$	VIII	60.59	60.92	0.33	7.12	7.35	0.23	32.29	31.73	−0.56			

TABLE 4. (Continued)

Sample[a]	Group	C wt % Theor	C wt % Exptl	C wt % Error	H wt % Theor	H wt % Exptl	H wt % Error	O wt % Theor	O wt % Exptl	O wt % Error	N wt % Theor	N wt % Exptl	N wt % Error
Tris(8-quinolinolato)-iron(III) $Fe(C_9H_6ON)_3$	VIII	74.99	74.93	−0.06	4.19	3.95	−0.24	11.10	11.42	0.32	9.72	9.70	−0.02
Cobalt(II) oxalate $CoC_2O_4 \cdot 2H_2O$	VIII	19.37	19.10	−0.27	3.25	3.21	−0.04	77.38	77.69	0.31			
Bis(anthranilato)-cobalt(II) $Co(C_7H_6O_2N)_2$	VIII	61.76	61.05	−0.71	4.44	4.51	0.07	23.51	23.99	0.48	10.29	10.44	0.15
Bis(8-quinolinolato)-cobalt(II) $Co(C_9H_6ON)_2 \cdot 2H_2O$	VIII	66.66	66.20	−0.46	4.97	4.92	−0.05	19.73	20.32	0.59	8.64	8.57	−0.07
Bis(2,3-butanedione dioximato)nickel(II) $Ni(C_4H_7O_2N_2)_2$	VIII	41.74	42.02	0.28	6.13	6.48	0.35	27.80	27.50	−0.30	24.34	24.00	−0.34
Bis(anthranilato)-nickel(II) $Ni(C_7H_6O_2N)_2$	VIII	61.76	61.25	−0.51	4.44	4.58	0.14	23.51	23.33	−0.18	10.29	10.83	0.54
Bis(8-quinolinolato)-nickel(II) $Ni(C_9H_6ON)_2$	VIII	74.99	74.62	−0.37	4.19	4.54	0.35	11.10	11.41	0.31	9.72	9.43	−0.29
Palladium(II) acetate $Pd(CH_3COO)_2$	VIII	40.68	40.15	−0.53	5.12	5.13	0.01	54.19	54.72	0.53			
Bis(2,3-butanedione dioximato)-palladium(II) $Pd(C_4H_7O_2N_2)_2$	VIII	41.74	41.58	−0.16	6.13	6.15	0.02	27.80	27.41	−0.39	24.34	24.85	0.51
Copper(II) oxalate CuC_2O_4	VIII	27.29	27.20	−0.09				72.71	72.80	0.09			
Copper(II) acetate $Cu(CH_3COO)_2 \cdot H_2O$	VIII	35.30	35.72	0.42	5.92	5.75	−0.17	58.78	58.53	−0.25			
(Benzoin oximato)-copper(II) $Cu(C_{14}H_{11}O_2N)$	VIII	74.65	74.09	−0.56	4.92	5.13	0.21	14.21	14.60	0.39	6.23	6.18	−0.05
Bis(salicylaldehyde oximato)copper(II) $Cu(C_7H_6O_2N)_2$	VIII	61.76	61.15	−0.61	4.44	4.26	−0.18	23.51	23.87	0.36	10.29	10.72	0.43
Bis(anthranilato)-copper(II) $Cu(C_7H_6O_2N)_2$	VIII	61.76	61.77	0.01	4.44	4.80	0.36	23.51	23.43	−0.08	10.29	10.00	−0.29
Bis(8-quinolinolato)-copper(II) $Cu(C_9H_6ON)_2$	VIII	74.99	75.00	0.01	4.19	4.16	−0.03	11.10	10.80	−0.30	9.72	10.06	0.34
Silver(I) acetate CH_3COOAg	VIII	40.68	40.64	−0.04	5.12	4.73	−0.39	54.19	54.63	0.44			
Bis(anthranilato)-zinc(II) $Zn(C_7H_6O_2N)_2$	II B	61.76	61.06	−0.70	4.44	4.41	−0.03	23.51	23.66	0.15	10.29	10.86	0.57
Bis(8-quinolinolato)-zinc(II) $Zn(C_9H_6ON)_2$	II B	74.99	75.01	0.02	4.19	4.12	−0.07	11.10	10.99	−0.11	9.72	9.88	0.16
Cadmium(II) oxalate CdC_2O_4	II B	27.29	27.18	−0.11				72.71	72.82	0.11			
Bis(anthranilato)-cadmium(II) $Cd(C_7H_6O_2N)_2$	II B	61.76	61.75	−0.01	4.44	4.48	0.04	23.51	22.80	−0.71	10.29	10.97	0.68
Bis(8-quinolinolato)-cadmium(II) $Cd(C_9H_6ON)_2 \cdot 2H_2O$	II B	66.66	66.28	−0.38	4.97	5.05	0.08	19.73	19.46	−0.27	8.64	9.22	0.58
Mercury(II) acetate $Hg(CH_3COO)_2$	II B	40.68	40.69	0.01	5.12	5.18	0.06	54.19	54.12	−0.07			
Tris(8-quinolinolato)-aluminium(III) $Al(C_9H_6ON)_3$	II B	74.99	78.05	3.06	4.19	4.57	0.37	11.10	7.12	−3.98	9.72	10.26	0.54

a) Metal atoms were neglected in the composition of metallo-organic compounds since they could not be determined.

in Table 3 correspond fairly well to those in Table 2. Since the ΔG° value of magnesium(II) oxide, titanium(IV) oxide, and silicon(III) oxide among the metal oxides are positive and large, it is understandable that these metal oxides show no reactivity to sulfur.

Analysis of Various Metallo-organic Compounds. Various metallo-organic compounds containing transition elements were analyzed (Table 4). Almost all the complex salts gave satisfactory results, but the complex salts of Ti, U, and Al gave a fairly negative error in the oxygen value. Because of the high stability and the difficult reduction of the oxides of titanium(IV), aluminium(III), and uranium(VI), the oxygen atom in their complex salts seems to be partly transferred into the residues, giving rise to error.

Magnesium(II) oxide does not react with sulfur, but bis(8-quinolinolato)magnesium(II)reacts quantitatively with sulfur to give an exact oxygen value without producing magnesium(II) oxide. In order to clarify the difference in the two cases, study was carried out on a series of magnesium salts (Table 5). Bis(2,4-pentanedionato)magnesium(II) as well as bis(8-quinolinolato) magnesium(II) gave expected results, while oxalate and acetate of magnesium(II) gave fairly low oxygen values (Table 5). This can be attributed to the shortage of carbon atom necessary for the prevention of the formation of magnesium(II) oxide. In conclusion, the present method gives satisfactory oxygen values when the number of carbon atom exceeds that of oxygen atom in magnesium compound.

Analysis of Organophosphorus Compounds. Various organophosphorus compounds were analyzed (Table 6). Carbon-rich compounds such as triphenylphosphine oxide give satisfactory oxygen values, while carbon-poor compounds such as guanidine phosphate gives fairly low oxygen value, which may be ascribed to the formation of polyphosphoric acid. It seems that carbon atoms prevent oxygen atoms from the formation of polyphosphoric acid as in magnesium compounds. Inorganic phosphorus compounds did not react quantitatively with sulfur, the whole amount of oxygen not being liberated.

Decomposition of Water. By the present method, N_2, carbon dioxide, hydrogen sulfide, carbonyl sulfide, water, SO_2, and carbon disulfide can be determined simultaneously under the experimental conditions. Since the tailing phenomenon is observed on the water peak, it is desirable to avoid the formation of water for accurate determination. The formation of water was observed with magnesium(II) oxalate tetrahydrate, magnesium(II) acetate tetrahydrate, and cobalt(II) oxalate dihydrate but not with the other componds containing water of crystallization such as sodium citrate dihydrate and oxalic acid dihydrate. It seems that water is decomposed with an increasing number of carbon atom

Table 5. Analytical results of magnesium compounds

Sample[a]	C wt %			H wt %			O wt %			N wt %		
	Theor	Exptl	Error	Theor	Exptl	Error	Theor	Exptl	Error	Theor	Exptl	Error
Magnesium oxalate $MgC_2O_4 \cdot 2H_2O$	19.37	21.88	2.51	3.25	3.69	0.44	77.38	74.43	−2.95			
Magnesium acetate $Mg(CH_3COO)_2 \cdot 4H_2O$	25.27	27.89	2.62	7.42	7.64	0.22	67.31	64.48	−2.83			
Bis(2,4-pentanedionato)-magnesium $Mg(C_5H_7O_2)_2 \cdot 2H_2O$	51.27	51.77	0.50	7.75	8.03	0.28	40.98	40.19	−0.79			
Bis(8-quinolonolato)-magnesium $Mg(C_9H_6ON)_2$	74.99	74.41	−0.58	4.19	4.54	0.35	11.10	11.23	0.13	9.72	9.81	0.09

a) Metal atoms were neglected in the composition of magnesium compound since they could not be determined.

Table 6. Analytical results of organophosphorus compounds

Sample[a]	C wt %			H wt %			O wt %			N wt %		
	Theor	Exptl	Error	Theor	Exptl	Error	Theor	Exptl	Error	Theor	Exptl	Error
Guanidine phosphate $(CH_5N_3)_2H_3PO_4$	12.97	15.25	2.28	7.08	8.15	1.07	34.54	21.31	−13.41	45.39	55.47	10.08
Di-*n*-octadecyl phosphate $(C_{18}H_{37}O)_2HPO_2$	75.59	75.77	0.18	13.22	13.28	0.06	11.19	10.95	−0.24			
Triphenylphosphine oxide $(C_6H_5)_3PO$	87.42	87.53	0.11	6.11	5.98	−0.13	6.47	6.49	0.02			
Tripenylphosphine $(C_6H_5)_3P$	93.46	93.51	0.05	6.54	6.49	−0.05						

a) Phosphorus atoms were neglected in the composition of organophosphorus compounds since they could not be determined.

TABLE 7. ANALYTICAL RESULTS OF ALKALI METAL COMPOUNDS

Sample[a]	C wt %			H wt %			O wt %			N wt %		
	Theor	Exptl	Error	Theor	Exptl	Error	Theor	Exptl	Error	Theor	Exptl	Error
Sodium oxalate $Na_2C_2O_4$	27.29	27.57	0.28				72.71	72.43	−0.28			
Sodium formate HCOONa	26.68	26.91	0.23	2.24	2.24	0	71.08	70.85	−0.23			
Sodium tartrate $Na_2C_4H_4O_6 \cdot 2H_2O$	26.10	26.41	0.31	4.38	4.02	−0.36	69.52	69.57	0.05			
Sodium citrate $Na_3C_6H_5O_7 \cdot 2H_2O$	32.01	31.58	−0.43	4.03	3.79	−0.24	63.96	64.63	0.67			
Sodium glutamate $NaC_5H_8O_4N \cdot H_2O$	36.59	36.45	−0.14	6.14	6.23	0.09	48.74	48.36	−0.38	8.53	8.96	0.43
Potassium hydrogen tartrate KHC_4H_5O	32.23	31.60	−0.63	3.38	3.27	−0.11	64.39	65.13	0.74			
Potassium hydrogen phthalate $KHC_8H_4O_4$	58.19	58.05	−0.14	3.05	2.82	−0.23	38.76	39.13	0.37			

a) Metal atoms were neglected in the composition of alkali metal compounds since they could not be determined.

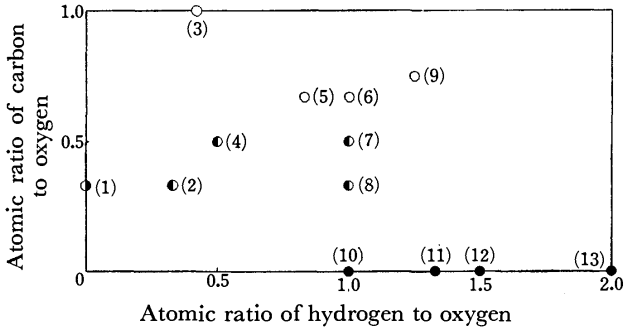

Fig. 1. Effect of the atomic ratio on the decomposition of water.
◐: H_2O produced, ◑: SO_2 produced, ●: both H_2O and SO_2 produced, ○: neither H_2O nor SO_2 produced.
(1): $SrCO_3$, (2): $KHCO_3$, (3): $[C_6H_2(NO_2)_3]_2NH_{(2,4,6)}$, (4): HCOONa, (5): $KHC_4H_4O_6$, (6): $C_4H_6O_6$, (7): $Na_2C_4H_4O_6 \cdot 2H_2O$, (8) $(COOH)_2 \cdot 2H_2O$, (9): $C_6H_8O_7 \cdot H_2O$, (10): HSO_3NH_2, (11): NH_4NO_3, (12): $(NH_2)_2 \cdot H_2SO_4$, (13): $(NH_4)_2SO_4$.

in the compound to form hydrogen sulfide and carbonyl sulfide similarly as in magnesium compounds. As shown in Fig. 1, no water is formed when the atomic ratio of carbon to oxygen exceeds 0.5, while excess oxygen which is not consumed by carbon forms SO_2 when the above ratio is less than 0.5, followed by the reaction between SO_2 and hydrogen sulfide and by the formation of water. The formation of water from SO_2 and hydrogen sulfide can be easily understood from the previous results.[2]

Analysis of Alkali Metal Compounds. It should be emphasized that organic alkali metal salts give satisfactory results. In the conventional elemental analysis using an oxygen combustion technique, alkali and alkaline earth metal compounds are apt to be converted into their carbonates. Vanadium(V) oxide has been added to prevent the formation of carbonate for the analysis of carbon. There are many alkali and alkaline earth metal compounds the analysis of which are of great importance. The present method provides a convenient tool for the elemental analysis, since no special procedure such as the addition of vanadium(V) oxide is necessary.

References

1) T. Hara, K. Fujinaga, and K. Tsuji, *Bull. Chem. Soc. Jpn.*, **51**, 1110 (1978).
2) K. Tsuji, K. Fujinaga, and T. Hara, *Bull. Chem. Soc. Jpn.*, **50**, 2292 (1977).
3) T. Matsumoto, *Bunseki Kagaku*, **3**, 307 (1954).
4) T. Matsumoto, *Bunseki Kagaku*, **7**, 346 (1958).
5) T. Matsumoto, *Bunseki Kagaku*, **3**, 221 (1954).
6) R. Berg, "Die Analytische Verwendung von *o*-Oxychinolin(Oxin) und seiner Derivate," translated by S. Uno, Kyoritsu-sha, Tokyo (1941), pp. 28—95.
7) M. Kitano, K. Yamagata, and Y. Yamazaki, *Nippon Kagaku Zasshi*, **90**, 190 (1969).
8) Y. Yamamoto, "Yukishiyaku ni yoru Bunribunsekiho (Ge)," ed by The Japan Society for Analytical Chemistry, Kyoritsu-shuppan, Tokyo (1964), pp. 183—237.
9) I. Barin and O. Knacke, "Thermochemical Properties of Inorganic Substances," Springer-Verlag, Berlin (1973), p. 10.

Aminocyclitols. 36. Chlorination and Dechlorination of Aminocyclitol and Inositol Derivatives. Preparation of Dideoxy- and Trideoxystreptamines[1a,b]

Seiichiro OGAWA,* Yuji HONGO, Hitoshi FUJIMORI, Keiji IWATA, Akira KASUGA, and Tetsuo SUAMI

Department of Applied Chemistry, Faculty of Engineering, Keio University, Hiyoshi, Yokohama 223

(Received September 27, 1977)

Chlorination of four aminocyclitol and six inositol derivatives with sulfuryl chloride gave the chloro substitution products, which were then dechlorinated by hydrogenolysis with Raney nickel or by treatment with tributyltin(IV) hydride giving the corresponding deoxy compounds. Several useful aminocyclitols, including 2,4-dideoxy- and 2,4,5-trideoxystreptamines, were prepared from 2-deoxystreptamine derivatives by these procedures.

The reaction of sulfuryl chloride with hexopyranoses and hexopyranosides had been extensively studied by Jones *et al.*[2] The mechanism and selectivity of the nucleophilic substitution of sulfate esters by chloride ions have been well established by both steric and electronic effects.[3] In the present paper, the reactions of aminocyclitol and inositol derivatives with sulfuryl chloride, and the preparation of dideoxy- and trideoxystreptamines by dechlorination of the corresponding chloro deoxy compounds are reported.

Inositol Derivatives. Treatment of 1,4,5,6-tetra-*O*-acetyl-*myo*-inositol (**1**)[4] with 3 mol equiv of sulfuryl chloride in pyridine at −10 °C for 0.5 h and subsequently at 5 °C overnight gave tetra-*O*-acetyl-2,3-dichloro-2,3-dideoxy-*myo*-inositol (**5**) in 45% yield. The structure of **5** was confirmed on the basis of the following evidence. In the ^{1}H NMR spectrum of **5** in deuteriochloroform ($CDCl_3$), the signals due to H-2 and H-3 were coupled and appeared as a triplet (δ 4.66) and a double doublet (δ 4.28) having 3-Hz splitting, and 3- and 10-Hz splitting, respectively. Hydrogenolysis of **5** with Raney nickel T-4[5] in ethanol in the presence of Amberlite IR-45 (OH^-) gave the known tetra-*O*-acetyl-1,3/2,4-cyclohexanetetrol (**9**)[6] in 67% yield.

Under similar conditions, the 3-*O*-benzoyl (**2**),[7] 3-*O*-mesyl (**3**),[7] and 3-*O*-tosyl derivatives (**4**)[8] of **1** were readily chlorinated to give the corresponding chloro deoxy compounds (**6**, **7**, and **8**) with inversion of configuration. Compound **6** could be hydrogenolyzed with Raney nickel analogously as described above to give the deoxy derivative (**10**) in 80% yield. Compounds **7** and **8** however gave **9** as the main product, together with a trace of the deoxy compounds (**11** and **12**), resulting from a cleavage of both the chlorine and sulfonyloxyl groups under these reduction conditions. Removal of only the chlorine atom of **8** was effected by treatment with tributyltin(IV) hydride in toluene in the presence of α,α′-azobisisobutyronitrile[9] and **12** was obtained in 87% yield.

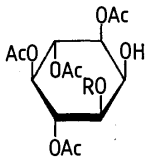

1 R=H
2 R=Bz
3 R=Ms
4 R=Ts

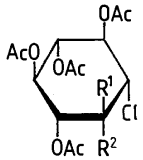

5 R^1=H, R^2=Cl
6 R^1=OBz, R^2=H
7 R^1=OMs, R^2=H
8 R^1=OTs, R^2=H

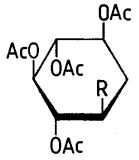

9 R=H
10 R=OBz
11 R=OMs
12 R=OTs

1,2-*O*-Cyclohexylidene-3,4,6-tri-*O*-tosyl-*myo*-inositol (**13**)[10] was similarly chlorinated to give the known chloro deoxy compound (**14**)[11] in 76% yield, which was subsequently reduced with tributyltin(IV) hydride to give the deoxy compound (**15**) in 55% yield.

1,4-Di-*O*-benzoyl-2,3-*O*-cyclohexylidene-*myo*-inositol (**16**),[11] when treated with sulfuryl chloride, gave the monochloro substitution product (**17**) in 62% yield. The acetyl derivative (**18**) of **17** was obtained by the conventional way. Acid hydrolysis of **17** followed by acetylation gave the penta-*O*-acetyl-chlorodeoxyinositol (**19**), which was reduced with tributyltin(IV) hydride to the known penta-*O*-acetyl-1,5/2,3,4-cyclohexanepentol (**20**)[12] in 77% yield. These results indicated that the C-5 hydroxyl group of **16** was selectively displaced by a chloride ion *via* the sulfate ester, establishing the structure of **17** as 1,4-di-*O*-benzoyl-5-chloro-2,3-*O*-cyclohexylidene-5-deoxy-*neo*-inositol.

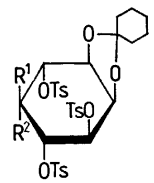

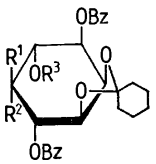

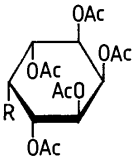

13 R^1=OH, R^2=H
14 R^1=H, R^2=Cl
15 R^1=R^2=H

16 R^1=OH, R^2=R^3=H
17 R^1=R^3=H, R^2=Cl
18 R^1=H, R^2=Cl, R^3=Ac

19 R=Cl
20 R=H

According to the above results, it was noted that an isolated hydroxyl group and both of the vicinal hydroxyl groups in the *cis*-relationship were easily displaced by chloride ions with inversion of configuration, but only one of the vicinal hydroxyl groups in the *trans* position was able to be displaced.

Aminocyclitol Derivatives. Deoxygenation of streptamine and 2-deoxystreptamine has been undertaken to prepare the deoxy derivatives of biological importance. Readily available 2-deoxystreptamine derivatives (**21**, **22**, **23**, and **33**) and streptamine derivative (**38**) were used as the starting materials.

Chlorination of 1,2-*O*-isopropylidene-(1,3/2,4,6)-4,6-bis(ethoxycarbonylamino)-1,2,3-cyclohexanetriol (**22**)[13] with 3 mol equiv of sulfuryl chloride in pyridine gave 1,2-*O*-isopropylidene-(1/2,3,4,6)-3-chloro-4,6-bis(ethoxycarbonylamino)-1,2-cyclohexanediol (**24**) in 63%

yield. The structure was confirmed by ^{1}H NMR, which revealed a narrow triplet at δ 4.69 attributable to H-3, indicating an inversion of the configuration at C-3. On treatment with 50% aqueous acetic acid at 80 °C followed by acetylation, **24** gave the di-*O*-acetyl derivative (**26**) in 83% yield. Similarly, the *N,N'*-diacetyl (**21**)[14] and *N,N'*-bis(benzyloxycarbonyl) derivatives (**23**)[14] of *O*-isopropylidene-2-deoxystreptamine were treated with sulfuryl chloride followed by mild acid hydrolysis and acetylation which gave the corresponding chloro deoxy compounds (**25** and **27**) in 48 and 34% yields, respectively.

Hydrogenolysis of **25** and **27** with Raney nickel in ethanol gave the deoxy compounds (**28** and **32**) in 56 and 89% yields, respectively. Compound **28** was shown to be identical with an authentic sample of tetra-*N,O*-acetyl-(1,3,5/2)-3,5-diamino-1,2-cyclohexanediol (2,4-dideoxystreptamine).[15] Hydrolysis of **28** with boiling 6 M hydrochloric acid gave the crystalline dihydrochloride (**29**) in 74% yield, which was further characterized by conversion into the *N,N'*-bis(ethoxycarbonyl) (**30**) and *N,N'*-bis(benzyloxycarbonyl)derivatives (**31**). Compound **30** was identical with the compound derived from **24** by mild acid hydrolysis and hydrogenolysis.

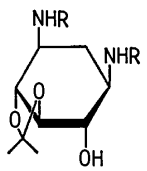

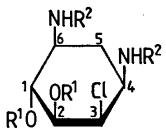

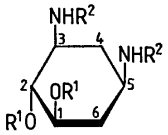

21 R=Ac
22 R=Cbe
23 R=Cbz

24 R^1, R^1=C(CH$_3$)$_2$ R^2=Cbe
25 R^1=R^2=Ac
26 R^1=Ac, R^2=Cbe
27 R^1=Ac, R^2=Cbz

28 R^1=R^2=Ac
29 R^1=R^2=H dihydrochloride
30 R^1=H, R^2=Cbe
31 R^1=H, R^2=Cbz
32 R^1=Ac, R^2=Cbz

The chlorination of *N,N'*-bis(ethoxycarbonyl)-2-deoxystreptamine (**33**)[13] was attempted to obtain the other chloro deoxy compounds. However, **33** gave, after acetylation, the cyclic sulfate ester (**34**, 28%) as the major product, together with **26** (17%). Thus, on chlorination, successive treatment with methanolic ammonia, and acetylation, **33** gave **26** in 61% yield.

In addition, the introduction of an amino function into 2-deoxystreptamine was carried out by reacting **26** with an azide ion. Treatment of **26** with an excess of sodium azide in *N,N*-dimethylformamide gave the azido deoxy compound (**35**) in 34% yield, which was reduced with Raney nickel to the 4-amino-4-deoxy derivative of 2-deoxystreptamine characterized as the *N*-acetyl derivative (**36**). Hydrolysis of **36** with boiling 48% hydrobromic acid followed by acetylation gave penta-*N,O*-acetyl-(1,3/2,4,6)-3,4,6-triamino-1,2-cyclohexanediol (**37**) whose ^{1}H NMR spectrum in dimethyl-d_6 sulfoxide revealed the presence of three equatorial acetamido groups [δ 1.76 (1) and 1.78 (2)] and two equatorial acetoxyl groups [δ 1.91 (1) and 1.92 (1)], establishing the proposed structure.

1,2-*O*-Isopropylidene-(1,3,5/2,4,6)-4,6-bis(ethoxycarbonylamino)-1,2,3,5-cyclohexanetetrol (**38**), when treated with sulfuryl chloride, gave two monochlorides (**39** and **40**) and one dichloride (**41**), which after separation by silica-gel chromatography gave yields of 19, 31, and 4%, respectively. Differentiation of **39** from **40** has been done by comparison of the ^{1}H NMR spectra. Thus, **39** showed two peaks of 2:1 ratio attributable to the three acetyl groups, while **40** showed three peaks for three individual acetyl groups. Finally, **40** was found to be identical with an authentic sample.[1a]

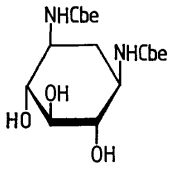

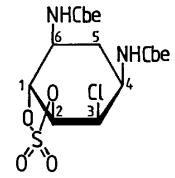

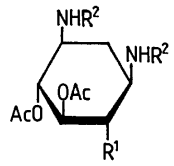

33 **34**

35 R^1=N$_3$, R^2=Cbe
36 R^1=NHAc, R^2=Cbe
37 R^1=NHAc, R^2=Ac

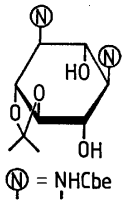

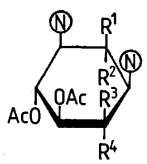

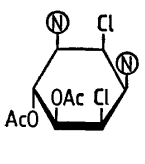

38

39 R^1=Cl, R^2=R^3=H, R^4=OAc
40 R^1=R^4=H, R^2=OAc, R^3=Cl

41

(1,2,3,5/4,6)-4,6-Bis(ethoxycarbonylamino)-1,2,3,5-cyclohexanetetrol (**42**) prepared from hexa-*N,O*-acetyl-*myo*-inosadiamine-4,6[16] by hydrolysis and subsequent ethoxycarbonylation was treated with 2,2-dimethoxypropane in *N,N*-dimethylformamide in the presence of an acid catalyst to give the 1,2-*O*-isopropylidene derivative, which was converted into 1,5-di-*O*-acetyl-2,3-*O*-isopropylidene-(1,2,3,5/4,6)-4,6-bis(ethoxycarbonylamino)-1,2,3,5-cyclohexanetetrol (**43**) in 25% overall yield. Chlorination of the hydroxy compound derived from **43** by *O*-deisopropylidenation gave the dichloro dideoxy compound (**44**) in 41% yield. The ^{1}H NMR spectrum of **44** was shown to be very similar to that of **5**, the protons attached to the carbon atoms bearing chlorine atoms. Dechlorination of **44** gave di-*O*-acetyl-(1,3/2,4)-2,4-bis(ethoxycarbonylamino)-1,3-cyclohexanediol (**45**) in 71% yield. The ^{1}H NMR spectrum supported the proposed structure.

Chlorination of **30** gave one monochloro substitution product (**46**) in 44% yield. The presence of the chlorine atom on C-1 was demonstrated by the appearance of the double doublet (δ 4.89) having 3.5- and 10-Hz

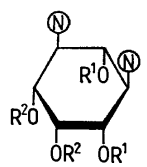

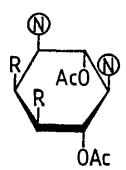

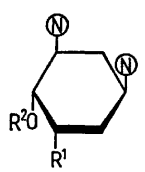

42 R^1=R^2=H
43 R^1=Ac R^2=C(CH$_3$)$_2$

44 R=Cl
45 R=H

46 R^1=Cl, R^2=Ac
47 R^1=H, R^2=Ac
48 R^1=R^2=H

splitting due to H-2. Dechlorination of **46** gave (1/2, 4)-1-acetoxy-2,4-bis(ethoxycarbonylamino)cyclohexane (**47**) in 63% yield, which was *O*-deacetylated to give *N,N'*-bis(ethoxycarbonyl)-2,4,5-trideoxystreptamine (**48**).

Experimental[17]

1,4,5,6-Tetra-O-*acetyl-2,3-dichloro-2,3-dideoxy*-myo-*inositol (5).* To a solution of 1,4,5,6-tetra-*O*-acetyl-*myo*-inositol (**1**)[4] (1 g) in dry pyridine (30 ml) was added sulfuryl chloride (0.7 ml, 3 molar equiv) at −15 °C with agitation. After stirring at the same temperature for 1 h, the reaction mixture was kept at 5 °C overnight. An insoluble matter was filtered off and washed with pyridine. The filtrate and washings were combined and evaporated to dryness, the residue dissolved in chloroform (30 ml), and the solution washed successively with aqueous sodium hydrogencarbonate and water, dried over anhydrous sodium sulfate and evaporated to dryness. The residue was crystallized from ethanol to give 0.48 g (45%) of **5**: mp 159—161 °C. Recrystallization from ethanol gave a pure sample: mp 160—160.5 °C; ^{1}H NMR ($CDCl_3$) δ 2.00 (s, 6), 2.07 (s, 3), and 2.11 (s, 3) (OAc), 4.28 (dd, 1, $J_{2,3}$=3 Hz, $J_{3,4}$=10 Hz, H-3), 4.66 (t, 1, $J_{1,2}$=3 Hz, H-2), 5.05 (dd, 1, $J_{1,6}$=10 Hz, H-1), 5.25 (t, 1, $J_{4,5}=J_{5,6}$=8 Hz, H-5), 5.50 (dd, 1) and 5.65 (dd, 1) (H-4 and H-6).

Found: Cl, 18.64%. Calcd for $C_{14}H_{18}O_8Cl_2$: Cl, 18.41%.

1,2,3,4-Tetra-O-*acetyl-5*-O-*benzoyl-6-chloro-6-deoxy*-scyllo-*inositol (6).* To a solution of 1,4,5,6-tetra-*O*-acetyl-3-*O*-benzoyl-*myo*-inositol (**2**)[7] (2 g) in dry pyridine (40 ml) was added sulfuryl chloride (1.3 ml, 3.5 molar equiv) at −10 °C with agitation. After 1 h at this temperature, the solution was stirred for a further 2.5 h at 5 °C. Then the reaction mixture was processed as described for the preparation of **5.** The product was crystallized from chloroform–ethanol to give 1.2 g (55%) of **6**: mp 241—244 °C; ^{1}H NMR ($CDCl_3$) δ 1.90 (s, 3), 2.04 (s, 3), 2.06 (s, 3), and 2.13 (s, 3) (OAc), 4.21 (t, 1, $J_{1,6}=J_{5,6}$=9 Hz, H-6).

Found: C, 53.27; H, 4.87; Cl, 7.70%. Calcd for $C_{21}H_{23}O_{10}Cl$: C, 53.57; H, 4.92; Cl, 7.53%.

1,2,3,4-Tetra-O-*acetyl-6-chloro-6-deoxy-5*-O-*mesyl*-scyllo-*inositol (7).* 1,4,5,6-Tetra-*O*-acetyl-3-*O*-mesyl-*myo*-inositol (**3**)[7] (0.51 g) was treated with sulfuryl chloride (0.4 ml, 2 molar equiv) in pyridine (15 ml) as described for the preparation of **5.** The crude product was crystallized from ethanol to give 0.26 g (49%) of **7**: mp 187.5—189 °C; ^{1}H NMR (Me_2SO-d_6) δ 1.98 (s, 3), 2.05 (s, 3), and 2.07 (s, 3) (OAc), 3.18 (s, 3, mesyl CH_3).

Found: C, 40.40; H, 4.65%. Calcd for $C_{15}H_{21}O_{11}SCl$: C, 40.49; H, 4.76%.

1,2,3,4-Tetra-O-*acetyl-6-chloro-6-deoxy-5*-O-*tosyl*-scyllo-*inositol (8).* 1,4,5,6-Tetra-*O*-acetyl-3-*O*-tosyl-*myo*-inositol (**4**)[8] (5 g) was treated with sulfuryl chloride (2.4 ml, 3 molar equiv) in pyridine (150 ml) as described for the preparation of **5.** The crystalline product was recrystallized from chloroform–ethanol to give 4.1 g (79%) of **8**: mp 200—201 °C; ^{1}H NMR ($CDCl_3$) δ 2.01 (s, 6), 2.06 (s, 3), and 2.08 (s, 3) (OAc), 2.47 (s, 3, tosyl CH_3), 4.00 (t, 1, $J_{1,6}=J_{5,6}$=10 Hz, H-6).

Found: C, 48.53; H, 4.88%. Calcd for $C_{26}H_{25}O_{11}SCl$: C, 48.42; H, 4.84%.

Tetra-O-*acetyl-1,3/2,4-cyclohexanetetrol (9).* A solution of **5** (0.1 g) in dioxane (10 ml) was hydrogenated in a Parr shaker apparatus in the presence of Raney nickel T-4[5] and Amberlite IR-45 (2 ml) under pressure (3.4 kg/cm^2) at room temperature for 2 days. The catalyst and resin were filtered off and the filtrate evaporated to dryness. The product was recrystallized from ethanol to give 0.06 g (67%) of **9**: mp 124.5—127 °C (lit,[6] 125.5—127 °C), identical with an authentic sample in all respects.

Dechlorination of 6. a) A solution of **6** (0.2 g) in ethanol (60 ml) was hydrogenated with Raney nickel catalyst as described above at room temperature overnight. The crude product was crystallized from ethanol to give 0.1 g (52%) of 1,2,3,4-tetra-*O*-acetyl-5-*O*-benzoyl-1,3,5/2,4-cyclohexanepentol (**10**): mp 168—169 °C; ^{1}H NMR ($CDCl_3$) δ 1.96 (s, 3) and 2.04 (s, 9) (OAc).

Found: C, 57.82; H, 5.52%. Calcd for $C_{21}H_{24}O_{10}$: C, 57.78; H, 5.55%.

b) Compound **6** (1 g) was treated with tributyltin(IV) hydride (1 ml) in toluene (30 ml) in the presence of α,α'-azobisisobutyronitrile (10 mg) at 80—90 °C under a stream of nitrogen for 3 h. The solution was evaporated to give a crystalline residue that was pulverized with ethanol and the crude crystals were collected by filtration. Recrystallization from ethanol gave 0.74 g (80%) of **10**: mp 168—170 °C.

Dechlorination of 7. A solution of **7** (1 g) in dioxane (20 ml) was hydrogenated with Raney nickel at room temperature overnight as described in the preparation of **9.** The product was crystallized from ethanol to give a crystalline mixture, which was fractionated on a silica gel column (40 g) with 1: 5 2-butanone–toluene. The main fraction was evaporated to give a syrup that crystallized from chloroform–ethanol to give 0.28 g (39%) of **9**: mp 124—126 °C. The minor component was crystallized from ethanol to give 0.04 g (4%) of 1,2,3,4-tetra-*O*-acetyl-5-*O*-mesyl-1,3,5/2,4-cyclohexanepentol (**11**): mp 218.5—219 °C; ^{1}H NMR ($CDCl_3$) δ 2.04 (broad s, 12, four OAc), 3.08 (s, 3, mesyl CH_3).

Found: C, 44.08; H, 5.36; S, 8.06%. Calcd for $C_{15}H_{22}O_{11}S$: C, 43.90; H, 5.40; S, 7.81%.

Dechlorination of 8. a) Compound **8** (0.2 g) was hydrogenated in dioxane (5 ml) in the presence of Raney nickel and Amberlite IR-45 (OH^-) (4 ml) at room temperature overnight. The product was crystallized from ethanol–ether to give 0.07 g (57%) of **9**: mp 134—135 °C, identical with an authentic sample[6] in all respects.

b) Compound **8** (3 g) was treated with tributyltin(IV) hydride (3 ml) in toluene (60 ml) in the presence of α,α'-azobisisobutyronitrile (30 mg) at 80—90 °C under a stream of nitrogen for 2 h. The reaction mixture was processed as described in the preparation of **10** to give crude crystals, which were recrystallized from chloroform–ethanol to give 2.34g (87%) of 1,2,3,4-tetra-*O*-acetyl-5-*O*-tosyl-1,3,5/2,4-cyclohexanepentol (**12**): mp 157.5—158.5 °C; ^{1}H NMR ($CDCl_3$) δ 1.84 (s, 3), 2.00 (s, 3), 2.02 (s, 3), and 2.05 (s, 3) (OAc), 2.50 (s, 3, tosyl CH_3).

Found: C, 51.85; H, 5.40; S, 6.43%. Calcd for $C_{21}H_{26}O_{11}S$: C, 51.84; H, 5.39; S, 6.59%.

5-Chloro-1,2-O-*cyclohexylidene-5-deoxy-3,4,6-tri*-O-*tosyl*-neo-*inositol (14).* To a solution of 1,2-*O*-cyclohexylidene-3,4,6-tri-*O*-tosyl-*myo*-inositol (**13**)[10] (0.5 g) in dry pyridine (15 ml) was added sulfuryl chloride (0.18 ml, 3 molar equiv) at −15 °C and the reaction mixture allowed to stand at this temperature for 1 h. The brown mixture was then poured into ice water and the solution evaporated to dryness. The residue was crystallized from ethanol to give 0.38 g (76%) of **14**: mp 182—183.5 °C (lit,[11] 182—183.5 °C). The IR spectrum was imposable with that of an authentic sample.

1,2-O-*Cyclohexylidene-5-deoxy-3,4,6-tri*-O-*tosyl*-myo-*inositol (15).* Compound **14** (0.2 g) was dechlorinated with tributyltin(IV) hydride in toluene as described in the preparation of **10.** The crude product was crystallized from chloroform–ethanol to give 0.11 g (55%) of **15**: mp 171—174 °C; ^{1}H NMR ($CDCl_3$) δ 2.48 (s, 9, three tosyl CH_3).

Found: C, 56.22; H, 5.41; S, 13.46%. Calcd for $C_{33}H_{38}$-

$O_{11}S_3$: C, 56.07; H, 5.42; S, 13.61%.

1,4-Di-O-benzoyl-5-chloro-2,3-O-cyclohexylidene-5-deoxy-neo-*inositol (17).* To a solution of 1,4-di-*O*-benzoyl-2,3-*O*-cyclohexylidene-*myo*-inositol (**16**)[11] (1 g) in dry pyridine (30 ml) was added sulfuryl chloride (1.04 ml, 6 molar equiv) at −15 °C and the mixture stirred at this temperature for 1 h and subsequently at 5 °C for 3 h. The reaction mixture was processed as described in the preparation of **5**, crude product being crystallized from ethanol to give 0.65 g (62%) of **17**: mp 194—196 °C.

Found: C, 63.89; H, 5.52; Cl, 7.51%. Calcd for $C_{26}H_{27}O_7Cl$: C, 64.13; H, 5.59; Cl, 7.28%.

Compound **17** (0.2 g) was treated with acetic anhydride (5 ml) and pyridine (5 ml) at room temperature overnight. The reaction mixture was evaporated and the residue crystallized from ethanol to give 0.19 g (87%) of the acetyl derivative (**18**): mp 180—181°C.

Found: C, 63.64; H, 5.50; Cl, 6.83%. Calcd for $C_{28}H_{29}O_8Cl$: C, 63.57; H, 5.53; Cl, 6.70%.

Penta-O-acetyl-5-chloro-5-deoxy-neo-*inositol (19).* A mixture of **18** (0.53 g), 12 M hydrochloric acid (30 ml), and ethanol (30 ml) was refluxed overnight, and then evaporated to give a crystalline product (0.16 g): mp 240—250 °C. Without further purification, the product was treated with acetic anhydride (10 ml) and pyridine (15 ml) at 60 °C for 2 h. The reaction mixture was evaporated and the residue crystallized from ethanol to give 0.14 g (82%) of **19**: mp 180—183 °C; ^{1}H NMR ($CDCl_3$) δ 1.99 (s, 6), 2.10 (s, 6), and 2.17 (s, 3) (OAc).

Found: C, 46.77; H, 5.08; Cl, 8.96%. Calcd for $C_{16}H_{21}O_{10}Cl$: C, 47.01; H, 5.18; Cl, 8.67%.

Penta-O-acetyl-1,5/2,3,4-cyclohexanepentol (20). Compound **19** (0.1 g) was dechlorinated with tributyltin(IV) hydride (0.3 ml) as described in the preparation of **10**. The product was crystallized from ethanol to give 0.07 g (77%) of **20**: mp 186—187 °C (lit,[12] 182 °C); ^{1}H NMR ($CDCl_3$) δ 1.45 (broad dd, 1, $J_{1,6ax\ (5,6ax)}=10$ Hz, $J_{6gem}=12$ Hz, H-6ax), 2.01 (s, 6), 2.03 (s, 6), and 2.18 (s, 3) (OAc), 2.50 (td, 1, $J_{1,6eq\ (5,6eq)}=5$ Hz, H-6eq), 4.99 (dd, 2, $J_{1,2\ (4,5)}=10$ Hz, $J_{2,3\ (3,4)}=2.5$ Hz, H-2 and H-4), 5.33 (dt, 2, H-1 and H-5), 5.65 (t, 1, H-3). (Found: C, 50.95; H, 5.74%).

1,2-O-Isopropylidene-(1/2,3,4,6)-3-chloro-4,6-bis(ethoxycarbonylamino)-1,2-cyclohexanediol (24). To a solution of 1,2-*O*-isopropylidene-(1,3/2,4,6)-4,6-bis(ethoxycarbonylamino)-1,2,3-cyclohexanetriol (**22**)[13] (0.57 g) in chloroform (5 ml) and pyridine (10 ml) was added sulfuryl chloride (0.4 ml, 3 molar equiv) at −15 °C, and the reaction mixture kept at 4 °C overnight. The mixture was processed as described in the preparation of **5**. The product was crystallized from ethyl acetate–ether to give 0.38 g (63%) of **24**: mp 189—190 °C; ^{1}H NMR ($CDCl_3$) δ 1.25 (t, 6, $J=7.5$ Hz, two ethoxycarbonyl CH_3), 1.46 (s, 6, two isopropylidene CH_3), 4.16 (q, 4, two ethoxycarbonyl CH_2), 4.69 (t, 1, $J_{2,3}=J_{3,4}=3$ Hz, H-3).

Found: C, 49.15; H, 6.71; N, 7.46; Cl, 9.92%. Calcd for $C_{15}H_{25}N_2O_6Cl$: C, 49.38; H, 6.91; N, 7.68; Cl, 9.72%.

Di-O-acetyl-(1/2,3,4,6)-3-chloro-4,6-bis(ethoxycarbonylamino)-1,2-cyclohexanediol (26). A mixture of **24** (1 g) in 50% aqueous acetic acid (80 ml) was heated at 70—80 °C for 2 h. The reaction mixture was evaporated to give a crystalline product that was directly treated with acetic anhydride and pyridine in the usual manner. The product was crystallized from ethyl acetate–ether to give 0.93 g (83%) of **26**: mp 154—155 °C; ^{1}H NMR ($CDCl_3$) δ 1.24 (t, 3) and 1.26 (t, 3) ($J=7$ Hz, ethoxycarbonyl CH_3), 2.07 (s, 3) and 2.11 (s, 3) (OAc), 4.15 (q, 2) and 4.18 (q, 2) (ethoxycarbonyl CH_2), 4.71 (m, 1, H-3).

Found: C, 47.05; H, 6.08; N, 6.77; Cl, 8.53%. Calcd for $C_{16}H_{25}N_2O_8Cl$: C, 47.00; H, 6.16; N, 6.85; Cl, 8.67%.

Di-O-acetyl-(1/2,3,4,6)-4,6-diacetamido-3-chloro-1,2-cyclohexanediol (25). 1,2-*O*-Isopropylidene-(1,3/2,4,6)-4,6-diacetamido-1,2,3-cyclohexanetriol (**21**)[14] (1 g) was treated with sulfuryl chloride in chloroform and pyridine as described in the preparation of **24**. The product was heated with 1 M hydrochloric acid (20 ml) at 70 °C for 20 min. The mixture was evaporated and the residual product acetylated in the usual manner to give, after crystallization from ethanol, 0.58 g (48%) of **25**: mp 223—224 °C; ^{1}H NMR (Me_2SO-d_6) δ 1.76 (s, 3), 1.85 (s, 3), 1.95 (s, 3), and 2.03 (s, 3) (OAc), 4.75 (broad s, 1, H-3), 5.14—5.25 (m, 2, H-1 and H-2).

Found: C, 48.09; H, 5.94; N, 7.84; Cl, 10.09%. Calcd for $C_{14}H_{21}N_2O_6Cl$: C, 48.21; H, 6.07; N, 8.03; Cl, 10.16%.

1,2-Di-O-acetyl-(1/2,3,4,6)-4,6-bis(benzyloxycarbonylamino)-3-chloro-1,2-cyclohexanediol (27). 1,2-*O*-Isopropylidene-(1,3/2,4,6)-4,6-bis(benzyloxycarbonylamino)-1,2,3-cyclohexanetriol (**23**)[13] (0.8 g) was chlorinated as described in the preparation of **24**. The product was treated with acid and acetylated as described above. Purification using a silica gel column (40 g) with 1:10 2-butanone–toluene gave 0.31 g (34%) of **27**: mp 128.5—129.5 °C; ^{1}H NMR (Me_2SO-d_6) δ 1.90 (s, 3) and 2.06 (s, 3) (OAc), 4.89 (m, 1, H-3), 5.17 (broad s, 4, two benzyloxycarbonyl CH_2).

Found: C, 58.78; H, 5.28; N, 5.08; Cl, 6.77%. Calcd for $C_{26}H_{29}N_2O_8Cl$: C, 58.59; H, 5.48; N, 5.26; Cl, 6.65%.

(1,3,5/2)-3,5-Bis(ethoxycarbonylamino)-1,2-cyclohexanediol [N,N′-*Bis(ethoxycarbonyl)-2,4-dideoxystreptamine*] *(30).* A mixture of **24** (0.16 g) in dioxane (5 ml) and 50% aqueous acetic acid (20 ml) was heated at 70 °C for 2 h, and then evaporated to dryness. The residue was crystallized from ethyl acetate to give 0.14 g (96%) of the dihydroxy compound: mp 120—123 °C. This compound was hydrogenated in ethanol (10 ml) as described in the preparation of **9** at room temperature for 27 h. The product was crystallized from ethanol to give 0.068 g (54%) of **30**: mp 185—186 °C; ^{1}H NMR (Me_2SO-d_6) δ 1.11 (t, 6, $J=7$ Hz, two ethoxycarbonyl CH_3), 3.78—4.15 (m, 4, two ethoxycarbonyl CH_2).

Found: C, 49.26; H, 7.39; N, 9.42%. Calcd for $C_{12}H_{22}N_2O_6$: C, 49.64; H, 7.64; N, 9.65%.

Di-O-acetyl-(1,3,5/2)-3,5-diacetamido-1,2-cyclohexanediol (N,N′-*Diacetyl-2,4-dideoxystreptamine*) *(28).* Compound **25** (0.4 g) was hydrogenated in ethanol (20 ml) as described in the preparation of **9** at room temeprature overnight. The product was crystallized from ethanol–ether to give 0.21 g (65%) of **28**: mp 247—249 °C (lit,[15] 231.5—233 °C). This compound was identified with an authentic sample[15] by comparison with IR and ^{1}H NMR spectra, and shown to be more homogeneous.

Di-O-acetyl-(1,3,5/2)-3,5-bis(benzyloxycarbonylamino)-1,2-cyclohexanediol (32). Compound **27** (0.075 g) was dechlorinated with tributyltin(IV) hydride (0.3 ml) as described in the preparation of **10**. The crude crystals were recrystallized from chloroform–petroleum ether to give 0.062 g (89%) of **32**: mp 180—182 °C; ^{1}H NMR ($CDCl_3$) δ 1.94 (s, 3) and 2.00 (s, 3) (OAc), 5.10 (broad s, 4, two benzyloxycarbonyl CH_2).

Found: C, 62.26; H, 6.04; N, 5.68%. Calcd for $C_{26}H_{30}N_2O_8$: C, 62.64; H, 6.07; N, 5.62%.

(1,3,5/2)-3,5-Diamino-1,2-cyclohexanediol Dihydrochloride (2,4-Dideoxystreptamine Dihydrochloride) (29). Compound **28** (0.46 g) was refluxed with 6 M hydrochloric acid (20 ml) for 3.5 h. The reaction mixture was evaporated and the residual syrup crystallized from ethanol–methanol–water to give 0.24 g (74%) of **29**: mp 247—249 °C (dec.).

Found: C, 32.69; H, 7.18; N, 12.72; Cl, 32.20%. Calcd for $C_6H_{16}N_2O_2Cl_2$: C, 32.89; H, 7.36; N, 12.78; Cl, 32.36%.

Compound **29** (0.44 g) was treated with ethyl chloroformate (0.76 ml) in acetone (12 ml) and water (12 ml) containing

sodium carbonate (2.2 g) under vigorous agitation at room temeprature overnight. The mixture was neutralized with 1 M hydrochloric acid and evaporated to dryness. The residue was extracted with hot dioxane (20 ml), the extract evaporated and crystallized from ethanol to give 0.45 g (78%) of **30**: mp 185—186 °C, identical with the compound obtained before.

(1,3,5/2)-3,5-Bis(benzyloxycarbonylamino)-1,2-cyclohexanediol [N,N'-*Bis(benzyloxycarbonyl)-2,4-dideoxystreptamine*] *(31)*. The crude **29** obtained from **28** (0.16 g) was treated with 30% toluene solution of carbobenzyloxy chloride (1.1 ml) in acetone (4 ml) and water (2 ml) in the presence of sodium hydrogencarbonate (0.19 g) at 5 °C overnight. The resulting crystals were collected and recrystallized from ethanol to give 0.15 g (73%) of **31**: mp 204—205 °C.

Found: C, 63.45; H, 6.46; N, 6.39%. Calcd for $C_{22}H_{26}N_2O_6$: C, 63.75; H, 6.32; N, 6.76%.

Chlorination of (1,3/2,4,6)-4,6-Bis(ethoxycarbonylamino)-1,2,3-cyclohexanetriol (33).[13] a) To a solution of **33** (1 g) in pyridine (40 ml) was added sulfuryl chloride (1.1 ml, 4 molar equiv) at −15 °C with stirring, and the mixture was kept at 4 °C for 4 h. TLC indicated the formation of two components (R_f 0.81 and 0.51, in 5:1 benzene–ethanol). The reaction mixture was processed as described in the preparation of **5** and the product acetylated in the usual manner. The mixture of two components (R_f 0.56 and 0.51, in 2:1 benzene–ethyl acetate) was fractionated using a silica-gel column (100 g) with 3:1 and 5:1 benzene–ethyl acetate as the eluate. The first fraction (R_f 0.56) was evaporated and crystallized from chloroform–ethyl acetate to give 0.33 g (28%) of (1/2,3,4,6)-3-chloro-4,6-bis(ethoxycarbonylamino)-1,2-cyclohexanediol 1,2-cyclic sulfate (**34**): mp 183 °C (dec) after melting and resolidification at 105—110 °C; ^{1}H NMR (Me_2SO-d_6) δ 1.19 (t, 6, J=7.5 Hz, two ethoxycarbonyl CH_3), 4.06 (q, 4, two ethoxycarbonyl CH_2), 5.06 (t, 1, $J_{1,2}=J_{1,6}=10$ Hz, H-1), 5.64 (dd, 1, $J_{2,3}=3$ Hz, H-2); IR 3300 (NH), 1700 and 1540 (amide), 1390 cm^{-1} (sulfate).

Found: C, 36.96; H, 4.79; N, 7.19%. Calcd for $C_{12}H_{14}N_2O_8SCl$: C, 37.24; H, 4.95; N, 7.24%.

The second fraction (R_f 0.51) was evaporated and crystallized from ethyl acetate–petroleum ether to give 0.23 g (17%) of **26**: mp 154—155 °C, identical with the compound obtained before.

b) Compound **33** (3 g) was treated with sulfuryl chloride (3.3 ml) in pyridine (100 ml) as described above. The syrupy mixture thus obtained was treated with methanol (100 ml) saturated with ammonia at 5 °C at room temperature for 4 days. The reaction mixture evaporated to dryness and the residue treated with 1 M hydrochloric acid (50 ml) at 80 °C for 15 h. Then the mixture was neutralized with sodium carbonate (2.6 g) and evaporated to give solid residue, which was extracted with hot dioxane (50 ml). The extract was evaporated and the residual product acetylated in the usual manner. The product was purified by passage through a short alumina column with chloroform and crystallized from ethyl acetate–petroleum ether to give 2.46 g (61%) of **26**: mp 153—155 °C.

Di-O-acetyl-(1,3/2,4,6)-3-azido-4,6-bis(ethoxycarbonylamino)-1,2-cyclohexanediol (35). A mixture of **26** (2 g), sodium azide (3.65 g), and *N,N*-dimethylformamide (30 ml) was heated at 100 °C under stirring overnight. An insoluble matter was filtered off and the filtrate evaporated to dryness. The residue was treated with acetic anhydride (20 ml) and pyridine (20 ml) at room temperature overnight. The reaction mixture was evaporated, and the residual product dissolved in chloroform and filtered through a short alumina column. The filtrate was evaporated and crystallized from chloroform–ether to give 0.86 g (34%) of **35**: mp 155—156 °C; ^{1}H NMR ($CDCl_3$) δ 1.23 (t, 3) and 1.27 (t, 3) (J=7 Hz, ethoxycarbonyl CH_3), 2.07 (s, 3) and 2.13 (s, 3) (OAc), 4.12 (q, 2) and 4.18 (q, 2) (ethoxycarbonyl CH_2).

Found: C, 46.14; H, 6.01; N, 16.84%. Calcd for $C_{16}H_{25}N_5O_8$: C, 46.26; H, 6.07; N, 16.86%.

Di-O-acetyl-(1,3/2,4,6)-3-acetamido-4,6-bis(ethoxycarbonylamino)-1,2-cyclohexanediol (36). Compound **35** (0.76 g) was treated with methanolic ammonia (20 ml) at room temperature overnight. The mixture was evaporated to give a white powder, which was hydrogenated in ethanol (20 ml) with Raney nickel as described in the preparation of **9**. The product was acetylated in the usual manner and crystallized from ethanol to give 0.42 g (54%) of **36**: mp 267—268 °C.

Found: C, 49.97; H, 6.56; N, 9.83%. Calcd for $C_{18}H_{29}N_3O_9$: C, 50.11; H, 6.77; N, 9.74%.

*Penta-*N,O-*acetyl-(1,3/2,4,6)-3,4,6-triamino-1,2-cyclohexanediol (37)*. Compound **36** (0.045 g) was refluxed with 48% hydrobromic acid (2 ml) for 3 h. The reaction mixture was evaporated and the residue dissolved in water. The solution was passed through a short column of Dowex 1×2 (OH^-) and the eluate was evaporated to give the free base, which on acetylation gave 0.032 g (83%) of **37**: mp 298—303 °C (dec); ^{1}H NMR (Me_2SO-d_6), see text.

Found: C, 51.65; H, 6.62; N, 11.34%. Calcd for $C_{16}H_{25}N_3O_7$: C, 51.74; H, 6.79; N, 11.34%.

1,2-O-Isopropylidene-(1,3,5/2,4,6)-4,6-bis(ethoxycarbonylamino)-1,2,3,5-cyclohexanetetrol (38). 1,5-Di-*O*-acetyl-2,3-*O*-isopropylidene-(1,3,5/2,4,6)-4,6-bis(ethoxycarbonylamino)-1,2,3,5-cyclohexanetetrol[18] (1 g) was treated with methanol (50 ml) saturated with ammonia at 5 °C. After standing at room temperature overnight, the reaction mixture was evaporated to dryness and the residue crystallized from ethanol to give 0.64 g (78%) of **38** as tiny needles: mp 228—230 °C, after sintering and resolidifying at 200—203 °C.

Found: C, 49.57; H, 7.03; N, 7.74%. Calcd for $C_{15}H_{26}N_2O_8$: C, 49.72; H, 7.23; N, 7.73%.

Chlorination of 38. To a solution of **38** (2 g) in pyridine (50 ml) was added sulfuryl chloride (2.7 ml, 4 molar equiv) at −20 °C with stirring, and then the mixture was kept at 4 °C for 6 h. The reaction mixture was diluted with chloroform (100 ml) and the solution washed successively with aqueous sodium hydrogencarbonate and water. After drying over anhydrous sodium sulfate, the organic layer was evaporated to give a syrup, which was dissolved in dioxane (10 ml) and heated with 50% aqueous acetic acid (10 ml) at 80 °C for 2 h. The reaction mixture was evaporated to dryness and the residue treated with acetic anhydride (10 ml) and pyridine (10 ml) at room temperature overnight. TLC indicated the formation of three components (R_f 0.58, 0.37, and 0.25 in 3:1 benzene–ethyl acetate). The reaction mixture was evaporated and the residual product was chromatographed on silica gel (100 g) with 4:1 benzene–ethyl acetate as an eluent.

The fraction (R_f 0.58) was evaporated and crystallized from ethanol to give 0.1 g (4%) of di-*O*-acetyl-(1/2,3,4,5,6)-3,5-dichloro-4,6-bis(ethoxycarbonylamino)-1,2-cyclohexanediol(**41**): mp 200—202 °C; ^{1}H NMR (Me_2SO-d_6) δ 1.19 (t, 6, J=7 Hz, two ethoxycarbonyl CH_3), 2.08 (s, 6, two OAc), 4.06 (q, 4, two ethoxycarbonyl CH_2), 4.72 (dd, 1, J=*ca.* 3 Hz, H-3 or H-5), 7.69 (d, 2, J=7 Hz, 2NH).

Found: C, 43.20; H, 5.29; N, 6.19; Cl, 16.00%. Calcd for $C_{16}H_{24}N_2O_8Cl_2$: C, 43.35; H, 5.46; N, 6.32; Cl, 15.99%.

The fraction (R_f 0.37) was evaporated and crystallized from ethanol to give 0.49 g (19%) of tri-*O*-acetyl-(1,3/2,4,5,6)-5-chloro-4,6-bis(ethoxycarbonylamino)-1,2,3-cyclohexanetriol (**39**): mp 195—196 °C; ^{1}H NMR (Me_2SO-d_6) δ 1.18 (t, 6, J=7 Hz, two ethoxycarbonyl CH_3), 1.92 (s, 3) and 1.97 (s, 6) (OAc), 4.07 (q, 4, two ethoxycarbonyl CH_2), 7.26 (d, 2, J=8

Hz, 2NH).

Found: C, 46.59; H, 5.69; N, 6.00; Cl, 7.77%. Calcd for $C_{18}H_{27}N_2O_{10}Cl$: C, 46.31; H, 5.38; N, 6.00; Cl, 7.59%.

The fraction (R_f 0.25) was evaporated and crystallized from ethanol to give 0.81 g (31%) of tri-*O*-acetyl-(1,3,5,6/2,4)-6-chloro-3,5-bis(ethoxycarbonylamino)-1,2,4-cyclohexanetriol (**40**): mp 183—184 °C; ^{1}H NMR (Me_2SO-d_6) δ 1.13 (t, 3) and 1.18 (t, 3) (J=7 Hz, ethoxycarbonyl CH_3), 1.97 (s, 6) and 2.03 (s, 3) (OAc), 3.99 (q, 2) and 4.05 (q, 2) (ethoxycarbonyl CH_2), 6.94 (d, 1) and 7.19 (d, 1) (J=8 Hz, NH). (Found: C, 46.57; H, 5.56; N, 6.06; Cl, 7.76%). This compound was identified with an authentic sample[1a] (mp 180—182 °C).

(1,2,3,5/4,6)-Bis(ethoxycarbonylamino)-1,2,3,5-cyclohexanetetrol [N,N′-*Bis(ethoxycarbonyl)*-myo-*inosadiamine-4,6*] (**42**). Hexa-*N,O*-acetyl-*myo*-inosadiamine-4,6[16] (1.33 g) was treated with 6 M hydrochloric acid (30 ml) at reflux temperature for 2 h. The reaction mixture was evaporated and the crude dihydrochloride obtained treated with ethyl chloroformate (1.2 ml) in 1 M sodium hydroxide solution (15 ml) at room temperature overnight. After neutralization with 1 M hydrochloric acid, the mixture was evaporated to dryness and the residue extracted with hot dioxane (30 ml). The extract was evaporated and the crystals recrystallized from dioxane to give 0.73 g (80%) of **42**: mp 247.5—248.5 °C.

Found: C, 45.01; H, 6.84; N, 8.39%. Calcd for $C_{12}H_{22}N_2O_8$: C, 44.71; H, 6.88; N, 8.69%.

Compound **42** was acetylated in the conventional way. The crude product was crystallized from ethanol to give the tetra-*O*-acetyl derivative: mp 247—248.5 °C; ^{1}H NMR ($CDCl_3$) δ 1.23 (t, 6, J=7 Hz, two ethoxycarbonyl CH_3), 2.02 (s, 6), 2.07 (s, 3), and 2.20 (s, 3) (OAc), 4.10 (q, 4, two ethoxycarbonyl CH_2), 4.21 (q, 2, $J_{1,6(3,4)}=J_{4,5(5,6)}=J_{4,NH(6,NH)}$ =10.5 Hz, H-4 and H-6), 5.07 (t, 1, H-5), 5.09 (dd, 2, $J_{1,2(2,3)}$ =2.5 Hz, H-1 and H-3), 5.23 (d, 2, 2NH), 5.62 (t, 1, H-2).

Found: C, 48.92; H, 6.22; N, 5.53%. Calcd for $C_{20}H_{30}N_2O_{12}$: C, 48.97; H, 6.17; N, 5.71%.

1,5-Di-O-acetyl-2,3-O-isopropylidene-(1,2,3,5/4,6)-4,6-bis(ethoxycarbonylamino)-1,2,3,5-cyclohexanetetrol (**43**). Compound **42** (0.4 g) was dissolved in *N,N*-dimethylformamide (20 ml), and 2,2-dimethoxypropane (5 ml) and *p*-toluenesulfonic acid (10 mg) were added. The mixture was heated at 80 °C for 10 min and then treated with Amberlite IRA-400 (OH^-) after cooling. The solution was evaporated and crystallized from ethanol to give 0.15 g (34%) of the *O*-isopropylidene derivative: mp 190—191 °C; ^{1}H NMR (Me_2SO-d_6) δ 1.22 (t, 6, J= 7 Hz, two ethoxycarbonyl CH_3), 1.33 (s, 3) and 1.53 (s, 3) (isopropylidene CH_3), 4.12 (q, 4, two ethoxycarbonyl CH_2).

A 0.1-g portion of the crystals was acetylated in the usual manner and the product crystallized from ethanol to give 0.1 g (74%) of **43**: mp 221—222 °C; ^{1}H NMR ($CDCl_3$) δ 1.22 (t, 6, J=7 Hz, two ethoxycarbonyl CH_3), 1.36 (s, 3) and 1.64 (s, 3) (isopropylidene CH_3), 2.05 (s, 3) and 2.13 (s, 3) (OAc), 4.11 (q, 4, two ethoxycarbonyl CH_2), 4.43 (t, 1, $J_{1,2}=J_{2,3}$=3 Hz, H-2), 4.95 (t, 1, $J_{4,5}=J_{5,6}$=10 Hz, H-5), 5.00 (d, 1, J= 10 Hz) and 5.19 (d, 1, J=9 Hz) (NH), 5.20 (dd, 1, $J_{1,6}$=11 Hz, H-1).

Found: C, 51.38; H, 6.89; N, 6.35%. Calcd for $C_{19}H_{30}N_2O_{10}$: C, 51.12; H, 6.77; N, 6.27%.

Di-O-acetyl-(1,3/2,4,5,6)-4,5-dichloro-2,6-bis(ethoxycarbonylamino)-1,3-cyclohexanediol (**44**). Compound **43** (0.057 g) was heated with 90% aqueous acetic acid (10 ml) at 80 °C for 30 min. The mixture was evaporated to give a syrupy dihydroxy compound. Without further purification, the product was treated with sulfuryl chloride (0.05 ml) in pyridine (5 ml) at 5 °C overnight. The reaction mixture was processed as described in the preparation of **5**. The product was recrystallized from ethanol to give 0.023 g (41%) of **44**: mp 218—219 °C; ^{1}H NMR ($CDCl_3$) δ 1.21 (t, 3) and 1.24 (t, 3) (J=7 Hz, ethoxycarbonyl CH_3), 2.07 (s, 3) and 2.10 (s, 3) (OAc), 4.11 (q, 2) and 4.15 (q, 2) (ethoxycarbonyl CH_2), 4.35 (dd, 1, $J_{3,4}$=10 Hz, $J_{4,5}$=3 Hz, H-4), 4.63 (t, 1, $J_{5,6}$=3 Hz, H-5), 5.14 (d, 1) and 5.26 (d, 1) (J=9 Hz, NH), 5.26 (t, 1, $J_{1,2}=J_{1,6}$=10 Hz, H-1), 5.38 (t, 1, $J_{2,3}$=10 Hz, H-3).

Found: C, 43.26; H, 5.41; N, 6.28; Cl, 15.95%. Calcd for $C_{16}H_{24}N_2O_8Cl_2$: C, 43.34; H, 5.46; N, 6.32; Cl, 16.00%.

Di-O-acetyl-(1,3/2,4)-2,4-bis(ethoxycarbonylamino)-1,3-cyclohexanediol [*Di-O-acetyl*-N,N′-*bis(ethoxycarbonyl)-4,5-dideoxystreptamine*] (**45**). Compound **44** (0.21 g) was hydrogenated in ethanol (15 ml) as described in the preparation of **9**. The product was crystallized from ethyl acetate–ether to give 0.13 g (71%) of **45**: mp 170 °C; ^{1}H NMR (Me_2SO-d_6) δ 1.15 (t, 6, J=7.5 Hz, two ethoxycarbonyl CH_3), 1.91 (s, 3) and 1.97 (s, 3) (OAc), 4.01 (q, 4, two ethoxycarbonyl CH_2), 4.71 (dd, 1, $J_{2,3}=J_{3,4}$=*ca.* 10 Hz, H-3).

Found: C, 51.33; H, 7.00; N, 7.48%. Calcd for $C_{16}H_{26}N_2O_8$: C, 51.13; H, 6.86; N, 7.28%.

(1,2/3,5)-2-Acetoxy-1-chloro-3,5-bis(ethoxycarbonylamino)cyclohexane (**46**). Compound **30** (0.09 g) was treated with sulfuryl chloride (0.15 ml) in pyridine (5 ml) at −20 °C for 10 min and then at 5 °C for 6 h. The reaction mixture was processed as described in the preparation of **5**. The product was acetylated in the usual manner and purified through a short column of alumina with chloroform. Recrystallization from chloroform–ether gave 0.047 g (44%) of **46**: mp 162—163 °C; ^{1}H NMR ($CDCl_3$) δ 1.21 (t, 6, J=7 Hz, two ethoxycarbonyl CH_3), 2.08 (s, 3, OAc), 4.10 (q, 4, two ethoxycarbonyl CH_2), 4.86 (dd, 1, $J_{1,2}$=3.5 Hz, $J_{2,3}$=10 Hz, H-2).

Found: C, 47.76; H, 6.42; N, 7.80; Cl, 10.07%. Calcd for $C_{14}H_{23}N_2O_6Cl$: C, 47.93; H, 6.61; N, 7.98; Cl, 10.11%.

(1/2,4)-1-Acetoxy-2,4-bis(ethoxycarbonylamino)cyclohexane (**47**). A solution of **46** (0.5 g) in ethanol (20 ml) was hydrogenated as described in the preparation of **9**. The product was crystallized from ethanol to give 0.28 g (63%) of **47**: mp 151—152 °C; ^{1}H NMR (Me_2SO-d_6) δ 1.17 (t, 1, J=7 Hz, two ethoxycarbonyl CH_3), 1.97 (s, 3, OAc), 4.03 (q, 4, two ethoxycarbonyl CH_2), 4.53 (ddd, 1, $J_{1,2}=J_{1,6ax}$=9 Hz, $J_{1,6eq}$=4 Hz, H-1).

Found: C, 52.89; H, 7.46; N, 8.99%. Calcd for $C_{14}H_{24}N_2O_6$: C, 53.15; H, 7.65; N, 8.85%.

(1/2,4)-2,4-Bis(ethoxycarbonylamino)-1-cyclohexanol [N,N′-*Bis(ethoxycarbonyl)-2,4,5-trideoxystreptamine*] (**48**). Compound **47** (0.22 g) was treated with methanolic ammonia (20 ml) at room temperature overnight. The reaction mixture was evaporated and recrystallized from ethanol–ether to give 0.17 g (88%) of **48**: mp 133—136 °C.

Found: C, 52.41; H, 7.98; N, 10.15%. Calcd for $C_{12}H_{22}N_2O_5$: C, 52.54; H, 8.09; N, 10.29%.

The authors wish to thank Dr. Shigeru Nishiyama for the preparation of compound **37** from **36**. This work was carried out with financial support from the Ministry of Education.

References

1) a) For paper 35 of this series, see S. Ogawa, T. Ueda, Y. Funaki, Y. Hongo, A. Kasuga, and T. Suami, *J. Org. Chem.*, **42**, 3083 (1977); b) In this paper, all the compounds except for meso compounds are racemic. All the formulas depict only one of the respective racemates.

2) B. T. Lawton, W. A. Szarek, and J. K. N. Jones, *Carbohydr. Res.*, **15**, 397 (1970).

3) H. J. Jennings and J. K. N. Jones, *Can. J. Chem.*, **43**, 2372 (1965).

4) S. J. Angyal, P. T. Gilham, and C. G. Mcdonald, *J.*

Chem. Soc., **1957**, 1417.
5) S. Nishimura, *Bull. Chem. Soc. Jpn.*, **32**, 61 (1959).
6) T. Suami, S. Ogawa, K. Yabe, and M. Uchida, *Bull. Chem. Soc. Jpn.*, **44**, 2804 (1971).
7) T. Suami, F. W. Lichtenthaler, and S. Ogawa, *Bull. Chem. Soc. Jpn.*, **30**, 170 (1966).
8) S. J. Angyal, P. T. Gilham, and G. T. H. Melrose, *J. Chem. Soc.*, **1965**, 5252.
9) H. Arita, N. Ueda, and Y. Matsushima, *Bull. Chem. Soc. Jpn.*, **45**, 567 (1972).
10) T. Suami, S. Ogawa, T. Tanaka, and T. Otake, *Bull. Chem. Soc. Jpn.*, **44**, 835 (1971).
11) T. Suami, S. Ogawa, K. Ohashi, and S. Oki, *Bull. Chem. Soc. Jpn.*, **45**, 3660 (1972).
12) G. E. McCasland, S. Furuta, L. F. Johnson, and J. N. Shoolery, *J. Am. Chem. Soc.*, **83**, 2335 (1961).
13) Y. Nishimura, T. Tsuchiya, and S. Umezawa, *Bull. Chem. Soc. Jpn.*, **43**, 2960 (1970).
14) A. Hasegawa, N. Kurihara, D. Nishimura, and M. Nakajima, *Agric. Biol. Chem.*, **32**, 1123 (1968).
15) T. Suami, S. Ogawa, H. Uchino, and Y. Funaki, *J. Org. Chem.*, **40**, 456 (1975).
16) T. Suami and S. Ogawa, *Bull. Chem. Soc. Jpn.*, **38**, 2026 (1965).
17) Melting points were determined in a capillary in a liquid bath and are uncorrected. Solutions were evaporated under diminished pressure at 40—50 °C. ^{1}H NMR spectra were measured at 60 MHz on a Varian A-60D spectrometer in $CDCl_3$ and dimethyl-d_6 sulfoxide with reference to tetramethylsilane as an internal standard and the peak positions are given in δ-values. Values given for coupling constants are of first-order. TLC was performed on silica gel (Wakogel B-10, Wako Pure Chemical Industries, Ltd.). Elemental analyses were performed by Mr. Saburo Nakada, to whom our thanks are due.

The Linearity of the Substituent-induced Carbon-13 Chemical Shifts of α-Carbons with Charge Densities in Aromatic Side Chains. Semi-empirical Calculations for 4-Substituted Derivatives of Styrenes, α-Methylstyrenes, and Biphenyls

Jun NIWA

College of General Education, Nagoya University, Chikusa, Nagoya 464

(Received October 31, 1977)

The contributions to ^{13}C shifts from the diamagnetic term of the neighboring carbon atom and from the "ring-current" have been estimated by means of the equations given in a previous paper (J. Niwa, *Bull. Chem. Soc. Jpn.*, **48**, 118 (1975)). A semi-empirical expression has been derived for the substituent-induced ^{13}C chemical shift in an aromatic side chain by considering such contributions in addition to the local diamagnetic and paramagnetic terms of the carbon atom in question. The applicability of the expression has been examined for α-carbons of 4-substituted derivatives of styrenes and α-methylstyrenes, and for 1′-carbons of 4-substituted biphenyls.

The linearity of ^{13}C nuclear shielding with electron density is widely accepted on the basis of the Karplus and Pople LCAO-MO theory of diamagnetism.[1] The attempt to interpret the ^{13}C chemical shift induced by substituents (SCS) along the lines of their approach has been successfully performed for the *para*-carbon of the benzene ring.[2] The SCS of the terminal carbon of a conjugated aromatic side chain can also be treated in the same way, whereas that of α-carbon is not always directly correlated with the electron density; for example, in the ^{13}C shielding of α- and β-carbons for the series of substituted styrenes, α-carbon absorbs over a relatively narrow range, about 2 ppm, while β-carbon differs by 10 ppm. The trend of the latter is clear; an electron-withdrawing substituent decreases the β-carbon shielding, while an electron-releasing substituent increases it. This trend has been nicely correlated with the electron density. In contrast to the β-carbon, the electron-withdrawing substituent tends to increase the α-carbon shielding. The effect, however, is small and is not linearly correlated with the electron density, as is shown in Fig. 1. Its interpretation awaits a more refined theory of ^{13}C nuclear shielding.

The dominant factor governing the ^{13}C shielding must be the local paramagnetic term, σ^{AA}_{para}, but the magnetic contributions from the rest of the molecule may also not be ignored for the SCS, the range of which is relatively narrow; in the case of styrenes, the failure of the linearity of the SCS of the α-carbon with the electron density may be attributed to ignoring the contributions from the neighboring carbon atoms and the long-range shielding effect of the "ring-current."

The premises of the present approach are: (i) it is based on the Saika-Slichter expression for the nuclear magnetic shielding;[3] (ii) it continues the use of Pople's average excitation energy approximation for the paramagnetic term;[1] (iii) it considers the magnetic contribution from the neighboring carbon atom which is situated at the site near to the substituent, and (iv) it takes the long-range shielding effect of the "ring-current" into account. In our preceding paper,[4] we derived the equations for estimating the contributions from the diamagnetic term of the neighboring carbon atom and from the "ring-current." We can derive a semi-empirical expression for obtaining the ^{13}C SCS in an aromatic side chain by considering such contributions in addition to the local diamagnetic and the local paramagnetic terms of the relevant carbon atom.

The aim of the present paper is to demonstrate the validity of the predictions by an expression for a variety of substituents in the series of 4-substituted derivatives of styrenes, α-methylstyrenes, and biphenyls and, in particular, to examine the propriety of the expression for understanding and predicting the SCS of α-carbons of the styrenes and the α-methylstyrenes, and those of 1′-carbons of the biphenyls.

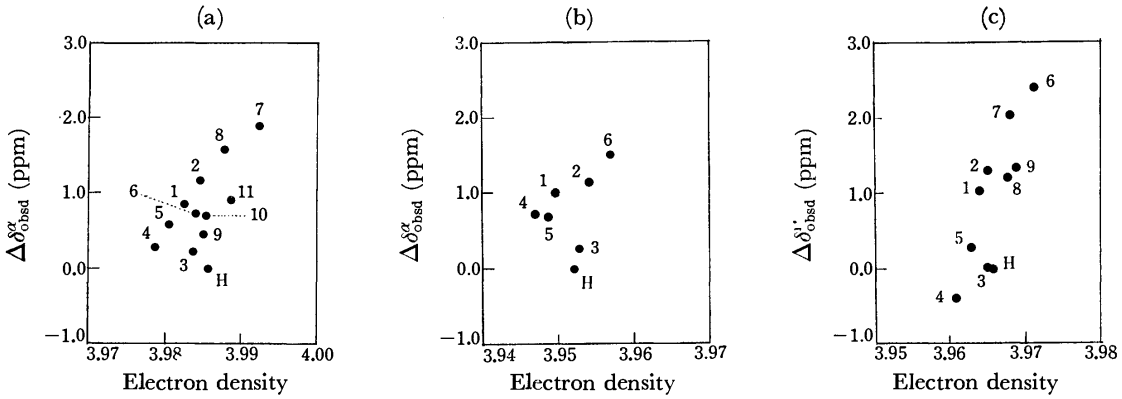

Fig. 1. Plots of $\Delta\delta_{obsd}$ against the electron density on α-carbon atom; (a) 4-substituted styrenes (b) 4-substituted α-methylstyrenes (c) 4-substituted biphenyls. Numbered points correspond to entries in Table 1.

Calculation, Results, and Discussion

The Saika-Slichter expression for obtaining a simple relationship for the nuclear magnetic shielding, σ^A, is given as[3]

$$\sigma^A = \sigma^{AA}_{dia} + \sigma^{AA}_{para} + \sum_{B\neq A}(\sigma^{AB}_{dia}+\sigma^{AB}_{para}) + \sigma^{A,ring}, \quad (1)$$

where σ^{AA} is the local diamagnetic and the local paramagnetic terms of the A atom in question; σ^{AB} is the contribution from currents on the B atom to the shielding of A, and $\sigma^{A,ring}$ is the contribution to the shielding of A from the "ring-current."

The local diamagnetic term, σ^{AB}_{dia}, is given by

$$\sigma^{AA}_{dia} = e^2/3mc^2\sum_i\langle r_i^{-1}\rangle, \quad (2)$$

where $\langle r_i^{-1}\rangle$ is the mean inverse distance of the i-th electron from a nucleus and where the summation is taken over all the electrons being considered; the diamagnetic shielding constant, σ_d', per 2s or 2p electron has been given by Yonezawa, Morishima, and Kato as[5]

$$\sigma_d'(2s \text{ or } 2p) = 4.45z^*,$$

where z^* is the "effective nuclear charge" estimated according to Slater's rules. The σ^{AA}_{dia} term has been defined in terms of the four valence electrons of a carbon atom:

$$\sigma^{AA}_{dia} = 4.45z^*q^A. \quad (3)$$

According to Pople's theory,[1] the zz-component of the local paramagnetic term, σ^{AA}_{para}, is given by

$$(\sigma^{AA}_{para})_{zz} = (-e^2\hbar^2/2m^2c^2\Delta E)\langle r^{-3}\rangle_{2p}\{(Q_{AA})_{zz} + \sum_{B\neq A}(Q_{AB})_{zz}\}, \quad (4)$$

where

$$(Q_{AA})_{zz} = 2-2(P_{xAxA}-1)(P_{yAyA}-1) + 2P_{xAyA}^2, \quad (5)$$

and

$$(Q_{AB})_{zz} = -2P_{xAxB}P_{yAyB} + 2P_{xAyB}P_{yAxB} \quad (6)$$

with corresponding expressions for other components. $\sum_{B\neq A}$ is a summation over all the atoms other than A, $\langle r^{-3}\rangle_{2p}$ is the mean inverse cube radius for carbon 2p orbitals, ΔE is the average electronic excitation energy, and $P_{\mu\nu}$ are elements of the charge density and the bond-order matrix in the MO theory of the unperturbed molecule. The suffixes xA, xB, yA, yB,$\cdots$ correspond to the various 2p atomic orbitals of the A and B atoms. The $\langle r^{-3}\rangle$ factor is given as[1,5]

$$\langle r^{-3}\rangle_{2p} = 1/24a_0^3\{3.25-0.35(P_{2p}-3)\}^3, \quad (7)$$

where a_0 is a Bohr radius and where $(P_{2p}-3)$ is the excess charge density of the 2p electron. The local paramagnetic term, σ^{AA}_{para}, becomes

$$\sigma^{AA}_{para} = -10.06/\Delta E\{3.25-0.35(P_{2p}-3)\}^3Q_{AB} \quad (8)$$

with $Q_{AB}=\sum_B\{(Q_{AA})_{\mu\mu}+\sum_{B\neq A}(Q_{AB})_{\mu\mu}\}$. The ΔE value has been assumed to be 8 eV to fit the chemical shifts observed for the α- and β-carbons of styrene and α-methylstyrene according to Pople's treatment.[1] In the same way, we have obtained 8.5 eV as the ΔE value for the 1′-carbon of biphenyl.

Table 1. Calculated and observed chemical shifts of α- and β-carbons in 4-substituted styrenes and 4-substituted α-methylstyrenes, and 1′-carbons in 4-substituted biphenyls[a]

	Substituent	$\Delta\sigma^{AA}_{dia}$ [b]	$\Delta\sigma^{AA}_{para}$ [b]	$\Delta\sigma^{AB}_{dia}$	$\Delta\sigma^{A,ring}$	$\Delta\delta_{calcd}$	$\Delta\delta_{obsd}$ [c,g]
(i) 4-Substituted styrenes[c]							
				a) α-Carbons[d]			
1	F	−0.025	−0.233	0.124	0.106	−0.03	0.85
2	Cl	−0.004	0.009	0.043	0.031	0.08	1.27
3	CH_3	−0.016	−0.257	0.060	0.034	−0.18	0.23
4	$N(CH_3)_2$	−0.056	−0.808	0.210	0.238	−0.42	0.29
5	OCH_3	−0.039	−0.504	0.168	0.124	−0.25	0.67
6	SCH_3	−0.012	−0.140	0.056	0.035[f]	−0.06	0.75
7	NO_2	0.056	0.863	−0.144	0.150	0.93	1.93
8	CN	0.016	0.236	−0.036	0.110	0.33	1.57
9	$CH=CH_2$	−0.003	−0.120	0.015	0.022[f]	−0.09	0.47
10	$C\equiv CH$	−0.001	−0.044	0.012	0.002[f]	−0.03	0.74
11	$COCH_3$	0.026	0.277	−0.080	0.128	0.35	0.89
				b) β-Carbons[e]			
1	F	0.024	0.377	−0.012	0.022	0.41	−0.23
2	Cl	−0.011	−0.149	−0.004	0.013	−0.15	−0.77
3	CH_3	0.027	0.401	−0.013	0.014	0.43	1.00
4	$N(CH_3)_2$	0.093	1.346	−0.047	0.099	1.49	4.27
5	OCH_3	0.057	0.837	−0.033	0.052	0.91	2.22
6	SCH_3	0.009	0.119	−0.010	0.015	0.13	0.56
7	NO_2	−0.123	−1.640	0.048	0.063	−1.66	−4.70
8	CN	−0.039	−0.481	0.014	0.046	−0.46	−3.85
9	$CH=CH_2$	0.003	0.086	−0.002	0.009[f]	0.10	0.00
10	$C\equiv CH$	−0.003	−0.006	−0.001	0.001[f]	−0.01	−1.24
11	$COCH_3$	−0.050	−0.826	0.022	0.053	−0.80	−2.71

TABLE 1. (Continued)

Substituent	$\Delta\sigma_{dia}^{AA}$ [b]	$\Delta\sigma_{para}^{AA}$ [b]	$\Delta\sigma_{dia}^{AB}$	$\Delta\sigma^{A,ring}$	$\Delta\delta_{calcd}$	$\Delta\delta_{obsd}$ [c,g]
(ii) 4-Substituted α-Methylstyrenes[c]						
			a) α-Carbons[d]			
1. F	−0.023	−0.192	0.124	0.106	0.02	0.98
2. Cl	−0.004	0.078	0.042	0.031	0.15	1.08
3. CH_3	−0.013	−0.180	0.059	0.034	−0.10	0.23
4. $N(CH_3)_2$	−0.044	−0.555	0.208	0.238	−0.15	0.69
5. OCH_3	−0.032	−0.361	0.161	0.124	−0.11	0.67
6. NO_2	0.037	0.499	−0.140	0.150	0.55	1.47
			b) β-Carbons[e]			
1. F	0.018	0.261	−0.019	0.023	0.28	0.04
2. Cl	−0.010	−0.150	−0.004	0.014	−0.15	−0.60
3. CH_3	0.020	0.279	−0.010	0.015	0.30	0.85
4. $N(CH_3)_2$	0.069	0.951	−0.036	0.106	1.09	3.48
5. OCH_3	0.043	0.592	−0.027	0.055	0.66	1.76
6. NO_2	−0.092	−1.182	0.031	0.067	−1.18	−3.69
(iii) 4-Substituted Biphenyls[g]						
			1′-Carbons[d]			
1. F	−0.017	−0.093	0.123	0.049	0.06	1.04
2. Cl	−0.005	0.083	0.041	0.029	0.15	1.32
3. CH_3	−0.011	−0.157	0.057	0.032	−0.08	0.04
4. NH_2	−0.045	−0.547	0.235	0.175	−0.18	−0.41
5. OCH_3	−0.027	−0.278	0.158	0.117	−0.03	0.29
6. NO_2	0.039	0.503	−0.138	0.141	0.55	2.40
7. CN	0.012	0.172	−0.035	0.104	0.25	2.05
8. $COCH_3$	0.017	0.206	−0.081	0.121	0.26	1.20
9. CO_2CH_3	0.021	0.271	−0.100	0.116[f]	0.31	1.28

a) All the values listed are relative to the unsubstituted compound, from the chemical shift of which upfield shifts are represented in ppm by positive values. b) For the α-carbon of styrene, σ_{dia}^{AA}: 57.733, σ_{para}^{AA}: −323.099 and for the β-carbon, σ_{dia}^{AA}: 58.262, σ_{para}^{AA}: −300.629. For the α-carbon of α-methylstyrene, σ_{dia}^{AA}: 57.459, σ_{para}^{AA}: −323.427 and for the β-carbon, σ_{dia}^{AA}: 58.453, σ_{para}^{AA}: −299.007. For the 1′-carbon of biphenyl, σ_{dia}^{AA}: 57.570, σ_{para}^{AA}: −325.839. c) Cited from Ref. 10, in which all the chemical shifts were measured in CCl_4 with 8% C_6D_{12}. d) The symbol A refers to the α-carbon (and the 1′-carbon), and the symbol B, to the C_1-carbon. e) The symbol A refers to the β-carbon, and the symbol B, to the α-carbon. f) The σ-values necessary to calculate the $\Delta\sigma^{A,ring}$, which had not been established from the reactivity data, were obtained from the correlation between the π-electron densities on *para*-carbons in monosubstituted benzenes and the known σ_π-values of the other substituents: $\sigma_\pi(-CH{=}CH_2)$, −0.05; $\sigma_\pi(-C{\equiv}CH)$, −0.005; $\sigma_\pi(SCH_3)$, −0.08; $\sigma_\pi(CO_2CH_3)$, 0.28. g) Cited from Ref. 12, in which all the chemical shifts were measured in acetone with 10% benzene.

The calculated values of the local diamagnetic (σ_{dia}^{AA}) and the local paramagnetic terms (σ_{para}^{AA}), relative to the unsubstituted compound, are summarized in Table 1. They are linearly correlated with the increments in the electron density on the carbon atom A:

$$\Delta\sigma_{dia}^{AA} + \Delta\sigma_{para}^{AA} = a\Delta q^A. \quad (9)$$

As has been shown in our preceding paper,[4] the diamagnetic contribution, σ_{dia}^{AB}, from the sp^2 hybridized carbon atom B to the A atom, to which the B atom is bonded, can be expressed as

$$\sigma_{dia}^{AB} = e^2/3mc^2\sum_I\langle r_{AB}^{-1}\rangle = e^2/3mc^2 r_{AB}^{-1}q^B, \quad (10)$$

where r_{AB}^{-1} is the inverse distance of the A atom from the point charge on the B atom and where q is the total (2s and 2p) electron density on the B atom. The expression of Eq. 10, relative to the unsubstituted compound, is given as

$$\Delta\sigma_{dia}^{AB} = b\Delta q^B. \quad (11)$$

The paramagnetic contribution, σ_{para}^{AB}, from the B atom has been calculated according to Pople's expression.[1] It remains almost constant for a series of compounds, so long as we assume the same average excitation energy and the same value of the integral $\langle r_{AB}^{-3}\rangle$ for the same series of compounds. Accordingly, the contribution of the paramagnetic term to the SCS can be ignored.

The "ring-current" effect on the SCS in an aromatic side chain can be expressed as[4,6]

$$\Delta\sigma^{A,ring} = -0.4f(\rho, z)|\sigma_\pi|, \quad (12)$$

where $f(\rho,z)$ is the Johnson-Bovey ring-current shift, which is expressed as a function of the geometric factor for the atom located at the cylindrical co-ordinates, ρ and z, and where σ_π is the Yukawa-Tsuno parameter for measuring the resonance ability of the substituent.

One might raise an objection that Eq. 12 should contain the magnetic contribution from the ring-carbon C_1, because the Johnson-Bovey ring-current

shift, $f(\rho,z)$, was originally estimated by measuring the difference in the ^1H chemical shift between benzene and ethylene; if so, according to the Saika-Slichter expression for the nuclear shielding, the $f(\rho,z)$ value for the ring proton might also contain the local diamagnetic term of the hydrogen atom, σ_{dia}^{AA}, and the magnetic contributions from the bonded carbon atom, σ_{dia}^{AB} and σ_{para}^{AB}, in addition to the effect of the "net" ring-current, $\sigma_{net.}^{A.ring}$,

$$\Delta\sigma = f(\rho,z) = \Delta\sigma_{dia}^{AA} + \Delta\sigma_{dia}^{AB} + \Delta\sigma_{para}^{AB} + \sigma_{net}^{A.ring}, \quad (13)$$

where $\Delta\sigma=\sigma(C_6H_6)-\sigma(C_2H_4)$. However, when the σ_{dia}^{AA} and σ_{net}^{AB} terms are calculated by means of the Eqs. 3 and 8 given in Ref. 4 and by using the CNDO/2 formalism:

$$\Delta\sigma_{dia}^{AA} = \sigma_{dia}^{AA}(C_6H_6) - \sigma_{dia}^{AA}(C_2H_4) = 0.355, \quad (14)$$

$$\Delta\sigma_{dia}^{AB} = \sigma_{dia}^{AB}(C_6H_6) - \sigma_{dia}^{AB}(C_2H_4) = -0.329. \quad (15)$$

The diamagnetic terms of benzene and ethylene almost cancel each other out; then Eq. 13 becomes

$$f(\rho,z) = \sigma_{para}^{AB}(C_6H_6) - \sigma_{para}^{AB}(C_2H_4) + \sigma_{net}^{A.ring}(C_6H_6). \quad (16)$$

Equation 16 shows that the $f(\rho,z)$ term does not depend on the nature of the resonating nucleus, A. The $f(\rho,z)$ term of monosubstituted benzene ($f(\rho,z)_X$) is given as

$$f(\rho,z)_X = \sigma_{para}^{AB}(C_6H_5X) - \sigma_{para}^{AB}(C_2H_4) + \sigma_{net}^{A.ring}(C_6H_5X). \quad (17)$$

On the other hand, the following relationship holds so long as we assume the same average excitation energy and the same value of the integral $\langle r_{AB}^{-3}\rangle$ for the same series of compounds:

$$\sigma_{para}^{AB}(C_6H_6) \fallingdotseq \sigma_{para}^{AB}(C_6H_5X). \quad (18)$$

Therefore, the difference in the $f(\rho,z)$ term between benzene and monosubstituted benzene is expressed as

$$f(\rho,z)_X - f(\rho,z) = \sigma_{net}^{A.ring}(C_6H_5X) - \sigma_{net}^{A.ring}(C_6H_6) = \Delta\sigma_{net}^{A.ring}(C_6H_5X). \quad (19)$$

The $(f(\rho,z)_X - f(\rho,z))$ term was empirically expressed by Eq. 12 on the basis of the correlation between the ^1H SCS of *m*-substituted aromatic side chains and the Hammett σ_m values reported by Yamada *et al.*[6] We showed in our preceding paper[4] that Eq. 12 can reasonably be applied to the calculation of the ^1H SCS in aromatic side chain. Therefore, Eq. 12 can be applied, just as it is, to the calculation of the ^{13}C SCS in aromatic side chains.*

The values of $f(\rho,z)$ for the α- and β-carbons of the styrenes and the α-methylstyrenes and for the 1′-carbons of the biphenyls have been graphically estimated by utilizing the table of the Johnson-Bovey ring-current shift.[7]

To estimate elements of the charge density and the bond-order matrix, the CNDO/2 formalism has been used.

The standard geometry of the styrenes is assumed to be planar in the present calculation.[8] The C_1–C_α bond length and the C_1–C_α–C_β valence angle are taken to be, respectively, 1.46 Å and 128°, and the phenyl-vinyl dihedral angle, θ, is taken to equal 0° on the basis of the MO calculations performed by Hehre, Radom, and Pople.[9] The geometry of α-methylstyrene may not be planar because of the steric repulsion between the phenyl ring and the methyl group of the side chain. For α-methylstyrene with an experimental dihedral angle $\theta=30°$, the C_1–C_α bond length is taken to be 1.46 Å and the C_1–C_α–C_β valence angle, to be 120°;[10] we have not attempted more rigorous energy optimizations. The respective values of the phenyl-phenyl dihedral angle and the C_1–$C_{1'}$ bond length of biphenyl are taken to be 45° and 1.48 Å.[11] The other bond angles and bond lengths for all the compounds are taken from the standard complications.[11] The carbons of the compounds examined were labeled as shown below:

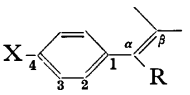

R: H or CH_3

4-Subustituted styrenes and α-methylstyrenes

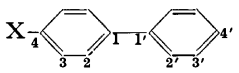

4-Substituted biphenyls

By combining Eqs. 3, 8, 10, and 12, we can calculate the ^{13}C SCS in an aromatic side chain. In Table 1, the calculated SCS values are compared with the observed SCS. In calculating the SCS of the α-carbon (and the 1′-carbon), the magnetic contribution from

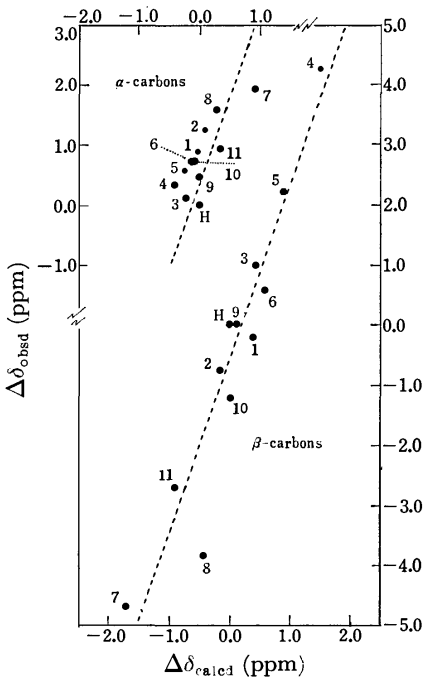

Fig. 2. Plots of $\Delta\delta_{obsd}$ against $\Delta\delta_{calcd}$ for α- and β-carbons of 4-substituted styrenes. Numbered points correspond to entries in Table 1.

* One of the referees expressed doubt about using the factor, −0.4 in Eq. 12 for the ^{13}C SCS because the factor was empirically estimated for the ^1H SCS; he advised determining the value of the factor, *c*, of the third term in the following equation by statistical treatment so as to make the slope of the correlation line between the observed and the calculated shift unity,

$$\Delta\delta_{calcd} = a\Delta q^A + b\Delta q^B + cf(\rho,z)|\sigma_z|,$$

where the values of *a* and *b* are taken from Table 2. However, this statistical treatment may result in overestimating the contribution of the 'ring-current' effect.

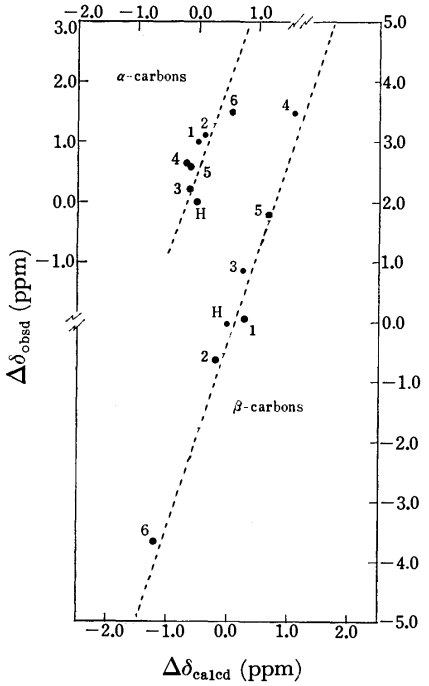

Fig. 3. Plots of $\Delta\delta_{obsd}$ against $\Delta\delta_{calcd}$ for α- and β-carbons of 4-substituted α-methylstyrenes. Numbered points correspond to entries in Table 1.

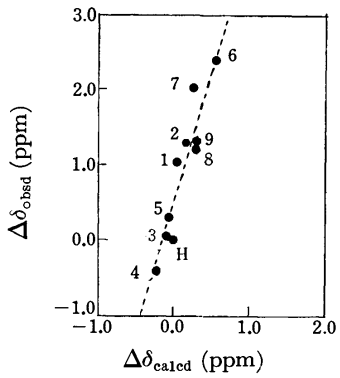

Fig. 4. Plots of $\Delta\delta_{obsd}$ against $\Delta\delta_{calcd}$ for 1'-carbons of 4-Substituted biphenyls. Numbered points correspond to entries in Table 1.

the β-carbon (and the 2'-carbon) has not been taken into account, because it may be small compared with that from the C_1-carbon. In Figs. 2—4, plots of the observed SCS are shown against the calculated SCS. As may clearly be seen in Table 1, the contributions from the diamagnetic term of the neighboring carbon atom, $B(\Delta\sigma^{AB}_{dia})$, and from the long-range shielding of the "ring-current" ($\Delta\sigma^{A,ring}$) can not be ignored in the case of the SCS of the α-carbons (and the 1'-carbon), while the local diamagnetic term ($\Delta\sigma^{AA}_{dia}$) can be ignored compared with the local paramagnetic term. The contributions of the $\Delta\sigma^{AB}_{dia}$ and the $\Delta\sigma^{A,ring}$ terms tend to almost cancel each other out in the case of the electron-withdrawing substituent, whereas both the $\Delta\sigma^{AB}_{dia}$ and the $\Delta\sigma^{A,ring}$ terms operate to cause a high-field shift in the case of the electron-releasing substituent.

We can express the SCS of the α-carbons of 4-substituted styrenes and α-methylstyrenes, and that of the 1'-carbons of 4-substituted biphenyls, by Eq. 20 in the same form as the expression derived for the ^1H SCS in an aromatic side chain, because the $\Delta\sigma^{AA}_{dia}$ and the $\Delta\sigma^{AA}_{para}$ terms are defined in terms of the electron density using Eq. 9:

$$\Delta\delta^{\alpha}_{calcd}(\text{or } \Delta\delta^{1'}_{calcd}) = a\Delta q^{A} + b\Delta q^{B} - 0.4f(\rho, z)|\sigma_{\pi}|. \quad (20)$$

The a, b, and $f(\rho,z)$ obtained are listed in Table 2.

TABLE 2. VALUES OF a, b AND $f(\rho, z)$ IN Eqs. 9, 11, AND 12 IN ppm

Compound		a	b	$f(\rho, z)$
Styrenes	α	124	6.43	−1.10
	β	121	7.01	−0.46
α-Methylstyrene	α	115	6.43	−1.10
	β	115	7.01	−0.49
Biphenyls	1'	108	6.35	−1.04

The results summarized in Table 1 show that the $\Delta\sigma^{AA}_{dia}$, the $\Delta\sigma^{AB}_{dia}$ and the $\Delta\sigma^{A,ring}$ terms do not make important contributions to the SCS of the β-carbons of the styrenes and the α-methylstyrenes. Therefore, the SCS of the β-carbon can be correlated only with the increments in the electron density on the β-carbon atom:

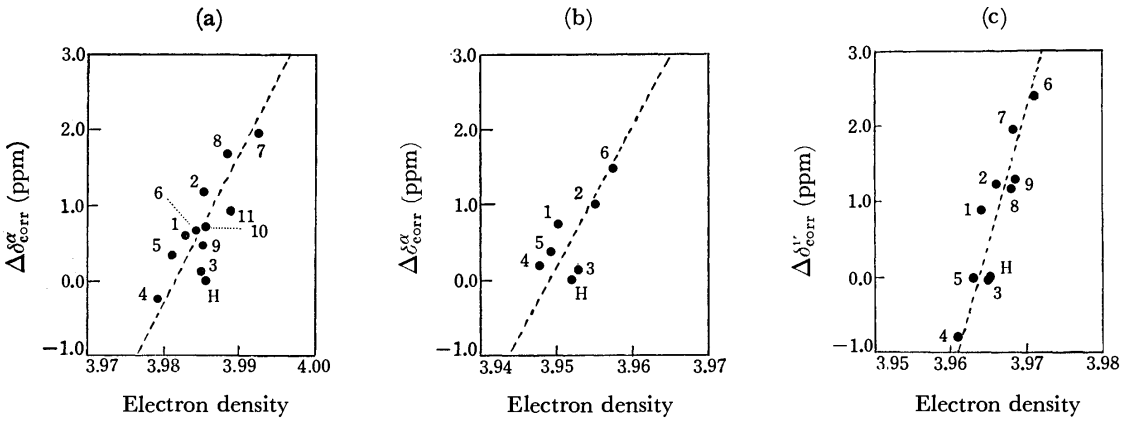

Fig. 5. Plots of $\Delta\delta_{corr}$ against the electron density on α-carbon (1'-carbon) atom; (a) 4-substituted styrenes (b) 4-substituted α-methylstyrenes (c) 4-substituted biphenyls. Numbered points correspond to entries in Table 1.

$$\Delta\delta^{\beta}_{\text{calcd}} = a\Delta q^{\text{A}}. \quad (21)$$

The calculated SCS values can reasonably reproduce all the observed SCS for the α- and β-carbons of the styrenes and the α-methylstyrenes, and for the 1'-carbons of the biphenyls, as is shown in Figs. 2—4. However, Figs. 2—4 also show that Eqs. 20 and 21 can not sufficiently reproduce the observed shifts. The shortcomings of Eqs. 20 and 21 may be attributed to adopting the same average excitation energy for all the derivatives in a series of compounds, as has been indicated by Bloor *et al.*,[2] who have calculated the SCS of ring-carbons of monosubstituted benzenes by the Karplus-Pople theory using $\delta^{13}\text{C(A)} = \sigma^{\text{AA}}_{\text{dia}} + \sigma^{\text{AA}}_{\text{para}}$**.

When the observed SCS of the α- and the 1'-carbons are corrected for the $\Delta\sigma^{\text{AB}}_{\text{dia}}$ and the $\Delta\sigma^{\text{A,ring}}$ terms, the corrected SCS values, $\Delta\delta^{\alpha}_{\text{corr}}$ (and $\Delta\delta^{\text{1'}}_{\text{corr}}$), come to be fairly well correlated with the electron densities on the α-carbons (and the 1'-carbons), as is shown in Fig. 5. This result implies that it may be appropriate to take the contributions of the $\Delta\sigma^{\text{AB}}_{\text{dia}}$ and the $\Delta\sigma^{\text{A,ring}}$ terms into consideration, so long as we interpret the SCS of α-carbon (and 1'-carbon) on the basis of the Saika-Slichter expression and Pople's average excitation energy approximation.

** For example, if it is permitted to assume empirically the appropriate ΔE value for each derivative within the range from 7.99 eV (for *p*-NMe_2) to 8.02 eV (for *p*-NO_2) for the α-carbons of the styrenes, the calculated shifts can reproduce the observed shifts fairly well. However, the MO Calculations (*e.g.*, the CNDO/2 and the INDO formalisms with the CI method) have not succeeded in reproducing the excitation energies to a degree of accuracy sufficient to examine the above assumption.

The CNDO/2 calculations were carried out on a FACOM-230 75 computer at the Nagoya University Computation Center.

References

1) J. A. Pople, *J. Chem. Phys.*, **37**, 53 (1962); M. Karplus and J. A. Pople, *ibid.*, **38**, 2803 (1963).
2) J. E. Bloor and D. L. Breen, *J. Phys. Chem.*, **72**, 716 (1968).
3) A. Saika and C. P. Slichter, *J. Chem. Phys.*, **22**, 26 (1954).
4) J. Niwa, *Bull. Chem. Soc. Jpn.*, **48**, 118, 1737 (1975); J. Niwa, *ibid.*, **50**, 979 (1977).
5) T. Yonezawa, I. Morishima, and H. Kato, *Bull. Chem. Soc. Jpn.*, **39**, 1398 (1965).
6) H. Yamada, Y. Tsuno, and Y. Yukawa, *Bull. Chem. Soc. Jpn.*, **43** 1459 (1970).
7) J. W. Emsley, J. Feeney, and L. H. Sutcliffe, "High Resolution Nuclear Magnetic Resonance Spectroscopy," Pergamon Press, Oxford (1965), Vol. 1, p. 595; G. E. Johnson and F. A. Bovey, *J. Chem. Phys.*, **29**, 1012 (1958).
8) P. L. Britton, C. L. Cheng, R. J. W. LeFevre, L. Radom, and G. L. Ritchie, *J. Chem. Soc., B*, 2100 (1971); M. Barfield, C. J. MacDonald, I. R. Peat, and W. F. Reynolds, *J. Am. Chem. Soc.*, **93**, 4195 (1971).
9) W. J. Hehre, L. Radom, and J. A. Pople, *J. Am. Chem. Soc.*, **94**, 1496 (1972).
10) G. K. Hamer, J. R. Peat, and W. F. Reynolds, *Can. J. Chem.*, **51**, 897, 915 (1973).
11) "Tables of Interactomic Distance and Configuration in Molecules and Ions," Chem. Soc., London, Spec. Publ., No. 11 (1958).
12) E. M. Schulman, K. A. Christensen, D. M. Grant, and C. Walling, *J. Org. Chem.*, **39**, 2686 (1974).

Studies of the Isomerization of Unsaturated Carboxylic Acids. IV. Base-catalyzed Rearrangements of β,γ-Unsaturated Esters to α,β-Isomers

Mutsuji SAKAI,* Shūji NISHIKAWA, Haruo KOIKE, Yasumasa SAKAKIBARA, and Norito UCHINO
Department of Fiber Chemistry, Kyoto Technical University, Matsugasaki, Sakyo-ku, Kyoto 606
(Received December 23, 1977)

Dimethyl methylenesuccinate, dimethyl citraconate, and dimethyl mesaconate mutually rearranged in the presence of triethylamine at room temperature. The rearrangement was found dependent on the polarity of the solvent and the basicity of the amine, and the rate was found to be first-order in both ester and amine. A mechanism has been proposed from a kinetic study.

In the preceding paper of this series, it was reported that such unsaturated dicarboxylic esters as dimethyl methylenesuccinate (**1**), dimethyl citraconate (**2**), and dimethyl mesaconate (**3**) mutually rearranged at high temperatures and that rearrangement would proceed by the mechanism involving carbanion intermediates formed under the general-base catalysis of methanol used as a solvent.[1] According to the above mechanism, the addition of a base, *e.g.*, tertiary amines, may accelerate the rearrangement. The base-catalyzed rearrangements of other unsaturated esters to their isomers have been reported in the literature.[2-5]

This paper deals with the interconversion between **1**, **2**, and **3** in the presence of a tertiary amine. The rearrangement of an unsaturated monocarboxylic ester, methyl 3-butenoate (**4**), has also been examined and compared with that of **1**.

Experimental

All the boiling points are uncorrected.

Materials. The organic solvents and amines were purified by ordinary methods. The following compounds were prepared by the methods described in the literature: dimethyl methylenesuccinate (dimethyl methylenebutanedioate) (**1**),[1] bp 111 °C/13 Torr; dimethyl citraconate (dimethyl (*Z*)-2-methyl-2-butenedioate) (**2**),[1] bp 116°C/15 Torr; dimethyl mesaconate (dimethyl (*E*)-2-methyl-2-butenedioate) (**3**),[1] bp 118 °C/16 Torr; methyl 3-butenoate (**4**),[6] bp 108 °C; methyl (*Z*)-2-butenoate (**5**),[7] bp 119 °C (contaminated with 23% of **6**); methyl (*E*)-2-butenoate (**6**),[6] bp 120 °C; dimethyl ethylidenesuccinate,[8] bp 112 °C/15 Torr; dimethyl isopropylidenesuccinate,[8] bp 115 °C/14 Torr.

Procedure. A mixture of the ester (12 mmol), tertiary amine (12 mmol), and solvent (15 ml) was placed in a test tube fitted with a stopcock and kept in a thermostated bath. The mixture was stirred with a magnetic stirrer. Aliquots (1 ml) of the mixture were taken at regular intervals, treated with aqueous hydrochloric acid (3 ml), and extracted with benzene (2 ml). The benzene extracts were washed with sodium hydrogencarbonate and subjected to GLC analysis.

Kinetics. The initial rate constants were calculated from the plot of $\ln[\text{ester}]_0/[\text{ester}]_t$ against time. The activation parameters were obtained from the Arrhenius plot for the rate of the disappearance of ester.

Reaction in Methanol-d. A mixture of **1** (12 mmol), triethylamine (12 mmol), and methanol-*d* (15 ml) was stirred and kept at 50 °C in a thermostated bath, and at appropriate intervals aliquots of the mixture were taken. The aliquots were treated with aqueous hydrochloric acid and extracted with carbon tetrachloride. The carbon tetrachloride extracts were subjected to GLC and NMR analyses. The NMR spectra were recorded on a Varian T-60A spectrometer.

Analysis. The extracts were analyzed by GLC using a 90 m BDS capillary column with Yanagimoto G-80 for the esters (**1**, **2**, and **3**), and a 4.5 m DNP column with Yanagimoto GCG-220 for the esters (**4**, **5**, and **6**). It was confirmed that no rearrangement took place in the course of the treatment and gas chromatographic analysis.

Results

It was observed that the β,γ-unsaturated esters, **1** and **4**, rearranged to the α,β-isomers in the presence of the tertiary amine at ambient temperature and that the α,β-esters, **2** and **3**, rearranged to the β,γ-isomer. The gas chromatogram of the reaction mixture revealed that the mixture contained only three isomers of each ester; no by-product was detected.

Effects of Solvent and Amine. The initial relative rates for the rearrangement of **1** with various solvents and amines were measured. An equimolecular amount of amine to **1** was employed in order to accelerate the reaction. The reaction rate was found sensitive to the dielectric constant of the solvent, as shown in Table 1. In a polar solvent such as dimethyl sulfoxide (DMSO), **1** rearranged rapidly to **3**. In the case of a nonpolar solvent, cyclohexane, however, the rearrangement was quite slow.

The effect of amine on the rate is shown in Table 2. Methanol was used as a solvent, since some amines were not soluble in DMSO and acetonitrile. Tertiary

Table 1. Effect of solvent on the rearrangement of **1**[a]

Solvent	Dielectric constant, D	Relative rate[b]
DMSO	46.7	1.00
Sulfolane	44.0	1.04
Acetonitrile	37.5	0.349
Methanol	32.6	0.163
THF	7.6	0.0127
Cyclohexane	2.0	0.00319

a) Ester **1**, 12 mmol; triethylamine, 12 mmol; solvent, 15 ml; temp, 50 °C.
b) The rate for the disappearance of **1** in DMSO ($k=2.21\times10^{-4}$ l mol^{-1} s^{-1}) is taken as 1.00.

Table 2. Effect of amine on the rearrangement of 1[a]

Amine	pK_a	Relative rate[b]
Tributylamine	10.9	0.700
N,N-Dimethylcyclohexylamine	10.7	1.93
Triethylamine	10.7	1.00
N-Ethylpiperidine	10.4	0.542
N-Methylpiperidine	10.1	0.810
N,N-Dimethylbenzylamine	8.9	0.129
Triallylamine	8.3	0.0136
Pyridine	5.2	0
N,N-Dimethylaniline	5.1	0

a) Ester **1**, 12 mmol; amine, 12 mmol; methanol, 15 ml; temp, 50 °C. b) The rate for the disappearance of **1** in the presence of triethylamine ($k=3.60\times10^{-5}$ l mol^{-1} s^{-1}) is taken as 1.00.

amines were suitable bases for the test of the effect of amine on the rearrangement. When primary or secondary amines were used for the reaction in methanol, the aminolysis of **1** by diethylamine occurred. Tertiary amines appear to act as specific bases and general acids for the reaction. The reactivity of tertiary amines examined increased approximately with increase in basicity. The results listed in Table 2 indicate that a steric factor, in addition to an electronic one, participates in determining the reactivity of the amine with **1**.

Equilibria. The equilibria of the three isomers in DMSO containing triethylamine were examined. The results of the rearrangement are summarized in Table 3, and as may be seen, the equilibrium composition was found to be 34% for **1**, 4% for **2**, and 62% for **3**. Under identical conditions, the values in the rearrangement of methyl butenoate, attempted for a comparison, were 0% for **4**, 4% for **5**, and 96% for **6**. The esters, **4** and **5**, rearranged practically to **6**. The effect of the alkyl substituent on the rearrangement was also examined. γ-Substituted **1**, dimethyl ethylidenesuccinate and dimethyl isopropylidenesuccinate, did not rearrange to their isomers.

Kinetics. Kinetic measurements for the rearrangement of **1** and **4** were undertaken in the temperature range from 30 to 50 °C and in the concentration range of triethylamine from 0.12 to 12 mmol. The total esters were recovered quantitatively without any side reactions even after a prolonged reaction time. The rate of the rearrangement was found to be first-order in both ester and amine,

$$\text{rate} = k[\text{ester}][\text{amine}].$$

A good first-order plot for the disappearance of ester was obtained over a conversion of 20% in all cases of the esters, **1**, **2**, **3**, and **4**. The rate of the disappearance of **1** may be regarded as the rate from **1** to **3**, because the rate from **1** to **2** is much slower than that from **1** to **3** and because the rate of the reverse reaction[9] from **3** to **1** is neglected at the initial stage of the reaction. The rates of the disappearance of **2** and **3** may be taken as the rate from **2** to **1** and that from **3** to **1**, respectively, because the direct interconversion between **2** and **3** may be negligible (*vide infra*). The activation parameters, $\Delta H^{\ddagger}$ and $\Delta S^{\ddagger}$, were 53.6 kJ mol^{-1} and −150 J K^{-1} mol^{-1} for **1**, 50.2 kJ mol^{-1} and −154 J K^{-1} mol^{-1} for **4**, respectively. In Table 4, these parameters are compared with those reported.[1,3] There are distinct differences between the values in the base-catalyzed and thermal rearrangements, the addition of a tertiary amine

Table 3. Equilibrium between 1, 2, and 3[a]

Starting ester	Time, h	Composition, %		
		1	**2**	**3**
1	1	61.8	0.3	37.9
1	12	33.7	2.7	63.6
2	12	29.5	41.8	28.7
3	1	20.1	0.1	79.8
3	12	36.5	3.4	60.1
1	54	34.7	3.1	62.2
1 : **3**=2 : 1	54	34.5	4.1	61.4
1 : **3**=1 : 1	54	34.3	4.1	61.6
1 : **3**=1 : 2	54	34.1	3.9	62.0
3	54	32.5	4.1	63.4
2	54	33.5	7.5	59.0

a) Ester, 12 mmol; triethylamine, 12 mmol; DMSO, 15 ml; temp, 50 °C.

Table 4. Kinetic data for the rearrangement[a]

Ester	Temp, °C	$k\times10^4$, 1 mol^{-1} s^{-1}
1	30±0.1	0.530
1	40	1.04
1	50	2.21 (2.30)[b]
2	50	0.415
3	50	1.19 (1.19)[b]
E_a=56.2 kJ mol^{-1}, $\Delta H^{\ddagger}$=53.6 kJ mol^{-1}, $\Delta S^{\ddagger}$=−150 J K^{-1} mol^{-1}.		
Thermal rearrangement of **1** to **3**[1]		
E_a=82.1 kJ mol^{-1}, $\Delta H^{\ddagger}$=77.8 kJ mol^{-1}, $\Delta S^{\ddagger}$=−184 J K^{-1} mol^{-1}.		
4	30	1.27
4	40	2.05
4	50	4.65
E_a=52.8 kJ mol^{-1}, $\Delta H^{\ddagger}$=50.2 kJ mol^{-1}, $\Delta S^{\ddagger}$=−154 J K^{-1} mol^{-1}.		
Reported[3] (ethyl ester, diethylamine, acetonitrile)		
E_a=43.9 kJ mol^{-1}, $\Delta H^{\ddagger}$=36.8 kJ mol^{-1}, $\Delta S^{\ddagger}$=−171 J K^{-1} mol^{-1}.		

a) Ester, 12 mmol; triethylamine, 12 mmol; DMSO, 15 ml. b) The value of k_f. See Ref. 9.

Table 5. The rearrangement of 2[a]

Time, min	Composition, %		
	1	**2**	**3**
40	6.0	93.1	0.9
60	7.8	90.3	1.9
80	9.5	87.6	2.9
100	10.4	85.7	3.9
120	12.5	82.4	5.1

a) Ester **2**, 12 mmol; triethylamine, 12 mmol; DMSO, 15 ml; temp, 50 °C.

accelerating the rearrangement significantly.

The steric effect of the ester group in methylenesuccinate on the rate was observed. The relative rate of diethyl and diisopropyl esters for **1** (1.0) were 0.75 and 0.36, respectively.

Deuterium Isotope Effect. When **1** was treated with triethylamine in methanol-*d* for 30 min, 50% of the hydrogen atoms in the α-methylene groups of the recovered **1** were replaced by deuterium atoms, whereas only 4% of **1** rearranged to **3**. The initial rate constant for the disappearance of **1** in methanol-*d*, k_{MeOD}, was measured and the ratio of k_{MeOH}/k_{MeOD} was found to be 2.5.

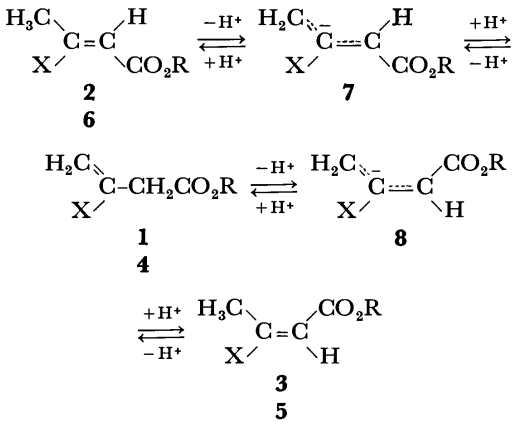

1, 2, 3 (X: $-CO_2CH_3$, R: $-CH_3$)
4, 5, 6 (X: –H, R: $-CH_3$)

Scheme 1.

Discussion

Tertiary amines accelerated the rearrangement remarkably as expected. In view of the kinetic study, the same mechanism as described in the thermal rearrangement[1] is proposed for the base-catalyzed rearrangements of the unsaturated esters, **1**, **2**, **3**, and **4**, as shown in Scheme 1. The formation of **3** from the carbanion (**8**) is the rate-determining step for the rearrangement of **1** supported by the following results; the second-order reaction dependent on ester and amine, the rate dependence on the polarity of the solvent and the basicity of the amine, a facile hydrogen-deuterium exchange of the hydrogen atoms in the α-methylene group of the recovered **1**, and the deuterium isotope effect observed on the reaction. The last two observations especially support the following equation,

$$\mathbf{1} + NR_3 \overset{\text{fast}}{\rightleftharpoons} \mathbf{8} + HN^+R_3 \overset{\text{slow}}{\longrightarrow} \mathbf{3} + NR_3.$$

The rate for the formation of **2** is slower than that of **3**, since the carbanion **8** may be more stable than **7**. In the carbanion **7** (X=$-CO_2CH_3$), there is a mutual repulsion between the two *cis*-oxygen atoms of the methoxycarbonyl groups. However, for the rearrangement of methyl butenoate, **8** (X=–H) is less stable than **7**, which can thus produce a *trans*-isomer. The equilibrium between **5** and **6** lies entirely to the left under the conditions, consequently, the thermodynamically stable esters, **3** and **6**, are the most favored products in the equilibria. The equilibrium composition in the base-catalyzed rearrangements of **1**, **2**, and **3** agrees very closely with that reported in the thermal rearrangement.[1] A large negative value of entropy appears to indicate that the carbanion exists in a stabilized planar structure. However, carbanions from γ-alkylsubstituted methylenesuccinates may be unstable and/or return to starting esters, judging from the fact that the γ-alkylsubstituted methylenesuccinates do not rearrange to their isomers.

The direct *cis-trans* isomerization between **2** and **3**, another route in the rearrangement, may be negligible, because **1** predominated over **2** and **3** at the initial stage of the rearrangement of **3** and **2**, as shown in Tables 3 and 5, respectively. The *cis*-ester, **2**, rearranged consecutively to the *trans*-isomer, **3**, *via* **1**.

Thus, the mechanism reported in the thermal rearrangement using methanol as a solvent is strongly supported by the above description.

The authors wish to thank Mr. Tsutomu Kashiwaya (Toray Inc.) for his assistance in the experimental work.

References

1) M. Sakai, *Bull. Chem. Soc. Jpn.*, **50**, 1232 (1977). Rearrangement is defined as the migration of a double bond.
2) D. J. Cram, "Fundamentals of Carbanion Chemistry," Academic Press, New York, N. Y. (1965).
3) Y. Mialhe and R. Vessière, *Bull. Soc. Chim. Fr.*, **1968**, 4181.
4) S. J. Rhoads, J. K. Chattopadhyay, and E. D. Waali, *J. Org. Chem.*, **35**, 3352, 3358 (1970).
5) J. Hine and N. W. Flachskam, *J. Am. Chem. Soc.*, **95**, 1179 (1973).
6) G. H. Jeffery and A. I. Vogel, *J. Chem. Soc.*, **1948**, 658.
7) a) C. Rappe, *Arkiv Kemi*, **21**, 503 (1963); *Acta Chem. Scand.*, **19**, 31 (1965); b) M. B. Hocking, *Can. J. Chem.*, **46** 466 (1968).
8) M. C. Kloetzel, *J. Am. Chem. Soc.*, **70**, 3571 (1948).
9) The values of the rate constant for the forward reaction, k_f, were obtained by means of the equation for the reversible first-order reaction, $A \underset{k_r}{\overset{k_f}{\rightleftharpoons}} B$,
and
$$([B]_e/[A]_0) \ln \{[B]_e/([B]_e - [B]_t)\} = k_f t\,[\text{amine}],$$
where $[B]_e$ is the concentration of B when equilibrium is reached; K. J. Laidler, "Chemical Kinetics," McGraw-Hill Book Company, New York, N. Y. (1965), p. 19.
The values of k do not differ from those of k_f, as shown in Table 4. Here, k is the sum of k_f and k_r.

An ^1H and ^{13}C NMR Spectroscopic Study of Ethyl 3-(2-Pyrimidylamino)crotonate, Ethyl 3-(5-Bromo-3-pyridylamino)crotonate, *N*-(2-Pyrimidyl)-3-(methylamino)crotonamide, and *N*-(4-Methyl-2-pyridyl)-3-(methylamino)crotonamide

Michio KONDO

Central Research Laboratories, Sankyo Co., Ltd., Hiromachi 1-2-58, Shinagawa-ku, Tokyo 140

(Received January 10, 1978)

It has been found, from the ^1H NMR spectra that two esters exist in an intramolecularly hydrogen bonded form (**Z**) in $CDCl_3$ and DMSO solutions. Two amides, on the other hand, have been found to exist as a mixture of the **Z** and **E** isomers in DMSO solutions. H/D exchange at the olefinic site has been found to occur by the addition of D_2O to the DMSO solutions of the amides, but not in the cases of the esters. The amide configurations are discussed. An interpretation of the ^{13}C NMR spectra of these compounds is also given.

It was found that esters[1,2] and amides[3] of 3-(alkylamino)crotonic acid exist as mixtures of the **Z** and **E** isomers, with the **Z** form preferred in various solvents. The **Z-E** equilibrium was found to be solvent-dependent.[3] It was also found that the H/D exchange at the olefinic site of these compounds is closely related to the **Z-E** tautomerism, which was assumed to proceed through enamine⇌imine tautomerization. These properties of enamine derivatives are expected to depend upon the double-bond character of the olefinic linkage, which is determined by the combination of electron-donating and electron-withdrawing substituents on the opposite ends of the olefinic bond.

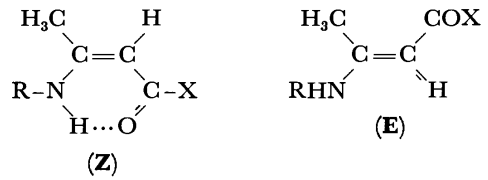

(**Z**)

(**E**)

1: R=2-Pyrimidyl, X=OEt, mp 76.2 °C
2: R=5-bromo-2-pyridyl, X=OEt, mp 90.0 °C
3: R=CH_3, X=2-pyrimidylamino, mp 178.5 °C
4: R=CH_3, X=4-methyl-2-pyridylamino, mp 165 °C.

This paper will be concerned with the ^1H and ^{13}C NMR spectroscopic study of the four title compounds in $CDCl_3$ and DMSO solutions.

Experimental

Compound **1** was prepared by heating an equimolar mixture of ethyl acetoacetate and 2-aminopyrimidine at about 130 °C for 5 h. The volatile components were removed under reduced pressure, and the residue was extracted with hot cyclohexane. The concentration of the extract gave crude **1**, which was then purified by recrystallization from cyclohexane.

Compound **2** was prepared in a similar way.

Compounds **3** and **4** were prepared by the condensation of methylamine with the corresponding crotonamides; 2-acetoacetamidopyrimidine was commercially available, and 2-acetoacetamido-4-methylpyridine was derived from 2-amino-4-methylpyridine and ethyl acetoacetate.[4]

All four compounds gave satisfactory results of elemental analyses.

The ^1H NMR spectra were recorded on a Varian XL-100A-15 spectrometer at the CW mode at room temperature (*ca.* 28 °C), using TMS as the internal standard. The sample concentration was 50 mg/ml unless otherwise noted. The ^{13}C NMR spectra were taken under the FT mode under these conditions: spectrometer frequency, 25.16 MHz; spectral width, 5,500 Hz; aquisition time, 2 s; pulse width, 20 μs; pulse delay, 1.6—5.2 s; number of transients, 1000—10000; with or without proton-noise decoupling (10 W of rf power).

Results and Discussion

Assignment of NMR Spectra. In each of the ^1H NMR spectra of these four compounds in $CDCl_3$, there was a broad signal which was concentration-insensitive. This implies the amino structure (**Z**), including the intramolecular hydrogen bond, NH···OC.

In DMSO, the ^1H NMR spectra of **1** and **2** can be well explained in terms of one molecular species (**Z** form), whereas those of **3** and **4** can be explained by assuming two molecular species (**Z** and **E**) coexisting in the solution. A similar DMSO-induced isomerization has been reported for enamino ketones[5] and 1-carbamoyl-5-fluorouracil.[6] The ^1H chemical shifts are summarized in Table 1.

Amide Configurations. It is noteworthy that the olefinic proton of **3** resonates at a field lower by as great as 1.15 ppm than that of **4** in $CDCl_3$, and that the former signal shows an upfield shift, whereas the latter shows a downfield shift, with the solvent change from $CDCl_3$ to DMSO. This solvent change induced a great downfield shift of the amide signals of both the compounds. These observations can be well explained by assuming that **3** exists predominantly in a *s-cis* form in $CDCl_3$ and in a *s-trans* form in DMSO, because a similar phenomenon was observed for 2-acetamidopyrimidine[7] and 2-acetoacetamidopyrimidine.[8] On the other hand, it seems that the amide configuration of **4** is *s-trans* and solvent-independent.

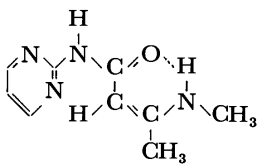

s-cis

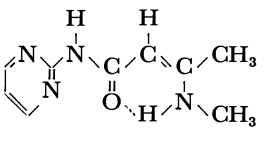

s-trans

TABLE 1. ^1H CHEMICAL SHIFTS OF VARIOUS KINDS OF PROTONS OF **1**, **2**, **3**, AND **4** IN $CDCl_3$ AND DMSO-d_6

	Solv.	CH_3	CH_2	$=CCH_3$	NCH_3	=CH	H-3′	H-4′	H-5′	H-6′	NHCO	NH	p[a]
1	$CDCl_3$	1.29	4.17	2.50	—	4.85	—	8.42	6.77	8.42	—	11.25	
	DMSO	1.23	4.11	2.48	—	4.89	—	8.55	7.01	8.55	—	11.17	
2	$CDCl_3$	1.30	4.16	2.43	—	4.80	6.67	7.61	—	8.27	—	11.02	
	DMSO	1.23	4.10	2.37	—	4.82	7.01	7.86	—	8.33	—	10.90	
3	$CDCl_3$	—	—	2.01	2.95	5.62	—	8.55	6.84	8.55	8.44	9.74	
	DMSO[b]	—	—	1.93	2.89	5.41	—	8.53	6.98	8.53	9.48	9.42	82
		—	—	2.24	2.62	5.22	—	c)	c)	c)		6.66	18
4	$CDCl_3$	—	—	1.91	2.91	4.47	8.01	(2.32)[d]	6.71	8.04	7.78	9.16	
	DMSO[b]	—	—	1.88	2.87	4.76	7.97	(2.28)[d]	6.73	8.04	9.38	9.06	70
		—	—	2.24	2.60	4.86	c)	c)	c)	c)	9.34	6.38	30

a) Population (±5%). b) The figures in the upper row correspond to the *Z* isomer, and those in the lower, to the *E* isomer. c) Not identified because of the overlap with the *Z*-signals. d) Methyl substituent at the 4′-position.

Hydrogen-deuterium Exchange at the Olefinic Site. The addition of about 5% v/v D_2O to the DMSO solutions of **3** and **4** caused a gradual disappearance of the olefinic proton signal as well as of the amino and amide proton signals, whereas the addition of D_2O to the DMSO solutions of **1** and **2** induced the disappearance of the amino proton signal only. This means that the coexistence of the **Z** and **E** isomers in the DMSO solutions of **3** and **4** is essential to the H/D exchange at the olefinic site.

^{13}C NMR Spectra. The signal assignment was rather simple when the relative intensity and multiplicity in the proton-coupled ^{13}C spectra were taken into account (Table 2). The ring carbon, 2′, in these compounds can be identified by its rather large spin-coupling constant of about 12 Hz with the ring proton, 6′.[9]

Paired signals corresponding to the **Z** and **E** isomers were observed for **3** and **4** dissolved in DMSO; this is consistent with the results obtained from the ^1H NMR spectroscopic study.

The chemical-shift difference between the two isomers (**Z** and **E**) is appreciable for the carbonyl and the olefinic C-3 only. These two carbons are more deshielded in the **Z** form than in the **E** form, probably because of the enhanced polarization of the carbonyl group by the

TABLE 2. ^{13}C CHEMICAL SHIFTS OF VARIOUS CARBONS OF **1**, **2**, **3**, AND **4**

Compd	**1**		**2**		**3**		**4**	
Solv.	$CDCl_3$	DMSO	$CDCl_3$	DMSO	$CDCl_3$	DMSO	$CDCl_3$	DMSO
C=O	169.3	168.8	170.1	168.9	168.8	167.8 (165.7)	169.1	168.9 (167.1)
C-2′	159.4	158.6	152.3	151.7	158.6	158.3 (158.7)	153.3	153.5 (153.9)
C-3′	—	—	114.9	115.5	—	—	113.9	113.0 (113.0)
C-4′	157.9	158.4	140.2	140.6	158.1	157.9 (157.9)	149.2	147.8 (147.8)
C-5′	114.4	115.2	112.6	112.5	114.3	114.6 (114.6)	119.1	118.4 (118.3)
C-6′	157.9	158.4	148.6	148.2	158.1	157.9 (157.9)	147.2	147.2 (147.8)
=C(3)N	156.0	156.1	157.2	156.6	164.2	162.9 (160.0)	161.9	161.1 (158.7)
=C(2)H	93.1	92.2	91.2	90.5	85.0	84.9 (84.6)	85.2	85.0 (84.8)
CH_2O	59.3	59.0	59.2	58.7	—	—	—	—
CH_3N	—	—	—	—	29.6	29.1 (29.3)	29.5	29.0 (29.3)
$CH_3C=$	22.9	22.4	22.4	21.7	19.6	19.2 (19.3)	21.4	20.9 (20.9)
CH_3(C-4′)	—	—	—	—	—	—	19.3	19.0 (18.9)
CH_3CH_2	14.5	14.3	14.5	14.6	—	—	—	—
Population					**Z** (**E**)	79±2 (21±2)		73±2 (27±2)

C-2′ means the ring carbon-2, for example. The values in parentheses correspond to the **E** isomer.

intramolecular hydrogen bonding. Another olefinic carbon, C-2, resonates at almost the same field in the either form of **Z** and **E**.

As has been mentioned before, it is very likely that the double-bond character of the C_2=C_3 linkage plays an important role in the isomerization and in the H/D exchange. An enhanced contribution of the canonical forms, **A** and **C**, to the ground state can be expected to reduce the double-bond character of the olefinic linkage and, as a consequence, to make the **Z-E** tautomerization as well as the H/D exchange easy.

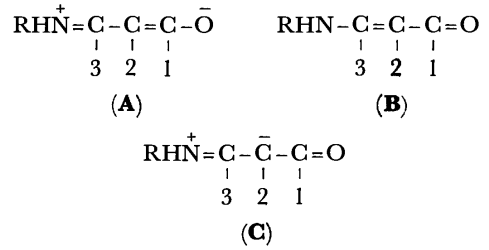

(**A**) (**B**)

(**C**)

It is noteworthy that the ^{13}C chemical shifts of the C-2 and C-3 of **1** and **2** are systematically different from those of **3** and **4**; C-3 is more shielded in **1** and **2** than in **3** and **4**, but C-2 is, on the contrary, more shielded in **3** and **4**. Since there is no appreciable difference among the chemical shifts of the carbonyl carbons of the four compounds, the above systematic difference is probably to be ascribed to the different substituents at the 3-position, which influence both C-2 and C-3 mainly by a mesomeric mechanism. Therefore, the more shielded nature of the C-2 in **3** and **4** implies a higher contribution of the polar canonical form **C** than in **1** and **2**. This in turn means an easier formation of the transient imino form and an easier occurrence of H/D exchange.

The carbon-proton spin-spin coupling constants, $^{1}J_{CH}$'s, are given in Table 3. The $^{1}J_{CH}(2)$ values for **1** and **2** are slightly but definitely greater than those for **3** and **4**, reflecting a smaller *s* character of the C-2 hybrid orbital in **3** and **4**. This is consistent with the above argument that the contribution of the canonical form **C** is to be considered larger in **3** and **4** than in **1** and **2**.

Table 3. $^{1}J_{CH}$ values for **1**, **2**, **3**, and **4** in $CDCl_3$

	1	**2**	**3**	**4**
CH(2)	166.1	166.1	163.5	160.2
CH_3(4)	126.8	126.9	128.1	127.4
NCH_3	—	—	137.7	136.5
CH(3′)	—	162.9	—	167.9
CH_3(C4′)	—	—	—	123.3
CH(4′)	179.1	166.3	180.3	—
CH(5′)	169.5	—	169.6	162.7
CH(6′)	179.1	186.6	180.3	175.9
OCH_2CH_3	146.8	146.5	—	—
OCH_2CH_3	129.8	129.9	—	—

References

1) G. O. Dudek and G. P. Volpp, *J. Am. Chem. Soc.*, **85**, 2697 (1963).
2) A. G. Sanchez, M. T. Aldave, and U. Scheideggar, *J. Chem. Soc., C*, **1968**, 2570.
3) M. Kondo, *Bull. Chem. Soc. Jpn.*, **50**, 2961 (1977).
4) M. Shur and S. S. Israelstam, *J. Org. Chem.*, **33**, 3015 (1968).
5) M. L. Filleux-Blanchard, H. Durand, M. T. Bergeon, F. Clesse, H. Quiniou, and G. J. Martin, *J. Mol. Struct.*, **3**, 351 (1969).
6) S. Ozaki, Y. Ike, H. Mizuno, K. Ishikawa, and H. Mori, *Bull. Chem. Soc. Jpn.*, **50**, 2406 (1977).
7) M. Kondo, *Bull. Chem. Soc. Jpn.*, **49**, 1443 (1976).
8) M. Kondo, *Bull. Chem. Soc. Jpn.*, **51**, 1905 (1978).
9) M. Hansen and H. J. Jacobsen, *J. Magn. Reson.* **10**, 74 (1973).

Stereochemical Studies of the Electrolytic Reactions of Organic Compounds. V.† The Electro-reductive Cyclization of 1-Acyl-8-benzoylnaphthalenes to 1,2-Acenaphthenediols

Tsutomu NONAKA* and Mitsuo ASAI

Department of Electronic Chemistry, Tokyo Institute of Technology, Nagatsuta-machi, Midori-ku, Yokohama 227

(Received February 9, 1978)

The electrolytic reductions of several 1-acyl-8-benzoylnaphthalenes were carried out by means of controlled potential electrolysis at a mercury cathode in various catholytes. The isomeric ratio of the *cis*- and *trans*-1,2-acenaphthenediols thus formed depended on the kind of acyl group, supporting electrolyte, organic solvent in the catholyte, and cathode potential applied. The mechanism of the reductive cyclization is discussed from the stereochemical point of view, and it is proposed that the cyclization may occur not only by the intramolecular coupling of the biradical intermediate, but also by the intramolecular nucleophilic addition of the anionic part of the carbanion intermediate to its unreacted carbonyl group.

A number of studies of the stereochemistry of *vic*-diols produced by the electro-reductive dimerization of aromatic ketones and aldehydes have been performed. For instance, Stocker and Jenevein[1,2] found that the *dl*/*meso* ratio of the diol derived from acetophenone ranged from 1.0 to 1.4 in acidic media and from 2.5 to 3.2 in alkaline media, under a wide variety of electolytic conditions. These facts were explained as resulting from hydrogen bonding between radical intermediates in the transition state favorable for the formation of the *dl* isomer.

On the other hand, there have been a few papers[3-5] dealing with the stereochemistry of cyclic *vic*-diols produced by the electro-reductive cyclization of diketones. Gourley and Grimshaw[3] reported that the *cis*/*trans* ratios of the cyclic *vic*-diols produced by the reductive cyclization of 1,5-bis(4-methoxybenzoyl)-pentane and 1,5-bis(4-hydroxybenzoyl)pentane in an alkaline medium were 21.6 and 0.9 respectively. These facts were explained as resulting from hydrogen bonding favorable for the formation of the *cis* isomer in the case of the former, and to the strong electrostatic repulsion between the two negatively charged aromatic rings in the case of the latter. They also obtained cyclic *vic*-diols in such *cis*/*trans* ratios as 1.5 and 2.3 from 2,2′-bis(4-methoxybenzoyl)biphenyl and 2,2′-bis(4-hydroxybenzoyl)biphenyl respectively. However, these facts contradict the above theory. There is also an ambiguous point in the reductive dimerization of hydroxy ketones.[1,6]

In a previous work,[5] several aromatic diketones were electrolytically reduced under a variety of conditions, and it was found that the distribution of the products, which were cyclic and non-cyclic *vic*-diols and secondary alcohols, depended on the molecular structure of the diketones and on the electrolytic conditions. Of the diketones used, 1,8-dibenzoylnaphthalene (**1a**) gave only the corresponding cyclic *vic*-diol (1,2-acenaphthenediol, **2a**).

In this work, in addition to **1a**, three kinds of 1-acyl-8-benzoylnaphthalenes (**1b**—**d**) were subjected to electrolysis in order to clarify the mechanism of the reductive cyclization from the stereochemical point of view. The diacylnaphthelenes, **1b**—**d**, are characterized by their unsymmetrical molecular structures.

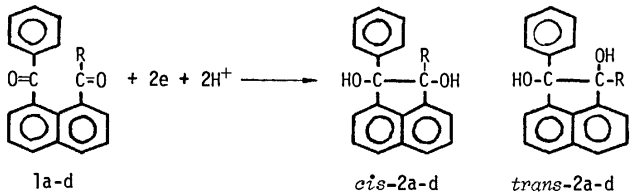

1a-d *cis*-2a-d *trans*-2a-d

a: R=C_6H_5
b: R=4-CH_3O-C_6H_4
c: R=4-HO-C_6H_4
d: R=CH_3

Results and Discussion

Synthesis of 1-Acyl-8-benzoylnaphthalenes (1a—d). 1,8-Dibenzoylnaphthalene (**1a**) was prepared according to the method of Beschke.[7] The routes of synthesizing the unsymmetrical diacylnaphthalenes (**1b**—**d**) were newly designed for this work.

At the first stage of the synthesis, 2-phenyl-2-hydroxy-1-acenaphthenone (**3**), which is an intermediate common to **1b**—**d**, was prepared from equimolar acenaphthenequinone and phenylmagnesium bromide in a 94% yield. The structure of the new compound, **3**, was determined by elemental analysis and by a study of the IR and mass spectra. At the second stage, **3** was converted into *trans*-1-phenyl-2-(4-methoxyphenyl)-1,2-acenaphthenediol (**2b**) and *trans*-rich 1-phenyl-2-methyl-1,2-acenaphthenediol (**2d**) by means of a Grignard reaction with 4-methoxyphenylmagnesium bromide and methylmagnesium iodide respectively. Finally, **2b** and **2d** were oxidized with chromium(VI) oxide to give 1-(4-methoxybenzoyl)-8-benzoylnaphthalene (**1b**) and 1-acetyl-8-benzoylnaphthalene (**1d**) respectively. 1-(4-Hydroxybenzoyl)-8-benzoylnaphthalene (**1c**) was prepared by the treatment of **1b** with boron tribromide.[8] The structures of the new compounds, **1b**—**d**, were established by elemental analysis and by a study of the IR and mass spectra.

† Part IV: *Bull. Chem. Soc. Jpn.*, **50**, 2965 (1977). Cathodic Crossed Hydrocoupling. Part 15. Part 14: *J. Chem. Soc., Perkin Trans. 2*, submitted for publication.

Determination of the Configuration of 1,2-Acenaphthenediol (2a—d). Since both *cis*-**2a**[7] and *trans*-**2a**[9] are known compounds, the measurement of their melting points served as the method of identification.

The diols, **2b—d**, are unknown compounds. The **2b** diol synthesized by the Grignard reaction differed from that synthesized by the magnesium reduction[10] of **1b** in its melting points, in the chemical shift of the methyl protons in the NMR spectra, and in the IR absorption bands of hydroxyl groups. Generally, the *cis* isomers of cyclic *vic*-diols, such as 1,2-acenaphthenediols and 9,10-dihydro-9,10-phenanthrenediols, showed higher melting points than the *trans* isomers.[9,10] Since the conformation of the phenyl and 4-methoxyphenyl groups of *cis*-**2b** shown in Scheme 1 seems to be more plausible than any other conformations in view of the steric requirement, the methyl protons of *cis*-**2b** are probably magnetically shielded by the phenyl group; consequently, a signal for the methyl protons would appear at a higher magnetic field in the NMR spectrum. From these considerations, the **2b** synthesized by the magnesium reduction, which melted at a higher temperature and which showed the NMR signal for methyl protons at a higher magnetic field than *trans*-**2b**, was considered to be the *cis* isomer. Both isomers also differed from one another in the IR spectrum in the OH-stretching band region. The *cis* isomer showed a broad band at about 3300 cm^{-1}. Such a low frequency seems to be the result of intramolecular hydrogen bonding. On the other hand, the *trans* isomer showed two sharper bands at 3550 and 3380 cm^{-1}. The higher-frequency band may be assigned to free hydroxyl groups, while the lower-frequency band may be the result of intermolecular hydrogen bonding.[12]

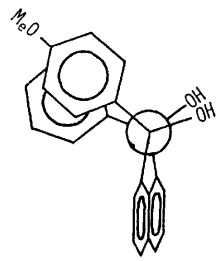

Scheme 1. Favorable conformation of *cis*-**2b**.

The *cis* and *trans* isomers of **2d** were separated by the fractional recrystallization of an isomeric mixture prepared by the Grignard reaction. The stereochemistry of the isomers was determined, similarly to the case of

Table 1. Electrolytic reduction of 1-acyl-8-benzoylnaphthalenes to 1,2-acenaphthenediols

Compound	Supporting electrolyte	Organic co-solvent	Cathode potential V *vs.* SCE	Quantity of electricity passed $\times 10^5$ C/mol	1,2-Acenaphthenediol Yield (%)	1,2-Acenaphthenediol *cis*: *trans* (%)
1a	H_2SO_4	THF	−0.75	1.9	87[a]	100: 0
1a	H_2SO_4	DMF	−1.00	1.7	72[a]	85: 15
1b	H_2SO_4	THF	−0.67	2.1	100	80: 20
1b	H_2SO_4	THF	−0.76	2.0	95	69: 31
1b	H_2SO_4	DMF	−1.16	2.1	100	70: 30
1b	H_2SO_4	DMF	−1.38	2.7	100[b]	59: 41
1c	H_2SO_4	THF	−0.74	2.7	70[c]	57: 43
1c	H_2SO_4	THF	−0.89	2.0	75[c]	50: 50
1c	H_2SO_4	THF	−1.13	1.7	78[c,d]	50: 50
1c	H_2SO_4	DMF	−0.88	2.5	70[c]	55: 45
1c	H_2SO_4	DMF	−0.97	1.6	75[c,d]	49: 51
1c	H_2SO_4	DMF	−1.10	2.5	92[c]	49: 51
1a	NaOH	THF	−1.50	2.0	84	0: 100
1a	NaOH	DMF	−1.70	1.8	87	0: 100
1b	NaOH	THF	−1.40	2.3	100	0: 100
1b	NaOH	THF	−1.50	2.7	100	0: 100
1c	NaOH	THF	−1.35	1.5	53[d]	9: 91
1c	NaOH	THF	−1.55	2.4	67[d]	12: 88
1c	NaOH	—	−1.30	1.5	—[d,e]	11: 89
1c	NaOH	—	−1.47	1.5	—[d,e]	19: 81
1a	AcONa	AcOH	−1.50	2.4	78[b]	59: 41
1b	AcONa	AcOH	−1.50	3.4	50[b,d]	66: 34
1b	AcONa	AcOH	−1.60	5.8	50[b,d]	62: 38
1c	AcONa	AcOH	−1.46	1.8	50[b,d]	77: 23
1c	AcONa	AcOH	−1.56	1.8	50[b,d]	73: 27
1d	AcONa	AcOH	−1.30	1.7	78[d]	95: 5
1d	AcONa	AcOH	−1.50	2.9	80[b,d]	85: 15

a) Yield after purification. b) A vigorous hydrogen evolution was observed. c) A part of the 1,2-acenaphthenediol formed underwent acid-catalyzed pinacol rearrangement during electrolysis. d) A considerable amount of the unreacted naphthalene was recovered. e) The yield was not estimated.

2b, from considerations of their melting points and by a study of their IR and NMR spectra.

Determination of the Isomeric Formation Ratio of 1,2-Acenaphthenediols (2a—d). The isomeric ratio of **2a** formed in electrolysis was determined by fractional precipitation. The isomeric ratios of **2b** and **2d** were determined from the intensity of NMR signals for their methyl protons. Because the direct determination of the isomeric ratio of **2c** was difficult, the determination was carried out after **2c** was converted into **2b** with methyl sulfate. It was confirmed by a repetition of a methylation-demethylation cycle that no isomerization occurred during the methylation.

Electrolytic Results. The electrolytic conditions and results are summarized in Table 1. The *cis/trans* ratio of the 1,2-acenaphthenediols formed depended on the substituent of the starting naphthalenes, the cathode potential applied, the supporting electrolyte, and the organic co-solvent added to the catholyte to dissolve the naphthalenes. No by-products, such as 1-acyl-8-(hydroxymethyl)naphthalenes or 1,8-di(hydroxymethyl)naphthalenes, could be separated by column chromatography.

As is shown in Table 1, **1a** and **1b** gave the *cis*-rich diols in strongly acidic media, while **1c** gave the *cis* and *trans* diols in almost equal quantities. A part of the diol from **1c** was rearranged by sulfuric acid into the corresponding pinacolone during electrolysis. Since the pinacol rearrangement of *cis*- and *trans*-1,2-acenaphthenediols proceeds at almost the same rate in a medium containing water,[11] the *cis/trans* ratio measured after electrolysis probably corresponds to the real formation ratio of the isomers.

The formation of the thermodynamically stable *trans* isomer was predominant in strongly alkaline media.

In an weakly acidic solution, **1a—d** gave the *cis*-rich diols. The naphthalene, **1d**, which was condensed by water elimination into 3-phenyl-1-phenalenone in strongly acidic and alkaline media, could be electrolyzed only in this solution.

Polarography. The naphthalenes, **1a—d**, mostly showed very complicated multiple reduction waves in their polarograms. The half-wave potentials for the first waves only, therefore, can be estimated from the polarograms.

Table 2. Half-wave potentials of the polarographic first waves of 1-acyl-8-benzoylnaphthalene[a]

Compound	Supporting electrolyte	Organic co-solvent	$E_{1/2}$ V *vs.* SCE
1a	H_2SO_4	DMF	−0.58
1b	H_2SO_4	THF	−0.56
1b	H_2SO_4	DMF	−0.63
1c	H_2SO_4	THF	−0.54
1c	H_2SO_4	DMF	−0.63
1a	AcONa	AcOH	−0.90
1b	AcONa	AcOH	−0.87
1c	AcONa	AcOH	−0.89
1d	AcONa	AcOH	−0.88
1a	NaOH	DMF	−1.23
1b	NaOH	THF	−1.26
1c	NaOH	—	−1.27

a) Measured in *ca.* 5×10^{-4} M of the concentration of the naphthalene in an electrolytic solution similar to one used for the macro electrolysis.

The reduction potential of an aromatic carbonyl compound generally depends on the substituents on its aromatic ring, and the dependence follows Hammet's rule.[13] For example, the polarographic half-wave potentials of 4-methoxy- and 4-hydroxybenzophenones are more negative by 100 and 170 mV respectively than that of unsubstituted benzophenone in an acidic medium. The half-wave potentials of **1a—d** were close to each other under the same conditions, as is shown in Table 2. This fact may suggest that the first one-electron transfer occurs at an unsubstituted benzoyl group in all of the naphthalenes.

Discussion of the Mechanism of the Reductive Cyclization from Stereochemical Aspects. The general reduction mechanism of carbonyl compounds was shown by Zuman[14,15] as follows:[16]

In acidic media;

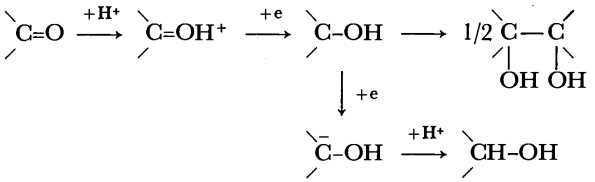

in the medium pH-range;

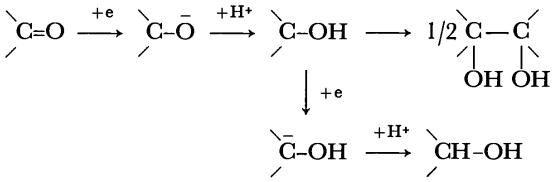

and in alkaline media;

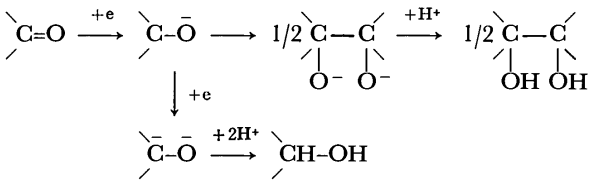

In the reduction of diketones, the second electron-transfer may occur not only at a radical carbon, but also at an unreacted carbonyl carbon. This problem could not be solved polarographically, because the naphthalenes, **1a—d**, showed multiple reduction waves which were ill-defined except for the first waves.

In Schemes 2, 3, and 4, two types of mechanisms for the cyclization are presented. One is based on the coupling of a biradical, and the other, on the nucleophilic addition of the carbanion.

Intramolecular hydrogen bonding in the intermediates would cause the formation of the *cis* isomer. The strength of the hydrogen bonding of a hydroxyl group with an other group containing an oxygen atom would increase in this order: $^+$HO=C, HO–C, O=C, and $^-$O–C, in view of the electron density on the oxygen atom.

As is shown in Table 1, in a strongly acidic medium a marked substituent effect on the isomeric ratio was

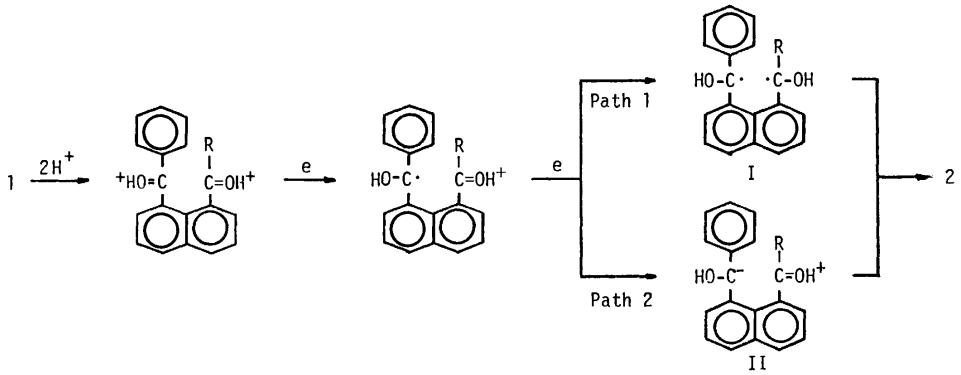

Scheme 2. Possible mechanisms in strongly acidic solutions.

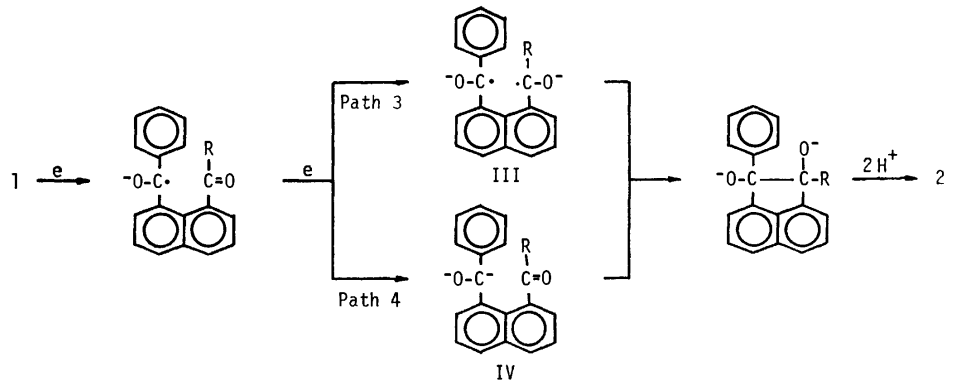

Scheme 3. Possible mechanisms in alkaline solutions

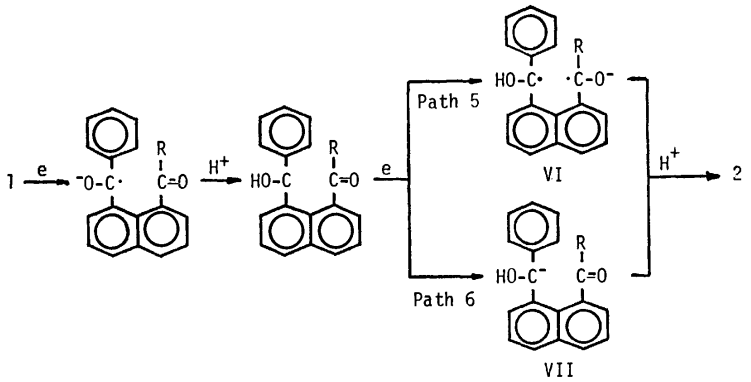

Scheme 4. Possible mechanisms in an weakyl acidic solution.

observed. An electron-releasing substituent on a substituted benzoyl group (R) would weaken the intramolecular hydrogen bonding in a carbanion intermediate (II) in Path 2 by promoting the protonation of the carbonyl group to decrease the ratio of the *cis* isomer, while such a substituent effect can not be expected in a biradical intermediate (I). The promotion of the protonation is essentially due to an increase in the basicity of the carbonyl group. The substituent effect observed suggests that Path 2 may be included in the cyclization process, but there is no experimental evidence for excluding Path 1. The influence of the cathode potential on the isomeric ratio may be explained as resulting from different potentials for the second electron-transfer in Paths 1 and 2, if the potential for the former is somewhat more positive than that for the latter. Whether the solvent effect is completely independent of the cathode potential is questionable.

In strongly alkaline media (see Scheme 3), where Paths 3 and 4 are possible, the *trans* isomers were predominantly formed. Since there is no contribution of hydrogen bonding in the cyclization process in either path, such electrolytic results seem reasonable. Path 3 may result in the formation of a larger amount of the *trans* isomer by the contribution of electrostatic repulsion between two negatively charged oxygen atoms than in Path 4. The exclusive formation of the *trans* isomers in the cases of **1a** and **1b** can be explained by Path 3.

Also, the formation of a small amount of the *cis* isomer in the case of **1c** may be explained as resulting from

another electrostatic repulsion, which would not be strong, between a phenolate anion (p-C_6H_4-O^-) and an oxygen anion at the opposite side of an intermediate (III) in Path 3. However, the influence of the cathode potential on the isomeric ratio can not be explained by Path 3. It seems that the reduction potential of a carbonyl group is more positive than that of the corresponding anion radical (Ċ–O^-) formed by one-electron transfer.[14,15] As the reduction potential of the carbonyl group shifts negatively when its basicity is increased by electron-releasing substituents,[13] the potential for the second electron-transfer in Path 3 may be very close to that in Path 4 in the case of **1c**, the substituent (p-C_6H_4-O^-) of which is a very strong electron-releasing group. The increase of the *cis* isomer in electrolysis at a more negative potential may be explained as resulting from the increase in the contribution of Path 4, which is competitive with Path 3, since in Path 4 the electrostatic repulsion should be weaker.

In acetic acid–sodium acetate, the manner of the substituent effect was similar to that in the alkaline media. Since the protonation of the carbonyl group would be very slight in this solution,†† the reduction mechanisms shown in Scheme 4 may be possible.[14] If the influence of the cathode potential on the isomeric ratio can be neglected compared with that of the substituent, Path 6 may be more favorable than Path 5 as an explanation of the electrolytic results. The predominant formation of the *cis* isomer in the case of **1d** may be the result of the overlapping of the strong electron-releasing and weak steric hindrance effects of the methyl group.

In summary it can be concluded from the above discussion that the nucleophilic addition process (Paths 2, 4, and 6) should be included in the reductive cyclization of 1,8-diacylnaphthalenes, without excluding the radical coupling process (Paths 1, 3, and 5); *i.e.*, the two processes are in competition with each other.

Experimental

*Synthesis of 1-Acyl-8-benzolylnaphthalenes (**1a—d**). 1,8-Dibenzoylnaphthalene (**1a**)*: *trans*-1,2-Diphenyl-1,2-acenaphthenediol (*trans*-**2a**) was prepared from one mole of acenaphthenequinone and two moles of phenylmagnesium bromide, and was then recrystallized from ethanol. Yield, 85%; mp 155—156 °C (lit,[7] 155—156 °C), and ν_{O-H} 3360 and 3420 cm^{-1}. The 1,2-acenaphthenediol obtained was oxidized with chromium (VI) oxide in acetic acid to give **1a** in a 30% yield. The crude product was recrystallized from a mixture of acetone and ethanol. Mp 187—190 °C (lit,[7] 190 °C), $\nu_{C=O}$ 1620 cm^{-1}, and *m/e* 336 (M^+). Found: C, 85.55; H, 4.56%. Calcd for $C_{24}H_{16}O_2$: C, 85.69; H, 4.79%.

*1-(4-Methoxybenzoyl)-8-benzoylnaphthalene (**1b**)*: A phenylmagnesium bromide solution, which has been prepared from 8.0 g of magnesium, 52.8 g of bromobenzene and 250 ml of THF, was added drop by drop, to 50 g of acenaphthenequinone suspended in 1500 ml of THF at room temperature. After stirring for 5 h, 50 ml of a saturated ammonium chloride solution was added to the reaction mixture, and then the resulting precipitates were filtered off. The filtrate was evaporated under reduced pressure. The residual red oil was extracted with 200 ml of benzene, and the benzene extract was washed with 500 ml of 5% sulfuric acid. The benzene solution was dried over anhydrous sodium sulfate and then evaporated to dryness under reduced pressure. The recrystallization of the residual solid from 2-propanol afforded 67 g (Yield 94%) of 2-phenyl-2-hydroxyl-1-acenaphthenone (**3**) as yellow plates. Mp 146—147 °C, $\nu_{C=O}$ 1710 cm^{-1}, ν_{O-H} 3500 cm^{-1}, and *m/e* 260 (M^+). Found: C, 83.31; H, 4.75%. Calcd for $C_{18}H_{12}O_2$: C, 83.06; H, 4.65%.

A 4-methoxyphenylmagnesium bromide solution, which had been prepared from 5.6 g of magnesium, 43.2 g of 4-methoxybromobenzene, and 200 ml of THF, was added to 20.0 g of **3** dissolved in 100 ml of THF. After stirring for 2 h, 20 ml of a saturated ammonium chloride solution was added to the reaction mixture, and then the resulting precipitates were removed by filtration. When the filtrate was evaporated, an oily substance remained. The oil was solidified by treatment with a small amount of methanol. The recrystallization of the solid from 2-propanol afforded 22.1 g (yield, 83%) of *trans*-1-phenyl-2-(4-methoxyphenyl)-1,2-acenaphthenediol (*trans*-**2b**)††† as white needles. Mp 111—112 °C, *m/e* 368 (M^+), ν_{O-H} 3380 and 3550 cm^{-1}, and δ for methyl protons 3.81 ppm. Found: C, 81.21; H, 5.23%. Calcd for $C_{25}H_{20}O_3$: C, 81.50; H, 5.47%.

Into 20.0 g of *trans*-**2b** dissolved in 100 ml of acetic acid we added drop by drop, 36.7 g of a 10% aqueous chromium(VI) oxide solution. After having been allowed to stand for 1.5 h, the reaction mixture was poured into cold water, and the resulting aqueous solution was repeatedly extracted with ether. The ethereal extract was washed with a saturated sodium carbonate solution and then with water. The ethereal solution was dried over anhydrous sodium sulfate and then evaporated. The resulting tar was solidified by treatment with a mixture of ethyl acetate and petroleum ether. The recrystallization of the solid from ethanol afforded 13.6 g (yield, 68%) of 1-(4-methoxybenzoyl)-8-benzoylnaphthalene (**1b**) as white needles. Mp 111—112 °C, $\nu_{C=O}$ 1650 and 1630 cm^{-1}, *m/e* 366 (M^+), and δ for methyl protons 3.86 ppm. Found: C, 81.96; H, 4.71%. Calcd for $C_{25}H_{18}O_3$: C, 81.95; H, 4.95%.

*1-(4-Hydroxybenzoyl)-8-benzoylnaphthalene (**1c**)*: In 500 ml of dichloromethane, 10.0 g of *trans*-**1b** was reacted with 20.0 g of boron tribromide at room temperature for 4 h. The reaction mixture was then poured into 500 ml of 5% sodium hydroxide. When the aqueous layer was neutralized with aqueous sulfuric acid, white solides were precipitated. Recrystallization from benzene afforded 8.0 g (yield, 80%) of **1c** as white needles. Mp 115 °C (dec), $\nu_{C=O}$ 1650 and 1630 cm^{-1}, ν_{O-H} 3260 cm^{-1}, and *m/e* 352 (M^+). Found: C, 81.74; H, 4.09%. Calcd for $C_{24}H_{16}O_3$: C, 81.80; H, 4.58%.

*1-Acetyl-8-benzoylnaphthalene (**1d**)*: A methylmagnesium iodide solution, which has been prepared from 4.2 g of magnesium, 25.0 g of methyl iodide, and 200 ml of ether, was added to 15.0 g of **3** dissolved in 50 ml of THF. The reaction mixture was refluxed for 3 h, and then a 100-ml portion of a saturated ammonium chloride solution was added. The organic layer was dried over anhydrous sodium sulfate and then evaporated. The residual red oil was solidified by treatment with a small amount of methanol. The recrystallization of the solid from a

†† It has been suggested, on the basis of the UV spectroscopic data, that a carbonyl compound is in protonation equilibrium in strongly acidic solutions.[17]

††† The *cis* isomer (*cis*-**2b**) was also prepared by the iodine-catalyzed magnesium reduction of **1b** in benzene at 80 °C. Yield, 100%; mp 177—178 °C, *m/e* 368 (M^+), and ν_{O-H} 3300 cm^{-1}, and δ for methyl protons 3.60 ppm. Found: C, 81.42; H, 5.24%.

mixture of methanol and water (2: 1 vol ratio) afforded 1.2 g (yield 8%) of *cis*-1-methyl-2-phenyl-1,2-acenaphthenediol (*cis*-**2d**) as prisms. Mp 161—162 °C, *m/e* 276 (M^+), ν_{O-H} 3300 cm^{-1}, and δ for methyl protons 1.00 ppm. Found: C, 82.25; H, 5.72%. Calcd for $C_{19}H_{16}O_3$: C, 82.58; H, 5.84%. On the other hand, the recrystallization from carbon tetrachloride of the solid obtained on evaporating the filtrate afforded 8.3 g (yield 52%) of *trans*-**2d** as white needles. Mp 111—112 °C, *m/e* 276 (M^+), ν_{O-H} 3320 and 3450 cm^{-1}, and δ for methyl protons 1.68 ppm. Found: C, 81.70; H, 5.84%.

A mixture of 3.0 g of *trans*-**2d**, 0.9 g of chromium(VI) oxide, 30 ml of acetic acid, and 9.1 ml of water was kept at 50 °C for 2 h. The reaction mixture was then poured into 70 ml of water and extracted with ether. The ethereal extract was washed with water and dried over anhydrous sodium sulfate. The red tar obtained by the evaporation of the ethereal solution under reduced pressure was solidified by treatment with a small amount of a mixture of ethyl acetate and petroleum ether. The subsequent recrystallization of the solid from 2-propanol afforded 2.8 g (yield 94%) of 1-acetyl-8-benzoylnaphthalene (**1d**) as white granules. Mp 110—111 °C, $\nu_{C=O}$ 1650 and 1680 cm^{-1}, and *m/e* 274 (M^+). Found: C, 83.26; H, 4.98%. Calcd for $C_{19}H_{14}O_2$: C, 83.19; H, 5.14%.

Conversion of ***1d*** *into 3-Phenyl-1-phenalenone.* To a DMF solution of **1d** we added a small amount of aqueous sulfuric acid or sodium hydroxide. After several minutes, the solution turned yellow. When a large amount of water was added to the solution, 3-phenyl-1-phenalenone was precipitated as yellow crystals. Mp 141—142 °C, $\nu_{C=O}$ 1630 cm^{-1}, and *m/e* 256 (M^+). Found: C, 89.39; H, 4.78%. Calcd for $C_{19}H_{12}O$: C, 89.04; H, 4.72%.

Electrolysis Procedure. An H-type electrolytic cell divided with a glass filter was used. A mercury pool (area, 12 cm^2) was used as the cathode, while the anode was a platinum disc (diameter, 2 cm). The catholyte and anolyte consisted of 60 ml of an organic solvent containing water in a concentration of 20 vol%. The supporting electrolytes were used in a concentration of 0.5 M except for sodium hydroxide, which was used in a concentration of 0.1 M. The starting diacylnaphthalene used for one run was 2.5 mmol. The catholyte was kept at 20 °C during the electrolysis, which was carried out by a controlled potential method.

Separation and Analysis of Products. General Procedure: After electrolysis, the catholyte was diluted with 300 ml of water and then neutralized with sulfuric acid or sodium hydroxide. The resulting solution was repeatedly extracted with ether, and the combined ethereal extract was dried over anhydrous sodium sulfate. The solids obtained by the evaporation of the ethereal solution were subjected to the following treatments for separation and analysis.

Electrolytic Products of ***1a***: The solid was dissolved in 30 ml of DMF, and the DMF solution was poured into 300 ml of water. When the resulting precipitate was recrystallized from ethanol, only unreacted **1a** crystallized out of the solution. The filtrate was evaporated, and the residue was recrystallized from acetic acid. The crystals thus obtained were *cis*-**2a**. The aqueous filtrate obtained at the first stage of this experiment was stored overnight in a refrigerator, and the resulting precipitate was filtered. The recrystallization of the precipitate from ethanol afforded pure *trans*-**2a**. The *cis*- and *trans*-**2a** thus obtained were identified with their authentic samples[7,9]** by mixed-melting point tests.

** The *cis* isomer (*cis*-**2a**) was also prepared using the method of Griegee.[9] Mp 174—175 °C (lit,[9] 176—177 °C) and ν_{O-H} 3220 cm^{-1}.

Electrolytic Products of ***1b***: Aliquorts of the solid obtained by the method described in *General Procedure* were subjected to NMR and IR spectroscopic analyses in order to determine the isomeric ratio of **2b** and to detect the unreacted **1b** respectively.

The unreacted **1b** was also recovered from the rest of the above solid by a method similar to that used in the case of **1a.** When the resulting isomeric mixture of **2b** was recrystallized from a small amount of aqueous methanol, *trans*-**2b** crystallized out of the solution. The crude *trans*-**2b** was recrystallized from 2-propanol. On the other hand, the recrystallization of the solids obtained by the evaporation of the methanolic filtrate from 2-propanol afforded *cis*-**2b**. The *cis*- and *trans*-**2b** thus obtained were identified with their authentic samples,†††,*** which were independently synthesized, by a mixed-melting point test.

Electrolytic Products of ***1c***: The solid obtained by the method described in *General Procedure* was dissolved in 100 ml of 0.5 M sodium hydroxide, and the resulting solution was stirred at room temperature for 12 h after the addition of 2.0 ml of dimethyl sulfate. The reaction mixture was repeatedly extracted with ether, and the combined ethereal extract was dried over anhydrous sodium sulfate. The subsequent evaporation of the etheral solution afforded methylated products‡ as white solids. These solids were analyzed much as in the case of **1b.** The methylated pinacol rearrangement product (2-phenyl-2-(4-methoxyphenyl)-1-acenaphthenone) was also detected using an IR spectroscopic method. This product was purely isolated by the use of a column chromatograph (silica gel, benzene). Mp 132—133 °C, $\nu_{C=O}$ 1720 cm^{-1}, *m/e* 350 (M^+), and δ for methyl protons 3.69 ppm. Found: C, 85.93; H, 5.05%. Calcd for $C_{25}H_{18}O_2$: C, 85.69; H, 5.18%.

Electrolytic Products of ***1d***: The solid obtained by the method described in *General Procedure* was subjected to the spectroscopic analyses of the products, and then unreacted **1d** was removed by a method similar to that used in the case of **1a** or **1b.** The recrystallization of the resulting isomeric mixture of **2d** from a mixture of methanol and water (2: 1 vol ratio) afforded *cis*-**2d.** On the other hand, the recrystallization from carbon tetrachloride of a solid obtained on evaporating the filtrate afforded *trans*-**2d.** The *cis*- and *trans*-**2d** thus obtained were identified with their authentic samples,‡‡ which were independently synthesized, by a mixed-melting point test.

The IR and NMR (90 MHz) spectra were measured in KBr tablets and in DMSO-d_6 solutions respectively, both at room temperature.

References

1) J. H. Stocker and R. M. Jenevein, *J. Org. Chem.*, **33**, 394 (1968).

2) J. H. Stocker and R. M. Jenevein, *J. Org. Chem.*, **33** 2145 (1968).

3) R. N. Gourley and J. Grimshaw, *J. Chem. Soc., C*, **1968**, 2388.

4) W. D. Hoffman, W. E. McEwen, and J. Kleinberg, *Tetrahedron*, **5**, 293 (1959).

5) T. Nonaka, A. Udagawa, and K. Odo, *Chem. Lett.*, **1975**, 2161.

*** See synthesis of 1-acyl-8-benzoylnaphthalene (**1a**—**d**), 1-(4-methoxybenzoyl)-8-benzoylnaphthalene (**1b**) in experimental.

‡ The products mainly consisted of **2b** and **1b.**

‡‡ See synthesis of 1-acyl-8-benzoylnaphthalenes (**1a**—**d**), 1-acethyl-8-benzoylnaphthalene (**1d**) in experimental.

6) J. Grimshaw and J. S. Ramsey, *J. Chem. Soc., C*, **1966**, 635.
7) E. Beschke, *Justus Liebigs Ann. Chem.*, **369**, 184 (1909).
8) J. F. McOmie and M. L. Watts, *Chem. Ind.*, **12**, 1658 (1963).
9) R. Griegee, L. Kraft, and B. Bank, *Justus Liebigs Ann. Chem.*, **507**, 195 (1933).
10) W. E. Bachmann, *J. Am. Chem. Soc.*, **54**, 1969 (1932).
11) P. D. Bartlett and R. F. Brown, *J. Am. Chem. Soc.*, **62**, 2927 (1940).
12) L. J. Bellamy, "The Infra-red Spectra of Complex Molecules," John Wiley & Sons, New York (1964), p. 95.
13) P. Zuman, "Substituent Effects in Organic Polarography," Plenum Press, New York (1967), p. 55.
14) P. Zuman, D. Barns, and A. Ryvolova-Kejharova, *Discuss. Faraday Soc.*, **45**, 202 (1968).
15) P. Zuman, *Collect. Czech. Chem. Commun.*, **33**, 2548 (1968).
16) In the present paper the theory of Zuman is modified in part.
17) S. Nagakura, A. Minegishi, and K. Stanfied, *J. Am. Chem. Soc.*, **79**, 1033 (1957).

The Decomposition of *N,N*-Dichlorourethane by Copper: A Comparison with the Photolysis of Ethyl Azidoformate

Noboru TORIMOTO,*,† Tadao SHINGAKI, and Toshikazu NAGAI

†*Science Education Institute of Osaka Prefecture, Karita-cho, Sumiyoshi-ku, Osaka 558*
College of General Education, Osaka University, Toyonaka, Osaka 560

(Received February 10, 1978)

The reactions of *N,N*-dichlorourethane (**1**) with substrates, such as hydrocarbons and ethers, gave *N*-substituted urethanes (**3**) and urethane (**4**) in the presence of copper or copper(I) chloride. The reactions with aromatic hydrocarbons and cyclic ethers possessing an alkyl group at the α-position, however, gave no azepine and no alkoxyurethane respectively, in contrast to those of ethoxycarbonylnitrene generated from the azide. The reactions with the tertiary C–H bonds of *cis*- and *trans*-1,4-dimethylcyclohexanes proceeded non-stereospecifically, contrary to those of the nitrene. The reactions with alcohols led to high yields of **4**, accompanied by the corresponding aldehydes, but afforded no O–H insertion product. The addition of a radical inhibitor, nitrobenzene, reduced the yield of **3**, while it had no appreciable effect on the yield of **4**. Furthermore, the reactions of *N*-chlorourethane with hydrocarbons also gave **3** and **4**. These results suggest that the reaction of **1** with substrates proceeds not by a nitrene mechanism, but by a metal-radical mechanism.

The α-elimination of certain compounds has been reported as a method of generating a nitrene intermediate other than by the photolysis or thermolysis of azides. For example, *N*-(*p*-nitrophenylsulfonyloxy)-urethane[1] was thermolyzed to give ethoxycarbonylnitrene. The decomposition of chloramine-T[2] and dichloramine-T[3] in the presence of zinc dust has also been advanced as a method of generating the sufonylnitrene. These α-eliminations afforded the same products as those produced by the photolyses or thermolyses of the corresponding azides.

On the other hand, the thermolysis of *N,N*-dichloromethanesulfonamide in benzene afforded methanesulfonamide (82% yield), but not mesylaniline.[4] This finding suggests that the reaction involves no nitrene. We reported, prior to Ref. 4, the thermolysis of *N,N*-dichloromethanesulfonamide in the presence of copper.[5,6] Therefore, we tentatively advanced the idea that the reaction proceeded by means of a radical mechanism involving no sulfonylnitrene. In that mechanism, although an intervention of *N*-chloromethanesulfonamide was postulated (Scheme 1), further experimental evidence for the postulate was not yet found because of the difficulty of preparing the monochloramide.

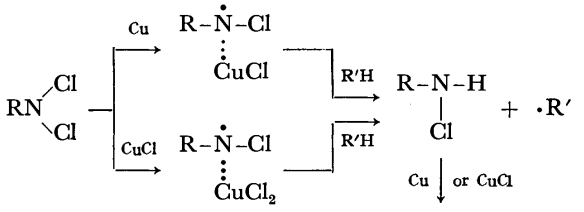

Scheme 1.

In this study, *N,N*-dichlorourethane was employed instead of *N,N*-dichloromethanesulfonamide to obtain further corroborating evidence about the radical mechanism in the dihaloamide–metal system. When the urethane is employed, *N*-chlorourethane, whose intervention is assumed in the dichlorourethane–metal system, is easy to prepare and can be utilized for the present investigation.

Results and Discussion

Reaction of N,N-*Dichlorourethane (1) with Hydrocarbons and Cyclic Ethers in the Presence of Copper.* Copper powder was suspended in a substrate (**5**), and **1** was added, drop by drop, into the suspension in a stream of nitrogen. The yields of the products are listed in Table 1 and compared with those of the photolyses of ethyl azidoformate (**2**).[7,8]

Each of the reactions of **1** with substrates gave the *N*-substituted urethane (**3**) and urethane (**4**).

$$\underset{(1)}{Cl_2NCOOEt} + \underset{(5)}{R'H} \xrightarrow{Cu} \underset{(3)}{R'NHCOOEt} + \underset{(4)}{NH_2COOEt}$$

The products, **3** and **4**, correspond formally to those resulting from insertion into the C–H bonds and from the abstraction of the hydrogen atoms respectively by ethoxycarbonylnitrene. In the reactions with cyclic ethers, **5f**, **5g**, and **5h**, the α-substituted derivatives were isolated. The preferential formation of the α-substituted derivatives in these reactions paralles that in the direct[7] and sensitized[8] photolyses of **2**. The reactions of **1** with small-membered cyclic ethers, **5d** and **5e**, gave large quantities of colorless, viscous substances whose IR spectra showed the respective strong O–H stretching absorptions. Contrary to the reactions of **1**, the reactions of **2** with **5d** and **5e** gave two ring-opening products, **3d** and **3e** respectively. In the reactions of **1** with aromatic hydrocarbons, azepines, whose formation is a typical nitrene reaction, were not detected, although they were obtained in the photolyses of **2**. In the reaction with **5c**, the product with a side-chain C–H bond was preferentially obtained. The ring-opening products (**3d** and **3e**) in **5d** and **5e** are formed by only singlet ethoxycarbonylnitrene *via* an O–N ylide mechanism.[6] In addition, singlet ethoxycarbonylnitrene adds to aromatic double bonds to give the aziridines, followed by the cleavage of C–C bonds to give the azepines.[9] Therefore, the generation of the singlet nitrene from **1** must be ruled out.

Table 1. Reaction of **1** and **2** with hydrocarbons and ethers

Substrate (**5**)	Product (%)[a] **3**			**4**
(**a**)	(**a**) 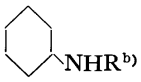 NHR[b] 1.4 (32.0)			57.2 (15.0)
(**b**)	(**b**$_1$) 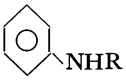 NHR 5.5 (1.7)	(**b**$_2$) 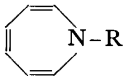 N–R ND[c] (20.8)		38.0 (7.6)
(**c**) 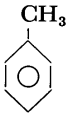	(**c**$_1$) 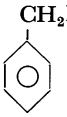 CH_2NHR 21.6 (1.8)	(**c**$_2$) 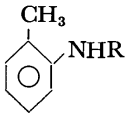 CH_3 NHR 1.4 (2.9)	(**c**$_3$) 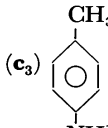 CH_3 NHR ND (1.1)	
	(**c**$_4$) 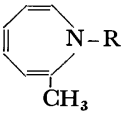 N–R CH_3 ND (6.7)	(**c**$_5$) 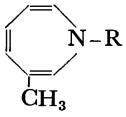 N–R CH_3 ND (9.0)	(**c**$_6$) 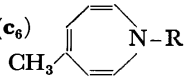 N–R CH_3 ND (6.2)	31.5 (5.0)
(**d**) 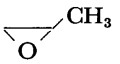	(**d**) CH_2=$CHCH_2ONHR$ ND (21.0)			34.3 (12.0)
(**e**) 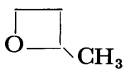	(**e**) CH_2=$CHCH_2CH_2ONHR$ ND (28.0)			85.9 (23.0)
(**f**)	(**f**) 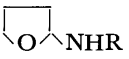 NHR 12.3 (25.0)			32.7 (21.0)
(**g**)	(**g**$_1$) 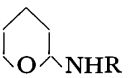 NHR 27.1 (25.0)	(**g**$_2$) 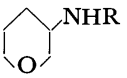 NHR ND (4.8)		32.0 (16.0)
(**h**)	(**h**) 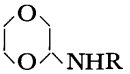 NHR 30.2 (32.8)			68.7 (22.2)

( ) Indicates the values resulting from the photolyses of **2**.[8,9] a) Calculated on the basis of the **1** used. b) R: $COOC_2H_5$. c) ND: not detected.

Stereochemistry. In order to compare the reaction of **1** with that of **2** in stereochemical behavior, the reactions of **1** were carried out in *cis*- and *trans*-1,4-dimethylcyclohexanes (*cis*-**5** and *trans*-**5**).

As can be seen in Table 2, the reaction of **1** with either *cis*-**5** or *trans*-**5** gave a mixture of *cis*-**3** and *trans*-**3** (stereoisomer), though the yield was low. Such non-stereospecific formation has also been observed in the reaction of *N*,*N*-dichloromethanesulfonamide with *cis*-**5** or *trans*-**5**, where the tertiary sulfonamides are isolated in moderate yields.[5,6]

The stereospecific formation of *cis*-**3** or *trans*-**3** in the photolyses of **2**, as shown in Table 2, indicates that triplet ethoxycarbonylnitrene does not lead to the formation of **3**. Thus, the non-stereospecific formation in the reaction of **1** means that neither the singlet nor the triplet nitrene takes part in the formation of **3**.

Reaction of 1 with Alcohols. The reaction of **1** with ethanol and 1-butanol gave urethane in yields of 84 and 86% respectively, accompanied by the corresponding aldehydes. None of the O–H insertion products was detected in these reactions. On the other hand, the photolyses of **2** in ethanol and 1-butanol gave O–H insertion products in yields of 11 and 27% respectively, accompanied by urethane.[8] The O–H insertion products have been formed by a singlet nitrene *via* an O–N ylide intermediate, but not by a triplet nitrene *via* a radical mechanism.[8]

Reaction of 1 in the Addition of Radical Inhibitors. The above-mentioned results suggest that some radical species is involved in the reaction of **1**. Therefore, the reactions of **1** with toluene and tetrahydropyran were carried out in the presence of a radical inhibitor, nitrobenzene. The results are displayed in Table 3.

Breslow and Edwards reported the effect of radical inhibitors, such as nitrobenzene, *m*-dinitrobenzene, and sulfur, on the decomposition of **2** in cyclohexane.[12] That is, decompositions in the presence of these inhibitors

Table 2. Reaction of **1** and **2** with *cis*- and *trans*-1,4-dimethylcyclohexanes

Substrate (5)	Product (%)[a]		
	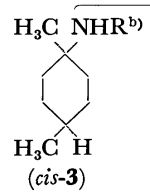 (*cis*-**3**)	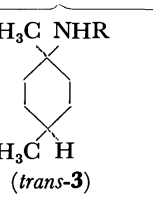 (*trans*-**3**)	**4**
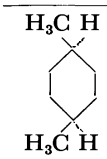 (*cis*)	1.0(14.0)	2.0(ND[c])	50.8(18.0)
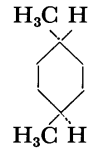 (*trans*)	1.2(ND)	2.3(11.0)	56.6(16.0)

( ) Indicates the values resulting from the photolyses of **2**.[10] a) b) c) See Table 1, footnotes.

Table 3. Reaction of **1** with substrate in the presence of nitrobenzene

Substrate (5)	Radical inhibitor	Product (%)[a]			
		3			**4**
	presence	**c**$_1$ 8.4	**c**$_2$	1.3	31.1
	absence	21.6		1.4	31.5
	presence	**g**$_1$ 13.8			30.0
	absence	27.1			32.0

a) See Table 1, footnotes.

gave *N*-cyclohexylurethane and urethane in yields of 56—76 and 12—21% respectively, while those in their absence gave *N*-cyclohexylurethane and urethane in yields of 52 and 25% respectively. These additives led to increased yields of the insertion, but to decreased yields of the abstraction. They gave the following interpretation of the findings. A radical, HNCOOEt, produced by the hydrogen abstraction of the triplet nitrene can catalyze the singlet-triplet intersystem crossing. The reaction of the radical with the additive decreases its radical concentration, resulting in a slow singlet-to-triplet conversion and, therefore, in a high yield of the product from the singlet. Contrary to the decomposition of **2**, in the reaction of **1** the addition of nitrobenzene led to decreased yields of the *N*-substituted urethanes, while it had no appreciable effect on the yield of urethane.

Reaction of N-*Chlorourethane.* The reaction of *N*-chlorourethane (**6**) with dioxane in the presence of copper gave the expected *N*-substituted urethane, **3h**, and urethane in yields of 18.1 and 71.2% respectively.

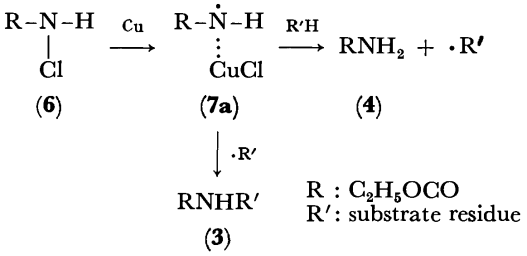

Scheme 2.

The reactions of **6** with either *cis*-**5** or *trans*-**5** gave a mixture of *cis*-**3** and *trans*-**3** non-stereospecifically, as in the case of **1**.

The decomposition of *N,N*-dichlorourethane (**1**) in the presence of copper leads to the formation of *N*-chlorourethane (**6**), as has been shown in Scheme 1. The chlorine atom of **6** is eliminated by copper to give a metal-radical complex (**7a**), as is shown in Scheme 2, followed by a hydrogen abstraction to give urethane (**4**). On the other hand, **7a** recombines with a substrate radical, ·R′, to afford the *N*-substituted urethane (**3**).

In the decomposition of the azide in hydrocarbons, the free HNCOOEt radical which resulted from triplet nitrene was not able to recombine with the substrate radical (·R′), but exclusively abstracted a hydrogen atom from the substrate. However, the HNCOOEt radical in the dichloramide– or chloramide–system may recombine with the substrate radical because of the stabilization produced by forming the metal-radical complex represented as **7a**.[6] In addition, a difference between the characteristics of the metal-radical and the free radical was shown also by the addition of the radical inhibitor, nitrobenzene. That is, the addition of the radical inhibitor caused a decreased yields of **3**, but had appreciable effect on the yield of **4** (Table 3). The substrate radical would be trapped by the inhibitor, while the metal-radical complex is not affected by the inhibitor, though the free radical can be captured by it.[12,13]

Reaction of **1** *and* **6** *in the Presence of Copper(I) Chloride.* As has been shown in Scheme 1, the copper-initiated decomposition of dichloramide should produce copper(I) chloride. This copper(I) chloride is expected to take part in the present reactions. The reaction of **1** with dioxane in the presence of copper(I) chloride gave the *N*-(1,4-dioxan-2-yl)urethane (**3h**) and urethane in yields of 6 and 64.4% respectively. The reactions with both *cis*-**5** and *trans*-**5** gave the *N*-substituted urethane isomer mixtures. The reaction of **6** with dioxane gave **3h** and urethane in yields of 9.6 and 65.4% respectively.

The reaction of **6** with a substrate in the presence

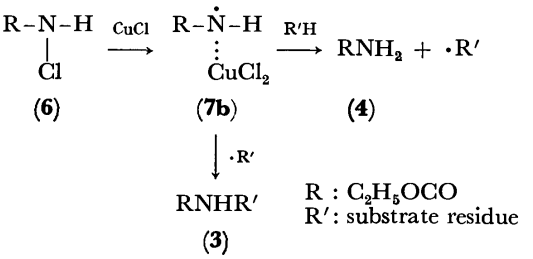

Scheme 3.

of copper(I) chloride is also outlined in Scheme 3. The metal-radical complex (**7b**) resulting from chlorine abstraction by copper(I) chloride abstracts a hydrogen atom from the substrate to give urethane. On the other hand, **7b** recombines with a substrate radical to afford **3**.

In Conclusion. In the absence of metals, the reactions of **1** with toluene and dioxane gave urethane in yields of 68 and 36% respectively, but not the C–H insertion products (**3**).

The formation of the insertion products from the chloramides is shown in Schemes 1—3, under the indispensable condition of the presence of copper or copper(I) chloride.

Experimental

The IR spectra were recorded on a Hitachi EP-S photometer and a Nippon Bunko (JASCO) Model IR-E photometer, while the NMR spectra were taken on Hitachi R-20 and Hitachi R-24 instruments, using tetramethylsilane as the internal standard. The gas chromatography (VPC) was done on Shimadzu GC-2C and Nippon Denshi (JEOL) JGC 20K units, employing as absorbents: A, 20% Apiezon Grease M on Neopak 1A (60—80 mesh); B, 20% Ucon Oil 5HB 2000 on Celite (60—80 mesh); C, 10% Polyethylene Glycol Succinate on Neopak 1A (60—80 mesh). The quantitative analyses of the products by VPC and the test for the stability of each product during VPC analysis have been done in the ways described in a previous paper.[14]

Materials. The *N,N*-dichlorourethane (**1**),[15] *N*-chlorourethane (**6**),[16] 2-methyloxetane,[7] and *cis*- or *trans*-1,4-dimethylcyclohexane (*cis*-**5** or *trans*-**5**)[17] were prepared by the methods already described. The propylene oxide, tetrahydrofuran, tetrahydropyran, 1,4-dioxane, cyclohexane, benzene, toluene, ethanol, and 1-butanol were used after purification by the methods recommended in the literature.[18]

Authentic Samples. The *N*-cyclohexylurethane (**3a**) was prepared by the method of Lwowski and Mattingly.[19] The *N*-phenylurethane (**3b**$_1$), *N*-benzylurethane (**3c**$_1$), *N*-(2-tolyl)-urethane (**3c**$_2$), and *N*-(4-tolyl)urethane (**3c**$_3$) were prepared from ethyl chloroformate and the corresponding amines in a way similar to that used in the preparation of *N*-cyclohexylurethane. **3a**: IR (Nujol, cm^{-1}): 3350, 1680, 1220. NMR (CCl_4, δ): 4.52 (NH, 1H, bs), 4.01 (2H, q), 3.40 (1H, m), 2.42—1.40 (ring-CH_2, 10H, m), 1.21 (3H, t). **3b**$_1$: IR (Nujol, cm^{-1}): 3350, 1700, 1240. NMR (CCl_4, δ): 7.80 (NH, 1H, bs), 7.64—6.75 (5H, m), 4.20 (2H, q), 1.21 (3H, t). **3c**$_1$: IR (Nujol, cm^{-1}): 3360, 1690, 1285. NMR (CCl_4, δ): 7.22 (5H, s), 5.36 (NH, 1H, bs), 4.21 (2H, d), 4.01 (2H, q), 1.67 (3H, t). **3c**$_2$: IR (Nujol, cm^{-1}): 3355, 1700, 1230. NMR (CCl_4, δ): 7.96—6.92 (4H, m), 6.68 (NH, 1H, bs), 4.20 (2H, q), 2.21 (3H, s), 8.71 (3H, t). **3c**$_3$: IR (Nujol, cm^{-1}): 3320, 1710, 1230. NMR (CCl_4, δ): 7.48—6.64 (5H, m), 4.10 (2H, q), 2.22 (3H, s), 1.19 (3H, t). The *cis* and *trans* isomers of *N*-(1,4-dimethylcyclohexyl)urethane (*cis*-**3** and *trans*-**3**) were prepared as follows. A mixture of the stereoisomers (*cis*-**3** and *trans*-**3**) was prepared from ethyl chloroformate and 1,4-dimethylcyclohexylamine (*cis-trans* mixture), which had been prepared in a way similar to that used in the preparation of 1-methylcyclohexylamine.[20] The urethanes were well separated into *cis* and *trans* isomers by using column B. The assignment of each stereoisomer was done by comparison with the products obtained from the stereospecific insertions of singlet ethoxycarbonylnitrene into the tertiary C–H bond of *cis*- and *trans*-1,4-dimethylcyclohexanes.[10] *cis*-**3**: IR (neat, cm^{-1}): 3340, 1710, 1230, NMR (CCl_4, δ): 4.80 (NH, 1H, bs), 4.22 (2H, q), 2.11—1.45 (ring-CH and CH_2, 9H, m), 1.38 (3H, s), 1.27 (3H, t), 0.98 (3H, d). *trans*-**3**: IR (neat, cm^{-1}): 3360, 1710, 1235. NMR (CCl_4, δ): 4.44 (NH, 1H, bs), 4.06 (2H, q), 2.50—1.40 (ring-CH and CH_2, 9H, m) 1.31 (3H, s), 1.22 (3H, t), 0.92 (3H, d). The IR and NMR spectral data of *N*-(2-tetrahydrofuryl)urethane (**3f**), *N*-(2-tetrahydropyranyl)urethane (**3g**$_1$), and *N*-(1,4-dioxan-2-yl)urethane (**3h**) have been described previously.[6,7]

Reaction of N,N-*Dichlorourethane (1) with Hydrocarbons and Ethers in the Presence of Copper.* Copper powder (4.8 g, 0.075 mol) was suspended in a substrate (0.5 mol of ethers and hydrocarbons), and *N,N*-dichlorourethane (**1**, 4 g, 0.025 mol) was added, drop by drop, into the suspension in a stream of nitrogen. The reactions with ethers and hydrocarbons were carried out at 20 and 50 °C respectively. After **1** had been added, the stirring was continued for about another 5 h, Then, the suspension was filtered, and the filtrate was concentrated under reduced pressure. The residue was analyzed by VPC on Columns B and C.

In Cyclohexane (5a), Benzene (5b), and Toluene (5c): **3a** (0.06 g), **3b**$_1$ (0.22 g), **3c**$_1$ (0.97 g), and **3c**$_2$ (0.06 g) were isolated.

In tetrahydrofuran (5f), Tetrahydropyran (5g), and 1,4-Dioxane (5h): **3f** (0.49 g), **3g**$_1$ (1.17 g), and **3h** (1.32 g) were isolated.

In cis-*1,4-Dimethylcyclohexane* (cis-*5*): *cis*-**3** (0.05 g) and *trans*-**3** (0.1 g) were isolated.

In trans-*1,4-Dimethylcyclohexane* (trans-*5*): *cis*-**3** (0.06 g) and *trans*-**3** (0.11 g) were isolated.

Reaction of 1 with Alcohols in the Presence of Copper. Copper powder (0.075 mol) was suspended in ethanol (0.5 mol) or 1-butanol (0.5 mol), and then **1** (4 g, 0.025 mol) was added, drop by drop, to the suspension kept at 5—7 °C in a stream of nitrogen. After the **1** had been added, the stirring was continued for about 5 h. Then, the suspension was filtered, and the excess substrate and the volatile product, aldehyde, were trapped in a flask immersed in a dry ice–methanol bath under reduced pressure. The trapped solution was added to a 2,4-dinitrophenylhydrazine solution, and the hydrazone was isolated.

Reaction of 1 with 5c and 5g in the Addition of Nitrobenzene. Copper powder (0.075 mol) was suspended in a mixture of substrate (0.5 mol) and nitrobenzene (0.025 mol), and then **1** (4 g, 0.025 mol) was added, drop by drop, into the suspension in a stream of nitrogen. The reactions with **5c** and **5g** were carried out at 50 and 20 °C respectively. Then, the reaction mixture was treated as has been described above. **3c**$_1$ (0.38 g) and **3c**$_2$ (0.06 g) were isolated in the reaction with **5c**, and **3g**$_1$ (0.6 g) was isolated in the reaction with **5g**.

Reaction of N-*Chlorourethane (6) with 5h and Hydrocarbons in the Presence of Copper.* Copper powder (0.075 mol) was suspended in a substrate (0.5 mol), and *N*-chlorourethane (**6**, 3.1 g, 0.025 mol) was added, drop by drop, into the stirred suspension at 20 °C (case of **5h**) or 50 °C (case of hydrocarbons) in a stream of nitrogen. Then, the reaction mixture was treated as has been described above.

In 5h: **3h** (0.8 g) was isolated.

In 5a: **3a** (0.08 g, 1.8%) and urethane (**4**, 50.0%) were isolated.

In cis-*5*: *cis*-**3** (0.06 g, 1.2%), *trans*-**3** (0.1 g, 2.1%), and **4** (50.4%) were isolated.

In trans-*5*: *cis*-**3** (0.05 g, 1.0%), *trans*-**3** (0.08 g, 1.6%), and **4** (63.7%) were isolated.

Reaction of 1 and 6 with 5h and Hydrocarbons in the Presence of Copper(I) Chloride. Copper(I) chloride (7.5 g, 0.075 mol) was suspended in a substrate (0.5 mol), and **1** or **6** (0.25 mol) was added to the suspension at 20 °C (case of **5h**) or 50 °C

(case of hydrocarbons) in a stream of nitrogen. Then, the reaction mixture was treated as has been described above.

In the Reaction of **1** *with* **5h**: **3h** (0.26 g) was isolated.

In the Reaction of **1** *with* cis-**5**: *cis*-**3** (0.06 g, 1.2%), *trans*-**3** (0.09 g, 1.8%), and **4** (62.0%) were isolated.

In the Reaction of **1** *with* trans-**5**: *cis*-**3** (0.09 g, 1.8%), *trans*-**3** (0.15 g, 3.0%), and **4** (54.8%) were isolated.

In the Reaction of **6** *with* **5h**: **3h** (0.42 g) was isolated.

Reaction of **1** *in the Absence of Copper.* The chloramide (**1**, 0.025 mol) was added, drop by drop, to **5h** (0.5 mol) kept at 20 °C or to **5c** (0.5 mol) kept at 50 °C in a stream of nitrogen. Then, the reaction mixture was treated as has been described above. Urethane was isolated in yields of 0.8 g and 1.51 g in **5h** and **5c** respectively.

Photolyses of Ethyl Azidoformate in Hydrocarbons. A solution of ethylazidoformate (0.02 mol) in hydrocarbon (0.5 mol) was irradiated using a low-pressure mercury lamp, with stirring and cooling at 0 °C until the evolution of nitrogen was no longer observed. The excess substrate was then removed under reduced pressure. The residue was analyzed by VPC on Colums B and C.

In 5a: **3a** (1.36 g) was isolated.

In 5b: $\mathbf{3b}_1$ (0.07 g) and *N*-(ethoxycarbonyl)azepine ($\mathbf{3b}_2$, 0.86 g) were isolated. $\mathbf{3b}_2$: IR (neat, cm^{-1}): 1715 (C=O), 1655 and 1630 (C=C). NMR ($CDCl_3$, δ): 6.12—5.18 (6H, m), 4.17 (2H, q), 1.25 (3H, t) (Found: C, 65.32; H, 6.62; N, 8.51%).

In 5c: $\mathbf{3c}_1$ (0.08 g), $\mathbf{3c}_2$ (0.13 g), $\mathbf{3c}_3$ (0.05 g), 2-methyl-*N*-(ethoxycarbonyl)azepine ($\mathbf{3c}_4$, 0.3 g), 3-methyl-*N*-(ethoxycarbonyl)azepine ($\mathbf{3c}_5$, 0.4 g), and 4-methyl-*N*-(ethoxycarbonyl)-azepine ($\mathbf{3c}_6$, 0.28 g) were isolated. $\mathbf{3c}_4$: IR (neat, cm^{-1}): 1710 (C=O), 1650 and 1630 (C=C). NMR ($CDCl_3$, δ): 6.35—5.63 (5H, m), 4.17 (2H, q), 2.07 (3H, s), 1.29 (3H, t) (Found: C, 67.21; H, 7.25; N, 7.76%). $\mathbf{3c}_5$: IR (neat, cm^{-1}): 1715 (C=O), 1660 and 1630 (C=C). NMR ($CDCl_3$, δ): 6.10—5.30 (5H, m), 4.22 (2H, q), 1.78 (3H, d, J=1.5 Hz), 1.32 (3H, t) (Found: C, 66.92; H, 7.41; N, 7.94%). $\mathbf{3c}_6$: IR (neat, cm^{-1}): 1720 (C=O), 1660 and 1630 (C=C). NMR ($CDCl_3$, δ): 6.10—5.14 (5H, m), 4.20 (2H, q), 1.80 (3H, s), 1.30 (3H, t) (Found: C, 67.30; H, 7.21; N, 7.95%). The IR and NMR data of $\mathbf{3c}_4$, $\mathbf{3c}_5$, and $\mathbf{3c}_6$ were assigned on the basis of those of 2-, 3-, and 4-methyl-*N*-(methoxycarbonyl)azepines.[21]

The authors are particularly indebted to Drs. Hisao Arakawa and Akira Matsumoto of the Science Education Institute of Osaka Prefecture for help in the preparation of this paper and for many useful suggestions.

References

1) W. Lwowski and T. J. Maricich, *J. Am. Chem. Soc.*, **87**, 3630 (1965).
2) D. Carr, T. P. Seden, and R. W. Turner, *Tetrahedron Lett.*, **1969**, 477.
3) D. S. Breslow and M. F. Sloan, *Tetrahedron Lett.*, **1969**, 5349.
4) R. A. Abramovitch, T. D. Bailey, T. Takaya, and V. Uma, *J. Org. Chem.*, **39**, 340 (1974).
5) T. Shingaki, N. Torimoto, M. Inagaki, and T. Nagai, *Chem. Lett.*, **1972**, 1181.
6) N. Torimoto, T. Shingaki, and T. Nagai, *Bull. Chem. Soc. Jpn.*, **50**, 2780 (1977).
7) N. Torimoto, T. Shingaki, and T. Nagai, *Bull. Chem. Soc. Jpn.*, **49**, 2572 (1976).
8) N. Torimoto, T. Shingaki, and T. Nagai, *Bull. Chem. Soc. Jpn.*, **50**, 1517 (1977).
9) W. Lwowski and T. J. Maricich, *J. Am. Chem. Soc.*, **87**, 3630 (1965).
10) T. Shingaki, M. Inagaki, N. Torimoto, and M. Takebayashi, *Chem. Lett.*, **1972**, 155.
11) J. M. Simon and W. Lwowski, *J. Am. Chem. Soc.*, **91**, 5107 (1969).
12) D. S. Breslow and E. I. Edwards, *Tetrahedron Lett.*, **1967**, 2123.
13) Y. Mori and J. Tsuji, *Kagaku No Ryoiki*, **27**, 197 (1973).
14) T. Shingaki, M. Inagaki, M. Takebayashi, and W. Lwowski, *Bull. Chem. Soc. Jpn.*, **45**, 3567 (1972).
15) T. A. Foglia and D. Swern, *J. Am. Chem. Soc.*, **31**, 3625 (1966).
16) D. Saika and D. Swern, *J. Org. Chem.*, **33**, 4548 (1968).
17) N. Torimoto, T. Shingaki, and T. Nagai, *J. Org. Chem.*, **43**, 631 (1978).
18) J. A. Riddic and W. B. Bunger, "Organic Solvents," in "Techniques of Chemistry," ed by A. Weissberger, Wiley-Interscience, New York, N. Y. (1970) Vol. VII.
19) W. Lwowski and T. W. Mattingly, Jr., *J. Am. Chem. Soc.*, **87**, 1947 (1965).
20) P. Kovacic and S. S. Chaudhary, *Org. Synth.*, Coll. Vol. V, 35 (1964).
21) L. A. Paquette, D. E. Kuhla, J. H. Barrett., and R. J. Haluska, *J. Org. Chem.*, **34**, 2866 (1969).

Layered Compounds. LII.[1] Syntheses of Eleven Anthracenophanes

Akio IWAMA, Toshihiro TOYODA, Misaku YOSHIDA, Tetsuo OTSUBO, Yoshiteru SAKATA, and Soichi MISUMI*

The Institute of Scientific and Industrial Research, Osaka University, Suita, Osaka 565

(Received February 20, 1978)

A series of layered cyclophanes where an anthracene ring is stacked in different modes with the same or other π-systems has been synthesized by the Hofmann elimination method or photodesulfurization for studying the transannular π-electronic interaction. Photochemical and thermal interconversions have been observed between *syn*-(1,4)anthracenophane and its isomer and have been discussed with reference to the X-ray crystal data. From the electronic spectra it has been established that the transannular interaction increases with overlapping between the two faced aromatic rings and that when the overlap between the two chromophores is the same, the interaction increases relative to the dimension of the faced chromophore.

Recently a wide variety of [2.2]phanes containing benzene or heteroaromatic rings has been synthesized in order to study the effect of transannular π-electronic interactions on their physical and chemical properties.[2] If one or two benzene rings are replaced by naphthalene or anthracene rings, which have a larger molecular surface and lower ionization potential than benzene, it is expected that such cyclophanes will show stronger transannular interactions. Various types of [2.2]naphthalenophanes[3] have been prepared for this purpose, but [2.2]anthracenophanes other than [2.2](9,10)-anthracenophane[4] have not been studied. Since the anthracene ring has a lower symmetry and more bridging points than the benzene ring, some isomeric anthracenophanes differing in stacking mode between the two chromophores are feasible. These isomers appear to be good models for studying the effect of the magnitude and/or the mode of overlapping between anthracene and other π-systems upon transannular π-electronic interaction. A series of anthracenophanes has been prepared along this line, *i.e.*, three isomers of both [2.2]anthracenophane (**1**—**3**) and [2.2]naphthalenoanthracenophane (**4**—**6**) and two isomers of both [2.2]paracycloanthracenophane (**7**, **8**) and its dimethyl derivative (**9**, **10**). In addition, a triple-layered anthracenophane **11** has also been synthesized.

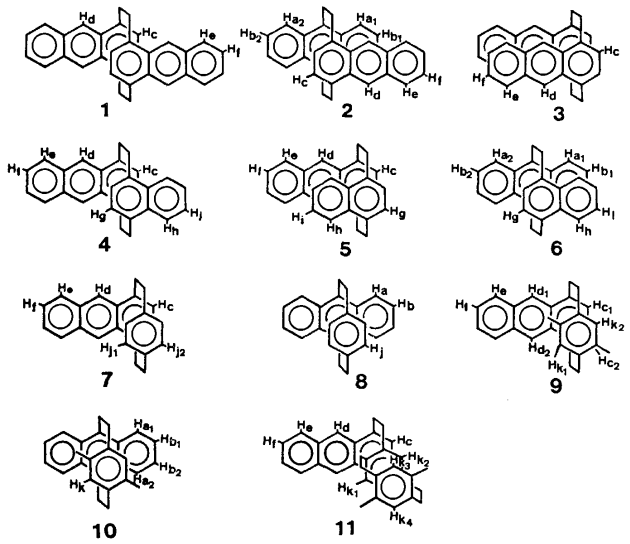

Results and Discussion

Syntheses. A quaternary ammonium salt **12** was prepared from 4-methylanthracene-1-carboxylic acid **17** as shown in Scheme 2. The other quaternary ammonium hydroxides **13**—**16** were obtained according to methods previously reported.[3c,3g,5] The syntheses of all the new cyclophanes **1**—**11** except for **9** and **10** were conducted as shown in Scheme 1 by the pyrolysis of the corresponding ammonium hydroxide or an equimolar mixture of two different bases in boiling xylene in the presence of a catalytic amount of phenothiazine. Yields of cyclophanes were relatively low as expected for the 1,6-Hofmann elimination. The synthesis of **9** and **10** was carried out by the coupling of 9,10- or 1,4-bis(halomethyl)anthracene with 2,5-bis(mercaptomethyl)-*p*-xylene,[6] followed by photodesulfurization in triethyl phosphite.

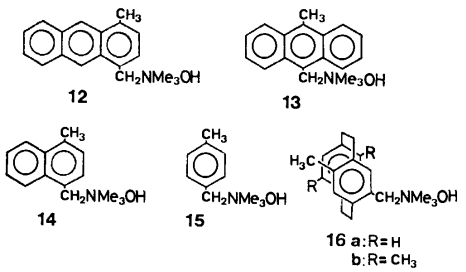

16 a: R=H
b: R=CH$_3$

12 ⟶ 1 + 3
12 + 13 ⟶ 2
12 + 14 ⟶ 4 + 5
13 + 14 ⟶ 6
12 + 15 ⟶ 7
13 + 15 ⟶ 8
12 + 16$_b$ ⟶ 11
13 + 16 ⟶ 23

Scheme 1.

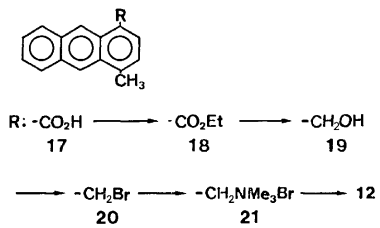

Scheme 2.

Separation and purification of the cyclophanes were achieved by careful column chromatography on silica gel and/or alumina followed by recrystallization. In the preparation of [2.2](1,4)anthracenophane and [2](1,4)naphthaleno[2](1,4)anthracenophane, both the *anti*- and *syn*-isomers, *i.e.*, **1** and **3**, and **4** and **5**, were isolated. The isomers are thermally stable and no interconversion between them was observed at room temperature. The structure of these isomers could be easily assigned by NMR analysis as described below. Pyrolysis of mixed ammonium bases, **13** and **15**, produced paracycloanthracenophane **8**. This was, however, not isolated in the reaction starting from [2.2]paracyclophane,[3c] probably due to an intramolecular Diels-Alder reaction as described below. Such instability of paracyclo(9,10)anthracenophane was observed in the attempted synthesis of the triple-layered (9,10)anthracenophane which is isomeric with **11**. Thus, the cross breeding reaction of **13** and **16** gave an unexpected, intramolecular Diels-Alder reaction product **23** instead of the desired triple-layered anthracenophane, the structure of which was determined by spectral data and X-ray crystallographic analysis.[5]

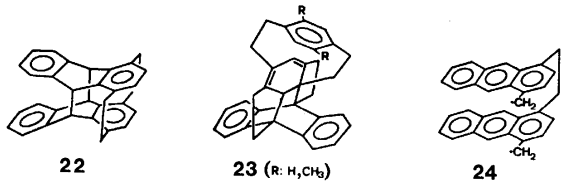

22 **23** (R: H,CH_3) **24**

Interconversion between 3 and 22. Pyrolysis of **12** and the succeeding work-up in the dark produced the *anti*- and *syn*-anthracenophanes (**1** and **3**). However, the same procedure in a bright room gave an unexpected mixture of **1** and its isomer **22**. The structure of **22** was confirmed by the absence of characteristic absorption bands in the electronic spectrum, NMR data, and finally by X-ray crystal structure analysis[1,7] as shown in Fig. 1. On the basis of the above results, it is reasonable to presume that the initially formed **3** might be isomerized to **22** by irradiation with scattered day light in the room, as in the photodimerization of anthracene to anthracene dimer (trivial name, dianthracene) (**25**). Irradiation with sunlight or monochromatic light (374 nm) of a solution of pure **3** gave immediately and quantitatively the photo-isomer **22**. The reverse reaction of **25** to anthracene is known to

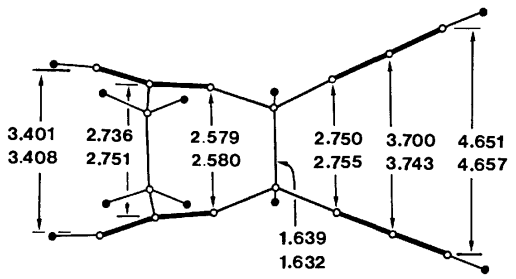

Fig. 1. Side view of **22**. Intramolecular nonbonding distances (Å) and single bond distances between bridgehead atoms are also given.

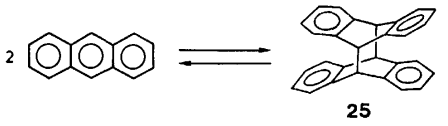

25

Table 1. Thermal isomerization of **22** to **3** in solid state

Temp (°C)	Reaction time (h)	Yield (%)	Decomposition product
196—203[a]	24	68.5	no
198—199[a]	6	quantitative	no
209—213[a]	6	69.4	exist
219—221[a]	6	23.9	exist
197—200[b]	6	83.2	trace
197—201[b]	6	85.1	trace

a) Under N_2. b) In sealed tube.

Table 2. Thermal isomerization of **22** to **1** and **3** in hexachlorobutadiene

	Reac. temp	199—201 °C		215—221 °C	
	Product ratio[a]	**1**/**22**	**3**/**22**	**1**/**22**	**3**/**22**
Reac. time (min)	5	0	0	0.14	0.14
	10	0	0.10	0.50	0.18
	15			0.98	0.31
	20	0.19	0.14		
	25			1.1	0.28
	30	0.43	0.20		
	45			3.8	0.30
	60	1.92	0.19		

a) Values were determined by the intensities in NMR spectra.

proceed at 200—270 °C.[8] The similar reverse reaction of **22** to **3** was performed under various pyrolytic conditions as shown in Tables 1 and 2. The optimum yield of **3** was achieved by heating **22** at 198—199 °C for 6 h under nitrogen stream (Table 1). However, when the pyrolysis was performed in solution (Table 2), a mixture of **1** and **3** was obtained and the ratio of **1**: **3** increased rapidly as the reaction proceeded. The difference in the pyrolytic reaction in the solid and in the solution can be understood as follows. In the solution an anthracene ring of biradical species **24**, which is formed by the homolytic cleavage of an sp^3-sp^3 single bond of **3**, can rotate to give thermodynamically stable *anti*-isomer **1**, while in the solid state the aromatic ring is unable to rotate due to less degrees of freedom for molecular motion and therefore more hindered *syn*-isomer **3** is afforded selectively. On the other hand, a photochemical interconversion was observed between **22** and **3**. Thus, when a solution of **22** in THF was exposed to monochromatic light (254 nm) for 10 min, **3** was observed in the resulting electronic spectrum and conversely, **3** to **22** by irradiation of 374 nm light.

The molecular structure of **22** and **3**[1] were determined by X-ray analysis, in order to clarify the reason for the easier interconversion between **22** and **3** than that between anthracene dimer and anthracene and to

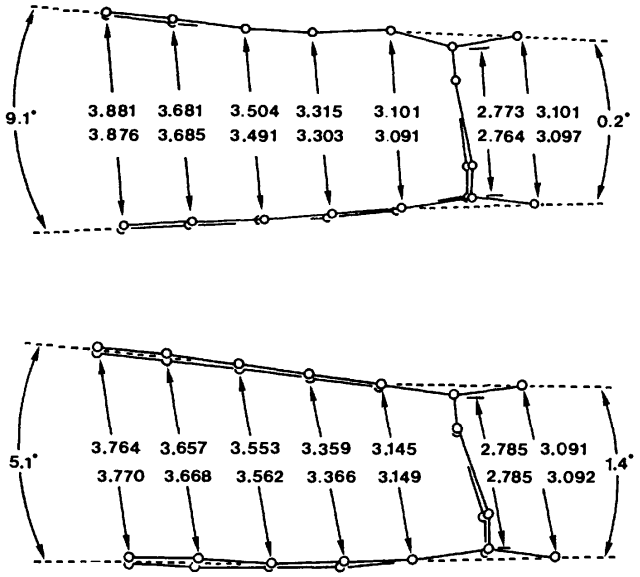

Fig. 2. Side view of the two anthracenophane molecules in crystal of **3**. Intramolecular nonbonding distances (Å) and dihedral angles are also given.

relate the structures of a series of anthracenophanes to their spectral data. Figure 1 shows marked elongation (1.632 and 1.639 Å) of the C_{sp^3}–C_{sp^3} bond in question from the normal value (1.54 Å) compared with the corresponding bond (1.61 Å) of anthracene dimer **25**,[9] indicating that there is greater strain in **22** causing easier breaking of the bond. Analysis of **3** showed two different anthracenophane molecules in each asymmetric unit of the crystal lattice. As seen in Fig. 2,[1] the non-bonding interatomic distances (3.315 and 3.303 Å) between the corresponding sp^2 carbon atoms in one of the two anthracenophane molecules are relatively shorter than the van der Waals distance, showing considerable overlap between the two $2P_z$ orbitals. In other words, it indicates easy formation of a covalent bond between the two carbon atoms. As a result the ready interconversion between **22** and **3** is understandable from the above analytical data.

NMR Spectra. NMR data of the compounds **1**—**11** are summarized in Table 3. The spectrum of *anti*-anthracenophane **1** was recorded in arsenic trichloride because of the low solubility in the usual

Table 3. NMR data of anthracenophanes (δ values in $CDCl_3$)

Compd	Aromatic proton		Calcd shift	Me
1[a]	H_c	5.47 (s)	−1.78	
	H_d	8.32 (s)	−0.24	
	H_e	8.13 (m)	+0.04	
	H_f	7.62 (m)	+0.08	
2	H_{a_1}	7.48 (A_2B_2)	−0.84	
	H_{a_2}	8.02 (A_2B_2)	−0.30	
	H_{b_1}	6.30 (A_2B_2)	−1.19	
	H_{b_2}	7.3—7.5 (m)		
	H_c	5.80 (s)	−1.39	
	H_d	7.84 (s)	−0.67	
	H_e	7.73 (A_2B_2)	−0.29	
	H_f	7.3—7.5 (m)		
3	H_c	6.71 (s)	−0.48	
	H_d	7.80 (s)	−0.71	
	H_e	7.39 (A_2B_2)	−0.63	
	H_f	6.96 (A_2B_2)	−0.52	
4	H_c	5.71 (s)	−1.48	
	H_d	8.23 (s)	−0.28	
	H_g	5.44 (s)	−1.71	
	H_e, H_f, H_h, H_i	7.3—8.1 (m)		
5	H_c	6.73 (s) or	−0.46 or	
		6.71 (s)	−0.48	
	H_d	7.87 (s)	−0.64	
	H_e	7.69 (A_2B_2)	−0.33	
	H_f	7.34 (A_2B_2)	−0.14	
	H_g	6.73 (s) or	−0.42 or	
		6.71 (s)	−0.44	
	H_h	7.25 (A_2B_2)	−0.71	
	H_i	6.30 (A_2B_2)	−1.16	
6	H_{a_1}, H_{a_2}, H_{b_1}	6.8—8.2 (m)		
6	H_{b_2}, H_h, H_i	6.8—8.2 (m)		
	H_g	5.81 (s)	−1.34	
7	H_c	6.69 (s)	−0.50	
	H_d	8.20 (s)	−0.31	
	H_e	7.97 (m)	−0.05	
	H_f	7.51 (m)	+0.03	
	H_{j_1}	5.29 (d)	−1.77	
	H_{j_2}	6.52 (d)	−0.54	
8	H_a	7.93 (m)	−0.39	
	H_b	7.30 (m)	−0.19	
	H_j	5.56 (s)	−1.50	
9	H_{c_1}	6.58 (AB)	−0.61	1.16 (s)
	H_{c_2}	6.90 (AB)	−0.29	2.16 (s)
	H_{d_1}	8.35 (s)	−0.16	
	H_{d_2}	8.17 (s)	−0.34	
	H_{k_1}	5.10 (s)	−1.80	
	H_{k_2}	6.14 (s)	−0.76	
	H_e	7.8—8.3 (m)		
	H_f	7.3—7.7 (m)		
10	H_{a_1}, H_{a_2}	7.7—8.3 (m)		1.56 (s)
	H_{b_1}, H_{b_2}	6.9—7.6 (m)		
	H_k	5.27 (s)	−1.63	
11	H_c	6.33 (s)	−0.86	1.81 (s)
	H_d	7.94 (s)	−0.57	1.54 (s)
	H_e, H_f	7.2—7.9		
	H_{k_1}	4.40 (s)	−2.50	
	H_{k_2}	5.70 (s)	−1.20	
	H_{k_3}	5.54 (s)	−1.36	
	H_{k_4}	5.51 (s)	−1.39	

a) in $AsCl_3$.

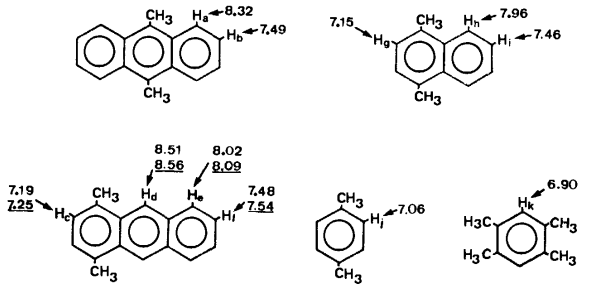

Fig. 3. NMR data of reference compounds, δ values in $CDCl_3$. Values with underline are in $AsCl_3$.

organic solvents. All the methylene proton signals appear separately as two groups of multiplets. The aromatic protons are assigned by reference to their coupling modes and the chemical shifts of non-layered compounds. The signals appear generally at higher field owing to the anisotropic effect of a faced aromatic ring or two benzene rings in the case of **11**, compared with those of the reference compounds. This effect was estimated by using the chemical shifts (Fig. 3) of the corresponding protons of 9,10- and 1,4-dimethylanthracenes, 1,4-dimethylnaphthalene, *p*-xylene, and durene as standards (Table 3). Of these values, marked upfield shifts (over 1 ppm) were observed for H_c's of **1**, **2**, and **4**, H_b, of **2**, H_g's of **4** and **6**, H_i of **5**, H_j, of **7**, H_j of **8**, H_k,'s of **9** and **11**, and H_k of **10**, all of which are located nearly above the center of the opposed aromatic ring. In triple-layered compound **11**, aromatic protons (H_{k_1}, H_{k_2}) of durene moiety absorb at higher field than the corresponding protons of double-layered compound **9** owing to the shielding effect of an additional benzene ring. *syn*- and *anti*-isomers [(**1** and **3**) and (**4** and **5**)] are easily distinguished by comparing the chemical shifts of H_c protons. Thus, H_c protons of the *anti*-forms (**1** and **4**) show high field shifts over 1 ppm, whereas those of the *syn*-forms (**3** and **5**) show only small high field shifts (0.48 ppm for **3**, 0.47 ppm for **5**). A slight down field shift was observed for H_e and H_f of **1** and H_f of **7**. These protons are situated far apart from the center of the opposite ring and hence, it is assumed that they are in the deshielding field of the transannular ring.

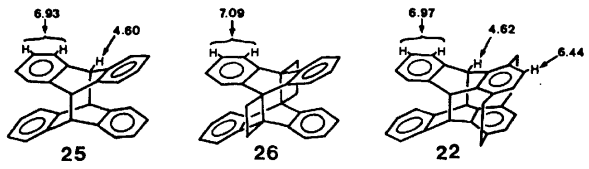

Fig. 4. NMR data of **22**, **25**, and **26** in $AsCl_3$.

NMR data of photo-adduct **22** are also shown in Fig. 4 together with those of two related compounds **25** and **26**. The chemical shifts of the corresponding protons reflect the similar molecular structure among the three compounds, *i.e.*, **22** (Fig. 1),[7] **25**,[9] and **26**.[10]

Electronic Spectra. The electronic spectra of anthracenophanes **1**—**11** are shown in Figs. 5—8 together with those of the reference compounds. Characteristic features of these spectra are eminent broadening of and considerable bathochromic and hypochromic shifts of ^1L_a band of anthracene chromophore compared with those of acyclic compounds, indicating obvious transannular π-electronic interaction. It may be easily understood from Fig. 6 that the magnitude of the transannular interaction is associated with the extent of overlap of the two chromophores. Thus, the longest wavelength bands of fully overlapped isomers **5** and **6** show large bathochromic shifts, while the spectrum of the least overlapped isomer **4** moderately resembles that of the reference compound. The same features are seen in Fig. 5. Anthracenophanes **2** and **3**, where two anthracene rings are stacked fully or appreciably, absorb in longer wavelength region than *anti*-isomer **1**.

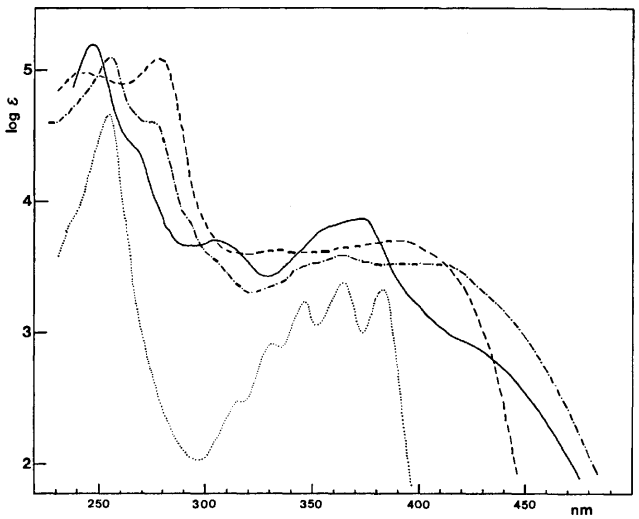

Fig. 5. Electronic spectra of **1** (----), **2** (·•·•·), **3** (——), and 1,4-dimethylanthracene (·····) in tetrahydrofuran. The curve of 1,4-dimethylanthracene is displaced downward by 0.5 log ε unit.

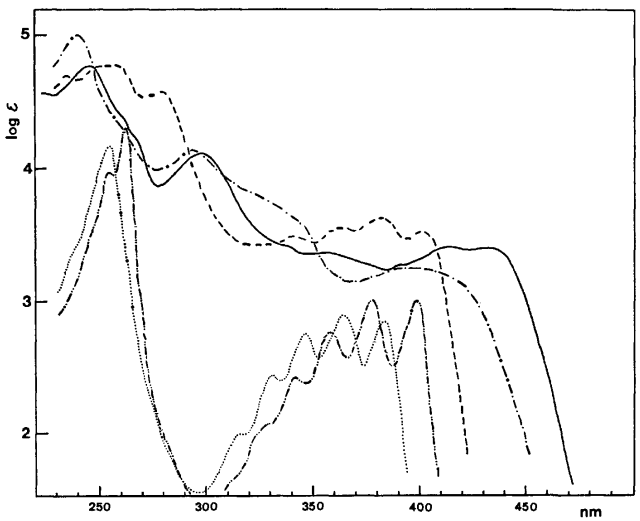

Fig. 6. Electronic spectra of **4** (----), **5** (·•·•·), **6** (——), 1,4-dimethylanthracene (·····), and 9,10-dimethylanthracene (-•••-) in tetrahydrofuran. The curves of two dimethylanthracenes are displaced downward by a log ε unit.

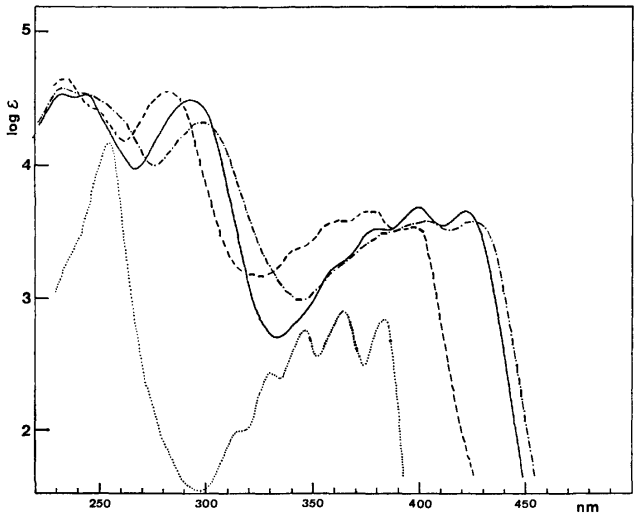

Fig. 7. Electronic spectra of **7** (----), **8** (——), **10** (·•··), and 1,4-dimethylanthracene (·····) in tetrahydrofuran. The curve of 1,4-dimethylanthracene is displaced downward by a log ε unit.

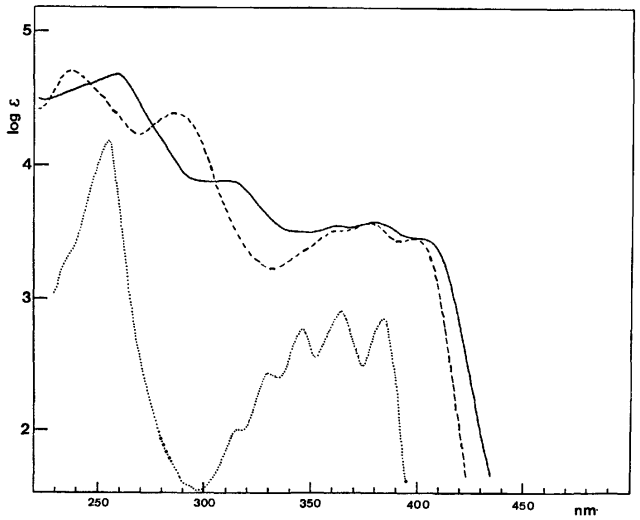

Fig. 8. Electronic spectra of **9** (----), **11** (——), and 1,4-dimethylanthracene (·····) in tetrahydrofuran. The curve of 1,4-dimethylanthracene is displaced downward by a log ε unit.

Let us consider an alternate groups of anthracenophanes, *i.e.*, compounds **1**, **4**, and **7**, which have the same degree of overlapping between the two faced rings and therefore probably the same degree of molecular strain. Of these three compounds, only **1** shows a structureless band in the region of 320—450 nm, indicative of extensive transannular interaction. The magnitude of the red shift of this band is largest for **1** and smallest for **7** compared with the reference compound. In other words, this implies that the transannular interaction increases in the order of **1**>**4**>**7**, that is, in the order of dimension of the faced chromophore. The same tendency is seen by comparing the spectrum of **2** with those of **5** and **6**. These observations may be interpreted by means of the exciton type interaction, which predicts that the smaller the difference in the transition energies of composite chromophores, the greater the configuration interaction between them; that is to say, the interaction is the strongest when the chromophores under consideration are the same. Theoretical treatment[11] of double-, triple-, and quadruple-layered cyclophanes has shown that their transannular bands in the longest wavelength region originate from the exciton interaction of composite chromophores with some degree of charge transfer character. Thus, it seems reasonable to assume the existence of similar excition interaction in anthracenophanes as above stated.

Triple-layered compound **11** absorbs at somewhat longer wavelength than double-layered one **9** (Fig. 8), indicating the increase of the transannular effect.

The fluorescence spectra of three isomeric anthracenophanes **1**—**3** are of particular interest in relation to the geometrical structure of excimers. This study has been reported in a separated paper.[12]

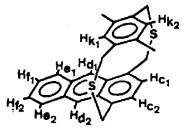

27

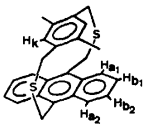

28

Experimental

All melting points are uncorrected. The NMR spectra were recorded on a Hitachi Perkin-Elmer R-20 or on a Varian XL-100. The UV and MS spectra were measured with a Hitachi EPS-3T and a Hitachi RMU-7, respectively.

Ethyl 4-Methylanthracene-1-carboxylate (18). Esterification of 4-methylanthracene-1-carboxylic acid (**17**)[13] was performed in the usual manner. **18**: yellow columns from petro-

Table 4. Analytical data, recrystallization solvents, and yields of anthracenophanes

Compound	Formula	Calcd %		Found %		Mp (°C)	Recryst solvent
		C	H	C	H		
2	$C_{32}H_{24}$	94.08	5.92	93.89	5.70	262.0—264.0	benzene
4	$C_{28}H_{22}$	93.81	6.19	93.70	5.91	246.5—247.5	toluene
5	$C_{28}H_{22}$	93.81	6.19	93.65	6.01	221.0—222.0	benzene–hexane (1:9)
6	$C_{28}H_{22}$	93.81	6.19	93.99	6.05	230.5—231.5	benzene
7	$C_{24}H_{20}$	93.46	6.54	93.23	6.41	172.0—173.5	benzene–hexane (1:9)
8	$C_{24}H_{20}$	93.46	6.54	93.51	6.40	168.5—173.0	benzene
11	$C_{36}H_{34}$	92.66	7.34	92.44	7.21	217.0—218.5	benzene–hexane (1:1)

leum ether, mp 66.0—66.5 °C.

Found: C, 81.67; H, 5.99%. Calcd for $C_{18}H_{16}O_2$: C, 81.79; H, 6.10%.

*4-Methyl-1-(bromomethyl)anthracene (**20**).* To a stirred suspension of $LiAlH_4$ (7.83 g) in dry ether (300 ml) was added dropwise a solution of **18** (74.8 g, 0.283 mol) in the same solvent (650 ml). After the addition was over, the mixture was stirred under reflux for 5 h, then at room temperature for 12 h. Water and 6 M aq HCl were successively added to the reaction mixture which was then extracted with ether and the organic layer was worked-up in the usual manner. Removal of the solvent gave yellow crystals (60.8 g, 96.8%) of **19**, which were used for the following reaction without further purification. To a stirred suspension of **19** (60.8 g, 0.274 mol) in CCl_4 (1 liter) was added a solution of PBr_3 (14 ml) in CCl_4 (200 ml). After the addition was over, the reaction mixture was heated at 50—53 °C for 10 h. Water (150 ml) was added and the mixture was extracted with CCl_4. The organic layer was worked-up in the usual manner and after recrystallization from CCl_4, pure **20** was obtained as yellow columns, 73.4% yield, mp 132.5—133.5 °C.

Found: C, 67.05; H, 4.34; Br, 27.79%. Calcd for $C_{16}H_{13}Br$: C, 67.38; H, 4.59; Br, 28.02%.

*(4-Methyl-1-anthrylmethyl)trimethylammonium Bromide (**21**).* An excess of trimethylamine (40 g) in ether was added with stirring to a cooled solution of **20** (49.2 g, 0.173 mol) in ether (5 l). After prolonged stirring, the resulting ppt was filtered, washed with ether, and dried. The yield of quaternary ammonium bromide **21** was 58.5 g (98.5%).

*Synthesis of **1**—**8** and **11** by the Hofmann Elimination Reaction.* All the coupling reactions of ammonium salts were undertaken according to the general procedure, which is described in detail for the case of (4-methyl-1-anthrylmethyl)trimethylammonium bromide **21** as follows.

An aq solution of **21** was passed through a column of anion exchange resin (Dowex 1-X8) to give an aq solution of ammonium base **12**. The soln thus obtained was added dropwise to a boiling solution of phenothiazine in xylene (0.2 g per 3 l of xylene) which was placed in a three-necked flask equipped with a condenser, mechanical stirrer, and water separator. After water separation was over, additional heating was continued for 24 h. The insoluble solid was filtered off and the filtrate dried over $MgSO_4$. The solvent was removed *in vacuo* until a small amount of the solvent was left. By this treatment *anti*-[2.2](1,4)anthracenophane **1** was precipitated from the solution. An additional amount of the compound **1** was obtained by benzene extraction of the insoluble solid above described. The total yield of **1** was about 60%. Recrystallization from xylene gave pure **1** as colorless prisms, dec over 300 °C.

Found: C, 93.95; H, 5.78%; M^+, 408. Calcd for $C_{32}H_{24}$: C, 94.08; H, 5.92%; M, 408.51.

The mother liquor was chromatographed on Al_2O_3 (Woelm, Activity I) to give **22** (1.9% yield). Recrystallization from AcOEt–EtOH gave pure **22** as colorless prisms, mp 242—243 °C with dec.

Found: C, 94.23; H, 5.82%; M^+, 408. Calcd for $C_{32}H_{24}$: C, 94.08; H, 5.92%; M, 408.51.

When the above reaction was carried out in the dark, **3** was obtained after filtration of the reaction mixture and evaporation of the solvent. Crude **3** was purified from the *anti*-isomer by the following manner. First it was recrystallized from benzene to give **3** containing 5% of **1**. Then, the crystals were dissolved in a minimum amount of benzene, the solution was frozen in a deep-freezer, and warmed up to room temperature. After most of the solid was dissolved, it was filtered as soon as possible to remove less soluble *anti*-isomer **1**. The above procedure was repeated once or twice and recrystallization from CCl_4 gave pure **3** as yellow plates, 250 °C dec.

Found: C, 93.91; H, 5.76%; M^+, 408. Calcd for $C_{32}H_{24}$: C, 94.08; H, 5.92%; M, 408.51.

Elemental analyses, melting points, recrystallization solvents, and yields of the other anthracenophanes are summarized in Table 4.

*5,8-Dimethyl-2,11-dithia[3.3]paracyclo(1,4)anthracenophane (**27**).* A solution of 1,4-bis(bromomethyl)anthracene[14] (1.82 g, 5.0 mmol) in benzene (300 ml) and a solution of 1,4-dimethyl-2,5-bis(mercaptomethyl)benzene[6] (0.99 g, 5.0 mmol) and sodium hydroxide (0.4 g) in 95% ethanol (50 ml) were added dropwise and simultaneously through dropping funnels into boiling ethanol (150 ml) over a period of 5 h under N_2 with vigorous stirring. After further heating and stirring for 18 h, the solvents were evaporated off and the residue was extracted with benzene. The benzene solution was passed through a short column of silica gel to yield a yellow solid. This was recrystallized from benzene to give pure dithiacyclophane **27** (1.09 g, 54.5%) as yellow prisms, dec>236 °C in a sealed tube.

Found: C, 78.06; H, 5.80; S, 15.92%; M^+, 400. Calcd for $C_{26}H_{24}S_2$: C, 77.95; H, 6.04; S, 16.01%; M, 400.58. NMR ($CDCl_3$, δ): 1.18 (s, 3, *endo*-Me), 2.38 (s, 3, *exo*-Me), 4.64—3.50 (m, 8, CH_2), 6.16 (s, 1, H_{k1}), 6.73 (s, 1, H_{k2}), 6.74 (AB, J=8 Hz, 1, H_{c1}), 7.04 (AB, J=8 Hz, 1, H_{c2}), 7.0—7.8 (m, 2, H_{f1} and H_{f2}), 7.8—8.4 (m, 2, H_{e1} and H_{e2}), 8.53 (s, 1, H_{d2}), 8.73 ppm (s, 1, H_{d1}).

*4,7-Dimethyl[2.2]paracyclo(1,4)anthracenophane (**9**).* A solution of dithiacyclophane **27** (2.0 g, 5.0 mmol) in benzene (400 ml) and triethyl phosphite (500 ml) was irradiated internally with a high pressure mercury lamp (400 W) for 9 h whilst a slow stream of N_2 was bubbled through. After removal of the solvents, the resulting solid was chromatographed on silica gel with benzene to yield the desired cyclophane **9** (1.24 g, 73.7%), yellow prisms from benzene, mp 235.0—235.5 °C with dec in a sealed tube.

Found: C, 92.59; H, 6.98%; M^+, 336. Calcd for $C_{26}H_{24}$: C, 92.81; H, 7.19%; M, 336.45.

*5,8-Dimethyl-2,11-dithia[3.3]paracyclo(9,10)anthracenophane (**28**).* A solution of 9,10-bis(chloromethyl)anthracene[15] (3.3 g, 12.0 mmol) in benzene (500 ml) and a solution of 2,5-bis(mercaptomethyl)-*p*-xylene (2.38 g, 12.0 mmol) and sodium hydroxide (1.0 g) in 90% ethanol were added dropwise and simultaneously through dropping funnels into boiling ethanol (200 ml) for 3.75 h under N_2. The mixture was refluxed for an additional 12 h and worked up in the same manner as in the synthesis of **27** to afford 3.06 g (63.7%) of **28**. It was recrystallized from benzene to give a yellow powder, dec>230 °C in a sealed tube.

Found: C, 77.94; H, 5.96; S, 15.79%; M^+, 400. Calcd for $C_{26}H_{24}S_2$: C, 77.95; H, 6.04; S, 16.01%; M, 400.58. NMR ($CDCl_3$, δ): 1.51 (s, 6, Me), 3.58 (AB, J=15 Hz, 2, CH_2 attached to durene moiety), 3.85 (AB, J=15 Hz, 2, CH_2 attached to durene moiety), 4.89 (bs, 4, CH_2 attached to anthracene moiety), 6.20 (s, 2, H_k), 7.3—7.8 (m, 4, H_{b1} and H_{b2}), 8.1—8.6 ppm (m, 4, H_{a1} and H_{a2}).

*4,7-Dimethyl[2.2]paracyclo(9,10)anthracenophane (**10**).* In the same manner as **9**, irradiation of a solution of disulfide **28** (4.0 g, 10 mmol) in 1 liter of benzene and triethyl phosphite (1:1) for about 5 h and purification by column chromatography on silica gel gave the cyclophane **10** (1.99 g, 59.2%), yellow needles from dichloromethane–petroleum ether, dec> 170 °C in a sealed tube.

Found: C, 92.15; H, 6.94%; M^+, 336. Calcd for $C_{26}H_{24}$: C, 92.81; H, 7.19%; M, 336.45.

We are greatly indebted to Mr. T. Fujino for microanalyses and to Mr. Y. Takai for NMR measurements. The present work was partly supported by a Grant-in-Aid for Scientific Research from the Ministry of Education.

References

1) Part LI: T. Toyoda and S. Misumi, *Tetrahedron Lett.*, **1978**, 1479.
2) S. Misumi, *Mem. Inst. Sci. and Ind. Res., Osaka Univ.*, **33**, 53 (1976); S. Misumi and T. Otsubo, *Acc. Chem. Res.*, **11**, 251 (1978).
3) a) W. Baker, F. Glockling, and J. F. W. McOmie, *J. Chem. Soc.*, **1951**, 1118; b) W. Baker, J. F. W. McOmie, and W. K. Warburton, *ibid.*, **1952**, 2991; c) D. J. Cram, C. K. Dalton, and G. R. Knox, *J. Am. Chem. Soc.*, **85**, 1088 (1963); d) G. W. Brown and F. Sondheimer, *ibid.*, **89**, 7116 (1967); e) H. J. Reich and D. J. Cram, *ibid.*, **91**, 3527 (1969); f) J. M. McBride, P. M. Keehn, and H. H. Wasserman, *Tetrahedron Lett.*, **1969**, 4147; g) H. H. Wasserman and P. M. Keehn, *J. Am. Chem. Soc.*, **91**, 2374 (1969); h) M. Haenel and H. A. Staab, *Tetrahedron Lett.*, **1970**, 3585; i) M. Haenel and H. A. Staab, *Chem. Ber.*, **106**, 2203 (1973); j) M. W. Haenel, *Tetrahedron Lett.*, **1974**, 3053; k) J. R. Davy and J. A. Reiss, *Aust. J. Chem.*, **29**, 163 (1976).
4) J. H. Golden, *J. Chem. Soc.*, **1961**, 3741.
5) T. Toyoda, A. Iwama, T. Otsubo, and S. Misumi, *Bull. Chem. Soc. Jpn.*, **49**, 3300 (1976).
6) F. Imashiro, M. Oda, T. Iida, Z. Yoshida, and I. Tabushi, *Tetrahedron Lett.*, **1976**, 371.
7) T. Toyoda, Dissertation, Osaka University, Osaka, 1976.
8) D. E. Applequist, R. L. Litle, E. C. Friedrich, and R. E. Wall, *J. Am. Chem. Soc.*, **81**, 452 (1959).
9) M. Ehrenberg, *Acta Crystallogr.*, **20**, 177 (1966).
10) M. Ehrenberg, *Acta Crystallogr.*, **20**, 182 (1966).
11) S. Iwata, K. Fuke, M. Sasaki, S. Nagakura, T. Otsubo, and S. Misumi, *J. Mol. Spectrosc.*, **46**, 1 (1973).
12) T. Hayashi, N. Mataga, Y. Sakata, S. Misumi, M. Morita, and J. Tanaka, *J. Am. Chem. Soc.*, **98**, 5910 (1976); M. Morita, T. Kishi, M. Tanaka, J. Tanaka, J. Ferguson, Y. Sakata, S. Misumi, T. Hayashi, and N. Mataga, *Bull. Chem. Soc. Jpn.*, in press.
13) R. Scholl, A. Keller, K. Meyer, and H. Penz, *Justus Liebigs Ann. Chem.*, **512**, 30 (1934).
14) K.-D. Gundermann and K.-D. Röker, *Justus Liebigs Ann. Chem.*, **1976**, 140.
15) M. W. Miller, R. W. Amidon, and P. O. Tawney, *J. Am. Chem. Soc.*, **77**, 2845 (1955).

Synthesis of [2-Serine, 8-Valine]-Human Calcitonin[1,2]

Sukekatsu NOZAKI

Department of Chemistry, College of Science, Rikkyo University, Nishi-Ikebukuro, Tokyo 171

(Received February 22, 1978)

The [2-serine, 8-valine]-analog of human calcitonin (**1**) was synthesized by the liquid phase method. Analog **1** was built up from five fragments with minimized protection for the side functional groups. These fragments were linked stepwise to the C-terminal fragments by the azide method. A gel filtration was effectively applied for the purification of the resulting peptide in each fragment condensation. Analog **1** had about the same hypocalcemic activity as that of human calcitonin. The result showed that the high activity of eel or salmon calcitonin 1 or 2 is not ascribable only to the amino acid sequence of their *N*-terminal decapeptide.

Among calcitonins isolated from various origins, salmon[3] and eel hormones[4] exhibit conspicuously high activity, about 20—50 times the hypocalcemic potency of any other calcitonin from mammalian species.[5-8] All the calcitonins so far isolated are composed of 32 amino acids with a disulfide bridge between two cysteinyl residues in positions 1 and 7. The structural homology of these calcitonins is found in the C-terminal prolinamide, glycine in position 28, and the region around the disulfide bridge; amino acids in positions 1, 3, 4, 5, 6, 7, and 9 are common to all the hormones. Salmon calcitonin 3 with methionine in position 8 exhibits the hormonal activity of one third of salmon calcitonin 2,[9] which has the same amino acid sequence but valine at this position. The oxidation of methionine in the same position as that of human calcitonin remarkably reduces the activity of the hormone,[7] but not the oxidation of the amino acid in position 25 of the porcine hormone.[5] Similarity in the N-terminal structure of calcitonins and the remarkable decrease of hormonal activity induced from the oxidation of methionine in position 8 suggests the presence of an "active site" around the disulfide bridge of the hormone.

Several analogs of human calcitonin have been synthesized but the structure-activity relationship of calcitonin has not been explained clearly.[10] To investigate the effect of variation of the primary structure around the disulfide bridge of the human hormone on its hypocalcemic activity, we synthesized [2-serine, 8-valine]-human calcitonin, **1** (Fig. 1), in which glycine in position 2 and methionine in position 8 of the original hormone are replaced by serine and valine, respectively. Analog **1** is a hybrid peptide consisting of the N-terminal decapeptide of eel calcitonin or salmon calcitonin (1 or 2), the hormones with the highest hypocalcemic potency, and the C-terminal decosapeptide amide of human calcitonin, the lowest potent hormone.

Results and Discussion

Analog **1** was built up from five subfragments prepared in the liquid phase method according to the routes illustrated in Schemes 1—5. The protection of the side functional groups of fragments was minimized in order to facilitate the application of various kinds of chromatography to the purification of elongated peptides. The subfragments were linked stepwise to the C-terminal fragments by Rudinger's modification of the azide method[11] as shown in Scheme 6. Each product of the azide coupling was purified after removal of its N-terminal protecting group. The restriction of the molecular size of the N-terminal fragment used in every coupling reaction to be sufficiently smaller than that of the resulting peptide made the gel filtration efficient in the purification of the product. When necessary, partition chromatography on Sephadex[12] was further applied to the purification of deprotected peptides. The yield and properties of N-protected intermediates are

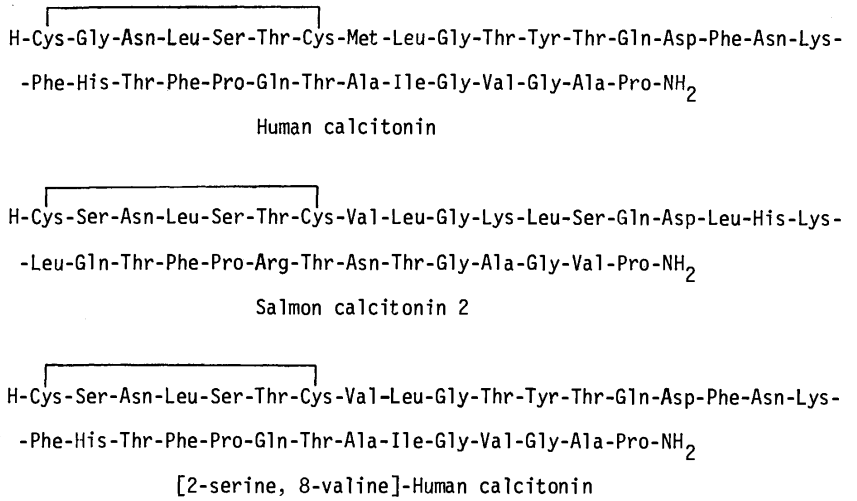

Fig. 1.

Table 1. Physical properties of N-protected peptides

Compd	Yield (%)	Mp (°C)	$[\alpha]_D$	Molecular formula	Elemental analysis (%) Found C	H	N	Calcd C	H	N
2[a]	94	oil	—		—	—	—	—	—	—
3[a]	86	168—169[b]	−89.1° (*c* 1.0, MeOH)[c]	$C_{16}H_{21}O_4N_3$	60.47	6.87	13.32	60.17	6.63	13.16
11	82	198—199	−9.6° (*c* 2.0, DMF)[d]	$C_{21}H_{31}N_3O_6$	60.08	7.66	10.11	59.84	7.41	9.97
13	74	224—226	−8.3° (*c* 1.0, DMF)[e]	$C_{35}H_{38}O_8N_4$	57.29	7.95	10.73	57.46	7.33	10.72
15	89	250	−4.9° (*c* 1.0, HMPA)[f]	$C_{30}H_{46}O_{10}N_6 \cdot 1/2H_2O$	54.27	7.14	12.80	54.61	7.19	12.74
17	88	243	−31.8° (*c* 1.0, HMPA)[g]	$C_{35}H_{53}O_{11}N_7 \cdot 1/2H_2O$	55.33	7.27	12.83	55.54	7.19	12.95
18	81	246—247	−13.6° (*c* 0.5, HMPA)[g]	$C_{33}H_{51}O_{11}N_9$	53.81	7.12	16.86	54.01	7.01	17.18
20[a]	82	251—252	−35.2° (*c* 1.0, DMF)[h]	$C_{48}H_{74}O_{14}N_{12}$	55.53	7.14	16.11	55.27	7.15	15.48
21	64	109—111	−3.3° (*c* 1.0, EtOH)[f]	$C_{23}H_{28}O_6N_2$	64.49	6.60	6.61	64.47	6.59	6.54
23	73	108—117	−2.8° (*c* 1.0, DMF)[h]	$C_{27}H_{35}O_7N_5$	61.55	6.41	12.43	61.58	6.24	12.38
24	70	204—205	−15.1° (*c* 1.0, DMF)[g]	$C_{27}H_{33}O_6N_7 \cdot H_2O$	57.00	6.18	17.27	56.93	6.19	17.21
27	82	120—123	−15.3° (*c* 1.0, MeOH)[e]	$C_{30}H_{41}O_7N_3$	64.44	7.50	7.57	64.85	7.44	7.56
29	42	176—177	−17.2° (*c* 1.0, DMF)[e]	$C_{30}H_{43}O_7N_9$	61.34	7.07	10.95	60.97	7.07	10.45
30	96	199—201	−36.0° (*c* 1.0, DMF)[g]	$C_{32}H_{45}O_8N_7$	58.39	6.87	14.79	58.61	6.92	14.95
34	80	169—171	−11.1° (*c* 1.0, DMF)[g]	$C_{23}H_{35}O_6N_3$	61.34	8.06	9.81	61.45	7.85	9.35
35	90	190—191	−52.2° (*c* 1.1, EtOH)[h]	$C_{21}H_{31}O_6N_3$	59.47	7.69	9.53	59.84	7.41	9.97
36	51	195—196	−16.5° (*c* 1.0, DMF)[g]	$C_{27}H_{34}O_8N_4$	59.62	6.46	10.00	59.77	6.32	10.33
37	83	152—154	−8.9° (*c* 1.0, DMF)[f]	$C_{30}H_{34}O_7N_2$	67.76	6.58	5.80	67.40	6.41	5.24
39	63	174—177	−5.1° (*c* 1.0, DMF)[j]	$C_{27}H_{35}O_9N_3$	59.29	6.44	7.66	59.44	6.47	7.70
41[a]	95	203—206	−14.1° (*c* 1.0, DMF)[j]	$C_{40}H_{58}O_{12}N_6 \cdot H_2O$	57.99	7.13	10.11	57.68	7.26	10.09
42	95	213—214	−12.6° (*c* 1.0, DMF)[j]	$C_{38}H_{56}O_{11}N_8$	57.29	7.33	13.82	56.99	7.05	13.99
43	99	75—81	−21.7° (*c* 1.0, DMF)[g]	$C_{33}H_{38}O_8N_4 \cdot 1/2H_2O$	63.42	6.26	8.22	63.14	6.26	8.93
45	77	176—178	−29.5° (*c* 1.0, DMF)[g]	$C_{31}H_{40}O_{10}N_6 \cdot 1/2H_2O$	55.65	6.03	12.39	55.93	6.21	12.62
47[a]	91	208—210	−17.7° (*c* 1.0, DMF)[g]	$C_{61}H_{86}O_{19}N_{12} \cdot 2H_2O$	54.60	6.62	13.18	55.19	6.83	12.66
48[a]	58	195—199	−14.8° (*c* 0.5, DMF)[j]	$C_{56}H_{79}O_{17}N_{12}Cl \cdot 3H_2O$	52.30	6.53	12.77	52.47	6.68	13.11
50	61	91—96	−22.8° (*c* 1.0, EtOH)[e]	$C_{20}H_{30}O_6N_2S$	56.68	7.07	6.77	56.32	7.09	6.57
51	90	163—166	−13.9° (*c* 1.0, DMF)[g]	$C_{18}H_{28}O_5N_4S \cdot 1/2H_2O$	51.36	6.62	13.76	51.29	6.93	13.29
52	70	117—119	−15.3° (*c* 1.0, DMF)[h]	$C_{19}H_{28}O_6N_2$	59.72	7.54	7.47	59.98	7.42	7.36
54	77	202—204	−24.7° (*c* 1.0, DMF)[g]	$C_{23}H_{34}O_8N_4$	55.71	7.06	12.07	55.86	6.93	11.33
56	70	212	−18.9° (*c* 1.0, DMF)[h]	$C_{33}H_{52}O_{11}N_6S \cdot 1/2H_2O$	51.92	7.08	11.20	52.23	7.09	11.08
57	75	204—205	−16.9° (*c* 1.0, DMF)[g]	$C_{31}H_{50}O_{10}N_8S \cdot H_2O$	50.33	6.96	14.86	49.99	7.04	15.04

Table 1. (Continued)

Compd	Yield (%)	Mp (°C)	$[\alpha]_D$	Molecular formula	Elemental analysis (%) Found C	H	N	Calcd C	H	N
58	44	139—141	−27.7° (*c* 1.0, DMF)[b]	$C_{24}H_{30}O_6N_2S$	60.50	6.12	5.84	60.73	6.37	5.90
60[a]	67	202	−23.2° (*c* 1.0, DMF)[j]	$C_{47}H_{70}O_{14}N_8S_2$	54.12	6.78	10.76	54.53	6.82	10.82
61	89	201—203	−21.0° (*c* 1.0, DMF)[g]	$C_{45}H_{68}O_{13}N_{10}S_2 \cdot 2H_2O$	51.42	6.75	12.88	51.12	6.68	13.25
62[a]	66	198	−25.2° (*c* 0.5, DMF)[g]	$C_{31}H_{54}O_{13}N_{10}S_2 \cdot CH_3COOH \cdot H_2O$	43.40	6.52	14.55	43.22	6.60	15.27

a) For details see Experimental. b) Lit,[14] mp 168—169°C. c) At 26 °C. d) At 23 °C. e) At 22 °C. f) At 18 °C. g) At 20 °C. h) At 21 °C. i) At 25 °C. j) At 24 °C.

given in Table 1.

Positions 23—32. Acylation of free proline with benzyloxycarbonylalanine *p*-nitrophenyl ester followed by a gel filtration on Sephadex LH-20 yielded benzyloxycarbonylalanylproline (**2**) nearly in a theoretical yield. The mixed anhydride prepared from **2** and isobutyl chloroformate was ammonolyzed in tetrahydrofuran to give benzyloxycarbonylalanylprolinamide (**3**) in a 86% yield. This route is applicable to the preparation of a dipeptide containing prolinamide, since it is much more convenient for preparation of **3** than other ones starting with prolinamide or *via* ammonolysis of benzyloxycarbonylalanylproline ethyl ester. The azide formation from benzyloxycarbonylprolylglutaminylthreonylalnanylisoleucylglycine hydrazide (**18**) was slow. The amine component, valylglycylalanylprolinamide (**19**), should be added to the azide solution after the hydrazide is consumed completely, in order to avoid serious difficulties in the separation of the desired decapeptide amide (**20**) from the remaining hydrazide.

Positions 20—32. Benzyloxycarbonylhistidylthreonylphenylalanine hydrazide (**24**) was converted into the azide, which was allowed to couple with the C-terminal decapeptide amide (**25**). The product was hydrogenated and applied to a gel filtration. Further purification was performed by means of partition chromatography on Sephadex with the system of 1-butanol–acetic acid–water. The eluate was monitored at 254 nm, three compounds (peptide A, B, and C) being obtained after removal of the solvent. The amino acid compositions in acid hydrolysates of those peptides agreed with the theoretical value for peptide **26**. By aminopeptidase M digestion, however, peptide A left undigested core of threonylphenylalanylprolylglutaminylthreonylalanine,

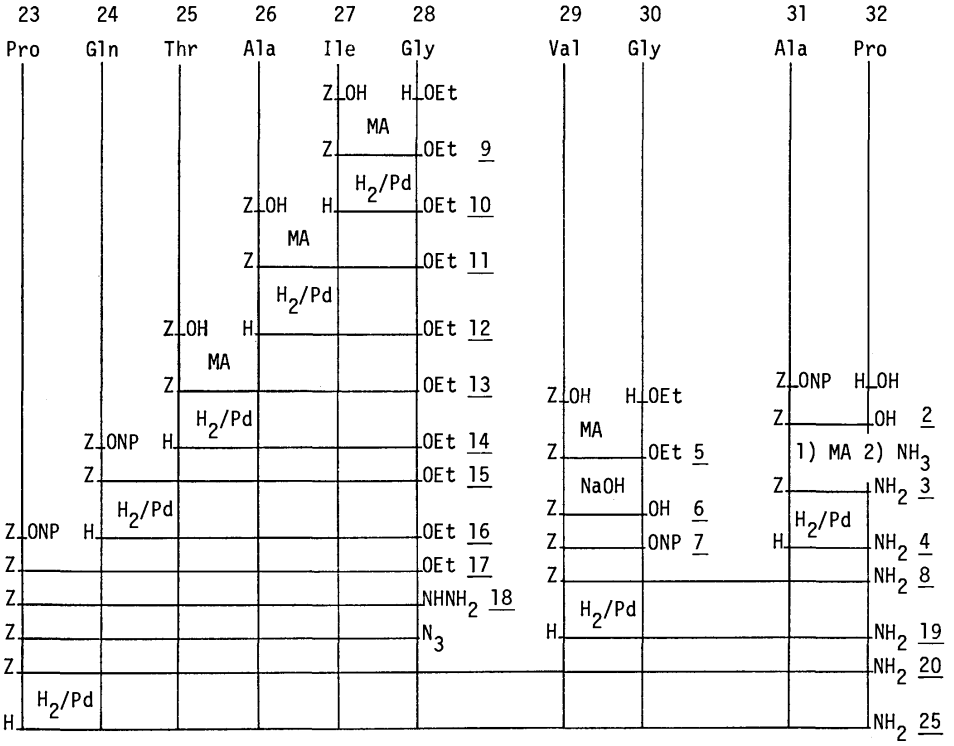

Scheme 1. Preparation of fragment positions at 17—32.

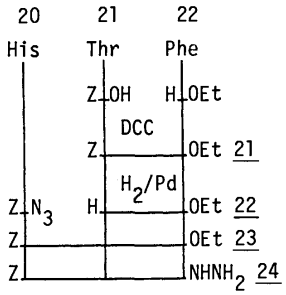

Scheme 2. Preparation of fragment positions at 20—22.

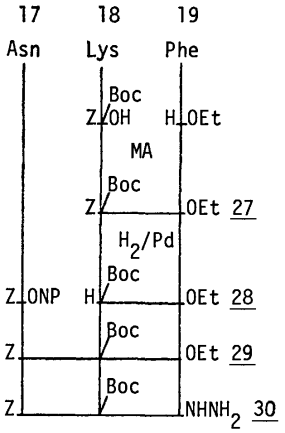

Scheme 3. Preparation of fragment positions at 17—19.

while peptides B and C gave the expected amino acid ratios. The results and other data[13] on aminopeptidase M from our laboratory suggest the presence of D-phenylalanine in peptide A. No difference was observed between peptide B and C on TLC with several solvent systems and between the results of Edman degradation. Peptide C was positive on Beilstein test, while B was negative. Thus, the two peptides, B and C, were thought to be the acetate and the hydrochloride, respectively, of the desired peptide (**26**) and were used for further elongation.

Positions 17—32. Rapid formation of cyclo-N^{ε}-*t*-butoxycarbonyllysylphenylalanyl occurred during the hydrogenolysis of N^{α}-benzyloxycarbonyl-N^{ε}-*t*-butoxycarbonyllysylphenylalanine ethyl ester (**27**) even in the presence of an equivalent amount of acetic acid. N^{ε}-*t*-butoxycarbonyllysylphenylalanine ethyl ester (**28**), the desired product, thus was obtained by use of excess acetic acid. The tridecapeptide (**26**) was acylated by the azide derived from benzyloxycarbonylasparaginyl-N^{ε}-*t*-butoxycarbonyllysylphenylalanine hydrazide (**30**). A gel filtration of the product after hydrogenolysis gave the hexadecapeptide amide (**31**).

Positions 8—32. Tyrosine was introduced to the peptide chain as *N*-benzyloxycarbonyl-*O*-benzyl ester. The protection of the side functional group was removed together with the N-protecting group prior to the further elongation. Benzyloxycarbonylvalylleucylglycine (**35**) was coupled with threonyltyrosylthreonine ethyl ester (**40**) by the two procedures. By the dicyclohexylcarbodiimide/*N*-hydroxysuccinimide method, the yield of the hexapeptide (**41**) was 69%, while the use of benzyloxycarbonylvalylleucylglycine *p*-nitrophenyl ester (**36**) improved the yield to 95%. In our preliminary experiments, benzyloxycarbonylvalylleucylglycylthreonyltyrosylthreonylglutaminyl-*β*-*t*-butylaspartylphenylalanine ethyl ester could not be converted into the hydrazide under mild conditions. The use of the protected hydrazide at the C-terminal of the nonapeptide made it difficult to find a suitable blocking group for *β*-carboxyl function of the aspartyl residue. The presence of the free *β*-carboxyl group in aspartylphenylalanine

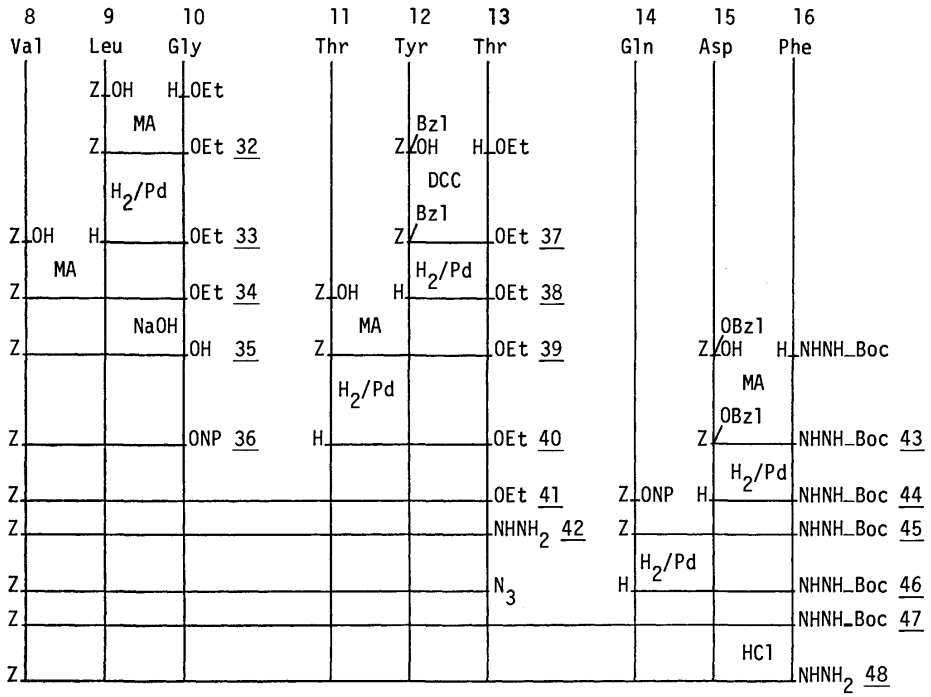

Scheme 4. Preparation of fragment positions at 8—16.

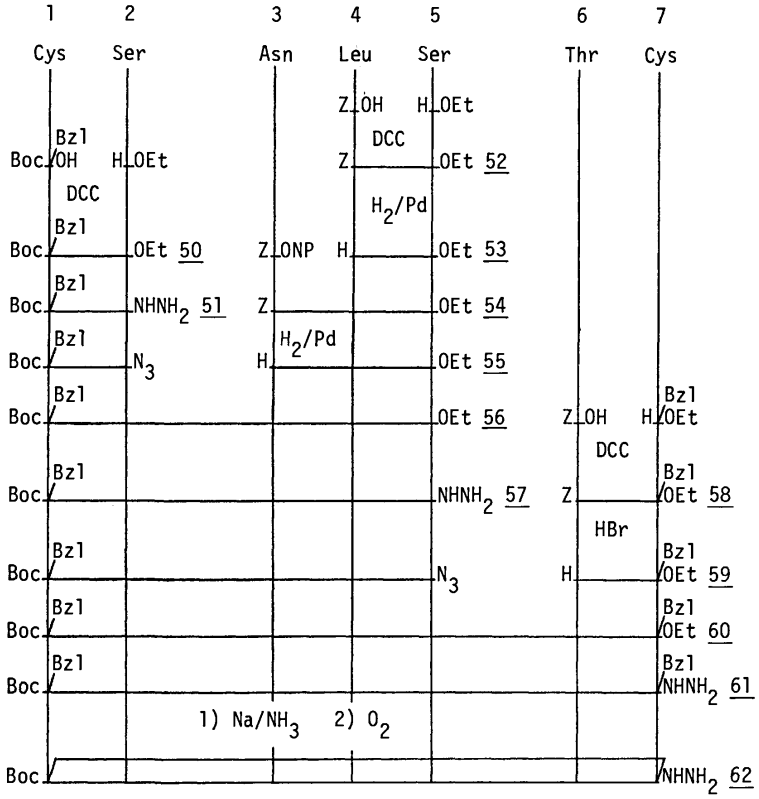

Scheme 5. Preparation of fragment positions at 1—7.

H-Val-Gly-Ala-Pro-NH_2 19

+ 18 1. azide coupling
2. H_2/Pd

H-Pro-Gln-Thr-Ala-Ile-Gly-Val-Gly-Ala-Pro-NH_2 25

+ 24 1. azide coupling
2. H_2/Pd

H-His-Thr-Phe-Pro-Gln-Thr-Ala-Ile-Gly-Val-Gly-Ala-Pro-NH_2 26

+ 30 1. azide coupling
2. H_2/Pd

H-Asn-Lys(Boc)-Phe-His-Thr-Phe-Pro-Gln-Thr-Ala-Ile-Gly-Val-Gly-Ala-Pro-NH_2 31

+ 48 1. azide coupling
2. H_2/Pd

H-Val-Leu-Gly-Thr-Tyr-Thr-Gln-Asp-Phe-Asn-Lys(Boc)-Phe-His-Thr-Phe-Pro-Gln-
-Thr-Ala-Ile-Gly-Val-Gly-Ala-Pro-NH_2 49

+ 62 1. azide coupling
2. HCl

1

Scheme 6. Preparation of [2-serine, 8-valine]-human calcitonin (**1**) by stepwise fragment condensation.

t-butoxyhydrazide (**44**), however, caused no difficulty for the construction of tripeptide (**45**) and the longer peptides. In the hydrogenolysis of the *t*-butoxycarbonylhydrazides, **43** and **45**, some by-products formed, especially after contact with hydrogen for a long time, but their amount was negligibly small when the hydrogenolysis was performed in a short period. The coupling of glutaminylaspartylphenylalanine *t*-butoxycarbonylhydrazide (**46**) with the azide derived from benzyloxycarbonylvalylleucylglycylthreonyltyrosylthreonine hydrazide (**42**) yielded protected nonapeptide (**47**). The *t*-butoxycarbonyl group of **47** was removed by concentrated hydrochloric acid. The use of trifluoroacetic acid for the deprotection unexpectedly gave a mixture showing multiple spots on TLC. Acylation of the hexadecapeptide amide (**31**) with the azide derived from **48** produced the pentacosapeptide amide, which was purified after removal of the N-protecting group by a gel filtration and succeeding partition chromatography on Sephadex to give **49**.

Positions 1—7. The azide prepared from *N-t*-butoxycarbonyl-*S*-benzylcysteinylserylasparaginylleucylserine hydrazide (**57**) was allowed to couple with threonyl-*S*-benzylcysteine ethyl ester (**59**) to yield the heptapeptide ester (**60**), which was led to the hydrazide (**61**) prior to the formation of disulfide bridge, lest the ester group should be ammonolysed during the course of sodium/ammonia treatment. After the removal of *S*-benzyl group, the thiols of cysteinyl residues were oxidized in a dilute solution by air to disulfide in a slightly basic region. In neutral or lower pH region, the thiol was not oxidized completely even after contact with air for a long time. Gel filtration on Sephadex LH-20 using DMF was successful for the purification of the product (**62**).

Positions 1—32. Two equivalent amount of the azide prepared from **62** was used for the acylation of pentacosapeptide amide (**49**). The *t*-butoxycarbonyl groups of the crude product were removed by concentrated hydrochloric acid treatment at −5 °C for 10 min to give **1**. Analog **1** was purified by gel filtration and carboxymethyl cellulose chromatography. The homogeneity of **1** was confirmed by tlc in several solvent systems and amino acid analyses of the acid hydrolysates, as well as of the aminopeptidase M digests.

Analog **1** exhibited hypocalcemic activity of 80—120 MRC units/mg. The potency is similar to or a little higher than that of human calcitonin but much lower than that of eel or salmon calcitonins. This suggests that the high activity of salmon or eel hormone is not ascribable only to the amino acid sequence of their N-terminal decapeptide and that the presence of methionine in position 8 of human calcitonin is not responsible by itself for the low potency of the hormone.

Experimental

Melting points are uncorrected. Amino acid analyses were carried out on a JLC-6AS automatic analyzer (JEOL) after acid hydrolysis with HCl of constant bp (110 °C, 16—20 h), or aminopeptidase M (Röhn and Haas Co.) digestion. The theoretical values of amino acid ratios are shown in parentheses after each result. Edman degradation was carried out with a JAC-47K automatic sequencer (JEOL). Biological activities were measured according to the method of Cooper *et al.*[15] The N-protected dipeptides, **5**,[16] **9**,[17] **21**, **27**, **32**,[18] **37**, **43**, **50**, **52**, and **58**, were prepared by the usual methods as shown in the Schemes. The longer peptides, **11**, **13**, **15**, **17**, **23**, **29**, **34**, **39**, **45**, and **54**, were synthesized by the stepwise elongation method. Compounds **8**[19] and **56** were prepared from the subfragments by the active ester method and the azide method, respectively. Hydrazides, **18**, **24**, **30**, **42**, **51**, **57**, and **61**, were obtained from the corresponding ethyl esters. The active esters, **7**[20] and **36**, were prepared from **6**[21] and **35** by the use of DDC. Compounds **6** and **35** were prepared from **5** and **34**, respectively, by saponification. The N-terminal free peptides, **10**, **12**, **14**, **16**, **19**, **22**, **33**, **38**, **40**, **44**, **46**, **53**, **55**, and **59**, were obtained by the usual catalytic hydrogenolysis of the corresponding benzyloxycarbonyl derivates. In TLC, silica gel G (Merck and Co.) plate (Sh), silica gel-precoated plate (Merck and Co.) (Sp) and cellulose-precoated plate (Avicel)(C) were used with the following solvent systems: chloroform–methanol, 95/15 (1a), 95/5 (1b); chloroform–methanol–acetic acid, 95/5/3 (2a), 36/4/1 (2b); 1-butanol–acetic acid–water, 4/1/1 (3a), 3/1/1 (3b), 10/1/1 (3c); 1-butanol–1 M acetic acid, 2/1 upper phase (4a), 1/1 upper phase (4b); 2-propanol–water, 4/1 (5); 1-butanol–pyridine–acetic acid–water, 16/3/1/4 (6); 2-butanol–15 M ammonia–water, 24/1/5 (7).

Cbz-Ala-Pro-OH (2). Cbz-Ala-ONP (6.50 g) was added to a suspension of proline (2.30 g) and triethylamine (2.78 ml) in DMF (50 ml). The mixture was stirred at room temperature for 4 days and the solvent was removed. The residue was dissolved in ethyl acetate and washed with 1 M HCl and water. An oil obtained after removal of solvent of the organic layer was dissolved in a small amount of ethanol. About half of the solution was applied onto a Sephadex LH-20 column (2.5×76 cm) and the product was eluted with ethanol. The colorless fractions containing the peptide were evaporated to give an oil. The rest of the ethanol solution was treated in the same way. The combined product was dried in reduced pressure; 5.70 g. R_f (Sh, 1b) 0.33.

Cbz-Ala-Pro-NH$_2$ (3). BCC (2.24 ml) was added with stirring to a solution of **2** (5.35 g) and *N*-methylmorpholine (1.69 g) in THF (200 ml) at −15 °C. After 5 min, dried ammonia was passed into the mixture at −15 °C for 20 min and then at ice-bath temperature for 1.5 h. The mixture was stirred for 2 h in the ice-bath and at room temperature for 2 days. The residue obtained after removal of the solvent was dissolved in chloroform–water (100 ml and 20 ml each), and the aqueous phase was extracted with chloroform (70 ml×2). The organic phases were combined and washed with water (10 ml×3). After removal of the chloroform the residue was recrystallized from ethyl acetate; 4.60 g. R_f (Sh, 2a) 0.67.

Cbz-Pro-Gln-Thr-Ala-Ile-Gly-Val-Gly-Ala-Pro-NH$_2$ (20). HCl/THF (3.08 M, 1.95 ml) was added dropwise to a suspension of **18** (1.47 g) in DMF (20 ml) at −40 °C. 1-Butyl nitrite (0.25 ml) was added to the suspension. The mixture was stirred for 40 min at −20 °C, and then cooled at −40 °C. Triethylamine (0.83 ml) was added to the azide solution followed by **19** (2 mM) and triethylamine (0.28 ml) in DMF (10 ml). The mixture was stirred at ice-bath temperature for 3 days. After removal of the solvent, the residue was triturated with water and the solid collected was washed with 1 M citric acid and water. The purified decapeptide amide was obtained by reprecipitation from DMF–ether; 1.69 g. R_f (Sh, 3a) 0.41, (Sh, 5) 0.52. Amino acid ratios in acid hydrolysate: Thr 0.88 (1), Glu 1.08 (1), Pro 2.05 (2), Gly 2.00 (2), Ala 2.08 (2), Val 1.01 (1), Ile 0.99 (1).

H-Pro-Gln-Thr-Ala-Ile-Gly-Val-Gly-Ala-Pro-NH_2 (25). The protected decapeptide amide, **20** (2.09 g), was hydrogenated in the presence of Pd black in DMF (200 ml) and water (40 ml) at 40—50 °C for 3 h. The mixture was diluted with additional water (40 ml) and the hydrogenolysis was continued at 40—50 °C for 3 h and at 70—80 °C for 1 h. After removal of the catalyst the solvent was evaporated to give a solid in a quantitative yield. R_f (Sh, 3b) 0.20.

H-His-Thr-Phe-Pro-Gln-Thr-Ala-Ile-Gly-Val-Gly-Ala-Pro-NH_2 Hydrochloride (26). HCl/THF (1.70 M, 5.56 ml) was added to a solution of **24** (2.40 mM, 1.32 g) in DMF (8 ml) at −40 °C. 1-Butyl nitrite (0.288 ml) was added dropwise and the mixture was stirred at −25 °C for 20 min and then cooled at −40 °C. To the azide solution thus obtained were added triethylamine (1.34 ml) and **25** (2.00 mM) in HMPA (10 ml) and DMF (6 ml). Stirring was continued at ice-bath temperature for 3 days and the solvent was removed. The residue was dissolved in water–saturated 1-butanol and washed with 5% $NaHCO_3$ and water. A syrup which remained after removal of the solvent was solidified by addition of ether. The solid (2.68 g) was hydrogenated in ethanol (100 ml) and water (20 ml) containing HCl. After removal of the catalyst and the solvent, the product was applied to a Sephadex G-10 column (3×32.5 cm) and eluted with water. Fractions of 5 ml each were collected and the desired peptide was obtained from fractions 13—20. The material from fractions 21—25 was rechromatographed on the same column, and an additional crop was obtained. Colorless powder (2.33 g), R_f (C, 4a) 0.18 and 0.14. A part of the product (0.996 g) was dissolved in a small amount of the upper phase of 1-butanol–acetic acid–water (5/1/5) and this was applied to a Sephadex G-25 column (3.5×42.5 cm) which had been equilibrated with the lower phase of the solvent system and then washed with the upper phase. The elution was carried out with the upper phase and the optical density of the eluate was observed at 254 nm to show three major peaks. Peptide A (0.119 g), B (0.079 g), and C (0.305 g) were obtained respectively from the fractions corresponding to the peaks. Peptide A: R_f (C, 4a) 0.18. Amino acid ratios in acid hydrolysate; His 1.17 (1), Thr 1.91 (2), Glu 1.02 (1), Pro 1.96 (2), Gly 1.99 (2), Ala 1.91 (2), Val 1.02 (1), Ile 1.01 (1), Phe 0.98 (1). Amino acid ratios in AP-M digest; His 1.00 (1), Thr 0.34 (2), Gln 0.15 (1), Gly 1.68 (2), Ala 0.48 (1), Val 0.90 (1), Ile 1.00 (1). Peptide B: R_f (C, 4a) 0.14. Amino acid ratios in acid hydrolysate; His 1.00 (1), Thr 1.89 (2), Glu 1.15 (1), Pro 2.17 (2), Gly 1.99 (2), Ala 1.98 (2), Val 0.93 (1), Ile 0.98 (1), Phe 0.91 (1). Amino acid ratios in AP-M digest; His 1.03 (1), Thr 1.88 (2), Gln 1.07 (1), Gly 2.08 (2), Ala 1.07 (1), Val 0.96 (1), Ile 0.91 (1). Peptide C: R_f (C, 4a) 0.14. Amino acid ratios in acid hydrolysate; His 1.07 (1), Thr 1.96 (2), Glu 1.14 (1), Pro 2.13 (2), Gly 1.93 (2), Ala 1.90 (2), Val 0.97 (1), Ile 0.96 (1), Phe 0.92 (1). Amino acid ratios in AP-M digest; His 1.03 (1), Thr 1.91 (2), Gln 1.12 (1), Gly 1.96 (2), Ala 1.05 (1), Val 0.96 (1), Ile 0.98 (1).

Peptide B (0.689 g) obtained by repeating a similar procedure was dissolved in 0.05 M HCl (24 ml). After removal of insoluble materials, the solvent was evaporated to give the hydrochloride, peptide C, as solid (0.644 g). Found: C, 47.96; H, 6.84; N, 15.94; Cl, 6.58%. Calcd for $C_{62}H_{95}O_{17}N_{18}\cdot 3HCl\cdot 5H_2O$: C, 47.46; H, 6.95; N, 15.95; Cl, 7.13%.

H-Lys(Boc)-Phe-OEt Acetate (28). The protected peptide (**27**) (7.50 g) was hydrogenated in ethanol (250 ml) and acetic acid (3.75 ml) to give the desired product. R_f (Sh, 3a) 0.75. However, when the hydrogenolysis was carried out with an equivalent amount of acetic acid, a product having high melting point and poor solubility was obtained. This was recrystallized from DMF and supposed to be cyclo-Lys(Boc)-Phe. R_f (Sh, 1a) 0.41. mp 246 °C. $[\alpha]_D^{20}$ −24.7° (*c* 0.6, DMF). (lit,[22]) mp 224—226 °C, $[\alpha]_D^{20}$ −24.7° (*c* 0.5, DMF). Found: C, 64.50; H, 7.90; N, 11.31%. Calcd for $C_{20}H_{28}O_4N_3$: C, 63.99; H, 7.78; N, 11.19%.

H-Asn-Lys(Boc)-Phe-His-Thr-Phe-Pro-Gln-Thr-Ala-Ile-Gly-Val-Gly-Ala-Pro-NH_2 Acetate (31). To the azide solution, prepared from **30** (0.36 mM, 0.237 g) in DMF (1 ml) as described for Z-His-Thr-Phe-N_3 in the preparation of **26**, was added a solution of **26** (0.30 mM, 0.410 g) and triethylamine (0.083 ml) in HMPA (3 ml) and DMF (3.5 ml). The mixture was stirred at ice-bath temperature for 4 days and the solvent was removed. The residue was washed and then solidified as in the preparation of **26**. The crude product (0.620 g) was hydrogenated in ethanol (50 ml) and water (10 ml) containing acetic acid (0.12 ml). After removal of the catalyst and the solvent, the product was applied to a Sephadex G-10 column (3×32.5 cm) and eluted with water. Fractions of 5 ml each were collected and the desired peptide was obtained from fractions 11—18. 0.375 g (57%). R_f (Sp, 6) 0.20 with a trace spot at 0.24, (Sp, 3a) 0.31 with a trace spot at 0.38. Amino acid ratios in acid hydrolysate: Asp 1.06 (1), Thr 1.94 (2), Glu 0.98 (1), Pro 1.94 (2), Gly 1.98 (2), Ala 1.97 (2), Val 1.01 (1), Ile 1.00 (1), Phe 2.01 (2), Lys 1.09 (1), His 1.09 (1).

Cbz-Val-Leu-Gly-Thr-Tyr-Thr-OEt (41). a) Triethylamine (0.695 ml) was added dropwise to an ice-cold solution of **36** (2.32 g) and **40** (5.0 mM) in DMF (20 ml). The mixture was stirred at room temperature for 2 days. After removal of the solvent the residue was dissolved in water–saturated 1-butanol and washed with 5% citric acid and water. The solvent was evaporated to give a solid, which was recrystallized from DMF–ether. 3.67 g. R_f (Sp, 1a) 0.27, (Sp, 2a) 0.08. b) DCC (0.825 g) in DMF (4 ml) was added in an ice-cold solution of **35** (1.69 g), **40** (3.76 mM) and HOSu (0.460 g) with triethylamine (0.523 ml) in DMF (25 ml). After 2.5 h, HOSu (0.460 g) was added and the mixture was stirred at room temperature overnight. The insoluble substances were removed and the filtrate was evaporated to give a solid, which was washed and reprecipitated from DMF–ether; 2.10 g (69%).

Cbz-Val-Leu-Gly-Thr-Tyr-Thr-Gln-Asp-Phe-NHNH-Boc (47). To an azide solution prepared from **42** (2.00 g) in DMF (8 ml) as in the preparation of **26** was added a solution of **46** (1.54 g) and triethylamine (0.417 ml) in DMF (12 ml). The mixture was stirred at ice-bath temperature for 4 days and the solvent was removed. After the usual treatment, the desired peptide was recrystallized from DMF–ether; 2.94 g. R_f (Sp, 3a) 0.69 (Sp, 6) 0.65. Amino acid ratios in acid hydrolysate: Asp 0.93 (1), Thr 2.05 (2), Glu 0.85 (1), Gly 0.95 (1), Val 0.99 (1), Leu 1.06 (1), Tyr 1.12 (1), Phe 1.06 (1).

Cbz-Val-Leu-Gly-Thr-Tyr-Thr-Gln-Asp-Phe-$NHNH_2$ Hydrochloride (48). The Boc-hydrazide (**47**) (0.30 g) was dissolved in ice-cold 12 M HCl. After 5 min, the solution was poured into NaCl-saturated water (30 ml) at ice-bath temperature. The resulting precipitate was collected and washed with saturated NaCl and with a small amount of water. The solid was dried *in vacuo* over NaOH pellets and recrystallized from DMF–ethyl acetate; 0.17 g. R_f (Sp, 3a) 0.51.

H-Val-Leu-Gly-Thr-Tyr-Thr-Gln-Asp-Phe-Asn-Lys(Boc)-Phe-His-Thr-Phe-Pro-Gln-Thr-Ala-Ile-Gly-Val-Gly-Ala-Pro-NH_2 (49). To the azide solution prepared from **48** (0.200 mM, 0.242 g) in DMF (0.8 ml) in the usual way was added a solution of **31** (0.173 mM, 0.320 g) and triethylamine (10% in DMF, 0.481 ml) in DMF (2.1 ml). The mixture was stirred at ice-bath temperature for 4 days and the solvent was

removed. The residue was dissolved in water-saturated 1-butanol and washed with water. The butanol solution was concentrated into a syrup, to which was added ether and the resulting precipitate was collected. 0.538 g. A part of the crude product (0.240 g) was hydrogenated in ethanol (50 ml) and water (10 ml) in the presence of acetic acid (0.09 ml). After removal of the catalyst and the solvent, the aqueous solution of the residue was applied to a Sephadex G-25 column (3×22 cm), and eluted with 0.05 M ammonium acetate. Fractions of 3 ml each were collected and the desired peptide was obtained from fractions 16—22. R_f (Sp, 3a) 0.47 with minor spots at 0.45 and 0.50. The peptide was further applied to a Sephadex G-25 column (3.5×41 cm), which had been equilibrated with 1-butanol−0.5 M acetic acid (1/1) in a similar way to that described in the preparation of **26**, and was eluted with the upper phase of the solvent system. Fractions of 3 ml each were collected and the purified peptide was obtained from fractions 52—68. 0.090 g. R_f (Sp, 6) 0.04, (Sp, 5) 0.74, (Sp, 3a) 0.43, (C, 4a) 0.05. Amino acid ratios in acid hydrolysate: Asp 1.96 (2), Thr 3.82 (4), Glu 1.91 (2), Pro 2.07 (2), Gly 3.18 (3), Ala 2.13 (2), Val 1.90 (2), Ile 1.04 (1), Leu 0.87 (1), Tyr 0.97 (1), Phe 3.01 (3), Lys 1.04 (1), His 1.11 (1).

*Boc-Cys(Bzl)-Ser-Asn-Leu-Ser-Thr-Cys(Bzl)-OEt (**60**).* To an azide solution prepared as usual from **57** (6.30 g) in DMF (50 ml) and THF (10 ml) was added a solution of **59** (9.25 mM) and triethylamine (1.29 ml) in DMF (50 ml). The mixture was stirred at ice-bath temperature for 3 days. Cold water (200 ml) was poured into the mixture and the resulting precipitate was collected and washed as usual; 6.00 g. R_f (Sh, 2b) 0.30 with a trace spot at 0.62. A part of the product (3.00 g) was applied to a silica gel column (3×38 cm) and eluted with chloroform-methanol (94/4). The purified peptide was obtained in a considerably low yield because of the strong adsorption of the peptide to the gel; 1.10 g. R_f (Sh, 2b) 0.30, (Sh, 3c) 0.75.

*Boc-Cys-Ser-Asn-Leu-Ser-Thr-Cys-NHNH$_2$ (**62**).* The heptapeptide hydrazide, **61** (0.256 g), was dissolved in liquid ammonia (about 50 ml). To the solution was added sodium in a small portions until the blue color of the solution remained for 10 min (0.087 g of sodium was required for a period of 25 min). NH_4Cl (0.282 g) was added to the mixture and the ammonia was evaporated under reduced pressure. The residue was dissolved in water (200 ml) and the solution (pH 8.05) was stirred vigorously in a stream of air for 3 h. The desired peptide was extracted with 1-butanol (40 ml×4, 20 ml×5). The combined organic phase was washed with water (20 ml) and acidified with acetic acid, and then the solvent was evaporated. The residue was applied to a Sephadex LH-20 column (3×32 cm) and eluted with DMF. Fractions of 3 ml each were collected and the desired peptide was located in fractions 21—24. The fractions were combined and concentrated to a small volume and ether was added. The resulting precipitate was collected and washed with ether; 0.139 g. R_f (Sp, 3a) 0.46 with a trace spot at 0.57. Amino acid ratios in the acid hydrolysate: Asp 1.14 (1), Thr 0.94 (1), Ser 1.94 (2), Cys_2 0.93 (1), Leu 1.11 (1).

*H-Cys-Ser-Asn-Leu-Ser-Thr-Cys-Val-Leu-Gly-Thr-Tyr-Thr-Gln-Asp-Phe-Asn-Lys-Phe-His-Thr-Phe-Pro-Gln-Thr-Ala-Ile-Gly-Val-Gly-Ala-Pro-NH$_2$ (**1**).* To the azide solution prepared from **62** (0.050 mM, 42.1 mg) in DMF (0.8 ml) was added a solution of **49** (0.025 mM, 71.7 mg) and triethylamine (10% in DMF, 0.07 ml) in DMF (0.6 ml). The mixture was stirred at ice-bath temperature for 4 days and the solvent was removed. The residue was solidified by the addition of ether. The solid was dissolved in 12 M HCl (1 ml) at −5 °C. After 10 min, ammonium hydrogencarbonate (950 mg) was added to the solution. The solution was diluted with water (about 12 ml), adjusted to pH 3.5 with formic acid and concentrated to about 5 ml volume. The resulting precipitate was separated (ppt fraction). The solution was applied to a Sephadex G-25 column (2.5×23 cm) and eluted with 0.05 M ammonium formate (pH 3.5). Fractions of 4 ml each were collected and the eluate in fractions 13—21 was lyophilized to give a solid. The crude product was further applied to a CM-cellulose column (Serva, 1.2×28 cm) and eluted with a linear gradient of ammonium formate buffer (0.01 M, pH 4.7—0.1 M, pH 5.2, 220 ml each). Fractions of 4 ml each were collected and the eluate in fractions 53—64 was lyophilized. The solid obtained was again desalted with a Sephadex G-10 column (1.5×14 cm) to give the desired peptide **1**; 2.27 mg. R_f (Sp, 3a) 0.45, (Sp, 6) 0.21, (Sp, 7) 0.17, (C, 4b) 0.21. $[\alpha]_{331}^{24}$ −1633° (*c* 0.2, 1 M acetic acid). Amino acid ratios in acid hydrolysate: His 0.98 (1), Lys 1.09 (1), Asp 3.16 (3), Thr 4.82 (5), Ser 2.19 (2), Glu 2.07 (2), Pro 2.24 (2). Gly 3.11 (3), Ala 2.22 (2), Cys_2 0.60 (1), Val 1.82 (2), Ile 1.11 (1), Leu 1.87 (2), Tyr 0.82 (1), Phe 2.96 (3). Average recovery of the amino acids was 90%. Amino acid ratios in AP-M digest: Asp 1.00 (1), Asn 1.99 (2), Thr 4.94 (5), Ser 2.13 (2), Gln 1.92 (2), Pro 0.11 (2), Gly 3.28 (3), Ala 1.53 (2), Cys_2 0.70 (1), Val 1.92 (2), Ile 1.36 (1), Leu 1.87 (2), Tyr 0.93 (1), Phe 2.35 (3), Lys 1.02 (1), His 1.12 (1). AP-M used in this analysis cleaved the peptide bond X-Pro (X=amino acid) very slowly. The low recoveries of Phe, Pro, and Ala are due to this. Hypocalcemic activity: 80—120 MRC units/mg. The product (18.96 mg), which still contained the amine component, positions 8—32, was recovered from the "ppt fraction" and the void volume fractions of CM-cellulose chromatography.

The author wishes to express his sincere thanks to Professor Ichiro Muramatsu for his kind guidance throughout this work. He also thanks the Research Laboratories of Toyo Jozo Co., Ltd. for the elemental and amino acid analyses, and for biological assay of the product. The sequence analyses of peptide **26** were kindly carried out in the Laboratory of JEOL Ltd.

References

1) Preceding paper: S. Nozaki and I. Muramatsu, *Chem. Lett.*, **1974**, 417.

2) Amino acids used are of L-configuration. The abbreviations for amino acids and peptides are in accordance with the rules of the IUPAC-IBU Commission on Biochemical Nomenclature. Other abbreviations are as follows; MRC=Medical Research Council, AP-M=aminopeptidase M, Cbz or Z=benzyloxycarbonyl, Boc=*t*-butoxycarbonyl, Bzl=benzyl, OBzl=benzyloxy, ONP=*p*-nitrophenyl, BCC=isobutyl chloroformate, DCC=dicyclohexylcarbodiimide, HOSu=*N*-hydroxysuccinimide, HMPA=hexamethylphosphoric triamide.

3) H. D. Niall, H. T. Keutmann, D. H. Copp, and J. T. Potts Jr., *Proc. Natl. Acad. Sci. U. S.*, **64**, 771 (1969).

4) M. Otani, H. Yamauchi, T. Meguro, S. Kitazawa, S. Watanabe, and H. Orimo, *J. Biochem.*, **79**, 345 (1976).

5) F. W. Kahnt, B. Riniker, I. MacIntyre, and R. Neher, *Helv. Chim. Acta*, **51**, 214 (1968).

6) J. Franz, J. Rosenthaler, K. Zehnder, W. Doepfner, H. Huguenin, and St. Guttmann, *Helv. Chim. Acta*, **51**, 218 (1968).

7) B. Riniker, R. Neher, R. Maier, F. W. Kahnt, P. G. H. Byfield, T. V. Gudmundsson, L. Galante, and I. MacIntyre, *Helv. Chim. Acta*, **51**, 1738 (1968).
8) H. B. Brewer, Jr., R. J. Schlueter, and J. P. Aldred, *J. Biol. Chem.*, **245**, 4232 (1970).
9) J. Pless, W. Bauer, H. Bossert, K. Zehnder, and St. Guttmann, *Nature (London), New Biol.*, **240**, 62 (1972).
10) R. Maier, B. Riniker, and W. Rittel, *FBES Lett.*, **48**, 68 (1974).
11) J. Honzl and J. Rudinger, *Collect. Czech. Chem. Commun.*, **26**, 2333 (1961).
12) D. Yamashiro, *Nature*, **201**, 76 (1964).
13) Y. Yaba, I. Muramatsu, and A. Hagitani, Preprint of 34th National Meeting of the Chemical Society of Japan, Hiratsuka, April 1976, p. 677.
14) P. Sieber, B. Riniker, M. Brugger, B. Kamber, and W. Rittel, *Helv. Chim. Acta*, **53**, 2135 (1970).
15) C. W. Cooper, P. F. Hirsch, S. U. Toverud, and P. L. Munson, *Endocrinology*, **81**, 610 (1967).
16) Mp 165—167 °C, lit; mp 166 °C, W. Grassman and E. Wünsch, *Chem. Ber.*, **91**, 449 (1958); L. Heslinga and J. F. Arens, *Recl. Trav. Chim. Pays-Bas*, **76**, 982 (1957).
17) Mp 152—154 °C, lit; mp 153.5—154.5 °C, S. Sakakibara and M. Fujino, *Bull. Chem. Soc. Jpn.*, **39**, 947 (1966).
18) Mp 101—103 °C, lit; mp 104—105 °C, D. W. Clayton, J. A. Farrington, G. W. Kenner, and J. M. Turner, *J. Chem. Soc.*, **1957**, 1398; W. Grassmann and E. Wünsch, *Chem. Ber.*, **91**, 449 (1958); M. A. Nyman and R. M. Herbst, *J. Org. Chem.*, **15**, 108 (1950).
19) Mp 207—209 °C, lit;[14] mp 209—211 °C.
20) Mp 201—204 °C, lit; mp 204—205 °C, K. Suzuki, *Chem. Pharm. Bull.*, **14**, 909 (1966).
21) Mp 143—145 °C, lit; mp 146 °C, W. Grassmann and E. Wünsch, *Chem. Ber.*, **91**, 449 (1958).
22) H. Klostermeyer, *Chem. Ber.*, **102**, 3617 (1969).

An ESR Study of *N*-Benzoyl- and *N*-Pivaloyl-*N*-(arylthio)aminyls[1)]

Yozo MIURA,* Yosuke KATSURA, and Masayoshi KINOSHITA

Department of Applied Chemistry, Faculty of Engineering, Osaka City University, Sumiyoshi-ku, Osaka 558

(Received February 27, 1978)

N-Benzoyl-*N*-(arylthio)aminyls, ArCONSAr', and *N*-pivaloyl-*N*-(arylthio)aminyls, *t*-BuCONSAr, were generated in benzene by hydrogen-abstraction from *N*-benzoyl- and *N*-pivaloylbenzenesulfenamides. The hyperfine coupling constants (*hfcc*) for the radicals are in the range of 6.80—7.57 G for the nitrogen nucleus and 1.68—1.97 G for the *S*-phenyl ring protons. However, *hfcc* due to the benzoyl and pivaloyl protons were not detected. The *g*-values lie in the range of 2.0081—2.0084. On the basis of these ESR parameters, it is suggested that the acylaminyls exist in a π-electronic ground state and that the unpaired electron is located predominantly on the nitrogen atom ($2p_z$ orbital) and the phenylthio group. From the decay kinetic study of the radicals, it was found that *N*-benzoyl-*N*-(4-chlorophenylthio)aminyl persisted for more than 3 h in benzene at 24 °C, and *N*-pivaloyl-*N*-(4-chlorophenylthio)aminyl decayed only a little, even after 20 h.

Acylaminyls are of interest as an important intermediate in such photochemical reactions as Hoffmann-Löffler type intramolecular rearrangements.[2)] Some ESR spectroscopic investigations of acylaminyls have been undertaken for the purpose of determining whether they can best be classified as π or σ radicals.[3-6)] Acylaminyls are generally known as transient radicals and are easily converted into the corresponding nitroxides in the presence of oxygen. Thus, the unequivocal identification of the radicals by ESR spectroscopy is difficult, and other radicals have often been misassigned as acylaminyls. Recent ESR spectroscopic investigations of acylaminyls have shown that they exist in a π-electronic ground state.[3)]

In the past years we have studied some nitrogen-centered free radicals in which one or two divalent sulfur atoms are adjacent to the radical center.[7)] In this report we will describe an ESR study of a new class of acylaminyls, *N*-acyl-*N*-(arylthio)aminyls (**2**).

Results and Discussion

Preparation of N-*Acylbenzenesulfenamides (**1**).* The sulfenamides were prepared by the reactions of benzamides or pivalamide with benzenesulfenyl chlorides in THF or ether in the presence of triethylamine. In the reactions of pivalamides, sulfenamides were afforded in relatively good yields (*ca.* 50%), but with benzamides the yields were low (8—28%). The structures of **1** were identified by means of elemental and instrumental analyses.

$$\mathrm{RCNH_2} + \mathrm{ArSCl} \xrightarrow[\text{in THF (ether)}]{\mathrm{Et_3N}} \mathrm{RCNHSAr} + \mathrm{Et_3N \cdot HCl}$$

1

Generation of Radicals. Acylaminyls, **2**, were generated by two procedures: a) the photolysis of a benzene solution of **1** using a high-pressure mercury lamp and b) the thermolysis of a benzene solution containing **1** and di-*t*-butyl diperoxyoxalate. In the former procedure, the radicals **2** seem to be generated by hydrogen-abstraction from **1** by the amidyl radicals which are formed by the photoinduced S–N bond fission of **1** (Scheme 1).[8,9)]

$$\mathbf{1} \xrightarrow{h\nu} \mathrm{RCNH\cdot} + \mathrm{ArS\cdot}$$

$$\mathrm{ArS\cdot} + \mathbf{1} \longrightarrow \mathrm{RCNH_2} + \mathrm{RCNSAr}\ (\mathbf{2})$$

Scheme 1.

The ESR spectra of **2** generated by Procedures a and b were in complete agreement with each other.

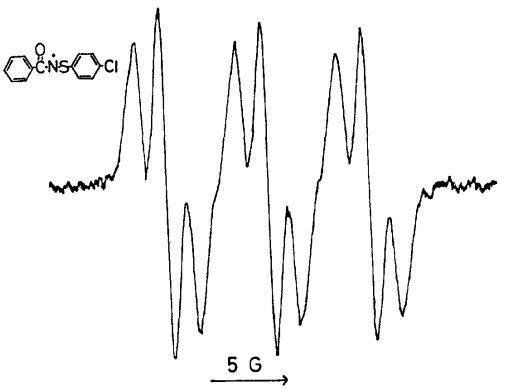

Fig. 1. An ESR spectrum of **2b** generated by photolysis of a benzene solution of **1b** at 24 °C.

The ESR spectrum (Fig. 1) of *N*-benzoyl-*N*-(4-chlorophenylthio)aminyl (**2b**) was split into a 1:1:1 triplet (7.16 G) by the interaction with one nitrogen nucleus, and each of the triplet was further split into a 1:2:1 triplet (1.72 G) by the interaction with two magnetically equivalent protons. The latter triplet is obviously due to the two ortho-protons in the *S*-phenyl ring, and no quartet splitting which could be expected on the basis of the benzoyl protons' participation could be detected. In order to confirm this assignment, an ESR spectrum of a *d*-labeled acylaminyl, **2g**, was measured. This ESR spectrum consisted of a simple 1:1:1 triplet (7.08 G), and no splitting due to the benzoyl protons was detected. The radicals **2c**, **2d**, and **2f** also showed spectra similar to that of **2b**. On the other hand, the spectra of *N*-benzoyl-*N*-(phenylthio)-aminyl (**2a**) and *N*-pivaloyl-*N*-(phenylthio)aminyl (**2e**) were constituted of 1:3:3:1 quartets (1.68—1.69 G)

Table 1. The ESR parameters for *N*-acyl-*N*-(arylthio)aminyls (**2**)[a]

	R–C(=O)–N•–S–R′		*S*-Phenyl ring			*g*-Value
	R	R′	a_N[b]	a_{o-H}[b]	a_{p-H}[b]	
2a	C_6H_5	C_6H_5	7.09	1.68	1.68	2.0081
2b	C_6H_5	4-ClC_6H_4	7.16	1.72	—	2.0083
2c	4-$CH_3OC_6H_4$	4-ClC_6H_4	7.38	1.73	—	2.0082
2d	4-$NO_2C_6H_4$	4-ClC_6H_4	6.80	1.97	—	2.0084
2e	*t*-C_4H_9	C_6H_5	7.49	1.69	1.69	2.0082
2f	*t*-C_4H_9	4-ClC_6H_4	7.57	1.69	—	2.0083
2g	C_6H_5	C_6D_5	7.08			2.0082

a) In benzene at 24 °C. b) In G.

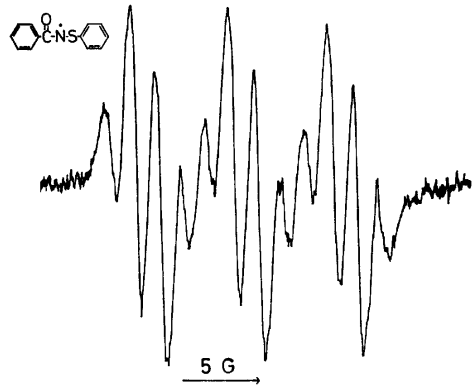

Fig. 2. An ESR spectrum of **2a** generated by photolysis of a benzene solution of **1a** at 24 °C.

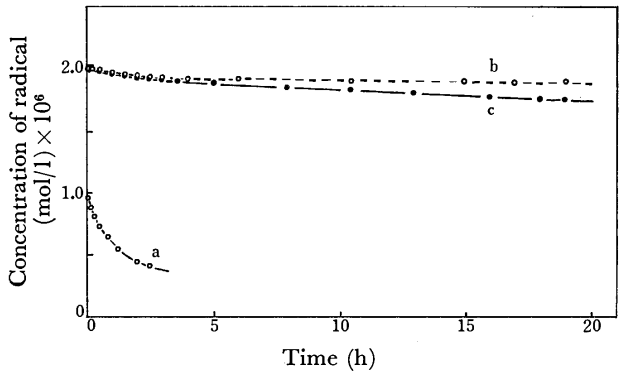

Fig. 3. Decay plots of *N*-acyl-*N*-(arylthio)aminyls (**2**) in benzene at 24 °C. a: **2b** in degassed benzene; b: **2f** in degassed benzene; c: **2f** in benzene saturated with air.

of a 1:1:1 triplet (7.09—7.49 G, see Fig. 2). The quartets were obviously due to the interaction with the magnetically equivalent two ortho- and one para-protons in the *S*-phenyl ring. The values of the coupling constants are listed in Table 1, together with the *g*-values.

It is well known that nitrogen-centered free radicals are easily converted into the corresponding nitroxides, even in the presence of such weak oxidants as atmospheric oxygen. In the present experiment, however, the possibility that **2** are identical with the corresponding nitroxides, **3**, may be excluded on the basis of the following points: 1) the *g*-values of **2** (2.0081—2.0084) are too high compared with those for nitroxides so far reported (*ca.* 2.006)[10] and 2) although, in *t*-BuNSAr, couplings due to the ring protons have never been detected,[11] in **2** relatively large couplings (a_H: 1.68—1.97 G) are observed.

3

Decay Kinetics. The decay kinetic study of **2** was carried out in benzene at 24 °C in the dark. The results are illustrated in Fig. 3. As can be seen from the figure, the radical **2b** persisted in degassed benzene for more than 3 h, and **2f** decayed only a little, even after one day. Moreover, the decay rate of **2f** was measured in benzene saturated with air in order to examine the influence of oxygen on the stability. As may be found from the figure, the decay rate is almost the same as that obtained under the degassed conditions, indicating that the life-time of the radical is little affected by oxygen. Since other acylaminyls are very short-lived and are significantly sensitive to oxygen,[3,12] these results are of interest.

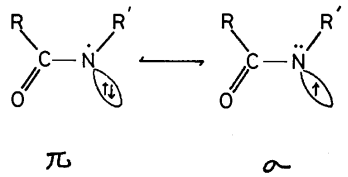

Fig. 4.

Consideration of ESR Parameters. Since, in acylaminyls, there is a carbonyl group which can potentially interact with the nitrogen lone-pair electrons, there has been considerable interest in determining whether they are π or σ radicals (Fig. 4). If in a σ-electronic ground state, they are expected to exhibit a large a_N value because the unpaired electron would reside in an orbital of an appreciable s character. Recent investigations of acylaminyls indicate that simple or *N*-alkoxyacylaminyls are π radicals, judging from the ESR parameters.[13]

With respect to the present radicals, the a_N values lie in the range of 6.80—7.57 G: they are considerably smaller than those observed for simple or *N*-alkoxyacylaminyls,[13] suggesting that **2** exist in a π-electronic ground state.

In **2a—d** and **2e**, no couplings due to the benzoyl protons were observed. Also, the replacement of the benzoyl groups in **2a** and **2b** by a pivaloyl group (**2a** or **2f**) increased the a_N values by only 0.4 G. Thus, in **2** there is a negligibly small delocalization of the unpaired electron onto the benzoyl aromatic ring.

When the a_H (1.68—1.97 G) and the *g*-values (2.0081—2.0084) for **2** are compared with those for *N*-(arylthio)-*t*-butylaminyls (**4**, a_H: 0.89—1.07 G, *g*-value: 2.0068—2.0072),[7] it is obvious that the extent of the delocalization of the unpaired electron onto the arylthio group in **2** is larger than in **4**. Since **4** is radical which the benzoyl or pivaloyl group in **2** is replaced by a *t*-butyl group with no ability to de-

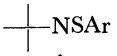

4

localize an unpaired electron, it is reasonable to think that, in **2**, the unpaired electron is little delocalized onto the carbonyl group.

The small a_N values observed for **2**, compared with those of other acylaminyls,[13] can be well explained in terms of the contribution of the resonance forms II and III, which reduce the spin density on the nitrogen. The contribution of II and III leads to an increase in

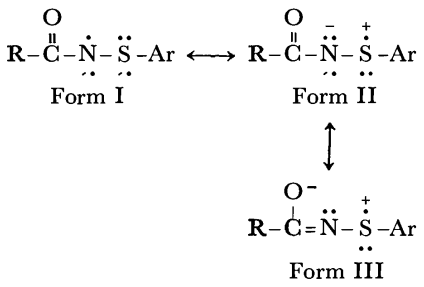

Form I Form II

Form III

the spin density on the sulfur atom possessing a large spin orbit coupling parameter,[15] resulting in the large *g*-values for **2**.

The contribution of II and III may become more important by the introduction of electron-withdrawing substituents into the benzoyl group, resulting in a reduction in the magnitude of the a_N value. In the *p*-nitro-substituted acylaminyl, **2d**, the a_N value is reduced by 0.36 G compared with that for **2b**. On the contrary, the introduction of electron-donating substituents may lead to an increase in the magnitude of the a_N value. In the *p*-methoxy-substituted acylaminyl, **2c**, the a_N value is increased by 0.22 G compared with that for **2b**.

From the results and discussion, it may be concluded that the acylaminyls **2** exist in a π-electronic ground state, and the unpaired electron is located predominantly on the nitrogen atom ($2p_z$ orbital) and the arylthio group.

Experimental

All the melting points are uncorrected. The IR spectra were run on a JASCO Model IR-G spectrometer, and the NMR spectra were recorded with a Hitachi-Perkin Elmer R-20 spectrometer, using TMS as an internal standard. Benzene-d_5-thiol[16] and di-*t*-butyl diperoxyoxalate[17] were prepared by the reported methods. The benzene used as a solvent in the ESR measurements was purified by the usual method.[18]

General Procedure for Preparation of N-*Acylbenzenesulfenamides (1).* Benzenesulfenyl chloride (0.024 mol) in dry THF [50 ml, or dry ether (50 ml) in the cases of **1e** and **1f**] was added dropwise to a stirred solution of amide (0.020 mol) and triethylamine (0.030 mol) in dry THF [250 ml, or dry ether (500 ml) in the cases of **1e** and **1f**] at 0 °C. After addition of the sulfenyl chloride, the reaction mixture was stirred for 3 h at 0 °C, and then for 10 h at room temperature. After the triethylamine hydrochloride thus formed was filtered off, the filtrate was concentrated under reduced pressure to give a powdery residue, which was subjected to column chromatography [alumina (E. Merck, Darmstate, Art 1097), column size 20×3 cm, eluent: benzene/ethanol: 100/1]. The **1** thus separated was recrystallized from the appropriate solvents.

N-*Benzoylbenzenesulfenamide (1a).* Colorless plates with mp 122—124 °C (from benzene/hexane: 2/1). Yield: 14%. IR (KBr): 3250 (NH) and 1635 cm^{-1} (CO). NMR (DMSO-d_6): δ 7.15—8.11 (m, aromatic, 10H) and 10.25 (br s, NH, 1H). Found: C, 67.77; H, 4.64; N, 5.88%. Calcd for $C_{13}H_{11}NOS$: C, 68.09; H, 4.84; N, 6.11%.

N-*Benzoyl-4-chlorobenzenesulfenamide (1b).* Colorless plates with mp 138—139 °C (from benzene/hexane: 2/1). Yield: 15%. IR (KBr): 3250 (NH), 1640 cm^{-1} (CO). NMR (DMSO-d_6): δ 7.19—8.10 (m, C_6H_4 and C_6H_5, 9H) and 10.33 (br s, NH, 1H). Found: C, 59.10; H, 3.70; N, 5.18%. Calcd for $C_{13}H_{10}NOClS$: C, 59.20; H, 3.82; N, 5.31%.

N-*(4-Methoxybenzol)-4-chlorobenesulfenemide (1c).* Colorless needles with mp 178—179 °C (from benzene). Yield: 13%. IR (KBr): 3200 (NH), 1650 cm^{-1} (CO). NMR (DMSO-d_6): δ 3.87 (s, CH_3, 3H), 7.12 and 8.04 (d, J=8 Hz, CO-C_6H_4, 4H), 7.25 and 7.49 (d, J=8 Hz, *S*-C_6H_4, 4H), and 10.12 (br s, NH, 1H). Found: C, 57.35; H, 4.25; N, 4.77%. Calcd for $C_{14}H_{12}NO_2ClS$: C, 57.24; H, 4.12; N, 4.77%.

N-*(4-Nitrobenzoyl)-4-chlorobenzenesulfenamide (1d).* Light yellow needles with mp 169—170 °C (from benzene). Yield: 8%. IR (KBr): 3250 (NH), 1660 cm^{-1} (CO). NMR (DMSO-d_6): δ 7.34 and 7.39 (s, *N*-C_6H_4, 4H), 8.16 and 8.41 (d, J=8 Hz, CO-C_6H_4, 4H), and 10.61 (br s, NH, 1H). Found: C, 50.57; H, 2.89; N, 9.09%. Calcd for $C_{13}H_9N_2O_3ClS$: C, 50.57; H, 2.94; N, 9.07%.

N-*Pivaloylbenzenesulfenamide (1e).* Colorless needles with mp 102—103 °C (from hexane). Yield 58%. IR (KBr): 3200 (NH), 1650 cm^{-1} (CO). NMR (CCl_4): δ 1.16 (s, *t*-Bu, 9H), 7.12 (s, C_6H_5, 5H), and 7.79 (br s, NH, 1H). Found: C, 62.95; H, 7.38; N, 6.65%. Calcd for $C_{11}H_{15}NOS$: C, 63.12; H, 7.22; N, 6.69%.

N-*Pivaloyl-4-chlorobenzenesulfenamide (1f).* Colorless plates with mp 119—120 °C (from hexane). Yield: 43%. IR (KBr): 3200 (NH) and 1650 cm^{-1} (CO). NMR (CCl_4): δ 1.20 (s, *t*-Bu, 9H), 7.00 and 7.13 (d, J=8 Hz, C_6H_4, 4H), and 7.66 (br s, NH, 1H). Found: C, 53.81; H, 6.08; N, 5.64%. Calcd for $C_{11}H_{14}NOClS$: C, 54.20; H, 5.79; N, 5.75%.

N-*Benzoylbenzenesulfenamide-2,3,4,5,6-*d_5 *(1g).* Colorless plates with mp 126—128 °C (from benzene/hexane: 2/1). Yield 28%. IR (KBr): 3250 (NH) and 1660 cm^{-1} (CO). NMR (DMSO-d_6): δ 7.25—8.22 (m, C_6H_5, 5H) and 10.44 (br s, NH, 1H). Found: C, 66.25; H, 4.50; N, 6.18%. Calcd for $C_{13}H_6NOD_5S$: C, 66.63; H, 4.74; N, 5.98%.

Generation of Radicals. a) Sulfenamide **1** (5.0 mg) and benzene (0.20 ml) were placed in an ESR tube. The solution

was degassed by three freeze-and-thaw cycles, and then sealed. The solution was directly irradiated in the cavity of an ESR instrument with an 100W high-pressure mercury lamp (JES-UV-1); b) **1** (5.0 mg), di-*t*-butyl diperoxyoxalate (10.0 mg), and benzene (0.20 ml) were placed in an ESR tube. The solution was degassed by the procedure described above, and then sealed. The ESR spectra from the solution were recorded at 24° C.

Decay Kinetics. The decay kinetic study of **2** was carried out in benzene at 24 °C in the dark. The sample was prepared as follows: **1** (5.0 mg) and benzene (0.20 ml) were placed in an ESR tube, degassed by the procedure described above, and then sealed. The solution was directly irradiated for *ca.* 20 min in the cavity of an ESR instrument with the mercury lamp, and then the light was turned off. The decay rates were followed by monitoring the ESR signal intensities, and the integration of the signals was carried out with a JES-ID-2 integrator, using a benzene solution of 3,4-dihydro-2,4,6-triphenyl-2*H*-1,2,4,5-tetrazin-1-yl (1,3,5-triphenylverdazyl)[19] as a standard.

The ESR spectra were recorded on a JES-ME-3X spectrometer, with an X-band microwave unit and 100 kHz field modulation. The hyperfine coupling constants *(hfcc)* and *g*-values for **2** were determined by comparing them with the *hfcc* (a_N: 13.09 G)[20] and *g*-value (2.0057)[21] of Fremy's salt.

References

1) Part VII of the series "ESR Studies of Nitrogen-centered Free Radicals," for Part VI, see Y. Miura, Y. Nakamura, and M. Kinoshita, *Bull. Chem. Soc. Jpn.*, **51**, 947 (1978).

2) a) R. S. Neale, *Synthesis*, **1971**, 1; b) S. F. Nelsen, "Free Radicals," ed by J. K. Kochi, John Wiley, New York, N. Y. (1973), Vol. II, p. 527.

3) W. C. Danen and F. A. Neugebauer, *Angew. Chem.*, **87**, 823 (1975).

4) T. Koenig, J. A. Hoobler, and W. R. Mabey, *J. Am. Chem. Soc.*, **94**, 2514 (1972).

5) W. C. Danen and R. W. Gellert, *J. Am. Chem. Soc.*, **94**, 6853 (1972).

6) W. C. Danen, C. T. West, and T. T. Kensler, *J. Am. Chem. Soc.*, **95**, 5716 (1973).

7) The ESR parameters for **4** are 11.70—11.89 G (a_N), 0.89—1.07 G ($a_{o\text{- and }p\text{-H}}$), and 2.0068—2.0072 (*g*-value); Y. Miura, H. Asada, and M. Kinoshita, *Bull. Chem. Soc. Jpn.*, **50**, 1855 (1977).

8) D. H. R. Barton, T. Nakano, and P. G. Sammes, *J. Chem. Soc., C*, **1968**, 322.

9) Arylthiyls have been assumed to have a poor ability for hydrogen-abstruction from other reagents; a) T. Sato, M. Abe, and T. Otsu, *Makromol. Chem.*, **178**, 1951 (1977); b) J. L. Kice, "Free Radicals," ed by J. K. Kochi, John Wiley, New York, N.Y. (1973), Vol. II, p. 711.

10) A. R. Forrester, J. M. Hay, and R. H. Thomson, "Organic Chemistry of Stable Free Radicals," Academic Press, New York, N.Y. (1968), p. 180.

11) I. H. Leaver and G. C. Ramsay, *Tetrahedron*, **25**, 5669 (1969).

12) In Ref. 4, *N*-alkoxyacylaminyls have been suggested to persist in the presence of oxygen.

13) The reported a_N values for acylaminys are 15.00—15.70 (RCONR′),[5] 9.60—10.50 (RCONOR′),[4] and 10.80 G (ROCONOR′).[6]

14) In 2-oxocyclohexyl, the contribution of the canonical structure with the unpaired electron on the oxygen has been reported to be *ca.* 15%; D. M. Camaioni, H. F. Walter, J. E. Jordan, and D. W. Pratt, *J. Am. Chem. Soc.*, **95**, 7978 (1973).

15) The spin-orbit coupling parameter of sulfur atom is 382 cm^{-1}; D. S. McClure, *J. Chem. Phys.*, **17**, 905 (1949).

16) Y. Miura and M. Kinoshita, *Bull. Chem. Soc. Jpn.*, **50**, 1142 (1977).

18) P. D. Bartlett, E. P. Benzing, and R. E. Pincock, *J. Am. Chem. Soc.*, **82**, 1762 (1960).

18) Y. Miura, N. Makita, and M. Kinoshita, *Bull. Chem. Soc. Jpn.*, **50**, 482 (1977).

19) R. Kuhn and H. Trischmann, *Monatsh. Chem.*, **95**, 457 (1964).

20) R. J. Faber and G. K. Fraenkel, *J. Chem. Phys.*, **47**, 2462 (1967).

21) J. E. Werz, D. C. Reitz, and F. Dravnieks, "Free Radicals in Biological Systems," Academic Press, New York, N.Y. (1961), p. 186.

Sulfenylation Accompanied by Dealkoxycarbonylation of β-Keto Esters, Geminal Diesters, and α-Cyano Ester in Hexamethylphosphoric Triamide (HMPA)

Morio ASAOKA,* Kazutoshi MIYAKE, and Hisashi TAKEI

Department of Life Chemistry, Tokyo Institute of Technology, Nagatsutacho, Midori-ku, Yokohama 227

(Received February 27, 1978)

In the presence of sodium iodide, diphenyl disulfide reacted with geminal diesters, β-keto esters, and α-cyano esters in hexamethylphosphoric triamide (HMPA) at 150—160 °C to give alkyl phenyl sulfides and α-phenylthio esters, ketones, and nitriles, respectively, along with evolution of carbon dioxide.

It is well-known that geminal diesters, β-keto esters, and α-cyano esters undergo dealkoxycarbonylation when heated with salt, such as sodium chloride or sodium cyanide, in a wet polar aprotic solvent.[1,2] The dealkoxycarbonylation was thought to involve carbanion as an intermediate. Our investigation was undertaken in order to utilize such carbanion for synthetic purposes. We previously reported the intermolecular and intramolecular alkylation of such carbanion.[3] In the present paper, we wish to report sulfenylation of the carbanion, since the sulfenylated compounds are known to be useful intermediates for a variety of organic compounds.[4]

Results and Discussion

When a solution of diethyl malonate, diphenyl disulfide, and sodium iodide in HMPA was heated to 150—160 °C for 1 h, the evolution of carbon dioxide was observed and the disappearance of diethyl malonate was recognized by TLC. From the reaction mixture, ethyl phenyl sulfide and ethyl (phenylthio)acetate were isolated in 40 and 46% yields, respectively, and unreacted diphenyl disulfide was recovered. At the same time, the formation of ethyl acetate was also confirmed. In this reaction, 1.1 equivalents of sodium iodide (which can be regarded as a catalyst) was used, but when 0.2 equivalent of sodium iodide was used, the reaction was found to proceed very slowly.

In order to find the most suitable reaction conditions

$$\underset{\mathbf{1}}{CH_2(COOEt)_2} + \underset{\mathbf{2}}{(PhS)_2} \xrightarrow[HMPA]{NaI} \underset{\mathbf{3}}{PhSCH_2COOEt} + \underset{\mathbf{4}}{PhSEt} + CO_2$$

and to elucidate the reaction mechanism, several experiments were carried out, using a variety of catalysts and solvents or changing the ratio of the reactants. These results are summarized in Table 1.

In view of these results the most effective catalyst is sodium iodide and the most suitable solvent is HMPA. When DMSO or sulfolane was used instead of HMPA, the dealkoxycarbonylation of diethyl malonate was very slow and considerable amounts of unreacted diethyl malonate and diphenyl disulfide were recovered.

Some of possible reaction sequences are shown in the following equations:

$$\underset{\mathbf{1}}{CH_2(COOEt)_2} + X^- \longrightarrow \underset{\mathbf{5}}{[EtOOCCH_2COO^-]} + EtX \quad (1)$$

$$\mathbf{5} \longrightarrow \underset{\mathbf{6}}{[\bar{C}H_2COOEt]} + CO_2 \quad (2)$$

$$\mathbf{6} + PhSSPh \longrightarrow \underset{\mathbf{7}}{PhSCH_2COOEt} + PhS^- \quad (3)$$

Table 1. Effect of metal halide, solvent, and molar ratio of reactants

Molar ratio $CH_2(COOEt)_2$	$(PhS)_2$	MX	Solvent	Time h	Yield (%)[a] $PhSCH_2COOEt$	Others	
1	1	1.3 (LiCl)	HMPA	1.0	4		
1	1	1.0 (LiI)	HMPA	1.0	25		
1	1	1.2 (NaBr)	HMPA	1.1	21		
1	1	1.2 (KI)	HMPA	1.1	35		
1	1	1.1 (NaI)	HMPA	1.1	46		
1	2	1.2 (NaI)	HMPA	1.3	44[b]		
1	1	5 (NaI)	HMPA	0.8	45		
2	1	1 (NaI)	HMPA	1.0	82	Et(PhS)CHCOOEt	8
2	1	2 (NaI)	HMPA	1.0	84	Et(PhS)CHCOOEt	9
1	1	1 (NaI)	DMSO	1.0	13	$CH_2(COOEt)_2$	63
1	1	1 (NaCl)	DMSO	1.0	5	$CH_2(COOEt)_2$	75
1	1	1 (NaI)	sulfolane	1.0	12	$CH_2(COOEt)_2$	65

a) Yields were calculated based on diphenyl disulfide. b) Yield was calculated based on diethyl malonate.

$$\mathbf{6} + CH_2(COOEt)_2 \longrightarrow CH_3COOEt + \underset{\mathbf{8}}{\bar{C}H(COOEt)_2} \quad (4)$$

$$\mathbf{8} + PhSSPh \longrightarrow \underset{\mathbf{9}}{PhSCH(COOEt)_2} + PhS^- \quad (5)$$

$$PhS^- + EtX \longrightarrow PhSEt + X^- \quad (6)$$

$$\mathbf{9} + X^- \longrightarrow \underset{\mathbf{10}}{PhS\bar{C}HCOOEt} + EtX + CO_2 \quad (7)$$

$$\mathbf{10} + EtX \longrightarrow Et(PhS)CHCOOEt \quad (8)$$

As shown in Table 1, use of 2 equivalents of diethyl malonate caused a great increase of the yield, though addition of excess sodium iodide or diphenyl disulfide scarcely affected the yield. These facts suggest that proton transfer (Eq. 4) and the succeeding sulfenylation (Eq. 5) might be involved in the major pathway for the formation of ethyl (phenylthio)acetate and the direct sulfenylation (Eq. 3) might be less important in this case. The formation of ethyl α-(phenylthio)butyrate in the reaction using 2 equivalents of diethyl malonate also supports the importance of the pathway which involves proton transfer (Eqs. 5, 7, and 8).

When ethyl acetoacetate was used instead of diethyl malonate, (phenylthio)acetone (**11**) (47%) was obtained along with α,α-bis(phenylthio)acetone (**12**) (8%). The formation of α,α-bis(phenylthio)acetone also shows the occurrence of proton transfer.

$$CH_3COCH_2COOEt + (PhS)_2 \xrightarrow[HMPA]{NaI} \underset{\mathbf{11}}{PhSCH_2COCH_3} + \underset{\mathbf{12}}{(PhS)_2CHCOCH_3} + PhSEt + CO_2$$

Table 2. Effect of reaction temperature

Reaction temperature (°C)	Yield (%)	
	11	**12**
140—145	35	4
160	47	8
175	34	7

Table 3. Sulfenylation of geminal diesters, β-keto esters, and ethyl cyanoacetate

Reactant	Product					
$PhCOCH_2COOEt$	$PhSCH_2COPh$	**13**	36%	$PhCOCH_3$		30%
$NCCH_2COOEt$	$PhSCH_2CN$	**14**	23%	$Et(PhS)CHCN$	**15**	15%
				$(PhS)_2CHCN$	**16**	3%
n-$BuCH(COOEt)_2$	*n*-$Bu(PhS)CHCOOEt$	**17**	40%			
$PhCH_2CH(COOEt)_2$	$PhCH_2(PhS)CHCOOEt$	**18**	46%			
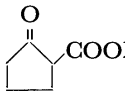	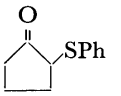	**19**	47%	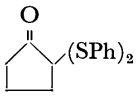	**20**	5%
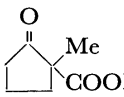	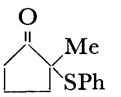	**21**	49%			
$Me(n\text{-}Pr)C(COOEt)_2$	$Me(n\text{-}Pr)C(PhS)COOEt$	**22**	60%			
$Me_2C(COOMe)_2$	$Me_2(PhS)CCOOMe$	**23**	71%			
$(PhCH)_2C(COOEt)_2$	$(PhCH_2)_2(PhS)CCOOEt$	**24**	66%			

Table 4. Physical properties and analytical data of the products

Product	IR, cm^{-1}	NMR, δ	Mp, (°C)	Ref.
3	1735 (C=O)	1.15 (3H, t), 3.48 (2H, s), 4.07 (2H, q), 7.00—7.52 (5H, m)	oil	5f
11	1710 (C=O)	2.18 (3H, s), 3.50 (2H, s), 7.20 (5H, s)	36—37	5c
12	1710 (C=O)	2.25 (3H, s), 3.75 (1H, s), 7.10—7.53 (10H, m)	42—43	5c
13	1670 (C=O)	4.10 (2H, s), 7.05—7.55 (8H, m), 7.68—8.15 (2H, m)	53—54	5d
14	2230 (C≡N)	3.45 (2H, s), 7.17—7.70 (5H, m)	oil	5e
15	2230 (C≡N)	1.15 (3H, t), 1.80 (2H, dq), 3.55 (1H, t), 7.20—7.81 (5H, m)	oil	
16	2220 (C≡N)	4.75 (1H, s), 7.17—7.85 (10H, m)	oil	
17	1735 (C=O)	1.12 (3H, t), 0.68—2.30 (9H, m), 3.85 (1H, t), 4.05 (2H, q), 7.05—7.55 (5H, m)	oil	5f
18	1730 (C=O)	1.02 (3H, t), 3.06 (2H, dd), 3.68—4.10 (1H, m) 3.94 (3H, q), 7.13—7.50 (5H, m), 7.18 (5H, s)	oil	5f
19	1740 (C=O)	1.60—2.50 (6H, m), 3.45 (1H, t), 7.05—7.65 (5H, m)	oil	5b
20	1740 (C=O)	1.60—2.50 (6H, m), 7.05—7.65 (10H, m)	oil	5b
21	1730 (C=O)	1.25 (3H, s), 1.57—2.73 (6H, m), 7.05—7.45 (5H, m)	oil	5a
22	1730 (C=O)	1.35 (3H, s), 1.17 (3H, t), 0.70—2.15 (7H, m), 4.07 (2H, q), 7.10—7.62 (5H, m)	oil	
23	1730 (C=O)	1.42 (6H, s), 3.56 (3H, s), 7.13—7.50 (5H, m)	41—43	
24	1730 (C=O)	1.08 (3H, t), 3.13 (4H, s), 3.98 (2H, q), 7.08 (10H, s), 7.00—7.52 (5H, m)	oil	

In order to increase the yield of **11** and the ratio of **11** to **12**, the influence of reaction temperature was examined, using HMPA and NaI as solvent and catalyst. Though the ratio scarcely changed, the highest yield of **11** was obtained at 160 °C (Table 2).

Then the reactions of various geminal diesters, β-keto esters, and ethyl cyanoacetate were carried out in HMPA in the presence of sodium iodide at 155—160 °C. α,α-Disubstituted malonic esters and β-keto esters gave the desired sulfenylated products in better yields than geminal diesters, β-keto esters, and α-cyano ester all of which possess active hydrogen. These results are summarized in Table 3. The NMR and IR spectral data of the sulfenylated compounds are also listed in Table 4.

In conclusion, the sulfenylation accompanied by dealkoxycarbonylation was proved to be a useful method for the synthesis of sulfenylated compounds, especially in the case of α,α-disubstituted malonic esters and β-keto esters.

Experimental

Materials. Alkali halides were used after drying at 110—120 °C for several hours in vacuo. HMPA was distilled over sodium hydride under reduced pressure.

Typical Example of the Sulfenylation. A mixture of dimethyl α,α-dimethylmalonate (320 mg, 2 mmol), diphenyl disulfide (436 mg, 2 mmol), sodium iodide (360 mg, 2 mmol), and HMPA (2 ml) was heated at 165—170 °C for 1 h. The mixture was then cooled to room temperature, poured into water (50 ml), and extracted with two portions of ether (50 ml). The organic layer was washed with water and dried over anhydrous sodium sulfate. After removal of the solvent under reduced pressure, the residue was separated by silica gel TLC (hexane–ether 6: 1), to give methyl α-(phenylthio)-isobutylate (**23**) (298 mg, 71%); mp 41—43 °C, IR(KBr) 1730 cm^{-1} NMR (CCl_4) δ= 1.4 (6H, s), 3.55 (3H, s), and 7.1—7.5 (5H, m). Found: C, 62.78; H, 6.63; S, 15.47%. Calcd for $C_{11}H_{14}O_2S$: C, 62.84; H, 6.71; S, 15.22%.

Ethyl α-benzyl-α-(phenylthio)hydrocinnamate (**24**) and ethyl α-methyl-α-(phenylthio)pentanoate (**22**) were obtained from the corresponding disubstituted malonates in a similar manner. Ethyl α-benzyl-α-(phenylthio)hydrocinnamate (**24**). Found: C, 76.37; H, 6.47; S, 8.26%. Calcd for $C_{23}H_{24}O_2S$; C, 76.57; H, 6.43; S. 8.50%. Ethyl α-methyl-α-(phenylthio)pentanoate (**22**). Found: C, 67.07; H, 7.89; S, 12.34%. Calcd for $C_{14}H_{20}O_2S$: C, 66.64; H, 7.99; S, 12.68%.

Other sulfenylated compounds were also obtained by practically the same method as described above. Their structures were confirmed by comparison of their spectral and elemental analyses with those of the authentic samples prepared according to the reported procedures.[5)]

References

1) A. P. Krapcho and A. J. Lovey, *Tetrahedron Lett.*, **1973**, 957.

2) A. P. Krapcho, G. A. Glynn, and B. J. Grenon, *Tetrahedron Lett.*, **1967**, 215.

3) M. Asaoka, K. Miyake, and H. Takei, *Chem. Lett.*, **1975**, 1149.

4) a) B. M. Trost and T. N. Salzmann, *J. Am. Chem. Soc.*, **95**, 6840 (1973); b) B. M. Trost and T. N. Salzmann, *J. Org. Chem.*, **40**, 148 (1975).

5) a) T. Kumamoto, S. Kobayashi, and T. Mukaiyama, *Bull. Chem,. Soc. Jpn.*, **45**, 866 (1972); b) S. Kobayashi, M. Thesis, Tokyo Institute of Technology, Tokyo, 1972; c) H. Iwasawa, M. Thesis, Tokyo Institute of Technology, Tokyo, 1975; d) L. M. Long, *J. Am. Chem. Soc.*, **68**, 2159 (1946); e) R. Dijikstra and H. J. Backer, *Recl. Trav. Chim. Pays-Bas*, **72**, 813 (1953); f) Authentic samples were synthesized by the action of sodium benzenethiolate on halo derivatives according to the procedures of L. M. Long or R. Dijkstra and H. J. Backer.

Synthesis of the Monoterpene Lactone from *Chrysanthemum flosculosum* L.

Shûichi YAMAGIWA, Hiroshi KOSUGI, and Hisashi UDA*

Chemical Research Institute of Non-Aqueous Solutions, Tohoku University, Katahira-2, Sendai 980

(Received March 2, 1978)

The synthesis of a lactonic constituent [(*Z*)-5-ethylidene-5,6-dihydro-3,6,6-trimethyl-2*H*-pyran-2-one] isolated from *Chrysanthemum flosculosum* L. is described. Dehydration of 5-ethyl-5,6-dihydro-5-hydroxy-3,6,6-trimethyl-2*H*-pyran-2-one derived from 5-ethyl-5,6-dihydro-6,6-dimethyl-3-phenylthio-2*H*-pyran-2-one *via* methylation, oxidation, [2,3]sigmatropic rearrangement, and saponification, gave the geoisomeric [(*E*)-5-ethylidene] lactone. Photochemical isomerization of the ethylidene side-chain furnished the natural lactone. The geometry of the ethylidene group in both isomers has been rigorously established.

The santolinyl group of monoterpenoids possesses the carbon skeleton **1**, which does not conform to the isoprene rule.[1] A representative member of this group of natural products is the crystalline lactone isolated as a minor polar constituent from *Chrysanthemum flosculosum* L.[2,3] Bohlmann and Grenz have assigned structure **2** to this lactone, but have not established the geometry of the ethylidene side-chain.[3,4]

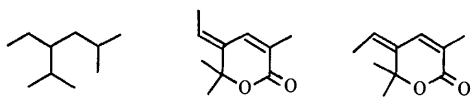

1 **2** **3**

The synthesis of both (*E*)- and (*Z*)-5-ethylidene isomers of this δ-lactone derivative, **2** and **3**, are reported which unambiguously establishes the structure of the natural lactone to be **3**. In view of the recent work on the reactions of (phenylthio)acetic acid and its ester,[5] and the rearrangement reactions of the α-phenylsulfinylacrylate derivatives,[6,7] the key intermediate chosen was the α-phenylthio-α,β-unsaturated δ-lactone **14**.

The Reformatsky reaction of ethyl α-bromobutyrate (**4**) with acetone in refluxing benzene gave the hydroxy ester **5** in 64% yield. Lithium aluminum hydride reduction of **5** afforded the glycol **6**, which was then transformed into the tetrahydropyranyloxy bromide **9** in 64% overall yield through the usual manner: monotosylation to **7**, substitution to the bromohydrin **8**, and finally tetrahydropyranylation (Scheme 1).

Methyl sodio(phenylthio)acetate (**10**), prepared from methyl (phenylthio)acetate by the action of sodium hydride in tetrahydrofuran and hexamethylphosphoric

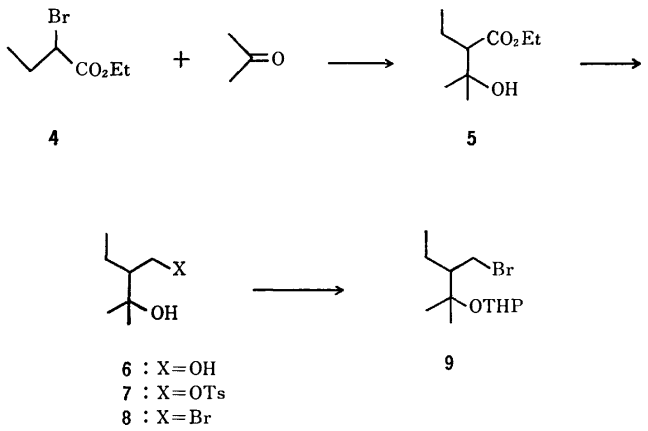

4 **5**

6 : X=OH
7 : X=OTs
8 : X=Br

9

Scheme 1.

triamide, reacted well with the bromide **9** to produce the substitution product **11**. Hydrolysis and lactonization by treating with *p*-toluenesulfonic acid, initially in boiling aqueous tetrahydrofuran and then in boiling benzene gave a 72% yield of a stereoisomeric mixture of the δ-lactone **12**. The lactone **12** was treated with sodium periodate in dilute methanol to give the sulfoxide **13**. Exposure of **13**, without purification, to trifluoroacetic anhydride in dichloromethane directly provided the desired intermediate **14**, mp 73—74 °C, in 80% yield from **12** through the spontaneous elimination of trifluoroacetic acid from the initially formed Pummerer rearrangement product, α-phenylthio-α-trifluoroacetoxy lactone (Scheme 2). The structure of **14** was verified by its analytical and spectroscopic properties.

The planned synthesis of **2** or **3** involved the one-step introduction of a methyl group at the α-position and of

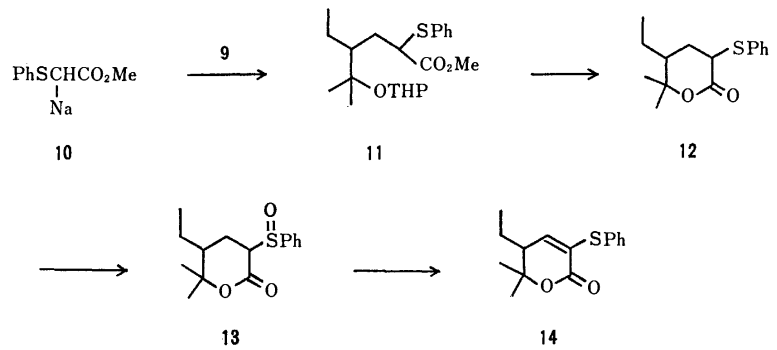

10 **11** **12**

13 **14**

Scheme 2.

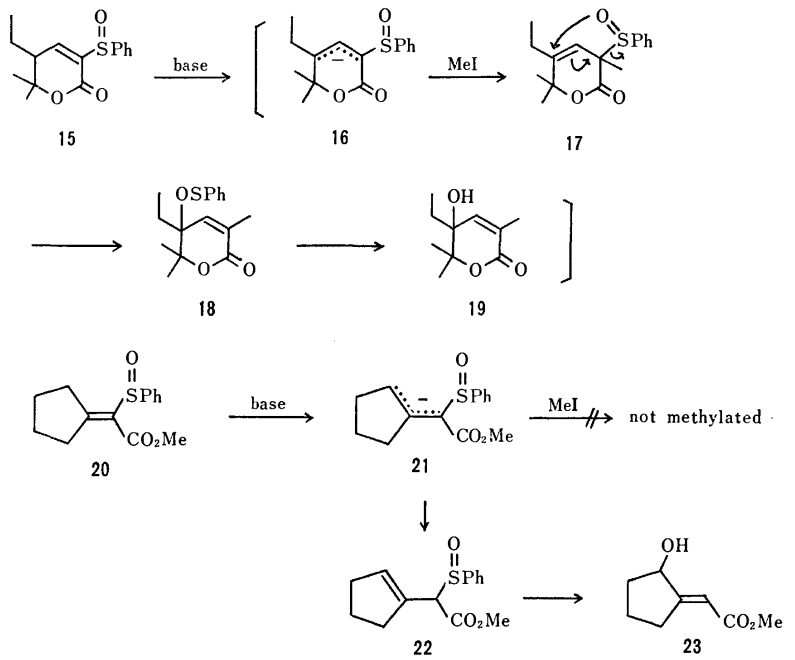

Scheme 3.

a hydroxyl group at the γ-position in the α-sulfinyl δ-lactone system **15** by applying the doubly double-bond migrating rearrangement reaction observed in the α-phenylsulfinylacrylate derivatives.[6,7] If the carbanion species **16** derived from **15** by an appropriate base reacts more rapidly with methyl iodide than the [2,3]-sigmatropic rearrangement of the sulfinyl group, the methylated sulfoxide **17** should be produced. Subsequent rearrangement and hydrolysis of the sulfenate **18** might give the precursor **19** of the natural product (Scheme 3). However, a number of preliminary experiments using methyl cyclopentylidene(phenylsulfinyl)acetate (**20**) as a model compound suggests that such a reaction process (alkylative rearrangement) is not applicable, since the migration of the double-bond of **20** and the [2,3]sigmatropic rearrangement of the resulting isomer **22** are extremely facile; methylation of the anion **21** did not take place, compound **23** being the only isolable product.[7]

The introduction of functional groups, methyl and hydroxyl, was then attempted in a stepwise manner (Scheme 4). Treatment of **14** with potassium *t*-butoxide in tetrahydrofuran and hexamethylphosphoric triamide and then with methyl iodide afforded the α-methylated product **24** in 72% yield. Oxidation of **24** with two equivalents of *m*-chloroperbenzoic acid in dichloromethane at 0 °C gave the rearranged sulfinyloxy lactone **27**. Compound **27** showed a very complicated pattern in the NMR spectrum, indicating that **27** was actually a mixture of diastereomers with respect to the γ-carbon and sulfur atoms. Compound **27** was treated with a catalytic amount of sodium methoxide in methanol to give a single crystalline hydroxy lactone **19**, mp 81—82 °C, in 65% yield from **24**; there was no indication of the presence of a translactonization product (γ-lactone). It should be noted that both the [2,3]sigmatropic rearrangement of the sulfoxide **25** and the oxidation of the resulting sulfenate **26** to the sulfinate **27** proceeded very rapidly. When one equivalent of *m*-chloroperbenzoic acid was employed in the oxidation of **24**, neither the sulfoxide **25** nor the sulfenate **26** was isolated; unchanged starting sulfide **24** and the sulfinate **27** were obtained in equal amounts.

We now considered the conformation of the ethyl

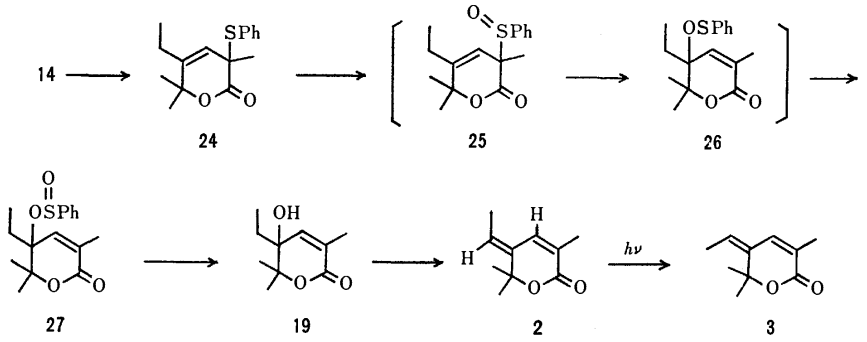

Scheme 4.

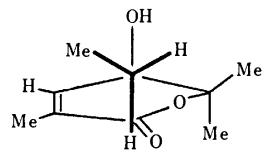

19a

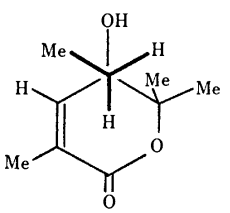

19b

group of **19** because this determined whether, at the next dehydration stage, the *E*- (**2**) or *Z*- (**3**) ethylidene group would be preferentially formed. Two conformations **19a** (quasi-equatorial ethyl) and **19b** (quasi-axial ethyl) are possible for the 2-pyrone ring of **19**. In both cases, if the conformation, in which the ring hydroxyl group and the one hydrogen atom of the ethyl-methylene are anti-periplanar, is the favorable one for dehydration, the methyl of the ethyl group would be apart from the gem-dimethyl group as a result of the severe steric interaction between these methyl groups. Furthermore, in the dehydration product the (*E*)-5-ethylidene isomer would be thermodynamically (or sterically) more stable than the (*Z*)-isomer due to the same steric interaction. Hence, dehydration of **19** would be expected to produce preferentially the isomer having the *E*-ethyliedne group.

Compound **19** was heated in boiling benzene containing a catalytic amount of *p*-toluenesulfonic acid and afforded a 63% yield of an unsaturated lactone **2** as the sole product. The lactone **2** was also obtained by treating **19** with thionyl chloride–pyridine at 0 °C. The spectral properties are fully in accord with the assigned structure **2** including the geometry of the ethylidene group. In the 100 MHz NMR spectroscopy, irradiation of the gem-dimethyl signal at δ 1.52 caused 11% of the NOE enhancement of the ethylidene olefinic proton signal at δ 5.72. Furthemore irradiation of the olefinic methyl signal centered at δ 1.92 resulted in 7% of the NOE enhancement of the ring olefinic proton signal at δ 7.00. Thus, the configuration of the ethylidene group of this lactone should be evidently *E*-geometry as expected.

It was found, however, that this compound **2** is oily and the spectral data (see Experimental section) is not entirely consistent with the reported values for the natural lactonic constituent. Consequently, the natural lactone must have the structure **3** possessing the *Z*-ethylidene side-chain, and the synthesis of **3** was achieved by photochemical isomerization. Irradiation of **2** in benzene with 100 W high-pressure mercury lamp through Pyrex provided the isomeric crystalline lactone **3**, mp 63.5—64.5 °C, in 73% yield. Although, the IR and UV absorption maxima [ν_{max} (CCl_4) 1710, 1640, and 1620 cm^{-1}; λ_{max} (EtOH) 276.5 nm (ε=17360)] are slightly different from the reported ones [ν_{max} (phase—not reported) 1725, 1650, and 1630 cm^{-1}; λ_{max} (solvent—not reported) 266.5 nm (ε=14900)], the melting point, the NMR spectrum [δ (CCl_4) 1.62 (s, 6H), 1.88 (s, 3H), 1.91 (d, J=7.0 Hz, 3H), 5.58 (q, J=7.0 Hz, 1H), and 6.42 (s, 1H)], and the mass spectrum [M^+ *m/e* 166 (35%), 151 (100%), and 123 (29%)] were consistent with the reported values for the natural lactone: mp 64.5 °C the NMR spectrum [δ (solvent—not reported) 1.60 (s, 6H), 1.87 (s, 3H), 1.89 (d, J=7.0 Hz, 3H), 5.57 (q, J=7.0 Hz, 1H), and 6.42 (s, 1H)], and mass spectrum [M^+ *m/e* 166 (25%), 151 (100%), and 123 (22%)].[8] From the present study, we conclude that the natural lactone has been assigned as (*Z*)-5-ethylidene-5,6-dihydro-3,6,6-trimethyl-2*H*-pyran-2-one.

Experimental

All the melting points were taken on a Yamato melting point apparatus and are uncorrected. Small amounts of liquid products were purified by evaporative short-path distillation; oil-bath temperatures are recorded. IR spectra were obtained with a Hitachi EPI-S2 or G2 spectrophotometer. A UV spectrum was taken on a Hitachi EPS-3T spectrometer. NMR spectra of solutions in carbon tetrachloride (unless otherwise indicated) were recorded with a JEOL PMX-60 (60 MHz) or PS-100 (100 MHz) instrument, with TMS as an internal standard; coupling constants are given in Hz. Mass spectra were taken with a Shimadzu LKB-9000 instrument. Microanalyses were carried out in the microanalytical laboratory of this Institute.

Tetrahydropyranyl Ether of 3-Bromomethyl-2-methyl-2-pentanol (8). To a slurry of zinc powder (11 g, 0.17 g atom) and iodine (a catalytic amount) in boiling anhydrous benzene (200 ml) was added dropwise over a period of 1 h a solution of ethyl α-bromobutyrate (26.5 g, 0.136 mol) and acetone (35 ml, 0.475 mol) in anhydrous benzene (40 ml), and the reaction mixture refluxed for 2 h. Dilute sulfuric acid (6 M, 150 ml) was added to the cooled reaction mixture, and the resulting solution vigorously stirred for 30 min at room temperature. The water layer was extracted twice with ether. The combined organic layers were washed twice with water and saturated brine, and dried. After removal of the solvent, the residual liquid was fractionated under reduced pressure, and the fraction of bp 62—63 °C/5 Torr (1 Torr≈133.322 Pa) collected to yield 15.22 g (64%) of ethyl 2-ethyl-3-hydroxy-3-methylbutyrate (**5**): IR (CCl_4) 3450, 1720 (sh), 1705, 1460, 1375, 1190, and 1160 cm^{-1}; NMR δ 0.89 (3H, t, J=7.0), 1.15 (6H, s), 1.27 (3H, t, J=7.0), 1.53 (2H, quint, J=7.0), 2.20 (1H, t, J=7.0), 2.81 (1H, s, OH), and 4.12 (2H, q, J=7.0).

To a slurry of lithium aluminum hydride (0.7 g, 18.5 mmol) in anhydrous ether (50 ml) was added dropwise a solution of **5** (1.74 g, 10 mmol) in anhydrous ether (20 ml) at room temperature under nitrogen, and the reaction mixture stirred for 30 min at room temperature. Ethyl acetate (10 ml) was added slowly to the mixture at 0 °C to decompose the excess hydride, and then a minimum amount of water was added until a jelly-like precipitate separated from the ether solution. The ether layer was decanted, and the precipitate thoroughly washed with ether. The combined ether solutions were evaporated under reduced pressure to give 1.32 g (100%) of 2-ethyl-3-methyl-1,3-butanediol (**6**): NMR δ 1.17 (3H, s), 1.28 (3H, s), 0.70—2.30 (6H, m), 3.74 (2H, m), and 4.70 (2H, m).

To a solution of **6** (660 mg, 5 mmol) in anhydrous pyridine (7 ml) was added portionwise *p*-toluenesulfonyl chloride (1.33 g, 7 mmol) at 0 °C, and the reaction mixture allowed to stand for 5 h at room temperature. Chopped ice was added to the mixture, and the resulting solution poured into a mixture of ether and water in a separatory funnel. The ether layer was washed with dilute HCl solution and twice with saturated brine. Evaporation of the ether left 1.22 g (86%) of 2-ethyl-3-hydroxy-3-methylbutyl *p*-toluenesulfonate (**7**): NMR δ 0.50—2.30 (6H, m), 1.13 (3H, s), 1.16 (3H, s),

1.97 (1H, br s), 2.46 (3H, s), 4.10 (2H, d, J=4.0), 7.24 (2H, d, J=8.0), and 7.74 (2H, d, J=8.0).

To a solution of sodium bromide (2.04 g, 20 mmol) in DMSO (15 ml) was added dropwise a solution of **7** (2.86 g, 10 mmol) in DMSO (7 ml) at 50 °C with stirring. After stirring at 60 °C for 30 min, more sodium bromide (2.5 g, 24 mmol) was added, and the reaction mixture was stirred for a further 2.5 h at 60 °C. The mixture was poured into water and extracted twice with ether. The combined ether extracts were washed twice with water and saturated brine. Evaporation of the ether gave 2.02 g (100%) of 3-bromomethyl-2-methyl-2-pentanol (**8**): bp 60—90 °C/47 Torr; IR (CCl_4) 3400, 1460, 1370, 1230, and 1115 cm^{-1}; NMR δ 0.50—2.30 (6H, m), 1.17 (3H, s), 1.21 (3H, s), 2.20 (1H, br s), and 3.27—3.83 (2H, m). Found: C, 42.96; H, 7.69; Br, 41.58%. Calcd for $C_7H_{15}OBr$: C, 43.09; H, 7.75; Br, 40.96%.

To a solution of **8** (2.5 g) and dihydropyrane (1.7 g) in CH_2Cl_2 (30 ml) was added a catalytic amount of anhydrous *p*-toluenesulfonic acid at 0 °C. After stirring for 30 min at room temperature, pyridine (2 drops) was added, and the mixture washed with saturated brine. The aqueous layer was further extracted with CH_2Cl_2. The combined organic layers were evaporated under reduced pressure and the residue chromatographed on silica gel (50 g) with petroleum ether to give 2.9 g (75%) of the tetrahydropyranyl ether **9**: NMR δ 0.60—2.50 (12H, m), 1.27 (6H, split s), 3.00—4.30 (4H, m), and 4.80 (1H, m).

*5-Ethyl-6,6-dimethyl-3-phenylthiotetrahydropyran-2-one (**12**).* To a slurry of sodium hydride (45% mineral oil dispersion, 2.2 g, washed three times with petroleum ether and once with anhydrous THF) in anhydrous THF (40 ml) was added dropwise a solution of methyl (phenylthio)acetate (5.5 g, 0.03 mol) in anhydrous THF (10 ml) at 0 °C under nitrogen, and the resulting mixture stirred for 1 h at 0 °C. A solution of **9** (14 g, 0.05 mol) in anhydrous THF (10 ml) and then HMPA (25 ml, 0.143 mol) were added dropwise to the above mixture. After stirring overnight at room temperature, the reaction mixture was poured into ice-water and extracted twice with ether. The combined extracts were washed twice with water and saturated brine. Evaporation of the ether left an oil (13.7 g), which was chromatographed on silica gel (150 g) with petroleum ether—petroleum ether–ether (gradient)—ether to give 9.2 g of methyl 4-[1-methyl-1-(tetrahydropyranyloxy)-ethyl]-2-phenylthiohexanoate (**11**): NMR δ 0.50—2.50 (20H, m), 3.00—4.20 (3H, m), 3.60 (3H, s), 4.80 (1H, m), and 7.00—7.70 (5H, m).

A solution of **11** (9.2 g) in dilute THF (80%, 50 ml) containing *p*-toluenesulfonic acid (0.1 g) was heated under reflux for 1 h. The reaction mixture was poured into ice-water and extracted twice with ether. The combined ether extracts were washed with brine and evaporated. The residue (8.53 g) was dissolved in anhydrous benzene (30 ml) containing anhydrous *p*-toluenesulfonic acid (a catalytic amount), and the solution heated under reflux for 40 min using a water separator. The reaction mixture was poured into ice-water, and the water layer extracted twice with ether. The combined organic layers were washed with saturated brine. After removal of the solvent, the residue (6.55 g) was chromatographed on silica gel (70 g) with petroleum ether—1: 2 petroleum ether-ether to give 5.7 g [72% based on methyl (phenylthio)-acetate] of **12**: bp 140 °C/1 Torr; IR (CCl_4) 1725, 1275, and 1125 cm^{-1}; NMR δ 1.03, 1.20, 1.34, and 1.40 (total 6H, each s), 0.50—2.80 (8H, m), 3.50—4.00 (1H, m), and 7.00—8.00 (5H, m). Found: C, 68.16; H, 7.63%. Calcd for $C_{15}H_{20}O_2S$: C, 68.49; H, 7.88%.

*5-Ethyl-5,6-dihydro-6,6-dimethyl-3-phenylthio-2H-pyran-2-one (**14**).* To a solution of **12** (1.27 g, 4.8 mmol) in methanol (30 ml) was added dropwise a solution of $NaIO_4$ (1.23 g, 5.75 mmol) in water (10 ml) at 0 °C, and the reaction mixture stirred for 18 h at room temperature. Inorganic material was removed by filtration, and the filtrate extracted twice with CH_2Cl_2. The combined extracts were washed with saturated brine. Evaporation of the solvent gave 1.34 g (99%) of 5-ethyl-6,6-dimethyl-3-phenylsulfinyltetrahydropyran-2-one (**13**): IR (CCl_4) 1720, 1275, 1135, 1085, and 1050 cm^{-1}; NMR δ 0.30—3.00 (14H, m), 3.40—4.50 (1H, m), and 7.00—8.30 (5H, m).

To a solution of **13** (1.14 g, 4.05 mmol) in CH_2Cl_2 (30 ml) was added dropwise a solution of trifluoroacetic anhydride (1 ml, 7.0 mmol) in CH_2Cl_2 (10 ml) at 0 °C. After stirring for 2 h at room temperature, the solvent was removed under reduced pressure. The residue (1.29 g) was chromatographed on silica gel (20 g) with 5: 1—1: 1 petroleum ether-ether to give 922 mg (86%) of **14**: mp 73—74 °C from petroleum ether-ether; IR ($CHCl_3$) 1710, 1600, 1140, and 1020 cm^{-1}; NMR ($CDCl_3$) δ 0.87 (3H, t, J=7.0), 1.00—1.80 (2H, m), 1.34 (3H, s), 1.45 (3H, s), 2.30 (1H, ddd, J=10.0, 4.0, and 4.0), 6.15 (1H, d, J=4.0), and 7.20—7.60 (5H, m). Found: C, 68.42; H, 6.99%. Calcd for $C_{15}H_{18}O_2S$: C, 68.68; H, 6.92%.

*5-Ethyl-3,6-dihydro-3,6,6-trimethyl-3-phenylthio-2H-pyran-2-one (**24**).* A solution of **14** (493 mg, 1.88 mmol) in anhydrous THF (4 ml) was added dropwise to a solution of potassium *t*-butoxide (260 mg, 2.3 mmol) in anhydrous THF (4 ml) at −60 °C under nitrogen, and the resulting solution was stirred for 1.5 h at −60——40 °C. Methyl iodide (0.5 ml, 8 mmol) and then HMPA (1 ml, 5.6 mmol) were added dropwise *via* syringes to the above solution at −60 °C. After stirring at −60——28 °C for 2 h, the reaction mixture was poured into ice-water, and the resulting aqueous solution extracted twice with ether. The combined extracts were washed with saturated brine and evaporatd. The residue (490 mg) was chromatographed on preparative TLC using silica gel with 1: 1 petroleum ether–ether to give 374 mg (72%) of **24**: bp 100 °C/1 Torr; IR (CCl_4) 1725. 1295, and 1150 cm^{-1}; NMR δ 1.10 (3H, t, J=7.0), 1.13 (3H, s), 1.36 (3H, s), 1.47 (3H, s), 2.01 (2H, q, J=7.0), 5.31 (1H, split s), and 7.17—7.60 (5H, m). Found: C, 69.70; H, 7.58%. Calcd for $C_{16}H_{20}O_2S$: C, 69.54; H, 7.30%.

*5-Ethyl-5,6-dihydro-5-hydroxy-3,6,6-trimethyl-2H-pyran-2-one (**19**).* To a solution of **24** (374 mg, 1.35 mmol) in CH_2Cl_2 (20 ml) was added portionwise *m*-chloroperbenzoic acid (80%, 640 mg, 3 mmol) at 0 °C. After stirring for 30 min at 0 °C, the reaction mixture was poured into a mixture of ice and dilute NaOH solution (3M), and the water layer extracted twice with CH_2Cl_2. The combined extracts were washed with water and saturated brine. Evaporation of the solvent gave 422 mg of 5-ethyl-5,6-dihydro-3,6,6-trimethyl-5-phenylsulfinyloxy-2*H*-pyran-2-one (**27**): IR (CCl_4) 1730 and 1150 cm^{-1}.

A solution of **27** in anhydrous methanol (2 ml) was added dropwise to a solution of sodium methoxide (a catalytic amount) in anhydrous methanol (3 ml) at 0 °C. After stirring at room temperature for 1 h, the mixture was poured into ice-water and extracted twice with ether. The combined extracts were washed with water and saturated brine, and evaporated. The residue (374 mg) was chromatographed on preparative TLC using silica gel with 1: 2 petroleum ether-ether to give 163 mg (66%) of **19**: mp 81—82 °C from petroleum ether-ether; IR ($CHCl_3$) 3570, 3400, 1700, 1120, and 1100 cm^{-1}; NMR ($CDCl_3$) δ 1.00 (3H, t, J=7.0), 1.38 (3H, s), 1.46 (3H, s), 1.60 (2H, q, J=7.0), 1.91 (3H, d, J=1.5), 3.27 (1H, br., OH), and 6.50 (1H, q, J=1.5). Found: C, 65.35; H, 8.42%. Calcd for $C_{10}H_{16}O_3$: C, 65.91; H, 8.75%.

(E)-5-Ethylidene-5,6-dihydro-3,6,6-trimethyl-2H-pyran-2-one (2). A solution of **19** (91 mg) in anhydrous benzene (7 ml) containing a trace of anhydrous *p*-toluenesulfonic acid was heated under reflux for 2 h using a water separator. The reaction mixture was diluted with ether, washed with water and brine, and evaporated. The residual liquid was chromatographed on preparative TLC using silica gel with 1:1 petroleum ether–ether to give 52 mg (63%) of **2**: bp 70 °C/1 Torr; IR (CCl_4) 1720 (sh), 1700, and 1115 cm^{-1}; NMR δ 1.52 (6H, s), 1.85 (3H, d, J=7.0), 1.98 (3H, s), 5.72 (1H, q, J=7.0), and 7.00 (1H, s); mass (70 eV) *m/e* 166 (M^+, 40%), 151 (100%), and 123 (25%). Found: C, 72.27; H, 8.73%. Calcd for $C_{10}H_{14}O_2$: C, 72.26; H, 8.49%.

(Z)-5-Ethylidene-5,6-dihydro-3,6,6-trimethyl-2H-pyran-2-one (3) = the Natural Lactone. A solution of **2** (67 mg) in anhydrous benzene (30 ml) in a Pyrex tube was externally irradiated for 3 h with a 100-W high-pressure mercury lamp under running water cooling and nitrogen. After removal of the solvent under reduced pressure, the residue was chromatographed on preparative TLC using silica gel with 1:1 petroleum ether–ether to give 18 mg (27%) of the recovered **2** and 51 mg (73%) of **3**: mp 63.5—64.5 °C from petroleum ether. Found: C, 72.60; H, 8.54%. Calcd for $C_{10}H_{14}O_2$: C, 72.26; H, 8.49%.

Acknowledgment is made to the Ministry of Education of Japan for financial support (a Grant-in-Aid for Scientific Research, No. 147028).

References

1) For a Review see S. Nozoe, "Natural Products Chemistry," ed by K. Nakanishi, T. Goto, S. Itô, S. Natori, and S. Nozoe, Kodansha, Tokyo, and Academic Press, New York (1974), Vol. 1, p. 42, and references cited therein.
2) F. Bohlmann and G. Florenz, *Chem. Ber.*, **99**, 990 (1966).
3) F. Bohlmann and M. Grenz, *Tetrahedron Lett.*, **1969**, 2413.
4) F. Bohlmann, private communication.
5) S. Yamagiwa, N. Hoshi, H. Sato, H. Kosugi, and H. Uda, *J. Chem. Soc., Perkin Trans. 1*, **1978**, 214.
6) H. Kosugi, H. Uda, and S. Yamagiwa, *J. Chem. Soc., Chem. Commun.*, **1975**, 192.
7) S. Yamagiwa, H. Sato, N. Hoshi, H. Kosugi, and H. Uda, *J. Chem. Soc., Perkin Trans. 1*, in press
8) We could not directly compare the physical properties of the synthetic sample with those of the natural one, because the physical data and a pure sample of the natural product were not available.[4)]

A New Catalyst for the Low Temperature Oxo Process with the Characteristic of Easy Separation[1)]

Akio MATSUDA,* Shigemitsu SHIN, Jun-ichi NAKAYAMA
Ken-ichiro BANDO, and Kazuhisa MURATA
National Chemical Laboratory for Industry, Mita, Meguro-ku, Tokyo 153
(Received March 6, 1978)

A new type of catalyst, a cobalt carbonyl-complex has been found for homogeneous hydroformylation. The complex has been prepared from $Co_2(CO)_8$ and the ethylene glycol diester of 3-(2-pyridyl)propionic acid as a ligand. The catalyst is active even at the low temperature of 50 °C and very low carbon monoxide pressure range of less than 1 kg/cm². On subsequent cooling it separates from the reaction product. The ligand was prepared by the hydroesterification of 2-vinylpyridine with carbon monoxide and methanol (or ethanol), followed by the transesterification with ethylene glycol. The effect of the partial pressures of carbon monoxide and hydrogen on the product composition and on the recovery of the catalyst was examined. The catalytic activity of the new complex is considerably higher than that of $Co_2(CO)_8$ at a lower temperature. The selectivity to linear aldehyde in the presence of new complex is significantly higher than in the presence of $Co_2(CO)_8$ when the hydrogen to carbon monoxide ratio (H_2/CO) in gas phase is high, but this difference in selectivity is small when the above gas ratio is normal. The new complex can be applied as catalyst for removal of carbon monoxide in hydrogen by means of oxo process.

Catalyst recovery and recycling in the homogeneously catalyzed oxo process are very important from an industrial point of view, and many reports have been published concerning the separation of the catalyst from the reaction product. In the cobalt catalyzed process, for example, Moffat has developed a catalyst recovery and recycling system consisting of a tetracarbonylhydridocobalt-poly(2-vinylpyridine) complex.[2,3)] In the case of the rhodium catalyzed oxo process, even more efforts have been devoted to catalyst recovery. Haag *et al.* have attempted to insolubilize the rhodium-oxo catalyst by complex formation with phosphin- or amine-polymer ligands;[4)] Bayer *et al.* have prepared a homogeneous rhodium-oxo catalyst attached to a soluble phosphine-polymer,[5)] a catalyst which is easily separated from the reaction product by filtration, *etc.*

Previously, it has been reported that a cobalt carbonyl-pyridine complex catalyst for the homogeneous hydroesterification spontaneously separates from the reaction product.[6)] The separated catalyst phase consisted of an ionic complex: $H_2Co_3(CO)_9(py)_5$, where py represents pyridine. This complex proved to be of an ion-pair structure: $\{Co(H^+)_2(py)_5(CO)\}\{Co(CO)_4^-\}_2$; it is insoluble in hydrocarbons and ether, but soluble in alcohols, ketones, aldehydes and pyridine. Although the complex can also be used for hydroformylation, it does not separate from the hydroformylation product, since it is soluble in aldehydes.

The present paper deals with a new oxo catalyst which is derived from $Co_2(CO)_8$ and ethylene bis-(3-(2-pyridyl)propionate) (hereafter abbreviated as EBP), and soluble under the reaction conditions, but which spontaneously separates from the reaction product on cooling to room temperature. Also an interesting feature of the new catalyst is that it is active in the low temperature range of 50 to 70 °C. As a result, the hydroformylation can be carried out under a very low carbon monoxide partial pressure, so that, it can be used as a catalyst for the removal of carbon monoxide in hydrogen by means of the oxo process. For example, when hydrogen containing 4 to 6% of carbon monoxide was allowed to react with excess olefin in the presence of the catalyst in a suitable solvent at 50 to 60 °C, carbon monoxide was almost completely consumed by the hydroformylation, reasonably pure hydrogen containing less than 0.1% of carbon monoxide being left in the gas phase as a result.

Experimental

Preparation of Ligand. EBP was prepared by the transesterification of methyl (or ethyl) 3-(2-pyridyl)propionate with ethylene glycol.

Hydroesterification of 2-Vinylpyridine with Carbon Monoxide and Methanol(or Ethanol): Hydroesterification was carried out in a 300 ml stainless steel autoclave equipped with a vertical agitator. After charging with 2-vinylpyridine, an alcohol, solvent, and $Co_2(CO)_8$, the autoclave was flushed and pressurized with carbon monoxide, and heated to the reaction temperature. The pressure was kept constant during the reaction by supplying carbon monoxide from a pressure storage vessel through a pressure regulator, while the temperature was kept constant by a temperature controller. After the solvent and alcohol were distilled off under normal pressure, unchanged 2-vinylpyridine and methyl (or ethyl) 3-(2-pyridyl)propionate were distilled under reduced pressure.

Methyl 3-(2-pyridyl)propionate: bp 118 °C/10 mmHg, IR spectrum 1730 cm^{-1} (ester).

Ethyl 3-(2-pyridyl)propionate: bp 122 °C/10 mmHg, IR spectrum 1730 cm^{-1} (ester).

Some typical results of the hydroesterification experiments are listed in Table 1.

Transesterification with Ethylene Glycol: Transesterification was carried out with ethlene glycol (0.1 mol) in the presence of excess methyl(or ethyl) 3-(2-pyridyl)propionate (0.22—0.4 mol) at 200 °C, the liberated methanol (or ethanol) being continuously distilled off. The reaction time necessary to attain 64 to 87% yield of diester based on ethylene glycol was 20 to 40 h in the absence of a catalyst, but decreased to 2 to 5 h in the presence of sodium methoxide (0.2—0.4 mmol).

Hydroformylation of 1-Decene. Reactions were carried out in the same apparatus by essentially the same procedure as in the hydroesterification experiments except that reactions in a lower pressure range (10—50 kg/cm²) were carried out

Table 1. Hydroesterification of 2-vinylpyridine

Exp. No.	Temp (°C)	Press. (kg/cm²)	Time (h)	Alcohol (mol)	Conv.[a] (%)	Yield[b] (%)	Bottom[c] (%)
1	150	100	5	CH_3OH (0.25)	80.0	49.0	31
2	170	100	5	CH_3OH (0.25)	96.2	58.0	38
3	170	70	5	CH_3OH (0.25)	71.4	45.2	26
4	120	40	2	C_2H_5OH (1)	76.0	33.6	42
5	140	50	2	C_2H_5OH (1)	86.3	64.8	21
6	170	70	2	C_2H_5OH (1)	94.7	66.4	28
7[d]	170	70	2	C_2H_5OH (2.7)	95.4	70.4	25

2-Vinylpyridine 0.25 mol, $Co_2(CO)_8$ 1 g, benzene (solvent) 100 ml. a) Conversion of 2-vinylpyridine. b) Yield of methyl (or ethyl) 3-(2-pyridyl)propionate (mol %) from 2-vinylpyridine. c) Yield (wt %) of resinous distillation bottom based on the amount of 2-vinylpyridine used. d) Experiment No. 7 was carried out in the absence of benzene.

in a 400 ml autoclave fitted with windows for observation during the reaction.

Aldehydes were obtained by distilling the reaction product under reduced pressure. The crude aldehyde obtained was separated into four fractions by distillation with a rectifying column of a spining band type, and each fraction identified by IR and ^{13}C-NMR spectra.

Fraction 1 (undecanal): bp 62 °C/2 mmHg.

Fraction 2 (2-methyldecanal): bp 57.5 °C/2 mmHg.

Fraction 3 (2-ethylnonanal): bp 53.2—53.5 °C/2 mmHg.

Fraction 4 (mixture of 2-propyl octanal and 2-butyl heptanal): bp 52 °C/2 mmHg. IR spectra of these fractions showed an absorption attributable to formyl group at 1735 cm^{-1}.

Identification by Means of ^{13}C-NMR Spectra. Spectra were measured with Varian XL 100.

Methyl 3-(2-pyridyl)propionate

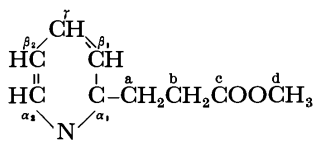

carbon	α_1	α_2	β_1	β_2	γ
ppm	160.5	149.6	123.3	121.7	136.7

a	b	c	d
33.0	33.0	173.5	51.5

Ethyl 3-(2-pyridyl)propinate

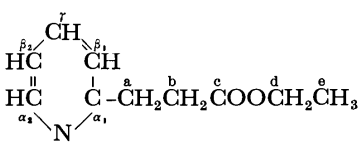

carbon	α_1	α_2	β_1	β_2	γ
ppm	160.8	149.8	123.3	121.7	136.5

a	b	c	d	e
33.5	33.5	173.0	60.4	14.5

Undecanal

$CH_3{}_{a}CH_2{}_{b}CH_2{}_{c}CH_2{}_{d}CH_2{}_{e}CH_2{}_{f}CH_2{}_{g}CH_2{}_{h}CH_2{}_{i}CH_2{}_{j}CHO{}_{k}$

carbon	a	b	c	d	e	f
ppm	14.5	23.4	32.7	30.3	30.3	30.3

g	h	i	j	k
30.3	30.3	22.8	44.3	200.6

2-Methyldecanal

$CH_3{}_{a}CH_2{}_{b}CH_2{}_{c}CH_2{}_{d}CH_2{}_{e}CH_2{}_{f}CH_2{}_{g}CH_2{}_{h}CH_2{}_{i}CH(CH_3){}_{j}CHO{}_{k}$

carbon	a	b	c	d	e	f
ppm	14.5	23.4	32.7	30.3	30.3	30.3

g	h	i	j	k
27.7	31.3	46.7	13.7	202.9

2-Ethylnonanal

$CH_3{}_{a}CH_2{}_{b}CH_2{}_{c}CH_2{}_{d}CH_2{}_{e}CH_2{}_{f}CH_2{}_{g}CH_2{}_{h}CH(CH_2CH_3){}_{i}{}_{j}CHO{}_{k}$

carbon	a	b	c	d	e	f
ppm	14.5	23.4	32.6	29.9	30.5	27.8

g	h	i	j	k
29.1	53.9	22.5	11.8	203.1

2-Propyloctanal

$CH_3{}_{a}CH_2{}_{b}CH_2{}_{c}CH_2{}_{d}CH_2{}_{e}CH_2{}_{f}CH_2{}_{g}CH(CH_2CH_2CH_3){}_{h}{}_{i}{}_{j}CHO{}_{k}$

carbon	a	b	c	d	e	f
ppm	14.4	23.5	32.7	30.0	27.7	29.6

g	h	i	j	k
52.4	31.8	21.0	14.4	203.1

2-Butylheptanal

$CH_3{}_{a}CH_2{}_{b}CH_2{}_{c}CH_2{}_{d}CH_2{}_{e}CH_2{}_{f}CH(CH_2CH_2CH_2CH_3){}_{g}{}_{h}{}_{i}{}_{j}CHO{}_{k}$

carbon	a	b	c	d	e	f
ppm	14.4	23.5	32.7	27.5	29.6	52.4

g	h	i	j	k
29.3	30.0	23.2	14.4	203.1

Isomerized decenes and decane formed by the isomerization and the hydrogenation of 1-decene were determined by gas chromatography (squalane, 0.25ϕ, 90 m, 90 °C). Dissolved cobalt in the reaction product was analyzed by heating an aliquot with 1.5M-sulfuric acid, followed by the chelate titration method.

Results

Effect of Recycling the Catalyst. Results of the hydroformylation of 1-decene carried out by recycling the initial catalyst are listed in Table 2.

TABLE 2. HYDROFORMYLATION OF 1-DECENE

Initial catalyst (run No. 1) was prepared *in situ* from 8 mmol of $Co_2(CO)_8$ and 20 mmol of EBP. $H_2/CO=1$, 1-decene 0.2 mol, liquid paraffin (solvent) 30 g.

Run No.		1	2	3	4
Temp (°C)		80	80	100	80
Press. (kg/cm²)		50	20	50	50
Time (h)		4	2	1	4
Conv. (%)		64.6	73.2	81.3	90.1
Select. (%)	A_1	65.8	47.9	54.9	64.1
	A_2	22.8	30.9	27.1	22.7
	A_3	5.2	9.7	8.0	6.2
	A_4	6.2	11.5	10.0	6.9
Dissolved Co (mg atom)		0.18	0.21	0.11	0.17
Co recovery (%)		98.9	98.7	99.4	98.9

Conv.; Conversion of 1-decene into aldehydes. Select.; Selectivity to each aldehyde determined by gas chromatography. A_1; undecanal. A_2; 2-methyl decanal. A_3; 2-ethylnonanal. A_4; 2-propyloctanal plus 2-butylheptanal. Dissolved Co; cobalt which remained dissolved in the reaction product. Co recovery; per cent of cobalt recovered and recycled.

It was observed through the windows of the reaction vessel that the catalyst complex was soluble during the reaction, but, on cooling to room temperature, separated as a dark red viscous liquid from the upper phase consisting of a solvent and reaction products. The remaining gas was discharged and the upper phase drained off; then 1-decene, the solvent, and the gas were charged again and the reaction repeated. The activity of the catalyst increased on repeated use as evident from a comparison of the results of the initial and the fourth runs.

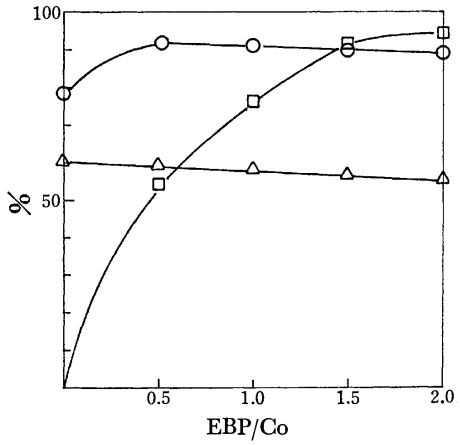

Fig. 1. Results plotted against the EBP/Co ratio.
1-Decene 0.2 mol, benzene 30 g, $Co_2(CO)_8$ 2 mmol, $H_2/CO=1$, 100 °C, 50 kg/cm², 1 h.
-○-: Conversion of decene (%), -△-: selectivity to linear aldehyde (%), -□-: Co recovery (%).

The Effect of the EBP to $Co_2(CO)_8$ Ratio. Results are plotted against the EBP/Co ratio in Fig. 1, where the amount of $Co_2(CO)_8$ was kept constant at 2 mmol.

The degree of conversion of decene increased by the addition of EBP, and reached a maximum when the ratio was 0.5, but slightly decreased as the ratio increased from 0.5 to 2.0. The selectivity to linear undecanal slightly decreased as the above ratio was increased. The catalyst did not separate at all from the reaction products in the absence of EBP, but began to separate as the ratio of EBP to $Co_2(CO)_8$ increased; Cobalt recovery reached near a maximum as the ratio increased to 1.5 and remained unchanged thereafter.

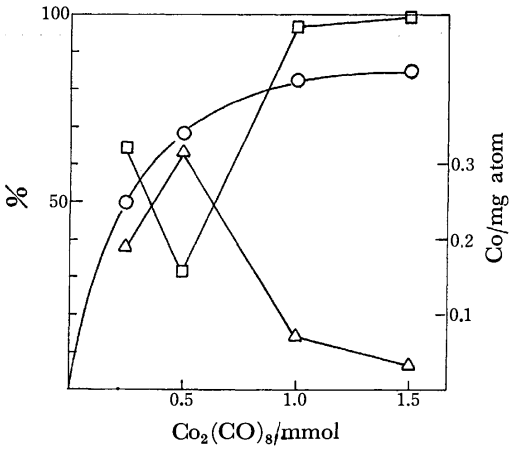

Fig. 2. Effect of catalyst concentration.
1-Decene 0.2 mol, liquid paraffin 30 g, $H_2/Co=1$, 100 °C, 50 kg/cm², 1 h, EBP: Co=4: 3.
-○-: Conversion of decene (%), -△-: dissolved Co (mg atom), -□-; Co recovery (%).

The Effect of Catalyst Concentration. In Fig. 2, the results are plotted against the amount of $Co_2(CO)_8$, where the EBP to $Co_2(CO)_8$ ratio was kept constant at 2.67, the ratio which corresponds to EBP 4: Co 3. The conversion of 1-decene after a definite reaction time increased as a natural result of increasing the amount of catalyst. Figure 2 shows, however, an unusual trend, *i.e.* a contrast between the amount of catalyst used and that of the cobalt remaining dissolved after the reaction. Thus, the larger the amount of catalyst employed, the better the separation of catalyst after the reaction.

The Effect of Pressure. The reactions were carried out under various partial pressures of hydrogen and carbon monoxide by recycling the initial catalyst, the results of which are summarized in Table 3.

The dissolved cobalt in the cooled reaction product decreased by increasing the ratio of hydrogen partial pressure(P_{H_2}) to that of carbon monoxide(P_{CO}); it decreased in the order: run No. 2 ($P_{H_2}/P_{CO}=0.25$)> No. 1($P_{H_2}/P_{CO}=1$)>No.4 ($P_{H_2}/P_{CO}=2$)>No.3($P_{H_2}/P_{CO}=4$)>No. 5($P_{H_2}/P_{CO}=9$). The selectivity to the linear aldehyde increased with the increase in partial pressure of hydrogen(No. 4<No. 3) and also increased with that of carbon monoxide(No. 7<No. 2). Nitrogen pressure did not affect the selectivity(No. 8). The rate constant

TABLE 3. HYDROFORMYLATION OF 1-DECENE UNDER VARIOUS HYDROGEN AND CARBON MONOXIDE PRESSURE

Initial catalyst was prepared *in situ* from 8 mmol of $Co_2(CO)_8$ and 16 mmol of EBP. Synthesis gas($H_2/CO=1$) was supplied during the reaction. 1-Decene 0.2 mol, diethyl ether (solvent) 30 g.

Run No.		1	2	3	4	5	6	7	8
P_{H_2} (kg/cm²)		25	10	40	20	45	45	10	10
Pco (kg/cm²)		25	40	10	10	5	5	10	10
P (kg/cm²)		50	50	50	30	50	50	20	50
Temp (°C)		70	70	70	70	60	50	70	70
Time (h)		4	20	2	2	3	15	5	10
Conv. (%)		51.2	73.4	70.0	68.4	64.5	59.1	70.0	52.3
Select. (%)	A_1	73.0	68.8	69.8	63.4	66.0	73.1	54.1	54.1
	A_2	18.8	21.1	20.1	23.4	22.4	18.5	28.5	28.5
	A_3	4.3	5.1	4.7	6.3	5.5	4.4	8.0	8.1
	A_4	3.9	4.9	5.4	6.9	6.1	4.0	9.4	9.4
$k\times 10$ min^{-1}		0.30	0.11	1.0	0.96	0.58	0.10	0.40	0.12
Decane (%)		0.05	0	2.6	0.49	0.18	0.83	1.98	0
Isomer (%)		1.5	2.7	2.7	4.1	2.1	0.9	7.0	3.9
Dissolved Co (mg atom)		1.92	2.24	0.94	1.01	0.19	0.22	1.54	0.87
Co recovery (%)		88.0	84.1	92.0	90.7	98.1	97.7	83.8	89.0

P; Total pressure, which is equal to $P_{H_2}+P_{CO}$, except in run No. 8, where nitrogen pressure ($P_{N_2}=30$) is employed. Conv.; Conversion of decene. k; Rate constant: $k=1/t$ ln $(100/100-x)$, where x is conv. at time t. Decane; Yield (%) of decane. Isomer; Total yield (%) of internal decenes. Other abbreviations: See footnote of Table 2.

increased with increasing partial pressure of hydrogen-(No. 7<No. 4<No. 3), but significantly decreased with that of carbon monoxide(No. 7>No. 2). The extent of isomerization of 1-decene into internal decenes increased as the carbon monoxide partial pressure decreased. Hydrogenation of decene to decane was also favored by lower carbon monoxide pressure.

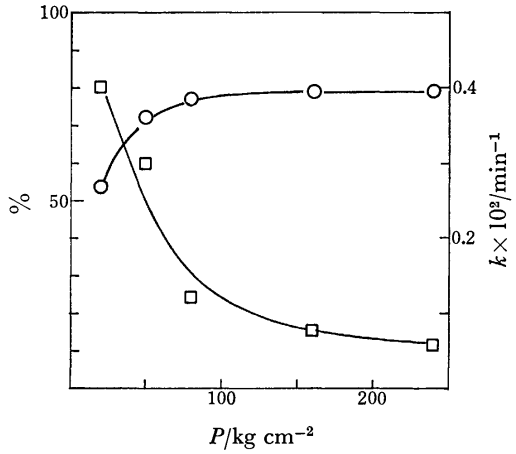

Fig. 3. Results plotted against total pressure.
1-Decene 0.2 mol, ether 30 g, $H_2/CO=ca.$ 1, 70 °C, EBP/Co=*ca.* 1.
-○-; Selectivity to linear aldehyde (%), -□-; rate constant k (min^{-1}).

Figure 3 illustrates the effect of the total pressure ($P_{H_2}+P_{CO}$) on the product composition and reaction rate. the selectivity to the linear aldehyde increased with increasing total pressure in the lower pressure range of 20 to 50 kg/cm², but leveled off thereafter. The rate constant decreased with increase in total pressure; this retarding effect of total pressure on the reaction rate was more pronounced in the lower pressure range.

Removal of Carbon Monoxide in Hydrogen by Means of the Oxo Process. Reactions were carried out by recycling the initial catalyst formed *in situ* from 4 mmol of $Co_2(CO)_8$ and 10.67 mmol of EBP. The autoclave was pressurized with hydrogen containing 4 to 6% of carbon monoxide to 100 kg/cm² (20 °C), then it was heated to 50 °C, and the reaction allowed to proceed, agitating at this temperature without supplying the synthesis gas. The results of consecutive experiments are listed in Table 4, the result of a control experiment carried out with 4 mmol of $Co_2(CO)_8$ but in the absence of EBP also being listed.

The activity of a catalyst formed *in situ* from $Co_2(CO)_8$ and EBP is initially very low, and the conversion of carbon monoxide into aldehyde is not complete even after 22 h reaction. The catalyst complex, however, gains in activity on recycling, attaining its highest activity when it has been recycled twice (after more than 40 h). Then, the carbon monoxide initially contained in the hydrogen is almost completely consumed by the hydroformylation in a few hours, and corresponding amount of aldehydes are formed in the liquid phase. The selectivity to the linear aldehyde in the presence of the recycled complex was 62%, which is significantly higher than that of the control experiment (53%) carried out with $Co_2(CO)_8$ in the absence of EBP. The separation of the catalyst after the reaction was in the range of 96 to 99%.

The conversion of carbon monoxide which was determined by analyzing the gas samples withdrawn at regular intervals in runs No. 4, No. 5, and No. 6 are

TABLE 4. HYDROFORMYLATION OF 1-DECENE UNDER PRESSURE OF HYDROGEN CONTAINING 4 TO 6 PER CENT OF CARBON MONOXIDE

Initial catalyst; $Co_2(CO)_8$ 4 mmol, EBP 10.67 mmol. Runs No. 1 to No. 5 were carried out recycling the initial catalyst. No. 6 is a controll experiment carried out with 4 mmol of $Co_2(CO)_8$ in the absence of EBP. 1-Decene 0.2 mol, ethyl acetate (solvent) 30 g, reaction temp 50 °C, initial pressure (20 °C) 100 kg/cm².

Run No.		1	2	3	4	5	6
CO content in hydrogen (%)	initial	4.2	5.5	5.2	5.3	4.8	4.8
	final	1.0	0.00	0.00	0.00	0.00	0.09
Time (h)		22	20	2	1.5	1.75	5
Conv. (%)		16.0	28.6	26.4	29.5	27.7	26.3
Select. (%)	A_1	58.4	61.6	62.4	62.6	62.4	53.6
	A_2	24.6	23.8	22.9	23.3	23.2	27.4
	A_3	7.7	6.5	6.7	6.4	6.8	8.9
	A_4	9.3	8.1	8.0	7.7	7.6	10.1
Decane (%)		0.45	2.0	1.2	3.9	4.5	3.0
Isomer (%)		0.63	34.2	50.8	49.0	60.9	57.8
Dissolved Co (mg atom)		0.25	0.31	0.21	0.059	0.095	—
Co recovery (%)		96.9	96.0	97.2	99.2	98.7	—

Abbreviations: See footnote of Table 3.

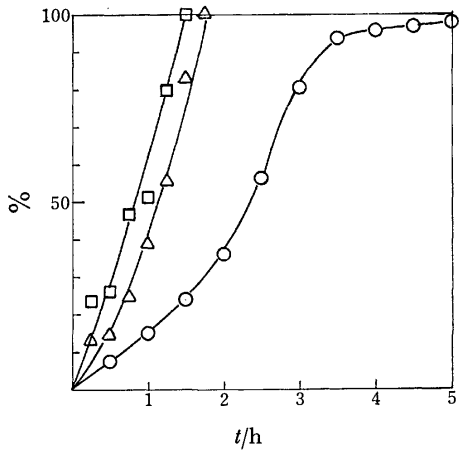

Fig. 4. Conversion of carbon monoxide *vs.* reaction time.
Mark Catalyst Run No. in Table 4
-○- $Co_2(CO)_8$ No. 6
-□- Recycled No. 4
-△- Recycled No. 5

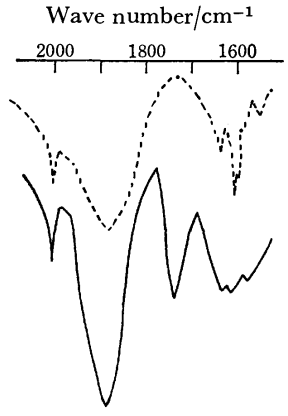

Fig. 5. Comparison of IR spectra.
Full line: New complex prepared from $Co_2(CO)_8$ and EBP in a molar ratio of 3: 8.
Dotted line; $H_2Co_3(CO)_9(Py)_5$.[6,7]

plotted against the reaction time in Fig. 4. Catalytic activities of the recycled complex in runs No. 4 and No. 5, according to Fig. 4, are markedly higher than that of $Co_2(CO)_8$ at the low temperature of 50 °C.

Infrared Spectrum of the New Complex. The complex, prepared from $Co_2(CO)_8$ (8 mmol) and EBP (21.3 mmol), and recycled several times as hydroformylation catalyst, was washed twice by agitating in petane (100 ml) at 100 °C, 40 kg/cm² ($H_2/CO=1$). A separated viscous phase was taken out of the autoclave after cooling and its IR spectrum together with that of a pyridine complex is shown in Fig. 5. The spectrum of the new complex shows the same absorptions at 2010 and 1890 cm⁻¹ as that of the pyridine complex, indicating the structural analogy of the new complex to $H_2Co_3(CO)_9(py)_5$.

Discussion

The complex, $H_2Co_3(CO)_9(py)_5$, is selectively produced by the reaction of $Co_2(CO)_8$ and pyridine in the molar ratio of one to four at 100 °C, 50 kg/cm² ($H_2/CO=1$), followed by cooling to room temperature.[7] A complex of an analogous structure should also be formed under similar conditions from $Co_2(CO)_8$ and EBP which has two pyridyl groups in the molecule, shown by a comparison of the IR spectra (Fig. 5). The catalyst structure and the mechanism of the catalyst separation can be understood by the model illustrated in Fig. 6, where EBP is represented by a mark N–N (N stands for nitrogen of the pyridyl group).

The higher the concentration of the unit complex during the reaction, the higher the possibility that the unit complex can be linked by N–N bridges with neighboring complexes after being cooled to room temperature, thereby becoming insoluble. This explains the unusual experimental results shown in Fig. 2, that the catalyst separation after cooling is improved by employing larger amounts of $Co_2(CO)_8$ and EBP in a fixed ratio of 3/2: 4, a ratio which corresponds to the

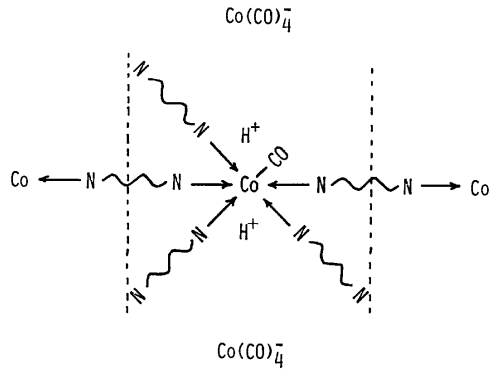

Fig. 6. Structural model of new complex, $H_2Co_3(CO)_9(EBP)_n$, when n is 4.

formula: $H_2Co_3(CO)_9(EBP)_4$. When the temperature is raised, on the other hand, the linking between unit complexes by N–N bridge will dissociate, at least partially, and the solubility of the complex will increase as a result. This explains the change in solubility of the complex with temperature observed through the windows of the reaction vessel.

As the ionic complex, $H_2Co_3(CO)_9(py)_5$, has been found to be in equilibrium with such non-ionic species as $Co_2(CO)_8$ at elevated temperatures,[6] there should also be an equilibrium relation as Eq. 1, in the case of the new complex.

$$H_2Co_3(CO)_9(EBP)_n + 3CO = H_2 + 3/2Co_2(CO)_8 + nEBP \quad (1)$$

The number n in Eq. 1 can be 4 or 3, since the separation takes place satisfactorily when the EBP to Co ratio is 4: 3 (Fig. 2) or 3: 3 (Table 3). The separation occurs only partially when the EBP/Co ratio is less than 1 (Fig. 1).

This complex, $H_2Co_3(CO)_9(EBP)_n$, is probably an active catalyst for hydroformylation under mild conditions, since the analogous pyridine complex, $H_2Co_3(CO)_9(py)_5$, has been found to react with an olefin even at room temperature.[7] The concentration of $H_2Co_3(CO)_9(EBP)_n$, according to Eq. 1, should increase as the hydrogen partial pressure is increased, but decrease as the carbon monoxide partial pressure is increased. This explains the accelerating effect of hydrogen, and the retarding effect of carbon monoxide, on the reaction rate (Table 3). The reaction rate decreases with increasing total pressure (Fig. 3), probably because its decrease due to an increase in P_{CO} is larger than its increase due to an increase in P_{H_2}. The retarding effect of nitrogen pressure on the reaction rate, however, remains unexplained. The fact that the catalyst separation is improved by employing a mixed gas with a higher ratio of hydrogen to carbon monoxide can be explained, since such non-ionic species as $Co_2(CO)_8$ which remain dissolved in the cooled reaction product, will decrease with increasing hydrogen pressure and decreasing carbon monoxide pressure, according to Eq. 1.

The foregoing argument, however, does not exclude the presence of other active species such as $HCo(CO)_4$ and $HCo(CO)_3$ which can also be in equilibrium with $Co_2(CO)_8$ under these reaction conditions. In this connection, it should be noted that the selectivity to the linear aldehyde under extreme conditions of very high P_{H_2}/P_{CO} ratios was remarkably higher in the presence of $H_2Co_3(CO)_9(EBP)_n$ than in the presence of $Co_2(CO)_8$ (Table 4). This strongly suggests that the active catalyst, at least under the extreme conditions of high P_{H_2}/P_{CO} ratios, is different from $HCo(CO)_4$ or $HCo(CO)_3$, and that the active catalyst in this case must be the complex, $H_2Co_3(CO)_9(EBP)_n$, the formation of which is favored by the high P_{H_2}/P_{CO} ratio.

The selectivity to the linear aldehyde under the normal gas ratio ($P_{H_2}/P_{CO}=1$) was, on the contrary, a little lower in the presence of the new complex than in the presence of $Co_2(CO)_8$ (Fig. 1). Therefore, still unidentified catalyst species different from $H_2Co_3(CO)_9(EBP)_n$, $HCo(CO)_4$, and $HCo(CO)_3$, must be taking part in this case.

The reasons for the selectivity to linear aldehyde increasing with increasing carbon monoxide pressure and increasing hydrogen pressure cannot be explained, because there are still unknown factors affecting the selectivity as discussed above. However, the effect of the total pressure on the selectivity to linear aldehyde is, evidently, a result of the co-effects of the respective partial pressures of carbon monoxide and hydrogen, since the increase in total pressure due to such inert gas as nitrogen does not affect the selectivity (Table 3).

The authors wish to express their thanks to Messrs. Toshiyuki Murakami and Ryuji Yamazaki for their assistance in the experimental work.

References

1) A part of this work is to be published in the Proc. 6th Internat. Conf. on High Pressure, Colorado (1977).
2) A. J. Moffat, *J. Catal.*, **18**, 193 (1970).
3) A. J. Moffat, *J. Catal.*, **19**, 322 (1970).
4) W. O. Haag and D. D. Whitehurst, Preprint, Proc. 5th Internat. Congr. on Catalysis, Amsterdam, 1972.
5) E. Bayer and V. Schurig, *Angew. Chem.*, **87**, 484 (1975).
6) A. Matsuda, K. Bando, S. Shin, and Y. Horiguchi, Proc. 4th Internat. Congr. on High Pressure, Kyoto, p. 725 (1974).
7) S. Shin, A. Matsuda, J. Nakayama, and K. Bando, *Chem. Lett.*, **1977**, 115.

Metal-catalyzed Organic Photoreactions. The Photooxidation of Olefins in the Presence of Uranyl Acetate[1)]

Eigoro MURAYAMA and Tadashi SATO*

Department of Applied Chemistry, Waseda University, Ookubo 3, Shinjuku-ku, Tokyo 160

(Received March 15, 1978)

The photooxidation of olefins in pyridine in the presence of uranyl acetate afforded β-hydroxy hydroperoxides. It was confirmed by spectroscopic studies and isotope-incorporation experiments that (1) the stereochemistry of the hydroxyl and hydroperoxyl groups in the β-hydroxy hydroperoxides was *trans*, (2) the hydroxyl group was added to the less substituted carbon of the double bond, and (3) the oxygen atom in the hydroxyl group originated mainly from the water molecule, while the oxygen atoms in the hydroperoxyl group originated mainly from molecular oxygen. From these results, we proposed a reaction scheme of: (i) the formation of the hydroxyl radical from water by uranyl acetate-catalyzed photolysis, (ii) the addition of the hydroxyl radical to the double bond, (iii) the combination of the resulted radical with molecular oxygen, and (iv) the hydrogen abstraction of the peroxyl radical to give the product. The scheme was further supported by the photoreaction of 2-methyl-2-butene with bromotrichloromethane in the presence of uranyl acetate, which afforded 3-bromo-3-methyl-2-butanol as the major product.

The dye-sensitized photooxidation and the autoxidation are two major types of the photooxidation of olefins, and they have been interpreted as involving the reaction of singlet oxygen and the initiation by a radical respectively.[2)] Recently several papers on photooxidation through novel types of mechanism have been published. Photooxidations sensitized by dicyanoanthracene,[3)] α-diketones,[4)] or Lewis acids[5)] are some examples.

In the course of our study of the metal-catalyzed organic photoreactions,[6)] we found that the photooxidation of olefins in pyridine in the presence of uranyl acetate proceeded in a way quite different from the oxidation processes known so far.

Results and Discussion

Solutions of limonene (**1**), 1,2-dimethylcyclohexene (**2**), or 2-methyl-2-butene (**3**) in pyridine, all containing an equivalent amount of uranyl acetate (dihydrate), were irradiated with Pyrex-filtered light while oxygen was bubbled through, and the products were separated on preparative TLC (silica gel). β-Hydroxy hydroperoxides, **4**, **5**, and **6**, were isolated in a fairly pure state in 14, 8, and 12% yields respectively. The yields of these products, as determined by NMR analyses of the crude reaction mixtures, amounted to 32, 11, and 18% respectively. The compounds **4** and **6** were further purified by vacuum distillation. The structures **4**, **5**, and **6** were assigned on the basis of the spectroscopic and elemental analyses[7)] and the following chemical processes.

Upon the hydrogenation on palladium–charcoal, the β-hydroxy hydroperoxides, **4**, **5**, and **6**, gave 1,2-diols, **7a**, **8**, and **9** respectively, while they afforded C–C bond cleavage products (**10** from **4**, **11** from **5**, and acetone and acetaldehyde from **6**) upon thermolysis or decomposition on silica gel. With a view to elucidating the stereochemistry of **7a**, we hydrogenated a stereoisomeric mixture of *trans*-diol **12**,[8)] and then isolated **7a** and **7b** on a preparative VPC. We assigned the stereochemistry of these isomers as indicated in view of the W_H=6 Hz value of H_a in **7a**, in contrast with the J values of 12 and 4 Hz (doublet of a doublet) for the corresponding proton in **7b**. The reduction product from **4** was identical with **7a**, thus establishing the stereochemistry of **4** to be as shown. The diols, **8** and **9**, were identical with authentic samples prepared by known methods.[9)]

The positional assignments of the substituents in **6** were deduced from the carbon-NMR analyses. While the chemical shifts of the secondary carbons (C_1) in compounds **6** and **9** were fairly close to each other (δ 70.5 for **6** and δ 74.2 for **9**), the signal of the tertiary carbon (C_2) in **6** appeared at a lower field (δ 85.1) than that of the corresponding carbon in **9** (δ 73.4). These observations would definitely support the tertiary

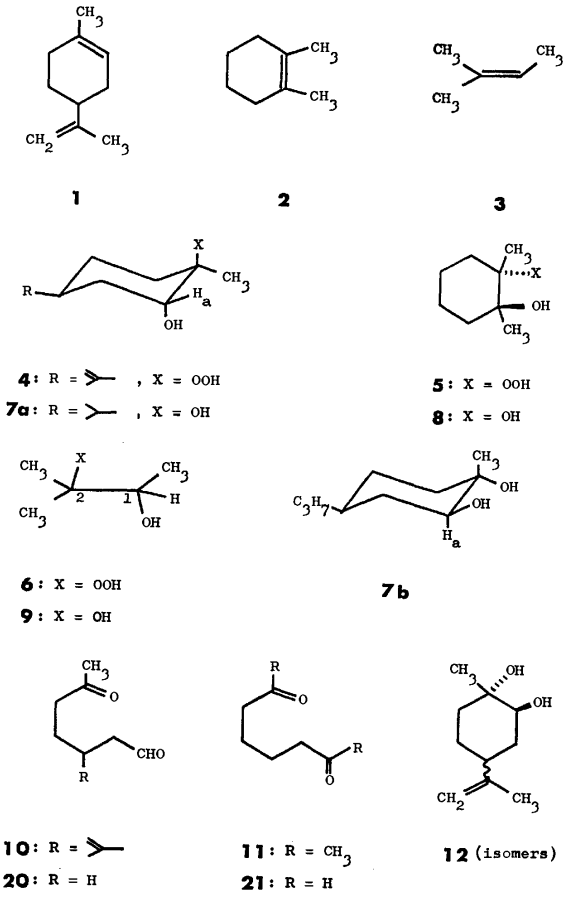

hydroperoxide structure for **6**, and the same regiochemistry was also postulated with compound **4**. Subramanyam *et al.* prepared several β-hydroxy hydroperoxides including **6**, which indicated spectroscopic data very close to ours.[10]

In order to gain an insight into the genuine character of the present reaction, the irradiated materials from **1** and **2** were directly treated with silica gel (to decompose β-hydroxy hydroperoxides) and the products were analyzed by a preparative VPC. A keto aldehyde, **10**, and a ketone, **13**, probable decomposition products of the β-hydroxy hydroperoxides from **1** at the 1,2- and 8,9-positions, were obtained from **1** in 26 and 2% yields respectively, along with three by-products, **12**, **14**, and **15** in 1, 1, and 3% yields respectively. Similarly, **11** was obtained in a 48% isolated yield from **2**, along with several by-products (**16**, **17**, and others; see Reference 2; total yield, 9%). In view of our previous observations,[2] it is evident that these by-products from **1** and **2** are formed through the radical-initiated oxidation. We have also reported that the allyl hydroperoxides, such as **18** and **19** are characteristic products of the singlet-oxygen oxidations of **1** and **2**, but these products were negligible in the present reactions. No observable amounts of any other products were isolated, but we have not examined whether the remainder becomes unextractable polymeric substances or remains intact as the original starting materials. The starting materials, even if they remained at the end of the reaction, could not be detected because they escaped during the work-up procedure of removing the pyridine solvent.

The possibility that the present oxidation might proceed through the uranyl acetate-catalyzed oxidation by singlet oxygen was ruled out in the following way. When solutions of **1** and **2** in *t*-butyl alcohol–water (1 : 1) or in pyridine, containing rose bengal as a sensitizer, were irradiated with a tungsten lamp, oxidation products were obtained with a product distribution typical of singlet-oxygen oxidation.[2] Under these conditions, however, no catalytic effect of uranyl acetate was observed. It was also shown by the experiment with **2** that the present oxidation is not affected by a radical scavenger (tri-*t*-butylphenol).

The same type of reaction seems to proceed with 1-methylcyclohexene and cyclohexene, because these olefins, under the same conditions of irradiation and succeeding decomposition on silica gel, afforded a keto aldehyde, **20**, and a dialdehyde, **21**, in 20 and 6% yields respectively. The yield of **21** was low because of the apparent polymerization during the work-up procedure.

Uranyl chloride in *t*-butyl alcohol–water (1 : 1) also catalyzed the present reaction, although the competitive radical-initiated oxidation process became appreciable under these conditions. However, no appreciable amounts of any products were observed when either of the metal compounds, light, or oxygen was lacking.

With a view to clarifying the reaction mechanism, the sources of the oxygen atoms in the product, **6**, were determined in the following way. The product, **6**, obtained by using oxygen-18 labelled water or molecular oxygen, was directly injected into a gas chromatograph-mass spectrometer, after which the isotope contents

Table 1. Incorporation of oxygen-18 into acetone and acetaldehyde

Condition	^{18}O in acetone (atom % excess)	^{18}O in acetaldehyde (atom % excess)
$^{18}O_2$ (30 atom % excess)–$UO_2(OAc)_2 \cdot 2H_2O$	27	7
O_2–$UO_2(OAc)_2 \cdot H_2{}^{18}O$ (30 atom % excess)	5	20

incorporated into acetone and acetaldehyde, the thermolyzed products from **6** in the gas chromatograph, were determined mass-spectrometrically. The results are shown in Table 1. Assuming that no oxygen migration occurs during the thermolysis step of **6**, as has been proposed for the fragmentation of α-hydroperoxy acid,[11] it was concluded that the oxygen atoms in the hydroperoxyl group originated mainly (90%) from molecular oxygen, while the oxygen atom in the hydroxyl group originated, in major part (67%), from the water molecule. We could scheme the major course of the reaction as: (i) the formation of the hydroxyl radical from water by uranyl acetate-catalyzed photolysis; (ii) the addition of the hydroxyl radical to the olefin so as to afford the more stable intermediate; (iii) the combination of the preceeding radical, **22**, with molecular oxygen, and (iv) the hydrogen abstraction of **23** to give the product (Scheme 1).

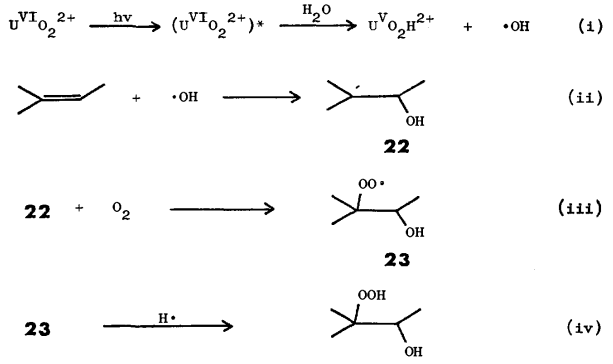

Scheme 1.

Although the stereo- and regio-chemistry of the present reaction are consistent with the scheme, the fact that the reaction under a lack of oxygen gives no observable products needs further consideration, because some products from the radical **22** (for instance, an alcohol, **24**, through the hydrogen abstraction) should be produced in view of the proposed scheme. The problem could be interpreted in the following way. First, we can assume that Step i is reversible and that, in the absence of oxygen, the back reaction is too fast to allow the hydroxyl radical to be involved in the further reaction. In the presence of oxygen, however, the back reaction might be inhibited due to the oxidation by oxygen of the low-valent uranium compound, and the hydroxyl radical could well survive to be involved in the next step. The reaction shown in Step i has been suggested by Burrows and Kemp[12] in

the uranyl compound-catalyzed photolyses of water, although they failed to detect the hydroxyl radical, supposedly because of the fast back reaction. Alternatively, we can assume that the hydroxyl radical produced in Step i could reversibly add to the olefin, but in the absence of any appropriate substance to trap the radical **22** effectively, the whole reaction does not proceed because of the back reaction in Step i. Presumably the second interpretation is preferable because we observed that the hydroxyl radical could be brought into the reaction, even in the absence of oxygen, as long as a suitable substance to trap the radical **22** is present. We found that bromotrichloromethane serves for this purpose. When a solution of **3** in pyridine containing uranyl acetate and bromotrichloromethane was irradiated with Pyrex-filtered light, two bromohydrins, **25** and **26**, were obtained as a 3: 1 mixture in a 18% yield, along with the addition product, **27**, in a 12% yield. When the irradiation was carried out in the absence of uranyl acetate, **27** was the sole product.[13] The structure of **25** was assigned on the basis of elemental and spectroscopic analyses, and by oxidizing the bromohydrin to α-bromoketone, **28**. The structures **26**[14] and **27**[13] were confirmed by comparing the compounds with authentic samples prepared by known procedures. We found that the ratios of **26**/**25** were independent (≈0.3) of the wavelength of the working light, the amounts of bromotrichloromethane and water, and the presence or absence of some additives, while the ratios of **27**/(**25**+**26**) changed from 0 to 1.2 depending upon the reaction conditions. Although the detailed results will be reported elsewhere, it can be suggested from these observations that **25** and **26** are formed *via* a common intermediate (probably a uranyl-substrate complex). A normal type of the addition of HOBr to the olefin, **3**, is known to occur so as to give **26** selectively;[14] therefore, the abnormal way of addition in the present reaction would be another support for the proposed scheme. Recently we found a photooxidation of olefins in the presence of iron(III) chloride to give chlorinated ketones. These reactions have been speculated[15] as proceeding in a way similar to that shown in the scheme proposed in this paper.

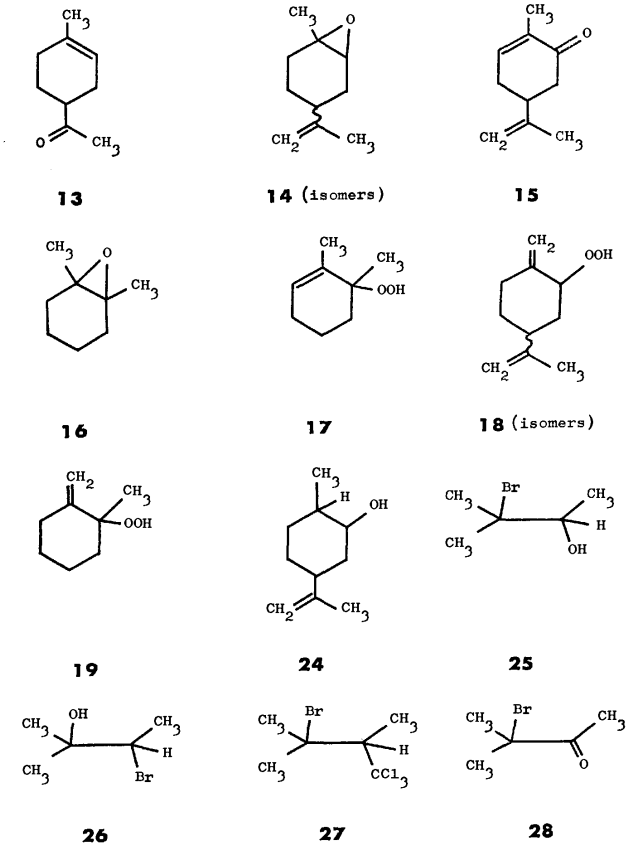

Experimental

General Procedures. The instrumentation was the same as has been described previously.[16] The carbon NMR spectra were determined in a $CDCl_3$ solution on a JEOL JNM-FX 100 spectrometer; the chemical shifts are represented in δ values relative to the internal TMS standard. The isotope incorporations were determined on a Hitachi RMU-6M mass spectrometer equipped with a gas chromatograph.

Unless otherwise stated, a pyridine solution (2—6 mmol, 0.02 M) of olefin containing an equivalent amount of uranyl acetate (dihydrate) was irradiated in Pyrex-glass test tubes with a high-pressure mercury vapor lamp (Ushio UM 452 (450 W)) for 10—90 min while oxygen was bubbled through. After the irradiation, the pyridine was removed *in vacuo* and the reaction products were extracted from the residue with carbon tetrachloride. The extract was filtered, and the solvent was removed *in vacuo*. The residual substance was treated as has been indicated below.

Materials. *a) Unhydrous Uranyl Acetate*: Commercially available uranyl acetate dihydrate (500 mg) was heated at 140 °C under reduced pressure for 30 min, and the resulting yellow powder (459 mg) was used directly for the reactions. *b) Oxygen-18 Labelled Water*: Commercially available $H_2{}^{18}O$ (96.5 atom% excess, Merck Sharp and Dohme Canada, Ltd., Lot No. B-863) was diluted with ordinary water to a concentration of 30 atom % excess of ^{18}O. *c) Oxygen-18 Labelled Molecular Oxygen*: Commercially available $^{18}O_2$ (70 atom % excess, B.O.C. Ltd.) was diluted with ordinary oxygen to a concentration of 30 atom % excess of ^{18}O.

Photooxidation of 1. When the crude oil from 272 mg of **1** was purified by preparative TLC (silica gel, chloroform), **4** was isolated (52 mg, 14%); this was then further purified by vacuum distillation. Bp 45—55 °C (≈10^{-5} mmHg). IR (neat), 3350, 3080, 2930, 1642, 1450, 1378, 1035, 890, and 840 cm^{-1}. NMR (CCl_4), δ 1.22 (3H, s), 1.70 (3H, s), 3.88 (1H, bs), 4.64 (2H, bs), and 4.6—5.9 (2H, bs, shifts upon dilution). Found:[7] C, 64.75; H, 9.11%. Calcd for $C_{10}H_{18}O_3$: C, 64.49; H, 9.74%.

When the crude oil was dissolved in chloroform and passed through a silica-gel column (10 cm), an oil was obtained from which five products, **10**, **12**, **13**, **14**, and **15**, were subsequently isolated by preparative VPC. The IR and NMR spectra of **10**[17] and **13**[18] were identical with those of the authentic samples obtained by the known methods. The IR and NMR spectra of **14** and **15** corresponded to those previously reported.[2] The IR and NMR spectra of **12** were identical with those of the samples described below.

Photooxidation of 2. The crude oil from 330 mg of **2** was dissolved in 20 ml water and then washed with hexane. After copper(II) sulfate (3.5 g) had been added to the aqueous layer, the solution was shaken with chloroform. The extract (Extract A) was dried (Na_2SO_4), and the solvent was removed

in vacuo. When the residual substance was purified by preparative TLC (silica gel, chloroform), **5** was isolated (38 mg, 8%). The NMR analysis indicated that the compound contained a small amount of **11**. **5**: in a state containing a small amount of **11**, IR (neat), 3380, 2935, 1372, 1120, and 1060 cm^{-1}. NMR (CCl_4), δ 1.21 (3H, s), 1.27 (3H, s), and 1.2—1.6 (m).

The Extract A obtained from 220 mg of **2** was applied on a silica-gel column (5 cm) and then eluted with chloroform. Upon removing the solvent *in vacuo* from the eluate, crystals of **11** were isolated in a pure state (137 mg, 48%). Mp 24—26 °C (lit,[19] mp 41—42.5 °C). NMR (CCl_4), δ 1.42 (4H, m), 2.03 (6H, s), and 2.33 (4H, dist. t). The IR spectrum was identical with that previously reported.[20]

From the hexane layer, the by-products[2] (40 mg) were obtained (9% total yield).

The same result was obtained (46% yield of **11**) when the reaction was carried out in the presence of tri-*t*-butylphenol (262 mg).

Photooxidation of 3. When the crude oil from 420 mg of **3** was distilled under reduced pressure, **6** was isolated in a pure state (59 mg, 12%). Bp 47—48 °C ($\approx 10^{-5}$ mmHg). IR (neat), 3320, 2980, 1387, 1110, and 835 cm^{-1}. NMR (CCl_4), δ 1.04 (3H, s), 1.07 (3H, d, J=6.4 Hz), 1.16 (3H, s), 3.92 (1H, q, J=6.4 Hz), and 4.8—7.7 (2H, bs, shifts upon dilution). Carbon-NMR ($CDCl_3$), δ 17.3 (q, J=126 Hz), 17.6 (q, J=127 Hz), 21.6 (q, J=126 Hz), 70.5 (d, J=145 Hz), and 85.1 (s). Found:[7] C, 51.20; H, 10.23%. Calcd for $C_5H_{12}O_3$: C, 49.98; H, 10.07%.

Isotope-incorporation experiments were carried out in the following way. A solution of **3** (14 mg) in unhydrous pyridine (10 ml), containing unhydrous uranyl acetate (68 mg) and $H_2{}^{18}O$ (30 atom% excess, 372 mg), was irradiated for 30 min while ordinary oxygen was bubbled through. The crude oil, obtained by means of the work-up described above, was directly injected into the gas chromatograph-mass spectrometer.

Hydrogenation of 4. A solution of **4** (15 mg) in ethanol (5 ml), containing 10% palladium–charcoal (10 mg), was stirred under an hydrogen atmosphere (1 atm) for two days. The oil which remained after the catalyst and solvent had been removed was almost pure **7a**. Preparative VPC gave a pure sample of **7a** which showed spectroscopic data identical with those of the sample described below.

Hydrogenation of 5. A solution of **5** (22 mg) in ethanol (2 ml) was stirred under a hydrogen atmosphere (1 atm) for 20 h in the presence of 10% palladium–charcoal (5 mg). An NMR analysis indicated that the oil remaining after the work-up was a mixture of **8** and **11** (1: 1). The separation was accomplished on a preparative VPC. The IR and NMR spectra of **8** were identical with those of an authentic sample.[9]

Hydrogenation of 6. The hydrogenation in the way described above gave a pure sample of **9**. The IR and NMR data were identical with those of an authentic sample.[9] Carbon-NMR ($CDCl_3$), δ 17.7 (q, J=125 Hz), 22.6 (q, J=125 Hz), 26.5 (q, J=125 Hz), 73.4 (s), and 74.2 (d, J=142 Hz).

Preparation of 7a. A solution of a stereoisomeric mixture of **14**[21] (200 mg) in *t*-butyl alcohol–water (1: 1 by volume, 20 ml), also containing 0.5 M-sulfuric acid (0.2 ml), was stirred at room temperature for 16 h. The reaction mixture was then poured into a saturated aqueous solution of sodium bicarbonate (40 ml) and shaken with chloroform. The extract was dried (Na_2SO_4), and the solvent was removed *in vacuo*. The residual substance was distilled to give a stereoisomeric mixture of **12** (141 mg).[8,22] Bp 95—97 °C (10 mmHg). A solution of the diol **12** obtained above (82 mg) in ethanol (5 ml), containing 10% palladium-charcoal (10 mg), was stirred under a hydrogen atmosphere (1 atm) for 17 h. Preparative VPC after the distillation (94—96 °C (4 mmHg)) gave two stereoisomers, **7a** and **7b**, in a pure state. **7a**: IR (CCl_4), 3650 cm^{-1}. NMR (CCl_4), δ 0.91 (6H, d, J=6 Hz), 1.19 (3H, s), and 3.57 (1H, bs, W_H=6 Hz). **7b**: IR (CCl_4), 3420 cm^{-1}. NMR (CCl_4), δ 0.91 (6H, d, J=6 Hz), 1.11 (3H, s), and 3.52 (1H, dd, J=12 and 4 Hz).

Thermolysis of 4. A solution of **4** (40 mg) in benzene (1 ml) was refluxed for 30 min, and then the solvent was removed *in vacuo*. From the IR, NMR, and VPC analyses, the major part of the residual oil was found to be **10**.,

Thermolysis of 5. A solution of **5** (16 mg) in benzene (2 ml) was refluxed for 1 h, and then the solvent was removed *in vacuo*. From the NMR analysis, the residual oil was found to be **11**.

Thermolysis of 6. A small amount of **6** was injected into a gas chromatograph-mass spectrometer (temperature of the injection port: 260 °C), and the decomposition products were directly analyzed on the mass spectrometer. The two products detected were identified as acetone and acetaldehyde from the mass spectra and the retention times on the VPC.

Photooxidation of 1-Methylcyclohexene. The crude oil from 288 mg of 1-methylcyclohexene was chromatographed on a silica-gel column (chloroform), and **20** (77 mg, 20%) was isolated. The IR and NMR spectra of **20** were identical with those of an authentic sample.[23]

Photooxidation of Cyclohexene. The crude oil from 246 mg of cyclohexene was treated in the way described above; the product thus obtained, **21** (39 mg, 6%), was accompanied by a small amount of a polymerization product of **21**. IR (neat), 2830, 2720, and 1720 cm^{-1}. NMR (CCl_4), δ 1.4—1.8 (4H, m), 2.2—2.8 (4H, m), and 9.57 (2H, t, J=1.5 Hz).

Photoreaction of 3 with Bromotrichloromethane. A solution of **3** (0.5 g) in pyridine (360 ml), containing uranyl acetate (3.1 g) and bromotrichloromethane (2.9 g), was irradiated with Pyrex-filtered light from a high-pressure mercury vapor lamp (Ushio UM 1000 (1 kW)) for 1 h. After the irradiation, the pyridine was removed *in vacuo*. The reaction products were extracted from the residue with chloroform, and the extract was passed through a Florisil column (6 cm) in a chloroform solution. The eluate was washed with a saturated aqueous solution of copper(II) sulfate, and dried over Na_2SO_4, and the solvent was removed *in vacuo*. The residual substance was dissolved in hexane, and the solution was shaken with a cold 2% aqueous solution of sodium bicarbonate. The aqueous layer was shaken with cold chloroform, the chloroform solution was dried (Na_2SO_4), and the solvent was removed *in vacuo* to give a yellow oil (220 mg). From NMR analysis, the oil was found to be a mixture of **25** and **26** (3: 1). The vacuum distillation (bp 40—41 °C (9 mmHg)) did not accomplish the complete separation of the two isomers, and so spectroscopic and elemental analyses were carried out on the mixture. Subtracting the spectra of **26**, which was prepared in a pure state according to the reported method,[14] the spectra of **25** were as follows: IR (neat), 3400, 2975, 1455, 1373, 1112, 942, and 702 cm^{-1}. NMR (CCl_4), δ 1.21 (3H, d, J=6 Hz), 1.68 (3H, s), 1.72 (3H, s), 3.04 (1H, bs), and 3.55 (1H, q, J=6 Hz). Found:[24] C, 36.63; H, 6.58%. Calcd for $C_5H_{11}OBr$: C, 35.95; H, 6.64%.

The hexane layer was dried over Na_2SO_4, and the hexane was removed *in vacuo*. The brown oil was mainly **27** identical with an authentic sample.[13] The yield of **27** was 12%, as determined by NMR analysis, using 1,1,2,2-tetrachloroethane as an internal reference.

Oxidation of 25. The oxidation of the mixture of **25** and **26** obtained above (40 mg) with a Jones reagent was

carried out according to the reported procedure.[14a] α-Bromoketone **28** was obtained, accompanied by unchanged **26**; the spectra of **28** were obtained by subtracting those of **26**. IR[25] (neat), 2975, 1710, 1372, 1360, 1138, and 1104 cm^{-1}. NMR[26] (CCl_4), δ 1.81 (6H, s) and 2.36 (3H, s).

References

1) Preliminary report: E. Murayama and T. Sato, *Tetrahedron Lett.*, **1977**, 4079.

2) T. Sato and E. Murayama, *Bull. Chem. Soc. Jpn.*, **47**, 715 (1974), and references cited therein.

3) J. Eriksen, C. S. Foote, and T. L. Parker, *J. Am. Chem. Soc.*, **99**, 6455 (1977).

4) N. Shimizu and P. D. Bartlett, *J. Am. Chem. Soc.*, **98**, 4193 (1976).

5) D. H. R. Barton and R. K. Haynes, *J. Chem. Soc., Perkin Trans. 1*, **1975**, 2065.

6) T. Sato, S. Yoshiie, T. Imamura, K. Hasegawa, M. Miyahara, S. Yamamura, and O. Ito, *Bull. Chem. Soc. Jpn.*, **50**, 2714 (1977), and references cited therein.

7) Errors in the elemental analyses were inevitable due to a slight decomposition during the distillation and contamination by a trace amount of the pyridine solvent.

8) M. Sumimoto, T. Suzuki, and T. Kondo, *Agr. Biol. Chem.*, **38**, 1061 (1974).

9) The two diols, **8** and **9**, were prepared from **2** and **3** respectively, according to the method which gives *trans*-1,2-cyclohexanediol from cyclohexene; A. Roebuck and H. Adkins, *Org. Synth.*, Coll. Vol. III, 217 (1965).

10) V. Subramanyam, C. L. Brizuela, and A. H. Soloway, *J. Chem. Soc., Chem. Commun.*, **1976**, 508, and private communication from Dr. Subramanyam.

11) W. Adam, A. Alzérreca, Ju-Chao Liu, and F. Yany, *J. Am. Chem. Soc.*, **99**, 5768 (1977).

12) H. D. Burrows and T. J. Kemp, *Chem. Soc. Rev.*, **3**, 139 (1974).

13) M. S. Kharasch and M. Sage, *J. Org. Chem.*, **14**, 537 (1949).

14) a) D. R. Dalton and V. P. Dutta, *J. Chem. Soc., B*, **1971**, 85; b) D. R. Dalton, V. P. Dutta, and D. G. Jones, *J. Am. Chem. Soc.*, **90**, 5498 (1968).

15) E. Murayama, A. Kohda, and T. Sato, *Chem. Lett.*, **1978**, 161.

16) T. Sato, K. Tamura, K. Maruyama, O. Ogawa, and T. Imamura, *J. Chem. Soc., Perkin Trans. 1*, **1976**, 779.

17) S. Kataoka and Y. Hamada, *Bull. Agr. Chem. Soc. Jpn.*, **20**, 223 (1956).

18) E. E. Lutz and G. M. Baily, *J. Am. Chem. Soc.*, **86**, 3889 (1964).

19) H. Adkins and C. Scanley, *J. Am. Chem. Soc.*, **73**, 2854 (1951).

20) "The Aldrich Library of Infrared Spectra," Aldrich Chemical Co., (1970), p. 195E.

21) T. Sato and E. Murayama, *Bull. Chem. Soc. Jpn.*, **47**, 1207 (1974).

22) W. F. Newhall, *J. Org. Chem.*, **29**, 185 (1964).

23) M. Barbier and M. F. Hügel, *Bull. Soc. Chim. Fr.*, **1961**, 951.

24) Errors in elemental analyses were inevitable due to the contamination by a trace amount of 2-bromopyridine.

25) L. Blanco, P. Amice, and J. M. Conia, *Synthesis*, **1976** 194.

26) R. A. Cox and J. Warkentin, *Can. J. Chem.*, **50**, 3242 (1972).

Fluorescence Spectra of 2-Pyridylbenzimidazoles. A Specific Interation of 2-(2-Pyridyl)benzimidazole with Ethanol

Michio KONDO

Central Research Laboratories, Sankyo Co., Ltd., Hiromachi, Shinagawa-ku, Tokyo 140

(Received March 17, 1978)

The fluorescence spectra of 2-(2-pyridyl)- (**1a**), 2-(3-hydroxy-2-pyridyl)- (**1b**), 1-methyl-2-(2-pyridyl)-, 2-(3-pyridyl)-, and 2-(4-pyridyl)-benzimidazole have been studied, and it has been found that their intensities are very strong, except for an ethanolic solution of **1a**. It is likely, therefore, that a specific interaction, probably a bridge-type complexation of **1a** with an ethanol molecule where imidazolic proton is explicitly involved, is responsible for the observed reduction in the fluorescence intensity for ethanol solutions. The fluorescence emission with a large Stokes' shift of **1b** is very strong, in ethanol as well as in other organic solvents tested, indicating a faster intramolecular proton transfer in the excited singlet state than intermolecular deactivation relaxation with ethanol molecules.

The fluorescence and phosphorescence intensities of an aromatic molecule are dependent on the relative alignment of the energy levels of its singlet and triplet states. Therefore, the fluorescence intensity of an aromatic molecule may differ much from those of the isomers. The emission nature of pyrazine, for example, is quite different from those of pyridazine and pyrimidine.[1]

It has been proved in some cases that intramolecular interactions, especially intermolecular hydrogen bonding, between a solvent and a solute molecule in the ground or excited state play an important role in fluorescence emission.[2] This type of interaction seems to be very important in the cases of heteroaromatic compounds, such as acridine, which have been proved to show a remarkable solvent dependence on the emission nature.[3,4]

Recently, it has been reported that pyrrolo[2,3-*b*]-pyridine shows two emission bands in a rather concentrated solution in non-polar solvents as well as in a dilute ethanol solution, and that the emission band at longer wavelengths can be attributed to the isomeric species produced *via* intermolecular proton transposition.[5]

This paper will be concerned with the fluorescence spectra of several 2-pyridylbenzimidazoles in various solvents.

Experimental

Materials. Four compounds, 2-(2-pyridyl)- (**1a**), 2-(3-hydroxy-2-pyridyl)- (**1b**), 2-(3-pyridyl)- (**2**), and 2-(4-pyridyl)-benzimidazole (**3**), were prepared by the condensation of *o*-phenylenediamine with an appropriate pyridinecarboxylic acid at elevated temperatures, according to the literature method.[6]

*1-Methyl-2-(2-pyridyl)benzimidazole (**1c**).* To a dried dimethyl sulfoxide solution (20 ml) containing sodium hydride (1/50 mol) was added **1a** (1/200 mol) under nitrogen purging. The solution was slowly heated up to 85 °C and, then kept for 30 min to yield a dark brown solution. To this solution, cooled in an ice-water bath, methyl iodide (1/50 mol) was added in portions, with care taken not to raise the solution temperature above 30 °C. The reaction mixture was then poured into water (500 ml), resulting in an oil-suspended aqueous solution. The oil was extracted with ethyl acetate. The subsequent evaporation of the solvent yielded a pale yellow oil which crystallized with treated with a glass rod. The pale yellow fine solids were charged on an alumina column and eluted with benzene. The evaporation of the solvent gave fine colorless crystals (**1c**): mp 64—65 °C; Found; C, 68.75; H, 5.30; N, 18.39%. Calcd for $C_{13}H_{11}N_3 \cdot H_2O$: C, 68.72; H, 5.72; N, 18.50%.

Spectral Measurements. The absorption and fluorescence spectra were recorded on a Hitachi spectrophotometer, Model 356, and a Hitachi fluorescence spectrophotometer, Model MPF-2, respectively, both at room temperature. Cyclohexane and 1,2-dichloroethane of a spectral grade and diethyl ether, benzene, and ethanol of a guaranteed grade were used without further purification.

TABLE 1. ABSORPTION AND FLUORESCENCE SPECTRAL DATA OF THREE 2-PYRIDYLBENZIMIDAZOLES (**1a**, **2**, AND **3**) IN VARIOUS SOLVENTS

Compd	Solvent[a]	Absorption		Fluorescence[b]	
		λ_{max}(nm)[c]	ε	λ_F (max)	I_{rel}[d]
1a	CH	311.5	25400	349.0	15
	Benzene	312.0	23100	357.0	11
	DCE	310.5	22600	359.0	10
	EE	310.0	23300	352.0	19
	Ethanol	309.0	20500	358.0	1
2	CH	314.5	20500	355.0	22
	Benzene	311.0	19700	352.5	15
	DCE	310.0	20000	354.5	17
	EE	309.0	21500	347.5	26
	Ethanol	312.0	20100	360.0	16
3	CH	310.0	20900	358.0	11
	Benzene	309.0	20900	357.0	9
	DCE	306.5	20900	363.0	13
	EE	306.0	23200	352.0	12
	Ethanol	306.5	20700	372.5	14

a) CH, DCE, and EE stand for cyclohexane, 1,2-dichloroethane, and ethyl ether respectively. b) The concentrations were 4.23×10^{-6}, 4.20×10^{-6}, and 4.22×10^{-6} M for **1a**, **2**, and **3** respectively. The excitation wavelength of 310 nm was selected. c) The vibrational structures in the absorption and emission spectra were observed for cyclohexane solutions, but not for most of the other solutions. Therefore, the $0 \rightarrow 1'$ and $0' \rightarrow 1$ transition components are recorded here as the band peak for the sake of easy comparison. d) The relative intensity was given as the ratio of the peak height to that for an ethanol solution of **1a**.

Results and Discussion

Fluorescence Spectra of Three 2-Pyridylbenzimidazoles, 1a, 2, and 3. Table 1 summarizes the results of the absorption and emission spectral measurements of **1a**, **2**, and **3** in various organic solvents.

The observed red shifts and the enhancement of the molar extinction coefficients for the first absorption bands of these compounds, as compared with those for benzimidazole,[7] indicate the complete conjugation of the pyridyl substituent with the benzimidazole moiety.

It is possible to say that the fluorescence bands of these compounds are not separated much from, and take mirror images with, the absorption band, indicating that the molecular conjugations in the excited singlet states differ little from those in the ground states. The fluorescence spectra were found to be independent of the excitation wavelengths and of the concentration.

The fluorescence intensities of these compounds are very strong and of the same order of magnitude, except for the case of **1a** in ethanol. It is noteworthy that benzene did not quench the fluorescence emission of these compounds, taking into account the quenching interactions between benzene and indole,[8] where the NH group has been suggested as being essential. The absence of any quenching effect of benzene in the present case is probably to be ascribed to: (i) the presence of a rather bulky pyridyl group, which is believed to prohibit the benzene molecule from interacting with the NH group and (ii) a stronger interaction of the NH group with the pyridine-N atom internally (**1a**) or intermolecularly (**2** and **3**) than with the benzene solvent molecules.

It is of interest that the fluorescence intensity of **1a** in an ethanol solution is much weaker than in cyclohexane. Figure 1 shows the quenching effect of ethanol on the fluorescence spectrum of **1a** in the binary solvent system of cyclohexane and ethanol. From the figure it is clear that ethanol molecules effectively quench the fluorescence emission of **1a**. By plotting the fluorescence intensities *versus* the quencher concentration, a value of 0.05 mol/l was obtained for the quencher efficiency of ethanol. This value is comparable with that reported for the chloroform–indole in cyclohexane.[8] On the other hand, ethanol molecules did not quench the emission of **2** and **3**. From these observations it is possible to assume that the fluorescence quenching by ethanol does not originate from a simple intermolecular hydrogen bonding, but from a specific bridge-type intermolecular hydrogen bonding, which is possible only for a combination of ethanol and **1a** which has two nitrogen atoms in a proper proximity. The specific bridge-type intermolecular hydrogen bonding is shown schematically in **A**. As can readily be expected from the figure, this type of intermolecular hydrogen bonding is impossible between an ethanol molecule and **2** or **3**.

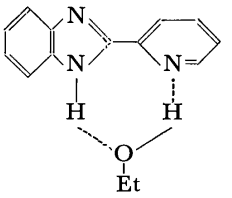

A

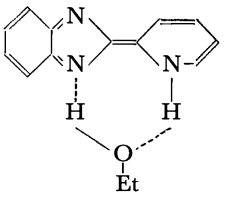

A'

A similar quenching effect, of course, is commonly observed for some alcoholic solutions of **1a**. The fluorescence intensity of **1a** in some alcoholic solutions is in this order: MeOH<EtOH<*n*-PrOH<*n*-BuOH (Table 2). This order is inversely proportional to the proton exchange activity of the hydroxyl group.

TABLE 2. SPECTRAL PARAMETERS OF **1a** IN VARIOUS ALCOHOLS AT ROOM TEMPERATURE (21±1 °C)[a]

Solvent	Absorption		Emission		
	λ_{max}	ε	λ_{ex}	λ_F(max)	I[b]
Methanol	308	21100	300	362	1.0
Ethanol	309	20500	300	358	1.4
Propanol	310	21100	300	356	1.7
Butanol	311	20800	300	354	2.1

a) Solutions were prepared by diluting a cyclohexane solution of **1a** with an appropriate alcohol, the resultant concentration being 1.48×10^{-5} M. b) The relative intensities of the emission bands were estimated from the ratio of the peak height to that of the methanol solution. The small difference in the molar extinction coefficients was neglected.

Molecular Mechanism of Fluorescence Quenching by Ethanol. Compound **1c** is similar to **1a** except for the replacement of the imidazolic proton by the methyl group. Consequently, it is unable to form a hydrogen-bonded complex like **A** with an ethanol molecule; thus it can serve as a convenient control for the experiments with **1a**. As would be expected, the absorption and fluorescence spectra of **1c** are very similar to those of **1a** (an ethanol solution; λ_{max}=304 nm, ε=20300, λ_F(max)=361 nm).

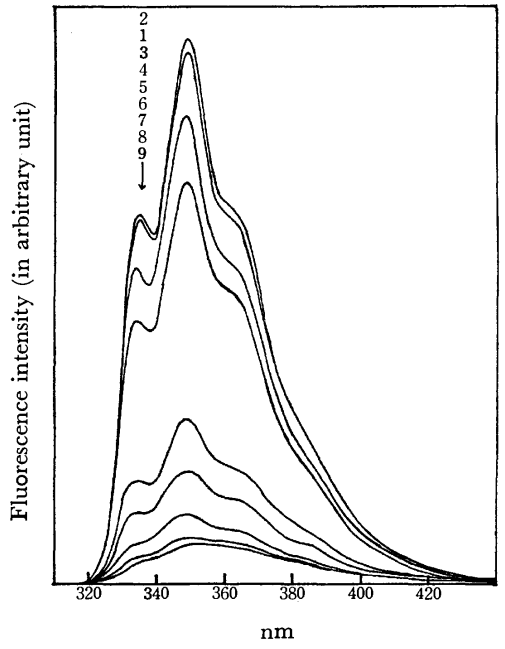

Fig. 1. Fluorescence spectrum of 2-(2-pyridyl)benzimidazole in cyclohexane–ethanol binary solvents (1.6×10^{-5} M, excitation at 310 nm). Ethanol contents are: 1, 0; 2, 0.01; 3, 0.05; 4, 0.1; 5, 0.5; 6, 1.0; 7, 2.0; 8, 5.0; and 9, 10.0.

This means that the molecular configuration of **1c** is very similar to that of **1a** in both the ground and the excited singlet states, except for the inability to form a specific bridge-type complex with an ethanol molecule. As expected, therefore, no serious fluorescence quenching by ethanol molecules was observed for **1c**, when solvents were changed from cyclohexane to ethanol.

It is clear, therefore, that the NH group in the imidazole moiety is explicitly involved in quenching the fluorescence of **1a** by ethanol.

A molecular complex like **A** has been proposed for pyrrolo[2,3-*b*]pyridine in ethanol. In that system, the second fluorescence band was observed at a longer wavelength and was ascribed to the isomeric species which was produced by proton transposition *via* the ethanol molecule being intermolecularly hydrogen bonded.[5] In the present case, however, it is not clear whether or not a similar isomerization occurs through intramolecular proton transposition like that, because no second fluorescence band was observed at any longer wavelength.

As a tentative explanation of the molecular mechanism in the fluorescence quenching of **1a** by ethanol, the present author proposes a proton exchange in the excited singlet state between the solute and solvent molecules in the bridge-type complex, **A**. In the case of ethanol solutions of **2** and **3**, an ethanol molecule can not form a bridge-type complex like **A**. Therefore, it is reasonable that no fluorescence quenching was observed for ethanol solutions of **2** and **3**.

Table 3. Relative fluorescence intensities (R) of **1a**, **2**, and **3** in phosphate buffers at pH 6.8

Compound	Concentration	Excitation	R[a]
1a	2.82×10^{-5} M	320 nm	0.73
2	2.05	300	0.44
3	2.21	320	0.90

a) The R value for an ethanol solution of **1a** at the same concentration was assumed to be 1. The difference in light intensities at 300 and 320 nm was taken into consideration in calculating R.

In the case of aqueous solutions of **1a**, **2**, and **3**, the fluorescence intensities are as weak as that of **1a** in ethanol (Table 3). This implies that a proton transposition-isomerization like that proposed for pyrrolo[2,3-*b*]-pyridine is not responsible for the fluorescence quenching in question, because such a proton-transposed isomer (like **A'**) can not be written for **2**. In aqueous solutions of **2** and **3**, the concerted operation of water molecules makes it possible to exchange protons through polymeric aggregates of water molecules.

Recently Kikuchi *et al.*[9] proposed a transient proton transfer as an internal conversion mechanism for the system of naphthol and pyridine.

Rapid Proton Transfer in the Excited Singlet State of ***1b***. The first absorption band and the fluorescence band of **1b** in various solvents are listed in Table **4**. The absorption band of **1b** is located at a longer wavelength than that of **1a** in any solvent, primarily because of the effect of the OH-group introduction, but also partly because of its intramolecular hydrogen bond between the

Table 4. Absorption and fluorescence spectral data of **1b** in various solvents

Solvent	Absorption[a]		Fluorescence[b]	
	$\lambda(0\rightarrow0')$	ε	λ_F(max)	I_{rel}
CH	344.5	30000	457	1.0
Benzene	342.5	28300	452	1.0
DCE	343.0	25300	448	1.3
EE	345.9	26700	450	1.4
Ethanol	342.0	25500	442	1.4

a) The concentration was 2.26×10^{-5} M. b) The concentration was 4.53×10^{-6} M.

phenolic hydroxyl and the N-3 atom. The observed large Stokes' shift (*ca.* 9000 cm^{-1}) of the emission band can be attributed to an isomeric species, **K**, which is formed by the intramolecular proton transfer shown schematically below:

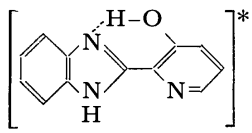

E

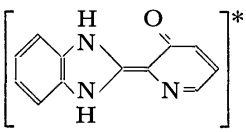

K

From the table it is clear that the fluorescence intensity of **1b** in ethanol is as strong as in the other solvents examined. This indicates that no serious quenching by ethanol operates and that the intramolecular proton transfer in the excited singlet state occurs in a very short period, within which hardly no quenching by ethanol occurs. In this connection, the rate of the intramolecular proton transfer has been reported to be 1.1×10^{10} s^{-1} for 2,4-bis(dimethylamino)-6-(2-hydroxy-5-methylphenyl)-1,3,5-triazine.[10] If the same proton-transfer rate is assumed in the present case, the ethanol-quenching rate can be roughly estimated as 1×10^{9} s^{-1} or less, because no quenching effect of ethanol was observed.

References

1) M. A. El-Sayed, *J. Chem. Phys.*, **36**, 573 (1962).

2) N. Mataga, Y. Kaifu, and M, Koizumi, *Nature*, **175**, 731 (1955); *Bull. Chem. Soc. Jpn.*, **29**, 115 (1956).

3) E. J. Bowen, N. J. Holder, and G. B. Woodger, *J. Phys. Chem.*, **66**, 2491 (1962).

4) N. Mataga and S. Tsuno, *Bull. Chem. Soc. Jpn.*, **30**, 368 (1957).

5) a) K. C. Ingham, M. Abu-Elqheit, and M. A. El-Bayoumi, *J. Am. Chem. Soc.*, **93**, 5022 (1971); b) K. C. Ingham and M. A. El-Bayoumi, *J. Am. Chem. Soc.*, **96**, 1674 (1974).

6) a) T. Hisano and M. Ichikawa, *Chem. Pharm. Bull.*, **22**, 1923 (1974); b) Y. Sasaki and T. Shigematsu, *Bull. Chem. Soc. Jpn.*, **46**, 3438 (1973); c) J. L. Walter and H. Freiser, *Anal. Chem.*, **26**, 217 (1954); d) D. Jerchel, M. Kracht, and K. Krucker, *Ann. Chem.*, **590**, 232 (1954).

7) K. Hoffmann, "Imidazole and its Derivatives. Part I," Interscience, New York (1951).

8) B. C. van Duuren, *J. Org. Chem.*, **26**, 2954 (1961).

9) K. Kikuchi, H. Watari, and M. Koizumi, *Bull. Chem. Soc. Jpn.*, **46**, 749 (1972).

10) H. Shizuka, K. Matsui, Y. Hirata, and I. Tanaka, *J. Phys. Chem.*, **80**, 2070 (1975).

The Binding and Catalytic Properties of a Positively Charged Cyclodextrin

Yoshihisa MATSUI* and Akihiko OKIMOTO

Department of Agricultural Chemistry, Shimane University, Nishikawazu, Matsue 690

(Received March 20, 1978)

In order to learn the significance of electrostatic interactions between charged groups in an enzymatic process, a positively charged cyclodextrin, mono-(6-trimethylammonio-6-deoxy)-β-cyclodextrin hydrogencarbonate (βCDtma), was prepared as a simple enzyme model, and its binding and catalytic properties were examined. The dissociation constant for an inclusion complex of βCDtma with an azo dye, sodium 4-(4-hydroxy-1-naphthylazo)-1-naphthalenesulfonate (**1**), was found to be 5.4×10^{-5} mol/dm^3 in an alkaline solution (pH 10.5, $I_c=0.0$ mol/dm^3) at 25 °C, the value being smaller than that for an inclusion complex of the parent β-cyclodextrin (βCD) with **1** by a factor of *ca.* 4. The catalytic effect of βCDtma on the alkaline hydrolyses of *o*-, *m*-, and *p*-acetoxybenzoic acids was significantly different from that of βCD. These observations were explained in terms of electrostatic and hydrophobic interactions between βCDtma and a guest molecule.

Cyclodextrin (CD) is a cyclic oligomer composed of six (αCD), seven (βCD), or more α-D-glucopyranose units linked 1→4 as in amylose. The interior cavity of the doughnut-shaped molecule provides a relatively hydrophobic environment into which an apolar molecule can be trapped.[1,2] Since the rate and stereochemistry of a reaction for an organic substrate are significantly changed by the formation of a CD–substrate adduct, CD has been utilized as a simple model for an enzymatic process.[2-4] However, an enzyme is a macromolecular electrolyte, whereas CD contains no charged group in the molecule. Electrostatic interactions between charged groups play an important role in an enzymatic system.[5-7] For example, they contribute not only to strengthening the binding of a specific substrate to an enzyme, but also to orienting the substrate properly in the active site of the enzyme.[8]

In the present work, a positively charged CD, mono-(6-trimethylammonio-6-deoxy)-β-cyclodextrin hydrogencarbonate (βCDtma), was prepared as a simple model of an enzyme containing a positively charged group in the vicinity of the active site. This molecule bears two binding sites, one being the hydrophobic cavity of the βCD ring, and the other, the cationic part of the ammonium ion. Focusing our attention on the cooperative action of the two binding sites, we examined the binding and catalytic properties of the modified CD in an aqueous solution. In this connection, Tabushi *et al.*[9] have recently reported that a CD flexibly capped with a metal ion can effectively bind a hydrophobic anion in such a manner as to facilitate cooperative double recognition.

Experimental

Materials. The βCD of a reagent grade was recrystallized from water and dried overnight *in vacuo* at 110 °C. Pyridine of a reagent grade was dried over calcium hydride and was distilled in the presence of fresh calcium hydride just before use. *p*-Toluenesulfonyl chloride of a reagent grade was used without further purification. *N,N*-Dimethylformamide (DMF) of a reagent grade was dried over K_2CO_3 and distilled in the presence of calcium hydride *in vacuo*. A solution of trimethylamine in DMF was prepared by introducing the gaseous trimethylamine to DMF. The concentration of trimethylamine in DMF was determined by titration with 0.1 mol/dm^3 oxalic acid. An azo dye, sodium 4-(4-hydroxy-1-naphthylazo)-1-naphthalenesulfonate (**1**), was prepared and purified as has been described previously.[10] *o*-Acetoxybenzoic acid (**2o**) of a reagent grade was used without purification. The *m*- and *p*-acetoxybenzoic acids (**2m** and **2p** respectively) were prepared by the reactions of the corresponding hydroxybenzoic acids with acetic anhydride in dry pyridine and were recrystallized from chloroform.

Thin-layer chromatography (TLC) was performed on silica gel G (Merck) with a mixed solvent of acetic acid–chloroform–water (80: 10: 10 (v/v)). A solution of diphenylamine (0.1 g), aniline (0.1 ml), and 85% phosphoric acid (1 ml) in acetone (10 ml) was used as a spray reagent to detect the parent and the modified βCD.

Apparatus. The absorption and NMR spectra were recorded using a Hitachi Model 124 spectrophotometer and a JEOL Model JNM-MH-100 NMR spectrometer respectively. The pH of each aqueous solution was measured by means of an Orion Model 801A digital pH/mV meter.

Preparation of βCDtma. A solution of *p*-toluenesulfonyl chloride (3.65 g, 19.1 mmol) in dry pyridine (30 ml) was added to a solution of βCD (29.60 g, 26.1 mmol) in dry pyridine (300 ml) cooled below 5 °C. After stirring overnight at room temperature, the mixture was evaporated *in vacuo* at 40 °C to dryness. Diethyl ether (700 ml) was added to the residue. The precipitate was collected and recrystallized three times from water to afford 10.37 g (8.0 mmol; yield, 31% based on βCD) of mono-(6-*O*-*p*-tolylsulfonyl)-β-cyclodextrin (βCDots). The TLC of the product gave a spot with R_f 0.38 (*cf.* R_f 0.26 for βCD). The monosubstitution of βCD was confirmed by the PMR spectra of the product in DMSO-d_6.[11] The βCDots (10.27 g, 7.9 mmol) was dissolved in 300 ml of DMF containing 3.2 mol/dm^3 trimethylamine. After being heated overnight at 90—100 °C in sealed tube, the mixture was evaporated *in vacuo* to dryness. The residue was dissolved in 10 ml of water and then chromatographed on a 4.5×43 cm carboxymethylcellulose column, with 0.05 mol/dm^3 ammonium hydrogencarbonate buffer as the eluant. One hundred and sixty fractions were taken, each being 10 ml. The fractions were assayed for carbohydrate by TLC. Fractions which gave only one spot with R_f 0.15 (the fractions from No. 75 to No. 150) were combined and evaporated to dryness at 40 °C *in vacuo* to afford 4.07 g (3.3 mmol; yield, 42% based on βCDots) of the product, βCDtma, as a white powder. The NMR spectra of the product in D_2O showed absorptions at $\delta=3.05$ due to the trimethyl hydrogens and at $\delta=4.97$ due to the anomeric hydrogens of the glucopyranose rings. The relative areas of these peaks were about 9: 7, indicating the monosubstitution of βCD.

An apparent dissociation constant (K_d) for a βCDtma-**1**

inclusion complex and an apparent acid-dissociation constant (K_a) for **1** in both the absence and presence of βCDtma were spectrophotometrically determined as has been described previously.[10] The aqueous buffer solutions used were citric acid–Na_2HPO_4 (pH 3—7), KH_2PO_4–$Na_2B_4O_7$ (pH 6—9), and $Na_2B_4O_7$–NaOH (pH 9—12).

Kinetics. The rates of the alkaline hydrolysis of acetoxybenzoic acids (**2**) were measured by following the appearance of the absorptions of the corresponding phenoxide anions at 300, 310, and 280 nm for **2o**, **2m**, and **2p** respectively in alkaline aqueous solutions. The ionic strength (I_c) of the solution was maintained at 0.65 mol/dm³ with Na_2SO_4. In a typical run, 2.00 ml of a base solution was pipetted into a pair of 1.00-cm quartz cells, one of which was used as the reference cell, and the other, as the sample cell, in a spectrophotometer. After thermal equilibrium at 25.0±0.1 °C had been reached, 5 to 8 μl of a 0.06 to 0.14 mmol/dm³ ester solution in ethanol was added to the sample cell and the change in absorbance was followed. The results for various reaction times were treated according to the ordinary first-order rate equation. The rate constants were graphically determined. All the reactions examined obeyed good first-order kinetics with respect to substrates in both the absence and presence of βCDtma.

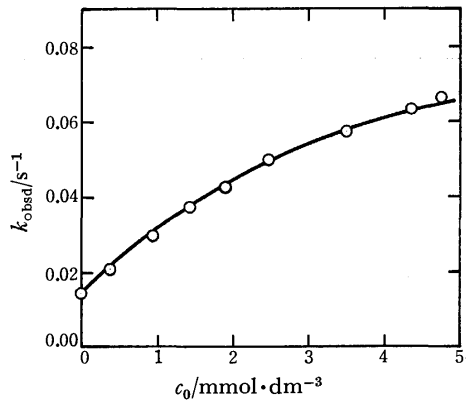

Fig. 1. The plot of k_{obsd} *vs.* c_0 for a βCDtma–**2m** system in 0.0105 mol/dm³ NaOH at 25 °C and I_c=0.65 mol/dm³.

Kinetic Determination of the Dissociation Constants and Rate Constants of βCDtma–2 Complexes. As is shown in Fig. 1 as an example, the observed first-order rate constant (k_{obsd}) for each substrate examined approached a maximum value as the βCDtma concentration (c_0) increased. This saturation behavior suggests that the rate process involves the prior formation of an inclusion complex of βCDtma with each substrate. Upon the assumption of the formation of a 1:1 βCDtma–**2** complex, k_{obsd} is represented by the following equation if c_0 is much higher than that of a substrate (s_0):

$$k_{obsd} = -\frac{K_d(k_{obsd}-k_{un})}{c_0} + k_c. \quad (1)$$

In this equation, k_d is the dissociation constant of an inclusion complex, and k_{un} and k_c, the rate constants for free and complexed substrates respectively. The plot of k_{obsd} *vs.* $(k_{obsd}-k_{un})/c_0$ was virtually linear for each βCDtma–**2** system; the values of K_d and k_c were calculated from the slope and intercept respectively of the line obtained by the use of the least-squares method.

Results and Discussion

Apparent Dissociation Constants for βCDtma–Azo Dye Inclusion Complexes. In order to learn the role of a positively charged group in the binding properties of βCDtma, the apparent dissociation constants (K_d) were determined for the βCDtma– and βCD–azo dye systems. Sodium 4-(4-hydroxy-1-naphthylazo)-1-naphthalenesulfonate (**1**) was used as an azo dye, since the dye shows a large spectral change upon being included within the βCD cavity.[10] In fact, the addition of βCDtma to an aqueous solution of **1** caused a large spectral change, one which is quite similar to that caused by the addition of the parent βCD. An isosbestic point was observed at 438 nm for a solution at pH 4.0 or at 445 nm for a solution at pH 10.5. These observations suggest that **1** forms a 1:1 inclusion complex with βCDtma in a manner similar to that with βCD in an aqueous solution. Table 1 shows the K_d values for the βCDtma– and βCD–**1** systems at the pH values of 4.0 and 10.5. The pK_a value of **1** is *ca.* 7.5 (see Table 2), so the acidic hydroxyl group of **1** is mostly undissociated at pH 4.0, while it is mostly dissociated at pH 10.5. The K_d value for a βCDtma–**1** system is larger than that for a βCD–**1** system at pH 4.0, whereas the former is smaller than the latter at pH 10.5.

Table 1. The K_d values for βCDtma– and βCD–**1** systems at 25 °C and I_c=0.03 mol/dm³

pH	K_d/(mmol/dm³)		K_d(βCD)/K_d(βCDtma)
	βCDtma	βCD	
4.0[a]	0.767	0.508	0.66
10.5[b]	0.096	0.195	2.03

a) Citric acid–Na_2HPO_4 buffer. b) $Na_2B_4O_7$–NaOH buffer.

The modification of βCD to the positively charged form resulted in a decrease in the stability of an inclusion complex with the undissociated form of **1**. A decrease in the hydrophobicity of the interior cavity of the CD ring, as well as a change in the geometry of the inclusion complex, with the modification of βCD may be the cause of the decrease in the stability of the inclusion complex. In this connection, we previously suggested[10] that the 4-hydroxy-1-naphthylazo moiety of **1**, rather than the 4-sulfonato-1-naphthylazo moiety, is bound to the βCD cavity, mainly through hydrophobic interactions. If βCDtma also includes the 4-hydroxy-1-naphthylazo moiety of **1**, a decrease in the hydrophobicity of the CD cavity, accompanied by the close location of a positive charge, may be responsible for the decrease in stability. In such a mode of binding, the negatively charged sulfonate group is too remote in position from the positive charge of βCDtma to enhance effectively the association of **1** with the host by means of the electrostatic force of attraction. It is also possible that the 4-sulfonato-1-naphthylazo moiety of **1**, instead of the 4-hydroxy-1-naphthylazo moiety, is included in the cavity of βCDtma. In this case, electrostatic interactions may contribute considerably to the association, while

the contribution of hydrophobic interactions to the association may significantly decrease. In either event, electrostatic interactions can scarcely cooperate with hydrophobic interactions in the present host-guest system.

On the other hand, the dissociated form of **1** is bound to the βCDtma *ca.* two times more strongly than the parent βCD. This fact suggests that electrostatic interactions between the positive charge of βCDtma and the negative charge of the naphthyloxide anion of **1** cooperate with hydrophobic interactions between the βCD cavity and the naphthylazo moiety in this case. A similar extent of binding enhancement due to electrostatic interactions has recently been reported in differently modified CD-substrate systems.[9]

Effect of the Ionic Strength on the K_d Values for the βCDtma- and βCD-1 Systems. In order to determine which electrostatic or hydrophobic interactions contribute more to the association of the modified βCD with **1**, the effect of the ionic strength (I_c) on the K_d values was examined for inclusion complexes at the pH values of 4.0 and 10.5. An increase in I_c generally weakens ion-ion and ion-dipole interactions,[12] while it strengthens hydrophobic interactions (salting-out effect).[13] Figures 2 and 3 show the plots of log K_d *vs.* $I_c^{1/2}$ for complexes of βCDtma and the parent βCD with **1** at pH 4.0 and at pH 10.5 respectively. Each plot is virtually linear. The K_d values increase with an increase in I_c for the βCDtma–**1** systems, whereas they decrease with an increase in I_c for the parent βCD–**1** systems at both pH's. These observations suggest that electrostatic, rather than hydrophobic, interactions play a dominant role in the association of βCDtma with **1**, while the reverse is true for the βCD–**1** systems. The extrapolation of the linear log K_d *vs.* $I_c^{1/2}$ plot to the intercept gives the K_d value (K_d°) at $I_c=0$ mol/dm³. The K_d° values for the βCDtma- and βCD–**1** systems at pH 10.5 were equal to 5.4×10^{-5} and 2.2×10^{-4} mol/dm³ respectively, indicating that the βCDtma binds the anionic **1** four times more strongly than the parent βCD does at $I_c=0$ mol/dm³.

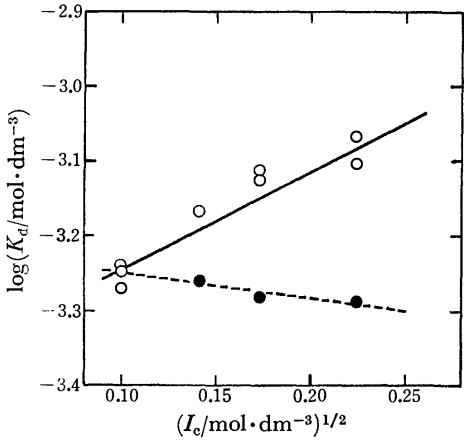

Fig. 2. The effect of I_c on the K_d value for βCDtma–**1** (○) and βCD–**1** (●) systems at pH 4.0 and 25 °C.

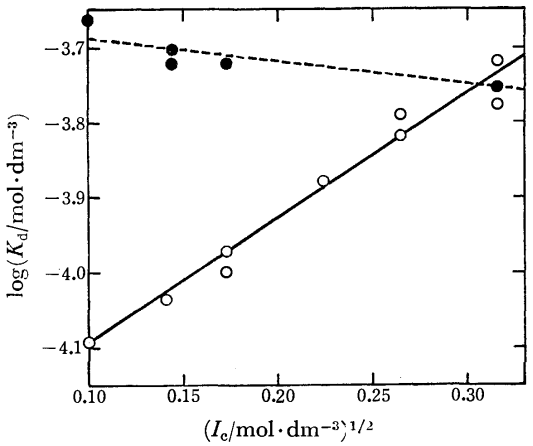

Fig. 3. The effect of I_c on the K_d value for βCDtma–**1** (○) and βCD–**1** (●) systems at pH 10.5 and 25 °C.

TABLE 2. THE EFFECT OF βCDtma ON THE pK_a VALUE OF **1** AT 25 °C AND I_c=0.04 mol/dm³

[βCDtma] / mmol/dm³	pK_a
0.00	7.50
0.48	7.00
0.95	6.87

Effect of βCDtma on the Apparent pK_a *Values of* **1**. In a protein–[14] or micellar–[15] dye system, it has frequently been shown that charged groups around a binding site significantly affect the pK_a value of a bound dye. The apparent pK_a values for **1** in the absence and in the presence of βCDtma were spectrophotometrically measured at I_c=0.04 mol/dm³ (Table 2). The observed pK_a values decrease with an increase in the βCDtma concentration. A similar decrease in pK_a has been observed in a βCD–**1** system at I_c=0.05 mol/dm³.[10] However, the extent of the decrease in pK_a is greater in a βCDtma–**1** system than in a βCD–**1** system. For example, the addition of only 0.95 mmol/dm³ βCDtma lowered the pK_a from 7.50 to 6.87, while the addition of 2.02 mmol/dm³ βCD decreased the pK_a only to 7.02. The pK_a value for an inclusion complex between βCDtma and **1** was calculated, by the use of Eq. 7 in Ref. 10, to be 6.60 at I_c=0.04 mol/dm³ (*cf.* pK_a=6.97 for a βCD–**1** complex at I_c=0.05 mol/dm³ [10]). It is apparent that the acid dissociation of **1** is facilitated to a greater extent by the formation of an inclusion complex with βCDtma than by the formation of a complex with the parent βCD. This fact may also be related to the electrostatic action of a positive charge in βCDtma.

Effect of βCDtma on the Alkaline Hydrolysis of **2**. In order to learn the effect of a positive charge on the catalytic properties of βCDtma, kinetic parameters were determined for the alkaline hydrolysis of **2** in the absence and in the presence of βCDtma. The substrates bear a carboxylate anion in alkaline solutions, so that it can be anticipated that the catalytic action of the positively charged βCDtma is significantly different from that of the parent βCD. The parameters for βCDtma and βCD systems are compared with each other in Table 3.

Table 3. Kinetic and equilibrium parameters for βCDtma- and βCD-acetoxybenzoic acid systems in alkaline solutions at 25 °C and I_c=0.65 mol/dm³

Substrate	Catalyst	$10^3 k_{un}$ / s^{-1}	$10^3 k_c$ / s^{-1}	k_c/k_{un}	K_d / mmol/dm³
2o[a]	βCDtma	1.89	4.25	2.25	2.29
2o	βCD	1.89	14.5	7.67	12.4
2m[b]	βCDtma	14.4	136	9.44	6.39
2m	βCD	14.4	58.1	4.03	4.40
2p[c]	βCDtma	1.51	1.99	1.32	0.528
2p	βCD	1.51	1.93	1.28	2.08

a) 0.0098 mol/dm³ NaOH. b) 0.0105 mol/dm³ NaOH. c) pH 10.84 ($Na_2B_4O_7$–NaOH buffer).

The effects of the modification of βCD on the kinetic and equilibrium parameters for the alkaline hydrolyses of **2o**, **2m**, and **2p** are markedly different from one another. The K_d values for the βCDtma–**2o** and –**2p** systems are smaller than those for the parent βCD–**2o** and –**2p** systems respectively, while the K_d value for a βCDtma–**2m** system is larger than that for the corresponding βCD system. An increase in the electrostatic attraction force does not always result in an increase in the stability of a host-guest complex. It seems that the K_d value depends on the geometry of the inclusion complex, in which electrostatic interactions contribute either favorably or unfavorably to the stabilization of the complex.

The k_c value for a βCDtma–**2o** system is smaller than that for a parent βCD–**2o** system, while that for a βCDtma–**2m** system is larger than that for the corresponding βCD system. The k_c values for βCDtma- and βCD–**2p** systems are virtually equal to each other. The value of k_c/k_{un} is a measure of the proximity between the catalytic and the reaction sites of an inclusion complex.[16] The catalytic site of the complex is an alkoxide ion derived by the acid dissociation of a secondary hydroxyl group of βCD. The reaction site is an ester carbonyl carbon. The significant change in the k_c/k_{un} ratio of the **2o** and **2m** systems with the modification of βCD indicates that the geometries of the βCDtma–**2o** and –**2m** complexes are considerably different from those of the parent βCD–**2o** and –**2m** complexes respectively. The geometry of a βCDtma–**2p** complex may be virtually the same as that of a βCD–**2p** complex. In this connection, the geometries of the βCD–**2o**, –**2m**, and –**2p** inclusion complexes, as well as the changes in the geometries accompanied by the modification of βCD to βCDtma, were presumed to be as is shown in Figs. 4, 5, and 6 respectively; these results

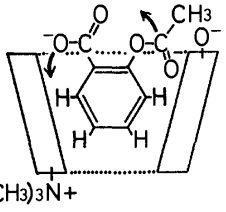

Fig. 4. The geometry of **2o** in the βCD cavity, suggested by the CPK molecular models.

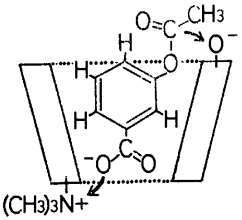

Fig. 5. The geometry of **2m** in the βCD cavity, suggested by the CPK molecular models.

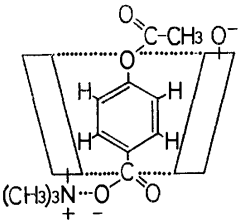

Fig. 6. The geometry of **2p** in the βCD cavity, suggested by the CPK molecular models.

were obtained by the use of the Corey-Pauling-Koltum molecular models. The acetyl groups of **2o** and **2m** may be located in the vicinity of the catalytically active alkoxide ion in their βCD complexes (the k_c/k_{un} values for these complexes are fairly large). In βCDtem–**2o** and –**2m** complexes, the carboxylate anions of the substrates may be electrostatically attracted to the cationic group of βCDtma, as is shown by the arrows in Figs. 4 and 5 respectively. At the same time, the acetyl group of **2o** may go far off from the alkoxide ion on the βCD ring, while that of **2m** may be brought closer to the alkoxide ion. In a βCD–**2p** system, the carboxylate anion of the substrate may lie close to the primary hydroxyl groups of βCD. The modification of one of the hydroxyl groups to the trimethylammonium group may cause little change in the geometry of the substrate in the βCD cavity. However, the electrostatic interaction between the ammonium cation and the carboxylate anion may serve to stabilize a complex of **2p** with βCDtma, compared with that of **2p** with βCD. Therefore, the above observations indicate that electrostatic interactions between a positive charge of βCDtma and a negative charge of a substrate affect not only the stability of the host-guest complex, but also the orientation of the guest in the host molecule. Although the detailed geometry of inclusion complexes remains to be determined, the present host-guest systems are interesting as simple model systems of an enzymatic process.

References

1) D. French, *Adv. Carbohyd. Chem.*, **12**, 189 (1957).
2) D. W. Griffiths and M. L. Bender, *Adv. Catal.*, **23**, 209 (1973).
3) R. Breslow, "Bioinorganic Chemistry," American Chemical Society Publications, Washington (1971), p. 21.
4) J. H. Fendler and E. J. Fendler, "Catalysis in Micellar and Macromolecular Systems," Academic Press, New York (1975), p. 450.
5) W. P. Jencks, "Catalysis in Chemistry and Enzymology," McGraw-Hill, New York (1969), p. 351.

6) F. R. N. Gurd, "Physical Principles and Techniques of Protein Chemistry," ed by S. J. Leach, Academic Press, New York (1970), Part B, p. 365.
7) K. J. Laidler and P. S. Bunting, "The Chemical Kinetics of Enzyme Action," 2nd ed, Clarendon Press, Oxford (1973), p. 272.
8) E. Zeffren and P. H. Hall, "The Study of Enzyme Mechanisms," John Wiley & Sons, New York (1973), p. 200.
9) I. Tabushi, N. Shimizu, T. Sugimoto, M. Shiozuka, and K. Yamamura, *J. Am. Chem. Soc.*, **99**, 7100 (1977).
10) Y. Matsui and K. Mochida, *Bull. Chem. Soc. Jpn.*, **51**, 673 (1978).
11) Y. Matsui, T. Yokoi, and K. Mochida, *Chem. Lett.*, **1976**, 1037.
12) H. Gutfreund, "Enzymes; Physical Principles," Wiley-Interscience, New York (1972), p. 32
13) H. von Hippel and T. Schleich, "Biological Macromolecules," ed by S. N. Timasheff and G. D. Fasman, Marcel Dekker, New York (1969), Vol. 2, p. 417.
14) C. E. Williamson and A. H. Corwin, *J. Colloid Interface Sci.*, **38**, 577 (1972).
15) C. E. Williamson and A. H. Corwin, *J. Colloid Interface Sci.*, **38**, 567 (1972).
16) R. L. VanEtten, J. F. Sebastian, G. A. Clowes, and M. L. Bender, *J. Am. Chem. Soc.*, **89**, 3242 (1967).

Stereospecific Synthesis of the C-9—C-16 Segment of Carbonolide B, the Aglycon of Carbomycin B†

Kuniaki TATSUTA,* Toyoaki YAMAUCHI, and Mitsuhiro KINOSHITA

Department of Applied Chemistry, Faculty of Engineering, Keio University, Hiyoshi, Kohoku-ku, Yokohama 223

(Received March 24, 1978)

Stereospecific synthetic routes to methyl (*R*)-7-hydroxy-(2*E*,4*E*)-octadienoate (**9**) and its (2*E*,4*Z*)-isomer (**16**), the former which can be a useful chemical precursor to the 16-membered-ring aglycon of carbomycin B (carbonolide B), are discussed. Compound **9**, corresponding to its C-9—C-16 segment, was synthesized starting with methyl 2-deoxy-α-D-*arabino*-hexopyranoside (**2**). The deoxysugar **2** was converted to the masked 2,4,6-trideoxy-D-*threo*-hexopyranose (**6**) *via* the 4,6-dichloro-2,4,6-trideoxy-α-D-*lyxo*-hexopyranoside derivative. Treatment of **6** with *p*-toluenesulfonyl chloride and triethylamine afforded 3-*O*-acetyl-1,5-anhydro-2,4,6-trideoxy-D-*threo*-hex-1-enitol, which by reaction with mercury(II) acetate was converted to (*R*)-5-hydroxy-(2*E*)-hexenal (**8**). Reaction of **8** with Wittig reagent gave the (2*E*,4*E*)-isomer **9**. Compound **16** was prepared by the Wittig reaction with the 2,3-unsaturated deoxysugar, 2,3,4,6-tetradeoxy-D-*glycero*-hex-2-enopyranose, which was derived from methyl 2,3-anhydro-4,6-dideoxy-α-D-*lyxo*-hexopyranoside by treatment with potassium selenocyanate followed by acid hydrolysis.

In the course of studies directed toward the total synthesis of 16-membered macrolide antibiotics, the regio- and stereoselective introduction of an aminodisaccharide onto the 16-membered aglycon has been reported.[1] Carbomycin B[2] is a representative antibiotic of the 16-membered-ring macrolides, and the structure of the aglycon, carbonolide B (**1a**), can be divided into two segments of C-1—C-8 and C-9—C-16. The latter is stereochemically related to methyl (*R*)-7-hydroxy-(2*E*,4*E*)-octadienoate (**9**), where the C-1 and C-8 carbon atoms correspond to the C-9 and C-16 of carbonolide B. This paper reports the stereospecific synthesis of **9** as an intermediate in the synthesis of carbonolide B using carbohydrates. Recently, a variety of carbohydrates have been used as chiral intermediate in the total synthesis[3,4] of and/or in the synthetic approach[5] to natural products.

The key process was the conversion of 3-*O*-acetyl-1,5-anhydro-2,4,6-trideoxy-D-*threo*-hex-1-enitol (**7**) by mercury(II) acetate to (*R*)-5-hydroxy-(2*E*)-hexenal (**8**), which reacted with Wittig reagent to give **9**. Methyl (*R*)-7-hydroxy-(2*E*,4*Z*)-octadienoate (**16**) was prepared by the Wittig reaction with 2,3,4,6-tetradeoxy-D-*glycero*-hex-2-enopyranose (**15**) in order to provide a reference for **9**.

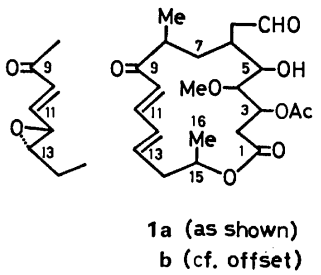

1a (as shown)
b (cf. offset)

Chart 1.

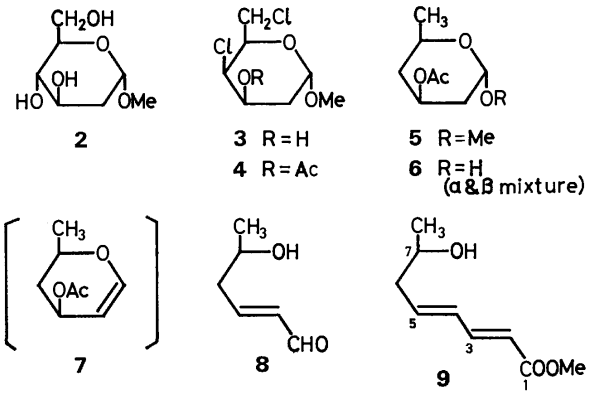

Chart 2.

Results and Discussion

The starting methyl 2-deoxy-α-D-*arabino*-hexopyranoside[6] (**2**) was treated with sulfuryl chloride in pyridine followed by treatment with sodium iodide in aqueous methanol, to give methyl 4,6-dichloro-2,4,6-trideoxy-α-D-*lyxo*-hexopyranoside (**3**). The corresponding 3-*O*-chlorosulfate, which could not be isolated, was considered to be an intermediate.[7] Acetylation of **3** gave a syrupy product **4**, which was dechlorinated with tributylstannane and successively hydrolyzed with dilute hydrochloric acid to give 3-*O*-acetyl-2,4,6-trideoxy-D-*threo*-hexopyranose (**6**). The intermediate methyl 3-*O*-acetyl-2,4,6-trideoxy-α-D-*threo*-hexopyranoside (**5**) was intractable because of its volatility. Conversion of the 2-deoxysugars to the corresponding glycals was achieved by treatment with *p*-toluenesulfonyl chloride in the presence of triethylamine.[1,8] The method was effectively applied to the preparation of 3-*O*-acetyl-1,5-anhydro-2,4,6-trideoxy-D-*threo*-hex-1-enitol (**7**) from **6**. Attempts were unsuccessful to prepare **7** from 2,3-di-*O*-acetyl-4,6-dideoxy-α-D-*xylo*-hexopyranosyl bromide by the usual manner.[9] As **7** was too labile to be purified, it was, without isolation, treated with mercury(II) acetate. This was followed by the addition of dilute sulfuric acid, which gave the syrupy (*R*)-5-hydroxy-(2*E*)-hexenal (**8**)

† Presented at the 37th National Meeting of the Chemical Society of Japan, Yokohama, April 2, 1978.

in a moderate overall-yield. The structure was supported by the characteristic, intense IR absorption at 1695 cm^{-1} and a weak absorption (shoulder) at 1650 cm^{-1}, complemented by a maximum at 223 nm in the UV spectrum. The NMR spectrum provided independent evidence for the open-chain structure of **8**, namely, the doublet at extremely low field (δ 9.62) for H-1, the well-resolved multiplets (δ 6.19 and 6.93) for H-2 and H-3, and the presence of a hydroxyl group (signal at δ 1.80, that disappeared upon addition of D_2O); the large value for $J_{2,3}$ (15.5 Hz) indicated the *trans* position of the olefinic protons. This transformation agrees with expectations based on the reaction of 3,4,6-tri-*O*-acetyl-D-glucal with acidic mercury(II) sulfate.[10] The Wittig reaction of **8** with methoxycarbonylmethylenetriphenylphosphorane provided an 80% yield of the dienoate **9**. The UV and NMR spectra of **9** were very similar to those of ethyl (2*E*,4*E*)-hexadienoate,[11] showing that **9** was a desired (2*E*,4*E*)-isomer implying not only the stereospecific synthesis of the C-9—C-16 segment of carbonolide B but also the utility of the key intermediate, the *trans*-unsaturated aldehyde **8**.

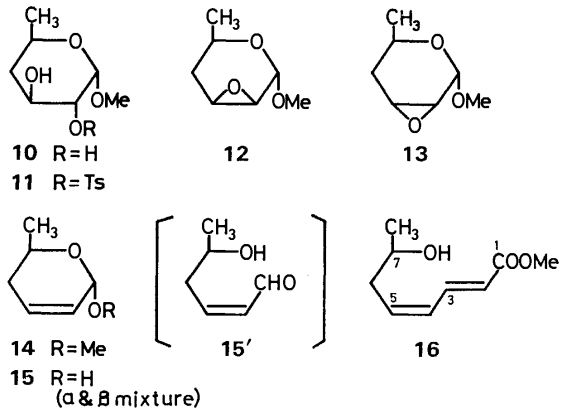

Chart 3.

The (2*E*,4*Z*)-isomer **16** was directly synthesized from the reducing sugar **15** by the Wittig reaction. Selective tosylation of the starting methyl 4,6-dideoxy-α-D-*xylo*-hexopyranoside[12] (**10**) gave predominantly the corresponding 2-*O*-*p*-toluenesulfonate **11** in 72% yield. Treatment of the crude *p*-toluenesulfonate **11**, containing a small amount of the 3-*O*-*p*-toluenesulfonate, with sodium methoxide gave a *ca.* 30: 1 mixture of methyl 2,3-anhydro-4,6-dideoxy-α-D-*lyxo*- and *ribo*-hexopyranosides (**12** and **13**), suggesting that the 3-*O*-*p*-toluenesulfonate was a very minor component. The product **12** could configurationally be a precursor of the C-11—C-16 segment of carbonolide A (**1b**), an aglycon of carbomycin A.[13] Compound **12**, which was isolated as needles, was treated with a boiling solution of potassium selenocyanate[14] in aqueous 2-methoxyethanol for twenty minutes to give methyl 2,3,4,6-tetradeoxy-α-D-*glycero*-hex-2-enopyranoside (**14**). The syrupy product **13**, however, required two hours for the complete reaction to give **14** in the same conditions as described above. Acid hydrolysis of **14** gave a syrupy compound **15**, which was subsequently treated with the Wittig reagent to give the (2*E*,4*Z*)-isomer **16** in 77% overall yield. The structure of **16** was confirmed by UV and NMR spectra in comparison with those of **9** and ethyl (2*E*,4*Z*)-hexadienoate.[11] It appears reasonable on the basis of the above results to suppose that, during the Wittig reaction, the *trans* and *cis* unsaturated aldehydo-forms **8** and **15′**, the latter of which is considered to take part in the reaction of **15** as an intermediate, do not suffer the *trans-cis* and *cis-trans* isomerizations, and the newly produced olefin groups possess the *trans* configuration in both cases.

The utility of the deoxy unsaturated carbohydrates **8** and **15** is thus demonstrated for stereospecific synthesis of α,β: γ,δ-unsaturated esters.

Experimental

Melting points were determined on a micro hot-stage Yanaco MP-S3 and are uncorrected. Specific rotations were measured (0.2-dm tube) with a Carl Zeiss Photoelectric Precision Polarimeter. The NMR spectra were determined with Varian A60, EM-390 or XL100 spectrometers. Unless otherwise stated, chloroform-*d* was used as a solvent and internal tetramethylsilane as a standard. Coupling constants were obtained by measuring spacings of spectra judged to be first-order. TLC and column chromatography were performed on silica gel Wakogel B-5 and Wakogel C-300, respectively. In general, concentration was carried out under reduced pressure below 30 °C.

The starting materials, methyl 2-deoxy-α-D-*arabino*-hexopyranoside[6] [**2**; which was recrystallized from ethyl acetate to give cubics; mp 94—95 °C; $[\alpha]_D^{16}+160°$ (*c* 1.0, CH_3OH)] and methyl 4,6-dideoxy-α-D-*xylo*-hexopyranoside[12] [**10**; which was purified by sublimation at 47 °C at 1 Torr††; mp 108—109 °C, $[\alpha]_D^{24}+179°$ (*c* 1.0, CH_3OH)] were prepared according to the published procedures.

1) Methyl 4,6-Dichloro-2,4,6-trideoxy-α-D-lyxo-hexopyranoside (3). To a stirred solution of **2** (8.91 g) in a dry mixture of pyridine (33 ml) and chloroform (82 ml), cooled in a Dry Ice–acetone bath, was added sulfuryl chloride (21.3 ml) drop by drop over 30 min. Cooling was continued for a further 2 h, after which the reaction mixture was allowed to stand at room temperature overnight. The resulting precipitate, possibly of pyridine salts, was filtered from the chloroform solution. The filtrate was washed successively with 10% sulfuric acid, saturated $NaHCO_3$ solution and water, dried (Na_2SO_4), and evaporated to give an oil. To a methanolic solution (200 ml) of the oil was added a solution of sodium iodide (6.60 g) in 50% aq methanol (16 ml). The mixture was vigorously stirred for 2 h at room temperature and then neutralized with $NaHCO_3$ (11.7 g). The resulting precipitate was removed by filtration, the filtrate evaporated, and the residue chromatographed on a column of silica gel (500 g) with benzene–ethyl acetate (3: 1). The eluate containing the major product (R_f 0.40 by TLC with the same solvent system) was evaporated to give a solid that was further purified by recrystallization from hexane, followed by sublimation at 67 °C under reduced pressure (12 Torr), to give crystals of **3** (4.4 g, 41%): mp 114—115 °C; $[\alpha]_D^{17}+175°$ (*c* 1.0, CH_3OH); NMR δ=1.6—2.6 (3H, m, CH_2-2 and OH-3), 3.39 (3H, s, OCH_3), 3.67 (2H, m, CH_2-5), 3.9—4.3 (2H, m, H-3 and 5), 4.45 (1H, m, H-4) and 4.85 (1H, t, $J_{1,2a}=J_{1,2e}\approx 2.5$ Hz, H-1).

Found: C, 39.15; H, 5.44; Cl, 32.72%. Calcd for C_7H_{12}-

†† Throughout this paper 1 Torr≈133.322 Pa.

O_3Cl_2: C, 39.09; H, 5.62; Cl, 32.97%.

2) Methyl 3-O-Acetyl-4,6-dichloro-2,4,6-trideoxy-α-D-lyxo-hexopyranoside (4). A solution of **3** (121 mg) in a mixture of acetic anhydride (0.11 ml) and pyridine (0.61 ml) was kept overnight at room temperature and, after addition of ethanol (0.11 ml), was concentrated *in vacuo* to give a residue that was chromatographed on a column of silica gel (10 g) with hexane–ethyl acetate (6: 1) to give an oil of **4** (143 mg, 93%). Micro-distillation of **4** at 35 °C at 1 Torr gave an analytically pure oil: $[\alpha]_D^{17}+153°$ (*c* 2.0, CH_3OH); NMR $\delta=1.6$—2.6 (2H, m, CH_2-2), 2.08 (3H, s, OAc), 3.37 (3H, s, OCH_3), 3.64 (2H, d, $J_{5,CH_2}=7$ Hz, CH_2-5), 4.15 (1H, dt, $J_{4,5}=1$ Hz, H-5), 4.59 (1H, m, H-4), 4.87 (1H, dd, $J=1$ and 3 Hz, H-1) and 5.30 (1H, m, H-3).

Found: C, 42.34; H, 5.41; Cl, 27.27%. Calcd for $C_9H_{14}O_4Cl_2$: C, 42.04; H, 5.49; Cl, 27.58%.

3) 3-O-Acetyl-2,4,6-trideoxy-D-threo-hexopyranose (6). To a solution of **4** (318 mg) in dry toluene (3.2 ml) under an argon atmosphere was added tributylstannane (792 mg) and α,α′-azobisisobutyronitrile (20 mg). The solution was stirred overnight at 100 °C and then concentrated to afford a residue, which was chromatographed on a column of silica gel with benzene–ethyl acetate (7: 1). The eluate containing the product (R_f 0.42 on TLC with the same solvent system) was carefully concentrated with an aspirator to give an oil **5**, which contained a little solvent: NMR $\delta=0.7$—2.4 (4H, m, CH_2-2 and 4), 1.23 (3H, d, $J=6.5$ Hz, CH_3-5), 2.02 (3H, s, OAc), 3.34 (3H, s, OCH_3), ≈3.9 (1H, m, H-5), 4.86 (1H, dd, $J=1$ and 3 Hz, H-1) and ≈5.1 (1H, m, H-3). The oil was kept in a desiccator under reduced pressure, where it was distilled away to disappear. Then, a solution of the oil in 10% aq acetic acid (5 ml) containing 1 M hydrochloric acid (1.7 ml) was kept at 40 °C for 3 h, after which TLC (hexane–ethyl acetate=1: 1) indicated that hydrolysis of the glycoside was complete. The solution was neutralized by addition of solid $NaHCO_3$ and extracted with ethyl acetate (10 ml×2). The extracts were combined, washed with saturated NaCl solution, dried ($MgSO_4$), and evaporated. The residue was chromatographed on a column of silica gel (10 g) with the same solvent system described above to give a solid of **6** (181 mg, 84%): mp 49—51 °C; $[\alpha]_D^{20}+13.8°\rightarrow+50.1°$ (*c* 1.0, CH_3OH, 26 h); NMR ($CDCl_3+D_2O$) $\delta=1.19$ and 1.29 (3H in total, each d, $J=7$ Hz, CH_3-5), 2.06 and 2.08 (3H in total, each s, OAc).

Found: C, 55.22; H, 8.02%. Calcd for $C_8H_{14}O_4$: C, 55.16; H, 8.10%.

4) (R)-5-Hydroxy-(2E)-hexenal (8). *p*-Toluenesulfonyl chloride (100 mg) was added to an ice-cold, stirred solution of **6** (60 mg) in dry acetonitrile (0.6 ml) containing triethylamine (0.15 ml). The mixture was allowed to stand at room temperature for 6 h and, after addition of a few drops of water, was poured into water (5 ml). The product was extracted with dichloromethane (2 ml×3). The combined extracts were washed with saturated NaCl solution, dried (Na_2SO_4), and evaporated to give an oil containing **7**. TLC with hexane–ethyl acetate (5: 1) clearly established the R_f of 0.60. Attempts to isolate pure **7** were unsuccessful. To a stirred solution of the oil in 50% aq acetone (2.4 ml) was added mercury(II) acetate (112 mg). After stirring at room temperature for 1 h, the mixture (pH 4) was acidified to pH 1 with dilute sufuric acid and again stirred overnight. The resulting solution, on TLC with hexane–ethyl acetate (1: 2), showed a major product at R_f 0.48. The solution was adjusted to pH 4 with barium carbonate and the suspension filtered and the filtrate extracted with dichloromethane (2.0 ml×5). The combined extracts were dried (Na_2SO_4) and evaporated to a residue, which was passed through a short column of Sephadex LH-20 with hexane–ethyl acetate (1: 2) to give a crude product of **8**. The crude product was further chromatographed on a column of silica gel (1g) to give an analytically pure oil of **8** (20 mg, 51%): $[\alpha]_D^{18}-23°$ (*c* 1.0, $CHCl_3$); IR (CCl_4) 3450 (OH), 1695 and 1650 cm^{-1} (C=C-CHO); UV_{max} (CH_3OH) 223 nm (ε 11,100); NMR $\delta=1.30$ (3H, d, $J=6.5$ Hz, CH_3-5), 1.80 (1H, OH-5), 2.52 (2H, t with a little long-range coupling, $J=7$ Hz, CH_2-4), ≈4.1 (1H, m, H-5), 6.19 (1H, dd, $J_{1,2}=7.5$ Hz, $J_{2,3}=15.5$ Hz, H-2), 6.93 (1H, dt, $J_{3,4}=7$ Hz, H-3) and 9.62 (1H, d, CHO-1).

Found: C, 62.92; H, 8.74%. Calcd for $C_6H_{10}O_2$: C, 63.13; H, 8.83%.

5) Methyl (R)-7-Hydroxy-(2E, 4E)-octadienoate (9). To a solution of **8** (16 mg) in dry benzene (1 ml) was added methoxycarbonylmethylenetriphenylphosphorane (52 mg), and the mixture refluxed for 1 h and then evaporated *in vacuo*. The residue was chromatographed on a column of alumina (Woelm neutral, 3.5 g) with chloroform–acetone (5: 1), followed by chromatography on a column of silica gel (2 g) with hexane–ethyl acetate (1: 1) to give an oil of **9** (20 mg, 83%): TLC (hexane–ethyl acetate 1: 1) R_f 0.50; $[\alpha]_D^{20}-17°$ (*c* 2.0, $CHCl_3$); IR ($CHCl_3$) 3460 (OH), 1720, 1705 (C=O), 1645, 1620 cm^{-1} (C=C-C=C); UV_{max} (CH_3OH) 260 nm (ε 27,800); NMR $\delta=1.23$ (3H, d, $J=6.5$ Hz, CH_3-7), 1.97 (1H, broad s, OH-7), 2.34 (2H, m, CH_2-6), 3.74 (3H, s, $COOCH_3$), 3.91 (1H, m, H-7), 5.83 (1H, d, $J_{2,3}=15$ Hz, H-2), 6.0—6.4 (2H, m, H-4 and 5) and 7.27 (1H, m, H-3).

Found: C, 63.46; H, 8.17%. Calcd for $C_9H_{14}O_3$: C, 63.51; H, 8.29%.

6) Methyl 4,6-Dideoxy-2-O-p-tolylsulfonyl-α-D-xylo-hexopyranoside (11). To an ice-cold, stirred solution of **10** (2.46 g) in pyridine (24 ml) was added *p*-toluenesulfonyl chloride (3.76 g), and the mixture allowed to stand at room temperature for 1 day. The mixture was then poured into agitated ice-water (70 ml), and the product extracted with chloroform (80 ml×2). The extracts were combined, washed successively with an ice-cold, saturated $KHSO_4$ solution, saturated $NaHCO_3$ solution and water, dried (Na_2SO_4), and evaporated. The residue was chromatographed on a column of silica gel (200 mg) with benzene–ethyl acetate (3: 1) to give an oil of **11** (3.46 g, 72%): $[\alpha]_D^{20}+99°$ (*c* 2.0, CH_3OH); NMR $\delta=1.18$ (3H, d, $J=6.5$ Hz, CH_3-5), 1.3—2.5 (3H, m, CH_2-4 and OH-3), 2.46 (3H, s, Ts-CH_3), 3.28 (3H, s, OCH_3), 3.5—4.3 (2H, m, H-3 and 5), 4.21 (1H, dd, $J_{1,2}=3$ Hz and $J_{2,3}=1.5$ Hz, H-2), 4.67 (1H, d, H-1), 7.37 and 7.87 (each 2H, AB quartet, $J=8.5$ Hz, Ts).

Found: C, 52.91; H, 6.38%. Calcd for $C_{14}H_{20}O_6S$: C, 53.15; H, 6.37%.

7) Methyl 2,3-Anhydro-4,6-dideoxy-α-D-lyxo- and ribo-Hexopyranosides (12 and 13). To a methanolic solution (2.8 ml) of a crude sample of **11** (817 mg) was added a 28% methanolic sodium methoxide solution (0.70 ml), and the solution refluxed for 1 h. After cooling, the solution was poured into ice-water (30 ml) and the product extracted with dichloromethane (35 ml×3). The combined extracts were washed with water, dried (Na_2SO_4), and evaporated. The residue was chromatographed on a column of silica gel (40 g) with benzene–ethyl acetate (7: 1) to give **12** (286 mg) and **13** (8 mg), which on TLC with the same solvent system gave R_f 0.48 and 0.31 respectively, in 79% total yield. Micro-distillation of **12** at 45—80 °C at 16 Torr gave analytically pure needles: mp 28—30 °C; $[\alpha]_D^{20}+70°$ (*c* 1.0, CH_3OH); NMR $\delta=1.15$ (3H, d, $J=6.5$ Hz, CH_3-5), 1.5—2.1 (2H, m, CH_2-4), 2.98 (1H, d, $J_{2,3}=4$ Hz, H-2), 3.40 (1H, m, H-3), 3.48 (3H, s, OCH_3), 3.88 (1H, m, H-5) and 4.91 (1H, s, H-1).

Found: C, 58.35; H, 8.31%. Calcd for $C_7H_{12}O_3$: C, 58.31; H, 8.39%. Compound **13** was an oil: NMR $\delta=1.15$ (3H, d, $J=6.5$ Hz, CH_3-5), 1.4—2.3 (2H, m, CH_2-4), 3.2—3.5 (2H, m, H-2 and 3), 3.46 (3H, s, OCH_3), 3.85 (1H, m, H-5) and 4.92 (1H, d, $J_{1,2}=3$ Hz, H-1).

8) Methyl 2,3,4,6-Tetradeoxy-α-D-glycero-hex-2-enopyranoside (14). To a solution of **12** (57 mg) in 90% aq 2-methoxyethanol (1.1 ml) was added 80% potassium selenocyanate (150 mg), and the mixture refluxed for 20 min. After cooling, the mixture was poured into water (5 ml) and the product extracted with dichloromethane (6 ml×3). The combined extracts were washed with water, dried ($MgSO_4$), and evaporated. The residue was chromatographed on a column of silica gel (3 g) with dichloromethane–chloroform (4: 1) to give an oil of **14** (21 mg, 42%): $[\alpha]_D^{16}-48°$ (*c* 2.0, $CHCl_3$); NMR $\delta=1.25$ (3H, d, $J=6.5$ Hz, CH_3-5), 1.7—2.2 (2H, m, CH_2-4), 3.45 (3H, s, OCH_3), 4.00 (1H, m, H-5), 4.87 (1H, dd, $J=1$ and 3 Hz, H-1), 5.74 (1H, m, H-2) and 6.01 (1H, dt, $J_{2,3}=10$ Hz, $J_{3,4}=4$ Hz, H-3).

Found: C, 65.42; H, 9.25%. Calcd for $C_7H_{12}O_2$: C, 65.59; H, 9.44%. Compound **13** was treated with potassium selenocyanate in a similar manner as above, except for a 2-h reaction time, to give **14** in 23% yield.

9) Methyl (R)-7-Hydroxy-(2E, 4Z)-octadienoate (16). A suspension of **14** (69 mg) in a mixture of 1 M hydrochloric acid (0.38 ml) and 50% aq acetone (3.4 ml) was stirred at room temperature for 2 min. The resulting solution was then neutralized with $NaHCO_3$ (90 mg) and extracted with dichloromethane (2 ml×6). The combined extracts were dried (Na_2SO_4) and evaporated to give a crude oil of **15** (56 mg), which on TLC with chloroform–acetone (9: 1) gave an R_f of 0.54: NMR $\delta=1.23$ and 1.24 (3H in total, d, $J=6.5$ Hz, CH_3-5), 1.58 (1H, sharp m, OH), 1.6—2.3 (2H, m, CH_2-4), 3.7—4.3 (1H, m, H-5), ≈5.4 (1H, m, H-1) and 5.5—6.2 (2H, m, H-2 and 3).

To a solution of the oil (56 mg) in benzene (1.0 mg) was added methoxycarbonylmethylenetriphenylphosphorane (180 mg), and the mixture was refluxed for 3 h, after which time TLC (chloroform–acetone=9: 1) indicated that the Wittig reaction was complete to give a single product (R_f 0.46). The solvent was evaporated, and the residue extracted with pentane (5 ml) under reflux for 30 min. After cooling, the pentane solution was decanted and evaporated. The residue was chromatographed on a column of silica gel (5 g) with chloroform–acetone (9: 1), followed by chromatography on a column of alumina (Woelm neutral, 10 g) with chloroform, to give an oil of **16** (71 mg, 77%): $[\alpha]_D^{15}+5.2°$ (*c* 2.0, $CHCl_3$); IR ($CHCl_3$) 3420 (OH), 1720, 1710 (C=O), 1640, 1605 cm^{-1} (C=C–C=C); UV_{max} (CH_3OH) 265 nm (ε 20,600); NMR $\delta=$ 1.24 (3H, d, $J=6.5$ Hz, CH_3-7), 1.84 (1H, s, OH), 2.50 (2H, t with a little long-range coupling, $J=6.5$ Hz, CH_2-6), 3.79 (3H, s, $COOCH_3$), 3.95 (1H, sextet, H-7), 5.7—6.2 (1H, m, H-5), 5.95 (1H, d, $J_{2,3}=15$ Hz, H-2), 6.32 (1H, t, $J_{3,4}=J_{4,5}=10.5$ Hz, H-4) and 7.65 (1H, dd, H-3).

Found: C, 63.39; H, 8.10%. Calcd for $C_9H_{14}O_3$: C, 63.51; H, 8.29%.

The authors are grateful to Emeritus Professor Sumio Umezawa for his helpful discussions and Mr. Saburo Nakada for the elemental analyses. This investigation was assisted in part financially by the Naito Research Grant for 1977.

References

1) K. Tatsuta, A. Tanaka, K. Fujimoto, M. Kinoshita, and S. Umezawa, *J. Am. Chem. Soc.*, **99**, 5826 (1977).
2) a) F. A. Hochstein and K. Murai, *J. Am. Chem. Soc.*, **76**, 5080 (1954); b) R. B. Woodward, *Angew. Chem.*, **69**, 50 (1957); c) R. B. Woodward, L. S. Weiler, and P. C. Dutta, *J. Am. Chem. Soc.*, **87**, 4662 (1965).
3) S. Aburaki and M. Kinoshita, *Chem. Lett.*, **1976**, 701.
4) S. Hanessian and P. Lavallee, *Can. J. Chem.*, **55**, 562 (1977).
5) M. Miljkovič, M. Gligorijevič, T. Satoh, and D. Miljkovič, *J. Org. Chem.* **39**, 1379 (1974).
6) W. G. Overend, M. Stacey, and J. Staněk, *J. Chem. Soc.*, **1949**, 2841.
7) H. J. Jennings and J. K. N. Jones, *Can. J. Chem.*, **40**, 1408 (1962).
8) K. Tatsuta, K. Fujimoto, M. Kinoshita, and S. Umezawa, *Carbohydr. Res.*, **54**, 85 (1977).
9) W. Roth and W. Pigman, *Methods Carbohydr. Chem.*, **2**, 405 (1963).
10) F. Gonzalez, S. Lesage, and A. S. Perlin, *Carbohydr. Res.*, **42**, 267 (1975).
11) F. Näf and P. Degan, *Helv. Chim. Acta*, **54**, 1939 (1971).
12) H. Paulsen, B. Sumfleth, and H. Redlich, *Chem. Ber.*, **109**, 1362 (1976).
13) S. Ōmura, A. Nakagawa, M. Otani, T. Hata, H. Ogura, and K. Furuhata, *J. Am. Chem. Soc.*, **91**, 3401 (1969).
14) T. van Es, *Carbohydr. Res.*, **5**, 282 (1967).

Studies of Reactions of Amines with Sulfur Trioxide. V.[1] Transsulfonation of Amine Salts of Some *N*-Substituted Amidosulfuric Acids

Fujio KANETANI* and Hachiro YAMAGUCHI

Department of Applied Chemistry, Hiroshima University, Senda-machi, Hiroshima 730

(Received March 27, 1978)

4-Methylanilinium butylamidosulfate, butylammonium (4-methylphenyl)amidosulfate, and 4-methylanilinium (4-methylphenyl)amidosulfate were heated separately under reduced pressure at different temperatures ranging from 80 to 180 °C. Butylammonium butylamidosulfate was heated with 4-methylaniline under atmospheric and reduced pressure. The product compositions were determined as functions of reaction time and temperature, and the components were separated and identified. At lower temperatures (4-methylphenyl)amidosulfate and 4-methylaniline-*N*,2-disulfonate were the major products, while at higher temperatures 4-methylaniline-2-sulfonate and 2,6-disulfonate were the major products. The ease of N–S bond cleavage of the amidosulfate salts ($RNHSO_3^-R'NH_3^+$) (**1**) depends largely on the basicity of both the parent amine (RNH_2) (**2**) and the salt-forming base ($R'NH_2$) (**3**). The results suggest that the initial step of the transsulfonation involves the dissociation of **1** into **3** and the free acid followed by an equilibration between $RNHSO_3H$ and $RNH_2^+SO_3^-$ (**4**). It is considered that **4** may be the sulfonating species and the free amines, **2** and **3**, should be the receptors of a sulfonate group. In contrast to the widely accepted scheme (transsulfonation and subsequent intramolecular rearrangement), our results show that both the transsulfonation and the rearrangement process occur concurrently and the same type of mechanism (a bimolecular displacement, *viz.*, $B^+: SO_3^- + B':\rightleftarrows B^+: + B^+: SO_3^-$) may be operative.

Paal and his co-workers first studied the reaction of amidosulfuric acid with a variety of amines.[2a-d] This reaction was later reinvestigated in detail by Quilico.[3] He found that amidosulfuric acid reacts at a water-bath temperature with an aromatic amine such as aniline, 4-methylaniline, or 1-naphthylamine, producing the corresponding ammonium arylamidosulfate, which in turn rearranges to the ring sulfonate at higher temperature (>150 °C). Recently, it has also been reported that the reaction of butyl- and cyclohexylamidosulfuric acids and their salts with a large excess of aniline, *N,N*-dimethylaniline, or anisole gave the corresponding *p*-sulfonic acids in high yields.[4] On the other hand, Saito, Dehara, and Manabe[5] demonstrated that the reaction between amidosulfuric acid and aniline gave a mixture of aniline-2- and 4-sulfonic acids along with a small amount of aniline-2,4- and 2,6-disulfonic acids whose composition depended on the reaction conditions.

Although it is well documented that arylamidosulfates rearrange to the corresponding ring sulfonates,[6,7] the mechanism of the rearrangement has been unsettled.[8-10] Furthermore, the intermediacy of phenylamidosulfuric acid in the sulfonation of aniline with concentrated sulfuric acid or by "baking" has been discussed for many years by many workers,[8-10] but so far phenylamidosulfuric acid has neither been isolated from such reactions nor been synthesized as such.[11]

We, therefore, undertook the thermal reaction of butylammonium and 4-methylanilinium salts of both butylamidosulfuric acid and (4-methylphenyl)amidosulfuric acid in order to gain an insight into the nature of the transsulfonation of *N*-substituted amidosulfates.

Results and Discussion

Isolation and Identification of the Reaction Products. 4-Methylanilinium butylamidosulfate (**5**), butylammonium (4-methylphenyl)amidosulfate (**9**), and 4-methylanilinium (4-methylphenyl)amidosulfate (**11**) were heated separately under reduced pressure at temperatures ranging from 80 to 180 °C. Butylammonium butylamidosulfate (**1**) was, in addition, heated with 4-methylaniline. The product composition depended on both the reaction time and temperature. Namely, (4-methylphenyl)amidosulfate (**9**) and 4-methylaniline-*N*,2-disulfonate (**13**)[12] were the major products at lower reaction temperatures, whereas 4-methylaniline-2-sulfonate (**12**) and 4-methylaniline-2,6-disulfonate (**15**) were the major products at higher temperatures. In no run was any chromatographic evidence obtained for the formation of 4-methylaniline-3-sulfonic acid and the 2,5-disulfonic acid. Each component was separated (as the sodium salts) by preparative liquid chromatography (cellulose Whatman CF-11, dioxane–H_2O 4: 1 and 5: 1 v/v as the developing solvent). **9** and **13** were then converted to the corresponding tetraphenylphosphonium salts and identified by elemental analysis, melting points (mixed mp), and comparison of their IR spectra with those of authentic samples. **12** and **15** were converted to the corresponding hexylammonium salts and identified similarly.

Product Analysis. Quantitative analysis of the reaction products was achieved by the combination of ion-exchange chromatography and chemical analysis (see the Experimental section). Use of quarternary ammonium-type resin-Amberlite CG 400 (Cl^- form) gave unsatisfactory results because this resin had excessively large distribution coefficients.

Thin-layer chromatography (TLC) was used in each run for qualitative analysis. The best resolution was obtained on cellulose with a dioxane–water (3: 1—4: 1 v/v) solvent system. The R_f values for isomeric 4-methylanilinemonosulfonic and disulfonic acids (spotted as their sodium salts) are listed in the Table.

Tetraphenylphosphonium Salts. The tetraphenylphosphonium salts of (4-methylphenyl)amidosulfuric

TABLE. R_f VALUES AND SPECTRAL DATA OF 4-METHYLANILINESULFONIC ACIDS

Compound	R_f[a)]	Color of spot	IR spectra (cm^{-1})
$4\text{-}MeC_6H_4NHSO_3Na$	0.63	orange	3260, 1512, 1198, 1061, 910, 810
$2\text{-}SO_3Na\text{-}4\text{-}MeC_6H_3NH_2$	0.54	reddish orange	3400, 3320, 1625, 1503, 1223, 1184, 1109, 1036, 817, 735, 701
$3\text{-}SO_3Na\text{-}4\text{-}MeC_6H_3NH_2$	0.42	red	1617, 1491, 1207, 1195, 1090, 1030, 886, 812, 717
$2\text{-}SO_3Na\text{-}4\text{-}MeC_6H_3NHSO_3Na$	0.34	reddish orange	1493, 1388, 1202, 1094, 1067, 1056, 1028, 914, 875, 832, 706
$2,6\text{-}(SO_3Na)_2\text{-}4\text{-}MeC_6H_2NH_2$	0.19	yellow	1630, 1475, 1182, 1123, 1039, 883, 807, 744
$2,5\text{-}(SO_3Na)_2\text{-}4\text{-}MeC_6H_2NH_2$	0.09	dark red	1481, 1395, 1203, 1132, 1033, 894, 655

a) 0.25 mm-thick cellulose plate; dioxane–water (15: 4 v/v). For details see the Experimental section.

acid and 4-methylaniline-*N*,2-disulfonic acid were soluble in non-polar solvents such as chloroform and carbon tetrachloride as well as in polar solvents. This solubility behavior is in marked contrast with that of the corresponding alkylammonium and metal salts. Furthermore, it is noteworthy that the phosphonium salts were remarkably stable toward hydrolysis, being comparable to the metal salts; that is, no hydrolysis was observed even after 0.5 h boiling of each saturated aqueous solution. This is in accord with the view that the amidosulfate ion ($R^1R^2NSO_3^-$) is indeed the unreactive species in the hydrolysis of the salts of amidosulfuric acid and its *N*-substituted derivatives, while the zwitterion ($R^1R^2NH^+SO_3^-$) is most probably the reactive species.[9]

Reaction of Butylammonium Butylamidosulfate (1) with 4-Methylaniline (6). When **1** was heated with **6** for 8 h under atmospheric pressure at different temperatures ranging from 120 to 180 °C, transsulfonation proceeded remarkably slowly. Thus, even after 8 h at 180 °C transsulfonation occurred only to the extent of 50%, to give (4-methylphenyl)amidosulfate (**9**) (40%) and 4-methylaniline-2-sulfonate (**12**) (6%) (Fig. 1). In marked contrast, the reaction was fast under reduced pressure. After 8 h at 150 °C **9** reached its maximum (80%) yield. At higher temperatures 4-methylaniline-2,6-disulfonate (**15**) as well as **12** were also formed at the expense of **9** (Fig. 1).

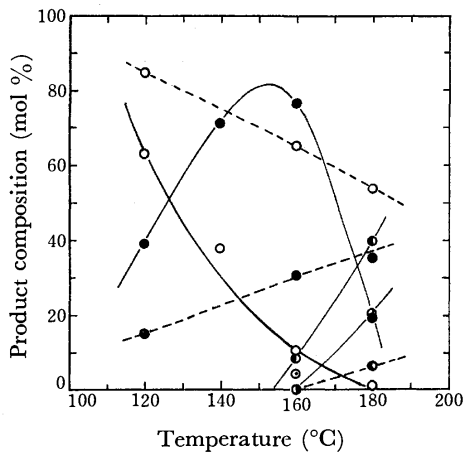

Fig. 1. Reaction of butylammonium butylamidosulfate with 4-methylaniline under atmospheric (----) and reduced (——) pressure.
Molar ratio 1: 1.1—1: 1.3, reaction time 8.5 h.
○: $BuNHSO_3^-$, ●: $MeC_6H_4NHSO_3^-$, ◐: $MeC_6H_3(SO_3^-)NH_2$, ⊙: $MeC_6H_3(SO_3^-)NHSO_3^-$, ◑: $MeC_6H_2(SO_3^-)_2NH_2$. The same symbols are used in all figures.

In order to gain a better understanding of the reaction path, the variation of product distribution with reaction time was followed (Fig. 2). In the first stage **1** was consumed rapidly and **9** was correspondingly formed. Two hours after the start of the reaction, the maximum (68%) yield of **9** was obtained. Beyond this point, **9** also decreased monotonically and **12** was formed instead. After 8.5 h **1** disappeared almost completely. **12** and **15** were the major products.

It is worthwhile noting the formation of 4-methylaniline-*N*,2-disulfonate (**13**), because the intermediacy of aniline-*N*,2- and *N*,4-disulfonic acids in the sulfonation of aniline with concentrated or fuming sulfuric acid has recently been discussed.[10] Although the formation of such compounds has already been reported,[7] no isolation was achieved. We isolated **13** successfully by preparative liquid chromatography.

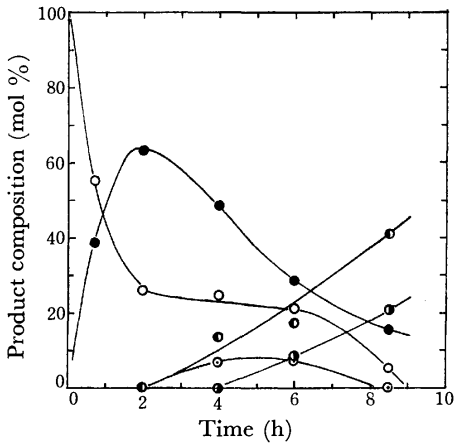

Fig. 2. Variation of product composition with reaction time in the reaction of butylammonium butylamidosulfate with 4-methylaniline at 180 °C under reduced pressure. Molar ratio 1: 1.1—1: 1.3.

Reaction of 4-Methylanilinium Butylamidosulfate (5). If the initial step both in the transsulfonation[13] and in the rearrangement[13] involves the dissociation into the free amidosulfuric acid (the reactive species) and the amine, it is to be expected that the rates of transsulfonation and rearrangement should increase with a decrease in the basicity of the salt-forming amine (to be discussed later).

As expected, transsulfonation of **5** was fast as compared with the reaction between **1** and **6**. Thus, the reaction

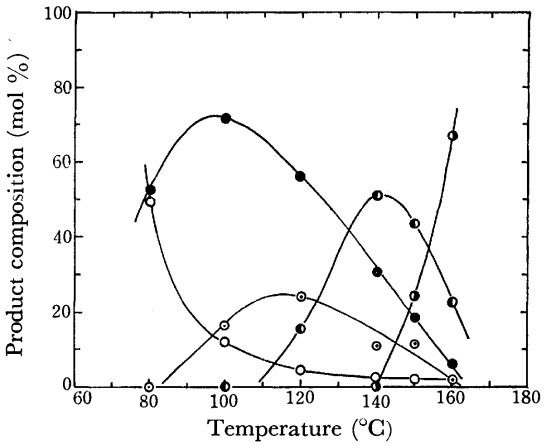

Fig. 3. Thermal reaction of 4-methylanilinium butylamidosulfate under reduced pressure. Reaction time 8.5 h.

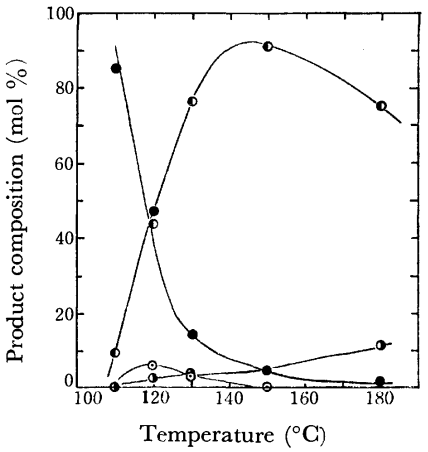

Fig. 5. Thermal reaction of 4-methylanilinium (4-methylphenyl)amidosulfate in *o*-dichlorobenzene. Reaction time 4 h. The reaction at 180 °C was conducted without solvent under reduced pressure.

of **5** at 80 °C for 8.5 h led to 52% conversion of **5** into **9**, and after 8.5 h at 120 °C **5** had disappeared almost completely (Fig. 3). It should be noted here that the reaction at 100 °C gave rise to the formation of **13** (17%), while no **12** was detected in the product mixture (TLC).

Thermal Rearrangement of Butylammonium (4-Methylphenyl)amidosulfate (9). **9** was heated for 8.5 h under reduced pressure in the temperature range 120—160 °C. The variation of product composition with reaction temperature is illustrated in Fig. 4. The rearrangement occurred only at temperatures above 120 °C, whereas with **5** the rearrangement to the ring sulfonate **13** took place far below 120 °C.

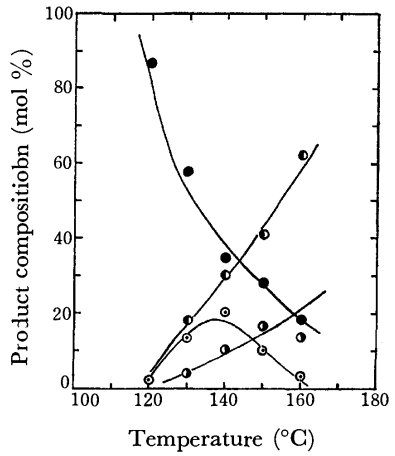

Fig. 4. Thermal reaction of butylammonium (4-methylphenyl)amidosulfate under reduced pressure. Reaction time 8.5 h.

12 and **15** increased with an increase in temperature. The total yield of **12** plus **15** amounted to 80% at 160 °C. **13** was also formed up to 20%.

Thermal Rearrangement of 4-Methylanilinium (4-Methylphenyl)amidosulfate (11). The rearrangement of **11** was very rapid as compared with that of **9** (Fig. 5); after 4 h at 120 and 130 °C **11** rearranged to the extents of 45 and 85% respectively, yielding **12** (main product) along with **13** and **15**. A maximum yield of **12** was obtained from the reaction at 150 °C for 4 h. At 180 °C, a considerable amount (11%) of **15** was formed. Shortening of the reaction period to 35 min improved the yield of **12** (95%); only a trace of **15** was formed. This fact suggests that **15** can be formed not only by direct sulfonation of **12** with **8** (Eq. 16), but also by disproportionation of **12** (Eq. 17).[7]

Mechanistic Considerations. It is well known[14] that anhydrous metal salts of amidosulfuric acid and its *N*-substituted derivatives are much less reactive[4,14-16] than the corresponding ammonium salts[4] and the free acids[3-5,11,17] towards nucleophilic N–S bond cleavage (sulfonation, sulfamation, sulfation, hydrolysis, *etc*). Striking differences in reactivity of the N–S bond between the ammonium or amine salts and the metal salts can be explained in terms of the thermal dissociation of the former salts into the free amidosulfuric acid and the base. For the latter salts such type of dissociation is impossible. However, if a proton donor such as anilinium chloride, water, or a mineral acid is added in the reaction system,[7,15,18] then metal salts can also undergo the N–S bond cleavage. It has been proved that the salts of amidosulfuric acids exist as the true amidosulfate ions ($R^1R^2NSO_3^-M^+$),[19a,b] whereas the corresponding free acids exist as the zwitterions ($R^1R^2NH^+SO_3^-$).[19a,b,d]

All these results strongly suggest that an amidosulfate ion as such is more or less stable, although its stability is dependent on the nature of the *N*-substituent, whereas its *N*-protonated form (the zwitterion) is most probably the reactive species in acid-catalyzed hydrolysis,[9] solvolysis,[20] and transsulfonation.[4,18] Undoubtedly the heterolysis of the N–S bond of the zwitterion should be facilitated by the positive charge on the amido-nitrogen atom, because R^1R^2NH (neutral molecule) is a much better leaving group than $R^1R^2N^-$ (amide ion).

The initial step in both the transsulfonation and the rearrangement of the amine salts of the amidosulfuric

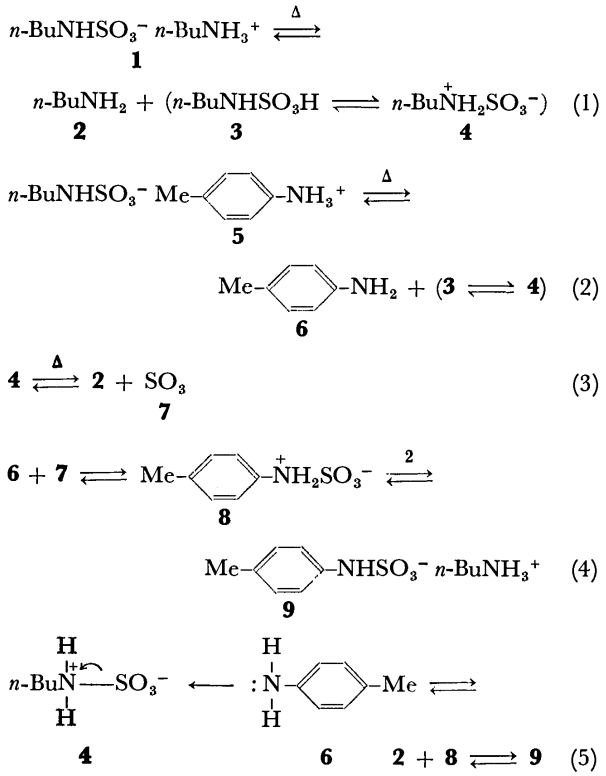

Scheme 1.

acids is presumably the dissociation of the salt into the amidosulfuric acid[21] and the salt-forming base (Eqs. 1, 2, 6, and 7). Support for this assertion was provided by the following observations: (1) in most of the runs carried out under reduced pressure, boiling of the reaction mixture and refluxing of **6** were observed immediately after the reaction had started; (2) under reduced pressure, transfer of the *N*-sulfonate group from **1** to **6** occurred much faster than it did under atmospheric pressure (Fig. 1); (3) the rates of transsulfonation and rearrangement increased with an increase in the acidity of the conjugate acid of the salt-forming base (compare Fig. 1 with Fig. 3, and Fig. 4 with Fig. 5).

Two possible types of mechanisms for the transsulfonation may be considered: (1) a dissociative mechanism (Eqs. 3 and 4) and (2) a bimolecular nucleophilic substitution (Eq. 5). It should be noted here that the transsulfonation with **5** occurred at such a low temperature that zwitterion **4** was quite stable. For example, at 100 °C for 8.5 h, **5** underwent transsulfonation to the extent of 80% to give **9** (72%) and **13** (16%).

Thermal decomposition of amidosulfuric acid[22] occurs only above its melting point (*i.e.*, at 210—220 °C). The most probable reaction has been considered to involve a chain condensation followed by cyclization to polysulfimide.[22] Cleavage of the N–S bond in this thermolysis probably takes place only through the hydrolysis with the water molecules released on the condensation and not through a pyrolytic process.

$$n\mathrm{NH_2SO_3H} \longrightarrow \mathrm{NH_2(SO_2NH)_{n-1}SO_3H} + (n-1)\mathrm{H_2O}$$
$$\longrightarrow (\mathrm{NHSO_2})_n + n\mathrm{H_2O}$$
$$\mathrm{NH_2SO_3H} + \mathrm{H_2O} \longrightarrow \mathrm{NH_4HSO_4}$$

The gas-phase reaction of sulfur trioxide with an amine such as trimethylamine is extremely exothermic.[23] Therefore, the N–S bond energy of $\mathrm{R^1R^2R^3N^+}$–$\mathrm{SO_3^-}$ must be very high. Accordingly the dissociative process seems to be unlikely.

On the other hand, it is well documented[20] that amidosulfuric acid and its *N*-substituted derivatives undergo cleavage of the N–S bond in a polar aprotic solvent such as pyridine, dioxane, DMF, *etc.* under mild conditions. It is, therefore, reasonable to assume that the transsulfonation proceeds through the latter process.

The rearrangement of phenylamidosulfuric acid to the ring sulfonic acid(s) has been performed by use of its salts under a variety of reaction conditions.[10] However, only a few papers have been published on the mechanism of thermal rearrangement of *neat* arylamidosulfates.[7]

Three possibilities may be considered for the mechanism of the rearrangement. The first possible mechanism is the intramolecular pathway postulated originally by Bamberger and Kunz[24] for the sulfonation of aniline. This scheme was later disproved experimentally.[25]

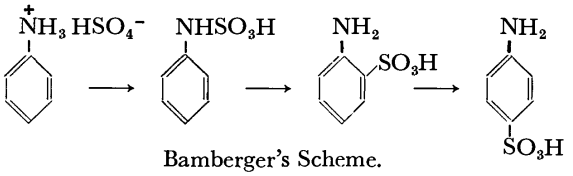

Bamberger's Scheme.

Furthermore, the formation of 2,6-dimethylaniline-4-sulfonate in the thermal rearrangement of 2,6-dimethylanilinium butylamidosulfate[26] cannot be explained by the intramolecular mechanism.

The second mechanism is an intermolecular process which involves thermal dissociation of **8** to **6** and **7**, followed by ring sulfonation of **6** with **7** (Eq. 8).

In view of the hydrolytic and thermal instability of **10**[11,14] thermal cleavage of the N–S bond may take place.

The third possible mechanism involves a bimolecular substitution at the sulfur atom (Eqs. 9 and 10). Since no traces of 4-methylaniline-3-sulfonate (*m*-sulfonation) could be detected (TLC) in the product mixture in any of our experiments, the free amine **6** and/or **10** but not the *N*-protonated species **8** must be the receptor of a rearranging *N*-sulfonate group.

Comparison of the data for the thermal rearrangment of **5** (Fig. 3) and **9** (Fig. 4) shows that conversion of **5** into **12** is much faster than that of **9** into **12**; thus, reaction of **5** at 120 °C for 8 h led to the formation of the rearrangement products **12** (16%) and **13** (24%), in addition to **9** (56%).[28] On the other hand reaction of **9** did not give **12** under the same conditions, and even after 8 h at 160 °C, 18% of **9** remained unchanged.

These results cannot be interpreted on the basis of the widely accepted sequence:[2c,3]

$$\mathrm{ArNH_2} + \mathrm{\overset{+}{N}H_3SO_3^-} \longrightarrow \mathrm{NH_2SO_3^-}\,\mathrm{ArNH_3^+} \longrightarrow$$
$$\mathrm{ArNHSO_3^-}\,\mathrm{NH_4^+} \longrightarrow o\text{- and/or } p\text{-Arenesulfonic acid}$$

A probable explanation involves concurrent pathways: The *N*-sulfonation of **6** with **4** to give **9** (Eq. 5) and the direct ring-sulfonation of **6** with **4** (Eq. 10) followed by sulfonate-group transfer from **4** and/or **8** to **12**

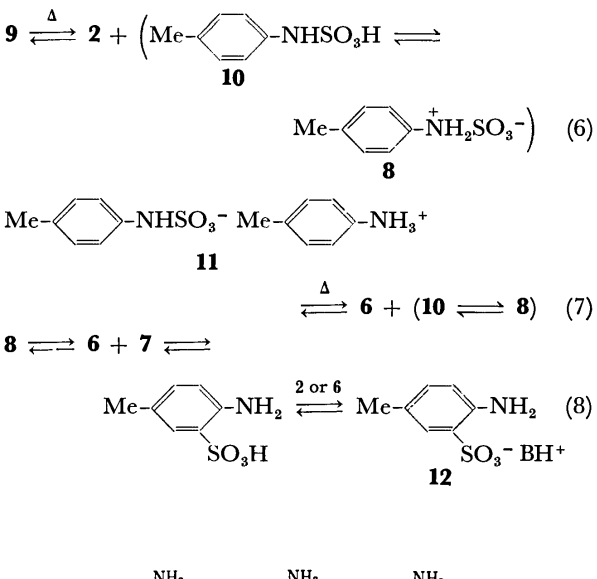

Scheme 2.

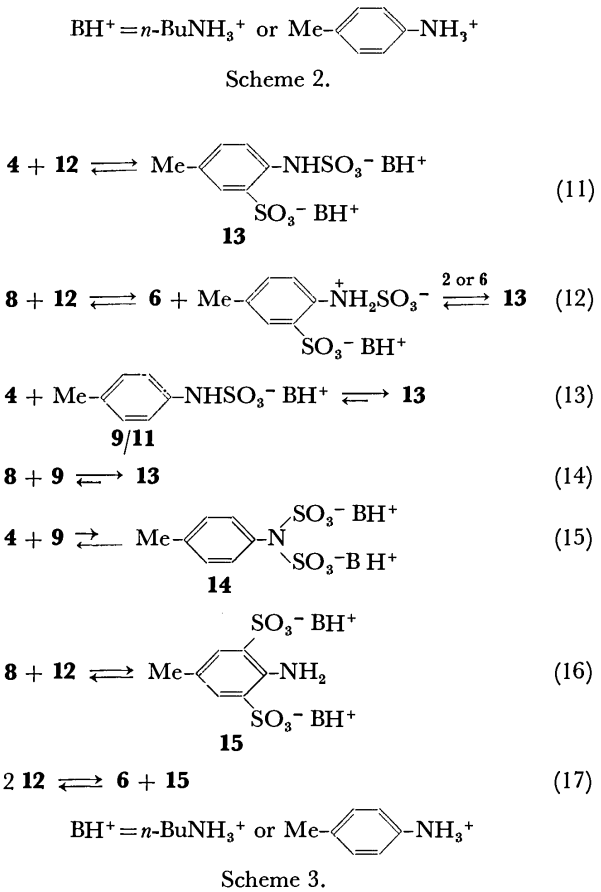

Scheme 3.

(Eqs. 11 and 12).

A dissociation equilibrium between the amidosulfate ion and the zwitterion should depend greatly on the acidity of the conjugate acid of the salt-forming amine; namely, this equilibrium shifts toward the zwitterionic form as the acidity of the conjugate acid of the amine increases[29] and thus the differences in reactivity between **5** and **9** can be accounted for by the following scheme:

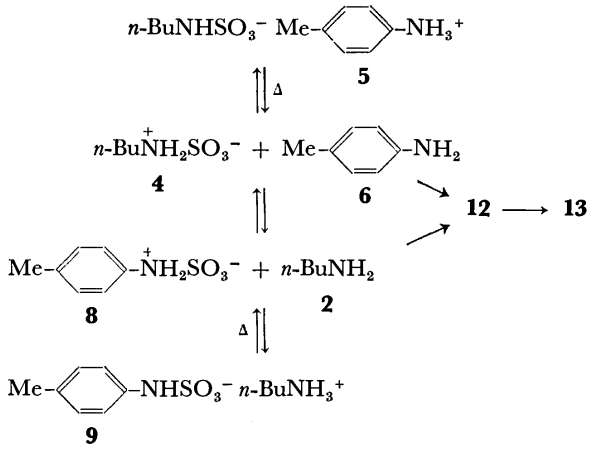

On the other hand, the strength of the N–S bond of an *N*-substituted amidosulfuric acid is expected to increase as the basicity of the parent amine increases. The considerable differences in the rate of rearrangement between **5** and **11** (Figs. 3 and 4) can be explained in terms of the differences in reactivity between the reactive species **4** and **8**.

Several pathways for the formation of **13** may be considered. However, it seems most probable that **13** is formed by reaction(s) between **4** and **12**, and/or between **8** and **12** (Eqs. 11 and 12), since it has been well known that, in the presence of a proton donor such as anilinium chloride, the *N*-sulfonate group on an aromatic amine is transferred readily to another aromatic amino-nitrogen.[7,18]

Ring sulfonation of **9** (Eqs. 13 and 14) at as low as 100 °C seems less probable, since **9** should be much less reactive than **12**. This process may, however, operate at higher temperatures.[27]

(4-Methylphenyl)imidobis(sulfate) (**14**) could neither be isolated nor detected. This can be accounted for in terms of the great degree of steric strain due to the over-crowding around the imido-nitrogen atom.[30]

Experimental

All the melting points were measured in sealed capillaries and uncorrected. The dioxane was of chromatographic grade. The butylamine and 4-methylaniline were guaranteed reagents and used as received. The IR spectra were recorded for KBr discs on a JASCO IR-S spectrophotometer. DEAE-cellulose (Serva, hydrochloride form) was suspended in deionized water and allowed to stand for 20—40 min, and the supernatant was discarded; this process was repeated several times. The exchanger was then suspended in 3M NaCl, packed in a column, and washed with water. Thin-layer chromatography was performed on 0.25 mm-thick cellulose plates (cellulose mikrokristallin, E. Merck) by use of a dioxane–water (15:4 v/v) solvent system. Components were located by inspection under UV light or by placing the plate in a container filled with nitrous gases, followed by spraying with 1-naphthol-4-sulfonic acid and subsequent exposure to ammonia gas.

Reaction Runs. In a test tube (150×14 mm) equipped with a stopcock was placed a weighed amount of a substrate (2 mmol). The test tube was evacuated (*ca.* 20 Torr) with a water aspirator for a very short period (*ca.* 10 s) and the stopcock was closed. The test tube was then heated in a thermostated oil bath. After the reaction was complete, the product mixture was cooled and dissolved in a dilute sodium hydroxide solution. The solution was extracted three times with 2-ml portions of benzene to remove the unreacted 4-methylaniline. The aqueous solution was evaporated *in vacuo*. The residual solid was dissolved in deionized water and the solution was passed through a column (180×9 mm i.d.) of Dowex 50WX4 (Na^+ form). The eluate was collected into a volumetric flask and diluted accurately up to 100 ml. Aliquots of this stock solution were employed for the following product analyses.

Determination of Product Composition. The quantities of each component (**A**—**F**) were calculated from the determinations given below: *n*-$BuNHSO_3Na$ (**A**), 4-$MeC_6H_4NHSO_3Na$ (**B**), 2-SO_3Na-4-$MeC_6H_3NHSO_3Na$ (**C**), 2-SO_3Na-4-$MeC_6H_3NH_2$ (**D**), 2,6-$(SO_3Na)_2$-4-$MeC_6H_2NH_2$ (**E**), Na_2SO_4 (**F**).

Butylamidosulfate and (4-Methylphenyl)amidosulfate: An aliquot (5 or 10 ml) was pipetted on a column (164×13 mm i.d.) of DEAE-cellulose. The column was rinsed with 0.5 ml of distilled water and then eluted with 0.15 M NaCl at a flow rate of 0.25—0.3 ml/min. The first fraction containing **A** was eluted at 30—37 ml and the second fraction containing **B** at 42—48 ml. Each fraction was treated with 3 M HCl (1 ml) and 6 M $NaNO_2$ (0.2 ml). Sulfate ion thus formed was precipitated with 0.01 M $BaCl_2$ (10 or 20 ml) and the excess of barium ion was back-titrated with 0.01 M EDTA; (**A** and **B**).

Total Sulfonate-group Bound to Aromatic Amino-nitrogen: To an aliquot (5 or 10 ml) was added 0.01 M $BaCl_2$ (10 or 20 ml). The volume of the solution was adjusted to *ca.* 20 ml by dilution or evaporation. 3 M HCl (1 ml) was then added and the solution was boiled for 20 min and cooled.[31] The barium sulfate was filtered off and the excess of barium ions in the filtrate titrated; (**B**+**C**+**F**).

Total N-Sulfonate Group: To an aliquot (5 or 10 ml) were added successively 3 M HCl (1 ml), 0.01 M $BaCl_2$ (10 or 20 ml), and 6 M $NaNO_2$ (0.2 ml). After the solution had been left for 1 h, urea (*ca.* 0.1 g) was added. The solution was left again for 1 h, and then heated for 30 min; the precipitate was removed by filtration; the excess of barium ion was titrated; (**A**+**B**+**C**+**F**).

Sulfate Ion Formed in the Reaction: To an aliquot (10 ml) 0.01 M $BaCl_2$ (10 ml) and 3 M HCl (1 ml) were added at room temperature. The solution was filtered directly into an Erlenmeyer flask containing 0.1 M Zn-EDTA (10 ml) and ammonium chloride buffer solution (pH 10) (1 ml). The excess of barium ion was titrated with 0.01 M EDTA; (**F**).

4-Methylaniline-N,2-disulfonate plus 4-Methylaniline-2-sulfonate and 4-Methylaniline-2,6-disulfonate: The remainder of the stock solution after the above analyses was concentrated to *ca.* 20 ml. After addition of 3 M HCl (2 ml), the mixture was boiled for 20 min, cooled, and evaporated *in vacuo*. The residue was dissolved in hot water (20 ml). Barium hydroxide was then added in a slight excess in order to remove sulfate ions. After filtration, the filtrate was passed through a cation-exchange column (Amberlite IR 120 H^+-form) and the eluate was evaporated to dryness. Trituration of the residue with a minimum volume of ethanol gave 4-methylaniline-2-sulfonic acid (**C**+**D**); evaporation of the ethanol solution gave 4-methylaniline-2,6-disulfonic acid (**E**). The 2- and 2,6-acids were then titrated with 0.05 M NaOH.

Material. Butylamidosulfuric Acid: This compound was prepared by the action of butylamine on chlorosulfuric acid in 1,2-dichloroethane at −10—0 °C; mp 173.5—174.5 °C (decomposed with effervescence) (lit,[32] 177—178 °C). IR: 3125 (N-H, br, s), 1527 (NH_2^+, m), 1299 (NH_2^+-SO_3^-, s), 1246 (NH_2^+-SO_3^-, s), 1080 (SO_3^-, m), 1066 (SO_3^-, m), 835 (m), 770 (m), and 715 cm^{-1} (S-N, m). Found: N, 9.12; S, 21.04%. Calcd for $C_4H_{11}O_3NS$: N, 9.14; S, 20.93%.

Butylammonium Butylamidosulfate (1): This was prepared by neutralization of the free acid with butylamine in methanol. After recrystallization from ethyl methyl ketone, it melted at 125.5—127 °C (lit,[32] 127—128 °C). IR: 2950 (NH_2^+, m), 1465 (m), 1186 (SO_3^-, s), 1041 (SO_3^-, s), 910 (w), and 740 cm^{-1} (br, w). Found: N, 12.36; S, 14.13%. Calcd for $C_8H_{22}O_3N_2S$: N, 12.38; S, 14.16%.

4-Methylanilinium Butylamidosulfate (5): A slight excess of 4-methylaniline was added to a solution of butylamidosulfuric acid in methanol. The mixture was evaporated *in vacuo* and the residual solid was washed three times with benzene and dried in a desiccator. Colorless *crystals;* the melting point depended on the rate of heating. IR: 3260 (N-H, w), 2930 (NH_2^+, br, s), 1187 (SO_3^-, s), 1043 (SO_3^-, br, s), and 817 cm^{-1} (2H, m). Found: N, 10.68; S, 12.35%. Calcd for $C_{11}H_{20}N_2O_3S$: N, 10.76; S, 12.31%.

Barium (4-Methylphenyl)amidosulfate: 4-Methylanilinium amidosulfate (30 g), prepared by neutralization of amidosulfuric acid with 4-methylaniline in methanol, was heated with 4-methylaniline (45 g) at 100 °C for 3.5 h. After cooling, benzene (50 ml) was added. The solid was collected, washed with benzene, and recrystallized from water to give the pure *ammonium salt*. This was dissolved in hot water and treated with a slurry of barium hydroxide. The mixture was filtered and the residue was washed repeatedly with hot water. The filtrate and washings were combined and evaporated to dryness *in vacuo*. The residual solid was dissolved again in hot water (500 ml) and carbon dioxide was passed through the solution to remove the excess of barium hydroxide. The filtered solution was left overnight at room temperature. The *product* separated out as needles, which were filtered and washed twice with cold water, yield 22.7 g. IR: 3200 (N-H, m), 1218 (SO_3^-, s), 1180 (SO_3^-, s), 1058 (SO_3^-, s), and 816 cm^{-1} (1,4-, w—m).

Butylammonium (4-Methylphenyl)amidosulfate (9): An aqueous solution of ammonium (4-methylphenyl)amidosulfate was passed through a column of Dowex 50W×4 (butylammonium form) and the eluate was evaporated to a small volume, giving colorless *crystals*. These were filtered, washed with cold water, and dried. IR: 1512 (m), 1185 (SO_3^-, s), 1041 (SO_3^-, s), 895 (m), 820 (1, 4-, m), and 696 cm^{-1} (br, m). Found: N, 10.67; S, 12.23%. Calcd for $C_{11}H_{20}O_3N_2S$: N, 10.76; S, 12.31%.

4-Methylanilinium (4-Methylphenyl)amidosulfate (11): An aqueous solution of bis(4-methylanilinium) sulfate was added slowly to a stirred solution of barium (4-methylphenyl)amidosulfate (4.35 g) in water (50 ml) until no more precipitate was formed. After stirring for a short period, the precipitate was filtered and the filtrate was evaporated to dryness. The *product* was washed repeatedly with ether and dried in a desiccator over silica gel; glistening flakes. IR: 2915 (NH_3^+, br, m), 1517 (m), 1205 (SO_3^-, s), 1050 (SO_3^-, s), 897 (w), and 815 cm^{-1} (1,4-, m). Found: N, 9.49; S, 10.77%. Calcd for $C_{14}H_{18}N_2O_3S$: N, 9.52; S, 10.89%. Mp: 168—169.5 °C (depended on the rate of heating).

Tetraphenylphosphonium Chloride (16): This salt was prepared according to the procedure of Horner *et al.*[33] with a slight modification. IR: 1620 (w), 1583 (w), 1480 (w,) 1434 ($C_6H_5P^+$, m), 1311 (w), 1107 ($C_6H_5P^+$, s), 998 (m), 763

(m), 722 (s), and 688 cm^{-1} (m). Found: Cl, 9.42; P, 8.18%. Calcd for $C_{24}H_{20}ClP$: Cl, 9.46; P, 8.26%.

Preparation of Authentic Compounds. Sodium (4-Methylphenyl)amidosulfate: The sodium salt was obtained from the foregoing ammonium salt by passing through a cation-exchanger (Na^+ form) column. Recrystallization from methanol gave the pure *salt*. IR: 3260 (N–H, m), 1512 (m), 1198 (SO_3^-, s), 1061 (SO_3^-, s), 910 (m), and 810 cm^{-1} (1,4-, m). Found: N, 6.78; S, 15.00%. Calcd for $C_7H_8O_3NNaS$: N, 6.70; S, 15.33%.

Tetraphenylphosphonium (4-Methylphenyl)amidosulfate: A hot solution of **16** (550 mg) in 20 ml of water was added to a stirred solution of sodium (4-methylphenyl)amidosulfate (300 mg). The mixture was boiled for a short time and cooled slowly. The phosphonium salt was collected by filtration. Repeated recrystallization from water furnished a pure *sample*. Found: N, 2.67; P, 5.75; S, 6.25%. Calcd for $C_{31}H_{28}O_3PS$: N, 2.67; P, 5.89; S, 6.10%. IR: 3225 (N–H, w), 1440 ($C_6H_5P^+$, m), 1395 (w), 1224 (SO_3^-, s), 1205 (SO_3^-, s), 1103 ($C_6H_5P^+$, s), 1033 (SO_3^-, s), 881 (m), 827 (2H, m), 761 (m), 722 (s), and 686 cm^{-1} (br, m).

4-Methylaniline-2,6-disulfonic Acid and Its Salts: 4-Methylaniline-2-sulfonic acid (commercial reagent) (5.00 g) and freshly distilled chlorosulfuric acid (2.4 g) were mixed and the mixture was heated at 120 °C for 2 h and then at 140 °C (for 2 h) until the evolution of hydrogen chloride had subsided. After cooling, cracked ice was added carefully to the reaction mass. The resulting solution was neutralized with slurries of barium hydroxide, heated to boiling, and filtered while hot; the precipitate was washed repeatedly with hot water. The combined filtrate and washings were evaporated to dryness. The solid was recrystallized twice from hot water, yielding the pure *barium salt*. This was then converted to the corresponding free acid by passing through a column of Amberlite IR-120B (H^+ form); the eluate was neutralized with aqueous sodium hydroxide. The neutralized solution was then concentrated to a small volume (*ca.* 12 ml). 3 M HCl (7.0 ml) and hot alcohol (10 ml) were added with stirring while hot. The mixture was left overnight at room temperature. *Monosodium 4-methylaniline-2,6-disulfonate* separated out as white glistening crystals. IR: 1500 (w), 1460 (w), 1235 (SO_3^-, s), 1180 (SO_3^-, s), 1122 (w), 1045 (SO_3^-, s), 882 (1H, w), and 805 cm^{-1} (m). Found: N, 4.25; S, 19.72%. Calcd for $C_7H_8O_6NNaS \cdot 2H_2O$: N, 4.31; S, 19.71%.

The *bis(hexylammonium) salt* was prepared by neutralization of the free acid with hexylamine. Recrystallization from ethyl acetate–isopropyl alcohol (5 : 2 v/v) gave a pure *specimen*; mp: 185—186 °C. IR: 1470 (m), 1210—1175 (br, s), 1028 (s), 886 (w), 802 (m), and 752 cm^{-1} (w). Found: N, 8.90; S, 13.68%. Calcd for $C_{19}H_{39}O_6N_3S_2$: N, 8.95; S, 13.65%.

4-Methylaniline-2,5-disulfonic Acid and Its Salts: This acid was prepared by the reaction between 4-methylaniline-3-sulfonic acid and chlorosulfuric acid. The product was isolated as the *barium salt* and purified by recrystallization from water.

The barium salt was converted into the sodium and bis(hexylammonium) salts by the same procedure as above *Monosodium salt*; IR: 1513 (w), 1483 (m), 1382 (w), 1225—1193 (SO_3^-, br, s), 1130 (s), 1030 (SO_3^-, s), 780 (w), and 650 cm^{-1} (s). Found: N, 4.28; S, 19.07%. Calcd for $C_7H_8NNaS_2 \cdot 2H_2O$: N, 4.31; S, 19.17%. *Bis(hexylammonium) salt*; mp: 195—196 °C. IR: 1480 (m), 1399 (m), 1202 (s), 1176 (s), 1118 (w), 1014 cm^{-1} (s). Found: N, 8.86; S, 13.34%.

Dipotassium, Disodium, and Bis(tetraphenylphosphonium) Salts of 4-Methylaniline-N,2-disulfonic Acid: Sulfur trioxide (2.14 g, 26.7 mmol) was dissolved in dry 1,2-dichloroethane (10 ml) and cooled in an ice–water bath. Dry 2-methylpyridine (3.0 ml) was added, drop by drop, with cooling and vigorous stirring. After stirring for 30 min, the solvent was removed *in vacuo* to give colorless crystals of 2-methylpyridine-sulfur trioxide adduct.

To the adduct was added in one portion an ice-cold solution of 4-methylaniline-2-sulfonic acid (4.60 g, 24.6 mmol) and potassium carbonate (3.70 g, 26.8 mmol) dissolved in water (40 ml). The mixture was allowed to warm to room temperature. Potassium carbonate (0.50 g, 3.6 mmol) was then added. After stirring at 35—40 °C for 30 min, the mixture was evaporated *in vacuo*, giving the solid. Recrystallization from 90% aqueous methanol gave the *potassium salt*. IR: 1485 (m), 1375 (w), 1281 (m), 1197 (SO_3^-, s), 1092 (s), 1047 (SO_3^-, s), 1027 (SO_3^-, s), 900 (w), 873 (w), 840 (w), and 706 cm^{-1} (m). Found: N, 3.50; S, 17.08%. Calcd for $C_7H_7O_6K_2NS_2 \cdot 2H_2O$: N, 3.69; S, 16.90%.

The dipotassium salt was converted to the disodium salt by cation-exchange. Recrystallization from aqueous ethanol yielded the pure *sodium salt*.[34] Found: N, 4.20; S, 19.47%. Calcd for $C_7H_7O_6NNa_2S_2 \cdot H_2O$: N, 4.25; S, 19.47%.

A solution of **16** (400 mg) in water (20 ml) was added to a stirred solution of the foregoing potassium salt (200 mg) in water and the mixture was boiled for a few minutes. After cooling, the crystals were filtered, washed with water, and recrystallized from water to give the pure *phosphonium salt* (340 mg); mp 210—211 °C (dec) (immersed in a bath preheated at 204 °C). IR: 1485 (m), 1439 ($C_6H_5P^+$, s), 1210 (SO_3^-, s), 1106 ($C_6H_5P^+$, s), 1036 (SO_3^-, s), 1019 (m), 898 (w), 847 (w), 834 (w), 762 (m), 721 (s), and 688 cm^{-1} (m). Found: P, 6.76; S, 6.81%. Calcd for $C_{55}H_{47}O_6NP_2S_2$: P, 6.56; S, 6.79%.

Isolation and Identification of the Reaction Products. Tetraphenylphosphonium (4-Methylphenyl)amidosulfate: The product mixture from the reaction of **8** at 100 °C for 17 h was dissolved in water (10—20 ml).[35] To the filtered solution was added **16** (200 mg) and the mixture was boiled for a short time. The clear solution was allowed to cool slowly[36] and left overnight at room temperature. The crystals which separated were collected by filtration and washed three times with cold water. Repeated recrystallization from water gave the pure *phosphonium salt*. The IR spectrum was entirely in accord with that of an authentic sample. Found: N, 2.58; P, 5.78; S, 6.26%. Calcd for $C_{31}H_{28}O_3NPS$: N, 2.67; P, 5.89; S, 6.10%.

Bis(tetraphenylphosphonium) 4-Methylaniline-N,2-disulfonate: Disodium 4-methylaniline-*N*,2-disulfonate[37] was isolated by liquid chromatography from the reaction of **5** at 130 °C for 8.5 h. To the filtered solution (20 ml) of this salt (0.205 g) was added **16** (0.504 g) and the mixture was boiled for a short period and allowed to cool slowly. The crystallized phosphonium salt was purified by repeated recrystallization from water; mp 210—211 °C. The mixed mp with an authentic specimen was not depressed. The IR spectrum agreed entirely with that of authentic material.

4-Methylaniline-2-sulfonic Acid and Its Hexylammonoum Salt: The sodium salt was separated by liquid chromatography from the product mixtures. To a hot solution (*ca.* 5 ml) of this salt (0.350 g) was added 3 M HCl (2 ml). The mixture was boiled for 20 min and cooled. The *free acid* separated out as colorless needles (hemihydrate). IR: 1550 (NH_3^+, w), 1498 (m), 1270—1290 (s, br), 1262 (w), 1092 (m), 1020 (s), 829 (m), and 698 cm^{-1} (m). Found: N, 7.12; S, 16.33%. Calcd for $C_7H_9O_3NS \cdot 1/2H_2O$: N, 7.14; S, 16.34%.

The free acid was neutralized with a methanolic solution of hexylamine. The solution was evaporated to dryness and the solid was recrystallized from EtOH–AcOEt (1 : 1 v/v) to

give the pure *hexylammonium salt*: mp 208—209 °C, mixed mp 208—208.5 °C. The IR spectrum agreed entirely with that of an authentic sample.

Bis(hexylammonium) 4-Methylaniline-2,6-disulfonate: The crude disodium salt (0.30 g) was dissolved in water and the solution was passed through a column of Dowex 50WX4 (H^+ form). The eluate was neutralized with a methanolic solution of hexylamine. After evaporation, the solid was recrystallized from *i*-PrOH–AcOEt (1: 5 v/v) to give the *bis-(hexylammonium) salt* as fine needles; mp 185—186 °C, mixed mp with an authentic sample: 185.5—186 °C. The IR spectrum was in agreement with that of an authentic specimen.

References

1) Part IV, F. Kanetani and H. Yamaguchi, *Bull. Chem. Soc. Jpn.*, **47**, 2713 (1974).

2) (a) C. Paal and F. Kretschmer, *Ber.*, **27**, 1241 (1894); (b) C. Paal and H. Jänicke, *ibid.*, **28**, 3160 (1895); c) C, Paal, *ibid.*, **34**, 2748 (1901); (d) C. Paal and M Hubaleck, *ibid.*, **50**, 1110 (1917).

3) A. Quilico, *Gazz. Chim. Ital.*, **56**, 620 (1926).

4) F. L. Scott, J. A. Barry, and W. J. Spillane, *J. Chem. Soc., Perkin Trans. 2*, **1972**, 2663.

5) M. Saito, M. Dehara, and O. Manabe, *Nippon Kagaku Kaishi*, **1972**, 380.

6) W. J. Spillane and F. L. Scott, *J. Chem. Soc., B*, **1968**, 779 and references cited therein.

7) Z. J. Allan and Z. Vrba, *Collect. Czech. Chem. Commun.*, **34**, 272 (1969) and references cited therein.

8) For early discussions see C. M. Suter, "The Organic Chemistry of Sulfur," John Wiley & Sons, Inc., New York (1944), p. 247; E. D. Hughes and C. K. Ingold, *Quart. Rev.*, **6**, 51 (1952).

9) For recent reviews on amidosulfuric acid and its derivatives see W. J. Spillane, *Int. J. Sulfur Chem.*, **8**, 469 (1973) and the two previous reviews of this series.

10) P. K. Maarsen and H. Cerfontain, *J. Chem. Soc., Perkin Trans. 2*, **1977**, 921 and references cited therein.

11) C. D. Hurd and N. Kharasch, *J. Am. Chem. Soc.*, **69**, 2113 (1947).

12) According to IUPAC rules this compound may be called (4-methyl-2-sulfophenyl)amidosulfate or *N*-(4-methyl-2-sulfophenyl)sulfamate.

13) The term "transsulfonation" in this paper refers to the transfer of a sulfonate group from one amino nitrogen to another amino nitrogen and the term "rearrangement" refers to the transfer of a sulfonate group from the aromatic amino-nitrogen to the aromatic ring.

14) For general reviews on amidosulfuric acid and its derivatives see L. F. Audrieth, M. Sveda, H. H. Sisler, and M. J. Butler, *Chem. Rev.*, **26**, 49 (1940): A. Dorlars, "Methoden der Organischen Chemie," Georg Thieme Verlag, Stuttgart (1958), 4. Aufl., Bd. XI/2, pp. 645—693 and Ref. 9.

15) E. R. Alexander, *J. Am. Chem. Soc.*, **70**, 1274 (1948).

16) D. J. Loder, U. S. Patent 2804472 (1957).

17) Abbott Laboratories, British Patent 662800 (1951).

18) R. Lantz and P. Obellianne, *C. R. Acad. Sci.*, **238**, 2243 (1954).

19) (a) A. M. Vuanagat and E. L. Wagner, *J. Chem. Phys.*, **26**, 77 (1957); (b) B. E. Cain and F. A. Kanda, *Z. Krystallogr., Krystallgeom., Krystallphys., Krystallchem.*, **135**, 253 (1972) and references cited therein; (c) E. Steger, *Z. Anorg. Allg. Chem.*, **325**, 89 (1963); (d) R. L. Sass, *Acta Crystallogr.*, **13**, 320 (1960) and references cited therein.

20) See for example: (a) K. Nagasawa and H. Yoshidome, *Chem. Pharm. Bull.*, **17**, 1316 (1969) and references cited therein; (b) Yu. B. Kagan, G. M. Pakhomova, N. A. Shimanko, A. Yu. Koshevnik, M. V. Shishkina, and R. G. Lokteva, *Kinet. Katal.*, **15**, 23 (1974).

21) Very recently, the protonation equilibria of various *N*-substituted amidosulfates have been studied in acidic aqueous solutions and their preferential *N*-protonation has been discussed: W. J. Spillane and N. Regan, *J. Chem. Soc., Perkin Trans. 2*, **1977**, 1180; See also Ref. 10.

22) J. Kubīk and W. Waněk, *Collect. Czech. Chem. Commun.*, **22**, 1446 (1957).

23) Unpublished data; see also, E. E. Gilbert, "Sulfonation and Related Reactions," Intercience Publishers, New York, N. Y. (1965) pp. 404—405.

24) E. Bamberger and J. Kunz, *Chem. Ber.*, **30**, 2274 (1897).

25) G. Illuminati, *J. Am. Chem. Soc.*, **78**, 2603 (1956).

26) To be published in a later paper.

27) It is expected that the electron-donating effect of the sulfamino group is much smaller than that of the amino group.

28) The formation of **13** can be accounted for in terms of the deficiency of **6** in the reaction mixture, *i.e.* $\mathbf{6}/SO_3 < 1$) caused by partial deposition of **6** on the cool wall of the reaction vessel.

29) The position of this equilibrium is, of course, dependent on the steric factors. 2,6-Dimethylanilinium salt of butylamidosulfuric acid, for example, is unstable and dissociates into the acid and 2,6-dimethylaniline even at room temperature. Accordingly, this salt undergoes trans-sulfonation and rearrangement to 2,6-dimethylaniline-4-sulfonic acid far more readily than **5**. See a later paper.

30) We succeeded, however, in isolating (2,4,6-trimethylphenyl)imidobis(sulfate) from the thermal reaction of 2,4,6-trimethylanilinium butylamidosulfate; see a later paper.

31) It was confirmed that both butylamidosulfate ion and the ring sulfonate group are not hydrolyzed under these conditions.

32) G. E. McCasland, *J. Am. Chem. Soc.*, **73**, 5507 (1951).

33) L. Horner, G. Mummenthey, H. Moser, and P. Beck, *Chem. Ber.*, **99**, 2782 (1966).

34) W. M. Lauer, M. M. Sprung, and C. M. Langkammerer, *J. Am. Chem. Soc.*, **58**, 225 (1936).

35) If the solution is acidic, it should be neutralized with 1 M ammonia.

36) If the phosphonium sulfonate tends to separate as an oil, sufficient water should be used for the crystallization and the solution should be seeded while hot.

37) This compound gave 4-methylaniline-2-sulfonic acid on acid hydrolysis.

Photochemical Reaction of 3,3-Dimethyl-1,2-indanedione with Xanthene

Kazuhiro MARUYAMA,* Atsuhiro OSUKA, and Yoshinori NARUTA
Department of Chemistry, Faculty of Science, Kyoto University, Kyoto 606
(Received April 22, 1978)

The photochemical reaction of 3,3-dimethyl-1,2-indanedione (DMID) with xanthene was investigated in detail. The products are 1-hydroxy-3,3-dimethyl-1-(9-xanthenyl)-2-indanone (**3a**) (49%), 2-hydroxy-3,3-dimethyl-1-indanone (13%), 1,1′-dihydroxy-3,3,3′,3′-tetramethyl-1,1′-biindan-2,2′-dione (**5a**) (23%), and 9,9′-bixanthenyl (**6**) (49%). The reaction proceeds *via* hydrogen abstraction by $^3(n\pi)^*$ of DMID leading to triplet radical pair composed of its semidione radical and 9-xanthenyl radical. The product **3a** is a combination product from the radical pair, while **5a** and **6** are escaping products from it. The hydrogen abstraction occurs at C-1 carbonyl group of DMID in a fairly efficient quantum yield ($\Phi=0.71$). Behavior of the DMID semidione radical is rather resemble those of open-chain semidione radicals than those of sterically hindered semidione radicals.

The photochemical reactions of a number of α-diketones in which the carbonyl groups are held in a somewhat rigid *cis*-configuration have been studied under various conditions.[1] *s-cis*-α-Diketone has been shown to undergo photo-hydrogen abstraction reaction in the presence of a hydrogen donor, and the resulting products can almost invariably be rationalized by taking into consideration a mechanistic pathway involving the initial hydrogen abstraction by photoexcited α-diketone *via* $^3(n\pi)^*$ excitation. For example, camphorquinone in methanol or in 2-propanol gives products derived from the initial hydrogen abstraction reaction from the solvent.[2] When 9,10-phenanthrenequinone is irradiated in hydrogen donating solvents, it yields 1,2-adduct or 1,4-adduct corresponding to the structures of the solvents.[3] In these light-induced reactions of camphorquinone and 9,10-phenanthrenequinone, intermediate radical pairs have been successfully detected by using CIDNP technique.[4] The light-induced hydrogen abstraction reactions of 3,3-dimethyl-1,2-indanedione (DMID), which is a nonenolizable aromatic α-diketone, have been investigated from the standpoint of comparing the photoreactivity with those of open-chain α-diketones.[5] The qualitative behaviors of photoexcited DMID in 2-propanol, diethyl ether, and toluene were reported by Rigaudy,[6] but the quantitative investigation has not been accomplished yet. In this investigation we have found that photoexcited DMID shows such a high reactivity to hydrogen donors as that of benzil.

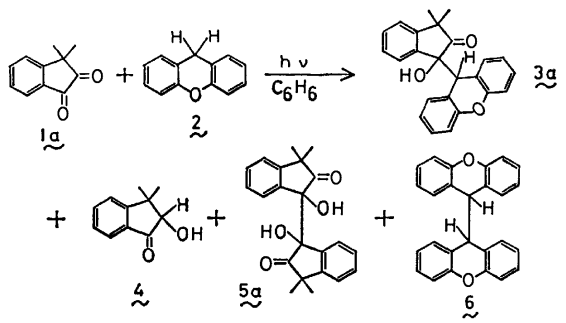

Scheme 1

Results and Discussion

a) Reaction Products. A degassed solution of DMID **1a** (0.04 M) and equimolar xanthene **2**, a good hydrogen donor, in benzene was irradiated for an hour, using a 300 W high-pressure mercury lamp. Separation of the products by column chromatography and preparative TLC gave 1-hydroxy-3,3-dimethyl-1-(9-xanthenyl)-2-indanone **3a** (49%), 2-hydroxy-3,3-dimethyl-1-indanone **4** (13%), and 9,9′-bixanthenyl **6** (46%). On the other hand, the ^{1}H NMR spectrum of this reaction mixture showed two characteristic signals at δ 0.92 and 1.26 corresponding to the dimethyl protons of 1,1′-dihydroxy-3,3,3′,3′-tetramethyl-1,1′-biindan-2,2′-dione **5a** (pinacol), indicating its yield of 23% besides those of photoreaction products mentioned above (Scheme 1). When silica gel chromatography was applied for the product separation, **5a** was not isolated owing to its high susceptibility to autoxidation on silica gel. The structures of these products were determined by their IR, UV, ^{1}H NMR, elemental analyses and chemical reactions.

The IR spectrum of **3a** showed characteristic bands at 3420 (hydroxy) and 1746 cm^{-1} (nonconjugated five membered ring ketone), the ^{1}H NMR spectrum ($CDCl_2$) showed signals at δ 0.40 (s, 3H), 1.18 (s, 3H), 2.70 (broad, 1H), 4.40 (s, 1H) and 6.60—7.75 (m, 12H), in agreement with the structure of **3a**.

The IR spectrum of **4** showed two characteristic absorptions of a hydroxyl group (3500 cm^{-1}) and a conjugated five membered ring ketone (1726 cm^{-1}). The ^{1}H NMR spectrum (CCl_4) of **4** showed signals at δ 1.13 (s, 3H), 1.54 (s, 3H), 4.17 (s, 1H), 4.10 (broad 1H) and 7.20—7.26 (m, 4H). The hydroxy ketone **4** was independently prepared by reduction of DMID with sodium borohydride, and compared with the photoreduction product. It is an interesting problem which one of two carbonyl groups is reduced in the photoreaction or in the hydride reduction. The problem was solved in the following way. Esterification of **4** with *p*-anisoyl chloride gave ester **A**, and its IR spectrum showed two characteristic bands at 1721 and 1757 cm^{-1} corresponding to the ester of a five membered ring ketone. On the other hand, irradiation of DMID with *p*-anisaldehyde in benzene gave a small amount (4%) of ester **B** besides various other products. The IR spectrum of the ester **B** showed two characteristic bands at 1723 and 1774 cm^{-1} corresponding to the ester of a five membered ring ketone, but clearly different from **A**; the esters, **A** and **B**, are regioisomers each other. Comparison of the IR spectra of these two isomers led

to a conclusion that **B** might have a nonconjugated carbonyl group and **A** a conjugated one. Surprisingly the alkaline hydrolysis of **B** gave a mixture of **4** and *p*-anisic acid as well as the hydrolysis of **A** (Scheme 2). The result observed in the hydrolysis of **B** was explained in terms of a series of equilibria involving a indenediol **8** as a common intermediate. The equilibria might favor rather **4** because of the stability of the conjugated ketone. This was confirmed in the oxidative hydrolysis of both 1-hydroxy-3,3-dimethylspiro(indan-2,2′-[1,3]-dithiolane) **9** and 2-hydroxy-3,3-dimethylspiro(indan-1,2′-[1,3]dithiolane) **10** with mercury(II) chloride; namely, both isomers gave only **4**.

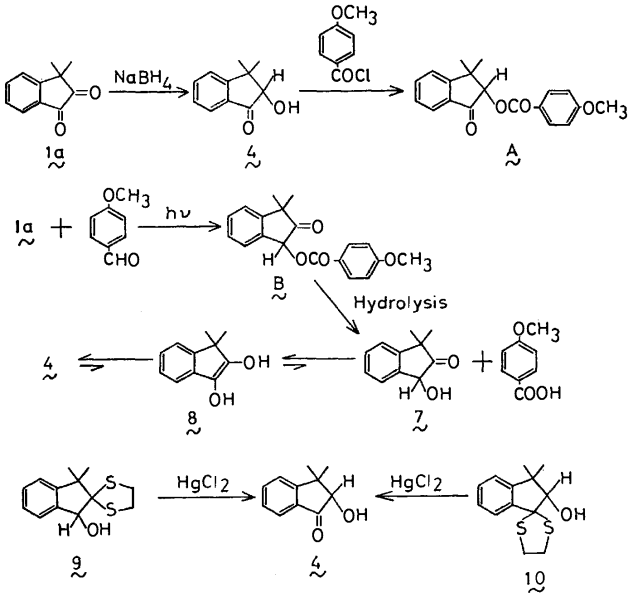

Scheme 2.

Irradiation of a degassed solution of 3,3-dimethyl-6-nitro-1,2-indanedione **1b** (NO_2–DMID) and xanthene for 6 h gave 1-hydroxy-3,3-dimethyl-6-nitro-1-(9-xanthenyl)-2-indanone **3b** in 70% yield and 1,1′-dihydroxy-3,3,3′,3′-tetramethyl-6-nitro-1,1′-biindan-2,2′-dione **5b** in 13% yield.

b) Reaction Mechanism. To investigate the reaction mechanism, we examined the photochemical reactions of DMID with xanthene in detail, changing the reaction conditions (Table 1).

Run 3 reveals that the pinacol **5a** photochemically decomposes to give two semidione radicals, which would regenerate **5a** by coupling or give DMID and hydroxy ketone by disproportionation. On irradiation, DMID thus formed would abstract a hydrogen atom from xanthene, giving **3a** and **6**. Run 4 shows obviously an occurrence of homolytic cleavage of photoexcited **3a**, yielding a semidione radical and 9-xanthenyl radical. However, exposure of a degassed solution of **5a** and **3a** in benzene to light of wavelength longer than 400 nm resulted in the nearly complete recovery of the starting materials (run 5 in the Table 1). When a solution of DMID and xanthene in benzene was irradiated with light of wavelength longer than 400 nm, DMID changed to give only **3a** and **5a** in yields of 13 and 27%, respectively, and **6** was formed in a yield of 29% (Run 2 in the Table 1).

The absence of hydroxy ketone in the reaction mixture of Run 2 might be ascribed to the much slower rate of disproportionation of the semidione radical than that of coupling of it. If **7** once would be produced from the semidione radical by disproportionation, **4** could be formed *via* the equilibria between **7** and **4** (Scheme 2).

In their stabilizing modes, the semidione radicals derived from α-diketones can be classified into two groups;[7] namely those derived from rigidly cis, sterically hindered α-diketones, which decay by disproportionation, and those derived from flexible α-diketones such as benzil or anisil, which terminate by coupling in rather faster decay rates. It is noteworthy that the *free* DMID semidione radical decays predominantly by coupling, resulting in the formation of **5a** in spite of its rigidly *cis*-fixed configuration.

c) Radical Pair as an Intermediate. The fact that DMID changes to give only **3a** and **5a** upon irradiation with light of wavelength longer than 400 nm is of value for examining the behaviors of the radical pair. That is, **3a** is a combination product of the semidione radical and 9-xanthenyl radical, whereas **5a** and **6** are escaping products from the initial solvent cage. We examined the effects of the concentration of xanthene and reaction temperature on the product distribution (Table 2). At three different temperature the ratio of **5a** to **3a** was

Table 1. Photochemical reaction of DMID **1a**, xanthene adduct **3a** and pinacol **5a** with xanthene in benzene. Photoreaction product distribution under various conditions

Run	Starting material	Irradiation condition	Products (%)				
			1	**3a**	**4**	**5a**	**6**
1	**1a**+**2**	A(1)	12	43	11	20	41
2	**1a**+**2**	B(3)	52	13	—	27	29
3	**5a**+**2**	A(6)	8	22	57	2	35
4	**3a**	A(6)	16	42	23	4	50
5	**3a**+**5a**	B(6)	—	98	—	96	—

A; usual irradiation, using high-pressure Hg lamp from outside. B; irradiation with light of wavelength longer than 400 nm. Yields were determined by ^{1}H NMR using durene as an internal standard.

Table 2. Photochemical reaction of DMID **1a** and xanthene **2** upon irradiation with light of wavelength (λ>400 nm). Effects of concentration of DMID and reaction temperature on the ratio of [**5a**]/[**3a**]

Temperature	5—7 °C		20—23 °C		30—34 °C	
[**2**]/[**1a**]	conv.	[**5a**]/[**3a**]	conv.	[**5a**]/[**3a**]	conv.	[**5a**]/[**3a**]
0.5	45(%)	1.2	47(%)	1.6	52(%)	2.3
1	48	1.2	48	1.8	43	2.4
3	56	1.4	46	1.9	42	2.1
5	68	1.0	53	2.0	58	2 0

a) Irradiation time is 2 h. b) [DMID]=9.83×10^{-3} M. c) Yields were determined by ^{1}H NMR with durene as an internal standard.

independent of the concentration of xanthene. This result suggests that neither the semidione radical nor 9-xanthenyl radical reacted with xanthene. In contrast, the ratio of **5a** to **3a** gradually increased with increasing reaction temperature. The increasing yield of the combination product **3a** with decreasing reaction temperature provides us a powerful support for the concept on the geminate combination of initially formed radical pair.

d) CIDNP Examination. Light-induced reactions of DMID and NO_2–DMID with xanthene were examined by means of CIDNP. As shown in Figure 1b, the methine proton of xanthenyl moiety of **3a** appeared at δ 4.40 as enhanced absorption signal 4, the dimethyl protons of DMID moiety of **3a** appeared at δ 0.40 and 1.18 as moderately enhanced absorption signals 1 and 2, and in addition the dimethyl protons of DMID appeared at δ 1.14 as enhanced emission signal 3. We can rationalized these polarized signals in terms of the initially formed triplet radical pair composed of the semidione radical **11a** and 9-xanthenyl radical **12**. The geminate combination of **11a** and **12** produces **3a**. On the other hand, **11a** escaping from the initial triplet radical pair reproduces DMID by donating a hydrogen atom to another DMID. The Kaptein's equation[8] (Eq. 1) allows us to predict the net effect of polarization, Γ_{ne}.

$$\Gamma_{ne} = \Delta g \varepsilon \mu A_i \quad (1)$$

if, $\Gamma_{ne}=+$, then absorption polarized signal,
$\Gamma_{ne}=-$, then emission polarized signal.

These parameters have their usual meanings. As to the enhanced absorption signal 4 in Fig. 1b, $\Delta g=-$, $\varepsilon=+$, and $A_i=-$ are to be considered, because **3a** is the geminate combination product, g-value of semidione radical is in general larger than that of carbon radical without exception, and the sign of hyperfine coupling constant A_i of α-hydrogen of carbon radical is assumed to be negative on the basis of the preceding reaction mechanism.[9] Thus, in Eq. 1, $+=-\cdot+\cdot\mu\cdot-$, then μ will be positive and the triplet radical pair was indicated.

The A_i sign of the dimethyl protons of **11a** was deduced to be positive from the direction of polarization of signals 1 and 2. Then, the observed enhanced emission signal 3 due to DMID itself led us to a conclusion that DMID was reproduced as the escaping product from the initial triplet radical pair. The hydrogen transfer process as designated e in Scheme 3 was similarly proposed in the photolysis of benzaldehyde[10] and the photochemical reaction of benzophenone in 2-propanol.[11]

In addition to the assigned polarized signals 1, 2, 3, and 4 observed in aliphatic region, other polarized signals in aromatic region remain unassigned in the reaction of DMID with xanthene due to their complicated spin-spin coupling. Photolysis of a solution of NO_2–DMID and xanthene provides us an invaluable information on this point. Figures 2a and 2b show the spectra of a solution of NO_2–DMID and xanthene in $CDCl_3$ before and during irradiation, respectively. The patterns of ^1H NMR signals in aromatic region of both NO_2–DMID and the xanthene-adduct **3b** are rather resemble each other. Thus, from comparison of their chemical shifts and coupling patterns each proton of these compounds was assigned as follows; H^3, δ 1.55

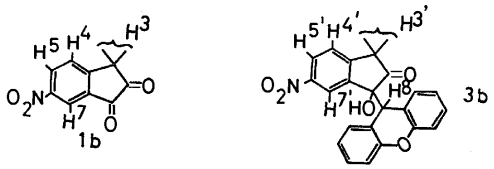

(s, 6H); H^4, 7.80 (d, J=8 Hz, 1H); H^5, 8.60 (dd, J=2 and 8 Hz, 1H); H^7, 8.66 (J=2 Hz, 1H) in **1b**, and $H^{3'}$, 0.46 (s, 3H) and 1.21 (s, 3H); $H^{4'}$, hidden in the signals of aromatic protons of xanthenyl moiety; $H^{5'}$, 8.18 (dd, J=2 and 8 Hz, 1H); $H^{7'}$, 7.76 (d, J=2 Hz, 1H); H^8, 4.46 (s, 1H). Based on these observation, we assigned polarized signals 1, 2, 4, 5, and 7 to $H^{3'}$, $H^{3'}$, H^8, $H^{7'}$, and $H^{5'}$, respectively, and polarized signals 3, 6, 8, and 9 to H^3, H^4, H^5, and H^7, respectively. Similar to the case of DMID, it was concluded according to Eq. 1 that **3b** was the geminate combination product from the initial triplet radical pair, and that there was reproduction of NO_2–DMID *via* the escaping semidione radical. Furthermore, consulting to Eq. 1 we can

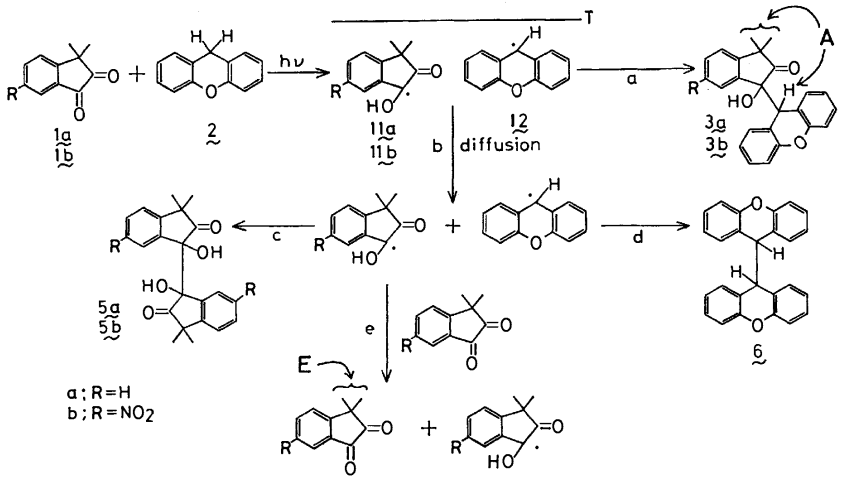

Scheme 3.

conclude from the direction of the polarized signals in aromatic region that the A_i signs of aromatic protons in the semidione radical **11b** were negative for the proton at C-7, negative for the proton at C-5, and positive for the proton at C-4, respectively.

e) Quantum Yield and Reaction Rate. The quantum yield for the disappearance of DMID in the presence of xanthene upon irradiation with light of 450 nm in a carefully degassed benzene solution was determined to be 0.71. The value of the quantum yield is significantly higher than the value of 0.07 ± 0.01 reported for the hydrogen abstraction reaction of camphorquinone with *p*-xylene,[2] but is nearly equal to the value of 0.7 reported for the reaction of benzil with toluene.[12] Although the carbonyl groups of DMID are rigidly fixed in a five membered ring, the C-1 carbonyl group is not suffering from such a high steric hindrance as the C-2 carbonyl group. Since in addition the C-1 carbonyl group is conjugated with the phenyl group, the π^* orbital of the C-1 carbonyl group in alkyl phenyl diketone may be stabilized by mixing with the benzene π^* orbitals and therefore contributes more to the lowest diketone π^* orbital.[13] Thus, the hydrogen abstraction of DMID could occur predominantly at the C-1 carbonyl group.

The lowest triplet $(n\pi)^*$ energy of DMID has been measured to be about 52 kcal/mol.[14] The photoreaction of DMID with xanthene was not quenched by phenanthrene (E_T=62 kcal/mol), but quenched by anthracene (E_T=42 kcal/mol) upon irradiation with 450 nm monochromatic light. There are some spectroscopic evidences[15] that the abstracting state is the lowest $^3(n\pi)^*$.

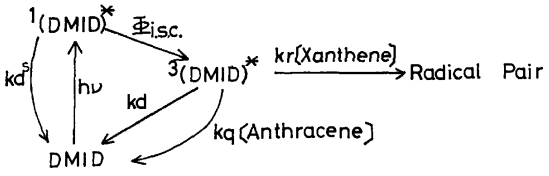

Scheme 4.

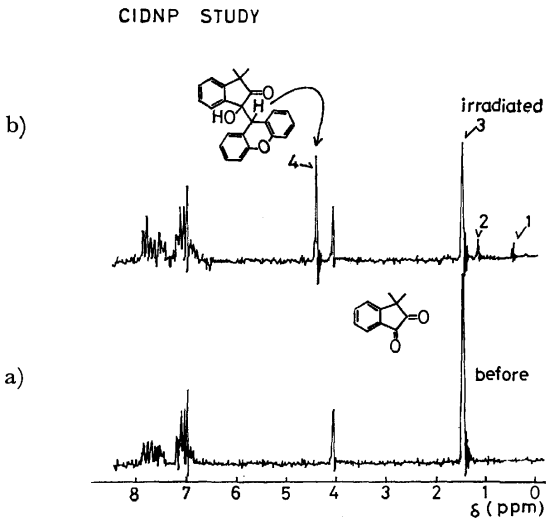

Fig. 1. ^{1}H NMR spectra observed in the photochemical reaction of DMID with xanthene in $CDCl_3$; a) before irradiation, b) during irradiation.

The possible reaction mechanism is described in Scheme 4, DMID in its ground state is excited to its $^3(n\pi)^*$ in the rate of $I\cdot\Phi_{isc}$: I; light intensity, Φ_{isc}; intersystem crossing yield. The ^{3}(DMID)* is consumed through two paths. The one is *via* self-decaying path (rate constant; k_d) involving both thermal and light emission, and the other is *via* hydrogen abstraction reaction from xanthene (rate constant; k_r). The hydrogen transfer process from the semidione radical to DMID can be neglected in Scheme 4, because there is no net change in the concentration of DMID. From the linear Stern-Volmer plots of Φ_d^{-1} *vs.* [xanthene]$^{-1}$ and Φ_d^{-1} *vs.* [anthracene], the quantum yield of

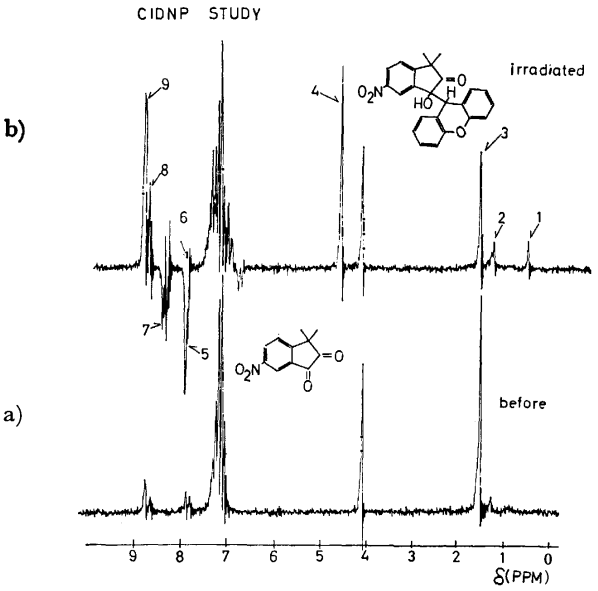

Fig. 2. ^{1}H NMR spectra observed in the photochemical reaction of NO_2–DMID with xanthene in $CDCl_3$; a) before irradiation, b) during irradiation.

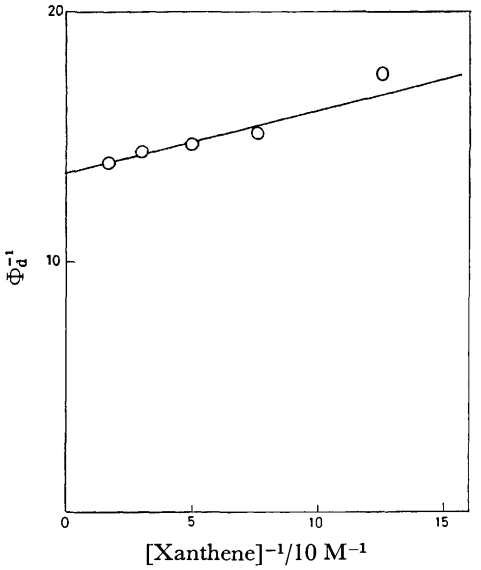

Fig. 3. Stern-Volmer plot of Φ_d^{-1} *vs.* [xanthene]$^{-1}$ in the photochemical reaction of DMID with xanthene.

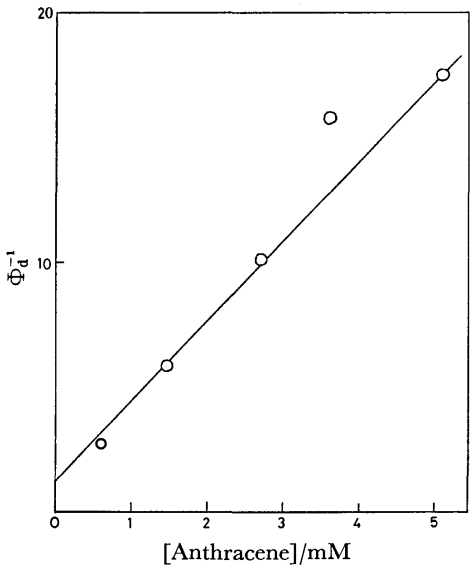

Fig. 4. Stern-Volmer quenching of the photochemical reaction of DMID and xanthene by anthracene.

intersystem crossing (Φ_{isc}) and the reaction rate constant (k_r) were estimated to $\Phi_{isc}=0.75$ and $k_r=5.7\times10^7$ M^{-1} s^{-1}, respectively.[16]

In conclusion, the hydrogen abstraction reaction of DMID with xanthene is a cosiderably fast process. The ^{3}(DMID)* shows high reactivity in the hydrogen abstraction reaction and behaves as one of aromatic α-diketones such as benzil rather than one of sterically hindered α-diketones.

Experimental

Apparatus. The melting points were measured with a Yanagimoto micro melting point apparatus and are uncorrected. Micro analyses were performed by the Micro analytical Laboratory of Kyoto University. IR spectra were recorded with a JASCO DS-402G spectrometer, and ^{1}H NMR spectra were taken with a JEOL PS-100 spectrometer with use of tetramethylsilane as an internal standard and the chemical shifts are expressed in δ value. UV irradiations were carried in a Pyrex glass tube at room temperature, using an Eikosha 300-W high-pressure mercury lamp.

Materials. 3,3-Dimethyl-1,2-indanedione (mp 104—105 °C) and 3,3-dimethyl-6-nitro-1,2-indanedione (mp 172—174 °C) were prepared by the method of Koelsh.[17] 1,1′-Dihydroxy-3,3,3′,3′-tetramethyl-2,2′-dioxo-1,1′-biindanyl (mp 123—125 °C) was prepared by the photoreduction of DMID in 2-propanol.

Photochemical Reaction of DMID with Xanthene. A degassed solution of DMID (1 mmol) and xanthene (1.2 mmol) in 30 ml of benzene was irradiated for an hour in a Pyrex glass tube, using a 300-W high-pressure mercury lamp from outside. After removal of the solvent, the residual oil was chromatographed on silica gel (Wakogel C-100). Elution with light petroleum ether (1%) gave colorless crystals of 9,9′-bixanthenyl **6** (46%). The isolated **6** was identified by comparison of IR and ^{1}H NMR spectra with those of the authentic sample. Elution with light petroleum ether (5%) gave colorless prisms of 1-hydroxy-3,3-dimethyl-1-(9-xanthenyl)-2-indanone **3a** (49%); mp 133—134 °C. Found: C, 80.72; H, 5.53%. Calcd for $C_{24}H_{20}O_3$: C, 80.86; H, 5.67%. Elution with light petroleum ether (10%) gave colorless oil of 2-hydroxy-3,3-dimethyl-1-indanone **4** (12%). Found: C, 74.72; H, 6.99% Calcd for $C_{11}H_{12}O_2$: C, 74.98; H, 6.86%. The hydroxy ketone **4** was also prepared by the reduction of DMID with $NaBH_4$ in ethanol in a yield of 68%.

Photochemical Reaction of 3,3-Dimethyl-6-nitro-1,2-indanedione. A degassed solution of **1b** (1 mmol) and xanthene (2 mmol) in 30 ml of benzene was irradiated for 6 houres in a Pyrex tube. White crystals were deposited and then filtered off (15%). The substance showed characteristic absorptions at 3500 (OH) and 1749 cm^{-1} (C=O), and changed to the starting **1b** on heating. The mass spectrum of it showed *m/e* at 219 and 221 corresponding to the molecular ions of NO_2–DMID and the hydroxy ketone, respectively, probably produced by disproportionation of the semidione cation radical. Therefore, the crystals were determined to be 1,1′-dihydroxy-3,3,3′,3′-tetramethyl-6,6′-dinitro-1,1′-biindan-2,2′-dione **5b** (pinacol). After removal of the solvent, the residual oil was chromatographed on silica gel column (Wakogel C-100). In addition to 9,9′-bixanthenyl **6** (75%), 1-hydroxy-3,3-dimethyl-6-nitro-1-(9-xanthenyl)-2-indanone **3b** (70%) was obtained. Colorless prisms; mp 170—171 °C; IR (KBr) 3520 (OH), 1725 (C=O), 1515 and 1250 cm^{-1}. Found: C, 71.80; H, 4.70; N, 3.52%. Calcd for $C_{24}H_{19}O_5$: C, 71.81; H, 4.77; N, 3.49%.

2-Anisoyloxyl-3,3-dimethyl-1-indanone; Ester A. A solution of **4** (1 mmol) in benzene (30 mL) was added *p*-anisoylchloride (1.1 mmol) at room temperature. The mixture was stirred for an hour, poured into water, and neutralized with $NaHCO_3$. Extraction with ether followed by drying (Na_2SO_4) and evaporation of the solvent afforded yellow oil. Separation on silica gel chromatography gave ester **A** (56%). Colorless needles; mp 98 °C; IR (KBr) 1757 (C=O), 1721 (ester), 1255 and 1032 cm^{-1}: ^{1}H NMR 1.24 (s, 3H), 1.64 (s, 3H), 3.38 (s, 3H), 5.56 (s, 1H), and 6.90—8.12 (m, 8H). Found: C, 73.45; H, 5.79%. Calcd for $C_{19}H_{18}O_4$: C, 73.53; H, 5.85%.

Photochemical Reaction of DMID with p-*Anisaldehyde.* A degassed solution of DMID (1 mmol) and *p*-anisaldehyde (1 mmol) in 30 ml of benzene was irradiated for 8 hours in a Pyrex tube. After removal of the solvent, the residual oil was chromatographed on silica gel (Wakogel C-200). 1-Anisoyloxy-3,3-dimethyl-2-indanone; ester **B** was obtained in 4% yield. Colorless oil; IR (CCl_4) 1774 (C=O), 1723 (ester), 1252 and 1034 cm^{-1}: ^{1}H NMR (CCl_4) 1.40 (s, 3H), 1.48 (s, 3H), 3.82 (s, 3H), 6.23 (s, 1H), and 6.78—8.01 (m, 8H). Found: C, 73.61; H, 5.89%. Calcd for $C_{19}H_{18}O_4$: C, 73.53; H, 5.85%.

Hydrolysis of Ester A and B. A solution of **A** or **B** (30 mg) in aqueous 50% ethanol was added to a solution of 0.1 N KOH (5 ml), neutralized with $NaHCO_3$, extracted with ether, dried, and chromatographed on preparative TLC. In addition to *p*-anisic acid (80%), the hydroxy ketone **4** was obtained in 60% and 56% yields in the reaction of the ester **A** and **B**, respectively.

3,3-Dimethylspiro(indan-1,2′-[1,3]dithiolan)-2-one ***13*** *and 3,3-Dimethylspiro(indan-2,2′-[1,3]dithiolan)-1-one* ***14***. A solution of DMID (1.0 mmol) and 1,2-ethanedithiol (1.1 mmol) in 20 ml of acetic acid was cooled at 0 °C and boron trifluoride etherate (1.1 mmol) was added with stirring. The mixture was allowed to stand 30 minutes at room temperature and was poured into water, and neutralized with $NaHCO_3$. Extraction with ether followed by drying with Na_2SO_4 and evaporation of the solvent afforded yellow semisolid oil. Separation on silica gel column chromatography gave **13** (67%); mp 77—78 °C: pale yellow needles. IR (KBr) 2970, 1774

(C=O), 1473, 1270, and 1047 cm^{-1}; ^1H NMR (CCl_4) 1.42 (s, 6H), 3.40—3.84 (m, 4H), and 7.04—7,32 and 7.48—7.64 (m, 4H). Found: C, 62.31; H, 5.60; S, 25.61%. Calcd for $C_{13}H_{14}OS_2$: C, 62.36; H, 5.64; S, 25.61%. And **14** (24%); pale yellow oil. IR (CCl_4) 2970, 1727 (C=O), 1608, 1543, 1255, and 1212 cm^{-1}; ^1H NMR (CCl_4) 1.54 (s, 6H), 3.12—3.60 (m, 4H), and 7.20—7.76 (m, 4H); Found: C, 62.45; H, 5.58; S, 25.75.%. Calcd for $C_{13}H_{14}OS_2$: C, 62.36 H, 5.64; S, 25.61%. The structures of these two regioisomers were determined by comparison of the characteristic bands due to the carbonyl group of **13** with that of **14**; namely, phenyl conjugated ketone **14** shows an absorption at smaller wave number compared with nonconjugated ketone **13.**

*2-Hydroxy-3,3-dimethylspiro(indan-1,2'-[1,3]dithiolane) **10** and 1-Hydroxy-3,3-dimethylspiro(indan-1,2'-[1,3]dithiolane) **9**.*
Both **13** and **14** were reduced with sodium borohydride in ethanol to give **10** (90%) and **9** (89%), respectively. Alcohol **10**; colorless needles; mp 72 °C; IR (KBr) 3490 (OH), 2990, 1545, 1133, and 1087 cm^{-1}: ^1H NMR (CCl_4) 1.08 (s, 3H), 1.33 (s, 3H), 2.86 (mobile, 1H), 3.30—3.41 (m, 4H), 4.12 (s, 1H), and 6.98—7.30 and 7.44—7.60 (m, total 4H). Found: C, 61.89; H, 6.65; S, 25.46%. Calcd for $C_{13}H_{16}OS_2$: C, 61.86; H, 6.39; S, 25.41%. Alcohol **9**; colorless oil: IR (CCl_4) 3490 (OH), 2990, 1547, and 1135 cm^{-1}: ^1H NMR (CCl_4) 1.31 (s, 3H), 1.51 (s, 3H), 3.02 (mobile, 1H), 2.09—3.40 (m, 4H), 5.18 (s, 1H), and 6.39—7.40 (m, 4H). Found: C, 62.53; H, 6.20; S, 25.09%. Calcd for $C_{13}H_{16}OS_2$: C, 61.86; H, 6.39; S, 25.41%.

*Oxidative Hydrolysis of **9** and **10**.* Both **9** and **10** were hydrolyzed with mercury(II) chloride by the method of Corey.[18] The hydroxy ketone **4** was obtained in 55% and 68% yields in the oxidative hydrolysis of **9** and **10**, respectively.

CIDNP Examination. PS-100 type NMR instruments equipped with ^1H NMR probe for irradiation (manufactured by JEOL) were used in CIDNP examinations. For irradiation, 1 kW super-high-pressure Xe lamp was applied.

Measurement of Quantum Yield. The absolute value of quantum yield for the disappearance of DMID in the reaction with xanthene was measured using 450 nm monochromatic light with application of both VY 42 and 45 KL filters (Toshiba). Disappearance of DMID in a carefully degassed benzene solution was measured at 505.7 nm. Light intensity was measured by means of tris(oxalato)ferrate(III) actinometry. In Stern-Volmer examination, we plotted the value calculated from relative quantum yields to the standard solution, using a merry-go-round.

References

1) B. M. Monroe, *Adv. Photochem.*, **8**, 77 (1971).

2) a) B. M. Monroe and S. A. Weiner, *J. Am. Chem. Soc.*, **91**, 450 (1961); b) M. B. Rubin and R. G. Labarge, *J. Org. Chem.*, **31**, 3283 (1966).

3) a) M. B. Rubin, *J. Org. Chem.*, **28**, 1949 (1963); b) M. B. Rubin and P. Zwitkowits, *ibid.*, **29**, 2362 (1964).

4) a) K. Maruyama nad T. Takahashi, *Chem. Lett.*, **1974**, 467; b) K. Maruyama and T. Takahashi, *Bull. Chem. Soc. Jpn.*, **49**, 3132 (1976); c) K. Maruyama, T. Ohtsuki, and T. Maruyama, *Bull. Chem. Soc. Jpn.*, **44**, 2756, 2789 (1971). d) K. Maruyama, T. Ohtsuki, and Y. Naruta, *Bull. Chem. Soc. Jpn.*, **49**, 791 (1976).

5) a) G. E. Gream, J. C. Paice, and C. C. R. Ramsey, *Aust. J. Chem.*, **20**, 1671 (1967); b) K. Maruyama, K. Ono, and J. Osugi, *Bull. Chem. Soc. Jpn.*, **45**, 847 (1972); c) K. Maruyama and A. Takuwa, *Bull. Chem. Soc. Jpn.*, **49**, 2790 (1976).

6) J. Rigaudy and N. Paillous, *Bull. der Soc. France*, **1971**, 576.

7) S. A. Weiner, E. J. Hamilton, Jr., B. M. Monroe, *J. Am. Chem. Soc.*, **91**, 6350 (1969).

8) a) R. Kaptain, *J. Chem. Soc., Chem. Commun.*, **1971**, 732; b) G. L. Closs and D. R. Paulson, *J. Am. Chem. Soc.*, **92**, 7229 (1970).

9) M. Cocivera and A. M. Trozzolo, *J. Am. Chem. Soc.*, **92**, 1772 (1970).

10) S. Marmor, *J. Org. Chem.*, **28**, 250 (1963).

11) J. N. Pitts, Jr. R. L. Latsiger, R. P. Traylor, J. M. Patterson, G. Recktenwald, and R. B. Martin, *J. Am. Chem. Soc.*, **81**, 1068 (1959).

12) D. L. Bunbury and T. T. Chuang, *Can. J. Chem.*, **47**, 2645 (1969).

13) a) S. Nakagura and J. Tanaka, *J. Chem. Phys.*, **22**, 236 (1954); b) P. J. Wagner, R. G. Zepp, K. C. Liu, M. Thomas, T. J. Lee, and N. J. Turro, *J. Am. Chem. Soc.*, **98**, 8125 (1976).

14) J. F. Arnett, G. Newkome, W. L. Mattice, and S. P. McGlymn, *J. Am. Chem. Soc.*, **96**, 4385 (1974).

15) Both of S_1-S_n absorption and T_1-T_n absorption were observed at 470—500 nm and 400—500 nm, respectively. Life time of T_1-T_n absorption was dramatically shortened in the presence of oxygen or xanthene, but xanthene had no effect on life time of S_1-S_n absorption. (Private communication from Dr. H. Hayashi; the Institute of Physical and Chemical Reseach, Saitama, Japan.)

16) The realtion between Φ_d and [xanthene] and the relation between Φ_d and [anthracene] were derived by application of the stationary state approximation to [^{3}(DMID)*].

$$\frac{1}{\Phi_d} = \frac{1}{\Phi_{isc}} + \frac{k_d}{\Phi_{isc} \cdot k_r \cdot [\text{xanthene}]} \quad (2)$$

$$\frac{1}{\Phi_d} = \frac{1}{\Phi_{isc}} + \frac{k_d}{\Phi_{isc} \cdot k_r \cdot [\text{xanthene}]} + \frac{k_q[\text{anthracene}]}{\Phi_{isc} \cdot k_r \cdot [\text{xanthene}]} \quad (3)$$

As the value of the quenching rate constant k_q in this experiment, we used the value of the quenching rate constant (5.6×10^9 M^{-1} s^{-1}) reported for benzophenone–naphthalene system in benzene at room temperature. (P. J. Wagner and I. Kochevar, *J. Am. Chem. Soc.*, **90**, 2232 (1968).)

17) C. F. Koelsh and C. D. Le Claire, *J. Org. Chem.*, **6**, 516 (1941).

18) E. J. Corey and B. W. Erickson, *J. Org. Chem.*, **23**, 3553 (1971).

Macrocyclic Formals. IV. Macrocyclic Formals as Complexing Agents

Yuhsuke KAWAKAMI,* Tomiya SUGIURA, and Yuya YAMASHITA
Department of Synthetic Chemistry, Faculty of Engineering, Nagoya University, Nagoya 464
(Received May 1, 1978)

Eleven to twenty membered macrocyclic formals have been synthesized from the corresponding polyethylene glycols and paraformaldehyde. Their activating efficiency has been measured in nucleophilic substitution reactions with alkali metal ions as counter ions. These macrocyclic formals were not as good complexing agents as crown ethers, but were much better than open chain polyethers which had the same number of oxygen atoms. In the reaction of butyl bromide with alkali metal acetate, 1,3,6,9,12,15-hexaoxacycloheptadecane was several times more effective than pentaethylene glycol dimethyl ether.

Macrocyclic compounds, such as crown ethers and cryptands, have been extensively studied in recent years as powerful complexing agents specially for alkali metal ions.[1–12] The authors have been interested in the polymerization reaction of macrocyclic formals having ether oxygens besides acetal oxygens. Macrocyclic oligomers were formed in the early stage, then high polymers were formed in the polymerization of macrocyclic formals.[13–17] There might be the possibility that the propagating cationic species was activated by macrocyclic oligomers already formed in the system through complexing in order to propagate. Thus, interest has been shown in the complexing ability of such macrocyclic formals with cations.

Macrocyclic formals from polyethylene glycols have the structure in which one of the ethylene groups of the crown ethers is replaced by a methylene group. They can be easily synthesized from the corresponding polyethylene glycols and paraformaldehyde by condensation and depolymerization at elevated temperatures in the presence of an acid *e.g.* *p*-toluenesulfonic acid. One of the advantages for macrocyclic formals as complexing agents is that they can be easily decomposed by mineral acids and can be separated from the products by simple extraction. From such a viewpoint, the effectiveness of crown ethers, macrocyclic formals and glymes as complexing agents were compared in a nucleophilic substitution reaction.

In this paper, complexing agents have been abbreviated according to the common crown ether nomenclature. For instance, 11-CF-4 stands for a 11-membered macrocyclic formal having four oxygen

crown ether
3*m*-CR-*m*

macrocyclic formal
(3*n*−1)-CF-*n*

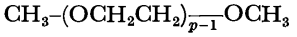

glyme
3*p*-GL-*p*

atoms and 18-GL-6 stands for a glyme consisting of 18 skeltal atoms including 6 ether oxygen atoms, namely, pentaethylene glycol dimethyl ether.

Experimental

Synthesis of Complexing Agents. 1,3,6,9-Tetraoxacycloundecane (11-CF-4), 1,3,6,9,12-pentaoxacyclotetradecane (14-CF-5), and 1,3,6,9,12,15-hexaoxacycloheptadecane (17-CF-6) were synthesized according to the reported methods.[16,18] The crude products were purified by fractional distillation over lithium aluminum hydride. Since, 1,3,6,9,12,15,18-heptaoxacycloeicosane could not be synthesized by a similar method, the method of ether linkage formation was used.

A 500 ml three-necked flask equipped with a mechanical stirrer, reflux condenser and addition funnel was charged with tetraethylene glycol (50 g, 0.26 mol) and tetrahydrofuran (200 ml). Stirring was commenced and aqueous potassium hydroxide (60%, 60 ml) solution was added and the solution was heated at 60 °C for one and a half hours. A solution of formaldehyde bis(2-chloroethyl) acetal[19] (44.6 g, 0.26 mol) in tetrahydrofuran (34 ml) was then added in a stream after which the solution was refluxed and stirred vigorously for 7 days. The solution was allowed to cool and the bulk of the tetrahydrofuran was evaporated on a rotary evaporator. The resulting slurry was diluted with dichloromethane (170 ml). The upper organic layer was separated and washed with water (40 ml) in order to remove unreacted tetraethylene glycol. This water layer (40 ml) was extracted twice with dichloromethane (10 ml) and the extract was combined with the organic layer. The combined organic solution was dried with calcium chloride and the solvent was evaporated off. The residue was distilled under reduced pressure to give 7.8 g of a crude product (152—165 °C/0.2 mmHg). The crude product was redistilled over lithium aluminum hydride.

20-CF-7: bp 142—144 °C/0.2 mmHg yield 3.4 g, 4.5%. IR (NaCl, cm^{-1}) 2930, 2870, 1460, 1360, 1300, 1255, 1180, 1120, 1030, 940, 850. NMR ($CDCl_3$, δ ppm) 4.80 (s, 2H, $-OC\underline{H}_2O-$), 3.78 (s, 8H, $-OC\underline{H}_2C\underline{H}_2OC\underline{H}_2O-$), 3.70 (s, 16H, $-OC\underline{H}_2-C\underline{H}_2O-$).

Found: C, 52.96; H, 8.22%. Calcd for $C_{13}H_{26}O_7$: C, 53.05; H, 8.90%. *M. W.* (VPO) 294.34 (302).

12-Crown-4 was synthesized from 1,8-dichloro-3,6-dioxaoctane and ethylene glycol according to the literature[20] and 2,5,8,11 14,17-hexaoxaoctadecane (18-GL-6) by the condensation between 1-chloro-3,6-dioxaheptane and triethylene glycol monomethyl ether sodium salt.

18-GL-6: bp 149—151 °C/2.5 mmHg. IR (NaCl, cm^{-1}) 2880, 1460, 1355, 1200, 1110. NMR ($CDCl_3$, δ ppm) 3.68 (s, 16H, $-C\underline{H}_2-O-C\underline{H}_2-$), 3.62 (broad s, 4H, $CH_3OC\underline{H}_2-$), 3.40 (s, 6H, $C\underline{H}_3O-$)

Found: C, 54.35; H, 9.56%. Calcd for $C_{12}H_{26}O_6$: C, 54.07; H, 9.84%. Other complexing agents, 15-CR-5, 18-CR-6, 12-GL-4, and 15-GL-5 were commercially supplied.

Determination of Reaction Rate in the Presence of Complexing Agent. A 20 ml round bottomed flask equipped with a reflux condenser was charged with alkali metal acetate (metal: K, Na, Li) (0.01 mol), butyl bromide (0.01 mol) a complexing agent (0.01 mol), toluene (1.0 ml) as internal standard for GLC and benzene (9 ml). The mixture was heated to reflux at a bath temperature of 90 °C. At a

given time interval, a small portion of the reaction system was extracted with a syringe and analyzed by GLC. The conversion of the reaction was determined by use of a calibration curve using toluene as an internal standard. The gas chromatograph was a Hitachi model K 23 connected with 2 m of stainless steel columns packed with 15% Apiezon grease M on Chromosorb. It was operated at 80 °C with 17 ml/min helium as the carrier gas.

Determination of Cation Binding Efficiency of Complexing Agents. The cation binding efficiency of the complexing agents was determined by measuring the extraction equilibrium of alkali metal picrate between dichloromethane and water. Twenty five ml of 0.1 M alkaline solution containing 8×10^{-5} mol of picric acid was extracted with 25 ml of dichloromethane and the system left to reach equilibrium. The concentration of picrate species present in the organic phase and water phase was determined by measuring the UV absorption of each phase at equilibrium using λ_{max} 357 nm (ε 15000) in water, λ_{max} 378 nm (ε 18000) in CH_2Cl_2.[21] The UV spectrophotometer used was a Hitachi Perkin Elmer model 139 using quartz cells.

Results and Discussion

Effect of Complexing Agents on the Reaction Rate. The effect of complexing agents in accelerating Reaction 1 was examined.

$$CH_3CO_2M + n\text{-}C_4H_9Br \xrightarrow[\text{Benzene reflux}]{\text{Complexing agent}} CH_3CO_2n\text{-}C_4H_9 + MBr \quad (1)$$

(M=K, Na, Li)

The conversion of butyl bromide or the yield of butyl acetate determined by GLC was plotted against time. A typical result has been shown in Figure 1. The conversion and the yield coincide with each other very well. The initial slope of the curve was taken as the initial rate V_0 of the reaction and the initial rates in the presence of various complexing agents have been shown in Table 1. Crown ethers were the best activating complexing agents for the reactions of potassium or sodium acetate. The initial rates decreased in the order of crown ethers, macrocyclic formals and glymes. In the case of lithium acetate, only 15-CR-5 slightly activated the reaction.

It is generally considered that the complexing agents

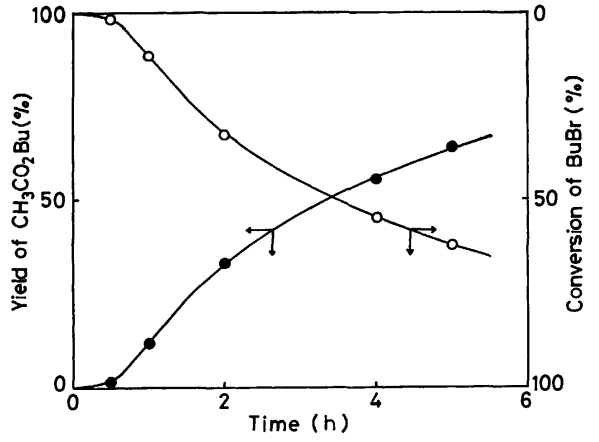

Fig. 1. Change in the quantity of *n*-BuBr and CH_3CO_2n-Bu with reaction time.

Table 1. Effects of complexing agent and cation on initial rate (V_0, mol/l s $\times 10^6$)

Complexing agent	K^+	Na^+	Li^+
None	0.0	0.0	0.0
20-CF-7	56	0.39	0.0
17-CF-6	15	2.3	0.0
14-CF-5	0.69	0.0	0.0
11-CF-4	0.0	0.0	0.0
18-CR-6	2600	12	0.0
15-CR-5	780	13	0.81
12-CR-4	1.4	0.44	0.0
18-GL-6	2.6	0.083	0.0
15-GL-5	1.0	0.0	0.0
12-GL-4	0.25	0.0	0.0

Metal acetate 0.01 mol, *n*-BuBr 0.01 mol, complexing agent 0.01 mol, toluene 1.0 ml, benzene 9.0 ml, 90 °C.

activate the reaction by complexing with the counter cation and separating the cation from the anion species. It is also well recognized that crown ethers have specific ring sizes to fit specific cations, for instance, 18-CR-6 has a specific size for the potassium cation. In the case of macrocyclic formals, 20-CF-7 appeared to be a much better activating agent than 17-CF-6 for the reaction with potassium as the counter cation. Moreover, 17-CF-6 was a better activating agent than 14-CF-5 or 20-CF-7 for the reaction with sodium as the counter cation. Thus, in case of macrocyclic formals, the specific ring size to fit an alkali metal cation might be one ethyleneoxy unit larger than that in case of crown ethers.

Thus, in comparing the effectiveness of complexing agents in accelerating Reaction 1, it would be reasonable to compare 20-CF-7 with 18-CR-6 and 18-GL-6 and 17-CF-6 with 15-CR-5 and 15-GL-5. For the potassium cation, the ratio of the initial rates among 18-CR-6, 20-CF-7, and 18-GL-6 was 46: 1.0: 0.046 and for the sodium cation, it was 31: 1.0: 0.21. The ratio among 15-CR-5, 17-CF-6, and 15-GL-5 was 52: 1.0: 0.067 for the potassium cation and 5.7: 1.0: 0.00 for the sodium cation. It was shown that the macrocyclic formals were not as good activating agents as the crown ethers, however, they were much better than the glymes. The difference in initial rate V_0 would reflect the effective concentration of the activated anion with its counter cation complexed. In order to clarify the difference in the effectiveness among complexing agents, the complexing agents' efficiency in the extraction equilibrium of alkali metal picrate between dichloromethane and water was examined and the results have been shown in Table 2. In determining the extraction efficiency, it was assumed that the picrate did not form a complex in the water phase and that the picrate was present only in the complexed form in the dichloromethane phase.[21] As shown in Table 2, percent picrate extracted in dichloromethane phase decreased in the order of crown ether, cyclic formal, and glyme. This was the same order as in the case of the activating of Reaction 1.

The efficiency of complexing agents in extracting

Table 2. Extraction of picrate salts by complexing agents in H_2O–CH_2Cl_2 (1 : 1, v/v) solvent system

Complexing agent	Percent of extracted picrate in dichloromethane		
	K^+	Na^+	Li^+
None	0.0	0.0	0.0
20-CF-7	14.2	1.4	0.7
17-CF-6	3.1	2.1	0.1
14-CF-5	0.1	0.1	0.0
11-CF-4	0.1	0.4	0.3
18-CR-6	88.4	7.5	2.6
15-CR-5	14.4	8.3	0.5
12-CR-4	0.5	1.3	0.1
18-GL-6	1.3	0.8	0.3
15-GL-5	0.4	0.1	0.1
12-GL-4	0.1	0.1	0.1

[Picric acid] $= 8 \times 10^{-5}$ M, [complexing agent] $= 35 \times 10^{-5}$ M, [metal hydroxide] $= 0.01$ M.

alkali metal cations would be controlled by ① the number of oxygen atoms in the complexing agent, ② the nature of the cation and anion of the salt, and ③ the structure of the complexing agent: cyclic or open chain and size of ring.

Let us consider a little more about these factors. Complexes are formed by the coordination of lone pair electrons of oxygen atoms to metal cations. The more oxygen atoms were contained in a complexing agent, the easier complex formation would be. When a salt is forming a complex, the easier the dissociation of the salt, the easier the complex formation. In Table 2, except 11-CF-4 and 12-CR-4, potassium picrate was extracted the most by all of the complexing agents, indicating that the ease of dissociation of the salt was the primary factor for complex formation.

The big advantage for symmetrical cyclic complexing agents in coordination is that all the oxygen atoms can participate equally. A crown ether is a cyclic oligomer of ethylene oxide and has a highly symmetrical structure. All the oxygen atoms in the ring are equivalent and the lone pair electrons can be equally directed towards the cation in complex formation. In open chain complexing agents, a pseudocyclic structure must be taken to make all oxygen atoms participate equally in coordination. This is a great disadvantage against open chain complexing agents in terms of entropy. Moreover, when it is difficult to take a pseudocyclic structure, only few oxygen atoms can participate in coordination leading to weak complex formation. In cyclic formal rings, the two acetal oxygens are not equivalent with other ether oxygens and the lone pair electrons on the acetal oxygens can only with difficulty coordinate to the metal cation. This means the effective oxygens for coordination are less than actual oxygens in the molecule.

It is also well recognized that the size of the ring is an important factor in order to form a strong complex. The ring sizes of 17-CF-6 and 14-CF-5 would be smaller than those of 18-CR-6 and 15-CR-5, respectively and the most suitable cyclic formals for potassium and sodium cations would be 20-CF-7 and 17-CF-6, respectively. This situation is well shown in Table 2. The percentages of potassium picrate extracted into the dichloromethane phase were 14.2 and 3.1, for 20-CF-7 and 17-CF-6, respectively. Moreover, the percentages of sodium picrate extracted were 1.4, 2.1, and 0.1 for 20-CF-7, 17-CF-6, and 14-CF-5, respectively. When the efficiency of cyclic formals was compared with that of the crown ethers, the low efficiency of the cyclic formals was apparent. This might indicate the importance of the exact agreement of the ring size with cation size and symmetry of the ring.

Table 3. Effects of complex concentration on initial rate, V_0/C (s^{-1})

Complexing agent	K^+	Na^+	Li^+
None	0.0	0.0	0.0
20-CF-7	4.7	0.33	0.0
17-CF-6	6.1	1.4	0.0
14-CF-5	6.9	0.0	0.0
11-CF-4	0.0	0.0	0.0
18-CR-6	36	2.0	0.0
15-CR-5	67	1.9	2.0
12-CR-4	3.3	0.44	0.0
18-GL-6	2.6	0.14	0.0
15-GL-5	3.3	0.0	0.0
12-GL-4	2.5	0.0	0.0

Assuming that the precentage of picrate extracted into the dichloromethane phase is proportional to the concentration of the complexed species in the reaction system, V_0/C (V_0: initial rate in Table 1, C: concentration of picrate extracted in Table 2) was taken as the relative standard of the reactivity of the complex, the values of which have been shown in Table 3. The values are in the order of 10^1 for the most effectively activated potassium-18-CR-6 or 15-CR-5 systems and in the order of 10^0 for the moderately activated potassium-20-CF-7 or 17-CF-6 and sodium-18-CR-6 or 15-CR-5 systems. The value was less than 1 for the other slow reaction systems. This might indicate that in the effectively activated systems, not only the concentration of the complex but also the reactivity of the complex was high. It would be reasonable to consider that the easier the dissociation of the salt was and the stronger the complexing agent coordinated to the cation, the higher the concentration of the complex was and the looser complexed ion pair became. The looser ion pair would have a higher degree of nucleophilicity and effectively activate the substitution reaction.

The effectiveness of the macrocyclic formals as complexing agents was not sufficiently high compared with the crown ethers in the nucleophilic substitution reactions. However, they were much more efficient complexing agents than the open chain polyethers.

This research was partially supported by a Grant-in-Aid from the Ministry of Education (No. 285199).

References

1) C. J. Pederson, *J. Am. Chem. Soc.*, **89**, 2495 (1967).

2) C. J. Pedersen, *J. Am. Chem. Soc.*, **89**, 7017 (1967).
3) C. J. Pedersen, *J. Am. Chem. Soc.*, **92**, 386, 391 (1970).
4) C. J. Pedersen, *J. Org. Chem.*, **36**, 254 (1971).
5) C. J. Pedersen, *J. Org. Chem.*, **36**, 1690 (1971).
6) B. Dietrich, J. M. Lehn, and J. P. Sauvage, *Tetrahedron Lett.*, **1969**, 2885, 2889.
7) J. M. Lehn and J. P. Sauvage, *J. Am. Chem. Soc.*, **92**, 2916 (1970).
8) J. M. Lehn and J. P. Sauvage, *J. Chem. Soc., B*, **1971**, 440.
9) B. Dietrich, J. M. Lehn, and J. P. Sauvage, *J. Chem. Soc., Chem. Commun.*, **1973**, 15.
10) B. Dietrich, J. M. Lehn, J. P. Sauvage, and J. B. Blanzat, *Tetrahedron*, **29**, 1629 (1973).
11) B. Dietrich, J. M. Lehn, and J. Simon, *Angew. Chem. Int. Ed. Engl.*, **13**, 406 (1974).
12) J. M. Lehn and M. E. Stubbs, *J. Am. Chem. Soc.*, **96**, 4011 (1974).
13) Y. Yamashita, Y. Kawakami, and K. Kitano, *J. Polym. Sci., Polym. Lett. Ed.*, **15**, 213 (1977).
14) Y. Kawakami and Y. Yamashita, *Polym. J.*, **9**, 227 (1977).
15) Y. Kawakami and Y. Yamashita, *Macromolecules*, **10**, 837 (1977).
16) Y. Kawakami, J. Suzuki, and Y. Yamashita, *Polym. J.*, **9**, 519 (1977).
17) Y. Yamashita and Y. Kawakami, *ACS Sympo. Ser.*, **59**, 99 (1977).
18) M. J. Astle, J. A. Zaslowsky, and P. G. Lafyatis, *Ind. Eng. Chem.*, **46**, 787 (1954).
19) R. M. Anker and A. H. Cook, *J. Chem. Soc.*, **1948**, 808.
20) F. L. Cook, T. C. Caruso, M. P. Byrne, C. W. Bowers, D. H. Speck, and C. L. Liotta, *Tetrahedron Lett.*, **46**, 4029 (1974).
21) S. Kopolow, T. E. Hogen Esch, and J. Smid, *Macromolecules*, **6**, 133 (1973).

NOTES

BULLETIN OF THE CHEMICAL SOCIETY OF JAPAN, VOL. 51 (10), 3057—3058 (1978)

$TiN_{0.07}O_{1.93}$ Semiconductor Electrodes for Photoassisted Oxidation of Water†

Taketsugu HIRAI,* Isao TARI, and Junichi YAMAURA

Department of Synthetic Chemistry, Faculty of Engineering, Okayama University, Tsushima, Okayama 700

(Received February 3, 1978)

Synopsis. As a new anode for the photoassisted oxidation of water, the $TiN_{0.07}O_{1.93}$ semiconductor electrode is proposed. Its photoanodic behavior in 0.1 M Na_3PO_4 was similar to those of n-type TiO_2 electrodes, but the photocurrent response was a little extended toward the long wavelength region. The electrode stability under the irradiation with ultraviolet light was good.

Much recent attention has been paid to the application of semiconductor electrodes to the photolysis of water and the direct conversion of solar to electrical energy. The n-type TiO_2 has been intensively studied as one of the most promising anode materials for such systems.[1-23] However, the n-type TiO_2 has a relatively wide band gap of *ca.* 3 eV[1,2,6] and thus makes inefficient use of solar energy. In addition, a certain deterioration of the photoanode characteristics of n-type TiO_2 under the irradiation from an artificial light source has been reported recently,[16,17] in opposition to the notion that the n-type TiO_2 electrode is chemically stable. Titanium nitride oxide $TiN_{0.07}O_{1.93}$, proposed here, is a novel photoanode material with the n-type semiconductivity. As shown by the formula of $TiN_{0.07}O_{1.93}$, this non-stoichiometric compound is one of the modified forms of TiO_2; it is easily prepared by the thermal treatment of metallic titanium substrate in a N_2–O_2 atmosphere. The idea of doping nitrogen together wtih oxygen into a titanium substrate is based on the fact that the titanium nitride TiN_x shows both good electronic conductivity and chemical stability, and on the possibility that the interstitial permeation of nitrogen atoms into the TiO_2 structure might produce some oxygen vacancies.

Experimental

Electrode Preparation. Commercial titanium plate (20 mm × 15 mm, 0.5 mm in thickness) with a short sleeve for the electrical connection to a leading wire was heated in a nitrogen gas atmosphere containing 0.5 vol % oxygen gas at 1100 °C for 3 h. Most electrodes thus obtained had a grayish appearance with a metallic luster. Prior to the measurement of the current-potential characteristics, the surface of the electrode was investigated by means of X-ray diffraction and ESCA (DuPont Model 650B) techniques. A copper lead wire was tied tightly around the sleeve of the electrode after the sleeve was scratched by a fine emery paper to expose the titanium substrate. The apparent working area for the photoanode was 1 × 1 cm^2 and the remaining portion was coated with solid paraffin.

Measurements of Current-potential Characteristics. The apparatus, comprising a light source, photoelectrochemical cell, and recording equipment, is shown in Fig. 1. A monochromatic light source was prepared by attaching an interference filter (Koshin Optics Ltd.) to a xenon lamp. The accelerated life testing for inspecting the stability of the electrode was performed under the ultraviolet irradiation from a 440 W high pressure mercury lamp.

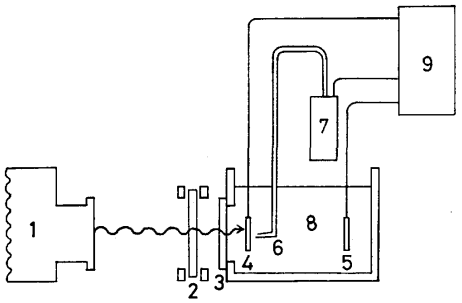

Fig. 1. Schematic representation of the experimental arrangement.
1: 450 W xenon lamp, 2: interference filter, 3: quartz window (3 mm thick), 4: working electrode, 5: Pt counter electrode, 6: Luggin capillary, 7: SCE reference electrode, 8: 0.1 M Na_3PO_4 (pH=6), 9: potentiostat and recorder.

Results

The X-ray diffraction analysis of the electrode surface gave mixed diffraction profiles of rutile, anatase, and titanium substrate. The ESCA spectra showed the presence of N, O, and Ti atoms in the thin surface layer of the electrode. The emission peaks of N 1s, O 1s, Ti 2p3/2, and Ti 2p1/2 electrons were observed at binding energies of 395.5 and 399.3, 529.1 and 531.3, 457.7, and 463.7 eV, respectively. From the summation of the corresponding peak areas on the ESCA spectra and the atomic sensitivity corrections for the photoelectron emission, the chemical composition of the outer surface layer of the electrode was estimated to be $TiN_{0.07}O_{1.93}$. Among a number of TiN_xO_y electrodes prepared under various atmospheric and thermal conditions, an electrode having a surface composition near $TiN_{0.07}O_{1.93}$ was found by a preliminary test to perform best as a photoanode.

The current-potential characteristics of the electrode in 0.1 M Na_3PO_4 (adjusted to pH 6 by addition of a small quantity of concd H_3PO_4) are shown in Fig. 2. From the comparison of curves A and B in Fig. 2, it is obvious that the electrode behaves as a photoanode. In addition, gas evolution at the electrode surface was

† A preliminary report of this work was presented at the 18th Battery Conference, Osaka, November 1977.

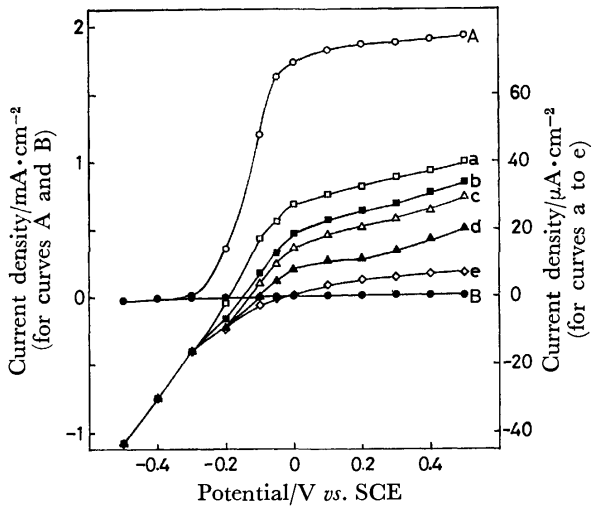

Fig. 2. Current-potential characteristics of $TiN_{0.07}O_{1.93}$ electrode in 0.1 M Na_3PO_4 (pH=6).
A: Under irradiation without interference filter, B: dark, a: under irradiation through a 400 nm interference filter, b: 440 nm, c: 420 nm, d: 450 nm, e: $\geqslant$460 nm.

observed in response to the passage of photocurrent. As shown by the curves a to e in Fig. 2, the electrode responded to the monochromatic light at wavelengths shorter than 460 nm, which corresponds to a band gap of *ca.* 2.7 eV. A small maximum of photocurrent at around 440 nm was a new feature of the electrode.

The accelerated stability test of the electrode was conducted in the following manner. Strong ultraviolet irradiation was directed, by use of a high pressure mercury lamp, onto the photoanode. This was short-circuited with the counter platinum cathode for 12 h and then operated with a constant anodic current density of 3.5 mA/cm² for 14 h. No significant change in the photocurrent-potential relation or in the electrode appearance was detected. These results demonstrate the stability of $TiN_{0.07}O_{1.93}$ electrode under ultraviolet irradiation.

Finally, the selection of Na_3PO_4 solution as electrolyte was due to its high pH-buffer action and its ability to detach the evolved bubbles from the electrode surface and move them into the bulk. In fact, the use of 0.1 M Na_2SO_4 as electrolyte caused a rapid decrease of the photocurrent with time.

We would like to thank Prof. Nobuatsu Watanabe and Dr. Tsuyoshi Nakajima of Kyoto University for their kind efforts in obtaining the ESCA spectra and for their helpful discussions.

References

1) A. Fujishima, K. Honda, and S. Kikuchi, *Kogyo Kagaku Zasshi*, **72**, 108 (1969).
2) A. Fujishima and K. Honda, *Bull. Chem. Soc. Jpn.*, **44**, 1148 (1971).
3) A. Fujishima and K. Honda, *Nature*, **238**, 37 (1972).
4) F. Möllers, H. J. Tolle, and R. Memming, *J. Electrochem. Soc.*, **121**, 1160 (1974).
5) A. Fujishima, K. Kohayakawa, and K. Honda, *Bull, Chem. Soc. Jpn.*, **48**, 1041 (1975).
6) M. Gleria and R. Memming, *J. Electroanal. Chem.*, **65**, 163 (1975).
7) K. L. Hardee and A. J. Bard, *J. Electrochem. Soc.*, **122**, 739 (1975).
8) J. Keeney, D. H. Weinstein, and G. M. Haas, *Nature*, **253**, 719 (1975).
9) A. J. Nozik, *Nature*, **257**, 383 (1975).
10) A. Fujishima, K. Kohayakawa, and K. Honda, *J. Electrochem. Soc.*, **122**, 1487 (1975).
11) T. Ohnishi, Y. Nakato, and H. Tsubomura, *Ber. Bunsenges. Phys. Chem.*, **79**, 253 (1975).
12) M. Shiozawa, K. Narita, Y. Fujita, S. Kurita, M. Takata, and H. Yanagida, *Yogyo Kyokai Shi*, **83**, 471 (1975).
13) H. Yoneyama, H. Sakamoto, and H. Tamura, *Electrochim. Acta*, **20**, 341 (1975).
14) J. H. Carey and B. G. Oliver, *Nature*, **259**, 555 (1976).
15) D. Laser and A. J. Bard, *J. Electrochem. Soc.*, **123**, 1027 (1976).
16) L. A. Harris and R. H. Wilson, *J. Electrochem. Soc.*, **123**, 1010 (1976).
17) J. O'M. Bockris and K. Uosaki, *J. Electrochem. Soc.*, **124**, 98 (1977).
18) K. Nakatani and H. Tsubomura, *Bull. Chem. Soc. Jpn.*, **50**, 783 (1977).
19) K. L. Hardee and A. J. Bard, *J. Electrochem. Soc.*, **124**, 215 (1977).
20) P. A. Kohl, S. N. Frank, and A. J. Bard, *J. Electrochem. Soc.*, **124**, 225 (1977).
21) L. A. Harris, K. R. Cross, and M. E. Gerstner, *J. Electrochem. Soc.*, **124**, 839 (1977).
22) J. Augustynski, J. Hinden, and Chs. Stalder, *J. Electrochem. Soc.*, **124**, 1063 (1977).
23) A. K. Ghosh H. P. Maruska, *J. Electrochem. Soc.*, **124**, 1516 (1977).

BULLETIN OF THE CHEIMCAL SOCIETY OF JAPAN, VOL. 51 (10), 3059—3060 (1978)

Charge-transfer Model in Considering the Reactivity of Heteroaromatic Nitriles with the Enolate Anion

Masumi YAMAKAWA, Tanekazu KUBOTA,* Yoshihiro TERUI, Tsunetoshi HONMA, and Yukio TADA

Shionogi Research Laboratory, Shionogi and Co., Ltd., Fukushima-ku, Osaka 553

(Received January 25, 1978)

Synopsis. The reactivity of heteroaromatic nitriles with the enolate anion to give the enamino ketones was discussed on the basis of a reaction index calculated by the charge-transfer model and also using the total electron densities. The results were reasonable in interpreting the reaction mechanism.

Recently Honma and Tada[1] have reported the very useful reaction of heteroaromatic nitriles with the enolate anion to prepare enamino ketones. The reaction is shown in Scheme 1. The reactivity will be considered using the molecular orbital (MO) description of the charge-transfer (CT) theory.[2,3] Supposing that the MO energies of the nitriles and enolate anion are related as Fig 1 shows, and that the CT occurs

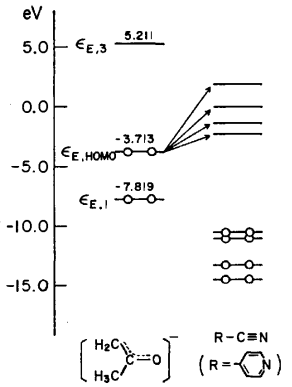

Fig. 1. Calculated MO energie of enolate anion and nitriles. The MO energies o heteroaromatic nitriles are more or less similar to th se given in this figure.

predominantly as shown by the arrows in Fig. 1, the stabilization energies due to CT can be written approximately by; $\Delta E_{rs}=2\sum_{k}^{VAC}[(C^{r}_{E.HO}\cdot C^{s}_{N.k})^2(H_{rs})^2/(\varepsilon_{E.HO}-\varepsilon_{N.k}+V^{E.HO}_{N.k})]$. $C^{r}_{E.HO}$ and $\varepsilon_{E.HO}$ are the πMO coefficients at the r-th atom in the highest occupied MO (HOMO) and the HOMO energy of the enolate anion respectively. Alternatively, $C^{s}_{N.k}$ and $\varepsilon_{N.k}$ stand for the πMO coefficient at the s-th atom in the k-th vacant πMO and the k-th πMO energy of nitriles respectively. H_{rs} is the resonance energy between the two πAO's. The intermolecular resonance interaction of the nitrile and the enolate anion was assumed to occur only through the two AO's. The electrostatic interaction energy between the MO's $\psi_{E.HO}$ and $\psi_{N.k}$ is expressed by $V^{E.HO}_{N.k}=\langle\psi^{*}_{E.HO}\cdot\psi^{*}_{N.k}|e^2/r|\psi_{E.HO}\cdot\psi_{N.k}\rangle$. For evaluating the $V^{E.HO}_{N.k}$ term, the geometrical configuration between each atom in nitriles and the enolate anion should be determined. Since this is quite difficult, we have disregarded the $V^{E.HO}_{N.k}$ term in the present calculation.[4] The reagent, the enolate anion, was always the same throughout the present experiments. Also assuming H_{rs} to be constant, we can now evaluate the value of $(CTA)_s=\sum_{k}^{VAC}[(C^{S}_{N.k})^2/(\varepsilon_{E.HO}-\varepsilon_{N.k})]$. The $\varepsilon_{E.HO}$ may be put as a constant in all the calculations.[4] Thus, the CTA value (charge-transfer ability) can be used as a measure of the selectivity of the reaction position, to which the first bond is formed to bring about the nucleophilic reaction of the enolate anion with nitriles. Note that the CTA value has a physical meaning very similar to the nucleophilic superdelocalizability.[5] The calculation was done using the PPP SCFMO method of π electron approximation. The parameters pertinent to each atom and each bond were determined by referring to many previous studies.[6] The π-electron energy for the enolate anion was obtained using the molecular model in Fig. 1; we know that the $\varepsilon_{E.HO}$ is shallow in energy,[7] so the CT to $\varepsilon_{N.k}$ from $\varepsilon_{E.HO}$ is the most important one, and, also, the CH_2-group carbon atom in the enolate anion may be the most likely to attack nitriles, because the MO corresponding to $\varepsilon_{E.HO}$ is mainly localized on the CH_2 group πAO.

The calculation results of the CTA values at each atom of various kinds of nitriles are given in Table 1. The nitrile, which has a CTA value at the nitrile carbon atom larger than $|\approx 0.195|$ throughout all the nitriles examined, and which is also larger than those of any other atoms in the nitrile in question, was quite reactive with the enolate anion in producing the final enamino ketone, according to the reasonable reaction shown in Scheme 1. However, in a case such as 3-cyanopyridine, the CTA values at the 2, 4, and 6 carbons were quite large compared with those of the other atoms in the molecule. Thus, there are three cases for the reaction of this kind of molecule with the enolate anion; the first two are the formation of byproducts caused by a reaction at the suitable ring atoms and a decrease in the yield of enamino ketones, while there is no reaction in the third case. In view of the above findings, the CTA values obtained here seem

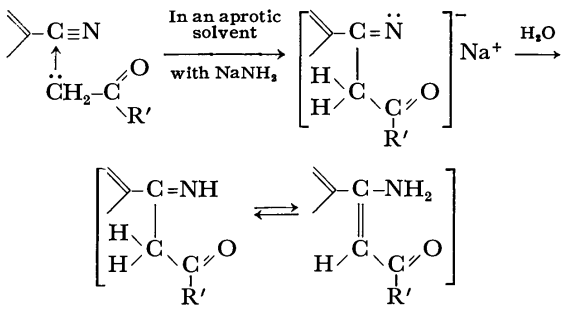

Scheme 1.

TABLE 1. THE CALCULATED RESULTS OF CTA VALUES (eV^{-1}) AT EACH ATOM, AND THE TOTAL ELECTRON DENSITIES IN THE $\overset{*}{\rangle C}-C\equiv N$ GROUP (ρ^t) AND AT THE C* ATOM (ρ^*)

Compound No.[a]		CTA[b] 1	2	3	4	5	6	7	8	$\rho^*(C^*)$[c]	ρ^t (C^*+C+N)[d]	Yield[e] (%)
I		0.177	0.200	0.175	0.201	0.175	0.200	0.195	0.177	3.961	13.045	g)
II	2CN	0.182	0.204	0.199	0.202	0.204	0.194	0.200	0.190	3.884	12.957	78.6
	3CN	0.159	0.220	0.179	0.230	0.177	0.226	0.198	0.181	3.984	13.064	g)
	4CN	0.185	0.199	0.205	0.209	0.205	0.199	0.207	0.198	3.929	13.007	48.7
III		0.217	0.214	0.223	0.189	0.238	0.202	0.205	0.197	3.907	12.976	g)
IV	2CN	0.180	0.229	0.180	0.222	0.204	0.222	0.205	0.201	3.811	12.868	40.5
	4CN	0.187	0.212	0.187	0.243	0.203	0.231	0.214	0.213	3.855	12.922	75.0 (2, 6-Me_2)[b]
	5CN	0.160	0.248	0.160	0.254	0.181	0.254	0.201	0.184	4.006	13.083	f, g) (2, 4-Me_2)[b]
V	2CN	0.065	0.149	0.165	0.124	0.176	0.196	0.172	—	3.860	12.930	90.0
	3CN	0.060	0.187	0.120	0.131	0.152	0.176	0.146	—	3.997	13.076	f)
VI	2CN	0.077	0.146	0.162	0.123	0.175	0.191	0.167	—	—	—	g, j)
	3CN	0.070	0.184	0.119	0.130	0.150	0.173	0.142	—	—	—	g, j)
VII	3CN	0.072	0.177	0.161	0.129	0.182	0.190	0.168	—	3.761	12.915	85.5 (5-Me)[b]
	4CN	0.072	0.142	0.166	0.121	0.222	0.181	0.150	—	3.954	13.173	f, g) (3, 5-Me_2)[b]
	5CN	0.081	0.168	0.160	0.169	0.186	0.211	0.196	—	3.927	12.857	85.6 (3-Me)[b]
VIII	2CN	0.072	0.180	0.146	0.127	0.173	0.210	0.194	—	3.850	12.822	73.8 (5-Me)[b]
	4CN	0.061	0.177	0.114	0.125	0.183	0.175	0.146	—	4.091	13.042	h)
	5CN	0.068	0.203	0.109	0.169	0.146	0.196	0.172	—	3.794	13.003	29.5 (2, 4-Me_2)[b]
IX	3CN	0.187	0.215	0.211	0.235	0.204	0.230	0.206	0.197	3.904	12.917	h, j)
	4CN	0.224	0.193	0.227	0.226	0.251	0.203	0.214	0.209	3.951	13.024	—
X		0.077	0.182	0.153	0.114	0.204	0.213	0.197	—	—	—	—
XI		0.093	0.226	0.175	0.172	0.179	0.198	0.180	—	3.919	12.979	88.2 (4-Me)[b]
XII	2CN	0.254	0.300	0.294	0.279	0.310	0.268	0.209	0.232	3.962	13.003	12.3[b]
	3CN	0.217	0.314	0.291	0.318	0.264	0.333	0.236	0.249	3.933	12.990	—
	4CN	0.280	0.282	0.306	0.319	0.306	0.282	0.242	0.263	3.980	13.056	—

a) The formula and numbering for each substance are as follows:

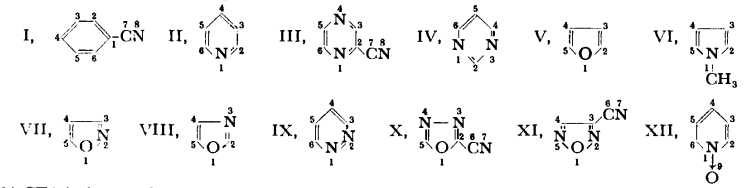

b) CTA is the negative value. The absolute values are given in this Table. c) CNDO/2 total electron density at the C* atom bound to the CN group. d) The sum of the CNDO/2 total electron density on each atom in the $\overset{*}{\rangle C}-C\equiv N$ group. e) See Reference 1 in text. f) Side reactions occurred. g) The starting nitrile was recovered. h) Ring cleavage occurred. i) These mean the methyl substituted compounds which were used as starting materials to prevent the ring cleavage in the reaction process. j) Unpublished data.[1]

to give a reasonable reaction index for interpreting the experimental results (Table 1) except for the cases of a few molecules. With 2- and 4-cyanopyrimidines, the largest CTA value is at the carbon (C*) to which the CN group is bound, in spite of the considerable yield of the enamino ketone. One reason for this may be the several approximations employed in deriving the CTA values, especially the hypothesis of a constant H_{rs}, since the geometrical configuration of the reaction intermediate would not be the same for all nitriles.[8] Another possibility is that the electron density, the CTA value, *etc.*, at the C* atom may also contribute more or less to the reaction process (*vide infra*). Alternatively, the CTA value (0.190) at the nitrile carbon atom of 3-cyanoisoxazole is less than 0.195 (*vide supra*), but the largest among those for the other atoms in the molecule. Since this molecule gives the enamino ketone, the reason may be that the total electron densities in the $\rangle C-C\equiv N$ group are quite small, as the calculations employing the CNDO/2 method *etc.* have shown (Table 1), so that the reaction centers of the enolate anion and the $C-C\equiv N$ group easily become close enough to initiate the reaction by the charge transfer-process.

References

1) T. Honma and Y. Tada, *Heterocycles*, **6**, 1985 (1977).

2) N. Mataga and T. Kubota, "Molecular Interactions and Electronic Spectra," Marcel Dekker, New York (1970), Chap. 6.

3) S. Iwata, J. Tanaka, and S. Nagakura, *J. Am. Chem. Soc.*, **88**, 894 (1966).

4) If the $V_{N\cdot k}^{E\cdot HO}$ term is taken into consideration, the absolute values of CTA become larger than those given in Table 1. As was found in the interpretation of a series of CT spectra,[2] the contribution from the electrostatic interaction energies may be put as a constant. Then, the conclusion derived from the present calculation may not change.

5) K. Fukui, T. Yonezawa, and C. Nagata, *Bull. Chem. Soc. Jpn.*, **27**, 423 (1954), *ect.*

6) M. Yamakawa, K. Ezumi, Y. Mizuno, and T. Kubota, *Bull. Chem. Soc. Jpn.*, **47**, 2982 (1974), *ect.*

7) a) S. Nagakura and J. Tanaka, *J. Chem. Phys.*, **22**, 563 (1954); b) S. Nagakura, *Tetrahedron*, **19**, Suppl. 2, 361 (1963).

8) Nagakura derived the other reaction indexes from the extension of the CT theory.[7] In the case of a nucleophilic reaction, the free valency, localization energy, *etc.* for the anion species of the reactant are important. An examination based on these indices would also be needed.

BULLETIN OF THE CHEMICAL SOCIETY OF JAPAN, VOL. 51 (10), 3061—3062 (1978)

Kinetic Evidence for the Participation of a Diatomic Oxygen Species in Vapor-Phase Oxidation of Butadiene over Silver Catalyst

Masamichi AKIMOTO* and Etsuro ECHIGOYA

Department of Chemical Engineering, Tokyo Institute of Technology, Ookayama, Meguro-ku, Tokyo 152

(Received February 15, 1978)

Synopsis. The participation of an adsorbed diatomic oxygen species in the oxidation of butadiene with O_2 or N_2O to maleic anhydride over silver catalyst was confirmed by the following finding: reaction order with respect to O_2 or N_2O is 0.83 or 1.95, respectively, whereas that to butadiene is negative.

Formation of O_2^- over reduced silver metal has been confirmed by means of ESR.[1-4] There are some observations showing that the diatomic oxygen species is active for epoxide formation.[4-7] However, no concrete evidence has been reported for the formation of the electronegative oxygen species during the course of oxidation of hydrocarbons over reduced silver metal. Our studies on the oxidation of furan over promoted anatase-titania catalyst revealed incorporation of oxygen atoms into maleic anhydride *via* the formation of O_2^-.[8] In this work, the formation of maleic anhydride in vapor-phase oxidation of butadiene with oxygen or nitrous oxide N_2O over silver catalyst has been kinetically investigated in order to confirm the formation of O_2^- during the oxidation.

Experimental

Vapor-phase catalytic oxidation of butadiene was carried out at 560—680 K using a conventional flow type fixed-bed reactor under atmospheric pressure. The shape of reactor and method of reaction were the same as those reported, and H_2O and CO_2 contained in air were removed in the same way as described.[8] Research grade butadiene (purity >99.9%) was used. Nitrogen, H_2, He and N_2O were supplied from commercial cylinders. Gas chromatographic analysis indicated a trace ($\approx$0.4 vol%) of O_2 in the N_2O. The silver catalyst was prepared by reacting $AgNO_3$ with NaOH in an aqueous medium followed by the reduction of the silver oxide formed with 36% formalin at pH=11$\pm$0.5.[9] The surface area was $<1.0\ m^2\ g^{-1}$. The catalyst was reduced with H_2 (100 NTPml min^{-1}) at 583 K for 1.0 h prior to the experiment. The gaseous effluent from the reactor was analyzed by gas chromatography.[8] Since maleic anhydride was confirmed to be the only acid formed, the anhydride was absorbed in water, followed by boiling of the solution in order to remove dissolved CO_2 and by titration with an aqueous solution of NaOH. Carbon monoxide was not analyzed. X-Ray diffraction study was carried out using nickel-filtered Cu $K\alpha$ radiation (30 kV, 20 mA).

Results

Table 1 shows the effect of reaction temperature on the oxidation of butadiene over silver catalyst. The reaction initiated at $\approx$560 K. However, butadiene was preferentially converted into CO_2 with low yields of 2,5-dihydrofuran (2,5-DHF), furan (F) and maleic anhydride (MA). The selectivity to 2,5-dihydrofuran was negligible above 602 K but that to furan decreased gradually in contrast to that to maleic anhydride.

Table 1. Effect of the reaction temperature on the oxidation of butadiene over silver catalyst[a]

Reaction temp (K)	Conversion of C_4'' (%)	Yield of CO_2 (%)	Selectivity (%)		
			2,5-DHF	F	MA
561	1.4	0.2	8.3	8.3	5.1
578	5.4	2.2	15.2	4.0	5.3
591	21.0	17.1	1.0	1.2	6.6
602	34.2	31.1	0.0	0.9	6.7
612	39.0	34.0	0.0	1.0	7.8
630	40.7	35.5	0.0	0.7	7.6

a) Feed concentration: C_4'' 3.82 vol %, O_2 10.0 vol%, Contact time W/F: 0.202 g-cat·h g-mol^{-1}.

The steady state of silver catalyst during the course of oxidation at 583 K, W/F=0.249 g-cat·h g-mol^{-1} and the feed concentration of butadiene 3.85 vol % and O_2 10.0 vol % was quenched by introduction of helium (200 NTPml min^{-1}) for 5 min to eliminate the reactant gas followed by rapid decrease in temperature. X-Ray diffraction revealed that the catalyst consists of silver metal (2θ=38.15, 44.34, and 64.45°) and a small amount of Ag_2O (2θ=26.71°) and Ag_2O_2 (2θ=34.20 and 37.26°). This structure was kept even when the feed concentration of O_2 was increased to 14.0 vol % and the temperature to 635 K. Oxidation of butadiene with Ag_2O at 551 K by means of pulse technique gave only CO_2 and a small amount of acrylaldehyde.

The rate of maleic anhydride formation was kinetically studied using a differential reactor:

$$r(\mathrm{MA}) = k_1[C_4'']^{-0.21}[O_2]^{0.83} \quad \text{at 573 K} \qquad \text{(A)}$$

overall activation energy=32.3 kcal g-mol^{-1}
C_4'': 3.3—7.8 vol %, O_2: 7.0—14.6 vol %

where

Table 2. Oxidation of butadiene with N_2O over silver catalyst[a]

Reaction temp (K)	Conversion of C_4'' (%)	Selectivity (%)		
		2,5-DHF	F	MA
606	7.9	0.8	0.0	2.0
633	13.4	1.2	0.0	4.1
637	17.7	1.3	0.0	4.6
660	49.1	1.1	0.0	4.9
679	45.6	0.8	0.0	4.1

a) Feed concentration: C_4'' 3.94 vol%, N_2O 20.0 vol%. Contact time W/F: 0.200 g-cat·h g-mol^{-1}. Yield of CO_2 was not determined because the retention times of CO_2 and N_2O were the same.

r(MA): initial rate of maleic anhydride formation,
k_1: overall reaction rate constant,
[ ]: concentration of butadiene or O_2 in the feed.

Formation of 2,5-dihydrofuran and maleic anhydride was also observed in the oxidation with N_2O (Table 2). Conversion of butadiene reached 49.1% at 660 K, but the selectivity to these oxidation products was low. The rate of maleic anhydride formation:

$$r(\mathrm{MA}) = k_2[\mathrm{C_4''}]^{-0.20}[\mathrm{N_2O}]^{1.95} \quad \text{at 613 K} \qquad (\mathrm{B})$$

overall activation energy = 28.5 kcal g-mol^{-1}
C_4'': 3.9—8.6 vol %, N_2O: 20.0—30.0 vol %

Discussion

The maximum conversion of butadiene (Tables 1 and 2) was attributed to the almost total consumption of O_2 or N_2O in the feed. 2,5-Dihydrofuran was postulated to be the first intermediate for maleic anhydride formation from butadiene: anhydride is formed from 2,5-dihydrofuran through two reaction paths, one *via* furan and the other *via* a direct path from 2,5-dihydrofuran.[10] Furan and maleic anhydride formation is in line with the above reaction mechanism. On the other hand, a negligible change was observed in the structure of silver catalyst with rise in oxygen concentration in the feed and with rise in temperature. No selective oxidation products in the reduction of Ag_2O with butadiene at 551 K suggests an important role of adsorbed oxygen species formed on metallic silver in the formation of 2,5-dihydrofuran, furan and maleic anhydride. Our previous studies on the formation of maleic anhydride from butadiene show that the activation energy for 2,5-dihydrofuran formation is the highest, the step thus being rate-determining.[10] Hence, the negative reaction order with respect to butadiene (A) indicates a competitive adsorption of butadiene with gaseous oxygen on the surface. The reaction of adsorbed species resulted in maleic anhydride formation. Accordingly, the reaction order with respect to gaseous oxygen, 0.83, is a strong indication of the reaction between an adsorbed diatomic oxygen species and adsorbed butadiene. Similarly, the negative reaction order with respect to butadiene (B) shows that the anhydride is formed through the Langmuir-Hinshelwood mechanism in the oxidation with N_2O as in the case with gaseous oxygen. Furthermore, as judged from the formation of O_2[11] and O_2^- [2] in the catalytic decomposition of N_2O over reduced silver metal, the reaction order of N_2O, 1.95 (B), is an evidence for the participation of an adsorbed diatomic oxygen species in the anhydride formation.

Olefinic hydrocarbons adsorbed on metal oxide generally have positive charge.[12] Since the surface of silver catalyst during the oxidation of butadiene is partially oxidized as shown elsewhere in this paper, the adsorbed butadiene species seems to be positively charged. It has not been clarified what kind of charge the adsorbed diatomic oxygen species has. However, judging from the ESR observation of O_2^- [1-4] and the addition of O_2^- to positively charged adsorbed furan species over promoted anatase-titania catalysts through a nucleophilic mechanism,[8] the diatomic oxygen species seems to be O_2^-. The reaction of adsorbed neutral oxygen molecule ($^3\Sigma_g^-$) with adsorbed butadiene seems to be less probable, since the former is electrophilic and less nucleophilic as judged from the electron affinity of 0.15 eV,[13] but it can not be denied either. The present work indicates the presence of an adsorbed diatomic oxygen species and its participation in the selective oxidation of butadiene over reduced silver catalyst. Oxygen atoms are possibly incorporated into maleic anhydride *via* the formation of this oxygen species. The oxygen species which promotes the complete oxidation of butadiene and serves to abstract hydrogen in maleic anhydride formation has not been clarified.

References

1) R. B. Clarkson and A. C. Cirillo, Jr., *J. Vac. Sci. Technol.*, **9**, 1073 (1972).
2) N. Shimizu, K. Shimokoshi, and I. Yasumori, *Bull. Chem. Soc. Jpn.*, **46**, 2929 (1973).
3) R. B. Clarkson and A. C. Cirillo, Jr., *J. Catal.*, **33**, 392 (1974).
4) S. Tanaka and T. Yamashina, *J. Catal.*, **40**. 140 (1975).
5) L. Ya. Margolis, *Adv. Catal.*, **14**, 429 (1967).
6) L. Imre, *Ber. Bunsenges. Phys. Chem.*, **72**, 863 (1968); **74**, 220 (1970).
7) S. Shikagawa, H. Tokunaga, and T. Seiyama, *Kogyo Kagaku Zasshi*, **74**, 819 (1971).
8) M. Akimoto and E. Echigoya, *J. Chem. Soc., Faraday Trans. 1*, **73**, 193 (1977).
9) T. Gotō, S. Shimatake, I. Hara, and Y. Aono, Japan Patent, 9259 (1963).
10) M. Akimoto and E. Echigoya, *Bull. Chem. Soc. Jpn.*, **48**, 3518 (1975).
11) W. Herzog, *Ber. Bunsenges. Phys. Chem.*, **74**, 216 (1970).
12) E. Kh. Enikeev, O. V. Isaev, and L. Ya. Margolis, *Kinet. Katal.*, **1**, 431 (1960).
13) R. S. Mulliken, *Phys. Rev.*, **115**, 1225 (1959).

BULLETIN OF THE CHEMICAL SOCIETY OF JAPAN, VOL. 51 (10), 3063—3064 (1978)

The Raman Spectra of Diazines Adsorbed on Silicas

Yoichiro YAMAMOTO and Haruka YAMADA*

Department of Chemistry, Kwansei Gakuin University, Nishinomiya 662

(Received March 14, 1978)

Synopsis. The Raman spectra of three diazines adsorbed on silicas have been measured. Spectra changes upon adsorption are interpreted as the result of hydrogen-bond formation between the surface OH group and the N atom of diazine. The order of the shifts of the Raman bands between three diazines is: 1,3-diazine>1,4-diazine>1,2-diazine.

Raman spectroscopy has recently been applied to the study of adsorbed species on solids, and the spectra of adsorbed pyridine have been measured considerably.[1-4] For the elucidation of the adsorption sites and the interactions between adsorbents and adsorbates, it is desirable to study the Raman spectra of several types of basic molecules in comparison with those of adsorbed pyridine. The present work will report on the Raman spectra of three diazines, 1,2-diazine (pyridazine), 1,3-diazine (pyrimidine), and 1,4-diazine (pyrazine), adsorbed on silicas.

Guaranteed reagents of 1,2-diazine and 1,3-diazine were obtained from the Tokyo Kasei Co. and a guaranteed reagent of 1,4-diazine, from the Nakarai Chem. Co.

Silica gel (*ca.* 20 mesh) was obtained from the Wako Chem. Co., and porous Vycor glass plate (Corning Glass No. 7930; 1 mm thick), from the Corning Glass Works. They were used after degassing, heating, and oxygen treatment, as has been described previously.[4,5] The surface area after the pretreatment was 620 m^2/g for the silica gel and 170 m^2/g for the porous Vycor glass. Gaseous diazine was adsorbed on the pretreated silica, and then the sample was evacuated for 0.5—30 min.

The Raman spectra were measured with a Jasco R-300 spectrophotometer equipped with an argon ion laser JEOL-04. The 488.0 nm excitation line and the 90° sample illumination were employed.[4]

The observed Raman spectra are shown in Fig. 1. The peak frequencies, with the relative intensities, are listed in Table 1, together with those of the liquids and CCl_4 solution (this work). The Raman spectrum of

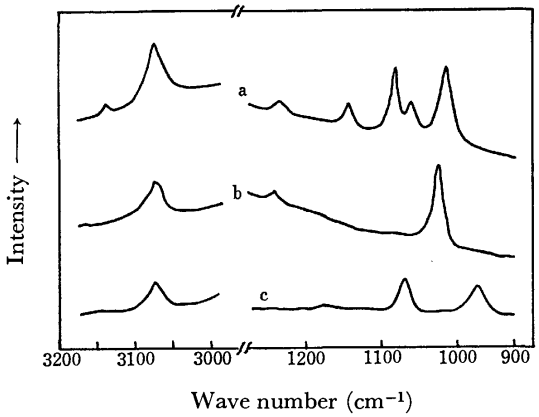

Fig. 1. Raman spectra of diazines adsorbed on silica gel; (a) 1,3-diazine, (b) 1,4-diazine, and (c) 1,2-diazine.

1,3-diazine adsorbed on the silica gel is quite similar to that of pyridine adsorbed on the silica gel. The ring-stretching band at 993 cm^{-1} shifts by 17 cm^{-1} to a higher frequency side from that of the liquid 1,3-diazine, while the CH stretching band at 3060 cm^{-1} shifts by 15 cm^{-1}. These shifts are a little larger than those observed for the pyridine adsorbed on the silica gel, 16 and 9 cm^{-1} respectively, and are interpreted as representing the hydrogen-bond formation between the surface OH group and the N atom of 1,3-diazine.

The shifts observed for 1,4-diazine and 1,2-diazine are smaller than those for 1,3-diazine. The spectra observed on the porous Vycor glass are almost the same as those observed on the silica gel. The Raman shifts observed, upon adsorption, on the silica gel are in the order of:

1,3-diazine > pyridine > 1,4-diazine > 1,2-diazine,

in agreement with the order of adsorption strength based on the upper limit temperatures of adsorption reported by Pichat:[6] 1,3-diazine 1,4-diazine 1,2-diazine. This

TABLE 1. RAMAN SPECTRA OF DIAZINES ADSORBED ON SILICA GEL (cm^{-1})

Assignment[a]	1,3-Diazine		1,4-Diazine		1,2-Diazine	
	Adsorbed	Liquid	Adsorbed	CCl_4 soln	Adsorbed	Liquid
Ring deform	681 (16)	680 (11)	703 (14)	708 (17)		670 (22)
Ring stretch	1010 (100)	993 (100)	1021 (100)	1019 (100)	968 (100)	968 (100)
Ring stretch	1056 (56)	1057 (36)				
CH deform	1078 (86)	1077 (35)			1068 (100)	1068 (103)
CH deform	1140 (18)	1142 (12)				1165 (62)
CH deform	1230 (21)	1231 (9)	1240 (10)	1235 (9)		1290 (10)
Ring stretch	1570 (12)	1570 (15)	1532 (14)	1531 (5)		
Ring stretch			1580 (9)	1580 (14)		1570 (23)
CH stretch	3075 (63)	3060 (53)	3075 (46)	3063 (50)	3075 (86)	3062 (118)

a) F. R. Dollish, W. G. Fateley, and F. F. Bentley, "Characteristic Raman Frequencies of Organic Compounds," Wiley Interscience, New York (1974), p. 274.

also corresponds to the order of the π-electron density of the N atom for the basic molecules,[7] but differs from the order of the first ionization potentials or the pK_a:[8]

pyridine $>$ 1,2-diazine $>$ 1,3-diazine $>$ 1,4-diazine.

Consequently, 1,3-diazine may be used, instead of pyridine, as a basic molecule for the study of adsorption on solid surfaces.

References

1) P. J. Hendra, *Spex Speaker*, **XIX**, 1 (1974); P. J. Hendra, J. R. Horder, and E. J. Loader, *J. Chem. Soc., A*, **1971**, 1766; P. J. Hendra and E. J. Loader, *Trans. Faraday Soc.*, **67**, 828 (1971).

2) R. P. Cooney, G. Curthoys, and N. T. Tam, *Adv. Catal.*, **24**, 293 (1975).

3) T. A. Egerton and A. H. Hardine, *Catal. Rev.*, **11**, 71 (1975).

4) T. Nagasao and H. Yamada, *Chem. Lett.*, **1974**, 1045.

5) T. Nagasao and H. Yamada, *J. Raman Spectrosc.*, **3**, 153 (1975).

6) P. Pichat, *J. Phys. Chem.*, **78**, 2376 (1974).

7) L. E. Orgel, T. L. Cottrell, W. Dick, and L. E. Sutton, *Trans. Faraday Soc.*, **47**, 113 (1951).

8) G.Briegleb,"Elektronen-Donator-Acceptor-Komplexe," Springer-Verlag, Berlin (1961), p. 156.

BULLETIN OF THE CHEMICAL SOCIETY OF JAPAN, VOL. 51 (10), 3065—3066 (1978)

Dipole Moments of Molecules Containing Single Chlorine Atoms

Masaaki SUGIE,* Harutoshi TAKEO, and Chi MATSUMURA

National Chemical Laboratory for Industry, Honmachi, Shibuya-ku, Tokyo 151

(Received April 4, 1978)

Synopsis. The dipole moments of CD_2ClF, CHDClF, CH_3CHClF, $CH_3CCl{=}CH_2$, and DCOCl have been determined from the $J=1\leftarrow0$ transitions of their microwave spectra. For the analyses of the Stark effects, the method of the intermediate field case proposed by Mizushima has been used.

In our laboratory the structures of halogeno-substituted hydrocarbons have been systematically investigated. These studies have clarified that the C–C, C–Cl, and C–F bond lengths are shortened regularly with further substitution of the chlorine or fluorine atoms for the hydrogen atoms,[1,2] and that the nuclear quadrupole coupling constants of Cl are mutually related to the bond lengths of C–Cl to a certain degree. It would be interesting to examine how the dipole moment of a molecule is influenced by the structure, whereas the informations on dipole moments are not enough for this purpose because of lack of the precise data for molecules containing atoms with nuclear quadrupoles. In the present work the dipole moments of some molecules containing single chlorine atoms are determined.

The Stark shift of the transition frequency was measured by using a d.c. voltage with a superimposed small a.c. voltage on the electrode plate inserted in the waveguide. Fluke 415B was used for the supply of a d.c. voltage, and the peak to peak height of an a.c. voltage was measured with Takeda TR-6334 digital voltmeter. The center frequency of a shifted spectral line was obtained as the zero-crossing point of the output of the phase-sensitive detector. The electrode spacing was calibrated by the Stark shift of the $J=2\leftarrow1$ transition of OCS[3] and determined to be 0.486 ± 0.002 cm.

From the viewpoint of analysis it is desirable to determine the dipole moment from the Stark shift of the $J=1\leftarrow0$ transition in the case of a molecule which has a rotational spectrum with hyperfine structure. Since the $J=1\leftarrow0$ transitions of CD_2ClF, CHDClF, CH_3CHClF, and $CH_3CCl{=}CH_2$ fall into a suitable frequency region, their dipole moments were determined in the present study. The dipole moment of DCOCl,[2] which had been determined with the weak field approximation, was re-determined in order to refine the value.

Generally speaking, the Stark components of asymmetric-top molecules shift proportionally to the square of the electric field strength. For a molecule with nuclear quadrupole coupling, the proportionality breaks down when the applied electric field is so strong that the Stark shift is comparable to or slightly larger than the splitting due to quadrupole coupling interaction.

The Stark effect of a molecule containing a single chlorine atom can be estimated by the method proposed by Mizushima, *i.e.*, the method of the intermediate field case.[4] The energy levels are characterized by the set of good quantum numbers J, I, M_J, M_I, and the pseudoquantum number τ. The shifts of an energy level due to the Stark effect are given as solutions of the following secular equation

$$|(J, \tau, I, M_J, M_I|H_Q|J, \tau, I, M_J', M_I') + (E_{J,\tau,I=0,M}-E)\delta_{M_J,M_J'}\delta_{M_I,M_I'}| = 0.$$

In the above equation, the first and the second terms represent the splitting due to nuclear quadrupole coupling and the Stark shift in case the nuclear quadrupole is absent, respectively. Kellogg *et al.* gave the matrix elements in the first term, which do not vanish only if $M_J+M_I=M_{J'}+M_{I'}$.[5] The secular equation is factorized into blocks for each value of $M(=M_J+M_I)$, which can be easily solved.

The dipole moment of DCOCl was determined from the measurements of the shifts for five Stark components of the $1_{11}\leftarrow0_{00}$ by a least squares fit. The result is given in Table 1, which shows a marked improvement of the accuracy compared to the values of $\mu_a=0.3(2)$ and $\mu_b=1.6(2)$ previously determined by using the weak field approximation.

The dipole moments of CD_2ClF, CHDClF, and CH_3CHClF were determined by observing $1_{11}\leftarrow0_{00}$ transitions with an electric field of 200—800 V/cm, and that of $CH_3CCl{=}CH_2$ was determined from the $1_{01}\leftarrow0_{00}$

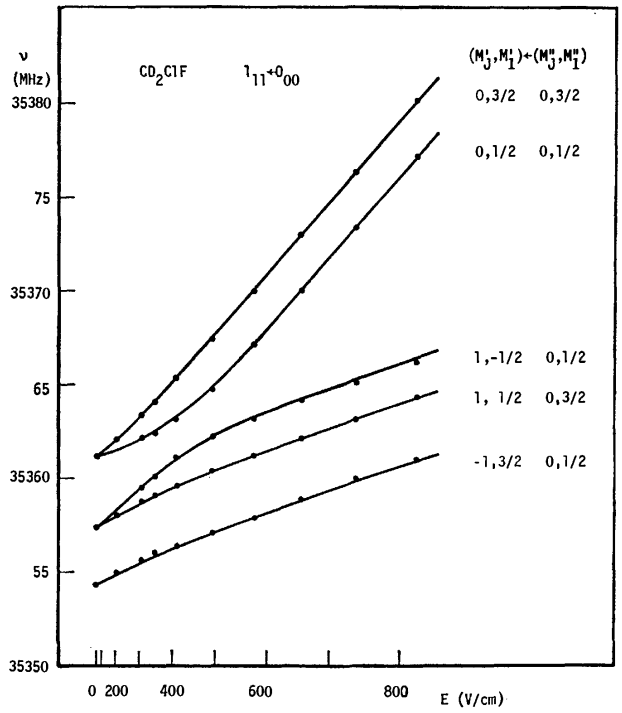

Fig. 1. The Stark shifts of CD_2ClF. The circles denote the measured displacements and the solid lines are theoretical ones.

Table 1. Dipole moments and their components (Debye)

Molecule	μ_a	μ_b	μ_c	μ_{total}
DCOCl	0.322(3)	1.780(15)	—	1.809(15)
CD_2ClF	0.302(3)	1.810(10)	—	1.834(10)
CHDClF	0.279(2)	1.787(10)	0.198(13)	1.819(10)
CH_3CHClF	0.953(8)	1.836(15)	0.013(24)	2.068(14)
$CH_3CCl{=}CH_2$	1.633(10)	0.211(14)	—	1.647(10)

transition with an applied field of 200—1000 V/cm. The Stark shifts of the $1_{11}\leftarrow 0_{00}$ transition for CD_2ClF are shown in Fig. 1 as a typical example. The dipole moments and their components determined by least squares fitting are given in Table 1. The limits of error were estimated by adding the errors due to the uncertainty of the applied electric fields to three times the standard deviations in the analysis.

The molecule which contains an atom with a nuclear quadrupole has the advantage that all the components of the dipole moment can be determined from the $J=1\leftarrow 0$ transition alone.[6] In addition, the analysis with the intermediate field approximation has been proved to give a sufficiently accurate dipole moment. In fact, the μ_c component of CHDClF could be determined, as shown in Table 1, although it has a rather large relative error because the energy levels which interact with the 0_{00} or 1_{11} level through the μ_c component are separated considerably. The dipole components of CHDClF obtained are consistent with the values calculated from those of CD_2ClF by rotation of the principal axes.

References

1) H. Takeo and C. Matsumura, *Bull. Chem. Soc. Jpn.*, **50**, 636 (1977).
2) H. Takeo and C. Matsumura, *J. Chem. Phys.*, **64**, 4536 (1976).
3) J. S. Muenter, *J. Chem. Phys.*, **48**, 4544 (1968).
4) M. Mizushima, *J. Chem. Phys.*, **21**, 539 (1953).
5) J. M. B. Kellogg, I. I. Rabi, N. F. Ramsey, Jr., and J. R. Zacharias, *Phys. Rev.*, **57**, 677 (1940).
6) E. Hirota and Y. Morino, *Bull. Chem. Soc. Jpn.*, **34**, 341 (1961).

BULLETIN OF THE CHEMICAL SOCIETY OF JAPAN, VOL. 51 (10), 3067—3068 (1978)

Solubility and Diffusion Coefficient of Sulfur in Silver

Kazuo FUEKI, Kenichiro OTA,* and Kohji KISHIO

Department of Industrial Chemistry, Faculty of Engineering, The University of Tokyo, Hongo, Bunkyo-ku, Tokyo 113

(Received April 10, 1978)

Synopsis. The solubility N_s and the diffusion coefficient D of sulfur in silver were determined at 604—752 °C by means of a previously proposed method.[1] The results can be represented by the following equations:

$$\log N_s(\text{atom fraction}) = -0.818 - \frac{2.28\times10^3}{T},$$

$$D = 2.34 \times 10^{-3} \exp\left(-\frac{26300}{RT}\right) \text{ cm}^2\text{ s}^{-1}.$$

In the high temperature oxidation of alloys, the rate is significantly affected by the formation of an internal oxidation layer. Since this internal oxidation is caused by the diffusion of oxygen atoms into the alloy from the metal-oxide interface and the formation of dispersed particles of the less noble constituent, the knowledge of the solubility and the diffusion coefficient of oxygen in the alloy are necessary in order to analyze the oxidation rate of alloys.

Similarly, the solubility and the diffusion coefficient of sulfur in metals must be known to study the sulfidation of alloys. The solubility of sulfur can be determined by the combustion method and the vacuum fusion method. The solubility and diffusion coefficient can be measured by means of the tracer method, X-ray diffraction method, and the electrochemical method using solid electrolytes. However, these methods are rather complicated.

Fueki and Ouchi have studied the solubility and the diffusion coefficient of sulfur in copper by a new method wherein a thin cuprous sulfide film was formed on copper specimens and the decrement of the film after diffusion annealing was determined by the coulometric method.[1] In the present study the solubility and the diffusion coefficient of sulfur in silver were determined by the method proposed by Fueki and Ouchi and compared with data obtained by other methods.

Experimental

The experimental method employed was similar to that of the study on the solubility and diffusion of sulfur in copper.[1] Rectangular silver specimens, 15 mm×6 mm in area and 0.015—0.02 mm in thickness, were used. The result of the chemical analysis of silver is given in Table 1. The specimens were polished with alumina polishing powder, rinsed in alcohol, and dried in a desiccator. The surface of the specimen was anodized in a 2 g/l-Na_2S solution at a current density of 10^{-1} mA/cm² to form a thin sulfide film. The surface film thickness was determined by means of the coulometric method.

Table 1. Results of chemical analysis

Impurity	Content (wt %)
Cu	0.060
Si	0.0039
Fe	0.00062

The silver specimen covered with silver sulfide was placed in a Vycor tube, which was then evacuated to 10^{-4} Torr and sealed. The sealed tube was placed in an electric furnace kept at the desired annealing temperature (within±2 °C). After a length of time the tube was taken out from the furnace and the thickness of the remaining sulfide film was determined coulometrically. The specimen was immersed in a 0.1M-KCl solution and the surface sulfide was reduced cathodically at a constant current density of 10^{-1} mA/cm². From the reflection point of the potential-time curve, the electric charge necessary for the reduction of sulfide was calculated.

During annealing, the silver sulfide on the surface decomposes into sulfur and silver and the sulfur diffuses into silver; thus

$$Ag_2S(\text{film}) = 2Ag + S(\text{in Ag}). \quad (1)$$

The amount of sulfur $\bar{N}_t$ (atom fraction) in silver after annealing was calculated from the difference between the initial and final amounts of sulfide film. The solubility of sulfur N_s was obtained from the saturation value of the $\bar{N}_t$-t plot.

When a silver specimen is covered with a thin sulfide film and sulfur is allowed to diffuse from both surfaces of the specimen, the diffusion is expressed by the following equation:[1]

$$\log\frac{N_s-\bar{N}_t}{N_s} = \log\left(\frac{8}{\pi^2}\right) - \frac{\pi^2 D}{2.303}\left(\frac{t}{l^2}\right), \quad (2)$$

where l is the thickness of the specimen and D is the diffusion coefficient of sulfur in silver. Therefore, the diffusion coefficient can be determined from the slope of the plot of log $\{(N_s-\bar{N}_t)/N_s\}$ against t/l^2.

Results and Discussion

Figure 1 shows the amount of sulfur in silver $\bar{N}_t$ plotted against t/l^2 and Fig. 2 gives the Arrhenius plots for N_s. The data obtained by the previous investigators are also plotted in the same figure. Barbouth *et al.* used the radio isotope ^{35}S to measure the solubility.[2] Raub

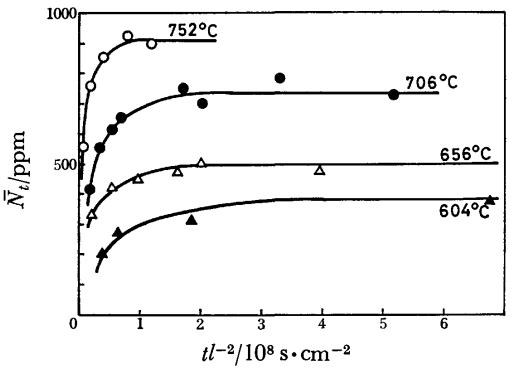

Fig. 1. Solubility of sulfur in silver.

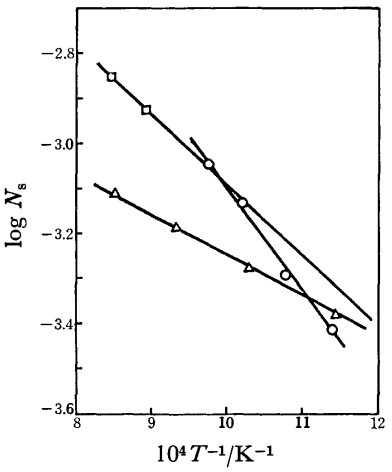

Fig. 2. Arrhenius plot of solubility of sulfur in silver.
○ This work, △ Barbouth,[2] □ Raub.[3]

measured the sulfide formation temperature during the cooling of a silver–sulfur solution and determined the solubility.[3] The data of the present work agree well with the other two. The solubility of the present work is represented by the following equation:

$$\log N_s = -0.818 - 2.28 \times 10^3 \left(\frac{1}{T}\right). \quad (3)$$

From Eq. 3 the enthalpy and entropy change for the dissolution of sulfur in silver were calculated. They are as follows:

$$\Delta H^\circ = 10.4 \text{ kcal/mol}$$

$$\Delta S^\circ = -3.74 \text{ cal/mol·deg.}$$

Figure 3 shows the relation between $\log\{(N_s - N_t)/N\}$ and t/l^2. The diffusion coefficient D of sulfur was determined from the slope of the plot. Figure 4 shows the Arrhenius plot of D. For comparison, Barbouth's results obtained by the tracer method[4] and Wang's results obtained by means of the relaxation method[5] are shown in the same figure. These results agree with each other. The Arrhenius equation for the present work is

$$D = 2.34 \times 10^{-3} \exp\left(-\frac{26300}{RT}\right) \text{ cm}^2 \text{ s}^{-1}, \quad (4)$$

where R is the gas constant (cal/mol·deg).

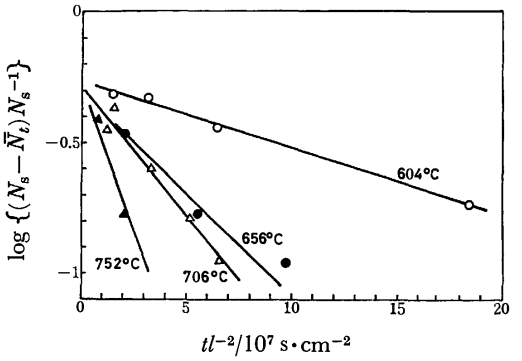

Fig. 3. Relation between $(N_s - \bar{N}_t)/N_s$ and t/l^2.

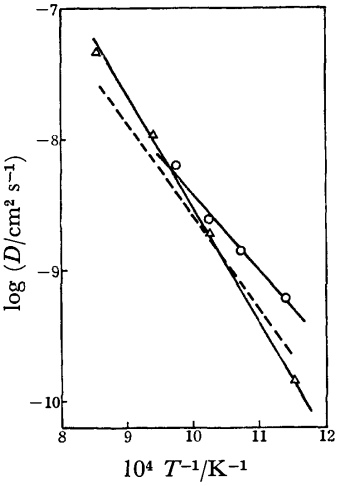

Fig. 4. Arrhenius plot of diffusion cofficient.
○ This work, △ Barbouth,[4] ---- Wang.[5]

References

1) K. Fueki and Y. Ouchi, *Bull. Chem. Soc. Jpn.*, **51**, 2234 (1978).
2) N. Barbouth and J. Oudar, *C. R. Acad. Sci. Paris*, **264**, 2120 (1967).
3) R. Raub, *Metall*, **25**, 7 (1971).
4) N. Barbouth, J. Oudar, and J. Cabane, *C. R. Acad. Sci. Paris*, **264**, 1029 (1967).
5) S. J. Wang and H. J. Grabke, *Z. Metallkd.*, **61**, 597 (1970).

BULLETIN OF THE CHEMICAL SOCIETY OF JAPAN, VOL. 51 (10), 3069—3070 (1978)

Homoconjugation in Bicyclo[3.2.1]octa-3,6-dien-2-yl and 6,9-Dihydro-5,9-methano-5*H*-benzocycloheptene-6-yl Radicals as Studied by Electron Spin Resonance[1)]

Takashi KAWAMURA,* Yoh'ichiro TAKEICHI, Shigeru HAYASHIDA, Masaaki SAKAMOTO, and Teijiro YONEZAWA

Department of Hydrocarbon Chemistry, Faculty of Engineering, Kyoto University, Sakyo-ku, Kyoto 606

(Received April 12, 1978)

Synopsis. The radicals in the title and the bicyclo[3.2.1]oct-3-en-2-yl radical are examined with ESR. The extent of the odd electron delocalization due to π-π homoconjugation in the bicyclo[3.2.1]octa-3,6-dien-2-yl radical is estimated to be in the order of a few per cent.

Brown and Occolowitz[2)] found an enhanced reactivity of bicyclo[3.2.1]octa-2,6-diene (**1h**) in a base-catalyzed allylic-proton exchange in comparison with that of bicyclo[3.2.1]oct-2-ene (**2h**). This was attributed to a strong π-π homoconjugation in the intermediate anion, **1a**. A similar but somewhat damped homodelocalization was reported for **3a** by Rosenthal and Winstein.[3)]

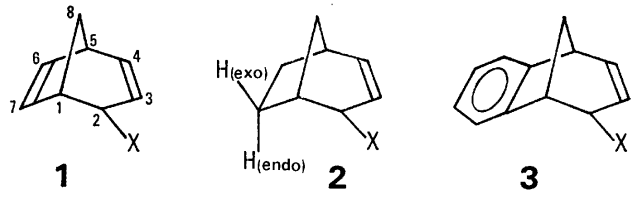

h: X = H, a: X = ⊖, r: X = •

Scheme 1.

Experimental evidence for the homodelocalization in **1a** was given by its ^{1}H NMR spectrum.[4)] However, Trimitsis and Tuncay[5)] reported that long-range π interactions can not be safely concluded by examining only the ^{1}H NMR of the anions.

We have now examined the homoconjugation involved in **1r** and **3r** by comparing their ESR spectra with that of **2r**. Toward the end of our study, a paper by Sustmann and Gellert[6)] appeared reporting a study similar to ours. Our analysis of the spectrum of **2r** is, however, somewhat different from that of Sustmann and Gellert, although the difference is not very important for the analysis of the homoconjugation.

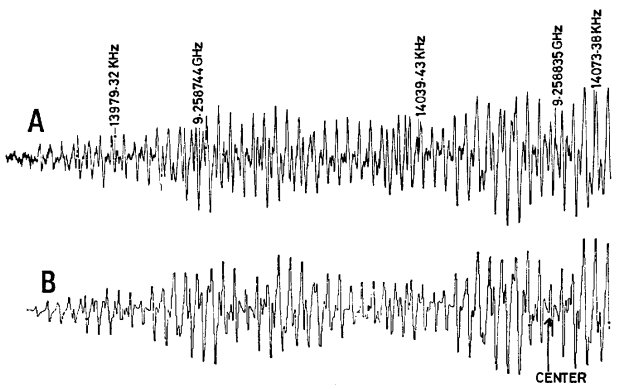

Fig. 1. Low-field half of observed (A) and simulated (B) spectra of **2r**. The numbers at markers in kHz and GHz units are ^{1}H NMR radio and ESR microwave frequencies, respectively.

An ESR spectrum of **2r** (Fig. 1) was observed during the photolysis of a cyclopropane solution of a mixture of **2h** and di-*t*-butyl peroxide at −120 °C. The spectrum was analyzed as 14.32 (2H), 4.93 (2H), 3.19 (1H), 1.80 (2H), 1.11 (1H), 1.02 (1H), and 0.54 G (2H). The *g* factor was 2.00256. A comparison of these hyperfine splitting constants (hfsc) with those of allylic cycloalkenyl radicals[7)] leads to the assignments of $a(H_2)=14.32$ and $a(H_3)=3.19$ G. The remaining two sets of doublets (1.11 and 1.02 G) are due to two protons on C_8. The hfsc of the triplet of 4.93 G is about a half of that of the exo-6 proton of the 2-norbornyl radical,[8)] suggesting an assignment to H_{6exo}. The triplet of 1.80 G is attributed to the bridgehead protons because triplet splittings of *ca.* 1.8 G were observed in the spectra of **1r**—**3r** (*vide infra*). The remaining triplet of 0.54 G is due to endo-6 and -7 protons. The **1r** and **3r** radicals were generated by the removal of a hydrogen atom by the *t*-butoxy radical from **1h** and **3h** respectively. The resolved hfsc's of **1r** and **3r** and their assignments are listed in Table 1, together with those of **2r**.

TABLE 1. OBSERVED hfsc's OF **1r**, **2r**, AND **3r**

Radical	*g*	a(H)[a)]				
		H_2	H_3	H_1	H_6	H_8
2r	2.00256	14.32	3.19	1.80	4.93[b)]	1.11
					0.54[c)]	1.02
3r	2.00272	14.23	3.19	1.78		1.21[d)]
1r	2.00276	14.07	3.25	1.87	1.35	1.35[d)]

a) In G units. b) *exo* protons. c) *endo* protons. d) Two nonequivalent protons have, accidentally, the same hfsc.

The hfsc of H_6 of **1r** has a magnitude between those of H_{6endo} and H_{6exo} of **2r**, in which the π-π homoconjugation is not involved. Thus, the extent of the homoconjugation can not be deduced directly from the hfsc of H_6 of **1r**. These is a shift in $a(H_2)$ in the order of **2r**>**3r**>**1r**. There exists a possibility that this is due to strain exerted on the allylic moiety, because this is the decreasing order of the bond length between C_6 and C_7. The hfsc's of the protons on the terminal carbon atoms of allylic moieties in the cyclohexenyl and in the more strained cyclopentenyl radicals are quite similar (14.35 and 14.30 G respectively),[7)] implying that the observed shift of $a(H_2)$ of **1r**—**3r** is not likely to originate

from the change in the geometry of the allylic moiety in these radicals.

Another possible origin of the shift of $a(H_2)$ is the delocalization of the odd electron from the allylic π system onto the etheno or benzo bridge. To examine this possibility, logarithms of the relative reactivities of **1h**—**3h** in the base-catalyzed allylic-proton exchange[2,3] were plotted against the values of the $a(H_2)$ of the corresponding radicals in Fig. 2. The fair correlation in Fig. 2 impies that the π-π homoconjugation in **1r** and **3r** is dominant, but not strong enough to exceed sufficiently other factors in shifting $a(H_2)$ and/or that the homoconjugation in anions is not linearly related to that in radicals.

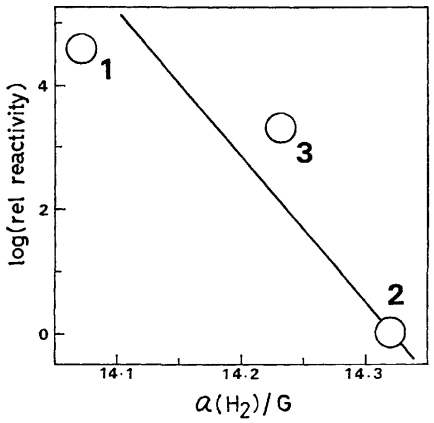

Fig. 2. Relation between kinetic acidity of olefin and hfsc of H_2 of the corresponding radical.

The odd electron density in the allylic π system can reasonably be expected to be proportional to $a(H_2)$; the odd electron density in the allylic π system of **1r** is estimated to be around 2% less than that of **3r**. This 2% decrease would more or less reflect the extent of the π-π homoconjugation in **1r**, as is suggested by the fair correlation between $a(H_2)$ and the kinetic acidity. Thus, we conclude that the extent of the odd electron delocalization from the allylic π system to the π system of the etheno bridge in **1r** is of the order of a few per cent, corresponding to the resonance integral (in Hückel approximation) between π atomic orbitals (AO) on C_2 and C_7 (β_{27}) of a magnitude of 5—20% of the integral between π AO's involved in a carbon-carbon double bond (β).

Experimental

Three hydrocarbons, **1h**,[9] **2h**,[9] and **3h**,[10] were prepared according to known procedures. The equipment and procedures for the photolysis-ESR experiments have been described earlier.[11]

References

1) A part of this study was presented at the 10th Symposium on Nonbenzenoid Aromatic Compounds, Matsuyama (1977).

2) J. M. Brown and J. L. Occolowitz, *Chem. Commun.*, **1965**, 376.

3) J. W. Rosenthal and S. Winstein, *Tetrahedron Lett.*, **1970**, 2683.

4) J. M. Brown, *Chem. Commun.*, **1967**, 638; S. Winstein, M. Ogliaruso, M. Sakai, and J. M. Nicholson, *J. Am. Chem, Soc.*, **89**, 3656 (1967).

5) G. B. Trimitsis and A. Tuncay, *J. Am. Chem. Soc.*, **98**, 1997 (1976).

6) R. Sustmann and R. W. Gellert, *Chem. Ber.*, **111**, 42 (1978).

7) J. K. Kochi and P. J. Krusic, "Essays on Free-radical Chemistry," ed by R. O. C. Norman, Chem. Soc. Spec. Pub. No. 24 (1970), Chap. 8.

8) T. Kawamura, Y. Sugiyama, and T. Yonezawa, *Mol. Phys.*, **33**, 1499 (1977).

9) R. W. Moore, W. R. Moser, and J. E. LaParade, *J. Org. Chem.*, **28**, 2200 (1963).

10) Z. Goldschmidt and U. Gutman, *Tetrahedron*, **30**, 3327 (1974).

11) T. Kawamura, M. Tsumura, Y. Yokomichi, and T. Yonezawa, *J. Am. Chem. Soc.*, **99**, 8251 (1977).

BULLETIN OF THE CHEMICAL SOCIETY OF JAPAN, VOL. 51 (10), 3071—3072 (1978)

Complex Isomerism in 7-Methylbenzo[*a*]phenazinium Tetracyano-*p*-quinodimethanide

Yoshio MATSUNAGA

Department of Chemistry, Faculty of Science, Hokkaido University, Sapporo 060

(Received May 1, 1978)

Synopsis. 7-Methylbenzo[*a*]phenazinium tetracyano-*p*-quinodimethanide is dark green when it is prepared in boiling ethanol and violet when it is prepared in acetonitrile. Examination of the electronic, vibrational, and ESR spectra revealed that the former form is essentially non-ionic, and the latter, ionic.

N-Methylphenazinium tetracyano-*p*-quinodimethanide, (NMP-TCNQ) is among the highest conducting TCNQ anion radical salts.[1] On the basis of the strong similarity of the electronic spectra of a wide variety of conducting TCNQ salts to each other and to $Cs_2(TCNQ)_3$ Torrance, Scott and Kaufman have suggested that NMP-TCNQ is not fully ionic.[2] The degree of ionicity has been estimated to be 0.94 by an NMR study and about 0.9 by measurements of the Seebeck coefficient.[3,4] These values are definitely larger than those reported for the well-known organic metal, TTF-TCNQ, 0.48—0.67.[5,6] Earlier, the present author demonstrated that the crystal charge-transfer complexes can be rather clearly classified into two groups, namely, non-ionic and ionic complexes.[7] NMP-TCNQ and TTF-TCNQ may be supposed to be in the region of non-ionic-to-ionic transitions of crystal charge-transfer complexes. Furthermore, it was shown that the probability of finding non-ionic complexes can be increased by choosing component molecules with larger differences in size and shape. Consequently, if the 7-methylbenzo[*a*]-phenazinium ion ($NMBP^+$) is employed in place of the

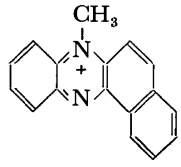

NMP^+ ion, a smaller degree of ionicity in the resulting complex may be foreseen. The recent work by Soos *et al.* indicating that phenazine–TCNQ systems are close to the non-ionic-to-ionic separation[8] prompted the present author to study the above-mentioned combination.

Benzo[*a*]phenazine was prepared by means of a condensation reaction between 1,2-naphthoquinone and *o*-phenylenediamine dissolved in 50% acetic acid at 0 °C,[9] and was purified by sublimation in a vacuum. NMBP methyl sulfate was obtained by boiling a benzene solution of the base and excess dimethyl sulfate for several hours. By the treatment of the methyl sulfate in hot absolute alcohol with a boiling ethanolic solution of one equivalent of LiTCNQ, dark green NMBP-TCNQ crystals were precipitated. Found: C, 77.14; H, 3.71; N, 18.52%. Calcd for $C_{17}H_{13}N_2$–$C_{12}H_4N_4$: C, 77.49; H, 3.81; N, 18.70%. Metathesis in aceto-nitrile instead of ethanol gave dark violet crystals. Found: C, 77.44; H, 3.64; N, 18.69%. The former form could be transformed into the latter by recrystallization from acetonitrile.

The electronic spectra recorded as Nujol mineral oil mulls are shown in Fig. 1. The sharp peaks located at 10.6 and $12.2\times10^3\ cm^{-1}$ in the spectrum of the

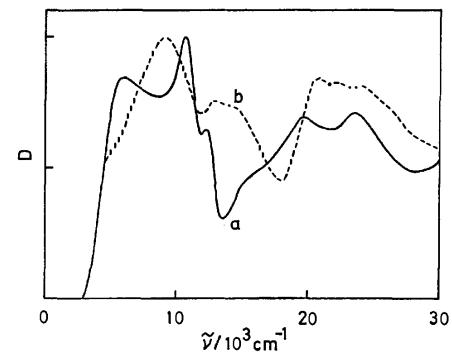

Fig. 1. Electronic spectra of 7-methylbenzo[*a*]phenazinium tetracyano-*p*-quinodimethanide, (a) the green form and (b) the violet form.

green form (Curve a) may be assigned to the monomeric $TCNQ^-$ anion radicals trapped in the crystals. Such peaks are not observed in the spectrum of the violet form. The shoulder appearing near $5\times10^3\ cm^{-1}$ suggests that the sample is contaminated with the green form. If this shoulder is ignored, the rest of the spectrum is that of a typical simple TCNQ salt, *e.g.*, pyridinium-TCNQ. Because of the close resemblance between this spectrum and that of the dimeric ion $(TCNQ)_2^{2-}$ in an aqueous solution,[10] the anion radicals in the violet form appear to be in predominantly pair-by-pair interaction. The two forms of NMBP-TCNQ exhibit spectra considerably different from each other. The lowest-energy absorption shown by the green form is at $6.0\times10^3\ cm^{-1}$. Assuming that this absorption arises from the charge transfer from 7-methylbenzo[*a*]phenazin-7-yl radical to TCNQ molecule, the ionization potential of the former species may be estimated to be about 6.6 eV. This value is so low that the combination can form an ionic complex provided the molecules are closely packed in the crystal.

The vibrational spectra of the green and violet forms examined as Nujol mulls are compared in Fig. 2. No band assignable to an N–H stretching vibration could be detected in the region from 3000 to $3500\ cm^{-1}$. Therefore, the reduction of the diamagnetic $NMBP^+$ ion to the $HNMBP^+$ cation radical during the course of preparation may be excluded from possible causes of the dimorphism. Although the relative intensities of

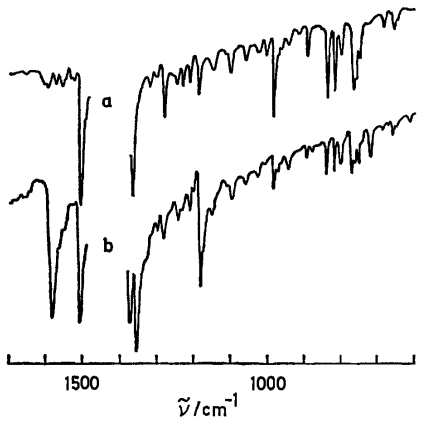

Fig. 2. Vibrational spectra of 7-methylbenzo[*a*]phenazinium tetracyano-*p*-quinodimethanide, (a) the green form and (b) the violet form.

bands are different, the locations in the region below 1300 cm^{-1} are rather similar to each other. In the spectrum of the violet form, strong bands appearing at about 1580, 1360, and 1180 cm^{-1} approximately constitute the pattern of the $TCNQ^-$ anion observed with the solid lithium salt. They are absent in the spectrum of the other form. However, no strong band is found in the latter spectrum near 1550 cm^{-1}, where solid TCNQ is known to give a relatively strong band.

The ESR spectra of the two forms were examined at the X-band. The green form gives a single resonance. The distance between the points of maximum slope is about 1.0 G. In addition to a strong narrow center line, three pairs of resonance lines characteristic of triplet-spin excitons were observed with the violet polycrystals. As the temperature is increased, the resonance lines broaden and the zero-field splitting parameters, $|D/g\beta|$ and $|E/g\beta|$, become smaller. The values obtained on the assumption that the isotropic g value is equal to the free electron value are 147 and 24 G at −30 °C and 140 and 20 G at 90 °C respectively. They are comparable to those reported for a number of the simple TCNQ salts, namely, 143—165 G for $|D/g\beta|$ and 17—25 G for $|E/g\beta|$.[11] The collapse of the three pairs into a single broad line was noted around 140 °C. The singlet-triplet separation was estimated to be 0.16 eV by relative-intensity measurements in the range from −30 to +10 °C.

The electrical resistivities measured with polycrystalline compactions were in the order of 10^5 ohm cm at room temperature for both the forms. The plots of the logarithm of the resistivity recorded between −125 and 110 °C against $1/T$ are not straight, indicating that the extrinsic conduction is dominant below room temperature. The activation energies for semiconduction were estimated to be about 0.3 eV for the high-temperature region. Thus, all the results presented above lead to the conclusion that the violet form of NMBP-TCNQ is essentially ionic, while the green form is not. The two forms may be called complex isomers, and this phenomenon, complex isomerism.

The author wishes to express his thanks to Mr. Nobuhiko Miyajima for the preparation of benzophenazine and to Mr. Shigeo Ikeura for the electrical resistivity measurements. The work was supported by a Grant-in-Aid for Scientific Research from the Ministry of Education (No. 234028).

References

1) L. R. Melby, *Can. J. Chem.*, **43**, 1448 (1965).
2) J. B. Torrance, B. A. Scott, and F. B. Kaufman, *Solid State Commun.*, **17**, 1369 (1975).
3) M. A. Butler, F. Wudl, and Z. G. Soos, *Phys. Rev. B*, **12**, 4708 (1976).
4) J. F. Kwak, G. Beni, and P. M. Chaikin, *Phys. Rev. B*, **13**, 641 (1976).
5) P. Coppens, *Phys. Rev. Lett.*, **35**, 98 (1975).
6) W. D. Grobman and B. D. Silverman, *Solid State Commun.*, **19**, 319 (1976).
7) Y. Matsunaga, *Bull. Chem. Soc. Jpn.*, **42**, 2490 (1969).
8) Z. G. Soos, H. J. Keller, W. Moroni, and D. Nöthe, *J. Am. Chem. Soc.*, **99**, 5040 (1977).
9) O. N. Witt, *Ber.*, **20**, 571 (1887).
10) R. H. Boyd and W. D. Phillips, *J. Chem. Phys.*, **43**, 2927 (1965).
11) T. Hibma, P. Dupuis, and J. Kommandeur, *Chem. Phys. Lett.*, **15**, 17 (1972).

BULLETIN OF THE CHEMICAL SOCIETY OF JAPAN, VOL. 51 (10), 3073—3074 (1978)

Magnetic Susceptibility of the So-Called Zero-Valent Aluminium Complex of 2,2′-Bipyridine, $[Al(bpy)_3]^0 \cdot 1/2THF$

Motomichi INOUE,* Tatsuo HORIBA,† and Ken-ichi HARA††
Department of Chemistry, Nagoya University, Chikusa, Nagoya 464

(Received May 15, 1978)

Synopsis. The magnetic susceptibility of tris(2,2′-bipyridine)aluminium(0) was determined between 4.2 and 300 K. It can be explained by a radical ion model in which three 2,2′-bipyridine radical ions are coordinated to an aluminium-(III) ion. Antiferromagnetic interaction operates between the radical ions with the exchange integral $J/k=-110$—115 K.

Tris(2,2′-bipyridine) complexes in apparently unusual valency states of metals have been prepared and characterized.[1] An electronic-spectrum study of the so-called zero-valent aluminium complex $[Al(bpy)_3]^0$ showed that bpy^- ions are involved in the complex molecules.[2] The magnetic susceptibility was found to obey the Curie-Weiss law between 80 and 300 K.[3] The magnetic moment $\mu=3.38$ B.M. evaluated from the Curie constant is inconsistent with the formula $[Al^0(bpy^0)_3]$, in which an unpaired electron exists in a molecule. From these, we can propose the formula $[Al^{3+}(bpy^-)_3]$ rather than $[Al^0(bpy^0)_3]$. If this is correct, magnetic interaction is presumed to operate between paramagnetic bpy^- ions within $[Al(bpy)_3]$. Thus, the proposed formula can be confirmed by getting information on the magnetic interaction. Therefore, we have determined the magnetic susceptibility down to 4.2 K, because the magnetic interaction may be effective at low temperatures.

Experimental

The material was prepared by the method reported by Herzog *et al.*[4] Recrystallization from THF yielded deep green crystals. On heating *in vacuo* at about 90 °C, the crystals librated THF gas. Weight loss amounted to 8.0%, indicating that the crystals were those of a THF adduct, $Al(bpy)_3 \cdot 1/2$ THF (Found: Al, 4.8; THF, 8.0%. Calcd: Al, 5.1; THF, 6.8%). The effective magnetic moment 2.38 B. M. at 290 K agreed with 2.32—2.44 B. M. reported for $Al(bpy)_3$.[3,4]

The magnetic susceptibility was determined by the Gouy method in the temperature range 80—300 K and by the Faraday method below 80 K. The molar magnetic susceptibility[5] was corrected for diamagnetic contributions (10^{-6} emu mol^{-1}) from 2,2′-bipyridine (−93) and THF (−55).[6]

Results and Discussion

The reciprocal molar susceptibility is plotted against temperature in Fig. 1. It obeys the Curie-Weiss law in the two temperature ranges, $T \gtrsim 180$ K and $T \lesssim 40$ K (broken lines in Fig. 1): the Curie and Weiss constants are determined as $C_h=1.31$ emu K mol^{-1} and $\theta_h=-244$ K for the high temperature range, and $C_l=0.37$ emu K mol^{-1} and $\theta_l=-9.7$ K for the low temperature range. Between 40 and 180 K, the magnetic susceptibility deviates from the Curie-Weiss law. This is confirmed by the temperature dependence of the signal intensity in the ESR powder spectrum (Fig. 1), which has an isotropic g factor equal to 2.003 and a peak-to-peak width equal to 1.5 mT.

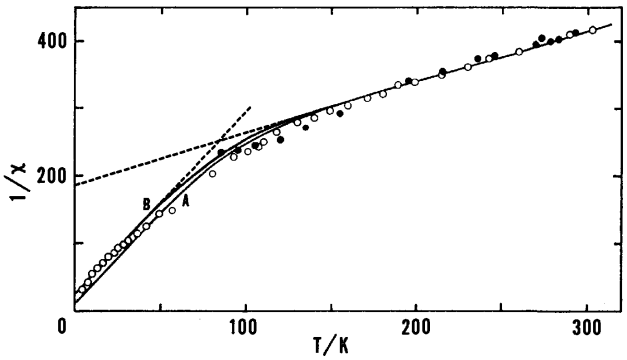

Fig. 1. Reciprocal magnetic susceptibility, $1/\chi$ in emu, (○) and relative ESR-signal intensity (●) of $[Al(bpy)_3]$ The curves A and B show theoretical susceptibilities calculated with the exchange integrals $J/k=-115$ K and -110 K, respectively, on the assumption of the formula $[Al^{3+}(bpy^-)_3]$.

The magnetic moment $\mu_h=3.24$ B.M. evaluated from C_h is nearly equal to $(3\times3)^{1/2}$ B.M. of a molecule having three independent unpaired electrons. The moment $\mu_l=1.72$ B.M. evaluated from C_l indicates that the ground state is doublet ($\mu_{s=1/2}=1.73$ B.M). This shows that the magnetic unit of the complex consists of three spins interacting antiferromagnetically with each other, supporting the proposed formula $[Al^{3+}(bpy^-)_3]$, in which each bpy^- ion carries an unpaired electron and aluminium is diamagnetic. For the spin system, eight spin functions are derived. Four of them correspond to $S=3/2(m_s=\pm3/2, \pm1/2)$ and the remaining four functions can be divided into two sets each corresponding to $S=1/2$ ($m_s=\pm1/2$). Because three bpy^- ions can be presumed to be equivalent with each other in a complex molecule, the magnetic susceptibility is given by[7]

$$\chi = \frac{Ng^2\mu_B^2}{4kT}\left[\frac{1+5\exp(3J/kT)}{1+\exp(3J/kT)}\right], \quad (1)$$

where J is the exchange integral, the absolute value of which is equal to one third of the energy separation between the doublet and quartet states. When magnetic interaction operates between complex ions, Eq. 1 can be rewritten as[8]

$$\chi = \frac{Ng^2\mu_B^2}{4k(T-\Delta)}\left[\frac{1+5\exp(3J/kT)}{1+\exp(3J/kT)}\right], \quad (2)$$

† Present address: Hitachi Research Laboratory, Hitachi Ltd., Hitachi 319-12.

†† Present address: Central Research Laboratory, Fuji Electric Co., Ltd., Yokosuka 240-01.

where Δ denotes the Weiss constant that takes into account the interaction. The solid curve A in Fig. 1 shows the magnetic susceptibility calculated from Eq. 2 with $J/k=-115$ K, $\Delta=-5$ K, and $g=2.00$, yielding the best fit to the observed data. When the Weiss constant Δ is assumed to be equal to θ_1, the curve B calculated with $J/k=-110$ K agrees well with the observed χ-T curve (Fig. 1).

The antiferromagnetic interaction between bpy^- ions takes place probably through aluminium atoms. Kobayashi *et al.*[9] propose a mechanism in which a charge transfer between bpy^- ions yields the antiferromagnetic interaction: the unpaired electron of a bpy^- ion can migrate to other bpy^- ions within an $[Al(bpy)_3]$ molecule through the vacant 3d orbitals of aluminium, and the resulting charge-transfer state stabilizes the doublet state rather than the quartet state. In this mechanism, aluminium 3d orbitals play an important part. Wulf and Herzog[3] determined the magnetic susceptibility of $[Sc(bpy)_3]^0$ between 80 and 350 K. It obeys the Curie-Weiss law in two temperature ranges: $\mu_h=3.67$ B.M. and $\theta_h=-667$ K for $T\gtrsim220$ K, and $\mu_l=1.76$ B.M. and $\theta_l=-20$ K for $T\lesssim134$ K. This magnetic behavior can be explained well with Eq. 2, the parameters being determined as $J/k=-200$ K, $\Delta=-20$ K, and $g=2.00$. Thus, three paramagnetic bpy^- ions are coordinated to a diamagnetic scandium(III) ion also in $[Sc(bpy)_3]^0$. The absolute J value of the scandium complex is larger than that of the aluminium complex. This arises from difference in the nature of central-metal d orbitals, because 3d orbitals contribute to metal-nitrogen bonding to a greater extent in the scandium complex. This provides evidence for the important role of the d orbitals in the magnetic interaction.

In our previous papers,[8,10,11] we reported that the magnetic susceptibilities of the $[M(bpy)_n]^0$ type complexes of manganese, beryllium, and magnesium can be explained by radical ion models in which bpy^- ions are coordinated to central-metal ions having normal oxidation states in the complexes. The present investigation along with the previous reports[8,10,11] has provided a convincing example in support of a conclusion that the "excess electrons" are localized mostly on the ligand molecules in the so-called zero-valent complexes of 2,2′-bipyridine.

References

1) W. R. McWhinnie and J. D. Miller, *Adv. Inorg. Chem. Radiochem.*, **12**, 135 (1969).
2) Y. Torii, S. Murasato, and Y. Kaizu, *Nippon Kagaku Zasshi*, **91**, 549 (1970).
3) E. Wulf and S. Herzog, *Z. Anorg. Allg. Chem.*, **387**, 81 (1972).
4) S. Herzog, K. Geisler, and H. Präkel, *Angew. Chem.* **75**, 94 (1963).
5) It is expressed in cgs emu in this paper. Multiplying it by $4\pi\times10^{-6}$ gives the corresponding susceptibility in SI units.
6) G. Foëx, "Constantes Sélectionés, Diamagnétisme et Paramagnétisme," Masson, Paris (1957).
7) S. Emori, M. Inoue, M. Kishita, M. Kubo, S. Mizukami, and M. Kono, *Inorg. Chem.*, **7**, 2419 (1968).
8) M. Inoue, K. Hara, T. Horiba, and M. Kubo, *Bull. Chem. Soc. Jpn.*, **47**, 2137 (1974).
9) H. Kobayashi, Y. Torii, Y. Kaizu, and H. Sekino, *Bull. Chem. Soc. Jpn.*, to be published. We are grateful to Professor Kobayashi, Tokyo Institute of Technology, for communicating us his theoretical results prior to the publication.
10) K. Hara, M. Inoue, and M. Kubo, *Chem. Lett.*, **1972**, 839.
11) T. Horiba, K. Hara M. Inoue, and M. Kubo, *Bull. Chem. Soc. Jpn.*, **47**, 1624 (1974).

BULLETIN OF THE CHEMICAL SOCIETY OF JAPAN, VOL. 51 (10), 3075—3076 (1978)

Gas-chromatographic Measurements of Nitrous Oxide(N_2O) in Air Using a Molecular Sieve Trap

Michio HIROTA

Meteorological Research Institute, Koenji-kita, Suginami-ku, Tokyo 166

(Received February 8, 1978)

Synopsis. The atmospheric mixing ratio of N_2O was measured at the MRI, Koenji (Tokyo), between May and September, 1977, by a gas-chromatographic method. The mean value was 0.32_7 ppm. Judging from the measurements over the last 10 years, the atmospheric N_2O seems to have increased about 20%.

The stratospheric ozone is produced by the photochemical reaction and destroyed by reactions with such tracer components as O, NO, NO_2, HO, HO_2, and halogen atoms. If such species are released in large quantities by man's activity (SST flights or the use of aerosol sprays and nitrogen fertilizer, for instance), the natural balance of the ozone will be damaged. The depletion of the stratospheric ozone will increase the biologically harmful UV radiation on the earth's surface, and will probably lead to the climatic change.[1,2]

The N_2O which is produced by micro-biological activity in soils and waters is the major source of the stratospheric NO. The N_2O released into the atmosphere is considered stable in the troposphere, at least stable under solar UV radiation,[3] and is transferred to NO mainly by Reaction 1 in the lower stratosphere.[4] In order to assess the influence of nitrogen fertilizer on the natural ozone balance, the atmospheric concentration and distribution of N_2O must also be examined.

$$N_2O + O(^1D) \longrightarrow 2NO \qquad (1)$$

The atmospheric N_2O is mainly measured by two methods, *i.e.*, the infrared spectroscopic and gas-chromatographic (GC) methods. In the latter case, N_2O is preconcentrated on a silica-gel trap[5] or, in many cases, on a molecular sieve trap.

The method of collecting N_2O on the molecular sieve trap was first adopted by Bock and Schütz,[6] and some improvements have since been made by Schütz *et al.*,[7] LaHue *et al.*,[8] and Hahn.[9,10] In the present paper, the results of some measurements at the MRI, Koenji (Tokyo), will be reported and compared with those of recent studies.

Experimental

Sampling of N_2O. Thirty litre of air was drawn through a series of three U-shaped adsorption tubes (i.d. 8 mm) at a flow rate of 30 l/h. The first tube was filled with drierite to remove the water vapor, the second with sodium asbestos to remove the CO_2, and the third with molecular sieve 5A(1/16 in. pellets, 10 g) to adsorb the N_2O. The third tube was submerged in a Dry Ice–ethanol bath (−72 °C). Impurities were excluded from the molecular sieve by heating the tube to 350 °C and by then passing He gas (99.99%) for 1 or 2 h.

Gas-chromatographic Analysis. GC measurements were performed using a Shimadzu Gas Chromatograph GC-6AM equipped with a thermald conductivity detector (90 °C). He gas was used as the carrier gas at a flow rate of 50 ml/min.

After the sampling, the molecular sieve tube was placed in a gas sampler (Shimadzu, MGS-4). The adsorbed N_2O was transferred from the tube to the GC column by heating the tube to 350 °C. Carrier gas was passed through for 7 min and then for 10 additional min after 8 min's interruption. The N_2O was again adsorbed at 65 °C on the glass column filled with 30/60 mesh molecular sieve 5A (3 mm i.d. × 1.5 m). The GC analysis was started by raising the column temperature to 245 °C at a rate of 15 °C/min. The peak of N_2O appeared 9 min after, and that of CO_2 appeared 1 min after that of N_2O.

The detector response was linear in the range from 3.9 to 30 μl of N_2O.* For the reference measurements, N_2O was injected directly into the column from the gas syringe (Terumo, GAN- 0.25).

Results and Discussion

In 10 reference measurements of 15 μl N_2O over three days, the standard deviation (SD) was 2.4%, while it was 3% in 15 measurements over three months. The error of the calibration curve in the range from 3.9 to 30 μl N_2O was ±4%.

The amount of molecular sieve in the tube was the same as that used by LaHue *et al.*[8] As the sampling time, however, was doubled, the tube was cooled (—72 °C) to ensure the quantitative collection of N_2O. The quantitative collection of N_2O was confirmed by the measurements of 20 μl N_2O which had been diluted with N_2** in a 30 l *aflon* bag and then trapped on the molecular sieve tube. Three measurements showed the value of 19.2±0.4 μl compared with the reference measurements of 20 μl N_2O. The total accuracy of the method was estimated as about ±7% because of 3% error of the flow meter.

Field measurements were performed 14 times between May and September, 1977, at the Meteorological Research Institute (Tokyo). The air was sampled at 1 m above a ground surface covered with weeds through a vinyl tube leading to the inside of the building.

The results were scattered widely between 0.24_8 and 0.45_4 ppm, and the mean was 0.32_7 ppm. The mean values of previous and the present studies are shown in Fig. 1. A wide distribution of the values have also been observed at Mainz, Schauinsland,[7] and Yokohama.[11] The values of 0.45_4 and 0.41_5 ppm were unusually high. Such high values have also been observed elsewhere.[11,12] The values observed over the sea and in the United

* Assuming the N_2O mixing ratio of 3×10^{-7}, 30 l of the sampled air contains 9 μl N_2O.

** The N_2 used was 99.9995%, and a molecular sieve tube (−72 °C) was placed before the bag.

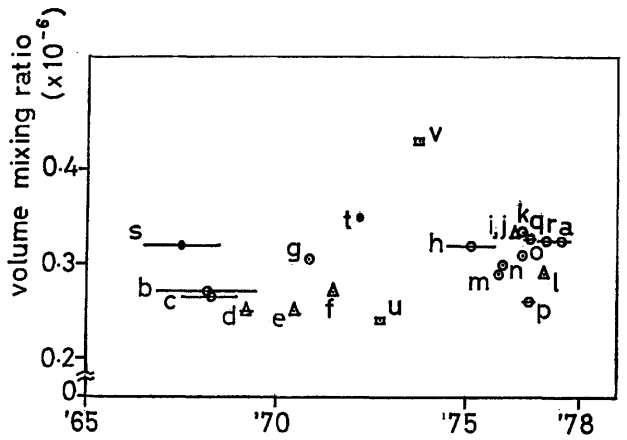

Fig. 1. Atmospheric mixing ratio of N_2O.
○; By GC method above the ground, △; by GC method over the sea, ●; by IR spectroscopic method, □; by mass spectrographic method.
(a) Present study, (b, c) Ref. 7, (d, e, f) Ref. 10, (g) Ref. 8, (h) Ref. 15, (i, j, k) Ref. 16, (l) Ref. 17, (m, n, o) Ref. 18, (p) Ref. 11, (q) Ref. 19, (r) Ref. 20, (s) Ref. 21, (t) Ref. 22, (u, v) Ref. 12.

TABLE 1. ATMOSPHERIC VOLUME MIXING RATIO OF N_2O AT THE METEOROLOGICAL RESEARCH INSTITUTE, KOENJI

Date (1977)	Sampling start	Mixing ratio (ppm)	Date (1977)	Sampling start	Mixing ratio (ppm)
23, May	10:40	0.30_9	30, Aug.	13:50	0.30_0
24, May	16:15	0.34_3	31, Aug.	13:40	0.29_4
25, May	14:10	0.45_4	31, Aug.	16:30	0.27_0
26, May	10:00	0.30_5	1, Sep.	9:10	0.25_8
4, July	14:55	0.38_9	1, Sep.	10:10	0.30_4
5, July	11:30	0.32_7	1, Sep.	13:45	0.24_8
6, July	15:05	0.35_9	1, Sep.	17:00	0.41_5

States, on the other hand, have shown a rather small distribution.[13] The distribution must be strongly dependent on the meteorological condition of the observatory and on the sampling platform (ground station, balloon, aircraft, *etc.*). According to Ehhalt *et al.*,[12] a surface station like that of Schütz *et al.* observes both surface air with a high value and free tropospheric air; therefore, the values would be scattered widely.

The values of 4 measurements on September 1 were scattered. A similar feature was also observed by Katou *et al.*[11] Brice *et al.* reported a regular diurnal variation of N_2O on the basis of measurements over 10 days.[14]

In comparison with the mean values, especially in Refs. 7, 19, and 20, it is evident that the atmospheric N_2O has increased over the last 10 years (about 20%), at least as shown by the GC data. The value was, however, exceptionally low in Ref. 11. This variation was considered significant because the SD was 10% in the measurements of Schütz *et al.*,[7] while those of the others were all less than 3.1%, though they were not shown in Ref. 10 and 15, and the values of Katou *et al.* and the present study were very scattered.

In the calculation of the mean, unusually high values which, according to Ehhalt *et al.*,[12] did not represent the tropospheric value were also used. This is because the ground surface is considered not only as the source of N_2O but also as its sink;[14] therefore, the lower value does not neccessarily represent the tropospheric value.

References

1) CIAP Monograph, DOT-TST-75-51 (1975).
2) "Fluorocarbons and the Environment, Report of Federal Task Force on Inadvertent Modification of the Stratosphere," (1975).
3) D. H. Stedman, R. J. Cicerone, W. L. Chameides, and R. B. Harvey, *J. Geophys. Res.*, **81**, 2003 (1976).
4) M. B. McElroy and J. C. McConnell, *J. Atmos. Sci.*, **28**, 1095 (1971).
5) H. Craig and L. I. Gordon, *Geochim. Cosmochim. Acta*, **27** 949 (1963).
6) R. Bock and K. Schütz, *Z. Anal. Chem.*, **237**, 321 (1968).
7) K. Schütz, C. Junge, R. Beek, and B. Albrecht, *J. Geophys. Res.*, **75**, 2230 (1970).
8) M. D. LaHue, H. D. Axelrod, and J. P. Lodge, Jr., *Anal. Chem.*, **43**, 1113 (1971).
9) J. Hahn, *Anal. Chem.*, **44**, 1889 (1972).
10) J. Hahn, *Tellus*, **26**, 160 (1974).
11) T. Katou, Y. Hanai, and M. Mimura, *Bull. Inst. Environ. Sci. Tech., Yokohama National Univ.*, **3**, 5 (1977).
12) D. H. Ehhalt, N. Roper, and H. E. Moore, *J. Geophys. Res.*, **80**, 1653 (1975).
13) P. J. Crutzen and D. H. Ehhalt, *AMBIO*, **6**, 112 (1977).
14) K. A. Brice, A. E. J. Eggleton, and S. A. Penkett, *Nature*, **268**, 127 (1977).
15) A. L. Schmeltekopf, D. L. Albritton, P. J. Crutzen, P. D. Goldan, W. J. Harrop, W. R. Henderson, J. R. McAfee, M. McFarland, H. I. Schiff, T. L. Thompson, D. J. Hofmann, and N. T. Kjome, *J. Atmos. Sci.*, **34**, 729 (1977).
16) R. A. Rasmussen, J. Kransec, and D. Pierotti, *Geophys. Res. Lett.*, **3**, 615 (1976).
17) Y. Cohen, *Anal. Chem.*, **49**, 1238 (1977).
18) H. B. Singh, L. Salas, H. Shigeishi, and A. Crawford, *Atmos. Environ.*, **11**, 819 (1977).
19) D. Pierotti and R. A. Rasmussen, *J. Geophys. Res.*, **82**, 5823 (1977).
20) P. D. Goldan, Y. A. Bush, F. C. Fehsenfeld, D. L. Albritton, P. J. Crutzen, A. L. Schmeltekopf, and E. E. Ferguson, *J. Geophys. Res.*, **83**, 935 (1978).
21) R. Goody, *Planet. Space Sci.*, **17**, 1319 (1969).
22) A. Goldman, D. G. Murcray, F. H. Murcray, and W. J. Williams, *J. Opt. Soc. Am.*, **63**, 843 (1973).

BULLETIN OF THE CHEMICAL SOCIETY OF JAPAN, VOL. 51 (10), 3077—3078 (1978)

Flux Growth of Double Oxides of Niobium and Rare-earth Elements (Ln_3NbO_7)

Yuichi YAMASAKI and Yoshinori SUGITANI*

Department of Chemistry, The University of Tsukuba, Sakura-mura, Ibaraki 300-31

(Received April 24, 1978)

Synopsis. Crystals of double oxides of rare-earth and niobium Ln_3NbO_7, where Ln=Ho, Y, Er, Dy, and La, and those of rare-earth and tantalum Ln_3TaO_7, where Ln=Y, Er, and Gd, were grown by Bi_2O_3–B_2O_3 and PbF_2–PbO fluxes for the Ln_3NbO_7, and by PbF_2–PbO flux for the Ln_3TaO_7. The composition of Ln_3NbO_7 or Ln_3TaO_7 is not yet known in natural minerals.

Double oxides of niobium (or tantalum) and a rare-earth element occur in nature as fergusonite $Y(Nb,Ta)O_4$ and samarskite $Y_4[(Nb,Ta)_2O_7]_3$ *etc.*[1] These compounds have high melting points of over 2000 °C, which depend mainly upon the component ratios between Nb and Ta in the solid solution. We reported that a series of compounds $LnNbO_4$[2,3] and $LnTaO_4$ were able to be grown by the flux method at lower temperatures than 1300 °C. These oxide compounds are attractive materials due to their electro-optical and/or ferroelastic characters,[4] in addition to the possibility of being a new laser matrix. We are now attempting the flux growth of compounds which have a different atomic ratio between the rare-earth element and niobium (or tantalum) than the naturally known minerals. This report describes the syntheses of Ln_3NbO_7 and Ln_3TaO_7 type compounds.

Mixtures of Ln_2O_3 (purity 4N) and Nb_2O_5 (purity 4N) with the molar ratio of 3: 1 were used as starting materials. Fluxes were added to the starting materials in the molar ratio of several to tens of times. The flux systems where we tried to grow Ln_3NbO_7 and Ln_3TaO_7 type crystals were PbF_2–PbO, Bi_2O_3–B_2O_3, B_2O_3–$Na_2B_4O_7$, Bi_2O_3–V_2O_5, and Li_2O–MoO_3. The purity of PbF_2 and PbO was 99.9%, and the others were all of the analytical reagent grade.

The starting material was put in a platinum crucible together with one of the flux materials, and was covered tightly by a platinum lid. This was placed in an electric muffle furnace at 1300 °C and was kept for 2 to 5 h at the same temperature. After that it was cooled slowly down to 900 °C in the rate of 1 to 5 °C/h by a programmed controller. At the final temperature it was taken out of the furnace and was air quenched to room temperature. Products in the crucible were washed with hot diluted HNO_3 for several hours. Crystals thus obtained were identified with the desired materials by X-ray powder diffraction.

The crystals of Y_3NbO_7 are shown as an example in Fig. 1. They are mostly octahedrons in shape and come to about 2 mm in the largest distance. Products obtained by the use of different fluxes are listed in Table 1. Crystals having Ln_3NbO_7 composition were obtained both from the flux systems of Bi_2O_3–B_2O_3 (the flux ratio ranges from 10: 0 to 8: 2) and from PbF_2–PbO (9: 1 to 7: 3). A list of Ln_3NbO_7 and Ln_3TaO_7 type compounds obtained in this work is given in Table 2. Compounds Ln_3TaO_7 were grown using the PbF_2–PbO flux system (from 9: 1 to 7: 3). The growth of crystals containing other rare-earth elements than those listed in Table 2 has not yet been successful. In the course of the runs, $Pb_2Nb_2O_7$ (pyrochlore type structure), $Pb_3Nb_2O_8$, and $LnNbO_4$ type crystals were obtained as by-products.

Precession and Weissenberg photographs show that the crystals given in Table 2, except for La_3NbO_7,

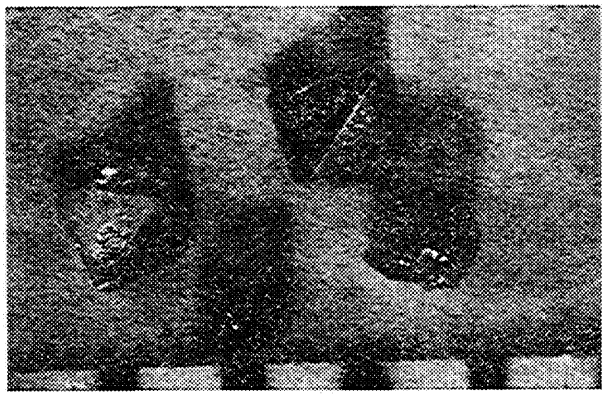

Fig. 1. Crystals of Y_3NbO_7.
(1 division=1 mm.)

Table 1. Flux systems used and their products (starting materials are Y_2O_3 and Nb_2O_5 in 3: 1 molar ratio)

Flux	Products
PbF_2–PbO	Y_3NbO_7, $YNbO_4$
Bi_2O_3–B_2O_3	Y_3NbO_7
B_2O_3–$Na_2B_4O_7$	$NaNbO_3$
Bi_2O_3–V_2O_5	$V_3Nb_{17}O_{50}$
Li_2O–MoO_3	$LiNbO_3$

Table 2. List of products having Ln_3NbO_7 and Ln_3TaO_7 composition

Compound	Color	Crystal system	Lattice parameter		
			a (Å)	*b* (Å)	*c* (Å)
Ho_3NbO_7	brown	cubic	5.243(3)		
Y_3NbO_7	yellow	cubic	5.238(3)		
Er_3NbO_7	pale brown	cubic	5.252(2)		
Dy_3NbO_7	brown	cubic	5.259(2)		
La_3NbO_7	brown	ortho-rhombic	7.615(2)	7.761(2)	11.14(2)
Y_3TaO_7	pale brown	cubic	5.240(2)		
Er_3TaO_7	pink	cubic	5.251(2)		
Gd_3TaO_7	yellow	cubic	5.321(2)		

belong to a cubic system with the space group of Fm3m. La_3NbO_7, however, belongs to the orthorhombic system with the space group of Pnma. Crystal structure analysis both for the products and for by-products are now in progress.

The authors are grateful to Professor Kozo Nagashima for his kind support of this work.

References

1) J. D. and E. S. Dana, "The System of Mineralogy," 7th ed John Wiley & Sons, Inc. London (1952); H. Strunz, "Mineralogische Tabellen," 5th ed Akad. Verlag, Leipzig (1970).
2) Y. Sugitani and K. Nagashima, *Miner. J.*, **8**, 66 (1975).
3) Y. Sugitani, *Bull. Chem. Soc. Jpn.*, **50**, 755 (1977).
4) S. Tsunekawa and H. Takei, *J. Phys. Soc. Jpn.*, **40**, 1523 (1976).

BULLETIN OF THE CHEMICAL SOCIETY OF JAPAN, VOL. 51 (10), 3079—3080 (1978)

Pyrolytic Sulfurization Gas Chromatography. IV. Removal of Trace Amounts of Organic Compounds in Sulfur by Refluxing with Oxides

Tadashi HARA,* Kaoru FUJINAGA, Katsuya TSUJI, and Fujio OKUI

Department of Applied Chemistry, Faculty of Engineering, Doshisha University, Karasuma Imadegawa, Kamigyo-ku, Kyoto 602

(Received May 12, 1978)

Synopsis. Oxides of aluminium, silicon, and titanium, instead of the magnesium oxide used in the Bacon-Fanelli method, were found to be effective for the elimination of trace amounts of organic compounds in sulfur. Prolonged refluxing in an inert gas atmosphere were especially favorable for the removal of organic compounds

The atomic ratio between C, H, O, and N in a sample can be simultaneously determined by pyrolytic sulfurization gas chromatography.[1] Since the high purity of sulfur was indispensable for the analysis, various purification methods such as distillation,[2] recrystallization, refluxing, decomposition of sodium thiosulfate, vacuum sublimation were investigated. The Bacon-Fanelli method[3] was found to be most promising for the present purpose. Sulfur was refluxed with several kinds of oxides including the magnesium oxide (MgO) in the Bacon-Fanelli method, its purity being examined gas chromatographically. Aluminium oxide(Al_2O_3), silicon oxide(SiO_2), and titanium oxide(TiO_2), which do not react with sulfur under the reaction conditions in a sealed quartz tube, were found to be effective for the elimination of carbonaceous impurities similarly to MgO. However, calcium oxide(CaO) and zinc oxide (ZnO), which react with sulfur to evolve sulfur dioxide (SO_2) under the same conditions as above, were unfavorable. Since the amounts of H, O, and N in the sulfur obtained by the present method, in which sulfur is refluxed with one of Al_2O_3, SiO_2, and TiO_2, were almost definite and small in comparison with those of carbonaceous impurities, the removal of carbonaceous impurities was exclusively investigated for the purification of sulfur.

Experimental

Reagents. Of the oxides, Al_2O_3 and SiO_2 were of GC-grade and MgO, TiO_2, ZnO, and CaO were of guaranteed grade. They were ignited at 950 °C for 1 h in the air before use. By this treatment, magnesium and calcium carbonates were expected to decompose with evolution of carbon dioxide (CO_2). Practically no CO_2 was detected in the gas chromatogram for the analysis of MgO. Sulfur as a starting material was of chemical grade.

Standard Procedure. About 100 g of sulfur was placed in a 300 ml four-hole flask with a reflux condenser and fused with an electric furnace, followed by addition of 1% (wt) MgO to sulfur. The contents were refluxed for about 24 h, and then the melts were filtered through the cylindrical glass filter held at 125 °C with a ribbon-heater. To the filtrate was added about 1% (wt) MgO and the same operation as above was repeated. About 75 g of sulfur was recovered after filtration. The oxides such as Al_2O_3, SiO_2, TiO_2, ZnO, and CaO were also used instead of MgO.

Analysis. The sulfur obtained in each purification step was analyzed by the same procedure as that given in the previous paper.[1] Twenty milligrams of sulfur was used for analysis. Carbonaceous impurities were determined as follows: A definite volume of a dilute glycine solution was taken in a reaction tube (a transparent quartz tube with one end closed) and evaporated to dryness in an oven at 65 °C, followed by addition of 20 mg of purified sulfur. The reaction tube was closed at the other end and the contents were analyzed. A calibration curve obtained on the basis of chromatograms was used for the determination of carbonaceous impurities.

Results and Discussion

Choice of Oxides. Since MgO did not react with sulfur, no SO_2 was evolved from MgO used in the Bacon-Fanelli method. The reaction between sulfur and oxides other than MgO was examined. Al_2O_3, SiO_2, and TiO_2 were found to be non-reactive with sulfur. Sulfur was purified by use of these oxides and the sulfur obtained was analyzed. The peaks of CO_2, carbonyl sulfide (COS), and carbon disulfide (CS_2) coming from carbon in the sample are shown in the gas chromatogram. The carbon content in the sulfur sample obtained in each purification step was determined by multiplying the correction factors[4] of CO_2, COS, and CS_2 by their peak areas and summing up the products. As seen from the relationship between the number of filtration and the content of carbonaceous impurities (Fig. 1), Al_2O_3, SiO_2, and TiO_2 are effective for the purification of sulfur similarly to the case of MgO, but not ZnO and CaO. Since the reaction

$$2AgNO_3 + 2S_2 \longrightarrow Ag_2S + 3SO_2 + N_2 \qquad (1)$$

reached completion, the relative conversion of the reaction between an oxide and sulfur was calculated from the amount of SO_2, based on the conversion of 1=1.0. There is a good correlation between the efficiency of the oxides (Fig. 1) and the relative conversion (Table 1). According to Bacon and Fanelli the effectiveness of MgO for the purification of sulfur is attributed to the basicity of MgO which shows an affinity to organic and inorganic acids in sulfur.[3] However, the reactivity of oxides to sulfur was concluded, on the basis of experimental results, to be more predominant than the basicity of the oxides.

Determination. The content of carbonaceous impurities in several sulfur samples was determined by means of the curve: 30—50 ppm in chemical grade sulfur, 3—6 ppm in sulfur purified with Al_2O_3, SiO_2, TiO_2, and MgO, and >100 ppm in commercial high purity sulfur (purity 99.9999%).

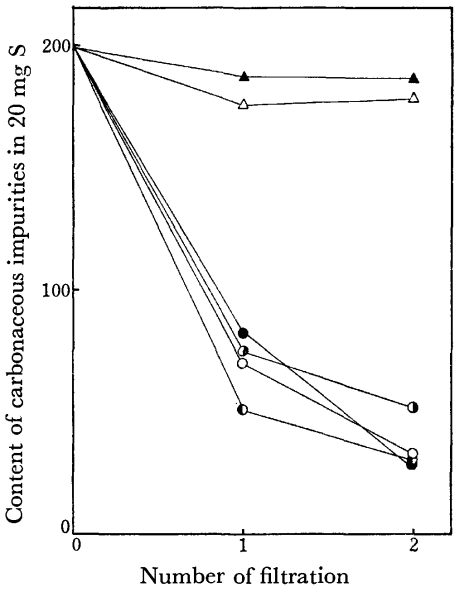

Fig. 1. The relationship between the number of filtration and the content of carbonaceous impurities.
○: MgO, ●: Al_2O_3, ◑: SiO_2, ◐: TiO_2, ▲: ZnO, △: CaO.

Table 1. Relative conversion in the reaction between an oxide and sulfur

Metal oxide	Relative conversion
MgO	0
Al_2O_3	0
SiO_2	0
TiO_2	0
CaO	0.67
ZnO	1.1

Organic Test. The spot test[3] to detect an organic substance in sulfur was applied to the sulfur obtained by refluxing with MgO, Al_2O_3, SiO_2, and TiO_2, but no black spot was hardly ever confirmed. However, a black spot appeared distinctly in the sulfur obtained by treatment with ZnO and CaO. This is in line with the results shown in Fig. 1. A fraction of the black spot was isolated and analyzed. Since the presence of carbonaceous impurities was confirmed gas chromatographically, the appearance of black color being attributed to the presence of an organic substance.

Reaction Time. Bacon and Fanelli pointed out that the organic substance in sulfur is isolated as a black cake during the course of refluxing and removed by filtration, a similar phenomenon to that above being also observed.[3] That is, sulfur was purified by refluxing for some time and by filtering a sludge in the absence of oxides. The effect of refluxing times 6 and 24 h on the removal of carbonaceous impurities was investigated by use of Al_2O_3 and the content of carbonaceous impurities was found to decrease with increase in refluxing time.

Effect of Oxygen. It was also found by use of Al_2O_3 that carbonaceous impurities are removed more effectively in nitrogen atmosphere than in the air. The result is contrary to what we expected. The reason remains unknown. A dark gray sludge sample obtained by refluxing sulfur with MgO in the air and by filtering the melts was analyzed and the peak area of CO_2 was found to be abnormally large.

From the results, it can be concluded that the purification of sulfur is mainly achieved by the adsorption of organic substances on the oxide, but not by the atmospheric oxidation of organic substances.

The authors wish to express their thanks to Mr. Hiroshi Suzuki, Dr. Masanori Nakae, and Dr. Yoshizo Miyake, Government Industrial Research Institute, Osaka, for the supply of purified sulfur sample.

References

1) Part I: K. Tsuji, K. Fujinaga, and T. Hara, *Bull. Chem. Soc. Jpn.*, **50**, 2292 (1977).
2) H. Suzuki, M. Nakae, and Y. Miyake, Japan Patent 617354 (1971).
3) R. F. Bacon and R. Fanelli, *Ind. Eng. Chem.*, **34**, 1043 (1942).
4) Part II: T. Hara, K. Fujinaga, and K. Tsuji, *Bull. Chem. Soc. Jpn.*, **51**, 1110 (1978).

BULLETIN OF THE CHEMICAL SOCIETY OF JAPAN, VOL. 51 (10), 3081—3082 (1978)

Reaction of α-Keto Sulfoxides with Hydrogen Chloride and Trichloroacetic Acid

Toshimitsu WAKUI, Yoshio NAKAMURA, and Shinichi MOTOKI*

Department of Chemistry, Faculty of Science, Science University of Tokyo, Kagurazaka, Shinjuku-ku, Tokyo 162

(Received December 22, 1977)

Synopsis. α-Keto sulfoxides (**1**) reacted with hydrogen chloride to afford chloroformates, disulfides, and thiosulfonates. **1** also reacted with trichloroacetic acid to give methyl trichloroacetate, disulfide and thiosulfonate.

α-Keto sulfoxides have been postulated as unstable intermediates in the thiocarboxylic *S*-acid oxidation with NBS, iodosobenzene,[1] and *m*-chloroperbenzoic acid[2] and isolated as stable compounds by oxidizing thiocarbonate *O,S*-diesters and related substances with *m*-chloroperbenzoic acid.[3] This new class of organic compounds are interesting and have attracted the attention of organic chemists to their chemical behavior.

Recent studies by Chaves das Neves and Machete have shown that ethoxycarbonyl benzyl sulfoxide reacts with thionyl chloride and *S*-benzyl *O*-ethyl thiocarbonate.[4] Furukawa and his co-workers also reported that benzyloxycarbonyl benzyl sulfoxide reacts with acetic anhydride to give 1-(acetylthio)benzyl sulfoxide together with other products.[5] In this note, the reactions of α-keto sulfoxides with hydrogen chloride and trichloroacetic acid will be reported.

Dry hydrogen chloride was bubbled at room temperature for 2 h into a solution of phenoxycarbonyl ethyl sulfoxide (**1a**) in dichloromethane. After the solution was stirred for an additional 20 h, it was shown by TLC that **1a** was consumed, and from the reaction mixture, phenyl chloroformate (**3a**), diethyl disulfide (**6a**) and *S*-ethyl ethanethiosulfonate (**7a**) were isolated in fairly good yields. The structures of the products were determined from their spectroscopic data.

In the reactions of methoxycarbonyl benzyl sulfoxide (**1b**), methoxycarbonyl phenyl sulfoxide (**1c**) and ethoxycarbonyl benzyl sulfoxide (**1d**) with hydrogen chloride, the yields of alkyl chloroformates (**3**) were determined by conversion into the alkyl phenyl carbonate derivatives. The disulfides (**6**) and the thiosulfonates (**7**) were separated by column chromatography using benzene–petroleum ether (1 : 1) as the eluent. The reaction of benzyloxycarbonyl benzyl sulfoxide (**1e**) with hydrogen chloride similarly gave benzyl chloroformate (**3e**), dibenzyl disulfide (**6e**) and *S*-benzyl toluene-α-thiosulfonate (**7e**). The yields of **3e** and **6e** were calculated by the integrated ratio of the PMR spectrum of the mixture since they could not be separated by ordinary column chromatography. The results are shown in Table 1.

Table 1. Reaction of α-keto sulfoxides **1** with hydrogen chloride

α-Keto sulfoxide	R_1	R_2	Yield (%)		
			3	**6**	**7**
1a	Ph	Et	74	63	76
1b	Me	$PhCH_2$	69	90	91
1c	Me	Ph	59	99	84
1d	Et	$PhCH_2$	57	92	93
1e	$PhCH_2$	$PhCH_2$	65	86	93

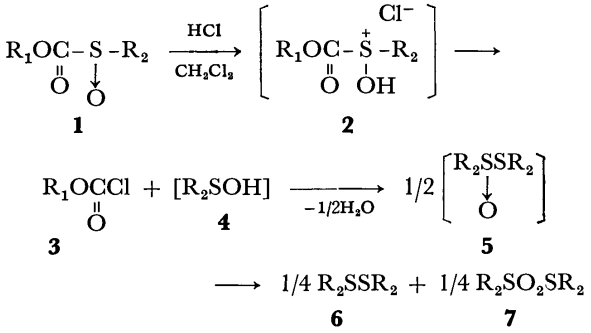

Scheme 1.

The reaction probably proceeds *via* an initial protonation of the sulfoxide **1** affording an unstable sulfonium ion such as **2** which is further converted to the alkyl (or aryl) chloroformate **3** and the sulfenic acid **4**. Then **4** may give the thiosulfinate **5** which disproportionates further to give the final products, the disulfide **6** and the thiosulfonate **7**. This scheme is based on the observation that the sulfenic acids afford water and the thiosulfinates through dimerization[6] while the thiosulfinates smoothly disproportionate in acidic conditions to the disulfides and the thiosulfonates.[7]

Both the reaction of **1d** with hydrogen chloride and with thionyl chloride gave closely similar products such

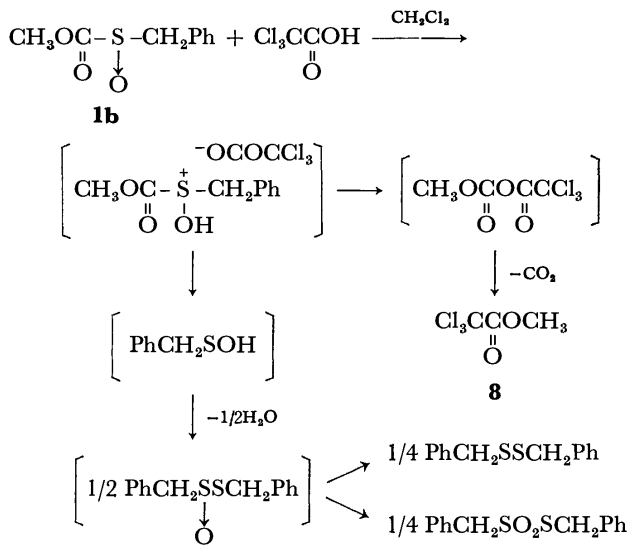

Scheme 2.

as ethyl chloroformate, dibenzyl disulfide, and *S*-benzyl toluene-α-thiosulfonate, but the yields of the products are better in the former case.

When a solution of **1b** and trichloroacetic acid in dichloromethane was refluxed for 15 h, methyl trichloroacetate (**8**, 42%), dibenzoyl disulfide (40%) and *S*-benzyl toluene-α-thiosulfonate (46%) were the products. These results may be rationalized according to Scheme 2.

Experimental

All the melting and boiling points are uncorrected. The IR spectra were obtained on a 260-10 Hitachi Model infrared spectrophotometer. PMR spectra were recorded with a JEOL JNM-PMX 60 spectrometer, in $CDCl_3$ solution with TMS as an internal standard.

Materials. α-Keto sulfoxides **1d** and **1e** were obtained by the methods described in the literature.[3] Other α-keto sulfoxides **1a**—**c** were prepared in a similar manner and their physical properties are as follows: **1a**: mp 67—69 °C; IR (Nujol): 1760 cm^{-1} (C=O); PMR (δ): 1.27 (t, 3H), 2.85 (q, 2H), 7.17 (s, 5H). **1b**: mp 81 °C; IR (Nujol): 1765 cm^{-1} (C=O); PMR (δ): 3.92 (s, 3H), 4.23 (s, 2H), 7.33 (s, 5H). **1c**: mp 77—78 °C; IR (Nujol): 1760 cm^{-1} (C=O); PMR (δ): 3.93 (s, 3H), 7.70 (m, 5H).

General Procedure for Reactions of α-Keto Sulfoxides (1) with Hydrogen Chloride. Dry hydrogen chloride was bubbled at room temperature for 2 h with stirring into a solution of **1** (3–23 mmol) in dichloromethane. The reaction mixture was stirred at the same temperature for 20 h and each product was separated as follows.

1a: After the solvent had been removed under reduced pressure, distillation of the residue gave 0.44 g (63%) of diethyl disulfide (**6a**), bp 50—60 °C/31 Torr, 2.68 g (74%) of phenyl chloroformate (**3a**), bp 60—62 °C/8 Torr, and 0.68 g (76%) of *S*-ethyl ethanethiosulfonate (**7a**), bp 90—100 °C/5 Torr.

1b: The solvent and methyl chloroformate (**3b**) were distilled under reduced pressure. The distillate was then added to a solution of phenol (0.94 g, 10 mmol) and triethylamine (5 g, excess) in ether (50 ml) and the mixture stirred for 5 h. Water (100 ml) was added to the mixture and the organic layer that separated, was successively washed with dilute sodium hydroxide solution, dilute hydrochloric acid, and water, dried over anhydrous sodium sulfate, and evaporated under reduced pressure to afford 0.95 g (69%) of methyl phenyl carbonate.

The residue obtained after the solvent and **3b** had been removed, was column chromatographed on silica gel C-200. Elution with benzene–petroleum ether (1 : 1) gave 0.50 g (90 %) of dibenzyl disulfide (**6b**), mp 68.5—69 °C, and 0.57 g (91 %) of *S*-benzyl toluene-α-thiosulfonate (**7b**), mp 108—109 °C.

1c, *1d*: The products obtained by the reactions of **1c** and **1d** with hydrogen chloride were isolated in a similar manner as above.

1e: After the solvent had been removed under reduced pressure, the residue was subjected to column chromatography on silica gel to afford the mixture of benzyl chloroformate (**3e**) and dibenzyl disulfide (**6e**), and 0.20 g (96%) of *S*-benzyl toluene-α-thiosulfonate (**7e**) by elution with benzene–petroleum ether (1 : 1). The yields of **3e** and **6e** (as determined by PMR) were 65 and 86%, respectively.

Reaction of 1b with Trichloacetic Acid. A mixture of **1b** (1.78 g, 9 mmol) and trichloroacetic acid (1.47 g, 9 mmol) in dichloromethane (30 ml) was refluxed for 15 h and the solvent removed under reduced pressure. The residue was distilled to give 0.63 g (42%) of methyl trichloroacetate (**8**), bp 50—56 °C/19 Torr. The residue obtained after distillation was dissolved in ether (100 ml) and the solution succesively washed with water, dilute sodium hydroxide solution, and water. After being dried over anhydrous sodium sulfate, the solvent was removed. The residue was column chromatographed on silica gel to afford 0.22 g (40%) of dibenzyl disulfide and 0.29 g (46%) of *S*-benzyl toluene-α-thiosulfonate, by elution with benzene–petroleum ether (1 : 1).

References

1) T. Kumamoto and T. Mukaiyama, *Bull. Chem. Soc. Jpn.*, **41**, 2111 (1968).

2) H. Minato, H. Kodama, T. Miura, and M. Kobayashi, *Chem. Lett.*, **1977**, 413.

3) D. H. R. Barton, D. P. Manly, and D. A. Widdowson, *J. Chem. Soc., Perkin Trans. 1*, **1975**, 1568.

4) H. J. Chaves das Waves and M. F. Machete, *Tetrahedron Lett.*, **1977**, 187.

5) N. Furukawa, T. Morishita, T. Akasaka, and S. Oae, *Tetrahedron Lett.*, **1977**, 1653.

6) J. R. Shelton and K. E. Davis, *J. Am. Chem. Soc.*, **89**, 714 (1967).

7) E. Brock and S. W. Weidman, *J. Am. Chem. Soc.*, **95**, 5046 (1973); D. Barnard, *J. Chem. Soc.*, **1957**, 4675; S. Oae and S. Kawamura, *Bull. Chem. Soc. Jpn.*, **35**, 1156 (1962).

BULLETIN OF THE CHEMICAL SOCIETY OF JAPAN, VOL. 51 (10), 3083—3084 (1978)

The Preparation of 6-Nitro-3-acetamidotoluene

Aoi ONO

Chemical Laboratory, Takada Branch, Faculty of Education, Niigata University, Nishishiro-cho, Joetsu 943

(Received February 3, 1978)

Synopsis. *m*-Acetamidotoluene was nitrated with fuming nitric acid in acetic acid or in a mixture of acetic and sulfuric acids at 20 °C, affording 6-nitro-3-acetamidotoluene in 38.6 and 53.7% yields respectively. The melting point of the product was found to be different from that reported in the literature.

In order to analyze mononitro acetamidotoluenes and toluidines by GLC, an authentic, pure sample of 6-nitro-3-acetamidotoluene was prepared by the simplest way. Noelting[1] reported that 6-nitro-3-aminotoluene could be obtained by the nitration of *m*-toluidine in a mixture of nitric and sulfuric acids. Coffey[2] nitrated *m*-acetamidotoluene with copper(II) nitrate. Cohen *et al.*[3] and Cook *et al.*,[4] nitrated *m*-acetamidotoluene with fuming nitric acid in acetic acid. Cohen *et al.*[5] and Morgan *et al.*[6] nitrated *m*-acetamidotoluene with a mixture of nitric and sulfuric acids. Morgan *et al.*,[7] Wibant,[8] and Cook *et al.*[4] compared the yields and ratios of 6- and 4-nitro-3-acetamidotoluenes formed under various conditions. However, the ratio of products (6- and 4-nitro-3-acetamidotoluenes) still remains ambiguous and the reported purification procedure seems unsatisfactory. The present author has, therefore, reinvestigated the procedure and found that an erroneous melting point of 6-nitro-3-acetamidotoluene was reported.

Experimental

The GLC analyses were performed on a 100 cm column (i.d. 3.0 mm) packed with C_{22} 60—80 mesh coated with 3% Silicone OV-17 or 20% Silicone KF-54 at 220 °C, using a Shimadzu GC-5A GC apparatus with FID. The IR and NMR spectra were recorded on a Hitachi EPI-S2 IR spectrophotometer and a Varian T-60 NMR spectrometer respectively. The measurement of the mp (corrected) and DTA were performed with a Yanagimoto Micro-Melting-Point Apparatus and a Rigaku Thermal TG-DTA M8075 respectively.

Reagent. The *m*-acetamidotoluene was prepared by refluxing a mixture of 70 g of *m*-toluidine (guaranteed grade, from the Nakarai Chemical Co.) and 300 ml of acetic acid (extra pure reagent, also from the Nakarai Chemical Co.) for 8 h. Fuming nitric acid (*d*, 1.50) and sulfuric acid (95%) of an extra pure reagent grade were purchased from the Nakarai Chemical Co.

Preparation. Part 1. Twenty grams of *m*-acetamidotoluene, suspended in 50 ml of acetic acid, were nitrated by adding 40 ml of fuming nitric acid (*d*, 1.50) over a period of 10 min with effective stirring below 20 °C. After the reaction, the contents were poured into 1 litre of ice water, and then the solid was filtered and dried. Pure 6-nitro-3-acetamidotoluene was obtained in a 38.6% yield after twice recrystallizations from 30% aqueous ethanol. Part 2. Twenty grams of *m*-acetamidotoluene were nitrated in a mixture of 30 ml of acetic and 30 ml of sulfuric acids with fuming nitric acid by the procedure described in Part 1. The yield was 53.7%. The melting point of the compound recrystallized from 30% aqueous ethanol or benzene was 117 °C, in contrast to the reported values of 101—102[9] and 103—104 °C.[3] Found: C, 50.98; H, 5.72; N, 13.49%. Calcd for $C_9H_{12}N_2O_4$: C, 50.94; H, 5.60; N, 13.20%. GLC retention time: 16.00 min on Silicone KF-54; 4.00 min on Silicone OV-17. TLC R_f; 0.50 on a silica gel plate; 0.80 on an alumina plate (solvent; carbon tetrachloride: ethyl acetate, 9: 1, v/v) at room temperature. IR; 3600—3200 (νNH_2), 1680 (νCO), 870 (δNO_2), and 750 cm^{-1} (δNH_2) NMR; δ (TMS, CD_3OD), 2.13 (s, 3H), 2.38 (s, 3H), 7.53—7.75 (m, 2H) and 7.90—8.11 (m, 1H).

6-Nitro-3-aminotoluene was obtained by the hydrolysis of 6-nitro-3-acetamidotoluene. Mp 136—138 °C (lit, 136—138,[5] 138—140 °C[7]); Found: C, 55.30; H, 5.29; N, 18.74%. Calcd for $C_7H_8N_2O_2$: C, 55.25; H, 5.30; N, 18.41%. GLC retention time; 6.00 min on Silicone KF-54; 1.00 min on Silicone OV-17. TLC R_f; 1.70 on a silica gel plate; 2.00 on an alumina plate (solvent: carbon tetrachloride: ethyl acetate, 9:1, v/v) at room temperature. IR; 3550, 3400 (νNH_2), 1620 ($\nu C{=}C$), 1300, 1250 (νNO_2), 850 (δNO_2), and 815 cm^{-1} (δNH_2). NMR; δ (TMS, CD_3OD), 2.61 (s, 3H), 6.56 (m, 2H), and 7.93—8.10 (m, 1H).

Results and Discussion

As has been mentioned in the Experimental section, when *m*-acetamidotoluene was nitrated in acetic acid or in a mixture of acetic and sulfuric acids (1: 1, v/v), 6-nitro-3-acetamidotoluene was obtained in a 38.6 or 53.7% yield respectively, after twice recrystallizations from 30% aqueous ethanol. The purity of the product was confirmed by GLC, TLC, IR, and NMR.

However, the melting point of the product was 117 °C, which is apparently different from that reported in the literature (lit, 101—102,[9] 103—104 °C[3]). Then DTA and elemental analyses were undertaken. The results of elemental analyses were reported in the Experimental section, the diagram of DTA had two peaks, at 117 and 102 °C, and the weight loss on DTA at 102 °C corresponded to the weight of one molecule of water. From these data, the prepared product was identified as 6-nitro-3-acetamidotoluene monohydrate. Details concerning the molecular structure of this prepared product will be reported elsewhere in the near future.

References

1) R. Noelting and L. Stoecklin, *Ber.*, **24**, 564 (1891).
2) S. Coffey, *J. Chem. Soc.*, **1926**, 3215.
3) J. B. Cohen and H. D. Dakin, *J. Chem. Soc.*, **83**, 331 (1903).
4) J. B. Cook and O. L. Brade, *J. Chem. Soc.*, **117**, 750 (1920).
5) J. B. Cohen and H. J. Hodsman, *J. Chem. Soc.*, **91**, 970 (1907).

6) G. T. Morgan and G. E. Scharff, *J. Chem. Soc.*, **105**, 117 (1914).
7) G. T. Morgan and F. M. G. Micklewait, *J. Chem. Soc.*, **103**, 1391 (1913).
8) M. J. P. Wibant, *Recl. Trav. Chim. Pays-Bas*, **32**, 287 (1913).
9) J. W. Cook and O. L. Brady, *J. Chem. Soc.*, **1920**, 750.

BULLETIN OF THE CHEMICAL SOCIETY OF JAPAN, VOL. 51 (10), 3085—3086 (1978)

(Hydroxyalkyl)pyridines as Bifunctional Catalysts. Dehydrobromination of 7-Bromocholesterol

Yoji TACHIBANA

Ueda Factory, Nisshin Chemical Co., Ltd., Kamishiodiri, Ueda-shi, Nagano 386

(Received March 8, 1978)

Synopsis. In the dehydrobromination of 7-bromocholesterol, the reactions catalyzed by 2- and 3-(hydroxyalkyl)-pyridines afforded 5,7-diene and 4,6-diene as the main product, respectively. The relative isomer ratio has been related to the position of the hydroxyalkyl group of the (hydroxyalkyl)pyridines. The results have been interpreted in terms of a concerted mechanism through a cyclic intermediate.

Increased attention has been paid to bifunctional catalysts in connection with biochemical reactions.[1-6] A selective rearrangement of penicillin *S*-oxide to isothiazolone using (hydroxyalkyl)pyridines as catalysts has been reported and the mechanism interpreted as a concerned reaction through a cyclic intermediate.[7] In the course of studies on the catalytic activities of (hydroxyalkyl)pyridines, it has been found that 2- and 3-(hydroxyalkyl)pyridines act as bifunctional catalysts in the dehydrobromination of 7-bromocholesterol.

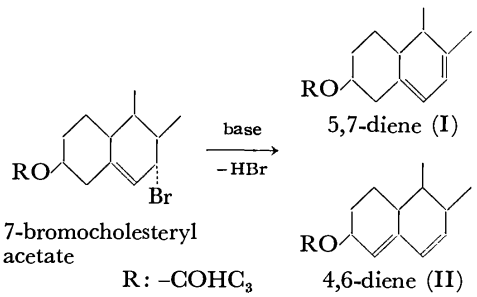

7-bromocholesteryl acetate

R: $-COHC_3$

It is known that the dehydrobromination of esters of 3-β-hydroxy-7-bromo-Δ^5-steroids gives a mixture of products, in which either a 5,7-diene or a 4,6-diene predominates, depending on the nature of the dehydrobrominating agent. Organic and inorganic bases do not act selectively and give mixtures of isomers.[8-10] When the dehydrobromination was carried out in the presence of 2-(hydroxyalkyl)pyridines, the 5,7-diene (I) was obtained as the main product. The reaction catalyzed by 3-(hydroxyalkyl)pyridines, on the other hand, afforded the 4,6-diene (II) selectively. The employment of 4-(hydroxyalkyl)pyridines showed no selectivity in the formation of (I) or (II) compared with the 2- and 3-(hydroxyalkyl)pyridines. The results are summarized in Table 1.

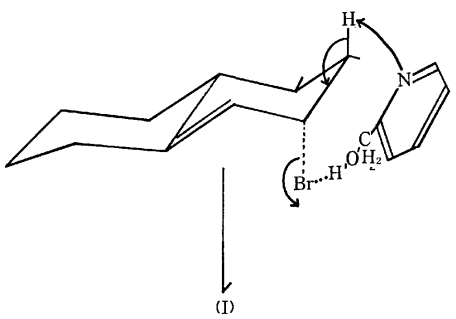

(I)

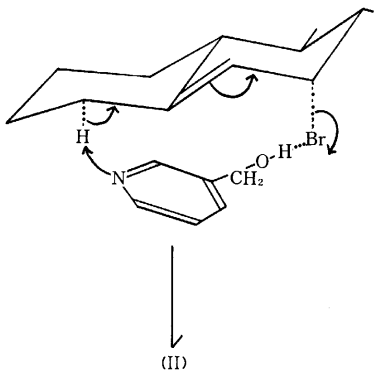

(II)

Table 1. Yield and relative ratio (I/II)

Base	Yield(%)[a] (I)	Yield(%)[a] (II)	Relative ratio[b] (I/II)
2-(Hydroxymethyl)pyridine	43.9	31.1	1.41
2,6-(Dihydroxymethyl)pyridine	44.1	30.8	1.43
2-(2-Hydroxyethyl)pyridine	46.1	29.0	1.59
2-(3-Hydroxypropyl)pyridine	41.9	31.2	1.34
Pyridine	23.4	35.4	0.66
2-Ethylpyridine	26.5	31.2	0.84
2-Propylpyridine	26.8	27.8	0.96
3-(Hydroxymethyl)pyridine	19.7	56.3	0.35
3-(3-Hydroxypropyl)pyridine	20.5	54.0	0.38
3-Ethylpyridine	22.6	35.9	0.63
4-(Hydroxymethyl)pyridine	24.6	49.3	0.50
4-(3-Hydroxypropyl)pyridine	25.8	49.7	0.53
4-Ethylpyridine	23.7	42.1	0.56
4-Propylpyridine	22.8	42.1	0.54

a), b) Yield and relative ratio were determined by GLC.

The interpretation is that a 5,7-diene (I) would be formed when the bromine atom on the carbon atom in position 7 is α, since hydrogen linked with the carbon atom in position 8 is always β. 7-Bromocholesteryl acetate employed in the reaction is considered to consist primarily of 7-α-bromocholesteryl acetate as suggested by Bernstein.[9] However, Jaworeska observed no relation between the configuration of the bromine atom in position 8 and the yield of 5,7-diene(I), and suggested the possibility of a rapid epimerization of the bromine atom.[11]

As can be seen in Table 1, 2- and 3-(hydroxyalkyl)-pyridines showed selectivity in the formation of (I) and (II) compared to the corresponding alkylpyridines. This

suggests that the steric and inductive effects are excluded and the hydroxyl group plays an important role in the selective formation of (I) and (II). The reported results above are most readily rationalized by a concerted mechanism involving a cyclic intermediate. The reaction may be initiated by the abstraction of a proton in position 8 or 4. The abstraction of the proton in position 8 competes with that in position 4, giving rise to the 5,7-diene (I) and the 4,6-diene (II), respectively. In the case of 2-(hydroxyalkyl)pyridines, the base abstracts the proton in position 8 and the reaction is considered to proceed through the cyclic intermediate by the interaction of the hydroxyl group with the bromine atom to give (I) as the main product.

When 3-(hydroxyalkyl)pyridines are employed, the preferential formation of (II) can be interpreted by assuming the selective abstraction of the proton in position 4 followed by the formation of a cyclic intermediate as depicted in the figure. It is highly probable that 4-(hydroxyalkyl)pyridines can not form cyclic intermediates since the interaction of the hydroxyl group with the bromine atom is considered to be difficult. This explains the absence of selectivity observed in the reaction catalyzed by 4-(hydroxyalkyl)pyridines compared with 2- and 3-(hydroxyalkyl)pyridines. The most plausible mechanism explaining the catalytic activities of 2- and 3-(hydroxyalkyl)pyridines is shown below.

Further work including a extension of the reaction and a mechanistic study of the reaction is now in progress.

Experimental

GLC was recorded on a Hitachi 023 gas chromatograph equipped with a flame ionizer detector.

A typical procedure is described for the reaction of cholesteryl acetate with 2-(hydroxymethyl)pyridine; A hexane solution (100 ml) of cholesteryl acetate (4.3 g, 10 mmol), *N*-bromosuccinimide (2.1 g, 12 mmol) and a catalytic amount of benzoyl peroxide was allowed to reflux for 1 h. After the reaction, the hexane solution was filtered to remove succinimide and the filtrate evaporated to dryness under reduced pressure. The residue was dissolved in butyl acetate (50 ml) and 2-(hydroxymethyl)pyridine (1.3 g, 12 mmol) was added. The mixture was heated under reflux for 1 h. The solution was washed with dilute hydrochloric acid and water, dried over anhydrous Na_2SO_4 and the extract condensed under reduced pressure. The residue was analyzed by GLC.

The author wishes to thank the Nisshin Chemical Co., Ltd., for permission to publish this report. The author is also grateful to Drs. K. Nakagawa and H. Fukawa of the Central Research Laboratory, Nisshin Flour Milling Co., Ltd., for their interest throughout this work.

References

1) T. H. Fife and B. M. Benjamin, *J. Am. Chem. Soc.*, **95**, 2059 (1973).
2) F. M. Menger, H. K. Rhee, and J. U. Rhee, *J. Am. Chem. Soc.*, **98**, 792 (1976).
3) P. Lochon and J. Schoenleber, *Tetrahedron*, **32**, 3023 (1976).
4) M. Feizon and P. Jaudon, *Tetrahedron*, **33**, 1619 (1977).
5) P. Wooley, *J. Chem. Soc., Chem. Commun.*, **1975**, 579.
6) L. Anoardi and U. Tonellato, *J. Chem. Soc., Chem. Commun.*, **1977**, 401.
7) Y. Tachibana, K. Nakagawa, and H. Fukawa, *Nippon Kagaku Kaishi*, **1976**, 148.
8) A. E. Bide, H. B. Henbest, E. R. H. Jones, R. W. Peevers, and P. A. Wilkinson, *J. Chem. Soc.*, **1948**, 1783.
9) S. Bernstein, L. J. Binovi, L. Dorfman, K. J. Sax, and Y. Subbarow, *J. Org. Chem.*, **14**, 433 (1949).
10) F. Hunziker and F. X. Mullner, *Helv. Chim. Acta*, **41**, 70 (1958).
11) R. Jaworska and M. Kocór, *Tetrahedron Lett.*, **1968**, 4341.

BULLETIN OF THE CHEMICAL SOCIETY OF JAPAN, VOL. 51 (10), 3087—3088 (1978)

The Oxidative Amination of Diethyl 2-Hydroxyazulene-1,3-dicarboxylate and Cycloheptimidazol-2(1*H*)-one

Katsuo KIKUCHI,* Yuji MAKI, and Noriyuki SAITO

Department of Chemistry, Faculty of Science, Yamagata University, Koshirakawa-cho, Yamagata 990

(Received March 22, 1978)

Synopsis. The reaction of diethyl 2-hydroxyazulene-1,3-dicarboxylate with morpholine, pyrrolidine, piperidine, and dimethylamine in the presence of copper(II) acetate gave the respective 6-aminoazulene derivatives. Similarly, the reaction of cycloheptimidazol-2(1*H*)-one with morpholine gave the 6-aminocycloheptimidazole derivative, while the reaction with pyrrolidine gave the 4-(or 5-)aminocycloheptimidazole derivative.

Azulene derivatives carrying amino groups on a seven-membered ring have usually been obtained by the nucleophilic substitution reaction,[1-3] by the Schmidt reaction on acetylazulene derivatives,[4] or by the reaction of acetamidotropolone with ethyl cyanoacetate.[5] Similarly, 4-, 5-, and 6-aminocycloheptimidazole derivatives have also been obtained by the nucleophilic substitution reaction,[6,7] Schmidt reaction,[8] or reduction of nitro group.[6] In the preceding paper,[9] we have reported that the reaction of tropone and tropolone with several kinds of amines in the presence of copper(II) salt afforded 2-aminotropones and 3- and 5-aminotropolones. In the course of the investigation of the oxidative amination of seven-membered aromatics, it was found that the title compounds were also aminated on treatment with amines, and these results will be reported in this paper.

When diethyl 2-hydroxyazulene-1,3-dicarboxylate (**1**) was heated with a solution of copper(II) acetate and morpholine in ethanol, a yellow crystalline product (**2a**), $C_{20}H_{23}O_6N$, was obtained in about 20% yield. The UV spectrum exhibited maxima at 234, 265, 348, 405, and 430 nm (sh), suggesting that **2a** is an azulenic compound. The NMR spectrum exhibited signals at 7.14 (C_5– and C_7–H, d, J=12 Hz) and 9.10 ppm (C_4– and C_8–H, d, J=12 Hz) besides the signals due to the hydroxyl, morpholino methylene, and ester ethyl groups. The elemental analysis and these spectral data indicate that **2a** is diethyl 2-hydroxy-6-morpholinoazulene-1,3-dicarboxylate. The treatment of **1** with pyrrolidine, piperidine, and dimethylamine under similar conditions gave 6-(1-pyrrolidinyl) (**2b**), 6-piperidino (**2c**), and 6-dimethylamino (**2d**) derivatives, respectively. The alkaline hydrolysis and decarboxylation of **2a** to obtain 2-hydroxy-6-morpholinoazulene failed, and the product obtained was ethyl 2-hydroxy-6-morpholinoazulene-1-carboxylate (**3a**). Similarly, monomethyl esters (**3b** and **3c**) were also obtained from **2b** and **2c**.

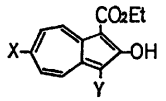

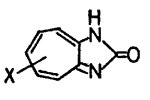

2a: X=morpholino Y=CO_2Et
2b: X=1-pyrrolidinyl Y=CO_2Et
2c: X=piperidino Y=CO_2Et
2d: X=dimethylamino Y=CO_2Et
3a: X=morpholino Y=H
3b: X=1-pyrrolidinyl Y=H
3c: X=piperidino Y=H

4: X=H
5a: X=6-morpholino
5b: X=4-(or 5-)-(1-pyrrolidinyl)

When cycloheptimidazol-2(1*H*)-one (**4**) was heated with a solution of copper(II) acetate and morpholine in methanol, a yellowish-orange crystalline product (**5a**), $C_{12}H_{13}O_2N_3$, mp 310 °C (dec) was obtained in about 15% yield. The UV spectrum of **5a** showed maxima at 255, 292, and 420 nm. The NMR spectrum (in trifluoroacetic acid) exhibited signals at 7.76 (C_5– and C_7–H, d, J=13.2 Hz) and 8.23 ppm (C_4– and C_8–H, d, J=13.2 Hz), indicating that **5a** is 6-morpholinocycloheptimidazol-2(1*H*)-one. On the other hand, when **4** was treated with pyrrolidine under similar conditions, yellow crystals (**5b**) $C_{12}H_{13}ON_3$, mp 297 °C (dec) were obtained. The NMR spectrum (in trifluoroacetic acid) exhibited signals due to aromatic protons at 7.3—8.1 ppm (4H) as a complex multiplet; the splitting pattern is quite different from that of **5a**. The UV spectrum, which shows maxima at 245, 279, 367, and 457 nm is also quite different from that of **5a**. Therefore, **5b** must be 4-(or 5-)(1-pyrrolidinyl)cycloheptimidazol-2(1*H*)-one.

Experimental

All the melting points were uncorrected. The NMR spectra were determined on a Hitachi H-60 instrument (Me_4Si), the UV spectra were recorded on a Hitachi EPS-3T spectrometer, and the IR spectra were taken on a Hitachi EPI-S spectrometer.

The Reaction of Diethyl 2-Hydroxyazulene-1,3-dicarboxylate (1) with Morpholine, Pyrrolidine, Piperidine, and Dimethylamine. To a solution obtained by dissolving copper(II) acetate (1.00 g) in ethanol (3 ml) and morpholine (3 ml), **1** (0.72 g) was added, and the mixture was heated at 70—75 °C for 48 h. The reaction mixture was diluted with water. The precipitate was collected, washed with water, and dried. Then it was dissolved in chloroform, hydrogen sulfide was passed through, and copper(II) sulfide was removed. After the solvent was evaporated, the residue was dissolved in benzene and passed through a silica gel column. The fraction eluted with benzene gave 380 mg of starting material, and the fraction eluted with a mixture of chloroform and ethanol (99: 1) gave 185 mg (20%) of diethyl 2-hydroxy-6-morpholinoazulene-1,3-dicarboxylate (**2a**) as yellow needles (from ethanol), mp 169.5—170.5 °C. UV (methanol) max: 234 (log ε 4.35), 265 (4.43), 348 (4.74), 405 (4.23), and 430 nm (sh, 4.10). Found: C, 64.07; H, 6.08; N, 3.71%. Calcd for $C_{20}H_{23}NO_6$: C, 64.33; H, 6.21; N, 3.75%.

The reaction of **1** with pyrrolidine, piperidine, and dimethylamine was carried out similarly.

Diethyl 2-hydroxy-6-(1-pyrrolidinyl)azulene-1,3-dicarboxy-

late (**2b**). Orange yellow prisms (from dioxane), mp 205—208 °C (dec). Yield, 23%. UV (methanol) max: 266 (log ε 4.44), 348 (4.77), 402 (4.25), and 431 nm (4.22). NMR ($CDCl_3$): δ, 6.60 (C_5- and C_7-H, d, J=12 Hz), and 8.90 (C_4- and C_8-H, d, J=12 Hz). Found: C, 67.51; H, 6.55; N, 3.56%. Calcd for $C_{20}H_{23}NO_5$: C, 67.21; H, 6.49; N, 3.92%.

Diethyl 2-hydroxy-6-piperidinoazulene-1,3-dicarboxylate (**2c**). Orange yellow prisms (from ethanol), mp 128—129 °C. Yield, 26%. UV (methanol) max: 232 (log ε 4.35), 266 (4.48), 351 (4.77), 402 (4.32), and 431 nm (4.25). NMR ($CDCl_3$): δ, 7.13 (C_5- and C_7-H, d, J=12 Hz), and 9.09 (C_4- and C_8-H, d, J=12 Hz). Found: C, 67.74; H, 6.68; N, 3.62%. Calcd for $C_{21}H_{25}NO_5$: C, 67.90; H, 6.78; N, 3.77%.

Diethyl 2-hydroxy-6-dimethylaminoazulene-1,3-dicarboxylate (**2d**). Orange prisms (from dioxane), mp 187—188 °C. UV (methanol) max: 230 (log ε 4.31), 265 (4.48), 347 (4.79), 402 (4.23), and 430 nm (4.17). NMR ($CDCl_3$): δ, 6.72 (C_5- and C_7-H, d, J=13 Hz), and 8.95 (C_4- and C_8-H, d, J=13 Hz). Found: C, 65.60; H, 6.50; N, 4.14%. Calcd for $C_{18}H_{21}NO_5$: C, 65.24; H, 6.39; N, 4.23%.

*The Alkaline Hydrolysis and Decarboxylation of **2a**, **2b**, and **2c**.* A solution of sodium hydroxide (150 mg) in water (1.5 ml) and ethanol (3 ml) was refluxed with **2a** (280 mg) for 5 h on a water bath. The mixture was diluted with water and acidified. The crystalline precipitate was washed with water and dried. The chromatographic separation on preparative TLC using Merck Silica Gel PF_{254} gave 80 mg of **2a** and 95 mg of ethyl 2-hydroxy-6-morpholinoazulene-1-carboxylate (**3a**), orange prisms (from dioxane), mp 166—168 °C. UV (methanol) max: 221 (log ε 4.45), 338 (4.76), and 400 nm (4.08). NMR ($CDCl_3$): δ, 6.57 (C_3-H, s), 7.0 (C_5- and C_7-H, m), 7.91 (C_4-H, d, J=12 Hz), and 8.77 (C_8-H, d, J=11 Hz). Found: C, 67.88; H, 6.50%. Calcd for $C_{17}H_{19}NO_4$: C, 67.76; H, 6.36%.

Ethyl 2-hydroxy-6-(1-pyrrolidinyl) azulene-1-carboxylate (**3b**). Orange yellow scales (from dioxane), mp 185—186 °C. UV (methanol) max: 219 (log ε 4.39), 241 (4.03), 345 (4.83), 406 (4.12), and 438 (3.98). NMR ($CDCl_3$): δ, 6.5 (C_3-, C_5-, and C_7-H, m), 7.77 (C_4-H, d, J=12 Hz), and 8.61 (C_8-H, d, J=12 Hz). Found: C, 71.79; H, 6.93%. Calcd for $C_{17}H_{19}NO_3$: C, 71.56; H, 6.71%.

Ethyl 2-hydroxy-6-piperidinoazulene-1-carboxylate (**3c**). Orange crystals (from ethanol), mp 114—115 °C. UV (methanol) max: 221 (log ε 4.41), 345 (4.73), and 409 nm (4.14). NMR ($CDCl_3$): δ, 6.45 (C_3-H, s), 6.9 (C_5- and C_7-H, m), 7.82 (C_4-H, d, J=12 Hz), 8.67 (C_8-H, d, J=11 Hz). Found: C, 72.57; H, 7.26%. Calcd for $C_{18}H_{21}NO_3$: C, 72.21; H, 7.07%.

*The Reaction of Cycloheptimidazol-2(1H)-one (**4**) with Morpholine and Pyrrolidine.* To a solution obtained by dissolving copper(II) acetate (2.00 g) in methanol (4 ml) and morpholine (4 ml), **4** (0.73 g) was added under stirring, and the mixture was heated at 70—75 °C for 48 h. Water was added to the reaction mixture and the precipitate was collected by filtration. The precipitate was dissolved in dilute hydrochloric acid, hydrogen sulfide was passed through the solution, and copper(II) sulfide was filtered off. The filtrate was neutralized with sodium hydrogencarbonate and the resulting crystalline precipitate was collected. Recrystallization from water gave 6-morpholinocycloheptimidazol-2(1*H*)-one (**5a**) as yellow needles, mp 310 °C (dec). Yield, 150 mg (15%). UV (methanol) max: 255 (log ε 4.37), 292 (sh, 3.78), and 420 nm (4.42). IR (KBr): 3300 and 1630 cm^{-1}. NMR (CF_3CO_2H): δ, 4.15 (morpholine CH_2, s, 8H), 7.76 (C_5- and C_7-H, d, J=13.2 Hz), and 8.23 (C_4- and C_8-H, d, J=13.2 Hz). Found: C, 62.33; H, 5.65; N, 18.07%. Calcd for $C_{12}H_{13}N_3O_2$: C, 62.32; H, 5.67; N, 18.07%.

A similar treatment of **4** with pyrrolidine (neutralization of the filtrate with sodium hydrogencarbonate, however, did not afford any precipitate and repeated extraction with chloroform was necessary) gave 4-(or 5-)(1-pyrrolidinyl)cycloheptimidazol-2(1*H*)-one (**5b**) as orange crystals, mp 297 °C (dec). Yield, 14%. UV (methanol) max: 245 (log ε 4.24), 279 (4.38), 367 (4.15), and 457 nm (4.09). IR (KBr): 3450 and 1625 cm^{-1}. NMR (CF_3CO_2H): δ, 2.1—2.6 (pyrrolidine CH_2, m, 4H), 3.9—4.4 (pyrrolidine CH_2, m, 4H), and 7.3—8.1 (aromatic H, m, 4H). Found: C, 67.09; H, 5.92; N, 19.04%. Calcd for $C_{12}H_{13}N_3O$: C, 66.95; H, 6.09; N, 19.52%.

References

1) T. Nozoe, K. Takase, and M. Tada, *Bull. Chem. Soc. Jpn.*, **38**, 247 (1965).
2) M. Tada, *Bull. Chem. Soc. Jpn.*, **39**, 1954 (1966).
3) K. Hafner, H. Patzelt, and H. Kaiser, *Ann. Chem.*, **656**, 24 (1962).
4) T. Nozoe, K. Takase, and M. Tada, *Bull. Chem. Soc. Jpn.*, **39**, 1948 (1966).
5) T. Nozoe, K. Takase, and M. Tada, *Bull. Chem. Soc. Jpn.*, **36**, 1006 (1963).
6) T. Nozoe, T. Mukai, and T. Asao, *Bull. Chem. Soc. Jpn.*, **35**, 1188 (1962).
7) G. Sunagawa and M. Watatani, *Chem. Pharm. Bull.*, **16**, 1308 (1968).
8) I. Murata, *Bull. Chem. Soc. Jpn.*, **34**, 580 (1961).
9) K. Kikuchi, Y. Maki, and K. Sato, *Bull. Chem. Soc. Jpn.*, **51**, 2338 (1978).

BULLETIN OF THE CHEMICAL SOCIETY OF JAPAN, VOL. 51 (10), 3089—3090 (1978)

Reversible Oxygen Transfer Reactions between Sulfoxides and Sulfides. Relative Stabilities of Acyloxysulfonium Ions

Rikuhei TANIKAGA,* Koji NAKAYAMA, Kazuhiko TANAKA, and Aritsune KAJI

Department of Chemistry, Faculty of Science, Kyoto University Kitashirakawa, Sakyo-ku, Kyoto 606

(Received April 14, 1978)

Synopsis. Sulfides and acyloxysulfonium ions generated from sulfoxides and trifluoroacetic anhydride undergo a reversible reaction at −80 °C. The acyloxysulfonium ions with electron-donating groups or less bulky groups were found to be more stable than those having electronwithdrawing or bulky substituents.

Intermolecular oxygen transfer reactions are known to occur between sulfoxides and sulfides. For example, the reaction between thiolane 1-oxide and dibenzyl sulfide in refluxing acetic acid gives dibenzyl sulfoxide,[1] and the refluxing of diaryl sulfides in dimethyl sulfoxide affords the corresponding sulfoxides in good yields.[2] Oae investigated an intramolecular oxygen migration reaction of *o*-(alkylthio)phenyl aryl sulfoxides in sulfuric acid, and proposed a mechanism involving the nucleophilic attack of the sulfide sulfur atom on the acyloxysulfonium sulfur atom.[3] Recently, we found a rapid reaction between sulfoxides and dimethyl sulfide in trifluoroacetic anhydride (TFAA), which can be applied for the convenient reduction of sulfoxides to the corresponding sulfides.[4] Interestingly, dimethyl sulfoxide is an oxidizing agent in one case, while dimethyl sulfide is a reducing agent in the other case. However, no reversible oxygen transfer reaction between sulfoxides and sulfides has yet been studied.

In extending our observation, we have studied the reversible oxygen transfer reactions between various sulfoxides and sulfides using TFAA, and determined the relative stabilities of acyloxysulfonium ions which had not been estimated.

Experimental

The NMR spectra were recorded on a JEOL PS-100 spectrometer. GLPC determination was performed on a Varian 920 apparatus, using 1.2 m × 6 mm column packed with 20% Silicone DC-550 on 40—60 mesh Celite support. Sulfoxides and sulfides employed were prepared by the known methods. Dichloromethane and acetonitrile were distilled over CaH_2 and P_2O_5, respectively. Commercially available TFAA was used without further purification.

Typical Procedure. A solution of TFAA (12 mmol) in dichloromethane (5 ml) and acetonitrile (5 ml) was added dropwise to a solution of methyl phenyl sulfoxide (**1f**, R=CH_3, R′=C_6H_5)(1.40 g, 10 mmol) and ethyl phenyl sulfide (**4**)(1.38 g, 10 mmol) in dichloromethane (10 ml) and acetonitrile (10 ml) during 5 min at −80 °C, and the mixture was stirred for 90 min. After addition of a small amount of aq NaOH, the mixture was stirred for 5 min at −80 °C and allowed to warm to room temperature. A saturated NaCl solution (50 ml) was added, the layers were separated, and the aq phase was washed with two 30 ml portions of dichloromethane. The combined organic phase was washed with aq $NaHCO_3$ and water, and dried over $MgSO_4$. Evaporation of the solvent gave a liquid (2.7 g). TLC GLPC revealed that the liquid contained four compounds: that is, **1f**, methyl phenyl sulfide (**2f**), ethyl phenyl sulfoxide (**3**), and **4**. No other compound was detected in the NMR spectrum of the liquid. The relative yield of each compound was determined by GLPC and NMR using the authentic samples: **2f/4**=53/47, and **3/1f**=53/47.

In order to determine whether quenching with aq NaOH was complete in 5 min at −80 °C, dimethyl sulfide (1.24 g, 20 mmol) was added to the mixture at −80 °C after stirring with aq NaOH for 5 min, but **1f**, **2f**, **3**, and **4** were obtained in the same yields as above.

Following a similar procedure, **2f/4**=51/49 was obtained from **2f** and **3**.

Results and Discussion

Since sulfoxides (**1**) were instantaneously reduced to sulfides (**2**) with TFAA and dimethyl sulfide at −80 °C,[4] the formation of acyloxysulfonium ions (I) from **1** is assumed to be very rapid and quantitative. When TFAA was added to a solution of **1f** in dichloromethane and acetonitrile at −80 °C, and after 90 min the reaction mixture was quenched with aqueous NaOH, **1f** was recovered quantitatively. This finding means that **1** never underwent the Pummerer rearrangement at −80 °C.

When TFAA was added to a solution of **1f** and **4** at −80 °C, and after 90 min the mixture was quenched with aqueous NaOH at −80 °C, **1f**, **2f**, **3**, and **4** were obtained, but no other product was detected. Upon similar treatments, **1f**, **2f**, **3**, and **4** were also obtained from **2f** and **3** in nearly the same yields. The relative yields of **2f/4** were found to be nearly equal to those of **3/1f**, suggesting that the following equilibrium exists:

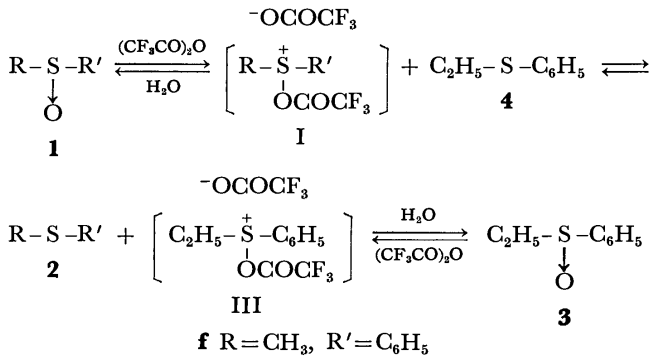

If **1f** and III were not quenched within a few minutes at −80 °C, dimethyl sulfide would rapidly react with **1f** and III to give **2f** and **4**, but not to give **1f** and **3**.[4] The addition of dimethyl sulfide during quenching, however, did not affect the yields of the products.

A NMR spectrum of **1f**, **4**, and TFAA (mol ratio: 1.0: 1.0: 1.2) in CH_2Cl_2–CD_3CN (v/v=1/1) at −80 °C

showed peaks at 2.7, 2.4, 1.2, 1.1 ppm corresponding to the methyl groups of **1f**, **2f**, III, and **4**, respectively. Although the relative yields of **2f**/**4** could not be determined because of overlapping of two methyl signals of III and **4**, those of **2f**/**1f** were found about 50/50.

The above findings mean that the III/**1f** ratio would be essentially the same as the **3**/**1f** (or **2f**/**4**) ratio.

The conceivable pathway from I and **4** to **2** and III (and *vice versa*) may involve the nucleophilc attack of the sulfide sulfur atom on the sulfonium sulfur atom.[3-5]

The results obtained with other sulfoxides, and **4**, are shown in Table 1.

Table 1. Relative yields of **2**/**4** from **1** and **4** (or **2** and **3**)

	R	R′	Yield ratio (**2**/**4**)
a	CH_3	CH_3	0/100
b	CH_3	n-C_6H_{13}	2/98
c	CH_3	p-CH_3O-C_6H_4	36/64
d	CH_3	p-CH_3-C_6H_4	47/53
e	CH_3	o-CH_3-C_6H_4	66/34
f	CH_3	C_6H_5	53/47
g	CH_3	p-Cl-C_6H_4	76/24
h	CH_3	o-Cl-C_6H_4	94/6
i	CH_3	p-NO_2-C_6H_4	100/0
j	i-C_3H_7	C_6H_5	54/46
k	CH_2Cl	C_6H_5	100/0
l	C_6H_5	C_6H_5	99/1

Since the above equilibrium is considered to depend on the relative stabilities of the acyloxysulfonium ions I and III, the smaller **2**/**4** ratio means that I is more stable. On this basis, the relative thermodynamic stabilities of I can readily be determined. Thus, we may reasonably conclude that an electron-donating group can make I more stable, and the steric bulkiness, for example, of an o-substituent makes I slightly unstable. The former conclusion also suggests that I obtained from basic **1** must be stable. In fact, the stabilities of I were found qualitatively to parallel the pK_a values of **1**,[6] though attempts to find out the exact relationships between them were unsuccessful.

The position of the equilibrium was little affected by the presence of 2,6-lutidine. The time necessary to attain the equilibrium varied from a few seconds (*i.e.*, from **2a** and **3**) to a few hours (*i.e.*, **1i** and **4**).

Since dimethyl sulfoxide forms the most stable acyloxysulfonium ion, other sulfoxides can be reduced with dimethyl sulfide in TFAA.[4] The intramolecular oxygen migration of o-alkylthiophenyl aryl sulfoxides also showed that alkyl(aryl)(oxy)sulfonium ions are more stable than diaryl(oxy)sulfonium ions.[3] When one component is removed in the equilibrium, the equilibrium can be displaced to the unfavorable direction. This is the case of the oxidation of sulfides with dimethyl sulfoxides.[2]

When trichloroacetic anhydride, trichloroacetyl chloride, and thionyl chloride were used in the place of TFAA, the **3**/**1** yield ratios were found to be 56/44, 55/45, and 55/45, respectively, and the order of the relative stabilities of the oxysulfonium ions was identical to that obtained with TFAA. When dichloroacetic anhydride was used, it took a much longer time to reach the equilibrium. No intermolecular oxygen exchange reaction of a sulfoxide and a sulfide took place in sulfuric acid at room temperature, or in acetic anhydride at 100 °C, unlike the intramolecular reaction.[3] Evidently such a decrease in reactivities corresponds to a decrease in the leaving group tendency; for example, $CF_3COO^- > CCl_3COO^- > CHCl_2COO^- > CH_3COO^-$.

The present work was partially supported by a Grant-in-Aid from the Ministry of Education (No. 254156).

References

1) F. G. Bordwell and B. M. Pitt, *J. Am. Chem. Soc.*, **77**, 572 (1955).
2) S. Searles, Jr., and H. R. Hays, *J. Org. Chem.*, **23**, 2028 (1958).
3) T. Numata and S. Oae, *Int. J. Sulfur Chem.*, *A*, **1**, 6 (1971).
4) R. Tanikaga, K. Nakayama, K. Tanaka, and A. Kaji, *Chem. Lett.*, **1977**, 395.
5) H. Minato, T. Miura, F. Takagi, and M. Kobayashi, *Chem. Lett.*, **1975**, 211.
6) D. Landini, G. Modena, G. Scorrano, and F. Taddei, *J. Am. Chem. Soc.*, **91**, 6703 (1969).

BULLETIN OF THE CHEMICAL SOCIETY OF JAPAN, VOL. 51 (10), 3091—3092 (1978)

Preparation of Fluorinated Imidazole Derivatives Using Hexafluoro-1,2-epoxypropane

Hamdy A. HAMMOUDA† and Nobuo ISHIKAWA*

Department of Chemical Technology, Tokyo Institute of Technology, Ookayama, Meguro-ku, Tokyo 152

(Received April 28, 1978)

Synopsis. Utilizing the reactivity of hexafluoro-1,2-epoxypropane, several new fluorine-containing imidazole derivatives were prepared. The reactions involve 2-mercaptobenzimidazole, 2-mercapto-4,5-diphenylimidazole, 2-imidazolidinethione, and 2-aminobenzamide.

It is well known that nucleophiles readily attack the central carbon atom of hexafluoro-1,2-epoxypropane (HFPO, hexafluoropropylene oxide), resulting in the formation of α-substituted tetrafluoropropionyl fluorides, which further react with an additional molecule of the nucleophiles to form esters and amides:[1-3]

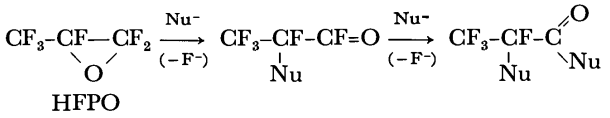

HFPO

Utilizing this reactivity of HFPO, we have previously reported on the preparation of several new benzo heterocyclic compounds containing CF_3 or C_2F_5 groups by allowing it react with ortho bifunctional benzenes:[4]

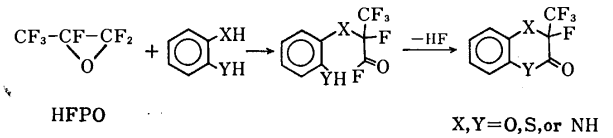

HFPO X,Y=O,S,or NH

This work has now been extended in order to search for more biologically active compounds; we wish here to report on the preparation of several new benzimidazole derivatives carrying a fluoroalkyl group.

As benzimidazole derivatives with a fused thiazole ring are known to be highly interesting from the physiological point of view, we first examined the preparation of fluorine-containing compounds of this type. 2-Mercaptobenzimidazole (or, better, its sodium salt) reacted with HFPO to give the acyl fluoride, **1**, which cyclized intramolecularly in aprotic solvents, such as dioxane or acetonitrile, to afford 2,3-dihydrothiazolo-[3,2-*a*]benzimidazol-3-one (**2**):

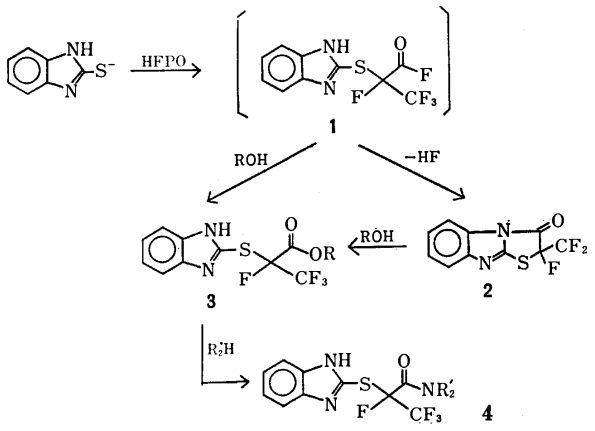

On the other hand, when the reaction was carried out in alcohols, the acid fluoride, **1**, acylated one molecule of the solvent immediately to give the esters, **3**, in good yields. These esters were also prepared from the cyclic compound, **2**, by heating it with alcohol for a short period.

As amides are generally more hydrophilic than esters, and are biologically more useful, we prepared various amides, **4**, by the aminolysis of the esters, **3**. For example, by heating the ethyl ester **3** (R=Et) with an excess of an aqueous ammonia, the amide **4** (R=H) was precipitated. The *N*-alkylated amides were obtained from the ethyl ester by allowing it to react with an excess of the alkylamine at room temperature.

Another group of similar compounds, **5** and **6**, was obtained by the reaction of HFPO with 2-mercapto-4,5-diphenylimidazole, as is shown below:

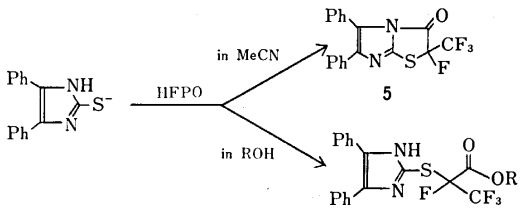

The all of the above compounds showed two characteristic signals, a doublet and a quartet at a 3:1 ratio of intensities, in their ^{19}F NMR spectra, thus supporting the presence of $\overset{CF_3}{\underset{F}{\diagdown C \diagup}}$ group. The ^1H NMR spectra data are also in agreement with the assigned structures (Table 1).

HFPO is known to isomerize to pentafluoropropionyl fluoride under the influence of a base such as triethylamine.[5] We have previously reported[6] a convenient method for the pentafluoropropionylation of amines, alcohols and thiols, which consists in allowing the nucleophile, triethylamine, and HFPO to react altogether in acetonitrile. By applying this procedure, 2-imidazolidinethione and 2-aminobenzamide were acylated to give the thioesters, **7**, and the amide, **8**,

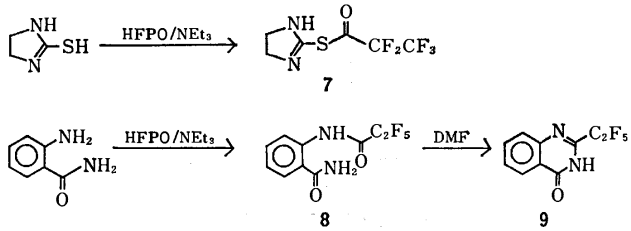

† UNESCO Post-graduate fellow on leave from the Department of Chemistry, Cairo University, Cairo, A. R. Egypt.

Table 1. Physical properties of the compounds[a)]

Compd No. (R or R')	Yield (%)	Mp °C (Solvent)[b)]	IR[c)] (cm^{-1})	NMR (ppm) ^{19}F	NMR (ppm) ^{1}H
2	55	90 (n-C_6H_{14})	1660(CO)	0.5(CF_3), 70.0(CF)	7.2—8.0m(ar)[e)]
3 (Me)	81	155 (aq MeOH)	1762(CO)	−2.0(CF_3), 67.0(CF)	3.8s(CH_3), 7.1—7.7m(ar), 10.1br(NH)[f)]
3 (Et)	89	159 (aq EtOH)	1762(CO)	−2.0(CF_3), 67.0(CF)	1.1t(CH_3), 3.1br(NH), 4.2q (OCH_2), 7.1—7.8m(ar)[f)]
3 (*i*-Pr)	77	162 (PhMe)	1750(CO)	−2.5(CF_3), 66.0(CF)	1.23d(CH_3), 5.0q(CH), 7.2—7.8m(ar)[e)]
3 (CH_2CH_2Cl)	72	117 (C_6H_{12})	1775(CO_2R)	−2.5(CF_3), 67.0(CF)	3.5t(CH_2Cl), 4.4t(OCH_2), 7.2—7.8m(ar)[g)]
4 (H)	60	197 (H_2O)	3400—3100(NH) 1705(CO)	−2.5(CF_3), 65.5(CF)	7.2—8.0m(ar), 12.2br (NH)[f)]
4 (H, Me)	65	214 (H_2O)	3325(NH), 1690(CO)	−3.8(CF_3), 67.0(CF)	
4 (Me_2)	62	181 (H_2O)	3320(NH), 1690(CO)	−3.0(CF_3), 64.0(CF)	
4 (H, Et)	67	199 (H_2O)	3320(NH), 1690(CO)	−4.2(CF_3), 66.0(CF)	0.8t(CH_3), 3.0m(CH_2), 7.2—7.9m(ar), 13.3br(NH)[h)]
5	60	115 (n-C_6H_{14})	1175(CO)	−4.0(CF_3), 59.0(CF)	7.2—7.4m(ar)[e)]
6 (Me)	82	168 (C_6H_{12})	3325(NH), 1765(CO)	−2.5(CF_3), 68.5(CF)	3.83s(OCH_3), 7.2—7.6m (ar), 12.4br(NH)[e)]
6 (Et)	85	167 (aq EtOH)	3400(NH), 1760(CO)	−2.5(CF_3), 67.5(CF)	
6 (*i*-Pr)	77	151 (C_6H_{12})	1755(CO)	−4.0(CF_3), 65.5(CF)	
7	65	83 (n-C_6H_{14})	3315(NH), 1710(CO)	5.7(CF_3), 45.2(CF_2)	3.7s(CH_2), 7.0br(NH)[g)]
8	73	145 (aq MeOH)	3425, 3200(NH), 1715, 1645(CO)	5.0(CF_3), 44.5(CF_2)	
9	76	205 (aq MeOH)	1680(CO), 1635(CN)	3.2(CF_3), 38.2(CF_2)	7.5—7.8m(ar)[h)]

a) The results of the elemental analysis (C, H, and N) for all compounds are in good agreement with the theoretical values. b) The solvents used for recrystallization are shown in parentheses. c) The IR spectra were taken in KBr. d) The chemical shifts of the ^{19}F and ^{1}H NMR spectra are given in δ ppm upfield from external trifluoroacetic acid, and downfield from internal tetramethylsilane, respectively. The ^{19}F NMR of **2**—**6** were run in acetone, while those of **7**—**9** were run in EtOH. The solvents used for ^{1}H NMR are indicated. e) In CCl_4. f) In acetone-d_6. g) In $CDCl_3$. h) In DMSO-d_6.

respectively. The latter compound, **8**, could be cyclized to the benzimidazole compound, 2-(pentafluoroethyl)-3,4-dihydroquinazolin-4-one (**9**), by heating it in *N,N*-dimethylformamide.

Experimental

2-Fluoro-2-(trifluoromethyl)-2,3-dihydrothiazolo[3,2-a]benzimidazol-3-one (2). HFPO (1.7 g, 0.01 mol) was bubbled into a stirred suspension of sodium 2-benzimidazolethiolate (1.7 g, 0.01 mol) in acetonitrile (20 ml) at −78 °C. The cooling bath was then removed, and stirring was continued for 4 h at room temperature using a Dry Ice condenser. The reaction mixture was filtered from a slight turbidity, and the filtrate was evaporated to dryness under a vacuum. The solid residue was dissolved in benzene and filtered from a trace of an insoluble material. The benzene was again removed, and the product was crystallized from hexane.

2-(2-Benzimidazolylthio)-2,3,3,3-tetrafluoropropionic Acid Esters (3): General Procedure. Sodium 2-mercaptobenzimidazolethiolate (0.01 mol) was stirred in the appropriate hydroxy compound. HFPO (0.01 mol) was then bubbled into the resulting, almost clear solution which was kept at −78 °C. The stirring was continued for 4 h at room temperature using a Dry Ice condenser. The reaction mixture was filtered, and the filtrate was poured into ice-cooled water. The crystalline material was collected, washed with water, and recrystallized from the proper solvent.

MS (*m/e*) for **3** (R=Et), 322 (M^+), 277 (M^+−OEt), 276 (M^+−EtOH), 229 (M^+−EtOH−CO−F), and 149 ($C_6H_4CHN_2S^+$).

2-(2-Benzimidazolylthio)-2,3,3,3-tetrafluoropropionamide (4, R'=H). The ethyl ester **3** (1 g) was stirred with a 25% aqueous ammonia (50 ml) for 2 h at room temperature. The reaction mixture was then boiled for a further 15 min and cooled in ice, and the separated crystals were collected and recrystallized from water.

The N-Alkyl Derivatives (4, R'=H, alkyl), The ethyl ester **3** (1 g) was stirred with an alkylamine solution (5 ml) (40% methylamine and 70% ethylamine solutions were used) for 5 h at room temperature. The clear solution was poured onto crushed ice and slightly acidified by adding a few drops of hydrochloric acid. The crystals that separated were collected, washed with water, dried well, and recrystallized.

The N,N-Dialkyl Derivatives (4, R'=alkyl). The ethyl ester **3** was stirred at room temperature with dimethylamine or diethylamine (3 ml). Exothermic dissolution first took place, followed by the precipitation of a white solid. After stirring for 5 h, the reaction mixture was poured on ice-cooled water, slightly acidified by adding a few drops of hydrochloric acid. The crystals that separated were filtered off, washed with water, dried well, and recrystallized.

2-Fluoro-2-(trifluoromethyl)-5,6-diphenyl-2,3-dihydroimidazolo-[2,1-b]thiazol-3-one (5). Sodium 4,5-diphenyl-2-imidazolethiolate (0.01 mol) was stirred with acetonitrile (20 ml) in a pressure tube. The mixture was then cooled to −78 °C, and liquefied HFPO (0.01 mol) was introduced. Stirring was continued for 4 h. The solvent was then evaporated under a vacuum, and the solid product was crystallized from hexane.

2-(4,5-Diphenyl-2-imidazolylthio)-2,3,3,3-tetrafluoropropionic Acid Esters (6): General Procedure. Liquefied HFPO (0.01 mol) was introduced into a solution of sodium 4,5-diphenyl-2-imidazolethiolate in the appropriate hydroxy compound (20 ml) at −78 °C. Stirring at room temperature was continued for 4 h. The reaction mixture was then filtered, and the filtrate was diluted with water. The precipitated crystals were filtered off, washed with water, dried, and recrystallized.

S-(2-Imidazolin-2-yl) Pentafluoropropanethioate (7). A mixture of 2-imidazolidinethione (1.02 g, 0.01 mol) and triethylamine (1.01 g, 0.01 mol) was stirred in acetonitrile (10 ml) at −78 °C. Liquefied HFPO (0.01 mol) was then introduced, and the stirring was continued for 30 min at room temperature. The reaction mixture was poured into ice-cooled water, and the crystals that separated were collected and recrystallized from hexane.

2'-Carbamoylpentafluoropropionanilide (8). 2-Aminobenzamide and HFPO were reacted in acetonitrile in the presence of triethylamine according to the procedure described above for the preparation of **7**. The product was recrystallized from aqueous methanol.

3,4-Dihydro-2-(pentafluoroethyl)quinazolin-4-one (9). The amide **8** (1 g) was refluxed in *N,N*-dimethylformamide (30 ml) for 3 h, cooled, and poured into cold water. The crystals that separated were filtered off, washed with water, dried, and recrystallized from aqueous methanol.

References

1) D. Sianesi, A. Pasetti, and F. Tarli, *J. Org. Chem.*, **31**, 2312 (1966).

2) A. Pasetti, F. Tarli, and D. Sianesi, *Gazz. Chim. Ital.*, **98**, 277, 290 (1968).

3) I. L. Knunyants, V. V. Shokina, and I. V. Galakhov, *Khim. Geterotsikl. Soedin.*, **1966**, 873.

4) N. Ishikawa and S. Sasaki, *Bull. Chem. Soc. Jpn.*, **50**, 2164 (1977).

5) Du Pont, Brit. Patent 1019788 (1966).

6) N. Ishikawa and S. Sasaki, *Nippon Kagaku Kaishi*, **1976**, 1954.

BULLETIN OF THE CHEMICAL SOCIETY OF JAPAN, VOL. 51 (10), 3093—3094 (1978)

The Nucleophilic Substitution Reaction of 1-Halogeno-2-methylsulfonylphenazine 5-Oxides

Masao TADA

The Research Institute for Tuberculosis and Cancer, Tohoku University, Seiryomachi, Sendai 980

(Received April 28, 1978)

Synopsis. The halogen atom in 1-halogeno-2-methylsulfonylphenazine 5-oxide is reactive toward the anionoid reagents through the activating effects of both the sulfone group and the *N*-oxide group. By the nucleophilic substitutions, some 1-substituted 2-methylsulfonylphenazine derivatives have been prepared in high yields.

In a previous paper,[1] it has been shown that direct comparison of the reactivities of the halogen atoms in 1- and 2-halogenophenazines and their *N*-oxides has confirmed the activating effect of the *N*-oxide group. The halogen-activating effects from the presence of oxide groups have been shown in other compounds.[2] Heppolette *et al.*[3] reported that the halogen displacement in 2-halogenonitrobenzene could be strongly promoted by the introduction of a sulfone group in the 4-position. The author's interest in the activating effects of both a sulfone group and a *N*-oxide group has led to the suggestion that a halogen atom of 1-halogeno-2-methylsulfonylphenazine 5-oxide will be reactive toward anionoid reagents. As part of the synthetic study of phenazines with potential biological activities, this note will describe the preparation and the reaction of 1-halogeno-2-methylsulfonylphenazine 5-oxides.

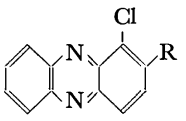

1: R=Cl
3: R=SCH_3
5: R=SO_2CH_3

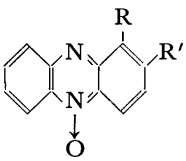

2: R=R′=Cl
4: R=Cl; R′=SCH_3
6: R=Cl; R′=SO_2CH_3
7: R=N⟨morpholine⟩; R′=SO_2CH_3
8: R=Br; R′=SO_2CH_3
9: R=N⟨morpholine⟩O; R′=SO_2CH_3
10: R=Cl; R′=H
11: R=OH; R′=SO_2CH_3
12: R=OC_2H_5; R′=SO_2CH_3
13: R=$CH(CO_2C_2H_5)_2$; R′=SO_2CH_3
14: R=$CHCNCO_2C_2H_5$; R′=SO_2CH_3

The reaction of 1,2-dichlorophenazine (**1**)[4] and its 5-oxide (**2**)[4] with an equimolecular quantity of sodium methanethiolate gave the corresponding methylthiophenazines, **3** and **4**. Compound **4** was deoxygenated by the treatment with zinc dust in acetic acid to give **3**, from which sulfone (**5**) was then prepared by the oxidation with a limited amount of hydrogen peroxide in acetic acid. The further oxidation of **5** with an excess of hydrogen peroxide afforded 1-chloro-2-methylsulfonylphenazine 5-oxide (**6**), which was also derived from **4** by the oxidation. The position of the chlorine atom in **6** was confirmed by the following piperidination. The refluxing of **6** with piperidine in ethanol for 2 h afforded 2-methylsulfonyl-1-piperidinophenazine 5-oxide (**7**), which was also derived from 1-bromo-2-methylsulfonylphenazine 5-oxide (**8**).[5]

The heating of **6** or **8** with morpholine in ethanol for 2 h gave 2-methylsulfonyl-1-morpholinophenazine 5-oxide (**9**), whereas **5** was unreactive toward morpholine under similar conditions. The reactivity to the amine of either **6** or **8** is in contrast with that of 1-chlorophenazine 5-oxide (**10**).[6] The treatment of **8** with aqueous ethanolic alkali for 1.5 h afforded both 1-ethoxy- (**11**) and 1-hydroxy-2-methylsulfonylphenazine 5-oxides (**12**). The former was also obtained by the reaction of **6** or **8** with sodium ethoxide in ethanol, and the latter was also derived from **6** or **8** by the treatment with aqueous alkali. The reaction of **8** with active methylene compounds, such as diethyl malonate and ethyl cyanoacetate, gave the corresponding products, **13** and **14**.

The results of these substitutions of 1-halogeno-2-methylsulfonylphenazine 5-oxide show that the displacement of a halogen group in Position 1 can be strongly promoted by the presence of a methylsulfonyl group in Position 2.

Experimental

The melting points, the appearances, the solvents of recrystallization, and the results of elemental analyses are all listed in Table 1. The infrared spectra were taken with a Hitachi Model EPI-S_2 spectrophotometer.

1-Chloro-2-methylthiophenazine (3). *From 1*: To a hot solution of **1** (2.5 g) in ethanol (0.5 l), a 20% aqueous solution of sodium methanethiolate (3 ml) was added. The mixture was refluxed for 10 h and diluted with water. The crystals thereby separated were chromatographed over alumina, using chloroform as the solvent, to give **3** (960 mg, 37%).

From 4: To a solution of **4** (150 mg) in acetic acid (30 ml), zinc dust (0.5 g) was added in small portions. The mixture was then warmed on a water bath for 5 min and filtered while hot. The filtrate was diluted with water to afford **3** (135 mg, 92%).

1-Chloro-2-methylthiophenazine 5-Oxide (4). To a hot solution of **2** (5.3 g) in ethanol (0.8 l), a 20% aqueous solution of sodium methanethiolate (6 ml) was added. The solution was refluxed for 5 h and diluted with water. The crystals which separated were chromatographed over alumina using chloroform as the solvent. From the effluent, **4** (3.54 g, 64%), **3** (550 mg, 11%), and 1,2-bis(methylthio)phenazine 5-oxide[7] (120 mg, 2%) were obtained.

1-Chloro-2-methylsulfonylphenazine (5). A solution of **3** (260 mg) in acetic acid (10 ml) and a 30% aqueous solution of hydrogen peroxide (2 ml) was warmed at 55 °C for 3 h to give **5** (270 mg, 93%).

1-Chloro-2-methylsulfonylphenazine 5-Oxide (6). *From 3*: To a solution of **3** (520 mg) in acetic acid (20 ml) and

Table 1. Properties of 1,2-disubstituted phenazine derivatives

Compound	Mp (°C)[a]	Appearance[b]	Recrystal. from	Molecular formula	Found (%)			Calcd (%)		
					C	H	N	C	H	N
3	179—180	Yellow n	C_6H_6–EtOH	$C_{13}H_9ClN_2S$	60.13	3.40	10.78	59.88	3.48	10.74
4	234—235 (dec)	Dull orange n	$CHCl_3$	$C_{13}H_9ClN_2OS$	56.50	3.08	9.87	56.42	3.28	10.12
5	202—203	Yellow n	DMF–EtOH	$C_{13}H_9ClN_2O_2S$	53.36	3.10	9.50	53.34	3.10	9.57
6	226—227 (dec)	Brown-yellow l	DMF	$C_{13}H_9ClN_2O_3S$	50.84	2.86	9.19	50.57	2.94	9.07
7	197—198 (dec)	Red-brown n	EtOH	$C_{18}H_{19}N_3O_3S$	60.37	5.30	11.70	60.49	5.36	11.76
9	212—213 (dec)	Red-orange n	C_6H_6–EtOH	$C_{17}H_{17}N_3O_4S$	57.07	4.74	11.59	56.81	4.77	11.69
11	236—237 (dec)	Brassy n	EtOH	$C_{13}H_{10}N_2O_4S$	53.75	3.35	9.79	53.79	3.47	9.65
12	182—183	Yellow n	EtOH	$C_{15}H_{14}N_2O_4S$			8.81			8.80
13	178—179 (dec)	Yellow n	EtOH	$C_{20}H_{20}N_2O_7S$	55.82	4.92	6.57	55.55	4.66	6.48
14	196—198 (dec)	Orange-yellow n	EtOH–$CHCl_3$	$C_{18}H_{15}N_3O_5S$	55.90	3.71	10.62	56.10	3.92	10.90

a) All the melting points are uncorrected. b) Needles and leaflets are abbreviated as n and l, respectively.

acetic anhydride (1 ml), a 30% aqueous solution of hydrogen peroxide (3 ml) was added. The mixture was warmed at 55 °C for 15 h to give **6** (600 mg, 97%).

From 4: **4** (550 mg) and a 30% aqueous solution of hydrogen peroxide (3 ml) were treated, following the procedure used in the preparation of **5**, to afford **6** (600 mg, 97%).

From 5: **5** (580 mg) was treated as in the case of the "From **3**" above to give **6** (590 mg, 95%).

2-Methylsulfonyl-1-piperidinophenazine 5-Oxide (7). From 6: A mixture of **6** (310 mg) and piperidine (0.5 ml) in ethanol (50 ml) was refluxed for 2 h and then diluted with water to give **7** (320 mg, 90%).

From 8: **8** (350 mg) was treated as in the case described above to give **7** (330 mg, 92%).

2-Methylsulfonyl-1-morpholinophenazine 5-Oxide (9). A mixture of **6** (310 mg) and morpholine (0.5 ml) in ethanol (50 ml) was refluxed for 2 h to afford **9** (300 mg, 84%). **8** (350 mg) was treated in a similar way to give **9** (310 mg, 86%).

1-Hydroxy-2-methylsulfonylphenazine 5-Oxide (11). A suspension of **8** (350 mg) in a 5% aqueous solution of potassium hydroxide (20 ml) was refluxed for 2 h, filtered, and acidified with diluted acetic acid to give **11** (250 mg, 86%). **6** (310 mg) was treated in a similar way to give **11** (240 mg, 83%). IR (KBr): 3120 cm^{-1}.

1-Ethoxy-2-methylsulfonylphenazine 5-Oxide (12). To a solution of **8** (350 mg) in absolute ethanol (50 ml), sodium (100 mg) was added. The resulting mixture was refluxed for 2 h to give **12** (285 mg, 90%). **6** was treated in a similar way to give **11** (85%).

To a suspension of **8** (530 mg) in ethanol (30 ml), a 10% aqueous solution of potassium hydroxide (10 ml) was added. The mixture was refluxed for 1.5 h and diluted with water. The resulting crystals gave **12** (250 mg, 52%); from the filtrate, **11** (180 mg, 41%) was obtained.

1-[Bis(ethoxycarbonyl)methyl]-2-methylsulfonylphenazine 5-Oxide (13). To a sodium ethoxide solution prepared from sodium (92 mg) and absolute ethanol (40 ml), diethyl malonate (640 mg) was added. **8** (706 mg) was then added to the mixture and the resulting mixture was refluxed for 1 h to give **13** (660 mg, 76%). IR (KBr): 1762 and 1724 cm^{-1}.

1-(1-Cyano-1-ethoxycarbonylmethyl)-2-methylsulfonylphenazine 5-Oxide (14). A mixture of **8** (706 mg) and ethyl cyanoacetate (432 mg) was treated, following procedure used in the preparation of **13**, to afford **14** (690 mg, 90%). IR (KBr): 2250 and 1751 cm^{-1}.

The author is grateful to Professor Atsushi Oikawa of Tohoku University for his encouragement.

References

1) H. Endo, M. Tada, and K. Katagiri, *Bull. Chem. Soc. Jpn.*, **42**, 502 (1969).
2) A. R. Katritzky and J. M. Lagowsky, "Chemistry of the Heterocyclic *N*-Oxides," Academic Press, London (1971), p. 406.
3) R. L. Heppolette and J. Miller, *Chem. Ind. (London)*, **1954**, 1457; *J. Chem. Soc.*, **1956**, 2329.
4) V. P. Chernetskii and A. I. Kiprianov, *Zh. Obshch. Khim.*, **23**, 1743 (1953); *Chem. Abstr.*, **48**, 13695 (1954).
5) M. Tada, *Bull. Chem. Soc. Jpn.*, **48**, 363 (1975).
6) H. Endo, M. Tada, and K. Katagiri, *Bull. Chem. Soc. Jpn.*, **42**, 506 (1969).
7) M. Tada, *Bull. Chem. Soc. Jpn.*, **47**, 1803 (1974).

BULLETIN OF THE CHEMICAL SOCIETY OF JAPAN, VOL. 51 (10), 3095—3096 (1978)

A Convenient Synthesis of 2-Substituted 3-Nitro-2*H*-chromene Derivatives[1)]

Tohru SAKAKIBARA,* Masaru KOEZUKA, and Rokuro SUDOH

Department of Chemistry, Faculty of Science, Tokyo Institute of Technology, Ookayama, Meguro-ku, Tokyo 152

(Received May 2, 1978)

Synopsis. On reaction with salicylaldehyde, ω-nitrostyrene and 4,6-dimethoxy-5-(2-nitrovinyl)pyrimidine gave a mixture of 3-nitro-4-hydroxyflavan and 3-nitro-2-phenyl-2*H*-chromene or 2-(4,6-dimethoxy-5-pyrimidinyl)-3-nitro-2*H*-chromene, respectively, whereas 4,6-dichloro-5-(2-nitrovinyl)-pyrimidine afforded substitution products: 4-chloro-6-(2-formylphenoxy)-5-(2-nitrovinyl)pyrimidine and 4,6-bis(2-formylphenoxy)-5-(2-nitrovinyl)pyrimidine.

C-Nucleosides frequently have interesting biological activities, and several synthetic studies on these compounds have been reported.[2)] In a series of studies on nucleophilic addition reactions to nitro olefin derivatives, we designed the synthesis of C-nucleosides from β-hydroxy aldehyde and nitro olefins. As a preliminary examination we have carried out the reaction of (2-nitrovinyl)pyrimidine derivatives with salicylaldehyde.

Treatment of salicylaldehyde (**1**) with ω-nitrostyrene (**2**) in the presence of triethylamine afforded a mixture of two cyclic compounds, 3-nitro-4-hydroxyflavan (**3**) and 3-nitro-2-phenyl-2*H*-chromene (**5**), in a *ca.* 1:1 ratio in 69% yield. The *trans-trans* structure of the nitro alcohol **3** was determined by the NMR spectrum of its nitro acetate **4**; $J_{2,3}=10$, $J_{3,4}=8.3$ Hz. The structure of 3-nitro-2-phenyl-2*H*-chromene (**5**) was deduced from analytical, IR, and NMR data.[3)]

To extend this ring formation, (2-nitrovinyl)-pyrimidine derivatives **9a** and **9b** were prepared from the corresponding 5-formylpyrimidine **6a** and **6b**, respectively. Nitromethane condensation of 4,6-dichloro-5-formylpyrimidine **6a**[4)] in the presence of sodium or potassium hydroxide, sodium methoxide, or triethylamine as a basic catalyst failed. However, in the presence of barium hydroxide the intended nitro alcohol **7a** was isolated in 62% yield. On the other hand, 4,6-dimethoxy-5-formylpyrimidine **6b**[5)] smoothly reacted with nitromethane in the presence of triethylamine, giving the nitro alcohol **7b**. Acetylation of the nitro alcohol **7a** and **7b** with acetic anhydride-boron trifluoride etherate and subsequent elimination of acetic acid with sodium hydrogencarbonate afforded the nitro olefins **9a** and **9b**, respectively.

Treatment of the nitro olefin **9a** with equimolar salicylaldehyde under various conditions (solvents, reaction temperature, and amounts of triethylamine) resulted in a colored solution, from which no desired product was isolated. When **9a** was treated with salicylaldehyde in the presence of *ca.* 1.4 equivalents of sodium 2-formylphenoxide in DMSO, 4-chloro-6-(2-formylphenoxy)-5-(2-nitrovinyl)pyrimidine (**10**) was isolated in 65% yield. A similar treatment of **9a** with 2.1 equivalents of sodium 2-formylphenoxide yielded 4,6-bis(2-formylphenoxy)-5-(2-nitrovinyl)pyrimid ine. These results showed that the chlorine atoms were more reactive to 2-formylphenoxide than the nitro olefin moiety under the conditions employed.

Under the conditions used for preparation of the flavan **3** and chromene **5**, the reaction of **9b** with salicylaldehyde did not occur, because **9b** was immediately precipitated when triethylamine was added. But treatment of **9b** with two equivalents of salicylaldehyde in the presence of 0.1 equivalent of sodium 2-formylphenoxide in DMSO at room temperature for 24 h gave the 2*H*-chromene derivative **12** as yellow crystals in 46% yield. Its IR spectrum showed the presence of a conjugated nitro group and characteristic absorption bands due to pyrimidine and benzene ring. The NMR spectrum supports the structure of **12.**

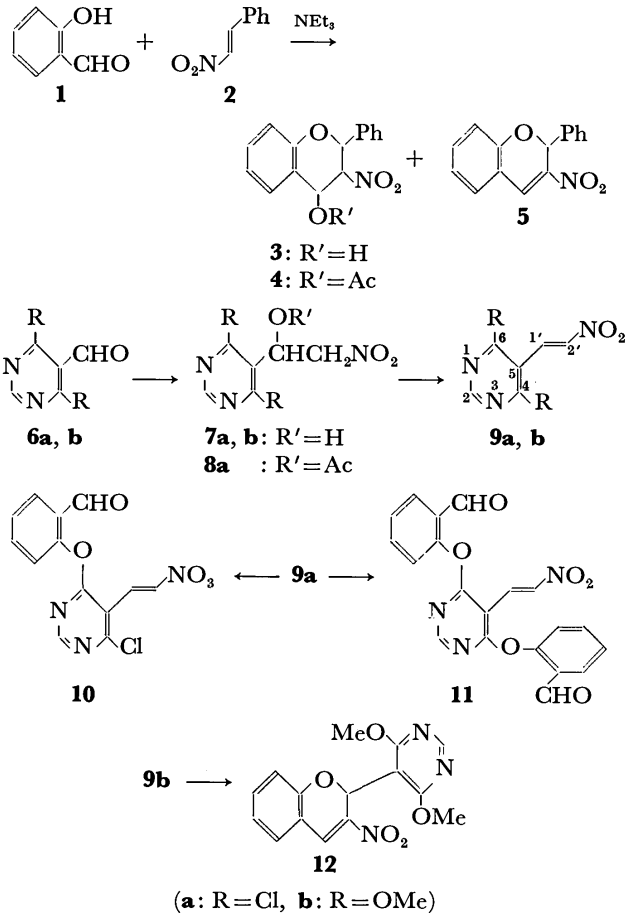

Experimental

Melting points were taken in capillaries and are uncorrected. NMR spectra were recorded at 60 MHz on a Varian T-60 spectrometer (except compound **4**, which was analyzed at 100 MHz on a JNM-4H-100 (JEOL) spectrometer), in chloroform-*d* using tetramethylsilane as internal standard.

t-*3-Nitro*-c-*2-phenyl*-r-*1-chromanol (3).* To a solution of **2** (3.0 g, 20 mmol) in **1** (7.5 g, 61.5 mmol) was added 0.2 g

(2 mmol) of triethylamine. The mixture, which gradually solidified, was allowed to stand for 16 h at room temperature. The resulting crystalline solid was broken up and dissolved in hot ethanol. The solution was filtered to remove insoluble material. After evaporation of the filtrate, the residue was washed several times with carbon tetrachloride and recrystallized from ethanol to give 1.68 g (31%) of **3** as colorless crystals: mp 138.5—139.5 °C; IR 3290 (OH), 1552, and 1376 cm^{-1} (NO_2). Found: C, 66.50; H, 4.79; N, 5.27%. Calcd for $C_{15}H_{13}NO_4$: C, 66.41; H, 4.83; N, 5.16%.

t-3-Nitro-c-2-phenyl-r-1-chromanyl Acetate (4). A solution of **3** (300 mg, 1.1 mmol) in 3 ml of acetic anhydride was left at room temperature for 6 h in the presence of catalytic amounts of boron trifluoride etherate. Addition of 20 ml of water to the reaction mixture gave a precipitate (312 mg, 90.5%), which was recrystallized from ethanol to give colorless needles of **4** (87%): mp 183—184 °C; IR 1738 (C=O), 1550 and 1368 cm^{-1} (NO_2); NMR δ 2.13 (Ac), 5.39 (1H, d, $J_{2,3}$= 10 Hz, H-2), 5.15 (1H, d, $J_{3,4}$=8.3 Hz, H-3), and 6.98 (1H, d, H-4). Found: C, 65.15; H, 4.79; N, 4.50%. Calcd for $C_{17}H_{15}NO_5$: C, 65.17; H, 4.82; N, 4.47%.

3-Nitro-2-phenyl-2H-chromene (5). The carbon tetrachloride solution obtained in the preparation of **3** was evaporated to give a yellow residue, which was recrystallized from ethanol to afford yellow crystals (1.9 g, 38%) of **5**: mp 92.5—93.5 °C (lit,[3] 87 °C); IR 1640 (C=C), 1502 and 1320 cm^{-1} (NO_2); NMR δ 6.59 (1H, s, H-2) and 8.09 (1H, s, H-4). Found: C, 70.86; H, 4.37; N, 5.73%. Calcd for $C_{15}H_{11}NO_3$: C, 71.14; H, 4.37; N, 5.53%.

4,6-Dichloro-5-(1-hydroxy-2-nitroethyl)pyrimidine (7a). To a mixture of **6a**[4] (500 mg, 2.8 mmol) and nitromethane (3.44 g, 56 mmol) in methanol (20 ml) at room temperature was added barium hydroxide octahydrate (221 mg, 0.7 mmol). The mixture was stirred for 3 h at 5 °C and then neutralized with cation-exchange resin (Mitsubishi Diaion SK 1). Evaporation of the solvent gave a solid residue, which was recrystallized from ethanol to yield colorless crystals of **7a** (419 mg, 62.4%): mp 102.5—103.5 °C; IR 3250 (OH), 1548 and 1377 cm^{-1} (NO_2). Found: C, 30.51; H, 2.09; N, 18.02%. Calcd for $C_6H_5Cl_2N_3$: C, 30.25; H, 2.10; N, 17.65%.

5-(1-Acetoxy-2-nitroethyl)-4,6-dichloropyrimidine (8a). A solution of **7a** (500 mg, 2.1 mmol) in 5 ml of acetic anhydride was allowed to stand for 6 h at room temperature in the presence of a catalytic amount of boron trifluoride etherate, and then poured into water (20 ml). The crystalline precipitate was collected and washed well with water. Recrystallization from ethanol gave colorless crystals of **8a** (511.6 mg, 87%): mp 87.5—88.5 °C; IR 1758 (C=O), 1548 and 1378 cm^{-1} (NO_2). Found: C, 34.29; H, 2.49; N, 15.24%. Calcd for $C_8H_7Cl_2N_3O_4$: C, 34.29; H, 2.50; N, 15.00%.

4,6-Dichloro-5-(2-nitrovinyl)pyrimidine (9a). To a solution of **8a** (500 mg, 1.79 mmol) in 30 ml of methanol was added solid sodium hydrogencarbonate (150 mg, 1.78 mmol). The mixture was stirred for 1 h at room temperature and then poured into 100 ml of water. The precipitate was collected and recrystallized from ethanol to give yellow crystals of **9a** (303 mg, 77%): mp 90.5—91.5 °C; IR 1642 (C=C), 1504, and 1340 cm^{-1} (NO_2); NMR δ 7.85 (1H, d, $J_{1',2'}$=14 Hz, H-2'), 8.22 (1H, d, H-1'), and 8.83 (1H, s, pyrimidine ring proton). Found: C, 33.00; H, 1.38; N, 19.31%. Calcd for $C_6H_3Cl_2N_3O_2$: C, 32.73; H, 1.36; N, 19.09%.

5-(1-Hydroxy-2-nitroethyl)-4,6-dimethoxypyrimidine (7b). To a mixture of **6b**[5] (500 mg, 2.97 mmol) and nitromethane (3.63 g, 59.5 mmol) in 50 ml of ethanol was added triethylamine (29 mg, 0.3 mmol). The mixture was allowed to stand for 4 h at room temperature and then evaporated to afford a solid residue, which was recrystallized from ethanol to give colorless crystals of **7b** (518 mg, 76%): mp 121—122 °C; IR 3200 (OH), 1550 and 1375 cm^{-1} (NO_2); NMR δ 4.45 (1H, q, J_{gem}=12.5, $J_{1a',2'}$=4 Hz, H-1a'), 4.92 (1H, q, $J_{1b',2'}$=9 Hz, H-1b'), 5.75 (1H, q, H-2'), and 8.45 (1H, s, pyrimidine ring proton). Found: C, 41.83; H, 4.95; N, 18.48%. Calcd for $C_8H_{11}N_3O_5$: C, 41.92; H, 4.84; N, 18.34%.

4,6-Dimethoxy-5-(2-nitrovinyl)pyrimidine (9b). Crude acetate obtained from **7b** (1.30 g, 5.67 mmol) under the same conditions as described above was directly treated with sodium hydrogencarbonate (510 mg, 6 mmol) in methanol at room temperature for 1 h. The mixture was evaporated to give a solid residue, which was washed completely with water and then recrystallized from ethanol to afford 791 mg (66%) of **9b** as light yellow crystals: mp 131—132 °C; IR 1620 (C=C) and 1500 cm^{-1} (NO_2); NMR δ 7.95 (1H, d, $J_{1',2'}$=14 Hz, H-2'), 8.32 (1H, d, H-1'), and 8.51 (1H, s, pyrimidine ring proton). Found: C, 45.38; H, 4.28; N, 20.04%. Calcd for $C_8H_9N_3O_4$: C, 45.50; H, 4.30; N, 19.90%.

4-Chloro-6-(2-formylphenoxy)-5-(2-nitrovinyl)pyrimidine (10). A solution of **9a** (220 mg, 1 mmol), sodium 2-formylphenoxide (196 mg, 1.36 mmol) and salicylaldehyde (1 ml) in DMSO (20 ml) was allowed to stand at room temperature for 20 h. The mixture was poured into water (50 ml) and the precipitate was collected and recrystallized from ethanol to give yellow crystals of **10** (65%): mp 126 °C; IR 1700 (C=O), 1633 (C=C), 1522 and 1340 cm^{-1} (NO_2). Found: C, 50.76; H, 2.81; N, 13.40%. Calcd for $C_{13}H_8ClN_3O_4$: C, 51.06; H, 2.62; N, 13.75%.

4,6-Bis(2-formylphenoxy)-5-(2-nitrovinyl)pyrimidine (11). A treatment of **9a** (220 mg) with sodium 2-formylphenoxide (300 mg, 2.1 mmol) similar to that described above gave yellow crystals of **11** (46%): mp 229—230 °C; IR 1692 (C=O), 1629 (C=C), and 1512 cm^{-1} (NO_2). Found: C, 60.93; H, 3.36; N, 10.64%. Calcd for $C_{20}H_{13}N_3O_6$: C, 61.38; H, 3.35; N, 10.74%.

2-(4,6-Dimethoxy-5-pyrimidinyl)-3-nitro-2H-chromene (12). To a solution of sodium 2-formylphenoxide (14.1 mg, 0.1 mmol) in DMSO (20 ml) were added **9b** (211 mg, 1 mmol) and **1** (183 mg, 1.5 mmol). The mixture was allowed to stand for 24 h at room temperature and then poured into ice-water. The precipitate was collected and recrystallized from ethanol to give 145 mg (46%) of **12** as yellow crystals: mp 143.5—144.5 °C; IR 1652 (C=C), 1502 and 1328 cm^{-1} (NO_2); NMR δ 3.82 (6H, s, 2×OMe), 7.27 (1H, s, H-2), 7.99 (1H, s, H-4), and 8.43 (1H, s, pyrimidine ring proton). Found: C, 56.97; H, 4.15; N, 13.39%. Calcd for $C_{15}H_{13}N_3O_5$: C, 57.14; H, 4.16; N, 13.33%.

References

1) T. Sakakibara, R. Sudoh, and M. Koezuka, 28 th National Meeting of the Chemical Society of Japan, Tokyo, April 1973, Abstr. p. 1731,

2) S. Hanessian and A. G. Pernet, *Adv. Carbohydr. Chem. Biochem.*, **33**, 111 (1976).

3) During our studies Rene and Royer synthesized 3-nitro-2-phenyl-2*H*-chromene (**5**) from **1** and **2** in pyridine in 34% yield; L. Rene and R. Royer, *Eur. J. Med. Chem.-Chim. Ther.*, **10**, 72 (1975).

4) H. Bredereck, G. Simchen, and A. A. Santos, *Chem. Ber.*, **100**, 1344 (1967).

5) W. Klotzer and M. Herberz, *Monatsh. Chem.*, **96**, 1573 (1965).

BULLETIN OF THE CHEMICAL SOCIETY OF JAPAN, VOL. 51 (10), 3097—3098 (1978)

The Bimolecular Reduction of Acridine and 9-Substituted Acridines by Sodium 1-Benzyl-1,4-dihydronicotinamide-4-sulfinate

Hiroo INOUE,* Ichiro SONODA, Nobuaki INOGUCHI, and Eiji IMOTO**

Department of Applied Chemistry, College of Engineering, University of Osaka Prefecture, Sakai, Osaka 591

(Received May 11, 1978)

Synopsis. Sodium 1-benzyl-1,4-dihydronicotinamide-4-sulfinate is found to undergo the bimolecular reduction of acridine or 9-substituted acridines to the corresponding 9,9′-biacridans.

The reducing behavior of sodium 1-benzyl-1,4-dihydronicotinamide-4-sulfinate (BNA-SO_2Na)[1] has received little attention. Recently we have found that BNA-SO_2Na reacts with various halogen compounds through the cleavage of its carbon-sulfur bond to give sulfones, olefins, and reduction products.[2] In order to explore further the chemical reactivity of BNA-SO_2Na, the reactions of BNA-SO_2Na were carried out with acridine (**1**) and its derivatives (**2**—**4**), with a methoxy, chloro, or cyano group at the 9-position. Herein, we wish to report our findings on these reactions.

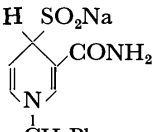

BNA-SO_2Na

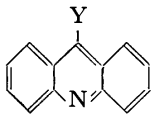

Y=H (**1**), CH_3O (**2**), Cl (**3**) and CN (**4**)

As Table 1 shows, the reaction of **1** with BNA-SO_2Na in 80 vol % aqueous methanol at 25 °C afforded 9,9′-biacridan (**5**), together with a small amount of acridan (**6**). In this reaction, BNA-SO_2Na was converted to 1-benzylnicotinamide hydroxide (BNA$^+$OH$^-$) and a sulfite ion. The formation of **5** along with an equivalent amount of BNA$^+$OH$^-$ constitutes the bimolecular reduction of **1** by BNA-SO_2Na. On the other hand,

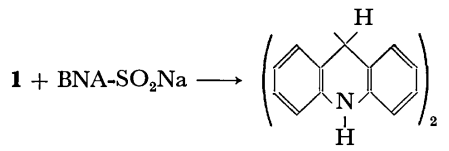

5 (major)

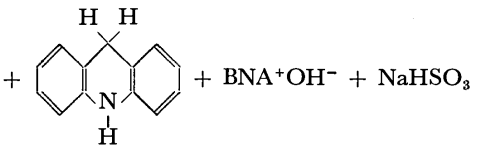

6 (minor)

the reaction of **1** with 1-benzyl-1,4-dihydronicotinamide (BNAH) or sodium dithionite afforded only **6**, without the formation of any **5**. Sodium dithionite would undergo the reduction of **1**, probably *via* the intermediary formation of an adduct (**7**), followed by the decomposition of **7** by water to give **6**.[3] Similar phenomena were also found in the reaction of 10-methylacridium chloride (**8**) with BNA-SO_2Na (Table 1). Thus, it is concluded that BNA-SO_2Na shows a reducing behavior different from that of BNAH and sodium dithionite.

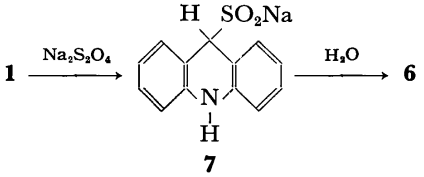

7

Table 1. The reductions of **1** and **8** with BNA-SO_2Na or $Na_2S_2O_4$[a]

Substrate	Reducing agent	Time h	Product, %[b] Biacridans	Acridans	BNA$^+$OH$^-$	SO_3^{2-}
1	BNA-SO_2Na	12	76	7	36	32
1	$Na_2S_2O_4$	2	0	75	—	—
8	BNA-SO_2Na	12	69	13	35	35
8	$Na_2S_2O_4$	2	12	41	—	—

a) Concentration of **1** and **8**: 6×10^{-2} mol/l. Solvent: 80 and 50 vol % MeOH–H_2O for BNA-SO_2Na and $Na_2S_2O_4$ respectively. Reducing agent/substrate molar ratio: 1. b) Biacridans% = {2 × biacridans (mol)/substrate (mol)} × 100. Acridans, BNA$^+$OH$^-$ and SO_3^{2-}% = {products (mol)/substrate (mol)} × 100.

Table 2. The reductions of **2**, **3**, and **4** with BNA-SO_2Na[a]

Substrate	Solvent	Time, h	Product (%)[b]
2	80% MeOH–H_2O	20	**9** (41), Acridone(6), BNA$^+$OH$^-$(43)[c]
3	EtOH	6	**10** (58), Acridone(37), BNA$^+$Cl$^-$(59)
4	DMF	3	**11** (91), BNA$^+$OH$^-$(100)

a) Concentration of **2**, **3**, and **4**: 6×10^{-2} mol/l. Reducing agent/substrate molar ratio = 1 (for **2** and **3**) and 2 (for **4**). b) **9** and **10**% = {2 × **9** and **10** (mol)/substrate (mol)} × 100. **11**, acridone, and BNA$^+$OH$^-$ (Cl$^-$) % = {products (mol)/substrate (mol)} × 100. c) Recovery% of **2**: 45%.

The reactions of 9-substituted acridines with BNA-SO_2Na were affected by the nature of the substituents. The reaction of **2** or **3** with BNA-SO_2Na afforded 9,9′-dimethoxy-9,9′-biacridan (**9**) or 9,9′-biacridine (**10**) respectively as the reduction product, as Table 2 shows. In both reactions, however, acridone was obtained as another product. In addition, in the case of **2**, the **2** was recovered in considerable amounts. On the other hand, BNA-SO_2Na was converted to BNA$^+$OH$^-$ (Cl$^-$) in larger amounts than those of **9** and **10**. Furthermore,

** Present address: Department of Industrial Chemistry, College of Engineering, Kyushu Sangyo University, Shokadai, Higashi-ku, Fukuoka 813.

the reduction of **2** with KBH_4 in 80 vol % aqueous methanol was found to afford acridone in a 40% yield, with a 45% recovery of **2**. These facts suggest that the 9,10-dihydro-compounds of **2** and **3**, which may be easily oxidized with air to acridone and the starting material, are produced in addition to **9** and **10**. In the reaction of **4** with BNA-SO_2Na, 9-cyanoacridan (**11**) was produced in a high yield, without the formation of any 9,9'-dicyano-9,9'-biacridan. Thus, the existence of an electron-withdrawing group, such as the cyano group, at the 9-position of the acridine ring favored the formation of a dihydro-compound by two-electron reduction.[4]

Experimental

Material. The BNA-SO_2Na was prepared according to the procedures described in our proceding paper.[2]

Reduction by BNA-SO_2Na. Acridine (1): A solution of a mixture of 3.06 mmol of **1** and 3.05 mmol of BNA-SO_2Na in 50 cm^3 of 80 vol% aqueous methanol was stirred under nitrogen at 25 °C for 12 h. A white precipitate (0.42 g, 76%) of **5** was formed and recrystallized from DMSO under nitrogen: mp 260—262 °C (lit,[5] 260—261 °C). (Found: C, 86.72; H, 5.26; N, 7.73%. Calcd for $C_{26}H_{20}N_2$: C, 86.63; H, 5.59; N, 7.77%). Its IR spectrum was identical with that of the authentic specimen. After the precipitate had been removed by filtration, 50 cm^3 of water was added to the filtrate to give 0.038 g (7%) of a white precipitate of **6** (mp 168—169 °C (lit,[5] 170 °C)). After the removal of **6** by filtration, the filtrate was acidified by concentrated hydrochloric acid to bring about the evolution of sulfur dioxide. The amount of sulfur dioxide evolved (32% was determined by the method described previously.[2] The solution thus acidified was evaporated *in vacuo*, and the residue was treated by the procedures described previously to yield 0.28 g (36%) of BNA$^+$Cl$^-$ (mp 230—233 °C (lit,[2] 236 °C)). Similar procedures were used for the reactions of **1** or **8** with BNAH, sodium dithionite, or BNA-SO_2Na. 10,10'-Dimethyl-9,9'-biacridan (mp 271—273 °C (lit,[5] 272—274 °C)) was obtained in a 69% yield. (Found: C, 86.65; H, 6.15; N, 6.96%. Calcd for $C_{28}H_{24}N_2$: C, 86.56; H, 6.23; N, 7.21%).

9-Methoxyacridine (2): To a solution of 1.49 mmol of **2** in 25 cm^3 of 80 vol% aqueous methanol, we added 1.5 mmol of BNA-SO_2Na. The solution was stirred under nitrogen at 25 °C for 20 h. A pale yellow precipitate which was thus deposited (0.13 g) was removed by filtration, washed under nitrogen with 80 vol% aqueous methanol, and dried *in vacuo*: mp>260 °C (The color turned to brown at 172 °C). The elementary analysis of the precipitate was carried out without purification, since it was oxidized easily with air in an organic solvent.

Found: C, 79.67; H, 5.60; N, 6.78%. Calcd for $C_{28}H_{24}N_2O_2$: C, 79.97; H, 5.75; N, 6.66%.

The pattern of its IR spectrum was similar to that of **5**. Its UV spectrum ($CHCl_3$) showed a peak at 280 nm, thus being similar to that of **5**. In contact with air, however, the UV spectrum changed completely to that of **2**, which had two peaks at 256 and 354 nm (ε: 1.4×10^5 and 8.3×10^3). Based on these facts, it was identified as **9**. Yield: 41%. On the other hand, the filtrate was concentrated to one-fifth of its original volume, and the orange precipitate thus deposited (0.31 g) was removed by filtration, washed with water, and dried *in vacuo*. The precipitate was chromatographed on silica gel. Elution with chloroform gave 0.14 g (45%) of **2** and 0.016 g (6%) of acridone. The combined filtrate was developed on an anion-exchange resin (Amberlite IRA-400) to yield 0.16 g (43%) of BNA$^+$Cl$^-$.

9-Chloroacridine (3): To a solution of 2.89 mmol of **3** in 50 cm^3 of ethanol, we added 3.11 mmol of BNA-SO_2Na. The mixture was stirred under nitrogen at 25 °C for 6 h. A pale yellow precipitate (**10**) thus deposited was removed by filtration, washed successively with ethanol and water, dried *in vacuo*, and recrystallized from toluene; mp>360 °C. Yield: 58%. Its IR spectrum was similar to that of **1**. (Found: C, 87.77; H, 4.83; H, 8.03%. Calcd for $C_{26}H_{16}N_2$: C, 87.61; H, 4.53; N, 7.86%). The filtrate was concentrated to one-fifth of its original volume, and 50 cm^3 of water was added. Extraction with dichloromethane gave 0.21 g (37%) of acridone. The aqueous layer was treated by a method similar to that used in the case of **1** to yield 0.42 g (59%) of BNA$^+$Cl$^-$.

9-Cyanoacridine (4): A solution of a mixture of 2.94 mmol of **4** and 6.01 mmol of BNA-SO_4Na in 50 cm^3 of DMF was stirred under nitrogen at 25 °C for 3 h. The solution immediately showed a red color, and then it turned orange. The reaction mixture was added to 200 cm^3 of water to give 0.55 g (91%) of a white precipitate of **11** (mp 146—147 °C (lit,[5] 146 °C)). Its IR spectrum was identical with that of the authentic specimen. After the removal of **11** by filtration, the filtrate was treated by a method similar to that used in the case of **1** to yield 0.73 g (100%) of BNA$^+$Cl$^-$.

References

1) J. F. Biellmann and H. J. Callot, *Bull. Soc. Chim. Fr.*, **1968**, 1154.

2) H. Inoue, N. Inoguchi, and E. Imoto, *Bull. Chem. Soc. Jpn.*, **50**, 197 (1977).

3) The reaction of acridine hydrochloride with sodium sulfite gives sodium acridan-9-sulfonate: R. M. Acheson and L. E. Orgel, "The Chemistry of Heterocyclic Compounds —Acridines," ed by A. Weissberger, Interscience Publishers, New York (1956), p. 255. In the preparation of BNAH from BNA$^+$Cl$^-$, BNA-SO_2Na is formed as an intermediate: W. S. Caughey and K. A. Schellenberg, *J. Org. Chem.*, **31**, 1978 (1966).

4) This reaction seems to be similar to the reduction of α-halo ketones with BNA-SO_2Na.[2]

5) Ref. 3, Chaps. 5 and 6, and the references cited therein; H. Goth, P. Cerutti, and H. Schmid, *Helv. Chim. Acta*, **48**, 1395 (1965); F. Mader and V. Zanker, *Chem. Ber.*, **94**, 2418 (1964).

BULLETIN OF THE CHEMICAL SOCIETY OF JAPAN, VOL. 51 (10), 3099—3100 (1978)

Unusual Reductive Deamination of 2,6-Dibromo-3,4,5-trimethylaniline by Alkyl Nitrites in *N,N*-Dimethylformamide. Simultaneous Side-chain Nitration[1]

Hitomi SUZUKI,* Tadashi MISHINA, and Terukiyo HANAFUSA

Department of Chemistry, Faculty of Science, Hiroshima University, Higashi-sendamachi, Hiroshima 730

(Received May 22, 1978)

Synopsis. Treatment of 2,6-dibromo-3,4,5-trimethylaniline with *t*-butyl nitrite in *N,N*-dimethylformamide at 60—65 °C was found to give a significant amount of a side-chain nitration product, 3,5-dibromo-2,6-dimethylphenylnitromethane, in addition to the expected 4,6-dibromo-1,2,3-trimethylbenzene.

In the course of our studies of the reactions of polyalkyl aromatics, it became necessary to prepare 4,6-dibromo-1,2,3-trimethylbenzene (**2**). The synthesis of this compound was performed along the five-step sequence shown in Scheme 1. The outcome in the last step was unexpected, however. The solid material obtained from the reaction of 2,6-dibromo-3,4,5-trimethylaniline (**1**) with *t*-butyl nitrite in *N,N*-dimethylformamide (DMF) according to the procedure of Doyle[2] was found to be a two-component mixture of an approximately 1 : 1 composition. Chromatography of this mixture over silica gel using hexane as eluant gave the expected **2** as early eluate, mp 143—144 °C, and a pale yellow solid as late eluate, mp 134—136 °C. The elemental analysis and molecular weight of the latter compound were consistent with the formula $C_9H_9NO_2Br_2$. Its IR spectrum showed strong bands at 1550 and 880 cm^{-1}, indicating the presence of an aliphatic nitro group. Its PMR spectrum contained peaks at δ 2.48, 5.66, and 7.89 ppm, with a relative intensity ratio of 6 : 2 : 1, indicating the presence of two methyl groups, one methylene group, and one aromatic proton. These analytical and spectral data agree with the structure of 3,5-dibromo-2,6-dimethylphenylnitromethane (**3**). Its mass spectrum showed all the features expected for the assigned structure: characteristic triplet peaks centered at *m/e* 323 (M^+) and 277 (M^+—NO_2; base peak), and fragment peaks of these at *m/e* 242 and 244 (M^+—Br), 196 and 198 (M^+—NO_2—Br), and 117 (M^+—NO_2—2Br). The phenylnitromethane obtained was not contaminated with the isomeric 2,3-dimethyl-4,6-dibromophenylnitromethane (**7**) in any detectable amount.

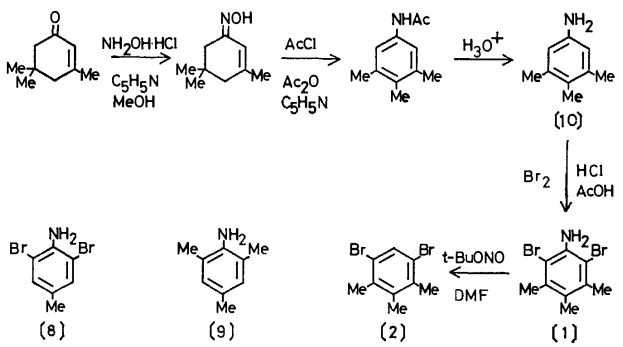

Scheme 1.

We tried to preclude this undesired side product by carrying out deamination in boiling tetrahydrofuran as a hydrogen donor.[3] The product obtained was nearly identical with those derived from the corresponding reaction in DMF. The replacement of *t*-butyl nitrite by butyl nitrite did not have much influence on the product composition. Since the compound **2** was inert to the reagent under the reaction conditions employed, the unusual product **3** should have been formed from **1** through a pathway competing with the normal deamination.

Alkyl nitrites have been successfully used in the aprotic diazotization of various arylamines.[4] To the best of our knowledge, however, no report seems to have appeared on the simultaneous deamination and side-chain nitration during the reaction of alkylanilines with alkyl nitrites. In order to ascertain the scope of this anomaly, several other methylanilines were treated in a similar manner. 2,6-Dibromo-4-methylaniline (**8**) gave 3,5-dibromotoluene in a 50% isolated yield. Spectral inspection of the crude product mixture indicated the presence of a side-chain nitration product which, however, could not be isolated due to its small quantity. Both 2,4,6- and 3,4,5-trimethylanilines (**9** and **10**) yielded the expected hydrocarbons together with considerable amounts of polymeric substances, proving the Doyle's method to be synthetically less useful for the deamination of these reactive amines. The PMR spectrum of the crude product from **9** contained a minor peak (δ 5.21 ppm) in the region where phenylnitromethanes usually absorb.[5] In contrast, no side-chain substitution product could be detected in the deamination product from **10**. The unusual course of deamination, therefore, seems to be important only for a narrow range of alkylanilines.

We have not made a mechanistic study of this unusual reaction, but a possible mechanism for the regiospecific side-chain nitration may be depicted by assuming the rearrangement of the hindered anilino radical (**4**) into the benzyl radical (**5**) (Scheme 2). Thus, alkyl nitrite decomposes homolytically to give alkoxyl radical and nitrogen oxide. The former abstracts a hydrogen atom from the amino group of arylamine, giving the assumed anilino radical intermediate **4**, while the latter is oxidized to nitrogen dioxide, as is evidenced by the liberation of brown fumes. In analogy to the conversion of hindered phenoxyl radicals to benzyl radicals,[6] **4** would isomerize to 4-aminobenzyl radical **5** which combines with nitrogen dioxide to form the amine **6**; this will undergo further reductive deamination,

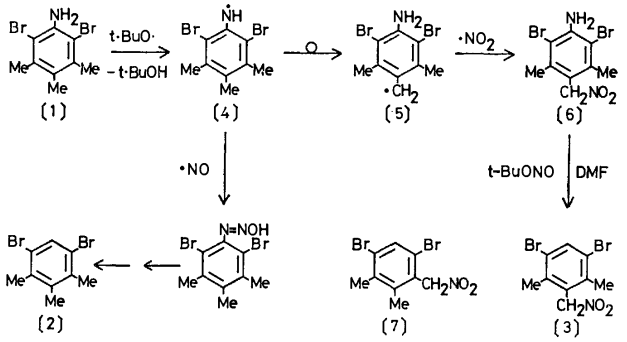

Scheme 2.

giving the arylnitromethane **3** as the final product. Although **6** could not be isolated as such, its intermediacy is highly probable.

Experimental

Melting points were determined on a hot stage apparatus and are uncorrected. IR spectra were obtained in Nujol mulls with a Hitachi 215 spectrophotometer. PMR spectra were run in deuteriochloroform on a Varian T-60 spectrometer using TMS as internal standard. Mass (MS) spectra were recorded on a Hitachi RMS-4 mass spectrometer with 70 eV ionizing current.

Butyl nitrites were prepared in the usual manner.[7] 2,4,6-Trimethylaniline (**9**; bp 145 °C/57 mmHg; lit,[8] bp 225—226 °C), 3,4,5-trimethylaniline (**10**; mp 77—78 °C; lit,[9] mp 78.5—79 °C), 2,6-dibromo-4-methylaniline (**8**; mp 74—75 °C; lit,[10] mp 79 °C), and 2,6-dibromo-3,4,5-trimethylaniline (**1**; mp 163—165 °C; lit,[9] mp 162.5—163.5 °C) were prepared as reported. *N,N*-Dimethylformamide was distilled from calcium hydride prior to its use.

Reaction of 2,6-Dibromo-3,4,5-trimethylaniline with t-Butyl Nitrite in DMF. To a stirred solution of *t*-butyl nitrite (0.74 g; 7.2 mmol) in dry DMF (10 ml) maintained at 60—65 °C, amine **1** (0.7 g; 2.4 mmol) in the same solvent (5 ml) was added dropwise over a 5 min period and the solution was stirred at this temperature for a further 20 min. After cooling, the mixture was diluted with ether (50 ml), washed successively with dilute hydrochloric acid, aqueous sodium hydrogencarbonate, and water, dried over sodium sulfate, and evaporated to leave a yellow residue (0.78 g), which was dried and chromatographed on silica gel. Elution with hexane gave **2** as early eluate; white needles, mp 143—144 °C. Yield, 0.28 g (42%). PMR: δ 2.31 (3H, s), 2.35 (6H, s), and 7.60 ppm (1H, aromatic H); IR: ν_{max} 1560, 1000, 900, and 850 cm^{-1}. Found: C, 38.72; H, 3.60%. Calcd for $C_9H_{10}Br_2$: C, 38.88; H, 3.63%.

Further elution with the same solvent gave **3** as straw-colored needles, mp 134—136 °C. Yield, 0.25 g (32%). The ratio **2** to **3** in the crude product mixture as determined by PMR analysis was approximately 10 to 11. Found: C, 33.65; H, 2.84; N, 4.27%. Calcd for $C_9H_9NO_2Br_2$: C, 33.47; H, 2.81; N, 4.34%.

In the corresponding reaction of 2,6-dibromo-4-methylaniline **8** with *t*-butyl nitrite, the reddish brown oil obtained on removal of the solvent was shown by PMR (singlet peak at δ 5.31 ppm) and IR spectra (strong band at 1560 cm^{-1}) to contain a nitromethyl compound which, however, could not be isolated due to its small quantity. After passage in a pentane solution through an alumina column, 3,5-dibromotoluene was obtained as colorless plates, mp 36—37 °C (lit,[11] mp 36.8—37 °C). Yield, 50%.

References

1) The reaction of polysubstituted aromatics. Part LI; Part L: H. Suzuki, K. Nakano, T. Mishina, and T. Hanafusa, *Nippon Kagaku Kaishi*, **1978**, 1049.

2) M. P. Doyle, J. F. Dellaria, Jr., B. Siegfried, and S. W. Bishop, *J. Org. Chem.*, **42**, 3494 (1977).

3) J. I. G. Cadogan and G. A. Molina, *J. Chem. Soc., Perkin Trans. 1*, **1973**, 541.

4) For the use of alkyl nitrites as *in situ* diazotizing agents, see *e.g.*, S. Huang, *Hua Hsüeh Pao*, **25**, 171 (1959); *Chem. Abstr.*, **54**, 4489 (1960); W. Zerweck, M. Schubert, and R. Fleischhauer, Ger. Patent 905014; *Chem. Abstr.*, **50**, 12111 (1956); J. I. G. Cadogan, *J. Chem. Soc.*, **1962**, 4257; L. Friedman and F. M. Logullo, *J. Am. Chem. Soc.*, **85**, 1549 (1963); M. Stiles, R. G. Miller, and U. Burckhardt, *ibid.*, **85**, 1792 (1963); J. I. G. Cadogan, D. A. Roy, and D. M. Smith, *J. Chem. Soc. C*, **1966**, 1249.

5) 3,4,5-Trimethylphenylnitromethane absorbs at δ 2.17 (3H, s), 2.30 (6H, s), 5.21 (2H, s), and 7.01 ppm (2H, s).

6) C. D. Cook, N. G. Nash, and H. R. Flanagan, *J. Am. Chem. Soc.*, **77**, 1783 (1955). In the side-chain nitration of polymethyl-1,4-dihydropyridines, dihydro-1-pyridyl cation radicals were assumed to isomerize into dihydropyridylmethyl radicals: J. Kuthan and A. Kurfürst, *Tetrahedron Lett.*, **1976**, 2073.

7) W. A. Noyes, *Org. Synth.*, Coll. Vol. II, 108 (1943).

8) R. Adams and L. J. Dankert, *J. Am. Chem. Soc.*, **62**, 2191 (1940).

9) F. M. Beringer and I. Ugelow, *J. Am. Chem. Soc.*, **75**, 2635 (1953).

10) G. Lock and R. Schreckeneder, *Chem. Ber.*, **72**, 511 (1939).

11) A. A. Maryott, M. E. Hobbs, and P. M. Gross, *J. Am. Chem. Soc.*, **62**, 2320 (1940).

BULLETIN OF THE CHEMICAL SOCIETY OF JAPAN, VOL. 51 (10), 3101—3102 (1978)

Structures of Copper(II) Complexes Which Deposit Copper in Chemical Copper-plating Bath

Seigo OHNO

Electron Device Laboratory, Oki Electric Industry Co., Ltd., 4-10-12 Shibaura, Minato-ku, Tokyo 108

(Received September 21, 1977)

Synopsis. The deposition of copper from alkaline solutions containing various copper(II) complexes and formaldehyde was studied. It was found that one-to-one copper(II) complexes of hepta-, hexa-, and quadridentate ligands deposit copper on reduced platinum by means of autocatalytic reduction, and that, under particular conditions, copper(I) oxide is deposited on oxidized platinum from the solutions containing quadridentate ligands.

It is well known that copper metal is catalytically deposited on the surfaces of noble metals from solutions which contain some kinds of copper(II) complexes and reducing agents. As the deposited copper also has a good catalytic activity, the reduction proceeds autocatalytically. This reduction method has been widely utilized as "chemical copper plating" in industry, especially in the manufacture of printed circuit boards.

For this reduction, several reaction mechanisms have been proposed. Saubestre[1] reported the following half-reactions for reductions in alkaline solutions containing the tartrate ion as the complexing agent and formaldehyde as the reducing agent:

$$HCHO + 3OH^- \longrightarrow HCOO^- + 2H_2O + 2e^- \quad (1\text{-a})$$

$$Cu^{2+} + 2e^- \longrightarrow Cu \quad (1\text{-b})$$

Although hydrogen gas is evidently generated on the plating surface, he discussed no details of the evolution of hydrogen. Tilley[2] and Lukes[3] proposed the following half-reactions:

$$2HCHO + 4OH^- \longrightarrow 2HCOO^- + H_2 + 2H_2O + 2e^- \quad (2\text{-a})$$

$$Cu^{2+} + 2e^- \longrightarrow Cu \quad (1\text{-b})$$

Konishi[4] and Saito[5] reported that not the hydrated copper(II) ion, but the copper(II) complex, participates in this reduction. It seems, however, that there is no direct evidence for what kind of copper(II) species deposits copper. A study has, therefore, been made to deepen our understanding of this reduction.

Experimental

Preparation of Plating Solutions. The following reagents were used as the complexing agents for the copper(II) ion: D-mannitol, D-sorbitol, dulcitol, ethylenediaminetetraacetic acid (H_4edta), 1,2-cyclohexanediaminetetraacetic acid (H_4-cdta), *N*-(2-hydroxyethyl)ethylenediaminetriacetic acid (H_3-hedta), diethylenetriaminepentaacetic acid (H_5dtpa), L-, D-, and *meso*-tartaric acids, *meso*-erythritol, ethylenediamine (en), diethylenetriamine (dien), and triethylenetetramine (trien). Known amounts of copper(II) sulfate, one of the above complexing agents, and sodium hydroxide were dissolved in deionized water in the above order. These mixtures were then kept at 29 °C for 24 h. Known amounts of a formaldehyde solution kept at 29 °C were added to the above mixtures before use. All the reagents used were of an A. R. grade.

Apparatus and Procedure. A cleaned platinum substrate (0.2 mm × 14 mm × 20 mm) was oxidized electrolytically in nitric acid (1 : 1) (oxidized substrate). In some runs, the substrate was reduced by immersing it in a 0.2 mol/dm^3 formaldehyde and 0.4 mol/dm^3 sodium hydroxide solution (reduced substrate) in order to differentiate the reactivities of the copper(II) complexes studied. Copper or copper(I) oxide was deposited on the substrates by immersing them in the plating solutions (250 cm^3) at 29 °C for 60 min. The amounts of deposits were determined by chelatometric titration. The amounts of hydrogen evolved during the deposition were measured by the use of the apparatus shown in Fig. 1 in the following manner. The apparatus, filled with a plating solution, was kept at 29.0 °C, and then the air in the apparatus and dissolved in the plating solution was replaced with hydrogen by bubbling. The substrate, S, was placed over the plating solution by means of a hanger, H, and a magnet, M, and then the plug, P, and the stopcoek, S, were closed. The substrate was immersed in the plating solution by moving the magnet. After an appropriate time, the substrate was raised and the pressure increase was measured by means of a water manometer, WM.

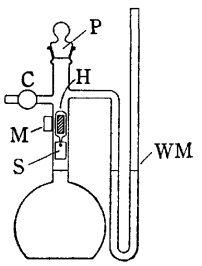

Fig. 1. Apparatus for measuring hydrogen evolution.

Results and Discussion

The deposition rate of copper on the oxidized substrate is shown in Fig. 2, with H_4edta used as the complexing agent. The rate was virtually independent of the concentration of H_4edta added. The rate on the reduced substrate was the same as that on the oxidized substrate within the limits of experimental errors.

It is well known that H_4edta forms a stable one-to-one complex with the copper(II) ion.[6] Therefore, the concentration of this complex must be almost constant under the present conditions, whereas the concentration of the hydrated copper(II) ion decreases steeply with an increase in the concentration of H_4edta as follows:

$$[Cu^{2+}] \approx c_c/K(c_l - c_c), \quad (3)$$

where K is the stability constant of the complex and where c_c and c_l represent the concentrations of copper(II) sulfate and the complexing agent respectively.

The above findings, therefore, suggest that not the hydrated copper(II) ion, but the copper(II) complex deposits copper. The slight decrease in the rate shown

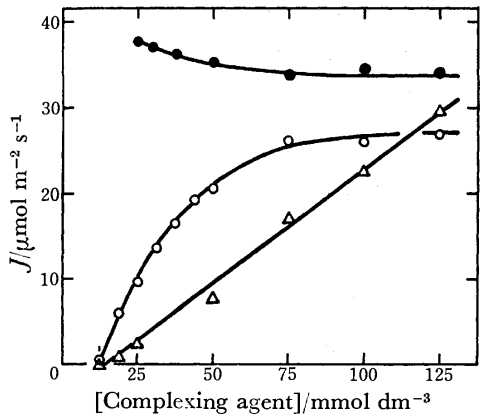

Fig. 2. Relations between the deposition rate of copper and the concentration of the compexing agent in Cu(II)–H_4edta (●), Cu(II)–D-mannitol (○), and Cu(II)–D-sorbitol (△) plating solutions. $CuSO_4$: 25, HCHO: 100 mmol/dm^3, pH: 12.8, Temp: 29 °C.

in Fig. 2 may be explained in terms of retardation due to the adsorption of edta^{4-}, Hedta^{3-}, *etc.*

Hexitols such as D-mannitol and D-sorbitol have six OH groups. These reagents may be expected to form two-to-one and/or one-to-one complexes with the copper(II) ion. Hence, the reactivity of their complexes was studied. As is shown in Fig. 2, the deposition of copper began just at $c_l/c_c=0.50$ in both plating solutions, and the rate increased with the increase in the c_l. In the range of $2c_l<c_c$, copper(II) hydroxide was precipitated. These findings indicate that D-mannitol and D-sorbitol react with the copper(II) ion as follows:

$$2Cu^{2+} + H_nL + 4OH^- \rightleftarrows [Cu_2H_{(n-4)}L] + 4H_2O, \quad (4)$$

$$Cu^{2+} + H_nL + 2OH^- \rightleftarrows [CuH_{(n-2)}L] + 2H_2O, \quad (5)$$

where H_nL represents a ligand, and that the one-to-one complex ($[CuH_{(n-2)}L]$) deposits copper.

In order to obtain further proof, the reactivities of various copper(II) complexes were studied. These complexes can be classified into three categories. The first-group complexes consist of the copper(II) ions and either hepta- or hexadentate ligands such as H_4edta, H_4cdta, H_3hedta, H_5dtpa, D-mannitol, D-sorbitol, and dulcitol and deposit copper by forming hydrogen, regardless of the surface state of the substrate. The second-group complexes are composed of the copper(II) ions and quadridentate ligands such as L-, D- and *meso*-tartaric acids, and *meso*-erythritol and deposit copper accompanied by the formation of hydrogen on the reduced substrate and copper(I) oxide, but not accompanied by the formation of hydrogen on the oxidized substrate under particular conditions ($c_l/c_c\approx2$). In this group, the species which give copper are probably one-to-one complexes, in view of the findings described in the preceding paragraphs. The formation of a one-to-one copper(II)–tartrate complex was previously verified by EPR under conditions similar to the present case.[7] The third-group complexes are those with the copper(II) ions surrounded by nitrogen atoms only (en, dien, and trien); they are completely inactive.

In all the cases of copper deposition, each plating solution gave almost the same rates for both oxidized and reduced substrates under the same conditions. It can, therefore, be suggested that the platinum oxide (PtO_x) formed on the oxidized substrate is quickly reduced when it is immersed in the plating solutions and that the reduced platinum catalyzes the deposition of copper.

The amounts of hydrogen formed during the deposition were measured in the plating solutions containing H_4edta. The H_2/Cu ratios ranged from 0.94 (pH=11.3) to 0.96 (pH=12.8), in agreement with Lukes' results.[3] It is well known that the formate ion, a product of Reaction 1-a or 2-a, is also a reducing agent. However, no deposits were obtained from the present solutions when sodium formate was used as the reducing agent. Accordingly, Reaction 2-a must be operative, at least in more than 94% of the total deposits.

From these results, it may be concluded that the one-to-one copper(II) complexes, whose general structures are shown in Fig. 3, are autocatalytically reduced by formaldehyde in an alkaline solution as follows:

$$PtO_x \xrightarrow{HCHO,\ OH^-} Pt \quad (6)$$

$$[CuH_{(n-2)}L] + 2HCHO + 4OH^- \xrightarrow{Pt,\ Cu} Cu + 2HCOO^- + H_2 + 2H_2O + H_{(n-2)}L^{2-}. \quad (7)$$

As has been described above, the second-group

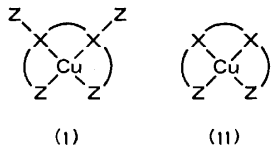

(I) (II)

Fig. 3. General structures of copper(II) complexes which deposit copper.
X's are N or O atoms. Z's are polar groups such as $-COO^-$, $-CH_2COO^-$, $-CH_2OH$ or $-CH(OH)CH_2OH$.

complexes gave copper(I) oxide on the oxidized substrate at $c_l/c_c\approx2$. This finding suggests that, under these conditions, PtO_x is not reduced, but catalyzes the partial reduction of some copper(II) species to deposit Cu_2O as:

$$\text{Cu(II)-species} \xrightarrow{HCHO,\ OH^-/PtO_x} Cu_2O. \quad (8)$$

A study of this deposition is now in progress.

References

1) E. B. Saubestre, *Proc. Am. Electroplaters' Soc.*, **46**, 264 (1959).
2) J. T. Tilley, *Trans. Inst. Metal Finishing*, **40**, 28 (1963).
3) R. M. Lukes, *Plating (East Orange, N. J.)*, **51**, 1066 (1964).
4) S. Konishi, *Kinzoku Hyomen Gijutsu*, **16**, 501 (1965).
5) M. Saito, *Kinzoku Hyomen Gijutsu*, **16**, 300 (1965); *ibid.*, **17**, 14 (1966).
6) L. G. Sillén and A. E. Martel, Compilers, "Stability Constants of Metal-Ion Complexes," 2nd ed, Chem. Soc., London (1964), p. 636.
7) L. N. Schoenberg, *J. Electrochem. Soc.*, **118**, 1571 (1971).

Correlation of Solvation Free Energy of Electron with Empirical Parameters of Solvents. A Criterion for Electrophilic Effects of Solvents

Hideo IMAI* and Kazuo YAMASHITA

Faculty of Integrated Arts and Sciences, Hiroshima University, Hiroshima 730

(Received January 5, 1978)

The solvation free energy of electrons in *N,N*-dimethylformamide, methanol, and water was estimated by means of electron photoemission into solution, and the data were compared with empirical parameters such as thermodynamic quantities, structural and kinetic parameters of solvents. It was confirmed that the interaction of an electron with solvent molecules is purely electrostatic and that the solvation free energy can be used as a tentative criterion of electrophilic properties of solvents.

The empirical parameters of solvents have been proposed as a measure of polarity or nucleophilic and electrophilic properties of solvents. These parameters were deduced from the solvent effects on the band shift of optical absorption spectra of particular solutes, NMR solvent shift, thermodynamic quantities of solvation, or kinetic parameters of solvent dependent processes.

The interaction of a solute with solvent molecules has been conceptualized from various points of view. Stengle *et al.*[1] proposed a three-region model: (1) the region of ordering effect of a solute on its immediate neighborhood, (2) the region of disordering of solvent structure, and (3) the bulk region where solvent structure is unperturbed. Cox *et al.*[2] classified the interaction into five types: (1) electrostatic interactions (either Born type or its modifications), (2) different hydrogen-bonding donor or acceptor properties of ions and solvents, (3) different types and extent of solvent structure, (4) dispersion force interactions, and (5) different Lewis acidity and basicity of ions and solvents. Some of these interactions are interrelated, *e.g.*, influence of hydrogen-bonding properties of solvents on their structure. The solvation effect would be more involved in kinetic processes where the structure of the activated complex plays an important role.

A solvent molecule and the usual solute are, in general, of dipolar character, so that the nucleophilic interaction occurs simultaneously with electrophilic interaction at different sites of a molecule depending the structural characteristics of the solute and solvent. However, a solvated electron is known to be the simplest entity with a unit negative charge held in a cavity created by dilated solvent molecules, so that the interaction of an electron with solvent molecules gives information on the simple electrostatic interaction.

The solvation free energy of an electron in polar solvents has been estimated by means of electron photoemission (EPE) into solution.[3] In this paper a discussion is given on how the solvation free energies of electrons in various polar solvents correlate with the empirical parameters of solvents and how these values can be used as a tentative criterion of electrophilic solvent effects.

Results and Discussion

Solvation Free Energy of Electron. The solvation free energy of a photoemitted electron was estimated by the EPE method. The photoemission current was measured in a cell equipped with a three-electrode system where the working electrode (mercury pool electrode) was illuminated by ultraviolet light (365 nm wavelength) under a controlled potential. The cell contained a highly concentrated supporting electrolyte solution saturated with dinitrogen oxide as an electron scavenger. The photoemission current, I_p, is expressed by the law of five-halves[4]

$$I_p = A(h\nu - h\nu_0 - e\phi)^{5/2}, \quad (1)$$

where A is a constant, $h\nu$ the energy of incident light, ν_0 the threshold frequency, and ϕ the electrode potential. The plot of $I_p^{0.4}$ *versus* ϕ gives a straight line, and extrapolation of the plot to $I_p=0$ gives the threshold potential, ϕ_0. Thus, we have $h\nu_0 = h\nu - e\phi_0$. The difference in energies required for the photoemission from mercury into vacuum and from mercury into solution gives the solvation free energy of the eletron ($\Delta G_s(e^-)$):

$$\begin{aligned} -\Delta G_s(e^-) &= W_{m-v} - h\nu_0 + e\Phi \\ &= W_{m-v} - h\nu + e(\phi_0 + \Phi), \end{aligned} \quad (2)$$

where W_{m-v} is the work function of electron photoemission from mercury into vacuum, Φ the Volta potential difference between mercury and solution.

The values of $\Delta G_s(e^-)$ thus obtained are the energy difference between electrons *in vacuo* and in solution, corresponding to those of the solvation free energy of ions estimated by Born-Haber cycle. It is noteworthy that the hydration energy of the fully hydrated electron was estimated to be 161[5] or 165[6] kJ mol^{-1} by radiation chemical studies, while our result is 108 kJ mol^{-1}. Our value presumably corresponds to the so-called damp or unlocalized electron, which is assumed to exist in solution only for a few tens picoseconds[7] before being fully solvated.

We had difficulty in estimating the values of $\Delta G_s(e^-)$ in various solutions due to the absence of information on the values of Volta potential difference for non-aqueous solutions. Only three data on *N,N*-

Table 1. Values of solvation free energy of electron, $\Delta G_s(e^-)$, and donor number (*DN*)

Solvent	DMF	MeOH	H_2O
$-\Delta G_s(e^-)$/kJ mol^{-1}	62	98	108
DN[a]	26.6	19.0	18.0

a) The values of *DN* are given in kcal mol^{-1} (1 cal = 4.184 J.

dimethylformamide (DMF), methanol (MeOH), and water (H_2O) are available (Table 1), which do not seem sufficient for a discussion of the general features of solvent effects. However, they are in line with the values estimated by a modified Born equation for fully solvated electrons in polar solvents.[8]

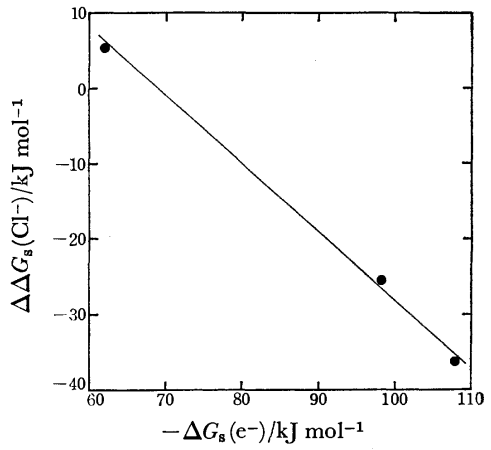

Fig. 1. Relationship between solvation free energy of electron, $\Delta G_s(e^-)$, and solvation free energy of chloride ion, $\Delta\Delta G_s(Cl^-)$ (reference solvent: acetonitrile).

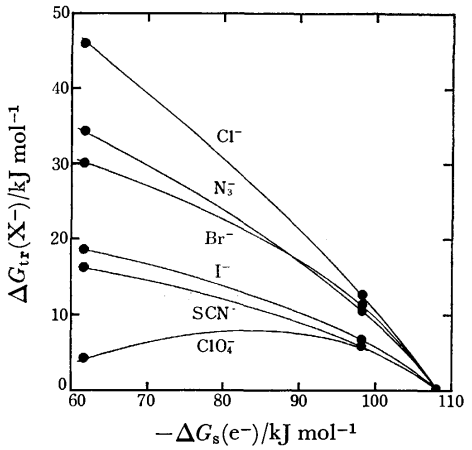

Fig. 2. Relationship between solvation free energy of electron, $\Delta G_s(e^-)$, and free energy of transfer of anions, $\Delta G_{tr}(X^-)$ (reference solvent: water).

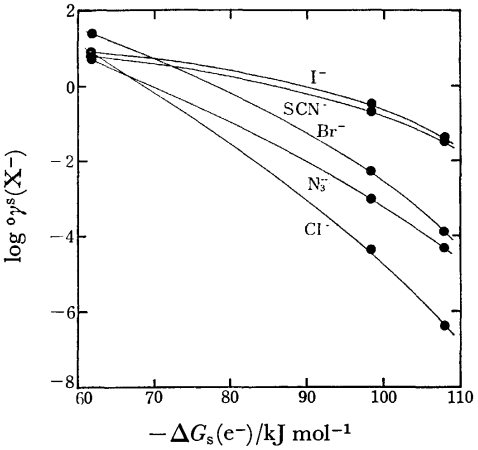

Fig. 3. Relationship between solvation free energy of electron, $\Delta G_s(e^-)$, and logarithm of solvent activity coefficient of anions, log $^{\circ}\gamma^s(X^-)$ (reference solvent; acetonitrile).

Correlation of $\Delta G_s(e^-)$ with Solvation Free Energy of Halide Ions. The values of $-\Delta G_s(e^-)$ are plotted against the solvation free energies of chloride ion in DMF, MeOH, and H_2O in Fig. 1, where $\Delta\Delta G_s(Cl^-)$ denotes the difference between the solvation free energy of Cl^- in a given solvent and that in acetonitrile.[9] The plot gives a straight line. When we plot the values of $-\Delta G_s(e^-)$ against the free energy of transfer, $\Delta G_{tr}(X^-)$, for several anions,[2] the plot of Cl^- is closest to a straight line, the deviation from linearity being pronounced in the order $Cl^- < N_3^- < Br^- < I^- < SCN^- < ClO_4^-$ (Fig. 2). The logarithm of the solvent activity coefficient, log $^{\circ}\gamma^s$, shows a similar trend (Fig. 3), where $^{\circ}\gamma^s$ is given in molar scale at 25 °C with acetonitrile as a reference solvent.[10] The order of deviation from linearity among the anions is the same as in the case of the free energy of transfer of anions, as can be predicted from the relation, $\Delta G_{tr} = -RT \ln {}^{\circ}\gamma^s$ and also from the valence-bond description. If we assume that chloride ion is the least polarizable anion among the anions considered and that the solvated electron is a simple entity with a unit negative charge in solution, the close correlation between the solvation free energy of chloride ion and that of electron is understandable.

The solvent shift of a halogen nucleus such as ^{35}Cl, ^{79}Br, or ^{127}I in respective halide ion[1] and also of ^{19}F in hexafluorophosphate ion, PF_6^-,[11] shows no trend of correlation with $\Delta G_s(e^-)$. Hall[12] suggested the origin of the NMR solvent shift as follows: (1) molecular volume and packing geometry, (2) hydrogen-bonding interactions, (3) charge transfer to solvent interactions, (4) orbital overlap with large atoms in solvent, and (5) charge distributions in solvent molecule. Stengle *et al.*[1] emphasized the prevailing effect of charge transfer interactions. It seems that the solvent shift depends primarily on short-range interactions, the solvent shift thus showing a considerable discrepancy from the trend of $\Delta G_s(e^-)$.

Correlation of $\Delta G_s(e^-)$ with AN-, E_T-, and Z-Values. The value of $\Delta G_s(e^-)$ will be discussed as a criterion of electrophilic properties of solvents in relation to several empirical parameters of solvents.

The acceptor number (*AN*) was proposed by Mayer *et al.*[13] as a measure of electrophilic property of solvents. The value is based on the measurement of NMR solvent shift of ^{31}P nucleus in triethylphosphine oxide, $(C_2H_5)_3PO$. The oxygen atom in $(C_2H_5)_3PO$ is attacked by solvent molecules, and the π-bonding character of the P–O bond is reduced. The effect, coupled with possible polarization of σ-bonding of the P–O bond, results in the decrease of the electron density of ^{31}P nucleus, causing NMR chemical shift. In order to standardize the *AN*-values, the chemical shift was extrapolated to null concentration of the substrate, the value of 1:1 adduct of $(C_2H_5)_3PO$ and $SbCl_5$ in 1,2-dichloroethane being taken as 100. The values of $-\Delta G_s(e^-)$ are plotted against *AN*-values (Fig. 4), the plot showing a straight line with only a slight deviation. The deviation can be attributed

either to the hydrogen-bonding of hydroxyl solvent or to the change in solvent structure caused by the nucleophilic substrate. It seems that the remaining coordination sites of phosphorus atom in $(C_2H_5)_3PO$ is almost completely blocked from the solvent attack. This effect is quite different from the case of carbonyl compounds. When we plot the values of $-\Delta G_s(e^-)$ against the chemical shift of ^{13}C or ^{17}O nucleus in acetone,[14-16] linearity is no longer observed (Fig. 5). Maciel and Ruben[14] attributed the predominant effect of hydroxyl solvents to the dipolar or Lewis base interaction coupled with intermolecular hydrogen-bonding. However, it is more likely that the coordination sites of the carbon atom in the carbonyl group are poorly shielded toward the nucleophilic attack of solvent molecules.

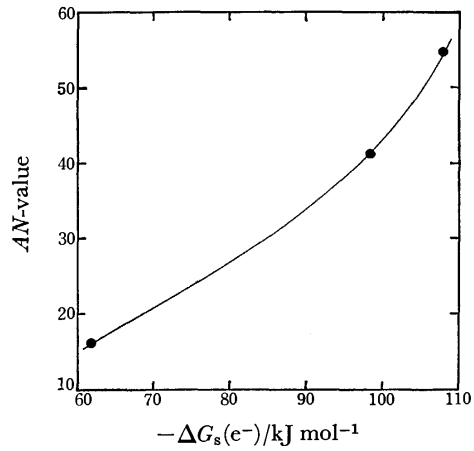

Fig. 4. Relationship between solvation free energy of electron, $\Delta G_s(e^-)$, and Mayer-Gutmann-Gerger's acceptor number (*AN*).

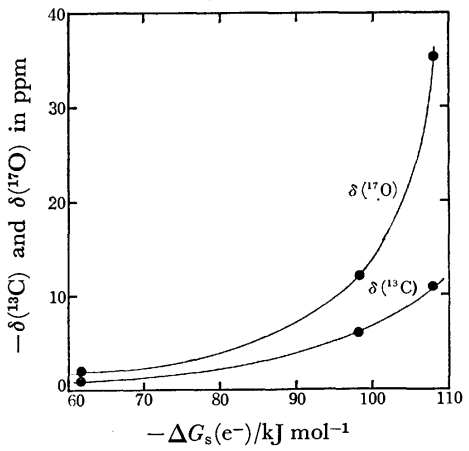

Fig. 5. Relationship between solvation free energy of electron, $\Delta G_s(e^-)$, and NMR solvent shift of ^{13}C and ^{17}O nuclei in acetone, $\delta(^{13}C)$ and $\delta(^{17}O)$.

A similar correlation to the case of *AN*-value can be seen in the plot of $-\Delta G_s(e^-)$ *versus* E_T- or *Z*-value (Fig. 6). The E_T-value was proposed by Dimroth *et al.*,[17] the value representing the energy of the lowest electronic transition of *p*-(1-pyridinio)-phenolate in various solvents. The oxygen atom of the solute is highly basic and sterically accessible for solvent molecules. The *Z*-value, proposed by Kosower[18] as a measure of solvent polarity, is the energy of charge transfer band of 1-ethyl-4-(methoxycarbonyl) piridinium iodide, the iodide ion of which is attacked by solvent molecules. Both E_T- and *Z*-values primarily represent the electrophilic properties of solvents, but from the curvilinear plots in Fig. 6 the effect of donicity or hydrogen-bonding of solvents seems to exist.

Correlation of $\Delta G_s(e^-)$ *with Kinetic Parameters of Solvent Dependent Processes.* A typical solvent parameter for a kinetic process is the *Y*-value proposed by Grunwald and Winstein[19] as a series of the ionizing power of solvents. This is defined as $Y=\log(k/k_0)$, where k and k_0 represent the first order solvolysis rate constant of *t*-butyl chloride at 25 °C in a given solvent and in a reference solvent (80% ethanol and 20% water), respectively. The plot of $-\Delta G_s(e^-)$ *versus Y* is shown in Fig. 7, where the datum of DMF is taken from the work of Mayer *et al.*[13] A set of data on the ionization rate constant, k_1, of 2-methyl-2-(*p*-methoxyphenyl)propyl *p*-toluenesulfonate is given by Smith *et al.*[20] The plot of $-\Delta G_s(e^-)$ *versus* $\log k_1$ is also shown in Fig. 7. Both plots show a remarkably

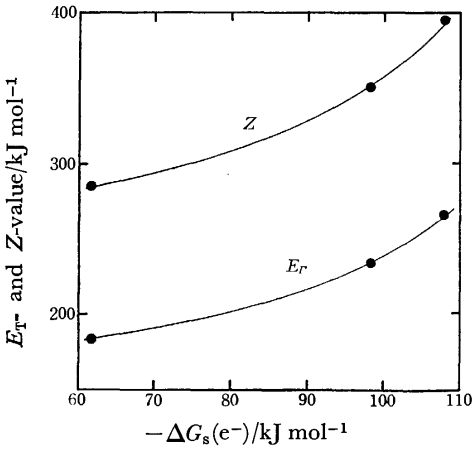

Fig. 6. Relationship between solvation free energy of electron, $\Delta G_s(e^-)$, and Dimroth-Reichardt-Siepmann-Bohlmann's E_T-value or Kosower's *Z*-value.

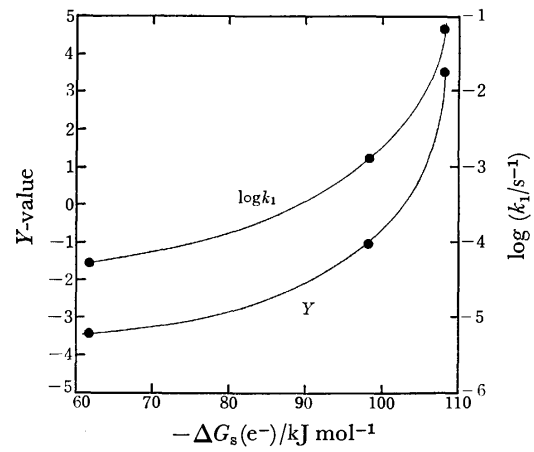

Fig. 7. Relationship between solvation free energy of electron, $\Delta G_s(e^-)$, and Grunwald-Winstein's *Y*-value or Smith-Fainberg-Winstein's log k_1-value.

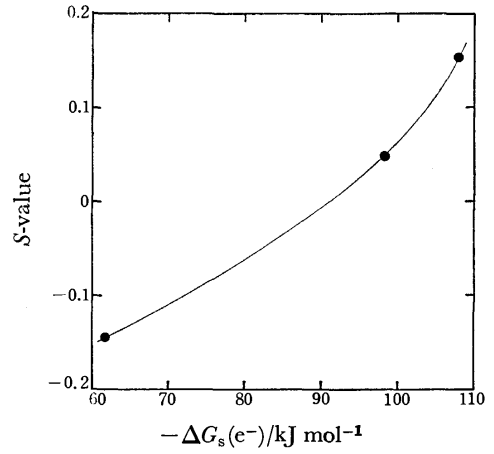

Fig. 8. Relationship between solvation free energy of electron, $\Delta G_s(e^-)$, and Brownstein's S-value.

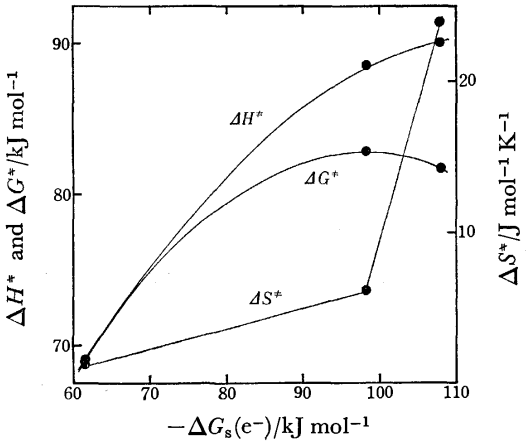

Fig. 9. Relationship between solvation free energy of electron, $\Delta G_s(e^-)$, and Arrhenius energy, ΔH^*, free energy of activation, ΔG^*, and entropy of activation, ΔS^*, for reaction, n-$C_4H_9Br+N_3^-=n$-$C_4H_9N_3+Br^-$.

curvilinear correlation, the effect of hydroxyl solvents being enhanced.

The S-value proposed by Brownstein[21] as a solvent dependent parameter was defined by the relation, $\log(k_{solvent}/k_{EtOH})=SR$, where k is a reaction rate constant, equilibrium constant or a function of spectral shift, and R a constant characteristic of the sensitivity of a given reaction. The plot of $-\Delta G_s(e^-)$ *versus* S-values also show a similar curvilinear trend to that of Y-values and log k_1-values (Fig. 8). The curvilinear correlation can be interpreted by taking the concerted effect of nucleophilic and electrophilic interactions into consideration. The nucleophilic attack of solvent is more pronounced in DMF (DN=26.6) than in MeOH or H_2O, while the electrophilic interaction is more enhanced in H_2O than DMF, MeOH being the intermediate (Table 1).

Delpuech[22] reported the Arrhenius energy for a substitution reaction, n-$C_4H_9Br+N_3^-=n$-$C_4H_9N_3+Br^-$, in various solvents. The plot of $-\Delta G_s(e^-)$ *versus* ΔH^*, ΔG^*, and ΔS^* is shown in Fig. 9. In this reaction the solvent attack on the anion seems to play a predominant role, stronger solvation requiring higher Arrhenius energy. It is noteworthy that the entropy of activation is fairly negative in the case of water. Thus, the free energy of activation is smaller in the case of water than in that of methanol. A possible hydrogen bonding of water molecule may increase the orderliness of the activated complex.

In view of the results obtained the solvent parameter can be expressed in terms of three effects: (1) nucleophilic effect represented by the donor number (2) electrophilic effect represented by the solvation free energy of electron, and (3) hydrogen-bonding energy. The three terms have the same dimension and can be expressed in the same unit, *e.g.* J mol^{-1}. Thus, we can estimate the overall solvent effect by the linear combination of the three terms provided the appropriate coefficients for each term are determined experimentally.

Science Research Grant B247008 of the Ministry of Education for this investigation is gratefully acknowledged.

References

1) T. R. Stengle, Y-C. E. Pan, and C. H. Langford, *J. Am. Chem. Soc.*, **94**, 9037 (1972).
2) B. G. Cox, G. R. Hedwig, A. J. Parker, and D. W. Watts, *Aust. J. Chem.*, **27**, 477 (1974).
3) K. Yamashita and H. Imai, *Bull. Chem. Soc. Jpn.*, **50**, 1066 (1977).
4) A. M. Brodsky and Yu. Ya. Gurevich, *Electrochim. Acta*, **13**, 1245 (1968).
5) J. Baxendale, *Radiat. Res. Suppl.*, **4**, 139 (1964).
6) J. Jortner and R. M. Noyes, *J. Phys. Chem.*, **70**, 770 (1966).
7) J. E. Aldrich, M. J. Bronskill, R. K. Wolf, and J. W. Hunt, *J. Chem. Phys.*, **55**, 530 (1971).
8) K. Yamashita, M. Kitamura, and H. Imai, *Chem. Lett.*, **1976** 1363.
9) U. Mayer, *Coord. Chem. Rev.*, **21**, 159 (1976).
10) R. Alexander, A. J. Parker, J. H. Sharp, and W. E. Waghorne, *J. Am. Chem. Soc.*, **94**, 1148 (1972).
11) W. J. DeWitte and A. I. Popov, *J. Solution Chem.*, **5**, 231 (1976).
12) C. Hall, *Quart. Rev., Chem. Soc.*, **25**, 87 (1971).
13) U. Mayer, V. Gutmann, and W. Gerger, *Monatsh. Chem.*, **106**, 1235 (1975).
14) G. E. Maciel and G. C. Ruben, *J. Am. Chem. Soc.*, **85**, 3903 (1963).
15) G. E. Maciel and J. J. Natterstad, *J. Chem. Phys.*, **42**, 2752 (1965).
16) H. A. Christ and P. Diel, *Helv. Phys. Acta*, **36**, 170 (1963).
17) K. Dimroth, Ch. Reichardt, T. Siepmann, and F. Bohlmann, *Ann. Chem.*, **661**, 1 (1963).
18) E. Kosower, *J. Am. Chem. Soc.*, **80**, 3253, 3261, 3267 (1958).
19) E. Grunwald and S. Winstein, *J. Am. Chem. Soc.*, **70**, 846 (1948).
20) S. G. Smith, A. H. Fainberg, and S. Winstein, *J. Am. Chem. Soc.*, **83**, 618 (1961).
21) S. Brownstein, *Can. J. Chem.*, **38**, 1590 (1960).
22) J-J. Delpuech, *Tetrahedron Lett.*, **25**, 2111 (1965).

Refractive Indices and Polarizabilities of Several Molten Rare Earth Chlorides

Junichi MOCHINAGA,* Kazuo IGARASHI, Toshio AOKI, and Yasuhiko IWADATE

Department of Synthetic Chemistry, Faculty of Engineering, Chiba University, Yayoi-cho, Chiba 280

(Received January 11, 1978)

Refractive indices of molten $LaCl_3$, $PrCl_3$, $NdCl_3$, $DyCl_3$, and YCl_3 were measured by the cylindrical lens method. The measurements were carried out with the lights of four wavelengths, and the refractive indices so obtained were represented by empirical equations as linear functions of temperature. From the data molar refractivities were calculated. The refractive indices at infinite wavelength were calculated by use of Cauchy's relation for dispersion, and electronic polarizabilities were obtained for the salt molecules in molten state, and also the electronic polarizabilities of La^{3+}, Pr^{3+}, Dy^{3+}, and Y^{3+} ions in the melts were obtained.

The refractive indices of molten salts are related to the polarizabilities, and especially the values extrapolated to infinite wavelength are directly related to the electronic polarizabilities of molecules or ions in the melts. But there are only a few available data of refractive indices for molten salts, because the experimental difficulties exist in such measurements. Zarzycki and Naudin[1] have reported the refractive indices of some alkali halides and alkali nitrates in molten states for the light of 546.1 nm, and Bloom *et al.* have reported the refractive indices[2] and other experimental data[3] of some nitrites, nitrates, chlorides, and binary chloride systems in molten states for the light of 589.3 nm, using the bent stick method. Marcoux[4,5] has measured the refractive indices of some gases in liquid and solid states and some molten ionic salts by the cylindrical lens method. Nakamura and Tanemoto[6] have also reported the refractive index of molten KCl measured by a He-Ne laser (632.8 nm).

In the present experiment, the refractive indices of molten $LaCl_3$, $PrCl_3$, $NdCl_3$, $DyCl_3$, and YCl_3 were measured by the cylindrical lens method with the lights of wavelengths, 656.3, 589.3, 486.2, and 434.1 nm.

Experimental

Preparations of $LaCl_3$, $PrCl_3$, $NdCl_3$, $DyCl_3$, and YCl_3. These rare earth chlorides were prepared by heating the mixtures of respective rare earth oxide and NH_4Cl according to the similar procedure in the previous paper.[7] Then, the crude chlorides were purified by sublimation, and their purities are shown in Table 1. The YCl_3 crystal had the similar purity as in the previous paper.[7]

Measurements of Refractive Indices. The apparatus used is based on that reported by Marcoux,[5] which measures the position of a focal point with a cylindrical lens. The schematic diagram of the apparatus is shown in Fig. 1, in which D is a transparent quartz cylinder tube of about 7 mm diameter. The distance between the center of the quartz tube and the position of the focal point depends on the refractive index of a liquid in the quartz tube. The distances were measured with a microscope by the precision of 1/100 mm for the several reference liquid materials of known refractive indices. The refractive index of a molten salt, therefore, can be obtained from the calibration curves in which the refractive indices of the reference materials were plotted against the measured distances. The calibration curves were drawn from the observed values at room temperature for CH_2I_2, $C_{10}H_7Br$, and CS_2 as the reference liquid materials, because the coefficient of expansion of quartz is very small (5.5×10^{-7}/deg). As the light source, a monochromator of UV-VIS spectrophotometer(HITACHI 139) was used, and the wavelengths

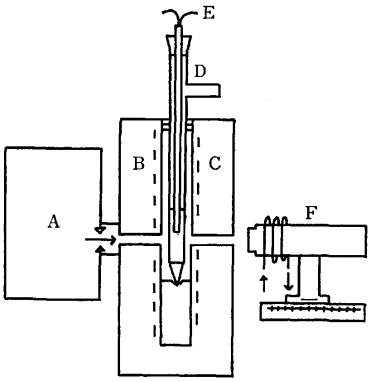

Fig. 1. Apparatus for measuring the refractive index of molten salts.
A: monochromator, B: electric furnace, C: Kanthal wire, D: quartz cell, E: C. A. thermocouple, F: microscope.

TABLE 1. IMPURITIES IN $LaCl_3$, $PrCl_3$, $NdCl_3$, AND $DyCl_3$

$LaCl_3$[a]		$PrCl_3$[b]		$NdCl_3$[b]		$DyCl_3$[a]	
Element	Content (ppm)	Element	Content (ppm)	Element	Content (ppm)	Element	Content (ppm)
Ce	<30	La	<30	La	<60	Y	60
Pr	110	Ce	<20	Ce	<60	Tb	<15
		Nd	<15	Pr	<20	Ho	<15
		Sm	<15	Sm	<15	Er	<15
				Eu	<20		

a) Emission spectrographic analysis. b) Fluorescence X-ray analysis.

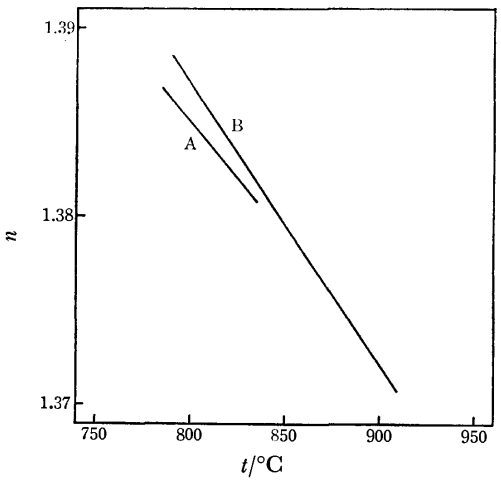

Fig. 2. Refractive indices of molten KCl (589.3 nm).
A: Literature,[2] $n=1.481-1.2\times10^{-4}t$, (785—835 °C),
B: this work, $n=1.507-1.5\times10^{-4}t$, (790—909 °C).

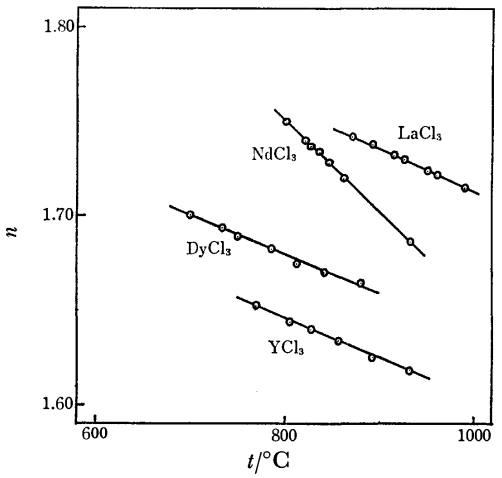

Fig. 3. Refractive indices of $LaCl_3$, $NdCl_3$, $DyCl_3$, and YCl_3 melts at 486.2 nm.

of lights used in this measurements were C(656.3 nm), D (589.3 nm), F(486.2 nm), and G(434.1 nm) lines. The refractive indices of the molten KCl observed in this apparatus were in fair agreement with the values in literature[2] as shown in Fig. 2.

Results and Discussion

As $PrCl_3$ and $NdCl_3$ melts have the absorption bands in the measured wavelengths, the refractive indices of $PrCl_3$ melt were measured at 656.3, 589.3, and 434.1 nm, and those of $NdCl_3$ melt at 486.2 nm only. The temperature dependence of refractive indices for these molten rare earth chlorides were linear at respective wavelength in the measured range of temperature. The results obtained at 486.2 nm are shown in Fig. 3. From the measured data, the refractive indices were represented by use of the method of least-squares as functions of temperature. The results are given in Table 2. In Table 2, σ is the standard error of estimate in refractive index equation. The relations of the refractive indices of $LaCl_3$, $PrCl_3$, $DyCl_3$, and YCl_3 melts *vs.* wavelength are shown in Fig. 4, in which the refractive indices slightly decrease in longer wavelength region, whereas in shorter wavelength region the dispersions of the refractive indices for $LaCl_3$, $PrCl_3$, and YCl_3 melts are observed.

Molar refractivity is one of the characteristic properties and is given by the following equation,

$$R_\lambda = \{(n_\lambda^2-1)/(n_\lambda^2+2)\}\times V_m,$$

where R_λ is the molar refractivity of the molten salt in cm^3, n_λ the refractive index of the molten salt for the light of wavelength λ, V_m the molar volume of the molten salt at the measured temperature, and λ represents C, D, F, or G line. The molar refractivities calculated are shown in Table 3. The molar refractivities are almost independent of temperature, and therefore the results in Table 3 are the averaged values over the measured temperature range.

The refractive indices at infinite wavelength can be calculated by Cauchy's approximate relation,

$$n_\lambda = A + B/\lambda^2,$$

where n_λ is the refractive index, A and B the constants for respective melt, and λ the wavelength. The electronic polarizabilities of molecules in a melt are given by the following equation,

$$\alpha_\infty^m = \{3/(4\pi N)\}\{(n_\infty^2-1)/(n_\infty^2+2)\}V_m,$$

where α_∞^m is the electronic polarizability of molecule in the melt, N Avogadro number, V_m the molar volume of the melt, and n_∞ the value of n_λ at $\lambda=\infty$. The obtained values of n_∞ and α_∞^m are shown in Table 4, in which n_∞ were calculated by the method of least-squares. As shown in Table 4, the order of magnitude in the electronic polarizabilities for the molten rare earth chlorides is in agreement with the order of the radii of cations contained in the molecules, and this fact satisfies the result of lanthanide contraction. The

Table 2. Refractive index equations
($n=a+b\times10^{-3}t$, t: °C)

	Wavelength (nm)	a	b	Temp range (°C)	σ ($\times10^{-2}$)
$LaCl_3$	434.1	2.1858	−0.4701	870—989	0.57
	486.2	1.9446	−0.2320	870—990	0.32
	589.3	1.8916	−0.1843	915—993	0.40
	656.3	1.9554	−0.2521	875—990	0.36
$PrCl_3$	434.1	2.0629	−0.3687	789—933	0.27
	589.3	2.0180	−0.3384	808—934	0.26
	656.3	1.9951	−0.3313	806—928	0.15
$NdCl_3$	486.2	2.1433	−0.4909	800—932	0.20
$DyCl_3$	434.1	1.9360	−0.3241	704—795	0.27
	486.2	1.8655	−0.2339	702—880	0.21
	589.3	1.8396	−0.2159	662—880	0.18
	656.3	1.8100	−0.1870	750—890	0.22
YCl_3	434.1	1.7685	−0.1339	721—934	0.10
	486.2	1.8137	−0.2099	768—932	0.14
	589.3	1.7788	−0.1804	768—928	0.11
	656.3	1.7667	−0.1585	788—925	0.19

Table 3. Molar refractivities (cm^3)

	R_C	R_F	R_D	R_C	Temp range (°C)
$LaCl_3$	31.7	31.2	30.9	30.9	900—980
$PrCl_3$	30.8	—	30.2	29.7	800—920
$NdCl_3$	—	30.0	—	—	800—920
$DyCl_3$	28.7[a)]	28.6	28.2	28.0	700—880
YCl_3	28.3	27.6	27.3	27.3	740—780

a) 720—780 (°C).

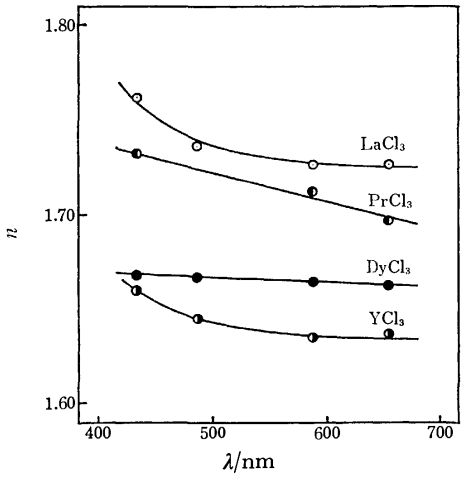

Fig. 4. Variation of the refractive index with wavelength.
○: $LaCl_3$ at 900 °C, ◐: $PrCl_3$ at 900 °C, ●: $DyCl_3$ at 800 °C, ◑: YCl_3 at 800 °C.

differences in electronic polarizabilities of molecules, therefore, are equal to those of cations, because the rare earth chloride molecules have chloride ion as a common anion. The values of polarizabilities for chloride ion in crystal at λ=589.3 nm(D-line) were reported by Tessman *et al.*[8] and by Kordes[9] to be 2.96 and 2.72 ($\times 10^{-24}$ cm^3), respectively, while that reported by Böttcher[10] for the same ion and wavelength in aqueous solution was 3.00×10^{-24} cm^3. The polarizabilities (α_D) of the rare earth cations in molten state calculated approximately using the above polarizabilities of chloride ion are shown in Table 5. Tessman *et al.*[8] have reported that the electronic polarizability was 2.97 ($\times 10^{-24}$ cm^3) for chloride ion in crystal, and Böttcher[11] reported the value 2.60 ($\times$ 10^{-24} cm^3) for chloride ion in aqueous solution. The electronic polarizabilities (α_∞) of the rare earth cations in molten state approximately calculated using these values are shown in Table 6. The values in Tables 5 and 6 were calculated by the following equation,

$$(n_\lambda^2-1)/(n_\lambda^2+2) = (4\pi/3)\sum N_i\alpha_{\lambda,i},$$

where N_i is the number of i-th ion per unit volume, and $\alpha_{\lambda,i}$ the polarizability of i-th ion at wavelength λ. According to Cauchy's relation, the longer the wavelength of light used in measurement is, the less polarizability of ion is obtained. The values of chloride ion in aqueous solution reported by Böttcher[10,11] are not appropriate for the estimation in molten state.

Table 4. n_∞ and α_∞^m of the rare earth chlorides in molten state

	Temp (°C)	Refractive index at $\lambda=\infty$ n_∞	Electronic polarizability of molecule α_∞^m ($\times 10^{-24}$ cm^3)
$LaCl_3$	920	1.696	11.91
	980	1.695	12.05
$PrCl_3$	820	1.702	11.52
	920	1.672	11.51
$DyCl_3$	720	1.663	10.92
	880	1.628	10.85
YCl_3	800	1.617	10.59
	920	1.594	10.50

Table 5. Polarizabilities of rare earth cations in molten state (α_D) calculated from data of chloride ion in literatures ($\times 10^{-24}$ cm^3)

Rare earth cation	Polarizability (α_D)[a)] calculated from		
	Tessman's value	Kordes' value	Böttcher's value
La^{3+}	3.38	4.10	3.26
Pr^{3+}	3.10	3.82	2.98
Dy^{3+}	2.31	3.03	2.19
Y^{3+}	1.95	2.67	1.83

a) The temperature ranges are the same as those in Table 3.

Table 6. Electronic polarizabilities of rare earth cations in molten state (α_∞) calculated from data of chloride ion in literatures ($\times 10^{-24}$ cm^3)

Rare earth cation	Electronic polarizability (α_∞) calculated from		Temp (°C)
	Tessman's value	Böttcher's value	
La^{3+}	3.00	4.11	920
Pr^{3+}	2.60	3.71	920
Dy^{3+}	1.94	3.05	880
Y^{3+}	1.59	2.70	920

The electronic polarizabilities of rare earth ions in molten state seem to be close to the values estimated from the chloride ion polarizability by Tessman *et al.*[8] *viz.* 2.97×10^{-24} cm^3. The estimations seem to yield good approximate polarizabilities of rare earth cations in molten state, though the chloride ion polarizabilities in different conditions were used.

Since the cylindrical lens method tends to give an error in the measurement of the focal distance for a substance with a large refractive index, it is desirable that the goniometry method reported by Nakamura and Tanemoto[6] is used.

Calculations were carried out with the computers in the University of Tokyo and Chiba University.

References

1) J. Zarzycki and F. Naudin, *C. R. Acad. Sci.*, **256**, 1282 (1963).
2) H. Bloom and D. C. Rhodes, *J. Phys. Chem.*, **60**, 791

(1956); H. Bloom and B. M. Peryer, *Aust. J. Chem.*, **18**, 777 (1965).
3) G. J. Janz, "Molten Salts Handbook," Academic Press, (1967), p. 89.
4) J. E. Marcoux, *J. Opt. Soc. Am.*, **59**, 998 (1969).
5) J. E. Marcoux, *Rev. Sci. Instrum.*, **42**, 600 (1971).
6) T. Nakamura and K. Tanemoto, *Jpn. J. Appl. Phys.*, **14**, 2089 (1975).
7) J. Mochinaga and K. Irisawa, *Bull. Chem. Soc. Jpn.*, **47**, 364 (1974).
8) J. R. Tessman, A. H. Kahn, and W. Shockley, *Phys. Rev.*, **92**, 890 (1953).
9) E. Kordes, *Z. Electrochem.*, **59**, 551 (1955).
10) C. J. F. Böttcher, *Recl. Trav. Chim. Pays-Bas*, **62**, 325 (1943).
11) C. J. F. Böttcher, *Recl. Trav. Chim. Pays-Bas*, **65**, 91 (1946).

Metal-ion Complexation of Noncyclic Poly(oxyethylene) Derivatives. III.[1] Complexation in Aprotic Solvent and Isolation of Their Solid Complexes†

Shozo YANAGIDA,* Kazutomo TAKAHASHI, and Mitsuo OKAHARA

Department of Applied Chemistry, Faculty of Engineering, Osaka University, Yamadakami, Suita, Osaka 565

(Received January 18, 1978)

The interaction of homogeneous polyethylene glycol(PEG)(EO*n*, *n*=1—8) with the alkali and magnesium metal cations and the ammonium cation was investigated on the basis of ^{1}H NMR(PMR) downfield shifts in acetone-d_6 or in acetonitrile-d_3. The specific complexations of EO4 with Mg^{2+}, EO6 with Na^+ and Ca^{2+}, and EO7 with K^+ were demonstrated by PMR studies, and their solid complexes were isolated. No specific interaction was detected for Rb^+ and Cs^+ in PMR studies. The magnesium ion interacts strongly with 15-crown-5, 18-crown-6, and PEG in acetone, and the $Mg(SCN)_2$-EO4 and the $Mg(SCN)_2$-above crown ether complexes were isolated. The terminal hydroxyl groups of PEG play an important role in the complexation with Li^+ and Mg^{2+} in acetone. The formation of the 1:1 complex with $Ca(SCN)_2$ was observed both for EO6 and for EO7. Strontium and barium thiocyanates formed solid complexes with PEG(EO*n*, *n*=2—8) and with glymes(tri- to octaglyme). Some novel complexes of 12-crown-4 and 15-crown-5 with NaSCN and $Ca(SCN)_2$ were also isolated. The mechanism of metal-ion complexation of poly(oxyethylene) derivatives is discussed in terms of the coordination geometry.

PMR spectroscopy has often been used to detect ligand-metal cation interactions[1-7] The changes in the PMR spectra induced by the typical metal cations are intrinsically complex phenomena. The use of the coordinating species as the solvent tends to mask the shifts, probably due to the competitive complexation. When aromatic anion salts such as tetraphenylborate[2] or fluorenyl salts[4] are used, the close proximity of the aromatic ring of the anion above the participating proton nuclei induces the upfield shifts, in spite of the complexation with the counter metal cation, which by itself would cause a downfield shift of the proton signals due to the increased electronegativity of the coordinating donor atom. Our previous study[1] revealed that the downfield shifts of PEG protons caused by the interaction with alkaline earth metal thiocyanates in methanol can be a qualitative measure of the extent of their complexation. On the basis of PMR downfield shifts, it was demonstrated that homogeneous PEG's with at least more than five oxyethylene units have strong complexing powers toward Ca^{2+}, Sr^{2+}, and Ba^{2+} in methanol; these are quite comparable with those of crown ethers, cyclic poly(oxyethylene). However, the downfield shifts induced by the alkali or magnesium metal cations or the ammonium ion were too small for either PEG or crown ethers to predict a complexing tendency. This phenomenon can be attributed to the competitive complexation of the methanol solvent. When a less polar nonaqueous solvent, *e.g.*, acetone or acetonitrile, is used, the downfield shifts are found to be large enough to evaluate the intrinsic complexing tendency.

On the basis of the previous and present PMR analyses, we have isolated solid complexes of PEG with alkali and alkaline earth metal salts. Further, we have attempted to point out some inconsistency in the ion-radius cavity concept regarding the metal complexation of the crown ethers.

† This work was presented at the 26th IUPAC Congress, Tokyo, September 1977.

Experimental

Materials. The following chemicals were obtained in the best available purity from the sources indicated; acetone-d_6 and acetonitrile-d_3 (CEA products through Nakarai Chemicals Ltd.), sodium tetraphenyl borate (Specially prepared reagent) (Nakarai Chemicals Ltd.), triethylene glycol monomethyl ether (Tokyo Kasei Kogyo Co., Ltd.).

Hexaethylene glycol monomethyl ether(MeEO6)(167—171 °C/0.15 mmHg) and octaethylene glycol monomethyl ether(MeEO8)(215 °C/0.16 mmHg) were prepared by the reaction of diethylene glycol 2-chloroethyl methyl ether with tetraethylene glycol and with pentaethylene glycol, respectively.

Other salts and poly(oxyethylene) derivatives were the same as in the previous paper.[1]

Measurement of Spectra. The PMR spectra were obtained using a JEOL LMN-PS-100 spectrometer(100 MHz) on an expanded scale (sweep width, 270 Hz), with 8% dioxane in benzene as the external reference, as previously described, except for weighing the thiocyanates:[1] thiocyanate concentration, 0.05 mol/kg; POE derivatives concentration, 1 wt %. Weighing the salts was done as follows: the acetone or methanol solution was injected in NMR tubes using a microsyringe and the NMR tubes were placed in a vacuum to evaporate the solvent. The chemical shifts for the split signals of EO7 and EO8 in acetonitrile-d_3 were averaged for the calculation of the downfield shifts.

The ^{13}C NMR spectra were obtained using a JEOL JNM-FX-60 spectrometer.

The IR spectra were recorded with a Japan Electroscopic IR-E spectrophotometer.

Isolation of Solid Complexes. Solid complexes of cyclic and noncyclic poly(oxyethylene) derivatives (POE) were isolated by the following methods. An anhydrous metal salt was powdered in a mortar and was heated with a slightly more than equimolecular quantity of POE without solvent until the pasty mixture became an entirely homogeneous solution. Generally, the complexes solidified on cooling. The resulting complexes were purified by recrystallization (Method 1), or were brodken up to pieces, washed throughly to remove excess POE or the salt, filtered, and dried under reduced pressure(Method 2).

It was found that some complexes could also be easily isolated from solution. Acetone or methanol was saturated with a salt and the stoichiometric quantity of POE was added to the above solution. The precipitation of the complexes was immediate(Method 3). The complexes were worked up as in Method 1 or in Method 2. The results are summarized in Tables 1, 2, and 4. The melting points were determined on a Büchi SMP-20 apparatus.

Typical examples are as follows.

Preparation of Crystalline KSCN Complex of Heptaethylene Glycol(EO7). Method 1. A mixture of 1.00 g(3.0 mmol) of EO 7 and 0.238 g(2.5 mmol) of powdered KSCN was melted in a test tube. The mixture solidified on cooling. The complex was broken up to pieces, washed with a small quantity of acetone, dried, and recrystallized twice from acetone. A crystalline 1 : 1 complex was obtained (0.47 g, 45% yield).

Preparation of $Ba(SCN)_2$ Complex of Tetraglyme(MeEO-4Me). Method 2. A mixture of 0.232 g (0.9 mmol) of powdered $Ba(SCN)_2$ and 0.210 g (0.95 mmol) of MeEO4Me was heated up in a test tube until the mixture become entirely homogeneous. After cooling, a mixture of benzene and acetone (9 : 1) was added to the mixture, giving the complex(0.12 g). When benzene was added to the filtrate, additional complex(0.13 g) was precipitated(total yield 58%).

Preparation of $Mg(SCN)_2$ Complex of Tetraethylene Glycol-(EO4). Method 2. A mixture of 0.228 g(1.0 mmol) of $Mg(SCN)_2 \cdot 4H_2O$ and 0.203 g (1.0 mmol) of EO4 was heated up in a test tube until the mixture became a clear solution. During the workup, the evolution of water and the complex formation were observed. The resulting complex was washed with acetone and dried in a vacuum. The complex(0.117 g) was obtained. Additional complex (0.076 g) was recovered from the filtrate(total yield 58%).

Preparation of $Mg(SCN)_2$ Complex of 15-Crown-5. Method 3. In acetone (1 g), 0.216 g (1.0 mmol) of $Mg(SCN)_2 \cdot 4H_2O$ was dissolved, and the solution was filtered. To the filtrate, 0.223 g(1.0 mmol) of 15-crown-5 was added. White crystals were immediately formed. After a while, some additional 15-crown-5(0.235 g, 1.1 mmol) was added, but no further precipitation was observed. The crystals were filtered, washed with acetone, and dried. The complex(0.231 g) was obtained(53% yield). The filtrate was concentrated in a rotary evaporator, yielding some additional complex (Table 4).

Preparation of $Ca(SCN)_2$ Complex of 12-Crown-4. Method 3. 12-Crown-4(0.128 g, 0.73 mmol) was dissolved in 0.364 g of methanol. The methanol solution of $Ca(SCN)_2$ prepared from 0.109 g of anhydrous $Ca(SCN)_2$ and 0.6 ml of methanol was added to the above solution. After a while, white crystals precipitated. After the workup, 0.155 g of the complex with water of crystallization were obtained (60% yield) (Table 4).

Results and Discussion

Complexation with Alkali Metal and Ammonium Cations in Aprotic Solvent. Recent studies on the structure of crown ether complexes have revealed their induced fit for metal cations, *i.e.*, their oxyethylene (EO) chains are flexible enough to coordinate to various metal cations in spite of their ring structure.[8-10] Thus, it seems appropriate to make use of the downfield shift for crown ethers as a probe to evaluate the complexation of acyclic POE derivatives.

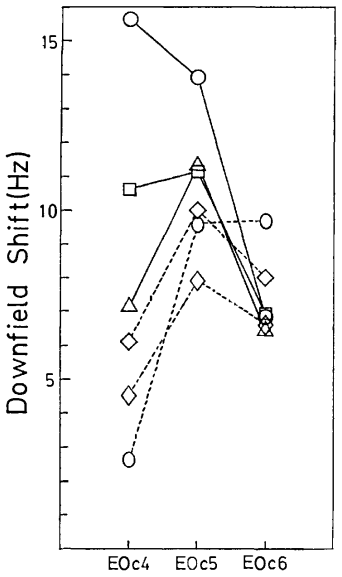

Fig. 1. Downfield shifts for crown ethers induced by alkali metal and ammonium cations in acetone-d_6. Thiocyanate concentration, 0.05 mol/kg; crown ether concentration, 1 wt %. △: Li^+, ○: Na^+, □: K^+, ◇: Rb^+, ◇: Cs^+, ○: NH_4^+.

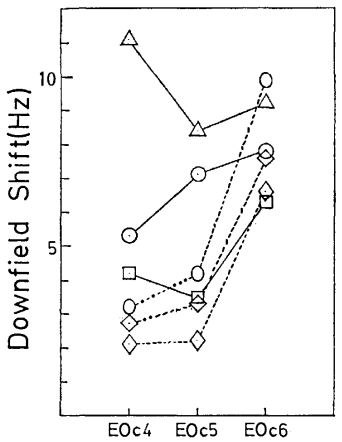

Fig. 2. Downfield shifts for crown ethers induced by alkali metal and ammonium cations in acetonitrile-d_3. The conditions and symbols used are identical with those in Fig. 1 and all of the following figures.

The downfield shifts of the crown ethers' protons by the complexation of the alkali metal and ammonium cations were measured both in acetone-d_6 and in acetonitrile-d_3. The results are shown in Figs. 1 and 2 as a function of the number of EO units. It is seen that the downfield shifts are generally larger in acetone-d_6 than in acetonitrile-d_3. And it is also seen that in acetonitrile the signals of 18-crown-6-(EOc6) show the largest shifts for most of the cations, while in acetone the largest shifts are observed mostly for 15-crown-5(EOc5). On careful examination, the chemical shift of 18-crown-6 in acetonitrile-d_3 was found to be *ca.* 5—7 Hz upfield, compared with those of the other crown ethers and PEG. The unusual upfield shift for 18-crown-6 is attributable to the magnetic anisotropy due to its specific interaction with the cyano group of acetonitrile.[11,12] Thus, the observed largest

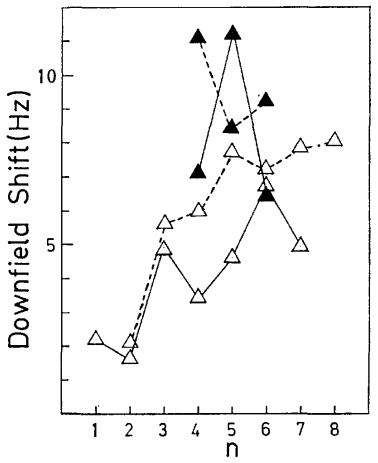

Fig. 3. Lithium-ion induced downfield shifts for the homogeneous PEG and crown ethers in acetone-d_6 and in acetonitrile-d_3. △—△: In acetone-d_6, △--△: in acetonitrile-d_3, ▲—▲: the shifts for the crown ethers in acetone-d_6, ▲--▲: the shifts for the crown ethers in acetonitrile-d_3.

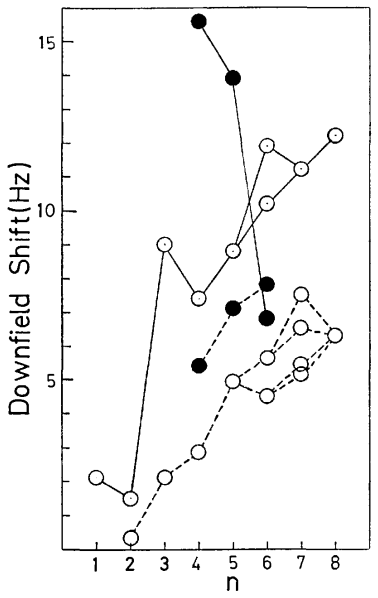

Fig. 4. Sodium-ion induced downfield shifts for the homogeneous PEG and crown ethers in acetone-d_6 and in acetonitrile-d_3. ○—○: In acetone-d_6, ○--○: in acetonitrile-d_3, ●—●: the shifts for the crown ethers in acetone-d_6, ●--●: the shifts for the crown ethers in acetonitrile-d_3.

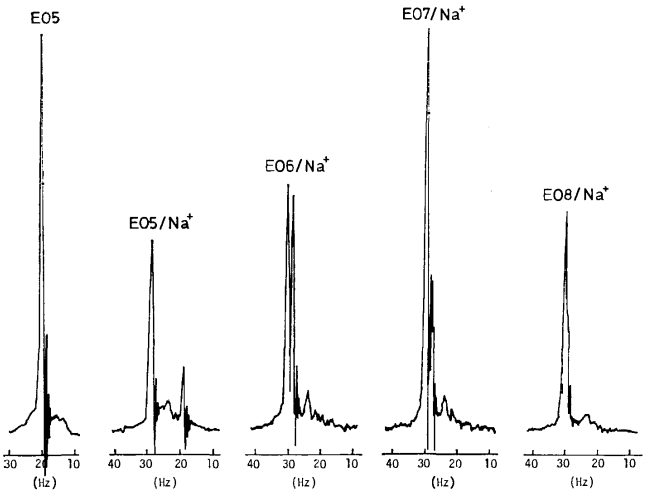

Fig. 5. PMR signals in acetone-d_6 of oxyethylene protons of the homogeneous PEG in the presence or the absence of sodium ion.

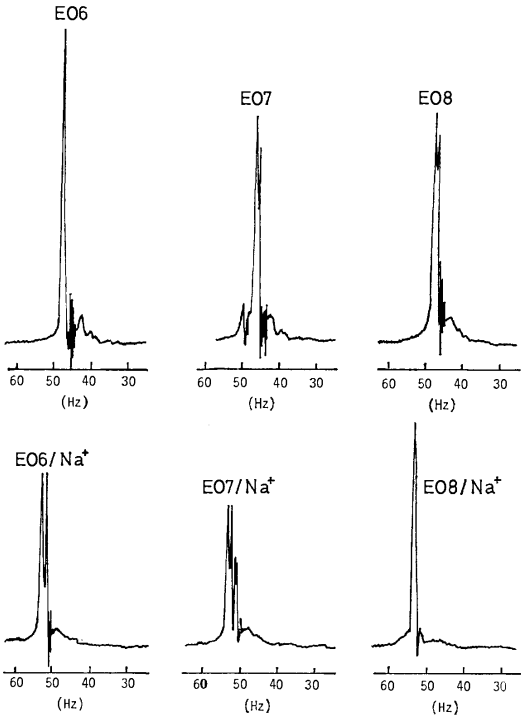

Fig. 6. PMR signals in acetonitrile-d_3 of oxyethylene protons of the homogeneous PEG in the absence and presence of sodium ion.

downfield shifts for 18-crown-6 in the presence of cations do not necessarily imply the strongest complexing power. It may be inferred that the specific interaction of 18-crown-6 with acetonitrile would easily disappear in the presence of cations.

On the basis of these large downfield shifts for the crown ethers in the presence of the cations, the corresponding shifts for a series of homogeneous PEG's were determined in acetone-d_6 and partly in acetonitrile-d_3; the results are plotted against the number of EO units in Figs. 3—4 and 7—10. The shifts for the crown ethers were also plotted in the respective figures for comparison. In general, the presence of the cations made the signals of ethylene glycol(EOl) broaden and also those of the diethylene glycol(EO2) complex, but with small downfield shifts.

In the interaction of EO*n* with Li^+ in acetone-d_6 (Fig. 3), the specific complexation of hexaethyle glycol (EO6) is to be noted. The shift for EO6 is far less than those of 12-crown-4 and 15-crown-5, but is quite comparable with that of 18-crown-6. Rather weak complexation of 12-crown-4 with Li^+ in acetone, implied by the small shift, can not be explained. In acetonitrile (Fig. 3), the larger shifts were observed for PEG with more than five EO units, but no specific complexation was observed. It should be noted

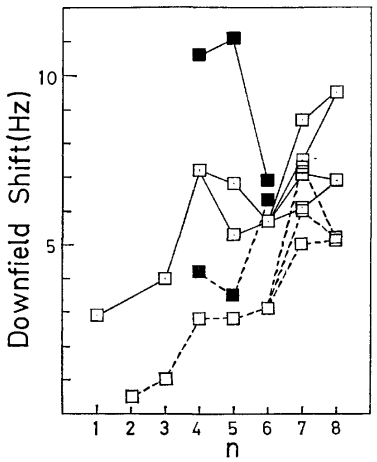

Fig. 7. Potassium-ion induced downfield shifts for the homogeneous PEG and crown ethers in acetone-d_6 and in acetonitrile-d_3. □—□: In acetone-d_6, □--□: in acetonitrile-d_3, ■—■: the shifts for the crown ethers in acetone-d_6, ■--■: the shifts for the crown ethers in acetonitrile-d_3.

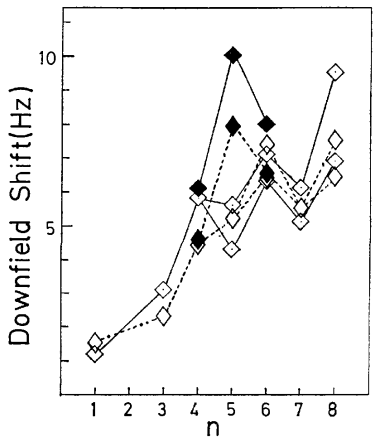

Fig. 8. Rubidium and caesium-ion induced downfield shifts for the homogeneous PEG and crown ethers in acetone-d_6. ◇: The shifts for the PEG in the presence of Rb^+, ◇: the shifts for the PEG in the presence of Cs^+, ◆: the shifts for the crown ethers in the presence of Rb^+, ◆: the shifts for the crown ethers in the presence of Cs^+.

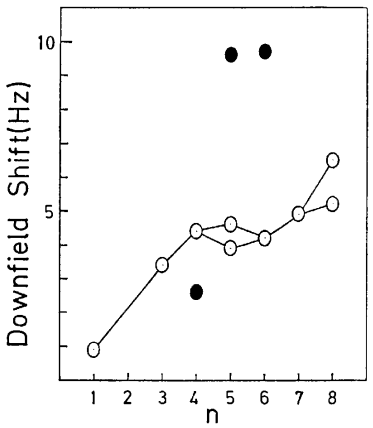

Fig. 9. Ammonium-ion induced downfield shifts for the homogeneous PEG and crown ethers in acetone-d_6. ●: The shifts for the crown ethers.

that the signals of heptaethylene glycol(EO7) and octaethylene glycol(EO8) were split into two peaks when measured in the absence of cations by an expanded scale (Fig. 6), and that the addition of LiSCN caused the coalescence of the signals with appreciable downfield shifts.

With regard to Na^+ in acetone-d_6(Fig. 4), the large shifts were observed for EO*n* with more than four EO units and the signal of EO6 was clearly split into two peaks with a larger downfield shift than that of 18-crown-6(Fig. 5). The shifts in acetonitrile-d_3 (Fig. 4) were not so large as those in acetone-d_6, but the clear splittings of the signals were observed not only for EO6 but also for EO7(Fig. 6). These splittings are in agreement with those observed in methanol-d_4,[1] but the splittings accompanying the downfield shifts suggest that EO6 and EO7 should take more rigid conformation on complexation with Na^+ in the aprotic solvent.

The study of K^+ in acetone-d_6(Fig. 7) found appreciable downfield shifts for EO*n* with more than four EO units. Pentaethylene glycol(EO5), EO7, and EO8 accompanied the splitting of the signals. EO7 gave the characterictic splitting which was observed in methanol-d_4.[1] The complexing power of EO*n* with more than four EO units, inferred from the large shifts, is far less than those of 12-crown-4 and 15-crown-5, but is quite comparable with that of 18-crown-6. This fact is quite consistent with the solid-liquid phase transfer catalysis of glymes with more than four EO units.[13] The shifts in acetonitrile-d_3(Fig. 7) make the specific complexation of EO7 with K^+ more apparent.

For Rb^+ and Cs^+ in acetone-d_6(Fig. 8), the large shifts comparable with those of the crown ethers were observed; splitting occurerd for EO*n* with more than four EO units. These are almost proportional to the number of EO units, suggesting their rather non-specific interactions.

For the ammonium ion in acetone-d_6(Fig. 9), no remarkable complexation comparable with those of 15-crown-5 and 18-crown-6 was observed among the PEG investigated. However, increasing the number of EO units seems to increase the tendency of complexation.

Complexation with Magnesium Cation in Acetone. The magnesium cation had been considered not to interact with any crown ethers, since the magnesium ion radii is apparently too small to fit the cavity of crown ethers larger than 12-crown-4. It has now been found that in acetone-d_6, the proton signal of 15-crown-5 shifts *ca.* 31 Hz downfield by the presence of $Mg(SCN)_2$ and the complex with the 1:1 composition precipitates under the conditions of the downfield shift measurment. Similarly, 18-crown-6 yielded the complex with the composition of 18-crown-6·$Mg(SCN)_2 \cdot 4H_2O$(see Table 4). It is surprising to note, however, that 12-crown-4 neither formed any solid complex nor showed any appreciable shift in the presence of Mg^{2+}. In the light of the ion-radius cavity concept, 12-crown-4 should have shown the

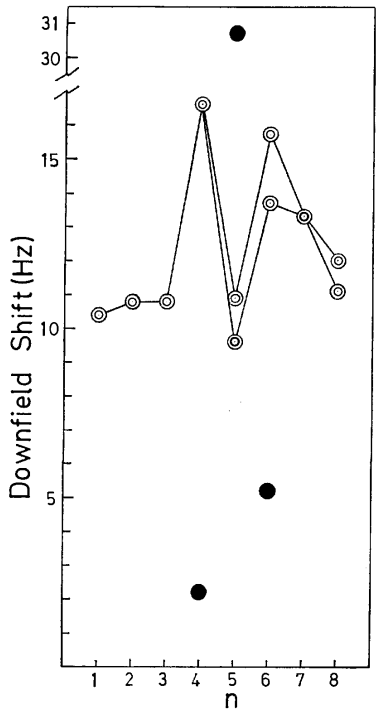

Fig. 10. Magnesium-ion induced downfield shifts for the homogeneous PEG and crown ethers in acetone-d_6.
●: The shifts for the crown ethers.

maximum interaction with Mg^{2+}. The fact is quite contradictory to the concept.

As is shown in Fig. 10, large downfield shifts were confirmed for a series of PEG's ranging from EO1 to EO8. Significant splitting or broadening of the signals were observed for PEG's with a longer chain than EO5. To our surprise, the 1:1 complex of EO4 with $Mg(SCN)_2$ was precipitated in acetone-d_6 just as those of 15-crown-5 and 18-crown-6. However, we could not succeed in isolating any other complexes of PEG. These facts indicate that Mg^{2+} interacts specifically with EO4.

The Role of Terminal Hydroxyl Groups in Complexation of PEG in Aprotic Solvents. Recently, a variety of noncyclic POE derivatives with chelating groups on the terminals have been reported to show remarkable complexing properties with metal cations.[14-16] The significance of these findings is that they demonstrate the importance of the terminal groups which stabilize the metal-ion complexation. In preceding papers,[1,17] however, we demonstrated that the TGT conformation of EO groups and the resulting helical conformation of the repeating EO units are the driving forces of the metal-ion complexation of noncyclic POE derivatives, and that the role of the terminal hydroxyl groups in the complexation of PEG varies with the properties of the metal cations and with the polarity of the solvent.

In this study, the effect of the terminal hydroxyl groups on complexation with Li^+, Na^+, K^+, and Mg^{2+} in aprotic solvent was also examined by comparing the downfield shifts of PEG with those of the methylated PEG. As is shown in Fig. 11, the hydroxyl groups of PEG play an important role in the effective complexation with Li^+ and Mg^{2+} in acetone. With regard to Na^+ in acetone(Fig. 12), the same is true for the tri-(oxyethylene) derivatives. In case of the hexa-(oxyethylene) derivatives, no drastic decrease in the shifts by methylation were observed, indiacting that the terminal hydroxyl groups are not necessarily so important for complexation with Na^+ in acetone. This also holds true for potassium ion complexation of the octa(oxyethylene) derivatives in acetonitrile(Fig. 12).

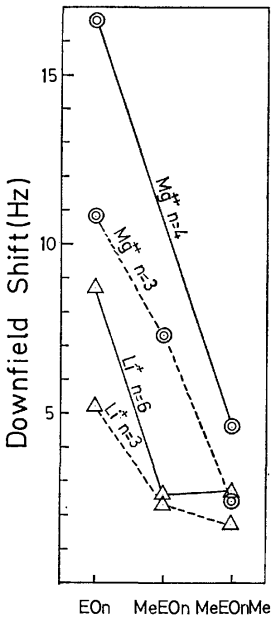

Fig. 11. Comparison of downfield shifts for PEG and methylated PEG induced by Lithium or magnesium ion. ◎: Mg^{2+} in acetone-d_6, △: Li^+ in acetone-d_6.

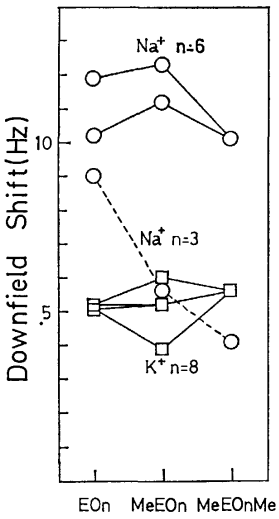

Fig. 12. Comparison of downfield shifts for PEG and methylated PEG induced by sodium or potassium ion. ○: Na^+ in acetone-d_6, □: K^+ in acetonitrile-d_3.

Isolation of Solid Complexes. Some polar compounds have recently been found to form solid complexes with metal salts under appropriate conditions.[18-20] Our previous and present studies of PMR indicated that some homogeneous PEG should react

TABLE 1. PREPARATION AND ANALYTICAL DATA OF COMPLEXES OF PEG

Salt	PEG	Stoichiometry Salt : POE : H_2O	Method[a] (solvent)	Mp (°C)	Infrared spectra (KBr disk)[b]			Found (Calcd) %		
					νOH	νSCN	νC-O-C	C	H	N
$NaBPh_4$	EO6	1 : 1 : 1/2	1(THF)	93.5—95.0	3550 3350		1120 sh, 1100, 1060 sh, 1030	69.09 (69.23)	7.68 (7.42)	
KSCN	EO7	1 : 1	2(Ac) 1(Be)	84.8—85.4	3360 3260 sh,	2065	1115, 1090 sh	42.38 (42.54)	7.32 (7.14)	3.30 (3.31)
KI	EO7	1 : 1	2(Ac)	101.0—101.5	3340		1115, 1100 sh, 1070 sh	34.00 (34.15)	6.29 (6.14)	
RbSCN	EO7	1 : 1	2(Ac/Be=1/1)	67.2—68.0	3380 3260 sh	2060	1115, 1090	37.90 (38.34)	6.98 (6.44)	2.25 (2.98)
NH_4SCN	EO7	1 : 1	2(EtAc)	50.2—51.2	3320 sh 3200	2050	1115, 1090 sh, 1075 sh	44.43 (44.76)	7.67 (8.51)	8.02 (6.96)
$Mg(SCN)_2$	EO4	1 : 1	2(Ac)	289.0—290.5	3280	2100	1115, 1085, 1050, 1035	35.70 (35.89)	5.33 (5.41)	8.30 (8.36)
$Ca(SCN)_2$	EO6	1 : 1	2(Ac/Be=1/1)	108.0—112.0	3360 3200 sh	2050	1110, 1090	39.44 (38.34)	6.05 (5.98)	6.07 (6.39)
$Ca(SCN)_2$	EO7	1 : 1	1(Ac)	123.3—123.7	3300	2040	1110 sh, 1085	39.75 (39.82)	6.35 (6.27)	5.90 (5.80)
$Ca(SCN)_2$	EO8	3 : 2	2(Ac)	212.2—213.0	3400 sh	2050	1105 sh, 1090 sh, 1075	38.05 (37.73)	5.68 (5.67)	6.72 (6.95)
$Sr(SCN)_2$	EO2	1 : 2	2(E)	140.0—159.0	3380	2060 2040 sh	1110, 1080, 1045	29.18 (28.87)	4.91 (4.85)	6.62 (6.73)
$Sr(SCN)_2$	EO3	1 : 2	2(E)	151.0—154.5	3300	2080 2050	1120 sh, 1100, 1080 sh, 1065, 1050 sh, 1030 sh	33.10 (33.36)	5.38 (5.60)	5.57 (5.56)
$Sr(SCN)_2$	EO4	3 : 4	2(Ac)	142.5—144.0	3360	2060	1110, 1080, 1050 sh, 1030 sh	32.73 (32.89)	5.25 (5.23)	5.95 (6.05)
$Sr(SCN)_2$	EO5	1 : 1	1(Ac)	215.0—218.0 (dec)	3400	2040	1110, 1080, 1040	32.46 (32.61)	5.05 (5.02)	6.42 (6.34)
$Sr(SCN)_2$	EO6	1 : 1	1(Ac)	169.0—170.0	3420 3280	2080	1110, 1085, 1050 sh, 1030 sh	34.49 (34.59)	5.39 (5.39)	5.58 (5.76)
$Sr(SCN)_2$	EO7	1 : 1	1(Ac)	187.0—187.5	3260 3060	2045	1085, 1052 sh, 1020 sh	36.20 (36.25)	5.63 (5.70)	5.24 (5.28)
$Sr(SCN)_2$	EO8	1 : 1	2(Ac/Be=1/1)	137.5—138.5	3400 3160	2045	1090	35.30 (34.91)	5.13 (5.34)	5.57 (5.81)
$Ba(SCN)_2$	EO2	1 : 2	2(E)	88.0—89.0 (dec)	3380	2060 2040 sh	1113, 1080, 1050	25.50 (25.79)	4.33 (4.33)	5.73 (6.02)
$Ba(SCN)_2$	EO3	1 : 1	2(Be)	210.5—213.5 (dec)	3380	2040	1130, 1100, 1075 sh, 1050 sh	23.96 (23.80)	3.54 (3.50)	6.73 (6.94)
$Ba(SCN)_2$	EO4	1 : 2	2(Ac)	158.0—159.0	3280 3160 sh	2060	1120, 1095, 1075 sh, 1055	33.61 (33.68)	5.52 (5.65)	4.57 (4.36)
$Ba(SCN)_2$	EO5	1 : 1	2(Ac)	156.2—157.3	3340	2040	1100 sh, 1080, 1045	29.30 (29.31)	4.68 (4.51)	5.70 (5.70)

Table 1. (Continued)

Salt	PEG	Stoichiometry Salt : POE : H_2O	Method[a] (solvent)	Mp (°C)	Infrared spectra (KBr disk)[b] νOH	νSCN	νC-O-C	Found (Calcd)% C	H	N
$Ba(SCN)_2$	EO6	1 : 1	1(Ac)	148.2—149.0	3310	2060	1105, 1080, 1050 sh, 1020	31.30 (31.38)	4.99 (4.89)	5.25 (5.23)
$Ba(SCN)_2$	EO7	1 : 1	1(Ac)	176.0—177.5	3340	2050	1120 sh, 1080, 1045 sh	32.79 (33.14)	5.28 (5.22)	4.88 (4.83)
$Ba(SCN)_2$	EO8	1 : 1	1(Ac)	151.5—152.0	3300 3120	2040	1090, 1060 sh	34.34 (34.65)	5.42 (5.49)	4.45 (4.49)
BaI_2	EO7	1 : 1	2(Ac)	247.0—251.0	3300		1090, 1075 sh, 1045 sh, 1025 sh	23.46 (23.44)	3.97 (4.21)	

a) See experimental section. THF=tetrahydrofuran, Ac=acetone, Be=benzene, EtAc=ethyl acetate, E=ether. b) sh=shoulder peak.

Table 2. Preparations and analytical data of complexes of glymes

Salt	Glyme	Stoichiometry Salt : POE : H_2O	Method[a] (solvent)	Mp (°C)	Infrared spectra (KBr disk)[b] δH_2O[c]	νSCN	νC-O-C	Found (Calcd)% C	H	N
$Sr(SCN)_2$	MeEO3Me	1 : 1 : 1/2	2(E)	179.0—181.0 (dec)	1620 (3400)	2050	1110, 1080, 1055, 1020, 1010	29.85 (30.71)	3.84 (4.90)	8.07 (7.16)
$Sr(SCN)_2$	MeEO4Me	1 : 1 : 1	2(E)	167.0—168.0	1620 (3320)	2050	1110, 1080, 1050, 1020	32.56 (32.45)	5.10 (5.45)	6.43 (6.31)
$Sr(SCN)_2$	MeEO5Me	1 : 1 : 1/2	2(E)	247.0—250.5 (dec)	1625 (3360)	2045	1095, 1085, 1060 sh, 1020	35.35 (35.09)	5.65 (5.68)	5.88 (5.85)
$Sr(SCN)_2$	MeEO6Me	1 : 1	2(E)	156.5—158.0		2040	1095, 1075 sh	37.07 (37.38)	5.80 (5.88)	5.51 (5.45)
$Sr(SCN)_2$	MeEO7Me	3 : 2	2(E)	138.5—142.0		2040	1080, 1055 sh	33.69 (34.57)	4.84 (5.19)	6.29 (6.37)
$Sr(SCN)_2$	MeEO8Me	2 : 1	2(E)	225.0 (dec)		2040	1080	33.21 (32.53)	4.97 (4.75)	6.24 (6.95)
$Ba(SCN)_2$	MeEO2Me	1 : 1	2(E)	144.5—154.0		2040	1110, 1090, 1065 sh	23.44 (24.79)	2.80 (3.64)	7.31 (7.23)
$Ba(SCN)_2$	MeEO3Me	1 : 1 : 1/2	2(E)	83.5—85.0	1620 (3380)	2030	1085, 1060, 1020	27.49 (24.79)	3.84 (3.64)	6.34 (6.36)
$Ba(SCN)_2$	MeEO4Me	1 : 1	2(E or Ac/Be)	144.0—145.0		2050	1105, 1085, 1060, 1020	30.21 (30.29)	4.36 (4.66)	5.86 (5.89)
$Ba(SCN)_2$	MeEO5Me	1 : 1 : 1	2(Ac)	162.0—164.4	1630 (3380)	2050	1090, 1055, 1020	31.39 (31.26)	5.28 (5.25)	5.19 (5.21)
$Ba(SCN)_2$	MeEO6Me	1 : 1	1(Ac)	171.5—172.5		2060 2040	1110, 1090, 1060 sh, 1020	33.90 (34.08)	5.44 (5.36)	4.80 (4.97)
$Ba(SCN)_2$	MeEO7Me	1 : 1	1(Ac/Be=3/25)	148.5—149.2		2040	1080, 1055 sh, 1030, 1020	35.43 (35.56)	5.71 (5.64)	4.57 (4.61)
$Ba(SCN)_2$	MeEO8Me	1 : 1	2(Ac)	89.8—90.7		2040	1090, 1020	36.53 (36.84)	5.98 (5.88)	4.33 (4.30)

a), b) See Table 1. The values in parentheses of δH_2O are those of νH_2O. c) The values in parentheses are νH_2O.

TABLE 3. ^{13}C NMR AND PROTON NMR OF SOME SOLID COMPLEXES

Complex	Solvent (concn %)	^{13}C NMR Chemical shift (ppm from TMS)		
		$\underline{C}H_2CH_2OH$	Other carbons	$CH_2\underline{C}H_2OH$
EO7	acetone-d_6 (20%)	61.9	71.0, 71.1	73.5
EO7-KSCN	acetone-d_6 (15%)	61.1	70.0, 70.2, 70.5	73.1
EO7-Sr(SCN)$_2$	methanol-d_4 (9%)	61.5	70.9, 71.3, 71.6, 71.8	73.5
EO7-Ba(SCN)$_2$	methanol-d_4 (12%)	62.4	71.3, 71.6, 71.9, 72.2	74.2
EO6-Ca(SCN)$_2$	methanol-d_4 (10%)	62.3	70.5, 70.9, 71.2, 71.8	73.3
EOc6-Ba(SCN)$_2$	methanol-d_4 (6%)	—	72.2	—

Complex	Solvent (concn %)	Proton NMR	
		Standard	Chemical shift
EO7-KSCN	methanol-d_4 (0.8%)	8% dioxane in benzene(external)	45.7, 47.2(Hz)[a]
EO7-KSCN	acetone-d_6 (15%)	TMS(internal)	3.64, 3.66, 3.67(ppm)
EO7-KSCN	acetonitrile-d_3 (17%)	TMS(internal)	3.57, 3.58, 3.59(ppm)
EO7-Ba(SCN)$_2$	methanol-d_4 (0.8%)	8% dioxane in benzene(external)	60.7(Hz)[a]

a) The chemical shift is expressed in Hz downfield. No correction of the bulk magnetic susceptibility was made. In the absence of metal cations, the chemical shift of EO7(*ca.* 1%) was in the range of 45—47 Hz.

TABLE 4. PREPARATIONS AND ANALYTICAL DATA OF NOVEL COMPLEXES OF CROWN ETHERS

Salt	Crown[a] ether	Stoichiometry salt : POE : H_2O	Method[b] (solvent)	Mp (°C)	Infrared spectra(KBr disk)[a] δH_2O	νSCN	νC-O-C	Found(Calcd)% C	H	N
LiSCN	EOc4	1 : 1	3(Ac)	260.0—261.0		2050	1134, 1087	44.64 (44.81)	6.77 (6.69)	5.71 (5.81)
NaSCN	EOc4	1 : 2 : 1/2	1(Ac)	138.0(dec)	1630 (3450)	2040 2060	1140, 1095	46.18 (46.13)	7.51 (7.51)	3.13 (3.17)
Mg(SCN)$_2$	EOc5	1 : 1	3(Ac)	360		2060	1090, 1060, 1040	39.80 (39.95)	5.56 (5.58)	7.71 (7.76)
Mg(SCN)$_2$	EOc6	1 : 1 : 4	1(AN)	360	1650 (3450)	2080	1140, 1110, 1090	34.89 (35.26)	6.64 (6.77)	5.84 (5.87)
Ca(SCN)$_2$	EOc4	1 : 1 : 2	3(M)	320	1620 (3380)	2080	1135, 1110, 1090	32.71 (32.60)	5.57 (5.47)	7.55 (7.60)
Ca(SCN)$_2$	EOc5	1 : 1 : 1	3(Ac)	310	1615 (3320) (3400 sh)	2090 2050	1120, 1095	36.57 (36.58)	5.74 (5.62)	7.08 (7.10)
Ca(SCN)$_2$	EOc6	1 : 1	3(Ac)	320		2045	1135, 1090	39.80 (39.98)	5.78 (5.75)	6.57 (6.66)
Ba(SCN)$_2$	EOc6	1 : 1	3(Ac)	270—300(dec)		2040	1085	31.95 (32.47)	4.32 (4.67)	5.39 (5.41)

a) EOc4=12-crown-4, EOc5=15-crown-5, EOc6=18-crown-6. b) See experimental section. Ac=acetone, AN=acetonitrile, M=methanol. c) The values in parentheses of δH_2O are those of νH_2O.

with alkali and alkaline earth metal thiocyanates to give stable solid complexes. However, our preliminary attempts of isolation using methanol as a solvent were unsuccessful. When a roughly 1 : 1 mixture of PEG and metal thiocyanates, which showed appreciable PMR downfield shifts, was heated up without solvent, some solid complexes were formed almost quantitatively, with a few exceptions(Table 1).

Among alkali metal thiocyanates, NaSCN gave a solid complex with EO6, while KSCN and RbSCN formed solid complexes with EO7. The complex with NaSCN was not isolated because of the difficulty in purification. The complex with $NaBPh_4$ was isolated and analyzed instead. Their compositions were all 1 : 1. Hexaethylene glycol(EO7) also produced a solid 1 : 1 complex with KI. Our attempts to isolate complexes with LiSCN and CsSCN, however, were all unsuccessful.

Ammonium thiocyanate gave a 1 : 1 complex with EO7, although two examples of the ammonium complexes with the diphenoxylated EO4 and EO6 have recently been reported.[19]

The magnesium complex with EO4 was confirmed to form on heating without solvent even when the thiocyanate has water of crystallization, and evolution of its water was observed during the complexation. Surprisingly, the resulting complex is no longer hygroscopic.

Calcium thiocyanate yielded the 1 : 1 complexes not only with EO6 but also with EO7. The solid complex

with EO8 was also isolated and its elemental analysis agreed with the 3:2 composition.

With $Sr(SCN)_2$ and $Ba(SCN)_2$, not only PEG with more than two EO units, but also glymes with more than two or three EO units gave the solid complexes with various compositions(Tables 1 and 2). As expected, the complex of EO7 with BaI_2 was also isolated.

Some of the above complexes could be recrystallized from aprotic solvent, suggesting that they are stable even in solution. This fact is also supported by ^{13}C NMR and PMR spectra of the complexes, in which, compared with the spectra of PEG, the splitting of signals or the shifts were observed especially in the PMR spectra(Table 3).

Remarkable differences between the IR spectra of PEG or glymes and those of their complexes may be noticed. The greatest changes are observed in the region 1000—1200 cm^{-1} which is assigned to the CH_2 rocking band and the C–C and C–O stretching bands.[21] It was reported[21] that the crystalline PEG's($n \geqq 3$) exhibit strong bands at about 1150, 1100—1115, and 1060—1065 cm^{-1}. Upon complexation, the bands are shifted to lower energy, giving one strong band which has a few shoulder peaks ranging from 1020—1080 cm^{-1}. The shifts are very similar to those of the crown ether complexes (see Table 4).[22] From these observations, it may be inferred that the structures of the complexes with PEG would be very similar to those of the crown ethers.[23]

Mechanism of Metal-ion Complexation of Poly(oxyethylene) Derivatives. From the ion-radius concept, it is widely recognized that the selective and strong metal-ion complexation of crown ethers is related to the relative sizes of the metal cations and the hole sizes of the crown ethers.[24–27] As is shown in Table 4, we have also succeeded in isolating some novel complexes of the crown ethers with thiocyanates of comparatively small ion-radius alkali and alkaline earth metals. The significance of these findings is that 12-crown-4, of which the cavity diameter is less than 1.2 Å, coordinate to both Li^+ (ion diameter 0.78 Å) and Ca^{2+}-(1.06 Å) with the 1 : 1 stoichiometry, but never to Mg^{2+} (0.78 Å). Further the 2 : 1 complex of 12-crown-4 with NaSCN including water of crystallization was found to form only in the presence of water, and could be recrystallized in acetone. The latter fact, implies along with the largest downfield shift on its complexation with Na^+ in acetone, that the complex is stable even in acetone. As was noted, $Mg(SCN)_2$ very easily gave the stable complexes with 15-crown-5 and 18-crown-6. Recently some magnesium complexes with benzo-15-crown-5 were reported.[28] From these various observations, it may be concluded that the cavity size of crown ethers is not the substantial factor governing their strong complexing properties. The poor complexing abilities of some rigid cyclic polyethers also support this conclusion.[29–32]

On the other hand, studies of the coordination geometry of the alkali metal cations based on PMR or metal element magnetic resonance experiments have attracted special interest recently. For the sodium ion, the existence of the four coordinated species were confirmed in THF,[3,33] DMSO,[34,35] or 1-methyl-2-pyrrolidone[35] by the PMR studies. Detellier and Laszlo[36] reported on the basis of the ^{23}Na NMR study that the tetracoordination and tetrahedral configuration of the sodium cation is of lowest energy. On the basis of the largest PMR downfield shifts, we have observed the strongest complexing ability of 15-crown-5 with the alkali and alkaline earth metal cations in acetone or methanol, with a few exceptions. Furthermore, it has been confirmed that there exists the specific interaction of PEG with the smaller metal cations, that is, Mg^{2+} with EO4, Na^+ and Ca^{2+} with EO6, and K^+ with EO7. These facts suggest that the fulfilment of the energetically favorable coordination geometry of the alkali and alkaline earth metal cations and the compatibility of the POE ligands should be the important factors governing the specific or the selective complexation. This mechanistic concept well explains an inclination of the induced fit of the crown ethers in complexation.[7,8]

The authors wish to express their thanks to Mrs. Y. Miyaji for her kind performance of the elaborate PMR measurements. They also wish to thank Miss J. Maenaka, Mr. and Mrs. Muneishi, and Miss Y. Sako for elemental analyses.

References

1) Part II in this series: S. Yanagida, K. Takahashi, and M. Okahara, *Bull. Chem. Soc. Jpn.*, **51**, 1294 (1978).
2) D. Nicholls and M. Szwarc, *J. Phys. Chem.*, **71**, 2727 (1967).
3) E. Schaschel and M. C. Day, *J. Am. Chem. Soc.*, **90**, 504 (1968).
4) K. Lie, *Macromolecules*, **1**, 308 (1968).
5) K. H. Wong, G. Konizer, and J. Smid, *J. Am. Chem. Soc.*, **92**, 666 (1970).
6) D. Live and S. I. Chan, *J. Am. Chem. Soc.*, **98**, 3769 (1976).
7) D. N. Reinhouldt, R. T. Gray, F. DeJong, and C. J. Smit, *Tetrahedron*, **33**, 563 (1977).
8) M. Dobler, J. D. Dunitz, and P. Seiler, *Acta Crystallogr., Sect B*, **30**, 2741 (1974).
9) J-M. Lehn, The 26th IUPAC Post Congress Symposium (Kyushu Symposium on Biomimetic Chemistry), September, 1977. See also *Kagaku*, **33**, 5 (1978).
10) M. R. Truter, *Struct. Bonding (Berlin)*, **16**, 71 (1973).
11) G. W. Gokel, D. J. Cram, C. L. Liotta, H. P. Harris, and F. L. Cook, *J. Org. Chem.*, **39**, 2445 (1974).
12) R. D. MacLachlan, *Spectrochim. Acta, Part A*, **30**, 2153 (1974).
13) S. Yanagida, Y. Noji, and M. Okahara, *Tetrahedron Lett.*, **1977**, 2893.
14) a) E. Weber and Vögtle, *Tetrahedron Lett.*, **1975**, 2415; b) F. Vögtle and H. Sieger, *Angew. Chem. Int. Ed. Engl.*, **16**, 396 (1977); c) B. Tummler, G. Maass, E. Weber, W. Wehner, and F. Vögtle, *J. Am. Chem. Soc.*, **99**, 4683 (1977); d) F. Vögtle and E. Weber, *Kontakte*, **1977**, 11.
15) N. N. L. Kirsch and W. Simon, *Helv. Chim. Acta*, **59**, 357 (1976).
16) R. Büchi and E. Pretsch, *Helv. Chim. Acta*, **58**, 1573 (1975).
17) S. Yanagida, K. Takahashi, and M. Okahara, *Bull.*

Chem. Soc. Jpn., **50**, 1386 (1977).
18) P. S. Gentle and T. A. Shankoff, *J. Inorg. Nucl. Chem.*, **27**, 2301 (1965).
19) C. Calzolari, L. Favretto, M. Pertodi, and L. Favretto Gabrielli, *Ann. Chim. (Rome)*, **64**, 463 (1974).
20) J. Smid and A. M. Grotens, *J. Phys. Chem.*, **77**, 2377 (1973).
21) H. Matsuura and T. Miyazawa, *Spectrochim. Acta, Part A*, **23**, 2433 (1967).
22) Lj. Tuŝek, H. Meider-Goricân, and P. R. Danesi, *Z. Naturforsch., Teil B*, **31**, 330 (1976).
23) For the complex of EO7 with $Sr(SCN)_2$, this speculation was supported by X-ray analysis.
24) C. J. Pedersen and H. K. Frensdorf, *Angew. Chem. Int. Ed. Engl.*, **11**, 16(1976).
25) a) J. J. Christensen, J. O. Hill, and R. M. Izatt, *Science*, **174**, 459 (1971); b) M. Izatt, D. J. Eatough, and J. J. Christensen, *Struct. Bonding (Berlin)*, **16**, 111 (1973); c) J. J. Christensen, D. J. Eatough, and R. M. Izatt, *Chem. Rev.*, **74**, 351 (1974).
26) J-M. Lehn, *Struct. Bonding (Berlin)*, **16**, 1 (1973).
27) M. Takagi and T. Matsuda, *Kagaku No Ryoiki*, **31**, 208 (1977).
28) N. S. Poonia, B. P. Yadav, and V. W. Bhagwat, *Inorg. Nucl. Chem. Lett.*, **13**, 119 (1977).
29) J. A. Elix, *Aust. J. Chem.*, **22**, 1951 (1969).
30) A. J. Coxon and J. F. Stoddart, *J. Chem. Soc., Perkin Trans. 1*, **1977**, 767.
31) D. E. Kime and J. K. Norymberski, *J. Chem. Soc., Perkin Trans. 1*, **1977**, 1048.
32) E. Buhleier and F. Vögtle, *Liebigs Ann. Chem.*, **1977**, 1080.
33) M. C. Day, *Pure Appl. Chem.*, **49**, 75 (1977).
34) A. T. Tsatsas, R. W. Stearns, and W. M. Risen, Jr., *J. Am. Chem. Soc.*, **94**, 5247 (1972).
35) J. L. Wuepper and A. I. Popov, *J. Am. Chem. Soc.*, **92**, 1493 (1970).
36) C. Detellier and P. Laszlo, *Helv. Chim. Acta*, **59**, 1333 (1976).

Microwave Spectrum, Structure, and Quadrupole Coupling Constant of *s-cis* *o*-Chlorophenol-*d*

Masao ONDA* and Ichiro YAMAGUCHI

Department of Chemistry, Faculty of Science and Technology, Sophia University, Tokyo 102

(Received February 8, 1978)

The microwave spectrum of *o*-chlorophenol-*d* has been observed in the frequency range 17—34 GHz. The rotational and centrifugal distortion constants have been obtained. The analysis of the hyperfine structure has given the following nuclear quadrupole coupling constants for the ^{35}Cl species: $\chi_{aa}=-67.1$, $\chi_{bb}=33.1$, and $\chi_{cc}=34.0$ (MHz). The spectrum assigned has been attributed to the *s-cis*-form (the hydroxyl hydrogen pointed toward the chlorine) from the consideration of the r_s-coordinates of hydrogen and chlorine atoms. The non-bonded Cl···H distance is 2.373±0.001 Å.

In the previous paper,[1] we suggested that the intense lines observed in the microwave spectrum of *o*-chlorophenol should be attributed to the *s-cis* form. In this paper, we report the spectrum of *o*-chlorophenol-*d*. Using the r_s-coordinates of the hydrogen and chlorine atoms, we have confirmed the *s-cis*-structure of the molecule, and determined the structural parameters which reproduce the observed rotational constants and the H···Cl non-bonded distance. We have also obtained the Cl quadrupole coupling constants.

Experimental

o-Chlorophenol-*d* was produced by mixing the normal species with D_2O. The obtained sample was dried over anhydrous calcium chloride, followed by trap-to-trap distillation *in vacuo*. The content of the *d*-species in the sample was estimated to be about 50% from the intensity ratio of the same rotational transition of the deuterated and normal species. The microwave spectrum was measured with a conventional spectrometer with 100 kHz square-wave Stark modulation. The D_2O vapor was introduced into the waveguide and pumped out for several hours, and then the sample was introduced. Measurements were made at *ca.* −20 °C with a sample pressure of 0.6—7 Pa.

Results and Discussion

Analysis of the Spectrum. The frequencies of the spectral lines were predicted from the structural models for both the regular and the distorted hexagonal skeleton structure of *s-cis* *o*-chlorophenol.[1] The initial step of the assignment was made for b-type Q-branch transitions with high-J values. The lines of several Q-branch series are the most intense in our observed frequency region. Their hyperfine structure is a clean doublet in which the separation of lines is a few MHz. The separation varies smoothly according as the J-value changes. The center of the doublet was taken as the unperturbed frequency, since only the first order perturbation was taken into account in the analysis of the hyperfine structure. To confirm the assignment of the Q-branch lines, the splitting widths observed were compared with the ones calculated from the χ-values obtained for *o*-$^{35}ClC_6H_4OH$[1] and the model structure.

The frequencies of the R-branch transitions were predicted from the values of κ and $(A-C)/2$ obtained from the analysis of the Q-branch transitions, together with an assumption of the molecular planarity. The hyperfine structure for the R-branch transitions, however, was not expected to be observed, because the magnitude of the hyperfine splitting was predicted to be smaller than the resolution of the spectrometer. A group of the a- and b-type transitions $J_{0,1}\leftarrow J-1_{1,J-1}$, $J_{1,J}\leftarrow J-1_{1,J-1}$, $J_{0,J}\leftarrow J-1_{0,J-1}$, and $J_{1,J}\leftarrow J-1_{0,J-1}$ was observed as a quartet for $J=9$ and 10. In the quartet, the intensities of a- and b-type transitions are comparable to each other. This indicates that the components of the dipole moment, μ_a and μ_b, of this molecule are comparable in magnitude, as observed for the normal species. The assigned transitions are given in Table 1. The rotational constants, and the centrifugal distortion constants constrained by the planarity conditions among $\tau_{aa\beta\beta}$'s, were obtained by the least-squares fitting and are given in Table 2. The values of the distortion constants obtained are fairly close to those for the normal species, but are smaller than those for most of the aromatic molecules studied.

Molecular Structure. The inertia defect for the isotopic species, *o*-$^{35}ClC_6H_4OD$, was almost the same as that for the normal species, *o*-$^{35}ClC_6H_4OH$,[1] and was found to be of very small positive value compared with those of other planar aromatic molecules. This fact is a strong indication of the planar configuration of this molecule. The isotopic substitution at the hydroxyl group, from H to D, reduces further the magnitude of the inertia defect. Therefore, a negative contribution to the inertia defect can be interpreted as coming from the OH torsion. The Kraitchman's equation was used to calculate the coordinates of the hydrogen atom. The values obtained are given in Table 3, where the errors come from those in the moments of inertia. A very small value of the c-coordinate has been obtained with a large error and it seems rather reasonable to consider that the hydrogen atom practically lies in the A-B plane. On the other hand, a very small imaginary value of the c-coordinate for the chlorine atom was obtained by applying the Kraitchman's equation for the two species, *o*-$^{35}ClC_6H_4OH$ and *o*-$^{37}ClC_6H_4OH$.[1] Therefore, the chlorine atom also lies effectively in the A-B plane. The planar structure of this molecule is plausible. No ambiguity in the sign of r_s-coordinates arises in this case, since the other choice of the sign of the H-coordinates leads to an impossible configuration, with too small a distance between the H atom and C–C bond of the

TABLE 1. OBSERVED FREQUENCIES AND QUADRUPOLE SPLITTING OF *s-cis* *o*-$^{35}ClC_6H_4OD$ (MHz)

Transition	Observed	Centrifugal correction	$\Delta\nu$(I)[a]	*hfs*	
				Obsd	$\Delta\nu$(II)[b]
$8_{0,8}-7_{1,7}$	17144.74	−0.06	−0.12		
$8_{1,8}-7_{1,7}$	17153.15	−0.06	0.04		
$8_{0,8}-7_{0,7}$	17166.35	−0.06	−0.06		
$8_{1,8}-7_{0,7}$	17174.77	−0.06	0.10		
$9_{0,9}-8_{1,8}$	19171.55	−0.09	−0.01		
$9_{1,9}-8_{1,8}$	19174.61	−0.09	−0.04		
$9_{0,9}-8_{0,8}$	19179.94	−0.09	0.12		
$9_{1,9}-8_{0,8}$	19183.11	−0.09	0.19		
$10_{0,10}-9_{1,9}$	21192.93	−0.12	0.01		
$10_{1,10}-9_{1,9}$	21194.07	−0.12	0.02		
$10_{0,10}-9_{0,9}$	21196.10	−0.12	0.09		
$10_{1,10}-9_{0,9}$	21197.14	−0.12	−0.00		
$9_{1,8}-8_{2,7}$	21041.50	−0.13	0.20		
$9_{2,8}-8_{2,7}$	21155.67	−0.13	−0.30		
$9_{1,8}-8_{1,7}$	21298.95	−0.13	0.08		
$9_{2,8}-8_{1,7}$	21413.54	−0.13	−0.00		
$11_{0,11}-10_{1,10}$	23212.22	−0.16	−0.02		
$11_{1,11}-10_{1,10}$	23212.72	−0.16	0.07		
$11_{0,11}-10_{0,10}$	23213.34	−0.16	−0.02		
$11_{1,11}-10_{0,10}$	23213.68	−0.16	−0.10		
$10_{1,9}-9_{2,8}$	23154.89	−0.17	0.05		
$10_{2,9}-9_{2,8}$	23203.49	−0.17	−0.02		
$10_{1,9}-9_{1,8}$	23269.46	−0.17	−0.05		
$10_{2,9}-9_{1,8}$	23318.17	−0.17	−0.01		
$12_{0,12}-11_{1,11}$	25230.90	−0.20	0.08		
$12_{1,12}-11_{1,11}$	25230.90	−0.20	−0.06		
$12_{0,12}-11_{0,11}$	25230.90[c]	−0.20	−0.32		
$12_{1,12}-11_{0,11}$	25230.90[c]	−0.20	−0.47		
$13_{0,13}-12_{1,12}$	27249.15	−0.25	0.01		
$13_{1,13}-12_{1,12}$	27249.15	−0.25	−0.04		
$13_{0,13}-12_{0,12}$	27249.15	−0.25	−0.13		
$13_{1,13}-12_{0,12}$	27249.15	−0.25	−0.18		
$14_{0,14}-13_{1,13}$	29267.39	−0.31	−0.00		
$14_{1,14}-13_{1,13}$	29267.39	−0.31	−0.02		
$14_{0,14}-13_{0,13}$	29267.39	−0.31	−0.05		
$14_{1,14}-13_{0,13}$	29267.39	−0.31	−0.07		
$15_{0,15}-14_{1,14}$	31285.71	−0.38	0.08		
$15_{1,15}-14_{1,14}$	31285.71	−0.38	0.08		
$15_{0,15}-14_{0,14}$	31285.71	−0.38	0.07		
$15_{1,15}-14_{0,14}$	31285.71	−0.38	0.06		
$16_{0,16}-15_{1,15}$	33303.64[c]	−0.46	−0.23		
$16_{1,16}-15_{1,15}$	33303.64[c]	−0.46	−0.23		
$16_{0,16}-15_{0,15}$	33303.64[c]	−0.46	−0.23		
$16_{1,16}-15_{0,15}$	33303.64[c]	−0.46	−0.24		
$24_{9,15}-24_{8,16}$	17029.17[d]	−2.01	0.06	−0.82	0.01
$24_{10,14}-24_{9,15}$	22299.30[d]	−2.54	−0.06	−2.27	0.08
$25_{10,15}-25_{9,16}$	20384.23[d]	−2.52	−0.03	−1.97	−0.03
$26_{10,16}-26_{9,17}$	19060.69[d]	−2.58	−0.01	−1.35	−0.02
$27_{10,17}-27_{9,18}$	18751.80[d]	−2.79	0.06	−0.69	−0.05
$28_{10,18}-28_{9,19}$	19684.25	−3.19	0.21		
$29_{10,19}-29_{9,20}$	21842.22[d]	−3.79	−0.10	0.36	−0.15
$30_{10,20}-30_{9,21}$	24958.86[d]	−4.56	−0.04	0.77	−0.00
$28_{11,17}-28_{10,18}$	21925.35[d]	−3.38	0.18	−1.76	−0.04
$29_{11,18}-29_{10,19}$	20641.42[d]	−3.47	−0.04	−1.12	0.01
$30_{11,19}-30_{10,20}$	20480.91[d]	−3.76	−0.32	−0.37	0.10

Table 1. (Continued)

Transition	Observed	Centrifugal correction	$\Delta\nu$(I)[a]	*hfs*	
				Obsd	$\Delta\nu$(II)[b]
$31_{11,20}-31_{10,21}$	21639.38	−4.30	−0.11		
$32_{11,21}-32_{10,22}$	24052.96[d]	−5.08	0.10	0.66	0.09
$31_{12,19}-31_{11,20}$	23423.99[d]	−4.41	−0.10	−1.51	0.01
$32_{12,20}-32_{11,21}$	22210.68[d]	−4.55	0.04	−0.82	0.13
$33_{12,21}-33_{11,22}$	22225.44	−4.95	0.13		
$34_{12,22}-34_{11,23}$	23626.73	−5.65	0.07		
$34_{13,21}-34_{12,22}$	24890.65[d]	−5.63	0.05	−1.32	0.04
$35_{13,22}-35_{12,23}$	23776.85[d]	−5.83	−0.01	−0.76	0.04
$36_{13,23}-36_{12,24}$	23990.67	−6.37	−0.08		

a) $\Delta\nu$(I) = observed − calculated, for the rotational transition. b) $\Delta\nu$(II) = observed − calculated, for the splitting. c) Not included in the least-squares fitting. d) Corrected for the quadrupole effect.

Table 2. Rotational constants(MHz), centrifugal distortion constants(kHz), and inertia defect (amu Å^2) of *s-cis* o-$^{35}ClC_6H_4OD$

A	2930.937±0.009[b]
B	1539.217±0.004
C	1009.203±0.002
τ_{aaaa}	−2.0±0.3
τ_{bbbb}	−0.36±0.03
τ_{aabb}	−0.1±0.2
τ_{abab}	−0.46±0.07
$I_c-I_a-I_b$	0.006±0.002
σ[a]	0.007

a) Standard deviation in frequencies(MHz) for lines fitted. b) Standard deviation.

benzene ring. The non-bonded H···Cl distance was obtained from the r_s-coordinates of Cl[1] and H, as shown in Table 3. The obtained H···Cl distance, 2.373 Å, implies that the assigned spectrum is of the *s-cis*-form of this molecule. As discussed in the previous paper,[1] the a- and b-components of the dipole moment for the *s-cis*-form are comparable in magnitude to each other. Therefore, the comparable intensities of the observed a- and b-type transitions also support the *s-cis*-form of the molecule studied here.

Assuming the rigid planar structure of this molecule, five structural parameters have been obtained from the three isotopic species, $^{35}ClC_6H_4OH$, $^{37}ClC_6H_4OH$, and $^{35}ClC_6H_4OD$. Here, the benzene ring was assumed to be of the same distorted skeleton as obtained for chlorobenzene from its complete r_s-coordinates analysis.[2] The parameters obtained are given in Table 4. These parameters reproduce the observed nine moments of inertia within 0.1 amu Å^2 and the r_s-non-bonded distance (Cl···H) within 0.01 Å. The structural parameters around the OH group are similar to those of phenol. The small differences in r_{OH}, $\angle C_1C_2O$, and $\angle C_2OH$, *i.e.*, the slightly longer bond length r_{OH} and the slightly narrower angles of the $\angle C_1C_2O$ and $\angle C_2OH$, where C_1 is bonded to Cl and C_2 to O, compared with those of phenol, suggest the existence of an intra-molecular hydrogen bonding.

Quadrupole Coupling Constants. The apparent splitting of the doublet was measured for each of the high-J b-type Q-branch transitions listed in Table 1. The hyperfine structures due to ^{35}Cl were analyzed, based on the first-order quadrupole correction computation using the rotational constants in Table 2. The quadrupole coupling constants in the principal inertia axis system, χ_{aa}, χ_{bb}, and χ_{cc}, were obtained using the least-squares method, as shown in Table 5. In this procedure, a quantity, the inverse of the squared standard deviation (in the measurements) for the splitting divided by the splitting width, was taken as the weight for each line. The uncertainties of the values in Table 5 were estimated from the error in the frequency measurements of the unresolved F components. Assuming that the principal z-axis of the χ-tensor lies along the C–Cl bond, the values of χ_{zz} and χ_{yy} are calculated as given in Table 5. The χ_{xx}, the component perpendicular to the molecular plane, is the same as χ_{cc}. The χ_{gg}-values (g=x,y, and z) of $^{35}ClC_6H_4OH$ was recalculated for the molecular structure obtained in this work. The ambiguity of the angle of θ_{za} was within ±0.1° when estimated from the structure in Table 4. The χ-values calculated for the normal and deuterated species coincide within the error limits. The value of χ_{zz}(−68.7 MHz) in this molecule is larger than that in chlorobenzene[3] (χ_{zz}=−71.10±0.50 MHz) by 2.4 MHz. This difference suggests an increase of ionicity of the Cl atom compared with that

Table 3. Principal axis coordinates of H and Cl (Å)

	$\|a\|$	$\|b\|$	$\|c\|$
H	1.4863±0.0003[b]	1.7874±0.0003	0.065 ±0.007
Cl[a]	2.0672±0.0001	0.5136±0.0005	$(-0.0004)^{1/2}$±0.011
H···Cl (in plane)		2.373±0.001	

a) Ref. 1. b) The errors came from those in the moments of inertia.

Table 4. Structural parameters[a]

	s-cis *o*-ClC_6H_4OH[b]	C_6H_5Cl[c]	C_6H_5OH[d]
r_{C-Cl} (Å)	1.721±0.001	1.7248	—
r_{C-O} (Å)	1.37±0.005	—	1.364
r_{O-H} (Å)	0.97±0.01	—	0.956
$\angle C_1C_2O$ (°)	121.0±0.5	—	122.2
$\angle C_2OH$ (°)	108.0±0.5	—	109.0

a) A distorted hexagon shape of the chlorobenzene molecule was assumed; Ref. 2. b) This work. c) Ref. 2. d) Ref. 4.

in chlorobenzene. The double bond character of the C–Cl bond should be negligible because the η-value is vanishingly small. This situation appears also in other chlorobenzene derivatives.[5]

Judging from the quadrupole coupling constant alone, the interaction between chlorine and hydrogen atoms is rather weak. The small difference in the χ_{zz} between *o*-chlorophenol and monochlorobenzene reveals no clear effect of hydrogen bonding on the nuclear quadrupole coupling constant of chlorine. The same conclusion had been obtained for 2-chloroethanol.[6]

Table 5. Quadrupole coupling constants of ^{35}Cl(MHz)

	$^{35}ClC_6H_4OH$[a]	$^{35}ClC_6H_4OD$[b]
χ_{aa}	−67.6±0.3	−67.1±2.0
χ_{bb}	33.3±0.1	33.1±0.2
χ_{cc}	34.3±0.4	34.0±2.2
θ_{za}[c]	5.87°	6.84°
χ_{zz}	−68.7±0.3	−68.6±2.0
χ_{yy}	34.4±0.1	34.6±0.2
χ_{xx}[d]	34.3±0.4	34.0±2.2
η[e]	0.00	0.01

a) Ref. 1. b) This work. c) θ_{za} is the angle between the principal inertial a-axis and the C-Cl bond axis. d) χ_{xx} is the component perpendicular to the molecular plane. e) $\eta=(\chi_{xx}-\chi_{yy})/\chi_{zz}$.

References

1) M. Onda, Y. Oshima, and I. Yamaguchi, *Bull. Chem. Soc. Jpn.*, **51**, 65 (1978).

2) G. Roussy and F. Michel, *J. Mol. Struct.*, **30**, 399 (1976); F. Michel, H. Nery, P. Nosberger, and G. Roussy, *J. Mol. Struct.*, **30**, 409 (1976).

3) R. Poynter, *J. Chem. Phys.*, **39**, 1962 (1963).

4) T. Pedersen, N. W. Larsen, and L. Nygaard, *J. Mol. Struct.*, **4**, 59 (1969).

5) M. Onda and I. Yamaguchi, *J. Mol. Struct.*, **34**, 1 (1976); M. Onda and I. Yamaguchi, *J. Mol. Struct.*, **36**, 158 (1977).

6) R. G. Azrak and E. B. Wilson, *J. Chem. Phys.*, **52**, 5299 (1970).

Chemisorption of Sulfur on Thermally Decomposed Copper and Iron Sulfides

Nakamichi YAMASAKI

Research Laboratory of Hydrothermal Chemistry, Faculty of Science, Kochi University, Asakura, Kochi 780

(Received February 10, 1978)

The chemisorption of sulfur on thermally decomposed copper and iron sulfides was studied and its application to the desulfurization process of heavy oil was attemped. Thermal decomposition of sulfides was carried out by calcining CuS and FeS_2 at 200—800 °C under 10^{-3} mmHg and with 5 °C/min. Sulfur was adsorbed on the calcined sulfides in toluene. Thermally decomposed copper sulfide (Cu/S: 1—2) easily chemisorbs free sulfur in toluene below 100 °C, but not iron sulfide (Fe/S: 1—0.5). The relationship between sulfur affinity and the structure of partially decomposed sulfide was discussed in terms of the kinetics of initial chemisorption of sulfur and the sulfur adsorption coefficient calculated from the ratio of the adsorbed sulfur to the sulfur required to reform starting CuS and FeS_2. The partially decomposed copper sulfide ($Cu_{1-2}S$) easily chemisorbs free sulfur in heavy oil. Chemisorption might be applied to the desulfurization of heavy oil.

The colloidal or dissolved sulfur in solvent is gradually oxidized by air, forming sulfur oxides. In industry, the sulfur oxides not only cause the corrosion of steel container or pipe line, but also produce substances harmful to human life. Active carbon or zeolite is used as an adsorbent of sulfur. The adsorption mechanisms of sulfur on active carbon and zeolite are explained by the physical trapping or van der Waals bonding. It is supposed that the thermally decomposed sulfides which partially release sulfur in a vacuum have the defect of sulfur atoms in crystal lattice. Such sulfides are expected to be strong adsorbents of sulfur reforming the chemical bonding of sulfur in defective positions of the crystal.

The partially decomposed sulfide in a vacuum generally has a skelton structure and is active to the reverse reaction, that is, adsorption. The thermal decomposition processes and phase diagrams of CuS and FeS_2 were discussed by Samsonov and Drozdova,[1] and the formation energies of CuS and FeS_2 were reported by Richardson and Jeffes.[2] However, no report seems to have appeared on the thermal decomposition of these sulfides in a vacuum and the chemisorption of sulfur. The relation between the sulfur release from starting sulfide and the chemisorption of sulfur is of interest as regards the development of new sulfur adsorbent.

The major sulfur compounds contained in heavy oil are mercaptan, disulfide and aromatic sulfide as thiophen. These sulfur compounds have analogy to H_2S in the redox-reaction. H_2S is easily oxidized by SO_2 even at room temperature, forming free sulfur. Sulfur compounds in heavy oil are also oxidized by SO_2 gas to sulfur at relatively high temperature or high pressure. Such free sulfur can be easily removed by adsorption on metal sulfide decomposed thermally in a vacuum.

In order to obtain a strong sulfur adsorbent, it is necessary to study the relationship between the various degree of decomposition of sulfide in a vacuum and the rate of chemisorption of sulfur.

Experimental

Preparations of Samples. The mode of the thermal decomposition of CuS and FeS_2 in a vacuum largely depends on the conditions of the preparation of starting materials. A distinct difference was observed between two kinds of CuS precipitated in alkaline and acidic solutions respectively, as regards the decomposition temperature in a vacuum. However, the two kinds of CuS have the same crystal structure.

Precipitation of starting materials was carried out as follows. FeS_2 was prepared by the dry method of Titarenko.[3] CuS was prepared by a wet method. An aqueous solution of Na_2S was added slowly to 10% aq solution of $Cu(NO_3)_2$ with stirring at 25 °C. The resulting precipitate (CuS) was aged on a hot plate for two hours with bubbling of nitrogen gas, filtered, and washed with ethanol, carbon disulfide, and then acetone. The product was kept to dry in a vacuum dessicator.

Thermal Decomposition. Proper calcination temperatures were selected from the results of TG-DTA. The starting FeS_2 or CuS was set in a quartz container in furmace, degassed slowly, and heated at a heating rate of 5 °C/min, under 10^{-3} mmHg, as in the case of TG-DTA. After the desired temperature of the container had been reached, the furnace was removed immediately and the container was cooled from outside with a fan. The samples calcined at various temperatures were subjected to elemental analysis, X-ray powder diffraction, and determination of specific surface area. The data of TG-DTA and specific surface area are shown in Figs. 1 and 2, and the X-ray powder patterns at various temperatures in Figs. 3 and 4. The preferable sulfur adsorbents selected according to the data of sulfur release and crystal structures are given in Table 1.

Elemental Analysis (Determination of Metal/S). In the Lunge method, the sample is dissolved in aqua regia on a steam bath. In order to suppress the formation of insoluble free sulfur, $KClO_3$ or Br_2 is added to the solution as an exhaustive oxidizing agent. In the present experiment, however, the sample was dissolved in nitric acid instead of aqua regia. After the evolution of H_2 gas had ceased, the solution was subjected to centrifugation and the insoluble residue separated was put into a glass tube, the liquid phase being kept for the subsequent procedure. A small amount of nitric acid centrifuged was added to the glass tube and sealed. The sealed tube was set in a micro-autoclave of inner volume of 25 ml. The outside of the tube was filled with water to prevent the breakdown of the glass tube. The autoclave was heated at 250 °C for a few minutes and cooled quickly. After the glass tube had been opened, the contents were added to the solution which had been centrifuged. The combined solution was treated according to a process similar to the Lunge method. Fe^{3+} was determined by colorimetry.[4]

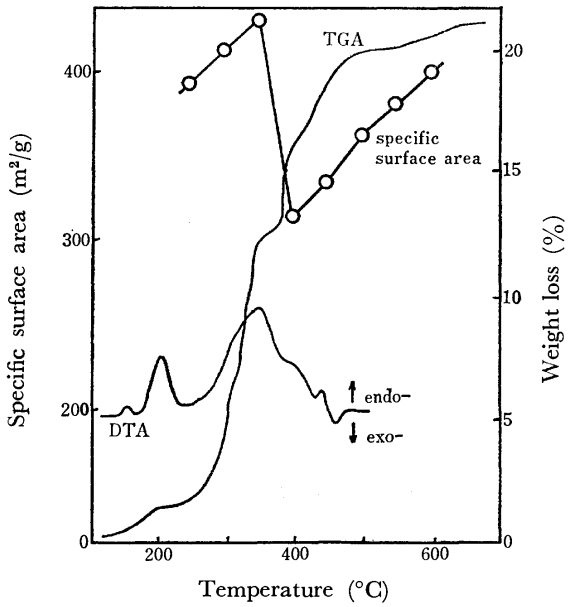

Fig. 1. Thermal decomposition pattern of CuS.

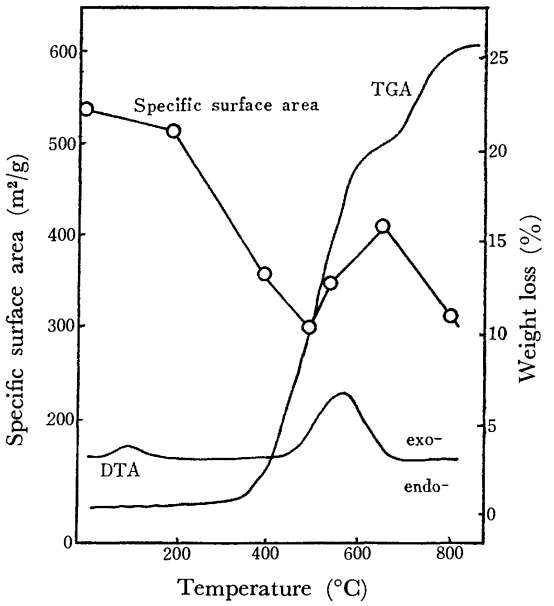

Fig. 2. Thermal decomposition pattern of FeS_2.

Sulfur Adsorption Procedure. The kinetics and quantities of sulfur adsorption were measured as follows.

The thermally decomposed iron sulfide adsorbed no sulfur in toluene under 100 °C. However, it reacted with sulfur vapor in a sealed glass tube at 200—260 °C.

A half gram of the decomposed iron sulfide was put into a glass tube with 0.5 g of sulfur (in excess), the tube then being sealed in a vacuum. This was heated in an electric furnace. After cooling, iron sulfide was washed with ethanol, acetone, and then CS_2, and dried in a vacuum oven. The quantity of the adsorbed sulfur was determined from the weight change and elemental analysis. The crystal structure was identified by means of X-ray diffraction.

The sulfur adsorption on active carbon was carried out as follows. Active carbon (animal charcoal) washed with 20% H_2SO_4 and 5 M NaOH solution was dried, and 1.000 g of the dried active carbon was added to 10 ml of toluene saturated with sulfur. Adsorption was carried out as in the case of copper sulfide.

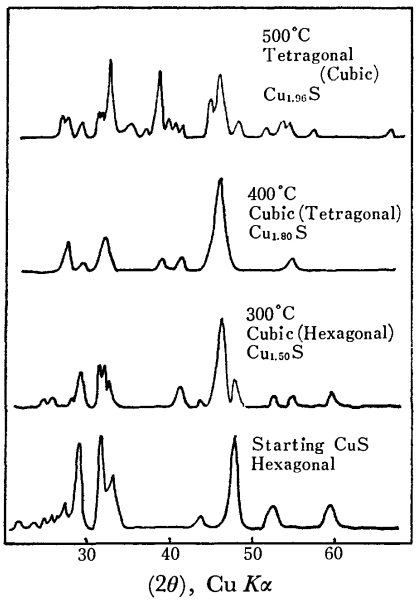

Fig. 3. X-Ray profiles of $Cu_{1-2}S$ at various calcined temperatures.

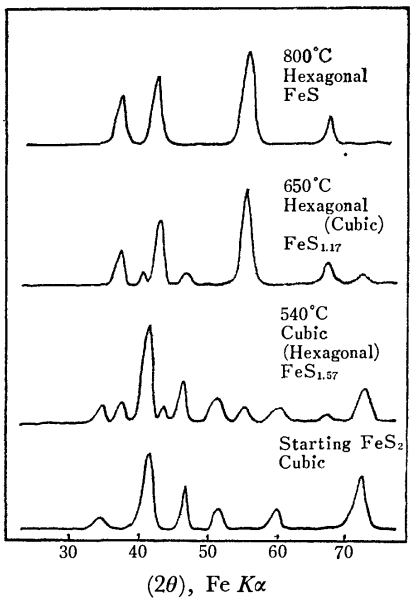

Fig. 4. X-Ray profiles of FeS_{1-2} at various calcined temperatures.

Application Procedure to Desulfurization Process of Heavy Oil. A B-class heavy oil (sulfur content 1.42%) was used as a starting material. The SO_2 gas of 2 kg/cm² and B-class heavy oil of 3 ml were introduced in a micro-autoclave shown in Fig. 5, and heated with stirring in a revolving furnace (Fig. 6) at 300 °C for 15 min. A half gram of thermally decomposed copper sulfide obtained by calcination of CuS in a vacuum at 500 °C for 90 min was added to the resulting heavy oil of 1.5 ml. The mixture was warmed on a water bath at 80 °C with stirring for 60 min. Heavy oil was separated from copper sulfide by filtration. The sulfur content of the heavy oil was determined by JIS K-2541, the desulfurization ratio being calculated. In order to confirm the chemisorption of sulfur, *viz.*, the formation of CuS ($Cu_2S+S=2CuS$), the crystal structure of the resulting copper sulfide was examined by means of X-ray diffraction.

Table 1. Ratios of metal/sulfur and structure at various calcined temperatures for sulfur adsorption

Calcined temp (°C)	Cu/S	Structure
100	1.00	hexagonal
250	1.20	hexagonal, (cubic)[a]
300	1.50	cubic, hexagonal
400	1.80	cubic
500	1.96	cubic, tetragonal
Calcined temp (°C)	**Fe/S**	**Structure**
100	0.50	cubic
540	0.64	cubic, (hexagonal)[a]
650	0.85	hexagonal, (cubic)[a]
800	1.02	hexagonal

a) ( ) is a meaning of small content.

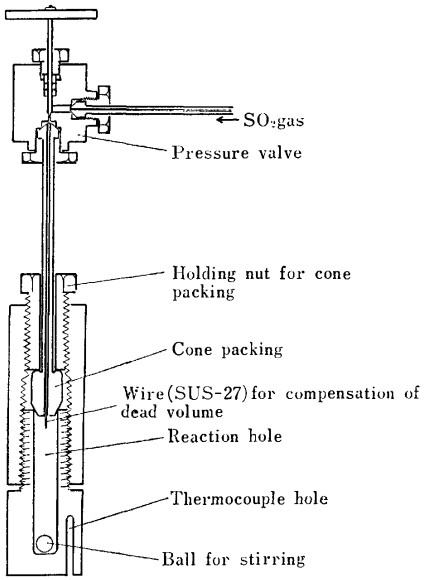

Fig. 5. Cross sectional view of micro-autoclave.

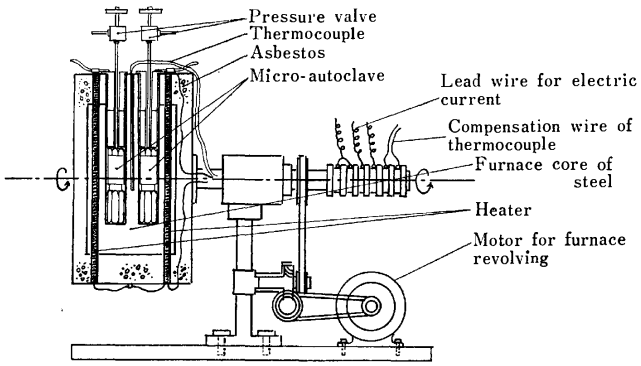

Fig. 6. Schema of revolving furnace.

Results and Discussion

The decomposition of CuS at 200—500 °C in a vacuum (Fig. 1) does not proceed linearly with the rise in temperature because of the existence of metastable state in the temperature range 380—400 °C. The crystal structure in the temperature range is cubic $Cu_{1.80}S$ (Fig. 3). On the other hand, the decomposition of FeS_2 is the constant release of sulfur in vacuum calcination (Figs. 2 and 4).

The ratios of metal/sulfur and the structures of decomposed sulfides at various temperatures are given in Table 1.

Transformation of Structure with Sulfur Chemisorption. The crystal structures of partially decomposed sulfides vary with sulfur adsorption (Figs. 7 and 8). The figures show that the process of sulfur chemisorption is opposite that of thermal decomposition in a vacuum. The tetragonal $Cu_{1.96}S$ calcined at 500 °C adsorbs sulfur 100 °C, forming hexagonal CuS through cubic $Cu_{1.80}S$. The X-ray profiles of Figs. 7 and 8 for the final product adsorbed sulfur show that the half value width of the X-ray peaks is about twice that of the starting CuS before thermal decomposition, and the crystalline size of the final product of copper sulfide is smaller than that of the starting materials. The results suggest that the starting CuS particles break in a vacuum at high temperature, new CuS particles being formed.

In the case of iron sulfide the chemisorption of sulfur occurs at high temperature above 200 °C, proceeding continuously.

Sulfur Adsorption Coefficient. The sulfur adsorption coefficient was calculated by means of the equation

$$K = (S_2/S_1) \times 100,$$

where K is adsorption coefficient, S_1 the amount of sulfur required to form starting sulfides CuS and FeS_2, and S_2 the amount of the adsorbed sulfur estimated from weight change and mole ratio of sulfur/metal by chemical analysis.

These coefficients increase with rise in adsorption temperature (Figs. 9 and 10). These data and results of X-ray anlysis (Figs. 7 and 8) show that the sulfur adsorption cause $Cu_{1.80}S$ or CuS. The adsorption is the reverse of the thermal decomposition of sulfide in a vacuum. Sulfur release is very small in copper sulfide calcined at 200 °C, and the sulfur adsorption coefficient (approximately 90% even at room temperature) is large as shown in Fig. 9. This suggests that the number of the empty site which can adsorb sulfur is small. However, the sample has a strong affinity to sulfur.

All the curves of adsorption coefficient for the samples calcined at above 300 °C are of similar form. This suggests that the mechanisms of sulfur adsorption at 400 and 500 °C are similar.

The adsorption temperatures of thermally decomposed copper sulfides are relatively lower than those of iron sulfides (Figs. 9 and 10). These results agree with those in which the formation energies for CuS and FeS_2 are −66.5 and +32 kcal/mol, respectively. The formation energy of CuS is endothermic, but that of FeS_2 is exothermic. The formation of CuS from $Cu_{1-2}S$ (released sulfur partially) occurs at relatively low temperature.

Activation Energies on Sulfur Adsorption. In general, the specific surface area is estimated by means of powder activity. In this experiment the copper

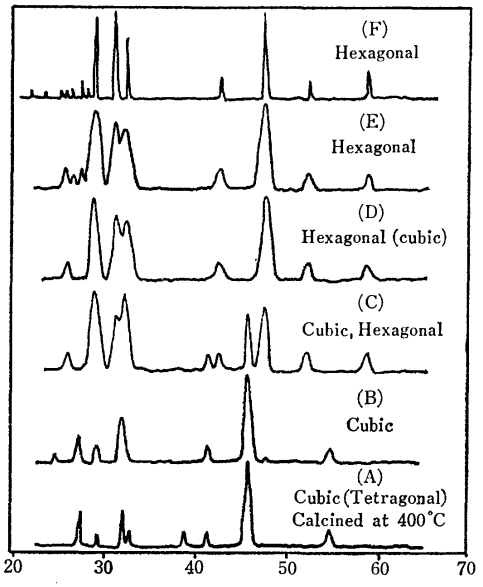

Fig. 7. X-Ray profiles of $Cu_{1-2}S$ at various sulfur adsorption temperatures of starting $Cu_{1.80}S$.
Adsorption time: 60 min, solvent: toluene.
A: Starting $Cu_{1.80}S$(calcined at 400 °C), B: adsorption temperature 25 °C, C: adsorption temperature 50 °C, D: adsorption temperature 75 °C, E: adsorption temperature 100 °C, F: $Cu_{1.00}S$(before thermal decomposition).

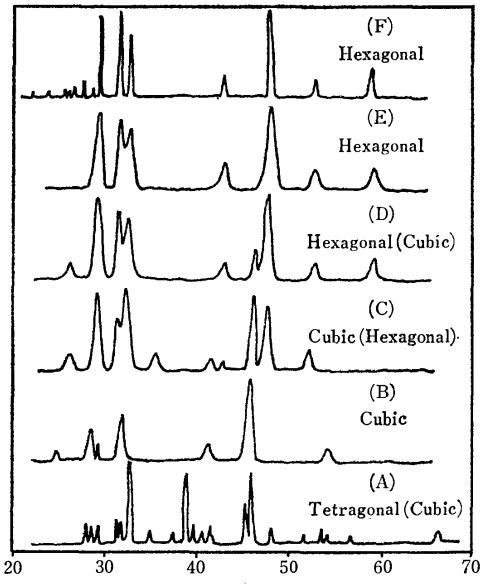

Fig. 8. X-Ray profiles of $Cu_{1-2}S$ at various sulfur adsorption temperatures of starting $Cu_{1.96}S$.
Adsorption time: 60 min, solvent: toluene.
A: Starting $Cu_{1.96}S$(calcined at 500 °C), B: adsorption temperature 25 °C, C: adsorption temperature 50 °C, D: adsorption temperature 75 °C, E: adsorption temperature 100 °C, F: $Cu_{1.00}S$(before thermal decomposition).

sulfide sample calcined at 400 °C gave the same adsorption coefficient as the one at 500 °C, but their crystal structures differ. Activation energies for

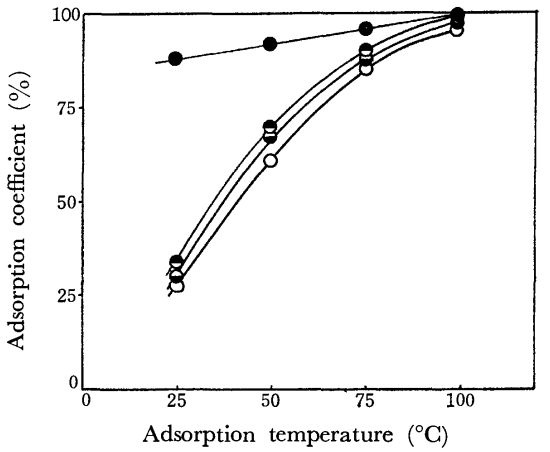

Fig. 9. Adsorption coefficient at various adsorption temperature (Comparison between different calcination temperature about $Cu_{1-2}S$).
Calcination temperature, ●: 250 °C, ◓: 300 °C, ◒: 400 °C, ○: 500 °C.

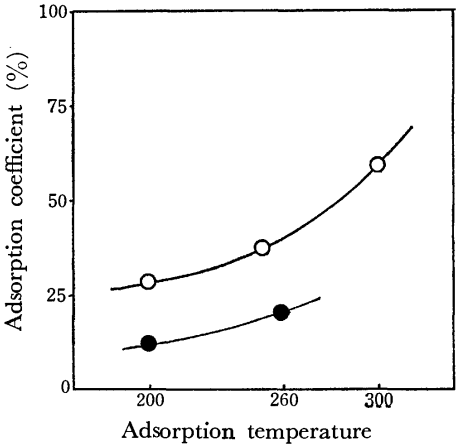

Fig. 10. Comparison of sulfur adsorption coefficient of FeS_{1-2} between different calcination temperature of 540 (○) and 800 °C (●).

sulfur adsorption were calculated from the adsorption kinetics of copper sulfides calcined at 400 and 500 °C and of iron sulfides calcined at 540 and 800 °C. The Arrhenius plots of sulfur adsorption on copper and iron sulfides are shown in Figs. 11 and 12, respectively. The activation energies of copper sulfides are 12.7 and 9.7 kcal/mol for the two calcination temperatures. The results show that the sample calcined at 400 °C is more stable than the one calcined at 500 °C. This suggests that the thermally decomposed sample which is more stable on thermal decomposition is less active for the reverse reaction, that is, sulfur adsorption. The specific surface area is an important factor for the facility of sulfur adsorption. The crystal strain or distortion seems to influence the sulfur adsorption. In order to estimate the effect of the surface area on reactivity, the activity of partially decomposed sulfide was defined as the product of unit formula weight per specific surface area and reciprocal of activation energy. The values estimated for copper sulfides calcined at 400 and 500 °C are 1.73×10^{-6} and 1.83×10^{-6} mol²/kcal·m², respectively. This suggests

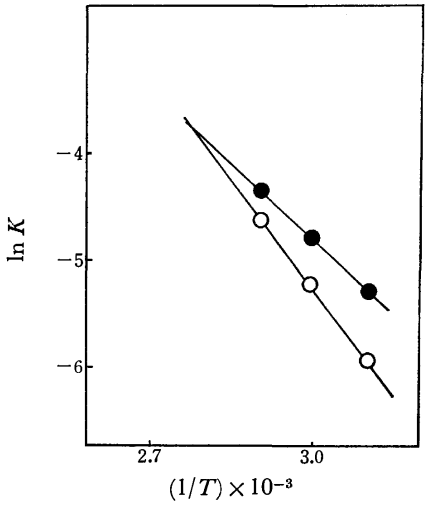

Fig. 11. Arrhenius plots of sulfur adsorption rates of $Cu_{1.80}S$, (○, calcined at 400 °C) and $Cu_{1.96}S$, (●, calcined at 500 °C).

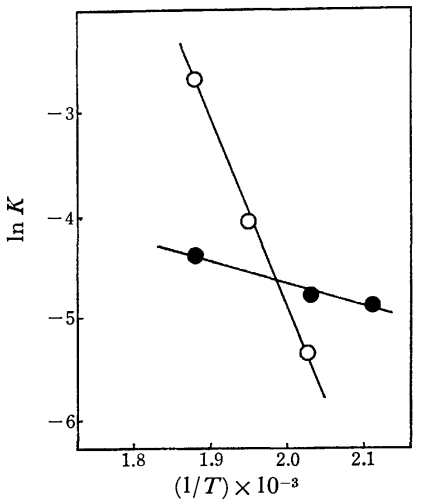

Fig. 12. Arrhenius plots of sulfur adsorption rates of $Fe_{0.64}S$ (○, calcined at 540 °C) and $Fe_{1.02}S$ (●, calcined at 800 °C).

that the sample calcined at 400 °C (cubic $Cu_{1.80}S$) is more stable than that calcined at 500 °C (mixed structure of cubic and tetragonal). Arrhenius plots of sulfur adsorption on iron sulfides calcined at 540 and 800 °C are shown in Fig. 12. The activation energies are 36.9 and 4.3 kcal/mol, respectively. This suggests that different adsorption mechanisms exits for the two species of iron sulfides. The sample calcined at 800 °C, in which the number of empty sites for bonding sulfur is large, has a low activation energy for the sulfur adsorption. This suggests that the diffusion of sulfur vapor is the rate-determing step in the adsorption kinetics.

Comparison with Active Carbon Used. The sulfur adsorbed on active carbon was washed out completely with CS_2. The amount of adsorbed sulfur was negligible. In the case of thermally decomposed copper sulfides the bond between sulfur and copper is chemical, but not that between sulfur and carbon.

Sulfur Adsorption in Heavy Oil on Thermally Decomposed Sulfide. A comparison of the sulfur contents and the desulfurization percentage of heavy oil by different treatment is given in Table 2. The heavy oil oxidized only with SO_2 has a higher sulfur content 1.61%, its desulfurization percentage being negative (−13.4%). The heavy oil washed with 5% H_2O_2 shows a 1.25% sulfur content decrease, the desulfurization percentage increasing by 12%. Asdorption on thermally decomposed copper sulfide ($Cu_{1.96}S$) gave the lowest sulfur content (1.13%) and the highest desulfurization percentage (20.4%). Results of a blank test without SO_2 gas treatment are given in Table 3. Adsorption by $Cu_{1.96}S$ as an adsorbent indicates 1.43% sulfur, almost the same value as in the case of no treatment. A comparison of the data given in Tables 2 and 3 shows the obvious effect of SO_2 on desulfurization. However, at 300 °C in an autoclave the sulfur content shows a slight decrease (Table 3). In copper sulfide after adsorption treatment partial existence of Cu(II)S was observed by means of X-ray diffraction (Table 2). It seems that the thermally decomposed copper sulfide does not react with sulfur compounds in heavy oil, but reacts with the free sulfur formed by SO_2 oxidation in heavy oil. The desulfurization percentage 20% is low for practical use. However, a higher percentage is expected by selection of temperature, pressure, mixing mole ratio, and by repetition of SO_2 oxidation and adsorption.

Table 2. Comparison of desulfurization percentage between two different treatments of B-class heavy oil being oxidized with SO_2 gas in autoclave

Treatment	Sulfur content (%)	Desulfurization percentage
No treatment	1.61	−13.4
Washing out with 5% H_2O_2	1.25	+12.0
Adsorption by $Cu_{1.96}S$	1.13	+20.4

Table 3. Blank test without SO_2 gas treatment

Treatment	Sulfur content (%)
No treatment (starting B-class heavy oil)	1.42
Washing out with 5% H_2O_2	1.24
Adsorption by $Cu_{1.96}S$ at atmospheric pressure	1.43
Adsorption by $Cu_{1.96}S$ with heating in micro-autoclave	1.37

The author wishes to express his thanks to Profs. K. Matsuoka and J. Yamasaki for valuable suggestions and to Messrs. S. Kanahara, M. Okazaki, M. Horibe, T. Kuroki, and A. Ishihara for their assistance.

References

1) G. V. Samsonov and S. V. Drozdova, "Sulfide" Moskva, Metallrurdija, (1972).
2) F. D. Richardson and J. H. E. Jeffes, *J. Iron Steel Inst.*, **171**, 162 (1952).
3) A. D. Titarenko, *Fiz. Khim. Tekhnol.*, Sb. Mater. Nauch. Tekh. Konf. Rab. Nauki Proizeod, 124—8, 1968 (Pub. 1969).
4) E. Sudo, *Nippon Kagaku Zasshi*, **75**, 100 (1954).

Solvochromism and Thermochromism of Cobalt(II) Complexes Solubilized in Reversed Micelles

Junzo SUNAMOTO* and Tomiko HAMADA

Department of Industrial Chemistry, Faculty of Engineering, Nagasaki University, Nagasaki 852

(Received March 2, 1978)

Configurational change takes place between tetrahedral and octahedral species, when cobalt(II) complexes are cosolubilized in reversed micelles formed by the cationic or ampholytic detergents in chloroform. This is accompanied by the elimination-addition reaction of ligand water from and to the metal ion in the reversed micellar core. The phenomenon is interpreted in terms of solvochromism and thermochromism. The nature and state of "*naked*" metal ion and "*free*" water molecule afforded in a highly restricted field of reversed micelles have been discussed on the basis of equilibrium constants and thermodynamic parameters for the configurational change, particular attention being given to the structure of micelles. Their resemblance to the active site of metalloenzymes is also discussed.

The resemblance of reversed micelles to hydrophobic pockets of enzymes or biomembranes has attracted much attention.[1] One of specific features of the reversed micelles is that some reversed micelles can solubilize a considerably large amount of water in their interior cores. Earlier works on fluorescent properties,[2] relaxation mechanisms in NMR,[3] electronic spectra,[4] and kinetics of reactions occurring in the micellar core[5] have demonstrated that the nature of water solubilized in reversed micelles differs a great deal from that of ordinary bulk water. Careful survey of these studies aroused our interest to investigate the properties of water in various reversed micelles paying particular attention to the coordination chemistry and metal ion catalysis. Elimination and addition of water molecules from and to the metal ion cosolubilized in the reversed micelles should be closely related to the nature of water present in a highly restricted field.

Cobalt(II) ion is only one of d^7 transition metal ions which show relatively easy octahedral-tetrahedral configuration change accompanied by the addition-elimination of ligands.[6] An octahedrally coordinated cobalt(II) ion should have three spin allowed d-d transitions, which are from the ground state, $^4T_1(F)$, to the states $^4T_2(\nu_1)$, $^4A_2(\nu_2)$, and $^4T_1(P)(\nu_3)$. The visible absorption of hexaaquacobalt(II) ion, $[Co(H_2O)_6]^{2+}$, is weak and the aqueous solution shows pale pink color. On the other hand, the visible absorption band of tetrahedrally coordinated cobalt(II) ion lies in the red part of the spectrum, giving intense blue color. This absorption band stems from the d-d transition from the $^4A_2$ ground state to the $^4T_1(P)$ state, and its fine structure results from spin-orbit coupling.[7] The octahedral-tetrahedral configuration change takes place in two ways. When cobalt(II) chloride is dissolved in water, octahedrally coordinated ion is formed. In alcohols or acetone, a blue color due to the tetrahedral species, $CoCl_2L_2$, is observed.[8,10c] This is interpreted in terms of the solvochromic effect. On the other hand, Swift and Connick found evidence of a tetrahedral species, $[Co(H_2O)_4]^{2+}$, near 100 °C by NMR relaxation studies.[9] Aqueous solutions of cobalt(II) chloride and bromide show a reversible color change from pink to violet in the temperature range 100—200 °C.[10] This was discussed in terms of the thermochromic effect.

Wells obtained an interesting result on the interior water pool of phosphatidylcholine micelles in ether by use of cobalt(II) chloride, attention being given to the correlation between the nature of bound water and the activity of phospholipase A_2 on the membrane surfaces.[11] In this work, we have studied the solvochromic and thermochromic behavior of the cobalt(II) complexes and the properties of bound and free water in the restricted field formed by various reversed micelles.

Experimental

Materials. Analytical grade samples of cobalt(II) chloride $CoCl_2 \cdot 6H_2O$, (Wako Pure Chemical Ind. Ltd.) and nitrate, $Co(NO_3)_2 \cdot 6H_2O$, (Nakarai Chemicals Ltd.) were used without further purification. The concentrations of their aqueous solutions were determined by the usual procedures with EDTA.

Commercial hexadecyltrimethylammonium bromide (CTAB)[12] and sodium 1,2-bis(2-ethylhexyloxycarbonyl)-1-ethanesulfonate (AOT)[13] were purified by recrystallization. Dodecylammonium propionate (DAP) was prepared and purified.[14] *N,N*-Dimethyl-*N,N*-dioctadecylammonium chloride (QD) was supplied by the Tokyo Institute of Kao Soap Co., Ltd. Egg lecithin was extracted from egg yolk and purified.[15]

Reagent grade chloroform was distilled and stored over a Linde type 4A molecular sieve, the water content of which being less than 4 ppm. Chloroform was chosen as the solvent since it is the only solvent which affords the completely homogeneous systems of reversed micelles cosolubilizing water and cobalt(II) complexes.

Spectrophotometric Measurements. All the visible and near infrared spectra were measured on a Hitachi 323 or Hitachi 124 recording spectrophotometer equipped with a thermoregulated cell compartment. Three milliliters of the detergent solution (about 0.20 M, M = mol dm^{-3}) in chloroform was placed in a cuvette. After the injection of 3.0 μl of aqueous cobalt(II) solution (about 3.0 M) into the cell, it was shaken on a Vortex mixer and kept in the thermostatted cell compartment for 20 min to attain equilibrium.

Results and Discussion

Solvochromic Effect. In aqueous solution the cobalt(II) ion is octahedrally complexed with water to afford $[Co(H_2O)_6]^{2+}$, giving pink coloration to the

TABLE 1. SPECTRAL DATA FOR TETRAHEDRAL COBALT(II) COMPLEXES IN VARIOUS REVERSED MICELLES

Micelles[a]	DAP		QD		CTAB		AOT		EL[c]		In water	
Salt[b]	I	II	I	II	I	II	I	II	I	II	I	II
Doublets cm^{-1} (ε)											20200[d] (5)	20200[d] (5)
ν_3 Band cm^{-1} (ε)	19200 (127)$_{sh}$	19200 (119)$_{sh}$	18700 (9)	18700 (8)	14600 (479)	15400 (324)	18900 (10)	18900 (13)	17200 (9)	18300 (1)		
	17200 (177)	17200 (165)	15700 (474)	15700 (443)	14400 (550)	14900 (716)			16700 (12)	17200 (1)		
			14300 (738)	14300 (670)	13900 (801)	14100 (1000)			16200 (13)	16700 (1)		
						13700 (1105)			15700 (14)	15900 (1)		
									15300 (14)			
ν_2 Band cm^{-1} (ε)	8403 (26)	8403 (20)	6061—4202 (92.3—69.2)	5917 (91.8)	5814—4255 (88.8)	5848—4545 (115.6)			7037—5128 (14)	4505 (1.4)	7843 (1.4)	7843 (1.4)
	4505 (16)	4878—4651 (14)		5348 (91.8)		4274 (115.6)					6494 (1.2)	6711—6494 (1.2)
	4444 (16)	4464 (19)		4808—4545 (61.2)								
	4255 (18)			4274 (20.4)								

a) Concentrations of water and detergent are 55.5×10^{-3} and 0.20 M, respectively, in all runs. b) I: $CoCl_2$, II: $Co(NO_3)_2$. c) EL stands for egg lecithin. d) Octahedral complex.

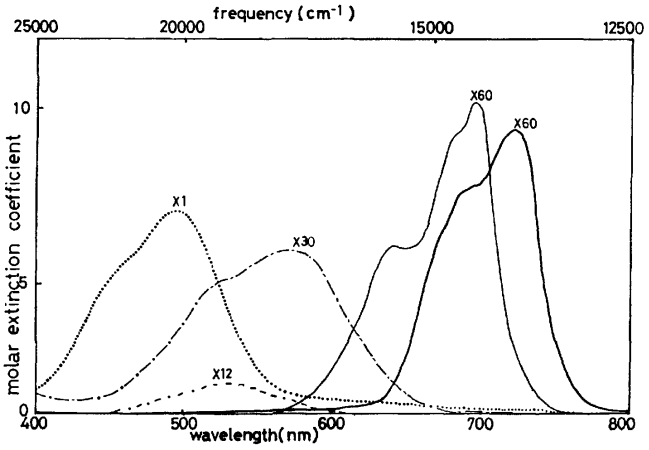

Fig. 1. Visible spectra of $CoCl_2$ in pure water (·····) and in reversed micelles formed by AOT (----), DAP (— - —), QD (——), and CTAB (——) in chloroform at 25 °C.

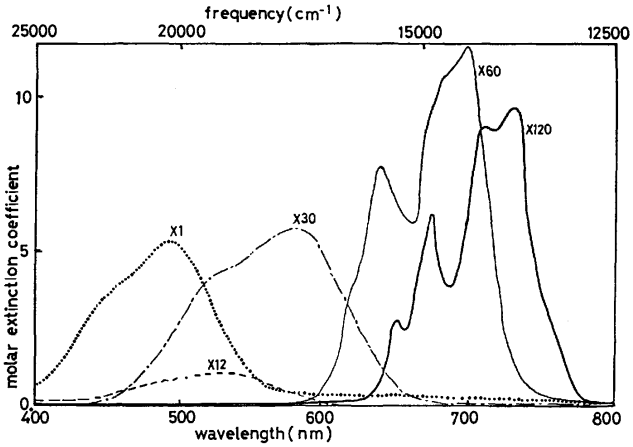

Fig. 2. Visible spectra of $Co(NO_3)_2$ in pure water (·····) and in reversed micelles formed by AOT (----), DAP (— - —), QD (——), and CTAB (——) in chloroform at 25 °C.

solution. When the concentrated aqueous solution of $CoCl_2$ or $Co(NO_3)_2$ is injected into the solutions of certain detergents in chloroform, it is readily dissolved, giving intense blue or violet solutions. Their visible spectra differ with detergent. When the cobalt(II) ion is cosolubilized in the DAP reversed micelles, the coloration is violet, while in the CTAB or QD micelles it is intensely blue. However, in AOT micelles, no color change from pink to blue is observed due to the cosolubilization of the cobalt(II) ion. In the anionic reversed micelles such as AOT, it is possible that the detergent molecules themselves coordinate to the metal ion forming stable octahedral complexes. The spectra in different reversed micelles are shown in Figs. 1 and 2. Spectral data are summarized in Table 1 for cobalt(II) chloride and nitrate.

The visible spectra of the cobalt(II) complexes in the CTAB or QD reversed micelles closely resemble those for the tetrahedral complex, $[CoX_4]^{2-}$, as reported by Cotton and his co-workers.[7] These cationic detergents carry halogen as counter anions. Thus the species formed in the micellar core may be $[CoBr_4]^{2-}$

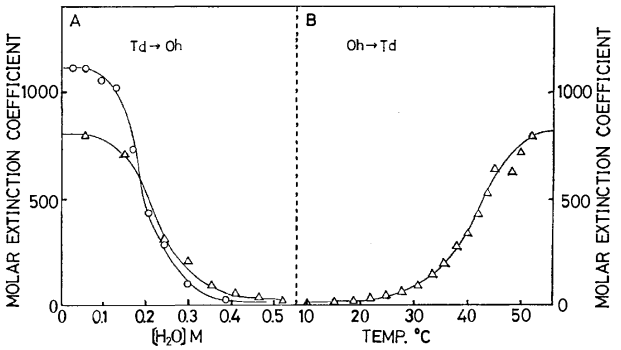

Fig. 3. The solvochromic effect with water (A) and thermochromic effect (B) for the configurational change of cobalt(II) complexes in the CTAB reversed micelles. —○—; $Co(NO_3)_2$, —△—; $CoCl_2$.

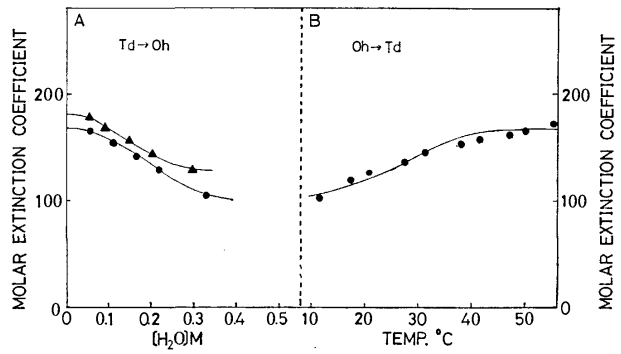

Fig. 4. The solvochromic effect with water (A) and thermochromic effect (B) for the configurational change of cobalt(II) complexes in the DAP reversed micelles. —▲—; $CoCl_2$, —●—; $Co(NO_3)_2$.

in the CTAB micelles and $[CoCl_4]^{2-}$ in the QD micelles. However, in view of the slight difference between the visible spectra of cobalt(II) chloride and nitrate in the CTAB micelles, we can not disregard the possibility of the coexistence of other mixed complexes[10c] such as $[Co(NO_3)_2Cl_2]^{2-}$, $[Co(NO_3)_2Br_2]^{2-}$, or $[CoCl_2Br_2]^{2-}$. The structures of complexes formed in each case can not be clarified at present. Contrary to what would be expected from the cloud expanding effect of ligands, halide ions are more strongly coordinating to the metal ion pushing away water molecules in the reversed micellar core.[16] This would be responsible for the effect of the very restricted field of the reversed micelles. Antipora-Karataeva and Vainshtein observed a similar phenomenon in different solvents such as methanol, ethanol, acetone, and ethyl methyl ketone, and pointed out the importance of chloride ion since solutions of $Co(NO_3)_2$ never become blue.[17] We found that even nitrate shows exactly the same phenomenon as that observed with chloride (Figs. 1 and 2).

When water is added to the reversed micelles cosolubilizing metal ions, the blue or violet color fades as reflected by the decrease in the molar absorbancy of the tetrahedral complex. Finally the solution becomes pale pink again, indicating the reproduction of an octahedral species. This configurational change from the tetrahedral complex to the octahedral one causes the spectral change with isosbestic points. As seen in Figs. 3-A and 4-A, configurational changes occur sigmoidally with water concentration. With both DAP and CTAB micelles, inflection points were observed around the point where the molar ratio of water to the detergent molecule is about unity. Inflection was more enhanced in the cationic CTAB reversed micelles than in the DAP micelles. The most plausible mechanism for the phenomena can be interpreted by the "two step hydration mechanism."[3,11] When water is first introduced into the reversed micelles, water tends to interact more strongly with the polar head group of the detergent rather than with the metal ion. Upon completion of the first hydration in the micellar core, water molecules start to coordinate to the metal ion, affording a octahedral complex with a concomitant decrease in intensity in red region of visible spectra. The strength of interaction of water in the first hydration stage with detergents should be affected by the kind of detergent molecule. Water molecules in the second hydration stage would behave differently from those of the first, *i.e.*, those tightly bound to detergents. The hydrolysis of norleucine *p*-nitrophenyl ester was significantly promoted by the copper(II) ion in the AOT reversed micelles.[18] The catalytic effect becomes maximum at the point where the water content is almost equivalent to the detergent concentration. When water concentration is less than that at the maximum, the formation constants of the complex between the copper(II) ion and substrate are surprisingly large ($\log K_f$=8—9 at 25 °C). At the maximum of catalytic effect in the reversed micelles, nucleophilic rate constants with water k_{H_2O} increase by about 10^3-fold as compared with those in bulk water.[18] This is closely related to the configurational change of metal complex in the reversed micelles. During the course of first hydration stage, the metal ion can easily form a complex with the substrate ester using vacant coordination sites of the metal ion. In the second hydration stage, water molecules start to coordinate to the metal ions or attack the substrate activated on complex formation with the metal ion. The "free" water molecules should be very reactive. The water further added in the second hydration stage finally tends to resemble pure bulk water.[3,11] A similar conclusion regarding the state of water in the AOT reversed micelles has recently been attained by Wong and his co-workers in NMR relaxion studies of water.[3]

Thermochromic Effect. When the pink solution was warmed after the completion of second hydration in the reversed micellar sphere, the intensely blue color appeared again. The thermochromism looks like a mirror image of the solvochromism shown in Fig. 3. The configurational change between the tetrahedral and octahedral complexes with temperatures was certainly reversible; upon cooling the solution, the original pink color appeared again. It is noteworthy that in the reversed micellar systems the reversible change of configuration occurs even at 10—60 °C, while much higher temperatures are necessary in aqueous solutions.[9,10]

Evaluation of Equilibrium Constant. The configu-

TABLE 2. EQUILIBRIUM CONSTANTS AND THERMODYNAMIC PARAMETERS FOR THE CONFIGURATIONAL CHANGE OF THE COBALT(II) COMPLEXES IN REVERSED MICELLES

In DAP reversed micelles;

$$\underset{T_d}{CoL_2X_2} + 2L \overset{K_1}{\rightleftharpoons} \underset{O_h}{CoL_4X_2}$$

$\ln K_1 = 1.17 \pm 0.18$ (25 °C) for chloride
$\ln K_1 = 1.10 \pm 0.06$ (25 °C) for nitrate
$\Delta G^0 = -0.69 \pm 0.11$ kcal mol^{-1}
$\Delta H^0 = -10.8 \pm 0.3$ kcal mol^{-1}
$\Delta S^0 = -33.6 \pm 1.0$ e.u.

In CTAB reversed micelles;

$$\underset{T_d}{[CoX_4]^{2-}} + 2L \overset{K_2}{\rightleftharpoons} \underset{O_h}{[CoX_4L_2]^{2-}}$$

$\ln K_2 = 6.64 \pm 0.50$ (25 °C) for nitrate
$\ln K_2 = 6.23 \pm 0.22$ (25 °C) for chloride
$\Delta G^0 = -3.69 \pm 0.13$ kcal mol^{-1}
$\Delta H^0 = -27.2 \pm 0.7$ kcal mol^{-1}
$\Delta S^0 = -72.2 \pm 2.2$ e.u.

rational change of the cobalt(II) complexes in the reversed micelles can be classified as follows.

(I) In the DAP micelles:

$$\underset{T_d}{CoL_2X_2} + 2L \overset{K_1}{\rightleftharpoons} \underset{O_h}{CoL_4X_2}, \quad (1)$$

where L is water and X is the halide ions or NO_3^-.

(II) In the CTAB micelles:

$$\underset{T_d}{[CoX_4]^{2-}} + 2L \overset{K_2}{\rightleftharpoons} \underset{O_h}{[CoX_4L_2]^{2-}}. \quad (2)$$

In the CTAB or QD micelles, other mixed complexes such as $[CoX_2Y_2]^{2-}$ or $[CoX_2Y_2L_2]^{2-}$ may be formed. Even if this is the case, the equilibrium of addition-elimination of water will be essentially similar to Eq. 2. Equilibrium constants K_1 and K_2 for the addition reactions (Eqs. 1 and 2) could be calculated by the procedure of Sacconi *et al.*[19]

$$K_1 = \frac{[CoL_4X_2]}{[CoL_2X_2][L]^2} \quad (3)$$

$$K_2 = \frac{[CoX_4L_2{}^{2-}]}{[CoX_4{}^{2-}][L]^2} \quad (4)$$

Modifying these we get the following equation which will be valid for different water concentrations:

$$\ln \frac{1-\alpha}{\alpha} = \ln K - 2 \ln [L]_f, \quad (5)$$

where α is the fraction of the tetrahedral complex of the total concentration of cobalt(II) ion adopted and $[L]_f$ is the concentration of the "free" ligand, the difference between the concentration of water initially added and twice the concentration of the adduct, the octahedral species. Figure 5 shows the reliability of equilibria 1 and 2. The maximum of the $\approx$17200 cm^{-1} band of the tetrahedral complexes was used for the concentration measurement. Corrections for the overlap by the absorption of the octahedral complexes are negligible because of the very much smaller molar extinction coefficients of the octahedral complexes (Table 1). From a comparison of the respective equilibrium constants for the two different types of micellar systems (Table 2), it seems that the second hydration occurs more easily in the CTAB reversed micelles than in the DAP micelles.

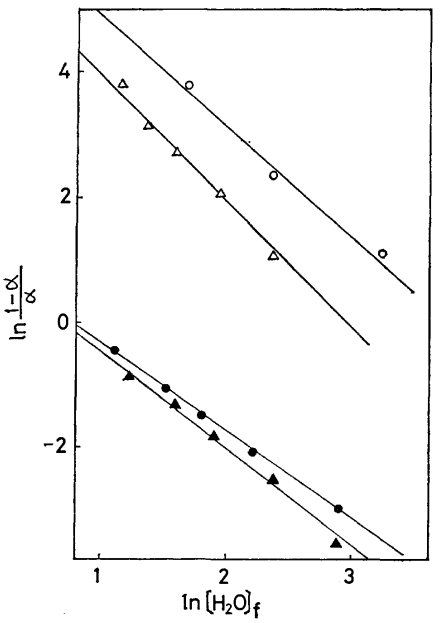

Fig. 5. Plots of $\ln (1-\alpha)/\alpha$ against $\ln [H_2O]_f$ related with the Eq. 5 in the text; $Co(NO_3)_2$(○) and $CoCl_2$(△) in the CTAB reversed micelles; $Co(NO_3)_2$(▲) and $CoCl_2$(●) in the DAP reversed micelles.

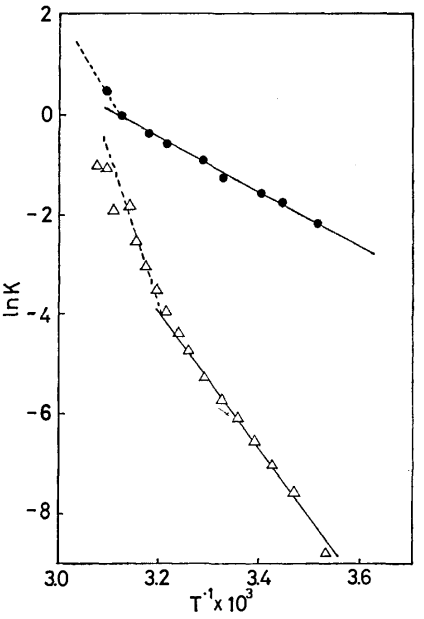

Fig. 6. Plots of $\ln K$ against $1/T$ for the thermochromism in the DAP reversed micelles cosolubilizing $Co(NO_3)_2$(●) and in the CTAB reversed micelles cosolubilizing $CoCl_2$(△).

The standard molar thermodynamic parameters are evaluated by means of the usual relationships $\Delta G^0 = -RT \ln K = \Delta H^0 - T \cdot \Delta S^0$ using the data of thermo-

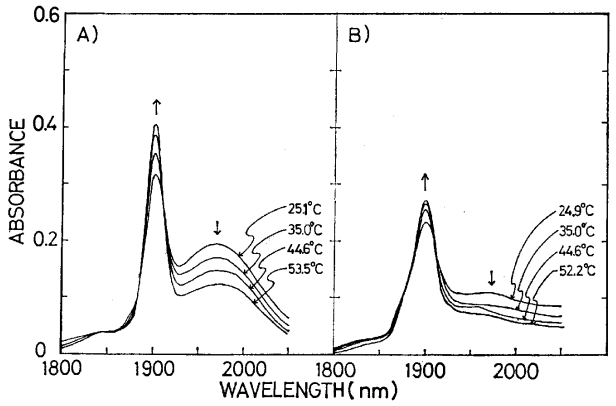

Fig. 7. The temperature effect on the near infrared spectra of water (0.203 M) solubilized in the 0.20 M CTAB (A) and in the 0.20 M DAP (B) reversed micelles formed in chloroform at different temperatures.

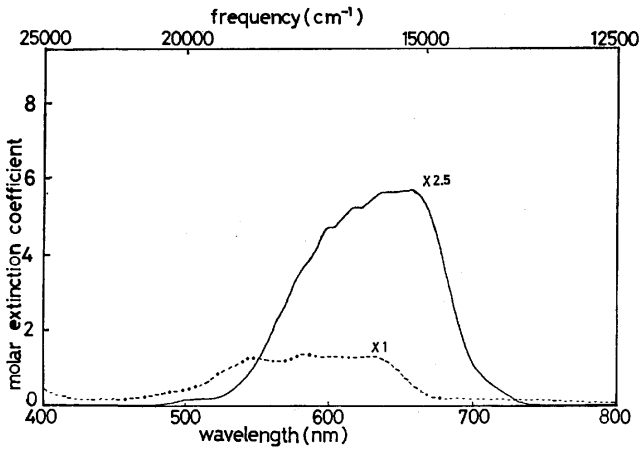

Fig. 8. Visible spectra of $CoCl_2$(——) and $Co(NO_3)_2$ (----) cosolubilized in the egg lecithin reversed micelles at 25 °C.

chromism for the configurational change. The results are given in Fig. 6 and parameters evaluated in Table 2. The data indicate that the addition reaction of water on the tetrahedral complex to afford the octahedral one is energetically more favorable in the CTAB micelles than that in the DAP micelles ($\Delta\Delta H^0 \fallingdotseq 16$ kcal mol^{-1}). On the basis of unfavorable entropy, on the other hand, we can imagine that the CTAB micelles may provide the more rigid hydration shell than the DAP micelles ($\Delta\Delta S^0 \fallingdotseq 38$ e.u.). Negative values of ΔG^0 are essential to form the more stable octahedral complexes. The values of parameters strongly resemble those obtained for the configurational equilibrium[10c] between Co(isoquinoline)$_2$Cl$_2$ and Co(isoquinoline)$_4$Cl$_2$,[20] Co(py)$_2$X$_2$ and Co(py)$_4$X$_2$[21,22] in chloroform, or $[Co(H_2O)_4]^{2+}$ and $[Co(H_2O)_6]^{2+}$ in aqueous solution.[23] Plots of $1/T$ against $\ln K$ indicate the presence of two energetically distinct equilibria. It was more obvious in the CTAB reversed micellar systems. The equilibrium in the partition of water molecules between the micellar core and bulk phase may play a role.

The near infrared spectra of water in the CTAB and DAP reversed micelles were determined over the range 1800—2000 nm. The water solubilized in the reversed micelles shows a relatively sharp band at 1902 nm and a broad band around 1970—1980 nm. The former band is ascribed to the free water dispersed in the bulk phase, and the latter to the water strongly bound to detergent molecules.[24] With temperature rise from 25 to 55 °C, the intensity of the band of free water increases, while that of the bound water decreases (Fig. 7). Rise in temperature causes the increase in the mobility of the water molecule encapsulated in the micellar core, resulting in easier dispersion into the bulk phase of organic solvent. The temperature effect on the equilibrium depends on the kind of micelle. It is more drastic in the CTAB micelles than in the DAP micelles. The results are in line with those observed in the thermochromism of the cobalt(II) complexes. The infrared spectra of the CTAB micellar system are sharper, relative amounts of bound water in the micellar core to those of free water in bulk appearing to be larger in the CTAB micelles than in the DAP ones.

The IR data might reflect the fact that in the micellar sphere the water interacts more strongly with CTAB than with DAP. The behavior of water molecules in the micelles closely correlates with the thermochromism and solvochromism of the cobalt(II) complexes.

Egg Lecithin Reversed Micelles. In all the reversed micelles except for egg lecithin micelles, no specific difference was observed in visible spectra between the chloride and nitrate. In the egg lecithin reversed micelles, however, there is much difference, especially in absorption maximum, as shown in Fig. 8. When cobalt(II) chloride was cosolubilized in the egg lecithin micelles, it gave a blue solution with a broad absorption at 620—670 nm, which was identical with the result in the phosphatidylcholine micelles obtained by Wells.[11] When nitrate was introduced into the same micelles, on the other hand, the broad absorption was observed at 540—640 nm range, its molar absorptivity being relatively small. In both cases, however, solvochromism and thermochromism were observed, though not distinctly.

We might conclude that in a very restricted field formed by reversed micelles, specifically reactive water molecule and "*naked*" metal ion can be afforded, where the situation resembles the hydrophobic pocket of metalloenzymes.

References

1) J. H. Fendler and E. J. Fendler, "Catalysis in Micellar and Macromolecular Systems," Academic Press, New York (1975); J. H. Fendler, *Acc. Chem. Res.*, **9**, 153 (1976); J. Sunamoto and H. Kondo, *Yukagaku*, **26**, 389 (1977).

2) U. K. A. Klein, D. J. Miller, and M. Hauser, *Spectrochim. Acta, Part A*, **32**, 379 (1976), Ref. 13.

3) M. Wong, J. K. Thomas, and T. Nowak, *J. Am. Chem. Soc.*, **99**, 4730 (1977).

4) M. Senō, K. Araki, and S. Shiraishi, *Bull. Chem. Soc. Jpn.*, **49**, 899 (1976).

5) C. J. O'Connor, E. J. Fendler, and J. H. Fendler, *J. Chem. Soc., Dalton Trans. 1*, **1974**, 625.

6) F. A. Cotton and G. Wilkinson, "Advanced Inorganic Chemistry, A Comprehensive Text," 2nd ed, John Wiley &

Sons, New York (1972), Part III, Chap. 29.
7) F. A. Cotton, D. M. L. Goodgame, and M. Goodgame, *J. Am. Chem. Soc.*, **83**, 4690 (1961).
8) W. C. Nieuwpoort, G. A. Wesselink, and E. H. A. M. van der Wee, *Recl. Trav. Chim. Pays-Bas*, **85**, 397 (1966).
9) T. J. Swift and R. E. Connick, *J. Chem. Phys.*, **37**, 307 (1962).
10) a) T. Katsurai and K. Sone, *Kolloid-Z.*, **163**, 70 (1959); b) M. Kato, T. Katsurai, K. Sone, and S. Utsuno, *Z. Phys. Chem. Neue Folge*, **35**, 348 (1962); c) K. Sone, Y. Fukuda, J. Mizusaki, and K. Moriyama, *Monatsh. Chem.*, **107**, 271 (1976).
11) M. A. Wells, *Biochemistry*, **13**, 4937 (1974).
12) E. F. Duynstee and E. Grunwald, *J. Am. Chem. Soc.*, **81**, 4540 (1959).
13) M. Wong, M. Grätzel, and J. K. Thomas, *J. Am. Chem. Soc.*, **98**, 2391 (1976).
14) A. Kitahara, *Bull. Chem. Soc. Jpn.*, **28**, 234 (1955); H. Kondo, K. Fujiki, and J. Sunamoto, *J. Org. Chem.*, **43**, 3584 (1978).
15) W. S. Singleton, M. S. Gray, M. L. Brown, and J. L. White, *J. Am. Oil Chem. Soc.*, **42**, 53 (1965); J. Sunamoto, H. Kondo, and A. Yoshimatsu, *Biochim. Biophys. Acta*, **510**, 52 (1978).
16) L. E. Orgel, "An Introduction to Transition-Metal Chemistry Ligand-Field Theory,' John-Wiley & Sons, New York (1967), p. 125.
17) I. I. Antipova-Karataeva and E. E. Vainshtein, *Zh. Neorg. Khim.*, **6**, 816 (1961).
18) J. Sunamoto, H. Kondo, and K. Akimaru, *Chem. Lett.*, **1978**, 821.
19) L. Sacconi, G. Lombardo, and P. Paoletti, *J. Chem. Soc.*, **1958**, 848.
20) H. C. A. King, E. Körös, and S. M. Nelson, *J. Chem. Soc.*, **1964**, 4832.
21) H. C. A. King, E. Körös, and S. M. Nelson, *J. Chem. Soc.*, **1963**, 5449.
22) S. M. Nelson and T. M. Shepherd, *J. Chem. Soc.*, **1965**, 3284.
23) T. J. Swift, *Inorg. Chem.*, **3**, 526 (1964).
24) O. D. Bonner and Y. S. Choi, *J. Phys. Chem.*, **78**, 1723 (1974); Ref. 4.

Monolayer Properties of Mixtures of Poly(octadecyl methacrylate) and Poly(butyl methacrylate) and Their Corresponding Copolymers†

Satoshi Yoshikawa,* Minoru Ueno, and Kenjiro Meguro
Department of Chemistry, Faculty of Science, Science University of Tokyo, 1-3 Kagurazaka, Shinjuku-ku, Tokyo 162
(Received March 10, 1978)

The monolayer properties of mixtures of poly(octadecyl methacrylate) and poly(butyl methacrylate) have been compared with those of their corresponding copolymers of octadecyl methacrylate and butyl methacrylate, using the measurements of their surface pressure-area isotherms at the air/water interface at 20 °C. The results showed that the isotherms of the mixed monolayers had three break points, and the surface pressures of the lower two break points agreed with those of poly(butyl methacrylate). This suggests that at lower surface pressures, the mixtures of the two homopolymers are compatible in a bidimensional state when each phase contains a small amount of the other homopolymer, and otherwise these are incompatible, while at higher surface pressures, up to 70 segment mol% of poly(octadecyl methacrylate) they are incompatible and above 80%, they are compatible. The copolymers showed characteristic isotherms different from those of the mixtures. The properties of the copolymers in the bidimensional state are affected by variations in the vitrified, liquid, or crystalline states with an increase in the mean lengths of the side chains in the three-dimensional state.

Monolayer studies of polymer mixtures or of copolymers of two kinds of monomers have been reported by many authors.[1–10] Kargin *et al.*[1] investigated the monolayer properties of the copolymers of methyl acrylate and hexadecyl acrylate in order to study the influence of the side chain at the air/water interface. Isemura *et al.*[2] showed that surface pressure-area isotherms of the copolymer monolayers of vinyl acetate and vinyl stearate above 50% of vinyl stearate content were almost consistent with the isotherm of poly(vinyl stearate), due to the strong cohesive interaction of octadecyl groups.

However, there have been few studies[3] about the difference of monolayer properties between copolymerized substances from two kinds of monomers, one of which has very long side chains and the other short ones, and mixtures of the corresponding two pure homopolymers.

In this paper, we have studied the monolayer properties of the mixtures of poly(octadecyl methacrylate) and poly(butyl methacrylate) (abbreviated as POMA and PBMA, respectively) and those of the copolymers of octadecyl methacrylate and butyl methacrylate (abbreviated as OMA and BMA, respectively) by surface pressure measurements. Further, the compatibility of the mixtures and the transition of the copolymers at a bidimensional state will also be discussed.

Experimental

Materials. OMA and BMA were supplied by Kyoei Oil Chemical Co., Ltd. These monomers were purified by reduced pressure distillation (nitrogen atmosphere). POMA, PBMA, and the various corresponding copolymers (abbreviated as COP OB-*n* for copolymer; *n*=segment mol % of OMA) were prepared by radical polymerization at 60 °C under a nitrogen gas flow. α,α′-Azobisisobutyronitrile was used as the initiator and benzene as the solvent. The products were purified by repeated precipitation from their benzene solutions into a large excess of methanol. The purified polymers were dried by the refrigeration method, and then the trace solvent was removed *in vacuo* at room temperature. The average molecular weights of these polymers were determined by viscosity measurements. Their average molecular weights were about 3.85 and 1.22×10^5 (g/mol) for POMA and PBMA, respectively. The composition ratios of the copolymers calculated from the results of the elemental analyses are listed in Table 1 with those of the mixtures (abbreviated as MIX OB-*m* for mixture; *m*=segment mol % of OMA).

Measurements. A modified Wilhelmy-type film balance was used to measure the surface pressure. The apparatus was enclosed in a chamber to allow thermostatic control at 20.0±0.5 °C. The water in the though was kept at 20.0±0.5 °C by circulating the water from the thermostat bath. The trough and the glass barriers were carefully coated with parafin wax. The distilled water used as the substrate had a pH of 5.0—6.0 at 20 °C. The monolayers of two homopolymers and corresponding copolymers were spread on the distilled water from their benzene solutions

Table 1. The composition ratios of copolymers and mixtures

Copolymer	Composition ratio/(segment mol %)	
	OMA	BMA
PBMA	—	100.0
COP OB-20	20.3	79.7
COP OB-45	45.3	54.7
COP OB-63	63.2	36.8
COP OB-82	82.0	18.0
POMA	100.0	—
Mixture	**POMA**	**PBMA**
MIX OB-10	10.0	90.0
MIX OB-20	20.0	80.0
MIX OB-30	30.0	70.0
MIX OB-40	40.0	60.0
MIX OB-50	50.0	50.0
MIX OB-60	60.0	40.0
MIX OB-70	70.0	30.0
MIX OB-80	80.0	20.0
MIX OB-90	90.0	10.0

† A preliminary report of this work was presented at the 34th National Meeting of the Chemical Society of Japan, Hiratsuka, April 1976.

(0.07 g polymer/100 ml) with an Alfa micro syringe. Thirty minutes were allowed for the solvent to evaporate before the start of film compression. The initial spreading area was 1100 (cm^2)/0.035 (mg). The rate of compression was 20.0 (cm^2/min). The measurement of the surface pressure was done at more than 5 min after the stop of every short compression so that the equilibrium was attained. The results were reproducible within the range of experimental errors.

Results and Discussion

1. Surface Pressure-area Isotherms of Pure and Mixed Polymer Monolayers. The surface pressure-area isotherms obtained for the monolayers of POMA, PBMA, and nine pairs of their mixtures with various ratios from 10 to 90 segment mol % of OMA on the water at 20 °C are shown in Fig. 1. The isotherm for POMA exhibited a collapse at high surface pressure of 52.6 (dyn/cm). On the other hand, the isotherm for PBMA exhibited two break points, corresponding to a transition and a complete collapse, at 14.3 and 16.7 (dyn/cm), respectively. POMA and PBMA monolayers gave the limiting areas of 24.8 and 32.8 (Å^2/residue), respectively, and formed a solid-condensed film and a liquid-condensed one, respectively. The monolayer properties characteristic of pure POMA and PBMA obtained here were in rather fair agreement with those obtained by Nakahara *et al.*[11,12] and Wu and Huntsberger,[4] respectively. The isotherms for the mixtures of two homopolymers, shown in Fig. 1, showed shapes similar to those of both POMA and PBMA, and exhibited three break points corresponding to transition or collapse at pressures of about 14, 17, and 44—52 (dyn/cm). For convenience, the three break points are denoted here as (A), (B), and (C) in the order of increasing pressures. Break points (A) and (B) were almost consistent with those for PBMA corresponding to the transition and the collapse at 14.3 and 16.7 (dyn/cm), respectively. On the other hand, break point (C) was located between the collapse pressures of the POMA and the PBMA isotherms. Three break points (A), (B), and (C) of the isotherms for the mixtures can be found clearly at each constant surface pressure up to 70 segment mol % of OMA, as shown in Fig. 2.

On the other hand, the isotherms for the MIX OB-80 and -90 did not show break points (A) and (B) but exhibited only one break point (C) corresponding to the collapse at higher surface pressures, as shown in Fig. 2; the values for their break point (C) increased along the ideal dotted line with an increase in the composition ratios of OMA. Crisp[5] has reported as a bidimensional phase rule that if two components are compatible in the monolayer, the surface pressure of the break point is dependent on the composition, and otherwise it is independent of the composition. It may be supported by this rule that, at higher surface pressures, the mixtures of POMA and PBMA are nearly incompatible up to 70 segment mol % of OMA, while they are compatible above 80% in the bidimensional state, as shown in Fig. 2. Such a phenomenon for the incompatible mixtures has also been reported by Gabrielli[6] and Wu and Huntsberger.[4]

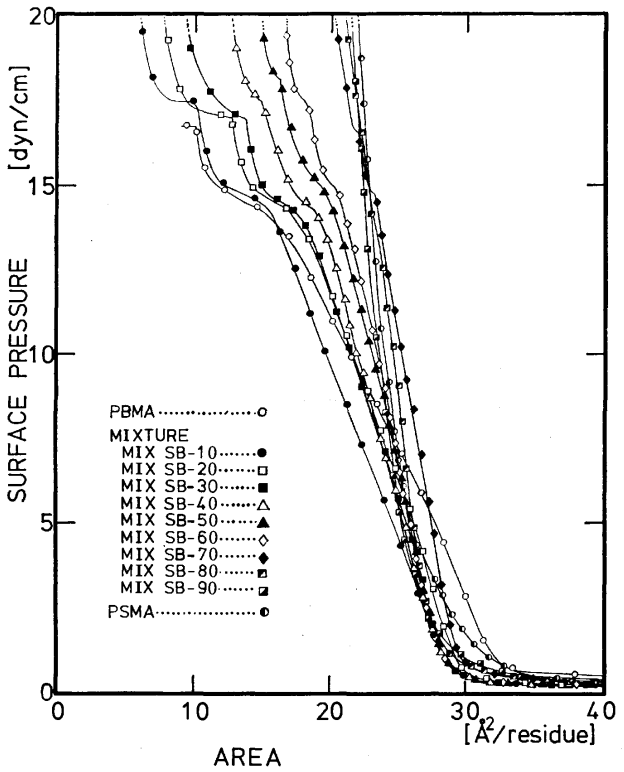

Fig. 1. Surface pressure-area isotherms of PSMA, PBMA, and their mixtures on distilled water at 20 °C.

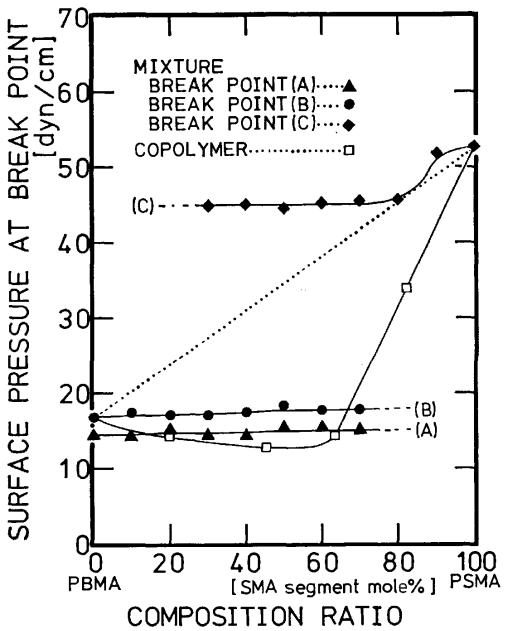

Fig. 2. Surface pressures at break points of copolymers (□) and mixtures (▲, ●, ◆) as a function of composition ratio.

In order to find the precise properties of the mixed monolayers in lower surface pressures, their limiting areas are plotted against the segment molar ratios of POMA in Fig. 3. The limiting areas for the mixtures containing a very small amount of POMA in PBMA exhibited intermediate values between those of POMA and PBMA, and then decreased

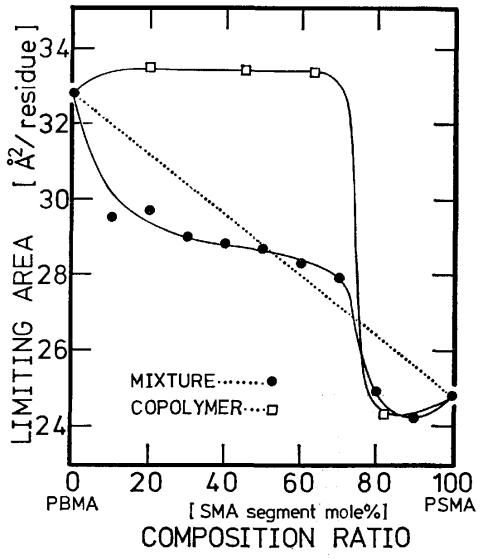

Fig. 3. Limiting areas of copolymers (□) and mixtures (●) as a function of composition ratio.

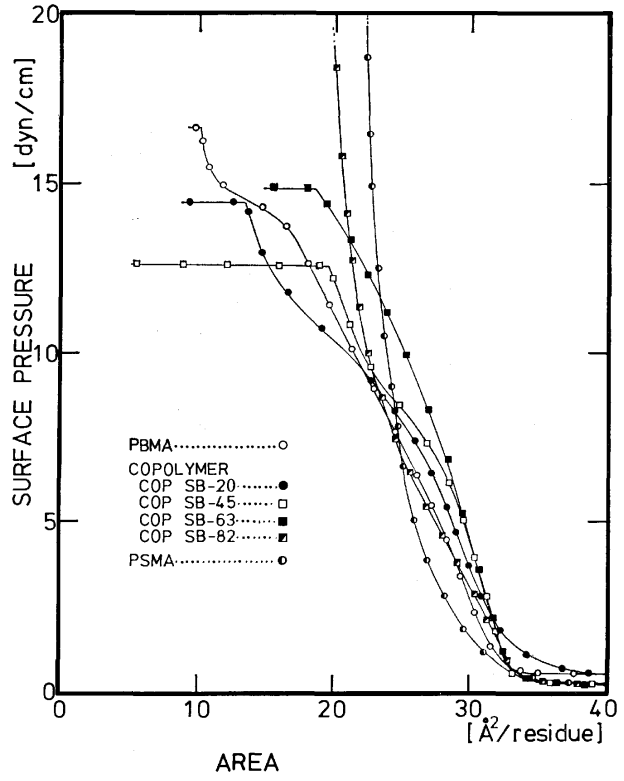

Fig. 4. Surface pressure-area isotherms of PSMA, PBMA, and copolymers of SMA and BMA on distilled water at 20 °C.

slightly with an increase in composition ratios of POMA up to 70 segment mol %. On the other hand, above 80%, their values were almost the same as that of POMA. These results imply that the mixtures containing small amounts of POMA are compatible in a bidimensional state at lower surface pressures, and become gradually incompatible with an increase in composition ratios of POMA up to 70 segment mol %, even at lower surface pressures, as shown in Fig. 3. These findings suggest that the mixed monolayers are gradually separated into one POMA rich film and another PBMA rich one with an increase in surface pressure, and near the collapse pressure of PBMA (break point (B)) the PBMA rich films are squeezed out from the incompatible monolayers, and then the other POMA rich films collapse completely at break point (C).

On the other hand, above 80%, the mixtures are considered to form more stable and compatible films due to the intermolecular cohesive forces of the large amount of octadecyl groups in POMA, at both lower and higher surface pressures, as shown in Figs. 2 and 3.

2. Surface Pressure-area Isotherms of Copolymer Monolayers. The surface pressure-area isotherms for four copolymers with various composition ratios of OMA and BMA on the water at 20 °C are shown in Fig. 4, together with those of POMA and PBMA for comparison. Their isotherms of the copolymers had only one break point, corresponding to the break point (B) or (C) for the mixtures, as shown in Fig. 2, and showed very different shapes from those of binary mixtures of homopolymers. With increasing OMA content of the copolymers the surface pressures corresponding to the break point decreased and then the long plateaus appeared at the break point. Subsequently, above 50 segment mol % of OMA the surface pressures corresponding to the break point increased again rapidly and the plateau disappeared gradually.

Each isotherm of COP OB-20, -45, and -63 formed liquid condensed films, while that of COP OB-82 formed a solid one similar to that of POMA. On the other hand, at the three-dimensional state, PBMA exhibited a vitrified state, and COP OB-20, -45, and -63 exhibited liquid states, while COP OB-82 and POMA exhibited solid cristalline ones at 20 °C. These results suggest that the properties in the bidimensional state are affected by those in the three-dimensional state.

The changes of the monolayer properties of copolymers from liquid condensed to solid states can be seen clearly from the curve in Fig. 2. These results imply that the transition from liquid condensed films to solid ones occurs at about 70 segment mol % of OMA. This transition is also recognized in Fig. 3. Up to 70% of OMA, their limiting areas gave approximately the same values as that of PBMA (32.8 Å²/residue), but above 80% of OMA, COP OB-82 gave the same limiting area as that of POMA (24.8 Å²/residue). From these results, the monolayer of COP OB-82 is considered to form a strongly condensed film, due to the intermolecular and intramolecular cohesive forces among a number of octadecyl groups in the same molecules, and also to have properties similar to the mixture monolayer having the same composition ratio.

Nakahara *et al.*[12] have reported that the poly(*n*-alkyl methacrylate) series form many kinds of films at 20 °C, depending on their side chain lengths, such as liquid ones for poly(nonyl, dodecyl, and tetradecyl

methacrylate), a solid one for POMA, and an intermediate one between liquid and solid state for poly(hexadecyl methacrylate). As COP OB-20, -45, -63, and -82 have the mean lengths of the side chains corresponding to 6.8, 10.3, 12.8, and 15.5 carbon numbers, respectively, their isotherms suggest the changes of the monolayer properties from liquid condensed to solid state due to the difference of the mean lengths of their side chains.

References

1) V. A. Kargin, Yu. M. Melinskii, and S. S. Mendredev, *Dokl. Obsch. Sobr. Akad. Nauk SSSR*, **96**, 307 (1954).
2) T. Isemura, H. Hotta, and T. Miwa, *Bull. Chem. Soc. Jpn.*, **26**, 380 (1953).
3) S. Hironaka, T. Kubota, and K. Meguro, *Bull. Chem. Soc. Jpn.*, **45**, 3267 (1972).
4) S. Wu and J. R. Huntsberger, *J. Colloid Interface Sci.*, **29**, 138 (1969).
5) D. J. Crisp, *Research (London) Suppl. Surface Chem.*, **17**, 23 (1947).
6) G. Gabrielli, *J. Colloid Interface Sci.*, **53**, 148 (1975).
7) D. J. Crisp, *J. Colloid Sci.*, **1**, **49**, 161 (1946).
8) A. Labbauf, *J. Appl. Polym. Sci.*, **10**, 865 (1966).
9) G. Gabrielli, M. Puggelli, and E. Ferroni, *J. Colloid Interface Sci.*, **47**, 145 (1974).
10) M. Puggelli and G. Gabrielli, *J. Colloid Interface Sci.*, **61**, 420 (1977).
11) T. Nakahara, K. Motomura, and R. Matuura, *J. Polym. Sci., Part A-2*, **4**, 649 (1966).
12) T. Nakahara, K. Motomura, and R. Matuura, *Bull. Chem. Soc. Jpn.*, **40**, 495 (1967).

The Study of Solutions of Alkali Halides in Acetone by Means of Vapor-pressure Osmometry and Conductometry

Ha Chung LEE and Yutaka MIYAHARA*
Department of Chemical Engineering, Faculty of Engineering, Nagoya University, Chikusa-ku, Nagoya 464
(Received March 13, 1978)

Vapor-pressure depressions and electric conductivities at 40.3 °C have been measured for LiCl, LiBr, NaI, KI, and RbI in acetone. The greatest care has been taken to minimize the contact of salts and their solutions with air. In order to account for the data of vapor-pressure osmometry (VPO) for lithium salts in acetone, the dissociation-association equilibria of the salts, MX, expressed as

$$M^+ + X^- \rightleftharpoons MX \rightleftharpoons 1/2(MX)_2$$

are proposed. The analysis of the conductance data of LiCl and LiBr, without considering the dimerization of the salts, leads to irrationally large values of the ionic association constants. For LiCl, NaI, and KI, VPO and conductometry give similar values of the dissociation constants, while for LiBr and RbI the agreement is not so satisfactory, though still within a factor of ten.

In a series of papers,[1-4] the vapor-pressure depression of various electrolytes in non-aqueous solutions has been measured by means of a vapor-pressure osmometer (VPO), and the concentration dependence of the activities of the salts has been analyzed, assuming the existence of a dissociation equilibrium.

In the first paper[1] (I) of this series, however, it has been reported that some lithium salts show an anomalous behavior in their acetone solutions. In order to account for it, it was assumed that an association equilibrium is present between the neutral salt molecules and their dimers.

In the present paper, the vapor-pressure depression of LiCl and LiBr in acetone is measured. Great care is taken to prevent moisture from coming in contact with the samples and their solutions, and measurements of the electric conductivity are also carried out in order to examine the existence of the dissociated ions. In order to account for the present data of VPO for lithium salts in acetone, an assumption of the existence of dissociation-association equilibria is proposed. Measurements of the VPO and conductometry for such salts as NaI, KI, and RbI are also made for the sake of reference.

Theoretical

When a salts, MX, dissolved in a non-aqueous solvent exhibits two-step equilibrium of dissociation and association as

$$M^+ + X^- \overset{K_d}{\rightleftharpoons} MX \overset{K_a}{\rightleftharpoons} 1/2(MX)_2 \qquad (1)$$

the Gibbs-Duhem equation becomes

$$\ln a_1 = -(1/N_1)(m_2+2m_4+m_d+2\int_0^{m_4} m_4 \, d\ln\gamma_4), \qquad (2)$$

$$\begin{aligned} m_3 &= m_4 = m\alpha, \\ m_2 &= m(1-\alpha-2\beta), \\ m_d &= m\beta, \end{aligned} \qquad (3)$$

where

a_1: the activity of the solvent,
N_1: the mole number of 1 kg of the solvent,
m: the molality of the salt as-a-whole,
m_2: the molality of undissociated or unassociated salt, MX,
m_3, m_4: the molalities of the M^+ and X^- ions, respectively,
m_d: the molality of the dimer, $(MX)_2$,
α, β: the degrees of dissociation and association respectively,
γ_4: the mean activity coefficient of the ions,
K_d: the equilibrium constant of dissociation,
K_a: the equilibrium constant of association.

In Eq. 2, the activity coefficients of MX and $(MX)_2$ are assumed to be unity. If we assume that the activity coefficients of the ions are represented by the Debye-Hückel limiting law, we obtain

$$2\int_0^{m_4} m_4 \, d\ln\gamma_4 = -\frac{4.604A}{3d_0}(\sqrt{m_4 d_0})\sigma(x), \qquad (4)$$

$$x = Ba_0\sqrt{m_4 d_0}, \qquad (5)$$

$$\sigma(x) = \frac{3}{x^3}\left\{(x+1) - \frac{1}{x+1} - 2\ln(x+1)\right\}. \qquad (6)$$

The notations in these equations are shown in the preceding paper[4] in detail. As in the previous papers, a function, h, defined as

$$h = \frac{N_1 \ln a_1}{m} + 1, \qquad (7)$$

was used for the analysis of the experimental results.

Experimental

Materials. LiCl, LiBr, KI, and RbI used were guaranteed pure-grade reagents supplied by the Merck Co., Ltd. (Germany). Before use, the salts were dried over a period of five days in a vacuum oven at 50 °C with molecular sieves 3 A (1/8 in. pellects). The molecular sieves were renewed each day. The dryness reached by this method was much the same as that obtained by heating in an oven at temperatures as high as 400 °C. The method used in preparing acetone, KCl, and conductivity water was the same as reported in the preceding paper.[4] To avoid the contact of salts and their solutions with moisture in the air, a dry box filled with nitrogen gas was used, as before.

Conductometry and Vapor-pressure Osmometry. The experimental methods were reported in the preceding paper[4] in detail. The measurements were made at 40.3 °C for

Table 1. h values of alkali halides in acetone at 40.3 °C

$m\times10^2$	h	$m\times10^2$	h	$m\times10^2$	h	$m\times10^2$	h
LiCl		LiCl		LiBr		KI	
0.0719	−0.1928	1.2558	0.0868	1.6477	−0.1251	0.1418	−0.8135
0.0986	0.0707	1.2891	0.1127	1.6552	−0.1279	0.2230	−0.7897
0.1021	−0.0137	1.5049	0.1299	1.6615	−0.1069	0.3729	−0.6725
0.1026	−0.1806	1.5152	0.1105	1.8049	−0.1145	0.3813	−0.6466
0.1033	−0.0015	1.5259	0.1206	1.8110	−0.0951	0.5525	−0.6156
0.1143	−0.1121	1.5774	0.1212	2.0080	−0.0872	0.5901	−0.5777
0.1268	−0.0957	1.6652	0.1178	2.0277	−0.1131	0.7691	−0.5549
0.1271	0.0002	1.7732	0.1182	2.0434	−0.1022	0.7786	−0.5185
0.1362	−0.1933	2.0600	0.1520	2.0842	−0.0849	1.0047	−0.5092
0.1439	−0.0888	2.0862	0.1471	2.2317	−0.0744	1.0581	−0.4888
0.1491	−0.1103	2.1291	0.1546	2.2862	−0.0950	1.2344	−0.4764
0.1844	−0.0823	2.3802	0.1829	2.4141	−0.0686	1.2702	−0.4501
0.1898	−0.0121	2.3888	0.1710	2.4835	−0.0921	1.3015	−0.4716
0.1993	−0.1122	2.4773	0.1851	2.5070	−0.0623	1.3102	−0.4574
0.2010	−0.0590	2.5625	0.1799	2.5194	−0.0817	1.5817	−0.4351
0.2244	−0.0801	2.6041	0.1885			1.6475	−0.4413
0.2477	−0.0622			NaI		1.7746	−0.4074
0.2683	−0.0905	LiBr		0.2017	−0.7761	1.7848	−0.4242
0.2719	−0.0870	0.1802	−0.4139	0.3666	−0.6852	2.0395	−0.3898
0.2748	−0.0973	0.2177	−0.3846	0.3828	−0.7000	2.0419	−0.3983
0.2903	−0.0754	0.2432	−0.2954	0.5826	−0.6134	2.2624	−0.3890
0.3401	−0.0169	0.3472	−0.3026	0.5852	−0.6262	2.2713	−0.3846
0.3896	−0.0243	0.3618	−0.2988	0.8112	−0.5740	2.4953	−0.3646
0.3989	−0.0224	0.4961	−0.2189	0.8176	−0.5437	2.5285	−0.3572
0.4151	0.0105	0.5582	−0.2538	1.0322	−0.5405		
0.4195	0.0347	0.5666	−0.2343	1.0708	−0.5044	RbI	
0.5002	−0.0104	0.6768	−0.2228	1.2558	−0.5016	0.1692	−0.8058
0.5190	0.0091	0.7415	−0.2102	1.2706	−0.4772	0.1782	−0.7880
0.5872	0.0085	0.7828	−0.2007	1.2775	−0.4742	0.3220	−0.6744
0.6129	−0.0031	0.9860	−0.1619	1.3679	−0.4844	0.3602	−0.6494
0.6271	−0.0040	0.9910	−0.1781	1.5909	−0.4602	0.3957	−0.6509
0.7915	0.0664	1.0036	−0.1680	1.6859	−0.4305	0.5794	−0.5844
0.8169	0.0592	1.0224	−0.1783	1.7895	−0.4403	0.6053	−0.5869
0.8181	0.0499	1.1772	−0.1439	1.9047	−0.4199	0.6277	−0.5624
0.8188	0.0651	1.1829	−0.1569	1.9961	−0.4230	0.8081	−0.5303
0.8274	0.0533	1.2504	−0.1550	2.0510	−0.4036	0.8247	−0.5160
0.9281	0.0414	1.2850	−0.1501	2.2351	−0.4150	1.0292	−0.4905
1.1032	0.0811	1.3624	−0.1411	2.2814	−0.3927	1.0474	−0.4703
1.1819	0.0922	1.3716	−0.1162	2.4623	−0.3972	1.2484	−0.4395
1.1913	0.0696	1.4618	−0.1234	2.5464	−0.3731	1.2622	−0.4378
1.2262	0.0985	1.4815	−0.1392	0.1978	−0.7780	1.2716	−0.4504
1.2549	0.0979	1.5820	−0.1064			1.3027	−0.4453

both methods.

Results and Discussion

The numerical values of h obtained by the VPO at 40.3 °C for the salts, NaI, KI, RbI, LiCl, and LiBr, are listed in Table 1, while the plots of h *vs.* the molality, m, are shown in Figs. 1 and 2. The profiles of the plots are similar to those reported in the preceding paper.[4] It should be noted, however, that the values of h for LiCl are positive at the concentrations higher than 3×10^{-3} mol kg^{-1}.

In the earlier paper (I), the values of h/m (not h) were plotted against m, and the curves obtained for LiCl and LiBr showed a tendency for h/m to increase with decrease in m at low concentrations. To account for this result, we assumed that an equilibrium

$$2MX \rightleftharpoons (MX)_2$$

prevails at these concentrations. According to this assumption,

$$\lim_{m\to0}\frac{h}{m} = K_a.^{8)}$$

In this paper, on the contrary, h tends to $-\infty$ at $m\to0$. This discrepancy is probably due to the in-

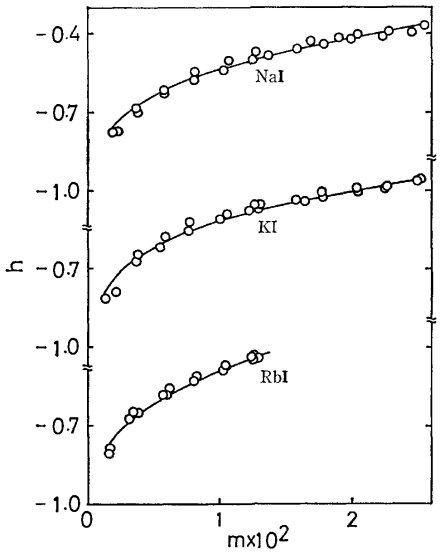

Fig. 1. Relationships between h and concentration for NaI, KI, and RbI at 40.3 °C.

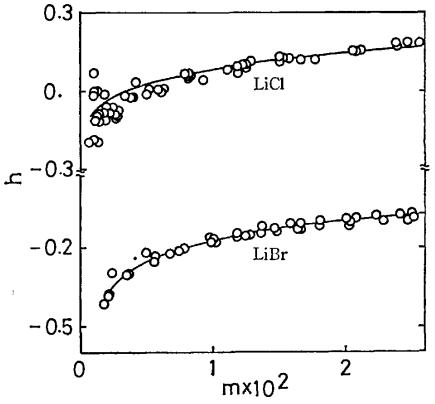

Fig. 2. Relationships between h and concentration for LiCl and LiBr at 40.3 °C.

complete drying of the lithium salts in the previous experiments.

In order to represent the experimental curves for LiCl and LiBr, we assume the two-step equilibria of Eq. 1. The dissociation equilibrium of the left-hand side is necessary in order to represent the shapes of curves at low concentrations, and the association equilibrium is inevitable to account for the fact that h is positive at moderate concentrations.

We have tried to estimate the most probable values of K_a and K_d by means of curve-fitting Eqs. 2, 3···, and 7. The curve-fitting was made by the method of non-linear least-squares. The results are shown in Table 2.

The measurements for NaI, KI, and RbI were also made for comparison. In the preceding paper,[4] the data were analyzed on the basis of the assumption that only the dissociation equilibrium exists, and the deviation from the ideality of undissociated molecules was taken in account. Similar analyses were carried out in the present investigation; the results are shown in Table 3, where β_2 is a parameter, given in the preceding paper, for compensating for the non-ideal behavior of the MX species in solution (not β in Eq. 3). The curves in Figs. 1 and 2 are theoretical ones calculated by the use of the parameters shown in the tables. The agreements with the experimental values are satisfactory.

Table 2. K_a and K_d for LiCl and LiBr (40.3 °C in molality scale)

	$K_d \times 10^3$	$K_a \times 10^3$	Standard deviation for the h function
LiCl	0.00952	18.8	0.047
LiBr	0.432	4.19	0.015

Table 3. Dissociation constant of NaI, KI, and RbI (40.3 °C in the molality scale)

	$K_d \times 10^3$	β_2	Standard deviation for the h function
NaI	10.99	29.6	0.017
KI	8.64	22.2	0.022
RbI	10.00	80.9	0.019

Table 4. Conductance parameters for acetone-alkali halide systems (Λ in $\Omega^{-1}\,cm^2\,mol^{-1}$)

	This research (40.3 °C)		Literature (25 °C)	
	K_A	Λ_0	K_A	Λ_0
LiCl	2114×10^2	227.1	3030×10^2	214 (6)
LiBr	5146	219.6	4570	194 (6)
NaI	157	218.7	160	184.4 (7)
KI	153.5	218.0	110	197.3 (7)
			179.5	197.5 (6)
RbI	254.8	224.3		

Table 5. Comparison of dissociation constants by VPO and conductometry at 40.3 °C (in terms of molality)

	VPO	Conductometry
LiCl	0.00952×10^{-3}	0.00617×10^{-3}
LiBr	0.432×10^{-3}	0.253×10^{-3}
NaI	10.99×10^{-3}	8.31×10^{-3}
KI	8.64×10^{-3}	8.49×10^{-3}
RbI	10.00×10^{-3}	5.11×10^{-3}

The electric conductances of the acetone solutions of LiCl, LiBr, NaI, KI, and RbI were measured at 40.3 °C. The results were analyzed by the use of Shedlovsky's equation.[5] The parameters, K_A and Λ_0, in Shedlovsky's equation, as obtained from our experimental results, are shown in Table 4, where those at 25 °C found in the literature[6] are also given for comparison. Shedlovsky's equation is

$$\frac{1}{\Lambda S(z)} = \frac{1}{\Lambda_0} + \frac{C\Lambda f_\pm^2 S(z) K_A}{\Lambda_0^2}, \tag{8}$$

$$S(z) = \left\{\frac{S\sqrt{C\Lambda}}{2\Lambda_0^{3/2}} + \left[1 + \left(\frac{S\sqrt{C\Lambda}}{2\Lambda_0^{3/2}}\right)^2\right]\right\}^2, \tag{9}$$

$$\ln f_\pm = -\frac{4.606 A\sqrt{C\alpha}}{1 + Ba_0\sqrt{C\alpha}}, \tag{10}$$

where Λ_0 is the equivalent conductance at an infinite dilution, K_A; the association constant ($=1/d_0K_d$, d_0 being the density of the solvent) has its usual meaning, and α is the degree of dissociation.

The values of K_A thus obtained are converted to K_d and are shown in Table 5, together with the values from VPO. In the table, the agreement between the values from VPO and conductometry is really satisfactory for LiCl, NaI, and KI. For LiBr and RbI, the agreement is not satisfactory, but it is still within a factor of ten.

In order to account for the profiles of the *h-m* plots for LiCl and LiBr, it is assumed that an equilibrium of the monomer-dimer exists at the higher concentration. The conductometry data can tell nothing about the presence of the dimer because of its electrically neutral nature. It should be emphasized here that the study with VPO is essentailly necessary for the study of the solution properties of non-aqueous solutions.

References

1) H. Nomura, M. Ando, and Y. Miyahara, *Nippon Kagaku Zasshi*, **90**, 1222 (1969).
2) H. Nomura, M. Ando, and Y. Miyahara, *Nippon Kagaku Zasshi*, **91**, 840 (1970).
3) M. Imura, H. Nomura, F. Kawaizumi, and Y. Miyahara, *Bull. Chem. Soc. Jpn.*, **47**, 2559 (1974).
4) H. C. Lee and Y. Miyahara, *Bull. Chem. Soc. Jpn.*, **51**, 1012 (1978).
5) R. M. Fuoss and T. Shedolovsky, *J. Am. Chem. Soc.*, **71**, 1496 (1949).
6) L. G. Savedoff, *J. Am. Chem. Soc.*, **88**, 664 (1966).
7) G. J. Janz and M. J. Tait, *Can. J. Chem.*, **45**, 1101 (1967).
8) Equation 13 in (I) should read $h/m=K_a+\cdots$.

Temperature Programmed Desorption Study of Water Adsorbed on Metal Oxides. I. Anatase and Rutile

Makoto EGASHIRA,* Shohachi KAWASUMI, Shuichi KAGAWA,† and Tetsuro SEIYAMA††

Department of Materials Science and Engineering, Faculty of Engineering, Nagasaki University, Nagasaki 852

† *Department of Industrial Chemistry, Faculty of Engineering, Nagasaki University, Nagasaki 852*

†† *Department of Materials Science and Technology, Faculty of Engineering, Kyushu University, Fukuoka 812*

(Received March 20, 1978)

The adsorbed state of water on TiO_2 was studied by temperature programmed desorption (TPD) in the range 0—1000 °C. Pure anatase and rutile samples, the TPD spectra of water from which were not affected by any contaminant, could be obtained by the hydrolysis of titanium oxalate and tetrachloride solutions, respectively. Two desorption peaks were observed for anatase with the peak maxima at 69—127 (I) and 191—256 °C (II), and three for rutile at 32—90 (I), 188—265 (II), and 310—356 °C (III). The sum of adsorbed amounts for peaks II, and III are within a monolayer coverage, that of peak I exceeding it. The enthalpies of adsorption were evaluated to be 36 and 55—69 $kJ \cdot mol^{-1}$ for peaks I and II of anatase, and 36, 64, and 104 $kJ \cdot mol^{-1}$ for peaks I, II, and III of rutile, respectively. From these results, the corresponding adsorbed species of peak I was tentatively assigned to physical adsorption, that of peak II to chemisorption on surface oxygen ion by hydrogen bond, and that of peak III to chemisortpion on Ti^{4+} by the coordination of oxygen atom of water molecule. The last species may be dissociated into surface OH groups.

Most metal oxides are covered with hydroxyl groups under normal conditions.[1] Since surface hydroxyl groups seem to have a great influence on the physical and chemical properties of metal oxide surface, it is important to have information on the adsorbed state of water on the surface.

The adsorbed state of water on titanium dioxide has been investigated by many authors by various methods: specific chemical reactions,[1] adsorption measurement,[2] infrared spectroscopy,[3] and temperature programmed desorption spectroscopy.[4-6] However, many problems remain unsolved: (1) whether surface hydroxyl groups are isolated freely or associated with each other through hydrogen bond, (2) whether there exists molecular species adsorbed by chemical or physical cohesion bond besides surface hydroxyl groups, (3) the amount and the adsorption bond strength of each adsorbed species, and (4) the difference between anatase and rutile. In the present work, these subjects were studied in detail by the temperature programmed desorption (TPD) technique.

Experimental

Materials. The crystal form of titanium dioxide prepared by the hydrolysis of titanium salts depends on the sort of electrolyte in the solution and on the calcination temperature.[7-9] Rutile is usually obtained by calcination above 900 °C. The rutile sample thus obtained, however, is not adequate for studying the surface phenomena because of its small surface area. In the present work, three kinds of anatase (A-1—3) and two kinds of rutile (R-1,2) samples were used (Table 1). Sample A-1 is of extra pure grade (Wako Pure Chemical Industries, Ltd.). Sample A-2 was prepared from titanium sulfate obtained by the reaction of titanium dioxide with concd H_2SO_4. The titanium sulfate solution was hydrolyzed with ammonia. The precipitate was washed with distilled water to remove sulfate ions thoroughly, and dissolved in an aqueous solution of oxalic acid. The hydrolysis of the titanium oxalate solution was then repeated twice with ammonia. Finally the washed precipitate was dried at 120 °C, and calcined at 600 °C in the air for 5 h. Sample A-3 was obtained by the hydrolysis of a titanium tetrachloride solution with ammonia in the presence of ammonium sulfate, followed by thorough washing, drying at 120 °C, and then calcination at 730 °C in the air for 3 h.

The hydrolysis of a titanium tetrachloride solution in the absence of ammonium sulfate gave rise to the formation of rutile crystals by calcination at 600 °C (the sample is denoted by R-1). Sample R-2 was also obtained by the hydrolysis of titanium tetrachloride, followed by washing with ammonium nitrate solution to improve the filtration yield.

The samples were confirmed by X-ray diffraction analysis to be pure anatase or rutile except sample R-2, which contains a small amount of anatase crystals. The surface areas of the samples were measured by the BET method with nitrogen as an adsorbate. Granules of 20—80 mesh were used for TPD experiments.

Apparatus. The apparatus used for the TPD experiments is essentially the same as that described previously.[10] Equipments added were a path of oxygen for pretreatment under oxygen atmosphere, and a water vapor supplier consisting of a saturated solution of sodium chloride held at 0 or 20 °C. Water vapor was supplied to the sample by passing a carrier gas through the supplier for a certain period. Helium was used as a carrier gas. Commercial helium and oxygen were dried with a phosphorus pentoxide column.

Procedure. A fixed amount of TiO_2 (0.25, 0.5, or 1.0 g) was loaded into the reactor. The sample was heated at 600 °C for 1 h under a stream of mixed gas of oxygen 10% and helium 90% (50 $cm^3 \cdot min^{-1}$) and then under a stream of helium for 1 h. After the sample had been cooled to 0 or 20 °C, the water vapor was supplied and adsorbed from the supplier for a certain period with a helium carrier (50 $cm^3 \cdot min^{-1}$). The partial pressure of water vapor was 0.61 or 2.34 kPa. The water vapor in gas phase was then purged by the helium carrier, programmed heating being started from 0 or 20 to 1000 °C at a constant rate of $b = 3.5$—25 $K \cdot min^{-1}$. Gas desorption during the course of heating was recorded as a TPD chromatogram with a conventional thermal conductivity detector. The desorbed species was identified by gas chromatography. The amount of desorbed species was calculated from the peak area of the TPD chromatogram.

Results and Discussion

Desorption Chromatogram. Figure 1 shows the TPD chromatograms from three kinds of anatase sam-

Table 1. TiO_2 Samples used

Sample	Preparation method	Calcination	Surface area/$m^2 \cdot g^{-1}$	X-Ray diffraction
A-1	Commercial TiO_2	600 °C-5 h	6.4	Anatase
A-2	Hydrolysis of $Ti(SO_4)_2$ → dissolve in $(COOH)_2$ → hydrolysis → washed by distd H_2O	600 °C-5 h	34.2	Anatase
A-3	Hydrolysis of $TiCl_4$ in the presence of $(NH_4)_2SO_4$ → washed by distd H_2O	730 °C-3 h	11.2	Anatase
R-1	Hydrolysis of $TiCl_4$ → washed by distd H_2O	600 °C-5 h	14.5	Rutile
R-2	Hydrolysis of $TiCl_4$ → washed by NH_4NO_3 soln	600 °C-5 h	15.4	Rutile (+Anatase)

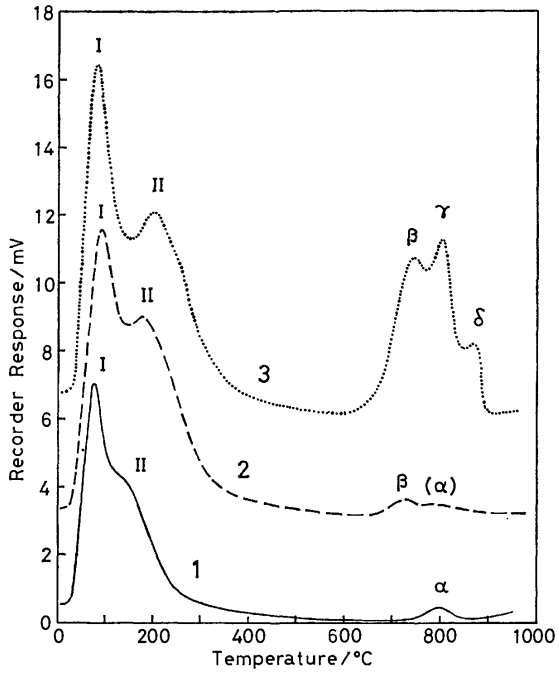

Fig. 1. TPD chromatograms from three anatase samples. Water vapor was fully preadsorbed at 0 °C after pretreated at 600 °C. Heating rate $b=15\ K \cdot min^{-1}$. 1: Sample A-1 1.0 g, 2: sample A-2 0.25 g, 3: sample A-3 0.5 g. For clarity, chromatograms 2 and 3 have been translated by 3 and 6 units along the ordinate, respectively.

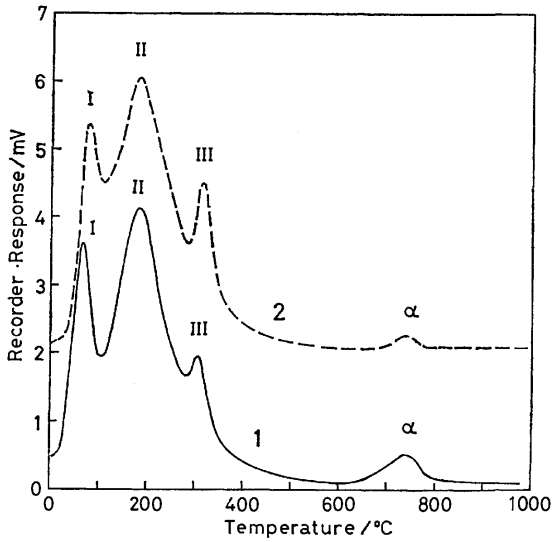

Fig. 2. TPD chromatograms from two rutile samples. Water vapor was fully preadsorbed at 0 °C after pretreated at 600 °C. $b=15\ K \cdot min^{-1}$. 1: Sample R-1 0.5 g, 2: sample R-2 0.5 g. For clarity, the chromatogram 2 has been translated by 2 units along the ordinate.

ples, which were pretreated at 600 °C and then allowed to adsorb water vapor at 0 °C, in the range 0—1000 °C. Similar results obtained from two kinds of rutile samples are shown in Fig. 2. The crystal structure of samples did not change with pretreatment. All samples pretreated showed no desorption peak up to 600 °C unless water was preadsorbed, but above 600 °C the same chromatograms were also observed without the preadsorption of water.

The chromatograms (Figs. 1 and 2) can be divided broadly into two groups; one with desorption peaks below and the other above 600 °C. The desorbed gases at lower temperatures were identified to be water alone by gas chromatography. Two desorption peaks I and II from sample A-2 well correspond to those from sample A-3. In the case of sample A-1, peak II was faintly observed as a shoulder of peak I. Munuera *et al.*[4] also reported two desorption peaks with the peak maxima at 175 and 215 °C. The rutile samples, on the other hand, gave three desorption peaks of water. Lower temperature peaks I and II correspond to those from anatase, no peak III being observed in the latter. The desorption peaks at 250 and 370 °C reported by Munuera and Stone[5,6] seem to be equivalent to peaks II and III (Fig. 2), though the peak temperatures are higher than the present results. Munuera[5] also reported another peak near 500 °C in the first TPD experiment using a fresh rutile sample evacuated at 400 °C, and attributed the peak to free OH groups from the original hydroxide. However, no such peak has been observed in the present work even though the sample was pretreated at 400 °C.

On the other hand, for the desorption peaks above 600 °C the desorbed gases were not water. Gas chromatographic analysis showed that peak α of sample

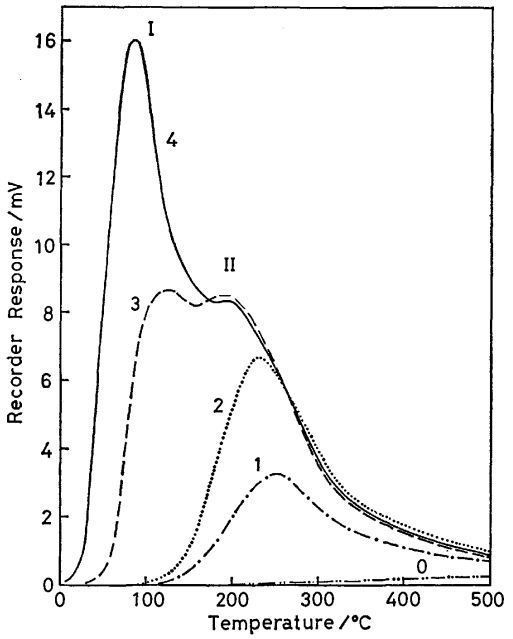

Fig. 3. The change of TPD chromatogram of water from sample A-2 (1.0 g) by the preadsorbed amount V_a of water. V_a value in each run is given in Table 2. $b=15$ K·min^{-1}. Run 0: no adsorption, 1: adsorption for 10 min, 2: 20 min, 3: 40 min, 4: 60 min.

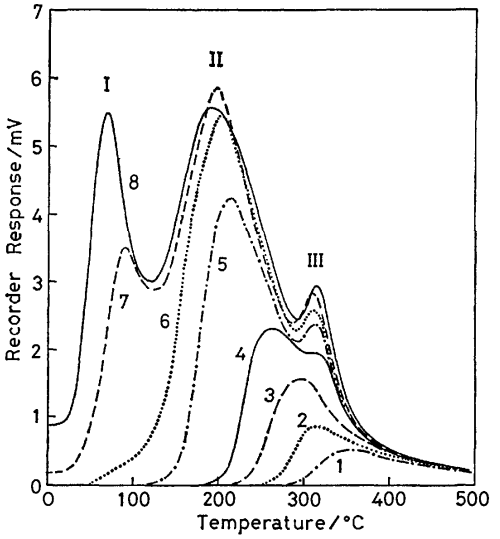

Fig. 4. The change of TPD chromatogram of water from sample R-1 (1.0 g) by the preadsorbed amount V_a of water. V_a value in each run is given in Table 3. $b=10$ K·min^{-1}. Run 1: adsorption for 1 min, 2: 1.5 min, 3: 2.5 min, 4: 4 min, 5: 9 min, 6: 12 min, 7: 15 min, 8: 21 min.

R-1 or R-2 at about 740 °C and peak α of sample A-1 at 800 °C arises from the desorption of surface oxygen. Several types of adsorbed oxygen species have been proposed over various metal oxides such as O_2^-, O^-, and O^{2-}. Peak α could be assigned to O^{2-} species since the former two species should be desorbed up to 600 °C.[10,11] The amount of α oxygen obtained from peak area of sample R-1 was evaluated to be 8.6×10^{-8} mol·m^{-2} of TiO_2 surface, corresponding to the surface coverage of *ca.* 1% with respect to surface titanium atoms. In the case of sample A-2, nitrogen was also detected in addition to oxygen as a desorbed gas. In particular most of peak β was due to the desorption of nitrogen. For large peaks β, γ, and δ from sample A-3 the desorbed gases were not oxygen, but nitrogen and unknown species. Lower calcination temperature caused the enlargement of these peaks as compared with peak II. From the results, it is concluded that the abnormally large, higher temperature peaks should correspond to the desorption with decomposition of ammonium sulfate residue used for preparation. Thus the preparation method of sample A-3 is not appropriate for pure anatase.

In the case of sample A-2, the coverage of impurity can be estimated to be only a few percent since the area of peak β is much smaller than that of peak II which corresponds to the adsorption amount within a monolayer coverage. When sample A-2 was pretreated at 850 °C to remove the impurity the feature of the desorption chromatogram of water was the same as the result in Fig. 1, though the recorder response was very low because of the decreased surface area. Thus, the influence of impurity for sample A-2 is negligible and the spectrum up to 600 °C (Fig. 1) can be taken to represent the desorption chromatogram of water from pure anatase surface.

Peak II of commercial sample A-1 represents a smaller peak area and a lower peak temperature than that of sample A-2. This may be caused by some impurities. Commercial sample is likely to contain some iron compounds or some phosphates.[12] Munuera *et al.*[4] reported that the addition of phosphate ions to anatase results in the disappearance of peak II.

Changes of Desorption Chromatograms by Adsorbed Amounts. Anatase and rutile show different TPD chromatograms; the former has two desorption peaks, the latter three. These peaks should reflect the different types of adsorbed states of water on the different surface sites. In order to obtain further information on the corresponding adsorbed states of these peaks, TPD chromatograms were measured at various amounts of water preadsorbed.

Figure 3 shows the TPD chromatograms from sample A-2 of anatase form after water vapor had been preadsorbed in various amounts at 0 °C. The amount of water preadsorbed was varied by passing helium carrier gas over the saturated solution of sodium chloride held at 0 °C for the periods 0—65 min. When the preadsorbed amount V_a was small, only one peak (II) appeared. With increasing V_a, peak II was enhanced, the peak temperature being lowered. However, the increase of peak II was saturated to a certain limit and another peak I appeared in the lower temperature region at $V_a=11.63$ μmol·m^{-2}. Similar results were also obtained in the case of sample A-1.

Figure 4 shows the results from sample R-1 of rutile form. Only one peak was observed for runs 1, 2, and 3, where the preadsorbed amount was less than 2.43 μmol·m^{-2}. The chromatogram started to separate into two peaks (II and III) at $V_a=3.53$ μmol·m^{-2} (run 4), the peak separation becoming clear by the further adsorption of water. At $V_a=9.08$ μmol·m^{-2}

Table 2. Analysis of TPD chromatograms of water from anatase A-2 sample

Run	V_a [a] / μmol·m^{-2}	Peak I			Peak II		
		T_M [b] / °C	V_d [c] / μmol·m^{-2}	ΔH [d] / kJ·mol^{-1}	T_M [b] / °C	V_d [c] / μmol·m^{-2}	ΔH [d] / kJ·mol^{-1}
1	3.56	—	0	—	256	3.56	—
2	6.75	—	0	—	233	6.75	69
3	11.63	127	3.89	—	191	7.74	—
4	19.58	88	11.99	36	204	7.59	55
5	23.33	69	15.81	—	199	7.52	—

a) Preadsorbed amount, the sum of V_d for peaks I and II. b) Temperature at peak maximum at $b=15$ K·min^{-1}. c) Amount of desorbed H_2O. d) Enthalpy of adsorption.

Table 3. Analysis of TPD chromatograms of water from rutile R-1 sample

Run	V_a [a] / μmol·m^{-2}	Peak I			Peak II			Peak III		
		T_M [b] / °C	V_d [c] / μmol·m^{-2}	ΔH / kJ·mol^{-1}	T_M [b] / °C	V_d / μmol·m^{-2}	ΔH / kJ·mol^{-1}	T_M [b] / °C	V_d / μmol·m^{-2}	ΔH / kJ·mol^{-1}
1	0.97	—	0	—	—	0	—	356	0.97	—
2	1.39	—	0	—	—	0	—	317	1.39	—
3	2.43	—	0	—	overlap					
4	3.53	—	0	—	265	1.59	—	316	1.94	—
5	7.67	—	0	—	212	5.56	—	313	2.11	—
6	9.08	—	0.29	—	203	6.56	—	310	2.23	—
7	12.66	90	2.48	—	197	7.86	—	310	2.32	—
8	13.58	68	3.66	36	190	7.69	64	315	2.23	104
9	17.68	54	7.57	—	188	7.90	—	313	2.21	—
10	25.33	32	15.37	—	191	7.65	—	315	2.31	—

a) Preadsorbed amount, the sum of V_d for peaks I, II, and III. b) At $b=10$ K·min^{-1}.

(run 6), both these peaks almost attained their saturated heights. Peak I appeared at a preadsorbed amount greater than $V_a=12.6$ μmol·m^{-2}. A comparison of peak temperatures suggests that peaks I and II of rutile correspond to two peaks of anatase; peak III is characteristic of rutile form.

Taking into account the long tailing of peak II from anatase, however, it is reasonable to consider that the adsorbed species corresponding to peak III from rutile should exist on the anatase surface. Smaller amount or lower desorption temperature than that of rutile may interfere with the appearance of a discrete peak.

Peak II of anatase and peaks II and III of rutile have attained the saturated adsorption. This indicates that the peaks should arise from the desorption of some species chemisorbed within a surface monolayer. For the sake of confirmation, the amounts of desorbed gas were determined from the peak areas of TPD chromatograms (Figs. 3 and 4). The results are given in Tables 2 and 3, respectively. The temperature at the minimum of chromatogram was taken as the boundary between two peaks. Assuming that every surface oxygen ion with the coordination number less than three is hydroxylated, the maximum amounts of desorbed water from the (100), (001), and (110) planes of anatase are calculated to be 9.28, 11.7, and 13.1 μmol·m^{-2}, respectively. For the (110), (101), and (001) planes of rutile, they amount to 8.64, 9.93, and 15.7 μmol·m^{-2}, respectively.

The maximum values observed for peak II of anatase and for peak II+III of rutile are in good agreement with the calculated values for low index planes. It is concluded that either peak II or III corresponds to chemisorbed species on the surface. On the other hand, the desorbed amount of peak I did not attain a saturated value, but increased over a monolayer coverage (Tables 2 and 3). It might be concluded that peak I corresponds to the physical adsorption species.

The Enthalpy of Adsorption. In order to estimate the adsorption strength of each species, the enthalpy of adsorption ΔH was measured for two peaks of sample A-2 and for three peaks of sample R-1. ΔH was determined according to the method of Konvalinka *et al.*[13] who extended the theory of Cvetanovic and Amenomiya.[14]

For the first order desorption from a homogeneous surface with freely occurring readsorption, peak temperature T_M of a desorption peak is correlated with ΔH and heating rate b by

$$2\log T_M - \log b = \frac{\Delta H}{2.303RT_M} + \log\frac{(1-\theta_M)^2 V_s \Delta H}{FAR}. \quad (1)$$

For second order desorption with freely occurring readsorption, Eq. 1 may be written as

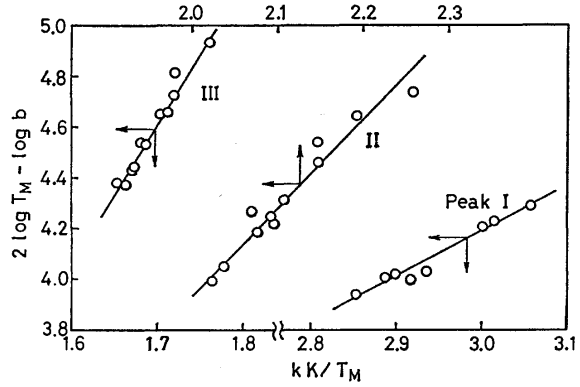

Fig. 5. Plots of (2 log $T_M - \log b$) *vs.* $1/T_M$ for three TPD peaks from sample R-1.

$$2\log T_M - \log b = \frac{\Delta H}{2.303RT_M} + \log\frac{(1-\theta_M)^2 V_s v_m \Delta H}{2\theta_M FAR}, \quad (2)$$

where R is the gas constant, V_s the volume of the solid phase, v_m the amount of gas adsorbed at full coverage per unit volume of the solid in a certain adsorbed state, F the flow rate of carrier gas, θ_M the coverage at $T = T_M$, and A is equal to $\exp(\Delta S/R)$, where ΔS is the entropy of adsorption. The flow rate of carrier gas 50 $cm^3 \cdot min^{-1}$ fulfills the condition with freely occurring readsorption, because desorption without readsorption cannot be realized unless the flow rate is set at 10^7 $cm^3 \cdot h^{-1}$ per gram of solid.[13] Since θ_M varies very slightly with heating rate, the slope of the plot of (2 log T_M $-\log b$) *vs.* $1/T_M$ should provide the enthalpy of adsorption at constant F and at constant initial surface coverage both for the first and second order desorption. Figure 5 shows the plots of (2 log T_M $-\log b$) *vs.* $1/T_M$ for three peaks of sample R-1. In all cases, a linear relation holds. ΔH's calculated from the slopes are also given in Tables 2 and 3.

Day *et al.*[15] reported the values 45—52 $kJ \cdot mol^{-1}$ for the heat of adsorption of water on rutile at 25 °C in the region of monolayer coverage. Morimoto *et al.*[16] obtained the values 79.5 and 105.4 $kJ \cdot mol^{-1}$ for the heats of hydration of rutile and anatase, respectively, from the measurement of heat of immersion in water. The values of Day *et al.* are intermediate between the ΔH values for peaks I and II. The values of Morimoto *et al.* are close to the present result for peak III of rutile, which is in good agreement with the result of Munuera and Stone.[6] However, Day *et al.* and Morimoto *et al.* paid no attention to the difference of adsorbed species. The different species should exhibit a different heat of adsorption or immersion.

Adsorbed State of Water. The ΔH value 36 $kJ \cdot mol^{-1}$ for peak I agrees with the heat of vaporization of water at 100 °C, 41 $kJ \cdot mol^{-1}$. The ΔH values for peak II are in the range 55—69 $kJ \cdot mol^{-1}$, greater than the heat of vaporization. Hydrogen bonds would participate in the adsorption of peak II species. From the fact that peak I arises after peak II has attained saturation, peak II can be assigned to the chemisorbed species held on the surface oxygen

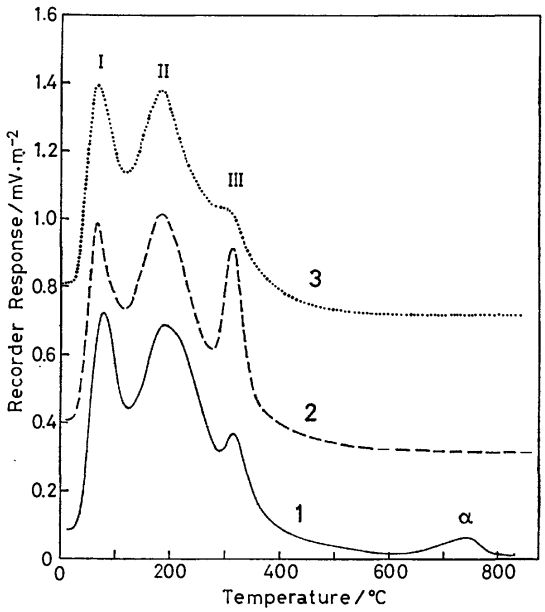

Fig. 6. The influence of pretreatment on the adsorption sites of sample R-1. 1: First run after pretreated at 600 °C, 2: second run after first TPD up to 830 °C, 3: third run after pretreated at 1000 °C for 30 min. Water was fully preadsorbed at 20 °C. $b = 10$ K·min^{-1}. For clarity, the chromatograms 2 and 3 have been translated by 0.3 and 0.7 units along the ordinate.

ions by hydrogen bond within a monolayer, and peak I to the multilayer physical adsorption on the chemisorbed water molecules. The hydrogen bond of water molecule with surface oxygen ion O^{2-} is considered to be stronger than that between water molecule since O^{2-} ion has a higher proton affinity than the oxygen atom of water molecule.

The ΔH value 104 $kJ \cdot mol^{-1}$ for peak III of rutile is considerably greater than that expected for the adsorption through hydrogen bond. On the other hand, it is indicated by infrared study[17] that free OH groups remain on the surface of silica gel or alumina even after evacuation at 650—950 °C. Thus free OH groups are likely to be able to desorb only at very high temperatures. Peak III can be tentatively assigned to the adsorbed species through the coordination of oxygen atom of water to the surface titanium ion.

In order to confirm the participation of Ti^{4+} ions in the peak III adsorption, the following experiments were carried out. After the surface oxygen (peak α) had been desorbed from sample R-1 by the first TPD procedure up to 830 °C (curve 1, Fig. 6), the sample was quenched to 20 °C in a stream of helium. Water was then readsorbed and the TPD chromatogram was recorded again. The result is shown in curve 2, where recorder response was plotted per unit area since the surface area decreased from 14.5 to 5.3 $m^2 \cdot g^{-1}$ by the first TPD run up to 830 °C. The magnitude of peak III markedly increased in the second run, that of peak II remaining almost unchanged. The increase of peak III is probably due to the increase of the number of Ti^{4+} sites by the desorption of surface oxygen ions. Elongated heat treatment above 800 °C caused a gradual decrease in surface area. The sintering

process would bring about the change of surface structure, in particular the decrease of the active Ti^{4+} sites, which results in the reduction of peak III. The result on sample R-1 pretreated at 1000 °C for 30 min, the surface area of which decreased to 1.65 $m^2 \cdot g^{-1}$, is given by curve 3. The reduction of peak III is considerable, but the magnitude of peak II per unit area remains unchanged. The results suggest the participation of Ti^{4+} sites in the adsorption of peak III species; the peak II species seem to be independent of Ti^{4+} sites. The possibility that reduced Ti^{3+} ions might be the peak III adsorption sites can be eliminated since in such a case curve 3, representing the run after pretreatment at the highest temperature in the inert gas, should exhibit the largest peak III.

Similar experiments were carried out on anatase sample A-2, but no clear peak III could be observed by any pretreatment. Thus the sites of Ti^{4+} on anatase are much fewer or weaker than those on rutile. This can be explained as follows. Since the cleavage of anatase crystal along (100), (001), and (110) planes produces 5-coordinate surface Ti^{4+} ions in each case, the oxygen atom of water molecule could be coordinated to only one Ti^{4+} ion at its vacant ligand position. In the case of rutile, a water molecule can be doubly coordinated to two adjacent 4-coordinate Ti^{4+} ions on the (100) and (110) planes. Such adsorption modes may be reflected in the difference of the desorption spectrum of peak III.

Primet *et al.*[3] suggested from infrared spectroscopic study that the surface of anatase and rutile evacuated at 200 or 300 °C for 20 h contains hydroxyl groups, and that OH groups bonded with each other by hydrogen bridges should be removed by evacuation at 350 °C and isolated OH groups at 400 °C. The former OH groups seem to be equivalent to peak III in the present work from the coincidence of desorption temperature. It is likely that a water molecule coordinated to Ti^{4+} ion would form the hydrogen bond with an adjacent surface O^{2-} ion, and dissociate into two OH groups by proton shift through hydrogen bond as follows:

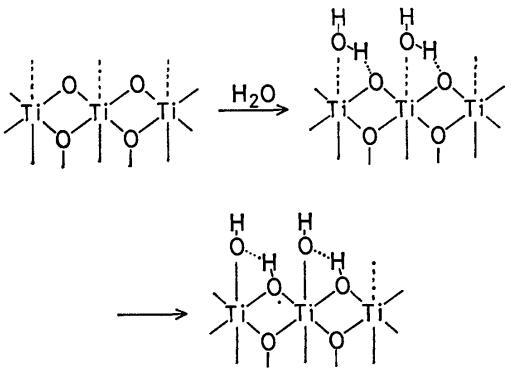

(3)

On the other hand, no desorption of free OH groups was observed as a peak in TPD chromatogram. However, it should be related to the long tailing part of chromatogram which starts at about 350 °C and continues above 600 °C, since the desorbed gas from a long tail was also found to be water. Thus the present results suggest the existence of some free OH groups still above 400 °C, contrary to the suggestion of Primet *et al.*[3]

Conclusion

The TPD chromatogram of water from anatase surface consists of two peaks, (I) T_M=69—127 °C, ΔH=36 kJ·mol^{-1} and (II) T_M=191—250 °C, ΔH=55—69 kJ·mol^{-1}, while that from rutile consists of three peaks, (I) T_M=32—90 °C, ΔH=36 kJ·mol^{-1}, (II) T_M=188—265 °C, ΔH=64 kJ·mol^{-1}, and (III) T_M=310—356 °C, ΔH=104 kJ·mol^{-1}. Peaks I and II from both samples well correspond to each other. Peak II of anatase and peaks II and III of rutile attain saturated adsorption within a surface monolayer coverage. On the other hand, the adsorption of peak I on both samples was not saturated but increased over a monolayer coverage. Three desorption peaks are concluded to correspond to the following adsorbed states.

peak I: Physically adsorbed species on surface hydroxyl groups or chemisorbed water molecules.

peak II: Chemisorbed species on surface oxygen ions through hydrogen bonds.

peak III: Chemisorbed species on Ti^{4+} ions through coordination bond. The species can be transformed into two OH groups by proton transfer to an adjacent surface oxygen ion.

References

1) H. P. Boehm, *Discuss. Faraday Soc.*, **52**, 264 (1971).
2) T. Morimoto, M. Nagao, and F. Tokuda, *Bull. Chem. Soc. Jpn.*, **41**, 1533 (1968).
3) M. Primet, P. Pichat, and M. V. Mathieu, *J. Phys. Chem.*, **75**, 1216, 1221 (1971).
4) G. Munuera, F. Moreno, and J. A. Prieto, *Z. Phys. Chem.*, **78**, 112 (1972).
5) G. Munuera, *J. Catal.*, **18**, 19 (1970).
6) G. Munuera and F. S. Stone, *Discuss. Faraday Soc.*, **52**, 205 (1971).
7) "Shin Jikken Kagaku Koza," ed by the Chemical Society of Japan, Maruzen, Tokyo (1976), Vol. 8-I, p. 269.
8) "Genso-betsu Shokubai Binran," ed by the Catalysis Society of Japan, Chijinshokan, Tokyo (1967), p. 253.
9) K. Funaki and Y. Saeki, *Kogyo Kagaku Zasshi*, **59**, 1291, 1295, 1297 (1956).
10) M. Iwamoto, Y. Yoda, M. Egashira, and T. Seiyama, *J. Phys. Chem.*, **80**, 1989 (1976).
11) K. Tanaka and G. Blyholder, *J. Phys. Chem.*, **76**, 3184 (1972).
12) "Kogyo Yakuhin Jiten," ed by S. Nagai and K. Kubo, Nikkan Kogyo Shinbun, Tokyo (1964), p. 542.
13) J. A. Konvalinka, J. J. F. Scholten, and J. C. Rasser, *J. Catal.*, **48**, 365 (1977).
14) R. J. Cvetanovic and Y. Amenomiya, *Adv. Catal.*, **17**, 103 (1967).
15) R. E. Day, G. D. Parfitt, and J. Peacock, *J. Colloid Interface Sci.*, **46**, 17 (1974).
16) T. Morimoto, M. Nagao, and T. Omori, *Bull. Chem. Soc. Jpn.*, **42**, 943 (1969); T. Omori, J. Imai, M. Nagao, and T. Morimoto, *ibid.*, **42**, 2198 (1969).
17) L. H. Little, "Infrared Spectra of Adsorbed Species," Academic Press, London (1966), Chap. 10.

Catalytic Activities of La_2O_3, Y_2O_3, and CeO_2 for Decomposition of 4-Hydroxy-4-methyl-2-pentanone and Isomerization of Butenes

Yasuo FUKUDA, Hideshi HATTORI, and Kozo TANABE*

Department of Chemistry, Faculty of Science, Hokkaido University, Sapporo 060

(Received March 31, 1978)

The decomposition of 4-hydroxy-4-methyl-2-pentanone and the isomerization of 1-butene were carried out over La_2O_3, Y_2O_3, and CeO_2. The activities for both types of reactions were in the following order; $La_2O_3 > Y_2O_3 > CeO_2$. With La_2O_3, the change in the activity for the decomposition with the pretreatment temperature of the catalyst correlated well with the change in basicity, the activity and basicity maxima being observed when the catalyst was pretreated at 500 °C. Yttrium sesquioxide showed a maximum activity for the decomposition when pretreated at 700 °C. For the isomerizations of 1-butene and *cis*-2-butene, La_2O_3 exhibited activity maxima when pretreated at 700 °C. The *cis*/*trans* selectivities from 1-butene were considerably greater than unity, and the *trans*/1 selectivities from 2-butene were less than unity. The coisomerization of *cis*-2-butene-d_0/d_8 revealed that the reaction involved an intramolecular H(or D) transfer. The isotope effects for the formation of 1-butene from *cis*-2-butene were 4—10, while those for the formation of *trans*-2-butene were about 1.

Rare earth oxides have recently been recognized as solid base catalysts. Rosynek *et al.* studied the surface properties and catalytic behavior of La_2O_3 and reported that basic sites on La_2O_3 were essential for the isomerization of butenes.[1-3] Minachev *et al.* investigated the catalytic action of rare earth oxides for the hydrogenation of ethylene and concluded that the basicity of the oxides correlated with the activity.[4] Although the basic property was thus regarded as an important property in catalytic actions, the number of basic sites has not yet been measured.

In this study, the number of basic sites of La_2O_3 was measured and correlated with the catalytic activities for the decomposition of 4-hydroxy-4-methyl-2-pentanone and the isomerization of butenes. In the isomerization of butenes, a mechanistic study was done by the coisomerization method.[5] For a comparison with La_2O_3, oxides of elements of the same IIIa group, Y_2O_3 and CeO_2, were also studied.

Experimental

The lanthanum sesquioxide (La_2O_3), Y_2O_3, and CeO_2 were obtained by the evacuation of each hydroxide at temperatures between 400 and 800 °C for 3 h. The final pressure was in the range of 10^{-2} Pa. The hydroxides were prepared by precipitation from nitrate solutions with aqueous ammonia.

The number of basic sites (basicity) on La_2O_3 were measured by titrating the sample suspended in dry benzene with a benzene solution of 0.1 mol/dm^3 benzoic acid, 2,4,6-trinitroaniline ($pK_{BH}=12.2$) being used as an indicator.[6] The suspension of the sample in dry benzene was performed under flowing dry nitrogen to prevent poisoning by air.

For the measurements of the IR spectra, $La(OH)_3$ was pressed into a disk and outgassed at various temperatures for 3 h *in situ*.

The decomposition of 4-hydroxy-4-methyl-2-pentanone was carried out at 30 °C in a liquid phase while magnetically stirring the reactant (10 ml) and the powdered catalyst. The reaction mixture (catalyst, reactant, and product; 1-ml portions) was periodically transferred into another vessel for the centrifugal separation of the catalyst from a solution. The solution was then analyzed by means of a gas chromatograph with a 1-m column containing polyethylene glycohol on Celite.

The isomerization of butenes was carried out in a closed circulation system (*ca.* 1370 ml) on *ca.* 0.1-g catalysts at temperatures between 0 and 200 °C and at an initial pressure of 46.6 kPa. For the coisomerization of *cis*-2-butene-d_0/d_8, a microcatalytic pulse reactor was employed and a mixture containing equal amounts of *cis*-2-butene-d_0 and *cis*-2-butene-d_8 was reacted at 0 °C. The products were gas-chromatographically separated and subjected to mass-spectrographic analysis.

Results

Basicity and IR Spectra of La_2O_3. The variations in the basicity as a function of the pretreatment temperature are shown in Fig. 1. The basicity of lanthanum sesquioxide increased on pretreatment above 400 °C, attained a maximum value when pretreated at 500 °C, and then gradually decreased as the pretreatment temperature was raised above 500 °C.

The IR spectra of La_2O_3 exhibited strong peaks around 1500—1300 cm^{-1}, which could be assigned to carbonate groups. A large number of carbonate

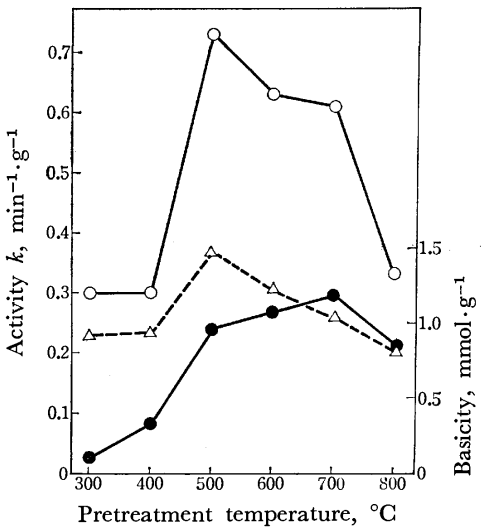

Fig. 1. Variations of basicity (—△—) of La_2O_3 as a function of pretreatment temperature and variations of activities of La_2O_3 (—○—) and Y_2O_3 (—●—) for decomposition of 4-hydroxy-4-methyl-2-pentanone at 30 °C.

Table 1. Catalytic activities and selectivities for the isomerization of 1-butene

Catalyst	Reaction temp °C	*cis*-2-Butene (%/m²·min)	*trans*-2-Butene (%/m²·min)	Selectivity
La_2O_3	0	8.6	3.3	2.8
Y_2O_3	0	2.2×10^{-2}	0.56×10^{-2}	3.9
CeO_2	0	0	0	—
CeO_2	200	3.1×10^{-2}	1.4×10^{-2}	2.2

groups still remained on the sample even when it was outgassed at 500 °C, and most of the carbonate groups was desorbed as CO_2 by raising the outgassing temperature from 500 to 600 °C.

Decomposition of 4-Hydroxy-4-methyl-2-pentanone. Only acetone was produced by the decomposition of 4-hydroxy-4-methyl-2-pentanone over La_2O_3, Y_2O_3, and CeO_2 at 30 °C. The decomposition followed the first-order rate equation with respect to the concentration of the reactant. The activity was represented by the first-order rate constant, k. Variations in the activities of La_2O_3 and Y_2O_3 on a unit of weight are also plotted as a function of the pretreatment temperature in Fig. 1. A maximum activity was obtained by pretreatment at 500 °C for La_2O_3 and at 700 °C for Y_2O_3. In the case of La_2O_3, the variation in the activity with the pretreatment temperature was similar to that of the basicity. The rate constants of CeO_2 pretreated at 700 and 800 °C were 1.02×10^{-2} and 1.17×10^{-2} $min^{-1}\cdot g^{-1}$ respectively. On comparing the maximum activities of La_2O_3 and Y_2O_3 to 1.17×10^{-2} $min^{-1}\cdot g^{-1}$ for CeO_2, the activities for the decomposition reaction are in the following order, $La_2O_3 > Y_2O_3 > CeO_2$.

Isomerization of Butenes. The activity was represented by a % conversion per min per unit weight or surface area of the catalyst in the initial stage of the reaction. The activities of La_2O_3, Y_2O_3, and CeO_2 pretreated at 700° for the isomerization of 1-butene are compared in Table 1 on the basis of a unit surface area, where the *cis*/*trans* selectivities in the initial stage of the reaction are also given. Cerium dioxide did not show any activity at 0 °C. The activity and the selectivity in the reaction at 200 °C are also given for the sake of comparison. The order of the activities is; $La_2O_3 > Y_2O_3 > CeO_2$. The *cis*/*trans* selectivities were greater than 2 for all catalysts.

The activity and *cis*/*trans* and *trans*/1 selectivities in the isomerizations of 1-butene and *cis*-2-butene are plotted against the pretreatment temperature in Figs. 2 and 3. The activities for both reactions appeared on pretreatment above 400 °C. The maximum activities were observed when La_2O_3 was pretreated at 700 °C for both reactions. The *cis*/*trans* and *trans*/1 selectivities were markedly changed by raising pretreatment temperature from 600 to 700 °C. In all cases, the *cis*/*trans* selectivities were greater than 2 and the *trans*/1 selectivities were less than 1.

The results of the coisomerization of *cis*-2-butene-d_0/d_8 over La_2O_3 pretreated at 600 and 700 °C are summarized in Table 2. Non-exchanged products were predominant. This indicates that the reaction

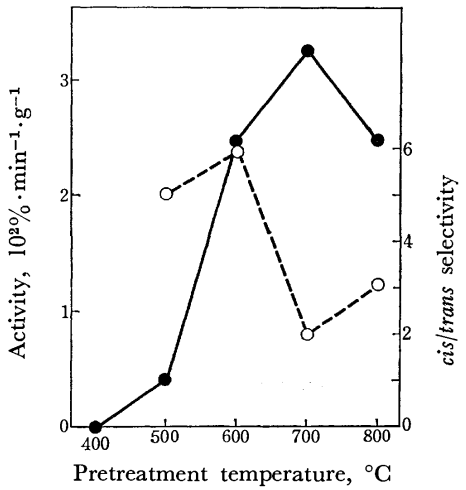

Fig. 2. Activity and *cis*/*trans* selectivity in isomerization of 1-butene over La_2O_3 at 0 °C. ●: Activity, ○: selectivity.

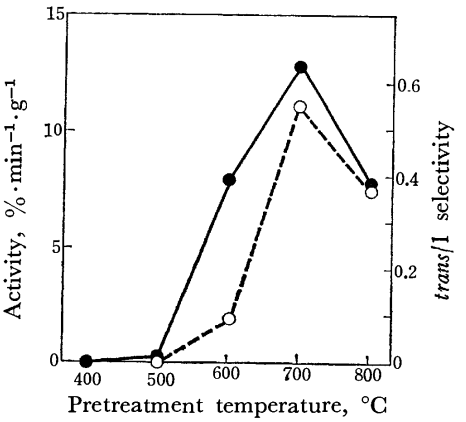

Fig. 3. Activity and *trans*/1 selectivity in isomerization of *cis*-2-butene over La_2O_3 at 0 °C. ●: Activity, ○: selectivity.

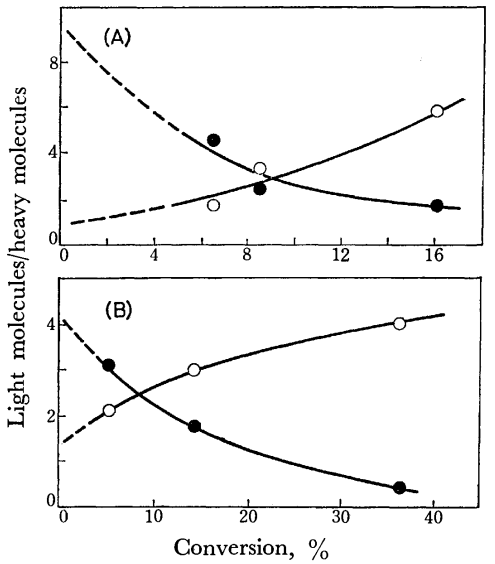

Fig. 4. Ratios of "light molecules" to "heavy molecules" produced in coisomerization of *cis*-2-butene-d_0/d_8. (A) La_2O_3 pretreated at 600 °C. (B) La_2O_3 pretreated at 700 °C. ●: 1-Butene, ○: *trans*-2-butene.

TABLE 2. DISTRIBUTION OF THE ISOTOPIC SPECIES IN THE PRODUCTS FOR THE COISOMERIZATION OF HEAVY (d_8) AND LIGHT (d_0) *cis*-2-BUTENE

	d_0	d_1	d_2	d_3	d_4	d_5	d_6	d_7	d_8
(a) On La_2O_3 evacuated at 600 °C.									
				6.5% conversion					
1-Butene	81.4	0.9	0	0	0	0	0	0.9	16.8
trans-2-Butene	60.7	0.4	0	0	0	0	0	0.1	38.8
cis-2-Butene	47.5	0.5	0	0	0	0	0	0.4	51.8
				8.4% conversion					
1-Butene	68.8	0.6	0	0	0	0	0	0.7	29.1
trans-2-Butene	75.0	1.8	0	0	0	0	0	1.7	21.6
cis-2-Butene	46.0	0.4	0	0	0	0	0	0.0	53.6
				16.0% conversion					
1-Butene	60.2	2.0	0	0	0	0	0	2.9	34.9
trans-2-Butene	74.3	10.0	0.8	0	0	0	0.4	3.1	11.4
cis-2-Butene	42.0	1.6	0	0	0	0	0	1.7	54.7
(b) On La_2O_3 evacuated at 700 °C.									
				5.1% conversion					
1-Butene	75.3	0.2	0	0	0	0	0	0.3	24.3
trans-2-Butene	67.3	1.8	0	0	0	0	0	1.3	29.5
cis-2-Butene	43.3	0	0	0	0	0	0	0	56.7
				12.1% conversion					
1-Butene	63.7	0.1	0	0	0	0	0	0.6	35.0
trans-2-Butene	69.6	4.5	0.6	0	0	0	0.7	4.1	20.5
cis-2-Butene	42.1	0.1	0	0	0	0	0	0.0	57.8
				36.4% conversion					
1-Butene	29.0	1.2	0	0	0	0	0	2.8	67.0
trans-2-Butene	76.1	4.0	0	0	0	0	0	3.0	16.9
cis-2-Butene	24.9	1.7	0	0	0	0	0	2.6	70.0

involves an intramolecular H(or D) transfer. The ratio of "light molecules (d_0—d_2)" to "heavy molecules (d_6—d_8)" is plotted against the conversion in Fig. 4. The zero conversion intercept gives an isotope effect. The isotope effects for the formation of 1-butene were about 10 and 4 for La_2O_3 pretreated at 600 °C and 700 °C respectively. On the contrary, the isotope effects for the formation of *trans*-2-butene were small (≈ 1) for both catalysts. The ratio for 1-butene decreased with an increase in the conversion, while the ratio for *trans*-2-butene increased. This is attributable to a large isotope effect for the conversion of 1-butene to *trans*-2-butene.

Discussion

The catalytic actions of La_2O_3, Y_2O_3, and CeO_2 in the decomposition of 4-hydroxy-4-methyl-2-pentanone and the isomerization of butenes could be attributed to their basic property as a decisive property. The good correlation of the basicity with the activity for the decomposition of 4-hydroxy-4-methyl-2-pentanone found on La_2O_3 is similar to that found on alkaline earth oxides.[7] The order of the activities of alkaline earth oxides on a unit surface area basis followed the order of strength of the basic sites, that is, BaO>SrO>CaO>MgO. Although the basic properties of Y_2O_3 and CeO_2 were not measured, the order of the activities on a unit surface area basis, $La_2O_3>Y_2O_3>CeO_2$, suggests that the basic strength of the active sites is also $La_2O_3>Y_2O_3>CeO_2$. The activity of La_2O_3 was one order of magnitude greater than that of MgO (1.4×10^{-3} min$^{-1}\cdot$m^{-2}).[7]

For the isomerization of 1-butene over La_2O_3, our results on the activity and selectivity are similar to those reported by Rosynek and Fox.[3] In their study, a maximum activity was obtained when the substance was pretreated at 650 °C, while it was obtained at 700 °C in our study. The *cis*/*trans* ratios were considerably higher than unity in both studies.

One of the criteria for the base-catalyzed isomerization of 1-butene is a high *cis*/*trans* selectivity.[8-11] The high selectivity observed for La_2O_3, combined with the existence of basic sites, seems to indicate that the isomerization is a base-catalyzed reaction, in which the initial step is an abstraction of an allylic H in the form of H^+ by a basic site to form an allyl carbanion. The *cis* form is much more stable than the *trans* form in the π-allyl carbanion. The H^+ thus abstracted transfers to the 1 carbon atom to form mainly *cis*-2-butene. In this case, an intramolecular H transfer can be observed provided that there are no H^+ around the carbanion other than the abstracted one. The observed result of an intramolecular H transfer also supports the idea that the isomerization is a base-catalyzed reaction.

There are two forms in the π-allyl carbanion, *syn* and *anti* π-allyls. Interconversion between the two allyls probably proceed by means of a σ-allyl. If the interconversion between two π-allyls is a slow step, the

conversion of *cis*-2-butene to *trans*-2-butene will be slow and the isotope effect for the formation of the *trans*-2-butene will be small. These were the observed sequences. Therefore, the slow step for the direct conversion of *cis*-2-butene to *trans*-2-butene is the conversion of *anti* π-allyl to *syn* π-allyl. The increase in the ratio of "light molecules" to "heavy molecules" for *trans*-2-butene as the reaction proceeded indicates that a large part of the *trans*-2-butene was produced *via* 1-butene in the intermediate stage of the reaction. The large isotope effect for the formation of 1-butene from *cis*-2-butene suggests that an H transfer is involved in the slow step. Provided that the initiation step is common for the formations of *trans*-2-butene and 1-butene from *cis*-2-butene, a small isotope effect for the formation of *trans*-2-butene shows that the abstraction of H^+ is not a slow step. Therefore, it may be considered that the migration of the H^+ to the 3 carbon atom is the slow step for the formation of 1-butene from *cis*-2-butene.

Rosynek and Fox[3] suggested, on the basis of the different activation energies for the formations of *cis*-2-butene and *trans*-2-butene, that the formations of two 2-butene isomers from the 1-butene reactant may occur on dissimilar sites. However, it does not seem necessary to postulate dissimilar sites, it is sufficient to assume different slow steps for the formations of the two 2-butene isomers.

A marked increase in the activity for the isomerizations of butenes by raising the outgassing temperature from 500 to 600 °C corresponded to an increase in the desorbed amount of carbonate groups. Therefore, it may be considered that the active sites for isomerization are generated by the removal of surface carbonate groups.

The active sites for the isomerization of butenes and for the decomposition of 4-hydroxy-4-methyl-2-pentanone may be dissimilar, because the pretreatment temperatures at which maximum activities were exhibited different for the two reactions and because basic sites generated by pretreatment at 400 °C catalyzed the decomposition, while they did not catalyze the isomerization. Perhaps, the isomerization needs stronger basic sites than the decomposition does.

References

1) M. P. Rosynek and D. T. Magnuson, *J. Catal.*, **46**, 402 (1977).
2) M. P. Rosynek and D. T. Magnuson, *J. Catal.*, **48**, 417 (1977).
3) M. P. Rosynek and J. S. Fox, *J. Catal.*, **49**, 285 (1977).
4) K. M. Minachev, Y. S. Khodakov, and V. S. Nakhshunov, *J. Catal.*, **49**, 209 (1977).
5) J. W. Hightower and K. W. Hall., *Chem. Eng. Prog. Symp. Ser.*, **63**, 122 (1967).
6) J. Take, N. Kikuchi, and Y. Yoneda, *J. Catal.*, **21**, 164 (1971).
7) Y. Fukuda, K. Tanabe, and S. Okazaki, *Nippon Kagaku Kaishi*, **1972**, 513.
8) N. F. Foster and R. J. Cvetanovič, *J. Am. Chem. Soc.*, **82**, 4274 (1960).
9) S. Bank, A. Schriesheim, and C. A. Rowe, *J. Am. Chem. Soc.*, **87**, 3224 (1975).
10) W. O. Haag and H. Pines, *J. Am. Chem. Soc.*, **82**, 2488 (1960).
11) C. C. Chang, W. C. Conner, and R. J. Kokes, *J. Phys. Chem.*, **77**, 1957 (1973).

The Photoreduction of the Silver Ion in a Zinc Oxide Suspension

Hiroshi HADA,* Hatsumi TANEMURA, and Yoshiro YONEZAWA

Department of Industrial Chemistry, Faculty of Engineering, Kyoto University, Yoshida, Kyoto 606

(Received April 1, 1978)

Quantum yields of from 0.235 to 0.385 have been determined for the reduction of Ag^+ by the irradiation of 365 nm light on a ZnO surface in aqueous solutions containing 5×10^{-5} to 1×10^{-3} M $AgClO_4$. It is proposed that these results can be interpreted by a reaction scheme based on the assumption that some conduction-band electron produced in the ZnO by the irradiation transfers to the Ag^+ adsorbed on the ZnO surface. The surface-energy barrier under the present experimental conditions was discussed with the aid of the electrochemical measurement of the ZnO sinter. The photoreduction of Ag^+ is optically sensitized by the addition of xanthene dyes, such as Uranine and Rhodamine B. In this case, it is observed that the photoreduction of Ag^+ is accompanied by the photolysis of dye molecules. The apparent quantum yields (the number of reacted molecules/the number of photons absorbed in the suspension) of the dye-sensitized photoreduction of Ag^+ and the photolysis of dye molecules are 0.015 and 0.007 for Uranine, and 0.003 and 0.0003 for Rhodamine B, respectively.

The electronic energy transfer in the semiconductor-aqueous solution interface is a fundamental process for semiconductor photochemistry and electrochemistry, and the detailed analysis of this process is closely related to the elucidation of related topics in photobiology, photographic science, and catalysis science, as well as the utilization of solar energy. Many reports[1–6] in which ZnO is used as a working electrode have been published in the fields of semiconductor electrochemistry. They cover the investigations of dye-sensitized photocurrents and the redox reactions as well as the construction of solar cells. In the photochemistry of ZnO powder, Cunningham *et al.*[7–13] have investigated the photoreduction of several molecules and ions on the ZnO–gas and ZnO–solution interfaces, and Dixon *et al.*[14] have reported on the photocatalytic reaction of H_2O on the ZnO–solution interface.

As to the photoreduction of metal ions, Tammann[15] has reported the darkening of an emulsion containing ZnO and Ag^+ under UV-irradiation. Recently, Fleischauer *et al.*[16,17] have investigated the photoreduction of $AgNO_3$ on the surface of ZnO and TiO_2 (rutile) single crystals by means of 365 nm light and obtained quantum yields of from 0.08 to 0.4 for the $AgNO_3$ concentrations of from 0.1 to 1.0 M respectively on the ZnO and also obtained quantum yields of from 0.016 to 0.03 for the $AgNO_3$ concentrations of from 0.001 to 0.01 M respectively on the TiO_2.

We have observed that the irradiation of an aqueous suspension of ZnO containing $AgClO_4$ by means of 365 nm light, which belongs to the fundamental absorption band of ZnO, produces colloidal silver adsorbed on the ZnO surface, and that this reaction can be optically sensitized by the addition of xanthene dyes. This reaction seems to be suitable for the study of the electron-transfer process in the interface because of its rather simple reaction. We have thus investigated the photoreduction of $AgClO_4$ in a ZnO aqueous suspension by means of 365 nm light and the optical sensitization of this reaction by two xanthene dyes, Uranine and Rhodamine B. It has been found that these dye molecules are decomposed in the course of the photoreduction of Ag^+. We also carried out preliminary measurements of the electrochemical properties of the ZnO–aqueous solution interface. Hence, we have obtained several significant conclusions regarding the reaction mechanism of the photoreduction of Ag^+ on the ZnO–aqueous solution interface.

Experimental

The ZnO used in the present study was a highly purified powder sample, labeled SAZEX-4000, which had been obtained by courtesy of the Sakai Kagaku Co., Ltd., Osaka. This material has a surface area of 4.6 m^2/g-ZnO, an average particle size of 0.5 μm, and very low impurities of Pb (0.002%) and Cd (0.0002%). $AgClO_4$, $AgNO_3$, and Uranine are of special grade, purchased from the Nakarai Chemicals Co., Ltd. The perchlorate salt of Rhodamine B was provided by the Nippon Kanko Shikiso Co., Ltd., Okayama. Distilled water was used for the preparation of all the aqueous suspensions of ZnO powder and of all the aqueous solutions employed in the study.

The reaction cell was a cylindrical quartz vessel of 4 cm in diameter and 20 cm in height. It was equipped with a flat window of 1.6 cm in diameter at the bottom for the irradiation of light and with a glass cap with a glass cock to introduce N_2 gas at the top. N_2 replacement was not carried out except when measuring the amount of dissolved oxygen in the suspension. All the parts of the reaction cell except for the flat window were covered with black cloth to avoid the entrance of any stray light. The aqueous suspensions were prepared in the dark. For the study of the dye-sensitized reduction, 0.5 g-ZnO powder was suspended in an 50 ml aqueous solution composed of $AgClO_4$ and xanthene dye. The buffer solution was not added in either case, because this might cause some undesirable reactions. The reaction mixture was rigorously mixed by a magnetic stirrer under a constant velocity throughout the reaction.

A 500 W xenon lamp, Type UXL-500D, with a Type DSB-500SS, power supply (Ushio Denki Co., Ltd.), was used as the light source. The monochromatic light for irradiation was selected by the combination of a monochromator (Shimadzu Seisakusho Co., Ltd.) and an appropriate glass filter (Toshiba Co., Ltd.). For the study of the unsensitized reduction, 365 nm light was used. For the study of the dye-sensitized reductions, 490 nm light was used for Uranine and 560 nm light for Rhodamine B (designated as dye-light). The irradiation was commenced after the adsorption equilibrium had been established. It takes about 30 min for the unsensitized system, and about 180 min for the dye-sensitized system, to attain the adsorption equilibrium. After the irradiation, the reaction mixture in the solid state was collected through a sintered glass filter, washed completely with a large excess of distilled water, dissolved by

HNO_3, and then submitted to the quantitative analysis of the Ag^+. The details of the silver analysis by means of the differential potentiometric titration method were presented in our previous paper.[18] The decomposition products of ZnO and dyes by HNO_3 did not hinder the analysis of the reduced silver.

The incident intensities of 365 nm light on the reaction vessel were measured by the use of the ferrioxalate actinometer, using the quantum yields determined by Parker.[19] Those of dye-light were determined with the aid of a photometer, Type IL-600 (International Light Co., Ltd.). In this work, the numbers of incident photons were 9.10×10^{14} photon/cm^2 s at 365 nm, 2.78×10^{15} photon/cm^2 s at 490 nm, and 1.89×10^{15} photon/cm^2 s at 560 nm. To calculate the number of photons absorbed by suspensions, the transmittance and the reflectance of suspensions were measured by the use of the spectrophotometers, MPS-5000 and QV-50 equipped with an integrating sphere (Shimadzu Seisakusho Co., Ltd.). The quantum yields of the photoreduction of Ag^+ for the unsensitized systems and the apparent quantum yield (the number of reacted molecules/the number of photons absorbed by suspension) for the dye-sensitized system were determined as follows:

$$\Phi = \frac{1}{Q}\cdot\frac{d[Ag]}{dt}, \quad (1)$$

where Φ is the quantum yield for the unsensitized system or the apparent quantum yield for the dye-sensitized system, $d[Ag]/dt$ the initial rate of the formation of the reduced silver (atom/s), and Q the number of photons absorbed by the suspension (photon/s). It is easy to determine the quantum yield for the unsensitized system by means of Eq. 1, because all the photons absorbed by the suspension at 365 nm are absorbed by ZnO itself. On the contrary, it is difficult to determine the quantum yield for the dye-sensitized system because some of the incident photons absorbed by free dye molecules in the solution, not by the dye adsorbed on ZnO, do not contribute to the photoreduction. Therefore, for the dye-sensitized system we have determined only the apparent quantum yield by means of Eq. 1.

The photobleach reactions of Uranine and Rhodamine B were studied in the suspensions described above. After the irradiation by dye-light, the suspension was filtered out and the optical density of the filtrate at this wavelength was measured. From this, the amount of dyes photobleached during the sensitized photoreduction was determined. The adsorption isotherm of Ag^+ adsorbed in equilibrium was determined after the ZnO powders had been immersed in 5×10^{-5} to 1×10^{-3} M solutions of $AgClO_4$ for 3 h under a constant stirring.

The electrochemical measurements of the ZnO sinter electrode were carried out in a conventional manner.[6,20] ZnO powder SAZEX-4000 was placed, in pellets, on a disk of 10 mm in diameter and 0.5 mm thick, and then sintered at 1000 °C for 2 h in air. After cooling to room temperature, it was activated at 550 °C under 1×10^{-4} mmHg for 3 h. The surface of ZnO electrode was etched by 85% H_3PO_4 and washed with distilled water before use. A platinum plate was used as the counter electrode, and a saturated KCl-Ag/AgCl electrode of the double-junction type was used as the reference electrode. The electrochemical measurements of the cell thus constructed were carried out by means of a potentiostat equipped with an electrometer, Type HA-104 (Hokuto Denko Co., Ltd.). The electrolyte solutions were composed of 0.5 M KNO_3 or of a mixed solution of 0.5 M KNO_3 and 1.0×10^{-4} M $AgClO_4$. Before the measurements, dissolved O_2 was purged by the introduction of high-purity N_2 gas.

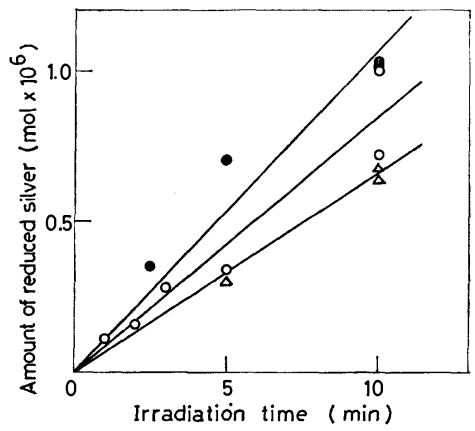

Fig. 1. Growth of the amount of reduced silver in ZnO suspension containing $AgClO_4$ with irradiation time. ●: $[AgClO_4]=1.0\times10^{-3}$ M, ○: 1×10^{-4} M, and △: 5×10^{-5} M.

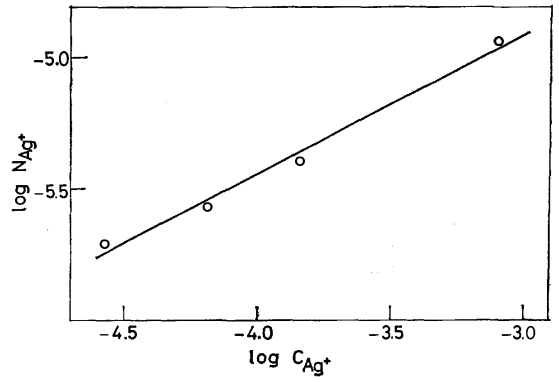

Fig. 2. Plots showing the Freundlich type adsorption for Ag^+ on ZnO surface. Index of adsorption is 0.53. N_{Ag^+}, and C_{Ag^+} denote the amount of adsorbed Ag^+ (mol/g-ZnO) and the concentration of Ag^+ in aqueous phase (mol/l).

Results

Photoreaction in the Unsensitized System. The dependence of the amount of reduced silver on the irradiation time of 365 nm light for the ZnO–$AgClO_4$ aqueous suspension is given in Fig. 1. The thermal reduction in the dark is negligible as compared with the photoreduction. From the rate of Ag^+ reduction obtained by means of the method of least squares in Fig. 1, and the number of photons absorbed at 365 nm in the suspensions, the quantum yield of the photoreduction of Ag^+ was calculated. The values are 0.385±0.016, 0.303±0.021, and 0.235±0.004 for $AgClO_4$ concentrations of 1.0×10^{-3}, 1.0×10^{-4}, and 5.0×10^{-5} M respectively. The pH values of the suspensions are 6.8, 6.6, and 6.5 for $AgClO_4$ concentrations of 1.0×10^{-3}, 1.0×10^{-4}, and 5.0×10^{-5} M respectively. The pH change during the irradiation was not remarkable after 30 min irradiation. The quantum yields obtained here are much larger than

those predicted by the extrapolation of the results of Fleischauer *et al.*[16] on the photoreduction of $AgNO_3$ on the ZnO single crystal. Cunningham *et al.*[10] reported that $NaNO_3$ is reduced to $NaNO_2$ by UV-light in the ZnO–aqueous suspension. Therefore, we have carried out the photoreduction of $AgNO_3$ by the same reaction system as $AgClO_4$. The quantum yields for $AgNO_3$ are nearly equal to that for $AgClO_4$. Therefore, these results seem to suggest the differences in the physicochemical properties of the ZnO employed by different investigators.

The adsorption isotherm of Ag^+ on the ZnO surface was measured at 20 °C. It is given in Fig. 2. In the equilibrium state, the concentration of Ag^+ in the aqueous phase, C_{Ag^+}, and the amount of adsorbed Ag^+ on the surface of 1.0 g-ZnO, N_{Ag^+}, satisfy Freundlich's adsorption formula:

$$N_{Ag^+} = \alpha(C_{Ag^+})^{1/n}, \tag{2a}$$

$$\log N_{Ag^+} = \log \alpha + \frac{1}{n} \log C_{Ag^+}. \tag{2b}$$

(α, n: constant)

The adsorption index, $1/n=0.53$, is a rather reasonable value.

We tried to clarify the behavior of the positive hole by the detection of the increases in the dissolved O_2 and Zn^{2+} in the aqueous phase during the photoreaction. A 50 ml aqueous suspension of 0.5 g of the ZnO and 1.0×10^{-3} M $AgClO_4$ was prepared. The dissolved O_2 was measured by the use of an oxygen meter, Model DO-2A (Toa Denpa Co., Ltd.). The amount of O_2 dissolved in the suspension is decreased by the introduction of N_2 gas in the dark under constant stirring. Then, the suspension was irradiated with 365 nm light for 40 min, and the increase of the dissolved O_2 was recorded. The observed value of 2.6×10^{-6} mol is nearly equal to the amount of photoreduced silver of 3.9×10^{-6} mol under the same reaction conditions. The increase in Zn^{2+} was examined by colorimetric analysis using Xylenol Orange as an indicator.[21-23] The same suspension described above was also irradiated by 365 nm light for 40 min and then filtered. 0.1% Xylenol Orange and a buffer solution (pH=5.6) were added to the filtrate, and the absorption spectra were recorded. A characteristic peak was observed at 571 nm which was not distinct in the unirradiated case. This surely implies that Zn^{2+} increases after the irradiation. From these results, the positive hole produced by 365 nm light can be thought to react with the chemisorbed oxygen ion or water molecule on the ZnO surface, as well as with the oxygen ion in the ZnO lattice.[14,24,25]

The current-voltage characteristics of the ZnO sinter electrode were also studied. The electrolyte solution was composed of either 0.5 M KNO_3 or a mixture of 0.5 M KNO_3 and 1.0×10^{-4} M $AgClO_4$. The polarization curves obtained are given in Figs. 3 and 4. The solid line and the dashed line indicate the currents measured under the irradiation and in the dark respectively. The dotted line indicates the partial anodic photocurrents.[26-28] This is obtained by the subtraction of the current in the dark from

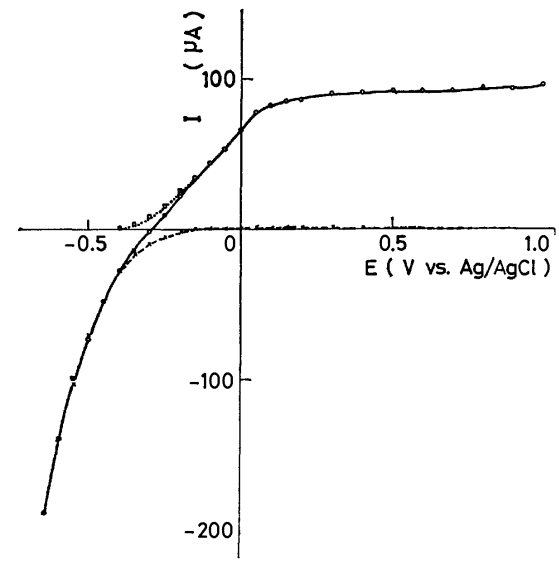

Fig. 3. Polarization curves of ZnO electrode in 0.5 M KNO_3 solution. ○——○: Measured currents under irradiation, ×----×: measured currents in the dark, □·····□: the partial anodic photocurrents defined in the text.

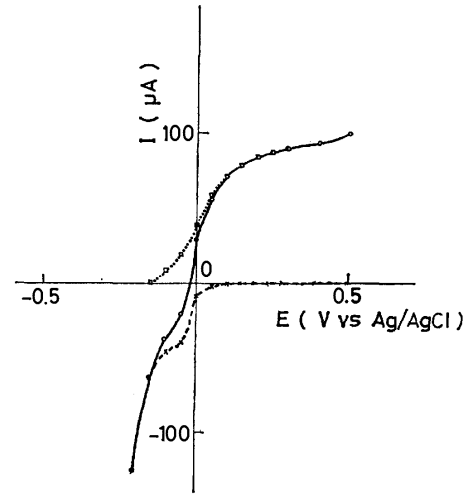

Fig. 4. Polarization curves of ZnO electrode in 0.5 M KNO_3 solution containing 1×10^{-4} M $AgClO_4$. ○——○: Measured currents under irradiation, ×----×: measured currents in the dark, □·····□: the partial anodic photocurrents defined in the text.

the current measured under the irradiation. Because the irradiation should not affect the cathodic current, the cathodic current measured in the dark is equal to that under the irradiation. Therefore, the partial anodic photocurrent indicates the real anodic element of the current under the irradiation.

Under the irradiation at the electrode potential of —0.030 V *vs.* Ag/AgCl in Fig. 4, the cathodic current cancels the anodic current on the ZnO sinter electrode, so the total current is zero (Zero-current-potential). The cathodic current at this potential is 24 μA in Fig. 4, but it is almost zero at this potential in Fig. 3. If all the cathodic current contributes to the reduction

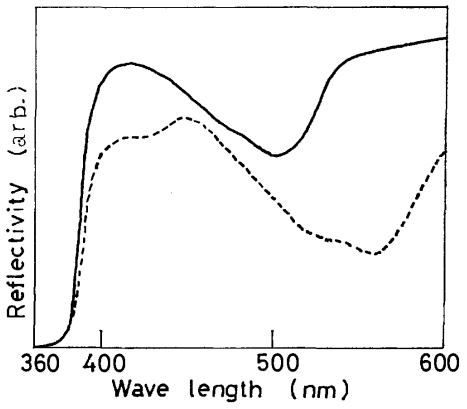

Fig. 5. Reflection spectra of ZnO-$AgClO_4$-Uranine (——) and ZnO-$AgClO_4$-Rhodamine B (----) aqueous suspensions.

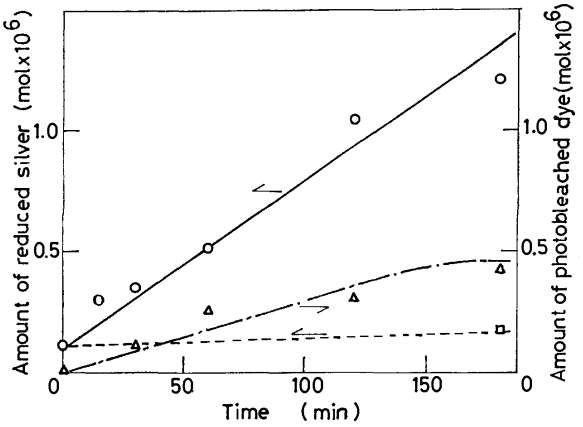

Fig. 6. Growth of the amount of reduced silver in ZnO suspension containing $AgClO_4$ and Uranine with irradiation of 490 nm light (O——O) and in the dark (□----□). Growth of the amount of photobleached dye is also given (△———△).

of Ag^+, we can determine the rate of photoreduction of Ag^+ on this electrode from this value. Indeed, the rate evaluated in this manner is in accord with the value obtained by the chemical-analysis method in the same electrode reaction system, within the limits of experimental error. Therefore, almost all the cathodic current at the zero-current-potential can be said to contribute to the photoreduction of Ag^+.

The onset point of the partial anodic photocurrents corresponds to the flat-band potential. We can see that this potential (—0.40 V *vs.* Ag/AgCl in Fig. 3) is shifted to a more positive value (—0.15 V *vs.* Ag/AgCl in Fig. 4) when $AgClO_4$ is added to the electrolyte solution.

Photoreaction in the Dye-Sensitized Systems. The diffuse reflection spectra of ZnO–$AgClO_4$ aqueous suspensions containing dye were recorded on a MPS-5000 spectrophotometer. The results are given in Fig. 5. The absorption band shorter than 385 nm corresponds to the fundamental absorption of ZnO. The monomer absorption maxima of dyes exist at 490 nm for Uranine and 560 nm for Rhodamine B. No peaks due to the dye aggregation were found.

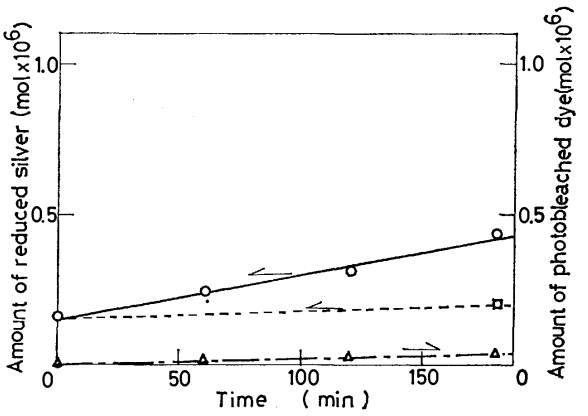

Fig. 7. Growth of the amount of reduced silver in ZnO suspension containing $AgClO_4$ and Rhodamine B with irradiation 560 nm light (O——O) and in the dark (□----□). Growth of the amount of photobleached dye is also given (△———△).

In the case of the Uranine system, the dependence of the amounts of photoreduced silver on the irradiation time is given in Fig. 6. The concentrations of $AgClO_4$ and dye are 1.0×10^{-4} and 1.0×10^{-5} M respectively. From the initial slope of the photoreduction curve and the number of absorbed photons, the apparent quantum yield of the photoreduction of Ag^+ is found to be 0.015. It is observed that a photobleach of the dye proceeds simultaneously with the Ag^+ reduction. The dependence of the amount of photobleached dye on the irradiation time is also shown in Fig. 6. The apparent quantum yield of this reaction is 0.007. We have found that the photoreduction of Ag^+ and the photobleach of the dye cannot occur in the absence of ZnO. Therefore, it is impossible that Ag^+ is directly reduced by the dye molecules without the participation of ZnO. The amount of reduced silver is about twice as large as the amount of Uranine which exists in the suspension at the beginning. This means that at least two Ag^+s are reduced by one Uranine molecule.

As to the Rhodamine B system, the amounts of reduced silver and photobleached dye are given in Fig. 7. The concentrations of $AgClO_4$ and dye are the same as in the Uranine system. The apparent quantum yields of 0.003 and 0.0003 were obtained for the photoreduction of Ag^+ and the photobleach of Rhodamine B respectively. These values are smaller than those in the Uranine system.

Discussion

Reaction Scheme. The amount of adsorbed Ag^+ plays a significant role in the photoreduction. We tried to interpret the dependence of the quantum yields on the $AgClO_4$ concentrations with the help of the simple reaction scheme of Fleischauer *et al*:[16]

$$ZnO + h\nu \xrightarrow{\theta} e(s) + p, \quad (3a)$$

$$e(s) + Ag^+(s) \xrightarrow{k_1} Ag(s), \quad (3b)$$

$$e(s) \xrightarrow{k_2} \text{non-reactive state}, \quad (3c)$$

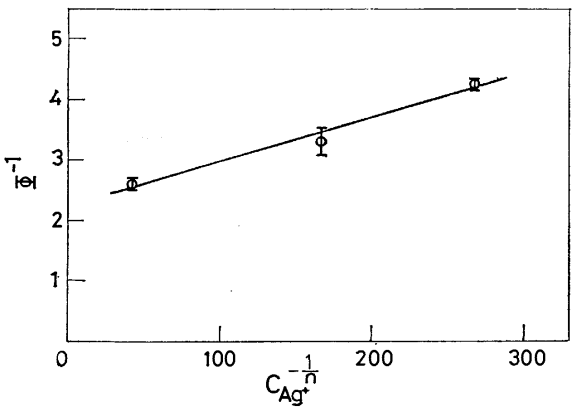

Fig. 8. Reciprocal plots between the quantum yield Φ and $(C_{Ag^+})^{1/n}$.

where e(s) and p denote the surface electron and the free hole produced by the light, and where $Ag^+(s)$ and Ag(s) denote the silver ion and the atom adsorbed on ZnO surface, respectively. In this scheme, the excitation of ZnO produces a surface electron with an efficiency of θ. This electron reacts with the adsorbed silver ion at the solid-liquid interface with the rate constant of k_1. Some part of this electron will be converted to the non-reactive state, with the average rate constant of k_2, by trapping, recombination, or reaction with some impurites on ZnO. Assuming the stationary concentration of e(s), the quantum yield of the Ag formation is expressed as

$$\Phi = \frac{\theta k_1 N_{Ag^+}}{k_2 + k_1 N_{Ag^+}}. \quad (4)$$

From Eqs. 2a and 4, we can obtain

$$\Phi^{-1} = \frac{k_2}{\alpha k_1 \theta}(C_{Ag^+})^{-1/n} + \frac{1}{\theta}. \quad (5)$$

The experimental relation between Φ^{-1} and $(C_{Ag^+})^{-1/n}$ given in Fig. 8. confirms our assumption that the adsorption equilibrium of Ag^+ on the ZnO surface is not perturbed very much in the earlier stage of the photoreaction and that the dependence of the quantum yield on the Ag^+ concentration can be interpreted by means of this scheme.

ZnO–Aqueous Solution Interface. It is well known[12,25,29] that there exists a surface-energy barrier for electrons in the space-charge layer of ZnO left in air due to electron localization on the surface-energy levels of the chemisorbed oxygen. When ZnO is in contact with an aqueous solution, the surface barrier will change with the pH or some other properties of the solution. In the aqueous suspension of ZnO studied here, both Ag^+ and ClO_4^-, as well as H^+, OH^-, and H_2O exist in the solution. Therefore, the surface barrier would be considerably changed from that in air.

Now, let us assume that the results of the ZnO suspension can be analyzed by an electrochemical study of the ZnO sinter. This is supported by the fact that the quantum yield of the photoreduction of Ag^+ on the ZnO sinter is almost the same as that in the ZnO suspension. First, let us consider the surface-energy barrier of the ZnO sinter in view of the results of the electrochemical measurements. In the "local cell model" of the photoreaction on the ZnO sinter, the electrode potential of the ZnO sinter immersed in the solution under the irradiation is equal to the zero-current-potential, noted before. We also found from the photopotential measurement of the ZnO electrode, that the electrode potential is indeed −0.030 V *vs.* Ag/AgCl under the irradiation and that it shifts to a more positive value (0.315 V *vs.* Ag/AgCl was measured), when the 365 nm light is cut off. According to the results of the photocurrent and the photopotential measurements cited above, it may be concluded that the upward band bending still exists in the space-charge layer of ZnO, because the flat-band potential of the ZnO electrode in the presence of Ag^+ is more negative than the electrode potential either in the dark or under the irradiation. It is evident that the bottom of the conduction band at the surface does not change so much as the electrode potential on the irradiation. From these facts, the surface barrier of the ZnO sinter in the $AgClO_4$ solution can surely be said to be much smaller under the irradiation of 365 nm light. This effect may be due to the rapid consumption of the positive hole, and the resultant accumulation of photoelectrons in the conduction band under the influence of the electric field of the space-charge layer. The photoelectrons in the conduction band can react with $Ag^+(s)$ over the surface barrier, which is considerably smaller than that in the dark. The rate of the photoreduction of Ag^+ is equal to the rate of hole consumption in the photostationary state. This corresponds to a "local cell model."[26–28]

In Figs. 3 and 4 the shift of the flat-band potential is observed upon the addition of $AgClO_4$. Lohmann[4] has demonstrated that the flat-band potential of a ZnO electrode is shifted as the pH of the solution is changed. The pH value of the solution containing 0.5 M KNO_3 is 5.1, and that of the solution containing 0.5 M KNO_3 and 1×10^{-4} M $AgClO_4$ is 5.2, so the shift of the flat-band potential observed in our case is much larger than that to be expected from the pH change by the addition of $AgClO_4$. Therefore, we can assume that when $AgClO_4$ is added, the pH change and also the specific adsorption of Ag^+ on the ZnO surface contribute to the shift of the flat-band potential. Ag^+ is specially adsorbed in the Helmholtz layer on the surface of ZnO and causes the changes in the physicochemical properties of the surface. This is not inconsistent with Freundlich's adsorption isotherm of Ag^+ on the surface of ZnO, which can be interpreted in terms of the assumption that the adsorbate can occupy various surface points whose adsorption energies are distributed exponentially. Morrison[3] reported that the flat-band potential of a ZnO electrode does not change when several other metal ions are added to the electrolyte solution. However, we think that Ag^+ may play a specific role, in contrast to the ions reported by him. The exact determination of the flat-band potential of the ZnO electrode by the impedance measurement when Ag^+ is added to the electrolyte solution is in progress. Our results will be published in forthcoming paper.

In the reaction scheme discussed in the previous section, it was assumed that the surface barrier under the irradiation does not change even if the concentrations of Ag^+ in the solution are varied. In fact, the differences between the flat-band potential and the electrode potential under the irradiation in Figs. 3 and 4 are almost the same. This means that, although the flat-band potential of the electrode is changed by the addition of $AgClO_4$, the surface barrier under the irradiation does not change very much by the addition of $AgClO_4$.

Cunningham *et al.*[7,10] have obtained that quantum yields of about 10^{-5} for the photoreduction of N_2O on the surface of ZnO powder and of 10^{-1} to 10^{-3} for the photoreduction of various molecules and ions in a ZnO aqueous suspension. They interpreted the greatly enhanced quantum efficientcies of the photoreaction at ZnO–water interface relative to the ZnO–gas interface, at least in part, by the assumption that there exists a rather downward band bending due to the predominance of H^+ over OH^- on the surface of ZnO at a neutral pH, but such bending would not be reasonable in our case. The much larger quantum yields and the relatively small dark reaction rates obtained by us must be mainly the result of the decrease in the surface barrier for the conduction-band electron, as has been described above.

The Mechanism of Dye Sensitization. There have been many studies of the dye sensitization of ZnO in terms of both photoelectric and electrochemical properties. In these studies, the external electric field was applied to the ZnO material, and the photocurrent caused by the energy transfer or the charge transfer from the dye in contact with them was measured. In our study, the photoelectron is moved by the electric field of the space-charge layer originally present in the ZnO–aqueous solution interface.

Because ZnO plays a decisive role in the dye-sensitized photoreduction of Ag^+, the following reaction mechanism seems probable. In the first step, the energy transfer or the charge transfer from the dye molecules adsorbed to ZnO occurs, and the concentration of the conduction-band electron increases, then the conduction-band electron in ZnO transfers to the Ag^+ adsorbed on the surface through the interface in the same manner as the unsensitized reduction of Ag^+. If we assume that the surface barrier of ZnO in the presence of $AgClO_4$ can hardly be affected by the addition of dyes, the quantum yield of the dye-sensitized photoreduction of Ag^+ would be of the same magnitude as the product of the quantum yields of the photocurrent generation and the unsensitized photoreduction of Ag^+. According to Tsubomura *et al.*,[20] the quantum yield of the photocurrent of a ZnO electrode by Rose Bengal, one of the xanthene dyes, is 0.22. In our study, the quantum yields of 0.23 to 0.50 have been determined for the reduction of Ag^+ by 365 nm light on the ZnO surface. Therefore, the apparent quantum yields of 0.015 and 0.003 obtained by us for the dye-sensitized photoreduction of Ag^+, which correspond to the minimum of the real quantum yields, are rather reasonable.

A large difference was found in quantum yields of the photobleach between the two dyes. The ratios of the apparent quantum yields of the photoreduction of Ag^+ by dyes to those of the photobleach of dyes are 2.2 for Uranine and 10 for Rhodamine B. It seems that these numbers show how many times one dye molecule contributes to the photoreduction of Ag^+. We think that the photobleach and the reproduction of dyes are related to the sensitization mechanism of a semiconductor.

The authors wish to thank the Nippon Kanko Shikiso Co., Ltd., Okayama, for kind providing the dyes, and the Sakai Kagaku Co., Ltd., Osaka, for the ZnO. This work was carried out with financial support from the Ministry of Education of Japan (Grant-in-Aid No. 147073).

References

1) H. Gerischer, M. E. Michel-Beyerle, F. Rebentrost, and H. Tributsch, *Electrochem. Acta*, **13**, 1509 (1968).

2) H. Gerischer and H. Tributsch, *Ber. Bunsenges. Phys. Chem.*, **72**, 437 (1968).

3) S. R. Morrison, *Surface Sci.*, **15**, 363 (1967).

4) F. Lohmann, *Ber. Bunsenges. Phys. Chem.*, **70**, 428 (1966).

5) A. Fujishima and K. Honda, *Denki Kagaku*, **43**, 606 (1975).

6) M. Matsumura, K. Yamamoto, and H. Tsubomura, *Nippon Kagaku Kaishi*, **1976**, 399.

7) J. Cunningham, J. J. Kelly, and A. L. Penny, *J. Phys. Chem.*, **74**, 1992 (1970).

8) J. Cunningham, J. J. Kelly, and A. L. Penny, *J. Phys. Chem.*, **75**, 617 (1971).

9) J. Cunningham and A. L. Penny, *J. Phys. Chem.*, **76**, 2353 (1972).

10) J. Cunningham and H. Zainal, *J. Phys. Chem.*, **76**, 2362 (1972).

11) J. Cunningham and A. L. Penny, *J. Phys. Chem.*, **78**, 870 (1974).

12) J. Cunningham, E. Finn, and N. Samman, *Discuss. Faraday Soc.*, **58**, 160 (1974).

13) J. Cunningham and S. Corkery, *J. Phys. Chem.*, **79**, 933 (1975).

14) D. R. Dixon and T. W. Healy, *Aust. J. Chem.*, **24**, 1193 (1971).

15) G. Tammann, *Z. Anorg. Chem.*, **114**, 15 (1920).

16) P. D. Fleischauer, H. K. Alan Kan, and J. R. Shepherd, *J. Am. Chem. Soc.*, **94**, 283 (1972).

17) A. W. Adamson and P. D. Fleischauer, "Concepts of Inorganic Photochemistry," John Wiley & Sons, New York (1975), p. 400.

18) H. Hada, Y. Yonezawa, A. Yoshida, and A. Kurakake, *J. Phys. Chem.*, **80**, 2728 (1976).

19) C. A. Parker, *Proc. R. Soc. London, Ser. A*, **220**, 104 (1953).

20) M. Matsumura, Y. Nomura, and H. Tsubomura, *Bull. Chem. Soc. Jpn.*, **50**, 2533 (1977).

21) Y. Ishihara, S. Naniwa, K. Yokokura, and S. Uchida, *Bunseki Kagaku*, **17**, 991 (1968).

22) T. Miyajima, *Bunseki Kagaku*, **13**, 256 (1964).

23) E. Ideno and K. Hozumi, *Bunseki Kagaku*, **17**, 727

(1968).
24) A. Fujishima and K. Honda, *Denki Kagaku*, **40**, 33 (1972).
25) T. Kwan, "Kagakuzokan, 20," ed by T. Kwan, M. Koizumi, and I. Tanaka, Kagaku Dojin, Kyoto (1965), p. 101.
26) H. Yoneyama, H. Toyoguchi, and H. Tamura, *J. Phys. Chem.*, **76**, 3460 (1972).
27) M. Miyake, H. Yoneyama, and H. Tamura, *Electrochim. Acta*, **21**, 1065 (1976).
28) F. Möllers, H. J. Tolle, and R. Memming, *J. Electrochem. Soc.*, **121**, 1160 (1974).
29) H. Kokado and T. Yamaguchi, *Kagaku To Kogyo*, **17**, 1344 (1964).

Crystal Structures of Dichlorobis(azocyclohexane)palladium(II) and Dichlorobis(azoisopropane)palladium(II)

Takashi YAMANE,* Tamaichi ASHIDA, Hiroharu SUZUKI,†
Kenji ITOH,†† and Yoshio ISHII†††

Department of Applied Chemistry and Department of Synthetic Chemistry, Faculty of Engineering, Nagoya University, Chikusa, Nagoya 464

(Received April 26, 1978)

The structures of dichlorobis(azocyclohexane)Pd(II) and dichlorobis(azoisopropane)Pd(II) have been determined. The crystallographic data are: dichlorobis(azocyclohexane)Pd(II), Im3, $a=16.538(2)$Å, $Z=6$, $R=8.9\%$ for 667 reflections; dichlorobis(azoisopropane)Pd(II), Pbca, $a=7.461(1)$, $b=17.096(1)$, $c=14.784(1)$Å, $Z=4$, $R=6.8\%$ for 1451 reflections. In dichlorobis(azocyclohexane)Pd(II), a disorder occurs at the azo group, and the coordination mode of the ligand is not clear. The structure of dichlorobis(azoisopropane)Pd(II) agrees with that of dichlorobis(azobenzene)Pd(II).

The transition-metal which generates a nitrene R–N has attracted much attention from both organic and inorganic chemists in the last decade. A possible precursor is *N,N*-dichloroamine, which may generate nitrenes or nitrenoids by a reductive elimination of two chlorine atoms with some low-valent transition-metal complexes. Little is known about this process. Previously, some of the present authors reported that *N,N*-dichloroamine or -amide generated nitrenoids by a reaction with $Fe_2(CO)_9$,[1] and that tetrakis(methoxycarbonyl)palladiacyclopentadiene, $[PdC_4(COOCH_3)_4]_n$,[2,3] induced a ring-opening of the palladole skeleton with *N,N*-dichloroacylamides.[4]

This paper will describe some X-ray structure analyses of dichlorobis(azocyclohexane)palladium(II), $PdCl_2(c\text{-}C_6H_{11}\text{–}N{=}N\text{–}C_6H_{11}\text{-}c)_2$ I, which was obtained by the reaction of $[PdC_4(COOCH_3)_4]_n$ and $c\text{-}C_6H_{11}\text{–}NCl_2$, and of the related dichlorobis(azoisopropane)-palladium(II), $PdCl_2(i\text{-}C_3H_7\text{–}N{=}N\text{–}C_3H_7\text{-}i)_2$ II, which was prepared by a ligand-exchange reaction between an excess of azoisopropane and dichlorobis(benzonitrile)palladium(II). The X-ray structure indicated unequivocally that the cyclohexylnitrene generated by the palladium complex was dimerized to azocyclohexane, which was then coordinated to the palladium(II). The azocyclohexane complex, I, exhibits a substantial disorder around the azo nitrogen atoms. However, the structure of the azoisopropane complex, II, has the lone-pair coordination of the azo group, in a fashion similar to the dichlorobis(azobenzene)-palladium(II).[5]

Experimental

Preparation of Dichlorobis(azocyclohexane)palladium(II) I. A benzene (2 ml) solution of *N,N*-dichlorocyclohexylamine (0.678 g, 4.04 mmol) was stirred into a benzene (10 ml) suspension of $[PdC_4(COOCH_3)_4]_n$ (0.359 g, 0.921 mmol) under an argon atmosphere at room temperature. The mixture turned to an orange solution, which was then stirred overnight. Ethyl ether (5 ml) was added to the mixture, resulting in the formation of a reddish brown solid of $c\text{-}C_6H_{11}NH_2\cdot HCl$, which was then filtered off. The brown filtrate was concentrated to *ca.* 2 ml under reduced pressure. A mixed solvent composed of ethyl ether and methanol (1:1 vol ratio) was added to the oily residue, and the mixture was kept in a refrigerator for a few days to give $PdCl_2(c\text{-}C_6H_{11}\text{–}N{=}N\text{–}C_6H_{11}\text{-}c)_2$ as yellow prisms in a 16.7% yield. Mp 159.5—160.0 °C. IR(KBr); 2930, 2850(C-H), 1596, 1433, and 338(Pd-Cl)cm^{-1}. NMR($CDCl_3$); δ 5.45(br, 2H, CH-N), 5.35(br, 2H, CH-N), 0.79—2.55(m, 40H, other cyclohexyl protons). CMR($CDCl_3$); δ 32.59(C(1)), 29.40, 29.29(C(2)), 25.41, 25.12, 24.03, and 23.84(C(3), C(4)).

Found: C, 51.05; H, 7.89; N, 9.74%. Calcd for $C_{24}H_{44}N_4Cl_2Pd$: C, 50.94; H, 7.84; N, 9.90%.

The same complex was prepared in a 55.2% yield by the reaction of dichlorobis(benzonitrile)palladium(II) (209.8 mg) with an excess of azocyclohexane (0.6 ml) in benzene (10 ml). The X-ray analysis indicated that this is the same as the above complex. Found: C, 50.96; H, 8.07; N, 9.72%.

Preparation of Dichlorobis(azoisopropane)palladium(II) II. An excess of azoisopropane (0.5 ml) was stirred, drop by drop, into a benzene (10 ml) solution of dichlorobis(benzonitrile)palladium(II) (198 mg, 0.517 mmol) at room temperature. The reaction took place instantaneously to give a pale yellow solution. The benzene and the excess azoisopropane were removed under reduced pressure after 1 h. The crude II was obtained quantitatively and was recrystallized from 8 ml of dry methanol to yield yellow prisms. Mp 136—137 °C. IR(KBr); 2960, 2920 (C–H), 1594, and 335(Pd–Cl)cm^{-1}. NMR($CDCl_3$); δ 5.60(brm, 2H, CH-N), 4.87(m, 2H, $J=7$ Hz, CH-N), and 1.51(d, 24H, $J=7$ Hz, CH_3).

Found: C, 35.49; H, 7.29; N, 13.92%. Calcd for $C_{12}H_{28}N_4Cl_2Pd$: C, 35.53; H, 6.96; N, 13.81%.

Crystallographic Procedure. The crystal data are as follows. Complex I; *F.W.*=566.0, Im3, $a=16.538(2)$Å, $Z=6$, $D_m=1.27$, $D_x=1.247$ g cm^{-3}, and μ(Mo $K\alpha$)=8.17 cm^{-1}. Complex II; *F.W.*=405.7, Pbca, $a=7.461(1)$, $b=17.096(1)$, $c=14.784(1)$Å, $Z=4$, $D_m=1.38$, $D_x=1.434$ g cm^{-3}, and μ(Mo $K\alpha$)=12.1 cm^{-1}.

For I, the intensity data were collected on a Hilger & Watts automatic diffractometer (at the Faculty of Science, Nagoya University) using Zr-filtered Mo $K\alpha$ radiation. 741 reflections with $2\theta\leq50°$ were measured by the θ-2θ step-scan technique. For II, 2148 reflections with $2\theta\leq55°$ were obtained by the use of a Rigaku automatic diffractometer (at the Institute for Protein Research, Osaka University), using Mo $K\alpha$ radiation and a Graphite-crystal monochro-

† Present address: Laboratories of Resources Utilization, Tokyo Institute of Technology, Nagatsuta, Midori, Yokohama 227.

†† Present address: School of Materials Science, Toyohashi University of Technology, Toyohashi, Aichi 440.

††† Present address: Department of Industrial Chemistry, Chubu Institute of Technology, Kasugai, Aichi 487.

TABLE 1. DICHLOROBIS(AZOCYCLOHEXANE)Pd(II): THE ATOMIC PARAMETERS AND THEIR ESTIMATED STANDARD DEVIATIONS($\times 10^4$)

The thermal parameters are in the form: $\exp(-\beta_{11}h^2-\beta_{22}k^2-\beta_{33}l^2-\beta_{12}hk-\beta_{13}hl-\beta_{23}kl)$.

	Wyckoff position[a]	x	y	z	β_{11}	β_{22}	β_{33}	β_{12}	β_{13}	β_{23}
Pd	b	5000	0	0	34(1)	38(1)	42(1)	0	0	0
Cl	e	5000	0	1392(3)	61(2)	76(3)	45(2)	0	0	0
N(1)	g	3811(13)	257(12)	0	32(8)	41(11)	44(8)	−1(12)	0	0
N(2)	g	3237(16)	−176(14)	0	40(9)	36(21)	70(12)	9(15)	0	0
C(1)	g	3506(11)	1079(11)	0	54(7)	53(7)	80(10)	49(13)	0	0
C(2)	h	3059(12)	1382(7)	748(6)	115(10)	44(4)	40(4)	29(11)	−10(11)	−8(7)
C(3)	h	3017(14)	2318(9)	754(10)	110(11)	51(5)	66(7)	37(13)	20(15)	−18(10)
C(4)	g	2600(18)	2597(17)	0	91(15)	84(13)	59(11)	75(22)	0	0

a) See Ref. 9.

TABLE 2. DICHLOROBIS(AZOCYCLOHEXANE)Pd(II): THE POSITIONAL PARAMETERS OF THE HYDROGEN ATOMS($\times 10^3$)

The standard deviations are given in parentheses.

	x	y	z
H(1)	401(13)	103(13)	0
H(21)	341(8)	109(8)	120(8)
H(22)	247(8)	99(10)	73(9)
H(31)	376(10)	250(7)	79(8)
H(32)	261(9)	249(8)	108(12)
H(41)	242(10)	331(13)	0
H(42)	198(16)	246(10)	0

mator (monochromator $2\theta=12.16°$). The θ-2θ scan was adopted . The crystals used for the data collection had the dimensions of $0.20\times0.25\times0.16$ mm for I and of $0.33\times0.30\times0.14$ mm for II. The intensity data were corrected for Lorentz and polarization effects, but no absorption correction was made.

Structure Determination

The structures were solved by the heavy-atom method. The refinement was carried out by the full-matrix least-squares method for I and by the block-diagonal least-squares method for II.[6] In the refinement, non-zero reflections were included and the weight $w=1/(\sigma^2(F)+a|F_o|+b|F_o|^2)$ was assigned, where $\sigma(F)$ is the standard deviation based on the counting statistics. The isotropic temperature factors for the H atoms were kept constant at 5.0 Å^2.

The space group of I is either Im3, I23, or $I2_13$, judging from the systematic absences of the reflections. However, $I2_13$ is excluded because the space group can not contain 6 molecules in a unit cell. If the space group is Im3, there exists an mmm symmetry in the complex, while in I23 a complex has a 222 symmetry. The refinement was carried out independently with Im3 and I23. The final R's for 667 reflections were: 8.9%(a=0.1181 and b=0.0062) for Im3 and 8.3% for I23. The R value with Im3 is inferior to that with I23. However, the structure of the cyclohexane group in I23 is greatly distorted from normal, while the structure in Im3 is reasonable. Thus the space group Im3 seems the more plausible. There is a disorder associated with the azo group. The correlation matrix, λ, shows that the correlation between the x parameters of N(1) and N(2) is significant ($\lambda_{jj'}=0.32$). The other correlations are insignificantly small.

The final R of II is 6.8% (a=0.0221 and b=0.0011) for 1451 reflections.

The atomic scattering factors were taken from "International Tables for X-Ray Crystallography," Vol. IV.[7] The calculations were carried out on the FACOM 230-60/75 computers at Nagoya University. The final atomic parameters are listed in Tables 1, 2, 3, and 4.[8]

TABLE 3. DICHLOROBIS(AZOISOPROPANE)Pd(II): THE ATOMIC PARAMETERS AND THEIR ESTIMATED STANDARD DEVIATIONS($\times 10^4$)

The thermal parameters are in the form: $\exp(-\beta_{11}h^2-\beta_{22}k^2-\beta_{33}l^2-\beta_{12}hk-\beta_{13}hl-\beta_{23}kl)$.

	x	y	z	β_{11}	β_{22}	β_{33}	β_{12}	β_{13}	β_{23}
Pd	0	0	0	173(1)	29(1)	35(1)	−2(1)	5(1)	−1(1)
Cl	2439(3)	694(1)	516(1)	201(3)	47(1)	54(1)	−38(3)	−11(3)	−15(1)
N(1)	1590(9)	−826(3)	−538(4)	228(13)	38(2)	36(2)	1(9)	30(10)	−3(4)
N(2)	2375(10)	−1380(4)	−168(4)	265(13)	35(2)	45(3)	26(11)	20(11)	5(4)
C(1)	1777(11)	−816(5)	−1558(4)	264(17)	51(3)	35(3)	26(13)	51(13)	13(5)
C(2)	2696(16)	−63(5)	−1800(4)	553(34)	57(4)	7(2)	−37(17)	109(15)	3(4)
C(3)	2516(14)	−1524(5)	−1950(5)	418(26)	49(3)	37(3)	3(17)	14(18)	−9(5)
C(4)	2132(11)	−1429(4)	820(5)	295(20)	37(3)	39(3)	33(12)	−12(13)	10(5)
C(5)	733(16)	−2032(6)	1013(6)	372(27)	72(5)	61(5)	−42(20)	55(21)	27(9)
C(6)	3952(16)	−1678(6)	1188(7)	410(31)	79(6)	66(6)	−38(23)	−67(23)	30(9)

Table 4. Dichlorobis(azoisopropane)Pd(II): the positional parameters of the hydrogen atoms($\times 10^3$)
The standard deviations are given in parentheses.

	x	y	z
H(1)	34(11)	−87(5)	−175(6)
H(21)	268(11)	−4(4)	−242(6)
H(22)	205(11)	40(5)	−137(6)
H(23)	380(13)	−9(4)	−138(7)
H(31)	239(10)	−151(5)	−259(5)
H(32)	177(12)	−197(5)	−173(6)
H(33)	389(12)	−155(5)	−171(6)
H(4)	175(12)	−90(5)	106(6)
H(51)	117(11)	−248(5)	72(6)
H(52)	−44(12)	−193(5)	73(7)
H(53)	58(12)	−215(5)	162(6)
H(61)	373(12)	−169(5)	180(6)
H(62)	463(11)	−124(5)	110(6)
H(63)	408(12)	−223(5)	99(6)

Table 5. Dichlorobis(azoisopropane)Pd(II): the best planes

(a) Equations of the best planes.

$X=ax$, $Y=by$, $Z=cz$

Plane I: Pd, Cl, N(1)
$-0.0293X-0.5090Y+0.8603Z=0$

Plane II: Pd, N(1), N(2)
$0.7978X+0.5830Y+0.1540Z=0$

Plane III: N(1), N(2), C(1), C(4)
$-0.8280X-0.5517Y-0.1006Z+0.1135=0$

Plane IV: C(1), C(2), C(3)
$0.6049X-0.1025Y+0.7897Z+0.8745=0$

Plane V: C(4), C(5), C(6)
$-0.2065X+0.4506Y+0.8685Z+0.3755=0$

(b) Dihedral angles(°) between the planes.

	I	II	III	IV
II	100.8			
III	102.6	176.1		
IV	135.5	123.0	121.6	
V	121.6	103.4	99.5	121.0

(c) Displacements($\times 10^3$ Å) of atoms from the planes.

The atoms with asterisks are not included in the best plane calculations.

II		III	
Pd	0	N(1)	−9
N(1)	0	N(2)	−27
N(2)	0	C(1)	17
C(1)*	−111	C(4)	21
C(4)*	32	Pd*	114

Description of Structures

Complex I. A disorder is observed at the azo group. A quarter part of the composite Fourier map is drawn in Fig. 1, where Cl is not drawn, since the Cl atom is in front of Pd. The two N atoms of the azo group are equivalent, and should be located at the d position of the space group Im3.[9] However, the Fourier and D-Fourier maps prepared with and without N(1) and N(2) made clear that the azo nitrogen atoms do not satisfy this situation. Therefore N(1) and N(2), with occupancies of 0.5 each, were located at the other special positions, g. This disordered model satisfies the symmetry, though no reasonable skeleton with proper covalent bonds can be proposed for this

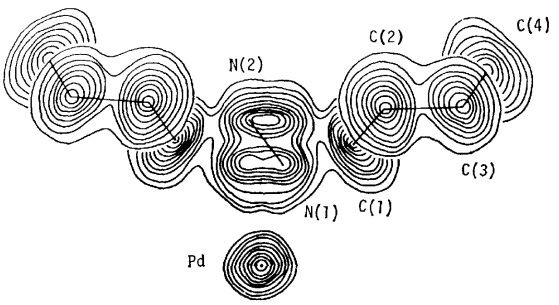

Fig. 1. Dichlorobis(azocyclohexane)Pd(II): The composite Fourier map. Cl is in front of Pd, and is not shown. For Pd, first contour 5 eÅ^{-3}, interval 10 eÅ^{-3}. For N and C, first contour 0.5 eÅ^{-3}, interval 0.5 eÅ^{-3}.

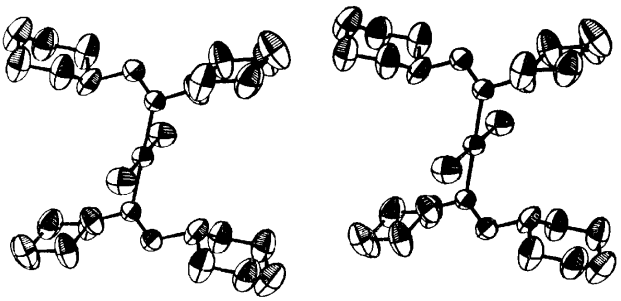

Fig. 2. Dichlorobis(azocyclohexane)Pd(II): The stereoscopic view of the model structure.

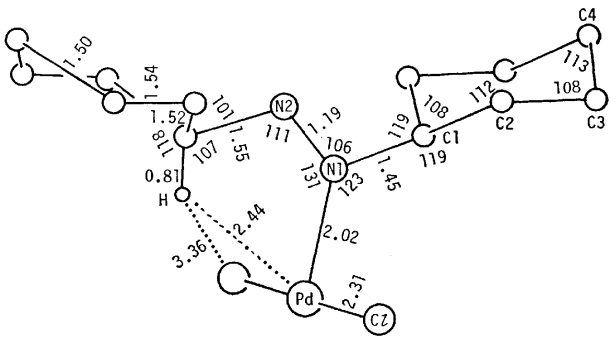

Fig. 3. Dichlorobis(azocyclohexane)Pd(II): Bond lengths(Å) and angles(°).

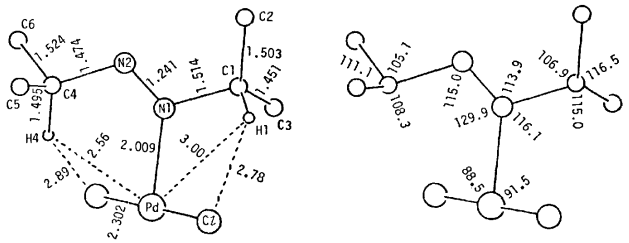

(a) (b)

Fig. 4. Dichlorobis(azoisopropane)Pd(II): (a) Bond lengths(Å). (b) Bond angles(°).

Table 6. Bond lengths and angles concerning the azo groups

	Dichlorobis(azo-isopropane)Pd(II)[a]	Dichlorobis (azobenzene)Pd(II)[b]	
(a) Bond lengths (Å)			
N(1)-N(2)	1.241	1.240	1.237
N(1)-C(1)	1.514	1.427	1.425
N(2)-C(4)	1.474	1.407	1.411
(b) Bond angles (°)			
Pd-N(1)-N(2)	129.0	129.0	129.3
Pd-N(1)-C(1)	116.1	117.8	117.7
N(2)-N(1)-C(1)	113.9	113.0	112.7
N(1)-N(2)-C(4)	115.0	118.7	118.1

a) This study. b) See Ref. 5.

complex. The refinement of the model structures gave the proper temperature factors for both N(1) and N(2), as compared with those of the other atoms. All the H atoms were found in the D-Fourier map. The H(1) peak is most prominent, with a height of 0.62 eÅ^{-3}. The other peaks ranged from 0.30 to 0.54 eÅ^{-3}. The stereoscopic view of one of the model structures drawn by ORTEP II[10] is shown in Fig. 2. The dimensions are given in Fig. 3. The e.s.d.'s are: 0.02—0.04 Å for bond lengths except for Pd–Cl (0.006 Å) and 1.7—2.2° for bond angles. The model shown in Figs. 2 and 3 is just a tentative one. Therefore, low-temperature work is desirable for this complex.

Complex II. The bond lengths and angles are given in Fig. 4. The e.s.d.'s are 0.007—0.014 Å for all the bond lengths except for Pd–Cl (0.002 Å), and 0.2—0.9° for the angles. The best planes and the related data are given in Table 5.

In II, there is no disorder, and a proper coordination mode is found which is similar to those of the other azo complexes. The symmetry of II is only a center of inversion. The two isopropyl groups are not equivalent to each other. The bond lengths and angles of the azo group of II are compared with those of dichlorobis(azobenzene)Pd(II), AZB,[5] in Table 6. The structures of the azo groups in both complexes are very similar to each other, though AZB has no symmetry in the molecule. The N(1)–C(1) length is larger than N(2)–C(4). The N–C bond lengths in AZB are much shorter than those in II. The bond angles concerning N(1), which coordinates to Pd, are in good agreement between II and AZB. However, the N(1)–N(2)–C(4) angles are significantly different in these complexes. The corresponding angle in II is smaller than that in AZB.

Short contacts involving the H atoms are found in these complexes. The H···Pd contacts are 2.56 Å in II, and 2.60 and 2.61 Å in AZB. Fairly short H···Cl contacts are observed: 2.78 Å in II, and 2.59 Å in AZB.

Discussion

When $[PdC_4(COOCH_3)_4]_n$[2,3] reacted with *N,N*-dichlorocyclohexylamine at room temperature, yellow-orange crystals with the composition of $PdCl_2(c\text{-}C_6H_{11}N)_4$, I, were obtained in a 16.7% yield. A complete elimination of the diene unit, $C_4(COOCH_3)_4$, from the palladiacyclopentadiene skeleton indicates the formation of a highly reactive Pd(0) state which abstracts two Cl atoms from *N,N*-dichlorocyclohexylamine to generate cyclohexylnitrene. The X-ray analysis of I made it clear that cyclohexylnitrene was dimerized to azocyclohexane, followed by the coordination of the dichloropalladium(II) moiety. The latter process was confirmed by the independent preparation of I from dichlorobis(benzonitrile)palladium(II) and azocyclohexane. This behavior is different from similar reactions between $[PdC_4(COOCH_3)_4]_n$ and several *N,N*-dichloroacyl amides,[4] which gave σ-4-chloro-1,2,3,4-tetrakis(methoxycarbonyl)buta-1,3-dienylpalladium complexes by the ring-opening of only one Pd–C bond of the palladiacyclopentadiene skeleton.

The NMR spectrum of I indicates two broad signals due to H(1) at δ 5.45 and 5.35; these signals show substantial low-field shifts from free azocyclohexane (δ 3.26) on coordination. The separation and intensive broadening of the two signals indicate that the two H(1)'s are not equivalent to each other in solution. The difference between the two cyclohexyl rings in solution is also consistent with the CMR spectrum of I, in which three signals corresponding to the C(2), C(3), and C(4) atoms are observed.

On the contrary, the NMR spectrum of II shows a well-separated multiplet(J=7 Hz) at δ 4.87, indicative of H(4), as well as a broad multiplet at δ 5.60, which is ascribed to H(1). This fact clearly suggests that the coordination mode of II in solution is consistently identical with that in the solid state.

The authors wish to express their thanks to Professor Masao Kakudo of Osaka University and Professor Jiro Tanaka of Nagoya University, who kindly allowed them to use the diffractometers in their laboratories. The authors are also grateful to Dr. Noritake Yasuoka of Osaka University for his helpful discussion.

References

1) H. Suzuki, K. Itoh, I. Matsuda, and Y. Ishii, *Chem. Lett.*, **1975**, 641.
2) K. Moseley and P.M. Maitlis, *J. Chem. Soc., Dalton Trans.*, **1974**, 169.
3) T. Ito, S. Hasegawa, Y. Takahashi, and Y. Ishii, *J. Organomet. Chem.*, **73**, 401 (1974).
4) H. Suzuki, K. Itoh, I. Matsuda, and Y. Ishii, *Chem. Lett.*, **1975**, 197.
5) G. P. Khare, R. G. Little, J. T. Veal, and R. J. Doedens, *Inorg. Chem.*, **14**, 2475 (1975).
6) All the programs used are in the "UNICS-Osaka" system, The Computation Center, Osaka University (1973).
7) "International Tables for X-Ray Crystallography," Kynoch Press, Birmingham (1974), Vol. IV, pp. 72—84.
8) The observed and calculated structure factors are available at the office of This Bulletin as Document No. 7837.
9) "International Tables for X-Ray Crystallography," Kynoch Press, Birmingham (1969), Vol. I, p. 314.
10) C. K. Johnson, "ORTEP II," Report ORNL-3794, Oak Ridge National Laboratory, Tennessee (1971).

Carrier Effect of Reversed Micelle on Imidazole Catalyst

Kijiro KON-NO, Ayao KITAHARA,* and Masami FUJIWARA
Science University of Tokyo, Kagurazaka, Shinjuku-ku, Tokyo 162
(Received May 10, 1978)

The reversed micelles of neither didodecyldimethyl ammonium bromide(DDAB) nor sodium 1,4-bis(2-ethylhexyl) 2-sulfonatosuccinate(AOT) catalyse the decomposition of *p*-nitrophenyl acetate(PNPA) by themselves. However, these reversed micelles increase the action of imidazole in the decomposition of PNPA by solubilizing it. This interesting carrier effect of the reversed micelle on imidazole was investigated in both anhydrous and hydrous systems. The carrier effect of DDAB was greater than that of AOT. This difference was related to the different interaction between imidazole and each of the surfactants. The existence of the different interaction was made clear from the investigation on the change of chemical shift of the H(1) proton of imidazole upon solubilization by the reversed micelle. The mechanism of the decomposition of PNPA was partially explained from NMR measurements. Aminolysis occurred in anhydrous systems and hydrolysis in hydrous systems. Water pooled in the reversed micelle was more effective than bulk water in enhancing the catalytic effect of imidazole.

It has been recently reported that oil-soluble surfactants such as alkylammonium carboxylate catalyse a variety of reactions in nonaqueous media.[1-4] It is thought that the reversed micelles formed by these oil-soluble surfactants play an important role in the catalysis. The reversed micelles can solubilize some oil-insoluble or oil-soluble ploar substances. Solubilized substances may affect the catalytic activity through their interaction with the surfactants. The effect of solubilized water on the catalytic activity of alkylammonium carboxylate has been previously published.[3-6] Also, the effect of methanol, propylamine or acetic acid solubilized by dodecylammonium propionate on the decomposition of PNPA has been reported by these authors.[7] Similarly, non-catalysing reversed micelles may change the catalytic properties of a solubilized catalyst through an interaction between the catalyst and micelle.

In this paper, the effects of the non-catalysing reversed micelle of cationic and anionic surfactants on the catalytic activity of imidazole for the decomposition of PNPA is studied in anhydrous and hydrous systems and these effects related to the interaction between the reversed micelle and imidazole. Because nonionic surfactants showed behavior differing from that of the ionic surfactants used here, studies on nonionic surfactants will be reported separately.

Experimental

Materials. Didodecyldimethyl ammonium bromide (DDAB) and sodium 1,4-bis(2-ethylhexyl) 2-sulfonatosuccinate(AOT) were used as typical oil-soluble cationic and anionic surfactants. Preparation and purification of the surfactants are described elsewhere.[8] The guranteed reagent grades of imidazole and *p*-nitrophenyl acetate(PNPA), the catalyst and the substrate, respectively, were utilized. Carbon tetrachloride (CCl_4) was used as the solvent for both UV and NMR measurements. The solvent was purified as usual and carefully dried with Molecular Sieve 4A. However, a small quantity of water in the reaction systems was inevitable because of the hydroscopicity of the surfactants. Water content measured with the Karl-Fischer method was approximately 2 mmol kg^{-1} for the DDAB system and 7 mmol kg^{-1} for the AOT system for the anhydrous systems.

Methods. The decomposition of PNPA was followed by measurement of the changes in UV absorption at 318 nm, the wavelength of maximum absorption for the *p*-nitrophenol produced by the reaction. The UV spectrometer was a Shimadzu Double Beam Spectrophotometer UV-200. The initial concentration of PNPA was always 6.45×10^{-4} mol kg^{-1}. The decomposition of PNPA was always observed to be a pseudo-first order for PNPA.

NMR spectra were taken with a Hitachi NMR Spectrometer R-21(60 MHz). Chemical shifts were obtained relatively to an external TMS standard.

UV and NMR spectra were taken at 30 and 35 °C, respectively. All of the concentrations were expressed in molality(m, mol kg^{-1}) except those in Fig. 1.

Results and Discussion

Anhydrous Systems. Changes in the observed rate constants (k_{obsd}) varying the concentration of imidazole and holding the surfactant concentration constant(0.1 m) were depicted in Fig. 1. Changes in the imidazole–dodecylammonium propionate(DAP) system were shown for comparison in the figure. Because the solubility of imidazole in CCl_4 is only 5 mmol kg,$^{-1}$ the increase of k_{obsd} with increased concentration of imidazole, as seen in Fig. 1, is due to solubilized imidazole. It is seen from Fig. 1 that

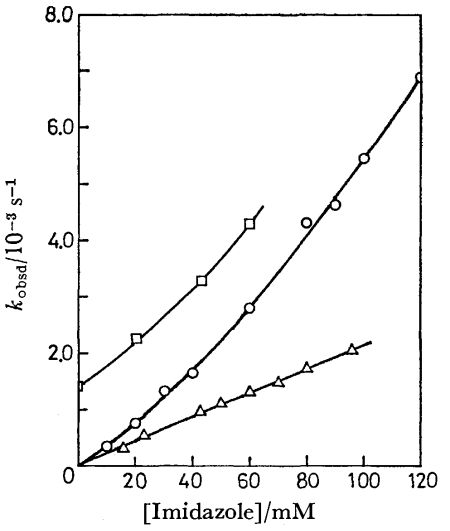

Fig. 1. Plots of k_{obsd} *versus* concentration of imidazole (mmol l^{-1}) at a fixed concentration of surfactants (0.1 m). —○—: DDAB, —△—: AOT, —□—: DAP.

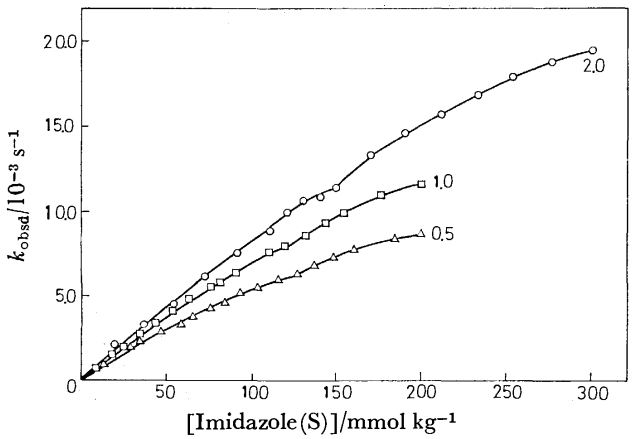

Fig. 2. Plots of k_{obsd} *versus* concentration of Imidazole-(S) in DDAB solutions. Figures show molar ratio of imidazole to DDAB.

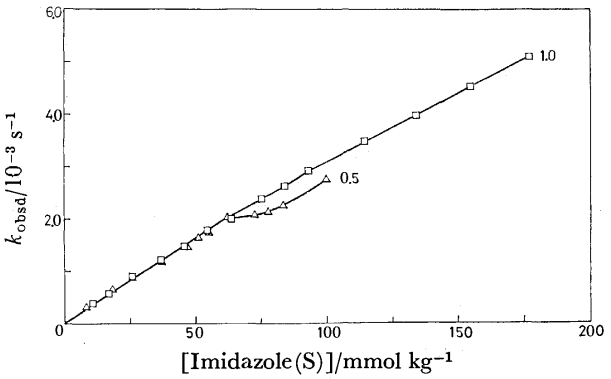

Fig. 3. Plots of k_{obsd} *versus* concentration of Imidazole-(S) in AOT solutions. Figures show molar ratio of imidazole to AOT.

DAP catalyzes the reaction in the absence of imidazole; however, neither DDAB nor AOT do so.

In order to investigate the effect of solubilization by non-catalsing micelle on the catalytic activity of imidazole, the systems solubilizing imidazole at a fixed ratio to a surfactnat were used and the change of reaction constant(k_{obsd}) with the concentration of solubilized imidazole was measured. The molar ratios of imidazole to the surfactant used were 0.5, 1.0, and 2.0. Imidazole solubilized at a fixed ratio is designated as "Imidazole(S)" or "Im(S)".

The relationship between k_{obsd} and the concentration of Im(S) for DDAB and AOT solutions is shown in Figs. 2 and 3. A linear relation can be seen at low concentration for both surfactant systems. The relation shows a curved line at higher concentration, some inflection appearing on the way. These changes may be due to changes in the size or shape of reversed micelles in this range. However, the present discussion forcuses on the lower concentration range.

The slope of the linear part gives the first order rate constant for Im(S), which was listed as k_1 in Table 1. To obtain the rate constant for imidazole dissolved in pure CCl_4, the rate constant for a small quantity of imidazole in the absence of any surfactant was measured. The rate constant obtained was designated as k_1°. The ratio, k_1/k_1° listed in Table 1 is a measure

Table 1. Rate constants for imidazole solubilized in anhydrous media

Surfactant	Molar ratio	k_1 (kg mol^{-1} s^{-1})	k_1/k_1° [a]
DDAB	0.5	0.067	5.4
	1.0	0.077	6.2
	2.0	0.080	6.4
AOT	0.5	0.033	2.6
	1.0	0.033	2.6

a) k_1°: the first order rate constant for imidazole in pure CCl_4: the value is 0.0124 kg mol^{-1} s^{-1}.

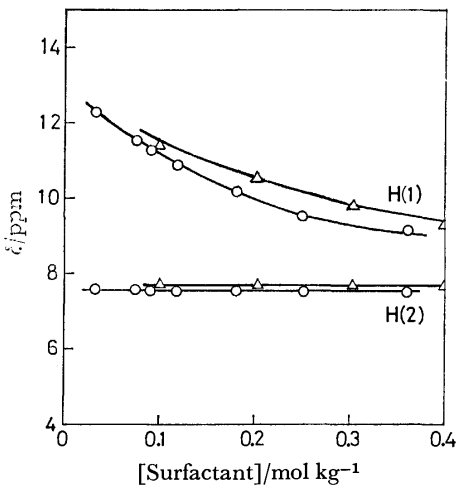

Fig. 4. Change of chemical shift of H(1) and H(2) protons of imidazole with concentration of surfactants. —○—: In DDAB solutions, —△—: in AOT solutions.

of the carrier effect of the surfactants. It is apparent that both surfactants show carrier effect for imidazole. DDAB shows a greater effect than AOT as seen in Table 1. Increase of the values of k_1/k_1° with increase of the molar ratios for DDAB as seen in Table 1 seems to show a concentrating effect of imidazole in the reversed micelle. It is considered that the difference in the observed rate constants of two surfactants is due to different interaction with imidazole.

The chemical shifts of the H(1) and H(2) protons of imidazole were measured in order to examine the interactions mentioned above. The result was shown in Fig. 4. It was observed that the chemical shift of the H(1) proton in both DDAB and AOT solutions shifts to higher field with increase of surfactant concentrations, though that of the H(2) proton does to minor extent. The high field shift shows the existence of the interaction of the H(1) proton with the polar part of the surfactant molecule in the reversed micelle. It is considered that the high field shift resulting from the interaction is due to electron-donation from bromide ion or sulfonate ion of each surfactant to the proton. Here bromide is more electron-donative(basic) than sulfonate, because the latter is partially hindered by neighboring sodium ion.

The interaction has been also discussed by NMR method on the solubilization of methanol and acetic acid by DDAB and other surfactants.[9] Higher field

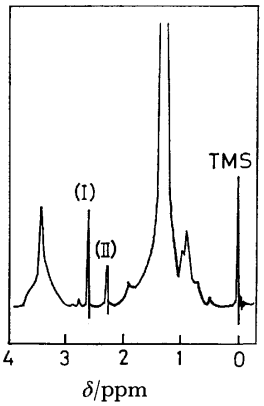

Fig. 5. NMR spectrum of DDAB–imidazole–PNPA solution in anhydrous CCl_4. Peak (I): $C\underline{H}_3CO$- of acetylimidazole, peak (II): $C\underline{H}_3CO$- of PNPA.

shifts correspond to higher interaction constants.[9] Therefore, the higher field shift of the H(1) proton in DDAB solution than that in AOT solution seen in Fig. 4 shows that the interaction of the H(1) proton with the reversed micelle is more intensive in the DDAB solution. This correlates with the higher values of $k_1/k_2^?$ for DDAB than AOT in Table 1. Minor change of the H(2) proton shows that the proton interacts with the surfactant in the micelle to minor extent.

NMR was further used to obtain some information on the reaction mechanism involved. Here, a higher concentration of PNPA was used in order to obtain a significant peak in the spectrum. A mixture of DDAB, imidazole and PNPA in CCl_4 (each component 0.1 m) was prepared and allowed to stand overnight. The NMR spectra of the mixture was shown in Fig. 5. The appearance of a peak corresponding to $C\underline{H}_3CO$– of 1-acetylimidazole(I) but none corresponding to acetic acid, shows that the reaction is a kind of aminolysis as shown in Eq. 1 and does not proceed to hydrolysis which may be expected from minor inevitable content of water.

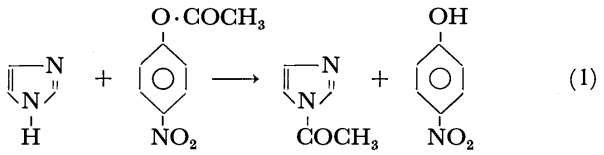

(1)

The NMR spectra of the AOT–imidazole–PNPA solution in CCl_4 were similar to those of DDAB solution. Similar aminolysis of the ester by benzamidine and piperidine has also been observed.[10,11] The proposed mechanism was further supported by the UV spectra of the mixture of AOT(0.1 m), imidazole(0.1 m), and PNPA(6.4×10^{-4}m) in hexane, which showed a gradual decrease of the peak corresponding to PNPA (263 nm) and the simultaneous increase of the peaks corresponding to *p*-nitrophenol(313 nm), and 1-acetylimidazole(220 nm) during the successive mixing for 4 h.

Acceleration of Reaction 1 by the reversed micelle may be due to combined catalytic action by imidazole and the basic part of the micelle(Br^- in DDAB or SO_3^- in AOT). This action is well known in aqueous solutions, as in the action of imidazole and hydroxide

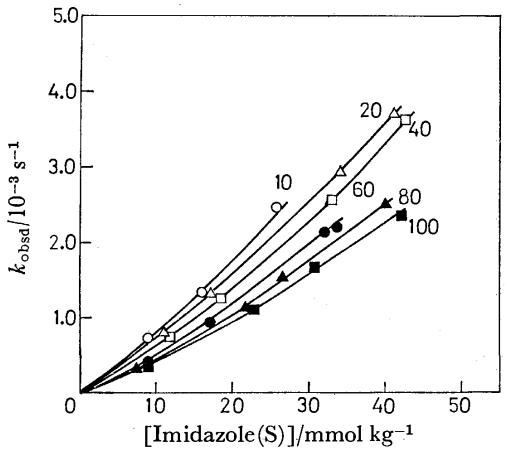

Fig. 6. Plots of k_{obsd} *versus* concentration of imidazole at a fixed concentration of water (0.020 m). Figures show concentration of DDAB (mmol kg^{-1}).

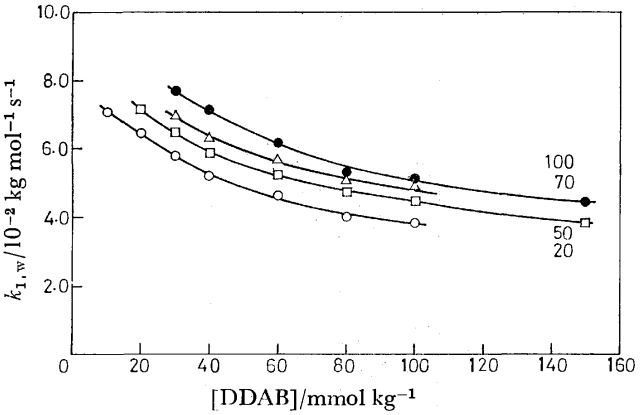

Fig. 7. Plots of $k_{1,w}$ *versus* concentration of DDAB. Figures show concentration of water(mmol kg^{-1}).

anion.[12] The existence of such an interaction between imidazole and the basic part of a reversed micelle can be seen from the remarkable shift of the H(1) proton in Fig. 4. Differences between DDAB and AOT with regards to interaction and acceleration of reaction may result from a difference in the structure of their reversed micelles. In the DDAB systems, the anion is exposed to the interior of the micelle, while in the AOT system, the anion is partially covered by Na^+. The effect of didodecyldimethyl ammonium chloride (DDAC) and iodide(DDAI) was compared with that of DDAB to check the basic activity. The order of the effects on both the rate and the chemical shift was DDAC>DDAB>DDAI. The order corresponds to that of the basicity of halogen ions.

Hydrous Systems. The quantity of water added to the reaction systems of imidazole–PNPA–surfactant in CCl_4 was of the same order as the surfactant. Because partition of water between the micelle and the solvent is of great advantage to the micelle, though the solubility of water in the solvent is 0.045 m at 30 °C, it was reasonably assumed that all of water added is solubilized in the reversed micelle and that water affects the imidazole catalyst under the state trapped in the interior of the micelle.

The change of k_{obsd} with concentration of imidazole

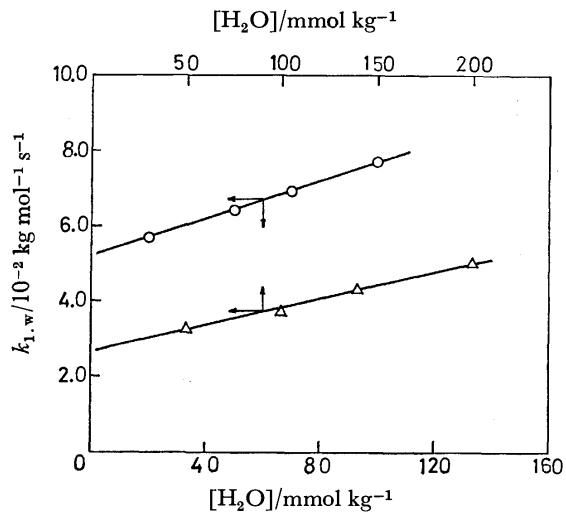

Fig. 8. Plots of $k_{1,w}$ *versus* concentration of water. —○—: solution of 30 mmol kg^{-1} of DDAB, —△—: solution of 20 mmol kg^{-1} of AOT.

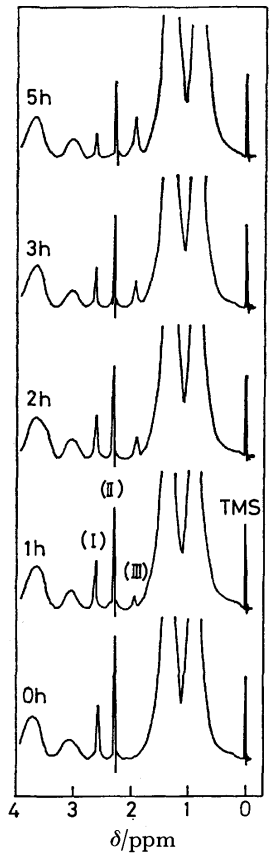

Fig. 9. NMR spectra of solution of DDAB-imidazole-PNPA-H_2O in CCl_4. Peak (I): $C\underline{H}_3CO$- of acetylimidazole, peak (II): $C\underline{H}_3CO$- of PNPA, peak (III): $C\underline{H}_3CO$- of acetic acid.

was measured by selecting the concentration of surfactant or water as a parameter. An example using the DDAB system(the concentration of water: 0.020 m) is given in Fig. 6. Similar plots were also obtained for 0.050, 0.070, and 0.100 m of H_2O. The initial slope of these plots is considered to be the first order rate constant for imidazole($k_{1,w}$), though the linearity is not complete. The values of $k_{1,w}$ were plotted against the concentration of DDAB,[DDAB], for various choices of the concentration of water, [H_2O], in Fig. 7. Relations quite similar to those shown in Figs. 6 and 7 were obtained for AOT system. The decrease of $k_{1,w}$ with increasing [DDAB] apparent in Fig. 7 shows the effect of dilution of the imidazole by the surfactant.

TABLE 2. RATE CONSTANT PARAMETERS FOR IMIDAZOLE IN HYDROUS MEDIA

Surfactant	Concentration of surfactant (mmol kg^{-1})	$k^{r}_{1,w}$ [a] (kg mol^{-1} s^{-1})	$k^{r}_{1,w}/k^{\circ}_{1,w}$ [b]
DDAB	30	13.9	21.5
	40	13.9	21.5
	60	10.9	16.9
	80	8.6	13.3
	100	8.4	13.0
AOT	20	4.1	6.3
	40	3.1	4.9
	60	1.9	2.9
	100	0.7	1.1

a) $k^{r}_{1,w}$: rate constant calculated for 1 kg of water solubilized. b) $k^{\circ}_{1,w}$: rate constant for imidazole in pure water (the value is 0.645 kg mol^{-1} s^{-1}).

In Fig. 8 were rearranged the relation of Fig. 7 as plots between $k_{1,w}$ and [H_2O]. The slope of the resulting lines in Fig. 8 shows the increment of $k_{1,w}$ relative to [H_2O] of 1 mmol kg^{-1} in the reversed micelles. Therefore, the reduced rate constant, $k^{r}_{1,w}$, could be calculated by multiplying the slope by the molar concentration of pure water, 55.5 mol kg.$^{-1}$ The values obtained are listed in Table 2.

The effect of water pooled in the reversed micelle on the catalytic activity of imidazole was estimated by comparing these reduced rate constants($k^{r}_{1,w}$) with the first order rate constants of the catalytic reaction of imidazole in pure water ($k^{\circ}_{1,w}$) which was measured separately. The values of the ratio, $k^{r}_{1,w}/k^{\circ}_{1,w}$ in Table 2 show that water pooled in the reversed micelle accelerates the catalytic effect of imidazole more markedly than free water. It is also seen in Table 2 that DDAB has a greater acceleration effect than AOT and that $k^{r}_{1,w}$ and $k^{r}_{1,w}/k^{\circ}_{1,w}$ decrease with increasing concentration of surfactants, showing the effects of the dilution of imidazole by the surfactants.

Again, to obtain some information on the reaction mechanism in hydrous systems, changes in the NMR spectra with time for the mixture of DDAB, imidazole, PNPA, and water in CCl_4, each component being 0.1 m, were measured. The result was shown in Fig. 9. Immediately after mixing, a peak corresponding to $C\underline{H}_3CO$- of 1-acetylimidazole appeared. As time elapsed, this peak(I) decreased and a peak corresponding to $C\underline{H}_3CO$- of acetic acid(III) appeared and gradually increased. Hence we can safely assign the following well known hydrolysis mechanism(Eqs. 2 and 3) to the systems solubilizing imidazole and considerable amount of water.

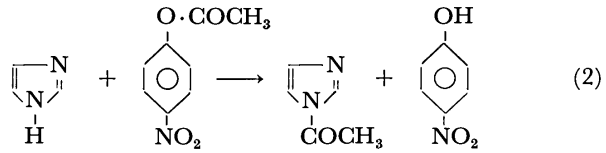

(2)

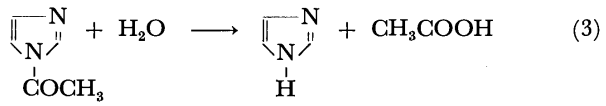

(3)

The rate of Eq. 2 was very fast due to the large quantity of PNPA used(0.1 m). Similar time dependence was observed in the NMR spectra of the AOT–imidazole–PNPA–H_2O system in CCl_4. However, it has not yet been determined how much water is necessary for Reaction 3 to proceed.

References

1) E. J. Fendler, J. H. Fendler, and R. T. Medary, *Chem. Commun.*, **1971**, 1497; J. H. Fendler, E. J. Fendler, and S. A. Chang, *J. Am. Chem. Soc.*, **95**, 3273 (1973); J. H. Fendler, R. T. Medary, and V. A. Woods, *J. Am. Chem. Soc.*, **94**, 7288 (1972).

2) K. Kon-no, K. Miyazawa, and A. Kitahara, *Bull. Chem. Soc. Jpn.*, **48**, 2955 (1975); K. Kon-no, T. Matsuyama, and A. Kitahara, *Nippon Kagaku Kaishi*, **1975**, 1857.

3) M. Seno, K. Araki, and S. Shiraishi, *Bull. Chem. Soc. Jpn.*, **49**, 899 (1976).

4) O. A. El Seoud, A. Martins, L. P. Barbur, M. J. da Silva, and V. Aldrigue, *J. Chem. Soc., Perkin Trans. 2*, **13**, 1674 (1977).

5) F. M. Menger, J. H. Donohue, and R. E. Williams, *J. Am. Chem. Soc.*, **95**, 286 (1973).

6) C. J. O'Conner, E. J. Fendler, and J. H. Fendler, *J. Am. Chem. Soc.*, **95**, 600(1973); **96**, 370 (1974).

7) A. Kitahara and K. Kon-no, "Micellization, Solubilization, and Microemulsion," ed by K. L. Mittal, Plenum Press, New York (1977), Vol. II, p. 675.

8) A. Kitahara and K. Kon-no, *J. Colloid Interface Sci.*, **29**, 1 (1969); **35**, 409 (1971).

9) A. Kitahara, K. Kon-no, and S. Fujiwara, *J. Colloid Interface Sci.*, **57**, 391 (1976); K. Kon-no and A. Kitahara, *J. Colloid Interface Sci.* in press.

10) F. M. Menger, *J. Am. Chem. Soc.*, **88**, 3081 (1966).

11) F. M. Menger and A. C. Vitale, *J. Am. Chem. Soc.*, **95**, 4931 (1973).

12) M. L. Bender and L. J. Brubacher, "Catalysis and Enzyme Action," McGraw-Hill, New York (1973), Chap. 3, Sec. 9.

The Crystal and Molecular Structure of Daphnetin 8-β-D-Glucopyranoside Dihydrate Isolated from *Daphne odora*

Katsuhiko UENO,* Norio SAITO,** and Mitsuhiko SATO***

Research Institute for Polymers and Textiles, Sawatari 4, Kanagawa-ku, Yokohama 221

*** Chemical Laboratory, Meiji-gakuin University, Minato-ku, Tokyo 108*

**** Department of Biology, Faculty of Science, Tokyo Metropolitan University, Setagaya-ku, Tokyo 154*

(Received May 13, 1978)

The crystal structure of daphnetin 8-β-D-glucopyranoside dihydrate has been determined by the X-ray method. The crystal is monoclinic, space group $P2_1$, with the lattice parameters $a=7.773(1)$, $b=22.478(5)$, $c=4.715(1)$ Å, $\beta=99.77(2)°$, and $Z=2$. The structure was determined by the direct method and refined by least-squares to a final R of 0.041 for 2690 observed reflexions. The daphnetin moiety is approximately planar, and little effect from glucosylation is observed in the bond lengths and angles, compared with daphnetin itself. The glucopyranoside is in C_1 chair conformation, with the ring torsion angles ranging from 48 to 66°. The anomeric C–O bond is twisted by 78.2° against the coumarin plane, which is the largest value in aromatic glycopyranosides so far reported and which is concomitant with a small valence angle, 114.4°, at the oxygen atom linking the coumarin and the glucose group.

During the course of studies on the biosyntheses of naturally occuring dihydroxycoumarins, Sato and Hasegawa found new enzymes from *Daphne odora* and *Cichorium intybus*. These enzymes show high substrate specificities for the hydrolysis and transglucosylation of dihydroxycoumarins and their glucosides.[1-4] As a part of investigations on the reaction mechanism of these enzymes, the structures of daphnetin (or 7,8-dihydroxycoumarin)[5] and esculetin(or 6,7-dihydroxycoumarin) have already been reported and some effects of the tautomerism were suggested in the molecular structures of 7-hydroxylated coumarins.[6] The present paper deals with the conformation of glucosylated coumarin and the effects of the glucosylation on the structure of the coumarin molecule.

Experimental

The crystals were obtained as transparent prisms by slow evaporation from an aqueous ethanol solution. The lattice constants and intensity data were obtained on a Rigaku four-circle diffractometer with graphite monochromated Mo $K\alpha$ radiation. A crystal $0.3\times0.2\times0.3$ mm in size was used. The scan mode of $2\theta/\omega$ was applied, with the scanning rate and range in ω of 2° min^{-1} and $(1.0+0.5\tan\theta)°$, respectively. Stationary background counts were made for 10 s before and after each scan. Of 3017 independent reflexions measured within $2\theta\leq65°$, 2690 had intensities greater than $3\sigma(|F_o|)$ and were used for the structure determination. No correction was made for absorption. The crystallographic data of daphnetin 8-β-D-glucopyranoside $2H_2O$ are: $C_{15}H_{16}O_9\cdot2H_2O$, $F.W.=376.3$. Monoclinic, $P2_1$, $a=7.773(1)$, $b=22.478(5)$, $c=4.715(1)$ Å, $\beta=99.77(2)°$. $Z=2$, $D_x=1.53$, $D_m=1.54$ g cm^{-3} (by flotation in a mixture of hexane and carbon tetrachloride). μ(Mo $K\alpha$) = 1.60 cm^{-1}. Systematic absence, $0k0$ with k odd.

Structure Determination

The structure was solved by the multi-solution method using 237 reflexions with $|E|\geq1.50$.[7,8] A phase set with the lowest R-value[9] gave an E-map which revealed the coumarin moiety. All the other non-hydrogen atoms emerged in successive Fourier maps. The structural parameters were refined by the block-diagonal least-squares method. The hydrogen atoms were located on a D-map at the stage of $R=0.09$ and their positional and isotropic thermal parameters were included in the refinement. The weighting scheme of $w=(20.0/|F_o|)$ if $|F_o|\geq20.0$, $w=1.0$ if $20.0>|F_o|\geq10.0$, and $w=(|F_o|/10.0)$ if $|F_o|<10.0$ was applied. The final R was 0.041 for 2690 observed reflexions. The atomic scattering factors were taken from International Tables for X-Ray Crystallography.[10] A list of observed and calculated structure factors is given in Table 1.[11] The final atomic parameters are shown in Table 2.

Results and Discussion

Molecular Geometry. The perspective drawing of the molecule with the numbering system is shown in Fig. 1. The bond lengths and angles are given in Fig. 2. The molecule is bent down at the glucosidic oxygen with a dihedral angle between the coumarin plane and the mean plane of the glucose ring of 116°. The daphnetin moiety is nearly planar. The equation of the best plane for the daphnetin moiety is given by

$$-0.3451X-0.5255Y-0.7777Z+8.3748=0.0,$$

where X, Y, Z refer to the crystallographic axes a, b, c* in Å units. The C(3), O(2), and O(1′) atoms show somewhat large deviations from this plane (−0.046, 0.045, and −0.038 Å, respectively). Compared with daphnetin,[5] the corresponding endocyclic bond lengths and angles deviate by no more than 0.01 Å and 0.7°, respectively, except for the angles around C(7) and, C(8); the C(6)–C(7)–C(8) angle is smaller by 2.0° the C(7)–C(8)–C(9) is larger by 1.5°, and the C(7)–C(8)–O(1′) is markedly larger by 3.4° than in daphnetin. The C(7)–O(7) bond is significantly shorter than those in other 7-hydroxylated coumarins, such as daphnetin, esculetin,[6] and 4-methylumbelliferone[12] (1.366, 1.358, and 1.393 Å, respectively). The C(8)–O(1′) bond is close to the bond length of the 8-methoxy group in xanthotoxin(1.375 Å).[13]

The glucopyranose moiety is in C_1 chair conformation and C–C bond lengths have similar values to those in other pyranoses observed in the X-ray studies.[14] Some relevant torsion angles are listed in

TABLE 2. FINAL ATOMIC PARAMETERS ($\times 10^4$) WITH THEIR STANDARD DEVIATIONS
The anisotropic thermal factors have the form exp $(-\beta_{11}h^2-\beta_{22}k^2-\beta_{33}l^2-\beta_{12}hk-\beta_{13}hl-\beta_{23}kl)$.

	x	y	z	β_{11}	β_{22}	β_{33}	β_{12}	β_{13}	β_{23}
O(1)	7574(2)	4208.3(7)	4094(4)	105(3)	10.2(3)	359(8)	3(2)	136(8)	10(3)
C(2)	8007(3)	4633.9(11)	2248(6)	133(4)	11.2(5)	354(12)	−15(2)	120(12)	2(4)
C(3)	6847(4)	5128.5(12)	1576(6)	166(5)	11.4(5)	437(15)	−6(3)	137(14)	40(4)
C(4)	5340(4)	5161.7(11)	2620(6)	153(5)	10.4(4)	373(13)	15(2)	60(13)	25(4)
C(5)	3342(3)	4706.3(11)	5675(6)	104(4)	10.5(4)	374(12)	19(2)	39(11)	−1(4)
C(6)	3016(3)	4263.6(12)	7507(6)	92(4)	13.6(5)	368(12)	10(2)	103(11)	−14(4)
C(7)	4216(3)	3798.7(10)	8239(5)	93(3)	10.8(4)	256(10)	0(2)	46(9)	−11(4)
C(8)	5735(3)	3785.4(10)	7027(5)	84(3)	8.6(4)	244(10)	3(2)	40(9)	−9(3)
C(9)	6046(3)	4240.8(10)	5206(5)	90(3)	9.3(4)	264(10)	0(2)	77(9)	−12(3)
C(10)	4878(3)	4709.3(10)	4507(5)	122(4)	9.0(4)	295(11)	9(2)	62(11)	−7(4)
O(2)	9369(2)	4544.2(9)	1346(3)	140(3)	15.2(4)	529(11)	−7(2)	265(10)	24(4)
O(7)	3986(2)	3358.7(8)	10063(4)	118(3)	15.0(4)	380(9)	9(2)	187(8)	38(3)
O(8)	6956(2)	3340.5(7)	7795(3)	97(3)	8.9(3)	267(7)	10(1)	31(7)	−10(3)
C(1′)	6948(3)	2890.6(10)	5697(5)	86(3)	8.8(4)	257(10)	1(2)	73(9)	1(3)
C(2′)	8446(3)	2478.4(10)	6858(5)	72(3)	10.2(4)	257(10)	3(2)	74(9)	10(3)
C(3′)	8403(3)	1909.3(10)	5086(5)	88(3)	9.0(4)	308(11)	8(2)	128(10)	6(3)
C(4′)	6589(3)	1635.9(10)	4591(5)	92(4)	8.8(4)	368(12)	1(2)	89(10)	−4(4)
C(5′)	5224(3)	2106.6(10)	3459(5)	90(4)	10.2(4)	319(11)	2(2)	82(10)	−14(4)
C(6′)	3361(3)	1882.9(12)	3132(6)	85(4)	16.2(6)	462(14)	−9(2)	50(12)	−40(5)
O(2′)	10096(2)	2766.2(7)	6861(4)	82(3)	13.6(3)	380(9)	−12(2)	88(7)	−16(3)
O(3′)	9586(2)	1483.2(8)	6537(4)	88(3)	12.2(3)	560(11)	20(2)	138(9)	38(3)
O(4′)	6420(3)	1173.1(9)	2518(5)	132(3)	14.8(4)	731(14)	8(2)	91(11)	−107(4)
O(5′)	5343(2)	2585.1(7)	5492(4)	77(2)	10.3(3)	341(8)	1(2)	77(7)	−21(3)
O(6′)	2875(3)	1778.6(11)	5449(5)	115(4)	27.0(6)	633(13)	−23(2)	202(11)	−10(5)
O(W1)	856(2)	3394.7(8)	11974(4)	121(3)	14.9(4)	372(9)	3(2)	159(8)	−14(3)
O(W2)	9260(4)	637.2(11)	10761(6)	353(7)	20.9(6)	853(17)	50(3)	764(18)	35(5)

	x	y	z	B(Å^2)		x	y	z	B(Å^2)
H(C3)	0.716(4)	0.542(1)	0.010(7)	2.4(7)	H(C6′a)	0.243(4)	0.216(1)	0.212(6)	1.3(6)
H(C4)	0.459(4)	0.545(2)	0.200(7)	2.6(8)	H(C6′b)	0.322(4)	0.149(1)	0.202(7)	2.6(7)
H(C5)	0.258(4)	0.502(1)	0.500(7)	2.7(8)	H(O2′)	1.026(5)	0.297(2)	0.850(7)	3.6(8)
H(C6)	0.197(4)	0.424(2)	0.819(7)	2.3(7)	H(O3′)	1.056(4)	0.156(2)	0.624(7)	2.8(8)
H(O7)	0.312(4)	0.338(2)	1.079(7)	2.7(7)	H(O4′)	0.734(4)	0.105(1)	0.235(7)	2.1(7)
H(C1′)	0.705(4)	0.305(1)	0.388(6)	0.9(6)	H(O6′)	0.298(5)	0.215(2)	0.696(8)	5.4(10)
H(C2′)	0.835(3)	0.237(1)	0.886(6)	0.7(6)	H(W1a)	0.049(4)	0.320(2)	1.319(7)	2.8(8)
H(C3′)	0.876(4)	0.199(1)	0.333(6)	1.5(6)	H(W1b)	0.040(4)	0.373(2)	1.169(7)	2.9(8)
H(C4′)	0.635(4)	0.152(1)	0.647(6)	1.4(6)	H(W2a)	0.956(6)	0.035(2)	0.968(10)	5.7(11)
H(C5′)	0.542(4)	0.225(1)	0.150(6)	1.2(6)	H(W2b)	0.954(5)	0.089(2)	0.955(8)	4.4(9)

Table 3. The endocyclic torsion angles vary from 48 to 66°. The pyranose ring has an approximate mirror symmetry normal to the mean plane of the ring and passing through the ring O and C(3′) atoms.[15] The maximum deviation from this pseudo mirror palne in torsion angle is 3.7°(between C(1′)–C(2′) and C(4′)–C(5′).) The conformation of the primary alcohol group is in a gauche-gauche orientation. although slightly distorted from the ideal 60° staggered form.

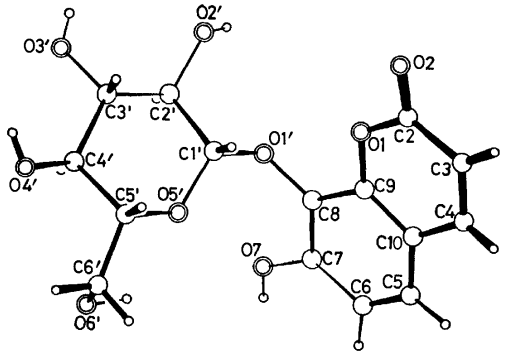

Fig. 1. Perspective drawing of the molecule with numbering system used.

Conformation of Glucosidic Bond. The bond lengths and angles in the sequence C(5′)–O(5′)–C(1′)–O(1′)–R have been discussed as an anomeric effect; it is expected that in the β-pyranose C(5′)–O(5′)≃O(5′)–C(1′)>C(1′)–O(1′), while in the α-anomer C(5′)–O(5′)>O(5′)–C(1′)≃C(1′)–O(1′).[14,16,17] In this crystal, however, C(5′)–O(5′) is significantly longer than O(5′)–C(1′) and C(1′)–O(1′). A similar geometry has been observed in some other aromatic β-pyranosides, such as *p*-nitrophenyl β-D-*N*-acetylglucosaminide[18] and 6-bromo-2-naphtyl β-D-glucopyranoside.[19] The relevant

valence angles are consistent with those in the β-anomer. Table 4 shows the geometry of the glycosidic bond lengths and angles in some pyranosides.

The valence angle of the oxygen atom linking the coumarin and glucose group is markedly smaller than those in the other aromatic glycopyranosides and is rather close to those in the methyl glucosides(Table 4).

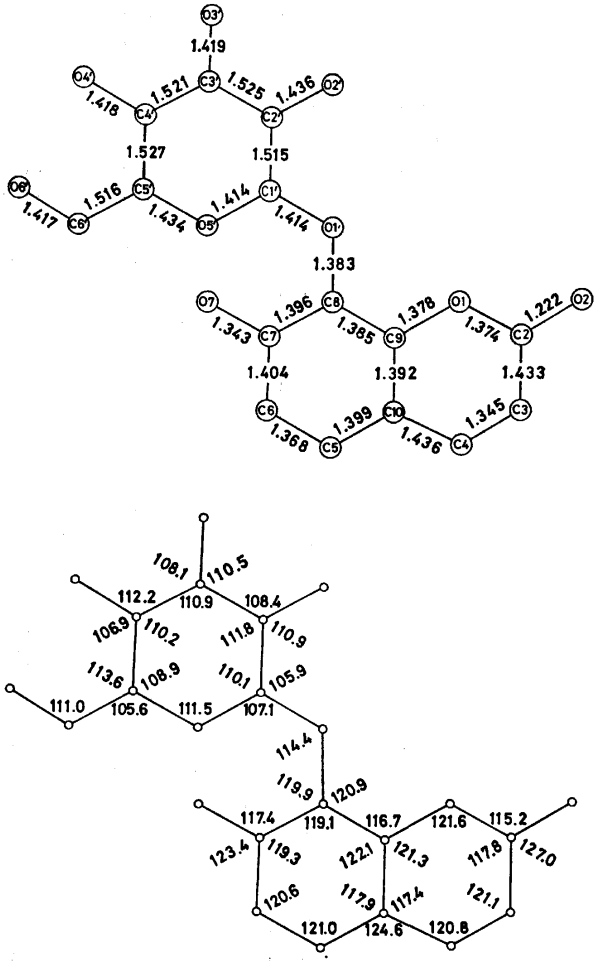

Fig. 2. Bond lengths (Å) and angles (°). The estimated standard deviations are 0.003—0.004 (Å) for lengths and 0.2—0.3 (°) for angles.

The O(1′)–C(1′) bond is twisted by 78.2° against the coumarin plane, which is the largest value in aromatic glycosides (φ in Table 4), probably owing to the repulsion between the O(7) and O(5′) atoms. The orientation of the O(1′)–C(8) bond is gauche and trans to the C(1′)–O(5′) and C(1′)–C(2′) bonds (−66.6 and 174.0°, respectively).

Crystal Structure. The crystal structure viewed down the c axis is shown in Fig. 3. The hydrogen bond lengths and angles are listed in Table 5. The O···O distances range from 2.716 to 2.918 Å. When a water molecule acts as a donor the lengths tends to be slightly larger than in other cases. This tendency is generally observed in the hydrogen bonds of amino acids and sugars.[24] The scheme of the three-dimensional hydrogen bond network is shown below:

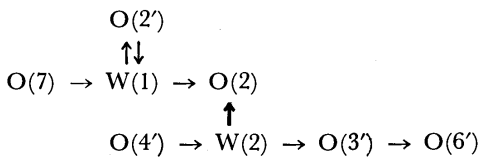

where → indicates the donor direction. The water molecule W(1) is concerned with four hydrogen bonds in a tetrahedral arrangement, whereas W(2) is concerned with three hydrogen bonds in a pyramid. The difference in the hydrogen bond modes may reflect the discrepancy between the thermal parameters of these water molecules. The hydroxyl group O(6′)H does not act as a hydrogen bond donor, although some weak interaction to intramolecular O(5′)

Table 3. Endo- and exocyclic torsion angles
Only for exocyclic angles is the whole sequence of atoms given.

Endocyclic		Exocyclic	
C(1′)C(2′)	54.3°	O(8)C(1′)C(2′)O(2′)	−69.3°
C(2′)C(3′)	−48.2	O(2′)C(2′)C(3′)O(3′)	69.4
C(3′)C(4′)	50.0	O(3′)C(3′)C(4′)O(4′)	−69.7
C(4′)C(5′)	−58.0	O(4′)C(4′)C(5′)C(6′)	62.5
C(5′)O(5′)	66.0	C(4′)C(5′)C(6′)O(6′)	69.4
O(5′)C(1′)	−63.9	O(5′)C(5′)C(6′)O(6′)	−49.9

Table 4. Geometry of anomeric C-O-C-O-R systems in some aromatic glycosides
Bond lengths and angles are denoted as $C(5')\overset{a}{-}O(5')\underset{\alpha}{\overset{b}{-}}C(1')\underset{\beta}{\overset{c}{-}}O(1')\underset{\gamma}{\overset{d}{-}}R$.

	a(Å)	b(Å)	c(Å)	d(Å)	α(°)	β(°)	γ(°)	θ(°)[a]	ϕ(°)[b]	Ref.
Daphnetin 8-β-glucoside	1.434	1.414	1.414	1.383	111.5	107.1	114.4	−66.6	78.2	this work
p-Nitrophenyl β-*N*-acetylglucosaminide	1.442	1.409	1.399	1.377	112.8	107.7	120.0	−80.9	16.4	18
p-Nitrophnyl β-xyloside	1.427	1.415	1.393	1.379	110.0	109.4	118.5	−75.1	23.6	19
6-Br-2-naphtyl β-glucoside	1.441	1.392	1.416	1.376	111.7	108.0	117.5	−78.3	0.7	20
Methyl β-glucoside	1.440	1.433	1.380	1.430	111.5	108.1	113.1	−73.2		21
Methyl α-glucoside	1.439	1.415	1.401	1.422	113.5	113.0	113.9	63.0		15
Novobiocin[c]	1.474	1.458	1.410	1.394	118.7	111.4	121.2	30	35	22
Phenyl α-maltoside	1.447 1.446	1.421 1.397	1.408 1.427	1.384 1.390	114.3 115.4	113.0 112.5	117.8 119.3	94 77	42 10	23

a) Torsion angle of O(5′)-C(1′)-O(1′)-R. b) Rotation angle around O(1′)-R. c) A derivative of coumarin 7-α-L-lyxoside.

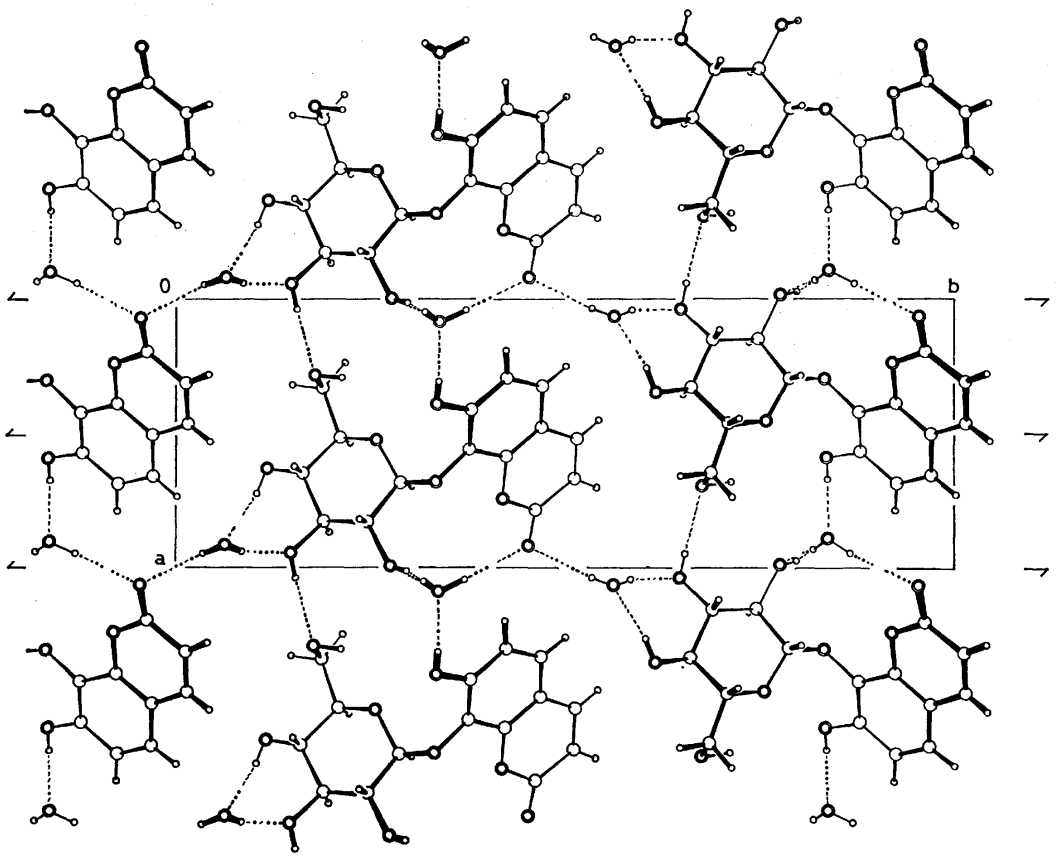

Fig. 3. The crystal structure viewed down the c axis. Hydrogen bonds are indicated by broken lines.

Table 5. Hydrogen bond distances (Å) and angles (°)

Donor atom (D)	(H)	Acceptor atom (A)		Distantances D···A	H···A	Angle D-H···A
O(7)	H(O7)	O(W1)	i	2.736(3)	1.94(4)	172(4)
O(2′)	H(O2′)	O(W1)	ii	2.770(3)	1.89(5)	174(3)
O(3′)	H(O3′)	O(6′)	ii	2.716(3)	1.91(4)	175(4)
O(4′)	H(O4′)	O(W2)	iii	2.764(4)	2.00(4)	162(4)
O(W1)	H(W1a)	O(2′)	iv	2.849(3)	2.05(4)	166(4)
O(W1)	H(W1b)	O(2)	v	2.826(3)	1.99(4)	175(4)
O(W2)	H(W2a)	O(2)	vi	2.918(4)	2.08(5)	157(4)
O(W2)	H(W2b)	O(3′)	i	2.797(4)	1.96(4)	166(4)

Symmetry code:
i) x, y, z, ii) $1+x, y, z$, iii) $x, y, -1+z$,
iv) $-1+x, y, z$, v) $-1+x, y, 1+z$, vi) $2-x, -1/2+y, 1-z$.

can be expected (distances of O(5′)–O(6′) and O(5′)–H(O6′) are 2.664 and 2.28 Å, respectively).

The authors are grateful to Professor Yoshio Sasada of Tokyo Institute of Technology for his valuable suggestions and encouragement.

References

1) M. Sato and M. Hasegawa, *Phytochemistry*, **8**, 1211 (1969); **11**, 657 (1972).
2) W. Z. Hassid, "Metabolic Pathways," ed by D. M. Greenberg, Academic Press, New York (1967), Vol. 2, p. 307.
3) M. Sato and M. Hasegawa, *Phytochemistry*, **10**, 2367 (1971).
4) M. Sato and M. Hasegawa, *Phytochemistry*, **11**, 3149 (1972).
5) K. Ueno and N. Saito, *Acta Crystallogr., Sect. B*, **32**, 946 (1976).
6) K. Ueno and N. Saito, *Acta Crystallogr., Sect. B*, **33**, 283 (1977).
7) J. Karle and H. Hauptman, *Acta Crystallogr.*, **9**, 635 (1956).
8) G. Germain and M. M. Woolfson, *Acta Crystallogr., Sect. B*, **24**, 91(1968).
9) J. Karle and I. L. Karle, *Acta Crystallogr.*, **21**, 849 (1966).
10) "International Tables for X-Ray Crystallography," Kynoch Press, Birmingham (1962), Vol. III, p. 201.
11) Table 1 is kept at the Chemical Society of Japan,

Kanda Surugadai, Chiyoda-ku, Tokyo (Document No. 7840).
12) S. Shimizu, S. Kashino, and M. Haisa, *Acta Crystallogr., Sect. B*, **31**, 1287 (1975).
13) N. R. Stemple and W. H. Watson, *Acta Crystallogr., Sect. B*, **28**, 2485 (1972).
14) S. Arnott and W. E. Scott, *J. Chem. Soc., Perkin Trans. 2*, **1972**, 324.
15) G. A. Jeffrey, R. K. McMullan, and S. Takagi, *Acta Crystallogr., Sect. B*, **33**, 728 (1977).
16) M. Sundaralingam, *Biopolymers*, **6**, 189(1968).
17) G. A. Jeffrey, J. A. Pople, and L. Radom, *Carbohydr. Res.*, **38**, 81 (1974): **25**, 117 (1972).
18) L. Brehm and J. Moult, *Proc. R. Soc. London, Ser. B*, **188**, 425 (1975).
19) K. Harata, *Acta Crystallogr., Sect. B*, **32**, 1932 (1975).
20) K. Harata, private communication.
21) G. A. Jeffrey and S. Takagi, *Acta Crystallogr., Sect. B*, **33**, 738 (1977).
22) M. O. Boles and D. J. Taylor, *Acta Crystallogr., Sect. B*, **31**, 1400 (1975).
23) I. Tanaka, N. Tanaka, T. Ashida, and M. Kakudo, *Acta Crystallogr., Sect B*, **32**, 155 (1976).
24) J. Mitra and C. Ramakrishnan, *Int. J. Pept. Protein Res.*, **9**, 27 (1977).

Absolute Configurations of Asperlin, a Metabolite of *Aspergillus nidulans*, and Its Related Compounds

Keiichi FUKUYAMA,* Yukiteru KATSUBE, Akihiro NODA,**
Takashi HAMASAKI,** and Yuichi HATSUDA**
Faculty of Engineering, Tottori University, Koyama, Tottori 680
***Faculty of Agriculture, Tottori University, Koyama, Tottori 680*
(Received May 26, 1978)

The structures of asperlin (**1**) $C_{10}H_{12}O_5$ and asperlinol (**2**) $C_{10}H_{14}O_6$, isolated from *Aspergillus nidulans*, and a chloro derivative of asperlin (**3**) $C_{10}H_{13}O_5Cl$ have been studied by the X-ray diffraction method. The absolute configuration of **3** has been determined by the Bijvoet method by utilizing the anomalous scattering of chlorine atom for Cu $K\alpha$ radiation. The present analysis has verified the configurations of the atoms in an $\alpha\beta$-unsaturated δ-lactone ring as suggested by spectroscopy. In each compound, the acetoxyl group occupies a quasi-axial and the three-carbon side chain a quasi-equatorial position on the lactone ring. All the crystals are orthorhombic, space group $P2_12_12_1$ with $Z=4$. The cell dimensions are $a=26.536$, $b=5.955$, $c=6.973$ Å for **1**, $a=25.496$, $b=7.097$, $c=6.329$ Å for **2**, and $a=26.050$, $b=5.899$, $c=7.548$ Å for **3**. The structures of **1**, **2**, and **3** were refined by the block-diagonal least-squares method to $R=0.068$ for 1084 reflections, $R=0.056$ for 1127 reflections, and $R=0.051$ for 831 reflections, respectively.

Extensive investigations have been made on the structures[1-4] and biosynthesis[5,6] of various kinds of lactone derivatives isolated from the genus *Aspergillus*. Although the configurations at the C(3) and C(7) atoms in asperlin (**1**), a metabolite isolated from *Aspergillus nidulans*, have been suggested by spectroscopy,[1,3] the whole stereochemistry has not yet been established. Recently we have isolated a new compound $C_{10}H_{14}O_6$ (**2**), named asperlinol, from *Aspergillus nidulans* together with asperlin. Asperlinol (**2**) was suggested to be one of the hydrated compounds of asperlin on the basis of spectroscopic evidence, but a definitive structure remained to be determined because of its instability in solution. For the establishment of the absolute configurations of these compounds, the chloro derivative (**3**) was prepared from asperlin to utilize the anomalous scattering of the chlorine atom for X-radiation. In this paper we report the results of the X-ray analyses of **1**—**3**.

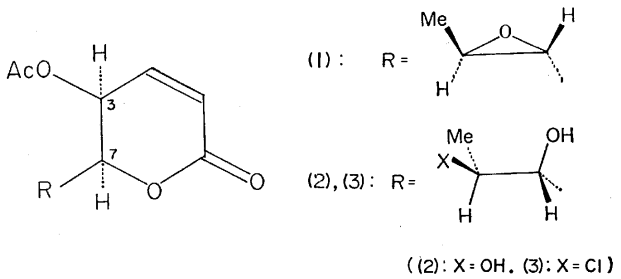

Experimental

Isolation of Asperlin (1) and Asperlinol (2). *Aspergillus nidulans* Wint. IFO 6390 was grown on malt extract medium in stationary culture at 24 °C for three weeks. The culture filtrate was adsorbed on activated carbon at pH 2—3 adjusted by hydrochloric acid. The carbon was extracted with acetone. Chloroform-soluble fraction of the acetone extract was concentrated, and chromatographed on a column of silicic acid. **1** was eluted with benzene, and **2** subsequently with benzene–acetone (9:1 v/v). **1** was recrystallized with ether to give colorless plates, which had physical constants identical with those for asperlin. **2** was further subjected to silicic acid column chromatography. The fraction eluted with benzene-acetone (4:1 v/v) yielded a colorless solid, which was recrystallized from an acetone–hexane solution to give colorless prisms (49 mg), mp 117—118 °C. Found: C, 52.38; H, 6.14%. Calcd for $C_{10}H_{14}O_6$: C, 52.18; H, 6.13%. $[\alpha]_D^{18}=220°$ ($c=0.9$, EtOH), λ_{max} (EtOH) 205(9200), ν_{max} (KBr) 3500, 3000, 2950, 1750, 1720, and 1640 cm^{-1}, δ(DMSO-d_6, 60 MHz) 7.07 (1H, dd, $J=6$ and 10 Hz), 6.12 (1H, d, $J=10$ Hz), 5.25 (1H, dd, $J=2.5$ and 6 Hz), 5.03 (1H, d, $J=5$ Hz), 4.48 (1H, d, $J=5$ Hz), 4.36 (1H, dd, $J=2.5$ and 9 Hz), 3.5—4.0 (2H, m), 2.01 (3H, s), and 1.03 (3H, d, $J=6$ Hz).

Preparation of Chloro Derivative (3). Asperlin (950 mg) was treated with hydrochloric acid (6 M, 10 ml) in diethyl ether (12 ml) at room temperature. Slow evaporation of ether gave colorless crystals from the aqueous solution, which were filtered and washed with water. Recrystallization with methanol gave chloro derivative (**3**) as colorless needles (440 mg), mp 187—189 °C. Found: C, 48.37; H, 5.46; Cl, 14.00%. Calcd for $C_{10}H_{13}O_5Cl$: C, 48.30; H, 5.27; Cl, 14.26%. $[\alpha]_D^{16}=280°$ ($c=0.9$, EtOH), λ_{max} (EtOH) 205 (10300), ν_{max} (KBr), 3450, 2980, 2925, 1750, 1720, and 1640 cm^{-1}, δ(DMSO-d_6, 60 MHz), 1.43 (3H, d, $J=6.5$ Hz), 2.02 (3H, s), 3.97 (1H, m, $J=2$, 6, and 10 Hz), 4.25 (1H, dq, $J=2$ and 6.5 Hz), 4.50 (1H, dd, $J=2.5$ and 10 Hz), 5.26 (1H, dd, $J=2.5$ and 6 Hz), 5.85 (1H, d, $J=6$ Hz), 6.15 (1H, d, $J=10$ Hz), and 7.08 (1H, dd, $J=6$ and 10 Hz).

Crystal Data. (a) Asperlin (**1**), $C_{10}H_{12}O_5$, $M=212.2$, orthorhombic, $P2_12_12_1$, $a=26.536(6)$, $b=5.955(4)$, $c=6.973(4)$ Å, $V=1101.9$ Å^3, $Z=4$, $D_x=1.279$ g cm^{-3}, $\mu=8.9$ cm^{-1} (for Cu $K\alpha$). (b) Asperlinol (**2**), $C_{10}H_{14}O_6$, $M=230.2$, orthorhombic, $P2_12_12_1$, $a=25.496(6)$, $b=7.097(4)$, $c=6.329(4)$ Å, $V=1145.2$ Å^3, $Z=4$, $D_x=1.335$ g cm^{-3}, $\mu=9.6$ cm^{-1} (for Cu $K\alpha$). (c) Chloro derivative of asperlin (**3**), $C_{10}H_{13}O_5Cl$, $M=248.7$, $a=26.050(7)$, $b=5.899(5)$, $c=7.548(5)$ Å, $V=1159.9$ Å^3, $Z=4$, $D_x=1.424$ g cm^{-3}, $\mu=29.9$ cm^{-1} (for Cu $K\alpha$).

Crystallographic Measurements. Preliminary photographic investigation showed all these crystals to be orthorhombic with the systematic absences uniquely characterizing $P2_12_12_1$. The approximate crystal size used for intensity measurement was $0.2\times0.4\times0.1$ mm^3 for **1**, $0.2\times0.3\times0.1$ mm^3 for **2**, and $0.2\times0.5\times0.2$ mm^3 for **3**. Each crystal was mounted with the b axis parallel to the ϕ axis of the diffractometer.

All the crystallographic measurements for **1** and **2** were

TABLE 1. FINAL ATOMIC COORDINATES WITH THEIR ESTIMATED STANDARD DEVIATIONS IN PARENTHESES

	x	y	z
(a) Asperlin (**1**)			
C(1)	0.2725(1)	−0.1478(13)	−0.0629(8)
C(2)	0.3098(1)	−0.2441(8)	0.0732(6)
C(3)	0.3921(1)	−0.1955(6)	0.2042(5)
C(4)	0.4298(1)	−0.2999(7)	0.0759(6)
C(5)	0.4674(1)	−0.1797(7)	0.0055(6)
C(6)	0.4714(1)	0.0637(7)	0.0429(5)
C(7)	0.4151(1)	0.0027(6)	0.3076(5)
C(8)	0.3768(1)	0.1440(6)	0.4079(5)
C(9)	0.3842(1)	0.2173(8)	0.6081(6)
C(10)	0.3567(2)	0.4238(10)	0.6823(8)
O(1)	0.3063(1)	−0.4202(7)	0.1544(6)
O(2)	0.3510(1)	−0.1128(4)	0.0857(4)
O(3)	0.4978(1)	0.1892(6)	−0.0474(5)
O(4)	0.4416(1)	0.1511(4)	0.1799(4)
O(5)	0.3523(1)	0.0297(5)	0.5621(4)
H(C1)	0.271(1)	0.022(7)	−0.037(7)
H(C1)	0.240(2)	−0.205(11)	−0.046(10)
H(C1)	0.285(2)	−0.172(10)	−0.196(8)
H(C3)	0.378(1)	−0.317(6)	0.312(5)
H(C4)	0.428(2)	−0.462(8)	0.031(6)
H(C5)	0.494(2)	−0.263(8)	−0.083(8)
H(C7)	0.440(1)	−0.075(7)	0.410(7)
H(C8)	0.355(1)	0.244(7)	0.311(6)
H(C9)	0.417(2)	0.251(8)	0.659(6)
H(C10)	0.377(2)	0.547(8)	0.687(6)
H(C10)	0.350(2)	0.364(9)	0.822(8)
H(C10)	0.323(2)	0.447(8)	0.594(7)
(b) Asperlinol (**2**)			
C(1)	0.2575(2)	0.1821(6)	0.4569(9)
C(2)	0.2819(1)	0.2972(5)	0.6237(8)
C(3)	0.3593(1)	0.4672(5)	0.7188(6)
C(4)	0.3880(1)	0.3498(6)	0.8779(6)
C(5)	0.4389(1)	0.3168(6)	0.8586(7)
C(6)	0.4677(1)	0.3768(5)	0.6689(6)
C(7)	0.3971(1)	0.5887(4)	0.5940(6)
C(8)	0.3730(1)	0.6737(5)	0.3964(6)
C(9)	0.4105(1)	0.7974(6)	0.2761(6)
C(10)	0.4249(2)	0.9774(6)	0.3864(7)
O(1)	0.2627(1)	0.3484(5)	0.7884(6)
O(2)	0.3319(1)	0.3433(3)	0.5732(5)
O(3)	0.5117(1)	0.3212(4)	0.6304(4)
O(4)	0.4434(1)	0.4844(3)	0.5275(4)
O(5)	0.3286(1)	0.7784(4)	0.4677(4)
O(6)	0.3854(1)	0.8404(4)	0.0778(4)
H(C1)	0.273(2)	0.059(7)	0.471(8)
H(C1)	0.216(2)	0.171(6)	0.487(7)
H(C1)	0.262(2)	0.211(6)	0.310(7)
H(C3)	0.333(2)	0.542(6)	0.804(7)
H(C4)	0.364(2)	0.294(6)	1.015(7)
H(C5)	0.463(2)	0.249(6)	0.970(7)
H(C7)	0.408(1)	0.701(5)	0.693(6)
H(C8)	0.363(1)	0.561(5)	0.301(6)
H(C9)	0.443(1)	0.717(6)	0.245(6)
H(C10)	0.441(2)	0.952(6)	0.502(7)
H(C10)	0.387(2)	1.049(7)	0.420(8)
H(C10)	0.448(1)	1.043(6)	0.299(6)
H(O5)	0.300(2)	0.710(6)	0.408(7)
H(O6)	0.415(2)	0.872(6)	0.006(7)
(c) Chloro derivative (**3**)			
Cl	0.3820(1)	−0.1920(3)	0.6565(2)
C(1)	0.4820(3)	0.1991(16)	−0.0588(9)
C(2)	0.4616(2)	0.3926(14)	0.0516(9)
C(3)	0.3885(2)	0.4995(11)	0.2261(8)
C(4)	0.3574(2)	0.6575(12)	0.1156(9)
C(5)	0.3093(2)	0.6182(13)	0.0863(10)
C(6)	0.2849(2)	0.3978(12)	0.1373(9)
C(7)	0.3543(2)	0.3686(11)	0.3520(8)
C(8)	0.3817(2)	0.1696(11)	0.4424(8)
C(9)	0.3468(2)	0.0503(11)	0.5731(9)
C(10)	0.3296(3)	0.1926(14)	0.7308(9)
O(1)	0.4820(2)	0.5660(10)	0.0869(8)
O(2)	0.4146(1)	0.3373(8)	0.1125(5)
O(3)	0.2455(2)	0.3340(9)	0.0797(8)
O(4)	0.3108(1)	0.2676(7)	0.2564(6)
O(5)	0.4250(2)	0.2622(8)	0.5282(6)
H(C1)	0.476(3)	0.060(14)	−0.009(12)
H(C1)	0.517(3)	0.268(13)	−0.060(11)
H(C1)	0.468(3)	0.255(13)	−0.180(10)
H(C3)	0.413(3)	0.549(13)	0.304(10)
H(C4)	0.388(3)	0.775(14)	0.063(11)
H(C5)	0.288(3)	0.729(12)	0.023(9)
H(C7)	0.339(2)	0.501(11)	0.428(9)
H(C8)	0.393(3)	0.054(13)	0.333(10)
H(C9)	0.313(3)	−0.032(13)	0.500(11)
H(C10)	0.310(3)	0.100(12)	0.826(10)
H(C10)	0.361(3)	0.251(13)	0.790(11)
H(C10)	0.313(3)	0.348(13)	0.668(9)
H(O5)	0.455(3)	0.171(13)	0.497(11)

made under the same experimental conditions. The cell constants were determined by least-squares treatement of the angular settings of 13 reflections measured on a Rigaku computer-controlled four-circle diffractometer with Ni-filtered Cu $K\alpha$ radiation. The intensities were measured by the θ-2θ scan technique with a scan speed of 2° min^{-1} in θ. The scan width for each reflection was calculated with the formula; $\Delta(\theta)=1.0°+0.15°\tan\theta$. The background counts were taken for 8 s at each end of the scan range. Attenuators were inserted automatically to keep the counting rate below 10^4 cps. The intensities of 1085 and 1127 independent reflections were collected for **1** and **2** respectively in the range $0<\sin\theta/\lambda<0.58$.

The cell constants of **3** were determined from Bragg angles of the reflections of (h00), (0k0), and (00l). The intensities were measured in the left-handed coordinate system on a Rigaku tape-controlled four-circle diffractometer with Ni-filtered Cu $K\alpha$ radiation. The θ-2θ scan technique was used with the scan speed of 2° min^{-1} in θ. The scan width was 1.2° in θ for all reflections and the backgrounds were counted for 5 s at both sides of the scan. The intensities of 831 independent reflections were measured in the range 0<

Table 2. Results of Bijvoet measurements

h	k	l	B_{th}	B_{ex}	DEL
1	1	4	0.102	−0.076	−0.75
1	1	5	0.081	−0.072	−0.89
3	2	1	0.179	−0.150	−0.84
5	1	2	−0.140	0.159	−1.14
5	1	3	−0.071	0.055	−0.77
5	1	5	−0.078	0.107	−1.37
6	2	4	−0.089	0.075	−0.84
7	2	3	−0.108	0.149	−1.38
7	1	4	0.104	−0.102	−0.98
8	1	2	0.083	−0.042	−0.51
8	1	3	−0.117	0.087	−0.74
8	1	4	0.104	−0.083	−0.80
9	1	1	0.100	−0.039	−0.39
11	2	3	−0.100	0.113	−1.13
12	1	1	−0.116	0.197	−1.70
12	1	2	−0.095	0.169	−1.78
14	1	3	0.110	−0.036	−0.33
15	2	1	0.081	−0.058	−0.72

$DEL=B_{ex}/B_{th}$, $B=2.0(Q-1)/(Q+1)$, $Q=F(hkl)/F(\bar{h}\bar{k}\bar{l})$. B_{ex} is the mean value of two B's observed individually. B_{th} has been calculated from the parameters at the final stage of the refinement including anomalous dispersion terms of chlorine atom; $\Delta f'_{Cl}=0.348$ and $\Delta f''_{Cl}=0.702$.

$\sin\theta/\lambda<0.53$.

The intensities were corrected for the Lorentz and polarization factors, but were not corrected for absorption.

Structure Determination and Refinement. *a)*: The structure of asperlin (**1**) was elucidated by MULTAN.[7] The 250 reflections with $|E|$ values greater than 1.2 were used for phase determination, and a set of phases of the highest figure of merit was chosen for the calculation of an E map. The map revealed the positions of all non-hydrogen atoms except the terminal methyl carbon atom; the atom was easily located by Fourier synthesis. The structure was refined by the block-diagonal least-squares method.[8] The atomic species and types of bonds were determined on the basis of temperature factors, and interatomic distances and angles as well as chemical information. The difference Fourier synthesis computed after the anisotropic refinement of the non-hydrogen atoms revealed the positions of hydrogen atoms. However, several minor residual peaks were found around the methyl gourp in the synthesis. The final refinement, including the contribution of these hydrogen atoms with isotropic temperature factors, reduced R to 0.068 for 1084 independent reflections ($R=0.052$ for non-zero reflections). The weighting scheme used in the final refinement was: $w=0.5$ for $F_o=0$ and $w=[\sigma^2(F_o)+0.004F_o^2]^{-1}$ for $F_o>0$, where the values of $\sigma(F_o)$ were calculated from counting statistics. However, zero weight was given for the strongest reflection, 601. The final atomic coordinates are given in Table 1(a).

b): The determination and the refinement of the structure of asperlinol (**2**) were made with the same way as that of asperlin. The final refinement, including the hydrogen atoms located in the difference Fourier synthesis with isotropic temperature factors, reduced R to 0.056 for 1127 independent reflections ($R=0.043$ for non-zero reflections). The weighting scheme used in the final refinement was $w=0.4$ for $F_o=0$ and $w=[\sigma^2(F_o)+0.03F_o]^{-1}$ for $F_o>0$.

Table 3. Bond lengths (Å) and angles (°) for non-hydrogen atoms with estimated standard deviations in parentheses

	1 (X=O(5))	**2** (X=O(6))	**3** (X=Cl)
Bond lengths			
C(1)-C(2)	1.485(9)	1.473(8)	1.510(13)
C(2)-O(1)	1.195(7)	1.208(6)	1.183(11)
C(2)-O(2)	1.348(6)	1.353(6)	1.348(10)
C(3)-C(4)	1.479(6)	1.497(6)	1.490(10)
C(3)-C(7)	1.511(5)	1.515(5)	1.515(9)
C(3)-O(2)	1.454(5)	1.454(5)	1.453(8)
C(4)-C(5)	1.323(6)	1.324(6)	1.294(10)
C(5)-C(6)	1.476(6)	1.471(6)	1.497(10)
C(6)-O(3)	1.202(6)	1.213(5)	1.177(9)
C(6)-O(4)	1.345(5)	1.330(5)	1.361(8)
C(7)-C(8)	1.493(5)	1.519(5)	1.534(9)
C(7)-O(4)	1.439(4)	1.455(4)	1.469(8)
C(8)-C(9)	1.475(6)	1.505(5)	1.516(9)
C(8)-O(5)	1.430(5)	1.428(5)	1.412(8)
C(9)-C(10)	1.521(8)	1.501(6)	1.523(11)
C(9)-X	1.438(6)	1.442(5)	1.812(7)
Bond angles			
C(1)-C(2)-O(1)	126.2(5)	127.8(5)	128.4(8)
C(1)-C(2)-O(2)	111.0(5)	111.3(4)	109.0(7)
O(1)-C(2)-O(2)	122.7(5)	120.9(5)	122.6(8)
C(4)-C(3)-C(7)	110.2(3)	110.9(3)	110.5(6)
C(4)-C(3)-O(2)	107.8(3)	108.9(3)	109.6(5)
C(7)-C(3)-O(2)	108.0(3)	108.7(3)	108.0(5)
C(3)-C(4)-C(5)	120.5(4)	121.0(4)	120.6(7)
C(4)-C(5)-C(6)	121.3(4)	120.9(4)	121.5(7)
C(5)-C(6)-O(3)	124.0(4)	122.1(4)	123.6(7)
C(5)-C(6)-O(4)	117.6(4)	118.8(3)	116.7(6)
O(3)-C(6)-O(4)	118.3(4)	118.9(4)	119.7(6)
C(3)-C(7)-C(8)	113.0(3)	113.4(3)	113.3(5)
C(3)-C(7)-O(4)	112.5(3)	112.2(3)	110.6(5)
C(8)-C(7)-O(4)	106.0(3)	107.0(3)	105.5(5)
C(7)-C(8)-C(9)	121.3(4)	113.0(3)	111.4(5)
C(7)-C(8)-O(5)	113.2(3)	105.5(3)	106.3(5)
C(9)-C(8)-O(5)	59.3(3)	111.1(3)	111.2(5)
C(8)-C(9)-C(10)	119.8(4)	114.6(3)	115.4(6)
C(8)-C(9)-X	58.8(3)	106.4(3)	106.8(5)
C(10)-C(9)-X	114.9(4)	109.5(3)	108.2(5)
C(2)-O(2)-C(3)	116.7(3)	116.7(3)	117.8(6)
C(6)-O(4)-C(7)	119.3(3)	118.4(3)	118.5(5)
C(8)-O(5)-C(9)	61.9(3)	—	—

The final atomic coordinates are given in Table 1(b).

c): The structure of chloro derivative (**3**) was solved by the heavy-atom method, and refined by the block-diagonal least-squares method in the same way as described above. After the absolute configuration of this molecule was determined (see below), the anomalous scattering factor of chlorine atom was included in the refinement. The positions of all hydrogen atoms were assigned from the difference Fourier synthesis. The final refinement, including the contribution of the hydrogen atoms with isotropic temperature factors, reduced R to 0.051 for 831 independent reflections, where the following weighting scheme was used; $w=0.5$ for $F_o=0$, $w=1.0$ for $0<F_o\leqq 15$, and $w=[1.0+0.4(F_o-15)]^{-1}$ for

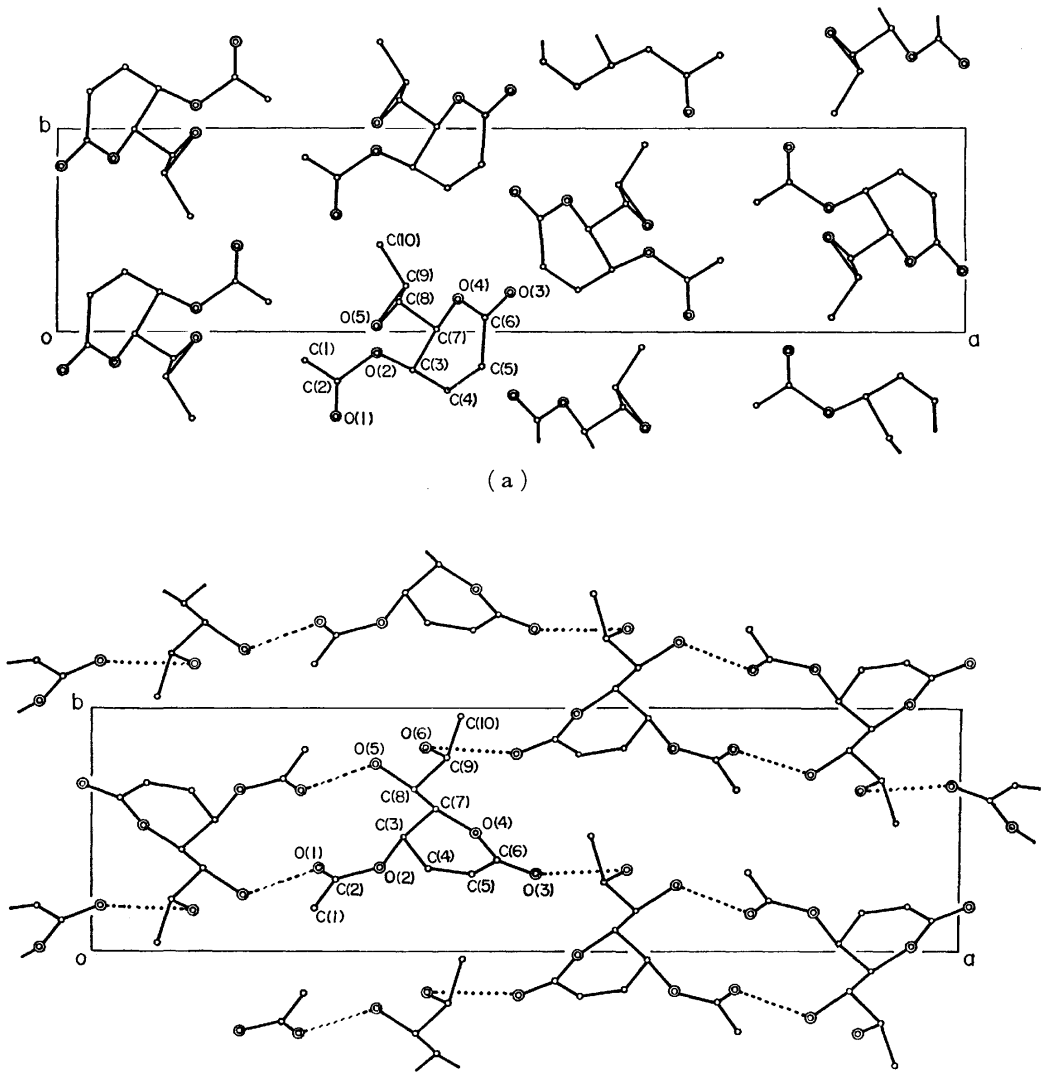

Fig. 1. (a) Projection of the crystal structure of asperlin (**1**). (b) Projection of the crystal structure of asperlinol (**2**). Broken lines indicate hydrogen bond. Hydrogen atoms are omitted for clarity.

TABLE 4. TORSION ANGLES (°)

	1 (X=O(5))	**2** (X=O(6))	**3** (X=Cl)		**1** (X=O(5))	**2** (X=O(6))	**3** (X=Cl)
C(7)-C(3)-C(4)-C(5)	−26.5	−19.7	−24.5	C(8)-C(7)-C(3)-O(2)	50.7	46.0	48.3
O(2)-C(3)-C(4)-C(5)	91.2	99.9	94.5	C(3)-C(7)-C(8)-C(9)	132.7	178.8	177.4
C(3)-C(4)-C(5)-C(6)	−3.6	−6.7	−9.5	O(4)-C(7)-C(8)-C(9)	−103.8	−57.0	−61.4
C(4)-C(5)-C(6)-O(4)	12.7	7.8	17.4	C(3)-C(7)-C(8)-O(5)	65.6	57.2	56.2
C(4)-C(5)-C(6)-O(3)	−163.6	−167.2	−162.3	O(4)-C(7)-C(8)-O(5)	−170.9	−178.6	177.4
C(5)-C(6)-O(4)-C(7)	12.1	20.1	12.1	C(7)-C(8)-C(9)-C(10)	157.2	−68.5	−64.1
O(3)-C(6)-O(4)-C(7)	−171.4	−164.7	−168.2	O(5)-C(8)-C(9)-C(10)	—	49.9	54.3
C(6)-O(4)-C(7)-C(3)	−42.8	−46.6	−45.3	C(7)-C(8)-C(9)-X	—	170.4	175.7
C(6)-O(4)-C(7)-C(8)	−166.7	−171.6	−168.1	O(5)-C(8)-C(9)-X	—	−71.2	−65.9
O(4)-C(7)-C(3)-C(4)	48.2	44.4	50.0	C(4)-C(3)-O(2)-C(2)	98.7	91.3	89.6
C(8)-C(7)-C(3)-C(4)	168.2	165.7	168.2	C(7)-C(3)-O(2)-C(2)	−142.3	−147.7	−149.9
O(4)-C(7)-C(3)-O(2)	−69.3	−75.3	−69.9				

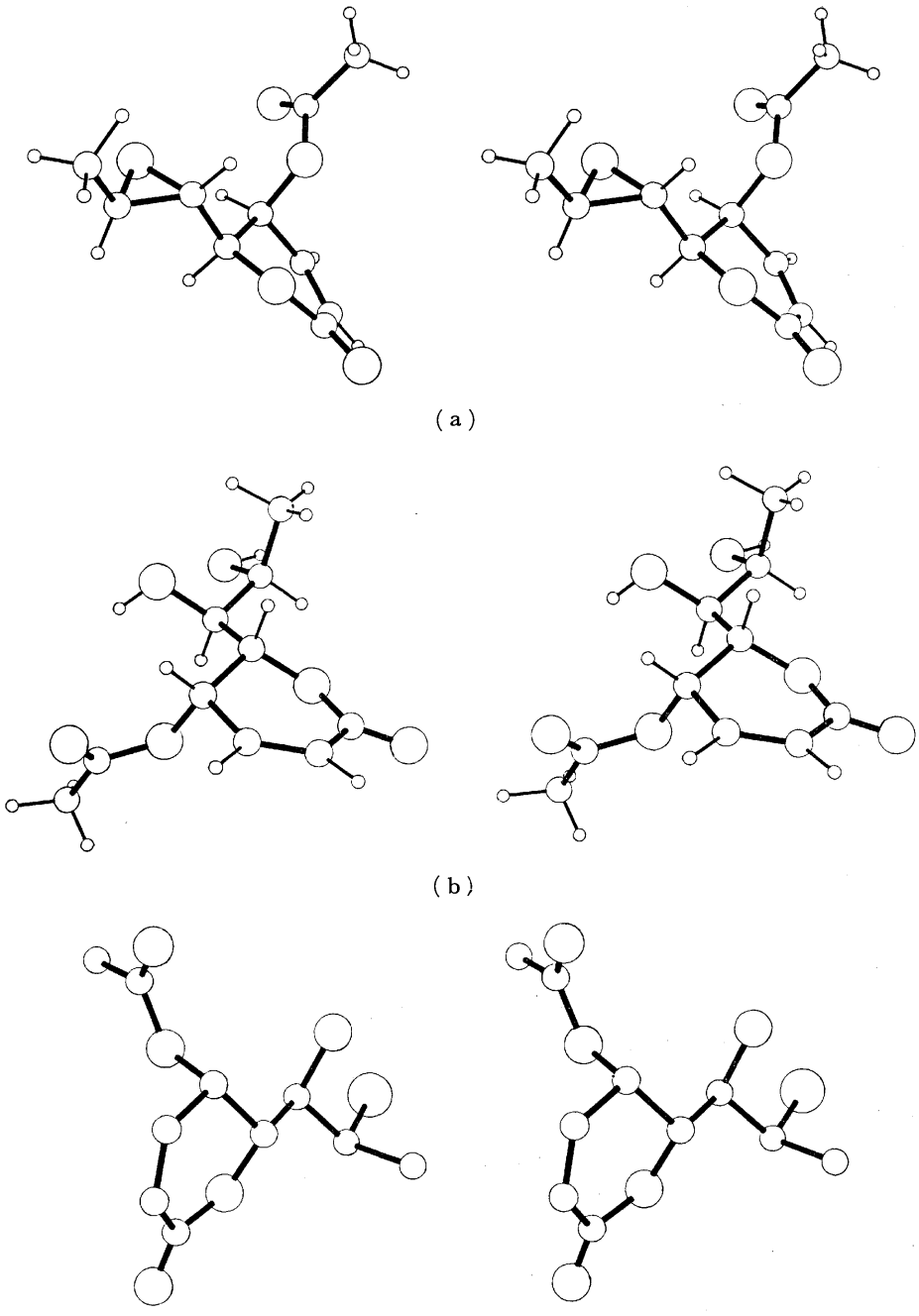

Fig. 2. (a) Stereoscopic view of asperlin (**1**). (b) Stereoscopic view of asperlinol (**2**). (c) Stereoscopic view of chloro derivative of asperlin (**3**). Each figure is drawn with the correct absolute configuration.

$15<F_o$. The final atomic coordinates are given in Table 1(c).

The temperature factors and the list of observed and calculated structure factors for each compound are kept as Document No. 7839 at the Chemical Society of Japan.

Absolute Configuration. The absolute configuration of **3** has been determined by the Bijvoet method.[9] The structure factors were calculated including anomalous scattering of chlorine atom for Cu $K\alpha$ radiation, and eighteen reflections sensitive to the choice of enantiomer were selected manually. The intensities of each pair of reflections, hkl and $h\bar{k}l$, were measured alternately twice. The experimental conditions for the Bijvoet measurement were the same as those for F_o-data collection previously described except the scan speed (1°/min in θ) and background counting time (10 s). The result of the Bijvoet measurement is given in Table 2. Since the measurement was made in a left-handed coordinate system, the absolute configuration of **3** is correctly represented by the atomic coordinates given in Table 1(c) referred to a right-handed coordinate system. Accordingly the absolute configurations of **1** and **2** have been established; the atomic coordinates in Table 1 in a right-handed coordinate system give the correct absolute configurations for **1** and **2**. The atomic scattering factors were taken from the International Tables for X-Ray Crystallography.[10]

TABLE 5. LEAST-SQUARES PLANES AND DEVIATIONS OF ATOMS FROM EACH PLANE

Each plane is represented by $lX+mY+nZ=p$, where X, Y, Z are Cartesian coordinates in Å, referred to the axes a, b, c.

	1	2	3
(a) Plane through the lactone group.			
l	0.730	0.356	0.482
m	−0.157	0.804	−0.456
n	0.665	0.476	−0.749
p	9.257	8.388	1.731
Deviation (Å)			
C(5)	0.006	0.008	−0.001
C(6)	−0.018	−0.025	0.002
O(3)	0.007	0.009	−0.001
O(4)	0.006	−0.009	−0.001
C(3)[a]	0.529	0.293	−0.523
C(4)[a]	0.296	0.223	−0.333
C(7)[a]	−0.210	−0.367	0.266
(b) Plane through the C(3)—C(6) atoms.			
l	0.568	0.242	0.303
m	−0.201	0.842	−0.434
n	0.798	0.482	−0.848
p	7.269	7.187	0.352
Deviation (Å)			
C(3)	−0.007	−0.012	0.009
C(4)	0.015	0.028	−0.048
C(5)	−0.015	−0.029	0.044
C(6)	0.007	0.013	−0.001
O(3)[a]	0.263	0.191	−0.221
O(4)[a]	−0.202	−0.049	0.224
C(7)[a]	−0.691	−0.590	0.751

a) Not included in least-squares calculations.

TABLE 6. INTERMOLECULAR DISTANCES FOR NON-HYDROGEN ATOMS LESS THAN 3.8 Å

(a) Asperlin (**1**)			
O(5)···C(1)^{I}	3.526	O(5)···O(2)^{I}	3.749
C(8)···O(1)^{II}	3.655	C(10)···O(5)^{II}	3.706
O(3)···C(4)^{II}	3.641	C(10)···C(2)^{III}	3.590
C(10)···C(4)^{III}	3.742	C(10)···O(1)^{III}	3.672
O(5)···C(1)^{V}	3.496	O(3)···C(7)^{VII}	3.410
O(4)···C(5)^{VII}	3.414	O(3)···C(5)^{VIII}	3.415
(b) Asperlinol (**2**)			
C(3)···O(6)^{I}	3.552	C(4)···O(6)^{I}	3.705
C(7)···O(6)^{I}	3.557	C(10)···C(6)^{II}	3.525
C(10)···O(2)^{II}	3.710	C(10)···O(3)^{II}	3.638
C(10)···O(4)^{II}	3.737	O(5)···C(1)^{II}	3.391
C(1)···O(1)^{VI}	3.536	C(2)···O(1)^{VI}	3.481
C(8)···O(1)^{VI}	3.529	O(2)···O(1)^{VI}	3.721
O(5)···C(2)^{VI}	3.600	O(5)···O(1)^{VI}	2.739[a]
O(6)···C(1)^{VI}	3.725	C(9)···O(3)^{VII}	3.253
O(6)···O(3)^{VII}	2.940[a]	C(5)···O(3)^{IX}	3.796
C(6)···O(3)^{IX}	3.441	C(7)···O(3)^{IX}	3.342
C(10)···O(3)^{IX}	3.632	O(3)···C(5)^{IX}	3.735
O(4)···O(3)^{IX}	3.423		
(c) Chloro derivative (**3**)			
C(10)···C(5)^{I}	3.713	C(10)···C(6)^{I}	3.499
C(10)···O(2)^{I}	3.732	C(10)···O(3)^{I}	3.527
O(5)···C(1)^{I}	3.472	C(3)···Cl^{II}	3.727
C(7)···Cl^{II}	3.539	O(5)···Cl^{II}	3.544
C(4)···Cl^{IV}	3.634	C(9)···O(3)^{V}	3.304
Cl···O(3)^{V}	3.474	O(3)···C(6)^{VI}	3.779
O(3)···C(7)^{VI}	3.576	O(3)···C(10)^{VI}	3.596
C(1)···Cl^{VII}	3.675	C(2)···O(5)^{VII}	3.720
O(1)···C(1)^{VII}	3.766	O(1)···C(2)^{VII}	3.650
O(1)···C(8)^{VII}	3.611	O(1)···O(5)^{VII}	2.822[a]
O(5)···C(1)^{VII}	3.544		

a) Hydrogen bond.

Roman numeral superscripts refer to the following transformations of the coordinates:

(I) $x, y, 1+z$ (II) $x, 1+y, z$
(III) $x, 1+y, 1+z$ (IV) $x, 1+y, -1+z$
(V) $1/2-x, -y, 1/2+z$
(VI) $1/2-x, 1-y, -1/2+z$
(VII) $1-x, 1/2+y, 1/2-z$
(VIII) $1-x, 1/2+y, -1/2-z$
(IX) $1-x, 1/2+y, 3/2-z$

Results and Discussion

The crystal structures and the numbering scheme of atoms used in this paper are shown in Fig. 1, and a stereoscopic view of each molecule plotted by a local version of PLUTO[11] in Fig. 2. The bond lengths and angles for non-hydrogen atoms are listed in Table 3, the selected torsion angles in Table 4, the equations of the least-squares planes and deviations of atoms from each plane in Table 5, and intermolecular distances less than 3.8 Å in Table 6.

The present X-ray crystallographic analysis has verified the configurations at the C(3) and C(7) atoms suggested by spectroscopy.[3] The hydrogen atoms in the epoxide ring of **1** are *trans*, the configurations at the C(8) and C(9) atoms being *S* and *R*, respectively. The configuration of the C(9) atom in **1** is opposite to that in **2** and **3**. This fact is consistent with the known mechanism that Walden inversion occurs at the atom to which nucleophile attack to open the epoxide ring.[12] The conformations found in the $\alpha\beta$-unsaturated δ-lactone rings are similar to each other. The planes of the lactone ring and olefinic double bond are not coplanar; the dihedral angles for **1**, **2**, and **3** are 12.4, 6.9, and 11.8°, respectively. The C(7) and O(4) atoms deviate to the same side of the plane of the olefinic double bond by different amounts. Such features are also found in related compounds.[13,14] As suggested by spectroscopy,[1,3,4] the hydrogen atoms at C(3) and C(7) are quasi-equatorial and quasi-axial, respectively. Since the NMR spectrum is reasonably explained by the results from the present crystallographic analysis, it is almost certain that the conformation of the lactone ring in solution is the same as that in the crystalline state. Beecham discussed the relationship between the chirality in the system C=C-C=O in an $\alpha\beta$-unsaturated lactone and the sign of the Cotton effect in the CD spectrum; he suggested that right or left-handed chirality causes a negative or positive Cotton effect in the $n\rightarrow\pi^*$ transi-

tion respectively.[13] In asperlin (**1**), the chirality in the system C=C-C=O in the crystalline state is left handed with the torsion angle being —163.6°. This fact is, according to Beecham's idea, consistent with the positive Cotton effect of **1**.[13]

In the crystals of **2** and **3**, an intermolecular hydrogen bond between one of the hydroxyl group(s) and the acetyl group, O(5)–H(O5)···O(1), connects molecules related by a screw axis. The distance of H(O5)··· O(1) is 1.81 Å for **2** and 1.87 Å for **3**, and the angle of O(5)–H(05)···O(1) is 163° for **2** and 166° for **3**, and that of H(O5)···O(1)–C(2) is 131° for **2** and 127° for **3**. The crystal structures of **2** and **3** are isotypic to each other (the b and c axes of **3** correspond to c and —b axes of **2** respectively), although **2** has an additional intermolecular hydrogen bond between the other hydroxyl group and the carbonyl oxygen atom of the lactone group, O(6)–H(O6)···O(3); the distance of H(O6)···O(3) is 2.08 Å, and the angles of O(6)–H(O6)···O(3) and H(O6)···O(3)–C(6) are 155° and 148° respectrively. There is no intramolecular hydrogen bond in the present three compounds. No abnormality in bond lengths and angles or in intermolecular distances is found in the crystals of **1**—**3**.

We wish to thank the staff of the Institute for Protein Research of Osaka University for the use of the Rigaku computer-controlled four-circle diffractometer. We are also indebted to Mr. Toshiaki Ogawa and Mr. Katsushi Tanikawa for valuable assistance in X-ray work.

References

1) A. D. Argoudelis and J. F. Zieserl, *Tetrahedron Lett.*, **1966**, 1969.
2) S. D. Mills and W. B. Turner, *J. Chem. Soc., C*, **1967**, 2242.
3) R. H. Evans, Jr., G. A. Ellestad, and M. P. Kunstmann, *Tetrahedron Lett.*, **1969**, 1791.
4) Wm. Rosenbrook, Jr. and R. E. Carney, *Tetrahedron Lett.*, **1970**, 1867.
5) M. Tanabe, T. Hamasaki, D. Thomas, and L. Johnson, *J. Am. Chem. Soc.*, **93**, 273 (1971).
6) M. Tanabe, M. Uramoto, T. Hamasaki, and L. Cary, *Heterocycles*, **5**, 355 (1976).
7) G. Germain, P. Main, and M. M. Woolfson, *Acta Crystallogr., Sect. A*, **27**, 368 (1971).
8) T. Ashida, HBLS-V, "The Universal Crystallographic Computing System-Osaka," The Computing Center, Osaka University, 1973, p.55.
9) J. M. Bijvoet, A. F. Peerdeman, and A. J. van Bommel, *Nature*, **168**, 271 (1951).
10) "International Tables for X-Ray Crystallography," Kynoch Press, Birmingham (1974), Vol. IV.
11) S. Motherwell, PLUTO, a Program for Plotting Molecular and Crystal Structures, Cambridge Crystallographic File User Manual, May, 1976.
12) For example, D. J. Cram and G. S. Hammond, "Organic Chemistry," McGraw-Hill, New York, (1970), p. 629.
13) A. F. Beecham, *Tetrahedron*, **28**, 5543 (1972).
14) P. J. Clarke and P. J. Pauling, *J. Chem. Soc., Perkin Trans. 2*, **1975**, 368.

Metachromasy. IV. The Simultaneous Determination of the Bound Dye Spectra and the Equilibrium Constants between Metachromatic Dyes and Various Polyelectrolytes by the Extended Principal Component Analysis Method

Kiwamu YAMAOKA* and Mineo TAKATSUKI

Faculty of Science, Hiroshima University, Higashisenda-machi, Hiroshima 730

(Received June 3, 1978)

Fourteen sets of visible absorption spectra of two metachromatic dyes, Crystal Violet (CV) and Trypaflavine (TF), were measured in the presence of seven widely different polyelectrolytes—sodium polyphosphate, polyacrylate, and poly(ethylenesulfonate), sodium and potassium poly(*p*-styrenesulfonate)s, and native and denatured calf thymus DNA—in polymer residue-to-dye ratios between 0 : 1 and about 1 : 1. The optical titration curves of these dye-polyanion systems showed either of two changes, sigmoidal or monotonous. The method of principal component analysis was applied to the observed spectra of each dye–polyanion system in order to determine both the equilibrium constant of the binding reaction and the pure spectrum of the bound dye. An empirical parameter α was introduced into the expression for the equilibrium constant in such a way that $K=[\text{complex}]/[\text{free dye}][\text{unoccupied binding site}]^{\alpha}$, by which the sigmoidal titration curves could be reproduced only with $\alpha>1$ and the monotonous ones, with $\alpha\leqq 1$. The spectra of bound CV and TF showed metachromasy bands, which depend on the functional group and the conformation of the polyanions, in wavelength regions both shorter and longer than the peak wavelength of the free dyes.

Metachromasy is the well known phenomenon of the spectral change in staining dyes in the presence of polyelectrolyte in aqueous solution. A new absorption band often appears in the wavelength region shorter than the peak wavelength of free dye; it is called the *metachromasy* band (hereafter denoted as the Meta band). Various types of metachromasy, however, have been observed for different combinations of dyes and polyelectrolytes.[1-30] For example, metachromatic changes in Crystal Violet (CV, a triphenylmethane dye)[2] and Trypaflavine (TF, an acridine dye)[3] have been shown to depend on the degree of polymerization of sodium polyphosphate (NaPP) in solution. A remarkable Meta band appears in the CV–NaPP system, whereas no such band is apparent in the TF–NaPP system. Shirai *et al.*[29,30] recently reported that the peak position of the Meta band of Methylene Blue depends on the functional group of polyanions. Since metachromasy is a complicated phenomenon involving a multiple binding between dye and polyanion, it is necessary to know the pure absorption spectrum of the bound dye and the equilibrium scheme between the reaction components for quantitative and systematic studies. Nevertheless, surprisingly few spectra of bound dyes have been unraveled so far,[16,22,31] although the spectra of dimeric dyes have been determined in the absence of polymers.[32-36]

The method of principal component analysis (the PCA method)[37-39] was previously extended and successfully applied to the absorption spectra of various dyes for the simultaneous determinations of not only the number of absorbing components involved in equilibrium mixtures, but also their molar absorption coefficients, and of the equilibrium constant for the acid-base or dimerization reaction.[32] In the PCA method, only the initial concentrations of components and a set of observed absorption spectra are needed as experimental data. It is not necessary to measure the equilibrium concentrations of the various components by experiments such as equilibrium dialysis,[12,16,31] the use of which is limited by the size of permeable molecules of a relatively low molecular weight, the ionic strength of solution, and the dyes extremely adsorbable to the dialysis membrane. The PCA method circumvents these difficulties and should be suited for the determination of an equilibrium scheme for the binding of dye to polyelectrolyte.

In this investigation, the PCA method was applied to fourteen dye–polyelectrolyte combinations in order to obtain information necessary for the quantitative study of metachromasy. As sample dyes, cationic CV and TF were chosen because of their different metachromatic behavior,[1-3] while anionic polyelectrolytes were selected from the point of view of their backbone structure, functional group, and counter-ion. The pure spectrum of the bound dye and the equilibrium constant for the binding reaction were estimated for each dye–polyanion complex system. The results revealed that, in each case, the spectrum of the bound dye has the Meta bands in the wavelength regions shorter and longer than the pronounced peak of the free dye. The peak positions of these bands were found to depend on the functional group and conformation of the polyanions. These are important findings for investigating metachromasy quantitatively in terms of the electronic states of bound dye.[9,40] The optical titration data showed two types of titration curves, sigmoidal and monotonous, depending on the particular combinations of CV or TF with polyanions. An empirical parameter α was introduced into the equilibrium expression for the binding reaction between a dye and a polyanion. By using the parameter α, which may characterize the binding process, the sigmoidal and monotonous optical titration curves could be reproduced successfully.

Experimental

Materials. The dyes, CV and TF, are the same samples as were reported previously.[2,32] The number-average degree of polymerization ($\bar{n}$) of sodium polyphos-

phate (NaPP) is 154, the highest refractionated sample in the previous study.[2] Purified sodium polyacrylate (NaPA, mol wt 7.24×10^5) was described elsewhere.[41] The sodium poly(ethylenesulfonate) (NaPES, $\bar{n}=65$) was a gift of Dr. Masamitsu Shirai of the University of Osaka Prefecture. The potassium poly(*p*-styrenesulfonate) (KPSS, mol wt *ca.* 7.5×10^5) was given by Dr. Koshiro Yoshioka of the University of Tokyo. Both samples were used without further purification. Native calf thymus DNA (nDNA) was purchased from Worthington Biochemical Corp. and was heat-denatured to prepare the denatured sample (dDNA).[31] Sodium poly(*p*-styrenesulfonate) (NaPSS) was prepared by dialyzing the KPSS, which had been dissolved in 3 M aqueous NaCl, against a 1 M NaCl aqueous solution for two days and then against distilled water for four days. All the polyanion samples except DNA were dried *in vacuo* at 56 °C for 6 h and used to prepare the stock solutions (*ca.* 10^{-2} M). Just prior to the absorption measurements, the stock solutions were diluted with distilled water to the desired concentrations.

Procedures. Two matched pairs of 1.0 and 2.0 cm quartz cells were used for CV and TF respectively. The inner wall of the sample cell was pre-equilibrated with a concentrated dye solution to avoid errors due to the adsorption of the dye. The dye adsorbed on the wall was calibrated against distilled water in a clean reference cell. The sample cell was dried and then filled with a fixed volume (3.5 and 7 ml for 1.0 and 2.0 cm cells respectively) of a dye solution. The concentration of the dye solution was optically determined from the molar absorption coefficient ε (9.20×10^4 at 592 nm for CV, 4.67×10^4 at 452 nm for TF) immediately before the addition of a polyanion solution, since the adsorption of dye to galssware is unavoidable and since the actual concentration of the stock dye solution was inevitably reduced in storage.

The series of the absorption spectra of a dye solution were measured by titrating it with a polyanion solution delivered through a microburet. The volume change of the titrate was made as small as possible so as not to shift the binding equilibrium. The volume correction was made for the observed absrobance A_{obsd} which was read out to the maximum of four digits:

$$A = A_{\mathrm{obsd}}\frac{v_{\mathrm{I}}+v_{\mathrm{add}}}{v_{\mathrm{I}}},$$

where v_{I} and v_{add} are the initial volume of the dye solution, and the volume of the polyanion solution added to it, respectively.

Measurements. A Hitachi Model EPS-3T recording spectrophotometer was used. The temperature of the cell holder was kept at 25 °C by circulating water through it. The solutions in the cells were always equilibrated for 5—10 min before measurements.

The Concept of the Extended Principal Component Analysis Method

A detailed description of the PCA method and of its application to the equilibrium systems of dye molecules was given in a previous paper;[32] therefore, the concept of the extended PCA method is described here only briefly. In an equilibrium system which contains p absorbing components out of a total of q components, m different absorption spectra can be measured by varying the compositions between these components. This suggests that some correlation must exist between the m absorption spectra because of the contribution from the p absorbing components. These m absorption spectra can be expressed by a data matrix **D** whose element, $D_{ij}(i=1,\ m \text{ and } j=1,\ n)$, denotes the absorption coefficient of the ith spectrum at the jth selected wavelength. According to Beer's law, the **D** matrix must be represented by the product of a concentration matrix **C** and an absorption coefficient matrix $\boldsymbol{\varepsilon}$:

$$\mathbf{D} = \mathbf{C}\boldsymbol{\varepsilon} = \begin{pmatrix} C_{11} \cdots C_{1j} \cdots C_{1p} \\ \cdots\cdots\cdots\cdots \\ C_{i1} \cdots C_{ij} \cdots C_{ip} \\ \cdots\cdots\cdots\cdots \\ C_{m1} \cdots C_{mj} \cdots C_{mp} \end{pmatrix} \begin{pmatrix} \varepsilon_{11} \cdots \varepsilon_{1j} \cdots \varepsilon_{1n} \\ \cdots\cdots\cdots\cdots \\ \varepsilon_{i1} \cdots \varepsilon_{ij} \cdots \varepsilon_{in} \\ \cdots\cdots\cdots\cdots \\ \varepsilon_{p1} \cdots \varepsilon_{pj} \cdots \varepsilon_{pn} \end{pmatrix} \tag{1}$$

where C_{ij} is the equilibrium concentration of the jth component in the ith solution, and ε_{ij} is the molar absorption coefficient of the ith component at the jth selected wavelength. The matrices, **C** and $\boldsymbol{\varepsilon}$, however, are not known *a priori* in most cases. Hence, the purpose of the application of the PCA method to chemical equilibria is to determine those unknown quantities simultaneously.

In the PCA method, the second moment matrix **A** is first constructed by the product of the **D** matrix and its transposed matrix. The eigenvectors $\boldsymbol{e}_i(i=1,\ n)$ and the eigenvalues $\Lambda_i(i=1,\ n)$ of the **A** matrix can then be calculated by diagonalization. The eigenvectors are the fundamental components which are common to the m absorption spectra, while the eigenvalues represent the contribution of the corresponding eigenvectors to the m spectra.[32] The relation between A_{jk}, Λ_i, and e_{ik} is given as

$$\sum_{j=1}^{n} A_{jk}e_{ij} = \Lambda_i e_{ik}. \tag{2}$$

The eigenvectors giving rise to extremely large eigenvalues are considered to be the principal components. When the eigenvalues are arranged in the order of magnitude, the following relation must hold for the data matrix **D** composed of p absorbing components:

$$\Lambda_1 \geqq \Lambda_2 \geqq \cdots \geqq \Lambda_p \gg \Lambda_{p+1} \geqq \cdots \geqq \Lambda_n > 0. \tag{3}$$

The **D** matrix can, then, be represented by a linear combination of p eigenvectors:

$$\mathbf{D} = \mathbf{f}\boldsymbol{e}, \tag{4}$$

where the **f** matrix of the (m,p) type is a linear combination coefficient matrix and can be calculated by the least-squares method. The $\boldsymbol{\varepsilon}$ matrix can also be related to the p eigenvectors by means of a transformation matrix **t** of the (p,p) type as follows:[32]

$$\boldsymbol{\varepsilon} = \mathbf{t}\boldsymbol{e}. \tag{5}$$

Therefore, the concentration matrix **C** can be computed as follows:

$$\mathbf{C} = \mathbf{f}\mathbf{t}^{-1}. \tag{6}$$

In order to determine the values of the elements of the **t** matrix, an appropriate equilibrium expression must be assumed for the system containing q components in which the absorbing components are p ($p \leqq q$). In the present work, the following general expression was assumed to describe the binding reaction between a dye and a polyanion:

$$K = \prod_{i=1}^{q} [\mathrm{X}_i]^{\nu_i}, \tag{7}$$

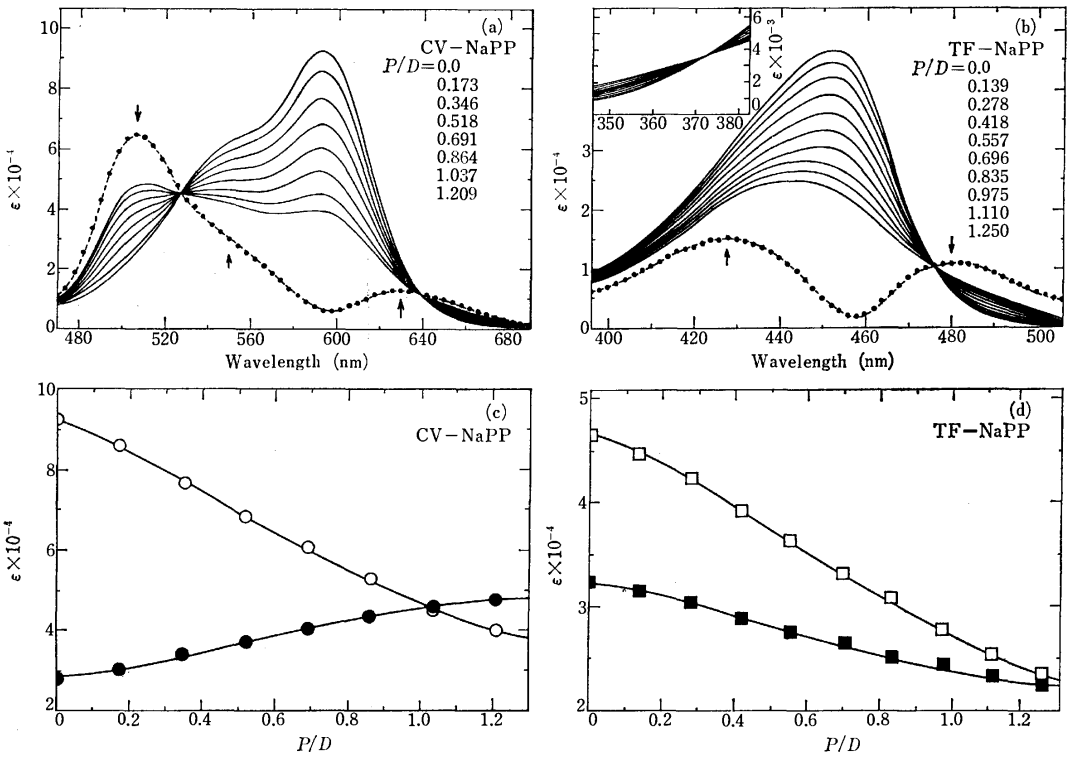

Fig. 1. Absorption spectra of CV and TF (solid curves) in the presence and absence of NaPP, the pure absorption spectra of bound dyes (closed circles) and optical titration curves.
The initial concentrations of CV and TF are 8.76 and 11.0 μM ((a) and (b)), respectively. The concentrations of NaPP are given in the respective figures in terms of *P/D*, the order of which corresponds to the order of the decrease in the maximum absorbances. The apparent molar absorption coefficients ε at 510 nm (●) and 592 nm (○) for CV and at 430 nm (■) and 450 nm (□) for TF are plotted against *P/D* in (c) and (d), respectively.

where K is the equilibrium constant, X_i is the ith absorbing or nonabsorbing component, and ν_i is the stoichiometric coefficient of X_i, whose equilibrium concentration is denoted by the brackets. The presence of nonabsorbing components in a given dye–polyanion system is subject to the equation of mass balance. Their equilibrium concentrations, therefore, can be calculated from their analytical concentrations and the **C** matrix if a set of the initial values for the elements of the **t** matrix is available. The substitution of m sets of the equilibrium concentrations in the right-hand side of Eq. 7 yields m different values for K, unless both the elements of the **t** matrix and the assumed equilibrium expression for the dye–polyanion system are correct. In order to discriminate the most probable **t** matrix and the equilibrium expression from the remainder, the coefficient of variation, S, is defined by Eq. 8 and used as a criterion:

$$S = \left(\frac{1}{m}\sum_{j=1}^{m}(K_j-\bar{K})^2\right)^{1/2}\Big/\bar{K}, \qquad (8)$$

where $\bar{K}$ denotes the mean value of K_j. The elements of the **t** matrix, and the equilibrium expression which yield the minimum S value can be determined by iterative calculations. The value of $\bar{K}$ corresponding to the minimized S value is considered as the most probable equilibrium constant. In this work, an acceptable upper limit of 0.15 was set for the minimized value of S in view of the experimental errors.[32]

Results

Application of the PCA Method to CV- and TF–NaPP Systems. The visible absorption spectra of CV and TF in the presence of NaPP are shown in Figs. 1(a) and (b) respectively. The spectra were measured at different stages of titration with the titrant NaPP solution up to the molar ratios of polymer residue-to-dye (*P/D*) of 1.21 and 1.25 for CV and TF respectively. The apparent molar absorption coefficients (ε) were calculated using the analytical concentrations of the dye in the solution. The spectra of CV–NaPP reveal a remarkable Meta band near 510 nm and three isosbestic points at 460, 529, and 639 nm (Fig. 1(a)), whereas TF–NaPP shows no such Meta band, but does show two isosbestic points at 371 and 476 nm (Fig. 1(b)). The apparent maximum absorption bands remain for CV, but are shifted gradually toward the shorter wavelengths for TF with an increase in the *P/D*.

The optical titration curves are plotted against *P/D* in terms of ε for CV and TF in Figs. 1(c) and (d) respectively. The titration curves were drawn at 510 and 592 nm for CV and at 430 and 450 nm for TF. It is clear from Figs. 1(c) and (d) that all these titration curves change with *P/D* sigmoidally but not monotonously. However, it can be expected from the existence of isosbestic points in the spectra of either

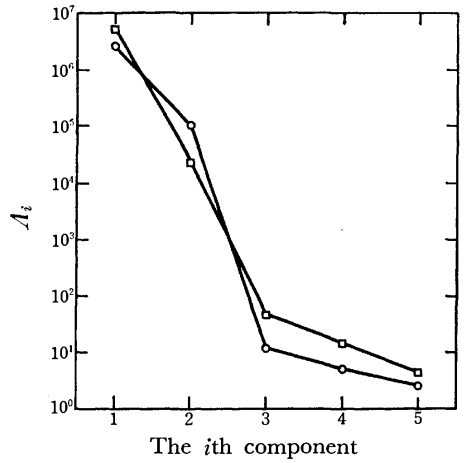

Fig. 2. Variation in eigenvalue Λ_i (i=1, 5) with the ith absorbing component. ○: CV–NaPP, □: TF–NaPP.

the CV– or TF–NaPP solution that there are two different absorbing components in the system. Such sigmoidal titration behavior was noted in the Acridine Orange–poly(α-L-glutamic acid) (PGA) system in the P/D range of 0—1 by Myhr and Foss.[15] They simply attributed the sigmoidal change to the equilibrium between three different absorbing components, *i.e.*, the free monomeric and dimeric dyes and the PGA-bound dye.

Since the advantage of the PCA method is that the likely number of the absorbing components involved in an equilibrium state can be determined by itself, it was applied to the sets of the observed spectra of dye-polyanion solutions over the entire P/D range shown in Figs. 1(a) and (b). The data matrix for CV–NaPP was composed of a set of absorbances at 56 selected wavelengths from 470 to 690 nm, at intervals of 4 nm, and a set of eight solutions differing in P/D, while the matrix for TF–NaPP was composed of a set of absorbances at 56 selected wavelengths from 396 to 512 nm, at intervals of 2 nm, and a set of ten solutions. The variations in eigenvalue Λ_i(i=1, 5) with the ith component are shown for both CV– and TF–NaPP systems in Fig. 2. It is clear that a large gap in eigenvalues exists between the second and third components for each system. This result confirms that the families of spectra in both Figs. 1(a) and (b) are composed of two, but not three, absorbing components, probably free and bound dyes. Schwarz[18] proposed a graphical method to analyze the absorption spectra of dye–polyion systems. The method, however, cannot be applied to sigmoidally changing titration curves like those of the CV– and TF–NaPP systems.

The extended PCA method is effective in analyzing the data of an unknown equilibrium system, since it assumes, successively, possible equilibrium schemes for a dye–polyanion system as *modus operandi*. Some specific equilibrium formulas based on Eq. 7 must first be considered for the equilibrium system. Three binding reactions frequently postulated for the system containing two absorbing components in the low P/D range are

$$D + P \rightleftharpoons DP, \quad K = \frac{[DP]}{[D][P]}, \tag{9}$$

$$2D + PP \rightleftharpoons DPDP, \quad K = \frac{[DPDP]}{[D]^2[PP]}, \tag{10}$$

and

$$D + 2P \rightleftharpoons PDP, \quad K = \frac{[PDP]}{[D][P]^2}, \tag{11}$$

where D is the free, unbound dye; P is the unoccupied binding site of polyanion; DP is the complex, *i.e.*, the bound dye; PP denotes two nearest-neighboring unoccupied sites; DPDP is the dimeric unit of bound dyes, and PDP is the complex in which a dye is bound to two nonneighboring polymer sites. The unknown absorbing components are DP, DPDP, and PDP, while the nonabsorbing components are P and PP. Unless otherwise stated, the computations were carried out under the assumption that the absorption spectrum of the free dye D is known. Equations 9 and 10 showed only monotonous titration curves, whereas Eq. 11 produced sigmoidal ones. In each of these three cases, the value of S in Eq. 8 could be minimized by varying the elements of the **t** matrix iteratively. However, the **t** matrix at this minimum S yielded some negative values for the molar absorption coefficient or the equilibrium concentration of the unknown absorbing component. Hence, the three schemes (9)—(11) should be concluded to be physically unsuitable for the experimental data.

Into the above three expressions, only the binding site P was taken as a nonabsorbing component which can not be directly detected as the eigenvector by the PCA method. In addition, solvent water and the counter-ions of the dye and NaPP, *i.e.*, Cl^- and Na^+, are all present in the solution as nonabsorbing components. Water is the solvent, so its concentration should be constant in equilibrium systems.[42] Consequently, the counter-ion Cl^- was taken into the fourth equilibrium scheme for the formation of a dye-polymer complex as follows:

$$D + Cl^- + P \rightleftharpoons DClP^-,$$

$$K = \frac{[DClP^-]}{[D][Cl^-][P]} = \frac{[DClP^-]}{[D]^2[P]}, \tag{12}$$

where $DClP^-$ is the complex and where $[D]=[Cl^-]$. No sigmoidal titration curve could be simulated with Eq. 12. Some K values calculated from the **t** matrix, which minimized S, deviated greatly from the mean value $\bar{K}$; moreover, some of them became negative. Thus, the equilibrium scheme (12) is also unsuitable for the CV– and TF–NaPP systems.

As the fifth equilibrium scheme, the participation of the counter-ion Na^+ was assumed:

$$D + Na^+ + P \rightleftharpoons DNaP^+, \quad K = \frac{[DNaP^+]}{[D][Na^+][P]}, \tag{13}$$

where $DNaP^+$ is the complex and an absorbing component with an absorption spectrum different from that of free dye. Since the initial concentration of Na^+ is equal to that of the binding site of NaPP, Eq. 13 is reduced to

$$K = \frac{[DNaP^+]}{[D][P]^2}, \tag{14}$$

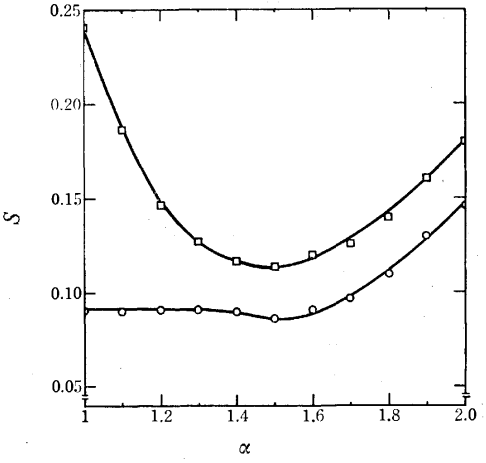

Fig. 3. Variation in the minimized S values with the empirical parameter α for the equilibrium formula (15) (see text). ○: CV–NaPP, □: TF–NaPP.

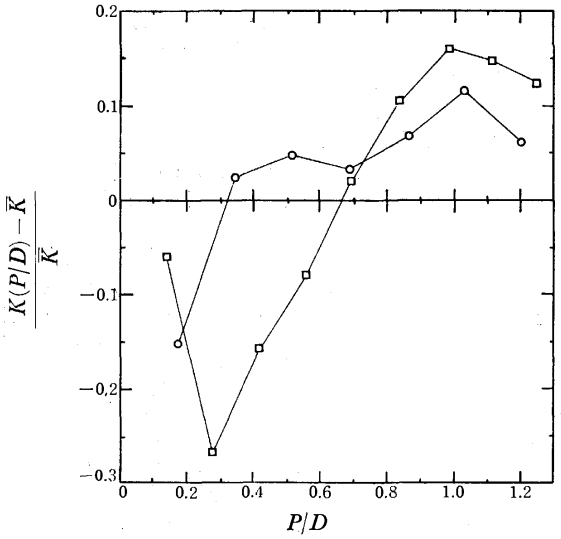

Fig. 4. Deviation of the equilibrium constant K from the mean value $\bar{K}$ at various P/D. The K values are computed with the optimum value of α in Eq. 15. ○: CV–NaPP, □: TF–NaPP.

A considerable sigmoidal change was manifested in the titration curve which was simulated with Eq. 14. Although the ε^b's of the bound dye and the values of K were always positive, the value of S was converged no less than 0.2, which exceeds the preset upper limit of 0.15.

The results of the above five equilibrium schemes led to the following conclusions. If the exponent of [D] is equal to, or larger than, that of [P], the optical titration data give rise to a monotonous curve. On the other hand, if the exponent of [P] is larger than that of [D], a sigmoidal titration curve results. Therefore, Eq. 14 is generalized by introducing an empirical parameter α into the equilibrium expression as

$$K = \frac{[DP^*]}{[D][P]^\alpha}, \qquad (15)$$

where DP* is the bound dye which differs from the free dye as regards the absorption spectrum. Both

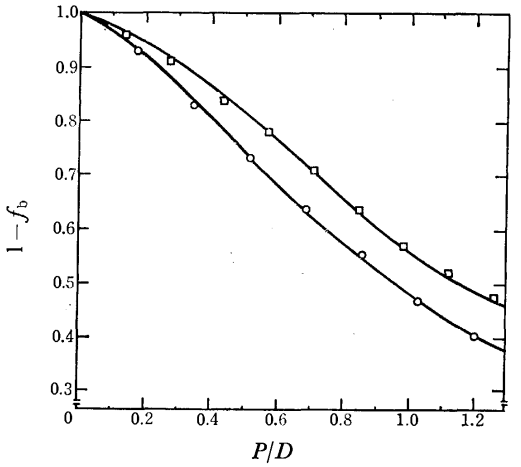

Fig. 5. Variation in the fraction of free dye $(1-f_b)$ with P/D for CV– and TF–NaPP. The fractions calculated at each P/D from Eq. 6 are represented by (—○—) and (—□—) for CV and TF, respectively. The fractions calculated from Eq. 15 with the values of α and the corresponding K given in Table 3 are drawn with solid curves.

monotonous and sigmoidal titration curves of various types can be produced from Eq. 15 by varying the parameter α.

Figure 3 shows the variations in the S values minimized by the **t** matrix with the empirical parameter α in Eq. 15 for both CV– and TF–NaPP systems. With an α value of 1.5, the values of S for the CV– and TF–NaPP systems reach the minimum points of 0.08 and 0.113 respectively. Both points are below the limit of 0.15. The variations in K with P/D at these points of S are shown in Fig. 4 for CV– and TF–NaPP. The scattering of each K from the mean value is only moderate, showing no systematic trend. These results suggest that equilibrium scheme (15) is acceptable for the binding reaction between NaPP and CV or TF if α is taken as 1.5.

The **t** matrix elements which minimized the S value are used for the calculation of the pure spectrum of the bound dye in terms of the molar absorption coefficient at the wavelength λ, ε^b_λ, determined in accordance with Eq. 5. The pure spectra of bound CV and TF are shown by closed circles in Figs. 1(a) and (b) respectively. The pure spectrum of bound CV reveals two peaks and a shoulder, while that of bound TF reveals two peaks (indicated by arrows). Although the Meta band of TF is not discernible at all in the observed spectra, the pure spectrum of bound TF demonstrates that a band does exist in the wavelength region shorter than the dominant peak of free TF. The characteristics of these spectra of bound dyes will be discussed later. Lastly, it should be noted that similar calculations were carried out with an assumption that the spectrum of the free dye D is unknown. The simulated spectrum of the free dye under this condition became identical to the observed one with $\alpha=1.5$ in Eq. 15.

The fraction of the bound dye, f_b, defined as C_b/C, could also be calculated at each P/D from the same

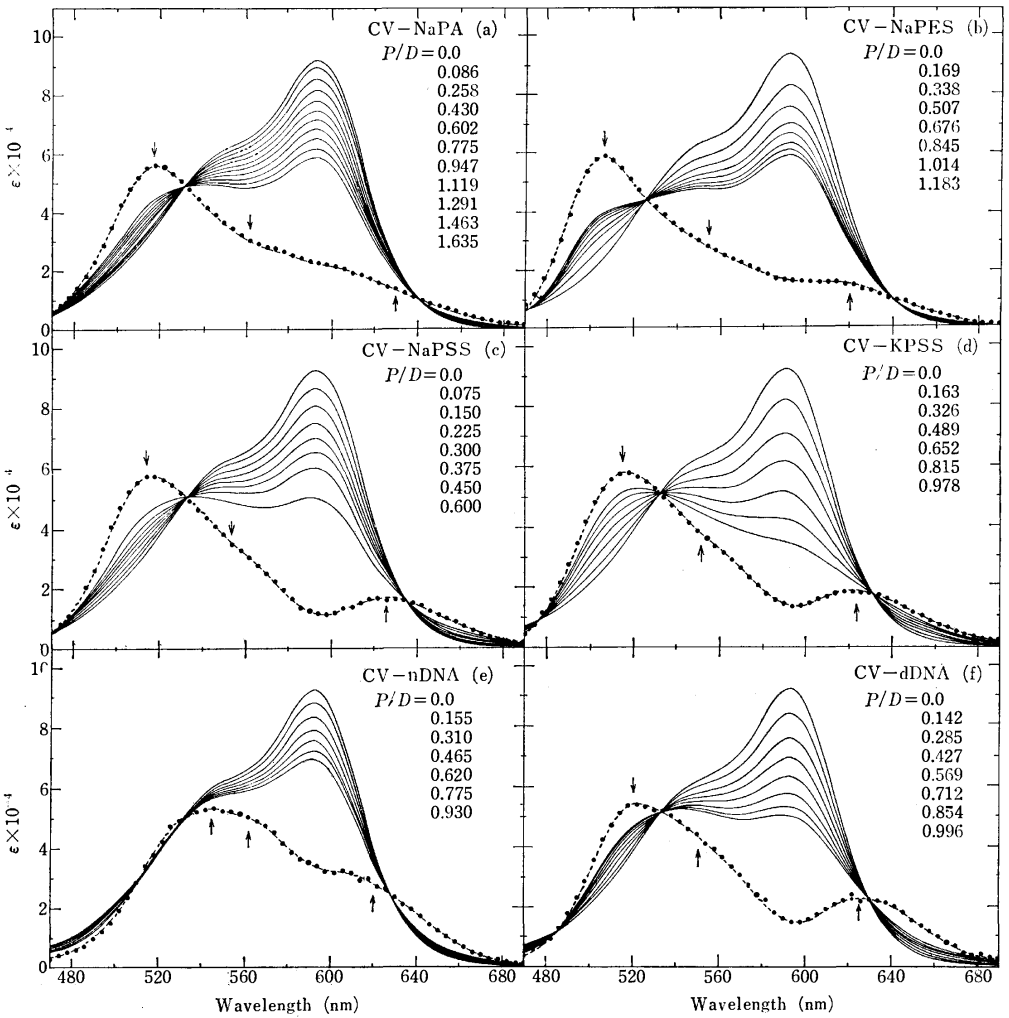

Fig. 6. Absorption spectra of CV in the presence and absence of polyanions (solid curves) and the pure absorption spectra of bound CV (closed circles).
Polyanions are; (a) NaPA, (b) NaPES, (c) NaPSS, (d) KPSS, (e) nDNA, and (f) dDNA. Neither polyanion nor dye solution contains neutral or buffer salts except for the DNA-dye solutions in which 1 mM NaCl is always present. The concentrations of CV are: (a) 8.33 μM, (b) 8.51 μM, (c) 8.67 μM, (d) 9.08 μM, (e) 9.05 μM, and (f) 11.9 μM. The concentrations of polyanions are listed in each figure in terms of P/D, the order of which corresponds to the order of the decrease in maximum absorbances. The isosbestic points are at (a) 476, 533, and 642 nm, (b) 460, 526, and 641 nm, (c) 473, 532, and 631 nm, (d) 473, 532, and 631 nm, (e) 628 nm, and (f) 486, 533, and 631 nm.

elements of the **t** matrix in accordance with Eq. 6, where C_b and C are the concentrations of the bound dye and the sum of the bound and free dyes respectively. The C_b at a given P/D is the mean of the C_b^λ values calculated from the observed spectrum at selected wavelengths, where C_b^λ is equal to $C(\varepsilon_\lambda - \varepsilon_\lambda^f)/(\varepsilon_\lambda^b - \varepsilon_\lambda^f)$. Therefore, the points in Fig. 5 represent the mean values of the normalized observed optical titration curves at selected wavelengths for CV- and TF-NaPP (circles and squares). These results are compared with the fractions of bound dye which were calculated from Eq. 15 with the values of α (=1.5) and K in Table 3; they are plotted with solid lines in Fig. 5. The agreement between them is excellent for both CV- and TF-NaPP. It should be noted that the sigmoidal decrease in the fraction of the unbound dye $(1-f_b)$ is quite clear.

Application of the PCA Method to Some CV–Polyelectrolyte Systems. Six polyelectrolytes, NaPA, NaPES, NaPSS, KPSS, nDNA, and dDNA, are chosen. The backbone structure of NaPA, NaPES, and NaPSS is identical, but their functional groups differ from one another. The difference between NaPSS and KPSS is only for the counter-ion, while nDNA and dDNA as biopolymers are different only in conformation. The absorption spectra of CV titrated with each polyanion are shown in Figs. 6(a)—(f). In all cases, the apparent ε at 592 nm decreases with the increase in P/D. The appearance of the Meta band in the observed spectra depends on the kind of polyanion; that is, a typical Meta band of CV appears near 510 nm in the presence of KPSS, whereas the Meta band appears only as a shoulder in the presence of NaPA, NaPES, and NaPSS. The presence of the Meta band is not manifested in the nDNA and dDNA. Two isosbestic points are clearly observed for each of the systems, suggesting

that two or more absorbing components are present. The eigenvalues of the second moment matrix were calculated from each set of spectra in Figs. 6(a)—(f). The ratios of the eigenvalues of the second, third, and fourth components to the eigenvalue of the first component are listed in Table 1. The ratios (expressed in terms of the logarithm) clearly indicate that a large gap exists between the second and third eigenvalues in each system, while the difference between the third and fourth eigenvalues is very small. These data verify that, in each CV–polyanion system, two absorbing components are involved in the binding reaction.

The pure spectra of bound CV are shown by closed circles in Figs. 6(a)—(f). For all the CV–polyanion systems, they exhibit two bands: a peak and a shoulder in the shorter-wavelength region and a band in the wavelength region longer than the peak position of free CV. These absorption bands will hereafter be abbreviated as follows: the Meta S_1 and Meta S_2 bands for the shorter-wavelength ones and the Meta L band for the longer-wavelength one (the numbering is from the one closest to the peak position of the free dye). The locations and ε^b's of the three Meta bands all depend on the polyanions, as is shown in Fig. 6 and Table 2. Especially, the Meta S_1 and S_2 bands of nDNA and dDNA seem to reflect their different conformations (the double helix *vs.* single-stranded coil).

TABLE 1. THE SECOND, THIRD, AND FOURTH EIGENVALUES NORMALIZED TO THE FIRST EIGENVALUE FOR CV- AND TF-POLYANION SYSTEMS

Dye	Polyanion	$\log(\Lambda_2/\Lambda_1)$	$\log(\Lambda_3/\Lambda_1)$	$\log(\Lambda_4/\Lambda_1)$
CV	NaPP	−1.39	−5.36	−5.72
	NaPA	−2.29	−5.46	−5.71
	NaPES	−2.14	−5.00	−5.60
	NaPSS	−2.09	−5.72	−5.91
	KPSS	−1.61	−4.90	−5.79
	nDNA	−2.90	−5.16	−5.68
	dDNA	−2.60	−4.97	−5.21
TF	NaPP	−2.34	−5.02	−5.55
	NaPA	−3.25	−5.80	−6.16
	NaPES	−2.68	−5.08	−5.74
	NaPSS	−2.17	−5.37	−5.69
	KPSS	−2.26	−5.59	−5.70
	nDNA	−2.89	−5.08	−6.02
	dDNA	−2.47	−4.63	−5.03

The optical titration curves of CV at 592 and 510 nm with six polyanions were found to be divided into two classes. Sigmoidal titration curves were observed for NaPA and KPSS just for NaPP (Fig. 5) and monotonous curves for NaPSS, NaPES, nDNA, and dDNA. The fractions of the bound dye, f_b, were calculated from Eq. 6; they are shown in Figs. 7(a)—(f). With the values of α and K which gave rise to the smallest S (the values are listed in Table 3 for each system), the observed titration curve can be reproduced quite excellently, as is indicated by the solid lines. It should be noted that the sigmoidal titration curve was observed whenever the value of α is greater than one, while a monotonous titration curve resulted when the value of α is equal to, or less than, one.

Application of the PCA Method to Some TF–Polyelectrolyte Systems. The same six polyanions are also

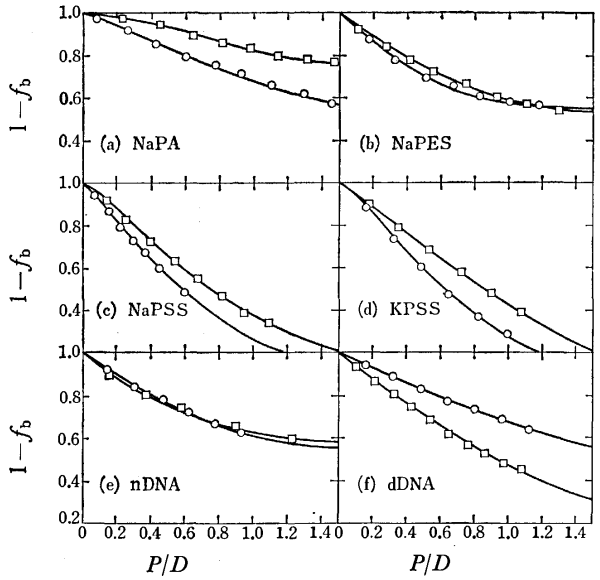

Fig. 7. Variation in the fraction of free dye ($1-f_b$) with P/D for six dye-polyanion systems. ○: CV-polyanions, □: TF-polyanions. For other details, see the caption of Fig. 5.

TABLE 2. THE MOLAR ABSORPTION COEFFICIENTS, ε^b, AND LOCATIONS OF METACHROMASY BANDS OF CV AND TF BOUND TO VARIOUS POLYANIONS

	Dye	CV (λ_{max}=592 nm; ε=9.20×10⁴)						TF (λ_{max}=452 nm; ε=4.67×10⁴)			
	Band	Meta S_2		Meta S_1[a]		Meta L		Meta S		Meta L	
		λ(nm)	$\varepsilon^b\times10^{-4}$	λ(nm)	$\varepsilon^b\times10^{-4}$	λ(nm)	$\varepsilon^b\times10^{-4}$	λ(nm)	$\varepsilon^b\times10^{-4}$	λ(nm)	$\varepsilon^b\times10^{-4}$
Polyanion	NaPP	506	6.48	550	2.97	630	1.26	428	1.53	480	1.08
	NaPA	518	5.41	550	3.54	630	1.53	430	1.35	475	1.17
	NaPES	506	5.78	555	2.72	620	1·52	430	1.85	476	0.96
	NaPSS	514	5.73	550	3.79	625	1.66	438	1.78	476	1.53
	KPSS	516	5.77	550	3.86	625	1.80	438	1.74	476	1.53
	nDNA	545	5.28	560	5.03	620	2.83	444	2.12	466	2.69
	dDNA	520	5.38	550	4.39	625	2.26	437	2.28	472	1.11

a) The position of this band is only approximate.

Table 3. Empirical parameters, α, and equilibrium constants, K and K', at 25 °C for CV- and TF-polyanion systems

	Dye	CV			TF		
		α	K [a]	K' [b]	α	K [a]	K' [b]
Polyanion	NaPP	1.5	$(1.0\pm0.1)\times10^{8}$	2.1×10^{5}	1.5	$(5.1\pm0.3)\times10^{7}$	1.3×10^{5}
	NaPA	1.2	$(8.8\pm0.9)\times10^{5}$	0.79×10^{5}	1.2	$(2.4\pm0.2)\times10^{5}$	0.24×10^{5}
	NaPES	0.6	$(1.1\pm0.1)\times10^{3}$	1.5×10^{5}	0.9	$(4.9\pm0.6)\times10^{4}$	1.7×10^{5}
	NaPSS	0.9	$(3.7\pm0.3)\times10^{5}$	13×10^{5}	1.5	$(2.6\pm0.1)\times10^{8}$	4.9×10^{5}
	KPSS	1.5	$(8.3\pm0.6)\times10^{8}$	12×10^{5}	1.3	$(1.6\pm0.2)\times10^{7}$	3.7×10^{5}
	nDNA	1.0	$(1.30\pm0.05)\times10^{5}$	1.3×10^{5}	1.0	$(7.4\pm0.6)\times10^{5}$	7.4×10^{5}
	dDNA	1.0	$(1.30\pm0.05)\times10^{5}$	1.3×10^{5}	1.0	$(1.8\pm0.3)\times10^{5}$	1.8×10^{5}

a) The dimension is given by $[\mathrm{l/mol}]^{\alpha}$. b) $K'=K\cdot[\mathrm{P}]^{\alpha-1}$ at $P/D=1$.

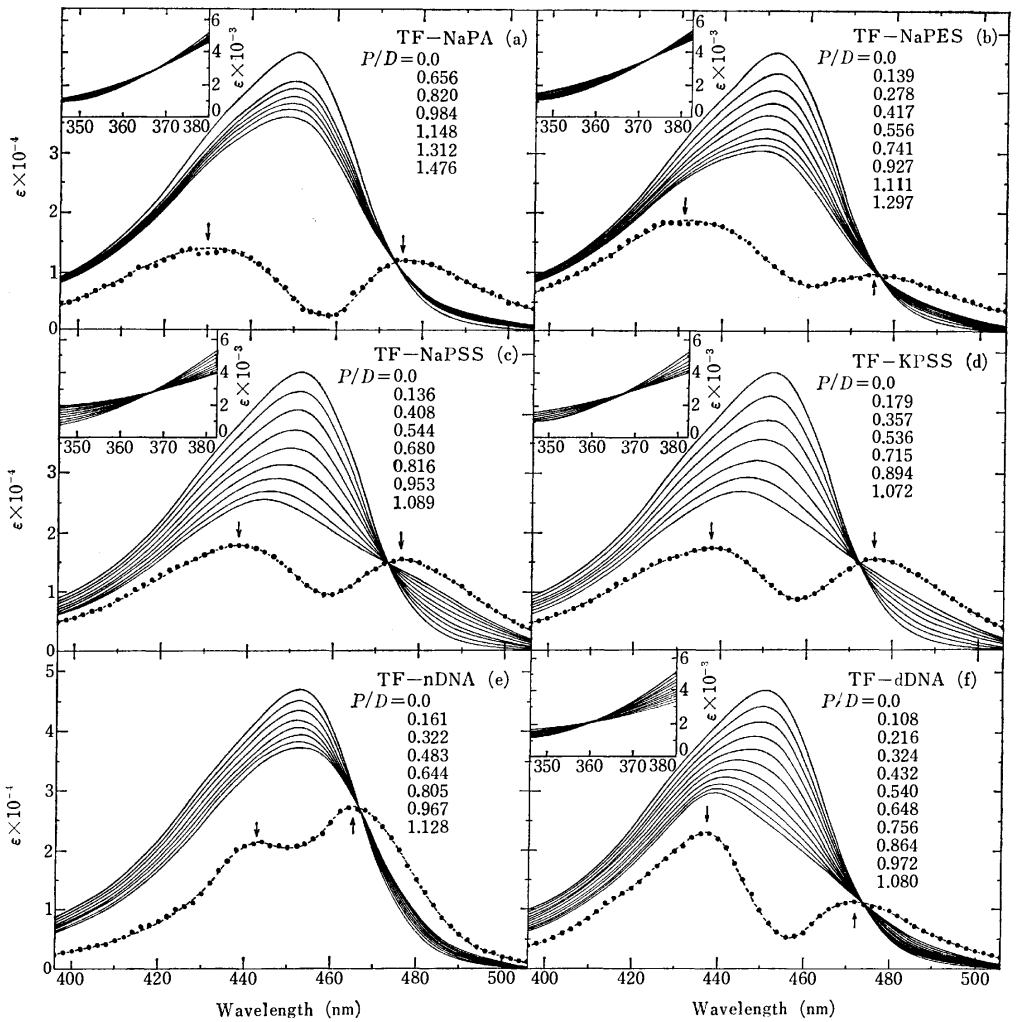

Fig. 8. Absorption spectra of TF in the presence and absence of polyanions (solid curves) and pure absorption spectra of bound TF (closed circles).
Polyanions are; (a) NaPA, (b) NaPES, (c) NaPSS, (d) KPSS, (e) nDNA, and (f) dDNA. Neither polyanion nor dye solution contains neutral or buffer salts except for the DNA–dye solutions in which 1 mM NaCl is always present. The concentrations of TF are: (a) 11.0 μM, (b) 7.77 μM, (c) 9.56 μM, (d) 8.28 μM, (e) 8.69 μM, and (f) 11.0 μM. The concentrations of polyanions are listed in each figure in terms of P/D, the order of which corresponds to the order of the decrease in maximum absorbances. The isosbestic points are at (a) 369 and 473.5 nm, (b) 372 and 476 nm, (c) 368 and 472 nm, (d) 368 and 472 nm, (e) 466 nm, and (f) 359 and 474.5 nm.

used for the titration of TF; the results are shown in Figs. 8(a)—(f). The spectra of all the TF–polyanion systems differ from those of the corresponding CV–polyanion systems in showing hypo- and hypsochromic effects without any Meta bands in the P/D range examined. The spectra of TF in the presence of polyanions show, without exception, an isosbestic point in the wavelength region longer than the peak position of the free TF. Another isosbestic point is also noted in the shorter-wavelength region (*cf.* the insert in each figure) except for the case of nDNA. Judged from the eigenvalues listed in Table 1, only two absorbing components are again sufficient to describe the spectral behavior in each TF–polyanion system. The pure spectra of bound TF are shown by closed circles in Figs. 8(a)—(f). Although none of the observed spectra manifests the presence of the Meta band, the bound spectra clearly show two such bands—the Meta S and Meta L bands — in all cases. The spectral profiles of the bound TF differ from those of the bound CV as regards the number of bands. The locations and ε^b's of those two Meta bands depend on the kinds of polyanions. They are listed in Table 2.

The empirical parameter α and the equilibrium constant K in Eq. 15 at the minimized S, which result from the application of the PCA method to the TF–polyanion spectra, are listed in Table 3 for all the systems. The values of α are, again, greater than one for those systems which yield the sigmoidal titration curves, whereas the values of α are equal to, or less than, one for those systems which produce the monotonous curves. As is shown in Figs. 7(a)—(f), the optical titration curves are sigmoidal for NaPA, NaPSS, and KPSS just for NaPP (*cf.* Fig. 5), while they are monotonous for NaPES, nDNA, and dDNA. The value of α obtained for the TF–polyanion system, however, is not necessarily identical with the value of α for the corresponding CV–polyanion system. This suggests that the value of α reflects the complexity and diversity of the binding reaction between a dye and a polyanion, the importance of the combination thereof, and the specificity of the chemical structure of the dye. It should also be noted in Fig. 7 that the fraction of the free, unbound dye decreases with the increase in the value of P/D, while no simple relation exists between TF and CV as regards their binding ability toward polyanions.

Discussion

The Method of Extended Principal Component Analysis. As has been described in a previous paper,[32] the PCA method has been proven to be exceedingly useful for an equilibrium system like dilute dye solutions composed of two or three absorbing components. In the equilibrium system of small molecules, the equilibrium schemes are relatively simple and the neglect of such a thermodynamic variable as activity coefficient may not affect the result too seriously. On the other hand, the binding of a dye to the polymer site is probably influenced by a large number of complicated factors in dye–polymer systems. In order to estimate the equilibrium scheme and the binding constant for these systems, and in order to evaluate the bound-dye spectrum, the equilibrium concentrations of the colored components have usually been determined by means of the absorption spectra and equilibrium dialysis combined.[12,16,20,27,31] Such a combined method, however, is difficult to apply to systems in which either a relatively small polymer cannot be retained by a semipermeable membrane, a dye is easily adsorbed on it, or the ionic strength imposes severe limitations as a result of the Donnan effect.

On the other hand, only the initial concentrations of the chemical species participating in a binding reaction and a set of the absorption spectra of solutions are needed in the PCA method; therefore, using it, a number of plausible equilibrium schemes can be tested successively. In order to determine the most probable absorption spectra of colored components and the equilibrium constant for the binding reaction, the only requirements are that the coefficient of variation S should reach a preset minimum value and that none of the spectra and equilibrium concentrations of the components should have a negative value. The latter condition is imposed by the physical restrictions and is quite useful for selecting appropriate parameters.[32] Thus, the only problem is concerned with the availability of adequate equilibrium expressions which describe the complicated binding processes between the dye and the polymer. In this work, an empirical parameter α was introduced into a relatively simple expression (Eq. 15) to circumvent the complexity. Since the PCA method could be applied to multicomponent dye systems,[32] its use may also be extended in the future to the dye–polyelectrolyte systems over the whole P/D range where more than two absorbing components coexist.

Absorption Spectra of Bound CV and TF. The term "metachromasy" has been used for the phenomenon of the hypo- and hypsochromic changes of the spectrum of a dye, often with a new band on the short-wavelength side which has been called the "metachromasy band." However, this concept of metachromasy is an oversimplification, as has been pointed out by a number of reports which more or less emphasize the simultaneous bathochromic effect of various polyelectrolytes on the spectrum of the dye.[1–3,43–45] The present work has proven that both bound CV and TF exhibit absorption spectra in which the new bands are clearly unraveled on the short- and long-wavelength sides of the peak of the corresponding free dyes (Figs. 1, 6, and 8). Fredericq and Houssier[16] have observed a similar result in the Acridine Orange–DNA system. The term "metachromasy band" may now be enlarged to include the long- and short-wavelength bands of a bound dye, both of which are abbreviated as "Meta bands."

The Meta S band for TF and the Meta L band for CV and TF are close to the peak of the free dyes and are simply hidden in the observed spectra, although their presence has been predicted from linear and circular dichroic studies.[44–47] The locations and ε^b's of the Meta bands for a given dye depend on the poly-

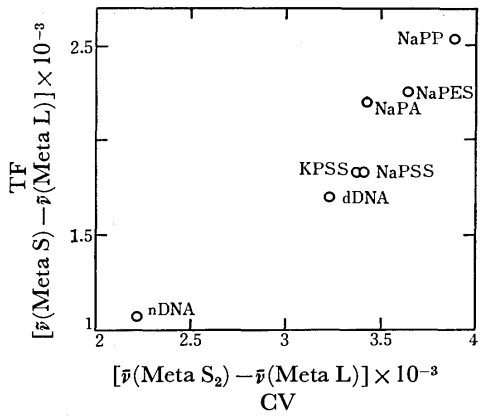

Fig. 9. Correlation between the energy separation between the Meta S_2 and L bands of CV and the separation between the Meta S and L bands of TF bound to seven polyanions. Scales are expressed in terms of wavenumbers $\bar{\nu}$.

anions (Table 2). The Meta bands of CV and TF bound to NaPA, NaPES, and NaPSS differ from one another depending on their functional groups, in spite of the fact that their backbone structure is identical. On the other hand, the Meta bands of nDNA and dDNA differ considerably in shape and position, although their backbone and functional groups are also identical. The Meta bands of either TF or CV are almost identical for NaPSS and KPSS. These results lead to the conclusion that the Meta bands sharply reflect the conformation of dye–polyanion complexes besides the functional group of the polyanions and that the kind of counter-ion scarcely affects the location and ε^b of the Meta bands.

A considerable positive correlation exists between the energy separation between the Meta S_2 and L bands of CV and the separation between the Meta S and L bands of TF, as is shown in Fig. 9; this indicates that the peak position of Meta bands depend mainly on the overall nature of the polyanions. The energy separation between the Meta S and L bands for a given dye may result from the different mean distance between the binding sites of a polyanion. The mean distance may, in turn, depend on the flexibility of the backbone in addition to the structure of the sidechain of the polyanion. The spectral aspects of the Meta band of bound dyes have now been clarified in sufficient detail. For a quantitative discussion of metachromasy, however, information is necessary on the electronic states and transition moments of dyes in the absence and presence of polyanions. The LCAO calculations may provide such information.

Empirical Parameter α and Equilibrium Constant. The absorption spectra of solutions containing both a dye and a polyanion vary in a complicated manner when a wide range of P/D is covered.[1-3] For example, the isosbestic points appear at different wavelengths depending on the P/D range, as has already been noted for CV– and TF–NaPP systems.[2,3] This strongly suggests that two or more of the absorbing components, *i.e.*, the bound dye species exclusive of the free dye, are present over the whole P/D range. In this work, the spectral changes in each dye–polyanion system are limited only in the low P/D range of 0—1, where a single set of isosbestic points is observed. In this P/D range, only a free dye and one kind of bound dye are present, as is confirmed by the eigenvalues of the second moment matrix (*cf.* Table 1). The empirical parameter α is indeed useful in simulating the optical titration curves and in classifying the dye–polyanion systems (Figs. 1 and 7). However, the values of the equilibrium constant K as such cannot be compared in order to characterize the different dye–polyanion systems, because the dimension of K $(=[\text{l/mol}]^{\alpha})$ now depends on α and is not identical in all the systems. The constant K defined in Eq. 15 may be related to the frequently granted equilibrium constant K' for the binding scheme (9) in such a way that $K'=[\text{DP}]/[\text{D}]\cdot[\text{P}]=K\cdot[\text{P}]^{\alpha-1}$. The values of K' calculated at $P/D=1$ using the K values listed in Table 3 are also given in the same table. Interestingly, these K' values compare favorably with the binding constants previously reported for various dye–polymer systems.[8,12,16,18,31]

The values of α for NaPA, NaPES, NaPSS, and KPSS differ from one another in ways reflecting the difference in the functional group or counter-ion of the polyanions (Table 3). Moreover, the α values also depend on the kind of dye to some extent. The difference in α-value between NaPSS and KPSS in the presence of either CV or TF suggests that the counter-ion plays some important role in the binding process of the dye to the polyanion, but does not affect the bound spectra. On the other hand, the values of α are unity for the dye–DNA systems and independent of the kinds of dyes and conformations of DNA, for which the distance between the charged sites of DNA appears to be responsible. Hence, the parameter α may be an indicator which reflects the local situation of the binding site of the polyanion, including the conformation, functional group, the counter-ion, and the structure and binding mode of the dye. Although the value of α is at present regarded as a constant in a low P/D range, it may be a function of P/D and could also represent the dependence of the activity coefficient of the polyelectrolyte on the residue concentration. Once the physical significance of the parameter α is clarified, it should be of great help for the better understanding of the metachromatic behavior of dye–polyelectrolytes. However, the parameter seems to contain many factors, such as temperature, counter-ion, and added salts. Thus, the clarification of the nature of α still awaits further quantitative studies.

Conclusions

The extended PCA method has now been demonstrated to be applicable to relatively complicated equilibrium systems between dyes and polyanions. By the use of this method, the quantitative studies of metachromasy are greatly facilitated as regards the number of dye species involved in dye–polyanion systems in equilibrium, the equilibrium constants, and the pure absorption spectra of the bound dye species. For each dye–polyanion system presently studied in

the low P/D range between zero and near one, only a single bound dye species is present besides a free, unbound dye. The pure spectra of bound CV and TF both show two remarkable metachromasy bands on the short- and long-wavelength sides of the absorption peak of free, unbound dyes. The spectral features of these bands are related to the functional group and the conformation of the polyanions. The equilibrium scheme between the bound and unbound absorbing components is not so simple as is often assumed, but requires an empirical parameter α to reproduce satisfactorily both the sigmoidal and monotonous optical titration curves of CV and TF. This parameter is probably an indicator of the local situation of the dye-bound polymer sites.

References

1) K. Yamaoka, T. Suenaga, A. Fujita, and M. Miura, *J. Sci. Hiroshima Univ., Ser. A*-II, **34**, 1 (1970).
2) K. Yamaoka, M. Takatsuki, Y. Yaguchi, and M. Miura, *Bull. Chem. Soc. Jpn.*, **47**, 611 (1974).
3) K. Yamaoka, M. Takatsuki, and M. Miura, *Bull. Chem. Soc. Jpn.*, **48**, 2739 (1975).
4) G. Weill and M. Calvin, *Biopolymers*, **1**, 401 (1963).
5) R. E. Kay, E. R. Walwick, and C. K. Gifford, *J. Phys. Chem.*, **68**, 1896 (1964).
6) R. C. Bean, W. C. Shepherd, R. E. Kay, and E. R. Walwick, *J. Phys. Chem.*, **69**, 4368 (1965).
7) T. Soda, and K. Yoshioka, *Nippon Kagaku Zasshi*, **87**, 22 (1966).
8) R. K. Tubbs, W. E. Ditmars, Jr., and Q. V. Winkle, *J. Mol. Biol.*, **9**, 545 (1964).
9) H. Ito and Y. J. I'Haya, *Int. J. Quantum Chem.*, **2**, 5 (1968).
10) V. Kleinwächter and J. Koudelka, *Biophysik*, **5**, 119 (1968).
11) D. G. Dalgleish, H. Fujita, and A. R. Peacocke, *Biopolymers*, **8**, 633 (1969).
12) D. G. Dalgleish, M. C. Feil, and A. R. Peacocke, *Biopolymers*, **11**, 2415 (1972).
13) M. K. Pal and M. Chauduri, *Makromol. Chem.*, **133**, 151 (1970).
14) M. K. Pal and M. Biswas, *Makromol. Chem.*, **151**, 121 (1972).
15) B. C. Myhr and J. G. Foss, *Biopolymers*, **10**, 425 (1971).
16) E. Fredericq and C. Houssier, *Biopolymers*, **11**, 2281 (1972).
17) G. Löber, H. Schütz, and V. Kleinwächter, *Biopolymers*, **11**, 2439 (1972).
18) G. Schwarz, S. Klose, and W. Balthasar, *Eur. J. Biochem.*, **12**, 454 (1970).
19) W. H. J. Stork, P. L. de Haseth, W. B. Schippers, C. M. Körmeling, and M. Mandel, *J. Phys. Chem.*, **77**, 1772 (1973).
20) W. H. J. Stork, J. A. M. Van Boxsel, A. F. P. M. de Goeij, P. L. de Haseth, and M. Mandel, *Biophys. Chem.*, **2**, 127 (1974).
21) S. C. Guhaniyogi and B. M. Mandel, *Makromol. Chem.*, **175**, 823 (1974).
22) V. Vitagliano, L. Costantino, and A. Zagari, *J. Phys. Chem.*, **77**, 204 (1973).
23) V. Vitagliano, L. Costantino, and R. Sartorio, *J. Phys. Chem.*, **80**, 959 (1976).
24) G. Löber, J. Koudelka, and E. Smekal, *Biophys. Chem.*, **2**, 158 (1974).
25) M. Tsuda, *Bull. Chem. Soc. Jpn.*, **48**, 1709 (1975).
26) S. Ichimura, *Biopolymers*, **14**, 1033 (1975).
27) J. S. Tan and R. L. Schneider, *J. Phys. Chem.*, **79**, 1380 (1975).
28) M. K. Salter, W. B. Rippon, and E. W. Abrahamson, *Biopolymers*, **15**, 1213 (1976).
29) M. Shirai, T. Nagatsuka, and M. Tanaka, *Chem. Lett.*, **1976**, 291.
30) M. Shirai, T. Nagatsuka, and M. Tanaka, *Makromol. Chem.*, **178**, 37 (1977).
31) K. Yamaoka and M. Masujima, *Biopolymers*, in press.
32) M. Takatsuki, and K. Yamaoka, *J. Sci. Hiroshima Univ. Ser. A*, **40**, 387 (1976).
33) W. H. J. Stork, G. J. M. Lippits, and M. Mandel, *J. Phys. Chem.*, **76**, 1772 (1972).
34) M. E. Lamm and D. M. Neville, Jr., *J. Phys. Chem.* **69**, 3872 (1965).
35) K. K. Rohatgi and G. S. Singhal, *J. Phys. Chem.*, **70**, 1695 (1966).
36) N. E. Sharpless, C. L. Greenblatt, and W. H. Jennings, *Trans. N. Y. Acad. Sci.*, **35**, 187 (1973).
37) W. H. Lawton and E. A. Sylvestre, *Technometrics*, **13**, 617 (1971).
38) N. Ohta, *Anal. Chem.*, **45**, 553 (1973).
39) T. W. Anderson, *Ann. Math. Statist.*, **34**, 122 (1963).
40) D. F. Bradley, I. Tinoco, Jr., and R. W. Woody, *Biopolymers*, **1**, 239 (1963).
41) S. Inoue, K. Yamaoka, and M. Miura, *J. Sci. Hiroshima Univ., Ser. A*, **39**, 27 (1975).
42) W. J. Moore, "Physical Chemistry," 3rd ed, Prentice-Hall, Englewood Cliff, N. J. (1962), Chap. 9.
43) J. A. Bergeron and M. Singer, *J. Biophys. Biochem. Cytol.*, **4**, 433 (1958).
44) K. Yamaoka and R. A. Resnik, *J. Phys. Chem.*, **70**, 4051 (1966).
45) K. Yamaoka and R. Resnik, *Nature*, **213**, 1031 (1967).
46) K. Yamaoka, *Chem. Lett.*, **1973**, 305.
47) K. Yamaoka and H. Hashimoto, *Chem. Lett.*, **1976**, 465.

Resonance Raman Spectra of *p*-Benzosemiquinone Anion Dimer

Satoshi YAMAGUCHI,* Kenji YOKOYAMA, and Shiro MAEDA
Research Laboratory of Resources Utilization, Tokyo Institute of Technology, Midori-ku, Yokohama 227

(Received June 21, 1978)

Resonance Raman specta have been observed for the dimer of *p*-benzosemiquinone anion. When the exciting-light frequency was exactly resonant with the absorption band characteristic of this dimer, a new polarized Raman line appeared at 177 cm^{-1} with a striking resonance enhancement. The resonant behavior and the frequency value both indicate that it can reasonably be assigned to the interradical stretching vibration of the parallel D_{2h} dimer molecule, much as in the case of the previous Würster's cation dimers.

The oxidation-reduction process between quinone and the corresponding hydroxy compound is known to proceed *via* an intermediate radical anion.[1] *p*-Benzosemiquinone anion (SQ^-) can be obtained by oxidizing hydroquinone dissolved in alkaline ethanol with air.[2] The solution is yellow at room temperature due to the absorption bands of SQ^- about 400 nm,[1-5] but it turns blue under −100 °C. The color change is due to the appearance of a new absorption band at 585 nm, as is shown in Fig. 1, which is associated with the formation of an ion dimer $(SQ^-)_2$.[2] The radical anion is also produced by irradiating UV light on a glassy ethanol matrix of hydroquinone at the temperature of liquid N_2.[2,4] The yellow glass thus obtained turns blue when it becomes fluid upon being warmed up to about −130 °C, but the blue color remaining unchanged after it cools down again, indicating the validity of presuming dimer formation.

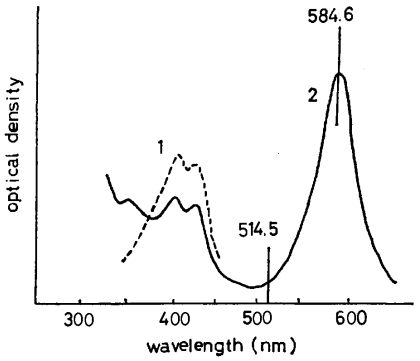

Fig. 1. Electronic absorption spectra of a SQ^- solution at room temperature (Curve 1) and at −196 °C (Curve 2). (from Ref. 2.)

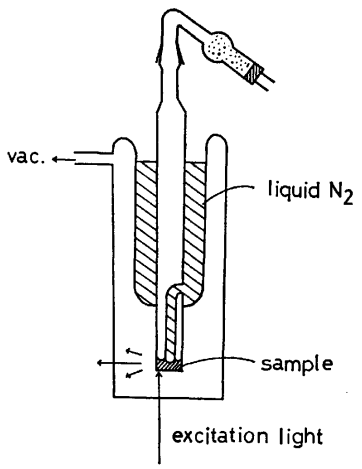

Fig. 2. Raman cell.

The long-wavelength absorption band has assigned to a dimer's transition characterized by interradical charge-transfer, which may affect the interradical binding considerably.[2] Accordingly, there is a good possibility of observing the interradical vibration of $(SQ^-)_2$ in the resonance Raman spectrum associated with the above absorption band, in much the same way as was previously reported for Würster's cation dimers.[6]

Experimental

SQ^- was prepared by oxidizing a 2 mM hydroquinone solution in alkaline ethanol (15 mM KOH) with ambient air. Before the further oxidation to quinone took place, the yellow solution was cooled with liquid N_2 in a proper rate to form a blue glassy matrix in a Raman cell, as is shown in Fig. 2. The Raman spectra were recorded on a JEOL JRS 400D spectrometer, with a CR 52G Ar^+ laser and a CR 590 dye laser (Rhodamine 6G). The dye laser is tuned by bireflingent filters and often brings weak satellite radiations, resulting in spurious lines in the spectra. Therefore, the exciting laser light was passed through a simple dispersing system to eliminate those satellite frequencies.

Results and Discussion

Figure 3 shows the Raman spectra of the blue glassy matrix obtained above by off-resonant 514.5 nm and exactly resonant 584.6 nm exciting radiations. Three Raman lines, at 177, 359, and 545 cm^{-1}, are polarized and are obviously enhanced by the resonance with the 585-nm absorption band. The most strikingly resonant line at 177 cm^{-1} is rather like, in all respects, the interradical vibration of *p*-phenylenediamine cation dimer reported previously,[6] and can probably be assigned to the SQ^--SQ^- stretching mode. We could not obtain a distinct spectrum of the monomer, probably because the resonance enhancement was insufficient to show up the Raman lines in the present dilute solution, but the resonance features of the Raman lines observed above seem to admit no other interpretation than dimer vibrations. The weakly resonant and relatively sharp 359 cm^{-1} and 545 cm^{-1} lines are probably due to such out-of-plane modes of SQ^- moieties that can couple with the interradical stretching, borrowing the intensity from the last mode.

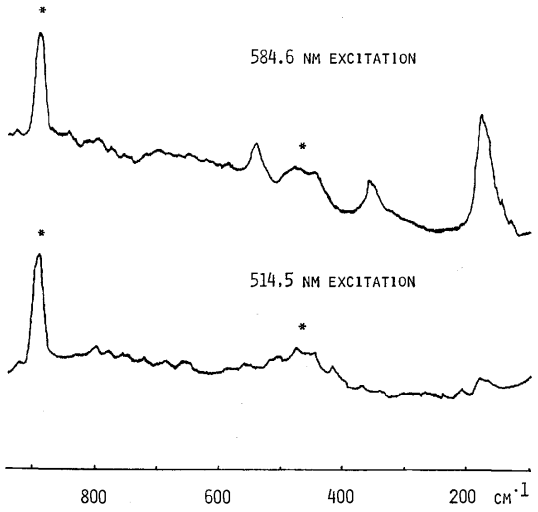

Fig. 3. Raman spectra of $(SQ^-)_2$ in ethanol matrix at −196 °C. * Ethanol lines.

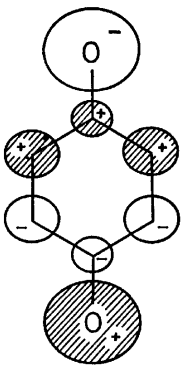

Fig. 4. Illustrated distribution of the b_{3g} molecular orbital of SQ^-.

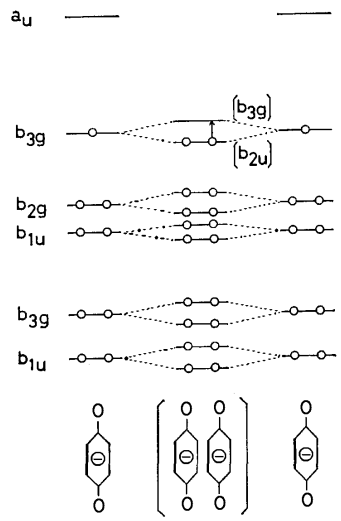

Fig. 5. MO energy scheme for SQ^- and $(SQ^-)_2$.

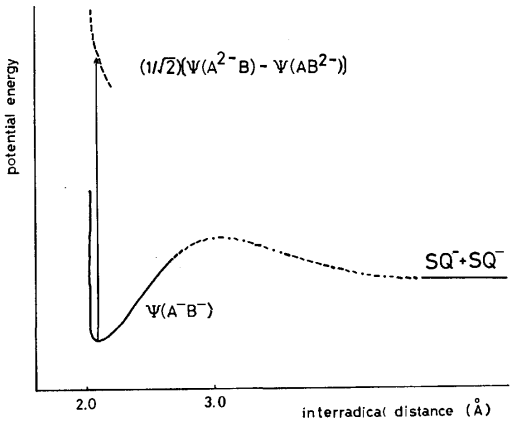

Fig. 6. The potential curve of $(SQ^-)_2$ for changing interradical distance.

The ground state of SQ^- has been shown[7] to be $^2B_{3g}$, principally represented by the π MO configuration:

$$(b_{1u})^2(b_{3g})^2(b_{1u})^2(b_{2g})^2(b_{3g}),$$

where the singly occupied b_{3g} MO has the form illustrated in Fig. 4. Therefore, the formation of the dimer may most reasonably be understood by considering the covalent interaction between the outer b_{3g} MO's for the parallel D_{2h} configuration, as is schematically shown in Fig. 5. The 585 nm absorption is thus assignable to the electron transition $[b_{2u}]\rightarrow[b_{3g}]$, which is characterized by a charge transfer between anion radicals:

$$\Psi(A^-\cdot B^-) \rightarrow (1/\sqrt{2})[\Psi(A^2\text{-}B) - \Psi(AB^{2-})],$$

where A and B represent each SQ monomer. The situation is quite like that of the previous *p*-phenylenediamine cation dimer.[5]

If the 177 cm^{-1} vibration is assumed to be entirely of an interradical stretching mode, the force constant can be calculated to be 1.09 md/Å, very close to the corresponding value of $(PPD^+)_2$.[6] Figure 6 gives the potential curve of $(SQ^-)_2$ for changing the interradical distance, where the part of trapping potential has been calculated by a CNDO approximation† and has been appropriately connected with the level of non-interacting monomer anions calculated on the CNDO basis. The dam in the transitional region is formed by the balance between the long-range electrostatic repulsion and the short-range binding interaction mentioned above. Although the present observed result is inevitably involved in the complex interaction with counter ions and solvent molecules, the binding aspect given above seems essentially applicable.

In conclusion, experimental evidence from vibrational spectroscopy has been given for the dimer formation of *p*-benzosemiquinone anion, indicating a close correspondence to *p*-phenylenediamine cation dimer, in accordance with the theoretical expectation.

References

1) Y. Harada and H. Inokuchi, *Mol. Phys.*, **8**, 265 (1964).

† This calculation was carried out on a HITAC 8800/8700 computer system at the Computer Center of the University of Tokyo, using the Y4CB04 library program based on the Q. C. P. E.[8] made by J. A. Pople, D. L. Beveridge, and P. A. Dobosh.

2) K. Kimura, H. Yamada, and H. Tsubomura, *J. Chem. Phys.*, **48**, 440 (1968).
3) S. Fukuzumi, Y. Ono, and T. Keii, *Bull. Chem. Soc. Jpn.*, **46**, 3353 (1973).
4) K. Kimura, K. Yoshinaga, and H. Tsubomura, *J. Phys. Chem.*, **71**, 4485 (1967).
5) H. Diebler, M. Eigen, and P. Matthies, *Z. Elektrochem.*, **65**, 634 (1961).
6) K. Yokoyama and S. Maeda, *Chem. Phys. Lett.*, **48**, 59 (1977).
7) Y. Harada, *Mol. Phys.*, **8**, 273 (1964).
8) J. A. Pople and D. L. Beveridge, "Approximate Molecular Orbital Theory," McGraw-Hill (1970).

Structural Study of Optical Resolution. VI. The Crystal Structure of $(+)_{589}$-*cis*-Chloroamminebis(ethylenediamine)cobalt(III) *d*-3-Bromocamphor-9-sulfonate Monohydrate

Masahiro KURAMOTO, Yoshihiko KUSHI, and Hayami YONEDA*

Department of Chemistry, Faculty of Science, Hiroshima University, Higashi-senda-machi, Hiroshima 730

(Received January 23, 1978)

The crystal structure of *cis*-chloroamminebis(ethylenediamine)cobalt(III) *d*-3-bromocamphor-9-sulfonate monohydrate, $(+)_{589}$-$[CoClNH_3(en)_2](d\text{-}BCS)_2\cdot H_2O$, has been determined by three-dimensional X-ray analysis. The deep red crystals are orthorhombic, space group $P2_12_12_1$, with four formula units in the unit cell of dimensions $a=34.97(2)$, $b=14.25(1)$, and $c=7.08(1)$ Å. The calculated density of 1.64 g·cm^{-3} compares well with the observed density 1.65 g·cm^{-3}. The structure has been refined by the block -diagonal least-squares method to an *R*-factor of 0.096 for 2662 reflection data points. In the complex cation, one of the two ethylenediamine chelate rings has a "50% *ob*, 50% *lel*" type disordered character in its conformation and the other ring is in a "*lel*" type. The absolute configuration of the complex cation is denoted as $\Lambda[(50\%\lambda, 50\%\delta)\delta]$, which was determined by comparison with that of the *d*-BCS anion. There are notable differences between the two crystallographically independent *d*-BCS anions with respect to their local packing modes.

Historically, *cis*-chloro- and -bromo-amminebis(ethylenediamine)cobalt(III) cations, *cis*-$[CoXNH_3(en)_2]^{2+}$ ($X=Cl^-$ and Br^-), were first resolved by Werner and King;[1] their hypothesis of octahedral coordination was thereby confirmed.[1,2] In their study of optical resolution, silver *d*-3-bromocamphor-9-sulfonate, *d*-BCS·Ag, was employed as a resolving agent. Since then, optical resolutions of many metal complexes were performed using this agent.[3]

Recently, we reported the crystal structure of *cis*-dichlorobis(ethylenediamine)cobalt(III) *d*-3-bromocamphor-9-sulfonate, $(+)_{589}$-$[CoCl_2(en)_2]d$-BCS, as a part of our structural studies of optical resolution,[4-8] and found an interesting "face-to-face type" close contact of the complex cation with the bromocamphor part of the *d*-BCS anion.

It is of interest to compare the structural features of the diastereoisomer, $(+)_{589}$-$[CoClNH_3(en)_2]$ $(d\text{-}BCS)_2\cdot H_2O$, with that of the previously determined $(+)_{589}$-$[CoCl_2(en)_2]d$-BCS. Moreover, the absolute configuration of *cis*-$[CoClNH_3(en)_2]^{2+}$ cation has not been determined by the X-ray method.[9] Therefore, the X-ray crystal structure analysis of the title compound was undertaken.

Experimental

The racemic *cis*-$[CoClNH_3(en)_2]Cl$ was prepared by the published method.[10] The racemic complex was resolved by the method of Garbett and Gillard, using *d*-BCS·NH_4 as a resolving agent.[9] The deep red crystals thus obtained were recrystallized from hot aqueous solution. Well formed crystals were separated out. Found: C, 33.01; H, 5.68; N, 7.98%. Calcd for $C_{24}H_{49}O_9N_5S_2ClBr_2Co$: C, 33.13; H, 5.68; N, 8.05%.

The unit cell dimensions were determined by the least-squares refinement of the *hk*0, *h*0*l*, 0*kl*, reflection data recorded on Weissenberg photographs. The sodium chloride diffraction lines were superimposed on the films for calibration. The crystal data are as follows: orthorhombic, $a=34.97(2)$, $b=14.25(1)$. $c=7.08(1)$ Å; $D_c=1.65$ g·cm^{-3} (by flotation in chloroform-bromoform mixture); $Z=4$; and $D_c=1.64$ g·cm^{-3}. From the systematic absence for *h*00 ($h=2n+1$), 0*k*0 ($k=2n+1$), and 00*l*($l=2n+1$), the space group is $P2_12_12_1$.

A crystal 0.65 mm long with a cross-sectional area of (0.20×0.23) mm^2 was adopted for recording the *hk*0—*hk*4 intensity data with Ni $K\alpha$ radiation, using the multiple-film equi-inclination Weissenberg technique. Another crystal, 0.42 mm long with (0.27×0.31) mm^2 cross-sectional area, was used to record the intensity data of *h*0*l*. The intensities were estimated visually with a calibrated intensity scale. The range of relative intensities was 1—3322. A total of 2662 independent reflections were used for the structure determination. Lorentz, polarization, and spot-shape corrections were applied in the usual manner; corrections for absorption were not made since the linear absorption coefficient, μ(Ni $K\alpha$), was 72.6 cm^{-1} ($\mu r=0.78$ for the former crystal).

Determination and Refinement of Crystal Structure

The structure was solved by the heavy-atom method. The positions of the two bromine atoms were easily found from the three-dimensional Patterson map. The subsequent Fourier synthesis revealed the positions of all the non-hydrogen atoms, excluding one water molecule. The position of the water molecule was found in the difference map which was synthesized at the stage of $R=0.16$ after the block-diagonal least-squares refinement of the other atoms for the 2662 observed reflections, where the *R*-value is $\Sigma||F_o|-|F_c||/\Sigma|F_o|$. The difference map showed a peak with the height of 4.0 e/Å^3 at the position $x=0.223$, $y=0.954$, and $z=0.275$. The presence of one water molecule was suggested by the elemental analysis for this compound. Thus, the peak was interpreted as due to a water molecule of crystallization.

Four cycles of further refinement with isotropic temperature factors for all the non-hydrogen atoms reduced the *R*-value to 0.14. The refinement(excluding the hydrogen atoms) was continued by applying anisotropic temperature factors for Br, Co, Cl, and S atoms and isotropic ones for O, N, and C atoms. After three cycles an *R*-value of 0.105 was obtained.

However, the value of the isotropic temperature factor of C(E2) was rather high($B=9.1$ Å^2) and the

TABLE 1. THE RATIOS(*ob* : *lel*) AND THE VALUES OF *R*-FACTORS, ISOTROPIC TEMPERATURE FACTORS, SELECTED BOND LENGTHS, AND BOND ANGLES

Ratios(*ob* : *lel*)	10 : 0	8 : 2	6 : 4	5 : 5	4 : 6	2 : 8
R-values(%)	10.49	9.81	9.64	9.63	9.64	9.83
Atoms			Temperature factors B(Å)^2			
C(E1A)(*ob*)	3.9	3.8	2.5	1.7	0.7	−1.6
C(E2A)(*ob*)	9.1	5.6	3.8	2.7	1.4	−0.9
C(E1B)(*lel*)	—	−0.2	1.5	2.5	3.2	4.2
C(E2B)(*lel*)	—	−1.0	2.2	3.6	4.6	6.5
C(E3)	2.6	2.6	2.6	2.6	2.6	2.5
C(E4)	2.7	2.8	2.8	2.8	2.8	2.8
			Distances (Å)			
N(1)-C(E1A)(*ob*)	1.52(4)	1.48(5)	1.48(5)	1.49(6)	1.50(6)	1.54(14)
N(1)-C(E1B)(*lel*)	—	1.56(13)	1.54(6)	1.53(6)	1.53(5)	1.51(5)
N(2)-C(E2A)(*ob*)	1.59(6)	1.53(5)	1.55(6)	1.56(6)	1.57(7)	1.62(14)
N(2)-C(E2B)(*lel*)	—	1.52(14)	1.50(8)	1.49(7)	1.49(6)	1.48(6)
C(E1A)-C(E2A)(*ob*)	1.32(6)	1.43(6)	1.48(7)	1.50(8)	1.52(9)	1.60(19)
C(E1B)-C(E2B)(*lel*)	—	1.51(19)	1.44(9)	1.42(8)	1.41(8)	1.37(7)
N(3)-C(E3)	1.45(4)	1.44(4)	1.44(4)	1.44(4)	1.44(4)	1.44(4)
N(4)-C(E4)	1.52(4)	1.52(4)	1.52(4)	1.52(4)	1.52(4)	1.52(4)
C(E3)-C(E4)	1.49(4)	1.45(4)	1.45(4)	1.45(4)	1.45(4)	1.45(4)
			Angles (°)			
Co-N(1)-C(E1A)(*ob*)	109(2)	109(2)	109(2)	110(2)	110(2)	110(5)
Co-N(1)-C(E1B)(*lel*)	—	110(5)	110(2)	109(2)	109(2)	109(2)
Co-N(2)-C(E2A)(*ob*)	106(2)	107(2)	107(2)	106(2)	106(3)	105(5)
Co-N(2)-C(E2B)(*lel*)	—	102(5)	104(3)	105(3)	105(3)	106(2)
Co-N(3)-C(E3)	112(2)	113(2)	113(2)	113(2)	113(2)	113(2)
Co-N(4)-C(E4)	108(2)	109(2)	109(2)	109(2)	109(2)	108(2)

resulting C(E1)–C(E2) distance, 1.32 Å, was fairly short. These results were observed also in several ethylenediamine metal complexes.[11]

Recently, Brouty *et al.* reported the crystal structure of the racemic tris(ethylenediamine)chromium(III) thiocyanate. They found the same character in its ethylenediamine ring, and tried to explain this anomaly more precisely.[12]

According to their approach, the difference map was recalculated after excluding the C(E1) and C(E2) atoms. Three peaks appeared in the map: two spherical peaks([peak I] 2.0 e/Å^3, x=0.202, y=0.770, z=0.935; [peak II] 2.2 e/Å^3, x=0.216, y=0.736, z=0.900) and one elongated peak([peak III] 3.2 e/Å^3, x=0.223, y=0.826, z=0.840). The occurrence of the "*ob-lel*" type disorder in the N(1)–C(E1)–C(E2)–N(2) ethylenediamine chelate ring[13] was thus suggested. The normal "*ob*" and "*lel*" models of the ethylenediamine ring were set up.[14] We tried to fit these models to the corresponding peaks in the difference map. The resulting positions of the four carbon atoms, C(E1A)–C(E2A) (*ob*) and C(E1B)–C(E2B) (*lel*), were included in the calculations for further refinement.

Five models with different ratios of the population of the C(E1A) and C(E2A) atoms to that of C(E1B) and C(E2B), (20% *ob*, 80% *lel*), (40, 60), (50, 50), (60, 40), and (80, 20), were refined. The starting values of the isotropic temperature factors of these four carbon atoms were set at 3.5 Å^2 (the average value of the other carbon atoms in this crystal at the stage of R=0.105). Hydrogen atom coordinates(excluded the water molecule and the methyl- and ammine- groups) were calculated(C–H 1.05, N–H 1.00 Å) assuming tetrahedral angles at carbon and nitrogen. Contributions from these forty hydrogen atoms with fixed positions and an isotropic temperature factor of B=3.5 Å^2 were also included in further least-squares iterations.

After three cycles of refinement based on the respective models, the best conventional *R*-value 0.096 was attained for the 50%-*ob*/50%-*lel* model. In the region of the corresponding four carbon atoms, a final difference map of this model showed no peak higher than 0.5 e/Å^3.

The final values of *R*-factors, isotropic temperature factors, and selected bond lengths and bond angles in the above five models are summarized in Table 1. These results suggest that the most probable ratio of conformational distribution of this ethylenediamine ring is 50%-*ob* and 50%-*lel*.

The quantity minimized was $w(|F_o|-k|F_c|)^2$ and the weighting scheme employed was w=1.0 for $F_o \geq 6.3(2.5\times F_{min})$ and w=0.5 for $F_o<6.3$. The atomic scattering factors for the Br^-, Co^{3+}, and Cl^- ions and for the neutral S, O, N, C, and H atoms were taken from Ref. 15. The dispersion effects were neglected.

All the computations were carried out by a HITAC-8700 computer at the Hiroshima University Computer Center. The computer programs used were FOUR-

TABLE 2. POPULATIONS(m) AND FINAL ATOMIC PARAMETERS AND TEMPERATURE FACTORS (with their e.s.d.'s)

Atom	m	x	y	z	B
Br(A)	1.0	0.0070(1)	0.4388(2)	0.7312(6)	a)
Br(B)	1.0	0.2073(1)	0.5114(2)	1.1067(6)	a)
Co	1.0	0.1647(1)	0.7793(3)	0.5904(7)	a)
Cl	1.0	0.2073(2)	0.6952(4)	0.4184(11)	a)
S(A)	1.0	0.0739(2)	0.6862(5)	0.0552(11)	a)
S(B)	1.0	0.1754(2)	0.0844(4)	0.9176(12)	a)
O(A1)	1.0	0.0860(5)	0.770(1)	0.154(3)	4.2(4)
O(A2)	1.0	0.0950(5)	0.603(1)	0.112(3)	5.0(4)
O(A3)	1.0	0.0734(5)	0.700(1)	−0.144(3)	4.2(4)
O(A4)	1.0	−0.0578(5)	0.601(1)	0.645(3)	4.8(4)
O(B1)	1.0	0.2010(5)	0.113(1)	1.066(3)	4.8(4)
O(B2)	1.0	0.1487(5)	0.010(1)	0.973(3)	3.7(4)
O(B3)	1.0	0.1984(5)	0.057(1)	0.751(3)	4.1(4)
O(B4)	1.0	0.1591(5)	0.515(1)	0.716(3)	3.6(4)
N(1)	1.0	0.2072(5)	0.862(1)	0.662(3)	2.3(3)
N(2)	1.0	0.1774(5)	0.707(1)	0.825(3)	2.8(4)
N(3)	1.0	0.1260(5)	0.856(1)	0.718(3)	2.7(4)
N(4)	1.0	0.1521(5)	0.859(1)	0.372(3)	2.8(4)
N(5)	1.0	0.1244(5)	0.684(1)	0.528(3)	2.2(3)
C(E1A)	0.5	0.2199(11)	0.839(3)	0.857(7)	1.7(8)
C(E2A)	0.5	0.2189(12)	0.735(3)	0.879(8)	2.7(9)
C(E1B)	0.5	0.2300(12)	0.817(3)	0.822(8)	2.5(9)
C(E2B)	0.5	0.2023(14)	0.771(4)	0.937(9)	3.6(10)
C(E3)	1.0	0.1042(6)	0.913(1)	0.589(4)	2.6(4)
C(E4)	1.0	0.1301(6)	0.944(2)	0.441(4)	2.8(4)
WO	1.0	0.2230(5)	0.954(1)	0.279(3)	4.2(4)
C(A1)	1.0	−0.0304(7)	0.607(2)	0.321(4)	3.1(5)
C(A2)	1.0	−0.0312(7)	0.591(2)	0.544(4)	3·2(5)
C(A3)	1.0	0.0093(6)	0.560(2)	0.611(4)	3.0(5)
C(A4)	1.0	0.0334(6)	0.560(1)	0.408(4)	2.2(4)
C(A5)	1.0	0.0193(6)	0.480(2)	0.293(4)	3.0(5)
C(A6)	1.0	−0.0255(7)	0.506(2)	0.246(5)	3.5(5)
C(A7)	1.0	0.0132(6)	0.647(2)	0.311(4)	2.8(5)
C(A8)	1.0	0.0168(7)	0.738(2)	0.420(5)	3.4(5)
C(A9)	1.0	0.0244(6)	0.665(2)	0.108(4)	3.0(5)
C(A10)	1.0	−0.0619(7)	0.661(2)	0.238(5)	3.5(5)
C(B1)	1.0	0.1364(6)	0.358(2)	0.791(4)	2.5(4)
C(B2)	1.0	0.1645(6)	0.440(2)	0.788(4)	3.0(5)
C(B3)	1.0	0.1986(7)	0.412(2)	0.915(5)	3.4(5)
C(B4)	1.0	0.1874(7)	0.319(2)	0.991(4)	3.7(6)
C(B5)	1.0	0.1502(8)	0.334(2)	1.126(5)	4.1(6)
C(B6)	1.0	0.1164(7)	0.364(2)	0.981(5)	3.9(6)
C(B7)	1.0	0.1665(6)	0.274(2)	0.813(4)	2.4(4)
C(B8)	1.0	0.1961(7)	0.264(2)	0.650(4)	3.5(5)
C(B9)	1.0	0.1459(6)	0.180(2)	0.852(4)	2.4(4)
C(B10)	1.0	0.1086(7)	0.353(2)	0.615(5)	3.9(6)

a) See Table 3.

TABLE 3. ANISOTROPIC TEMPERATURE FACTORS($\times 10^3$) EXPRESSED IN THE FORM $\exp[-2\pi^2(U_{11}h^2a^{*2}+U_{22}k^2b^{*2}+U_{33}l^2c^{*2}+2U_{12}hka^*b^*+2U_{13}hla^*c^*+2U_{23}klb^*c^*)]$.

Atom	U_{11}	U_{22}	U_{33}	U_{12}	U_{13}	U_{23}
Br(A)	80(2)	71(2)	37(2)	3(2)	14(4)	17(2)
Br(B)	117(3)	45(1)	73(3)	−8(2)	−44(3)	−7(2)
Co	55(2)	47(2)	36(3)	−1(2)	2(2)	−2(2)
Cl	44(3)	41(3)	26(5)	6(3)	4(3)	−10(4)
S(A)	40(3)	61(4)	12(5)	−12(3)	4(3)	3(4)
S(B)	47(3)	25(3)	38(6)	1(2)	−10(4)	−4(4)

TABLE 4. BOND DISTANCES AND ANGLES(e.s.d.'s in parentheses)
The values of BCS(B) is shown in square brackets.

(a) Bond lengths (Å)			
Co-N(1)	1.96(2)	S(A)-O(A1)	1.45(2)[1.44(3)]
Co-N(2)	2.00(2)	S(A)-O(A2)	1.45(3)[1.47(2)]
Co-N(3)	1.96(2)	S(A)-O(A3)	1.42(2)[1.48(2)]
Co-N(4)	1.97(2)	S(A)-C(A9)	1.80(3)[1.78(3)]
Co-N(5)	2.00(2)	O(A4)-C(A2)	1.18(4)[1.19(4)]
Co-Cl	2.27(1)	Br(A)-C(A3)	1.93(3)[1.99(3)]
N(1)-C(E1A)	1.49(6)	C(A1)-C(A2)	1.60(4)[1.53(4)]
N(1)-C(E1B)	1.53(6)	C(A2)-C(A3)	1.56(4)[1.55(4)]
N(2)-C(E2A)	1.56(6)	C(A3)-C(A4)	1.67(4)[1.48(5)]
N(2)-C(E2B)	1.49(7)	C(A4)-C(A5)	1.49(4)[1.63(5)]
N(3)-C(E3)	1.44(4)	C(A5)-C(A6)	1.64(4)[1.62(5)]
N(4)-C(E4)	1.52(4)	C(A1)-C(A6)	1.55(4)[1.52(4)]
C(E1A)-C(E2A)	1.50(8)	C(A1)-C(A7)	1.63(4)[1.61(4)]
C(E1B)-C(E2B)	1.42(8)	C(A1)-C(A10)	1.47(4)[1.58(5)]
C(E3)-C(E4)	1.45(4)	C(A4)-C(A7)	1.58(4)[1.60(4)]
		C(A7)-C(A8)	1.52(4)[1.55(4)]
		C(A7)-C(A9)	1.51(4)[1.54(4)]
(b) Bond angles (°)			
N(1)-Co-N(2)	86(1)	N(1)-Co-Cl	88(1)
N(3)-Co-N(4)	84(1)	N(2)-Co-Cl	92(1)
N(1)-Co-N(5)	174(1)	N(3)-Co-Cl	175(1)
N(2)-Co-N(5)	90(1)	N(4)-Co-Cl	92(1)
N(3)-Co-N(5)	90(1)	N(5)-Co-Cl	89(1)
N(4)-Co-N(5)	93(1)		
Co-N(1)-C(E1A)	110(2)	N(1)-C(E1A)-C(E2A)	108(4)
Co-N(1)-C(E1B)	109(2)	N(1)-C(E1B)-C(E2B)	105(4)
Co-N(2)-C(E2A)	106(2)	N(2)-C(E2A)-C(E1A)	104(4)
Co-N(2)-C(E2B)	105(3)	N(2)-C(E2B)-C(E1B)	112(5)
Co-N(3)-C(E3)	113(2)	N(3)-C(E3)-C(E4)	107(2)
Co-N(4)-C(E4)	109(2)	N(4)-C(E4)-C(E3)	108(2)
C(A2)-C(A1)-C(A6)	102(2)[106(2)]	C(A2)-C(A1)-C(A7)	96(2)[99(2)]
C(A2)-C(A1)-C(A10)	117(3)[115(2)]	C(A6)-C(A1)-C(A7)	102(2)[105(2)]
C(A6)-C(A1)-C(A10)	116(3)[115(3)]	C(A7)-C(A1)-C(A10)	120(3)[116(2)]
O(A4)-C(A2)-C(A1)	127(3)[126(3)]	O(A4)-C(A2)-C(A3)	124(3)[127(3)]
C(A1)-C(A2)-C(A3)	109(2)[107(2)]	Br(A)-C(A3)-C(A2)	111(2)[109(2)]
Br(A)-C(A3)-C(A4)	114(2)[116(2)]	C(A2)-C(A3)-C(A4)	101(2)[104(3)]
C(A3)-C(A4)-C(A5)	108(2)[108(3)]	C(A3)-C(A4)-C(A7)	99(2)[101(2)]
C(A5)-C(A4)-C(A7)	102(2)[99(2)]	C(A4)-C(A5)-C(A6)	105(2)[104(2)]
C(A1)-C(A6)-C(A5)	104(2)[102(2)]	C(A1)-C(A7)-C(A4)	97(2)[94(2)]
C(A1)-C(A7)-C(A8)	111(2)[115(2)]	C(A1)-C(A7)-C(A9)	110(2)[111(2)]
C(A4)-C(A7)-C(A8)	114(2)[108(2)]	C(A4)-C(A7)-C(A9)	115(2)[115(2)]
C(A8)-C(A7)-C(A9)	109(2)[112(2)]	S(A)-C(A9)-C(A7)	118(2)[116(2)]
O(A1)-S(A)-C(A9)	109(1)[109(1)]	O(A2)-S(A)-C(A9)	107(1)[105(1)]
O(A3)-S(A)-C(A9)	103(1)[108(1)]	O(A1)-S(A)-O(A2)	113(1)[114(1)]
O(A1)-S(A)-O(A3)	112(1)[109(1)]	O(A2)-S(A)-O(A3)	113(1)[112(1)]

MMM(Fourier synthesis)[16] and HBLS-IV (Least-squares calculation) with slight modification.[17]

The final atomic parameters, temperature factors (with their estimated standard deviations) and populations(m) are listed in Tables 2 and 3. Complete lists of the $5F_o$ and $5F_c$ values and the final atomic parameters of the hydrogen atoms have been preserved by the Chemical Society of Japan(Document No. 7835).

Results and Discussion

Cation and Anion Geometries. Figure 1 shows the crystal structure viewed along the c-axis. The crystal is built up of discrete $(+)_{589}$-*cis*-$[CoClNH_3(en)_2]^{2+}$ cations, two kinds of *d*-BCS anions(denoted as *d*-BCS(A) and *d*-BCS(B)), and water molecules. The bond distances and bond angles are listed in Table 4.

In the complex cation, the bond distances and bond angles around the cobalt atom are in good agreement with those found in the previous studies.[4,18] There are two ethylenediamine rings in the complex cation. The conformation of one ethylenediamine ring(N(1)–C(E1)–C(E2)–N(2)) is in "50% *ob*(N(1)–C(E1A)–

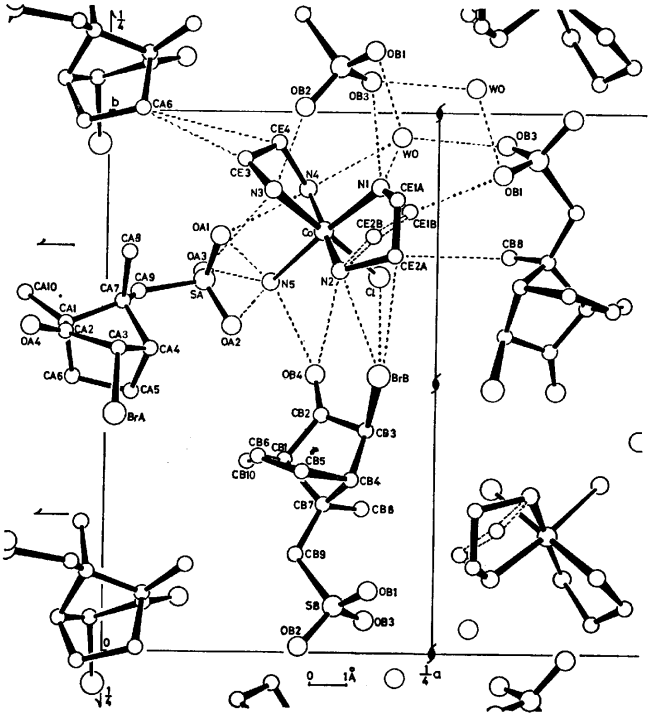

Fig. 1. A perspective drawing of the contents of the unit cell along the c-axis. Possible hydrogen bonds and short contacts are indicated by broken lines. The round brackets in the numbering scheme of the atoms are omitted.

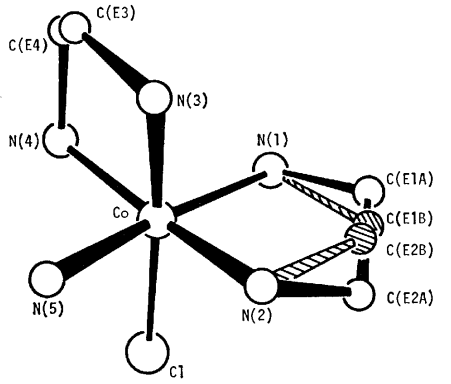

Fig. 2. The absolute configuration of the complex cation.

C(E2A)–N(2)), 50% *lel*(N(1)–C(E1B)–C(E2B)–N(2)),” as described in the refinement part. The other ethylenediamine ring(N(3)–C(E3)–C(E4)–N(4)) is in the *lel* conformation. Thus the conformation of the two ethylenediamine rings is designated as a “(50% *ob*, 50% *lel*), *lel*” type.

The absolute configuration of the complex cation was assigned as *Λ* for the $(+)_{589}$-isomer, based on the *d*-BCS anion as an internal reference.[19] This configuration is in accordance with the result previously reported on the basis of spectral evidence.[9] Thus, the absolute configuration of the complex cation is denoted as *Λ*[(50% *λ*, 50% *δ*)*δ*],[13] as illustrated in Fig. 2.

Table 5. Selected intermolecular distances(≤3.53 Å)

N-H···B	N···B (Å)	H···B (Å)	∠N-H···B (°)
N(1)-H2[b]···O(B1)^{IV}	3.30	2.50	137
N(1)-H10···O(B1)^{IV}	3.30	2.63	125
N(1)-H1···O(B3)^{I}	2.87[a]	1.95	152
N(1)-H9···O(B3)^{I}	2.87[a]	1.93	156
N(1)-H2···WO	3.06[a]	2.53	113
N(1)-H10···WO	3.06[a]	2.25	138
N(2)-H3···O(B4)	2.92[a]	1.95	164
N(2)-H11···O(B4)	2.92[a]	2.27	121
N(3)-H6···O(A3)^{II}	3.05[a]	2.08	162
N(3)-H5···O(B2)^{I}	2.95[a]	1.99	159
N(4)-H7···O(A1)	3.05[a]	2.10	157
N(4)-H8···WO	2.90[a]	1.97	155
N(5)···O(A1)	3.21[a]	—	—
N(5)···O(A2)	3.32	—	—
N(5)···O(A3)^{II}	2.94[a]	—	—
N(5)···O(B4)	3.01[a]	—	—
C(E1A)-H14···O(B1)^{IV}	3.52	2.87	120
C(E1A)-H13···O(B3)^{I}	3.28	3.03	94
C(E1A)-H13···WO^{II}	3.41	2.69	126
C(E1A)-H14···WO^{II}	3.41	3.23	91
C(E1B)-H17···O(B1)^{IV}	3.18	3.05	88
C(E1B)-H18···O(B1)^{IV}	3.18	2.81	101
C(E3)-H21···O(B2)^{I}	3.43	3.01	104
C(E4)-H23···O(B2)^{III}	3.51	2.84	122
C(E4)-H24···WO	3.45	3.05	103
Br(B)···Cl^{II}	3.43	—	—
WO···O(B1)^{III}	2.83[a]	—	—
WO···O(B1)^{IV}	3.48	—	—
WO···O(B2)^{III}	3.48	—	—
WO···O(B3)^{IV}	2.76[a]	—	—
O(B2)···O(A4)^{V}	3.53	—	—
C(B9)-H39···O(A4)^{V}	3.28	2.83	106
C(B9)-H40···O(A4)^{V}	3.28	2.83	106
C(A3)-H25···O(A3)^{II}	3.47	2.48	156

Roman numerals as superscripts refer to the following equivalent positions relative to the reference molecule at *x*, *y*, *z*:
I (*x*, 1+*y*, *z*), II (*x*, *y*, 1+*z*)
III (*x*, 1+*y*, −1+*z*), IV (1/2−*x*, 1−*y*, −1/2+*z*)
V (−*x*, −1/2+*y*, 3/2−*z*)

a) Possible hydrogen bonds. b) H1, H2, H3, H13, and H14 belong to the *ob* conformation and H9, H10, H11, H17, and H18 to the *lel*.

The bond distances and bond angles in both *d*-BCS anions are summarized in Table 4. The structures of both *d*-BCS anions are in accordance with each other and also with the results reported in the previous studies.[4,19] The bromine atoms are in the *endo* position on C(A3) and C(B3). The sulfonate groups are attached to C(A9) and C(B9), that is in *trans-π* position to the keto group. Selected intermolecular bond distances are summarized in Table 5.

The Local Packing Modes of the d*-BCS Anions.* There are notable differences between the two crystallographically independent *d*-BCS anions with respect to their local packing modes in this crystal.

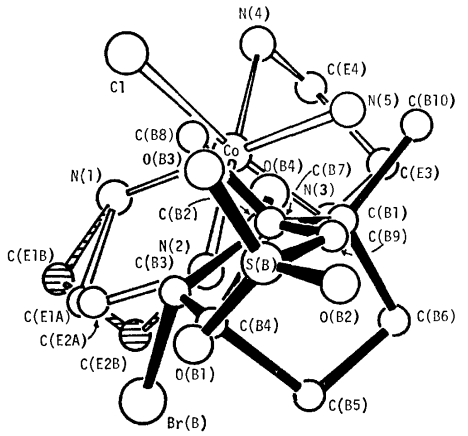

Fig. 3. A projected sketch displaying the spacial arrangement of the *d*-BCS anion and the complex cation.

In the *d*-BCS(A) anion, only the sulfonate group has short contacts with the complex cation. The distances are O(A1)···N(4) 3.05, O(A1)···N(5) 3.21, O(A2)···N(5) 3.32, O(A3)(x, y, $1+z$)···N(3) 3.05 and O(A3)(x, y, $1+z$)···N(5) 2.94 Å, suggesting the existence of the hydrogen bonds shown in Fig. 1. The bromocamphor part of the *d*-BCS(A) anion has no short contacts with the complex cation, though a few van der Waals contacts are present. These distances are C(A6)($-x$, $1/2+y$, $1/2-z$)···C(E3) 3.86 and C(A6)($-x$, $1/2+y$, $1/2-z$)···C(E4) 3.99 Å.

On the other hand, the packing mode around the *d*-BCS(B) anion bears a resemblance to that of the *d*-BCS anion in $(+)_{589}$-$[CoCl_2(en)_2]$*d*-BCS.[4] Namely, the sulfonate group tightly links the adjacent complex cations through the O···H–N hydrogen bonds and the bromocamphor part has short contacts with the complex cation. Figure 3 shows the sketch of the "$[CoClNH_3(en)_2]$*d*-BCS (B)" group projected on the "N(2), N(5), Cl" plane of the complex cation. The distances of the bromocamphor part(*d*-BCS(B)) to the complex cation are O(B4)···N(2) 2.92, O(B4)···N(5) 3.01, Br(B)···N(2) 3.59, Br(B)···C(E2A) 3.59, and Br(B)···Cl(x, y, $1+z$) 3.43 Å.

Though the bromocamphor part(*d*-BCS(B)) comes near to the "N(2), N(5), Cl" triangular facet of the octahedral complex cation, the distinct "three-to-four type" close contact found in our previous structural studies of $(+)_{589}$-$[CoCl_2(en)_2]$*d*-BCS[4] and tris(ethylenediamine)metal(III) *d*-tartrate systems[5,6,8] is not formed between the $[CoClNH_3(en)_2]^{2+}$ cation and the *d*-BCS(B) anion.

Including the "N(1), N(3), N(4)" plane of the complex cation, a hydrogen bond network is built up among the sulfonate groups of the *d*-BCS(B) anions and water molecules, as shown in Fig. 1. The hydrogen bond distances are O(B2)(x, $1+y$, z)···N(3) 2.95, O(B3)(x, $1+y$, z)···N(1) 2.87, O(B1)(x, $1+y$, $-1+z$)···WO 2.83, WO···N(1) 3.06, and WO···N(4) 2.90 Å.

Several van der Waals contacts also exist between the complex cations and the bromocamphor part of the *d*-BCS(B) anions along the b-axis, as shown in Fig. 1; C(E1B)···O(B1)($1/2-x$, $1-y$, $-1/2+z$) 3.18 and C(E2A)···C(B8)($1/2-x$, $1-y$, $1/2+z$) 3.54 Å.

The Packing of the Water of Crystallization. Hydrogen bonds in a right-handed spiral chain are formed between the sulfonate groups of the *d*-BCS(B) anions and the waters of crystallization along the twofold screw axis parallel to c($x=1/4$, $y=1$). The sequence of the chain is as follows; WO···O(B3)–S(B)–O(B1)($1/2-x$, $1-y$, $-1/2+z$)···WO($1/2-x$, $2-y$, $1/2+z$)···O(B3)–S(B)–O(B1)(x, $1+y$, z)···WO(x, y, $1+z$). The bond distances of hydrogen bonds are WO···O(B1)(x, $1+y$, $-1+z$) 2.83 and WO···O(B3) ($1/2-x$, $1-y$, $-1/2+z$) 2.76 Å.

Analogy between d-*BCS Systems and* d-*Tartrate Systems.* The ratios of the complex cation to the resolving agent-(*d*-BCS) in the crystals of $(+)_{589}$-$[CoCl_2(en)_2]$*d*-BCS and $(+)_{589}$-$[CoClNH_3(en)_2]$ $(d\text{-BCS})_2\cdot H_2O$ are 1 : 1 and 1 : 2 respectively.

It is found that the bromocamphor part of the *d*-BCS anion has a close contact with one triangular facet of the octahedral complex cation in both crystal structures. Another crystallographically independent *d*-BCS anion is present in the $(+)_{589}$-$[CoClNH_3(en)_2]$ $(d\text{-BCS})_2\cdot H_2O$, but the bromocamphor part of this anion(*d*-BCS(A)) is apart from any triangular facet of the complex cation. For a diastereomeric discrimination, the key-and-lock type association model was proposed by Fischer,[20] in which two chiral species make a compact fit. If this model is valid, the above results suggest that, though there are two *d*-BCS anions in the $(+)_{589}$-$[CoClNH_3(en)_2]$ $(d\text{-BCS})_2\cdot H_2O$, one of the *d*-BCS anions, *d*-BCS(B), plays a more important role in the diastereomeric discrimination.

Recently, three crystal structures of tris(ethylenediamine)metal(III) *d*-tartrate complexes, $(+)_{589}$-$[Co(en)_3]Br\cdot d\text{-tart}\cdot 5H_2O$, $Li\{(+)_{589}\text{-}[Cr(en)_3]\}(d\text{-tart})_2\cdot 3H_2O$, and $H\{(+)_{589}\text{-}[Co(en)_3]\}(d\text{-tart})_2\cdot 3H_2O$, have also been determined as a part of our structural studies of optical resolution.[5,6,8] The ratios of the complex cation to the resolving agent are 1 : 1, 1 : 2, and 1 : 2, respectively. Comparing the crystal structure of the 1 : 1 compound with that of the 1 : 2, we found as a common characteristic a "face-to-face type" close contact between the triangular facet of the complex cation and one *d*-tartrate anion. Moreover, though another crystallographically independent *d*-tartrate anion is present in $Li\{(+)_{589}\text{-}[Cr(en)_3]\}(d\text{-tart})_2\cdot 3H_2O$ and $H\{(+)_{589}\text{-}[Co(en)_3]\}(d\text{-tart})_2\cdot 3H_2O$ crystals, one of the two –COO groups of this *d*-tartrate anion takes the place of the bromine atom in $(+)_{589}$-$[Co(en)_3]Br\cdot d\text{-tart}\cdot 5H_2O$.[5,6,8] These results again imply that one of the *d*-tartrate anions probably plays a more important role in the diastereomeric discrimination in the above 1 : 2 type salts.

It is worthy of note that only one resolving agent probably plays a more dominant role in the diastereomeric discrimination in both *d*-tartrate and *d*-BCS systems in which two crystallographically independent resolving agents are contained.

We thank the Hiroshima University Computer Center for a generous allocation of computer time and acknowledge a Grant-in-Aid for Scientific Research from the Ministry of Education.

References

1) A. Werner and V. L. King, *Ber.*, **44**, 1890 (1911).
2) G. B. Kauffman, *Coord. Chem. Rev.*, **12**, 105 (1974).
3) J. C. Bailar, Jr., and R. W. Auten, *J. Am. Chem. Soc.*, **56**, 774 (1934); K. Garbett and R. D. Gillard, *J. Chem. Soc., A*, **1966**, 802.
4) Y. Kushi, M. Kuramoto, and H. Yoneda, *Chem. Lett.*, **1976**, 663.
5) Y. Kushi, M. Kuramoto, and H. Yoneda, *Chem. Lett.*, **1976**, 135.
6) Y. Kushi, M. Kuramoto, and H. Yoneda, *Chem. Lett.*, **1976**, 339.
7) M. Kuramoto, Y. Kushi, and H. Yoneda, *Chem. Lett.*, **1976**, 1133.
8) T. Tada, Y. Kushi, and H. Yoneda, *Chem. Lett.*, **1977**, 379.
9) K. Garbett and R. D. Gillard, *J. Chem. Soc.*, **1965**, 6084.
10) A. Werner, *Ann.*, **386**, 165 (1912).
11) S. Baggio and L. N. Becka, *Acta Crystallogr., Sect. B*, **25**, 946 (1969); M. Iwata, K. Nakatzu, and Y. Saito, *ibid.*, **25**, 2562 (1969); R. J. Williams, A. C. Larson, and D. T. Cromer, *ibid.*, **28**, 858 (1972); Y. Kanazawa and T. Matsumoto, *ibid.*, **32**, 282 (1976); H. Shintani, S. Sato, and Y. Saito, *ibid.*, **32**, 1184 (1976).
12) P. C. Brouty, P. Spinat, A. Whuler, and P. Herpin, *Acta Crystallogr., Sect. B*, **33**, 1913 (1977).
13) The notation "*lel, ob*" was introduced by J. Corey and J. C. Bailar, Jr., (E. J. Corey and J. C. Bailar, Jr., *J. Am. Chem. Soc.*, **81**, 2620 (1959)) and "δ, λ" was proposed by IUPAC (*Inorg. Chem.*, **9**, 1 (1970)).
14) C. J. Hawkins, "Absolute Configuration of Metal Complexes," Wiley-Interscience, New York (1971), p. 129.
15) "International Tables for X-Ray Crystallography," Kynoch Press, Birmingham (1968), Vol. III, pp. 201—206.
16) Y. Kushi, unpublished work.
17) T. Ashida, "The Univeral Crystallographic Computation Program System," ed by T. Sakurai, The Crystallographic Society of Japan (1967).
18) J. A. Stanco and I. C. Paul, *Inorg. Chem.*, **6**, 486 (1967).
19) J. A. Wunderlich, *Acta Crystallogr.*, **23**, 846 (1967).
20) E. Fischer, *Ber.*, **32**, 3617 (1899).

Solution Equilibria of Ternary α-Amino Acid–Copper(II) Complexes with Electrostatic Ligand-Ligand Interactions

Takeshi SAKURAI, Osamu YAMAUCHI, and Akitsugu NAKAHARA*

Institute of Chemistry, College of General Education, Osaka University, Toyonaka, Osaka 560

(Received February 16, 1978)

The stability constants for the parent and mixed copper(II) complexes involving an acidic α-amino acid (aspartic acid or glutamic acid, abbreviated as A) and/or a basic α-amino acid (arginine, lysine, or ornithine, abbreviated as B) have been determined by potentiometric titration at 25 °C in 0.1 and 0.03 M KNO_3 (M=mol dm^{-3}). The protonated ternary species Cu(L-A)(L-B)(H) and Cu(D-A)(L-B)(H) (species 1111) have essentially the same stability constants, the log β_{1111} values being in the range 25.0—27.5. The species distribution curves for the systems Cu(II)–L- or D-glutamic acid–L-lysine at the ionic strength I=0.1 and 0.03 reveal that species 1111 is more predominant at I=0.03 than at I=0.1, suggesting that electrostatic ligand-ligand interactions between the carboxylate group in the side chain of A and the ammonium or the guanidinium group in the side chain of B are reinforced in solution at lower ionic strength to favor the ternary complex formation. The constants for deprotonation from species 1111 to form 1110, *e.g.* Cu(L-A)(L-B), are given by the difference log β_{1111} − log β_{1110}, which is higher for the Cu(II)–A–B systems than for the systems containing alanine in place of A. The results indicate that intramolecular electrostatic interactions are present in the ternary species 1111, stabilizing them under favorable conditions.

Ternary metal complexes have been extensively studied because of their possible significance as models for biological processes assisted by metal ions. Since non-covalent interactions are supposed to be an important source of specificity or selectivity in biological reactions,[1] mixed ligand copper(II) complexes involving aromatic ring stacking[2] and electrostatic ligand-ligand interactions[3] have attracted considerable attention.

On the basis of the electrostatic enzyme-substrate interactions found in the carboxypeptidase A–glycyl-L-tyrosinate complex, we designed mixed amino acid–copper(II) complex systems capable of forming intramolecular electrostatic bonds between the two amino acids, and inferred from synthetic and spectroscopic studies that such ligand-ligand interactions exist in the systems containing an acidic and a basic amino acid.[3] The IR spectra of the isolated complexes[3b] and successful optical resolution of acidic and basic amino acids *via* complex formation[5] indicate that the diastereomers Cu(L-A)(L-B)(H) and Cu(D-A)(L-B)(H), where A refers to aspartate (asp) or glutamate (glu), B to argininate (arg), lysinate (lys), or ornithinate (orn), and H to proton, are probably *cis-trans* isomers arising from the steric requirements for the ligand-ligand interactions (Scheme 1).

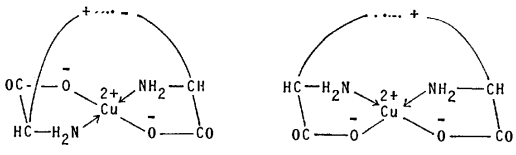

Cu(L-A)(L-B)(H) Cu(D-A)(L-B)(H)

Scheme 1.

Brookes and Pettit[6] determined the stability constants for the ternary systems containing copper(II), L- or D-histidine (L- or D-his), and a basic amino acid (L-B), and found the stability differences between the complexes Cu(L-his)(L-B)(H) and Cu(D-his)(L-B)(H), which they ascribed to the intramolecular electrostatic bonding. Steric hindrance has been reported to give rise to stereoselectivity in the ternary copper(II) complexes of *N*-substituted α-amino acids with α-amino acids.[7] Although many other mixed amino acid–copper(II) systems have been studied potentiometrically,[8] no systematic investigations of the ternary systems, copper(II)–L-A–L-B, seem to have been reported. In order to clarify the effects of electrostatic ligand-ligand interactions on the stability of the metal complexes in solution and the factors affecting the optical resolution of DL-A and DL-B, we have carried out a potentiometric study of the ternary amino acid–copper(II) complexes containing A and B.

Experimental

Materials. L-Arginine hydrochloride, L-lysine hydrochloride, L-ornithine hydrochloride, L- and D-aspartic acid, and L- and D-glutamic acid of grade A from Nakarai Chemicals, Ltd. were dried *in vacuo* over P_4O_{10} before use. All other chemicals used were of highest grade available. Water was distilled and deionized.

pH *Titrations.* *Reagents*: Carbonate-free potassium hydroxide (0.1 M, M=mol dm^{-3}) was prepared by the method of Armstrong,[9] standardized against potassium hydrogen phthalate, and stored under a nitrogen atmosphere. Copper(II) nitrate (0.01 M) was prepared by dissolving copper(II) nitrate trihydrate in water and standardized against standard zinc by chelatometric titration.

Apparatus: An Orion Research 801A digital pH meter equipped with a 90-01-00 glass electrode and a 91-02-00 double junction reference electrode was used for measuring the pH values after standardization with Horiba standard buffer solutions (pH 4.01, 6.86, and 9.18).

Procedure: For determination of the acid dissociation constants of the ligands, an aqueous solution (4×10^{-3} M) of protonated A or B was titrated with 0.1 M KOH at 25± 0.05 °C under a nitrogen atmosphere. For determination of the stability constants of the binary and the ternary systems, 1:2 copper(II)–A or B and 1:1:1 copper(II)–A–B solutions, respectively, were titrated with 0.1 M KOH at a constant copper(II) concentration of 2×10^{-3}M under the same conditions. Titration was carried out in the presence of 0.1 or 0.03 M KNO_3. Aliquots of A and B to be titrated were taken from stock solutions freshly prepared before use. The

pH value was measured for each addition of a small amount of 0.1 M KOH. The apparent ion products of water, pK_w', at the ionic strength $I=0.1$ and 0.03 were determined to be 13.90 and 14.02, respectively, by titration of 0.01 M HNO_3 with 0.1 M KOH, which also gave the hydrogen ion concentrations, $[H^+]$, as $10^{-pH}/0.865$ at $I=0.1$ and $10^{-pH}/0.902$ at $I=0.03$.

Results and Discussion

Calculations. The equilibria of binary and ternary systems and the stability constants β_{pqrs} are expressed by

$$pCu + qA + rB + sH \overset{\beta_{pqrs}}{\rightleftharpoons} Cu_pA_qB_rH_s, \quad (1)$$

$$\beta_{pqrs} = \frac{[Cu_pA_qB_rH_s]}{[Cu]^p[A]^q[B]^r[H]^s},$$

where p, q, r, and s denote the numbers of copper(II), A, B, and H, respectively, contained in the complex (charges are omitted). Each species will be represented as *pqrs* hereinafter.

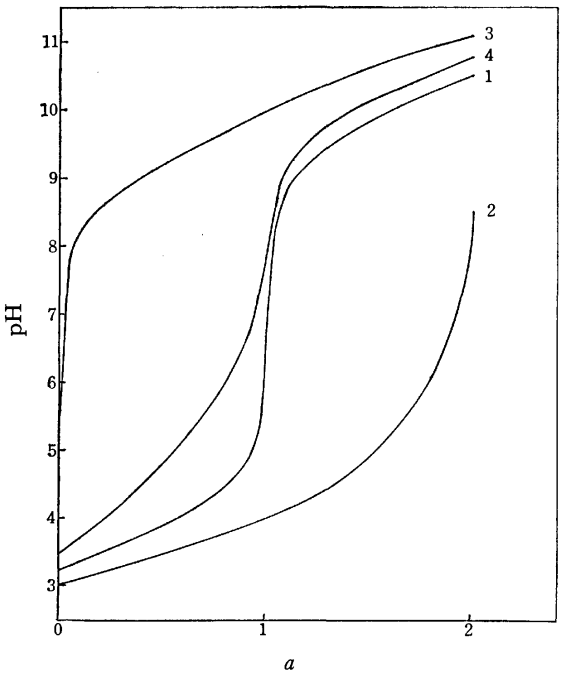

Fig. 1. Typical titration curves for ligands and 1:2 binary systems, Cu(II)-A or B(25 °C; $I=0.1$(KNO_3)). Total concentrations: ligand=0.004000 M; Cu(II)=0.002016 M.
Curves 1—4 correspond to the following systems: 1, L-asp; 2, Cu(II)-L-asp; 3, L-lys; 4, Cu(II)-L-lys.
a: Moles of alkali added per mole of ligand.

The stability constants were calculated from the pH titration data by non-linear least-squares refinement with the use of the computer program SCOGS.[10] The initial estimates for the refinements were taken from the literature[11] or guessed from the values for analogous systems. At the final stage of refinement the difference between experimental and calculated titers were well within 0.02 ml in the pH ranges considered. The acid dissociation constants (pK_a) of the ligands were calculated separately with the aid of a computer.

Stability Constants of Binary Copper(II) Complexes. Typical titration curves for the systems with a ligand alone and with copper(II) and a ligand are shown in Fig. 1. Table 1 summarizes the pK_a values of the amino acids, most of which are in good agreement with the reported values.[6b,11] To avoid erroneous results suspected at low concentrations of solutions,[9] we did not determine the constants for the α-carboxyl groups of all the amino acids whose acid dissociation occurs at around pH 2. For calculations of the stability constants, such pK_a values were taken from the litera-

Table 1. Acid dissociation constants of ligands (25 °C; $I=0.1$(KNO_3))[a]

Ligand	pK_{a_1}	pK_{a_2}
L-asp	9.75	3.79
D-asp	9.79	3.77
L-glu	9.61	4.15
D-glu	9.68	4.21
L-arg	12.11	9.07
L-lys	10.85	9.14
L-orn	10.52[b]	8.75[b]

a) Standard deviations of all the constants are within ±0.01. b) Taken from Ref. 6b.

Table 2. Stability constants for binary copper(II) complexes containing acidic amino acids (25 °C; $I=0.1$ (KNO_3))[a]

Ligand	Stability		
	$\log\beta_{1101}$	$\log\beta_{1100}$	$\log\beta_{1200}$
L-asp	12.72(0.009)	9.00(0.004)	15.84(0.010)
D-asp	12.70(0.009)	8.97(0.004)	15.81(0.009)
L-glu	12.50(0.003)	8.30(0.001)	14.80(0.003)
D-glu	12.49(0.005)	8.32(0.003)	14.86(0.005)

a) Standard deviations are shown in parentheses.

Table 3. Stability constants for binary copper(II) complexes containing basic amino acids (25 °C; $I=0.1$ (KNO_3))[a]

Ligand	Stability				pK_{c_1}	pK_{c_2}
	$\log\beta_{1011}$	$\log\beta_{1022}$	$\log\beta_{1021}$	$\log\beta_{1020}$		
L-arg	19.55(0.06)	37.91(0.08)	—	—	—	—
L-lys	18.46(0.007)	35.63(0.008)	25.64(0.010)	15.07(0.008)	9.99	10.57
L-orn	17.95(0.006)	34.65(0.007)	25.73(0.008)	15.71(0.008)	8.92	10.02

a) Standard deviations are shown in parentheses.

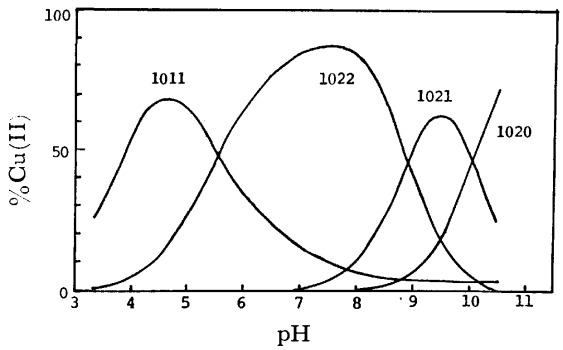

Fig. 2. Species distribution curves for the 1 : 2 Cu(II)-L-orn system (25 °C; I=0.1(KNO_3)).
Total concentrations: L-orn=0.004000 M; Cu(II)=0.002016 M.

ture[11] when necessary. However, they did not affect the present calculations seriously.

The stability constants for the binary complexes are shown in Tables 2 and 3. The titration curves for the binary copper(II)–A systems were satisfactorily reproduced by considering species 1101, 1100, and 1200 excluding the protonated bis-complexes 1202 and 1201. Although Clarke and Martell[12] detected species 1021 in the Cu(II)–arg system at pH ≈11, the present results are explained by the protonated species 1011 and 1022, deprotonation from which was not observed because of precipitation around this pH. On the other hand, the deprotonated species were found to be formed appreciably in the systems Cu(II)–orn and Cu(II)–lys at pH>8, which is illustrated in the species distribution for the 1 : 2 Cu(II)–L-orn system plotted against pH (Fig. 2). The standard deviations expressed in titer were usually larger for the systems with arg than for the systems with the other ligands probably owing to the errors in the pH measurement in a strongly alkaline solution.

Deprotonations from species 1022, where the proton is bound to the ω-amino group, to give 1021 and 1020 are represented by

$$Cu(L\text{-}B)_2(H)_2 \overset{K_{c1}}{\rightleftharpoons} Cu(L\text{-}B)_2(H) + H, \quad (2)$$

$$Cu(L\text{-}B)_2(H) \overset{K_{c2}}{\rightleftharpoons} Cu(L\text{-}B)_2 + H. \quad (3)$$

The dissociation constants pK_{c_1} (=$-\log K_{c_1}$) and pK_{c_2} are given by the differences $\log\beta_{1022}-\log\beta_{1021}$ and $\log\beta_{1021}-\log\beta_{1020}$, respectively. The pK_{c_1} values are lower than the pK_{a_1} values of orn and lys (Tables 1 and 3), and the Cu(II)–orn system has a smaller pK_{c_1} value than that of the Cu(II)–lys system, indicating that orn coordinates to copper(II) at the apical position through its δ-amino group, whereas lys does not coordinate in the same way. This is in line with the ORD[13] and CD[3a,14] spectral behaviors of these systems. Because the pK_{c_2} values for both systems do not differ very much from the respective pK_{a_1} values, they suggest that the δ-amino group of the second orn is not effectively involved in the apical coordination.

Stability Constants of Ternary Copper(II) Complexes. The stability constants for the systems were obtained from the titration curves such as those shown in Fig. 3 by the least-squares refinement starting from known

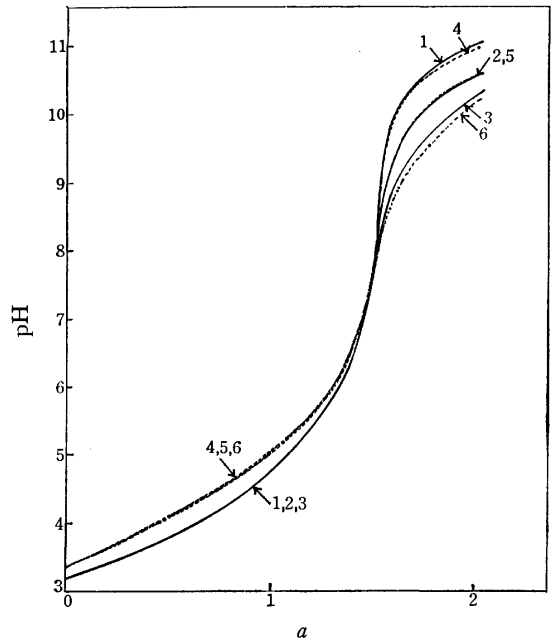

Fig. 3. Titration curves for the 1 : 1 : 1 ternary systems, Cu(II)-L-A-L-B(25 °C; I=0.1(KNO_3)).
Total concentrations: each ligand=0.002000 M; Cu(II)=0.002016 M.
Curves 1—6 correspond to the following systems: 1, Cu(II)-L-asp-L-arg; 2, Cu(II)-L-asp-L-lys; 3, Cu(II)-L-asp-L-orn; 4, Cu(II)-L-glu-L-arg; 5, Cu(II)-L-glu-L-lys; 6, Cu(II)-L-glu-L-orn.
a: Moles of alkali added per mole of ligand.

Table 4. Stability constants for ternary copper(II) complexes (25 °C; I=0.1 (KNO_3))[a]

Ligand		Stability	
B	A	$\log\beta_{1111}$	$\log\beta_{1110}$
L-arg	L-asp	27.43(0.08)	—
L-arg	D-asp	27.47(0.02)	—
L-arg	L-glu	26.61(0.13)	—
L-arg	D-glu	26.61(0.08)	—
L-lys	L-asp	26.32(0.01)	15.82(0.02)
L-lys	D-asp	26.27(0.03)	15.67(0.06)
L-lys	L-glu	25.60(0.01)	15.08(0.02)
L-lys	D-glu	25.60(0.01)	15.14(0.02)
L-lys	L-ala	25.52(0.04)	15.59(0.03)
L-orn	L-asp	25.65(0.04)	15.29(0.13)
L-orn	D-asp	25.66(0.04)	15.28(0.17)
L-orn	L-glu	24.93(0.05)	14.68(0.26)
L-orn	D-glu	24.88(0.06)	—
L-orn	L-ala	24.86(0.07)	15.37(0.09)
L-lys	L-glu	25.92(0.02)[b]	15.85(0.03)[b]
L-lys	D-glu	25.98(0.02)[b]	15.95(0.03)[b]

a) Standard deviations are shown in parentheses. b) Determined at I=0.03(KNO_3).

stability constants for protonated ligands and binary complexes and estimated constants for ternary complexes. The refined values are given in Table 4 together with those of the systems involving L-alanine (L-ala) in place of L-A.[15]

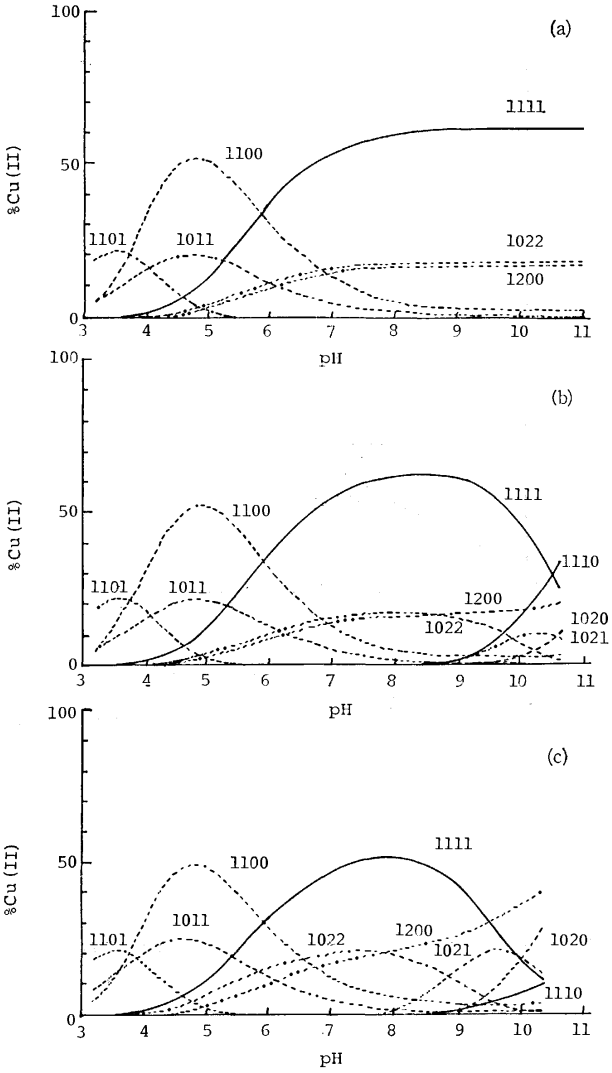

Fig. 4. Species distribution curves for the 1:1:1 Cu(II)–L-asp–L-B systems (25 °C; I=0.1 (KNO_3)).
Total concentrations: each ligand=0.002000 M; Cu(II)=0.002016 M.
(a): Cu(II)–L-asp–L-arg, (b): Cu(II)–L-asp–L-lys, (c): Cu(II)–L-asp–L-orn.

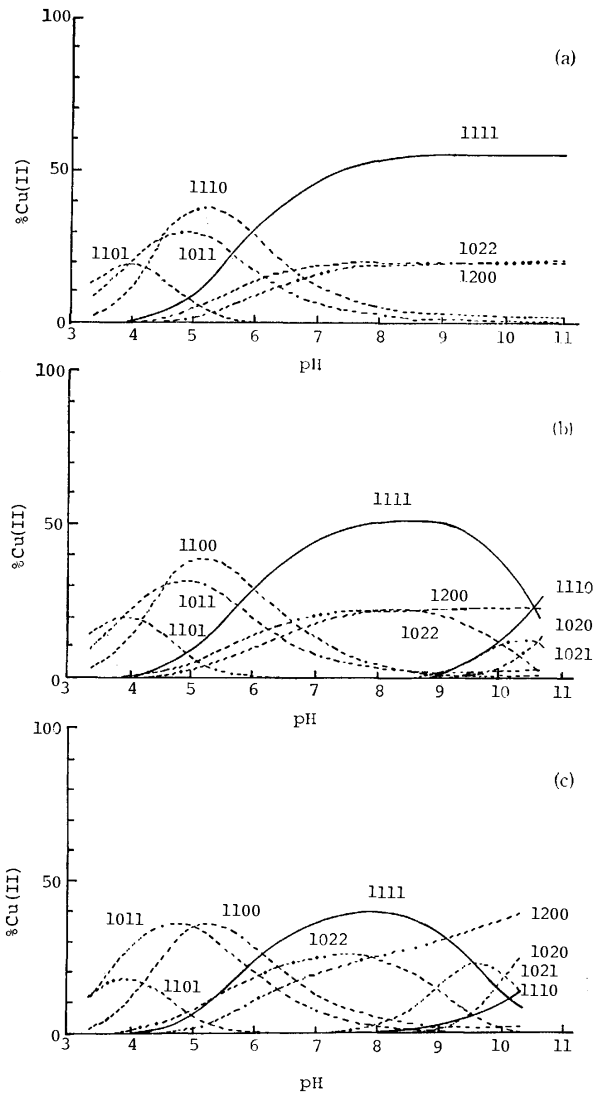

Fig. 5. Species distribution curves for the 1:1:1 Cu(II)–L-glu–L-B systems (25 °C; I=0.1 (KNO_3)).
Total concentrations: each ligand=0.002000 M; Cu(II)=0.002016 M.
(a): Cu(II)–L-glu–L-arg, (b): Cu(II)–L-glu–L-lys, (c): Cu(II)–L-glu–L-orn.

The only ternary species detected in the Cu(II)–L-A–L-arg systems is 1111 because of the tight association of the proton in the guanidinium group, whereas for the other systems both protonated (1111) and deprotonated (1110) species were found to be formed at neutral—alkaline pH. Figures 4 and 5 show the species distribution curves for the Cu(II)–L-asp–L-B and Cu(II)–L-glu–L-B systems, respectively. Although considerable amounts of the binary species are present in the latter systems as compared with the former, the ternary species 1111 are predominant at neutral pH in all the systems. We may take this as evidence supporting the previous assumption that the CD magnitude enhancements are ascribable to the ternary complexes (1111) with increased rigidity resulting from ligand-ligand interactions.[3]

A comparison of the stability constants with the statistically estimated values may offer another measure of preferential formation of the ternary species. The statistical values for species 1111 and 1110 are given by[16]

$$\log \beta_{1111(\mathrm{calcd})} = \frac{1}{2}(\log \beta_{1200} + \log \beta_{1022}) + \log 2, \quad (4)$$

$$\log \beta_{1110(\mathrm{calcd})} = \frac{1}{2}(\log \beta_{1200} + \log \beta_{1020}) + \log 2. \quad (5)$$

For most systems the experimental $\log \beta_{1111}$ values are greater than the calculated ones, substantiating the stabilization of species 1111, whereas the deprotonated species 1110 are usually less stable than expected from Eq. 5 (Table 5). The differences, $\log \beta_{1111} - \log \beta_{1110}$, are greater for Cu(L-A)(L-lys) and Cu(L-A)(L-orn) than for Cu(L-ala)(L-lys) and Cu(L-ala)(L-orn), probably reflecting the intramolecular electrostatic bonding.

Stereoselectivity in Solution. Optical resolution of

TABLE 5. COMPARISON OF THE STABILITY CONSTANTS WITH THE STATISTICALLY ESTIMATED VALUES

Ligand		Stability				$\log\beta_{1111}-\log\beta_{1110}$
B	A	$\log\beta_{1111}$	$\log\beta_{1111(calcd)}$ [a]	$\log\beta_{1110}$	$\log\beta_{1110(calcd)}$ [b]	
L-arg	L-asp	27.43	27.18	—	—	—
L-arg	L-glu	26.61	26.66	—	—	—
L-lys	L-asp	26.32	26.04	15.82	15.76	10.50
L-lys	L-glu	25.60	25.52	15.08	15.24	10.52
L-lys	L-ala	25.52	25.58	15.59	15.30	9.93
L-orn	L-asp	25.65	25.55	15.29	16.08	10.36
L-orn	L-glu	24.93	25.03	14.68	15.56	10.25
L-orn	L-ala	24.86	25.09	15.37	15.61	9.49

a) Calculated according to Eq. 4. b) Calculated according to Eq. 5.

racemic A and B has established that the systems Cu(II)–DL-A–L-B and Cu(II)–L-A–DL-B preferentially give the *meso* complexes as crystals incorporating the D-enantiomers of A and B with various optical purities, respectively.[5] We see from Table 4 that the diastercomers, which may exist as geometric isomers (Scheme 1), have virtually the same stability constants and that no stereoselectivity is detected at least in the solution with $I=0.1$. Therefore, the optical resolution may be primarily due to the solubility difference and not to the stability difference between the diastereomers in solution under the conditions used.[5]

Effects of Ionic Strength on Ternary Complex Formation. In the Cu(II)–L-glu–L-lys system the stability constants for the ternary species 1111 and 1110 at lower ionic strength (0.03) were found to be higher than those at $I=0.1$ (Table 4), the increments being 0.32 for 1111 and 0.77 for 1110. The diastereomeric system Cu(II)–D-glu–L-lys exhibited the same stability increase at $I=0.03$. A similar observation was made by Nagypál *et al.*,[17] who found that the stability difference between experimental and statistical values for the copper(II)–glycine–aspartic acid complex varies with the ionic strength because of the change in charge on complex formation. The distributions of the ternary species in the present system are more predominant at lower ionic strength regardless of the enantiomers of A and B used.[18] Since such a trend is also expected for the other ternary systems and the CD spectral magnitude decrease due to increased ionic strength[3a,3c] has confirmed its effect on the electrostatic ligand-ligand interactions, the above result indicates that the stabilities of the complexes in aqueous solution are enhanced as the ligand-ligand interactions are reinforced.

In a hydrophobic region, such as is found in biological systems, electrostatic interactions as well as hydrogen bonds are certainly of importance, and elucidation of the complex formation *in vivo* will require further information on such non-covalent interactions, which might be more effective in biofluids than in experimental aqueous media.

This work was supported in part by a grant from the Ministry of Education.

References

1) E. Frieden, *J. Chem. Educ.*, **52**, 754 (1975).
2) C. F. Naumann, B. Prijs, and H. Sigel, *Eur. J. Biochem.*, **41**, 209(1974); C. F. Naumann and H. Sigel, *J. Am. Chem. Soc.*, **96**, 2750 (1974); H. Sigel, *Angew. Chem. Int. Ed. Engl.*, **14**, 394 (1975); H. Sigel, *J. Am. Chem. Soc.*, **97**, 3209 (1975); P. Chaudhuri and H. Sigel, *ibid.*, **99**, 3142 (1977); H. Sigel, *J. Inorg. Nucl. Chem.*, **39**, 1903 (1977).
3) a) O. Yamauchi, Y. Nakao, and A. Nakahara, *Bull. Chem. Soc. Jpn.*, **48**, 2572 (1975); b) T. Sakurai, O. Yamauchi, and A. Nakahara, *ibid.*, **49**, 169 (1976); c) T. Sakurai, O. Yamauchi, and A. Nakahara, *ibid.*, **49**, 1579 (1976).
4) W. N. Lipscomb, G. N. Reeke, J. A. Hartsuck, F. A. Quiocho, and P. H. Bethge, *Phil. Trans. R. Soc. London, Ser B*, **257**, 177 (1970); W. N. Lipscomb, *Acc. Chem. Res.*, **3**, 81 (1970).
5) T. Sakurai, O. Yamauchi, and A. Nakahara, *J. Chem. Soc., Chem. Commun.*, **1976**, 553; O. Yamauchi, T. Sakurai, and A. Nakahara, *Bull. Chem. Soc. Jpn.*, **50**, 1776 (1977).
6) a) G. Brookes and L. D. Pettit, *J. Chem. Soc., Chem. Commun.*, **1975**, 385; b) G. Brookes and L. D. Pettit, *J. Chem. Soc., Dalton Trans.*, **1977**, 1918.
7) B. E. Leach and R. J. Angelici, *J. Am. Chem. Soc.*, **91**, 6296 (1969); V. A. Davankov and P. R. Mitchell, *J. Chem. Soc., Dalton Trans.*, **1972**, 1012; R. V. Snyder and R. J. Angelici, *J. Inorg. Nucl. Chem.*, **35**, 523 (1973); R. Nakon, P. R. Rechani, and R. J. Angelici, *Inorg. Chem.*, **12**, 243 (1973); V. A. Davankov, S. V. Rogozhin, A. A. Kurganov, and L. Ya. Zhuchkova, *J. Inorg. Nucl. Chem.*, **37**, 369 (1975); S. A. Bedell, P. R. Rechani, R. J. Angelici, and R. Nakon, *Inorg. Chem.*, **16**, 972 (1977).
8) R. -P. Martin, M.M. Pettit-Ramel, and J. P. Scharff, "Metal Ions in Biological Systems," ed by H. Sigel, Marcel Dekker, New York (1973), Vol. 2.
9) A. Albert and E. P. Serjeant, "Ionization Constants of Acids and Bases," Methuen and Co., London (1962).
10) I. G. Sayce, *Talanta*, **15**, 1397 (1968).
11) a) L. G. Sillén and A. E. Martell, "Stability Constants of Metal-Ion Complexes, Supplement No. 1," Special Publication No. 25, The Chemical Society, London (1971); b) A. E. Martell and R. M. Smith, "Critical Stability Constants," Plenum Press, New York (1974), Vol. 1.
12) E. P. Clarke and A. E. Martell, *J. Inorg. Nucl. Chem.*, **32**, 911 (1970).
13) K. M. Wellman, T. G. Mecca, W. Mungall, and C. R. Hare, *J. Am. Chem. Soc.*, **90**, 805 (1968).
14) E. W. Wilson, Jr., M. H. Kasperian, and R. B. Martin, *J. Am. Chem. Soc.*, **92**, 5365 (1970).

15) The pK_a values of L-ala and the $\log \beta$ values of the binary copper(II) complexes were taken from Ref. 11b.

16) V. S. Sharma and J. Schubert, *J. Chem. Educ.*, **46**, 506 (1969).

17) I. Nagypál, A. Gergely, and E. Farkas, *J. Inorg. Nucl. Chem.*, **36**, 699 (1974).

18) The distribution of 1111 species increased from 52% at $I=0.1$ to 60% at $I=0.03$. The pK_a values and the stability constants for the binary species at $I=0.03$ are as follows: L-Glu: $pK_{a_1}=9.67$ (0.001), $pK_{a_2}=4.20$ (0.001), $\log \beta_{1100}=8.48$ (0.005), $\log \beta_{1101}=12.64$ (0.006), and $\log \beta_{1200}=15.05$ (0.007); L-Lys: $pK_{a_1}=10.83$ (0.001), $pK_{a_2}=9.12$ (0.001), $\log \beta_{1022}=35.65$ (0.02), $\log \beta_{1021}=25.74$ (0.03), $\log \beta_{1020}=15.35$ (0.02), and $\log \beta_{1100}=18.41$ (0.02).

Fluxional Behavior of Palladium(II) and Platinum(II) Complexes Containing both a Metal–Aryl Bond and a Pyrazole-derived Ligand†

Masayoshi ONISHI,* Koji SUGIMURA, and Katsuma HIRAKI*

Department of Industrial Chemistry, Faculty of Engineering, Nagasaki University, Bunkyo-machi, Nagasaki 852

(Received February 22, 1978)

New (acetophenone oximato, 2-*C,N*)- and (benzophenone oximato, 2-*C,N*)palladium(II) complexes containing poly(1-pyrazolyl)borato ligand (BPz_4 or $HBPz_3$, Pz=1-pyrazolyl) or poly(1-pyrazolyl)methane (CPz_4 or $HCPz_3$) were prepared and investigated by means of ^{1}H-NMR spectroscopy. For the BPz_4 complexes, the tumbling motion of the BPz_4 ligand averaged the environments of all four pyrazolyl groups to give spectroscopic equivalence above 65 °C, and was virtually frozen at *ca.* −9 °C. With regard to the $HBPz_3$, CPz_4, and $HCPz_3$ complexes, all pyrazolyl groups were equivalent at high temperature exhibiting stereochemical nonrigidity. The well-defined slow-exchange limiting spectra were not obtained at *ca.* −34 °C. In addition, new (acetophenone oximato, 2-*C,N*)platinum(II) complexes involving the BPz_4 or $HBPz_3$ ligand were prepared. The bidentate coordination of the BPz_4 ligand in the BPz_4 platinum(II) complex was stereochemically rigid in the range of 29 to 110 °C in DMSO-d_6. Three pyrazolyl groups in the $HBPz_3$ platinum(II) complex were equivalent at 85 °C in DMSO-d_6, while the fluxional motion was fairly restricted at room temperature.

Trofimenko[1,2] synthesized π-allylpalladium(II) complexes, $[Pd(\pi\text{-}C_3H_5)(PBz_4)]$ (Pz=1-pyrazolyl) and $[Pd(\pi\text{-}C_3H_5)(CPz_4)]PF_6$, reported that each of the 3-, 4-, and 5-H's of the four pyrazolyl groups in these complexes showed only one signal in the ^{1}H-NMR spectra at room temperature, and explained the fluxional behavior in terms of a "tumbling process."[1]

It is interesting to compare the fluxional behavior of the pyrazole-derived chelate ligands in the other square-planar complexes with those of the π-allylpalladium(II) complexes[1,2] and related platinum(II) complexes.[3] In a previous paper,[4] the fluxional behavior has been reported for several polypyrazolylborato palladium(II) complexes, which were prepared from dimeric cyclopalladated complexes derived from *N,N*-dimethylbenzylamine, azobenzene, 2-phenylpyridine, and benzo[*h*]quinoline.

This paper will deal with several new polypyrazolylborato (BPz_4 or $HBPz_3$) and polypyrazolylmethane (CPz_4 or $HCPz_3$) palladium(II) complexes, derived from cyclopalladated complexes, di-μ-chloro-bis(acetophenone oximato, 2-*C,N*)dipalladium(II)[5] $[\{PdCl(apo)\}_2]$ {apo=$-C_6H_4-C(=NOH)CH_3$,2-*C,N*} or di-μ-chloro-bis(benzophenone oximato, 2-*C,N*)dipalladium(II)[5] $[\{PdCl(bpo)\}_2]$ {bpo=$-C_6H_4-C(=NOH)C_6H_5$, 2-*C,N*}, and with the fluxional behavior of the pyrazole-derived ligands in these complexes by means of ^{1}H-NMR spectroscopy.

New platinum(II) complexes, $[Pt(apo)(BPz_4)]$ and $[Pt(apo)(HBPz_3)]$ were also obtained and compared with the corresponding polypyrazolylborato palladium(II) complexes.

Experimental

General Procedures. Melting points were determined on a Yanagimoto MP-S3 microstage apparatus and are uncorrected. IR spectra were recorded on a Hitachi model 285 spectrometer. ^{1}H-NMR spectra were run on a Japan Electron Optics Laboratory model JNM-MH-100 (100 MHz) spectrometer using tetramethylsilane as the internal standard. The temperatures of the NMR samples were determined with methanol or 1,3-propanediol.

$[\{PdCl(apo)\}_2]$,[5] $[\{PdCl(bpo)\}_2]$,[5] $[PtCl(apo)(Hapo)]$,[5] sodium tetrakis(1-pyrazolyl)borate {$Na(BPz_4)$},[6] sodium hydrotris(1-pyrazolyl)borate {$Na(HBPz_3)$},[6] CPz_4,[2] and $HCPz_3$[7] were prepared and purified according to the methods described in the literature.

Syntheses of the BPz_4 Palladium(II) Complexes. $[\{PdCl(bpo)\}_2]$ (1.6 g) and $Na(BPz_4)$ (1.5 g) were mixed in ethanol (80 ml) and the suspension stirred at room temperature for *ca.* 20 h. The precipitate was extracted with hot benzene, the solvent evaporated, and the residue recrystallized from ethanol to give yellow crystals of $[Pd(bpo)(BPz_4)]\cdot C_2H_5OH$, 0.9 g. This complex was converted into the non-solvated complex (**1**), by recrystallization from benzene.

The acetophenone oxime analogue, (**2**) and the ethanol monosolvate were obtained by a similar method.

Syntheses of the $HBPz_3$ Palladium(II) Complexes. A solution of $Na(HBPz_3)$ (0.9 g) in ethanol (20 ml) was added dropwise to a stirred suspension of $[\{PdCl(bpo)\}_2]$ (1.3 g)

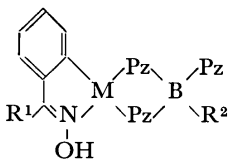

1 $R^1=C_6H_5$, $R^2=Pz$, M=Pd
2 $R^1=CH_3$, $R^2=Pz$, M=Pd
3 $R^1=C_6H_5$, $R^2=H$, M=Pd
4 $R^1=CH_3$, $R^2=H$, M=Pd
9 $R^1=CH_3$, $R^2=Pz$, M=Pt
10 $R^1=CH_3$, $R^2=H$, M=Pt

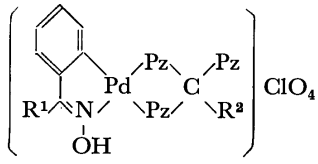

5 $R^1=C_6H_5$, $R^2=Pz$
6 $R^1=CH_3$, $R^2=Pz$
7 $R^1=C_6H_5$, $R^2=H$
8 $R^1=CH_3$, $R^2=H$

† Presented in part at the 27th Symposium on Coordination Chemistry, Matsumoto, Japan, September 1977.

Table 1. Properties and elemental analyses of the new complexes

	Yield[a] (%)	Color	Mp[b] (°C)	Found (Calcd) (%) C	H	N
1	21	Pale yellow	167—169	51.82(51.62)	3.90(3.81)	21.39(21.67)
2	28	Pale yellow	181—184	45.88(46.23)	3.89(3.88)	23.93(24.26)
3	55	Pale yellow	170—173[c]	51.09(51.24)	3.90(3.91)	18.95(19.01)
4	25	Pale yellow	159—162[c]	44.71(45.02)	3.94(4.00)	21.59(21.62)
5	36	Yellow	183—215	46.14(45.76)	3.31(3.25)	18.63(18.47)
6	44	Pale yellow	197—200	40.59(40.66)	3.12(3.25)	20.05(20.32)
7	41	Yellow	142—152	44.54(44.82)	3.20(3.27)	15.83(15.91)
8	41	Pale yellow	209—212	39.13(39.01)	3.24(3.27)	17.58(17.69)
9	40	Orange	230—233	39.59(39.49)	3.21(3.31)	20.73(20.72)
10	50	Orange	218—220	37.70(37.65)	3.29(3.35)	18.17(18.08)

a) Based on the starting palladium(II) or platinum(II) complexes. b) All complexes decomposed without melting. c) Measured in dinitrogen atmosphere.

in ethanol (10 ml). After stirring for *ca.* 20 h, the suspension was filtered and the precipitate washed with dichloromethane and methanol to yield a pale yellow powder of [Pd(bpo)-($HBPz_3$)] (**3**), 1.1 g: IR (Nujol) 2410 and 2425 cm^{-1} (ν_{BH}).

The complex [Pd(apo)($HBPz_3$)] (**4**) was prepared similarly except the washing was conducted with dichloromethane: IR (Nujol) 2425 and 2440 cm^{-1} (ν_{BH}).

Syntheses of the CPz_4 Palladium(II) Perchlorate Complexes. A mixture of CPz_4 (0.1 g) and [{PdCl(bpo)}$_2$] (0.12 g) in methanol–water (35 ml) (1:3), was stirred for *ca.* 20 h at room temperature.

The mixture was filtered and a solution of sodium perchlorate in methanol–water added to the filtrate. The resulting precipitate was recrystallized from methanol to give a yellow solid of [Pd(bpo)(CPz_4)]ClO_4 (**5**), 0.09 g.

The complex [Pd(apo)(CPz_4)]ClO_4 (**6**) was prepared in a similar method as described for **5**, where the corresponding precipitate was washed with benzene, dichloromethane, and water in place of recrystallization.

Syntheses of the $HCPz_3$ Palladium(II) Perchlorate Complexes. A mixture of [{PdCl(bpo)}$_2$] (0.37 g) and $HCPz_3$ (0.24 g) in methanol–water (30 ml) (1:3) was stirred for 5 h at room temperature and the reaction mixture filtered. Sodium perchlorate was added to the filtrate, and the resulting precipitate was recrystallized from methanol to afford a yellow solid of [Pd(bpo)($HCPz_3$)]ClO_4 (**7**) 0.28 g: IR (KBr) 3000 cm^{-1} (ν_{CH} of $HCPz_3$).

The complex [Pd(apo)($HCPz_3$)]ClO_4 (**8**) was prepared similarly: IR (KBr) 2990 cm^{-1} (ν_{CH} of $HCPz_3$).

Syntheses of [Pt(apo)(BPz_4)] and [Pt(apo)($HBPz_3$)]. After a mixture of Na(BPz_4) (0.3 g) and [PtCl(apo)(Hapo)] (0.41 g) was stirred for *ca.* 20 h in benzene (20 ml), the solvent was removed. The residue was extracted with dichloromethane and the extract evaporated to dryness. The resulting solid was washed with diethyl ether and ethanol to yield an orange powder of [Pt(apo)(BPz_4)] (**9**), 0.2 g.

The complex [Pt(apo)($HBPz_3$)] (**10**) was obtained similarly, and recrystallized from methanol: IR(Nujol) 2430 and 2410 cm^{-1} (ν_{BH}).

Results and Discussion

Physical Properties. The analytical data and the physical properties of the new palladium(II) and platinum(II) complexes are summarized in Table 1. The BPz_4 palladium(II) complexes, **1** and **2** were soluble in chloroform and DMSO, and slightly soluble in ethanol and benzene. The $HBPz_3$ palladium(II) complexes, **3** and **4**, were less soluble than the corresponding BPz_4 complexes, **1** and **2**, respectively. The ^{1}H-NMR spectrum of **3** was not obtainable. The complexes were stable in the solid state. However, complex **4** decomposed slowly in dichloromethane to give metallic palladium. The cationic palladium(II) complexes, **5**, **6**, **7**, and **8** involving polypyrazolylmethane were insoluble in common organic solvents except for acetonitrile and methanol. The polypyrazolylmethane complexes were thermally more stable than the corresponding polypyrazolylborato ones in the solid

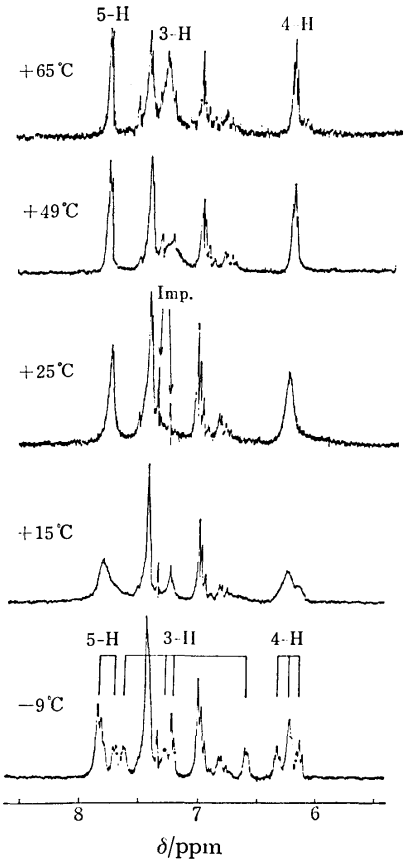

Fig. 1. ^{1}H-NMR spectra of **1** in $CDCl_3$. Two impurities are $CHCl_3$ and C_6H_6.

Table 2. Solvent effects on the chemical shifts of pyrazolyl protons[a)]

Proton	[Pd(bpo)(BPz_4)]			[Pd(apo)(BPz_4)]		
	DMSO-d_6	C_6D_6	$CDCl_3$[b)]	DMSO-d_6	C_6D_6	$CDCl_3$[b)]
3-H	7.19	7.49	7.28	7.01	7.46	7.27
4-H	6.38	6.08	6.22	6.21	6.10	6.24
5-H	7.84	7.80	7.76	7.70	7.75	7.71

a) δ-Values relative to TMS, at 76 °C unless noted elsewhere. b) At 65 °C.

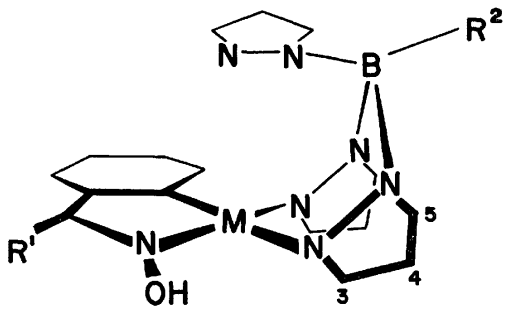

Fig. 2. The proposed geometrical arrangement.

state, complexes, **5** and **6** decomposing in acetonitrile at 80 °C.

The polypyrazolylborato platinum(II) complexes, **9** and **10** were stable in the solid state, slightly soluble in DMSO at room temperature, and insoluble in other common organic solvents.

Each of the ν(BH) bands in the $HBPz_3$ complexes consisted of two peaks, which were associated with $\nu(^{10}BH)$ and $\nu(^{11}BH)$ corresponding to the natural abundance of boron isotopes.

^{1}H-NMR Spectra of the BPz_4 Palladium(II) Complexes. Figure 1 shows the ^{1}H-NMR spectra of **1** in $CDCl_3$ at several temperatures between −9 and 65 °C. The line shapes of the three signals at δ 7.44 (5H), 7.01 (3H), and 6.80 (1H) were independent of temperature, and were unaffected by the exchange process. The first signal was assigned to the phenyl protons, and the remaining two to the metallated *o*-phenylene group. The protons of the four pyrazolyl groups showed signals which were remarkably temperature-dependent. At 65 °C, a signal at δ 6.22 (4H) exhibited a triplet and was ascribed to 4-H's. Signals at δ 7.28 (4H) and 7.76 (4H) were associated with 3-H's and 5-H's, respectively, on the basis of the temperature-dependency of each signal (*vide infra*). At this temperature, each of the three kinds of protons belonging to the four pyrazolyl groups exhibited spectroscopic identity, indicating a tumbling motion of the BPz_4 group as observed for [Pd(π-C_3H_5)(BPz_4)].[1)]

The signal for the 5-H's became gradually broader on cooling and separated into two signals at δ 7.79 (3H) and 7.66 (1H) at −9 °C. The signal for the 3-H's was apparently missing at 25 °C, and reappeared at δ 7.56, 7.26, 7.21, and 6.64 at −9 °C. These facts indicate that at this temperature the four pyrazolyl groups are spectroscopically unequal, and the BPz_4 ligand is coordinated to the central metal in a stereochemically rigid state. In this state, one can expect that the differences in environments and chemical shifts among the four 3-H's are larger than those among the 5-H's, respectively, by considering the proposed arrangement shown in Fig. 2. At 45 °C, a broad peak at δ 5.15 was observed in $CDCl_3$ and ascribed to an oxime proton, since it disappeared with the addition of D_2O.

Table 2 shows the NMR data of the pyrazolyl protons of **1** recorded at 76 °C in C_6D_6 and DMSO-d_6, and indicates an appreciable degree of solvent effect on the chemical shifts of the 3-H's, in contrast to that of the 5-H's. This confirms the above-mentioned assignment of the 3-H's.

At −16 °C, complex **2** exhibited a low-temperature limiting spectrum, in which a signal at δ 7.58 was attributed to two protons overlapping each other, assignable to one of the 3-H's and one of the 5-H's. The other signals of **2** exhibited very similar patterns to those of **1**.

In the BPz_4 complexes, the tumbling motion averages the environments of all four pyrazolyl groups to give spectroscopic equivalence at high temperature. The motion is thought to involve the coordination of one uncoordinated pyrazolyl group to the axial site of palladium accompanied instantaneously by the dissociation of one previously coordinated group and the inversion of the Pd–(N–N)$_2$–B boat-type six-menbered ring. In consideration of the proposed conformation shown in Fig. 2, it is reasonably expected that one uncoordinated pyrazolyl group easily approaches the axial site of the palladium atom. The tumbling motion is probably restricted to an appreciable degree in these aromatic oximato complexes, in which the *trans* positions of the BPz_4 ligand are coordinated with nitrogen donor and aryl group, in contrast to the π-allyl analogue. The comparatively weak *trans* influence of the nitrogen donor in the cyclometallated moiety of **1** and **2** possibly resulted in a moderately strong binding of Pd–Pz bond *trans* to the nitrogen donor and in an easy fixation of tumbling motion of the BPz_4 ligand.

^{1}H-NMR Spectra of the Other Palladium(II) Complexes. In the NMR spectra of [Pd(apo)($HBPz_3$)], the three pyrazolyl groups were spectroscopically equivalent at 36 °C, indicating the fluxional motion of the $HBPz_3$ ligand. The peaks for pyrazolyl groups began to broaden at −24 °C. At *ca.* −34 °C, a new peak appeared near δ 6.5, which was tentatively ascribed to one proton of 3-H's. However, a slow-exchange limiting spectrum was not obtained even at this temperature. The fluxional motion of the $HBPz_3$ complex was more hardly fixed than that of the corresponding BPz_4 complex.

Each signal for the 3-, 4-, and 5-H's of the CPz_4

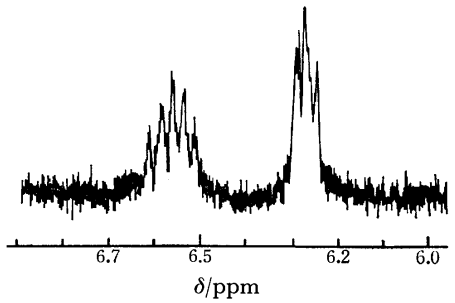

Fig. 3. 4-H's signals in ^{1}H-NMR spectrum of **9** in DMSO-d_6 at 30 °C.

complexes, **5** and **6**, showed only one signal at *ca.* 50 °C in CD_3CN, demonstrating the spectroscopic equivalence of all four pyrazolyl groups and the tumbling motion of the CPz_4 ligand. The signals for the 3- and 5-H's of the pyrazolyl groups became broad at temperatures below −10 °C, and began to separate at *ca.* −30 °C. In contrast to the polypyrazolylborate ligands, the fixation of the fluxional motion of the polypyrazolylmethane ligands was comparatively difficult.

The $HCPz_3$ complexes, **7** and **8**, at room temperature gave well-defined fast-exchange limiting spectra, showing spectroscopic equivalence of the three pyrazolyl groups and stereochemical nonrigidity.

^{1}H-NMR Spectra of Platinum(II) Complexes. Coordination of the BPz_4 ligand in the platinum(II) complex **9** was stereochemically rigid even at 110 °C on the basis of the ^{1}H-NMR spectra, and the compound decomposed at *ca.* 130 °C in DMSO-d_6. No fluxional behavior was observed. The 4-H's resonances showed a triplet at δ 6.28 and a multiplet at δ 6.55 in the ratio of 2:2, as shown in Fig. 3. The apparent multiplet was assigned to the 4-H protons with attendant ^{195}Pt satellites in two coordinated pyrazolyl groups, indicating that the BPz_4 ligand acted as a bidentate ligand and the complex was four-coordinated. For the ^{1}H-NMR spectra of methyl(polypyrazolylborato)platinum(II) complexes, similar ^{195}Pt satellites were observed for the 4-H protons of the pyrazolyl groups coordinated to platinum.[3]

In the $HBPz_3$ platinum(II) complex **10**, three signals, a slightly broad peak (3H) at δ 7.89, a doublet (3H) at δ 7.74, and a triplet (3H) at δ 6.37 were observed for the pyrazolyl protons at *ca.* 85 °C and the triplet was assigned to the 4-H's. Three pyrazolyl groups were spectroscopically equivalent at this temperature showing stereochemical nonrigidity of the $HBPz_3$ ligand. At room temperature, the 4-H's signal separated into two signals in a 2:1 intensity ratio and the coordination of the $HBPz_3$ ligand became comparatively rigid on the NMR time scale. The slow-exchange limiting spectrum was not obtained due to poor solubility of **10** below room temperature. The fluxional motion of the $HBPz_3$ platinum(II) complex was easily fixed in contrast to that of the corresponding palladium(II) complexes.

Table 3. Fast-exchange limiting ^{1}H-NMR spectra[a] of pyrazolyl groups in the $HBPz_3$, CPz_4, and $HCPz_3$ complexes

Complex	Temp (°C)	4-H	3-H or 5-H
4[b]	36	6.28(t, 2.0)	7.68(d, 1.9)[c]
5	61	6.76[d]	7.52(d, 3.0) 8.19[d]
6	75	6.80(t, 2.5)	7.58(d, 2.8) 8.22[d]
7	28	6.73(t, 2.5)	8.09(d, 2.1) 8.27(d, 3.0)
8	29	6.63(t, 2.5)	7.96(d, 2.0) 8.13(d, 2.7)

a) δ-Values relative to TMS; multiplicities and coupling constants in Hz are given in parentheses; in CD_3CN, unless noted elsewhere; s=singlet, d=doublet, t=triplet. b) In CD_2Cl_2. c) Overlapping occurred. d) Coupling constants could not be detected.

References

1) S. Trofimenko, *J. Am. Chem. Soc.*, **91**, 588, 3183 (1969).
2) S. Trofimenko, *J. Am. Chem. Soc.*, **92**, 5118 (1970).
3) H. C. Clark and L. E. Manzer, *Inorg. Chem.*, **13**, 1996 (1974), and the references cited therein.
4) M. Onishi, Y. Ohama, K. Sugimura, and K. Hiraki, *Chem. Lett.*, **1976**, 955.
5) H. Onoue, K. Minami, and K. Nakagawa, *Bull. Chem. Soc. Jpn.*, **43**, 3480 (1970).
6) S. Trofimenko, *J. Am. Chem. Soc.*, **89**, 3170 (1967).
7) H. Bretshneider, *Ber.*, **70**, 2024 (1937).

Mixed Ligand Complexes Derived from the Reactions of Diaquabis-(3-hydroxy-2-methyl-4-pyronato)-cobalt(II), -nickel(II), and -zinc(II) with Pyridine and 4-Substituted Pyridines

Hideyoshi MORITA,* Shigeru SHIMOMURA, and Shinichi KAWAGUCHI†

Faculty of Pharmaceutical Sciences, Tokushima University, Shomachi, Tokushima 770

†*Department of Chemistry, Faculty of Science, Osaka City University, Sumiyoshi-ku, Osaka 558*

(Received April 3, 1978)

The pyridine(py), 4-methylpyridine(4-Me-py) and 4-cyanopyridine(4-CN-py) adducts of bis(3-hydroxy-2-methyl-4-pyronato) complexes (ML_2) of cobalt(II), nickel(II), and zinc(II) have been synthesized: $CoL_2(py)_n$ (where $n=2$ or 3), $NiL_2(py)_3$, $ZnL_2(py)$, $ML_2(4\text{-Me-py})_2$ (where M=Co(II), Ni(II), and Zn(II)), $ML_2(4\text{-CN-py})$ (where M=Co(II) and Zn(II)), and $NiL_2(4\text{-CN-py})_2$. Based on the magnetic, spectral, and thermogravimetric data, three of these complexes, $ZnL_2(py)$ and $ML_2(4\text{-CN-py})$ (where M=Co(II) and Zn(II)), are presumed to have a five-coordinate structure, while the other complexes are presumed to be octahedral. In the case of the 4-cyanopyridine complexes, the infrared spectra show that the pyridine-ring nitrogen is linked to the metal ion and that the nitrogen atom of the nitrile group is not coordinated.

In previous papers it was reported that, when treated with 2,2′-bipyridine(bpy) or 1,10-phenanthroline (phen), the aqua ligands of the diaquabis(3-hydroxy-2-methyl-4-pyronato) complexes of Co(II), Ni(II), and Zn(II) were replaced by the base,[1] whereas bis(3-hydroxy-2-methyl-4-pyronato)palladium(II) gave mixed ligand complexes, $[PdL(bpy)]ClO_4$ and $[PdL(phen)]ClO_4$.[2] On the other hand, an aliphatic amine, such as ethylenediamine(en), propylamine(pa), and benzylamine(ba), replaced both of the ligands in $[PdL_2]$ to afford a complex containing 3-hydroxy-2-methyl-4-pyronate (Fig. 1) as counter ions, $[Pd(en)_2]L_2\cdot 2H_2O$,[2] $[Pd(pa)_4]L_2$, or $[Pd(ba)_4]L_2$.[3] In the course of our studies it was noticed that pyridine and 4-substituted pyridines react with diaquabis-(3-hydroxy-2-methyl-4-pyronato) complexes of Co(II), Ni(II), and Zn(II) to produce five- or six coordinate mixed-ligand complexes containing the pyronate anion and the base.

This paper will report on the syntheses and structural studies of the pyridine, 4-methylpyridine, and 4-cyanopyridine adducts of bis(3-hydroxy-2-methyl-4-pyronato) complexes of Co(II), Ni(II), and Zn(II).

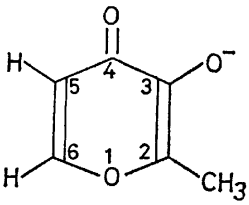

Fig. 1. 3-Hydroxy-2-methyl-4-pyronate anion.

Experimental

Materials. The preparation of three diaquabis(3-hydroxy-2-methyl-4-pyronato) complexes of Co(II), Ni(II), and Zn(II), $(CoL_2(OH_2)_2$, $NiL_2(OH_2)_2$, and $[ZnL_2(OH_2)_2]\cdot 1/2H_2O)$ has previously been reported.[1] Reagent-grade pyridine, 4-methylpyridine, and 4-cyanopyridine were used without further purification. The ethanol was purified by the fractional distillation of the ternary azeotrope, benzene–ethanol–water. The mercury(II) tetrakis(isothiocyanato)-cobalt(II) was prepared according to the literature[4] and was used as a referecne substance for the magnetic measurements.

*Preparation of Complexes. Bis(3-hydroxy-2-methyl-4-pyronato)bis(pyridine)cobalt(II) Pyridine, $[CoL_2(py)_2](py)$ (**1**):* In 10 ml of hot pyridine–ethanol (1 : 2 by volume) we dissolved 1.0 g of $CoL_2(OH_2)_2$, the solution was then heated on a hot-plate for 10 min with stirring and stored overnight in a refrigerator. The brown precipitate thus obtained was filtered and dried *in vacuo* at room temperature. The yield was 1.4 g (87%).

*Bis(3-hydroxy-2-methyl-4-pyronato)bis(pyridine)cobalt(II), $[CoL_2(py)_2]$ (**2**):* This compound was produced when Complex **1** was kept at *ca.* 95 °C for 2 h in an atmosphere of flowing nitrogen (50 ml/min).

The corresponding pyridine adducts of Ni(II) and Zn(II), $[NiL_2(py)_2](py)$ (**3**) and $[ZnL_2(py)]$ (**4**), were also prepared, by the method used for Complex **1** using $NiL_2(OH_2)$ and $[ZnL_2(OH_2)_2]\cdot 1/2H_2O$ instead of $CoL_2(OH_2)_2$, in 92 and 93% yields respectively.

*Bis(3-hydroxy-2-methyl-4-pyronato)bis(4-methylpyridine)cobalt-(II), $[CoL_2(4\text{-Me-py})_2]$ (**5**):* One gram of $CoL_2(OH_2)_2$ was added little by little to 5 ml of 4-methylpyridine with stirring. The mixture was heated on a hot-plate with stirring for 15 min, and then cooled to room temperature. The brown precipitate thus obtained was filtered, washed with ethanol and petroleum ether, and dried *in vacuo* at room temperature. The yield was 1.3 g (91%).

In a similar fashion, $[NiL_2(4\text{-Me-py})_2]$ (**6**) and $[ZnL_2(4\text{-Me-py})_2]$ (**7**) were obtained in 98 and 86% yields respectively.

*(4-Cyanopyridine)bis(3-hydroxy-2-methyl-4-pyroanato)cobalt(II), $[CoL_2(4\text{-CN-py})]$ (**8**):* To an ethanol solution (120 ml) of 4-cyanopyridine (0.52 g, 0.005 mol) we added 1.72 g (0.005 mol) of $CoL_2(OH_2)_2$. The mixture was heated on a hot-plate with stirring. The solution was concentrated to begin the formation of a precipitate, and was then left standing overnight in a refrigerator. The brown precipitate thus obtained was filtered, washed with ethanol, and dried *in vacuo* at room temperature. The yield was 1.4 g (67%).

The corresponding 4-cyanopyridine adducts of Ni(II) and Zn(II), $[NiL_2(4\text{-CN-py})_2]$ (**9**) and $[ZnL_2(4\text{-CN-py})]$ (**10**), were also prepared by the reaction of $NiL_2(OH_2)_2$ or $[ZnL_2(OH_2)_2]\cdot 1/2H_2O$ respectively with two or three times as many moles of 4-cyanopyridine in a manner similar to that used for Complex **8**. The yields were 81% and 80 respectively.

Analyses and Measurements. The metal contents in these complexes were determined by atomic absorption spectroscopy. The visible and ultraviolet reflection spectra were

Table 1. Color and analytical data of the isolated complexes

Complex		Color	Found (Calcd), % C	H	N	M	Magnetic moment B. M. (K)
$[CoL_2(py)_2](py)$	**1**	brown	59.19 (59.35)	4.60 (4.61)	7.74 (7.69)	10.49 (10.78)	4.84 (289)
$[CoL_2(py)_2]$	**2**	yellow brown	56·38 (56.54)	4.46 (4.31)	6.14 (5.99)	12.86 (12.61)	5.02 (302)
$[CoL_2(4\text{-Me-py})_2]$	**5**	brown	57.86 (58.19)	4.80 (4.88)	5.55 (5.65)	11.76 (11.90)	4.87 (302)
$[CoL_2(4\text{-CN-py})]$	**8**	brown	52.15 (52.32)	3.53 (3.41)	6.63 (6.78)	13.97 (14.26)	4.66 (301)
$[NiL_2(py)_2](py)$	**3**	green	59.53 (59.37)	4.65 (4.61)	7.58 (7.72)	10.66 (10.75)	3.17 (303)
$[NiL_2(4\text{-Me-py})_2]$	**6**	green	57.90 (58.22)	4.70 (4.89)	5.64 (5.66)	11.57 (11.86)	3.23 (303)
$[NiL_2(4\text{-CN-py})_2]$	**9**	green	55.69 (55.75)	3.53 (3.51)	10.72 (10.83)	11.26 (11.35)	3.16 (303)
$[ZnL_2(py)]$	**4**	white	51.64 (51.74)	3.86 (3.83)	3.48 (3.55)	16.59 (16.57)	
$[ZnL_2(4\text{-Me-py})_2]$	**7**	pale yellow	57.48 (57.44)	4.81 (4.82)	5.56 (5.58)	12.71 (13.03)	
$[ZnL_2(4\text{-CN-py})]$	**10**	yellow	51.45 (51.51)	3.24 (3.36)	6.36 (6.67)	15.17 (15.58)	

obtained with a Shimadzu MPS-5000 recording sepctrophotometer. The infrared spectra (4000—200 cm^{-1}) were obtained with a Jasco DS-701G infrared spectrophotometer in Nujol mull between CsI plates. The magnetic susceptibility was determined at room temperature by the Faraday method with an automatically recording magnetic balance (Shimadzu Seisakusho Co., Ltd.). Mercury(II) tetakis(isothiocyanato)cobaltate(II) was used as a reference substance. The diamagnetic corrections were calculated from Pascal's constants. The thermogravimetric curves were obtained with a Shimadzu TGA-20B thermobalance at a heating rate of 5 °C/min in an atmosphere of nitrogen flowing at 50 ml/min. The PMR spectra were measured in $CDCl_3$ at 100 MHz with a JNM-PS-100 spectrometer (Japan Electron Optics Lab. Co., Ltd.) using tetramethylsilane as the internal reference. The molecular weight was determined in chloroform at 35 °C with a vapor-pressure osmometer of the Hitachi Perkin-Elmer 115 type, employing benzil as a reference substance.

Results and Discussion

Ten mixed-ligand complexes isolated are listed in Table 1, together with their colors and analytical and magnetic data. As may be seen in Table 2, the observed molecular weights of Complexes **5**—**10** are remarkably smaller than the calculated values, indicating that these complexes dissociate extensively in solution. Furthermore, the electronic spectra of the nickel(II) and cobalt(II) complexes in ethanol (**1**, **2**, **3**, **5**, and **6**) or chloroform (**8** and **9**) changed on the addition of the corresponding base to the solution, suggesting again the dissociation of these complexes in solution. Therefore, the structural study of the complexes was done mainly on the basis of thermogravimetic, IR, reflection-spectral, and magnetic data in the solid state.

Thermogravimetric Data. The thermogravimetric (TG) curves for the pyridine, 4-methylpyridine, and 4-cyanopyridine complexes are given in Figs. 2 and 3.

Table 2. Molecular weight data in chloroform

Compound		Calcd	Found
$[ZnL_2(py)]$	**4**	394.7	390,[a] 410[b]
$[CoL_2(4\text{-Me-py})_2]$	**5**	495.4	283[a]
$[NiL_2(4\text{-Me-py})_2]$	**6**	495.2	342[a]
$[ZnL_2(4\text{-Me-py})_2]$	**7**	501.8	337[b]
$[CoL_2(4\text{-CN-py})_2]$	**8**	413.3	335,[a] 339[c]
$[NiL_2(4\text{-CN-py})_2]$	**9**	517.1	248,[a] 295[c]
$[ZnL_2(4\text{-CN-py})_2]$	**10**	419.7	299,[b] 300[c]

a) At 1.0×10^{-3} M. b) At 1.5×10^{-3} M. c) At 2.0×10^{-3} M.

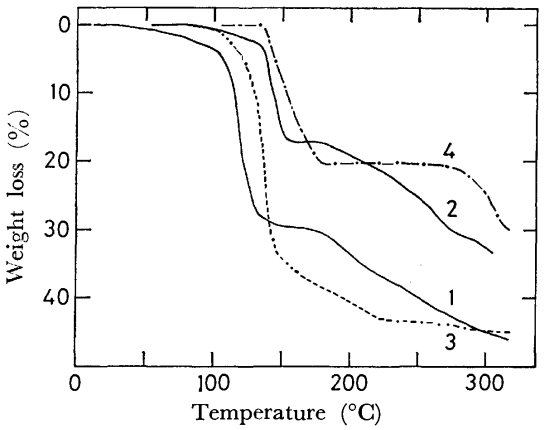

Fig. 2. The TG curves for complexes **1**(1), **2**(2), **3**(3), and **4**(4).

Complex **1** begins to liberate pyridine at around 30 °C and loses two molecules up to *ca.* 160 °C to give $CoL_2(py)$ (weight loss at 160 °C; found: 29.54%, calcd for 2 py: 28.95%.). The TG curve does not show distinctly whether or not the two pyridine molecules are liberated in two steps, but Complex **2** was

Table 3. Characteristic IR bands (cm^{-1}) of the isolated complexes

Complex		ν(C=O)	ν(C=C)		ν(M-O)	Base				
$[CoL_2(py)_2](py)$	**1**	1600 vs	1572 vs	1512 s	443m	624m	603w	430w	421m	413 vw
$[CoL_2(py)_2]$	**2**	1595 vs	1571 vs	1518 s	451m	619m	421m			
$[NiL_2(py)_2](py)$	**3**	1598 vs	1570 vs	1510 s	450m	628m	604m	438m	427w	413 vw
$[ZnL_2(py)]$	**4**	1601 vs	1568 vs	1510 vs	470m	640m	420m			
$[CoL_2(4\text{-Me-py})_2]$	**5**	1602 vs	1577 vs	1514 s	443m	1017m	723m	526m	493m	488m
$[NiL_2(4\text{-Me-py})_2]$	**6**	1601 vs	1572 vs	1510 s	448m	1019m	723m	529m	496m	489m
$[ZnL_2(4\text{-Me-py})_2]$	**7**	1603 vs	1569 vs	1518 s	447m	1017m	724m	527m	494m	488m
$[CoL_2(4\text{-CN-py})]$	**8**	1604 vs	1579 vs	1511 s	458m	2230m	1613 sh[a]	1095 sh	1061 vw	1016w
$[NiL_2(4\text{-CN-py})_2]$	**9**	1595 vs	1575 vs	1516 s	460w	2238m	1608 sh[a]	1092w	1060w	1018w
$[ZnL_2(4\text{-CN-py})]$	**10**	1600 vs	1582 vs	1515 s	463m	2241m	1615 sh[a]	1605 sh[a]	1094 sh	1063w 1017m

a) The band overlaps with the ν(C=O) band of the pyronate ligand.

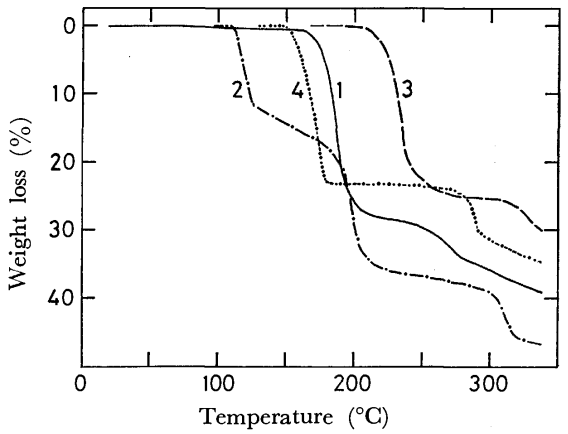

Fig. 3. The TG curves for complexes **5**(1), **7**(2), **8**(3), and **10**(4).

obtained by keeping Complex **1** at *ca.* 95 °C for 2 h in an atmosphere of flowing nitrogen. Complex **2** loses a further pyridine molecule in the same temperature range in which Complex **1** loses two pyridine molecules (weight loss at 160 °C; found: 17.14%, calcd for py: 16.93%.). Based on these results and on the IR spectral data, which indicate that an uncoordinated pyridine molecule is contained in Complex **1**, but not in Complex **2**, it may be concluded that the former complex loses an uncoordinated pyridine molecule most easily. The pyridine in the residual compound, $CoL_2(py)$, seems to be held much more tightly. Complex **3** begins to decompose at *ca.* 80 °C, and no stable intermediate is detected. Complex **4**, on the other hand, begins to liberate pyridine at 120 °C to give ZnL_2 in the temperature range of 160—250 °C to give ZnL_2 (weight loss at 200 °C; found: 20.31%, calcd for py: 20.04%.).

The TG curve for Complex **7** shows that the liberation of 4-methylpyridine takes place in three steps: *i.e.*, $ZnL_2 \cdot 2B \xrightarrow[110-125\,^\circ C]{-0.6B} ZnL_2 \cdot 1.4B \xrightarrow[125-190\,^\circ C]{-0.4B} ZnL_2 \cdot B \xrightarrow[190-250\,^\circ C]{-1B} ZnL_2$ (where B is 4-methylpyridine), although the metastable intermediate compounds have not been isolated. The TG curves for Complexes **8** and **10** indicate that these complexes lose 4-cyanopyridine in a single step (weight loss of **8** at 290 °C; found: 25.28%, calcd for 4-CN-py: 25.19%, and weight loss of **10** at 270 °C; found: 24.12%, calcd for 4-CN-py: 24.81%.).

For the five-coordinate complexes, a rough order of thermal stability, is estimated from the temperature at which the complexes begin to lose weight, is: $ZnL_2(py) \leq ZnL_2(4\text{-CN-py}) < CoL_2(4\text{-CN-py})$.

Infrared Spectral Data. The infrared spectral data for the isolated complexes are shown in Table 3. In all of these complexes, the 3-hydroxy-2-methyl-4-pyronate ligand is coordinated to the metal ion through the two oxygen atoms of the carbonyl and hydroxyl groups, since the frequencies of the C=O and C=C stretching vibrations are smaller by *ca.* 50 cm^{-1} than those in the free ligand.[1] The coordination of pyridine can be readily inferred from the shift of the 604 (an inplane ring deformation) and 405 cm^{-1} (an out-of-plane ring deformation) bands for uncoordinated pyridine to about 625 and 420 cm^{-1} respectively.[5-7] The magnitude of the frequency shift depends on the stereochemistry of the complex and on the radii of the metal ions.[6] For Complexes **1** and **3**, the bands due to both the coordinated and uncoordinated pyridines are observed. However, Complex **2** shows bands due to coordinated pyridine only. From these results, which are consistent with those of the thermogravimetric analysis, it may be concluded that two of the pyridine molecules in Complexes **1** and **3** are coordinated, while one is uncoordinated. Clark and Williams indicated that the 604 cm^{-1} band is more sensitive to the stereochemistry of the complex, but the frequencies of both the 604 and 405 cm^{-1} bands increase with a decrease in the ionic radius of the metal for the series of polymeric octahedral chloro compounds, $M(py)_2Cl_2$, where M=Mn(II), Fe(II), Co(II), Ni(II), and Cu(II).[7] Complex **4** shows absorption at 640 and 420 cm^{-1}; the position of the former band is apparently higher than those of the other pyridine complexes. This difference may stem from the difference in stereochemistry, since the zinc complex has a five-coordinate structure, while the others are octahedral.

For the 4-methylpyridine complexes of metal halides, Gill and Kingdon previously noted that the bands due to 4-methylpyridine move to higher frequencies except for the band at 728 cm^{-1}, which moves to

Table 4. PMR spectra of the zinc(II) complexes in chloroform solution (δ, ppm)

Compound	L⁻				py or 4-Me-py		
	CH_3	H^5	H^6	$J_{5,6}$	H^2, H^6	H^3, H^5	H^4 or CH_3
py					8.54	7.19	7.57
4	2.42	6.49	7.68	5.2 Hz	8.59	7.34	7.78
4-Me-py					8.41	7.06	2.31
7	2.47	6.53	7.69	5.2 Hz	8.42	7.12	2.34

a lower frequency.[8] They further pointed out that the magnitude of the shift of the bands in the monomeric octahedral complexes increases with the series from the manganese to the nickel complexes, particularly for the 996, 515, and 484 cm^{-1} bands of the free ligand. Table 3 shows that these tendencies are also observed in Complexes **5**, **6**, and **7** obtained in the present study, revealing that both of the 4-methylpyridine molecules are coordinated to the metal ion in these complexes.

With regard to the 4-cyanopyridine complexes, it is well known that, when the nitrile nitrogen is coordinated to a metal ion, the stretching frequency of the nitrile group moves to a higher value than that for the free ligand.[9-12] On the other hand, when the pyridine ring nitrogen is coordinated to the metal ion, the ν(CN) band at 2242 cm^{-1} suffers little influence, but the bands (1081, 1075sh, and 988 cm^{-1}) due to the ring-breathing mode suffer appreciable shifts.[9-12] In complexes **8**, **9**, and **10**, the nitrile stretching frequency is decreased a little and the ring-breathing frequencies are shifted (Table 3). These data suggest that 4-cyanopyridine in these complexes is coordinated to the metal ion *via* the ring nitrogen.

The metal-oxygen stretching bands are assigned tentatively by reference to the literature.[1,13]

PMR Spectra of Zn(II) Complexes. The PMR data for Complexes **4** and **7** in $CDCl_3$ solutions are shown in Table 4. The assignments are based on the relative peak areas and on a comparison with the spectra of $[ZnL_2(OH)_2]\cdot 1/2H_2O$,[1] pyridine, and 4-methylpyridine.[14] In the spectrum of Complex **4**, the resonance peaks due to pyridine are shifted downfield on ligation as compared to those of free pyridine. The shifts for the 2 and 6 protons are much smaller than those for the 3, 5, and 4 protons. The molecular weight of this complex was determined to be 400± 10 in chloroform, very close to the calculated value of 394.7, indicating that the compound is stable and retains the five-coordinate structure in chloroform. However, it is not certain whether the complex has a square pyramidal structure or a trigonal bipyramidal structure. In the case of Complex **7**, only one set of resonance peaks due to the pyrone and 4-methylpyridine was observed, although the data of the molecular weight of this complex indicated that the complex dissociates extensively in chloroform. This result suggests that the dissociation and addition reactions of 4-methylpyridine in **7** are so rapid as to average the magnetic environments. The magnitudes of the downfield shift of the 2 and 6 protons of pyridine and 4-methylpyridine are considerably small as compared with those of the 3 and 5 protons of the base. This might be attributable to the operation of the magnetic anisotropy effect of the carbonyl group of the pyronate ligand on the 2 and 6 protons. Unfortunately, Complex **10** is not soluble enough to give a PMR spectrum in nondonor common solvents.

The analogous pyridine or 4-methylpyridine adducts of bis(acetylacetonato)zinc(II) have been previously reported by Graddon and Weeden.[15] Their measurement of the molecular weight of the compounds showed that the mono-adducts, $[Zn(acac)_2(py)]$ and $[Zn(acac)_2(4\text{-Me-py})]$, are monomeric in benzene and triphenylmethane, whereas $[Zn(acac)_2(4\text{-Me-py})_2]$ dissociates in these solutions to form a five-coordinate mono-adduct, while $[Zn(acac)_2(py)_2]$ is extremely unstable, losing pyridine rapidly even in the solid state to give monopyridine compound. From these properties of the adducts and the absence of crystal-field stabilization in the octahedral zinc(II) complexes, they inferred that the five-coordinate adduct is more favorable for Zn(II) than the octahedral bis-adduct.[15] In the present pyridine, 4-methylpyridine, and 4-cyanopyridine adducts of bis(3-hydroxy-2-methyl-4-pyronato)zinc(II), the five-coordinate adducts seem also to be favorable, although we could not isolate $[ZnL_2(4\text{-Me-py})]$.

Electronic Spectra and Magnetic Data. The reflection spectra of the cobalt(II) and nickel(II) complexes are shown in Figs. 4 and 5 respectively, their magnetic moments being listed in Table 1. Complexes **2**, **5**, and **8** show bands at 7.4(sh), 8.7, 17.8, and *ca.* 23.0 kK; 9.3, 16.8(sh), 17.8, and 21.7 kK; and 8.0, *ca.* 17.5, *ca.* 20.0, and 22.2 kK, respectively. From the spectra and the observed magnetic moments of **2**(5.02 B.M.), **5**(4.87 B.M.), and **8**(4.66 B.M.), it may be inferred that Complexes **2** and **5** are octahedral and Complex **8** is octahedral or five-coordinated, since the magnetic moments previously reported for the high-spin octahedral and five-coordinate cobalt(II) complexes lie in the ranges of 4.7—5.2 and 4.3—5.5 B.M. respectively.[16] However, taking account of the IR data for Complex **8**, which show that 4-cyanopyridine is coordinated to the cobalt ion solely with the ring nitrogen, the possibility of an octahedral structure for Complex **8** seems to be excluded. Furthermore, it has been reported that, for high-spin metal complexes, the five-coordination is favored in the order of: Co(II), Cu(II), Zn(II)>Fe(II), Ni(II)>Mn(II).[17] In the present work, the 4-CN-py adduct of cobalt(II) and Zn(II) complexes have one 4-CN-py moleucle, while the corresponding nickel(II) adducts has two 4-CN-py molecules, in conformity with the above series,

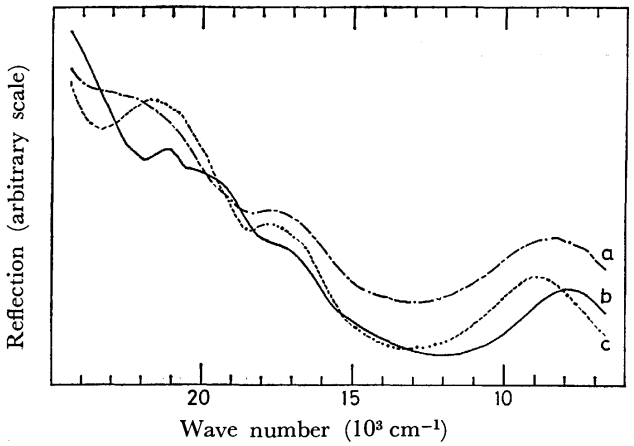

Fig. 4. The reflection spectra of complexes **2**(a), **8**(b), and **5**(c).

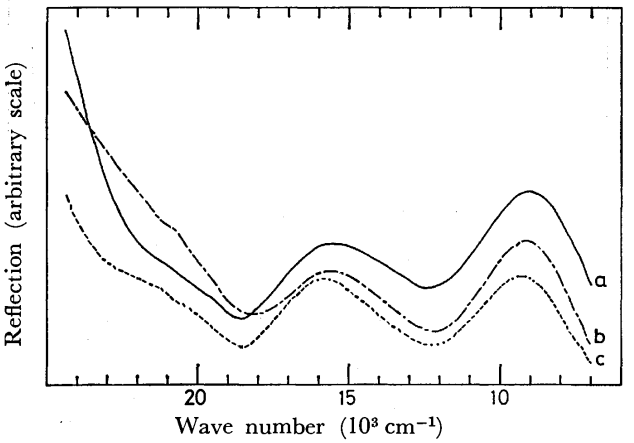

Fig. 5. The reflection spectra of complexes **9**(a), **3**(b), and **6**(c).

The reflection spectra of Complexes **9**, **3**, and **6** in the 20—7 kK region exhibit bands at 9.0 and 15.5 kK; 9.2 and 15.6 kK, and 9.3 and 15.8 kK respectively. The order of the increasing wave numbers of the bands is consistent with the order of the increasing ligand-field strength of the base, (4-CN-py<py<4-Me-py). The spectra and the observed magnetic moments of **3**(3.17 B.M.), **6**(3.23 B.M.), and **9**(3.16 B.M.) suggest that these complexes are octahedral.

The authors wish to express their thanks to Dr. Shunji Utsuno of Shizuoka University for lending the facilities for the measurement of the reflection spectra. We would also like to thank Miss Noriko Onishi and Miss Sachiko Takahara for their experimental assistance. The present work was partially supported by a Grant-in-Aid for Scientific Research from the Ministry of Education.

References

1) H. Morita, S. Shimomura, and S. Kawaguchi, *Bull. Chem. Soc., Jpn.*, **49**, 2461 (1976).
2) H. Morita, H. Sakurai, S. Shimomura, and S. Kawaguchi, *Transition Metal Chem.*, **2**, 210 (1977).
3) H. Morita, S. Shimomura, and S. Kawaguchi, 27th Symposium on the Chemistry of Metal Coordination Compounds, Nagano, Sept., 1977.
4) B. N. Figgis and R. S. Nyholm, *J. Chem. Soc.*, **1958**, 4190.
5) N. S. Gill, R. H. Nutall, D. E. Saife, and D. W. A. Sharp, *J. Inorg. Nucl. Chem.*, **18**, 79 (1961).
6) R. V. Biagetti and H. M. Haendler, *Inorg. Chem.*, **5**, 383 (1966).
7) R. J. H. Clark and C. S. Williams, *Inorg. Chem.*, **4**, 350 (1965).
8) N. S. Gill and H. J. Kingdon, *Aust. J. Chem.*, **19**, 2197 (1966).
9) F. Farha and R. T. Iwamoto, *Inorg. Chem.*, **4**, 844 (1965).
10) R. A. Walton, *J. Inorg. Nucl. Chem.*, **28**, 2229 (1966).
11) L. C. Nathan, *J. Chem. Educ.*, **51**, 285 (1974).
12) I. S. Ahuja and R. Singh, *J. Inorg. Nucl. Chem.*, **36**, 1505 (1974).
13) K. Nakamoto, C. Udovich, and J. Takemoto, *J. Am. Chem. Soc.*, **93**, 3973 (1970).
14) T. J. Batterham, "NMR Spectra of Simple Heterocycles," John Wiley & Sons, New York (1973), Chap. 2.
15) D. P. Graddon and D. G. Weeden, *Aust. J. Chem.*, **16**, 980 (1963).
16) R. L. Carlin, "Transition Metal Chemistry," Marcel Dekker, New York (1965), Vol. 1, p. 20.
17) P. Paoletti and M. Ciampolini, *Inorg. Chem.*, **6**, 64 (1967).

The Computer-assisted Characterization of Terpenes and Related Compounds by the Use of Combined Spectrometric Data

Shin-ichi SASAKI,* Hidetsugu ABE,*** Keiji SAITO,** and Yoshiaki ISHIDA**
Miyagi University of Education, Aoba, Sendai 980
(Received April 10, 1978)

Basic research to prepare a combined retrieval system based on three different sets of spectrometric data, infrared, mass, and ^{1}H NMR, for terpenes and related compounds is described. The system may be used either for searching all three types of spectra, for two, or for one only. The results of 112 test searches are presented. The combined method is proved to be a good tool for the identification of such compounds, especially those in a structurally close relationship.

A number of search systems for the structure characterization of chemical compounds have been reported, but most of them are designed for a single type of spectra.[1-29] However, to improve the possibility of identification, several kinds of combined retrieval systems based on different spectrometric data have also been developed.[30-37] The present authors are doing basic research to make a new searching system combining three different sets of spectrometric data (NMR, IR, and MS) to characterize organic compounds as a link in the study of the CHEMICS system (a computer program system for the structural elucidation of organic compounds).[38] In this paper the identification of terpenes and the related compounds will be described. The spectrometric data of these compounds, which number over, 110, were taken from a spectral atlas;[39] all of the data were packed in a computer in the form of normalized data. The normalization of the spectrometric data was carried out in a manner to be described later. The sorting experiment was implemented by the successive comparison of one of the stored compounds with all of them. The results given by the combined comparison are shown to be completely reliable.

Data Base. Numerals, 1, 2, 3,···, and 112 were given for each terpene and related compound, as is shown in Table 1. Their NMR, IR, and mass spectra were normalized and recorded in a computer. The normalization of spectra was performed as follows: the NMR was converted into G and S values according to Eqs. 1 and 2, where G stands for the center of gravity of a whole spectrum, and S, the standard deviation of each signal to the center:[40]

$$G = \sum_{i=1}^{n} (W_i A_i) / \sum_{i=1}^{n} A_i, \quad (1)$$

$$S = \left(\sum_{i=1}^{n} (W_i - G)^2 A_i / \sum_{i=1}^{n} A_i \right)^{1/2}. \quad (2)$$

Here, A_i and W_i express the weight of the proton(s) and the position of the ith signal, respectively. For example, the NMR of β-selinene (101)(Fig. 1) is converted into $G(=1.778)$ and S $(=1.121)$.

The IR is normalized by expressing it with the positions and intensities of the absorption bands. The spectral region of 4000 to 650 cm^{-1} is divided into 18 main divisions, at 3200, 2800, 2300, 2000, 1900, 1800, 1700, 1600, 1500, 1400, 1300, 1200, 1100, 1000, 900, 800, and 700 cm^{-1}. Further, each division is divided into 10 equal parts to make subdivisions, 1—10. The position (P) of the strongest band in each division is expressed numerically with the number of the subdivision where the top of the band is located. To code the band intensity (I), the following equations (Eqs. 3 and 4) are necessary to convert the apparent transmittance (T) into A' *via* the pesudo absorbance (A):

$$A = -\log T \quad (3)$$

$$A' = A/A_{max} \times 100 \quad (4)$$

Here, T, A, and A_{max} stand for the apparent transmittance based on the base line of the spectral chart, the pseudo absorbance, and the intensity of the strongest band in the whole spectrum respectively. The numerals 1, 2, and 3 are given for the intensity (I) when $A' \leqq 30$, $30 < A' \leqq 70$, and $A' > 70$ respectively.

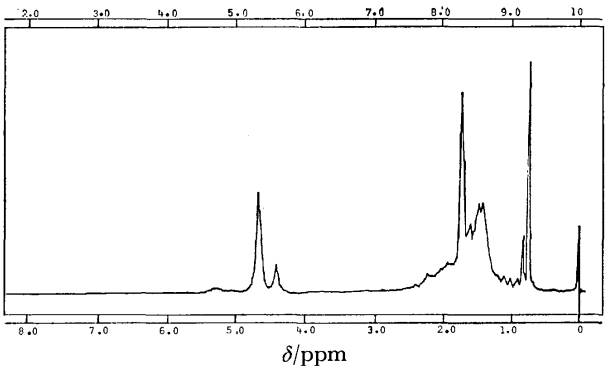

Fig. 1. NMR of β-selinene.

A line of numerals is given for the IR of β-selinene (101)(Fig. 2) as follows: 0 307 102 0 0 0 103 206 0 206 203 104 106 106 107 303 103 110. In numeral 307, the first figure 3 stands for the intensity and the last figure 7 the location of the strongest band in the division of 3200—2800. A band located just on the boundary is regarded as being in the higher division.

The mass spectrum was normalized by expressing it with the position and intensity of the two most intense peaks at 14 m.u. intervals, starting at m/e 40. To express the intensity, 1, 2, and 3 are given for the peak in accordance with its relative intensity, $\leqq 35\%$, $>35\%$ and $\leqq 75\%$, and $>75\%$, respectively. The mass spectrum of β-selinene (101)(Fig. 3) was converted into a numerically normalized state as follows: 413 131 532 552 672 691 793 813 912 933 1053 1073 1192 1212 1332 1351 1472 1491 1612 1751

** Present Address: Ube Industries Ltd., Ube, Yamaguchi 755.
*** Present Address: Toyohashi University of Technology, Tempaku, Toyohashi, Aichi 440.

Table 1. Results given by the use of either three types of spectra, two, or one only
(N, I, and M stand for the ^1H NMR, IR, and mass spectrometric data, respectively.
The numeral in each column indicates the number of noise(s).[a])

No.	Compound	N	I	M	N+I	N+M	I+M	N+I+M
1	Acoradiene	0	5	1	0	0	0	0
2	Anethole	0	0	0	0	0	0	0
3	Angelic acid	0	0	1	0	0	0	**0**
4	Aromadendrene	2	0	7	0	0	0	0
5	Ascaridole	0	0	0	0	0	0	0
6	Auraptene	0	0	0	0	0	0	0
7	β-Bisabolene	0	4	2	0	0	0	0
8	Borneol	1	0	1	0	0	0	0
9	Bornyl acetate	2	0	1	0	1	0	0
10	Isobornyl acetate	3	0	1	0	1	0	0
11	Calamenene	0	0	0	0	0	0	0
12	Camphene	0	0	6	0	0	0	0
13	Camphor	2	2	2	1	0	0	0
14	3-Carene	0	2	4	0	0	1	0
15	*cis*-Carveol	1	4	0	1	0	0	0
16	*trans*-Carveol	0	4	0	0	0	0	0
17	*d*-Carvone	0	1	0	0	0	0	0
18	Carvotanacetone	2	0	1	0	0	0	0
19	Caryophyllene	0	0	8	0	0	0	0
20	α-Cedrene	2	3	1	0	0	0	0
21	Cedrol	0	1	0	0	0	0	0
22	β-Chamigrene	0	3	2	0	0	1	0
23	1,4-Cineol	0	3	1	0	0	0	0
24	1,8-Cineol	0	0	1	0	0	0	0
25	Citronellal	0	0	0	0	0	0	0
26	β-Citronellol	0	3	2	0	0	0	0
27	α-Copaene	2	2	0	0	0	0	0
28	Cuparene	0	0	0	0	0	0	0
29	*p*-Cymene	0	1	1	0	0	1	0
30	Dihydroactinidiolide	1	1	0	0	0	0	0
31	Dihydrocarvone	0	0	0	0	0	0	0
32	Diosphenol	0	0	0	0	0	0	0
33	β-Elemene	0	2	5	0	0	1	0
34	Elemol	0	0	4	0	0	0	0
35	Eucarvone	0	0	2	0	0	0	0
36	β-Eudesmol	2	0	0	0	0	0	0
37	Eugenol	0	0	1	0	0	0	0
38	Isoeugenol	0	0	1	0	0	0	0
39	Farnesol	0	1	0	0	0	0	0
40	Fenchone	0	0	0	0	0	0	0
41	Fenchyl alcohol	2	5	0	0	0	0	0
42	Geraniol	0	2	0	0	0	0	0
43	Guaiazulene	0	0	0	0	0	0	0
44	3-Hexen-1-ol	—	0	0	—	—	0	—
45	α-Humulene	0	0	0	0	0	0	0
46	Hydroxycitronellol	2	0	0	0	0	0	0
47	Isoimperatorin	0	0	0	0	0	0	0
48	α-Ionone	0	4	0	0	0	0	0
49	β-Ionone	0	1	0	0	0	0	0
50	α-Irone	1	0	0	0	0	0	0
51	Hinokitiol	0	0	0	0	0	0	0
52	Lavandulol	1	3	1	1	0	0	0
53	α-Limonene	0	5	4	0	0	0	0
54	Linalool	0	5	4	0	0	0	0

Table 1. (Continued)

No.	Compound	N	I	M	N+I	N+M	I+M	N+I+M
55	*cis*-Linalool oxide	0	0	2	0	0	0	0
56	*trans*-Linalool oxide	0	0	2	0	0	0	0
57	Linalyl acetate	0	2	3	0	0	0	0
58	Longifolene	0	1	6	0	0	0	0
59	Maltol	0	0	0	0	0	0	0
60	Mayurone	0	0	0	0	0	0	0
61	1,8-Menthanediol hydrate	0	0	0	0	0	0	0
62	Menthofuran	0	0	1	0	0	0	0
63	Isomenthol	0	3	4	0	0	2	0
64	l-Menthol	3	3	3	0	0	2	0
65	Neomenthol	1	2	3	0	0	2	0
66	Neoisomenthol	1	4	4	0	0	0	0
67	Menthone	2	4	1	1	0	0	0
68	Isomenthone	0	4	1	0	0	0	0
69	Methyl anthranilate	0	0	0	0	0	0	0
70	2-Hydroxy-3-methyl-2-cyclopenten-1-one	0	0	0	0	0	0	0
71	6-Methyl-5-hepten-2-one	0	3	2	0	0	0	0
72	Myrcenol	1	1	2	0	0	0	0
73	Myristicin	0	0	0	0	0	0	0
74	Myrtenal	0	0	2	0	0	0	0
75	Myrtenol	0	1	1	0	0	0	0
76	Nerol	0	3	10	0	0	0	0
77	Nerolidol	0	1	1	0	0	0	0
78	Nezukone	0	0	0	0	0	0	0
79	1-Nonene	0	0	0	0	0	0	0
80	Nootkatone	1	1	0	0	0	0	0
81	Occidentalol	0	0	0	0	0	0	0
82	Ocimene	0	0	5	0	0	0	0
83	1-Octen-3-ol	0	1	0	0	0	0	0
84	α-Patchoulene	2	1	0	0	0	0	0
85	β-Patchoulene	1	0	1	0	0	0	0
86	γ-Patchoulene	2	4	4	0	0	1	0
87	Patchouli alcohol	0	2	5	0	0	0	0
88	Perillaldehyde	0	0	3	0	0	0	0
89	Perillyl alcohol	0	1	3	0	0	0	0
90	α-Pinene	2	1	6	0	0	1	0
91	β-Pinene	0	2	9	0	0	0	0
92	Isopinocamphone	0	3	1	0	0	0	0
93	Piperitenone oxide	0	1	0	0	0	0	0
94	Piperitone	0	1	1	0	0	0	0
95	Piperonal	0	0	0	0	0	0	0
96	Pulegone	0	2	0	0	0	0	0
97	*cis*-Rose oxide	0	1	1	0	0	0	0
98	*trans*-Rose oxide	0	1	1	0	0	0	0
99	Sabinene hydrate	1	3	5	0	0	0	0
100	Safrole	0	0	0	0	0	0	0
101	β-Selinene	1	9	8	0	0	3	0
102	α-Terpinene	1	2	3	0	0	0	0
103	γ-Terpinene	1	1	1	0	0	1	0
104	Terpinen-4-ol	0	5	2	0	0	0	0
105	α-Terpineol	1	6	1	0	0	0	0
106	β-Terpineol	0	4	2	0	0	0	0
107	Thyjopsene	1	0	3	0	0	0	0
108	Thymol	0	0	0	0	0	0	0
109	Tiglic acid	0	0	1	0	0	0	0

TABLE 1. (Continued)

No.	Compound	N	I	M	N+I	N+M	I+M	N+I+M
110	Valeranone	0	0	0	0	0	0	0
111	Vanillin	0	0	0	0	0	0	0
112	Verbenone	0	4	0	0	0	0	0
	Maximum of noise	3	9	10	1	1	3	0
	Minimum of noise	0	0	0	0	0	0	0
	Sum total of noise	48	151	177	4	2	14	0
	Average	0.432	1.348	1.580	0.036	0.018	0.125	0.000

a) Noise stands for an inappropriate response for the sample taken.

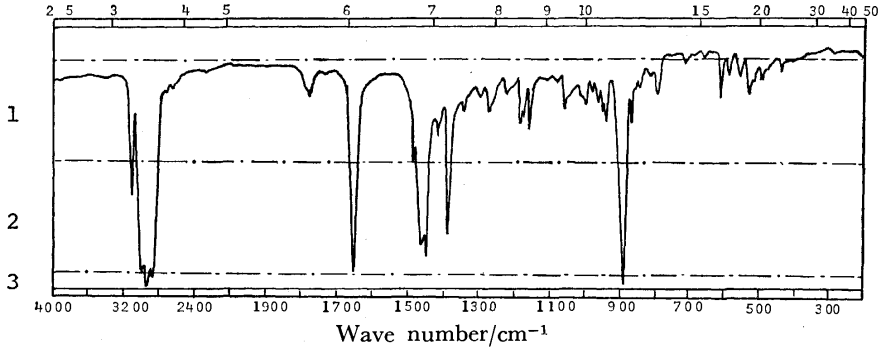

Fig. 2. IR of β-selinene.

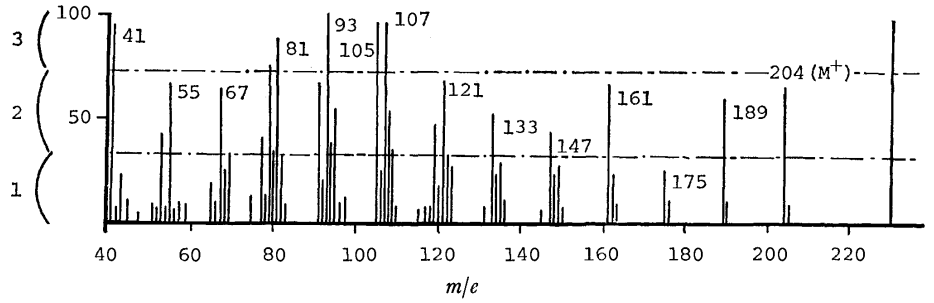

Fig. 3. MS of β-selinene.

1761 1892 1901 2042 2051. The last figure of each numeral indicates the intensity.

These normalized data of the NMR, IR, and MS of each compound are stored, with its code number (instead of compound name) in the computer.

Comparison of Spectra. On NMR comparison, when the conditions of $|G_y-G_x| \leqq 0.03$ and $|S_y-S_x| \leqq 0.04$ are satisfied, the x spectrum is judged to be equal to the y spectrum, where G_x and G_y mean the G values, and where S_x and S_y mean the S values, of the x and y spectra, respectively.

A parameter (E) defined by Eq. 5 is used for the IR comparison, where P_{xi} and P_{yi} mean the position of the strongest band in the ith main division of a

$$E = \sum_i |P_{xi}-P_{yi}| \quad (5)$$

spectrum registered in the file, and that of the spectrum to be compared, respectively. When two spectra were compared, another parameter (M) was also used; this parameter represents the sum of the main divisions which have similar P values but different I values. As the most appropriate value, 20 for E and 6 for M are chosen by trial and error.

Two kinds of parameters (D and Q) are used in the MS comparison. D is the number of peaks which have a similar mass but a different intensity in the comparison of an unknown with each of the stored compounds. Q is the number of peaks which are lacking in the spectrum of an unknown but which are present in that of to be compared. The spectra of 10 compounds collected arbitrarily were measured at several different conditions in order to decide the most appropriate threshold values of D and Q. As a result, it was observed that D is distributed within the range from 0 to 3, and Q, within that from 0 to 4. Thus, taking a sufficient allowance into account, 5 and 7 were selected as the threshold values of D and Q, respectively. When D and Q are observed to be below the thresholds in the sorting upon MS, the two spectra are regarded as identical.

Results

The data base consists of terpenes and related compounds. They are in a structurally close relationship with each other, and a similar type of pattern

is observed for their spectra in many cases. If sorting can discriminate one spectrum from all the other spectra in the system containing such kinds of compounds, the method may be considered to be a good tool for structure identification. Indeed, the sorting by the combined spectrometric data of NMR, IR, and MS gave excellent results.

Table 1 shows the sorting results afforded by the use of either all three types of spectra, of two, or of one only. As is shown in the table, one completely correct compound is retrieved by sorting either NMR, IR, or MS alone for almost one-third (2, 5, 6, 11, 25, 28, 31, 32, 40, 43, 44, 45, 47, 51, 59, 60, 61, 69, 70, 73, 78, 79, 81, 95, 100, 108, 110, and 111) of the registered compounds. The remaining two-thirds are contaminated with noise(s) when sorted with a single set of spectrometric data. However, the number of these compounds accompanied by contamination rapidly diminishes by sorting with either two or three types of spectra. For example, compound 101 is contaminated with one (145), nine (3, 15, 31, 33, 45, 67, 107, 173, and 183), and eight (9, 39, 45, 67, 117, 173, and 175) noises by sorting with only NMR, IR, or MS respectively. However, sorting with two types of spectra (NMR+IR, NMR+MS) gives no noise, though sorting with IR and MS gives three noises (45, 67, 173). Furthermore, as is shown in the most right column of Table 1, when three types of spectra are used, only one correct answer is always obtained for all compounds. The fact that nothing was retreived when three types of spectra of α-pseudowiddrene, which had not yet been registered in the data base, were compared with the store also proves the authors' method to be completely reliable.

References

1) R. A. Sparks, "Storage and Retrieval of WYANDOTTE-ASTM Infrared Spectral Data Using an IBM 1401 Computer," American Society for Testing Materials, Philadelphia, Pa. (1964).
2) D. H. Anderson, and G. L. Covert, *Anal. Chem.*, **39**, 1288 (1967).
3) D. S. Erley, *Anal. Chem.*, **40**, 894 (1968).
4) F. E. Lytle and T. L. Brazie, *Anal. Chem.*, **42**, 1532 (1970).
5) G. A. Massios, *Am. Lab.*, **3**, 55 (1971).
6) R. W. Sebasta and G. G. Johnson, Jr., *Anal. Chem.*, **44**, 260 (1972).
7) C. S. Rann, *Anal. Chem.*, **44**, 1669 (1972).
8) J. Zupan, D. Hadzi, and M. Penca, *Kem. Ind.*, **23**, 275 (1974).
9) E. C. Penski, D. A. Padowski, and J. B. Bouck, *Anal. Chem.*, **46**, 955 (1974).
10) K. Schaarschmidt, R. Riemer, and E. Steger, *Z. Chem.*, **14**, 374 (1974).
11) H. B. Woodruff, S. R. Lowry, and T. L. Isenhour, *J. Chem. Inf. Comput. Sci.*, **15**, 207 (1975).
12) R. C. Fox, *Anal. Chem.*, **48**, 717 (1976).
13) J. Zupan, D. Hadzi, and M. Penca, *Comput. Chem.*, **1**, 71 (1976).
14) E. M. Kirby, R. N. Jones, and D. G. Cameron, *CODATA Bull.*, **21**, 18 (1976).
15) J. Zupan, J. T. Clerc, and D. Hadzi, *Vestn. Slov. Kem. Drus.*, **23**, 73 (1976).
16) B. Pettersson and R. Ryhage, *Ark. Kemi.*, **26**, 293 (1967).
17) L. R. Crawford and J. D. Morisson, *Anal. Chem.*, **40**, 1464 (1968).
18) S. L. Grotch, *Anal. Chem.*, **42**, 1214 (1970).
19) B. A. Knock, I. C. Smith, D. E. Wright, R. G. Ridley, and W. Kelly, *Anal. Chem.*, **42**, 1526 (1970).
20) H. S. Hertz, R. A. Hites, and K. Beiemann, *Anal. Chem.*, **43**, 681 (1971).
21) S. L. Grotch, *Anal. Chem.*, **43**, 1362 (1971).
22) L. E. Wangen, W. S. Woodward, and T. L. Isenhour, *Anal. Chem.*, **43**, 1605 (1971).
23) S. R. Heller, "DCRT/CIS, MSSS User's Manual," Division of Computer Research and Technology, Bethesda, Md. (1972).
24) S. R. Heller, *Anal. Chem.*, **44**, 1951 (1972).
25) S. R. Heller, H. M. Fales, and G. W. A. Milne, *Org. Mass Spectrom.*, **7**, 107 (1973).
26) S. L. Grotch, *Anal. Chem.*, **45**, 2 (1973).
27) P. R. Naegeli and J. T. Clerc, *Anal. Chem.*, **45**, 739A (1974).
28) R. Schwarzenbach, J. Meili, H. Konitzer, and J. T. Clerc, *Org. Magn. Res.*, **8**, 11 (1976).
29) R. J. Feldman, S. R. Heller, K. P. Shapiro, and R. S. Heller, *J. Chem. Doc.*, **12**, 41 (1972).
30) J. T. Clerc, C. Jost, T. Meier, and R. Schwarzenbach, *Chimia*, **27**, (12) 665 (1973).
31) J. T. Clerc and F. Erni, *Top. Curr. Chem.*, **39**, 91 (1973).
32) J. T. Clerc, "Computers in Chemical Research and Education, Proceedings," D. Hadzi, ed, Elsevier Publishing Co., Amsterdam (1973), Vol. 2, pp. 3/109.
33) L. A. Gribov, V. A. Dementyev, M. E. Elyashberg, and E. Z. Yakupov, *J. Mol. Struct.*, **22**, 161 (1974).
34) V. A. Koptyug, *Z. Chem.*, **15**, 41 (1975).
35) N. A. Gray, *Anal. Chem.*, **47**, 2426 (1975).
36) The NIH-EPA Chemical Information Systems, Status Report No. 4, Dec., 1976.
37) J. Zupan, M. Penca, D. Hadzi, and J. Marsel, *Anal. Chem.*, **49**, 2145 (1977).
38) S. Sasaki, Y. Kudo, H. Abe, and T. Yamasaki: "Computer-assisted Structure Elucidation," ACS Symposium Series, (1977), No. 54, p. 108.
39) "Spectral Atlas of Terpenes and the Related Compounds," ed by Y. Yukawa and Sho Ito, Hirokawa Publishing Co., Tokyo (1973).
40) S. Sasaki, Y. Yotsui, and S. Ochiai, *Bunseki Kagaku*, **24**, 213 (1975).

Phase Equilibria in Europium(III) Oxide–Titanium(IV) Oxide System at Temperatures from 900 to 1400 °C

Bunji Iwasaki

Research Institute of Underground Resources, Mining College, Akita University, Tegata-Gakuen machi, Akita 010

(Received April 13, 1978)

The phase equilibria in the Eu_2O_3–TiO_2 system has been established at temperatures from 900 to 1400 °C in air using coprecipitated gels as starting materials. In this system, Eu_2O_3, TiO_2, Eu_2TiO_5, and $Eu_2Ti_2O_7$ are stable. The stoichiometric $Eu_2Ti_2O_7$ has a cubic pyrochlore type structure with $a=1.0210(3)$ nm, and forms a solid solution with TiO_2. The TiO_2 contents and the lattice constants of these solid solutions equilibrated with TiO_2 at different temperatures were [given as mol %, a/nm, θ/°C]: 70.4(5), 1.0187(1), 1409(9); 69.5(5), 1.0193(1), 1292(8); 68.9(5), 1.0197(1), 1191(9); 68.4(5), 1.0200(1), 1099(2); 68.1(5), 1.0202(1), 996(4); and 68.0(5), 1.0203(1), 898(3). Numbers in parentheses are errors in the last digits.

Europium(II) titanium(IV) trioxide (perovskite type), $EuTiO_3$, is an interesting compound in field of inorganic chemistry and geochemistry, because it forms an extensive solid solution with respect to oxygen.[1] It may be used as an oxygen barometer, according to the principle that it is formed from dieuropium(III) dititanium(IV) heptaoxide, $Eu_2Ti_2O_7$, at a given temperature and oxygen fugacity.[2] In order to furnish thermodynamic data on the $EuTiO_3$ solid solution at high temperatures, a phase diagram for the system europium(III) oxide[3]–titanium(IV) oxide[4] is required. This binary system has not been systematically studied, while the europium–titanium–oxygen system at 1400 °C including this binary system has been reported McCarthy *et al.*[1] On the other hand, dieuropium(III) titanium(IV) pentaoxide, Eu_2TiO_5,[5] and $Eu_2Ti_2O_7$[6] have been observed in this binary system.

The purposes of this study are to establish the phase relations in this binary system in the temperature range between 900 and 1400 °C in air, to determine the solubility of titanium(IV) oxide in $Eu_2Ti_2O_7$, and to obtain the phase diagram of this binary system.

Experimental

Materials. The samples prepared by the coprecipitation method were used as starting materials. Both the stock solutions of europium and titanium were prepared separately as follows: (i) the freshly ignited Eu_2O_3 having a purity of 99.9% was dissolved in conc. hydrochloric acid; (ii) Guaranteed reagent-grade $TiCl_4$ was dissolved in 3 mol/dm^3 hydrochloric acid solution at a temperature below 65 °C.[7] Both the metals in the 1 mol/dm^3 hydrochloric acid solution prepared by mixing the stock solutions in the desired ratios were coprecipitated with aqueous ammonia. After being washed thoroughly with water, these coprecipitates were dried at about 100 °C for 12 h, heated at about 400 °C for 12 h, and finely ground by an agate mortar.

Furnaces and Temperature Control. Vertical tube quench furnaces with a 60%Pt-40%Rh winding were used for the equilibration runs.

Furnace temperatures were kept constant within the temperature range given in Table 1 by means of an electric controller activated by a Pt-(87%Pt-13%Rh) thermocouple inserted close to the hot spot of the furnace. The actual temperatures within the furnace were measured with the other thermocouple which was calibrated within ±0.5 °C against the melting points of diopside, 1394 °C, and gold, 1064 °C.

General Procedure. About 0.1-g powdered starting material was placed in a 60%Pt-40%Rh foil envelope, about 0.05 mm in thickness and 10×10 mm in area, and heated in air at the temperatures listed in Table 1. After heated during the reaction time given in Table 1, the samples were quenched rapidly to the temperature of ice by burning away the thin Pt wire with an electric current. In a single run, 10 or 12 charges were heated together by suspending these envelopes over the hooks of a 60%Pt-40%Rh wire netting.

Identification of Phases and Determination of Lattice Constants. The phases present in the starting materials and the quenched samples were identified by X-ray powder diffraction method using a scintillation counter diffractometer with Ni-filtered Cu $K\alpha$ radiation.

Lattice constants were determined by the same method with a scanning rate of 1/4° or 1/8° per min and with an internal standard of high-purity silicon.

Chemical Analysis. The titanium content in the titanium stock solution was determined by precipitating as titanium(IV) oxide hydrate in the presence of acetic acid, and igniting the precipitates to titanium(IV) oxide.

After the freshly ignited starting materials and the quenched samples were fused with potassium disulfate, the cold melt obtained was dissolved in sulfuric acid solution. The europium content in the sulfuric acid solution was determined by precipitating as europium(III) oxalate and igniting the precipitates to europium(III) oxide, while the titanium content in the solution was determined photometrically by the hydrogen peroxide method.[8]

Table 1. Temperature and reaction time

A group[a]		B group	
θ/°C	t/d	θ/°C	t/d
901±1	32.8	898±3	29.9
998±2	30.8	996±4	26.8
1100±1	19.8	1099±2	23.8
1209±10	14.9	1191±9	14.9
1295±6	9.9	1292±8	9.8
1406±6	7.9	1409±9	6.9

a) The samples with different chemical compositions were divided into two groups, according to the period when the samples were prepared. One group is composed of 10 or 12 samples heated together at constant temperature.

Table 2. Results of equilibration runs in the temp range between 900 and 1400 °C

No.[a]	Materials		Phase[b]
	TiO_2(mol %)	Eu_2O_3(mol %)	
B-1[c]	15.4	84.6	E + Y
B-2	30.6	69.4	E + Y
A-1	35.9	64.1	E + Y
B-3	49.8	50.2	Y
A-2	55.8	44.2	Y + P
A-3	57.8	42.2	Y + P
A-4	62.6	37.4	Y + P
B-4	67.4	32.6	Ps
A-5	72.4	27.6	Ps + R
A-6	74.2	25.8	Ps + R
A-7	77.1	22.9	Ps + R
A-8	81.4	18.6	Ps + R

a) The samples labeled as A and B, respectively, belong to A group and B group in Table 1. For example, the sample of A-1 was heated at the temperatures and for the reaction times given as A group in Table 1. b) E=Eu_2O_3, Y=Eu_2TiO_5, P=$Eu_2Ti_2O_7$, Ps=$Eu_2Ti_2O_7$ solid solution, R=TiO_2. c) Only one of the most intense reflections of Eu_2TiO_5 in addition to reflections of Eu_2O_3 was detected in the sample heated at 898 °C.

Results and Discussion

Reaction Time for Equilibration. According to preliminary experiments, in which, Eu_2TiO_5, the poorest crystalline substance in this system, was synthesized from oxide mixtures, trace amounts of $Eu_2Ti_2O_7$ and europium(III) oxide in addition to Eu_2TiO_5 were detected in the sample heated at 1200 °C for 13.6 d, and further heat treatment was necessary to obtain Eu_2TiO_5 as a single phase. Therefore, the samples prepared by the coprecipitation method were selected as starting materials in order to shorten the time of equilibration.

More than both phases were not detected in all the quenched samples obtained in this study (Table 2). Furthermore, Eu_2TiO_5 was definitely identified in all the quenched samples expected to contain this phase, except in the sample B-1 heated at 900 °C. Each reaction time listed in Table 1 is thought to be sufficient as the reaction time needed for equilibrium.

Chemical Composition. The ratios of europium to titanium in the starting materials were in agreement with those in the quenched samples within the limit of analytical errors. The chemical compositions of the samples listed in Table 2 are based on chemical analyses.

Phases in Starting Materials. Most of the starting materials indicated an amorphous condition. Small amounts of europium(III) chloride oxide, EuClO,[9] were identified in a few of the starting materials, *e.g.* B-3. The occurrence of this compound may be attributed to the thermal decomposition of europium(III) chloride dihydroxide, $EuCl(OH)_2$, precipitated from the mixtures of both the stock solutions. Trace amounts of $Eu_2Ti_2O_7$ were detected in few of them, *e.g.* B-7.

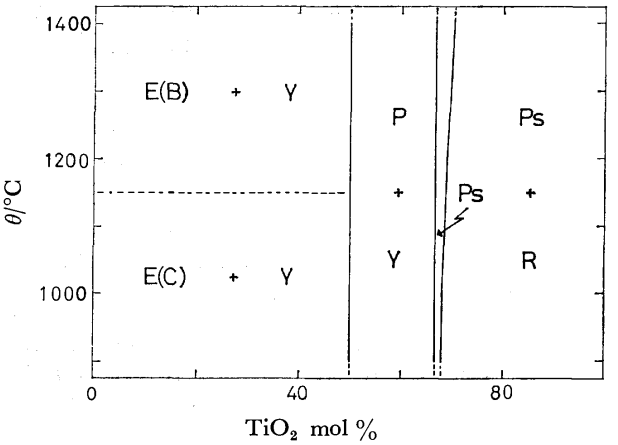

Fig. 1. Phase diagram for Eu_2O_3–TiO_2 system. Abbreviations are the same as those in Table 2 except for the followings: E(B)=Eu_2O_3(B-form), E(C)=Eu_2O_3 (C-form).

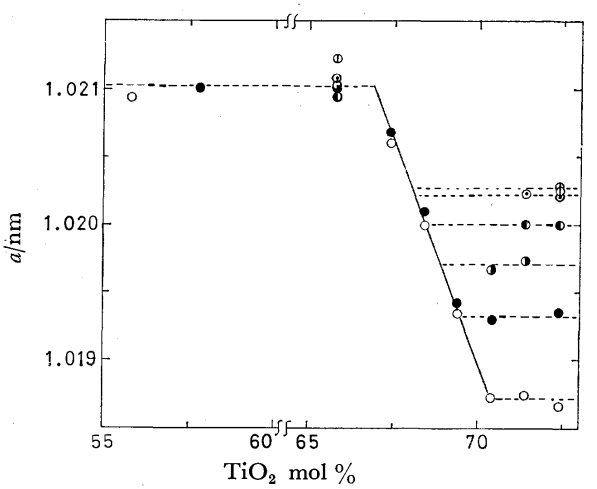

Fig. 2. Lattice constant, *a*, of $Eu_2Ti_2O_7$ solid solution *vs.* chemical composition.
○: 1409 °C, ●: 1292 °C, ◑: 1191 °C, ◐: 1099 °C, ⊙: 996 °C, ⓓ: 898 °C, ◔: 1409 and 1191 °C.

Phases and Phase Relations. The equilibrium data obtained at temperatures ranging from 900 to 1400 °C are summarized in Table 2, and illustrated graphically in Fig. 1 together with the addtiona data shown in Fig. 2.

In the present system, four compounds were stable: Eu_2O_3, TiO_2, Eu_2TiO_5, and $Eu_2Ti_2O_7$.

Europium(III) Oxide: This oxide[3] found in this study occurred in a cubic C-type form below 1100 °C, and crystallized in a monoclinic B-type structure above 1200 °C. Warshaw and Roy[10] have reported that trace amounts of the C-form were converted to the B-form after 30 h at 1105 °C. The present findings are compatible with their observations.

Titanium(IV) Oxide: The tetragonal rutile type structure of this oxide,[4] which is believed to be thermodynamically stable,[11] was observed under the present experimental conditions.

Dieuropium(III) Titanium(IV) Pentaoxide: This compound[5] found in this study had an orthorhombic

TiY_2O_5 type structure. The lattice constants were $a=1.054(1)$* nm, $b=1.133(1)$ nm, $c=0.376(1)$ nm, and $V=0.449$ nm^3, which is in good agreement with those reported by McCarthy *et al.*[5] ($a=1.054$ nm, $b=1.132$ nm, $c=0.378$ nm, and $V=0.451$ nm^3.)

The lattice constants of this compounds equilibrated with europium(III) oxide and with $Eu_2Ti_2O_7$ were identical with each other, irrespective of temperature. Therefore, there is the possibility that this compound is stoichiometric.

Dieuropium(III) Dititanium(IV) Heptaoxide: This compound[6] with a cubic pyrochlore type structure was stable in this study, and formed a solid solution with titanium(IV) oxide.

Figure 2 shows the relationship between the titanium(IV) oxide contents in the samples and the lattice constants of this solid solution. The lattice constants of this solid solution within the region for the coexistence of both $Eu_2Ti_2O_7$ and Eu_2TiO_5 phases were identical with each another within the limit of experimental errors, regardless of temperature. The datum was $a=1.0210(3)$ nm, while this compound has been reported to have a lattice constants of $a=1.0193$ nm.[6] The data within the $Eu_2Ti_2O_7$-stable region showed such a straight line as represented by the equation

$$a = 1.0648 - 0.0654X(TiO_2), \quad (1)$$

where a and $X(TiO_2)$, respectively, represent the lattice constant and the titanium(IV) oxide content given in mol% of $Eu_2Ti_2O_7$. The data on $Eu_2Ti_2O_7$ within the region for the coexistence of both $Eu_2Ti_2O_7$ and titanium(IV) oxide phases were identical with each other at constant temperature, and decreased with an increase in temperature.

The chemical composition of this solid solution equilibrated with Eu_2TiO_5 was calculated to be 66.9 mol%TiO_2, by substituting the a-value given above in Eq. 1, indicating good agreement with the stoichiometric value, 66.7 mol % TiO_2. The chemical compositions of these solid solutions equilibrated with titanium(IV) oxide at each temperature have been calculated according to the same treatment reported above, and illustrated in Fig. 1.

Solubility of Titanium(IV) Oxide in Dieuropium(III) Dititanium(IV) Heptaoxide. The equation for the solution of rutile in the pyrochlore phase may be written as

$$TiO_2(\text{rutile}) = TiO_2(\text{in pyrochlore}), \quad (2)$$

for which the equilibrium constant is

$$K = \frac{a(TiO_2)^p}{a(TiO_2)^r}, \quad (3)$$

where $a(TiO_2)^p$ and $a(TiO_2)^r$, respectively, indicates the activity of titanium(IV) oxide in the pyrochlore phase and in the rutile phase. As the rutile is considered to be pure, the activity of rutile may be taken as unity; also the solubility of rutile is low as given below, and the activity of titanium(IV) oxide in the pyrochlore phase may be assumbed to be proportional to the mole fraction, if Henry's law is applicable.

* Numbers in parentheses here and elsewhere are estimated experimental errors in limits of the last significant digit.

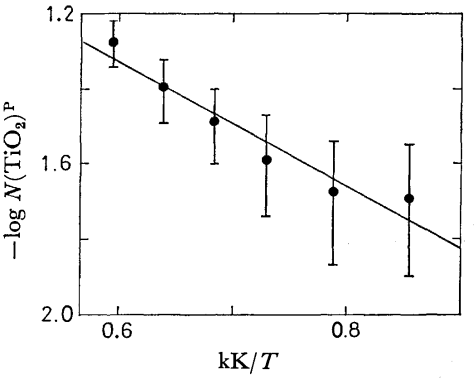

Fig. 3. Change of the solubility of TiO_2 in $Eu_2Ti_2O_7$ with temperature.

Hence,

$$K = kN(TiO_2)^p, \quad (4)$$

where k is the Henry's constant, and $N(TiO_2)^p$ denoted the mole fraction of titanium(IV) oxide in the pyrochlore phase.

The solubility of rutile in $Eu_2Ti_2O_7$, calculated from such chemical compositions of these solid solutions equilibrated with rutile as obtained above, are given as $N(TiO_2)^p$, θ/°C: 0.020(8), 898; 0.021(8), 996; 0.026(8), 1099; 0.033(8), 1191; 0.040(8), 1292; and 0.053(8), 1409. Figure 3 shows the relationship between temperature and the solubility of rutile in $Eu_2Ti_2O_7$. It may be seen from Fig. 3 that the amount of rutile increases with an increase in temperature, while a linear relationship exists between them, as predicted from the equation

$$\left[\frac{\partial \ln K}{\partial(1/T)}\right]_P = -\frac{\Delta H}{R}, \quad (5)$$

where T is the absolute temperature, P is the pressure, ΔH indicates the enthalpy change of Eq. 2, which corresponds to the relative partial enthalpy of solution,[12] and R is the gas constant. This line may be represented by the equation

$$\log N(TiO_2)^p = -\frac{1700}{T} - 0.33, \quad (6)$$

corresponding to $\Delta H=33(2)$ kJ.

The Phase Diagram. The present results obtained are shown as a phase diagram in Fig. 1. A comparison of this phase diagram with those of the systems M_2O_3–TiO_2 (M=La,[13] Gd,[13] Dy,[15] Yb[16]) shows that the present phase diagram is the most similar to that for the Gd_2O_3–TiO_2 system among them. The similarity in phase diagrams may be due to the similarity in ionic radii.

We wish to express our sincere thanks to Dr. Takashi Katsura, Professor of the Tokyo Institute of Technology for his encouragement throughout the present study.

References

1) G. J. McCarthy, W. B. White, and R. Roy, *J. Inorg. Nucl. Chem.*, **31**, 329 (1969).
2) B. Iwasaki, Abstr. C-11, Symposium on Geochemistry

held by the Geochemical Society of Japan, Tokyo, Oct. 1974.

3) V. M. Goldschmidt, F. Ulrich, and T. Barth, *Skrifter, Norske Videnskap-Akad. Oslo, (I), Mat. Naturv. Kl.*, No. 5, 5 (1925).

4) M. E. Straumanis, T. Ejima, and W. J. James, *Acta Crystallogr., Sect. B*, **14**, 493 (1961).

5) J. L. Waring and S. J. Schneider, *J. Res. Natl. Bur. Std.*, **69A**, 255 (1965); X-Ray powder data file, Card 22—1100, J. C. P. D. S.; *Cf.* Ref. 1.

6) L. H. Brixner, *Inorg. Chem.*, **3**, 1065 (1964).

7) N. Mizutani, A. Kitazawa, and M. Kato, *Nippon Kagaku Zasshi*, **1974**, 1623.

8) E. B. Sandell, "Colorimetric Determination of Traces of Metals," 3rd ed, Interscience Publishers Inc., New York (1959), p. 874.

9) X-Ray powder data file, Card 12—163, J. C. P. D. S.

10) J. Warshaw and R. Roy, *J. Phys. Chem.*, **65**, 2048 (1961).

11) L. Brewer, *Chem. Rev.*, **52**, 1 (1953).

12) G. N. Lewis and M. Randall, "Thermodynamics," revised by K. S. Pitzer and L. Brewer, McGraw-Hill Book Company, New York (1961), p. 393.

13) J. B. MacChesney and H. A. Sauer, *J. Am. Ceram. Soc.*, **45**, 416 (1962).

14) F. Queyroux, *Bull. Soc. Fr. Mineral. Cristallogr.*, **86**, 295 (1963); *Cf.* Ref. 5.

15) F. Queyroux, *C. R. Acad. Sci.*, **259**, 1527 (1964).

16) F. Queyroux, *Bull. Soc. Fr. Mineral. Cristallogr.*, **88**, 521 (1965).

X-Ray Diffraction Studies on the Structures of Tetraammine- and Triamminemonochlorozinc(II) Ions in Aqueous Solution

Toshio YAMAGUCHI and Hitoshi OHTAKI*

Department of Electronic Chemistry, Tokyo Institute of Technology at Nagatsuta, Nagatsuta-cho, Midori-ku, Yokohama 227

(Received April 14, 1978)

X-Ray scattering measurements have been carried out on ammoniacal aqueous solutions of zinc(II) chloride at the NH_3/Zn mole ratios of 3.8, 5.0, and 6.6. The radial distribution curves show that the tetraamminezinc(II) complex is formed as the main species, the ammonia molecules within the complex being tetrahedrally coordinated to zinc(II) ion at a distance of (2.03±0.02) Å. Analysis of the radial distribution curve obtained for the solution at the NH_3/Zn ratio of 3.8 indicates formation of the mixed complex $ZnCl(NH_3)_3^+$, the Zn–NH_3 and Zn–Cl bond lengths being (2.00±0.03) and (2.30±0.03) Å, respectively.

According to the results of formation constants,[1] enthalpic and entropic measurements[1] and spectrophotometry,[2] a zinc(II) ion combines with four ammonia molecules at most, the structure of the tetraamminezinc(II) complex presumably being in a tetrahedral form. However, no X-ray crystallographic data are available because of the difficulty in the preparation of a stable single crystal.

In the present investigation we have attempted to determine the structure of the tetraamminezinc(II) complex as well as other zinc(II)–ammine complexes in ammoniacal aqueous solutions with various NH_3/Zn mole ratios (3.8, 5.0, and 6.6) by the X-ray diffraction method. Raman spectroscopic measurements were also carried out as a supplement to the structural determination of the main complex.

Experimental

Preparation and Analysis of Sample Solutions. The sample solutions were prepared by dissolving zinc(II) chloride (Wako Pure Chemicals, Co., reagent grade), which had been recrystallized twice from water, in a concentrated aqueous ammonia solution (Wako Pure Chemicals, Co., reagent grade, 28%). The concentration of ammonia was adjusted to the desired value by introducing gaseous ammonia (99.99%) into the sample solutions.

The concentration of zinc(II) ion was determined by EDTA titration and electrogravimetry. The results obtained by the two methods were found to agree with each other within 0.2%. Ammonia content in the sample solutions was determined by the Kjeldahl method. Concentration of the chloride ion was determined from the stoichiometry of the zinc(II) chloride.

The density of the solutions was determined pycnometrically.

The composition of the sample solutions is given in Table 1.

X-Ray Scattering Measurements. X-Ray scattering measurements were carried out by using a θ-θ JEOL diffractometer in a room thermostated at (25±1) °C. Mo $K\alpha$ Radiation (λ=0.7107 Å) was used. The diffracted beam was monochromatized with a Johansson-type LiF crystal and then a pulse height analyzer. The accessible range of scattering angle (2θ) was 2—140°, corresponding to the range 0.31 Å^{-1}<s<16.6 Å^{-1} ($s=4\pi\lambda^{-1}\sin\theta$). The time required for counting 40000 counts was recorded at each angle. The measurements over the whole angle range were carried out twice for each solution. The divergence of the measured intensities was within ±2%. The average intensities thus measured at each scattering point were used in the subsequent calculations. Details of the measurements are described in previous papers.[3,4]

Raman Spectroscopic Measurements. Raman spectra for the sample solutions were measured with a JEOL laser Raman spectrophotometer JRS-S1 with use of the 4880 Å excited line of Ar^+ laser.

Treatment of Intensity Data. The measured intensities $I(s)$ were corrected in the usual way for absorption and polarization of the X-ray beam.[3-5] The corrected intensities were normalized to electron units by the conventional methods,[6,7] from which the incoherent scatterings $\sum n_i\phi(s)I_i^{inco}(s)$ were subtracted (n_i=the number of atom i, $\phi(s)$=the fraction of the incoherent radiation reaching the counter). The Breit-Dirac effect was taken into account. Correction for double scattering[8] was made, which did not exceed 4% of scattered intensities of solutions investigated. The values of coherent, incoherent and anomalous scatterings of all atoms were the same as those used previously[9] except for N, the values of which were taken from the literature.[10] The coherent intensities $I^{coh}(s)$ thus obtained are shown in Fig. 1 for each sample solution.

The radial distribution function $D(r)$ was calculated by

$$D(r) = 4\pi r^2\rho_0 + \frac{2r}{\pi}\int_0^{s_{max}} si(s)M(s)\sin(rs)\mathrm{d}s, \qquad (1)$$

where ρ_0 is the average scattering density in the stoichiometric volume V containing one Zn atom, s_{max} the maximum s-value attained in the measurements (s_{max}=16.7 Å^{-1}). $M(s)$ represents the modification function

$$[\sum n_i\{(f_i(0)+\Delta f_i')^2+(\Delta f_i'')^2\}/\sum n_i\{(f_i(s)+\Delta f_i')^2 + (\Delta f_i'')^2\}]\exp(-0.01s^2), \qquad (2)$$

where $f_i(0)$ and $f_i(s)$ denote the scattering factors of atom i at angle 0 and s, respectively. $\Delta f_i'$ represents the real part of the anomalous dispersion, whereas $\Delta f_i''$ is the imaginary one. The reduced intensity $i(s)$ is given by

$$i(s) = I^{coh}(s) - \sum n_i\{(f_i(s)+\Delta f_i')^2+(\Delta f_i'')^2\}. \qquad (3)$$

Before the Fourier transform, the reduced intensities experimetally obtained were smoothed by use of spline function.[11] Spurious peaks appearing below 1 Å in the radial distribution curves were eliminated by the reported method.[9] Curve (a) in Fig. 2 represents the $(D(r)-4\pi r^2\rho_0)$ curve obtained by a Fourier transform of the reduced intensities of solution C after a correction for only spurious peaks within the hard-core radius (<1 Å). The curve still shows periodic ripples in the range of large r values. The ripples were eliminated when the intensity data were further corrected by the smoothing procedure (Fig. 2, curve (b)). Thus, the data-smoothing procedure in combination with a hard-core correction is needed to correct spurious peaks in $D(r)$

TABLE 1. THE COMPOSITION (g-atoms/dm³) AND STOICHIOMETRIC VOLUME V PER ZINC ATOM IN THE SOLUTIONS

Solution	Zn	Cl	N	O	H	$\frac{NH_3}{Zn}$	$\frac{V}{Å^3}$	Density / g cm^{-3}
A	2.679	5.359	10.09	37.99	106.3	3.8	619.7	1.217
B	2.364	4.727	11.79	32.30	99.96	5.0	702.4	1.170
C	2.217	4.434	14.66	32.61	109.2	6.6	749.0	1.139

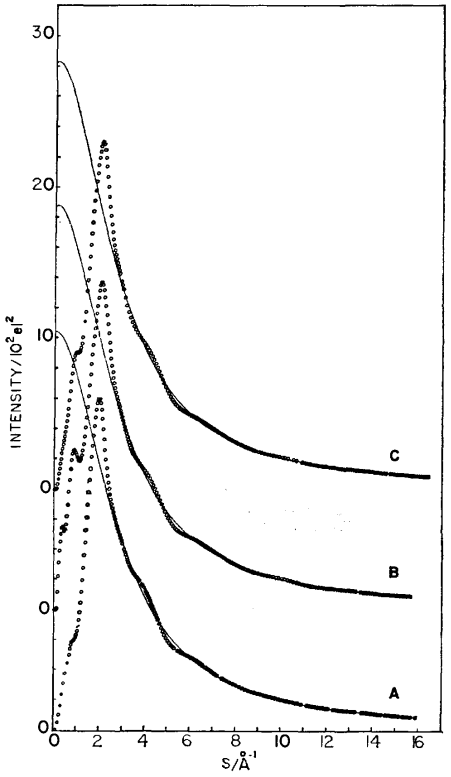

Fig. 1. X-Ray diffraction patterns for the sample solutions A, B, and C. Experimental coherent scattering intensities $I^{coh}(s)$ are shown by circles and calculated independent scattering intensities by solid lines.

curves over the whole angle range measured. It should be noted that the smoothing procedure leads sometimes to erroneous results when the intervals between data points are large. The separation between the points should be less than 0.3 Å^{-1} in s. For solutions containing heavy atoms the smoothing correction for the scattered intensities might be unnecessary.

The $s\cdot i(s)$, $D(r)$, and $(D(r)-4\pi r^2\rho_0)$ curves obtained after the smoothing correction are shown in Figs. 3, 4, and 5, respectively, for each solution.

The theoretical peak shape of an atom pair i-j was estimated from the calculated reduced intensity:

$$i_{calc}(s) = n_{ij}\{(f_i(s)+\Delta f_i')(f_j(s)+\Delta f_j')+(\Delta f_i'')(\Delta f_j'')\} \times \frac{\sin(r_{ij}s)}{(r_{ij}s)}\exp(-b_{ij}s^2), \quad (4)$$

where r_{ij}, b_{ij}, and n_{ij} denote the distance, the temperature factor and the frequency factor of the atom pair i-j, respectively.

All calculations were performed with the aid of electronic computers HITAC 8700 and M 180 by means of the KUR-VLR program.[12]

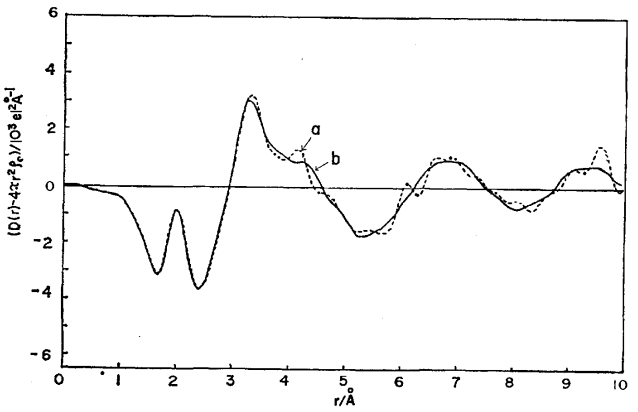

Fig. 2. The $(D(r)-4\pi r^2\rho_0)$ curves obtained after the hard-core correction alone (curve (a)) and further data-smoothing correction (curve (b)) for solution C.

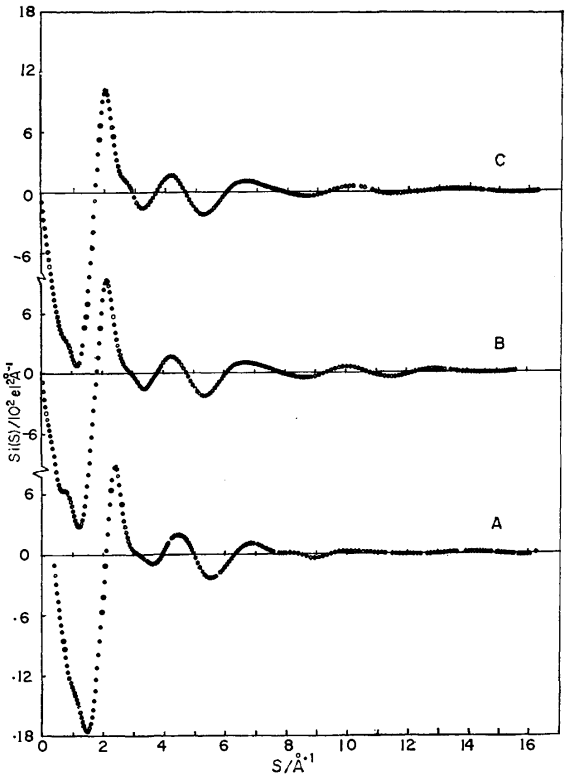

Fig. 3. The reduced intensities $i(s)$ multiplied by s for solutions A, B, and C.

Results and Discussion

Structure of Tetraamminezinc(II) Ion. Solutions B and C (Table 1) predominantly contain the tetraamminezinc(II) complex according to the formation con-

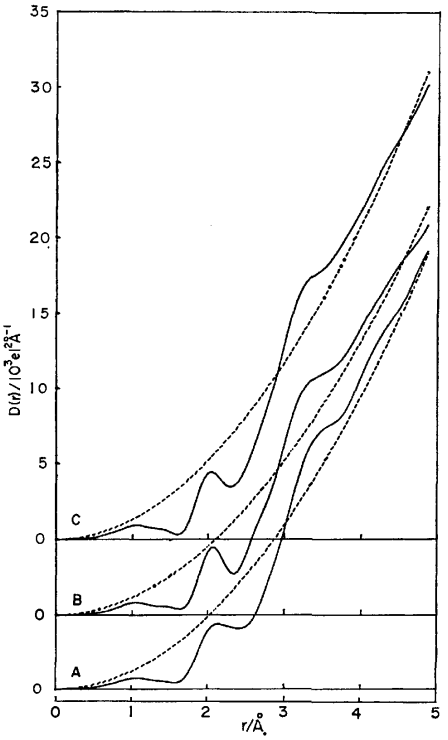

Fig. 4. The radial distribution curves, $D(r)$, for solutions A, B, and C. The curves of $4\pi r^2\rho_0$ are shown by dashed lines.

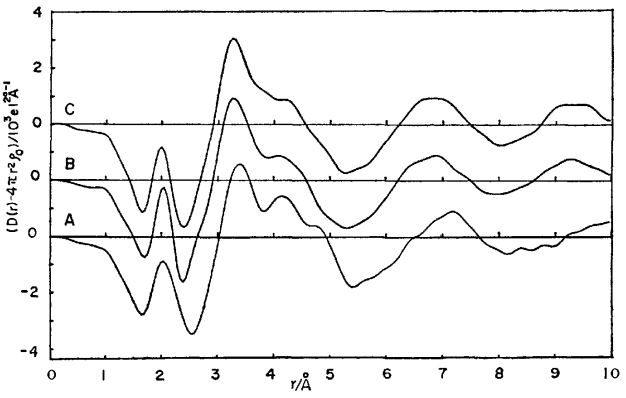

Fig. 5. The $(D(r)-4\pi r^2\rho_0)$ curves for solutions A, B, and C.

stants so far reported.[1] Therefore, the data obtained from these solutions are assessed to the tetraamminezinc(II) species rather than triammineaquazinc(II) and other amminezinc(II) complexes, although nitrogen and oxygen atoms coordinated to the metal ion are undistinguishable by the X-ray method. In each $D(r)$ curve four peaks appear around 1.0, 2.0, 3.3, and 4.2 Å (Fig. 4). The small and broad peak at about 1.0 Å is due to the O–H bonds in water. The N–H bonds in ammonia molecules may partly contribute to the peak. The second peak located at 2.0 Å can be ascribed to the interaction between the zinc(II) ion and the nearest ammonia molecules as is expected from the sum of the sizes of a Zn^{2+} ion and an ammonia molecule. The third peak at about 3.3 Å is mainly due to the Cl–O contacts.[13–16] The fourth peak found

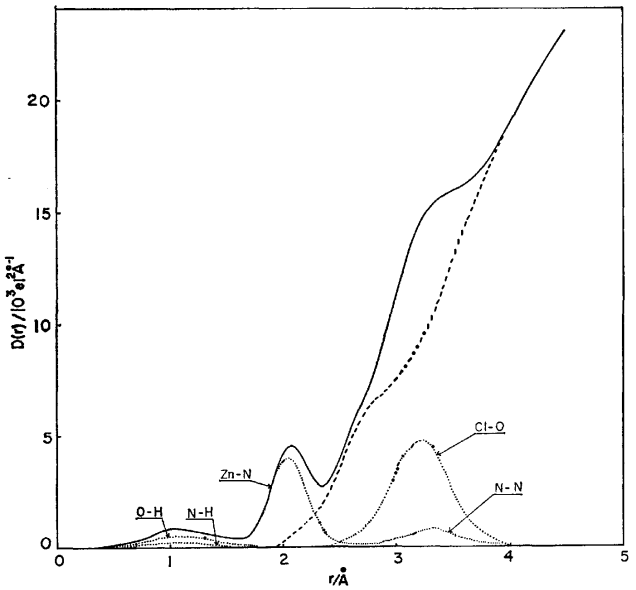

Fig. 6. The radial distribution curve for solution B. The dashed line shows the residual curve after subtraction of the theoretical peaks calculated for the O–H and N–H bonds within H_2O and NH_3, the Zn–N and N···N contacts within $Zn(NH_3)_4^{2+}$ and the Cl–O pair within $Cl(H_2O)_6^-$ from $D(r)$ curve.

around 4.2 Å may be due to the interactions between the zinc(II) ion and the molecules in the second coordination sphere.[17]

The $D(r)$ curve of solution B is essentially the same as that of solution C. The area under the peak at 2.0 Å gives about four ammonia molecules bonded to the zinc(II) ion. The area and the location of the peak rule out the existence of the $Zn(NH_3)_4(OH_2)_2^{2+}$ species of the octahedral form and the formation of the contact ion pair between zinc(II) and chloride ions, the peak maximum due to the Zn–Cl atom pair being expected to appear at about 2.3 Å.[16] The position and the area of the peak are not affected by increase in the NH_3/Zn ratio. The Zn–N bond length within the tetraamminezinc(II) ion was determined by the trial-and-error method so as to obtain a smooth background curve with no indication of any other intramolecular interactions within the first coordination layer of the zinc(II) ion. The temperature factor calculated from the half-width of the peak at 2.0 Å in $D(r)$ was 0.002—0.003 Å^2, which is in good agreement with 0.0022 Å^2 obtained from spectroscopic data.[18] The length of the Zn–N bond was finally determined to be (2.03±0.02) Å. The results are shown in Fig. 6, together with the contribution from the hydrated chloride ion to the $D(r)$ curve calculated by using the distance and the temperature factor of the Cl–O bond within the $Cl(H_2O)_6^-$ ion reported by Narten *et al.*[13] There is no appreciable peak in the residual curve (Fig. 6, dashed line) in the range $r<4$ Å except for a broad peak around 2.8 Å which corresponds to the adjacent O–O bond of bulk water and N–O bond of dissolved ammonia.[19]

Structure of Triamminemonochlorozinc(II) Ion. Solution A might contain a small amount of triammine-

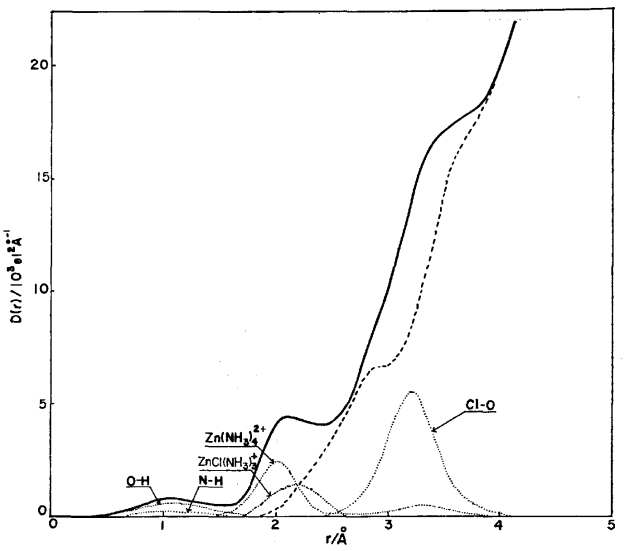

Fig. 7. The radial distribution curve for solution A. The dashed line shows the difference between the $D(r)$ curve and theoretical peak shapes calculated for the O–H and N–H bonds within H_2O and NH_3, the Zn–N and N···N contacts within $Zn(NH_3)_4^{2+}$, the Zn–N and Zn–Cl bonds within $ZnCl(NH_3)_3^+$ and Cl–O pair within $Cl(H_2O)_6^-$.

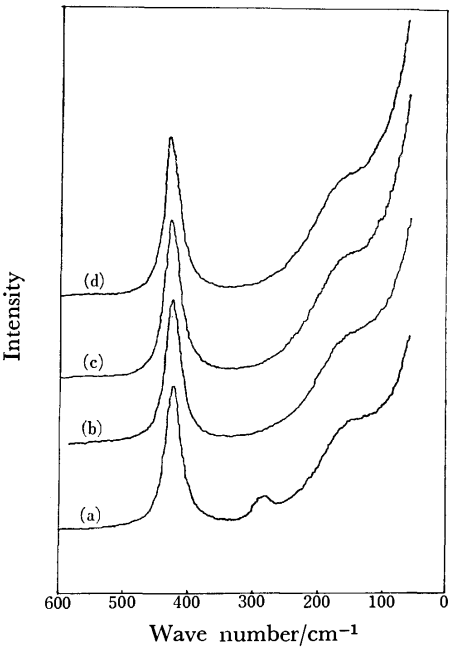

Fig. 8. Raman spectra of solutions. (a) Solution A; (b) solution B; (c) solution C; (d) solution at NH_3/Zn ratio=10.

zinc(II) complex besides the predominant tetraamminezinc(II) ion. Since the solution contains a large amount of chloride ions, mixed chloro-ammine complexes may be formed in the solution. Although no formation constants of the mixed chloro-ammine complexes of zinc(II) ion have been reported, the formation constants can be estimated by an appropriate equation for the formation equilibria of the mixed complexes. The equilibrium for the formation of a mixed complex $ZnCl_v(NH_3)_y^{(2-v)+}$ is written as follows:

$$Zn^{2+} + vCl^- + yNH_3 = ZnCl_v(NH_3)_y^{(2-v)+}. \quad (5)$$

If we use Dyrssen's equation[20] for the calculation of the equilibrium constant of the complex, we obtain β_{1vy} as follows:

$$\log \beta_{1vy} = \log \frac{(v+y)!}{v!y!} + \frac{v}{v+y} \log \beta_{1,v+y,0} + \frac{y}{v+y} \log \beta_{1,0,v+y}, \quad (6)$$

where the constant β_{1vy} is defined as $[ZnCl_v(NH_3)_y^{(2-v)+}]/[Zn^{2+}][Cl^-]^v[NH_3]^y$. Thus, the stepwise formation constant $K=[ZnCl(NH_3)_3^+]/[Zn(NH_3)_3^{2+}][Cl^-]$ is given by

$$Zn(NH_3)_3^{2+} + Cl^- = ZnCl(NH_3)_3^+,$$
$$K = \beta_{113}/\beta_{103}. \quad (7)$$

The value of β_{113} was estimated by insertion of the values of β_{104} and β_{140}[1] into Eq. 6 (β_{103} was also quoted from the same literature). The stepwise formation constant K thus evaluated was 1.2. The composition of solution A was estimated to be 60 mol % of $Zn(NH_3)_4^{2+}$, 34 mol % of $ZnCl(NH_3)_3^+$ and 6 mol % of $Zn(NH_3)_3(OH_2)^{2+}$.

The theoretical peaks of the radial distribution curve of solution A were calculated on the basis of the composition of the complexes. The peak shapes for each atom pair are shown in Fig. 7. The parameter values of the $Zn(NH_3)_4^{2+}$ ion used were those obtained in the previous section. The parameter values of the structure of the $ZnCl(NH_3)_3^+$ complex were obtained by the trial-and-error method. The formation of the $Zn(NH_3)_3(OH_2)^{2+}$ ion was neglected, because of its small amount and the structure practically undistinguishable from $Zn(NH_3)_4^{2+}$ by means of X-ray. The distances of the Zn–NH_3 and Zn–Cl bonds within the $ZnCl(NH_3)_3^+$ complex thus determined were (2.00±0.03) and (2.30±0.03) Å, respectively. The smooth background curve, except for a broad peak around 2.8 Å due to the structure of bulk water, indicates no significant intramolecular interaction being left within the first coordination shell of the zinc(II) ion.

Raman spectra have been observed in a solution containing the tetraamminezinc(II) ion[21] and in the solid $[Zn(NH_3)_4]I_2$ compound having the tetrahedral $Zn(NH_3)_4^{2+}$ moiety.[2] In aqueous solution the only totally symmetric Zn–NH_3 frequency was found at 428 cm^{-1}, the band being almost identical to the 431.2 cm^{-1} band of the solid state. In the spectra of all the solutions A, B, and C, a totally symmetric Zn–NH_3 stretching vibration appeared at (429±1) cm^{-1} (Fig. 8). No change in the Raman spectrum was observed even in a solution of $NH_3/Zn=10$ prepared by introduction of gaseous ammonia into solution C. The results suggest that the tetraamminezinc(II) ion is the main species in solutions of an NH_3/Zn ratio larger than 3.8 and that no higher-ammine–zinc(II) complexes can be formed even in solutions of high ammonia content. In solution A, a small polarized band was observed at *ca.* 285 cm^{-1} (Fig. 8). In Raman spectroscopic studies of zinc(II) chloride solution in the presence of ammonium chloride at various pH

values, Beer *et al.* assigned the band at 284 cm^{-1} observed for the solutions at high pH values to the Zn–Cl stretching frequency of the chloro-ammine complexes.[22] Perchard and Novak[23] reported on the Raman spectra of the $ZnCl_2(NH_3)_2$ crystal and assigned the bands at 420 and 283 cm^{-1} to the Zn–NH_3 and Zn–Cl stretching frequencies, respectively. The band around 285 cm^{-1} might be due to the symmetric Zn–Cl stretching vibration of the triamminemonochlorozinc(II) ion present in the solution, the Zn–N stretching frequency overlapping the 429 cm^{-1} band of the predominant tetraamminezinc(II) ion.

As is seen in Fig. 1, a small peak appears at about 0.8 $Å^{-1}$ in s in all the X-ray diffraction patterns. According to Dorosh and Skryshevskii[24] and Marques and Marques,[25] the peak is due to the "superarrangement" of cations in the solution. The distance between the cations, R_c, is calculated by

$$R_c = 7.73/s_m, \quad (8)$$

where s_m denotes the s-value of the peak maximum. The distance R_c thus calculated is about 9Å, in good agreement with the calculated zinc(II)–zinc(II) distance from the stoichiometric volume given in Table 1. The distances are 8.5, 8.9, and 9.1 Å for the solutions A, B, and C, respectively.

The present work was partially supported by a Grant-in-Aid for Scientific Research from the Ministry of Education.

References

1) L. G. Sillén and A. E. Martell, "Stability Constants," Spec. Publ. No. 17 and Supplement No. 1, Spec. Publ. No. 25, The Chemical Soc., London (1964) and (1971).
2) K. H. Schmidt and A. Müller, *Coord. Chem. Rev.*, **19**, 41 (1976).
3) H. Ohtaki and M. Maeda, *Bull. Chem. Soc. Jpn.*, **47**, 2197 (1974).
4) H. Ohtaki, M. Maeda, and S. Ito, *Bull. Chem. Soc. Jpn.*, **47**, 2217 (1974).
5) H. A. Levy, M. D. Danford, and A. H. Narten, ORNL-3960 (1966).
6) K. Furukawa, *Rep. Progr. Phys.*, **25**, 395 (1962).
7) J. Krogh-Moe, *Acta Crystallogr.*, **2**, 951 (1956).
8) B. E. Warren and R. L. Mozzi, *Acta Crystallogr.*, **21**, 459 (1966).
9) H. Ohtaki, T. Yamaguchi, and M. Maeda, *Bull. Chem. Soc. Jpn.*, **49**, 701 (1976).
10) D. T. Cromer and J. T. Waber, *Acta Crystallogr.*, **18**, 104 (1965); D. T. Cromer, *J. Chem. Phys.*, **50**, 4857 (1969); D. T. Cromer and D. Lieberman, *J. Chem. Phys.*, **53**, 1891 (1970).
11) K. Ichida, F. Yoshimoto, and T. Kiyono, *Joho Shori*, **15**, 414, 477 (1974).
12) G. Johansson and M. Sandström, *Chem. Scripta*, **4**, 195 (1973).
13) A. H. Narten, F. Vaslow, and H. A. Levy, *J. Chem. Phys.*, **58**, 5017 (1973).
14) D. L. Wertz, *J. Solution Chem.*, **1**, 489 (1972).
15) R. Caminiti, G. Licheri, G. Piccaluga, and G. Pinna, *J. Chem. Phys.*, **65**, 3134 (1976).
16) D. L. Wertz and J. R. Bell, *J. Inorg. Nucl. Chem.*, **35**, 37 (1973).
17) W. Bol, G. J. A. Gerrits, and C. L. van Panthaleon van Eck, *J. Appl. Crystallogr.*, **3**, 486 (1970).
18) S. J. Cyvin, B. N. Cyvin, and R. Andreassen, *J. Mol. Struct.*, **25**, 141 (1975).
19) A. H. Narten, *J. Chem. Phys.*, **49**, 1962 (1968).
20) D. Dyrssen, D. Janger, and F. Wengelin, "Computer Calculation of Ionic Equilibria and Titration Procedures," Almquist and Wilksell, Stockholm (1968).
21) K. Nakamoto, J. Takemoto, and T. L. Chow, *Appl. Spectrosc.*, **25**, 352 (1971).
22) J. Beer, D. R. Crow, R. Grzeskowiaki, and I. D. M. Turner, *Inorg. Nucl. Chem. Lett.*, **9**, 35 (1973).
23) C. Perchard and A. Novak, *Spectrochim. Acta, Part A*, **26**, 871 (1970).
24) A. K. Dorosh and A. F. Skryshevskii, *Russ. J. Struct. Chem.*, **8**, 300 (1966).
25) M. A. Marques and M. I. D. B. Marques, *Proc. N. Ned. Akad. Wet., Part B*, **77**, 286 (1974).

The Partition Mechanism of Thenoylacetone and Thenoyltrifluoroacetone in Water/Alcohol Systems

Nobuo SUZUKI,* Hidenori SHIBUYA, and Hitoshi WATARAI
Department of Chemistry, Faculty of Science, Tohoku University, Sendai 980
(Received April 17, 1978)

The apparent partition coefficients of thenoylacetone (TA) in ten alcohol/water systems and the enol fractions of TA in both phases were determined. Comparing the results with those of thenoyltrifluoroacetone (TTA), the substituent effect of methyl and trifluoromethyl groups on the partition behavior of the β-diketones in the alcoholic partition systems was examined. The experimental results showed that the apparent partition coefficient of TA is larger than that of TTA, while the partition coefficient of the enol form of TA is smaller than that of TTA. This was related to the differences in the partitioning species of TA and TTA; that is, TA is in keto and enol forms, while TTA is in enol, hydrate, and hemiacetal forms. The partition coefficient of each species was discussed in terms of the solubility parameter of alcohol.

The two-phase system composed of alcohol and water is known to be effective for the extraction of a neutral metal complex which is co-ordinatively unsaturated. For example, the Co(II)–TTA complex can be extracted more effectively by butanol than by benzene.[1] In such extraction studies, TTA has frequently been used as an extractant. However, our information about the partition behavior of TTA in alcohol/water systems is limited. The purpose of our present study is to elucidate the partition mechanism of TTA. In a previous study,[2] the chemical species of TTA in wet higher alcohols are identified as of the enol, hydrate, and hemiacetal forms, and the high reactivity of TTA with hydroxylic solvents was interpreted in terms of the electron-withdrawing effect of the trifluoromethyl group. Such a characteristic property of TTA is expected to affect its partition behavior. In this study, we obtain the partition equilibrium data for TA in alcohol/water systems and examine the substituent effect of the trifluoromethyl group by comparing the partition data of TA with those of TTA.[3]

Experimental

Materials. The TA was synthesized by the Claisen acylation of acetylthiophene.[4] The crude product was purified by the copper salt method[5] and by subsequent vacuum sublimation. The elemental analysis of the purified reagent showed: C: 57.24% and H: 4.79% (calcd for C: 57.11%, H: 4.80%), while the mp is 33.7—34.5 °C. The alcohols were purified by the method described previously.[2] The β-naphthol was purified by recrystalization from ethanol and by vacuum sublimation. The other reagents were used as purchased in the reagent-grade.

Partition Experiment. Five ml of a water-saturated alcohol solution of TA (0.002 M) and an equal volume of the alcohol-saturated aqueous phase (I=0.1 by $NaClO_4$, pH=3.5) were agitated for over 3 h at 25±0.5 °C. After centrifugation, an aliquot of the aqueous phase was pipetted out into a quartz cell and the concentration of TA was determined photometrically (295 nm, $\varepsilon=7.94\times10^3$). The concentration in the aqueous phase and the initial concentration allowed the calculation of the apparent partition coefficient of TA. The experiment was repeated six times for each partition system. On the other hand, the apparent partition coefficients of TTA were reported previously by one of the authors for most alcohols except for heptanol,[3] for which we determined the partition coefficient by a procedure similar to that described above.

Bromination. The enol fractions and the enolization rate constants of TA in several water-saturated alcohols were determined by Meyer's bromination method.[6] The procedure was as follows. A 0.01 M solution of TA in water (I=0.1, pH=3)-saturated alcohol was prepared. After the solution has stood for over 6 h, 5 ml of the solution was mixed with an equal volume of a 0.1 M alcoholic solution of bromine. After a certain interval, the bromination reaction was stopped by adding a 0.05 M ethanol solution of β-naphthol. Subsequently, after 50 ml of ethanol and 10 ml of the aqueous solution of potassium iodide has been added, and after the mixture had stood for 30 min, the iodine was titrated with a sodium thiosulfate solution. The end point was determined from the vanishing of the color of iodine. The sodium thiosulfate solution used in the titration was standardized by potassium iodate. By this procedure, the enol concentration at a certain time after the initiation of bromination was determined. Hence, the enol fraction at equilibrium was obtained from the enol concentration at reaction time zero, and the enolization rate constant from the slope of the plot of the logarithmic enol concentration against the time.

UV Absorption Measurement. The UV spectra of alcoholic solutions of TA show two absorption maxima, at 264 and 320 nm. The maximum at the longer wavelength is thought to be due to the enol form.[7] The absorption coefficient at the wavelength was determined for each water-saturated alcohol and for each alcohol-saturated aqueous solution. In order to estimate the enol fraction of TA in an aqueous solution, the following measurements were carried out. An alkaline (pH=11.6) solution of TA(2×10^{-5} M) in which TA (pK_a=8.1) dissociates entirely and diluted perchloric acid were rapidly mixed by means of a sample-mixing device (Union Co. Type MX-7), and the subsequent increase in the transmittance at 340 nm was recorded on a Hitachi 356 spectrophotometer. At the time of mixing, TA is thought to be in the enol form completely.[8,9] Hence, the ratio of the absorbances at time zero and at equilibrium refers to the enol fraction. Furthermore, from the absorption change, the tautomerization rate constant of TA in an aqueous solution was obtained.

Results

Apparent Partition Coefficients. The observed partition coefficients of TA are shown in Table 1, together with those of TTA. The value for TA is larger than that for TTA in every alcohol–water pair.

Enol Fractions and Tautomerization Rate Constants. The enol fractions and the enolization rate constants of TA, which were determined by bromination tech-

Table 1. The apparent partition coefficients of TA and TTA at 25±0.5 °C

Solvent	P(TA)[a]	P(TTA)[b]
1-Butanol	32.1	30.9
1-Pentanol	52.4	43.7
1-Hexanol	55.6	38.9
1-Heptanol	55.0	37.4[a]
1-Octanol	49.6	28.8
2-Ethyl-1-hexanol	44.8	29.5
2-Octanol	51.4	22.9
3-Methyl-1-butanol	43.3	38.0
Cyclohexanol	48.4	33.9
2-Methyl-1-propanol	28.2	26.9
Benzyl alcohol	—	56.2

a) This work. b) Ref. 3.

Table 2. The enol fractions and the enolization rate constants of TA in water-saturated alcohols and the enol fractions in alcohol-saturated water[c] at 25 °C

No.	Solvent	Enol fraction	Enolization rate constant ($\times 10^{-2}$ s^{-1})
1	1-Butanol[a]	0.812 (0.184)	2.46
2	1-Pentanol[a]	0.878 (0.150)	2.77
3	1-Octanol[a]	0.899 (0.136)	2.87
4	3-Methyl-1-butanol[a]	0.834 (0.150)	2.27
5	1-Hexanol[b]	0.879 (0.141)	
6	1-Heptanol[b]	0.885 (0.136)	
7	2-Ethyl-1-hexanol[b]	0.894 (0.137)	
8	2-Octanol[b]	0.887 (0.137)	
9	Cyclohexanol[b]	0.823 (0.156)	
10	2-Methyl-1-propanol[b]	0.829 (0.182)	

a) Bromination. b) Enol fraction $=0.566\varepsilon_{max}$.
c) Shown in parentheses.

nique, are listed in Table 2 for four alcohols. In the other alcohols, reproducible results were not obtained; therefore, the following convenient method was adopted. A simple correlation between the enol fraction of TA in the four alcohols and the absorption coefficients at the absorption maximum, ε_{max}, was obtained:

$$\text{Enol fraction} = 0.566\varepsilon_{max}. \quad (1)$$

The enol fractions for the other alcohols were calculated from Eq. 1; they are listed in Table 2. The enol fraction in an aqueous solution was obtained as 0.13_4 from the kinetic experiment. From the experiment, the enolization rate constant, 1.62×10^{-2} s^{-1}; the ketonization rate constant, 1.19×10^{-1} s^{-1}, and the absorption coefficient of the enol form at 340 nm, $\varepsilon_e=1.78\times10^4$, were also obtained. The enol fractions of TA in alcohol-saturated water were estimated by the ratio of the apparent absorption coefficient to ε_e, they are shown in Table 2.

Discussion

The Tautomerization of TA in Aqueous and Alcoholic Phases. As is shown in Table 2, the enol fractions

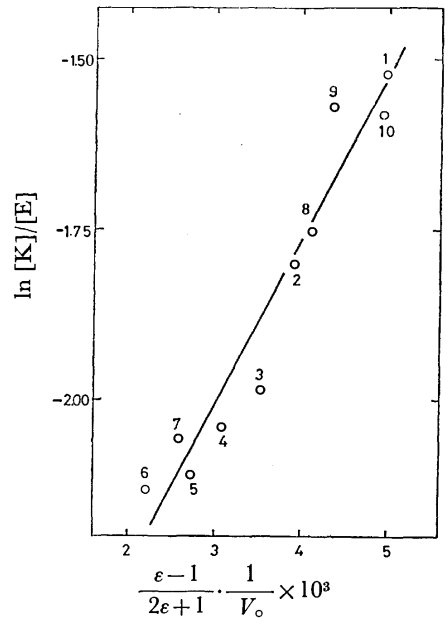

Fig. 1. Correlation between the keto-enol equilibrium constant and the solvent quantity $(\varepsilon-1)/V_o(2\varepsilon+1)$. The numbers correspond to those in Table 2.

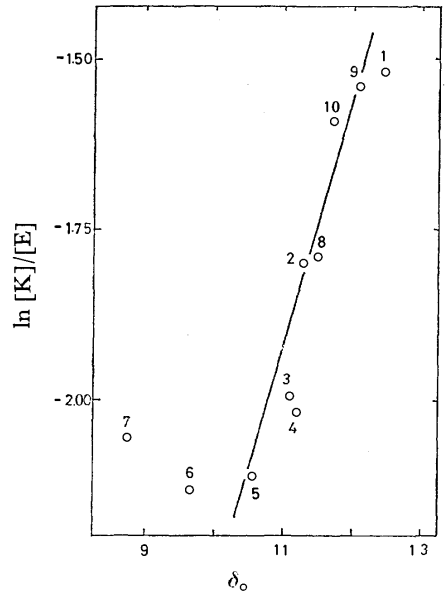

Fig. 2. Correlation between the keto-enol equilibrium constant and the solubility parameter of alcohol. The numbers correspond to those in Table 2.

of TA in water-saturated alcohols seem to increase with a decrease in the solvent polarity. This tendency was also noted in the case of TTA, as was reported in a previous paper,[2] in which the solvent effect was discussed in terms of electrostatic theory and the regular solution theory. The electrostatic theory proposes that an equilibrium constant depends on the dielectric constant, ε, of the solvent through the terms of $(\varepsilon-1)/V_o(2\varepsilon+1)$, in which V_o is the molar volume of the solvent.[10] On the other hand, the regular solution theory relates an equilibrium constant to the solubility parameter of the solvent.[11] The dependencies of the keto-enol equilibrium constant on the dielectric factor

Table 3. The partition coefficients of the enol (P_E) and the keto (P_K) forms of TA and those of the enol (P_E) and the hydrate (P_H) forms of TTA at 25 °C

No.	Solvent	TA		TTA	
		P_E	P_K	P_E	P_H
1	1-Butanol	143	7.06	961	19.4
2	1-Pentanol	300	8.75	1820	23.8
3	1-Hexanol	347	7.83	1860	19.1
4	1-Heptanol	357	7.32	1870	17.4
5	1-Octanol	325	6.19	1640	11.7
6	2-Ethyl-1-hexanol	293	5.49	1420	8.5
7	2-Octanol	333	6.74	1780	13.6
8	3-Methyl-1-butanol	246	7.50	1480	19.7
9	Cyclohexanol	256	10.11	1160	27.4
10	2-Methyl-1-propanol	128	5.88	812	16.3
11	Benzyl alcohol	—	—	1950	36.3

$(\varepsilon-1)/V_o(2\varepsilon+1)$ and on the solubility parameter of alcoholic phase are shown in Figs. 1 and 2 respectively. In both figures, satisfactory relationships are obtained. The positive sign of the slopes of the figures seems to be related to the more dipolar character of the keto form than the enol form. The enolization rate constant of TA is about 2.5×10^{-2} s^{-1} for most alcohols, and no significant solvent dependency is observed, different from the enolization rate of the hemiacetal form of TTA.[2]

The Partition Coefficient of Each Species of TA and TTA. The TTA in the alcohol phase is in the enol, the hydrate and the hemiacetal forms, while in the aqueous phase, it is in the enol and hydrate forms. On the other hand, TA is thought to be in the enol and the keto forms in both phases. Consequently, the partition schemes of the two diketones are considerably different and can be drawn as follows:

$$\begin{array}{lcl} \text{TA;} & \text{K}\rightleftharpoons\text{E} & \text{org.} \\ & \Updownarrow\ \Updownarrow & \\ & \text{K}\rightleftharpoons\text{E} & \text{aq} \end{array} \qquad \begin{array}{lcl} \text{TTA;} & \text{H}\rightleftharpoons\text{E}\rightleftharpoons\text{A} & \text{org.} \\ & \Updownarrow\ \Updownarrow & \\ & \text{H}\rightleftharpoons\text{E} & \text{aq} \end{array} \qquad (2)$$

Here E, K, H, and A refer to the enol, keto, hydrate, and hemiacetal forms respectively. On the basis of the above schemes, the partition coefficients of the enol (P_E), keto (P_K), and hydrate (P_H) forms can be represented by

$$P_E=\frac{f_o}{f}P,\quad P_K=\frac{1-f_o}{1-f}P,\quad P_H=\frac{g_o}{1-f}P, \qquad (3)$$

where f, f_o, and g_o refer to the enol fraction in the aqueous phase, the enol fraction in the organic phase, and the hydrate fraction in the organic phase respectively, and where P refers to the apparent partition coefficient. The values of P_E and P_K for TA and those of P_E and P_H for TTA are shown in Table 3. The order of the magnitude of the partition coefficient is: $P_E(\text{TTA})>P_E(\text{TA})>P_H(\text{TTA})>P_K(\text{TA})$.

For the solvent effect of alcohol on the partition coefficients, it is difficult to draw out any regularity instantaneously. In an earlier work, one of the present authors demonstrated the utility of the regular solution theory for an interpretation of the solvent effect in

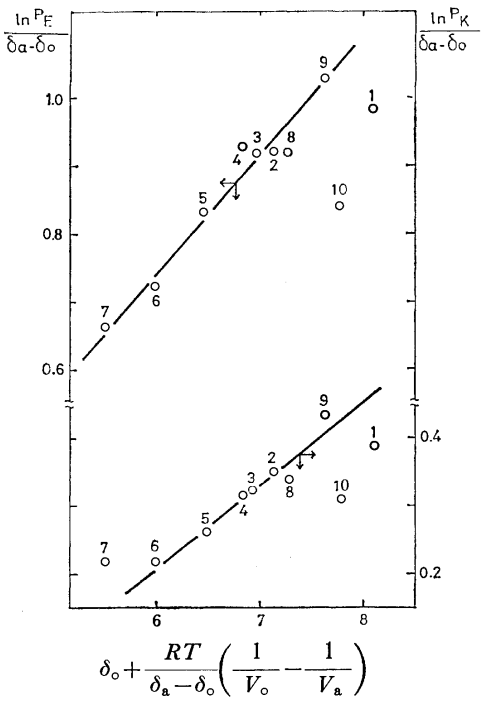

Fig. 3. Correlation between the partition coefficients of the keto (P_K) and the enol (P_E) forms of TA and the solubility parameter of alcoholic phase. The numbers correspond to those in Table 3.

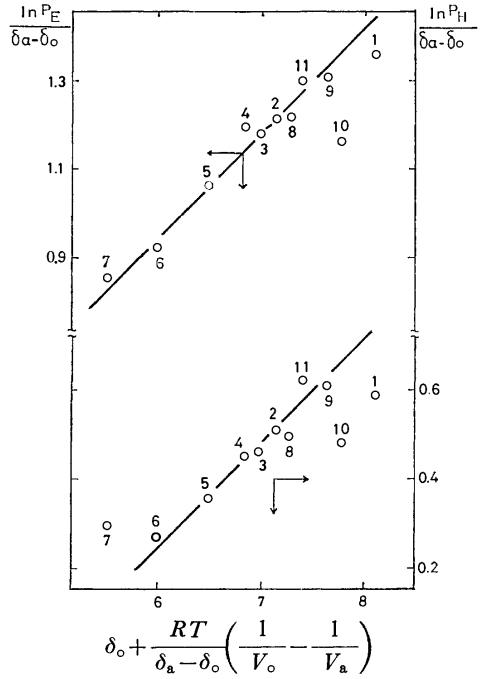

Fig. 4. Correlations between the partition coefficients of the enol (P_E) and the hydrate (P_H) forms of TTA and the solubility parameter of alcoholic phase. The numbers correspond to those in Table 3.

alcohol/water systems.[3] Hence, we employed this treatment for the partition coefficient of each species of TA and TTA. On a certain species, i, the following equation is derived from the regular solution approximation for the present partition system:[3]

$$\frac{\ln P_i}{\delta_a-\delta_o}=\frac{V_i}{RT}\left\{\delta_o+\delta_a-2\delta_I+\frac{RT}{\delta_a-\delta_o}\left(\frac{1}{V_o}-\frac{1}{V_a}\right)\right\}, \qquad (4)$$

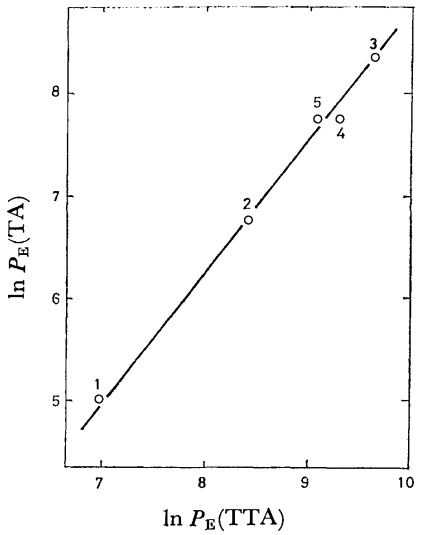

Fig. 5. Correlation between ln P_E(TA) and ln P_E-(TTA). The numbers correspond to those in Table 3.

where P is the partition coefficient; V, the molar volume and δ, solubility parameter, and where the subscripts i, and o refer to the solute i, the aqueous phase, and the organic phase respectively. Figures 3 and 4 show the plots based on the above relation. A satisfactory correlation is obtained in each case.

Comparison of the Partition Coefficients of TA with Those of TTA. As is shown in Table 3, P_E(TTA) is larger than P_E(TA). In addition, a linear correlation appears between ln P_E(TTA) and ln P_E(TA), as is shown in Fig. 5. This relationship may be understood from the point of view of the linear free-energy relationship. The partition coefficient is related to a transfer free energy, ΔG, from the aqueous phase to the organic phase by the following equation:

$$-RT \ln P = \Delta G. \tag{5}$$

Assuming an additivity of group-transfer free energy,[12] the ΔG of the enol forms of TA and TTA can be represented as

$$\begin{aligned} \Delta G(\mathrm{TA}) &= \Delta G(\mathrm{CH_3}) + \Delta G(\mathrm{R}), \\ \Delta G(\mathrm{TTA}) &= \Delta G(\mathrm{CF_3}) + \Delta G(\mathrm{R}), \end{aligned} \tag{6}$$

where R refers to the group of $-\mathrm{COCHCOC_4H_3S}$. Hence, the partition coefficients are

$$\begin{aligned} \ln P(\mathrm{TA}) &= \ln P(\mathrm{CH_3}) + \ln P(\mathrm{R}), \\ \ln P(\mathrm{TTA}) &= \ln P(\mathrm{CF_3}) + \ln P(\mathrm{R}). \end{aligned} \tag{7}$$

Equation 7 provides

$$\ln P(\mathrm{TA}) - \ln P(\mathrm{TTA}) = \ln P(\mathrm{CH_3}) - \ln P(\mathrm{CF_3}). \tag{8}$$

Equation 8 and the intercept in Fig. 5 allow the estimation of $\Delta G(\mathrm{CH_3}) - \Delta G(\mathrm{CF_3})$ as 1.4 kcal/mol. Similar analysis has been performed for the previous results in apolar solvent/water systems;[13] the free energy difference was estimated as 2.1 kcal/mol. The larger value for the apolar system corresponds to a general tendency for a fluorocompound to show a high solubility in an apolar solvent.

Finally, let us discuss the effect of the solution species on the apparent partition coefficient. On the basis of the scheme of Eq. 2, the apparent partition coefficient of TA can be represented by

$$P(\mathrm{TA}) = \frac{[\mathrm{E}]_o + [\mathrm{K}]_o}{[\mathrm{E}] + [\mathrm{K}]} = \frac{[\mathrm{E}]_o}{[\mathrm{E}] + [\mathrm{K}]} + \frac{[\mathrm{K}]_o}{[\mathrm{E}] + [\mathrm{K}]} = P'(\mathrm{E}) + P'(\mathrm{K}). \tag{9}$$

Since the ratio of $P'(\mathrm{K})/P'(\mathrm{E})$, which is identical with the keto-enol equilibrium constant in the alcoholic phase, is much smaller than unity, it may be concluded that the magnitude of P_E(TA) is primarily governed by that of P'(E). On the other hand, the apparent partition coefficient of TTA can be separated into the following terms:

$$P(\mathrm{TTA}) = \frac{[\mathrm{E}]_o}{[\mathrm{E}] + [\mathrm{H}]} + \frac{[\mathrm{H}]_o}{[\mathrm{E}] + [\mathrm{H}]} + \frac{[\mathrm{A}]_o}{[\mathrm{E}] + [\mathrm{H}]} = P'(\mathrm{E}) + P'(\mathrm{H}) + P'(\mathrm{A}). \tag{10}$$

The relative magnitude among P'(E), P'(H), and P'(A) is equal to that among $[\mathrm{E}]_o$, $[\mathrm{H}]_o$, and $[\mathrm{A}]_o$ (*cf.* Table 1 in the preceding paper).[2] Hence, we found that the contribution of P'(H), or approximately $P_H = [\mathrm{H}]_o/[\mathrm{H}]$, to P(TTA) is the most important because the major species of TTA in the alcohol phase is the hydrate form in most cases. However, in 2-ethyl-1-hexanol P'(A) plays the most important role because of the high fraction (50%) of the hemiacetal form in the solvent. In conclusion, we can state that P(TA) is governed by P'(E), and P(TTA) by P_H and P'(A). Although P_E(TTA) is larger than P_E(TA), because of the small contribution of P_E(TTA) P(TA) is larger than P(TTA).

References

1) I. P. Alimarin and Yu. A. Zolotov, *Talanta*, **9**, 891 (1962).
2) H. Shibuya, H. Watarai, and N. Suzuki, *Bull. Chem. Soc. Jpn.*, **51**, 2932 (1978).
3) N. Suzuki, K. Akiba, T. Kanno, and T. Wakahayashi, *J. Inorg. Nucl. Chem.*, **26**, 2521 (1964).
4) F. W. Swamer and C. R. Hauser, *J. Am. Chem. Soc.*, **72**, 1352 (1950).
5) J. T. Adams and C. R. Hauser, *J. Am. Chem. Soc.*, **66**, 1220 (1944).
6) K. H. Meyer, *Ber.*, **45**, 2843 (1912).
7) E. L. King and W. H. Reas, *J. Am. Chem. Soc.*, **73**, 1806 (1951).
8) L. G. Uitert and B. E. Douglas, *J. Am. Chem. Soc.*, **75**, 455 (1953).
9) M. Eigen, *Pure Appl. Chem.*, **6**, 97 (1963).
10) J. Powling and H. J. Bernstein, *J. Am. Chem. Soc.*, **73**, 4353 (1951).
11) J. H. Hildebrand and R. L. Scott, "The Solubility of Nonelectrolytes," 3rd ed, Dover, New York, p. 131.
12) A. Leo, C. Hansch, and D. Elkins, *Chem. Revs.*, **71**, 525 (1971).
13) T. Wakahayashi, S. Oki, T. Omori, and N. Suzuki, *J. Inorg. Nucl. Chem.*, **26**, 2255 (1964).

Binuclear Metal Complexes. XXIV.[1] Synthesis and Magnetism of Binuclear Cobalt(II) Complexes in Mixed-spin State[2]

Naoyuki TORIHARA, Hisashi OKAWA,* and Sigeo KIDA

Department of Chemistry, Faculty of Science, Kyushu University, Hakozaki, Higashi-ku, Fukuoka 812

(Received May 1, 1978)

Binuclear cobalt(II) complexes, $Co_2(fsaR)(py)_3$ and $Co_2(fsaR)MeOH\cdot 1/2H_2O$ with 3-formylsalicylic acid-diamine Schiff bases, H_4fsaR (R=en, pn, bn, ch, and ph), were prepared and characterized. Mixed-spin states of these complexes were demonstrated by the cryomagnetic measurements and no spin-exchange interaction was observed between high-spin and low-spin cobalt(II) ions. The absence of spin-exchange interaction in these complexes was discussed on the basis of the electronic configuration of the low-spin cobalt(II) ion and in comparison with the antiferromagnetic Cu(II)–Co(II) ($s=3/2$) complexes with the same ligands.

Binuclear metal complexes are classified into four types: homo-metal binuclear complexes (*e.g.*, Cu(II)–Cu(II)), mixed-spin binuclear complexes (*e.g.*, Ni(II)-($s=0$)–Ni(II)($s=1$)), mixed-valence binuclear complexes (*e.g.*, Cu(I)–Cu(II)), and hetero-metal binuclear complexes (*e.g.*, Cu(II)–Ni(II)). Among these complexes homo-metal binuclear complexes have been most extensively studied because of the ease of preparation. Recently much attention has been denoted to the mixed-valence and the hetero-metal binuclear complexes in connection with metalloenzymes and homogeneous catalysis. On the other hand, there are very few characterized binuclear complexes in mixed-spin state.

Although there have been obtained some binuclear complexes with high-spin cobalt(II) ion,[3–8] no mixed-spin binuclear cobalt(II) complexes have yet been obtained. In the previous papers of this series,[9–13] the mixed-spin binuclear nickel(II) complexes[9] and the hetero-metal binuclear complexes[10–13] were obtained by use of 3-formylsalicylic acid-diamine Schiff bases (H_4fsaR). In $CuCo(fsaR)(H_2O)_{2-3}$ complexes with these ligands,[11,12,14] the high-spin cobalt(II) ion is bonded to the "outside" coordination site with two water molecules at the apical positions. On the other hand, the "inside" coordination site of these ligands quite resembles the coordination site of *N,N'*-disalicylideneethylenediamine and its homologues capable of forming low-spin cobalt(II) complexes. Thus, we aimed in this study to prepare mixed-spin binuclear cobalt(II) complexes with 3-formylsalicyclic acid-diamine Schiff bases and to investigate the spin-exchange interaction between high-spin and low-spin cobalt(II) ions.

The 2:1 condensation product of 3-formylsalicyclic acid with ethylenediamine, propylenediamine, 2,3-butanediamine, 1,2-cyclohexanediamine and *o*-phenylenediamine are abbreviated as H_4fsaen, H_4fsapn, H_4fsabn, H_4fsach, and H_4fsaph, respectively.

Experimental

Synthesis. 3-Formylsalicylic acid-diamine Schiff bases, H_4fsaR (R=en, pn, bn, ch, and ph), were obtained as yellow prisms by the reaction of 3-formylsalicylic acid and a diamine in ethanol in the 2:1 mole ratio. Syntheses of complexes were carried out in an atmosphere of nitrogen by means of a VAC Inert Atmosphere & Vacuum Deposition Equipment Model HE-43-2.

$Co_2(fsaen)(py)_3$. Cobalt(II) acetate tetrahydrate (500 mg) and H_4fsaen (350 mg) were dissolved in pyridine (20 ml) to form a deep red solution. When the solution was stirred at 60 °C for 30 min red prisms separated. Stirring was continued for additional two hours at 100 °C and the reaction mixture was allowed to stand overnight to give red-purple prisms. They were collected and dried at ordinary pressure.

In the same way as the above $Co_2(fsapn)(py)_3$, $Co_2(fsabn)(py)_3$, $Co_2(fsach)(py)_3$, and $Co_2(fsaph)(py)_3$ were obtained.

$Co_2(fsaen)MeOH\cdot 1/2H_2O$. To a solution of H_4fsaen (700 mg) in methanol (50 ml) was added cobalt(II) acetate tetrahydrate (1.0 g) and the mixture was stirred under reflux for 24 h. After the reaction mixture was left standing overnight, red fine-crystals which separated were collected and dried.

$Co_2(fsach)MeOH\cdot 1/2H_2O$ and $Co_2(fsaph)MeOH\cdot 1/2H_2O$ were obtained by the procedures similar to that for $Co_2(fsaen)MeOH\cdot 1/2H_2O$. Syntheses of metal complexes with H_4fsach and H_4fsabn were also carried out. Red prisms obtained became black on exposure to air. Composition of black product was assumed to be $Co_2(fsaR)(MeOH)_2\cdot O_2\cdot 1/2H_2O$ (R=pn, bn).

Elemental analyses of the complexes are tabulated in Table 1.

Measurements. Infrared spectra of the complexes were measured with a Hitachi Infrared Spectrophotometer Model 215 on a KBr disk. Electronic spectra were measured with a Shimadzu Multipurpose Spectrophotometer Model MSP-5000 by the reflection on a powder sample. ESR spectra were measured with a JES-ME-3 Spectrometer by the X-band. Magnetic susceptibility was measured by the Faraday method in the temperature range from liquid nitrogen temperature to room temperature. The apparatus was calibrated by use of $HgCo(NCS)_4$. Magnetic moments were calculated by the expression, $\mu_{eff}=2.828(\chi_M\times T)^{1/2}$, where χ_M is the magnetic susceptibility per molecule corrected for diamagnetism by use of Pascal's constants.

Results and Discussion

Reaction of H_4fsaR with cobalt(II) acetate in pyridine always resulted in the formation of $Co_2(fsaR)(py)_3$. Since in $CuCo(fsaR)(H_2O)_{2-3}$ the cobalt(II) ion is in the "outside" coordination site and has a pseudo-octahedral configuration with water molecules at the apical positions[14], it is likely that the "outside" cobalt(II) in $Co_2(fsaR)(py)_3$ also has a pseudo-octahedral structure coordinated by pyridine at the apical positions. It is known[15] that *N,N'*-disalicylidene-ethylenediaminatocobalt(II) (Co(salen)) reacts with pyridine

Table 1. Elemental analyses of complexes

	Found (%)				Calcd (%)			
	C	H	N	Co	C	H	N	Co
$Co_2(fsaen)(py)_3$	56.24	3.98	10.01	16.88	56.03	3.85	9.90	16.66
$Co_2(fsapn)(py)_3$	56.13	4.03	9.55	16.11	56.60	4.05	9.71	16.34
$Co_2(fsabn)(py)_3$	57.15	4.31	9.66	16.23	57.16	4.25	9.52	16.03
$Co_2(fsach)(py)_3$	58.59	4.59	9.65	15.58	58.36	4.37	9.20	15.48
$Co_2(fsaph)(py)_3$	58.82	3.71	9.36	15.29	58.82	3.71	9.27	15.60
$Co_2(fsaen)MeOH\cdot 1/2H_2O$	44.29	3.19	5.29	23.30	44.64	3.35	5.42	23.06
$Co_2(fsapn)(MeOH)_2\cdot O_2\cdot 1/2H_2O$	48.39	3.93	4.90	19.70	48.87	4.10	4.96	20.00
$Co_2(fsabn)(MeOH)_2\cdot O_2\cdot 1/2H_2O$	49.17	3.02	5.02	19.60	49.40	3.06	5.01	19.28
$Co_2(fsach)MeOH\cdot 1/2H_2O$	42.36	3.68	4.53	21.00	42.75	3.93	4.75	20.85
$Co_2(fsaph)MeOH\cdot 1/2H_2O$	43.59	3.95	4.35	20.75	43.22	4.12	4.58	21.08

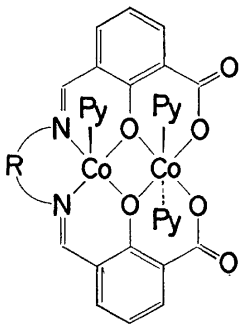

Fig. 1.

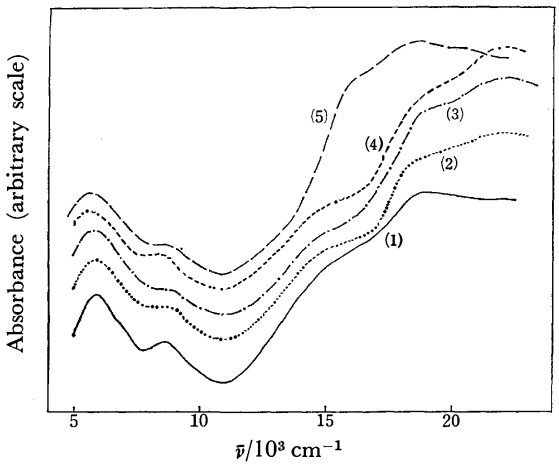

Fig. 2. Reflectance spectra of (1) $Co_2(fasen)(py)_3$, (2) $Co_2(fsapn)(py)_3$. (3) $Co_2(fsabn)(py)_3$, (4) $Co_2(fsach)(py)_3$, and (5) $Co_2(fsaph)(py)_3$.

to form Co(salen)py, where the cobalt(II) is in the low-spin state and has a tetragonal-pyramidal geometry with pyridine at the apex. Therefore, it is likely that $Co_2(fsaR)(py)_3$ has a binuclear structure composed of a low-spin tetragonal-pyramidal and a spin-free pseudo-octahedral cobalt(II) ions (Fig. 1). Coordination of pyridine was demostrated by the infrared absorption band around 700 cm^{-1}.

Reflectance spectra of $Co(fsaR)(py)_3$ are shown in Fig. 2. Each spectrum possesses several absorption bands in the region 5000—25000 cm^{-1}. The spectrum must be the superposition of the spectra of the "inside" and the "outside" cobalt(II) chromophores. Despite the difference in the apical ligands, the "outside" cobalt(II) in $Co_2(fsaR)(py)_3$ should display a spectrum similar to that of the "outside" cobalt(II) in $CuCo(fsaR)(H_2O)_{2-3}$, because pyridine does not differ much from water in the ligand field strength. In $CuCo(fsaR)(H_2O)_{2-3}$ d-d bands due to the "outside" cobalt(II) were found at 8300, 11000, and 19200 cm^{-1}.[12] On the other hand, the spectrum of the "inside" cobalt(II) in $Co_2(fsaR)(py)_3$ should be similar to that of Co(salen)py, which has d-d bands at 6000, 9000, 13500, and 16000 cm^{-1}.[16,17] Accordingly the spectra shown in Fig. 2 can be interpreted in terms of the superposition of the spectra of the five-coordinate "inside" cobalt(II) and the six-coordinate "outside" cobalt(II) ions.

Two types of complexes, $Co_2(fsaR)MeOH\cdot 1/2H_2O$ (R=en, ch, ph) and $Co_2(fsaR)(MeOH)_2\cdot O_2\cdot 1/2H_2O$ (R=pn, bn), were obtained by the reaction in methanol. The latter is tentatively assumed to be an oxygen-carrying complex, since its color turned black from red when exposed to air and its elemental analysis quite agrees with the formula shown above. It is to be noted that the oxygen-carrying complexes contain two molecules of methanol, while the complexes lacking oxygen-carrying ability contain one molecule of methanol. Since low-spin cobalt(II) complexes with the quadridentate Schiff bases usually exhibit the oxygen-carrying ability when coordinated by a base at the fifth position,[18] it is supposed that one of the methanol molecules in $Co_2(fsaR)(MeOH)_2\cdot O_2\cdot 1/2H_2O$ coordinates to the "inside" cobalt(II) ion.

Reflectance spectra of $Co_2(fsaR)MeOH\cdot 1/2H_2O$ are not well resolved and exhibit broad bands around 6000, 12000—14000, and 18000 cm^{-1}. Because of the complexity in the composition and in the visible spectra, we could not deduce a difinite structure to $Co_2(fsaR)MeOH\cdot 1/2H_2O$.

Magnetic moments of $Co_2(fsaR)(py)_3$ and $Co_2(fsaR)MeOH\cdot 1/2H_2O$ at room temperature are in the range 4.9—5.6 B.M. Since low-spin cobalt(II) and high-spin cobalt(II) (octahedral) have magnetic moments of 1.9—2.8 and 4.3—5.2 B.M.,[19] respectively, the magnetic moments expected for high-spin binuclear cobalt(II), mixed-spin binuclear cobalt(II) and low-spin binuclear cobalt(II) complexes are 6.1—7.4, 4.7—5.9, and 2.7—4.0 B.M. respectively, provided that no

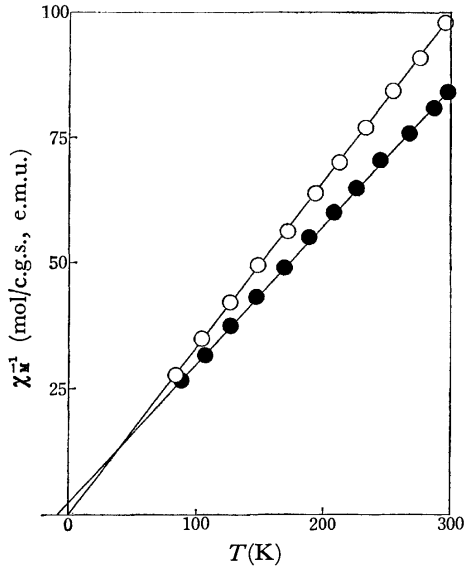

Fig. 3. Temperature variations of inverse magnetic susceptibilities of (○) Co_2(fsaen)$(py)_3$ and (●) Co_2-(fsaen)MeOH·1/2H_2O.

TABLE 2. EFFECTIVE MAGNETIC MOMENTS NEAR LIQUID NITROGEN TEMPERATURE AND AT ROOM TEMPERATURE, AND WEISS CONSTANT OF COMPLEXES

	μ_{eff}(T) (BM)		θ (K)
Co_2(fsaen)$(py)_3$	4.91(82.9)	4.92(297.4)	≈0
Co_2(fsapn)$(py)_3$	5.32(81.2)	5.34(297.4)	≈0
Co(fsabn)$(py)_3$	5.31(90.3)	5.29(296.8)	≈0
Co_2(fsach)$(py)_3$	5.44(82.8)	5.58(298.3)	−8
Co_2(fsaph)$(py)_3$	5.24(81.7)	5.31(296.8)	−4
Co_2(fsaen)MeOH·1/2H_2O	5.18(87.4)	5.34(297.8)	−10
Co_2(fsach)MeOH·1/2H_2O	5.09(81.7)	5.15(289.3)	−3
Co_2(fsaph)MeOH·1/2H_2O	5.23(84.6)	5.34(296.6)	−4

spin-exchange interaction is operating between the cobalt(II) ions. Thus, the present complexes may be mixed-spin binuclear complexes or magnetically coupled high-spin binuclear complexes. As already mentioned above electronic spectra of Co_2(fsaR)$(py)_3$ are in favor of a mixed-spin binuclear structure. Mixed-spin state for Co_2(fsaR)$(py)_3$ as well as Co_2(fsaR)-MeOH·1/2H_2O was further demonstrated by the magnetic susceptibility measurements down to liquid nitrogen temperature. Plots of inverse magnetic susceptibility *versus* temperature obey the Curie law or the Curie-Weiss law with a very small negative Weiss constant; some representatives of the $1/\chi_M$ *vs.* T plot being shown in Fig. 3. In Table 2 the magnetic moments at room temperature and near liquid nitrogen temperature and the Weiss constants determined by the Curie-Weiss plot are given. It is evident that the magnetic moments of the present complexes are almost independent on the temperature. Thus, it is concluded that Co_2(fsaR)$(py)_3$ and Co_2(fsaR)MeOH·1/2H_2O are mixed-spin binuclear complexes and no spin-exchange interaction is operating between the low-spin and the high-spin cobalt(II) ions.

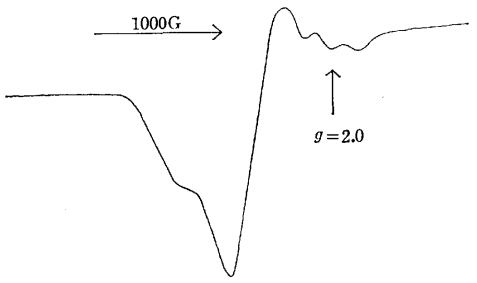

Fig. 4. ESR spectrum of CoMg(fsaen)$(py)_3$ (in DMF at liq. nitrogen temperature).

Since a considerably strong antiferromagnetic spin-exchange interaction was observed for CuCo(fsaR)-$(H_2O)_{2-3}$,[11,12] the difference in magnetic exchange interaction between the Cu(II) (s=1/2)–Co(II) (s=3/2) and the Co(II) (s=1/2)–Co(II) (s=3/2) systems may be attributed to the difference in the ground-state electronic configuration between copper(II) and low-spin cobalt(II) ions. In general copper(II) has an unpaired electron on $d_{x^2-y^2}$ orbital (x and y axes are taken on the donating atoms in the tetragonal plane). On the other hand, in low-spin cobalt(II) complexes an unpaired electron is in either a d_{yz} or d_{z^2} orbital. It is known that in Co(salen) an unpaired electron occupies d_{yz} orbital, while Co(salen)py has the ground-state electron configuration in which an unpaired electron occupies d_{z^2} orbital.[17,20-22] The main difference between the "inside" cobalt(II) of Co_2(fsaR)$(py)_3$ and Co(salen)py is in the donating phenolic oxygen; a bridging oxygen in the former while a simply donating oxygen in the latter. It is unlikely that a considerable change in the electronic configuration is brought about when the phenolic oxygen acts as a bridge.

In order to determine precisely the electronic configuration of the "inside" cobalt(II) ion, we measured ESR spectra of Co_2(fsaR)$(py)_3$ and their related complex, CoMg(fsaen)$(py)_3$. Although no ESR signal was detected for Co_2(fsaR)$(py)_3$ owing to the "outside" high-spin cobalt(II) ion, an *N*,*N*-dimethylformamide solution of CoMg(fsaen)$(py)_3$ displayed a well defined ESR spectrum, in which g_x, g_y, and g_z are found to be *ca.* 2.40, 2.25, and 2.00, respectively (Fig. 4). Three-lined hyperfine structure with hyperfine splitting constant of *ca.* 90 G around g=2.00 clearly indicates that pyridine is coordinated to the "inside" cobalt(II) ion. This ESR spectrum is quite similar to the spectrum of Co(salen)py[17] and can be interpreted in terms of a d_{z^2} ground-state electronic configuration. Based on these facts we may conclude that the "inside" cobalt(II) ion in Co_2(fsaR)$(py)_3$ has an unpaired electron in d_{z^2} orbital. Thus, it is presumed that no spin-exchange interaction in Co_2(fsaR)$(py)_3$ and Co_2(fsaR)MeOH·1/2H_2O is attributed to a negligibly small overlapping between the metal d_{z^2} orbital and the bridging oxygen orbital.[23]

The authors are grateful to the Ministry of Education for a Scientific Research Grant-in-Aid. We also thank to Mr. Y. Nonaka for the measurement of ESR spectra.

References

1) Part XXIII: Ref. 14.
2) This work was presented at the 27th Symposium of Coordination Chemistry, Matsumoto, September 28, 1977.
3) N. H. Pilkington and R. Robson, *Aust. J. Chem.*, **23**, 2225 (1970).
4) D. P. Graddon and I. T. Townsend, *Aust. J. Chem.*, **22**, 505 (1969).
5) M. Kuszaj, B. Tolonovic, D. P. Murtha, R. L. Lindvedt, and M. D. Glick, *Inorg. Chem.*, **12**, 1297 (1973).
6) J. A. Bertrand and A. R. Kalyanaraman, *Inorg. Chim. Acta*, **5**, 167 (1971).
7) G. O. Carlisle and L. J. Theriot, *J. Inorg. Nucl. Chem.*, **35**, 2093 (1973).
8) M. E. Brown, J. N. Brown, and L. M. Trefonas, *Inorg. Chem.*, **11**, 1836 (1972).
9) M. Tanaka, M. Kitaoka, and S. Kida, *Bull. Chem. Soc. Jpn.*, **46**, 2464 (1973).
10) H. Okawa, M. Tanaka, and S. Kida, *Chem. Lett.*, **1974**, 987.
11) H. Okawa, Y. Nishida, M. Tanaka, and S. Kida, *Bull. Chem. Soc. Jpn.*, **50**, 127 (1977).
12) N. Torihara, H. Okawa, and S. Kida, *Inorg. Chim. Acta*, **26**, 97 (1978).
13) N. Torihara, H. Okawa, and S. Kida, *Chem. Lett.*, **1978**, 185.
14) M. Mikuriya, H. Okawa, S. Kida, and I. Ueda, submitted to Bull. Chem. Soc. Jpn.
15) M. Calligaris, D. Minichelli, G. Nardin, and L. Randaccio, *J. Chem. Soc., A*, **1970**, 2411.
16) C. Busetto, F. Cariati, P. Fantucci, D. Galizzioli, and F. Morazzoni, *J. Chem. Soc., Dalton Trans.*, **1973**, 1712.
17) M. A. Hitchman, *Inorg. Chem.*, **16**, 1985 (1977).
18) G. McLendon and A, E, Martell, *Coord. Chem. Rev.*, **19**, 1, (1976).
19) A. T. Casey and S. Mitra, in "Theory and Application of Molecular Paramagnetism," ed by E. A. Boudreaux and L. N. Mulay, John Wiley & Sons, New York (1976), pp. 214, 221, 223.
20) B. M. Hoffman, D. L. Diemente, and F. Basolo, *J. Am. Chem. Soc.*, **92**, 61 (1970).
21) B. M. Hoffman, F. Basolo, and D. L. Diemente, *J. Am. Chem. Soc.*, **95**, 6497 (1973).
22) E. I. Ochiai, *J. Inorg. Nucl. Chem.*, **35**, 1727 (1973).
23) A. B. Blake and L. R. Fraser, *J. Chem. Soc., Dalton. Trans.*, **1974**, 2554.

Chemical Vapor Deposition of Titanium Disulfide

Seiji MOTOJIMA,* Kazuaki ITOH, Yasutaka TAKAHASHI, and Kohzo SUGIYAMA

Department of Synthetic Chemistry, Faculty of Engineering, Gifu University, Kakamigahara, Gifu 504

(Received May 15, 1978)

Chemical vapor deposition of TiS_2 was examined. TiS_2 was deposited on a quartz substrate above 300 °C from a gas mixture of $TiCl_4$, H_2S, and Ar. Maximum deposition rate was attained at 700—800 °C for a 0.7 gas flow ratio $H_2S/(TiCl_4+H_2S)$ irrespective of temperature. Crystal morphology and composition were strongly affected by temperature and gas compositions. Well-formed TiS_2 crystals were grown either at 600 °C or from a gas mixture of low flow ratio 0.2 of $H_2S/(TiCl_4+H_2S)$. Single phase of TiS_2 was deposited in the temperature range 400—850 °C.

There are several non-stoichiometric compounds in the system Ti–S. Of these, titanium disulfide has a CdI_2-type structure and is of interest as a dry-lubricant,[1] catalyst,[2] electrical contact operating under friction,[3] reversible electrode,[4] and cathode material for electric vehicle propulsion.[5,6]

Titanium disulfide has been prepared by the reaction between the elements,[7–10] reaction of titanium with hydrogen sulfide,[9,11] titanium dioxide with hydrogen sulfide and carbon,[12] and by chemical transport technique in closed ampoules,[13–18] and in open flow system.[19] Single crystals of titanium disulfide have so far been prepared only by chemical transport in a closed system.

The aim of the present study is to examine the growth conditions of titanium disulfide crystals by the chemical vapor deposition in an open flow system. Over-all reaction used is as follows, unless otherwise stated.

$$TiCl_4 + 2H_2S = TiS_2 + 4HCl. \quad (1)$$

Experimental

Materials. Commercial GR grade titanium and chlorine were used without further purification. Hydrogen was dehydrated by passing over calcium chloride and phosphorus pentaoxide, successively. Argon and hydrogen were also dehydrated by passing through concentrated sulfuric acid. Titanium tetrachloride was prepared *in situ (vide infra)*.

Growth Apparatus and Procedure. The apparatus is shown in Fig. 1. A quartz tube, outer dia. 7 mm, length 70 mm, was used as a substrate, into which a silicon carbide heater was inserted. The substrate was held in a vertical quartz tube, inner diam. 19 mm, heated with a nichrome heater from the outside. Titanium tetrachloride was prepared by chlorination of titanium sponge at 350—400 °C and carried by argon into the upper inlet of the reaction tube. Hydrogen sulfide was introduced through an uppermost inlet and allowed to mix with the stream of titanium tetrachloride just above the substrate. The surface temperature of the substrate was measured with an infrared thermometer (Japan Sensor Co., Model TSS-2P) through an observation window. The temperature had been calibrated with a chromel-alumel thermocouple. The flow rate of titanium tetrachloride was calculated from that of the chlorine stream to a bed of titanium sponge assuming full conversion.

Analysis of Crystals. Titanium content in the crystals was determined by the gravimetric method. A collection of crystallites was pulverized, weighed, and oxidized to titanium dioxide in an air flow at 1000 °C for an hour. Non-stoichiometry number x of TiS_x was calculated by the following equation:

$$x = \frac{W_{TiS_x} - W_{TiO_2}\dfrac{A.W.\,(Ti)}{M.W.\,(TiO_2)}}{A.W.\,(S)} \Bigg/ \frac{W_{TiO_2}\dfrac{A.W.\,(Ti)}{M.W.\,(TiO_2)}}{A.W.\,(Ti)} = \frac{1}{32.06}\left(79.90\frac{W_{TiS_x}}{W_{TiO_2}} - 47.90\right),$$

where W_{TiS_x} and W_{TiO_2} are weights of titanium disulfide sample and its oxidized product, respectively, and $A.W.$(i) and $M.W.$(j) are the atomic weight of element i and the molecular weight of compound j, respectively.

Thermoelectric Power. With use of silver conducting paint, a plate-like crystal of titanium disulfide was contacted to two copper plates (3×5 mm) separated 1 mm from each other, one of which was heated by a nichrome heater. The temperature difference of two sides of the crystal was measured with a 100 μm dia. chromel-alumel thermocouple. Thermoelectric power was measured in an argon atmosphere.

Results and Discussion

Effects of Substrate Temperature. Deposition rates of titanium disulfide crystals plotted against the temperature of substrate are shown in Fig. 2. The sum of the flow rates of titanium tetrachloride and hydrogen sulfide, and total gas flow rate were kept at 0.4 and

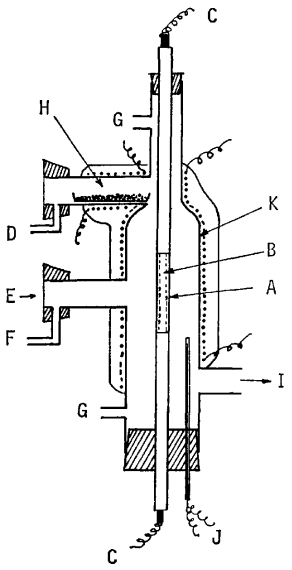

Fig. 1. Apparatus. A) Substrate (quartz, 7 mm o.d., 70 mm long), B) SiC heater, C) electrodes (graphite), D) Cl_2, Ar inlet, E) window for observation, path of the optical pyrometer, F) Ar inlet , G) H_2S inlet, H) Ti sponge, I) gas outlet, J) CA thermocouple, K) reaction tube (quartz tube, 19 mm i.d.).

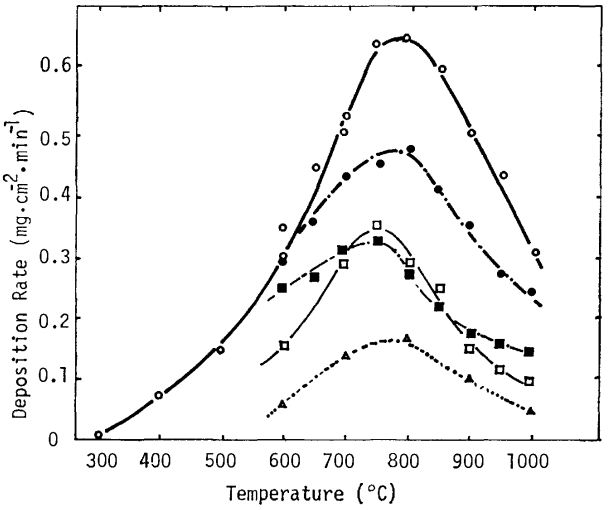

Fig. 2. Effect of substrate temperature on the deposition rate. Reaction time: 15 min, $H_2S+TiCl_4$: 0.4 cm³/s, total flow rate: 6.0 cm³/s, $H_2S/(TiCl_4+H_2S)$: (■) 0.9, (●) 0.8, (○) 0.7, (□) 0.5, (△) 0.3.

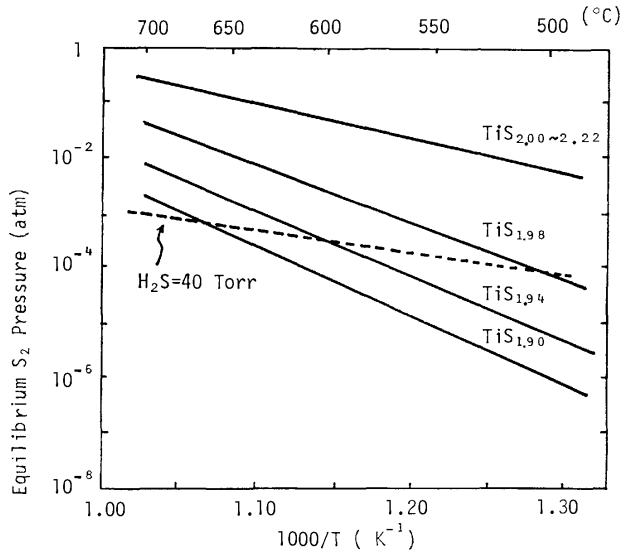

Fig. 3. Equilibrium partial pressure of sulfur *versus* temperature. (——) Partial pressures of sulfur equilibriated with nonstoichiometrical titanium disulfide quoted from Ref. 24, (----) partial pressure of sulfur formed by dissociation of H_2S.

6.0 cm³/s, respectively (linear velocity at room temperature, 2.4 cm/s). The deposition rate reached a maximum at 700—800 °C. The temperature range 700—800 °C corresponding to that of maximum growth rate has been used in chemical vapor transport.[17] Saeki,[18] Biltz *et al.*,[19] and Winn and Steele[20] reported on the equilibrium partial pressure of diatomic sulfur over the non-stoichiometric titanium disulfide. The pressure[20] is shown in Fig. 3, together with that of diatomic sulfur formed in dissociation of hydrogen sulfide in the case of inlet partial pressure of hydrogen sulfide of 40 Torr. Although the pressure of titanium disulfide is very low[21] in comparison with the disulfur pressure in the temperature range of the present work, the equilibrium sulfur pressure increases steeply with

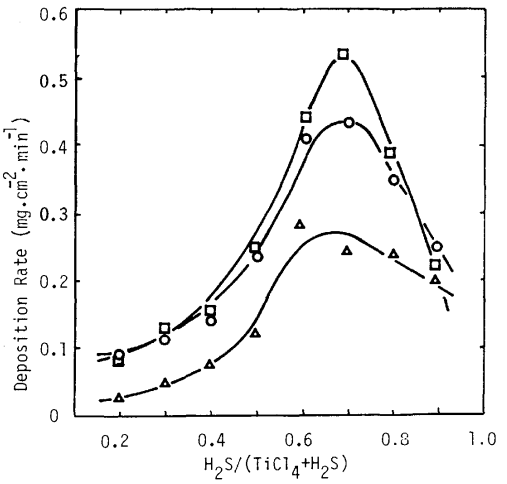

Fig. 4. Effect of gas flow ratio of $H_2S/(TiCl_4+H_2S)$ on the deposition rate. Reaction time: 15 min, $TiCl_4+H_2S$: 0.4 cm³/s, Ar: 5.6 cm³/s, substarte temperature: (△) 600 °C, (○) 700 °C, (□) 800 °C.

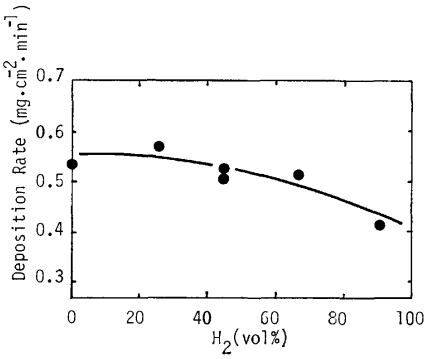

Fig. 5. Effect of hydrogen flow rate on the deposition rate. Reaction time: 15 min, H_2S: 0.1 cm³/s, $TiCl_4$: 0.1 cm³/s, H_2+Ar: 2.2 cm³/s, substrate temperature: 800 °C.

the increase of the sulfur content in titanium disulfide and with the increase of temperature especially above 800 °C. Thus, the decrease of the deposition rate above 800 °C can be attributed to the degradation of titanium disulfide to a lower sulfide phase and disulfur. The maximum deposition efficiency of titanium disulfide with respect to the feed of titanium tetrachloride was estimated to be about 20 per cent.

Effects of Gas Composition and Flow Rate. The effects of gas flow ratio $H_2S/(TiCl_4+H_2S)$ ("H_2S" ratio hereafter) on the deposition rate of titanium disulfide, with substrate temperature used as parameter, are shown in Fig. 4. The deposition rate increases with increase in the H_2S ratio, reaching a maximum at the ratio of *ca.* 0.7, which is roughly in agreement with the stoichiometrical ratio (0.67) of Reaction 1. The optimum H_2S ratio shifts to the lower value when hydrogen is introduced in the input gas. For example, H_2S ratio corresponding to the maximum deposition rate varies to 0.5 when hydrogen is introduced up to 80 per cent. The deposition rates of titanium disulfide increase with increase in the sum of the flow rates of titanium tetrachloride and hydrogen sulfide, attaining

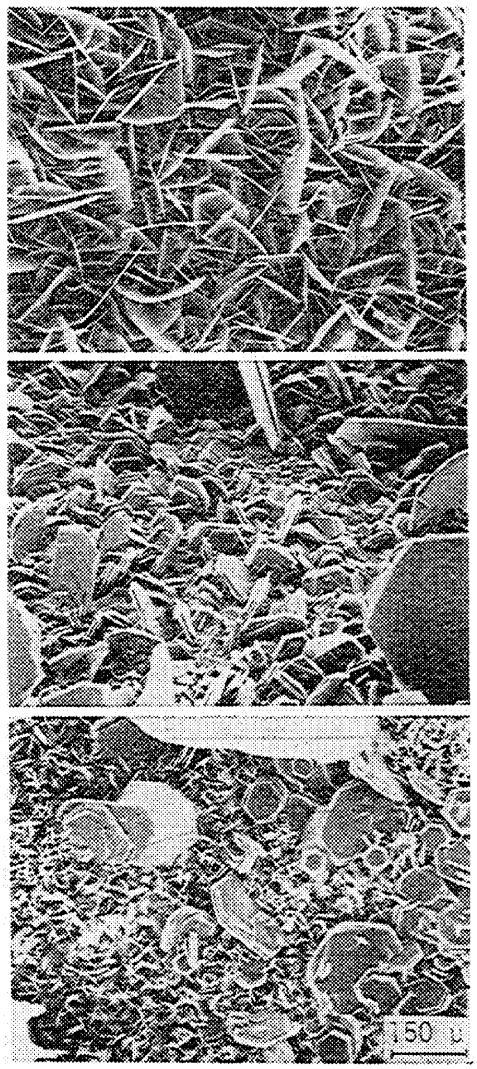

Fig. 6. Morphologies of TiS_2 crystals (1). $H_2S/(TiCl_4+H_2S)$: 0.2, substrate temperature: (A) 600 °C, (B) 800 °C, (C) 1000 °C.

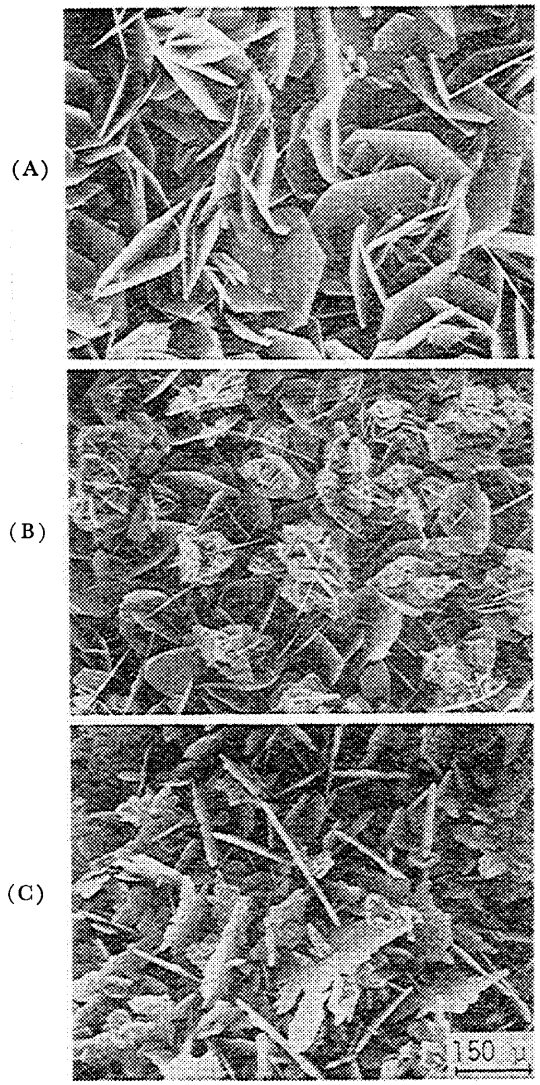

Fig. 7. Morphologies of TiS_2 crystals (2). $H_2S/(TiCl_4)$: 0.5, substrate temperature: (A) 600 °C, (B) 800 °C, (C) 1000 °C.

a constant value for the flow rate above 0.2 cm^3/s, irrespective of substrate temperature. Introduction of hydrogen resulted in negative effect on the deposition rate of titanium disulfide as shown in Fig. 5, probably due to the depression of the dissociation of hydrogen sulfide. The dissociation degree of hydrogen sulfide is estimated to be 7.4 per cent at 800 °C.[22]

Effect of Growth Time. The deposition rate of titanium disulfide became roughly constant after an induction period of 3—5 min. Hexagonal plate-like crystals of average diagonal of 2 mm having mirror faces were formed after an hour growth.

Effects of Temperature and Gas Composition on Crystal Morphology. The morphology of titanium disulfide is affected by substrate temperature and H_2S ratio as shown in Figs. 6, 7, and 8. Thin plate-like crystals up to 1 μm thick grew vertically to the surface of the substrate at 600 °C. The growth rate in direction *c* is very low as compared with that in direction *a*. However, at a low H_2S ratio such as 0.2, crystals grew appreciably in direction *c*, hexagonal crystals of 20 μm thick being obtained (Figs. 6B and 6C). Under a high H_2S ratio (Figs. 7B and 7C) or high substrate temperature (Figs. 8B and 8C) secondary deposition is apt to take place. Strotzer *et al.*[23] reported on the color-change of the Ti–S system compounds in connection with the sulfur content. The crystals grown in the present study were golden-yellow independent of the substrate temperature and gas compositions.

Effects of Temperature and Gas Composition on Crystal Compositions. X-Ray diffraction profiles of titanium sulfides grown at various temperature with the H_2S ratio kept at 0.7 are shown in Fig. 9. Peaks of titanium trisulfides (TiS_3) and sesquisulfide (Ti_3S_4) are found only on the profiles of the crystals grown below 350 °C and at 1000 °C, respectively (Figs. 9C and 9D). On the profiles of crystals grown at 400—850 °C, only the peaks of titanium disulfide are seen irrespective of the H_2S ratio (Fig. 9B).

Titanium disulfide is a well-known non-stoichiometric compound. From the results of gravimetric analysis of titanium in relation with growth temperature and H_2S ratio, the atomic ratio of sulfur to titanium (S/Ti) in crystals was determined as shown in Fig. 10. The

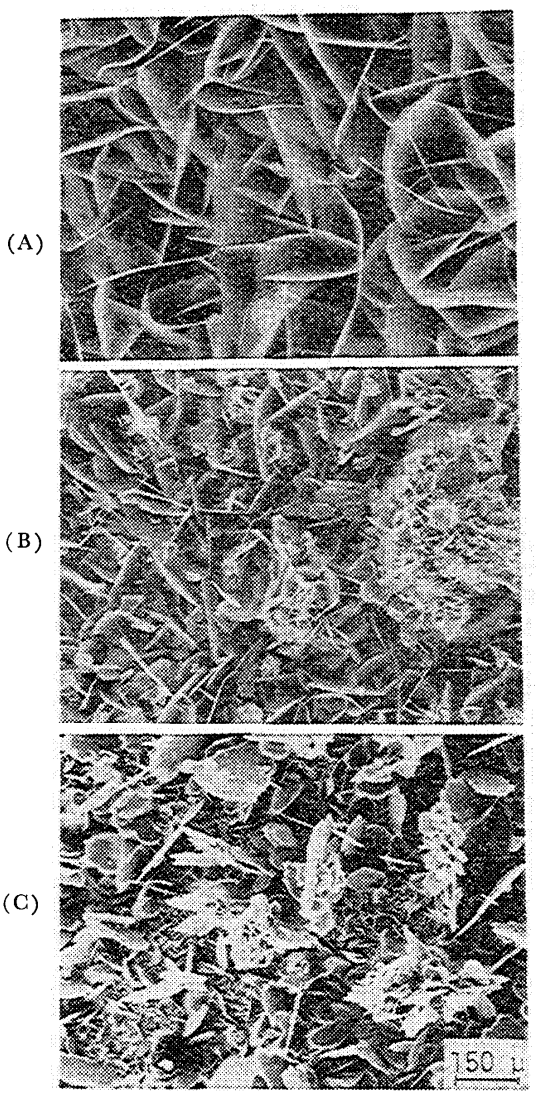

Fig. 8. Morphologies of TiS_2 crystals (3). $H_2S/(TiCl_4+H_2S)$: 0.8, substrate temperature: (A) 600 °C, (B) 800 °C, (C) 1000 °C.

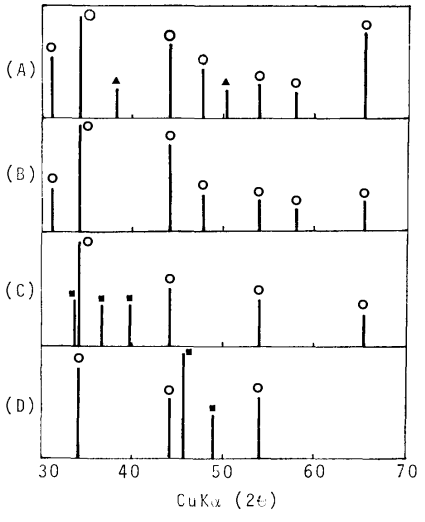

Fig. 9. X-Ray diffraction profiles.
$H_2S/(TiCl_4+H_2S)$: 0.7, substrate temperature: (A) 1000 °C, (B) 700 °C, (C) 350 °C, (D) 300 °C, (○) TiS_2, (▲) Ti_3S_4, (■) TiS_3.

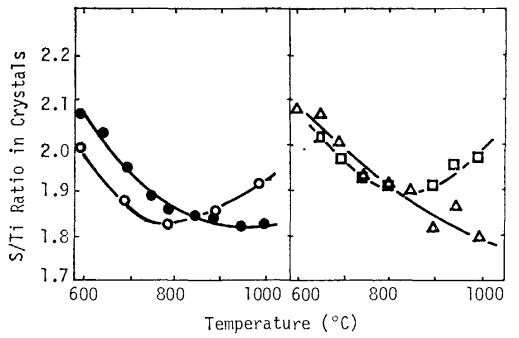

Fig. 10. Effects of temperature and gas composition on crystal composition. $H_2S/(TiCl_4+H_2S)$: (○) 0.2, (●) 0.4, (△) 0.6, (□) 0.8.

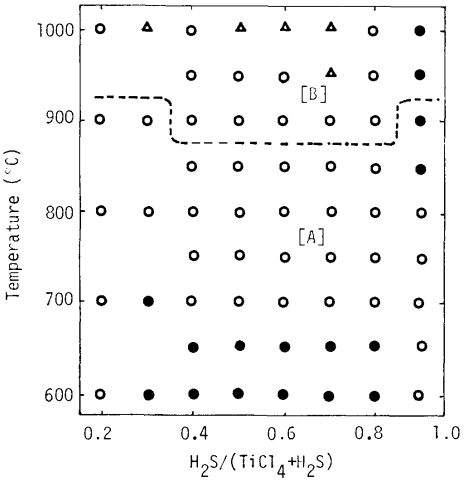

Fig. 11. Deposition region of TiS_2. (●) S/Ti>2.00, (○) 1.81≤S/Ti≤2.00, (△) S/Ti<1.81; [A] single TiS_2-phase, [B] mixed phase of TiS_2 and Ti_3S_4.

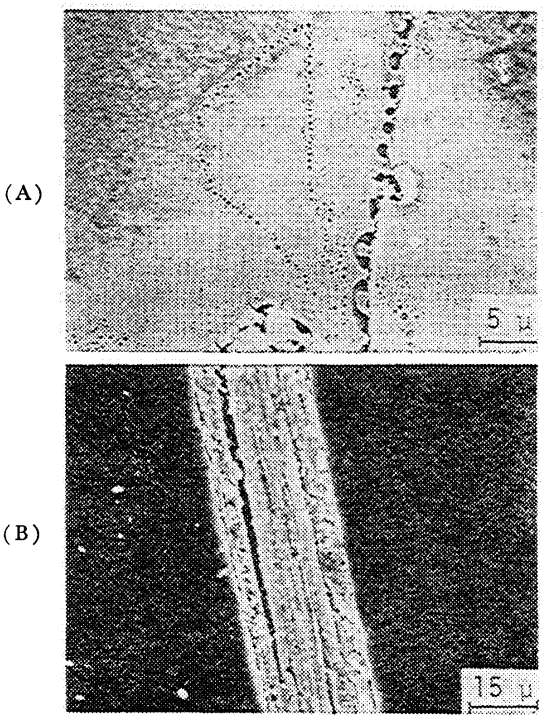

Fig. 12. Etching patterns. (A) Surface, (B) cross section.

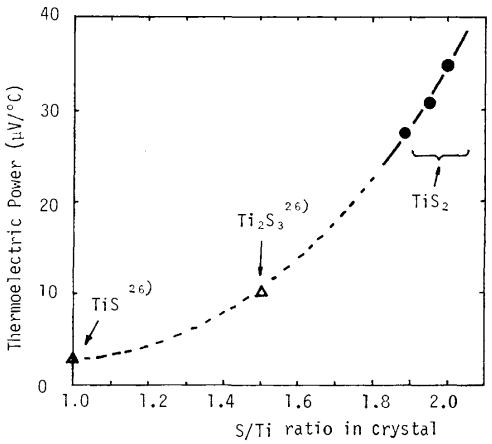

Fig. 13. Thermoelectric power of TiS_2 crystal.

atomic ratio of S/Ti decreases with increase in temperature, attaining a maximum of 1.83—1.90 at *ca.* 800 °C and increasing above 800 °C, except for that of crystals grown from a gas mixture of the H_2S ratio 0.6. Crystals having a high atomic ratio of 2.07—2.09 were grown at 600 °C with H_2S ratio of 0.4—0.7. Rimmington and Balchin,[17] Jeannin,[24] and Bartran[25] reported the limit of atomic ratio of S/Ti for titanium disulfide phase as 1.96—1.89, 1.98—1.81, and 2.00—1.50, respectively. Deposition limits of the single phase of titanium disulfide are shown in relation with growth temperature and gas flow ratio in Fig. 11, in which compositions of crystals are divided into three regions according to the phase limits.[24]

The lattice parameters of titanium disulfide crystals of S/Ti of 1.98 were determined to be 3.407 Å for *a* and 5.712 Å for *c*. The former agrees with those of $TiS_{1.96\pm0.03}$.[17] However, the latter is higher than those reported by Rimmington and Balchin[17] and lower than that reported by Norrby and Franzen.[28]

Etching Patterns. A titanium disulfide crystal grown at 850 °C from a gas mixture of H_2S ratio 0.5 was etched by 3 mol/dm³ nitric acid for 5 min at room temperature. The etching pattern on a (001) face is shown in Fig. 12A. Loop or open etch-pit arrays are observed with the order of density 10^2—10^3/cm². Cross section of a plate-like crystal was polished with abrasive paper and chromium trioxide powder, and etched (Fig. 12B). As expected, a plane vertical to the *c*-plane is weak against etching, cleavages of 0.5—2 μm thick being observed.

Thermoelectric Power. The thermoelectric power of titanium disulfide crystal is shown in Fig. 13 together with that reported on the titanium sulfides. Thermoelectric power of the crystals of S/Ti ratio 2.00 and 1.89 are 35 and 28 μV/°C at 20 °C, respectively, increasing linearly with increasing temperature. The thermoelectric power of the titanium sulfides was reported by Dubrovskaya and Oranesyan[26] to be 3.4 μV/°C (TiS) and 10 μV/°C (Ti_2S_3) and McTaggart[27] to be 200 μV/°C ($TiS_{1.95}$) and 600 μV/°C (TiS_3) on the pressed samples of fine powder. Thermoelectric power of the titanium sulfides increases with increase in sulfur content irrespective of the crystallographic nature, as in the Zr–S system.[27]

Conclusion

Crystals of titanium disulfide were grown by chemical vapor deposition in an open flow system.

1) Deposition rate reached a maximum at 700—800 °C. The flow ratio $H_2S/(TiCl_4+H_2S)$ near that of reaction stoichiometry, 0.67, resulted in the maximum rate irrespective of temperature.

2) Titanium trisulfide and sesquisulfide were found among the disulfide deposits below 350 °C and at 1000 °C, respectively.

3) It was found that well-formed hexagonal crystals grow either at low temperature such as 600 °C or from a gas mixture of a 0.2 flow ratio of $H_2S/(TiCl_4+H_2S)$.

4) Atomic ratio of S/Ti in grown crystals decreased to 1.83—1.90 with increase of temperature up to 800 °C.

5) Thermoelectric power of the crystals with the S/Ti ratios 2.00 and 1.89 was determined to be 35 and 28 μV/°C at 20 °C, respectively.

References

1) A. J. Haltner and C. S. Oliver, *J. Chem. Eng. Data*, **6**, 128 (1961).
2) A. I. Goncharov, V. A. Obolonchik, L. M. Prokoshina, S. V. Radzikuskaya, and A. A. Yasinski, *Ukr. Khim. Zh.*, **37**, 426 (1971); *Chem. Abstr.*, **75**, 53748le (1971).
3) Firma Dr. Eugen Duerrwaechter, DODUCO, Fr. Patent 1437951 (1966).
4) D. W. Murphy and F. A. Trumbore, *J. Cryst. Growth*, **39**, 185 (1977).
5) M. S. Whittinghan, *Science*, **192**, 1126 (1976).
6) L. H. Gaines, R. W. Francis, G. H. Newman, and B. M. L. Rao, 11th IECEC, Lake, Tahoe, September 1976.
7) H. Hahn and B. Harder, *Z. Anorg. Allg. Chem.*, **288**, 241 (1956).
8) H. Hahn and P. Ness, *Z. Anorg. Allg. Chem.*, **302**, 2 (1959).
9) K. Ohta, K. Fueki, and T. Mukaibo, *Denki Kagaku*, **41**, 697 (1973).
10) J. E. Dutrizac, *J. Less-Common Metals*, **51**, 283 (1977).
11) S. Toesca and J. C. Colson, *C. R. Acad. Sci., Ser. C*, **270**, 2101 (1970).
12) B. T. Kaminskii and A. S. Plygunov, *Ukr. Khim. Zh.*, **39**, 1224 (1973); *Chem. Abstr.*, **80**, 77814c (1974).
13) R. Nitsche, *J. Phys. Chem. Solids*, Suppl. No. 1, 215 (1967).
14) L. E. Conroy, *Inorg. Syn.*, **12**, 158 (1970).
15) H. Schafer, *J. Cryst. Growth*, **9**, 17 (1971).
16) H. P. B. Rimmington, A. A. Balchin, and B. K. Tanner, *J. Cryst. Growth*, **15**, 51 (1972).
17) H. P. B. Rimmington and A. A. Balchin, *J. Cryst. Growth.*, **21**, 171 (1974).
18) M. Saeki, *J. Cryst. Growth*, **36**, 77 (1976).
19) W. Biltz, P. Ehrlich, and K. Meisel, *Z. Anorg. Allg. Chem.*, **234**, 7 (1937).
20) D. A. Winn and B. C. H. Steele, *Mater. Res. Bull.*, **11**, 551 (1976).
21) J. G. Edwards, H. F. Franzen, and P. W. Gilles, *J. Chem. Phys.*, **54**, 545 (1971).
22) D. Alexejeff, *J. Chim. Phys.*, **23**, 415 (1926).
23) E. F. Strotzer, W. Biltz, and K. Meisel, *Z. Anorg. Allg. Chem.*, **242**, 249 (1939).
24) Y. Jeannin, *Ann. Chim.*, **7**, 57 (1962).
25) S. Bartran, *Dissertation Abstr.*, **19**, 1216 (1958).
26) G. N. Dubrovskaya and V. Kh. Oranesyan, *Izv. AN Armyansnkoi CCR*, **17**, 387 (1964).
27) F. K. McTaggart, *Aust. J. Chem.*, **11**, 471 (1958).
28) L. Norrby and H. Franzen, *J. Solid State Chem.*, **2**, 36 (1970).

Asymmetric Induction on the Reaction of Prochiral Olefins with Chloro-L-aminocarboxylato-η^2-ethyleneplatinum(II)

Yoshiro TERAI,** Hiroaki KIDO, Kazuo KASHIWABARA,*** and Kazuo SAITO*

Chemistry Department, Faculty of Science, Tohoku University, Aramaki, Aoba, Sendai 980

(Received May 17, 1978)

Addition of a large excess of *trans*-2-butene (tbn) or 2-methyl-2-butene (mbn) to an acetone solution of *cis*- or *trans*(*N*, ethylene)[PtCl(L-am)(C_2H_4)] (L-am, 9 kinds of L-aminocarboxylate) gave first increase and then gradual decrease in CD strength in the region $\simeq$26500 cm^{-1}. The kinetic optical yield amounted to 53% whereas that at the equilibrated state was much less (up to 27% for *cis*(*N*, olefin) complexes and 6 to 12% for trans complexes). *trans*-2-Butene gives larger yields than mbn. Kinetic analysis of the growth and decay curve of the CD strength disclosed that the first fast increase in CD reflects the greater rate of substitution of the prochiral olefins for ethylene in *S*-configuration than that in *R*-configuration. The second step seems to involve the exchange of coordinated tbn or mbn catalyzed by ethylene which was made free in the first step. The mechanism of asymmetric induction has been discussed from both steric and electronic viewpoints. Asymmetry of the coordinated nitrogen seems to give a dominating effect.

Corradini, Paiaro, and Pununzi observed asymmertic coordination of *trans*-2-butene (tbn) on the reaction between *cis*[$PtCl_2$((*S*)- or (*R*)-α-methylbenzylamine)(tbn)] and free tbn, and claimed that the selectivity is thermodynamically controlled.[1] We found that the replacement of coordinated *S,S*- or *R,R*-tbn in *trans*(*N*, olefin) [PtCl(L-pro)(*S,S*- or *R,R*-tbn[^3H])] (L-pro, L-prolinate) by free tbn in acetone takes place more easily with retention than with inversion of configuration. The stereoselectivity is considered to be caused by the steric interaction between the incoming tbn and the coordinated tbn and/or L-prolinate.[2] In order to clarify the source of such a stereoselective olefin exchange, we investigated the exchange of tbn between [$PtCl_3$(*S,S*-tbn[^3H])]$^-$ and free tbn, and found that the main source of asymmetric induction is in the interaction between the coordinated and the free tbn in the square pyramidal transition state.[3] However, this complex anion gives smaller ratio of rates of olefin exchange with retention and with inversion of the configuration than *trans*(*N*, olefin) [PtCl(L-am)(*S,S*-tbn)]. This suggests the significant role of L-aminocarboxylate ligand in the stereoselective substitution. This paper deals with the kinetics of substitution reaction of tbn and 2-methyl-2-butene(mbn) for the ethylene in *trans*- and *cis*(*N*, olefin) [PtCl(L-am)(C_2H_4)] and the accompanying thermodynamic and kinetic stereoselectivity, which is dependent on the geometrical isomerism of the complex and the variety of L-aminocarboxylates.

Experimental

Materials. All the complexes [PtCl(L-am)(ethylene)] were prepared according to previously reported methods.[4,5] The following ligands were employed; *trans*(*N*, olefin) complexes: L-am's are L-prolinate (L-pro), 4-hydroxy-L-prolinate (L-hyp), allo-4-hydroxy-L-prolinate (L-ahyp), *N*-methyl-L-prolinate (*N*-me-L-pro), *N*-methyl-4-hydroxy-L-prolinate (*N*-me-L-hyp), *N*-ethyl-L-prolinate (*N*-et-L-pro), *N*-benzyl-L-prolinate (*N*-bz-L-pro), *N*-benzyl-L-valinate (*N*-bz-L-val), L-valinate (L-val) and L-alaninate (L-ala); *cis*(*N*, olefin) complex; L-am is L-pro.

allo-4-Hydroxy-L-proline was prepared from 4-hydroxy-L-proline.[6,7] The *N*-substituted L-aminocarboxylic acids, *N*-me-L-proH, *N*-me-L-hypH, *N*-et-L-proH, *N*-bz-L-proH and *N*-bz-L-valH were synthesized by the reported methods.[8,9] The new *trans*(*N*, ethylene) complexes and their tbn and mbn derivatives containing L-ahyp, *N*-me-L-hyp, *N*-et-L-pro, *N*-bz-L-val were identified by elemental analysis of C, H, and N, and ultraviolet (UV) absorption spectra in acetonitrile (AN).

Results and Kinetic Analysis

Overall Progress of the Substitution Reaction between the Ethylene Complex and tbn. The change in CD pattern of *trans*(*N*, olefin) [PtCl(*N*-me-L-pro)(C_2H_4)] in the presence of a large excess of tbn is shown in Fig. 1. The change in CD strength at 26300 cm^{-1} is plotted against time in Fig. 2. The CD strength increases at the initial stage of the reaction to reach a maximum ($\Delta\varepsilon_{max}$) (first step). The UV absorption spectrum

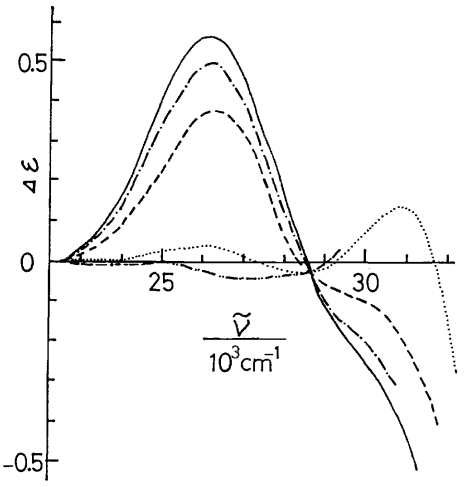

Fig. 1. Change of the CD spectrum with time on the reaction of *trans*(*N*,ethylene)[PtCl(*N*-me-L-pro)(C_2H_4)] (0.00154 mol dm^{-3}) with *trans*-2-butene (0.279 mol dm^{-3}) in acetone at −28.0 °C; dotted line: the original ethylene complex, broken line: 1 min, broken line with a dot: 2 min, solid line: 4 min, broken line with double dotts: infinite time.

**Present address: The Institute of Physical and Chemical Research, Hirosawa, Wako-shi, Saitama 351.

***Present address: Chemistry Department, Faculty of Science, Nagoya University, Chikusa, Nagoya 464.

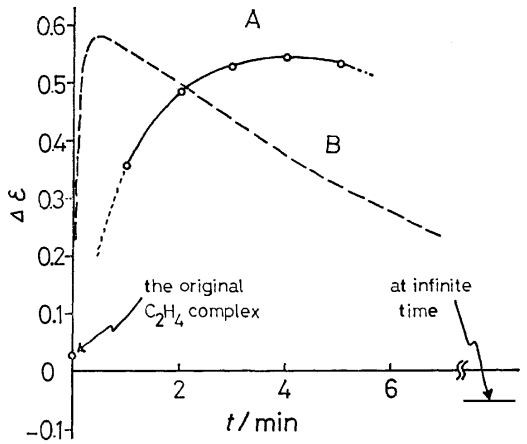

Fig. 2. Change in the CD strength with time on the reaction of *trans*(*N*,ethylene)[PtCl(*N*-me-L-pro)(C_2H_4)] with *trans*-2-butene in acetone.
A: Open circles correspond to the CD strength at the peak (26300 cm^{-1}) of the curves in Fig. 1.
B: The broken line represents the CD strength at 26300 cm^{-1} recorded continuously by the method reported in Ref. 4. ([complex]=0.00164 mol dm^{-3}, [*trans*-2-butene]=0.268 mol dm^{-3}, at 8.0 °C).

in the 32000—45000 cm^{-1} region of the original ethylene complex slightly changes simultaneously and approaches that of the tbn complex. This step should involve a stereoselective formation of the *S,S*-tbn complex by the substitution of tbn for the coordinated ethylene shown by

$$[PtCl(L\text{-am})(C_2H_4)] + tbn \rightarrow [PtCl(L\text{-am})(tbn)] + C_2H_4. \quad (1)$$

By the end of the first step, almost all the ethylene should have been replaced by tbn (*vide infra*). In the second step, the CD strength at 26300 cm^{-1} gradually decreases, while the UV absorption spectrum remains unchanged. The first step proceeds faster than the second step, and their kinetics can be studied separately. All the other ethylene complexes gave similar changes in CD and UV spectra except that for L-ala and L-val complexes, which gave change in the UV pattern but not in CD strength.

The apparent optical yields in the first step (p_{max}) were calculated by[10]

$$p_{max} = (\Delta\varepsilon_{max}-\Delta\varepsilon_{vic})/(\Delta\varepsilon_{resolv}-\Delta\varepsilon_{vic}), \quad (2)$$

where $\Delta\varepsilon_{resolv}$ is the CD peak strength in the region 26000—27000 cm^{-1} of the resolved tbn complex, and $\Delta\varepsilon_{vic}$ the CD strength due to the vicinal effect of L-aminocarboxylate (L-am), which is represented by the CD strength of the ethylene complex at the same wave number. The p_{max} values for a variety of L-aminocarboxylate complexes are shown in Table 1.

The second step gives no change in UV absorption spectrum, and hence is considered to be the replacement of asymmetrically coordinated tbn by free tbn toward a thermodynamically equilibrated state:

$$[PtCl(L\text{-am})(S,S\text{-tbn})] + tbn \rightarrow [PtCl(L\text{-am})(R,R\text{-tbn})] + tbn. \quad (3)$$

The optical yields at the equilibrium were calculated by

$$p_{eq} = (\Delta\varepsilon_{eq}-\Delta\varepsilon_{vic})/(\Delta\varepsilon_{resolv}-\Delta\varepsilon_{vic}), \quad (4)$$

where $\Delta\varepsilon_{eq}$ is the CD strength in the equilibrated state. The p_{eq} values are given in Table 1.

When mbn was used in place of tbn, similar changes in UV and CD spectra were observed. Equations 2[9] and 4 are applicable to the mbn complexes, the optical yields being given in Table 1.

Kinetic Analysis of the First Step. The increase in the CD strength ($\Delta\varepsilon_t$) at $\bar{\nu}_{max}$ (Table 1) in the first step obeyed the following first order kinetic formula 5 for all the complexes,

$$k_{obsd,i} = -\ln[(\Delta\varepsilon_t-\Delta\varepsilon_{max})/(\Delta\varepsilon_1-\Delta\varepsilon_{max})]/t, \quad (5)$$

where $\Delta\varepsilon_1$ is the initial CD strength in this step. $k_{obsd,i}$ increases linearly with increase in free tbn concentration to give

$$Rate_i = k_{obsd,i}[complex] = k_{2,i}[tbn][complex]. \quad (6)$$

The $k_{2,i}$ values are given in Table 2. The Reaction (1) should consist of two reactions,

$$[PtCl(L\text{-am})(C_2H_4)] + tbn \xrightarrow[k_{2[ES]}]{} [PtCl(L\text{-am})(S,S\text{-tbn})] + C_2H_4$$
$$\xrightarrow[k_{2[ER]}]{} [PtCl(L\text{-am})(R,R\text{-tbn})] + C_2H_4. \quad (7)$$

The relation between $k_{2[ES]}$, $k_{2[ER]}$, the optical yield p_{max} and $k_{2,i}$ is given by

$$(1+p_{max})/(1-p_{max}) = k_{2[ES]}/k_{2[ES]}, \quad (8)$$

$$k_{2,i} = k_{2[ES]} - k_{[ER]}. \quad (9)$$

The formation rate constants of the *S,S*- and *R,R*-tbn complexes from the ethylene complex, $k_{2[ER]}$ and $k_{2[ER]}$, can be calculated by Eqs. 8 and 9. (Table 2).

Kinetic Analysis of the Second Step. The rate of decrease in the CD strength ($\Delta\varepsilon_t$) at time t is expressed by the first order kinetic formula

$$k_{obsd,d} = -\ln[(\Delta\varepsilon_t-\Delta\varepsilon_{eq})/(\Delta\varepsilon_2-\Delta\varepsilon_{eq})]/t, \quad (10)$$

where $\Delta\varepsilon_2$ denotes the initial CD strength in this step. The $k_{obsd,d}$ is independent of the concentration of free tbn, but dependent on that of the complex:

$$k_{obsd,d} = k_{2,d}[complex]. \quad (11)$$

Since $k_{obsd,d}$ was obtained by the first order kinetic treatment with respect to the complex concentration, the rate of decrease in the CD strength is apparently proportional to the square of platinum(II) complex concentration:

$$Rate_d = k_{2,d}[complex]^2. \quad (12)$$

Such a kinetic formula is unusual for the substitution of a square planar complex, but can be accounted for by considering the catalytic action of ethylene liberated by Eq. 1 (*vide infra*). The concentration of free ethylene in the presence of a large excess of tbn should be equal to that of the initial complex, so that Eq. 12 can be rewritten as

$$Rate_d = k_{2,d}[complex][C_2H_4]. \quad (13)$$

In order to verify this, addition of a known amount of ethylene is desirable, but not practicable. Alternatively various amounts of *trans*(*N*, olefin) [PtCl(L-ala)-

TABLE 1. KINETIC AND THERMODYNANIC OPTICAL YIELDS OF *trans*(*N*, olefin)[PtCl(L-am)(olefin)] ON THE REACTION OF THE CORRESPONDING ETHYLENE COMPLEX WITH OLEFINS, ALONG WITH CIRCULAR DICHROISM DATA FOR THE COMPLEXES

L-am	$\bar{\nu}_{max}$ / 10^{-3} cm^{-1}	$\Delta\varepsilon_{resolv}$ [a]	$\Delta\varepsilon_{vle}$ [b]	Condition [c]	$\Delta\varepsilon_{max}$	p_{max} [d] / %	$\Delta\varepsilon_{eq}$	p_{eq} [e] / %
				with *trans*-2-butene				
L-pro	27.0[g]	1.05	−0.04		0.34	35	0.09	12(*S*,*S*)
				−27.5	0.32	34		
N-me-L-pro	26.3[g]	−1.06[h]	0.03		0.59	53	−0.05	−6(*R*,*R*)
				−28.0	0.55	49		
N-et-L-pro	26.3	1.0	0		0.52	*ca.* 50	0	0
N-bz-L-pro	26.0[g]	1.00	−0.19		0.10	24	−0.20	*ca.* −1(*R*,*R*)
				DCM	0.14	28		
				15.0	0.13	27	−0.16	3(*S*,*S*)
N-bz-L-val	26.3	1.00	−0.16		0.30	40	−0.28	−10(*R*,*R*)
					0.30	40[i]		
				AN	0.29	39	−0.27	−9(*R*,*R*)
				MA	0.25	35		
L-val	26.7[g]	−1.06[h]	−0.06	−30.0	k)	0		
L-ala	27.0[g]	1.09	−0.04	−30.0	k)	0		
L-hyp	27.0	1.04	−0.01		0.38	37	0.07	8(*S*,*S*)
N-me-L-hyp	26.3	−1.06[h]	0.02		0.34	32	−0.07	−7(*R*,*R*)
L-ahyp	27.0	1.09	0.04		0.43	37	0.10	6(*S*,*S*)
L-pro[f]	27.8[g]	1.14	0.12		0.46	33		
				AN	0.52	39		
				−13.0	0.47	34	−0.16	−27(*R*,*R*)
				with 2-methyl-2-butene				
L-pro	26.3	0.67	−0.04		0.008	7	0.004	6(*S*)
L-hyp	26.3	0.67	−0.03		0.01	6	(0.002)[j]	(3)[j] (*S*)
L-ahyp	26.3	0.70	0.00		0.14	19	0.05	7(*S*)
N-me-L-pro	25.6	0.74	0.04		0.09	7	0.03	*ca.* −1(*R*)
N-me-L-hyp	25.6	0.67	−0.03		−0.01	3	−0.03	0

a) $\Delta\varepsilon$ values for the resolved olefin complexes at $\bar{\nu}_{max}$ in acetone. b) $\Delta\varepsilon$ values for the ethylene complexes at $\bar{\nu}_{max}$ in acetone. c) In acetone at 8.0 °C unless otherwise stated; DCM: in dichloromethane, AN: in acetonitrile, MA: in L-menthylacetate; figures denote temperature in °C. d) From Eq. 2, always formation of (*S*,*S*)-*trans*-2-butene and (*S*)-2-methyl-2-butene complexes is preferred. e) From Eq. 4, *S* and *R* in parentheses indicate the configuration of olefin in the preferred diastereomer at the equilibrium. f) *cis*(*N*, olefin) isomers. g) Ref. 4. h) For the *R*,*R*-isomers; the other for the (*S*,*S*)-*trans*-2-butene or (*S*)-2-methyl-2-butene isomers. i) In the presence of *trans*-(*N*, ethylene) [PtCl(L-ala)(C_2H_4)] (see the text). j) Very sparingly soluble in acetone, and only an appoximate value is given. k) Not observed.

(C_2H_4)] were added to mixtures of *trans*(*N*, olefin)-[PtCl(*N*-bz-L-val)(C_2H_4)] and tbn in acetone at 8.0 °C, and the changes in the CD strength at 26300 cm^{-1} with time were measured. The rate of decrease in the CD strength in the second step is represented by

$$Rate_d = k_{2,d}[N\text{-bz-L-val complex}]([N\text{-bz-L-val complex}] + [\text{L-ala complex}]). \quad (14)$$

The L-ala complex undergoes rapid replacement of ethylene by free tbn without stereoselectivity (*cf.* Table 2). Thus the substrate complex for giving the CD change should be the *N*-bz-L-val complex alone. Under the given experimental conditions, practically all the ethylene should have been liberated from both the complexes during the first step of the reaction, and should be present as free ethylene in the reaction mixture. Thus, the term in parentheses in Eq. 14 is represented by the ethylene concentration [C_2H_4], so that Eq. 13 holds for this system. The $k_{2,d}$ values obtained from Eqs. 12 and 14 are 1.09 and 1.15 s^{-1}-mol^{-1} dm^3, respectively, for the *N*-bz-L-val complex at 8 °C, indicating the legitimacy of such a kinetic treatment.

The $k_{2,d}$ values can be compared to the k_2 values for the pure epimerization of *trans*(*N*, olefin) [PtCl-(L-am) (*S*,*S*-tbn)] in the presence of tbn under similar conditions.[4] The larger values for $k_{2,d}$ than for k_2 may be interpreted by considering the catalytic action of ethylene as in the following.

Catalytic Action of Ethylene in the Second Step. Less bulky olefins give larger values of k_2 on the substitution for tbn in *trans*(*N*, olefin) [PtCl(L-pro)(tbn)].[2] Hence, ethylene should be a more effective nucleophile than tbn towards [PtCl(L-am)(*S*,*S*- or *R*,*R*-tbn)], and the contribution of direct substitution of tbn can be ignored. Individual second order rate constants for the ethylene-

TABLE 2. INDIVIDUAL SECOND ORDER RATE CONSTANTS OF THE REACTION OF *trans*(*N*,ethylene)-[PtCl(L-am)(C_2H_4)] WITH *trans*-2-BUTENE[a]

L-am	Condition[b]	$k_{2,i}$[c]	$\frac{p_{max}}{\%}$	$k_{2[ES]}$[c]	$k_{2[ER]}$[c]	$k_{2,d}$[d]	$\frac{p_{eq}}{\%}$	$k_{2[SE]}$[d]	$k_{2[RE]}$[d]
L-pro		fast	35			6.1	12	8.3	5.1
	−27.5	(450)[g]	34	(890)	(440)				
N-me-L-pro		fast	53			1.1	−6	2.5	0.68
	−28.0	(75)[g]	49	(114)	(39)				
N-et-L-pro		10	50	15	5	slow	0		
N-bz-L-pro		8.2	24	21.2	13.0	slow	*ca.* −1		
	DCM	8.0	28	18.3	10.3	slow			
	15.0	15.3	27	36.0	20.7	0.018	<3	0.024	0.015
N-bz-L-val		fast	40			1.09	−10	2.0	0.70
		fast	40			1.15		(2.1)	(0.74)
	AN	fast	39			1.18	−9	2.1	0.77
	MA	fast	35			1.0		(1.9)	(0.66)
L-val	−30.0	not obsd	0				0		
L-ala	−30.0	not obsd	0				0		
L-hyp		fast	37			10.8	8	15.8	8.5
N-me-L-hyp		fast	32			2.4	−7	3.8	1.7
L-ahyp		fast	37			3.8	6	5.7	3.0
L-pro[e]		(20)[h]	33	(40)	(20)				
	AN	(50)[h]	39	(90)	(40)				
	−13.0	(2)[g,h]	34	(4)	(2)		−27		
L-pro[f]		fast	7			2.77	6	2.80	2.75

a) The error in k_2 values is ±5 on the last figures of individual data on 70% confidence level unless otherwise stated. b) *Cf.* footnote c in Table 1. c) In 10^{-3} s^{-1} mol^{-1} dm^3. d) In s^{-1} mol^{-1} dm^3. e) Reaction of *cis*(*N*,ethylene) isomer. f) Reactions with 2-methyl-2-butene. g) Only from one datum. h) *Cf.* footnote, j in Table 1.

catalyzed epimerization

$$\begin{array}{l}[PtCl(L\text{-am})(S,S\text{-tbn})] + C_2H_4 \\ \qquad\qquad \nwarrow\!\searrow\ k_{2[SE]} \\ \qquad k_{2[ES]}\ \searrow\!\nwarrow \qquad [PtCl[(L\text{-am})(C_2H_4)] \\ \qquad k_{2[RE]}\ \nearrow\!\swarrow\ k_{2[ER]} \qquad\qquad + \text{tbn}, \quad (15) \\ [PtCl(L\text{-am})(R,R\text{-tbn})] + C_2H_4\end{array}$$

are written as follows:

$$d[S]/dt = k_{2[ES]}[E][\text{tbn}] - k_{2[SE]}[S][C_2H_4], \quad (16)$$

$$d[E]/dt = k_{2[SE]}[S][C_2H_4] - (k_{2[ES]}+k_{2[ER]})[E][\text{tbn}] + k_{2[RE]}[R][C_2H_4], \quad (17)$$

$$d[R]/dt = k_{2[ER]}[E][\text{tbn}] - k_{2[RE]}[R][C_2H_4], \quad (18)$$

$$[C] = [S] + [E] + [R], \quad (19)$$

where [E], [S], and [R] represent the concentrations of the ethylene, *S,S*-tbn and *R,R*-tbn complexes containing a given L-am, respectively; [C] is their total. Under the present experimental conditions where the free tbn overwhelms the initial ethylene complex and the first step has reached completion, the ethylene complex should be present only as an intermediate in Eq. 15, and a steady state treatment can be applied to Eq. 17, *i.e.* $d[E]/dt=0$. Hence the rate of decrease of [S] can be written by

$$-d[S]/dt = (k_{2[SE]}k_{2[ER]}[S] - k_{2[RE]}k_{2[ES]}[R]) \times [C_2H_4]/(k_{2[ES]}+k_{2[ER]}). \quad (20)$$

Integrating, we get

$$-\ln\left\{\frac{[S]-(k_{2[RE]}k_{2[ES]}[R]/k_{2[SE]}k_{2[ER]})}{[S]+[R]}\right\}\Big/t = (k_{2[SE]}k_{2[ER]} + k_{2[RE]}k_{2[ES]})[C_2H_4]/(k_{2[ES]}+k_{2[ER]}) \quad (21)$$

In the equilibrated state, the left side of Eq. 20 should be zero, and we obtain

$$K_{RS} = [S]_\infty/[R]_\infty = k_{2[RE]}k_{2[ES]}/k_{2[SE]}k_{2[ER]}. \quad (22)$$

Expressing [S], [R], $[S]_\infty$, and $[R]_\infty$ in Eqs. 21 and 22 in terms of $\Delta\varepsilon_t$, $\Delta\varepsilon_2$, and $\Delta\varepsilon_\infty$, we have

$$-\ln\{(\Delta\varepsilon_t-\Delta\varepsilon_\infty)/(\Delta\varepsilon_2-\Delta\varepsilon_\infty)\}/t = (k_{2[SE]}k_{2[ER]}+k_{2[RE]}k_{2[ES]})[C_2H_4]/(k_{2[ES]}k_{2[ER]}). \quad (23)$$

This corresponds to the experimental kinetic formula Eq. 13, $k_{2,d}$ being written as

$$k_{2,d} = (k_{2[SE]}k_{2[ER]}+k_{2[RE]}k_{2[ES]})/(k_{2[ES]}/k_{2[ER]}). \quad (24)$$

From Eqs. 8, 16, 22, and 24, individual rate constants were calculated by use of the following equations:

$$k_{2[SE]} = (1-p_{eq})k_{2,d}/(1-p_{max}), \quad (25)$$

$$k_{2[RE]} = (1+p_{eq})k_{2,d}/(1+p_{max}). \quad (26)$$

The data for tbn and mbn complexes are given in Table 2.

Discussion

Stereoselectivity in the Equilibrium State. The p_{eq} value for the tbn complexes in the equilibrium state (end point of the second step) can be reckoned as to

reflect the difference of stability between the *S,S*- and the *R,R*-tbn complexes. The stability should be directly related to the structure of both isomers. Table 1 indicates that the *cis*(*N*, olefin) complex gives a rather large negative p_{eq}. Molecular models of the two optical isomers of *cis*(*N*, olefin) [PtCl(L-pro)(tbn)] suggest that the coordinated *S,S*-tbn is subject to a larger steric hindrance than *R,R*-tbn is, giving a large negative p_{eq} value (favorable for *R,R*-configuration).

trans(*N*, tbn)-Complexes with various L-aminocarboxylates containing asymmetric nitrogens give larger $|p_{eq}|$ values than those without asymmetric nitrogens. Molecular model studies cannot account for such a selectivity. An indirect influence coming from solvent molecules does not seem significant, since similar optical yields were observed for the *N*-bz-L-pro and *N*-bz-L-val complex in different solvents (Table 1). There can be an electronic effect from the asymmetric nitrogen to the coordinated tbn through platinum(II) d-orbitals. We studied the CD spectra of *trans*(*N*, olefin)[PtCl(L-am)(*S,S*-tbn)], and suggested an electronic perturbation from asymmetric nitrogen upon coordinated tbn.[11] However, the L-pro, L-hyp, and L-ahyp complexes give positive, and the *N*-me-L-pro, *N*-me-L-hyp and *N*-bz-L-val complexes negative signs. The reason for such a difference cannot be understood at the present stage.

A similar trend in p_{eq} values is observed for the mbn complexes, the signs being the same as those for the tbn complexes. However, the figures for the mbn complexes are smaller than those for the tbn complexes with given L-aminocarboxylates.

Asymmetric Induction on the Substitution of tbn. The *S,S*-tbn complexes are formed from the corresponding ethylene complexes more readily than the *R,R*-tbn complexes. The extent can be represented by the p_{max} values. The complexes containing asymmetric nitrogens give p_{max} values from 20 to 55%, while the L-ala and L-val complexes without asymmetric nitrogens fail to give appreciable optical yields. Thus the asymmetric induction should be governed by the symmetry of the coordinated amino nitrogen. The energy diagram for the forward process of Eq. 7 can be written as shown in Fig. 3. The $\delta\Delta G^*$ is expressed by

$$-\delta\Delta G^* = RT\ln[(1+p_{max})/(1-p_{max})] = RT\ln(k_{2[ES]}/k_{2[ER]}). \quad (29)$$

The sign of p_{max} is not always equal to that of p_{eq} for a given complex. The sequence of magnitude of p_{max}'s of the complexes containing various aminocarboxylates is neither parallel to that of p_{eq}'s. The difference between $k_{2[ES]}$ and $k_{2[ER]}$ for a given complex cannot be interpreted by the difference in stability between the *S,S*- and *R,R*-tbn complexes. The transition state on the substitution reaction should be considered.

Substitution reactions of square-planar complexes are understood to proceed *via* five coordinated transition states. The kinetic ease of formation of the *S,S*- and *R,R*-tbn complexes should reflect the stability of the transition state. Two possible structures are considered for the five coordinated transition state.[12] Whenever a trigonal bipyramidal structure is formed as intermediate or transition state, the ligand to be replaced is reckoned to be located at the basal position. In the present complex either amino nitrogen or carboxyl oxygen occupies the basal position depending on the trans or cis isomerism of the original complex, respectively. The mutual location between the incoming tbn, which always occupies one of the basal positions, and the asymmetric nitrogen, which should play the most important role in determining the selectivity, should differ depending on the geometrical isomerism. In the square pyramidal structure, on the other hand, the mutual locations between nucleophilic tbn and asymmetric nitrogen do not differ much for both geometrical isomers. From our experimental results, however, the p_{max} values are almost equal for the formation of *trans* and *cis*(*N*, olefin) [PtCl(L-pro)(*S,S*-tbn)], indicating that the transition state would be more appropriately apporoximated by the square pyramidal structure. This interpretation is in line with the suggestion made for the isotopic exchange between [$PtCl_3$(tbn[^3H])] and tbn.[3]

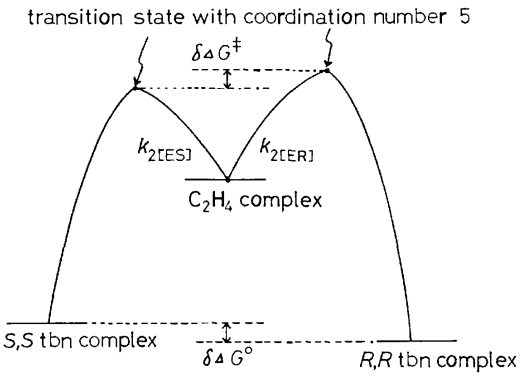

Fig. 3. Schematic diagram of the change in Gibbs free energy on the reaction of *trans*(*N*,ethylene)[PtCl(L-am)(C_2H_4)] with prochiral olefins.

Detailed structure of the transition state cannot be discussed at the present stage, but the side from which the incoming olefin approaches platinum(II) plane might be as follows. The substituent on the amino nitrogen in the complex extends to the opposite side of the square plane to that where the pyrrolidine ring of L-prolinate does. The p_{max} values depend on the variety of the *N*-substituent, but the location of hydroxyl group on the 4-position of the pyrrolidine ring (L-hyp and L-ahyp) affects neither the p_{max} nor the rate constant. Thus the incoming tbn will approach platinum(II) from the opposite side to that occupied by the pyrrolidine. The bulkiness of the substituent on amino nitrogen of the aminocarboxylate affects the p_{max} in different ways depending on the kind of aminocarboxylate; *e.g.* introduction of benzyl group on L-valinate increases whereas that on L-prolinate decreases the p_{max}. Studies with molecular models suggest that the approach of tbn to the platinum(II) bound to *N*-substituted aminocarboxylate would be easier in *S,S*-configuration than in *R,R*-configuration. More than one factor should affect the p_{max} and $k_{2,d}$ values.

Asymmetric Induction on the Reaction with mbn. The p_{max} values for the formation of *S*-mbn complexes are

smaller than those of tbn complexes (Table 1). The transition state for the reactions with mbn should be similar to those with tbn. Free mbn has two methyl groups on one side of C=C double bond axis, and one methyl group and methine hydrogen on the other side. When the former side is directed to the coordinated L-amino nitrogen in the transition state, no difference is expected in the steric interactions, regardless of the orientation of the methine hydrogen. Such an attack does not result in a stereoselective substitution. When the other side faces the asymmetric nitrogen, a stereoselective formation can be expected to give p_{max} values similar to those on the attack of tbn. Participation of these two different transition states should be responsible for the smaller values of p_{max} on the substitution of mbn than those on reaction with tbn.

Comparison of Overall Rate Constants and the Contribution by the Substituents of the Coordinated L-Aminocarboxylates. Table 2 indicates that the individual rate constants, $k_{2[ES]}$, $k_{2[ER]}$, $k_{2[SE]}$, and $k_{2[RE]}$ are largely dependent on the variety of L-aminocarboxylate. However, an overall trend is obvious; *i.e.* the second order rate constants decrease in the following sequence, which is equal to that for the exchange of tbn in *trans*(*N*, olefin) [PtCl(L-am)(*S*,*S*-tbn)].[4]

L-hyp > L-pro > L-ahyp > *N*-me-L-hyp > *N*-bz-L-val >

N-me-L-pro > *cis*(*N*, olefin) L-pro > *N*-bz-L-pro

Introduction of trans OH (L-hyp) on 4-position of pyrrolidine ring increases whereas that of cis OH(L-ahyp) decreases the k_2 values both for L-pro and *N*-me-L-pro complexes. However, this effect is smaller than that of the introduction of *N*-substituents on the L-aminocarboxylates. Thus, the reaction rates of individual courses of olefin exchange is largely controlled by the moiety around amino nitrogen, and to a less extent by the substituents on the 4-position of the pyrrolidine ring. Such a trend seems to be interpreted by the stereochemistry of the transition state mentioned above.

References

1) P. Corradini, G. Paiaro, and A. Pununzi, *J. Am. Chem. Soc.*, **88**, 2863 (1966); A. Pununzi and G. Paiaro, *J. Am. Chem. Soc.*, **88**, 4843 (1966).
2) Y. Terai, H. Kido, J. Fujita, and K. Saito, *Bull. Chem. Soc. Jpn.*, **48**, 1233 (1975).
3) Y. Terai and K. Saito, *Bull. Chem. Soc. Jpn.*, **51**, 503 (1978).
4) Y. Terai, H. Kido, K. Kashiwabara, J. Fujita, and K. Saito *Bull. Chem. Soc. Jpn.*, **50**, 150 (1977).
5) J. Fujita, K. Konya, and K. Nakamoto, *Inorg. Chem.*, **9**, 2794 (1970).
6) A. A. Patchett and B. Witokop, *J. Am. Chem. Soc.*, **79**, 185 (1957).
7) F. Irreverre, K. Morita, A. V. Robertson, and B. Witokop, *J. Am. Chem. Soc.*, **85**, 2824 (1963).
8) P. Quitt, J. Hellerbach, and K. Vogler, *Helv. Chim. Acta*, **46**, 327 (1963).
9) A. B. Mauger and B. Witokop, *Chem. Rev.*, **66**, 48 (1966).
10) ($\Delta\varepsilon_{resolv} - \Delta\varepsilon_{vlc}$) values of the tbn complexes are *ca.* 1—1.1 for various coordinated L-aminocarboxylates, whereas those of the mbn complexes are 0.7.
11) Y. Terai, H. Kido, and K. Saito, *Bull. Chem. Soc. Jpn.*, **50**, 3265 (1977).
12) L. Cattalini, *Prog. Inorg. Chem.*, **13**, 263 (1970).

Structural Study of Optical Resolution. IV-b.** The Crystal Structure of $(+)_{589}$-Oxalatobis(ethylenediamine)cobalt(III) Hydrogen-*d*-tartrate Monohydrate and Its Thermal Behavior

Masahiro KURAMOTO, Yoshihiko KUSHI, and Hayami YONEDA*

Department of Chemistry, Faculty of Science, Hiroshima University, Higashi-senda-machi, Hiroshima 730

(Received May 24, 1978)

The crystal structure of $(+)_{589}$-oxalatobis(ethylenediamine)cobalt(III) hydrogen-*d*-tartrate monohydrate, $(+)_{589}$-[Co(ox)en_2]H-*d*-tart·H_2O, has been determined by three-dimensional X-ray analysis. The red crystals are monoclinic, space group $P2_1$, with two molecules in a unit cell of dimensions $a=8.27(1)$, $b=14.60(1)$, $c=7.02(1)$ Å, and $\beta=104.8(2)°$. The structure was solved by Patterson and Fourier methods, and refined by anisotropic block-diagonal least-squares to a conventional R-value of 0.100 for the 1265 independent reflections observed. In the diastereoisomer, the optically active complex cation is locked by the $\{H\text{-}d\text{-tart}\}_\infty$ units of the right-handed spiral chains formed along the b-axis. The TG and DSC measurements have been carried out on both less- and more-soluble diastereoisomers of oxalatobis(ethylenediamine)cobalt(III) hydrogen-*d*-tartrate; the difference of their thermal behavior is discussed.

As parts of our structural studies of optical resolution,[1-6] we reported the structures of several diastereoisomers in crystals containing *d*-tartrate anion (*d*-tart^{2-}; *d*-$C_4H_4O_6^{2-}$)[2-4] as the resolving agent. In these compounds, "face-to-face" close contacts between a triangular face of the octahedral complex cation and the *d*-tart^{2-} anion were found.[2-4] The results seem to support the famous "key and lock" hypothesis of Fischer for the diastereomeric discrimination.[7]

Recently, optical resolutions of several complex cations were effected by using hydrogen-*d*-tartrate (H-*d*-tart$^-$; *d*-$C_4H_5O_6^-$) anion as a resolving agent.[8-12] Among them, a simple one-step resolution which provides both optical isomers of oxalatobis(ethylenediamine)cobalt(III) cation, $[Co(ox)en_2]^+$, in high yield was established.[10]

We thought it would be worthwhile to compare the packing manner of the H-*d*-tart$^-$ anion in the above-mentioned diastereoisomers with those of the *d*-tart^{2-} anion in the previous studies. Thus, three-dimensional X-ray analysis of the less-soluble $(+)_{589}$-[Co(ox)en_2]H-*d*-tart·H_2O has been undertaken.

Besides the single crystals of the less-soluble diastereoisomer, the single crystals of the more-soluble isomer, $(-)_{589}$-[Co(ox)en_2]H-*d*-tart·$2H_2O$, could also be obtained, and the thermal behavior of these two diastereoisomers has been examined.

A preliminary communication of this study has already been published.[1]

Experimental

Preparation of Compound. *(a) $(+)_{589}$-[Co(ox)en_2] H-d-tart·H_2O*: The less-soluble diastereoisomer was prepared by the method of Jordan *et al.*[10] Recrystallization from hot aqueous solution of the diastereoisomer gave red crystals. The crystals have a trapezoidal rod shape. Found: C, 27.40; H, 5.32; N, 12.58%. Calcd for $(+)_{589}$-[Co(ox)en_2]H-*d*-tart·H_2O: C, 27.56; H, 5.30; N, 12.90%. The optical purity of these crystals was also checked by the CD-measurement(a JASCO Model J-40CS spectrophotometer with 1 cm cell. ($\Delta\varepsilon_{520}=+2.70$).

(b) $(-)_{589}$-[Co(ox)en_2]H-d-tart·$2H_2O$: After removal of the precipitated crystals of the $(+)_{589}$-diastereoisomer,[10] the filtrate solution was evaporated for 2—3 days at room temperature. The filtration of the $(+)_{589}$-diastereoisomer was continued. This step was repeated three times. As a result, the red crystals of more-soluble $(-)_{589}$-diastereoisomeric salt dihydrate were separated out. The crystals have an octagonal rod shape. Found: C, 26.65; H, 5.64; N, 12.59%. Calcd for $(-)_{589}$-[Co(ox)en_2]H-*d*-tart·$2H_2O$: C, 26.55; H, 5.57; N, 12.39%. The optical purity of these crystals was also checked by the CD-measurement ($\Delta\varepsilon_{523}=-2.18$).

X-Ray Data Measurement. *(a) The Less-soluble Diastereoisomer*: Weissenberg photographs indicated a monoclinic unit cell with systematic extinctions for $0k0$, $k=2n+1$. Of the two possible space groups, $P2_1$ and $P2_1/m$, the latter was eliminated because of the optical activity of the compound. The unit cell dimensions were determined by the least-squares refinement of the $hk0$, $h0l$, and $0kl$ reflection data recorded on Weissenberg photographs. The sodium chloride diffraction lines were superimposed on the films for calibration. The crystal data are as follows: monoclinic, space group $P2_1$, $a=8.27(1)$, $b=14.60(1)$, $c=7.02(1)$ Å, $\beta=104.8(2)°$, $D_m=1.74$ g/cm^3 (by flotation in chloroform-bromoform mixture), $Z=2$, and $D_c=1.76$ g/cm^3.

A crystal 0.80 mm long with a cross-sectional area of (0.40×0.35) mm^2 was selected for obtaining the $hk0$—$hk5$ intensity data with Ni $K\alpha$ radiation, using the multiple-film equi-inclination Weissenberg technique. Another crystal, 0.25 mm long with (0.25×0.38) mm^2 cross-sectional area, was used to obtain the intensity data $0kl$—$2kl$. The intensities were estimated visually with a calibrated intensity scale. A total of 1318 independent reflections were collected. Among them 1265 reflections were observed ($|F_o|>0$) and used for the structure determination. Lorentz, polarization, and spot-shape corrections were applied in the usual manner; corrections for absorption were not made since the value of linear absorption coefficient, μ(Ni $K\alpha$), was 26.7 cm^{-1}.

(b) The More-soluble Diastereoisomer: The crystal data of the more-soluble diastereoisomer were determined similarly. They are as follows: orthorhombic, space group $P2_12_12$, $a=16.56(1)$, $b=14.14(1)$, $c=7.39(1)$ Å, $D_m=1.72$ g/cm^3, $Z=4$, and $D_c=1.74$ g/cm^3.

Thermogravimetric Analysis(TG). TG data were obtained by using a Rigaku Thermal Analyzer Model 8005. A heating rate of 3 °C/min and a static air atmosphere were employed and 9.36—9.71 mg samples were used in each run.

Differential Scanning Calorimetry(DSC). A Rigaku Differential Scanning Calorimeter(Model-8055Cl) was used to

**Ref. 1 corresponds to "Structural Study of Optical Resolution IV-a."

TABLE 1. FINAL ATOMIC PARAMETERS WITH THEIR e.s.d.'s

Atom	x	y	z
Co	0.5556(2)	0.2500(2)	0.5807(2)
O(X1)	0.462(1)	−0.003(1)	0.689(2)
O(X2)	0.542(1)	0.101(1)	1.033(1)
O(X3)	0.514(1)	0.121(1)	0.530(1)
O(X4)	0.575(1)	0.221(1)	0.846(1)
O(T1)	0.190(2)	0.178(1)	0.838(2)
O(T2)	0.119(2)	0.216(1)	1.111(2)
O(T3)	0.232(1)	−0.002(1)	0.960(2)
O(T4)	−0.125(1)	0.055(1)	0.836(2)
O(T5)	−0.123(2)	−0.118(1)	0.932(2)
O(T6)	0.044(1)	−0.101(1)	1.234(2)
O(W)	0.043(2)	0.026(1)	0.535(2)
N(1)	0.314(2)	0.271(1)	0.537(2)
N(2)	0.791(2)	0.230(1)	0.617(2)
N(3)	0.551(1)	0.274(1)	0.305(2)
N(4)	0.583(1)	0.379(1)	0.656(2)
C(E1)	0.278(2)	0.371(1)	0.545(2)
C(E2)	0.831(2)	0.221(1)	0.428(2)
C(E3)	0.728(2)	0.292(1)	0.296(2)
C(E4)	0.425(2)	0.408(1)	0.711(3)
C(X1)	0.501(2)	0.078(1)	0.679(2)
C(X2)	0.543(2)	0.134(1)	0.874(2)
C(T1)	0.157(2)	0.159(1)	0.992(2)
C(T2)	0.154(2)	0.061(1)	1.064(2)
C(T3)	−0.029(2)	0.030(1)	1.027(2)
C(T4)	−0.033(2)	−0.072(1)	1.068(2)

measure the DSC curves. In order to determine the ΔH values of dissociation of the water of crystallization for both diastereoisomers, the instrument was calibrated using the ΔH values of fusion of pure indium, tin, and lead metals as standards. Weights of samples were 8.03 to 13.1 mg. A heating rate of 10 °C/min was used in each run. The dry nitrogen gas(25 ml/min) was used as a furnace atmosphere.

Determination and Refinement of Crystal Structure

The structure was solved by the heavy-atom method. The position of the cobalt atom was determined from the three-dimensional Patterson map. The subsequent Fourier synthesis revealed the positions of all the non-hydrogen atoms. Refinement employing these atomic positions with isotropic thermal parameters converged to a conventional R factor of 0.132 for the 1265 observed reflections, where the R value is $\Sigma||F_o|-|F_c||/\Sigma|F_o|$.

Hydrogen atom co-ordinates, excluding the water molecule and the glycolic hydroxyl and carboxyl groups of H-*d*-tart anion, were calculated (C–H 1.08, N–H 1.00 Å) assuming tetrahedral angles at carbon and nitrogen atoms. Refinement with anisotropic temperature factors for all the non-hydrogen atoms and with fixed hydrogen atom contributions(the isotropic temperature factor $B=3.0$ Å^2 was used) was continued. After four cycles an R value of 0.100 was obtained and the refinement was terminated. The quantity minimized was $w(|F_o|-k|F_c|)^2$ and Cruickshank's weighting scheme[13] was used, where $w=1/(a+|F_o|+b|F_o|^2)$ with $a=5.80$ and $b=0.037$. The atomic scattering factors from the International Tables[14] were used. The dispersion effects were neglected.

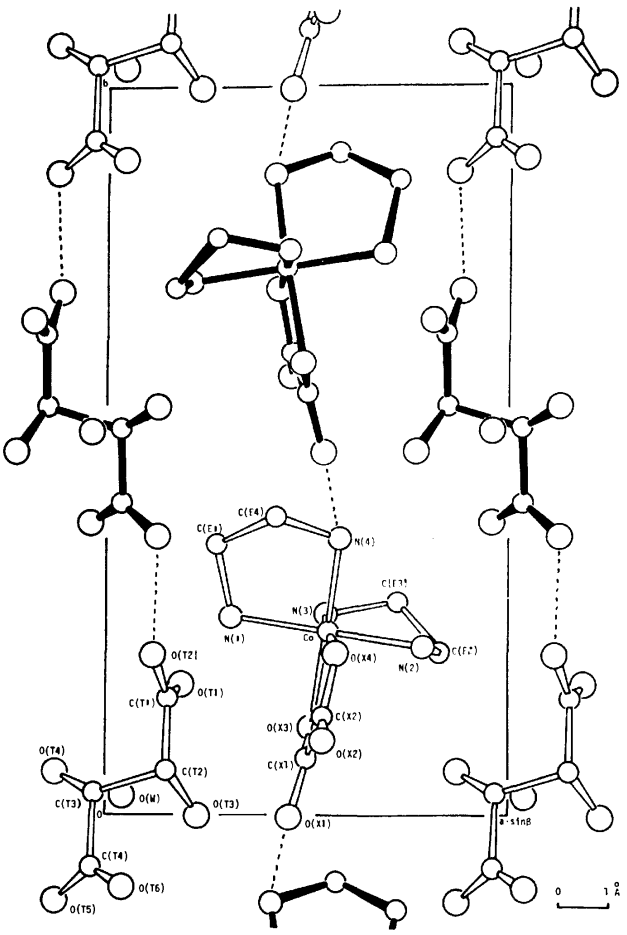

Fig. 1. A perspective drawing of the contents of the unit cell viewed along the c-axis.

All the computations were carried out by a HITAC-8700 computer at the Hiroshima University Computer Center. The computer programs used were FOUR-2/M(Fourier synthesis)[15] and HBLS-IV(Least-squares calculation) with a slight modification.[16]

The final atomic parameters and temperature factors(with their estimated standard deviations) are listed in Tables 1 and 2. Complete lists of the $10F_o$ and $10F_c$ values and the final atomic parameters of the hydrogen atoms have been preserved by the Chemical Society of Japan (Document No. 7838).

Results and Discussion

The crytsal structure consists of discrete $(+)_{589}$-$[Co(ox)en_2]^+$ cations, H-*d*-tart anions, and water molecules. Figures 1 and 2 show the projections of the crystal structure along the c- and b-axis, respectively. Bond distances and angles within the complex cation and the H-*d*-tart anion are listed in Table 3. The water molecules exist around the twofold screw axis at (0, y, 1/2). Each complex cation is surrounded by eight H-*d*-tart anions in a deformed cubic environment.

Cation Geometry. All distances and angles

TABLE 2. ANISOTROPIC TEMPERATURE FACTORS($\times 10^3$) EXPRESSED IN THE FORM $\exp[-2\pi^2(U_{11}h^2a^{*2}+U_{22}k^2b^{*2}+U_{33}l^2c^{*2}+2U_{12}hka^*b^*+2U_{13}hla^*c^*+2U_{23}klb^*c^*)]$.

Atom	U_{11}	U_{22}	U_{33}	U_{12}	U_{13}	U_{23}
Co	40(1)	29(1)	34(1)	−3(1)	4(1)	0(1)
O(X1)	49(6)	13(4)	42(6)	−12(4)	14(5)	−5(4)
O(X2)	52(7)	30(5)	20(5)	−5(5)	11(5)	5(4)
O(X3)	31(5)	29(5)	18(5)	−2(4)	2(4)	0(4)
O(X4)	32(5)	13(4)	22(4)	−8(3)	−3(4)	3(3)
O(T1)	57(7)	27(5)	61(8)	2(5)	29(6)	18(6)
O(T2)	85(9)	16(5)	47(7)	−1(5)	7(7)	4(5)
O(T3)	39(6)	18(5)	59(7)	8(4)	15(5)	−3(5)
O(T4)	29(5)	22(4)	39(6)	4(4)	−2(4)	8(4)
O(T5)	73(9)	17(5)	51(7)	−8(5)	−9(6)	8(5)
O(T6)	41(6)	18(4)	31(5)	−1(4)	6(4)	5(4)
O(W)	76(11)	65(10)	58(9)	4(8)	16(8)	−13(8)
N(1)	34(6)	37(7)	24(6)	−4(5)	0(5)	−6(5)
N(2)	38(6)	14(5)	27(6)	4(4)	0(5)	4(4)
N(3)	24(5)	35(7)	17(5)	−4(4)	0(5)	−1(4)
N(4)	24(5)	27(5)	22(6)	−4(4)	3(5)	−3(5)
C(E1)	28(7)	43(9)	40(9)	2(6)	4(7)	−8(7)
C(E2)	30(7)	33(7)	28(7)	−3(5)	1(6)	0(6)
C(E3)	38(8)	21(6)	26(7)	−3(5)	11(6)	5(5)
C(E4)	41(9)	30(7)	46(10)	5(6)	13(7)	−13(7)
C(X1)	39(7)	20(6)	30(7)	−1(5)	13(6)	−7(5)
C(X2)	35(7)	23(6)	18(7)	−1(5)	5(6)	6(5)
C(T1)	24(7)	29(7)	34(8)	−5(5)	−8(6)	11(6)
C(T2)	30(7)	17(6)	31(7)	4(5)	11(6)	−1(5)
C(T3)	26(7)	18(6)	33(8)	6(5)	13(6)	13(5)
C(T4)	29(7)	23(7)	38(8)	−7(5)	3(6)	0(6)

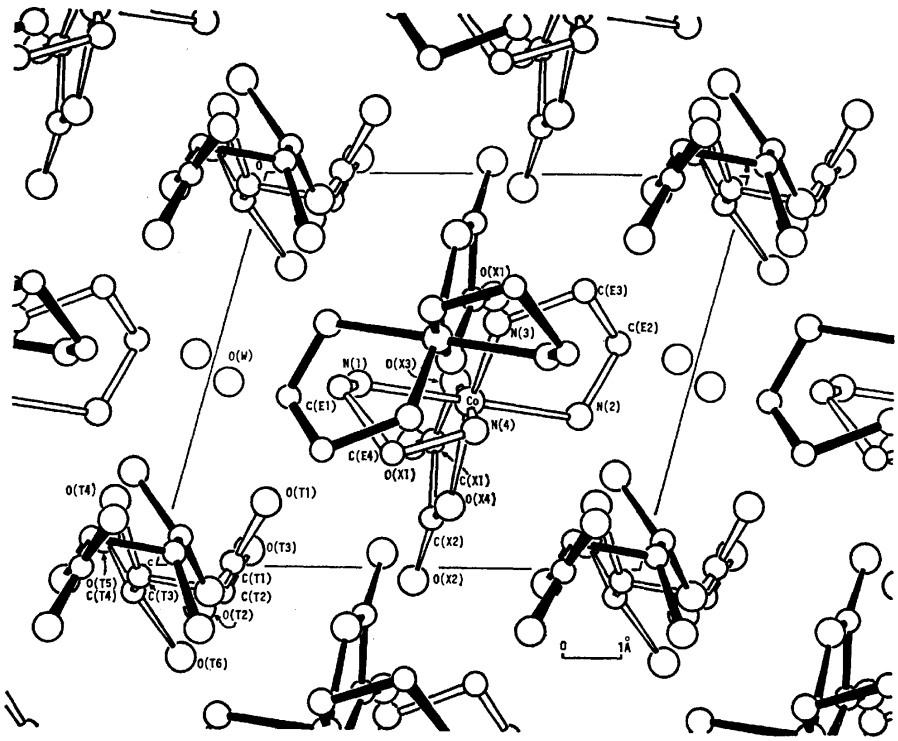

Fig. 2. A projection of the crystal structure along the b-axis.

TABLE 3. BOND DISTANCES AND ANGLES (e.s.d.'s in parentheses)

(a) Bond lengths(Å)					
Co-N(1)	1.96(1)	O(X1)-C(X1)	1.23(2)	O(T1)-C(T1)	1.21(2)
Co-N(2)	1.92(1)	O(X2)-C(X2)	1.22(2)	O(T2)-C(T1)	1.29(2)
Co-N(3)	1.96(1)	O(X3)-C(X1)	1.25(2)	O(T3)-C(T2)	1.43(2)
Co-N(4)	1.95(1)	O(X4)-C(X2)	1.32(2)	O(T4)-C(T3)	1.42(2)
Co-O(X3)	1.94(1)	C(E1)-C(E4)	1.55(3)	O(T5)-C(T4)	1.25(2)
Co-O(X4)	1.88(1)	C(E2)-C(E3)	1.50(2)	O(T6)-C(T4)	1.24(2)
N(1)-C(E1)	1.50(2)	C(X1)-C(X2)	1.57(2)	C(T1)-C(T2)	1.52(2)
N(2)-C(E2)	1.46(2)			C(T2)-C(T3)	1.53(2)
N(3)-C(E3)	1.50(2)			C(T3)-C(T4)	1.52(2)
N(4)-C(E4)	1.52(2)				

(b) Bond angles(°)			
N(1)-Co-N(4)	86(1)	N(1)-C(E1)-C(E4)	104(1)
N(2)-Co-N(3)	86(1)	N(2)-C(E2)-C(E3)	106(1)
O(X3)-Co-O(X4)	86(0)	N(3)-C(E3)-C(E2)	105(1)
Co-N(1)-C(E1)	111(1)	N(4)-C(E4)-C(E1)	105(1)
Co-N(2)-C(E2)	111(1)	O(X1)-C(X1)-C(X2)	117(1)
Co-N(3)-C(E3)	108(1)	O(X2)-C(X2)-C(X1)	122(1)
Co-N(4)-C(E4)	107(1)	O(X3)-C(X1)-C(X2)	115(1)
Co-O(X3)-C(X1)	113(1)	O(X4)-C(X2)-C(X1)	113(1)
Co-O(X4)-C(X2)	113(1)	O(X1)-C(X1)-O(X3)	128(1)
		O(X2)-C(X2)-O(X4)	125(1)
O(T1)-C(T1)-O(T2)	126(2)	O(T5)-C(T4)-O(T6)	127(1)
O(T1)-C(T1)-C(T2)	122(1)	O(T2)-C(T1)-C(T2)	112(1)
O(T5)-C(T4)-C(T3)	115(1)	O(T6)-C(T4)-C(T3)	118(1)
C(T1)-C(T2)-O(T3)	113(1)	C(T4)-C(T3)-O(T4)	114(1)
O(T3)-C(T2)-C(T3)	106(1)	O(T4)-C(T3)-C(T2)	112(1)

within the complex cation are in good agreement with those in the previous studies.[17,18] The absolute configuration of the complex cation was assigned as *Λ*-*δλ* for the $(+)_{589}$-$[Co(ox)en_2]^+$ cation, based on the H-$(+)_{589}$-tartrate anion as an internal reference.[19] Therefore, the geometry of the complex cation is the mirror image of those reported by Aoki *et al.*[17] and Toriumi *et al.*[18]

Recently, it has been reported that, in the $[M(en)_3]^{3+}$ complex cations, the *lel-lel-ob* conformation of three ethylenediamine molecules is the most stable form.[20] Three independent crystal structure analyses are available at present for the $[Co(ox)en_2]^+$ cation, including the present result.[17,18] If these structures were projected down the quasi-threefold axis of the complex cation, a *lel-ob* conformation of the two ethylenediamine molecules was found in every case, though the sizes of the counter anions(Br^-,[17] $(+)_{589}$-$[Co(CN)_2(mal)(NH_3)_2]^-$,[18] and H-*d*-tart$^-$) vary considerably. These results suggest that, in the $[Co(ox)en_2]^+$ cation, the *lel-ob* conformation is the most stable form.

Anion Geometry. The projected sketch of the H-*d*-tart anion is illustrated in Figs. 1 and 2. The O(T1)C(T1)O(T2) group with bond distances C(T1)–O(T1)(1.21 Å) and C(T1)–O(T2)(1.29 Å) and with bond angles O(T1)–C(T1)–C(T2)(122°) and O(T2)–C(T1)–C(T2)(112°) is asymmetric with regard to the C(T1)–C(T2) axis, and obviously this group is considered to be the non-ionized side of the H-*d*-tart anion. In contrast, another O(T5)C(T4)O(T6) group with distances 1.25 and 1.24 Å and with angles 115 and 118° is considered to be the ionized side. These bond distances and angles are in accordance with the previously reported values in H-*d*-tart anions.[19,21–23] Additionally, a short intermolecular distance, O(T2)···O(T5)′ 2.44 Å, was observed. Therefore, the hydrogen atom on the non-symmetrical carboxyl group is possibly bound to O(T2).

The planes including tht five non-hydrogen atoms of each α-hydroxycarboxylate moiety are approximately coplanar. The equations of the least-squares planes are expressed by $-0.840x-0.153y-0.520z+3.464=0$ for the [C(T1), C(T2), O(T1), O(T2), O(T3)] plane and by $0.920x-0.150y-0.361z+4.498=0$ for the [C(T3), C(T4), O(T4), O(T5), O(T6)] plane respectively. The angle between the two planes is slightly less than the corresponding angles of H-*d*-tart anions in other crystals (55.8 *vs.* 62.0,[19] 58.9,[21] 68.7,[22] and 72,1°[23]).

Crystal Packing. In the crystal, H-*d*-tart anions are arranged to make a specific chain structure along the b-axis; they are linked to each other through the hydrogen bonding as shown in Fig. 1. The hydrogen bond distance O(T2)···O(T5) ($-x$, $1/2+y$, $2-z$) is 2.44 Å. This hydrogen bond distance is slightly shorter than those of (−)-adrenaline hydrogen-*d*-tartrate,[21] (+)-[(−)-1-methyl-3-benzoylpiperidinium hydrogen-*d*-tartrate]H_2O,[22] and (−)-[(−)-1-methyl-3-ethyl-3-benzoylpiperidinium hydrogen-*d*-tartrate][23] (2.49, 2.63, and 2.49 Å respectively).

Along the b-axis, there is another chain of complex

cations, which are also joined by the hydrogen bond; N(4)···O(X1)($1-x$, $1/2+y$, $1-z$) 2.92 Å. Both chains have the right-handed twofold screw symmetry along the b-axis, as is shown in Fig. 2. Besides, these screw chains are mutually in contact with the following short distances: O(T1)···N(1) 2.91, O(T1)···C(X2) 2.94, O(T1)···O(X2) 3.10, O(T3)···O(X1) 3.01, O(T3)···O(X2) 2.90, O(T4)($1+x$, y, z)···N(2) 2.97, O(T4)($1+x$, y, z)···C(X2) 3.06, O(T4)($1+x$, y, z)···C(X1) 3.02, O(T6)($1-x$, $1/2+y$, $2-z$)···N(2) 2.89, and O(T6)($1-x$, $1/2+y$, $2-z$)···N(4) 3.00 Å.

Table 4. Intermolecular distances($\leq$3.25 Å)

N-H···B	N···B (Å)	H···B (Å)	∠N-H···B
N(1)-H1···O(T1)	2.91[a]	1.91	178
N(1)-H2···O(T2)^{I}	3.12[a]	2.12	171
N(2)-H3···O(T4)^{II}	2.97[a]	1.97	176
N(2)-H4···O(T6)^{III}	2.89[a]	1.92	164
N(3)-H6···O(X2)^{I}	3.17[a]	2.26	150
N(3)-H5···O(X1)^{IV}	3.25[a]	2.50	131
N(4)-H7···O(X1)^{IV}	2.92[a]	1.97	158
N(4)-H8···O(T3)^{III}	3.24	2.45	136
N(4)-H8···O(T6)^{III}	3.00[a]	2.28	128
O(X1)···O(T3)	3.01[a]	—	—
O(X2)···O(T1)	3.10[a]	—	—
O(X2)···O(T3)	2.90[a]	—	—
O(X4)···H14-C(E3)^{V}	3.25	2.41	137
C(X1)···O(T4)^{II}	3.02	—	—
C(X2)···O(T1)	2.94	—	—
C(X2)···O(T4)^{II}	3.06	—	—
O(T2)···O(T5)^{VI}	2.44[a]	—	—
O(W)···O(T1)	3.10	—	—
O(W)···O(T3)	3.03[a]	—	—
O(W)···O(T4)	2.84[a]	—	—
O(W)···O(T6)^{I}	2.81[a]	—	—

Roman numerals as superscripts refer to the following equivalent positions relative to the reference molecule at x, y, z:

I(x, y, $-1+z$), II($1+x$, y, z)
III($1-x$, $1/2+y$, $2-z$), IV($1-x$, $1/2+y$, $1-z$)
V(x, y, $1+z$), VI($-x$, $1/2+y$, $2-z$)

a) Possible hydrogen bonds.

Moreover, along the c-axis, adjacent H-*d*-tart chains are linked by the water molecules with the hydrogen bond distances; O(W)···O(T1) 3.10, O(W)···O(T3) 3.03, O(W)···O(T4) 2.84, and O(W)···O(T6)(x, y, $-1+z$) 2.81 Å. Thus around the water molecule a distorted tetrahedral environment is formed by these four oxygen atoms, and this water molecule has no short contact with the complex cation. Selected intermolecular bond distances and angles are summarized in Table 4.

Difference between d-*Tart*$^{2-}$ *and H-*d*-tart*$^{-}$ *Systems.* Figure 3 shows the arrangement of the $(+)_{589}$-[Co(ox)en_2]$^{+}$ cation and the H-*d*-tart anions projected down the quasi-threefold axis of the complex cation. The adjacent distances between the complex cation and H-*d*-tart anion are: N(1)···O(T2)(x, y, $-1+z$) 3.12, N(2)···O(T6)′($1-x$, $1/2+y$, $2-z$) 2.89, N(4)···O(T6)′($1-x$, $1/2+y$, $2-z$) 3.00, and N(4)···O(T3)′($1-x$, $1/2+y$, $2-z$) 3.24 Å. In this case, there-

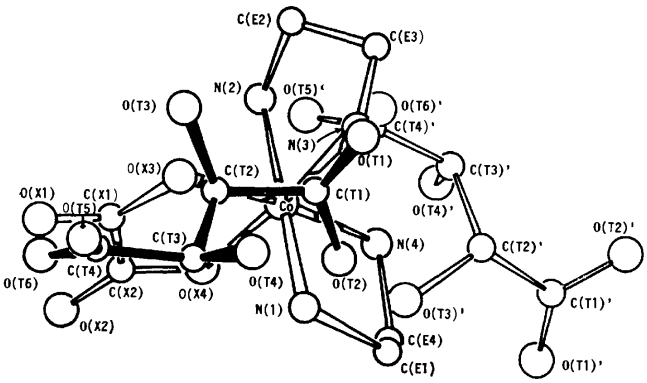

Fig. 3. The arrangement of the complex cation and H-*d*-tart anions projected down the quasi-threefold axis of the complex cation.

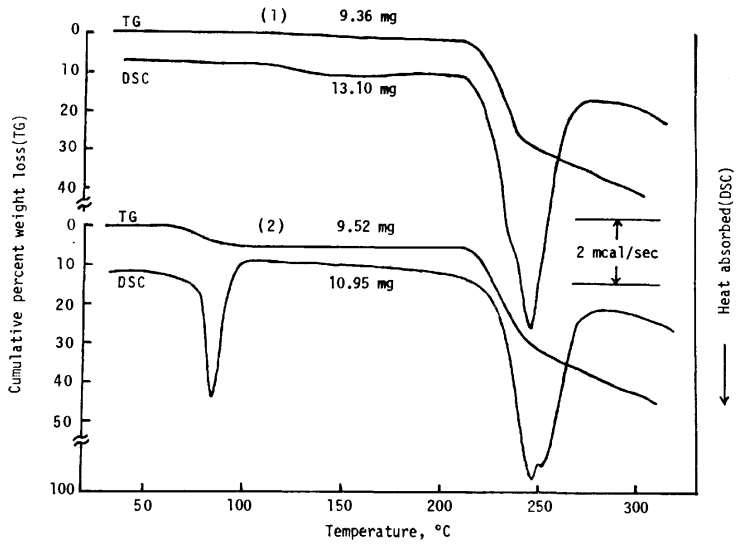

Fig. 4. TG and DSC curves of both diastereoisomers:
(1) $(+)_{589}$-[Co(ox)en_2]H-*d*-tart·H_2O; (2) $(-)_{589}$-[Co(ox)en_2]H-*d*-tart·$2H_2O$.

fore, the characteristic "face-to-face" close contact does not exist between the triangular facet of the octahedral complex cation and the H-*d*-tart anion. Thus, it is suggested that, in the optical resolution process, the discriminative role of the H-*d*-tart anion to the complex cation is quite different from that of the *d*-tartrate anion in the $[M(en)_3]^{3+}\cdots d\text{-tart}^{2-}$ system.[2-4] In other words, in the case of the H-*d*-tart anion, the diastereomeric discrimination is effected even without the "face-to-face" compact fit proposed by Fischer.[7] In the present diastereoisomer the optical-active complex cation, $\Lambda\text{-}\delta\lambda\text{-}(+)_{589}\text{-}[Co(ox)en_2]^+$, is locked by the right-handed spiral chain of $\{\text{H-}d\text{-tart}\}_\infty$ units formed along the b-axis. Then, it seems that the discrimination of optical isomers in this crystal originates in the formation of such a "lock-in-column" mode bonding through the strong hydrogen-bond network.

Thermal Behavior. It is supposed that the thermal behavior of the water of crystallization in both diastereoisomers reflects the difference of the crystal packing modes in these compounds. Therefore, the TG and DSC measurements of both diastereoisomers have been performed. These results are shown in Fig. 4.

The results clearly show that the crystals of the less-soluble diastereoisomer are thermally more stable than those of the more-soluble diastereoisomer. In fact, the water of crystallization is stable up to about 115 °C in the less-soluble salt, the release of the water molecule proceeds very slowly, and no DSC peak is observed. On the other hand, the crystals of the more-soluble salt begin to release the water of crystallization at about 78 °C and the process ceases at 90 °C. The weight loss accompanying this thermal transition is found to be 5.8%. This value is very close to the expected value of the dehydration of $1.5H_2O$(6.0%). A distinct endothermic DSC peak is also observed, as shown in Fig. 4. The ΔH value for the dehydration step is found to be 12.8 kcal/mol(53.6 kJ/mol), which is quite silmilar to those of $(\pm)\text{-}[Co(en)_3]Cl_3\cdot nH_2O$[24] and $(\pm)\text{-}[Cr(en)_3](NCS)_3\cdot H_2O$.[25] Both diastereoisomers are decomposed at about the same temperature(228 °C). Consequently, it is thought that the water of crystallization in the more-soluble salt is more loosely packed crystallographically than that of the less-soluble salt.

Recently, the solubilities of both salts were studied by Shimura and Tsutsui.[26] They mentioned that the solubility of the more-soluble salt, $(-)_{589}\text{-}[Co(ox)en_2]\text{H-}d\text{-tart}\cdot 2.5H_2O$, is three times larger than that of the less-soluble salt, $(+)_{589}\text{-}[Co(ox)en_2]\text{H-}d\text{-tart}\cdot H_2O$, at 25 °C. Moreover, the result of the three-dimensional crystal structure analysis of the more-soluble salt[27] also revealed that the waters of crystallization in this crystal were packed more loosely than those of the less-soluble salt.

We thank the Hiroshima University Computer Center for a generous allocation of computer time and acknowledge a Grant-in-Aid for Scientific Research from the Ministry of Education. We are also grateful to Dr. Kozo Akabori, Hiroshima University, for TG and DSC measurements and for his valuable suggestions.

References

1) M. Kuramoto, Y. Kushi, and H. Yoneda, *Chem. Lett.*, **1976**, 1133.
2) Y. Kushi, M. Kuramoto, and H. Yoneda, *Chem. Lett.*, **1976**, 135.
3) Y. Kushi, M. Kuramoto, and H. Yoneda, *Chem. Lett.*, **1976**, 339.
4) T. Tada, Y. Kushi, and H. Yoneda, *Chem. Lett.*, **1977**, 379.
5) Y. Kushi, M. Kuramoto, and H. Yoneda, *Chem. Lett.*, **1976**, 663.
6) M. Kuramoto, Y. Kushi, and H. Yoneda, *Bull. Chem. Soc. Jpn.*, in press.
7) E. Fischer, *Chem. Ber.*, **32**, 3617 (1899); S. F. Mason, *Ann. Rep.*, **73**, 53 (1976); K. Bernauer, *Topics Current Chem.*, **65**, 1 (1976).
8) J. I. Legg, D. W. Cooke, and B. E. Douglas, *Inorg. Chem.*, **6**, 700 (1967).
9) W. T. Jordan and B. E. Douglas, *Inorg. Chem.*, **12**, 403 (1973).
10) W. T. Jordan, B. J. Brennan, L. R. Froebe, and B. E. Douglas, *Inorg. Chem.*, **12**, 1827 (1973).
11) J. C. Dabrowiak and D. W. Cooke, *Inorg. Chem.*, **14**, 1305 (1975).
12) K. Yamanari, J. Hidaka, and Y. Shimura, *Bull. Chem. Soc. Jpn.*, **50**, 2299 (1977).
13) D. W. J. Cruickshank, "Computing Methods and the Phase Problem in X-Ray Crystal Analysis," ed by R. Pepinsky, J. M. Robertson, and J. C. Speakman, Pergamon Press, Oxford (1961), p. 45.
14) "International Tables for X-Ray Crystallography," Kynoch Press, Birmingham (1968), Vol. III, pp. 201—206.
15) Y. Kushi, unpublished work.
16) T. Ashida, "The Universal Crystallographic Computation Program System," ed by T. Sakurai, The Crystallographic Society of Japan (1967).
17) T. Aoki, K. Matsumoto, S. Ooi, and H. Kuroya, *Bull. Chem. Soc. Jpn.*, **46**, 159 (1973).
18) K. Toriumi, S. Sato, and Y. Saito, *Acta Crystallogr., Sect. B*, **33**, 1378 (1977).
19) A. J. van Bommel and J. M. Bijvoet, *Acta Crystallogr.*, **11**, 61 (1958).
20) R. E. Cramer and J. T. Huneke, *Inorg. Chem.*, **17**, 365 (1978).
21) D. Carlstrøm, *Acta Crystallogr., Sect. B*, **29**, 161 (1973).
22) G. Hite and J. R. Soares, *Acta Crystallogr., Sect. B*, **29**, 2935 (1973).
23) J. R. Ruble, G. Hite, and J. R. Soares, *Acta Crystallogr., Sect. B*, **32**, 136 (1976).
24) H. Chihara and K. Nakatsu, *Bull. Chem. Soc. Jpn.*, **32**, 903 (1956).
25) W. H. Lee and M. F. C. Lord, *Prog. Solid. State Chem.*, **3**, 265 (1967); J. E. House, Jr., and J. C. Bailar, Jr., *J. Inorg. Nucl. Chem.*, **38**, 1791 (1976).
26) Y. Shimura and K. Tsutsui, *Bull. Chem. Soc. Jpn.*, **50**, 145 (1977).
27) M. Kuramoto, Y. Kushi, and H. Yoneda, Presented at the 26th Annual Meeting on Coordination Chemistry of Japan, Sapporo, August 1976, Abstructs 2M04.

An X-Ray Photoelectron Spectroscopic Study of Dioxime Metal Complexes

Tooru YOSHIDA

Osaka Prefectural Industrial Research Institute, Enokojima, Nishi-ku, Osaka 550

(Received June 13, 1978)

The O(1s) and N(1s) electron-binding energies were measured for the dioxime complexes of several transition metals by means of the X-ray photoelectron spectroscopic method. On the basis of their chemical shifts, the strength of the intramolecular hydrogen bonds and the charge distribution around the nitrogen atoms in the complexes are discussed. Two kinds of oxygen atoms were observed for all the complexes, and their binding energy differences were in the range of 1.3—1.9 eV. This difference was found to decrease with the increase in the strength of the hydrogen bonds. However, only one kind of nitrogen atom was observed for all the compounds except one. The N(1s) chemical shifts were in the range of 0.2—0.8 eV, and were found to increase slightly in the order of Cu^{II}< Ni^{II}<Pd^{II}<Pt^{II}.

It is well known that dimethylglyoxime is the first selective organic reagent[1] applied in the analyses of metals. In order to establish the structure of dimethylglyoxime complexes of transition metals, several complexes have been investigated by X-ray diffraction,[2-7] infra-red spectrophotometry,[8-14] magnetic[15-17] and stability[18,19] measurements. These investigations confirmed the square planar structure of the dimethylglyoxime complexes with a metal-ligand ratio of 1:2 of nickel, palladium, platinum, and copper. Furthermore, these investigations proved more important factors stabilizing the dioxime complexes to be the intramolecular hydrogen bonds in the planar configuration and the metal→ligand donor-acceptor π bonds in the chelate rings.

There have been two different opinions regarding the intramolecular hydrogen bonds in the Ni complex of dimethylglyoxime; one is that they are symmetric,[2,8,14,20] and the other that they are unsymmetric.[11] These conflicting results are due to the complexity of assigning the band of a hydroxyl group in IR. The former opinion is based only on the apparent centrosymmetric structure of the complex, the short O–O distance, and the low OH stretching frequency. No direct location of the protons has been carried out.

It has been known that X-ray photoelectron spectroscopy (XPS) is suitable for the detection of a protonated atom.[21] The purpose of the present study is to examine the hydrogen bonds and the π bonds in several dioxime complexes of transition metals by means of XPS.

Experimental

The X-ray photoelectron spectra were measured on an AEI ES200 spectrometer. Al $K\alpha$ (1486.6 eV) X-ray radiation was used as the excitation source. Samples were ground to a powder and then dusted onto a double-backed adhesive tape. The measurements were run at room temperature under a vacuum of about 10^{-7} Torr. Dimethylglyoxime, benzil dioxime, 1,2-cyclohexanedione dioxime (abbreviated as LH, L'H, and L''H) were used as ligands, and nickel(II), palladium(II), platinum(II), copper(II), and cobalt(III), as metal ions. All the free ligands were commercially available and of an analytical grade, and were used without further purification. All the complexes were prepared by the literature methods, and were checked by elemental analysis.

All the C(1s) electron spectra showed nearly symmetrical single peaks with the full-width at a half-maximum height (FWHM) of 1.8—2.0 eV for benzil dioxime and 1,2-cyclohexanedione dioxime and their metal complexes, and of 2.0—2.2 eV for dimethylglyoxime and its metal complexes. It is reasonable to assume that the C(1s) binding energy is nearly constant within the complexes with the same ligand. Furthermore, as only the relative binding energies were considered in the present study, the binding energy of the C(1s) peak was used as the energy standard throughout the experiments; it was taken to be 285.0 eV. The reproducibilities of the values thus obtained were within ±0.1 eV.

Results

The O(1s) and N(1s) electron-binding energies measured are given in Table 1.

The O(1s) Spectra. The O(1s) electron spectra of the dimethylglyoxime complexes are shown in Figs.

TABLE 1. MEASURED BINDING ENERGIES

Compound[a]	Binding energy (eV)			N(1s) chemical shift (eV)[c]
	N(1s)	O(1s)	ΔE[b]	
PtL_2	400.8	532.8; 531.0	1.8	0.8
PdL_2	400.7	532.8; 531.0	1.8	0.7
NiL_2	400.5	532.5; 531.2	1.3	0·5
CuL_2	400.3	532.8; 531.1	1.7	0.3
$Co^{III}L_3$	400.3	532.9; 531.0	1.9	0.3
$[Co^{III}(NH_3)_2L_2]Cl$	400.7; 399.4	532.6; 531.2	1.4	0.7
$HCo^{III}L_2Cl_2$	400.7	532.8; 531.2	1.6	0.7
PtL_2'	401.4	533.4; 531.7	1.7	0.6
PdL_2'	401.2	533.4; 531.7	1.7	0.4
NiL_2'	401.1	533.0; 531.7	1.3	0.3
CuL_2'	401.0	533.4; 531.7	1.7	0.2
PtL_2''	400.9	533.1; 531.2	1.9	0.7
PdL_2''	400.8	533.1; 531.2	1.9	0.6
NiL_2''	400.6	532.6; 531.2	1.4	0.4
CuL_2''	400.4	533.0; 531.1	1.9	0.2
LH	400.0	532.8		
L'H	400.8	533.5		
L''H	400.2	533.0		

a) LH, L'H, and L''H indicate dimethylglyoxime, benzil dioxime, and 1,2-cyclohexanedione dioxime respectively. b) The binding-energy difference of the two O(1s) peaks. c) The N(1s) binding-energy difference of a complex and a free ligand.

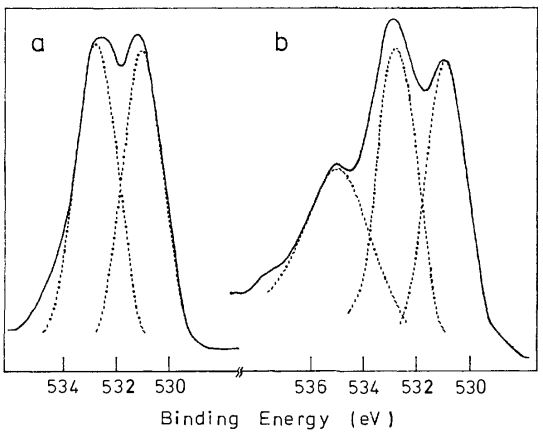

Fig. 1. O(1s) electron spectra.
a: PtL_2, b: PdL_2.

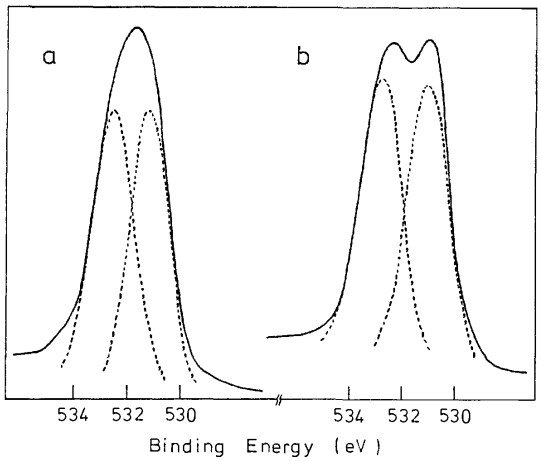

Fig. 2. O(1s) electron spectra.
a: NiL_2, b: CuL_2.

1—3. All the spectra showed multiple peaks, or one broad peak with the FWHM of 2.7—2.9 eV. The peaks with the FWHM of about 1.8 eV, indicated by the broken lines in the figures, were obtained by a graphical resolution. The peak with the highest binding energy of the three peaks in Fig. 1b can be assigned to the $Pd(3p_{3/2})$ electron. As is seen in Figs. 1—3, at least two kinds of oxygen atoms were observed for all the complexes. The intensity ratio of the two kinds of oxygens was nearly 1:1 for all the complexes except for $HCoL_2Cl_2$, for which the ratio was about 3:1.

The O(1s) spectra of the benzyl dioxime and 1,2-cyclohexane-dione dioxime complexes of each metal ion were very similar in appearance to that of the corresponding dimethylglyoxime complex. The O(1s) spectra of all the free ligands showed nearly symmetrical single peaks with an FWHM of 2.0—2.1 eV.

The N(1s) Spectra. Figure 4 shows the N(1s) spectra of NiL_2 and $[Co(NH_3)_2L_2]Cl$. The peaks indicated by the broken lines were obtained as in the case of the O(1s) spectra.

The N(1s) spectrum of NiL_2 showed a single main peak with an FWHM of 1.6 eV and a broad satellite with a low intensity in the region of higher energies

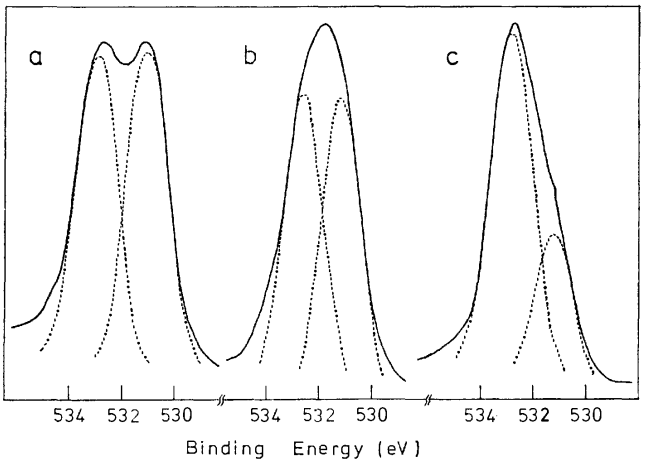

Fig. 3. O(1s) electron spectra.
a: CoL_3, b: $[Co(NH_3)_2L_2]Cl$, c: $HCoL_2Cl_2$.

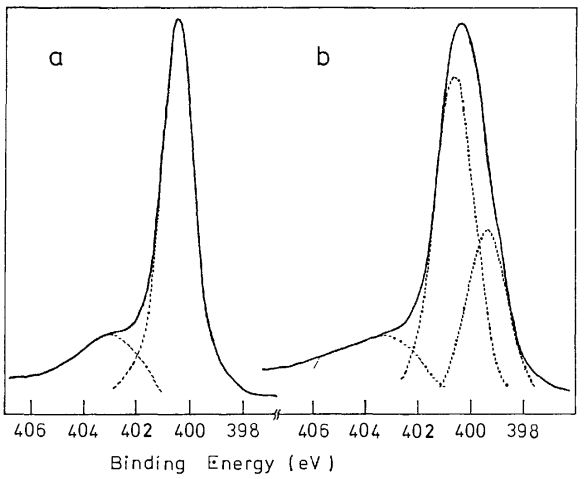

Fig. 4. N(1s) electron spectra.
a: NiL_2, b: $[Co(NH_3)_2L_2]Cl$.

than the main peak. The N(1s) spectra of all the other compounds were similar in appearance to that of NiL_2 except for the $[Co(NH_3)_2L_2]Cl$ shown in Fig. 4b. This indicates the presence of only one kind of nitrogen atom in all the compounds studied here except for $[Co(NH_3)_2L_2]Cl$.

The N(1s) spectrum of $[Co(NH_3)_2L_2]Cl$ showed an unsymmetrical broad peak with an FWHM of 2.3 eV (Fig. 4b). This suggests the presence of two kinds of nitrogen atoms. The intensity ratio of about 2:1 of the two peaks clearly indicates that the peak with the higher binding energy is due to the nitrogen atom of dimethylglyoxime, and the other, to the nitrogen of ammonia.

Discussion

The O(1s) Spectra. For all the metal complexes of the three ligands, the peaks with high and low binding energies may be assigned to the protonated and deprotonated oxygen atoms, –OH and $–O^-$ respectively, because the binding energy of the former was close to that of the free ligand.

The magnitude of the O(1s) binding-energy differ-

ences between the above two peaks may be correlated with the difference in the electronic charge between the two oxygen atoms. That is, the binding energy difference becomes large as the charge difference becomes large.

An increase in the strength of an OH···O hydrogen bond results in decreases in the O–O distance and the charge difference between the two oxygen atoms, giving rise to a small binding-energy difference between the two O(1s) peaks. Therefore, it may be considered that the hydrogen bond in the Ni complex, which has the smallest binding-energy difference, is stronger than those of the Pt and Pd complexes. This coincides with the results previously obtained by X-ray analysis[2–4] and IR studies.[8,20]

The O–O distances of the Pt, Pd, and Ni complexes of dimethylglyoxime, as determined by the X-ray analyses, were 3.03, 2.59, and 2.44 Å respectively.[2–4]

It is striking that the binding-energy differences of the two peaks for both the Pt and Pd complexes of dimethylglyoxime are the same, while there is an appreciable difference in the O–O distance between the two complexes.

The binding-energy difference between the two peaks for $[Co(NH_3)_2L_2]^+$, in which the O–O distance is 2.65 Å,[6] is 1.4 eV. The binding-energy differences between the two peaks in the O(1s) spectra for *o*- and *p*-aminobenzoic acids,[22] in which the O–O distances of the intermolecular hydrogen bonds are 2.54[23] and 2.61—2.64 Å,[24] were 1.4 and 1.5 eV respectively. Therefore, it seems that the binding-energy difference for PdL_2 was fairly large compared with those for the compounds stated above with O–O distances similar to that of PdL_2. Though the reason for this cannot be explained clearly as yet, it is possibly due to the difference in the bonding type of the hydrogen bond, such as a bent or straight hydrogen bond. That is, the former type may be supposed for the Pd complexes, and the latter type, for the complexes quoted above as comparison and the Pt complexes.

It seems reasonable that the binding-energy differences observed in the complexes in Table 1 which have the intramolecular hydrogen bonds are equal to or smaller than that for CoL_3, in which the presence of a hydrogen bond analogous to those in the above complexes cannot be expected.[10a,10c]

It is very interesting that the present experiment for the three Ni complexes showed the presence of two kinds of oxygen atoms. In a symmetrical O···H··· O hydrogen bond, the equivalence of the two oxygen atoms may be expected, because the proton occupies a central position between the two oxygen atoms. Therefore, it seems that the hydrogen bonds in the three Ni complexes are unsymmetrical.

The crystal-structure analysis[5] of CuL_2 showed that this complex exists as a dimer bridged by two oxygen atoms, and that it involves two kinds of intramolecular hydrogen bonds: weak and strong ones. Therefore, four kinds of oxygen atoms should be present in the complex. However, the O(1s) spectrum for CuL_2 could roughly be divided into only two peaks, like the other two Cu complexes.

It is clear from the dominant presence of the protonated oxygen atom over the deprotonated one, as may be seen in Fig. 3c, that, in the $HCoL_2Cl_2$ complex, an additional proton exists near an oxygen atom. This agrees with the results obtained by IR studies[10c,12] of the complex.

In the intramolecular hydrogen bonds studied here, the protons may be considered to be rapidly changing in their position from near one oxygen atom to near the other. In general, the lifetime of proton tautomers is much longer than the time (10^{-16}—10^{-18} s) needed in an ionization process in XPS.[25] Therefore, it was considered that the two kinds of oxygen atoms, the individual tautomers could easily be detected in this experiment.

The N(1s) Spectra. The N(1s) spectra of all the complexes were expected to show two well-resolved peaks or a single broad peak, because the complexes contain two kinds of nitrogen atoms bonded with different groups, –OH and $-O^-$. However, only a single peak with almost the same FWHM as the free ligand was observed in the N(1s) spectrum for all the complexes. This is probably due to the cyclic delocalization[13,18,19,26] based upon the metal→ligand donor-acceptor π bond in the five-membered rings. Such delocalization is considered to equalize the charges on the four nitrogen atoms.

The positive N(1s) chemical shift, which is the difference between the N(1s) binding energies of the complex and the free ligand, is, in all the complexes, considered to be due to the change in the electron density on the nitrogen atom caused by the coordination of lone-pair electrons of the nitrogen atom to the metal and the above-stated cyclic delocalization of electrons.

The magnitudes of the N(1s) chemical shifts were found to increase gradually in the order of Cu<Ni< Pd<Pt complexes. This indicates that, of the four complexes, the electron density around the nitrogen atom is the smallest in the Pt complex and the largest in the Cu complex. This order corresponds well to the decreasing order of the C=N frequencies of these complexes, where fewer frequencies indicate more conjugation in a chelate ring.[13]

The weak peak observed about 2.5 eV on the higher-energy side of the main peak, as is seen in Fig. 4, may be partly assigned to the shake-up satellite peak, which is mainly due to the co-excitations of valence electrons (L-L transition) on the ejection of the innner electrons, on the basis of the following facts. Such a weak peak was also observed in the N(1s) spectrum of each free ligand in the present study. In our laboratory, such peaks have previously been observed in the N(1s) spectra only of compounds containing unsaturated nitrogen groups in addition to the compounds listed in Table 1.[27] Furthermore, the electron spectra of the compounds containing the unsaturated bonds with a hetero-atom in the molecule generally show the absorption bands due to n-π^*, π-π^* transitions in a region of about $(10—50)\times10^3$ cm^{-1}.[28] In the case of NiL_2, such bands are observed in the vicinity of 20×10^3 and 40×10^3 cm^{-1},[29,30] which approximately correspond to 2.5 and 5.0 eV respectively.

The Estimation of the Charge Difference. In the point charge model,[31] a core-binding energy can be expressed by

$$Eb = kq_i + V_i + l + E_r, \quad (1)$$

where Eb is the binding energy for a particular core level in a given atom (the "ionized" atom), q_i is the charge of the ionized atom, $V_i(=\sum_{i\neq j} q_j/R_{ij})$ is the Coulomb potential energy at the site of the ionized atom due to the other charged atoms of the molecule, k and l are empirical constants for the studied atom, and E_r is the relaxation energy associated with the shift of electrons toward the core hole.

The O(1s) binding energies of two oxygen atoms in the nickel dimethylglyoxime complex can be given by

$$\text{B. E.}(O_1) = k_O q_{O_1} + V_{O_1} + l_O + E_r, \quad (2)$$

$$\text{B. E.}(O_2) = k_O q_{O_2} + V_{O_2} + l_O + E_r. \quad (3)$$

The following equation can be obtained by using the interatomic distances previously reported[2] and by considering the D_{2h} symmetry of the complex:

$$\Delta q = \frac{1}{k_O - 0.42}\{\Delta E - q_H(1/R_{O_1H} - 1/R_{O_2H})\}, \quad (4)$$

where $\Delta q = q_{O_1} - q_{O_2}$ and where $\Delta E = \text{B.E.}(O_1) - \text{B.E.}(O_2) = 1.3$ eV. By substituting $R_{O_1H} = 1.15$Å and $R_{O_2H} = 1.29$ Å, obtained by the application of Lippincott's model equation,[32] and $k_O = 25.8$ eV/(unit charge), determined empirically by Siegbahn *et al.*,[33] into Eq. 4, Δq was estimated as follows:

$$\Delta q = \frac{1}{25.4}(1.3 - 0.003q_H) \approx \frac{1}{25.4} \times 1.3 \fallingdotseq 0.051.$$

Therefore, it seemed that the intramolecular hydrogen bond of the nickel dimethylglyoxime complex was slightly unsymmetrical, with a charge difference of about 0.05 unit charge.

The author wishes to thank Drs. Kiyoshi Yamasaki and Shigemasa Sawada for their many helpful discussions and suggestions during this work, and Mr. Taichiro Hirohara for the elemental analysis of all the samples.

References

1) L. Tshugaeff, *Z. Anorg. Chem.*, **46**, 144 (1905).
2) L. E. Godycki and R. E. Rundle, *Acta Crystallogr.*, **6**, 487 (1953).
3) D. E. Williams, G. Wohlauer, and R. E. Rundle, *J. Am. Chem. Soc.*, **81**, 755 (1959).
4) E. Frasson, C. Panattoni, and R. Zannetti, *Acta Crystallogr.*, **12**, 1027 (1959).
5) a) E. Frasson, R. Bardi, and S. Bezzi, *Acta Crystallogr.*, **12**, 201 (1959). b) A. Vaciago and L. Zambonelli, *J. Chem. Soc., A*, **1970**, 218.
6) K. S. Viswanathan and N. R. Kunchur, *Acta Crystallogr.*, **14**, 675 (1961).
7) a) E. Frasson and C. Panattoni, *Acta Crystallogr.*, **13**, 893 (1960); b) R. H. Bowers, C. V. Banks, and R. A. Jacobson, *Acta Crystallogr., Sect. B*, **28**, 2318 (1972).
8) R. E. Rundle and M. Parasol, *J. Chem. Phys.*, **20**, 1487 (1952).
9) J. Fujita, A. Nakahara, and R. Tsuchida, *J. Chem. Phys.*, **23**, 1541 (1955).
10) a) A. Nakahara, *Bull. Chem. Soc. Jpn.*, **27**, 560 (1954); b) A. Nakahara, *ibid.*, **28**, 207 (1955); c) A. Nakahara, *ibid.*, **28**, 473 (1955); d) A. Nakahara, J. Fujita, and R. Tsuchida, *ibid.*, **29**, 296 (1956).
11) a) R. Blinc and D. Hadzi, *J. Chem. Soc.*, **1958**, 4536; b) R. Blinc and D. Hadzi, *Spectrochim. Acta*, **16**, 853 (1960).
12) R. D. Gillard and G. Wilkinson, *J. Chem. Soc.*, **1963**, 6041.
13) K. Burger, I. Ruff, and F. Ruff, *J. Inorg. Nucl. Chem.*, **27**, 179 (1965).
14) J. E. Caton, Jr., and C. V. Banks, *Inorg. Chem.*, **6**, 1670 (1967).
15) S. Sugden, *J. Chem. Soc.*, **1932**, 246.
16) J. B. Willis and D. P. Mellor, *J. Am. Chem. Soc.*, **69**, 1237 (1947).
17) C. V. Banks, R. V. Vander Hass, and R. P. Wander Val., *J. Am. Chem. Soc.*, **77**, 324 (1955).
18) K. Burger and I. Ruff, *Talanta*, **10**, 329 (1963).
19) I. Ruff and K. Burger, *Acta Chim. Acad. Sci. Hung.*, **47**, 143 (1966).
20) K. Nakamoto, M. Margoshes, and R. E. Rundle, *J. Am. Chem. Soc.*, **77**, 6480 (1955).
21) a) K. Siegbahn *et al.*, "ESCA Applied to Free Molecules," North-Holland Publ. Co., Amsterdam (1969), pp. 109—127; b) D. B. Adams, D. T. Clark, A. D. Baker, and M. Thompson, *Chem. Commun.*, 1600 (1971); c) B. C. Lane, J. E. Lester, and F. Basolo, *ibid.*, 1618 (1971); d) L. E. Cox, J. J. Jack, and D. M. Hercules, *J. Am. Chem. Soc.*, **94**, 6575 (1972); e) R. L. Martin and D. A. Shirley, *ibid.*, **96**, 5299 (1974); f) Y. Niwa, H. Kobayashi, and T. Tsuchiya, *J. Chem. Phys.*, **60**, 799 (1974).
22) T. Yoshida and S. Sawada, *Bull. Chem. Soc. Jpn.*, **49**, 3319 (1976).
23) C. J. Brown, *Proc. R. Soc. London, Ser. A*, **302**, 185 (1968).
24) T. F. Lai and R. E. Marsh, *Acta Crystallogr.*, **22**, 885 (1967).
25) Paratt, L. G., *Rev. Mod. Phys.*, **31**, 616 (1959).
26) E. Bayer, H. Fiedler, K. L. Hock, D. Otterbach, G. Schenk and W. Voelter, *Angew. Chem.*, **76**, 76 (1964).
27) T. Yoshida, unpublished data.
28) Jaffe and Orchin, "Theory and Applications of Ultraviolet Spectroscopy," John Wiley & Sons, New York (1964).
29) L. L. Ingraham, *Acta Chem. Scand.*, **20**, 283 (1966).
30) C. V. Banks and D. W. Barnum, *J. Am. Chem. Soc.*, **80**, 4767 (1958).
31) Ref. 21a, p. 108.
32) E. R. Lippincott and R. Schroeder, *J. Chem. Phys.*, **23**, 1099 (1955).
33) Ref. 21a, p. 136.

Synthetic Approach to 2,3,5-Triamino-2,3,5-trideoxy-D-arabonic Acid Derivatives from 3,4,6-Triazido-3,4,6-trideoxy-1,2-*O*-isopropylidene-α-D-glucopyranose

Mitsuhiro KINOSHITA,* Shinpei ABURAKI, Yasuyuki KAWADA, Takumi YAMASAKI, Yoshiharu SUZUKI, and Yoichi NIIMURA

Department of Applied Chemistry, Faculty of Engineering, Keio University, Hiyoshi, Kohoku-ku, Yokohama 223

(Received January 14, 1978)

3,6-Diazido-3,6-dideoxy-1,2-*O*-isopropylidene-α-D-glucofuranose was converted into the corresponding derivative of α-D-glucopyranose, which was transformed into 3,4,6-triazido-3,4,6-trideoxy-1,2-*O*-isopropylidene-α-D-glucopyranose (**7**) through the sequence of reactions involving displacement of sulfonate ester function with benzoate, followed by debenzoylation, sulfonylation, and nucleophilic substitution. Hydrogenolysis of **7** afforded the corresponding triamino derivative **8**. The tri-*N*-benzyloxycarbonyl derivative of **8** was *O*-deisopropylidenated and oxidized with periodate to afford the piperidinose derivative **11**, deformylation of which yielded 2,3,5-tris(benzyloxycarbonylamino)-2,3,5-trideoxy-D-arabinopyranose (**13**). "Pfitzner-Moffatt" oxidation of **11** failed to give the corresponding lactam **15**. Condensation of the 6-*N*-benzyloxycarbonyl derivative of **8** (**18**) with cyanogen bromide afforded the cyclic guanidine derivative (**20**) hydrobromide. The triazido derivative **7** was converted into 3,4,6-tris(benzyloxycarbonylamino)-3,4,6-trideoxy-D-glucitol (**23**), which was then oxidized successively with periodate and chromium trioxide–acetic acid–pyridine to give 2,3,5-tris(benzyloxycarbonylamino)-2,3,5-trideoxy-D-arabono-1,4-lactone (**25**); this was further transformed into 2,3,5-trianimo-2,3,5-trideoxy-D-arabono-1,5-lactam (**16**).

2,3,5-Triamino-2,3,5-trideoxy-D-arabono-1,5-lactam (**16**) has proved to be a useful intermediate for the synthesis of 2,3,5-triamino-2,3,5-trideoxy-D-arabonic acid derivatives, such as streptolidine[1,2] (**21**) and streptolidine lactam[3] (**27**). Synthesis of the lactam **16** was first accomplished from D-ribose through 2,3,5-triacylamino-2,3,5-trideoxy-D-arabinofuranose.[1,2] Recently **16** has been prepared through a new stereospecific route from 3,4-anhydro-D-iditol derivative.[3]

In view of the preparation of lactam **16**, we were interested in some synthetic approaches to the triamino-D-arabonic acid derivatives from 3,4,6-triazido-3,4,6-trideoxy-1,2-*O*-isopropylidene-α-D-glucopyranose (**7**) which was synthesized from 3,6-diazido-3,6-dideoxy-1,2-*O*-isopropylidene-α-D-glucofuranose[4] (**1**). The following approaches were attempted: (i) transformation of 3,4,6-tris(benzyloxycarbonylamino)-3,4,6-trideoxy-D-glucopyranose derived from **7** to **16** *via* 2,3,5-tris(benzyloxycarbonylamino)-2,3,5-trideoxy-D-arabinopyranose derivative (**11**) (Chart 2), (ii) conversion of triamino glucopyranose derivative **8** into streptolidine **21** (Chart 3), and (iii) transformation of **7** into 2,3,5-tris(benzyloxycarbonylamino)-2,3,5-trideoxy-D-arabono-1,4-lactone (**25**) which can be converted into **16** (Chart 4).

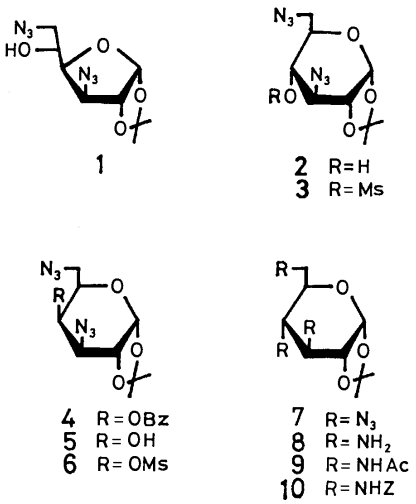

Chart 1.

3,4,6-Triazido-3,4,6-trideoxy-1,2-O-isopropylidene-α-D-glucopyranose (7). 3,6-Diazido-3,6-dideoxy-1,2-*O*-isopropylidene-α-D-glucofuranose[4] (**1**) was converted into 3,6-diazido-3,6-dideoxy-1,2-*O*-isopropylidene-α-D-glucopyranose (**2**) in 55% overall yield by *O*-deisopropylidenation of **1** with warm aqueous acetic acid and the subsequent 1,2-*O*-isopropylidenation with 2,2-dimethoxypropane in hot DMF in the presence of *p*-toluenesulfonic acid.

Kiso and Hasegawa[5a] reported that isopropylidenation of D-glucose with 2,2-dimethoxypropane–DMF–*p*-toleuensulfonic acid gives no 1,2-*O*-isopropylidene-α-D-glucopyranose. The result is not in line with ours. They also reported[5b] that isopropylidenation of D-xylose with the same reagent gives 1,2-*O*-isopropylidene-α-D-xylopyranose as a minor product in 16% yield. Meyer zu Reckendorf and Bischef[6] reported that treatment of 3-(*N*-methylbenzamido)-3-deoxy-D-xylose with the same reagent affords the corresponding 1,2-*O*-isopropylidene-D-xylopyranose derivative in 40% yield. The difference between isopropylidenation of D-glucose and of 3,6-diazido-3,6-dideoxy-D-glucose, in which the hydroxyl groups at C-3 and C-6 position of D-glucose are absent, may thus be explained.

O-Mesylation of **2** afforded the corresponding 4-*O*-mesylate **3** (90% yield), which was allowed to react with sodium benzoate in boiling DMF to give 3,6-diazido-4-*O*-benzoyl-3,6-dideoxy-1,2-*O*-isopropylidene-α-D-galactopyranose (**4**) in 84% yield. Debenzoylation of **4** with sodium methoxide in methanol afforded **5**, the 4-epimer of **2**, in 93% yield. The 4-*O*-mesylate **6** prepared from **5** in 89% yield, was heated with sodium azide in DMSO to give 3,4,6-triazido-3,4,6-trideoxy-1,2-*O*-isopropylidene-α-D-glucopyranose

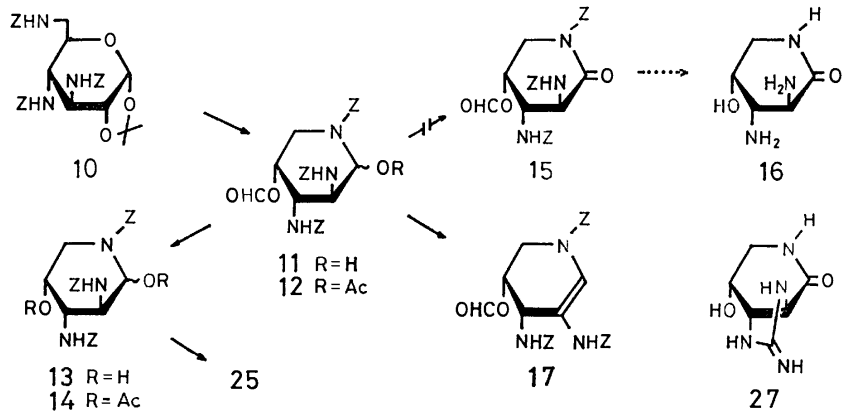

Chart 2.

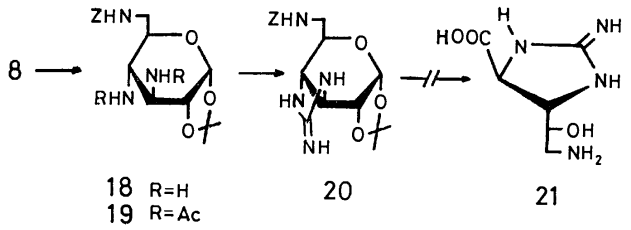

Chart 3.

(**7**) as a syrup in 69% yield after being subjected to chromatography.

Synthetic Approach to Triamino Arabono-1,4-lactam ***16*** *from Triazido Glucose Derivative* ***7***. Hydrogenolysis of **7** over palladium black afforded 3,4,6-triamino-3,4,6-trideoxy-1,2-*O*-isopropylidene-α-D-glucopyranose (**8**) as a colorless syrup, which led to the crystalline tri-*N*-acetyl derivative **9** on treatment with acetic anhydride in methanol. The crystalline tri-*N*-benzyloxycarbonyl derivative **10** was also obtained by the reaction of **8** with benzyl chloroformate in pyridine in 70% yield after being subjected to chromatography. Compounds **8**, **9**, and **10** are the derivatives of the new triamino glucose.

The 1,2-*O*-isopropylidene group of **10** was removed with warm aqueous acetic acid and the resulting free sugar was subjected to periodate oxidation in aqueous acetone to afford a crystalline piperidinose derivative, 4-*O*-formyl-2,3,5-tris(benzyloxycarbonylamino)-2,3,5-trideoxy-D-arabinopyranose (**11**) in 71.5% yield. Compound **11** was converted into the 1-*O*-acetate **12** in good yield. Deformylation of **11** with ammonia in aqueous dioxane gave **13** as crystals (93% yield), which could be converted into the 1,4-di-*O*-acetate **14**.[2b] The PMR spectra of **11**, **12**, **13**, and **14** showed signals in line with piperidinose structure.[7]

Transformation of **11** into **16** was attempted. However, no desired lactam **15** was obtained on treatment with DMSO–DCCI–pyridine–trifluoroacetic acid.[8] Instead, only 2,3,5-tris(benzyloxycarbonylamino)-1,2,3,5-tetradeoxy-4-*O*-formyl-D-*erythro*-pent-1-enopyranose (**17**), the dehydration product, was obtained in 82% yield. The structure of **17** was confirmed by PMR spectroscopy (singlet at δ 7.48 due to the H-1 olefinic proton) and by elemental analysis. When **11** was treated with DMSO–trifluoroacetic anhydride in dichloromethane at —70 °C according to the method of Huang *et al.*[9] no reaction product was detected in TLC, but when the mixture was warmed up to room temperature, the formation of **17** was observed. Oxidation of **11** with chromium trioxide–acetic acid–pyridine,[10] with bromine–water, or with *N*-bromosuccinimide in dioxane afforded only the unchanged material.

*Attempt to Synthesize Streptolidine (****21****) from Triamino Glucose Derivative* ***8***. Selective *N*-benzyloxycarbonylation of **8** with *N*-(benzyloxycarbonyloxy)-succinimide[11] in aqueous DMF yielded the 6-*N*-benzyloxy-carbonylated product **18** as a major product in 46% yield after being subjected to chromatography. Acetylation of **18** afforded the di-*N*-acetyl derivative **19**, whose PMR spectrum showed signals at δ 3.03 (H-3) and 2.53(H-4); those of **18** being shifted to downfield by acetylation.

Treatment of **18** with one equivalent of cyanogen bromide in water gave the cyclic guanidine derivative **20** as crystalline hydrobromide in 93% yield after being subjected to chromatography. *O*-Deisopropylidenation of **20** followed by successive oxidation with periodate and with bromide–water afforded no expected product from which streptolidine (**21**) could be derived. Periodate oxidation of the *O*-deisopropylidenation product might have yielded a piperidinose derivative as an intermediary product which resists oxidation with bromine–water as in the case of **11**.

Transformation of Triazido Glucose Derivative ***7*** *into Triamino Sugar Lactam* ***16***. A synthetic approach to triamino sugar lactam **16** involving the conversion of the triazido D-glucose derivative **7** into the glucitol derivative **23** was performed. *O*-Deisopropylidenation of **7** with 20% aqueous acetic acid, followed by sodium borohydride-reduction in aqueous ethanol, afforded 3,4,6-triazido-3,4,6-trideoxy-D-glucitol (**22**) in 60% yield. Hydrogenolysis of **22** over palladium black and subsequent *N*-benzyloxycarbonylation with *N*-(benzyloxycarbonyloxy)succinimide gave the crystalline 3,4,6-tris(benzyloxycarbonylamino)-3,4,6-trideoxy-D-glucitol (**23**) in 98% yield. Periodate-oxidation of **23** afforded the furanose derivative **24**[2b] whose TLC showed a single spot having R_f-value differing from that of piperidinose derivative **13**. With-

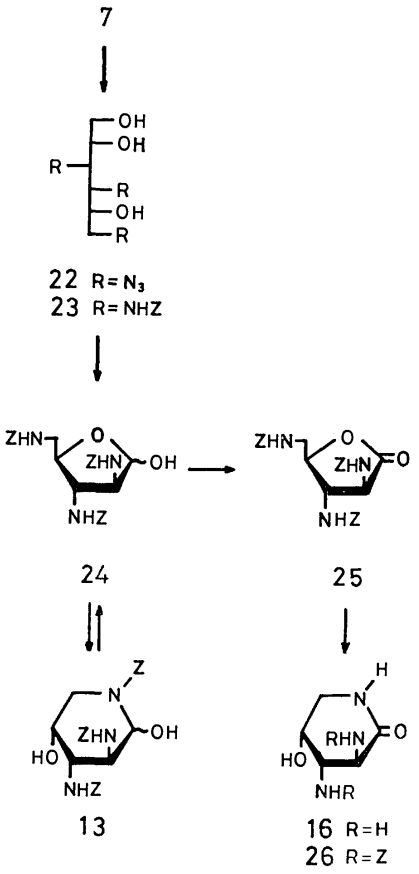

Chart 4.

out purification, **24**, was oxidized with chromium trioxide–acetic acid–pyridine to give the corresponding crystalline 1,4-lactone **25**[2b] as the sole product in 66% yield from **23** after being subjected to chromatography. When the oxidation of **24** was carried out with bromine–water[3] instead of the chromium trioxide reagent, a considerable amount of **13** was isolated together with **25** on column chromatography of the reaction product. During the slow oxidation reaction with bromine–water, **24** might have partially been converted into **13** which resisted bromine-oxidation.

Lactone **25** was also obtained in 42% yield by oxidation of **13** with chromium trioxide reagent. Hydrogenolysis of **25** over palladium black gave **16**, whose structure was confirmed by conversion into 2,3-di-*N*-benzyloxycarbonylated triamino sugar lactam **26**.[3]

Experimental

Melting points were determined on a micro hot-stage and are uncorrected. IR spectra were taken on a Hitachi 225 spectrophotometer, PMR spectra on a Varian A-60D spectrometer using TMS as an internal standard. Specific rotations were determined with a Zeiss Photoelectric polarimeter. TLC was performed on Wakogel B-5 and column chromatography on Wakogel C-200. Hydrogenolysis was conducted under bubbling with hydrogen at room temperature. Concentration was carried out below 40 °C under reduced pressure.

3,6-Diazido-3,6-dideoxy-1,2-O-isopropylidene-α-D-glucopyranose (2). A mixture of 3,6-diazido-3,6-dideoxy-1,2-*O*-isopropylidene-α-D-glucofuranose (**1**)[4] (31.5 g) and 50% aqueous acetic acid (320 ml) was heated at 90—100 °C for 6.5 h, the resulting solution being evaporated to give free sugar as pale yellow crystals (24.6 g, 92%). A mixture of the product (24.6 g), dry DMF (246 ml), 2,2-dimethoxypropane (64 ml), and *p*-toluenesulfonic acid (3.53 g) was kept at 60 °C for 2.5 h, the reaction mixture being poured into cold water (250 ml) and extracted with chloroform (250 ml × 3). The combined extracts were washed with saturated NaCl solution, dried, and evaporated. The residual syrup (31.6 g) was chromatographed on silica gel (1.3 kg) with benzene–ethyl acetate (15:1) to afford a homogeneous sample of **2** (17.2 g, 60%) as a colorless syrup. Chromatography also gave **1** (0.19 g, 0.7%) and a mixture of **1** and **2** (2.0 g, 7%). **2**: $[\alpha]_D^{14}$ +95° (*c* 1.4, $CHCl_3$); $\delta(CDCl_3)$ 1.41 and 1.62 [each s, 6H, $C(CH_3)_2$], 3.6—3.9(m, 5H, H-3,4,5,6,6′), 4.18(dd, H-2 $J_{1,2}$=4.8, $J_{2,3}$=5.9 Hz), and 5.63 (d, H-1).

Found: C, 40.15; H, 5.09; N, 30.77%. Calcd for $C_9H_{14}N_6O_4$: C, 40.00; H, 5.22; N, 31.10%.

3,6-Diazido-3,6-dideoxy-1,2-O-isopropylidene-4-O-mesyl-α-D-glucopyranose (3). A sample of **2** (17.1 g) was mesylated with mesyl chloride (5.36 ml) in pyridine (86 ml) at room temperature for 5 h. Work-up of the reaction mixture in the usual way afforded a practically pure syrup of the 4-*O*-mesylate (**3**) in quantitative yield (22.0 g). Analytical sample of **3** was obtained in 90% yield after being subjected to chromatography on silica gel with benzene–ethyl acetate (12:1); $[\alpha]_D^{17}$ +80° (*c* 1.9, $CHCl_3$); $\nu_{max}^{CCl_4}$ (0.1 M) 2100 (N_3), 1380 and 1185 cm^{-1} (SO_3); $\delta(CDCl_3)$ 1.39 and 1.60 [each s, 6H, $C(CH_3)_2$], 3.12(s, 3H, OMs), *ca.* 3.6(m, 2H, H-6,6′), *ca.* 4.1(m, 1H, H-5), 4.12(dd, 1H, H-3, $J_{2,3}$=4.2, $J_{3,4}$=8.8 Hz), 4.29(dd, 1H, H-2, $J_{1,2}$=4.6 Hz), 4.68(dd, 1H, H-4, $J_{4,5}$=4.3 Hz), and 5.63(d, 1H, H-1).

Found: C, 34.76; H, 4.47; N, 23.83; S, 9.42%. Calcd for $C_{10}H_{16}N_6O_6S$: C, 34.47; H, 4.62; N, 24.12; S, 9.20%.

3,6-Diazido-4-O-benzoyl-3,6-dideoxy-1,2-O-isopropylidene-α-D-galactopyranose (4). A mixture of **3** (669 mg), sodium benzoate (1.39 g), and dry DMF (62 ml) was refluxed for 4 h. The cooled reaction mixture was filtered, and the insoluble matter was washed with ethyl acetate (65 ml). The combined filtrate and washings were evaporated to a syrup, which was dissolved in chloroform, washed with water and saturated NaCl solution, dried and evaporated. The residual yellow syrup was chromatographed on silica gel with benzene–ethyl acetate (12:1) to afford colorless syrup of **4** (604 mg, 84%): $[\alpha]_D^{20}$ +156° (*c* 1.6, $CHCl_3$); ν_{max}^{liq} 2100 (N_3), 1730 cm^{-1} (ester); $\delta(CDCl_3)$, 1.46 and 1.61[each s, 6H, $C(CH_3)_2$], *ca.* 3.5(m, 2H, H-6,6′), 4.01(dd, 1H, H-3, $J_{2,3}$=6.2, $J_{3,4}$=4.0 Hz), *ca.* 4.3(m, 1H, H-5), 4.32(dd, 1H, H-2, $J_{1,2}$=4.6 Hz), 5.58(dd, 1H, H-4, $J_{4,5}$=3.2 Hz), and 5.74(d, 1H, H-1).

Found: C, 51.12; H, 4.56; N, 22.25%. Calcd for $C_{16}H_{18}N_6O_5$: C, 51.33; H, 4.85; N, 22.45%.

3,6-Diazido-3,6-dideoxy-1,2-O-isopropylidene-α-D-galactopyranose (5). A 0.82 M methanolic sodium methoxide solution (2.95 ml) was added to a solution of **4** (604 mg) in methanol (12 ml) and the mixture was kept at room temperature for 3 h. The solution was neutralized with 20% acetic acid and evaporated. The residue was dissolved in ethyl acetate, washed with water and saturated NaCl solution, dried, and evaporated. The residual yellow syrup was chromatographed on silica gel with benzene–ethyl acetate (12:1) to afford **5** as a syrup (406 mg, 93%): $[\alpha]_D^{18}$ +91° (*c* 1.4, $CHCl_3$); $\delta(CDCl_3)$ 1.43 and 1.57[each s, 6H, $C(CH_3)_2$], 2.45(1H, OH), 3.4—4.1(m, 5H, H-3,4,5,6,6′), 4.32(dd, 1H, H-2, $J_{1,2}$=4.6, $J_{2,3}$=7.0 Hz), and 5.71(d, 1H, H-1).

Found: C, 40.22; H, 5.26; N, 31.25%. Calcd for $C_9H_{14}N_6O_4$: C, 40.00; H, 5.22; N, 31.10%.

*3,6-Diazido-3,6-dideoxy-1,2-O-isopropylidene-4-O-mesyl-α-D-galactopyranose (**6**).* A sample of **5** (382 mg) was mesylated in the usual way to afford **6** (493 mg) in quantitative yield. Analytical sample was obtained by silica gel column chromatography with benzene-ethyl acetate (12:1) in 89% yield as a pale yellow syrup: $[\alpha]_D^{20}$ +74° (*c* 2.0, $CHCl_3$); $\nu_{max}^{CHCl_3}$ (0.1 M) 2100(N_3), 1360 and 1175 cm^{-1} (SO_3); δ($CDCl_3$) 1.42 and 1.57[each s, 6H, $C(CH_3)_2$], 3.18(s, 3H, OMs), 3.53(m, 2H, H-6,6'), 3.88(dd, 1H, H-3, $J_{2,3}$=6.5, $J_{3,4}$= 2.8 Hz), *ca.* 4.2(m, 1H, H-5), 4.21(dd, 1H, H-2, $J_{1,2}$=4.2 Hz), 4.94(dd, 1H, H-4, $J_{4,5}$=3.8 Hz), and 5.61(d, 1H, H-1).

Found: C, 34.73; H, 4.65; N, 24.10; S, 9.03%. Calcd for $C_{10}H_{16}N_6O_6S$: C, 34.47; H, 4.62; N, 24.12; S, 9.20%.

*3,4,6-Triazido-3,4,6-trideoxy-1,2-O-isopropylidene-α-D-glucopyranose (**7**).* A mixture of **6** (375 mg), sodium azide (211 mg) and dry DMSO (7.6 ml) was heated under stirring at 95—100 °C for 1.5 h and then poured into cold water (7.7 ml). The mixture was extracted with chloroform and the combined extracts were washed with saturated NaCl solution, dried, and evaporated. The residual brown syrup was chromatographed on silica gel with benzene-ethyl acetate (30:1) to afford a pale yellow syrup of **7** (218 mg, 69%). A part of this sample was again chromatographed on silica gel with hexane-ethyl acetate (20:1) to give an analytical sample: $[\alpha]_D^{20}$ +239° (*c* 1.47, $CHCl_3$); $\nu_{max}^{CHCl_3}$ 2110 cm^{-1} (N_3); δ($CDCl_3$) 1.42 and 1.59[each s, 6H, $C(CH_3)_2$], 3.5—3.9(m, 5H, H-3, 4,5,6,6'), 4.19(dd, 1H, H-2, $J_{1,2}$=4.8, $J_{2,3}$=5.0 Hz), 5.67(d, 1H, H-1).

Found: C, 36.84; H, 4.49; N, 42.48%. Calcd for $C_9H_{13}N_9O_3$: C, 36.61; H, 4.44; N, 42.70%.

*3,4,6-Triamino-3,4,6-trideoxy-1,2-O-isopropylidene-α-D-glucopyranose (**8**).* The triazido compound **7** (114 mg) was hydrogenolized over palladium black in methanol to afford the triamino derivative **8** (77.3 mg, 92%), which was used for the subsequent reaction without purification.

*Tri-N-acetyl Derivative (**9**):* Acetylation of **8** (69.1 mg) with acetic anhydride (0.09 ml) in methanol at room temperature for 1 h gave **9** (91.3 mg, 84%) as needles after silica gel chromatography (5:1, chloroform-methanol): mp 253 °C (dec); $[\alpha]_D^{22}$ +59°(*c* 0.59, MeOH); ν_{max}^{KBr} 1645 and 1533 cm^{-1} (amide).

Found: C, 52.24; H, 7.25; N, 12.04%. Calcd for $C_{15}H_{25}N_3O_6$: C, 52.47; H, 7.34; N, 12.24%.

*Tri-N-benzyloxycarbonyl Derivative (**10**):* A sample of **8** (244 mg) was *N*-benzyloxycarbonylated with benzyl chloroformate (0.64 ml) in dry pyridine (4 ml) at −40——35 °C for 3 h. The reaction mixture was diluted with water and extracted with chloroform. The extracts were washed with saturated NaCl solution, dried, and evaporated. The residue was chromatographed on silica gel with benzene-acetone (10:1) to afford **10** (490 mg, 71%) as crystals. Recrystallization from ethyl acetate-petroleum ether gave a pure sample: mp 124—125 °C; $[\alpha]_D^{18}$ −28°(*c* 1.21, $CHCl_3$); ν_{max}^{KBr} 3320 (NH), 1690 and 1530 cm^{-1} (amide); δ($CDCl_3$) 1.32 and 1.55[each s, 6H, $C(CH_3)_2$], 3.7—4.3(m, 6H, H-2,3, 4,5,6,6'), 5.20(s, 6H, CH_2Ph), *ca.* 5.5(3H, NH), 5.63(d, 1H, H-1, $J_{1,2}$=4.8 Hz), and 7.48(s, 15H, Ph).

Found: C, 63.83; H, 6.11; N, 6.63%. Calcd for $C_{33}H_{37}N_3O_9$: C, 63.96; H, 6.02; N, 6.78%.

*2,3,5-Tris(benzyloxycarbonylamino)-2,3,5-trideoxy-O-formyl-D-arabinopyranose (**11**).* Treatment of **10** (1.78 g) with 67% aqueous acetic acid (26.7 ml) at 55—60 °C for 4.5 h afforded a crystalline free sugar (1.60 g, 96%), which was suspended in acetone (48 ml) to which added a solution of sodium metaperiodate (1.77 g) in water (18 ml). The mixture was stirred at 33°C for 40 h, and the resulting precipitates were collected by filtration and washed with acetone and water to give **11** as a colorless powder (1.14 g, 72%). A part of this product was chromatographed on silica gel with chloroform-ethyl acetate (10:1) to afford an analytical sample: mp 198—199 °C(dec); $[\alpha]_D^{17}$ −20°(constant for 48 h, *c* 0.75, dioxane); ν_{max}^{KBr} 3430 (OH), 3300 (NH), 1718 (OCHO), 1680 and 1540 cm^{-1} (urethane); δ(DMSO-d_6) *ca.* 3.2—4.1(m, 4H, H-2,3,5,5'), 5.10 and 5.18(each s, 6H, OCH_2Ph), *ca.* 5.2(m, 1H, H-4), *ca.* 5.8(m, 1H, H-1), *ca.* 6.5, 7.2, and 7.5(m, 3H, NH and OH), 7.45(s, 15H, Ph), and 8.27(s, OCHO); δ(pyridine-d_5) 3.82(m, 1H, H-5, $J_{5,5}$ = 14.2 Hz), *ca.* 4.4—5.3(m, 5H, H-1,2,3,5', and OH), 5.18(s, 6H, OCH_2Ph), 5.75(m, 1H, H-4), *ca.* 6.7 and 7.4(m, 2H, NH), and 8.10(s, 1H, OCHO).

Found: C, 62.48; H, 5.52; N, 7.09%. Calcd for $C_{30}H_{31}N_3O_9$: C, 62.38; H, 5.41; N, 7.28%.

*1-O-Acetyl Derivative (**12**).* A sample of **11** (35.6 mg) was acetylated with acetic anhydride (0.02 ml) in pyridine (0.36 ml) to afford colorless powder of **12** (32.9 mg, 86%): mp 194—198 °C (MeOH); $[\alpha]_D^{19}$ −43° (*c* 1.8, $CHCl_3$); δ($CDCl_3$) 2.10(s, 3H, OAc), *ca.* 3.3 and 4.2—4.5(m, 4H, H-2,3,5,5'), 5.08(s, 4H, OCH_2Ph at 2- and 3-N), 5.21(ABq, OCH_2Ph at 5-N), 5.0—5.4(br, 3H, two NH, H-4), 7.05(m, H-1), 7.37(s, 15H, Ph), and 7.98(s, 1H, OCHO).

Found: C, 62.24; H, 5.51; N, 6.70%. Calcd for $C_{32}H_{33}N_3O_{10}$: C, 62.03; H, 5.37; N, 6.78%.

*2,3,5-Tris(benzyloxycarbonylamino)-2,3,5-trideoxy-D-arabinopyranose (**13**).* A mixture of **11** (47.4 mg), dioxane (0.5 ml), and 10% aqueous ammonia (0.1 ml) was kept at room temperature for 2 h. The reaction mixture was evaporated to dryness and the residue was washed with ethanol to afford **13** as a powder (41.9 mg, 93%): R_f 0.64(silica gel, 3:1 benzene-acetone); mp 204—206 °C; δ(DMSO-d_6) *ca.* 3.2(m, 1H, H-5), 3.8—4.0(m, 4H, H-2,3,4,5'), 5.12 and 5.19(each s, 6H, OCH_2Ph), 5.75(m, 1H, H-1), *ca.* 6.6(m, 2H, NH), *ca.* 7.4(m, 1H, NH), and 7.41(s, 15H, Ph); δ(pyridine-d_5) 3.79(m, 1H, H-5, $J_{5,5}$=13.2 Hz), 4.4—5.3(m, 7H, H-1, 2,3,4,5', OH) 5.18 and 5.21(each s, OCH_2Ph), *ca.* 6.6 and 7.8(2H, NH), and 7.26(s, 15H, CH_2Ph).

Found: C, 63.22; H, 5.85; N, 7.47%. Calcd for $C_{29}H_{31}N_3O_8$: C, 63.38; H, 5.69; N, 7.65%.

*1,4-Di-O-Acetyl Derivative (**14**).* A sample of **13** (15 mg) was acetylated with acetic anhydride (0.025 ml) in pyridine (0.15 ml) for 48 h. The crystalline product was recrystallized from chloroform-hexane to afford the pure sample of **14** (12.1 mg, 70%): mp 192.5—194.5 °C (lit,[2b] 186—186.5 °C); $[\alpha]_D^{19}$ −41°(*c* 2.05, $CHCl_3$); δ(DMSO-d_6) 1.92 and 2.11(each s, 6H, CH_3CO), 3.19(dd, 1H, H-5, $J_{5,5'}$= 15 Hz), 4.2—4.4(m, 3H, H-2,3,5'), 5.0—5.2(m, 9H, CH_2Ph, H-4, NH), 6.99(m, 1H, H-1), 7.35—7.40(each s, Ph).

Found: C, 62.52; H, 5.62; N, 6.46%. Calcd for $C_{33}H_{35}O_{10}N_3$: C, 62.55; H, 5.57; N, 6.63%.

*2,3,5-Tris(benzyloxycarbonylamino)-1,2,3,5-tetradeoxy-4-O-formyl-D-erythro-pent-1-enopyranose (**17**).* A mixture of dry DMSO, dry pyridine, and trifluoroacetic acid (10:1:0.473 by volume) (3.12 ml) was added to a solution of **11** (1.00 g) in dry DMSO (10 ml). DCCI (1.07 g) was then added to the mixture, and stirred at room temperature for 1 day. The reaction mixture was poured into ice-water (15 ml). The pale yellow precipitates formed were collected by filtration and washed with water. The dried solid was dissolved in dioxane, the insoluble matter was filtered off, and the filtrate was evaporated to afford a colorless solid of **17** (793 mg, 82%). The analytical sample was obtained by silica gel chromatography with benzene-ethyl acetate (6:1): mp 174—177 °C (dec); $[\alpha]_D^{18}$ +90°(*c* 0.5, dioxane); ν_{max}^{KBr} 3320 (NH), 1730(ester), 1695 and 1525 cm^{-1}(amide); δ(DMSO-d_6) 3.4—3.9(m, 3H, H-3,5,5'), *ca.* 4.9(m, 1H, H-4), 5.22 and 5.37(each

s, 6H, CH_2Ph), 7.3—7.8(m, 2H, NH), 7.48(s, 1H, H-1), 7.60(s, 15H, Ph), and 8.42(s, CHO).

Found: C, 64.14; H, 5.30; N, 7.23%. Calcd for $C_{30}H_{29}N_3O_8$: C, 64.39; H, 5.08; N, 7.23%.

*3,4-Diamino-6-(benzyloxycarbonylamino)-3,4,6-trideoxy-1,2-O-isopropylidene-α-D-glucopyranose (**18**).* A solution of *N*-(benzyloxycarbonyloxy)succinimide (810 mg) in DMF (7.1 ml) was added dropwise to a solution of **8** (706 mg) in 75% DMF-water (14.1 ml) at −30——20 °C under stirring over a period of 30 min. After being kept at room temperature for 1 h, the reaction mixture was evaporated, the resulting syrup was dissolved in chloroform (20 ml), washed with saturated $NaHCO_3$ and saturated NaCl solution successively, dried, and evaporated. The syrupy residue (1.4 g) was chromatographed on silica gel (140 g) with chloroform-methanol (5:1) to afford a homogeneous sample of the 6-*N*-benzyloxycarbonylated product **18** (527 mg, 40%) as a colorless syrup, which was used for subsequent synthesis without further purification: $\nu_{max}^{CHCl_3}$ (0.1 M) 3400 (NH), 1710 and 1510 cm^{-1}(amide); δ ($CDCl_3$) 1.37 and 1.56 [each s, 6H, $C(CH_3)_2$], 1.66(s, 4H, NH) 2.53(dd, 1H, H-4, $J_{3,4}$=6.0, $J_{4,5}$=8.3 Hz), 3.03(dd, 1H, H-3, $J_{2,3}$=5.0 Hz), 3.6—3.8(m, 3H, H-5,6,6'), 4.07(dd, 1H, H-2, $J_{1,2}$=5.0 Hz), 5.21(s, 2H, CH_2Ph), *ca.* 5.4(m, 1H, NH), 5.63(d, 1H, H-1), and 7.48(s, 5H, Ph).

*3,4-Di-*N*-acetyl Derivative (**19**).* A sample of **18** (33.6 mg) was acetylated with acetic anhydride (0.02 ml) in methanol (0.67 ml) at room temperature for 20 min. Evaporation of the reaction mixture followed by chromatography on silica gel (4 g) with chloroform-methanol (20:1) afforded the pure sample of **19** as a glassy solid (38.5 mg, 93%): $[\alpha]_D^{25}$ +38°(*c* 0.66, $CHCl_3$); ν_{max}^{KBr} 3300 (NH), 1700, 1650 and 1530 cm^{-1}(amide); δ($CDCl_3$) 1.37 and 1.59[each s, 6H, $C(CH_3)_2$], 1.96 and 1.99(each s, 6H, NAc), 3.4—4.5(m, 6H, H-2,3,4,5,6,6'), 5.21(s, 2H, CH_2Ph), 5.65(d, 1H, H-1, $J_{1,2}$=4.8 Hz), *ca.* 5.7 and 6.3(3H, NH), and 7.47(s, 5H, Ph).

Found: C, 57.63; H, 6.58; N, 9.42%. Calcd for $C_{21}H_{29}N_3O_7$: C, 57.92; H, 6.71; N, 9.65%.

*3,4-(1,3-Guanidinediyl)-6-benzyloxycarbonylamino-3,4,6-trideoxy-1,2-O-isopropylidene-α-D-glucopyranose (**20**) Hydrobromide.* Cyanogen bromide (138 mg) was added to a solution of **18** (458 mg) in water (4.6 ml) under stirring. After being left to stand at room temperature for 1 h, the reaction mixture was evaporated and the residue was chromatographed on silica gel (60 g) with chloroform-ethanol (5:1) to afford the crystalline hydrobromide of **20** (555 mg, 93%): mp 122—125 °C (dec); ν_{max}^{KBr} 3400—3000 (NH^+), 1700 and 1530(amide), 1675 cm^{-1} (guanidium I); $[\alpha]_D^{20}$ +59°(*c* 0.55, MeOH); δ($CDCl_3$) 1.36 and 1.52[each s, 6H, $C(CH_3)_2$], 3.7—4.4(m, 6H, H-2,3,4,5,6,6'), 5.23(s, 2H, CH_2Ph), *ca.* 5.7(1H, H-1), *ca.* 6.2(br, 1H, NH), 7.2—7.7(br, 4H, guanidinium), and 7.46(s, 5H, Ph).

Found: C, 47.39; H, 5.72; N, 12.41; Br, 17.14%. Calcd for $C_{18}H_{25}N_4O_5Br$: C, 47.27; H, 5.51; N, 12.25; Br, 17.47%.

*3,4,6-Tris(benzyloxycarbonylamino)-3,4,6-trideoxy-D-glucitol (**23**).* A mixture of **7** (916 mg) and 20% acetic acid (27.5 ml) was heated at 100—110 °C for 1.5 h and then evaporated. The residual brown syrup was chromatographed on silica gel (43 g) with benzene–ethyl acetate(2:1) to afford 3,4,6-triazido-3,4,6-trideoxy-D-glucose (682 mg, 86.2%) A solution of sodium borohydride (57 mg) in 80% ethanol (1.0 ml) was added to a solution of free sugar (682 mg) in ethanol (5.1 ml) under ice-cooling. The mixture was stirred at the same temperature for 0.5 h, and then warmed up to room temperature, stirring being continued for 3 h, and neutralized with Amberlite IR-120(1.5 ml). The resulting solution was evaporated and the residue was chromatographed on silica gel (65 g) with benzene-ethyl acetate (1:1) to give a colorless syrup of **22** (415 mg, 60%). Triazido compound **22** (632 mg) was hydrogenolized over palladium black in methanol (12 ml) for 4 h to afford the triamino compound as a pale yellow syrup. A solution of *N*-(benzyloxycarbonyloxy)succinimide (2.0 g) in DMF (4 ml) was added to a solution of the triamino compound (450 mg) in DMF (4 ml) and water (0.2 ml). After being kept at room temperature, the reaction mixture was poured into ice-water (150 ml). The precipitates formed were collected by filtration, washed with water, and dried to yield a colorless crystalline solid of **23** (1.43 g, 98% from **22**). Recrystallization from methanol afforded an analytical sample: mp 148.5—149.5 °C; $[\alpha]_D^{20}$ +53°(*c* 0.94, DMF).

Found: C, 62.11; H, 6.04; N, 7.20%. Calcd for $C_{30}H_{35}N_3O_9$: C, 61.95; H, 6.07; N, 7.23%.

*2,3,5-Tris(benzyloxycarbonylamino)-2,3,5-trideoxy-D-arabono-1,4-lactone (**25**).* (a) A solution of sodium metaperiodate (273 mg) in water (2 ml) was added to a solution of **23** (430 mg) in acetone (9 ml), and the mixture was stirred at room temperature for 1 h. The mixture was diluted with acetone (9 ml). The precipitates were filtered off, and the filtrate was evaporated to afford 2,3,5-tris(benzyloxycarbonylamino)-2,3,5-trideoxy-D-arabinofuranose (**24**) (404 mg) as a colorless solid: R_f 0.56(silica gel, 3:1 benzene-acetone). Furanose **24** (404 mg) was oxidized with the chromium trioxide-acetic acid-pyridine reagent** (9.2 ml) at room temperature for 1.5 h. The reaction mixture was diluted with water (20 ml), extracted with chloroform, the extracts being washed with saturated NaCl solution, dried, and evaporated. The syrupy residue (300 mg) was chromatographed on silica gel (30 g) with benzene-acetone (6:1) to give **25** (265 mg, 66%) as a colorless solid: mp 89—91 °C (benzene); $[\alpha]_D^{18}$ −26° (*c* 0.97, $CHCl_3$); ν_{max}^{KBr} 3320 (NH), 1785 (1,4-lactone), 1680 and 1510 cm^{-1}(amide); δ($CDCl_3$) *ca.* 3.6, 4.3, and 4.7(m, 5H, H-2,3,-4,5,5'), 5.10(s, 6H, CH_2Ph), *ca.* 5.8(br, 3H, NH), and 7.32(s, 15H, Ph).

Found: C, 63.70; H, 5.47; N, 7.49%. Calcd for $C_{29}H_{29}N_3O_8$: C, 63.61; H, 5.34; N, 7.68%.

(b) A sample of **13** (10.8 mg) was treated with the chromium trioxide-acetic acid-pyridine reagent (0.25 ml) at room temperature for 3 h. The reagent (0.25 ml) was added to the mixture. After being stirred for 30 min, the reaction mixture was worked up as described in (a) to afford a sample of **25** (4.1 mg, 42%) as a semicrystalline solid, whose IR spectrum was identical with that of the sample of **25** prepared from **24**.

*5-Amino-2,3-bis(benzyloxycarbonylamino)-2,3,5-trideoxy-D-arabono-1,5-lactam (**26**).* A sample of **25** (209 mg) was hydrogenolized in methanol (6 ml) over palladium black for 5 h. During the course of reaction a fresh catalyst was added every hour. The crude triamino sugar lactam **16** was purified by silica gel chromatography with chloroform-methanol-17% aqueous ammonia (6:6:1) to afford a practically pure sample of **16** (39.7 mg, 72%). Treatment of the sample of triamino sugar lactam **16** with 3 equivalent of *N*-(benzyloxycarbonyloxy)succinimide in aqueous DMF gave a crystalline sample of **26** in 85% yield after being subjected to chromatography with chloroform-methanol (10:1). The sample was identical with the authentic sample[3] of **26**.

The authors wish to thank Mr. Saburo Nakata for carring out the microanalyses.

**The reagent[10] is composed of chromium trioxide (1 g), acetic acid (30 ml) and pyridine (1 ml).

References

1) T. Goto and T. Ohgi, *Tetrahedron Lett.*, **1974**, 1413.
2) (a) S. Kusumoto, S. Tsuji, K. Shima, and T. Shiba, *Tetrahedron Lett.*, **1974**, 1417; (b) S. Kusumoto, S. Tsuji, and T. Shiba, *Bull. Chem. Soc. Jpn.*, **47**, 2690 (1974).
3) M. Kinoshita and Y. Suzuki, *Bull. Chem. Soc. Jpn.*, **50**, 2375 (1977).
4) W. Meyer zu Reckendorf, *Chem. Ber.*, **101**, 3082 (1968).
5) (a) M. Kiso and A. Hasegawa, *Carbohydr. Res.*, **52**, 87 (1976); (b) *ibid.*, **52**, 95 (1976).
6) W. Meyer zu Reckendorf and E. Bischef, *Tetrahedron Lett.*, **1970**, 2475.
7) H. Paulsen, *Angew. Chem. Int. Ed. Engl.*, **5**, 495 (1966).
8) K. E. Pfitzner, J. G. Moffatt, *J. Am. Chem. Soc.*, **85**, 3027 (1963); *ibid.*, **87**, 5661 (1965); H. Yanagisawa, M. Kinoshita, S. Nakata and S. Umezawa, *Bull. Chem. Soc. Jpn.*, **43**, 246 (1970).
9) S. L. Huang, K. Omura, and D. Swern, *J. Org. Chem.*, **41**, 3339 (1976).
10) J. C. Sheehan, H. G. Zachan, and W. B. Lawson, *J. Am. Chem. Soc.*, **80**, 3349 (1958).
11) H. Kawaguchi, T. Naito, S. Nakagawa, and K. Fujisawa, *J. Antibiot.*, **25**, 695 (1972).

Aromatic Solvent-induced Shifts (ASIS). II. Interpretation of Benzene and Hexafluorobenzene Induced Shifts by Means of the Electrostatic Interaction Model

Kunio NIKKI* and Naoya NAKAGAWA

The University of Electro-Communications, Chofu, Tokyo 182

(Received January 31, 1978)

The relationships between the ASIS in proton magnetic resonance and charge distribution in the solute and solvent molecules were studied. The results obtained are as follows. Protons lying in the positive charge-region of the solute dipole showed an up-field shift in C_6H_6 and a down-field shift in C_6F_6, while protons lying in the negative charge-region showed a down-field shift in C_6H_6 and an up-field shift in C_6F_6. There exists a linear relationship between the ASIS and the solute dipole moments of monosubstituted methanes, *t*-butyl derivatives, and para substituted toluenes. Shifts of para substituted toluenes and 4-methyl-4′-nitrobiphenyl are in good agreement with those expected from the electrostatic interaction model.

Aromatic solvent-induced shifts (ASIS) in ^1H NMR spectroscopy have been well investigated.[1,2] The benzene-induced shifts observed for carbonyl compounds are conveniently explained by an empirical rule, the so-called "Carbonyl plane rule."[3]

In the earlier models of ASIS, *i.e.*, the dipole-induced dipole interaction model, the quadrupole-induced quadrupole interaction model,[4] and in the H-bond interaction model,[5] the nature of intermolecular interactions was discussed without much success.

Since then, two models have been proposed to explain ASIS. One is the solute–solvent specific 1:1 complex model and the other is the time-averaged cluster model. In the former model Williams *et al.* assumed the existence of solvent molecules with favorable distances and orientations to the solute molecules; these would show the feature of ASIS.[1] Laszlo *et al.* pointed out in the latter model that the solute dipole should be the cause of clustering.[2] They did not discuss, however, the nature of the solute-solvent interaction.

In our previous paper,[6] benzene-induced shifts of methyl protons on *d*-camphor were discussed in terms of the electrostatic dipole(*d*-camphor)-quadrupole-(benzene) interaction. The results were in good agreement with the experimental ASIS values. If the main interaction between solute molecule and solvent mole cules is assumed as the electrostatic interaction, the flat surface of benzene molecules near the positive charge end of the dipole are likely to face to the positive end. Thus, benzene molecules induce up-field shifts due to their magnetic anisotropy for the protron near the positive end. On the other hand, the periphery part of benzene molecules near the negative charge end of the dipole are likely to face to the negative end. Thus, they induce down-field shifts for the proton near the negative end. These favorable orientations are similar to those proposed by Williams[1] and Ledaal.[7]

Recently, it was shown that a different solvent effect was induced by hexafluorobenzene, which generally shows shifts opposite to those induced by benzene.[8-17] The carbonyl plane rule for that solvent was also proposed,[16] but the nature of the intermolecular interaction was not discussed.

The main purpose in this paper is to clarify the mechanism of ASIS: these shifts are caused by the orientation of solvent molecules around the dipole due to intermolecular electrostatic interactions. Furthermore, it will be shown that the hexafluorobenzene(which has a different charge distribution than benzene)-induced shifts were also caused mainly by the electrostatic interaction, as in the case of benzene-induced shifts.

Thus the aromatic solvent-induced shifts (ASIS) in benzene and hexafluorobenzene of monosubstituted methanes, *t*-butyl derivatives, para substituted toluenes, and 4-methyl-4′-nitrobiphenyl were determined. Besides these determinations, the observed ASIS values of para substituted toluenes and 4-methyl-4′-nitrobiphenyl were calculated on the basis of the electrostatic interaction between solute and solvent molecules.

Experimental

ASIS(C_6H_6) and ASIS(C_6F_6) of the compounds given in Table 1 were measured with a Hitachi R-20B spectometer operating at 60 MHz as 1 mol % solutions, with cyclohexane as the internal reference. Carbon tetrachloride was assumed to be inert. The ASISs were defined by

$$\mathrm{ASIS}(C_6H_6) = \delta_{C_6D_6} - \delta_{CCl_4},$$

$$\mathrm{ASIS}(C_6F_6) = \delta_{C_6F_6} - \delta_{CCl_4},$$

where $\delta_{C_6D_6}$, δ_{CCl_4}, and $\delta_{C_6F_6}$ are the chemical shifts in benzene-d_6, carbon tetrachloride, and hexafluorobenzene from the internal reference of cyclohexane, respectively. The chemical shifts were determined by the sideband method with the aid of a frequency counter. The standard deviation in all cases was less than ± 0.01 ppm.

Calculation

The electric charge distributions in benzene and hexafluorobenzene molecules were approximately

TABLE 1. SOLUTE MOLECULES

	Compound	Substituent
(I)	CH_3-X	X=NO_2, CN, CCl, I, SCN
(II)	$(CH_3)_3C$-X	X=CN, Cl, Br, NH_2, OCH_3, OH
(III)	*para*-$CH_3C_6H_4$-X	X=$\begin{cases}NO_2, CN, CHO, Br, Cl, I\\ OCH_3\ NH_2, N(CH_3)_2\end{cases}$
(III′)	$CH_3C_5H_4N$(4-methyl pyridine)	
(IV)	$CH_3C_6H_4C_6H_4NO_2$(4-methyl-4′-nitrobiphenyl)	

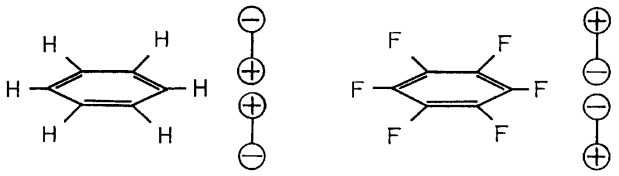

a) C_6H_6 b) C_6F_6

Fig. 1. Benzene molecule(a) and hexafluorobenzene molecule(b) are approximately expressed by electric bar-quadrupoles.

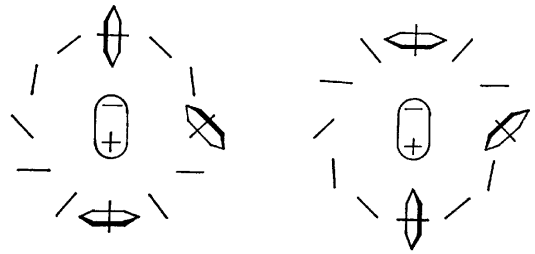

C_6H_6 C_6F_6

Fig. 2. The most stabel orientation of solvent molecules around a solute molecules due to the dipole (solute)-quadrupole(solvent) interaction ($U \propto \mu Q/r^4$).

represented by electric bar-quadrupoles (see Fig. 1). The principal values of the quadrupole moment tensor, with the Z-principal axis along with the six-fold molecular axis, and the anisotropy of the magnetic susceptibility ($\Delta\chi = \chi_{\parallel} - \chi_{\perp}$; the subscripts $\parallel$ and $\perp$ here mean parallel and perpendicular to the highest axis of symmetry of the molecule) are given in Table 2. Then the ASIS value of a polar solute molecule induced by these solvents can be calculated if the orientation of these quadrupoles (solvent) around the solute dipole is assumed.

The most stable orientation of benzene molecules and hexafluorobenzene molecules around a dipole is shown in Fig. 2. The calculation of ASIS based on the electrostatic dipole(solute)-quadrupole(solvent) interaction was reported in detail in the previous paper of this series.†,[6]

The calculations were performed by computer with the HITAC 8300 at the University of Tokyo.

† We found some errors in Figs. 2 and 4 in the previous paper.[6]

The expressions of the dihedral angle (ϕ) between the plane containing $\vec{\mu}$ and $\vec{r}$ and that containing $\vec{r}$ and $\vec{B}$ in Figs. 2 and 4 should be corrected as follows:

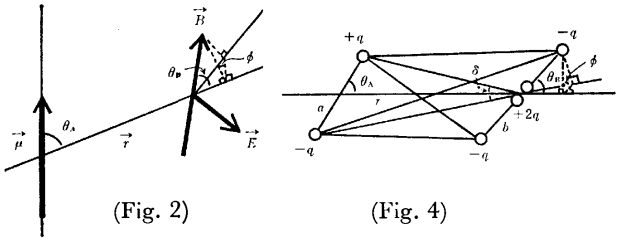

(Fig. 2) (Fig. 4)

Fig. 3. Errata (Fig. 2): A benzene molecule in a permanent dipole field of a solute molecule.
(Fig. 4): Electrostatic interaction between bar-dipole and bar-quadrupole.

Table 2. Quadrupole moments and magnetic anisotropies of solvent molecules

Solvent	Quadrupole moment[18] (10^{-26} esu) Obsd	Quadrupole moment[18] (10^{-26} esu) Calcd	Magnetic anisotropies[19] (10^{-30} emu)
C_6H_6	Q_{XX} +2.8±1.4	+3.3	89±4
	Q_{YY} +2.8±1.4	+3.3	
	Q_{ZZ} −5.6±2.8	−6.6	
C_6F_6	Q_{XX} ——	−8.6	53±2
	Q_{YY} ——	−8.6	
	Q_{ZZ} ——	+17.2	

Results and Discussion

The ASIS of methyl protons *versus* dipole moments of monosubstituted methanes(I) and *t*-butyl derivatives(II) are plotted in Fig. 4. The ASIS values *versus* their dipole moments for methyl-protons and *ortho*-protons of para substituted toluenes(III) are plotted in Fig. 5. The experimental values and the calculated ones of these ASIS are summarized, together with those of the dipole moments, in Tables 3(a)—(b).

There exists a linear relationship between the ASIS and the solute dipole moments in benzene solutions. Of the protons in question, those on solute molecules lying in the positive-charge region of the solute dipole exhibit up-field shifts, while the protons lying in the negative-region exhibit down-field shifts or only minor up-field shifts.

For the convenience of further discussion, the substituted molecules can be classified into two groups according to the directions of their dipole moments. (see Table 4.) In the proposed classification, group (A) consists of protons of the methyl group and those on the aromatic ring of p-$CH_3C_6H_4X_A$ which are lying in the positive-region of the solute dipole and show up-field shifts, while group (B) consists of those which show down-field shifts or only slight up-field shifts.

ASIS(C_6H_6) values of molecules of (III), (III'), and (IV) expressed as a function of the distance between the proton in question and the carbon on the base of the substituent are plotted in Fig. 6. The "sense" of the shifts is quite different for group (A) and group (B) molecules. In order to express this difference, the "Carbonyl plane rule" is conveniently extended to other polar substituents, and renamed as the "Dipole plane rule." A dipole plane can be assumed on the polar substituents, as illustrated in Fig. 7(a). Protons lying in the positive region of the dipole are assumed to show up-field shifts. However, the dipole planes of 4-methylpyridine (III') and 4-methyl-4'-nitrobiphenyl(IV) are located near the center of these molecules.

Conversely, in hexafluorobenzene solutions, sensor protons lying in the positive-region of the solute dipole showed down-field shifts while the protons in the negative-region showed up-field shifts. Therefore, a dipole plane can be illustrated as in Fig. 7(b). Here the protons lying in the positive-region of the dipole are assumed to show down-field shifts.

The experimental "Dipole plane rule" can, though

Table 3(a). ASIS(C_6H_6) and ASIS(C_6F_6) values and dipole moments of molecules of (I) and (II)

Substituent(X)	δ_{CCl_4}	ASIS(C_6H_6)	ASIS(C_6F_6)	Dipole moment[20]
(I) CH_3-X				
CN	0.52 ppm	+1.18 ppm	−0.17 ppm	3.92 D
NO_2	2.83	+1.18	−0.17	3.46
SCN	1.17	+1.26	−0.20	3.34
I	0.71	+0.67	−0.07	1.64
CCl_3	1.29	+0.59	−0.07	1.66
(II) $(CH_3)_3C$-X				
CN	−0.07 ppm	+0.53 ppm	−0.13 ppm	3.65 D
Cl	+0.17	+0.22	−0.03	2.15
Br	+0.35	+0.26	−0.04	2.21
SH	−0.01	+0.18	−0.00	—
OH	−0.23	+0.10	+0.02	1.67
OCH_3	−0.31	+0.02	+0.03	1.23
NH_2	−0.34	+0.07	+0.03	1.32

Table 3(b). ASIS values (ppm) and dipole moments of molecules (III), (III′), and (IV)

X	CH_3			*ortho*-H			*meta*-H			μ^{20} (D)
	δ_{CCl_4}	C_6H_6	C_6F_6	δ_{CCl_4}	C_6H_6	C_6F_6	δ_{CCl_4}	C_6H_6	C_6F_6	
CN	1.00	+0.60 (+0.36)	−0.17 (−0.28)	5.80	+0.66 (+0.41)	−0.18 (−0.30)	6.05	+0.47 (+0.09)	+0.07 (+0.07)	4.40
NO_2	1.04	+0.63 (+0.35)	−0.21 (−0.28)	5.85	+0.69 (+0.41)	−0.17 (−0.30)	6.65	+0.26 (+0.10)	+0.11 (+0.06)	4.47
CHO	1.00	+0.47	−0.13	5.84	+0.41	−0.08	6.28	+0.17	+0.13	3.24
Br	0.87	+0.40	−0.12	5.23	+0.37	−0.10	6.33	+0.07	+0.22	1.98
Cl	0.88	+0.38 (+0.16)	−0.11 (−0.16)	5.60	+0.33 (+0.19)	−0.01 (−0.18)	5.72	+0.05 (+0.04)	+0.12 (+0.03)	1.96
I	0.86	+0.40	−0.13	5.43	+0.35	−0.05	6.07	+0.07	+0.17	1.73
OCH_3	0.83	+0.10	+0.01	5.23	−0.15	+0.05	5.52	−0.03	−0.03	1.21
$N(CH_3)_2$	0.79	−0.04	+0.06	5.45	−0.20	+0.16	5.10	−0.12	+0.24	1.29
NH_2	0.76	+0.02 (−0.11)	+0.04 (+0.19)	5.39	−0.11 (−0.12)	+0.12 (+0.22)	4.99	+0.05 (+0.01)	+0.15 (+0.05)	1.61
(III′)	0.88	+0.12	−0.12	5.55	+0.38	−0.04	6.92	−0.14	+0.26	2.60

	CH_3			3-H			2-H			2′-H			3′-H		
	δ_{CCl_4}	C_6H_6	C_6F_6	δ_{CCl_4}	C_6H_6	C_6F_6	δ_{CCl_4}	C_6H_6	C_6F_6	δ_{CCl_4}	C_6H_6	C_6F_6	δ_{CCl_4}	C_6H_6	C_6F_6
(IV)	0.98	+0.26 (+0.29)	−0.09 (−0.25)	6.22	+0.55 (+0.42)	−0.14 (−0.33)	6.79	+0.30 (+0.26)	−0.01 (−0.12)	6.00	+0.27 (+0.13)	+0.09 (+0.03)	5.90	−0.06 (+0.21)	+0.02 (−0.12)

( ): represent calculated values.

Table 4. Classification of solute molecules

Group (A)			Group (B)		
Positive-charge region		Negative-charge region	Negative-charge region		Positive-charge region
CH_3	—	X_A			
$(CH_3)_3$	—	X_A			
$CH_3C_6H_4$	—	X_A	$CH_3C_6H_4$	—	X_B
X_A=CN		large	X_B=OCH_3		
NO_2		↑	NH_2		
CHO		|	$N(CH_3)_2$		
Br		|			
Cl		|			
I		μ[a)]			

a) μ represents a dipole moment.

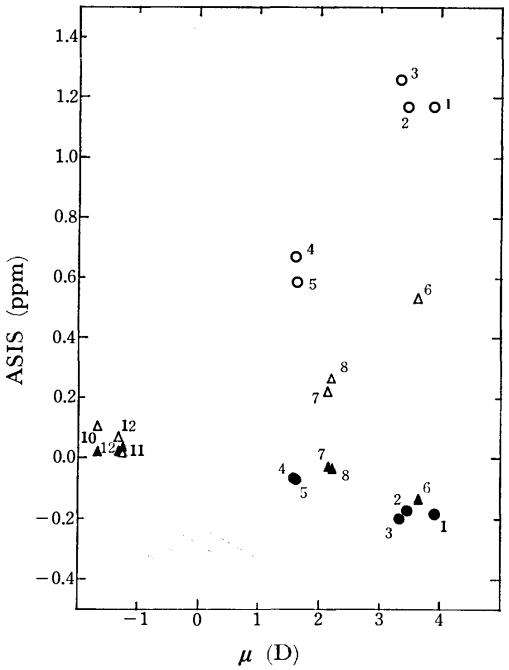

Fig. 4. ASIS values of methyl-protons *vs.* dipole moments(μ) of monosubstituted methanes (○: in C_6H_6, ●: in C_6F_6, and substituent; 1: CN, 2: NO_2, 3: SCN, 4: I, 5: CCl_3) and *t*-butyl derivatives (△: in C_6H_6, ▲: in C_6F_6, and substituent; 6: CN, 7: Cl, 8: Br, 9:SH, 10: OH, 11: OCH_3, 12: NH_2).

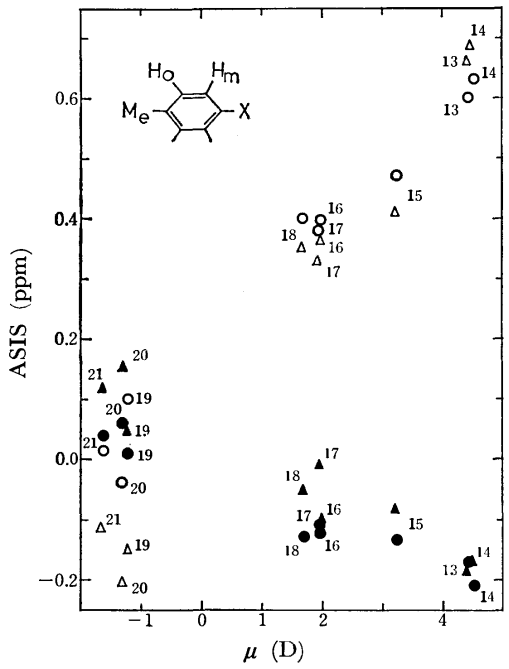

Fig. 5. ASIS values of methyl-protons (○: in C_6H_6 and ●: in C_6F_6) and *ortho*-protons (△: in C_6H_6 and ▲: in C_6F_6) *vs.* dipole moments (μ) for para substituted toluenes)(substituent; 13: CN, 14: NO_2, 15: CHO, 16: Br, 17: Cl, 18: I, 19: OCH_3, 20: $N(CH_3)_2$, 21: NH_2).

only in a qualitative manner, express ASIS values except for the proton near the dipole plane.

Figure 6 indicates that significiant differences between ASIS (C_6H_6) and ASIS(C_6F_6) are in the "sense" of the shifts and the position of the dipole planes. In hexafluorobenzene, the plane should be placed between the substituent and the center of the molecules.

As a general feature of the shifts, the magnitude of up-field shifts is larger than those of down-field shifts in benzene, while the magnitude of up-field shifts is comparable with down-field shifts in hexafluorobenzene, and the magnitude of ASIS(C_6H_6) is larger than those of ASIS(C_6F_6) for the same solute molecules. Those features of the ASIS are explainable in terms of the electrostatic interaction model. In a benzene solution, the more stable orientation of a solvent molecule around the solute dipole takes configuration (C) on the positive-charge region of the solute dipole while it takes configuration (D) on the negative-charge (see Figs. 2 and 8). As both benzene and hexafluorobenzene molecules have a flat, disk-like shape, the distance from the center of the solute dipole to the center of the solvent quadrupole is shorter in configuration (C) than in (D) ; furthermore the distance from the proton in question of the solute to the solvent molecules is also shorter in configuration (C) than in (D).

The stabilization energy of configuration (C) on the positive region is thus greater than that of (D) on the negative-region(see our previous paper[6]). In view of the known magnetic anisotropy of the benzene ring, configuration (C) should give an up-field shift,

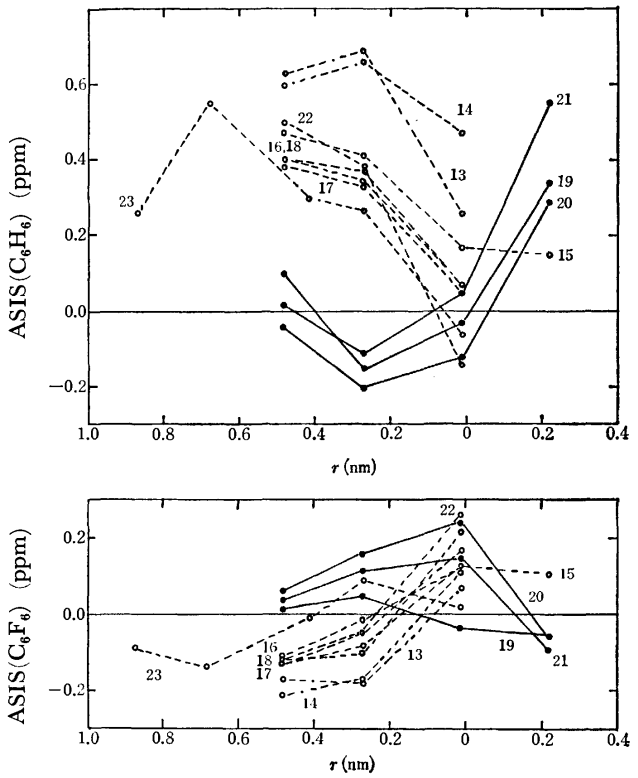

Fig. 6. The relations between ASIS values and the position of protons on para substituted toluenes and on 4-methyl-4′-nitrobiphenyl in C_6H_6 and in C_6F_6 (----: group (A) molecules and ——: group (B) molecules, substituent; 13: CN, 14: NO_2, 15: CHO, 16: Br, 17: Cl, 18: I, 19: OCH_3, 20: $N(CH_3)_2$, 21: NH_2, and molecules; 22: III′, 23: IV).

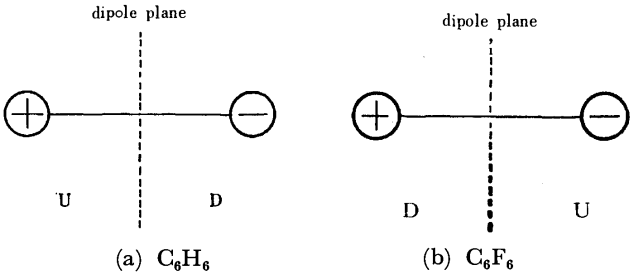

Fig. 7. A dipole plane rule in C_6H_6 (a) and in C_6F_6 (b). (U: up-field shift region and D: down-field shift region.)

while (D) should give a down-field shift for solute protons. Therefore the up-field shifts should show larger values than the down-field shifts.

In hexafluorobenzene solutions, however, the most stable orientation are configuration (D) on the positive-region of the solute dipole and configuration (C) on the negative-region. And the stabilized energy due to the dipole-quadrupole interaction on the positive-region is less than that on the negative-region; the effect of down-field shifts on the positive-region, is however, comparable with the up-field shifts on the negative-region, since the other attractive interaction between the local positive charge of the solute dipole and the localized dipole of C–F bond is not so small.

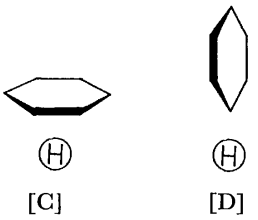

Fig. 8.

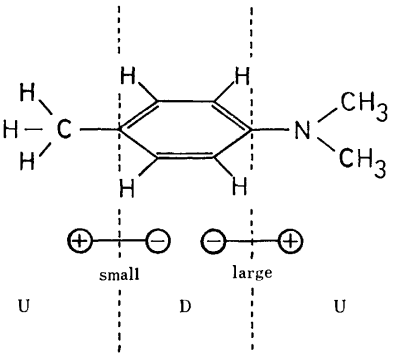

Fig. 9. Dipole plane rule on a *N*,*N*-dimethyl-*p*-toluidine. (U: up-field shift region and D: down-field shift region.)

Almost all the ASIS are interpreted by the orientation of the quadrupoles(solvent moleucles) around the solute dipole due to the electrostatic interaction, and are in good accord with the dipole plane rule. However, three exceptions were found.

One is the ASIS of methyl protons of the molecules in (III) when X=OCH_3, NH_2, or $N(CH_3)_2$. The ASIS values of these molecules showed a very slight up-field shift with hexafluorobenzene. These molecules are classified in group (B) and so the Hammett's σ_p values of the methyl group has the same sign as the Hammett's σ_p values of the OCH_3, NH_2, $N(CH_3)_2$ groups, but the direction of the bond dipole of the methyl group is opposite to that of the substituents in group (B). In this case, the effect of the bond dipole on the ASIS of the methyl group must be taken into consideration. This effect is especially great in the case of benzene solution, because benzene molecules around methyl protons are located in the positive-region of the methyl dipole, and so their more stable orientation gives large up-field shifts.(See Fig. 9.)

The second exception is a remarkable up-field shift found in the ASIS(C_6F_6) of *meta*-protons of the molecules in (III) in which X=$N(CH_3)_2$. As $N(CH_3)_2$ is a bulky substituent, no other solvent molecules are permitted to exist within it. As the exclusion space is located in the positive-region, the proton in question is not influenced by solvents that will cause down-field shifts. Herein the proton is considered to be influenced mainly by solvents in the negative-region and to show up-field shifts.

The third exception is that both solvents will induced a large up-field shift of protons on NH_2 on a group (III) molecule. It is presumed that the up-field shift is caused by the hydrogen bond-like interaction between the NH_2 group and π-electrons of the

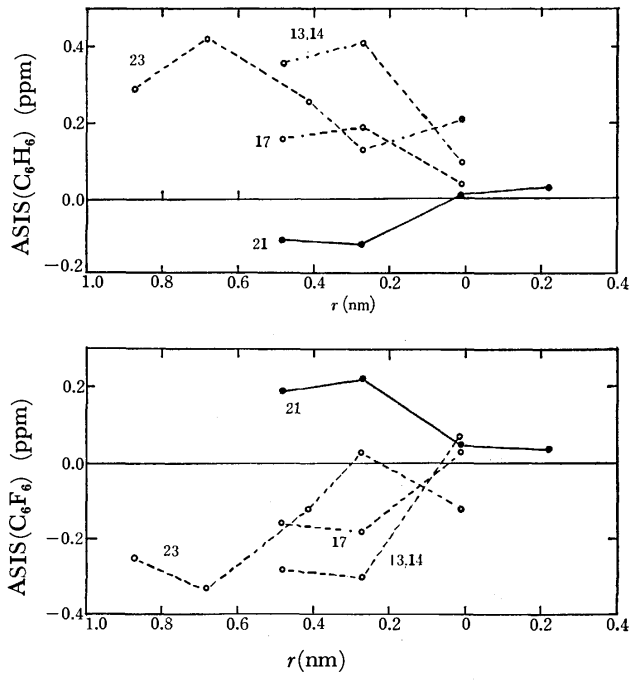

Fig. 10. The relations between calculated ASIS values and the position of protons on para substituted toluenes and on 4-methyl-4′-nitrobiphenyl in C_6H_6 and in C_6F_6 (substituent; 13: CN, 14: NO_2, 17: Cl, 21: NH_2, and molecule; 23: IV).

aromatic ring.

The calculated ASIS values of protons on para-substituted toluenes and 4-methyl-4′-nitrobiphenyl with benzene and hexafluorobenzene are illustrated in Fig. 10.

These exceptions are mostly due to the point-dipole and point-quadrupole approximations. Our model is, however, much more quantitative than the arbitrary models of Williams,[1] Ledaal,[7] and Verkade *et al.*[8-17] There is no need to say that a 1:1 complex is highly unlikely.

Our calculation is performed based on real physical numerical quantities without using the arbitary parameters such as in Laszlo *et al.*[2] The calculated values are in a good agreement with the observed values in the "sense" and in the order of magnitude. And the magnitude of shifts on the same molecule or on the molecules with a similar shape can be compared.

Thus, the ASIS of various solute molecules in ^1H NMR caused by benzene and hexafluorobenzene can be explained by the orientation of solvent molecules around a polar solute molecule(see Fig. 2) due to electrostatic interaction.

The authors wish to express their thanks to Dr. Yosito Takeuchi of the University of Tokyo for his helpful advice.

References

1) J. Ronayne and D. H. Williams, *Ann. Rev. Nucl. Magn. Reson. Spectrosc.*, **2**, 97 (1969).
2) E. M. Engler and P. Laszlo, *J. Am. Chem. Soc.*, **93**, 1317 (1971).
3) J. D. Connolly and McCrindle, *Chem. Ind. (London)*, 379 (1965); D. H. Williams and N. S. Bacca, *Tetrahedron*, **21**, 2021 (1965).
4) W. G. Schneider, *J. Phys. Chem.*, **66**, 2653 (1962).
5) J. V. Hatton and W. G. Schineider, *Can. J. Chem.*, **40**, 1285 (1962).
6) K. Nikki, N. Nakagawa, and Y. Takeuchi, *Bull. Chem. Soc. Jpn.*, **48**, 2902 (1975).
7) T. Ledaal, *Tetrahedron Lett.*, **1968**, 1683.
8) R. D. Bertrand, R. D. Comton, and J. G. Verkade, *J. Am. Chem. Soc.*, **92**, 2702 (1970).
9) J. A. Mosbo, J. R. Pipal, and J. G. Verkade, *J. Magn. Reson.*, **8**, 243 (1972).
10) J. A. Mosbo and J. G. Verkade, *J. Magn. Reson.*, **8**, 250 (1972).
11) A. H. Cowley, M. C. Damasco, J. A. Mosbo, and J. G. Verkade, *J. Am. Chem. Soc.*, **94**, 6715 (1972).
12) E. Farnworth and J. M. Miller, *Can. J. Spectroscopy*, **17**, 103 (1972).
13) R. S. Armstrong, M. J. Aroney, R. K. Duffin, H. J. Stootman, and R. J. W. Le Fevre, *J. Chem. Soc., Perkin Trans. 2*, **1973**, 1362.
14) K. Nikki and N. Nakagawa, *Chem. Lett.*, **1974**, 699.
15) K. Nikki, N. Nakahata, and N. Nakagawa, *Tetrahedron Lett.*, **1975**, 3811.
16) K. Tori, I. Horibe, H. Sigemoto, and K. Umemoto, *Tetrahedron Lett.*, **1975**, 2199.
17) I. Horibe, H. Sigemoto, and K. Tori, *Tetrahedron Lett.*, **1975**, 2852.
18) T. D. Gierke, H. L. Tigelaar, and W. H. Flygare, *J. Am. Chem. Soc.*, **94**, 330 (1972).
19) M. P. Bogaard, A. D. Buckingham, M. G. Corfield, D. A. Dummur, and A. H. White, *Chem. Phys. Lett.*, **12**, 558 (1972).
20) A. L. McGlellan, "Tables of Experimental Dipole Moments," W. H. Freeman and Co., San Francisco (1963).

The Formation of Ethers from Unsaturated Aliphatic Alcohols in the Presence of Boron Trifluoride Etherate

Kimiko NAGAI,* Mitsuru NAKAYAMA,** and Shûichi HAYASHI**

Yasuda Women's University, Kamiyasu, Yasufuruichi-cho, Hiroshima 731-01

** *Department of Chemistry, Faculty of Science, Hiroshima University, Higashisenda-machi, Hiroshima 730*

(Received February 3, 1978)

Unsaturated acyclic alcohols of carbon numbers four and five reacted with boron trifluoride etherate to give eight ethers. Of these ethers, novel acyclic di- and tri-ethers were found in the reaction products of 2-methyl-2-propen-1-ol. Boron trifluoride etherate catalyzes double-bond migration, allylic rearrangement, intermolecular dehydration, and Markownikov addition reactions in unsaturated aliphatic alcohols.

In previous papers it has been reported that ethers of several types were obtained by reactions of monoterpene alcohols, of allylic geraniol,[1] nerol,[2] homoallylic *l*-isopulegol,[3] saturated bicyclic *d*-borneol,[4] and *dl*-isoborneol[4] with boron trifluoride etherate in the acid-catalyzed intermolecular dehydration of these alcohols and/or their isomers. Citronellol, in which one double bond is at the ζ-position for the hydroxyl group, gave cyclic and acyclic ethers upon intermolecular addition.[5]

In the present work, studies of analogous acid-catalyzed reactions of four unsaturated acyclic alcohols, allylic 3-methyl-2-buten-1-ol (**1**), 2-methyl-3-buten-2-ol (**2**), 2-methyl-2-propen-1-ol (**3**), and homoallylic 3-methyl-3-buten-1-ol (**4**), will be reported.

Results and Discussion

Upon treatment with boron trifluoride etherate at room temperature, **1** of a primary alcohol was dimerized to give two ethers, one symmetrical and one unsymmetrical, in yields of 4 and 32% respectively, by means of the intermolecular dehydration of the starting material and/or its isomer. On the other hand, **2** of a tertiary alcohol gave only a unsymmetrical ether in a 40% yield. The structures of these ethers were determined to be bis(3-methyl-2-butenyl) ether (**5**) for the symmetrical ether and 3-methyl-2-butenyl 1,1-dimethyl-2-propenyl ether (**6**) for the other one on the basis of their spectral data and chemical behavior.

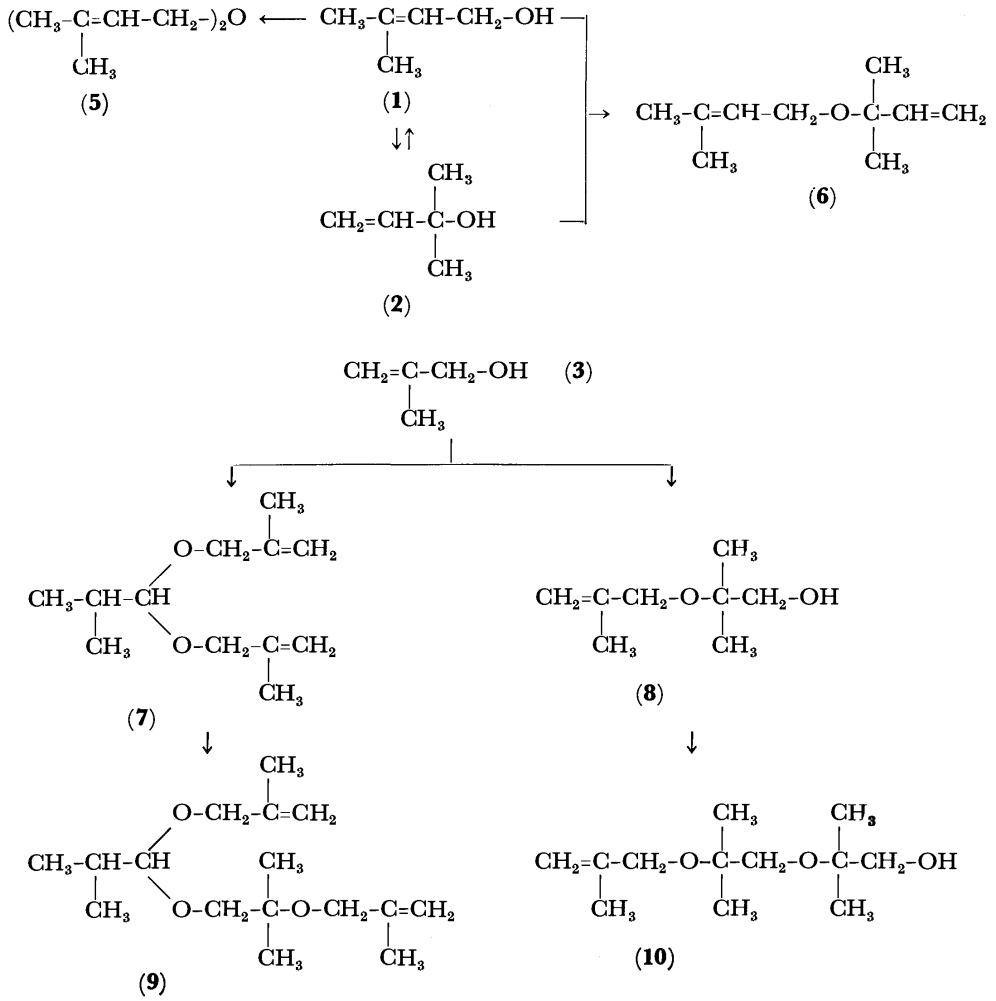

In these reactions, on double-bond migration occurs, the allylic rearrangement of the hydroxyl group takes place at a high rate, and the equilibrium is probably shifted from **1** to **2**.

2-Methyl-2-propen-1-ol (**3**), which contains a isopropenyl group, gave two kinds of polyethers (**7** and **9**) and two kinds of hydroxyl ethers (**8** and **10**). The novel ethers (**7** and **9**) are thought to be produced by the method of double-bond migration, followed by the dehydration condensation with **3** *via* the aldehyde form. On the other hand, the hydroxyl ethers appear to be formed by the Markownikov addition of the hydroxyl group to the double bond.

On the other hand, 3-methyl-3-buten-1-ol (**4**), which has two methylene groups between the double bond and the hydroxyl group, gave two hydroxyl ethers (**11** and **12**) according to the Markownikov rule and no di- or tri-ether (**7** or **9**), as has been mentioned in the case of the **3** alcohol.

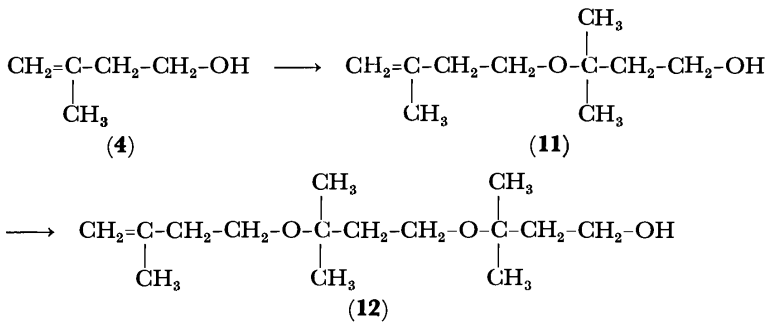

TABLE 1. REACTION CONDITIONS AND REACTION PRODUCTS OF UNSATURATED ALIPHATIC ALCOHOLS WITH BORON TRIFLUORIDE ETHERATE

Reaction conditions					Reaction products		
Sample	(g)	$BF_3 \cdot Et_2O$ (ml)	React temp (°C)	React period (h)	Product	Yield (%)	n_D (°C)
1	10	0.6	20	24	**5**	4	1.4491 (22)
					6	32	1.4415 (22)
2	10	0.6	20	24	**6**	40	1.4403 (20)
3	10	0.5	23	72	**7**	12	1.4272 (20)
					8	28	1.4315 (20)
					9	5	1.4329 (20)
					10	20	1.4340 (20)
4	10	0.5	28	72	**11**	35	1.4371 (20)
					12	5	1.4427 (20)

Experimental

Apparatus. The GLC analyses were carried out using a Hitachi-063 apparatus, equipped with an FID detector, a stainless-steel separating column (3 mm×3 m) packed with Carbowax 6000 (10%) on Diasolid L (60—80 mesh) and Carbowax 20 M (10%) on Diasolid L (60—80 mesh); the flow rate of the nitrogen carrier gas was 20 ml/min. The mass spectra were recorded on a Hitachi RMS-4 spectrometer at an ionization voltage of 80 eV, an ion-accelerating voltage of 1800 eV, and an ionization chamber temperature of 100 °C. The PMR spectra were measured in CCl_4 solutions using a 60 MHz spectrometer, Hitachi R-20, with TMS as the internal reference. The CMR spectrum was obtained in a $CDCl_3$ solution on a JEOL FX-60 spectrometer under those conditions: pulse repetition, 3 s; accumulation, 1200 times, and frequency range, 4 kHz. The preparative-GLC separations were carried out by means of a Yanagimoto G-80 apparatus, with Carbowax 20 M (10%) on Diasolid L (6 mm×2 m); temperature program: 5 °C/min, from 150 °C to 200 °C.

Materials. Commercial **2**, **3**, and **4** were used without purification. These alcohols exhibited single peaks in GLC with DEGS and Carbowax 6000.

$BF_3 \cdot Et_2O$ of a chemical grade (BF_3 47%) was used without any purification.

*1) Reaction of **1** with $BF_3 \cdot Et_2O$.* Ten grams of **1**[6] were submitted to a reaction with $BF_3 \cdot Et_2O$ (0.6 ml) at room temperature (*ca.* 20 °C) for 24 h, and then extracted with ether after being diluted with water (50 ml). The extract was washed with a 10% aqueous solution of sodium carbonate and then with water, and dried over anhydrous sodium sulfate. The reaction mixture showed the presence of two compounds upon GLC and TLC, these compounds (**5** and **6**) were separated by means of a silica-gel column using a mixed solvent of hexane containing 5% ethyl acetate.

*Bis(3-methyl-2-butenyl) Ether (**5**):* One of the above-mentioned compounds was isolated as a colorless oil: Rast's molecular weight, 158 (Calcd, 154); IR (liq.) 1070 (C–O–C), 1675, 830 cm^{-1} (–CH=$\overset{|}{C}$–); PMR (CCl_4) δ 1.61, 1.70 (each 6H, br s, CH_3–$\overset{|}{C}$=$\overset{|}{C}$–×4), 3.79 (4H, d, J=7 Hz, –$\overset{|}{C}$=CH–CH_2–O–×2), 5.24 ppm (2H, m, –CH=$\overset{|}{C}$–×2).

*Catalytic Hydrogenation of **5**:* Compound **5** (250 mg) was hydrogenated over PtO_2 (25 mg) in acetic acid (5 ml) to take up two equivalent moles of hydrogen. The spectral data of tetrahydro-**5** were superimposable on those of the diisopentyl ether synthesized from 3-methyl-1-butanol (1.0 g)

and diisopentyl bromide (0.5 g). Colorless oil; bp 171—172 °C, d_4^{20} 0.776. IR (liq.) 1385, 1371 (CH_3–CH–CH_3), 1130, 1111 cm^{-1} (C–O–C); PMR (CCl_4) δ 0.89 (12H, d, J= 6 Hz, CH_3–CH–CH_3 ×2), 1.49 (4H, t, J=7 Hz, –CH–CH_2 –CH_2– ×2), 1.30—1.78 (2H, m, CH_3–CH–CH_3 ×2), 3.40 ppm (4H, t, J=7 Hz, –CH_2–CH_2–O– ×2).

*3-Methyl-2-butenyl 1,1-Dimethyl-2-propenyl Ether (**6**)*: The second compound was obtained as a colorless oil. Rast's molecular weight (155) and the molecular ion (M^+ 154) in the mass spectrum corresponded to a molecular formula of $C_{10}H_{18}O$. Mass *m/e* 41 (75%), 55 (20), 57 (25), 69 (base), 85 (33), 110 (15), 124 (24), 137 (7, M^+-CH_3), 154 (5, M^+, $C_{10}H_{18}O$); IR (liq.) 1145, 1060 (C–O–C), 1680, 830 (–CH=C–), 3080, 1645, 1001, 920 cm^{-1} (CH_2=CH–); PMR (CCl_4) δ 1.20 (6H, s, –O–C(CH_3)$_2$–C=C–), 1.62, 1.71 (6H, br s, CH_3–C=C– ×2), 3.82 (2H, d, J=7 Hz, =CH–CH_2–O–), 4.91—5.80 ppm (4H, q and m, CH_2=CH– and –CH=C–).

*Tetrahydro Derivative of **6***: Colorless oil. IR (liq.) 1390, 1371, 1368 (CH_3–CH–CH_3), 1088 cm^{-1} (C–O–C); PMR (CCl_4) δ 0.82 (3H, t, J=6 Hz, CH_3–CH_2–C–), 0.88 (6H, d, J=6 Hz, CH_3–CH–CH_3), 1.10 (6H, s, $(CH_3)_2$–C–O–), 1.43 (2H, t, J=6 Hz, $(CH_3)_2$–CH–CH_2–CH_2–), 3.31 ppm (2H, t, J=6 Hz, –O–CH_2–CH_2–).

*2) Reaction of **2** with $BF_3 \cdot Et_2O$.* The **2** alcohol (10 g) was allowed to react with $BF_3 \cdot Et_2O$ (0.6 ml) according to the procedure previously described. A colorless oil was thus obtained; Rast's molecular weight, 156 (Calcd, 154). The spectral data of the compound and its tetrahydro derivative were identical with those of Compound **6** and its tetrahydro-**6** respectively.

*3) Reaction of **3** with $BF_3 \cdot Et_2O$.* The **3** alcohol (10 g) was submitted to a reaction with $BF_3 \cdot Et_2O$ (0.5 ml) at room temperature (*ca.* 20 °C) for 72 h. The reaction mixture showed the presence of four compounds (**7**, **8**, **9**, and **10**) by GLC with Carbowax 20 M; these compounds were separated into individual compounds by means of preparative-GLC.

*2,8-Dimethyl-5-isopropyl-4,6-dioxa-1,8-nonadiene (**7**)*: The first compound was isolated from the reaction mixture as a colorless oil. The molecular formula corresponded to $C_{12}H_{22}O_2$, judging from the molecular weight (Rast's 200; Calcd, 198). Mass *m/e* 55 (base), 71 (31%, C_4H_7O), 127 (9, M^+-CH_2=C(CH_3)–CH_2–O–), 155 (12H, $M^+-C_3H_7$), 198 (trace, $C_{12}H_{22}O_2$); IR (CCl_4), 3081, 1665, 905 (CH_2=C(CH_3)–), 1397, 1380 (CH_3–CH–CH_3), 1311, 1111, 1071, 1041 cm^{-1} (C–O–C); PMR (CCl_4) δ 0.91 (6H, d, J=7 Hz, CH_3–CH–CH_3), 1.75 (6H, br s, CH_3–C=C– ×2), 1.70—2.10 (1H, m, $(CH_3)_2$–CH–CH–), 3.84 (4H, br s, –O–CH_2–C=C– ×2), 4.09 (1H, d, J=7 Hz, –O–CH(O–)–CH–), 4.81, 4.91 ppm (each 2H, br s, CH_2=C– ×2). The CMR spectrum of the compound was reasonably explained by the following assignments.

*Tetrahydro Derivative of **7***: Colorless oil. Mass *m/e* 57 (base), 73 (28%, C_4H_9O), 125 (10, $M^+-(CH_3)_2$–CH–CH_2–O–); IR (CCl_4) 1384, 1370 (CH_3–CH–CH_3), 1080, 1050 cm^{-1} (C–O–C); PMR (CCl_4) δ 0.89, 0.92 (12H and 6H, each d, J=6 Hz, CH_3–CH–CH_3 ×3), 1.51—2.05 (3H, m, $(CH_3)_2$–CH–CH_2 ×2 and $(CH_3)_2$–CH–CH–), 3.10 (4H, d, J=6 Hz, –CH–CH_2–O– ×2), 4.09 ppm (1H, d, J=7 Hz, –O–CH(O–)–CH–).

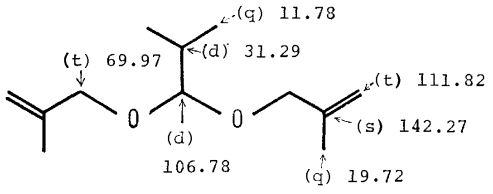

*2,2,5-Trimethyl-3-oxa-5-hexen-1-ol (**8**)*: The second compound was isolated as a colorless oil. The Rast's molecular weight, 145 (Calcd, 144), corresponded to the molecular formula of $C_8H_{16}O_2$. Mass *m/e* 55 (base), 113 (32%, M^+-CH_2OH), 126 (3, M^+-H_2O), 144 (trace, M^+, $C_8H_{16}O_2$); IR (liq.) 3480, 1155 (–OH), 1103, 1060 (C–O–C), 3080, 1664, 905 (CH_2=C–), 1380, 1370 cm^{-1} (CH_3–CH–CH_3); PMR (CCl_4) δ 1.15 (6H, s, CH_3–C–CH_3), 1.72 (3H, br s, CH_3–C=C–), 1.91 (1H, br s, –OH), 3.30 (2H, s, –C–CH_2–OH), 3.47 (2H, br s, =C–CH_2–O–), 4.78, 4.90 ppm (each 1H, br s, CH_2=C–).

*Acetyl Derivative of **8***: The acetylation of Compound **8** (300 mg) was carried out with acetic anhydride (1 ml) in dry pyridine (3 ml) at room temperature for 72 h. Colorless oil. IR (CCl_4) 1746, 1236 (CH_3COO–), 3080, 1660, 901 (CH_2=C–), 1100, 1050 cm^{-1} (C–O–C); PMR (CCl_4) δ 1.10 (6H, s, –O–C(CH_3)$_2$–), 1.72 (3H, br s, CH_3–C=C–), 2.00 (3H, s, CH_3COO–), 3.75 (2H, br s, –C=C–CH_2–O–), 3.92 (2H, s, CH_3COO–CH_2–C–), 4.73, 4.92 ppm (each 1H, br s, CH_2=C–).

*Dihydro Derivative of **8***: Colorless oil. IR (CCl_4) 3580, 3420, 1152 (–OH), 1080, 1057 (C–O–C), 1383, 1371 cm^{-1} (CH_3–CH–CH_3); PMR (CCl_4) δ 0.90 (6H, d, J=6 Hz, CH_3–CH–CH_3), 1.17 (6H, s, CH_3–C(O–)–CH_3), 1.60—2.01 (1H, m, $(CH_3)_2$–CH–CH_2–), 2.20 (1H, br s, –OH), 3.10 (2H, d, J=6 Hz, –CH–CH_2–O–), 3.40 ppm (2H, m, –C–CH_2–OH.)

*2,5,5,11-Tetramethyl-8-isopropyl-4,7,9-trioxa-1,11-dodecadiene (**9**)*: The third compound was also obtained as a colorless oil. The molecular formula had $C_{16}H_{30}O_3$ from Rast's molecular weight, 274 (Calcd, 270). Mass *m/e* 55 (base), 71 (15%), 81 (7), 101 (12), 115 (27), 155 (31), 227 (2, $M^+-C_3H_7$), 270 (trace, M^+, $C_{16}H_{30}O_3$); IR (CCl_4) 1110, 1060 (C–O–C), 3080, 1165, 903 (CH_2=C–), 1391, 1380, 1370 cm^{-1} (CH_3–CH–CH_3); PMR (CCl_4) δ 0.92 (6H, d, J=7 Hz, CH_3–CH–CH_3), 1.20 (6H, s, –CH–C–O–), 1.65 (6H, br s, –C(CH_3)$_2$=C– ×2), 1.76—2.10 (1H, m, $(CH_3)_2$–CH–CH–), 3.22, 3.40 (each 1H, d, J_{AB}=12 Hz, –O–CH_2–C(CH_3)–O–), 3.69, 3.89 (each 2H, s, =C–CH_2–O– ×2), 4.09 (1H, d, J=7 Hz, –O–CH–CH–), 4.80, 4.90 ppm (each 2H, br s, CH_2=C(O–)– ×2).

*Tetrahydro Derivative of **9***: Colorless oil. IR (CCl_4) 1390, 1384, 1370 (CH_3–CH–CH_3 and CH_3–C–CH_3), 1111, 1058 cm^{-1} (C–O–C); PMR (CCl_4) δ 0.89, 0.91 (18H, each d, J=6 Hz, CH_3–CH–CH_3 ×3), 1.19 (6H, s, CH_3–C–CH_3), 1.70—2.05 (3H, m, $(CH_3)_2$–CH–CH– ×3), 3.15 (4H, d, J=

6 Hz, -O-C**H**$_2$-CH-×2), 3.20, 3.39 (each 1H, d, J_{AB}= 12 Hz, -O-C**H**$_2$-C-O-), 4.09 ppm (1H, d, J=7 Hz, -O-CH-C**H**-).

*2,2,5,5,8-Pentamethyl-3,6-dioxa-8-nonen-1-ol (**10**)*: The last compound was isolated as a colorless oil; Rast's mol wt, 220 (Calcd, 216, $C_{12}H_{24}O_3$). Mass *m/e* 55 (base), 73 (22%), 101 (9), 113 (28), 127 (7), 143 (4), 185 (4, M^+-CH_2OH), 216 (trace, M^+, $C_{12}H_{24}O_3$); IR (liq.) 3480, 1071 (-OH), 1170, 1095, 1068 (C-O-C), 3080, 1662, 903 (CH$_2$=C-), 1397, 1370 cm^{-1} (CH$_3$-C-CH$_3$); PMR (CCl_4) δ 1.10, 1.16 (each 6H, s, C**H**$_3$-C-C**H**$_3$×2), 1.73 (3H, br s, C**H**$_3$-C=C-), 2.33 (1H, br s, -O**H**), 3.18 (2H, s, -C-C**H**$_2$-O-), 3.28 (2H, s, -C-C**H**$_2$-OH), 3.78 (2H, br s, -C=C-C**H**$_2$-O-), 4.76, 4.90 ppm (each 1H, br s, C**H**$_2$=C-).

*Acetyl Derivative of **10***: Colorless oil. IR (CCl_4) 1746, 1235 (CH$_3$COO-), 1170, 1095, 1045 (C-O-C), 3080, 1660, 900 cm^{-1} (CH$_2$=C-); PMR (CCl_4) δ 1.10, 1.18 (each 6H, s, -O-C-(C**H**$_3$)$_2$×2), 1.73 (3H, br s, C**H**$_3$-C=C-), 2.01 (3H, s, C**H**$_3$COO-), 3.15 (2H, s, -C-C**H**$_2$-O-), 3.78 (2H, br s, =C-C**H**$_2$-O-), 3.96 (2H, s, CH$_3$COO-C**H**$_2$-C-), 4.78, 4.93 ppm (each 1H, br s, C**H**$_2$=C-).

*Dihydro Derivative of **10***: Colorless oil. IR (CCl_4) 3470, 1070 (-OH), 1088, 1060 (C-O-C), 1389, 1375 cm^{-1} (CH$_3$-C-CH$_3$ and CH$_3$-CH-CH$_3$); PMR (CCl_4) δ 0.90 (6H, d, J=6 Hz, C**H**$_3$-CH-C**H**$_3$), 1.13, 1.18 (each 6H, s, C**H**$_3$-C-C**H**$_3$×2), 1.65—1.98 (1H, m, (CH$_3$)$_2$-C**H**-CH$_2$-), 2.24 (1H, br s, -O**H**), 3.10 (2H, d, J=7 Hz, -CH-C**H**$_2$-O-), 3.17 (2H, br s, -C-C**H**$_2$-O-C-), 3.40 ppm (2H, m, -C-C**H**$_2$-OH).

*4) Reaction of **4** with $BF_3 \cdot Et_2O$.* The reaction of **4** (10 g) was carried out with $BF_3 \cdot Et_2O$ (0.5 ml) according to the procedure described above.

*3,3,7-Trimethyl-4-oxa-7-octen-1-ol (**11**)*: The compound from the first eluate was obtained as a colorless oil. The molecular formula was $C_{10}H_{20}O_2$ (M^+ 172, Rast's mol wt, 176). Mass *m/e* 31 (41%), 41 (30), 59 (6), 69 (base), 87 (22), 99 (16), 117 (5), 127 (5), 155 (3), 172 (2, M^+, $C_{10}H_{20}O_2$); IR (CCl_4) 3510, 1145 (-OH), 1170, 1075, 1035 (C-O-C), 1652, 899 (CH$_2$=C-), 1380, 1369 cm^{-1} (CH$_3$-C-CH$_3$); PMR (CCl_4) δ 1.27 (6H, s, (C**H**$_3$)$_2$-C-O-), 1.65 (2H, t, J=6 Hz, -C-C**H**$_2$-CH$_2$-OH), 1.72 (3H, br s, C**H**$_3$-C=C-), 2.20 (2H, t, J=6 Hz, -CH$_2$-C**H**$_2$-C=C-), 2.67 (1H, br s, -O**H**), 3.47 (2H, t, J=6 Hz, -CH$_2$-C**H**$_2$-O-), 3.62 (2H, t, J=6 Hz, -CH$_2$-C**H**$_2$-OH), 4.80 ppm (2H, br s, C**H**$_2$=C-).

*Acetyl Derivative of **11***: Colorless oil. IR (CCl_4) 1745, 1245, 1239 (CH$_3$COO-), 1387, 1378 (CH$_3$-C-CH$_3$), 3081, 1653, 893 (CH$_2$=C-), 1171, 1035 cm^{-1} (C-O-C); PMR (CCl_4) δ 1.26 (6H, s, (C**H**$_3$)$_2$-C-O-), 1.65 (2H, t, J=6 Hz, -C-C**H**$_2$-CH$_2$-), 1.70 (3H, br s, -C=C-), 2.00 (3H, s, C**H**$_3$COO-), CH$_3$

2.20 (2H, t, J=6 Hz, =C-C**H**$_2$-CH$_2$-), 3.40 (2H, t, J= 6 Hz, -CH$_2$-C**H**$_2$-O-), 4.10 (2H, t, J=6 Hz, -CH$_2$-C**H**$_2$-COOCH$_3$), 4.68 ppm (2H, br s, C**H**$_2$=C-).

*Dihydro Derivative of **11***: Colorless oil. Mass *m/e* 41 (32%), 43 (85), 59 (55), 69 (43), 70 (11), 71 (base), 89 (18), 129 (59, $M^+-(CH_2-CH_2-OH)$), 159 (7, M^+-CH_3), 174 (trace, M^+, $C_{10}H_{22}O_2$); IR (CCl_4) 3490, 1148 (-OH), 1079 (C-O-C), 1391, 1371 cm^{-1} ((CH$_3$)$_2$-CH-, CH$_3$-C-CH$_3$); PMR (CCl_4) δ 0.90 (6H, d, J=6 Hz, (C**H**$_3$)$_2$-CH-), 1.23 (6H, s, (C**H**$_3$)$_2$-C-O-), 1.50 (2H, t, J=6 Hz, -CH-C**H**$_2$-CH$_2$-O-), 1.66 (2H, t, J=6 Hz, -O-C-C**H**$_2$-CH$_2$-OH), 2.16 (1H, br s, -O**H**), 3.40 (2H, t, J=6 Hz, -CH$_2$-C**H**$_2$-O-), 3.78 ppm (2H, t, J=6 Hz, -CH$_2$-C**H**$_2$-OH).

*3,3,7,7,11-Pentamethyl-4,8-dioxa-11-dodecen-1-ol (**12**)*: As the second compound, a colorless oil was isolated. The molecular formula was determined to be $C_{15}H_{30}O_3$ (M^+ 258, Rast's 263). Mass *m/e* 31 (6%), 41 (32), 43 (13), 59 (6), 69 (base), 99 (20), 105 (12), 115 (7), 127 (5), 139 (6), 173 (5), 258 (1, M^+, $C_{15}H_{30}O_3$); IR (CCl_4) 3400, 1143 (-OH), 1075, 1025 (C-O-C), 3075, 1655, 900 (CH$_2$=C-), 1380, 1369 cm^{-1} (CH$_3$-CH-CH$_3$ and CH$_3$-C-CH$_3$); PMR (CCl_4) δ 1.13, 1.20 (each 6H, s, CH$_3$-C-CH$_3$×2), 1.65 (4H, t, J=6 Hz, -O-C-C**H**$_2$-CH$_2$-O- and -O-C-C**H**$_2$-CH$_2$-OH), 1.73 (3H, br s, C**H**$_3$-C=C-), 2.18 (2H, t, J=6 Hz, =C-C**H**$_2$-CH$_2$-), 2.50 (1H, br s, -OH), 3.38 (4H, t, J=6 Hz, -CH$_2$-C**H**$_2$-O-×2), 3.52 (2H, t, J=6 Hz, -CH$_2$-C**H**$_2$-OH), 4.70 ppm (2H, br s, C**H**$_2$=C-).

*Acetyl Derivative of **12***: Colorless oil. IR (CCl_4) 1740, 1240, 1225 (CH$_3$COO-), 1075, 1030 (C-O-C), 3078, 1650, 889 cm^{-1} (CH$_2$=C-); PMR (CCl_4) δ 1.17, 1.21 (each 6H, s, (C**H**$_3$)$_2$-C-O-×2), 1.65 (4H, t, J=6 Hz, -O-C-C**H**$_2$-CH$_2$-O- and -O-C-C**H**$_2$-CH$_2$-OH), 1.75 (3H, br s, C**H**$_3$-C=C-), 2.00 (3H, s, C**H**$_3$COO-), 2.20 (2H, t, J=6 Hz, =C-C**H**$_2$-CH$_2$-), 3.40 (4H, t, J=6 Hz, -CH$_2$-C**H**$_2$-O-×2), 4.10 (2H, t, J=6 Hz, -CH$_2$-C**H**$_2$-COOCH$_3$), 4.70 ppm (2H, br s, C**H**$_2$=C-).

*Dihydro Derivative of **12***: Colorless oil. IR (CCl_4) 3500, 1145 (-OH), 1078 (C-O-C), 1386, 1370 cm^{-1} (CH$_3$-CH-CH$_3$ and CH$_3$-C-CH$_3$); PMR (CCl_4) δ 0.90 (6H, d, J= 6 Hz, CH$_3$-CH-C**H**$_3$), 1.22 (12H, s, (C**H**$_3$)$_2$-C-O-×2), 1.50 (2H, t, J=6 H, (CH$_3$)$_2$-CH-C**H**$_2$-CH$_2$-O-), 1.65 (4H, t, J=6 Hz, -O-C-C**H**$_2$-CH$_2$-O- and -O-C-C**H**$_2$-CH$_2$-OH), 2.30 (1H, br s, -O**H**), 3.41 (4H, t, J=6 Hz, -CH$_2$-C**H**$_2$-O-×2), 3.77 ppm (2H, t, J=6 Hz, -CH$_2$-C**H**$_2$-OH).

References

1) K. Nagai, *Chem. Pharm. Bull.*, **18**, 2123 (1970).
2) K. Nagai, *Bull. Chem. Soc. Jpn.*, **48**, 2317 (1975).
3) K. Nagai, *J. Soc. Hiroshima Univ., Ser. A*, **38**, 141 (1974).
4) K. Nagai, M. Nakayama, A. Matsuo, S. Eguchi, and S. Hayashi, *Bull. Chem. Soc. Jpn.*, **47**, 1193 (1974).
5) K. Nagai, *Bull. Chem. Soc. Jpn.*, **49**, 265 (1976).
6) W. M. Bandaranayake, L. Crombie, and D. A. Whiting *J. Chem. Soc., C*, **1971**, 811.

Studies on 5—8 Fused Ring Compounds. II. The Crystal and Molecular Structure of 7-Bromo-4,4-dimethylbicyclo[6.3.0]undecane-2,6-dione

Misao UMEHARA,* Hiroaki TAKAYANAGI,** Haruo OGURA,** and Shinzaburo HISHIDA***

Department of Chemistry, Keio University, Hiyoshi 4-1-1, Kohoku-ku, Yokohama 223

** *School of Pharmaceutical Sciences, Kitasato University, Shirokane, Minato-ku, Tokyo 108*

***Naka Works, Hitachi Ltd., Ichige, Katsuta, Ibaraki 312*

(Received February 16, 1978)

The crystal structure of 7-bromo-4,4-dimethylbicyclo[6.3.0]undecane-2,6-dione has been determined in order to elucidate the configuration and the conformation of 4,4-dimethylbicyclo[6.3.0]undecane-2,6-dione. The crystals of this compound are triclinic with space group $P\bar{1}$ and the unit cell dimensions are, $a=7.178$, $b=16.934$, $c=6.091$ Å, $\alpha=96.22$, $\beta=100.91$, $\gamma=115.39°$, and $Z=2$. The crystal structure was solved by the heavy-atom method and refined by the block-diagonal least-squares method. The final R value for 1473 non-zero reflexions was 0.067. The ring fusion of this compound is *trans* and the 8-membered ring has a boat-chair conformation.

In a previous paper,[1] it was reported that 4,4-dimethylbicyclo[6.3.0]undecane-2,6-dione (I) is given by the retro-aldol cleavage of 2-acetoxy-4,4-dimethyltricyclo[6.3.0.$0^{2,7}$]undecane-6-one which is the photoadduct of cyclopentene with the enol acetate of dimedone. This compound (I) has a fused ring system consisting of a five-membered ring and an eight-membered ring. No study concerning the conformations on such 5—8 fused ring compounds has been reported. Furthermore, no report concerning the relative stabilities of the *cis* and *trans* isomers of the 5—8 fused ring systems has appeared. Consequently the configuration of I at the ring juncture has not been assigned. In this work ^{1}H-NMR spectroscopy is not available for stereochemical study, because the ^{1}H-NMR spectra of I does not exhibit much difference in chemical shift and the definite assignment of each proton is not possible. In order to elucidate the conformation of I and to know whether the ring fusion is *cis* or *trans*, X-ray analysis of the monobromo derivative of I, 7-bromo-4,4-dimethylbicyclo[6.3.0]undecane-2,6-dione (II)†,[2] has been conducted, because II forms more suitable crystals for X-ray analysis than I. Since II is easily debrominated[3] by zinc dust in acetic acid at room temperature giving rise to the original dione (I), the ring fusion of I is probably the same as that of II.

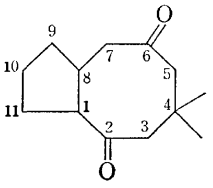

(I)

Experimental

7-Bromo-4,4-dimethylbicyclo[6.3.0]undecane-2,6-dione (II) was synthesized by the bromination of I with pyridinium bromide perbromide in ethanol.[2] Crystals of suitable quality for X-ray analysis were obtained from hexane in the form of colourless plates elongated along the b axis. The three-dimensional intensity data were collected on a Rigaku automatic four-circle diffractometer with graphite-monochromatized Cu $K\alpha$ radiation. The density was measured by the flotation method in a mixture of carbon tetrachloride and petroleum ether. The cell dimensions were determined by the least-squares method using the 2θ values of 20 strong reflexions in the range $36°\leqq 2\theta \leqq 50°$.

Crystal Data. 7-Bromo-4,4-dimethylbicyclo[6.3.0]-undecane-2,6-dione, $C_{13}H_{19}O_2Br$, *F.W.* 287.2, mp 111—113 °C, triclinic, $a=7.178$ (3), $b=16.934$ (8), $c=6.091$ (3) Å, $\alpha=96.22$ (4), $\beta=100.91$ (3), $\gamma=115.39$ (4)°, $V=642$ Å^3, $D_m=1.49$ g/cm^3, $D_c=1.486$ g/cm^3, $Z=2$, space group $P\bar{1}$.

The three dimensional intensity data were collected with a $\omega/2\theta$ scan technique at a constant scanning rate of 2 deg/min. Reflexions having an intensity exceeding the corresponding standard deviations by three times were treated as observed. 1473 reflexions with $2\theta \leqq 140°$ were retained and corrected for Lorentz and polarization factors but not for absorption and extinction factors.

Determination of the Structure

From the three dimensional Patterson map, the position of the bromine atom could easily be deduced. On the basis of the coordinates of the bromine atom, and from the Fourier synthesis all the 15 non-hydrogen light atoms in the asymmetric unit were deduced. The R-value was 0.52 at this stage. Refinement was conducted by the block-diagonal least-squares method. After several cycles of the refinement, the R-value was reduced to 0.295. Three cycles of calculations assuming the anisotropic thermal vibration for all the atoms gave an R-value of 0.098. From a second Fourier map, all hydrogen atoms except the five hydrogen atoms (H(5), H(8), H(11), H(13), and H(17)), were deduced. Three more cycles of refinement were performed using anisotropic temperature factors for the bromine, oxygen and carbon atoms and isotropic temperature factors for the hydrogen atoms. The final R-value for 1473 non-zero reflexions was 0.067. The scattering factors for bromine were taken from the International Tables for X-Ray Crystallography.[4] For these calculations, computer programs made by Stewart *et al.*[5] were used. The complete F_o-F_c tables are kept by the office of the Chemical Society of Japan (Document No. 7833).

The final values of the positional and thermal parameters are given in Tables 1 and 2. The molecular structure and the numbering of 7-bromo-4,4-dimethylbicyclo[6.3.0]undecane-2,6-dione (II) determined by the present analysis is shown in Fig. 1. Figure 2 shows

† II was assumed to be the 5-bromo derivative in a previous paper,[2] but this analysis showed it to be the 7-bromo derivative.

TABLE 1. FRACTIONAL ATOMIC COORDINATES ($\times 10^4$) AND ANISOTROPIC THERMAL PARAMETERS ($\times 10^4$) OF THE NON-HYDROGEN ATOMS

The estimated standard deviations are given in parentheses. The anisotropic temperature factors are of the form: $\exp[-2\pi^2(a^{*2}h^2U_{11}+b^{*2}k^2U_{22}+c^{*2}l^2U_{33}+2a^*b^*hkU_{12}+2a^*c^*hlU_{13}+2b^*c^*klU_{23})]$.

Atom	x	y	z	U_{11}	U_{22}	U_{33}	U_{12}	U_{13}	U_{23}
Br	1484(2)	4361(1)	765(2)	588(7)	569(7)	727(9)	390(6)	95(6)	65(7)
C(1)	4697(14)	2727(6)	387(16)	295(48)	485(57)	237(60)	233(45)	25(44)	47(51)
C(2)	3244(15)	1878(7)	−1142(17)	393(53)	624(68)	332(65)	403(54)	102(49)	97(58)
C(3)	1132(13)	1250(7)	−808(18)	258(44)	502(62)	442(69)	210(45)	47(45)	180(57)
C(4)	−879(14)	1257(7)	−2353(17)	244(45)	454(58)	351(62)	155(44)	24(44)	86(53)
C(5)	−810(14)	2183(7)	−1922(17)	270(46)	575(59)	390(65)	226(45)	135(46)	179(55)
C(6)	1018(14)	2944(7)	−2403(16)	333(48)	527(60)	312(58)	318(47)	92(44)	129(52)
C(7)	2763(16)	3639(7)	−557(17)	428(56)	486(61)	249(60)	281(52)	1(49)	−13(53)
C(8)	3684(14)	3299(6)	1391(16)	323(48)	493(58)	247(57)	278(46)	76(44)	21(51)
C(9)	5517(16)	4008(7)	3389(18)	431(57)	652(68)	392(67)	250(54)	−56(52)	16(59)
C(10)	6765(18)	3526(9)	4416(20)	590(68)	817(92)	261(74)	400(69)	−232(59)	−207(72)
C(11)	5913(16)	2608(8)	2645(18)	419(57)	744(79)	491(68)	435(60)	−28(51)	57(63)
C(12)	−1113(18)	946(8)	−4854(19)	504(68)	647(79)	400(69)	332(64)	46(57)	−47(64)
C(13)	−2823(16)	595(8)	−1657(22)	342(53)	601(71)	753(90)	171(52)	113(58)	224(69)
O(1)	3758(11)	1627(6)	−2847(14)	456(43)	859(61)	617(57)	395(44)	145(41)	18(50)
O(2)	1100(11)	2972(6)	−4387(12)	548(44)	801(56)	338(44)	303(43)	92(37)	189(44)

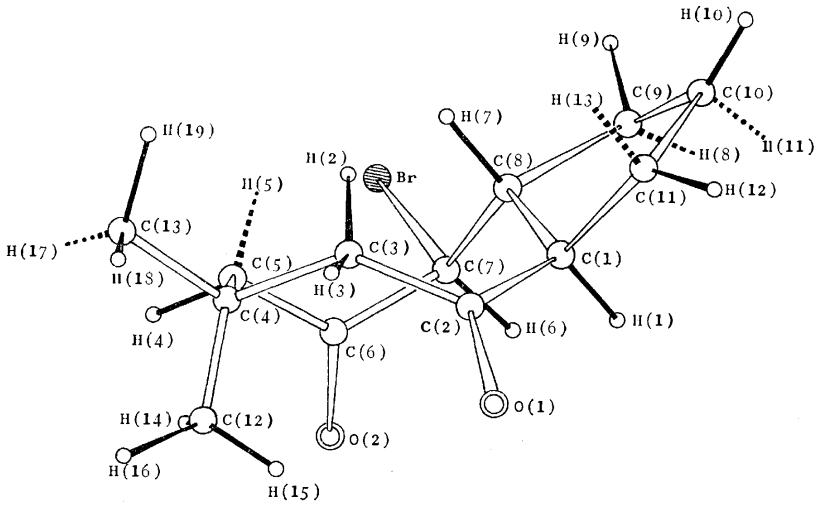

Fig. 1. Molecular structure and numbering of II. Projection of II along the b axis. (Hydrogen atoms connected with dot lines were not deduced.)

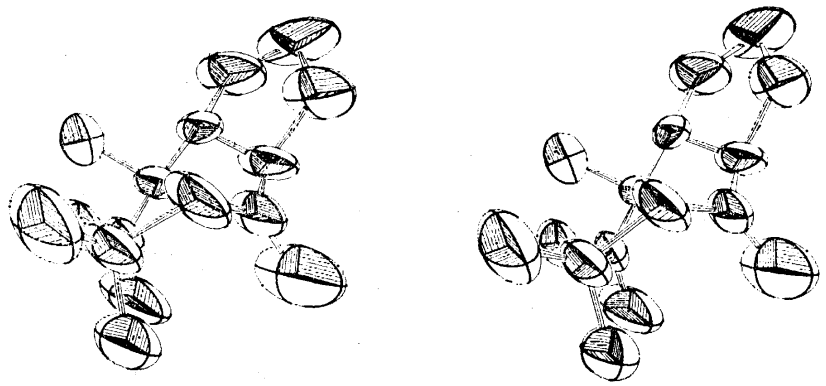

Fig. 2. A stereoscopic ORTEP drawing[6] of the molecule. Thermal ellipsoids are drawn at the 50% probability level.

Table 2. Fractional coordinates ($\times 10^3$) and thermal parameters ($\times 10^2$) for hydrogen atoms
The estimated standard deviations are in parentheses.

	x	y	z	U[a]
H(1)	573(12)	303(5)	−61(14)	6(2)
H(2)	93(12)	137(5)	72(14)	7(2)
H(3)	78(12)	57(5)	−127(14)	3(2)
H(4)	−218(12)	207(5)	−308(14)	3(2)
H(6)	398(12)	412(5)	−133(14)	3(2)
H(7)	248(12)	294(5)	242(14)	4(2)
H(9)	510(12)	434(5)	483(14)	7(2)
H(10)	765(12)	369(5)	599(14)	9(2)
H(12)	709(12)	254(5)	254(14)	6(2)
H(14)	−132(12)	36(5)	−495(14)	7(2)
H(15)	27(12)	137(5)	−531(13)	7(2)
H(16)	−248(12)	87(5)	−596(14)	6(2)
H(18)	−284(12)	−3(5)	−221(14)	6(2)
H(19)	−260(12)	73(5)	21(14)	5(2)

a) U is defined by: $\exp(-8U\pi^2 \sin^2\theta/\lambda^2)$.

Table 3. Bond lengths and bond angles
Standard deviations are given in parentheses.

Bond lengths (1/Å)			
C(1)-C(2)	1.442(12)	C(10)-C(11)	1.589(17)
C(2)-C(3)	1.500(13)	C(11)-C(1)	1.566(16)
C(3)-C(4)	1.572(15)	C(1)-C(8)	1.576(17)
C(4)-C(5)	1.540(17)	C(4)-C(12)	1.510(15)
C(5)-C(6)	1.498(13)	C(4)-C(13)	1.539(15)
C(6)-C(7)	1.461(11)	C(2)-O(1)	1.257(15)
C(7)-C(8)	1.534(16)	C(6)-O(2)	1.226(13)
C(8)-C(9)	1.542(11)	C(7)-Br	2.004(13)
C(9)-C(10)	1.545(21)		
Bond angles (φ/°)			
C(1)-C(2)-C(3)	124.0(10)	C(11)-C(1)-C(8)	100.7(8)
C(2)-C(3)-C(4)	115.4(9)	C(11)-C(1)-C(2)	111.7(10)
C(3)-C(4)-C(5)	112.1(7)	C(1)-C(2)-O(1)	119.3(9)
C(4)-C(5)-C(6)	117.1(10)	C(3)-C(2)-O(1)	116.7(8)
C(5)-C(6)-C(7)	121.6(9)	C(3)-C(4)-C(12)	110.9(10)
C(6)-C(7)-C(8)	115.3(9)	C(3)-C(4)-C(13)	106.1(9)
C(7)-C(8)-C(1)	108.5(8)	C(5)-C(4)-C(12)	110.4(10)
C(8)-C(1)-C(2)	117.0(8)	C(5(-C(4)-C(13)	107.9(10)
C(1)-C(8)-C(9)	103.9(8)	C(12)-C(4)-C(13)	109.3(7)
C(7)-C(8)-C(9)	117.2(9)	C(5)-C(6)-O(2)	119.6(7)
C(8)-C(9)-C(10)	105.2(10)	C(7)-C(6)-O(2)	118.8(8)
C(9)-C(10)-C(11)	106.5(9)	C(6)-C(7)-Br	104.9(8)
C(10)-C(11)-C(1)	104.7(11)	C(8)-C(7)-Br	107.6(7)

the conformation and thermal vibration of the molecule drawn by the ORTEP.[6] The bond lengths and angles of the molecule, calculated from the coordinates given in Table 1, are shown in Table 3. Important torsion angles are shown in Table 4. The projection of the crystal structure along the c axis is shown in Fig. 3.

Discussion

For the conformation of 8-membered rings, a boat-chair (BC) form was shown by the calculation of strain

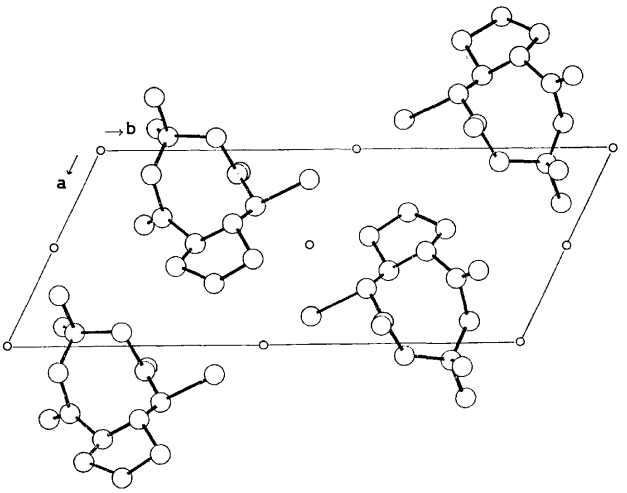

Fig. 3. Crystal structure projected along the c axis.

energies to be the most stable.[7] Cyclooctane and its simple derivatives have been found to be exist predominantly in the BC form,[8–10] however, since the energy differences from other conformations are small, the cases with crown family conformations (crown, chair-chair, and twist-chair-chair) are also reported.[10,11] For 8-membered ring ketones, Anet *et al.*[12] showed by NMR studies at low temperature that cyclooctanone and 1,5-cyclooctanedione exist in BC-3 (or BC-7) and BC-3,7 forms, respectively.

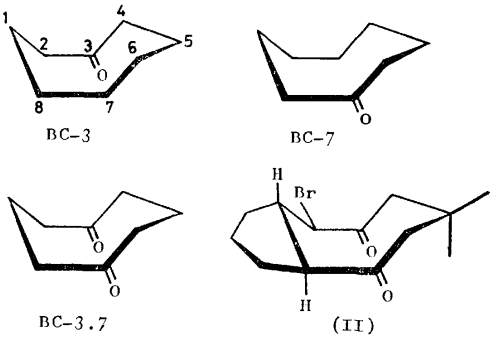

According to the results of this study, it has been shown that the 8-membered ring of II has a BC-3,7 conformation. In Table 5, the conformation of the 8-membered ring in II is shown in terms of torsion angles.[13] In these values, the torsion angles around the ring juncture and C(4) bearing two methyl groups, that is, C(8)–C(1), C(3)–C(4), and C(4)–C(5) deviated from the values of *cis*- and *trans*-1,2-cyclooctanedicarboxylic acids[8] and the calculated values for cyclooctane,[7] while the others are similar. When the 8-membered ring of II has a BC form, it is expected that the transannular repulsions occur between the three hydrogen atoms H(2), H(5), and H(7) which are directed towards the inside of the 8-membered ring. Although H(5) was not located the H(2)···H(7) interatomic distance was determined to be 2.4 Å. Since the interatomic distance is not small, these transannular interactions perhaps are weak, if any, in the crystalline

Table 4. Torsion angles (φ/°)

Torsion angles in the 8-membered ring		Torsion angles in the 5-membered ring	
C(1)-C(2)-C(3)-C(4)	102.0	C(1)-C(8)-C(9)-C(10)	−35.0
C(2)-C(3)-C(4)-C(5)	−60.6	C(8)-C(9)-C(10)-C(11)	11.9
C(3)-C(4)-C(5)-C(6)	61.4	C(9)-C(10)-C(11)-C(1)	15.5
C(4)-C(5)-C(6)-C(7)	−107.1	C(10)-C(11)-C(1)-C(8)	−35.9
C(5)-C(6)-C(7)-C(8)	46.5	C(11)-C(1)-C(8)-C(9)	44.0
C(6)-C(7)-C(8)-C(1)	63.2		
C(7)-C(8)-C(1)-C(2)	−69.4		
C(8)-C(1)-C(2)-C(3)	−39.5		
Other torsion angles			
C(2)-C(1)-C(8)-C(9)	165.2	C(1)-C(8)-C(7)-Br	180.0
C(2)-C(1)-C(11)-C(10)	−160.8	C(5)-C(6)-C(7)-Br	−71.7
C(6)-C(7)-C(8)-C(9)	−179.5	C(9)-C(8)-C(7)-Br	−62.8
C(7)-C(8)-C(9)-C(10)	−154.6	O(1)-C(2)-C(1)-H(1)	15.8
C(7)-C(8)-C(1)-C(11)	169.4	O(1)-C(2)-C(3)-H(2)	163.6
C(2)-C(3)-C(4)-C(12)	63.5	O(1)-C(2)-C(3)-H(3)	36.6
C(2)-C(3)-C(4)-C(13)	−178.1	O(2)-C(6)-C(5)-H(4)	−43.0
C(6)-C(5)-C(4)-C(12)	−62.8	O(2)-C(6)-C(7)-H(6)	0.0
C(6)-C(5)-C(4)-C(13)	177.8	O(2)-C(6)-C(7)-Br	110.8
C(4)-C(3)-C(2)-O(1)	−79.3	H(1)-C(1)-C(8)-H(7)	177.2
C(4)-C(5)-C(6)-O(2)	70.3	H(6)-C(7)-C(8)-H(7)	167.0
C(8)-C(1)-C(2)-O(1)	141.8	H(7)-C(8)-C(7)-Br	51.6
C(8)-C(7)-C(6)-O(2)	−131.0		

Table 5. Conformations for 8-membered rings in terms of torsion angles around carbon framework[13]
According to the accepted notation, the axis or plane of symmetry is represented by a horizontal symmetry line.

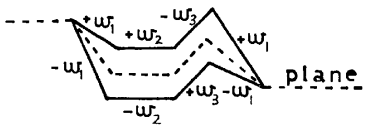

	$+\omega_1$	$+\omega_2$	$-\omega_3$	$+\omega_1$
	$-\omega_1$	$-\omega_2$	$+\omega_3$	$-\omega_1$
Compound II	63.2	46.5	−107.1	61.4
	−69.4	−39.5	102.0	−60.6
cis-1,2-Cyclooctanedicarboxylic acid[8]	68.8	38.0	−96.1	65.7
	−60.1	−48.2	104.8	−67.4
trans-1,2-Cyclooctanedicarboxylic acid[8]	63.0	43.4	−100.9	70.3
	−62.0	−46.8	105.9	−70.8
Cyclooctane, BC form (calculated by Englar *et al.*[7])	64.0	43.4	−101.1	68.1
	−65.0	−41.9	100.3	−68.3
Cyclooctane, BC form (calculated by Hendrickson[7])	65.0	44.7	−102.2	65.0
	−65.0	−44.7	102.2	−65.0

state.

The C–C–C bond angles in the 8-membered ring at C(1), C(3), C(5), and C(7) which are at α-positions of the carbonyl groups are 115—117 °C. Although these values are larger than the normal values of 109.5°, they are similar to the values observed in the 8-membered ring of 1,2-cyclooctanedicarboxylic acid.[8] As shown in Table 3, the four C–C bond lengths containing carbonyl carbon atoms (C(2) and C(6)) are C(1)–C(2)=1.442 Å, C(2)–C(3)=1.500 Å, C(5)–C(6)=1.498 Å, and C(6)–C(7)=1.461 Å, respectively. In these values, the C(1)–C(2) bond length is significantly shorter than that for the usual C_{sp^2}–C_{sp^3} single bond (1.501 Å).[14] The value of the C(2)–O(1) bond length s 1.257 Å which is longer than the characteristic value for the C=O double bond length. In the 8-membered ring, the distance between the two carbonyl carbon atoms, C(2)···C(6) is 2.951 Å and this is considerably shorter than the other distances between two carbon atoms in the 1,5 positions: C(1)···C(5)=3.598 Å, C(3)···C(7)=3.673 Å, C(4)···C(8)=3.693 Å.

The ring fusion of the 5-membered ring and the 8-membered ring in II is *trans* because the torsion angle H(1)–C(1)–C(8)–H(7) is 177.2° as shown in Table 5. Therefore the ring fusion of I may be assumed to be *trans*.

As shown in Figs. 1 and 2, the bromine atom in II was found to be bonded to C(7) in disagreement with what was assumed in a previous paper,[2] *i.e.* bromine substitution at C(5). Also in a previous paper[2] it was reported that the C=O at position 6 and C–Br in II greatly deviated from co-planarity on the basis of IR and UV data. This is consistent with the result of this study because the torsion angle O(2)–C(6)–C(7)–Br is 110.8°, whereas the torsion angle O(2)–C(6)–C(7)–H(6) is 0.0°.

Thus the 8-membered ring of II has a BC-3,7 conformation which appears to be the most stable. Consequently it may be assumed that I has a similar conformation.

The authors are grateful to Professor Yoichi Iitaka, University of Tokyo, for his valuable discussion.

References

1) M. Umehara, T. Oda, Y. Ikebe, and S. Hishida, *Bull. Chem. Soc., Jpn.*, **49**, 1075 (1976).
2) M. Umehara, S. Hishida, K. Fujieda, and H. Sasaki, *Bull. Chem. Soc. Jpn.*, **50**, 1074 (1977).
3) M. Umehara, S. Hishida, K. Fujieda, H. Ogura, and H. Takayanagi, *Bull. Chem. Soc. Jpn.*, **51**, 2449 (1978).
4) "International Tables for X-Ray Crystallography," Kynoch Press, Birmingham (1962), Vol. III, p. 202.
5) J. M. Stewart *et al.*, Technical Report TR-192 (June, 1972), The X-Ray System of Crystallographic Programs for Any Computer, Computer Science Center, University of Maryland.
6) C. K. Johnson, ORTEP, Report ORNL-3794, Oak Ridge National Laboratory, Oak Ridge, Tennessee, U. S. A. (1965).
7) J. B. Hendrickson, *J. Am. Chem. Soc.*, **89**, 7036 (1967); E. M. Engler, J. D. Andose, and P. von R. Schleyer, *ibid.*, **95**, 8005 (1973).
8) M. Dobler, J. D. Dunitz, and A. Mugnoli, *Helv. Chim. Acta*, **49**, 2492 (1966); H. B. Bürgi and J. D. Dunitz, *ibid.*, **51**, 1514 (1968).
9) F. A. L. Anet and M. St. Jacques, *J. Am. Chem. Soc.*, **88**, 2585, 2586 (1966); J. E. Anderson, E. S. Glazer, D. L. Griffith, R. Knorr, and J. D. Roberts, *ibid.*, **91**, 1386 (1969).
10) H. J. Schneider, T. Keller, and R. Price, *Org. Magn. Reson.*, **4**, 907 (1972); F. A. L. Anet and V. J. Basus, *J. Am. Chem. Soc.*, **95**, 4424 (1973).
11) G. Ferguson, D. D. MacNicol, W. Oberhansli, R. A. Raphael, and J. A. Zabkiewicz, *Chem. Commun.*, **1968**, 103.
12) F. A. L. Anet, M. St. Jacques, P. M. Henrichs, A. K. Cheng, J. Krane, and L. Wong, *Tetrahedron*, **30**, 1629 (1974).
13) J. B. Hendrickson, *J. Am. Chem. Soc.*, **86**, 4854 (1964).
14) D. R. Lide, Jr., *Tetrahedron*, **17**, 125 (1962).

Structural Studies on Anthglutin, an Inhibitor of γ-Glutamyl Transpeptidase, from *Penicillium Oxalicum*

Takeshi KINOSHITA* and Sadamasa MINATO†

Central Research Laboratories, Sankyo Co., Ltd., Hiromachi, Shinagawa-ku, Tokyo 140

† *Fermentation Research Laboratories, Sankyo Co., Ltd., Hiromachi, Shinagawa-ku, Tokyo 140*

(Received February 23, 1978)

Anthglutin, a new γ-glutamylphenylhydrazine and an inhibitor of γ-glutamyl transpeptidase, has been isolated from the cultured medium of *Penicillium oxalicum*. Spectral studies indicate that it has the structure of 1-γ-L-glutamyl-2-(2-carboxyphenyl)hydrazine.

γ-Glutamyl transpeptidase [EC 2.3.2.2] is an enzyme widely distributed in the tissues and body fluids of animals,[1] microorganisms,[2] plants,[3] and coelenterates.[4] Serum γ-glutamyl transpeptidase activity is assayed in clinical diagnosis.[5] A strong inhibitor of γ-glutamyl transpeptidase has been isolated from the cultured medium of *Penicillium oxalicum* SANK 10477 and named anthglutin.[6] The new compound anthglutin is a competitive and specific inhibitor for γ-glutamyl transpeptidase. This paper deals with the structure determination of anthglutin.

Experimental

Spectra. IR spectra were obtained with a JASCO IRA-2 spectrometer, and NMR spectra with a Varian A-60D spectrometer using tetramethylsilane as an internal standard. GLC analyses were carried out on a JEOL JGC-20KFP gas chromatograph and GC-MS analyses on a JEOL JMS D-100 gas chromatograph mass spectrometer. Field desorption mass spectra (FD-MS) were obtained with a double focusing JEOL JMS-OlSG instrument equipped with a combined f.d.f.i.e.i. ion source. Conventional low and high resolution mass spectra were taken on a JEOL JMS-OlSG spectrometer, using a direct insertion probe and an ionization energy of 75 eV.

Material. Anthglutin was obtained by the method described in a previous paper.[6] The result of elemental analysis agreed with the formula $C_{12}H_{15}N_3O_5$.

Found: C, 51.07; H, 5.51; N, 14.65; O, 28.87%. Calcd for: C, 51.24; H, 5.38; N, 14.94; O, 28.44%.

Preparation of Derivatives. Trimethylsilyl (TMS), perdeuteriotrimethylsilyl (TMS-d_9), and trifluoroacetyl (TFA) derivatives of anthglutin (I) were prepared according to methods in literature.[7-10] *N*-[(Dimethylamino)methylene] methyl ester derivatives of amino acids were also prepared according to the reported method.[11]

Results and Discussion

The formula $C_{12}H_{15}N_3O_5$ of anthglutin (I) was substantiated by high resolution mass measurement on the quasi-molecular ion $(M+H)^+$ at *m/e* 282 in the field desorption mass spectrum (Fig. 1). The NMR spectrum of I in D_2O at basic pD is shown in Fig. 2. The signals at δ 6.8—8.2 correspond to four aromatic hydrogens, indicating the presence of an *ortho*-disubstituted benzene. The remaining signals consist of a triplet at δ 3.90 (1H, J=6 Hz) and a complex pattern centered at δ 2.5 (4H), corresponding to those of L-glutamic acid whose occurence in I was expected by bioassay and amino acid analysis.[6] The IR spectrum (Nujol) of I exhibits absorption bands which can be attributed to >N-H (3290 cm^{-1}), >C=O (1675, 1655 cm^{-1}), and *ortho*-disubstituted benzene (760 cm^{-1}).

Major structure analysis was carried out by means of fragmentation analysis of the mass spectra. A strong peak is seen at *m/e* 134 ($C_7H_6N_2O$, *M.W.* obsd=134.0475, *M.W.* calcd=134.0480) corresponding to $[M-C_5H_9NO_4]^+$ ion (Fig. 3). Since the atomic composition of $C_5H_9NO_4$ is identical to that of glutamic acid and the NMR spectrum of I suggests the presence of an *ortho*-disubstituted benzene ring, the structure of this fragment ion at *m/e* 134 should be one of the following:

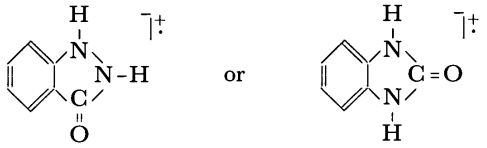

II or III

As shown in Fig. 2, the signals in the down-field of the NMR spectrum of I resemble those of *o*-aminobenzoic acid very closely in chemical shifts and spectral

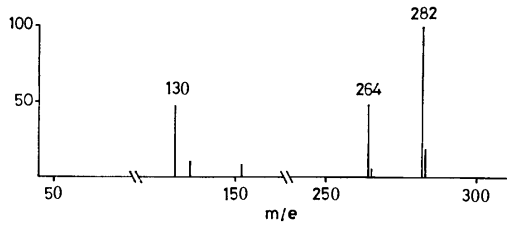

Fig. 1. The field desorption mass spectrum of **I**: heating current 17 mA, *m/e* 282=$C_{12}H_{16}N_3O_5$ (*M.W.* calcd=282.1088, *M.W.* obsd=282.1079).

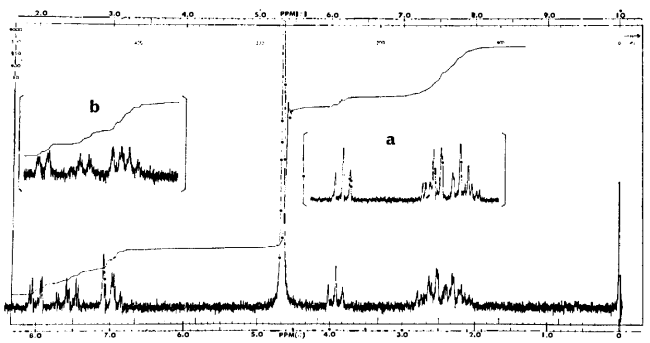

Fig. 2. The NMR spectrum of **I** in D_2O containing a small amount of NaOH; the spectra in brackets: (a) L-glutamic acid in D_2O and (b) *o*-aminobenzoic acid in $(CD_3)_2CO$: D_2O (3:1).

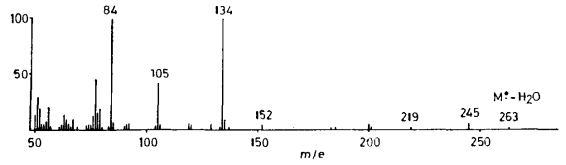

Fig. 3. Mass spectrum of **I**.

patterns. Thus, structure II seems more likely. The fragment ion at *m/e* 134 can be derived from one of the structural units of the following types in which X plus Y should be $C_5H_9NO_4$.

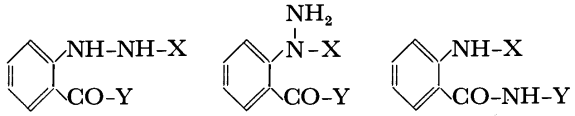

In order to determine the whole structure, the reactions of I with some reagents were carried out. The product derived from the reaction of I with *N,N*-dimethylformamide dimethyl acetal (DMF–DMA)[11] is labile even at 230 °C (Fig. 4). Gas chromatography mass spectrometry (GC-MS) was applied for further analysis to the products derived from the partial pyrolysis at the injection port of a gas chromatograph.

The mass spectrum of GLC peak A in Fig. 4 is identical to that of the product (VII) from the reaction of L-glutamic acid with DMF–DMA (Fig. 5-(a)).

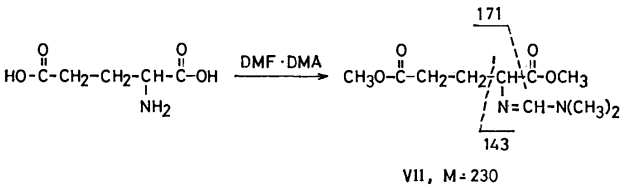

VII, M=230

The structural assignment for peak B is based on its mass spectrum which is analogous in fragmentation patterns to that of VII as shown below.

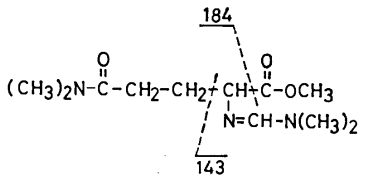

VIII, M=243

Peak C seems to be derived from compound IX as indicated by its mass spectrum (Fig. 5-(b)).

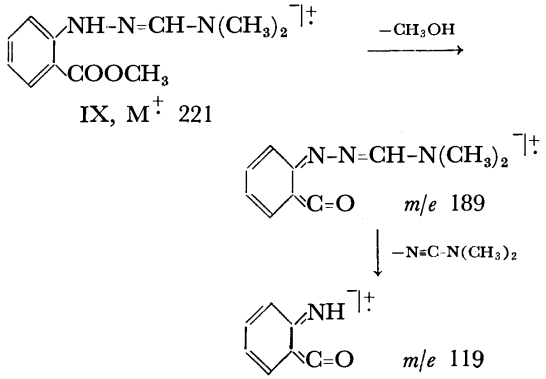

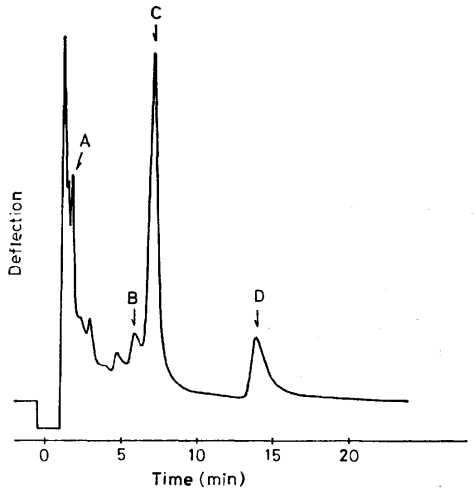

Fig. 4. Gas chromatogram of the reaction products of **I** with DMF-DMA taken by total ion current of GC-MS. Column of 2% Silicone OV-1 on Chromosorb G, 1 m×2 mm i.d. glass column, col. temp: 145 °C, inj. temp: 230 °C, flow rate: 23 ml/min He.

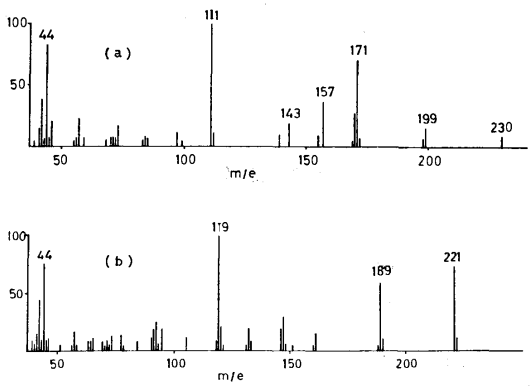

Fig. 5. Mass spectra of peak A (a) and peak C (b).

For peak D, the assignment was done by the analysis of the corresponding GC-MS spectrum which is analogous in fragmentation modes to that of IX.

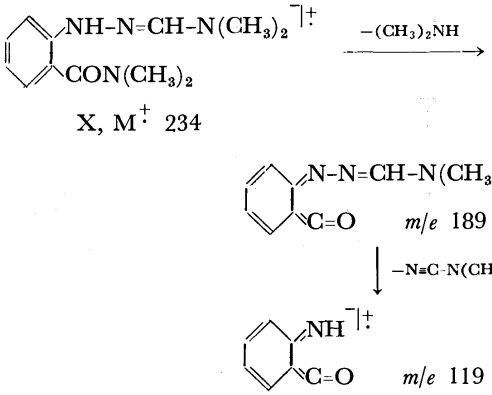

The above data suggest that the structure of I should be one of the following five structures XI—XV.

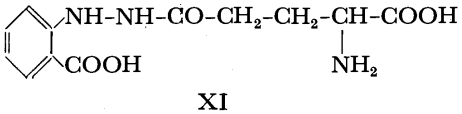

XI

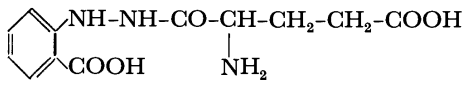

XII

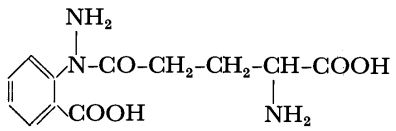

XIII

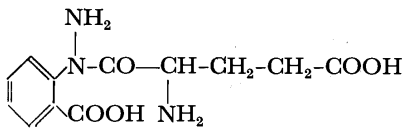

XIV

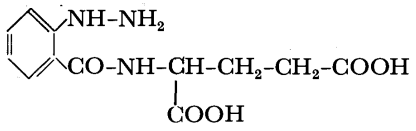

XV

Further information was obtained by a study of the mass spectra of the trimethylsilyl (TMS) and the perdeuteriotrimethylsilyl (TMS-d_9) derivatives of I (Figs. 6 and 7). The occurrence of the fragment ions at *m/e* 219 and 237 (Figs. 6 and 7) suggests that I has an α-amino acid moiety as part of its structure.

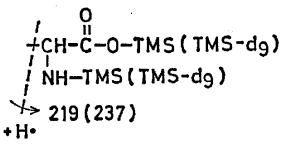

The result of the color reaction of I with ninhydrin, a strong purple color being obtained at elevated temperature, also suggests that a free α-amino acid moiety might occur in I. Thus, of the five possible structures, only structures XI and XIII seem likely. The information for differentiating XI and XIII was obtained from the mass spectrum of the *N*-trifluoroacetyl-*O*-trimethylsilyl (*N*-TFA-*O*-TMS) derivative of I. *N*-TFA-*O*-TMS derivatives are easily prepared by trimethylsilylation with *N,O*-bis(trimethylsilyl)trifluoroacetamide (BSTFA) followed by selective *N*-acylation with *N*-methylperfluorodiacetamide (MPFDA).[9]

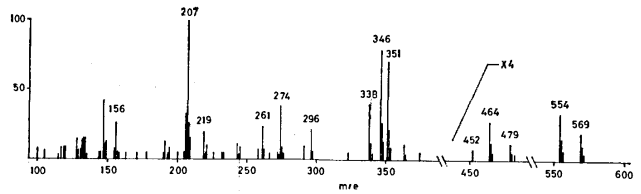

Fig. 6. Mass spectrum of the TMS derivative of **I**.

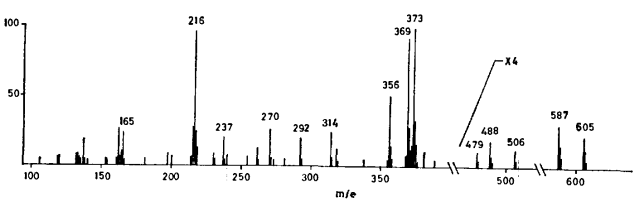

Fig. 7. Mass spectrum of the TMS-d_9 derivative of **I**.

TABLE 1. HIGH RESOLUTION MASS MEASUREMENTS OF PRINCIPAL IONS IN MASS SPECTRUM OF TMS DERIVATIVE OF I

Observed	Calculated	Formulae
569.2619	569.2591	$C_{24}H_{47}N_3O_5Si_4$
554.2370	554.2356	$C_{23}H_{44}N_3O_5Si_4$
479.2067	479.2090	$C_{21}H_{37}N_3O_4Si_3$
464.1832	464.1855	$C_{20}H_{34}N_3O_4Si_3$
452.2201	452.2219	$C_{20}H_{38}N_3O_3Si_3$
351.1573	351.1559	$C_{16}H_{27}N_2O_3Si_2$
346.1709	346.1729	$C_{14}H_{32}NO_3Si_3$
338.1574	338.1587	$C_{15}H_{26}N_2O_3Si_2$
296.1394	296.1375	$C_{13}H_{24}N_2O_2Si_2$
274.1315	274.1294	$C_{11}H_{24}NO_3Si_2$
261.1066	261.1059	$C_{13}H_{17}N_2O_2Si$
219.1093	219.1109	$C_8H_{21}NO_2Si_2$
207.0962	207.0954	$C_{10}H_{15}N_2OSi$
206.0885	206.0876	$C_{10}H_{14}N_2OSi$
156.0832	156.0844	$C_7H_{14}NOSi$

Subsequent acylation of the TMS derivative of I with MPFDA gave a mass shift of the molecular ion of 24 mass units as compared with the original derivative (Fig. 8). This indicates that the TMS derivative of I has only one *N*-trimethylsilyl group. It can be concluded that the *N*-TFA-*O*-TMS derivative of I is XVI and not XVII.

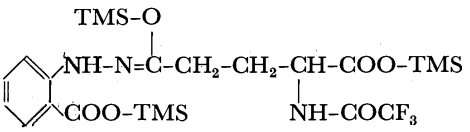

XVI, M=593

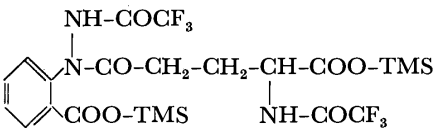

XVII, M=617

Consequently, the proposed structure of anthglutin (I) is 1-γ-L-glutamyl-2-(2-carboxyphenyl)hydrazine (XI). The structural assignments of fragment ions of the TMS derivative of I (Fig. 6) were confirmed by high resolution mass measurements (Table 1) and by comparison with the mass spectrum of the TMS-d_9 derivative of I. The peaks at *m/e* 569, 452, 351, 346, 338, and 219 in the mass spectrum of the TMS derivative shifted to *m/e* 605, 479, 369, 373, 356, and 237, respectively, in that of the TMS-d_9 derivative (Fig. 7). These peaks decide the selection of structure XI as the most likely structure for I. The formation of these ions can be illustrated as shown in Fig. 9.††

The major fragmentation routes of I in its mass spectrum (Fig. 3) are shown in Scheme 1. High resolution measurements of these fragment ions have been carried out (Table 2). A similar strong ion

†† Substituting a TMS group for the hydrogen atom of –NH–N=C< in the TMS derivative of I seems to be difficult because of the steric hindrance of the bulky group, –CO–O–TMS, at the *ortho* position in the phenyl group.

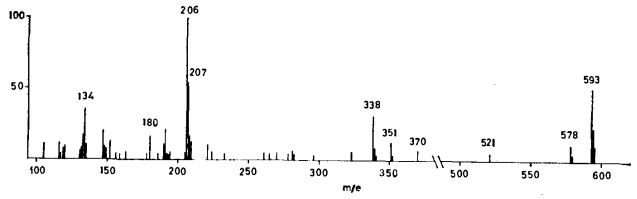

Fig. 8. Mass spectrum of the TMS derivative of **I** followed by *N*-acylation with MPFDA.

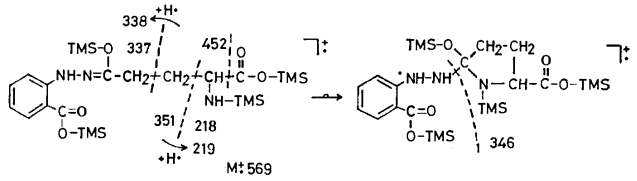

Fig. 9. Mass spectral fragmentation modes of the TMS derivative of **I**.

peak at *m/e* 84 (C_4H_6NO) was also observed in the mass spectra of glutamic acid and its derivatives such as glutamine, 4-(γ-L-glutaminyl)phenol,[12] and glutamic acid diethyl ester.[13]

The proposed structure of the fragment ion at *m/e* 84 is in line with the results showing that in the case of the TMS and the TMS-d_9 derivatives of I, the corresponding ions appear at *m/e* 156 and 165, respectively.

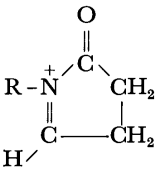

R=TMS, *m/e* 156
R=TMS-d_9, *m/e* 165

It can be said that the structural assignment for the strongest fragment ion of *m/e* 134 derived from the ion of *m/e* 152 as shown in Scheme 1 is supported by the fact that *o*-hydrazinobenzoic acid is easily converted into indazolone.[14]

A synthetic investigation of 1-γ-L-glutamyl-2-(2-carboxyphenyl)hydrazine (XI) is in progress.

We are grateful to Dr. Chihiro Tamura for his valuable discussions. Thanks are also due to Mr. Hidemi Nagaki for his assistance in obtaining field desorption spectra.

Table 2. High resolution mass measurements of principal ions in mass spectrum of I

Observed	Calculated	Formulae
263.0889	263.0905	$C_{12}H_{13}N_3O_4$
245.0795	245.0800	$C_{12}H_{11}N_3O_3$
219.1021	219.1008	$C_{11}H_{13}N_3O_2$
152.0597	152.0585	$C_7H_8N_2O_2$
134.0475	134.0480	$C_7H_6N_2O$
129.0454	129.0427	$C_5H_7NO_3$
105.0438	105.0452	$C_6H_5N_2$
84.0433	84.0449	C_4H_6NO
56.0479	56.0500	C_3H_6N

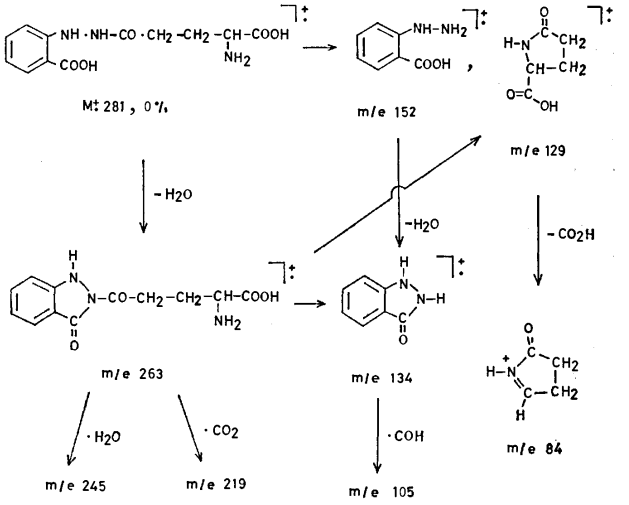

Scheme 1.

References

1) S. B. Rosalki, "Advances in Clinical Chemistry," ed by O. Bodansky and A. L. Latner, Academic Press, New York (1975), Vol. 17, p. 53.

2) W. J. Williams and C. B. Thorne, *J. Biol. Chem.*, **210**, 203 (1954).

3) M. Y. Goore and J. F. Thompson, *Biochim. Biophys. Acta*, **132**, 15 (1967).

4) J. Danner, H. M. Lenhoff, M. Houston-Cobb, W. Heagy, and G. R. Marshall, *Biochem. Biophys. Res. Commun.*, **73**, 180 (1976).

5) S. Minato, H. Tamaoki, S. Takei, and K. Fujisawa, *Clin. Chim. Acta*, **65**, 21 (1975).

6) S. Minato, A. Terahara, and T. Kinoshita, Japan Patent, Application No. (77)-41166., 1977.

7) F. Shahrokhi and C. W. Gehrke, *J. Chromatogr.*, **36**, 31 (1968).

8) K. Bergström, J. Gürtler, and R. Blomstrand, *Anal. Biochem.*, **34**, 74 (1970).

9) M. Donike, *J. Chromatogr.*, **115**, 591 (1975).

10) H. Miyazaki, M. Ishibashi, M. Itoh, and T. Nambara, *Biomed. Mass Spectrom.*, **4**, 23 (1977).

11) J. P. Thenot and E. C. Horning, *Anal. Lett.*, **5**, 519 (1972).

12) R. F. Weaver, K. V. Rajagopalan, P. Handler, D. Rosenthal, and P. W. Jeffs, *J. Biol. Chem.*, **246**, 2010 (1971).

13) W. Vetter, "Biochemical Applications of Mass Spectrometry," ed by G. R. Waller, Wiley-Interscience, New York (1972), p. 387.

14) E. C. Horning, *Org. Synth.*, Coll. Vol. III, 475 (1955).

Solvent Effects on Intramolecular Photocycloaddition of Poly(1-vinylnaphthalene)

Takao KAMIJO, Masahiro IRIE,* and Koichiro HAYASHI
The Institute of Scientific and Industrial Research, Osaka University, Suita, Osaka 565
(Received February 24, 1978)

Photocycloaddition reaction of naphthalene side groups in poly(1-vinylnaphthalene) was studied in cyclohexane, benzene, and dichloromethane. In cyclohexane the reaction proceeds following the first order kinetics to a high conversion of 70%, while in dichloromethane the reaction levels off at a very low conversion of 20%. The reaction behavior in benzene is intermediate between cyclohexane and dichloromethane. Quenching and sensitizing experiments proved that a triplet mechanism is predominant in cyclohexane, while in dichloromethane a singlet mechanism, presumably excimer mechanism, takes place. The solvent effect was interpreted by the formation of ground state dimer due to the conformational change of the polymer chain in poor solvents.

Photocycloaddition of aromatic compounds, in particular anthracene and acenaphthylene, is of interest from photochemical and photophysical points of view.[1] It has been assumed that the excimer state is the intermediate state in the formation of cyclodimers of anthracene derivatives.[2] Recently, experimental evidence of the mechanism has accumulated by use of a single crystal of the anthracene dimer[3] or the bichromophoric systems.[4]

In the case of photocycloaddition of acenaphthylene, however, other schemes have been proposed in addition to the singlet excimer mechanism[1f] *e.g.* bimolecular reaction between triplet state and ground state molecules, and pseudounimolecular photo-reaction of a ground state associated dimer. Although the latter unimolecular mechanism has attracted little attention[1e] because of the absence of the spectroscopic evidence of the postulated ground state dimer, it is worthwhile to reconsider this mechanism since several non-conjugated bichromophoric systems have recently been reported to undergo intramolecular cycloaddition *via* excitation of ground state complexes.[4,5]

In a previous paper[6] a report was given on spectroscopic evidence for the formation of a ground state dimer in poly(1-vinylnaphthalene) and 1,3-di-1-naphthylpropane in fluid and solid cyclohexane, respectively. This paper deals with the cycloaddition mechanism of naphthalene side groups in poly(1-vinylnaphthalene), especially the effect of solvent on the reaction, and a consideration on the role of the ground state dimer in the cycloaddition reaction. The intramolecular cyclodimerization of 1,3-di-1-naphthylpropane was also carried out as a model system of the polymer. These studies are expected to give valuable information on the precursors of the cycloaddition process of naphthalene and its homologes.[7]

Experimental

Preparation and purification methods of poly(1-vinylnaphthalene) have been described.[6] Cyclohexane and dichloromethane were of spectrograde. All samples were degassed by the freeze-pump-thaw-cycles under a reduced pressure less than 10^{-5} mmHg in the dark.

A super high pressure mercury lamp (1 kW) was used as a radiation source. Wavelengths longer than 280 nm were selected with a Toshiba UV-29 filter. Absorption and emission spectra were measured with a Shimadzu UV-200 spectrophotometer and a Hitachi MPF-2A spectrofluorometer, respectively.

Quantum yields of the cycloaddition reaction were determined with a chemical actinometer of potassium ferioxalate system. The mercury line of 297 nm was isolated with a grating monochrometer (Ritsu MC-20), the initial concentration being so controlled as to make the absorbance at 297 nm less than 0.1.

Results and Discussion

Photocycloaddition in Solutions. Poly(1-vinylnaphthalene) exhibits monomer, dimer, and excimer emissions in dichloromethane, while in cyclohexane a dimer emission becomes predominant, the excimer emission not being discerned.[6,8] This indicates that the dimer conformation is stable even in the excited state in cyclohexane, though the excimer conformation is favorable in dichloromethane. The absorption spectrum in cyclohexane also notably differs from the spectrum in dichloromethane, indicating the formation of the ground state dimer in a cyclohexane solution.[6] The conformation of the polymer in poor solvents is conceived to be more rigid as compared to conformation in good solvents, the conformational change in the excited state being restricted. On the other hand, higher mobility of the chain in good solvents makes it possible to attain the most stable conformation, an excimer conformation, in the excited state.

Photoillumination of poly(1-vinylnaphthalene) in the two solvents, cyclohexane and dichloromethane, results in a photochemical reaction of the naphthalene side groups. The photochemical reaction was followed by measurements of the absorption spectra of the naphthalene side groups in the 250—350 nm region (Figs. 1 and 2). In both cases the intensity of the absorption decreases with photoillumination.

Addition of a trace amount of trifluoroacetic acid to the illuminated sample restores the initial absorbance.[7a] The recovery indicates that the decrease in absorbance induced by photoillumination is due to the photocycloaddition of the naphthalene side groups as shown in the following:

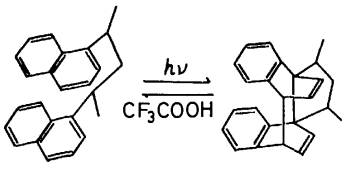

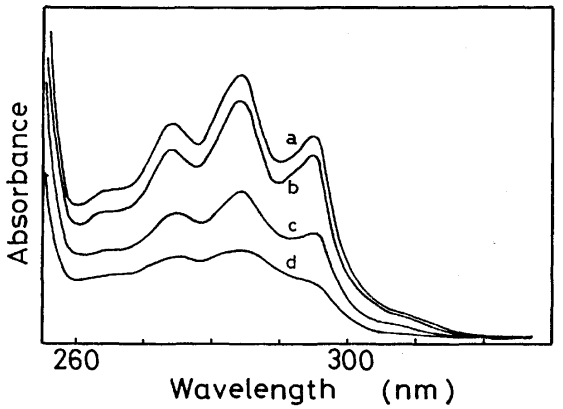

Fig. 1. Absorption spectra of poly(1-vinylnaphthalene) in cyclohexane before and after photoillumination by the light passed through Toshiba UV-29 filter ($\lambda >$ 280 nm) at 20 °C. Illumination times are (a) 0, (b) 0.2, (c) 11 and (d) 36 min. Initial concentration of poly(1-vinylnaphthalne) is 5×10^{-5} M.

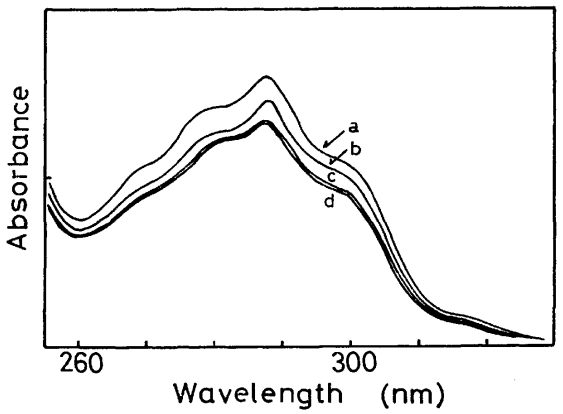

Fig. 2. Absorption spectra of poly(1-vinylnaphthalene) in dichloromethane before and after photoillumination at 20 °C. Illumination times are (a) 0, (b) 0.5, (c) 4 and (d) 20 min. Initial concentration of poly(1-vinylnaphthalene) is 5×10^{-5} M.

In order to confirm the cycloaddition reaction, NMR spectra of the sample were measured before and after photoillumination (Fig. 3). The intensity ratio of aromatic and vinyl protons to the alkyl proton is 2.23 before photoillumination, while it decreases to 1.64 after illumination for 3 h. The corresponding theoretical values before and after the cycloaddition should be 2.33 and 1.50, respectively. Although the values include some errors even before photoillumination probably due to chain end groups, the value after illumination is located between the initial and theoretical values. In addition to the above ratio the NMR spectrum after illumination shows a new peak at 6.1 τ attributable to methine proton.[7c] These results indicate that the photochemical reaction of poly(1-vinylnaphthalene) corresponds to the cycloaddition.

Figure 4 shows the relative changes in absorbance of naphthalene side groups in cyclohexane, dichloromethane and benzene during the course of photolysis. The photocycloaddition of 1,3-di-1-naphthylpropane in cyclohexane is also shown for the sake of comparison

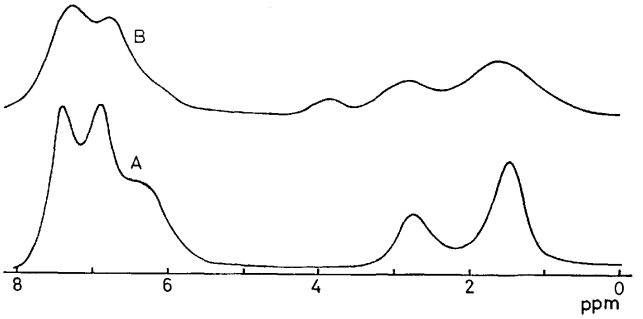

Fig. 3. NMR spectra of poly(1-vinylnaphthalene) (A) before and (B) after photoillumination for 3 h in benzene at 20 °C. $CDCl_3$ was used as a solvent.

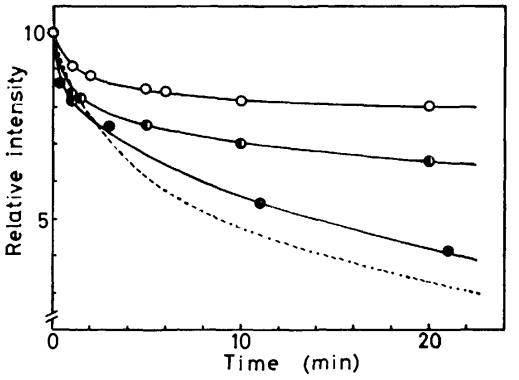

Fig. 4. Photocycloaddition of poly(1-vinylnaphthalene) in (○) dichloromethane, (◐) benzene and (●) cyclohexane and of 1,3-di-1-naphthylpropane (---) in cyclohexane at 20 °C. The reaction was followed by measurements of absorbance at 295 nm.

with the corresponding polymer system. In this experiment the concentrations of the polymer and 1,3-di-1-naphthylpropane were so controlled as to have the same absorbance at 297 nm. In cyclohexane the reaction proceeds following the first order kinetics except in the very early stage. The behavior is similar to the reaction of 1,3-di-1-naphthylpropane.[7c] This suggests that the cycloaddition of naphthalene side groups in cyclohexane occurs between the isolated dimer pairs, which are formed stably in the ground state. A statistical calculation predicts the degree of pairing of the side groups to be 84.46% when the side groups make a pair randomly.[9] In a real polymer system, however, the degree of pairing is naturally less than the theoretical prediction due to the conformational restriction. Thus, the conversion of 70% is explained by the dimerization of the naphthalene pairs formed in the ground state independent of each other.

On the other hand, in dichloromethane the reaction levels off at a very low conversion of *ca.* 20%. The flexibility of the polymer chain in dichloromethane makes the reaction possible between nonadjacent naphthalenes.[5] The reaction between the nonadjacent molecules presumably produces the macro-ring to make the polymer chain rigid. The regidity thus formed is considered to prevent the reaction between the residual side groups, giving rise to the low conversion.

The reaction behavior in benzene is intermediate between cyclohexane and dichloromethane. The

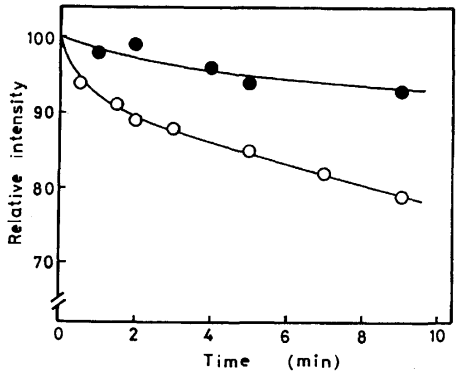

Fig. 5. Photocycloaddition reaction of poly(1-vinylnaphthalene) in cyclohexane in the absence (○) and in the presence (●) of 5×10^{-4} M of 1,3-pentadiene at 20 °C.

cycloaddition reaction proceeds up to 40% conversion but after that it levels off. The intensity of the dimer absorption in benzene is weaker than that in cyclohexane, though it is much higher than in dichloromethane. The higher conversion in benzene is attributable to the photo-reaction of the ground state dimers.

The quantum yields of cycloaddition by the mercury line of 297 nm were measured to be 0.04 and 0.02 in cyclohexane and dichloromethane, respectively, at 20 °C. The yield in dichloromethane is the value in the initial stage at 2×10^{-5} M, since it decreases with time and finally becomes very small after prolonged illumination. The higher value in cyclohexane indicates that the rigid dimer conformation is favorable to the cycloaddition reaction in comparison with the mobile conformation in dichloromethane.

Reaction Mechanism. The difference in the reaction behavior in cyclohexane and dichloromethane was further confirmed by quenching and sensitizing experiments. Figure 5 shows the effect of the addition of 1,3-pentadiene upon the cycloaddition reaction in cyclohexane. The reaction is suppressed by 1,3-pentadiene in cyclohexane. In this experiment very low concentration of 1,3-pentadiene (5×10^{-4} M) was adopted in order to avoid the addition reaction between the naphthalene side groups in the excited singlet state and 1,3-pentadiene.[10] In dichloromethane, however, no noticeable difference was observed in the reaction even in the presence of the same concentration of 1,3-pentadiene.[11] The quenching experiment confirmed that the solvent alters the reaction mechanism. In cyclohexane a triplet excited state is mainly responsible for the reaction. The reaction was suppressed not only by 1,3-pentadiene but also by oxygen which is a typical triplet quencher. Ineffectiveness of 1,3-pentadiene in dichloromethane suggests a singlet mechanism, since the triplet state of naphthalene is known to be effectively quenched by 1,3-pentadiene.

In order to substantiate the triplet mechanism in cyclohexane, the triplet sensitization by benzophenone was carried out as shown in Fig. 6. The reaction was followed by the fluorescence intensity of the naphthalene moiety. Decrease in intensity was observed even when the excitation wavelength was restricted to the

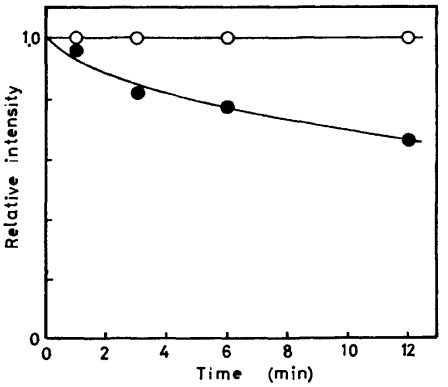

Fig. 6. Photosensitized cycloaddition of poly(1-vinylnaphthalene) in (●) cyclohexane and (○) dichloromethane in the presence of benzophenone by excitation wavelengths longer than 340 nm at 20 °C. The reaction was followed by measurements of the fluorescence intensity of the naphthalene moiety. The areas of the whole spectra plotted against wave number scale were compared.

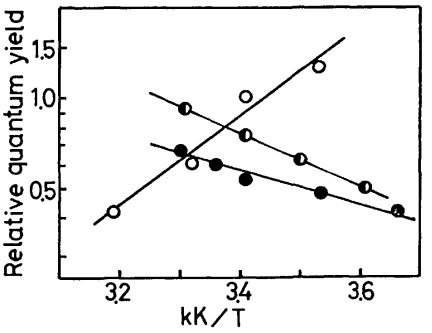

Fig. 7. Temperature dependence of relative quantum yields of photocycloaddition of poly(1-vinylnaphthalene) in (○) cyclohexane and (●) dichloromethane and of 1,3-di-1-naphthylpropane in cyclohexane(◐).

absorption of benzophenone ($\lambda>390$ nm). The decrease is not due to the reaction between a naphthyl side group and benzophenone, since the fluorescence of 1-methylnaphthalene retains the same intensity even after prolonged photoillumination in the presence of benzophenone. The result provides unambiguous evidence that the cycloaddition reaction in cyclohexane occurs in the triplet excited state.

On the other hand, the fluorescence intensity shows no decrease in a dichloromethane solution by photosensitization with benzophenone under identical conditions. The result confirms the singlet mechanism, presumably excimer mechanism, of the cycloaddition reaction in dichloromethane.

The temperature dependence of the quantum yield of cycloaddition is shown in Fig. 7. The slope in dichloromethane gave an activation energy of 2.0 kcal/mol, which is smaller than the value 4.3 kcal/mol for 1,3-di-1-naphthylpropane. The difference suggests that in this temperature range polymer chains assist the cycloaddition reaction. The enthalpy change associated with the excimer formation is conceived to be similar both in the polymer and 1,3-di-1-naphthylpropane, while the activation energy necessary to attain

the excimer conformation or dimer conformation is considered to depend on the chain length. The low activation energy in the polymer system indicates that the naphthyl side groups, which are in a favorable conformation to make the cyclodimer, react in the initial stage of the reaction in dichloromethane.

The temperature dependence in cyclohexane, on the other hand, gave a negative value of −5.7 kcal/mol. The reaction scheme in cyclohexane can be expressed as follows:

$$\mathrm{N} + \mathrm{N} \underset{k_m,}{\overset{k_d}{\rightleftharpoons}} (\mathrm{N{\cdot}N}) \quad (1)$$

$$(\mathrm{N{\cdot}N}) \xrightarrow{h\nu} {}^1(\mathrm{N{\cdot}N})^* \qquad I_0, \quad (2)$$

$${}^1(\mathrm{N{\cdot}N})^* \longrightarrow {}^3(\mathrm{N{\cdot}N})^* \qquad k_{ISC}, \quad (3)$$

$${}^1(\mathrm{N{\cdot}N})^* \longrightarrow \mathrm{N} + \mathrm{N} \qquad k_f + k_n, \quad (4)$$

$${}^3(\mathrm{N{\cdot}N})^* \longrightarrow \mathrm{N{-}N} \qquad k_D, \quad (5)$$

$${}^3(\mathrm{N{\cdot}N})^* \longrightarrow \mathrm{N} + \mathrm{N} \qquad k_p + k_n'. \quad (6)$$

Here, N, (N·N) and N–N are a naphthalene side group, an associated dimer and a photodimer, respectively. Equations 4 and 6 involve all deactivation processes in the excited singlet and triplet states, respectively. Using the steady-state approximation, the quantum yield of the cycloaddition reaction, Φ_D, is given by

$$\Phi_D = k_{ISC} \cdot k_D \cdot \tau_1 \cdot \tau_3 \cdot \frac{k_d \bar{\varepsilon}_d}{k_d \bar{\varepsilon}_d + k_m \bar{\varepsilon}_m},$$

where τ_1 and τ_3 are lifetimes of singlet and triplet excited states, respectively, $\bar{\varepsilon}_d$ and $\bar{\varepsilon}_m$ average extinction coefficients of dimer and monomer, respectively, at the excitation wavelength. The negative activation energy is attributable to τ_3 and $k_d\bar{\varepsilon}_d/(k_d\bar{\varepsilon}_d + k_d\bar{\varepsilon}_m)$, since other terms are insensitive or have positive temperature coefficient. The increase in the mobility of polymer chain at higher temperatures is considered to cause the decrease of the triplet state lifetime due to the increase in the rates of non-radiative deactivation processes and prevent the formation of cyclodimer, giving a low quantum yield.

References

1) *Cf. e.g.*, a) O. L. Chapman and K. Lee, *J. Org. Chem.*, **34**, 4166 (1969); b) R. Calas and R. Lalande, *Bull. Soc. Chim. Fr.*, 148 (1960); c) E. J. Bowen, *Adv. Photochem.*, **1**, 23 (1963); d) R. S. L. Shou, D. O. Cowan, and W. W. Schmiegel, *J. Phys. Chem.*, **79**, 2087 (1975); e) D. O. Cowan and J. C. Koziar, *J. Am. Chem. Soc.*, **97**, 249 (1975); f) R. Livingston and K. S. Wei, *J. Phys. Chem.*, **71**, 541 (1967).

2) R. L. Barnes and J. B. Birks, *Proc. R. Soc., London, Ser. A*, **291**, 570 (1966).

3) a) J. Ferguson and A. W. H. Man, *Mol. Phys.*, **27**, 377 (1974); b) J. Ferguson and S. E. H. Miller, *Chem. Phys. Lett.* **36**, 635 (1975).

4) N. Boens, M. De Brackeleire, J. Huybrechts, and F. C. De Schryver, private communication.

5) a) F. C. De Schryver, N. Boens, and J. Put, *Adv. Photochem.*, in press; b) F. C. De Schryver, J. Put, L. Leenders, and H. Loos, *J. Am. Chem. Soc.*, **96**, 6994 (1974).

6) M. Irie, T. Kamijo, K. Hayashi, M. Aikawa, T. Takemura, and H. Baba, *J. Phys. Chem.*, **81**, 1571 (1977).

7) a) J. S. Bradshaw and G. S. Hammond, *J. Am. Chem. Soc.*, **85**, 3953 (1963); b) T. W. Mattingly, Jr., J. E. Lancaster, and A. Zweig, *Chem. Commun.*, 595 (1971); c) E. A. Chandross and C. J. Dempster, *J. Am. Chem. Soc.*, **92**, 703, 704 (1970); d) J. S. Bradshaw, N. B. Nielsen, and D. P. Ress, *J. Org. Chem.*, **33**, 259 (1968).

8) Monomer emission signifies the fluorescence from isolated naphthalene side groups excited to its first excited singlet state. Dimer emission is the fluorescence emitted from an excited dimer produced by excitation of the associated dimer of the side groups with its conformation in the ground state essentially unchanged. Excimer signifies a kind of excited dimer the conformation of which is suitable for strong interaction in the excited state between the side groups but repulsive in the ground state. This conformation clearly differs from that of the associated dimer formed in the ground state.

9) P. J. Flory, *J. Am. Chem. Soc.*, **72**, 5052 (1950).

10) N. L. Yang, J. Libman, and M. F. Savitzky, *J. Am. Chem. Soc.*, **94**, 9227 (1972).

11) External heavy atom effect of the solvent is negligible. Dichloromethane scarcely alters the triplet lifetime of the polymer. Conversely, low viscosity of dichloromethane increases the collision frequency between the polymer and the quencher.

Oxidative Degradation of Polymers. VI. Photooxidation of Polystyrene Powder and Some Model Compounds

Takeo SHIONO,* Etsuo NIKI, and Yoshio KAMIYA
Department of Reaction Chemistry, Faculty of Engineering, The University of Tokyo, Hongo, Tokyo 113

(Received March 1, 1978)

The rates and products of photooxidation of polystyrene powder were studied at 70 °C under irradiation of a 30W low pressure mercury lamp. It was found that the rate of oxidation is remarkably high but the amount of oxygen incorporated into the polystyrene chain is very small. About a half of the absorbed oxygen appeared as carbon dioxide, independent of the conversion, irradiation time, oxygen pressure, and molecular weight. A trace amount of phenol was detected by GLC. The isotachophoretic analysis showed the formation of formic acid, oxalic acid, and glyoxylic acid. It was found that the mechanism of photooxidation is dependent on the state of the substrate, *i.e.*, crystalline solid, melt(viscous liquid) or solution. It is concluded that the polystyrene powder is photooxidized from its surface and aromatic ring of polystyrene is cleaved to give carboxylic acids. It was suggested that ozone played an important role in the photooxidation of polystyrene. The conclusions are supported by the results obtained in the photooxidation of some model compouds such as 1,2-diphenylethane, hexamethylbenzene, azobenzene, and phenylazotriphenylmethane.

Although it is accepted that the oxidation of polymers proceeds by a similar mechanism to that in the oxidation of simple hydrocarbons, the modes of polymer oxidation are complicated and need to be clarified.[1] Photochemical oxidation of polymers has been studied by numerous investigators mostly on films.[2,3] Formation of hydrogen molecule was observed when polystyrene films were irradiated with 253.7 nm light *in vacuo*.[4,5] On the other hand, water and carbon dioxide were found as the only volatile products in the photooxidation of polystyrene films at 28 °C with 253.7 nm light.[6] Rabek and Rånby[7] proposed a new mechanism in the photooxidation of polystyrene as film or in benzene, where the cleavage of benzene ring plays an important role in the reaction pathway. They suggested the contribution of singlet oxygen molecule as a reactive species.

We have found that isotactic polypropylene powder is oxidized quite rapidly by irradiation with a 30 W low pressure mercury lamp, approximately half of the oxygen absorbed appearing as carbon dioxide independent of the extent of oxidation.[8] As an extension we have studied the photooxidation of polystyrene powder using a low pressure mercury lamp as a light source. The principal object is to measure rates and products of oxidation with particular attention on the absorbed oxygen balance. Polystyrene powder has an advantage over polypropylene powder in that it is soluble in organic solvents, making analyses of the oxidized polystyrene easier than for polypropylene. The data on the quantitative product analyses are lacking, but they are apparently most needed for the understanding of the nature of the reaction. Photooxidation of several relevant model compounds has also been carried out in order to elucidate the mechanism of the photooxidation of polystyrene.

Experimental

Materials. Polystyrene powders obtained from Pressure Chemical Co. were used, the molecular weight being 4000, 9000, and 20400. 1,2-Diphenylehtane (mp 52.5 °C) and azobenzene (mp 58 °C) were recrystallized twice from ethanol and benzene, respectively. Reagent grade hexamethylbenzene powder was used. The electronic spectrum of azobenzene in benzene solution shows two distinct maximum transition regions at 318 and 435 nm in the π-π^* and n-π^*, respectively. Thus the azobenzene is trans.[9] Phenylazotriphenylmethane was used without futher purification. Commercial azobisisobutyronitrile(AIBN) and azobiscyclohexanecarbonitrile (ACN) were recrystallized from methanol and used as a radical initiator. Water was purified by passing through an ion-exchange resin.

A 30W low pressure mercury lamp was used as an ultraviolet light source, the main emission being the resonance lines of 184.9 and 253.7 nm.

Procedure. Fifty or one hundred mg polystyrene powder was weighed into a 50 ml quartz vessel. 10 ml of water was then introduced. The vessel was connected to a vacuum line and degassed by freeze and thaw cycles. Oxygen was then introduced. Amounts of initial and final gases were determined with use of a Toepler pump and by subsequent gas analysis by means of gas chromatography.[8]

After the oxidation and analysis of the final gases noncondensable at −80 °C had been carried out, the vessel was opened and the reaction mixture was filtered with a glass filter 1G-4. The polystyrene powder recovered was washed several times with water, dried in a vacuum at 70 °C, weighed, and then analyzed by IR, NMR,[10] gel permeation chromatography[11] and elemental analysis. The filtrate was analyzed by iodometric and neutralization titration. Low-boiling products were determined by gas liquid chromatography (GLC, Porapak-Q, 2 m, 50/80 mesh; PEG 20 M, 20 wt %, 7 m, 80/100 mesh). Low molecular weight acids were determined by isotachophoretic analysis with a Shimadzu Isotachophoretic analyzer IP-1B. Aqueous solution of 0.01 M gultamic acid was used as a terminal solution and aqueous solution containing 0.01 M L-histidine and 0.01 M L-histidine hydrochloride as a leading solution.

Results and Discussion

Photooxidation of Polystyrene Powder. The results of photooxidation of polystyrene powder of different molecular weight at different irradiation time are summarized in Table 1. Photooxidation was carried out under atmospheric pressure of oxygen. The rate of oxidation is remarkably great, the average rate of oxygen absorption being *ca.* 0.2 mol O_2/mol PS/h. The amount of oxygen absorbed per monomer unit of poly-

Table 1. Photooxidation of polystyrene powder at 70 °C in 10 ml water

Run No.	1	2	3	4	5	6	7	8	9
$[PS]_0$, μmol[a]	495	471	490	490	978	954	960	960	961
Molecular weight	4000	4000	4000	4000	4000	4000	4000	9000	20400
Time, h	1/6	1.5	3	6	1.5	3	4.5	3	3
ΔO_2, μmol	18	190	385	718	322	509	1013	554	436
$-dO_2/dt$, mol O_2/mol PS/h[b]	0.218	0.269	0.262	0.244	0.219	0.178	0.234	0.192	0.151
$\Delta O_2/[PS]_0$, mol/mol[c]	0.037	0.402	0.785	1.466	0.33	0.531	1.06	0.576	0.453
ΔCO_2, μmol	12	67	190	448	153	248	545	296	280
$\Delta CO_2/\Delta O_2$	0.67	0.36	0.49	0.62	0.48	0.49	0.54	0.54	0.64
PS recovery,[d] μmol		454	468	426	971		888	898	917
Calculated recovery,[e] μmol		463	466	434	960		892	892	925

a) Initial polystyrene by monomer unit. b) Average rate of oxygen absorption by polystyrene monomer unit. c) The amount of oxygen absorbed per monomer unit. d) Polystyrene powder recovered after oxidation. e) See text for calculation.

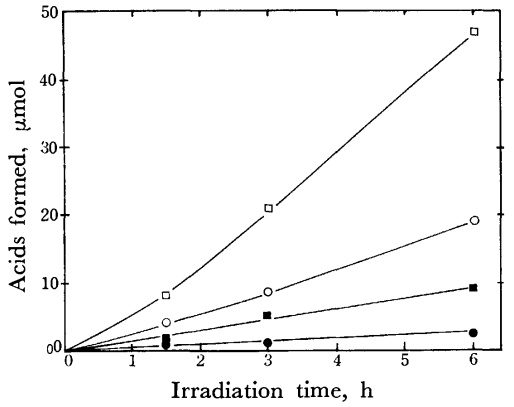

Fig. 1. Formation of carboxylic acids in the photooxidations of polystyrene powder (Runs 2, 3, and 4). □: Total acid, ○: formaic acid, ■: glyoxylic acid, ●: oxalic acid.

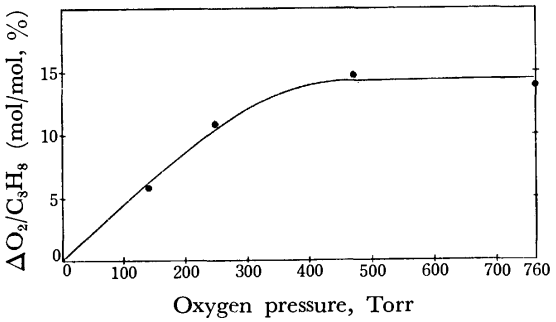

Fig. 2. Effect of oxygen pressure on the rate of photooxidation of polystyrene powder at 70 °C for 1 h.

styrene is as high as 0.80 mol/mol in 3 h and 1.50 mol/mol in 6 h (Runs 3 and 4). Nevertheless, approximately 90% of polystyrene powder could be recovered after photooxidation. This significance will be discussed later. About half of the absorbed oxygen was found as carbon dioxide. This is true even at 3.7% conversion, independent of irradiation time or the extent of oxidation. The effect of molecular weight of polystyrene is small both on rate and products of oxidation(Table 1).

It was found by isotachophoretic analyses that carboxylic acids such as formic, glyoxylic and oxalic acids

Table 2. Elemental analysis of initial and photooxidized polystyrenes

Run No.	Initial PS		2	3	4
	Calcd	Obsd			
C, %	92.26	92.16	91.60	90.31	91.00
H, %	7.74	8.06	8.06	8.01	8.05
O, %[a]	0		0.34	1.68	0.95
C/H	1/1.01	1/1.05	1/1.06	1/1.07	1/1.06
$\Delta O_2/C_8H_8$ obsd[b]			0.001	0.056	0.031
$\Delta O_2/C_8H_8$ calcd[c]			0.402	0.785	1.466

a) Oxygen content by difference. b) Calculated from the results of elemental analysis. c) Calculated from oxygen absorbed.

Table 3. Ratio of aromatic hydrogens in initial and photooxidized polystyrenes by ^{1}H-NMR

		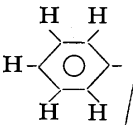	/	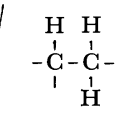
Initial PS	Calcd	1	/	0.600
	Obsd	1	/	0.616
Run 5		1	/	0.621
7		1	/	0.610

are formed and their amounts increase with increasing irradiation time (Fig. 1). Hydroperoxide and hydrogen peroxide were also detected by iodometric titration in the presence and absence of catalase: for example, 6.8 μmol(2.1% based on absorbed oxygen) and 30.5 μmol(9.5%), respectively in Run 4. A trace amount of phenol was also found by GLC analysis.

The rate of oxidation increases with increasing oxygen pressure up to 400 Torr, further increase in oxygen pressure showing little effect(Fig. 2). Even at low oxygen pressures, carbon dioxide is the only gaseous product, about a half of the oxygen absorbed appearing as carbon dioxide.

Figure 3 shows the relation between conversion and the ratio of carbon dioxide formed to the oxygen absorbed. Although there is some scatter of data, the yield of carbon dioxide is approximately 50% of

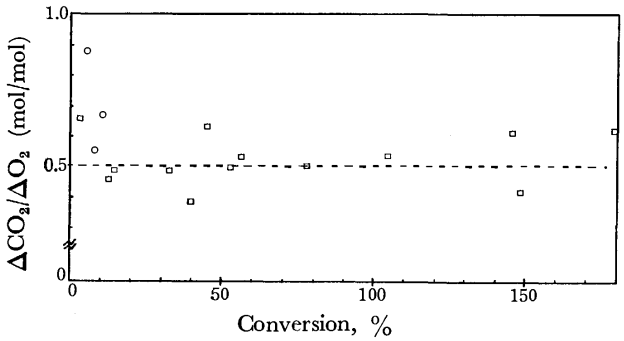

Fig. 3. Relation between $\Delta CO_2/\Delta O_2$ and conversion in the photooxidation of polystyrene powder. □: Po_2=1 atm, ○: Po_2=reduced pressure.

the absorbed oxygen independent of conversion.

The results of elemental analyses of the initial and photooxidized polystyrene powders are summarized in Table 2. Although the amount of oxygen absorbed per monomer unit is quite high, the amount of oxygen incorporated into the polymer chain is exceedingly small, the ratio of carbon to hydrogen remaining constant. For example, 0.4 mol oxygen is absorbed per monomer unit, but little oxygen remained in the polystyrene(Run 2).

The ratio of aromatic to aliphatic proton for the initial and photooxidized polystyrenes obtained by integration of proton NMR spectra is given in Table 3. About 100 mg of polystyrene powder with molecular weight 4000 was used for analysis. The conversion based on monomer unit was 33 and 106% for 1.5 and 4.5 h irradiation, respectively. The ratio of aromatic to aliphatic proton remains constant.

Figure 4 shows the gel permeation chromatograms of initial and photooxidized polystyrene with molecular weight of 4000. Molecular weight distribution was shifted by oxidation to higher fractions rather than to

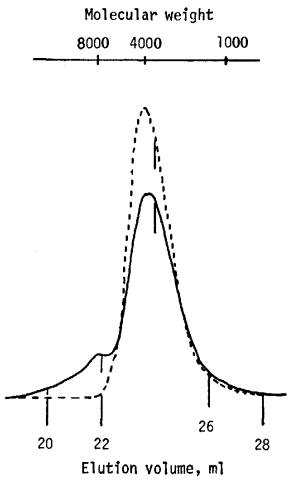

Fig. 4. Gel permeation chromatograms of photooxidized polystyrene powder. Molecular weight: 4000. ----: Initial polystyrene, ——: photooxidized polystyrene.

lower fractions. Similar results were obtained for polystyrene with molecular weight of 9000 and 20400. The results indicate that crosslinking prevails over chain scission.

The results of photooxidation of polystyrene powder observed differ remarkably from those of thermal[12,13] or even γ-ray[14] oxidation of polystyrene at moderate temperature, where the major products are hydroperoxide, benzaldehyde and acetophenone with little carbon dioxide or carbon monoxide.

Oxidation of Model Compounds. In order to clarify the nature of the photooxidation of polystyrene powders, the photooxidation of several relevant model compounds was performed under similar conditions. 1,2-Diphenylethane and hexamethylbenzene were used as model compounds for aromatic hydrocarbons containing benzylic hydrogen(Table 4) while azobenzene

TABLE 4. OXIDATION OF 1,2-DIPHENYLETHANE(DPE) AND HEXAMETHYLBENZENE

Run No.	10	11	12	13	14	15	16	17[c]
DPE	Crystal[a]	Crystal[a]	Melt[b]	Solution	Solution	Solution	Solution	Powder
μmol	505	502	520	1118	1050	1928	1935	635
Solvent	Water	Water	Water	Benzene	Benzene	Benzene	PhCl	Water
ml	10	10	10	5	5	3	3	10
Initiator						AIBN	ACN	
μmol						136	135	
Temp, °C	30	30	70	30	70	70	90	30
Time, h	1/6	2	2	2	2	4	4	2
Oxidation	Photo	Photo	Photo	Photo	Photo	Thermal	Thermal	Photo
ΔO_2, μmol	73	481	661	251	257	162	244	257
ΔO_2/DPE	0.14	0.96	1.27	0.22	0.24	0.08	0.13	0.40
ΔN_2, μmol	0	0	0	0	0	83	83	0
ΔCO_2, μmol	29	229	176	51	17	0	0	120
$\Delta CO_2/\Delta O_2$	0.40	0.48	0.27	0.20	0.07	0	0	0.48
ΔCO, μmol	0	0	60	90	107	0	0	0
Total acid, μmol		99	195	20	40	12	22	85[d]
Total peroxide, μmol		31	77	6	6	75	82	29

a) DPE crystal floating on the water surface. b) Viscous liquid of DPE floating on the water surface.
c) Hexamethylbenzene. d) 9.6 μmol formic acid and 50.8 μmol acetic acid were observed.

Table 5. Photo and thermal oxidation of azobenzene and PAT

Run No.	18	19	20	21	22
Substrate, RH	Azobenzene	Azobenzene	PAT	PAT	PAT
Substrate, μmol	515	515	297	502	1375
Solvent	Water[a)]	Water[b)]	Water[a)]	Benzene	Benzene
[RH], M				0.167	0.458
Oxidation	Photo	Photo	Photo	Thermal	Thermal
Temp, °C	30	70	30	70	70
Time, h	2	2	2	2	3
ΔN_2, μmol	30	42	44	527	1477
ΔO_2, μmol	178	509	221	532	802
ΔCO_2, μmol	96	234	72	0	0
ΔCO, μmol	0	4	0	5	Trace
$\Delta CO_2/\Delta O_2$	0.54	0.46	0.33	0	0
Recovered RH, μmol	483	433	284		
Total acid, μmol	29[c)]	90[d)]	56[e)]		
Peroxide, μmol	16	81			
Carbonyl, μmol	Trace	Trace			

a) Substrate floating on the water surface. b) At 70 °C, azobenzene is a viscous liquid and forms a thin layer on the water surface. c) Formic acid 14, glyoxylic acid 3, and oxalic acid 4 μmol. d) Formic acid 48, glyoxylic acid 12, oxalic acid 3, 2,4-hexadienedioic acid 6 μmol. e) Formic acid 34, glyoxylic acid 10, oxalic acid 4, 2,4-hexadienedioic acid 2 μmol.

and phenylazotriphenylmethane were used as model compounds that give phenyl radical(Table 5).

1,2-Diphenylethane is a crystal at 30 °C, its photooxidation proceeding rapidly, and absorbs approximately equimolar oxygen in 2 h(Table 4, Run 11). The most striking result is that carbon dioxide is formed as a major product, its yield being as high as 40% of oxygen absored in spite of low reaction temperature and low conversion(Run 10). Essentially the same results were obtained at higher conversion (Run 11). After the photooxidation of 1,2-diphenylethane crystal, the reaction mixture was filtered and the recovered 1,2-diphenylethane washed and dried in a vacuum. The recovered diphenylethane was found to be identical with the initial, unoxidized 1,2-diphenylethane by GLC, NMR, IR, and elemental analyses. However, the formation of carbon dioxide decrease as 1,2-diphenylethane changes from crystal to melt and to solution, whereas the formation of carbon monoxide increase. The thermal oxidation initiated by AIBN or ACN gave neither carbon dioxide nor carbon monoxide and the major product was peroxide, the reaction being typical autoxidation. From the results of photooxidation of hexamethylbenzene powder (Table 4), oxidation is seen to be similar to that of polystyrene and 1,2-diphenylethane crystal. The rate is high, about half of the oxygen absorbed appearing as carbon dioxide. Carboxylic acids were another major product (33% based on oxygen uptake). Formation of acetic and formic acids suggests the cleavage of aromatic ring.

Azobenzene powder(515 μmol) was floated on the water surface and irradiated with a low pressure mercury lamp at 30 °C under atmospheric pressure of oxygen (Run 18). After 2 h, 178 μmol oxygen was absorbed and 30 μmol nitrogen and 96 μmol carbon dioxide evolved. The isotachophoretic analysis of the aqueous phase showed the presence of 14 μmol formic acid, 3 μmol glyoxylic acid, and 4 μmol oxalic acid. These acids account for three quarters of the total acid observed by titration. After the oxidation was over, the powder floating on the water surface was collected, washed, and dried at room temperature in a vacuum. 483 μmol Azobenzene was recovered, 99.6% of nitrogen being accounted for. The NMR, UV, IR, and elemental analyses for the recovered azobenzene gave identical results with those of the initial azobenzene. Thus, azobenzene should cleave photolytically to give nitrogen and phenyl radicals, which cleave to give eventually acids, carbon dioxide and other products.

The photooxidation of azobenzene was also carried out at 70 °C(Run 19). Azobenzene becomes a viscous liquid when warmed to 70 °C, forming a thin layer on the water surface. The nitrogen evolution did not increase appreciably with rise in temperature from 30 to 70 °C. However, the amount of oxygen absorption at 70 °C was about three times as much as that at 30 °C. This can be ascribed partly to the phase change but mostly to the temperature difference. The temperature did not affect the product distribution, 46% of absorbed oxygen being found as carbon dioxide.

Phenylazotriphenylmethane(PAT) was oxidized either photochemically or thermally. Photooxidation was carried out with solid PAT, and thermal oxidation in benzene solution. The results show that considerable carbon dioxide was formed by photochemical oxidation, while in contrast, none was observed by thermal oxidation even at higher conversion(Table 5).

Mechanism and Active Species in the Photooxidation of Polystyrene Powder. Polystyrene powder is oxidized remarkably fast by irradiation with a 30 W low pressure mercury lamp. Approximately half of the oxygen absorbed gives carbon dioxide even at low temperature and low conversion. The yield for carbon dioxide remains constant independent of the extent of oxidation.

TABLE 6. PHOTOOXIDATION OF POLYSTYRENE WITH AND WITHOUT H_2O FILTER[a]

Run No.	23		24	
PS,[b] μmol	960		978	
H_2O, ml	10		10	
H_2O filter	Yes		No	
Temp, °C	24		24	
Time, h	9		9	
ΔO_2, μmol	298		882	
ΔO_2/PS, %	31		90	
ΔCO_2, μmol	81		404	
$\Delta CO_2/\Delta O_2$, %	27		46	
ΔCO, μmol	37		0	
Recovery, μmol	923		910	
Peroxide, μmol	5		149	
Total acid,[c] μmol	80		130	
Formic acid, μmol	40		45	
Glyoxylic acid, μmol	15		16	
Oxalic acid, μmol	3	68 μmol (85%)	21	92 μmol (71%)
Malealdehyde, μmol	7		6	
Maleic acid and/or 2,4-hexadienedioic acid, μmol	3		4	

a) 2.3 cm H_2O filter was placed between light source and quartz cell(3 cm). b) By monomer unit, molecular weight=4000. c) By titration.

That the photooxidation of polystyrene powder takes place exclusively on its surface is supported by the following results: (1) the oxygen incorporated into polymer chain is quite small in spite of high oxygen uptake(Table 2), and (2) much of the powders of polystyrene, azobenzene, PAT and 1,2-diphenylethane is recovered after photooxidation.

If we assume that one styrene monomer unit yields eight molecules of carbon dioxide and four molecules of water, then the remaining polystyrene is estimated by

$$\text{Calculated recovery } (\%) = 100 \times \frac{[PS]_0 - \Delta CO_2/8}{[PS]_0},$$

where $[PS]_0$ is the initial amount of polystyrene and ΔCO_2 is carbon dioxide formed. As shown in Table 1, the calculated recovery agrees well with the observed recovery. On the other hand, if we assume that aromatic carbons are not oxidized to carbon dioxide and only two molecules of carbon dioxide are formed from one monomer unit, the agreement between calculated and observed recoveries is poor.

Formation of low molecular weight carboxylic acids and the importance of crosslinking observed in this study indicate the contribution of ozone, since they resemble the ozonation of polystyrene[10] and aromatic compounds.[15] 184.9 nm light converts oxygen molecule into ozone,[16] which is decomposed to $O(^1D)$ and singlet oxygen molecule by 253.7 nm light.[17] Since 184.9 nm light is absorbed by air, it was first assumed that only monochromatic 253.7 nm light would be introduced into the vessel.

In order to study the effect of wavelength of the incident light and contribution of ozone, photooxidation

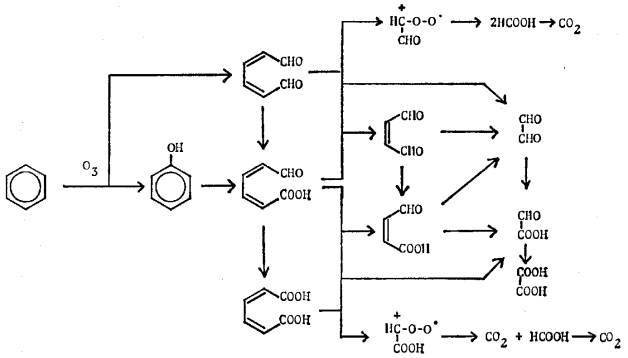

Fig. 5. Ozonation of aromatic ring. Substituents are neglected.

was carried out in the presence and absence of a water filter placed between light source and quartz vessel. The main emission of the light source is the resonance lines of 184.9 and 253.7 nm. The former should be absorbed by water. The results of photooxidation of polystyrene powder with and without a water filter are given in Table 6. We see that the water filter decreases both rate of oxidation and formation of carbon dioxide.

It should be noted that photooxidation of polystyrene gives formic acid, glyoxylic acid, oxalic acid, malealdehyde, and maleic acid and/or 2,4-hexadienedioic acid. The products are similar to the ozonation products from aromatic compounds,[10,15] strongly indicating the contribution of ozone in the cleavage of aromatic ring.[18] These products should be formed according to the scheme shown in Fig. 5. The formation of ozone in the reaction vessel was confirmed by passing the gas through an aqueous solution of potassium iodide.

However, it is not clear how carbon dioxide is formed in as high as 50% yield and why the yield decreases when the state of substrate changes from solid to melt and to solution.

Conclusion

Polystyrene powder was found to be oxidized rapidly when irradiated with a low pressure mercury lamp. The major product was carbon dioxide with approximately 50% yield based on oxygen absorbed. The yield is independent of irradiation time, oxygen pressure and molecular weight. The molecular weight did not decrease appreciably by oxidation, crosslinking being observed instead. Formic acid and other low molecular weight carboxylic acids were also observed. It was suggested that ozone plays an important role as an active species, especially in the cleavage of aromatic ring.

The authors are grateful to the Shimadzu Seisakusho for permission to use their isotachophoretic analyzer.

References

1) Y. Kamiya and E. Niki, "Aspects of Degradation and Stabilization of Polymers," ed by H. H. G. Jellinek, Elsevier, Amsterdam (1977), Chap. 3.

2) N. S. Allen and J. F. McKellar, *Chem. Soc. Rev.*, **4**,

533 (1975); F. H. Winslow, *Pure Appl. Chem.*, **49**, 495 (1977).

3) B. Rånby and J. F. Rabek, "Photodegration, Photooxidation and Photostabilization of Polymers," Wiley, London (1975).

4) N. Grassie and N. A. Weir, *J. Appl. Polym. Sci.*, **9**, 975 (1965).

5) N. A. Weir, *J. Appl. Polym. Sci.*, **17**, 401 (1973).

6) N. Grassie and N. A. Weir, *J. Appl. Polym. Sci.*, **9**, 987 (1965).

7) J. F. Rabek and B. Rånby, *J. Polym. Sci., Polym. Chem. Ed.*, **12**, 273(1974.)

8) T. Shiono, E. Niki, and Y. Kamiya, *J. Jpn. Petrol. Inst.*, **21**, 63(1978).

9) H. Zollinger, "Azo and Diazo Chemistry, Aliphatic and Aromatic Compounds," Interscience, New York (1961); J. Griffiths, *Chem. Soc. Rev.*, **1**, 481 (1972).

10) T. Saito, E. Niki, T. Shiono, and Y. Kamiya, *Bull. Chem. Soc. Jpn.*, **51**, 1153 (1978).

11) T. Shiono, E. Niki, and Y. Kamiya, *J. Appl. Polym. Sci.*, **21**, 1635 (1977).

12) Le Khac Bi and Y. Kamiya, *J. Polym. Sci., Part A-1*, **7**, 1131 (1969).

13) G. A. George and D. K. C. Hodgeman, *Eur. Polym. J.*, **13** 63 (1977).

14) C. Crouzet and J. Marchal, *Makromol. Chem.*, **177**, 2819 (1976).

15) T. Saito, E. Niki, and Y. Kamiya, unpublished results.

16) J. G. Calvert and J, N. Pitts, "Photochemistry," John Wiley & Sons,, New York, N. Y. (1966), p. 782.

17) I. T. N. Jones and R. P. Wayne, *Proc. R. Soc. London, Ser, A*, **319**, 273 (1970); I. T. N. Jones, U. B. Kaczmar, and R. P. Wayne, *ibid.*, **316**, 431 (1970); I. T. N. Jones and R. P. Wayne, *ibid.*, **321**, 409 (1971).

18) Recently, Weir[19] reported that the reaction of hydroxy radical with polystyrene induces cleavage of the aromatic ring to give mucondialdehydes.

19) N. A. Weir, *Eur. Polym. J.*, **14**, 9(1978).

A New Synthesis of L-4-Amino-2-hydroxybutyric Acid. Carboxyl-Assisted Nitrile Synthesis from Primary Amides

Toshio YONETA,* Seiji SHIBAHARA, Shunzo FUKATSU, and Shigeo SEKI

Central Research Laboratories, Meiji Seika Kaisha, Ltd., Morooka-cho, Kohoku-ku, Yokohama 222

(Received March 11, 1978)

L-2-Hydroxysuccinamic acid prepared from L-asparagine was dehydrated with acetic anhydride in pyridine, affording the respective ω-cyano acid, which, on catalytic hydrogenation, gave the title compound. Similarly, the amide groups of some other β- and γ-amic acids were dehydrated to give the respective cyano acids in good yields.

Butirosin B,[1,2] an antibiotic produced by *Bacillus circulans*, is a derivative of ribostamycin acylated with the title acid (**1**) at the C-1 amino group of the 2-deoxystreptamine moiety, and it is active against ribostamycin- and kanamycin-resistant organisms, including *Pseudomonas* strains. Kawaguchi *et al.*[3] synthesized amikacin (BB-K8) by the condensation of kanamycin A with **1** at the C-1 amino group of the deoxystreptamine moiety. Amikacin is also active against kanamycin-resistant organisms. On the basis of these facts, **1** is presumed to be a valuable amino acid in chemical-modification studies of amino-sugar antibiotics.

Although **1** had previously been synthesized by the partial deamination of L-2,4-diaminobutyric acid[2,4] or by the Hofmann degradation of L-2-hydroxyglutaramic acid[5] prepared from L-glutamine, we have searched for other potential methods which might be more convenient and adequate for large-scale perparation. We wish now to describe a three-step synthesis of **1** using L-asparagine as the starting material.

L-Asparagine was first converted to L-2-hydroxysuccinamic acid (**2**) by treatment with sodium nitrite.[6] Then we attempted to transform the amide group of **2** into the nitrile group without the protection of the other functional groups. Among several known dehydration methods of primary amides into nitriles, *p*-toluenesulfonyl chloride–pyridine[7] or trifluoroacetic abhydride–pyridine[8] methods were assumed to be adequate. However, the treatment of **2** with these reagents according to the described procedures afforded no cyano derivatives, but only a tarry product. Pyriadi *et al.*[9] reported that *N*-alkylmaleamic acids were easily converted to 4-(alkylimino)-2-butenolides with an acetic anhydride–triethylamine or acetyl chloride–triethylamine mixture. This fact prompted us to consider that the 3-iminophthalide produced from primary amide and carboxylate by the above methods might be convertible to nitrile and carboxyl groups as is shown in Scheme 1. As expected, the treatment of ammonium phthalamate (**3**) with two equivalents of acetic anhydride in pyridine afforded the *o*-cyanobenzoic acid (**5**) as a single product. Under similar conditions, benzamide was not converted to benzonitrile, but was recovered unchanged. Judging from these experimental results, the reaction is likely to proceed through the intermediary 3-iminophthalide (**4**), as is shown in Scheme 1. Indeed, the treatment of **2** with acetic anhydride in pyridine at room temperature afforded L-2-acetoxy-3-cyanopropionic acid (**6**). The hydrogenation of **6** with platinum oxide in aqueous ethanol under acidic conditions afforded **1** in a 30% yield form L-asparagine. As **6** was unstable,[10,11] the structure was confirmed as that of the corresponding benzhydryl ester (**7**).

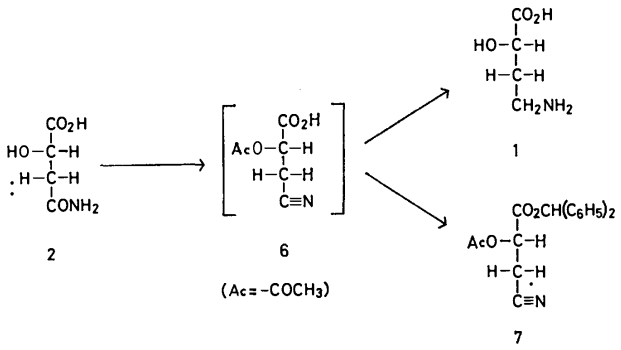

Scheme 2.

In order to extend this dehydration reaction further, we treated N^2-benzyloxycarbonyl-L-asparagine with acetic anhydride in pyridine. The product isolated in an 83% yield was identical with authentic *N*-benzyloxycarbonyl-3-cyano-L-alanine (**8**).[13] Similary, N^2-benzyloxycarbonyl-L-glutamine gave L-2-(benzyloxycarbonylamino)-4-cyanobutyric acid (**9**) in a good yield as a thick syrup. The hydrogenation of **9** gave ornithine and a trace amount of proline, both of which were identified by paper chromatography.[13]

The mild conditions, easy dehydration, and reasonable yields of **5**, **6**, **8**, and **9** indicate that this dehydration method would be useful for the synthesis of various β- and γ-cyano carboxylic acids.

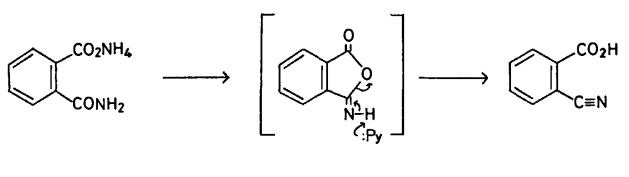

Scheme 1.

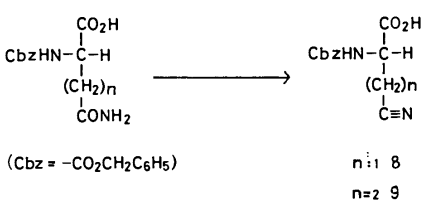

Scheme 3.

Experimental

The melting points are uncorrected. The optical rotation were measured with a Perkin-Elmer Model 241 polarimeter. The NMR spectra were recorded at 60 MHz with a Varian S-60T spectrometer.

o-Cyanobenzoic Acid (5). A solution of ammonium phthalamate (**3**) (165 mg) and acetic anhydride (0.2 ml) in pyridine (4 ml) was kept at room temperature for 1 h. Almost all of the solvent was then removed by evaporation under reduced pressure, and the residue was diluted with ethyl acetate (15 ml). The resulting solution was washed with 1M-hydrochloric acid and a saturated aqueous sodium chloride solution, and dried over sodium sulfate. The solution was subsequently concentrated to give a white powder (105 mg). Recrystallization from ethyl acetate afforded a white granule of **5** (72 mg); mp 227—228 °C (lit,[10] mp 226—230 °C); IR (KBr): 1690 (COOH) and 2240 cm^{-1} (CN).

Found: C, 65.19; H, 3.50; N, 9.78%. Calcd for $C_8H_5NO_2$: C, 65.30; H, 3.43; N, 9.52%.

L-4-Amino-2-hydroxybutyric Acid (1). A solution of L-2-hydroxysuccinamic acid (**2**)[6] (532 mg) and acetic anhydride (1.5 ml) in pyridine (15 ml) was kept at room temperature for 1 h. The solution was then concentrated to thick syrup under reduced pressure. The resulting crude L-2-acetoxy-3-cyanopropionic acid (**6**) was dissolved in a mixture of ethanol (20 ml), water (5 ml), and concd hydrochloric acid (1 ml), and hydrgenated with platinum oxide (50 mg) for 6 h under a pressure of 3 atm. After the removal of the catalyst, the filtrate was concentrated to a thick syrup, which was dissolved in water (10 ml) and chromatographed on Dowex 50W-X4 resine (H^+ form). After being washed with water, the column was developed with 0.5M-ammonium hydroxide. The eluted fraction was concentrated to give a crude compound, **1** (291 mg). This was dissolved in a mixture of methanol (9.6 ml) and water (2.3 ml) and then stored at 5 °C overnight. The crystals thus precipitated were collected and dried. 177 mg (37.2%); mp 197—198.5 °C, $[\alpha]_D^{25}$ −28.2° (*c* 1.2, water) (lit, mp 203—206 °C,[2] 200—200.5 °C,[4] $[\alpha]_D^{25}$ −28.2° (*c* 1.22, water),[2] −29.1° (*c* 1.0, water)[4]); NMR (D_2O): δ 1.97 (2H, m, CH_2), 3.16 (2H, t, N-CH_2), 4.16 (1H, q, C<u>H</u>(OH)COOH).

Found: C, 40.27; H, 7.65; N, 12.01%. Calcd for $C_4H_9NO_3$: C, 40.33; H, 7.62; N, 11.76%.

Benzhydryl L-2-Acetoxy-3-cyanopropionate (7). To a solution of crude **6**, obtained from **2**, (775 mg) as described for **1**, in acetone (16 ml), we added diazodiphenylmethane[12] (2 g) in acetone (6 ml). The solution was then allowed to stand at room temperature for 2 h. After working up with acetic acid, almost all of the solvent was removed under reduced pressure, and the residue was diluted with benzene (50 ml). The resulting solution was washed with water and dried over sodium sulfate. The solution was concentrated to *ca.* one-fifth in volume, and this residue was chromatographed on silica gel. Subsequent elution with benzene–ethyl acetate (50:1) afforded a thick syrup of **7** (1.5 g, 84%) on evaporation, $[\alpha]_D^{25}$ −36.3° (*c* 1.2, methanol); NMR ($CDCl_3$) : δ 2.13 (3H, s, $COCH_3$), 2.85 (2H, d, CH_2CN), 5.37 (1H, t, C<u>H</u>($OCOCH_3$)), 6.87 (1H, s, $CH(C_6H_5)_2$), 7.30 (10H, s, C_6H_5). IR (KBr): 2260 cm^{-1} (CN). Found: *m/e* 323.1163. Calcd for $C_{19}H_{17}NO_4$: M, 323.1157.

N-Benzyloxycarbonyl-3-cyano-L-alanine (8). A solution of N^2-benzyloxycarbonyl-L-asparagine (2.66 g). in acetic anhydride (1.2 ml) and pyridine (30 ml) was kept at room temperature for 1 h. The solution was then concentrated to a thick syrup under reduced pressure, and the residue was diluted with 1M-hydrochloric acid to give colorless needles of **8** (2.05 g, 83%). Recrystallization from 1,2-dichloroethane afforded pure **8**; mp 129—131.5 °C, $[\alpha]_D^{25}$ −18.7° (*c* 1.27, methanol) (lit,[13] mp 131—134 °C, $[\alpha]_D^{25}$ −19.0° (*c* 1.25, methanol)); IR (KBr): 1745 (COOH) and 2280 cm^{-1} (CN); NMR (C_5D_5N–D_2O): δ 3.43 (2H, d, CH_2CN), 5.11 (1H, t, C<u>H</u>(COOH)).

Found: C, 58.33; H, 4.91; N, 11.23%. Calcd for $C_{12}H_{12}N_2O_4$: C, 58.05; H, 4.88; N, 11.29%.

L-2-(Benzyloxycarbonylamino)-4-cyanobutyric Acid (9). A solution of N^2-benzyloxycarbonyl-L-glutamine (1 g) in acetic anhydride (0.44 ml) and pyridine (15 ml) was kept at room temperature overnight. Most of the solvent was then removed under reduced pressure, and the residue was diluted with elthyl acetate (50 ml). The solution was washed with 1M-hydrochloric acid and a saturated aqueous sodium chloride solution, and then dried over sodium sulfate. The solution was concentrated to *ca.* 5 ml, which quantity was chromatographed over silica gel. Elution with chloroform–methanol (5 : 1) afforded a thick syrup of **9** (855 mg, 91%) on evaporation, $[\alpha]_D^{25}$ −12.5° (*c* 1.18, methanol); IR (film): 2245 cm^{-1} (CN). Found: *m/e* 262.0931. Calcd for $C_{13}H_{14}N_2O_4$: M, 262.0953.

The hydrogenation of this compound with palladium on charcoal in the presence of hydrochloric acid led to ornithine and proline, the structure of which were confirmed by paper chromatography.

References

1) P. W. K. Woo, H. W. Dion, G. L. Coffey, S. A. Fusari, and G. Senos, Ger. Offen., 1914527 (1969).
2) P. W. K. Woo, H. W. Dion, and O. R. Bartz, *Tetrahedron Lett.*, **1971**, 2617.
3) H. Kawaguchi, T. Naito, S. Nakagawa, and K. Fujisawa, *J. Antibiot.*, **25**, 695 (1972).
4) Y. Horiuchi, E. Akita, and T. Ito, *Agric. Biol. Chem.*, **40**, 1649 (1976).
5) T. Naitoh *et al.*, Japan Patent 504019 (1975).
6) T. Miyazawa, E. Akita, and T. Ito, *Agric. Biol. Chem.*, **40**, 1651 (1976).
7) M. Zaoral and J. Rudinger, *Collect. Czech. Chem. Commun.*, **24**, 1933 (1959).
8) F. Campagna, A. Carotti, and G. Gassini, *Tetrahrdron Lett.*, **1977**, 1813.
9) T. M. Pyriadi and H. J. Harwood, *J. Org. Chem.*, **36**, 821 (1971).
10) S. Wideqvist, *Arkiv. Kemi.*, **2**, 383 (1950).
11) S. Wideqvist, *Arkiv. Kemi.*, **3**, 281 (1951).
12) J. R. Adamson, R. Bywood, D. T. Eastlick, G. Gallagher, D. Walker, and E. M. Wilson, *J. Chem. Soc., Perkin Trans. 1*, **1975**, 2030.
13) M. Wilcheck, S. Ariely, and A. Patchornik, *J. Org. Chem.*, **33**, 1258 (1968).

The Crystal and Molecular Structure of Dichlorobis(2-pyridinethiolato)tin(IV)

Mitsuo MASAKI,* Satoshi MATSUNAMI, and Hideo UEDA†

Polymer Research Laboratory, Ube Industries, Ltd., Minami-Kaigan, Goi, Ichihara, Chiba 290

†*Central Research Laboratory, Ube Industries, Ltd., Nishihon-Machi, Ube, Yamaguchi 755*

(Received March 16, 1978)

The crystal and molecular structures of dichlorobis(2-pyridinethiolato)tin(IV) have been determined by X-ray analysis. The crystal belongs to the triclinic system: $a=8.340(8)$, $b=12.456(7)$, $c=7.178(3)$ Å, $\alpha=86.46(4)$, $\beta=111.06(5)$, $\gamma=99.18(6)°$, space group $P\bar{1}$ with $Z=2$. The structure was determined by the heavy atom method and refined by the block-diagonal least-squares method ($R=0.058$). The complex is a distorted octahedral complex in which 2-pyridinethiolato ligands act as bidentate ligands, two four-membered (Sn, S, C, and N) chelate rings being present. Two Sn–Cl bonds are *cis*, two Sn–N bonds are *cis*, and two Sn–S bonds are *trans* configuration.

The synthesis of dichlorobis(2-pyridinethiolato)-tin(IV) (**1**) and its possible structures were described in a previous report.[1] Complex (**1**) is very stable. However, bis(benzenethiolato)dichlorotin(IV)[1] or dichlorobis(4-pyridinethiolato)tin(IV)[2] could not be isolated probably because of its instability. On the basis of IR spectral observation[1] the stability of complex (**1**) is ascribed to the intramolecular four-membered chelate ring formation for the six-coordination of the tin atom.

2-Pyridinethiolato ligand acts as a uni- or bi-dentate or a bridging ligand in rhodium,[3] iridium,[4] and ruthenium(II)[5,6] complexes.

This paper describes the crystal and moleuclar structures of **1** obtained by X-ray analysis: octahedral structure with four-membered chelate ring condensed with pyridine ring.

Experimental

Dichlorobis(2-pyridinethiolato)tin(IV) (**1**) was prepared by the reaction of di-2-pyridyl disulfide and tin(II) chloride in benzene in the presence of perhydroazepin-2-one.[1] The crystal for the X-ray analysis was obtained by recrystallization from acetonitrile solution.

The crystal system was determined as triclinic from the oscillation and Weissenberg photographs. The density was measured by the flotation method in an aqueous solution of ZnI_2. The unit-cell parameters were determined by the least-squares method, using 20 reflections carefully measured on a Syntex model $P2_1$ four-circle diffractometer with graphite-monochromatized Mo $K\alpha$ radiation ($\lambda=0.71069$ Å). The intensity data were collected on a diffractometer with the 2θ-ω scanning mode ($2\theta\leqq50°$). The variable-scan method was used, the minimum and maximum scan rates being 1° and 24° min^{-1}, respectively. Background was counted for half the scan time on each side of a reflection. The size of the crystal was $0.2\times0.1\times0.4$ mm. In order to confirm the stability of the crystal and the counting system, the intensities of three standard reflections were measured every 99 reflections. The standard reflections were stable to 1.0% from their mean values. Neither absorption nor extinction correction was made. This might reduce the accuracy of the structure obtained.

TABLE 1. CRYSTAL DATA

$C_{10}H_8Cl_2N_2S_2Sn$
M. W.: 409.91
Crystal system: $P\bar{1}$; $Z=2$
$a=8.340(8)$, $b=12.456(7)$, $c=7.178(3)$ Å,
$\alpha=86.46(4)$, $\beta=111.06(5)$, $\gamma=99.18(6)°$
$D_m=1.992$, $D_c=2.000$ g·cm^{-3}

Determination and Refinement of the Structure

The structure was determined by the heavy atom method. The coordinates of the tin atom were obtained from the Patterson map. Other atoms were found by successive Fourier synthesis. Refinement of the structure was performed by the block-diagonal least-squares method with 2209 independent reflections of $|F_o|\geqq3\sigma$. The final refinement was carried out with anisotropic thermal parameters for all the atoms. The strongest reflections at low scattering angles were omitted from the refinement in order to exclude extinction effects. The R-index converged to 0.058 with an equal weight for each reflection. The atomic scattering factors were taken from the International Tables for X-Ray Crystallography.[7] The program ORTEP coded by Johnson[8] was used for drawing Figs. 1 and 2. The observed and calculated structure factors are given in Table 2.[9]

Results and Discussion

The positional and thermal parameters with their standard deviations are given in Tables 3 and 4, respectively. The molecular structure for **1** and the numbering scheme of atoms are shown in Fig. 1. Bond lengths and bond angles with their standard deviations are given in Tables 5 and 6, respectively. The tin atom is six-coordinated and two 2-pyridinethiolato ligands act as bidentate ligands, forming two four-membered (Sn, S, C, and N) chelate rings. Two Sn–Cl bonds are of *cis* configuration as suggested by IR spectral data.[1] Two Sn–N bonds are of *cis* and two Sn–S bonds are of *trans* configurations.

Deviations of ligand atoms from several least-squares planes are given in Table 7. Considerable deviations are observed from the mean plane (A) of five atoms (Sn, two Cl, and two N atoms), mean plane (B) of five atoms [Sn, Cl(1), N(1), and two S atoms], and mean plane (C) of five atoms [Sn, Cl(2), N(2), and two S atoms]. The angles of three pairs of *trans* bondings, Cl(1)–Sn–N(1), Cl(2)–Sn–N(2), and S(1)–Sn–S(2) are 161.1, 162.9, and 154.2°, respectively. The data show a distorted octahedral structure of **1**.

The lengths of C–S bonds of two 2-pyridinethiolato ligands in **1** are greater than the C–S bond of 2(1*H*)-pyridinethione (1.68 Å),[10] while the lengths of C–N bonds in the ligands are samller than the C–N bond length in 2(1*H*)-pyridinethione (1.39 Å).[10] This suggests that the ligands act as bidentate ligands forming four-membered chelate rings. The same phenomena have been observed for the corresponding ruthenium complex.[5a]

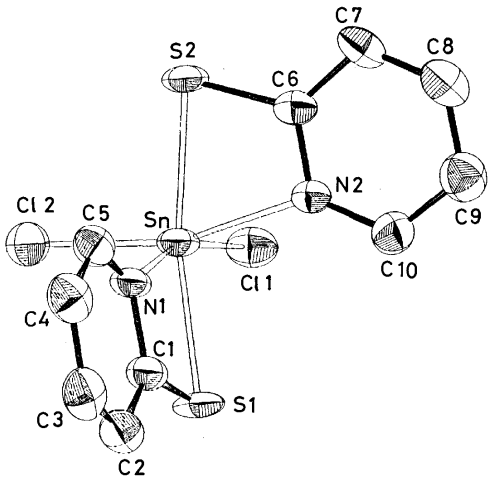

Fig. 1. The molecular structure for **1** and the numbering scheme of atoms. The ellipsoid encloses the region in which the center of the atom is found with probability 50%.

The bond lengths of two Sn–S bonds and two Sn–N bonds in **1** are nearly equal to the lengths of Sn–S bond [2.496(1) Å] and Sn–N bond [2.217(3) Å], respectively, in [2-[[(2-mercaptophenyl)imino]methyl]-phenolato]diphenyltin(IV), in which sulfur and nitrogen atoms are bonded to the tin atom forming five-membered chelate ring.[11] On the other hand, the lengths of two Sn–S bonds and two Sn–N bonds in **1** are smaller than those of the Sn–S bond [2.576(7) Å] and the Sn–N bond [2.62(2) Å], respectively, in triphenyl(4-pyridinethiolato)tin(IV), which has a polymeric structure formed by the intermolecular bridging through the nitrogen atom of the pyridine ring.[12] This suggests that two 2-pyridinethiolato ligands are bonded to the central tin atom through both nitrogen and sulfur atoms.

The deviation of S(1) atom from plane (D) of the pyridine ring [C(1—5) and N(1)] is 0.07 Å and that of S(2) from plane (E) of the pyridine ring [C(6—10) and N(2)] is 0.03 Å (Table 7). The sulfur atom lies practically on the same plane as the pyridine ring plane to which the atom is bonded. The deviations

Table 3. Atomic coordinates and their standard deviations

	x	*y*	*z*		*x*	*y*	*z*
Sn	0.2796(1)	0.2354(1)	0.0323(1)	C(3)	0.7090(16)	0.1216(10)	0.6520(18)
Cl(1)	0.2124(3)	0.3237(3)	−0.2869(4)	C(4)	0.5413(16)	0.1048(10)	0.6677(17)
Cl(2)	0.1955(4)	0.0560(3)	−0.1005(5)	C(5)	0.4064(15)	0.1344(9)	0.5063(16)
S(1)	0.5961(3)	0.2586(3)	0.1085(5)	C(6)	0.1265(12)	0.3752(9)	0.1894(16)
S(2)	0.0174(3)	0.2446(3)	0.1093(4)	C(7)	0.0605(15)	0.4546(10)	0.2573(17)
N(1)	0.4322(10)	0.1780(7)	0.3428(13)	C(8)	0.1648(17)	0.5528(11)	0.3098(19)
N(2)	0.2831(10)	0.3936(7)	0.1720(13)	C(9)	0.3311(17)	0.5739(11)	0.2932(19)
C(1)	0.5920(13)	0.1967(9)	0.3292(16)	C(10)	0.3873(14)	0.4906(10)	0.2245(18)
C(2)	0.7364(14)	0.1657(10)	0.4888(17)				

Table 4. Anisotropic thermal factors[a] ($\times 10^4$) and their standard deviations

	B_{11}	B_{22}	B_{33}	B_{12}	B_{23}	B_{31}
Sn	65(1)	55(1)	173(2)	24(1)	−21(1)	82(2)
Cl(1)	120(5)	78(3)	179(6)	48(5)	19(6)	87(9)
Cl(2)	148(5)	56(2)	244(8)	12(5)	−54(7)	141(10)
S(1)	60(4)	80(3)	240(8)	27(5)	14(7)	125(9)
S(2)	67(4)	65(3)	240(7)	7(5)	−55(7)	132(9)
N(1)	70(13)	51(7)	197(22)	26(15)	−36(19)	77(27)
N(2)	81(13)	46(7)	183(21)	24(15)	−10(18)	82(27)
C(1)	89(16)	51(9)	206(27)	19(18)	−52(24)	86(34)
C(2)	104(18)	59(10)	202(28)	30(21)	−48(25)	−11(36)
C(3)	168(23)	57(10)	198(29)	27(24)	−51(26)	−21(41)
C(4)	181(24)	61(10)	183(27)	38(24)	−49(26)	83(41)
C(5)	156(21)	52(9)	179(26)	30(21)	−37(23)	165(38)
C(6)	86(16)	56(9)	172(25)	31(19)	4(22)	78(32)
C(7)	149(21)	68(10)	187(27)	88(23)	−33(25)	104(38)
C(8)	180(24)	70(11)	246(33)	88(26)	−14(29)	126(46)
C(9)	181(25)	65(11)	228(31)	34(25)	−27(28)	116(45)
C(10)	125(20)	54(10)	235(30)	16(21)	−6(26)	88(39)

a) The anisotropic thermal factors are of the form $\exp\{-(h^2B_{11}+k^2B_{22}+l^2B_{33}+hkB_{12}+hlB_{31}+klB_{23})\}$.

Table 5. Bond lengths and their standard deviations

Sn-Cl(1)	2.396(3) Å	Sn-Cl(2)	2.382(3) Å
Sn-S(1)	2.467(3)	Sn-S(2)	2.462(3)
Sn-N(1)	2.271(9)	Sn-N(2)	2.256(9)
S(1)-C(1)	1.729(12)	S(2)-C(6)	1.751(12)
N(1)-C(1)	1.352(15)	N(1)-C(5)	1.337(15)
N(2)-C(6)	1.340(15)	N(2)-C(10)	1.356(16)
C(1)-C(2)	1.420(17)	C(2)-C(3)	1.342(18)
C(3)-C(4)	1.425(19)	C(4)-C(5)	1.372(18)
C(6)-C(7)	1.394(17)	C(7)-C(8)	1.369(19)
C(8)-C(9)	1.416(20)	C(9)-C(10)	1.386(19)

Table 6. Bond angles and their standard deviations

Cl(1)-Sn-Cl(2)	94.8(1)°	Cl(1)-Sn-S(1)	95.6(1)°
Cl(1)-Sn-S(2)	101.6(1)	Cl(1)-Sn-N(1)	161.1(3)
Cl(1)-Sn-N(2)	89.6(3)	Cl(2)-Sn-S(1)	100.7(1)
Cl(2)-Sn-S(2)	96.9(1)	Cl(2)-Sn-N(1)	93.2(3)
Cl(2)-Sn-N(2)	162.9(3)	S(1)-Sn-S(2)	154.2(1)
S(1)-Sn-N(1)	66.2(3)	S(1)-Sn-N(2)	95.3(3)
S(2)-Sn-N(1)	94.1(3)	S(2)-Sn-N(2)	66.0(3)
N(1)-Sn-N(2)	87.7(3)	Sn-S(1)-C(1)	81.8(4)
Sn-S(2)-C(6)	81.9(4)	Sn-N(1)-C(1)	98.1(7)
Sn-N(1)-C(5)	140.1(8)	C(1)-N(1)-C(5)	121.8(10)
Sn-N(2)-C(6)	100.0(7)	Sn-N(2)-C(10)	138.8(8)
C(6)-N(2)-C(10)	121.1(10)	S(1)-C(1)-N(1)	113.9(8)
S(1)-C(1)-C(2)	126.4(9)	N(1)-C(1)-C(2)	119.8(11)
C(1)-C(2)-C(3)	117.9(11)	C(2)-C(3)-C(4)	122.0(12)
C(3)-C(4)-C(5)	117.0(12)	N(1)-C(5)-C(4)	121.4(11)
S(2)-C(6)-N(2)	112.2(8)	S(2)-C(6)-C(7)	125.7(9)
N(2)-C(6)-C(7)	122.1(11)	C(6)-C(7)-C(8)	116.9(12)
C(7)-C(8)-C(9)	121.9(13)	C(8)-C(9)-C(10)	117.7(13)
N(2)-C(10)-C(9)	120.2(12)		

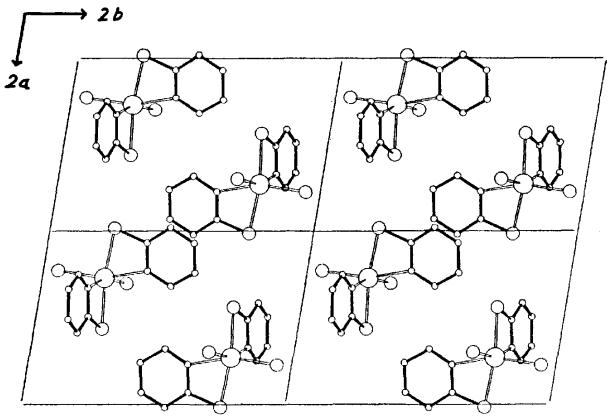

Fig. 2. The crystal structure of **1**.

of tin atom from planes (D) and (E) are 0.12 and 0.16 Å, respectively. The values of deviation seem to be comparatively small. This is supported by the fact that eight atoms [C(1—5), N(1), S(1), and Sn] are nearly on plane (F) within a deviation of 0.07 Å. The deviations of eight atoms [C(6—10), N(2), S(2), and Sn] from the mean plane (G) are also small (Table 7). This is in line with the IR spectral observation that the absorption bands due to pyridine ring vibrations and C–H out of plane bending vibrations in **1** appear in

Table 7. Deviations of ligand atoms from least-squares plane

Plane A: Sn, Cl(1), Cl(2), N(1), N(2)
$0.9866X-0.0019Y-0.3939Z-2.2135=0$

Sn	−0.009 Å	Cl(1)	0.339 Å	Cl(2)	−0.322 Å
N(1)	0.371	N(2)	−0.379		

Plane B: Sn, Cl(1), N(1), S(1), S(2)
$-0.0281X+0.9179Y+0.3659Z-2.9247=0$

Sn	−0.214	Cl(1)	−0.028	N(1)	−0.090
S(1)	0.177	S(2)	0.155		

Plane C: Sn, Cl(2), N(2), S(1), S(2)
$0.0078X-0.4128Y+0.8442Z+0.8144=0$

Sn	−0.183	Cl(2)	−0.070	N(2)	−0.149
S(1)	0.181	S(2)	0.220		

Plane D: C(1), C(2), C(3), C(4), C(5), N(1)
$-0.1132X+0.9186Y+0.4109Z-2.6490=0$

C(1)	0.014	C(2)	−0.007	C(3)	−0.004
C(4)	0.009	C(5)	−0.002	N(1)	−0.009
Sn[a]	−0.124	S(1)[a]	0.067		

Plane E: C(6), C(7), C(8), C(9), C(10), N(2)
$0.1308X-0.3423Y+0.8259Z+0.3438=0$

C(6)	0.005	C(7)	−0.003	C(8)	0.003
C(9)	−0.004	C(10)	0.005	N(2)	−0.006
Sn[a]	−0.164	S(2)[a]	−0.032		

Plane F: C(1), C(2), C(3), C(4), C(5), N(1), S(1), Sn
$-0.1395X+0.9223Y+0.4134Z-2.5394=0$

C(1)	0.009	C(2)	−0.042	C(3)	−0.032
C(4)	0.017	C(5)	0.034	N(1)	0.020
S(1)	0.060	Sn	−0.064	Cl(1)[a]	0.080
S(2)[a]	0.575				

Plane G: C(6), C(7), C(8), C(9), C(10), N(2), S(2), Sn
$0.1492X-0.3651Y+0.8099Z+0.4770=0$

C(6)	0.029	C(7)	−0.019	C(8)	−0.031
C(9)	−0.016	C(10)	0.033	N(2)	0.040
S(2)	0.022	Sn	−0.058	Cl(2)[a]	−0.118
S(1)[a]	0.674				

a) Omitted from the least-squares plane calculation.

a higher spectral region than those in di-2-pyridyl disulfide, suggesting the depletion of π-electron density of the pyridine ring.[1] The four-membered chelate ring condensed with the pyridine ring seems to be stabilized by mesomeric effect. The results support the assumption that the stability of **1** is based on the intramolecular chelation for six-coordination of the tin atom.[1]

The crystal structure is shown in Fig. 2. Intermolecular contacts are normal.

References

1) M. Masaki and S. Matsunami, *Bull. Chem. Soc. Jpn.*, **49**, 3274 (1976).
2) M. Masaki and S. Matsunami, unpublished results.
3) R. W. Mitchell, J. D. Ruddick, and G. Wilkinson, *J. Chem. Soc., A*, **1971**, 3224.

4) I. P. Evans and G. Wilkinson, *J. Chem. Soc., Dalton Trans.*, **1974**, 946; C. K. Brown, D. Georgiou, and G. Wilkinson, *ibid.*, **1973**, 929.

5) (a) S. R. Fletcher and A. C. Skapski, *J. Chem. Soc., Dalton Trans.*, **1972**, 635; (b) P. Powell, *J. Organomet. Chem.*, **65**, 89 (1974).

6) J. D. Gilbert and G. Wilkinson, *J. Chem. Soc., A*, **1969**, 1749.

7) "International Tables for X-Ray Crystallography," Birmingham, Kynoch press (1974), Vol. IV, pp. 72—98.

8) C. K. Johnson, ORTEP, Report ORNL-3794, Oak Ridge National Laboratory, Tennessee, 1965.

9) Table 2 is kept at the office of the Chemical Society of Japan, Kanda, Surugadai, Chiyodaku, Tokyo. (Document No. 7834).

10) B. R. Penfold, *Acta Crystallogr.*, **6**, 707 (1953).

11) H. Preut, H. J. Haupt, F. Huber, R. Cefalu, and R. Barbieri, *Z. Anorg. Allg. Chem.*, **407**, 257 (1974).

12) N. G. Bokii, Yu. T. Struchkov, D. N. Kravtsov, and E. M. Rokhlina, *Zh. Strukt. Khim.*, **14**, 502 (1973).

The Effect of Surfactants and β-Cyclodextrin on the Photooxidation of Stable Carbanions

Kazutoshi YAMADA,* Kiyoshi SHIGEHIRO, Tetsuo TOMIZAWA, and Hirotada IIDA

Department of Industrial Chemistry and Synthetic Chemistry, Faculty of Engineering, Chiba University, Yayoi-cho, Chiba 280

(Received March 27, 1978)

The micellar effect on the photochemistry of α-(4-hydroxyimino-2,5-cyclohexa-dienylidene)-α-phenylacetonitrile and its derivatives has been studied. 4-Nitrobenzophenone derivatives were obtained by the irradiation of ethanolic alkaline aqueous solutions of the oximes. 4-Nitrosobenzophenone derivatives formed as an intermediate were thermally oxidized to give the corresponding nitro compounds. The reaction was found to be the photochemical oxidation by singlet oxygen. The addition of an anionic surfactant (sodium dodecyl sulfate) and a nonionic surfactant (Tween #80) to the reaction solution scarcely changed the pK_a values of oximes, whereas the addition of a cationic surfactant such as hexadodecyltrimethylammonium bromide (HTAB) caused a considerable decrease. This indicates that HTAB promotes the formation of a stable carbanion. The presence of HTAB enhanced the rate of photooxidation by a factor of 10^2. The catalytic effect becomes maximum at the pH value of the reaction solution near the pK_a measured in the presence of HTAB or β-CDX.

Various chemical reactions modeled to the specific enzymatic interactions have been carried out in recent years. The reactions in certain aqueous micellar systems and the kinetics of organic reactions have been dealt with as a model for the enzymatic interaction. In the photooxidation of chlorophyll-a the addition of a nonionic sufactant to the reaction solution increased the rate of photooxidation ($k_{obsd}/k_0=21$).[1] Luciferin has been found to be chemiluminescent in the presence of a micellar cationic surfactant, but not in an anionic ones.[2] Cationic surfactants enhance the stability of anions, and anionic ones stabilize cations by forming micelles with them.

Minch *et al.*[3] reported that (4-nitrophenyl)phenyl acetonitrile is converted into the stable carbanion form in an aqueous alkaline solution, the addition of HTAB to this solution greatly enhancing the formation of its carbanion. In order to study the micellar effects on the photochemical reactions of the ionic species, carbanions, we used the derivatives of α-(4-hydroxyimino-2,5-cyclohexadienylidene)-α-phenylacetonitrile (**1**) which dissociate to form stable carbanion in alkaline solution. The synthetic method of these oximes was reported by Davis and his co-workers.[4] They also reported that the hydrogen peroxide oxidation of these oximes in methanolic alkaline solution gives 4-nitrobenzophenones. This paper provides

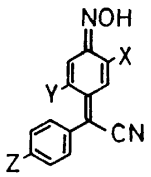

Compd	1	2	3	4	5	6	7	8	9	10
X	H	H	CH_3	CH_3	Cl	Cl	Cl	H	H	CH_3
Y	H	H	CH_3	CH_3	Cl	Cl	H	CH_3	Cl	H
Z	H	Cl	H	Cl	H	Cl	H	Cl	H	H

Chart.

detailed information on the photooxidation of stable carbanions formed by the ionization of the oxime compounds, and the catalytic effects of various surfactants (hexadecyltrimethylammonium bromide (HTAB), sodium dodecyl sulfate (SDS), Tween #80, and β-cyclodextrin (β-CDX)). The kinetic has also been studied.

Results and Discussion

Photoreaction of Oxime Derivatives. 4-Nitrobenzophenone derivatives and its dimers (4,4'-diaroylazoxybenzenes) were obtained as photoreaction products by irradiation of an ethanolic alkaline aqueous solution of oximes **1** and **2**. The structures of products were determined by comparison of mp, NMR and mass spectra with those of authentic samples. The photooxidation was carried out by irradiating an ethanolic alkaline aqueous solution of the oxime with a high pressure mercury lamp under aerobic conditions. The photooxidation was followed by means of UV spectroscopy (Fig. 1). The maximum absorbance of the oxime **1** at 405 nm decreased during the course of irradiation, a new maximum having an isosbestic point at 334 nm appearing at 288 nm. The maximum at 288 nm shifted to 264 nm which corresponds to that of 4-nitrobenzophenone. A new small absorbance corresponding to that of the dimer of oxime appeared at 345 nm together with one at 264 nm. The shift of

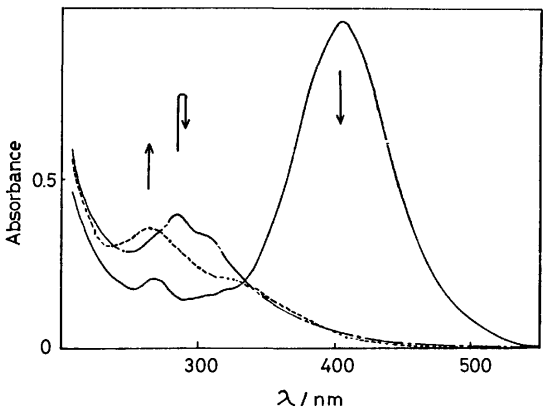

Fig. 1. Spectra of a 10% ethanolic aqueous buffer solution (pH 9.20) of oxime **1**. ——: Before irardiation, ———: after 80 min of irradiation, ---: after 240 min of irradiation.

the maximum at 288 nm to 264 was observed both under irradiation and in the dark. The first band appearing at 288 nm agrees very closely with the characteristic absorbance (λ_{max} 283 nm) of nitrosobenzene. 4-Nitrosobenzophenone seems to be formed as an intermediate.

Source of the Oxidizing Agent. Photochemical oxidation with oxygen is known in bioorganic chemistry. Chlorophyll-a was photooxidized by a molecular oxygen.[1] The photooxidation of bilirubin proceeds with singlet oxygen, bilirubin acting as a sensitizer to form singlet oxygen. As a source of energy to form the highly reactive species, singlet oxygen, the triplet dye was recognized in many oxygenation reactions.[6] The mechanism of the present photooxidation is considered as that of the photooxidation of bilirubin.

Table 1. Effect of β-CDX and HTAB on the visible spectra[a]

Compd	λ_{max} nm	λ_{max}^{CDX} [b] nm	λ_{max}^{HTAB} [c] nm
1	371, 407	372, 417	378, 440
2	376, 418	377, 423	377, 435
3	368, 413	368, 416	369, 424
4	369, 419	370, 420	372, 433
5	369, 418	372, 428	372, 448
6	378, 441	378, 442	379, 455
7	375, 415	375, 417	377, 433
8	371, 414	373, 417	373, 436
9	374, 420	377, 423	377, 440
10	374, 417	376, 417	377, 433

a) A left line of λ_{max}; in neutral solution. A right line of λ_{max}; in alkaline solution. b) In 2.81×10^{-3} M β-CDX. c) In 10^{-2} M HTAB.

Table 2. Effect of β-CDX and HTAB on the acid dissociation of oximes

Compd	pK_a	$\Delta pK_{a\,CDX}$[a]	$\Delta pK_{a\,HTAB}$[b]
1	8.60	0.24	1.44
2	9.36	0.30	1.07
3	10.10	0.32	0.51
4	9.88	0.08	0.60
5	8.01	0.30	1.61
6	7.99	0.08	1.00
7	8.33		0.98
8	9.09		1.40
9	7.88		0.94
10	9.23		0.56

a) $pK_a - pK_{a\,CDX}$; in 5×10^{-3} M β-CDX. b) $pK_a - pK_{a\,HTAB}$; in 10^{-2} M HTAB.

Table 3. Effect of SDS and Tween #80 on the acid dissociation of oximes

Compd	$\Delta pK_{a\,SDS}$[a]	$\Delta pK_{a\,Tween}$[b]
1	−0.48	−0.12
2	0.53	0.32

a) $pK_a - pK_{a\,SDS}$; in 10^{-2} M SDS. b) $pK_a - pK_{a\,Tween}$; in 6.6×10^{-2} g/dl Tween #80.

The photooxidation proceeds extremely slowly in the absence of oxygen. In the presence of β-carotene (1.27×10^{-5} M), which is a singlet oxygen quencher,[7] the quantum yield of the reaction decreases by a factor of 5. However, it increases considerably in the presence of Rose Bengal (7.70×10^{-6} M), a photosensitizer to form singlet oxygen,[6a] by a factor of 12. In the presence of a free radical inhibitor such as 2,6-di-*t*-butylphenol (up to 1×10^{-2} M),[6a,8] the reaction is not suppressed. It is obvious that the reaction is photochemical oxidation by singlet oxygen.

The Effect of Surfactant on Visible Spectra. Remarkable micellar effects of HTAB are observed in the visible spectra of the oxime. The addition of HTAB to the neutral and alkaline solution containing the oxime causes a red shift of the λ_{max} values for the neutral and anion form of the oxime. A similar effect was also observed on addition of β-CDX. The λ_{max} values for the neutral and anion forms of the oxime in 25—10% ethanolic water, aqueous HTAB, and β-CDX are given in Table 1.

The Effects of Surfactants on the pK_a Value. The pK_a values determined in 25—10% ethanolic aqueous solution with and without surfactants are given in Tables 2 and 3. The pK_a values of all oximes decrease when the micellar concentration of HTAB is used. This is also the case for β-CDX. On the other hand, the pK_a values of the oximes are random in the case of SDS and Tween #80. The decrease in the pK_a values results from the stabilization of the anion form of the substrates, arising from (a) an electrostatic interaction with cationic head groups of HTAB and the anion form, and (b) an electron delocalization by the hydrogen bond between an adjacent hydroxyl group of β-CDX and an oxygen atom of 4-nitroso group of the substrate which forms 1:1 inclusion complex with β-CDX.

Effects of Surfactants on Quantum Yields. The quantum yields of the catalytic action of the HTAB (Φ_2) in the photooxidation of oximes were analyzed by means of a modified form of Lineweaver-Burk equation.[14] Φ_0 and Φ_{obsd} are the quantum yields for the formation of oxidized products in the absence and presence of the HTAB. The quantum yield (Φ_2) increased by a factor of 370 in the presence of

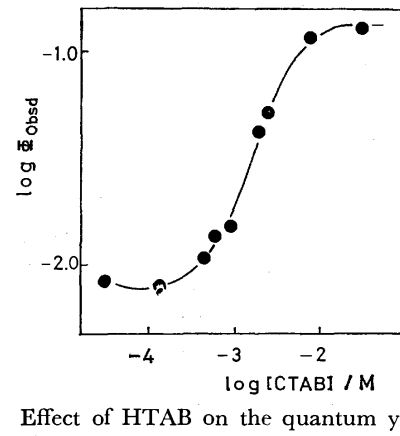

Fig. 2. Effect of HTAB on the quantum yield for the photooxidation of 5.18×10^{-5} M of oxime **1** in 10% ethanolic aqueous buffer (pH 7.31).

TABLE 4. THE QUANTUM YIELDS AND ASSOCIATION CONSTANTS FOR THE PHOTOOXIDATION OF **1** IN THE PRESENCE OF HTAB AND β-CDX

Surfactant	HTAB[a)]	β-CDX[c)]
$\Phi_0 \times 10^4$	1.66	77.7
$\Phi_{obsd}^{max} \times 10^3$	62.4[b)]	9.67[d)]
$\Phi_2 \times 10^2$	3.64	1.03
Φ_{obsd}^{max}/Φ_0	370	1.24
Φ_2/Φ_0	220	1.33
$K \times 10^{-2}/M^{-1}$	327	4.16

a) In 20% ethanolic buffer (pH 7.31, H_3BO_3-NaCl). b) [HTAB]$=3\times10^{-2}$ M. c) In 20% ethanolic water (0.01 M NaOH). d) [β-CDX]$=7\times10^{-3}$ M.

TABLE 5. THE RELATIVE RATE CONSTANTS AND ASSOCIATION CONSTANTS OF THE COMPOUNDS HAVING CHLORO-SUBSTITUENT[a)]

Compd	X	Y	Z	k_0	k_{obsd}[b)]	k_2	K	k_2/k_0
1	H	H	H	1.0	1.0	1.0	1.0	1.0
7	Cl	H	H	1.2	1.1	1.5	0.032	1.2
9	H	Cl	H	0.045	0.025	0.046	0.0079	1.0
2	H	H	Cl	0.65	0.76	0.76	0.47	1.2

a) In 25% ethanolic buffer (pH 9.20). b) In the presence of 10^{-2} M of HTAB.

HTAB (1×10^{-2} M). The critical micellar concentration (CMC) of HTAB in the photooxidation of **1** is estimated to be 6×10^{-4} M from the plot of $\log \Phi_{obsd}$ *vs.* $\log C_D$(surfactant concentration) as shown in Fig. 2. The quantum yield of this photooxidation becomes maximum at the surfactant concentration of 10^{-2} M. The value of Φ_{obsd} varies with the concentration of β-CDX, reaching maximum at a certain concentration. Such a phenomenon is characterized in the enzyme reaction which follows Michaelis-Menten kinetics. A general mechanism involving the micell-substrate complex similar to that used for an enzymatic catalysis[9] was applied. The effect of HTAB and β-CDX at a particular pH value was examined according to the Scheme (Experimental), using a technique worked out by Colter *et al.*[10] The results are given in Table 4. The quantum yield for the photooxidation of **1** in the micellar phase is large by a factor of 220 as compared with that in aqueous phase.

pH-Dependence. Stabilization of carbanion was examined in the photooxidation of oxime **1**, and was confirmed by measuring the quantum yields Φ_0 and Φ_{obsd} in the pH 3 to 12 region in the presence of HTAB, β-CDX, SDS, and Tween #80, respectively. As shown in Fig. 3, the presence of HTAB increases the quantum yield over the whole pH region. In the pH region above the pK_a value of oxime, the quantum yield increases irrespective of the presence or absence of the surfactant (Fig. 3). This indicates that the formation of the carbanion agrees with the increase in quantum yield. In the case of β-CDX, a similar phenomenon was observed. The extent of the catalytic effect of HTAB and β-CDX depends on the pH values of the reaction solution (Fig. 4). The catalytic effect

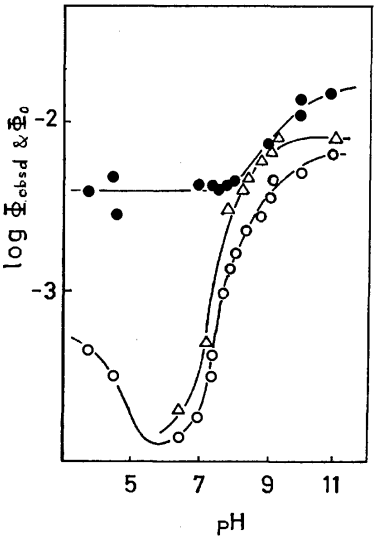

Fig. 3. pH-Dependence on the photooxidation of oxime **1** in a 10% ethanolic aqueous buffer (○), in the presence of 7.10×10^{-4} M HTAB (●), and 4.85×10^{-3} M β-CDX (△).

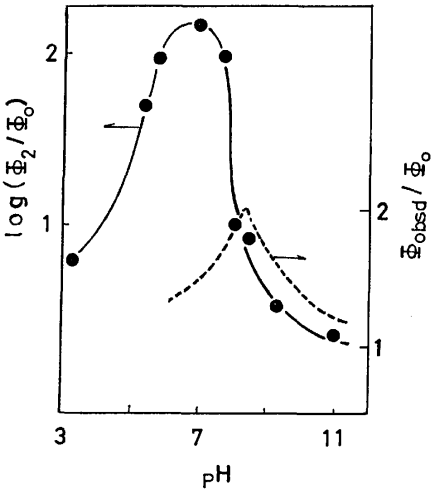

Fig. 4. pH-Dependence on the photooxidation of oxime **1** in the presence of HTAB (-●-) and β-CDX (——).

become maximum in the pH value around the pK_a's of the oxime determined in the presence of surfactant. On the other hand, the relation of the pH value and the quantum yield is not clear when SDS and Tween #80 were used. From the results, the mechanism is considered as follows. The stabilization of the carbanion in the hydrophobic cavity of β-CDX does not increase the quantum yield as in HTAB. This is because the steric hindrance of β-CDX inhibits the attack of singlet oxygen on the carbanion. HTAB does not inhibit the approach of singlet oxygen for the loosely bound carbanion. Consequently the stabilization of the carbanion in the presence of HTAB is reflected on the increase in the quantum yield.

Effect of Chloro-Substituent on the Rate Constant and the Association Constant. There is some difference in the reactivity of three oximes having a chloro-substituent. The rate constants of the photooxidation of the oxime

were determined in the presence or absence of HTAB. The rate constant k_2 for the formation of the product in the micellar phase and the association constants were calculated by means of Eq. 2. The relative values against those of **1** are given in Table 5. The steric hindrance is responsible for the least reactivity of the 2-chloro-substituted oxime. The catalytic effect of a cationic surfactant is recognized to be nearly equal to that observed for all the oximes, independent of the position of the chloro-substituent.

Experimental

All melting points were measured with a Yanagimoto micro melting point apparatus and are uncorrected. The ultraviolet spectra were taken on Hitachi EPS-3T and Shimadzu UV-200 spectrometers, mass spectra on a Hitachi RMU-6E mass spectrometer. The pH was measured with a TOA Electronics, Ltd., model HM-5A pH meter. Buffer solutions were chosen[11] according to the required pH region. CH_3-COOH (pH 3), M/15 KH_2PO_4-Na_2HPO_4 (pH 4—6), M/20 H_3BO_3-$Na_2B_4O_7$ (pH 6—8), M/20 H_3BO_3-KCl-NaOH (pH 8—10), and M/20 Na_2HPO_4-NaOH (pH 10—12). Column chromatography separation was carried out with Merck silica gel Art. 7734.

Materials. Commercial HTAB and SDS were recrystallized twice from methanol-ether and ethanol, respectively.[12,13] Other materials were used without further purification. All the compounds of oximes **1**—**10** were prepared from substituted nitrobenzene and substituted phenylacetonitriles by the procedure of Davis *et al.*[4a,b] The products were recrystallized twice from benzene.

*Irradiation of **1** and **2**.* A solution of 1 g of **1** in 2 liter of ethanol–aqueous alkaline (NaOH) solution was irradiated with an Ushio UM-452 450W high pressure mercury lamp for 10 h. After irradiation, the solvent was removed with rotary evaporators, the oily residue being chromatographed on silica gel to give two products. These were identified as nitrobenzophenone, mp 126 °C (lit,[4] 120 °C) and MS, *m/e* 227 (M^+); and 4,4′-dibenzoylazoxybenzene, mp 198—199 °C (lit,[4] 202—203 °C) and MS, *m/e* 406 (M^+). Irradiation of **2** in a similar manner gave 4-chloro-4′-nitrobenzophenone, mp 99 °C (lit,[4] 100—101 °C) and MS, *m/e* 261 (M^+), and 263 ($M^+ +2$); and 4,4′-bis(*p*-chlorobenzoyl) azoxybenzene, mp 292—296 °C (lit, [4] 291—293 °C) and MS, *m/e* 475 (M^+) and 477 ($M^+ +2$).

pK_a *Values.* The pK_a values of all the compounds were calculated by means of the equation,[3]

$$pK_a = pH_{obsd} + \log \frac{A_{max} - A_{obsd}}{A_{obsd}}. \quad (1)$$

The pH_{obsd} is the pH value at the inflection point estimated from the plot of absorbance *vs.* pH value of the solution. A_{max} and A_{obsd} are the absorption values for fully dissociated and partially dissociated (at pH_{obsd}) solutions of the oximes. The pK_a values of oximes in 5×10^{-3} M *β*-CDX, in 10^{-2}M HTAB, in 10^{-2} M SDS and in 6.6×10^{-2} g/dl Tween ♯80 were determined in a similar manner. All the compounds were dissolved in a small amount of ethanol before dilution with water, the final solution containing 25—10% ethanol.

Kinetic Method. In numerous kinetic runs, the sample kept in the dark showed no measurable change in absorption at λ_{max} of carbanion during the course of run ($\leq$5 h). A solution of 2.51×10^{-5} M of **1** in 10% ethanolic aqueous buffer reached equilibrium within for a few minutes. The solution kept for 2 days in the air still retained 97% of its absorbance at λ_{max} of carbanion, showing no change in th mode of absorption.

All the photoreactions were followed under pseudo-first-order kinetics conditions by monitoring the consumption of reactant at the λ_{max} of the carbanion.

After argon gas had been bubbled in the reactant solution for 1 h to remove dissolved oxygen, it was irradiated and the rate was measured. The k_{obsd} obtained was less than in the presence of dissolved oxygen by a factor of 50. The result indicates that dissolved oxygen participates in the photooxidation.

Various concentrations of *β*-carotene, Rose Bengal, and 2,6-di-*t*-butylphenol were dissolved in the reactant solutions. The rate of the photooxidation of these solutions was compared with that of the original solution.

The effect of HTAB at a particular pH region was examined according to the Scheme. SH, unionized and ionized, is

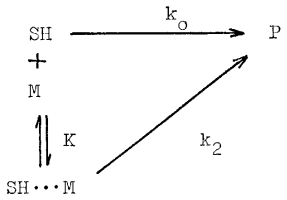

Scheme.

the total substrate present. Variation of surfactant concentration gave the rate constants for the product formation in the micellar phase, k_2, and the association constants for the substrate-micelle complex, K, by calculation by means of Eq. 2. The value of CMC obtained previously and the aggregation number (N 61 at HTAB) were used:

$$\frac{1}{k_{obsd}-k_0} = \frac{1}{k_2-k_0} + \frac{1}{k_2-k_0}\cdot\frac{N}{K(C_D-CMC)}. \quad (2)$$

C_D is the total concentration of the surfactant, k_0 the rate constant in the bulk solvent, and k_{obsd} the observed rate constant in the presence of HTAB. The estimated rate constant values were converted into the quantum yield.[14]

The effect of *β*-CDX was also examined according to the Scheme. The value of K, association constant of *β*-CDX-substrate complex, and k_2, the rate constant for the product formation in the bound species, were obtained by

$$\frac{1}{k_{obsd}-k_0} = \frac{1}{k_2-k_0} + \frac{1}{k(k_2-k_0)[CDX]}. \quad (3)$$

References

1) M. G. Shaposhnikova, N. N. Drozdova, and A. A. Krasnovskii, *Biochemistry*, **36**, 592 (1971).

2) T. Goto and H. Fukatsu, *Tetrahedron Lett.*, **1969**, 3873.

3) M. J. Minch, M. Giaccio, and R. Wolff, *J. Am. Chem. Soc.*, **97**, 3766 (1975).

4) (a) R. B. Davis, L. C. Pizzini, and J. D. Benigini, *J. Am. Chem. Soc.*, **82**, 2913 (1960); (b) R. B. Davis, L. C. Pizzini, and E. J. Bara, *J. Org. Chem.*, **26**, 4270 (1961); (c) R. B. Davis and J. D. Benigni, *J. Org. Chem.*, **27**, 1605 (1962).

5) (a) R. Bonnett and J. C. M. Stevart, *Biochem. J.*, **130**, 895 (1972); *J. Chem. Soc., Chem. Commun.*, **1972**, 596; (b) C. S. Foote and T. Y. Ching, *J. Am. Chem. Soc.*, **97**, 6209 (1975).

6) (a) C. S. Foote, S. Wexler, and W. Ando, *Tetrahedron*

Lett., **1965**, 4111; (b) R. S. Davidson and K. R. Trethewey, *J. Am. Chem. Soc.*, **98**, 4008 (1976).

7) C. S. Foote, Y. C. Chang, and R. W. Denny, *J. Am. Chem. Soc.*, **92**, 5216 (1970).

8) C. Ouannes and T. Wilson, *J. Am. Chem. Soc.*, **90**, 6527 (1968); 2,6-di-*t*-butylphenol, 0.04 M, stops the autoxidation. Conversely, this free-radical inhibitor does not suppress the singlet oxygen oxygenation, according to Foote *et al.*[6a] although it seems to have a small inhibitory effect (at high concentration: 0.3 M) on the photooxidation of rubrene.

9) J. H. Fendler and E. J. Fendler, "Catalysis in Micellar and Macromolecular Systems," Academic Press, New York (1975), p. 86.

10) A. K. Colter, S. S. Wang, G. H. Megerle, and P. S. Ossip, *J. Am. Chem. Soc.*, **86**, 3106 (1964).

11) "Jikken Kagaku Koza," ed by the Chemical Society of Japan, Maruzen, Tokyo (1958), Vol. 24, p. 204.

12) E. F. J. Duynstee and E. Grunwald, *J. Am. Chem. Soc.*, **81**, 4540 (1959).

13) P. Mukerjee and K. J. Mysels, *J. Am. Chem. Soc.*, **77**, 2937 (1955).

14) K. Yamada, S. Kohmoto, and H. Iida, *Bull. Chem. Soc. Jpn.*, **49**, 1171 (1976).

Synthesis of 6-*O*-Mycoloyl-*N*-acetylmuramyl-L-alanyl-D-isoglutamine with Antitumor Activity[1)]

Tetsuo SHIBA,* Satoshi OKADA, Shoichi KUSUMOTO,
Ichiro AZUMA,† and Yuichi YAMAMURA†
Department of Chemistry, Faculty of Science, Osaka University, Toyonaka, Osaka 560
†*The Third Department of Internal Medicine, Medical School, Osaka University, Fukushima-ku, Osaka 553*
(Received March 27, 1978)

N-Acetylmuramyl-L-alanyl-D-isoglutamine corresponding to the minimum structure responsible for the immunoadjuvant activity of bacterial cell walls was acylated at the 6-hydroxyl group with various mycolic acids of long carbon chains in order to test their possible antitumor effects. Mycolic acids used were extracted from cell walls of *Mycobacterium*, *Nocardia*, and *Corynebacterium*. All the mycoloyl derivatives synthesized show antitumor activity based on a principle of immunotherapy.

In the course of synthetic studies on immunoadjuvant active *N*-acetylmuramyl-L-alanyl-D-isoglutamine (**1**), we attempted to synthesize a novel compound which would exhibit antitumor activity based on the principle of immunotherapy of cancer. Since *Mycobacterium bovis* Bacille de Calmette-Guérin (BCG) cell wall is highly effective in tumor immunotherapy, it was expected that a modification of the structure of **1**, the key substance in immuno reactions, might turn out to be desirable substance by simulation of the structure of the cell wall. An outer layer of the BCG cell wall consists of mycoloyl arabinogalactan which is linked with the peptidoglycan.[2)] The antitumor effect of the cell wall might be attributed to the lipophilic character of mycolic acid moiety connected with the adjuvant activity of muramyl peptide moiety.

We have prepared several lipophilic derivatives of **1** by acylation of the 6-hydroxyl group of the muramic acid residue.[3)] However, no antitumor effect was observed even in 6-*O*-stearoyl-*N*-acetylmuramyl-L-alanyl-D-isoglutamine,[4)] which possesses the maximum adjuvant activity among 6-*O*-acyl derivatives prepared so far.[5)] We have thus extended our synthetic program to preparation of more lipophilic derivative coupled with the natural mycolic acid isolated from *Mycobacterium*. 6-*O*-Mycoloyl-*N*-acetylmuramyl-L-alanyl-D-isoglutamine (**2a**) thus obtained[1)] showed distinct activity in a suppression test of hepatoma in mice.[6)] In the present paper, we report the details of the synthesis of the mycoloyl derivative (**2a**) as well as two other 6-*O*-acyl derivatives of **1** prepared by using mycolic acid analogs originated from cells of *Nocardia* and *Corynebacterium*.

The general name "mycolic acid" represents α-branched β-hydroxylated fatty acids of high molecular weight (Fig. 1). They are involved in mycobacterial cell walls as typical constituents, being always present as a homologous mixture of some subgroups.[7)] The mycolic acid from *Mycobacterium tuberculosis* strain Aoyama B[8)] was found to have an average molecular formula $C_{80}H_{158}O_{3.5}$ on the basis of acid titration and elemental analysis.

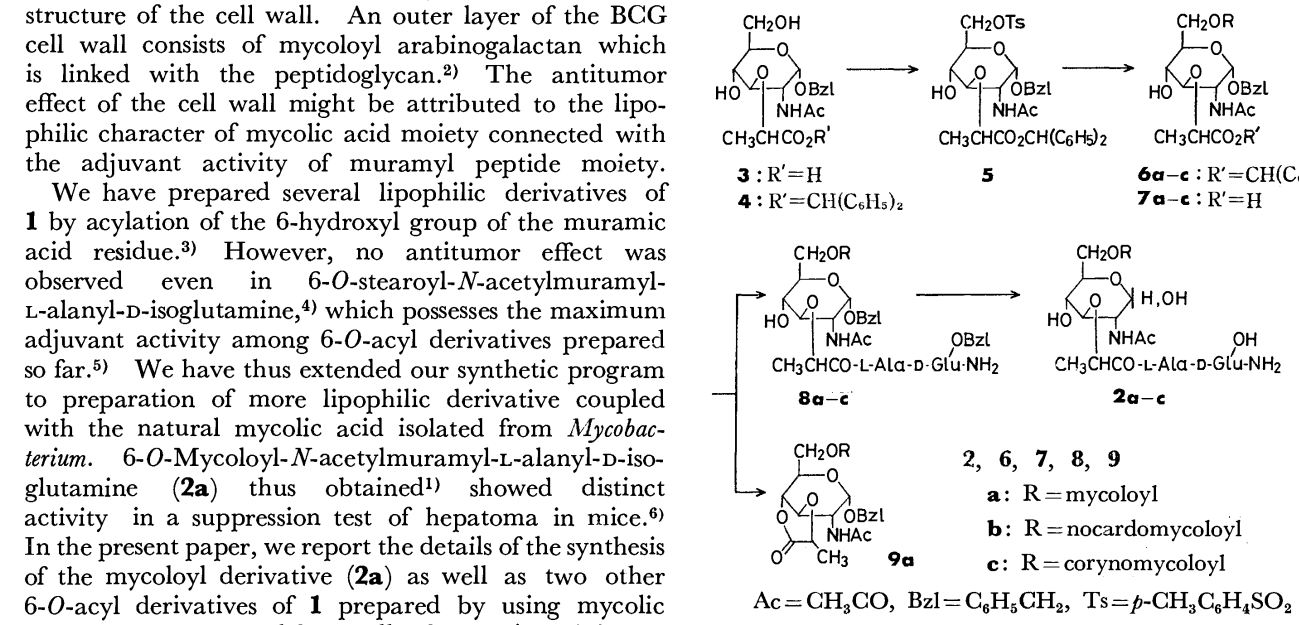

Fig. 1. The basic structure of mycolic acid analogs.

The synthetic route for 6-*O*-mycoloyl-*N*-acetylmuramyl-L-alanyl-D-isoglutamine (**2a**) is depicted in the scheme. It differs from the previous method for

the 6-*O*-stearoyl derivative in the following points. For introduction of the mycoloyl group into the muramic acid moiety, the acid chloride method, which was successfully used for the stearoyl derivative, should be avoided because of the presence of β-hydroxyl function in mycolic acid. An exchange reaction of 6-*O*-tosylate of a muramic acid derivative with potassium mycolate was employed for this purpose. Since the reaction conditions in this step are drastic, using a strongly basic reagent at high temperature, the peptide moiety had to be coupled after the reaction.

Benzyl *N*-acetyl-α-muramide (**3**)[3)] was converted with diphenyldiazomethane into the diphenylmethyl ester (**4**), which was then treated with excess tosyl chloride (11 mol equivalent) in pyridine under ice-cooling. Tosylation occurred almost exclusively at

TABLE 1. AVERAGE MOLECULAR WEIGHTS AND MOLECULAR FORMULAE OF MYCOLIC ACID ANALOGS USED IN THIS STUDY

	Average molecular weight[a]	Elemental analysis[b]		Average molecular formula calculated			
		C%	H%		C%	H%	mol wt
Mycolic acid	1180	81.45	13.55	$C_{80}H_{158}O_{3.5}$	81.70	13.54	1176
Nocardomycolic acid	766	79.84	12.76	$C_{51}H_{97}O_{3.6}$	79.77	12.73	768
Corynomycolic acid	483	76.97	12.38	$C_{31}H_{59}O_{3.3}$	76.83	12.27	485

a) Determined by acid titration, see Experimental. b) Mean values of two individual analyses.

the primary hydroxyl group, so that 6-*O*-monotosylate (**5**) was isolated in 89% yield after chromatographic purification. The exchange reaction of the tosylate with potassium mycolate proceeded smoothly in boiling benzene in the presence of 18-crown-6 to afford 1-α-*O*-benzyl-6-*O*-mycoloyl-*N*-acetylmuramic acid diphenylmethyl ester (**6a**). Although this reaction can also be performed without the crown ether in *N*,*N*-dimethylformamide (DMF) at higher temperature,[9] the yield became appreciably low. The diphenylmethyl group in the ester **6a** was then selectively removed with trifluoroacetic acid to give 1-α-*O*-benzyl-6-*O*-mycoloyl-*N*-acetylmuramic acid (**7a**), which was then subjected to the successive coupling reaction with the dipeptide moiety.

When the mycoloyl muramic acid (**7a**) was coupled with L-alanyl-D-isoglutamine benzyl ester[10] by means of the dicyclohexylcarbodiimide (DCC)–*N*-hydroxysuccinimide (HONSu) method, the desired product, 1-α-*O*-benzyl-6-*O*-mycoloyl-*N*-acetylmuramyl-L-alanyl-D-isoglutamine benzyl ester (**8a**), was obtained. However, the yield was rather low (38%) because of a competitive formation of an intramolecular ester (**9a**) (26%). The situation was somewhat improved by employing the following alternative procedure, in which an active ester of **7a** was prepared by ester-exchange reaction without use of dehydrating agent.[11] Thus, when **7a** was converted with pentachlorophenyl trichloroacetate into the pentachlorophenyl ester and then treated with the dipeptide benzyl ester under ice-cooling, formation of the internal ester (**9a**) was suppressed (17%) and the desired product (**8a**) was obtained in 47% yield. The final hydrogenolytic deprotection of **8a** was carried out in tetrahydrofuran (THF) in the presence of palladium black catalyst to afford 6-*O*-mycoloyl-*N*-acetylmuramyl-L-alanyl-D-isoglutamine (**2a**) in a good yield.

The mycoloyl-*N*-acetylmuramyl dipeptide (**2a**) thus obtained gave a positive antitumor effect.[6] When a suspension of **2a** in phosphate-buffered saline was administered intradermally with MH134 hepatoma cells to syngeneic mice, a distinct suppression of the tumor growth was observed. Accordingly, we synthesized two more analogs of **2a** with use of nocardomycolic acid and corynomycolic acid with different ranges of carbon numbers in order to estimate the influence of chain length in fatty acids on the antitumor activity.

Cells of *Nocardia* and *Corynebacterium*, closely related to *Mycobacterium* taxonomically, contain nocardomycolic (or nocardic) and corynomycolic acid, respectively, which have similar α-branched β-hydroxylated structures but with smaller carbon numbers than in the mycolic acid from *Mycobacterium*. Extraction of cells of *Nocardia asteroides* 131 and *Corynebacterium diphtheriae* PW8 afforded the corresponding nocardomycolic and corynomycolic acid, whose average molecular formulae were deduced to be $C_{51}H_{97}O_{3.6}$ and $C_{31}H_{59}O_{3.3}$, respectively, on the basis of elemental analyses and acid titrations. Average molecular weights and molecular formulae of the mycolic acid analogs are given in Table 1.

TABLE 2. SUPPRESSION OF MH-134 HEPATOMA WITH 6-*O*-MYCOLOYL-*N*-ACETYLMURAMYL DIPEPTIDES (**2a**—**c**)[6]

Compound	Dose (μg)	No. of mice tested	Tumor-free mice /mice survived[a]
2a	20	10	3/8
2b	20	10	5/9
2c	20	10	6/7
Control[b]	—	10	0/1

a) At 49 days. b) Only tumor cells were inoculated.

The syntheses of nocardomycoloyl- and corynomycoloyl-*N*-acetylmuramyl-L-alanyl-D-isoglutamine (**2b** and **c**) were performed in a similar way to that for **2a**. In the coupling reaction of nocardomycoloyl- and corynomycoloyl-*N*-acetylmuramic acid (**7b** and **c**) with the dipeptide moiety, 1-α-*O*-benzyl-6-*O*-nocardomycoloyl- and corynomycoloyl-*N*-acetylmuramyl-L-alanyl-D-isoglutamine benzyl ester (**8b** and **c**) could be obtained in better yields as compared to that for mycoloyl derivative (**8a**). In these cases, the intramolecular esters of type **9** were not formed from **7b** and **c**, although the DCC–HONSu method was employed under similar conditions to those for the coupling of mycoloyl derivative (**7a**).[12] Hydrogenolysis of **8b** and **c** afforded the final products, 6-*O*-nocardomycoloyl and corynomycoloyl-*N*-acetylmuramyl-L-alanyl-D-isoglutamine (**2b** and **c**). However, one of the two benzyl groups in **8b** and **c** resisted the cleavage at room temperature below 20 °C in this reaction. Thus, hydrogenolysis was carried out at 28—30 °C for 3 or more days to complete deprotection.[13,14]

The results of an antitumor test of the compounds synthesized in this study are summarized in Table 2.[6] Nocardomycoloyl and corynomycoloyl muramyl dipeptides (**2b** and **c**) also showed similar or even stronger activity to mycoloyl derivative (**2a**). Although the activity seemed to be less significant than natural BCG cell wall and not sufficient for practical use, this is the first case in which synthetic substances suppressed growth of a tumor on the basis of their im-

munoadjuvant activities. In order to clarify the role of the unique structure of mycolic acid, we are now preparing other acyl derivatives of *N*-acetylmuramyl dipeptide (**1**) using various kinds of synthetic fatty acids of high molecular weights.

Experimental

All melting points are uncorrected. Silica gel 60 (0.063-0.2 mm) and silica gel G, Merck, were used for column chromatography and TLC, respectively.

Preparation of Mycolic Acid, Nocardomycolic Acid, and Corynomycolic Acid from the Cells of Mycobacterium tuberculosis *Aoyama B*, Nocardia asteroides *131, and* Corynebacterium diphtheriae *PW8*. The cells[15] were defatted by repeated extraction with ether–ethanol (1:1) and $CHCl_3$–methanol (2:1), and then hydrolyzed by heating with 2.5% KOH in benzene–methanol (1:1) under reflux for 23 h. After the reaction mixture had been filtered, the filtrate was concentrated to dryness *in vacuo*, acidified with HCl and extracted with hexane. The solvent was removed from the extract by evaporation and the residue was heated in 2.5% HCl–methanol for 5 h. The products were subjected to column chromatography on silica gel and eluted with hexane–ether to afford methyl mycolates (1.7—2.2% from defatted cells). The free acids could be regenerated by hydrolysis of the corresponding methyl esters with 3 M KOH in methanol–benzene under reflux for 3 h.

Determination of the Average Molecular Formulae of Mycolic Acids and Preparation of Their Potassium Salts. i) Mycolic Acid: Mycolic acid (0.500 g) from *Mycobacterium* was dissolved in $CHCl_3$ (5 ml) and titrated with 0.176M KOH in methanol against phenolphthalein. After the solvent had been evaporated *in vacuo*, the residual potassium mycolate was washed with methanol and filtered; yield, 0.51 g (99%).

From the amount of alkali consumed (2.41 ml), the average molecular weight was deduced to be 1180. The average molecular formula $C_{80}H_{158}O_{3.5}$ was obtained from this molecular weight and the results of elemental analyses (Table 1).

ii) Nocardomycolic Acid: Nocardomycolic acid (0.870 g) in $CHCl_3$ (10ml) was titrated with 0.46 M KOH in methanol. The consumed volume of the solution to neutrality was 2.47 ml. After evaporation of the solvent *in vacuo*, the residue was treated with ether and insoluble material was filtered off. Evaporation of the solvent afforded the potassium salt as waxy residue; yield, 0.88 g (96%) (Table 1).

iii) Corynomycolic Acid: Corynomycolic acid (0.420 g) in $CHCl_3$ (10 ml) was titrated with 3.41 ml of 0.255M KOH in methanol and the resulting potassium salt was isolated as described in (ii); yield, 0.44 g (97%) (Table 1).

1-α-O-Benzyl-N-acetylmuramic Acid Diphenylmethyl Ester (4). Diphenyldiazomethane (0.80 g, 4.1 mmol) in THF (5 ml) was added to a stirred solution of benzyl *N*-acetyl-α-muramide (**3**) (1.00 g, 2.6 mmol) in THF (10 ml). After being left to stand at room temperature overnight, the solvent was evaporated *in vacuo*. The residue crystallized on trituration with hexane. The crystals were washed with hexane to remove excess diphenyldiazomethane and then recrystallized from ethyl acetate–hexane: yield, 1.30 g (91%); mp 151—153 °C. An analytical sample was again recrystallized from the same solvent system; mp 155—156°C; $[\alpha]_D^{22}$ +122° (*c* 1, $CHCl_3$).

Found: C, 67.62; H, 6.50; N, 2.52%. Calcd for $C_{31}H_{35}O_8N$: C, 67.74; H, 6.42; N, 2.55%.

1-α-O-Benzyl-6-O-tosyl-N-acetylmuramic Acid Diphenylmethyl Ester (5). Tosyl chloride (1.20 g, 6.3 mmol) was added to an ice-cooled solution of **4** (0.30 g, 0.55 mmol) in pyridine (3 ml) with stirring. After 1 h, excess reagent was decomposed with ice-water and the mixture was extracted with ethyl acetate. The organic layer was washed successively with 0.3 M NaOH, H_2O, 1 M HCl, and H_2O, dried ($MgSO_4$) and evaporated *in vacuo*. The residue was purified with silica gel column chromatography (benzene–ethyl acetate, 5:1). Fractions containing only the main product (monitored with TLC) were collected and evaporated *in vacuo* to afford colorless powder; yield, 0.34 g, (89%); mp 68—73 °C; $[\alpha]_D^{22}$ +84.4° (*c* 0.5, $CHCl_3$).

Found: C, 64.68; H, 5.92; N, 1.93; S, 4.31%. Calcd for $C_{38}H_{41}O_{10}NS$: C, 64.85; H, 5.87; N, 1.99; S, 4.56%.

1-α-O-Benzyl-6-O-mycoloyl-N-acetylmuramic Acid Diphenylmethyl Ester (6a). i) In Benzene and in the Presence of 18-Crown-6: A mixture of **5** (325 mg, 0.46 mmol), potassium mycolate (375 mg, 0.31 mmol) and 18-crown-6 (18 mg, 0.07 mmol) in anhydrous benzene (15 ml) was heated under reflux for 3 h. After evaporation of the solvent *in vacuo*, acetone-soluble material in the residue was subjected to silica gel column chromatography. Elution with hexane–ethyl acetate (5:1) gave a mixture of the product (**6a**) and a small amount of recovered mycolic acid. The mixture was treated with diazomethane and again chromatographed on silica gel. Elution with benzene–ethyl acetate (10:1) afforded pure **6a**; yield, 0.32 g (60%); mp 55—56 °C; $[\alpha]_D^{22}$ +32.6° (*c* 0.5, $CHCl_3$).

Found: C, 78.34; H, 11.48; N, 0.85%. Calcd for $C_{111}H_{191}O_{10.5}N$: C, 78.07; H, 11.27; N, 0.82%.

ii) In DMF: A mixture of potassium mycolate (49 mg, 0.040 mmol) and **5** (39 mg, 0.055 mmol) in DMF (1 ml) was heated at 125 °C for 19 h. The mixture was acidified with 0.5M H_2SO_4 under ice-coling and then neutralized with aqueous $NaHCO_3$. After evaporation of the solvent *in vacuo*, the product was isolated by means of preparative TLC on silica gel(benzene-ethyl acetate, 2 : 1), the main band of R_f 0.6—0.8 was extracted with ethyl acetate. The residue obtained by evaporation of the solvent was triturated with methanol and filtered; yield, 28 mg (41%); mp 50—56 °C. This product was identified with **6a** obtained in (i) on TLC.

1-α-O-Benzyl-6-O-mycoloyl-N-acetylmuramyl-L-alanyl-D-isoglutamine Benzyl Ester (8a). i) The DCC–HONSu Method: Trifluoroacetic acid (3 ml) was added to an ice-cooled solution of **6a** (0.30 g, 0.18 mmol) and anisole (1 ml) in $CHCl_3$ (20 ml) with stirring . After being stirred in an ice bath for 1 h, the mixture was diluted with acetone (100 ml) and the solvent was removed *in vacuo*. Trituration of the resulting syrup with ethanol gave **7a** as white powder, which was collected by filtration. To a solution of **7a** thus obtained in THF (10 ml) were added L-alanyl-D-isoglutamine benzyl ester hydrochloride (65 mg, 0.19 mmol), triethylamine (0.024 ml, 0.18 ml) and HONSu (75 mg, 0.65 mmol). To the mixture cooled in an ice bath was added DCC (37 mg, 0.18 mmol). After being stirred overnight, *N,N'*-dicyclohexylurea and triethylamine hydrochloride were filtered off; the filtrate was evaporated *in vacuo*, and the residue was triturated with methanol. The insoluble materials were subjected to silica gel column chromatography. A mixture of benzene–acetone (1:1) eluted the intramolecular ester (**9a**) in an early fraction; yield, 0.07 g (26%); mp 46—51 °C (Found: N, 0.86%. Calcd for $C_{98}H_{179}O_{9.5}N$: N, 0.92%). Further elution with the same solvent and recrystallization from benzene–methanol afforded **8a**; yield, 0.12 g (36%); mp 171—172 °C; $[\alpha]_D^{22}$ +30.2° (*c* 0.5, $CHCl_3$).

Found: C, 73.63; H, 11.05; N, 3.18%. Calcd for $C_{113}H_{200}O_{13.5}N_4$: C, 74.13; H, 11.01; N, 3.06%.

ii) The Pentachlorophenyl Ester Method: A solution of **6a**

(0.33 g, 0.19 mmol) and anisole (1 ml) in $CHCl_3$ (20 ml) was treated with trifluoroacetic acid (3 ml) and worked up as in (i). Resulting **7a** and pentachlorophenyl trichloroacetate[11] (0.20 g, 0.49 mmol) were dissolved in a mixture of DMF and THF (1:1, 15 ml), triethylamine (0.038 ml, 0.27 mmol) being added under ice-cooling. After being stirred at this temperature for 2.5 h, benzene was added and the mixture was washed with water, dried ($MgSO_4$) and evaporated *in vacuo*. Trituration of the residue with acetone gave the pentachlorophenyl ester of **7a** as powder. This was dissolved in THF (10 ml) and added to a mixture of L-alanyl-D-isoglutamine benzyl ester hydrochloride (76 mg, 0.22 mmol) and triethylamine (0.031 ml, 0.22 mmol) in THF (3 ml). After being stirred at room temperature for 3 h, triethylamine hydrochloride was filtered off, the filtrate was concentrated *in vacuo*, and the residue was chromatographed on silica gel as in (i). After **9a** (yield, 0.05 g (17%); mp 45—50 °C), **8a** was eluted. This was recrystallized from ether–methanol; yield, 0.17 g (47%); mp 171—172 °C.

6-O-Mycoloyl-N-acetylmuramyl-L-alanyl-D-isoglutamine (2a). Compound **8a** (76 mg, 0.04 mmol) in THF (20 ml) was hydrogenolyzed in the presence of palladium black catalyst. After removal of the catalyst and evaporation of the solvent *in vacuo*, the residue was recrystallized from ether–ethanol; yield, 64 mg (93%); mp 137—160 °C (dec); $[\alpha]_D^{22}$ +25.8° (*c* 0.4, THF–H_2O, 50: 1, after 20 h).

Found: C, 71.08; H, 11.40; N, 3.26%. Calcd for $C_{99}H_{188}O_{13.5}N_4 \cdot H_2O$: C, 71.26; H, 11.48; N, 3.36%.

1-α-O-Benzyl-6-O-nocardomycoloyl-N-acetylmuramic Acid Diphenylmethyl Ester (6b). A mixture of **5** (0.35 g, 0.50 mmol), potassium nocardomycolate (0.30 g, 0.37 mmol) and 18-crown-6 (19 mg, 0.07 mmol) in anhydrous benzene (15 ml) was heated under reflux for 3 h. After addition of benzene (15 ml), the resulting solution was washed with 0.1 M HCl and water, dried (Na_2SO_4) and then concentrated *in vacuo*. The residue was chromatographed on silica gel. Elution with benzene–ethyl acetate (5:1) and complete evaporation of the solvent afforded **6b** as waxy residue; yield, 0.34 g (70%); $[\alpha]_D^{27}$ +46.7° (*c* 1, $CHCl_3$).

Found: C, 75.38; H, 10.15; N, 1.03%. Calcd for $C_{82}H_{130}O_{10.6}N$: C, 75.79; H, 10.08; N, 1.08%.

1-α-O-Benzyl-6-O-nocardomycoloyl-N-acetylmuramyl-L-alanyl-D-isoglutamine Benzyl Ester (8b). To an ice-cooled solution of **6b** (0.24 g, 0.18 mmol) and anisole (0.1 ml) in CH_2Cl_2 (10 ml) was added trifluoroacetic acid (1.5 ml) with stirring. After 30 min, the solvent was removed *in vacuo* and the residue was chromatographed on a silica gel column ($CHCl_3$–methanol, 5:1) to afford **7b**. This was added to a suspension of L-alanyl-D-isoglutamine benzyl ester hydrochloride (75 mg, 0.22 mmol) and triethylamine (0.030 ml, 0.22 mmol) in THF (5 ml). To the mixture cooled in an ice-salt bath (−13 °C) were added HONSu (36 mg, 0.31 mmol) and DCC (39 mg, 0.19 mmol) with stirring. After 1 h, the cold bath was removed and the mixture was stirred at room temperature overnight. The insoluble materials were filtered off, the filtrate was evaporated *in vacuo* and the residue was chromatographed on silica gel. Elution with $CHCl_3$–methanol (30:1) and recrystallization from methanol–water gave **8b**; yield, 0.14 g (53%); mp 164—167 °C; $[\alpha]_D^{17}$ +44.7 ° (*c* 1, $CHCl_3$).

Found: C, 71.05; H, 9.87; N, 3.65%. Calcd for $C_{84}H_{139}O_{13.6}N_4$: C, 70.91; H, 9.85; N, 3.94%.

6-O-Nocardomycoloyl-N-acetylmuramyl-L-alanyl-D-isoglutamine (2b). Compound **8b** (84 mg, 0.06 mmol) in THF (5 ml) was hydrogenolyzed in the presence of palladium black at 28 °C for 3 days. After the usual work-up, the product was recrystallized from $CHCl_3$–acetone; yield, 51 mg (68%); mp 154—157 °C (dec); $[\alpha]_D^{20}$ +30.0° (*c* 1, THF–H_2O, 50: 1, after 24 h).

Found: C, 66.07; H, 10.58; N, 4.26%. Calcd for $C_{70}H_{127} \cdot O_{13.6}N_4 \cdot 1.5H_2O$: C, 66.23; H, 10.32; N, 4.41%.

1-α-O-Benzyl-6-O-corynomycoloyl-N-acetylmuramic Acid Diphenylmethyl Ester (6c). A solution of **5** (0.48 g, 0.68 mmol), potassium corynomycolate (0.31 g, 0.59 mmol), and 18-crown-6 (30 mg, 0.11 mmol) in anhydrous benzene (15 ml) was heated under reflux for 3 h. The mixture was then treated as for **6b** and subjected to column chromatography on silica gel. Elution with benzene–ethyl acetate (5 : 1) yielded **6c** as waxy solid; yield, 0.30 g (50%); $[\alpha]_D^{25}$ +58.4° (*c* 1, $CHCl_3$).

Found: C, 72.85; H, 9.27; N, 1.40%. Calcd for $C_{62}H_{92}O_{10.3}N$: C, 73.28; H, 9.13; N, 1.38%.

1-α-O-Benzyl-6-O-corynomycoloyl-N-acetylmuramyl-L-alanyl-D-isoglutamine Benzyl Ester (8c). This compound was prepared in a similar way to that for nocardomycoloyl derivative (**8b**). After the diphenylmethyl group of **6c** (0.52 g, 0.51 mmol) had been removed with trifluoroacetic acid, the resulting **7c** was mixed with L-alanyl-D-isoglutamine benzyl ester hydrochloride (0.21 g, 0.61 mmol) and triethylamine (0.087 ml, 0.62 mmol) in THF (10 ml). HONSu (101 mg, 0.88 mmol) and DCC (100 mg, 0.49 mmol) were added to the mixture under cooling and worked up as above. The product (**8c**) was isolated and purified by silica gel column chromatography followed by recrystallization from methanol–water; yield, 0.28 g (48%); mp 172—175 °C; $[\alpha]_D^{14}$ +53.7° (*c* 1, $CHCl_3$).

Found: C, 67.16; H, 9.08; N, 4.99%. Calcd for $C_{64}H_{101}O_{13.3}N_4$: C, 67.47; H, 8.94; N, 4.92%.

6-O-Corynomycoloyl-N-acetylmuramyl-L-alanyl-D-isoglutamine (2c). Compound **8c** (127 mg, 0.11 mmol) in THF (10 ml) was subjected to hydrogenolysis in the presence of palladium black at 28 °C for 3 days. After evaporation of the solvent, the residue was dissolved in a mixture of ether–methanol (1:1). On addition of acetone, white powder precipitated; yield, 77 mg (71%); mp 156—159 °C (dec); $[\alpha]_D^{18}$ +33.0° (*c* 1, THF–H_2O, 50:1, after 24 h).

Found: C, 61.64; H, 9.48; N, 5.59%. Calcd for $C_{50}H_{89}O_{13.3}N_4 \cdot H_2O$: C, 61.46; H, 9.39; N, 5.73%.

Determination of Antitumor Activity.[6] A mixture of tumor cells of MH 134 hepatoma (1×10^5) and **2a**, **b**, or **c** (20 μg) suspended in phosphate-buffered saline was inoculated intradermally into C3H mice and tumor growth was observed in inoculated sites.

The work was carried out with a Grant-in-Aid for Scientific Research from the Ministry of Education.

References

1) This work was presented at the 36th Natinal Meeting of the Chemical Society of Japan, Osaka, April 1977; II, p. 1233 and reported in a preliminary form: S. Kusumoto, S. Okada, T. Shiba, I, Azuma, and Y. Yamamura, *Tetrahedron Lett.*, **1976**, 4287.

2) I. Azuma, Y. Yamamura, and K. Fukushi, *J. Bacteriol.*, **96** 1885 (1968).

3) S. Kusumoto, S. Okada, K. Yamamoto, and T. Shiba, *Bull. Chem. Soc. Jpn.*, **51**, 2122 (1978).

4) I. Azuma, K. Sugimura, T. Taniyama, M. Yamawaki, Y. Yamamura, S. Kusumoto, S. Okada, and T. Shiba, *Infect. Immun.*, **14**, 18 (1976).

5) S. Kotani, F. Kinoshita, I. Morisaki, T. Shimono, T. Okunaga, H. Takada, M. Tsujimoto, Y. Watanabe,

K. Kato, T. Shiba, S. Kusumoto, and S. Okada, *Biken J.*, **20**, 95 (1977).

6) Y. Yamamura, I. Azuma, K. Sugimura, M. Yamawaki, M. Uemiya, S. Kusumoto, S. Okada, and T. Shiba, *Proc. Jpn. Acad.*, **53**, 63 (1977).

7) Mycolic acids can be classified according to the type of modification in the α-branched β-hydroxylated structure. Thus, typical subgroups contain double bonds, cyclopropane rings, or methoxy substituents in the main chains. Each subgroup exists again as a mixture of homologs with various chain lengths. J. Asselineau, "The Bacterial Lipids," Herman, Paris (1966).

8) The natural mycolic acid was used without separation into subgroups.[7]

9) These reaction conditions were described by G. Brochere-Ferreol and J. Polonsky in the synthesis of trehalose 6,6′-di-*O*-mycolate (the so-called cord factor) *via* the same type of substitution. *Bull. Soc. Chim. Fr.*, **1958**, 714.

10) S. Kusumoto, Y. Tarumi, K. Ikenaka, and T. Shiba, *Bull. Chem. Soc. Jpn.*, **49**, 533 (1976).

11) M. Fujino and C. Hatanaka, *Chem. Pharm. Bull.*, **16**, 929 (1968).

12) Internal ester formation was observed in the preparation of neither 6-*O*-stearoyl-,[3] nocardomycoloyl- nor corynomycoloyl-*N*-acetylmuramyl-L-alanyl-D-isoglutamine derivatives. It seems that the ease of ester (**9a**) formation from **7a** can be attributed to the length of mycolic acid, which keeps the molecule in a certain conformation in the solution to make contact between the active ester and the dipeptide difficult.

13) The trouble was not encountered in the case of preparation of **2a**, when the ambient temperature was over 25 °C.

14) When the reaction was interrupted before completion, the product had to be purified by means of column chromatography first on silica gel ($CHCl_3$–methanol–acetic acid, 5:1:0.01) then on Sephadex LH20 (THF). The latter column was necessary to remove the trace of inorganic materials eluted from silica gel.

15) Cells of *M. tuberculosis* and *N. asteroides* were cultured in Sauton's synthetic medium, while those of *C. diphtheriae* were in the medium of Mueller and Miller. For details, see: I. Azuma, F. Kanetsuna, T. Taniyama, Y. Yamamura, H. Hori, and Y. Tanaka, *Biken J.*, **18**, 1 (1975).

Reactions of Azomethine Derivatives. IV.[1] The Synthesis of 2,3,5-Trisubstituted 2-Pyrrolin-4-ones and Their Oxidation to 2,4,5-Trisubstituted 1,3-Oxazin-6-ones

Masahiko TAKAHASHI,* Nobuyuki INABA, Hiroji KIRIHARA, and Shin-ichi WATANABE

Department of Industrial Chemistry, Faculty of Engineering, Ibaraki University, Hitachi, Ibaraki 316

(Received March 28, 1978)

The reaction of aromatic azines with diphenylcyclopropenone in refluxing toluene gave 5-aryl-2,3-diphenyl-2-pyrrolin-4-ones (**4**) in moderate yields *via* initial [2+3] 1:1 cycloaddition and subsequent elimination of an aromatic nitrile from the adducts. Treatment with phosphorus pentasulfide deoxygenated the compounds **4** to 5-aryl-2,3-diphenyl-pyrroles. The same compounds **4** were oxidized to 2-aryl-4,5-diphenyl-1,3-oxazin-6-ones (**11**) by refluxing the pyridine solution in a stream of oxygen, by treatment with hydrogen peroxide, or by irradiation of the chloroform solution in a stream of oxygen. Treatment with alkali in aqueous pyridine converted **4** into 3-aroylamino-2,3-diphenylacrylic acids. These were also obtained from the hydrolysis of **11**. When *p*-dimethylaminobenzaldehyde azine reacted with diethyl azodicarboxylate in refluxing toluene, a 1:2 conjugated adduct, 3,6-bis(*p*-dimethylaminophenyl)-1,2,7,8-tetrakis(ethoxycarbonyl)-1,2,4,5,7,8-hexaaza-3,5-octadiene, and a 1:1 conjugate adduct, 3,6-bis(*p*-dimethylaminophenyl)-1,2-bis(ethoxycarbonyl)-1,2,4,5-tetraaza-3,5-hexadiene, were obtained.

The cycloaddition reactions of azines with various dipolarophiles generally give criss-cross 1:2 adducts.[2] Eicher *et al.* have reported [2+3] cycloaddition reactions of aldimines,[3] ketimines,[4] guanidines,[5] and benzamidines[5] with diphenylcyclopropenone to give 2,3-diphenyl-2-pyrrolin-4-ones as reaction intermediates or products. When appropriately substituted amidines and guanidines were used for the reaction, 5,6-dihydropyrimidin-4-ones were produced.[6]

In the course of our study of cycloaddition reactions of heterodienes containing azomethine groups,[1] these publications prompted us to investigate the reaction of azines **1** with diphenylcyclopropenone (**2**); we obtained 5-aryl-2,3-diphenyl-2-pyrrolin-4-ones (**4**).[7] These pyrrolinones **4** were found to be oxidized by oxygen, by hydrogen peroxide, or by irradiation in a stream of oxygen to 2-aryl-4,5-diphenyl-1,3-oxazin-6-ones (**11**). Although many oxidation reactions of pyrroles have been reported,[8] little is known concerning the oxidation reactions of 2-pyrrolin-4-ones: 2,5-dimethyl-1-phenyl-2-pyrrolin-4-one was reported to be oxidized to 5-hydroxy derivative,[9] and 2,3-dimethyl-2-pyrrolin-4-one was found to be oxidized to tetramethylpyrrole indigo[10] or 3-pyrrolin-5-one derivative.[11] To the best of our knowledge the oxidative ring-enlargement of 2-pyrrolin-4-ones has not been reported. Moreover, the resulting oxadinones **11** belong to relatively rare derivatives of 1,3-oxazines.[12]

When azines **1** reacted with diethyl azodicarboxylate, similar cycloaddition reactions were not observed; the 1:2 and 1:1 conjugate addition products (**13** and **14**, respectively) were obtained in the case of **1e**.

Results and Discussion

When a mixture of *p*-methoxybenzaldehyde azine (**1a**) and diphenylcyclopropenone (**2**) in toluene was refluxed, a yellow crystalline product was obtained in 55% yield. The molecular formula $C_{23}H_{19}O_2N$ was confirmed on the basis of the elemental analysis and the mass spectrum (M^+, 341). The IR spectrum showed NH and CO absorptions at 3200 and 1640 cm^{-1}, respectively. These data suggest that the product is not an expected product such as a criss-cross 1:2 adduct **5a** or a [2+3] 1:1 adduct **3a**, but an addition-elimination product **4a** or **6a** (Scheme 1).

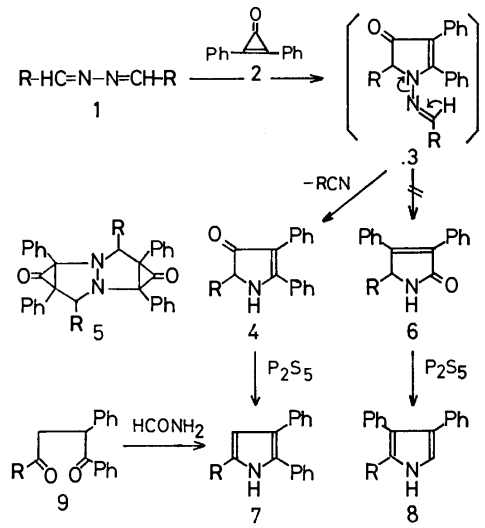

a: R=*p*-$MeOC_6H_4$ **b**: R=*p*-MeC_6H_4
c: R=*p*-$Me_2CHC_6H_4$ **d**: R=C_6H_5
e: R=*p*-$Me_2NC_6H_4$

Scheme 1.

In order to distinguish between two regioisomers, **4a** and **6a**, conversion of the product into the known pyrrole derivative was attempted. Thus, treatment of the product with phosphorus pentasulfide in refluxing benzene gave a deoxygenated product, which seemed to be (*p*-methoxyphenyl)diphenylpyrrole (**7a**) or (**8a**). An authentic specimen **7a**[13] prepared from **9a** was identical with the deoxygenated product; this proved that the addition-elimination product was not **6a** but 5-(*p*-methoxyphenyl)-2,3-diphenyl-2-pyrrolin-4-one (**4a**).

Other 2-pyrrolin-4-ones (**4b**—**e**) were also obtained in a similar manner from **1b**—**e** in moderate yields (35—87%). The compounds **4b** and **4d** were converted

into the corresponding pyrroles **7b** and **7d**, whose structures were identified by comparison with the authentic samples prepared from **9b** and **9d**, respectively.

As shown in Scheme 1, the reaction is considered to proceed *via* the formation of a [2+3] cycloadduct **3**, followed by elimination of RCN. A similar process involving the initial cycloaddition to azomethine group of azine followed by elimination of RCN has been reported in the case of the reaction of azines with diphenylketene.[14]

In the course of the structure elucidation of **4a**, a mixture of **4a** in acetic acid and acetic anhydride was heated for acetylation. A product was separated in 23% yield by column chromatography. This compound showed no NH absorption and a new carbonyl absorption at 1738 cm^{-1} in the IR spectrum, but the absorption at 1640 cm^{-1} present in **4a** disappeared. These data imply that the product is not the desired acetate **10** but an auto-oxidation product, 2-(*p*-methoxyphenyl)-4,5-diphenyl-1,3-oxazin-6-one (**11a**) (Scheme 2). The compound **11a** was identical with the authentic sample prepared from **7a** by oxidation with hydrogen peroxide, according to the literature method.[15] These results suggest the possibility that **4** are generally oxidized by oxygen to 1,3-oxazin-6-ones (**11**). In fact, when the solutions of **4a—d** in pyridine were refluxed in a stream of oxygen, **11a—d** were obtained in 38—50% yields. The structures of **11b—d** were established by spectral data or by comparison with the samples derived from **7**.

Oxidations of **4** to **11** in different manners were further examined. When the solutions of **4** in chloroform were irradiated by a mercury lamp in a stream of oxygen, photooxidation products **11a** (21%), **11b** (14%), and **11c** (16%) could be isolated by column chromatography, but pure products were not obtained from **4d** and **4e**. Oxidation of **4** by hydrogen peroxide in acetic acid proceeded smoothly only in the cases of **4a** and **4c** to yield **11a** (85%) and **11c** (32%), respectively.

When a solution of **4a** in aqueous pyridine containing potassium hydroxide was stirred at room temperature, an acidic product (36%) was produced, accompanied by a mixture of neutral products, whose structures could not be determined because of low yields and difficulties in purification. The IR spectrum of the acidic product showed carboxyl absorptions at 3020 and 1688 cm^{-1} and an amide absorption at 1640 cm^{-1}. Consideration of the mass and the NMR spectra suggested that the acidic products was 3-(*p*-methoxybenzamido)-2,3-diphenylacrylic acid (**12a**). The structure of **12a** was further confirmed by comparing the samples obtained by the alkaline hydrolysis of **11a** under the same conditions. The compounds **12b** (25%), **12c** (26%), and **12d** (41%) were similarly obtained, and their structures were assigned by the spectral data or by comparison with the samples derived from **11**.

To explain the formation of 3-aroylamino-2,3-diphenylacrylic acids and indenone derivatives from aldimines and diphenylcyclopropenone, Eicher *et al.*[3] proposed a mechanism where the initially formed

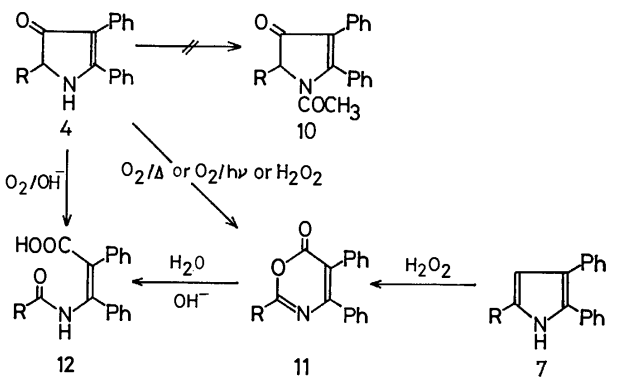

a: R=*p*-$MeOC_6H_4$ **b**: R=*p*-MeC_6H_4
c: R=*p*-$Me_2CHC_6H_4$ **d**: R=C_6H_5

Scheme 2.

2-pyrrolin-4-ones were oxidized by air to 1,3-oxazin-6-ones, which subsequently underwent hydrolysis to acrylic acids or ring-opening, followed by cyclization to indenones. Taking into account this explanation and our experiments on the hydrolysis of **11** to **12**, the oxidative cleavage of **4** to **12** appears to proceed *via* **11**. On the other hand, for the formation of **11**, the following pathway seems plausible: 2-pyrrolin-4-ones (**4**) are first cleaved to acrylic acids **12**, which are subsequently dehydrated to **11**. This pathway, however, may not be possible, since treatment of **12d** under the same conditions as the oxidation of **4** to **11**, that is, heating of **12d** in pyridine in a stream of oxygen, yielded **11d**, but the corresponding **11a—c** were not formed in the cases of **12a—c**, which gave unidentified products. To clarify the oxidation mechanism more detailed experiments will be needed.

During further studies of the reaction of azines, diethyl azodicarboxylate was found to add to *p*-dimethylaminobenzaldehyde azine (**1e**) in refluxing toluene, although no reaction occurred in the cases of **1b—d** and purification of the products from **1a** was difficult. Chromatographic separation of the reaction mixture from **1e** afforded two products. The first and the second eluated products proved to be a 1:2 adduct and a 1:1 adduct, respectively, on the basis of the elemental analyses and the mass spectra. The NMR spectrum of the 1:2 adduct **13** showed a singlet peak at δ 3.08 ppm due to two equivalent dimethylamino groups, suggesting a symmetrical structure. On the other hand, the NMR spectrum of the 1:1 adduct **14** showed two singlet peaks at δ 3.00 and 3.07 ppm due to two non-equivalent dimethylamino groups, suggesting an unsymmetrical structure. Moreover, the UV spectra of both **13** and **14** were very similar

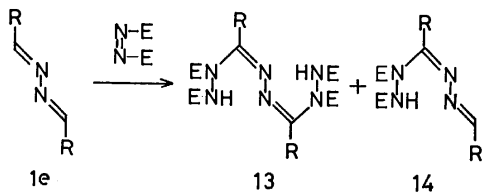

R=*p*-$Me_2NC_6H_4$ E=$CO_2C_2H_5$

Scheme 3.

to those of the starting azine **1e**. From the above observations it was concluded that both **13** and **14** were not the anticipated cycloadducts, but 1,4-conjugate adducts. Although Marchetti *et al.*[16] reported the reactions of ketazines with diethyl azodicarboxylate, that is, the formation of 2-[*N*,*N'*-bis(ethoxycarbonyl)-hydrazino]cyclohexanone azines from cyclohexanone azines by conjugate addition, no reactions of aldazines have appeared in the literature.[2]

Experimental

The measurements of IR, UV, and NMR spectra and the elemental analyses were performed with the same instruments as previously described.[1b]

Preparation of 5-Aryl-2,3-diphenyl-2-pyrrolin-4-ones (4). General Procedure: A mixture of **1** (1.0 mmol) and **2** (1.2 mmol) in toluene (10 ml) was refluxed for 18—48 h. After cooling the precipitates were collected by filtration and recrystallized to give yellow needles **4**.

*Compound **4a***: Reaction time 18 h. Yield 55%. Mp 282—285 °C (C_6H_6). IR (KBr): 3200, 1640, 1600, 1580, 1540, 1507 cm^{-1}. UV (MeOH) nm (log ε): 243 (4.35), 383 (3.88), 250 sh (4.34). MS *m/e* (%): 341 (M^+, 42), 339 (M^+-H_2, 28), 326 (M^+ —NH, 28), 298 (326—CO, 5.1), 178 (PhC≡CPh, 100). Found: C, 81.30; H, 5.23%. Calcd for $C_{23}H_{19}O_2N$: C, 80.91; H, 5.61%.

*Compound **4b***: Reaction time 48 h. Yield 49%. Mp 269—271 °C (C_6H_6). IR (KBr): 3230, 1640, 1605, 1582, 1540, 1508 cm^{-1}. UV (MeOH) nm (log ε): 254 (4.33), 383 (3.84). Found: C, 85.01; H, 5.64%. Calcd for $C_{23}H_{19}ON$: C, 84.89; H, 5.89%.

*Compound **4c***: Reaction time 48 h. Yield 42%. Mp 274—275 °C (THF–MeOH). IR (KBr): 3240, 2960, 1640, 1605, 1582, 1542, 1510 cm^{-1}. UV (MeOH) nm (log ε): 255 (4.32), 378 (3.81). Found: C, 85.00; H, 6.23%. Calcd for $C_{25}H_{23}ON$: C, 84.95; H, 6.56%.

*Compound **4d***: Reaction time 24 h. Yield 35%. Mp 279—284 °C (sublimation) (DMF). IR (KBr): 3230, 1640, 1605, 1580, 1540, 1512 cm^{-1}. UV (MeOH) nm (log ε): 254 (4.31), 385 (3.84). Found: C, 84.81; H, 5.26%. Calcd for $C_{22}H_{17}ON$: C, 84.86; H, 5.50%.

*Compound **4e***: Reaction time 18 h. Yield 87%. Mp 244—247 °C (C_6H_6). IR (KBr): 3200, 3040, 2880, 2800, 1633, 1600, 1580, 1540, 1510 cm^{-1}. UV (MeOH) nm (log ε): 261 (4.35), 400 (4.09). Found: C, 81.47; H, 5.84%. Calcd for $C_{24}H_{22}ON_2$: C, 81.32; H, 6.26%.

Preparation of 5-Aryl-2,3-diphenylpyrroles (7). General Procedure: A mixture of **4** (0.50 mmol) and powdered phosphorus pentasulfide (1.0 mmol) in C_6H_6 (10 ml) was refluxed for 3 h. After cooling the undissolved materials were removed from the mixture by decantation, and the solvent was removed under reduced pressure. The resulting residue was washed with a small amount of MeOH and recrystallized once to give **7**. In the case of **7d** the residue was purified by column chromatography on silica gel with $CHCl_3$.

*Compound **7a***: Yield 70%. White prisms; mp 180—182 °C (MeOH) (lit,[13] 180 °C). IR (KBr): 3370, 3050, 1605, 1530 cm^{-1}. MS *m/e* (%): 325 (M^+, 100). NMR ($CDCl_3$): δ 3.80 (s, 3H, OMe), 6.5—7.6 (m, 15H, ArH), 8.32 (braod s, 1H, NH).

*Compound **7b***: Yield 26%. White needles; mp 116—118 °C (MeOH). IR (KBr): 3460, 3020, 2920, 1603, 1493 cm^{-1}. NMR ($CDCl_3$): δ 2.35 (s, 3H, Me), 6.6—7.5 (m, 15H, ArH), 8.35 (broad s, 1H, NH). Found: C, 89.14; H. 6.11%. Calcd for $C_{23}H_{19}N$: C, 89.28; H, 6.19%.

*Compound **7d***: Yield 31%. Pale yellow plates; mp 137—138 °C (C_6H_6-petroleum ether) (lit,[17] 140 °C).

*Preparation of **7** from **9***. Compounds **7a** (73%), **7b** (26%), and **7d** (24%) were prepared from the corresponding **9a**, **9b**, and **9d**, respectively, according to the literature method,[13] and showed the same mps and IR spectra as those of **7** prepared from **4**.

*Treatment of **4a** with a Mixture of AcOH and Ac_2O.* A solution of **4a** (300 mg) in a mixture of AcOH (30 ml) and Ac_2O (0.3 ml) was refluxed for 10 h. The solvent was removed under reduced pressure and the resulting residue was purified by column chromatography on silica gel with $CHCl_3$ to give 2-(*p*-methoxyphenyl)-4,5-diphenyl-1,3-oxazin-6-one (**11a**) (93 mg, 23%). Recrystallization from MeOH–THF afforded yellow needles; mp 204—205 °C. IR (KBr): 1738, 1598, 1570, 1535, 1510 cm^{-1}. NMR (CF_3COOH): δ 4.03 (s, 3H, OMe), 7.1—8.5 (m, 14H, ArH). MS *m/e* (%): 355 (M^+, 53), 327 (M^+ —CO, 53), 135 (100). Found: C, 77.88; H, 4.88%. Calcd for $C_{23}H_{17}O_3N$: C, 77.73; H, 4.82%.

*Oxidation of **4** by Oxygen. General Procedure*: A solution of **4** (1.0 mmol) in pyridine (10 ml) was refluxed for 6—11 h in a stream of oxygen. After removal of the solvent under reduced pressure, the resulting residue was washed with a small amount of MeOH and recrystallized to give 2-aryl-4,5-diphenyl-1,3-oxazin-6-ones (**11**).

*Compound **11a***: Reaction time 6 h. Yield 46%. The mp and the IR spectrum were identical with those described above.

*Compound **11b***: Reaction time 9 h. Yield 38%. Yellow needles; mp 203—204 °C (MeOH). IR (KBr): 1730, 1610, 1600, 1570, 1545, 1505 cm^{-1}. NMR ($CDCl_3$): δ 2.45 (s, 3H, Me), 7.3—8.4 (m, 14H, ArH). Found: C, 81.17; H, 5.01%. Calcd for $C_{23}H_{17}O_2N$: C, 81.39; H, 5.05%.

*Compound **11c***: Reaction time 11 h. Compound **11c** was separated from the residue by column chromatography on silica gel with $CHCl_3$. Yield 50%. White needles; mp 131—134 °C (MeOH–THF). IR (KBr): 2960, 1732, 1610, 1600, 1565, 1548 cm^{-1}. NMR ($CDCl_3$): δ 1.28 (d, J=6.8 Hz, 6H, 2Me), 2.99 (m, 1H, CH), 7.2—8.3 (m, 14H, ArH). Found: C, 81.75; H, 5.77%. Calcd for $C_{25}H_{21}O_2N$: C, 81.72; H, 5.76%.

*Compound **11d***: Reaction time 9 h. Yield 45%. Yellow needles; mp 206—207 °C (MeOH–THF). The mp and the IR spectrum were identical with those of an authentic specimen prepared according to the literature.[15]

*Preparation of **11** from **7***. Compounds **11a** (36%), **11b** (30%), and **11d**(14%) were prepared from the correponding **7a**, **7b**, and **7d**, respectively, according to the literature method.[15] The mps and the IR spectra were identical with those described above.

*Photooxidation of **4**. General Procedure*: A solution of **4** (0.50 mmol) in $CHCl_3$ (200 ml) was irradiated by means of a 100W high-pressure mercury arc lamp with stirring in a stream of oxygen for 4 h. Removal of the solvent followed by column chromatography on silica gel with $CHCl_3$ gave the products **11**. Compounds **11a** (21%), **11b** (14%), and **11c** (16%) were obtained. The mps and the IR spectra were identical with those described above.

*Oxidation of **4** by Hydrogen Peroxide.* To a suspension of **4a** (340 mg, 1.0 mmol) in AcOH (10 ml) was added 30% H_2O_2 (0.45 g, 4.0 mmol) and the mixture was stirred at room temperature. After one day another equal amount of 30% H_2O_2 (0.45 g) was added and the reaction mixture was stirred for an additional day. The precipitates were

collected by filtration, washed with a small amount of MeOH, and recrystallized to give **11a** (290 mg, 85%). In the case of **4c** the reaction mixture was evaporated to dryness and the residue was chromatographed on silica gel with $CHCl_3$ to give **11c** (32%). The mps and the IR spectra were identical to those described above.

*Alkali Treatment of **4**.* General procedure: A solution of **4** (1.0 mmol) in a mixture of 1.0 M KOH (4.0 ml) and pyridine (16 ml) was stirred at room temperature for 2—3 h. The reaction mixture was poured into water (200 ml) and the precipitates were filtered off. The filtrate was acidified with dil HCl and allowed to stand. The separated precipitates were collected by filtration and once recrystallized to give 3-aroylamino-2,3-diphenylacrylic acids (**12**).

*Compound **12a***: Reaction time 2 h. Yield 36%. White prisms; mp 189—192 °C (MeOH). IR (KBr): 3020 (broad), 1688, 1640, 1600, 1584, 1560 cm^{-1}. NMR (DMSO-d_6) : δ 3.86 (s, 3H, OMe), 7.0—8.1 (m, 14H, ArH). MS *m/e* (%): 373 (M^+, 8.1), 355 ($M^+ - H_2O$, 4.2), 329 ($M^+ - CO_2$, 41), 222 (7.8), 135 (100). Found: C, 73.68; H, 5.25%. Calcd for $C_{23}H_{19}O_4N$: C, 73.98; H, 5.13%.

*Compound **12b***: Reaction time 2 h. Yield 25%. White needles; mp 190—191 °C (MeOH). IR (KBr): 3180, 1655, 1610, 1595, 1575 cm^{-1}. NMR (DMSO-d_6): δ 2.38 (s, 3H, Me), 7.1—9.1 (m, 14H, ArH). Found: C, 77.49: H, 5.67%. Calcd for $C_{23}H_{19}O_3N$: C, 77.29; H, 5.36%.

*Compound **12c***: Reaction time 3 h. Yield 26%. White needles; mp 197—198 °C (MeOH). IR (KBr): 3160, 2960, 1670, 1605, 1595, 1575 cm^{-1}. NMR (DMSO-d_6): δ 1.23 (d, J=6.8 Hz, 6H, 2Me), 2.95 (m, 1H, CH), 7.8—8.0 (m, 14H, ArH). Found: C, 77.79; H, 6.22%. Calcd for $C_{25}H_{23}O_3N$: C, 77.90; H, 6.01%.

*Compound **12d***: Reaction time 2 h. Yield 41%. White needles; mp 151—152 °C (EtOH). IR (KBr): 3060, 2860, 1690, 1650, 1615, 1593 cm^{-1}. Found: C, 73.01; H, 5.19%. Calcd for $C_{22}H_{17}O_3N \cdot H_2O$: C, 73.11; H, 5.30%.

*Alkali Treatment of **11***. Compounds **11** were treated with alkali in the same manner as described in the case of **4**. Compounds **12a** (65%), **12b** (63%), and **12d** (20%) were obtained and their mps and IR spectra were identical to those described above.

*Reaction of **1e** with Diethyl Azodicarboxylate.* A mixture of **1e** (1.30 g, 4.5 mmol) and diethyl azodicarboxylate (1.58 g, 9.1 mmol) in toluene (30 ml) was refluxed for 5 h. After removal of the solvent the resulting residue was subjected to column chromatography on silica gel with $CHCl_3$–AcOEt (1:1). Both the first and the second eluated fractions gave oils **13** (1.1 g, 77%) and **14** (430 mg, 42%), respectively, which crystallized upon adding a small amount of MeOH.

*3,6-Bis(p-dimethylaminophenyl)-1,2,7,8-tetrakis(ethoxycarbonyl)-1,2,4,5,7,8-hexaaza-3,5-octadiene (**13**).* Yellow powders; mp 188—189 °C (MeOH–H_2O). IR (KBr) : 3180, 2960, 1735, 1705, 1585, 1518 cm^{-1}. NMR (DMSO-d_6) : δ 0.92—1.35 (m, 12H, 4Me), 3.08 (s, 12H, $2NMe_2$), 3.83—4.15 (m, 8H, $4CH_2$), 8.58 (s, 2H, 2NH), 6.95 (d, J=9.0 Hz, 4H, 4*m*-H of ArH), 7.72 (d, J=9.0 Hz, 4H, 4*o*-H of ArH). UV (MeOH) nm (log ε): 241 (4.22), 320 sh (4.25), 382 (4.65).[18] MS *m/e* (%): 642 (M^+, 9.4), 467 (42), 454 (23), 351 (13), 294 (22), 280 (100), 266 (21), 175 (42). Found: C, 56.07; H, 6.54%. Calcd for $C_{30}H_{42}O_8N_8$: C, 56.06; H, 6.59%.

*3,6-Bis(p-dimethylaminophenyl)-1,2-bis(ethoxycarbonyl)-1,2,4,5-tetraaza,-3,5-hexadiene (**14**).* Yellow powders; mp 120—122 °C (MeOH–H_2O). IR (KBr): 3280, 2980, 2920, 1735, 1710, 1680, 1600, 1557, 1520 cm^{-1}. NMR ($CDCl_3$): δ 1.20 (t, J=7.5 Hz, 3H, Me), 1.27 (t, J=7.5 Hz, 3H, Me), 3.00 (s, 6H, NMe_2), 3.07 (s, 6H, NMe_2), 4.14 (q, J=7.5 Hz, 2H, CH_2), 4.22 (q, J=7.5 Hz, 2H, CH_2), 5.17 (s, 1H, CH), 6.70 (d, J=9.0 Hz, 2H, 2*m*-H of ArH), 6.85 (d, J=9.0 Hz, 2H, 2*o*-H of ArH), 7.70 (d, J=9.0 Hz, 4H, 2*o*- and 2*m*-H of ArH), 8.56 (s, 1H, NH). UV (MeOH) nm (log ε): 243 (4.26), 325 sh (4.28), 388 (4.61). Found: C, 61.31; H, 6.94%. Calcd for $C_{24}H_{32}O_4N_6$: C, 61.52; H, 6.88%.

The authors wish to express their thanks to Dr. Masatoshi Hirayama and Mr. Mamoru Sekine for the NMR measurements, and to Sankyo Co., Ltd., for the mass measurements.

References

1) The previous papers in this series: a) M. Takahashi, N. Suzuki, and Y. Igari, *Bull. Chem. Soc. Jpn.*, **48**, 2605 (1975); b) M. Takahashi, H. Ishida, and M. Kohmoto, *Bull. Chem. Soc. Jpn.*, **49**, 1725 (1976); c) M. Takahashi, S. Yamaguchi, and N. Igari, *Chem. Lett.*, **1977**, 1497.

2) T. Wagner-Jauregg, *Synthesis*, **1976**, 349.

3) T. Eicher and J. L. Weber, *Tetrahedron Lett.*, **1973**, 1541.

4) T. Eicher and J. L. Weber, *Tetrahedron Lett.*, **1974**, 1381.

5) T. Eicher, F. Abdesaken, G. Franke, and J. L. Weber, *Tetrahedron Lett.*, **1975**, 3915.

6) T. Eicher, G. Franke, and F. Abdesaken, *Tetrahedron Lett.*, **1977**, 4067.

7) A preliminary report, Ref 1c.

8) G. P. Gardini, "Advances in Heterocyclic Chemistry," ed by A. R. Katritzky and A. J. Boulton, Academic Press, New York and London (1973), Vol. 15, p. 67.

9) J. Davoll, *J. Chem. Soc.*, **1953**, 3802.

10) H. Bauer, *Angew. Chem.*, **80**, 758 (1968).

11) H. Bauer, *Chem. Ber.*, **104**, 259 (1971).

12) a) R. L. Mckee, "The Chemistry of Heterocyclic Compounds," ed by A. Weissberger, Interscience Publishers, New York and London (1962), Vol. 17, p. 327; b) Z. Eckstein and T. Urbański, "Advances in Heretocyclic Chemistry," ed by A. R. Katritzky, Academic Press, New York and London (1963), Vol. 2, p. 311.

13) W. Neugebauer and H. R. Stumpf, Ger. Patent, 1105714 (1959); *Chem. Abstr.*, **56**, 8215h (1962).

14) S. Satsumabayashi, S. Motoki, and H. Nakano, *J. Org. Chem.*, **41**, 156 (1976).

15) V. Sprio, *Gazz. Chim. Ital.*, **85**, 569 (1955); *Chem. Abstr.*, **50**, 4910b (1956).

16) a) L. Marchetti, *Ann. Chim. (Rome)*, **57**, 575 (1967); *Chem. Abstr.*, **67**, 53961d (1967); b) L. Marchetti and P. Bruni, *Ann. Chim. (Rome)*, **56**, 923 (1966); *Chem. Abstr.*, **66**, 55083x (1967).

17) V. Sprio and I. Fabra, *Ann. Chim. (Rome)*, **51**, 135 (1961); *Chem. Abstr.*, **55**, 19934e (1961).

18) UV spectrum (MeOH) of **1e**. nm (log ε): 244 (4.21), 330 sh (4.28), 393 (4.61).

Reactive Troponoids and *o*-Aminophenol. II. The Formation of Cyclohepta[*b*][1,4]benzoxazine and 11*H*-Cyclohepta[*b*][1,4]benzoxazin-10-one Derivatives from Isomeric Isopropyl-2-chlorotropones

Tetsuo Nozoe and Taichi Someya*

Central Research Laboratory of Takasago Perfumery Co., Ltd., Kamata, Ohta-ku, Tokyo 144

(Received March 30, 1978)

The reactions of three isomeric isopropyl-2-chlorotropones with *o*-aminophenol were investigated. 8-Isopropylcyclohepta[*b*][1,4]benzoxazine was obtained from 5-isopropyl-2-chlorotropone, while 4- and 6-isopropyl-derivatives gave the same mixture of 7- and 9-isopropylcyclohepta[*b*][1,4]benzoxazine. These facts showed that the amino group of *o*-aminophenol attacked both the C-1 and C-2 positions of 2-chlorotropones. Also 6-, 7-, and 8-isopropyl-11*H*-cyclohepta[*b*][1,4]benzoxazin-10-ones were obtained as the minor products of these reactions.

In the preceding paper,[1] we reported the formation of 2-(*o*-hydroxyanilino)tropone (**3a**) and cyclohepta[*b*]-[1,4]benzoxazine (**4**) by the reaction of 2-chloro- (**1a**) or 2-methoxytropone (**1b**) with *o*-aminophenol (**2a**). Since the reaction of **1a, b** with *o*-methoxyaniline (**2b**) resulted in the formation of a small amount of 1-(*o*-methoxyanilino)-7-(*o*-methoxyphenylimino)-1,3,5-cycloheptatriene (**5**), besides the corresponding aminotropone (**3b**), it has been shown that the amino group of *o*-aminophenol reacted not only with C-2 (or C-7), but also with the carbonyl group (C-1).[2]

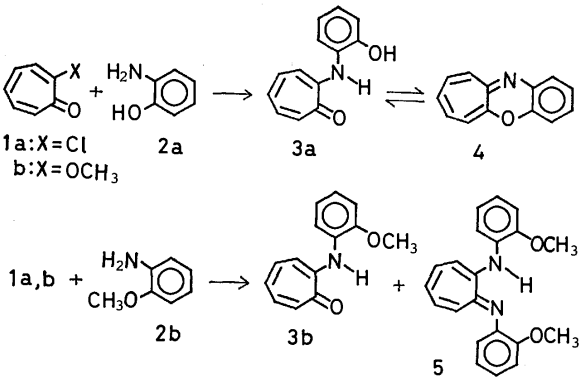

In order to confirm the position attacked by the amino group of the reagent on the seven-membered ring, we investigated the reactions of three isomeric isopropyl-2-chlorotropones (**7a—c**) with *o*-aminophenol. From the kinds of products obtained and their ratio, the amino group of the reagent was found to attack both the C-1 and C-2 positions of 2-chlorotropones approximately equally.

Results and Discussion

The most popular method of the synthesis of 2-chlorotropone is to treat tropolone with thionyl chloride,[3] but this method is not convenient when using alkyltropolones. We found the reaction of 2-tosyloxytropone with dry hydrogen chloride in dioxane[4] is most advantageous in such a case. By the use of this method,

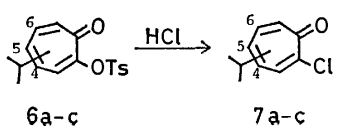

three isomeric isopropyl-2-chlorotropones (**7a—c**) were obtained in about a 90% yield from the corresponding tosylates (**6a—c**),[5] which indicated that normal replacement has taken place in these reactions.

The reaction of 2-chloro-5-isopropyltropone (**7b**) with *o*-aminophenol in acetic acid afforded **8b** (78%) and **9b** (0.5%). The heating of **8b** with 2 eq. of ethanolic alkali resulted in the quantitative formation of **10b**, along with a minute amount of **9b**, and **10b** reverted to **8b** quantitatively when heated in acetic

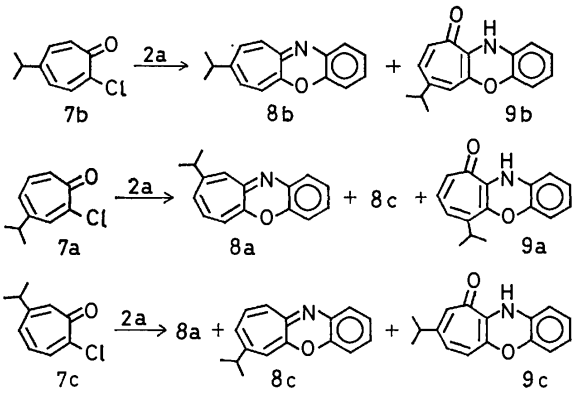

Scheme 1.

Table 1. NMR spectral data of isopropylcyclohepta-[*b*][1,4]benzoxazines (100 MHz in $CDCl_3$)

Proton	Chemical shift δ in ppm		
	7-*i*-Pr (**8c**)	8-*i*-Pr (**8b**)	9-*i*-Pr (**8a**)
6	5.40(d)[a]	5.37(d)[c] (6.74)[h]	5.37(d d)[e]
7		5.79(d)[d] (7.10)[h]	5.90(d d)[f]
8	5.66(d)[b]		5.68(br d)[g]
9	6.02(m, 2H)	6.07(d, 2H) (7.32)[h]	
10			6.04(br s)
4	6.37(m)	6.34(m) (6.54)[h]	6.37(m)
1—3	6.71(m)	6.70(m) (6.81)[h]	6.72(m)

a) J=1.1 Hz. b) J=7.0 Hz. c) J=9.7 Hz. d) J=9.7 Hz. e) J=9.0 and 1.1 Hz. f) J=11.3 and 9.0 Hz. g) J=11.3 Hz. h) In CF_3COOD.

acid in the presence of concd sulfuric acid. From these results, and from their elemental analytical and spectral data, **8b** was determined to be 8-isopropylcyclohepta[*b*][1,4]benzoxazine and **10b** as 5-isopropyl-2-(*o*-hydroxyanilino)tropone.

The reaction of 2-chloro-4-isopropyltropone (**7a**) with *o*-aminophenol afforded **8a** (40%) and **8c** (38%), besides **9a** (0.5%). In the same reaction, 2-chloro-6-isopropyltropone (**7c**) also gave **8a** (36%) and **8c** (42%), besides **9c** (0.5%). The structures of **8a** and **8c** were determined to be 9-isopropyl- (**8a**) and 7-isopropylcyclohepta[*b*][1,4]benzoxazine (**8c**) from their NMR spectra, shown in Table 1.

When **8a** was heated with 2 eq. of ethanolic alkali, **10a** was obtained quantitatively, along with traces of **9a**. In the same manner, **10c** and traces of **9c** were obtained from **8c**. **10a** and **10c** were reverted to **8a** and **8c** respectively by heating in acetic acid in the presence of concd sulfuric acid. From these results, **10a** and **10c** were determined to be 4-isopropyl- and 6-isopropyl-2-(*o*-hydroxyanilino)tropone, respectively (Scheme 2).

The NMR spectral measurement of **8b** in trifluoroacetic acid, which exists as a cation, **11**, shows, as in the case of the parent **4**,[1] shifts of the seven-membered ring protons by 1.22—1.37 ppm and those of the benzene-ring protons by 0.11—0.20 ppm to a lower magnetic field (Table 1).

It should be noted in these reactions that the same mixture of **8a** and **8c** was obtained from both **7a** and **7c**, indicating that the amino group of *o*-aminophenol attacked both C-2 and C-1 positions to the same extent. It is clear from the formation of these products that the so-called cine-reaction[6] (abnormal substitution at C-7 instead of C-2) has not taken place. Tropones act as tropylium ions in an acidic medium, so C-1 positions also seem liable to be attacked by nucleophiles.

The three products (**9a**—**c**) obtained in small amounts were found to be isomers with the same formula of $C_{16}H_{15}NO_2$, and their IR absorptions at 3200—3250 cm^{-1} (NH) and 1607—1610 cm^{-1} (C=O) agree with those at 3218 cm^{-1} (NH) and at 1607 cm^{-1} (C=O) in the 11*H*-cyclohepta[*b*][1,4]benzothiazin-10-one (**12a**) obtained earlier.[7]

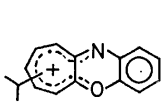

11

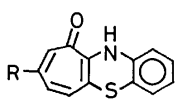

12 a: R = H
b: R = iPr

In the NMR spectrum of **9c**, the broad singlet at δ 6.98 ppm was considered to be the proton on C-9, next to the carbonyl group in the seven-membered ring; this agrees well with the absorption at δ 7.05 ppm (br s, C_9–H) in the NMR spectrum of 11*H*-8-isopropylcyclohepta[*b*][1,4]benzothiazin-10-one (**12b**).[8] From this evidence, **9c** was determined to be 11*H*-8-isopropylcyclohepta[*b*][1,4]benzoxazin-10-one. It was considered that **9c** was formed by the dehydrogenation of the intermediate B, derived from the cyclization of **10c** at the C-3 position. A similar explanation can be put forward for the formation of 11*H*-6-isopropyl- (**9a**) and 11*H*-7-isopropylcyclohepta[*b*][1,4]benzoxazin-10-one (**9b**) from **10a** and **10b** respectively. Interconversion between **8** and **10** obviously proceeds *via* the hydrated intermediate, A (Scheme 2).

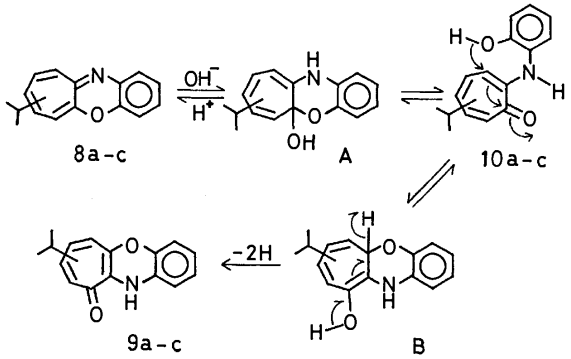

Scheme 2.

Experimental

All the melting points are uncorrected. TLC and preparative TLC were carried out on Kiesel gel 60 F_{254} (Merck) and Wakogel BF-5 (Wako) respectively, developed with benzene, and spots were detected with an UV lamp. The IR and UV spectra were taken on a Hitachi EPI-G2 and a Hitachi 124 spectrophotometer respectively. The UV spectra in an acidic or basic medium were measured by adding three drops of 1 M HCl or 1 M NaOH to the sample solution. The NMR spectra were recorded on a 60 MHz Hitachi-R-24A and a 100 MHz Varian HA-100 spectrometer, with TMS as the internal standard. The mass spectra were recorded on a Hitachi RMU-6M mass spectrometer operating at 75 eV.

2-Chloro-5-isopropyltropone (7b). A solution of 5-isopropyl-2-tosyloxytropone (**6b**)[5] (1.6 g, 5.0 mmol) in dry dioxane (30 ml) was refluxed by passing dry hydrogen chloride through for 20 min. After the dioxane has been removed under reduced pressure, the residue was dissolved in ether. The ether solution was passed through an alumina column to give 0.9 g (97%) of **7b** as a pale yellow oil.

By the same procedure, 2-chlorotropone was obtained from 2-tosyloxytropone in a 96% yield.

2-Chloro-4-isopropyltropone (7a) and 2-Chloro-6-isopropyltropone (7c). 4-Isopropyl- (**6a**) and 6-isopropyl-2-tosyloxytropone (**6c**) were prepared from β-thujaplicin by the reported method.[5] By the method described above, from **6a** (2.1 g, 6.6 mmol) 1.1 g (90%) of **7a** were obtained as a pale yellow oil. Similarly, 3.3 g (94%) of **7c** were obtained from **6c** (6.2 g, 19.5 mmol); subsequent recrystallization from hexane afforded pale yellow needles; mp 48 °C. (Lit,[5] 46.5—48.5 °C)

8-Isopropylcyclohepta[b][*1,4*]*benzoxazine (8b).* A mixture of **7b** (0.8 g, 4.4 mmol), **2a** (0.8 g, 7.3 mmol), and acetic acid (4 ml) was refluxed for 2 h. After the removal of the acetic acid under reduced pressure, 30 ml of water was added to the residue, and it was extracted with $CHCl_3$. The extract was evaporated, the residue of dark brown oil was dissolved in EtOH, and an EtOH solution of picric acid was added. When the resulting picrate was filtered and washed with ether, 1.46 g were obtained; mp 193—196 °C. The picrate was stirred with EtOH (5 ml) and 1M NaOH (25 ml) for 20 min at room temp. The mixture was then extracted with benzene. The extract was washed with water, dried over Na_2SO_4, and evaporated. The recrystallization of the residue from hexane gave 0.76 g (78%) of **8b** as dark

brown plates; mp 105 °C; λ_{max}^{MeOH} nm (log ε): 214 (4.24), 263 (4.31), 270 (4.27), and 418 (3.99); $\lambda_{max}^{MeOH+HCl}$ nm (log ε): 221 (4.27), 265 (4.32), 273 (4.46), 320 (3.80), and 436 (3.82); NMR (see Table 1). Found: C, 81.00; H, 6.41; N, 6.07%; M^+, 237. Calcd for $C_{16}H_{15}NO$: C, 80.98; H, 6.37; N, 5.90%; M, 237. Picrate: brown needles (from EtOH); mp 198 °C (dec).

11H-7-Isopropylcyclohepta[b][*1,4*]*benzoxazin-10-one* (**9b**). From the filtrate of the preparation of the picrate, 50 mg of **7b** and 6 mg (0.5%) of **9b** were obtained by preparative TLC. Recrystallization from ethyl acetate gave red needles; mp 114 °C; λ_{max}^{MeOH} nm (log ε): 208 (4.39), 228 (4.45), 257 (4.35), 268 (4.34), 285 (4.25), 420 (3.79)^{sh}, and 480 (3.97); $\lambda_{max}^{MeOH+HCl}$ nm (log ε): 208 (4.37), 228 (4.48), 260 (4.28), 270 (4.29), 286 (4.36), 325 (3.85), and 470—490 (3.93); IR (KBr): 3240 (NH) and 1610 cm^{-1} (C=O). Found: C, 75.65; H, 6.01; N, 5.58%; M^+, 253. Calcd for $C_{16}H_{15}NO_2$: C, 75.87; H, 5.97; N, 5.53%; M, 253.

Reaction of **7a** *with* **2a**. A mixture of **7a** (1.0 g, 5.5 mmol), **2a** (1.0 g, 9.2 mmol), and acetic acid (4 ml) was refluxed for 2 h. By a method similar to the reaction of **7b** with **2a**, 3g of dark brown crystals were obtained. These crystals were shown by TLC to be a mixture of two components. Then **8a** (0.52 g, 40%) and **8c** (0.49 g, 38%) were obtained by preparative TLC. From the filtrate which the picrate was separated, 7 mg (0.5%) of **9a** were obtained by preparative TLC.

9-Isopropylcyclohepta[b][*1,4*]*benzoxazine* (**8a**): Dark brown needles (from hexane); mp 63 °C; λ_{max}^{MeOH} nm (log ε): 207 (4.17), 215 (4.17), 263 (4.31), 270 (4.29), and 414 (3.95); $\lambda_{max}^{MeOH+HCl}$ nm (log ε): 205 (4.13), 227 (4.20), 265 (4.24)^{sh}, 275 (4.28), 316 (3.83), and 435—450 (3.82); NMR (see Table 1). Found: C, 80.77; H, 6.27; N, 6.13%; M^+, 237. Picrate: brown needles (from EtOH); mp 221—222 °C (dec).

7-Isopropylcyclohepta[b][*1,4*]*benzoxazine* (**8c**): Dark brown needles (from hexane); mp 109 °C; λ_{max}^{MeOH} nm (log ε): 207 (4.23), 215 (4.24), 263 (4.31), 270 (4.29), and 415 (3.96); $\lambda_{max}^{MeOH+HCl}$ nm (log ε): 206 (4.22), 226 (4.33), 265 (4.25)^{sh}, 275 (4,28), 317 (3.84), and 435—450 (3.84); NMR (see Table 1). Found: C, 80.73; H, 6.23; N, 5.90%; M^+, 237. Picrate: brown needles (from EtOH), mp 201—202 °C (dec).

11H-6-Isopropylcyclohepta[b][*1,4*]*benzoxazin-10-one* (**9a**): Orange red needles (from EtOAc); mp 141 °C; λ_{max}^{MeOH} nm (log ε): 207 (4.36), 230 (4.45), 257 (4.34), 269 (4.33), 286 (4.28), 410 (3.76)^{sh}, and 470 (3.98); $\lambda_{max}^{MeOH+HCl}$ nm (log ε): 207 (4.34), 228 (4.49), 260 (4.28), 270 (4.31), 288 (4.37), 325 (3.82)^{sh}, and 450—470 (3.93); IR (KBr): 3200 (NH) and 1610 cm^{-1} (C=O); NMR (100 MHz in $CDCl_3$): δ 6.90 (m, 1H, C_9-H), 6.38—6.78 (m, 6H), 3.24 (m, 1H, CH), and 1.19 ppm (d, 6H, J=7.0 Hz, CH_3). Found: C, 75.75; H, 6.03; N, 5.57%; M^+, 253.

Reaction of **7c** *with* **2a**. A mixture of **7c** (3.0 g, 16.4 mmol), **2a** (3.0 g, 27.5 mmol), and acetic acid (20 ml) was refluxed for 2 h. After the treatment described above, **8a** (1.3 g, 36%), **8c** (1.5 g, 42%), **9c** (19 mg, 0.5%), and **7c** (0.25 g) were obtained.

11H-8-Isopropylcyclohepta[b][*1,4*]*benzoxazin-10-one* (**9c**): Red needles (from EtOAc); mp 172 °C; λ_{max}^{MeOH} nm (log ε): 205 (4.34), 233 (4.45), 258 (4.35), 270 (4.35), 283 (4.22) 415 (3.76)^{sh}, and 480 (3.97); $\lambda_{max}^{MeOH+HCl}$ nm (log ε): 205 (4.34), 230 (4.46), 260 (4.32)^{sh}, 270 (4.35), 285 (4.36), 322 (3.80)^{sh}, and 450—485 (3.94); IR (KBr): 3250 (NH), and 1607 cm^{-1} (C=O); NMR (100 MHz in $CDCl_3$): δ 6.98 (br s, 1H, C_9-H), 6.28—6.68 (m, 6H), 2.60 (m, 1H, CH), and 1.13 ppm (d, 6H, J=7.0 Hz, CH_3). Found: C, 75,73; H, 5.92; N, 5.54%; M^+, 253.

4-Isopropyl-2-(o-hydroxyanilino)tropone (**10a**). A solution of **8a** (0.5 g, 2.1 mmol) in ethanol (10 ml) and 1M NaOH (5 ml) was refluxed for 1 h. After the subsequent removal of the ethanol, the residue was dissolved in water (5 ml) and adjusted to make it slightly acidic with 1M HCl. The resulting precipitate was filtered and dried in a desiccator. Recrystallization from hexane afforded 0.47 g (88%) of **10a** as yellow needles; mp 170 °C. From the mother liquor, 2 mg of **9a** was obtained by preparative TLC. **10a**: λ_{max}^{MeOH} nm (log ε): 208 (4.45), 235(4.28), 255 (4.18), 343 (3.88), and 400 (4.07); $\lambda_{max}^{MeOH+HCl}$ nm (log ε): 208 (4.25), 245 (4.32), 257 (4.30), and 378 (3.92); $\lambda_{max}^{MeOH+NaOH}$ nm (log ε): 235 (4.85), 340 (3.62)^{sh}, and 410 (4.00); IR (KBr): 3300 (NH), 3050 (OH), and 1590 cm^{-1} (C=O); NMR (60 MHz in $CDCl_3$): δ 9.70 (br s, 1H, OH), 8.75 (br s, 1H, NH), 6.50—7.30 (m, 8H), 2.72 (m, 1H, CH), and 1.15 ppm (d, 6H, J=7.0 Hz, CH_3). Found: C, 75.23; H, 6.73; N, 5.55%; M^+, 255. Calcd for $C_{16}H_{17}NO_2$: C, 75.27; H, 6.71; N, 5.49%; M, 255.

5-Isopropyl-2-(o-hydroxyanilino)tropone (**10b**). By the method described above, 0.48 g (89%) of **10b** and 2 mg of **9b** were obtained from 0.5 g of **8b**. **10b**: Orange yellow needles (from hexane); mp 181 °C; λ_{max}^{MeOH} nm (log ε): 208 (4.38), 236 (4.42), 346 (3.96), and 409 (4.07); $\lambda_{max}^{MeOH+HCl}$ nm (log ε): 241 (4.41) and 382 (3.96); $\lambda_{max}^{MeOH+NaOH}$ nm (log ε): 236 (4.64), 346 (3.65), and 418 (4.00); IR (KBr): 3250 (NH), 3050 (OH), and 1600 cm^{-1} (C=O); NMR (60 MHz in $CDCl_3$): δ 9.60 (br s, 1H, OH), 8.60 (br s, 1H, NH), 6.70—7.25 (m, 8H), 2.75 (m, 1H, CH), and 1.16 ppm (d, 6H, J=8.0 Hz, CH_3). Found: C, 75.05; H, 6.74; N, 5.41%; M^+, 255.

6-Isopropyl-2-(o-hydroxyanilino)tropone (**10c**). By the method described above, 0.48 g (89%) of **10c** and 2 mg of **9c** were obtained from 0.5 g of **8c**. **10c**: Orange yellow needles (from hexane); mp 181 °C; λ_{max}^{MeOH} nm (log ε): 236 (4.28), 250 (4.28), 345 (3.87), and 400 (4.08); $\lambda_{max}^{MeOH+HCl}$ nm (log ε): 245 (4.20), 255 (4.19), and 383 (3.88); $\lambda_{max}^{MeOH+NaOH}$ nm (log ε): 235 (4.27) and 410 (3.88); IR (KBr): 3300 (NH), 3000 (OH), and 1590 cm^{-1} (C=O); NMR (60 MHz in $CDCl_3$): δ 9.30 (br s, 1H, OH), 8.50 (br s, 1H, NH), 6.45—7.20 (m, 8H), 2.70 (m, 1H, CH), and 1.10 ppm (d, 6H, J=7.0 Hz, CH_3). Found: C, 75.16; H, 6.58; N, 5.53%; M^+, 255.

Conversion of **10a—c** *into* **8a—c**. A solution of **10** (0.2 g) in acetic acid (2 ml) and one drop of concd H_2SO_4 was refluxed for 15 min. The solution turned dark brown. After the removal of the acetic acid, the residue was extracted with benzene. The extract was washed with aq $NaHCO_3$ and water, dried over Na_2SO_4, and evaporated. The recrystallization of the residue from hexane gave **8**. The yields were **8a** (90%), **8b** (89%), and **8c** (90%) respectively.

The authors wish to express their thanks to Professor Shô Itô and Dr. Yoshimasa Fukazawa (Tohoku University) for the assignment of the NMR spectra, and also to Dr. Masao Sugimura and the Sankyo Co., Ltd., for measuring some of the mass spectra and 100 MHz NMR spectra and for their elemental analyses.

References

1) T. Nozoe, H. Okai, and T. Someya, *Bull. Chem. Soc. Jpn.*, **51**, 2185 (1978).

2) It has been known that, in the reactions of reactive troponoids (**1**) with amines, usually the amino group of

the reagents attacks not at the carbonyl carbon (C-1), but at C-2 or C-7 position exclusively. *Cf.* T. Nozoe, "Daiyuki Kagaku," Asakura, Tokyo (1961), Vol. 13, p. 187.

3) T. Nozoe, S. Seto, S. Itô, M. Sato, and K. Kotono, *Proc. Jpn. Acad.*, **28**, 488 (1952).

4) H. Matsumura, *Nippom Kagaku Kaishi*, **82**, 623 (1961).

5) T. Sato, *Nippon Kagaku Kaishi*, **80**, 1056, 1058 (1959).

6) As for cine-substitution, see, for example, T. Nozoe, *Pure Appl. Chem.*, **28**, 239 (1971).

7) T. Nozoe, T. Asao, and K. Takahashi, *Bull. Chem. Soc. Jpn.*, **34**, 146 (1961).

8) Kindly measured by Dr. Kazuko Takahashi (Tohoku University).

Peptides. VII. Some Sulfonates of Strongly Acidic *N*-Hydroxy Compounds as Novel Coupling Reagents[1)]

Masumi ITOH,* Hiroshi NOJIMA, Jiyoji NOTANI, Daijiro HAGIWARA, and Kuniaki TAKAI

Research Laboratories, Fujisawa Pharmaceutical Co., Ltd., Kashima-cho, Yodogawa-ku, Osaka 532

(Received April 1, 1978)

Sulfonates of strongly acidic *N*-hydroxy compounds such as 6-chloro-1-(*p*-chlorophenylsulfonyloxy)benzotriazole have been found to be excellent coupling reagents for amide bond formation. Amides can be prepared through either an active ester or a mixed anhydride according to the chosen procedure. Several active esters and protected di- and tripeptides prepared are listed in the Tables. Racemization, possible side reactions, and reaction pathways of the amide bond formation have also been discussed.

Many reports on coupling methods and reagents for peptide synthesis have been published. Many of these reagents can be added directly to a mixture of a carboxyl and an amino components to simplify the technique. Of these, dicyclohexylcarbodiimide (DCC) is the most versatile and widely utilized one, although it has the following disadvantages:[2)] 1) the rearrangement of the active intermediate, *O*-acyl-*N*,*N*'-dicyclohexylisourea, to the inactive *N*-acyl-*N*,*N*'-dicyclohexylurea, 2) the contamination of products by *N*,*N*'-dicyclohexylurea which is to a certain extent soluble in many organic solvents, 3) the dehydration from the side chain amide group of *N*-protected asparagine or glutamine to the corresponding cyano group, 4) the racemization *via* oxazolone formation, and 5) the allergic property to humans. A recent investigation revealed that DCC might lead histidine-containing peptides to their N^{im}-(*N*,*N*'-dicyclohexylamidino) derivatives.[3)] The present authors wish to report some new sulfonate-type coupling reagents which promise the simple operation, high purity and high yield of products, and seem to be superior to DCC at the points mentioned above.

It has been reported that some carbonates of strongly acidic *N*-hydroxy compounds activated carboxylic acids by the formation of mixed anhydride-type intermediates which were subsequently transformed to esters in good yield by eliminating carbon dioxide. One of these carbonates, ethyl 2-(isobutoxycarbonyloxyimino)-2-cyanoacetate, may be employed as a coupling reagent in the mixed anhydride method.[4)] These results prompted the preparation of ethyl 2-(methylsulfonyloxyimino)-2-cyanoacetate (**3a**)[5)] and its potency as a coupling reagent was examined. Preliminary experiments showed that the coupling of a carboxylic acid with an amine proceeded smoothly by the use of **3a** and triethylamine at room temperature affording an amide in excellent yield. To demonstrate the superiority of **3a** to methanesulfonyl chloride (**1a**) itself or a combination of **1a**/ethyl 2-hydroxyimino-2-cyanoacetate (**2a**), ethyl *N*-benzyloxycarbonyl-L-prolyl-L-leucinate (**5**) was prepared using the above mentioned reagents. *N*-Benzyloxycarbonyl-L-proline (**6**) was allowed to react with the reagents in the presence of triethylamine in chloroform for 15 min at 0 °C, then a solution of ethyl L-leucinate (**7**) in chloroform was added to the resulting mixture. After stirring for 18 h at room temperature, **5** was obtained in 61.5, 76.9, and 80.2% yield by the use of **1a**, the combination of **1a**/**2a**, and **3a**, respectively. These results indicated the value of preparing other sulfonates of *N*-hydroxy compounds. The sulfonates were prepared by the reaction of alkane- or arenesulfonyl chlorides (**1**) with *N*-hydroxy compounds (**2**) under the conditions of the Schotten-Baumann reaction, and were stable, easy to prepare, and highly reactive crystalline materials. Some sulfonates were difficult to isolate such as 1-(trichloromethylsulfonyloxy)-benzotriazole. The sulfonates of *N*-hydroxy compounds prepared are listed in Tables 1 and 2. Most of the sulfonates are stable crystalline materials unless

TABLE 1. SOME SULFONATES OF VARIOUS *N*-HYDROXY COMPOUNDS

$$R^1\text{-}SO_2\text{-}ON\begin{matrix}R^2\\R^3\end{matrix} \quad (3)$$

	R^1	R^2 R^3	Solvent	Base	Yield(%)	Mp(°C)	Recrysted from
3a	Me	NC-C(-)-COOEt	C_6H_6	TEA	96.3	79—81	C_6H_6/pet. ether
b	Me- 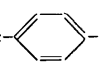	NC-C(-)-COOEt	EtOAc	TEA	93.9	84—87	EtOAc/c. hexane
c	Me	NC-C(-)-$CONH_2$	H_2O/EtOAc	NaOH	76.4	143—145	Diox./EtOAc/pet. ether
d	Me	$-CO(CH_2)_2-CO-$	C_6H_6/Diox.	TEA	32.6	150—152	EtOAc/pet. ether
e	Me	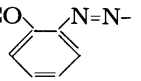	C_6H_6	TEA	77.2	132—134	C_6H_6/pet. ether
f		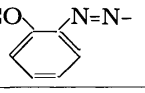	H_2O/EtOAc	NaOH	88.9	132—134	C_6H_6

Table 2. Sulfonates of 1-hydoxybenzotriazoles

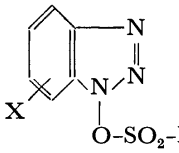

(4)

4	R^1	X	Solvent	Base	Yield (%)	Mp (°C)	Crystd from
a	Me	H	H_2O/EtOAc	NaOH	99.0	90—92	A
b	Bu(*n*)	H	C_6H_6	TEA	96.8	oil	
c	CH_2-(DL) O	H	CH_2Cl_2	TEA	35.8	148—150	B
d	CH_2-	H	H_2O/ether	NaOH	46.7	65—67	A
e	-	H	H_2O	NaOH	85.5	83—84	B
f	-Me	H	H_2O/ether	NaOH	86.1	84—86	C
g	-Cl	H	C_6H_6	TEA	98.6	94—95	D
h	$-NO_2$	H	H_2O	NaOH	43.8	119.5—121.5	E
i	Me_3(2,4,6)	H	CH_2Cl_2	TEA	68.9	130—131	F
j	N	H	H_2O/ether	NaOH	70.0	98	
k	-CH=CH-	H	CH_2Cl_2	TEA	75.0	102—103	B
l	Me	NO_2(6)	H_2O/EtOAc	NaOH	72.0	117—118	B
m	CH_2-(DL) O	NO_2(6)	CH_2Cl_2	TEA	89.0	157—159	B
n	-	NO_2(6)	EtOAc	TEA	53.1	122—124	B
o	-Me	NO_2(6)	EtOAc	TEA	56.1	144	B
p	Me	Cl(6)	C_6H_6	TEA	82.9	174—175(dec)	D
q	Bu(*n*)	Cl(6)	EtOAc	TEA	88.9	72—74	G
r	CH_2-(DL) O	Cl(6)	C_6H_6	TEA	89.6	151—153	H
s	CH_2-	Cl(6)	H_2O/ether	NaOH	57.3	126.5—127.5	H
t	-	Cl(6)	H_2O/ether	NaOH	83.0	110—110.5	H
u	-Me	Cl(6)	C_6H_6	TEA	77.8	94—96	I
v	-Cl	Cl(6)	H_2O/ether	NaOH	91.4	125—127	A
w	Me	Cl(4)	C_6H_6	TEA	79.2	71—74	D

Recrystallization solvents: A=benzene/petroleum ether; B=ethyl acetate/hexane; C=ethanol; D=ethyl acetate/peteoleum ether; E=benzene; F=dichloromethane/hexane; G=tetrachloromethane/petroleum ether; H=benzene/hexane; I=terachloromethane.

exposed to atmospheric moisture for a long period, and are storable in a closed brown bottle without decomposition for three years. Some representative sulfonates were subjected to a rough comparison of their reactivity in the coupling of **6** or *N*-benzyloxycarbonyl-L-phenylalanine (**8**) with **7** at room temperature (Table 3). It is apparent from the table that the reactivity of each sulfonate is largely dependent on the acidity of both the parent *N*-hydroxy compound and the sulfonic acid. Electron-withdrawing substituents on the nuclei of both benzotriazole and benzenesulfonic acid increased the reactivity of the corresponding sulfonate. In contrast with the reactive sulfonates, the sulfonates of phenols such as the methanesulfonate[6] of 2,4-dinitrophenol (pK_a 4.11) showed far less reactivity.

Table 3. An approximate comparison of the reactivity of representative sulfonates

Z-AA-OH + H-Leu-OEt ⟶ Z-AA-Leu-OEt

Z-AA-OH	Reagent	Procedure	Base	Solvent	Yield (%)
Z-Phe-OH	**3a**	A	TEA	CH_2Cl_2	80
Z-Phe-OH	**3a**	B	TEA	CH_2Cl_2	80
Z-Phe-OH	**3d**	A	TEA	CH_2Cl_2	trace
Z-Phe-OH	**4a**	B	TEA	CH_2Cl_2	83
Z-Phe-OH	**4e**	B	TEA	CH_2Cl_2	80
Z-Phe-OH	**4v**	B	TEA	CH_2Cl_2	75
Z-Pro-OH	**3a**	B	TEA	$CHCl_3$	72
Z-Pro-OH	**3b**	B	TEA	$CHCl_3$	trace
Z-Pro-OH	**3e**	B	NMM	$CHCl_3$	67
Z-Pro-OH	**3f**	B	NMM	$CHCl_3$	67

NMM = *N*-Methylmorpholine.

Table 4. Comparison of reactivity and stability of the sulfonates

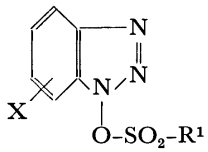

(**4**)

4	R^1	X	Reaction time required (min)	Stability to[a] moisture
a	Me	H	10	poor
c	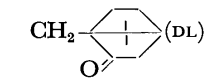 (DL)	H	180	excellent
d	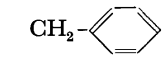	H	—	poor
e	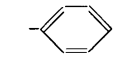	H	60	poor
f	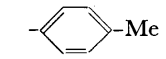	H	360	—
g	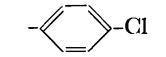	H	25	good
h	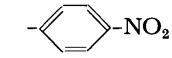	H	20	—
i	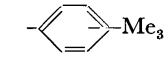	H	120	—
j	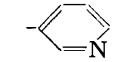	H	20	—
k	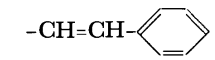	H	45	poor
m	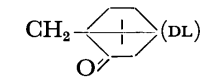 (DL)	NO_2(6)	3	excellent
n	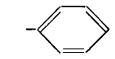	NO_2(6)	10	good
o	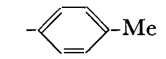	NO_2(6)	10	excellent
p	Me	Cl(6)	10	excellent
t	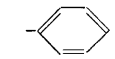	Cl(6)	20	good
u	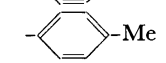	Cl(6)	45	—
v	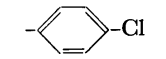	Cl(6)	5	good

a) Poor: decomposed within 3 days; good: unchanged after more than 3 days; excellent: unchanged after more than a week.

Table 5. Active esters of several carboxylic acids $R^4\text{-}COON\begin{matrix}R^2\\R^3\end{matrix}$

R^4-CO-	R^2 R^3	Reagent	Base	Solvent	Yield (%)	Mp (°C)	Recrystd from
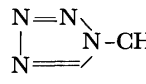	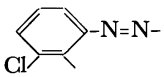	**4v**	TEA	$CHCl_3$	70	171—172 (dec)	$CHCl_3$
Z-Val-	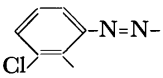	**4v**	TEA	$CHCl_3$	84	96—96.5	ether/hexane
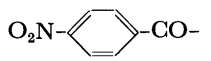	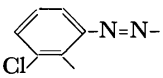	**4v**	TEA	$CHCl_3$	69.6	198—199 (dec)	$CHCl_3$
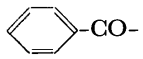	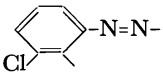	**4v**	TEA	CH_2Cl_2	83	132	CCl_4/ pet. ether
H_3C-CO-	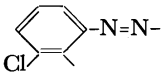	**4v**	TEA	$CHCl_3$	83	141—142	EtOH
H_3C-CO-	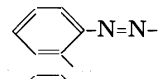	**4a**	TEA	CH_2Cl_2	84.6	102—106	C_6H_6
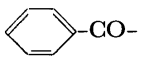	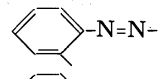	**4g**	TEA	$CHCl_3$	81	77—79	ether/ cyclohexane
Z-Phe-	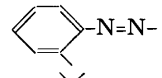	**4a**	TEA	EtOAc	62	120—125	2-propanol
Z-Phe-	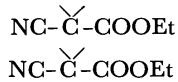	**3a**	TEA	EtOAc	95	oil[a)]	
Z-Pro-		**3a**	TEA	EtOAc	100	oil[a)]	

a) Solidifiied on standing.

In another series of preliminary experiments, it was observed that **3a**, 3-(methylsulfonyloxy)- and 3-(phenylsulfonyloxy)-1,2,3-benzotriazine-4-ones (**3e** and **3f**) induced colored impurities into the products, whereas the sulfonates of the benzotriazole series gave satisfactory results. Consequently, the reagents of the benzotriazole series were subsequently studied. To select the most prominent one from the sulfonates, the reactivity in the coupling of **6** (5 mmol) and **7** hydrochloride (2.5 mmol) by the use of triethylamine (7.5 mmol) and the sulfonates (5 mmol) were compared by recording the time required for the disappearance of free **7** in the reaction mixture. At the same time, the stability to atmospheric moisture was examined by infrared and thin layer chromatography. Most of the sulfonates adsorbed atmospheric moisture gradually during exposure and showed partial decomposition to some extent. Table 4 summarizes the results, and it is clearly shown that the stability of the reagents has no relation to their reactivity, but with their hygroscopic characters. In consideration of the reactivity, stability and accessibility, 6-chloro-1-(*p*-chlorophenylsulfonyloxy)benzotriazole (**4v**) was finally chosen as the prominent member of the series.

Using the sulfonates of acidic *N*-hydroxy compounds, amides can be prepared by the following two procedures: (A) activation of a carboxyl component with a reagent prior to the addition of an amine component, and (B) the direct addition of the reagent into a mixture of the carboxyl and the amine components. The use of an equimolar amount of tertiary amine is essential in both procedures.

Procedure A:

$$R^1\text{-}SO_2\text{-}ON\begin{matrix}R^2\\R^3\end{matrix} + R^4\text{-}COOH \xrightarrow{\text{Base}}$$

$$R^4\text{-}COON\begin{matrix}R^2\\R^3\end{matrix} + R^1\text{-}SO_3H\cdot\text{Base}$$

$$\downarrow H_2N\text{-}R^5$$

$$R^4\text{-}CONH\text{-}R^5 + HON\begin{matrix}R^2\\R^3\end{matrix}$$

Procedure B:

$$R^1\text{-}SO_2\text{-}ON\begin{matrix}R^2\\R^3\end{matrix} + R^4\text{-}COOH + H_2N\text{-}R^5 \xrightarrow{\text{Base}}$$

$$R^4\text{-}CONH\text{-}R^5 + R^1\text{-}SO_3H\cdot\text{Base} + HON\begin{matrix}R^2\\R^3\end{matrix}$$

Scheme 1.

In procedure A, the active ester formation is rapid and is usually completed within one hour using triethylamine in chloroform or ethyl acetate at room temperature. When pyridine is employed as a base, a polar solvent such as acetonitrile is necessary to produce a smooth reaction. The active ester formed in this stage can be isolated in good yield, some examples of which are listed in Table 5. Aminolysis of the active esters is also completed within a few hours at room temperature.

In procedure B, the reaction mixture tends to be

Table 6. Preparation of protected di- and tripeptides

Acylamino acid	Amino acid ester salt	Reagent	Procedure	Base/Solvent	Reaction time (h)	Yield (%)	Ref.
Boc-Arg(NO_2)-OH	Tos-OH·H-Tyr-OBzl	**4a**	B	2TEA/$CHCl_3$	20	70.3[a)]	
Z-Arg(NO_2)-OH	HCl·H-Gly-OEt	**4a**	B	2NMM/DMF-$CHCl_3$	18	73.1	8
Z-CyS(Bzl)-OH	HCl·H-Gly-OEt	**4a**	B	2TEA/$CHCl_3$	18	58.1	9
Z-Gln-OH	2HCl·H-His-OMe	**4a**	B	3TEA/$CHCl_3$	18	58.0	10
Z-Gln-OH	2HCl·H-His-OMe	**4q**	B	3TEA/$CHCl_3$	18	82.8	
Z-Gln-OH	Tos-OH·H-Tyr-OBzl	**4q**	A	2TEA/MeCN	0.5/18	71.8	11
Z-Phe-OH	HCl·H-Leu-OEt	**4a**	B	2TEA/$CHCl_3$	8	73.2	12
Z-Phe-OH	HCl·H-Leu-OEt	**4a**	B	3TEA/$CHCl_3$[b)]	2	73.2	
Z-Phe-OH	HCl·H-Ile-OEt	**4a**	B	2TEA/CH_2Cl_2	40	81.2	13
Z-Pro-OH	HCl·H-Leu-OEt	**4a**	B	2TEA/$CHCl_3$	15	74.3	14
Z-Pro-OH	HCl·H-Leu-OEt	**4f**	B	2TEA/$CHCl_3$	18	82.0	
Z-Pro-OH	HCl·H-Leu-OEt	**4q**	B	TEA-Pyr/CH_2Cl_2	18	77.4	
Z-Pro-OH	HCl·H-Ser-OMe	**4t**	B	2TEA/$CHCl_3$	18	85.7	15
Z-Val-OH	HCl·H-Gly-OEt	**4a**	B	2TEA/$CHCl_3$	65	77.3	11
Z-Val-OH	HCl·H-Val-OEt	**4a**	B	2TEA/CH_2Cl_2	72	80.4	16
Z-Val-OH	HCl·H-Val-OEt	**4o**	B	2TEA/CH_2Cl_2	48	74.0	
Z-Gly-Phe-OH	HCl·H-Gly-OEt	**4a**	B	2TEA/$CHCl_3$	18	72.5	17

a) Hemihydrate; mp 79—80 °C(dec). b) Periodic neutralization was done.

Table 7. Preparation of model peptides using **4v**

Acylamino acid	Amino acid ester salt	Procedure	Base/Solvent	Reaction time (h)	(%) Yield	Ref.
Z-Arg(NO_2)-OH	HCl·H-Gly-OEt	B	2NMM/MeCN	2	71.2	8
Z-Arg(NO_2)-OH	HCl·H-Pro-OBzl	B	2NMM/$CHCl_3$	4	41.7	18
Boc-Arg(NO_2)-OH	Tos-OH·H-Tyr-OBzl	A	Pyr-NMM/DMF-MeCN	2/18	63.7	
Boc-Asn-OH	HCl·H-Phe-OEt	B	2TEA/DMF-$CHCl_3$	18	69.8	
Z-CyS(Bzl)-OH	HCl·H-Gly-OEt	B	2TEA/$CHCl_3$	18	85.0	9
(Z-CyS-OH)$_2$	HCl·H-Gly-OEt	B	TEA-Pyr/CH_2Cl_2	48	88.5	19
Z-Gln-OH	2HCl·H-His-OMe	B	2NMM/MeCN	18	80.9	10
Z-Gln-OH	2HCl·H-His-OMe	B	TEA-NMM/MeCN	3.5	67.1	
Z-Pro-OH	HCl·H-Leu-OEt	B	2TEA/$CHCl_3$	18	84.1	14
Z-Pro-OH	HCl·H-Leu-OEt	B	2NMM/EtOAc	8	81.8	
Z-Pro-OH	HCl·H-Ser-OMe	B	2TEA/$CHCl_3$	18	77.8	15
Boc-Pro-OH	H-Gly-OH	B	NMM/Diox-H_2O	18	16.5	
Z-Ser-OH	HCl·H-Phe-OEt	B	2Pyr/MeCN-DMF	6	48.2	
Z-Ser-OH	HCl·H-Phe-OEt	B	2Pyr/MeCN-DMF	18	72.4	
Z-Ser-OH	HCl·H-Phe-OEt	B	2Pyr/DMF	72	68.5	
Z-Val-OH	HCl·H-Gly-OEt	B	TEA-Pyr/CH_2Cl_2	60	82.1	11
Z-Val-OH	HCl·H-Val-OEt	B	2TEA/CH_2Cl_2	72	84.6	16
Z-Gly-Phe-OH	H-Gly-OEt	B	Pyr/MeCN	18	67.7	17
Boc-Pro-OH	HCl·H-Ser(Bzl)Gly-OBzl	B	2TEA/EtOAc	8	84.2	20
Z-Pro-OH	HCl·H-Leu-OEt	B	3MWA-1/CH_2Cl_2	72	85.8	
Z-Pro-OH	HCl·H-Leu-OEt	B	2MWA-1/$CHCl_3$	24	49.0	
Z-Pro-OH	HCl·H-Ser-OMe	B	3MWA-1/CH_2Cl_2-DMF	72	52.8	

MWA-1 = Dowex macroporous weak cation exchanger. The yields recorded are of recrystallized products. Melting points and optical rotations of the products are within the limits of experimental error.

acidic by the formation of the *N*-hydroxy compound resulting in a retardation of the aminolysis of active intermediates, and 6 to 8 h is required for completion of the reaction by the use of triethylamine or *N*-methylmorpholine in chloroform or ethyl acetate, and 2 to 3 h in acetonitrile. When pyridine is employed as the tertiary base, the reaction may require nearly 2 days or more for completion even in acetonitrile. In general, neutralization of the acidic reaction mixture with extra an amount of tertiary base promoted the reaction. For example, the conventional coupling of **6** and **7** by the use of 1-(methylsulfonyloxy)benzotri-

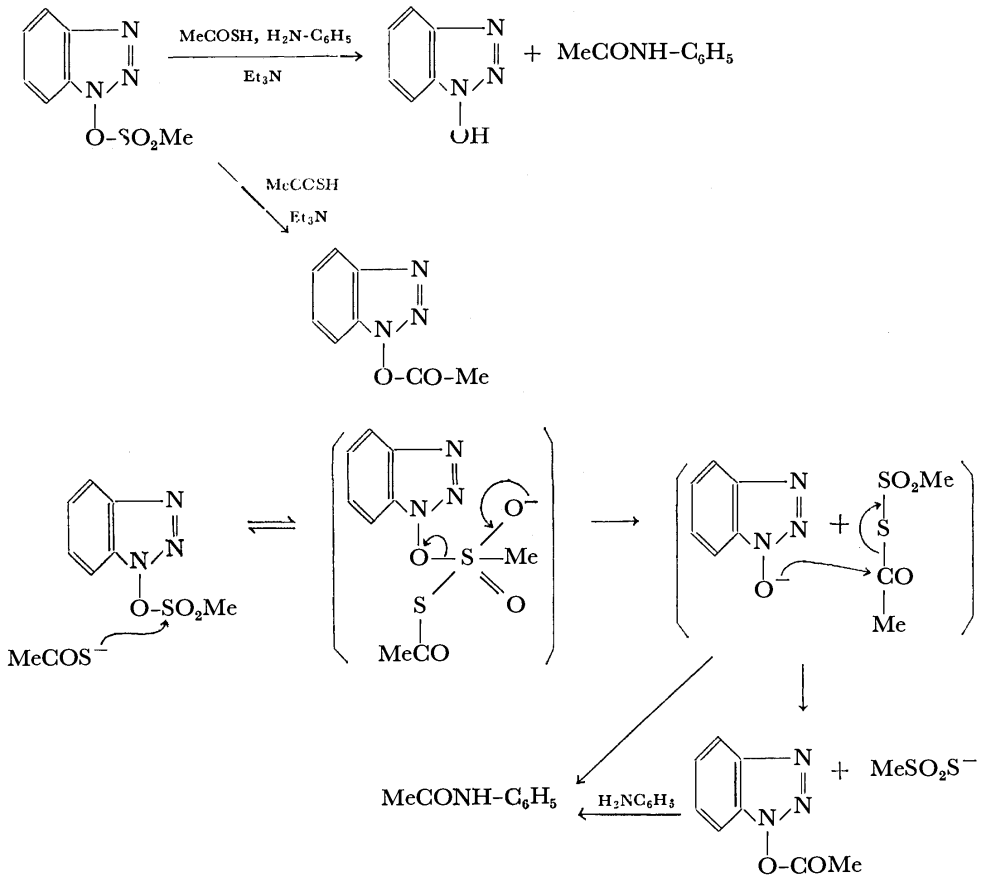

Scheme 2.

azole (**4a**) required 8 h, while the same reaction was completed within 2 h by the periodic addition of an extra amount of triethylamine.

Reaction conditions employed and yields of model peptides are summarized in Tables 6 and 7. In the coupling of *N*-protected L-asparagine and L-glutamine with amine components, no dehydration from the ω-amide to the cyano group was detected in the infrared spectra of the crude products. Free hydroxy or imino groups did not cause any difficulty in the preparation of serine-, tyrosine- or histidine-containing peptides, and no racemate was detected in the preparation of ethyl *N*-benzyloxycarbonylglycyl-L-phenylalanylglycinate by fractional crystallization.

The use of **4v** appeared to be advantageous with oily products or products less soluble in organic solvents. Methyl *N*-benzyloxycarbonyl-L-glutaminyl-L-histidinate prepared by the DCC method was separated from *N,N'*-dicyclohexylurea by extraction with 2 M hydrochloric acid, whereas **4v** gave the product in excellent yield by a simple operation. The coupling of *N*-*t*-butoxycarbonyl-L-proline with benzyl *O*-benzyl-L-serylglycinate is another example to demonstrate the superiority of **4v** over DCC. In the DCC method the product can be isolated only with the help of counter current distribution to eliminate *N,N'*-dicyclohexylurea,[20] whereas the use of **4v** gave the pure product by the following conventional procedure.

A combination of **4v** with a macropolous cation exchange resin was examined in order to test a new technique for peptide synthesis in the liquid-solid phase method. Unlike common solid phase methods, this is designed to leave only the neutral product in the liquid phase after completion of the reaction, while the acidic by-products and unreacted carboxyl components are adsorbed on the resin. That is, a carboxylate anion on the resin is allowed to react with **4v** and forms an active intermediate first, which subsequently reacts with the free amine liberated from an amine hydrochloride on the resin affording an amide in the liquid phase. All the acidic by-products, hydrochloric acid, *p*-chlorobenzenesulfonic acid, 6-chloro-1-hydroxybenzotriazole, and unreacted carboxyl components will be retained on the resin enabling separation of the products. A mixture of an equimolar amount of **6**, the hydrochloride of **7**, **4v**, and 3 equivalents of the resin (Dowex MWA-1) in dichloromethane or chloroform was allowed to stand for 72 h with occasional stirring. The thin layer chromatogram of the liquid phase showed the presence of a large amount of **5** and trace amounts of impurities. Pure **5** was easily obtained by evaporation of the solvent and the recrystallization of the crude product. The results obtained are summarized at the bottom of Table 7.

A possible side reaction, which may occur due to the use of the sulfonates only in procedure B but not in procedure A, is sulfonamide formation from the sulfonates and the amine components. In practice the sulfonamide formation is so slow that it is not detectable in most cases. For instance, a mixture of equimolar amounts of **7** and **4a** in chloroform showed no sulfonamide formation at room temperature unless

Table 8. Racemization test

Z-Phe-Ile-OH + H-AA-OR·HCl ⟶ Z-Phe-Ile-AA-OR

Reagent	H-AA-OR	Procedure	Base/Solvent	Temp (°C)	Yield (%)	D-Alloisoleucine (%)
4g	H-Pro-OBzl	B	2NMM/DMF	r. t.	83.8	25.4
4v	H-Pro-OBzl	B	2NMM/DMF	r. t.	100	23.9
4v	H-Pro-OBzl	B	2NMM/DMF	0—+5	98	12.2
4v	H-Pro-OBzl	B	2Pyr/DMF	r. t.	66.4	18.2
4v	H-Pro-OBzl	B	2Pyr/DMF	−10	72.8	6.8
4v	H-Pro-OBzl	B	2NMM/EtOAc	r. t.	96.5	12.0
4v	H-Pro-OBzl	B	2NMM/$CHCl_3$	r. t.	93.4	14.5
4v	H-Pro-OBzl	B	2MWA-1/DMF[a]	r. t.	89.0	19.7
4v+**2a**[b]	H-Pro-OBzl	B	2NMM/DMF	r. t.	94.5	11.3
4v+**2a**	H-Pro-OBzl	B	2NMM/DMF	0—+5	92.8	7.6
4v+**2b**[c]	H-Pro-OBzl	B	2NMM/DMF	r. t.	95.1	21.3
4v	H-Pro-OBzl	A[d]	2NMM/DMF	r. t.	98.9	42.6
4v	H-Pro-OBzl	A[e]	2Pyr/DMF	r. t.	59.8	33.2
4v+**2a**	H-Pro-OBzl	A[d]	2NMM/DMF	r. t.	100	14.4
4v	H-Leu-OEt	B	2NMM/DMF	0—+5	85.5	10.4
4v	H-Leu-OEt	B	2NMM/EtOAc	0—+5	95.6	6.1
4v+**2a**	H-Leu-OEt	B	2NMM/DMF	0—+5	96.9	3.1
4v+**2a**	H-Leu-OEt	B	2NMM/$CHCl_3$	0—+5	97.2	0.5
DCC	H-Pro-OBzl	—	NMM/DMF	r. t.	95.6	43.3
DCC+**2a**	H-Pro-OBzl	—	NMM/DMF	r. t.	97.4	17.7
EEDQ	H-Pro-OBzl	—	2NMM/DMF	r. t.	57	24.0
DPPA	H-Pro-OBzl	—	2NMM/DMF	r. t.	94.4	16.3

a) The mixture was allowed to react for 24 h. b) Ethyl 2-(hydroxyimino)-2-cyanoacetate (1.2 equivalent). c) 6-Chloro-1-hydroxybenzotriazole (1.2 equivalent). d) Z-Phe-Ile-OH, **4v**, and *N*-methylmorpholine in DMF were allowed to react for 15 min before the addition of a solution of benzyl L-prolinate hydrochloride and *N*-methylmorpholine in DMF. e) Z-Phe-Ile-OH was allowed to react with **4v** for 1.5 h before the addition of benzyl L-prolinate solution.

triethylamine was added. The only exception was when 2-[3,5-bis(benzyloxy)phenyl]ethylamine (**9**) was acylated with **8** by the use of the arenesulfonates of 1-hydroxybenzotriazoles and triethylamine in dichloromethane. For example, the 41% yield of *N*-(*p*-chlorophenylsulfonyl)-2-[3,5-bis(benzyloxy)phenyl]ethylamine (**10**), accompanied by the 33% yield of *N*-(*N*-benzyloxycarbonyl-L-phenylalanyl)-2-[3,5-bis(benzyloxy)phenyl]ethylamine (**11**) was obtained in the acylation of **9** with **8** using **4v**. On the other hand, the alkanesulfonates of 1-hydroxybenzotriazole such as **4a** or 6-chloro-1-(methylsulfonyloxy)benzotriazole (**4p**) produced far less sulfonamide (**10**) than **4v** did. The use of *N*-methylmorpholine or pyridine in the place of triethylamine greatly assisted the suppression of sulfonamide formation even when **4v** was used. The isolation of pure **11** in high yield posed no practical problems. The effect of weaker bases may be due to the selective activation of the carboxyl group of **8** prior to the gradual liberation of free **9** from the hydrochloride.

To elucidate the reaction path of amide formation, **4a** was treated with a mixture of either thioacetic *S*-acid and triethylamine, or thioacetic *S*-acid, aniline and triethylamine. In the former case 1-acetoxybenzotriazole[21] (**13**) was obtained in 85% yield, and in the latter, acetanilide and 1-hydroxybenzotriazole (**2b**) were obtained in 89 and 88.7% yields, respectively. These results suggest that the thioacetate anion, carboxylate anion alike, attacks the sulfur atom of the sulfonate first, forming thioacetic methanesulfonic anhydride. The mixed anhydride may directly be aminolyzed with aniline affording acetanilide and **2b**, or be converted to **13**, which is subsequently aminolyzed to acetanilide or isolated in the absence of aniline.

The active intermediate in procedure A is doubtlessly 1-acyloxybenzotriazole, but specification of the intermediate in procedure B remains difficult. As described before the active ester formation is completed within 1 h, whereas the coupling reaction in procedure B requires 6 to 8 h under the same conditions unless the mixture is neutralized periodically. This suggests that a substantial portion of amides can be produced through 1-acyloxybenzotriazole, which is also a possible active intermediate of recently reported reagents, tris(dimethylamino)(1-benzotriazolyloxy)phosphonium hexafluorophosphonate[22] and tris(dimethylamino)(1-benzotriazolyloxy)phosphonium tetrafluoroborate.[23] The reaction mechanism of **4v** and related compounds in coupling reaction has been discussed in detail by Horiki and Murakami.[24]

The tendency toward racemization of **4v** was compared with those of DCC, 1-ethoxycarbonyl-2-ethoxy-1,2-dihydroquinoline (EEDQ) and diphenoxyphosphinyl azide (DPPA).[26] The racemization test was conducted using a modification of Bodanszky's method reported

by Fujino *et al.*[27] Coupling of *N*-benzyloxycarbonyl-L-phenylalanyl-L-isoleucine (**14**) with benzyl L-prolinate (**15**) or **7** was carried out mainly in *N,N*-dimethylformamide, in which significant racemization occurs. The contents of D-alloisoleucine (**16**) in the protected tripeptide preparations were determined by subjecting the hydrolyzates to amino acid analysis. The results obtained are summarized in Table 8. As Fujino *et al.*[27] have reported, severe racemization in the coupling of **14** with **15** in DCC method, **15** caused markedly more racemization than the other amino acid esters did. DCC produced 43.3% of **16**, which was suppressed to 17.7% by the addition of **2a**. **4v** and EEDQ showed the same extent of racemization, giving 23.9 and 24.0% of **16**, respectively. The use of **2a** with **4v** lowered the formation of **16** to 11.3%, but the use of 6-chloro-1-hydroxybenzotriazole, which was an effective additive in DCC method and a component of **4v**, was not so effective. DPPA which is said to proceed the coupling reaction through carboxylic azide formation gave 16.3% of **16**. The use of pyridine in place of *N*-methylmorpholine gave more satisfactory results in racemization suppression, although it usually required a longer reaction time. An unexpected result was that severe racemization comparable to DCC method was observed in procedure A, but was again suppressed with **2a** to 14.4%.

The conditions employed are suitable only for the detection of racemization, but not for practical coupling. Reactions need to be carried out using weak bases and amine components whose *N*-terminal amino acid residue is other than proline at low temperature. These results suggest that **4v** is a much superior reagent than DCC in racemization, especially when it is used with **2a**.

Experimental

Melting points were measured on a Hoover "Uni-Melt" apparatus and are uncorrected. The optical rotations were determined with a JEOLCO Model DIP-4.

Materials. Commercially available methane-, 1-butane-, benzene-, *p*-toluene-, *p*-chlorobenzene-, *p*-nitrobenzene- and 2,4,6-trimethylbenzenesulfonyl chlorides, *N*-hydroxysuccinimide, and 3-hydroxy-1,2,3-benzotriazin-4-one were used for the preparation of the sulfonates of *N*-hydroxy compounds. Phenylmethane-,[28] *dl*-10-camphor-,[29] β-styrene-,[30] and 3-pyridinesulfonyl chloride,[31] ethyl 2-hydroxyimino-2-cyanoacetate,[32] 2-hydroxyimino-2-cyanoacetamide,[32] 1-hydroxybenzotriazole,[33] 6-chloro-1-hydroxybenzotriazole,[34] and 6-nitro-1-hydroxybenzotriazole[35] were prepared according to the literature.

4-Chloro-1-hydroxybenzotriazole. A mixture of 2,3-dichloronitrobenzene (25 g, 0.13 mol) and hydrazine hydrate (19.5 g, 0.39 mol) in 99% ethanol (40 ml) was refluxed for 24 h. After removal of the solvent *in vacuo*, the residue was dissolved in 10% sodium carbonate solution. The solution was washed with ether and acidified with concentrated hydrochloric acid to precipitate the product, which was washed with water on a filter and dried; 20.6 g (93.4%); mp 160—166 °C. A part of the product was recrystallized from methanol (MeOH); mp 170—172 °C.

Found: C, 42.74; H, 2.27; N, 24.89%. Calcd for $C_6H_4ON_3Cl$: C, 42.50; H, 2.38; N, 24.80%.

*1-(Phenylsulfonyloxy)benzotriazole (**4e**). General Procedure for the Preparation of the Sulfonates of* N*-Hydroxy Compounds*: To a solution of 1-hydroxybenzotriazole (6.6 g, 0.049 mol) in 1 M-sodium hydroxyide solution (49 ml) was added dropwise benzenesulfonyl chloride (8.8 g, 0.05 mol) with stirring under ice-cooling. After stirring for 1 h, the product was extracted with ethyl acetate (EtOAc), and the extract was washed with water and dried over magnesium sulfate. Evaporation of the solvent *in vacuo* gave a residue, which was triturated in hexane and filtered to give 11.5 g (85.2%) of **4e**; mp 83—84 °C.

Found: C, 52.30; H, 3.09; N, 15.13%. Calcd for $C_{12}H_9O_3N_3S$: C, 52.35; H, 3.30; N, 15.27%.

Other sulfonates were prepared by similar procedures under conditions cited in Tables 1 and 2. Triethylamine (TEA) was used in place of sodium hydroxide when organic solvents were employed.

*1-(*N*-Benzyloxycarbonyl-*L*-phenylalanyloxy)benzotriazole. General Procedure for the Preparation of the Active Esters*: To an ice-cooled solution of *N*-benzyloxycarbonyl-L-phenylalanine (1.50 g, 5 mmol) and TEA (0.70 ml, 5 mmol) in EtOAc (15 ml) was added 1-(methylsulfonyloxy)benzotriazole (1.1 g, 5 mmol). The mixture was stirred for 1 h and allowed to stand overnight. After the addition of EtOAc and water, the organic layer was washed with water and dried over magnesium sulfate. Evaporation of the solvent and subsequent trituration of the residue with ether gave the product; mp 120—125 °C; 1.3 g (62%). IR (Nujol, cm^{-1}) 3330, 1735, 1690.

General Procedures for the Coupling of Amino and Carboxyl Components. Procedure A: To a solution of *N*-benzyloxycarbonyl-L-glutamine (1.40 g, 5 mmol) and TEA (0.70 ml, 5 mmol) in dry acetonitrile (MeCN)(10 ml) was added 1-(butylsulfonyloxy)-6-chlorobenzotriazole (1.47 g, 5 mmol) at room temperature. The mixture solidified immediately. On standing for 30 min, a solution of benzyl L-tyrosinate *p*-toluenesulfonate (2.20 g, 5 mmol) and TEA (0.70 ml, 5 mmol) in dry MeCN(20 ml) was added to the mixture with stirring. The reaction mixture was allowed to react for a total of 18 h, and clarified by the addition of water. After evaporation of MeCN *in vacuo* the residue was extracted with EtOAc. The extract was washed with water, 1 M hydrochloric acid, water, 5% sodium hydrogencarbonate solution, and water, dried over magnesium sulfate, and concentarted to dryness *in vacuo*. Recrystallization of the residue from MeOH gave 1.92 g (71.8%) of benzyl *N*-benzyloxycarbonyl-L-glutaminyl-L-tyrosinate; mp 173—174 °C (lit,[11] mp 174—175 °C).

Procedure B: To an ice-cooled solution of *N*-benzyloxycarbonyl-L-proline (1.25 g, 5 mmol), methyl L-serinate hydrochloride (0.78 g, 5 mmol) and TEA (1.40 ml, 10 mmol) in dry chloroform ($CHCl_3$)(20 ml) was added 1-(phenylsulfonyloxy)-6-chlorobenzotriazole (**4t**) (1.50 g, 5 mmol). The mixture was stirred for 1 h at room temperature and allowed to stand for a further 17 h. After the addition of EtOAc and water the organic layer was worked-up in the usual manner and concentrated to dryness *in vacuo*. The residue was triturated with a mixture of ether and petroleum ether, filtered, and recrystallized from EtOAc/petroleum ether to give 1.5 g (85.7%) of methyl *N*-benzyloxycarbonyl-L-prolyl-L-serinate; mp 97—100 °C (lit,[15] mp 103—104 °C).

Other protected peptides prepared by the procedures A and B are listed in Tables 6 and 7.

N-t-*Butoxycarbonyl-*L*-prolylglycine.* A solution of *N*-*t*-butoxycarbonyl-L-proline (1.08 g, 5 mmol), glycine (0.375 g, 5 mmol) and *N*-methylmorpholine (NMM)(0.60 ml) in water (7.5 ml) was adjusted to pH 7.0 by the addition of a

small amount of 1-hydroxybenzotriazole. A solution of 6-chloro-1-(*p*-chlorophenylsulfonyloxy)benzotriazole (**4v**) (1.72 g, 5 mmol) in dioxane (14 ml) was added to the solution described above under ice-cooling and the whole mixture stirred for 2.5 h at room temperature. After evaporation of dioxane *in vacuo*, the residue was dissolved in water, washed with EtOAc, acidified to pH 2 and extracted with EtOAc. The extract was washed with water, dried over magnesium sulfate and concentrated to dryness. The residue was dissolved in $CHCl_3$ and adsorbed on a silica gel column (Merck Kieselgel 60, 40 g). The column was eluted with 5% MeOH-containing $CHCl_3$ (150 ml) and then with 10% MeOH-containing $CHCl_3$ (200 ml). Evaporation of the second eluate gave the product (302 mg), which was recrystallized from $CHCl_3$ and petroleunm ether,; 225 mg (16.5%); 165—167 °C (dec).

Found: C, 52.88; H, 7.42; N, 10.33%. Calcd for $C_{12}H_{20}O_5N_2$: C, 52.93; H, 7.40; N, 10.29%.

The Coupling Reaction of N-*Benzyloxycarbonyl-*L-*proline with Ethyl* L-*Leucinate Using* **4v** *and the Macropolous Ion Exchanger.* To an ice-cooled mixture of *N*-benzyloxycarbonyl-L-proline (1.25 g, 5 mmol), ethyl L-leucinate hydrochloride (1.00 g, 5 mmol) and Dowex MWA-1 ion exchange resin (3.8 g, ≈15 mmol, dried over phosphorus pentoxide in a vacuum desiccator for 24 h) in dichloromethane (CH_2Cl_2) (20 ml) was added **4v** (1.72 g, 5 mmol) with occasional stirring. The mixture was allowed to react for 72 h with occasional stirring, and was then filtered. The resin was extracted five times with a small amount of CH_2Cl_2. The filtrate and the extracts were combined and evaporated to dryness, and the residue triturated with a small amount of hexane and filtrered; 1.676 g (85.8%); mp 65—67 °C.

N-(N-*Benzyloxycarbonyl-*L-*phenylalanyl)-2-[3,5-bis(benzyloxy)-phenyl]ethylamine (**11**) and* N-(p-*chlorophenylsulfonyl)-2-[3,5-bis(benzyloxy)phenyl]ethylamine (**10**).* To a mixture of *N*-benzyloxycarbonyl-L-phenylalanine (2. 99 g, 10 mmol), 2-[3,5-bis(benzyloxy)phenyl]ethylamine hydrochloride (3.69 g, 10 mmol) and TEA (2.80 ml, 20 mmol) in CH_2Cl_2 (25 ml) was added a solution of **4v** (3.44 g, 10 mmol) in CH_2Cl_2 (15 ml) under ice-cooling. After stirring at room temperature for 5.5 h, water and EtOAc were added to the reaction mixture which was subsequently filtered to remove insoluble material; mp 144—152 °C; 2.1 g. Recrystallization from MeOH gave pure **11**; mp 153—154.5 °C; 2.0 g (32. 6%).

Found: C, 75.88; H, 6.15; N, 4.56%. Calcd for $C_{39}H_{38}O_5N_2$: C, 76.20; H, 6.23: N, 4.56%.

The filtrate was concentrated to dryness and the residue (3.0 g) was recrystallized from MeOH to give **10**; mp 102—103.5 °C; 2.1 g (41.3%).

Found: C, 65.96; H, 5.05; N, 2.80; S, 6.58; Cl, 6.96%. Calcd for $C_{28}H_{26}NO_4SCl$: C, 66.19; H, 5.16; N, 2.76; S, 6.31; Cl, 6.98%.

11 was prepared in 73.0% yield by following procedure A in MeCN.

*The Reaction of 1-(Methylsulfonyloxy)benzotriazole (**4a**) with Thioacetic* S-*Acid.* To a mixture of thioacetic *S*-acid (0.36 ml) and TEA (0.70 ml) in CH_2Cl_2 (10 ml) was added **4a** (1.07 g) under ice-cooling. The mixture was stirred for 1 h and allowed to stand overnight. Water and EtOAc were added to the mixture and the organic layer separating out was washed with 1 M sodium hydrogencarbonate solution, water, 1 M hydrochloric acid and water, dried over magnesium sulfate and evaporated to dryness. The residue was triturated with an ether–petroleum ether mixture and recrystallized from the same solvents; mp 82—100 °C; 0.6 g. The product was identical with the one obtained from the reaction between acetyl chloride and 1-hydroxybenzotriazole or from **4a** and acetic acid.

*The Reaction of **4a** with Thioacetic* S-*Acid and Aniline.* The same reaction described above was carried out in the presence of an equimolar amount of aniline (0.5 g). After the addition of water and EtOAc, the organic layer was washed with 1 M sodium hydrogencarbonate, water, 1 M hydrochloric acid, and water, dried over magnesium sulfate and evaporated *in vacuo*. The residue was triturated with petroleum ether and filtered to give acetanilide; 0.60 g; mp 110—112 °C. The 1 M sodium hydrogencarbonate washing was acidified with hydrochloric acid, and extracted with 10% dioxane-containing EtOAc. The extract was washed with water, dried over magnesium sulfate and concentrated *in vacuo*. The residue was triturated with petroleum ether and filtered to give 1-hydroxybenzotriazole; 0.6 g (88.7%); mp 151—154.5 °C.

Modified Bodanszky's Test.[27] A typical example is as follows: To a solution of benzyl L-prolinate hydrochloride (241.7 mg, 1 mmol), *N*-benzyloxycarbonyl-L-phenylalanyl-L-isoleucinate (394.5 mg, 1 mmol), ethyl 2-hydroxyimino-2-cyanoacetate (170.5 mg, 1.2 mmol) and NMM (0.22 ml, 2 mmol) in dry *N,N*-dimethylformamide (5.0 ml) was added **4v** (344.2 mg, 1 mmol) under ice-cooling. The mixture was stirred for 3 h at 0—5 °C. After evaporation of the *N,N*-dimethylformamide under nitrogen, the residue was extracted with EtOAc. The extract was washed with water, 1 M sodium hydrogencarbonate (4 times), water, 1 M hydrochloric acid and water, dried over magnesium sulfate and concentrated to dryness. A part of the residue was hydrolyzed by 6 M hydrochloric acid at 105 °C in a sealed tube for 16 h. The hydrolyzate was subjected to amino acid analysis to determine the D-alloisoleucine content. Reaction conditions and the results are given in Table 8.

The authors wish to express their deep gratitude to Professor Nobuo Izumiya of Kyushu University and Dr. Shumpei Sakakibara, Director of the Peptide Institute, Protein Research Foundation, for their kind advice and encouragement.

References

1) A part of this study has been reported in a preliminary form: M. Itoh, H. Nojima, J. Notani, D. Hagiwara, and K. Takai, *Tetrahedron Lett.*, **1974**, 3089, and has also been presented at the 12th Symposium on Peptide Chemistry, Kyoto, Nov. 2, 1974.

2) Y. S. Klausner and M. Bodanszky, *Synthesis*, **1972**, 453.

3) H. Rink and B. Riniker, *Helv. Chim. Acta*, **57**, 831 (1974).

4) M. Itoh, *Bull. Chem. Soc. Jpn.*, **47**, 471 (1974).

5) J. -M. Biehler, J.-P. Fleury, J. Perchais, and A. Regent, *Tetrahedron Lett.*, **1968**, 4227.

6) J. H. Looker, *J. Org. Chem.*, **17**, 510 (1952).

7) C. D. Campbell and C. W. Rees, *J. Chem. Soc., C*, **1969**, 742.

8) H. Gibian and E. Schröder, *Ann. Chem.*, **642**, 145 (1961).

9) E. Schnabel, *Ann. Chem.*, **688**, 238 (1965).

10) H. Kappeler, *Helv. Chim. Acta*, **44**, 476 (1961).

11) H. Determann, O. Zipp, and T. Wieland, *Ann. Chem.*, **651**, 172 (1962).

12) C. -S. Yang, K. Blaha, and J. Rudinger, *Collect. Czech. Chem. Commun.*, **29**, 2633 (1964).

13) E. Sandrin and R. A. Boissonnas, *Helv. Chim. Acta*, **46**, 1637 (1963).
14) M. Zaoral and J. Rudinger, *Collect. Czech. Chem. Commun.*, **20**, 1183 (1955).
15) K. Lübke, E. Schröder, R. Schmiechen, and H. Gibian, *Ann. Chem.*, **679**, 195 (1964).
16) E. Klieger and H. Gibian, *Ann. Chem.*, **649**, 183 (1961).
17) G. W. Anderson and F. M. Callahan, *J. Am. Chem. Soc.*, **80**, 2902 (1958).
18) J. Kovacs and M. Q. Ceprini, *Chem. Ind. (London)*, **1965**, 2100.
19) L. Zervas and I. Photaki, *J. Am. Chem. Soc.*, **84**, 2887 (1962).
20) M. Bodanszky, N. Chaturvedi, D. Hudson, and M. Itoh, *J. Org. Chem.*, **37**, 2303 (1972).
21) N. J. Leonard and K. Golankiewicz, *J. Org. Chem.*, **34**, 359 (1969).
22) I. J. Galpin, P. F. Gordon, R. Ramage, and W. D. Thorpe, *Tetrahedron*, **32**, 2417 (1976).
23) B. Castro, J. R. Dormoy, G. Evin, and C. Seleve, *Tetrahedron Lett.*, **1975**, 1219.
24) K. Horiki and A. Murakami, 15th Symposium on Peptide Chem., Osaka, Nov. 4th, 1977.
25) B. Belleau and G. Malek, *J. Am. Chem. Soc.*, **90**, 1651 (1968).
26) T. Shioiri, K. Ninomiya, and S. Yamada, *J. Am. Chem. Soc.*, **94**, 6203 (1972).
27) M. Fujino, S. Kobayashi, T. Fukuda, M. Obayashi, and S. Shinagawa, *Proc. of the 10th Symposium on Peptide Chem.*, p. 7, 1972.
28) T. B. Johnson and J. M. Sprague, *J. Am. Chem. Soc.*, **58**, 1348 (1936).
29) A. Raoul Poggi and G. Serchi, *Sperimentale, Sez. Chim. Biol.*, **3**, 6 (1952); *Chem. Abstr.*, **47**, 6382 (1953).
30) B. M. Culbertson and S. Dietz, *J. Chem. Soc., C*, **1968**, 992.
31) M. F. Zienty, *J. Am. Pharm. Assoc., Sci. Ed.*, **37**, 97 (1948).
32) M. Conrad and A. Schulze, *Ber.*, **42**, 735 (1909).
33) W. König and R. Geiger, *Chem. Ber.*, **103**, 788 (1970).
34) S. S. Joshi and D. S. Deorha, *J. Indian Chem. Soc.*, **29**, 545 (1952).
35) A. K. Macbeth and J. R. Price, *J. Chem. Soc.*, **1937**, 982.

Hydrogenation and Hydrogenolysis. XVI.[1] The Reactions of Two Isomeric Enol Ethers of 3-Methylcyclohexanone over Platinum Group Metals

Shigeo NISHIMURA,* Kunihiro KAGAWA, and Nobuo SATO

Department of Industrial Chemistry, Tokyo University of Agriculture and Technology, Koganei, Tokyo 184

(Received April 8, 1978)

The two isomeric enol ethers of 3-methylcyclohexanone, 1-ethoxy-3-methyl-, and 1-ethoxy-5-methylcyclohexenes (**5** and **6**), have been hydrogenated in ethanol with six platinum group metals as catalysts. Palladium, rhodium, and platinum efficiently catalyzed the addition of ethanol to the enol ethers to give the corresponding acetal, while iridium and ruthenium catalyzed it only slightly. Osmium was moderately active for the acetal formation. Extensive isomerization between **5** and **6** occurred over all catalysts. In addition, isomerization to an allyl ether, 3-ethoxy-1-methylcyclohexene (**9**), was observed with **5** over the metals other than palladium. Hydrogenation of **5** and **6** with palladium gave the *trans*-ether predominantly. With the other metals, the *cis*-ether was formed in large excess from **5** and the *trans*-ether in slight excess from **6** at the initial stage of hydrogenation. Hydrogenolysis of the ethoxyl group occurred extensively over platinum but only slightly with palladium and ruthenium. These results are compared with those obtained with the corresponding dimethylcyclohexenes and allyl ether **9**.

Previously we have studied the hydrogenation of the enol ethers of 2- and 4-methylcyclohexanone **1**, **2**, and **3** with platinum group metals as catalysts.[2,3] Hydrogenation of **3** in ethanol was accompanied by formation of the corresponding acetal which depended on the catalyst metal employed. Palladium, platinum, and rhodium catalyzed the acetal formation efficiently, while ruthenium, osmium, and iridium were only poor catalysts for this reaction. Hydrogenolysis of the ethoxyl group occurred extensively over platinum, while it was very slight with palladium and ruthenium. The order of activity of the platinum metals toward hydrogenolysis has been explained in terms of the activity of ionized adsorbed hydrogen on the catalyst surface which was estimated by the activity for the acetal formation and of the strength of olefin adsorption which was assumed to increase with decreasing activity for olefin isomerization. With palladium enol ethers **1**, **2**, and **3** all gave saturated *cis*-ethers with high stereoselectivity. This stereochemistry of hydrogenation has been explained on the basis of the selective formation of the half-hydrogenated states with the adsorption bond at the carbon bearing the ethoxyl group, together with the assumption that the product-controlling step is formation of the saturated ethers. Selective formation of such half-hydrogenated states has been supported by the fact that isomerization of enol ether **1** occurred extensively to the isomeric enol ether **2** but not to an isomeric allyl ether **4**.[3]

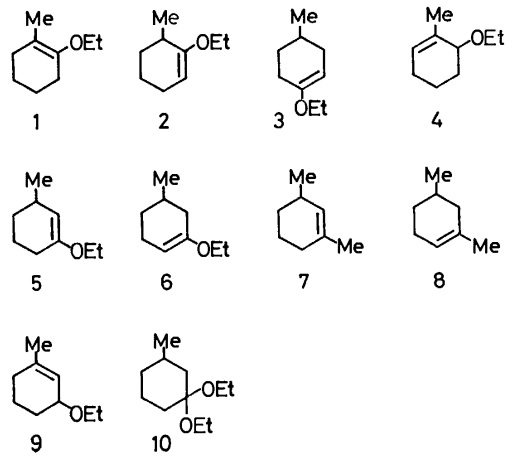

This paper reports the hydrogenation of the two isomeric enol ethers of 3-methylcyclohexanone, 1-ethoxy-3-methyl- and 1-ethoxy-5-methylcyclohexenes (**5** and **6**) that has been studied in ethanol with six platinum group metals as catalysts. Since the enol ethers were extensively isomerized to each other during hydrogenation, characteristic behaviors of **5** and **6** were observable only at the initial stage of hydrogenation. For this reason, the selectivities of platinum metals for acetal formation, isomerization, stereochemistry of hydrogenation and hydrogenolysis are discussed on the results at the initial stage of hydrogenation which were obtained by extrapolation. Further, the results have been compared with those obtained with the corresponding dimethylcyclohexenes **7** and **8** for isomerization and stereochemistry of hydrogenation and also with those on an isomeric allyl ether **9** with respect to hydrogenolysis.

Experimental

*1-Ethoxy-3-methyl- and 1-Ethoxy-5-methylcyclohexenes (**5** and **6**).* A mixture of **5** and **6** was prepared by heating 3-methylcyclohexanone diethyl acetal with a catalytic amount of ammonium dihydrogenphosphate.[4] Bp 171.5—172.5 °C. Pure **5** and **6** were obtained by purification on a preparative GLPC employing a column of PEG 20M. Enol ether **5**: n_D^{25} 1.4533; ^{1}H NMR (60 MHz, CCl_4), δ=0.93 (d, 3H, >CHC$\underline{H}_3$), 1.19 (t, 3H, OCH$_2$C$\underline{H}_3$), 1.33—2.33 (m, 7H, saturated ring protons), 3,52 (q, 2H, OC$\underline{H}_2$CH$_3$) and 4.27 ppm (d, 1H, olefinic proton). Enol ether **6**: n_D^{25} 1.4514; ^{1}H NMR (60 MHz, CCl_4), δ=0.93 (d, 3H, >CHC$\underline{H}_3$), 1.19 (t, 3H, OCH$_2$OC$\underline{H}_3$), 1.33—2.33 (m, 7H, saturated ring protons), 3.52 (q, 2H, OC$\underline{H}_2$CH$_3$) and 4.38 ppm (t, 1H, olefinic proton). The structures of **5** and **6** were determined from their NMR specta: the olefinic proton of **5** showed a doublet at a higher field (4.27 ppm) while that of **6** gave a triplet at a lower field (4.38 ppm). The structures thus assigned were supported by the occurrence of the isomerization of **5** to the allyl ether **9** and its absence with **6** during hydrogenation, and also by the similarities in stereochemistry of hydrogenation of **5** and **6** to the corresponding dimethylcyclohexenes **7** and **8**, respectively, as observed over the metals of low isomerization (Ru, Os,

Ir, Pt) (see Table 3).

1,3- and 1,5-Dimethylcyclohexenes (7 and 8). **8** was obtained by purification on a preparative GLPC of a mixture of **7** and **8** prepared by dehydrating 1,3-dimethylcyclohexanol with iodine.[5] **7** was prepared by pyrolysis of 2,6-dimethylcyclohexanol acetate at 400 °C[6] followed by purification on a preparative GLPC.

3-Ethoxy-1-methylcyclohexene (9). This is a known compound and was prepared by the method of Spangler and Hennis[7] followed by purification on a preparative GLPC.

All the compounds described above were obtained in greater than 99% purity by GLPC analysis.

Solvent. S. S. G. ethanol of Wako Pure Chemical Industries was dehydrated by refluxing with sodium metal and diethyl phthalate.[8]

Catalysts. All the catalysts used in this study were unsupported metals and prepared by reducing the corresponding metal hydroxides (Ru, Rh, Pd, Ir, Pt) or oxide (Os) with hydrogen in water at atmospheric or high pressure.[2,9] Great care was taken to remove traces of alkaline or acidic substances with repeated reductions and washings.[9]

Hydrogenations. All hydrogenations were carried out in a small glass bottle at 25 °C and atmospheric pressure. A high purity hydrogen gas (Nippon Sanso Co.) was used without further purification. The catalyst (1.5—4 mg) was shaken with hydrogen in ethanol (2 ml) for the time which differed with the catalyst metal used (15—20 min for Pd, Pt, and Rh; 1 h for Ir and Os; 2 h for Ru), and then the substance to be hydrogenated (0.04 ml) was added with a microsyringe through a silicone rubber stopper.

Product Analysis. The reaction mixture was taken into a microsyringe through the silicone rubber stopper during the course of hydrogenation and subjected to GLPC analysis (column: PEG 20 M, programmed at 2°C/min in the temperature range of 50 to 160 °C for the products from **5**, **6**, and **9**; TXP at 60 °C for the products from **7** and **8**). The peaks of *cis*- and *trans*-1-ethoxy-3-methylcyclohexanes were identified by comparison with those of a *cis*-rich sample of the ethers which was obtained by ethylating a *cis*-rich 3-methylcyclohexanol with sodium hydride and ethyl iodide in tetrahydrofuran.[10] The peak at a longer retention time was found to be that of the *cis* isomer. Other peaks were identified by comparison of their retention times with those of authentic samples.

Results and Discussion

In Figs. 1 and 2 are shown the changes in composition of reaction mixture during the course of hydrogenation of enol ethers **5** and **6** in ethanol. All hydrogenations were performed at 25 °C and atmospheric pressure with unsupported metals as catalysts. Although ethanol used as the solvent had been carefully dehydrated, some amounts of a hydrolysis product, 3-methylcyclohexanone, was formed together with the acetal **10** over rhodium and palladium and to a lesser extent over platinum. Since the hydrolysis is considered to be related to the acetal formation,[2,11] the ketone formed is included in the acetal in the figures. Usually hydrogenation of the acetal proceeded very slowly and did not go to completion.

Acetal Formation. As seen in Figs. 1 and 2, the extent of the acetal formation greatly depends on the catalyst metal used and to some extent on the enol ether hydrogenated as well. Table 1 summarizes the ratios of the acetal formed to the enol ether hydrogenated at initial stage of hydrogenation. The tendency of the platinum metals for the acetal formation is consistent in both the enol ethers. Thus palladium, rhodium and platinum are definitely more active for the acetal formation than the other platinum

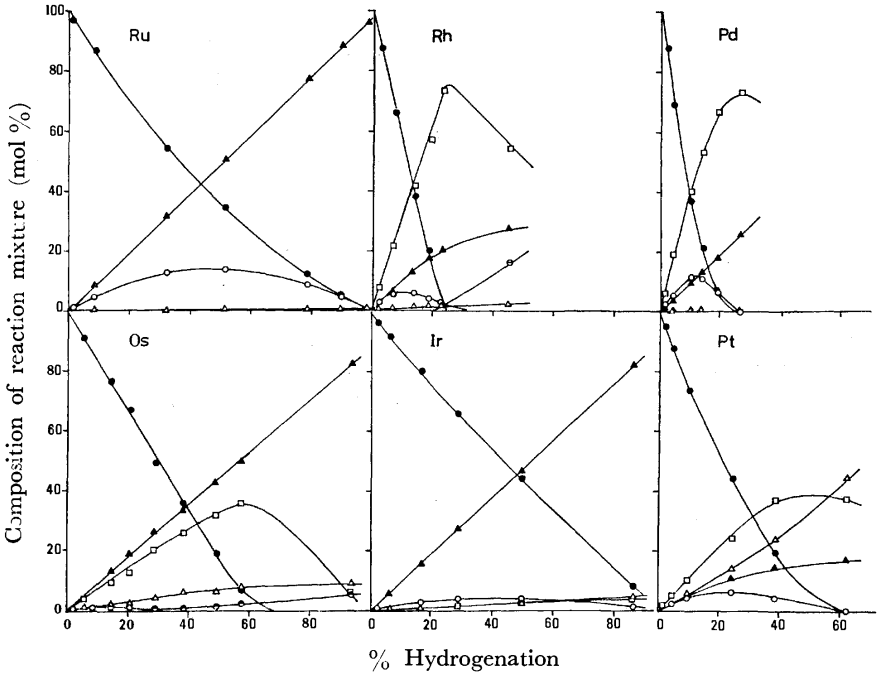

Fig. 1. Hydrogenation of enol ether **5** in ethanol.
●: Enol ether **5**, ○: enol ether **6**, ▲: saturated *cis*- and *trans*-ether, △: methylcyclohexane, □: acetal **10** and 3-methylcyclohexanone, ⊖: 3-methylcyclohexanol.

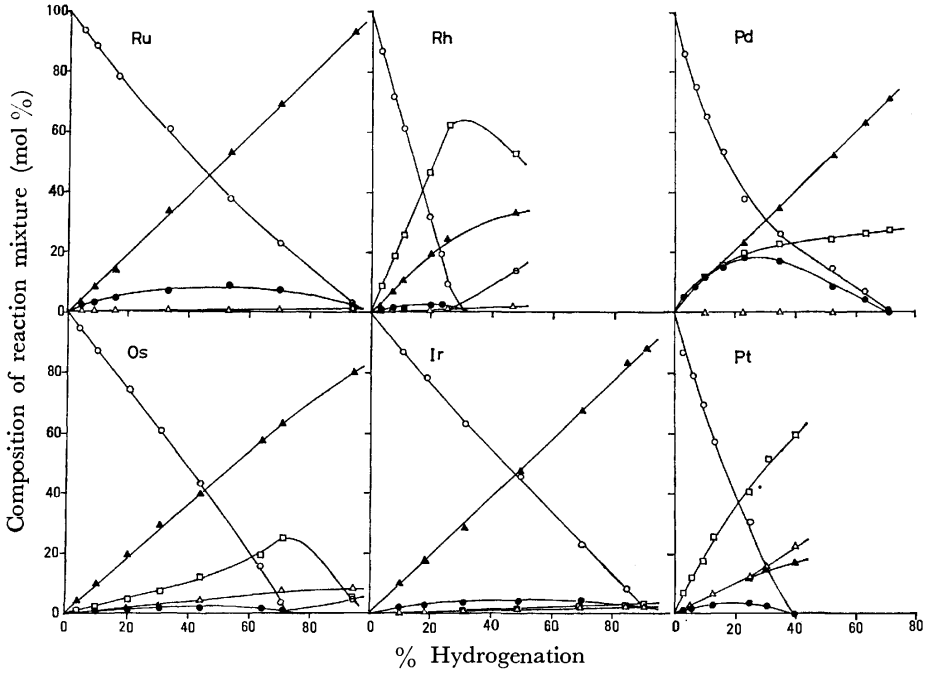

Fig. 2. Hydrogenation of enol ether **6** in ethanol.
For indications, see the footnotes in Fig. 1.

TABLE 1. INITIAL RATIO OF ACETAL FORMATION TO HYDROGENATION WITH ENOL ETHERS **5** AND **6**[a)]

Catalyst	Enol ether	
	5	**6**
Ru	0	0
Rh	3.0	2.5
Pd	4.5	2.0
Os	0.70	0.25
Ir	0.05	0.06
Pt	1.2	2.4

a) Hydrogenation including hydrogenolysis.

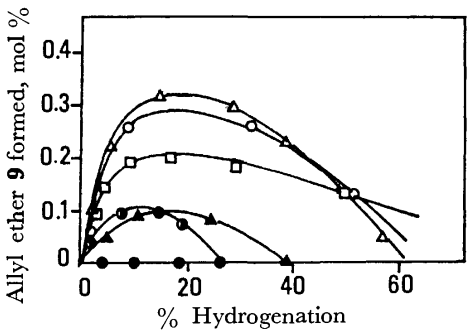

Fig. 3. Isomerization of enol ether **5** to allyl ether **9**.
△: Os, ○: Ru, □: Ir, ◑: Rh, ▲: Pt, ●: Pd.

metals. Iridium and ruthenium cause little or no acetal formation. Osmium is moderately active for this reaction and lies between the two extreme groups of the metals. The acetal formation is very sensitive to the preparations of catalyst metals, and therefore great care was taken to remove traces of alkaline or acidic substances according to the procedures described previously.[9)] The trend of the platinum metals shown in Table 1, however, is in good agreement with that reported previously with enol ether **3** except in a few cases. The acetal formation is an acid-catalyzed reaction and therefore it is considered that the high activity of palladium, rhodium, and platinum results from the presence of ionized hydrogen on the surfaces of these metals, as discussed previously.[2,11)]

Isomerization. As previously shown with enol ethers **1** and **2**, isomeric enol ethers are very liable to isomerization to each other.[3)] Enol ethers **5** and **6** also isomerized extensively to each other as seen in Figs. 1 and 2. In addition, with enol ether **5** the isomerization to an isomeric allyl ether **9** was observed over the metals other than palladium (see Fig. 3), although it was much less extensive than the isomerization to the isomeric enol ether. The isomerization of an enol ether to an allyl ether as observed here could not be detected previously in the hydrogenation of enol ether **1**.[3)] The initial ratios of isomerized product to enol ether hydrogenated are summarized in Table 2. The comparable data obtained with the corresponding cycloolefins **7** and **8** are also included in Table 2. Although the observed isomerization of enol ethers might be decreased by the acetal formation, it is seen that isomerization occurs much more extensively in the enol ethers than in the cycloolefins. With palladium, however, isomerization in the cycloolefins was as much or even more extensive. It is to be noted that isomerization occurs more easily from **5** to **6** than from **6** to **5**. Similar trend is also seen with cycloolefins **7** and **8**. It appears that more isomerization in **5** and **7** than in **6** and **8** may be related to the stereochemistry of hydrogenation of these compounds. As will be described later, with most catalysts both **5** and **7** give much greater amounts of *cis* isomers than **6** and **8**. If isomerization between **5** and **6** or **7** and **8** occurs *via* the

Table 2. Initial ratio of isomerization to hydrogenation with enol ethers **5** and **6**[a] and with corresponding cycloolefins **7** and **8**

Catalyst	Enol ether			Cycloolefin	
	5		**6**	**7**	**8**
	Isomer to **6**	Isomer to **9**	Isomer to **5**	Isomer to **8**	Isomer to **7**
Ru	0.52	0.044	0.34	0.052	0.026
Rh	1.05	0.025	0.20	0.18	0.044
Pd	2.2	0.0	1.8	3.0	1.9
Os	0.16	0.051	0.046	0.035	0.028
Ir	0.34	0.038	0.29	0.043	0.022
Pt	0.76	0.010	0.29	0.055	0.010

a) Hydrogenation including hydrogenolysis.

common half-hydrogenated states **11** and **12**, the one which will lead to the formation of *cis* isomers on further hydroegnation (**11**) is considered to be more unstable than that which will give rise to *trans* isomers (**12**), as presumed from the conformations shown in Fig. 4. Accordingly, the reversal of the half-hydrogenated states leading to isomerization may be expected to occur more easily in **11** than in **12**. More isomerization in **5** and **7** than in **6** and **8** may be accounted for by considering a more significant contribution of the half-hydrogenated state **11** in **5** and **7**.

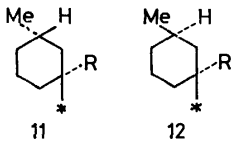

R = OEt or Me

The ratio of the isomerizations **5** to **6** and **5** to **9** is informative on the nature of catalyst metals. It increases in the order: Os (3.1)<Ir (8.9)<Ru (12)≪ Rh (42)<Pt (76)<Pd (∞). It is pointed out that the metals which are active for acetal formation (Rh, Pt, Pd) isomerize **5** very selectively to the isomeric enol ether **6**. It is further noted that isomerization to **6** is three times more extensive than isomerization to **9** even over osmium which causes the latter isomerization more extensively than any other metals investigated. The selective isomerization of enol ethers is probably directed by the electron-releasing ethoxyl group which will force to form the half-hydrogenated state with an adsorption bond at the carbon bearing the ethoxyl group. The fact that the selectivity is especially high with platinum and palladium is consistent with the observation by Teratani and Takagi[12,13] that deuteration of 4-*t*-butyl-1-methoxycyclohexene gave the exchanged products with deuterium atoms at C_2 and C_6 but no deuterium at C_3 and C_5 in the cases of platinum and palladium.

Stereochemistry of Hydrogenation. Initial *cis*/*trans* isomer ratios of the saturated ether from hydrogenation of **5** and **6** are shown in Table 3, in comparison with those obtained with the cycloolefins **7** and **8**.

The results with palladium are characteristic in that both **5** and **6** give the *trans*-ether predominantly

Table 3. Initial *cis*/*trans* isomer ratio of saturated product from hydrogenation of enol ethers **5** and **6** and corresponding cycloolefins **7** and **8**

Catalyst	Compound hydrogenated			
	5	**6**	**7**	**8**
Ru	5.3	0.69	11	0.70
Rh	1.4	0.26	3.0	0.85
Pd	0.26	0.18	5.2	4.2
Os	12	0.89	12	0.80
Ir	9.0	0.72	8.2	0.73
Pt	3.0	0.58	4.2	0.81

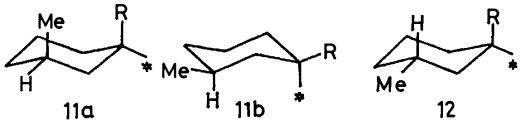

Fig. 4. Conformations of the half-hydrogenated states **11** and **12** (R=OEt or Me).

and, in contrast, the *cis* isomer is formed from both **7** and **8** with high selectivity. Previously it was shown that hydrogenation of the enol ethers **1**, **2**, and **3** with palladium give the *cis*-ethers with high stereoselectivity. The results have been explained on the basis of the preferential formation of the half-hydrogenated states with adsorption bonds at the carbons carrying the ethoxyl group, together with the assumption that the product-controlling step is formation of the saturated ethers. Application of the same explanation to the hydrogenation of enol ethers **5** and **6** expects a predominant formation of the *trans*-ether from both **5** and **6**, since the half-hydrogenated state leading to the *trans*-ether (**12**, R=OEt) will be more stable than that producing the *cis*-ether (**11**, R=OEt). The results shown in Table 3 are in accord with this expectation and may give further support for the explanation made previously for the stereochemistry of hydrogenation of enol ethers **1**, **2**, and **3**.

The predominant formation of the *cis* isomer in the cycloolefins **7** and **8** with palladium is consistent with the results by other investigators.[14] In these cases the stereochemistry of hydrogenation has been explained by assuming that the stability of the half-hydrogenated states decreases with increasing steric requirement at the adsorbed carbon.[14,15]

As in the case of palladium, the selective formation of the half-hydrogenated states **11** and **12** from **5** and **6** may also be considered over the other metals, as has been indicated by the extensive isomerization between **5** and **6**. However, in contrast to palladium, the stereochemistry of hydrogenation is not similar for **5** and **6**. In general the *cis*-ether is formed in large excess from **5** while the *trans*-ether is produced in slight excess from **6**. Further it should be noted that the stereochemistry is very similar for **5** and **7** and for **6** and **8**. These results suggest that the product-controlling step may be the same for the enol ethers and the cycloolefins, probably it being either adsorption of the substrates or formation of half-hydrogenated

TABLE 4. INITIAL AMOUNT OF HYDROGENOLYSIS WITH ENOL ETHERS **5** AND **6** AND WITH ALLYL ETHER **9** (mol %)[a)]

Catalyst	Compound hydrogenated		
	5	**6**	**9**
Ru	0.4	1.2	1.6
Rh	6.5	4.4	9.8
Pd	3.0	0.2	18
Os	13	8.1	4.5
Ir	6.0	2.7	2.5
Pt	50	43	21.5

a) Proportion of hydrogenolysis in mol % in hydrogenation and hydrogenolysis.

states.[16)] The stereoselective formation of *cis* isomers from **5** and **7** may be a result of a steric interaction between the methyl group at the allylic position and the catalyst surface, because the methyl group is considered to be in a quasi-axial conformation and may increase the addition of hydrogen from the opposite side to the methyl group.[17)] The *cis*/*trans* product ratios from **5** and **6** are rather small in the case of rhodium, although greater than with palladium. This is indicative that the rhodium catalyzed hydrogenation of enol ethers has some aspect similar to the hydrogenation with palladium.

Hydrogenolysis. The hydrogenation of enol ethers is accompanied by the hydrogenolysis of alkoxyl group which depends largely on the catalyst metal and solvent.[2)] The initial amounts of the hydrogenolysis products with **5** and **6** in ethanol are summarized in Table 4, together with the results obtained with an isomeric allyl ether **9** for comparison.

In agreement with the previous results on enol ether **3**,[2)] platinum is definitely more active for the hydrogenolysis than the other platinum metals. On the other hand, palladium and ruthenium show the least tendency toward the hydrogenolysis. Osmium, iridium and rhodium are intermediately active in this reaction. The order of the platinum metals in catalyzing the hydrogenolysis of an enol ether has previously been explained in terms of two factors: the activity of ionized adsorbed hydrogen and the strength of olefin adsorption. The former factor was estimated from the activity of catalyst metal for acetal formation in the presence of adsorbed hydrogen and for the latter it has been assumed that the strength of olefin adsorption increases with decreasing tendency of catalyst metal for olefin isomerization. On the basis of this explanation, the extremely high activity of platinum toward the hydrogenolysis can be accounted for by its high activity for acetal formation and its low activity for olefin isomerization. Only small amounts of hydrogenolysis with palladium is attributed to its extremely high acitivity for olefin isomerization which may surpass its high activity for acetal formation. Differences in the amounts of hydrogenolysis between osmium and iridium might result from their differences in acetal formation activity, rather than in olefin isomerization activity.

The factors that control the hydrogenolysis of an allyl ether appear not the same as in the hydrogenolysis of an enol ether. As seen in Table 4, the metals which are active for the hydrogenolysis of allyl ether **9** (platinum, palladium, and rhodium) are all those which are active for acetal formation (see Table 1). This result suggests that the action of ionized hydrogen may be the most important factor in the hydrogenolysis of an allyl ether. This consideration is also consistent with the fact that the hydrogenolysis of allyl and benzyl ethers is greatly promoted by the presence of acid.[18)]

The authors are grateful to Prof. Hiizu Iwamura of Institute for Molecular Sciences and Dr. Michiko Tsuchimoto of Tokyo University of Agriculture and Technology for the interpretation of the NMR spectra. The authors are also indebted to Mr. Noboru Naito, Mr. Fumitaka Imamura, and Mr. Koji Horii for the experiments with the dimethylcyclohexenes and allyl ether.

References

1) Part XV: S. Nishimura, T. Takaoka, and Y. Maekawa, *Bull. Chem. Soc. Jpn.*, **48**, 3648 (1975).
2) S. Nishimura, M. Katagiri, T. Watanabe, and M. Uramoto, *Bull. Chem. Soc. Jpn.*, **44**, 166 (1971).
3) S. Nishimura and Y. Kano, *Chem. Lett.*, **1972**, 565.
4) H. O. House and V. Kramar, *J. Org. Chem.*, **28**, 3362 (1963).
5) F. K. Signaigo and P. L. Cramer, *J. Am. Chem. Soc.*, **55**, 3326 (1933).
6) J.-F. Sauvage, R. H. Baker, and A. S. Hussey, *J. Am. Chem. Soc.*, **82**, 6090 (1960).
7) C. W. Spangler and R. P. Hennis, *J. Org. Chem.*, **36**, 917 (1971).
8) L. F. Fieser, "Experiments in Organic Chemistry," 3rd ed, D. C. Heath and Company, Boston (1955), p. 285.
9) S. Nishimura, M. Ishige, and M. Shiota, *Chem. Lett.*, **1977**, 535.
10) C. A. Brown, D. Barton, and S. Sivaram, *Synthesis*, **1974**, 434.
11) S. Nishimura, T. Itaya, and M. Shiota, *Chem. Commun.*, **1967**, 422.
12) S. Teratani and Y. Takagi, *Shokubai*, **15**, 140P (1973).
13) Y. Takagi and S. Teratani, *J. Catal.*, **34**, 490 (1974).
14) S. Mitsui, S. Imaizumi, A. Nanbu, and Y. Senda, *J. Catal.*, **36**, 333 (1975).
15) S. Siegel and G. V. Smith, *J. Am. Chem. Soc.*, **82**, 6087 (1960).
16) S. Siegel and G. V. Smith, *J. Am. Chem. Soc.*, **82**, 6082 (1960).
17) S. Nishimura, H. Sakamoto, and T. Ozawa, *Chem. Lett.*, **1973**, 855, and references cited therein.
18) P. N. Rylander, "Catalytic Hydrogenation over Platinum Metals," Academic Press Inc., New York (1967), pp. 433—465.

3β-Angeloyloxy-10β-hydroxy-9β-senecioyloxyfuranoeremophilane and 3β-Angeloyloxy-10β-hydroxyfuranoeremophilane. New Furanoeremophilane Derivatives from *Farfugium japonicum* Kitamura[1)]

Hajime NAGANO and Takeyoshi TAKAHASHI*

Department of Chemistry, Faculty of Science, The University of Tokyo, Bunkyo-ku, Tokyo 113

(Received April 22, 1978)

Two new furanoeremophilane derivatives isolated from *Farfugium japonicum* Kitamura have been shown to be 3β-angeloyloxy-10β-hydroxy-9β-senecioyloxyfuranoeremophilane and 3β-angeloyloxy-10β-hydroxyfuranoeremophilane.

In the previous papers[2,3)] we have reported the isolation and structure determination of furanosesquiterpenes from *Farfugium japonicum* Kitamura (= *Ligularia tussilaginea* Makino). Two additional furanoeremophilane derivatives have now been isolated from the same plant. In this paper we wish to present evidence leading to 3β-angeloyloxy-10β-hydroxy-9β-senecioyloxyfuranoeremophilane (**1**) and 3β-angeloyloxy-10β-hydroxyfuranoeremophilane (**2**) for these new sesquiterpenes.

Compound **1**, a viscous oil, was positive to the Ehrlich test. The IR, UV, PMR, and mass spectra (*cf.* Experimental and Table 1) suggest the presence of a β-methyl-substituted furan ring with an α-proton, a tertiary hydroxyl, an angeloyloxyl, and a senecioyloxyl group.[3)] The PMR spectrum also shows the presence of a secondary and a tertiary methyl group. This sesquiterpene (**1**) was converted in five steps into the known acetoxy ketone (**3**) as follows.

Reduction of **1** with lithium aluminium hydride gave a triol (**4**), which was oxidized with active manganese dioxide[4)] in benzene to yield a dihydroxy ketone (**5**). Acetylation of **5** with acetic anhydride in pyridine at room temperature gave a monoacetate (**6**), whose IR spectrum still shows an absorption due to a tertiary hydroxyl group. The tertiary hydroxyl group of **6** was replaced by bromine atom using phosphorus tribromide in dichloromethane[5)] to give an α-bromo ketone (**7**). Debromination of **7** with active zinc dust in acetic acid[6)] afforded an acetoxy ketone (**3**), which was found to be identical (mp, mmp, $[\alpha]_D$, IR, PMR, and mass spectra) including absolute configuration with 3β-acetoxy-9-oxo-10α*H*-furanoeremophilane (**3**) prepared from epieuryopsonol[3,7)] (**8**; 3β-hydroxy-9-oxo-10α*H*-furanoeremophilane). Thus a 9-oxygenated furanoeremophilane skeleton with 3β-hydroxyl or 3β-acyloxyl group was shown for this series of compounds (**1**, **3**—**7**). The absolute configuration at C-3 was further confirmed as *S* by applying the Horeau's method[8)] to **5** (esterification 36%; optical yield (−) 62%).

The 9-oxo structure for both the dihydroxy ketone (**5**) and the monoacetate (**6**) received support from their UV spectra (λ_{max} 283—285 nm, ε 8800—9300).[3,9)] The tertiary hydroxyl group of **6** could only be placed on either C-10 or C-4. As the PMR spectrum of **6** shows the presence of a secondary methyl group (at C-4), this tertiary hydroxyl group must be located on C-10. Therefore, the triol (**4**) should be 3β, 6ξ, 10ξ-trihydroxyfuranoeremophilane. To confirm this result, the triol (**4**) was treated with chromium trioxide in pyridine to give 10ξ-hydroxy-3,9-dioxofuranoeremophilane (**9**); in the PMR spectrum of **9** a doublet due to a secondary methyl group (at C-4) was observed.

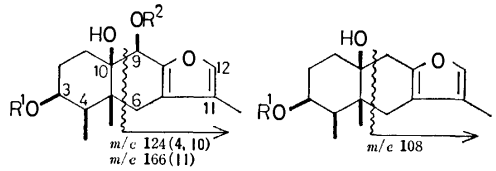

	R¹	R²
1	-CO-C(CH₃)=CH-CH₃	-CO-CH=C(CH₃)-CH₃
4	H	H
10	-CO-C(CH₃)=CH-CH₃	H
11	-COCH₃	-COCH₃

	R¹
2	-CO-C(CH₃)=CH-CH₃
14	H
16	-COCH₃

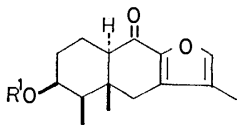

	R¹
3	-COCH₃
8	H

Treatment of **1** with ethanolic potassium hydroxide at room temperature gave a partially hydrolyzed compound (**10**). Spectral data of **10** show the presence of a secondary hydroxyl group and the absence of a senecioyloxyl group. Compound **10** is thus a decenecioyl derivative of **1**. In the PMR spectrum of **10** an allylic proton on hydroxyl-bearing carbon atom resonates at δ (C_6D_6) 4.31, while the corresponding allylic proton signal of **1** at δ (C_6D_6) 6.05. This observation shows that the hydroxyl group of **10** and the senecioyloxyl group of **1** are located on C-9. Therefore, **1** must be 3β-angeloyloxy-10ξ-hydroxy-9ξ-senecioyloxyfuranoeremophilane. The configurations at C-9 and at C-10 were determined as follows.

Acetylation of **4** with acetic anhydride in pyridine gave a diacetate (**11**). In the PMR sepctrum of **11** at 25 °C, two broad signals due to $C_{(9)}$–H and $C_{(12)}$–H appear at δ (CS_2) 5.48 and 6.97, respectively. At −40 °C these signals changed into a pair of signals at δ (CS_2) 5.26 (half-band width: $W_{1/2}$=3 Hz) and 6.02 ($W_{1/2}$=5 Hz) and δ (CS_2) 6.96 and 6.86 in a ratio of *ca.* 5:1, respectively; this indicates that **11** has

TABLE 1. PMR SPECTRAL DATA (δ values)[a]

	1		2	
	CCl_4	C_6D_6	CCl_4	C_6D_6
$C_{(4)}$-CH_3	1.06m		1.05 d J=6	1.08 d J=6
$C_{(5)}$-CH_3	1.18 s	1.31 s	1.08 s	1.03 s
$C_{(11)}$-CH_3	1.90	1.65 d J=1	1.90	1.75 d J=1.5
$C_{(3)}$-H	5.20m	5.22m	5.20m	5.20m
$C_{(9)}$-H	5.70m	6.05m		
$C_{(12)}$-H	7.04m	6.92m	6.93m	6.99m
CH_3(H)C=C(CO-CH_3)	1.90	1.90	1.90m	1.82m
CH_3(H)C=C(CO-CH_3)	1.98	1.99 d J=8	1.99 d J=7	2.02 d J=7
CH_3(CH_3)C=C(CO-H)	2.18	2.07m	—	—
CH_3(CH_3)C=C(CO-H)	1.90	1.31 d J=1.5	—	—
CH_3(H)C=C(CO-CH_3)	5.95	5.72 q J=8	5.98 q J=7	5.75 q J=7
CH_3(CH_3)C=C(CO-H)	5.65m	5.55m	—	—

a) Coupling constants are expressed in Hz. s: singlet, d: doublet, q: quartet, m: multiplet.

a *cis*-AB-ring junction and exists in two interchangeable conformational isomers, so-called "steroid-like" (**11-A**) and "non-steroid-like" (**11-B**) chair-chair conformer.[10] A broad signal ($W_{1/2}$=*ca.* 22 Hz; axial proton) at δ (CS_2) 4.92 assigned to the 3α-proton in **11** suggests that **11** has predominantly the "non-steroid-like" conformation (**11-B**) at −40 °C.

Reduction of **5** with lithium aluminium hydride gave **4** and its C-9 epimer (**12**) in a ratio of 1:1. Acetylation of **12** with acetic anhydride in pyridine afforded a diacetate (**13**). In the PMR spectrum of **13** at 25 °C a broad signal of the C-12 proton was observed at δ (CS_2) 6.93. When the temperature was lowered to −40 °C this signal changed into a pair of signals at δ (CS_2) 6.89 and 6.97 in a ratio of 5:1. The broad signal ($W_{1/2}$=*ca.* 22 Hz) at δ (CS_2) 5.03 due to the C-3 proton indicates that the "non-steroid-like" conformer is the major one. The half-band width (5 Hz) observed for the PMR signal δ (CS_2) 5.52 of C-9 proton in **13** is larger than that (3 Hz) for the signal δ (CS_2) 5.26 of C-9 proton in **11**. This implies that the C-9 proton in **13** has a quasi-axial nature ("non-steroid-like" conformation) and that the C-9 proton in **11** has a quasi-equatorial nature ("non-steroid-like" conformation).[11] Therefore, the acetoxyl group at C-9 of **11** and **13** are in β- and α-configuration, respectively. The structure including absolute configuration of **1** is represented by 3β-angeloyloxy-10β-hydroxy-9β-senecioyloxyfuranoeremophilane.

Compound **2** was also positive to the Ehrlich test. From the UV, IR, PMR, and mass spectra **2** is assumed to be the desenecioyloxyl derivative of **1** (*cf.* Experimental and Table 1).

Reduction of **2** with lithium aluminium hydride in ether gave a diol (**14**), which was also obtained by alkaline hydrolysis of **2**.

Oxidation of **14** with chromium trioxide in pyridine gave a hydroxy ketone (**15**). Deuterium-exchange reaction of **15** with CH_3OD in the presence of a trace of alkali afforded a mixture of deuterated products (**15**-d_3 and **15**'-d_3), whose mass spectrum shows an incorporation of three deuterium atoms. A doublet at δ 0.94 due to the secondary methyl in **15** changed into a pair of singlets at δ 0.94 (**15**-d_3) and δ 1.01 (**15**'-d_3). The carbonyl group of **15** and hence the secondary hydroxyl group of **14** could be placed on C-3, provided that these compounds have a furanoeremophilane skeleton.

Carbon skeleton including absolute configuration of the above compounds was determined on the basis of the following transformation. Reduction of **11** with lithium in ethylamine[12] yielded 3β,10β-dihydroxyfuranoeremophilane. Its spectroscopic data (IR, PMR, and mass spectra) are in complete accord with those of **14**. The absolute configuration (*S*) at C-3 in **14** was further confirmed by the Horeau's method[8] (esterification 100%; optical yield (−) 28%). Compounds **2**, **14**, and **15** were thus shown to be 3β-angeloyloxy-10β-hydroxyfuranoeremophilane, 3β,10β-dihydroxyfuranoeremophilane, and 10β-hydroxy-3-oxofuranoeremophilane, respectively.

In further support for the proposed structures, the intense peak at *m/e* 108 due to the *retro*-Diels-Alder fragmentation in ring B[13] was observed for the furanoeremophilane derivatives (**2**, **14**, and **16**), and the corresponding peaks at *m/e* 124, *m/e* 166, and *m/e* 122 for the compounds with 9-hydroxyl (**4** and **10**), 9-acetoxyl (**11** and **13**), and 9-oxo (**3**, **5**, **6**, and **9**) group, respectively.

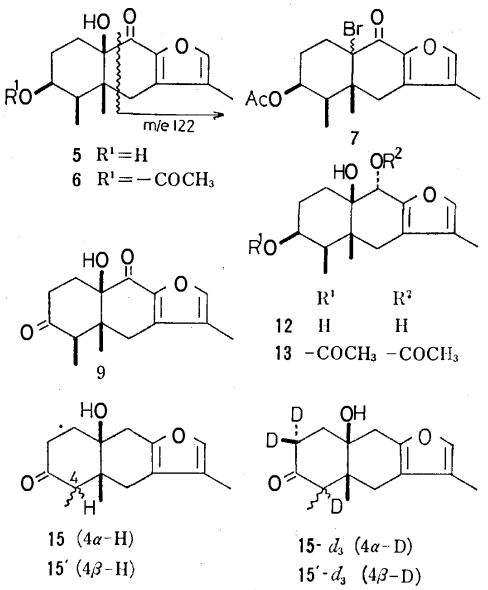

In the PMR spectra (Table 2) of the hydroxy ketone (**15**), a remarkable pyridine-induced solvent shift[14] ($\delta^{CDCl_3}-\delta^{C_5H_5N}=-0.17$) of the tertiary methyl at C-5 arising from preferential association of pyridine with the hydroxyl group was observed. The carbonyl group at C-3 would cause[15] a small and positive solvent shift of the tertiary methyl signal for both structures

Table 2. Chemical shifts (δ values) and solvent shifts (Δ values) of methyl protons for compounds **15** and **15′-d_3**

Compound	Solvent	$C_{(4)}$-CH_3	$C_{(5)}$-CH_3	$C_{(11)}$-CH_3
15	CCl_4	0.94	0.92	1.87
	C_6H_6	0.94	0.76	1.73
	$\Delta^{CCl_4}_{C_6H_6}$	0.00	+0.16	+0.14
	$CDCl_3$	1.02	0.99	1.95
	C_5H_5N	1.10	1.16	1.92
	$\Delta^{CDCl_3}_{C_5H_5N}$	−0.08	−0.17	+0.03
15′-d_3	CCl_4	1.01	1.04	1.84
	C_6H_6	1.05	0.84	1.63
	$\Delta^{CCl_4}_{C_6H_6}$	−0.04	+0.21	+0.21

$\Delta^{CDCl_3}_{C_5H_5N}=\delta^{CDCl_3}-\delta^{C_5H_5N}$, $\Delta^{CCl_4}_{C_6H_6}=\delta^{CCl_4}-\delta^{C_6H_6}$.

with *cis*- and *trans*-AB-ring junction. The extent of the negative solvent shift value for the tertiary methyl suggests the structure with a *cis*-AB-ring junction for **15**, in which the dihedral angle between the hydroxyl group and the tertiary methyl would be approximately 60°, while a small solvent shift ($\delta^{CDCl_3}-\delta^{C_5H_5N}$ = *ca.* −0.04) is expected for the structure with a *trans*-AB-ring junction. This shows that the solvent shift is applicable for the structure determination of these compounds.

A small benzene-induced solvent shift[16] (Table 2) for the C-4 methyl signal adjacent to carbonyl group was observed in the PMR spectra of **15** and **15′-d_3**; this suggests equatorial nature for the secondary methyl. **15** and **15′-d_3** must exist preferably in a "steroid-like" (**15-A**) and in a "non-steroid-like" (**15′-d_3-B**) conformation, respectively.

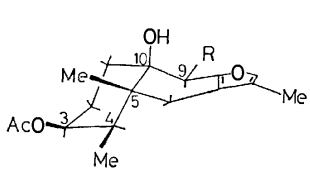

11-A (R=OAc)
16-A (R=H)

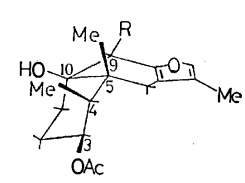

11-B (R=OAc)
16-B (R=H)

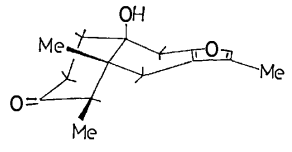

15-A

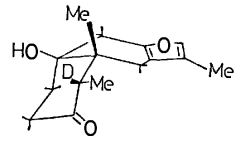

15′-B

Acetylation of **14** with acetic anhydride in pyridine gave a monoacetate (**16**). The PMR spectrum in carbon disulfide at 30 °C showed a signal at δ 5.06 (quintet, J=*ca.* 4 Hz) due to the proton at C-3. As the temperature was lowered the signal broadened and at −46 °C the signal changed into a pair of signals at δ 4.78 (s, $W_{1/2}$ *ca.* 8 Hz) and δ 5.07 (quintet, J=*ca.* 5.5 Hz) in a ratio of 1:3, which are assigned to the C-3α proton (equatorial) in the "steroid-like" conformation (**16-A**) and the C-3α proton (axial) in the "non-steroid-like" conformation (**16-B**), respectively. An equilibrium between the "steroid-like" (**A**) and "non-steroid-like" (**B**) conformations on PMR time scale at room temperature was thus shown for **16**.

Experimental

IR, UV, and mass spectra were measured using a Hitachi EPI-G2, a Hitachi EPS-3, and a Hitachi RMU-6-Tokugata, spectrometers, respectively. Optical rotations, $[\alpha]_D$, were measured with a JASCO DIP-SL spectrometer. PMR spectra were taken on a JEOL PS-100 (100 MHz), a Hitachi R-20 (60 MHz), or a Hitachi R-24 (60 MHz) spectrometer. Chemical shifts are expressed in δ (TMS as an internal standard), and coupling constants in Hz. All melting points were determined on a hot block and reported uncorrected. Merck Kieselgel G and Kieselgel 60 PF_{254} were used for analytical and preparative TLC, respectively. For column chromatography, silica gel (Wakogel C-200) was used.

Isolation of 3β-Angeloyloxy-10β-hydroxy-9β-senecioyloxyfuranoeremophilane (1) and 3β-Angeloyloxy-10β-hydroxyfuranoeremophilane (2). The roots of *Farfugium japonicum* Kitamura (15 kg) were extracted with ether at room temperature for 3 days. The extract was then filtered, dried over anhydrous sodium sulfate, and the solvent was evaporated to give a viscous oil (80 g). The oil (36 g) was chromatographed on silica gel (500 g) using light petroleum–ether (10:1) as eluent. The eluted fractions (each 400 ml) were collected and examined by TLC. Fractions 10 and 11 gave a viscous oil (959 mg), containing **1**, which was purified by preparative TLC. Fractions 15—17 gave a viscous oil (1.06 g). The oil was purified by preparative TLC to afford **2**.

3β-Angeloyloxy-10β-hydroxy-9β-senecioyloxyfuranoeremophilane (1). Compound **1** (one spot on TLC), an oil, $[\alpha]_D^{16}$ +79° (*c* 1.05, EtOH), was positive to the Ehrlich test (pink in color). Characterization of **1** is as follows; UV (MeOH): λ_{max} 220 nm (ε 37000); IR(neat): 3500, 1710, and 1642 cm^{-1}; PMR (Table 1); MS: *m/e* 430 [1%, M^+ ($C_{25}H_{34}O_6$)], 412 (3%, $[M-H_2O]^+$), 83 (100%, $[CH_3CH=C(CH_3)CO]^+$ and $[(CH_3)_2C=CHCO]^+$) and 55 (42%, $[CH_3CH=CCH_3]^+$ and $[(CH_3)_2C=CH]^+$).

3β-Angeloyloxy-10β-hydroxyfuranoeremophilane (2). Compound **2** (one spot on TLC) was a viscous oil, $[\alpha]_D^{24}$ −13° (*c* 0.88, EtOH). Its spot on TLC plate showed purple color to the Ehrlich test. Spectral data of **2** are as follows; UV (MeOH): λ_{max} 218.5 nm (ε 19000); IR (CCl_4): 3500, 1710, 1645, and 1565 cm^{-1}; PMR (Table 1); MS: *m/e* 332 [6%, M^+ ($C_{20}H_{28}O_4$)], 124 (41%), 109 (100%), 108 (75%, *retro*-Diels-Alder fragment[13]), 83 (89%, $[CH_3CH=C(CH_3)CO]^+$), and 55 (64%, $[CH_3CH=CCH_3]^+$).

Reduction of 1 with Lithium Aluminium Hydride. To a suspension of lithium aluminium hydride (100 mg) in dry ether (6 ml) a solution of **1** (125 mg) in dry ether (6 ml) was added and the mixture was refluxed for 2.5 h under a nitrogen atmosphere. An excess of lithium aluminium hydride was decomposed with water and the product was extracted with ether. The usual treatment of the extract gave a crystalline product (86 mg), which was purified by preparative TLC (developed with ether) to afford 3β,9β,10β-trihydroxyfuranocremophilane (**4**: 34 mg), mp 158—159 °C (dec), $[\alpha]_D^{25}$ −5° (*c* 1.0, MeOH); UV (MeOH): λ_{max} 224 nm (ε 4200); IR (Nujol): 3250—3460 cm^{-1}; PMR ($CDCl_3$): δ 1.10 (d, J=6.5 Hz, $C_{(4)}$-CH_3), 1.21 (s, $C_{(5)}$-CH_3), 1.90 (d, J=1.2 Hz, $C_{(11)}$-CH_3), 2.15 (d, J=17 Hz, $C_{(6)}$-H),

2.53 (d, J=17 Hz, $C_{(6)}$-H), 4.02 (m, $C_{(3)}$-H), 4.47 (br s, $C_{(9)}$-H), and 7.12 (q, J=1.2 Hz, $C_{(12)}$-H); MS: *m/e* 124 (100%, *retro*-Diels-Alder fragment). A molecular ion peak at *m/e* 266 ($C_{15}H_{22}O_4$) was not observed. Found: C, 67.74; H, 8.17%. Calcd for $C_{15}H_{22}O_4$: C, 67.84; H, 8.33%.

Oxidation of ***4*** *with Active Manganese Dioxide.* To a solution of **4** (40 mg) in benzene (30 ml) was added active manganese dioxide (70 mg) and the mixture was stirred for 8 h under a nitrogen atmosphere. After filtration, the solvent was removed to give 3β,10β-dihydroxy-9-oxofuranoeremophilane (**5**; 26 mg); negative to the Ehrlich test; mp 138 °C (recrystallized from light petroleum–ether), $[\alpha]_D^{25}$ −18° (c 0.59, MeOH); UV (MeOH): λ_{max} 283 nm (ε 8800); IR (Nujol): 3450, 3340, 1670, 1605, and 1530 cm^{-1}; MS: *m/e* 264 [20%, M^+ ($C_{15}H_{20}O_4$)] and 122 (100%, *retro*-Diels-Alder fragment). Found: C, 68.43; H, 7.56%. Calcd for $C_{15}H_{20}O_4$: C, 68.16; H, 7.63%.

Acetylation of ***5*** *with Acetic Anhydride in Pyridine.* Compound **5** (140 mg) was treated with acetic anhydride (1.5 ml) and pyridine (3 ml) overnight at room temperature. Methanol (2 ml) was added to decompose an excess of acetic anhydride. Evaporation of the solvent gave an oily residue which was chromatographed on silica gel (7 g) using hexane–ether (2:1; 75 ml) as eluent to yield the monoacetate, 3β-acetoxy-10β-hydroxy-9-oxofuranoeremophilane (**6**; 157 mg; one spot on TLC), an amorphous solid, IR (Nujol): 3450, 1735, and 1675 cm^{-1}; PMR (CCl_4): δ 0.98 (s, $C_{(5)}$-CH_3), 1.08 (d, J=*ca.* 7 Hz, $C_{(4)}$-CH_3), 2.00 (s, $C_{(11)}$-CH_3 and -OCOCH_3), 5.20 (m, $C_{(3)}$-H), and 7.37 (br s, $C_{(12)}$-H); MS: *m/e* 306 [6%, M^+ ($C_{17}H_{22}O_5$)], 263 (5%, [M−CH_3-CO]$^+$), 246 (11%, [M−CH_3COOH]$^+$), 124 (66%), 123 (63%), and 122 (100%, *retro*-Diels-Alder fragment).

Treatment of ***6*** *with Phosphorus Tribromide.* To a solution of **6** (73 mg) in dichloromethane (9 ml) was added a solution of phosphorus tribromide (0.1 ml) in dichloromethane (0.9 ml) and the reaction mixture was heated under reflux for 4 h under a nitrogen atmosphere. The reaction mixture was then cooled to 0 °C and a saturated aqueous solution of sodium hydrogencarbonate (5 ml) was added dropwise. The product was extracted three times with ether and a combined ethereal solution was washed with water and with saturated brine, and dried over anhydrous sodium sulfate. Evaporation of the solvent gave an oily product, 3β-acetoxy-10 ξ-bromo-9-oxofuranoeremophilane (**7**; 56 mg; one spot on TLC), IR (neat): 1730 and 1670 cm^{-1}; PMR (CCl_4): δ 1.00 (d, J=*ca.* 7 Hz, $C_{(4)}$-CH_3), 1.11 (s, $C_{(5)}$-CH_3), 1.99 (s, $C_{(11)}$-CH_3 and -OCOCH_3), 4.98 (m, $C_{(3)}$-H, $W_{1/2}$=*ca.* 12 Hz), and 7.34 (m, $C_{(12)}$-H); MS: *m/e* 370 [13%, M^+ ($C_{17}H_{21}O_4Br$)], 368 (13%, M^+), 289 (24%, [M−Br]$^+$), and 229 (100%, [M−Br−CH_3-COOH]$^+$).

Debromination of ***7*** *with Active Zinc Dust in Acetic Acid.* To a solution of **7** (56 mg) in acetic acid (3 ml) was added active zinc dust (107 mg) and the mixture was allowed to stir for 3.5 h at room temperature under a nitrogen atmosphere. Ether was then added. After filtration the solvent was evaporated under reduced pressure to give an oily residue, which was chromatographed on silica gel (7 g). Elution with hexane–ether (2:1, 100 ml) and hexane–ether (1:1, 80 ml) gave colorless crystals (30 mg). Recrystallization from hexane–ether afforded 3β-acetoxy-9-oxo-10α*H*-furanoeremophilane (**3**; 17 mg) as colorless needles, mp 172—174 °C, $[\alpha]_D^{28}$ +27° (c 0.55, MeOH), IR (Nujol): 1720 and 1655 cm^{-1}; PMR ($CDCl_3$): δ 0.98 (s, $C_{(5)}$-CH_3), 1.04 (d, J=*ca.* 7 Hz, $C_{(4)}$-CH_3), 2.00 (d, J=*ca.* 1 Hz, $C_{(11)}$-CH_3), 2.06 (s, -OCOCH_3), 5.01 (m, $C_{(3)}$-H), and 7.37 (m, $C_{(12)}$-H); *m/e* 290 [35%, M^+($C_{17}H_{22}O_4$)], 230 (58%, [M−CH_3COOH]$^+$), 215 (51%, [M−CH_3COOH−CH_3]$^+$), 162 (100%), and 122 (77%, *retro*-Diels-Alder fragment). This compound was found to be identical (mp, mixed mp, IR, PMR, and mass spectra) with **3** prepared from **8** (*vide infra*).

Acetylation of ***8*** *with Acetic Anhydride in Pyridine.* A solution of epieuryopsonol (**8**; 22 mg) in acetic anhydride (2 ml) and pyridine (3 ml) was allowed to stand overnight at room temperature to yield **3**, colorless needles (recrystallization from hexane–ether), mp 173—175 °C, $[\alpha]_D^{28}$ +28° (c 0.53, MeOH), IR (Nujol): 1720 and 1655 cm^{-1}; PMR ($CDCl_3$): δ 0.98 (s, $C_{(5)}$-CH_3), 1.04 (d, J=*ca.* 7 Hz, $C_{(4)}$-CH_3), 2.00 (d, J=*ca.* 1 Hz, $C_{(11)}$-CH_3), 2.06 (s, -OCOCH_3), 5.03 (m, $C_{(3)}$-H)1 and 7.36 (m, $C_{(12)}$-H); MS: *m/e* 290 [32%, M^+($C_{17}H_{22}O_4$)], 230 (54%, [M−CH_3COOH]$^+$), 215 (48%, [M−CH_3COOH−CH_3]$^+$), 162 (100%), and 122 (77%. *retro*-Diels-Alder fragment). Found: C, 70.33; H, 7.90%. Calcd for $C_{17}H_{22}O_4$: C, 70.34; H, 7.64%.

Application of the Horeau's Method to ***5****.* A solution of **5** (20.6 mg, 0.078 mmol) in pyridine (0.3 ml) was allowed to stand with α-phenylbutyric anhydride (85.0 mg, 0.259 mmol) overnight. The reaction mixture was then heated with one drop of water. After benzene was added, the mixture was titrated with 0.1 M potassium hydroxide solution in the presence of phenolphthalein. The aqueous layer was acidified with dilute sulfuric acid and then extracted with benzene. After usual treatment of the extract, the solvent was distilled off to give α-phenylbutyric acid. The optical rotation value (α_D −0.027°) was observed for benzene solution (1.5 ml) of the acid using a 0.1 dm cell. Esterification 36%; optical yield (−) 62%.

Oxidation of ***4*** *with Chromium Trioxide in Pyridine.* To a solution of chromium trioxide (419 mg) in pyridine (6 ml) was added a solution of **4** (193 mg) in pyridine (3 ml) with stirring at 0 °C. The mixture was allowed to stand for 24 h at room temperature under a nitrogen atmosphere, diluted with a mixture of ice and water, and extracted with ether. The extract was washed with water and dried over anhydrous sodium sulfate. The solvent was removed to give a residue (77 mg) which was chromatographed on silica gel (5 g; eluent: light petroleum–ether, 1:1) to give 10β-hydroxy-3,9-dioxofuranoeremophilane (**9**; 25 mg), mp 121—122 °C (recrystallization from light petroleum–ether); UV (EtOH): λ_{max} 285 nm (ε 9300); IR (Nujol): 3430, 1700, 1655, and 1530 cm^{-1}; PMR ($CDCl_3$): δ 1.05 (s, $C_{(5)}$-CH_3), 1.33 (d, J=7.5 Hz, $C_{(4)}$-CH_3), 1.97 (d, J=1 Hz, $C_{(11)}$-CH_3), 3.73 (s, OH; this signal disappeared on addition of D_2O), and 7.48 (q, J=1 Hz, $C_{(12)}$-H); MS: *m/e* 262 [34%, M^+($C_{15}H_{18}O_4$)], 178 (41%), and 122 (100%, *retro*-Diels-Alder fragment). Found: C, 68.57; H, 6.85%. Calcd for $C_{15}H_{18}O_4$: C, 68.68; H, 6.92%.

Partial Hydrolysis of ***1*** *with Ethanolic Potassium Hydroxide.* A solution of potassium hydroxide (50 mg) in 95% ethanol (1 ml) was added to **1** (33 mg), and the solution was allowed to stand at room temperature for 3 h. To the reaction mixture was added water (10 ml), and the resulting aqueous solution was extracted with ether (each 30 ml) three times. A combined ethereal solution was washed with 10% hydrochloric acid (10 ml), saturated aqueous solution of sodium hydrogencarbonate (10 ml), and with water (20 ml), and finally dried over anhydrous sodium sulfate. Evaporation of the solvent gave a residue (23 mg), which was passed through a column of silica gel (200 mg) (eluent: light petroleum–ether, 2:1) to give partially hydrolyzed product (**10**; one spot on TLC), a viscous oil; IR (neat): 3450, 1710, 1640, and 1560 cm^{-1}; PMR (C_6D_6): δ 1.10 (m, $C_{(4)}$-CH_3), 1.17 (s, $C_{(5)}$-CH_3), 1.73 (d, J=*ca.* 1 Hz, $C_{(11)}$-CH_3), 1.95

(m, $-COC(CH_3)=CHCH_3$), 2.05 (d, $J=7$ Hz, $-COC(CH_3)=CHCH_3$), 4.31 (br s, $C_{(9)}$-H), 5.30 (m, $C_{(3)}$-H), 5.80 (q, $J=7$ Hz, $-CO(CH_3)C=CHCH_3$), and 7.05 (m, $C_{(12)}$-H); MS: *m/e* 348 [0.8%, M^+ ($C_{20}H_{28}O_5$)]. 330 (0.6%, [$M-H_2O$]$^+$), 124 (100%, *retro*-Diels-Alder fragment), 83 (20%, [$COC(CH_3)=CHCH_3$]$^+$), and 55 (21 %, [$C(CH_3)=CHCH_3$]$^+$).

Acetylation of ***4*** *with Acetic Anhydride in Pyridine.* A mixture of **4** (51 mg), acetic anhydride (0.2 ml), and pyridine (0.5 ml) was allowed to stand overnight at room temperature. After addition of methanol (1 ml), the solvent was removed under reduced pressure to give a residue. From the residue 3*β*, 9*β*-diacetoxy-10*β*-hydroxyfuranoeremophilane (**11**; one spot on TLC), an oil, was isolated by preparative TLC (developed with light petroleum–ether, 1:1). Spectral data of **11** are as follows ; IR (neat): 3480, 1735, and 1560 cm^{-1}; PMR (CCl_4): δ 1.05 (d, $J=7$ Hz, $C_{(4)}$-CH_3), 1.13 (s, $C_{(5)}$-CH_3), 1.92 (d, $J=ca.$ 1 Hz, $C_{(11)}$-CH_3), 2.00 (s, $-OCOCH_3$), 2.10 (s, $-OCOCH_3$), 5.10 (m, $C_{(3)}$-H), 5.65 (m, $C_{(9)}$-H), and 7.08 (q, $J=1$ Hz, $C_{(12)}$-H); PMR (CS_2): δ 0.99 (d, $J=7$ Hz, $C_{(4)}$-CH_3), 1.06 (s, $C_{(5)}$-CH_3), 1.88 (d, $J=ca.$ 1 Hz, $C_{(11)}$-CH_3), 1.91 (s, $-OCOCH_3$), 2.00 (s, $-OCOCH_3$), 4.94(m, $C_{(3)}$-H), 5.48 (m, $C_{(9)}$-H), and 6.97 (q, $J=ca.$ 1 Hz, $C_{(12)}$-H); MS: *m/e* 350 [1%, M^+ ($C_{19}H_{26}O_6$)], 332 (3%, [$M-H_2O$]$^+$), 290 (3%, [$M-CH_3COOH$]$^+$), 230 (4%, [$M-2CH_3COOH$]$^+$), 166 (37%, *retro*-Diels-Alder fragment), 124 (100%), and 43 (36%, [CH_3CO]$^+$).

Reduction of ***5*** *with Lithium Aluminium Hydride.* To a suspension of lithium aluminium hydride (97 mg) in dry ether (3 ml) was added a solution of **5** (52 mg) in dry ether (3 ml) and the mixture was stirred for 3.5 h at room temperature under a nitrogen atmosphere. An excess of lithium aluminium hydride was decomposed by addition of water and the product was extracted with ether. The usual treatment of the extract gave a residue, which was chromatographed on silica gel (300 mg) using ether as eluent to afford 3*β*,9*β*,10*β*-trihydroxyfuranoeremophilane (**4**; 21 mg) and 3*β*,9*α*,10*β*-trihydroxyfuranoeremophilane (**12**; 27 mg). The latter compound (**12**) showed a higher R_f value than that of **4** on TLC (silica gel) developed with ether. The separated compound (**12**) without further purification was used for acetylation.

Acetylation of ***12*** *with Acetic Anhydride in Pyridine.* A solution of **12** (27 mg), acetic anhydride (0.2 ml), and pyridine (0.5 ml) was allowed to stand overnight at room temperature. After addition of methanol (1 ml), the solvent was removed under reduced pressure. The residual oil was subjected to separation by preparative TLC (developed with light petroleum–ether, 3:5) to give 3*β*,9*α*-diacetoxy-10*β*-hydroxyfuranoeremophilane (**13**; 18 mg; one spot on TLC), an oil, IR (Nujol): 3460, 1730, and 1560 cm^{-1}; PMR (CCl_4): δ 1.11 (d, $J=7$ Hz, $C_{(4)}$-CH_3), 1.11 (s, $C_{(5)}$-CH_3), 1.92 (d, $J=ca.$ 1 Hz, $C_{(11)}$-CH_3), 2.00 (s, $-OCOCH_3$), 2.19 (s, $-OCOCH_3$), 5.25 (m, $C_{(3)}$-H), 5.70 (m, $C_{(9)}$-H), and 7.05 (q, $J=ca.$ 1 Hz, $C_{(12)}$-H); PMR (CS_2): δ 1.00 (s, $C_{(5)}$-CH_3), 1.04 (d, $J=7$ Hz, $C_{(4)}$-CH_3), 1.86 (d, $J=ca.$ 1 Hz, $C_{(11)}$-CH_3), 1.90 (s, $-OCOCH_3$), 2.07 (s, $-OCOCH_3$), 5.08 (dt, $J=11$ Hz and $J=5$ Hz, $C_{(3)}$-H), 5.54 (s, $C_{(9)}$-H), and 6.93 (q, $J=ca.$ 1 Hz, $C_{(12)}$-H); MS: *m/e* 350 [1%, M^+ ($C_{19}H_{26}O_6$)], 332 (7%, [$M-H_2O$]$^+$), 290 (4 %, [$M-CH_3COOH$]$^+$), 230 (6%, [$M-2CH_3COOH$]$^+$),), 215 (9%), [$M-2CH_3COOH-CH_3$]$^+$), 166 (31%, *retro*-Diels-Alder fragment), 124 (100%), and 43 (71%, [CH_3CO]$^+$).

Alkaline Hydrolysis of ***2****.* A solution of potassium hydroxide (250 mg) in ethanol (5 ml) was added to **2** (37 mg) and the mixture was refluxed for 1 h under a nitrogen atmosphere. After the solvent was distilled off, the residue was recrystallized from ether to give colorless crystals, **14**, mp 153—154 °C (dec). This compound was found to be identical (mp, IR, PMR, and mass spectra) with **14**, obtained from **2** by treatment with lithium aluminium hydride (*vide infra*).

Reduction of ***2*** *with Lithium Aluminium Hydride.* To a suspension of lithium aluminium hydride (210 mg) in dry ether (6 ml), an oil (893 mg) containing **2** as the major component was added and stirred for 4 h at room temperature under a nitrogen atmosphere. An excess of lithium aluminium hydride was decomposed by addition of water and the product was extracted with ether. The ethereal solution was dried over anhydrous sodium sulfate and the solvent was evaporated to give a residue(519 mg), which was chromatographed on silica gel (30 g). Fractions 8—10 eluted with light petroleum–ether (1:1) (each fraction 50 ml) gave a crystalline product (129 mg), which was recrystallized from acetone–diisopropyl ether to afford 3*β*,10*β*-dihydroxyfuranoeremophilane (**14**), mp 151—153 °C, $[\alpha]_D^{21}$ −11° (*c* 1.0, MeOH). Spectral data of **14** are as follows; UV (MeOH): λ_{max} 220 nm (ε 5800); IR (Nujol): 3425, 1655, and 1560 cm^{-1}; PMR ($CDCl_3$): δ 1.10 (d, $J=7$ Hz, $C_{(4)}$-CH_3), 1.14 (s, $C_{(5)}$-CH_3), 1.89 (d, $J=1.5$ Hz, $C_{(11)}$-CH_3), 4.02 (m, $C_{(3)}$-H), and 7.03 (m, $C_{(12)}$-H); MS: *m/e* 250 [14%, M^+ ($C_{15}H_{22}O_3$)], 109 (100%), and 108 (62%, *retro*-Diels-Alder fragment). Found: C, 72.16; H, 8.68%. Calcd for $C_{15}H_{22}O_3$: C, 71.97; H, 8.68%.

Oxidation of ***14*** *with Chromium Trioxide in Pyridine.* To a solution of chromium trioxide (102 mg) in pyridine (6 ml) was added a solution of **14** (95 mg) in pyridine (2 ml) with stirring at 0 °C. The mixture was allowed to stand at room temperature for 2.5 h under a nitrogen atmosphere, diluted with a mixture of crashed ice and water, and extracted with ether. The extract was washed with water and dried over anhydrous sodium sulfate. The solvent was removed to give a residue (77 mg). From the residue **14** (14 mg) and **15** (47 mg) were separated by preparative TLC (developed with light petroleum–ether, 1 : 4). 10*β*-Hydroxy-3-oxofuranoeremophilane (**15**; one spot on TLC); an oil, $[\alpha]_D^{24}$ +10° (*c* 1.07, MeOH); UV (EtOH): λ_{max}219 nm (ε 4500); IR (neat): 3450, 1700, 1645, and 1560 cm^{-1}; PMR (CCl_4): δ 0.92 (s, $C_{(5)}$-CH_3), 0.94 (d, $J=7$ Hz, $C_{(4)}$-CH_3), 1.87 (d, $J=1.5$ Hz, $C_{(11)}$-CH_3), and 6.96 (m, $C_{(12)}$-H); MS: *m/e* 248 [<5%, M^+ ($C_{15}H_{20}O_3$)] and 108 (100%, *retro*-Diels-Alder fragment).

Deuterium-exchange Reaction of ***15****.* A solution of **15** (25 mg) in CH_3OD (1 ml) was warmed at 70 °C in the presence of a trace of NaOD for 10 h in a sealed tube. The reaction mixture was diluted with water and the extracted with ether. The extract was washed with dilute hydrochloric acid, water, aqueous solution of sodium hydrogencarbonate, and then with water. The ethereal solution was dried over anhydrous sodium sulfate and the solvent was evaporated to give a residue. The residue was submitted once more to deuterium-exchange reaction in a similar manner. The resulting oil was purified by preparative TLC to afford a mixture of **15**-d_3 and **15′**-d_3(1 : 5). This mixture showed one spot on TLC developed with light petroleum–ether (1 : 1). Signals due to **15′**-d_3 in the PMR spectrum of the mixture are as follows; δ (CCl_4) 1.01 (s, $C_{(4)}$-CH_3), 1.04 (s, $C_{(5)}$-CH_3), 1.84 (d, $J=1.5$ Hz, $C_{(11)}$-CH_3), and 6.92 (m, $C_{(12)}$-H). Treatment of the mixture with sodium hydroxide in methanol gave a mixture of **15** and 10*β*-hydroxy-3-oxo-4*βH*-furanoeremophilane (**15′**), whose PMR spectra show a doublet due to the C-4 methyl in **15′** at δ (CCl_4) 1.00 (d, $J=7$ Hz) and δ (C_6H_6) 1.05 (d, $J=7$ Hz).

Reduction of ***11*** *with Lithium in Ethylamine.* To a solution of **11** (123 mg) in ethylamine (10 ml) cooled to −78 °C

was added lithium (80 mg) and the reaction mixture was stirred at this temperature. When the reaction mixture changed to blue in color saturated aqueous solution of ammonium chloride (10 ml) was added. The resulting solution was extracted with ether for three times and a combined ethereal solution was washed with dilute hydrochloric acid, water, and with saturated brine, and dried over anhydrous sodium sulfate. The crude product (65 mg) was chromatographed on silica gel (6 g). Elution with hexane–ether (1:1; 200 ml) yielded 3β,10β-dihydroxyfuranoeremophilane (**14**; 36 mg), mp 152—154 °C (recrystallization from acetone–diisopropyl ether), $[\alpha]_D^{28}$ −9° (*c* 1.3, MeOH), IR (Nujol): 3425 cm^{-1}; PMR ($CDCl_3$): δ 1.10 (d, J=7 Hz, $C_{(4)}$–CH_3), 1.15 (s, $C_{(5)}$–CH_3), 1.90 (d, J=*ca.* 1 Hz, $C_{(11)}$–CH_3), 4.02 (m, $C_{(3)}$–H), and 7.05 (m, $C_{(12)}$–H); MS: *m/e* 250 [10%, M^+ ($C_{15}H_{22}O_3$)], 109 (100%), and 108 (64%, *retro*-Diels-Alder fragment). This compound was found to be identical (mp, $[\alpha]_D$ IR, PMR, and mass spectra) with **14** prepared from **2**.

*Application of the Horeau's Method to **14**.* A solution of **14** (14 mg, 0.056 mmol) in pyridine (0.3 ml) was allowed to stand overnight with α-phenylbutyric anhydride (67.7 mg, 0.218 mmol) at room temperature. The reaction mixture was treated by a similar manner described above. Esterification 100%; optical yield (−) 28% (optical rotation α_D −0.027°, cell length 0.1 dm, benzene solution 1.5 ml).

*Acetylation of **14** with Acetic Anhydride in Pyridine.* A mixture of **14** (22 mg), acetic anhydride (0.5 ml), and pyridine (4 ml) was allowed to stand overnight at room temperature. After addition of methanol the solvent was evaporated under reduced pressure to afford a residue. The residue was passed through a silica gel column (2 g) (light petroleum–ether, 10:1) to give **16** (one spot on TLC), an oil, IR (neat): 3450 and 1735 cm^{-1}; PMR (CS_2 at 30 °C): δ 1.00 (d, J=8 Hz, $C_{(4)}$–CH_3), 1.04 (s, $C_{(5)}$–CH_3), 1.88 (d, J=*ca.* 1 Hz, $C_{(11)}$–CH_3), 1.97 (s, –$OCOCH_3$), 5.06 (quintet, J=4 Hz, $C_{(3)}$–H), and 6.94 (m, $C_{(12)}$–H); MS: *m/e* 292 [7%, M^+ ($C_{17}H_{24}O_4$)], 206 (76%), 109 (80%), 108 (51%, *retro*-Diels-Alder fragment), and 43 (100%, $[CH_3CO]^+$).

References

1) A part of this work was presented at the 30th National Meeting of the Chemical Society of Japan, Higashiosaka, April 1974, Abstr. Vol. III, p. 1373.

2) H. Nagano, Y. Moriyama, Y. Tanahashi, T. Takahashi, M. Fukuyama, and K. Sato, *Chem. Lett.*, **1972**, 13; H. Nagano, Y. Moriyama, Y. Tanahashi, and T. Takahashi, *Bull. Chem. Soc. Jpn.*, **47**, 1994 (1974); H. Shirasaki, H. Komatsu, H. Nagano, Y. Moriyama, Y. Tanahashi, and T. Takahashi, *Bull. Chem. Soc. Jpn.*, **46**, 2818 (1973).

3) H. Nagano, Y. Tanahashi, Y. Moriyama, and T. Takahashi, *Bull. Chem. Soc. Jpn.*, **46**, 2840 (1973).

4) J. Attenburrow, A. F. B. Cameron, J. H. Chapman, R. M. Evans, B. A. Hems, A. B. A. Jansen, and T. Walker, *J. Chem. Soc.*, **1952**, 1094.

5) E. Borgstrom and T. F. Gallagher, *J. Biol. Chem.*, **177**, 951 (1949).

6) H. E. Zimmerman and A. Mais, *J. Am. Chem. Soc.*, **81**, 3644 (1959).

7) D. E. A. Rivett and G. R. Woolard, *Tetrahedron*, **23**, 2431 (1967).

8) A. Horeau and H. B. Kagan, *Tetrahedron*, **20**, 2431 (1964).

9) L. Novotný, Ch. Tabačíkova-Wlotzká, V. Herout, and F. Šorm, *Collect. Czech. Chem. Commun.*, **29**, 1922 (1964); 6-oxofuranoeremophilanes exhibit an UV absorption at λ_{max} 269 nm (ε *ca.* 4000).

10) M. Tada and T. Takahashi, *Tetrahedron Lett.*, **1973**, 5169; T. Sato, M. Tada, T. Takahashi, I. Horibe, H. Ishi, T. Iwata, K. Kuriyama, Y. Tamura, and K. Tori, *Chem. Lett.*, **1977**, 1191; T. Sato, M. Tada, T. Takahashi, I. Horibe, H. Ishi, and K. Tori, *Tetrahedron Lett.*, **1977**, 3895.

11) J. T. Pinhey and S. Sternhell, *Tetrahedron Lett.*, **1963**, 275.

12) A. S. Hallsworth, H. B. Henbest, and T. I. Wrigley, *J. Chem. Soc.*, **1957**, 1969.

13) Q. N. Porter and J. Baldas, "Mass Spectrometry of Heterocyclic Compounds," Wiley-Interscience, a Division of John Wiley Sons, New York (1971), pp. 128 and 129.

14) P. V. Demarco, E. Farkas, D. Doddrell, B. L. Mylari, and E. Wenkert, *J. Am. Chem. Soc.*, **90**, 5480 (1968).

15) D. H. Williams, *Tetrahedron Lett.*, **1965**, 2305.

16) N. S. Bhacca and D. H. Williams, "Application of NMR Spectroscopy in Organic Chemistry," Holden-Day, San Francisco (1964), pp. 77 and 165.

Preparation and Diels-Alder Reactions of 3-Substituted 3-Sulfolenes

Katsuhiko INOMATA,* Hideki KINOSHITA, Hisayo TAKEMOTO,
Yasue MURATA, and Hiroshi KOTAKE
Department of Chemistry, Faculty of Science, Kanazawa University, Kanazawa 920

(Received May 10, 1978)

It was found that 3-(*p*-tolylsulfonyl)- and 3-(*p*-tolylsulfinyl)-3-sulfolenes prepared from 3-sulfolene react with various dienophiles to give the corresponding Diels-Alder cycloadducts in good yields, and that only the "para" substituted cycloadducts are obtained with monofunctionalized (CHO, $COCH_3$, CO_2CH_3, CN, and C_6H_5) ethylenes and methyl 2-methylpropenoate, respectively.

Readily available 3-sulfolene (2,5-dihydrothiophene 1,1-dioxide) loses SO_2, giving pure butadiene on heating at 110—130 °C.[1] However, only a few reports have been given on the preparation of substituted dienes starting from 3-sulfolene.[2] In this paper we wish to report on the preparation and the reactions of 3-(*p*-tolylsulfonyl)- and 3-(*p*-tolylsulfinyl)-3-sulfolenes (**2** and **9**) which produce the electron-deficient dienes, 2-(*p*-tolylsulfonyl)- and 2-(*p*-tolylsulfinyl)-1,3-butadienes, respectively.

*Preparation and Reaction of 3-(*p*-Tolylsulfonyl)-3-sulfolene.* 3-(*p*-Tolylsulfonyl)-3-sulfolene (**2**) was readily prepared by the reaction of *trans*-3,4-dibromosulfolane (**1**) obtained by the bromination of 3-sulfolene[3] with sodium *p*-toluenesulfinate tetrahydrate and sodium hydroxide in methanol, in a one-pot substitution-elimination reaction as shown in the following scheme.

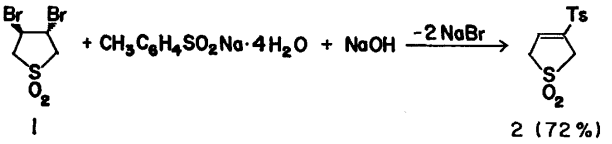

In order to confirm the reaction in which **2** thus obtained produces 2-(*p*-tolylsulfonyl)-1,3-butadiene (**3**) on heating, a solution of **2** in xylene was refluxed for 3 h. Evolution of SO_2 was confirmed by the color change in the universal indicator. However, the final product was not the expected **3** but its dimer **4** (97% yield). The structure of **4** was confirmed by elemental analysis and spectral data including ^{13}C-NMR spectrum of its reduction product. The fact that the dimer **4** was obtained in such an excellent yield indicates that the intermediate **3** is reactive to a dienophile. It was found that the reaction is accelerated by the addition of pyridine to capture SO_2.

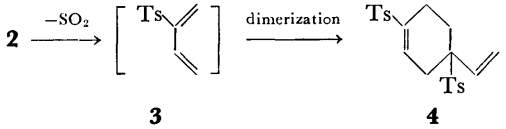

Hence the Diels-Alder reaction of **2** with various dienophiles **5a**—**i** was attempted. Since the monofunctionalized ethylenes **5e**—**i** and methyl 2-methylpropenoate (**5d**) are liable to polymerize, the reactions were carried out in the presence of a catalytic amount of hydroquinone and pyridine (as a scavenger of SO_2, equimolar with **2**) in a sealed tube. It was found that the Diels-Alder reaction of **2** with dienophiles **5a**—**i** gives the corresponding cycloadducts **6a**—**i** in excellent yields in all cases except **5b,g** (Table 1).

All the products **6d**—**i** and dimer **4** are "para" substituted cycloadducts. Their structures were confirmed by elemental analyses and spectral data including ^{13}C-NMR spectra of their reduction products, which indicate four peaks assigned to the "para" substituted cyclohexanes. It is evident that the Diels-Alder reaction of **2** with the dienophiles **5d**—**i** proceeds regioselectively. The reaction of **2** with dienophiles **5a**—**c** is stereospecific.

*Preparation and Reaction of 3-(*p*-Tolylsulfinyl)-3-sulfolene.* 3-(*p*-Tolylsulfinyl)-3-sulfolene (**9**) was prepared in three steps from **1** as follows: 4-bromo-2-sulfolene (**7**), prepared from **1** by the procedure of Bailey and Cummins,[3] was reacted with sodium *p*-toluenethiolate to give 4-(*p*-tolylthio)-2-sulfolene (**8**). Oxidation of **8** by sodium periodate gave the desired **9** accompanied by the isomerization of the double bond.

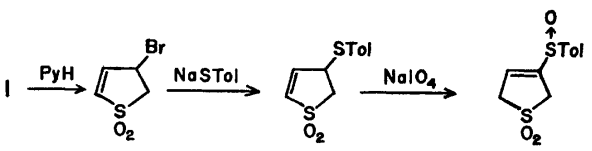

The Diels-Alder reaction of **9** with various dienophiles **5b**—**g** was attempted in a similar manner. It was found that the reaction also proceeds regioselectively to give the corresponding "para" substituted cycloadducts **10d**—**g** (Table 2).

It is apparent that both the Diels-Alder reactions of 3-(*p*-tolylsulfonyl)- and 3-(*p*-tolylsulfinyl)-3-sulfolenes (**2** and **9**) give the corresponding "para" regioisomers in good yields *via* 2-substituted butadienes. These results are in line with those predicted by means of Houk's generalization.[4]

Experimental

All the melting points are uncorrected. The ^{1}H- and ^{13}C-NMR spectra were recorded on JEOL JNM/MH-60 and JEOL PFT/PS-100 NMR spectrometers, respectively. The chemical shifts are reported in the δ scale relative to TMS as an internal standard. The IR spectra were taken with JASCO IRA-1 diffraction grating infrared spectrometer.

Materials. All the solvents were distilled according to the usual methods and stored over a drying agent. Thin-layer chromatography (TLC) was performed on Merck's Kieselgel 60 PF_{254} (Art. 7749) using a mixture of benzene and ethyl acetate as an eluent, unless otherwise stated.

Table 1. Cycloadducts of 3-(*p*-tolylsulfonyl)-3-sulfolene (**2**) with various dienophiles

	Dienophile	Molar ratio **5/2**	Condition[a]	Isolated yield (%)[b] **6a—i**
5a	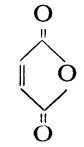	10	A	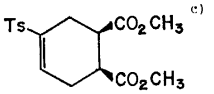 99
5b	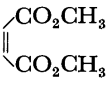	10	A	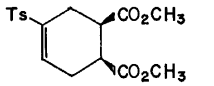 50[d]
5c	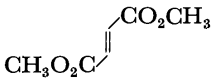	10	A	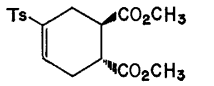 98
5d	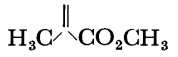	20	B	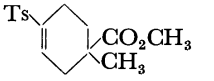 93
5e		20	B	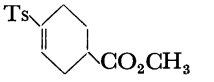 quant.
5f		20	B	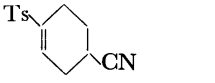 89[e]
5g	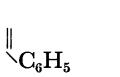	10	C	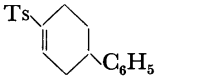 64[f]
5h		20	B	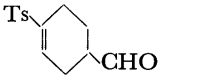 84
5i		20	B	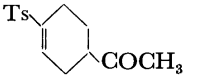 quant.

a) A: Refluxed in xylene for 3 h. B: Heated in a sealed tube at 140—150 °C in xylene for 2 h in the presence of catalytic amount of hydroquinone and pyridine (1 equiv). C: Toluene was used in the place of xylene in B at 110—120 °C. b) Based on **2**. c) Initial product subjected to hydrolysis followed by esterification with diazomethane in THF-ether. d) Dimer **4** isolated in 42% yield. e) Dimer **4** isolated in 11% yield. f) Dimer **4** isolated in 32% yield.

*3-(*p*-Tolylsulfonyl)-3-sulfolene (2).* To a methanol solution (300 ml) of sodium hydroxide (1.760 g, 44 mmol) were added sodium *p*-toluenesulfinate tetrahydrate (50 g, 200 mmol) and 3,4-dibromosulfolane (**1**, 11.118 g, 40 mmol).[3] After being refluxed for 5 h, the reaction mixture was poured over ice to give the crude **2** (8.596 g, mp 108—110 °C), which was recrystallized from ethanol (7.848 g, 72%): mp 125—126 °C; IR 1315, 1307, 1298, 1142, 1125 cm^{-1}; NMR ($CDCl_3$) δ 2.44 (s, 3H), 3.84 (m, 2H), 4.02 (m, 2H), 6.98 (m, 1H), 7.34 (d, 2H, J=9 Hz), 7.73 (d, 2H, J=9 Hz). Found: C, 48.63; H, 4.51; S, 23.24%. Calcd for $C_{11}H_{12}O_4S_2$: C, 48.53; H, 4.44; S, 23.51%.

*1,4-Bis(*p*-tolylsulfonyl)-4-vinylcyclohexene (4).* To a xylene solution (6 ml) of **2** (273 mg, 1 mmol) were added pyridine (79 mg, 1 mmol) and a catalytic amount of hydroquinone (*ca.* 5 mg). The mixed solution was heated at 140—150 °C in a sealed tube for 2 h. After addition of ethyl acetate and 1 M HCl, the organic layer was washed with a saturated solution of NaCl, dried over Na_2SO_4, filtered, and evaporated to dryness under reduced pressure. The crystalline residue was separated by preparative TLC to afford **4** (417 mg, mp 166—170 °C) in a nearly quantitative yield. Recrystallization from ethanol gave pure **4** (404 mg, 97%): mp 198—199 °C; IR 1280, 1145 cm^{-1}; NMR ($CDCl_3$) δ 1.7—3.0 (m, 6H), 2.40 (s, 6H), 4.87 (d, 1H, J=17 Hz), 5.23 (d, 1H, J=11 Hz), 5.63 (dd, 1H, J=11 and 17 Hz), 6.90 (m, 1H), 7.25 (m, 4H), 7.59 (d, 4H, J=8 Hz). Found: C, 63.52; H, 5.79; S, 15.35%. Calcd for $C_{22}H_{24}O_4S_2$: C, 63.45; H, 5.81; S, 15.37%.

Dimethyl cis*-4-(*p*-Tolylsulfonyl)-4-cyclohexene-1,2-dicarboxylate (6a).* A suspension of **2** (91 mg, 1/3 mmol) and maleic anhydride (**5a**, 10/3 mmol) in xylene (2 ml), which became a clear solution on heating, was refluxed for 3 h. After evaporation of the solvent, excess **5a** was removed by sublimation. The residue was treated with 6 M HCl and tetrahydrofuran (THF) to hydrolyze the product followed by concentration. The residue was redissolved in THF and dried over Na_2SO_4 followed by addition of an ethereal solution of diazomethane. After evaporation of the solvent, the residue was separated by preparative TLC to afford **6a** (116 mg) in a 99% yield. Recrystallization from ethanol gave pure **6a**: mp 144—146 °C; IR 1720, 1295, 1285, 1240, 1205, 1145 cm^{-1}; NMR ($CDCl_3$) δ 2.39 (s, 3H), 2.4—3.3 (m, 6H), 3.44 (s, 3H), 3.66 (s, 3H), 6.93 (m, 1H), 7.24 (d, 2H, J=9 Hz), 7.64 (d, 2H, J=9 Hz). Found: C, 57.86; H, 5.61; S, 9.24%. Calcd for $C_{17}H_{20}O_6S$: C, 57.95; H, 5.72; S, 9.08%.

In a similar manner except for esterification with diazomethane, other cycloadducts **6b** (=**6a**) and **6c** were obtained from **2** and the corresponding dienophiles **5b** and **5c**.

Table 2. Cycloadducts of 3-(*p*-tolylsulfinyl)-3-sulfolene (**9**) with various dienophiles

	Dienophile	Molar ratio **5**/**9**	Condition[a]	Isolated yield (%)[b] **10b—g**
5b	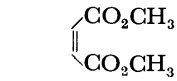	10	A	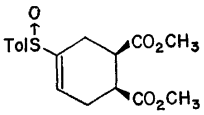 66
5c	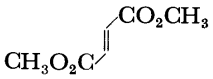	10	A	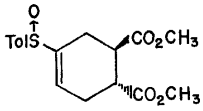 89
5d	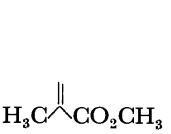	20	B	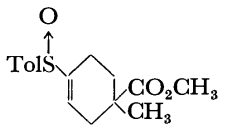 74
5e		20	B	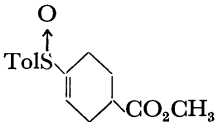 97
5f		20	B	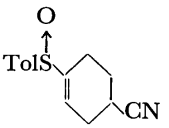 63[c]
5g		10	C	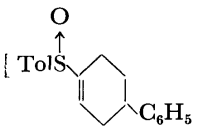 56

a) As in Table 1. b) Based on **9**. c) Consists of two diastereoisomers isolated in 29 and 34% yields, respectively.

6c: Mp 110—112 °C; IR 1720, 1300, 1200, 1140 cm^{-1}; NMR ($CDCl_3$) δ 1.6—3.2 (m, 6H), 2.43 (s, 3H), 3.61 (s, 3H), 3.66 (s, 3H), 6.97 (m, 1H), 7.30 (d, 2H, J=9 Hz), 7.69 (d, 2H, J=9 Hz). Found: C, 58.11; H, 5.62; S, 9.11%. Calcd for $C_{17}H_{20}O_6S$: C, 57.95; H, 5.72; S, 9.08%.

*Methyl 1-Methyl-4-(*p*-tolylsulfonyl)-3-cyclohexene-1-carboxylate (**6d**).* A mixture of **2** (273 mg, 1 mmol), methyl 2-methylpropenoate (**5d**, 2.002 g, 20 mmol), pyridine (79 mg, 1 mmol), and a catalytic amount of hydroquinone in xylene (5 ml) was heated at 140—150 °C in a sealed tube for 2 h. After addition of ethyl acetate, the solution was washed with water, dried over Na_2SO_4, and concentrated under reduced pressure. The residue was separated by preparative TLC to afford **6d** (287 mg) in 93% yield. Recrystallization from hexane gave pure **6d**: mp 72.5—73 °C; IR 1720, 1300, 1155, 1125 cm^{-1}; NMR ($CDCl_3$) δ 1.15 (s, 3H), 1.5—3.1 (m, 6H), 2.39 (s, 3H), 3.53 (s, 3H), 6.95 (m, 1H), 7.27 (d, 2H, J=9 Hz), 7.68 (d, 2H, J=9 Hz). Found: C, 62.38; H, 6.56%. Calcd for $C_{16}H_{20}O_4S$: C, 62.32; H, 6.54%.

In a similar manner, cycloadducts **6e—i** were obtained from **2** and the corresponding dienophiles **5e—i** in good yields (Table 1).

6e: Mp 58—60 °C; IR 1728, 1300, 1290, 1145 cm^{-1}; NMR ($CDCl_3$) δ 1.2—2.7 (m, 7H), 2.42 (s, 3H), 3.62 (s, 3H), 6.96 (m, 1H), 7.27 (d, 2H, J=9 Hz), 7.69 (d, 2H, J=9 Hz). Found: C, 61.14; H, 6.14%. Calcd for $C_{15}H_{18}O_4S$: C, 61.21; H, 6.17%.

6f: Mp 110—111 °C; IR 2230, 1285, 1140 cm^{-1}; NMR ($CDCl_3$) δ 1.6—3.2 (m, 7H), 2.39 (s, 3H), 6.90 (m, 1H), 7.30 (d, 2H, J=9 Hz), 7.69 (d, 2H, J=9 Hz). Found: C, 64.37; H, 5.70; N, 5.34%. Calcd for $C_{14}H_{15}NO_2S$: C, 64.36; H, 5.79; N, 5.36%.

6g: Mp 126—127 °C; IR 1295, 1280, 1145 cm^{-1}; NMR ($CDCl_3$) δ 1.5—3.2 (m, 7H), 2.45 (s, 3H), 7.16 (m, 1H), 7.32 (m, 5H), 7.43 (d, 2H, J=9 Hz), 7.91 (d, 2H, J=9 Hz). Found: C, 72.98; H, 6.47%. Calcd for $C_{19}H_{20}O_2S$: C, 73.06; H, 6.45%.

6h: Oil; IR 1725, 1290, 1150 cm^{-1}; NMR ($CDCl_3$) δ 1.5—2.7 (m, 7H), 2.38 (s, 3H), 6.95 (m, 1H), 7.24 (d, 2H, J=9 Hz), 7.64 (d, 2H, J=9 Hz), 9.55 (s, 1H). *Semicarbazone of **6h***: mp 217—218 °C (dec). Found: C, 55.95; H, 6.15; N, 13.03%. Calcd for $C_{15}H_{20}N_3O_3S$: C, 55.89; H, 6.25; N, 13.04%.

6i: Oil; IR 1700, 1310, 1295, 1280, 1140 cm^{-1}; NMR ($CDCl_3$) δ 1.2—2.7 (m, 7H), 2.12 (s, 3H), 2.38 (s, 3H), 6.94 (m, 1H), 7.23 (d, 2H, J=8 Hz), 7.63 (d, 2H, J=8 Hz). *Semicarbazone of **6i***: mp 218—219 °C. Found: C, 57.39; H, 6.35; N, 12.39%. Calcd for $C_{16}H_{21}N_3O_3S$: C, 57.30; H, 6.31; N, 12.53%.

*Reduction of **6d**.* A methanol solution of **6d** (155 mg, 0.5 mmol) and boron trifluoride etherate (142 mg, 1 mmol) was shaken vigorously under hydrogen atmosphere in the presence of Pd-C as a catalyst. After the usual treatment, the reduction product, methyl 1-methyl-4-(*p*-tolylsulfonyl)-1-cyclohexanecarboxylate, was separated by preparative TLC in a 71% (111 mg) yield. Recrystallization from hexane gave the pure compound: mp 122—123 °C; IR 1735, 1300, 1145 cm^{-1}; ^{13}C-NMR ($CDCl_3$) δ 21.6 (q, 1C), 23.1 (t, 2C), 27.7 (q, 1C), 34.3 (t, 2C), 42.8 (s, 1C), 51.9 (q, 1C), 62.7 (d, 1C), 128.9 (d, 2C), 129.6 (d, 2C), 134.2 (s, 1C), 144.5 (s, 1C), 176.3 (s, 1C). Found: C, 62.06; H, 7.04%. Calcd for $C_{16}H_{22}O_4S$: C, 61.92; H, 7.15%.

Similarly, the reduction product of **6e**, methyl 4-(*p*-tolyl-

sulfonyl)-1-cyclohexanecarboxylate, was obtained: mp 102—104 °C; IR 1728, 1285, 1150 cm^{-1}; ^{13}C-NMR ($CDCl_3$) δ 21.6 (q, 1C), 22.3 (t, 2C), 25.8 (t, 2C), 38.3 (d, 1C), 51.8 (q, 1C), 62.6 (d, 1C), 128.9 (d, 2C), 129.7 (d, 2C), 134.3 (s, 1C), 144.5 (s, 1C), 174.2 (s, 1C). Found: C, 61.04; H, 6.95%. Calcd for $C_{15}H_{20}O_4S$: C, 60.80; H, 6.80%.

The structures of **6f** and **6h** were confirmed by transformation into **6e**. They were hydrolyzed or oxidized to 4-(*p*-tolylsulfonyl)-3-cyclohexene-1-carboxylic acid giving **6e** by subsequent esterification with diazomethane. Their melting points and spectral data were identical with those of **6e**.

*Reduction of **6g**.* To a solution of **6g** (56 mg, 0.18 mmol) in THF-methanol (1:1) was added excess sodium borohydride at room temperature until **6g** disappeared on TLC. After the usual treatment, the reduction product, 1-phenyl-4-(*p*-tolylsulfonyl)cyclohexane, was separated by preparative TLC in a nearly quantitative yield (56 mg). Recrystallization from ethanol gave the pure compound: mp 153—154 °C; IR 1305, 1270, 1140 cm^{-1}; ^{13}C-NMR ($CDCl_3$) δ 21.6 (q, 1C), 25.9 (t, 2C), 32.6 (t, 2C), 43.1 (d, 1C), 63.0 (d, 1C), 126.3 (d, 1C), 126.5 (d, 2C), 128.4 (d, 2C), 129.0 (d, 2C), 129.7 (d, 2C), 134.3 (s, 1C), 144.5 (s, 1C), 145.7 (s, 1C). Found: C, 72.27; H, 7.02%. Calcd for $C_{19}H_{22}O_2S$: C, 72.59; H, 7.05%.

Similarly, the dimer **4** was reduced to 1,4-bis(*p*-tolylsulfonyl)-4-vinylcyclohexane: mp 226—228 °C; IR 1280, 1140 cm^{-1}; ^{13}C-NMR ($CDCl_3$) δ 20.9 (t, 2C), 21.6 (q, 2C), 27.2 (t, 2C), 62.0 (d, 1C), 67.0 (s, 1C), 123.8 (t, 1C), 128.8 (d, 2C), 129.1 (d, 2C), 129.8 (d, 2C), 130.9 (d, 2C), 131.5 (s, 1C), 132.6 (d, 1C), 134.1 (s, 1C), 144.8 (s, 1C). Found: C, 62.97; H, 6.02%. Calcd for $C_{22}H_{26}O_4S_2$: C, 63.15; H, 6.26%.

1-Acetyl-4-(p-tolylsulfonyl)cyclohexane. To a methanol solution of ***6i*** (278 mg, 1 mmol) was added excess sodium borohydride at room temperature. After evaporation, water and then ethyl acetate were added to the residue. The organic layer was separated, dried over Na_2SO_4, and concentrated to give crude 1-[4-(*p*-tolylsulfonyl)cyclohexyl]ethanol, which was further oxidized with Jones reagent. After the usual treatment, 1-acetyl-4-(*p*-tolylsulfonyl)cyclohexane was separated by preparative TLC in a 96% (268 mg) yield. Recrystallization from aqueous ethanol gave the pure compound: mp 110—112 °C; IR 1705, 1280, 1140 cm^{-1}; ^{13}C-NMR ($CDCl_3$) δ 21.6 (q, 1C), 24.8 (t, 2C), 26.9 (t, 2C), 28.2 (q, 1C), 49.7 (d, 1C), 62.5 (d, 1C), 128.9 (d, 2C), 129.7 (d, 2C), 134.0 (s, 1C), 144.7 (s, 1C), 210.2 (s, 1C). Found: C, 64.18; H, 7.26%. Calcd for $C_{15}H_{20}O_3S$: C, 64.27; H, 7.19%.

*4-(p-Tolylthio)-2-sulfolene (**8**).* To a methanol solution (4 ml) of **7** (394 mg, 2 mmol) prepared according to the procedure of Bailey and Cummins[3] was added dropwise a mixture of *p*-toluenethiol (248 mg, 2 mmol) and 1 M NaOH (2 ml, 2 mmol) with stirring at room temperature. After being stirred for 3 h, the reaction mixture was concentrated. Dichloromethane was added to the concentrate which was then washed with water, and dried over Na_2SO_4. The residue obtained by evaporation was separated by preparative TLC to afford **8** in a 69% (331 mg) yield: oil; IR 1305, 1145 cm^{-1}; NMR ($CDCl_3$) δ 2.31 (s, 3H), 3.09 (dd, 1H, J=5 and 14 Hz), 3.55 (dd, 1H, J=8 and 14 Hz), 4.30 (m, 1H), 6.55 (m, 2H), 7.05 (d, 2H, J=8 Hz), 7.27 (d, 2H, J=8 Hz).

*3-(p-Tolylsulfinyl)-3-sulfolene (**9**).* To a methanol solution (4 ml) of **8** (440 mg, 1.8 mmol) was added dropwise an aqueous solution (2 ml) of sodium periodate (385 mg, 1.8 mmol) with stirring at room temperature. After being stirred for 3 days, the resulting precipitate was removed by filtration, and the filtrate was evaporated under reduced pressure. The residue was redissolved in dichloromethane, and the solution was dried over Na_2SO_4. After concentration, the residue was separated by preparative TLC to afford **9** in a 75% (354 mg) yield. Recrystallization from ethanol gave the pure compound: mp 146—147 °C; IR 1300, 1130, 1050 cm^{-1}; NMR (DMSO-d_6) δ 2.36 (s, 3H), 3.63 (m, 2H), 4.08 (m, 2H), 6.81 (m, 1H), 7.31 (d, 2H, J=9 Hz), 7.50 (d, 2H, J=9 Hz). Found: C, 51.54; H, 4.43%. Calcd for $C_{11}H_{12}O_3S_2$: C, 51.56; H, 4.72%.

*Diels-Alder Reaction of **9**.* The Diels-Alder reaction of **9** with dienophiles **5b**—**g** was carried out in a similar manner to that for **2**. The structure of cycloadducts **10b**—**g**, all of which were oil, containing diastereoisomers based on the chiral center of sulfoxide group, were confirmed by transformation into the corresponding sulfones **6b**—**g** by oxidation with a mixture of acetic acid and hydrogen peroxide. The melting points and spectral data of the oxidation products were the same as those of the authentic **6b**—**g** prepared by Diels-Alder reaction of **2**.

Particularly in the case of 4-(*p*-tolylsulfinyl)-3-cyclohexene-1-carbonitrile (**10f**), two diastereoisomers were isolated by TLC in 29% and 34% yields, respectively. They were converted into 4-(*p*-tolylsulfonyl)-3-cyclohexene-1-carbonitrile (**6f**) by the oxidation in nearly 95% yields.

We wish to thank Dr. Y. Itatani for the determination of the ^{13}C-NMR spectra and for valuable discussions.

References

1) M. Fieser and L. Fieser, "Reagents for Organic Synthesis," John Wiley & Sons, New York (1969), Vol. 2, p. 389.

2) W. L. Mock, "Pericyclic Reactions," ed by A. P. Marchand and R. E. Lehr, Academic Press, New York (1977), Vol. 2, p. 142.

3) W. J. Bailey and E. W. Cummins, *J. Am. Chem. Soc.*, **76**, 1932 (1954).

4) K. N. Houk, *J. Am. Chem. Soc.*, **95**, 4092 (1973).

Dehydroannulenes. VIII. Synthesis of Position Isomers of Di-*t*-butyl-diphenyl-1,8-bisdehydro[14]annulene and Dimethoxy Derivative

Tateo NOMOTO, Shin'ichi NAKATSUJI, and Masazumi NAKAGAWA*

Department of Chemistry, Faculty of Science, Osaka University, Toyonaka, Osaka 560

(Received May 15, 1978)

Two position isomers of di-*t*-butyl-diphenyl-1,8-bisdehydro[14]annulene corresponding to *o*- and *m*-isomers of terphenyl have been prepared by a stepwise reaction sequence, and their physical properties were compared with those of 3,10-di-*t*-butyl-7,14-diphenyl-1,8-bisdehydro[14]annulene which corresponds to the *p*-isomer of terphenyl. The marked difference in electronic spectra between *o*-, *m*-, and *p*-isomers of terphenyl could not be observed in the spectra of "*ortho*"-, "*meta*"-, and "*para*"-isomers of the [14]annulene. Dimethoxy derivative of the "*para*"-isomer, 3,10-di-*t*-butyl-6,13-dimethoxy-7,14-diphenyl-1,8-bisdehydro[14]annulene, has been synthesized.

As reported in the previous papers, increase in the number of phenyl substituents on bisdehydro[14]-[1], tetrakisdehydro[18]-,[2] and tetrakisdehydro[22]annulene rings[3] caused appreciable bathochromic shifts of their electronic spectra indicating conjugative effect of π-electrons in the phenyl group on the annulene nucleus. Considering the remarkable difference in electronic spectral properties between position isomers of terphenyl,[4] we have carried out the synthesis of di-*t*-butyl-diphenyl-1,8-bisdehydro[14]annulenes (**1** and **2**) corresponding to *o*- and *m*-isomers of terphenyl.[5] The synthesis of 7,14-di-*t*-butyl-3,10-diphenyl-1,8-bisdehydro[14]annulene (**3**) which corresponds to *p*-terphenyl has been reported previously.[1]

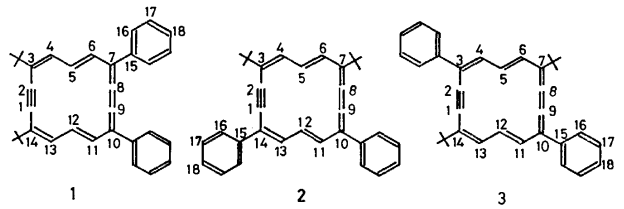

1 2 3

Synthesis. As outlined in Scheme 1, 3-*t*-butyl-2-penten-4-ynal diethyl acetal[3b,c] was converted into lithio derivative (**4**) on treatment with phenyllithium. The reaction of the lithio derivative (**4**) with dienyne ketone (**5**) gave hydroxy acetal (**6**) in a high yield. Hydroxy aldehyde (**7**) was obtained on treatment of the acetal (**6**) in ethanol with an aqueous solution of tartaric acid. The aldol condensation of the hydroxy aldehyde (**7**) with methyl ketone yielded hydroxy ketone (**8**). A solution of the hydroxy ketone (**8**) in tetrahydrofuran was added to a suspension of finely powdered potassium hydroxide in liquid ammonia. The products were passed through a short column of alumina. Slightly crude cyclic glycol (**9**) thus obtained was subjected without further purification to the subsequent reaction. Treatment of the cyclic glycol (**9**) in ether with a solution of tin(II) chloride dihydrate in the same solvent saturated with hydrogen chloride at −15——17 °C afforded position isomers of di-*t*-butyldiphenyl-1,8-bisdehydro[14]annulene, (**1**) or (**2**).

In order to obtain further information on the effect of substituent on the electronic spectrum of 1,8-bisdehydro[14]annulene, dimethoxy derivative (**14**) of the isomer (**3**) has been prepared according to Scheme 2. The aldol condensation of 3-*t*-butyl-2-penten-4-ynal (**10**)[2b,6] with α-methoxyacetophenone (**11**)[7] gave

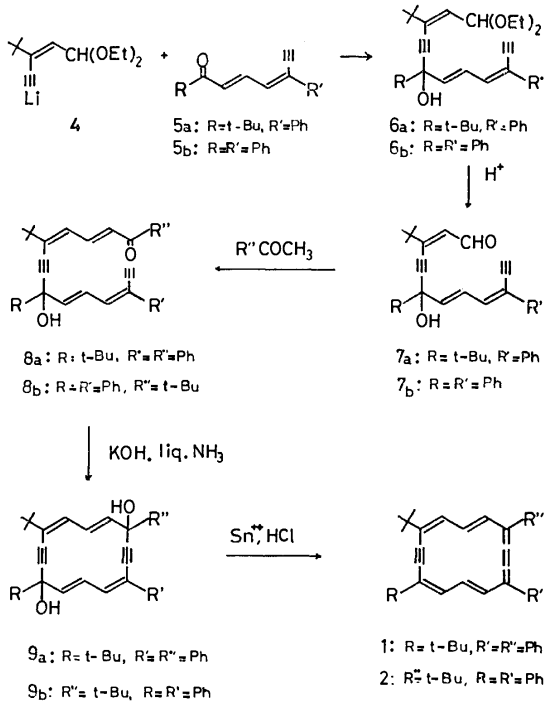

Scheme 1.

methoxydienyne ketone (**12**). Another geometrical isomer (**15**) can be considered for the methoxy ethynyl ketone. NMR spectroscopy of the ketone, *i.e.*, difference in chemical shift between carbon tetrachloride and deuteriobenzene solutions[8] and the NOE of H^3 or H^4 on irradiation of methyl protons in methoxyl groups, afforded no confirmative information on the discrimination between **12** and **15**. However, formation of the cyclic glycol (**13**) seemed to suggest the *trans* disposition of the methoxyl group with respect to H^3. Treatment of the methoxy ethynyl ketone (**12**) with a suspension of potassium hydroxide in liquid ammonia gave the cyclic glycol (**13**). Reductive dehydroxylation of the cyclic glycol (**13**) by tin(II) chloride dihydrate in ether saturated with hydrogen chloride yielded 3,10-di-*t*-butyl-7,14-diphenyl-6,13-dimethoxy-1,8-bisdehydro[14]annulene (**14**).

Properties. The color of crystals, melting points and ^1H NMR parameters of the position isomers of di-*t*-butyl-diphenyl-1,8-bisdehydro[14]annulene (**1** and **2**) and the dimethoxy derivative (**14**) are shown in Table 1 together with those of the other position isomer

TABLE 1. COLOR OF CRYSTALS, MELTING POINTS AND 100 MHz ^{1}H NMR PARAMETERS OF **1**, **2**, **3**, AND **14**

	"*ortho*" **1**	"*meta*" **2**	"*para*" **3**	Di-MeO- **14**
Color	deep reddish violet	reddish green	brownish violet	deep geen
Mp(°C) (dec)	248.0—249.0	200.8—202.0	284.0—284.5	281.5—282.7
Inner-H	13.51(t, J=13.5)	13.54(t, J=13.5) 13.65(t, J=13.5)	13.54(t, J=13.5)	13.76(t, J=13.5)
t-Bu	8.10(s)	8.07(s)	8.06(s)	8.15(s)
MeO				6.09(s)
m,*p*-H of Ph	2.38(m)	2.40(m)	2.43(m)	2.43(m)
o-H of Ph	1.37(m)	1.41(m)	1.42(m)	1.51(m)
Outer-H adjacent to *t*-Bu	0.58(d, J=13.5)	0.64(d, J=13.5)	0.56(d, J=13.5)	0.49(d, J=13.5)
Outer-H adjacent to Ph	0.26(d, J=13.5)	0.17(d, J=13.5)	0.26(d, J=13.5)	

TABLE 2. ^{13}C NMR PARAMETERS OF **1**, **2**, **3**, AND TETRA-*t*-BUTYL ANALOGUE (**16**)[a]

tetra-*t*-Bu **16**		"*ortho*"- **1**		"*meta*"- **2**		"*para*"- **3**	
t-Bu	32.2, 37.8	*t*-Bu	32.1, 37.9	*t*-Bu	32.3, 38.0	*t*-Bu	32.3, 37.8
C^1	116.7	C^1, C^8	115.1	C^1, C^2	114.3, 116.5	C^1, C^2	114.7, 115.7
C^3	131.3	C^3, C^7, C^{15}	119.8, 133.6, 139.7	C^3, C^{10}, C^{15}	119.4, 134.4, 139.9	C^3, C^7, C^{15}	119.8, 133.7, 139.9
C^4	131.3	C^4, C^6	130.4, 130.6	C^4, C^{11}	131.5, 131.7	C^4, C^6	130.3, 130.7
C^5	129.0	C^5	132.1	C^5, C^{12}	129.4, 131.3	C^5	132.3
		C^{16}, C^{17}	128.3, 128.7	C^{16}, C^{17}	120.8, 128.8	C^{16}, C^{17}	128.0, 128.7
		C^{18}	127.3	C^{18}	127.3	C^{19}	127.3

a) The spectra were obtained on a Varian XL-100 spectrometer operated at 25.2 MHz with deuteriochloroform internal lock using TMS as an internal standard.

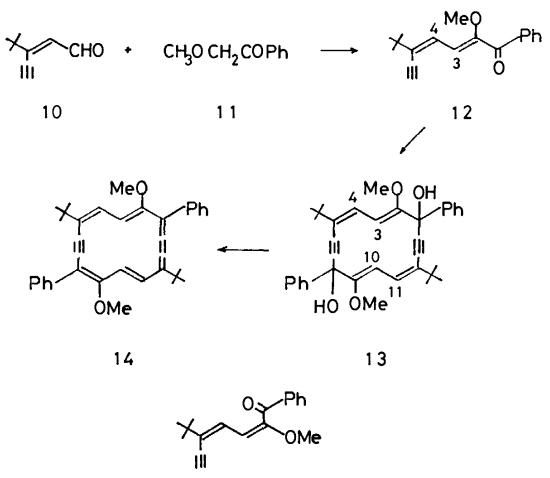

Scheme 2.

(**3**).[1]

The position isomers and the dimethoxy derivative (**1**, **2**, **3**, and **14**) were found to be strongly diatropic showing the signals of inner protons at high field and those of outer protons at low field. The close similarity of ^{1}H NMR behavior between the position isomers (**1**, **2**, and **3**) indicates that the difference of position of substituent group does not exert prominent effect on the π-electron system in the annulene nucleus at the ground state. Introduction of two methoxyl groups also exerts no essential change in NMR characteristics, although the group has both of electron attractive and donating property in the inductive and mesomeric modes. The low field shift of *ortho*-protons of phenyl groups as compared with that of *meta*- and *para*-protons can be reasonably attributed to the deshielding effect of diamagnetic ring current induced in the annulene ring. Inversely, the low field shift of outer protons of annulene ring adjacent to phenyl substituent indicates the ring current effect of benzene nucleus.

The ^{13}C NMR parameters are summarized in Table 2 together with those of tetra-*t*-butyl analogue (**16**). The assignment was made on the basis of chemical shifts, off resonance technique and the magnitude of NOE. The coupling constants are found to be J_{CH}=150—152 Hz, J_{CCH}=5 Hz and $J_{CCCH}\simeq$10 Hz. The fact that the sp-hybridized carbon atoms in the position isomers (**2** and **3**) exhibit two signals can be attributed to the difference of electron density between C^1 and C^2 which is caused by the difference of inductive effect between *t*-butyl and phenyl groups. However, it should be noted that the sp-hybridized carbon atoms in the isomer (**1**) showed only a signal in the corresponding

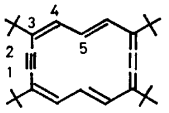

16

region. It is also to be noted that the sp-carbon exhibits siganl at an intermediate region of acetylene and cumulene reflecting the hybrid nature of the linkage incorporated in the aromatic system.

Remarkable difference in electronic spectra between the position isomers (**2** and **3**) was anticipated, because

Table 3. Electronic spectra of **1**, **2**, **3**, and **14** in THF. (λ_{max} in nm)[a]

	"*ortho*"-**1**		"*meta*"-**2**		"*para*"-**3**		di-MeO **12**	
	λ_{max}	ε	λ_{max}	ε	λ_{max}	ε	λ_{max}	ε
I	624	1800	624	1270	623	1640	637	4540
	573	538	574	352	571	590	590	698
II	507	37200	499	36430	508	52600	492	35000
	480*	18600	474*	19300	478*	1260		
III	360	215000	367	187000	357	195000	356	177000
	347*	78500	352*	87100	345*	76300	344*	8900
	331*	37600	335*	37000	332*	41100	321*	29700
	315*	22500	315*	19900	315*	27900		
IV	278	12900	275*	12800	270*	10800	264	11100
	239	14500			260	13400	253*	10900
	228*	12700			234	14300	236	10900
					226*	12300		

a) For absorption curves, see, Ref. 4. * Asterisk denotes shoulder.

the dipolar structure (**17**) may contribute in the excited state of (**3**) just as the case of *p*-terphenyl (**18**), and the contribution of such type of dipolar structure can be excluded in (**2**). However, in fact as shown in Table 3, the electronic spectra of the position isomers (**1**,**2** and **3**) and the dimethoxy derivative (**14**) showed close similarity except for the hyperchromism and bathochromic shift of the longest wavelength absorption band (I) of the dimethoxy derivative (**14**). The marked difference in electronic spectra between *p*- and *m*-terphenyls could not be observed in the spectra of the position isomers (**3** and **2**). This fact seems to be ascribable to the large difference in the stability of π-electron system between benzene nucleus and the 14-membered ring, and the general tendency that the electronic spectrum of a large conjugated system such as condensed benzenoid compound is less sensitive to the introduction of substituent group(s).

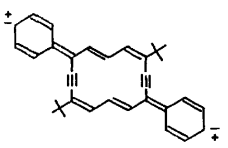

17

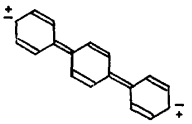

18

At first sight, the intensification of the longest wavelength band (I) in **14** seemed to suggest that the direction of polarization of the longest wavelength band (I) is perpendicular to the long axis of the bisdehydro[14]annulene nucleus.[5] However, the measurements of fluorescence excitation spectra of tetra-*t*-butyl-bisdehydro[14]annulene (**16**) and the position isomer (**3**), and the theoretical calculation by PPP and RPA methods performed by Tanaka *et al.* revealed the nature of electronic transitions and the direction of polarization.[9] Namely as shown in Fig., the longest wavelength band (I) is ^1L_b species and the direction of polarization is parallel to the long axis, the medium wavelength band (II) is ^1L_a species having perpendicular polarization and the short wavelength band (III) consists of parallel polarized ^1B_b species and perpendicular polarized ^1B_a species.

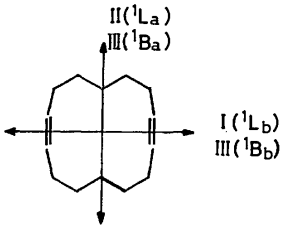

Fig. Direction of polarization of bisdehydro[14]-annulene.

Experimental

All the melting and boiling points are uncorrected. The melting points were measured an a Mettler FP-2 apparatus. The IR spectra were obtained on a Hitachi EPI-G3 or EPI-2 spectrophotometer by neat liquid film or KBr-disk method. Strong, medium, weak and broad bands were denoted by s, m, w and br, respectively. The electronic spectra were measured in THF using Hitachi EPS-3T spectrophotometer. The NMR spectra were obtained on one of the Varian spectrometerss of XL-100, A-60D, T-60 or a Hitachi R-24, and the parameters are given in τ-values with respect to TMS as an internal standard. The mass spectra were measured with a Hitachi RM-50 spectrometer (ionization potential 70 eV). The adsorbents used in the column chromatography are alumina (Merck, activity II-III or Woelm, activity I) and silica gel (Wako gel C-200). Evaporation of the solvent was performed under reduced pressure.

*3,6-Di-t-butyl-6-hydroxy-10-phenyl-2,7,9-dodecatriene-4,11-diynal Diethyl Acetal (**6a**).* 3-*t*-Butyl-2-penten-4-ynal diethyl acetal[3c] (0.9274 g, 0.00442 mol) in ether (80 ml) was mixed with 0.8 M of phenyllithium in ether (6.9 ml, 0.0055 mol) at −15——18 °C under nitrogen atmosphere to give the lithio derivative (**4**). After bing stirred for 10 min, a solution of the ketone (**5a**, 1.00 g, 0.0042 mol)[10] in ether (80 ml) was added dropwise over 1 h-period at the same temperature. After the mixture had been stirred for 1 h at 0 °C, stirring was continued overnight at room temperature. Cracked ice was added to the reaction mixture under external cooling. The organic layer was separated and the aqueous layer was extracted with ether. The combined ethereal solution was thoroughly washed with water and dried (K_2CO_3). Dark red liquid (2.1 g) obtained on evaporating the solvent was chromatographed on alumina (Merck,

100 g). The column was eluted with cyclohexane and benzene–cyclohexane (1:9) to remove a minor amount of starting material and by-product. Elution with benzene–cyclohexane (1:1) followed by benzene yielded **6a** as a pale yellow liquid, 1.21 g, 64%, IR(neat): 3425 (br, m, OH), 3300 (m, C≡CH), 1120, 1060, 960 (s, C–O–C) cm^{-1}. Further elution with ether–benzene (1:9) afforded **7** as a pale yellow viscous liquid (0.365 g, 23.2%).

*3,6-Di-t-butyl-6-hydroxy-10-phenyl-2,7,9-dodecatriene-4,11-diynal (**7a**).* A mixture of **6a** (2.9 g, 0.0065 mol), ethanol (290 ml), tartaric acid (1.5 g) and water (150 ml) was stirred for 3 h under ice-cooling and then for 2 h at 12 °C. The mixture was extracted with ether. The extract, after being washed with water and an aqueous solution of sodium hydrogencarbonate, was dried (K_2CO_3). A yellow viscous liquid (2.35 g) obtained on evaporating the solvent was dissolved in carbon tetrachloride and the solution was passed through a column of alumina (Merck, 95 g). Elution with benzene and ether–benzene (1:9) yielded a pale yellow viscous liquid (2.30 g, 95%) which was triturated with hexane to give **7a** as colorless crystals, mp 101.2—102.1 °C, 2.21 g, 91.3%, IR(KBr): 3450 (s, OH), 3280 (s, C≡CH), 1670 (s, C=O), 1580 (s, aromatic C=C) cm^{-1}, NMR(CCl_4): τ 8.90 (9H, d, *t*-Bu), 8.75 (9H, s, *t*-Bu adjacent to OH), 7.22 (1H, br s, C≡CH), 3.88 (1H, d, J=15 Hz, H^7), 8.83 (1H, d, J=8 Hz, H^2), 3.08 (1H, d, J=11 Hz, H^9), 2.75 (4H, m, *m,p*-H of Ph and H^8), 2.43 (2H, m, *o*-H of Ph), −0.16 (1H, d, J=8 Hz, CHO).

Found: C, 83.44; H, 8.10%. Calcd for $C_{26}H_{30}O_2$: C, 83.88; H, 8.07%.

*5,8-Di-t-butyl-1,12-diphenyl-8-hydroxy-2,4,9,11-tetradecatetraene-6,13-diyn-1-one (**8a**).* To a stirred solution of **7a** (1.24 g, 0.003 mol) and acetophenone (0.475 g, 0.004 mol) in ethanol (15 ml) was added at −5 °C a solution of sodium hydroxide (0.15 g, 0.38 mol) in water (1 ml) and ethanol (1 ml) under nitrogen atmosphere. After being stirred for 1 h at −5——10 °C, for 2 h at 2 °C and then for 1 h at 14 °C, the mixture was extracted with ether. A reddish liquid (1.7 g) obtained on evaporation of the ethereal extract, after being washed and dried (K_2CO_3), was dissolved in benzene–cyclohexane (1:9) and chromatographed on alumina (Merck, 70 g). Excess of acetophenone was removed on elution with benzene–cyclohexane (2:8—5:5). Further elution with benzene and ether–benzene (2:8) afforded a pale yellow viscous liquid (1.12 g, 71.2%) which crystallized on trituration with hexane to give **8a**, pale yellow needles, mp 88.5—89.5 °C, 1.09 g, 69.3%, IR(KBr): 3430 (m, OH), 3300 (m, C≡CH), 1655 (s, C=O), 1590 (s, aromatic C=C) cm^{-1}, NMR(CCl_4): 8.90 (9H, s, *t*-Bu), 8.77 (9H, s, *t*-Bu adjacent to OH), 7.15 (1H, s, disappeared on addition of D_2O), 6.67 (1H, s, C≡CH), 3.95—3.00 (6H, m, olefinic·H), 2.83—1.93 (10H, m, aromatic-H).

Found: C, 85.38; H, 7.56%. Calcd for $C_{34}H_{36}O_2$: C, 85.67; H, 7.61%.

*5,8-Di-t-butyl-1,12-diphenyl-2,4,9,11-cyclotetradecatetraene-6,13-diyn-1,8-diol (**9a**).* A solution of **8a** (0.45 g, 0.0009 mol) in THF (90 ml) was added over 8 h-period to a suspension of finely powdered potassium hydroxide (2.0 g) in liquid ammonia (280 ml) at −45——35 °C. After the mixture had been stirred for 12 h, powdered ammonium chloride (7.0 g) was added at −50——55 °C. After 15 min, the cooling bath was removed and the ammonia was allowed to evaporate. The residue was repeatedly extracted with ether. The extract was washed with saturated ammonium chloride solution and dried (K_2CO_3). The product obtained on evaporating the solvent was dissolved in ether–benzene (3:7) and passed through a column of alumina (Woelm, 10 g). Slightly crude **9a**, pale yellow fine crystals, 0.41 g, was used without further purification in the following reaction.

*3,14-Di-t-butyl-7,10-diphenyl-1,8-bisdehydro[14]annulene (**1**).* To a stirred solution of **9a** (410 mg) in ether (50 ml) was added at −12——15 °C a solution of tin(II) chloride dihydrate (500 mg) in the same solvent saturated with hydrogen chloride (10 ml). After being stirred for 3 min, cold water was added to the mixture. The organic layer was washed successively with water, aqueous sodium hydrogencarbonate solution and water, and dried (K_2CO_3). The crude product obtained on evaporating the solvent was chromatographed on alumina (Merck, 40 g) and eluted with ether–hexane (2:8). Rechromatography on alumina (Merck, 30 g) and elution with benzene afforded **1**, deep reddish violet crystals, 231 mg, 55.3% based on **8a**, which were recrystallized from ether–hexane (3:7) to give pure **1**, reddish violet plates with deep green metallic luster, mp 248.0—249.0 °C (dec).

Found: C, 92.12; H, 7.83%. Calcd for $C_{34}H_{34}$: C, 92.26; H, 7.74%.

*3-t-Butyl-6-hydroxy-6,10-diphenyl-2,7,9-dodecatriene-4,11-diynal Diethyl Acetal (**6b**).* To a stirred and cooled (ice–salt bath) solution of the lithio derivative (**4**), prepared from *t*-butyl-pentenynal diethyl acetal (2.10 g, 10 mmol) in ether (150 ml) on treatment with an ethereal phenyllithium solution (0.74 M, 18.5 ml, 13.7 mmol), was added under nitrogen atmosphere a solution of **5b** (3.00 g, 11.6 mmol)[2] in the same solvent (120 ml) over a period of 1.5 h. After being stirred for 15 min at 0 °C, and then for 14.5 h at a room temperature, the reaction mixture was poured onto ice-water. The organic layer was washed successively with cold water, cold brine and cold water, and dried (K_2CO_3). Reddish brown liquid (5.88 g) obtained on evaporation of the solvent was chromatographed on silica gel (160 g). 3-*t*-Butyl-pentenynal diethyl acetal was eluted with benzene–cyclohexane (1:1) and benzene. Further elution with ether–benzene(1:1) yielded **6b**, yellowish red powder, 4.05 g, 84.4%, IR(neat): 3380 (m, OH), 3303 (m, C≡CH), 2090 (w, C≡C), 1120, 1053, 972 (C–O–C) cm^{-1}, NMR($CDCl_3$): 2.31 (4H. m, *o*-H of Ph), 2.81 (7H, m, *m,p*-H of Ph and H^8), 4.17 (1H, d, J=7 Hz, H^2), 4.68 (1H, d, J=7 Hz, H^1), 6.32 (4H, m, CH_2), 6.47 (1H, s, C≡CH), 7.24 (1H, s, OH), 8.75 (9H, s, *t*-Bu), 8.78 (6H, t, J=7 Hz, CH_3).

The attempts to crystallize **6a** were unsuccessful.

*3-t-Butyl-6-hydroxy-6,10-diphenyl-2,7,9-dodecatriene-4,11-diynal (**7b**).* A solution of **6b** (3.03 g, 6.47 mmol) in ether (250 ml) and THF (10 ml) was added over 1 h-period to an ice-cooled aqueous solution of tartaric acid (1%, 150 ml). After being stirred for 2.5 h at 0—12 °C, the reaction mixture was poured onto ice-water and extracted with ether. The extract, after washing with brine and drying (K_2CO_3), was concentrated to give a reddish yellow solid (2.54 g), which was chromatographed on alumina and recrystallized from carbon tetrachloride and from cyclohexane to give pure **7b**, mp 84.3—85.7 °C, pale yellow plates, IR(KBr): 3325 (m, OH), 3290 (m, C≡CH), 1658 (s, C=O), 1580 (w, C=O) cm^{-1}, NMR($CDCl_3$): 8.74 (9H, s, *t*-Bu), 7.08 (1H, br, s, OH, disappeared on addition of D_2O), 6.38 (1H, s, C≡CH), 3.80 (1H, d, J=14 Hz, H^7), 3.70 (1H, d, J=8 Hz, H^2), 2.99 (1H, d, J=11 Hz, H^9), 2.61 (7H, m, *m,p*-H of Ph and H^8), 2.27 (4H, m, *o*-H of Ph), −0.16 (1H, d, J=8 Hz, H^1).

*7-t-Butyl-2,2-dimethyl-10,14-diphenyl-10-hydroxy-4,6,11,13-hexadecatetraene-8,15-diyn-3-one (**8b**).* A solution of sodium hydroxide (0.23 g, 5.75 mmol) in 50% aqueous ethanol (3.0 ml) was added under nitrogen atmosphere to an ice-cooled solution of **7b** (2.04 g, 5.18 mmol) and pinacolone (4.80 g, 47 mmol) in ethanol (25 ml). After being stirred for 2 h at 0 °C and for 24 h at a room temperature,

the reaction mixture was poured onto ice–water and extracted with ether. The extract was washed with water, brine and water, successively, and dried (K_2CO_3). A red liquid obtained on evaporation of the solvent was chromatographed on silica gel (Wako, 120 g) and eluted with cyclohexane–benzene–ether to give **8a**, a yellow solid, 1.97 g, IR(KBr): 3320 (m, OH), 3250 (m, C≡CH), 1675 (m, C=O), 1590 (s, C=C) cm^{-1}, NMR(CCl_4): 8.88 (9H, s, *t*-Bu), 8.76 (9H, s, *t*-Bu adjacent to C=O), 6.65 (1H, s, C≡CH), 3.83 (1H, d, J=16 Hz, H^{11}), 3.61 (1H, d, J=13 Hz, H^6), 3.45 (1H, d, J=15 Hz, H^4), 2.71 (8H, m, *m,p*-H of Ph and $H^{5,12}$), 2.40 (4H, m, *o*-H of Ph).

Crystallization of **8b** could not be achieved.

*1,5-Di-*t*-butyl-8,12-diphenyl-2,4,9,11-cyclotetradecatetraene-6,13-diyne-1,8-diol (**9b**).* A solution of **8b** (400 mg, 0.84 mmol) in THF (120 ml) was added to a stirred suspension of potassium hydroxide (3.0 g, 54 mmol) in liquid ammonia (700 ml) over a period of 22.5 h at −60——38 °C. After being stirred for further 3 h at −38——30 °C, powdered ammonium chloride was added to the reaction mixture and the ammonia was allowed to evaporate. The residue was mixed with water and extracted with ether. After being washed with a saturated solution of ammonium chloride, the extract was dried ($MgSO_4$). Removal of the solvent yielded a yellow solid, which gave IR and NMR spectra consistent with the 14-membered cyclic glycol (**9b**). The crude **9b** was used without further purification in the following reaction.

*3,7-Di-*t*-butyl-10,14-diphenyl-1,8-bisdehydro[14]annulene (**2**).* To a solution of crude **9b** in ether (40 ml) cooled in an ice–salt bath was added a solution of tin(II) chloride dihydrate (1.2 g) in the same solvent saturated with hydrogen chloride (15 ml). After being stirred for 15 min, ether was added to the reaction mixture, and the ethereal solution was washed successively with water and brine, and dried ($MgSO_4$). Deeply colored solid obtained on working up the extract was chromatographed on alumina (Merck, 30 g). Greenish violet crystals (8.2 mg, 20.5% based on **8b**) obtained on elution with hexane–ether were rechromatographed on alumina (Woelm) to give pure **2**, reddish green needles, mp 200.8—202.0 °C (dec).

Found: C, 92.17; H, 7.71%, mass (*m/e*): 442 (M^+). Calcd for $C_{34}H_{34}$: C, 92.26; H, 7.74%, mol wt: 442.612.

*5-*t*-Butyl-2-methoxy-1-phenyl-2,4-heptadien-6-yn-1-one (**12**).* To an ice-cooled solution of 3-*t*-butyl-2-penten-4-ynal (**10**, 6.7 g, 49 mmol)[2c,5] and ω-methoxyacetophenone (**11**, 7.6 g, 51 mmol)[6] in ethanol (250 ml) was added over 1 h-period a solution of sodium hydroxide (2.5 g, 83 mmol) in 50% aqueous ethanol (100 ml) under nitrogen atmosphere. After the resulting deep red solution had been stirred for 49 h at 12 °C, water was added to the mixture and extracted with ether. The extract was washed successively with water, brine and sodium hydrogencarbonate solution, and dried ($MgSO_4$). A yellow liquid obtained on evaporation of the solvent was chromatographed on alumina (Merck, 120 g). Elution with ether–hexane (1:9 to 2:8) gave **12**, a yellow liquid, 10.6 g, 80%, mass (*m/e*): 268 (M^+), Calcd for $C_{18}H_{21}O_2$: 268.348, IR(neat): 3290 (m, C≡CH), 2079 (w, C≡C), 1649 (s, C=O), 1598 (s, C=C), 1450 (s, O–CH_3), 1125 (s, C–O–C) cm^{-1}. The ^1H NMR parameters are given in Table 4. The ketone (**12**) was found to be rather unstable in neat, but can be kept for a month without appreciable decomposition in an ether solution under argon atmosphere at a room temperature. Distillation of **12** (bp 110—120 °C/ 7×10^{-5} Pa) accompanied with a remarkable decomposition.

*5,12-Di-*t*-butyl-1,8-diphenyl-2,9-dimethoxy-2,4,9,11-cyclotetradecatetraen-6,13-diyn-1,8-diol (**13**).* A solution of **12** (429 mg, 1.60 mmol) in THF (30 ml) was added to a suspension of potassium hydroxide (2.0 g, 56 mmol) in liquid ammonia (200 ml) over a period of 2.5 h at −64——63 °C. After stirring for 16 h at −64——30 °C, ammonium chloride was added to the reaction mixture at −60 °C, and the ammonia was allowed to evaporate. Water was added to the residue and the mixture was extracted with ether. The extract was worked up in the usual manner. Evaporation of the solvent afforded a brown liquid, which was chromatographed on alumina (Merck, 40 g). After being eluted thoroughly with cyclohexane–benzene (1:1) to remove the starting materials, the solvent was replaced by ether–benzene (1:9). Concentration of the eluate yielded a diastereomer of **13**, mp 247.9—249.1 °C (dec), colorless crystals, 68 mg, 17%. Elution with ether–benzene (1:1) gave another diastereomer of **13**, mp 265.2—266.1 °C (dec), colorless crystals, 128 mg, 30%, NMR($CDCl_3$): 8.83 (9H, s, *t*-Bu), 8.72 (1H, s, OH), 6.35 (3H, s, OCH_3), 3.46 (1H, d, J=11 Hz, H^3), 3.24 (1H, d, J=11 Hz, H^4), 2.77 (3H, m, *m,p*-H of Ph), 2.52 (2H, m, *o*-H of Ph).

Table 4. ^1H NMR parameters of **12**

	CCl_4	C_6D_6
o-H of Ph	2.20(2H, m)	2.21(2H, m)
m,p-H of Ph	2.57(3H, m)	2.87(3H, m)
H^4	3.10(1H, dd, J=0.6, 11)	2.86(1H, dd, J=0.6, 11)
H^3	3.39(1H, d, J=11)	3.06(1H, d, J=11)
OCH_3	6.28(3H, s)	6.46(3H, s)
C≡CH	6.70(1H, d, J=0.6)	7.04(1H, d, J=0.6)
t-Bu	8.80(9H, s)	8.87(9H, s)

Although the mass spectrum of the high melting isomer showed the presence of impurities, the material was subjected to the following conversion without further purification. Both of the diastereomers gave **14**.

*3,10-Di-*t*-butyl-6,13-dimethoxy-7,14-diphenyl-1,8-bisdehydro-[14]-annulene (**14**).* A diastereomeric mixture of crude **13** prepared from **12** (271 mg, 1.01 mmol) by the above-stated procedure was dissolved in ether (20 ml). A solution of tin(II) chloride dihydrate (1.4 g, 8.9 mmol) in ether saturated with hydrogen chloride (13 ml) was added to the stirred solution of **13** at −60 °C. After 2 min, the resulting deep reddish violet solution was poured onto ice–water, and extracted with ether. The extract, after being washed successively with water, brine, sodium hydrogencarbonate solution and water, and dried (K_2CO_3), was concentrated to give a black solid, which was chromatographed on alumina (Merck, 30 g). Elution with hexane and THF–hexane (0.5:9.5) gave **14**, green crystals, 84 mg, 33% based on **12**. Rechromatography on alumina (Woelm) followed by recrystallization from benzene–hexane (1:5) gave analytical specimen of **14**, deep green plates, mp 281.5—282.7 °C (dec).

Found: C, 85.97; H, 7.60%, mass (*m/e*): 502 (M^+). Calcd for $C_{36}H_{38}O_2$: C, 86.01; H, 7.62%, mol wt: 502.664.

References

1) a) K. Fukui, T. Nomoto, S. Nakatsuji, and M. Nakagawa, *Tetrahedron Lett.*, **1972**, 3157; b) K. Fukui, T. Nomoto, S. Nakatsuji, S. Akiyama, and M. Nakagawa, *Bull. Chem. Soc. Jpn.*, **50**, 2758 (1977).

2) a) K. Fukui, T. Okamoto, and M. Nakagawa, *Tetrahedron Lett.*, **1971**, 3121; b) T. Katakami, K. Fukui, T. Okamoto, and M. Nakagawa, *Chem. Lett.*, **1972**, 225; c) T. Katakami, K. Fukui, T. Okamoto, and M. Nakagawa

Bull. Chem. Soc. Jpn., **49**, 297 (1976).

3) a) S. Akiyama, T. Nomoto, M. Iyoda, and M. Nakagawa, *Bull. Chem. Soc. Jpn.*, **49**, 2579 (1976); b) M. Iyoda, H. Miyazaki, and M. Nakagawa, *J. Chem. Soc., Chem. Commun.*, **1972**, 431; c) M. Iyoda, H. Miyazaki, and M. Nakagawa, *Bull. Chem. Soc. Jpn.*, **49**, 2306 (1976).

4) A. E. Gillam and D. H. Hey, *J. Chem. Soc.*, **1939**, 1170; G. F. Wood, A. L. van Artsdale, and R. T. Reed, *J. Am. Chem. Soc.*, **72**, 3221 (1950); J. Derkosch and F. Langer, *Monatsh. Chem.*, **86**, 924 (1955).

5) For a preliminary report, see, T. Nomoto, S. Nakatsuji, and M. Nakagawa, *Chem. Lett.*, **1974**, 839.

6) S. Tomita and M. Nakagawa, *Bull. Chem. Soc. Jpn.*, **49**, 302 (1976).

7) R. B. Moffett and R. L. Shriner, *Org. Synth.*, Coll. Vol. III, 562 (1955).

8) a) Y. Fujise and S. Ito, *Chem. Pharm. Bull.*, **14**, 797 (1966); b) C. J. Timmons, *Chem. Commun.*, **1965**, 576.

9) J. Tanaka, M. Tanaka, and M. Morita, to be published.

10) T. Nomoto, K. Fukui, and M. Nakagawa, *Tetrahedron Lett.*, **1972**, 3253; T. Nomoto, K. Fukui, and M. Nakagawa, *Bull. Chem. Soc. Jpn.*, **49**, 305 (1976).

Dehydroannulenes. IX. Effects of Substituents on the ^{1}H NMR Spectra of Tetrakisdehydro[18]- and Bisdehydro[14]annulenes

Shuzo AKIYAMA,† Masahiko IYODA, Kiyoshi YOSHITSUGU, Masatoshi FUKUOKA, and Masazumi NAKAGAWA*

Department of Chemistry, Faculty of Science, Osaka University, Toyonaka, Osaka 560

(Received May 15, 1978)

In order to obtain information on the cause of low field shift of ^{1}H NMR signals of 'acetylene-cumulene'-dehydroannulenes on introduction of substituents, the syntheses of 1,8-bisdehydro[14]- and 6,8,15,17-tetrakisdehydro[18]annulenes bearing *p*-substituted phenyl group(s) have been performed. The examination of their ^{1}H NMR spectra indicates that the low field shift of NMR signals can be regarded as a superposition of three effects, *i.e.*, 1) decrease of ring current in annulene nucleus by perturbation of substituent group(s), 2) Deshielding effect of ring current in aryl substituent(s) exerted on annulene protons, and 3) Electronic effect of *p*-substituent in phenyl group(s) transmitted to annulene ring.

Replacement of the methyl groups in 1,5,10,14-tetramethyl-6,8,15,17-tetrakisdehydro[18]annulene (**1a**)[1] by *t*-butyl groups to give tetra-*t*-butyl derivative (**1b**)[2] resulted in appreciable down field shifts of both of the outer and inner proton signals of the annulene ring. As pointed out in previous papers of this series,[3] further down field shifts of annulene protons were observed on successive replacement of the methyl groups in **1a** or *t*-butyl groups in **1b** by phenyl groups to give **1c**[3] or **1d**[4]. Furthermore, tetraphenyltetrakisdehydro[18]annulene (**1e**)[3] exhibits both of the inner and outer proton signals at even more low field than those of **1c** or **1d**.

Preparation of tetrasubstituted 1,8-bisdehydro[14]annulenes bearing various substituents has revealed the similar substituent effects on the chemical shifts of protons in 1,8-bisdehydro[14]annulene ring. Substitution of the hydrogens at 3,7,10 and 14-positions in the parent bisdehydro[14]annulene (**2a**)[5] by *t*-butyl groups (**2b**) resulted in an appreciable down field shifts of inner protons (H^5 and H^{12}) accompanying with slight high field shifts of the outer protons (H^4, H^6, H^{11}, and H^{13}). The H^1 NMR spectra of position isomers of di-*t*-butyl-diphenyl-1,8-bisdehydro[14]annulene, (**2c**),[6] (**2d**),[7] (**2e**),[7] and the tetraphenyl derivative (**2f**)[6] exhibit also low field shift of both of the inner and outer protons in the annulene ring as compared with those of **2b**.

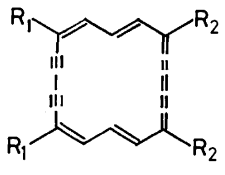

1

a: $R_1 = R_2 = Me$
b: $R_1 = R_2 = t\text{-}Bu$
c: $R_1 = Me$, $R_2 = Ph$
d: $R_1 = t\text{-}Bu$, $R_2 = Ph$
e: $R_1 = R_2 = Ph$
f: $R_1 = R_2 = p\text{-}MeO\text{-}Ph$

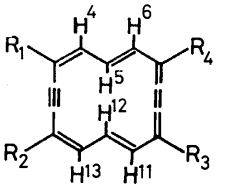

2

a: $R_1 = R_2 = R_3 = R_4 = H$
b: $R_1 = R_2 = R_3 = R_4 = t\text{-}Bu$
c: $R_1 = R_3 = t\text{-}Bu$, $R_2 = R_4 = Ph$
d: $R_1 = R_2 = t\text{-}Bu$, $R_3 = R_4 = Ph$
e: $R_1 = R_4 = t\text{-}Bu$, $R_2 = R_3 = Ph$
f: $R_1 = R_2 = R_3 = R_4 = Ph$

In order to get further insight into the effect of substituents, we have carried out the syntheses of tetrasubstituted 'acetylene-cumulene'-dehydroannulenes bearing *p*-substituted phenyl group(s).

Syntheses. 3,7,10,14-Tetrasubstituted 1,8-bisdehydro[14]annulenes (**2g—m**) were obtained by a similar reaction sequence used in the preparation of other analogues (**2b, c**) outlined in Scheme 1.

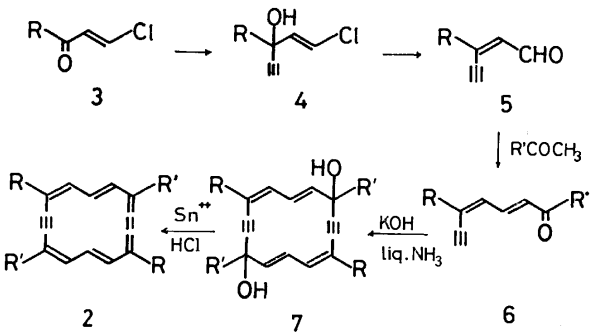

g: R = R' = p-MeO-Ph, h: R = Ph, R' = p-MeO-Ph
i: R = t-Bu, R' = p-MeO-Ph, j: R = t-Bu, R' = p-Br-Ph
k: R = t-Bu, R' = p-Cl-Ph, l: R = t-Bu, R' = p-Me-Ph
m: R = t-Bu, R' = p-MeOOCPh

Scheme 1.

The stepwise sequence of reactions employed for the preparation of "*ortho*"- (**2d**) and "*meta*"-isomers (**2e**)[7] was adopted to the synthesis of tri-*t*-butyl (*p*-methoxycarbonylphenyl)-1,8-bisdehydro[14]annulene (**2n**) (Scheme 2). Crude product of the aldol condenstation of the hydroxy aldehyde (**8**)[8] with *p*-acetyl-benzoic acid was converted into the methyl ester (**9**). The hydroxy ketone (**9**) was treated with potassium hydroxide in liquid ammonia and the product was methylated by diazomethane to give 14-membered cyclic glycol (**10**). Reductive dehydroxylation of **10** by means of tin(II) chloride dihydrate in ether saturated with hydrogen chloride yielded **2n**.

The tetrakis(*p*-methoxyphenyl)tetrakisdehydro[18]annulene (**1f**) was synthesized by the method used for the preparation of other analogous tetrakisdehydro[18]annulenes (**1a—e**).[1-4] The reaction sequence is outlined in Scheme 3. The diketone

† Present address: Faculty of Pharmacy, Nagasaki University, Bunkyo-cho, Nagasaki 852.

Table 1. Color of crystals, melting points and electronic spectra of **2g**—**n** and **1f**

	Color of crystals mp (°C) (dec)	Electronic spectra in THF λ_{max} in nm and (ε)
2g	deep violet >280	247.5(21600), 285(33600), 333(19200), 350(25700), 408(298000), 576(57400), 665(2270)
2h	deep violet >250	245(19300), 261*(20500), 283(27100), 330(17100), 347(24700), 395(278000), 563(52100), 665(4800)
2i	deep violet >230	240(14400), 267(16000), 316(30500), 334(20700), 367(176000), 524(60500), 625(2240)
2j	dark brick red >275	231(14620), 239(16580), 269(14250), 315(30350), 332(45160), 348*(78470), 361(191700), 514(57740), 574(879), 628(2270)
2k	dark copper red >280	229.5(13800), 237.5(16200), 267.5(14600), 332(48000), 360(196200), 512(58400), 570(540), 623(2120)
2l	dark reddish violet >280	237.5(14600), 264(13900), 330.5(41900), 361(192100), 513(54800), 571(680), 624(1580)
2m	deep violet >320	235(17300), 275.5(15200), 317(32400), 334(46100), 351(69500), 365(186000), 525(61100), 578(1560), 616(2950)
2n	reddish brown >270	234.5(11300), 255*(10300), 267.5(11600), 305*(22500), 326*(42600), 340*(77500), 354.5(161000), 491(36800), 561(695), 612(1800)
1f	deep green 169—171	282(31700), 305(30200), 329(22400), 358(23400), 381(36300), 453(288500), 670(115000), 784(3900)

* Asterisk indicates shoulder.

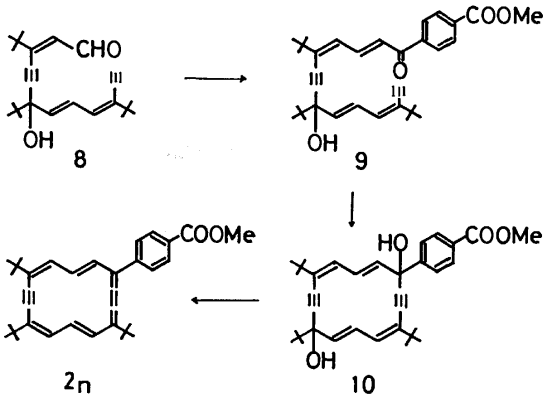

Scheme 2.

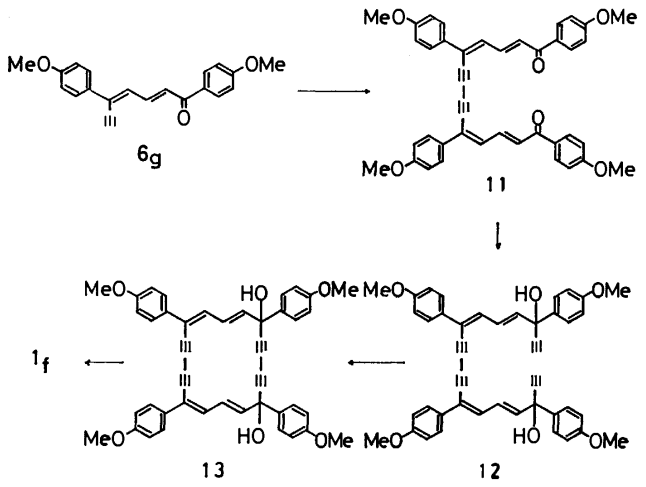

Scheme 3.

(**11**) obtained by the oxidative coupling of dienyne ketone (**6g**) by cupric acetate in pyridine was allowed to react with lithium acetylide-ethylenendiamine complex[9] in THF to give the acetylenic glycol (**12**). Oxidative coupling of **12** by cupric acetate in pyridine under high dilution conditions yielded the cyclic glycol (**13**), which could be converted into the tetrakis(*p*-methoxyphenyl)tetrakisdehydro[18]annulene (**1f**) on treatment with tin(II) chloride dihydrate in ether saturated with hydrogen chloride.

The color of crystals, melting points and the electronic spectral data of **2g**—**n** and **1f** are summarized in Table 1.

Discussion. The effect of alkyl groups on the chemical shifts of protons on 'acetylene-cumulene'-dehydroannulene rings is summarized in Table 2. The most remarkable change caused by the replacement of hydrogens by *t*-butyl groups (**2a**→**2b**) or methyl by *t*-butyl groups (**1a**→**1b**) is the appreciable low field shifts of inner protons signals. The essentially planar structures of tetra-*t*-butylbisdehydro[18]-[10] and [22]annulenes[11] have been proved by the X-ray structure analyses, and the almost temperature independent ^{1}H NMR spectra of this series of 'acetylene-cumulene'-dehydroannulenes indicate their high conformational stability.[1,3,14] Also the examination of molecular models of *t*-butylsubstituted derivatives reveals that they have no steric interference between the *t*-butyl group and the adjacent outer hydrogen atom. In view of the rather high diatropicity of **1** and **2**, it seemed to be reasonable to assume that the annulenes (**1** and **2**) hold essentially planar conformation in solution just as in crystalline state. Therefore, the marked low field shifts of inner protons seems to be difficult to ascribe solely to the deformation of annulene perimeter caused by introduction of substituent groups. Also the remarkable low field shifts can not be attributed to the change of electron density of the annulene ring induced by the introduction of substituent groups, becaues the ^{1}H NMR spectra of **14a**[12] and **14b**[12] bearing electron attractive acetyl

Table 2. Effects of alkyl and acyl substituents

R	Outer-H		Inner-H		Me	*t*-Bu	Solvent
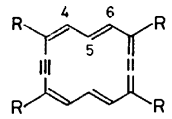 2							
a: H[5]	$H^{4,6}$	0.45	H^5	15.54			$CDCl_3$
b: *t*-Bu[6]	$H^{4,6}$	0.58	H^5	13.39		8.10	THF-d_8
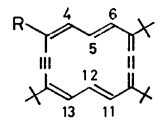 14							
a: $COCH_3$[12]	H^6	0.05	H^5	14.16		8.13	$CDCl_3$
	H^4	0.48	H^{12}	13.88		8.11	
	$H^{11,13}$	0.68, 0.66				8.09	
b: COOH[12]	H^4	−0.12	H^5	14.29		8.04	$CDCl_3$
	H^6	0.40	H^{12}	14.07		8.09	
	$H^{11,13}$	0.61					
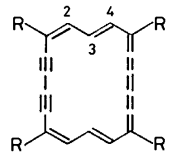 1							
a: Me[1]	$H^{2,4}$	0.34	H^3	15.24	7.42		THF-d_8
b: *t*-Bu[2]	$H^{2,4}$	0.02	H^3	14.92		7.98	THF-d_8

Table 3. Effects of aryl substituents on tetrakisdehydro[18]annulenes

	R_1	R_2	Outer-H		Inner-H		Aryl-H *o*-	Aryl-H *m p*-	*t*-Bu	Me	Solvent
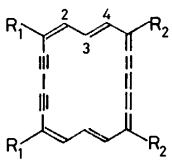 1											
a:	Me	Me	$H^{2,4}$	0.34	H^3	15.24				7.42	$CDCl_3$
b:	*t*-Bu	*t*-Bu	$H^{2,4}$	0.04	H^3	14.89			7.98		$CDCl_3$
c:	Ph	Me	H^2	0.12	H^3	14.20	1.36	2.60		6.56	
			H^4	0.54							
d:	Ph	*t*-Bu	H^2	−0.40	H^3	13.90	1.13	2.37	7.93		THF-d_8
			H^4	0.01							
e:	Ph	Ph	$H^{2,4}$	−0.31		13.19	1.30	2.40			THF-d_8
f:	$R_1=R_2=p$-$MeOC_6H_4$		$H^{2,4}$	−0.04	H^3	13.00	1.21	*ca.* 2.7*		5.98	$CDCl_3$

* Submerged in $CHCl_3$ peak.

Table 4. ^1H NMR parameters of diaryl-di-*t*-butyl-1,8-bisdehydro[14]annulene (**2**) in THF-d_8. τ-values

	R_1	R_2	R_3	R_4	Outer-H		Inner-H		Aryl-H *o*-	Aryl-H *m p*-	*t*-Bu	Lit
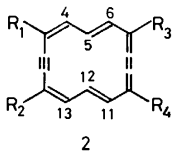 2												
b:	*t*-Bu	*t*-Bu	*t*-Bu	*t*-Bu	$H^{4,6}$	0.58	H^5	14.39			8.10	6)
c:	*t*-Bu	Ph		*t*-Bu	H^6	0.16	H^5	13.45	1.39	2.39	8.05	6)
					H^4	0.49						
d:	*t*-Bu	*t*-Bu	Ph	Ph	$H^{4,13}$	0.58	H^5	13.51	1.37	2.38	8.10	7)
					$H^{6,11}$	0.26						
e:	*t*-Bu	Ph	*t*-Bu	Ph	$H^{1,13}$	0.64	H^5	13.65	1.41	2.40	8.07	7)
					$H^{6,11}$	0.17	H^{12}	13.54				
i:	*t*-Bu	*p*-$MeOC_6H_4$		*t*-Bu	H^6	0.27	H^5	13.40	1.47	2.81	8.05	present paper
					H^4	0.58						
j:	*t*-Bu	*p*-BrC_6H_4		*t*-Bu	H^6	0.04	H^5	13.45	1.50	2.22	8.07	present paper
					H^4	0.39						
k:	*t*-Bu	*p*-ClC_6H_4		*t*-Bu	H_6	0.14	H^5	13.48	1.35	2.33	8.05	present paper
					H^4	0.44						
l:	*t*-Bu	*p*-MeC_6H_4		*t*-Bu	H^6	0.22	H^5	13.46	1.52	2.57	8.07	present paper
					H^4	0.53						
m:	*t*-Bu	*p*-$MeOOCC_6H_4$		*t*-Bu	H^6	0.04	H^5	13.36	1.24	1.68	8.04	present paper
					H^4	0.32						

Table 5. ^{1}H NMR parameters of tetraaryl- and tri-*t*-butyl-*p*-methoxycarbonylphenyl-1,8-bisdehydro[14]annulenes

2	R_1	R_2	$H^{4,6}$	H^5	Aryl-H *o*-	Aryl-H *m,p*-	OCH_3	*t*-Bu	Solvent
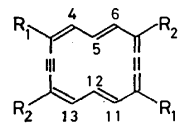	**f**: Ph	Ph	0.06	12.56	1.30	2.35			THF-d_8
	g: $R_1=R_2=p$-$MeOC_6H_4$		0.44	12.60	1.54	2.80	6.04		$CDCl_3$
	h: Ph	*p*-$MeOC_6H_4$	0.21	12.50	1.40	2.50	6.08		THF-d_8
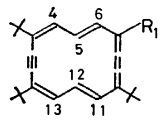	**n**: *p*-$MeO_2CC_6H_4$	H^6 0.25 H^4 0.55 $H^{11,13}$ 0.66	H^5 13.93 H^{12} 13.95		1.34	1.69	5.99	8.10(18H) 8.07(9H)	$CDCl_3$

or carboxyl group exhibit essentially the same NMR trend as compared with **2a** and **2b** having hydrogen or electron donating alkyl groups.

The ^{1}H NMR parameters of aryl substituted tetrakisdehydro[18]annulene derivatives are recorded in Table 3 together with those of tetramethyl and tetra-*t*-butyl derivatives (**1a** and **1b**) as references. The ^{1}H NMR parameters of bisdehydro[14]annulenes bearing two aryl groups are summarized in Table 4 together with tetra-*t*-butyl derivative (**2b**) as a reference. It is to be noted that the position isomers of di-*t*-butyldiphenylbisdehydro[14]annulenes (**2c**, **2d**, and **2e**) show quite similar ^{1}H NMR spectra. This fact indicates that decrease of ring current by the contribution of dipolar structures such as **15a** or **15b** can be ignored in the ground state of 1,8-bisdehydro[14]-annulene system.[13]

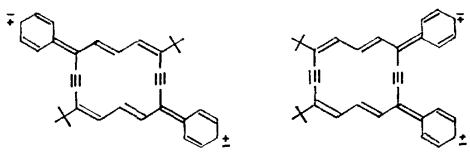

15a 15b

As schematically illustrated in Fig., the magnitude of low field shifts of H^{15} and H^{16} in **2c**, **i**, **j**, **k**, **l**, and **2m** caused by the substituent group at the *p*-position of phenyl group is found to be in the same sequence with the corresponding positions ($H^{m'}$ and $H^{o'}$) in monosubstituted benzenes. This fact suggests that the perturbation of bisdehydro[14]annulene ring on benzene nucleus is not sufficiently large enough to alter the electronic state or electron density of the *p*-substituted phenyl group. Interestingly, as shown in Fig., low field shifts of outer protons of the annulene nuclei (H^4 and H^6), although in less extent being maximum values 0.19 and 0.23 ppm for H^4 and H^6, respectively, are found in the same sequence of H^{16} and $H^{o'}$. This fact indicates a transmission of the effects of *p*-substituent group to the annulene nuclei.

The ^{1}H NMR parameters of tetraaryl-1,8-bisdehydro[14]annulenes (**2f**, **g**, **h**) and tri-*t*-butyl(*p*-methoxycarbonylphenyl)-1,8-bisdehydro[14]annulene (**2n**) are recorded in Table 5. The tetraaryl derivatives (**2f**, **g**, **h**) showed inner proton signals at lower field

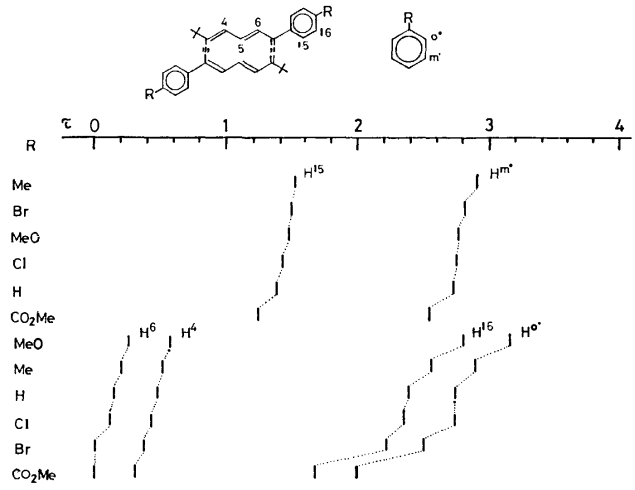

Fig. ^{1}H NMR chemical shifts of bis(*p*-substituted-phenyl)-di-*t*-butyl-1,8-bisdehydro[14]annulenes (**2c**, **i**—**m**) and corresponding monosubstuitedt benzenes.

than those for diaryl derivatives (Table 4). On the other hand, high field shifts of both of the inner and outer proton signals were observed in the monoaryl-derivative (**2n**) as compared with the diaryl derivatives (**2c**, **d**, **e**, **i**, **j**, **k**, **l**, **m**) shown in Table 4. This trend seems to indicate that the diamagnetic ring current induced in the aryl substituent(s) exerts deshielding effect on the outer and inner protons of the annulene nuclei.

The deshielding effect of phenyl group in di-*t*-butyl-diphenyl-1,8-bisdehydro[14]annulene (**2c**) on the annulene protons has been calculated assuming coplanar conformation of the phenyl groups with the annulene ring by the Johnson-Bovey's method. The low field shifts due to the diamagnetic ring current in phenyl groups were estimated to be as follows : H^6 -0.60—-0.50; $H^4 < -0.15$; H^5 -0.15——-0.20 ppm. In view of the observed much larger down field shifts, this results seem to indicate that some other effects cooperate with the deshielding effect of aryl substituents.

It is well recognized that the signals of inner protons show remarkable shifts on minor variation of diamagnetic ring current in contrast to rather insensitive outer proton signals.[14] Because as pointed out previ-

Table 6. Preparation of heptadienyne ketones (**6h—m**)

6	Starting materials				Reaction		Heptadienyne ketone **6**			
	Aldehyde **5**	$R'COCH_3$	Solvent	Base	Temp (°C)	Time (h)	Color	Mp (°C)	Yield (%)	Found (Calcd), %
h	R=Ph 0.888 g 5.69 mmol	R'=*p*-$MeOC_6H_4$ 0.858 g 5.71 mmol	EtOH 65 ml	NaOH 0.3 g H_2O 2 ml	0	overnight	pale yellow	125	1.05 (63.7)	C, 83.15(83.31); H, 5.55(5.59)
i	R=*t*-Bu 5.5 g 40.4 mmol	R'=*p*-$MeOC_6H_4$ 6.0 g 40.4 mmol	EtOH 200 ml	NaOH 2.0 g H_2O 4 ml EtOH 50 ml	5	overnight	yellow	54.7— 55.7	2.1 (65.0)	C, 80.30(80.50); H, 7.36(7.51)
j	R=*t*-Bu 3.8 g 28 mmol	R'=*p*-BrC_6H_4 5.6 g 30 mmol	EtOH 30 ml	NaOH 1.6 g H_2O 2 ml EtOH 10 ml	5	overnight	greenish yellow	109	4.5 (64.0)	C, 64.23(64.27); H, 5.45(5.35); Br, 25.09(25.15)
k	R=*t*-Bu 1.09 g 8 mmol	R'=*p*-ClC_6H_4 1.16 g 7.5 mmol	EtOH 15 ml	NaOH 0.32 g H_2O 3 ml	0	2	pale yellow	119— 121	1.96 (96.0)	C, 75.04(74.86); H, 6.26(6.24); Cl, 13.06(13.00)
l	R=*t*-Bu 1.09 g 8 mmol	R'=*p*-MeC_6H_4 1.07 g 8 mmol	EtOH 15 ml	NaOH 0.32 g H_2O 3 ml	0	3	pale yellow	93— 94	1.60 (79.0)	C, 85.70(85.67); H, 7.90(7.99)
m[a]	R=*t*-Bu 1.27 g 9.3 mmol	R'=*p*-$HOOCC_6H_4$ 1.56 g 9.5 mmol	EtOH 15 ml	NaOH 1.24 g H_2O 36 ml	r. t.	20	yellow	109.9— 111.0	0.723 (27.0)	C, 76.91(77.00); H, 6.78(6.80)

a) The product of the aldol condensation was treated with diazomethane to give the methyl ester (**6m**).

Table 7. Prepartion of tetrasubstituted 1,8-bisdehydro[14]annulene (**2g—m**)

	Heptadienyne ketone **6**		Cyclic dimerization				Reductive dehydroxylation			Annulene **2**		
	g (mmol)	THF (ml)	Time[a] (h)	KOH (g)	NH_3 (ml)	Temp (°C)	Time[b] (h)	Sn^{2+} [c] (g)	Solvent-H^+	Temp (°C)	Mp (°C) (dec)	Yield mg(%)	Found (Calcd), %
g	R=R'=*p*-$MeOC_6H_4$ 0.456 (1.43)	90	3	18.0	250	*ca.* −35	overnight	1.3	THF-Et_2O-HCl	−59	>280	176(58.4)	C, 83.61(83.70); H, 5.62(5.62)
h	R=Ph, R'=*p*-$MeOC_6H_4$ 0.448 (1.55)	60	4	16.0	250	*ca.* −35	overnight	0.6	CH_2Cl_2-HCl	−15	>250	93(22)	C, 88.30(88.53); H, 5.52(5.57)
i	R=*t*-Bu, R'=*p*-$MeOC_6H_4$ 0.924 (3.45)	100	4	19.0	250	−35——40	24	2.0	Et_2O-HCl	−66	>230	100(11.6)	C, 85.76(86.01); H, 7.62(7.62)
j	R=*t*-Bu, R'=*p*-BrC_6H_4 0.475 (1.50)	50	8	17.0	250	*ca.* −35	24	2.0	Et_2O-HCl	−58	>275	98.3(21.9)	C, 67.85(68.01); H, 5.35(5.37); Br, 26.50(26.62)
k	R=*t*-Bu, R'=*p*-ClC_6H_4 0.50 (1.80)	60	4	15.0	400	−35——40	5	0.5	Et_2O-HCl	−15	>280	140(31)	C, 79.75(79.83); H, 6.30(6.31); Cl, 13.78(13.86)
l	R=*t*-Bu, R'=*p*-MeC_6H_4 0.50 (1.83)	60	4	15.0	400	−35——40	5	0.5	Et_2O-HCl	−15	>280	130(33)	C, 91.73(91.86); H, 8.15(8.14)
m[d]	R=*t*-Bu, R'=*p*-$MeOOCC_6H_4$ 0.20 (0.67)	15	8	5.0	500	−35——40	1	1.0	CH_2Cl_2-Et_2O-HCl	−50	>320	98(52)	C, 81.16(81.69); H, 6.94(6.86)

a) Over this period, the THF solution of **6** was added. b) After the addition of THF solution, the mixture was stirred over this period. c) The amount of tin(II) chloride dihydrate. d) The crude cyclic glycol was treated with diazomethane to reconvert into the dimethyl ester (**7m**).

ously, steric effects of the substituent groups seem to be insufficient to explain the marked ^1H NMR change, a decrease of ring current as a result of perturbation of substituent(s) may be largely responsible for the marked low field shifts of the inner proton signals, although the nature of perturbation is not clear yet and the low field shift of outer protons in **1b** can not be explained in terms of decrease of ring current.[15] The diamagnetic ring current induced in aryl substituent exerts deshielding effect on both of inner and outer protons of annulene ring. Inversely, the deshielding effect of ring current induced in annulene ring is reflected in the low field shifts of *o*-protons of aryl substituent as compared with that of *m*-protons. Also the outer protons of annulene ring suffer a minor electronic effect of *p*-substituent in phenyl group as illustrated in Fig. The interesting ^1H NMR characteristics observed in substituted 'acetylene-cumulene'-dehydroannulenes should arise from the superposition of these various effects.

Experimental

The melting points were measured on a Mettler FP-2 apparatus and uncorrected. The IR spectra were obtained on a Hitachi EPI-G3 or a JASCO DS-402G spectrophotometer. The NMR spectra were measured on a Varian A-60D or XL-100 spectrometer, and the parameters were given in τ-values with respect to TMS used as an internal standard. The electronic spectra were obtained in THF on a Hitachi EPS-3T spectrophotometer. The adsorbents used in column chromatography are silica gel (Merck) and alumina (Merck, Act. II-III and Woelm Act. I). Evaporation of solvent was performed under reduced pressure.

2,2-Dichloroethyl p-*Methoxyphenyl Ketone.* To a stirred solution of *p*-methoxybenzoyl chloride (45.5 g, 0.266 mol) in 1,2-dichloroethane (500 ml) was added dropwise a solution of anhydrous aluminium chloride (41.0 g, 0.307 mol) in nitromethane (75 ml) under bubbling of vinyl chloride. After being stirred for 2 h, the reaction mixture was poured onto cracked ice. The organic layer was washed with sodium hydrogencarbonate solution. The crystals obtained on evaporation of the solvent were washed with ethanol to give fairly pure dichloroethyl ketone, pale yellow crystals, mp 58 °C (dec), 32.4 g, 52.2%, IR(KBr-disk): 1670 (C=O), 706 (C–Cl) cm^{-1}, NMR(CCl_4): 6.13 (3H, s, CH_3), 6.23 (2H, d, J=6 Hz, CH_2), 3.70 (1H, t, J=6 Hz, $CHCl_2$); 3.07 (2H, d, J=10 Hz, aromatic-H), 2.08 (2H, d, J=10 Hz, aromatic-H).

Found: C, 51.58; H, 4.29; Cl, 30.02%. Calcd for $C_{10}H_{10}Cl_2$: C, 51.53; H, 4.32; Cl, 30.42%.

2-Chlorovinyl p-*Methoxyphenyl Ketone (**3g**).* A solution of triethylamine (17.0 g, 0.086 mol) in ether (40 ml) was added at 5 °C to a solution of 2,2-dichloroethyl *p*-methoxyphenyl ketone (20.0 g, 0.086 mol) in the same solvent (260 ml). After being stirred for 3 h at the same temperature, the reaction mixture was kept in a refrigerator overnight. The amine hydrochloride deposited was removed by filtration. Crystalline solid obtained on concentrating the filtrate was extracted with petroleum ether (bp 35—60 °C). Evaporation of the solvent yielded pure **3g**, pale yellow crystals, mp 47 °C (dec), 17.0 g, quantitative, IR(KBr-disk): 1665 (C=O), 940 (CH=CH), 758 (C–Cl) cm^{-1}, NMR(CCl_4): 6.13 (3H, s, CH_3), 2.66 (1H, s, vinyl-H), 2.63 (1H, s, vinyl-H), 2.99 (2H, d, J=10 Hz, aromatic-H), 2.15 (2H, d, J=10 Hz, aromatic-H).

Found: C, 61.68; H, 4.75; Cl, 17.87%. Calcd for $C_{10}H_9O_2Cl$: C, 61.40; H, 4.64; Cl, 17.61%.

*1-Chloro-3-(*p-*methoxyphenyl)-1-penten-4-yn-3-ol (**4g**).* A solution of **3g** (16.9 g, 86.2 mmol) in THF (190 ml) was added to a stirred solution of lithium acetylide (prepared from lithium, 0.81 g, 0.12 g atm) in liquid ammonia (250 ml) over a period of 5 h at −60 °C. After the ammonia was allowed to evaporate, saturated ammonium chloride solution (100 ml) was added to the residue at −20 °C. The aqueous layer was extracted with ether and the extract was combined with the organic layer and dried (Na_2SO_4). Evaporation of the solvent yielded crude **4g**, reddish brown liquid, 19.0 g. Because attempted high vacuum distillation resulted in decomposition, the crude material was subjected to a chromatography on silica gel to give fairly pure **4g**, IR(neat): 3425 (O–H), 3300 (C≡CH), 2120 (C≡C), 1608 (CH=CH), 940 (CH=CH), 734 (C–Cl) cm^{-1}, NMR(CCl_4): 7.33 (1H, s, C≡CH), 6.30 (3H, s, CH_3), 6.63 (1H, s, OH), 4.00 (1H, d, J=13 Hz, vinyl-H), 3.51 (1H, d, J=13 Hz, vinyl-H), 3.26 (2H, d, J=9 Hz, aromatic-H), 2.59 (2H, d, J=9 Hz, aromatic-H).

*3-(*p-*Methoxyphenyl)-2-penten-4-ynal (**5g**).* A solution of **4g** (34.9 g, 0.12 mol) in THF (100 ml) was mixed with 1.5 M sulfuric acid (450 ml) and the mixture was stirred under nitrogen atmosphere for 3 days at 18 °C. The organic layer was separated and the aqueous layer, after neutralization with an aqueous sodium hydroxide solution, was extracted successively with ether and benzene. The combined organic solution was washed with brine and dried (Na_2SO_4). Crude brown crystals obtained on concentration of the solution were recrystallized from ethanol to give pure **5g**, yellow crystals, mp 120 °C (dec), 5.5 g, 26%, IR(KBr-disk): 3210 (C≡CH), 2080 (C≡C), 1670 (C=O) cm^{-1}, NMR($CDCl_3$): 6.23 (1H, s, C≡CH), 6.16 (3H, s, CH_3), 3.23 (1H, d, J= 8 Hz, vinyl-H), 3.06 (2H, d, J=10 Hz, aromatic-H), 2.26 (2H, d, J=10 Hz, aromatic-H), −0.24 (1H, d, J=8 Hz, CHO). **5g** was found to be rather unstable decomposing gradually in a dark at low temperature and gave less satisfactory elemental analysis.

Found: C, 77.05; H, 5.41%. Calcd for $C_{12}H_{10}O_2$: C, 77.40; H, 5.41%.

*1,5-Bis(*p-*methoxyphenyl)-2,4-heptadien-6-yn-1-one (**6g**).* A solution of sodium hydroxide (0.5 g, 12.5 mmol) in 50% aqueous ethanol (4 ml) was added at 5 °C to a stirred solution of *p*-methoxyacetophenone (1.53 g, 0.2 mmol) and **5g** (1.90 g, 10.2 mmol) in ethanol (70 ml). After being stirred overnight, deposited crystals were collected and washed successively with water and ethanol to give **6g**, yellow crystals, mp 111—112 °C, 1.95 g, 62%, IR(KBr-disk): 3230 (C≡CH), 2100 (C≡C), 1650 (C=O) cm^{-1}, NMR($CDCl_3$): 6.33 (1H, s, C≡CH), 6.18 (3H, s, CH_3), 6.13 (3H, s, CH_3), 3.10 (2H, d, J=9.0 Hz, aromatic-H), 3.05 (2H, d, J=9.0 Hz, aromatic-H), 2.31 (2H, d, J=9.0 Hz, aromatic-H), 2.05 (2H, d, J=9.0 Hz, aromatic-H), 2—3(3H, m, vinyl-H).

Found: C, 79.19; H, 5.70%. Calcd for $C_{21}H_{18}O_3$: C, 79.22; H, 5.69%.

*Preparation of 1,5-disubstituted 2,4-Heptadien-6-yn-1-one (**6h**—**m**).* Because the heptadienyne ketones (**6h**—**m**) were prepared by the aldol condensation of methyl ketones with 3-substituted-2-penten-4-ynals (**5**, R=Ph[3] and R=*t*-Bu[2]) under similar reaction conditions used in the synthesis of **6g**, the reaction conditions, physical properties, yields and elemental analyses are tabulated in Table 6. The IR and NMR spectra of **6h**—**m** were found to be consistent with the assigned structures.

*Preparation of 3,7,10,14-Tetrasubstituted 1,8-Bisdehydro[14]annulenes (**2g**—**m**).* The preparation of **2g**—**m** were per-

formed by the previously reported procedure.[7] Because the cyclic glycols (**7g**—**m**) were obtained as amorphous solids and found to be difficult to crystallize, the crude materials were subjected to the reductive dehydroxylation to give **2g**—**m**. The products were purified by chromatography on alumina (Merck or Woelm). The reaction conditions, melting points and analytical data are summarized in Table 7. The yields of **2g**—**m** were calculated on the basis of **6g**—**m**.

*1-(*p*-Methoxycarbonylphenyl)-5,8,12-tri-*t*-butyl-2,4,9,11-tetradecatetraene-6,13-diyn-1-one (**9**).* To a stirred solution of *p*-acetylbenzoic acid (0.5240 g, 3.19 mmol) in water (4 ml) containing sodium hydroxide (0.34 g, 8.5 mmol) was added under argon atmosphere at 15 °C a solution of hydroxy aldehyde[9] (**8**, 0.939 g, 2.65 mmol) in methanol (30 ml). After being stirred for 44.5 h, 1 M hydrochloric acid was added to the reaction mixture, and the resulting turbid yellow mixture was extracted with ether. Yellow solid obtained on working up the extract was treated with an ethereal solution of diazomethane. Chromatography of the product on alumina (Merck, 70 g) followed by elution with hexane–benzene (1:1) and ether afforded **9**, yellow solid, 523 mg, 38%, IR(KBr-disk): 3480 (O–H), 3300 (C≡CH), 2081 (C≡C), 1727 (C=O ester), 1655 (C=O), 1585 (CH=CH) cm^{-1}, NMR(CCl_4): 8.91 (9H, s, *t*-Bu), 8.83 (9H, s, *t*-Bu), 8.77 (9H, s, *t*-Bu), 7.00 (1H, s, OH), 6.80 (1H, s, C≡CH), 6.11 (3H, s, $COCH_3$), 4.13—1.89 (10H, m, olefinic and aromatic-H).

Attempts to crystallize **9** were unsuccessful.

*3,10,14-Tri-*t*-butyl-7-(*p*-methoxycarbonylphenyl)-1,8-bisdehydro[14]annulene (**2n**).* A solution of **9** (105.7 mg, 0.205 mmol) in THF (20 ml) was added over 6.5 h-period to a stirred suspension of powdered potassium hydroxide (4.0 g, 71.4 mmol) in liquid ammonia (300 ml) at −35—−40 °C. After the mixture had been stirred for further 15 h, ammonium chloride (4.0 g, 74.7 mmol) was added and the ammonia was allowed to evaporate. The residue was mixed with water and extracted with ether. The aqueous layer was acidified with 1 M hydrochloric acid and extracted with ether. The combined extract, after being washed successively with water and brine, and dried ($MgSO_4$), was concentrated in a small volume. An ethereal solution of diazomethane was added to the concentrate. As the purification of **10** was found to be difficult, the crude **10** in ether (10 ml) was treated with a solution of tin(II) chloride dihydrate (0.5 g) in the same solvent saturated with hydrogen chloride (10 ml) at −15 °C. After 5 min, the resulting deep reddish brown solution was poured on an aqueous solution of sodium hydrogencarbonate, and extracted with ether. The crude product obtained on working up the extract was chromatographed on alumina (Merck, 50 g). Elution with hexane–benzene (1:1) gave **2n**, reddish brown crystals, mp> 270 °C (dec), 93.2 mg, 32% based on **9**, IR (KBr-disk): 2075 (C–C≡C–C ↔ C=C=C=C=), 1714 (C=O), 1604 (CH=CH), 970 (*trans* CH–CH) cm^{-1}, mass (*m/e*): 480 (M^+), calcd for $C_{34}H_{40}O_2$: mol wt 480.66.

*1,5,10,14-Tetra-*p*-methoxyphenyl-2,4,10,12-tetradecatetraene-6,8-diyne-1,14-dione (**11**).* A solution of copper(II) acetate monohydrate (12.0 g) in pyridine–methanol (1:1, 200 ml) was added to a stirred solution of **6g** (5.4 g, 17 mmol) in the same solvent (200 ml) at 5 °C. The mixture was stirred overnight at a room temperature. Yellow crystals deposited were collected and washed successively with water and ethanol to give pure **11**, yellow crystals, mp 156.8 °C, 5.3 g, 98%, IR(KBr-disk): 2830 (C–H in O–CH_3), 1645 (C=O), 983 (CH=CH) cm^{-1}, NMR($CDCl_3$): 6.13 (12H, s, OCH_3), 3.10 (4H, d, J=9 Hz, aromatic-H), 2.86 (4H, d, J=9 Hz, aromatic-H), 2.33 (4H, d, J=9 Hz, aromatic-H), 2.03 (4H, J=9 Hz, aromatic-H), 1.9—2.3 (6H, m, olefinic-H).

Found: C, 79.44; H, 5.44%. Calcd for $C_{42}H_{34}O_6$: C, 79.48; H, 5.40%.

*3,7,12,16-Tetra-*p*-methoxyphenyl-4,6,12,13-octadecatetraene-1,8,10,17-tetrayne-3,6-diol (**12**).* A solution of **11** (2.050 g, 3.23 mmol) in THF (330 ml) was added over 2 h-period at 15—17 °C to a stirred suspension of lithium acetylide-ethylenediamine complex (4.2 g, 45.5 mmol) in the same solvent (50 ml) under bubbling of acetylene. After being stirred for further 4 h, saturated aqueous solution of ammonium chloride (50 ml) was added to the reaction mixture at −15 °C. The aqueous layer was extracted with benzene and combined with the organic layer, which was worked up to give a light brown solid. The material was chromatographed on alumina (Merck, 20 g) to give slightly crude **12**, 1.980 g, which was used without further purification in the subsequent reaction.

*1,5,10,14-Tetra-*p*-methoxyphenyl-6,8,15,17-tetrakisdehydro[18]annulene (**1f**).* To a vigorously stirred solution of copper(II) acetate monohydrate (3.7 g) in pyridine (60 ml), methanol (30 ml) and ether (180 ml) was added a solution of crude **12** (2.23 g) in pyridine (40 ml), methanol (20 ml) and ether (10 ml) over a period of 14 h at 40—45 °C. The residue obtained on evaporation of the solvent was digested with benzene. The benzene solution was washed successively with brine, sodium hydrogencarbonate solution and brine, and dried ($MgSO_4$). Evaporation of the solvent yielded brown crystalline solid, which was washed with benzene to give sufficiently pure **13**, pale yellow fine crystals, 0.514 g, 23.2% based on **11**.

A solution of tin(II) chloride dihydrate (1.0 g, 4.4 mmol) in ether saturated with hydrogen chloride (5 ml) was added at −78 °C to a stirred solution of **13** (100 mg, 0.15 mmol) in ether (20 ml) and THF (5 ml). After being stirred for 10 min at the same temperature, water (100 ml) was added to the reaction mixture. Crystals deposited were washed successively with ethanol and acetone to give fairly pure **1f**, deep green crystals, mp 169—171 °C (decomposed without fusion), 76 mg, 77%. A specimen obtained by passing repeatedly a solution of **1f** in THF through a column of alumina (Woelm) gave rather unsatisfactory elemental analysis.

Found: C, 84.38; H, 5.33%. Calcd for $C_{46}H_{34}O_4$: C, 84.90; H, 5.27%.

References

1) J. Ojima, T. Katakami, G. Nakaminami, and M. Nakagawa, *Tetrahedron Lett.*, **1968**, 1115; J. Ojima, T. Katakami, G. Nakaminami, and M. Nakagawa, *Bull. Chem. Soc. Jpn.*, **49**, 292 (1972).

2) a) T. Katakami, S. Tomita, K. Fukui, and M. Nakagawa, *Chem. Lett.*, **1972**, 225; b) S. Tomita and M. Nakagawa, *Bull. Chem. Soc. Jpn.*, **49**, 302 (1976).

3) a) K. Fukui, T. Okamoto, and M. Nakagawa, *Tetrahedron Lett.*, **1971**, 3121; b) T. Katakami, K. Fukui, T. Okamoto, and M. Nakagawa, *Bull. Chem. Soc. Jpn.*, **49**, 297 (1976).

4) T. Nomoto, K. Fukui, and M. Nakagawa, *Tetrahedron Lett.*, **1972**, 3253; T. Nomoto, K. Fukui, and M. Nakagawa, *Bull. Chem. Soc. Jpn.*, **49**, 305 (1976).

5) F. Sondheimer and Y. Gaoni, *J. Am. Chem. Soc.*, **82**, 5765 (1960); F. Sondheimer, Y. Gaoni, L. M. Jackman, N. A. Bailey, and R. Mason, *ibid.*, **84**, 4595 (1962).

6) a) K. Fukui, T. Nomoto, S. Nakatsuji, and M. Nakagawa, *Tetrahedron Lett.*, **1972**, 3157; b) K. Fukui, T. Nomoto, S. Nakatsuji, S. Akiyama, and M. Nakagawa,

Bull. Chem. Soc. Jpn., **50**, 2758 (1977).

7) a) T. Nomoto, S. Nakatsuji, and M. Nakagawa, *Chem. Lett.*, **1974**, 839; b) T. Nomoto, S. Nakatsuji, and M. Nakagawa, *Bull. Chem. Soc. Jpn.*, **51**, 3345 (1978).

8) S. Nakatsuji, M. Morigaki, S. Akiyama, and M. Nakagawa, *Tetrahedron Lett.*, **1975**, 1233.

9) D. F. Beumel, Jr. and R. F. Harries, *J. Org. Chem.*, **29**, 1872 (1964).

10) C. Kabuto, Y. Kitahara, M. Iyoda, and M. Nakagawa, *Tetrahedron Lett.*, **1976**, 2791.

11) C. Kabuto, Y. Kitahara, M. Iyoda, and M. Nakagawa, *Tetrahedron Lett.*, **1976**, 2787.

12) T. Satake, S. Nakatsuji, M. Iyoda, S. Akiyama, and M. Nakagawa, *Tetrahedron Lett.*, **1976**, 1881.

13) Contribution of such type dipolar structures of **2c** and **2d** seemed to be negligible even in their excited states, because the electronic spectra of **2c**, **2d**, and **2e** were found to be almost identical. See, Ref. 7a) and the preceding paper.

14) M. Nakagawa, *Pure Appl. Chem.*, **44**, 885 (1975).

15) It was puzzling that *trans*-15,16-dihydropyrene showed smaller ring current than *trans*-15,16-dimethyldihydropyrene. The ESR studies on radical anion of *trans*-15,16-dihydropyrene provide a strong evidence for an exceptionally large hyperconjugative effect of inner hydrogen atoms (C. Elschenbroich, F. Gerson, and V. Boekelheide, *Helv. Chim. Acta*, **58**, 1245 (1975)), and the reduction of ring current of *trans*-15,16-dihydropyrene has been considered to be attributable to the hyperconjugative effect (T. Otsubo, R. Gray, and V. Boekelheide, *J. Am. Chem. Soc.*, **100**, 2449 (1978)). In the case of methyl or *t*-butyl substituted 'acetylene-cumulene'-dehydroannulenes, the possibility can not be excluded that the hyperconjugation of C–H bond in methyl or C–CH_3 bond in *t*-butyl group disposed in parallel direction with the *p*-orbital of adjacent sp^2-hybridized carbon atom of annulene ring is responsible for the ^1H NMR behavior of the 'acetylene-cumulene'-dehydroannulenes.

Dehydroannulenes. X. Synthesis and Properties of 3,9,12,18-Tetrasubstituted-1,10-bisdehydro[18]annulenes

Masahiko IYODA, Shuzo AKIYAMA,† and Masazumi NAKAGAWA*

Department of Chemistry, Faculty of Science, Osaka University, Toyonaka, Osaka 560

(Received May 15, 1978)

The cyclic dimerization of 1,7-disubstituted-1-oxo-2,4,6-nonatrien-8-ynes on treatment with a suspension of potassium hydroxide in liquid ammonia to give tetrasubstituted 18-membered cyclic glycols has been achieved. The cyclic glycols could be converted into 3,9,12,18-tetrasubstituted 1,10-bisdehydro[18]annulenes which were found to be conformationally stable and strongly diatropic.

As reported in previous papers,[1] 1,5-disubstituted 1-oxo-2,4-heptadien-6-ynes gave 14-membered cyclic glycols on treatment with a suspension of potassium hydroxide in liquid ammonia, and the cyclic glycols could be converted into 3,7,10,14-tetra-substituted 1,8-bisdehydro[14]annulenes by reductive dehydroxylation. The finding seemed to open a new route leading to higher members of bisdehydro[4n+2]annulenes provided that the cyclic dimerization can be realized for higher ethynylpolyene ketones.

In this paper we wish to report the cyclic dimerization of ethynyltriene ketones (**2**) to give 18-membered cyclic glycols (**3**) and their transformation into tetrasubstituted bisdehydro[18]-annulenes (**4**).[1]

Synthesis. The ethynyltriene ketones (**2a**[3,4] and **2c**[5]) were prepared by the reported methods. The trienyne ketone (**2b**) was obtained by the aldol condensation of acetophenone with 3-*t*-butyl-2,4-heptadien-6-ynal (**1a**).[3,4] A solution of ethynyltriene ketone (**2**) in tetrahydrofuran was added to a stirred suspension of finely powdered potassium hydroxide in liquid ammonia at *ca.* −35 °C. The cyclic glycol (**3a**) was obtained as a 1:1 mixture of diastereomers and could be separated into a high melting and a low melting isomers on chromatography on silica gel. Because the 18-membered cyclic glycols (**3b** and **3c**) were found to be difficult to purify, slightly crude materials were subjected to the following reductive dehydroxylation.

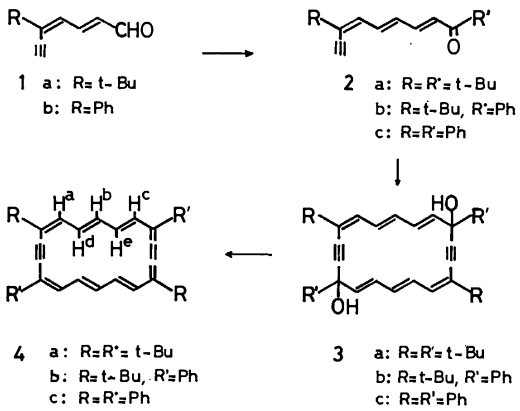

Scheme.

Finely powdered tin(II) chloride dihydrate was added to a stirred solution of **3a** in ether saturated with hydrogen chloride at −60 °C under nitrogen atmosphere. Resulting deeply colored solution was worked up and the product was chromatographed on alumina to give 3,9,12,18-tetra-*t*-butyl-1,10-bisdehydro[18]annulene (**4a**) as reddish violet crystals in 93% yield. Catalytic hydrogenation of **4a** over platinum catalyst yielded tetra-*t*-butyl-cyclooctadecane.

3,12-Di-*t*-butyl-9,18-diphenyl-1,10-bisdehydro[18]-annulene (**4b**) was obtained by a similar procedure as deep violet crystals.

Taking the poor solubility of **3c** and presumably of **4c** into account, a dilute solution of **3c** in dichloromethane was mixed with a solution of tin(II) chloride dihydrate in concentrated hydrochloric acid at −15 °C. 3,9,12,18-Tetraphenyl-1,10-bisdehydro[18]annulene (**4c**) was obtained as deep violet crystals in 59% yield. Full hydrogenation of **4c** over platinum catalyst yielded tetraphenylcyclooctadecane.

Properties. The bisdehydro[18]annulenes (**4a, b, c**) were found to be fairly stable being much stable than the corresponding tetrakisdehydro[18]annulenes.[6] 2,4,7-Trinitrofluorenone gave 1 : 1 CT complexes with **4a** and **4b**. However, CT complex with a definite composition could not be obtained with **4c**.

The electronic spectra of **4a, b, c** consist of three main absorption maxima characteristic of aromatic [4n+2]annulenes and showed close similarity to each other except for bathochromic shift along with the increase of phenyl substitution.[7] The numerical data of the electronic spectra are recorded in Table 1.

The ^{1}H NMR spectra of **4a, b, c** revealed that they sustain strong diamagnetic ring current exhibiting the inner proton signals at high field and those of outer protons at low field. The ^{1}H NMR parameters are summarized in Table 2. Replacement of *t*-butyl group by phenyl caused low field shift of inner and outer proton signals in **4b** and **4c**, which can be attributed, at least partly, to the deshielding effect of the diamagnetic ring current induced in phenyl groups. On the other hand, low field shift of *o*-proton signal of phenyl group as compared with that of *m,p*-protons indicate that the ring current in annulene ring exerts deshielding effect on the phenyl protons, and the *o*-protons suffer pronounced shift owing to their proximate position to the annulene nucleus. As recorded in Table 3, the ^{1}H NMR spectra of **4a** were found to be temperature independent being essentially unchanged up to 110 °C. This fact indicates the conformational stability of the tetrasubstituted 1,10-bisdehydro[18]annulene system. An attempted measurement of the NMR spectrum at 150 °C in deuteriobromo-

† Present address: Faculty of Pharmacy, Nagasaki University, Bunkyo-cho, Nagasaki 852.

Table 1. Electronic spectra of **4a, b, c** in THF (λ_{max} in nm (ε))

4a	217(11300), 255*(5810), 267.5(8360), 342*(44400), 356(94400), 372(447000), 464*(4790), 499(10600), 539(19100), 607(100), 646*(89), 669(116), 681(116), 720*(138), 751(316)
4b	240*(12900), 249.5(14000), 267*(12000), 281.5(16200), 367*(51800), 389*(171000), 401(330000), 534*(17900), 574(48000), 673*(150), 701(231), 785(980)
4c	261(25000), 293(26300), 411(106300), 431(506800), 572(20600), 615(48600), 735(270), 826(1560)

Table 2. ^{1}H NMR spectra of **4a** in deuteriobromoform

Temp (°C)	$H^{a,c}$	H^{b}	$H^{d,e}$	*t*-Bu
36	0.68, d J=13 Hz	0.18, t J=13 Hz	13.64, t J=13 Hz	8.09, s
70	0.78, d J=13 Hz	0.30, t J=13 Hz	13.46, t J=13 Hz	8.10, s
110	0.81, d J=13 Hz	0.44, t J=13 Hz	13.28, t J=13 Hz	8.10, s

form resulted in a rapid decomposition of **4a**. Because the planar structure of **4a** has been revealed by the X-ray structure analysis,[8] the minor high field and low field shifts of outer and inner proton signals at higher temperature should be a reflection of increasing deviation of the annulene perimeter from the mean molecular plane owing to the increase of thermal vibration at higher temperature.

It has been generally recognized that dehydroannulenes have higher conformational stability than the corresponding annulenes. The conformational stability of dehydroannulene, which is rendered by the rigid and straight nature of acetylenic bond, is favorable for the study of aromaticity of annulene system. But, on the other hand, the diatropicity of dehydroannulene is suppressed by the perturbation of acetylenic linkage. On the contrary, dehydroannulenes containing an acetylenic and a cumulenic bonds ('acetylene-cumulene'-dehydroannulenes), such as 1,8-bisdehydro[14]annulene[9] and its tetrasubstituted derivatives[1] and **4a,b,c**, showed strong diatropicity and high conformational stability being the most adequate tool for the study of aromaticity of macrocyclic system. Because the acetylenic and cumulenic bonds in 1,8-bisdehydro[14]annulene[10] and in **4a**[8] have been proved to be identical by the X-ray structure analyses being a hybrid of acetylene and butatriene, the strong diatropicity in 'acetylene-cumulene'-dehydroannulene can be attributed to the presence of equivalent valence-bond structures such as **5a**↔**5b**.

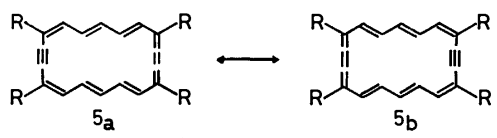

Experimental

All melting points were measured on a Mettler FP-2 apparatus and uncorrected. The IR spectra were obtained on a Hitachi EPI-2 or EPI-G3 spectrophotometer and only the significant absorptions were recorded (s=strong, m=medium and w=weak). The NMR spectra obtained on a Varian A-60 or XL-100 spectrometer were recorded in τ-values with respect to TMS used as an internal standard. The mass spectra were obtained on a Hitachi RM-50 spectrometer (ionization potential=70 eV). TLC was performed on Kieselgel GF_{254}(Merck) plates. The adsorbents used in column chromatography were silica gel (Merck, Kieselgel 60) or alumina (Merck, act. II—III), unless stated otherwise. Evaporation of solvent was performed under reduced pressure.

1,4,10,13-Tetra-t-butyl-4,6,8,13,15,17-cyclooctadecahexaene-2,11-diyne-1,10-diol (3a). To a stirred suspension of finely powdered potassium hydroxide (900 mg, 1.60 mmol) in liquid ammonia (180 ml) was added at −34 °C a solution of **2a** (320 mg, 1.13 mmol) in THF (30 ml) over a period of 5 h. After being stirred for further 3 h at the same temperature, ammonium chloride (1.80 g, 33.6 mmol) was added and the ammonia was allowed to evaporate. Water and ether (20 ml) were added to the residue. The aqueous layer was washed successively with water and brine, and dried ($MgSO_4$). Evaporation of the solvent yielded pale yellow crystals, which were washed with hexane to give a mixture of diastereomers of **3a**, colorless crystals, 212 mg, 66.3%. The mixture was chromatographed on silica gel. Elution with benzene gave the high melting isomer of **3a**, colorless crystals, mp 230.5—231.5 °C; mass (*m/e*): 488 (M^+), 470 (M^+-18), 431 (M^+-57), 57 (*t*-Bu, base peak); IR(KBr-disk): 3560 m (OH), 2180 vw (−C≡C−), 1563 w (C=C), 985 vs (*trans* −CH=CH−) cm^{-1}; NMR($CDCl_3$): 2.75—4.20 (10H, m, olefinic), 8.2 (2H, br s, OH), 8.80 (18H, s, *t*-Bu), 8.92 (18H, s, *t*-Bu); UV: $\lambda_{max}^{99\%EtOH}$ (ε): 230 (21100), 280.5 (86900), 291 (113000), 327.5 (13800) nm.

Found: C, 83.53; H, 9.93%. Calcd for $C_{34}H_{48}O_2$: C, 83.55; H, 9.90%.

Elution with benzene–ether (19:1) gave the low melting isomer of **3a**, colorless crystals, mp 170.0—171.0 °C; mass (*m/e*): 488 (M^+), 470 (M^+-18), 431 (M^+-57), 57 (*t*-Bu, base peak); IR(KBr-disk): 3480 m, 3340 m (OH), 2180 vw (−C≡C−), 1563 w (C=C), 985 vs (*trans* −CH=CH−) cm^{-1}; NMR($CDCl_3$): 2.75—4.20 (10H, m, olefinic), 8.01 (2H, s, OH), 8.80 (18H, s, *t*-Bu), 8.92 (18H, s, *t*-Bu); UV: $\lambda_{max}^{99\%EtOH}$ (ε) 230 (18200), 280.5 (76300), 291 (98400), 327.5 (12300) nm.

Found: C, 83.72; H, 10.76%. Calcd for $C_{34}H_{48}O_2$: C, 83.55; H, 9.90%.

3,9,12,18-Tetra-t-butyl-1,10-bisdehydro[18]annulene (4a). To a solution of the diastereomeric mixture of **3a** (105 mg, 0.215 mmol) in ether saturated with hydrogen chloride (10 ml) was added at −60 °C under nitrogen atmosphere finely powdered tin(II) chloride dihydrate (400 mg, 1.77 mmol). The mixture was vigorously stirred at the same temperature for 10 min. The reaction mixture was poured onto ice-cooled sodium hydrogencarbonate solution. The mixture was extracted with ether and the ethereal solution was dried (K_2CO_3). Evaporation of the solution furnished dark red crystals, which were chromatographed on alumina (Woelm, act. I) and eluted with hexane–dichloromethane (19:1) to afford pure **4a**, dark reddish violet crystals, 91 mg, 93%. The crystals obtained on rechromatography on alumina were

Table 3. ^{1}H NMR parameters of **4a, b, c** at 36 °C[a)]

	H^a, H^c	H^b	H^d, H^e	*t*-Bu	*o*-H of Ph	*m,p*-H of Ph
4a, 60 MHz $CDCl_3$	0.62, d, 4H J=13 Hz	0.13, t, 2H J=13 Hz	13.42, t, 4H J=13 Hz	8.03, s, 36H		
4b, 60 MHz $CDCl_3$	−0.21—0.62, m, 6H		13.28, m, 4H	7.98, s, 18H	1.33, m, 4H	2.33, m, 6H
4c, 100 MHz-FT, THF-d_8	−0.04, d J=13 Hz	−0.20, t J=13 Hz	12.70, t J=13 Hz		1.24, d	2.07—2.80, m

a) For NMR charts of **4a** and **4c**, see Ref. 2.

washed successively with ether and hexane to give analytical specimen of **2a**, mp 260 °C (dec); mass (*m/e*): 454 (M^+), 397 (M^+-57), 57 (*t*-Bu, base peak); IR(KBr-disk): 3030 w, 2950 s, 2000 vw (−C≡C−↔−C=C=), 1041 m, 987 vs, 878 w cm^{-1}.

Found: C, 89.72; H, 10.18%. Calcd for $C_{34}H_{46}$: C, 89.80; H, 10.20%.

*CT Complex of **4a** with 2,4,7-Trinitrofluorenone.* A solution of **4a** (31.5 mg, 0.0694 mmol) in benzene–methanol (1:1, 40 ml) was mixed with a solution of the trinitrofluorenone (43.5 mg, 0.138 mmol) in benzene–methanol (2 : 1, 9 ml) at 40—50 °C. The solution was kept at 0 °C to deposite the CT complex, deep violet needles, mp *ca.* 260 °C, 41 mg, 77%.

Found: C, 73.37; H, 6.63; N, 5.43%. Calcd for $C_{34}H_{46}\cdot C_{13}H_5N_3O_7$: C, 73.32; H, 6.68; N, 5.46%.

The CT complex was found to be more stable and less soluble in organic solvents than **4a**. The electronic spectrum of the complex showed no CT band being a superposition of the spectra of components.

*Catalytic Hydrogenation of **4a**.* A solution of **4a** (42 mg, 0.0924 mmol) in ethyl acetate (25 ml) was added to platinum catalyst (from 150 mg of platinum(IV) oxide) in acetic acid (25 ml). The mixture was vigorously stirred at room temperature under hydrogen atmosphere for 2.5 h and the catalyst was removed by filtration and washed with ether (50 ml). The combined organic layer was washed successively with water, sodium hydrogencarbonate solution and brine, and dried ($MgSO_4$). Evaporation of the solvent gave a crystalline solid, which was chromatographed on alumina (Woelm, act. I) and eluted with hexane to yield 1,4,10,13-tetra-*t*-butyl-cyclooctadecane, 40 mg, 91%. An analytical specimen was prepared by recrystallization from ethyl acetate–methanol, colorless crystals, mp 151—154 °C; mass (*m/e*): 476 (M^+), 419 (M^+-57), 57 (*t*-Bu, base peak); IR(CCl_4): 2940 s, 2860 m, 1475 m, 1393 m, 1365 m cm^{-1}; NMR(CCl_4): 8.63 (32H, br s, $-CH_2-$, −CH=), 9.11 (36H, s, *t*-Bu).

Found: C, 85.62; H, 14.13%. Calcd for $C_{34}H_{68}$: C, 85.63; H, 14.37%.

*6-t-Butyl-1,3,5-octatrien-7-ynyl Phenyl Ketone (**2b**).* To a solution of sodium hydroxide (0.88 g, 0.022 mol) in aqueous ethanol (1:1, 6 ml) was added at 0 °C a solution of **1a** (3.56 g, 0.0219 mol) and acetophenone (2.64 g, 0.0220 mol) in ethanol (30 ml) under nitrogen atmosphere. The mixture was kept at the same temperature for 3 h and then acidified with 1 M sulfuric acid (20 ml). The mixture was extracted with ether (50 ml×3). The combined extract was washed successively with water, saturated sodium hydrogencarbonate solution and brine, and dried ($MgSO_4$). The residue obtained on evaporating the solvent was chromatographed on silica gel and eluted successively with hexane, benzene and ether–benzene to give **2b**, 4.41 g, 76%. Recrystallization of the material from petroleum ether (bp 40—60 °C) afforded an analytical specimen of **2b**, yellow crystals, mp 59.5—60.0 °C; mass (*m/e*): 264 (M^+); IR($CHCl_3$): 3320 m (C≡CH), 2060 vw (−C≡C−), 1658 s (C=O), 1590 s, 1550 s (C=C), 1016 s, 1002 s (*trans* −CH=CH−) cm^{-1}; NMR($CDCl_3$): 1.98—3.72 (10H, m, olefinic and aromatic), 6.50 (1H, s, C≡CH), 8.81 (9H, s, *t*-Bu); UV: $\lambda_{max}^{99\%EtOH}$ (ε) 225* (8710), 267.5 (10300), 359 (39100) nm.

Found: C, 86.27; H, 7.56%. Calcd for $C_{38}H_{38}$: C, 86.32; H, 7.63%.

*3,12-Di-t-butyl-9,18-diphenyl-1,10-bisdehydro[18]annulene (**4b**).* A solution of **2b** (350 mg, 1.32 mmol) in THF (50 ml) was added over 8 h-period to a stirred suspension of powdered potassium hydroxide (1.00 g, 17.8 mmol) in liquid ammonia (200 ml) at −34 °C. After being stirred for further 2 h at the same temperature, ammonium chloride (2.00 g, 37.4 mmol) was added and the ammonia was allowed to evaporate. The residue was mixed water and ether (20 ml). The aqueous layer was extracted with ether (15 ml×2). The combined organic layer was washed successively with water and brine, and dried ($MgSO_4$). Evaporation of the solvent yielded crude **3b**, light brown solid, *ca.* 350 mg. As the formation of **3b** was confirmed by spectroscopy and TLC analysis and the purification of **3b** was found to be difficult, the crude **3b** was used in the following reaction.

To a solution of the crude **3b** (*ca.* 350 mg) in ether (10 ml) was added at −60 °C ether saturated with hydrogen chloride (10 ml) and finely powdered tin(II) chloride dihydrate (1.00 g, 4.43 mmol). The mixture was vigorously stirred for 10 min at the same temperature and then poured onto an ice-cooled solution of sodium hydrogencarbonate. Ether was added to the mixture and the organic layer was separated, and dried (K_2CO_3). Evaporation of the solvent yielded violet crystals, which were chromatographed on alumina (Woelm, act. I) and eluted with hexane–benzene (4:1—1:1) to give pure **4b**, deep violet crystals, 108 mg, 33% based on **2b**. An analytical specimen was obtained on recrystallizing the crystals from benzene–methanol, mp 235 °C (dec); mass (*m/e*): 494 (M^+), 57 (*t*-Bu, base peak); IR(KBr-disk): 3025 w, 2950 m, 2010 vw (−C≡C−↔−C=C=), 1595 m (C=C), 983 s (*trans* −CH=CH−), 766 s (phenyl) cm^{-1}.

Found: C, 92.16; H, 7.67%. Calcd for $C_{38}H_{38}$: C, 92.26; H, 7.74%.

*CT Complex of **4b** with 2,4,7-Trinitrofluorenone.* A solution of **4b** (45.3 mg, 0.0916 mmol) in benzene–methanol (1:1, 40 ml) kept at 40 °C was mixed with a solution of the trinitro compound (57.7 mg, 0.183 mmol) in the same solvent (20 ml). The mixture was allowed to stand at 0 °C to deposite the CT complex, deep violet needles, mp *ca.* 250 °C (dec), 46.6 mg, 62.8%.

Found: C, 75.06; H, 5.23; N, 5.49%. Calcd for $C_{38}H_{38}\cdot C_{13}H_5N_3O_7$: C, 75.63; H, 5.35; N, 5.19%.

*3,9,12,18-Tetraphenyl-1,10-bisdehydro[18]annulene (**4c**).* A solution of **2c** (0.150 g, 0.77 mmol) in THF (40 ml) was added over 3 h-period at −34 °C to a stirred suspension of potassium hydroxide (3.00 g, 5.36 mmol) in liquid ammonia (200 ml). After the mixture had been stirred overnight at the same temperature, ammonium chloride (6.0 g, 0.113 mol)

was added. The residue obtained after being allowed the ammonia to evaporate was extracted with benzene (200 ml). The extract was washed with water, and dried ($MgSO_4$). Light solid (0.148 g) obtained on evaporating the solvent was dissolved in a small amount of benzene. Hexane was added to the benzene solution to precipitate **3c**, crystalline solid, 76 mg, 53%, which was found to be difficult to purify. A solution of tin(II) chloride dihydrate (0.30 g) in concentrated hydrochloric acid (5.0 ml) was added at −15 °C to a solution of the crude cyclic glycol (**3c**, 76 mg, 0.13 mmol) in dichloromethane (200 ml). After being stirred for 10 min at the same temperature, a solution of sodium carbonate was added to the mixture. The organic layer was washed with water, and dried ($MgSO_4$). The solution was passed through a short column of alumina (10 g). The residue obtained on concentrating the filtrate was triturated with benzene-hexane and the crystals deposited were washed with the same solvent to give **4c**, dark violet needles, mp 250 °C (dec), 41 mg, 59%. The tetraphenyl derivative (**4c**) was found to be sparingly soluble and stable compound. The crystals were recrystallized from THF and repeatedly chromatographed on alumina (Woelm, act. I) to give an analytical sample, mass (*m/e*): 534 (M^+); IR (KBr-disk): 2040 (−C≡C−↔−C=C=), 1595 (C=C), 980 (*trans* −CH=CH−), 761 (phenyl) cm^{-1}.

Found: C, 94.37; H, 5.61%. Calcd for $C_{42}H_{30}$: C, 94.34; H, 5.66%.

Catalytic Hydrogenation of ***4c***. Platinic oxide (100 mg) was added to a solution of **4c** (30 mg) in THF–ethyl acetate (1:1, 30 ml), and the mixture was vigorously stirred under hydrogen atmosphere for 3 h. The catalyst was removed by filtration and washed with benzene. The residue obtained on evaporation of the filtrate and washing was dissolved in hexane (5 ml) and passed through a thin layer of silica gel (0.2 g). Evaporation of the filtrate afforded colorless crystals, 27 mg, 90%, which were recrystallized twice from hexane–pentane to give 1,4,10,13-tetraphenylcyclooctadecane, mp 146—152 °C; mass (*m/e*): 556 (M^+); NMR(CD_2Cl_2): 2.83 (20H, s, aromatic), 7.35 (4H, m, −CH=), 8—9 (28H, m, $-CH_2-$).

Found: C, 90.80; H, 9.49%. Calcd for $C_{42}H_{52}$: C, 90.59; H, 9.41%.

References

1) K. Fukui, T. Nomoto, S. Nakatsuji, and M. Nakagawa, *Tetrahedron Lett.*, **1972**, 3157; K. Fukui, T. Nomoto, S. Nakatsuji, S. Akiyama, and M. Nakagawa, *Bull. Chem. Soc. Jpn.*, **50**, 2758 (1977).

2) For a preliminary report, see, M. Iyoda and M. Nakagawa, *Tetrahedron Lett.*, **1972**, 3161.

3) M. Iyoda, H. Miyazaki, and M. Nakagawa, *J. Chem. Soc., Chem. Commun.*, **1972**, 431.

4) M. Iyoda, H. Miyazaki, and M. Nakagawa, *Bull. Chem. Soc. Jpn.*, **49**, 2306 (1976).

5) S. Akiyama, T. Nomoto, M. Iyoda, and M. Nakagawa, *Bull. Chem. Soc. Jpn.*, **49**, 2574 (1976).

6) K. Fukui, T. Okamoto, and M. Nakagawa, *Tetrahedron Lett.*, **1971**, 3121; T. Katakami, S. Tomita, K. Fukui, and M. Nakagawa, *Chem. Lett.*, **1972**, 225; T. Katakami, K. Fukui, T. Okamoto, and M. Nakagawa, *Bull. Chem. Soc. Jpn.*, **49**, 297 (1976); S. Tomita and M. Nakagawa, *Bull. Chem. Soc. Jpn.*, **49**, 302 (1976); T. Nomoto, K. Fukui, and M. Nakagawa, *Tetrahedron Lett.*, **1972**, 3253; T. Nomoto, K. Fukui, and M. Nakagawa, *Bull. Chem. Soc. Jpn.*, **49**, 305 (1976).

7) For the absorption curves of **4a,b,c**, see, M. Nakagawa, *Pure Appl. Chem.*, **44**, 885 (1975).

8) C. Kabuto, Y. Kitahara, M. Iyoda, and M. Nakagawa, *Tetrahedron Lett.*, **1976**, 2791.

9) F. Sondheimer and Y. Gaoni, *J. Am. Chem. Soc.*, **82**, 5765 (1960); F. Sondheimer, Y. Gaoni, L. M. Jackman, N. A. Bailey, and R. Mason, *J. Am. Chem. Soc.*, **84**, 4595 (1962).

10) N. A. Bailey and R. Mason, *Proc. Chem. Soc.*, **1963**, 180; N. A. Bailey and R. Mason, *Proc. R. Soc. London, Ser. A*, **290**, 94 (1966).

Dehydroannulenes. XI. Synthesis and Properties of 3,11,14,22-Tetra-*t*-butyl-1,12-bisdehydro[22]annulene

Masahiko IYODA and Masazumi NAKAGAWA*

Department of Chemistry, Faculty of Science, Osaka University, Toyonaka, Osaka 560

(Received May 15, 1978)

7-*t*-Butyl-9-trimethylsilyl-2,4,6-nonatrien-8-ynal prepared from 5-*t*-butyl-7-trimethylsilyl-2,4-heptadien-6-ynal diethyl acetal was converted into 8-*t*-butyl-1,3,5,7-decatetraen-7-ynyl *t*-butyl ketone. Treatment of the tetraenyne ketone with potassium hydroxide in liquid ammonia gave 22-membered cyclic glycol in a high yield. Reductive dehydroxylation of the cyclic glycol by tin(II) chloride and hydrogen chloride yielded tetra-*t*-butylbisdehydro[22]annulene in good yield. The [22]annulene was found to be strongly diatropic and conformationally stable.

The stable nature, strong diatropicity and high conformational stability observed in 3,9,12,18-tetrasubstituted 1,10-bisdehydro[18]annulenes[1] provide a stimulus to further efforts to synthesize higher analogues of this series of bisdehydro[4n+2]annulenes.

In this paper we wish to report the synthesis and properties of 3,11,14,22-tetra-*t*-butyl-1,12-bisdehydro-[22]annulene (**9**).

Synthesis. The synthesis of the bisdehydro[22]-annulene (**9**) has been achieved by the reaction sequence shown in Scheme. Because the diethyl acetal of 5-*t*-butyl-2,4-heptadien-6-ynal[2] was found to be rather unstable, 5-*t*-butyl-3-ethoxy-4-hepten-6-ynal diethyl acetal (**1**)[1] was converted into the trimethylsilyl derivative (**2**) in 92% yield on successive treatment with ethylmagnesium bromide and trimethylchlorosilane. Treatment of **2** with an aqueous acetic acid containing sodium acetate afforded trimethylsilyl derivative of 5-*t*-butyl-2,4-heptadien-6-ynal (**3**) in a yield of 89%, which was converted into the diethyl acetal (**4**) in the usual method. The reaction of ethyl vinyl ether with **4** in benzene in the presence of boron trifluoride etherate[2,3] gave ethoxy acetal (**5**) in 86% yield. Trimethylsilyltrienyne aldehyde (**6**) was obtained on treatment of **5** with an aqueous acetic acid containing sodium acetate. The trienyne aldehyde (**6**) was found to be fairly stable and could be isolated on rapid distillation *in vacuo* in a yield of 87%.

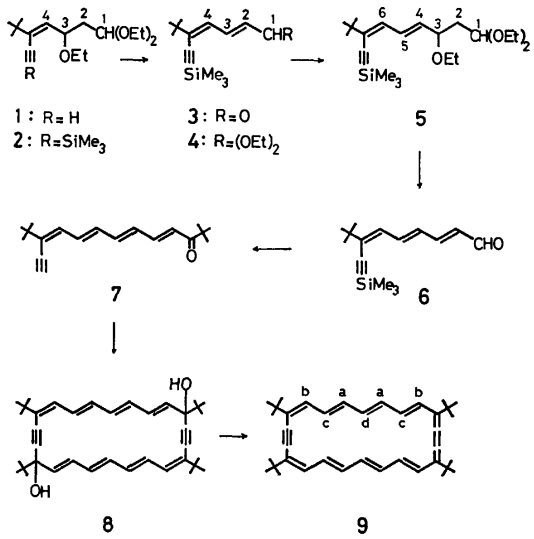

Scheme.

The aldol condensation of pinacolone with the trienyne aldehyde (**6**) under alkaline conditions resulted in tetraenyne ketone (**7**) in 60% yield accompanying the cleavage of trimethylsilyl group.

A diluted solution of the tetraenyne ketone (**7**) in tetrahydrofuran was added slowly to a stirred suspension of finely powdered potassium hydroxide in liquid ammonia. The 22-membered cyclic glycol (**8**) was obtained as a mixture of diastereomers which could be separated into the high melting isomer (**8a**, 31%) and the low melting isomer (**8b**, 58%) upon chromatography on alumina. The diastereomers (**8a**, and **8b**) gave identical electronic and NMR spectra, but slight difference was observed between their IR spectra measured by KBr-disk method.

Finely powdered tin(II) chloride dihydrate was added at −60 °C to a stirred suspension of the diastereomeric mixture of cyclic glycol (**8**) in ether containing hydrogen chloride under nitrogen atmosphere. The reaction mixture was worked up in the usual way and purified by chromatography on alumina to give 3,11,14,22-tetra-*t*-butyl-1,12-bisdehydro[22]annulene (**9**) in a yield of 94%.

Full hydrogenation of **9** in ethyl acetate and acetic acid over platinum catalyst at −15——20 °C afforded crystalline tetra-*t*-butylcyclodocosane as a mixture of stereoisomers. Recrystallization of the mixture resulted in a crude separation of stereoisomers. The bisdehydro[22]annulene (**9**) gave 1 : 1 CT complex with 2,4,7-trinitrofluorenone.

Properties. The tetra-*t*-butylbisdehydro[22]annulene (**9**) was found to be rather stable compound and could be kept without decomposition in a dark place at room temperature for a long period.

The electronic spectrum of **9** showed representative aromatic characteristic exhibiting three distinct main absorption bands. As illustrated in Fig. 1, the spectrum of **9** shows close similarity with those of 3,9,12,18-tetra-*t*-butyl-1,10-bisdehydro[18]annulene (**10**)[1] and 1,6,12,17-tetra-*t*-butyl-2,4,13,15-tetrakisdehydro[22]annulene (**11**).[2]

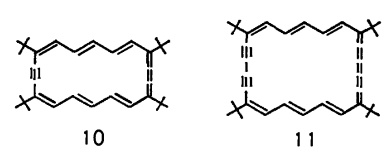

The ^{1}H NMR spectrum and the parameters are shown in Fig. 2 and Table, respectively. The minor

Table. ^{1}H NMR parameters of **9** in $CDCl_3$

	Temp/°C	H^a	H^b	*t*-Bu	H^c	H^d
60 MHz	30	0.79, t J=13 Hz	1.24, d J=13 Hz	8.18, s	10.82, m	
	70	0.81, t J=13 Hz	1.26, d J=13 Hz	8.21, s	10.68, m	
100 MHz	35	0.84, t J=13 Hz	1.28, d J=13 Hz	8.20, s	10.87, t J=13 Hz	10.83, t J=13 Hz
	0	0.80, t J=13 Hz	1.25, d J=13 Hz	8.19, s	10.99, t J=13 Hz	10.94, t J=13 Hz
	−30	0.74, t J=13 Hz	1.20, d J=13 Hz	8.18, s	11.10, t J=13 Hz	11.04, t J=13 Hz
	−50	0.69, t J=13 Hz	1.17, d J=13 Hz	8.17, s	11.18, t J=13 Hz	11.11, t J=13 Hz

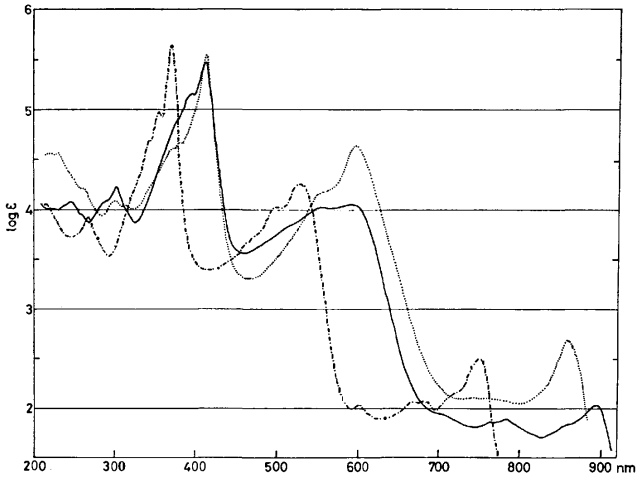

Fig. 1. Electronic spectra of **9** (——), **10** (—·—·) and **11** (·····) in THF.

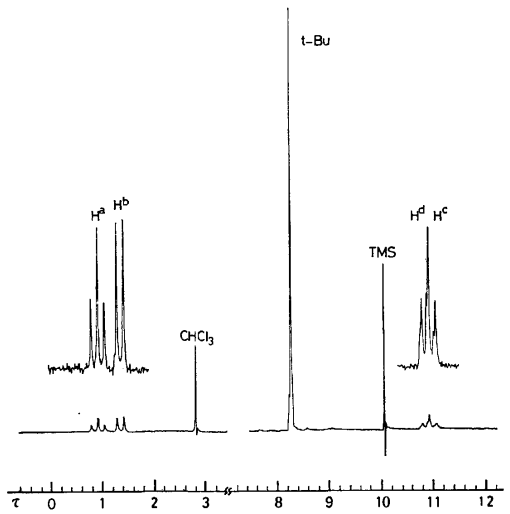

Fig. 2. 100 MHz ^{1}H NMR spectrum of **9** in $CDCl_3$ at 35 °C.

difference between the spectra measured at various temperatures indicates the conformational stability of **9**. An attempted measurement at 80 °C in deuteriobromoform resulted in a rapid decomposition of **9**. The ^{1}H NMR spectrum reveals that the bisdehydro[22]annulene (**9**) is strongly diatropic being stronger than that of monodehydro[22]annulene.[4] It has been reported that the parent [22]annulene[5] gave high-field multiplet at τ 10.4—11.2 (inner protons) and low-field multiplets at τ 0.35—0.7 and 0.9—1.5 (outer protons) at −90 °C being almost the same with the parameters of **9** obtained at 36 °C. However, obvious high-field and low-field shifts of outer and inner proton signals of **9** were observed as compared with those of the lower analogues, *i.e.*, 3,7,10,14-tetra-*t*-butyl-1,8-bisdehydro[14]annulene[6] and 3,9,12,18-tetra-*t*-butyl-1,10-bisdehydro[18]annulene (**10**).[1] The X-ray structure analysis of **9** revealed that the polyene parts in **9** have slight bond-alternation, and also one of the sp-sp linkages in **9** has more acetylenic and the other has more cumulenic character in contrast to the highly symmetrical structure of tetra-*t*-butylbisdehydro[18]annulene (**10**).[8] It has been predicted theoretically that the resonance energies per π-electron of [4n+2]annulenes should decrease and the bond-alternation should increase along with the increase of ring size.[9] Also the decrease of ring current in larger ring has been concluded theoretically.[9b,d,10] Consequently, the results obtained on bisdehydro[18]- and [22]annulenes (**10** and **9**) provide experimental supports to justify the theoretical prediction.

Experimental

All melting points were determined on a Mettler FP-2 apparatus and uncorrected. IR spectra were measured on a Hitachi EPI-2 or EPI-G3 spectrophotometer and only significant maxima are recorded. The intensities are denoted by the following abbreviation: strong=s, medium=m and weak=w. Electronic spectra were obtained on a Hitachi EPS-3T spectrophotometer and the shoulder was indicated by an asterisk. The NMR spectra were measured on a Varian A-60 or a XL-100 spectrometer using TMS as an internal standard and recorded in τ-unit. The mass spectra were obtained on a Hitachi RM-50 spectrometer operated at 70 eV of ionization potential. The TLC was performed on Kiesel Gel GF_{254} (Merck) plates. Silica gel (Merck, Kiesel Gel 60) or alumina (Merck, act. II-III) were used in the column chromatography, unless otherwise stated. Evaporation of the solvent was performed under reduced pressure.

5-t-Butyl-2,4-heptadien-6-ynal Diethyl Acetal. A solution of *p*-toluenesulfonic acid monohydrate (300 mg, 1.58 mmol) in ethanol (1 ml) was added to a solution of 5-*t*-butyl-2,4-heptadien-6-ynal[2] (2.88 g, 0.0178 mol) in triethyl ortho-

formate (7.70 g, 0.0520 mol). After being stirred overnight, the reaction mixture was worked up in the usual way. The residue obtained on evaporation of the solvent was distilled through a short column to furnish the diethyl acetal, a yellow liquid, bp 105 °C/267 Pa, 2.60 g, 62%; NMR(CCl_4): 3.27 (1H, dd, J=10.0, 15.5 Hz, H^{β}), 3.79 (1H, d, J=10 Hz, H^{γ}), 4.47 (1H, dd, J=5.0, 15.5 Hz, H^{α}), 5.09 (1H, d, J=5.0 Hz, acetal-H), 6.46 (4H, q, J=7.0 Hz, $-CH_2-$), 6.52 (6H, q, J=7.0 Hz, CH_3), 8.85 (9H, s, *t*-Bu).

*5-t-Butyl-3-ethoxy-7-trimethylsilyl-4-hepten-6-ynal Diethyl Acetal (**2**).* To a stirred solution of ethylmagnesium bromide (prepared from magnesium, 1.91 g, 0.0786 mol, ethyl bromide, 10.30 g, 0.0945 mol and THF, 30 ml) was added dropwise at 10—20 °C under nitrogen atmosphere a solution of the ethoxy acetal[2] (**1**, 14.80 g, 0.0524 mol) in the same solvent (30 ml) under ice-cooling. The mixture was stirred at 20 °C for further 30 min and then chilled on an ice-bath. Trimethylchlorosilane (10.26 g, 0.0945 mol) was added to the mixture at 0 °C. After being stirred for 1 h at the same temperature, ammonium chloride solution was added to the reaction mixture. The aqueous layer was extracted with ether (50 ml×3) and the extracts were combined with the organic layer. The combined organic layer was washed successively with water and brine, and dried ($MgSO_4$). The residue obtained on evaporation of the solvent was distilled *in vacuo* to give **2**, pale yellow liquid, bp 122—130 °C/333 Pa, 17.02 g, 91.6%; mass (*m/e*): 354 (M^+); IR(neat): 2125 m ($-C\equiv C-$), 1616 vw (C=C), 1250 s ($Si-CH_3$), 875 s, 842 vs, 758 m (Si–C) cm^{-1}; NMR(CCl_4): 4.45 (1H, d, J=8.5 Hz, H^4), 5.43 (1H, t, J=6.0 Hz, H^2), 5.67 (1H, m, H^3), 6.56 (6H, m, $O-CH_2-$), 8.32 (2H, t, J=6.0 Hz, H^2), 8.84 (9H, t, J=7.0 Hz, $-CH_3$), 8.88 (9H, s, *t*-Bu), 9.80 (9H, s, $-SiMe_3$).

Found: C, 67.48; H, 10.58%. Calcd for $C_{20}H_{38}O_3Si$: C, 67.75; H, 10.80%.

*5-t-Butyl-7-trimethylsilyl-2,4-heptadien-6-ynal (**3**).* A mixture of **2** (6.74 g, 0.0190 mol), sodium acetate (6.50 g, 0.0792 mol), acetic acid (56 ml) and water (4 ml) was stirred at 80 °C for 6 h under nitrogen atmosphere, and then allowed to stand overnight at room temperature. The reaction mixture was poured onto saturated sodium carbonate solution and extracted with ether (50 ml×2). The extracts were washed successively with saturated sodium carbonate and sodium chloride solutions, and dried ($MgSO_4$). The product obtained on evaporation of the solvent was distilled using a short-path appratus to give **3**, a yellow liquid, bp 105—108 °C/333 Pa, 3.98 g, 89.3%; mass (*m/e*): 234 (M^+); IR(neat): 2810 w (CHO), 2120 m, ($-C\equiv C-$), 1687 vs (CHO), 1613 vs (C=C), 1244 s, 1221 m ($Si-CH_3$), 878 vs, 843 vs, 759 s (Si–C) cm^{-1}; NMR(CCl_4): 0.42 (1H, d, J=8.0 Hz, H^1), 2.49 (1H, dd, J=11.5, 15.5 Hz, H^3), 3.50 (1H, d, J=11.5 Hz, H^4), 3.88 (1H, dd, J=8.0 Hz, 11.5 Hz, H^2), 8.78 (9H, s, *t*-Bu), 9.70 (9H, s, $Si-Me_3$).

The trimethylsilyl aldehyde (**3**) was more stable than 5-*t*-butyl-2,4-heptadien-6-ynal, but gradually decomposed on standing in air under diffused light at room temperature. Less satisfactory elemental analysis was obtained owing to the unstable nature.

*2,4-Dinitrophenylhydrazone of **3**.* A solution of 2,4-dinitrophenylhydrazine (95 mg, 0.48 mmol) in phosphoric acid (1 ml) and ethanol (1 ml) was added to a solution of **3** (56 mg, 0.24 mmol) in ethanol (15 ml). After the mixture had been allowed to stand at room temperature for 30 min, red precipitate deposited was collected by filtration and washed with ethanol to give the hydrazone, 62 mg, 63%, which was recrystallized from ethyl acetate to give red crystals, mp 201—202 °C (dec).

Found: C, 57.81; H, 6.39; N, 13.27%. Calcd for $C_{20}H_{26}N_2O_4Si$: C, 57.95; H, 6.32; N, 13.52%.

*5-t-Butyl-7-trimethylsilyl-2,4-heptadien-6-ynal Diethyl Acetal (**4**).* To a mixture of **3** (3.98 g, 0.017 mol) and triethyl orthoformate (30 ml) was added a solution of *p*-toluenesulfonic acid monohydrate (400 mg, 2.10 mmol) in ethanol (4 ml). After being stirred for 20 h at room temperature, the reaction mixture chilled in an ice-bath was poured onto an ice-cooled sodium carbonate solution, and extracted with ether (30 ml×3). The extracts were washed successively with saturated sodium carbonate and sodium chloride solutions, and dried (K_2CO_3). The residue obtained on evaporation of the solvent was distilled under reduced pressure to yield **4**, a pale yellow liquid, bp 118—120 °C/333 Pa, 4.92 g, 94%; mass (*m/e*): 308 (M^+), 263 (M^+-45); IR (neat): 2125 m ($-C\equiv C-$), 1644 vw (C=C), 1248 s, 1227 w ($Si-CH_3$), 881 vs, 842 vs, 760 m (Si–C) cm^{-1}; NMR(CCl_4): 3.20 (1H, dd, J=11.0, 15.5 Hz, H^3), 3.77 (1H, d, J=11.0 Hz, H^4), 4.37 (1H, dd, J=5.0, 15.5 Hz, H^2), 5.07 (1H, d, J=5.0 Hz, H^1), 6.49 (4H, m, $-CH_2-$), 8.83 (6H, t, J=7.0 Hz, $-CH_3$), 8.85 (9H, s, *t*-Bu), 9.76 (9H, s, $Si-Me_3$).

Found: C, 70.50; H, 10.30%. Calcd for $C_{18}H_{32}O_2Si$: C, 70.08; H, 10.46%.

*7-t-Butyl-3-ethoxy-9-trimethylsilyl-4,6-nonadien-8-ynal Diethyl Acetal (**5**).* A mixture of borontrifluoride etherate (20 mg) in benzene (1 ml) was added at 35 °C to a solution of **4** (4.92 g, 0.0159 mol) in the same solvent (20 ml), and a solution of ethyl vinyl ether (1.40 g, 0.0194 mol) in the same solvent (5 ml) was slowly added at the same temperature. After the mixture had been kept at the same temperature for 20 min, finely powdered potassium carbonate (1.0 g) was added. The inorganic material was removed by filtration and washed with ether. The residue obtained on evaporation of the filtrate and washings was distilled *in vacuo* to give **5**, a pale yellow liquid, bp 120—124 °C/1.2 Pa, 5.20 g, 86%; mass (*m/e*): 380 (M^+), 334 (M^+-46); IR(neat): 2120 m ($-C\equiv C-$), 1640 vw (C=C), 1248 s ($Si-CH_3$), 880 vs, 842 vs, 758 m (Si–C) cm^{-1}; NMR(CCl_4): 3.39 (1H, dd, J=10.5, 14.5 Hz, H^5), 3.81 (1H, d, J=10.5 Hz, H^6), 4.42 (1H, dd, J=7.0, 14.5 Hz, H^4), 5.44 (1H, t, J=5.5 Hz, H^1), 6.04—6.88 (7H, m, $O-CH_2-$, O–CH–), 8.29 (2H, m, H^2), 8.85 (18H, t, J=7.0 Hz, $-CH_3$), 8.86 (9H, s, *t*-Bu), 9.78 (9H, s, $Si-Me_3$).

Found: C, 69.14; H, 10.38%. Calcd for $C_{22}H_{40}O_3Si$: C, 69.42; H, 10.59%.

*7-t-Butyl-9-trimethylsilyl-2,4,6-nonatrien-8-ynal (**5**).* A mixture of **5** (2.00 g, 5.26 mmol), sodium acetate (2.00 g, 24.4 mmol), acetic acid (18 ml) and water (2 ml) was stirred for 6 h at 60 °C, and then allowed to cool to room temperature. The reaction mixture was poured onto saturated sodium carbonate solution and extracted with ether (20 ml×3). The extracts were washed successively with saturated sodium carbonate and sodium chloride solutions, and dried ($MgSO_4$). The residue obtained on concentration of the extracts was distilled *in vacuo* using a short-path apparatus to give **6**, a viscous yellow liquid, bp 111—114 °C/2.7 Pa, 1.19 g, 86.9%; mass (*m/e*): 260 (M^+); IR(neat): 2810 w, 2725 w (CHO), 2120 m ($-C\equiv C-$), 1683 vs (C=O), 1612 s, 1597 s (C=C), 1247 s ($Si-CH_3$), 1007 m, 987 m (*trans* –CH=CH–), 880 vs, 843 vs, 759 m (Si–C) cm^{-1}; NMR (CCl_4): 0.43 (1H, d, J=4.0 Hz, CHO), 2.56—4.13 (5H, m, olefinic), 8.81 (9H, s, *t*-Bu), 9.72 (9H, s, $Si-Me_3$).

*2,4-Dinitrophenylhydrazone of **6**.* To a solution of **6** (134 mg, 0.515 mmol) in ethanol (8 ml) was added a solution of 2,4-dinitrophenylhydrazine (119 mg, 0.601 mmol) in phosphoric acid (1 ml) and ethanol (1 ml). After the mixture was allowed to stand for 30 min at room temperature, reddish

brown precipitate formed was filtered and washed with ethanol to give the hydrazone, 164 mg, 72.3%, which was dissolved in benzene and passed through a short column of silica gel. The crystals obtained from the filtrate were recrystallized from hexane–benzene (1:1) to yield pure 2,4-dinitrophenylhydrazone of **6**, reddish brown crystals, mp 208—211 °C.

Found: C, 60.09; H, 6.38; N, 12.69%. Calcd for $C_{22}H_{28}N_4O_4Si$: C, 59.98; H, 6.41; N, 12.72%.

8-t-Butyl-1,3,5,7-decatetraen-9-ynyl t-Butyl Ketone (8). A solution of sodium hydroxide (209 mg, 5.22 mmol) in 50% aqueous ethanol (2 ml) was added to a solution of **6** (1.00 g, 3.84 mmol) and pinacolone (522 mg, 5.21 mmol) in ethanol (10 ml) at 0 °C under nitrogen atmosphere. After being kept at room temperature for 24 h, the mixture was acidified with 3 M hydrochloric acid (10 ml) and extracted with ether (20 ml×3). The extracts were washed successively with sodium hydrogencarbonate solution and brine, and dried ($MgSO_4$). The residue obtained on concentration of the extracts was chromatographed on alumina. Elution with hexane–benzene (9:1) afforded crystals, which were washed with methanol to give **7**, 618 mg, 59.5%. Recrystallization of the crystals from methanol gave analytical specimen of **7**, yellow crystals, mp 133.5—134.0 °C; mass (*m/e*): 270 (M^+); IR (CCl_4): 3325 m (–C≡CH), 2060 vw (–C≡C–), 1684 s (C=O), 1607 s (C=C), 1574 vs (C=C), 1070 vs, 1003 vs (*trans* –CH=CH–) cm^{-1}; NMR(CCl_4): 2.52—3.92 (7H, m, olefinic), 6.63 (1H, s, –C≡CH), 8.82 (9H, s, *t*-Bu), 8.86 (9H, s, *t*-Bu); UV: $\lambda_{max}^{99\%EtOH}$ (ε) 261 (5870), 359* (52000), 369 (53000) nm.

Found: C, 84.74; H, 9.75%. Calcd for $C_{19}H_{26}O$: C, 84.39; H, 9.69%.

1,4,12,15-Tetra-t-butyl-4,6,8,10,15,17,19,21-cyclodocosaoctaene-2,13-diyne-1,12-diol (8). A solution of the tetraenyne ketone (**7**, 160 mg, 0.592 mmol) in THF (60 ml) was added very slowly through a Hershberg dropping funnel over a period of 8 hr to a stirred suspension of finely powdered potassium hydroxide (2.00 g, 35.7 mmol) in liquid ammonia (150 ml) at −34 °C. After being stirred for further 6 h at the same temperature, ammonium chloride (4.00 g, 0.0748 mol) was added to the reaction mixture, and the ammonia was allowed to evaporate. The residue was treated with water and ether (20 ml). The aqueous layer was extracted with ether (15 ml×2). The combined organic layer was washed successively with water and brine, and dried ($MgSO_4$). The yellow crystals obtained on evaporation of the solvent were chromatographed on alumina (40 g). Elution with ether–benzene (1:49—1:19) afforded high melting isomer (**8a**), colorless crystals, 56 mg, 31%, which were washed thoroughly with ethyl acetate to give pure specimen, mp 252 °C (dec); mass (*m/e*): 540 (M^+), 483 (M^+-57), 57 (*t*-Bu^+, base peak); IR(KBr-disk): 3570 m (–OH), 2190 vw (–C≡C–), 1638 vw, 1607 w (C=C), 1001 vs, 977 vs, 960 s (*trans* –CH=CH–) cm^{-1}; NMR($CDCl_3$): 2.8—4.2 (14H, m, olefinic), 8.35 (2H, s, –OH, disappeared on addition of D_2O), 8.79 (18H, s, *t*-Bu), 8.90 (18H, s, *t*-Bu); UV: $\lambda_{max}^{99\%EtOH}$ (ε) 248.5 (22600), 292* (50600), 307 (120000), 320 (137000), 341* (34800), 359 (27800) nm.

Found: C, 84.15; H, 9.61%. Calcd for $C_{38}O_{52}O_2$: C, 84.39; H, 9.69%.

Further elution with ether–benzene (1:3) gave low melting isomer (**8b**), colorless crystals, 105 mg, 58%, which were washed with ethyl acetate to give pure material, mp 220—221 °C; mass (*m/e*): 540 (M^+), 483 (M^+-57, base peak), 57 (*t*-Bu^+); IR(KBr-disk): 3530 m, 3465 m (–OH), 2180 vw (–C≡C–), 1634 w, 1590 vw (C=O), 993 vs (*trans* –CH=CH–) cm^{-1}; NMR($CDCl_3$): 2.8—4.2 (14H, m, olefinic), 8.31 (2H, s, –OH, disappeared on addition of D_2O), 8.80 (18H, s, *t*-Bu), 8.90 (18H, s, *t*-Bu); UV: $\lambda_{max}^{99\%EtOH}$ (ε) 248.5 (22200), 292* (45400), 307 (109000), 320 (160000), 341* (34200), 359 (26100) nm.

Found: C, 84.56; H, 9.84%. Calcd for $C_{38}H_{52}O_2$: C, 84.39; H, 9.69%.

3,11,14,22-Tetra-t-butyl-1,12-bisdehydro[22]annulene (9). To a suspension of **8** (a mixture of diastereomers, 136 mg, 0.251 mmol) in ether (10 ml) was added ether saturated with hydrogen chloride (10 ml) at −60 °C under nitrogen atmosphere. Finely powdered tin(II) chloride dihydrate (600 mg, 2.66 mmol) was added to the mixture at the same temperature. After being stirred vigorously for 15 min at −60 °C, the reaction mixture was poured onto ice-cooled sodium carbonate solution, and extracted with dichloromethane. The extract, after being washed with brine, and dried (K_2CO_3), was chromatographed on alumina (Woelm, act. I). Elution with carbon tetrachloride–dichloromethane (19:1) afforded pure **9**, 120 mg, 94.2%. An analytical specimen was prepared on recrystallization from benzene–methanol, dark violet crystals, mp *ca.* 230 °C (dec); mass (*m/e*): 506 (M^+), 449 (M^+-57), 57 (*t*-Bu^+, base peak); IR(KBr-disk): 3020 w, 2950 s, 992 vs, 881 w; UV: λ_{max}^{THF} (ε) 221.5 (10400), 248 (11900), 261* (8810), 277* (9200), 290 (12100), 302.5 (17100), 316.5* (9610), 377* (7720), 395 (147000), 412.5 (300000), 512* (6640), 556 (10400), 591 (11300), 712* (83), 757* (72), 782 (77), 853* (66), 895 (106) nm.

Found: C, 90.38; H, 9.92%. Calcd for $C_{38}H_{50}$: C, 90.05; H, 9.95%.

CT Complex of 9 with 2,4,7-Trinitrofluorenone. To a solution of **9** (25 mg, 0.049 mmol) in benzene–methanol (1:1, 40 ml) was added a solution of 2,4,7-trinitrofluorenone (31 mg, 0.098 mmol) in the same solvent (10 ml). The mixture was allowed to stand at 18 °C to deposite the CT complex, black violet crystals, mp *ca.* 260 °C (dec), 32 mg, 79%.

Found: C, 74.39; H, 6.67; N, 5.14%. Calcd for $C_{38}H_{50}\cdot C_{13}H_5N_3O_7$: C, 74.52; H, 6.74; N, 5.11%.

Catalytic Hydrogenation of 9. A mixture of **9** (32 mg, 0.063 mmol) and platinum(IV) oxide (100 mg) in acetic acid–ethyl acetate (1:1, 40 ml) was vigorously stirred under hydrogen at −15—−20 °C overnight. The catalyst was removed by filtration and washed with ether (30 ml). The organic layer and washing were washed successively with water, saturated sodium carbonate and sodium chloride solutions, and dried ($MgSO_4$). Evaporation of the solvent gave a crystalline residue, which was chromatographed on alumina (Woelm, act. I) and eluted with hexane to give a mixture of stereoisomers of 1,4,12,15-tetra-*t*-butylcyclodocosane, 31 mg, 92%. Recrystallization of the crystals from ethyl acetate–methanol yielded colorless crystals, 15 mg, mp 104—112 °C; mass (*m/e*): 532 (M^+), 475 (M^+-57), 57 (*t*-Bu^+, base peak); IR(KBr-disk): 2930 vs, 2860 s, 1475 m, 1393 m, 1360 m cm^{-1}; NMR(CCl_4): 8.72 (40H, br s, $-CH_2-$, –CH–), 9.05 (36H, s, *t*-Bu).

Found: C, 85.35; H, 14.19%. Calcd for $C_{38}H_{76}$: C, 85.63; H, 14.37%.

The mother liquor of the recrystallization was concentrated, and the crystals deposited were recrystallized from ethyl acetate–methanol to give colorless crystals, 8 mg, mp 91—95 °C.

References

1) M. Iyoda and M. Nakagawa, *Tetrahedron Lett.*, **1972**, 3161; M. Iyoda, S. Akiyama, and M. Nakagawa, the preceding paper.

2) M. Iyoda, H. Miyazaki, and M. Nakagawa, *J. Chem.*

Soc., Chem. Commun., **1972**, 1003; M. Iyoda, H. Miyazaki, and M. Nakagawa, *Bull. Chem. Soc. Jpn.*, **49**, 2306 (1976).

3) M. Müller-Cunradi and K. Pieroth, U. S. Pat., 2165962 (1936); R. Rüegg, M. Montavon, G. Ryser, G. Saucy, U. Schwieter, and O. Isler, *Helv. Chim. Acta*, **42**, 854 (1959) and the preceding papers.

4) R. M. McQuilkin and F. Sondheimer, *J. Am. Chem. Soc.*, **92**, 6341 (1970).

5) R. M. McQuilkin, B. W. Metcalf, and F. Sondheimer, *Chem. Commun.*, **1971**, 338.

6) K. Fukui, T. Nomoto, S. Nakatsuji, and M. Nakagawa, *Tetrahedron Lett.*, **3157**; K. Fukui, T. Nomoto, S. Nakatsuji, S. Akiyama, and M. Nakagawa, *Bull. Chem. Soc. Jpn.*, **50**, 2758 (1977).

7) C. Kabuto, Y. Kitahara, M. Iyoda, and M. Nakagawa, *Tetrahedron Lett.*, **1976**, 2787.

8) C. Kabuto, Y. Kitahara, M. Iyoda, and M. Nakagawa, *Tetrahedron Lett.*, **1976**, 2791.

9) a) H. C. Longuet-Higgins and L. Salem, *Proc. R. Soc. London, Ser. A*, **251**, 172 (1954); b) H. C. Longuet-Higgins and L. Salem, *ibid.*, **257**, 445 (1960); c) C. A. Coulson and W. T. Dixon, *Tetrahedron*, **17**, 215 (1962); d) M. J. S. Dewar and G. J. Gleicher, *J. Am. Chem. Soc.*, **87**, 685 (1965).

10) F. Baer, H. Kuhn, and W. Regel, *Z. Naturforsch.*, **22a**, 103 (1967); T. Nakajima and S. Kohda, *Bull. Chem. Soc. Jpn.*, **39**, 804 (1966); J. A. Pople and K. G. Untch, *J. Am. Chem. Soc.*, **88**, 4811 (1966); H. P. Feyges, "Topics in Carbocyclic Chemistry," ed by D. Lloyd, Logos Press, London (1969), Vol. 1, p. 269.

Asymmetric Synthesis Based on (2*R*,3*S*)-3,4-Dimethyl-2-phenylperhydro-1,4-oxazepine-5,7-dione. Synthesis of Highly Optically Active β-Substituted Alkanoic Acids

Teruaki MUKAIYAMA,* Takeshi TAKEDA, and Katsumi FUJIMOTO

Department of Chemistry, Faculty of Science,
The University of Tokyo, Hongo, Bunkyo-ku, Tokyo 113

(Received May 30, 1978)

A general method was worked out for the preparation of highly optically pure β-substituted alkanoic acids from aldehydes with use of (2*R*,3*S*)-6-alkylidene-3,4-dimethyl-2-phenylperhydro-1,4-oxazepine-5,7-diones(**2**) as key intermediates. Oxazepines(**2**) were prepared in high yields by treating aldehydes with (2*R*,3*S*)-3,4-dimethyl-2-phenylperhydro-1,4-oxazepine-5,7-dione(**1**) in the presence of titanium tetrachloride. The conjugate addition of Grignard reagents to **2** in the presence of nickel chloride, followed by hydrolysis and decarboxylation afforded highly enantiomerically pure β-substituted alkanoic acids in good yields. The addition of lithium dialkylcuprate to **2** was examined. It was found that (*S*)-(+)-3-phenylheptanoic acid is obtained by the reaction of lithium dibutylcuprate with (*E*)- and (*Z*)-6-benzylidene derivatives of **1**, respectively.

Synthesis of optically active alkanoic acids is important in organic synthesis, and many works have appeared so far. Inouye and Walborsky[1] and Kawana and Emoto[2] reported that partial asymmetric induction is achieved by the addition of Grignard reagents to crotonic or cinnamic esters of (−)-menthol or some sugar derivatives, respectively. Tsuchihashi *et al.* reported that optically active 3-phenylbutanoic acid is obtained by the reaction of optically pure vinyl sulfoxide with diethyl malonate, followed by reduction, hydrolysis, and decarboxylation.[3] Recently, the syntheses of highly optically pure α-and β-substituted alkanoic acids were achieved with the use of optically active oxazoline derivatives.[4]

In a previous paper,[5] a report was given on the preparation of an almost optically pure 3-phenylheptanoic acid in high yield by the conjugate addition of butylmagnesium bromide to (*Z*)-(2*R*,3*S*)-6-benzylidene-3,4-dimethyl-2-phenylperhydro-1,4-oxazepine-5,7-dione (**2a**) in the presence of a catalytic amount of nickel chloride, followed by hydrolysis and decarboxylation of the adduct (**3**). It was thus shown that the 6-alkylidene derivatives of (2*R*,3*S*)-3,4-dimethyl-2-phenylperhydro-1,4-oxazepine-5,7-dione(**1**) are the key intermediates for the preparation of optically active β-substituted alkanoic acids. We have attempted to establish a general route for the synthesis of optically active alkanoic acids starting from aldehydes as in the following.

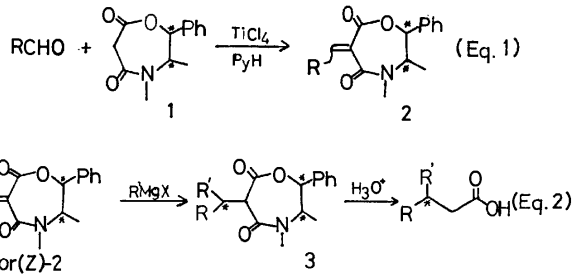

The first step consists of the condensation of aldehydes with the cyclic compound(**1**)[6] (Eq. 1). The reaction was carried out in the presence of titanium tetrachloride and pyridine using tetrahydrofuran(THF) as a solvent as in the method for the preparation of alkylidenemalonic esters reported by Lehnert.[7] The IR and NMR spectral data of the product(**2b**) obtained from benzaldehyde and **1** do not agree with those of (*Z*)-6-alkylidene derivative(**2a**).[5] In order to determine the configuration of **2b**, **2a** and **2b** were treated with phenylmagnesium bromide (Eq. 3). The NMR and IR spectra of the adducts (**4a** and **b**) were identical, the

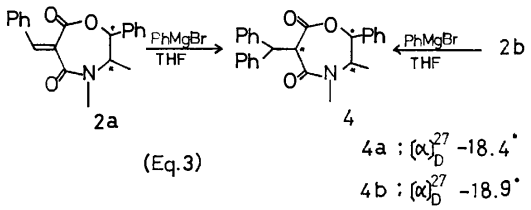

value of the specific rotation of **4a** being the same as that of **4b**. Thus, the structure of **2b** was determined to be *E* isomer of **2a**. The configuration of the alkylidene group of **2c—f** was also determined by a comparison of its IR and NMR spectra with those of **2a** and **2b**. It was confirmed that a small amount of *Z*-isomer is produced in the preparation of **2c—f**, almost pure *E* isomer of **2c—f** being obtained by recrystallization of the product. The yields and properties of the products(**2**) are summarized in Table 1.

The conjugate addition of Grignard reagents to **2a** was carried out under various conditions at −78 °C for 3 h (Table 2). Alkanoic acids were obtained by hydrolysis and decarboxylation of the crude adducts(**3**) in 3 M sulfuric acid and acetic acid (Eq. 2). The result shows that the optical purity of the acids depends on the conditions of the addition reaction. The best result was obtained when the reaction was carried out in the presence of a catalytic amount of nickel chloride at low temperature. Though the role of the metal salt in the conjugate addition remains to be resolved,

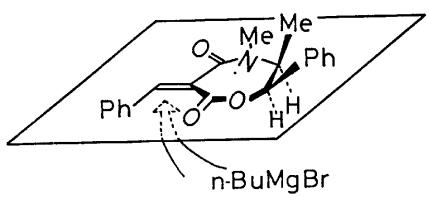

Fig. 1.

Table 1. Yields and properties of (2*R*,3*S*)-6-alkylidene-3,4-dimethyl-2-phenylperhydro-1,4-oxazepine-5,7-diones (**2**)

	R	Yield (%)	*E* : *Z*[a]	Mp (°C)[b]	$[\alpha]_D^{\circ}$[c] (*t* °C, *c*)	Found (Calcd) (%) C	H	N
2a	(*Z*)Ph-[8]			188—189	−182 (29, 7.59)	74.98 (74.74)	5.89 (5.96)	4.39 (4.36)
2b	(*E*)Ph-	99[d]	100 : 0	195—196	+59.5 (24, 8.45)	74.61 (74.74)	5.79 (5.96)	4.14 (4.36)
2c	(*E*)CH_3-	99[e]		150—151	−150 (27, 1.01)	69.47 (69.48)	6.75 (6.61)	5.44 (5.40)
2d	(*E*)CH_3CH_2-	76	85 : 15	122—124	−146 (26, 1.01)	70.39 (70.31)	7.17 (7.01)	5.13 (5.15)
2e	(*E*)$CH_3(CH_2)_3$-	94	90 : 10	79— 80	−129 (26, 0.776)	71.68 (71.73)	7.90 (7.69)	4.39 (4.65)
2f	(*E*)$(CH_3)_2CH$-	84		123—125	−130 (24, 1.21)	71.27 (71.05)	7.65 (7.37)	4.60 (4.87)

a) Determined by NMR spectrum. b) Melting points uncorrected. c) Measured after recrystallization, dichloromethane being used as a solvent. d) An equimolar amount of aldehyde used. e) Two equimolar amounts of aldehyde used.

Table 2. Effects of added metal salts and/or solvent change in the asymmetric synthesis of 3-substituted alkanoic acids by the reaction of Grignard reagents with **2a**

Entry	RMgX	MX_n	Solvent	Yield (%)	$[\alpha]_D^{\circ}$[a] (*t* °C, *c*)	Optical purity (%)
1	*n*-BuMgBr	—	THF	85	−30.4[b] (24, 8.25)	88[d]
2		—	THF-HMPT[c]	68	−21.2[b] (26, 8.16)	62[d]
3		$NiCl_2$	THF	92	−34.0[b] (24, 8.03)	99[d]
4		$ZnCl_2$	THF	76	−29.3[b] (25, 8.09)	85[d]
5		$FeCl_3$	THF	70	−20.6[b] (26, 8.00)	60[d]
6	$PhCH_2MgCl$	—	THF	75	+ 5.65 (30, 1.93)	9[e]
7		$NiCl_2$	THF	78	+ 4.17 (29, 1.92)	7[e]
8		$ZnCl_2$	THF	85	+ 8.81 (26, 1.93)	15[e]
9		$FeCl_3$	THF	62	+10.6 (30, 1.93)	18[e]
10		—	THF-HMPT[c]	68	−43.7 (24, 1.92)	73[e]
11		$NiCl_2$	THF-HMPT[c]	76	−44.7 (26, 1.94)	75[e]
12		CuI[f]	THF-HMPT[c]	64	−42.4 (27, 1.92)	71[e]
13[g]		CuI[f]	THF-HMPT[c]	55	−44.9 (22, 1.92)	75[e]

a) Benzene used as a solvent. b) $[\alpha]_{578}$. c) A mixture of THF (15 ml) and HMPT (4 ml) used as a solvent for 1.5 mmol of **2a**. d) Based on $[\alpha]_{578}$ −34.4° (*c* 8, benzene) for enantiomerically pure acid.[4c] e) The reported $[\alpha]_D^{28}$ max −60° (*c* 1.92, benzene) determined by resolution method.[2] f) Four mol % amounts of the salt used. g) Addition carried out at −100 °C.

the absolute configuration of (*R*)-(−)-3-phenylheptanoic acid indicates that the Grignard reagent attacks from the opposite side of the phenyl and methyl groups of the oxazepine ring as shown in Fig. 1.

In the same manner, various highly optically active β-substituted alkanoic acids were obtained in high yields utilizing **2a**—**f** (Table 3).

The relation between the absolute configuration of the alkanoic acid and the configuration of **2** is clearly shown in entries 2 and 5; (*R*)-(−)-3-phenylheptanoic acid was obtained by the reaction of the (*Z*)-6-benzylidene derivative of **1** with butylmagnesium bromide.

TABLE 3. SYNTHESIS OF OPTICALLY ACTIVE ALKANOIC ACIDS BY THE REACTION OF GRIGNARD REAGENTS WITH **2**

Entry	R	R′	Yield (%)	$[\alpha]_D^{\circ}$ a) (t °C, c)	Lit $[\alpha]_D^{\circ}$ a) (c)	Optical purity (%)	Absolute configuration
1	(*Z*)Ph-	CH_3CH_2-	94	−49.2 (25, 7.04)	−49.66[9] (7)	99	*R*
2		$CH_3(CH_2)_3$-	92	−34.0[b] (24, 8.03)	−34.4[b),4c)] (8)	99	*R*
3	(*E*)Ph-	CH_3-	85	+52.6 (26, 9.81)	−57.2[10] (9.80)	92	*S*
4		CH_3CH_2-	94	+49.8 (28, 7.07)		>99	*S*
5		$CH_3(CH_2)_3$-	92	+32.1[b] (24, 8.39)		93	*S*
6	(*E*)CH_3-	$(CH_3)_2CH$-	55	+10.5 (25, neat)	+12.8[11] (neat)	82	*R*
7		$CH_3(CH_2)_3$-	82	− 3.74 (23, neat)	−4.2[12] (neat)	89	*S*
8		Ph-	88	−51.1 (28, 9.84)		89	*R*
9	(*E*)CH_3CH_2-	$CH_3(CH_2)_3$-	78	− 2.91 (23, neat)	+4.69[c),13)] (neat)	62	*S*
10		Ph-	84	−49.5 (28, 7.11)		>99	*R*
11	(*E*)$(CH_3)_2CH$-	CH_3-	73	−11.9 (24, neat)		93	*S*
12	(*E*)$CH_3(CH_2)_3$-	CH_3CH_2-	77	+ 2.70 (24, neat)		58	*R*

a) Benzene used as a solvent. b) $[\alpha]_{578}$. c) Meyers noted that there is some doubt as to the reliability of the reported rotation.[4a)]

TABLE 4. SYNTHESIS OF OPTICALLY ACTIVE ALKANOIC ACIDS BY THE REACTION OF LITHIUM DIALKYLCUPRATE WITH **2**

Entry	R	R′	Yield (%)	$[\alpha]_D^{\circ}$ a) (t °C, c)	Optical purity (%)	Absolute configuration
1	(*Z*)Ph-	$CH_3(CH_2)_3$-	76	+34.4[b] (24, 8.12)	>99	*S*
2	(*E*)Ph-	$CH_3(CH_2)_3$-	64	+33.9[b] (25, 7.90)	99	*S*
3	(*E*)CH_3-	$CH_3(CH_2)_3$-	70	−3.78 (25, neat)	90	*S*
4		Ph-	79	−37.6 (20, 9.82)	66	*R*
5	(*E*)CH_3CH_2-	$CH_3(CH_2)_3$-	73	−2.64 (24, neat)	56	*S*
6		Ph-	66	−32.4 (19, 7.29)	65	*R*
7	(*E*)$CH_3(CH_2)_3$-	Ph-	66	−23.2[b] (23, 8.12)	67	*R*

a) Benzene used as a solvent. b) $[\alpha]_{578}$.

On the other hand, the (*S*)-(+) acid was obtained when the *E* isomer was employed.

It was found that the absolute configuration of the carboxylic acid obtained from **2** possessing the substituent R and Grignard reagent R′MgX differs from that of the carboxylic acid obtained from **2** having the substituent R′ and Grignard reagent RMgX(for example, entries 3 and 8). The results show that the Grignard reagent stereoselectively attacks **2** regardless of the configuration of the alkylidene group or the substituent R of **2**.

Asymmetric addition of lithium dialkylcuprate was also examined. A typical reaction is shown in the following: Lithium dialkylcuprate in diglyme was prepared according to the method for the preparation of the cuprate in ether reported by Whitesides *et al.*[14] The 6-alkylidene derivative of **1** in THF and diglyme was then added at −78 °C. The usual work-up gave the adduct (**3**). The corresponding optically active β-substituted alkanoic acid was obtained in good yield by hydrolysis and decarboxylation of the adduct (**3**) (Eq. 4). The results are summarized in Table 4.

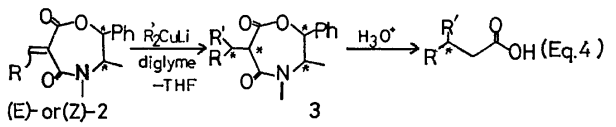

Contrary to the results obtained in the reaction of Grignard reagents, alkanoic acids having the same absolute configuration were produced, regardless of the configuration of the starting 6-alkylidene-1,4-oxazepine(**2**), *viz.*, (*S*)-(+)-3-phenylheptanoic acid was obtained by the reaction of lithium dibutylcuprate with either (*E*)- or (*Z*)-6-benzylidene derivatives of **1**. This can be explained by assuming the existence of the radical anion intermediate(**5**) (Eq. 5).[15]

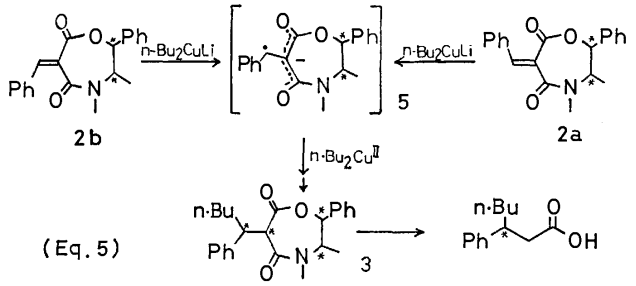

In conclusion, a general method for the preparation of highly optically pure β-substituted alkanoic acids from aldehydes was established by the use of (2*R*,3*S*)-3,4-dimethyl-2-phenylperhydro-1,4-oxazepine-5,7-dione-(**1**).

Experimental

*Reaction of Propionaldehyde with (2*R*,3*S*)-3,4-Dimethyl-2-phenylperhydro-1,4-oxazepine-5,7-dione(**1**).* Titanium tetrachloride (1.3 ml, 12 mmol) was added to a THF (53 ml) solution of **1**(2.33 g, 10 mmol), propionaldehyde (0.697 g, 12 mmol), and pyridine (2 ml) at −78 °C under an argon atmosphere with vigorous stirring. After being stirred at room temperature overnight, the reaction mixture was poured into a phosphate buffer solution (pH 7). The resulting white precipitate was filtered off through Celite and washed with dichloromethane. The aqueous mixture was extracted with dichloromethane. The combined dichloromethane solution was dried over anhydrous Na_2SO_4 and condensed under reduced pressure. The residue was chromatographed on silica gel (CH_2Cl_2–Et_2O) and (2*R*,3*S*)-3,4-dimethyl-2-phenyl-6-propylideneperhydro-1,4-oxazepine-5,7-dione(**2d**)(2.08 g, 76%) was obtained. Recrystallization (benzene–hexane) gave the pure *E* isomer: IR(KBr) 1725, 1640, 1600 cm^{-1}. NMR($CDCl_3$) δ 1.06 (t, *J*=8 Hz, 3 H), 1.18(d, *J*=7 Hz, 3 H), 2.0—2.7 (m, 2H), 3.05 (s, 3H), 3.67 (q, *J*=7 Hz, 1 H), 5.93 (s, 1 H), 7.28 (t, *J*=8 Hz, 1H), 7.42 (s, 5 H). The oxazepines (**2b—f**) were prepared from **1** and the corresponding aldehydes in a similar manner. The IR and NMR spectra of these compounds were in line with the assigned structures; **2b**;IR(KBr) 1750, 1640, 1600 cm^{-1}. NMR($CDCl_3$)δ 1.23 (d, *J*=7 Hz, 3H), 3.10 (s, 3H), 3.70 (q, *J*=7 Hz, 1 H), 6.20 (s, 1 H), 7.1—7.6(m, 10 H), 7.93 (s, 1 H). **2c**; IR(KBr) 1740, 1642, 1600 cm^{-1}. NMR($CDCl_3$)δ 1.17 (d, *J*=6 Hz, 3 H), 1.96 (d, *J*=7 Hz, 3 H), 3.02 (s, 3 H), 3.62 (q, *J*=6 Hz, 1 H), 5.85 (s, 1 H), 7.4—7.7 (m, 6 H). **2e**; IR(KBr) 1722, 1642, 1605 cm^{-1}. NMR($CDCl_3$)δ 0.6—1.8 (m, 10 H), 2.0—2.7 (m, 2H), 3.05 (s, 3 H), 3.3—3.8 (m, 1 H), 5.89 (s, 1H), 6.8—7.9 (m, 6H). **2f**; IR(KBr) 1725, 1640, 1605 cm^{-1}. NMR($CDCl_3$)δ 0.7—1.5 (m, 9 H), 2.4—2.8 (m, 1 H), 3.01 (s, 3H), 3.2—3.9 (m, 1 H), 5.80 (s, 1 H), 7.01 (d, *J*=10 Hz, 1H), 7.36 (s, 5H).

*Preparation of (S)-(−)-3-Methylheptanoic Acid by the Reaction of (E)-(2R,3S)-6-Ethylidene-3,4-dimethyl-2-phenylperhydro-1,4-oxazepine-5,7-dione(**2c**) with Butylmagnesium Bromide.* To a THF (14 ml) solution of **2c** (0.547 g, 2.0 mmol) and nickel chloride (0.013 g, 0.10 mmol) was added a THF solution (3.5 ml) of butylmagnesium bromide (2.45 mmol) at −78 °C under an argon atmosphere. After being stirred for 3 h, the reaction mixture was poured into a phosphate buffer solution (pH 7). The organic layer was extracted with dichloromethane and the extract was dried over anhydrous Na_2SO_4. Evaporation of the solvent gave the adduct, which was dissolved in acetic acid (20 ml) and 3M H_2SO_4 (40 ml). The reaction mixture was then refluxed for 6 h. The resulting oily substance was extracted with dichloromethane and the extract was dried over anhydrous Na_2SO_4. After the extract had been condensed under reduced pressure, the residue was distilled according to the Kugel-Rohr method (150—160 °C (bath temperature)/15 mmHg) to give (*S*)-(−)-3-methylheptanoic acid (0.236 g, 82%). The acids (Table 3) were obtained in a similar manner and the structures of the compounds identified by their IR and NMR spectra.

*Preparation of (S)-(+)-3-Phenylheptanoic Acid by the Reaction of (E)-(2R,3S)-6-Benzylidene-3,4-dimethyl-2-phenylperhydro-1,4-oxazepine-5,7-dione (**2b**) with Lithium Dibutylcuprate.* To a diglyme (10 ml) suspension of cuprous iodide (0.343 g, 1.8 mmol) was added a hexane solution (2.2 ml) of butyllithium (3.43 mmol) at −50 °C under an argon atmosphere. After 2 min, the reaction mixture was cooled to −78 °C. The oxazepine (**2b**) (0.482 g, 1.5 mmol) in THF (5 ml) and diglyme (5 ml) was added dropwise and the mixture was stirred for 2 h. It was then warmed to room temperature and poured into a phosphate buffer solution (pH 7). The resulting insoluble materials were filtered off through Celite and washed with dichloromethane. The aqueous mixture was extracted with dichloromethane. The combined dichloromethane solution was dried over anhydrous Na_2SO_4 and condensed under reduced pressure. The residue was chromatographed on silica gel (CH_2Cl_2–Et_2O) to give a mixture of diastereomers. The adducts were hydrolized and decarboxylated according to the above procedure to give the crude acid which was purified by silica gel chromatography (CH_2Cl_2–Et_2O) to yield 0.193 g (64%) of (*S*)-(+)-3-phenyheptanoic acid. It was then distilled for measurement of specific rotation by the Kugel-Rohr method (180—190 °C (bath temperature)/1.5 mmHg).

The acids (Table 4) were obtained in a similar manner and the structures of the compounds identified by their IR and NMR spectra.

The present work was partially supported by a Grant-in-Aid for Scientific Research from the Ministry of Education.

References

1) Y. Inouye and H. M. Walborsky, *J. Org. Chem.*, **27**, 2706 (1962).
2) M. Kawana and S. Emoto, *Bull. Chem. Soc. Jpn.*, **39**, 910 (1966).
3) G. Tsuchihashi, S. Mitamura, S. Inoue, and K. Ogura, *Tetrahedron Lett.*, **1973**, 323.
4) a) A. I. Meyers and C. E. Whitten, *J. Am. Chem.*

Soc., **97**, 6266 (1975); b) A. I. Meyers and E. D. Mihelich, *Angew. Chem. Int. Ed. Engl.*, **15**, 270 (1976); c) A. I. Meyers and C. E. Whitten, *Heterocycles*, **4**, 1687 (1976).

5) T. Mukaiyama, T. Takeda, and M. Osaki, *Chem. Lett.*, **1977**, 1165.

6) T. Mukaiyama, Y. Hirako, and T. Takeda, *Chem. Lett.*, **1978**, 461.

7) W. Lehnert, *Tetrahedron Lett.*, **1970**, 4723.

8) The procedure for the preparation of **2a** was described in Ref. 5. The spectral data are as follows; IR(KBr) 1745, 1640, 1600 cm^{-1}; NMR ($CDCl_3$)δ1.21 (d, J=7 Hz, 3H), 2.85 (s, 3 H), 4.18 (dq, J=2 and 7 Hz, 1 H), 5.73 (d, J= 2 Hz, 1 H), 7.30 (s, 10 H), 7.52 (s, 1 H).

9) L. Lardicci, R. Menicagel, and P. Salvadori, *Gazz. Chim. Ital.*, **98**, 738 (1968).

10) H. Rupe, *Justus Liebigs Ann. Chem.*, **369**, 311 (1969).

11) P. A. Levene and R. E. Marker, *J. Biol. Chem.*, **111**, 299 (1935).

12) P. A. Levene and R. E. Marker, *J. Biol. Chem.*, **95**, 153 (1932).

13) P. A. Levene and R. E. Marker, *J. Biol. Chem.*, **115**, 401 (1936).

14) G. M. Whitesides, W. F. Fisher, Jr., J. S. Filippo, Jr., R. W. Bashe, and H. O. House, *J. Am. Chem. Soc.*, **91**, 4871 (1969).

15) a) H. O. House and M. J. Umen, *J. Am. Chem. Soc.*, **94**, 5495 (1972); b) H. O. House and P. D. Weeks, *ibid.*, **97**, 2770 (1975).

Syntheses and Some Properties of 9,2′:7′,9″-, 9,2′:9′,9″-, and 9,4′:9′,9″-Terfluorene

Masahiro MINABE,* Masaaki YOSHIDA, and Kazuo SUZUKI

Department of Industrial Chemistry, Faculty of Engineering, Utsunomiya University, Ishiicho, Utsunomiya 321-31

(Received June 5, 1978)

Three kinds of terfluorene and 9,4′:9′,9″:4″,9‴-quaterfluorene were synthesized. The ^{1}H-NMR spectrum of 9′- and 9″-methine protons of 9,4′:9′,9″-terfluorene shows an AB spin pattern at room temperature, and that of 9,2′:9′,9″-terfluorene has an A_2 pattern. The π-π^* red shift of the UV spectra of some fulvalenes are in the order of 9,9′-bifluorenylidene, 4-(9-fluorenyl)-, and 4,4′-di(9-fluorenyl)-9,9′-bifluorenylidene. A homoconjugation effect was also observed in an alcohol series: 9-fluorenol, 4,9′-bifluoren-9-ol, and 9,4′:9′,9″-terfluoren-9′-ol.

The synthesis and properties of the crowded molecule, 9,9′:9′,9″-terfluorene (**1**) have been reported in detail.[1] However, other types of terfluorenes have not been studied.

The present paper deals with the syntheses of 9,2′:7′,9″- (**2**), 9,2′:9′,9″- (**3**), and 9,4′:9′,9″-terfluorene (**4**) and also with the spectral properties of these terfluorenes in comparison with those of **1**.

Results and Discussion

Syntheses of Terfluorenes. A new terfluorene, **2** was obtained as one of by-products in the synthesis of 2,9′-bifluorene (**5**)[2] by condensation of fluorene (**6**) and 9-fluorenol (**7**). The oxidation of **2** with sodium dichromate afforded the corresponding dicarboxylic acid (**8**), which was identical with the compound obtained by oxidation of 2,7-di(*o*-toluoyl)fluorene (**9**). The oxidation of known 2,7-dibenzoylfluorene (**10**)[3] gave 2,7-dibenzoyl-9-fluorenone (**11**) derived from decarboxylation of the acid **8** (Scheme 1).

The reaction of 9-lithiofluorene with 9′-hydroxy-2,9′-bifluoren-9-one (**12**) yielded 9,2′:9′,9″-terfluorene-9,9′-diol (**13**), which was reduced to **3**. Also, the reaction of 9-lithiofluorene with 4,9′-bifluoren-9-one (**14**)[4] afforded 9,4′:9′,9″-terfluoren-9′-ol (**15**) and

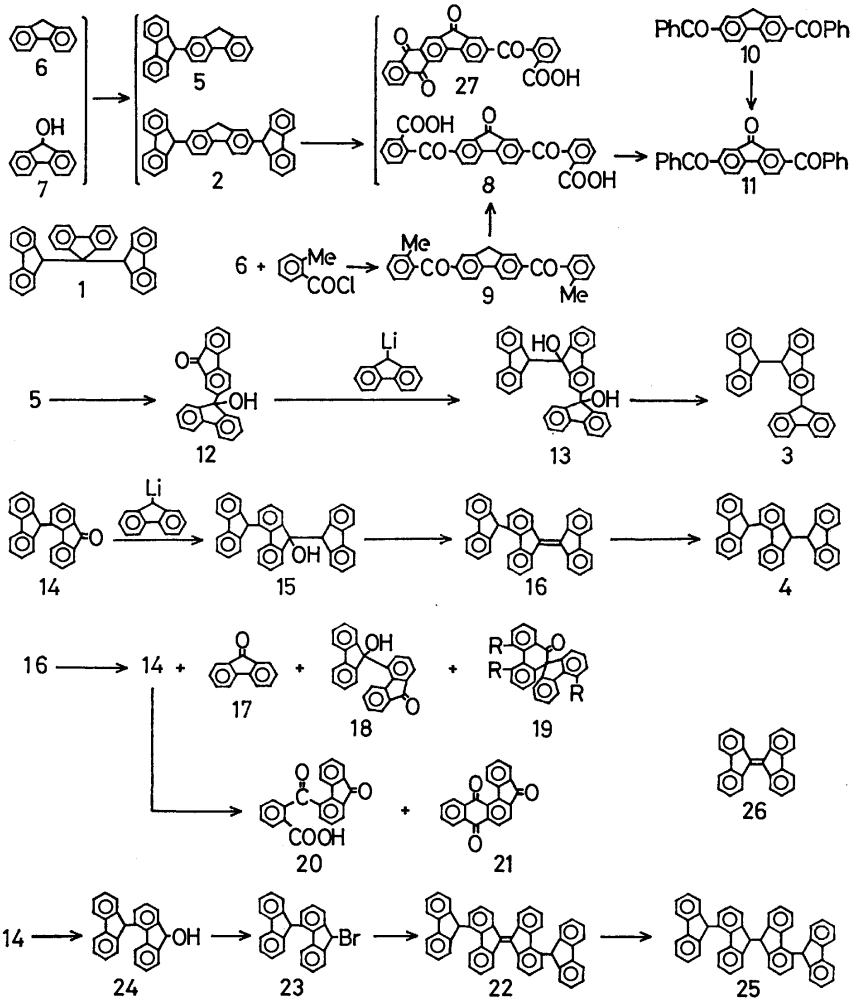

Scheme 1. Compound **19**: One of R is 9-fluorenyl and the others are H.

TABLE 1. PROTON NMR SPECTRA OF SOME TERFLUORENES IN C_6D_6

Compd	Methine	Methylene	Aromatic
1	5.36(2H, s)		5.58—8.34(24H, m)
2	4.94(2H, s)	3.16(2H, s)	6.95—7.80(22H, m)
3	4.46(2H, s) 4.74(1H, s)		6.41(1H, s) 6.62—7.75(22H, m)
4	4.69(2H, q) 6.10(1H, s)		6.60—8.09(23H, m)

4-(9-fluorenyl)-9,9′-bifluorenylidene (**16**), and the latter was reduced to **4**.

Oxidative cleavage at the central 9—9′ carbon-carbon double bond on **16** gave **14**, 9-fluorenone (**17**), and 9′-hydroxy-4,9′-bifluoren-9-one (**18**),[4] and a compound (**19**) having a melting point of 332—333 °C. The structure of **19** has not been determined, but **19** should be formed through the pinacol-pinacolone rearrangement of 4-(9-fluorenyl)-9,9′-bifluorene-9,9′-diol. Further oxidation of **14** yielded the corresponding carboxylic acid **20** and an anthraquinone derivative, **21**. This suggests that the ring closure of **20** occurs at the 3-position to form **21**, but not the 5-position.

One of the quaterfluorenes, 4,4′-di(9-fluorenyl)-9,9′-bifluorenylidene (**22**), was obtained by condensation of 9-bromo-4,9′-bifluorene (**23**), which was prepared from alcohol **24**. Hydrogenation of **22** afforded hydrocarbon **25**.

Spectral Observation of Terfluorenes and Their Derivatives. Table 1 shows the ^{1}H-NMR spectral data of **2**, **3**, and **4** in comparison with that of **1**.[1] Methine protons of 9′- and 9″-positions on **3** appears at 4.46 ppm as an A_2 spin pattern. This finding suggests that the 9′- and 9″-protons of **3** are magnetically equivalent to each other, as in the case of 9,9′-bifluorene (4.61 ppm).[1] On the contrary, those of **4** are shown at 4.69 ppm as an AB quartet (J=3.6 Hz, $\Delta\nu$=6.2 Hz) at room temperature. The splitting of the methine protons may be caused by the dihedral angle between H–$C_{9'}$–$C_{9'}$ and $C_{9'}$–$C_{9''}$–H. This quartet of **4** is changed with elevation of the temperature and the spectrum at 134.5 °C was observed as an A_2 singlet.

The methine proton on the 9-position of **4** appears at a lower field than that of the 9-position of **3** and than those of the 9- and 9″-positions of **2**. The rotation around the sp^3-sp^2 C–C single bond at 9—4′ positions of **4** may be hindered because of collisions between the adjacent hydrogen atoms on the 9- and 4′-fluorene planes. Therefore, the 9-methine proton of **4** could be situated on the deshielding zone of the 9′-fluorene plane, which shifts the signal to a lower field as in the case of the 4- or 5-proton of **6**[5] and also as in the cases of the 1,8,1′, and 8′-protons of **26**.[6] Actually, the 9′-methine proton of **14** has been observed at 5.89 ppm (CCl_4).[4]

Figure 1 shows the UV spectra of **1**,[7] **2**, **3**, **4**, and **25**. The spectra of **3** and **4** are very similar to that of **1**, but are somewhat different from that of **2**. Compound **2** has no 9—9′ C–C bond and the homoconjugation effect of **2** may be expected to be larger than

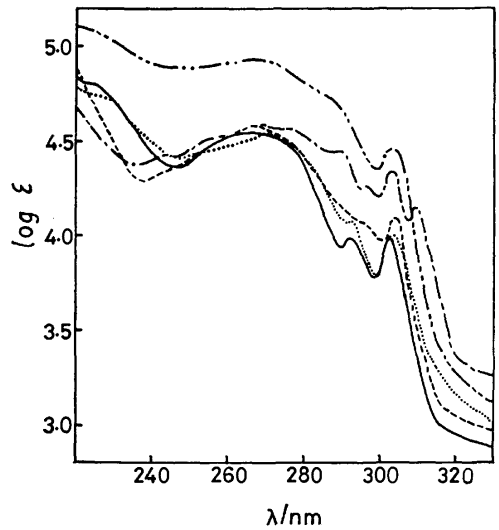

Fig. 1. UV spectra of **1** (——), **2** (— — —), **3** (----), **4** (·····), and **25** (— — —).

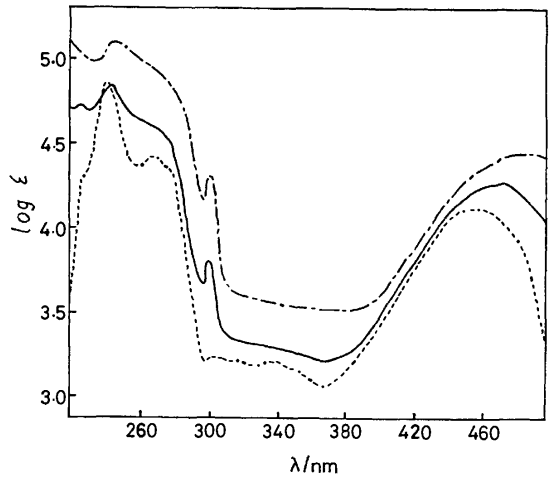

Fig. 2. UV and visible spectra of **16** (——), **22** (— — —), and **26** (----).

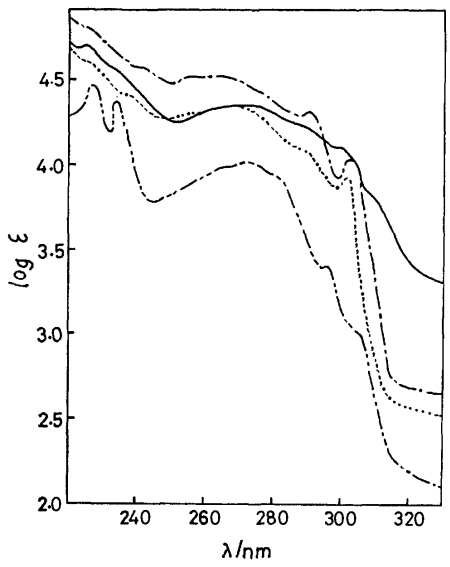

Fig. 3. UV spectra of **7** (— — —), **13** (——), **15** (— — —), and **24** (----).

that of the other terfluorenes. The spectrum of **25** suggests that the increase of absorbance is brought about by the substitution of the 9-fluorenyl group to the 4″-position of **4**, despite the fact that the coplanarity may be prevented at this position.

The UV and visible spectra of fulvalenes, **16**, **22**, and **26**[8-10] are given in Fig. 2. The π-π^* red shift and an increase of absorbance due to the central 9—9′ double bond are observed in the order of the increase of fluorene moiety: **26** (λ_{max} 455 nm, log ε 4.11); **16** (477 nm, 4.24); **22** (490 nm, 4.44). An additive property by the homoconjugation effect may also be postulated in an alcohol series, **7**, **13**, **15**, and **24**, as shown in Fig. 3.

Experimental

All the melting points are uncorrected. The UV, IR, ^{1}H-NMR, and MS spectra were obtained with a ORD/UV-5 apparatus (JASCO) in cyclohexane (scanning speed 0.76 s/nm), an IR-G spectrophotometer (JASCO) as KBr-pellets, a JNM-C60HL spectrometer (60 MHz) (JEOL), using TMS as an internal reference at 21 °C, and a RMU-6E apparatus (Hitachi) by means of a direct-inlet system, respectively.

*9,2′:7′,9″-Terfluorene (**2**).* A mixture of **6** (2.0 g) and **7** (4.0 g) in acetic acid (30 ml) was refluxed with concd sulfuric acid (0.15 ml) for 5 h. After being poured into cold water, the precipitate was collected and recrystallized from pyridine to give 0.10 g (2%) of **2**: mp 299—300 °C; NMR (C_5D_5N) δ=3.64 (2H, s), 5.27 (2H, s), and 7.15—8.10 (22H, m); MS, *m/e*, 494 (M^+), 329, and 165. Found: C, 94.54; H, 5.23%. Calcd for $C_{39}H_{26}$: C, 94.70; H, 5.30%.

The mother liquor was evaporated to dryness and the residue was recrystallized from benzene to afford 1.22 g (34%) of **5**: mp 225—226 °C (lit,[2] mp 225—226 °C).

*Structural Proof of **2**.* *a) Oxidation of **2***: An acetic acid (950 ml) solution of **2** (494 mg) was refluxed with sodium dichromate (19.0 g) for 3.5 h. Upon evaporation to dryness, the residue was extracted with aqueous alkaline and the extract was neutralized with dilute hydrochloric acid. The precipitate was collected and recrystallized from acetic acid to yield 73 mg (15%) of 2,7-bis(*o*-carboxybenzoyl)-9-fluorenone (**8**): mp 299—300 °C (dec); IR, 3420 (OH), 1715, and 1680 cm^{-1} (C=O); MS, *m/e*, 476 (M^+), 432, 388, 355, 311, and 283. Found: C, 73.23; H, 3.49%. Calcd for $C_{29}H_{16}O_7$: C, 73.11; H, 3.39%.

Additionally, 3 mg (1%) of *o*-[6,11,13-trioxo-13*H*-indeno-[1,2-*b*]anthracen-2-ylcarbonyl]benzoic acid (**27**) was isolated from the mother liquor: mp 340 °C (dec); IR, 3430 (OH), 1710, and 1670 cm^{-1} (C=O); MS, *m/e*, 458 (M^+), 414, 337, and 208. Found: C, 76.29: H, 2.70%. Calcd for $C_{29}H_{14}O_6$: C, 75.98; H, 3.08%.

*b) Synthesis and Oxidation of 2,7-Di(o-toluoyl)fluorene (**9**)*: The Friedel-Crafts reaction of **6** (1.66 g) and *o*-toluoyl chloride (3.90 g) was carried out at 120 °C in nitrobenzene (55 ml) during a period of 4 h in the presence of anhydrous aluminum chloride (3.33 g) to give 2.34 g (58%) of **9**: mp 175—176 °C (recrystallized from ethyl acetate); IR, 1650 cm^{-1} (C=O); NMR ($CDCl_3$) δ=2.36 (6H, s), 3.99 (2H, s), and 7.22—8.08 (14 H, m). Found: C, 86.65; H, 5.34%. Calcd for $C_{29}H_{22}O_2$: C, 86.54; H, 5.51%.

A solution of **9** (2.00 g) in pyridine (60 ml) was stirred with potassium permanganate (7.20 g) for 6.5 h at room temperature. The reaction mixture yielded 1.88 g (91%) of 2,7-di(*o*-toluoyl)-9-fluorenone: mp 197—199 °C; IR, 1718, 1663, and 1650 cm^{-1} (C=O); NMR ($CDCl_3$) δ=2.36 (6H, s) and 7.20—8.30 (14H, m); MS, *m/e*, 416 (M^+) and 401. Found: C, 83.44; H, 4.56%. Calcd for $C_{29}H_{20}O_3$: C, 83.63; H, 4.84%.

The foregoing fluorenone (827 mg) in benzene (80 ml) was refluxed with *N*-bromosuccinimide (2.12 g) for 1.5 h. Upon cooling, the reaction mixture was washed with water and evaporated to dryness. The residue was dissolved in acetic acid (40 ml) containing sodium dichromate (5.96 g) and refluxed for 3 h to yield 220 mg (25%) of **8**, which was identical in all respects with that obtained in a).

*c) 2,7-Dibenzoyl-9-fluorenone (**11**)*: A solution of **10** (480 mg) in pyridine (20 ml) was stirred with potassium permanganate (300 mg) at room temperature for 22 h giving 420 mg (84%) of **11**: mp 227—228 °C (recrystallized from ethyl acetate); IR, 1716 and 1648 cm^{-1} (C=O); MS, *m/e*, 388 (M^+) and 311. Found: C, 83.44; H, 4.54%. Calcd for $C_{27}H_{16}O_3$: C, 83.49; H, 4.15%.

*d) Decarboxylation of **8***: The foregoing dicarboxylic acid **8** (210 mg) was dissolved in quinoline (30 ml) and the solution was refluxed with copper bronze (200 mg) for 16 h. After cooling, the reaction mixture was filtered, then the filtrate was added to dilute hydrochloric acid and extracted with benzene. The extract was dried and chromatographed on an alumina column; 58 mg (34%) of **11** was obtained from the yellow band on the column. The compound was identical in all respects with that obtained in method c).

*Oxidation of 2,9′-Bifluorene (**5**).* Hydrocarbon **5** (3.00 g) in pyridine (150 ml) was stirred at 15—25 °C for 4 h in the presence of Triton B (40%, 0.5 ml) with gentle introduction of oxygen. The reaction mixture gave 2.83g (87%) of **12**: mp 184—185 °C; IR, 3550 (OH) and 1708 cm^{-1} (C=O); NMR ($CDCl_3$) δ=2.58 (1H, s) and 7.05—7.74 (15H, m); MS, *m/e*, 360 (M^+), 344, 315, and 180. Found: C, 86.67; H, 4.74%. Calcd for $C_{26}H_{16}O_2$: C, 86.65; H, 4.47%.

*9,2′:9′,9″-Terfluorene-9,9′-diol (**13**).* Alcohol **12** (720 mg) in xylene (60 ml) was allowed to react with 9-lithiofluorene (prepared from 1.32 g of **6**) under reflux for 1 h to afford 231 mg (22%) of **13**: mp 195—197 °C (dec) from benzene–cyclohexane (1:1); IR, 3580 and 3450 cm^{-1} (OH); NMR ($CDCl_3$) δ=2.34 (1H, s), 2.46 (1H, s), 4.70 (1H, s), and 6.85—7.67 (23H, m); MS, *m/e*, 526 (M^+), 509, 494, and 492. Found: C, 89.23; H, 4.72%. Calcd for $C_{39}H_{26}O_2$: C, 88.95; H, 4.98%.

*9,2′:9′,9″-Terfluorene (**3**).* Diol **13** (100 mg) was reduced with hydroiodic acid (57%, 3 ml) and red phosphorus (3 g) in acetic acid (50 ml) under reflux for 20 h, giving 65 mg (69%) of **3**: mp 214.5—216.5 °C (dec); NMR (C_5D_5N) δ=4.94 (2H, s), 5.01 (1H, s), 6.70 (1H, s), and 6.96—8.03 (22H, m); MS, *m/e*, 494 (M^+), 329, and 165. Found: C, 95.00; H, 5.12%. Calcd for $C_{39}H_{26}$: C, 94.70; H, 5.30%.

*9,4′:9′,9″-Terfluoren-9′-ol (**15**).* To a 9-lithiofluorene solution (prepared from 1.66 g of **6** in xylene), **14** (1.73 g) in xylene (100 ml) was added for 10 min at room temperature and then the reaction mixture was stirred at 70 °C for an additional 1 h to yield 1.82 g (72%) of **15**: mp 233—235 °C (dec); IR, 3550 cm^{-1} (OH); NMR ($CDCl_3$) δ=2.57 (1H, s), 4.81 (1H, s), 5.58 (1H, s), and 6.44—8.12 (23H, m); MS, *m/e*, 510 (M^+), 494, 492, 347, and 329. Found: C, 91.95; H, 5.19%. Calcd for $C_{39}H_{26}O$: C, 91.74; H, 5.13%.

Under different conditions, the reaction mixture was refluxed for 1 h; 0.23 g (9%) of **15** and 1.52 g (62%) of **16** were isolated: mp of **16**, 272—274 °C (dec) from ethyl acetate; NMR ($CDCl_3$) δ=6.14 (1H, s) and 6.33—8.61

(23H, m); MS, *m/e*, 492 (M^+) and 330. Found: C, 94.91; H, 5.22%. Calcd for $C_{39}H_{24}$: C, 95.09; H, 4.91%.

*9,4′:9′,9″-Terfluorene (**4**).* A solution of **16** (1.00 g) in benzene–ethanol (50 ml and 30 ml) was shaken with Raney nickel (W-7, 1.5 g) for 2 h at room temperature under an atmosphere of hydrogen. The reaction mixture was filtered, the filtrate was concentrated to a small volume, and 0.84 g (84%) of **4** crystallized out: mp 253—254 °C (dec); NMR (C_5D_5N) δ=5.06 (2H, q, J=3.6 Hz, $\Delta\nu$=5.3 Hz), 6.28 (1H, s), and 6.59—8.39 (23H, m); MS, *m/e*, 494 (M^+) and 329. Found: C, 94.98; H, 5.41%. Calcd for $C_{39}H_{26}$: C, 94.70; H, 5.30%.

*Oxidation of **16**.* A mixture of **16** (980 mg) and sodium dichromate (2.40 g) in acetic acid (150 ml) was refluxed for 1 h; **17** (170 mg, 47%, mp 82—84 °C), **14** (100 mg, 15%, mp 216—218 °C, lit,[4] mp 216.5—218.0 °C), and **18** (110 mg, 15%, mp 207.5—209.0 °C, lit,[4] mp 207.5—209.0 °C) were isolated by means of alumina-column chromatography.

In addition, 80 mg (8%) of **19** was obtained: mp 332—333 °C; IR, 1682 cm^{-1} (C=O); MS, *m/e*, 508 (M^+). Found: C, 92.28; H, 4.80%. Calcd for $C_{39}H_{24}O$: C, 92.10; H, 4.76%.

*Oxidation of 4,9′-Bifluoren-9-one (**14**).* A mixture of **14** (1.03 g) and sodium dichromate (19.6 g) in acetic acid (50 ml) was refluxed for 3.5 h to afford 530 mg (54%) of *o*-(9-oxofluoren-4-ylcarbonyl)benzoic acid (**20**): mp 210—212 °C; IR, 3070 (OH), 1722, and 1688 cm^{-1} (C=O); MS, *m/e*, 328 (M^+) and 207. Found: C, 76.83; H, 3.34%. Calcd for $C_{21}H_{12}O_4$: C, 76.82; H, 3.68%.

Additionally, 50 mg (5%) of 8*H*-indeno[1,2-*a*]anthracene-5,8,13-trione (**21**) was isolated: mp 321—323 °C (dec); IR, 1714 and 1687 cm^{-1} (C=O); MS, *m/e*, 310 (M^+), 282, and 254. Found: C, 80.98; H, 3.17%. Calcd for $C_{21}H_{10}O_3$: C, 81.28; H, 3.25%.

*9-Bromo-4,9′-bifluorene (**23**).* *a)*: A solution of **14** (500 mg) in benzene–ethanol (30 ml and 10 ml) was shaken at room temperature for 2.5 h in the presence of Raney nickel (W-7, 0.5 g) under an atmosphere of hydrogen to give 460 mg (92%) of 4,9′-bifluoren-9-ol (**24**): mp 195—196 °C; IR, 3385 cm^{-1} (OH); NMR (C_6D_6) δ=1.46 (1H, d, J=9.00 Hz), 5.40 (1H, d), 5.97 (1H, s), and 6.65—7.97 (15H, m); MS, *m/e*, 346 (M^+), 181, and 165. Found: C, 90.25; H, 5.37%. Calcd for $C_{26}H_{18}O$: C, 90.14; H, 5.24%.

The foregoing **24** (300 mg) was treated with hydrogen bromide in acetic acid to yield 310 mg (87%) of **23**: mp 192—193 °C (dec); NMR (C_6D_6) δ=5.70 (1H, s), 5.85 (1H, s), and 6.56—7.93 (15H, m); MS, *m/e*, 410, 408 (M^+), and 330. Found: C, 76.55; H, 3.98%. Calcd for $C_{26}H_{17}Br$: C, 76.29; H, 4.19%.

b): A mixture of 4,9′-bifluorene[7] (1.98 g) and *N*-bromosuccinimide (1.16 g) in benzene (75 ml) was refluxed for 6 h to give 1.75 g (72%) of **23**, which was identical in all respects with that obtained in a).

*Formation of 4,4′-Di(9-fluorenyl)-9,9′-bifluorenylidene (**22**).* A solution of **23** (1.10 g) in acetone (170 ml) was treated with potassium hydroxide (0.20 g) in methanol (10 ml) at −15 °C to afford 136 mg (15%) of **22**: mp 290—291 °C (dec); NMR (C_5D_5N) δ=6.28 (2H, s) and 6.53—8.63 (30H, m) (measured at 53 °C). Found: C, 94.91; H, 5.00%. Calcd for $C_{52}H_{32}$: C, 95.09; H, 4.91%.

*Reduction of **22**.* Olefin **22** (100 mg) in benzene (120 ml) was shaken for 3 h at room temperature with Raney nickel (W-4, 0.5 g) under an atmosphere of hydrogen, giving 71 mg (71%) of 9,4′:-9′,9″:4″,9‴-quaterfluorene (**25**): mp 292—293 °C (dec). Found: C, 94.52; H, 5.20%. Calcd for $C_{52}H_{34}$: C, 94.80; H, 5.20%.

The authors thank to Mr. Norio Eda and Miss Katsuko Nakada for their helpful assistance.

References

1) For example: M. Minabe and K. Suzuki, *J. Org. Chem.*, **40**, 1298 (1975).
2) K. Suzuki, *J. Org. Chem.*, **27**, 2224 (1962).
3) K. Dziewonski and A. Obtulowicz, *Bull. Intern. Acad. Pol., A*, 399 (1930); *Chem. Abstr.*, **25**, 5157 (1931).
4) T. Ooya, M. Minabe, and K. Suzuki, *Bull. Chem. Soc. Jpn.*, **51**, 1473 (1978).
5) K. D. Bartle and D. W. Jones, *J. Mol. Struct.*, **1**, 131 (1967—1968).
6) M. Rabinovitz, I. Agranat, and E. D. Bergmann, *Tetrahedron Lett.*, **1965**, 1265.
7) K. Suzuki, *Technol. Rep. Tohoku Univ.*, **19**, 63 (1955).
8) A. Pullman and B. Pullman, *Discuss. Faraday Soc.*, **1950**, 46.
9) E. D. Bergmann, G. Berthier, E. Fischer, Y. Hirshberg, D. Lavie, E. Loewenthal, and B. Pullman, *Bull. Soc. Chim. Fr.*, **1952**, 78.
10) G. J. Heeres and H. Wynberg, *Tetrahedron*, **28**, 5237 (1972).

NOTES

BULLETIN OF THE CHEMICAL SOCIETY OF JAPAN, VOL. 51 (11), 3377—3378 (1978)

Fluorescence of the Proton Transferred Excited Species between 4-Amino-2-methyl-5*H*-[1]benzopyrano[3,4-*c*]pyridin-5-one and Acetic Acid. Time-Resolved Fluorescence Spectra and Solvent Effects

Akira FUJIMOTO* and Hiroshi HIROSE†

Department of Applied Science, Faculty of Technology, Tokyo Denki University, Kanda, Chiyoda-ku Tokyo 101

†*Naka Works, Hitachi Ltd., Katsuta, Ibaragi 312*

(Received January 23, 1978)

Synopsis. The nanosecond time-resolved spectra and apparent lifetime for the fluorescence of the proton transferred excited species (tautomer) between 4-amino-2-methyl-5*H*-[1]benzopyrano[3,4-*c*]pyridin-5-one (BPP) and acetic acid have been measured in isooctane (2,2,4-trimethylpentane) at room temperature. It has been established that the rising time of the tautomer fluorescence was *ca.* 15 ns and the time required for the excited hydrogen-bonded species-tautomer equilibrium was *ca.* 40 ns. Solvent effects upon the fluorescence characteristics of the tautomer have also been investigated.

Recently, El-Bayoumi *et al.*[1] and Shizuka *et al.*[2] have measured the fluorescence with large Stokes shifts for 7-azaindole (7AI) and for 6-(2-hydroxy-5-methylphenyl)-*s*-triazines (TH), respectively. It has been suggested that the fluorescence of the former originates from a tautomer formed by a fast intermolecular double proton transfer reaction of the excited hydrogen-bonded dimer of 7AI.[1] In the latter case the fluorescence has been attributed to a tautomer (keto form) formed by a fast intramolecular proton transfer reaction of the excited hydrogen-bonded species (enol form) of TH.[2]

Previous studies have reported the fluorescence with a large Stokes shift, besides the fluorescence of hydrogen-bonded species for the BPP–acetic acid system in isooctane.[3] Accordingly, from the similarity of tautomer fluorescences for 7AI and TH, it is reasonable to assume that the fluorescence of the present system with a large Stokes shift corresponds to that from the tautomer (T*) formed *via* the intermolecular double proton transfer in the excited state of the doubly hydrogen-bonded species (H) as follows:

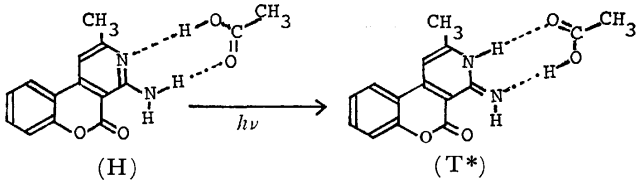

(H) (T*)

In addition, from the absorption spectra it has been shown that substantially all BPP molecules are present as H in isooctane when the concentration of BPP is 3.5×10^{-5} M and that of acetic acid 2.0×10^{-1} M.[3] In the present study, nanosecond time-resolved fluorescence spectral techniques were applied to the problem of the double proton transfer reaction between BPP in the lowest excited singlet state and acetic acid under the conditions as stated above.

Results and Discussion

The time-resolved fluorescence spectra of the BPP–acetic acid system in isooctane solution are given in Fig. 1. As shown in Fig. 1 two fluorescence bands with peaks at *ca.* 384 nm and 458 nm appear, which correspond to the emission bands of the hydrogen-bonded and proton transferred species[3] (tautomer) respectively. The fluorescence band maxima of these two species are scarcely shifted with a delay time (t). It seems that an equilibrium between H* and T* is established in the excited state as follows:

$$\text{H}^* \rightleftarrows \text{T}^*$$

where H* signifies the excited hydrogen-bonded species. The tautomer fluorescence at $t\approx15$ ns has the greatest intensity as seen in Fig. 1. The rising time of T* is *ca.* 15 ns. Figure 2 shows the plot of I_2/I_1 *vs.* t for the BPP–acetic acid system, where I_1 and

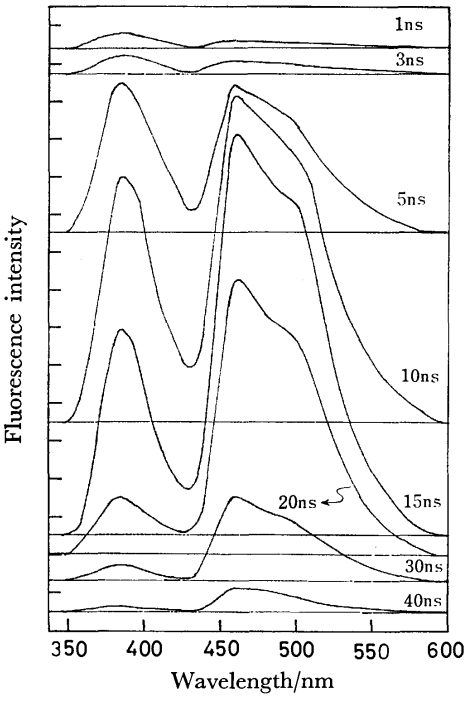

Fig. 1. Time-resolved fluorescence spectra of the BPP-acetic acid system in an isooctane solution at room temperature.

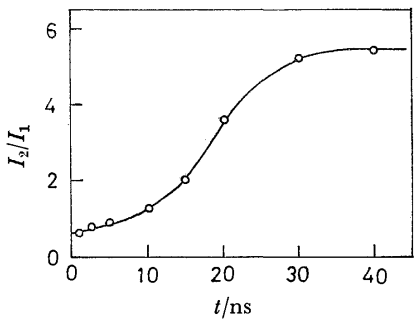

Fig. 2. The polt of I_2/I_1 *vs.* t.

I_2 represent the fluorescence intensities at 384 nm and 458 nm respectively. At first, I_2/I_1 increases with t and then is virtually invariant at $t \approx 40$ ns. Furthermore, the time-resolved fluorescence spectra at *ca.* 40 ns were the same as those in the stationary state of the BPP–acetic acid system. These results show that it takes about 40 ns to establish the H*–T* equilibrium. It should be noted that the rate of proton transfer in the excited state is generally fast,[1,2] while in the case of the system studied here that of proton transfer is relatively slow and the reaction takes time to reach the H*–T* equilibrium.

The fluorescence lifetime calculated from the integrated absorption intensity and the fluorescence quantum yield ($\Phi=0.14$[4]) of BPP in isooctane without acetic acid was estimated to be 1.0 ns. The lifetime of BPP in isooctane could not be obtained because it was shorter than the response time (few ns) of the apparatus. Nevertheless, the apparent fluorescence lifetimes (τ_T) of the tautomer T* in various solvents could be measured at room temperature. These was no wavelength effect upon the apparent lifetimes of T*. The values of τ_T at 470 nm in various solvents are listed in Table 1.

The other characteristics (the wave numbers of the band maxima and quantum yields) of the tautomer fluorescence measured in non-polar and slightly polar solvents are also given in Table 1 with dielectric constants. It is to be noted that with an incerase in the polarity of solvent the tautomer fluorescence band maximum shifted towards the red with a decrease in the fluorescence quantum yield, The apparent lifetime also decreases with an increase in the solvent polarity.

Experimental

The sample of BPP[6] was the same as reported previously.[3] The sample was recrystallized from pyridine and further purified by vacuum sublimation. Acetic acid and quinine bisulfate of extra pure grade were used without further purification. The solvent used here were commercially available and when purification was needed, they were further purified by distillation. The time-resolved fluorescence spectra and lifetimes were measured with a Hitachi MPF-4 spectrophotometer equipped with a time-resolved photometer at room temperature. An ultraviolet D_2 pulser was used for the excitation of the species. The pulse given by this lamp had a life-duration less than 5 ns. For the measurement of ordinary emission intensity, a Hitachi MPF-2A fluorescence spectrophotometer was used.

Table 1. Wave numbers (ν_T) of the band max., fluorescence quantum yields (Φ_T), and apparent fluorescence lifetimes (τ_T) of the tautomer T* in the BPP–acetic acid system measured in solvents having different polarity at room temp

Solvent	Dielectric const	ν_T $\times 10^3$ cm^{-1}	Φ_T[4]	τ_T ns
Hexane	1.88	21.8	0.088	8.1
Isooctane	1.95	21.8	0.081	8.0
Benzene	2.28	21.5	0.053	7.3
Chloroform	5.15	21.4	0.051	7.2
Chlorobenzene	5.53	21.4	0.050	7.1
Dichloromethane	8.90	21.3	0.036	6.7
Dichloroethane	10.37	21.3	0.035	6.4

This work was supported by grants from the Tokyo Denki University Research Fund. The authors wish to express their thanks to Prof. Kozo Inuzuka and Dr. Akio Sakurai for their kind advice during this study.

References

1) K. C. Ingham and M. A. El-Bayoumi, *J. Am. Chem. Soc.*, **96**, 1674 (1974); M. A. El-Bayoumi, P. Avouris, and W. R. Ware, *J. Chem. Phys.*, **62**, 2499 (1975).

2) H. Shizuka, K. Matsui, Y. Hirata, and I. Tanaka, *J. Phys. Chem.*, **80**, 2070 (1976); *ibid.*, **81**, 2243 (1977).

3) A. Fujimoto, A. Sakurai, H. Midorikawa, and E. Iwase, *Nippon Kagaku Kaishi*, **1974**, 1.

4) The fluorescence quantum yields were measured by comparison with a quinine bisulfate solution ($\Phi=0.55$ at 27 °C, see Ref. 5).

5) G. G. Guilbault, "Practical Fluorescence Theory, Methods, and Techniques," Marcel Dekker, Inc., New York (1973), p. 12.

6) A. Sakurai, H. Midorikawa, and Y. Hashimoto, *Bull. Chem. Soc. Jpn.*, **43**, 2925 (1970).

BULLETIN OF THE CHEMICAL SOCIETY OF JAPAN, VOL. 51 (11), 3379—3380 (1978)

The Carbon-13 NMR Spectra of Barbituric-acid Derivatives

Shozo ASADA and Jujiro NISHIJO*
Kobe Women's College of Pharmacy, Higashinada-ku, Kobe 658

(Received December 19, 1977)

Synopsis. The ^{13}C nuclear magnetic resonance spectra of thirty kinds of barbituric-acid derivatives were measured, and the chemical shifts of each carbon were assigned. The correlation between chemical shifts of the ring skeletal carbon and the pK_a values was examined.

There have been several reports concerning the ^{13}C nuclear magnetic resonance (NMR) spectra of barbituric-acid derivatives. Okada *et al.*[1] have measured the ^{13}C NMR spectra of some 5-monosubstituted barbituric-acids (I). They pointed out that (I) dissociated by releasing the hydrogen at the 5-position and that there was a good linear correlation between the ^{13}C chemical shifts of C-5 and the pK_a values. In 5,5-disubstituted and 1-methyl-5,5-disubstituted barbituric-acids (II) and (III), however, dissociation may be more complicated, as is shown in Chart 1. In order to gain a clew with regard to those dissociation schemes, we tried to assign the chemical shifts of each carbon for (II) and (III) and examined the correlation of the ^{13}C shifts of the ring skeletal carbons with the pK_a values of these compounds.

Experimental

Materials. The barbituric-acids used for the measurement of the ^{13}C NMR spectra are listed in Table 1. Compounds **2**, **3**, **7**, **9**, **10**, **11**, **13**, **14**, **28**, and **29** were synthesized by the methods described in the literature.[2,3] Compound **30** was synthesized by the methylation of **15** with CH_2N_2. The other compounds were those reported in the preceeding paper.[4]

Measurements of the Acid-dissociation Constants and the ^{13}C NMR Spectra of Barbituric-acid Derivatives. The apparent acid-dissociation constants, pK_a, were determined by means of a Hitachi model UV-200 spectrophotometer at 20 °C in an ionic strength of 0.75. The pK_a values of the new compounds were as follows : **2**=7.94, **3**=7.85, **7**=8.14, **9**=7.53, **10**=8.05, **11**=7.77, **13**=7.87, **14**=7.61, **28**=7.85, and **29**=7.90. The ^{13}C NMR spectra were measured at room temperature by means of a NEVA NV-21 (22.6 MHz) spectrometer. All the samples were dissolved in dimethyl-d_6 sulfoxide (1M). The chemical shifts were expressed in ppm downfield from tetramethylsilane (TMS).

Results and Discussion

Table 1 shows the ^{13}C chemical shifts of the ring skeletal carbons, assigned by using the off-resonance technique or by comparing them with the values in the literature.[1,5] The mean value of the chemical shifts of *N*-methyl carbon for (III) was given as 27.09±0.25 (n=15).

We attempted to correlate the ^{13}C shifts with the pK_a values as follows. The results of regression analyses concerning Eq. 1 are summarized in Table 2.

$$pK_a = a_0 + a_1\delta_c(\text{ring position}), \quad (1)$$

where δ_c indicates the ^{13}C shift of the ring skeletal

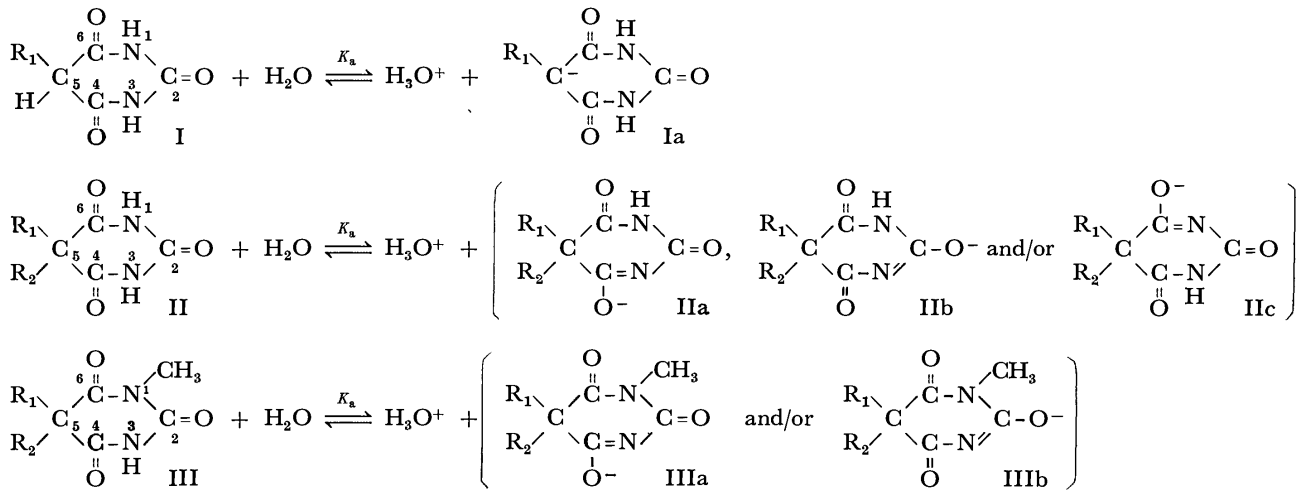

Chart 1.

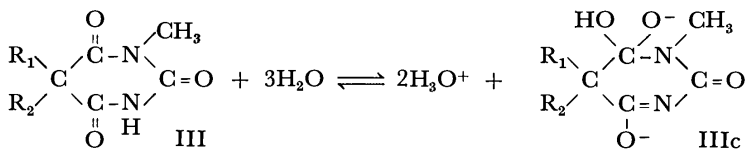

Chart 2.

Table 1. Compound number and ^{13}C chemical shift (δ_C) in ppm of barbituric-acid derivatives

Compound No.	Substituent[a]		δ_C[b]				
			Ring				N-CH_3
	R_1	R_2	C-2	C-4	C-6	C-5	
II, (R_3=R_4=H) series							
1	Ethyl	Ethyl	150.0	173.1×2		56.6	
2	Ethyl	Allyl	149.8	172.4×2		55.8	
3	Ethyl	Propyl	149.9	173.1×2		55.9	
4	Ethyl	3-Methylbutyl	149.9	173.1×2		55.8	
5	Ethyl	1-Methylbutyl	150.1	(173.1)	(172.8)[c]	59.3	
6	Ethyl	Cyclohexen-1-yl	150.0	171.5×2		61.5	
7	Ethyl	Cyclohexyl	150.1	172.7×2		59.5	
8	Ethyl	Phenyl	149.9	171.6×2		60.0	
9	Ethyl	Benzyl	149.4	172.5×2		57.8	
10	Ethyl	α-Methylbenzyl	149.4	(172.8)	(171.7)[c]	60.1	
11	Ethyl	Cinnamyl	149.3	(172.4)	(171.6)[c]	57.7	
12	Allyl	Allyl	149.7	171.9×2		55.1	
13	Propyl	Propyl	149.8	173.2×2		55.2	
14	Benzyl	Benzyl	148.9	172.1×2		59.1	
III, (R_3=CH_3, R_4=H) series							
15[d]	Ethyl	Ethyl	149.9	171.8	171.3	56.9	27.1[e]
16	Ethyl	Allyl	149.8	171.4	170.8	56.2	27.1
17	Ethyl	Propyl	149.8	171.9	171.3	56.2	27.1
18	Ethyl	3-Methylbutyl	149.8	171.9	171.3	56.1	27.1
19	Ethyl	1-Methylbutyl	150.0	171.8	171.2	59.7	27.1
20	Ethyl	Cyclohexen-1-yl	149.9	170.5	169.8	61.7	27.4
21	Ethyl	Cyclohexyl	150.6	172.1	171.5	60.3	26.8
22	Ethyl	Phenyl	149.8	170.4	169.9	60.3	27.6
23	Ethyl	Benzyl	149.3	171.4	170.8	58.3	27.0
24	Ethyl	α-Methylbenzyl	149.7	172.0	170.5	61.0	27.0
25	Ethyl	Cinnamyl	150.2	171.9	171.2	56.9	27.4
26	Ethyl	Phenylpropyl	150.2	172.4	171.8	56.3	27.2
27	Allyl	Allyl	149.6	170.8	170.1	55.4	27.0
28	Benzyl	Benzyl	149.1	171.5	170.7	59.7	26.8
29	Benzyl	α-Methylbenzyl	149.2	171.4	170.3	61.8	26.6
IV, (R_3=R_4=CH_3) series							
30	Ethyl	Ethyl	150.9	171.4×2		57.4	28.2×2

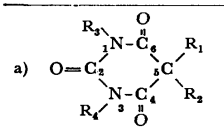

a) b) Symbol "×2" means twice the intensity. c) In Compounds **5**, **10**, and **11**, which have no *N*-methyl group, equivalent signals of carbons at the 4- and 6-positions split off in two. d) The δ_c 171.8 is the signal to C-4, and the δ_c 171.3 is that to C-6, which is situated nearer the *N*-methyl group. In **1**, δ_c 173.1×2 is assigned as the signals to C-4 and C-6. In **30**, these signals appear at a higher field, δ_c 171.4×2. e) The ^{13}C signal of the *N*-methyl group was shown as a quartet in the partial proton-decoupling state.

carbons for (II) and (III), and where a_0 and a_1 are constants. In a series of (II), it was found that the regression of pK_a with δ_c (4 and/or 6 position) was significant at the 5% level concerning the F-test for the variance ratio, as is shown in Eq. 3. On the other hand, the regression of pK_a with δ_c(2) or of pK_a with δ_c(5) was less significant, as is shown in Eq. 2 or Eq. 4. Thus, the ionization of (II) may produce (IIa) and/or (IIc). Further, in the (III) series, the regression of pK_a with δ_c(4) was highly significant,

Table 2. Regression analyses[a] between pK_a and δ_c of ring carbon for two barbituric-acid derivatives, (II) and (III)

Series	a_0 +	a_1 (t value)	δ_c	γ Correlation coeff.	Ve Variance	$F_{1,n-2}$ Variance ratio	Equation
II	−8.06	0.106(0.52)	δ_c(2)	0.149	0.066	0.274	2
	−41.4	0.285(2.92*)	δ_c(4 and/or 6)	0.697	0.038	8.49*	3[b]
	9.28	−0.026(0.80)	δ_c(5)	0.224	0.064	0.632	4
III	−15.06	0.153(1.09)	δ_c(2)	0.291	0.044	1.20	5
	−44.21	0.304(5.36**)	δ_c(4)	0.830	0.015	28.8**	6
	−30.25	0.223(3.17**)	δ_c(6)	0.666	0.026	10.4**	7
	7.85	0.001(0.02)	δ_c(5)	0.006	0.048	0.001	8

a) pK_a=a_0+$a_1\delta_c$ (ring position). b) No. of samples: n=11 (No. 1—No. **14** except Nos. **5**, **10**, and **11**). Symbol ** indicates a substance to be significant at the 1% level, *, to be significant at the 5% level.

as had been expected (Eq. 6), while that of pK_a with δ_c(2) or of pK_a with δ_c(5) had little significance (Eq. 5 or Eq. 8). The regression of pK_a with δ_c(6) was also significant at the 1% level relative to the F-test (Eq. 7). It seems that this result is inconsistent with Chart 1. In this connection, Eriksson *et al.*[6] have reported that a tetrahedral substrate–hydroxide ion complex of 1-methylbarbituric-acid was formed in an alkaline solution. Accordingly, the ionization form (IIIc) shown in Chart 2 may be useful in predicting a good correlation of Eq. 7. A complete explanation must be left to further study because pK_a is related to the ^{13}C chemical shifts at the 4 and/or 6 position of 5,5-disubstituted barbituric-acid derivatives.

The authors wish to express their thanks to Miss Makiko Sugiura for the measurement of the ^{13}C NMR spectra.

References

1) J. Okada and T. Esaki, *Yakugaku Zasshi*, **93**, 1014 (1973).

2) a) J. B. Dickey and A. R. Gray, *Org. Synth.*, Coll. Vol. II, 60 (1943); b) G. A. Neville, H. W. Avdovich, and A. W. By, *Can. J. Chem.*, **48**, 2274 (1970).

3) T. Itai and B. Hashimoto, *Eiseishikensho Iho*, **61**, 11 (1943).

4) S. Asada, A. Kashimoto, and T. Yamada, *Yakugaku Zasshi*, **96**, 1169 (1976).

5) J. B. Stothers, "Carbon-13 NMR Spectroscopy," Academic Press, New York and London (1972).

6) S. O. Eriksson and C. G. Regårdh, *Acta Pharm. Suec.*, **5**, 457 (1968).

BULLETIN OF THE CHEMICAL SOCIETY OF JAPAN, VOL. 51 (11), 3381—3382 (1978)

Mass-transfer Experiment through the Water–Benzene Interface in a Capillary Tube

Teruya SHIMBASHI

Department of Chemical Engineering, Tokyo Institute of Technology, Meguro-ku, Tokyo 152

(Received February 17, 1978)

Synopsis. In order to confirm a previous discussion of a mass-transfer experiment that indicated a high interfacial resistance, an experiment using a capillary tube was done for the transfer process of butylamine through the water–benzene interface at 50 °C. The results obtained agree with the preceding ones.

In a preceding paper,[1] it was described that the resistance ($\Delta F^*_{d2}=18$ kcal/mol, 50 °C) against which propylamine and butylamine molecules were transferred through the water–benzene interface agreed well with the results of another study[2] about the transfer rates of fatty acids through liquid-liquid interfaces. However, the experiment described in the preceding paper showed confused results that the diffusion coefficients measured with the same apparatus as in the transfer experiment were much larger than the values estimated from the literature, and that their concentration dependences could not be disregarded; the author ascribed this discrepancy to the large sectional-area of mass transfer and to the existence of a gas-liquid interface.

In the present paper, the results and its subsequent analysis of an experiment done in order to confirm the discussion in the preceding paper, are described for the transfer process of butylamine through the water–benzene interface at 50 °C, using a capillary tube so as to get diffusion coefficients nearly equal to the literature values.

Experimental and Results

The mass-transfer cell used is a U-shaped glass-tube on the whole, one arm of which has a 1.5 mm (ID) capillary with three Teflon cocks—at both ends and at the middle point; the part from the middle cock to the upper end is called the first capillary, which is to be filled with a benzene solution, while the lower half is called the second capillary, which is to be filled with water. The second capillary is equipped with an array of six pairs of platinum electrodes for determination of electric conductivity.

In order to obtain the temperature constancy and electric insulation of the leading wires, the cell is set in a cylindrical glass-container filled with chemically pure xylene, and then the whole is set in a thermostat.

Opening the middle cock of the cell causes the transfer of the solute (butylamine) from the first phase (benzene) to the second (water). The electrode circuits are automatically switched on and off in turn, and the conductivities are recorded.

In the case of the measurement of the diffusion coefficients in water, aqueous solutions were used instead of benzene solutions, but in the same manner. The electrode sensitivity (equivalent to the cell constant) for each pair of electrodes was referred to the conductivity for an 0.02 M aqueous solution of potassium chloride.

As a result of the transfer experiments, the time dependences of the conductivity of each pair of electrodes were obtained, and were then translated to the concentration changes. The concentration distributions in the second phase at various times were obtained by the interpolation of the concentration changes, and the fitting curves of the concentration distributions were obtained by means of the least squares; the amounts of transfer at the assigned times were obtained by the integration of the fitting curves.

In the measurement of the diffusion coefficients of butylamine in water at 30 and 50 °C, both values calculated from the time dependence of the concentration at the pair of electrodes nearest to the water–benzene interface and calculated from the change in the amount of transfer agreed well with that estimated by Wilke's method[3] from the literature; the diffusion coefficients in benzene were not measured because of the difficulty of determining them. In the calculation of the interfacial resistance, the diffusion coefficients estimated from the literature were used (D_1 (in benzene)$=3.21\times10^{-5}$, D_2 (in water)$=1.79\times10^{-5}$ cm^2/s).

Two points of special attention were found in this experiment. (1) When the initial concentration in the first phase was sufficiently high, the analysis became difficult, because the change in concentration tended to be complicated; this means that a turbulence, presumably caused by the Marangoni effect,[4] occurred and continued for a long time. Consequently, it was necessary to select an initial concentration low enough so as to get a normal pattern of the concentration change ($c_{10}<0.01$ M). (2) When the electrode sensitivities that had been determined in advance were used for obtaining the transfer amount after a long time (about 20 days), unreasonably large values[5] were obtained; this may signify that the electrode sensitivity gradually increased in this experiment. Nevertheless, a relative comparison of the transfer amounts after a long time is considered to be feasible,[6] because the variation in the electrode sensitivity may become negligible after a certain time.

The results of determination are indicated in Table 1. Here, suffixes a and b have the following meanings. When the transfer amount was computed by integration from the concentration-distribution observed, $c=a_1+a_2x+a_3x^2$ in (a) and $c=a_1+a_2x+a_3x^2+a_4x^3$ in (b) were used for the functional mode of concentration (c: concentration; x: distance from the interface; a_i:

Table 1. Results of determination

Sample	l [cm]	$c_{10}\times10^{6}$ [mol/cm^3]	$t_1\times10^{-6}$ [s]	$t_2\times10^{-6}$ [s]	$t_3\times10^{-6}$ [s]	q_1/q_3	q_2/q_3
1a	8.48	8.22	0.968	1.200	1.500	0.813	0.911
1b	8.48	8.22	1.000	1.200	1.400	0.837	0.927
2a	10.35	5.00	0.900	1.200	1.400	0.904	0.969
2b	10.35	5.00	1.000	1.200	1.400	0.926	0.969

Table 2. Results of calculation

Sample	$k_{d2}\times10^{9}$[mol/cm^2 s]	$c'_{20}\times10^{7}$[mol/cm^3]
1a	1.4	1.3
1b	0.7	0.8
2a	1.9	5.5
2b	1.0	5.7

parameters); l: depth of both phases; c_{10}: initial concentration of solute in the first phase; t_1, t_2, and t_3: contact times; q_1, q_2, and q_3: transfer amount of the solute at t_1, t_2, and t_3 respectively (mol/cm^2).

Estimation of the Interfacial Resistance

Assigning an arbitrary value to q_1 (or q_3) on the condition that q_1/q_3=const. determines a pair of values, q_1 and q_3, and enables one to compute the desorption rateconstant (k_{d2}) of the solute from the interface to the second phase and the average concentration (c'_{20}) in the second phase immediately after the cessation of an abnormally rapid process, if any, after the procedure described in the preceding paper. The computation was repeatedly made on varied values of q_1 so as to get Curve A on the k_{d2}-c'_{20} plane; Curve B was obtained in the same manner on the condition that q_2/q_3= constant.

As may be seen from drawing Curve A and Curve B from a theoretical change in the transfer amount on definite conditions, Curve A is a tangent which touches Curve B at a point representing the k_{d2} and c'_{20} given as the conditions. We take the k_{d2} sought to be at the minimum point of the difference, c'_{20}(B)-c'_{20}(A), where c'_{20}(A) and c'_{20}(B) are the values of c'_{20} on Curve A and Curve B respectively, corresponding to an assigned value of k_{d2}; the c'_{20} sought is also taken to be the average of c'_{20}(A) and c'_{20}(B) corresponding to the obtained k_{d2}.

The results of calculation are shown in Table 2.

Strictly speaking, the k_{d2} should be obtained by extrapolating the value to $c_{10}=0$,[1] but the values obtained above may be nearly equal to the extrapolated value, because the values of c_{10} are quite small in Table 1. We take the activation free energy of desorption from the interface to the second phase to be ΔF^{*}_{d2}=18.6 kcal/mol, converting the average value of k_{d2} in Table 2, 1.2×10^{-9} mol/cm^2 s;[7] this agrees with the result in the preceding paper.

The author is indebted to Professors Hikoji Inazumi and Tadao Shiba of this Institute for their helpful discussions concerning this subject.

References

1) T. Shimbashi, *Nippon Kagaku Kaishi*, **1976**, 373.
2) T. Shimbashi and T. Shiba, *Nippon Kagaku Zasshi*, **92**, 676 (1971).
3) C. R. Wilke, *Chem. Eng. Progr.*, **45**, 218 (1949).
4) C. V. Strenling and L. E. Scriven, *AIChE J.*, **5**, 514 (1959).
5) For example, a value larger than the amount of solute in the transfer equilibrium.
6) According to the graph used for obtaining the concentrations from the conductivities, the ratio of concentrations on a curve of a constant electrode sensitivity, corresponding to the fixed conductivities, has a change of only about 5% when the concentration that corresponds to a fixed conductivity has been changed + 100%.
7) T. Shimbashi, *Bull. Chem. Soc. Jpn.*, **48**, 626 (1975).

BULLETIN OF THE CHEMICAL SOCIETY OF JAPAN, VOL. 51 (11), 2283—3384 (1978)

Excitation Wavelength Dependence of Quinoline Phosphorescence Lifetime†

I-Fu HUNG,*,** Tadashi OKAMURA,*** Sam SUGAMORI, and R. W. YIP
Division of Chemistry, National Research Council of Canada, Ottawa, Canada
(Received April 19, 1978)

Synopsis. The quinoline phosphorescence lifetime in several rigid media at 77 K has been found to be dependent on excitation wavelength. The change of lifetime is especially remarkable in hydroxylic solvents. This observation has been attributed to the inhomogeneous broadening of spectral lines caused by the distribution of solvent environments around quinoline molecules.

The quinoline phosphorescence lifetime has been shown to be solvent dependent with the ones observed in hydrocarbons being shorter than in hydroxylic solvents.[1,2] These results were interpreted by Lim and Yu[1] as due to the solvent effect on the second order perturbation including spin-orbit coupling and vibronic interaction among the excited singlet and triplet states. This was supported from the polarization measurement where the phosphorescence is found to be more in-plane polarized in hydrocarbon than in hydroxylic solvents outside the 0,0 band. In order to examine such a solvent effect more in detail, the measurement of quinoline phosphorescence lifetime in several solvents has been conducted with the excitation wavelength varied across the first absorption band.

The results of lifetime measurements are listed in Table 1 and also shown in Fig. 1. It is clearly seen that the quinoline phosphorescence lifetime observed in hydroxylic solvents is markedly dependent upon the excitation wavelength whereas those measured in hydrocarbon solvents show only slight dependence. The lifetimes observed in hydroxylic and hydrocarbon solvents by excitation at the long wavelength edge (red edge) of the first absorption band are very similar except for the one in ethyl alcohol excited at 317.5 nm which is shorter than those for other solvents. Itoh and Azumi[3] observed a slight but significant spectral shift of quinoline phosphorescence in EPA by red edge excitation. In the present work as shown in Fig. 2, the phosphorescence spectra measured in ethyl alcohol show very little change in spectral profile and peak position with excitation outside the red edge region, except for a slight change in relative peak height which is barely observable under the experimental conditions (apparent 0,0 peak was observed at 314.5 nm in phosphorescence excitation spectrum). In consideration of these observations, it is not unlikely that the considerable change of phosphorescence lifetime observed by the red edge excitation is caused by the same sort of effect they observed, though the origin of such red edge effect has not been consistently interpreted for all molecules studied so far.[3,4]

Johnson and Levin[5] reported the excitation wavelength dependent phosphorescence lifetime of benzene and naphthalene in nonpolar rigid media and attributed such observations mainly to the change in the radiationless transition rate caused by the presence of a distribution of local environment for the solute molecules which shows up as an inhomogeneous line

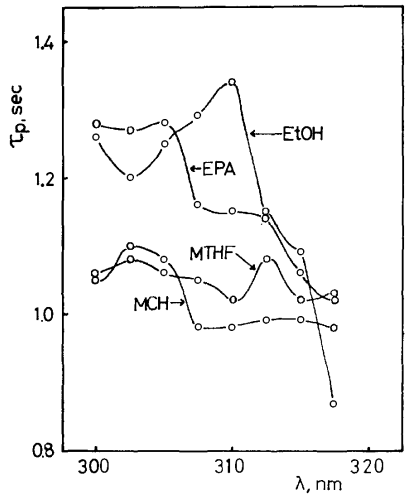

Fig. 1. Excitation wavelength dependence of the phosphorescence lifetime of quinoline at 77 K. Solvents used are indicated by arrows.

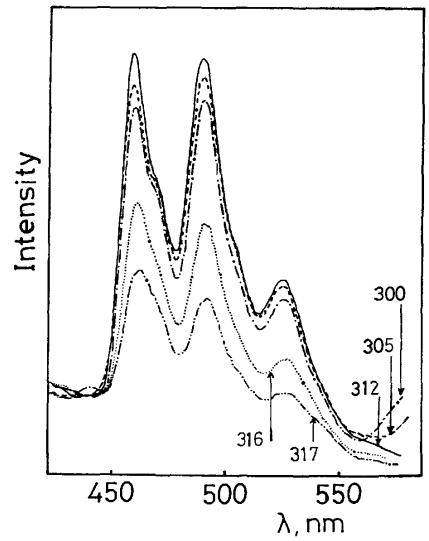

Fig. 2. Phosphorescence spectra of quinoline in ethyl alcohol excited at different wavelength region. Excitation wavelength in nm is given by following the arrows.

† Issued as NRCC No. 16903.

** Present address: Department of Epidemiology and Health, McGill University, Montreal, Quebec, Canada.
*** N. R. C. Research Associate, 1975—1976. Present address: Laboratory of Chemistry, Tokyo Zokei University, Motohachioji, Hachioji, Tokyo, Japan.

Table 1. Phosphorescence lifetimes of quinoline as a function of excitation wavelength[a)]

Excitation wavelength (nm)	Phosphorescence lifetime (s)			
	EtOH	EPA	MTHF	MCH
275	—	1.24±0.07	—	1.05±0.09
300	1.26±0.04	1.28±0.11	1.06±0.05	1.05±0.04
302.5	1.20±0.04	1.27±0.08	1.08±0.04	1.10±0.07
305	1.25±0.05	1.28±0.06	1.06±0.06	1.08±0.06
307.5	1.29±0.06	1.16±0.08	1.05±0.05	0.98±0.08
310	1.34±0.08	1.15±0.09	1.02±0.08	0.98±0.06
312.5	1.15±0.10	1.14±0.10	1.08±0.04	0.99±0.05
315	1.09±0.06	1.06±0.12	1.02±0.11	0.99±0.05
317.5	0.87±0.03	1.02±0.12	1.03±0.11	0.98±0.08

a) Solvents: EtOH: ethyl alcohol; EPA: ethanol-isopentane-diethyl ether, 2 : 5 : 5; MTHF: 2-methyltetrahydrofuran; MCH: methylcyclohexane.

broadening of the molecule. While the effect of solvent perturbation on the radiationless transition rate has been observed recently in anthracenes in the low temperature region,[6] it is not clear as to what extent this effect might have on both the radiative and the radiationless transition rate of the quinoline molecule. The greater change in lifetime observed in hydroxylic solvents appears to indicate the enhancement of inhomogeneous line broadening in hydroxylic solvents, though the effect of using a narrower bandwidth can not be entirely discounted. It is also worth noting that in a recent study of diphenylanthracence fluorescence in EtOH low temperature glass,[7] the fluorescence band shift with the excitation wavelength has been attributed to the effect caused by the inhomogeneous line broadening.

Thus, in view of these results, it is concluded that the excitation wavelength dependence of quinoline phosphorescence lifetime observed in this study is most likely due to the solvent induced inhomogeneous line broadening effect on both the radiative and the radiationless relaxation processes of the lowest triplet state.

Experimental

Quinoline used for the measurement of phosphorescence lifetime and spectrum was laboratory reagent (BDH Chemicals) and guaranteed reagent (Tokyo Kasei) respectively and these were further purified by successive vacuum distillation. Spectrograde ethyl alcohol was used as received for the measurement of phosphorescence spectrum and the other solvent used for the lifetime measurement were treated with activated charcoal to remove luminescent impurities. Quinoline solutions of 10^{-3} M concentration were all degassed and sealed in the supracil tubes. The phosphorescence lifetime was calculated from the oscilloscope trace obtained by using a xenon flash lamp excitation source of 5 microsecond duration which was coupled with a 1/4 meter B & L monochromator. Both the entrance and the exit slit widths were set at 1.0 mm (bandwidth of 7.4 nm) for measurement in EtOH and EPA solvents and 1.5 mm (bandwidth of 11.1 nm) for those measured in methylcyclohexane and 2-methyltetrahydrofuran. A Corning 3-73 filter was used in front of the photomultiplier to eliminate scattered light. Phosphorescence spectra were measured using a fluorescence spectrometer Hitachi MPF-2A with the spectral resolution set at 10 nm.

The authors are grateful to Professor T. Azumi for the reprints on subjects relevant to this study.

References

1) E. C. Lim and J. M. H. Yu, *J. Chem. Phys.*, **47**, 3270 (1967).
2) M. F. Anton and W. R. Moomaw, *J. Chem. Phys.*, **66**, 1808 (1977).
3) K. Itoh and T. Azumi, *J. Chem. Phys.*, **62**, 3431 (1975).
4) W. C. Galley and R. M. Purkey, *Proc. Natl. Acad. Sci. U. S. A.*, **67**, 1116 (1970); W. Klopffer, *Chem. Phys. Lett.*, **11**, 482 (1971); P. R. Callis and R. W. Wilson, *ibid.*, **13**, 417 (1972); O. S. Khalil, C. J. Seliskar, and S. P. McGlynn, *J. Chem. Phys.*, **58**, 1607 (1973).
5) P. M. Johnson and D. Levin, *Mol. Photochem.*, **6**, 263 (1974).
6) I. F. Hung and B. R. Henry, *Chem. Phys.*, **27**, 263 (1978).
7) G. Flatscher, K. Fritz, and J. Friedrich, *Z. Naturforsch., Teil A*, **31**, 1220 (1976).

BULLETIN OF THE CHEMICAL SOCIETY OF JAPAN, VOL. 51 (11), 3385—3386 (1978)

Polymorphism and the Structure of Bis(dichloromethylene)succinic Acid as Studied by Chlorine NQR

Masao HASHIMOTO,* Koichi MANO,** and Akira FUJINO**

Department of Chemistry, Faculty of Science, Kobe University, Nada-ku, Kobe 657

*** Research Institute for Atomic Energy, Osaka City University, Sugimoto-cho, Sumiyoshi-ku, Osaka 558*

(Received April 28, 1978)

Synopsis. It was found that bis(dichloromethylne) succinic acid (BDCSA) has two crystal forms, the molecule having an *s-trans* conformation in each form. A frequency drop of about 1 MHz found for BDCSA might be explained in terms of a short intramolecular contact between the chlorine and oxygen atoms.

The ^{35}Cl NQR frequencies were measured for bis(dichloromethylene)succinic acid (BDCSA), its anhydride (BDCSAA), trichloroacrylic acid (TCAA), and methyl trichloroacrylate (MTCA) in order to investigate the structure of BDCSA. Details of NQR experiments and methods of preparation of the compound studied were reported.[1,2]

Crystals of BDCSA obtained by recrystallizations from ether gave NQR two lines (designated as α-spect rum), while a specimen crystallized from water afforded four lines (β-spectrum). It is evident that BDCSA has two crystal forms.[3] The resonance frequencies for these two spectra are given in Table 1, together with those for the related compounds. The spectra are also shown as stick diagrams in Fig. 1. Both α-and β-spectra exhibit considerably large frequency splittings of about 1 MHz. In the β-spectrum, the four lines seem to be devided into two frequency groups, a higher (38.430 MHz, average of ν_1 and ν_2) and a lower (37.535 MHz, average of ν_3 and ν_4).

As to the structure of BDCSA, there are two conformational possibilities, *i.e.*, *s-trans* (I) and *s-cis* (II)

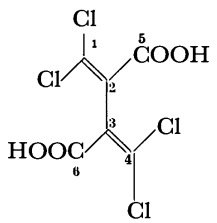

(I)

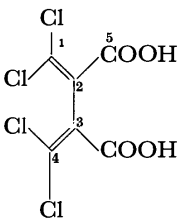

(II)

forms.[4] If BDCSA has an *s-cis* form in both crystalline modifications, the NQR spectrum is expected to be similar to that for BDCSAA being forced to have an *s-cis* form. However, the lower frequency group of the former is situated far below the average (38.238 MHz) of ν_1 and ν_2 of the latter (Fig. 1). This suggests that BDCSA has an *s-trans* form.

From a comparison of the spectrum for TCAA with that of MTCA, their ν_2 and ν_3's can be assigned to geminal vinylic chlorine atoms. The NQR spectra of these two compounds and BDCSAA indicate that the geminal vinylic chlorine atoms in BDCSA would afford their NQR lines in a region, 38.2±0.3 MHz. The higher-frequency lines in BDCSA (ν_a in the α-, and ν_1 and ν_2 in the β-spectrum) appear in this anticipated region, but the lower-frequency lines lie in a frequency region significantly lower by about 1 MHz. Since both α- and β-spectra show a similar pattern, the large frequency drop might be attributed to an intramolecular phenomenon. The abnormal drop causes one to imagine an intramolecular hydrogen-bond formation between one of the chlorine atoms at C-1 position and the carboxyl group (at C-3 position) on the same side.[5] If this is correct, the magnitudes of the temperature coefficient of resonance frequencies for the lower-frequency lines should be smaller than those for the higher-frequency lines.[5] However, no such tendency was observed (Table 2).

Thus, the hydrogen-bond model does not seem to be applicable to the explanation of the large frequency drop. An alternative and most likely interpretation

TABLE 1. THE ^{35}Cl NQR FREQUENCIES (f) FOR BIS(DICHLOROMETHYLENE)SUCCINIC ACID AND RELATED COMPOUNDS AT 77 K

Compounds		No. of lines	f/MHz
BDCSA	α-spectrum	ν_a	38.489
		ν_b	37.478
	β-spectrum	ν_1	38.530
		ν_2	38.330
		ν_3	37.772
		ν_4	37.299
BDCSAA		ν_1	38.370
		ν_2	38.106
TCAA		ν_1	39.245
		ν_2	38.549
		ν_3	37.933
MTCA		ν_1	39.648
		ν_2	38.230
		ν_3	38.160

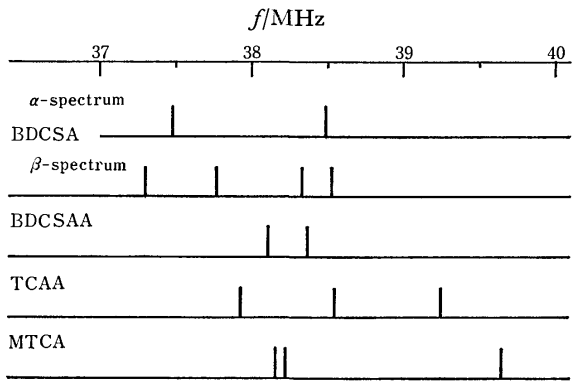

Fig. 1. The ^{35}Cl NQR spectra of bis(dichloromethylene)succinic acid and related compounds at 77 K.

Table 2. Temperature coefficients of resonance frequency (df/dT) in bis(dichloromethylene)-succinic acid

No. of lines	$\frac{df/dT}{kHz/K}$
ν_a	−2.20
ν_b	−3.14
ν_1	−2.45
ν_2	−1.83
ν_3	−2.43
ν_4	−4.05

for the frequency drop would be a short contact between the chlorine atom on position 1 and an oxygen atom in the carboxyl group on 6. A similar frequency drop was reported in the case of chloral hydrate.[6]

References

1) M. Hashimoto, *Bull. Chem. Soc. Jpn.*, **50**, 1746 (1977).

2) A. Fujino, Y. Nagata, and T. Sakan. *Bull. Chem. Soc. Jpn.*, **38**, 295 (1965).

3) Both the elementary analysis (Found: C, 25.74; H, 0.69%. Calcd for $C_6Cl_4H_2O_4$: C, 25.75; H, 0.72%) and the IR data support the absence of water of crystallization for the one crystallized from water. This polymorphism was also confirmed by X-ray diffraction method.

4) No planarity was found in the two double bonds on the basis of the UV spectra of BDCSA (Ref. 2).

5) A. Sasane, T. Matuo, D. Nakamura, and M. Kubo, *Bull. Chem. Soc. Jpn.*, **43**, 1908 (1970).

6) H. Chihara and N. Nakamura, *Bull. Chem. Soc. Jpn.*, **45**, 3530 (1972).

BULLETIN OF THE CHEMICAL SOCIETY OF JAPAN, VOL. 51 (11), 3387—3388 (1978)

Surface Nonstoichiometry and Isoelectric Point of Manganese Oxide

Tetsuo MORIMOTO, Hidetoshi NAKAHATA, and Shigeharu KITTAKA*,†

Department of Chemistry, Faculty of Science, Okayama University, Tsushima, Okayama 700

† *Department of Chemistry, Faculty of Science, Okayama College of Science, 1-1 Ridaicho, Okayama 700*

(Received May 18, 1978)

The isoelectric point and the nonstoichiometric composition of the surface layer were measured for manganese oxide samples treated *in vacuo* or in air at elevated temperatures. It was found that the surface composition of most samples tested was oxygen-deficient with reference to the bulk composition, and that the IEP was determined by the bulk structure rather than the surface composition. This was ascribed to the fact that the surface is heterogeneous and the dissolution of the solid will take place preferentially at surfaces which involve defect structures or Mn(II) ions.

Transition metals form a variety of nonstoichiometric compounds not only in the interior but also on the surface of the solids. Accordingly, the oxygen content on the surface of such metal compounds as oxides is liable to be excessive or deficient with reference to the bulk composition, as revealed from ESR study[1,2] or the test of the oxidizing power of the solid surface.[3–5] This situation should affect significantly the physical and chemical properties of solid surfaces, but few quantitative relationships between the nonstoichiometry and the properties of solid surfaces have been disclosed. Several authors studied surface excess oxygen in NiO,[3,6] Cr_2O_3,[4,7,8] and MnO_2[5] in connection with their catalytic activity.

In the preceding paper[9] the isoelectric point (IEP) of manganese oxide was studied as a function of pretreatment temperature. The results showed that the IEP of manganese oxide had a value characteristic of the bulk composition of the solid, which changed in three stages with increasing temperature of treatment; the results obtained were interpreted in terms of the idea that the IEP is governed by the valency and the coordination number of surface manganese ions. The IEP of samples treated at temperatures lower than 300 °C had such small values that the existence of Mn(IV) ions with the coordination number 4 on the surface was suggested.

We can naturally expect a drastic change in surface composition when a sample is treated *in vacuo* at elevated temperatures. This paper is concerned with the effect of evacuation treatment on the IEP value of manganese oxide and on the surface composition.

Experimental

Materials. The original sample of manganese oxide used in this study was prepared by the pyrolysis of guaranteed grade $Mn(NO_3)_2 \cdot 6H_2O$ at 160 °C for 400 h in an electric oven.[9] Powdered oxide was washed sufficiently with distilled water and finally electrodialyzed until the electrical conductivity of the supernatant solution was approximately equal to the value of deionized water (1.43×10^{-6} $\mho cm^{-1}$). Then it was dried at 110 °C for 24 h in an electric oven, followed by the evacuation for 5 h at 300, 800, or 1000 °C in a vacuum of 1.33×10^{-3} Pa (M-300, M-800, and M-1000).

Another series of samples were also prepared by heating the samples M-300, M-800, and M-1000 for 5 h in air at 300, 800, and 1000 °C, respectively (M-300A, M-800A, and M-1000A).

Reaction of Surface Layer with KI. The reactivity of the solid surface with KI was examined in a vessel with the capacity of 300 cm^3, equipped with a breaking system of an ampoule containing the powdered sample. The sample was introduced into an ampoule by 2 m^2, evacuated at room temperature, and sealed. The ampoule was mounted on the ampoule holder and immersed in 100 cm^3 of a buffer solution containing 1.0 g KI. The space above the solution in the vessel was filled with N_2 to avoid the influence of air, and the vessel was thermostatted at 45 °C. After the equilibration of the system, the ampoule was broken and a vigorous shaking of the solution was started. For the preparation of buffer solutions the combination of $Na_2B_4O_7 \cdot 10H_2O$ and KH_2PO_4, which covers the wide range of pH values 5.4—9.0, was selected, because a preliminary test showed that a different combination of constituents of buffer solutions somewhat alters the reactivity of manganese oxide. After the attainment of reaction equilibrium, the amount of iodine was determined by titrating the solution with a standard $Na_2S_2O_3$ solution (1×10^{-3} mol/dm^3) by use of starch as an indicator. At the same time, the amount of Mn(II) ions dissolved was determined spectroscopically after treating the solution with 2% oxine.[10]

Measurement of IEP. The IEP value was measured by means of the streaming potential method, as described previously.[11]

Results and Discussion

Figures 1, 2, and 3 give the amounts of iodine and Mn(II) ions which were formed by the reaction of KI with manganese oxide surfaces, as a function of pH. The results obtained show that the amount of reaction products decreases exponentially with increasing pH and vanishes at pH 8. Under the present conditions, the dissolution of manganese oxide takes place according to the following reactions:

$$MnO + 2H^+ \longrightarrow Mn^{2+} + H_2O \quad (1)$$

$$MnO_2 + 4H^+ + 2I^- \longrightarrow Mn^{2+} + I_2 + 2H_2O \quad (2)$$

$$O(s) + 2H^+ + 2I^- \longrightarrow I_2 + H_2O \quad (3)$$

Reaction 1 implies the dissolution of Mn(II) oxide, which is an oxygen-deficient compound possibly formed on the surface of manganese oxide, and Reaction 3 the dissolution of excess oxygens on MnO_2 surfaces. If the surface composition of a sample is somewhat smaller in oxygen content than MnO_2, Reactions 1 and 2 will take place simultaneously, whereas if it is somewhat larger than MnO_2, Reactions 2 and 3 will occur simultaneously. The fact that the dissolved amounts of both iodine and Mn(II) ions

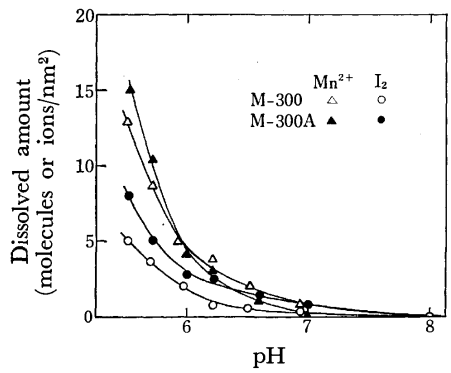

Fig. 1. pH dependence of the amounts of I_2 and Mn(II) ions formed from sample M-300 and M-300A.

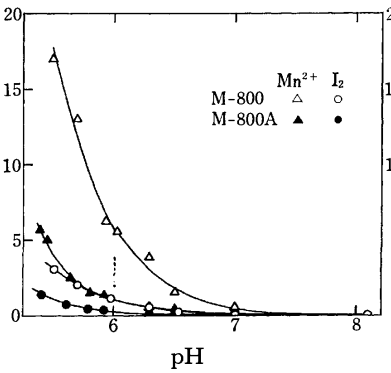

Fig. 2. pH dependence of the amounts of I_2 and Mn(II) ions formed from the sample M-800 and M-800A.

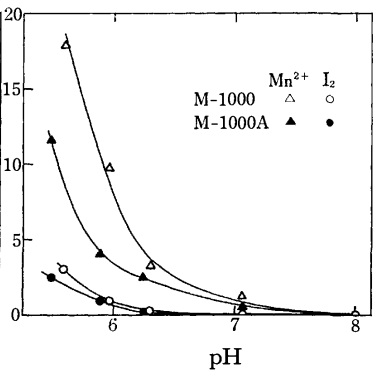

Fig. 3. pH dependence of the amounts of I_2 and Mn(II) ions formed from sample M-1000 and M-1000A.

TABLE 1. COMPOSITION OF SURFACE LAYER OF MANGANESE OXIDE

Sample	Surface area[a] ($m^2\ g^{-1}$)	Crystal structure[b]	pH	x value in MnO_x					*IEP*
				5.4 | 5.5	5.6 | 5.7	5.9 | 6.0	6.2 | 6.3	6.5 | 6.6	
M-300	2.24	β-MnO_2		1.40	1.37	1.36	1.30	1.19	<3
M-300A	1.86	β-MnO_2		1.53	1.55	1.66	1.94	2·44	<3
M-800	0.960	Mn_3O_4		1.19	1.16	1.16	1.15	1.14	4.54
M-800A	1.31	α-Mn_2O_3		1.27	1.27	1.25	1.21	1.22	8.17
M-1000	0.536	Mn_3O_4		—	1.16	1.07	1.03	—	3.30
M-1000A	0.605	Mn_3O_4		1.15	—	1.12	1.11	—	3.22

a) Measured by N_2-adsorption, assuming the molecular area to be 0.162 nm^2.
b) Determined by X-ray analysis.

increase rapidly with decreasing pH is due to the increase in solubility and oxidation potential of manganese oxide with pH, as shown in Eqs. 1, 2, and 3.

The data in Figs. 1—3 permit the calculation of the composition of dissolved substances, as given in Table 1, where the x value in MnO_x is listed. In addition, the thickness of the dissolved layer can be estimated. It was found to be about 2.4 layers at maximum at pH 5.5 (Fig. 1) by assuming that the real surfaces are mainly composed of the (110) plane,[12] which has a Mn(IV) ion density of 5.55 nm^{-2}. Table 1 indicates that the surface composition of samples evacuated at elevated temperatures is deficient in oxygen with reference to the bulk composition, and that the succeeding treatment in air at the same temperature as before does not give such a large increment in surface oxygen. Thus the surface is still kept deficient in oxygen with respect to the bulk composition, except for the case of M-300A.

In Table 1, the *IEP* values of samples are also listed. Here, one can see that the sample treated *in vacuo* at 800 °C exhibits a small *IEP* value 4.54, but this increases to 8.17 when treated in air, and is accompanied by the conversion from Mn_3O_4 to α-Mn_2O_3 of the bulk composition. The present results, including this finding, have the same tendency as those obtained in the previous work:[9] manganese oxide gives *IEP* values characteristic of the bulk structure, which changes with heat treatment at different temperatures. Admittedly, no intimate correlation was found between surface composition and *IEP*. It seems at first sight strange that the *IEP* does not depend on the surface composition, but is determined by the bulk structure. This may be due to the fact that the solid surface is heterogeneous, and consequently the reaction with KI or the dissolution of the solid takes place preferentially at the surface, which involves defect structures or Mn(II) ions. On the same surface, a more stable structure which is dissolved only with difficulty should also be present: manganese ions on this part of the surface will determine the *IEP* of samples.

Finally, the extremely small *IEP* values of the 300-treated samples, *i.e.* less than 3, still have not been elucidated in this study; but there remains the possibility of the existence of Mn(IV) ions with the coordination number 4, which comes from the oxygen-deficient states of the surface.

References

1) R. D. Iyenger and M. Codell, *Adv. Colloid Interface Sci.*, **3**, 365 (1972).
2) Y. Mizokawa and S. Nakamura, *Jpn. J. Appl. Phys.*, **14**, 779 (1975).
3) T. Uchijima, M. Takahashi, and Y. Yoneda, *Bull. Chem. Soc. Jpn.*, **40**, 2767 (1967).
4) S. Weller and S. E. Voltz, *J. Am. Chem. Soc.*, **76**, 4695 (1954).
5) Y. Inoue, S. Hasegawa, and T. Kawaguchi, *Nippon Kagaku Zasshi*, **91**, 1034 (1970).
6) T. Uchijima, M. Takahashi, and Y. Yoneda, *J. Catal.*, **9**, 403 (1967).
7) J. Deren, J. Haber, A. Podgorecka, and J. Burzyk, *J. Catal.*, **2**, 161 (1963).
8) J. Deren and J. Haber, *J. Catal.*, **4**, 22 (1965).
9) T. Morimoto and S. Kittaka, *Bull. Chem. Soc. Jpn.*, **49**, 1586 (1974).
10) K. Motojima, H. Hashitani, and T. Imahashi, *Anal. Chem.*, **34**, 571 (1962).
11) S. Kittaka, *J. Colloid Interface Sci.*, **48**, 327 (1974).
12) L. G. Berry and B. Mason, "Mineralogy," W. H. Freeman and Co., San Francisco (1959), p. 373.

BULLETIN OF THE CHEMICAL SOCIETY OF JAPAN, VOL. 51 (11), 3389—3390 (1978)

The Reaction of Phenylacetonitriles with Benzaldehydes in Hexamethylphosphoric Triamide Solution Containing the Sodium Salt of α,α-Dimethylbenzyl Hydroperoxide[1,2]

Kazumasa TAKAHASHI,* Kazutoshi YAMADA, and Hirotada IIDA
Department of Synthetic Chemistry, Chiba University, Yayoi-cho, Chiba 280

(Received December 5, 1977)

Synopsis. Treatment of phenylacetonitriles with *p*-substituted benzaldehydes in hexamethylphosphoric triamide solution containing the sodium salt of α,α-dimethylbenzyl hydroperoxide gave α-benzoyl-α-phenylacetamides as major products.

The reaction of phenylacetonitriles with *p*-substituted benzaldehydes was carried out in hexamethylphosphoric triamide (HMPA) solutions containing the sodium salt of α,α-dimethylbenzyl hydroperoxide (I). α-Benzoyl-α-phenylacetamide derivatives (II) were obtained as major products (Scheme 1 and Table 1). However, the treatment of diphenylacetonitrile and α-phenylpropionitrile having substituents in the α-position with *p*-anisaldehyde gave oxidation products of the starting materials, but not the corresponding benzoyl-acetamides. I has both strongly basic and oxidative properties. However, no report seems to have been made on the use of these properties of I in reactions. The properties were found to act effectively in an HMPA solution.

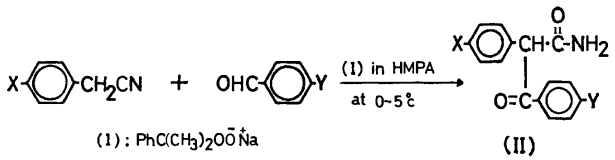

Scheme 1.

Results and Discussion

The reactions of phenylacetonitriles with *p*-substituted benzaldehydes were carried out in HMPA solutions in the presence of I, giving benzoyl-acetamides (II) in 40—55% yield (Table 1). The reaction of phenylacetonitrile with *p*-nitrobenzaldehyde, however, gave various products, but no product of type II. In all cases except the case of *p*-nitrobenzaldehyde, the color of the reaction solution was reddish orange. In the case of *p*-nitrobenzaldehyde, it was purple-blue, characteristic of nitrobenzene radical anions.[3]

The treatment of diphenylacetonitrile with *p*-anisaldehyde gave oxidation products, benzophenone and *p*-anisic acid. The yield of benzophenone was 78%. The expected benzoyl-acetamide was not obtained. Likewise, the treatment of α-phenylpropionitrile with *p*-anisaldehyde gave acetophenone and *p*-anisic acid, but not the corresponding benzoyl-acetamide either.

The mechanism for the formation of the benzoyl-acetamides (II) is assumed as follows. The acidic α-hydrogen of phenylacetonitrile is abstracted by I and the α-cyanophenylmethanide ion thus formed nucleophilically attacks the carbonyl group of benzaldehydes to give III (Eqs. 1 and 2, Scheme 2). Intermediate III is oxidized by the hydroperoxide shown in Eq. 1 or by I to give α-benzoyl-α-phenylacetamide II. The problem is how III is oxidized to give benzoyl-acetamide (II). The reaction of 2-cyano-1,2-diphenylethanol (III'), which is the protonated form of the hypothetical intermediate (III), was assumed to react with I. However, various attempts to synthesize III' were unsuccessful. It was presumed that the cyano group of α-cyanodeoxybenzoin (V) (Eq. 2) is oxidized by I. However, when α-cyanodeoxybenzoin (V) synthesized[4] was treated with I, no oxidation of the cyano group took place. When (*E*)-α-phenylcinnamonitrile (IV) obtained as a minor product in *ca.* 10% yield was treated with I, the corresponding benzoyl-acetamide (II) was obtained in 39% yield. The treatment of phenylacetonitrile and benzaldehyde using a base such as sodium hydroxide or sodium ethoxide has been reported to give IV in 87—97% yield.[10] The low yield of IV in the present work is due to the further conversion of IV into benzoyl-acetamide (II). The formation of the benzoyl-acetamide (II) is accounted for by both the nucleophilic reaction of I to the double bond, and the hydrolysis of the cyano group. The nucleophilic reaction is most likely caused by the complex of ROONa (I) with ROOH produced (Eq. 1), which is more reactive than ROONa itself.[11] The mechanism (Scheme 2) is further supported by the fact that the reaction with use of diphenylacetonitrile or α-phenylpropionitrile, which cannot form an intermediate such as IV, gave no products corresponding to the compound II.

The mechanism by which the reaction with use of diphenylacetonitrile or α-phenylpropionitrile gave the corresponding ketone is shown in Eqs. 3 and 4 (Scheme 2). The nucleophilic addition of a carbanion to a carbonyl group is thought to be a reversible process.[5] Since VI cannot undergo a process leading to the formation of α-phenylcinnamonitrile, the oxidation process to give benzophenone or acetophenone would proceed efficiently.

Experimental

All the melting points were uncorrected. The sodium salt of α,α-dimethylbenzyl hydroperoxide (I) was prepared from technical-grade α,α-dimethylbenzyl hydroperoxide according to the procedure of Belyaev and Nemtsov.[6] The peroxide content of I was estimated to be 65% by iodometric titration. *p*-Tolylacetonitrile and *p*-chlorophenylacetonitrile were synthesized by the reaction of *p*-methylbenzyl and *p*-chlorobenzyl chlorides with sodium cyanide.[7]

Table 1. Yields and physical data of new compounds (IIa—IIg)[a]

Compd	Yield %	Mp °C	IR(KBr), cm^{-1} ν_{NH}	IR(KBr), cm^{-1} ν_{CO}	UV(EtOH) λ nm	UV(EtOH) $\varepsilon\times10^{-4}$	Mass M^+	NMR, δ units (DMSO-d_6)	Calcd(Found)% C	H	N
IIa	41	181—	3400	1690	206	1.52	269	7.61(2H, m), 7.5—7.3(7H,	71.36	5.61	5.20
X=H		181.5	3300	1660	235	1.88		m), 6.91(2H, d, J=9 Hz),	(71.47)	(5.55)	(5.15)
Y=OCH_3			3150					4.20(1H, s), 3.79(3H, s)			
IIb	55	181—	3400	1690	205	2.39	253	7.61(2H, m), 7.5—7.0(9H,	75.87	5.97	5.53
X=H		182	3250	1660	236	2.18		m), 4.15(1H, s), 2.30(3H,	(75.82)	(5.97)	(5.49)
Y=CH_3			3150					s)			
IIc[b]	45	205—	3400	1680	206	2.00	239	7.60(2H, b·m), 7.37(10H,	75.30	5.48	5.85
X=H		207	3250	1660	226	1.99		s-like), 4.28(1H, s)	(75.23)	(5.51)	(5.82)
Y=H			3150								
IId	43	189.5	3400	1660	205	2.56	273	7.65(2H, b·m), 7.5—7.2	65.82	4.42	5.12
X=H		—190	3300	(broad)	230	2.35		(9H, s-like), 4.30(1H, s)	(65.96)	(4.35)	(5.25)
Y=Cl			3200								
IIf	37	192—	3350	1690	205	2.39	283	7.55(2H, s-like), 7.5—	72.06	6.05	4.94
X=CH_3		193	3260	1660	236	2.18		7.1(6H, m), 6.85(2H, d,	(72.35)	(6.03)	(4.88)
Y=OCH_3			3150					J=9 Hz), 4.10(1H, s),			
								3.75(3H, s), 2.30(3H, s)			
IIg	40	211—	3370	1660	211	2.10	304	7.70(2H, m), 7.6—7.2(6H,	63.27	4.65	4.61
X=Cl		212	3260	(broad)	237	2.52		m), 6.85(2H, d, J=9 Hz),	(63.16)	(4.46)	(4.55)
Y=OCH_3			3150					4.25(1H, s), 3.75(3H, s)			

a) The product corresponding to IIe (X=H, Y=NO_2) was not obtained. b) The compound (IIc) is a known compound. However, all its physical data are given since the melting point differs from that (178 °C) reported.[9]

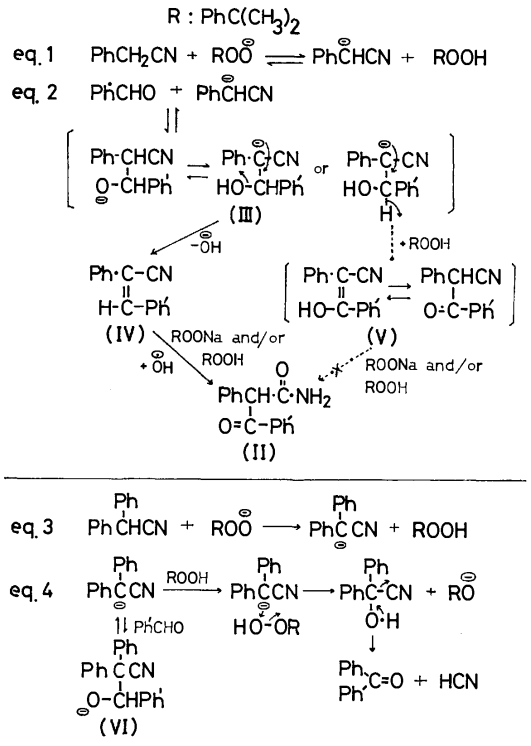

Scheme 2.

α-Cyanopropionitrile was prepared by the reaction of phenylacetonitrile with methyl bromide.[8]

Synthesis and Physical Properties of II. Into a 100-ml four-necked flask equipped with a thermometer and inlet and outlet tubes for nitrogen gas was placed 5.36 g(0.02 mol) of I dissolved in 25 ml of HMPA. To the solution maintained at 0—5 °C was added a mixture of 0.585 g(0.005 mol) of phenylacetonitrile and 0.682 g(5.5 mmol) of *p*-anisaldehyde in 5 ml of HMPA under nitrogen atmosphere. The mixture was stirred at 0—5 °C for 4 h and then poured into an aqueous solution of ammonium chloride . The aqueous layer was extracted several times with ether and then with benzene (*ca.* 200 ml each). The combined extracts were washed with water and dried over anhydrous sodium sulfate. After the solvents had been evaporated, compound IIa was separated as white crystals and recrystallized from benzene. Other acetamides (IIa—g) except IIe were prepared in a similar way. Their structures were confirmed by UV and IR spectra, MS and elementary analyses (Table 1).

α-Cyanodeoxybenzoin (V). The benzoin was synthesized by a modification of the procedure of Coan and Becker[4] and recrystallized from ethanol; mp 93—94.5 °C (lit,[9] 90 °C), MS: M^+ 221, IR(KBr): νC=O 1690 cm^{-1}, νCN 2250 cm^{-1}, UV: λ_{max}^{EtOH} 292 nm $\varepsilon=1.25\times10^4$. The benzoin (0.553 g, 2.5 mmol) was treated with (I) (2.68g, 2.5 mmol) dissolved in 15 ml of HMPA. However, no reaction took place, most of V being recovered.

(E)-*α-Phenylcinnamonitrile (IVc).* The physical properties of IVc (mp 83—84 °C), isolated together with the benzoyl-acetamide (IIc), agreed with those (mp 86 °C) of the known sample synthesized according to the procedure of Wawzonek and Smolin.[10] The cinnamonitrile (0.683 g, 3.3 mmol) was treated with I (3.57 g, 13 mmol) dissolved in 20 ml of HMPA at 0—5 °C for 4 h. The corresponding benzoyl-acetamide (IIc) was obtained in 39% yield.

References

1) This paper forms part X of "Studies on the Base-catalyzed Reaction."

2) Part IX . K. Takahashi, T. Okamoto, K. Yamada, and H. Iida, *Synthesis*, **1977**, 58.

3) G. A. Russell, E. G. Janzen, and E. T. Strom, *J. Am. Chem. Soc.*, **86**, 1807 (1964); H. Iida, M. Yamazaki, K. Takahashi, and K. Yamada, *Nippon Kagaku Kaishi*, **1976**, 138.

4) S. B. Coan and E. I. Becker, *Org. Syn.* Coll. Vol. **4**, 174 (1963).

5) E. M. Kaiser and C. R. Hauser, *J. Org. Chem.*, **31**, 3317 (1966).

6) V. A. Belyaev and M. S. Nemtsov, *Zh. Obshch. Khim.*, **31**, 3855(1961).

7) R. Adams and A. F. Thal, *Org. Syn.*, Coll. Vol. I, 107 (1967).

8) M. Makosza and B. Serafin, *Rocz. Chem.*, **39**, 1401 (1965); *Chem. Abst.*, **64**, 17474 g.

9) E. F. J. Atkinson, H. Ingham, and J. E. Thorpe, *J. Chem. Soc.*, **91**, 592 (1907).

10) S. Wawzonek and E. M. Smolin, *Org. Syn.*, Coll. Vol. III, 715 (1965).

11) V. A. Belyaev and M. S. Nemtsov, *Zh. Obshch. Khim.*, **32**, 3113 (1962).

BULLETIN OF THE CHEMICAL SOCIETY OF JAPAN, VOL. 51 (11), 3391—3392 (1978)

The Chemistry of Isocyanic Acid and Its Derivatives. Part V.[1] The Oxidative Coupling of Ethyl Carbamate and Urea with Cyclohexene, Tetrahydrofuran, and Cyclooctadiene Effected by Palladium(II) Chloride[2]

Shoichiro OZAKI* and Akihiro TAMAKI

Research Center, Mitsui Toatsu Chemicals, Inc., Kasama-cho, Totsuka-ku, Yokohama 247

(Received December 16, 1977)

Synopsis. The reaction of ethyl carbamate with cyclohexene promoted by $PdCl_2$ gave ethyl 1-cyclohexenylcarbamate. The reaction of ethyl carbamate and tetrahydrofuran gave ethyl 2-tetrahydrofurylcarbamate. Ethyl carbamate and 1,5-cyclooctadiene–$PdCl_2$ complex (**4**) reacted to give ethyl 4-cyclooctenylcarbamate. The reaction of urea and **4** afforded cyclooctylurea and 4-cyclooctenylurea.

Although various compounds bearing active hydrogens are known to undergo oxidative coupling reactions by the aid of palladous chloride,[3] the reactions of carbamates and ureas have been little studied. The communications by Kasahara *et al.* on the *intra*molecular cyclization reactions of unsaturated amides[4] and ureas[5] prompted the present authors to publish the results of their studies[2] of the *inter*molecular oxidative coupling reactions of ethyl carbamate and urea with cyclic olefins.

Ethyl 1-cyclohexenylcarbamate (**1**) and ethyl phenylcarbamate (**2**) were obtained by heating a mixture of cyclohexene, ethyl carbamate, and palladium(II) chloride.[2a]

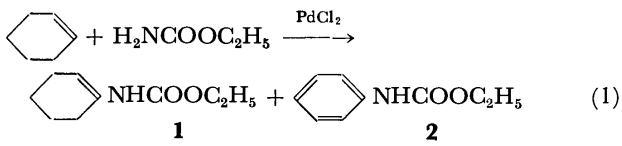

(1)

It is of interest that ethyl carbamate did not attack the allylic position of cyclohexene, while CN^- [6] and AcO^- [7] did. The hydrogen-transfer reaction, *e.g.*, Eq. 2, might be responsible for the formation of **2**:

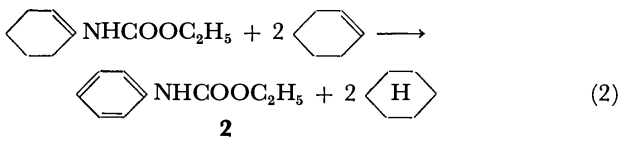

(2)

An attempted reaction of the same mixture in tetrahydrofuran did not give the expected products, but instead gave ethyl 2-tetrahydrofurylcarbamate (**3**) in a 30% yield.[2b]

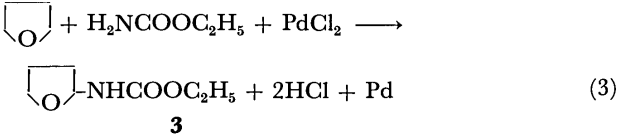

(3)

This reaction is a new type of oxidative coupling, in which tetrahydrofuran, instead of olefin, is activated by palladium(II) chloride. Attempted reactions in benzene, diethyl ether, anisole, ethanol, or *N,N*-dimethylformamide, did not give any oxidative coupling products.

Ethyl carbamate also reacted with the 1.5-cyclooctadiene palladous chloride complex (**4**) to afford ethyl 4-cyclooctenylcarbamate (**5**).[2c]

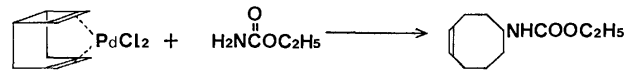

(4)

Urea did not give any coupling product with cyclohexene, in either the presence or absence of a solvent. Urea-olefin coupling products, cyclooctylurea (**6**) and 4-cyclooctenylurea (**7**), however, were obtained when **4** was made to react with urea in *N,N*-dimethylacetamide.

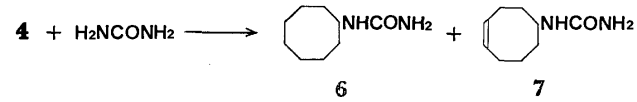

(5)

Experimental

Reaction of Cyclohexene with Ethyl Carbamate. Cyclohexene (15 g, 0.183 mol), ethyl carbamate (30 g, 0.337 mol), and palladium(II) chloride (1 g, 0.00562 mol) were mixed and stirred at 60 °C for 23 h. After agitation under an hydrogen atmosphere for 3 h, the reaction mixture was extracted with petroleum benzine, the solvent was removed by evaporation, and the residue was distilled under reduced pressure to give two fractions. The first fraction (0.39 g; 38.1%, based on palladium(II) chloride; bp 64 °C/0.18 mmHg) was found to be **1** by means of an NMR measurement [(neat) δ 1.22 (3H, triplet, CH_3), 1.17 (8H, multiplet, CH_2-ring) 4.02 (2H, quartet, OCH_2–C), 5.12 (1H, singlet, NH), 5.54 (1H, multiplet, –CH=)], and elemental analysis. Found: C, 64.13; H, 9.01; N, 7.97%. Calcd for $C_9H_{15}NO_2$: C, 63.88; H, 8.94; N, 8.28%. The second fraction (0.53 g; 53.0%; bp 78—82 °C/0.14 mmHg) was found to be **2** by means of an NMR measurement [(neat) δ 1.25 (3H, triplet, CH_3), 4.15 (2H, quartet, O–CH_2–C), 7.25 (5H, multiplet, C_6H_5+ NH)], and elemental analysis. Found: C, 65.22; H, 7.00; N, 8.19%. Calcd for $C_9H_{11}NO_2$: C, 65.44; H, 6.71; N, 8.48%.

*Ethyl 2-Tetrahydrofurylcarbamete (**3**).* A mixture of tetrahydrofuran (41 g, 0.5 mol), palladium(II) chloride (1.0 g, 0.0056 mol), ethyl carbamate (0.89 g, 0.01 mol), and disodium hydrogenphosphate (1.6 g, 0.0112 mol) was stirred for 1 h at room temperature, and then cyclohexene (5.0 ml, 0.049 mol) was added; there after the mixture was stirred for additional 17 h at room temperature and subsequently exposed to a hydrogen atmosphere for 4 h. The mixture was then filtered, and the filtrate was concentrated and, after the addition of a small amount of water, extracted with benzene and ether. The extract was dried with anhydrous sodium sulfate and distilled under reduced pressure. The

product (0.267 g, 30%) (bp 71—5 °C/0.08 mmHg), which slowly solidified at room temperature and which melted at 44—46 °C, was found to be **3** by means of an NMR measurement [(in $CDCl_3$) δ 1.24 (3H, triplet, CH_3), 1.92 (4H, multiplet, CH_2-ring), 3.87 (2H, quartet, OCH_2-ethyl), 4.14 (2H, triplet, OCH_2-ring) 5.53 (2H, multiplet, CH=NH)] and elemental analysis. Found: C, 53.01; H, 8.26; N, 8.68%. Calcd for $C_7H_{13}NO_3$: C, 52.81; H, 8.23; N, 8.80%.

Ethyl 4-Cyclooctenylcarbamate (5). A mixture of **4** (2.0 g, 7 mmol), ethyl carbamate (1.50 g, 16.9 mmol), sodium carbonate (0.787 g, 7.3 mmol), and *N,N*-dimethylacetamide (40 ml) was stirred for 5 h at room temperature. Calcium hydride (3 g) was then added, and the mixture was agitated for an additional 10 h. The precipitated palladium black was filtered off, and the filtrate was concentrated and distilled under reduced pressure. Ethyl 4-cyclooctenylcarbamate (**5**) (0.811 g, 58.7% based on **4**) was thus obtained as a viscous oil; bp 110 °C/0.2 mmHg; NMR ($CDCl_3$) δ 1.23 (3H, t, CH_3), 1.58 (6H, m, CH_2), 2.25 (4H, m, =CH-$\underline{CH_2}$), 3.75 (1H, m, CH), 4.02 (2H, m, O-CH_2), 5.68 (3H, m, CH=CH+NH); IR (KBr), 3360, 2925., 1964, 1528, 1468, 1245, 1100, 1050, 780 cm^{-1}. Found: C, 67.16; H, 10.07; N, 7.35%. Calcd for $C_{11}H_{19}NO_2$: C, 66.97; H, 9.71; N, 7.10%.

Reaction of **4** *with Urea.* Urea (7.5 g, 0.125 mol), **4** (15 g, 0.052 mol), and anhydrous sodium carbonate (5.6 g, 0.052 mol) were added to *N,N*-dimethylacetamide (150 ml), and the mixture was stirred for 6.5 h at room temperature; palladium black separated in the meantime. Agitation was continued for an additional 41 h while calcium hydride (18 g) was added in small portions. The mixture was then filtered, and the filtrate was concentrated and extracted with chloroform at 50 °C. The subsequent evaporation of the solvent left 5.48 g of a white, crystalline solid (mp 144—155 °C), which was a mixture of cyclooctylurea (**6**) and cyclooctenylurea (**7**); on hydrogenation over the Pd–C catalyst, it gave **6** (5.21 g, 58.3% based on **4**); mp 175.5—176 °C; NMR (DMSO-d_6) δ 1.51 (14H, multiplet, CH_2), 3.53 (1H, multiplet, CH), 5.20 (3H, multiplet, NH+NH_2); molecular weight by vapor-pressure osmometry, 171 (Calcd, 170.23). Found: C, 63.43; H, 10.85; N, 16.39%. Calcd for $C_9H_{18}N_2O$: C, 63.49; H, 10.66; N, 16.45%.

References

1) For Paper IV in this series, see Y. Miyake, S. Ozaki, and Y. Hirata, *J. Polym. Sci., Part A1*, 899 (1969).

2) The authors have applied for Japanese Patents on their results. (a) Jpn. Patent 44-4541 (1969); *Chem. Abstr.* **71**, 60852c (1969); (b) Jpn. Patent 44-28900 (1969); *Chem. Abstr.* **72**, 43412q (1970); (c) Jpn. Patent 46-29844 (1971), *Chem. Abstr.* **76**, 140059v (1972).

3) P. M. Maitlis, "The Organic Chemistry of Palladium", New York, Academic Press, (1971), and the references therein.

4) A. Kasahara and T. Saito, *Chem. Ind.*, **1975**, 745.

5) A. Kasahara and N. Fukuda, *Chem. Ind.*, **1976**, 485.

6) J. Odaira, T. Oishi, T. Yukawa, and S. Tsutsumi, *J. Am. Chem. Soc.*, **88**, 4105 (1966).

7) W. Kitching, Z. Rappoport, S. Winstein, and W. G. Young, *J. Am. Chem. Soc.*, **88**, 2054 (1966).

BULLETIN OF THE CHEMICAL SOCIETY OF JAPAN, VOL. 51 (11), 3393—3394 (1978)

The Synthesis of Several Dipivaloylpolymethylbenzenes[1)]

Hitomi SUZUKI,* Yasuo AOMORI, Tadashi MISHINA, and Terukiyo HANAFUSA

Department of Chemistry, Faculty of Science, Hiroshima University, Higashi-sendamachi, Hiroshima 730

(Received February 7, 1978)

Synopsis. 2,4-Dipivaloyl-1,3,5-trimethylbenzene, 4,6-dipivaloyl-1,2,3,5-tetramethylbenzene, and 3,6-dipivaloyl-1,2,4,5-tetramethylbenzene were prepared by the Friedel-Crafts dipropionylation of the corresponding polymethylbenzenes, followed by the exhaustive methylation of the resulting diketones with potassium *t*-butoxide and methyl iodide in boiling benzene–*t*-butyl alcohol. The PMR and IR spectra are reported for these new compounds.

In connection with our work on the non-conventional reactions of polysubstituted aromatics, we needed hindered ketones of the (**8**) type, bearing a methyl group at the position flanked both sides by the bulky electron-withdrawing groups. To our knowledge, there is no published preparation of ketones with this particular structure. The traditional method for the direct synthesis of pivalophenones (2,2-dimethyl-1-phenyl-1-propanones) involves the reaction of pivaloyl chloride with arylmagnesium halides[2)] or with arenes in the presence of the Friedel-Crafts catalyst,[3)] and the reaction of pivalonitrile] with the appropriate Grignard reagent.[4)] Our attempts to convert hindered polymethylpivalophenones to the title diketones by the Friedel-Crafts method led to extensive deacylation as well as the formation of a complicated mixture of hydrocarbons and polymeric substances. The reactions of pivaloyl chloride with the Grignard reagent[5)] derived from bromopolymethylpivalophenones resulted only in the recovery of the parent polymethylpivalophenones. Likewise, attempts to prepare the diketones by the reaction of polymethylbenzenedicarbonitriles with *t*-butylmagnesium chloride failed, since no reaction took place.

Next we planned to prepare the diketones starting from polymethylbenzene-1,3-dicarboxylic acids and following the reaction sequence: diacids — diacid dichlorides — dipivaloylbenzenes. In a search for a simple procedure for converting the hindered acid chloride groups into pivaloyl groups, we examined the reaction of several polymethylbenzoyl chlorides with *t*-butylmagnesium chloride with or without the use of transition metal catalysts.[6)] The results were unpromising, however. When polymethylbenzoyl chloride (**1b—c**) was treated with an excess of the Grignard reagent, the reductive 1,2-addition occurred sluggishly, giving an ester as the sole product.[7)] The analytical and spectral data of this compound were consistent with the highly crowded structure (**4b—c**) (Table 1). As expected, neither attempts to saponify this ester by heating it with ethanolic potassium hydroxide or concentrated hydrochloric acid, nor attempts to obtain an authentic specimen from the reaction of alcohol (**5**) and acid chloride (**1**), were successful. However, this ester underwent reductive cleavage with lithium aluminum hydride in boiling tetrahydrofuran, giving two benzylic alcohols (**5** and **6**) in accord with the assigned structure **4**. Two possible mechanisms for the formation of the ester are given in Scheme 1. In order to differentiate between these two pathways, the aldehyde (**2b**) and ketone (**3b**) were each treated with *t*-butylmagnesium chloride under the same conditions. The latter compound was recovered unchanged, while the former gave the expected alcohol **5b**, supporting the first mechanism, in which the reaction proceeds *via* the aldehyde as intermediate.

Finally, we have found that the compounds of the **8** and **10** types are accessible *via* an indirect route involving the Friedel-Crafts dipropionylation of polymethylbenzenes,[8)] followed by the treatment of the resulting diketones with potassium *t*-butoxide and methyl iodide in boiling benzene/*t*-butyl alcohol (Scheme 2).[9)] The exhaustive methylation of the ketones, **7** and **9**, proceeded with ease, and the concurrent formation of the enol ethers was not significant.

All the dipivaloylpolymethylbenzenes obtained are well-crystallized solids melting between 128 and 232 °C with partial sublimation. They are moderately soluble in benzene, chloroform, and ether, and slightly soluble in carbon tetrachloride, hexane, and methanol. The PMR signals for pivaloyl groups in **8a,b** and **10** showed a slight splitting ($\Delta\delta<0.02$ ppm), and those for ring methyl groups appeared as a somewhat broad singlet, suggesting the occurrence of stereoisomerism as a result of the restricted rotation about the sp^2-sp^2 carbon-carbon bond at room temperature. Ring methyl signals for each pair of diketones **7/8** or **9/10** appeared nearly at the same chemical shifts, indi-

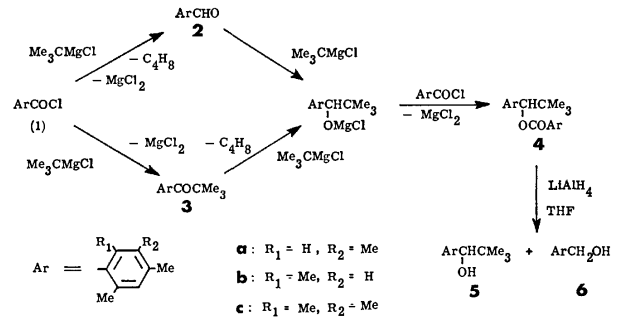

Scheme 1.

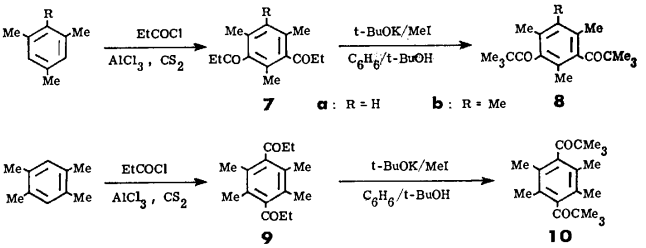

Scheme 2.

Table 1. Physical data for some diacylbenzenes and 1-aryl-2,2-dimethylpropyl benzoates

Compound	Mp (°C)	IR (ν_{max}, cm^{-1})	PMR (δ)	Yield[a] (%)
2,4-Dipropionyl-1,3,5-trimethylbenzene (**7a**)	99—101	865, 930, 1140, 1240, 1345, 1695	1.13(6H, t; J=7 Hz), 1.95(3H, s), 2.57(4H, q; J=7 Hz), 6.75(1H, s)	51
4,6-Dipropionyl-1,2,3,5-tetramethylbenzene (**7b**)	99—100	775, 930, 1110, 1340, 1400, 1690	1.13(6H, t; J=7 Hz), 1.90(3H, s), 2.07(6H, s), 2.13(3H, s), 2.57(4H, q; J=7 Hz)	65
3,6-Dipropionyl-1,2,4,5-tetramethylbenzene[b] (**9**)	170—172	945, 1000, 1113, 1335, 1405, 1700	1.18(6H, t; J=7 Hz), 2.05(12H, s), 2.60(4H, q; J=7 Hz)	26
2,4-Dipivaloyl-1,3,5-trimethylbenzene (**8a**)	128—130	865, 930, 1100, 1230, 1685	1.22(9H, s), 1.23(9H, s), 1.97(3H, s), 2.15(6H, s), 6.82(1H, s)	39
4,6-Dipivaloyl-1,2,3,5-tetramethylbenzene (**8b**)	166—168	910, 930, 1100, 1300, 1690	1.18(9H, s), 1.20(9H, s), 1.93(3H, s), 2.08(6H, s), 2.15(3H, s)	33
3,6-Dipivaloyl-1,2,4,5-tetramethylbenzene[b] (**10**)	230—232	948, 1085, 1270, 1680	1.22(9H, s), 1.23(9H, s), 2.07(12H, s)	40
1-(2,4,5-Trimethylphenyl)-2,2-dimethypropyl 2,4,5-trimethylbenzoate (**5a**)	208—209	1035, 1136, 1265, 1720	1.06(9H, s), 2.18(6H, s), 2.24(6H, s), 2.44(3H, s), 2.54(3H, s), 5.95 (1H, s), 6.89(1H, s), 6.96(1H, s), 7.14(1H, s), 7.76(1H, s)	~5
1-(2,4,6-Trimethylphenyl)-2,2-dimethylpropyl 2,4,6-trimethylbenzoate (**5b**)	126—128	1075, 1162, 1260, 1725	1.09(6H, s), 2.16(6H, s), 2.24(6H, s), 2.37(3H, s), 2.57(3H, s), 6.07 (1H, s), 6.80(4H, s)	56
1-(2,3,4,6-Tetramethylphenyl)-2,2-dimethylpropyl 2,3,4,6-tetramethylbenzoate (**5**)	130—131	1028, 1150, 1270, 1725	1.03(9H, s), 2.00(6H, s), 2.07(6H, s), 2.20(6H, s), 2.27(3H, s), 2.50 (3H, s), 6.35(1H, s), 6.70(2H, s)	50

a) Based on the isolated product. All new compounds gave satisfactory analyses. b) The PMR spectra were measured in deuteriochloroform.

cating that the preferred conformations of all the pairs of compounds are very similar.

On treatment with nitric acid in dichloromethane, **8b** underwent preferential attack upon the 2-methyl group at the most hindered position. This and other aspects of the reaction of this new compound will be reported in detail separately.

Experimental

The melting points were taken on a hot-stage apparatus and are uncorrected. The IR spectra were run as Nujol mulls on a Hitachi 215 spectrophotometer, and only prominent peaks were recorded. The PMR spectra were measured in carbon tetrachloride with a Varian T-60 spectrometer, using TMS as the internal standard, unless otherwise stated. The mass (MS) spectra were obtained on a Hitachi RMS-4 mass spectrometer with an ionizing potential of 70 eV.

The polymethylbenzoyl chlorides (**1a—c**) were prepared from the corresponding benzoic acids[10] by treatment with thionyl chloride. The dipropionylpolymethylbenzenes (**7a—b** and **9**) were prepared from the corresponding hydrocarbons according to the Perrier procedure of the Friedel-Crafts acylation.[8] The aldehyde (**2b**) and ketone (**3b**) were prepared as has previously been reported.[3,11] The physical properties and yields of dipropionyl- and dipivaloylpolymethylbenzenes (**7a—b** and **9**, and **8a—b** and **10**, respectively), and 1-(polymethylphenyl)-2,2-dimethylpropyl polymethylbenzoates (**4a—c**) obtained are summarized in Table 1. The general preparation of the hindered diketones and esters is illustrated below by the synthesis of **8b** and **4b**.

4,6-Dipivaloyl-1,2,3,5-tetramethylbenzene (8b). A mixture of the **7b** diketone (1.5 g; 0.006 mol), potassium *t*-butoxide (5.5 g; 0.050 mol), benzene (15 ml), and *t*-butyl alcohol (6 ml) was stirred, and then a solution of methyl iodide (15 g; 0.102 mol) in benzene (30 ml) was slowly added during the course of 30 min. Stirring was continued for 4 h under reflux, and then the reaction mixture was treated with water. The organic layer was separated and washed thoroughly with water, and the solvent was removed under reduced pressure. The residue was purified over a column of silica gel (hexane), giving **8b** as colorless plates (0.6 g; 33%); mp 166—168 °C. MS: *m/e* 302 (M^+), 287 (M^+-CH_3), and 245 (base peak; $M^+-C_4H_9$). Found: C, 79.67; H, 10.15%. Calcd for $C_{20}H_{30}O_2$: C, 79.42; H, 10.00%.

Compounds **8a** and **10** were obtained in a similar manner from 1,3,5-trimethylbenzene and 1,2,4,5-tetramethylbenzene respectively. **8a**: Found: C, 79.19; H, 9.74%. Calcd for $C_{19}H_{28}O_2$: C, 79.12; H, 9.78%. **10**: Found: C, 79.48; H, 10.13%. Calcd for $C_{20}H_{30}O_2$: C, 79.42; H, 10.00%.

1-(2,4,6-Trimethylphenyl)-2,2-dimethylpropyl 2,4,6-Trimethylbenzoate (4b). Into a solution of the Grignard reagent prepared from *t*-butyl chloride (5.0 g; 0.054 mol) and magnesium (1.3 g; 0.054 atom) in ether (30 ml), 2,4,6-trimethylbenzoyl chloride (5.9 g; 0.032 mol) in ether (20 ml) was stirred under ice-water cooling during the course of 0.5 h. After the acid chloride had then been added, the mixture was gently refluxed for 4 h and then treated with aqueous ammonium chloride. The organic layer was separated, and the aqueous layer was extracted with ether. The combined extracts were washed successively with aqueous sodium hydrogencarbonate and water, dried over magnesium sulfate, and evaporated. After standing overnight in a refrigerator, the oily residue gave an ester as a white solid which, on several recrystallizations from hexane, melted at 126—128 °C. Yield, 3.2 g (56%). MS: *m/e* 352 (M^+) and 295 (base peak; $M^+-C_4H_9$). Found: C, 82.05; H, 9.19%. Calcd for $C_{24}H_{32}O_2$: C, 81.77; H, 9.14%.

References

1) The reaction of polysubstituted aromatics. Part XLIX. Part XLVIII: H, Suzuki, A. Inoue, M. Koge, and T. Hanafusa, *Bull. Chem. Soc. Jpn.*, **51**, 1172 (1978).

2) J. H. Ford, C. D. Thompson, and C. S. Marvel, *J. Am. Chem. Soc.*, **57**, 2619 (1935).

3) E. Rothstein and R. W. Saville, *J. Chem. Soc.*, **1949**, 1950; H. Suzuki, H. Wada, K. Maruyama, and R. Goto, *Bull. Chem. Soc. Jpn.*, **39**, 1201 (1966).

4) D. E. Pearson, *J. Am. Chem. Soc.*, **72**, 4169 (1950).

5) A. G. Pinkus, J. I. Riggis, Jr., and S. M. Broughton, *J. Am. Chem. Soc.*, **90**, 5043 (1968). The authors are grateful to Dr. A. G. Pinkus for sending us the experimental details of the preparation of this reagent.

6) W. C. Percival, R. B. Wagner, and N. C. Cook, *J. Am. Chem. Soc.*, **75**, 3731 (1953); J. E. Dubois, M. Chastrette, and E. Schunk, *Bull. Soc. Chim. Fr.*, **1967**, 2011; J. E. Dubois and M. Boussu, *Tetrahedron Lett.*, **1970**, 2523.

7) For a review of reduction by the Grignard reagent, see T. Eicher, "The Chemistry of the Carbonyl Group," ed by S. Patai, Interscience, London (1966), p. 621; K. Nützel, "Houben-Weyl Methoden der Organischen Chemie," XIII/2a ed by E. Müller, Georg Thieme, Stuttgart (1973), p. 297, 413; F. Wingler, *ibid.*, VII/2a, Part 1 (1973), p. 575.

8) P. H. Gore, "Friedel-Crafts and Related Reactions," ed by G. A. Olah, Interscience, London (1964), Vol. III, Part 1, p. 4; P. H. Gore and J. A. Hoskins, *J. Chem. Soc., C*, **1970**, 517.

9) This combination was preferred because of its higher yield and simpler manipulation. The alkylation of alkyl aryl ketones with sodium amide and alkyl iodide constitutes the first stage of the Haller-Bauer method for the synthesis of tertiary carboxamides. C. L. Carter and S. N. Slater, *J. Chem. Soc.*, **1946**, 130; A. Friedman, W. Gugic, and E. I. Becker, *J. Org. Chem.*, **24**, 516 (1959).

10) G. A. Varvoglis and N. E. Alexandrou, *Chim. Chronika (Athens)*, **26**, 137 (1961); H. Suzuki, *Nippon Kagaku Zasshi*, **91**, 484 (1970).

11) A. Rieche, H. Gross, and E. Höft, *Org. Synth.*, Coll. Vol. V, 49 (1973).

BULLETIN OF THE CHEMICAL SOCIETY OF JAPAN, VOL. 51 (11), 3395—3396 (1978)

The Sesquiterpenes of *Dendropanax trifidus*

Kazuo YOSHIHARA* and Yoshio HIROSE

The Institute of Food Chemistry, Wakayamadai, Shimamoto-cho, Mishima-gun, Osaka 618

(Received March 16, 1978)

Synopsis. The volatile oils of the leaves, cortex and fruits of *Dendropanax trifidus* were investigated. Germacrene-D is enantiomeric, sesquiterpenes of other series, such as caryophyllene and selinenes, optically corresponding to those in higher plants.

Some volatile oils of *Aralia* species have simple compositions, consisting of germacrene-D, caryophyllene, humulene, *etc.*[1] We have studied the volatile oils of *Dendropanax trifidus*.

The volatile oils of the leaves, cortex and fruits were obtained by steam distillation, the components being isolated by silica gel column and gas chromatography. The isolated compounds and their $[\alpha]_D$ values are given in Table 1. Caryophyllene (**1**) was the major component in the leaf oil, the series, α- and β-neoclovenes(**2** and **3**) and β-panasinsene (**4**) being detected. The occurrence of **4** in nature is significant since it has been suggested to be a key intermediate in the caryophyllene-neoclovene conversion reaction.[2] Cadalene-type compounds (**6**—**9**) and selinenes (**10** and **11**) were also detected. In contrast to the leaf oil, only a trace of caryophyllene was found in the cortex oil, germacrene-D (**5**), a potential precursor of cadalene-type compounds, bourbonenes, *etc.*,[3] being the major component. These serial compounds were also detected. Selinenes were found in small amounts. In the fruit oil, almost all caryophyllene disappeared and no germacrene-D was present. However, various derivatives such as cadinenes (**6** and **7**) and muurolenes (**8** and **9**) were found together with neoclovenes and selinenes. A large amount of humulene was found in this oil. It is probable that caryophyllene and germacrene-D were further transformed into compounds, **2**, **3** and **6**—**9** for final storage in the fruits.

It is noteworthy that germacrene-D in the plant is dextrorotatory, containing an α-isopropyl group as shown in Fig. 1. The optical rotations show that the compounds of the germacrene-D series have also α-isopropyl groups, being enantiomers of those occurring in higher plants.[3] On the other hand, the selinenes have β-isopropyl groups. Thus, in this plant, germacrene-D series compounds and selinenes, which may be derived from a common germacrene-type precursor (**12**), have enantiomeric isopropyl configurations.

TABLE 1. COMPOUNDS ISOLATED FROM *D. trifidus*

Compounds	Leaf oil (%)	Cortical oil (%)	Fruit oil (%)	$[\alpha]_D$ (°)
Caryophyllene series				
caryophyllene (**1**)	63	trace	trace	−14
α-neoclovene (**2**)	2	—	4	−50
β-neoclovene (**3**)	3	—	6	−30
β-panasinsene (**4**)	2	trace	trace	
isocaryophyllene	2	—	—	
caryophyllene oxide	1	—	—	
Germacrene-D series				
germacrene-D (**5**)	—	73	—	+305
γ-cadinene (**6**)	3	6	8	−62
δ-cadinene (**7**)	2	3	23	−53
α-muurolene (**8**)	1.5	2	1	+58
γ-muurolene (**9**)	5	7	3	−2
β-bourbonene	trace	—	—	
β-copaene	trace	—	—	
calamenene	—	1	—	
Selinene series				
α-selinene (**10**)	2	trace	3	+68
β-selinene (**11**)	3	1.5	7	+49
Others				
δ-elememe	trace	—	—	
β-farnesene	1.5	—	2	
α-humulene	2	—	32	

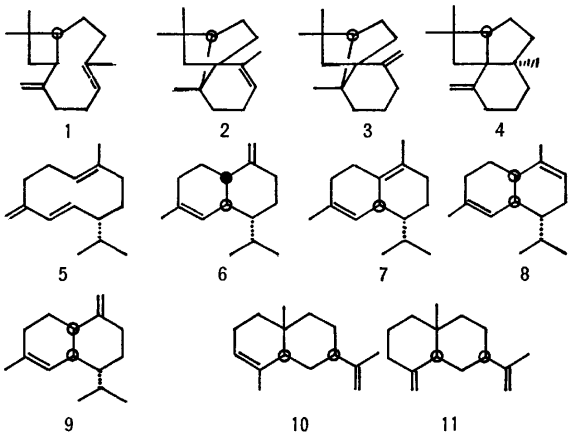

Fig. 1. Structures of selected compounds from Table 1.

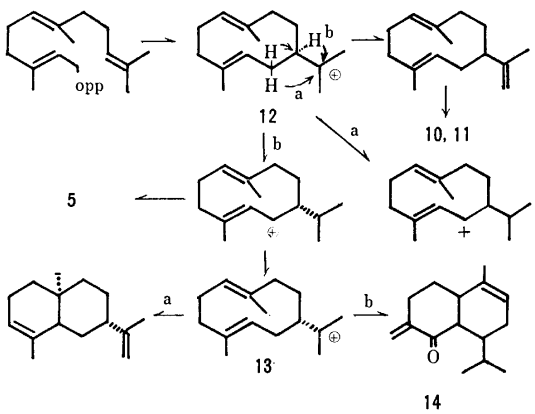

Fig. 2. Possible biosynthetic route involving enantiomeric germacrenoidal precursors (see the text).

Such coexistence of enantiomeric germacrene-D series and normal selinene-type compounds in a higher plant does not seem to have been found. A similar case was reported for a sort of liverwort, *Chiloscyphus polyanthus*, in which, in contrast to *D. trifidus*, α-selinene has an α-isopropyl group, and chiloscyphone (**14**), a cadalene-type ketone, has a β-isopropyl group.[4] Andersen *et al.* suggested that α-selinene and chiloscyphone in *C. polyanthus* are derived from enantiomeric germacrenoidal precursors (**12** and **13**, respectively). However, an alternative biogenetic route is also possible, *i.e.*, a single 1,3-hydride shift (path a) and two concerted 1,2-hydride shifts (path b) in the germacrenium-cation (**12**) can occur, resulting in an opposite orientation of the isopropyl group. If this is the case, the unusual coexistence of chiloscyphone with other enantiomeric compounds in *C. polyanthus* can be explained by the inversion of its isopropyl group through path b. Thus, *C. polyanthus* resembles other liverworts producing enantiomeric terpenes. The coexistence of enantiomeric germacrene-D series compounds in *D. trifidus* appears to support this view.

Experimental

Analytical Instrument. Analytical gas chromatography was carried out on a Hitachi-063-type apparatus fitted with a HB-2000 capillary column. Measurements of physical data were taken on a Hitachi EPI-G-2-type IR absorption spectrometer with NaCl cell, a JEOL-JNM-C-60-type NMR spectrometer and a Perkin-Elmer's 141-type polarimeter.

Isolation. The materials were collected in Osaka prefecture. 5.2 g of leaf oil (from 25 kg, 0.02%), 2.7 g of the cortical oil (from 12 kg, 0.02%), and 11.7 g of the fruit oil (from 8 kg, 0.146%) were obtained by steam distillation. Each oil was chromatographed on silica gel using hexane–ether as the carrier. Each eluted fraction was separated into pure compounds by means of a Varian MODEL-90-P-type gas chromatograph fitted with a Carbowax 20 M column.

References

1) K. Yoshihara and Y. Hirose, *Phytochemistry*, **12**, 468 (1973).

2) K. Yoshihara and Y. Hirose, *Bull. Chem. Soc. Jpn.*, **48**, 2078 (1975); W. Parker, R. A. Raphael, and J. S. Roberts, *Tetrahedron Lett.*, **1965**, 2313.

3) K. Yoshihara, Y. Ohta, T. Sakai, and Y. Hirose, *Tetrahedron Lett.*, **1969**, 2263.

4) A. Matsuo, *Tetrahedron*, **28**, 1203 (1972); N. H. Andersen, B. Shunk, and C. R. Costin, *Experientia*, **29**, 645 (1973).

BULLETIN OF THE CHEMICAL SOCIETY OF JAPAN, VOL. 51 (11), 3397—3398 (1978)

Transformation of *o*-Nitrobenzenes to Quinolines with Tetracarbonylhydridoferrate

Yoshihisa WATANABE,* Kunihiko TAKATSUKI, Sang Chul SHIM, Take-aki MITSUDO, and Yoshinobu TAKEGAMI

Department of Hydrocarbon Chemistry, Faculty of Engineering, Kyoto University, Sakyo-ku, Kyoto 606

(Received March 20, 1978)

Synopsis. Condensates of *o*-nitrobenzaldehyde with carbonyl compounds are reduced with tetracarbonylhydridoferrate under mild conditions to give quinolines in good yields.

Derivatives of tetracarbonylferrate such as hydrido-,[1] acyl-,[2] alkyl-,[3] and carbamoyl-[4] are powerful reducing reagents for the conversion of nitro compounds into the corresponding amines, amides and ureas. The present study deals with the applicability of tetracarbonylhydridoferrate to the synthesis of *N*-heterocycles from condensates of *o*-nitrobenzaldehyde and *o*-nitroaniline with carbonyl compounds and/or primary amines.

Experimental

Infrared spectra were measured with a 215 Hitachi Model spectrophotometer. Nuclear magnetic resonance spectra were measured with a JEOL-JNM-PM-60 NMR spectrometer in deuteriochloroform with Me_4Si as an internal standard. Melting points were uncorrected.

Materials. *o*-Nitrocinnamaldehyde, *o*-nitrobenzaldehyde, *o*-nitroaniline, 1-naphthylamine, acetophenone, iron pentacarbonyl and solvents were all commercial products and were used without further purification. *N*-(*o*-Nitrobenzylidene)-1-naphthylamine(**3a**), *N*-(*o*-nitrobenzylidene)-*p*-anisidine(**3b**) and *p*-chloro-*N*-(*o*-nitrobenzylidene)aniline (**3c**) were prepared from *o*-nitrobenzaldehyde and 1-naphthylamine, *p*-anisidine and *p*-chloroaniline, respectively. *o*-Nitro-*N*-benzylideneaniline(**6a**) and *o*-nitro-*N*-(*p*-chlorobenzylidene)aniline(**6b**) were prepared from *o*-nitroaniline and benzaldehyde and *p*-chlorobenzaldehyde, respectively. Potassium tetracarbonylhydridoferrate was prepared according to the method described in a previous paper.[5]

General Reaction Procedure. To the ferrate(11 mmol) in moist ethanol (50—100 ml), a nitro compound(11 mmol) was added and the mixture stirred under an argon atmosphere at room temperature for 1 h. Reaction products, quinoline, quinaldine and 2-phenylquinoline were analyzed by GLC using internal standards: a column(0.3 cm ϕ, 3 m) packed with 10% Versamid on Neopak 60—80 mesh. Other products were detected by chromatography on alumina, silica gel or florisil, IR and PMR spectroscopy and elemnetal analysis.

Condensates of *o*-nitrobenzaldehyde with acetaldehyde, acetone or acetophenone were prepared *in situ* and submitted for further reaction: a mixture of *o*-nitrobenzaldehyde(11 mmol) and a carbonyl compound(13 mmol) in ethanol (20 ml) was stirred in the presence of a certain amount of potassium hydroxide under an argon atmosphere at room temperature for 3—23 h and then to this mixture were added iron pentacarbonyl(11 mmol) and 1 M potassium hydroxide(30—33 mmol) solution in ethanol.

Reaction of o-*Nitro*-N-*benzylideneaniline(**6a**) with* $KHFe(CO)_4$. The brown reaction mixture obtained was filtered and evaporation of the filtrate gave a brown residue which was chromatographed on florisil (3 × 30 cm) using dichloromethane as an eluant. A yellow orange band fraction gave 2-phenylbenzimidazole(**7a**) as yellow crystals in 10% yield. The reaction of *o*-nitro-*N*-(*p*-chlorobenzylidene)aniline(**6b**) gave 2-(*p*-chlorophenyl)benzimidazole(**7b**) as yellow orange crystals in 16% yield.

Preparation of N-*(o-Nitrobenzylidene) Amines (**3**).* A mixture of *o*-nitrobenzaldehyde(20 mmol), a primary amine (20 mmol) and ethanol(15 ml) was stirred at room temperature for 5 h to give yellow or orange precipitates, which were separated by filtration and recrystallized from chloroform-ethanol. *N*-(*o*-Nitrobenzylidene)-1-naphthylamine(**3a**), yield 45%, yellow crystals. PMR($CDCl_3$): δ 9.0(s, 1, -C<u>H</u>=N-), 7—8.5(m, 11, Ar). IR(KBr): $\nu_{C=N}$ 1620 cm^{-1}. *N*-(*o*-Nitrobenzylidene)-*p*-anisidine(**3b**), 85%, orange crystals. PMR($CDCl_3$): δ 8.9(s, 1, -C<u>H</u>=N-), 6.8—8.4(m, 8, Ar), 3.8(s, 3, -OC<u>H</u>$_3$). IR(KBr): $\nu_{C=N}$ 1620 cm^{-1}. *p*-Chloro-*N*-(*o*-nitrobenzylidene)aniline(**3c**), 75%, yellow crystals. PMR($CDCl_3$): δ 8.9(s, 1, -C<u>H</u>=N-), 7—8.4(m, 8, Ar). IR(KBr): $\nu_{C=N}$ 1610 cm^{-1}.

Reaction of N-*(o-Nitrobenzylidene)amines (**3**) with* $KHFe(CO)_4$. A mixture of **3**, the ferrate and moist ethanol (100 ml) was stirred under argon at room temperature for 3 h. The reaction products, *N*-(*o*-aminobenzylidene) amines (**4**) were isolated by evaporating the filtered solution to dryness and purified by recrystallization from chloroform-ethanol.

N-(*o*-Aminobenzylidene)-1-naphthylamine(**4a**), yield 50%, yellow crystals mp 80.5—81.5 °C. PMR($CDCl_3$): δ 8.5 (s, 1, -C<u>H</u>=N-), 6.3—8.4(m, 13, Ar and -N<u>H</u>$_2$). IR (KBr): ν_{NH_2} 3370, $\nu_{C=N}$ 1620 cm^{-1}. Found: C, 83.04; H, 5.66; N, 11.08%. Calcd for $C_{17}H_{14}N_2$: C, 82.90; H, 5.73; N, 11.37%.

N-(*o*-Aminobenzylidene)-*p*-anisidine(**4b**), 8%, yellow crystals, mp 122.0—123.5 °C. PMR($CDCl_3$): δ 8.5 (s, 1, -C<u>H</u>=N-), 6.2—7.7(m, Ar and -N<u>H</u>$_2$), 3.8(s, 3, -OC<u>H</u>$_3$). IR(KBr): ν_{NH_2} 3470, $\nu_{C=N}$ 1620 cm^{-1}. Found: C, 73.96; H, 6.09; N, 12.30; O, 7.62%. Calcd for $C_{14}H_{14}N_2O$: C, 74.31; H, 6.24; N, 12.38; O, 7.07%.

p-Chloro-*N*-(*o*-aminobenzylidene)aniline(**4c**), 9%, white yellow crystals, mp 108.5—110.0 °C. PMR($CDCl_3$): δ 8.4(s, 1, -C<u>H</u>=H-), 6.1—7.9 (m, 10, Ar and -N<u>H</u>$_2$). IR (KBr): ν_{NH_2} 3460, $\nu_{C=N}$ 1620 cm^{-1}. Found: C, 67.99; H, 4.69; N, 12.13; Cl, 15.38%. Calcd for $C_{13}H_{11}N_2Cl$: C, 67.68; H, 4.81; N, 12.14; Cl, 15.37%.

Results and Discussion

Alcoholic tetracarbonylhydridoferrate has high reactivity for the conversion of condensates of *o*-nitrobenzaldehyde with carbonyl compounds into the corresponding 2-alkylquinolines under mild conditions. The results are summarized in Table 1.

o-Nitrocinnamaldehyde readily reacted with the ferrate to give quinoline quantitatively which appeared to be formed by an intramolecular cyclization of

Table 1. The reduction of *o*-nitrobenzenes to quinolines with $KHFe(CO)_4$[a]

Run	Nitro compound	Carbonyl compound	Condensation[b] KOH[c]	Condensation[b] Time (h)	Product	Yield %
1	*o*-Nitrocinnamaldehyde	—	—	—	Quinoline	100
2	*o*-Nitrobenzaldehyde	Acetaldehyde	0.49	10	Quinoline	33
3	*o*-Nitrobenzaldehyde	Acetone	0.06	3	Quinaldine	55
4	*o*-Nitrobenzaldehyde	Acetone	0.06	23	Quinaldine	45
5	*o*-Nitrobenzaldehyde	Acetophenone	0.06	23	2-Phenylquinoline	17

a) At room temperature under argon for 1—3 h. b) *o*-Nitrobenzaldehyde was treated with carbonyl compounds at room temperature and then the condensates obtained *in situ* were reduced. c) Molar ratio, potassium hydroxide/carbonyl compound.

o-aminocinnamaldehyde. *o*-Nitrocinnamaldehyde is a condensate of *o*-nitrobenzaldehyde with acetaldehyde. Two succesive treatments of *o*-nitrobenzaldehyde with such carbonyl compounds as acetaldehyde, acetone or acetophenone in the presence of potassium hydroxide and then with the ferrate gave quinoline(**2a**), quinaldine(**2b**) and 2-phenylquinoline(**2c**) in good yields, respectively. The potassium hydroxide used appears to play two roles, a catalyst for the aldol condensation of *o*-nitrobenzaldehyde with the carbonyl compounds and a reagent for the formation of the ferrate.

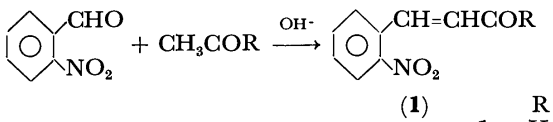

(**1**)

	R
1a	H
1b	CH_3
1c	Ph

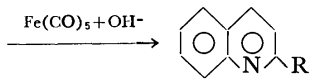

(**2**)

These results show that *o*-nitrobenzaldehyde combined with carbonyl compounds and with the ferrate as a reducing reagent can provide a simple route to a variety of 2-alkylquinolines.

N-(*o*-Nitrobenzylidene)amines(**3**), condensates of *o*-nitrobenzaldehyde with 1-naphthylamine, *p*-anisidine and *p*-chloroaniline, gave only the corresponding *N*-(*o*-aminobenzylidene)amines(**4**) in good to poor yields. The expected *N*-heterocycles, 2-alkylbenzopyrazoles(**5**), could not be detected.

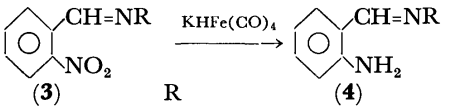

(**3**)

	R
3a	1-naphthyl
3b	*p*-$CH_3OC_6H_4$
3c	*p*-ClC_6H_4

(**4**)

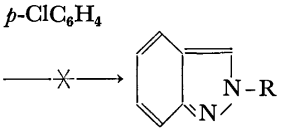

(**5**)

On the other hand, *o*-nitro-*N*-benzylideneaniline(**6**), condensates of *o*-nitroaniline with benzaldehyde or *p*-chlorobenzaldehyde, gave benzimidazoles(**7**) but in poor yields.

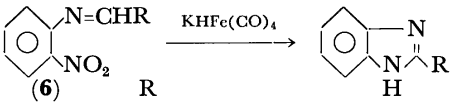

(**6**)

	R
6a	Ph
6b	*p*-ClC_6H_4

(**7**)

References

1) Y. Watanabe, T. Mitsudo, M. Yamashita, and Y. Takegami, *Bull. Chem. Soc. Jpn.*, **48**, 1478(1975), and the references therein.

2) M. Yamashita, Y. Watanabe, T. Mitsudo, and Y. Takegami, *Tetrahedron Lett.*, **1976**, 1585.

3) Y. Watanabe, K. Taniguchi, M. Suga, T. Mitsudo, and Y. Takegami, 37th National Meeting of the Chemical Society of Japan, Tokyo, April 1978, Abstr. No. 4, L37.

4) M. Yamashita, K. Mizushima, Y. Watanabe, T. Mitsudo, and Y. Takegami, *J. Chem. Soc., Chem. Commun.*, **1976**, 670.

5) Y. Takegami, Y. Watanabe, H. Masada, and I. Kanaya, *Bull. Chem. Soc. Jpn.*, **40**, 1456 (1967).

BULLETIN OF THE CHEMICAL SOCIETY OF JAPAN, VOL. 51 (11), 3399—3400 (1978)

Synthesis of Chromenochlalcone Glucosides

Shigetoshi YAMADA,* Futara ONO, Takao KATAGIRI† and Juntaro TANAKA†

Department of Industrial Chemistry, Junior College of Technology, Shizuoka University, Hamamatsu 432

†*Department of Synthetic Chemistry, Faculty of Engineering, Shizuoka University, Hamamatsu 432*

(Received March 29, 1978)

Synopsis. Some chromenochalcone glucosides were synthesized in 24—62% yields from 6-acetyl-5,8-dihydroxy-2,2-dimethylchromene and various (β-glucosyloxy)-benzaldehydes.

Chalcones containing isoprene units which have biological activities[1,2] have been isolated from various plants[3-7] and synthesized.[8]

We reported the synthesis of Flemichapparin-A isolated from *Flemingia Chappar* ham (Legminosae),[9] and attempted to synthesize chromenochalcone glucosides.

As regards chalcone glucosides, many chalcones and flavonoids containing glucose moiety in ring A such as phloridzin[10-12] have been found in various species of plants. However, only a few chalcones and flavonoids containing glucose moiety in ring B such as Epimedoside-B have been found.[13,14] We wish to report on the synthesis of the latter compounds which are expected to have biological activities.

The Claisen-Schmidt condensation of 6-acetyl-5,8-dihydroxy-2,2-dimethylchromene (**1**) with helicin (**2**), 2-(β-glucosyloxy)-1-naphthaldehyde (**3**), isovanillinβ-D-glucoside (**4**), and *p*-(β-glucosyloxy)benzaldehyde (**5**) was carried out, chromenochalcone glucosides (**6**), (**7**), (**8**), and (**9**) being obtained in fair yields. Dihydrochalcone glucoside (**10**) which tastes sweet was obtained by the catalytic hydrogenation of (**6**) with palladium–carbon in 10% aq KOH.

Experimental

1 was prepared by the previous method.[9] **2** (mp 173.5—174 °C. 51% yield), **3** (mp 182.5—184.5 °C, 62% yield), **4** (mp 190.5—192 °C, 33% yield) and **5** (mp 162—163 °C, 57% yield) were prepared by Robertson's method.[15] The products were identified by means of mp and spectral data. The physical data of **2**, **4**, and **5** agreed with those found in literatures.[15-17]

3: mp 182—184.5 °C (brown amorphous). IR (cm^{-1}, KBr disk): 3300, 1650, 1240, 1050, 740, 710. Found: C, 61.47; H, 5.53%. Calcd for $C_{17}H_{18}O_7$: C, 61.07; H, 5.43%.

*Reaction of **1** with **2**.* On cooling, 50% alcoholic KOH (4 ml) was added to a stirred solution of **1** (300 mg) and **2** (284 mg) in ethanol (4 ml) under nitrogen and the mixture was stirred at room temperature for a week. The mixture was acidified with 0.5M HCl and extracted with ether. Chromatography of the ether extract on silica gel eluted by benzene-ethylacetate (22 : 3 v/v) afforded **6** in 56% yield.

*Reaction of **1** with **3**.* 60% Alcoholic KOH (4 ml) was added to a stirred solution of **1** (234 mg) and **3** (324 mg) in ethanol (4 ml) and the mixture was stirred at 60 °C for three days under nitrogen. By the same work-up as above, **7** was obtained in 33% yield.

*Reaction of **1** with **4**.* 40% Alcoholic KOH (4 ml) was added to a stirred solution of **1** (234 mg) and **4** (295 mg) in ethanol (4 ml) and the mixture was stirred at 60 °C for two days under nitrogen. By the same work-up as above, **8** was obtained in 24% yield.

*Reaction of **1** with **5**.* 60% Alcoholic KOH (4 ml) was added to a stirred solution of **1** (234 mg) and **5** (284 mg) in ethanol (4 ml) and the mixture was stirred at 60 °C for two days under nitrogen. By the same work-up as above, **9** was obtained in 62% yield.

The products were identified by means of their analytical and spectral data (Table 1).

*Hydrogenation of **6**.* **6** (200 mg) was dissolved in 10% aq KOH (2 ml) and the solution was cooled to 0 °C. To this solution was added 10% palladium–carbon catalyst

TABLE 1. PHYSICAL PROPERTIES OF REACTION PRODUCTS

Products	Mp (°C)	IR (cm^{-1}, KBr disk)	NMR (CD_3OD, δ)	Found (Calcd) C (%)	Found (Calcd) H (%)
6	145.5—147 orange	3400, 1640, 1240, 1160, 1075, 960, 760	1.48(6H, s), 3.23—3.60(7H, m), 5.67 (1H, d, J=10.0 Hz), 6.70(1H, d, J=10.0 Hz), 7.0—7.52(5H, m), 7.74 (1H, d, J=15.5 Hz), 8.25(1H, d, J=15.5 Hz)	62.69 (62.39)	5.42 (5.64)
7	223—224 redish-brown	3400, 1640, 1150, 1060, 950, 770	1.48(6H, s), 3.25—3.70(7H, m), 5.79 (1H, d, J=10.0 Hz), 6.84(1H, d, J=10.0 Hz), 7.35—8.15(7H, m), 8.20(1H, d, J=15.5 Hz), 8.68 (1H, d, J=15.5 Hz)	65.72 (65.44)	5.28 (5.49)
8	214—216 orange	3400, 1660, 1240, 1170, 1060, 930, 750	1.50(6H, s), 3.22—3.70(7H, m), 3.90 (3H, s), 5.65(1H, d, J=10.0 Hz), 6.80(1H, d, J=10.0 Hz), 7.35—7.80 (6H, m)	61.24 (61.13)	5.91 (5.70)
9	140—142 orange	3500, 1670, 1070, 1035, 935, 735	1.50(6H, s), 3.20—3.65(7H, m), 5.65 (1H, d, J=10.0Hz), 6.67(1H, d, J=10.0 Hz), 7.48—7.85(7H, m)	62.21 (62.39)	5.67 (5.64)

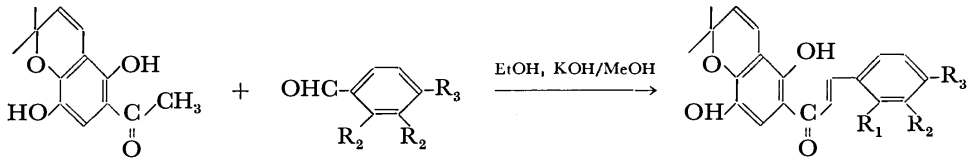

1 **2, 4, 5** **6, 8, 9**

2, 6 R_1=β-glucosyloxy, R_2=R_3=H
4, 8 R_1=H, R_2=β-glucosyloxy, R_3=OCH_3
5, 9 R_1=R_2=H, R_3=β-glucosyloxy

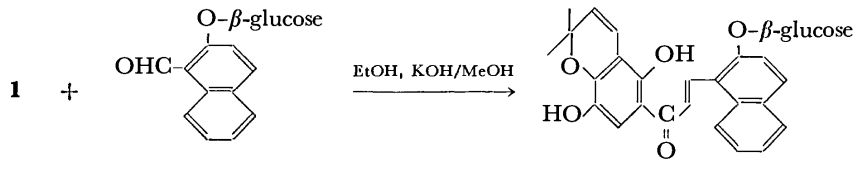

3 **7**

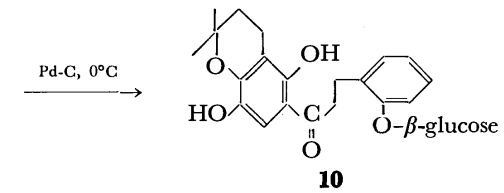

10

(50 mg), the mixture being kept at room temperature for 2 h under hydrogen with stirring. The product was filtrated and acidified with concd HCl. When the solution was kept at 0 °C overnight, the hydrogenated product was crystallized and washed with cold water. (110 mg, 55% yield) mp 123—127 °C (amorphous). IR (cm^{-1}, KBr disk): 3400, 1620, 1602, 1250, 1070. NMR (δ, CD_3OD): 1.40 (6H, s), 1.65—2.05(4H, m), 2.05—2.95 (4H, m), 3.17—3.75(7H, m), 7.20—7.50(5H, m). Found: C, 61.72; H, 6.69%. Calcd for $C_{26}H_{32}O_{10}$: C, 61.89; H, 6.39%.

References

1) K. Kyogoku, K. Hatayama, S. Yokomori, and T. Seki, *Japan Patent Kokai* 50-140430; *ibid.*, 50-24258; *ibid.*, 52-78856; *ibid.*, 52-7857; *ibid.*, 52-7858.

2) A. Lupi and M. G. Delle, *Farmaco. Ed. Sci.*, **32**, 261 (1977).

3) K. Kyogoku, K. Hatayama, K. Suzuki, S. Yokomori, K. Maejima, and M. Komatsu, *Chem. Pharm. Bull.*, **21**, 1192, 1436, 1777, 2733 (1973).

4) N. Adityachaudhury, D. Ghosh, A. Chaudhury, and C. L. Kirtaniya, *J. Indian Chem. Soc.*, **50**, 363 (1973).

5) B. S. Bajba, P. L. Khanna, and T. R. Seshadri, *Curr. Sci.*, **41**, 815 (1972).

6) K. Subrahmanyam, J. M. Rao, and K. V. J. Rao, *Indian J. Chem., Sect. B*, **15**, 12, 105 (1977).

7) L. O. Goncalves, M. E. Montogomery, and H. Arn, *Gazz. Chim. Ital.*, **103**, 771 (1973).

8) K. Kyogoku, K. Hatayama, S. Yokomori, T. Seki, and I. Tanaka, *Agric. Biol. Chem.*, **39**, 133 (1975); *ibid.*, **38**, 2291 (1974).

9) S. Yamada, F. Ono, T. Katagiri, and J. Tanaka, *Bull. Chem. Soc. Jpn.*, **48**, 2391 (1975).

10) V. K. Ahluwalium and N. Rani, *Indian J. Chem., Sect. B*, **14**, 594 (1976).

11) M. E. Montogomery and H. Arn, *J. Insect Physiol.*, **20**, 413 (1974).

12) A. F. Debons, I. Krimty, A. From, and H. Pattinian, *Am. J. Physiol.*, **226**, 574 (1974).

13) A. J. Kahra, M. Krishnamurti, and T. R. Seshadri, *Indian J. Chem.*, **12**, 1040 (1974).

14) Y. Tokuoka, K. Daigi, and T. Takemoto, *Yakugaku Zasshi*, **95**, 321 (1975).

15) A. Robertson and R. B. Waters, *J. Chem. Soc.*, **1930**, 2729.

16) P. Casparis, *Pharm. Acta Helv.*, **21**, 341 (1946).

17) Mauthner, *J. Prakt. Chim.*, **85**, 568 (1912).

BULLETIN OF THE CHEMICAL SOCIETY OF JAPAN, VOL. 51 (11), 3401—3402 (1978)

The Preparation of Isoxazole Derivatives from a Nitro Sugar with Dimethylsulfonium Phenacylide

Tohru SAKAKIBARA and Rokuro SUDOH

Department of Chemistry, Faculty of Science, Tokyo Institute of Technology, Ookayama, Meguro-ku, Tokyo 152

(Received May 2, 1978)

Synopsis. The reaction of methyl 4,6-*O*-benzylidene-2,3-dideoxy-3-nitro-α-D-*erythro*-hex-2-enopyranoside or 5-benzoyl(methyl 4,6-*O*-benzylidene-2,3-dideoxy-α-D-*erythro*-hexopyranosido)[3,2-*c*]isoxazoline *N*-oxide with dimethylsulfonium phenacylide gave 5-benzoyl-3-(1,3-*O*-benzylidene-D-*erthro*-glyceryl)-4-isoxazolecarbaldehyde in a fairly good yield.

Recently we reported that the reaction of methyl 4,6-*O*-benzylidene-2,3-dideoxy-3-nitro-α-D-*erythro*-hex-2-enopyranoside (**1**) (0.2 mmol) with dimethylsulfonium phenacyclide (0.25 mmol) afforded the isoxazoline *N*-oxide **2** in a good yield.[1] However, when this reaction was carried out on a larger scale, the isoxazole, **3**, was formed. The determination of the structure of **3** and the conversion of the isoxazoline *N*-oxide **2** into **3** is described herewith.

The treatment of **1** (293 mg, 1 mmol) with dimethylsulfonium phenacylide (1.5 mmol) in THF (10 ml) at room temperature for 3 h gave a NMR spectroscopically pure syrup, **3** (315 mg), with the odor of dimethyl sulfide. The IR spectrum showed the absorption bands for a hydroxyl (3400 cm^{-1} broad) and α,β-unsaturated carbonyl group (1670 cm^{-1}). The NMR spectrum revealed that **3** had lost the glycosidic methoxyl group, but retained the benzylidene group. The presence of 10-protons in the aromatic region suggested the presence of a benzoyl group. The two 1-proton signals at δ 9.15 and 3.00 (broad) were assigned to the formyl proton and the OH proton respectively. The H-1′ signal appeared as a doublet due to vicinal coupling with H-2′ ($J_{1',2'}$=9 Hz). The acetylation of **3** with acetic anhydride–sodium acetate gave the crystalline acetate, **4**, the NMR spectrum of which showed that the hydroxyl group attached originally at C-2′, since the signal of H-2′ had moved remarkably downfield as a result of the deshielding effect of the acetate group. The results of the elemental analysis of the acetate, **4**, agreed with the formula of $C_{23}H_{19}NO_7$, indicating that the products, **3** and **4**, have not a isoxazoline *N*-oxide ring, but a isoxazole.

The conversion of the isoxazoline *N*-oxide **2** into **3** was observed when **2** was treated with dimethylsulfonium phenacylide at 0 °C for 3 h, whereas the similar treatment of **2** with dimethyl sulfide resulted in the recovery of **2**. The reinvestigation[1] of the reaction between **1** and dimethylsulfonium ethoxycarbonylmethylide under similar conditions gave no evidence for the formation of an isoxazole corresponding to **3**. Furthermore, the treatment of the isoxazoline *N*-oxide, **5**, with dimethylsulfonium ethoxycarbonylmethylide or dimethyl sulfide afforded unchanged **5** in a quantitative yield.

On the basis of the mechanism proposed for the conversion of isoxazoline *N*-oxide into isoxazole[2] and the reports[3] in the literature that the hydrolysis of a pyranose derivative with unsaturated functional groups at the 2 position is facile and that the hydrolyzed product tends to exist in the open-chair aldehyde-form rather than with the pyranoside structure, the route shown in Scheme seems to be most plausible. In this reaction, the abstraction of the proton at C-5 (the isoxazoline ring proton) is probably the crucial step. Dimethylsulfonium phenacylide is basic enough for **2**, but dimethyl sulfide is not, and dimethylsulfonium ethoxycarbonylmethylide is not a sufficient base for **5** because the hydrogen atom (H-5) of **5** is less acidic than that of **2**.

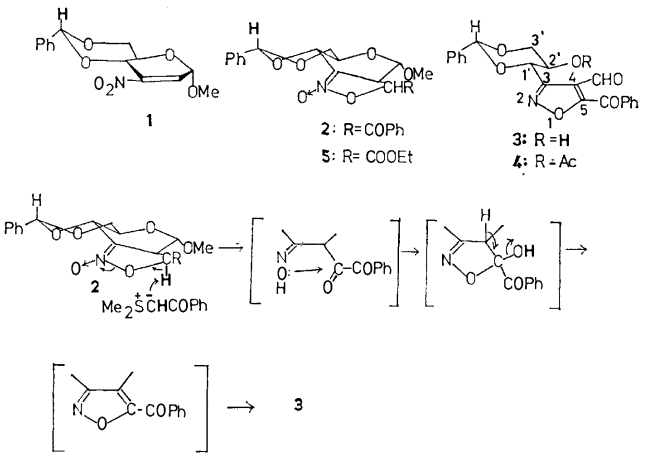

Scheme.

Experimental

The melting point was determined in capillary and is uncorrected. The NMR spectra were determined for solutions in chloroform-*d* (with tetramethylsilane as the internal standard) with a JNM-4H-100 (JEOL) spectrometer.

*5-Benzoyl-3-(1,3-O-benzylidene-*D-erythro*-glyceryl)-4-isoxazolecarbaldehyde (3).* (a) To a solution of **1**[4] (293 mg, 1 mmol) in THF (10 ml), dimethylsulfonium phenacylide (270 mg, 1.5 mmol) was added at room temperature. The mixture was kept at the same temperature for 3 h and then evaporated under reduced pressure to give a dark orange syrup, which was subsequently extracted with benzene. The extract was washed with water, dried (Na_2SO_4), and evaporated to give an orange syrup (465 mg). Its MNR spectrum suggested that it was fairly pure; IR (NaCl) 3400 (broad, OH) and 1670 cm^{-1} (α,β-unsaturated CO); NMR δ=9.15 (s, 1, CHO), 5.60 (s, 1, PhCH), 5.20 (d, 1, H-1′), 4.45 (m, 1, H-2′),4.55 (q, 1, H-3e′), 3.76 (t, 1, H-3a′) and 3.00 (broad, s, 1, OH).

Without further purification the syrup was acetylated.

(b) To a solution of dimethylsulfonium phenacylide (13 mg, 0.07 mmol) in THF (0.22 ml) in either the presence

or absence of dimethyl sulfide (0.07 mmol), the isoxazoline *N*-oxide **2** (0.07 mmol) was added at 0 °C. The mixture was kept at 0 °C for 3 h and then evaporated at reduced pressure to give a syrup. Its NMR spectrum showed the complete conversion of **2** into **3**.

The treatment of **2** (0.07 mmol) with dimethyl sulfide in the absence of dimethylsulfonium phenacylide resulted in the recovery of **2**, as judged by NMR spectroscopy.

*3-(2-O-Acetyl-1,3-O-benzylidene-*D*-erythro-glyceryl)-5-benzoyl-4-isoxazolecarbaldehyde (**4**).* The crude isoxazole **3** (62 mg) was warmed in a water bath (90 °C) with sodium acetate (62 mg) in acetic anhydride (2 ml) for 1 h. The mixture was then poured into ice water, and the precipitate was collected and washed with water and chromatographed on silica gel (15×70 mm) with benzene. The eluate was evaporated to give a solid residue, which was subsequently recrystallized from ethanol to give 32 mg (46.4%) of colorless crystals of **4**; mp 123.5—124.5 °C; $[\alpha]_D^{20}$ −18.6° (*c* 1, $CHCl_3$); IR (KBr) 1740 (OAc) and 1670 cm^{-1} (α,β-unsaturated COPh and CHO); NMR δ=9.18 (s, 1, CHO), 5.70 (m, 1, H-2′, $J_{1',2'}$=10, $J_{2',3a'}$=10, $J_{2',3e'}$=5.0 Hz), 5.67 (s, 1, PhCH), 5.40 (d, 1, H-1′), 4.55 (q, 1, H-3e′, $J_{3a',3e'}$=10 Hz), 3.79 (t, 1, H-3a′), and 1.97 (s, 3, OAc).

Found: C, 65.60; H, 4.67; N, 3.06%. Calcd for $C_{23}H_{19}NO_7$: C, 65.55; H, 4.54; N, 3.32%.

References

1) T. Sakakibara and R. Sudoh, *Bull. Chem. Soc. Jpn.*, **51**, 1193 (1978).

2) A. Quilico,"The Chemistry of Heterocyclic Compounds, Five and Six-Membered Compounds with Nitrogen and Oxygen," ed by R. H. Wiley, Interscience Publishers, New York (1962), Chap. I.

3) P. M. Collins, D. Gardiner, S. Kumar, and W. G. Overend, *J. Chem. Soc., Perkin Trans. 1*, **1972**, 2611; B. Fraser-Reid and B, Radatus, *J. Am. Chem. Soc.*, **92**, 5288 (1970).

4) H. H. Baer and F. Kienzle, *Can. J. Chem.*, **45**, 983 (1967).

BULLETIN OF THE CHEMICAL SOCIETY OF JAPAN, VOL. 51 (11), 3403—3404 (1978)

The Photochemical SO Extrusion of 2,2,4,4-Tetraacylthietane 1-Oxides

Shoei Iro* and Jun-ichi Mori**

Department of Chemistry, Faculty of Science, Hirosaki University, Hirosaki 036

(Received May 10, 1978)

Synopsis. The irradiation of a benzene solution of 2,2,4,4-tetraacylthietane 1-oxides, which had been prepared from dimedone-aldehyde derivatives with SCl_2, followed by oxidation with peracid, was carried out to give the corresponding 1,1,2,2-tetraacylcylopropanes(**4**) or a mixture of **4** and the corresponding dihydrofuran derivative, depending on the C_3 substituent on the 1-oxides and wavelength.

Photochemical studies of various sulfoxides, one of them is the photoisomerization of 2-phenyl-2*H*-naphto-[1,8-*b*,*c*]thiophene 1-oxide to the corresponding sulfenate, have been undertaken.[1] However, few attempts seem to have been made for the photolysis of thietane 1-oxides.

An attempt to prepare an 3,3,5,5-tetraacyl-1,2-oxathiolane by the photoisomerization of the corresponding 2,2,4,4-tetraacylthietane 1-oxide was carried out. However, no 1,2-oxathiolane was obtained, although photodesulfurization occurred.

In this paper we wish to describe the photochemical reactions of 2,2,4,4-tetraacylthietane 1-oxide using 3,3,11,11-tetramethyl-7-thiadispiro[5.1.5.1]teradecane-1,5,9,13-tetrone 7-oxide(**3a**) and its 14-methyl(**3b**) and 14-isopropyl(**3c**) derivatives as model compounds.

The reaction of 2,2′-methylenebis[5,5-dimethyl-1,3-cyclohexanedione] (**1a**) and its derivatives(**1b**—**1d**) with an equimolar amount of sulfur dichloride in ethyl acetate or dichloromethane gave thietane derivatives (**2a**—**2d**) in good yields. The conversion of **2** into the dioxide was unsuccessful except for the case of **2d**, which also failed to be converted into the monoxide.

A water-cooling dilute solution of **3a** in benzene open to air was irradiated with a Toshiba 75 W high-pressure mercury lamp for 1 h through a Pyrex filter. The product was identified as 3,3,10,10-tetramethyldispiro[5.0.5.1]tridecane-1,5,8,12-tetrone(**4a**) by comparison with the reported spectral data[2] and the elemental analysis. The photolysis of **2a** was also carried out in oxygen-free benzene both in a sealed vessel and in an atmosphere of nitrogen in a manner similar to that describes above to afford **4a** quantitatively.

Therefore, the possibility of sulfur monoxide extrusion upon the irradiation open to air *via* the formation of sulfone by photooxidation, followed by sulfur dioxide extrusion, can be ruled out.

On the other hand, the exposure of a dilute benzene solution of **2a** to light through a quartz filter open to air for 1 h gave **3a**, together with 4,5,6,7-tetrahydro-4′,4′,6,6-tetramethylspiro[benzofuran-2(3*H*),1′-cyclohexane]-2′,4,6′-trione(**5a**), which was readily formed by the treatment of **1a** with bromine in acetic acid. These results are summarized in Table 1, together with the results for other 1-oxides(**3b** and **3c**). Unfortunately, a comparative study with the corresponding 1,1-dioxides(**6a**—**6c**) was not undertaken because of the failure to prepare the dioxides. Thietane **2a** gave only a resinous substance under similar reaction conditions.

Table 1. Photoreactions of **3**

No.	Products (%)		No.	Products (%)	
	4	**5**		**4**	**5**
3a(P)	100		**3b**(P)	50	15
3a(P)[a]	100		**3b**(Q)	50	20
3a(P)[b]	100		**3c**(P)	100	
3a(Q)	70	20	**3c**(Q)	50	20

P: Pyrex filter, Q: Quartz filter, a) In oxygen-free benzene (in a sealed vessel). b) Under nitrogen.

On the other hand, sulfone **6d** afforded neither the corresponding cyclopropane(**4d**) nor dihydrofuran(**5d**), but gave the octahydroxanthene derivative(**7d**) under similar reaction conditions.

No decomposition of **3a** occurred upon prolonged heating in boiling xylene, while the pyrolysis of **3a** in a sealed tube at the melting point resulted in the formation of only a resinous substance which could not be purified by column chromatography.

Chow *et al.* reported that the SO moiety of dibenzo-[*b*,*f*][1,4,6]thiadiazepin 1-oxide(**8**) was extruded in benzene or chloroform under reflux to give benzocinnoline, but no decomposition was observed when a benzene solution of **8** was irradiated in a Pyrex apparatus.[3] The difference in photolysis between **3** and **8** may be attributed to the low bond-dissociation energy of the carbon–sulfur bond of **3** caused by the four acyl groups. The photolysis of **3** presumably proceeds *via* a sulfenate-intermediate which, upon further photolysis, gives **4** and **5**, with SO extrusion by means of a concerted mechanism. Furthermore, the inability of compound **3** to form a thiiran 1-oxide may be responsible for the thermal stabitity of the compound.

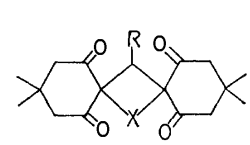

2 X=S, **3** X=SO, **6** X=SO_2

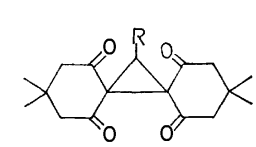

4

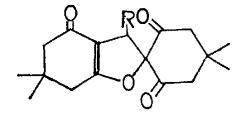

5

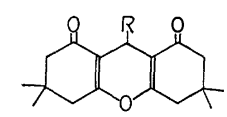

7

a: R=H, **b**: R=CH_3, **c**: R=$CH(CH_3)_2$, **d**: R=C_6H_5.

** Present address: Department of Chemistry, Faculty of Science, Hokkaido University, Sapporo 060.

TABLE 2. MELTING POINTS AND ELEMENTAL ANALYSES OF **2**—**4** AND **6d**

Compd No.	IR (KBr) (cm^{-1})	MS (70 eV) (m/e)	NMR (in $CDCl_3$) (δ)
2a	1700, 1730	322 (M^+)	0.82 (6H, s), 1.09 (6H, s), 2.38—2.65 (8H, m), 3.83 (2H, s)
2b	1700, 1720	336 (M^+)	0.97 (12H, s), 1.52 (3H, d, J=7.5 Hz), 2.25—3.01 (8H, m), 4.34 (1H, q, J=7.5 Hz)
2c	1705, 1730	364 (M^+)	0.65 (6H, d, J=6.0 Hz), 1.08 (12H, s), 2.28—2.78 (8H, m), 3.65 (1H, m), 4.65 (1H, d, J=11.5 Hz)
2d	1705, 1730	398 (M^+)	0.90 (12H, s), 1.85—2.93 (8H, m), 5.01 (1H, s), 7.35 (5H, s)
3a	1720, 1740	338 (M^+)	0.84 (6H, s), 1.25 (6H, s), 2.73 (8H, s), 3.50 (2H, s)
3b	1720, 1740	352 (M^+)	0.85 (6H, s), 1.22 (6H, s), 1.66 (3H, d, J=7.5 Hz), 2.40—3.04 (8H, m), 4.55 (1H, q, J=7.5 Hz)
3c	1720, 1740	380 (M^+)	0.75 (6H, d, J=6.0 Hz), 0.89 (6H, s), 1.19 (6H, s), 2.40—3.04 (8H, m), 3.83 (1H, m), 4.30 (1H, J=11.5 Hz)
4a	1690 (sh), 1705* 1720, 1730	290 (M^+)	1.03 (6H, s), 1.15 (6H, s), 2.23 (2H, s), 2.60 (8H, s)
4b	1690 (sh), 1705* 1735	304 (M^+)	1.00 (6H, s), 1.08 (6H, s), 1.38 (3H, d, J=7.5 Hz), 2.13—2.50 (1H, m), 2.58 (8H, s)
4c	1688 (sh), 1705* 1735	332 (M^+)	1.06 (6H, d, J=6.0 Hz), 1.09 (12H, s), 1.90—2.32 (2H, m), 2.50 (8H, s)
6d	1690, 1720	430 (M^+)	1.01 (6H, s), 1.24 (6H, s), 2.50—3.10 (8H, m), 5.78 (1H, s), 6.45—7.20 (5H, m)

(sh) shoulder, * the strongest peak. UV: λ_{max}^{EtOH}; **2a** 245 (ε 3000), 258 (max, 3200), 270 (2510), 300 nm (1000). **3a** 230 (sh, ε 3500), 270 (900), 300 nm (700)

TABLE 3. SPECTRAL DATA OF **2**—**4** AND **6d**

No.	Mp, °C (a)	Molecular formula	Found (Calcd), % C	H
2a	220—221 (Ethanol)	$C_{17}H_{22}O_4S$	63.21 (63.34)	6.76 (6.88)
2b	179—180 (Ethyl acetate)	$C_{18}H_{24}O_4S$	63.92 (64.27)	7.35 (7.19)
2c	198—199 (Ethanol)	$C_{20}H_{28}O_4S$	65.62 (65.91)	7.85 (7.74)
2d	201—202 (Ethanol)	$C_{23}H_{34}O_4S$	69.05 (69.33)	6.62 (6.58)
3a	238—240 (Benzene)	$C_{17}H_{22}O_5S$	60.05 (60.34)	6.42 (6.55)
3d	215—217 (Benzene)	$C_{18}H_{24}O_5S$	61.64 (61.35)	6.99 (6.86)
3c	218—220 (Benzene)	$C_{20}H_{28}O_5S$	63.42 (63.14)	7.34 (7.42)
4a	175—176 (Ethanol) [b]	$C_{17}H_{22}O_4$	70.54 (70.32)	7.82 (7.64)
4b	110—111 (Methanol) [c]	$C_{18}H_{24}O_4$	71.42 (71.02)	8.05 (7.95)
4c	167—168 (Ethanol)	$C_{20}H_{28}O_4$	72.17 (72.26)	8.36 (8.49)
6d	183—184 (Benzene)	$C_{23}H_{26}O_6S$	63.95 (64.17)	6.12 (6.09)

a) Recrystallization solvent. b) Lit,[3] 147—148 °C. c) Lit,[3] 109—110 °C.

Experimental

General. All the melting points are uncorrected. The IR spectra were recorded with a JASCO-DS-601F spectrophotometer. The UV spectra were obtained on a Hitachi EPS-2 spectrophotometer. The NMR spectra were obtained on a JNM-C-60HL spectrometer, using TMS as the internal standard. The mass spectra were measured on a Hitachi RMU-6 spectrometer.

Materials. The *m*-chloroperbenzoic acid and sulfur dichloride were obtained commercially. The purity of *m*-chloroperbenzoic acid was determined by iodometry.

Irradiation. All the irradiations were carried out externally with a high-pressure mercury lamp (Toshiba SHL-100UV, 75 W) at the temperature of running water.

Preparation of ***2****.* *General Procedure*: To a stirred solution of the aldehyde-dimedone derivative (0.01 mol) in ethyl acetate (100 ml), cooled in an ice bath, a solution of sulfur dichloride (0.01 ml) in ethyl acetate (10 ml) was added, drop by drop, over a 20-min period. After additional stirring for 2 h at this temperature, the mixture was stirred at room temperature for 10 h. The evaporation of the solvent under reduced pressure afforded white crystals. Yields: **2a** (80%); **2b** (80%); **2c** (80%); **2d** (75%). The recrystallization solvents, mps, and elemental analyses are summarized in Table 2.

Oxidation of ***2*** *with* m-*Chloroperbenzoic Acid. General Procedure*: To a stirred solution of **2** (2 mmol) in benzene (100 ml), cooled in an ice bath, a solution of *m*-chloroperbenzoic acid (2 mmol) in benzene (50 ml) was added, drop by drop, over a 10-min period. After additional stirring for 1 h at this temperature, the mixture was stirred at room temperature for 19 h. The precipitate (*m*-chlorobenzoic acid) was then filtered off, and the filtrate was washed with a 5% cold $NaHCO_3$ solution and then with cold water. The evaporation of the solvent from the dried solution (Na_2SO_4) gave a solid substance which was fractionated by recrystallization. Yields: **3a** (63%); **3b** (30%); **3c** (45%); **6d** (20%). The recrystallization solvents, mps, and elemental analyses of the monoxides **3a**—**3c** and the dioxide **6d** are summarized in Table 2.

Preparation of ***5****.* Compounds **5a**—**5c** were prepared according to the previously reported method.[4] **5a**: Mp 210—212 °C (lit, 211—213 °C), **5b**: mp 197—198 °C (lit, 197—198 °C), **5c**: mp 186—187 °C, Found: C, 71.52; H, 9.06%. Calcd for $C_{20}H_{30}O_4$: C, 71.82; H, 9.04%.

*Irradiation of Thietane Monoxide(****3****) in Benzene. General Procedure*: A solution of **3** in benzene (0.006 M) was irradiated in a Pyrex vessel or a quartz vessel for 1 h. The subsequent evaporation of the solvent afforded a white solid, which was then recrystallized from an appropriate solvent. When a mixture was given, it was chromatographed on silica gel, using hexane, hexane–benzene, and then benzene. The results are summarized in Table 1.

Irradiation of ***3a*** *in Oxygen-free Benzene.* A benzene solution of **3a** was degassed at −70 °C under a high vacuum and then sealed. The irradiation of the solution was carried out in a manner similar to that described above.

Irradiation of ***3a*** *under Nitrogen.* Nitrogen gas was allowed to pass through a benzene solution of **3a** during the course of irradiation.

Irradiation of ***6d*** *in Benzene.* A solution of **6d** in benzene (0.006 M) was irradiated in a Pyrex vessel for 1 h. The subsequent evaporation of the solvent afforded a white solid, which was identified as the corresponding octahydroxanthene derivative (**7d**) by direct comparison with an authentic sample (yield, 95%).

References

1) A. G. Shultz and R. H. Schlessinger, *Chem. Commun.*, **1970**, 1294.

2) K. Ohkata, T. Sakai, Y. Kubo, and T. Hanafusa, *J. Chem. Soc., Chem. Commun.*, **1974**, 581.

3) Y. L. Chow, J. N. S. Tam, and J. E. Blier, *Chem. Commun.*, **1970**, 1604.

4) I. Lielbriedis and E. Gudriniece, *Lativ. PSR Zinat. Akad. Vestis, Kim. Ser.*, **1968**, 192; *Chem. Abstr.*, **69**, 9955 (1968).

BULLETIN OF THE CHEMICAL SOCIETY OF JAPAN, VOL. 51 (11), 3405—3406 (1978)

A Synthesis of (±)-epi-Seychellene

Kiyoyuki YAMADA,* Yoshinori KYOTANI, Shunichi MANABE, and Masaaki SUZUKI

Department of Chemistry, Faculty of Science, Nagoya University, Chikusa, Nagoya 464

(Received May 15, 1978)

Synopsis. Starting from a mixture of two diastereomeric ketols, (±)-seychellene and (±)-epi-seychellene were synthesized in six steps.

Patchouli alcohol (**1**)[1] and seychellene (**2**),[2] constituents of patchouli oil, contain commonly the novel carbon framework, a tricyclo[5.3.1.$0^{3,8}$]undecane skeleton, and their synthetic studies have actively been carried out.[3]

In the previous investigation[4] we reported a method of constructing a tricyclo[5.3.1.$0^{3,8}$]undecane skeleton in one step by intramolecular cyclization of a conjugated cyclohexenone derivative. We have recently made a total synthesis of patchouli alcohol **1** and seychellene **2** in racemic form utilizing this method of cyclization:[5] a 1:1 mixture of the diastereomeric α,β-enones (**4**) was cyclized with potassium *t*-butoxide in *t*-butyl alcohol to afford two ketols, (**5**) (23%) and (**6**) (3%), only the former being obtained in pure form.[5] These ketols, **5** and **6**, were deduced to be diastereomers regarding C-4. Stereochemical assignments of **5** and **6** were made by consideration of the steric course of cyclization[5] and confirmed by the synthesis of the sesquiterpenes of defined structures, **1** and **2**, employing the major isomer **5**.[5]

In this note a synthesis of (±)-epi-seychellene (**3**) together with a synthesis of (±)-**2** is described, starting from a mixture of two diastereomers, **5** and **6**, and this result provides an additional evidence for the validity of the assigned stereochemistry of **5** and **6**. A synthesis of (±)-epi-seychellene was previously carried out by Fráter.[3d]

The mixture of the two ketols, **5** and **6**, was converted to a mixture of two thioacetals, (**7**) and (**9**), under the standard conditions, which was desulfurized with W-2 Raney nickel in ethanol under reflux,

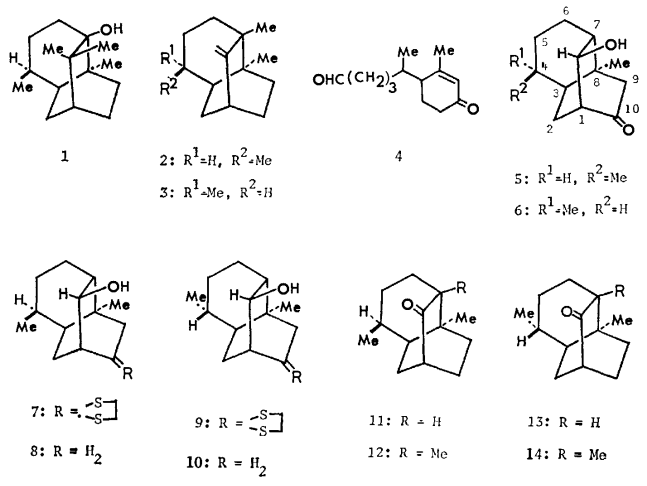

affording a mixture of two diastereomeric alcohols, (**8**) and (**10**) in 99% overall yield. On oxidation with chromium trioxide in pyridine, a mixture of **8** and **10** gave a mixture of the corresponding ketones, (**11**) and (**13**) in 95% yield. Treatment of a mixture of the two ketones, **11** and **13** with lithium diisopropylamide (LDA) in tetrahydrofuran (THF) followed by reaction with methyl iodide at —50 °C afforded a mixture of two ketones, (**12**) and (**14**) in 93% yield. The mixture was separated by preparative gas chromatography (GC) to give (±)-norseychellanone **12** (liquid) identified by spectral (IR and NMR) data of the authentic specimen and the crystalline ketone **14**, mp 145—146 °C. Reaction of the mixture of **12** and **14** with methyllithium in ether and subsequent dehydration with thionyl chloride in pyridine–benzene produced a mixture of two olefins in 85% yield, which was purified by preparative GC to give (±)-seychellene **2** (liquid) and (±)-epi-seychellene **3**, mp 145—147 °C. The spectral (IR and NMR) data of the latter was in agreement with those[3d] of (±)-epi-seychellene reported.

Experimental

Melting points were uncorrected. IR spectra ($CHCl_3$) were recorded with JASCO Model IRS and JASCO DS-402G instruments. NMR spectra ($CDCl_3$) were obtained on a Varian HA-100D spectrometer using TMS as an internal standard. Low resolution and high resolution mass spectra were determined on Hitachi RMU-6C and JEOLCO GMS-01SG mass spectrometers, respectively. A Varian 1820-4 gas chromatograph was used for GC (5 ft. $\times$0.25 in. column packed with 5% SE-30 on Celite 545; helium as the carrier gas). For TLC silica gel 60 F_{254} and 60 PF_{254} (E. Merck, A. G., Germany) were used. Organic solutions were washed with saturated NaCl solution, dried over anhydrous Na_2SO_4, and evaporated by a vacuum rotary evaporator.

*Alcohols, **8** and **10**.* A solution of the 1 : 1 mixture of **5** and **6**[5] (200 mg) and $BF_3\cdot OEt_2$ (0.24 ml, distilled from CaH_2) in 1,2-ethanedithiol (10 ml) was stirred at room temperature for 20 min and diluted with a saturated $NaHCO_3$ solution. The mixture was extracted with $CHCl_3$ (4$\times$20 ml). The residue obtained on evaporation of the $CHCl_3$ extracts was dissolved in toluene and the solution was concentrated for complete removal of 1,2-ethanedithiol. Purification of the residue by preparative TLC ($CHCl_3$–EtOAc, 10:1) gave a mixture of thioacetals, **7** and **9** (273 mg) as a colorless liquid: IR 3520, 3360 cm^{-1}; NMR (δ) 0.77 and 1.10 (total 3H, d each, J=7.0 Hz), 0.88 and 0.96 (total 3H, s each), 2.9—3.6 (4H, complex m), 3.78 and 3.98 (total 1H, m each). To a solution of the mixture of **7** and **9** (273 mg) in EtOH (32 ml) was added W-2 Raney nickel (*ca.* 5.2 g). The suspension was refluxed for 30 min and filtered. The filtrate was evaporated, giving a mixture of alcohols, **9** and **10** (185 mg, 99% from the ketols, **5** and **6**) as a colorless liquid: IR 3550, 3400 cm^{-1}; NMR (δ) 0.76 and 1.10 (total 3H, d each, J=6.0 Hz), 0.86 and 0.95 (total 3H, s each), 3.65 and 3.73 (total 1H, dd each, J=2.0, 4.0 Hz); MS 194(M^+). Found: *m/e* 194.1666. Calcd for $C_{13}H_{22}O$:

194.1671.

*Ketones, **11** and **13**.* A suspension of CrO_3 (230 mg) in dry pyridine (5.6 ml, distilled from BaO) was added to a solution of the mixture of **8** and **10** (190 mg) in dry pyridine (2.5 ml). The mixture was stirred at room temperature for 6 h and diluted with ether (50 ml). The precipitates were filtered and washed with ether (40 ml). The combined filtrates were washed with 1M HCl (5×10 ml) and H_2O (3×10 ml), dried, and concentrated. The residue was purified by preparative TLC ($CHCl_3$), affording a mixture of **11** and **13** (181 mg, 95%) as a colorless liquid: IR 1715 cm^{-1}; NMR (δ) 0.80 and 1.17 (total 3H, d each, J=7.0 Hz), 1.10 and 1.11 (total 3H, s each); MS 192 (M^+). Found: *m/e* 192.1522. Calcd for $C_{13}H_{20}O$: 192.1514.

*(±)-Norseychellanone **12** and Ketone **14**.* To a stirred solution of *i*-Pr_2NH (0.66 ml, distilled from NaH) in dry THF (8.7 ml, distilled from potassium–benzophenone ketyl under nitrogen) at −78 °C was added under nitrogen a solution (2.6 ml) of 1.6M BuLi in hexane. A solution of the mixture of **11** and **13** (53 mg) in dry THF (2.6 ml) was added dropwise over a period of 20 min to the above LDA solution at −78 °C. The mixture was stirred at −50 °C for 20 min. Then MeI (0.87 ml, distilled from $CaCl_2$) was added at −50 °C. After 30 min NH_4Cl was added. The mixture was diluted with H_2O (1 ml). The cooling bath was removed. After 5 min the mixture was concentrated, diluted with H_2O (2 ml), and extracted with benzene (3×10 ml). The benzene extracts were dried and concentrated. The residue was purified by preparative TLC ($CHCl_3$–EtOAc, 200:1), giving a mixture of **12** and **14** (53 mg, 93%) as a colorless liquid. The mixture was separated by preparative GC (120 °C, 160 ml/min) to give (±)-**12** (retention time 14 min) and **14** (retention time 16 min). **14**: mp 145—146 °C (sealed tube); IR 1710 cm^{-1}; NMR (δ) 0.98 (3H, s), 1.04 (3H, s), 1.15 (3H, d, J=7.5 Hz), 2.31 (1H, m); MS 206 (M^+). Found: *m/e* 206.1690. Calcd for $C_{14}H_{22}O$: 206.1671.

*(±)-Seychellene **2** and (±)-epi-Seychellene **3**.* To a stirred solution of the mixture of **12** and **14** (10 mg) in dry ether (0.07 ml, distilled from Na) was added a solution (0.40 ml) of 1.15 M MeLi in ether under nitrogen. The mixture was stirred at room temperature for 4 h. Water (1 ml) was added and the mixture extracted with ether (4×10 ml). The ethereal extracts were dried and concentrated. The residue (10.8 mg) was dissolved in dry benzene (0.23 ml, distilled from Na)–dry pyridine (0.15 ml). To the cooled (0 °C) solution was added $SOCl_2$ (4.7 μl, freshly distilled) in dry benzene (0.14 ml). The mixture was stirred for 35 min at 0 °C, poured into ice–water (2 ml), and extracted with benzene (4×10 ml). The benzene extracts were dried and concentrated. The residue was purified by preparative TLC (pentane), affording a mixture of **2** and **3** as a colorless oil (8.5 mg, 85%). Separation of the mixture was made by preparative GC (110 °C, 150 ml/min) to give (±)-**2** (retention time 15 min) and (±)-**3** (retention time 17 min). (±)-**3**: mp 145—147 °C (sealed tube); IR (neat) 3060, 3000(sh), 2920, 2860, 1640, 1460, 1380, 1370, 1110, 1102, 1060, 1020, 980, 970 945, 888(strong) cm^{-1}; NMR (δ) 0.93 (3H, s), 0.96 (3H, s), 1.08 (3H, d, J=7.5 Hz), 4.61 (1H, d, J=1.5 Hz), 4.81 (1H, d, J=1.5 Hz); MS 204 (M^+). Found: *m/e* 204.1883. Calcd for $C_{15}H_{24}$: 204.1878.

The authors wish to thank Professor Y. Hirata for his encouragement and Professor A. Yoshikoshi, Tohoku University, for providing us with the spectral data of (±)-norseychellanone.

References

1) M. Dobler, J. D. Dunitz, B. Gubler, H. P. Weber, G. Büchi, and J. Padilla, *Proc. Chem. Soc.*, **1963**, 383.

2) a) N. Tsubaki, K. Nishimura, and Y. Hirose, *Bull. Chem. Soc. Jpn.*, **40**, 597 (1967); b) G. Wolff and G. Ourisson, *Tetrahedron Lett.*, **1968**, 3849; c) G. Wolff and G. Ourisson *Tetrahedron*, **25**, 4903 (1969).

3) Total synthesis of seychellene: a) E. Piers, W. de Waal, and R. W. Britton, *J. Am. Chem. Soc.*, **93**, 5113 (1971); b) R. N. Mirrington and K. J. Schmalzl, *J. Org. Chem.*, **37**, 2877 (1972); c) N. Fukamiya, M. Kato, and A. Yoshikoshi, *J. Chem. Soc., Perkin Trans. 1*, **1973**, 1843; d) G. Fráter, *Helv. Chim. Acta*, **57**, 172 (1974).

4) K. Yamada, M. Aratani, Y. Hayakawa, H. Nakamura, H. Nagase, and Y. Hirata, *J. Org. Chem.*, **36**, 3653 (1971).

5) K. Yamada, Y. Kyotani, S. Manabe, and M. Suzuki, submitted for publication in *Tetrahedron*.

BULLETIN OF THE CHEMICAL SOCIETY OF JAPAN, VOL. 51 (11), 3407—3408 (1978)

The σ-Bonded Palladium(II) Complexes of 4-Chromanone Oxime Derivatives

Taeko IZUMI, Takao KATOU, Akira KASAHARA,* and Kaoru HANAYA,**

Department of Applied Chemistry, Faculty of Engineering, Yamagata University, Yonezawa 992

***Department of Chemistry, Faculty of Science, Yamagata University, Yamagata 990*

(Received May 22, 1978)

Synopsis. In the presence of sodium acetate, the reaction of 4-chromanone oxime with lithium tetrachloropalladate(II) affords an *ortho*-palladated binuclear complex. The reaction of the complex with carbon monoxide in methanol was also examined.

Following the first observation by Cope and Siekman[1] that azobenzene reacts with palladium(II) chloride to give an intramolecular *ortho*-palladation product with a carbon-to-metal σ-bond, considerable interest developed in this area.[2] Moreover, Onoue *et al.*[3] reported a reaction of aromatic ketoximes with palladium(II) chloride giving a dimeric σ-bonded complex. Herein, we wish to report on the *ortho*-metalation of 4-chromanone oxime (**1a**) with palladium(II) chloride and the reaction of the metalation product with carbon monoxide in methanol.

In the presence of sodium acetate, the reaction of **1a** with lithium tetrachloropalladate(II) in methanol gave a binuclear complex with palladium-carbon σ-bonding: di-μ-chloro-bis[4-chromanone oxime-5-*C*,*N*]dipalladium(II) (**2a**). Under the same conditions, flavanone oxime (**1b**) and 2-methyl-4*H*-1-benzothiopyran-4-one oxime (**1c**) also reacted with lithium tetrachloropalladate(II) to afford the *ortho*-palladated complexes, di-μ-chloro-bis[flavanone oxime-5-*C*,*N*]-dipalladium(II) (**2b**) and di-μ-chloro-bis[2-methyl-4*H*-1-benzothiopyran-4-one oxime-5-*C*,*N*]dipalladium-(II) (**2c**) respectively. On the basis of the microanalytical and spectroscopic data and the molecular weight, the **2a**—**c** complexes were shown to be intramolecularly *ortho*-palladated complexes. The molecular weights in chloroform are consistent with the values calculated for the binuclear complexes. The treatment of **2a**—**c** with triphenylphosphine gives results typical of a chlorine-bridged binuclear complex, affording the monomeric triphenylphosphine derivatives (**3a**—**c**). The IR spectra of **2a**—**c** showed the characteristic OH stretching frequency in the 3450—3350 cm^{-1} region and the characteristic deformation mode of 1,2,3-trisubstituted benzene at 790—785 cm^{-1} region, as shown in Table 1. Moreover, the C=N stretching frequency shifted to a slightly lower wave number (**2a**, 1635; **2b**, 1635; **2c**, 1620 cm^{-1}), characteristic of nitrogen lone-pair donation, as has been found for *ortho*-palladated aryloxime complexes.[3] In the far-infrared spectra of **2a**—**c** there are typicaly two bridged Pd–Cl stretching absorptions at 278—275 and 250—245 cm^{-1}. The NMR spectra of the **2a**—**c** complexes were in good agreement with the proposed structures. For example, the spectrum of **2a** has four bands: a triplet at 2.96 (J=6.0 Hz, 4H), a triplet at 4.24 (J=6.0 Hz, 4H), a multiplet at 6.60—7.40 (6H), and a broad singlet at 10.15 ppm (2H), the bands corresponding to $-CH_2-C=N$, $-O-CH_2-$, aromatic **H**, and **OH** respectively. These results and the IR spectral data show that one aromatic ring proton *ortho* to the C=N group was replaced by palladium(II). Similarly, the NMR spectra of **2b** and **2c** provide evidence for the occurrence of *ortho*-metalated aromatic rings (see Table 1).

The carbonylation of *ortho*-palladated products of azobenzene, Schiff bases, and tertiary benzylamines usually gives a variety of heterocyclic compounds.[4,5] In addition, it was found that benzophenone oxime gave 3-phenyl-1-isoindolinone by carbonylation in the presence of dicobalt octacarbonyl[6] or palladium(II) chloride in benzene.[3] We also studied the carbonylation of **2a**—**c** complexes. The attempted carbonylation of **2a**—**c** was unsuccessful, even at 100 °C; however, the triphenylphosphine derivatives, **3a**—**c**, in methanol were readily carbonylated at 100 °C to produce uncyclized and deoxymated esters (**4a**—**c**) in 28—45% yields. Maeda *et al.*[7] have recently shown that the C=N bond of ketoximes can be cleaved in the presence of the Pd(O) complex, with the subsequent formation of free ketone. The results of the carbonylation of **3a**—**c** complexes clearly suggest that a deoxymation of carbonylated intermediates with palladium species occurs.

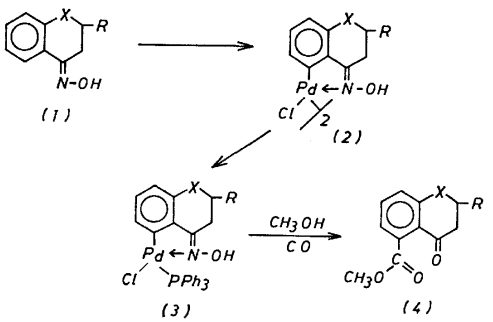

1a, **2a**, **3a**, **4a**: R=H, X=O
1b, **2b**, **3b**, **4b**: R=Ph, X=O
1c, **2c**, **3c**, **4c**: R=CH_3, X=S

Fig. 1.

Experimental

Materials and Measurement. All the melting points are uncorrected. The **1a**[8] and **1b**[9] compounds were prepared by the method prevously reported. The **1c** compound (mp 136—138 °C) was prepared by the usual oxymation of the corresponding carbonyl compound. The IR spectra were measured on KBr disks (4000—650 cm^{-1}) or in nujol mulls mounted on thin polythene windows (700—200 cm^{-1}). The NMR spectra were observed in $CDCl_3$ or in DMSO-d_6 at 90 MHz, using TMS as the internal standard. The molecular weight was determined in $CHCl_3$, using a Hitachi 115

Table 1. The *ortho*-palladation of oximes (**1a—c**)

Oxime	Product (mp (dec), yield)	Found (Calcd) % and mol wt	IR and NMR (in DMSO-d_6) spectra
1a	**2a** (215—218 °C, 90%)	C, 35.27 (35.53) H, 2.51 (2.63) N, 4.48 (4.60) Mol wt 591 (608)	IR: 3400 (OH), 1635 (C=N), 790 (1,2,3-trisubstituted aromatic ring), 275 and 250 cm^{-1} (bridged Pd-Cl). NMR: δ 2.96 (t, 4H, -C**H**$_2$-C=N), 4.24 (t, 4H, -O-C**H**$_2$-), 6.60—7.40 (m, 6H, aromatic **H**), and 10.15 ppm (br s, 2H, **OH**).
1b	**2b** (260—265 °C, 82%)	C, 47.25 (47.38) H, 2.93 (3.15) N, 3.29 (3.42) Mol wt 748 (760)	IR: 3450 (OH), 1635 (C=N), 790 (1,2,3-trisubstituted aromatic ring), 275 and 245 cm^{-1} (bridged Pd-Cl). NMR: δ 2.58—3.45 (m, 4H, -C**H**$_2$-C=N), 5.25 (d-d, 2H, -O-C**H**-), 6.60—7.81 (m, 16H, aromatic **H**), and 10.60 ppm (s, 2H, **OH**).
1c	**2c** (228—230 °C, 90%)	C, 35.78 (35.90) H, 2.83 (2.99) N, 4.06 (4.19) Mol wt 650 (668)	IR: 3350 (OH), 1620 (C=N), 785 (1,2,3-trisubstituted aromatic ring), 278 and 245 cm^{-1} (bridged Pd-Cl). NMR: δ 1.28 (d, 6H, -C**H**$_3$), 2.55—3.33 (m, 4H, -C**H**$_2$-C=N), 4.85 (m, 2H, S-C**H**-), 6.68—7.55 (m, 6H, aromatic **H**), and 10.45 ppm (br s, 2H, **OH**).

Table 2. The triphenylphosphine derivatives (**3a—c**)

Complex	Mp (dec) (yield)	Found (Calcd) % and mol wt	IR and NMR (in $CDCl_3$) spectra
3a	214—215 °C (70%)	C, 57.08 (57.25) H, 3.91 (4.06) N, 2.27 (2.47) Mol wt 548 (566)	IR: 3200 (OH), 1640 (C=N), 790 (1,2,3-trisubstituted aromatic ring), 305 cm^{-1} (terminal Pd-Cl). NMR: δ 3.05 (t, J=6.0 Hz, 2H, -C**H**$_2$-C=N), 4.25 (t, J=6.0 Hz, 2H, -O-C**H**$_2$-), 6.00—6.50 (m, 3H, aromatic **H**), 7.50)m, 15H, aromatic **H**), and 10.40 ppm (br s, 1H, **OH**).
3b	210—212 °C (75%)	C, 61.55 (61.69) H, 3.97 (4.20) N, 2.03 (2.18) Mol wt 625 (642)	IR: 3200 (OH), 1640 (C=N), 790, 740, 690 (aromatic ring), and 305 cm^{-1} (terminal Pd-Cl). NMR: δ 3.04 (d-d, J=17 and 12 Hz, 1H, -C**H**-C=N), 3.65 (d-d, J=17 and 3.5 Hz, 1H, -C**H**-C=N), 5.10 (d-d, J=12 and 3.5 Hz, 1H, O-C**H**-), 6.05 (m, 1H, aromatic **H**), 6.60 (m, 2H, aromatic **H**), 7.60 (m, 20H, aromatic **H**), and 10.50 ppm (br s, 1H, **OH**).
3c	208—210 °C (65%)	C, 56.16 (56.38) H, 4.05 (4.19) N, 2.27 (2.36) Mol wt 585 (596)	IR: 3200 (OH), 1640 (C=N), 785 (1,2,3-trisubstituted aromatic ring), and 310 cm^{-1} (terminal Pd-Cl). NMR: δ 1.25 (d, 3H, -C**H**$_3$), 2.97 (d-d, J=16 and 12 Hz, 1H, -C**H**-C=N), 3.55 (d-d, J=16 and 4 Hz, 1H, -C**H**-C=N), 4.68 (m, J=12 and 4 Hz, 1H, -C**H**-O), 6.11—6.58 (m, 3H, aromatic **H**), 7.50 (m, 15 H, aromatic **H**), and 10.40 ppm (br s, 1H, **OH**).

Table 3. The carbonylation products (**4a—c**)

Compound	Mp (yield)	Found (Calcd) % and mol wt	IR, NMR (in $CDCl_3$), and MS spectra
4a	38—40 °C (45%)	C, 63.38 (63.45) H, 5.88 (5.81) Mol wt (208)	IR: 1735 (ester), 1695 (C=O), 785 cm^{-1} (1,2,3-trisubstituted aromatic ring). NMR: δ 2.82 (t, 2H, -C**H**$_2$C=O), 3.94 (s, 3H, -COOC**H**$_3$), 4.56 (t, 2H, -C**H**$_2$-O), 7.05 (m, 2H, aromatic **H**), and 7.45 ppm (m, 1H, aromatic **H**). MS: *m/e* 208 (M^+).
4b	44—46 °C (28%)	C, 72.21 (72.33) H, 4.86 (5.00) Mol wt (282)	IR: 1735 (ester), 1695 (C=O), 790, 740, and 690 cm^{-1} (aromatic ring). NMR: δ 2.96 (m, 2H, -C**H**$_2$-CO), 3.93 (s, 3H, -COOC**H**$_3$), 5.48 (d-d, 1H, -O-C**H**-), and 6.98—7.90 ppm (m, 8H, aromatic **H**). MS: *m/e* 282 (M^+).
4c	50—52 °C (32%)	C, 60.95 (61.01) H, 5.03 (5.12) Mol wt (236)	IR: 1735 (ester), 1695 (C=O), 790 cm^{-1} (1,2,3-trisubstituted aromatic ring). NMR: δ 1.26 (d, 3H, -C**H**$_3$), 2.78 (m, 2H, -C**H**$_2$-CO), 3.87 (s, 3H, -COOC**H**$_3$), 4.78 (m, 1H, -C**H**-O-), and 7.01—7.54 ppm (m, 3H, aromatic **H**). MS: *m/e* 236 (M^+).

vapor-pressure osmometer.

*General Procedure of the Preparation of Complexes **2a—c**.* A solution of 5 mmol of the **1a—c** oximes in methanol (50 ml) was added to a mixture of lithium tetrachloropalladate (II) (1.31 g, 5 mmol) and sodium acetate trihydrate (0.68 g, 5 mmol) in methanol (50 ml). The resulting mixture was stirred for 24 h at room temperature. The pale yellow precipitate thus formed was filtered off and purified by recrystallization from chloroform-hexane or by column chromatography (SiO_2–$CHCl_3$). The results are listed in Table 1.

*General Procedure for the Preparation of Triphenylphosphine Derivatives **3a—c**.* Triphenylphosphine (0.26 g, 1 mmol) and the **2a—c** complexes (0.5 mmol) were dissolved in benzene, and then the mixture was stirred for 6 h at room temperature. The solvent was removed under reduced pressure, and the products were obtained as pale yellow crystals from chloroform-hexane. The results are summarized in Table 2.

*The Carbonylation of The **3a—c** Complexes.* In 50 ml of methanol, the **3a—c** complexes were carbonylated at 100 °C under a carbon monoxide pressure of 60 atm for 20 h with shaking. The product was then isolated by filtering to remove a precipitated palladium and distilling under reduced pressure to remove the solvent. The residue was dissolved in hexane or benzene and chromatographed on silica gel to afford colorless crystals, which can be identified as 5-methoxycarbonyl derivatives (**4a—c**). The results are summarized in Table 3.

References

1) A. C. Cope and R. W. Siekman, *J. Am. Chem. Soc.*, **87**, 3272 (1965).

2) P. M. Maitlis, "The Organic Chemistry of Palladium," Academic Press, New York (1971), Vol. 1, p. 82; J. Tsuji, *Yuki Gosei Kagaku Kyokai Shi*, **35**, 10 (1977).

3) H. Onoue, K. Minami, and K. Nakagawa, *Bull. Chem. Soc. Jpn.*, **43**, 3480 (1970).

4) H. Takahashi and J. Tsuji, *J. Organometal. Chem.*, **10**, 511 (1967).

5) J. M. Thompson and R. F. Heck, *J. Org. Chem.*, **40**, 2667 (1975).

6) A. Rosenthal, R. F. Astbury, and A. Hubscher, *J. Org. Chem.*, **33**, 1037 (1958).

7) K. Maeda, I. Moritani, T. Hosikawa, and S.-I. Murahashi, *Tetrahedron Lett.*, **1974**, 797.

8) A. Arndt and G. Kallner, *Ber.*, **57**, 202 (1924).

9) A. Kasahara, *Nippon Kagaku Zasshi*, **80**, 416 (1959).

BULLETIN OF THE CHEMICAL SOCIETY OF JAPAN, VOL. 51 (11), 3409—3410 (1978)

Racemization during the Synthesis of Histidine-containing Peptides

Shigeyuki TERADA, Akira KAWABATA,** Nobuo MITSUYASU,***
Haruhiko AOYAGI, and Nobuo IZUMIYA*

Laboratory of Biochemistry, Faculty of Science Kyushu University 33,, Higashi-ku, Fukuoka 812

(Received May 25, 1978)

Synopsis. A convenient test for racemization using an amino acid analyzer was developed and applied to examine the effects of several *im*-protecting groups and synthesis of histidyl peptides.

Urethane protected L-amino acid moieties are recognized to be free from racemization under the usual conditions of peptide synthesis. Jorgensen *et al.*, however, observed appreciable racemization of *t*-butoxycarbonyl-N^{im}-benzyl-L-histidine during the course of synthesis of an analog of angiotensin.[1] They separated a diastereomeric mixture of DL-His(Bzl)-L-Glu[2] by an amino acid analyzer, and applied the procedure to determine the extent of racemization during the course of coupling of Boc-L-His(Bzl) and L-Glu(OBzl)-OBzl or L-Glu(OBzl)-resin.[3] After the examination of seven DL-histidyl-dipeptides (DL-His-L-A where A=Asp, Glu, Val, Leu, Ile, Ser, and Ala), we found that His-Ser and His-Ala are also suitable systems for the amino acid analyzer detection of as little as 0.1% racemization.[4] Using the His-Ser system, we have examined the relationships between the extent of racemization and various *im*-protecting groups, as well as various coupling conditions.

The results for the conventional peptide synthesis are given in Table 1. With use of the DCC method, *im*-Z, *im*-Ts, and *im*-Boc on urethane protected L-histidines gave little racemization in CH_2Cl_2 or DMF (entries 1—3). However, *im*-Bzl led to a slightly higher level (entry 4). Insufficient masking of the basicity of the imidazole function by Bzl group seemed to be the main reason for the higher degree of racemization. Low levels of racemization (0.2—0.3%; entries 5 and 7) were observed in the usual MA method. The activation of Z-L-His(Z) under the strict conditions introduced by Anderson *et al.*[5] suppressed the racemization to below 0.1% (entry 6). Windridge and Jorgensen reported 24% racemization by Woodward's reagent during the course of coupling of Boc-L-His(Bzl) and L-Glu(OBzl)-OBzl using DMF as a solvent.[3] The present study showed only 0.4% racemization by this method (entry 8) in the coupling of Z-L-His(Z) and L-Ser(Bzl)-OBzl in CH_3CN. The azide method is considered free from racemization; however, Z-L-His-N_3 causes a slight degree of racemization (entry 9), which might be due to the basicity of free imidazole moiety.

The results of racemization during the solid-phase method are also given in Table 1. More appreciable racemization takes place in synthesis carried out by the solid-phase method than that by the conventional method. The remarkably high racemization (37%; entry 13) of Z-L-His(Bzl) coincides with the result of Windridge and Jorgensen.[3] The use of Z-L-His also causes appreciable racemization (4.8%). Racemization was reduced to 0.9% with Z-L-His(Ts). Lin *et al.* observed almost no racemization of Boc-L-His(Ts) in the synthesis of [L-His(Ts)^{119}, Ile^{120}]-ribonuclease decapeptide in contrast to 2.3% racemization of His^{119} when Boc-L-His was used.[6] Addition of either HOSu or HOBt with DCC resulted in an extensive reduction of racemization to 0.2% (entry 11). Weygand *et al.* reported the occurrence of less than 1% racemization with DCC plus HOSu.[7] König and Geiger also reported suppressed racemization by the DCC method in the presence of HOBt.[8]

Experimental

Preparation of Diastereomers (DL-His-L-A). Amino Acid Derivatives: Z-DL-His(Z)·EtOH (**1**) was prepared in a similar way to that for the L-isomer;[9] yield, 54%; mp 92—94 °C. L-Ser(Bzl)-OBzl·TsOH (**2**) was prepared following the general procedure by Izumiya and Makisumi;[10] yield, 72%; mp 120—122 °C; $[\alpha]_D^{20}$ −19.0° (*c* 2, MeOH).

*Z-DL-His(Z)-L-Ser(Bzl)-OBzl (**3**)*: IBCF (1 mmol) was added to a chilled solution (−15 °C) of **1** (1 mmol) and TEA (1 mmol) in THF (4 ml). After 10 min, a mixture of **2** (1 mmol), TEA (1 mmol) and THF (4 ml) was added to the chilled solution. The reaction mixture was allowed to stand at 0 °C for 1 h and at 20 °C for 19 h, and evaporated. The residue was dissolved in EtOAc and the solution was washed with 2% HCl, 4% $NaHCO_3$, and dried (Na_2SO_4). Evaporation of the filtrate afforded an oil (**3**).

DL-His-L-Ser: A part (0.5 mmol) of the crude oil (**3**) dissolved in a mixture (6 ml) of AcOH-MeOH-H_2O (6:3:1, v/v) was treated with H_2 in the presence of Pd black. The filtrate from the catalyst was evaporated, and the residue (DL-His-L-Ser) was used in an experiment with the analyzer.

Other diastereomers (DL-His-L-A) were prepared in the same manner as described above.

Separation of DL-His-L-A by the Amino Acid Analyzer: A part (1 μmol) of the residue (DL-His-L-A) was dissolved in 0.2 M citrate buffer (pH 2.2) and analyzed on a Hitachi amino acid analyzer: column, 0.6×10 cm; solvent, standard 0.2 M citrate buffer (pH 4.25); flow rate, 60 ml/h; jacket temperature, 55 °C. Pure diastereomers of His-Ser were prepared for the identification of peaks, and for the determination of color yields by ninhydrin reaction.

Diastereomers of His-Ser. Z-L(or D)-His(Z)-L-Ser(Bzl)-OBzl (**4,5**): Z-D-His(Z)·EtOH was prepared as described for **1**; yield, 71%; mp 93—95 °C; $[\alpha]_D^{23}$ −30.4° (*c* 2, EtOAc). Compounds **4** and **5** were prepared from Z-L(or D)-His(Z)·EtOH and **2** as described for **3**. Crude products were recrystallized from EtOAc-petroleum ether.

*L(or D)-His-L-Ser (**6,7**)*: Compounds **4** and **5** were hy-

**Present address: Mitsubishi Kasei Co., Kurashiki, Okayama 712.

***Present address: Laboratory of Chemistry, College of General Education, Saga University, Saga 840.

Table 1. Extent of recemization in conventional (entries 1—9) and solid-phase method (entries 10—14)

Entry	Coupling reagent	Acid component	Solvent	Reaction time (h)	Reaction temp (°C)	Extent of racemization (%)[a]
1	DCC	Z-L-His(Ts)	CH_2Cl_2	20	0, 20	0.3
2	DCC	Boc-L-His(Boc)	CH_2Cl_2	20	0, 20	0.4
3	DCC	Z-L-His(Z)	DMF	20	20	0.6
4	DCC	Z-L-His(Bzl)	DMF	20	20	1.8
5	IBCF	Z-L-His(Z)	THF	20	0, 20	0.2[b]
6	IBCF	Z-L-His(Z)	THF	20	0, 20	<0.1[c]
7	IBCF	Boc-L-His(Boc)	THF	20	0, 20	0.3[b]
8	Woodward's reagent	Z-L-His(Z)	CH_3CN	20	0, 20	0.4
9	Isopentyl nitrite	Z-L-His-$NHNH_2$	DMF	48	0	0.8
10	DCC	Boc-L-His(Boc)	CH_2Cl_2	4	20	1.5
11	DCC/HOSu or HOBt	Boc-L-His(Boc)	CH_2Cl_2	4	20	0.2
12	DCC	Z-L-His(Ts)	CH_2Cl_2	4	20	0.9
13	DCC	Z-L-His(Bzl)	DMF	4	20	37
14	DCC	Z-L-His	DMF	4	20	4.8

a) Defined as [100(D-L isomer)]/[(L-L isomer)+(D-L isomer)]. b) MA was prepared with TEA at −15 °C for 10 min and reacted at 0 °C for 1 h and at 20 °C for 19 h. c) MA was prepared with *N*-methylmorpholine at −15 °C for 1 min.

Table 2. Yields and physical constants of compounds **4**—**7**

Compounds[a]	Yield (%)	Mp (°C)	$[\alpha]_D^{20}$ (*c* 2)
Z-L-His(Z)-L-Ser(Bzl)-OBzl (**4**)	66	109—110	+23.5°[b]
Z-D-His(Z)-L-Ser(Bzl)-OBzl (**5**)	69	131—132	−32.7°[b]
L-His-L-Ser (**6**)[c]	69	192—193 (dec)	+4.1°[d]
D-His-L-Ser·H_2O (**7**)	67	197—198 (dec)	−6.0°[d]

a) Satisfactory elemental analyses were obtained for all compounds. b) Solvent, $CHCl_3$. c) G. Losse and G. Müller, *Chem. Ber.*, **94**, 2768 (1961), synthesized **6** from Trt-L-His(Trt)-L-Ser and afforded mp 138—141 °C. d) Solvent, 0.1 M NaOH.

drogenated as described for DL-His-L-Ser, and the crude products were recrystallized from water–EtOH. Melting points and other data of **4**—**7** are summarized in Table 2. Each dipeptide was subjected to analysis as described before; **6** was eluted at 85 ml of effluent volume, and **7** at 115 ml.

Detection of Racemization during the Conventional Method. Several acyl-L-histidines (1 mmol each) were coupled with **2** (1 mmol) by DCC,[11] IBCF,[5] Woodward's reagent,[12] and by the azide method.[13] The solvent of the reaction mixture was evaporated and the residue was worked up as described for **3**. The crude product was deblocked by a suitable method to afford His-Ser, a part (5 μmol) of which was subjected to analysis.

Detection of Racemization during the Solid-phase Method. Coupling was performed manually.[14] L-Ser(Bzl)-resin derived from Boc-L-Ser(Bzl)-resin (0.20 g, 0.06 mmol) was treated with four equivalents of DCC and a protected histidine (*e.g.*, Boc-L-His(Boc)). In some cases HOSu or HOBt (fourfold) was used together with DCC. The acyl-dipeptide-resin obtained was treated with HF (3 ml) at 0 °C for 1 h in the presence of anisole (0.3 ml). After removal of HF, the crude peptide was extracted with 1% AcOH, the extract being washed with ether and evaporated. The residue (His-Ser) was subjected to analysis.

References

1) E. C. Jorgensen, G. C. Windridge, and T. C. Lee, *J. Med. Chem.*, **13**, 352 (1970).

2) Abbreviations according to IUPAC-IUB commission, *J. Biol. Chem.*, **247**, 977 (1972), are used throughout. Additional abbreviations: DMF, *N*,*N*-dimethylformamide; HOBt, *N*-hydroxybenzotriazole; HOSu, *N*-hydroxysuccinimide; IBCF, isobutyl chloroformate; MA, mixed anhydride; OBzl, benzyl ester; TEA, triethylamine; EtOH, ethanol; THF, tetrahydrofuran; TsOH, *p*-toluenesulfonic acid.

3) G. C. Windridge and E. C. Jorgensen, *Intra-Sci. Chim. Rep.*, **5**, 375 (1971); *Chem. Abstr.*, **76**, 86129 (1972).

4) M. Bodanszky and L. E. Conklin, *Chem. Commun.*, **1967**, 773; N. Izumiya, M. Muraoka, and H. Aoyagi, *Bull. Chem. Soc. Jpn.*, **44**, 3391 (1971).

5) G. W. Anderson, J. E. Zimmerman, and F. M. Callahan, *J. Am. Chem. Soc.*, **89**, 5012 (1967).

6) M. C. Lin, B. Gutte, D. G. Caldi, S. Moore, and R. B. Merrifield, *J. Biol. Chem.*, **247**, 4768 (1972).

7) F. Weygand, D. Hoffmann, and E. Wünsch, *Z. Naturforsch.*, **21b**, 426 (1966).

8) W. König and R. Geiger, *Chem. Ber.*, **103**, 788 (1970).

9) A. Patchornik, A. Berger, and E. Katchalski, *J. Am. Chem. Soc.*, **79**, 6416 (1957).

10) N. Izumiya and S. Makisumi, *Nippon Kagaku Zasshi*, **78**, 662, 1768 (1957).

11) J. C. Sheehan and G. P. Hess, *J. Am. Chem. Soc.*, **77**, 1067 (1955).

12) R. B. Woodward, R. A. Olofson, and H. Mayer, *J. Am. Chem. Soc.*, **83**, 1010 (1961).

13) J. Honzl and J. Rudinger, *Collect. Czech. Chem. Commun.*, **26**, 2333 (1961).

14) H. Takashima, V. du Vigneaud, and R. B. Merrifield, *J. Am. Chem. Soc.*, **90**, 1323 (1968).

Microwave Spectrum, Barrier to Internal Rotation, and Dipole Moment of Methyl Selenocyanate

Takeshi SAKAIZUMI,* Yoshio KOHRI, Osamu OHASHI, and Ichiro YAMAGUCHI

Department of Chemistry, Faculty of Science and Technology, Sophia University, Kioi-cho, Chiyoda-ku, Tokyo 102

(Received January 17, 1978)

Microwave rotational spectra of five isotopic species of methyl selenocyanate (CH_3SeCN with ^{82}Se, ^{80}Se, ^{78}Se, ^{77}Se, and ^{76}Se) in the ground vibrational state, and two isotopic species of methyl selenocyanate-d_3 (CD_3SeCN with ^{80}Se and ^{78}Se) in the ground and first excited states of the methyl torsional mode have been assigned in the 8.0 to 35.5 GHz frequency range. For the most abundant species in the ground vibrational state, the rotational constants determined are $A_A=10147\pm2$, $B_A=3483.57\pm0.04$, and $C=2631.58\pm0.04$ MHz for $CH_3{}^{80}SeCN$ and $A=8322.57\pm0.81$, $B=3308.06\pm0.02$, and $C=2436.92\pm0.01$ MHz for $CD_3{}^{80}SeCN$. The A-E splittings due to the methyl internal rotation were observed for the rotational transitions in the ground vibrational state for the normal species and in the first excited state of the methyl torsional mode for the deuterated species. Analysis of the splittings gave a barrier height to the methyl internal rotation of 1241 ± 50 and 1228 ± 50 cal/mol for the CH_3 and CD_3 species, respectively. Stark measurements yielded the principal axis dipole moments of $\mu_a=4.35\pm0.04$, $\mu_b=0.76\pm0.10$, and the total dipole moment of $\mu=4.42\pm0.05$ D for $CH_3{}^{80}SeCN$, and $\mu_a=4.31\pm0.04$, $\mu_b=0.67\pm0.07$, and $\mu=4.36\pm0.04$ D for $CD_3{}^{80}SeCN$. The direction of the dipole moment in the molecule is discussed.

The microwave spectra of alkyl compounds having an isocyanato (–N=C=O) or an isothiocyanato (–N=C=S) group have been studied: ethyl isocyanate (CH_3CH_2NCO)[1] and ethyl isothiocyanate (CH_3CH_2NCS).[2] There have been several studies of the microwave spectra of molecules having a C–Se bond which is an axis of internal rotation, *e.g.*, CH_3SeH[3] and $(CH_3)_2Se$.[4]

Studies of the microwave spectra of a series of compounds, CH_3SeH,[3] CH_3SH,[5] and CH_3OH,[6] have been made. Among the series, methane selenol had the lowest potential barrier hindering the methyl internal rotation and the longest bond which is the internal rotation axis (see Table 13). The potential barrier of methanethiol is higher than that of methanol, while the C–S bond in methanethiol is longer than the C–O bond in methanol. There seems no simple parallelism between the height of the potential barrier and the bond length for this series, but for a series of dimethyl compounds, $(CH_3)_2Se$,[4] $(CH_3)_2S$,[7] and $(CH_3)_2O$,[8] it does exist as shown in Table 13.

Therefore, it is of interest to study the potential barrier of methyl selenocyanate and to compare it with those of the related compounds in relation to the bond length. In this paper, the spectrum of methyl selenocyanate will be reported, and the barrier height and dipole moment will be discussed.

Experimental

Methyl selenocyanate was prepared by mixing methyl iodide with a cold solution of potassium selenocyanate in ethanol.[9] An exothermic reaction occurred immediately after adding the iodide followed by the deposition of potassium halides. The mixture was mildly refluxed for 4 h after standing for 30 min at room temperature. The solvent was removed by distillation in a stream of nitrogen and the resultant slurry steam-distilled, giving crude yellow methyl selenocyanate (40 to 50% yield). Reduced pressure distillation with a nitrogen leak yielded a pale yellow product. Methyl selenocyanate-d_3 (CD_3SeCN) was prepared by reacting 99% enriched CD_3I (E. Merk Co., Ltd.) with KSeCN according to the method of normal species. The normal species was identified by the IR and proton NMR spectra, while the deuterated one only by the IR.

The rotational spectra were obtained in the frequency region from 8.0 to 35.5 GHz with a conventional 100-kHz squares-wave Stark modulation spectrometer. The waveguide was cooled with Dry Ice. Transition frequencies were measured with a Hewlett-Packard Model 5245L electronic counter with a 5257A transfer oscillator.

Results and Discussion

Assignment of Spectrum of CH_3SeCN. A model of the molecular structure was constructed based upon the following known molecular parameters: methyl group and C–N bond in CH_3SCN,[10] Se–CH_3 bond in CH_3SeH,[3] Se–CN bond in selenophene,[11] and angle C–Se–C in dimethyl selenide.[4] The assumed structural parameters are listed in Table 1. The assumed molecular structure and bond moment considerations indicated that the CH_3SeCN molecule should be an asymmetric prolate rotor ($\kappa=-0.77$) with a large component of the dipole moment lying along the a-principal axis. A search for the a-type R-branch transitions, $3_{13}\leftarrow2_{12}$, $3_{03}\leftarrow2_{02}$, and $3_{12}\leftarrow2_{11}$, in the predicted frequency range was fruitful. The transitions of the K-doublet ($K_{-1}=1$ and 2) on the higher frequency side with respect to the $K_{-1}=0$ line split into A and E components due to the hindered internal rotation of the methyl group. A characteristic A-E splitting of the $J=4\leftarrow3$ transition with $K_{-1}=3$ was observed for $CH_3{}^{80}SeCN$ as shown in Fig. 1. The assignments of the lines for the isotopic species (^{82}Se, ^{80}Se, ^{78}Se, ^{77}Se, and ^{76}Se) were made

Table 1. Assumed structural parameters

Length(Å)		Angle(°)	
C–H :	1.093[a]	H–C–H:	109.4[a]
C≡N :	1.156[a]	H–C–Se :	109.6[a]
C–Se :	1.958[b]	C–Se–C :	97.06[d]
Se–CN:	1.832[c]	Se–C≡N :	180

a) Ref. 10. b) Ref. 3. c) Ref. 11. d) Ref. 4.

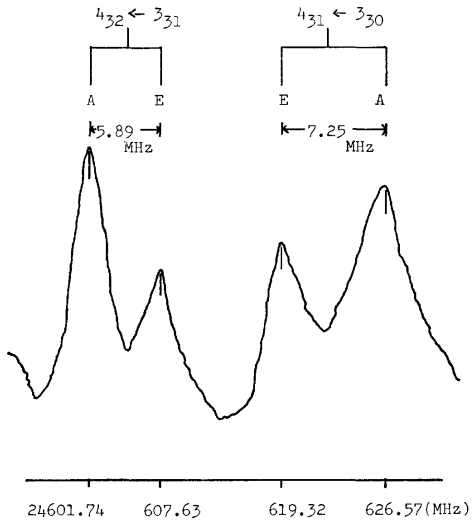

Fig. 1. Observed spectrum of $4_{32}\leftarrow3_{31}$ and $4_{31}\leftarrow3_{30}$ transitions in $CH_3{}^{80}SeCN$ showing their characteristic A-E splitting.

based on the Stark effects and the relative intensities corresponding to the natural abundances (9.1, 49.8, 23.5, 7.5, and 9.0%, respectively). The observed and calculated frequencies are in good agreement for transitions up to $J=5\leftarrow4$ of CH_3SeCN in the ground vibrational state as shown in Table 2. The rotational constants in the ground vibrational state of the A-species were obtained by the least-squares method and are listed in Table 3. Almost a constant value of $\Delta I(=I_c-I_b-I_a)$ was obtained for the ^{82}Se, ^{80}Se, ^{78}Se, ^{77}Se, and ^{76}Se isotopic species as shown in Table 3, indicating that the selenium atom is in the molecular symmetry plane as expected. The constant ΔI value also ensures the assignment of the transition lines.

The observed values of ΔI, -2.83 to -2.85 amu Å^2, are smaller than the values, -3.12 to -3.26 amu Å^2, usually obtained for molecules with a planar framework and a methyl group whose axis of symmetry lies in the plane.

Deuterated Species. The assignment of the spectrum for the ^{80}Se species was made by the same procedure as for the normal species. The absorption lines due to the excited state of the ^{80}Se species were found in the vicinity of the ground state as shown by the broken lines in Fig. 2. The assignment for the ^{78}Se species was made bearing in mind the Stark effects and the isotopic shifts

Table 2. Observed transition frequencies of methyl selenocyanate (A-species) (MHz)

Transition	$CH_3{}^{82}SeCN$		$CH_3{}^{80}SeCN$		$CH_3{}^{78}SeCN$		$CH_3{}^{77}SeCN$		$CH_3{}^{76}SeCN$	
	Obsd	$\Delta\nu$	Obsd	$\Delta\nu$	Obsd	$\Delta\nu$	Obsd	$\Delta\nu$	Obsd	$\Delta\nu$
$2_{12}\leftarrow1_{11}$	11344.57	0.25	11378.56	0.20	11414.04	0.27	—	—	11449.95	−0.49
$2_{02}\leftarrow1_{01}$	12118.59	−0.48	12153.57	−0.16	12189.47	−0.22	12207.79	−0.29	12226.85	−0.20
$2_{11}\leftarrow1_{10}$	—	—	13082.20	−0.11	13117.69	−0.19	13136.31	0.07	13154.17[a]	−0.82
$3_{13}\leftarrow2_{12}$	16970.81	0.46	17021.91	0.29	17075.29	0.26	17102.12	0.05	17130.53	0.23
$3_{03}\leftarrow2_{02}$	17989.90	−0.29	18043.21	0.06	18098.25	0.07	18126.14	−0.18	18155.80	0.47
$3_{22}\leftarrow2_{21}$	18294.60	0.49	18345.58	0.08	18399.00	0.26	—	—	—	—
$3_{21}\leftarrow2_{20}$	18597.79	−0.22	18647.65	−0.19	18699.24	−0.05	18726.40[a]	0.83	18752.82	0.01
$3_{12}\leftarrow2_{11}$	19521.58	0.34	19573.37	0.11	19626.88	−0.04	19654.50	−0.11	19682.57	0.34
$4_{14}\leftarrow3_{13}$	22546.97	0.07	22615.80	0.16	22687.33	0.05	22723.24	−0.30	22761.63	0.22
$4_{04}\leftarrow3_{03}$	23657.13	−0.14	23729.34	0.02	23804.29	−0.07	23843.17	0.40	23881.99	−0.25
$4_{23}\leftarrow3_{22}$	24331.79	0.34	24400.77	−0.19	24472.24	−0.08	24508.97	0.17	24545.93[a]	−0.53
$4_{32}\leftarrow3_{31}$	24534.59[a]	0.71	24601.74	0.03	24671.14[a]	0.64	24709.16[a]	1.38	24745.37[a]	0.48
$4_{31}\leftarrow3_{30}$	24557.26[a]	−2.71	24626.57[a]	−0.95	24695.26[a]	−1.79	24731.32[a]	−1.79	24768.57[a]	−1.49
$4_{22}\leftarrow3_{21}$	25066.45	−0.34	25131.99	−0.11	25199.01	−0.39	25233.35	−0.41	25269.64	0.18
$4_{13}\leftarrow3_{12}$	25927.86	0.04	25998.11	0.33	26069.97	−0.03	26107.06	−0.22	26145.76	0.42
$5_{15}\leftarrow4_{14}$	28066.48	−0.05	28152.89	−0.03	28242.87	−0.17	28288.78	0.11	28336.11	−0.15
$5_{05}\leftarrow4_{04}$	29109.70	0.13	29200.83	−0.20	29296.70	0.18	29345.50	0.14	29395.70	0.16
$5_{24}\leftarrow4_{23}$	30318.92	−0.26	30405.52	−0.20	30495.37	−0.13	30541.28	−0.11	30588.43	−0.33
$5_{23}\leftarrow4_{22}$	31698.27	0.11	31778.89	−0.01	31862.22	0.25	31904.82	0.44	31948.30	−0.15
$5_{14}\leftarrow4_{13}$	32235.14	0.13	32323.58	0.04	32415.27	0.20	32462.41	0.08	32510.66	0.16

$\Delta\nu=\nu_{obsd}-\nu_{calcd}$. a) Not used for the least-squares fit.

Table 3. Rotational constants (MHz) and moments of inertia (amu Å^2)[a]

	$CH_3{}^{82}SeCN$	$CH_3{}^{80}SeCN$	$CH_3{}^{78}SeCN$	$CH_3{}^{77}SeCN$	$CH_3{}^{76}SeCN$
A_A	10096 ±4	10146 ±2	10199 ±3	10230 ±4	10257 ±4
B_A	3474.89±0.08	3483.57±0.04	3492.48±0.06	3497.12±0.07	3501.81±0.09
C	2623.14±0.08	2631.58±0.04	2640.42±0.06	2644.85±0.07	2649.53±0.08
I_a^A	50.057	49.809	49.547	49.396	49.269
I_b^A	145.436	145.074	144.704	144.512	144.318
I_c	192.660	192.042	191.399	191.079	190.741
ΔI	−2.832	−2.840	−2.851	−2.828	−2.846

a) Conversion factor: 505376 MHz amu Å^2, ΔI(amu Å^2)$=I_c-I_b-I_a$.

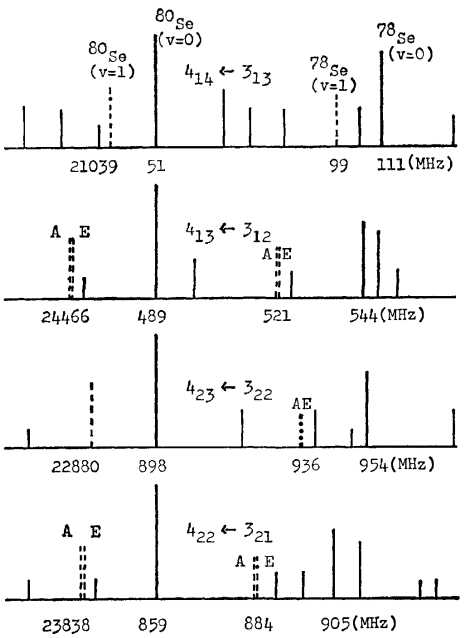

Fig. 2. Observed spectrum of $J=4\leftarrow3$ transitions in CD_3SeCN.

of the lines predicted from the model. In this spectrum the strong satellite lines due to the vibrationally excited state appeared in the vicinity of the ground state line. The observed lines for the excited state of the ^{78}Se species are also shown by the broken lines in Fig. 2. The broken lines were assigned to the first excited state of the methyl torsional mode because of the splitting of the A-E doublet. The observed and calculated frequencies for CD_3SeCN in the ground and first excited vibrational states of the A-species are in good agreement as given in Table 4. The rotational constants in the ground and excited states of the A-species are listed in Table 5.

$r_s(H\cdots H)$ Distance. The distance between the out-of-plane H atoms was determined from the moments of inertia for the normal and deuterated species. The distance between the H atoms is related to the effective moments of inertia as follows,

$$I_a^\circ + I_b^\circ - I_c^\circ = m_H r_e^2 - \Delta_c, \quad (1)$$

where r_e is the equilibrium distance between the two out-of-plane H atoms. The major contribution to Δ_c arises from the low-frequency in-plane motions of the heavy atom skeleton[12] and hence the effect of isotopic substitution of the out-of-plane hydrogen atoms on Δ_c should be small. The contribution of the in-plane vibration may be estimated by using the following approximate equation,[12]

$$\Delta_c = 4K/\omega, \quad (2)$$

where ω is the frequency of the lowest in-plane vibration in cm^{-1} and $K=h/8\pi^2=16.863$ amu Å^2 cm^{-1}. Equation 2 is given for planar molecules, but it is suitable for such cases as non-planar molecules (X_2YZ_2 and CH_3CXO) with a heavy planar skeleton.[12] Substitution of the infrared data for the C–Se–C bending mode ($\omega=166$ cm^{-1})[13] into Eq. 2 gives $\Delta_c=0.406$ amu Å^2. Using Eqs. 1 and 2 for ^{80}Se and ^{78}Se species the values of $r_e(H\cdots H)$ and $r_e(D\cdots D)$ obtained are listed in Table 6.

The change in the moments of inertia from the normal to the deuterated species gives the following relation,

Table 4. Observed frequencies of methyl selenocyanate-d_3 (MHz)

Transition	$CD_3{}^{80}SeCN$				$CD_3{}^{78}SeCN$			
	($v=0$)		($v=1$)		($v=0$)		($v=1$)	
	Obsd	$\Delta\nu$	Obsd	$\Delta\nu$	Obsd	$\Delta\nu$	Obsd	$\Delta\nu$
$3_{13}\leftarrow2_{12}$	15866.83	0.08	15857.27	0.21	15911.01	−0.38	15902.06	0.29
$3_{03}\leftarrow2_{02}$	16828.84	0.18	16816.53	0.28	16875.04	0.24	16862.49	0.23
$3_{22}\leftarrow2_{21}$	17235.14	0.18	17221.05	0.38	17276.66	0.17	17261.97	−0.12
$3_{21}\leftarrow2_{20}$	17641.04	−0.22	17625.38	0.14	17678.14	−0.02	17661.85	−0.08
$3_{12}\leftarrow2_{11}$	18472.66	0.30	18454.22	0.21	18512.17	−0.13	18493.85	0.08
$4_{14}\leftarrow3_{13}$	21050.96	−0.24	21039.10	0.11	21111.83	0.01	21099.58	0.14
$4_{04}\leftarrow3_{03}$	22018.99	0.10	22003.87	−0.23	22084.48	0.23	22069.43	0.12
$4_{23}\leftarrow3_{22}$	22898.96	0.14	22880.30	0.07	22955.03	−0.11	22936.43	0.09
$4_{22}\leftarrow3_{21}$	23859.47	0.08	23836.72	0.09	23906.00	0.26	23882.93	0.24
$4_{13}\leftarrow3_{12}$	24489.53	0.23	24465.73	0.24	24544.66	0.23	24520.39	0.01
$5_{15}\leftarrow4_{14}$	26166.45	0.08	26151.80	0.07	26243.60	0.13	26228.46	−0.15
$5_{05}\leftarrow4_{04}$	26981.59	0.02	26965.04	−0.11	27066.38	0.02	27049.92	0.13
$5_{24}\leftarrow4_{23}$	28494.17	−0.06	28471.54	−0.03	28566.28	0.12	28543.09	−0.14
$5_{23}\leftarrow4_{22}$	30233.47	−0.26	30203.59	−0.21	30290.03	−0.15	30259.80	−0.08
$5_{14}\leftarrow4_{13}$	30362.72	0.02	30334.08	−0.03	30435.20	0.12	30405.84	−0.36
$6_{16}\leftarrow5_{15}$	31215.53	0.02	31198.76	0.08	31309.43	0.03	31291.93	−0.39
$6_{06}\leftarrow5_{05}$	31809.11	−0.01	31791.45	0.10	31911.62	−0.08	31893.76	0.02
$6_{25}\leftarrow5_{24}$	34006.48	−0.32	33979.83	−0.60	34094.70	−0.52	34068.82	0.26
$5_{14}\leftarrow5_{15}$	12853.76	0.30	12810.06	−0.11				
$6_{15}\leftarrow6_{16}$	17671.20	0.02	17612.15	−0.19				
$7_{16}\leftarrow7_{17}$	22906.80	−0.20	22832.15	0.14				

$\Delta\nu=\nu_{obsd}-\nu_{calcd}$.

Table 5. Rotational constants (MHz) and moments of inertia (amu Å²)

	$CD_3{}^{80}SeCN$		$CD_3{}^{78}SeCN$	
	$(v=0)$	$(v=1)^{a)}$	$(v=0)$	$(v=1)^{a)}$
A	8322.31±0.81	8307.45±0.98	8374.37±1.08	8359.77±1.85
B	3308.06±0.02	3304.21±0.02	3314.17±0.02	3310.28±0.05
C	2436.92±0.01	2436.03±0.02	2444.65±0.02	2443.74±0.04
I_a	60.725	60.834	60.348	60.453
I_b	152.771	152.949	152.489	152.669
I_c	207.383	207.459	206.727	206.804
ΔI	−6.113	−6.324	−6.110	−6.317

a) A-species, $\Delta I(\text{amu Å}^2)=I_c-I_b-I_a$.

$$\Delta I_a^\circ + \Delta I_b^\circ - \Delta I_c^\circ = (m_D - m_H)r_s^2, \quad (3)$$

where $\Delta I_a^\circ = I_a^\circ(CD_3) - I_a^\circ(CH_3)$, *etc.* In Eq. 3, the vibrational effect is effectively cancelled if Δ_c is the same for the CH_3 and CD_3 isotopic species.[14] The values of r_s obtained using Eq. 3 for ^{80}Se and ^{78}Se species are listed in Table 6.

Table 6. Nonbonded H···H distance (Å) in methyl group

	$CH_3{}^{80}SeCN$	$CH_3{}^{78}SeCN$
r_s	1.802±0.009	1.798±0.012
r_e(D–D)	1.799±0.001	1.798±0.001
r_e(H–H)	1.795±0.004	1.799±0.006

Tabel 7. Comparison of the H···H distance (Å)

Molecule	r_s
CH_3SeCN	1.800[a)]
CH_3CHO	1.776[b)]
CH_3CFO	1.770[b)]
CH_3CClO	1.768[b)]
CH_3COOH	1.774[b)]
CH_3COCN	1.766[b)]

a) This work. b) Ref. 14.

Table 7 shows a comparison of the H···H distance in some related molecules. The r_s in CH_3SeCN obtained in this work is larger than that in the other molecules.

The Bond Length $r_{Se-C(methyl)}$. The r_s-coordinate of the carbon atom in the methyl group could not be determined, because the spectrum of the $^{13}CH_3$ species was not observed. However the bond length r_{Se-C} may be obtained using the moments of inertia of the four isotopic species ($CH_3{}^{80}SeCN$, $CH_3{}^{78}SeCN$, $CD_3{}^{80}SeCN$, and $CD_3{}^{78}SeCN$). If the methyl group is assumed to have C_{3v} symmetry, r_{Se-C} is expressed by the relation (see Appendix),

$$r_{Se-C} = \sqrt{1/3}\, r_{C-H}\left[\sqrt{\cos\theta - 1 + (Z/r_{C-H}^2)} - \sqrt{2\cos\theta + 1}\right], \quad (4)$$

where θ and r_{C-H} are the angle H–C–H and the C–H bond length in the methyl group and Z is a quantity calculated from the observed moments of inertia (I_c) of the four isotopic species and their molecular weights. Assuming r_{C-H} to be 1.085 Å as in the case of the CH_3SeH molecule, the H–C–H angle θ may be obtained as 112° from the r_s(H···H) distance determined (Table 6). With these values, the bond distance, r_{Se-C}, may be estimated from Eq. 4 to be 1.950 Å. The error in r_{Se-C} depends on the estimation of r_{C-H} distance. If the estimation error of r_{C-H} is ±0.008 Å, the error of r_{Se-C} is ±0.025 Å.

The remaining parameters, $r_{C\equiv N}$, r_{Se-CN}, and the angle C–Se–C, have been fitted to all the observed moments of inertia (except for I_a in normal species). The obtained structural parameters are listed in Table 8 and the observed and calculated moments of inertia are shown in Table 9.

Table 8. Structural parameters

Lengh(Å)	Angle(°)
C≡N: 1.160	H–C–H: 112.0
Se–CN: 1.851	C–Se–C: 95.57
C–Se: 1.950	Se–C≡N: 180(assumed)
C–H: 1.085(assumed)	

Table 9. The observed and calculated moments of inertia (amu Å²)

		Obsd	Calcd	Δ
$CH_3{}^{82}SeCN$	I_a	50.057	50.086	−0.029
	I_b	145.436	145.820	−0.384
	I_c	192.660	192.645	0.015
$CH_3{}^{80}SeCN$	I_a	49.809	49.836	−0.027
	I_b	145.074	145.439	−0.365
	I_c	192.042	192.013	0.029
$CH_3{}^{78}SeCN$	I_a	49.547	49.575	−0.028
	I_b	144.704	145.047	−0.343
	I_c	191.399	191.361	0.038
$CH_3{}^{77}SeCN$	I_a	49.396	49.441	−0.045
	I_b	144.512	144.848	−0.336
	I_c	191.079	191.028	0.051
$CH_3{}^{76}SeCN$	I_a	49.269	49.304	−0.035
	I_b	144.318	144.645	−0.327
	I_c	190.741	190.688	0.053
$CD_3{}^{80}SeCN$	I_a	60.725	60.705	0.020
	I_b	152.771	152.745	0.026
	I_c	207.383	206.932	0.451
$CD_3{}^{78}SeCN$	I_a	60.348	60.336	0.012
	I_b	152.489	152.443	0.046
	I_c	206.727	206.261	0.466

Δ=Obsd−Calcd.

TABLE 10. INTERNAL ROTATION SPLITTING (MHz) OF METHYL SELENOCYANATE

Transition	$CH_3{}^{82}SeCN$		$CH_3{}^{80}SeCN$		$CH_3{}^{78}SeCN$		$CH_3{}^{77}SeCN$		$CH_3{}^{76}SeCN$	
	Obsd	$\Delta\nu$[a]	Obsd	$\Delta\nu$[a]	Obsd	$\Delta\nu$[a]	Obsd	$\Delta\nu$[a]	Obsd	$\Delta\nu$[a]
$3_{21}\leftarrow2_{20}$	1.31	−0.38	1.70	0.15	1.63	−0.09	1.44	−0.26	—	—
$4_{22}\leftarrow3_{21}$	—	—	0.95	−0.19	1.08	−0.14	—	—	1.15	−0.08
$4_{31}\leftarrow3_{30}$	—	—	7.25	−0.06	7.81	0.18	7.86	0.30	7.81	0.14
$4_{32}\leftarrow3_{31}$	−6.34	−0.41	−5.89	−0.17	−5.99	−0.04	−5.72	0.19	−5.89	0.09
$4_{13}\leftarrow3_{12}$	0.96	0.14	1.04	0.01	0.95	−0.14	1.03	−0.04	1.08	−0.01
$5_{23}\leftarrow4_{22}$	1.37	−0.13	1.31	−0.09	1.38	−0.10	1.43	−0.03	1.27	−0.22
$5_{24}\leftarrow4_{23}$	0.52	−0.33	0.57	−0.23	0.61	−0.24	0.59	−0.24	0.63	−0.22
$5_{14}\leftarrow4_{13}$	1.34	0.05	1.10	−0.11	1.14	−0.14	1.31	0.05	1.44	0.15

a) $\Delta\nu=(\nu_A-\nu_E)_{obsd}-(\nu_A-\nu_E)_{calcd}$.

TABLE 11. INTERNAL ROTATION SPLITTING (MHz) OF METHYL SELENOCYANATE-d_3

Transition	$CD_3{}^{80}SeCN$ ($v=1$)		$CD_3{}^{78}SeCN$ ($v=1$)	
	Obsd	$\Delta\nu$[a]	Obsd	$\Delta\nu$[a]
$3_{12}\leftarrow2_{11}$	−1.37	−0.10	−1.25	0.03
$4_{04}\leftarrow3_{03}$	−0.60	0.01	—	—
$4_{23}\leftarrow3_{22}$	—	—	−1.20	0.03
$4_{22}\leftarrow3_{21}$	−1.73	−0.12	−1.43	0.19
$4_{13}\leftarrow3_{12}$	−1.68	−0.09	−1.65	−0.03
$5_{23}\leftarrow4_{22}$	−2.19	0.06	−2.02	0.25
$5_{14}\leftarrow4_{13}$	−1.99	−0.17	−2.33	−0.49
$6_{25}\leftarrow5_{24}$	−1.57	−0.10	−1.48	−0.01
$5_{14}\leftarrow5_{15}$	−4.12	0.07		
$6_{15}\leftarrow6_{16}$	−5.44	0.13		
$7_{16}\leftarrow7_{17}$	−6.91	−0.04		

a) $\Delta\nu=(\nu_A-\nu_E)_{obsd}-(\nu_A-\nu_E)_{calcd}$.

Barrier to Internal Rotation. The A-E splittings due to internal rotation of the methyl group were measured for each isotopic species and are shown in Tables 10 and 11. Analysis of the A-E splittings was achieved using the principal axis method (PAM) developed by Herschbach.[15] The Hamiltonians used in this analysis contained perturbation terms up to second order for A-species and up to third order for E-species. The values of the perturbation coefficients, $W_{v\sigma}^{(n)}$ ($v=0$ or 1 and $\sigma=$A or E) were taken from Hayashi and Pierce.[16] The assignment of the E-species transitions was made with the aid of the internal rotation calculation. The parameters required to compute the A-E splitting of the rotational transitions in the PAM formalism are A, B, C, I_α, λ_a, and s. The rotational constants A, B, and C were fixed to the effective values obtained from the least-squares fit of the A-species lines. Assuming r(C–H)=r(C–D), the value of the moment of intertia of the CH_3 group about its axis of symmetry, I_α, was determined using the following relation:

$$I_\alpha(CH_3) = [m_H/(m_D-m_H)][(I_a+I_b-I_c)_{CD_3} - (I_a+I_b-I_c)_{CH_3}]. \quad (5)$$

The values of $I_\alpha(CH_3)$ for the two pairs of isotopic species, $CH_3{}^{80}SeCN$-$CD_3{}^{80}SeCN$ and $CH_3{}^{78}SeCN$-$CD_3{}^{78}SeCN$ were determined, independently, using Eq. 5 and found to be in good agreement (within 0.017 amu Å^2). The average value of $I_\alpha(CH_3)=3.267$ amu Å^2 was used in the internal rotation analysis involving the methyl group. The moment of inertia of the deuterated methyl group, $I_\alpha(CD_3)$, was obtained from $I_\alpha(CH_3)$ using the relationship

$$I_\alpha(CD_3) = (m_D/m_H)I_\alpha(CH_3) \quad (6)$$

based on the assumption that CH_3 and CD_3 groups are identical except for the differing masses of the hydrogen and deuterium atoms. Substitution of the values of $I_\alpha(CH_3)=3.267$ amu Å^2 into Eq. 6 yields $I_\alpha(CD_3)=6.529$ amu Å^2, which was used in the internal rotation analysis of the methyl selenocyanate-d_3 species. The direction cosine, $\lambda_a(\lambda_a=\cos\varphi$, where φ is the angle between the axis of symmetry of the threefold symmetric top and the a-principal axis), may be obtained from the structural parameters listed in Table 8, assuming that the axis of symmetry of the CH_3 and CD_3 groups coincides with the C–Se bond. From the assigned transitions of the A- and E-species, an approximate value of s, a parameter of the Mathieu equation, could be evaluated. Using the approximate values of s and the internal rotation parameters, the transitions of the E-species were predicted. The E-species lines were observed in the vicinity of the predicted frequencies and consequently were assigned. The observed and calculated A-E splittings of CH_3SeCN and CD_3SeCN are in good agreement as shown in Tables 10 and 11. The s values for the various isotopic species were obtained by the least-squares fit to the observed A-E splittings. The results of the internal rotation analysis are listed in Table 12. The resulting barriers to the methyl internal rotation are 1241±50 and 1228±50 cal/mol for the CH_3 and CD_3 species, respectively.

TABLE 12. INTERNAL ROTATION PARAMETERS[a] OF METHYL SELENOCYANATE

	F (GHz)	λ_a	s	V_3 (cal/mol)
$CH_3{}^{82}SeCN$	158.941	0.316087	36.1±1.0	1234
$CH_3{}^{80}SeCN$	158.968	0.319147	36.6±0.4	1251
$CH_3{}^{78}SeCN$	158.996	0.322314	36.3±0.6	1238
$CH_3{}^{77}SeCN$	159.012	0.323935	36.4±0.5	1242
$CH_3{}^{76}SeCN$	159.027	0.325592	36.3±0.4	1239
$CD_3{}^{80}SeCN$	81.638	0.376662	70.1±0.6	1229
$CD_3{}^{78}SeCN$	81.666	0.380020	70.0±1.4	1227

a) $I_\alpha(CH_3)=3.267$amu Å^2; $I_\alpha(CD_3)=6.529$ amu Å^2.

Table 13. Barrier heights (cal/mol) about C–Se, C–S, and C–O bonds (Å) in some related molecules

		M=Se	M=S	M=O
CH_3MH	V_3	1001±50[a]	1270±29[b]	1070[c]
	r(C–M)	1.959±0.010[a]	1.819±0.005[b]	1.427±0.007[c]
CH_3MCN	V_3	1241±50[d]	1600±80[e]	
	r(C–M)	1.950[d]	1.818[e]	
CH_3MCH_3	V_3	1500±20[f]	2132±2[g]	2720[h]
	r(C–M)	1.943±0.001[f]	1.802±0.002[g]	1.410±0.003[h]

a) Ref. 3. b) Ref. 5. c) Ref. 6. d) This work. e) Ref. 10. f) Ref. 4. g) Ref. 7. h) Ref. 8.

Table 13 shows a comparison of the potential barrier in some related molecules. In the series of $(CH_3)_2Se$, $(CH_3)_2S$, and $(CH_3)_2O$, the potential barrier becomes higher as the C–M bond length (M=Se, S, and O) becomes shorter. The same trend holds for the series of CH_3SeCN and CH_3SCN. However, this trend does not hold for the series of CH_3SeH, CH_3SH, and CH_3OH.

Inspection of the data in Table 13 revealed a quantitative trend that the replacement of a hydrogen atom of the selenol group in CH_3SeH by a cyano group to make CH_3SeCN results in an increase of the barrier by about 240 cal/mol. This increment is consistent with the same replacement from CH_3SH to CH_3SCN.

Table 14. Stark coefficients[a] and dipole moment (D)

Transition	M	$CH_3{}^{80}SeCN$ Obsd	$CH_3{}^{80}SeCN$ Calcd	$CD_3{}^{80}SeCN$ Obsd	$CD_3{}^{80}SeCN$ Calcd
$2_{02}\leftarrow1_{01}$	0	−11.2	−11.7		
	1	10.3	10.2		
$2_{11}\leftarrow1_{10}$	0	9.52	9.11		
$3_{03}\leftarrow2_{02}$	0	−2.04	−2.06	−2.15	−2.16
	1	−0.514	−0.518	−0.559	−0.555
	2	4.06	4.12	4.26	4.25
$3_{12}\leftarrow2_{11}$	0	−1.19	−1.13	−0.467	−0.469
	1	−5.30	−4.89	−3.95	−4.03
	2	−14.9	−15.9	−13.8	−14.7
μ_a:		4.35±0.04		4.31±0.04	
μ_b:		0.76±0.10		0.67±0.07	
μ_{total}:		4.42±0.05		4.36±0.04	

a) $[MHz/(V/cm)^2]\times10^{-5}$.

Stark Effect and Dipole Moment. The dipole moments in the ground vibrational state were determined from the Stark coefficients of the $2_{02}\leftarrow1_{01}$, $2_{11}\leftarrow1_{10}$, $3_{03}\leftarrow2_{02}$, and $3_{12}\leftarrow2_{11}$ transitions for $CH_3{}^{80}SeCN$ and the $3_{03}\leftarrow2_{02}$ and $3_{12}\leftarrow2_{11}$ transitions for $CD_3{}^{80}SeCN$. The c-component of the dipole moment was assumed to be zero because of the plane of symmetry of the molecule as discussed above. The electric-field strength in the absorption cell was calibrated using the dipole moment of OCS, 0.71521 D[17] and the results are given in Table 14. The total dipole moment (4.42 D) is larger than the value of 3.91 D obtained from the dielectric measurement.[18] The same trend is noted for methyl thiocyanate, where the dipole moment obtained by the rotational spectrum is 4.03 D[10] while that obtained from the dielectric measurement is 3.59 D.[18] The replacement of the selenol hydrogen atom by a cyano group results in an increase of the dipole moment by about 3.1 D. This increment is consistent with that of 2.5 D found in changing from CH_3SH to CH_3SCN.

The direction of the dipole moment in the molecule was determined using the values of the dipole moment for both the normal and deuterated species. The observed value of γ ($\cos\gamma=\mu_a/\mu_{total}$), the angle between the direction of the dipole moment and the a-principal axis, is 10.2°±2° for the normal species. Therefore, two directions of the dipole moment are possible in the molecule as shown by two broken lines in Fig. 3. The angle between the a-principal axis for the normal species, CH_3SeCN, and for the deuterated species, CD_3SeCN, was calculated to be 3.8° from the structural parameters in Table 8. Two predicted directions, γ, in CD_3SeCN are 14.0 and 6.4°. The angle γ obtained from the observed data for CD_3SeCN is 8.6°. This is consistent with a predicted value 6.4±2° rather than the other one. Taking account of the electronegativities of the elements (or groups) in this molecule, the above discussion leads to the conclusion that the dipole moment of the molecule lies along the thick arrow shown in Fig. 3.

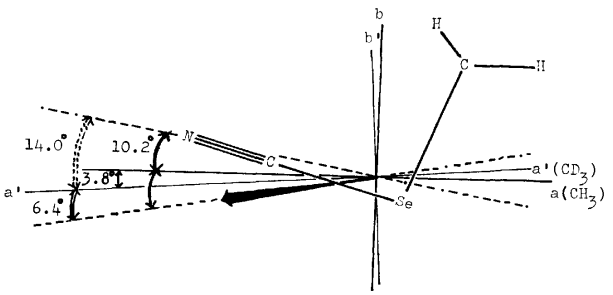

Fig. 3. The direction of dipole moment in methyl selenocyanate.

The authors wish to thank Dr. Teruhiko Ogata, Shizuoka University, for the use of a computer program for the PAM analysis.

Appendix

The molecules studied have a plane of symmetry. If the z axis is chosen as perpendicular to the plane of symmetry, the principal moment of inertia, I_z, is represented by the following equation,

$$I_z=\sum_i m_i r_i^2 - M(X^2+Y^2) \quad \text{(A1)}$$

the origin of the coordinate system being taken at an arbitrary point in the molecule, where m_i is the mass of the i-th atom in

the normal species and M is the total mass of the molecule. r_i represents the distance of the i-th atom from the origin. X and Y are the coordinates of the center of mass from the origin.

The z axis has been chosen as the principal axis c for the molecules studied in this work. If the selenium atom in the molecule is chosen as the origin of the coordinate system, the moment of inertia, I_c, are given by

$$I = \sum_i m_i r_i^2 - M(X^2+Y^2) \quad \text{(A2)}$$

for $CH_3{}^{80}SeCN$ and $CH_3{}^{78}SeCN$ molecules and

$$I = \sum_i m_i r_i^2 - M(X^2+Y^2) + \Delta m(r_4^2+2r_5^2) \quad \text{(A3)}$$

for $CD_3{}^{80}SeCN$ and $CD_3{}^{78}SeCN$ molecules, respectively, where the subscript c of I has been eliminated as unnessessary. In Eqs. A2 and A3, the summation is over all atoms in the molecules. r_i's can be identified in Fig. 4. Δm is the difference between the masses of deuterium and hydrogen atoms. The first terms in Eqs. A2 and A3 are identical for molecules with the same Se isotopic species. The coordinates of the center of mass, X and Y, are given by

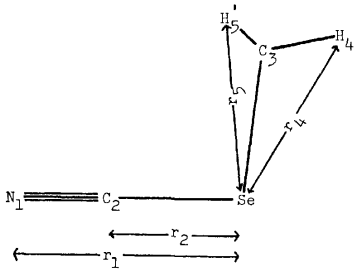

Fig. 4. Model for the calculation of the bond length of $r(Se–CH_3)$.

$$X = \sum_i m_i x_i / \sum_i m_i, \qquad Y = \sum_i m_i y_i / \sum_i m_i \quad \text{(A4)}$$

for $CH_3{}^{80}SeCN$ and $CH_3{}^{78}SeCN$, and

$$\left.\begin{aligned} X &= [\textstyle\sum_i m_i x_i + \Delta m(x_4+2x_5)]/(\sum_i m_i + 3\Delta m) \\ Y &= [\textstyle\sum_i m_i y_i + \Delta m(y_4+2y_5)]/(\sum_i m_i + 3\Delta m) \end{aligned}\right\} \quad \text{(A5)}$$

for $CD_3{}^{80}SeCN$ and $CD_3{}^{78}SeCN$. x_i and y_i are the coordinates of the i-th atom in the molecule and the summation in Eqs. A4 and A5 is over all the atoms in the molecules. The numerator in Eq. A4 and the first term of the numerator in Eq. A5 are equivalent for the molecules with the same Se isotopic species. From Eqs. A2, A3, A4, and A5, the following relation is obtained,

$$(r_4^2+2r_5^2) = [\mu\Delta I_A - \mu'\Delta I_B - (\mu/M_{A'} - \mu'/M_{B'}) \times (M\Delta I_{AB} + M'\Delta I_{A'B'})]/\Delta m(\mu-\mu'), \quad \text{(A6)}$$

where

$$1/\mu = 1/M_A + 1/M_{A'}, \qquad 1/\mu' = 1/M_B + 1/M_{B'},$$
$$1/M = 1/M_A - 1/M_B, \qquad 1/M' = 1/M_{A'} - 1/M_{B'},$$
$$\Delta I_A = I_{A'} - I_A, \qquad \Delta I_B = I_{B'} - I_B$$
$$\Delta I_{AB} = I_A - I_B, \qquad \Delta I_{A'B'} = I_{A'} - I_{B'}.$$

M_A, $M_{A'}$, M_B, and $M_{B'}$ are the total masses and I_A, $I_{A'}$, I_B, and $I_{B'}$ the principal moments of inertia, I_c, of $CH_3{}^{80}SeCN$, $CD_3{}^{80}SeCN$, $CH_3{}^{78}SeCN$, and $CD_3{}^{78}SeCN$, respectively.

Expressing the right side of Eq. A6 as Z, rewriting the left side in terms of $r_{Se-C(methyl)}$, r_{C-H}, and θ, and assuming that the methyl group has C_{3v} symmetry and the symmetry axis coincides with the Se–C(methyl) bond, then Eq. A6 leads to Eq. 4.

References

1) T. Sakaizumi, O. Yamada, K. Ushida, O. Ohashi, and I. Yamaguchi, *Bull. Chem. Soc. Jpn.*, **49**, 2908 (1976).
2) T. Sakaizumi, O. Ohashi, and I. Yamaguchi, *Bull. Chem. Soc. Jpn.*, **49**, 948 (1976).
3) C. H. Thomas, *J. Chem. Phys.*, **59**, 70 (1973).
4) J. F. Beecher, *J. Mol. Spectrosc.*, **21**, 414 (1966).
5) T. Kojima and T. Nishikawa, *J. Phys. Soc. Jpn.*, **12**, 680 (1957).
6) E. V. Ivash and D. M. Dennison, *J. Chem. Phys.*, **21**, 1804 (1953).
7) L. Pierce and M. Hayashi, *J. Chem. Phys.*, **35**, 479 (1961).
8) P. H. Kasai and R. J. Myers, *J. Chem. Phys.*, **30**, 1096 (1959).
9) W. J. Franklin and R. L. Werner, *Tetrahedron Lett.*, **34**, 3003 (1965).
10) S. Nakagawa, S. Takahashi, T. Kojima, and C. C. Lin, *J. Chem. Phys.*, **43**, 3583 (1965); R. G. Lett and W. H. Flygare. *J. Chem. Phys.*, **47**, 4730 (1967).
11) R. D. Brown, F. R. Burden, and P. D. Godfrey, *J. Mol, Spectrosc.*, **25**, 415 (1968).
12) D. R. Herschbach and V. W. Laurie, *J. Chem. Phys.*, **40**, 3142 (1964).
13) W.J. Franklin, R.L. Werner, and R.A. Ashby, *Spectrochim. Acta*, **30**, 387 (1974).
14) V. W. Laurie, *J. Chem. Phys.*, **28**, 704 (1958).
15) D. R. Herschbach, *J. Chem. Phys.*, **31**, 91 (1959).
16) J.E. Wollrab "Rotational Spectra and Molecular Structure," Academic Press, New York and London (1967), Appendix 12.
17) J. S. Muenter, *J. Chem. Phys.*, **48**, 4544 (1968).
18) S. Millefiori and A. Foffani, *Tetrahedron*, **22**, 803 (1966).

A Shock Tube Study on the Pyrolysis of Acetylene in the Presence of Nitrogen Oxide

Hiroo OGURA

Institute of Space and Aeronautical Science, The University of Tokyo, Komaba, Meguro-ku, Tokyo 153

(Received Feburary 3, 1978)

The pyrolysis of acetylene in the presence of nitrogen oxide has been investigated by use of a single-pulse shock tube in the temperature range 1100—1650 K. The hydrocarbons produced in the presence of nitrogen oxide were quite the same as those obtained from the pyrolysis of acetylene by itself. The yield-temperature plots of 1-buten-3-yne showed that at temperatures below 1350 K the formation rate of 1-buten-3-yne is reduced by the addition of nitrogen oxide. The retarding effect of nitrogen oxide on the 1-buten-3-yne formation was interpreted in terms of the reactions of nitrogen oxide with 1-ethynylvinyl and 2-ethynylvinyl radicals to yield propynenitrile and hydrogen cyanide, respectively. An illustrative radical chain mechanism was presented for the pyrolysis of acetylene in line with the experimental results obtained from the pyrolysis inhibited by nitrogen oxide. The radical chain is initiated by the bimolecular reaction of acetylene, *viz.* $2C_2H_2 \rightarrow C_4H_3 + H$, ethynyl and 2-ethynylvinyl radicals being the chain carriers, where C_4H_3 is 1-ethynylvinyl radical.

Since the work by Staveley and Hinshelwood on the inhibiting effect of nitrogen oxide on the decomposition of hydrocarbons,[1] the technique of nitrogen oxide addition has been utilized to confirm the existence of chain processes in the systems of decomposing hydrocarbons.

Nitrogen oxide addition method was also applied to the pyrolysis of acetylene. Below 800 K the addition of nitrogen oxide to acetylene system inhibited the consumption of acetylene.[2,3] On the other hand, nitrogen oxide was found to have no effect on the pyrolysis of acetylene at *ca.* 2000 K.[4] It seems of interest to examine an inhibiting effect by nitrogen oxide on the pyrolysis of acetylene at intermediate temperatures.

Hardly any analysis of reaction products containing nitrogen and oxygen atoms has been made in pyrolysis experiments. Sherwood and Gunning investigated the mercuryphotosensitized decomposition of acetylene in the presence of nitrogen oxide by the analysis of the reaction products involving nitrogen and oxygen atoms. From their study on the substituted vinyl radical reactions with nitrogen oxide, they concluded that a radical mechanism is operative in the system.[5,6]

Analysis of the inhibiting effect of nitrogen oxide on the pyrolysis products together with that of the reaction products containing nitrogen and oxygen atoms will make it possible to identify the substituted vinyl radicals assumed in the radical chain mechanism.[7]

Experimental

Apparatus and Procedure. The apparatus and procedure were essentially the same as those described in previous papers.[7-9] A 4-cm single-pulse shock tube was used, the driven section being 277 cm and the driver section 128.5 cm in length. The ultimate vacuum was *ca.* 6.4×10^{-5} Torr, the leak plus outgassing rate being *ca.* 1.5×10^{-5} Torr/min. Prior to the introduction of gases under investigation into the driven section, the tube was flushed with argon several times. Helium was used as a driver gas. Shocks were fired within five minutes after the driven section had been filled with gases.

Materials. Seven mixtures were prepared in a glass vessel of 10-l volume with the ratios $C_2H_2/NO/Ar = 10/0.2/89.8$; 10/1/89; 10/2/88; 5/1/94; 5/2/93; 1/1/98; and $C_2H_2/Ar = 10/90$. The gases were stirred with a glass fan located in the glass flask for at least four hours before use.

Nitrogen oxide (Matheson Co.) was purified at first by bulb-to-bulb distillation, and then passed through a silica gel column cooled with a Dry Ice–acetone bath.

The standard gas mixtures for the calibration of gas chromatography were the same as those used in the pyrolysis experiments. Carbon monoxide (research grade, Matheson Co.) was used.

Hydrogen cyanide was generated in a vacuum by pouring concd sulfuric acid onto potassium cyanide powder.[10] The crude hydrogen cyanide was purified by bulb-to-bulb distillation at *ca.* −50 °C.

Propynenitrile (cyanoacetylene) was prepared by the method of Moureu and Bongrand:[11]

$$H\text{-}C{\equiv}C\text{-}COOCH_3 \xrightarrow[-10\,^\circ C]{NH_4OH} H\text{-}C{\equiv}C\text{-}CONH_2$$

$$\xrightarrow[\text{vac. } 120\,^\circ C]{P_2O_5,\ \text{sand}} H\text{-}C{\equiv}C\text{-}C{\equiv}N.$$

Propynal (propiolaldehyde) was prepared from propynol.[12] Cyanogen was generated by pouring an aqueous sodium cyanide solution onto copper(II) sulfate pentahydrate at 50 °C, and dried by passing through diphosphorus pentaoxide.[13] Formaldehyde was prepared by the distillation of paraformaldehyde at *ca.* 120 °C. All the gases synthesized were purified by trap-to-trap distillation at Dry Ice–acetone temperature. The purified gases were diluted with argon gas and used as reference gases for gas-chromatographic analysis.

Analytical. The reaction products were analyzed by gas chromatography.. The details of the hydrocarbon analysis were reported.[7] Propynenitrile, cyanogen, and propynal were analyzed in the same way as in the hydrocarbons. The order of elution was CH_4, C_2H_4, C_2H_2, allene, propyne, 1,3-butadiene, 1-buten-3-yne, 1,3-butadiyne, propynenitrile, cyanogen, and propynal at the temperature of 140 °C. The propynenitrile was identified by gas-chromatographic comparison with the synthesized gas. Cyanogen, however, has the same retention time as that of propynenitrile at 140 °C. Thus propynenitrile cannot be seperated from cyanogen on a Porapak N column at other temperatures.

Hydrogen cyanide and formaldehyde were analyzed at 60 °C on a 3 mm × 0.8 m column packed with Porapak Q using helium ionization detector. When water is contained in the test gas and shock heated sample gas, it interferes with the analysis of hydrogen cyanide and formaldehyde. However, neither sample gas nor the shock heated gas contained water

in detectable amounts. Carbon monoxide was analyzed at room temperature with a thermal conductivity cell, on a 1.2 m column packed with molecular sieve 13 X(80—100 mesh). Carbon monoxide appeared at the tail end of the nitrogen oxide peak, but no difficulty was encountered in the analysis, analytical error being larger at low concentration of carbon monoxide in the shock heated gas.

Results

The mixtures were subjected to shock heating in the temperature range 1100—1650 K. The total densities behind the reflected shock waves were *ca.* 2.67×10^{-5} mol/cm^3, the reaction times being *ca.* 900 μs. The shock heated samples were extracted into evacuated bulbs of 60 ml volume, and analyzed by gas chromatography.

Product analyses for the hydrocarbons produced in the presence and absence of nitrogen oxide showed that the hydrocarbons formed in the C_2H_2–NO system and in the C_2H_2–Ar system are quite the same; CH_4, C_2H_4, C_2H_6, allene, propyne, 1,3-butadiene, 1-buten-3-yne, 1,3-butadiyne, and benzene being generated. The major products were also 1-buten-3-yne, 1,3-butadiyne and hydrogen in the presence of nitrogen oxide, the shapes of their yield-temperature plots being similar to those in the absence of nitrogen oxide. The minor products were CH_4, C_2H_4, allene, propyne, and benzene, trace products being C_2H_6 and 1,3-butadiene as in the case of the pyrolysis of acetylene alone.

Besides the hydrocarbons, hydrogen cyanide and carbon monoxide were formed as the major products containing nitrogen and oxygen atoms in the temperature range studied. Propynenitrile was found in much smaller amounts. No other products containing nitrogen and/or oxygen atoms such as N_2, N_2O, CO_2, O_2, and H_2O were found in large amounts. Since the amount of carbon monoxide was approximately equal to that of hydrogen cyanide (Fig. 1), there would be no missing

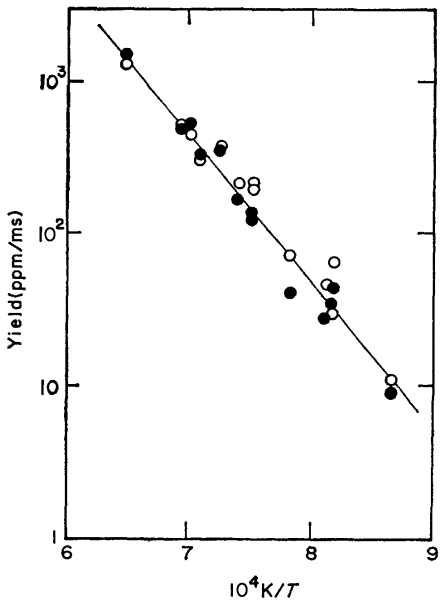

Fig. 1. Yields of carbon monoxide and hydrogen cyanide as a function of temperature (C_2H_2/NO/Ar=10/2/88). ●: Carbon monoxide, ○: hydrogen cyanide.

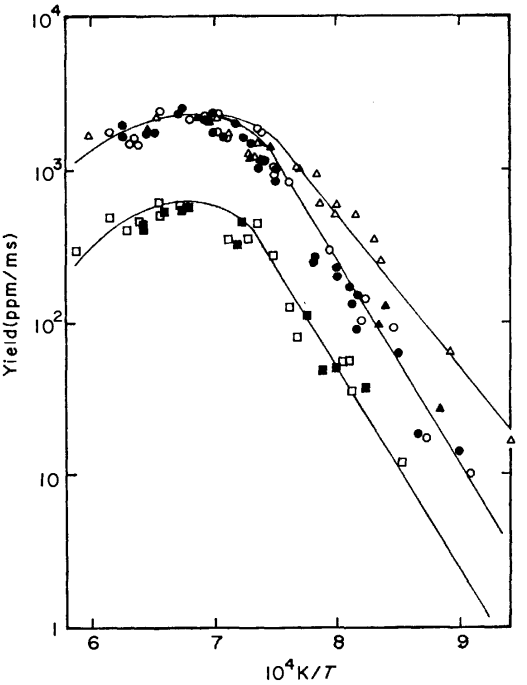

Fig. 2. Effect of nitrogen oxide on the rate of 1-buten-3-yne formation.
△: C_2H_2/Ar=10/90, ▲: C_2H_2/NO/Ar=10/0.2/89.8, ○: C_2H_2/NO/Ar=10/1/89, ●: C_2H_2/NO/Ar=10/2/88, □: C_2H_2/NO/Ar=5/1/94, ■: C_2H_2/NO/Ar=5/2/93.

products involving nitrogen and oxygen atoms. Thus the amount of nitrogen oxide consumed in the pyrolysis should be nearly equal to the yields of carbon monoxide and hydrogen cyanide.

Inhibited Rate of 1-Buten-3-yne Formation. The yields of 1-buten-3-yne for five mixtures with different composition of C_2H_2 and NO are plotted as a function of temperature in Fig. 2. The yield-temperature plots of 1-buten-3-yne show that at temperatures below 1350 K the yield decreases with the addition of nitrogen oxide, and that above 1350 K the yield is almost the same as that in the C_2H_2–Ar system. The rates of 1-buten-3-yne formation are also of second-order with respect to acetylene, and depend little on the amount of nitrogen oxide added at both lower and higher temperatures. The decrease in the yield of 1-buten-3-yne at lower temperatures can be attributed to the inhibition by nitrogen oxide added. An apparent second-order rate constant for the inhibited 1-buten-3-yne formation at temperatures below 1350 K was derived from 38 experiments by the least-squares method:

$$k_1(\mathrm{cm^3\ mol^{-1}\ s^{-1}}) = (4.5\pm2.4) \times 10^{15} \exp\{(-55700\pm2100)^*/RT\} \quad (1)$$

the errors denoting the standard deviation of the least-squares method. The Arrhenius plot of the second-order rate constants is shown in Fig. 3. The frequency factor in k_1 is considerably greater than that in the normal second-order rate constant.

* The activation energy is expressed in cal/mol (1 $\mathrm{cal_{th}}$ = 4.184 J).

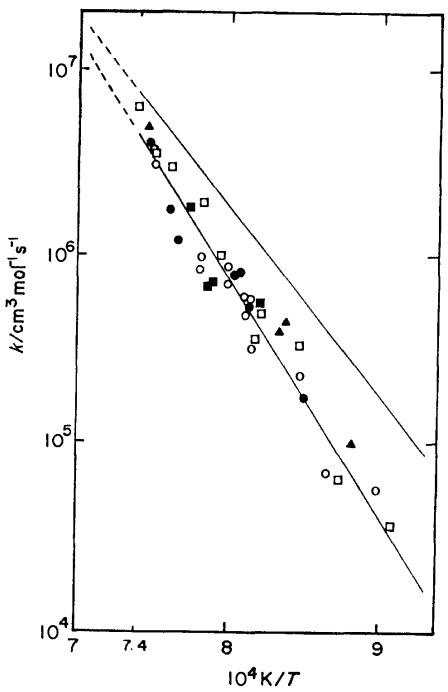

Fig. 3. Arrhenius plots of the second-order rate constants for 1-buten-3-yne formation inhibited by nitrogen oxide, the upper straight line showing the second-order rate constant obtained previously.[7]
▲: C_2H_2/NO/Ar=10/0.2/89.8, ○: C_2H_2/NO/Ar=10/1/89, ●: C_2H_2/NO/Ar=10/2/88, □: C_2H_2/NO/Ar=5/1/94, ■: C_2H_2/NO/Ar=5/2/93.

Rate of Hydrogen Cyanide Formation. Simultaneously with the reduction of 1-buten-3-yne yield, hydrogen cyanide and carbon monoxide were formed in approximately equal amounts. In order to determine the concentration dependence of hydrogen cyanide formation on acetylene and nitrogen oxide, the yields of

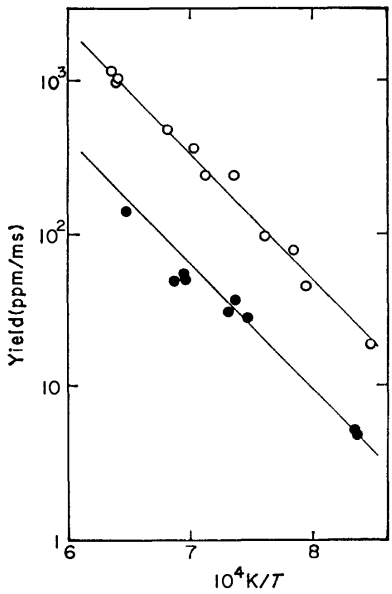

Fig. 4. Dependence of hydrogen cyanide formation rate on nitrogen oxide concentration.
○: C_2H_2/NO/Ar=10/1/89, ●: C_2H_2/NO/Ar=10/0.2/89.8.

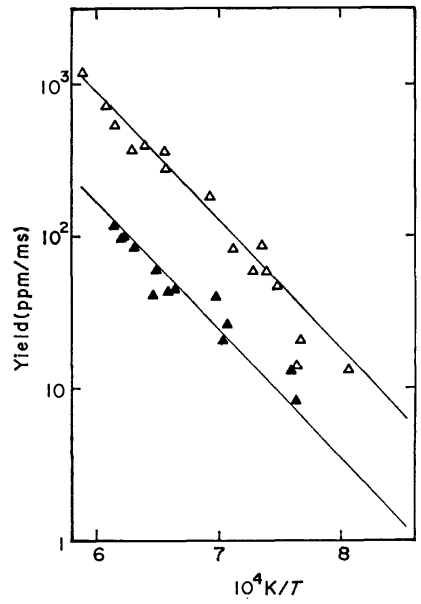

Fig. 5. Dependence of hydrogen cyanide formation rate on acetylene concentration.
△: C_2H_2/NO/Ar=5/1/94, ▲: C_2H_2/NO/Ar=1/1/98.

hydrogen cyanide for four mixtures, *viz.* C_2H_2/NO/Ar=10/0.2/89.9; 10/1/89; 5/1/94; and 1/1/98; are plotted against temperature in Figs. 4 and 5. We see that the rate of hydrogen cyanide formation is nearly of first-order in both acetylene and nitrogen oxide. An apparent second-order rate expression was fitted to the data (61 points obtained from the shock heated mixtures of C_2H_2/NO/Ar=10/0.2/89.8; 10/1/89; 10/2/88; 5/1/94; and 1/1/98) by the least-squares method:

$$k_2(\mathrm{cm^3\ mol^{-1}\ s^{-1}}) = (5.4\pm1.6) \times 10^{12} \exp\{(-37700\pm1300)/RT\}. \quad (2)$$

The Arrhenius plot of the second-order rate constants

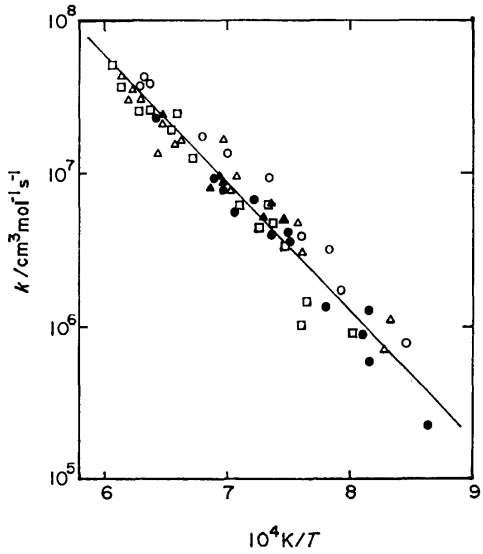

Fig. 6. Arrhenius plots of the second-order rate constants for hydrogen cyanide formation.
▲: C_2H_2/NO/Ar=10/0.2/89.8, ○: C_2H_2/NO/Ar=10/1/89, ●: C_2H_2/NO/Ar=10/2/88, □: C_2H_2/NO/Ar=5/1/94, △: C_2H_2/NO/Ar=1/1/98.

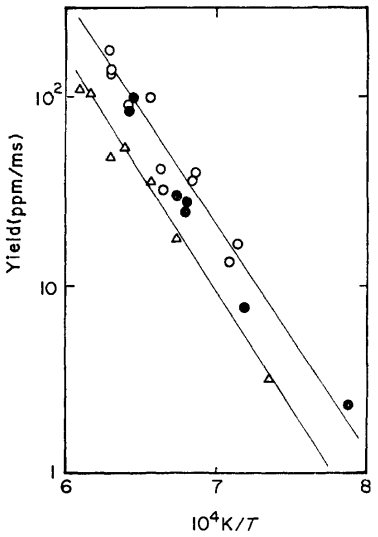

Fig. 7. Dependence of propynenitrile formation rate on acetylene and nitrogen oxide concentrations.
○: C_2H_2/NO/Ar=10/1/89, ●: C_2H_2/NO/Ar=5/2/93, △: C_2H_2/NO/Ar=5/1/94.

is shown in Fig. 6. Hydrogen cyanide and carbon monoxide continue to increase in the temperature range studied, whereas the yield of 1-buten-3-yne reaches its maximum at *ca.* 1500 K with a subsequent decrease.

Rate of Propynenitrile Formation. Propynenitrile was found at slightly higher temperatures and in smaller amounts than hydrogen cyanide. In determing the concentration dependence of acetylene and nitrogen oxide, the data obtained from the runs for the mixtures of C_2H_2/NO/Ar=10/1/89; 5/1/94; and 5/2/93 were adopted, since the yields of propynenitrile for the mixtures of C_2H_2/NO/Ar=10/0.2/89.8 and 1/1/98 were very small, involving large error. The rates of propynenitrile formation as a function of temperature are plotted in Fig. 7. The rate of propynenitrile generation is of the second-order with respect to acetylene. Although the data obtained from the runs for the mixture of C_2H_2/NO/Ar=5/2/93 scatter considerably, the rate of propynenitrile formation is expected to be also of the first-order with respect to nitrogen oxide by analogy with that of hydrogen cyanide production. An apparent second-order rate constant was derived by the least-squares method:

$$k_3(\mathrm{cm^3\ mol^{-1}\ s^{-1}}) = (9.9\pm2.3) \times 10^{13} \exp\{(-53300\pm2500)/RT\}. \quad (3)$$

For derivation, only the data in Fig. 7 (25 points) were adopted. The Arrhenius plot of the second-order rate constants is shown in Fig. 8.

Effects on the Other Products. The influence of added nitrogen oxide on the formation of hydrogen is illustrated in Fig. 9. The shape of yield-temperature plots for hydrogen is similar to that in the absence of nitrogen oxide. The yield of hydrogen increases considerably at higher temperatures, and appears to depend little on the concentration of nitrogen oxide added. The same is true for the yield-temperature plots of the other major and minor products.

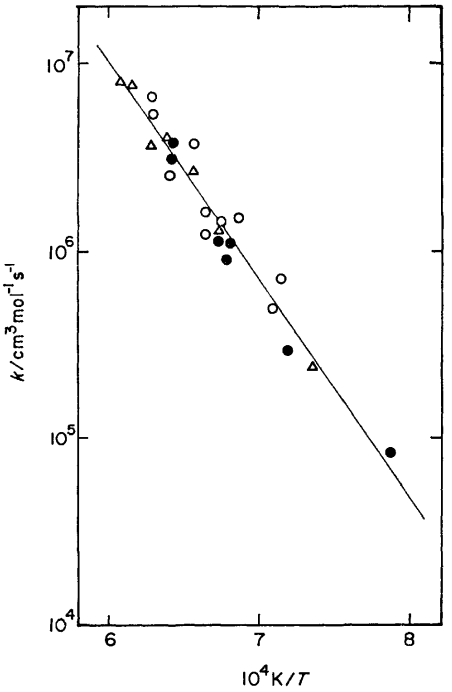

Fig. 8. Arrhenius plots of the second-order rate constants for propynenitrile formation.
○: C_2H_2/NO/Ar=10/1/89, ●: C_2H_2/NO/Ar=5/2/93, △: C_2H_2/NO/Ar=5/1/94.

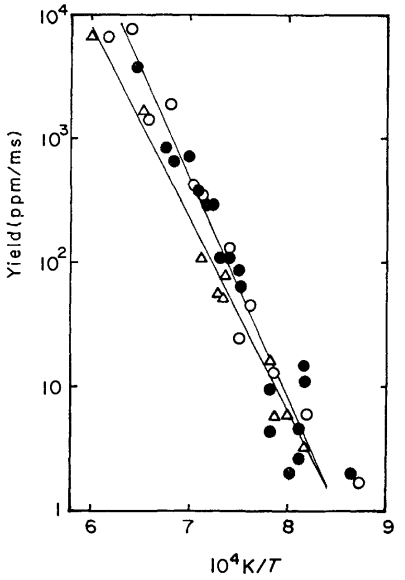

Fig. 9. Effect of nitrogen oxide on the yield of hydrogen.
△: C_2H_2/Ar=10/90, ○: C_2H_2/NO/Ar=10/1/89, ●: C_2H_2/NO/Ar=10/2/88.

Discussion

The same reaction product formation as in the absence of nitrogen oxide and similar shapes of the yield-temperature plots suggest that a similar mechanism is operative for the formation of the hydrocarbons in the C_2H_2–NO system. A mechanism for the pyrolysis of acetylene in the absence of nitrogen oxide was proposed from a thermochemical point of view:[7]

$$2C_2H_2 \longrightarrow C_4H_3 + H, \quad (4)$$
$$C_4H_3 + C_2H_2 \longrightarrow C_6H_5, \quad (5)$$
$$C_6H_5 + C_2H_2 \longrightarrow C_4H_4 + C_4H_3, \quad (6)$$
$$H + C_2H_2 \longrightarrow C_2H_3, \quad (7)$$
$$C_2H_3 + C_2H_2 \longrightarrow C_4H_4 + H, \quad (8)$$
$$2C_6H_5 \longrightarrow \text{termination}, \quad (9)$$
$$2C_2H_3 \longrightarrow \text{termination}, \quad (10)$$

where C_4H_3 radical is supposed to be 1-ethynylvinyl ($H_2C=\dot{C}-C_2H$) radical. Hereafter 1-ethynylvinyl and 2-ethynylvinyl($C_2H-CH=\dot{C}H$) radicals will be denoted by $C_4H_3(1)$ and $C_4H_3(2)$, respectively.

Initiation Step. Probable initiation steps for the radical chain mechanism of the pyrolysis of acetylene alone are as follows:

$$2C_2H_2 \longrightarrow C_4H_3(1) + H, \quad \Delta H^\circ = 46.2, \quad (4)$$
$$\longrightarrow C_4H_3(2) + H, \quad \Delta H^\circ = 67.1, \quad (11)$$
$$\longrightarrow C_2H_3 + C_2H, \quad \Delta H^\circ = 65.3. \quad (12)$$

In the presence of nitrogen oxide the abstraction reaction of H atom by nitrogen oxide could also be a probable initiation step:

$$C_2H_2 + NO \longrightarrow C_2H + HNO, \quad \Delta H^\circ = 62.0. \quad (13)$$

In the calculation of the heats of reaction, the heats of formation are based on the observed or estimated values.[14] At present stage, Reaction 4 is the most probable initiation step in view of the heat of reaction. Another probable initiation is the bimolecular reaction of nitrogen oxide when added in a large amount:

$$2NO \longrightarrow N_2O + O, \quad \Delta H^\circ = 36.0. \quad (14)$$

The rate constants of Reactions 4 and 14 are estimated to be[7,15]

$$k_4(\text{cm}^3\ \text{mol}^{-1}\ \text{s}^{-1}) = 3.5\times10^{13}\exp(-47400/RT), \quad (15)$$
$$k_{14}(\text{cm}^3\ \text{mol}^{-1}\ \text{s}^{-1}) = 1.3\times10^{12}\exp(-63800/RT). \quad (16)$$

The rate constant of Reaction 14 is much smaller than that of Reaction 4 in the temperature range studied. Thus Reaction 4 is the most predominant initiation step in the C_2H_2–NO system.

Mechanism of 1-Buten-3-yne Formation. The reduction of 1-buten-3-yne formation rate at temperatures below 1350 K is accompanied by the formation of hydrogen cyanide and carbon monoxide. No other products containing nitrogen and/or oxygen atoms are found except for the propynenitrile in much smaller amount. It seems likely that the hydrogen cyanide and carbon monoxide in nearly equal amounts are produced simultaneously or *via* the same intermediate. We have tried to interpret the inhibiting effect of nitrogen oxide on 1-buten-3-yne formation by the reactions of nitrogen oxide with the chain carrier radicals present in the above pyrolysis mechanism.

Examination of the Proposed Mechanism for the Pyrolysis: Sherwood and Gunning showed experimentally that C_2H_3 and $C_4H_3(2)$ radicals react with nitrogen oxide to generate formaldehyde, propynal, and hydrogen cyanide.[5] In general the reaction between the substituted vinyl radical and nitrogen oxide can be written as $XYC=\dot{C}Z + NO \longrightarrow XYC=O + ZCN$,

where X, Y, and Z are functional groups of hydrocarbons. Thus the radicals in the proposed mechanism are expected to react with nitrogen oxide as follows:

$$C_4H_3(1) + NO \longrightarrow H_2CO + C_2HCN, \quad \Delta H^\circ = -60.0, \quad (17)$$
$$C_6H_5 + NO \longrightarrow C_4H_3CHO + HCN, \quad (18)$$
$$H + NO \longrightarrow HNO, \quad \Delta H^\circ = -49.9, \quad (19)$$
$$C_2H_3 + NO \longrightarrow H_2CO + HCN, \quad \Delta H^\circ = -76.6, \quad (20)$$

where C_6H_5 is assumed to have the structure of $H_2C=C(C_2H)-CH=\dot{C}H$. In the present analysis, hydrogen cyanide and propynenitrile have been detected as compounds containing nitrogen atom. Accordingly, the substituted vinyl radicals scavenged by nitrogen oxide should be C_2H_3, $C_4H_3(1)$, and C_6H_5 radicals in the proposed scheme.

If the chain propagation of Reaction 7 and 8 were mainly responsible for the formation of 1-buten-3-yne, the same amount of H_2CO as that of HCN would be produced. Therefore, as in the absence of NO, nearly equal amounts of hydrogen and carbon monoxide would be produced by the reaction

$$H_2CO \longrightarrow H_2 + CO, \quad \Delta H^\circ = 1.3. \quad (21)$$

As shown in Figs. 1 and 9, the yield of hydrogen is smaller than that of carbon monoxide at lower temperatures. Tadasa *et al.* reported that in the pyrolysis of H_2CO with a large excess of NO at 773 K the amount of hydrogen is very small as compared with that of carbon monoxide; water and nitrogen are formed instead.[16] In the present experiments, however, no detectable amounts of water and nitrogen have been found in the shock heated samples. In any event the chain propagation step of Reactions 7 and 8 can be concluded to have minor importance in the formation of 1-buten-3-yne. The same result has been obtained from the analysis of the isotopic distributions of C_2H_2 and C_4H_4 in the mixtures of C_2H_2 and D_2.[8]

On the other hand, if the chain propagation process, $C_4H_3(1)$ and C_6H_5 radicals as the chain carriers, is predominant, propynenitrile along with hydrogen cyanide should be detected. This is the case in the present experiments. Applying the steady-state treatment to Reactions 4, 5, 6, and 9, the steady-state concentrations of $C_4H_3(1)$ and C_6H_5, $[C_4H_3(1)]_{ss}$ and $[C_6H_5]_{ss}$, are given approximately by

$$[C_4H_3(1)]_{ss}/[C_6H_5]_{ss} \cong k_6/k_5, \quad (22)$$
$$= 1.3\times10^2\exp(-16100/RT). \quad (22')$$

The rate constants adopted are as follows:[7,17]

$$k_5(\text{cm}^3\ \text{mol}^{-1}\ \text{s}^{-1}) = 6.3\times10^{11}\exp(-6500/RT), \quad (23)$$
$$k_6(\text{cm}^3\ \text{mol}^{-1}\ \text{s}^{-1}) = 7.9\times10^{13}\exp(-22600/RT). \quad (24)$$

Equation 22′ would hold approximately even in the presence of nitrogen oxide, assuming the rate constants k_{17} and k_{18} have the same order of magnitude because of the similarity of both reactions. Thus the rates of propynenitrile and hydrogen cyanide formation could be expressed by

$$R_{C_4HCN}/R_{HCN} \simeq (k_{17}[C_4H_3(1)]_{ss}[NO])/(k_{18}[C_6H_5]_{ss}[NO])$$
$$\simeq [C_4H_3(1)]_{ss}/[C_6H_5]_{ss}. \quad (25)$$

However, the above rate ratio obtained experimentally was

$$R_{C_2HCN}/R_{HCN} = 18 \exp(-15600/RT). \quad (26)$$

The observed rate for the formation of propynenitrile is much smaller than that predicted from the above mechanism. The chain propagation step of Reactions 5 and 6 is open to question; Reaction 6 particularly seems uncertain. The validity of the above discussion is based on the reliability of the rate constants used.

Alternative Mechanism for the Pyrolysis: An alternative chain propagation process is as follows:[17]

$$C_2H + C_2H_2 \longrightarrow C_4H_3(2), \quad \Delta H^\circ = -44.8, \quad (27)$$

$$C_4H_3(2) + C_2H_2 \longrightarrow C_4H_4 + C_2H, \quad \Delta H^\circ = 11.7. \quad (28)$$

The reaction of $C_4H_3(2)$ with NO produces HCN by

$$C_4H_3(2) + NO \longrightarrow C_2HCHO + HCN. \quad (29)$$

The C_2H radical is reported not to react with NO.[5] A fast conversion process of $C_4H_3(1)$ into $C_4H_3(2)$ or C_2H is essential for the above chain propagation step to be compatible with the most predominant initiation step, Reaction 4.

If the isomerization of $C_4H_3(1)$ to $C_4H_3(2)$ such as

$$C_4H_3(1) \longrightarrow C_4H_3(2), \quad \Delta H^\circ = 20.9 \quad (30)$$

were fast enough, the equilibrium would be established at an early stage of the reaction, since the reverse reaction would also be fast. The equilibrium concentrations are dominated by the heat of reaction because of the small entropy change of Reaction 30. At the present temperatures the equilibrium concentration of $C_4H_3(1)$ should be greater than that of $C_4H_3(2)$. This implies that the yield of propynenitrile should also be greater than that of hydrogen cyanide, which conflicts with the present observation. Thus the direct conversion of $C_4H_3(1)$ into $C_4H_3(2)$ will be too slow to be the initiation step.

Another process is the conversion of $C_4H_3(1)$ into C_2H radical. The H atom abstraction reaction of $C_4H_3(1)$ from C_2H_2 is an ineffective path to generate C_2H radical in view of the heat of reaction:

$$C_4H_3(1) + C_2H_2 \longrightarrow C_4H_4 + C_2H, \quad \Delta H^\circ = 32.6. \quad (31)$$

The following path seems most promissing. The addition of $C_4H_3(1)$ to C_2H_2 is much faster than Reaction 31 with the rate constant of k_5 (Eq. 23):

$$C_4H_3(1) + C_2H_2 \longrightarrow H_2C{=}C(C_2H){-}CH{=}\dot{C}H, \quad \Delta H^\circ = -20.5. \quad (5)$$

A successive H atom shift and the C–C bond rupture will occur:

$$H_2C{=}C(C_2H){-}CH{=}\dot{C}H \longrightarrow H\dot{C}{=}C(C_2H){-}CH{=}CH_2,$$

$$\longrightarrow HC{\equiv}C{-}CH{=}CH_2 + C_2H, \quad \Delta H^\circ = 53.1. \quad (32)$$

The radical chain mechanism of 1-buten-3-yne formation is completed by

$$2C_4H_3(2) \longrightarrow \text{termination}. \quad (33)$$

Application of steady-state approximation to $C_4H_3(1)$, $C_4H_3(2)$, C_6H_5, and C_2H radicals gives the following equations:

$$R_{C_4H_4} = k_{28}(k_4/2k_{33})^{1/2}[C_2H_2]^2, \quad (34)$$

$$[C_4H_3(1)]_{ss} = (k_4/k_5)[C_2H_2], \quad (35)$$

$$[C_4H_3(2)]_{ss} = (k_4/2k_{33})^{1/2}[C_2H_2]. \quad (36)$$

As in the mechanism previously proposed, the second-order rate of 1-buten-3-yne formation is also derived from the revised mechanism. The heat of reaction for Reaction 28 is smaller than the activation energy estimated for Reactions 6 and 8 (*ca.* 18—23 kcal/mol).[7] Consequently Reaction 28 is likely to occur as the alternative to Reaction 6 forming 1-buten-3-yne. Substituting the rate constants in the right-hand side of Eqs. 35 and 36 for estimated ones, the ratio of the two ethynylvinyl radicals is calculated. The rate constant k_{33} adopted is as follows:[7]

$$k_{33}(\text{cm}^3\ \text{mol}^{-1}\ \text{s}^{-1}) = 2.0 \times 10^{12}. \quad (37)$$

The estimated values of $[C_4H_3(1)]_{ss}/[C_4H_3(2)]_{ss}$,

$$[C_4H_3(1)]_{ss}/[C_4H_3(2)]_{ss} = 19 \exp(-17200/RT), \quad (38)$$

agrees with the observed value of R_{C_2HCN}/R_{HCN}. This suggests that the revised mechanism is most probable one for the formation of 1-buten-3-yne in the presence and absence of nitrogen oxide.

Mechanism of Inhibited Pyrolysis. A radical chain mechanism for the inhibited formation of 1-buten-3-yne will be set up to be in line with that for the pyrolysis of acetylene by itself. Propynenitrile was not distinguished from cyanogen by the gas-chromatographic analysis. Shock tube experiments showed that the secondary reaction of hydrogen cyanide and that with acetylene and nitrogen oxide can be ignored in the temperature range studied.[18] Thus the propynenitrile originates from the reaction of nitrogen oxide with acetylene.

The characteristic features of inhibited 1-buten-3-yne formation by nitrogen oxide can be explained by the following radical chain mechanism:

$$2C_2H_2 \longrightarrow C_4H_3(1) + H, \quad (4)$$

$$C_4H_3(1) + C_2H_2 \longrightarrow C_6H_5, \quad (5)$$

$$C_4H_3(1) + NO \longrightarrow C_2HCN + H_2CO, \quad (17)$$

$$C_6H_5 \longrightarrow C_4H_4 + C_2H, \quad (32)$$

$$C_2H + C_2H_2 \longrightarrow C_4H_3(2), \quad (27)$$

$$C_4H_3(2) + C_2H_2 \longrightarrow C_4H_4 + C_2H, \quad (28)$$

$$C_4H_3(2) + NO \longrightarrow C_2HCHO + HCN, \quad (29)$$

$$C_2HCHO \longrightarrow C_2H + CHO, \quad (39)$$

$$CHO \longrightarrow CO + H \quad \Delta H^\circ = 28.6, \quad (40)$$

$$2C_4H_3(2) \longrightarrow \text{termination}. \quad (33)$$

Assuming the steady-state concentrations of the radicals in the above mechanism, we can derive

$$R_4 = 2R_{33} + (R_{29} - R_{39}). \quad (41)$$

Here the small effect of NO with $C_4H_3(1)$ radical on the reduction of 1-buten-3-yne formation rate is neglected. In the absence of nitrogen oxide Eq. 41 is reduced to

$$R_4 = 2R_{33}. \quad (41')$$

When the rate of Reaction 29 is greater than that of Reaction 39, the steady-state concentration of $C_4H_3(2)$ in the presence of nitrogen oxide ($[C_4H_3(2)]_{ss}^{NO}$) is lower than that in its absence ($[C_4H_3(2)]_{ss}$; the inhibition by nitrogen oxide occurs. The observed second-order rates with and without nitrogen oxide are directly

proportional to the steady-state concentrations of $C_4H_3(2)$ radical present in the systems:[7]

$$[C_4H_3(2)]^{NO}_{ss}/[C_4H_3(2)]_{ss} = R^{NO}_{C_4H_4}/R_{C_4H_4}, \quad (42)$$

$$= 18 \exp(-9300/RT). \quad (42')$$

It is observed that the inhibited rates of 1-buten-3-yne formation are hardly affected by the amounts of nitrogen oxide added (Fig. 2). The attainment of "limiting rate" can be easily accounted for by the above mechanism. When the amount of nitrogen oxide is increased to some extent, the rate of propynal generation is accelerated by Reaction 29 to the same extent, and in turn by Reaction 39 the same amount of the C_2H radical is regenerated as that of $C_4H_3(2)$ radical scavenged by Reaction 29 at a definite temperature. The C_2H radical is quickly converted into $C_4H_3(2)$ radical by Reaction 27. Thus the steady-state concentration of the $C_4H_3(2)$ radical is not affected by further addition of nitrogen oxide at a definite temperature. The present results are in agreement with those obtained at lower temperatures by Cullis *et al.*[3]

With increase in temperature the rate of Reaction 39 increases up to that of Reaction 29. In this case (Eq. 41') no inhibition occurs, the steady-state concentration of $C_4H_3(2)$ radical being the same as that in the absence of nitrogen oxide. Actually, however, the 1-buten-3-yne begins to decompose at around 1350 K. The yield-temperature plots of 1-buten-3-yne are almost the same as those in the C_2H_2–Ar system above 1350 K. This suggests that the radical concentrations relevant to its formation and decomposition remain unchanged in the presence of nitrogen oxide.

The rate of propynenitrile formation is given by

$$R_{C_4HCN} = k_{17}[C_4H_3(1)]_{ss}[NO]. \quad (43)$$

Since the yields of propynenitrile are very small as compared with those of hydrogen cyanide, the steady-state concentration of $C_4H_3(1)$ can be approximated by Eq. 35. Equation 43 is then expressed by

$$R_{C_4HCN} = (k_4k_{17}/k_5)[C_2H_2][NO]. \quad (43')$$

The rate expression of propynenitrile formation is the same in both inhibited and uninhibited regions. On the other hand, within the present errors the yield-temperature plots of hydrogen cyanide are fitted to a single straight line in the temperature range studied. For the sake of simplicity, the rate expression in the uninhibited region is extended to the inhibited region:

$$R_{HCN} = k_{29}[C_4H_3(2)]_{ss}[NO]$$

$$= k_{29}(k_4/2k_{33})^{1/2}[C_2H_2][NO]. \quad (44)$$

Since Reaction 17 and 29 are of the same type, k_{17} and k_{29} are expected to be nearly equal. As shown by Eqs. 43 and 44, the steady-state concentrations are related to the observed rates:

$$[C_4H_3(1)]_{ss}/[C_4H_3(2)]_{ss} = R_{C_4HCN}/R_{HCN}. \quad (45)$$

The validity of the discussion on the pyrolysis mechanism is verified under the above conditions. The agreement between the observed and calculated values (Eqs. 26 and 38) is excellent.

By a comparison with the observed rates for propynenitrile and hydrogen cyanide formation, k_{17} and k_{29} are estimated from Eqs. 43' and 44, respectively:

$$k_{17}(\mathrm{cm^3\ mol^{-1}\ s^{-1}}) = 1.8\times10^{12} \exp(-12400/RT), \quad (46)$$

$$k_{29}(\mathrm{cm^3\ mol^{-1}\ s^{-1}}) = 2.3\times10^{12} \exp(-14900/RT). \quad (47)$$

The small inhibiting effect of NO with $C_4H_3(1)$ radical being neglected, k_{17} is compared with k_{29} obtained in the inhibited region. The activation energy and frequency factor have approximately equal values in k_{17} and k_{29}. In the derivation of Eq. 45 (analogously Eq. 25), k_{17} was assumed to be equal to k_{29}, which is supported by Eqs. 46 and 47. It is noteworthy that the observed second-order rate constant for propynenitrile generation (k_3) has higher activation energy than that of hydrogen cyanide (k_2), whereas the activation energy of k_{17} is nearly the same as that of k_{29}. As can be seen from Eqs. 43 and 44, the difference between k_2 and k_3 results from the fact that in the present radical chain mechanism the steady-state concentration of $C_4H_3(1)$ is related to that of $C_4H_3(2)$ such as Eq. 38. Gay *et al.*[20] and Bopp and Kern[21] detected C_4H_3 radical in the pyrolysis of acetylene at temperatures above 1700 K by use of a time-of-flight mass spectrometer. The C_4H_3 radical as detected with mass spectrometer at $m/e=51$, however, cannot be distinguished among the C_4H_3 radical isomers. On the contrary, the addition of nitrogen oxide revealed that the C_4H_3 radicals are $C_4H_3(1)$ and $C_4H_3(2)$, both radicals being responsible for the formation of 1-buten-3-yne. Reaction 4 was predicted to be the most predominant initiation step on the basis of the heat of reaction. Detection of propynenitrile formation upon the addition of nitrogen oxide would provide experimental support for the occurrence of Reaction 4 as the initiation step.

Formation Mechanism for the Other Products. No significant change appears in the shape of yield-temperature plots of hydrogen (Fig. 9) and other major and minor products with appreciable increase in their yields at higher temperatures. The formation reactions will be unaltered, whereas the concentrations of the radicals relevant to their formation would increase considerably by the addition of nitrogen oxide.

As to the major products, the hydrogen will be generated by

$$H + C_2H_2 \longrightarrow H_2 + C_2H, \qquad \Delta H^\circ = 7.7, \quad (48)$$

and 1,3-butadiyne will be formed by

$$C_2H + C_2H_2 \longrightarrow C_4H_2 + H, \qquad \Delta H^\circ = -4.8. \quad (49)$$

H and C_2H are not scavenged by nitrogen oxide. Increase in H atom concentration will cause the increase of hydrogen and 1,3-butadiyne yields by Reactions 48 and 49, respectively. The H atom responsible for the increase in the yields of major and minor hydrocarbons will be generated by the decomposition of formyl radical:

$$CHO \longrightarrow H + CO. \quad (40)$$

Thus the concentration of H atom is increased by the presence of nitrogen oxide. H atom participated in all the secondary reactions to form ethylene, allene, propyne, and benzene such as[7]

$$H + C_2H_2 \longrightarrow C_2H_3 \xrightarrow{C_2H_2} C_2H_4,$$

$$C_2H_3 + C_2H_2 \longrightarrow C_4H_5 \xrightarrow{C_2H_2} C_6H_7,$$

$$C_6H_7 \longrightarrow C_3H_3 \xrightarrow{C_2H_2} C_3H_4,$$

$$\longrightarrow C_6H_6.$$

As can be seen from Fig. 9, the yields are hardly dependent on the amounts of nitrogen oxide added. At lower temperatures the yields of the above products are hardly increased by the addition of nitrogen oxide. The steady-state concentration of H atom in the absence of nitrogen oxide will be great enough relative to its increase by the addition of nitrogen oxide. With increase in temperature the H atom concentration increases gradually. The H atom, however, is converted into larger radicals by the subsequent reactions with acetylene. Thus the effect of the increase in the H atom concentration is averaged over the relevant radicals, the influence of the amounts of added nitrogen oxide being small.

The reactions mentioned above are too simple to give explicit formulas of major and minor hydrocarbons generation in the presence of nitrogen oxides. However, the main feature of the inhibited pyrolysis of acetylene can be interpreted by the present mechanism.

The author is grateful to Prof. Kenji Kuratani, Tokyo University, for his interest in this work and for his valuable discussions. Thanks are also due to Mr. Yoshinori Sano for the purification of nitrogen oxide and for the preparation of hydrogen cyanide.

References

1) L. A. K. Staveley and C. N. Hinshelwood, *J. Chem. Soc.*, **1937**, 1568.
2) C. G. Silcocks, *Proc. R. Soc. London, Ser. A*, **242**, 411 (1957).
3) C. F. Cullis, G. J. Minkoff, and M. A. Nettleton, *Trans. Faraday Soc.*, **58**, 1117 (1962).
4) C. F. Aten and E. F. Greene, *Combust. Flame*, **5**, 55 (1961).
5) A. G. Sherwood and H. E. Gunning, *J. Am. Chem. Soc.*, **85**, 3506 (1963).
6) A. G. Sherwood and H. E. Gunning, *J. Phys. Chem.*, **69**, 1732 (1963).
7) H. Ogura, *Bull. Chem. Soc. Jpn.*, **50**, 1044 (1977).
8) H. Ogura, *Bull. Chem. Soc. Jpn.*, **50**, 2051 (1977).
9) H. Ogura, *Bull. Chem. Soc. Jpn.*, **50**, 2242 (1977).
10) K. Ziegler, *Org. Synth.*, Coll. Vol. 1, 314 (1956).
11) MM. C. Moureu and J. Ch. Bongrand, *Ann. Chim. (Paris)*, **14**, 47 (1920).
12) J. C. Sauer, *Org. Synth.*, Coll. Vol. 4, 8131 (1963).
13) G. J. Janz, *Inorg. Synth.*, Vol. 5, 43 (1957).
14) The heats of reaction, $\Delta H°$(kcal/mol), are calculated at 298 K. a) The heats of formation for C_4H_4, C_4H_2, and C_4H_3 (1) are 75.3, 111.3, and 102.5 kcal/mol. M. Cowperwaite and S. H. Bauer, *J. Chem. Phys.*, **36**, 1743 (1962); b) The heat of formation for C_4H_3(2) is 123.4 kcal/mol;[7] c) The heat of formation for C_2H_3 is 59.6 kcal/mol. F. P. Lossing, *Can. J. Chem.*, **49**, 357 (1971); d) The heat of formation for C_6H_6 (H_2C=C(CH=CH_2)–C≡CH) is estimated to be 84.31 kcal/mol using the Group Additivity method of Benson. Taking the C–H bond dissociation energy to be equal to 104 kcal/mol, the heat of formation for C_6H_5(H_2C=C(C_2H)–CH=$\dot{C}$H) is calculated to be 136.21 kcal/mol. S. W. Benson, "Thermochemical Kinetics," Wiley, New York (1968); e) The heat of formation for C_2HCN is 91.8 kcal/mol. J. D. Cox and G. Pilcher "Thermochemistry of Organic and Organometallic Compounds," Academic Press, New York, N. Y. (1970); f) The heats of formation for C_2H_2, C_2H_4, C_2H, H_2CO, CHO, CO, O, H, NO, N_2O, HNO, and HCN are 54.2, 12.5, 114, −27.7, −2.9, −26.4, 59.6, 52.1, 21.6, 19.6, 23.8, and 32.3 kcal/mol. "JANAF Thermochemical Tables," 2nd ed, National Bureau of Standards NSRDS-NBS 37, U. S. Government printing Office, Washington D. C. (1971).
15) D. L. Baulch, D. D. Drysdale, and D. G. Horne, "Evaluated Kinetic Data for High Temperature Reactions," Butterworths, London (1973), Vol. 2.
16) K. Tadasa, N. Imai, and T. Inaba, *Bull. Chem. Soc. Jpn.*, **47**, 548 (1974).
17) M. H. Back, *Can. J. Chem.*, **49**, 2119 (1971).
18) The mixture of 2670 ppm HCN in Ar diluent was shock heated, the reaction time and total density being nearly the same as those of the pyrolysis in the C_2H_2–NO system. No detectable amounts of cyanogen were found at 1620 and 1700 K. The test mixture of 4370 ppm HCN and 2.15% NO in Ar diluent was subjected to shock heating at 1482, 1540, and 1715 K, no appreciable amounts of cyanogen being detected. It is reported that hydrogen cyanide reacts with acetylene to yield propynenitrile.[19] A mixture of 1300 ppm HCN and 10% C_2H_2 in Ar was pyrolyzed at 1422, 1586, 1605, and 1656 K, the amounts of propynenitrile generated being 1.6, 21.8, 36.0, and 39.3 ppm/ms, respectively. The amounts of propynenitrile in the C_2H_2–HCN system were less than about one tenth of those in the C_2H_2–NO system.
19) L. J. Krebaum, U. S. Patent 3079424 (1963); *Chem. Abstr.*, **59**, 3777h (1963).
20) I. D. Gay, G. B. Kistiakowsky, J. V. Michael, and H. Niki, *J. Chem. Phys.*, **43**, 1720 (1965).
21) A. F. Bopp and R. D. Kern, *J. Phys. Chem.*, **79**, 2579 (1975).

The Reaction of Hydrogen Chloride with Nitrogen Oxide in Shock Waves

Tetsuo HIGASHIHARA, Ko SAITO,* and Ichiro MURAKAMI
Department of Chemistry, Faculty of Science, Hiroshima University, Higashisenda-machi, Hiroshima 730
(Received March 1, 1978)

The reaction of hydrogen chloride with nitrogen oxide in the temperature range 2670—3850 K and in the pressure range 2.5—3.5 atm has been studied behind reflected shock waves by monitoring the IR emission of HCl. When nitrogen oxide was added to the HCl–Ar system, the rate of HCl dissociation was found to be accelerated. For the early stage of reaction, the rate equation obtained was $-\mathrm{d[HCl]}/\mathrm{d}t = 10^{11.7} \exp(-33\ \mathrm{kcal}/RT)[\mathrm{HCl}]^{1.3}[\mathrm{NO}]^{0.5}$ mol cm^{-3} s^{-1}. As the initiation step, Reaction 1 was found to be more important than Reaction 2 under these experimental conditions:

$$\mathrm{HCl} + \mathrm{NO} \longrightarrow \mathrm{HNO} + \mathrm{Cl}, \quad (1)$$

$$\mathrm{HCl} + \mathrm{Ar} \longrightarrow \mathrm{H} + \mathrm{Cl} + \mathrm{Ar}. \quad (2)$$

The rate constant of Reaction 1 was determined to be $k_1 = 10^{13.2} \exp(-50.2\ \mathrm{kcal}/RT)$ cm^3 mol^{-1} s^{-1}.

The reactions of NO with H_2 or NH_3 have been studied by several investigators.[1-5] Asaba and coworkers[1,2] found the initiation step to be the abstraction of a hydrogen atom by nitrogen oxide, and determined its rate constant. This is the only datum available for the abstraction reaction by nitrogen oxide at high temperatures. In this paper, in order to clarify the role of nitrogen oxide in the decomposition of hydrogen containing compounds, we studied the reaction of hydrogen chloride with nitrogen oxide in shock waves by monitoring the IR emission of HCl.

Experimental

The shock tube was 5 cm in internal diameter, as described previously.[6] All experiments were performed behind reflected shock waves. The IR emission from the fundamental vibration-rotation bands of HCl at 3.45 μm was detected by an AuGe detector through a CaF_2 window which was placed at a position 2 cm upstream from the end plate. The appropriate wavelength was selected by a grating monochromator. The output signal was amplified and recorded on an oscilloscope. The mole fractions of the samples were as follows: 4% HCl–96% Ar, 8% HCl–92% Ar, 4% HCl–4% NO–92% Ar, 4% HCl–8% NO–88% Ar, 8% HCl–4% NO–88% Ar, and 8% HCl–8% NO–84% Ar. The post-shock pressure (P_5) and temperature (T_5) were in the ranges 2.5—3.5 atm and 2670—3850 K, respectively.

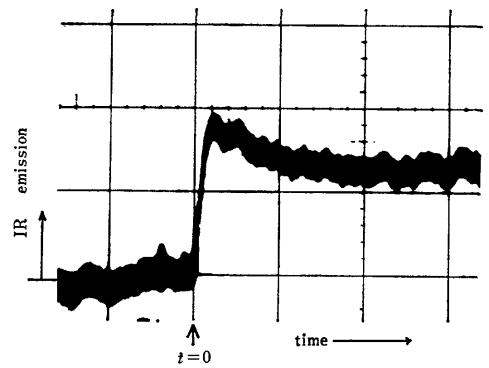

Fig. 1. A typical oscillogram of the IR emission at 3.45 μm. Run No. 231; conditions are summarized in Table 2. Sweep time=50 μs/division.

Results and Discussion

A typical oscillogram is shown in Fig. 1 (Run No. 231). This figure shows the IR emission at 3.45 μm, whose intensity corresponds to the concentration of HCl. The slow rise of the IR emission is due to the relatively long time constant (about 10 μs) of the AuGe detector. The rate of HCl dissociation ($-\mathrm{d[HCl]}/\mathrm{d}t$) was obtained from the initial gradient of the IR emission intensity. The Arrhenius plots of $-\mathrm{d[HCl]}/\mathrm{d}t$ obtained for four different mixtures are shown in Fig. 2. It is found that the rate of HCl dissociation was influenced by the initial concentrations of HCl and NO. The reaction orders with respect to the initial concentrations of HCl and NO were determined to be about 1.3 and 0.5, respectively. Thus,

$$-\mathrm{d[HCl]}/\mathrm{d}t = k_{\mathrm{overall}}[\mathrm{HCl}]^{1.3}[\mathrm{NO}]^{0.5}.$$

The Arrhenius plot of k_{overall} thus obtained is shown in Fig. 3. The best fit line gives the overall rate constant as

$$k_{\mathrm{overall}} = 10^{11.7} \exp(-33\ \mathrm{kcal}/RT)\ \mathrm{cm}^{2.4}\ \mathrm{mol}^{-0.8}\ \mathrm{s}^{-1}.$$

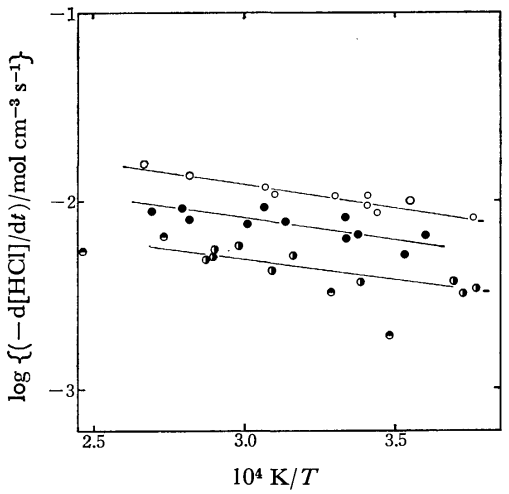

Fig. 2. Arrhenius plots of $-\mathrm{d[HCl]}/\mathrm{d}t$ obtained for different mixtures. ○: 8% HCl–8% NO–84% Ar, ●: 8% HCl–4% NO–88% Ar, ◑: 4% HCl–8% NO–88% Ar, ◓: 4% HCl–4% NO–92% Ar.

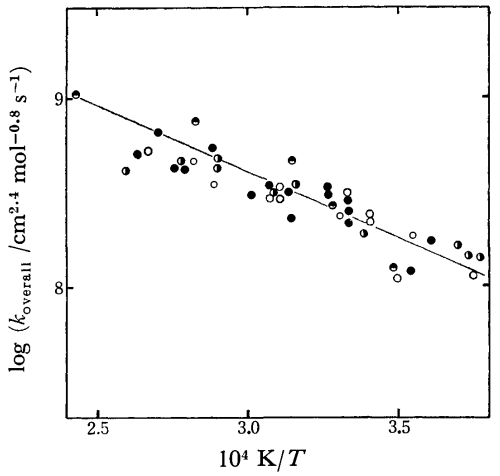

Fig. 3. Arrhenius plot of $k_{overall}$. Symbols are the same as in Fig. 2.

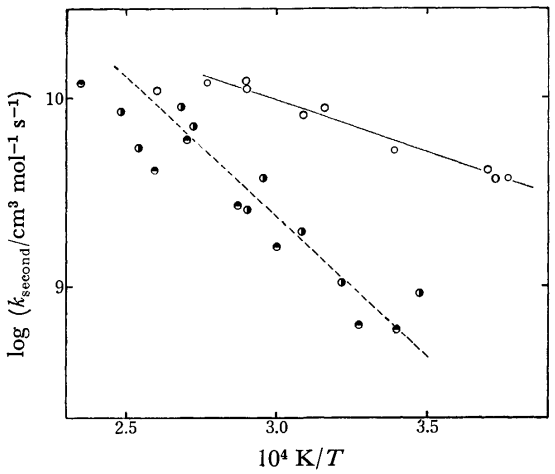

Fig. 4. Arrhenius plots of k_{second} for the mixtures with NO (○) and without NO (◑, ◓). ○: 4% HCl–8% NO–88% Ar, ◑: 4% HCl–96% Ar, ◓: 8% HCl–92% Ar, ---: Jacobs *et al.*[7]

In order to check the experimental method used in this work, HCl–Ar mixtures were also shock-heated and the rates of HCl dissociation were measured similarly. In Fig. 4, the second order rate constants, k_{second}= (—d[HCl]/dt)/[HCl][Ar], are plotted in the Arrhenius form for mixtures with and without NO. In this figure, the data obtained by Jacobs *et al.*[7] are also shown by a broken line. In spite of different experimental conditions and methods of the data reduction in the two works, our rate data for the HCl dissociation without NO are in good agreement with those of Jacobs. It was also found, as seen in Fig. 4, that the rate of HCl dissociation was accelerated by the addition of NO, and this effect was more remarkable at lower temperatures.

To clarify the dissociation kinetics of hydrogen chloride in the system involving nitrogen oxide, 26 elementary reactions (Mechanism I) were selected and tabulated in Table 1. Values of the rate constants for Reactions 2—26 were cited from the references. The numerical integrations of simultaneous rate equations for 15 species listed in Table 1 were performed on an

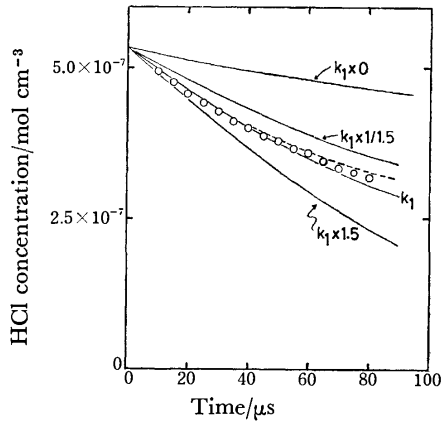

Fig. 5. Time histories of HCl calculated with various k_1 values for the conditions of Run No. 322. ○: Observed history, —: calculated histories for Mechanism I, ---: calculated history for Mechanism II. The best fit value of k_1 is 3.00×10^9 cm^3 mol^{-1} s^{-1}. The value of k_1 is varied from 0 to 1.5 times the best value.

Table 1. Elementary reactions and assigned rate constants, $k=AT^B \exp(-E/RT)$

	Reaction	log A[a]	B	E (kcal/mol)	Ref.
1	HCl+NO→HNO+Cl	13.2	0.0	50.2	This work
2	HCl+Ar→H+Cl+Ar	12.82	0.0	70.0	7
3	HNO+Ar→H+NO+Ar	16.5	0.0	49.0	11
4	HCl+H→H_2+Cl	13.36	0.0	3.5	12, 14
5	H_2+Cl→HCl+H	13.68	0.0	5.26	13
6	HCl+Cl→H+Cl_2	13.85	0.0	48.0	14, 15
7	Cl_2+H→HCl+Cl	14.2	0.0	1.96	15
8	Cl_2+Ar→2Cl+Ar	13.94	0.0	44.8	16
9	H_2+Ar→2H+Ar	14.34	0.0	96.0	11
10	H+NO→OH+N	13.7	0.0	48.7	2
11	N+NO→N_2+O	13.2	0.0	0.0	11
12	O+HCl→OH+Cl	12.76	0.0	5.9	17
13	OH+HCl→H_2O+Cl	12.98	0.0	1.0	18
14	H_2O+H→H_2+OH	13.97	0.0	20.6	11
15	OH+H→H_2+O	9.5	1.0	7.0	11
16	2H+Ar→H_2+Ar	17.81	−1.0	0.0	11
17	2Cl+Ar→Cl_2+Ar	13.3	0.0	−11.3	16
18	H_2+O→OH+H	10.25	1.0	9.96	11
19	H_2+OH→H_2O+H	13.35	0.0	5.2	11
20	2O+Ar→O_2+Ar	15.78	−0.5	0.0	11
21	O_2+Ar→2O+Ar	14.41	0.0	108.0	11
22	H+O_2→OH+O	14.34	0.0	0.0	11
23	OH+O→H+O_2	13.1	0.0	0.0	11
24	NO+O→N+O_2	9.18	1.0	38.5	11
25	O+Cl_2→ClO+Cl	12.8	0.0	3.6	19
26	O+ClO→O_2+Cl	13.5	0.0	0.0	20

a) Units: mol cm^{-3} for concentration, s for time.

electronic computer to obtain the time histories of the concentrations of the reactants and products. There are no data for the rate constant of Reaction 1. Thus in the calculations the value of k_1 was varied in the range 10^9—2×10^{10} cm^3 mol^{-1} s^{-1}, and the value of k_1 was determined as the value at which the calculated history of HCl agreed best with that obtained from experiment. The fit of the calculations to the experiment is shown

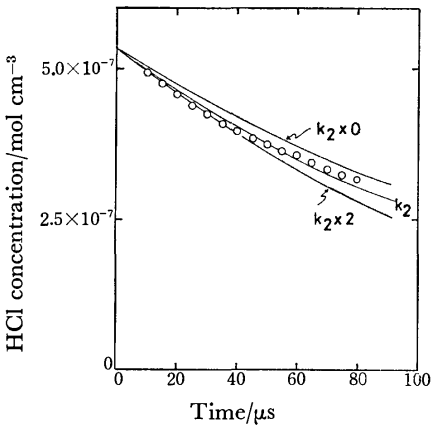

Fig. 6. Time histories of HCl calculated with various k_2 values for the conditions of Run No. 322. ○: Observed history, —: calculated histories for Mechanism I. The best fit value of k_2 is $k_2=10^{12.82}$ exp $(-70$ kcal/$RT)$[7] cm^3 mol^{-1} s^{-1} (middle curve). The value of k_2 is varied from 0 to 2 times the best-fit value.

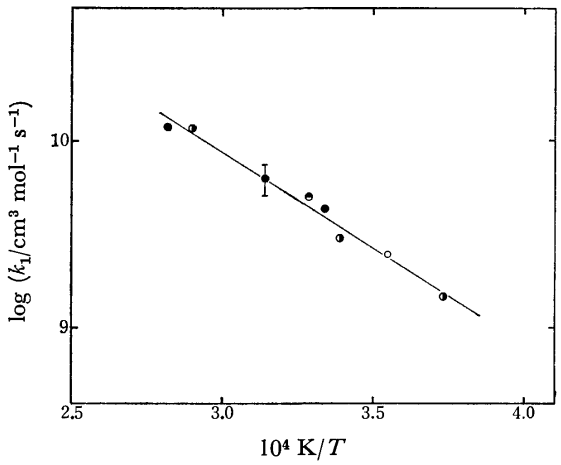

Fig. 7. Arrhenius plot of k_1. The error bar indicates the ±25% maximum uncertainty. Symbols are the same as in Fig. 2.

in Fig. 5 for Run No. 322 as an example. For checking the sensitivity, the value of k_1 was varied from 0 to 1.5 times the best value, and the histories of HCl were recalculated by using these values. The histories thus obtained are also shown in Fig. 5. From Fig. 5, it appears that the rate of HCl dissociation is strongly influenced by the value of k_1. The sensitivity of k_2 to the overall rate of HCl dissociation was also checked. The value of k_2 was varied from 0 to 2 times that listed in Table 1. Figure 6, which shows the results of the calculations for Run No. 322, reveals that the variation in k_2 has very little effect on the overall rate. Therefore, Reaction 1 is found to be predominant as the initiation step. The experimental conditions used for the estimation of k_1 and the values of k_1 determined at various temperatures are listed in Table 2. The Arrhenius plot of k_1 is shown in Fig. 7. The best fit line of the plot gives the rate expression as

$$k_1 = 10^{13.2} \exp(-50.2 \text{ kcal}/RT) \text{ cm}^3 \text{ mol}^{-1} \text{ s}^{-1}.$$

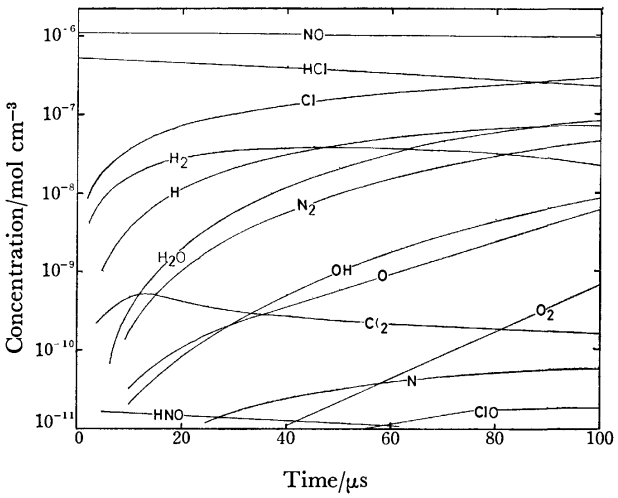

Fig. 8. Time dependent concentration changes of chemical species calculated with Mechanism I for the conditions of Run No. 322.

Figure 8 shows the time variation of the concentration of each chemical species for Run No. 322. The figure implies that Mechanism I can be reduced to only the first eight elementary reactions (1—8) (Mechanism II), since in the initial stage of reaction nitrogen oxide does not decrease largely and thus H_2O, OH, N_2, O, N, *etc.* are neglected. The calculated history of HCl for Mechanism II is shown by the broken line in Fig. 5.

Since the experimentally determined reaction orders were the average values in the initial stage (from 0 to about 30 μs), the reaction orders for HCl and NO, which were averaged between 0 and 30 μs, were calculated by using Mechanism I. The values calculated for HCl and NO were 1.06 and 0.62, respectively. Thus, the calculated reaction orders are comparable to the values determined experimentally. The rate of HCl

Table 2. Experimental conditions and determined rate constants

Run No.	Temp (K)	HCl (mol cm^{-3})	NO (mol cm^{-3})	Ar (mol cm^{-3})	$-$d[HCl]/dt (mol cm^{-3} s^{-1})	k_1 (cm^3 mol^{-1} s^{-1})
231	3185	9.295×10^{-7}	4.647×10^{-7}	1.023×10^{-5}	7.62×10^{-3}	6.23×10^{9}
232	2996	10.18	5.089	1.119	6.36	4.30
235	3544	8.062	4.031	0.887	8.02	11.6
261	3044	5.100	5.100	1.173	3.29	4.95
281	2819	11.94	11.94	1.253	10.6	2.46
321	2678	5.859	11.72	1.289	3.26	1.48
322	2949	5.345	10.69	1.176	3.75	3.00
331	3447	4.301	8.602	0.946	5.29	11.5

dissociation in Mechanism II is expressed as

$$-\mathrm{d[HCl]}/\mathrm{d}t = \underbrace{k_1[\mathrm{HCl}][\mathrm{NO}]}_{\text{term A}} + \underbrace{k_2[\mathrm{HCl}][\mathrm{Ar}]}_{\text{term B}} + \underbrace{(k_4[\mathrm{H}][\mathrm{HCl}] - k_5[\mathrm{H_2}][\mathrm{Cl}])}_{\text{term C}} + \underbrace{(k_6[\mathrm{Cl}][\mathrm{HCl}] - k_7[\mathrm{Cl_2}][\mathrm{H}])}_{\text{term D}}.$$

The contributions of terms A, B, C, and D to the rate of HCl dissociation are shown in Fig. 9 as a function of time for the conditions of Run No. 322. From this figure, it is found that terms A and C are important for the HCl consumption.

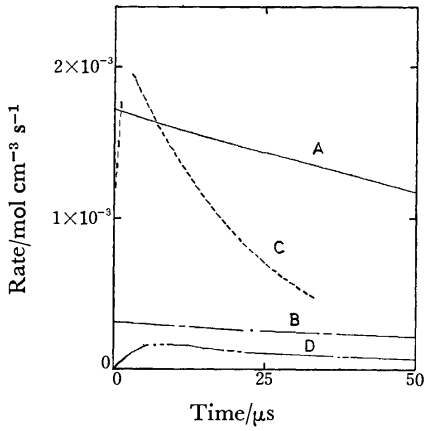

Fig. 9. Time variations of rate terms which contribute to the HCl dissociation. Symbols A, B, C, and D are explained in the text.

As the initiation step, the following three reactions are possible:

$$\mathrm{HCl} + \mathrm{NO} \longrightarrow \mathrm{HNO} + \mathrm{Cl}, \quad \Delta H^\circ_{298} = 53.2 \text{ kcal mol}^{-1}, \tag{1}$$

$$\mathrm{HCl} + \mathrm{NO} \longrightarrow \mathrm{H} + \mathrm{ClNO}, \quad \Delta H^\circ_{298} = 65.0 \text{ kcal mol}^{-1}, \tag{1'}$$

$$\mathrm{HCl} + \mathrm{Ar} \longrightarrow \mathrm{H} + \mathrm{Cl} + \mathrm{Ar}, \quad \Delta H^\circ_{298} = 103.1 \text{ kcal mol}^{-1}, \tag{2}$$

where the standard enthalpy changes (ΔH°_{298}) were calculated from JANAF Thermochemical Tables.[21] Reactions 1 and 1′ are not distinguishable because the decomposition rates of HNO and ClNO are very fast. However, because Reaction 1′ is more endothermic by 12 kcal mol^{-1} than Reaction 1, it seems to be reasonable to neglect Reaction 1′ as the initiation step. As shown in Fig. 6, even if Reaction 2 was ruled out, the rate of HCl dissociation did not change very much. Therefore, Reaction 1 was confirmed to be a more important initiation step than Reaction 2.

The activation energy of Reaction 1 was calculated by the bond-energy-bond-order (BEBO) method, which was developed by Johnston and Parr,[22,23] as 52.7 kcal mol^{-1}. The activation energy which was obtained in this work, 50.2 kcal mol^{-1}, is very close to this calculated value. It is interesting to compare the rate constant with that for a similar reaction

$$\mathrm{H_2} + \mathrm{NO} \longrightarrow \mathrm{HNO} + \mathrm{H}. \tag{27}$$

The rate constant of Reaction 27 was obtained as[2]

$$k_{27} = 10^{13.5} \exp(-55.2 \text{ kcal}/RT) \text{ cm}^3 \text{ mol}^{-1} \text{ s}^{-1}.$$

This activation energy is nearly equal to the standard enthalpy change (54.3 kcal mol^{-1}) of the reaction. The value of the A factor for k_{27} is larger than for k_1 by a factor of about 2. This difference is greater than the experimental error of ±25% maximum uncertainty in the determination of k_1. Since the ratio of the collision number for the H_2–NO system to that for the HCl–NO system was calculated as

$$Z_{\mathrm{H_2-NO}}/Z_{\mathrm{HCl-NO}} = 2.7,$$

the difference of the A factor may be due to the difference of collision numbers for Reactions 1 and 27.

The authors wish to thank Professor T. Asaba and Dr. N. Fujii of the University of Tokyo for providing us with the computer program.

References

1) M. Koshi, H. Ando, M. Oya, and T. Asaba, 15th Symp. (Int.) Combust., 1975, p. 809.
2) H. Ando and T. Asaba, *Int. J. Chem. Kinet.*, **8**, 259 (1976).
3) J. Duxbury and N. H. Pratt, 15th Symp. (Int.) Combust., 1975, p. 843.
4) W. L. Flower, R. K. Hanson, and C. H. Kruger, 15th Symp. (Int.) Combust., 1975, p. 825.
5) J. N. Bradley and P. Craggs, 15th Symp. (Int.) Combust., 1975, p. 833.
6) T. Higashihara, K. Saito, and H. Yamamura, *Bull. Chem. Soc. Jpn.*, **49**, 965 (1976).
7) T. A. Jacobs, N. Cohen, and R. R. Giedt, *J. Chem. Phys.*, **46**, 1958 (1967).
8) D. J. Deery and C. T. Bowman, *J. Chem. Phys.*, **48**, 4314 (1968).
9) R. L. Belford and R. A. Strehlow, *Ann. Rev. Phys. Chem.*, **20**, 260 (1969).
10) R. D. Kern and G. G. Nika, *J. Phys. Chem.*, **75**, 171 (1971).
11) D. L. Baulch, D. D. Drysdale, D. G. Home, and A. C. Lloyd, "Evaluated Kinetic Data for High Temperauture Reactions," Butterworths, London (1972), Vol. 1; (1973), Vol. 2; D. L. Baulch, D. D. Drysdale, J. Duxbury, and S. Grant, *ibid.*, (1976), Vol. 3.
12) A. A. Westenberg and N. de Hass, *J. Chem. Phys.*, **48**, 4405 (1968).
13) S. W. Benson, F. R. Cruickshank, and R. Shaw, *Int. J. Chem. Kinet.*, **1**, 29 (1969).
14) D. L. Tompson, H. H. Suzukawa, and L. M. Raff, *J. Chem. Phys.*, **62**, 4727 (1975).
15) F. S. Klein and M. Wolfsberg, *J. Chem. Phys.*, **34**, 1494 (1961).
16) A. C. Lloyd, *Int. J. Chem. Kinet.*, **3**, 39 (1971).
17) R. D. H. Brown and I. W. M. Smith, *Int. J. Chem, Kinet.*, **7**, 301 (1975).
18) I. W. M. Smith and R. Zellner, *J. Chem. Soc., Faraday Trans. 2*, **70**, 1045 (1974).
19) J. N. Bradley and D. A. Zaleski, *J. Chem. Soc., Faraday Trans. 1*, **69**, 1251 (1973).
20) P. P. Bemand, M. A. A. Clyne, and R. T. Watson, *J. Chem. Soc. Faraday Trans. 1*, **69**, 1356 (1973).
21) JANAF Thermochemical Tables, 2nd ed, Natl. Bur. Stand., 1971.
22) H. S. Johnston and C. Parr, *J. Am. Chem. Soc.*, **85**, 2544 (1963).
23) H. S. Johnston, "Gas Phase Reaction Rate Theory," Ronald, New York (1966).

The Reaction of Hydrogen Bromide with Nitrogen Oxide in Shock Waves

Tetsuo HIGASHIHARA, Ko SAITO,* and Ichiro MURAKAMI

Department of Chemistry, Faculty of Science, Hiroshima University, Higashisenda-machi, Hiroshima 730

(Received March 9, 1978)

The reaction of hydrogen bromide with nitrogen oxide in the temperature range 2000—3300 K and in the pressure range 0.7—3.8 atm has been studied behind reflected shock waves by monitoring the IR emission of HBr. For the early stage of the reaction, the rate equation obtained was $-d[HBr]/dt = k_{overall}[HBr]^{1\pm0.3}[NO]^{0.7\pm0.2}[Ar]^{0\pm0.1}$, where $k_{overall} = 10^{10.4\pm0.2} \exp\{-(23.2\pm3.0)\ \text{kcal}/RT\}\ \text{cm}^{2.1}\ \text{mol}^{-0.7}\ \text{s}^{-1}$. As the initiation step, Reaction 1 was found to be more important than Reaction 2:

$$HBr + NO \longrightarrow HNO + Br, \quad (1)$$

$$HBr + Ar \longrightarrow H + Br + Ar. \quad (2)$$

The rate constant of Reaction 1 was determined to be $k_1 = 10^{12.8} \exp(-30\ \text{kcal}/RT)\ \text{cm}^3\ \text{mol}^{-1}\ \text{s}^{-1}$.

There have been a few previous shock-tube investigations of the reactions of nitrogen oxide with other compounds. Asaba and coworkers[1,2] studied the reaction between H_2 and NO, and determined the initiation step and its rate constant to be

$$H_2 + NO \longrightarrow HNO + H, \quad (A)$$

$$k_A = 10^{13.5} \exp(-55.2\ \text{kcal}/RT)\ \text{cm}^3\ \text{mol}^{-1}\ \text{s}^{-1}.$$

In the previous paper,[3] we studied the reaction of HCl with NO. In that work, we found that when nitrogen oxide was added to the HCl–Ar mixture the rate of HCl disappearance was significantly accelerated. On the basis of these experimental results, we discussed the role of NO in the HCl disappearance and determined the initiation step and its rate constant to be

$$HCl + NO \longrightarrow HNO + Cl, \quad (B)$$

$$k_B = 10^{13.2} \exp(-50.2\ \text{kcal}/RT)\ \text{cm}^3\ \text{mol}^{-1}\ \text{s}^{-1}.$$

In order to make the role of NO in the disappearance rate of hydrogen halide more clear, we studied the reaction of hydrogen bromide with nitrogen oxide. Since the rate constant of Reaction 2 was determined in the HBr–Ar system by Giedt *et al.*[4] in the temperature range 2100—4200 K:

$$HBr + Ar \longrightarrow H + Br + Ar, \quad (2)$$

the influence of NO on the rate of HBr disappearance could be investigated by adding NO to the HBr–Ar system.

Experimental

The shock tube was 5 cm in internal diameter, and had a 3.8 cm long test section. The side of the tube was fitted with a CaF_2 window mounted flush with the interior surface at a position 2 cm upstream from the end plate. The shocks were generated by high pressure hydrogen in a 1.7 m long driver section. The system was pumped off by an oil-diffusion pump to less than 1×10^{-4} Torr before each run. All experiments were performed behind reflected shock waves.

The concentration change of hydrogen bromide was monitored by 3.93 μm emission, which was detected by an AuGe detector at 77 K. The detector was coupled to an amplifier, whose output was displayed directly on an oscilloscope.

Hydrogen bromide was produced by dropping bromine on tetrahydronaphthalene.[5] The gas thus obtained was solidified and degassed at the temperature of liquid N_2–ethanol slush and purified by trap to trap distillation at this temperature. Argon and nitrogen oxide from commercial cylinders were used without further purification.

The gas mixtures studied and the experimental conditions are listed in Table 1. Fig. 1 shows a typical oscillogram of

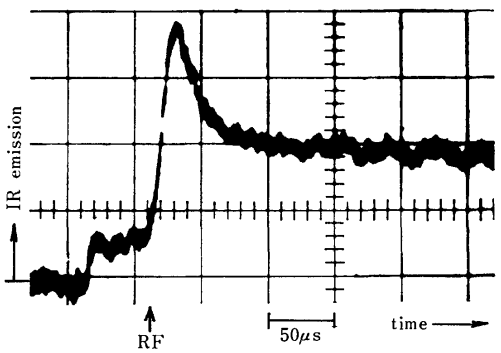

Fig. 1. Typical oscillogram of the experiments. Run No. 181; $T = 2977$ K, HBr $= 5.955 \times 10^{-7}$ mol/cm³, NO $= 2.975 \times 10^{-7}$ mol/cm³, Ar $= 7.400 \times 10^{-6}$ mol/cm³. The trace shows the IR emission at 3.93 ± 0.1 μm. RF indictes the time at which reflected shock front reached the window.

TABLE 1. SAMPLES AND EXPERIMENTAL CONDITIONS

	HBr (%)	NO (%)	Ar (%)	Total mol/cm³	Pressure (atm)	Temperature (K)	Symbol
1)	8	8	84	$3.4—5.5 \times 10^{-6}$	0.7—0.95	2000—3030	○
2)	4	4	92	6.7—10	1.6—1.81	2180—2894	◑
3a)	2	2	96	6.7—10.2	1.6—1.95	2244—3237	◐
3b)	2	2	96	17—22	3.4—3.8	2104—2485	◐
4)	2	4	94	7.1—11.3	1.9—2.2	2140—3000	◓
5)	8	4	88	7.4—13	1.8—2.2	2050—3350	◒
6)	2	7.1	90.9	7.7—12.6	1.8—2.2	2150—3150	●

the experiments. The slow rise of IR emission is due to the relatively long time constant of the AuGe detector. From the signals of two piezo-gauges, the shock speed was calculated.

Results and Discussion

The rate of HBr disappearance ($-$d[HBr]/dt) was obtained from the gradient of the IR emission intensity in an early stage of reaction. Figures 2, 3, and 4 show the Arrhenius plots of $-$d[HBr]/dt for pairs of different samples. In Fig. 2, in each of these samples at about the same temperature the concentrations of NO and Ar are almost equal, but there are two- and four-fold differences in the concentration of HBr. In Fig. 3, there are differences in the concentration of NO, and in Fig. 4, the argon density is varied about two- and four-fold, holding the concentrations of the other reactants constant. The reaction orders with respect to the initial concentrations of HBr, NO, and Ar were obtained from these figures at 2500 K to be 1 ± 0.3, 0.7 ± 0.2, and 0 ± 0.1, respectively. The fact that the reaction order with respect to Ar is small, nearly zero, implies that Reaction 2 becomes unimportant with the addition of NO. Later, we will find that this value of

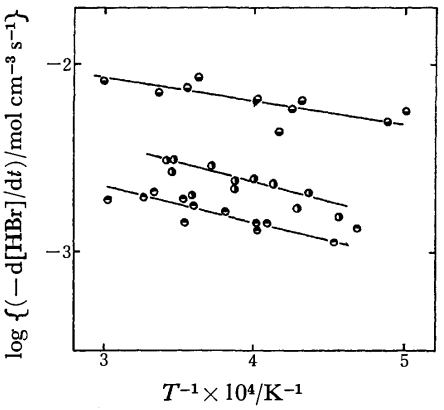

Fig. 2. Arrhenius plot of the rate of HBr disappearance for samples 2), 4), and 5). This figure shows that the reaction order for HBr is 1 ± 0.3 at 2500 K. Symbols are summarized in Table 1.

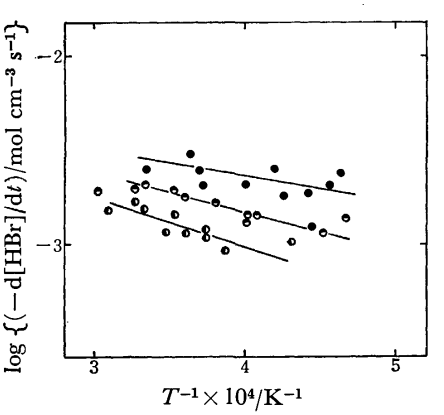

Fig. 3. Arrhenius plot of the rate of HBr disappearance for samples 3a), 4), and 6). This figure shows that the reaction order for NO is 0.7 ± 0.2 at 2500 K. Symbols are summarized in Table 1.

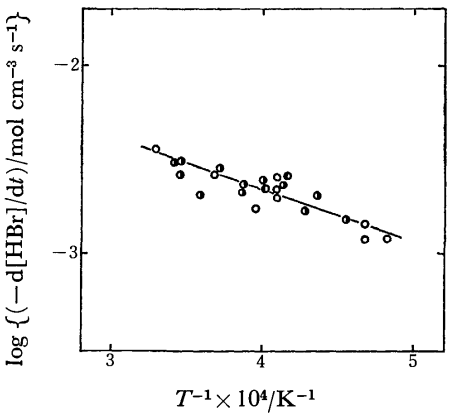

Fig. 4. Arrhenius plot of the rate of HBr disappearance for samples 1), 2), and 3b). This figure shows that the reaction order for Ar is 0 ± 0.1 at 2500 K. Symbols are summarized in Table 1.

the reaction order is in good agreement with the value (0—0.1) which was estimated from the calculations with an assumed reaction mechanism. From Fig. 3, the reaction order with respect to NO seems to decrease slightly with increasing temperature. This may be explained qualitatively by the fact that at higher temperatures Reaction 2 begins to contribute gradually to the rate of HBr disappearance (see Fig. 6). Thus, the overall rate equation can be expressed as

Table 2. Elementary reactions and kinetic parameters, $k=AT^B\exp(-E/RT)$

	Reaction	log A[a)]	B	E (kcal/mol)	Ref.
1	HBr+NO→HNO+Br	12.8	0.0	30.0	This work
2	HBr+Ar→H+Br+Ar	12.19	0.0	50.0	4
3	HNO+Ar→H+NO+Ar	16.5	0.0	49.0	6
4	HBr+H→H_2+Br	13.1	0.0	0.9	7
5	H_2+Br→HBr+H	14.43	0.0	19.7	8
6	HBr+Br→H+Br_2	13.4	0.0	41.8	8
7	Br_2+H→HBr+Br	14.18	0.0	0.9	9
8	Br_2+Ar→2Br+Ar	11.33	0.5	31.3	10
9	H_2+Ar→2H+Ar	14.34	0.0	96.0	6
10	H+NO→OH+N	13.7	0.0	48.7	1
11	N+NO→N_2+O	13.2	0.0	0.0	6
12	O+HBr→OH+Br	12.38	0.0	2.7	11
13	OH+HBr→H_2O+Br	12.5	0.0	0.0	12
14	H_2O+H→H_2+OH	13.97	0.0	20.6	6
15	OH+H→H_2+O	9.5	1.0	7.0	6
16	2H+Ar→H_2+Ar	17.81	−1.0	0.0	6
17	2Br+Ar→Br_2+Ar	12.9	0.0	−10.8	10
18	H_2+O→OH+H	10.25	1.0	9.96	6
19	H_2+OH→H_2O+H	13.35	0.0	5.2	6
20	2O+Ar→O_2+Ar	15.78	−0.5	0.0	6
21	O_2+Ar→2O+Ar	14.41	0.0	108.0	6
22	H+O_2→OH+O	14.34	0.0	16.9	6
23	OH+O→H+O_2	13.1	0.0	0.0	6
24	NO+O→N+O_2	9.18	1.0	38.5	6
25	O+Br_2→BrO+Br	12.71	0.0	0.0	13
26	O+BrO→O_2+Br	13.61	0.0	0.0	14

a) Units: mol cm^{-3} for concentration, s for time.

$$-d[HBr]/dt = k_{overall}[HBr]^{1\pm0.3}[NO]^{0.7\pm0.2}[Ar]^{0\pm0.1}.$$

It is to be noted that this equation can be applied in an early stage of reaction. Reaction orders change with time, because Reactions 4—7, which are shown in Table 2, become predominant with time. Calculations of the reaction orders with time are discussed later and shown in Fig. 11. Figure 5 shows the Arrhenius plot of $k_{orerall}$ for all data obtained under various experimental conditions. It is found that all data points fall around one straight line. The best fit line gives the rate expression as

$$k_{overall} = 10^{10.4\pm0.2} \exp\{-(23.2\pm3.0)\ \text{kcal}/RT\}\ \text{cm}^{2.1}\ \text{mol}^{-1}\ \text{s}^{-1}.$$

To ascertain the influence of NO on the rate of HBr disappearance, a 4% HBr–96% Ar mixture was also shock-heated, and the second order rate constants, $k_{second}=(-d[HBr]/dt)/[HBr][Ar]$, were compared between the mixtures with and without NO (Fig. 6). In this figure, the data obtained by Giedt *et al.*[4] for HBr–Ar mixture are also shown by a broken line. In spite of the different experimental conditions and methods of data reduction in the two works, our rate data for HBr disappearance without NO are in good agreement with those of Giedt *et al.* It is also found, in Fig. 6, that the rate of HBr disappearance is accelerated by the addition of NO; this effect is remarkable at lower temperatures. Similar facts for HCl–NO–Ar mixtures[3] were also found in previous work.

To clarify the kinetics of HBr disappearance for mixtures involving NO, 26 elementary reactions (Mechanism I) were selected and tabulated in Table 2. Using tabulated rate constants for Reactions 2—26, concentration changes of HBr were calculated and were compared with the histories of HBr (IR intensity) obtained experimentally, where the emission intensity at zero time was determined by extrapolating the emission trace to the reflected shock front. In the calculations, since there are no rate data for Reaction 1, the value of k_1 was varied and then determined so as to fit the experimental histories of HBr at various temperatures. The value of k_1 thus determined is expressed as

$$k_1 = 10^{12.8} \exp(-30\ \text{kcal}/RT)\ \text{cm}^3\ \text{mol}^{-1}\ \text{s}^{-1}.$$

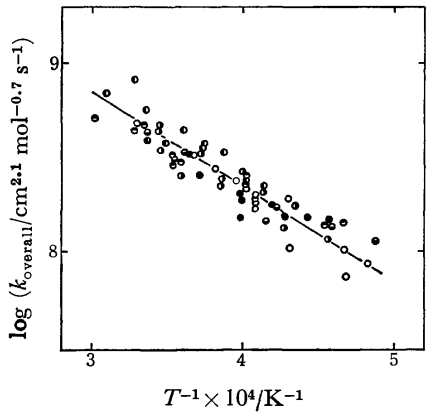

Fig. 5. Arrhenius plot of $k_{overall}$. Symbols are summarized in Table 1.

Examples of a fitting between the calculated and observed history are shown in Figs. 7a, b, c, and d for four cases under various experimental conditions. Figure 8 shows the time variations of the concentrations of HBr, NO, and the main products. As shown in this figure, NO does not decompose remarkably and the concentrations of N, O, OH, H_2O, and BrO are very low, at least in the early stages of reaction. Therefore, Mechanism I can be reduced to only the first eight elementary reactions (Mechanism II). The histories of HBr were also calculated by using Mechanism II and no discrepancy was found with those calculated with Mechanism I, implying that the rate of HBr disappearance was mainly governed by Reactions 1—8.

Sensitivity checks were performed on k_1 and k_2 for

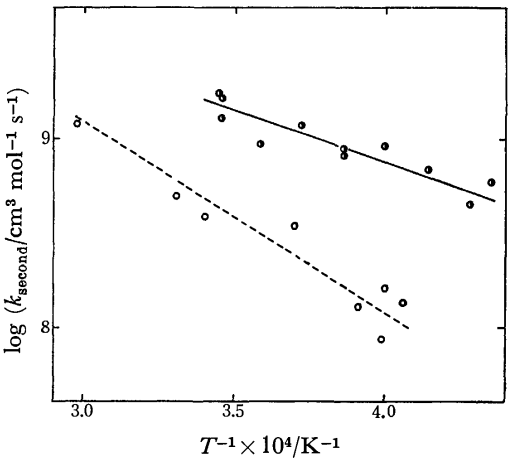

Fig. 6. Arrhenius plot of k_{second} for the mixtures with NO and without NO. ◑: 4% HBr–4% NO–92% Ar, ○: 4% HBr–96% Ar, —: calculated from the data of Giedt *et al*[4].

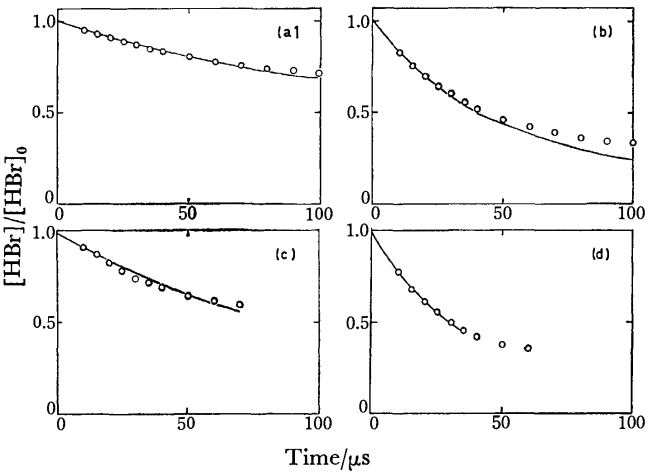

Fig. 7. Comparison of the histories of HBr obtained experimentally with those calculated. ○: Experiment, —: calculation. (a) Run No. 113; T=2142 K, HBr=3.661×10^{-7} mol/cm^3, NO=3.661×10^{-7} mol/cm^3, Ar=4.576×10^{-6} mol/cm^3. (b) Run No. 204; T=2508 K, HBr=1.784×10^{-7} mol/cm^3, NO=6.337×10^{-7} mol/cm^3, Ar=8.925×10^{-6} mol/cm^3. (c) Run No. 110; T=2529 K, HBr=2.705×10^{-7} mol/cm^3, NO=2.075×10^{-7} mol/cm^3, Ar=3.381×10^{-6} mol/cm^3. (d) Run No. 181; conditions are the same as Fig. 1.

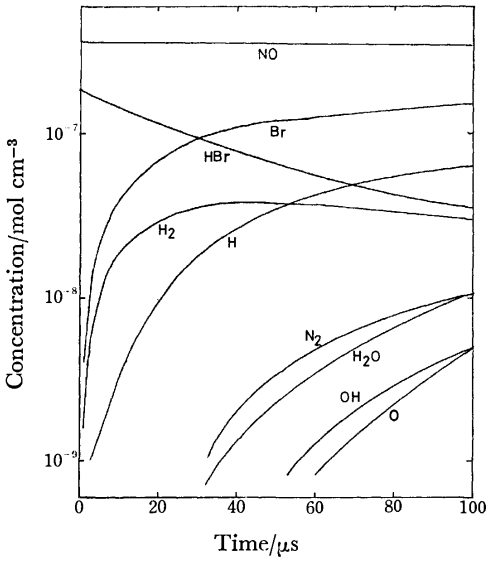

Fig. 8. Time dependent concentration changes of chemical species for Run No. 166. $T=2828$ K, HBr$=1.867\times10^{-7}$ mol/cm^3, NO$=3.735\times10^{-7}$ mol/cm^3, Ar$=9.337\times10^{-6}$ mol/cm^3.

the purpose of examining how the overall rate of HBr disappearance was influenced by k_1 and k_2. The values of k_1 and k_2 were varied in the ranges of 0 to 1.5 times and 0 to 2 times, respectively. The results of the calculations at temperatures 2179 and 2977 K are shown in Figs. 9 and 10, respectively. These figures show that the rate of HBr disappearance is remarkably influenced by the value of k_1. On the other hand, at 2179 K the influence of the variation of k_2 is very little, while at 2977 K it becomes slightly appreciable. These facts suggest that Reaction 1 is more important than Reaction 2 for the rate of HBr disappearance at least in the low temperature region, and that the importance of Reaction 2 increases with increasing temperature.

Figure 11 shows the time variations of reaction orders with respect to the concentrations of HBr, NO, and Ar; these were calculated by using Mechanism I for the conditions of Run No. 110. When the reaction order for HBr was calculated, for example, the initial concentration of HBr was changed by a factor of 2 and those of NO and Ar were not changed, then the rate of HBr disappearance was calculated and compared with that for the conditions of Run No. 110, where the rates were obtained as an average over every 2 μs intervals, *i.e.*, $-\mathrm{d[HBr]}/\mathrm{d}t=([\mathrm{HBr}]_t-[\mathrm{HBr}]_{t-2})/2$. From Fig. 11, in the initial stage, the reaction orders are 1, 0.5—0.9, and 0—0.1 with respect to HBr, NO, and Ar, respectively. These calculated reaction orders are in good agreement with those determined experimentally, as mentioned already. Several calculated results showed that the reaction orders with respect to NO and Ar were dependent on the value of k_1. That is, as the value of k_1 decreases, the reaction order for NO decreases and that for Ar increases. The agreement of the reaction orders between the calculation and the observation implies that the value of k_1 determined is reasonable.

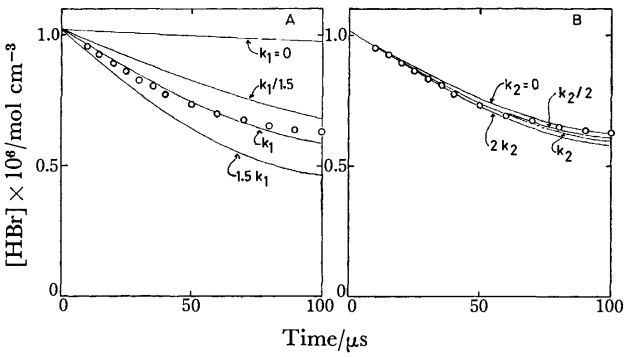

Fig. 9. Sensitivity of calculated HBr concentration to the value of k_1 (Fig. A) and k_2 (Fig. B) for Run No. 189. $T=2179$ K, HBr$=1.022\times10^{-6}$ mol/cm^3, NO$=5.112\times10^{-7}$ mol/cm^3, Ar$=1.278\times10^{-5}$ mol/cm^3. ○: Experimental history, —: histories calculated by using various values of k_1 and k_2.

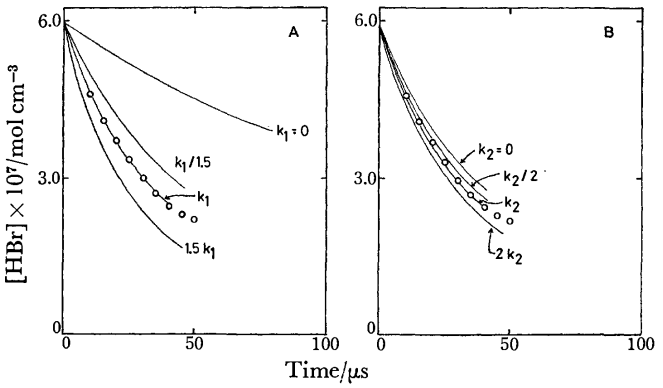

Fig. 10. Sensitivity of calculated HBr concentration to the values of k_1 (Fig. A) and k_2 (Fig. B) for Run No. 181. Conditions are the same as Fig. 1. ○: Experimental history, —: histories calculated by using various values of k_1 and k_2.

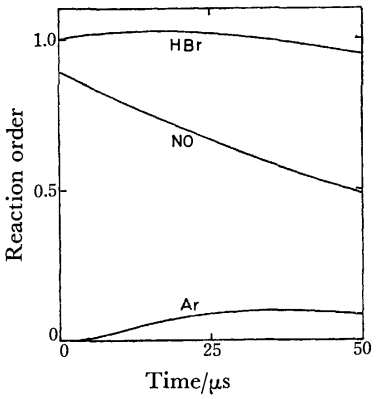

Fig. 11. Time variations of the reaction orders with respect to the initial concentrations of HBr, NO, and Ar for Run No. 110. Conditions are the same as Fig. 7 (c).

The rate of HBr disappearance in Mechanism II is expressed as

$$-\mathrm{d[HBr]}/\mathrm{d}t=\underbrace{k_1[\mathrm{HBr}][\mathrm{NO}]}_{\text{term A}}+\underbrace{k_2[\mathrm{HBr}][\mathrm{Ar}]}_{\text{term B}}+\underbrace{k_4[\mathrm{H}][\mathrm{HBr}]-k_5[\mathrm{H_2}][\mathrm{Br}]}_{\text{term C}}$$

$$+ \underbrace{k_6[HBr][Br] - k_7[Br_2][H]}_{\text{term D}}.$$

The contributions of terms A, B, C, and D to the rate of HBr disappearance are shown in Fig. 12 as a function of time for the conditions of Run No. 110. This figure shows that terms A and C are dominant in the rate of HBr disappearance, comfirming the importance of Reactions 1, 4, and 5.

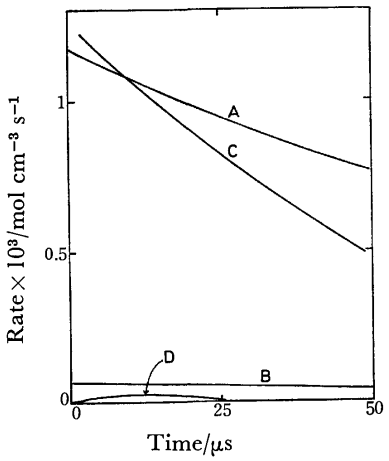

Fig. 12. Time variations of the rate terms which contribute to HBr disappearance for Run No. 110. Conditions are the same as Fig. 7(c). Terms A, B, C, and D are explained in the text.

Reaction B and Reaction 1 are expected to have similar activated complexes. According to the transition state theory, the ratio of k_B to k_1 is expressed as

$$k_B/k_1 = (F_{(HBr)}/F_{(HCl)}) \times (F^{\neq}_{(HCl-NO)}/F^{\neq}_{(HBr-NO)}) \times \exp\{-(E_{0(B)} - E_{0(1)})/RT\} \quad (I)$$

where $F_{(X)}$ is the partition function of species X, E_0 is the activation energy, and superscript $\neq$ denotes activated complex. Assuming that the electronical and vibrational partition functions are canceled out, Eq. I can be rewritten as

$$\begin{aligned} k_B/k_1 &= (f_{t(HBr)}/f_{t(HCl)}) \times (f_{r(HBr)}/f_{r(HCl)}) \\ &\quad \times (f^{\neq}_{t(HCl-NO)}/f^{\neq}_{t(HBr-NO)}) \times (f^{\neq}_{r(HCl-NO)}/f^{\neq}_{r(HBr-NO)}) \\ &\quad \times \exp\{-(E_{0(B)} - E_{0(1)})/RT\} \\ &= (M_{(HBr)}/M_{(HCl)})^{3/2} \times (I_{(HBr)}/I_{(HCl)}) \\ &\quad \times (M_{(HCl-NO)}/M_{(HBr-NO)})^{3/2} \\ &\quad \times (I_{A(HCl-NO)} I_{B(HCl-NO)} I_{C(HCl-NO)} / \\ &\quad I_{A(HBr-NO)} I_{B(HBr-NO)} I_{C(HBr-NO)})^{1/2} \\ &\quad \times \exp\{-(E_{0(B)} - E_{0(1)})/RT\}, \end{aligned} \quad (II)$$

where f_t and f_r are the translational and rotational partition functions, respectively, M is the mass of the molecule or activated complex, and I is the moment of inertia. Activation energies and bond lengths of activated complexes were calculated by the BEBO method. In the calculations, the bond angles of the complexes were assumed to be 108.6° for O–N–H and 180° for N–H–X. Thus, from Eq. II we obtain

$$\begin{aligned} (k_B/k_1)_{cal.} &= (81/36.5)^{3/2} \times (3.30/2.71) \times (66.5/111)^{3/2} \\ &\quad \times \{(1.72 \times 38.95 \times 40.67)/ \\ &\quad (1.82 \times 56.5 \times 58.36)\}^{1/2} \\ &\quad \times \exp\{-(52.7 - 36.7)\ \text{kcal}/RT\} \\ &= 1.26 \exp(-16.0\ \text{kcal}/RT). \end{aligned} \quad (III)$$

The ratio determined experimentally is

$$(k_B/k_1)_{exp.} = 2.51 \exp(-20.2\ \text{kcal}/RT). \quad (IV)$$

The agreement between the calculated and experimental ratios seems very good.

References

1) H. Ando and T. Asaba, *Int. J. Chem. Kinet.*, **8**, 259 (1976).
2) M. Koshi, H. Ando, M. Oya, and T. Asaba, 15th Symp. (Int.) Combst., 1975, p. 809.
3) T. Higashihara, K. Saito, and I. Murakami, *Bull. Chem. Soc. Jpn.*, **51**, 3426 (1978).
4) R. R. Giedt, N. Choen, and T. A. Jacobs, *J. Chem. Phys.*, **50**, 5374 (1969).
5) *Inorg. Synth.*, **1**, 150 (1939).
6) D. L. Baulch, D. D. Drysdale, D. G. Home, and A. C. Lloyd, "Evaluated Kinetic Data for High Temperaure Reactions," Butterworths, London (1972), Vol. 1; (1973), Vol. 2; D. L. Baulch, D. D. Drysdale, J. Duxbury, and S. Grant, *ibid.*, (1976), Vol. 3.
7) J. M. White, *J. Chem. Phys.*, **58**, 4482 (1973).
8) G. C. Fettis and J. H. Knox, *Prog. React. Kinet.*, **2**, 27 (1964).
9) B. A. Thrush, *Prog. React. Kinet.*, **3**, 88 (1965).
10) M. Warshay, *J. Chem. Phys.*, **54**, 4060 (1971).
11) R. D. H. Brown and I. W. M. Smith, *Int. J. Chem. Kinet.*, **7**, 301 (1975).
12) G. A. Takacs and G. P. Glass, *J. Phys. Chem.*, **77**, 1060 (1972).
13) M. A. A. Clyne and H. W. Cruse, *Trans. Faraday Soc.*, **67**, 2869 (1971).
14) M. A. A. Clyne and H. W. Cruse, *Trans. Faraday Soc.*, **66**, 2227 (1970).

Oxidation of Propylene Adsorbed on Metal Oxides. Oxygen Species in Catalytic Oxidation

Yutaka KUBOKAWA* and Takehiko ONO

Department of Applied Chemistry, University of Osaka Prefecture, Sakai, Osaka 591

(Received March 18, 1978)

Adsorption of ethylene and propylene has been investigated volumetrically with various oxide catalysts. From the results together with those of oxidation of propylene adsorbed on oxides, it is concluded that the difference between the characteristics of oxidation of propylene adsorbed on the oxide catalysts for complete or selective oxidation is attributable to the difference in the oxygen species responsible for oxidation rather than that in the adsorbed state of propylene. A comparison of characteristics of the oxidation of adsorbed propylene in the presence of gaseous oxygen and in a vacuum suggests that on the catalysts for complete oxidation, adsorbed oxygen plays a significant role in the oxidation because of its higher activity as compared to that of lattice oxygen.

In order to obtain information on the mechanism of catalytic oxidation, investigation was carried out on the oxidation of olefins adsorbed on oxide catalysts by analysis of reaction products as well as by IR techniques.[1-3] In the case of ZnO, adsorbed propylene was converted into surface formate and acetate ions as well as OH groups with oxygen uptake, which were oxidized successively to CO_2 and H_2O. A marked difference in the oxidation of adsorbed propylene was observed with catalysts for selective oxidation such as V_2O_5[2] and Sn–Mo oxide.[4] For understanding the difference between the characteristics of oxidation of olefins adsorbed on oxides, it seems necessary to obtain information on how the oxygen species responsible for the oxidation as well as the nature of adsorbed state of olefins varies on going from one oxide to another. Work along this line has been undertaken in the present study.

As regards the adsorbed state of olefins, IR studies seem to be most promising. However, IR data are available only for a limited range of oxides such as ZnO,[5] Sn–Mo oxide,[4] and copper oxides[6] because of the inherent difficulties in the IR measurements of adsorbed species. Accordingly, volumetric adsorption measurements have been carried out for all the oxide catalysts for which the oxidation of adsorbed propylene was examined.[1,2]

Experimental

Details of apparatus, procedure and materials were reported.[1,2] The adsorption of ethylene and propylene as well as the oxidation or desorption was investigated with a closed circulation apparatus. In the case of the oxidation of adsorbed propylene, the temperature of the catalysts containing a known amount of adsorbed propylene was raised stepwise in the presence of oxygen. The amount of oxygen consumed and that of the reaction products were determined.

The surface area of the catalysts determined by the BET method using argon were as follows; Co_3O_4, 10.0; NiO, 3.3; CuO, 12.5; V_2O_5, 2.0; ZnO, 3.1; Fe_2O_3, 16.2; TiO_2, 2.0; MoO_3, 1.3 m^2/g.

Results and Discussion

Adsorption of Ethylene and Propylene on Oxides. The results of olefin adsorption experiments with various oxide catalysts are shown in Fig. 1. The amount of olefins adsorbed per unit area of the catalyst surface at 0 °C and 30 Torr as well as that of olefins remaining after evacuation at 0 °C are given. From these data we can obtain information on the activity of oxides toward the chemisorption of olefins. The strength of adsorption can be estimated from the remaining amount of adsorbed propylene after evacuation to the total amount adsorbed at 30 Torr. It is seen that both Co_3O_4 and ZnO exhibit the highest activity towards olefin chemisorption. The highest strength of adsorption of propylene is observed with Co_3O_4 and the lowest strength of adsorption with TiO_2 and MoO_3.

For the oxides such as ZnO, Fe_2O_3, and TiO_2 the amount of adsorbed propylene remaining after evacuation is larger than the corresponding amount of ethylene, while for the oxides such as Co_3O_4, NiO, CuO, and V_2O_5 the amounts of both olefins remaining are roughly the same. This suggests that the nature of the strong adsorption of olefins differs between both groups of oxide catalysts. Dent and Kokes[5] found that propylene undergoes adsorption to form π-allyl on ZnO while ethylene undergoes adsorption to form π-complex. They explained the difference between the remaining amounts of adsorbed propylene and ethylene.

On increasing the desorption temperature olefins adsorbed on ZnO desorbed as such without undergoing oxidation, while most olefins adsorbed on Co_3O_4 desorbed as CO_2 and H_2O. Thus, the difference between the nature of olefins adsorbed on both groups of oxides is confirmed.

Oxidation of Propylene Adsorbed on Oxides. The behavior of catalysts containing adsorbed propylene in the presence of oxygen, observed on raising the temperature, was described in previous papers.[1,2] In the case of ZnO one mole of the strongly adsorbed propylene took up two moles of oxygen to form surface formate and acetate ions,[1,3] which were oxidized successively to CO_2 and H_2O. A similar oxygen uptake was observed with other oxides such as Co_3O_4, NiO, Fe_2O_3, and CuO. On NiO, formation of carboxylate ions similar to that on ZnO was confirmed by IR techniques.[7] On the other hand, the interaction of oxygen with strongly adsorbed propylene on V_2O_5 led to little or no oxygen uptake, formation of water being observed at lower temperatures as compared to the cases of oxides such as Co_3O_4, ZnO, *etc.*[2] IR studies on Sn–Mo oxide[4] show that the interaction of oxygen with strongly adsorbed propylene causes formation of surface OH groups alone,

no surface carboxylate ions being observed. The results indicate that the behavior observed with the catalysts for complete oxidation, such as Co_3O_4 and ZnO, differs from that with the catalysts for selective oxidation, such as V_2O_5 and Sn–Mo oxide.

The results of oxidation of the propylene adsorbed are compared with those of the adsorption of olefins. Although there is a striking difference in the nature of propylene adsorbed on Co_3O_4 and ZnO, both exhibit a similar behavior in the oxidation of adsorbed propylene, *i.e.*, formation of carboxylate species with oxygen uptake occurs during the course of oxidation. Irrespective of a marked difference in the behavior of Co_3O_4 and V_2O_5 in the oxidation of adsorbed propylene, there seems little difference in the features of olefin adsorption, *e.g.*, for both oxides the amount of adsorbed ethylene remaining is roughly the same as the corresponding amount of propylene (Fig. 1).

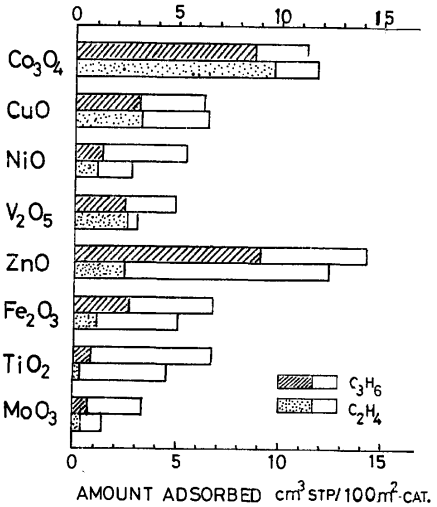

Fig. 1. Adsorption of propylene and ethylene on various oxides. Shaded parts show the fraction of the remaining amounts after evacuation. Temperature, 0 °C; Olefin pressure, 30 Torr (1 Torr=133.3 Pa); Adsorption time, 3 h.

Instead of propylene, acetone was adsorbed on NiO[8] and Sn–Mo oxide.[4] The oxidation of adsorbed acetone was carried out in a similar manner. Formation of surface carboxylate ions was observed for NiO, but not for Sn–Mo oxide. Essentially the same difference between the behavior of both oxides in the oxidation was observed as that with propylene adsorbed. It seems that the features of the oxidation of adsorbed propylene are not closely associated with its adsorbed state. Such a difference in the features of the oxidation could be attributed to the difference in the oxygen species responsible for oxidation.

Oxygen Species Responsible for Catalytic Oxidation.
A number of workers[9] have discussed the difference between the characteristics of the oxide catalysts for selective oxidation such as V_2O_5, MoO_3, and Bi–Mo oxide and for complete oxidation such as Co_3O_4, NiO, and Fe_2O_3 from the viewpoint of the type of metal–oxygen bonds.

The present paper is concerned with the relative roles of adsorbed and lattice oxygen in the oxidation on these oxide catalysts. The following experiments were carried out: The temperature of catalysts containing the strongly adsorbed propylene was raised stepwise in a vacuum, *i.e.*, desorption experiments were carried out. The amount of CO_2 formed during the course of temperature rise was compared with the corresponding amount in the presence of oxygen at 30 Torr. The results are shown by plots R *vs.* T, where R=(the amount of CO_2 formed during the temperature rise from 0 to T °C)/(the amount of propylene strongly adsorbed at 0 °C)$\times 3$.

In the case of Co_3O_4 the plots R *vs.* T in the presence of oxygen shift to a lower temperature by about 150 °C as compared with that in a vacuum, suggesting participation of adsorbed oxygen in the oxidation (Fig. 2). A similar behavior is observed with Fe_2O_3 (Fig. 3). On ZnO, most part of adsorbed propylene was removed in a vacuum without undergoing oxidation, in contrast

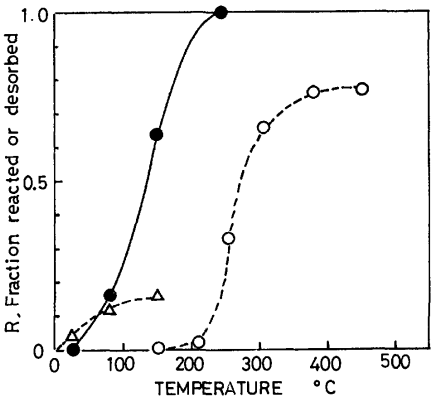

Fig. 2. Comparison of oxidation with desorption of propylene adsorbed on Co_3O_4.
—●—, CO_2 formed in the oxidation; ···○···, CO_2 formed in the desorption; —△—, C_3H_6 desorbed in the desorption. Experimental conditions in Figs. 2, 3, 4, and 5; Reaction time at each temperature in the oxidation, 3 h; oxygen pressure, 30 Torr; desorption time, 3 h; amounts of propylene adsorbed are shown in Fig. 1.

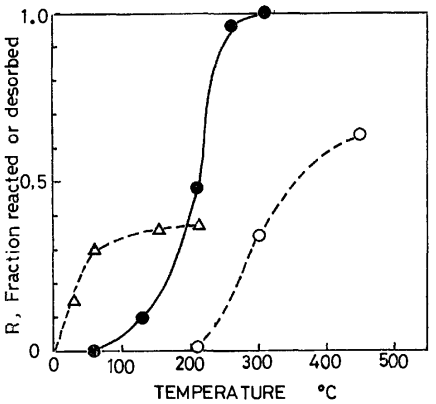

Fig. 3. Comparison of oxidation with desorption of propylene adsorbed on Fe_2O_3.
Symbols are the same as Fig. 2.

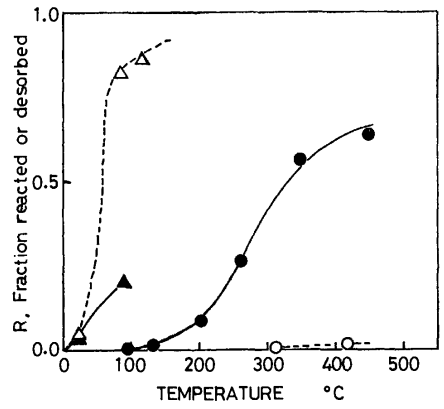

Fig. 4. Comparison of oxidation with desorption of propylene adsorbed on ZnO.
-▲-, C_3H_6 desorbed in the oxidation; other symbols are the same as Fig. 2.

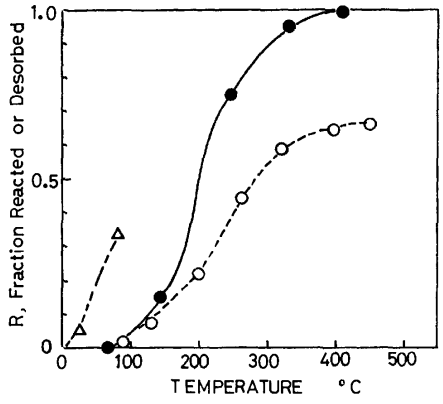

Fig. 5. Comparison of oxidation with desorption of propylene adsorbed on V_2O_5.
Symbols are the same as Fig. 2. Since in the case of V_2O_5 CO is formed in addition to CO_2, R values refer to formation of $CO+CO_2$. The amount of oxygen required for the oxidation of adsorbed propylene corresponded to about 30% of the surface oxygen layer.

with the case in the presence of oxygen where most part of adsorbed propylene was oxidized to CO_2 and H_2O (Fig. 4). Such a behavior suggests that surface lattice oxygen has no oxidizing power, *i.e.*, the oxidation proceeds *via* adsorbed oxygen alone.

For V_2O_5, the oxidation of adsorbed propylene in a vacuum occurs in about the same temperature range in the presence of oxygen (Fig. 5). The presence of gaseous oxygen has no effect on oxidation, *i.e.*, the surface lattice oxygen participates in the oxidation, in line with the conclusion reached by various workers.[10,11]

On the oxides which are effective for complete oxidation, active adsorbed oxygen is formed, which attacks olefins to form carboxylate ions, leading to the oxygen uptake by the catalysts. The absence of adsorbed oxygen on the catalysts for selective oxidation has been demonstrated by Seiyama,[14] who carried out the thermal desorption of oxygen adsorbed on various oxides. Haber and Grzybowska[15] reached similar conclusions from available data on the activity in oxygen isotopic exchange of various oxide catalysts. The general characteristic feature of the oxides effective for complete oxidation is that adsorbed oxygen plays a significant role in the oxidation because of its higher activity as compared with that of surface lattice oxygen.

References

1) Y. Kubokawa, T. Ono, and N. Yano, *J. Catal.*, **28**, 471 (1973).
2) T. Ono, T. Tomino, and Y. Kubokawa, *J. Catal.*, **31**, 167 (1973).
3) K. Hata, S. Kawasaki, Y. Kubokawa, and H. Miyata, *Proc. 6th Int. Cong. Catal.*, London, (1976), Vol. 2, p. 1102.
4) T. Ono and Y. Kubokawa, *J. Catal.*, **52**, 412 (1978).
5) A. L. Dent and R. J. Kokes, *J. Am. Chem. Soc.*, **92**, 6709, 6718 (1970).
6) S. V. Gerei, E. V. Rozhkova, and Ya. B. Gorokhovatsky, *J. Catal.*, **28**, 341 (1973).
7) S. Kawasaki, H. Miyata, and Y. Kubokawa, unpublished results.
8) H. Miyata, M. Wakamiya, and Y. Kubokawa, *J. Catal.*, **34**, 117 (1974).
9) E. R. S. Winter, *J. Chem. Soc., A*, **1968**, 2889; J. Novakova, *Catal. Rev.*, **4**, 77 (1971); F. Trifiro and I. Pasquon, *J. Catal.*, **12**, 412 (1968).
10) *E.g.*, K. Hirota, Y. Kera, and S. Teratani, *J. Phys. Chem.*, **72**, 3133 (1968); W. M. H. Sachtler, G. J. H. Dorgero, J. Fahrenfort, and R. J. H. Voorhoeve, *Proc. 4th Int. Cong. Catal.*, Moscow, (1968), Vol. 1, p. 454.
11) In the case of supported V_2O_5 catalysts, adsorbed oxygen participates in the oxidation of olefins.[12] A similar behavior has been observed with another group of catalysts for selective oxidation such as Ag_2O and Cu_2O. For Ag_2O, participation of adsorbed oxygen appears to be established.[13]
12) S. Yoshida, T. Matsuzaki, T. Kashiwazaki, K. Mori, and K. Tarama, *Bull. Chem. Soc. Jpn.*, **47**, 1564 (1974).
13) P. A. Kilty, N. C. Rol, and W. M. H. Sachtler, *Proc. 5th Int. Cong. Catal.*, Florida, (1972), Vol. 2, p. 929.
14) "Kinzoku-sankabutsu To Sono Shokubai-sayo," ed by T. Seiyama, Kodansha, Tokyo (1978), p. 169.
15) J. Haber and B. Grzybowska, *J. Catal.*, **28**, 489 (1973).

Ionic Motion and Phase Transition in Potassium Hydrogendifluoride KHF_2 Studied by Pulsed NMR

Yoshihiro FURUKAWA* and Hideko KIRIYAMA

The Institute of Scientific and Industrial Research, Osaka University, Yamadakami, Suita 565

(Received May 8, 1978)

Nuclear spin-lattice relaxation times, T_1 and $T_{1\rho}$, have been measured above room temperature for ^1H and ^{19}F nuclei in powdered KHF_2 and its deuterated analogue. Below 400 K and in the high-temperature β-phase (T_t=469.8 K), the magnetization recovery for both nuclei in KHF_2 is strongly non-exponential owing to the heteronuclear H–F interaction. In the low-temperature α-phase the T_1 *vs.* $1/T$ curves show broad minima ascribable to the 180°-flip motion of linear $[FHF]^-$ anions. The activation energy E_a of this motion was determined to be 50.5 ± 2 kJ/mol. The phase transition, which is defined by discontinuous changes in both T_1 and $T_{1\rho}$, is associated with diffusional disorder superimposed on rapid isotropic reorientation of the HF_2^- ion. The relaxational process in the β-phase is governed by self-diffusion of the anions with an E_a of 80 ± 6 kJ/mol deduced from the $T_{1\rho}$ data. In contrast to the earlier suggestion from electrical measurements, the NMR results indicate that the dominantly mobile species in the conducting high-temperature β-phase are not single F^- ions but complex $[FHF]^-$ anions.

Potassium hydrogendifluoride KHF_2 has been studied extensively by diffraction, spectroscopic and other physical methods, on account of its hydrogen bond forming unique difluoride ion $[F\cdots H\cdots F]^-$. In all cases, except for early infrared studies, the HF_2^- ion was found to be linear and centro-symmetric with an unusually short F–F distance of 2.29 Å.[1-6]

The compound KHF_2 is tetragonal with cell constants a=5.672, c=6.801 Å and Z=4 in the room-temperature α-phase.[3] The linear HF_2^- ions are arranged in planes (001). In these planes the $[FHF]^-$ ionic axes are directed alternately parallel to either [110] or [$\bar{1}$10]. At the transition temperature T_t (196.7 °C), the crystal transforms to the cubic β-phase. This is accompanied by large changes in volume and entropy, the cell constants being a=6.36 Å and Z=4.[1,7,8] In the high-temperature phase the F–F axis may orient parallel to any of the four body-diagonals [111] of the cubic cell with equal probability to attain higher symmetry. It seemed worthwhile to clarify whether such a disordered structure is dynamic or static by means of nuclear magnetic resonance (NMR) techniques.

Also of interest is the fact that the ionic conductivity of the compound increases sharply at T_t by about two orders of magnitude, when T_t is approached from a low temperature.[9,10] This strongly suggests that dynamical disorder or migration of ions takes place in the β-phase. Furthermore, electromotive force and electrolysis experiments show that the F^- ions contribute dominantly to the ionic conduction in the high-temperature phase.[11]

The purpose of this study is to determine the type of molecular motion associated with phase transition and ionic conduction by measuring proton and fluorine NMR relaxation times. Kriger *et al.* have reported the spin-lattice relaxation times, T_1, of KHF_2[12] and $CsHF_2$.[13] Our independent experiments, however, include a more detailed study of the temperature dependence of T_1 and the rotating-frame relaxation time, $T_{1\rho}$, in KHF_2 and its deuterated analogue. The results and discussion presented here disagree to some extent with those of Kriger *et al.*

Experimental

Commercial potassium hydrogendifluoride was twice recrystallized from water and dried over P_2O_5. Deuterated KDF_2 was prepared by repeated crystallization from saturated heavy-water solutions of the salt in a closed bottle. Polyethylene wares were used in order to avoid the reaction of HF acid with silicate glass. For the NMR measurement on the α-phase the powdered KHF_2 was placed in an 8 mm diam. glass tube, which was evacuated and then sealed. When the sample was kept below T_t for several days, the wall of the tube was hardly corroded at all by gaseous HF, but when the sample was transformed to the waxy β-phase, it became corroded at the contact surface. For the relaxation measurements on the β-phase, several pieces of single crystals with dimensions of about $4\times4\times1$ mm^3 were wrapped in Teflon tape and then sealed in a glass tube. It was thought that the use of Teflon would not interfere with the measurements since the ^{19}F FID (free induction decay) signal in the β-phase is long as compared with that in Teflon. Actually, the Teflon coated sample gave almost the same relaxation data as those of the sample coated with vacuum-pump-oil. The samples used were identified from the X-ray powder patterns at room temperature before and after NMR measurements. No extra diffraction peaks, especially those assignable to crystalline KF, were recognized after the sample had been heated at about 500 K for ten hours.

T_1 and $T_{1\rho}$ were measured with a Bruker pulsed NMR spectrometer B-KR 322s by the conventional methods. The Larmor frequencies were 20 and 18.814 MHz for ^1H and ^{19}F, respectively. Since the FID signal in the α-phase was very short, its height was obtained from the solid echo[14] and was averaged on a NIC 1074 signal averager. The sample temperature controlled within ±1 K was measured with a copper-constantan thermocouple.

Results and Discussion

The proton and fluorine relaxation times of KHF_2 are summarized in Fig. 1 as a semilogarithmic plot *versus* inverse temperature. Below 400 K the T_1 behavior for both nuclei was somewhat complicated by the presence of heteronuclear H–F interactions. In the region below the temperatures of the T_1 minima, the relaxations of ^1H and ^{19}F became markedly non-

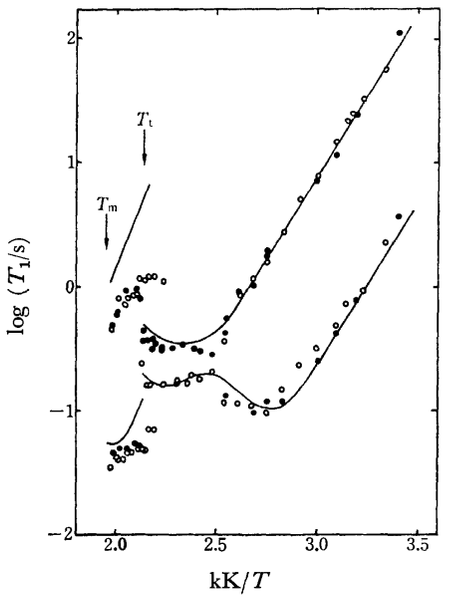

Fig. 1. Temperature dependences of the spin-lattice relaxation times, T_1, in KHF_2. ●: ^1H, ○: ^{19}F. Below 400 K and in the β-phase two components of T_1 are shown because of the non-exponential magnetization recovery. The solid lines in the α-phase are calculated on the basis of a model of 180°-flipping HF_2^- ions.

exponential. Each recovery curve of magnetization was manually resolved into two components, one of which (the short component) was characterized by a short relaxation time T_1', and the other by a long relaxation time T_1''.[15] As shown in Fig. 1, the relaxations for ^1H and ^{19}F have the same pair of T_1' and T_1'' below 400 K. On the other hand, at temperatures between 400 K and T_t (469.8 K), both relaxations are nearly exponential, the minimum value of $T_1(H)$ being about twice as long as that of $T_1(F)$. The results differ from those of Kriger *et al.*[12] as regards (1) the non-exponential behavior, (2) the absence of a temperature region in which $T_1(H)<T_1(F)$, and (3) the slope of log T_1 *vs.* $1/T$ curve in the high-temperature β-phase.

T_1 in the α-Phase of KHF_2. In this system, since the heteronuclear dipole interaction between ^1H and ^{19}F cannot be neglected, the observed relaxation rates of both nuclei are the eigenvalues of the following relaxation matrix:[15,16]

$$\begin{pmatrix} R_{HH}+R_{HF} & R_{HF}' \\ R_{FH}' & R_{FF}+R_{FH} \end{pmatrix} \quad (1)$$

The element R_{HF} represents the proton relaxation rate *via* the dipolar interaction between ^1H and ^{19}F spins. The relative magnitudes of these matrix elements are expected to govern the non-exponential behavior and the depths of the T_1 minima for ^1H and ^{19}F.[15]

$T_{1\,min}(F)<T_{1\,min}(H)$ indicates that $(R_{FF}+R_{FH})>(R_{HH}+R_{HF})$, suggesting that the two-fold reorientation or 180° flip of HF_2^- ions takes place rapidly in the α-phase. Look and Lowe derived a formula for the relaxation rate of flipping water molecules in a hydrated single crystal.[17] It is also applicable to R_{FF} in the case of 180°-flipping HF_2^- ions. Thus, we obtain

$$R_{FF}=\frac{3\gamma_F^4\hbar^2I_F(I_F+1)}{16N}\sum_{i\neq j}\left[\eta_{ij}^1\frac{\tau_f}{1+0.25\omega_{0F}^2\tau_f^2}+(2\xi_{ij}^1+\eta_{ij}^2)\frac{\tau_f}{1+\omega_{0F}^2\tau_f^2}+2\xi_{ij}^2\frac{\tau_f}{1+4\omega_{0F}^2\tau_f^2}\right], \quad (2a)$$

$$\eta_{ij}^q=\frac{1}{2}|\chi_{ij}^q(\beta\beta)+\chi_{ij}^q(\delta\delta)-\chi_{ij}^q(\beta\delta)-\chi_{ij}^q(\delta\beta)|^2, \quad (2b)$$

$$\xi_{ij}^q=|\chi_{ij}^q(\beta\beta)-\chi_{ij}^q(\delta\delta)|^2+|\chi_{ij}^q(\beta\delta)-\chi_{ij}^q(\delta\beta)|^2, \quad (2c)$$

where the symbols are those of Look and Lowe.[17] Since our sample was powdered, Eq. 2 was used after spatial averaging.[18]

On the other hand, the relaxation rate due to the heteronuclear H–F interactions was derived for a flipping model, in which the central H atom is fixed and each terminal F atom jumps between two equilibrium lattice sites. Only its spatially averaged form is presented here:

$$R_{HF}=\gamma_H^2\gamma_F^2\hbar^2/40\sum_F[r_{HF}(\beta)^{-6}+r_{HF}(\delta)^{-6}-r_{HF}(\beta)^{-3}r_{HF}(\delta)^{-3}\times(3\cos^2\Delta_{\beta\delta}-1)]g(\omega_{0H},\omega_{0F},\tau_f), \quad (3a)$$

$$R_{HF}'=\gamma_H^2\gamma_F^2\hbar^2/40\sum_F[r_{HF}(\beta)^{-6}+r_{HF}(\delta)^{-6}-r_{HF}(\beta)^{-3}r_{HF}(\delta)^{-3}\times(3\cos^2\Delta_{\beta\delta}-1)]g'(\omega_{0H},\omega_{0F},\tau_f), \quad (3b)$$

$$g(\omega_{0H},\omega_{0F},\tau_f)=\frac{\tau_f}{1+(\omega_{0H}-\omega_{0F})^2\tau_f^2}+\frac{3\tau_f}{1+\omega_{0H}^2\tau_f^2}+\frac{6\tau_f}{1+(\omega_{0H}+\omega_{0F})^2\tau_f^2}, \quad (3c)$$

$$g'(\omega_{0H},\omega_{0F},\tau_f)=-\frac{\tau_f}{1+(\omega_{0H}-\omega_{0F})^2\tau_f^2}+\frac{6\tau_f}{1+(\omega_{0H}+\omega_{0F})^2\tau_f^2}. \quad (3d)$$

Symbols β and δ denote the two possible sites for a given F atom and $\Delta_{\beta\delta}$ the angle between two H–F vectors of $r_{HF}(\beta)$ and $r_{HF}(\delta)$. It can readily be shown from the atomic arrangements that $R_{HH}=0$, whereas the other components are $R_{FH}=(1/2)R_{HF}$ and $R_{FH}'=(1/2)R_{HF}'$.[16]

The summation was taken over 14 neighboring HF_2^- ions about a central HF_2^- ion in Eq. 2, and over 6 neighbors in Eq. 3, within the tetragonal structure. Diagonalizing Eqs. 1—3 and using the Arrhenius relation, we can calculate the temperature dependences of $T_1(H)$ and $T_1(F)$. Simulated T_1 curves are represented by the solid lines in Fig. 1, with an activation energy E_a of 50.5 kJ/mol deduced from the linear region on the low-temperature side of the $T_{1\,min}$. Agreement between the observed and calculated $T_{1\,min}$ values indicates that the 180°-flip motion of the $[FHF]^-$ ion is responsible for the T_1 process in the α-phase. On the low-temperature side of $T_{1\,min}$, the off-diagonal elements in the relaxation matrix become comparable in magnitude with the diagonal elements, as anticipated from the non-exponential behavior. On the other hand, above and near the temperature of $T_{1\,min}$ both relaxations for ^1H and ^{19}F are exponential, since the off-diagonal elements can be neglected in comparison with the diagonal elements. The 180°-flip motion of linear $[FHF]^-$ ions was also found in $CsHF_2$.[13] The activation energy E_a of 50.5 kJ/mol for KHF_2 is much larger than that of 14.9 kJ/mol for $CsHF_2$. The room-temperature phase of $CsHF_2$ (T_t=61 °C) is isomorphous with

the α-phase of KHF_2, but the cell dimensions of the former are appreciably larger than those of the latter. Thus, the difference in E_a is attributable primarily to the cation-size effect.

T_1 and $T_{1\rho}$ in the β-Phase of KHF_2. At the phase transition both T_1 and $T_{1\rho}$ change abruptly, the FID signals of ^1H and ^{19}F becoming very long as in a liquid above T_t. The T_2 value defined as the time necessary for the FID to fall to 1/e of its initial value is of the order of a millisecond, demonstrating that the HF_2^- ions are very mobile. Thus, the static disordered model is excluded in view of motional narrowing. The T_1 and $T_{1\rho}$ data for the β-phase are given in Fig. 2 against an expanded scale of inverse temperature. The magnetization recovery for the T_1 process again becomes non-exponential, but not that for the $T_{1\rho}$ process. This is in line with the positive and negative slopes of the T_1 and $T_{1\rho}$ *vs.* $1/T$ curves, respectively. As shown in Fig. 2, the β-phase was often supercooled down to 445 K, some indication on the $T_{1\rho}$ minimum being recognized in the supercooled region.

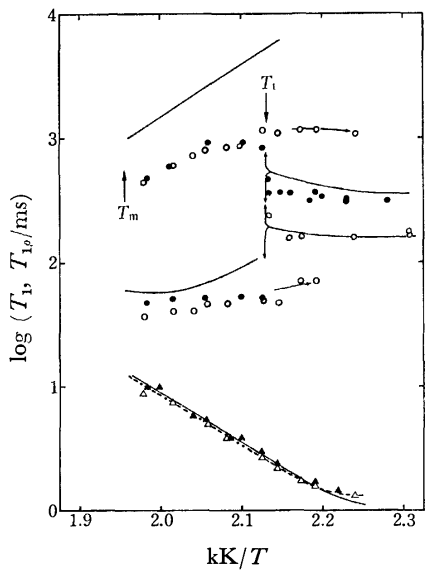

Fig. 2. The T_1 and $T_{1\rho}$ in the β-phase of KHF_2, plotted against an expanded scale of inverse temperature. ●: ^1H T_1, ○: ^{19}F T_1, ▲: ^1H $T_{1\rho}$ (H_1=10 G), △: ^{19}F $T_{1\rho}$ (H_1=10.6 G). The solid and broken lines represent the calculated ^1H and ^{19}F $T_{1\rho}$ curves, respectively. The self-diffusion of the HF_2^- ions is assumed. The phase transition and thermal hysteresis are indicated by arrows.

The dominant relaxation mechanism in the high-temperature phase cannot be assigned to isotropic reorientation of HF_2^- ions, since the experimental second moments estimated from the FID shapes are much smaller than the calculated ones for this model. The primary process is ascribable to the self-diffusion of HF_2^- ions. The rate of process is usually calculated by means of correlation functions derived and tabulated by Torrey[19] and Sholl.[20] Their derivations involve only the homonuclear dipole interactions for a random walk model, where jumping motion occurs between the nearest-neighbor sites. In the case of KHF_2, however, the interactions are complicated since they include the heteronuclear H–F as well as the H–H and F–F interactions, the magnitudes of which are comparable.

For the sake of simplicity, we start from an approximate expression to analyze the relaxation and correlation times for the diffusion process. In the temperature region where $T_1 > T_{1\rho}$, the $T_{1\rho}$ can be approximated by the following equation:[15]

$$T_{1\rho}(\mathrm{I})^{-1} = \frac{2}{3}\gamma_I^2 M_{II}\left(\frac{3}{2}\frac{\tau_d}{1+4\omega_{1I}^2\tau_d^2}\right) + \frac{1}{2}\gamma_I^2 M_{IS}\left\{\frac{2\tau_d}{1+\omega_{1I}^2\tau_d^2}+\frac{1}{2}\frac{\tau_d}{1+(\omega_{0I}-\omega_{0S})^2\tau_d^2}\right\}, \quad (4)$$

where subscripts I and S stand for H and F or *vice versa*, and M_{IS} is the second moment of the I-spin absorption spectrum due to I–S dipolar interaction prior to diffusional narrowing.

The motion of a linear $[FHF]^-$ ion would be expected to be thermally activated in the sequence of the 180° flip, the isotropic reorientation, and the diffusion with an increase in temperature. In the present case, however, the reorientational motion could not be separated from the other motions; it was probably prevented by the occurrence of the phase transition. On this supposition the values of the second moments in Eq. 4 were taken as those calculated for the rapid isotropic reorientation of the HF_2^- ions. The second moments were estimated on the basis of the NaCl-type structure of the β-phase and using the approximation that the two fluorine atoms of each HF_2^- ion are effectively located at the center of the ion; they are M_{HH}=0.626, M_{HF}=0.491, M_{FF}=1.105, and M_{FH}=0.278 G^2.

By substituting these values into Eq. 4 and by taking an activation energy of 80 kJ/mol from the experimental $T_{1\rho}$ *vs.* $1/T$ curve, the temperature dependence of the ^1H and ^{19}F $T_{1\rho}$'s was simulated. The results together with the corresponding T_1' and T_1'' are shown in Fig. 2. The agreement between the calculated and experimental curves for both $T_{1\rho}$'s supports the relaxation model used in the present analysis. On the other hand, the experimental curves for T_1' and T_1'' are significantly depressed from the calculated ones; the departure increases with decreasing temperature in the β-phase. This indicates that the rapid reorientation and the slow diffusional motion are superposed in this region. The correlation time for the reorientation is roughly estimated to be 10^{-12} s at the transition point. The motional parameters are summarized in Table 1.

Table 1. Summary of relaxational parameters

Phase	E_a/(kJ mol^{-1})	τ_0/s	Motion
α-Phase	50.5±2	6.4×10^{-15}	180° flip
β-Phase	80 ±6	5×10^{-16}	diffusion

T_1 and $T_{1\rho}$ in KDF_2. In order to confirm the relaxation mechanism, the T_1 and $T_{1\rho}$ of ^{19}F were measured on deuterated KDF_2 (Fig. 3). Since the isotope exchange of ^1H with ^2H nuclei almost extinguishes the heteronuclear dipole interaction, the relaxa-

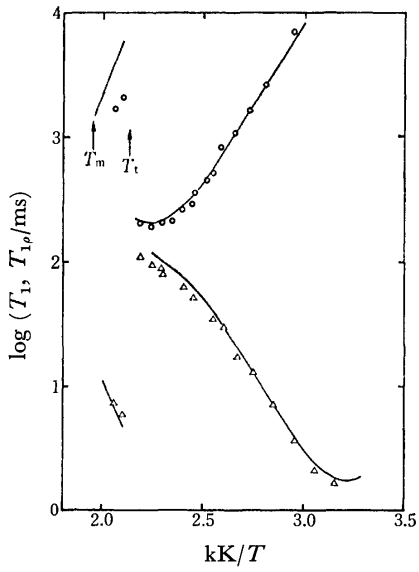

Fig. 3. Temperature dependences of T_1 and $T_{1\rho}$ for ^{19}F in KDF_2 ($H_1=10.6$ G). The solid lines represent the expected dependences based on relaxation processes similar to those in KHF_2 (see text).

tion becomes exponential for all temperatures studied. The T_1 value in the α-phase of KDF_2 is nearly equal to the long component T_1'' (Fig. 1). The $T_{1\,min}$ value is only 1.2 times that for ^{19}F in KHF_2. This shows that the T_1'' in KHF_2 is mainly due to the F–F dipolar interaction; of course both are modulated by 180°-flipping of the HF_2^- ion. Therefore, the T_1 and $T_{1\rho}$ values were calculated from Eq. 2 and the corresponding formulae derived by Look and Lowe,[17] respectively, using the same values as those found in KHF_2, except $\tau_0=7\times10^{-15}$ s. The results are shown by solid lines in Fig. 3. Agreement between the calculated and experimental T_1 and $T_{1\rho}$ curves furnishes additional evidence for the relaxation due to the flipping of the HF_2^- ion.

On the other hand, the ^{19}F relaxation times in the β-phase of KDF_2 were markedly affected by the isotope exchange, *viz.*, $T_1(KDF_2)\approx2\times T_1''(KHF_2)$ and $T_{1\rho}(KDF_2)\approx2\times T_{1\rho}(KHF_2)$. The calculation based on Eq. 4, taking $M_{FH}=0$, supports the results. However, the absolute value of the ^{19}F T_1 in the β-phase is in poor agreement with the experimental one, possibly for the same reason as that for KHF_2.

Phase Transition. At the phase transition the relaxation times change discontinuously with accompanying thermal hysteresis. This suggests a first-order phase transition. The compounds containing linear XY_2^- ions are often transformed into cubic phases at high temperatures. The azides of rubidium and caesium have the same structure as that of KHF_2 at room temperature, *viz.*, a tetragonally distorted CsCl-type structure with space group I4/mcm. On heating, the azides undergo phase transitions to cubic Pm3m phases.[21] Such I4/mcm-Pm3m transition involves a small displacement of the anion. The transition entropies of 7.9 for Rb- and 7.5 J/(K mol) for Cs-azides were interpreted in terms of random orienting N_3^- ions parallel to three cube-edges. Caesium hydrogendifluoride also shows an I4/mcm-Pm3m transition having a transition entropy of 8.4 J/(K mol), which is nearly equal to the expected $R\ln3$.[22]

On the other hand, the phase transition of KHF_2 is somewhat different from those described above. The high-temperature β-phase has an NaCl-type structure with space group Fm3m, and the HF_2^- ions are directed at random along four body-diagonals. The I4/mcm-Fm3m transition is associated with a large ionic displacement as well as disordering of the HF_2^- ions, as evidenced from the large increase in volume at the transition point.[8] The present NMR study on KHF_2 and KDF_2 suggests that the rapid flip motion triggers the phase transition and the spherical reorientation of the linear HF_2^- ion causes the symmetry of the anion to be effectively cubic in the β-phase. However, the diffusive motion of the HF_2^- ion can also be correlated with the I4/mcm-Fm3m transition, since the transition entropy of 23.8 J/(K mol),[7] is much larger than $R\ln4$ expected for pure orientational disorder in the β-phase.

Mobile Ions in the β-Phase. A number of hydrogen-bonded crystals have been studied as proton conductors with special interest centering on the identity of charge carriers and the mechanism of ionic migration.[23] The ionic conduction in KHF_2, where the hydrogen atom is located inside an isolated anion, becomes substantial only in the high-temperature β-phase. Bruinink and Kosmeijer determined the ionic transport numbers from changes in chemical composition on electrolysis as follows: $t_F\approx0.75$, $t_K\approx0.25$, and $t_H\approx0$ in the β-phase, while $t_H\approx1$ in the α-phase.[11] They explained the relatively high conductivity in the β-phase in terms of the migration of F^- (and to a smaller extent K^+) ions but not of H^+ ions.

The results of ^1H and ^{19}F T_1 are evidence for self-diffusion of the ions in the conducting β-phase, affording valuable information on the mobile ion-species. If the hydrogen ions are essentially immobile in this phase, as suggested from the electrolysis experiments, then the calculated $T_{1\rho}$ for ^1H should be about two times that for ^{19}F except near the $T_{1\rho}(H)$ minimum. The estimation is not compatible with the observation that $T_{1\rho}(H)\approx T_{1\rho}(F)$. Thus, the HF_2^- ion diffuses as a whole; at least H^+ and F^- ions move with almost equal correlation times, which is not in agreement with the results of electrolysis. On the other hand, the activation energy (80 kJ/mol) for the self-diffusion found from the NMR study is in fairly good agreement with the value of 86 kJ/mol deduced from the electric conductivity measurements.[10] Both values are much smaller than the hydrogen-bond energy, 240 kJ/mol, estimated for $[F\cdots H\cdots F]^-$ ions.[24] It can be concluded that the most mobile charge carriers in the conducting high-temperature β-phase are not single F^- ions but complex $[FHF]^-$ anions.

The authors are grateful to Professor Emeritus Ryôiti Kiriyama for his continued interest and stimulating discussions. This work was partly supported by a Grant-in-Aid for Scientific Research from the Ministry of Education (No. 047076).

References

1) R. Kruh, K. Fuwa, and T. E. McEver, *J. Am. Chem. Soc.*, **78**, 4256 (1956).
2) J. A. Ibers, *J. Chem. Phys.*, **40**, 402 (1964).
3) H. L. Carrell and J. Donohue, *Israel J. Chem.*, **10**, 195 (1972).
4) J. S. Waugh, F. B. Humphrey, and D. M. Yost, *J. Phys. Chem.*, **57**, 486 (1953).
5) J. C. Pratt and J. A. S. Smith, *J. Chem. Soc., Faraday Trans. 2*, **71**, 596 (1975).
6) P. Van Hecke, H. W. Spiess, and V. Haeberlen, *J. Magn. Reson.*, **22**, 93 (1976).
7) M. L. Davis and E. F. Westrum, Jr., *J. Am. Chem. Soc.*, **65**, 338 (1961).
8) R. W. Fink and E. F. Westrum, Jr., *J. Phys. Chem.*, **60**, 800 (1956).
9) J. M. Pollock and M. Sharan, *J. Chem. Phys.*, **47**, 4064 (1967).
10) J. Bruinink and G. H. J. Broers, *J. Phys. Chem. Solids*, **33**, 1713 (1972).
11) J. Bruinink and B. Kosmeijer, *J. Phys. Chem. Solids*, **34**, 897 (1973).
12) Yu. G. Kriger, N. K. Moroz, and S. P. Gabuda, *Fiz. Tverd. Tela*, **18**, 891 (1976) [*Sov. Phys. Solid State*, **18**, 514 (1976)].
13) Yu. G. Kriger, S. P. Gabuda, and N. K. Moroz, *Fiz, Tverd. Tela*, **17**, 3420 (1975) [*Sov. Phys. Solid State*, **17**, 2239 (1976)].
14) J. G. Powles and J. H. Strange, *Proc. Phys. Soc.*, **82**, 6 (1963).
15) D. E. O'Reilly, E. M. Peterson, and T. Tsang, *Phys. Rev.*, **160**, 333 (1967).
16) A. Abragam, "The Principles of Nuclear Magnetism," Oxford Univ. Press, (1961), Chap. 8.
17) D. C. Look and I. J. Lowe, *J. Chem. Phys.*, **44**, 2995 (1966).
18) K. Sagisawa, H. Kiriyama, and R. Kiriyama, *Bull. Chem. Soc. Jpn.*, **51**, 1942 (1978).
19) H. C. Torrey, *Phys. Rev.*, **92**, 962 (1953); **96**, 690 (1954).
20) C. A. Sholl, *J. Phys. C*, **7**, 3378 (1974); **8**, 1737 (1975); W. A. Barton and C. A. Sholl, *ibid.*, **9**, 4315 (1976).
21) H. J. Mueller and J. A. Joebstl, *Z. Kristallogr., Kristallgeom., Kristallphys., Kristallchem.*, **121**, S385 (1965).
22) A. J. C. White and C. W. F. T. Pistorius, *J. Chem. Phys.*, **56**, 4318 (1972).
23) L. Glasser, *Chem. Rev.*, **75**, 21 (1975).
24) T. C. Waddington, *Trans. Faraday Soc.*, **54**, 25 (1958); W. Van Gool, J. Bruinink, and P. H. Bottelberghs, *J. Inorg. Nucl. Chem.*, **34**, 3631 (1972).

An Analysis of the Through-bond Interaction Using the Localized Molecular Orbitals. I. Interactions between Lone-pair Orbitals in Azines: Pyridazine, Pyrimidine, and Pyrazine

Masaru OHSAKU, Akira IMAMURA,*,† and Kimihiko HIRAO†

Department of Chemistry, Faculty of Science, Hiroshima University, Higashisenda-machi, Hiroshima 730
† *Department of Chemistry, Shiga University of Medical Science, Setatsukinowa-cho, Otsu, Shiga 520-21*

(Received May 11, 1978)

The CNDO/2 and INDO calculations were performed on three azines: pyridazine, pyrimidine, and pyrazine. In order to check the validity of the lone-pair orbital energies, the calculated orbital energies were compared with those obtained by *ab initio* calculations. These molecules have two lone-pairs, which can be transformed into symmetric and antisymmetric combinations. In pyridazine and pyrimidine, the symmetric one is lower than the antisymmetric one in energy, while in pyrazine the reverse is true. These results were subjected to an analysis from the standpoint of the through-bond interaction. That is, we transformed the canonical molecular orbitals obtained by the CNDO/2 method into localized molecular orbitals. By the use of the localized molecular orbitals thus obtained, the variation in the lone-pair orbital energies of these molecules was estimated in terms of the through-bond (and/or the through space) interaction according to a method which selectively considered the particular interaction between the specified localized molecular orbitals in a molecule. As a result of this analysis, it was found that the relative order of the lone-pair orbital energies was determined by the different types of interactions from molecule to molecule, and the energy variation in the lone-pair orbitals was elucidated in terms of the specified through-bond and through-space interactions.

From the early days of the molecular orbital theory, such azines as pyridazine, pyrimidine, and pyrazine have been studied. Most of the previous works were examined by the semi-empirical methods.[1] Recently, *ab initio* molecular orbital methods have also been applied to these molecules.[2]

These molecules are characterized by their two lone-pair orbitals (LPO). These two LPO should be classified into symmetric and antisymmetric combinations on the basis of their symmetry properties. Hoffmann and his coworkers attempted to explain the separation between two lone-pair orbital energies (LPOE)[3] generally in terms of the "through-space" and the "through-bond" interactions in the cases of benzyne and its related compounds.[4] Many researches in this direction have been reported. However, the explicit calculations of the through-bond interactions have never been carried out, although data have been accumulated for the through-space interactions.[5] In the present article, we attempted to evaluate quantitatively the through-bond interactions by using the localized molecular orbitals (LMO) transformed from the canonical molecular orbitals (CMO). There is an advantage for chemists to understanding chemical phenomena in using the LMO- rather than the usual CMO-bases wave function, since the LMO can often be chosen so as to be localized in a certain space region, whereas the CMO are delocalized in most cases.

There are two LPO, n_1 and n_2, in the molecules treated here. These two LPO n_1 and n_2 can be classified into a symmetric or an antisymmetric combination from their symmetry properties, as was mentioned in the previous paragraph. There is an interest in the order of these LPOE, since there are intimate relations between this order and the assignments of the ionization potentials (IP's) and the $n\rightarrow\pi^*$ transition in the photoelectron or absorption spectra. For the IP's and the spectra of these molecules, there are many references available.[6] In connection with this, the order of the LPOE is different from molecule to molecule. Therefore, we have investigated the dominant factors in determining the order of the LPOE by using the LMO; that is, the order of the LPOE was successfully explained in terms of the through-space and the specified through-bond interactions.

Method of Calculations

There are fifteen occupied orbitals in the azines now under consideration. Among them, three are π-molecular orbitals. As a result, twelve occupied σ-orbitals were localized by minimizing the off-diagonal exchange energy according to the procedure of Edmiston-Ruedenberg.[7] The occupied π and all of the virtual orbitals were not transformed into the LMO. The original CMO were obtained from the CNDO/2

TABLE 1. NUCLEAR COORDINATES (in Å units) OF THE AZINES

		x	y	z
Pyridazine[a]	N	0	±0.665	0
	C	−1.18236	±1.32	0
	C	−2.41	±0.6875	0
	H	−1.16619	±2.40988	0
	H	−3.29671	±1.24986	0
Pyrimidine[b]	N	±1.182650	0.668858	0
	C	0	1.243153	0
	C	±1.165980	−0.668858	0
	C	0	−1.393466	0
	H	0	2.293153	0
	H	±2.080520	−1.184725	0
	H	0	−2.443466	0
Pyrazine[c]	N	0	0	±1.404814
	C	0	±1.125714	±0.689018
	H	0	±2.032340	±1.218801

a) From Ref. 6c. b) Recalculated in the light of Ref. 10. c) From Ref. 2c.

calculations,[8] since an *ab initio* calculation consumes a lot of computation time. The INDO calculations[9] were also carried out in order to compare the order of the LPOE with the *ab initio* one. The atomic coordinates used are summarized in Table 1.[2c,6c,10]

Pyridazime, pyrimidine, and pyrazine belong to the C_{2v}, C_{2v}, and D_{2h} point groups respectively. In order to express the symmetric character of the LPO, only the two-fold axis, which bisects the LPO and interchanges n_1 and n_2 with the symmetry operation, is used. The two symbols, S(Symmetric) and A(Antisymmetric), are named according to their symmetry properties in terms of the transformation around the two-fold axis.

When there is no interaction between n_1 and n_2, the two LPOE should be equal. If there are some interactions between them, S and A should be separated into two different energy levels; the separation width $\Delta = |E(S)-E(A)|$ expresses the magnitude of the interactions between them.

Now we will attempt to explain the procedure for estimating the effect of a particular through-bond interaction in the molecule. For the purpose of this procedure, the atomic orbital, χ_r, is represented by a linear combination of the LMO in the CNDO or INDO approximation, as is shown below. That is, the LMO, ϕ_i, is given by

$$\phi_i = \sum_s c_{is}\chi_s. \tag{1}$$

Equation 1 is multiplied by the coefficient, c_{ir}, for all the i and the equations are added:

$$\sum_i c_{ir}\phi_i = \sum_i c_{ir}\sum_s c_{is}\chi_s = \sum_s \chi_s \sum_i c_{ir}c_{is} = \sum_s \chi_s \delta_{rs}. \tag{2}$$

Thus,

$$\chi_r = \sum_i c_{ir}\phi_i. \tag{3}$$

By using Eq. 3, we can represent a core resonance integral between atomic orbitals, χ_r and χ_s, as the summation of the core resonance integrals between the LMO, ϕ_i and ϕ_j:

$$I^\circ_{rs} = \int \chi_r h^\circ \chi_s d\tau = \sum_i \sum_j c_{ir}c_{js}\int \phi_i h^\circ \phi_j d\tau = \sum_i \sum_j c_{ir}c_{js}I_{ij}, \tag{4}$$

where I°_{rs} and I_{ij} are the core resonance integral between the atomic orbitals, χ_r and χ_s, and that between the LMO, ϕ_i, and ϕ_j, respectively, and where h° denotes a one-electron Hamiltonian. By modifying Eq. 4, we can obtain the value of the core resonance integral between the atomic orbitals which gives zero for the core resonance integrals between the specified LMO, and which gives the core resonance integral between the other LMO correctly. That is,

$$I_{rs} = I^\circ_{rs} - \sum_{(i_1-j_1)} (c_{i_1,r}c_{j_1,s} + c_{i_1,s}c_{j_1,r})I_{i_1,j_1}, \tag{5}$$

where $(i_1\text{-}j_1)$ means that the summation should cover only definite pairs of the specified LMO. It can easily be proved that the core resonance integral, I_{rs}, obtained by Eq. 5 gives zero for the core resonance integral between the specified LMO, $I_{i_1j_1}$, and the correct values for the others as is shown below.

$$\begin{aligned} I'_{ij} &= \sum_r \sum_s c_{ir}c_{js}\int \chi_r h^\circ \chi_s d\tau = \sum_r \sum_s c_{ir}c_{js}I_{rs} \\ &= \sum_r \sum_s c_{ir}c_{js}I^\circ_{rs} - \sum_r \sum_s c_{ir}c_{js}\sum_{(i_1-j_1)} (c_{i_1,r}c_{j_1,s} \\ &\quad + c_{i_1,s}c_{j_1,r})I_{i_1,j_1} \\ &= I_{ij} - \sum_{(i_1-j_1)} I_{i_1,j_1}[(\sum_r c_{ir}c_{i_1,r})(\sum_s c_{js}c_{j_1,s}) \\ &\quad + (\sum_r c_{ir}c_{j_1,r})(\sum_s c_{js}c_{i_1,s})] \\ &= I_{ij} - \sum_{(i_1-j_1)} I_{i_1,j_1}(\delta_{ii_1}\delta_{jj_1} + \delta_{ij_1}\delta_{ji_1}), \\ &\begin{cases} = 0 & (i = i_1,\ j = j_1 \text{ or } i = j_1,\ j = i_1) \\ = I_{ij} & (\text{otherwise}). \end{cases} \end{aligned} \tag{6}$$

Equation 6 indicates that I'_{ij} is equal to zero when $i = i_1$, $j = j_1$, or $i = j_1$, $j = i_1$, and is equal to the correct value otherwise. Consequently, when the LMO, ϕ_i and ϕ_j, which specified the bonds i and j, are picked up in Eq. 5, the core resonance integral between ϕ_i and ϕ_j should be cut off; that is, the through-bond interaction between the bonds i and j can be considered to be cut off.[11] Thus, the SCF calculations using the core resonance integrals in Eq. 5 give the total energy without the appropriate through-bond interactions. The difference between the total energies calculated with and without the specified through-bond interactions should be a measure of the specified through-bond interactions.[12]

Previously, in order to describe the π-hyperconjugative interactions, the through-space and the through-bond interactions were treated separately by removing the core resonance integrals by the use of the semi-empirical method;[5] the present procedure is the first attempt to analyze the LPO interactions including a σ-system quantitatively.

Results and Discussion

The LPOE of these molecules, as calculated by the CNDO/2 and INDO methods, together with an *ab initio* calculation,[2f] are summarized in Table 2. From this table we can see that the order of S and A, and the separation width between them as calculated by the semi-empirical method, correspond with the results of the *ab initio* calculations. The tendencies of the separation width between S and A are also very similar to each other in the cases of the semi-empirical and non-empirical methods. Therefore, we can recognize that

Table 2. Orbital energies (au) for the lone-pairs in the azines[a]

		CNDO/2	INDO	*ab initio*[b]
Pyridazine		−0.5091 S	−0.4732 S	−0.4727 S
		−0.4705 A	−0.4036 A	−0.3919 A
	Δ	0.0386	0.0696	0.0808
Pyrimidine		−0.5075 S	−0.4676 S	−0.4621 S
		−0.4689 A	−0.4139 A	−0.4039 A
	Δ	0.0386	0.0537	0.0582
Pyrazine		−0.6128 A	−0.5362 A	−0.4900 A
		−0.4582 S	−0.3996 S	−0.3953 S
	Δ	0.1546	0.1366	0.0947

a) S: Symmetric; A: Antisymmetric; $\Delta = |E(S)-E(A)|$.
b) From Ref. 2f.

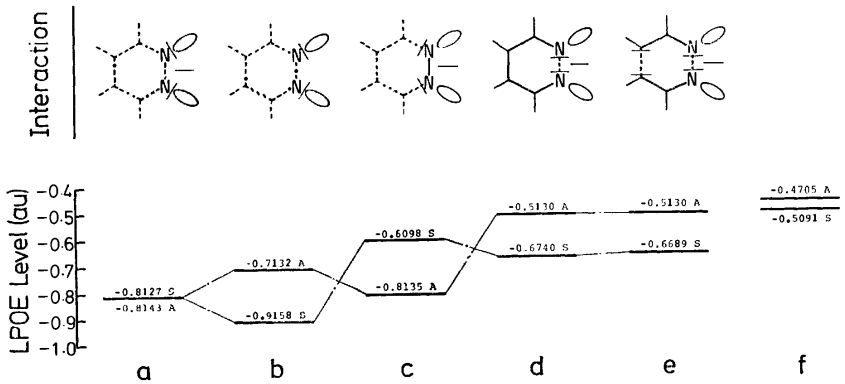

Fig. 1. LPO interaction diagram for pyridazine.
a: LPO are "cut off", **b**: LPO are "cut off" and N···N direct-through space interaction is allowed, **c**: short path is allowed, **d**: long path is allowed, **e**: short path is "cut off" and long path is "cut off" at the C–C bond parallel to the N–N bond, **f**: CMO level.

the semi-empirical method used here is sufficient to explain the energy variation in the LPOE or the change in the symmetry property of the LPO in these molecules.

Figure 1 shows the variation in the LPO energy levels of pyridazine.

a. When both LPO n_1 and n_2 were cut off from the interactions, S and A go to considerably lower energy levels. In this case, the N···N direct through-space interaction is not allowed. From the LPOE we can see that there is no interaction between n_1 and n_2.

b. Then the N···N direct through-space interaction was added to the **a** state; under these circumstances, A goes up about 0.1 au, while S lowers. This gives the magnitude of the direct through-space interaction between the LPO.

c. When the through-bond interaction *via* the N–N direct path (short path) was taken into consideration, S was found to go drastically up, but A scarcely varies from the **a** state. From the consideration of the orbital symmetry, it seems that this type of through-bond interaction does not have any effect on the energy level of A, as has already been pointed out by Hoffmann *et al.*[4]

d. When the interaction through the path N–C–C–C–C–N (long path) is taken into consideration, A goes up to around the CMO level, but S does not. The order of S and A is reversed from the **c** state.

e. In addition to the **d** state, the long path is cut off at the C–C bond parallel to the N–N bond; both S and A levels scarcely vary from the **d** state. Accordingly, it is obvious that the LPOE in the **d** state are not due merely to the through-bond interaction, but to a combination of the through-bond and through-space interactions, as will be discussed later in detail.

Figure 2 shows the variation in the LPO energy levels of pyrimidine.

a. Two LPO, n_1 and n_2, were cut off from the interactions; when this happens the energy levels of the LPO go lower, and S and A degenerate.

b. When we added the N···N direct through-space interaction to the **a** state, there were no variations in the energies of S and A from the **a** state. This shows that the N···N direct through-space interaction between two N atoms at the meta-position is almost zero. The same is true in pyrazine, as will be shown later.

c. Only the short path is allowed; S and A go upper,

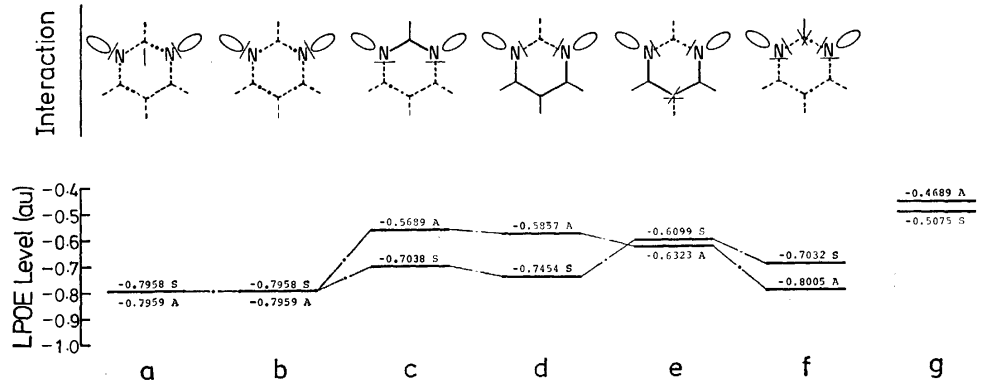

Fig. 2. LPO interaction diagram for pyrimidine.
a: LPO are "cut off", **b**: LPO are "cut off" and N···N direct through-space interaction is allowed, **c**: short path is allowed, **d**: long path is allowed, **e**: short path is "cut off" and long path is "cut off" at its central point, moreover C–H bond bonded at this point is "cut off", **f**: long path is "cut off" and short path is "cut off", but one C–H interaction with two LPO in the short path is allowed, **g**: CMO level.

but the variation is larger in A than in S. Therefore, it is noteworthy that the present situation is quite different from that in pyridazine.

d. The long path is allowed; both S and A vary from the **b** state. However, the variation in this case is less than that of the **c** state. One of the differences between the **c** and **d** states may be a result of the difference of the through-bond interactions *via* two and four bonds.

e. The short path is cut off, and the long path is cut off at its central point; moreover, the C–H bond combined at this point is cut off from the interactions. With this state, A goes lower than the **d** state, but S goes up. The energy difference between S and A becomes fairly small, and the order of S and A is reversed from the **d** state. From the **d** and **e** states, it is obvious that the energy variation in the LPO of the **e** state from the **d** state is caused by the through-bond interaction itself. This situation is also quite different from that of the **d** and **e** states in pyridazine.

f. The long path is cut off, as is the short path, but in the short path one C–H interaction is allowed. Therefore, in this state, only the through-space interaction between the two LPO (indirect through-space interaction) is allowed *via* the central C–H bond. With this interaction, S goes up from the **b** state; this new S level is nearly the same in energy as that of the **c** state. By comparing the energy levels in the **c** and **f** states, the variation in energy of S should mainly be derived not from the through-bond interaction (short path), but from the through-space interaction *via* the central C–H bond, while the variation of A is mostly the result of the through-bond interaction.

Figure 3 shows the variation in the LPO energy levels of pyrazine.

a. Two LPO on N atoms are cut off from the interactions; the energy levels of two LPO then go to lower levels and degenerate.

b. Even when we added the N···N direct through-space interaction to the **a** state, S and A showed no change in energy. The same phenomena had already been seen in pyrimidine.

c. When we cut off the right-hand side of C–C bond from the interactions (the same is true on the left-hand side), A goes up to the CMO level, but S does partly.

d. When the C–C bonds on both sides are cut off from the interactions, A does not vary from the **c** state, but S goes lower. The energy difference between the **c** and **d** states shows the magnitude of the C–C direct through-bond interaction. The order of S and A is reversed from the **c** state. From the **c** and **d** states, the energy level of S depends much on the through-bond interaction, while that of A does not, as is predicted from the consideration of the orbital symmetry. It is also noteworthy that the through-space interaction is not responsible for the energy difference between S and A, since the energy difference in the **d** state is rather small. This situation is quite different from that shown in pyridazine.

e. When the interactions were permitted only between the "cut-off" LPO and their neighboring four N–C bonds, A goes beyond the CMO level, but S still retains much below the CMO level. This result indicates that the energy level of S is determined not only by the direct through-bond interaction, but also by the through-space interaction combined with the through-bond interaction, since the energy level for S in the **e** state is much different from that of CMO, and the **e** state can be considered to include only the direct through-bond interaction.

Now we will discuss the roots of the LPO interactions. In the case of pyridazine, S is mainly destabilized through the short path, whereas A mainly interacts with the long path. Moreover in this molecule, the direct through-space interaction between n_1 and n_2 is larger than that of pyrimidine or pyrazine. Let us examine in more detail the **c**, **d**, and **e** states of Fig. 1. A indeed goes up by means of interactions *via* the long path. However, in comparison with the **d** and **e** states, both S and A retain nearly the same levels in spite of their different interactions. Therefore, in this molecule, it may be concluded that the interactions between the upper half and the lower half of a molecule *via* the through-space interaction are very important, as was

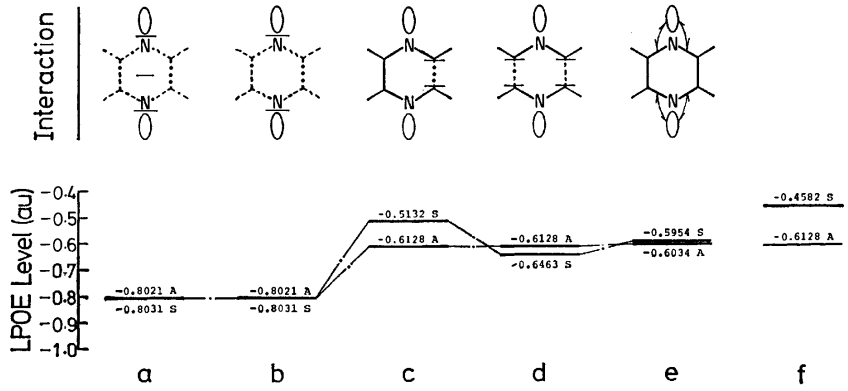

Fig. 3. LPO interaction diagram for pyrazine.
a: LPO are "cut off", **b**: LPO are "cut off" and N···N direct through-space interaction is allowed, **c**: one path is allowed but the other path is "cut off" at the C–C bond, **d**: both C–C bonds are "cut off", **e**: LPO are "cut off" and interactions between LPO and four N–C bonds are allowed, **f**: CMO level.

a b

Fig. 4. **a**: Through-space interaction, and **b**: through-bond interaction, in pyridazine. After combining **a** and **b**, it becomes the "through-space interaction after through-bond" or "through-bond interaction after through-space".

mentioned above. In the case, the through-bond interaction is also included, of course. That is, in other words, this may be named the "through-space after through-bond" or "through-bond after through-space" interaction. Some of interaction courses are shown in Fig. 4.

We shall now return to the discussion of pyrimidine by examining the **d**, **e**, and **f** states of Fig. 2 in more detail. In the case of pyridazine, we have already shown that the LPOE in the **d** and **e** states do not vary very much, as is shown in Fig. 1. However, in the case of pyrimidine, the LPOE are different in the **d** and **e** states, as is shown in Fig. 2. From this we can conclude that, in pyrimidine, the through-bond interaction *via* the N–C–C–C–N course is one of the most important interaction courses, unlike the case of pyridazine. That is, by cutting off the interactions between the C_1–C_2 and C_2–C_3 bonds, and the interaction of C_2–H in the N–C_1–C_2–C_3–N group, the LPO become less interactive.

With pyrazine from the **c** and **d** states shown in Fig. 3, we can recognize that S interacts intimately with the central C–C bonds. Usually the LPO energy order is S<A, but in pyrazine this order is reversed. Hoffmann *et al.*[4] have explained that this reverse order is attributable to the destabilization of the S level as a result of the interaction with the parallel σ C–C levels. Hackmeyer and Whitten[2c] have described that, in the case of the $n\rightarrow\pi^*$ transition, the two combinations of LPO n_1 and n_2 correspond to the $S\simeq n_1+n_2+\lambda\sigma$ and $A\simeq n_1-n_2$ relations. They have also concluded that the higher energy of S is attributable to the interaction with the pyrazine-ring σ system. The case in which the LPO do not interact with the σ C–C bond is shown by, for example, **d** of Fig. 3. In this case the energy order is S<A, indicating that the lack of interaction between the LPO and the central σ C–C bonds leads to a reversion of the levels of S and A. Therefore, the reverse order of S and A in pyrazine is explained quantitatively by the present analysis, and the present analysis confirms the previous hypotheses. In the **d** state, the LPOE are −0.6463 S and −0.6128 A (au), with a difference Δ= 0.0335 (au). The order of the difference agrees well with those of the CMO levels of pyridazine and pyrimidine, although the reason for it remains obscure.

The reversion of S and A is, of course, to be seen in pyridazine and pyrimidine also. In these molecules, however, the reversion cannot be explained only by the hypotheses of Hoffmann and his coworkers.[4] For example, with a pyridazine-type molecule, they proposed that the "through-space" interaction between LPO is dominant and that this lowers the S combination. According to the present analysis, it was found that the N–N direct through-bond interaction also plays an important role (the **c** state in Fig. 1), and in the **d** and **e** states of Fig. 1, the order is S below A even though the N···N direct through-space interaction is cut off.

Palmer *et al.* have reported on the photoelectron spectra of oxygen, sulfur, and nitrogen heterocycles, and they have discussed the variations in the LPOE at O, S, and N atoms.[13] In their paper they suggested that the "through-bond" interactions may play an important role in azines. In that paper, however, we cannot obtain a clear image of the interactions. The present investigation showed that the interactions between LPO are indeed very complicated. However, the interactions can be investigated very simply and clearly using the present procedure.

In conclusion, the present procedure for analyzing orbital interactions is very helpful to analyze the interactions between or among LPO in other molecules with very clear chemical images. The procedure is also applicable to analyzing the orbital interactions in such diradicals as benzynes. For such molecules the analyses are now in progress. This method will also be applied in an *ab initio* calculation. The details will be published elsewhere in the near future.

This work was supported in part by a Grant-in-Aid for Scientific Research from the Ministry of Education, for which we express our gratitude. We would like to acknowledge the continuing encouragement of Professor Hiromu Murata. The computations were carried out on a FACOM M190 of the Data Processing Center, Kyoto University.

References

1) a) R. Pariser and R. G. Parr, *J. Chem. Phys.*, **21**, 767 (1953); b) T. Yonezawa, H. Katô, and H. Kato, *Theor. Chim. Acta*, **13**, 125 (1969), and the references cited theirin. See also Refs. 2c, 2g, 6a, and 6d.

2) a) E. Clementi, *J. Chem. Phys.*, **46**, 4737 (1967); b) J. D. Petke, J. L. Whitten, and J. A. Ryan, *ibid.*, **48**, 953 (1968); c) M. Hackmeyer and J. L. Whitten, *J. Chem.* Phys., **54**, 3739 (1971); d) D. W. Genson and R. E. Christoffersen, *J. Am. Chem. Soc.*, **94**, 6904 (1972); e) T.-K. Ha and C. T. O'Konski, *Int. J. Quantumn Chem.*, **7**, 609 (1973); f) J. Almlöf, B. Roos, U. Wahlgren, and H. Johansen, *J. Electron Spectrosc. Relat. Phenom.*, **2**, 51 (1973); g) M. H. Palmer, A. J. Gaskell, and R. H. Findlay, *J. Chem. Soc., Perkin Trans. 2*, **1974**, 778.

3) In the present article, the following abbreviations are used: LPO; lone-pair orbitals, LPOE; lone-pair orbital energies.

4) a) R. Hoffmann, A. Imamura, and W. J. Hehre, *J. Am. Chem. Soc.*, **90**, 1499 (1968); b) R. Hoffmann, *Acc. Chem. Res.*, **4**, 1 (1971).

5) a) N. C. Baird, *Theor. Chim. Acta*, **16**, 239 (1970); b) H. L. Hase and A. Schweig, *Tetrahedron*, **29**, 1759 (1973); c) H. Schmidt, A. Schweig, F. Manthey, and G. Müller, *ibid.*, **31**, 1287 (1975); d) H. Schmidt and A. Schweig, *Z. Naturforsch. A*, **31**, 215 (1976).

6) a) M. Ito, R. Shimada, T. Kuraishi, and W. Mizushima, *J. Chem. Phys.*, **26**, 1508 (1957); b) J. A. Merritt and K. K.

Innes, *Spectrochim. Acta*, **16**, 945 (1960); c) K. K. Innes and R. M. Lucas, Jr., *J. Mol. Spectrosc.*, **24**, 247 (1967); d) R. Gleiter, E. Heilbronner, and V. Hornung, *Helv. Chim. Acta*, **55**, 255 (1972).

7) C. Edmiston and K. Ruedenberg, *Rev. Mod. Phys.*, **35**, 457 (1963).

8) a) J. A. Pople, D. P. Santry, and G. A. Segal, *J. Chem. Phys.*, **43**, S129 (1965); b) J. A. Pople and G. A. Segal, *ibid.*, **43**, S136 (1965); c) J. A. Pople and G. A. Segal, *ibid.*, **44**, 3289 (1966).

9) J. A. Pople, D. L. Beveridge, and P. A. Dobosh, *J. Chem. Phys.*, **47**, 2026 (1967).

10) P. J. Wheatley, *Acta Crystallogr.*, **13**, 80 (1960).

11) Strictly speaking, the through-space and through-bond interactions, as defined in the present article, do not include the exchange energy, but include only the effect due to the core resonance intergrals. Although the through-space and through-bond interactions usually involve the exchange energy, the through-bond interaction with the exchange energy is dufficult to define by using the LMO; moreover, the problem treated in the present article is not essentially affected by omitting the exchange energy in the definitions of the though-space and through-bond interactions.

12) The through-space and/or through-bond interactions used in the present article are named on the basis of the LMO. Therefore, the definition used here is one of convenience.

13) M. H. Palmer, R. H. Findlay, and R. G. Egdell, *J. Mol. Struct.*, **40**, 191 (1977).

Electronic Absorption and Fluorescence Spectra of [2.2]Anthracenophanes

Masaharu MORITA,† Tohru KISHI,†† Masashi TANAKA, Jiro TANAKA,*
James FERGUSON,** Yoshiteru SAKATA,*** Soichi MISUMI,***
Toyoharu HAYASHI,**** and Noboru MATAGA****

Department of Chemistry, Faculty of Science, Nagoya University, Chikusa, Nagoya, 464
***Research School of Chemistry, Australian National University, Canberra, A.C.T. 2600 Australia*
****The Institute of Scientific and Industrial Research, Osaka University, Suita, Osaka, 565*
*****Department of Chemistry, Faculty of Engineering Science, Osaka University, Toyonaka, Osaka, 560*

(Received May 4, 1978)

The absorption and the fluorescence spectra of four [2.2]anthracenophanes were investigated at low temperatures. A theoretical calculation of the energy levels was performed by including the charge resonance and the exciton type interactions. The fluorescence excitation polarization spectra were recorded for all absorption bands at low temperatures, the directions of the transition moment of the excimer type emission bands being estimated by the *p*-values and the established transition directions of anthracene chromophores. The assignments of the absorption bands are presented based on these results.

The sandwich dimer is formed by photocleavage of dianthracene in rigid glass at low temperatures. Chandross *et al.*[1] and Ferguson *et al.*[2] found that the dimer shows excimer type emission at low temperatures but the absorption spectra slightly differ from a monomer spectrum and are correlated by a weak coupling vibronic theory. Ferguson and Mau[3] found the absorption of the anthracene sandwich pairs in dianthracene crystal.[3] In studies on the emission spectra of 9,10-dichloroanthracene crystal, Tanaka and Shibata[4] found that only the β crystalline form emits an excimer type emission, suggesting that a favorable geometrical arrangement of molecules in the crystal is necessary for formation of the excimer.

As a next step it is important to study the dimer interaction with a rigid molecule, *viz.*, anthracenophanes. Anthracenophanes have two anthracene chromophores separated by two ethylene bridges with a fixed or limited motion of composite rings; thus the inter-ring interaction should be more precisely investigated. Recently accurate X-ray crystal structure analyses of two anthracenophanes were carried out, the geometry and interatomic distances of these molecules being determined.[5,6] We have investigated the absorption and fluorescence spectra of four anthracenophanes at room temperature and low temperatures, and recorded the polarization of the fluorescence excitation spectra. A part of the emission work was published.[7] A theoretical calculation of the excited levels of these molecules was performed, and the assignments of the spectra are presented. It has been shown that the exciton type and the charge resonance type interactions between two chromophores are very important in molecules of close ring contact.[8–10] The structure of the excimer of anthracene is discussed from the reslults of the absorption and emission spectra of anthracenophanes.

† Former Research Fellow of Research School of Chemistry, Australian National University.
Present address: Matsumoto Dental College, Shiojiri, Nagano
†† Visiting researcher from The Institute of Police Science, Tokyo.

Experimental

The materials were synthesized by the methods reported.[11,12] The shape and name of molecules are shown in Fig. 1. The solvent 2-methyltetrahydrofuran of spectrograde was distilled with sodium metal after treatment with potassium hydroxide.

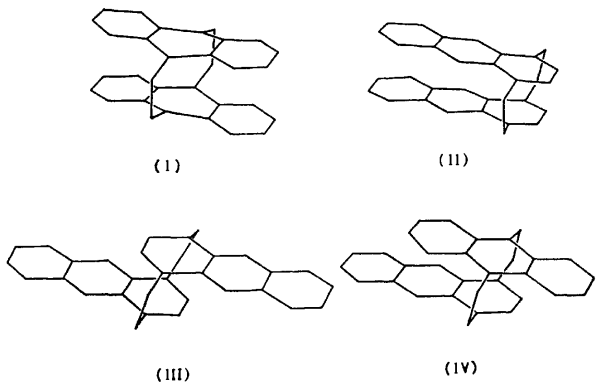

Fig. 1. [2.2]Anthracenophanes: (I) [2.2](9,10)anthracenophane; (II) *syn*-[2.2](1,4)anthracenophane; (III) *anti*-[2.2](1,4)anthracenophane; (IV) [2.2](1,4)(9,10)-anthracenophane.

The absorption spectra were recorded with a Cary 15 spectrophotometer with a Cryo-tip refrigerator for the low temperature measurement. A Cary 17 spectrophotometer at Australian National University was also used with a flow type cryostat. The fluorescence spectra were measured on a Carl-Zeiss M4QIII spectrofluorometer with a HTV R446 photomultiplier tube. The sample was excited with a 1 kW Xe lamp through a Carl-Zeiss monochromator set at right angles to the entrance slit of the fluorometer. Measurements of emission were also made with a 3/4 m Spex spectrometer, a cooled ITT-FW130 photomultiplier being used. The light from a 150W Varian xenon illuminator dispersed by a Carl-Zeiss MM 12 double monochromator was used as exciting source.[2,3] The intensity of fluorescence was corrected by comparison with that of quinine bisulfate solution in 0.1 N H_2SO_4 and of *o*-dichlorobenzene solution of 4-dimethylamino-4′-nitrostilbene. The polarization of the emission (PF) and the excitation (APF) was measured with the same system combined with calcite and pola-coat polarizers, the polarization character of the system

being cheked beforehand. The lifetime of the emission band was measured with a pulsed nitrogen gas laser combined with a Tektronix synchroscope of 465 type or a Tektronix sampling scope 564-3S2-3T77A system. The NMR spectra were recorded on JEOL JNM-TS-100 at 23, −50, −95, and −100 °C.

Theoretical Calculation

A SCF MO of each anthracene chromophore was calculated by the P-P-P method[13,14] with Nishimoto-Mataga potential.[15] The calculation was based on the structures determined by X-ray crystal analysis.[5,6] For molecules whose structures have not been determined by the X-ray method, model structures were constructed from the known forms.

The ground state wavefunctions of each ring are written as follows.

$$\begin{aligned} \Phi_0 &= |\varphi_1\bar{\varphi}_1 \cdots \varphi_7\bar{\varphi}_7| \\ \Theta_0 &= |\theta_1\bar{\theta}_1 \cdots \theta_7\bar{\theta}_7| \end{aligned} \tag{1}$$

The energies of the excited states were calculated from configuration interactions, where the intergroup charge resonance (CR) and the exciton interactions are included. The matrix elements between the locally excited (LE) and CR states were calculated by using the following formulas.

$$\begin{aligned} &\langle\varphi_m\varphi_n|H|\varphi_m\theta_n\rangle \\ &\quad= \frac{1}{2}\langle\{|\cdots\varphi_m\bar{\varphi}_n\cdots|+|\cdots\varphi_n\bar{\varphi}_m\cdots|\} \\ &\qquad||H||\{|\cdots\varphi_m\bar{\theta}_n\cdots|+|\cdots\bar{\theta}_n\varphi_m\cdots|\}\rangle \\ &\quad= \langle\varphi_n|F|\theta_n\rangle + 2(\varphi_m\theta_n|\varphi_m\varphi_n) - (\varphi_m\varphi_m|\varphi_n\theta_n), \\ &\langle\varphi_m\varphi_n|H|\theta_m\varphi_n\rangle \\ &\quad= \frac{1}{2}\langle\{|\cdots\varphi_m\bar{\varphi}_n\cdots|+|\cdots\varphi_n\bar{\varphi}_m\cdots|\} \\ &\qquad||H||\{|\cdots\theta_m\bar{\varphi}_n\cdots|+|\cdots\varphi_n\bar{\theta}_m\cdots|\}\rangle \\ &\quad= -\langle\varphi_m|F|\theta_m\rangle + 2(\varphi_m\varphi_n|\theta_m\varphi_n) - (\varphi_m\theta_m|\varphi_n\varphi_n), \end{aligned} \tag{2}$$

where Coulomb hybrid integrals are denoted by

$$(\varphi_m\theta_m|\varphi_n\varphi_n) = \int\varphi_m(1)\theta_m(1)\frac{1}{r_{12}}\varphi_n(2)\varphi_n(2)dv_1dv_2.$$

The hybrid integrals are calculated by using Mulliken's approximation

$$(\varphi_m\theta_m|\varphi_n\varphi_n) = \frac{1}{2}S_{mm}\{(\varphi_m\varphi_m|\varphi_n\varphi_n)+(\varphi_n\varphi_n|\theta_m\theta_m)\},$$

$$S_{mm} = \langle\varphi_m|\theta_m\rangle = \int\varphi_m(1)\theta_m(1)dv_1.$$

The one-electron integrals extending over two rings are taken as proportional to the overlap integrals:

$$\langle\varphi_n|F|\theta_n\rangle = kS_{nn}. \tag{4}$$

The proportionality constant, k, was so chosen as to obtain the best fit of calculated results with the observed values of transition energies and set to −14.0 eV. All computations were carried out on a Facom 230-60 computer at Nagoya University Computation Center.

Feature of Anthracenophane Excited State. Anthracene monomers have three excited states in the 25000—48000 cm^{-1} region, two of which are observed as allowed transitions. The lower energy transition in the 25000 cm^{-1} region is the short-axis polarized band ($^1B_{2u}$ state, ^1L_a band). It is composed of the electronic excitation from the highest occupied MO (φ_7, HOMO) to the lowest unoccupied MO (φ_8, LUMO). We can abbreviate the wavefunction of this state to

$$\Phi_1 = \frac{1}{\sqrt{2}}\{|\cdots\varphi_7\bar{\varphi}_8|+|\cdots\varphi_8\bar{\varphi}_7|\}. \tag{5}$$

The higher and stronger absorption is the long-axis polarized transition to the $^1B_{3u}$ state (^1B_b band); the wavefunction of the state is described by a linear combination of the excitation of an electron from the second HOMO (φ_6) to the LUMO (φ_8) and from the HOMO (φ_7) to the second LUMO (φ^9) as

$$\begin{aligned} \Phi_2 = \frac{1}{2}\{&|\cdots\varphi_6\bar{\varphi}_8\cdots|+|\cdots\varphi_8\bar{\varphi}_6\cdots| \\ &+|\cdots\varphi_7\bar{\varphi}_9|+|\cdots\varphi_9\bar{\varphi}_7|\}. \end{aligned} \tag{6}$$

A forbidden transition (^1L_b band) is composed of antisymmetric combination of the same excitation orbitals and is expected in the region of the first band, however, it has never been observed in the anthracene molecule.

When two anthracenophane chromophores approach each other, the CR configuration and the exciton type interaction become significant. The wavefunction of the exciton type state of the short-axis polarized first band is written as

$$\begin{aligned} \mathrm{ER}_1(+) &= \frac{1}{\sqrt{2}}\{\Phi_1\Theta_0+\Phi_0\Theta_1\}, \\ \mathrm{ER}_1(-) &= \frac{1}{\sqrt{2}}\{\Phi_1\Theta_0-\Phi_0\Theta_1\}. \end{aligned} \tag{7}$$

If the two chromophores are related by an inversion symmetry, the $ER_1(+)$ state is forbidden and the $ER_1(-)$ state allowed.

The CR configuration of the same symmetry type are given by

$$\begin{aligned} \mathrm{CR}_1(+) &= \frac{1}{\sqrt{2}}\{\Phi_1^+\Theta_1^- + \Phi_1^-\Theta_1^+\} \\ \text{and} \\ \mathrm{CR}_1(-) &= \frac{1}{\sqrt{2}}\{\Phi_1^+\Theta_1^- - \Phi_1^-\Theta_1^+\}. \end{aligned} \tag{8}$$

The energies of these configurations may be nearly degenerate, and the configuration interaction between the same symmetry levels should be considered. The resultant states can be approximately written as

$$\begin{aligned} \text{forbidden states} &\begin{cases} \mathrm{ER}_1(+) + \mathrm{CR}_1(+) \\ \mathrm{ER}_1(+) - \mathrm{CR}_1(+) \end{cases} \\ \text{allowed states} &\begin{cases} \mathrm{ER}_1(-) + \mathrm{CR}_1(-) \\ \mathrm{ER}_1(-) - \mathrm{CR}_1(-). \end{cases} \end{aligned} \tag{9}$$

The exciton states of the long-axis polarized transition are given by a linear combination of each LE state as

$$\begin{aligned} \mathrm{ER}_2(+) &= \frac{1}{\sqrt{2}}(\Phi_2\Theta_0+\Phi_0\Theta_2), \\ \mathrm{ER}_2(-) &= \frac{1}{\sqrt{2}}(\Phi_2\Theta_0-\Phi_0\Theta_2). \end{aligned} \tag{10}$$

The charge resonance excited levels of the same orbital type are written as $\Phi_2^+\Theta_2^-$. They are combined to give two CR states as

Table 1. Calculated and observed energy levels of [2.2](9,10)anthracenophane

	State	Energy (cm^{-1}) Calcd (Obsd)	Intensity (f) Calcd (Obsd)	Wave function
1	Ground	0		$0.98\Phi_0\Theta_0+0.10\phi_6\theta_8+0.11\theta_6\phi_8-0.08\theta_7\phi_9+0.07\phi_7\theta_9$
2	$ER_1(+)+CR_1(+)$	17950 (19000)	0.0002 (0.002)	$0.50\phi_7\phi_8+0.46\theta_7\theta_8+0.47\phi_7\theta_8+0.49\theta_7\phi_8$
3	$ER_1(-)+CR_1(-)$	25250 (24000)	0.008 (0.03)	$0.16\phi_7\phi_8-0.18\theta_7\theta_8+0.62\phi_7\theta_8-0.59\theta_7\phi_8$
4	$ER_1(-)-CR_1(-)$	28060 (26247)	0.19 (0.05)	$0.51\phi_7\phi_8-0.65\theta_7\theta_8-0.25\phi_7\theta_8+0.21\theta_7\phi_8$
5	$ER_2(+)+CR_2(+)$	29800 (31300)	0.002 (0.01)	$0.49\phi_7\phi_9+0.45\theta_7\theta_8+0.23\phi_6\phi_8+0.27\theta_6\theta_8+0.34\phi_7\theta_9+0.34\theta_7\phi_9+0.26\phi_6\theta_8+0.27\theta_6\phi_8$
6	$CR_2(-)$	34757 (34000)	0.09 (0.03)	$0.33\phi_7\theta_9-0.31\theta_7\phi_9-0.44\phi_6\theta_8+0.40\theta_6\phi_8$
7	$CR_2'(-)$	36660 (35600)	0.08 (0.16)	$0.53\phi_7\theta_9-0.46\theta_7\phi_9+0.40\phi_6\theta_8-0.45\theta_6\phi_8$
8	$ER_2(-)-CR_2(-)$	39620 } (39000)	0.87 } (0.86)	$0.29\phi_7\phi_9-0.29\theta_7\theta_9+0.28\phi_6\phi_8-0.32\theta_6\theta_8-0.16\phi_7\theta_9+0.17\theta_7\phi_9+0.16\phi_6\theta_8-0.08\theta_6\phi_8+0.35\phi_6\phi_{10}-0.26\theta_6\theta_{10}-0.30\phi_5\phi_9+0.20\theta_5\theta_9$
9	$ER_2(-)+CR_2(-)$	41400	1.10	$0.48\phi_7\phi_9-0.18\theta_7\theta_9+0.27\phi_6\phi_8-0.37\theta_6\theta_8-0.03\phi_7\theta_9-0.43\theta_7\phi_9-0.07\phi_6\theta_8+0.33\theta_6\phi_8$

Table 2. Calculated and observed energy levels of *syn*-[2.2](1,4)anthracenophane

	State	Energy (cm^{-1}) Calcd (Obsd)	Intensity (f) Calcd (Obsd)	Wave function
1	Ground	0		$0.98\Phi_0\Theta_0+0.14\phi_6\theta_8-0.08\theta_6\phi_8+0.11\phi_7\theta_9+0.05\theta_7\phi_9$
2	$ER_1(+)+CR_1(+)$	20250 (20500)	6×10^{-4}	$0.44\phi_7\phi_8+0.45\theta_7\theta_8+0.35\phi_7\theta_8+0.52\theta_7\phi_8$
3	Coupled $^1B_{3u}$	26030 (24500)	1.5×10^{-3} (0.01)	$0.49\phi_6\theta_8-0.40\theta_6\phi_8-0.40\phi_7\theta_8+0.32\theta_7\theta_9+0.23\phi_6\theta_8-0.32\theta_6\phi_8+0.20\phi_7\theta_8-0.16\theta_7\phi_8+0.14\phi_7\theta_9-0.21\theta_7\phi_9$
4	$CR_1(-)$	26980 (26300)	4.4×10^{-3}	$0.19\phi_7\phi_8+0.29\theta_7\theta_8+0.55\phi_7\theta_8-0.37\theta_7\phi_8-0.42\phi_5\theta_8-0.10\theta_5\theta_8-0.04\phi_5\theta_8-0.35\theta_5\phi_8$
5	$ER_1(-)$	28590 (26800)	0.18 (0.085)	$0.63\phi_7\phi_8-0.54\theta_7\theta_8+0.02\phi_7\theta_8+0.17\theta_7\phi_8-0.06\phi_5\phi_8+0.25\theta_5\theta_8-0.36\phi_5\theta_8-0.04\phi_5\phi_8$
6	$ER_2(-)+CR_2(-)$	31530 (33000)	0.027 (0.057)	$0.30\phi_7\phi_9+0.36\theta_7\theta_9-0.18\phi_7\theta_9-0.27\theta_8\phi_8-0.07\phi_7\phi_8-0.24\theta_7\theta_8+0.26\phi_6\phi_8-0.25\theta_6\theta_8+0.10\phi_6\theta_8+0.42\theta_6\phi_8$
7	Mixed higher ER+CR	36470 (37740)	0.12 (0.104)	$0.13\phi_7\phi_8+0.23\theta_7\theta_8-0.14\phi_7\theta_8-0.29\theta_7\phi_8+0.19\phi_7\theta_9+0.18\theta_7\phi_9-0.42\phi_6\theta_8-0.26\theta_6\phi_8+0.16\phi_5\theta_8+0.35\theta_5\phi_8+0.11\phi_5\phi_8-0.35\theta_5\theta_8$
8	$ER_2(-)-CR_2(-)$	42420 (40650)	1.62 (1.06)	$0.47\phi_7\phi_9-0.36\theta_7\theta_9-0.19\phi_7\theta_9+0.21\theta_7\phi_9+0.52\phi_6\phi_8-0.24\theta_6\theta_8-0.27\phi_6\theta_8-0.08\theta_6\phi_8-0.17\phi_6\phi_9+0.22\theta_6\theta_9$

Table 3. Calculated and observed energy levels of *anti*-[2.2](1,4)anthracenophane

	State	Energy (cm^{-1}) Calcd (Obsd)	Intensity (f) Calcd (Obsd)	Wave function
1	Ground	0		$0.99\Phi_0\Theta_0+0.10\phi_7\theta_9+0.10\theta_7\phi_9$
2	$ER_1(+)+CR_1(+)$	23200 (23900)	0.011 (0.009)	$0.47\phi_7\phi_8+0.16\theta_7\theta_8+0.58\phi_7\theta_8+0.20\theta_7\phi_8+0.15\phi_5\phi_8+0.26\theta_5\theta_8+0.31\phi_5\theta_8+0.22\theta_5\phi_8$
3	$ER_1(-)+CR_1(-)$	23300 (24750)	0.064 (0.08)	$0.23\phi_7\phi_8-0.51\theta_7\theta_8+0.29\phi_7\theta_8-0.62\theta_7\phi_8$
4	$ER_1(-)-CR_1(-)$	29623 (25250)	0.135 (0.06)	$0.52\phi_7\phi_8-0.44\theta_7\theta_8-0.21\phi_7\theta_8+0.17\theta_7\phi_8+0.18\phi_5\phi_8-0.14\theta_5\theta_8-0.33\phi_5\theta_8+0.30\theta_5\phi_8$
5	Higher CR	33130 (30000)	4×10^{-4} (0.02)	$0.29\phi_5\phi_8+0.36\theta_5\theta_8-0.39\phi_7\theta_8-0.42\theta_7\phi_8+0.33\phi_5\theta_8+0.23\theta_5\phi_8$
6	$ER_2(-)+CR_2(-)$	35100 } (35300)	0.59 } (1.30)	$0.24\phi_7\phi_9-0.27\theta_7\theta_9+0.11\phi_7\theta_9-0.11\theta_7\phi_9+0.16\phi_6\phi_8-0.18\theta_6\theta_8+0.50\phi_6\theta_8-0.52\theta_6\phi_8$
7	$ER_2(-)+CR'_2(-)$	37000	1.12	$0.22\phi_7\phi_9-0.25\theta_7\theta_9+0.33\phi_7\theta_9-0.35\theta_7\phi_9+0.36\phi_6\phi_8-0.38\theta_6\theta_8-0.08\phi_6\theta_8+0.09\theta_6\phi_8$
8	$ER_2(-)-CR_2(-)$	39200 (39500)	0.40 (1.00)	$0.25\phi_6\phi_8-0.22\theta_6\theta_8-0.31\phi_6\theta_8+0.31\theta_6\phi_8-0.42\phi_6\phi_{10}+0.41\theta_6\theta_{10}+0.29\phi_5\phi_9-0.28\theta_5\theta_9$

Table 4. Calculated and observed energy levels of [2.2](1,4)(9,10)anthracenophane

	State	Energy Calcd (Obsd)	Intensity (f) Calcd (Obsd)	Wave function
1	Ground	0		$0.99\Phi_0\Theta_0+0.07\phi_7\theta_9+0.08\theta_7\phi_9-0.05\phi_6\theta_8+0.09\theta_6\phi_8$
2	$ER_1(+)+CR_1(+)$	17160 (22500)	1×10^{-4} (0.002)	$0.41\phi_7\phi_8+0.41\theta_7\theta_8+0.51\phi_7\theta_8+0.34\theta_7\phi_8+0.10\phi_5\phi_8+0.35\theta_5\theta_8+0.12\phi_5\theta_8+0.25\theta_5\phi_8$
3	$ER_1(-)+CR_1(-)$	21850 (23800)	0.059 (0.077)	$0.18\phi_7\phi_8-0.54\theta_7\theta_8+0.45\phi_7\theta_8-0.56\theta_7\phi_8-0.17\phi_5\phi_8+0.27\theta_5\theta_8-0.12\phi_5\theta_8$
4	$ER_1(-)-CR_1(-)$	26920 (27600)	0.16 (0.10)	$0.56\phi_7\phi_8-0.47\theta_7\theta_8-0.22\phi_7\theta_8+0.32\phi_7\theta_8+0.10\phi_5\phi_8-0.21\theta_5\theta_8-0.12\phi_5\theta_8-0.31\theta_5\phi_8$
5	$ER_2(-)+CR_2(-)$	34440 (35500)	0.42 (0.87)	$0.22\phi_7\phi_9-0.28\theta_7\theta_9+0.35\phi_7\theta_9-0.29\theta_7\phi_9-0.19\theta_6\theta_8+0.54\phi_6\theta_8-0.45\theta_6\phi_8$
6	$ER_2(-)-CR_2(-)$	39620 (39000)	1.47 (1.15)	$0.32\phi_7\phi_9-0.46\theta_7\theta_9+0.39\theta_7\phi_9+0.33\phi_6\phi_8-0.48\theta_6\theta_8+0.27\theta_6\phi_8$

$$CR_2(+)=\frac{1}{\sqrt{2}}(\Phi_2^+\Theta_2^-+\Phi_2^-\Theta_2^+),$$
$$CR_2(-)=\frac{1}{\sqrt{2}}(\Phi_2^+\Theta_2^--\Phi_2^-\Theta_2^+). \quad (11)$$

Since the energy levels of the ER_2 and the CR_2 states do not differ a great deal, the same symmetry levels are coupled to give new states as given by Eq. 9.

The calculated results on the energy levels for each molecule are given in Tables 1—4. Only allowed transtions are compiled, assignments by abbreviated notations being given in the first column. The results show that the excited levels of anthracenophanes are described by a complex linear combination of LE and CT transitions of each anthracene chromophore. Actually the structure of the molecule deviates from an inversion symmetry, so that the calculated MO and the state functions lose symmetric properties. Lowering of molecular symmetry makes some transitions allowed, which were originally forbidden in anthracene molecule. Weak transitions appear as a result of the inter-chromophore interactions.

In spite of these complication the feature of anthracenophane absorption bands is characterized by the allowed states of Eq. 9 and allowed combinations of $ER_2(-)\pm CR_2(-)$. The excimer emission state is related to the lowest forbidden state of Eq. 9, which includes nearly a half $CR_1(+)$ state.

Results and Discussion

[2.2](9,10)Anthracenophane (I). The absorption spectra measured at room temperature and 77 K are shown in Fig. 2. A number of absorption peaks were found, at least six excited levels being discerned. The lowest energy transition was found in the range 19000—23000 cm^{-1} with weak intensity and broad band shape. Since the intensity is very weak and the level is much lower than other levels, the band is assigned to a forbidden transition to a mixed state of the $CR_1(+)$ and $ER_1(+)$. Murrell and Tanaka[8] represented this excited level as a mixed state of $^1E_g-{}^1R_g$, where ^1E_g and ^1R_g correspond to $ER_1(+)$ and $CR_1(+)$, respectively. In earlier studies on anthracene dimer or anthracene crystals, no such forbidden band had been observed in this region. Recently such transitions have been observed in bridged anthracene derivatives.[3] The

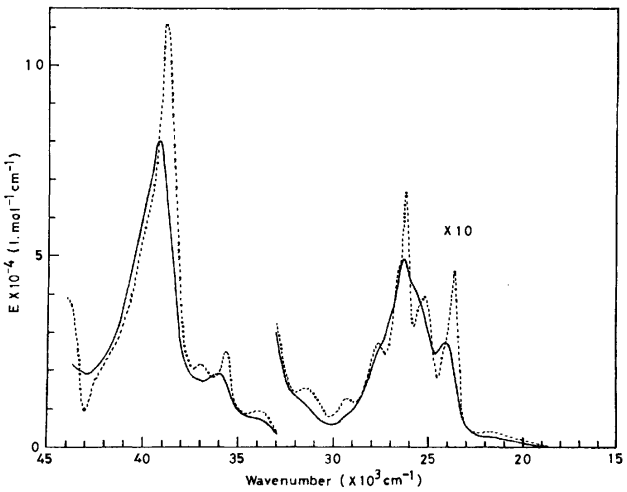

Fig. 2. Absorption spectra of I at 298 K (full line) and at 77 K (broken line) in MTHF.

inter-ring contact of this molecule is very close in the ground state, hence such type band is observed. The absorption band may be correlated with the excimer type emission of anthracene dimer, but the molecule gives no fluorescence even at 4 K. The absence of emission is ascribed to an efficient photochemical reaction and radiationless transitions.[7,16]

In the allowed transitions observed in the succeeding

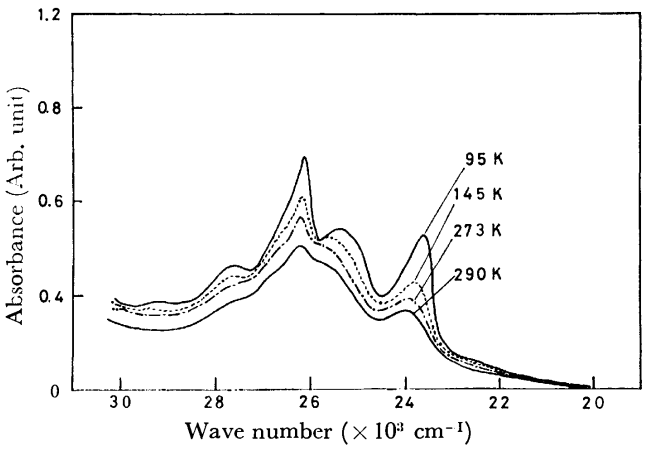

Fig. 3. Absorption spectra of I at various temperaures in MTHF.

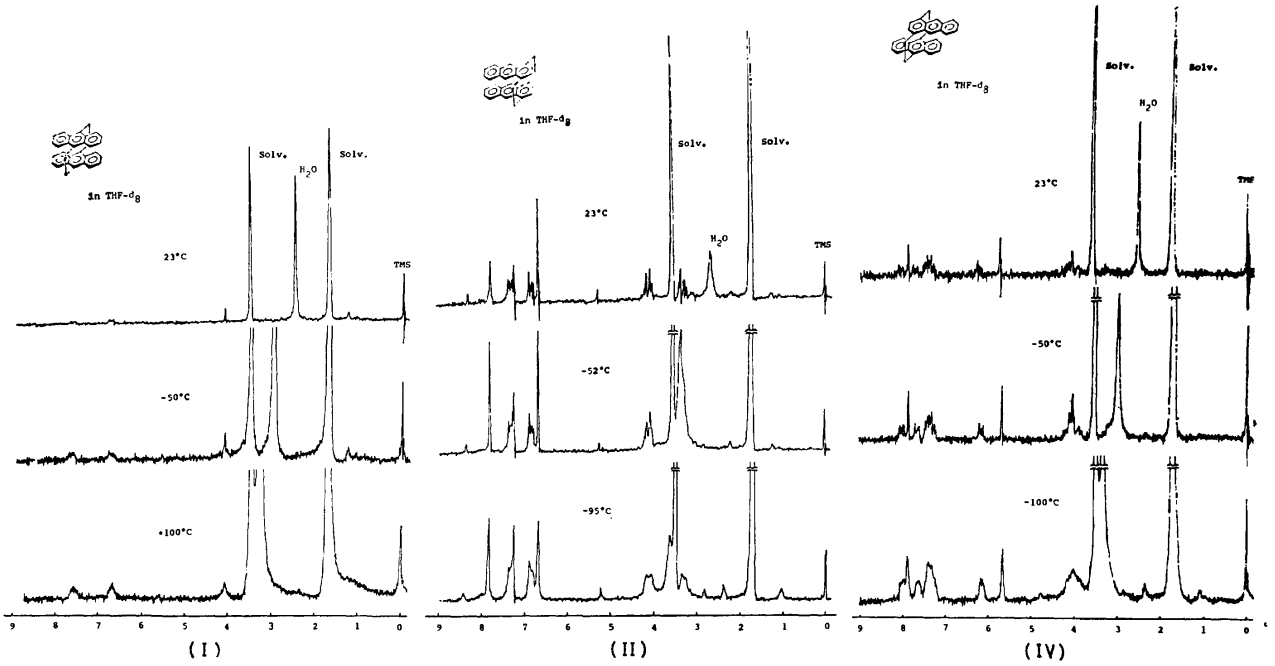

Fig. 4. NMR spectra of I, II, and IV at various temperatures.

region, the band at 24000 cm^{-1} is assigned to the transition of $ER_1(-)+CR_1(-)$. The next band at 25510 cm^{-1} shows strange spectral behavior with lowering in temperature; its intensity does not increase as compared to nearby transitions which are enhanced significantly. The intensity of this band is recorded as a guest in the single crystal of the photoisomer host, its intensity being much larger at 10 K as compared to that at 206 K.[17] The temperature change of solution spectra in this region shows that the 25510 cm^{-1} band behaves differently as compared to the neighboring bands (Fig. 3). Such unusual spectral behavior may be accounted for by assigning the band to the conformational isomer whose spectrum differs from that of the major conformer in this region.[18] The X-ray data on *syn*-[2.2](1,4)anthracenophane show the presence of two conformational isomers in the crystal.[5] Moreover, the NMR spectra of (I) (δ=4.05) at low temperature (Fig. 4) indicate that the methylene proton signals are broadened. It seems that a twisting around the methylene bridges causes the conformers.

The next peak at 26247 cm^{-1} is due to the transition to the $ER_1(-)-CR_1(-)$ state. The band shows regular vibrational progressions at 27624 and 29412 cm^{-1}. The appearance of sharp vibrational progressions indicates that the molecule has a relatively rigid structure. In the following region, several absorption bands were found at 31300, 33800, and 35600—37000 cm^{-1}. The 31300 cm^{-1} band may be due to a transition to the forbidden state of the coupled long-axis transition, $ER_2(+)+CR_2(+)$. The bands at 34000 and 35600 cm^{-1} region are assigned to the CR_2 type bands. The strongest absorption band observed at 38800 cm^{-1} is assigned to the strongly allowed long-axis transition of the coupled dimer, namely to the $ER_2(-)\pm CR_2(-)$ state. It appears from the calculation that two closely situated levels exist in this region.

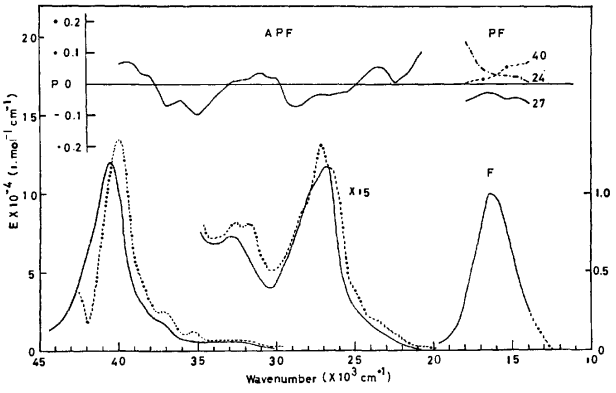

Fig. 5. Absorption spectra of II at 298 K (full line) and at 77 K (broken line) in MTHF with emission spectrum, PF, and APF measured at 77 K. APF monitored at 16000 cm^{-1}.

syn-[*2.2*]*(1,4)Anthracenophane (II).* The absorption spectra measured at room temperature and 77 K are shown in Fig. 5. There are at least seven transitions in the region 20000—45000 cm^{-1}. The lowest band is assigned to a forbidden transition to the $ER_1(+)+CR_1(+)$ state. No absorption related to the excimer emission has been observed in anthracene dimer prepared by photolysis at low temperature. The band can be assigned to the transition to the Franck-Condon state of the excimer level from the ground state. The excimer type fluorescence appears at 16000 cm^{-1}.

Several strong absorption bands were found in the range 24000—29000 cm^{-1} where there are at least three transitions. They are assigned to the coupled $^1B_{3u}$ state (forbidden long-axis polarized band in anthracene, ^1L_b band), $CR_1(-)$ and $ER_1(-)$ bands, respectively. The vibrational progressions are blurred off since the anthracene rings are hinged at the terminal benzene rings and the molecular structure seems to be flexible.

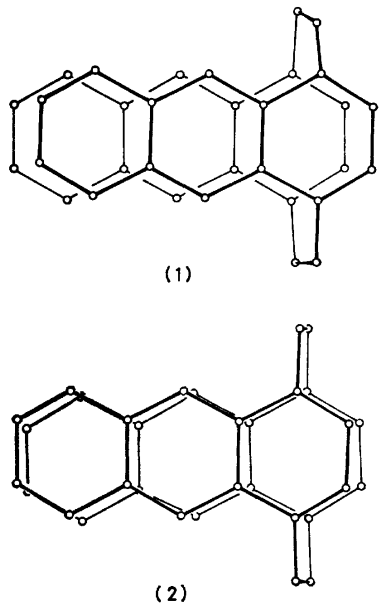

Fig. 6. Molecular structures of II at 124 K.
(1) Slipped form; (2) eclipsed form.

Toyoda and Misumi[5] determined the crystal structure of this molecule at −149 °C and found that two independent molecules are included in a unit cell, taking noticeably different conformations as shown in Fig. 6. One has an approximately symmetric faced conformation, while the other has a displaced or slipped conformation. NMR spectra at low temperature indicate that the methylene protons at $\delta=4$ ppm are broadened in (II) (Fig. 4). This indicates that the methylene bridges are not completely rigid and different conformers may exist at this temperature. The fluorescence spectra of (II) produced by the photocleavage of the photoisomer at 80 K show a peak at 16130 cm^{-1}. It turns into two peaks at 16130 and 16670 cm^{-1} at 140 K and finally is transformed into a single peak centered at 16580 cm^{-1} with enhancement of an intensity of three times. The results also show the presence of conformers at low temperatures.

In the higher energy region several absorption bands were found at 31000—34000, 35000—37000, and 39000—41000 cm^{-1}. The 31000—34000 cm^{-1} band is assigned to the $ER_2(-)$—$CR_2(-)$ band, which may have long-axis polarization. The band at around 37000 cm^{-1} is calculated to be the mixed higher CR and ER states. The strongest band in the 39000—41000 cm^{-1} region corresponds to the transition to the $ER_2(-)+CR_2(-)$ state.

For assignment of the absorption bands, the analysis of fluorescence polarization spectra would be of most value. The fluorescence spectra were measured at room temperature and 77 K as shown in Fig. 5, the broad excimer type emission band being observed with a peak at 16500 cm^{-1}. The excitation spectra for the red emission are consistent with the absorption spectra of (II), and the excitation efficiency is particularly large at 22000 cm^{-1} where the transition is to the Franck-Condon excimer state of $ER_1(+)+CR_1(+)$. The fluorescence excitation polarization spectra (APF) were measured by observing the fluorescence at 16500 cm^{-1}. The result is shown in Fig. 5 together with the absorption spectra. The first absorption band in the range 21000—22000 cm^{-1} shows the highest positive p value of 0.1. This indicates that the Franck-Condon excited state has nearly the same character as that of the excimer emission, but still the p-value is not high enough to show parallelism of the absorption and emission transition moments. It is very probable that the molecule is deformed in the excited state and the polarization direction of the emission is not exactly the same as of the absorption band. The emissive transition is originally forbidden; it might thus borrow the transition moment from other allowed transitions.

Although the internal molecular motion may occur in the excited state, we can estimate the direction of the transition moment of the emission band based on the p-value of APF for each absorption band at low temperature where the translational molecular motion is frozen. If the excimer state has the strict symmetry of D_{2h}, a radiative transition to the ground state is forbidden, and no emission can be expected. As a matter of fact the fluorescence is observed, hence the symmetry of the excited state should be lowered. However, no polarization study has been published on the excimer state formed by the encounter process in solution. Subudhi, Kanamaru and Lim[19] measured the polarization property on anthracene sandwich dimer and found that the excimer state includes both the short axis component of anthracene $^1B_{2u}(^1L_a)$ type state and the out of plane constituent of CR_1 type state.

In anthracenophanes the emission might appear as a result of the deformation of the molecule in the excited state. Several levels might be mixed to make the transition allowed with a definite polarization direction. The direction might be estimated by correlating the p-value to the long and the short axes polarized transition of anthracene chromophore in anthracenophane. We use the relation of angles between the transition moments of the absorption and the emission:[20]

$$p=\frac{3\cos^2\alpha-1}{3+\cos^2\alpha}, \tag{12}$$

where α is the angle between the emission and the absorption bands.

The direction of the transition moment of the strongest band at 40000 cm^{-1} is certainly along the long-axis; the excimer emission shows positive p-value to the long-axis polarized band. This can occur since the emission state involves the long-axis polarization component. The angle between the transition moment of the emission band and the long-axis is estimated at 48° by Eq. 12. The absorption band in the range 27300—29000 cm^{-1} may have the short-axis polarization (Table 2). The p-value is −0.08 and the angle is found as 60° to the short-axis. The direction of the excimer emission band is thus estimated by using these angles as shown in Fig. 7. In the 26500 cm^{-1} region the p-value is −0.04 and the angle between the absorption and emission transition moments is estimated to be 57° by Eq. 12. The transition of $CR_1(-)$ type may have the polarization in the out of plane direction, and the direction

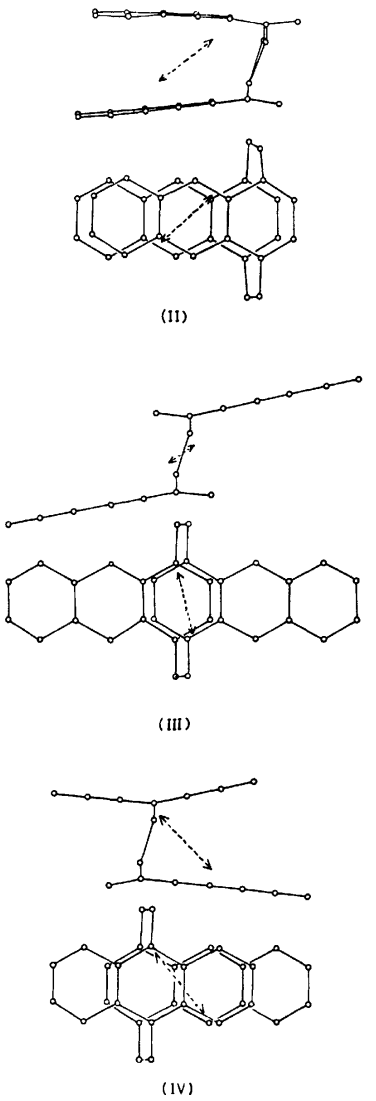

Fig. 7. The directions of the transition moment of emission bands of II, III, and IV estimated from polarization measurements.

makes 56° with the estimated direction of the excimer transition moment. The agreement seems satisfactory.

A positive hump of *p*-value was observed in the 23000—25000 cm^{-1} range, weak shoulders being detected in the absorption spectra. According to theoretical calculation, these weak transitions are attributed to the forbidden transition of the long-axis polarized band originated from anthracene $^1B_{3u}^-$ state (^1L_b type). The 31000 cm^{-1} band shows positive *p*-value, consistent with the assignment of $ER_2(-)+CR_2(-)$, since ER_2 component may have large contribution. In the range 35000—38000 cm^{-1}, the *p*-value is negative. This is reasonable since the transition takes place toward higher CR and the short-axis polarized ER states.

The polarization of the fluorescence band (PF) was measured with excitations fixed at 40000, 27000 and 24000 cm^{-1}, respectively, and the *p*-values were found nearly constant for the 27000 cm^{-1} excitation, varying slightly for the 24000 and 40000 cm^{-1} excitations. This indicates that the excited state involved for the emission band has a mixed character.

The lifetime of the emission was 70 ns, which may be short because of photochemical reaction. It seems that the molecule in the excited state is so deformed that a mixing of an allowed component occurs extensively and both the radiative and the radiationless transitions are enhanced.

anti-[*2.2*]*(1,4)Anthracenophane (III).* The absorption spectra measured at room temperature and 77 K are shown in Fig. 8. The first absorption band consisting of three different bands starts at 23000 cm^{-1} and extends to 31000 cm^{-1}. By lowering the temperature to 77 K, the lowest transition is red-shifted to 23900 cm^{-1}. This is assigned to the $ER_1(+)+CR_1(+)$ state. Several vibrational progressions are observed in the succeeding region. They are classified into two series at 24750, 26180, and 27620 cm^{-1} and 25250, 26740 and 28170 cm^{-1}. Theoretical calculation showed that these are the transitions to the $ER_1(-)\pm CR_1(-)$ states. The splitting of these levels was experimentally estimated as 500 cm^{-1}, while theoretical calculation showed a much larger value. For the molecule with a weak coupling, the present treatment should be modified considering the vibronic effect. The origin of the succeeding band series is not clear and the band at 30000 cm^{-1} is assigned to the higher CR state.

The strongest absorption band is found at 35300 cm^{-1}. This is an allowed long-axis polarized transition which is red-shifted from monomer transition by the exciton type interaction. The red shift as compared to I and II occurred because the arrangement of chromophore is of a head to tail type. The result of calculation shows that two allowed transitions coexist in the 35000—37000 cm^{-1} region, which are regarded to be of $ER_2(-)+CR_2(-)$ type. Another transition was observed at 39500 cm^{-1}, which is ascribed to the long-axis polarized transition of $ER_2(-)-CR_2(-)$.

The fluorescence and the APF spectra measured at 77 K are shown in Fig. 8. The Stokes shift for the

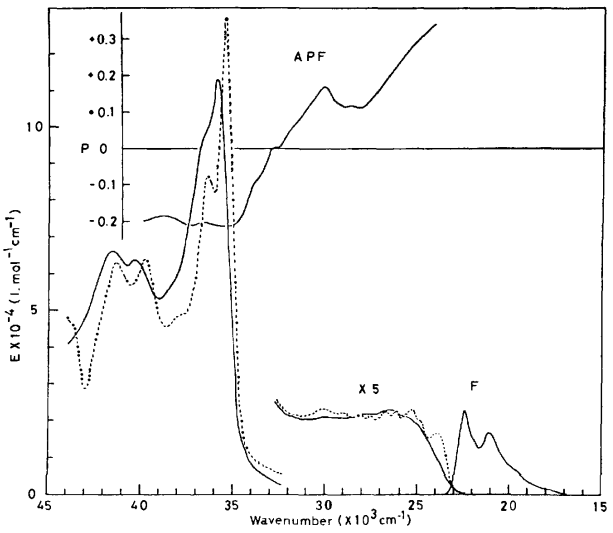

Fig. 8. Absorption spectra of III at 298 K (full line) and at 77 K (broken line) along with emission spectrum and APF at 77 K. APF monitored at 22000 cm^{-1}.

emission is 1500 cm^{-1}, which is smaller than in II and IV but fairly large to indicate the contribution of the CR interaction in the excited state. The APF spectra were measured at 22000 cm^{-1} emission band and the first absorption band at 26000 cm^{-1} shows a high p-value of 0.4. The angle between the emission and the first absorption is estimated to be 23° by Eq. 12, but actually it may be nearly parallel because of inherent experimental error. The bands at 25000—29000 cm^{-1} show positive p-values and the angle is estimated to be about 40°. The two band series are derived from the $ER_1(-)\pm CR_1(-)$ states; the mixing of the CR state with ER state makes the transition moments have an appreciable deviation from the short-axis. In the region of the long-axis polarized transitions, the p-values are all negative, being in line with the assignment of the transitions. The angle between the emission and the long-axis is estimated to be about 71°. By using these angles the direction of the transition moment is estimated as shown in Fig. 7. The lifetime of the emission is 8 ns which is very close to the value of anthracene derivatives. It is consistent with a relatively small shift of the energy level by the dimer type interaction.

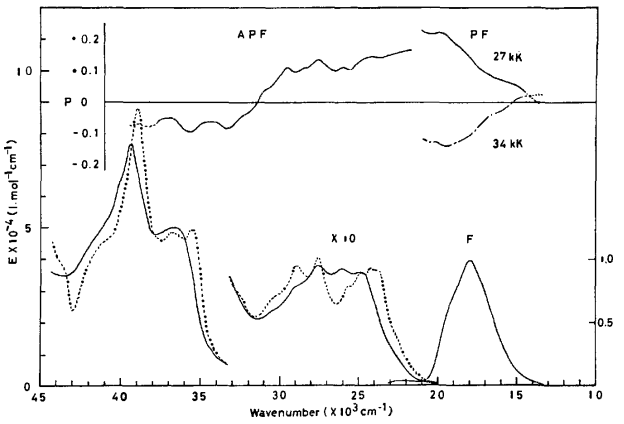

Fig. 9. Absorption spectra of IV at 298 K (full line) and at 77 K (broken line) with emission spectrum, PF, and APF mesured at 77 K. APF monitored at 17500 cm^{-1}.

[2.2](1,4)(9,10)Anthracenophane (IV). The absorption spectra measured at room temperature and 77 K are shown in Fig. 9. The spectra show a conspicuous change at 77 K as compared to that at room temperature, particularly in the lowest energy region. At 22500 cm^{-1} a faint shoulder is observed, but it is not clear whether it is correlated to the lowest calculated level of $ER_1(+)+CR_1(+)$. The strong bands observed at 23800, 24200, 24800, and 25600 cm^{-1} are assigned to the transitions to the $ER_1(-)+CR_1(-)$ state. The succeeding bands found at 27600, 29000, and 30500 cm^{-1} are considered as the transition to the $ER_1(-)-CR_1(-)$ state. The red-shift of the 23800—25600 cm^{-1} bands at low temperature can be explained by a conformational change of the molecule. The NMR spectra (Fig. 4) at low temperature show a broadening of the methylene protons at $\delta=4$ ppm which may be due to the conformational changes. According to a theoretical calculation, a slight change in molecular conformation may cause a significant change in energy levels, therefore a slight change in molecular structure may induce a conspicuous change in absorption spectra. The state which involves the CR configuration will be particularly influenced by a conformational change. The red shift of the 24000 cm^{-1} band can be reasonably understood by a contribution of the CR state to this level.

In the ranges 31500—34000 and 35500—37000 cm^{-1}, the absorption bands detected are ascribed to the $ER_2(-)+CR_2(-)$ state and the higher CR states. The strongest absorption band observed in the 39000—40000 cm^{-1} region is assigned to the $ER_2(-)-CR_2(-)$ state, which is polarized along the long-axis.

The fluorescence and APF spectra measured at room temperature and 77 K are shown in Fig. 9. At low temperature the fluorescence is of a typical excimer type, the Stokes shift being *ca.* 5000 cm^{-1}. APF spectra show positive p-values in the ranges 21500—26000 and 27000—31000 cm^{-1} for the emission band detected at 17500 cm^{-1}.

The results indicate that the polarization of the emission is inclined to the short-axis. In the higher energy region above 32000 cm^{-1}, the p-value is negative. By using Eq. 12 and these p-values, the direction of the transition moment of emission band is estimated as shown in Fig. 7.

The polarization of the fluorescence (PF) is not constant for the whole range of emission bands; the p-value is much more positive in the higher than the lower energy region. A similar result was reported by Subudhi *et al.*[19] for the sandwich dimer formed by the photocleavage of dianthracene in a rigid media. The lifetime of this emission at 77 K is 150—170 ns, typical of the excimer type emission.

Concluding Remarks

The absorption spectra of anthracenophanes show a remarkable change as compared to the sandwich dimer prepared by the photolysis of dianthracene at low temperature. This implies that the inter-ring interaction between anthracene chromophore is much stronger than in the sandwich dimer because the inter-ring distance is shorter than that of normal van der Waals contact. Moreover the planes of the anthracene rings in anthracenophanes are so deformed by ethylene bridges that some fordidden transitions in anthracene appear with lowering in molecular symmetry.

Relative arrangement of the faced rings greatly affects the pattern of the absorption spectra. The charge resonance and exciton type interactions are found to be most important for the interaction between the faced aromatic rings. The absorption bands corresponding to the excimer emission state were observed with weak intensities at the lowest energy region.

The excimer type fluorescence spectra of *syn*-[2.2](1,4)anthracenophane and [2.2](1,4)(9,10)anthracenophane do not differ much from that of the sandwich dimer. A large electron overlap is necessary for the stabilization of the excited state. An overlap of more than two benzene rings is sufficient for the excimer type emission to appear. A large Stokes shift from the

absorption to the fluorescence maximum suggests that the molecules are further deformed in the excited state to cause the stabilization of the excited level and the destabilization of the ground state. The excimer emission state was found to involve nearly a half CR state besides the lowest exciton states of the short- and the long-axis polarization.

References

1) E. A. Chandross, J. Ferguson, and E. G. McRae, *J. Chem. Phys.*, **45**, 3546 (1966).

2) J. Ferguson, A. W.-H. Mau, and J. M. Morris, *Aust. J. Chem.*, **26**, 91 (1973).

3) J. Ferguson and A. W.-H. Mau, *Mol. Phys.*, **27**, 377 (1974).

4) J. Tanaka and M. Shibata, *Bull. Chem. Soc. Jpn.*, **41**, 34 (1968).

5) T. Toyoda and S. Misumi, *Tetrahedron Lett.*, in press.

6) A. Wada and J. Tanaka, *Acta Crystallogr., Sect. B*, **33**, 355 (1977).

7) T. Hayashi, N. Mataga, Y. Sakata, S. Misumi, M. Morita, and J. Tanaka, *J. Am. Chem. Soc.*, **98**, 5910 (1976).

8) J. N. Murrell and J. Tanaka, *Mol. Phys.*, **7**, 363 (1964).

9) T. Azumi, A. T. Armstrong, and S. P. McGlyn, *J. Chem. Phys.*, **41**, 3839 (1964).

10) A. K. Chandra and E. C. Lim, *J. Chem. Phys.*, **48**, 2589 (1968).

11) (a) T. Toyoda, I. Otsubo, T. Otsubo, Y. Sakata, and S. Misumi, *Tetrahedron Lett.*, **1972**, 1731; (b) A. Iwama, T. Toyoda, T. Otsubo, and S. Misumi, *ibid.*, **1973**, 1725; (c) A. Iwama, T. Toyoda, M. Yoshida, T. Otsubo, Y. Sakata, and S. Misumi, *Bull. Chem. Soc. Jpn.*, **51**, 2988 (1978).

12) J. H. Golden, *J. Chem. Soc.*, **1961**, 3741.

13) R. Pariser and R. G. Parr, *J. Chem. Phys.*, **21**, 466 (1953); *ibid.*, **21**, 767 (1953).

14) J. A. Pople, *Trans. Faraday Soc.*, **49**, 1375 (1953).

15) N. Mataga and K. Nishimoto, *Z. Phys. Chem., N.F.*, **13**, 140 (1957).

16) G. Kaupp, *Angew. Chem. Int. Ed. Engl.*, **11**, 313 (1972).

17) J. Ferguson, M. Morita, and M. Puza, *Chem. Phys. Let·.*, **42**, 288 (1976).

18) J. Ferguson, M. Morita, and M. Puza, *Chem. Phys. Lett.*, **49**, 265 (1977).

19) P. C. Subudhi, N. Kanamaru, and E. C. Lim, *Chem. Phys. Lett.*, **32**, 503 (1975).

20) (a) F. Perrin, *Ann. Phys.*, **12**, 169 (1929); (b) A. Jablonski, *Z. Phys.*, **96**, 236 (1935); (c) Th. Förster, "Floreszenz organischer Verbindungen," Vandenhoeck u. Ruprecht, Göttingen (1951).

Electronic Spectra and Electronic Structures of a Series of Bisdehydroannulenes

Jiro TANAKA,* Masashi TANAKA, Masaharu MORITA,** Masazumi NAKAGAWA,† and Masahiko IYODA†

Department of Chemistry, Faculty of Science, Nagoya University, Chikusa, Nagoya 464
†*Department of Chemistry, Faculty of Science, Osaka University, Toyonaka, Osaka 560*

(Received May 15, 1978)

Electronic absorption spectra of tetra-*t*-butylbisdehydro[14], [18], [22], [26], and [30]annulenes were investigated experimentally and theoretically. SCF MO calculations were carried out by the P-P-P method and random phase approximation (RPA). An assignment of spectra is presented. Fluorescence excitation polarization spectra of tetra-*t*-butylbisdehydro[14]annulene and the crystalline reflection spectra of tetra-*t*-butylbisdehydro[18]annulene were studied in order to determine the polarization of the spectra. The assignment was confirmed by these methods.

Recently a series of bisdehydroannulenes were synthesized by Nakagawa and coworkers.[1,2] The molecules were shown to have a symmetrical conjugated system. Among interesting physicochemical properties of these molecules, the electronic absorption spectra and fluorescence spectra are of particular interest, since they show a characteristic pattern of conjugated system.

In this paper we will present the assignment of the electronic transitions for bisdehydro[14], [18], [22], [26], and [30]annulenes based on the polarization analyses of the absorption bands with the aid of a crystalline reflectance measurement. The fluorescence polarization technique was also used for determination of the polarization direction. A theoretical calculation of the excited state has been performed, the effect of the bond alternation being examined.

Experimental

The synthesis of the compounds used in this investigation has been described elsewhere.[2] The visisble and UV absorption spectra were measured with a Carl Zeiss spectrophotometer PMQ II, and the fluorescence spectra were recorded with a Carl Zeiss spectrofluorometer. The polarization of the fluorescence was measured with a pola-coat polarizer placed parallel and perpendicular to the fluorescence cell, which was excited by light passed through a calcite polarizer. Reflectivity of a crystal was measured with a reflecting microscope constructed in this laboratory. Calculation of the energy levels of the excited states was carried out by the standard method of Pariser and Parr[3] and Pople[4] with CI calculation and the RPA method developed by Tanaka and Tanaka.[5] All the calculations were performed at Nagoya University Computation Center.

Results and Discussion

Absorption Spectra. The electronic spectra of tetra-*t*-butylbisdehydro[14], [18], [22], [26], and [30]-annulenes were measured in THF solutions in the range 10000—50000 cm^{-1}, four or five allowed transitions being found (Fig. 1). The intensities of these bands are weak, medium, very strong, and strong in the order of increasing energy. Although the location and shape of bands differ for each compound, a common spectral pattern conformable to the spectrum of naphthalene is observed.

We will use the notations used in the classification of polyacene spectra, and call the transitions ^1L_b, ^1L_a, ^1B_b, and ^1B_a bands in the order of increasing energy. A group theoretical classification of the states is also used assuming that the molecule has a D_{2h} symmetry.

Molecular Structure and Theoretical Calculation of Energy Levels. The electronic energy level of a large conjugated system is critically dependent on the precise structure of the molecule. According to the X-ray crystal analysis of Bailey and Mason,[6] and of Kabuto *et al.*[7] the crystals of bisdehydro[14] and [18]annulenes have symmetrical structures, where the center of the molecule is situated in the ceneter of the symmetry of the crystal. Although this does not necessarily indicate a symmetrical structure of the molecule, it is very probable that the molecules have a fully conjugated double bond system. However, according to Kabuto *et al.*[8] bisdehydro[22]annulene shows bond alternation in the crystal which suggests that the larger ring system is stable for the alternate bond structure. A theoretical calculation was carried out for all bisdehydroannulenes assuming that the symmetrical D_{2h} structure has cyclic delocalized double bonds. For bisdehydro[30]annulene, calculation was also carried out with alternate double bond lengths. The results are given in Table 1 together with the observed transition energies and intensities. A comparison of the calculated and observed values gives the following results:

(1) For bisdehydro[14] and [18]annulenes results obtained by the P-P-P and RPA methods are in excellent agreement except that the ^1B_b and ^1B_a transitions are reversed in sequence. The RPA method gives better results with respect to intensity. The ^1B_b and ^1B_a bands are assigned with reference to absorption intensity. The assignment for the ^1B_a band of bisdehydro[18]-annulene is based on the crystalline absorption measurement.

(2) For bisdehydro[22]annulene the agreement is not so good as comapred to small ring molecules. The ^1B_a band is calculated to be low in energy as compared to the observed 33000 cm^{-1} peak. A shoulder around 25000 cm^{-1} region can be assigned to the ^1B_a band.

(3) For bisdehydro[26]annulene the calculated values

** Present address: Matsumoto Dental College, Shiojiri, Nagano.

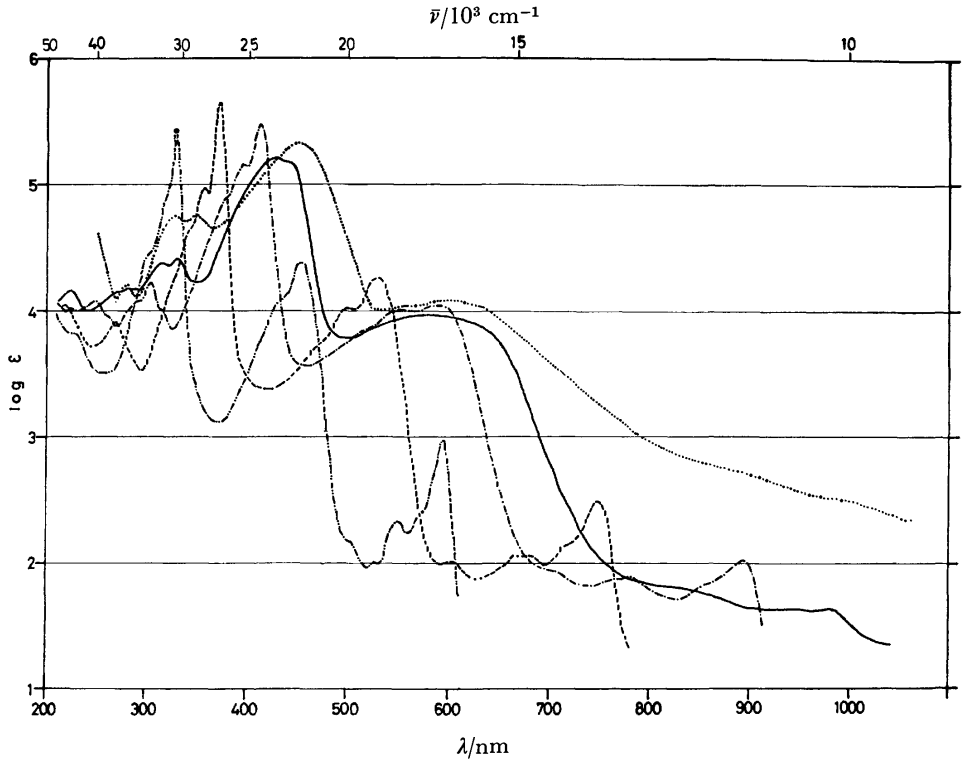

Fig. 1. Electronic absorption spectra of a series of bisdehydroannulenes.
–·–·–: [14], – – –: [18], –·–·–: [22], ——: [26], ·····: [30]annulene.

Table 1. Calculated and observed electronic transitions of bisdehydroannulenes

Number of ring atoms	Calculated transitions: PPP CI energy (cm^{-1})	f	PPA energy (cm^{-1})	f	Symmetry	Notation	Observed transitions: Energy (cm^{-1})	f	Polarization
[14]	17040	0	15590	0	B_{2u}	^1L_b	16800	0.003	*l*
	21530	0.026	21280	0.034	B_{3u}	^1L_a	21980	0.17	*s*
	33620	2.75	29510	1.39	B_{2u}	^1B_b	30550	1.21	*l*
	32830	2.62	28670	1.34	B_{3u}	^1B_a	34000	0.20	*s*
[18]	13270	0	11490	0	B_{2u}	^1L_b	13300	0.001	*l*
	16820	0.012	16450	0.016	B_{3u}	^1L_a	19000	0.25	*s*
	29020	4.45	24240	2.08	B_{2u}	^1B_b	26800	1.80	*l*
	27980	2.53	23760	1.17	B_{3u}	^1B_a	29400	0.20	*s*
[22]	10910	0	8930	0	B_{2u}	^1L_b	11200	0.004	*l*
	13840	0.007	13360	0.009	B_{3u}	^1L_a	16600	0.27	*s*
	26100	6.34	21630	2.79	B_{2u}	^1B_b	24200	2.30	*l*
	24090	2.32	19920	1.00	B_{3u}	^1B_a	33000	0.23	*s*
[26]	9310	0	7200	0	B_{2u}	^1L_b	10180	0.0002	*l*
	11790	0.005	11230	0.006	B_{3u}	^1L_a	15600	0.20	*s*
	23800	8.23	19420	3.47	B_{2u}	^1B_b	22500	2.20	*l*
	21240	2.14	17210	0.88	B_{3u}	^1B_a	30200	0.55	*s*
[30]	(Sym. structure)								
	8170	0	5980	0	B_{2u}	^1L_b			
	10310	0.004	9690	0.004	B_{3u}	^1L_a			
	21930	10.1	17690	4.13	B_{2u}	^1B_b			
	19080	2.0	15200	0.78	B_{3u}	^1B_a			
	(Deform. structure)								
	10860	0	9440	0	B_{2u}	^1L_b	10000	2×10^{-4}	*l*
	10570	0.002	10290	0.001	B_{3u}	^1L_a	15200	0.21	*s*
	21240	7.61	18470	3.93	B_{2u}	^1B_b	22200	2.50	*l*
	18250	1.42	15860	0.73	B_{3u}	^1B_a	28400	0.60	*s*

are smaller than the observed values. The ^1B_a band is calculated to be too low in energy; it might be buried under the strong band around 24000 cm^{-1} region. If this is the case the 30200 cm^{-1} band should be assigned to another origin.

(4) For bisdehydro[30]annulene the calculated results are also lower in energy than the observed bands; the symmetrical model gives much lower energies than the alternate deformed model. It appears that the molecule has actually an alternate bond structure.

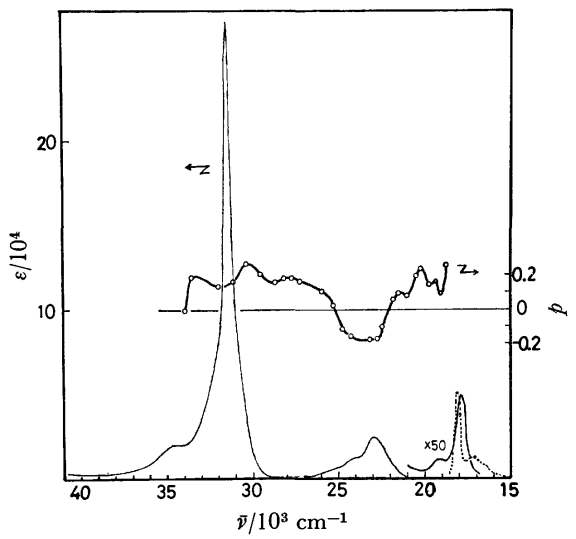

Fig. 2. Electronic absorption (——), fluorescence (……), and fluorescence excitation polarization (APF) spectra (-∘-∘-) of bisdehydro[14]annulene. p-Values are in the middle of the figure.

Fluorescence Excitation Polarization Spectra. The fluorescence excitation polarization (AFP) of bisdehydro[14]annulene was measured in 2-methyltetrahydrofuran solution at 77 K. The fluorescence was detected at 17100 cm^{-1}. The result is shown in Fig. 2. The fluorescence peak at 77 K was noticeably blue shifted as compared to the absorption peak at room temperature. The polarization of the excitation band defined by $p=I_{//}-I_{\perp}/I_{//}+I_{\perp}$ is also shown. The p-value for the first absorption band is positive (0.25—0.10), while that for the second band (^1L_a band) around 22000 cm^{-1} is negative (−0.19). For the strongest absorption region around 30000 cm^{-1}, the p-value is positive (0.25—0.13), becoming zero at around 33000 cm^{-1}. A theoretical calculation showed the polarization character; the first and the strongest bands are long-axis polarized, the second band is short-axis polarized and another short-axis polarized transition exists at above 30000 cm^{-1}. The result from AFP measurement confirms the theoretical assignment of polarization if we assume that the lowest transition is long-axis polarized. This was confirmed by the crystalline spectra of bisdehydro[18]annulene, and we use this result for bisdehydro[14] and other bisdehydro annulenes. A preliminary result on di-*t*-butyldiphenylbisdehydro[14]-annulene was reported.[1)]

Crystalline Spectra of Bisdehydro[18]annulene. In order to find a more reliable assignment of the spectra,

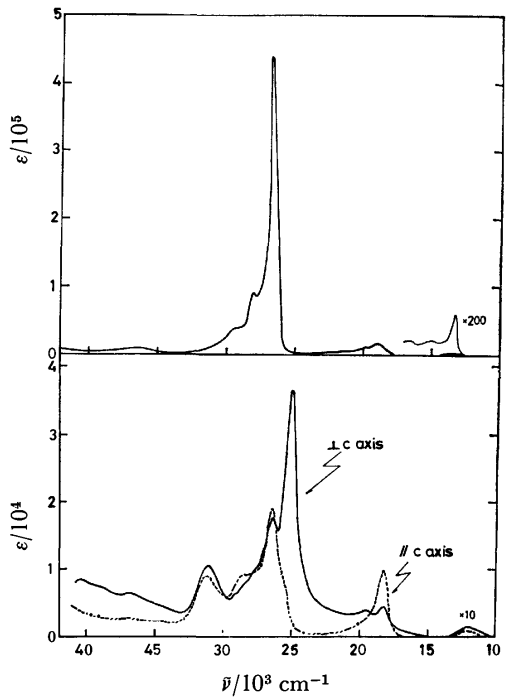

Fig. 3. Solution and the crystalline (110) face spectra of bisdehydro[18]annulene

the single crystal polarization spectra of bisdehydro[18]-annulene were measured by a reflection method. The solution spectra in 2-methyltetrahydrofuran and the crystalline spectra of bisdehydro[18]annulene are shown in Fig. 3; the crystalline spectra were obtained for the (110) face by the Kramers-Kronig transform of reflectivity. For the first absorption region the absorption was too weak to be measured by means of reflectivity and the transmission measurement was employed.

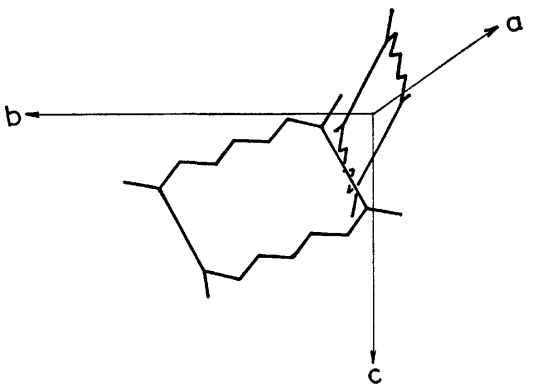

Fig. 4. Projection of molecules onto the (110) face of bisdehydro[18]annulene obtained from Ref. 7.

The projection of molecules onto the developed (110) face is shown in Fig. 4. From the crystalline projection it is easily seen that the short molecular axis of two molecules in a unit cell has a larger component along the c-axis than along the ⊥ c-axis. The long-axis of one of the molecules has a larger component along the ⊥ c-axis on this face, while another molecule has a smaller component. Thus the long-axis polarized transition will

appear mainly along the ⊥ c-direction.

The observed spectra clearly show the polarization character of each transition. The first absorption band in the 12000 cm^{-1} region is the weakest one. Such a transition is easily perturbed by the nearby transition. However, the first band shows its own polarization character in which its intensity is stronger along the ⊥ c-axis than along the // c-axis. This means that the first band has long-axis polarization. The second absorption band at 18200 cm^{-1} shows stronger absorption along the // c-axis than along the ⊥ c-axis. Thus it is assigned to the short-axis polarized transition. The third transition, which is the strongest of all transitions, shows peaks at 25000 (0-0), 26400 (0-1) and 27600 (0-2) cm^{-1} along the ⊥ c-axis, and at 26400 (0-0) and 27900—28400 (0-1, 0-2) cm^{-1} along the // c-axis. The splitting of 1400 cm^{-1} for the 0-0 band is due to a Davydov type crystalline splitting. The intensity is stronger along the ⊥ c-axis than along the // c-axis, hence it is assigned to the long-axis polarized band. The fourth absorption band appearing around 31000 cm^{-1} is considered to be the shifted one of 29400 cm^{-1} band in solution. It shows similar strengths of intensity along the ⊥ c and // c directions, and the ⊥ c band may be intensified since the tail of the third band is overlapped with the fourth band. Thus the fourth band is assigned to the short-axis polarized transition. The polarization of transitions was determined from these results (Table 1).

Concluding Remarks

Recently Kolc, Michl, and Vogel[9] studied the electronic spectra of bridged [14]annulenes and calculated excited energies of hypothetical planar [14]annulene. They obtained a similar result similar to ours which shows that the polarization of transitions are along long-, short-, short-, and long-axis in the order of increasing energy. Our theoretical results show a similar tendency, but it is not in harmony with experiment as regard to the third and fourth bands. A reason for this discrepancy may be that the valence state energies of the sp hybridized carbon atoms in the conjugated triple bonds are much larger than those of the sp^2 hybridized carbon atoms; this point was not considered in the present calculation.

References

1) M. Nakagawa, *Pure Appl. Chem.*, **44**, 885 (1975).
2) K. Fukui, T. Nomoto, S. Nakatsuji, and M. Nakagawa, *Tetrahedron Lett.*, **1972**, 3157; K. Fukui, T. Nomoto, S. Nakatsuji, S. Akiyama, and M. Nakagawa, *Bull. Chem. Soc. Jpn.*, **50**, 2758 (1977); M. Iyoda and M. Nakagawa, *Tetrahedron Lett.*, **1972**, 3161; M. Iyoda and M. Nakagawa, *J. Chem. Soc., Chem. Commun.*, **1972**, 1003; M. Iyoda and M. Nakagawa, *Tetrahedron Lett.*, **1972**, 4253; M. Iyoda and M. Nakagawa, *ibid.*, **1973**, 4743.
3) R. Pariser and R. G. Parr, *J. Chem. Phys.*, **21**, 466 (1953); *ibid.*, **21**, 767 (1953).
4) J. A. Pople, *Trans. Faraday Soc.*, **49**, 1375 (1953).
5) M. Tanaka and J. Tanaka, *Theor. Chim. Acta*, **30**, 81 (1973).
6) N. A. Bailey and R. Mason, *Proc. R. Soc., London, Ser A*, **290**, 94 (1966).
7) C. Kabuto, Y. Kitahara, M. Iyoda, and M. Nakagawa, *Tetrahedron Lett.*, **1976**, 2791.
8) C. Kabuto, Y. Kitahara, M. Iyoda, and M. Nakagawa, *Tetrahedron Lett.*, **1976**, 2787.
9) J. Kolc, J. Milch, and E. Vogel, *J. Am. Chem. Soc.*, **98**, 3935 (1976).

Electrical Properties of Langmuir Films of Fatty Acid Salts and Carotenoic Acid

Naoto YAMAMOTO, Toshihiro OHNISHI, Masahiro HATAKEYAMA, and Hiroshi TSUBOMURA*

Department of Chemistry, Faculty of Engineering Science, Osaka University, Toyonaka, Osaka 560

(Received May 26, 1978)

Electric conductivities have been studied for Langmuir molecular layers of barium salt of fatty acids and for the layers of barium arachidate mixed with *all-trans-β-apo-8'*-carotenoic acid. These results have been interpreted based on an electron tunneling model taking account of the mirror image force. The conduction levels of the layers have thereby been estimated to be 1.00 eV for barium stearate, 1.31 eV for barium arachidate and 1.45 eV for barium behenate below vacuum level. The conduction level of the carotenoic acid has been derived to be 1.9 eV from these results. The structure of these layers has been discussed from the above mentioned experimental results, together with those on surface pressure, absorption spectrum and electric capacitance.

Recently, the physicochemical properties of Langmuir films were extensively investigated by Kuhn *et al.*[1,2] They showed from electric conductivity measurements of fatty acid layers that electron tunneling predominantly contributes to the conductivity through the monomolecular layers. They estimated the conduction levels of these fatty acid salts from a theoretical equation for the tunneling current and their experimental results.[3,4]

We have investigated electrical and spectroscopic properties of molecular layers of fatty acid mixed with *all-trans-β*-carotene.[5] It has been shown that, contrary to our expectation, *β*-carotene molecules lie parallel to the plane of the molecular layer and are aggregated.

All-trans-β-apo-8'-carotenoic acid is expected to form a stable mixed monolayer with fatty acids in which the molecules are perpendicular to the layer because of its hydrophobic chain and the hydrophilic end group. It is of interest to investigate the electrical properties of the surfaces, where long π-conjugated chain molecules are perpendicularly aligned, in connection with the action of carotenoids in biological electron transport. We have studied the surface pressure, the absorption spectrum and the electric conductivity of the monolayers of fatty acid salts with and without the carotenoic acid in order to clarify the structure of these layers and the mechanism of their electric conduction.

Experimental

The method for the preparation of aluminum/Langmiuir film/aluminum junctions was described in detail in a previous paper.[5] The surface pressure of monolayer spread at an air–water interface was kept constant at 30 dynes/cm during transferring the monolayer onto a substrate by use of a compression barrier automatically driven by a servomotor combined with a Wilhelmy balance.

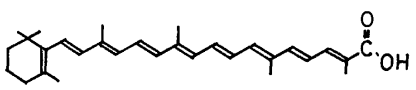

carotenoic acid

All-trans-β-apo-8'-carotenoic acid (carotenoic acid) ethyl ester was obtained from F. Hoffmann-La Roche and Co.† Carotenoic acid was prepared by hydrolysis of the ester, followed by recrystallization from a benzene solution according to Isler *et al.*[6] Absorption spectrum of the purified carotenoic acid in hexane was confirmed to agree with that reported in benzene solution.[7] No band ascribable to the cis-isomer was found in the spectrum.[8] Arachidic acid from P-L Biochemicals, Inc. was purified by recrystallization twice from an ethanol solution. Other materials were prepared and purified in the same procedures as described previously.[5]

The dc conductivity was measured with a Keithley 414S picoammeter and a Shimadzu VM101 voltmeter. The dc voltage was applied by coupling a potentiometer and a dry cell. Capacitance measurement was made with a Yokogawa-Hewlett-Packard 4265B bridge at 1 kHz, 20 mV peak-to-peak. The visible-UV absorption spectra of the films were measured with an ultra sensitive spectrophotometer constructed in our laboratry.[9]

All measurements and preparation of the mixed layers of the carotenoic acid were performed in an atmosphere of nitrogen under red light.

Results and Discussion

Structure of the Mixed Layers. Figure 1 shows the surface pressure (π) *versus* the area per molecule (A) of the monolayers of carotenoic acid mixed with arachidic acid in various molar fractions at the air–water interface. The π-A curves consist of two components: the slow rising part below 10—20 dyn/cm and the steep part in the higher pressure region. The limiting areas per molecule, A_0, were derived by extrapolating the steep part in the curves at zero-pressure. The value of A_0 was obtained to be 28 Å^2 for the pure carotenoic acid monolayer, which was between the polyene chain cross section (about 20 Å^2) and the *β*-ionone ring cross section (about 50 Å^2). This result strongly suggests that carotenoic acid molecules are standing perpendicularly at the water surface. A linear relationship between the A_0 value and the molar fraction was found for the mixed monolayers, also implying that carotenoic acid molecules are perpendicularly standing in the mixed monolayers.

Figure 2 shows the electronic absorption spectra of carotenoic acid dissolved in hexane and those incorporated in cadmium arachidate monolayers at various molar ratios deposited on slide glass. The absorption spectra of the carotenoic acid in the mixed layers are somewhat broader than that of the solution. The

† The authors wish to express their gratitude to F. Hoffmann-La Roche and Co. for the kind donation of *all-trans-β-apo-8'*-carotenoic acid ester.

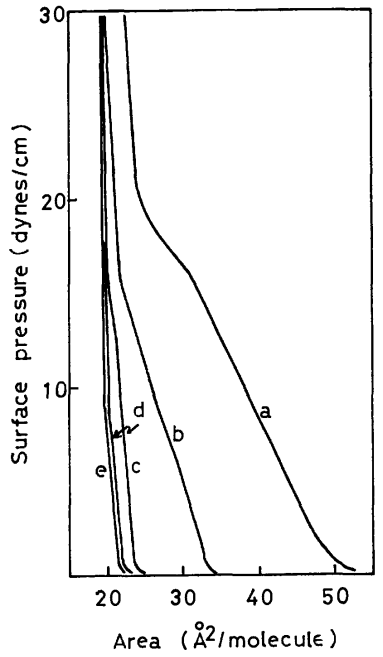

Fig. 1. The surface pressure-area curves for mixed layers of carotenoic acid and arachidic acid on the surface of solution containing 3×10^{-5} mol/l barium chloride and 4×10^{-4} mol/l potassium bicarbonate. The molar fractions of carotenoic acid were 1.0 for a, 0.464 for b, 0.0709 for c, 0.017 for d, and 0 for e, respectively.

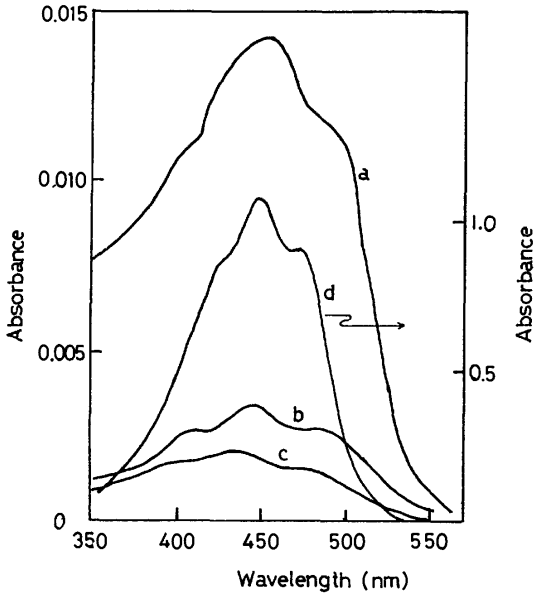

Fig. 2. Absorption spectra of the mixed monolayers of carotenoic acid and cadmium arachidate at normal incidence. The molar fractions of carotenoic acid are 1.0 for curve a, 0.194 for curve b, and 0.0973 for curve c. Curve d is for the 10^{-5} mol/l hexane solution of carotenoic acid.

spectra of the films show a slight blue-shift with decreasing molar fraction of carotenoic acid.

The "molar" extinction coefficient of carotenoic acid in the layers at the absorption peak may be defined by $\varepsilon_m=A/\Gamma$ mol^{-1} cm^2 where A is the absorbance of the monolayer and Γ is the number of moles of carotenoic acid per 1 cm^2 of the film. Taking A to be 0.014 from the maximum of curve a in Fig. 2 and Γ to be 5.9×10^{-10} mol cm^{-1}, corresponding to the value of 28 Å^2/molecule obtained for pure carotenoic acid layer, we obtain $\varepsilon_m=2.4\times10^7$ mol^{-1} cm^2. If the carotenoic acid molecules were to lie randomly in the pure carotenoic acid monolayer, ε_m would take the value of *ca.* 1.1×10^8 mol^{-1} cm^2, corresponding to the maximum molar extinction coefficient measured in the hexane solution. The experimental ε value obtained is 5 times as small as the latter. As the direction of the transition moment for the absorption band is thought to be parallel to the polyene chain, no absorption band should be observed in the wavelength region measured if the molecules are aligned in an exactly perpendicular array in the film. Simple calculation by use of our result leads to the conclusion that the carotenoic acid molecules in the pure film on an average make an angle of 20° with the line normal to the film plane. Curves b and c in Fig. 2 also indicate that the molecules are similarly oriented in the mixed films as well.

The capacitance measurements for the mixed films with various number of monolayers revealed that a good linear relationship between the reciprocal of capacitance and the number of the monolayers was observed. The value of thickness of the mixed monolayer divided by its relative permittivity was obtained to be 11.2 Å from the slope. Assuming that the electric polarization of the film is a simple sum of those due to the fatty acid and the carotenoic acid and taking the relative permittivities for the fatty acid and carotenoic acid to be 2.41[5] and 3.6[10] respectively, the thickness of carotenoic acid array was estimated to be 28 Å, corresponding to the length of the molecule, by the same methods as employed for the layers of fatty acid salt mixed with β-carotene.[5] This result also confirms that the carotenoic acid molecules are perpendicularly standing in the mixed monolayers deposited on the solid substrate. The conclusion on the molecular orientation of carotenoic acid in the layers agrees with that reported by Reich[11] and Engelsen.[7]

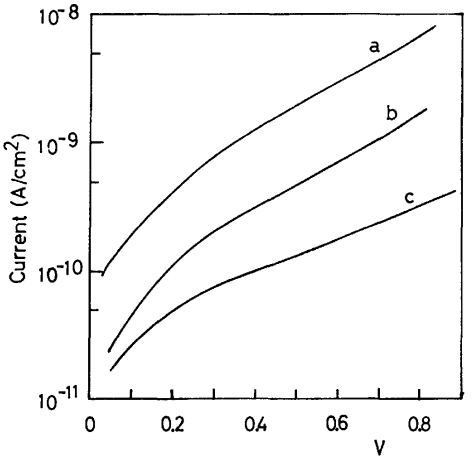

Fig. 3. The current-voltage curves for the monolayers of fatty acid salts: (a) barium stearate, (b) barium arachidate, and (c) barium behenate.

Conductivity Measurements. The current-voltage (j-V) curves obtained for the fatty acid salt monolayers at room temperature are shown in Fig. 3. The magnitude of current decreased with increasing fatty acid chain length, *i.e.*, in the order of barium stearate, barium arachidate and barium behenate. Each of the currents was proportional to the applied voltage in the low voltage region ($V<0.1$ V), but increased exponentially above 0.3 V. The currents obtained were about 100 times as small as those measured for Al/fatty acid salt/metal junctions by Kuhn *et al.*,[3,4] though the shapes of our j-V curves were very similar to theirs. The currents for 3-, 5-, 7-, and 9-layer films were much smaller than that for the monolayer, and proportional to the voltage up to about 0.8 V. The dc conductivity, σ_0, calculated from this ohmic behavior of the multilayer films was 2.3×10^{-16} Ω^{-1} cm^{-1} for barium stearate, 1.1×10^{-16} Ω^{-1} cm^{-1} for barium arachidate and 4.8×10^{-17} Ω^{-1} cm^{-1} for barium behenate. The σ_0 values fall into the range of conductivities of paraffin in the solid state.[12] This fact indicates that the fatty acid multi-layer films prepared have no substantial pinholes.

TABLE 1. TUNNELING CONDUCTIVITY, POTENTIAL BARRIER HEIGHT AND CONDUCTION LEVEL OF FATTY ACID SALT MONOLAYERS AND CAROTENOIC ACID ARRAY IN THE MIXED MONOLAYER

Material	σ_t (Ω^{-1} cm^{-1})	$\bar{\phi}$(eV)	V_0(eV)	d(Å)
Barium stearate	2.7×10^{-16}	2.53	1.00	25.8[a]
Barium arachidate	8.7×10^{-17}	2.26	1.31	28.0[a]
Barium behenate	1.96×10^{-17}	2.05	1.45	30.2[a]
Carotenoic acid	1.95×10^{-14}	1.7	1.9	28

a) Taken from Ref. 4.

The j-V curves obtained for the monolayers are reasonably explained by the electron tunneling model given for thin oxide films by Simmons.[13] The tunneling conductivity, σ_t, for the fatty acid salt monolayers was derived by subtracting σ_0 from the conductivity obtained for the monolayers at low voltage region and listed in Table 1. According to a Simmons' equation for a rectangular potential barrier in the low voltage region,[13] the tunneling current, j_t, can be expressed as a function of potential barrier height, $\bar{\phi}$, as follows:

$$j_t = [(2m\bar{\phi})^{1/2}/d](e/h)^2 \cdot V \cdot \exp[-4\pi d/h \cdot (2m\bar{\phi})^{1/2}], \quad (1)$$

where m and e are the electron mass and charge, respectively, h is Planck's constant and d the thidkness of monolayer. The $\bar{\phi}$ values calculated from the σ_t values using Eq. 1 are listed in Table 1. Assuming that $\bar{\phi}$ is simply represented by the difference between the work function of the metal electrode and the electron conduction level of the monolayer, V_0, the V_0 values of 1.7—2.1 eV were calculated for these fatty acid salts taking 4.2 eV as the work function of aluminum.[14] On the other hand, if one takes account of a mirror image force due to the metal electrodes, the V_0 values as listed in Table 1 were obtained with the aid of Simmons' method (Eqs. 48 and 49 in Ref. 13).

Figure 4 shows j-V curves measured for mono- and multi-layer films of barium arachidate with and without carotenoic acid at room temperature. The current measured for the mixed monolayer was much higher than that for the barium arachidate monolayer. The electric conductivity of the mixed monolayers is considered to be a sum of those by the barium arachidate array and the carotenoic acid array, so that the current in the mixed monolayer is caused mainly by electron flowing through the carotenoic acid array. The σ_0 and V_0 values were roughly estimated to be 1.1×10^{-13} Ω^{-1} cm^{-1} and 1.73 eV for the mixed monolayer, respectively.[15]

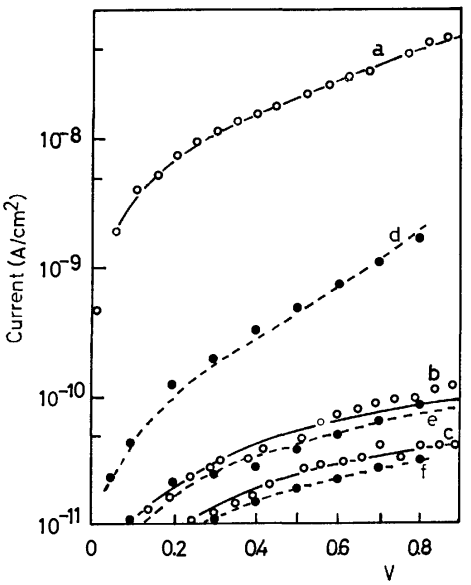

Fig. 4. The current-voltage curves for mono- and multilayer films of arachidic acid salt with and without carotenoic acid. Curves a, b, and c; for 1-, 5-, and 7-layer films of arachidic acid salt mixed with carotenoic acid, respectively (○). Curves d, e, and f; for 1-, 5-, and 7-layer films of arachidic acid salt, respectively (●). Solid and dotted lines are calculated curves (Ref. 15). Molar fraction of carotenoic acid in the mixed layers is 0.0709.

In the case of multi-layer films, the increase in the current due to the addition of carotenoic acid was small. The conductivity of the multi-layer films of barium arachidate mixed with carotenoic acid was obtained to be 1.3×10^{-16} Ω^{-1} cm^{-1} from the j-V curves shown in Fig. 3.

The conduction band level of a dry electron has been estimated to be almost zero for alkanes,[16,17] and the depth of electron trap in alkane matrices and benzene matrices have been obtained to be 0.26 eV[17-19] and 0.5 eV,[19] respectively. Our V_0 values are somewhat larger than either of these values.

The Simmons' equations have been derived for the tunneling current at 0 K.[13] At higher temperatures, the metal electrons should be populated in the higher electronic states of the electrode metal according to the Fermi distribution. It is, therefore, expected that part of the metal electrons are allowed to have kinetic energies much more than the average thermal energy ($kT\approx0.03$ eV) at room temperature. Though the number of

electrons in such highly excited states are relatively few according to the Fermi distribution, they can contribute largely in the tunnel current by the exponential dependence of the effective barrier height. Consequently, it becomes likely that our room temperature experiment brings about the larger V_0 value.

Inelastic electron tunneling process coupled with vibrational excitation and polarization of molecules has been investigated at low temperature.[20] It has been pointed out that an inelastic process for a monolayer of simple organic molecules adsorbed on metal oxide surface changes the conductance by *ca.* 1%,[21] and that the inelastic tunneling channels increase with applied voltage. In the inelastic processes, the electrons either lose or gain energy by interactions with the film material. In the first case, electrons should have excess energy to compensate the energy loss due to the inelastic processes in order to reach another electrode. In the second case, the film material should be in a higher lattice vibration-rotation states. Therefore, in either case, the probability of the inetastic tunneling is increased at higher temperature. It is, therefore, suggested that such an inelastic process, giving more important contributions at higher temperature, makes the experimental V_0 values larger than those corresponding to the conduction band levels for the alkane matrices obtained by other experimental methods.

References

1) H. Kuhn, D. Möbius, and H. Bücher, "Techniques of Chemistry," ed by A. Weissberger and B. W. Rossitor, Wiley, New York (1972), Vol. 1, Part 3B, p. 577.

2) H. Bücher, K. H. Drexhage, M. Fleck, H. Kuhn, D. Möbius, F. P. Schäfer, J. Sondermann, W. Sperling, P. Tillmann, and J. Wiegand, *Mol. Cryst.*, **2**, 199 (1967).

3) B. Mann, H. Kuhn, and L. V. Szentpály, *Chem. Phys. Lett.*, **8**, 82 (1971).

4) B. Mann and H. Kuhn, *J. Appl. Phys.*, **42**, 4398 (1971).

5) T. Ohnishi, M. Hatakeyama, N. Yamamoto, and H. Tsubomura, *Bull. Chem. Soc. Jpn.*, **51**, 1714 (1978).

6) O. Isler, W. Guex, R. Rüegg, G. Ryser, G. Saucy, U. Schwieter, M. Walter, and A. Winterstein, *Helv. Chim. Acta*, **42**, 864 (1959).

7) D. den Engelsen and B. de Koning, *J. Chem. Soc., Faraday Trans. 1*, **70**, 2100 (1974).

8) W. Vetter, G. Englert, N. Rigassi, and U. Schwieter, "Carotenoids," ed by O. Isler, Birkhauser Verlag, Basel (1971), p. 195.

9) N. Yamamoto, T. Sawada, and H. Tsubomura, to be published.

10) The relative permittivity, ε, was estimated to be 3.5 ± 0.2 by Reich *et al.* in Ref. 11. The value of refractive index, n, of carotenoic acid was reported to be 1.91 by Engelsen *et al.* in Ref. 7. From the relation: $\varepsilon=n^2$, the ε value is also estimated to be 3.6 for carotenoic acid.

11) R. Reich and K.-U. Sewe, *Photochem. Photobiol.*, **26**, 11 (1977).

12) F. M. Farmer, "International Critical Tables of Numerical Data, Physics, Chemistry and Technology," ed by E. W. Washburn, Mc Graw-Hill, New York (1972), Vol. 2, p. 310.

13) J. G. Simmons, *J. Appl. Phys.*, **34**, 1793 (1963).

14) J. C. Rivière, "Solid State Surface Science," ed by M. Green, Dekker, New York (1969), Vol. 1, p. 179.

15) Calculated j-V curves were obtained by summing the ohmic current $(\sigma_0 V/d)$ and tunneling current, j_t, which was calculated by using Eq. 27 in Ref. 13 and $\bar{\phi}$ values.

16) N. R. Kestner and J. Jortner, *J. Chem. Phys.*, **59**, 26 (1973); R. A. Holroyd, S. Tames, and A. Kennedy, *J. Phys. Chem.*, **70**, 2857 (1975).

17) S. Noda, L. Kevan, and K. Fueki, *J. Phys. Chem.*, **79**, 2866 (1975).

18) R. Schiller, *J. Chem. Phys.*, **57**, 2222 (1972).

19) Y. Nakato, M. Ozaki, and H. Tsubomura, *J. Phys. Chem.*, **76**, 2105 (1972).

20) R. C. Jaklevic and J. Lambe, *Phys. Rev. Lett.*, **17**, 1139 (1966).

21) D. J. Scalapino and S. M. Marcus, *Phys. Rev. Lett.*, **18**, 459 (1967); B. F. Lewis, M. Mosesman, and W. H. Weinberh, *Surface Sci.*, **41**, 142 (1974).

NMR Studies on Zerovalent Metal π-Complexes of Dibenzylideneacetone. I. Ligand Conformation and Bonding in the Binuclear Palladium Complex

Hiroshi KAWAZURA,* Hisao TANAKA, Koh-ichi YAMADA, Toshio TAKAHASHI,** and Yoshio ISHII**

Faculty of Pharmaceutical Sciences, Josai University, Sakado, Saitama 350-02
***Department of Synthetic Chemistry, Faculty of Engineering, Nagoya University, Chikusa, Nagoya 464*

(Received June 9, 1978)

To elucidate the ligand conformation and the metal–olefin bonding nature in the binuclear palladium complex of dibenzylideneacetone, $Pd_2[(C_6H_5CH{=}CH)_2CO]_3$, ^1H NMR studies have been performed on the deuteriated complexes $Pd_2[(C_6D_5CH{=}CH)_2CO]_3$, $Pd_2[(C_6D_5CD{=}CH)_2CO]_3$, and $Pd_2[(C_6D_5CH{=}CD)_2CO]_3$. Examination of the spectra has revealed that the three dibenzylideneacetone ligands which triply bridge the two Pd atoms are all in the *s-cis,trans* conformation. The most probable bonding scheme of the three ligands to the two Pd atoms is as follows: one Pd atom is ligated by one *s-trans* and two *s-cis* olefinic moieties and hence the other by one *s-cis* and two *s-trans* to yield a metal–olefin bonding stronger in the former combination than in the latter. A linear correlation between the couplings and the mean chemical shifts of the *trans* olefinic protons suggests a dominant role of metal to olefin π-back donation in differentiating the olefinic moieties in their bonding strength to the metal atoms and in retaining the characteristic rigid structure of the complex.

Concurrently reported X-ray structural analyses[1–3] of the binuclear Pd complexes of dibenzylideneacetone (dba), $(C_6H_5CH{=}CH)_2CO$, of the formula $Pd_2(dba)_3$(solvent) showed an interesting disparity in the conformations of the dba ligands. Pierpont and Mazza[1,2] conducted a structural analysis on a crystal of $Pd_2(dba)_3(CH_2Cl_2)$ and found two dba molecules in the *s-cis,trans* conformation and one in the more symmetric *s-trans,trans* conformation, whereas the analysis[3] of a crystal of $Pd_2(dba)_3(CHCl_3)$ indicated all three to be in the *s-cis,trans* conformation. The $Pd_2(dba)_3$ molecule in both crystals possesses essentialy the same configurational arrangement, *i.e.*, the two olefinic double bonds of a given dba ligand coordinate separately to Pd atoms (Pd–Pd distance 3.24 Å) to form a binuclear complex in which each of the Pd atoms exhibits trigonal coordination. The fact that the solvent molecules of crystallization in the $Pd_2(dba)_3$ molecule play a decisive role in changing the conformation of the dba ligand in the crystals prompted us to elucidate the ligand conformation of $Pd_2(dba)_3$ in solutions.

Another motive of this study emerged from a desire to elucidate the metal to olefin bonding nature. The $Pd_2(dba)_3$ molecule can provide genuine information on the π-olefin–metal bonding since the molecule contains a ligand in which only the olefinic portions are involved in bonding to the metal atoms.

With the above interests, we have performed a ^1H NMR study on the $Pd_2(dba)_3$ molecule. Examination of the NMR parameters for the olefinic moieties of the ligands has led to a clarification of the ligand conformation and suggested the bonding nature of the ligands to the Pd atoms.

Results and Discussion

Analysis of the ^1H NMR Spectrum of $Pd_2(dba)_3$.
As earlier reported,[3] the signals of the olefinic protons in $Pd_2[(C_6H_5CH{=}CH)_2CO]_3(CHCl_3)$ are partially obscured by those of the phenyl protons, although they are spread considerably to high field as a direct consequence of coordination. The whole pattern of olefinic protons was observed in the spectrum of $Pd_2[(C_6D_5CH{=}CH)_2CO]_3(CHCl_3)$ in $CDCl_3$ (Fig. 1A). The interpretation of this intricate spectrum was assisted by the availability of the spectra of $Pd_2[(C_6D_5CD{=}CH)_2CO]_3(CHCl_3)$ and $Pd_2[(C_6D_5CH{=}CD)_2CO]_3(CHCl_3)$ in $CDCl_3$ (Fig. 1C and D). These well resolved spectra were obtained through a number of pattern accumulations carried out by a pulsed 100 MHz NMR system in the Fourier transform mode. The fast pulsed scans greatly reduced the measurement time, so that liberation of the coordinated dba was minimized. The resonances

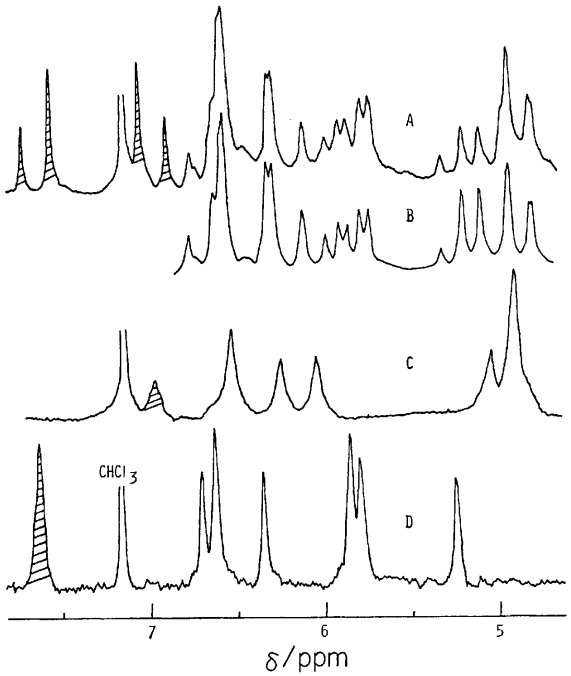

Fig. 1. ^1H NMR spectra measured in $CDCl_3$ at 25 °C. A: $Pd_2[(C_6D_5CH{=}CH)_2CO]_3$, C: $Pd_2[(C_6D_5CD{=}CH)_2CO]_3$, and D: $Pd_2[(C_6D_5CH{=}CD)_2CO]_3$ and B: the computer-simulated spectrum of $Pd_2[(C_6D_5CH{=}CH)_2CO]_3$.

originating from the free dba are shown with striped lines in Fig. 1. The spectra of Fig. 1C and D explicitly gave the resonance positions of the olefinic protons on the carbonyl side (H_A) and those of the olefinic protons on the phenyl side (H_B), respectively, in the coordinated dba. The chemical shifts of H_A and H_B (δ_A and δ_B) were used to assign the olefinic AB quartet families by spin decoupling in the spectrum of Fig. 1A, and then to simulate the spectrum by providing the coupling constants (J_{AB}) as small variables. An optimal simulation spectrum (Fig. 1B) was obtained to give the ^1H NMR parameters of the six olefinic moieties in the dba ligands (Table 1).

Table 1. ^1H NMR parameters of the olefinic protons of dba in $Pd_2(dba)_3$ in $CDCl_3$ at 25 °C

Olefin	J_{AB}/Hz	δ_A/ppm	δ_B/ppm	δ_{AB}/ppm	$\bar{\delta}_H$/ppm
a	14.2	6.619	6.688	0.069	6.654
b	13.7	6.134	6.765	0.631	6.450
c	13.8	6.322	6.422	0.100	6.372
d	12.7	4.935	5.900	0.965	5.418
e	12.7	4.916	5.853	0.937	5.385
f	12.3	5.057	5.243	0.186	5.150

δ_A and δ_B; in ppm with tetramethylsilane. $\delta_{AB}=\delta_B-\delta_A$ and $\bar{\delta}_H=(\delta_A+\delta_B)/2$. For free dba (in $CDCl_3$ at 25 °C): J_{AB}; 16.0 Hz, δ_A; 7.090, δ_B; 7.750, δ_{AB}; 0.660, and $\bar{\delta}_H$; 7.420 ppm.

From the Table, it can be seen that the six olefinic moieties which manifest various AB quartet patterns divide into two distinct and separate groups of three with respect to either the coupling J_{AB} or mean chemical shift $\bar{\delta}_H[=(\delta_A+\delta_B)/2]$ of the olefinic protons in the *trans* configuration; the three olefinic moieties **a**, **b**, and **c** with J_{AB} of *ca.* 14.0 Hz are located on the low field side ($\bar{\delta}_H$; *ca.* 6.5 ppm) and the other three **d**, **e**, and **f** with J_{AB} of *ca.* 12.5 Hz on the high field side ($\bar{\delta}_H$; *ca.* 5.3 ppm). The high field shift of the olefinic proton signals upon coordination has been observed for many metal–olefin π-complexes, especially for low valency transition metal complexes[4] and has been directly related to the amount of metal to olefin π-back donation.[5,6] It follows that the olefinic moieties **d**, **e**, and **f** are stronger in the π-bonding with the Pd atom than the other olefinic moieties **a**, **b**, and **c**.[10]

The six olefinic moieties can also be divided into another two distinct groups of three with respect to the internal chemical shift $\delta_{AB}(=\delta_B-\delta_A)$; the three olefinic moieties **a**, **c**, and **f** with δ_{AB} smaller than 0.2 ppm and the other three **b**, **d**, and **e** with δ_{AB} larger than 0.6 ppm. It should be noted that the former group contains two of the olefinic moieties with $\bar{\delta}_H$ of *ca.* 6.5 ppm and so the latter contains only one of them. Therefore the separation of the olefinic moieties with respect to δ_{AB} must differ in its origin from the separation with respect to $\bar{\delta}_H$.

Conformation of the dba Ligands. In the preceding paper[12] it has been shown that the parameter δ_{AB} is a good measure of the conformation of the olefinic moiety of dba. Thus it has been fully proven that the *s-cis* form of the olefinic moiety must have a minimum value of δ_{AB} (0.5 ppm) which increases slightly by a deformation towards the *s-skew* form, while the *s-trans* form must have a maximum value of δ_{AB} (1.5 ppm) which decreases rapidly even by a small deformation towards the *s-skew* form. From the above relation between the δ_{AB} value and the form of the olefin, it can be said that the six olefinic moieties of the coordinated dba molecules consist of three in the *s-cis* form (olefins **a**, **c**, and **f**) and three in the *s-trans* form (olefins **b**, **d**, and **e**).[13]

The existence of an equal number of both forms in the olefinic moieties necessarily demands at least one of the dba ligands with *s-cis,trans* conformation. In mutual allocation between H_A of one of the two olefinic portions of dba and H_B of the other, only the allocation between H_A of the *s-cis* olefin and H_B of the *s-trans* olefin in the *s-cis,trans* conformation brings about the closest proximity between H_A and H_B (Fig. 2); hence an intramolecular NOE will be a maximum for one of

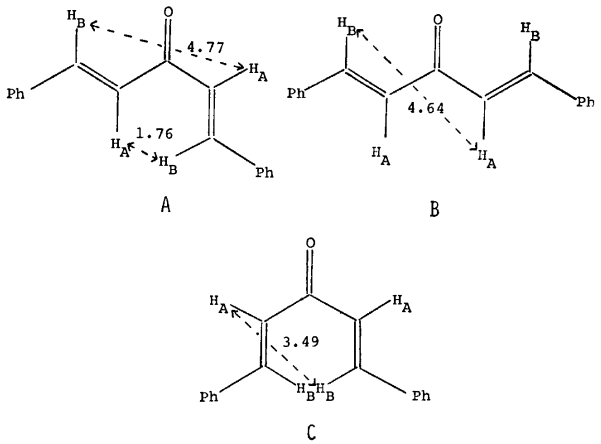

Fig. 2. Three basic conformations of dba. A: *s-cis, trans* B: *s-cis, cis*, and C: *s-trans, trans* and distances (in Å), between H_A and H_B in the different olefinic moiety in a given dba, estimated from the bond lengths and angles assumed in the preceding paper.[12]

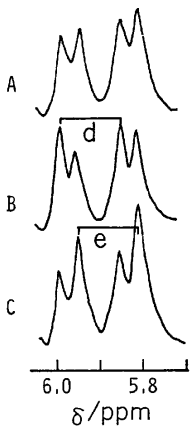

Fig. 3. NOE effects. A: Ordinary signals of H_B's of olefins **d** and **e** near 5.9 ppm in the spectrum of $Pd_2[(C_6D_5CH{=}CH)_2CO]_3$, B: enhancement of H_B signal of olefin **d** on an irradiation of H_A of olefin **a**, and C: enhancement of H_B signal of olefin **e** on an irradiation of H_A of olefin **c**. These spectra were successively taken under identical conditions.

these proton signals when the other is saturated. Figure 3 shows the results of irradiation of the H_A protons in the olefinic moieties. As expected, the irradiation of H_A in the *s-cis* olefin **a** caused an appreciable enhancement of the signal intensity of H_B in the *s-trans* olefin **d**. This indicates that the *s-cis* olefin **a** and *s-trans* olefin **d** are linked to constitute one *s-cis,trans* dba ligand. The signal enhancement of H_B in olefin **e** was also observed on irradiation of H_A in olefin **c** to show the existence of another dba ligand of *s-cis,trans* conformation. Thus the remainder, the *s-trans* olefin **b** and *s-cis* olefin **f** should combine to give the third *s-cis,trans* ligand. Thus it may be concluded that the $Pd_2(dba)_3$ molecule in solution retain the three dba ligands in a *s-cis,trans* conformation as in the crystalline state.

If the conformations of the dba ligands in the crystal could be conserved in solution as in $Pd_2(dba)_3(CHCl_3)$, for $Pd_2(dba)_3(CH_2Cl_2)$ an ^1H NMR spectrum differing from that of $Pd_2(dba)_3(CHCl_3)$ would be expected. The ^1H NMR spectrum of $Pd_2[(C_6D_5CH{=}CH)_2CO]_3$-$(CH_2Cl_2)$ prepared by the recrystallization of Pd_2-$[(C_6D_5CH{=}CH)_2CO]_3(CHCl_3)$ in CH_2Cl_2 was measured in CD_2Cl_2. The spectrum showed that the resonance pattern of the olefinic protons was completely identical with that of $Pd_2[(C_6D_5CH{=}CH)_2CO]_3(CHCl_3)$ in $CDCl_3$, implying that in solution, the sterically repulsive *s-trans,trans* dba ligand[12] in the crystalline $Pd_2[(C_6D_5$-$CH{=}CH)_2CO]_3(CH_2Cl_2)$ changes to the less repulsive *s-cis,trans* form. The appearance of the *s-trans,trans* form in the crystal may be due to a packing requirement on the crystallization involving the solvent molecule.

In consideration of the bonding scheme of the three dba ligands to the two Pd atoms, the three ligands may be denoted as **a**(*cis*)–**d**(*trans*), **c**(*cis*)–**e**(*trans*), and **f**(*cis*)–**b**(*trans*) according to the binding manner of the olefinic moieties as already determined. The following four bonding schemes will be considered:

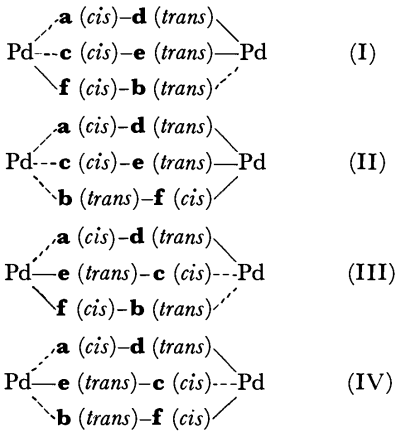

Here, the π-bonding strengths, as estimated already, between the olefinic moieties and the Pd metal are indicated by the solid line for the stronger bonds and by the broken line for the weaker ones. Although there is no direct method for determining the ligand allocation because of an absence of spin interaction between the ligands, schemes III or IV would be prefered from circumstantial evidence: the first scheme in which each Pd atom is attached by three *s-cis* or three *s-trans* olefins is improbable since the allocation differs from that[3] in the crystalline $Pd_2(dba)_3(CHCl_3)$. Indeed in scheme I the three olefinic moieties around each Pd atom must be equivalent in all the NMR parameters contrary to the experimental results. The remaining three all satisfy the allocation of the ligands in the crystalline complex. Some differences in the δ_{AB} values of ligand **b**–**f** from those of the other two ligands may be considered to come from a difference in the spatial location of the olefinic protons towards the carbonyl group[17] of the neighbouring ligand. In this respect scheme II is not compatible, since a molecular model indicates that the two ligands in inverse conformational allocation, *e.g.* **b**–**f** and **a**–**d** or **b**–**f** and **c**–**e** in II, must be similar to each other in spatial location.[18] The results of the decomposition process of the complex are against scheme II. Figure 4 shows the spectra of $Pd_2[(C_6D_5CD{=}$

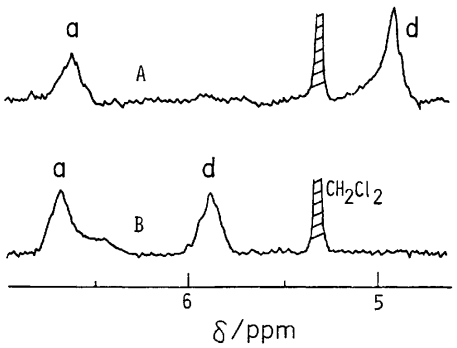

Fig. 4. ^1H NMR spectra of $Pd_2[(C_6D_5CD{=}CH)_2CO]_3$ (A) and $Pd_2[(C_6D_5CH{=}CD)_2CO]_3$ (B) measured in CD_2Cl_2 at 40 °C.

$CH)_2CO]_3$ and $Pd_2[(C_6D_5CH{=}CD)_2CO]_3$ in CD_2Cl_2 at 40 °C, where the broadened signals resulting from only the ligand **a**–**d** can be observed. This may indicate a slower elimination of the one specific ligand in the complex in accordance with the results of the thermogravimetric analysis.[3] The above behaviour of ligand **a**–**d** is difficult to understand in scheme II where ligands **a**–**d** and **c**–**e** are similar in both bonding and conformational allocation to the two Pd atoms. In the scheme III or IV the ligand **a**–**d** is different from the other two in either bonding or conformational allocation. Thus it may be justifiably said that the allocation of the three ligands in the complex is that in III or IV. Both schemes lead to the conclusion that the Pd atom coordinated by one *s-trans* and two *s-cis* olefins binds the olefins more strongly than does the one coordinated by one *s-cis* and two *s-trans* olefins. It should be reasonable to expect a difference in the Pd–olefin bonding between the conformation of *cis-trans-trans* and that of *cis-cis-trans*.

Pd–Olefin Bonding Nature. It has been already shown that either the chemical shift $\bar{\delta}_H$ or coupling J_{AB} classifies the six olefinic moieties into two groups of three with respect to their π-bonding strengths to the metal atoms. The parallel correlation between J_{AB} and $\bar{\delta}_H$ can be seen in Fig. 5 where the correlation is embodied in a line passing near the point for the free dba molecule (J_{AB}; 16.0 Hz and $\bar{\delta}_H$; 7.42 ppm in $CDCl_3$ at 25 °C) showing that the reduction of J_{AB} causes

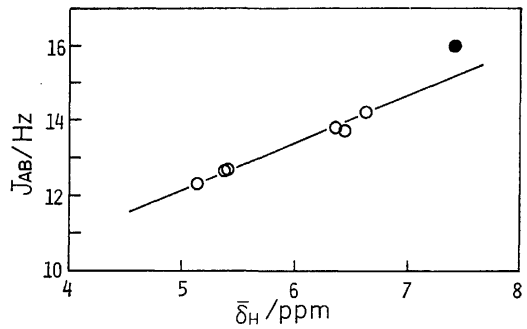

Fgi. 5. A correlation between J_{AB} and δ_H of olefinic protons of dba. ○: $Pd_2(dba)_3$ and ●: free dba.

the high field shift of $\bar{\delta}_H$. This suggests[19] that the coupling is mainly influenced by the same source as that for the chemical shift $\bar{\delta}_H$, *i.e.* the amount of π-back donation. A similar result has also been discussed with the divalent Pt–olefin complexes.[20]

The reason for differing degrees of π-back donation in the olefinic moieties requires discussion. In $Pd_2(dba)_3$, the factors affecting the strength of π-bonding may be limited to the geometries around the metal–olefin bond. Two geometrical factors emerge from the structural data[2] on a crystal of $Pd_2(dba)_3(CH_2Cl_2)$.[21] The first one is the tilt angle of the olefinic double bond to the trigonal plane which the metal atom makes with the centers of the three olefinic double bonds. These angles are 9, 17, 21, and 37° for the *s-trans* olefins as compared to 67 and 80° for the *s-cis* olefins. The molecular models of the binuclear systems generally suggest that the double bonds of the *s-trans* and those of the *s-cis* olefin are forced parallel and perpendicular to the trigonal plane, respectively, due to conformational constraints. The recent molecular orbital treatment[22] of tris-(ethylene)nickel $Ni(C_2H_4)_3$ has shown that the "in plane" configuration is more effective in the π-back donation than the "up right" configuration. If this rule could be immediately applied to the present case the *s-trans* olefin would form the stronger π-bonding with the Pd atom than the *s-cis* olefin. However, as already seen it was not always so. Therefore the double bond tilting may not be the main factor in determining the strength of each metal–olefin π-bonding in $Pd_2(dba)_3$. The second factor, the distance between the olefinic double bond and the Pd atom, may be responsible for the π-bonding strength. The distances measured with the average of the metal–olefinic carbon distances fall into two ranges of 2.19—2.22 Å for the three *s-trans* and 2.28—2.30 Å for the one *s-trans* and two *s-cis* olefins. It is to be expected that the shorter ones cause better π-back donation through the improved overlapping of the metal hybridized orbital with the olefin π^*-orbital. For example, in the complexes such as $[PtCl_3(olefin)]^+$,[23] $PtCl_2$(4-methylpyridine *N*-oxide)(olefin),[24] and PtX-(acac)(olefin)(X=Cl, Br)[25] stronger shielding of the olefinic proton has been observed in ethylene as compared with the substituted ethylenes. This may be explained in terms of an easing of approach of the small ethylene molecule to the metal atom.[4] Thus it may be infered that the same mechanism operates for the present binuclear complex in solution, where the olefinic moieties **d**, **e**, and **f** with the stronger π-back bonding are closer and the olefinic moieties **a**, **b**, and **c** are more distant from the Pd atom.

The asymmetric allocation, probably forced by the minimal potential requirement, in the conformations of the dba molecules to the Pd atoms results in a slight distortion of the trigonal symmetry, and makes the olefinic moieties maintain their individual characteristics even in solution. The characteristics in the π-bonding occur from the geometry around each metal–olefin bond, especially the metal–olefin distance settled by the total configuration of the complex rather than the direction of the olefinic double bond to the trigonal plane.

Experimental

Materials. 1,5-Di(phenyl-d_5)-1,4-pentadien-3-one $(C_6D_5CH{=}CH)_2CO$, 1,5-di(phenyl-d_5)-1,4-pentadien-3-one-1,5-d_2 $(C_6D_5CD{=}CH)_2CO$, and 1,5-di(phenyl-d_5)-1,4-pentadien-3-one-2,4-d_2 $(C_6D_5CH{=}CD)_2CO$ were prepared by the same method as described elsewhere.[12] Tris[1,5-di(phenyl-d_5)-1,4-pentadien-3-one]dipalladium(chloroform) $[(C_6D_5CH{=}CH)_2CO]_3Pd_2(CHCl_3)$ was prepared according to the procedure in the preceding paper.[3] Tris[1,5-di(phenyl-d_5)-1,4-pentadien-3-one]dipalladium(dichloromethane) $[(C_6D_5CH{=}CH)_2CO]_3Pd_2(CH_2Cl_2)$ was prepared by allowing a dichloromethane solution of $[(C_6D_5CH{=}CH)_2CO]_3Pd_2(CHCl_3)$ to deposit deep violet needle-like crystals; mp 137—138 °C. Tris[1,5-di(phenyl-d_5)-1,4-pentadien-3-one-1,5-d_2]dipalladium(chloroform) $[(C_6D_5CD{=}CH)_2CO]_3(CHCl_3)$ and tris[1,5-di(phenyl-d_5)-1,4-pentadien-3-one-2,4-d_2]dipalladium(chloroform) $[(C_6D_5CH{=}CD)_2CO]_3Pd_2(CHCl_3)$ were also prepared by a method similar to that used to prepare $[(C_6D_5CH{=}CH)_2CO]_3Pd_2(CHCl_3)$. These gave deep violet needle-like crystals; mp 126—128 °C and 125—127 °C in 85 and 95% yield, respectively.

^1H NMR Measurements. A NMR sample was prepared as a solution containing a saturated amount of a deuteriated complex (smaller than 1%) and a trace of tetramethylsilane in the respective deuteriated solvent. The ^1H NMR spectrum was recorded on a JEOL PS-PFT 100/EC 100 pulsed Fourier transform system operating at 100 MHz with an internal deuterium lock. Typically, 8192 data points were taken over a 1 kHz spectral width at a tilt angle 45°, repeated at 4.2 s intervals. An EC 100 computer was also used, in addition to its ordinary use for the Fourier transformation, pattern accumulation, and data reduction, to simulate an observed spectrum by following a program written by JEOL. The sample used for the NOE experiment was degassed by repeated freezing and thawing under vacuum and measured at low temperature (−50 °C) set by a variable temperature unit VT-3C attached to the spectrometer.

The authors are grateful to Professors P. M. Maitlis of the University, Sheffield and J. A. Ibers of Northwestern University for helpful discussions.

References

1) M. C. Mazza and C. G. Pierpont, *J. Chem. Soc., Chem. Commun.*, **1973**, 207.

2) C. G. Pierpont and M. C. Mazza, *Inorg. Chem.*, **13**, 1891 (1974).

3) T. Ukai, H. Kawazura, Y. Ishii, J. J. Bonnet, and J. A. Ibers, *J. Organomet. Chem.*, **65**, 253 (1974).

4) M. Herberhold, "Metal π-Complexes," Elsevier, New York (1974), Vol. 2, pp. 31—69.

5) S. Cenini, R. Ugo, and G. La Monica, *J. Chem. Soc.*, *A*, **1971**, 409.

6) A high field shift of olefinic proton signals on coordination may be attributed to π-back bonding[7] rather than σ-dative bonding in the Dewar-Chatt-Duncanson model:[8,9] the high field shift is remarkable (2—3 ppm) in Pd^0 and Pt^0 complexes where the π-bonding plays a major role in the overall metal–olefin bond, while the shift is relatively small (0.5—1.5 ppm) in Pd^{II} and Pt^{II} complexes showing nearly equal contribution of the π and σ-bonding. There is almost no shift or a slightly low field shift in Ag^I and Au^I adducts of olefin where the σ-bonding is operative.

7) L. Malatesta and S. Senini, "Zerovalent Compounds of Metals," Academic Press, New York (1974), pp. 28—47.

8) M. J. S. Dewar, *Bull. Soc. Chim. Fr.*, **18**, 79 (1951).

9) J. Chatt and L. A. Duncanson, *J. Chem. Soc.*, **1953**, 2939.

10) Although the amount of up field shift of the $\bar{\delta}_H$ values thus varies significantly, the average up field shift is 1.51 ppm, being small in comparison with the shifts (*loc. cit.*) in the other zerovalent Pd-olefin complexes.[11] This implies that the Pd–olefin bonding, as a whole, in $Pd_2(dba)_3$ is comparatively weak. It explain well the comparatively long Pd-olefin distance averaged as 2.25 Å.[2]

11) S. Takahashi and N. Hagihara, *Nippon Kagaku Zasshi*, **88**, 1306 (1967).

12) H. Tanaka, K. Yamada, and H. Kawazura, *J. Chem. Soc., Perkin Trans. 2*, **1978**, 231.

13) This criterion may be a generality for other dba complexes. For example, in (pentamethylcyclopentadienyl) (dibenzylideneacetone) rhodium (C_5Me_5) (dba) Rh the δ_{AB} value has been found to be 1.30 ppm,[14] indicating an *s-trans* form for the olefinic moiety of the dba ligand. Indeed X-ray analysis[15] of the complex has shown the dba ligand to be in the *s-trans, trans* conformation. As indicated by the above example and observed for the other dba complexes,[16] both the δ_{AB} values of the coordinated *s-cis* and *s-trans* olefin, in most cases, tend to become somewhat small compared with the corresponding values for the free dba (0.5 for *s-cis* and 1.5 ppm for *s-trans*). Probably this is because the intrinsic term[12] of δ_{AB} which is independent of the conformational change is reduced as a consequence of the decrease of the π-bond nature in the olefinic double bond upon coordination.

14) H. B. Lee and P. M. Maitlis, *J. Organomet. Chem.*, **57**, C87 (1973).

15) J. A. Ibers, *J. Organomet. Chem.*, **73**, 389 (1974).

16) The complexes are $Pt_2(dba)_3$, $Pt(dba)_3$, and $Pd(dba)_3$ (to be published).

17) The carbonyl group contributes to the long range shielding of the olefinic protons.[12]

18) Framework molecular model (Prentice Hall) was successively used to derive the rule, and also showed that the schemes III and IV do not violate the rule.

19) Both J_{AB} and $\bar{\delta}_H$ were found to be independent of the conformational change between *s-cis* and *s-trans* forms.[12]

20) C. E. Holloway, G. Hulley, B. F. G. Johnson, and J. Lewis, *J. Chem. Soc., A*, **1970**, 1653.

21) No discernible geometrical factors on $Pd_2(dba)_3(CHCl_3)$ crystals has been obtained owing to disorder or excessive thermal motion.[3]

22) N. Rosch and R. Hoffmann, *Inorg. Chem.*, **13**, 2656 (1974).

23) H. P. Fritz, K. E. Schwarzhans, and D. Sellman, *J. Organomet. Chem.*, **6**, 551 (1966).

24) P. D. Kaplan and M. Orchin, *Inorg. Chem.*, **6**, 1096 (1967).

25) C. E. Holloway, G. Hulley, B. F. G. Johnson, and J. Lewis, *J. Chem. Soc., A*, **1969**, 53.

Solution Properties of Phycocyanin. V. Studies of the Self-association Reaction of Phycocyanin in a pH 5.4 Solution†

Takahide SAITO, Naomichi Iso, Haruo MIZUNO,* and Ichiro KITAMURA

Department of Food Science and Technology, Tokyo University of Fisheries, Konan, Minato-ku, Tokyo 108

(Received June 16, 1978)

The self-association of phycocyanin in a buffer solution of pH 5.4 with an ionic strength of 0.1 has been studied by sedimentation equilibrium measurements in the temperature range from 5.0 to 25.0 °C. The thermodynamical treatment is also presented. The self-association of phycocyanin molecules proceeds with a decrease in the temperature. The concentration dependence of the apparent weight-average molecular weight of phycocyanin is interpreted in terms of a monomer⇌hexamer equilibrium system. It is clear from the thermodynamic parameters, ΔG^0, ΔH^0, and ΔS^0, that the self-association reaction is spontaneous in the solution of pH 5.4. In the association process, the formation of hydrophobic bonds is suggested by the large positive entropy change accompanying association reaction of phycocyanin molecules.

The dissociation-association properties of phycocyanin have been studied by many investigators. Some investigations in regard to the dissociation-association reaction system have also been reported in publications from this laboratory. Especially, it was suggested that the dissociation-association reacting state was precisely a monomer⇌hexamer system at pH 5.4, and also a monomer⇌trimer at pH 6.8 in relatively low concentrations.[1,2] In the higher concentration region, however, the existence of various aggregates higher than trimer was presumed from the osmotic pressure measurements under pH 6.8. The molecular weight of phycocyanin has been obtained as 2.56×10^5 from the osmotic pressure measurements at pH 5.4. The value was considered to be the molecular weight of the higher aggregate(hexamer) of phycocyanin.[3] The electron micrographic pattern of phycocyanin showed that the phycocyanin molecule was homogeneous and quite stable in the pH region 4.0—5.6, while, in contrast, it was unstable at a higher pH region.[4]

In the previous paper,[5] we postulated, from the results of the sedimentation equilibrium measurements under various temperature conditions at pH 6.8 and at the ionic strength of 0.1, that the dissociation-association behavior of phycocyanin could be explained by assuming a monomer⇌trimer⇌tetramer equilibrium system at this pH and ionic strength. Moreover, it was suggested from an analysis of the thermodynamic parameters, such as the Gibbs free energy change, ΔG^0, the enthalpy change, ΔH^0, and the entropy change, ΔS^0, that the associating reaction was analogous to the ordinary crystallization.

This work was undertaken in order to study the dissociation-association behavior of phycocyanin in solution at pH 5.4 and at the ionic strength of 0.1. In order to determine the equilibrium constants of phycocyanin under various temperature conditions, sedimentation equilibrium measurements in an acetate buffer solution at the ionic strength of 0.1 were performed at 5.0, 15.0, 20.0, and 25.0 °C. From the thermodynamic quantities, the ΔG^0, ΔH^0, ΔS^0 values, accompanied with the dissociation-association reaction, were estimated, and the mechanism of the dissociation-association of phycocyanin was discussed based on these quantities.

† Some of the experimental results in this paper were presented at the 26th Annual Meeting of The Society of Polymer Science, Japan, Kyoto, May 25, 1977.

Experimental

Protein Preparation. The crystalline phycocyanin from *Porphyra tenera* used in this study was isolated and purified as has been described previously.[1] The acetate buffer solution was used as a solvent, and the ionic strength was limited to 0.1. The ionic strength was the same as that previously used in the sedimentation equilibrium measurements performed at pH 6.8. The purity of the phycocyanin was ascertained from the measurements of the absorbance at 620 nm and at 280 nm in a phosphate buffer solution. The ratio of absorbance at 620 nm to that at 280 nm has usually been used as a criterion for judging the purity of phycocyanin; when the ratio is greater than 4.0, the protein has been considered to have a high purity.[6] The value of the ratio measured was greater than 4.7 for the phycocyanin obtained in this work. Therefore, the phycocyanin used in this study was a highly purified sample.

Sedimentation Equilibrium Measurements. Sedimentation equilibrium experiments were performed on the phycocyanin-buffer solutions at 5.0, 10.0, 20.0, and 25.0 °C respectively, using a Hitachi Model UCA-1 ultracentrifuge with an interference optics. The rotor speeds were set at approximately 8000—9000 rpm. All the runs were made at a given speed for approximately 24 h so as to ensure that an equilibrium was established in about a 2-mm liquid column. The apparent weight-average molecular weights at several radial positions in the solution column were evaluated by the method reported previously.[5] The solvent densities at 15.0, 20.0, and 25.0 °C were deterined in a 10-ml pycnometer. Since it was difficult to determine the solvent densities at low temperatures, the densities at 5.0 and 10.0 °C were estimated by the linear extrapolation of the values of the densities at 15.0, 20.0, and 25.0 °C repectively. By the same method, the solution densities at 5.0 and 10.0 °C were estimated. The partial specific volume of phycocyanin, $\bar{v}$, was calculated by the usual method from the densities of the solvents and solutions at 25.0 °C; the value of 0.749 ml/g was thus obtained. The variation in the partial specific volume with the temperature was very small;[7] therefore, the value of 0.749 ml/g was used in all the calculations of the molecular weight of phycocyanin in this work. This value is in good agreement with that of 0.744 ml/g(pH 5.3—7.0) reported by Hattori *et al.*[8]

Results and Discussion

Figure 1 shows a plot of the apparent weight-average molecular weight *versus* the concentration of protein in the solution column of the ultracentrifuge cell for the sedimentation experiment at 25.0 °C. As shown in this figure, the apparent weight-average molecular weights increase with an increase in the solute concentration in the low concentration region, and the molecular weight reaches a saturated value in the higher concentration region. This behavior is characteristic of a self-association system. Similar results were obtained from the measurements performed under the other temperature conditions; the saturated values of the molecular weight in the higher concentrations obtained from these measurements increased slightly as the temperature fell.

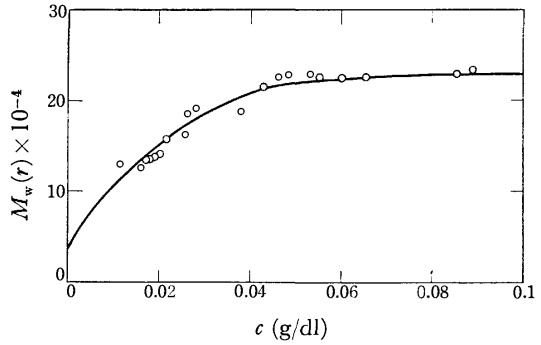

Fig. 1. Plot of apparent weight-average molecular weight as a function of concentration for phycocyanin solution at pH 5.4, $\mu=0.1$, and 25 °C.

In the equilibrium mixture system, the apparent weight fraction of the monomer, f_a, is related to $M_w^{app}(r)$ as follows:[9]

$$\ln f_a = \int_0^c \left(\frac{M_1}{M_w^{app}(r)} - 1\right)\frac{dc}{c}, \quad (1)$$

where

$$\ln f_a = \ln f_1 + BM_1c. \quad (2)$$

In these relations, $M_w^{app}(r)$ represents the apparent weight-average molecular weight at a radial position, r, in the sedimentation equilibrium cell; M_1 is the molecular weight of the monomer; f_1, the weight fraction of the monomer, and B, the non-ideal parameter. The value for M_1 was assumed to be 4.20×10^4 from the previous result of the osmotic pressure measurements performed at pH 5.4, which was about one-sixth of the molecular weight of the phycocyanin hexamer.[3] It becomes clear from previous works that the phycocyanin solution may be considered to be a pseudo-ideal solution.[3,5] Therefore, the non-ideal parameter, B, in relation (2) may be neglected, Therefore, f_a can be replaced by f_1. Once f_1 is determined, the concentration of the monomer in solution, c_1, is obtained from the following relation:

$$c_1 = c\cdot f_1. \quad (3)$$

In the monomer$\rightleftharpoons$$n$-mer type of self-association, the concentration of n-mer, c_n, is expressed as follows:

$$c_n = c - c_1. \quad (4)$$

This relation can be rewritten as

$$c - c_1 = K_n\cdot c_1^n, \quad (5)$$

where K_n represents the equilibrium constant on the weight-concentration scale of the monomer$\rightleftharpoons$$n$-mer system. If the value of n arbitrarily chosen is suitable, the plot of $(c-c_1)$ versus c_1^n will give a straight line which passes through the point of origin. In this study, such a plot could be obtained over the whole temperature range when the n-value was assumed to be 6, as is shown in Fig. 2. It may be concluded from the result described just above that the type of self-association of phycocyanin used in this study is a monomer$\rightleftharpoons$hexamer system at pH 5.4.

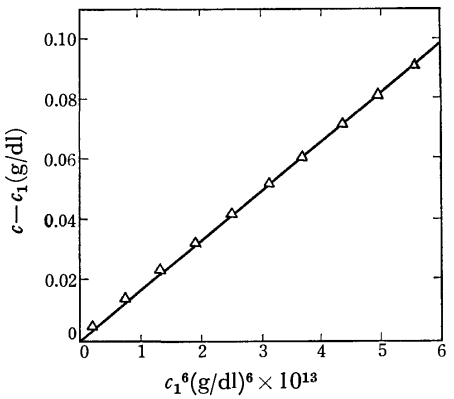

Fig. 2. Plot of $c-c_1$ *versus* c_1^6. The slope of this plot gives the equilibrium constant, K_6.

Table 1. Equilibrium constants at different temperatures

Temp (°C)	K_6(dl/g)^5	k_6(1/mol)^5
25.0	2×10^{11}	4×10^{28}
20.0	6×10^{11}	1×10^{29}
15.0	5×10^{11}	1×10^{29}
10.0	10×10^{11}	2×10^{29}
5.0	23×10^{11}	5×10^{29}

The molar equilibrium constant, k_6(1/mol)^5, was calculated by means of this relation: $k_6=\frac{1}{6}\cdot\left(\frac{M_1}{10}\right)^5\cdot K_6$.

Figure 2 shows the plot of $(c-c_1)$ *versus* c_1^6 at 25.0 °C. The equilibrium constant, K_6, can be evaluated from the slope of such a plot. Thus, the equilibrium constants at 5.0, 10.0, 20.0, and 25.0 °C were obtained. These values are summarized in Table 1. From the value of K_6, it is reasonable to say that the self-associating reaction of phycocyanin is practically hexamerization at pH 5.4 and the ionic strength of 0.1; this tendency becomes more outstanding with the decrease in the temperature. As is shown in Fig. 3, the characteristic dependence of the self-association on the temperature is clear from the van't Hoff plot, which is the relationship between the logarithm of the equilibrium constant on the molar scale and the reciprocal of the absolute temperature. The value of the equilibrium constant on the molar scale, k_6, is calculated from that on the weight-concentration scale by using the following relation:

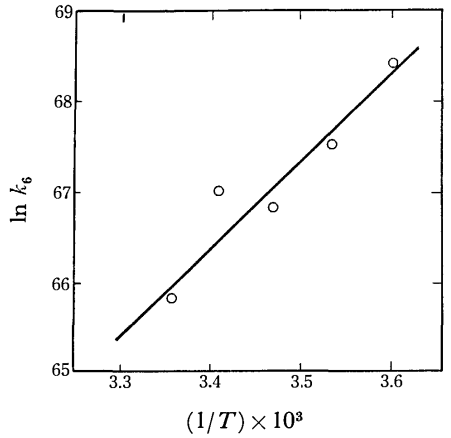

Fig. 3. The van't Hoff plot, $\ln k_6$ *versus* $1/T$, for the phycocyanin systems at five temperatures. The slope of this plot, calculated by a linear regression analysis, is $-\Delta H^0/R$.

$$k_6 = \frac{1}{6}\cdot\left(\frac{M_1}{10}\right)^5\cdot K_6 .$$

The ΔH^0 is evaluated as -19 kcal/mol from the van't Hoff plot, and the association reaction of phycocyanin is exothermic. It was concluded in a previous report[5] that the association reaction of phycocyanin at pH 6.8 was exothermic and that the value of ΔH^0 for the monomer⇌tetramer was -3.8 kcal/mol. Therefore, the difference in the enthalpy change shows that, from the viewpoint of energetics, the polymerization to a hexamer at pH 5.4 is more favorable than that to a tetramer at pH 6.8.

Table 2. Thermodynamic parameters at different temperatures

Temp (°C)	ΔG^0 (kcal/mol)	ΔS^0 (cal/K mol)
25.0	−39	67
20.0	−39	68
15.0	−38	66
10.0	−38	67
5.0	−38	68

$\Delta H^0 = -19$(kcal/mol).

The Gibbs free energy change, ΔG^0, and the entropy change, ΔS^0, accompanied by the dissociation-association of phycocyanin, can be calculated by using the following relations:

$$\Delta G^0 = -RT\ln K, \tag{6}$$

$$\Delta S^0 = \frac{\Delta H^0 - \Delta G^0}{T}. \tag{7}$$

The ΔG^0 and ΔS^0 values are calculated to be -38——-39 kcal/mol and 66—68 cal/K mol respectively. These values are listed in Table 2. If the aggregate at pH 5.4 is assumed to be a hexamer, the ΔG^0 value for the monomer unit is evaluated to be -6.5 kcal/mol from one-sixth of ΔG^0 for the hexamer. This result is not so different from the value of ΔG^0 reported for the monomer unit of phycocyanin at pH 6.8 (-5.0——5.3 kcal/mol).[5]

In other proteins, similar values have been reported for the ΔG^0 — for example, α-amylase (pH 7, 20 °C), -6.3 kcal/mol, and hemerythrine (pH 7, 5 °C), -5.8 kcal/mol.[10]

In the previous report,[5] the value of ΔS^0 for the monomer⇌tetramer at pH 6.8 was calculated to be 59—60 kcal/K mol. The value of ΔS^0 for the monomer ⇌hexamer at pH 5.4 in this study is 66—68 cal/K mol, almost the same order as that for the monomer⇌ tetramer.

From the negative values of ΔH^0 and ΔG^0 and the positive value of ΔS^0 for the phycocyanin aggregation obtained in this study, it is clear that the self-association reaction of phycocyanin is spontaneous under the solution conditions of pH 5.4 and an ionic strength of 0.1.

In the association reaction, the loss in entropy is expected to be quite high because of the increase in the restriction for the motion of molecules. However, the value of the entropy change of the phycocyanin obtained in this work is a large positive one. Scherga and his co-workers have studied the thermodynamic properties of hydrophobic bonds in protein.[11–13] They suggested that the positive entropy change accompanying the association reaction of protein is due to the changes in the water structure around the side chain which are caused by the formation of hydrophobic bonds, and that the hydrophobic bonds can contribute to the stabilization of protein structures. Cann has observed a large entropy change caused by the antigen-antibody reaction, and suggested that it is a result of the release of bound water from antigen and antibody molecules.[14]

As described above, the formation of a hydrophobic bond produces a reduction of the water in contact with the protein molecules and the destruction of that structure, and the freedom of water molecules increases. This brings about an increase in the entropy of the reaction system. The positive changes of entropy accompnying the association are currently interpreted as being due to the formation of a hydrophobic bond between monomers and also to the change in the water structure around a polymer. Scott and Berns have suggested that the hydrophobic bonding force and electrostatic force are involved in the interaction of phycocyanin molecules.[15] MacColl *et al.* have reported that the phycocyanin hexamer appears to be more stabilized by hydrophobic force than the trimer.[16]

Although it does not necessarily mean that the positive change of entropy is wholly attributable to the formation of the hydrophobic bond and the change in the water structure, the large value of ΔS^0 observed in this study suggests a change in conformation, with the cooperative formation of many bonds between monomers.

Nagasawa and Holtzer proposed an interesting method for the estimation of the non-electrostatic part of the standard free energy change accompanying the dissociation reaction of protein from the experimental potentiometric curve.[17] Their method will be of great help in attacking the aggregation mechanism of phycocyanin.

References

1) T. Saito, N. Iso, and H. Mizuno, *Bull. Chem. Soc. Jpn.*, **47**, 1375 (1974).
2) H. Mizuno, T. Saito, and N. Iso, *Bull. Chem. Soc. Jpn.*, **48**, 3496 (1975).
3) A. Kotera, T. Saito, N. Iso. H. Mizuno, and N. Taki, *Bull. Chem. Soc. Jpn.*, **48**, 1176 (1975).
4) H. Mizuno, T. Saito, N. Iso, K. Hirate, and I. Kitamura, *J. Tokyo Univ. Fish.*, **63**, 1 (1976).
5) N. Iso, H. Mizuno, T. Saito, N. Nitta, and K. Yoshizaki, *Bull. Chem. Soc. Jpn.*, **50**, 2892 (1977).
6) R. MacColl, J. J. Lee, and D. S. Berns, *Biochem. J.*, **122**, 421 (1971).
7) H. Bull and K. Breese, *J. Phys. Chem.*, **72**, 1817 (1968).
8) A. Hattori, H. L. Crespi, and J. J. Katz, *Biochemistry*, **41**, 1225 (1965).
9) E. T. Adams, Jr., and J. W. Williams, *J. Am. Chem. Soc.*, **86**, 3454 (1964).
10) I. M. Klotz, N. R. Langerman, and D. W. Darnall, *Ann. Rev. Biochem.*, **39**, 25 (1970).
11) H. A. Scheraga, *J. Phys. Chem.*, **65**, 107 (1961).
12) G. Némethy and H. A. Scheraga, *J. Phys. Chem.*, **66**, 1773 (1962).
13) I. Z. Steinberg and H. A. Scheraga, *J. Biol. Chem.*, **238**, 172 (1963).
14) J. R. Cann, "Interacting Macromolecules," Academic Press, New York (1970), p. 140.
15) E. Scott and D. S. Berns, *Biochemistry*, **4**, 2597 (1965).
16) R. MacColl, D. S. Berns, and N. Koven, *Arch. Biochem. Biophys.*, **146**, 477 (1971).
17) M. Nagasawa and A. Holtzer, *J. Am. Chem. Soc.*, **93**, 606 (1971).

Depolarized Rayleigh Wings of the Liquids and Solutions of Some Symmetric Top Molecules

Keiji KAMOGAWA

Department of Chemistry, Faculty of Science, Tohoku University, Aramaki, Aoba, Sendai 980

(Received July 17, 1978)

Spectra of depolarized Rayleigh wings were observed for the liquids and CCl_4 solutions of C_6H_6, CH_3CN, and $CHCl_3$. The spectral band shape can be reproduced very well by a Lorentz function for the low frequency wing component and a Gauss function for the far wing component. The functions for neat liquids gave the relaxation times for orientational motion, which support free rotation models. The relaxation times of the solutions were found to be independent of concentration, the integrated intensities showing a linear dependence on concentration. The results for the wing component are in marked contrast to those found for the central component of the spectra. The difference is discussed in terms of dynamical structure of the liquids.

The depolarized Rayleigh scattering spectrum of liquids usually appears in the frequency region less than 100 cm^{-1}, consisting of a sharp line at the exciting frequency and a broad wing spread over a wide frequency region. The spectrum is caused by fluctuations in the polarizability anisotropy of the molecules and provides information on the molecular motion and local structure of the liquid. The sharp line arises from the fluctuation caused by rotational diffusion motion of time scale $\approx$1 ps. The broad wing reflects the fluctuation of shorter time scale of 0.1 ps which is probably due to librational motion (rotational oscillation)[1-3] or collisional motion of the molecules.[4,5] Thus, the sharp line and broad wing correspond to the diffusional motion and bounded motion, respectively.

In order to clarify the dynamical behavior of molecules in the usual liquid, it is important to study the concentration (N) dependence of the Rayleigh scattering spectrum. For the liquids of symmetric top molecules, the concentration dependence has been studied theoretically and experimentally for the sharp line component and for the total Rayleigh intensity, the results being interpreted in terms of the rotational diffusion and the pair correlation.[6-13] However, there seems to be no study on the concentration dependence of the broad wing. In the present work, the concentration dependence of the wing components of several symmetric top molecules, C_6H_6, CH_3CN, and $CHCl_3$, was studied in their carbon tetrachloride solutions. The results provide information on the orientational correlation function between the solute molecules of the short time scale of 0.1 ps. By combining the results with the information of the longer time scale motions available from the analysis of the central component, the whole aspect of the dynamical structure of the liquid can be made clear.

Experimental

The experimental arrangement for Rayleigh scattering is almost the same as that for Raman spectral measurements. An argon ion laser operating at 514.5 nm was used as a light source. The incident light was chopped by a rotating sector at 20 Hz to avoid thermal lensing effect. After being passed through a Glan-Thomson prism, the light was focused with a long focusing lens into a sample cell kept at 30.0±0.1 °C. The light scattered at 90° with a small solid angle of 10^{-4} radian was observed along the direction parallel to that of the electric polarization of incident light and collected to a Nalumi double monochromator scanning with instrumental width of 1 cm^{-1}. The signal detected by an HTV R585 or cooled R649 photomultiplier was counted with an ORTEC Model 9315 photoncounter with time constant 5—10 s and digitally recorded with an interval of 0.6—1.2 cm^{-1}. The signals were averaged after several repeated measurements. The whole scattering intensity of solution was determined relative to the intensity of the neat liquid which was taken to be 100. The observed intensities thus obtained were not corrected for spectral sensitivity of the detection system because of the narrow frequency region. The spectra obtained were usually symmetric except for the Boltzmann factor, the intensity maxima being taken as $\omega=0$. The measurements were carried out from the intensity maxima to lower frequency region. The samples were neat liquids of C_6H_6, CH_3CN, $CHCl_3$, and CS_2 and their mixtures with CCl_4. They were of spectral grade and used without further purification. Just before the spectral measurements, the samples were filtered with 0.2 μm millipore membrane filter to remove suspended dusts. The refractive indices of the solutions were measured with an Abbe refractometer.

Results and Band Shape Analysis

The depolarized Rayleigh scattering spectrum of liquid CH_3CN is shown in Fig. 1. The spectrum consists of a sharp component at the center and a broad

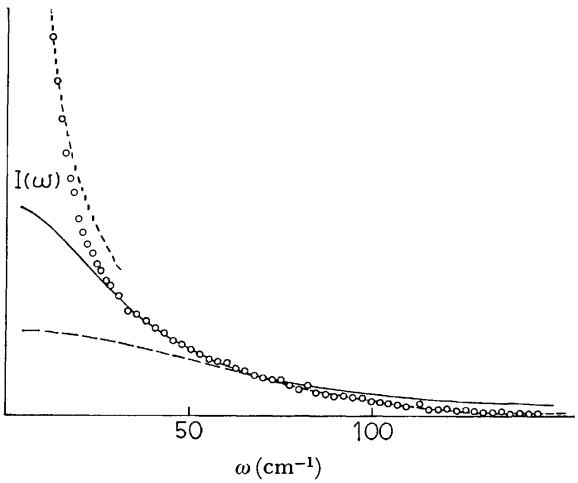

Fig. 1. The observed spectrum of liquid CH_3CN (circles) and analysis of the band shape by wing Lorentzian (full line), wing Lorentzian plus center Lorentzian (dotted line) and far wing Gaussian (broken line).

wing. In order to analyze the band shape, it is useful to assume reasonable analytical function.

Depolarized Rayleigh scattering originates from fluctuation in the local polarizability anisotropy α. Three kinds of fluctuations; rotational diffusion, libration (rotational oscillation in a potential well) and collision of the molecules; seem to contribute to the intensity $I(\omega)$ through the polarizability correlation function $<\alpha(t)\alpha(0)>$. According to Keyes and Kivelson[6] and Alms *et al.*,[7] the rotational diffusion of symmetric top molecule gives the spectrum expressed by the Lorentz function

$$I_r(\omega) = \frac{A}{15n^2\pi}\left[\frac{n^2+2}{3}\right]^4\beta^2N(1+fN)\frac{6D'}{\omega^2+(6D')^2},$$
$$D' = \left(\frac{(1+gN)}{(1+fN)}\right)D, \qquad (1)$$

where n, N, β, and D are the refractive index,[12] density of liquid, optical anisotropy of the molecule and rotational diffusion constant, respectively. f is the static orientational pair correlation function given by

$$f = \frac{<\alpha_o^i(0)\alpha_o^i(0)>}{<\alpha_o^i(0)\alpha_o^i(0)>}, \qquad (2)$$

where $\alpha_o^i(0)$ and $\alpha_o^j(0)$ are the polarizability anisotropies of the rigid rotating molecules i and j at $t=0$. g is the dynamical pair correlation function (Eq. B6, Ref. 6). The integrated intensity of Eq. 1 is given by

$$I_r = \frac{A}{15n^2}\left[\frac{n^2+2}{3}\right]^4\beta^2N(1+fN). \qquad (3)$$

It is well established that the rotational diffusion contributes to most of the intensities of narrow wave number region around the center of the Rayleigh scattering, giving rise to the sharp band of Lorentzian shape.

On the other hand, based on the librational scattering models, Starunov[1] obtained a modified Lorentzian spectrum expressed by

$$I(\omega) = \frac{I^0}{(1-I_\perp\omega^2/\mu)^2+\zeta^2\omega^2/\mu^2}, \qquad (4)$$

while Prorvin[2] and Sechkarev and Nikolaenko[3] gave on nearly the same model a squared Lorentzian

$$I(\omega) = \frac{I^0}{(1+\tau_2^2\omega^2)^2} \qquad \tau_2^2 = \frac{1}{1/\tau_0^2+z^2}. \qquad (5)$$

In Eqs. 4 and 5, I^0 is the peak intensity at $\omega=0$, ζ the internal friction constant of the molecule in the liquid, μ the elastic constant, $I_\perp$ the moment of inertia of the molecule perpendicular to the principal axis, τ_0 the average half-period of the libration, and z an average frequency of intermolecular interactions. Although it is assumed in both models that the scattering comes from the librational motion of individual molecules ($f=0$), Starunov's model is based on the stable librators of different sites in the liquid. Thus, different molecules contribute to the central and wing components. On the other hand, Sechkarev and Nikolaenko assumed that the librator is a temporary one appearing and disappearing by jump diffusion from one potential well to another and the two components of the spectrum come from the same molecules in different time periods. Thus, the band shape of the modified Lorentzian (Eq. 4) or the squared Lorentzian (Eq. 5) is expected if the librational fluctuations are predominant.

The collisional motion of the pairing molecules is known to give the spectrum of a modified exponential type[4] of Eq. 6 or a sum or a combination of exponential functions.[5,14]

$$I(\omega) = \omega^{2(m-7)/7}\exp(-\omega/\omega_0). \quad (\omega>\omega_0) \qquad (6)$$

ω_0 is an average frequency of translational oscillation and m has the value of 9 or 13 according to whether the fluid is an atomic or molecular fluid. Equation 6 holds on the assumption that collisionally induced polarizability $\Delta\alpha$ depends on the intermolecular distance r as follows:

$$\Delta\alpha \propto r^{-m}. \qquad (7)$$

In many liquids the librational and collisional motions give a broad spectrum, the Rayleigh wing, spread over a wide frequency region. In liquids composed of symmetric top molecules, both the modified Lorentzian and the squared Lorentzian reproduce the observed wing better than the modified exponential type.[15,16] We thus start analysis of the observed wing on the basis of the librational models. Both Eqs. 4 and 5 give a Lorentzian in the low frequency region. First we look for the low frequency region of the wing component where the spectrum can be expressed by a Lorentzian $I_L(\omega)$. Second, the central component obtained by subtraction of $I_L(\omega)$ from the observed intensities will be examined by another Lorentzian $I_r(\omega)$ corresponding to Eq. 1. A typical example of the analysis is shown in Fig. 1 for neat CH_3CN liquid. In the low frequency wing region 25—60 cm^{-1}, the spectrum can be reproduced by a Lorentzian $I_L(\omega)$ (called wing Lorentzian in this study). The spectral region less than 20 cm^{-1} can be reproduced by addition

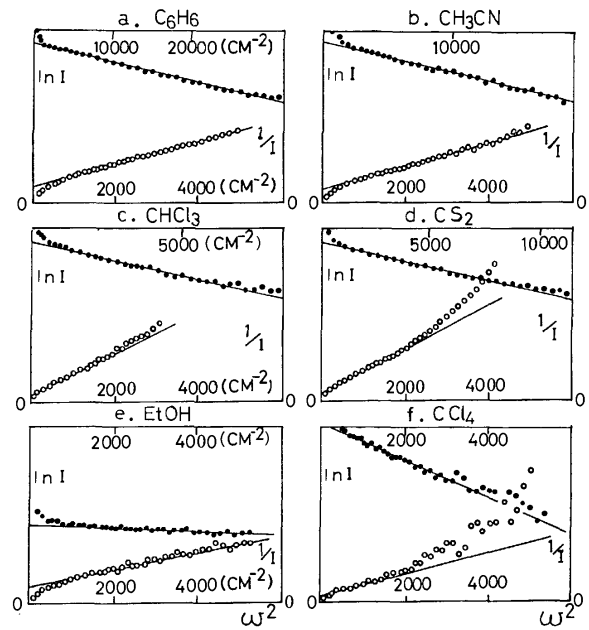

Fig. 2. Band shape analyses for neat liquids. A line drawn for the plots ○ of $1/I$ against ω^2 corresponds to the wing Lorentzian and a line drawn for the plots ● of ln I against ω^2 to the far wing Gaussian.

of the Lorentzian $I_L(\omega)$ plus another Lorentzian $I_r(\omega)$. The observed points for this frequency region are few and $I_r(\omega)$ involves a considerable ambiguity. No attempt was made to deduce physical quantities from $I_r(\omega)$. In this way, for all the liquids except for CCl_4, the spectra over the central and low frequency wing regions can be reproduced by a Lorentzian $I_L(\omega)$ and the central component which has a form close to that of Lorentzian $I_r(\omega)$. The results of the analysis are shown in Fig. 2.

However, the spectrum of the far wing region cannot be reproduced by the above analysis. As seen in Fig. 1, the spectrum deviates appreciably "downward" from the Lorentzian $I_L(\omega)$ in the frequency region higher than 65 cm^{-1}. The "downward" deviation cannot be reproduced by addition of another Lorentzian. As far as the spectral region is concerned, the spectrum can be expressed very well by a Gauss function. The Gauss function changes smoothly to the Lorentzian $I_L(\omega)$. The same is true for the far wing regions of all the liquids studied here (Fig. 2). The Gauss function is called far wing Gaussian $I_g(\omega)$ in this study. The central region of the Rayleigh scattering spectrum is explained by overlapping of the central component lying close to the Lorentzian $I_r(\omega)$ given by Eq. 1 and the wing Lorentzian $I_L(\omega)$. The low frequency wing region is expressed practically by $I_L(\omega)$, since the contribution from the central component is negligibly small in this region. For the far wing region, the spectrum can be reproduced very well by the far wing Gaussian $I_g(\omega)$ only. We assume that $I_L(\omega)$ does not necessarily extend to the far wing region.

Band shape analysis by the above method is successful for the symmetric top molecules, C_6H_6, CH_3CN, $CHCl_3$, and CS_2 (Figs. 2a—2d), and also for EtOH which is an asymmetric top and highly associative molecule (Fig. 2e). For these molecules, the deviation of the observed intensities from the analytical ones were within $\pm 2\%$ for the whole wing region. On the other hand, the Lorentzian analysis for the low frequency wing of CCl_4 shows appreciable deviation from the observed shape while a Gaussian for the far wing gives a good fit (Fig. 2f). The inadequacy of the Lorentzian analysis for the low frequency wing seems to be characteristic of isotropic molecules, for which only the collisional mechanism gives depolarized Rayleigh scattering.

We should compare the present analysis for the wing with the analysis based on the single function of the squared Lorentzian proposed by Prorvin[2] and Sechkarev and Nikolaenko.[3] Figure 3 shows the plots of $I(\omega)^{-1/2}$ *vs.* ω^2 for the wings of C_6H_6 and CH_3CN. The frequency

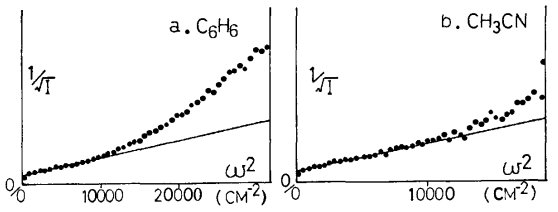

Fig. 3. Band shape analyses for liquid C_6H_6 and CH_3CN. A line drawn corresponds to the squared Lorentzian.

Table 1. Frequency regions of the wing (cm^{-1}) for which the observed spectrum is reproduced by the assumed functions

	CH_3CN	C_6H_6	CS_2	$CHCl_3$
Lorentzian	27—65	36—73	17—46	15—41
Gaussian	57—146	44—163	46—86	42—76
Squared Lorentzian	32—94	30—105	16—66	20—57

regions where the observed band shape is well described by the squared Lorentzian are summarized in Table 1 together with the regions of the good fit obtained by the present analysis. Although the squared Lorentzian reproduces the observed band shape fairly well over a wide wing region, considerable deviation occurs in the far wing region especially for C_6H_6. Measurements of Rayleigh scattering carried out by many workers are usually limited in the frequency region up to 100 cm^{-1}.[2,3,17] In this frequency region, the spectra can be reproduced fairly well by a single function of the squared Lorentzian. However, it is evident from our data that it is impossible to have a good fit with a single function for wider frequency region. It seems adequate to adopt a combination of a Lorentzian and a Gaussian for the wing in a wide frequency region.

From the slopes and the intercepts of the straight lines (Fig. 2) band widths and integrated intensities can be obtained for the low frequency wing and for the far wing. When the functions are given by

$$I_L(\omega) = \frac{1}{a_L + b_L\omega^2},$$
$$I_g(\omega) = \exp(a_g - b_g\omega^2), \tag{8}$$

the widths and the integrated areas for them are

$$\omega_L = \sqrt{\frac{a_L}{b_L}}, \quad \omega_g = \sqrt{\frac{1}{b_g}},$$
$$\int_0^{\omega_c} I_L(\omega)d\omega = \frac{1}{\sqrt{a_L b_L}} \tan^{-1}\left[\frac{\omega_c}{\omega_L}\right],$$
$$\int_{\omega_c}^{\infty} I_g(\omega)d\omega = \exp[a]\int_{\omega_c}^{\infty} \exp[-b_g\omega^2]d\omega, \tag{9}$$

where the two functions are joined at $\omega = \omega_c$. Although ω_c is arbitrary, the value does not affect the total wing intensity as far as $I_L(\omega)$ smoothly changes to $I_g(\omega)$ around the region $\omega \approx \omega_c$ (Fig. 1). Integration of $I_g(\omega)$ can be carried out by use of a numerical table for the error function. The relaxation time τ_L can be calculated from the half band width ω_L of the wing Lorentzian by $\tau_L = 1/2c\pi\omega_L$, while the relaxation time

Table 2. Observed band width and relaxation time for the neat liquids

	CH_3CN	EtOH	C_6H_6	CS_2	$CHCl_3$	CCl_4
ω_g cm^{-1}	74	66	76	48	45	37
τ_2^{-1} cm^{-1}	66	—	76	40	38	—
τ_g ps	0.14	0.16	0.14	0.22	0.24	0.29
ω_L cm^{-1}	34	48	43	18	19	21
τ_L ps	0.16 (0.15)[a]	0.11	0.12	0.30	0.28	0.25

a) Schwarz and Wang.[16]

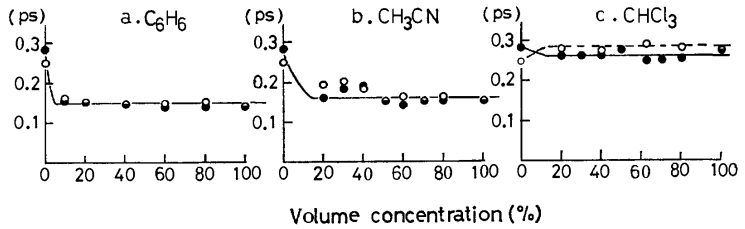

Fig. 4. Experimental relaxation times τ_g (●) and τ_L (○) for carbon tetrachloride solutions of C_6H_6, CH_3CN, and $CHCl_3$ at various volume concentrations.

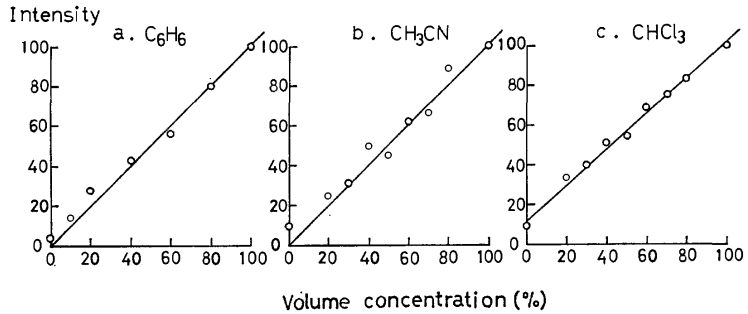

Fig. 5. Concentration dependence of the integrated intensity $\left(I/\frac{1}{n^2}\left(\frac{n^2+2}{3}\right)^4\right)$ for carbon tetrachloride solutions of C_6H_6, CH_3CN, and $CHCl_3$ (I is given by I_L+I_g).

τ_g can be calculated from the band width ω_g of the far wing Gaussian by means of $\tau_g=1/c\pi\omega_g$. The widths and relaxation times obtained are given in Table 2. Both τ_L and τ_g are as short as the order of 0.1 ps for all the liquids. τ_g corresponds to the time in which the correlation function $<\alpha(t)\alpha(0)>$ decays to $1/e$ according to

$$\langle\alpha(t)\alpha(0)\rangle \propto 1-t^2/\tau_g^2+O(t^4) \approx \exp[-t^2/\tau_g^2]. \quad (10)$$

τ_L is the time in which the correlation function decays exponentially to $1/e$.

The above are the results for the neat liquids. The relaxation times were also obtained from the analysis of the solution spectra at various concentrations. The observed τ_g and τ_L of the carbon tetrachloride solutions of C_6H_6, CH_3CN, and $CHCl_3$ at various concentrations are plotted against the concentrations in Fig. 4. We see that τ_g and τ_L remain unchanged over all the concentrations except for the region less than 10%. The sudden increases for C_6H_6 and CH_3CN at concentrations less than 10% are due to the appearance of CCl_4 spectrum whose relaxation time is 0.29 ps. According to Alms *et al.*,[7] in contrast to τ_L and τ_g, the relaxation time for the central component τ_c varies depending on the concentration and kind of the solvent. They found that τ_c varies from 2.91 to 1.79 ps for C_6H_6 in isopentane and from 2.95 to 1.74 ps for $CHCl_3$ in CCl_4 with change in volume concentration from 100 to 20%. They also found that the relaxation time obtained from NMR of $CHCl_3$ in CCl_4 remains constant at 1.5 ps over a wide concentration range, which is also close to the time obtained from NQR. The concentration independence of τ_g and τ_L is similar to the concentration behavior of the relaxation times obtained from NMR and NQR but differs from the concentration dependence of the central component.

The observed integrated intensities of the wing components I_L+I_g at various concentrations are given for the carbon tetrachloride solutions of C_6H_6, CH_3CN, and $CHCl_3$ in Fig. 5. The wing components of C_6H_6 show almost linear dependence on the concentration. The observed points lie near the straight line passing through the origin. This indicates that there is no orientational correlation ($f=0$) among the solute molecules, if Eq. 3 is applied to the wing component, I_L+I_g. The wing components of CH_3CN and $CHCl_3$ also show similar concentration dependence.†

On the other hand, the central component seems to show a concentration dependence differing from that of the wing component. $f=-0.2$ for the central component of C_6H_6 and $f=+0.9$ for that of $CHCl_3$ reported by Bauer *et al.*,[12,18] are different from $f\approx 0$ obtained for the wing components.

Discussion

Collisional Scattering. Let us first examine the possibility of the collisional process as a cause of the wing component. The collisional process can be tested by the observed relaxation time, its concentration dependence and the integrated intensity of the spectrum.

† In contrast, ethanol solution of CCl_4 shows quite different solute concentration dependence of the integrated intensity, which is non-linear in concentration. The non-linear dependence seems to be expressed by the sum of the part proportional to the square of the CCl_4 concentration and that of linear concentration dependence of EtOH.

The collisional interval time τ_{BC} is considered to be an average time interval between collisions and given by[19]

$$\tau_{BC} = 1/\bar{v}[V_m^{1/3} - \sigma], \quad (11)$$

where V_m is the average molecular volume, σ the collision diameter and $\bar{v}$ the average velocity of the molecules. τ_{BC} is not the exact relaxation time for collisional scattering determined by the correlation function for the intermolecular separation and its orientation of a pair molecule. However, τ_{BC} corresponds to the librational half period of the pair molecules so that it will be a measure of the collisional relaxation time. τ_{BC} given by Bartoli and Litovitz[19] are compared with τ_g obtained in the present study in Table 3. Although qualitative correlation seems to exist between them, τ_{BC} differes from τ_g by a factor of 5. The collisional interval time τ_{BC} should be dependent on the concentration, since τ_{BC} (Eq. 11) changes with the changes in the reduced mass of the colliding pair and $V^{1/3}$. Actually, such a change was experimentally confirmed by Dill *et al.*[20] for the angular velocity correlation time (τ_j) which is a measure of τ_{BC}. However, τ_g as well as τ_L are found to be almost independent of concentration. If the spectrum is caused by the binary collision process, the integrated intensity of the wing should change with the square of the concentration. However, the intensity of the wing component has linear dependence on the concentration for C_6H_6, CH_3CN, and $CHCl_3$.

Thus, the observed relaxation time, its concentration dependence and the integrated intensity do not support the collisional scattering process. It seems that the wing component comes from dynamical process of the single molecule rather than collision process between pairing molecules.

Librational Scattering. The observed spectra of the far wing region are reproduced by a Gauss function. The far wing spectrum corresponds to the motion of short time period which seems to be inertial. There are two types of rotational motions in liquids according to the classification by Atkins,[21] conditional and unconditional free rotations, which give a Lorentzian shape and a Gaussian shape, respectively. The former exists in the first stage of orientational motion of the molecule in homogeneous media having weak intermolecular torque. The correlation function for this process was given by Steel,[22] Gordon,[23] and Atkins[21] as follows.

$$\langle \alpha_o(t)\alpha_o(0)\rangle \propto 1 - \frac{l(l+1)kT}{2I_\perp}t^2 + O(t^4) \approx \exp\left[-\frac{l(l+1)kT}{2I_\perp}t^2\right], \quad (12)$$

where $l=2$ for light scattering and NMR process. The relaxation time, τ_{FR}, for Eq. 12, is given by $\sqrt{I_\perp/3kT}$, corresponding to Gaussian relaxation time. Another definition of the relaxation time for the unconditional free rotation was given by Bartoli and Litovitz[19] as the time in which a molecule rotates 41° based on the fact that the correlation function is the second Legendre polynomial. It is given by $41/360 \cdot 2\pi\sqrt{I_\perp/kT}$. Both τ_{FR} should be proportional to $I_\perp^{1/2}$. Figure 6 shows the plot of τ_g *vs.* $I_\perp^{1/2}$, which gives a straight line with zero intercept. This provides strong evidence that the far wing component arises from the unconditional free rotation of the molecule. However, τ_{FR} calculated by $\sqrt{I_\perp/3kT}$ differs from τ_g by a factor of 2 as shown in Table 3.

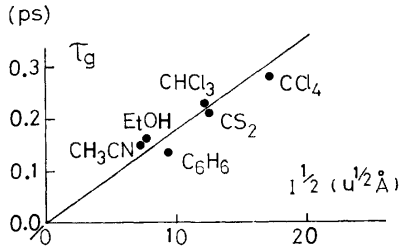

Fig. 6. Correlation between the relaxation time τ_g and $I_\perp^{1/2}$ ($I_\perp$: moment of inertia of the molecule).

Table 3. Observed and calculated relaxation times and moment of inertia of the molecules

	CH_3CN	EtOH	C_6H_6	CS_2	$CHCl_3$	CCl_4
τ_g ps	0.14	0.16	0.14	0.22	0.24	0.29
τ_{BC}[a] ps	0.026	—	0.023	0.074	0.071	0.114
τ_{FR} ps	0.27	0.29	0.34	0.46	0.44	0.63
$I_\perp$ aumA[2c]	54.9	57.8	88.9	155.9	148.1	295.7
τ_L ps	0.16	0.11	0.12	0.30	0.28	0.25
τ_{LC} ps	0.19	0.19	0.17	0.32	0.22	0.36

a) Bartoli and Litovitz.[19] b) "Landolt-Börnstein," ed by K. H. Hellwege, Springer-Verlag, Berlin (1976), New Series II 7. c) lamu = 1.66056×10^{-27} kg.

The conditional free rotation would be of importance in the media where the intermolecular torques are appreciable. In such circumstances, free rotation occurs only in the local part of the media such as lattice defect, but it is inhibited in other parts of the liquid. The orientational correlation function for such conditional free rotation shows an exponential decay[21] on the assumption that the free rotation is caused by fast formation and destruction of the lattice defects, the rates being proportional to time t. The relaxation time of this model is given by

$$\tau_{LC} = \sqrt{\frac{I_\perp}{3kT}}\left(\frac{\alpha}{1+2\alpha}\right)^{1/2} P_d^{-1}, \quad (13)$$

where α is given by $I_\perp/I_\parallel$, a ratio of the moments of inertia perpendicular and parallel to the principal axis of the related symmetric top molecule, and P_d is the probability of finding the molecule in the lattice defects, being equal to 1 at the limit of weak intermolecular torques. The observed τ_L values obtained from the wing Lorentzian $I_L(\omega)$ are compared with τ_{LC} calculated by means of Eq. 13 at the limit of $P_d=1$, in Table 3. We see that the correlation between τ_L and τ_{LC} is fairly good. It seems that the orientational motions of the molecules are mostly free in the first stage to give the far wing Gaussian, the free rotation undergoing weak intermolecular interactions in the next stage to give the wing Lorentzian. This is the reason why the wing component can be separated into the Lorentzian and Gaussian parts as shown in the band analysis. The

concentration independence of τ_g and τ_L is important. In the orientational diffusion process, the concentration dependence of the relaxation time is determined by the pair correlation as shown by Eq. 1. If the process is of single molecular nature, the relaxation time should be independent of the concentration as found in NMR and NQR for the mixture of $CHCl_3$ and CCl_4. Our result confirms the view that the motion corresponding to the broad wing should be of single molecular nature with no correlation between different molecules. The orientational pair correlation f is expressed by[24]

$$f = \frac{1}{2}\langle 3\cos^2 \Psi_{ij}(0) - 1\rangle, \tag{14}$$

where $\Psi_{ij}(0)$ is the angle between the principal axis of molecule i and that of molecule j at arbitrary instant. From Eq. 14 we see that a negative value of f indicates perpendicular orientation of the two molecules, a positive value of f parallel orientation and $f=0$ random orientation. The concentration dependence of integrated intensities suggests that f is nearly zero in the short time period of 0.1 ps; the random orientation is realized in this short time scale. This is quite in contrast to the appreciable correlation in the long time period $\approx$2 ps known for C_6H_6[25] and $CHCl_3$,[26] showing perpendicular and parallel correlations, respectively.

Origin of Different f Values. We obtained $f\approx 0$ for the wing component from both the relaxation times and the integrated intensity, while $f\neq 0$ is shown by many workers for the central component. We should consider the cause of this difference, since f should be independent of time according to Eq. 2. The orientational pair correlation function f is as follows.[24]

$$\langle \alpha_0(t)\alpha_0(0)\rangle = \sum_{i,j}\langle \alpha_0^i(t)\alpha_0^j(0)\rangle$$
$$\propto \sum_i \langle P_2[\cos\theta_i(t)]P_2[\cos\theta_i(0)]\rangle \sum_j \langle 3\cos^2\Psi_{ij}(0) - 1\rangle \frac{1}{2}, \tag{15}$$

where $P_2[\cos\theta]$ is the second Legendre polynomial and $\Psi_{ij}(0)$ is given by Eq. 14. The ensemble average $1/2\langle 3\cos^2\Psi_{ij}(0) - 1\rangle$ should be replaced by a time average for finite time T as follows.

$$\bar{f}^T = \frac{1}{2}(3\cos^2\Psi_{ij}(0) - 1)^T = \frac{\frac{1}{2}\int_0^T (3\cos^2\Psi_{ij}(t) - 1)\mathrm{d}t}{T}, \tag{16}$$

where T is the duration time of the motion.

We assume that T can be replaced by relaxation time. The central and the wing component have different relaxation time τ_c and τ_L or τ_g, respectively. The pair correlation function for the central component might differ from that for the wing component. The different pair correlation function (f) indicates that the molecules in the different time scale are in different non-stationary states with regard to orientation. There should be a finite time τ_r in which the molecule has a preferential orientation in average relative to the neighbors. τ_r should be at least the period of libration in a potential well ($2\tau_0$, Eq. 5) and also a few times greater than τ_g (Eq. 5 and Table 2). Since the central component reflects the rotational diffusion, τ_c should be greater than τ_r. Thus, we have

$$\tau_c > \tau_r > \tau_g.$$

The rapid process with the relaxation time τ_g cannot reflect the stationary state, since the stationary state requires a relaxation time greater than τ_r.[27] In other words, the relaxation process for the wing scattering is too rapid for a molecule to follow average orientation of neighboring molecules. Such a rapid process gives random orientation corresponding to non-correlation ($f=0$).

Another interpretation for the different f values is possible when the liquid consists of two different portions, one giving the center spectrum and the other the broad wing spectrum. Transition from one portion to another may be fast or slow depending on the stability of the inhomogeneous liquid structure. The most unstable structure corresponds to the conditional free rotation model. The different orientational pair correlations will be obtained by assuming an inhomogeneous model. For the portion giving the wing scattering, intermolecular torques are weak enough to allow free rotation, the molecules taking random orientation without pair correlation. However, in another portion, the molecules are packed to the extent that they undergo diffusional motion as a whole. The pair correlation function for this portion will be positive or negative depending on the orientation of the pairing molecules. So far we have not sufficient evidence to make a choice from the two models.

The author sincerely thanks Prof. Mitsuo Ito and Dr. Yasuo Udagawa for their valuable advice, and Assist. Prof. Tohru Azumi for his help in the experimental setup.

References

1) V. S. Starunov, *Opt. Spektrosk.*, **18**, 165 (1965).
2) A. I. Prorvin, *Opt. Spektrosk.*, **24**, 380 (1968).
3) A. V. Sechkarev and P. T. Nikolaenko, *Soviet. Phys. DOK.*, **13**, 888 (1969).
4) J. A. Bucaro and T. A. Litovitz, *J. Chem. Phys.*, **54**, 3846 (1971).
5) H. A. Posch and T. A. Litovitz, *Mol. Phys.*, **32**, 1559 (1976).
6) T. Keyes and D. Kivelson, *J. Chem. Phys.*, **56**, 1057 (1972).
7) G. R. Alms, D. R. Bauer, J. I. Brauman, and R. Pecora, *J. Chem. Phys.*, **58**, 5570 (1973); **59**, 5310 (1973).
8) D. J. Coumou, J. Hijmans, and E. L. Mackor, *Trans. Faraday Soc.*, **60**, 2244 (1974).
9) M. S. Malmberg and E. R. Lippincott, *J. Colloid. Interface Sci.*, **27**, 591 (1968).
10) P. Bothorel, C. Such, and C. Clement, *J. Chim. Phys. Phys.-Chim. Biol.*, **69**, 1443 (1972).
11) G. Dezelic and N. Segudovic, *Croat. Chim. Acta*, **45**, 407 (1973).
12) D. R. Bauer, J. I. Brauman, and R. Pecora, *J. Chem. Phys.*, **63**, 53 (1975).
13) G. D. Patterson and J. E. Griffth, *J. Chem. Phys.*, **63**, 2406 (1975).
14) P. A. Fleury, W. B. Daniels, and J. M. Worlock, *Phys. Rev. Lett.*, **27**, 1493 (1971).
15) J. H. K. Ho and G. C. Tabisz, *Can. J. Phys.*, **51**, 2025 (1973).

16) M. Schwarz and C. H. Wang, *Chem. Phys. Lett.*, **29**, 383 (1974).
17) B. Simic-Glavaski and D. A. Jackson, *J. Phys. (Paris)*, **33**, 183 (1972).
18) D. R. Bauer, J. I. Brauman, and R. Pecora, *Ann. Rev. Phys. Chem.*, **27**, 443 (1976).
19) F. J. Bartoli and T. A. Litovitz, *J. Chem. Phys.*, **56**, 413 (1972).
20) J. F. Dill, T. A. Litovitz, and J. A. Bucaro, *J. Chem. Phys.*, **62**, 3839 (1975).
21) P. W. Atkins, *Mol. Phys.*, **17**, 321 (1969); **17**, 329 (1969).
22) A. Steel, *J. Chem. Phys.*, **38**, 2411 (1963).
23) R. G. Gordon, *J. Chem. Phys.*, **43**, 1307 (1965).
24) D. A. Pinnow, S. J. Candau, and T. A. Litovitz, *J. Chem. Phys.*, **49**, 347 (1968).
25) A. H. Harten, *J. Chem. Phys.*, **67**, 2102 (1977).
26) P. R. Ireland, R. Mason, and A. I. M. Rae, *Mol. Phys.*, **24**, 17 (1972).
27) K. B. Tolpigo, "Termodinamika i Statisticheskaya Fizika," Kiev Univ., (Japanese translation) (1966).

Photoelectron Angular Distribution Measurements for Some Pyridines

Chikatoshi UTSUNOMIYA,† Tsunetoshi KOBAYASHI,†† and Saburo NAGAKURA*,†,††

†*The Institute for Solid State Physics, The University of Tokyo, Roppongi, Minato-ku, Tokyo 106*

††*The Institute of Physical and Chemical Research, Wako, Saitama 351*

(Received July 20, 1978)

The angular distributions for the He I photoelectron spectra of pyridine, pentafluoropyridine, and 2,6-lutidine have been measured in order to solve the ambiguities on the band assignment of pyridine. It has been concluded that the first band of pyridine is assigned to the a_1n orbital and the fifth band to the lowest occupied $b_1\pi$ orbital.

The photoelectron differential cross-section $(d\sigma/d\Omega)$ for an unpolarized light and an ensemble of randomly oriented molecules or atoms is given by

$$d\sigma/d\Omega \propto 1 + 0.5\beta(1.5\sin^2\theta - 1), \quad (1)$$

where β is an asymmetry parameter and θ is the angle between the direction of an ejected photoelectron and that of an incoming photon.[1,2] The asymmetry parameter β depends on the kinetic energy of the photoelectron and the character of the molecular orbital from which the photoelectron is ejected. Therefore, the determination of the β value is useful for interpretation of photoelectron spectra. Especially, it is useful for the assignments of the overlapping bands which are difficult to be assigned solely by analysis of the ionization energies.

We reported in a previous paper[3] that the second and third bands of benzene, the assignments of which were in dispute, were assigned to the $e_{2g}\sigma$ and $a_{2u}\pi$ orbitals, respectively, by the comparison of the β values of benzene with those of hexafluorobenzene. In this paper the He I photoelectron angular distributions for pyridine, pentafluoropyridine, and 2,6-lutidine are reported and the assignments of the photoelectron spectral bands of pyridine are discussed.

Historically, concerning the assignments of the first three photoelectron spectral bands of pyridine there have been some conflicting proposals[4–12] (see also references 13—16). At present, however, there is no doubt that the broad band around 9.7 eV contains the a_1n and $a_2\pi$ bands and that the third band around 10.6 eV is related with the $b_1\pi$ orbital.[7,9–12,16] As for the band order of the first and second bands Heilbronner and co-workers assigned the first band to the a_1n orbital and the second band to the $a_2\pi$ orbital on the basis of band shape consideration and also of the methyl and trimethylsilyl-substituent effect.[7,9–11] On the other hand, King and co-workers prefer the reverse order on the basis of the fluoro-substituent effect.[12] In order to solve this problem we compare the photoelectron angular distributions for pyridine with those for 2,6-lutidine the band assignments of which are definite.[11] In addition to this, we examine the photoelectron angular distributions for the fourth and fifth bands of pyridine to certify their assignments by comparison with those of pentafluoropyridine.

Concerning the photoelectron angular distribution measurement for pyridine, Ames *et al.* presented crude data for the first three bands without giving the asymmetry parameter values.[17] Their data will be compared later with the present results.

Experimental

The details of the photoelectron spectrometer used for the photoelectron angular distribution measurements in this study were described in the previous paper.[3] The β values were obtained according to formula (1) using the intensities measured at the two angles, $\theta = 45°$ and 90°. The measurements were carried out at room temperature and the vapour pressure of the samples was kept constant at 4×10^{-4} Torr.

Results and Discussion

The ionization potentials (IP) and the β values of pyridine, pentafluoropyridine, and 2,6-lutidine are summarized in Table 1. The error limits for β values in Table 1 denote mean square errors. The first, second, and third bands of the photoelectron spectra of pyridine and 2,6-lutidine are shown in Figs. 1(a) and (b), respectively, with the β values plotted against IP.

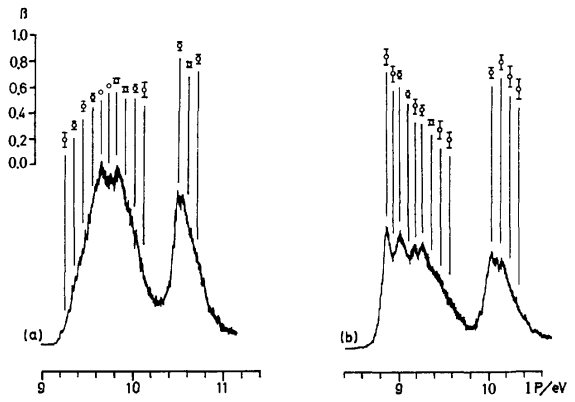

Fig. 1. The first, second, and third bands of the photoelectron spectra of pyridine (a) and 2,6-lutidine (b) and their β values.

We can see from Fig. 1 and Table 1 that the β values of the first and second bands of pyridine increase with increasing IP while the reverse is the case for 2,6-lutidine. This suggests that the order of the first and second bands of pyridine is reverse to that of 2,6-lutidine. The first band of 2,6-lutidine is the $a_2\pi$ band and the second band is the a_1n band.[11] Therefore, the first band of pyridine is assigned to the a_1n orbital and the second band to the $a_2\pi$ orbital. The β values of the first and second bands of pyridine estimated from the values in the regions in which the band overlap is small are $\approx$0.2 and $\approx$0.6, respectively (see Fig. 1(a) and Table 1), while those of 2,6-lutidine are $\approx$0.8 and

Table 1. The ionization potentials (IP in eV) and asymmetry parameters (β) of pyridine, pentafluoropyridine, and 2,6-lutidine

Pyridine		Pentafluoropyridine		2,6-Lutidine	
IP[a]	β	IP[a]	β	IP[a]	β
first and second bands		first band		first and second bands	
9.26	0.19±0.06	10.07	0.63±0.03	8.87	0.83±0.06
9.36	0.30±0.03	10.25	0.61±0.03	8.94	0.70±0.06
9.46	0.45±0.04	10.44	0.57±0.05	9.02	0.69±0.03
9.56	0.52±0.03	10.63	0.57±0.04	9.12	0.54±0.03
9.66(I)	0.56±0.01			9.21	0.45±0.06
9.73	0.61±0.01	second band		9.28	0.42±0.04
9.80(II)	0.65±0.02	11.14	0.71±0.08	9.38	0.32±0.02
9.90	0.58±0.02	11.34	0.67±0.07	9.48	0.27±0.07
10.00	0.59±0.03	11.54	0.65±0.05	9.58	0.19±0.06
10.10	0.58±0.06				
		third band		third band	
third band		11.84	0.63±0.04	10.03	0.71±0.04
10.54	0.91±0.03	11.94	0.69±0.04	10.14	0.79±0.06
10.64	0.77±0.02	12.04	0.64±0.06	10.24	0.68±0.08
10.74	0.81±0.04	12.14	0.67±0.04	10.34	0.58±0.08
		12.24	0.65±0.03		
fourth band					
12.37	−0.16±0.03	fourth band			
12.48	−0.31±0.01	13.44	0.57±0.08		
12.65	−0.35±0.01	13.61	0.55±0.08		
12.75	−0.14±0.07	13.78	0.54±0.08		
		13.95	0.54±0.05		
fifth band					
13.07	0.12±0.04	fifth band			
13.17	0.26±0.03	14.22	0.33±0.05		
13.27	0.27±0.06	14.39	0.37±0.05		
13.37	0.27±0.02	14.56	0.33±0.04		
13.47	0.37±0.03	14.73	0.33±0.05		

a) The IP's underlined are the vertical ionization potentials.

≈0.2, respectively (see Fig. 1(b) and Table 1). The β value of the first band of pyridine corresponds to that of the second band of 2,6-lutidine and the β value of the second band of pyridine is nearly equal to that of the first band of 2,6-lutidine. This fact also supports the above assignments.

Ames *et al.* presented crude photoelectron angular distribution data for pyridine and diazabenzenes without giving β values.[17] Their data indicate a general tendency that the band assignments for the first two bands of pyridine are consistent with the present conclusion.

IP (I) and IP (II) in Table 1 have so far been adopted as the vertical ionization potentials of the a_1n and $a_2\pi$ orbitals, respectively.[7,9–11,18] The β value of band peak (I) or (II) largely deviates from that for the a_1n band (≈0.2) and is nearly equal to the value for the $a_2\pi$ band. This indicates that IP (I) in Table 1 corresponds to the vertical ionization potential of the $a_2\pi$ band. The vertical ionization potential of the a_1n band may be smaller than IP (I) although it can not be decided precisely on account of the overlap of the bands.

We can see from Fig. 1 and Table 1 that the β values of the third bands of pyridine and 2,6-lutidine are ≈0.8 and ≈0.7, respectively, and are nearly equal to each other. This supports Heilbronner and co-workers' assignments of the third bands of pyridine and 2,6-lutidine.[7,9–11]

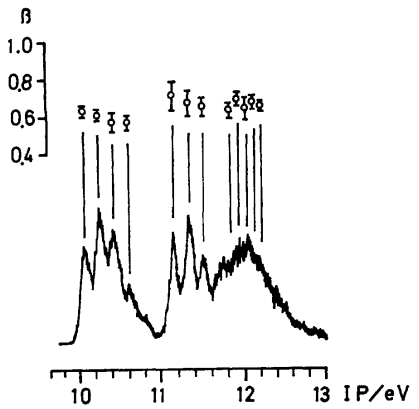

Fig. 2. The first, second, and third bands of the photoelectron spectrum of pentafluoropyridine and their β values.

The first three bands of the photoelectron spectrum of pentafluoropyridine are shown in Fig. 2 and the β values in Table 1 are also plotted against IP in Fig. 2. Brundle and co-workers assigned the first, second, and

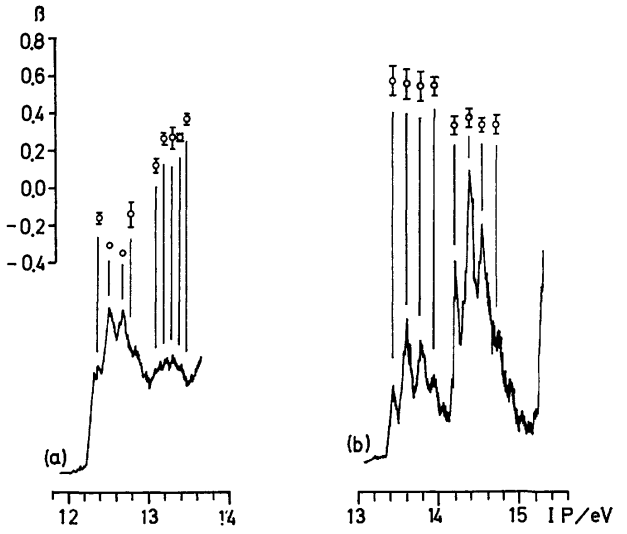

Fig. 3. The fourth and fifth bands of the photoelectron spectra of pyridine (a) and pentafluoropyridine (b) and their β values.

third bands to the $a_2\pi$, $b_1\pi$, and a_1n orbitals, respectively.[18] As is seen in Fig. 2 and Table 1, the β values of the $a_2\pi$ and $b_1\pi$ bands are $\approx$0.6 and $\approx$0.7, respectively. These values are nearly equal to those of the corresponding bands of pyridine, respectively. This also supports the above assignments. The β value ($\approx$0.6) of the a_1n band of pentafluoropyridine, however, differs largely from that ($\approx$0.2) of the corresponding a_1n band of pyridine (see Figs. 1(a), 2, and Table 1). This suggests that the character of the a_1n orbital of pyridine has been considerably changed by the perfluorination.

The fourth and fifth bands of the photoelectron spectra of pyridine and pentafluoropyridine are shown in Figs. 3(a) and (b), respectively, and the β values in Table 1 are also plotted against IP in Fig. 3. Brundle and co-workers assigned the fifth band of pyridine and the fourth band of pentafluoropyridine to the lowest occupied $b_1\pi$ orbitals and the fourth band of pyridine and the fifth band of pentafluoropyridine to the $b_2\sigma$ orbitals mainly from the perfluoro effect.[18] The result of our angular distribution measurements supports this assignment as described below.

The β value of the $b_1\pi$ band (fourth band) of pentafluoropyridine is $\approx$0.6 while the β values of the fourth and fifth bands of pyridine are —0.14——0.35 and 0.12—0.37, respectively. Comparing these β values, the $b_1\pi$ band of pentafluoropyridine should be correlated with not the fourth band but the fifth band of pyridine. Therefore, the fifth band of pyridine is assigned to the lowest occupied $b_1\pi$ orbital. The fourth band of pyridine is necessarily assigned to the $b_2\sigma$ orbital.

We can see that the β value of the $b_2\sigma$ band of pyridine is largely different from that of pentafluoropyridine (see Fig. 3 and Table 1). This indicates that the character of the $b_2\sigma$ orbital of pyridine has been changed by the perfluorination.

In conclusion, the five lower-energy bands of the photoelectron spectrum of pyridine can be assigned to the a_1n, $a_2\pi$, $b_1\pi$, $b_2\sigma$, and $b_1\pi$ orbitals from the lower IP side, respectively, and it is found that the β values of the a_1n and $b_2\sigma$ bands of pyridine are considerably changed by perfluorination while those of the π bands of pyridine are scarcely changed by it.

References

1) J. C. Tully, R. S. Berry, and B. J. Dalton, *Phys. Rev.*, **176**, 95 (1968).
2) J. W. McGowan, D. A. Vroom, and A. R. Comeaux, *J. Chem. Phys.*, **51**, 5626 (1969).
3) T. Kobayashi and S. Nagakura, *J. Electron Spectrosc.*, **7**, 187 (1975).
4) D. W. Turner, *Tetrahedron Lett.*, **35**, 3419 (1967).
5) B.-Ö. Jonsson, E. Lindholm, and A. Skerbele, *Int. J. Mass Spectrom. Ion Phys.*, **3**, 385 (1969).
6) M. J. S. Dewar and S. D. Worley, *J. Chem. Phys.*, **51**, 263 (1969).
7) E. Heilbronner, V. Hornung, H. Bock, and H. Alt, *Angew. Chem.*, **81**, 537 (1969).
8) D. W. Turner, C. Baker, A. D. Baker, and C. R.Brundle, "Molecular Photoelectron Spectroscopy," Wiley-Interscience, London (1970).
9) R. Gleiter, E. Heilbronner, and V. Hornung, *Angew. Chem.*, **82**, 878 (1970).
10) R. Gleiter, E. Heilbronner, and V. Hornung, *Helv. Chim. Acta*, **55**, 255 (1972).
11) E. Heilbronner, V. Hornung, F. H. Pinkerton, and S. F. Thames, *Helv. Chim. Acta*, **55**, 289 (1972).
12) G. H. King, J. N. Murrell, and R. J. Suffolk, *J. Chem. Soc., Dalton Trans.*, **1972**, 564.
13) M. F. A. El-Sayed, M. Kasha, and Y. Tanaka, *J. Chem. Phys.*, **34**, 334 (1961).
14) K. Higasi, I. Omura, and H. Baba, *J. Chem. Phys.*, **24**, 623 (1956); I. Omura, H. Baba, K. Higasi, and Y. Kanaoka, *Bull. Chem. Soc. Jpn.*, **30**, 633 (1957).
15) M. R. Basila and D. J. Clancy, *J. Phys. Chem.*, **67**, 1551 (1963).
16) W. von Niessen, G. H. F. Diercksen, and L. S. Cederbaum, *Chem. Phys.*, **10**, 345 (1975).
17) D. L. Ames, J. P. Maier, F. Watt, and D. W. Turner, *Faraday Discuss. Chem. Soc.*, No. 54, 277 (1973).
18) C. R. Brundle, M. B. Robin, and N. A. Kuebler, *J. Am. Chem. Soc.*, **94** 1466 (1972).

Studies on the Ammonium Form of Crystalline Zirconium Phosphate. III.[1,2] Ammonium-Hydrogen Ion-exchange on α-Zirconium Phosphate Prepared by the Direct Precipitation Method

Yoshitsugu HASEGAWA* and Motomasa KUWAYAMA**

Department of Industrial Chemistry, Faculty of Technology, Tokyo University of Agriculture and Technology, Nakamachi, Koganei, Tokyo 184

(Received November 7, 1977)

The ammonium-hydrogen ion-exchange on α-zirconium phosphate prepared by the direct precipitation method has been investigated by means of pH titration and X-ray diffractometry. In the forward process (α-zirconium phosphate to the ammonium form) the ion-exchange reaction took place in one stage at the equilibrium pH of 5.9—6.0 and the α-zirconium phosphate exchanger was directly converted into the ammonium form. In the reverse process (the ammonium form to α-zirconium phosphate) the reaction proceeded in three stages, that is, the ammonium form→ a half-exchanged form→ an intermediate form→ α-zirconium phosphate. The chemical composition of the half-exchanged form has been represented as $Zr(NH_4PO_4)(HPO_4)\cdot nH_2O$ ($n>0.5$). A small amount of ammonium ions in the exchanger could not be easily replaced with protons in the solution.

The properties of α-zirconium phosphate as an ion-exchanger have been studied by several workers in recent years. It is well known that the ion-exchange reaction on α-zirconium phosphate is strongly affected by its crystal structure, since the largest opening into the crystal would allow a spherical cation with a diameter of 2.63 Å to diffuse into the crystal. Experimentally, Li^+, Na^+, and K^+ exchanged in acidic solution.[3] Although the ionic radius of the ammonium ion is larger than 1.32 Å, the ammonium-hydrogen ion-exchange took place on α-zirconium phosphate.[4,5] In the hydrogen–lithium ion-exchange system the titration curve exhibited two clear inflections at 50 and 66% exchange on α-zirconium phosphate prepared by the direct precipitation (d.p.) and the long refluxing,[6,7] while only one inflection was observed at 66% exchange on α-zirconium phosphate prepared by the ordinary reflux method.[8] Thus the ammonium-hydrogen ion-exchange on α-zirconium phosphate depends on the degree of crystallinity.

To date the ordinary reflux method has been employed in the course of a survey of ammonium form exchangers, but α-zirconium phosphate of high crystallinity could not be obtained by this method.[9] The present investigation has been undertaken using α-zirconium phosphate prepared by the d.p. method in order to avoid the gelatinous characteristics of the compound.

While the manuscript of this paper was in preparation, Alberti *et al.*[10] have reported the ammonium ion and ammonia uptake on α-zirconium phosphate prepared by the d.p. method.

Experimental

Preparation of the α-Zirconium Phosphate Ion-exchanger. α-Zirconium phosphate, $Zr(HPO_4)_2\cdot H_2O$, was prepared by a modification of Horsley and Nowell's method.[11] Zirconium dichloride oxide octahydrate (32 g) was dissolved in water (1050 ml), and hydrofluoric acid (40%, 22 ml) added slowly followed by orthophosphoric acid (about 85%, 77 ml) under continuous stirring. When gelatinous zirconium phosphate precipitated, a small amount of hydrofluoric acid was added until the precipitate was redissolved. The mixture was placed in a water bath (50 °C) and prehumidified air passed through it for 24—30 h. The precipitated α-zirconium phosphate was decantated with distilled water and separated by centrifugation.

pH *Titrations.* The titrations were carried out in batch. A weighed amount of α-zirconium phosphate (100 mg) was placed in contact with the solution of ammonium chloride–aqueous ammonia (10.0 ml) in a thermostat regulated at 25 °C in the forward titration. The composition of the solution was adjusted so that the total ammonium ion was equal to 0.1 M with a varying ratio of NH_4Cl to aqueous NH_3 in the range from 1 to 0. After the mixture was shaken continuously for a specified period of time, the value of the supernatant solution was measured using a pH meter with a glass electrode. Since the chemical composition of the ammonium form is represented as $Zr(NH_4PO_4)_2\cdot H_2O$, the ammonium form (112 mg) was placed in contact with NH_4Cl–HCl solution (10.0 ml) in the reverse titration. The concentration of ammonium chloride was kept constant (3.36×10^{-2} M) and the amount of hydrochloric acid varied.

For the forward process, the titration was also carried out with ammonium acetate–aqueous ammonia solution.

Analytical Procedure. The structural change of the exchanger during the ion-exchange process was measured by X-ray diffractometry. The powder patterns of the exchangers were obtained with a Geigerflex X-ray diffractometer with nickel filtered copper radiation. To avoid obscurity due to overlap and instability of peaks the powder pattern of one sample was recorded under wet and dry conditions. The wet sample was covered with a Mylar film to prevent evaporation after mounting on a glass holder. The dried sample was prepared over a saturated sodium chloride solution (relative humidity about 75% at room temperature). Thermogravimetric and differential scanning calorimetric data were obtained on a Rigaku scanning calorimetric balance TG-DSC standard unit. The chemical analysis of the exchanger was carried out according to the methods described previously.[4]

Results and Discussion

Characterization of the α-zirconium phosphate ion-exchanger was made by X-ray diffraction pattern, TG, DSC data, pH titration with LiCl-LiOH solution, and chemical analysis. The interplanar spacings (*d*-values)

** Present address: New Japan Surveyors and Sworn Measurers Association, 541 Chitose, Takatsu-ku, Kawasaki 211.

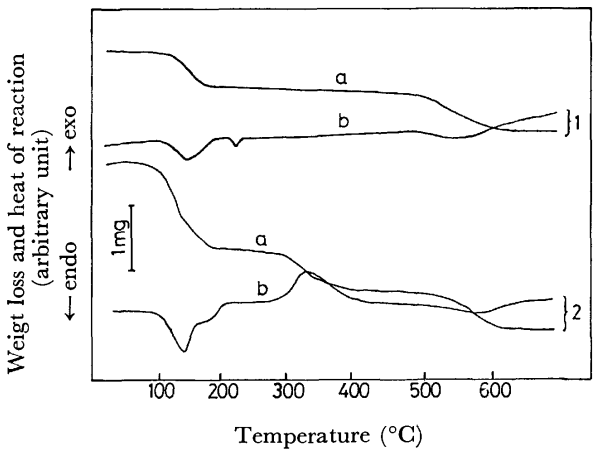

Fig. 1. Thermoanalytical curves. 1: α-Zirconium phosphate in H^+ form, 2: the ammonium form, (a) thermogravimetric and (b) scanning calorimetric curve.

agreed with those given in the literature.[11] The results of thermal analysis are shown in Fig. 1(1). The titration curve for the lithium ion agreed with those reported previously.[6,7] The chemical composition was as follows; Found: Zr, 30.2; PO_4, 63.7; ignition loss, 12.0%. Calcd for $Zr(HPO_4)_2 \cdot H_2O$: Zr, 30.0; PO_4, 63.0; ignition loss, 12.0%. The above results show that the α-zirconium phosphate ion-exchanger used was highly crystalline and essentially identical to that prepared by long refluxing.[5]

The chemical composition of the ammonium form was as follows: Found: Zr, 27.2; PO_4, 57.6; NH_4, 10.8; ignition loss, 20.9%. Calcd for $Zr(NH_4PO_4)_2 \cdot H_2O$: Zr, 27.2; PO_4, 56.7; NH_4, 10.8; ignition loss, 20.9%. The results of thermal analysis for the ammonium form are shown in Fig. 1(2). The curves agreed with those reported for the reflux method.[12] The exothermic peak at about 400 °C might be caused by the oxidation of the evolved ammonia on platinum surface of a crucible.[13]

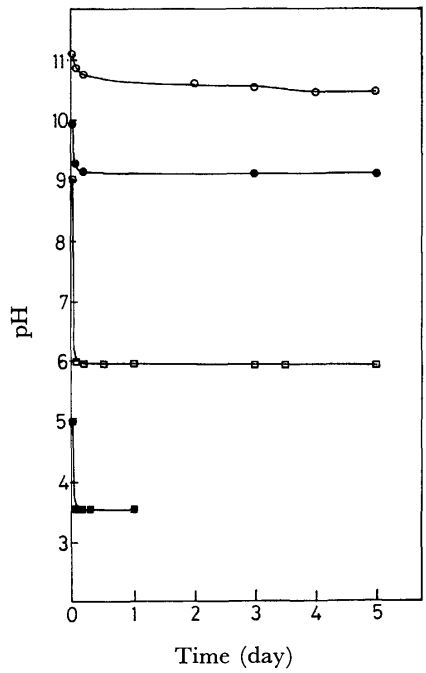

Fig. 2. pH dependence on time.
OH^- meq/g α-zirconium phosphate; ■ 0, □ 3, ● 7, ○ 10.

pH *Titrations.* To determine the equilibration time the pH values of the solutions were measured at specific intervals of time. Figure 2 shows that the ion-exchange reaction proceeded rapidly initially and then the pH value gradually fell to an equilibrium value. It took about 5 days to attain equilibrium for 0.1 M aqueous ammonia, compared to 6 h for 0.1 M ammonium chloride solution. In the reverse titration the pH values were measured at 6.00 and 3.00 meq H^+/g α-zirconium phosphate. The observed equilibrium was attained within one day for both solutions. Thus, a reaction time of 2—5 days was chosen in the forward process and 2 days in the reverse one.

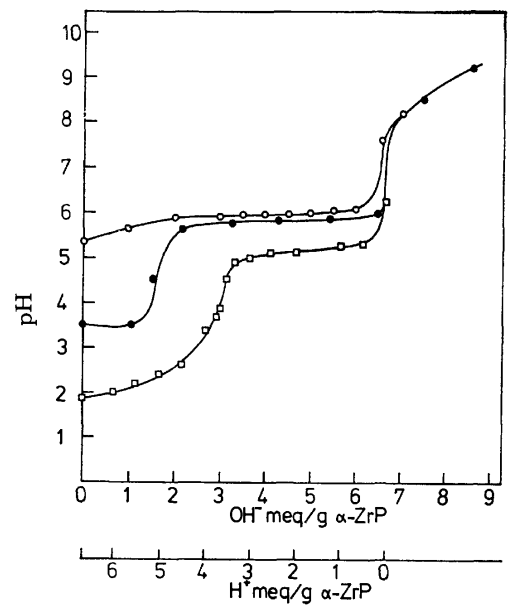

Fig. 3. pH titration curves.
(a) ● Forward titration NH_4Cl–NH_3(aq), (b) ○ forward titration NH_4CH_3COO–NH_3(aq), (c) □ reverse titration NH_4Cl–HCl.

The pH titration curves obtained are shown in Fig. 3. The curve (a) shows that in the forward process the ammonium–hydrogen ion-exchange reaction took place at a pH of about 3.5 until approximately $OH^- = 1.0$ meq, whereupon the pH rose sharply to the equilibrium pH of 5.9. The lowering of the pH in the initial stage may be ascribed to the selective uptake of the ammonium ion on α-zirconium phosphate. Figure 3(b) demonstrates that in ammonium acetate–aqueous ammonia solution the equilibrium pH and the ion-exchange capacity were almost equal to those observed for the chloride solution. In the initial stage of curve (b) compared with the curve (a) higher pH values are due to the bufferring action of the ammonium acetate solution. The α-zirconium phosphate ion-exchanger behaved as a monobasic exchanger with a capacity of 6.64 meq/g. The equilibrium pH was found to be approximately 5.9—6.0.

The titration curve of the reverse process is shown in

Fig. 3(c). It appears that the ion-exchange reaction took place in two stage, that is, in the first stage 50% of the ammonium ions in the exchanger were replaced with hydrogen ions and in the second stage the remaining ammonium ions were involved in the reaction. The reaction proceeded in a more acidic solution than for the forward titration, especially in the second stage. At the hydrogen ion addition of 6.0 and 6.6 meq the pH values of the solutions were found to be 2.03 and 1.88. The low pH value indicates that some hydrogen ions remained in the solution phase and the ionic mole fraction of the ammonium ion in the exchanger, $\bar{X}_{NH_4^+}$, was higher than expected from the forward process. Assuming that the apparent value of pH on a pH meter is equal to $-\log [H^+]$, the hydrogen ion concentration can be calculated to be 9.3×10^{-3} and 1.3×10^{-2} mol/l and this corresponds to the fact that hydrogen ions of 5.2 and 5.4 mmol/g α-zirconium phosphate exchanged with the ammonium ions in the exchanger. Consequently, $\bar{X}_{NH_4^+}$ is estimated to be 0.22 and 0.19. This demonstrates that the α-zirconium phosphate exchanger has a strong affinity for the ammonium ion especially when the exchanger is loaded by a small amount of ammonium ion. A similar behavior has been observed in another system.[14]

The titration curves, (a) and (c) in Fig. 3, indicate the irreversible ion-exchange reaction for the ammonium–hydrogen ion-exchange system.

Since the α-zirconium phosphate exchanger and its salt form have a layered structure, the structural change of solid phase is revealed in comparison with the reflections of the powder patterns at lower diffraction angles.[15] A similar phenomena may be expected, because the ammonium form also has a layered structure.[16]

Table 1. Phases present in the forward titration

OH^- meq/gZrP	Medium	
	Cl^-	CH_3COO^-
0	H	H
1.0	H	H + A
2.2	H + A	H + A
3.2	H + A	H + A
4.3	A + H	A + H
5.4	A + H	A + H
6.4	A + H	A + H
6.5		A
7.6	A	

H=Hydrogen form $Zr(HPO_4)_2 \cdot H_2O$,
A=Ammonium form $Zr(NH_4PO_4)_2 \cdot H_2O$.

Table 1 shows the structural change in the exchanger in the forward process. At the beginning of the ion-exchange reaction only the α-zirconium phosphate phase was present. Two phases, the α-zirconium phosphate and the ammonium phase, coexisted in the range of $\bar{X}_{NH_4^+}$=0.33—0.91. The intensity of the diffraction peak of α-zirconium phosphate decreased with an increase in $\bar{X}_{NH_4^+}$. Table 1 also shows that the structural change of the exchanger was similar in the chloride and acetate solution. At the initial stage of the ion-exchange the reaction proceeded further in the acetate solution than in the chloride solution, because the solution phase of acetate had higher pH value. α-Zirconium phosphate was directly converted into the ammonium form. These data support the validity of the interpretation of the titration curves given above.

Table 2. Phases present in the reverse titration

H^+ meq/gZrP	Phase
0	A
0.05	A + A′
2.00	A + A′
2.50	A′ + A
3.30	A′ + A
3.50	A′

A=Ammonium form, A′=A phase having peaks at 11.5 and 10.5° ($I_{11.5}/I_{10.5}$=8/5).

A complicated change was observed on the X-ray diffraction patterns of the solid phases during the reverse titration. In the first stage, 0—50% of the ion-exchange, four peaks were observed for the wet samples at a range of lower angles. The intensity of the peak at 2θ=8.6° was strongly affected by the water content of the sample. When the same sample was dried over a saturated sodium chloride solution, three peaks were observed on the powder pattern. On the assumption that the number of phases does not change on drying out of the solid sample, assignment of the peaks was conducted. The peak at 9.4° originated from the ammonium form and its intensity decreased with an increase in the mole fraction of hydrogen ion in the exchanger, $\bar{X}_{H^+}$. This peak was found in both wet and dry samples up to H^+=3.30 meq/g α-zirconium phosphate. The intensity of other two peaks at 11.5° and 10.5° increased as the ion-exchange process proceeded. In consideration of the inflection point of the titration curve (Fig. 3(c)) and the phase rule,[9] only two phases must be present in this region. Hence, the two peaks may be assigned as one phase, namely the half-exchanged form. A similar change was reported for α-zirconium phosphate prepared by long refluxing.[5] The ammonium ion and water contents of the half-exchanged form were determined by elemental analysis after drying. Found: N, 4.32; H, 1.84; ignition loss at 950 °C (100—ash), 13.4%. Calcd for $Zr(NH_4PO_4)(HPO_4) \cdot 0.5H_2O$: N, 4.53; H, 1.96; ignition loss, 14.3%. The half-exchanged form had more waters of hydration in solution than in the dry condition.

In the second stage of the reverse titration, the dried exchanger had two peaks at 11.5 and 10.5°. The intensity of the peak at 11.5° decreased with increase in $\bar{X}_{H^+}$ and the peak was observed as a shoulder of the peak at 10.5°. Subsequently the intensity of the peak at 11.5° increased again with the reaction above the hydrogen ion addition of 4.5 meq suggesting that a half-exchanged and an intermediate form were present in the region of H^+=3.6—4.5 meq. An intermediate and α-zirconium phosphate coexisted above H^+=4.5 meq (Table 3). At the final stage of the reverse titration an intermediate form was still present. This indicates

TABLE 3. CHANGE OF THE INTENSITY RATIO IN THE SECOND STAGE OF THE REVERSE TITRATION

H^+ meq/gZrP	$I_{11.5}/I_{10.5}$	Phase
3.50	8/5	A′
4.00	5/6	A′, A″
4.50	1/20	A′, A″ or A″, H
5.00	4/11	A″, H
6.00	5/3	A″, H
6.60	11/7	A″, H

A″=A phase deduced having a peak only at 10.5°, H=Hydrogen form.

that the ion-exchange reaction does not proceed stoichiometrically and that the ammonium ion was held by the exchanger.

The conclusion drawn are as follows. (1) Highly crystalline zirconium phosphate ion-exchanger was prepared under the mild conditions employed and the exchanger was essentially identical to that prepared by long refluxing. (2) The α-zirconium phosphate ion-exchanger behaved as a monobasic acid to aqueous ammonia and was converted into the ammonium form. In the reverse process the ion-exchange reaction took place in three stages. (3) A small amount of ammonium ion in the exchanger could not be replaced easily with hydrogen ion.

The authors are grateful to Professor Shuji Abe for his continuing interest and encouragement. They also wish to thank Mrs. Michiko Asuke for her assistance in the elemental analysis.

References

1) Part II. Y. Hasegawa and Y. Komiyama, *Bull. Chem. Soc. Jpn.*, **51**, 2302 (1978).
2) A part of this work was presented at the 26th International Congress on Pure and Applied Chemistry, Tokyo, Japan, September, 1977.
3) A. Clearfield, G. H. Nancollas, and R. H. Blessing, "Ion Exchange and Solvent Extraction," ed by J. A. Marinsky and Y. Marcus, Marcel Dekker, New York (1973), Vol. 5, pp. 21—28.
4) Y. Hasegawa and H. Aoki, *Bull. Chem. Soc. Jpn.*, **46**, 836 (1973).
5) A. Clearfield and R. A. Hunter, *J. Inorg. Nucl. Chem.*, **38**, 1085 (1976).
6) G. Alberti, U. Costantino, S. Alluli, M. A. Massucci, and M. Pelliccioni, *J. Inorg. Nucl. Chem.*, **34**, 1347 (1973).
7) A. Clearfield and D. A. Tuhtar, *J. Phys. Chem.*, **80**, 1296 (1976).
8) A. Clearfield and J. Troup, *J. Phys. Chem.*, **74**, 314 (1970).
9) A. Clearfield and A. S. Medina, *J. Phys. Chem.*, **75**, 3750 (1971); A. Clearfield, A. Oskarsson, and C. Oscarsson, *Ion Exchange Membrane*, **1**, 91 (1972).
10) G. Alberti, R. Bertrami, U. Costantino, and J. P. Gupta, *J. Inorg. Nucl Chem.*, **39**, 1057 (1977).
11) S. E. Horsley and D. V. Nowell, *J. Appl. Chem. Biotechnol.*, **23**, 215 (1973).
12) Y. Hasegawa, *Bull. Chem. Soc. Jpn.*, **46**, 3296 (1973).
13) T. Flora, *Acta Chem. Acad. Scientiarum Hungacae, Tomus*, **69**, 1 (1971).
14) Y. Hasegawa, *J. Inorg. Nucl. Chem.*, **38**, 319 (1976).
15) A. Clearfield, W. L. Duax, A. S. Medina, G. D. Smith, and J. R. Thomas, *J. Phys. Chem.*, **73**, 3424 (1969).
16) A. Clearfield and J. M. Troup, *J. Phys. Chem.*, **77**, 243 (1973).

Syntheses and Electronic Spectra of 2,2′-Isopropylidenedi-8-quinolinol, Its Nickel(II), and Copper(II) Chelates

Yoshinori YAMAMOTO,* Akira MIURA, Akira KAWAMATA, Masayoshi MIURA, and Shinsuke TAKEI

Department of Industrial Chemistry, Faculty of Engineering, Ibaraki University, Nakanarusawa-cho, Hitachi 316

(Received November 14, 1977)

The title ligand, which contains two 8-quinolinol (oxine) functions in one molecule, and the Ni(II) and Cu(II) chelates have been synthesized and characterized. Visible and ultraviolet spectra of the chelates and the ligand in several solvents have been measured. Square-coordination of the ligand to the metal has been revealed by a comparison of the d-d bands between the chelates and quadridentate Schiff base chelates in the literature. Intra-ligand transition bands of the title chelates and the solvent effects on the frequency shifts have been compared with those of the ligand, 8-hydroxy-1-methylquinolinium hydroxide, bis(8-quinolinolato)palladium(II), -copper(II), and -nickel(II), and have been discussed.

The quadridentate ligand, 2,2′-isopropylidenedi-8-quinolinol, abbreviated as ipdq, has been prepared in our laboratory, in expectation of forming such type of stable metal chelates as *cis*-bis(8-quinolinolato)metal. The synthetic pathway is outlined in Scheme 1. It has been shown that ipdq readily reacts with both nickel(II) and copper(II) to give the crystalline compounds, Ni(ipdq) and Cu(ipdq), respectively. These chelates are sufficiently soluble in many organic solvents to examine the d-d absorption bands, which provide significant information regarding the coordinating structure. This paper presents the absorption data of Ni(ipdq) and Cu(ipdq) in eight solvents in the ultraviolet and visible regions, and the spectra have been compared with those of related compounds.

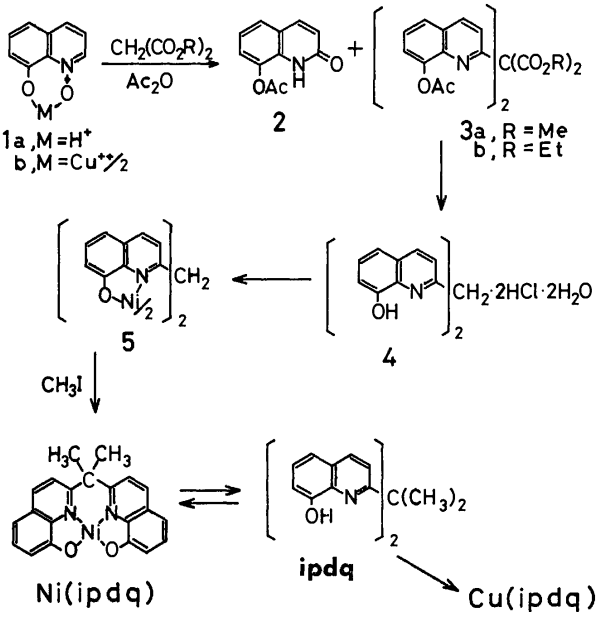

Scheme 1.

The chief purpose of this work was to determine the effect of the metal ion on the spectra of the 8-quinolinol-type ligand, of value from the viewpoint of the development of analytical colorimetric reagents, and in connection with the spectra of the corresponding 8-quinolinol chelates, NiQ_2 and CuQ_2.[1] It is known that the position of the lowest energy intra-ligand band of CuQ_2 is highly dependent upon the solvent[2] and the spectrum of NiQ_2 changes drastically with solvent.[3-7] The low solubility, however, restricts the elucidation of the relationship among the spectra, coordinating structure, and nature of solvent.

Results

Preparations. As shown in Scheme 1, Ni(ipdq) has been obtained from 8-quinolinol *N*-oxide (**1a**) or its copper(II) complex (**1b**) in a four-step process. The intermediate compounds (**3**—**5**) have also been isolated and characterized, the detailed procedures and results of which are given in the experimental section.

The malonates, **3a** and **3b**, have been prepared by a method similar to that reported by Hamana and Yamazaki[8] for the synthesis of diethyl di-2-quinolylmalonate by the treatment of quinoline *N*-oxide with diethyl malonate in the presence of acetic anhydride (Ac_2O). It is known that the treatment of **1a** with Ac_2O at room[9] or bath-temperature[10,11] affords 8-acetoxy-2-

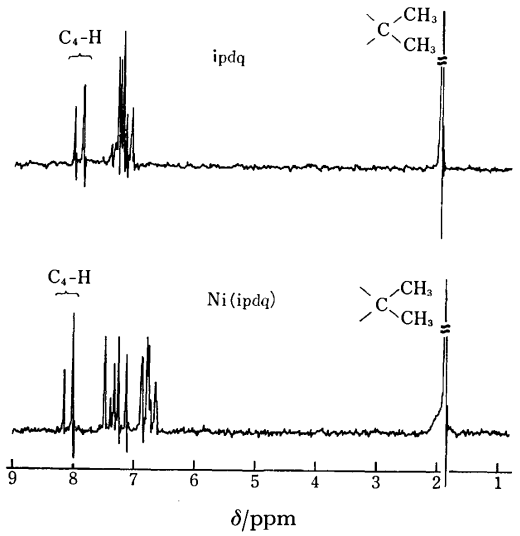

Fig. 1. The 60 MHz PMR spectra of ipdq and Ni(ipdq) in $CDCl_3$. For the spectrum of Ni(ipdq) (29 mg/0.6 cm³), the relative intensity are 3 (siglet), 4 (multiplet), and 1 (doublet). For the spectrum of ipdq (40 mg/0.6 cm³), those are 3, 4.4, and 1.2, respectively, and the latter two contain probably the phenolic proton.

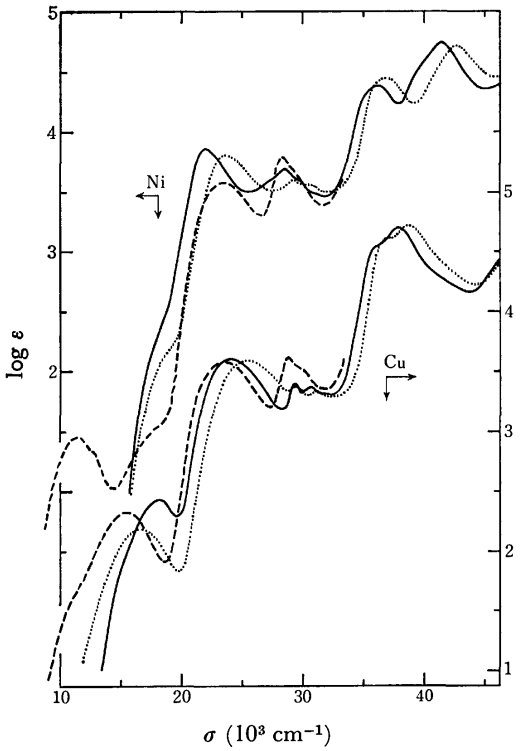

Fig. 2. The absorption spectra of Ni(ipdq) in MeOH (·····), in THF (——), and in pyridine (------), and the spectra of Cu(ipdq) in MeOH (·····), in 1,2-dichloroethane (——), and in pyridine (------).

quinolone (**2**) in high yield. It has been found, however, that the addition of dimethyl or diethyl malonate to the above system gives a mixture of **3** (**a** or **b**) and **2**, and that, on lowering the temperature, the yield of **3** increases at the expense of **2** as given in Table 4 in the experimental section.

The chelate, **5**, is not suitable for the present purpose, since in many common solvents it is not sufficiently soluble. However, **5** readily reacts with two moles of methyl iodide to yield a higher soluble chelate, Ni(ipdq). The PMR spectra of Ni(ipdq) and the metal-free ligand, ipdq, are shown in Fig. 1. The similarity of these spectra to those of 2-methyl-8-quinolinol and its Al(III) complex[12] supports the structure shown in Scheme 1.

Absorption Spectra. Absorption data obtained are set out in Tables 1—3. The spectra of some representative species are shown in Fig. 2. The intra-ligand transition bands have been divided into three parts, in an analogy with those of the 8-quinolinolate.[2,3,13] In this paper these bands have been denoted by A-, B-, and C- in the order of decreasing frequency.

The spectra of ipdq (Table 1) are comparable to those of 8-quinolinol[2,3,14] and its 2-methyl derivative.[3,15] A weak shoulder near 450 nm for ipdq in methanol (MeOH) is similar to a band for 8-quinolinol at 430 nm (ε: 51)[14c,f,h,i] in water or at 450 nm in MeOH (shoulder, log ε: −0.34),[14f] which is known to be due to the presence of the zwitter ionic form.[14c,h,i]

The spectrum of the 8-hydroxy-1-methylquinolinium salt in basic solvent is known to be a good model for the absorption characteristics of the zwitter ionic form of 8-quinolinol.[14c,g,i,j] The 8-hydroxy-1-methylquinolinium hydroxide (the isomer of 1-methylquinolinium-8-

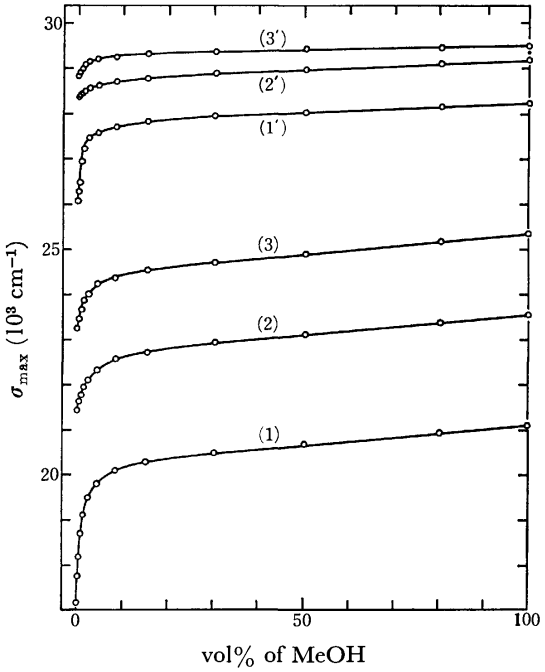

Fig. 3. Variation of the positions of the C- (1—3) and B-bands (1'—3') of the compounds in benzene–MeOH mixtures as a function of the vol% of MeOH; (1) 8-hydroxy-1-methylquinolinium hydroxide, (2) Ni-(ipdq), and (3) Cu(ipdq).

TABLE 1. THE ABSORPTION DATA[a,b] OF ipdq AND 8-HYDROXY-1-METHYLQUINOLINIUM CHLORIDE (N–CH_3)

Compound	Solvent	A-band σ_{max} (log ε)	B-band σ_{max} (log ε)	C-band σ_{max} (log ε)
ipdq	Cyclohexane	39.18 (4.94)	32.13 (3.83)	31.1 (sh 3.77)
	MeOH	39.64 (4.91)	32.39 (3.81)	31.3 (sh 3.73) 22.5 (sh −0.42)[c]
	0.1 M aq NaOH	37.91 (4.79)	29.59 (3.84)	28.3 (sh 3.77)
	0.1 M KOH–MeOH	37.88 (4.74)	29.41 (3.80)	28.0 (sh 3.72)
	1.0 M aq HCl	37.49 (4.82)	30.53 (3.92)	26.9 (3.49)
N–CH_3	0.1 M aq NaOH	36.56 (4.52)	28.9 (3.11)	22.4 (3.21)
	0.05 M KOH–MeOH	35.91 (4.52)	28.3 (3.30)	21.1 (3.19)

a) The wave numbers are given in 10^3 cm^{-1} units, and sh means a shoulder band. b) Only the main peaks are tabulated. c) A 10 cm cell was used.

TABLE 2. THE ABSORPTION DATA[a,b] OF 8-HYDROXY-1-METHYLQUINOLINIUM HYDROXIDE (N-CH_3, OH) AND THE METAL CHELATES

Compound	Band		Solvent							
			MeOH	2-PrOH[c]	DMF	DCE[d]	Pyridine	$CHCl_3$[e]	THF	Benzene
N-CH_3, OH	A	σ_{max}	35.91	35.46		34.36		34.31	34.31	
	B	σ_{max}	28.3	27.9	26.3	26.5	26.0	26.7	26.3	26.1
		(log ε)	(3.31)	(3.39)	(3.66)	(3.66)	(3.71)	(3.53)	(3.64)	f)
	C	σ_{max}	21.1	20.2	18.2	18.0	17.7	18.3	17.5	17.2
		(log ε)	(3.16)	(3.16)	(3.12)	(3.16)	(3.12)	(3.09)	(3.09)	f)
CuQ_2[g]	A	σ_{max}[h]	38.83	38.61		37.95		38.02	37.95	
	B	σ_{max}	29.90	29.81	29.63	29.74	29.4	29.72	29.56	29.56
		(log ε)	(3.36)	f)	(3.49)	(3.38)	(3.51)	(3.34)	(3.50)	(3.42)
	C	σ_{max}	25.5	25.1	24.2	24.0	24.2	24.3	23.9	23.6
		(log ε)	(3.73)	f)	(3.76)	(3.77)	(3.77)	(3.78)	(3.77)	(3.77)
Cu(ipdq)	A	σ_{max}	38.69	38.31		37.88		37.74	37.66	
	B	σ_{max}	29.50	29.4	29.1	29.2	28.8	29.1	28.9	28.8
		(log ε)	(3.37)	(3.37)	(3.53)	(3.41)	(3.61)	(3.36)	(3.54)	(3.48)
	C	σ_{max}	25.4	24.6	24.2	24.0	23.5	23.7	23.5	23.3
		(log ε)	(3.59)	(3.60)	(3.61)	(3.61)	(3.58)	(3.60)	(3.58)	(3.56)
	d-d	σ_{max}	16.5	17.1	16.6	18.1	15.5	18.2	16.9	17.9
		(log ε)	(2.19)	(2.24)	(2.30)	(2.43)	(2.33)	(2.43)	(2.35)	(2.47)
PdQ_2	A	σ_{max}[i]	40.82	40.65		39.80		39.76	39.76	
		σ_{max}[j]	37.52	37.24		36.63		36.83	36.63	
	B	σ_{max}	29.63	29.67	29.46	29.46	29.3	29.4	29.4	29.2
		(log ε)	(3.31)	(3.31)	(3.44)	(3.42)	(3.51)	(3.38)	(3.48)	(3.52)
	C	σ_{max}	—	—	23(sh)	23(sh)	23(sh)	—	23(sh)	23(sh)
		σ_{max}	24.0	23.6	22.6	22.5	22.3	23.0[k]	22.1	22.0
		(log ε)	(3.84)	(3.83)	(3.83)	(3.82)	(3.84)	(3.82)	(3.85)	(3.88)
Ni(ipdq)	A	σ_{max}	42.68	42.28		41.67		41.67	41.41	
		σ_{max}	36.87	36.70		36.23		36.28	36.10	
	B	σ_{max}	29.2	28.9	28.7	28.7	28.3	28.6	28.5	28.4
		(log ε)	(3.60)	(3.59)	(3.68)	(3.66)	(3.79)	(3.67)	(3.69)	(3.72)
	1)	σ_{max}		28(sh)	28(sh)	28(sh)	—	28(sh)	27(sh)	27(sh)
				24(sh)	24(sh)	24(sh)	—	23(sh)	23(sh)	23(sh)
	C	σ_{max}								
		σ_{max}	23.6	22.9	22.5	22.3	23.4	22.1	21.8	21.4
		(log ε)	(3.81)	(3.81)	(3.88)	(3.85)	(3.57)	(3.85)	(3.86)	(3.83)
NiQ_2[m]	C[n]	σ_{max}	25.9[p]	25.8	24.6	26.1	24.4[q]	26.0	25.6	25.9
		(log ε)	(3.72)	f)	(3.67)	r)	(3.77)	r)	r)	r)
	C[o]	σ_{max}	—			23(sh)	—	23(sh)	22(sh)	22(sh)
		σ_{max}	—	23(sh)	22(sh)	21.6	—	21.7	21.4	21.2

a) The wave numbers are given in 10^3 cm^{-1} units, and sh means shoulder band. b) Only the main bands are tabulated; see in Fig. 2. c) 2-Propanaol. d) 1,2-Dichloroethane. e) Containing 0.5 vol% EtOH. f) A saturated soln. g) *Cf.* Refs. 2 and 3. h) log ε is *ca.* 4.83. i) log ε is 4.6—4.7. j) log ε is *ca.* 4.5. k) *Cf.* K. Sone, *J. Am. Chem. Soc.*, **75**, 5207 (1953); E. Sekido, *Nippon Kagaku Zasshi*, **80**, 871 (1959). l) A new band. See text. m) *Cf.* Refs. 2—7. n) Of one form in an equilibrium mixture, presumed to be a polymeric species (ref. 22) or solvent-coordinated species. o) Of another form, presumed to be a planar species. p) The A-band: 38.54 (4.74), the B-band: 29.72 (3.59). q) The B-band: 28.9 (3.81). r) Immediately after suspension, filtration, and dilution. After one day standing considerable amounts of ppt were deposited.

olate monohydrate) is known as one of the solvatochromic compounds exhibiting large color changes with solvent polarity.[16,17] The band positions of this hydroxide in MeOH (Table 2) are seen to be almost the same as that of the corresponding chloride salt in MeOH–KOH (Table 1). From these results, the chloride in a basic solvent and the hydroxide in an organic solvent can best be utilized to establish the spectral behavior of the zwitter ionic form of ipdq.

The plots of the positions of the B- and C-bands of the hydroxide, Ni(ipdq), and Cu(ipdq) in benzene–MeOH mixtures *vs.* the vol% of MeOH are shown in Fig. 3.

Discussion

The coordinating structure of Cu(ipdq) in eight solvents can be classified into three groups according to the positions and the shapes of the d-d bands (Fig. 2 and Table 2). On the basis of the data of (*N,N'*-disalicylidene-1,2-propanediaminato)copper(II) which has been shown to be square-planar in chloroform

TABLE 3. THE d-d ABSORPTION DATA[a] OF THE NICKEL CHELATES[b,c]

Chelate	Solvent	Band I σ_{max} (log ε)	Singlet band σ_{max} (log ε)	Band II σ_{max} (log ε)
$NiQ_2 \cdot 2H_2O$	MeOH	9.71 (1.12)	13.0 (0.50)	16.3 (0.97)
NiQ_2	MeOH[d]	9.8	13.0	16.3
	solid(mull)	9.76	13.0 (sh)	16.0
	Pyridine[e]	10.70 (1.03)	12.8 (sh 0.72)	18.3 (1.44)
Ni(ipdq)[c]	Pyridine	11.43 (1.45)	12.8 (sh 1.35)	18.5 (sh 1.54)

a) The wave numbers are given in 10^3 cm^{-1} unit, and sh means a shoulder band. b) *Cf.* Ref. 21, the data of $KNiQ_3$. c) The d-d data of Ni(ipdq) in the other seven solvents are omitted. The spectra in MeOH and in THF shown in Fig. 2 are representative. d) A saturated soln, and a 10 cm cell was used. e) *Cf.* Refs. 3, 5, and 6.

(d-d_{max}: 17760 cm^{-1}) and forming a five-coordinated monoadduct in pyridine (max: 16860),[18] it can be deduced that the benzene, chloroform, and 1,2-dichloroethane solutions of Cu(ipdq) involve a planar monomeric species; the tetrahydrofuran, *N,N*-dimethylformamide, and two alcoholic solutions involve a five-coordinated copper(II); and the pyridine solution involves a six-coordinated copper(II). The five-coordination in the solutions does not mean a dimeric structure since even in such an inert solvent as benzene the chelate is a monomer. Any relationship between the solvent-induced frequency shifts of the d-d band of Cu(ipdq) and those of the A-, B-, or C-band could not be found. The position of the C-band shifts linearly with the E_T value known as a solvent polarity parameter[19] with small deriation for the pyridine solution.

By comparing the d-d bands of Ni(ipdq) (Fig. 2 and Table 3) with those of the quadridentate Schiff base chelates of nickel(II),[20] it has been concluded that the pyridine solution involves a solvent-coordinated species and the other seven solutions involve a planar monomeric species. The difference in band position and intensity between the first d-d band of NiQ_2 in pyridine and that of Ni(ipdq) may be correlated with the difference in coordinated environment between *trans*-O_2N_4 and *cis*-O_2N_4 with a similar discussion of the d-d bands for *mer*- and *fac*-$KNiQ_3$.[21] From the band positions of the nickel chelates (Table 3), the form of NiQ_2 in MeOH and in the solid state have been assigned as solvent-coordinated O_4N_2 and oxygen-bridged polymeric O_4N_2, respectively. The latter is consistent with previous conclusions[22] of one form in an equilibrium mixture of NiQ_2 in inert solvent.

The shapes of the A-, B-, and C-bands of planar Ni(ipdq), and possibly those of planar NiQ_2 also, differ markedly from those of the copper chelates and the six-coordinated nickel chelates, which are similar to those of the ligand cation[3,13,14a] and the zwitter ion (Fig. 2 and Table 2). The bands of the planar nickel chelates, however, may be correlated to those of the other chelates by an inspection of the spectra of PdQ_2 (Table 2), since PdQ_2 has intermediate spectral properties between the copper chelates and the planar nickel chelates. Thus, with change from the copper chelates to PdQ_2 or the planar nickel chelates, the A-band appears to be split into two strong bands and the C-band becomes sharper and more intense, shifting to the red. Planar Ni(ipdq) shows an additional band near $27—28 \times 10^3$ cm^{-1}, and there is no corresponding band in the spectra of PdQ_2. In this sence, the band is clearly a new one.

It has been noted that the frequency shifts of the C-band of planar Ni(ipdq) induced by the solvents are almost the same as those of Cu(ipdq). These shifts may be correlated to the solvatochromism of the *N*-methyl compound, in regard to the strong blue shift by the addition of a small amount of MeOH in the benzene solutions (Fig. 3) and to the approximately linear relationship with the E_T value[19] (Table 2). These facts suggest that the nature of the C-bands, *i.e.* the first π-π^* bands, of these species are similar to each other, and throw doubt upon the explanation[3] for the C-band of planar NiQ_2 in terms of a strong mixing of charge transfer from the metal to the ligand with the intra-ligand transition.

Burton and Davis have studied the spectrum of 8-quinolinol and explained that the lowest energy band of the neutral molecule involves a movement of the electronic charge from the phenol ring to the pyridine ring, and that an increase in the electron density in the phenol ring (*e.g.* by the formation of the dissociated anion) or a decrease in the electron density in the pyridine ring (*e.g.* by the formation of the protonated cation) will move the transition to lower energies.[23] Hence the strong red shift of the C-band of the zwitter ion is explained.

In CuQ_2 *etc.*, the considerable delocalization of the negative charge on the phenol ring has been suggested from the bond-length between the carbon at 8-position and the phenolic oxygen[24] and the electrophilic reaction.[25] The delocalization and good σ-bonding character[3,13] of the metal–nitrogen bond can bring the C-band positions of the chelates listed in Table 2 between those of the zwitter ion and protonated cation of the ligand. As suggested from the study of the hydroxide,[17] the sensitivity of the C-band to the protic solvent, shown in Fig. 3, may be ascribed in most part to a decrease in the degree of delocalization of the negative charge to the phenol ring, possibly due to the formation of the H-bond between the protic solvent and the anionic oxygen in the chelates.

While the position of the C-band of the copper chelates is near to that of the solvent-coordinated nickel chelates, a blue shift of the C-band of the polymeric NiQ_2 relative to CuQ_2 (*e.g. ca.* 2000 cm^{-1}, in benzene) has been observed. In analogy with the formation of

the H-bond, the blue shift may be explained on the basis that the delocalization of the negative charge decreases due to the bonding of the phenolic oxygen to the two metal ions.

On changing from solvent-coordinated NiQ_2 to planar Ni(ipdq), the C-band is displaced to the red (*e.g. ca.* 2000 cm^{-1}, in MeOH). Although detailed analysis is not yet possible, the better σ-bonding character of the N–Ni (low spin) bond in the planar chelate may contribute much to this shift.

Experimental

Preparation of the Compounds. The spectral sample of NiQ_2 was obtained by heating $NiQ_2 \cdot 2H_2O$ at 140—150 °C for 10 h, which showed the bands (IR: KBr, in part) at 744, 737 (sh), and 731 cm^{-1}. A sample dehydrated by heating at lower temperature showed the single and somewhat broader peak at 730 cm^{-1} in this region.[26] The other MQ_2 were prepared by the usual method.[27]

8-Hydroxy-1-methylquinolinium chloride was prepared in a manner similar to the preparation of its perchlorate salt[14j] and recrystallized.[28] Mp 237—238 °C (lit,[28] 233 °C) (lit,[16] 197 °C). Found: C, 61.44; H, 5.27%. 8-Hydroxy-1-methylquinolinium hydroxide was prepared by the reported method.[17] Mp(dec) 117 °C (lit,[17] 115 °C) (lit,[16] 119 °C).

8-Quinolinol N-*Oxide (**1a**)*: The reported methods[29,30] were modified in the following way. To a hot solution of 8-quinolinol (73 g) dissolved in AcOH (200 cm^3), 30% aq H_2O_2 was added (50 cm^3). The mixture was heated at 75—80 °C, for 6 h. Additional peroxide (100 cm^3) was added in five equal portions, while heating, at hourly intervals. After cooling, the reaction mixture was concentrated with a rotary evaporator at 40—50 °C, and water (50 cm^3) added when the residue decreased. The resulting solution was concentrated again, and this procedure repeated three or four times until a solid separated. The resulting mixture was extracted with 150-, 100-, 100-, and 50 cm^3 of $CHCl_3$ and the combined extracts were washed with 2 M aq NH_3 (200- and 200 cm^3), water, 1 M aq HCl (200 cm^3), and finally water. The solvent of the organic layer, without drying, was distilled and the residual yellow solids were recrystallized from 50 vol% aq EtOH (210 cm^3) to give 47 g (58%) of **1a** as fine yellow needles; mp 138—139 °C (lit,[29] 138 °C) (lit,[30] 139 °C).

Bis(8-quinolinol N-*oxidato)copper(II) (**1b**)*: The reported method[10] was modified for large scale preparation. To a hot solution of $Cu(NO_3)_2 \cdot 3H_2O$ (25 g) dissolved in water (500 cm^3), concd aq NH_3 (24 cm^3) was added, followed by **1a** (32 g) dissolved in 50 vol% aq EtOH (300 cm^3) with vigorous stirring. After continued heating and stirring at *ca.* 60 °C for 4 h, the resulting suspension was allowed to stand overnight at room-temperature. The light-green product was collected, washed with 1.5 M aq NH_3 (*ca.* 200 cm^3) and water, and dried at 110 °C until the color changed to a yellowish brown to give 37 g (97%) of **1b**; mp (dec) 257—262 °C. IR(KBr): 3100, 3060, 1584, 1567, 1510, 1453, 1388, 1350, 1313, 1301, 1052, 1034, 821, 789, 745, 715, and 512 cm^{-1}. Found: C, 55.77; H, 3.11; Cu, 16.56%. This complex was slightly soluble in aq NH_3.

*Dimethyl and Diethyl Bis(8-acetoxy-2-quinolyl)malonate (**3a** and **3b**)*: See text. The following procedure is representative. A suspended mixture of **1b** (19 g), $CH_2(COOMe)_2$ (12 g), and Ac_2O (40 cm^3) in a flask equipped with a $CaCl_2$ tube, was stirred for periods and bath-temperature's as given in Table 4. To the resulting deep-green suspension, MeOH (25 cm^3) was added, and after stirring for 2 h at room-temperature, water (50 cm^3) was added in limited amounts with continuous stirring for complete precipitation of the desired products. The collected precipitate was washed with 50 vol% aq AcOH (*ca.* 100 cm^3) and water to remove the AcOH and the copper salt, and dried at 110 °C. The solids were suspended in hot $CHCl_3$ (50 cm^3), and the crude quinolone (**2**) filtered off. The filtrate was distilled off and the pale brown residual solids were dissolved in boiling acetone (150 cm^3 per 10 g). After cooling a small amount of **2** separated. The new filtrate was warmed, and an equal volume of hot water added portionwise to separate the crystalline powder of **3a**. After cooling, the collected powder was washed with water and dried. Concentration and cooling of the mother liquor yielded a small amount of a mixture of **2** and **3a**, which were separated by acetone. The combined crude quinolone (**2**) was recrystallized from AcOH by adding water (30- and 30 cm^3 per 10 g) to give light-tan leaflets; mp 247—249 °C, the yield of which is given in Table 4. Recrystallization from EtOH gave pale yellow leaflets; mp 249—251 °C (lit,[11] 252—254 °C), whose IR spectrum was virtually identical with that given in the lit.[9] The combined crude malonate (**3a**) was recrystallized from $CHCl_3$ by adding MeOH (25- and 75 cm^3 per 10 g) to give colorless needles; mp 211.5—213 °C, the yield of which is given in Table 4. Recrystallization from MeOH (100 cm^3 per 0.8 g) gave an analytical sample of the colorless needles; mp 211.5—213 °C. IR(KBr): 1759 and 1741 cm^{-1} (C=O); PMR ($CDCl_3$): δ=2.49 (6H, s, $-OCOCH_3$), 3.91 (6H, s, $-COOCH_3$), 7.29—8.10 (10H, m). Found: C, 64.47; H, 4.43%. Calcd for $C_{27}H_{22}N_2O_8$: C, 64.54; H, 4.41%. The estimated solubility of **2** and **3a** in hot $CHCl_3$ were 0.7 g and 20 g per 50 cm^3, and in acetone at a room-temperature were 0.07 g and 3.5 g per 50 cm^3, respectively.

The treatment of **1a** (16 g) with the methyl ester and the treatment of **1a** or **1b** with $CH_2(COOEt)_2$ (14 g) in a similar manner gave the results given in Table 4. The two samples of **3a** obtained from **1a** and **1b** had identical IR spectra with each other and the mp of a mixture of the two samples was not depressed. The same was found with the two samples of **3b**.

The colorless leaflets of **3b** recrystallized from MeOH; mp 237.5—239 °C. IR(KBr): 1763 and 1736 cm^{-1} (C=O); PMR ($CDCl_3$): δ=1.30 (6H, t, J=7 Hz, $-CH_3$ of the ethyl ester), 2.49 (6H, s, $-OCOCH_3$), 4.43 (4H, q, J=7 Hz, $-CH_2-$), 7.24—8.13 (10H, m). Found: C, 65.96; H, 4.73%. Calcd for $C_{29}H_{26}N_2O_8$: C, 65.65; H, 4.94%.

Table 4. The yields of **3** and **2**

N-oxide	Malonic ester	Temp[a] (°C)	Time (days)	Yield (%) **3**	Yield (%) **2**
1a	Dimethyl malonate	15	21	40	31
		25	7	36	36
		35	5	29	45
		45	4	25	51
	Diethyl malonate	25	8	17	62
		35	5	15	66
		45	4	12	70
1b	Dimethyl malonate	15	33	55	10
		25	16	49	9
		35	10	43	14
		45	6	38	20
	Diethyl malonate	25	21	46	18
		35	13	40	25
		45	7	35	30

a) Bath temp, ±3 °C.

2,2'-Methylenedi-8-quinolinol Dihydrochloride Dihydrate (4): This was prepared in a similar way to the conversion of di-2-quinolylmalonate into 2,2'-methylenediquinoline.[8] A suspension of **3a** (10.1 g) in 20% aq HCl (700 cm³) was heated under reflux for 2 h producing a yellow solution. While hot, a small amount of reddish material was filtered off, and the filtrate allowed to stand overnight at room-temperature. The separated yellow solid was collected, washed with acetone, dried at room-temperature under reduced pressure, and recrystallized from MeOH (150 cm³) containing concd HCl (1.5 cm³) by adding concd HCl (15 cm³) to give the yellow crystals of **4**, which were washed with 20% HCl and then with acetone. The yield was 7.8 g (95%). Further recrystallization from 20% HCl (100 cm³ per 2.5 g) gave an analytical sample of the yellow plates, salmon-pink above 110 °C, dec at 255—270 °C. IR(KBr): 3360, 3180—2500, 1631, 1599, 1502, 1422, 1391, 1302, 1090, 863, 848, 837, 821, 748, 574, and 564 cm⁻¹. Found: C, 55.27; H. 4.80%. Calcd for $C_{19}H_{20}N_2O_4Cl_2$: C, 55.49; H, 4.90%. The weight loss after heating at 110 °C for 15 h was 17.64%, corresponding to the release of one molecule of HCl and two molecules of H_2O (Calcd: 17.63%). The treatment of **3b** was effected also with 20% HCl (10.6 g per 700 cm³) under reflux for 3 h, resulting in a 95% yield of **4**. The IR spectrum was identical with that prepared from **3a**.

(2,2'-Methylenedi-8-quinolinolato)nickel(II) (5): To a hot solution of $Ni(OAc)_2 \cdot 4H_2O$ (4.7 g) dissolved in MeOH (100 cm³), **4** (7.8 g) was added with stirring and heating at *ca.* 60 °C. When the reddish brown precipitate disappeared producing a sky-blue precipitate and deep-green mother liquor (after *ca.* 30 min), a hot solution of $NaOAc \cdot 3H_2O$ (7.8 g) dissolved in water (200 cm³) was added portionwise. After heating and stirring for 2 h, the resulting yellowish brown solid was collected, washed with hot water, and dried at 110 °C to give 6.8 g (quantitative) of **5**; mp above 280 °C. IR(KBr): 3040, 2870, 1574, 1502, 1458, 1439, 1395, 1369, 1333, 1302, 1279, 1138, 1108 (C–O),[31] 904, 828, 818, 768, 743, 729, 631, 536, and 525 cm⁻¹. Found: C, 63.84; H, 3.18; Ni, 16.37%. Calcd for $C_{19}H_{12}N_2O_2Ni$: C, 63.56; H, 3.27; Ni, 16.35%.

The structure of **5** was deduced from its characteristic visible spectra. This yellowish brown powder showed similar visible spectra (mull method, max: 445 nm, sh: 540 nm) to that of Ni(ipdq) discussed in the text. However, the solution spectra (*ca.* 4×10^{-4} M, a 0.1 cm cell) showed three sharp peaks near 500 nm (Scheibe's A-band).[32] Thus in DMF at 452.5 nm (ε: 4700), 482 (9400), 515 (17600), and in 0.01 M methanolic NaOH at 447.5 (6400), 477 (15600), 511 (33200), these are similar to the metal chelates with 2,2'-methylenediquinoline.[32] A spectral change with time was observed, probably due to air-oxidation.

(2,2'-Isopropylidenedi-8-quinolinolato)nickel(II), Ni(ipdq): To a warmed suspension of **5** (1.8 g) in MeOH (100 cm³), CH_3I (5 cm³) was added, followed by NaOH (0.5 g) dissolved in water (45 cm³) with stirring and heating at 45—50 °C under reflux, to give a reddish black mixture. Soon a brown solid separated out. After continuous stirring and heating for 30 min, the reaction mixture was poured into hot water (200 cm³) with stirring with caution against the remaining iodide. The precipitated reddish brown solids were collected, washed with hot water, dried at 110 °C (yield: 1.9—1.8 g), extracted with boiling MeOH (250 cm³), and the residual solids (0.3—0.2 g) filtered off. After cooling the filtrate for some time, a small amount of the precipitated black material was filtered off, and the new filtrate allowed to stand at *ca.* 5 °C overnight. The crystals separated were collected, washed with MeOH, and dried to give 1.0 g (and 0.3 g from the mother liquor, total 67%) of Ni(ipdq). Repeated recrystallizations from MeOH (100 cm³ per 0.8 g) gave an analytical and spectral sample as reddish brown leaflets (sometime gave needles having a virtually identical IR spectrum). PMR and UV: see in the text. TGA-DTA (5 °C/min, in air): a sharp endothermic peak at 336 °C, followed by a weight loss. IR(KBr): 3040, 2970, 1567, 1501, 1468, 1447, 1395, 1334, 1296, 1110 (C–O),[31] 832, 772, 740, 638, and 551 cm⁻¹. Found: C, 65.21; H, 4.04; Ni, 15.16 %. Calcd for $C_{21}H_{16}N_2O_2Ni$: C, 65.16; H, 4.17; Ni, 15.17%.

2,2'-Isopropylidenedi-8-quinolinol, ipdq: To a suspension of Ni(ipdq) (2.0 g) in EtOH (20 cm³), concd HCl (4 cm³) was added with swirling to give a clear deep-green solution, to which hot water (80 cm³) was added in limited amounts, separating out the yellow leaflets (probably the hydrochloride of ipdq). The mixture was allowed to stand at *ca.* 5 °C overnight. The crystals were collected, washed with 1 M aq HCl, air-dried at room-temperature, and dissolved in hot EtOH (40 cm³). To this solution a half portion of a hot solution of $NaOAc \cdot 3H_2O$ (2 g) in water (40 cm³) was added to produce turbidity which was followed by crystallization. With continuous warming, the remaining portion of the acetate solution was added portionwise with swirling, followed by the addition of water (20 cm³). After cooling, the crystals were collected, washed with water, air-dried, and recrystallized from hexane (40 cm³) to give 1.4 g (and 0.1 g from the mother liquor, total 88%) of ipdq as colorless plates; mp 101.5—102.7 °C. Recrystallization from MeOH by adding water (40- and 100 cm³ per 1.4 g) gave an analytical and spectral sample as colorless leaflects; mp 102.0—102.7 °C. IR(KBr): 3460, 3425, 3040, 2975, 2925, 1599, 1568, 1498, 1470, 1454, 1433, 1317, 1252, 1230, 1193, 1098, 1077, 838, 756, 719, 607, and 560 cm⁻¹. PMR and UV: see in the text. Found: C, 76.22; H, 5.33%. Calcd for $C_{21}H_{18}N_2O_2$: C, 76.35; H, 5.49%.

(2,2'-Isopropylidenedi-8-quinolinolato)copper(II), Cu(ipdq): To a hot solution of ipdq (1.0 g) dissolved in EtOH (40 cm³), a warmed solution of $Cu(OAc)_2 \cdot H_2O$ (0.6 g) in water (40 cm³) was added to give a clear deep-green solution. Very soon green crystals separated out. After heating at *ca.* 60 °C for 30 min, the mixture was allowed to stand at *ca.* 5 °C overnight. The crystals were collected, washed with water, and dried at 110 °C to give 1.2 g (quantitative) of Cu(ipdq). Repeated recrystallizations from MeOH (100 cm³ per 0.75 g) gave an analytical and spectral sample as deep-green needles. TGA-DTA (5 °C/min, in air): a sharp exothermic peak at 346 °C, accompanied by a weight loss. IR(KBr): 3040, 2980, 1601, 1552, 1494, 1432, 1383, 1343, 1333, 1309, 1272, 1107 (C–O),[31] 826, 746, 605, 535, and 521 cm⁻¹. UV: see in the text. Found: C, 63.91; H, 4.18; Cu, 16.23%. Calcd for $C_{21}H_{16}N_2O_2Cu$: C, 64.36; H, 4.12; Cu, 16.21%.

Ni(ipdq) from ipdq: To a hot solution of ipdq (1.0 g) dissolved in MeOH (30 cm³), a hot solution of $Ni(OAc)_2 \cdot 4H_2O$ (0.75 g) in water (30 cm³) was added to make the solution turbid. Soon the crystals separated out. After heating at *ca.* 60 °C for 1 h, the mixture was worked up in a manner similar to that of Cu(ipdq). The sample obtained had an identical IR spectrum with that prepared from **5**.

Measurements. All the melting points were uncorrected. The IR and PMR spectra were recorded with a JASCO IRA-2 and a Hitachi R-20 spectrometer respectively. The TGA-DTA measurements were carried out with a Rigaku-denki TG-DSC apparatus. The electronic spectra were measured with a Simadzu MPS-50L spectrometer at room-temperature, using a 0.1 cm cell for the ultraviolet region, a 1.0 cm cell for the near-ultraviolet and visible region, except PdQ_2 in MeOH (a 2.0 cm cell), and a 1.0 or 5.0 cm cell for the d-d region, unless otherwise stated. The solvents used were dried and distilled except DMF, THF, 1,2-dichloroethane, and cyclohexane which were of spectroscopic grade and used without further purification.

Analyses: A Shimadzu UM-3B apparatus was used for the elemental analyses. The metal contents in the complexes were determined gravimetrically, after the complete decomposition with H_2SO_4–HNO_3.

The authors wish to thank Mr. Masahiko Takahashi for the elemental analyses and Dr. Masatoshi Hirayama for the PMR measurements.

References

1) In this paper, MQ_n represents the metal 8-quinolinolate (oxinate), where n is the valence state of the metal ion M.

2) H.-H. Perkampus and K. Kortüm, *Fresenius' Z. Anal. Chem.*, **190**, 111 (1962).

3) L. Morpurgo and R. J. P. Williams, *J. Chem. Soc., A*, **1966**, 73.

4) Y. Moriguchi and K. Ueno, *Bull. Chem. Soc. Jpn.*, **43**, 1053 (1970).

5) F. G. Beltran, A. Roy, L. A. Oro, and F. Palacio, *Rev. Acad. Cienc. Exactas, Fis.-Quim. Natur. Zaragoza*, **26**, 565 (1971); *Chem. Abstr.*, **76**, 146929a (1972).

6) N. N. Kazanova, I. I. Antipova-Karataeva, O. M. Petrukhin, and Yu. A. Zolotov, *Izv. Akad. Nauk. SSSR, Ser. Khim.*, **1974**, 15.

7) E. Sekido and K. Kunikida, *Anal. Chim. Acta*, **92**, 183 (1977).

8) M. Hamana and M. Yamazaki, *Chem. Pharm. Bull.*, **11**, 415 (1963); M. Hamana, *Kagaku No Ryoiki, Zokan*, **94**, 39 (1971).

9) J. P. Phillips, E. M. Barrall, and R. Breese, *Trans. Kentucky Acad. Sci.*, **17**, 135 (1956); *Chem. Abstr.*, **51**, 11349b (1957).

10) I. Murase, *Nippon Kagaku Zasshi*, **75**, 1180 (1954).

11) G. R. Pettit, W. C. Fleming, and K. D. Paull, *J. Org. Chem.*, **33**, 1089 (1968).

12) P. R. Scherer and Q. Fernando, *Anal. Chem.*, **40**, 1938 (1968).

13) O. Popovych and L. B. Rogers, *Spectrochim. Acta*, **21**, 1229 (1965).

14) a) T. Moeller and F. L. Pundsack, *J. Am. Chem. Soc.*, **76**, 617 (1954), and earlier papers summarized therein; b) H. Irving and H. S. Rossotti, *J. Chem. Soc.*, **1954**, 2910; c) S. F. Mason, *ibid.*, **1957**, 5010; d) W. E. Ohnesorge and L. B. Rogers, *Spectrochim. Acta*, **14**, 27 (1959); O. Popovych and L. B. Rogers, *J. Am. Chem. Soc.*, **81**, 4469 (1959); e) N. Matsuoka, Y. Shimura, and R. Tsuchida, *Nippon Kagaku Zasshi*, **82**, 1637 (1961); f) J. Szoke, *Acta Chim. Hung. Tomus*, **35**, 179 (1963); g) R. E. Ballard and J. W. Edwards, *J. Chem. Soc.*, **1964**, 4868; h) P. D. Anderson and D. M. Hercules, *Anal. Chem.*, **38**, 1702 (1966); i) S. Schulman and Q. Fernando, *Tetrahedron*, **24**, 1777 (1968); j) M. Goldman and E. L. Wehry, *Anal. Chem.*, **42**, 1178 (1970).

15) a) J. P. Phillips, *J. Am. Chem. Soc.*, **74**, 552 (1952), and references therein; b) O. Popovych and L. B. Rogers, *Spectrochim. Acta*, **14**, 584 (1959).

16) J. P. Phillips and R. W. Keown, *J. Am. Chem. Soc.*, **73**, 5483 (1951). *Cf.* J. W. Faller and J. P. Phillips, *Talanta*, **11**, 641 (1964).

17) J. P. Saxena, W. H. Stafford, and W. L. Stafford, *J. Chem. Soc.*, **1959**, 1579.

18) R. S. Downing and F. L. Urbach, *J. Am. Chem. Soc.*, **91**, 5977 (1969).

19) K. Dimroth, C. Reichardt, T. Siepmann, and F. Bohlmann, *Justus Liebigs Ann. Chem.*, **661**, 1 (1963).

20) a) G. Maki, *J. Chem. Phys.*, **29**, 1129 (1958); b) R. H. Holm, *J. Am. Chem. Soc.*, **82**, 5632 (1960); c) G. M. Mockler, G. W. Chaffey, E. Sinn, and H. Wong, *Inorg. Chem.*, **11**, 1038 (1972); d) M. D. Hobday and T. D. Smith, *Coord. Chem. Rev.*, **9**, 311 (1972—3), and references therein; e) S. Yamada, H. Nishikawa, and H. Kuma, *Sci. Rep., Col. Gen. Educ. Osaka Univ.*, **22**, 45 (1973); *Chem. Abstr.*, **81**, 32676p (1974).

21) Y. Yamamoto, *Bull. Chem. Soc. Jpn.*, **46**, 331 (1973).

22) E. Butter, H. Singer, and H. Holzapfel, *Z. Chem.*, **5**, 149 (1965).

23) R. E. Burton and W. J. Davis, *J. Chem. Soc.*, **1964**, 1766.

24) Bonds *et al.* pointed out that this bond-length for one group, including CuQ_2, PdQ_2, and $ZnQ_2 \cdot 2H_2O$ *etc.*, is shorter than that of another group including QH_2–$SeOCl_3$ *etc.*, and suggested that this discrepancy reflects the degree of the C–O multiple bonding. W. D. Bonds, Jr., R. D. Archer, and W. C. Hamilton, *Inorg. Chem.*, **10**, 1764 (1971); the structural data of the individual complexes are given in the lit. cited therein.

25) From the study of the reactivity at 5- and/or 7-position of MQ_n and HQ including CuQ_2, Jones concluded that the –OH group attracts the electron from the aromatic ring more strongly than the –OM group. M. M. Jones, "Ligand Reactivity and Catalysis," Academic Press (1968); Japanese Translation by H. Kobayashi and Y. Torii, "Haiishi no Hannosei to Shokubai-sayo," Tokyo Kagaku Dojin, Tokyo (1973), p. 73; *Cf.* N. K. Chawla and M. M. Jones, *Inorg. Chem.*, **3**, 1549 (1964).

26) *Cf.* J. E. Tackett and D. T. Sawyer, *Inorg. Chem.*, **3**, 692 (1964).

27) *E.g.* A. S. Bailey, R. J. P. Williams, and J. D. Wright, *J. Chem. Soc.*, **1965**, 2579.

28) H. Vogt, *Arch. Pharm. (Weinheim, Ger.)*, **282**, 27 (1944); *Chem. Abstr.*, **40**, 6759^6 (1946).

29) I. Murase and Y. Demura, *Memo. Fac. Sci. Kyushu Univ., Ser. C*, **3**, 175 (1961); *Chem. Abstr.*, **58**, 3390b (1963).

30) a) K. Ramaiah and V. R. Srinivasan, *Proc. Indian Acad. Sci., Sect. A*, **55**, 360 (1962); *Chem. Abstr.*, **59**, 567b (1963); b) M. N. Al-Zagoum and C. G. Warren, *J. Inorg. Nucl. Chem.*, **31**, 3465 (1969).

31) In the IR spectra of MQ_n, the C–O stretching vibration is known as the 9 μm peak. R. G. Charles, H. Freiser, R. Friedel, L. E. Hilliard, and W. D. Johnston, *Spectrochim. Acta*, **8**, 1 (1956).

32) It is well established that 2,2′-methylenediquinoline and its metal complexes exhibit such characteristic spectra as dyestuffs of the pseudoisocyanine type, which is due to the dissociation of the carbon-acid in the methylene group. G. Scheibe and W. Riess, *Chem. Ber.*, **92**, 2189 (1959); G, Scheibe and H. J. Friedrich, *Z. Elektrochem.*, **64**, 720 (1960); G. Scheibe and E. Daltrozzo, *Adv. Heterocycl. Chem.*, **7**, 153 (1966), and references therein.

Photometric Determination of a Trace Amount of Nitrite by Its Kinetic Effect†

Satori UTSUMI, Tadao OKUTANI, Akio SAKURAGAWA,* and Akira KENMOTSU**

College of Science and Technology, Nihon University, 1-8, Kanda-Surugadai, Chiyoda-ku, Tokyo 101

(Received January 30, 1978)

A new photometric method has been developed for determining nitrite ions. This method is based on the kinetic effect of nitrite ions on the color-fading of the iron(III) thiocyanate complex in dilute nitric acid solution in the presence of iodide ions. The reaction is initiated by adding an ammonium iron(III) sulfate solution to the sample solution containing a mixture of potassium thiocyanate and potassium iodide at 25 °C. A concentration of nitrite ions, ranging from 0.0005 to 10 ppm can be determined by measuring the absorbance at 460 nm at a given time after the initiation using four appropriate calibration curves. Silver, mercury(II), iron(II), sulfide, sulfite, thiosulfate, chromate and cyanide ions in the concentration range from 0.1 to 1 ppm level interfered with the determination.

It has been established that the orange color of iron(III) thiocyanate, which was formed by the reaction with potassium thiocyanate and an excess of iron(III) salt in dilute nitric acid solution, faded more rapidly in the presence of iodide than in its absence.[1] The catalytic action of iodide ions on this reaction has been studied colorimetrically, and a new micro-determination method for iodide ions established.[1,2] It was also found that the catalytic reaction was characterized by an induction period, the length of which depended on the nitrite ion concentration.[2,3] This kinetic effect has been utilized to determine the amounts of iodide ions in the presence of nitrite ions.[4] Iodides in silicate rocks,[5] and iodide and iodate ions in sea water[6] have also been determined.

Successive investigations on the behavior of nitrite ions have shown that the kinetic effect can be applied to the determination of nitrite ions. This paper proposes a new method for the determination of nitrite ions on the basis of the kinetic effect mentioned above.

The proposed method gives accurate results for nitrite ions ranging from 0.0005 to 10 ppm. The determination can be made by measuring the absorbance at a given time after the addition of an ammonium iron(III) sulfate solution using calibration curves obtained under identical conditions.

Experimental

Apparatus. A Hirama IIC type photometric colorimeter with a 460 nm filter and 10 mm glass cells was used to measure the absorbance. The reaction was performed at 25.00±0.05 °C using a water bath with a Komatsu-Yamato Coolnicks circulator Model CTE/CTR-120 unit.

Reagents. All of the chemicals used were of guaranteed reagent grade. The ion-exchanged water was distilled in a borosilicate still prior to use.

Standard Nitrite Solution: Sodium nitrite (1.4997 g) was dissolved in distilled water, diluted to exactly 1 litre (1000 ppm NO_2^-), and stored in a brown glass bottle. The working solution was diluted as required.

Potassium Thiocyanate Solution (0.01 M): A potassium thiocyanate solution(0.1 M), standardized by Volhard's method, was diluted to 0.01 M and stored in a brown glass bottle.

Potassium Iodide Solution (2×10^{-3} M): A potassium iodide solution (0.1 M), standardized by Volhard's method, was diluted to 2×10^{-3} M and stored in a brown glass bottle.

Potassium Thiocyanate–Potassium Iodide Mixed Reagent Solution (Mixed Reagent Solution): The mixed reagent solution was prepared by mixing potassium thiocyanate solution (0.01 M) with an equal volume of potassium iodide solution (2×10^{-3} M) just before the experiment was started.

Ammonium Iron(III) Sulfate–Nitric Acid Solution (Iron(III) Reagent Solution): The iron(III) reagent solution was prepared by dissolving ammonium iron(III) sulfate (6.0 g) in nitric acid (7.0 M), and then diluting to 100 ml with 7.0 M nitric acid. After urea (10 mg) was added to the solution, it was heated in boiling water with a reflux condenser for 10 min and then cooled rapidly in water. This reagent solution was stored in a brown glass bottle at room temperature, and could be used for approximately 30 days.

Procedure and Calibration Curves. The sample solution (10 ml) was placed in a 20 ml glass tube fitted with a stopper. The mixed reagent solution (1 ml) was then added and the glass tube placed in a water bath at 25.00±0.05 °C for 10

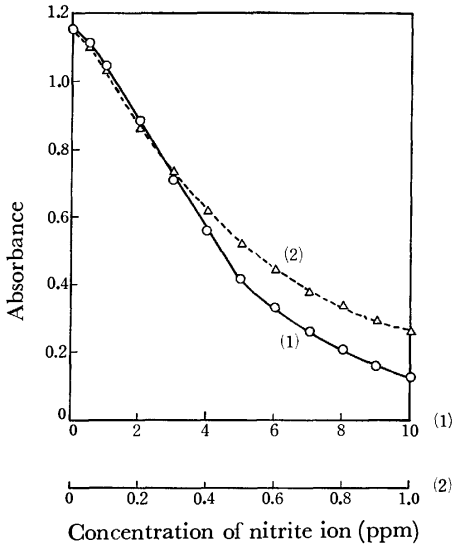

Fig. 1. Calibration curves 1.
(reaction temperature: 25 °C)
(1) Reaction time: 7 min, (2) reaction time: 13 min.

† Presented at the 21th National Meeting of the Chemical Society of Japan, Osaka, April 1968, and at the 25th Annual Meeting of the Japan Society for Analytical Chemistry, Niigata, October 1976.

** Present address: Nippon Electronics Engineering College, 5-23-22, Nishi-Kamata, Ohta-ku, Tokyo 144.

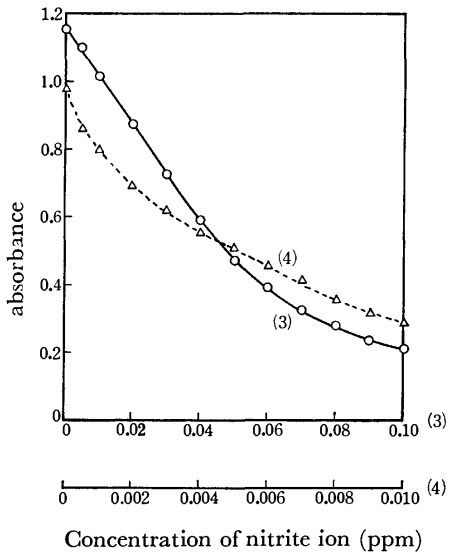

Fig. 2. Calibration curves 2.
(reaction temperature: 25 °C)
(3) Reaction time: 19 min, (4) reaction time: 24 min.

min. The reaction was initiated by adding the iron(III) reagent solution (2 ml, at the same temperature), mixing thoroughly and then replacing the glass tube in the water bath. The absorbance was measured at 460 nm using water as a reference at a given time after the addition of the iron(III) reagent solution. It is recommended that the solution in the glass tube is removed from the water bath and poured into the cell 20 s before measurement of the absorbance. By employing 7, 13, 19, or 24 min of reaction time, nitrite ions in the concentration range of 0.5—10, 0.05—1, 0.005—0.1, or 0.0005—0.01 ppm, respectively, could be determined. The calibration curves shown in Figs. 1 and 2 were obtained by the procedure described above.

Results and Discussion

The Reaction Rate Curves. The kinetic reactions were examined for each solution (10.0 ml) containing 10, 1, 0.1, or 0.01 ppm nitrite ions, and for distilled water. The curves shown in Fig. 3 were obtained by measuring the absorbances of these solutions at various reaction times. In the absence of nitrite ions (curve 5 in Fig. 3), the color-fading of the iron(III) thiocyanate complex began approximately 20 min after the initiation and after 32 min, the solution became almost colorless. In the presence of nitrite ions, the color-fading was accelerated with an increase in the concentration of nitrite ions. These results indicate that the length of the induction period is greatly affected by the concentration of nitrite ions, and that nitrite ions ranging in concentration from 0.0005 to 10 ppm can be determined by measuring the absorbances at different reaction times.

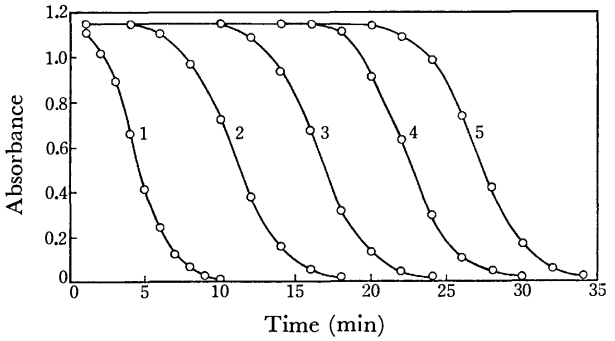

Fig. 3. The changes in absorbances of iron(III) thiocyanate solution with time in the presence of various concentrations of nitrite ions.
(reaction temperature: 25 °C)
1: 10 ppm, 2: 1 ppm, 3: 0.1 ppm, 4: 0.01 ppm, 5: distilled water.

The Effect of Iodide Ion Concentration in the Mixed Reagent Solution. The concentration of potassium thiocyanate in the mixed reagent solution was chosen as 5×10^{-3} M, which was the same value as in a previous paper.[4] Three concentrations of iodide ion (5×10^{-4}, 1×10^{-3}, and 2×10^{-3} M) were adopted to examine the effect of the iodide ion concentration in the mixed reagent solution on the color-fading. It was found that, as the concentration of iodide ion increased, the start of the color-fading was delayed, but once initiated the speed of the color-fading increased. For example, in the reagent blank, the color-fading of the iron(III) thiocyanate complex began approximately 19 min after the initiation at a concentration of 5×10^{-4} M of iodide ions, whereas it began approximately 24 min after the initiation at 2×10^{-3} M of iodide ions. In the present work, the concentration of iodide ions was adjusted to 1×10^{-3} M to make four calibration curves effective for the concentration range from 0.0005 to 10 ppm of nitrite ions. Consequently, the mixed reagent solution used was of 5×10^{-3} M potassium thiocyanate and 1×10^{-3} M potassium iodide.

The Effect of the Concentration of Nitric Acid in Iron(III) Reagent Solution. This effect was studied using the three reagent solutions in which ammonium iron(III) sulfate was dissolved in 6.00, 7.00, or 8.00 M nitric acid, the experimental results of which are shown in Fig. 4. With regard to the sensitivity and the length of time required to determine the amounts of nitrite ions, the iron(III) reagent solution prepared from 7.00 M of nitric acid was selected. Figure 4 illustrates the effect of nitric acid on the color-fading which is remarkable. Therefore, it is necessary to accurately adjust the concentration of nitric acid.

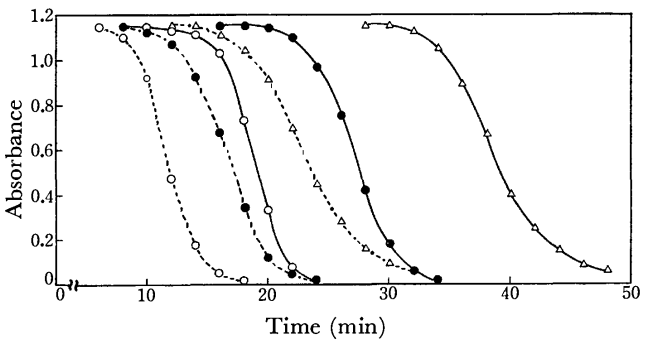

Fig. 4. Effect of concentration of nitric acid in the iron(III) reagent solution.
(reaction temperature: 25 °C)
——: Blank, ------: 0.1 ppm NO_2^-.
Nitric acid: △: 6.00 M, ●: 7.00 M, ○: 8.00 M.

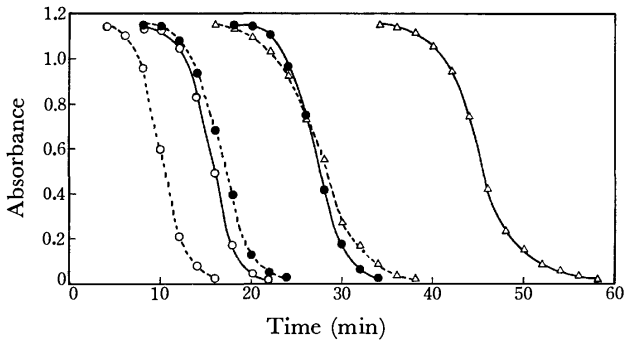

Fig. 5. Effect of the temperature.
——: Blank, ------: 0.1 ppm NO_2^-.
Reaction temperature: △: 20 °C, ●: 25 °C, ○: 30 °C.

Table 1. Effect of urea on absorbance of solution

Amount of urea[a] (mg/100 ml)	Absorbance 24 min	Absorbance 28 min
0[b]	0.652	0.161
2	0.865	0.260
5	0.921	0.327
10	0.987	0.426
20	1.009	0.445

a) Urea mg/100 ml iron(III) reagent solution, heated for 10 min in boiling water. b) Untreated.

Table 2. Effect of the heating period on absorbance

Time (min)	Absorbance 24 min	Absorbance 28 min
—[a]	0.886	0.280
5	0.967	0.390
10	0.987	0.426
20	0.833	0.227

10 mg urea/100 ml iron(III) reagent solution.
a) Untreated.

Table 3. The treatment with urea on the various grades of nitric acid

Grade of nitric acid	Absorbance 24 min Untreated	Absorbance 24 min Urea treated	Absorbance 28 min Untreated	Absorbance 28 min Urea treated
SSG[a]	0.648	0.987	0.162	0.426
JIS-GR[b]	0.580	0.983	0.110	0.423
JIS-EP[c] 1	0.550	0.975	0.105	0.420
JIS-EP 2	0.535	0.979	0.100	0.415

10 mg urea/100 ml iron(III) reagent solution, heated for 10 min in boiling water.
a) Super Special Grade. b) Guaranteed Reagent of Japanese Industrial Standards. c) Extra Pure Japanese Industrial Standards.

The Effect of Temperature. Measurements were made at temperatures 20, 25, and 30 °C to study the effect of temperature. The induction period of the color-fading decreased with an increase in temperature. For example, in the reagent blank, the color-fading of the iron(III) thiocyanate complex began approximately 20 min after the initiation at 25 °C, and 36 min after the initiation at 20 °C (Fig. 5). A temperature of 25.00±0.05 °C was used throughout this work.

The Removal of Nitrite Ions in Nitric Acid. Commercially available nitric acid usually contains trace amounts of nitrite ions as impurity. If such nitric acid is used as a reagent, nitrite ion concentration of less than 0.01 ppm in the sample will prove impossible to determine. Thus, several attempts were made to remove the trace amounts of nitrite ions in the iron(III) reagent solution. It was found that the nitrite ion was readily decomposed

Table 4. Effect of various ions on the determination of nitrite

Ion	Added as	Concn (ppm)	Absorbance (19 min) Blank	Absorbance (19 min) 0.05 ppm NO_2^-
None			1.155	0.475
Cl^-	NaCl	1000	1.119	0.372
		500	1.149	0.470
Br^-	KBr	1000	1.143	0.393
		500	1.149	0.480
F^-	NaF	100	1.119	0.456
		10	1.143	0.472
NO_3^-	KNO_3	1000	1.108	0.403
		500	1.149	0.472
SO_4^{2-}	K_2SO_4	1000	1.137	0.527
		500	1.149	0.472
ClO_4^-	$KClO_4$	1000	1.149	0.472
$H_2PO_4^-$	$NaH_2PO_4 \cdot 2H_2O$	500	1.108	0.461
		200	1.149	0.472
CO_3^{2-}	Na_2CO_3	500	1.137	0.502
		250	1.155	0.475
S^{2-}	$Na_2S \cdot 9H_2O$	0.1	1.137	0.620
		0.01	1.143	0.484
SO_3^{2-}	Na_2SO_3	1	1.155	0.551
		0.1	1.149	0.482
CN^-	KCN	1	1.155	0.602
		0.1	1.149	0.480
CrO_4^{2-}	K_2CrO_4	1	1.114	0.416
		0.1	1.143	0.469
$S_2O_3^{2-}$	$Na_2S_2O_3 \cdot 5H_2O$	0.1	1.155	0.509
		0.05	1.155	0.479
Al^{3+}	$Al(NO_3)_3 \cdot 9H_2O$	100	1.149	0.467
Mg^{2+}	$MgSO_4 \cdot 7H_2O$	100	1.149	0.479
Ca^{2+}	$Ca(NO_3)_2 \cdot 4H_2O$	100	1.149	0.479
Cu^{2+}	$CuSO_4 \cdot 5H_2O$	100	1.155	0.472
Zn^{2+}	$Zn(NO_3)_2 \cdot 6H_2O$	100	1.155	0.472
Pb^{2+}	$Pb(NO_3)_2$	100	1.149	0.474
Cd^{2+}	$CdSO_4$	100	1.149	0.471
Mn^{2+}	$MnSO_4$	100	1.155	0.474
Co^{2+}	$Co(NO_3)_2 \cdot 6H_2O$	100	1.155	0.476
Ni^{2+}	$Ni(NO_3)_2 \cdot 6H_2O$	100	1.149	0.478
Ag^+	$AgNO_3$	1	1.149	0.526
		0.1	1.149	0.478
Hg^{2+}	$HgSO_4$	1	1.119	0.513
		0.1	1.137	0.482
Fe^{2+}	$FeSO_4 \cdot 7H_2O$	10	1.149	1.032
		1	1.143	0.480

by the addition of urea. Therefore urea was added to the iron(III) reagent solution, and the solution heated in boiling water under different conditions. As Table 1 illustrates, the absorbance of the reagent blank increases with an increase in the amount of urea. As shown in Table 2, maximum absorbance was obtained after a heating period of 10 min. Heating of the solution over 10 min, causes the complete decomposition of urea, which is succeeded by the decomposition of nitric acid to produce the nitrite ion. By using 10 mg of urea and a heating period of 10 min, nitrite ions can be almost completely decomposed (Table 3). Less than 0.1 ppm of the nitrite ion in the iron(III) reagent solution can also be removed by treating the solution in the same way. The iron(III) reagent solution thus treated could be used for at least 30 days.

The Effect of Various Ions. To establish the effect of various ions on the proposed method, experiments were conducted, both in the presence of nitrite ion (0.05 ppm) and its absence. The experimental results are given in Table 4.

Metal ions, such as silver, mercury(II), and iron(II) interfered with the determination of nitrite ion. Oxidizing or reducing anions, such as sulfide, sulfite, thiosulfate, chromate, and cyanide at 0.1 to 1 ppm level also interfered.

The present work was partially supported by a Grant-in-Aid for Scientific Research from the Ministry of Education.

References

1) I. Iwasaki, S. Utsumi, and T. Ozawa, *Bull. Chem. Soc. Jpn.*, **26**, 108 (1953).
2) S. Utsumi, *Nippon Kagaku Zasshi*, **74**, 298 (1953).
3) I. Iwasaki, S. Utsumi, and T. Ozawa, *Nippon Kagaku Zasshi*, **78**, 474 (1957).
4) S. Utsumi, M. Shioda, N. Yonehara, and I. Iwasaki, *Nippon Kagaku Zasshi*, **85**, 32 (1964).
5) N. Yonehara, M. Yoshida, and I. Iwasaki, *Bull. Chem. Soc. Jpn.*, **43**, 3796 (1970).
6) N. Yonehara, *Bull. Chem. Soc. Jpn.*, **37**, 1101 (1964).

Kinetic Studies on the Stability Enhancement of Mixed Ligand Copper(II) Complexs with 2,2′-Bipyridyl and Acetylacetonate

Megumu MUNAKATA* and Katsumi YAMADA

Department of Chemistry, Kinki University; Kowakae, Higashi-Osaka-Shi, Osaka 577

(Received March 9, 1978)

The rate constants for the formation and dissociation of the binary Cu^{2+}-acetylacetonate($acac^-$) complex and the ternary 2,2′-bipyridyl(bpy)-Cu^{2+}-$acac^-$ complex have been determined by the temperature-jump method. For the reactions $Cu^{2+}+acac^- \underset{k_{-1b}}{\overset{k_{1b}}{\rightleftharpoons}} Cu(acac)^+$, $Cu(acac)^+ + acac^- \underset{k_{-2b}}{\overset{k_{2b}}{\rightleftharpoons}} Cu(acac)_2$, and $Cu(bpy)^{2+} + acac^- \underset{k_{-1t}}{\overset{k_{1t}}{\rightleftharpoons}} Cu(bpy)(acac)^+$, the rate constants are $k_{1b}=9.0\times10^8\ M^{-1}\ s^{-1}$, $k_{-1b}=3.2\ s^{-1}$, $k_{2b}=7.0\times10^7\ M^{-1}\ s^{-1}$, $k_{-2b}=13\ s^{-1}$, $k_{1t}=1.1\times10^9\ M^{-1}\ s^{-1}$ and $k_{-1t}=1.9\ s^{-1}$. A comparison of the reactions shows that the forward rate for the Cu(bpy)(acac)$^+$ formation is larger than that for $Cu(acac)^+$ and, subsequently, the rate of the complex formation between $Cu(bpy)^{2+}$ and $acac^-$ is enhanced by the coordinating bpy. On the other hand, the reverse rate for the ternary complexation reaction is smaller than for the binary. This illustrates that the dissociation of $acac^-$ of Cu(bpy)(acac)$^+$ becomes more difficult owing to the coordination of the bpy. The above two effects of the bpy may be driving forces producing high stability, *i.e.*, a positive value of $\Delta \log K$ $\left(K=\dfrac{[Cu(bpy)[L]}{[Cu(bpy)][L]}\right)$ for the ternary copper(II) complexes with bpy and other ligands containing O as donor atoms.

It has been reported[1-9] that ligands containing O as donor atoms form stabler complexes with 2,2′-bipyridyl copper(II) ion (Eq. A) than with the hydrated Cu^{2+} ion (Eq. B).

$$Cu(bpy) + L \rightleftharpoons Cu(bpy)L$$

$$K^{Cu(bpy)}_{Cu(bpy)L} = \frac{[Cu(bpy)L]}{[Cu(bpy)][L]} \quad (A)$$

$$Cu + L \rightleftharpoons CuL \quad K^{Cu}_{CuL} = \frac{[CuL]}{[Cu][L]} \quad (B)$$

$$\Delta \log K = \log K^{Cu(bpy)}_{Cu(bpy)L} - \log K^{Cu}_{CuL} \quad (C)$$

The value of $\Delta \log K$ is, therefore, positive for ligands containing O donor atoms. This is especially noticeable in view of the fact that the value expected for $\Delta \log K$ is generally negative, since more coordination positions are available for bonding of the first ligand than for the second ligand to a given metal ion. Table 1 shows the $\Delta \log K$ values for some ternary complexes. The most important driving force for stabilization of the ternary complex (*i.e.*, the positive value of $\Delta \log K$) is considered to be the electronic effect due to π bonding formation in the complex.[3] However, little evidence is available which clarifies the electronic effect.

TABLE 1. STABILITIES OF SOME TERNARY Cu^{2+} COMPLEXES (25 °C, I=0.1)

Complex	$\Delta \log K$[a]
2,2′-Bipyridyl-Cu^{2+}-acetylacetonate	+0.32 (+0.51[b])
2,2′-Bipyridyl-Cu^{2+}-malonate	+0.27[c]
2,2′-Bipyridyl-Cu^{2+}-glycinate	−0.35[c]
2,2′-Bipyridyl-Cu^{2+}-ethylenediamine	−1.29[c]

a) *Cf.* Eq. 3. b) 60% dioxane (Ref. 9). c) Ref. 3.

One method of elucidating the high stability of ternary bpy-Cu^{2+}-O ligand complexes is a kinetic study of the complexation reaction of the ternary complexes. No kinetics on the complexation reaction of Cu^{2+}-O ligand complexes have however been reported. In this paper the relaxation effects of the complexation of bpy-Cu^{2+}-acetylacetone and Cu^{2+}-acetylacetone (Hacac) have been investigated using temperature-jump techniques. On the basis of the kinetic data the high stability for the ternary bpy-Cu^{2+}-$acac^-$ complex has been discussed.

Experimental

Kinetic experiments were conducted using a Union Giken co-axial cable temperature-jump apparatus RA-1200. A discharge of 30 KV, through two electrodes in 1.0 ml sample solution, from a 0.05 μF condenser, corresponding to an increase in temperature of about 5 °C was used in all experiments. Wako Pure Chemical reagent grade $Cu(NO_3)_2\cdot 3H_2O$, KNO_3, 2,2′-bipyridyl, acetylacetone, Chlorophenol Red, and Protein Research Foundation glycine were used without further purification. The concentration of a copper stock solution was determined by an EDTA titration. Experimental solutions containing 1.00×10^{-4} M Chlorophenol Red were maintained at 0.1 ionic strength using KNO_3 and adjusted to the desired pH value with NaOH and/or HNO_3 solution. The temperature of this study was 25 °C. Each relaxation time was estimated from the relaxation graph which was the accumulation of five oscilloscope traces recorded using a Union Giken kinetic data processer RA-450 equipped with an X-Y recorder. The relative error for these measurements was ±5%. The analysis of the temperature-jump data required the appropriate equilibrium constants, which were determined by the titration technique. The titration procedure was essentially the same as in a previous paper.[9] The equilibrium constants obtained are given in Table 2.

TABLE 2. EQUILIBRIUM CONSTANTS (25 °C and μ=0.1)

Symbol	log K
K_a	−9.33
K_{1b}	8.45
K_{2b}	6.73
K_{1t}	8.77
K_{1n}	−6.00[a]

a) HIn=Chlorophenol Red (Kolthoff, *J. Phys. Chem.*, **34**, 1466 (1930)).

Results

Ternary Complex. No relaxation effect was observed for solutions containing equal concentrations of Cu^{2+} and bpy under the conditions of these experiments, as had been reported.[10] In the pH range which was studied here, 5.50—5.80, the reaction

$$Cu^{2+} + bpy \rightleftharpoons Cu(bpy)^{2+} \quad (1)$$

is effectively complete and a 5 °C temperature-jump does not appreciably perturb it. It the complexation reactions 2—4 of the ternary bpy-Cu-acetylacetone system, no complexation reaction 4 needs to be considered, since the copper(II) ion is square planar and not a distorted octahedron as in the complex with acetylacetone (Hacac).[10]

$$Cu(bpy)^{2+} + acac^- \underset{k_{-1t}}{\overset{k_{1t}}{\rightleftharpoons}} Cu(bpy)(acac)^+, \quad (2)$$

where

$$k_{1t}/k_{-1t} = K_{1t} = \frac{[Cu(bpy)(acac)^+]}{[Cu(bpy)^{2+}][acac^-]},$$

$$Cu(bpy)^{2+} + Hacac \underset{k'_{-1t}}{\overset{k'_{1t}}{\rightleftharpoons}} Cu(bpy)(acac)^+ + H^+, \quad (3)$$

$$Cu(bpy)(acac)^+ + acac^- \rightleftharpoons Cu(bpy)(acac)_2, \quad (4)$$

where K_{1t} is the stability constant of the ternary $Cu(bpy)(acac)^+$ complex. These reactions are coupled to the more rapid protonation processes 5 and 6.

$$Hacac \underset{}{\overset{K_a}{\rightleftharpoons}} acac^- + H^+,$$

$$K_a = [acac^-][H^+]/[Hacac], \quad (5)$$

$$HIn \underset{}{\overset{K_{In}}{\rightleftharpoons}} In^- + H^+,$$

$$K_{In} = [In^-][H^+]/[HIn], \quad (6)$$

where HIn, K_{1n} and K_a are the acidic form of Chlorophenol Red and the dissociation constants of H_{In} and Hacac, respectively.

By applying the standard techniques[10-12] for deriving relaxation time τ expressions, it can be shown that

$$1/\tau = Ak_{1t} + Bk'_{1t}, \quad (7)$$

where

$$A = \frac{[Cu(bpy)^{2+}]}{1+\alpha} + [acac^-] + \frac{1}{K_{1t}}, \quad (8)$$

$$B = \frac{\alpha[Cu(bpy)^{2+}]}{1+\alpha} + [Hacac] + \frac{1}{K_{1t}K_a}\left([H^+] + \frac{\alpha\beta[Cu(bpy)(acac)^+]}{1+\alpha}\right), \quad (9)$$

$$\alpha = \frac{[H^+]}{K_a + \beta[acac^-]}, \quad (10)$$

$$\beta = \frac{K_{In} + [H^+]}{K_{In} + [In^-] + [H^+]}. \quad (11)$$

The experimental conditions, equilibrium concentrations and observed relaxation times for the bpy-Cu^{2+}-acetylacetone system are shown in Table 3 and $(\tau B)^{-1}$ plotted against A/B is shown in Fig. 1, where the data was handled on the assumption that

$$[Cu^{2+}]_{total} = [bpy]_{total} = [Cu(bpy)^{2+}] \quad (12)$$

The assumption of complete formation of Cu^{2+}-bpy 1 : 1 complex has been demonstrated.[10] The slope of the line in Fig. 1 represents k_{1t} and the intercept k'_{1t} and from the plots, $k_{1t} = 1.1 \times 10^9\ M^{-1}\ s^{-1}$ and $k'_{1t} = 0—2 \times 10^{-4}\ M^{-1}\ s^{-1}$. This demonstrates that Hacac is remarkably unreactive towards $Cu(bpy)^{2+}$ and possibly towards Cu^{2+}.

Binary Complex. Two complexation reactions

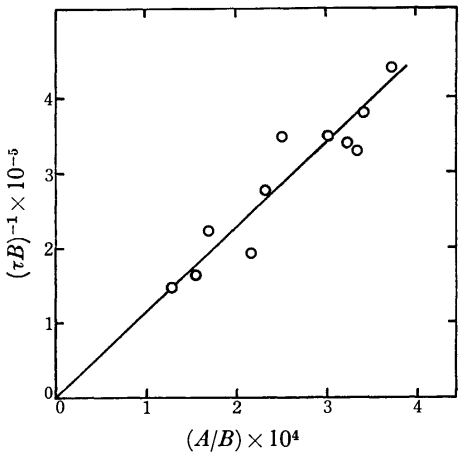

Fig. 1. A plot of $(\tau B)^{-1}$ *vs.* A/B for the 2,2′-bipyridyl-Cu^{2+}-acetylacetone system.
$k_{1t} = 1.1 \times 10^9\ M\ s^{-1}$; $k'_{1t} = 0—2 \times 10^{-4}\ M^{-1}\ s^{-1}$,; $k_{-1t} = 1.9\ s^{-1}$

Table 3. Equilibrium concentrations and relaxation times for 2,2′-bipyridyl-Cu^{2+}-acetylacetone solutions

$[Cu(bpy)^{2+}]_{tot}$ /10^{-4}	$[Hacac]_{tot}$ /10^{-4}	$[H^+]$ /10^{-6}	[Hacac] /10^{-4}	$[acac^-]$ /10^{-8}	$[Cu(bpy)^{2+}]$ /10^{-6}	$[Cu(bpy)(acac)^+]$ /10^{-5}	τ^{-1} /10 s^{-1}
1.00	2.00	1.57	1.05	3.14	5.13	9.49	6.26
3.00	5.00	1.25	2.06	7.72	6.46	29.4	16.3
5.00	5.00	2.15	0.586	1.28	58.7	44.1	13.8
5.00	10.0	3.48	5.12	6.88	12.1	48.8	15.5
8.00	10.0	2.74	2.37	3.98	32.7	76.7	19.7
8.00	8.00	1.40	1.23	4.09	31.9	76.8	17.0
10.0	10.0	1.28	0.659	2.41	65.9	93.4	16.1
30.0	30.0	1.83	1.38	3.53	138	282	13.1
50.0	50.0	1.77	1.76	4.66	176	482	45.0
50.0	100	2.10	50.1	112	7.60	499	117
80.0	80.0	1.39	1.98	6.68	198	780	108

All concentrations are molar. $\mu = 0.1M(KNO_3)$. Temperature = 25 °C.

between Cu^{2+} and acetylacetonate have been considered:

$$Cu^{2+} + acac^- \underset{k_{-1b}}{\overset{k_{1b}}{\rightleftharpoons}} Cu(acac)^+,$$

$$K_{1b} = \frac{[Cu(acac)^+]}{[Cu^{2+}][acac^-]}, \quad (13)$$

$$Cu(acac)^+ + acac^- \underset{k_{-2b}}{\overset{k_{2b}}{\rightleftharpoons}} Cu(acac)_2,$$

$$K_{2b} = \frac{[Cu(acac)_2]}{[Cu(acac)^+][acac^-]}. \quad (14)$$

A general treatment for obtaining relaxation time expressions in metal-ligand systems represented by Eqs. 13 and 14 has already been given.[13,14] The reciprocals of the two relaxation time are

$$\frac{1}{\tau_{+,-}} = \frac{1}{2}\{a_{11}+a_{22} \pm \sqrt{(a_{11}+a_{22})^2 - 4(a_{11}a_{22}-a_{21}a_{12})}\}, \quad (15)$$

where

$$a_{11} = k_{1b}\left([acac^-] + \frac{[Cu^{2+}]}{1+\alpha} + \frac{1}{K_{1b}}\right), \quad (16)$$

$$a_{12} = k_{1b}\left(\frac{1}{K_{1b}} - \frac{[Cu^{2+}]}{1+\alpha}\right), \quad (17)$$

$$a_{21} = k_{2b}\left([acac^-] - \frac{[Cu(acac)^+]}{1+\alpha}\right), \quad (18)$$

$$a_{22} = k_{2b}\left([acac^-] + \frac{[Cu(acac)^+]}{1+\alpha} + \frac{1}{K_{2b}}\right). \quad (19)$$

The plus and minus signs give the short and long relaxation times, respectively. Generally the short relaxation time, τ_+, was observed.[14] Equations 5, 6, and 10—19 were applied to the data of Table 4. The values of τ_{calc}^{-1} were fitted to the best values of k_{1b} and k_{2b} by inserting a large number of combinations for the two unknown constants into a computer program and comparing predicted values for τ_+^{-1} with those (τ_{obsd}^{-1}) observed experimentally. The best fit was determined by minimizing the quantity σ,[15]

$$\sigma = \sum\{(\tau_{calcd}^{-1} - \tau_{obsd}^{-1})/\tau_{obsd}^{-1}\}^2. \quad (20)$$

The best fit forward rate constants are given in Table 4.

Discussion

The kinetics of the complexation reactions of nickel(II), cobalt(II), and copper(II) ions have been extensively studied using a variety of rapid reaction techniques.[16] It has been concluded that the substitution reactions of nickel(II), cobalt(II), and copper(II) ions proceed *via* the rate determining mechanism in which a water molecule dissociates from the inner coordination sphere of a thermodynamically stable species. There have been some reports in which the rate-determining is chelate ring closure, when there is steric hindrance of the ligand to the chelate ring closure.[14] In the case of the fully hydrated copper(II) ion and a normal bidentate ligand, A–B, such as $acac^-$, the complexation reactions may be written as follows:

$$M_{aq} + A\text{-}B_{(aq)} \overset{K_{01}}{\rightleftharpoons} \underset{\text{ion pair}}{W_2MW_1, A\text{-}B}, \quad \text{very rapid,}$$

$$W_2MW_1, A\text{-}B \underset{k_{-01}}{\overset{k_{01}}{\rightleftharpoons}} W_2M\text{-}A\text{-}B + H_2O, \quad \text{slow,}$$

$$W_2M\text{-}A\text{-}B \underset{k'_{-01}}{\overset{k'_{01}}{\rightleftharpoons}} M\begin{matrix}A\\|\\B\end{matrix} + H_2O, \quad \text{fast.}$$

where W_1 and W_2 represent the two water molecules in the inner coordination sphere replaced by A–B. The rate-determining step in the transition from the ion pair to the final complex is the dissociation of a water molecule from the inner coordination sphere of the metal ion. The rate constant for complex formation is then

$$k_{1b} = K_{01}k_{01}, \quad (21)$$

where K_{01} is the ion pair formation constant (Eq. 22) and k_{01} is the rate constant for water dissociation.

$$K_{01} = \frac{[W_2MW_1, A\text{-}B]}{[W_2MW_1][A\text{-}B(aq)]}. \quad (22)$$

Theoretical values of K_{01} can be estimated from Eq. 23,[13] where $U(a)$ is the Debye-Hückel interaction potential and a is the distance between the centers of the ion-pair partners.

TABLE 4. EQUILIBRIUM CONCENTRATIONS AND RELAXATION TIMES FOR Cu^{2+}-ACETYLACETONE SOLUTIONS

$[Cu]_{tot}$ /10^{-4}	$[Hacac]_{tot}$ /10^{-4}	$[H^+]$ /10^{-6}	[Hacac] /10^{-5}	$[acac^-]$ /10^{-8}	$[Cu^{2+}]$ /10^{-5}	$[Cu(acac)^+]$ /10^{-4}	$[Cu(acac)_2]$ /10^{-5}	τ_{obsd}^{-1} /10 s^{-1}	τ_{calcd}^{-1} /10 s^{-1}
1.00	2.00	3.29	8.12	1.16	2.24	0.730	0.453	9.79	8.95
2.00	3.00	1.94	11.1	2.67	2.08	1.57	2.25	9.29	8.83
3.00	4.00	1.69	10.5	2.91	2.87	2.35	3.66	20.2	17.4
4.00	4.00	1.94	5.75	1.39	7.68	3.01	2.25	17.5	18.0
5.00	5.00	2.55	7.43	1.36	9.77	3.75	2.74	20.5	21.5
5.00	4.00	2.22	3.75	0.789	15.1	3.35	1.42	17.3	18.8
5.00	6.00	2.03	9.84	2.27	6.12	3.91	4.77	22.0	25.3
6.00	6.00	3.00	8.80	1.37	11.6	4.50	3.32	27.1	25.2
7.00	7.00	1.98	7.08	1.67	11.4	5.38	4.82	23.6	26.9
$k_{1b}=9.0\times10^8\ M^{-1}\ s^{-1}$					$k_2=7.0\times10^7\ M^{-1}\ s^{-1}$			$\sigma=0.188$	
$k_{-1b}=3.2\ s^{-1}$					$k_{-2b}=13\ s^{-1}$				

All concentrations are molar. $\mu=0.1M(KNO_3)$. Temperature=25 °C.

$$K_{01} = \frac{4\pi Na^3}{3000} \exp\left(-\frac{U(a)}{kT}\right). \quad (23)$$

Choosing $a=5$ Å (under the conditions $\mu=0.1$ and 25 °C) leads to a value of $K_{01}=0.8$ for +1, −1 interactions; 2 for +2, −1 and +1, −2; 0.3 when one of the reactants is uncharged.

The values of the forward rate constant, k_{1b}, for the binary complex formation between Cu^{2+} and acetylacetonate (O, O ligand) is 9.0×10^8 M^{-1} s^{-1} and is smaller than the value for glycinate (N, O ligand)[10] 4.0×10^9 M^{-1} s^{-1} and ethylendiamine (N, N ligand)[17] 3.8×10^9 M^{-1} s^{-1}. This can be interpreted as the easier entrance of the N-donor atom of the ligand in the ion pair into the inner coordination sphere than the O-donor atom.

A similar mechanism may be proposed for the formation of ternary complexes with bpy and higher order complexes.[10]

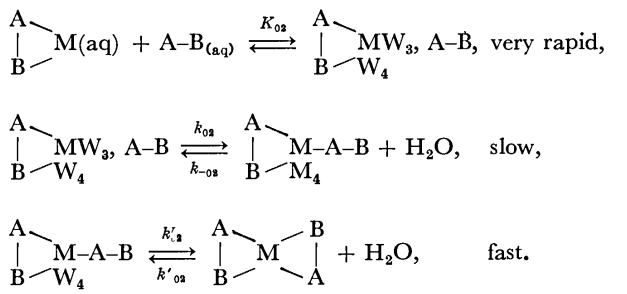

The observed forward rate constant, k_{1t}, is given by

$$k_{1t} = SK_{02}k_{02}, \quad (24)$$

where S is a statistical factor which can be computed from the number of independent attacking sites available for the ligand. For the first bidentate $acac^-$ substituting on the distorted octahedron of hydrated copper(II) ion there are 12 edges. This is because the rate constant[18] for the internal inversion between the axial water molecules and the equatorial water molecules, 10^{11} s^{-1}, is about two orders of magnitude greater than the rate constant of water dissociation, 4.5×10^8 s^{-1} (calculated for the complexation reaction between Cu^{2+} aq and acac from Eq. 21) and subsequently the six coordinating waters are equally attacked by the ligand. The attacking sites of $Cu(bpy)^{2+}$ for the second bidentate ligand is one, since $Cu(bpy)^{2+}$ is square planar rather than a distorted octahedron. A more satisfactory statistical factor therefore may be 1/12 rather than 1/8 as described in Ref. 10.

It is surprising that the forward rate for the ternary copper complexation reaction 2 is larger than for the binary complexation reaction 13. Furthermore, from a consideration of the statistical factors, the forward rate for the ternary complex formation should be about 15 times that for the binary, where the ion pair formation constants are assumed to be the same in both cases. It has been reported[10] that the forward rate for the $Cu(bpy)(gly)^+$ formation (Eq. 26) is also larger than that for the $Cu(gly)^+$ (Eq. 25) by a factor of about 3 (for $S=1/8$) and by a factor of about 5 if $S=1/12$.

$$Cu^{2+} + gly^- \underset{22\ s^{-1}}{\overset{4\times10^9\ M^{-1}\ s^{-1}}{\rightleftharpoons}} Cu(gly)^+ \quad (25)$$

$$Cu(bpy)^{2+} + gly^- \underset{19\ s^{-1}}{\overset{1.4\times10^9\ M^{-1}\ s^{-1}}{\rightleftharpoons}} Cu(bpy)(gly)^+ \quad (26)$$

These facts suggest that the forward rate for the ternary copper(II) complexation reaction between $Cu(bpy)^{2+}$ and a ligand is increased by the bpy coordinating to the copper(II). The enhancement ratio of the forward rate for the $Cu(bpy)(acac)^+$ formation is larger than that for the $Cu(bpy)(gly)^+$ formation. This corresponds to the increasing order in the $\Delta \log K$ values: $\Delta \log K=-0.35$ for $Cu(bpy)(gly)^+$; 0.32 for $Cu(bpy)(acac)^+$.

The most important factor for the possitive values of $\Delta \log K$ for the ternary copper(II) complexes with bpy and $acac^-$ with O as donor atoms is apparently the remarkable increase in the forward rate for the complexation reaction. The increase indicates that the activation energy of formation of the ternary complex is smaller than that of the binary complex. If the square planar $Cu(bpy)^{2+}$ easily leads to a transition state, *i.e.*, the five coordination state,[19] in which the d-orbitals of the copper(II) ion combine more preferably with O donor atoms than the hydrated copper(II) ions, the forward rate for the reaction between $Cu(bpy)^{2+}$ and a ligand with O donor atoms must be larger than that between hydrated Cu^{2+} and the ligand.

Both reverse rate constants for the ternary $Cu(bpy)L^+$ and binary CuL^+ complexation reactions are statistically the same, since in both cases there is only one way to remove L and the charges are the same. In fact, both the constants for $Cu(bpy)^+$ and $Cu(bpy)(gly)^+$ are the same.[10] On the other hand, the value of the reverse rate constant, 1.9 s^{-1}, for the ternary $Cu(bpy)(acac)^+$ complexation reaction is smaller than 3.2 s^{-1} for the binary $Cu(acac)^+$. The ratio of the former to the latter is 0.6. This illustrates the greater difficulty of dissociation of the Cu-acac bond in the ternary complex than that in the binary complex. The copper-ligand bond may be stabilized by the π-bond interaction between the two ligands through the copper(II).[3,20] The stability constant of the ternary copper(II) complex is slightly enhanced by a small decrease in the dissociation rate. In conclusion, the high stability of the mixed ligand copper(II) complex with 2,2′-bipyridyl and acetylacetonate is largely attributed to the remarkable enhancement of the forward rate for the complexation reaction.

References

1) H. Sigel, K. Becker, and D. B. McCormik, *Biochim. Biophys. Acta*, **148**, 655 (1967)
2) P. R. Huber, R. Griesser, B. Prijs, and H. Sigel, *Eur. J. Biochem.*, **10**, 238 (1969).
3) R. Griesser and H. Sigel, *Inorg. Chem.*, **9**, 1238 (1970).
4) P. R. Huber, R. Griesser, and H. Sigel, *Inorg. Chem.*, **10**, 945 (1971).
5) H. Sigel, P. R. Huber, and R. F. Pasternack, *Inorg. Chem.*, **10**, 2226 (1971).
6) R. Griesser and H. Sigel, *Inorg. Chem.*, **10**, 2229 (1971).
7) H. Sigel, P. R. Huber, R. Griesser, and B. Prijs, *Inorg. Chem.*, **12**, 1198 (1973).

8) H. Sigel, R. Caraco, and B. Prijs, *Inorg. Chem.*, **13**, 462 (1974).
9) M. Munakata, M. Harada, and S. Niina, *Inorg. Chem.*, **15**, 1727 (1976).
10) R. F. Pasternack and H. Sigel, *J. Am. Chem. Soc.*, **92**, 6146 (1970).
11) R. F. Pasternack, K. Kustin, L. A. Hughes, and E. Gibbs, *J. Am. Chem. Soc.*, **91**, 4401 (1969).
12) R. F. Pasternack, E. Gibbs, and J. C. Cassatt, *J. Phys. Chem.*, **73**, 3814 (1969).
13) G. G. Hammes and J. I. Sternfeld, *J. Am. Chem. Soc.*, **84**, 4639 (1962).
14) K. Kustin, R. F. Pasternack, and E. M. Weinstock, *J. Am. Chem. Soc.*, **88**, 4610 (1966).
15) J. W. Brubaker, A. F. Pearlmutter, J. E. Stuehr, and T. V. Vu, *Inorg. Chem.*, **13**, 559 (1974).
16) M. Eigen and R. G. Wilkins "Mechanism of Inorganic Reactions," Advances in Chemistry Series, No 49, American Chemical Society, Washington, D. C. (1965).
17) L. J. Kirschenbaum and K. Kustin *J. Chem. Soc., A*, **1970** 684.
18) R. Poupko and Z. Luz, *J. Chem. Phys.*, **57**, 3311 (1972).
19) Though a number of the five coordination states for the copper(II) complex are known, few three coordination states have been reported. The transition state on the complex formation may be the former rather than the latter.
20) F. A. Walker, M. Sigel, and D. B. McCormick, *Inorg. Chem.*, **11**, 2756 (1972).

Circular Dichroism Spectra of Cobalt(III) Complexes of the $[Co(O,O)_2(N)_2]^-$-Type[1]

Satoru MURAMOTO, Kenji KAWASE, and Muraji SHIBATA*

Department of Chemistry, Faculty of Science, Kanazawa University, Kanazawa 920

(Received March 31, 1978)

The $[Co(O,O)_2(N)_2]^-$-type complexes, $[Co(ox)(mal)(en)]^-$, *cis*-$[Co(CO_3)(mal)(NH_3)_2]^-$, *cis*-$[Co(ox)(mal)(NH_3)_2]^-$ and *cis*-$[Co(mal)_2(NH_3)_2]^-$, have been prepared and resolved. The CD spectra of various complexes of this type including these new complexes have been measured. The assignments of the absolute configurations have been carried out by means of the CD comparison. The CD patterns in the first absorption band region have revealed regular change with the varied O,O ligands (O,O=CO_3^{2-}, ox^{2-}, and mal^{2-}), and from this fact a criterion for the assignments of the absolute configurations for the complexes of the present type has been established.

It is known[2,3] that in the $[Co(O,O)_2(N,N)]^-$-type complexes, which contain two of a bidentate O-donor ligand such as oxalato (ox) or malonato (mal) and one of a bidentate N-donor ligand such as ethylenediamine (en) or trimethylenediamine (tn), the variations of the O-donor ligands cause marked changes in the CD spectra; the CD spectra of the $(+)_{546}[Co(ox)_2(en)]^-$ [2] and $(+)_{546}[Co(ox)_2(tn)]^-$ [3] complexes show two CD peaks of the same sign, (—, —), in the first absorption band region, while the spectra of the $(-)_{546}[Co(mal)_2(en)]^-$ [2] and $(-)_{546}[Co(mal)_2(tn)]^-$ [3] complexes show three CD peaks of alternating sign, (+, —, +), in the first absorption band region. On account of this change, it is difficult to correlate the absolute configurations of these complexes with the observed CD spectra. Thus, it was thought that the CD spectrum of a complex such as $[Co(ox)(mal)(en)]^-$, which is a transient intermediate between the bis(oxalato) and bis(malonato) complexes, would help in the understanding of such CD spectral changes.

From this standpoint, the preparation and optical resolution of the $[Co(O,O)_2(en)]^-$-type complexes containing a variety of O,O ligands (CO_3^{2-}, ox^{2-}, and mal^{2-}) have been conducted. The work was then extended to the corresponding diammine complexes, *cis*-$[Co(O,O)_2(NH_3)_2]^-$, and the bis(pyridine) complexes, *cis*-$[Co(O,O)_2(py)_2]^-$. The present paper deals with the CD studies of the complexes of the $[Co(O,O)_2(N)_2]^-$-type ($(N)_2$=en, $2NH_3$, and 2py).

Experimental

Preparation and Resolution. *a) Sodium Ethylenediaminemalonatooxalatocobaltate(III) Monohydrate, Na[Co(ox)(mal)(en)]·H_2O*: To a solution of $K[Co(CO_3)(ox)(en)]\cdot H_2O$[4] (32 g, 0.1 mol, in 150 cm³ H_2O) was added dropwise a solution of malonic acid (15 g, 0.15 mol, in 50 cm³ H_2O) with stirring at room temperature. The mixed solution was stirred at 40 °C for 2 h. The final product was filtered and the filtrate charged on a column containing Dowex 1-X 8 resin in Cl^- form (100—200 mesh, 7×20 cm). By elution with a 0.1 M NaCl aqueous solution, three bands colored red-violet descended and the three fractions were collected. The second desired fraction was concentrated under reduced pressure and, after filtration, kept in a refrigerator. The product obtained was recrystallized from a minimum amount of warm water (*ca.* 40 °C) and the yield was 3 g. The products from the first and third fractions were $Na[Co(mal)_2(en)]$ and $Na[Co(ox)_2(en)]$, respectively. Found: C, 23.84; H, 3.36; N, 8.07%. Calcd for $Na[Co(C_2O_4)(C_3H_2O_4)(C_2H_8N_2)]\cdot H_2O$: C, 24.04; H, 3.45; N, 8.00%.

The iodide complex, $(-)_{589}[Co(ox)(en)_2]$ I (4 g, 0.01 mol) was converted into the acetate with silver acetate (2.0 g, 0.012 mol) according to the literature.[5] To a solution of this resolving agent in H_2O (40 cm³, 40 °C) was added the above racemate (7.2 g, 0.02 mol) with constant stirring. A pink diastereoisomer containing the $(-)_{589}$-form of the malonatooxalato complex crystallized out on cooling the solution in an ice-bath (*ca.* 30 min). The crude product was recrystallized from a minimum amount of warm water (40 °C) producing fine scale-like crystals (yield 1.5 g). Found: C, 21.33; H, 4.91; N, 18.08%. Calcd for $[Co(C_2O_4)(C_2H_8N_2)_2]\cdot[Co(C_2O_4)(C_3H_2O_4)(C_2H_8N_2)]\cdot 2H_2O$: C, 21.44; H, 4.91; N, 18.19%.

When $(-)_{589}[Co(NO_2)_2(en)_2](C_2H_3O_2)$ was used as a resolving agent,[5] the same form of the complex formed the less soluble diastereoisomer.

b) Potassium Carbonatoethylenediamineoxalatocobaltate(III) Monohydrate, K[Co(CO₃)(ox)(en)]·H_2O: This complex was prepared by the literature method,[4] and resolved with $(-)_{589}[Co(ox)(en)_2](C_2H_3O_2)$. The less soluble diastereoisomer containing the $(-)_{589}$-form of the carbonatooxalato complex was recrystallized from water by the addition of ethanol. Found: C, 22.85; H, 4.98; N, 14.54%. Calcd for $[Co(C_2O_4)(C_2H_8N_2)_2]\cdot[Co(CO_3)(C_2O_4)(C_2H_8N_2)]\cdot 2.5H_2O$: C, 22.81; H, 5.05; N, 14.51%.

c) cis-*Diaquaethylenediamineoxalatocobalt(III) Nitrate*, cis-*[Co(ox)(en)(H₂O)₂]NO₃*: To a solution of $K[Co(CO_3)(ox)(en)]\cdot H_2O$ (13 g, 0.04 mol, in 30 cm³ H_2O) was carefully added 6 M HNO_3 until the evolution of CO_2 ceased. The resulting solution was kept in a refrigerator overnight. The crude product thus obtained was recrystallized from warm water yielding 8 g. Found: C, 15.98; H, 3.93; N, 13.69%. Calcd for *cis*-$[Co(C_2O_4)(C_2H_8N_2)(H_2O)_2]NO_3$: C, 15.75; H, 3.96; N, 13.77%.

To a solution of this racemate (9.2 g, 0.03 mol, in 50 cm³ H_2O, *ca.* 40 °C) was added $(+)_{546}Na[Co(ox)_2(en)]$[2] (5 g, 0.015 mol) as the resolving agent. The mixture was cooled in an ice-bath for 1 h, whereupon the less soluble diastereoisomer containing the $(+)_{589}$-form of the diaqua complex precipitated. Recrystallization from water yielded 2 g. Found: C, 20.89; H, 3.97; N, 9.93%. Calcd for $[Co(C_2O_4)(C_2H_8N_2)(H_2O)_2]\cdot[Co(C_2O_4)_2(C_2H_8N_2)]\cdot 2H_2O$: C, 20.92; H, 4.21; N, 9.76%.

The complex, $(+)_{546}Na[Co(edta)]$[2] was also useful for the resolution of this complex, where the $(+)_{589}$-isomer also formed the less soluble diastereoisomer.

d) Potassium Dicarbonatoethylenediaminecobaltate(III) Monohydrate, K[Co(CO₃)₂(en)]·H_2O: This complex was prepared by a modification of the procedure reported previously.[4] To a cold, green solution of tricarbonatocobaltate(III) ($Co(NO_3)_2\cdot 6H_2O$, 30 g, 0.1 mol scale) was added ethylenediamine (9 cm³,

0.13 mol), and the mixture was then stirred at *ca.* 5 °C for half an hour. Ethanol (*ca.* 100 cm³) was added to the solution, and the solution cooled in an ice-bath for half an hour. The solution, once filtered, was kept in a refrigerator and powdery purple crystals separated out. The material was recrystallized from warm water yielding 8 g.

This racemate was resolved with $(-)_{589}$[Co(ox)(en)$_2$]($C_2H_3O_2$). The less soluble diastereoisomer containing the $(+)_{589}$-form of the dicarbonato complex was recrystallized from a minimum amount of cold water (*ca.* 10 °C). The yield was 1 g. Found: C, 21.08; H, 5.59; N, 14.64%. Calcd for [Co(C_2O_4)($C_2H_8N_2$)$_2$]·[Co(CO_3)$_2$($C_2H_8N_2$)]·3H_2O: C, 21.06; H, 5.30; N, 14.74%.

e) Lithium cis-*Diamminedicarbonatocobaltate(III)*, cis-*Li*[Co(CO_3)$_2$(NH_3)$_2$]: The preparation of this complex and the isolation of its active lithium salt have been reported in an earlier communication.[6] The active complex, $(-)_{589}$Li[Co(CO_3)$_2$(NH_3)$_2$] was precipitated from a mixed solution of the racemic lithium salt and $(-)_{589}$[Co(ox)(en)$_2$]($C_2H_3O_2$), while the $(+)_{589}$ complex was precipitated in the presence of $(+)_{589}$-[Co(ox)(en)$_2$]($C_2H_3O_2$).

f) Potassium cis-*Diamminecarbonatooxalatocobaltate(III) Monohydrate*, cis-*K*[Co(CO_3)(ox)(NH_3)$_2$]·H_2O: This complex was prepared according to the literature.[4] A solution of the racemate (6 g, 0.02 mol, in 50 cm³ H_2O) was poured into a column of Dowex 50W-X 8 resin in Li^+ form (100—200 mesh, 5×10 cm) in order to convert the potassium salt into the lithium one. The effluent was added to a solution of $(-)_{589}$-[Co(ox)(en)$_2$]($C_2H_3O_2$) (4 g, 0.01 mol, in 20 cm³ H_2O) and the mixed solution evaporated to reduce the volume (*ca.* 15 cm³). The concentrated solution was kept in a refrigerator until the less soluble diastereoisomer containing the $(-)_{589}$-form of the carbonatooxalato complex precipitated. Recrystallization was carried out from water. Found: C, 20.03; H, 4.40; N, 15.50%. Calcd for [Co(C_2O_4)($C_2H_8N_2$)$_2$]·[Co(CO_3)-(C_2O_4)(NH_3)$_2$]·1.5H_2O: C, 20.19; H, 4.71; N, 15.71%.

g) Potassium cis-*Diamminebis(oxalato)cobaltate(III) Monohydrate*, cis-*K*[Co(ox)$_2$(NH_3)$_2$]·H_2O: This was prepared by the method in the literature.[4] The racemate was resolved with $(-)_{589}$[Co(ox)(en)$_2$]($C_2H_3O_2$). The less soluble diastereoisomer containing the $(+)_{589}$-form of the bis(oxalato) complex was recrystallized from a minimum amount of warm water. Found: C, 19.45; H, 5.21; N, 13.57%. Calcd for [Co(C_2O_4)-($C_2H_8N_2$)$_2$]·[Co(C_2O_4)$_2$(NH_3)$_2$]·4.5H_2O: C, 19.45; H, 5.06; N, 13.62%.

h) Sodium cis-*Diamminemalonatooxalatocobaltate(III) 2.5-Hydrate*, cis-*Na*[Co(ox)(mal)(NH_3)$_2$]·2.5H_2O: This was prepared and resolved in the same manner as that for the corresponding ethylenediamine complex. Found: C, 17.11; H, 3.73; N, 7.98%. Calcd for Na[Co(C_2O_4)($C_3H_2O_4$)(NH_3)$_2$]·2.5H_2O: C, 17.25; H, 3.75; N, 8.13%. Found: C, 22.18; H, 4.95; N, 14.32%. Calcd for [Co(C_2O_4)($C_2H_8N_2$)$_2$]·[Co(C_2O_4)(C_3H_2-O_4)(NH_3)$_2$]·2.5H_2O: C, 22.02; H, 4.91; N, 14.12%.

i) Potassium cis-*Diamminebis(malonato)cobaltate(III) 2.5-Hydrate*, cis-*K*[Co(mal)$_2$(NH_3)$_2$]·2.5H_2O: To a solution of *cis*-K[Co(CO_3)$_2$(NH_3)$_2$]·H_2O (28 g, 0.1 mol, in 150 cm³ H_2O) was added dropwise a solution of malonic acid (25 g, 0.25 mol, in 100 cm³ H_2O) with mechanical stirring in ice. The solution was then stirred at *ca.* 40 °C until the evolution of CO_2 ceased. The solution was neutralized with an aqueous KOH solution and further stirred at *ca.* 50 °C for half an hour. The resulting solution was evaporated to *ca.* 100 cm³ and the concentrated solution kept in a refrigerator overnight. The crude product thus obtained was recrystallized from warm water yielding 10 g. Found: C, 18.90; H, 3.83; N, 7.38%. Calcd for K[Co($C_3H_2O_4$)$_2$(NH_3)$_2$]·2.5H_2O: C, 18.96; H, 3.97; N, 7.37%.

The complex was resolved with $(-)_{589}$[Co(ox)(en)$_2$](C_2H_3-O_2). The less soluble diastereoisomer containing the $(+)_{589}$-form of the bis(malonato) complex was recrystallized from warm water. Found: C, 23.55; H, 4.91; N, 13.77%. Calcd for [Co(C_2O_4)($C_2H_8N_2$)$_2$]·[Co($C_3H_2O_4$)$_2$(NH_3)$_2$]·2.5H_2O: C, 23.69; H, 5.14; N, 13.81%.

j) Bis(ethylenediamine)oxalatocobalt(III) cis-*Diamminecarbonatomalonatocobaltate(III) Dihydrate*, [Co(ox)(en)$_2$]·cis-[Co(CO_3)-(mal)(NH_3)$_2$]·2H_2O: An appropriate amount of 30% $HClO_4$ was added dropwise to a solution of K[Co(CO_3)$_2$(NH_3)$_2$]·H_2O (28 g, 0.1 mol, in 100 cm³ H_2O) in order to adjust the pH to 5.0 in ice. After filtration, potassium malonate (20 g, 0.1 mol) was added to the filtrate and the mixture stirred at 40 °C for 1 h. Perchloric acid (30%) was again added to adjust the pH to 1.0. The solution was then filtered and the filtrate chromatographed on a column of Dowex 50W-X 8 resin in H^+ form (100—200 mesh, 7×15 cm) using 0.2 M NaCl as the eluting solution. Two red-violet bands came out from the column and were collected in fractions. The first fraction was concentrated to *ca.* 50 cm³ with simultaneous removal of NaCl precipitated by filtration. To the filtrate was added $NaHCO_3$ in order to adjust the pH to 9.0. To this solution was added an aqueous solution of [Co(ox)(en)$_2$]($C_2H_3O_2$) and the mixture kept in a refrigerator until reddish brown crystals precipitated. The crude product was recrystallized from water yielding 2 g. Found: C, 21.51; H, 5.05; N, 15.05%. Calcd for [Co(C_2O_4)-($C_2H_8N_2$)$_2$]·[Co(CO_3)($C_3H_2O_4$)(NH_3)$_2$]·2H_2O: C, 21.36; H, 4.87; N, 15.10%.

This complex (3 g, 0.005 mol) was ground in a mortar with water (10 cm³) and sodium iodide (0.83 g, 0.005 mol) added. The mixture was then filtered to remove the sparingly soluble [Co(ox)(en)$_2$]I. To this filtrate was added a solution of $(-)_{589}$[Co(ox)(en)$_2$]($C_2H_3O_2$) (1.0 g, 0.0025 mol, in 15 cm³ H_2O), and the mixture kept in a refrigerator. The less soluble diastereoisomer containing the $(+)_{589}$-form of the carbonatomalonato complex recrystallized yielding 0.1 g. Found: C, 20.99; H, 4.90; N, 14.90%. Calcd for [Co(C_2O_4)($C_2H_8N_2$)$_2$]·[Co(CO_3)($C_3H_2O_4$)(NH_3)$_2$]·2.5H_2O: C, 21.17; H, 5.15; N, 14.81%.

k) Potassium cis-*Dicarbonatobis(pyridine)cobaltate(III) Trihydrate*, cis-*K*[Co(CO_3)$_2$(*py*)$_2$]·3H_2O: This complex was prepared according to the method in the literature.[7] The optical resolution was performed with $(-)_{589}$[Co(ox)(en)$_2$]($C_2H_3O_2$). The less soluble diastereoisomer containing the $(+)_{589}$-form of the dicarbonato complex was recrystallized from cold water. Found: C, 32.82; H, 4.99; N, 12.60%. Calcd for [Co(C_2O_4)-($C_2H_8N_2$)$_2$]·[Co(CO_3)$_2$(C_5H_5N)$_2$]·3H_2O: C, 32.83; H, 4.89; N, 12.77%.

l) Lithium cis-*Bis(oxalato)bis(pyridine)cobaltate(III) Monohydrate*, cis-*Li*[Co(ox)$_2$(*py*)$_2$]·H_2O: This salt was prepared by the method in the literature.[8] The resolution was carried out in the same manner as that for the corresponding dicarbonato complex. The less soluble diastereoisomer contains the $(+)_{589}$-form of the bis(oxalato) complex. Found: C, 31.67; H, 4.85; N, 11.02%. Calcd for [Co(C_2O_4)($C_2H_8N_2$)$_2$]·[Co-(C_2O_4)$_2$(C_5H_5N)$_2$]·5.5H_2O: C, 31.63; H, 4.91; N, 11.07%.

Measurements. The absorption spectra in aqueous solution were recorded with a Hitachi 323 recording spectrophotometer. In the case of the *cis*-[Co(CO_3)(mal)(NH_3)$_2$]$^-$ complex, the spectrum was measured with a solution treated with a cation exchange resin in Na^+ form in order to remove the counter [Co(ox)(en)$_2$]$^+$ ion. The spectrum of the diaqua complex, after the corresponding carbonato complex was acid-hydrolyzed with 10% perchloric acid, was measured.

For the circular dichroism (CD) spectra and optical rotation measurements, a JASCO J-40CS automatic recording spectropolarimeter with a JASCO Model J-DPZ data processor for

CD, and a JASCO Model DIP-SL automatic polarimeter were used, respectively, with samples converted into the same cations as those of the corresponding racemates by means of ion-exchange techniques.

Solubility measurements of the *cis*-Li[$Co(CO_3)_2(NH_3)_2$] complex were conducted as follows; a 0.2 M aqueous solution of $(-)_{589}[Co(ox)(en)_2](C_2H_3O_2)$ (20 cm^3) containing an excess of the complex to be measured was mechanically stirred at 25 °C for a minute and, after filtering, an appropriate volume of the filtrate was withdrawn with a pipet. The solution was passed through a column containing cation exchange resin (Na^+ form) and the effluent diluted to the appropriate volume. The concentration of the complex was measured at the maximum wavelength of the first absorption band (587 nm).

Gaussian Analysis. Some of the CD spectra measured were fitted to the two best gaussian on a wavelength scale using a computer. The expression of the gaussian formula employed was $E \cdot e^{-\delta(\Delta\lambda)^2}$, where E stands for the intensity of a calculated gaussian, δ a measure of the curve band-width, and $\Delta\lambda$ the difference in wavelength between the peak position of the gaussian and an arbitrary position.

Results and Discussion

Preparation and Resolution. In a previous paper,[9] it was reported that the *cis*(a),*cis*(N)-[$Coa_2(O,O)(N)_2$]$^-$-type complexes (a=CN^- or NO_2^-, $(N)_2$=en or $2NH_3$) could be prepared based on the *cis* substitution of the ligating carbonate ion in a starting complex by the desired ligand. The synthesis of the present *cis*-[$Co(O,O)_2(N_2)$]$^-$-type complexes ($(N)_2$=en or $2NH_3$) is analogous and Scheme 1 represents the pathway.

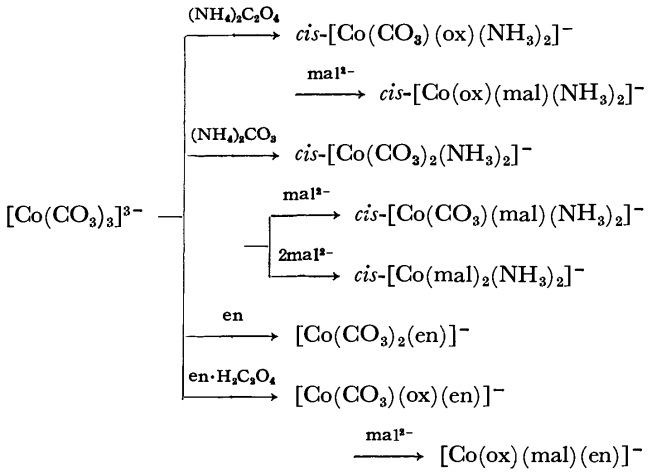

Scheme 1. Preparation of bis(dicarboxylato) complexes.

For the optical resolution of the complexes synthesized in this work, two kinds of resolving agents, $(-)_{589}$-$[Co(ox)(en)_2]^+$ and $(-)_{589}[Co(NO_2)_2(en)_2]^+$ were successfully used. The $[Co(CO_3)_2(NH_3)_2]^-$ complex, however, was an exceptional case; its active lithium salt, $(-)_{589}$Li[$Co(CO_3)_2(NH_3)_2$] being precipitated from a mixed aqueous solution of the racemic lithium salt and $(-)_{589}[Co(ox)(en)_2](C_2H_3O_2)$. In the presence of $(+)_{589}[Co(ox)(en)_2](C_2H_3O_2)$, the $(+)_{589}$ lithium salt was precipitated. The fact[6] that the yield of the active lithium salt was about 70% suggests that an asymmetric synthesis is achieved in the system. The complex obtained was optically labile such that its optical rotation decreased, in aqueous solution, with a half-life *ca.* 3 min at room temperature. The solubilities of the

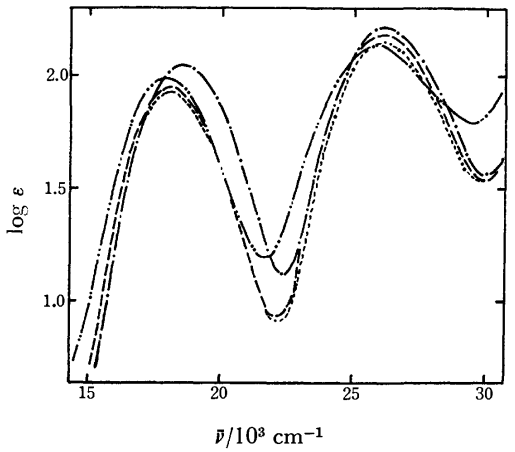

Fig. 1. Absorption spectra of —·—[Co(ox)(mal)(en)]$^-$, —··—*cis*-[$Co(CO_3)(mal)(NH_3)_2$]$^-$, ——*cis*-[Co(ox)(mal)-$(NH_3)_2$]$^-$, and ------*cis*-[$Co(mal)_2(NH_3)_2$]$^-$.

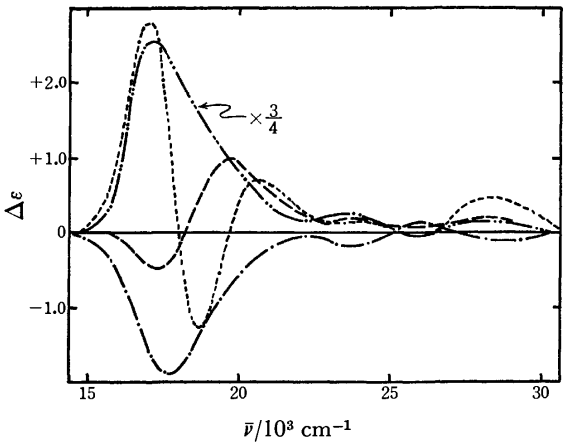

Fig. 2. CD spectra of —·—$(+)_{589}[Co(CO_3)_2(en)]^-$, —··—$(-)_{589}[Co(CO_3)(ox)(en)]^-$, ——$(+)_{589}$[Co(ox)-$(en)(H_2O)_2]^+$, and ------$(-)_{589}[Co(ox)(mal)(en)]^-$.

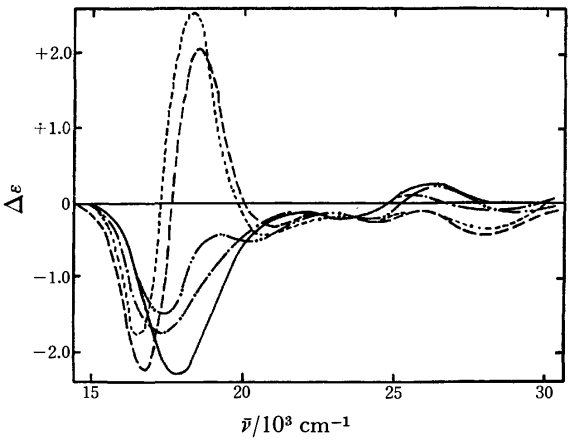

Fig. 3. CD spectra of ——$(-)_{589}[Co(CO_3)_2(NH_3)_2]^-$, —·—$(-)_{589}[Co(CO_3)(ox)(NH_3)_2]^-$, —··—$(+)_{589}$[Co-$(ox)_2(NH_3)_2]^-$, ——$(+)_{589}$[Co(ox)(mal)$(NH_3)_2]^-$, and ------$(+)_{589}[Co(mal)_2(NH_3)_2]^-$.

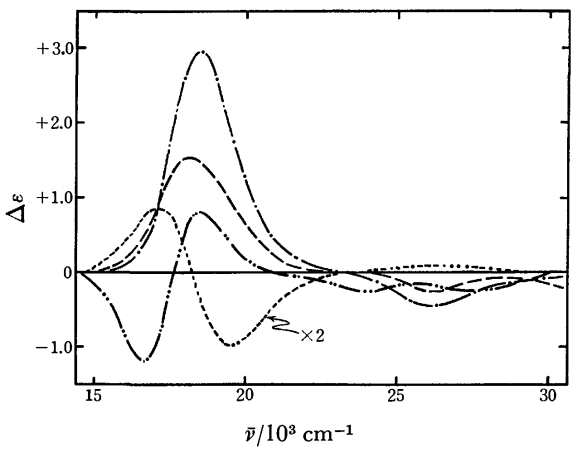

Fig. 4. CD spectra of —·—$(+)_{589}[Co(CO_3)_2(py)_2]^-$, ---$(+)_{589}[Co(ox)_2(py)_2]^-$, —··—$(+)_{589}[Co(CO_3)(mal)(NH_3)_2]^-$, and ------$(-)_{589}[Co(mal)(NH_3)_2(H_2O)_2]^+$.

racemic, $(+)_{589}$ and $(-)_{589}$ lithium salts in 0.2 M $(-)_{589}[Co(ox)(en)_2](C_2H_3O_2)$ aqueous solution were found to be approximately 0.35, 0.26, and 0.24 mol/l, respectively. From these facts, the poorer solubilities of the active salts than that of the racemate, the different solubilities between the enantiomeric salts, and the rapid racemization of the more soluble enantiomer are assumed as the conditions for the present asymmetric synthesis. For the documented asymmetric synthesis of metal complexes, the essential conditions are optical lability and the formation of the less soluble diastereoisomer in the presence of a resolving agent.[10]

Table 1. Spectral data and absolute configurations

Complex	Absorption $\bar{\nu}_{max}$ [a] (log ε)	CD $\bar{\nu}_{max}$ [a] (Δε)	Confign.
$(+)_{589}[Co(CO_3)_2(en)]^-$ [b]	17.5 (2.17)	17.6 (−1.91)	Δ
	25.6 (2.23)	23.5 (−0.22)	
		26.8 (+0.10)	
		28.8 (−0.09)	
$(-)_{589}[Co(CO_3)(ox)(en)]^-$ [b]	18.1 (2.16)	17.2 (+3.43)	Δ
	25.6 (2.25)	23.9 (+0.33)	
		25.9 (−0.07)	
		28.3 (+0.21)	
$(+)_{589}[Co(ox)(en)(H_2O)_2]^+$	18.7 (1.94)	17.3 (−0.47)	Δ
		19.7 (+0.99)	
	26.2 (2.06)	23.8 (+0.16)	
		27.9 (+0.18)	
$(-)_{589}[Co(ox)(mal)(en)]^-$	18.5 (2.04)	17.0 (+2.80)	Δ
		18.0 (−1.29)	
		20.6 (+0.71)	
	26.0 (2.20)	23.6 (+0.13)	
		25.8 (−0.06)	
		27.0 (+0.48)	
$(+)_{589}[Co(CO_3)_2(py)_2]^-$ [c]	17.7 (2.24)	18.4 (+2.94)	Δ
	25.5 (2.34)	26.1 (−0.42)	
$(+)_{589}[Co(ox)_2(py)_2]^-$ [c]	18.2 (2.06)	18.2 (+1.53)	Δ
	25.8 (2.29)	26.2 (−0.42)	

a) $\bar{\nu}_{max}$ values in 10^3 cm^{-1}. b) Absorption spectral data are in Ref. 4. c) Absorption spectral data are in Ref. 8.

Table 2. Spectral data and absolute configurations

Complex	Absorption $\bar{\nu}_{max}$ [a] (log ε)	CD $\bar{\nu}_{max}$ [a] (Δε)	Confign.
$(-)_{589}[Co(CO_3)_2(NH_3)_2]^-$ [b]	17.3 (2.13)	17.8 (−2.32)	Δ
	25.4 (2.40)	23.6 (−0.19)	
		26.1 (+0.26)	
$(-)_{589}[Co(CO_3)(ox)(NH_3)_2]^-$ [b]	17.7 (2.09)	17.3 (−1.74)	Δ
	25.7 (2.18)	23.6 (−0.22)	
		25.8 (+0.11)	
		28.3 (−0.09)	
$(+)_{589}[Co(ox)_2(NH_3)_2]^-$ [b]	18.0 (2.04)	17.3 (−1.52)	Δ
		20.2 (−0.46)	
	26.1 (2.30)	23.0 (−0.11)	
		26.4 (+0.26)	
		28.8 (−0.08)	
$(+)_{589}[Co(ox)(mal)(NH_3)_2]^-$	18.0 (1.95)	16.7 (−2.25)	Δ
		18.5 (+2.06)	
		20.9 (−0.31)	
	26.0 (2.19)	24.2 (−0.23)	
		27.8 (−0.42)	
$(+)_{589}[Co(mal)_2(NH_3)_2]^-$	18.0 (1.92)	16.5 (−1.74)	Δ
		18.3 (+2.52)	
		20.6 (−0.41)	
	26.0 (2.14)	24.2 (−0.17)	
		28.2 (−0.31)	
$(+)_{589}[Co(CO_3)(mal)(NH_3)_2]^-$	17.8 (2.00)	16.5 (−1.21)	Δ
		18.4 (+0.81)	
	25.7 (2.14)	23.9 (−0.28)	
		27.2 (−0.26)	
$(-)_{589}[Co(mal)(NH_3)_2(H_2O)_2]^+$	18.3 (1.72)	17.0 (+0.43)	Λ
		19.4 (−0.49)	
	26.4 (1.89)	26.1 (+0.04)	

a) In 10^3 cm^{-1}. b) Absorption spectral data are in Ref. 4.

CD Spectra. The absorption spectra of the new complexes are shown in Fig. 1 and the CD spectra for the $[Co(O,O)_2(en)]^-$-type, $[Co(O,O)_2(NH_3)_2]^-$-type, and $[Co(O,O)_2(py)_2]^-$-type complexes are shown in Figs. 2—4, the spectral data being summarized in Tables 1 and 2. The observed CD spectra may be grouped into four types from the patterns in the first absorption band ($\bar{\nu}_I$) region; 1) only one peak, 2) two peaks of opposite sign, 3) two peaks of the same sign, and 4) three peaks of alternating sign.

The $(+)_{589}[Co(CO_3)_2(en)]^-$, $(-)_{589}[Co(CO_3)_2(NH_3)_2]^-$ and $(+)_{589}[Co(CO_3)_2(py)_2]^-$ complexes exhibit the patterns of type 1. These peaks are almost symmetrical and the maximum position of each peak shifts to the higher-frequency-side compared with the corresponding absorption maximum ($\bar{\nu}_{I\,max}$). The $(-)_{589}[Co(CO_3)(ox)(en)]^-$ and $(-)_{589}[Co(CO_3)(ox)(NH_3)_2]^-$ complexes also have only one peak, which is unsymmetrical.

The $(+)_{589}[Co(CO_3)(mal)(NH_3)_2]^-$ complex exhibits the pattern of type 2. The acid hydrolysis of this carbonato complex to give the $(-)_{589}[Co(mal)(NH_3)_2(H_2O)_2]^+$ species brings about a reversal of the signs. Similar changes in CD sign has been reported with such diaqua complex species as $(+)_{589}[Co(ox)(NH_3)_2$-

$(H_2O)_2]^+$, $(+)_{589}[Co(CN)_2(NH_3)_2(H_2O)_2]^+$, and $(+)_{589}$-$[Co(NO_2)_2(NH_3)_2(H_2O)_2]^+$.[9,11]

The $(-)_{546}[Co(ox)_2(en)]^-$ [2] and $(+)_{589}[Co(ox)_2$-$(NH_3)_2]^-$ complexes have the patterns of type 3, whereas the $(+)_{589}[Co(ox)_2(py)_2]^-$ complex has that of type 1, but its peak position is compatible with the observed $\bar{\nu}_{I\,max}$.

The $(-)_{589}[Co(ox)(mal)(en)]^-$ and $(+)_{589}[Co(ox)$-$(mal)(NH_3)_2]^-$ complexes have the patterns of type 4, where the dominant peak in each pattern is at the lowest-frequency-side (that is, the first peak). The patterns of $(-)_{546}[Co(mal)_2(en)]^-$,[2] $(+)_{589}[Co(mal)_2$-$(NH_3)_2]^-$ also belong to type 4, but in these cases the middle peaks have greater intensities than the first peak intensities, or comparable ones to those.

The CD spectra in the second absorption band ($\bar{\nu}_{II}$) region also reveal patterns of the four types; the spectra of $(+)_{589}[Co(CO_3)_2(py)_2]^-$ and $(+)_{589}[Co(ox)_2(py)_2]^-$ show one peak, the spectrum of $(-)_{589}[Co(CO_3)_2$-$(NH_3)_2]^-$ show two peaks of opposite sign, those of $(+)_{589}[Co(ox)(mal)(NH_3)_2]^-$ show two peaks of the same sign, and those of $(+)_{589}[Co(ox)_2(NH_3)_2]^-$, $(+)_{589}[Co(CO_3)_2(en)]^-$ and $(-)_{589}[Co(ox)(mal)(en)]^-$ show three peaks of alternating sign. Further discussion can not be given about the CD spectra in the $\bar{\nu}_{II}$ region, but it may be noted that the sign of the lowest frequency peak in this region is consistent with that of the lowest one in the $\bar{\nu}_I$ region for complexes of the type $[Co(O,O)_2$-$(N)_2]^-$ except for the bis(pyridine) and diaquaoxalato complexes.

Absolute Configurations. Since the absolute configuration of the $(+)_{546}[Co(ox)_2(en)]^-$ complex has been known to be *Δ*,[2] the absolute configuration of the $(+)_{589}[Co(ox)_2(NH_3)_2]^-$ complex is determined to be *Δ*, since both complexes have CD patterns of type 3. As for the complexes whose CD patterns belong to type 1, the absolute configurations are assumed to be that the (−) sign refers to *Δ* and the (+) sign to *Λ* compared with the *Δ*$(+)_{546}[Co(ox)_2(en)]^-$ complex exhibiting the (−, −) signs. The $(+)_{589}[Co(ox)(mal)$-$(NH_3)_2]^-$, $(+)_{589}[Co(mal)_2(NH_3)_2]^-$, and $(-)_{589}[Co$-$(ox)(mal)(en)]^-$ complexes are assigned with *Δ*, *Δ*, and *Λ* configurations, respectively, from a comparison of the CD patterns with that of the $(-)_{546}[Co(mal)_2(en)]^-$ complex whose absolute configuration has been shown to be *Λ*.[12] Douglas *et al.*[2] used the $(-)_{546}[Co(edta)]^-$ complex for the assignment of the $(+)_{546}[Co(ox)_2(en)]^-$ and $(-)_{546}[Co(mal)_2(en)]^-$ complexes as the reference. In the same manner, the $(+)_{589}[Co(CO_3)(mal)(NH_3)_2]^-$ complex has tentatively been assigned to be the *Δ* configuration. The $(-)_{589}[Co(mal)(NH_3)_2(H_2O)_2]^+$ species derived from the above $(+)_{589}[Co(CO_3)(mal)$-$(NH_3)_2]^-$ complex may have an *S*[13] configuration, which is equivalent to the *Δ* configuration of the parent complex, since the acid hydrolysis should proceed with retention of configuration. The CD pattern of the $(+)_{589}[Co(ox)(en)(H_2O)_2]^+$ species derived from the $(-)_{589}[Co(CO_3)(ox)(en)]^-$ complex is the same as that of the $(+)_{589}[Co(ox)(en)(H_2O)_2]^+$ complex resolved using the $(+)_{546}[Co(ox)_2(en)]^-$ complex. Hence the *Λ* configuration is assigned to this diaqua complex. All the absolute configurations thus assigned are summarized in Tables 1 and 2.

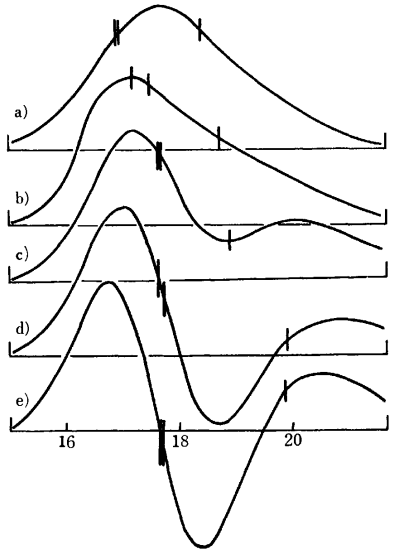

Fig. 5. CD spectral change in the $[Co(O,O)_2(en)]^-$-type complexes of *Λ* configuration.
a) $(-)_{589}[Co(CO_3)_2(en)]^-$, b) $(-)_{589}[Co(CO_3)(ox)$-$(en)]^-$, c) $(-)_{546}[Co(ox)_2(en)]^-$, d) $(-)_{589}[Co(ox)$-$(mal)(en)]^-$, e) $(-)_{546}[Co(mal)_2(en)]^-$. c) and e) Ref. 2.

In order to illustrate the changes of the CD patterns, in the $\bar{\nu}_I$ region, with the varied O,O ligands, the patterns of the complexes having *Λ* configuration have been collected and are shown in Fig. 5. The peak intensity, however, is arbitarily taken in each pattern, because the discussion is limited only to the shape of the pattern. The short vertical lines on each CD curve indicate the band positions calculated by means of Yamatera's predictions:[14] δ_I(en-CO_3)=5800, δ_I(en-ox)=4730, and δ_I(en-mal)=4830 cm^{-1}.

It is clear that there are regular changes of the shapes of the patterns over the range of complexes. The CD peak for the *Λ*-$[Co(CO_3)_2(en)]^-$ complex is situated in a middle position of the predicted band positions, the peak for the *Λ*-$[Co(CO_3)(ox)(en)]^-$ complex being apart considerably from a mean position of the predicted band positions. The two CD peaks for the *Λ*-$[Co(ox)_2$-$(en)]^-$ complex lie on both sides of the predicted two positions. With respect to the *Λ*-$[Co(ox)(mal)(en)]^-$ and *Λ*-$[Co(mal)_2(en)]^-$ complexes, their three CD peaks correspond incorrectly to the calculated components.

A similar change in CD pattern can be observed in the case of the *Λ*-$[Co(O,O)_2(NH_3)_2]^-$-type complexes, and also of the corresponding bis(pyridine) complexes although the bis(oxalato) complex exhibits only one peak.

In order to understand these regular changes of the CD patterns, an attempt has been made to analyze the patterns into Gaussian curves. Douglas *et al.*[2] resolved the CD curve of the $[Co(O,O)_2(en)]^-$ complex (O,O= ox or mal) into three components with respect to both the $\bar{\nu}_I$ and $\bar{\nu}_{II}$ regions, and claimed an effective rhombic field for each of the complexes. In this computation, the CD curve in $\bar{\nu}_I$ region was resolved into two com-

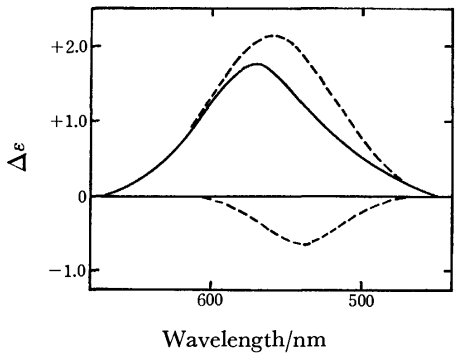

Fig. 6. Gaussian resolution of the CD spectrum of $(+)_{589}[Co(CO_3)(ox)(NH_3)_2]^-$.
——: Observed CD spectrum, ------: calculated gaussian curves.

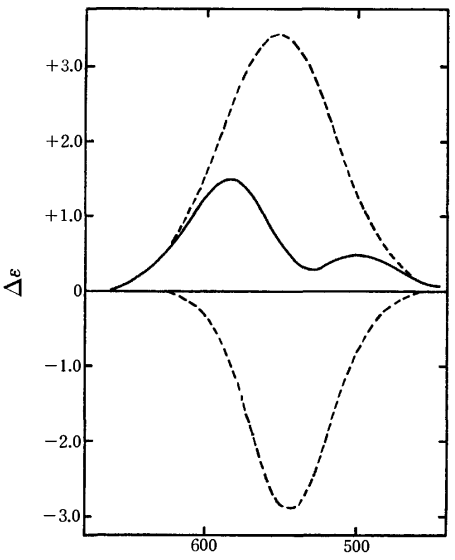

Fig. 7. Gaussian resolution of the CD spectrum of $(-)_{589}[Co(ox)_2(NH_3)_2]^-$.
——: Observed CD spectrum, ------: calculated gaussian curves.

ponents with opposite signs. The results obtained are shown in Figs. 6—8 with respect to the *Λ*-$[Co(O,O)_2(NH_3)_2]^-$-type complexes.

It is seen, from the Gaussian analysis, that every pattern is a resultant curve from the mutual cancellation of a (+) component at a lower frequency and a (−) component at a higher frequency. The separation between the two components is very small, unfortunately the correspondences of the peak positions of the Gaussians with the predicted band positions being too poor. However, the observed regular change in the CD spectra can be qualitatively understood from these results. It is evident that the CD sign at the shorter-wavelength is altered by the mutual cancelation, but the sign at the longest-wavelength remains unchanged. On the basis of this the absolute configurations of the $[Co(O,O)_2(N)_2]^-$-type complexes can be assigned from

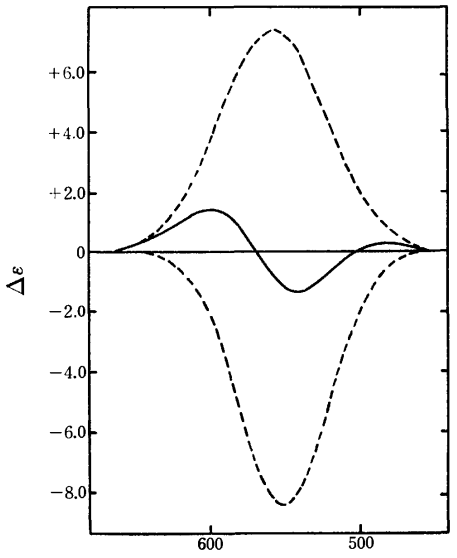

Fig. 8. Gaussian resolution of the CD spectrum of $(-)_{589}[Co(ox)(mal)(NH_3)_2]^-$.
——: Observed CD spectrum, ------ calculated gaussian curve.

the sign of the lowest-frequency peak; the (+) sign refers to *Λ* and the (−) sign to *Δ*. The results of the assignments from this criterion agree with those in Tables 1 and 2. However, this criterion is inapplicable to the $[Co(O,O)(N)_2(H_2O)_2]^+$-type complexes, where the (−) sign of the lowest-frequency peak relates to the *Λ* configuration of the corresponding $[Co(O,O)(CO_3)(N)_2]^-$ complex.

References

1) Presented in part at the 27th Symposium on Coordination Chemistry, Matsumoto, September 29, 1977.
2) B. E. Douglas, R. A. Haines, and J. G. Brushmiller, *Inorg. Chem.*, **2**, 1194 (1963).
3) B. J. Brennan, K. Igi, and B. E. Douglas, *J. Coord. Chem.*, **4**, 19 (1974).
4) M. Shibata, *Nippon Kagaku Zasshi*, **87**, 771 (1966).
5) F. P. Dwyer, J. K. Reid, and F. L. Garvan, *J. Am. Chem. Soc.*, **83**, 1285 (1961).
6) S. Muramoto and M. Shibata, *Chem. Lett.*, **1977**, 1499.
7) Y. Ida, K. Kobayashi, and M. Shibata, *Chem. Lett.*, **1974**, 1299.
8) Y. Ida, S. Fujinami, and M. Shibata, *Bull. Chem. Soc. Jpn.*, **50**, 2665 (1977).
9) T. Ito and M. Shibata, *Inorg. Chem.*, **16**, 108 (1977).
10) "Chelating Agents and Metal Chelates," ed by F. P. Dwyer and D. P. Mellor, Academic Press, New York and London (1964), Chap. 5, p. 195.
11) Y. Enomoto, T. Ito, and M. Shibata, *Chem. Lett.*, **1974**, 423.
12) K. R. Bulter and M. R. Snow, *Chem. Commun.*, **1971**, 550.
13) R. S. Cahn, C. K. Ingold, and V. Prelog, *Angew. Chem., Int. Ed. Engl.*, **5**, 385 (1966).
14) H. Yamatera, *Bull. Chem. Soc. Jpn.*, **31**, 95 (1958).

Syntheses and Properties of Some Trimethylantimony(V) Complexes of Dithiocarbonate Derivatives

Akira OUCHI,* Mamoru SHIMOI, Fujio EBINA, Takashi UEHIRO, and Yukichi YOSHINO

Department of Chemistry, College of General Education, The University of Tokyo, Komaba, Meguro, Tokyo 153

(Received April 7, 1978)

New stable trimethylantimony(V) complexes of some dithiocarbonate derivatives, $(CH_3)_3SbL_2$, where HL= secondary amine-*N*-carbodithioic acid or *O*-alkyl dithiocarbonic acid, have been synthesized by the metathetical reaction between dibromotrimethylantimony(V) and the alkali salts of ligands. In these compounds, the antimony is kept quinquevalent. The ^{1}H-NMR peak of the methyl protons of all of these compounds appears as a singlet even at −60 °C. Therefore, the most probable structure for these compounds is the trigonal bipyramidal one, where two unidentate dithiocarbonate derivative ligands bond to antimony from the apical directions.

The R_3SbL_2 type quinquevalent organoantimony compounds, where R=alkyl or aryl, and HL= carboxylic acid, are well-known compounds, and are obtained by the metathetical reaction from dibromo- or dichlorotrialkyl(or triaryl)antimony(V).[1,2] However, the same type compounds where the antimony bonds to the ligands through sulfur atoms are not easily synthesized. Although the organoantimony(V) compounds, such as thioglycolates,[3] monothiocarboxylates,[4] alkanethiolates,[5] and thiophenolates,[5] where the ligands bond to antimony through sulfur, have already been synthesized, their complexes of dithiocarbonate derivatives, such as dialkyldithiocarbamates, and *O*-alkyl dithiocarbonates, have not been reported yet. Meinema and Noltes[6] reported about the dialkyldithiocarbamato derivatives of the types $RSbL_2$ and R_2SbL (where R= phenyl or alkyl, and HL=dialkyldithiocarbamic acid), but they are all tervalent antimony compounds.

The authors have investigated the metathetical reaction of R_3SbBr_2 (R=methyl or phenyl) with some alkali salts of secondary amine-*N*-carbodithioic acids as well as with *O*-alkyl dithiocarbonic acids, and obtained some stable trimethylantimony(V) compounds of dithiocarbonate derivatives, although the corresponding complexes of triphenylantimony(V) could not be isolated. They are not air sensitive, and do not decompose after several weeks in a refrigerator (5 °C).

During an attempt to synthesize trialkyl(or triaryl)-antimony(V) complexes of dithiocarboxy derivatives, the antimony(III) compounds of the type R_2SbL, where R=phenyl or methyl, were obtained when a little excess of the ligand was used. This fact shows that trialkyl(or triaryl)antimony(V) is readily reduced by such sulfur-containing ligands. Therefore when dibromo- or dichlorotriarylantimony(V) was treated with a large excess of dialkyldithiocarbamates, some of the aryl groups bonded to antimony were removed.

Experimental

Dibromotrimethylantimony(V) was obtained by the standard technique found in the references.[7–9] Sodium salts of piperidine- and pyrrolidine-*N*-carbodithioic acids were synthesized from each amine, carbon disulfide, and sodium hydroxide by the literature method.[10] Sodium *O*-benzyl dithiocarbonate was synthesized from benzyl alcohol, carbon disulfide, and sodium hydroxide applying the synthetic technique for other *O*-alkyl dithiocarbonates.[11,12] Potassium salts of *O*-propyl, isopropyl, and isobutyl dithiocarbonic acids were the GR of Tokyo Kasei Kogyo Co., Ltd., and other reagents were all GR of Wako Pure Chemicals Ltd. They were used without further purification.

Infrared and ^{1}H-NMR spectra were obtained using a JASCO 403G infrared spectrophotometer and a JEOL JNM-MH-100 (100 MHz) NMR spectrometer.

*Synthesis of Bis(pyrrolidine-*N*-carbodithioato)trimethylantimony(V).* To 0.96 g (3 mmol) of dibromotrimethylantimony(V) and 1.02 g (6 mmol) of soduim pyrrolidine-*N*-carbodithioate was added 20 ml of benzene–acetonitrile mixture (5/1= v/v). The mixture was stirred for about 1 h at room temperature (about 20 °C). Special air shielding was not necessary. The precipitated sodium bromide was filtered off, and the filtrate was evaporated using a water jet pump, at a temperature lower than 60 °C. After the residue thus obtained was dissolved in 7 ml of chloroform, 20 ml of petroleum ether was added, and the mixture was ice cooled. The product precipitated slowly. The yield was, on the average, 0.6 g (50%). The piperidine-*N*-carbodithioato complex was obtained by almost the same technique.

Synthesis of Bis(O-benzyl dithiocarbonato)trimethylantimony(V). To 20 ml of an isopropyl alcohol–water (1/1=v/v) mixture were added 0.96 g (3 mmol) of dibromotrimethylantimony(V) and 1.24 g (6 mmol) of sodium *O*-benzyl dithiocarbonate. The mixture was stirred for 2 h. The solvent was removed and sodium bromide was washed away with cold water. The residue was recrystallized from diethyl ether. The yield after the recrystallization was 0.9 g (58%). Other *O*-alkyl dithiocarbonates of trimethylantimony(V) were obtained by almost the same technique. However, the *O*-methyl and *O*-ethyl dithiocarbonates obtained by this process were hardly purified even by the repeated recrystallizations. As the products thus obtained decompose easily at high temperature, they must not be heated beyond 60 °C.

It should be noted that the synthetic technique used for the secondary amine-*N*-carbodithioates could not be applied for *O*-alkyl dithiocarbonates, and *vice versa*.

Results and Discussion

The elementary analyses, the calculated values from the expected chemical formulae, and melting points of these trimethylantimony(V) complexes of dithiocarbonate derivatives are shown in Table 1. All of them have the general formula $(CH_3)_3SbL_2$. These products were colorless or slightly yellow crystalline powders. All of them were soluble in organic solvents such as acetone, chloroform, and benzene, but insoluble in water.

The wave numbers of some infrared spectral bands of

Table 1. Analyses of $(CH_3)_3SbL_2$ (%) and their melting points

L⁻		C	H	N	Mp[a] (°C)
$(CH_2)_5NCS_2^-$	Calcd	36.96	6.00	5.75	
	Found	36.95	5.95	5.72	109
$(CH_2)_4NCS_2^-$	Calcd	33.99	5.49	6.10	
	Found	33.88	5.40	6.09	110
n-$PrOCS_2^-$	Calcd	30.05	5.27		
	Found	30.16	5.31		79
i-$PrOCS_2^-$	Calcd	30.05	5.27		
	Found	30.06	5.24		98
i-$BuOCS_2^-$	Calcd	33.55	5.83		
	Found	33.60	5.81		71
$BzOCS_2^-$	Calcd	42.78	4.35		
	Found	42.77	4.31		69

a) Probably decomposed at the mp or very near to it. *n*-Pr: $CH_3(CH_2)_2$; *i*-Pr: $(CH_3)_2CH$; *i*-Bu: $(CH_3)_2CHCH_2$; Bz: $C_6H_5CH_2$.

dithiocarboxy derivatives (organoantimony complexes and alkali salts) are shown in Table 2. In the infrared spectra of secondary amine-*N*-carbodithioates, a strong band assigned as ν(C=N) appears at about 1460 cm^{-1}, which is an intermediate wave number between 1600 cm^{-1} (for ν(C=N)) and 1100 cm^{-1} (for ν(C–N)). The wave numbers of the bands of the trimethylantimony(V) derivatives are about 20—50 cm^{-1} lower than those of the 3d transition metal dialkyldithiocarbamates,[13,14] and are almost the same as those of the alkali salts. This fact shows that the double bond character of C=N bond does not increase much when the ligand bonds to antimony.

The ν(C–N) band of both these types of compounds easily mixes with other vibrational modes. Consequently, the assignments of the bands are difficult and the opinions of many authors are controversial.[15-18] A pure ν(C=S) band should appear at about 1200 cm^{-1},[19] but, in the infrared spectra of these products, three strong bands are found in 1250—980 cm^{-1} region. The ν(C=S) bands of these complexes are easily mixed with those from other modes. The band seems to be mixed with the ν(COC) mode one in the *O*-alkyl dithiocarbonates, and with some amine ring deformational modes in the piperidine- and pyrrolidine-*N*-carbodithioates. As a result, very little information about the bond type or its strength could be obtained from the data, although the general features of these spectra clearly show that these compounds are the complexes of dithiocarbonate derivatives.

The ν(Sb–S) band is expected to appear in the 350—410 cm^{-1} region, judging from the data about trialkyl(or triaryl)antimony(V) thiocarboxylates[4] as well as about tris(alkanethiolato)antimony(III).[20] In the cases of these complexes, however, the intensity of this band is not high. The wavenumbers of the tentatively assigned peaks are about 405 cm^{-1} for secondary amine-*N*-carbodithioates and about 360 cm^{-1} for *O*-alkyl dithiocarbonates, as shown in Table 2.

A characteristic band of dibromotrimethylantimony(V) at about 867 cm^{-1}, which is assigned as the skeletal vibration $\nu(C_3Sb)$, shifts to about 850 cm^{-1} in the complexes of dithiocarbonate derivatives.

The ^{1}H-NMR spectra of trimethylantimony(V) secondary amine-*N*-carbodithioates and *O*-alkyl dithiocarbonates, as well as their alkali salts, are shown in Table 3.

The methyl proton peak of all of these complexes was a sharp singlet at room temperature, and even at —60 °C; no broadening of the peak was found during the temperature lowering. Therefore, neither the coexisting of isomers nor the existence of nonequivalent methyl groups in a organoantimony complex are probable, provided that the exchange rates of the bonding groups are low enough.

Consequently, for these complexes, the most probable structure is the penta-coordinated trigonal bipyramidal one, where three methyl groups bond from equatorial directions, and two unidentate dithiocarboxy derivative ligands from apical directions. In penta-coordinate complexes, however, Berry's pseudo-rotation may occur,[21] and in such a case the exchange of ligands in a different positions is too rapid to be distinguished by NMR, even at low temperature.[22,23] Therefore, the

Table 2. Infrared spectra of $(CH_3)_3SbL_2$ and alkali salts of their ligands (cm^{-1})

A. Secondary amine-*N*-carbodithioates.

L⁻		ν (C=N)	ν (C=S) and others			ν (CNC)	$\nu(C_3Sb)$	ν (Sb–S)
$(CH_2)_5NCS_2^-$	NaL	1465	1220	1128	1002	965		
	Me_3SbL_2	1468	1223	1113	987	946	848	405
$(CH_2)_4NCS_2^-$	NaL	1455	1243	1159	992	940		
	Me_3SbL_2	1450	1243	1160	998	947	850	407

B. *O*-Alkyl dithiocarbonates.

L⁻		ν (C=S), ν (COC)				$\nu(C_3Sb)$	ν (Sb–S)
n-$PrOCS_2^-$	KL	1151	1108	1058			
	Me_3SbL_2	1188	1128	1052	1036	848	365
i-$PrOCS_2^-$	KL	1180	1136	1050			
	Me_3SbL_2	1200	1139	1080—1030		846	369
i-$BuOCS_2^-$	KL	1181	1145	1105			
	Me_3SbL_2	1195	1170	1055		848	357
$BzOCS_2^-$	NaL	1227	1120	1060			
	Me_3SbL_2	1211	1158	1047		835	369

TABLE 3. ^{1}H-NMR OF $(CH_3)_3SbL_2$ AND THE FREE LIGANDS (alkali salts) (δ: ppm, TMS=0 or DSS=0 for $CDCl_3$ or D_2O solutions, respectively.)

L$^-$	ML (M=Na,K) in D_2O			$(CH_3)_3SbL_2$ in $CDCl_3$ (TMS=0)			
	L			L			CH_3
$(CH_2)_5NCS_2^-$	4.29	1.66		4.12	1.68		2.03
$(CH_2)_4NCS_2^-$	3.79	2.04		3.66	2.01		2.49
n-$PrOCS_2^-$	4.42	1.78	0.98	4.48	1.87	1.03	2.40
i-$PrOCS_2^-$	5.12	1.34		5.70		1.45	2.37
i-$BuOCS_2^-$	4.15	2.01	0.99	4.25	2.10	1.03	2.36
$BzOCS_2^-$	7.35	5.52		7.35	5.49		2.22

possibility of other penta-coordinate structures cannot be denied.

If the dithiocarboxy derivative ligands, one or both, work as the bidentates, the central antimony must be hexa- or hepta-coordinated. In such a case, the complex is expected to be rigid enough, and the exchange rate of the bonding bidentates should be low. Consequently, three methyl groups in the complex must be in unequal positions, and some splitting of the peak is expected. Some hexa-coordinated organoantimony(V) derivatives show fast pseudo-rotation even at low temperature, but even in such a case, some broadening of the peak is expected at −60 °C.[24]

When pyrrolidine was added to a $CDCl_3$ solution of dibromotrimethylantimony(V) containing carbon disulfide, a new peak appeared at about 2.49 ppm, besides the original 2.69 ppm one, due to the formation of the pyrrolidine-*N*-carbodithioate. This peak did not disappear even when the solution was dried up and redissolved into the same solvent. On the other hand, when pyrrolidine was added to a $CDCl_3$ solution of dibromotriphenylantimony(V) containing carbon disulfide at 25 °C, one new peak at 7.30 ppm, which is likely the peak of the triphenylantimony(III) proton, appeared. When more than three times the amounts of the amine (in moles) was added to the dibromotriphenylantimony(V), the original phenyl proton peaks at 8.23 and 7.58 ppm dissapeared. This change is probably due to the reduction of organoantimony(V) to (III), owing to the instability of secondary amine-*N*-carbodithioates of triphenylantimony(V).

References

1) A. Ouchi, H. Honda, and S. Kitazima, *J. Inorg. Nucl. Chem.*, **37**, 2559 (1975).

2) M. Shindo and R. Okawara, *J. Organomet. Chem.*, **5**, 537 (1966).

3) Y. Matsumura, M. Shindo, and R. Okawara, *J. Organomet. Chm.*, **27**, 357 (1971).

4) J. Otera and R. Okawara, *J. Organomet. Chem.*, **17**, 353 (1969).

5) H. Schmidbauer and K. H. Mitschke, *Chem. Ber.*, **104**, 1837 (1971).

6) H. A. Meinema and J. G. Noltes, *J. Organomet. Chem.*, **25**, 139 (1970).

7) H. Landolt, *J. Prakt. Chem.*, [**1**], **84**, 334 (1861).

8) F. F. Blicke, V. O. Oakdale, and F. D. Smith, *J. Am. Chem. Soc.*, **53**, 1025 (1931).

9) W. J. Dyke and W. J. Jones, *J. Chem. Soc.*, **1930**, I, 1921.

10) G. Marcotrigiano, G. C. Pellacini, and C. Preti, *J. Inorg. Nucl. Chem.*, **36**, 3709 (1974).

11) A. K. Das and D. V. Ramana Rao, *Indian J. Chem.*, **13**, 620 (1975).

12) H. L. Klopping and G. J. M. Van der Kerk, *Recl. Trav. Chim. Pay-Bas*, **70**, 917 (1951).

13) K. Nakamoto, T. Fujita, R. A. Condrate, and M. Morimoto, *J. Chem. Phys.*, **39**, 423 (1963).

14) G. M. C. Higgins and B. Saville, *J. Chem. Soc.*, **1963**, 2812.

15) K. A. Jensen, B. M. Dahl, P. H. Nielsen, and G. Borch, *Acta Chem. Scand.*, **26**, 2241 (1971).

16) L. H. Little, G. W. Poling, and J. Leja, *Can. J. Chem.*, **39**, 745 (1961).

17) G. E. Manoussakis and C. A. Tsipis, *J. Inorg. Nucl. Chem.*, **35**, 743 (1973).

18) M. Honda, M. Komura, Y. Kawasaki, T. Tanaka, and R. Okawara, *J. Inorg. Nucl. Chem.*, **30**, 3231 (1968).

19) L. J. Bellamy "The Infrared Spectra of Complex Molecules," 3rd ed, Chapman and Hall, London (1975), p. 394.

20) T. B. Brill and N. C. Campbell, *Inorg. Chem.*, **12**, 1884 (1973).

21) I. Ugi, D. Marquarding, H. Klusacek, and P. Gillespie, *Acc. Chem. Res.*, **4**, 288 (1971).

22) J. L. Sharpley and J. A. Osborn, *Acc. Chem. Res.*, **6**, 305 (1973).

23) P. Meakin, E. L. Muetterties, and J. P. Jesson, *J. Am. Chem. Soc.*, **94**, 5271 (1972).

24) H. A. Meinema, E. Rivarola, and J. G. Noltes, *J. Organomet. Chem.*, **17**, 71 (1969).

Studies on Mixed Valence Complexes of Platinum and Palladium. II.[1] The Crystal Structures of $[Pt(tn)_2][PtCl_2(tn)_2](BF_4)_4$, $[Pt(tn)_2][PtBr_2(tn)_2](ClO_4)_4$, and $[Pt(tn)_2][PtBr_2(tn)_2](BF_4)_4$

Naohide MATSUMOTO, Masahiro YAMASHITA, and Sigeo KIDA*

Department of Chemistry, Faculty of Science, Kyushu University 33, Hakozaki, Fukuoka 812

(Received February 6, 1978)

The crystal structures of Pt(II)-Pt(IV) complexes, $[Pt(tn)_2][PtCl_2(tn)_2](BF_4)_4$ (**1**), $[Pt(tn)_2][PtBr_2(tn)_2](ClO_4)_4$ (**2**), and $[Pt(tn)_2][PtBr_2(tn)_2](BF_4)_4$ (**3**) have been determined by the single-crystal X-ray diffraction method, where tn denotes trimethylenediamine. The crystals of these complexes are isomorphous with one another and the space group is A222 with $a=10.790(2)$, $b=13.872(2)$, $c=10.287(1)$ Å for **1**, $a=11.003(6)$, $b=13.979(6)$, $c=10.355(4)$ Å for **2**, and $a=10.925(3)$, $b=13.862(3)$, $c=10.291(1)$ Å for **3**. The structures were determined by the heavy atom method and refined by the block-diagonal least-squares method to give the disagreement factor 0.082, 0.089, and 0.086 for **1**, **2**, and **3**, respectively. Each crystal comprises infinite $Pt^{II}\cdots X-Pt^{IV}-X\cdots$ chains running parallel to the a-axis. In the chain, tetragonal bipyramidal $[Pt^{IV}X_2(tn)_2]^{2+}$ (X=Cl or Br) and square planar $[Pt^{II}(tn)_2]^{2+}$ units are stacked alternately. Two of the fluorine or oxygen atoms of the counter anion are hydrogen-bonded to the nitrogen atoms of the ligand, contributing to the formation of an infinite chain.

In the preceding paper,[1] we reported the preparation of a number of mixed-valence complexes, $[Pt(AA)_2][PtX_2(AA)_2]Y_4$, $[Pd(AA)_2][PtX_2(AA)_2]Y_4$, and $[Pd(AA)_2][PdX_2(AA)_2]Y_4$, (AA = ethylenediamine(en), propylenediamine(pn), trimethylenediamine(tn); X= Cl, Br, I; Y=ClO_4, BF_4). In the visible region, the complexes show a characteristic broad band assigned to the charge-transfer transition from Pt(II) to Pt(IV). They are of interest in connection with the oxidation states of the platinum atoms and the charge-transfer mechanism between platinum atoms.

In this work, the crystal structures for three complexes, $[Pt(tn)_2][PtCl_2(tn)_2](BF_4)_4$, $[Pt(tn)_2][PtBr_2(tn)_2](ClO_4)_4$, and $[Pt(tn)_2][PtBr_2(tn)_2](BF_4)_4$ have been determined by the single-crystal X-ray diffraction method in order to verify the mixed valence state and to discuss the oxidation state of each platinum atom in more detail.

Experimental

Single-crystals for X-ray work were obtained by recrystallization from a dilute perchloric acid or tetrafluoroboric acid solution at room temperature. Red needle crystals of $[Pt(tn)_2][PtCl_2(tn)_2](BF_4)_4$ show remarkable dichroism; they are dark-red for polarized light along the needle axis and almost colorless for polarized light perpendicular to the axis. $[Pt(tn)_2][PtBr_2(tn)_2](ClO_4)_4$ and $[Pt(tn)_2][PtBr(tn)_2](BF_4)_4$ are lustrous dark-green needle crystals, and also show strong dichroism; they are dark-green parallel to, and light-green perpendicular to the needle axis.

Rotation and Weissenberg photographs about the needle axis (a-axis) were taken for each compound. In contrast to the even layer lines, the odd layer lines are weak in intensity. Similar phenomena were found in Wolffram's red salt,[2] $PtBr_3en$,[3] and related compounds,[4-7] consisting of infinite chains, $\cdots Pt^{II}\cdots X-Pt^{IV}-X\cdots$.

Approximate unit-cell parameters were obtained from the Weissenberg photographs, and refined later by a least-squares procedure using 2θ values of 15 high-angle reflections ($25° < 2\theta < 45°$) measured on a Syntex P$\bar{1}$ diffractometer. Bond's method[8] was applied to ground the crystals. However, no spherical crystals favorable for X-ray work could be obtained owing to the brittleness of the crystals. Hence, a nearly cubic crystal with dimensions *ca.* $0.3\times0.3\times0.3$ mm was used for the intensity measurement. Intensity data were collected on a Syntex P$\bar{1}$ automated four-circle diffractometer by the 2θ-θ scan technique with a variable scan rate in the range 4.0°—24.0°/min using Mo $K\alpha$ radiation monochromoated by a

TABLE 1. CRYSTAL DATA

Compound	$[Pt(tn)_2][PtCl_2(tn)_2](BF_4)_4$	$[Pt(tn)_2][PtBr_2(tn)_2](ClO_4)_4$	$[Pt(tn)_2][PtBr_2(tn)_2](BF_4)_4$
Formula	$Pt_2Cl_2F_{16}N_8C_{12}B_4H_{40}$	$Pt_2Br_2Cl_4O_{16}N_8C_{12}H_{40}$	$Pt_2Br_2F_{16}N_8C_{12}B_4H_{40}$
M.W.	1103.9	1244.2	1193.6
Color	Red-needle	Dark green needle	Dark green needle
Crystal system	Orthorhombic	Orthorhombic	Orthorhombic
Space group	A222	A222	A222
a(Å)	10.790(2)	11.003(6)	10.925(3)
b(Å)	13.872(2)	13.979(6)	13.862(3)
c(Å)	10.287(1)	10.355(4)	10.291(1)
V(Å^3)	1539.8(5)	1572.8(14)	1558.5(6)
D_{cal}(g cm^{-3})	2.382	2.594	2.543
Z	2	2	2
μ(cm^{-1})(Mo $K\alpha$)	107.0	132.1	132.0
F(000)	984	1180	1116
$2\theta_{max}$	60	54	60
N ref(obsd)	1260	1034	1287

graphite plate. Three standard reflections were monitored after each measurement of 50 reflections, their intensities showing good stability. The Lorentz and polarization corrections were applied to the intensity data. Since the present structure analysis was focussed on the determination of the arrangement of heavier atoms and their interatomic distances, no correction was made for absorption. The crystal data are given in Table 1.

Structure Determination and Refinement

The structures were determined by the heavey-atom method, and refined by the block-diagonal least-squares method. The function minimized was $\sum\omega(|F_o|-k|F_c|)^2$, where k is a scale factor and $\omega=1$ for $|F_o|>5.0$ and $\omega=0$ for $|F_o|<5.0$. The space group, in each case, was determined as A222 unequivocally based on the Patterson maps. Atomic scattering factors were taken from International Tables for X-Ray Crystallography.[9] Anomalous dispersion corrections were applied to Pt and Br atoms. All calculations were carried out on a FACOM 230-75 computer in the Computer Center of Kyushu University, the UNICS Program System being used.[10] The final positional and thermal parameters with their estimated standard deviations are given in Table 2. The tables of observed and calculated structure factors are deposited in the office of the Chemical Society of Japan as a Document No. 7842.

$[Pt(tn)_2][PtCl_2(tn)_2](BF_4)_4$. The Patterson function gave the positions of platinum and chlorine atoms. The minimum function based on the platinum and chlorine positions revealed the positions of the nitrogen and boron atoms. In this stage the space group was unequivocally determined to be A222 on the basis of restrictions on crystal packing of the counter ions. Successive Fourier synthesis revealed all the remaining non-hydrogen atoms. The atomic positions and isotropic temperature factors were refined by the block-diagonal least-squares method, the disagreement factor (R) being reduced to 9.3%. Refinement was carried out with anisotropic temperature factors for the Pt and Cl atoms and isotropic ones for all the remaining non-hydrogen atoms, the final R value being 8.2%.

$[Pt(tn)_2][PtBr_2(tn)_2](ClO_4)_4$. The structure was determined by a procedure similar to that for $[Pt(tn)_2][PtCl_2(tn)_2](BF_4)_4$, the final R value being 8.9%.

$[Pt(tn)_2][PtBr_2(tn)_2](BF_4)_4$. Since this compound was thought to be isomorphous with $[Pt(tn)_2][PtBr_2(tn)_2](ClO_4)_4$, the positional parameters of the perchlorate and the over-all temperature factor calculated from Wilson's plot were used as the initial parameters of the refinement. After 5 cycles of the refinement, the R value was reduced to 10.5%. Refinement was then

Table 2. Positional and thermal parameters with their estimated standard deviations in parentheses ($\times 10^4$) (Anisotropic thermal parameters are expressed in the form $\exp[-(B_{11}h^2+B_{22}k^2+B_{33}l^2+B_{12}hk+B_{13}hl+B_{23}kl)]$.)

$[Pt(tn)_2][PtCl_2(tn)_2](BF_4)_4$

	x/a	y/b	z/c	B(Å^2)
Pt(1)	0	0	0	—
Pt(2)	1/2	0	0	—
Cl	2870(7)	0	0	—
N(1)	171(26)	1076(16)	1393(22)	3.8(4)
N(2)	5169(33)	1062(15)	1403(21)	3.1(4)
C(1)	546(24)	928(19)	2609(28)	2.5(4)
C(2)	0	0	3291(63)	6.8(9)
C(3)	5557(38)	920(34)	2614(53)	6.0(8)
C(4)	1/2	0	3320(53)	6.8(11)
B	2548(42)	3052(27)	793(35)	3.7(6)
F(1)	1471(23)	2539(22)	510(24)	7.2(6)
F(2)	3578(22)	2601(20)	233(31)	8.1(6)
F(3)	2597(20)	3885(14)	−133(26)	6.2(4)
F(4)	2390(29)	3264(19)	2025(26)	8.1(6)

	B_{11}	B_{22}	B_{33}	B_{12}	B_{13}	B_{23}
Pt(1)	37(1)	22(0)	44(1)	0	0	0
Pt(2)	39(1)	20(0)	39(1)	0	0	0
Cl	55(5)	21(2)	42(4)	0	0	−26(15)

$[Pt(tn)_2][Pt\,Br_2(tn)_2](ClO_4)_4$

	x/a	y/b	z/c	B(Å^2)
Pt(1)	0	0	0	—
Pt(2)	1/2	0	0	—
Br	2686(7)	0	0	—
Cl	2518(12)	3055(7)	738(10)	—
N(1)	−139(24)	1045(19)	1432(23)	1.3(5)
N(2)	4976(61)	1055(29)	1363(36)	4.1(7)
C(1)	636(38)	937(32)	2624(42)	2.3(7)
C(2)	0	0	3343(82)	9.8(21)
C(3)	5362(68)	923(61)	2701(65)	7.5(18)
C(4)	1/2	0	3273(60)	4.2(11)
O(1)	1487(43)	2522(38)	503(43)	8.6(11)
O(2)	3610(40)	2561(35)	−87(62)	7.4(9)
O(3)	2802(29)	3902(22)	126(40)	4.3(7)
O(4)	2379(50)	3167(34)	2066(42)	7.4(9)

	B_{11}	B_{22}	B_{33}	B_{12}	B_{13}	B_{23}
Pt(1)	17(1)	21(1)	37(2)	0	0	0
Pt(2)	22(1)	18(1)	28(1)	0	0	0
Br	132(8)	37(2)	49(4)	0	0	5(12)
Cl	59(8)	32(4)	100(11)	1(20)	−46(23)	8(13)

$[Pt(tn)_2][PtBr_2(tn)_2](BF_4)_4$

	x/a	y/b	z/c	B(Å^2)
Pt(1)	0	0	0	—
Pt(2)	1/2	0	0	—
Br	2674(5)	0	0	—
N(1)	191(27)	1068(18)	1426(24)	2.1(4)
N(2)	5226(28)	1072(21)	1459(29)	2.8(5)
C(1)	600(32)	890(31)	2646(43)	3.1(6)
C(2)	0	0	3252(61)	4.6(10)
C(3)	5569(35)	923(36)	2662(50)	3.9(8)
C(4)	1/2	0	3335(46)	3.1(7)
B	2557(28)	3077(28)	776(42)	3.1(7)
F(1)	1520(28)	2588(23)	637(32)	6.1(7)
F(2)	3548(21)	2569(25)	240(43)	7.2(8)
F(3)	2626(30)	3887(18)	−82(50)	6.9(6)
F(4)	2291(41)	3264(29)	2026(29)	7.9(9)

	B_{11}	B_{22}	B_{33}	B_{12}	B_{13}	B_{23}
Pt(1)	18(1)	12(0)	32(1)	0	0	0
Pt(2)	19(1)	11(0)	29(1)	0	0	0
Br	121(4)	24(1)	55(3)	0	0	−30(7)

Table 3. Interatomic bond distances $[Pt(tn)_2]$ (l/Å) and angles (ϕ/°) with their estimated standard deviations in parentheses

$[Pt(tn)_2][PtCl_2(tn)_2](BF_4)_4$			
Pt(1)–Cl	3.096(6)	N(2)–C(3)	1.33(5)
Pt(2)–Cl	2.299(6)	C(3)–C(4)	1.58(5)
Pt(1)–N(1)	2.07(2)	B–F(1)	1.39(5)
N(1)–C(1)	1.33(3)	B–F(2)	1.39(4)
C(1)–C(2)	1.58(4)	B–F(3)	1.49(4)
Pt(2)–N(2)	2.07(2)	B–F(4)	1.31(4)
N(1)–Pt(1)–N(1)[a]	88.1(8)	N(2)–C(3)–C(4)	115(4)
N(1)–Pt(1)–N(1)[b]	92.7(8)	C(3)–C(4)–C(3)[a]	125(4)
Pt(1)–N(1)–C(1)	124(1)	F(1)–B–F(2)	110(3)
N(1)–C(1)–C(2)	111(4)	F(1)–B–F(3)	106(3)
C(1)–C(2)–C(1)[a]	127(4)	F(1)–B–F(4)	103(3)
N(2)–Pt(2)–N(2)[a]	89.2(8)	F(2)–B–F(3)	92(3)
N(2)–Pt(2)–N(2)[b]	91.6(8)	F(2)–B–F(4)	126(3)
Pt(2)–N(2)–C(3)	125(2)	F(3)–B–F(4)	117(3)
$[Pt(tn)_2][PtBr_2(tn)_2](ClO_4)_4$			
Pt(1)–Br	2.955(7)	N(2)–C(3)	1.46(7)
Pt(2)–Br	2.546(7)	C(3)–C(4)	1.47(8)
Pt(1)–N(1)	2.08(2)	Cl–O(1)	1.37(5)
N(1)–C(1)	1.50(5)	Cl–O(2)	1.62(5)
C(1)–C(2)	1.66(5)	Cl–O(3)	1.37(3)
Pt(2)–N(2)	2.04(3)	Cl–O(4)	1.39(4)
N(1)–Pt(1)–N(1)[a]	89.4(9)	N(2)–C(3)–C(4)	114(5)
N(1)–Pt(1)–N(1)[b]	91.9(9)	C(3)–C(4)–C(3)[a]	132(5)
Pt(1)–N(1)–C(1)	118(2)	O(1)–Cl–O(2)	106(2)
N(1)–C(1)–C(2)	102(3)	O(1)–Cl–O(3)	124(2)
C(1)–C(2)–C(1)[a]	126(5)	O(1)–Cl–O(4)	98(2)
N(2)–Pt(2)–N(2)[a]	87(1)	O(2)–Cl–O(3)	87(2)
N(2)–Pt(2)–N(2)[b]	92(1)	O(2)–Cl–O(4)	130(3)
Pt(2)–N(2)–C(3)	124(4)	O(3)–Cl–O(4)	112(2)
$[Pt(tn)_2][PtBr_2(tn)_2](BF_4)_4$			
Pt(1)–Br	2.921(5)	N(2)–C(3)	1.31(5)
Pt(2)–Br	2.541(5)	C(3)–C(4)	1.59(5)
Pt(1)–N(1)	2.09(2)	B–F(1)	1.33(5)
N(1)–C(1)	1.35(5)	B–F(2)	1.40(5)
C(1)–C(2)	1.53(5)	B–F(3)	1.43(5)
Pt(2)–N(2)	2.12(2)	B–F(4)	1.34(5)
N(1)–Pt(1)–N(1)[a]	90.0(9)	N(2)–C(3)–C(4)	115(4)
N(1)–Pt(1)–N(1)[b]	91.0(9)	C(3)–C(4)–C(3)[a]	126(3)
Pt(1)–N(1)–C(1)	123(2)	F(1)–B–F(2)	111(3)
N(1)–C(1)–C(2)	112(3)	F(1)–B–F(3)	111(3)
C(1)–C(2)–C(1)[a]	131(4)	F(1)–B–F(4)	91(3)
N(2)–Pt(2)–N(2)[b]	90(1)	F(2)–B–F(3)	96(3)
N(2)–Pt(2)–N(2)[b]	91(1)	F(2)–B–F(4)	129(4)
Pt(2)–N(2)–C(3)	126(2)	F(3)–B–F(4)	116(3)

a) Key $\bar{x}, \bar{y}, z$. b) Key $\bar{x}, y, \bar{z}$.

Table 4. Hydrogen bond distances (Å)

Compound	A[a] N(2)–F(2) or (N(2)–O(2))	B[a] N(2)[b]–F(2) (N(2)[b]–O(2))	C[a] N(1)–F(1) (N(1)–O(1))
$[Pt(tn)_2][PtCl_2(tn)_2](BF_4)_4$	2.99(4)	3.03(4)	2.63(4)
$[Pt(tn)_2][PtBr_2(tn)_2](ClO_4)_4$	2.99(7)	2.93(7)	2.89(5)
$[Pt(tn)_2]$ $[PtBr_2(tn)_2](BF_4)_4$	3.03(4)	3.02(4)	2.68(4)

a) Hydrogen bonds depicted in Fig. 2. b) Key, $\bar{x}, y, \bar{z}$.

carried out with anisotropic temperature factors for the Pt and Br atoms, the final R value being 8.6%.

Description of the Structure

The crystal structure of $[Pt(tn)_2][PtCl_2(tn)_2](BF_4)_4$ and the atom numbering systems are shown in Fig. 1. Bond distances and bond angles with their estimated standard deviations are given in Table 3, hydrogen bond distances in Table 4.

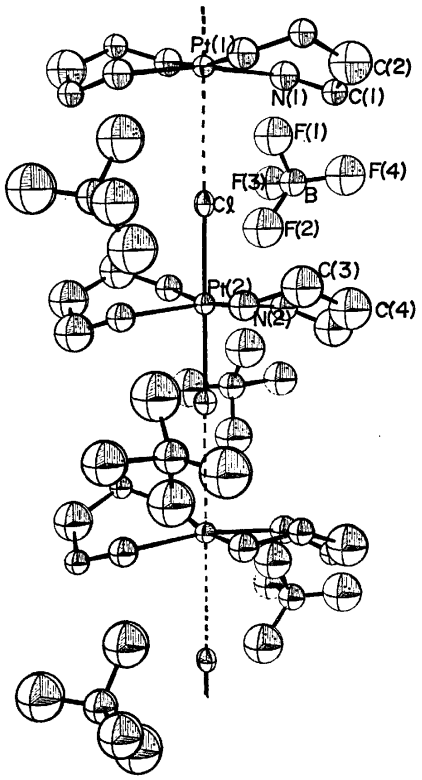

Fig. 1. A perspective view of $[Pt(tn)_2][PtCl_2(tn)_2](BF_4)_4$ and the numbering system of atoms. The vibrational spheres and ellipsoids are drawn at the 50% probability.[14]

$[Pt(tn)_2][PtCl_2(tn)_2](BF_4)_4$. The crystal contains infinite ···Pt(1)···Cl–Pt(2)–Cl··· chains running parallel to the a-axis. Pt(1) and Pt(2) occupy (0,0,0) and (1/2,0,0), respectively. Hence, the Pt(1)–Pt(1) and Pt(2)–Pt(2) distances correspond to the length of the a-axis.

Each platinum atom is coordinated with four nitrogen atoms of diamines in a square planar configuration with normal Pt–N distances of Pt(II) and Pt(IV) complexes. However, the Pt(1)–Cl (3.096(6) Å) and Pt(2)–Cl (2.299(6) Å) distances are quite different. The latter is close to the value (2.32 Å) of the Pt–Cl distance in *trans*-$[PtCl_2(NH_3)_4]Cl_2$,[11] which is a discrete Pt(IV) complex, and is also near the value (2.27 Å) calculated from atomic radii.[12] On the other hand, the former distance is greater than the normal covalent Pt–Cl distance, though it is still small enough to bring about some interaction between Pt(1) and Pt(2), as evidenced by the characteristic visible absorption.[13] Thus, the compound can be regarded to comprise square planar $[Pt^{II}(tn)_2]^{2+}$ and tetragonal bipyramidal $[Pt^{IV}Cl_2(tn)_2]^{2+}$ units which are stacked alternately in the chain.

The distances N(1)–F(1) (or –O(1)), N(2)–F(2) (or –O(2)), and N(2)[b]–F(2) (or –O(2)) (Table 4 and Fig. 2) indicate that the atoms are hydrogen-bonded. These hydrogen bonds seem to serve for the formation of the complexes of this type.

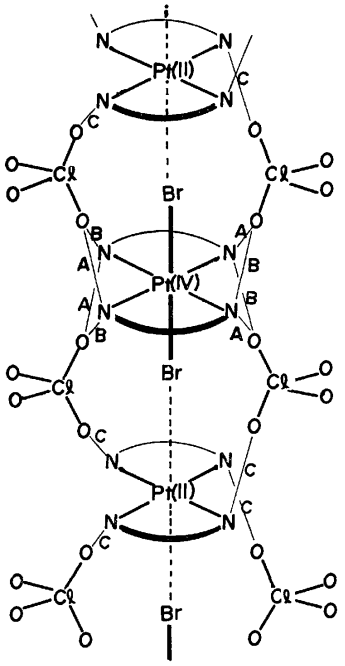

Fig. 2. A schematic representation of the hydrogen bonds. (A, B, and C refer to Table 4.)

$[Pt(tn)_2][PtBr_2(tn)_2](ClO_4)_4$ and $[Pt(tn)_2][PtBr_2(tn)_2](BF_4)_4$. The crystal structures are essentially the same as that of $[Pt(tn)_2][PtCl_2(tn)_2](BF_4)_4$. The Pt–Br distances are 2.546(7) and 2.955(7) Å for $[Pt(tn)_2][PtBr_2(tn)_2](ClO_4)_4$, and 2.541(5) and 2.921(5) Å for $[Pt(tn)_2][PtBr_2(tn)_2](BF_4)_4$, respectively. The Pt(2)–Br bond distances (2.546(7), 2.541(5) Å) are greater than the sum of the covalent bond radii 2.43 Å.[12] They are also greater than the corresponding distances in the related compounds, $[Pt(ea)_4][PtBr_2(ea)_4]Br_4\cdot 4H_2O$ (2.447 Å)[5] and $[Pt(ea)_4][PtBr_2(ea)_4]Br_4$ (2.42 Å),[4] where ea denotes ethylamine. The Pt(1)–Br distances (2.955(7), 2.921(5) Å) are smaller than those in the related complexes $[Pt(ea)_4][PtBr_2(ea)_4]Br_4\cdot 4H_2O$ (3.107, 3.139 Å)[5] and $[Pt(ea)_4][PtBr_2(ea)_4]Br_4$ (3.19, 4.07 Å).[4]

Discussion

The crystal structure is exactly in accord with what we had expected.[1] The fact that the ···Pt^{II}···X–Pt^{IV}–X··· chains array along the needle axis of crystal is also in line with our prediction deduced from the consideration of the polarization of the visible absorption.[1]

The relation between ν_{max} of the visible absorption and the Pt–halogen distances has not been clarified. The difference in Pt–Br distances between the per-

TABLE 5. ABSORPTION MAXIMUM AND PLATINUM-HALOGEN DISTANCES

Compound	ν_{max}(kcm^{-1})	Pt^{IV}–X(Å)	Pt^{II}–X(Å)	a(Å)	$\rho=(Pt^{IV}–X)/(Pt^{II}–X)$
$[Pt(tn)_2][PtCl_2(tn)_2](BF_4)_4$	20.62	2.299(6)	3.096(6)	10.790(2)	0.74
$[Pt(tn)_2][PtBr_2(tn)_2](ClO_4)_4$	16.53	2.546(7)	2.955(7)	11.003(6)	0.86
$[Pt(tn)_2][PtBr_2(tn)_2](BF_4)_4$	14.08	2.541(6)	2.921(5)	10.925(3)	0.87

chlorate and the tetrafluoroborate seems to be too small to account for the remarkable red-shift of the visible band (Table 5).

It is of interest to examine the oxidation states of the platinum atoms in the crystal in terms of the ratio of interatomic distances between platinum and halogen, $\rho=$(Pt(IV)–X)/(Pt(II)–X). In the case $\rho<1$, there is a difference in oxidation state between platinum atoms. When ρ approaches unity, the difference decreases to zero; the oxidation states of platinum atoms being leveled out at $\rho=1$. All the ratios are less than unity, and the ρ value of the bromo-complexes is larger than that of the chloro-complex (Table 5). This indicates that the extent of leveling of oxidation states of platinum atoms is greater in bromo-complexes than in the chloro-complex, as a result of the stronger Pt(II)$\cdots$ Br–Pt(IV) interaction. In this connection, it is of interest to consider the ρ value of the iodo-homologs expected to assume a value greater than that of bromo-homologs. The single-crystal X-ray analysis of $[Pt(tn)_2][PtI_2(tn)_2](ClO_4)_4$ is in progress, preliminary data showing $\rho\approx0.91$.

The authors are grateful to Prof. I. Ueda and Assoc. Prof. S. Kawano, Kyushu University, for their valuable advice and for use of their programs. Thanks are also due to Prof. T. Komori for use of the Syntex $P\bar{1}$ automated diffractometer.

References

1) Part I. N. Matsumoto, M. Yamashita, and S. Kida, *Bull. Chem. Soc. Jpn.*, **51**, 2334 (1978).
2) B. M. Craven and D. Hall, *Acta Crystallogr.*, **14**, 475 (1961).
3) T. D. Ryan and R. E. Rundle, *J. Am. Chem. Soc.*, **83**, 2814 (1961).
4) B. M. Craven and D. Hall, *Acta Crystallogr.*, **21**, 177 (1966).
5) K. L. Brown and D. Hall, *Acta Crystallogr., Sect. B*, **32**, 279 (1976).
6) J. Wallen, C. Brosset, and N. Vannerberg, *Arkiv für Kemi*, **18**, 541 (1962).
7) C. Brosset, *Arkiv Kemi, Min., Geol.*, **25A**, No. 19 (1968).
8) W. L. Bond, *Rev. Sci. Instr.*, **22**, 344 (1951).
9) "International Tables for X-Ray Crystallography," Kynoch Press, Birmingham (1962), Vol. III.
10) "Universal Crystallographic Computation Program System (UNICS)," ed by T. Sakurai, The Crystallographic Society of Japan, Tokyo (1967).
11) M. A. Porai-Koshits and E. M. Romanova, *Neorg. Khim., Akad. Nauk SSSR*, **28**, 282 (1954); *Chem. Abstr.*, **50**, 644C, (1956).
12) T. Moeller, "Inorganic Chemistry," John-Wiley, New York (1952).
13) S. Yamada and R. Tsuchida, *Bull. Chem. Soc. Jpn.*, **29**, 894 (1956); **29**, 421 (1956).
14) C. K. Johnson, ORTEP, Oak Ridge National Laboratory Report ORNL-3794 (1965).

On the Behavior of Mercury in Some Polluted Seawater

Katsuhiko MATSUNAGA,* Hiroaki TSUJIOKU, Sigeru FUKASA, and Kiyoshi HASEBE**

Department of Chemistry, Faculty of Fisheries, Hokkaido University, Hakodate 041

***Department of Chemistry, Faculty of Science, Hokkaido University, Sapporo 060*

(Received March 17, 1978)

Most of the mercury in coastal seawater polluted with waste water including mainly organic suspended matter is associated with suspended matter, especially particulate organic matter. The amount of mercury adsorbed on a given amount of particulate organic matter nearly obeys Freundlich's adsorption isotherm at mercury concentrations less than 15 ppm in particulate organic matter. The mercury in suspended matter is not much reduced by the addition of tin(II) chloride. Thus, to get the total value of the mercury concentration, the water samples must be heated with the addition of a sulfuric and nitric acid mixture to decompose the suspended matter.

Measurements of the mercury concentration in seawater have been made by several investigators; the values, however, are widely scattered. It may be most significant that almost all the samples were kept in polyethylene bottles after acidification. Matsunaga[1] has found that mercury at the nanogram level is given off from such bottles during sample storage, increasing the initial mercury level by a factor of 2 to 100, even if the container has been acid-rinsed. The mercury concentrations in uncontaminated natural waters are generally lower than 5 ng dm^{-3},[2-6] and that in the oceans was found to be constant at 5 ng dm^{-3}.[2,3] In studying the behavior of mercury in contaminated seawater, Carr and Wilknis[7] have reported a desorption rate of mercury from suspended matter. They added ^{197}Hg into seawater including a high concentration of suspended matter (7 mg dm^{-3}) and adjusted the pH of the water to 1.

Here we report on the behavior of mercury in coastal seawater polluted with waste water including mercury and fish meal.

Experimental

Reagents. 1000 ppm $HgCl_2$ stock solution: 1.345 g $HgCl_2$ was dissolved in distilled water; the volume was filled up to 1 dm^3. NaCl: To eliminate any contaminant mercury in the sodium chloride, the reagent was heated in a furnace at 500 °C for 2 h. 10 ppb $HgCl_2$ solution: Sodium chloride and sulfuric acid were added into the adequate amounts of the stock solution to become 3.5% and 0.2 mol dm^{-3}, respectively. This solution is stable for at least 3 months. Tin(II) chloride solution: 50 g $SnCl_2 \cdot 2H_2O$ was dissolved in 1 dm^3 of 1 mol dm^{-3} hydrochloric acid. The mercury in tin(II) chloride solution was eliminated by passing nitrogen gas at a flow rate of 1.4 dm^3 min^{-1} for 1 h. H_2SO_4 and HNO_3: Both the chemicals are of the analytical special reagent grade for measurements of toxic metals produced by Wako Chemicals Inc. Mercury contents in both acids were below 0.1 ppb in most cases, but we had to determine the amount before using because there is a difference of mercury concentration between lots.

Apparatus. Absorbances were measured on a Jarrell-Ash atomic absorption spectrophotometer, AA-780, with a quartz cell (2.0-cm diameter, 20-cm length).

Sampling and Analytical Methods. *Sampling Method*: About 30 samples of surface seawater were collected in the Hakodate Bay with a plastic bucket during a period from June to September 1976 at a station shown by the star mark in Fig. 1. Immediately after collection the sample was acidified to 0.2 mol dm^{-3} with sulfuric acid, and stored in a glass bottle. The mercury contents in the samples were analysed at the laboratory within 1 h. Samples were also collected vertically in the bay with a Van Dorn bottle on 12 August, 1976 at stations shown by a circle mark in Fig. 1.

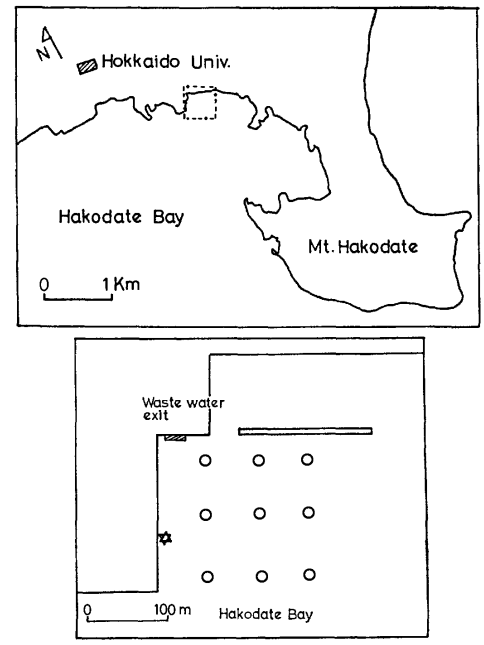

Fig. 1. Sampling stations for polluted seawater. Sampling station ☆: about 30 surface seawater samples were collected from Jun. to Sep. 1976, ○: samples were vertically collected at 12 Aug. 1976.

Analytical Method. *Ionic Mercury*: The outline of the analytical method is as follows:[8] Ionic mercury in 0.2—0.8 dm^3 sample is reduced with tin(II) chloride and the mercury vapor generated is transferred to gold particles, packed in a glass tube, by a stream of nitrogen gas. The metal is then heated to 500 °C in a furnace, and the vaporized mercury is determined with an atomic absorption spectrophotometer.

Total Mercury: To a 0.5 dm^3 sample solution, sulfuric acid (2 cm^3) and nitric acid (5 cm^3) are added, and the solution is heated with a reflux condenser for 2 h to decompose particulate phases. The leached mercury is determined according to the procedure of ionic mercury determination. The acid decomposition method was compared with the decomposition method with potassium permanganate for the same samples. Table 1 shows that there is no significant difference between two methods for the significance level $(1-\alpha)=95\%$, $(\alpha=0.05)$.

Mercury in Suspended Matter: The sample was filtered through an HA type Millipore filter with a 0.45 μm pore size, and then

TABLE 1. THE COMPARISON OF TOTAL MERCURY CONCENTRATIONS DETERMINED BY TWO OXIDATION METHODS

Batch	Oxidant	
	NHO_3–H_2SO_4	$KMnO_4$
	[Hg] (ng dm^{-3})	
1	64.3	54.5
2	11.5	9.6
3	420	414
4	9.3	15.8
5	44.4	44.5
6	12.0	13.5
7	5.8	5.3
8	4.4	3.5
9	23.3	19.3
10	15.1	12.9

$t_0 = 1.25 < t(9, 0.05) = 2.26$.

the residue was decomposed with sulfuric and nitric acid mixture by heating. The mercury was determined by AAS, following the procedure described above.

Suspended Matter and Loss on Ignition: After the sample solution was filtered using the Millipore filter, the filter paper was rinsed with 100—150 cm^3 H_2O to remove sea salt, and dried in a desiccator until the weight of each filter reached a constant value within $\pm$0.2 mg. After weighing, the total weight of suspended matter was obtained using the difference in weight before and after filtration, and then the filter was ignited at 500 °C for 2 h. After weighing, the loss on ignition, assumed to be a measurement of the particulate organic matter, was determined from the difference in the values of the weight.

Results and Discussion

Student's *t*-test is useful to compare the data obtained by the use of two different methods. As already mentioned above, there is no significant difference between the two sets of data given in Table 1, for $\alpha = 0.05$. Therefore, the method with sulfuric and nitric acid mixture can be applied to decompose suspended matters present in the samples in a simple and easy way. Some results on different forms are shown in Table 2. For the samples containing more than 10 mg dm^{-3} of suspended matter, quantities of mercury less than 11% of total mercury were detected in ionic form. Judging from the concentrations of mercury in suspended matters, evidently the rest of the mercury in those samples is adsorbed on, or coagulated with, suspended matter. Figure 2 shows the relationship between ionic mercury concentration and total mercury concentration. A remarkable deviation form the line which indicates the 1 : 1 relationship is observed with increasing the amounts of suspended matters. This means that the concentrations of ionic mercury decreased with

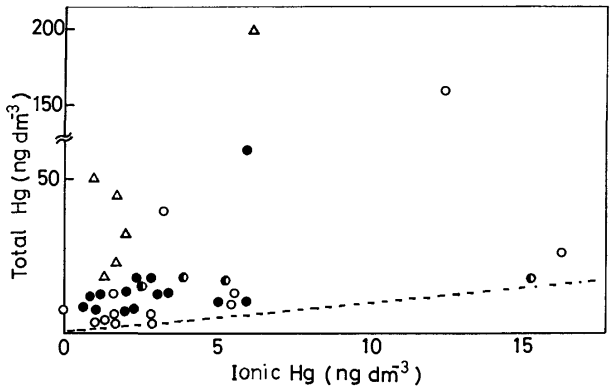

Fig. 2. The relationship between ionic mercury and total mercury. Marks denote the amounts of suspended matter.
○ 0—5; ● 5—10; ◐ 10—20; △ >20 mg dm^{-3}.

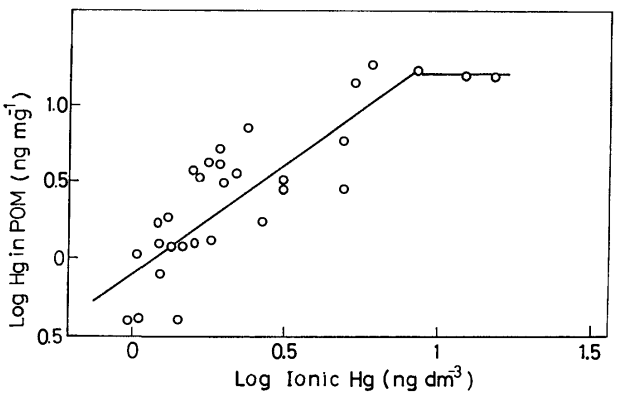

Fig. 3. Freundlich's adsorption isotherm between ionic mercury and mercury in particulate organic matter.

TABLE 2. MERCURY CONCENTRATIONS IN SEVERAL FORMS

Sample	Ionic Hg (ng dm^{-3})	Total Hg (ng dm^{-3})	Hg on a filter (ng dm^{-3})	SM[a] (mg dm^{-3})	Hg in SM (ppm)	POM[b]/SM (%)
1	1.7	45	45	76.4	0.59	72.4
2	8.9	416	370	28.2	13.12	87.9
3	13.0	122	106	12.6	8.41	63.4
4	5.3	11	9.1	2.2	4.14	36.4
5	1.1	11	6.5	8.2	0.79	73.2
6	1.8	8.2	6.4	4.2	1.52	89.6
7	3.3	42	41	15.0	2.73	76.0
8	3.3	12	10	6.8	1.47	58.8
9	1.8	4.0	3.6	3.6	1.00	33.3
10	1.4	23	19	14.4	1.32	90.2

Sampling was done at the station shown by the star mark in Fig. 1 from June to Sept. 1976. a) SM means suspended matter. b) POM means particulate organic matter.

increasing the amounts of suspended matters. Figure 3 shows the relationship between mercury concentrations in ionic form and in particulate organic matters. The amount of mercury adsorbed on particulate organic matters per unit weight nearly obeys Freundlich's adsorption isotherm at the concentrations lower than 15 ppm mercury.

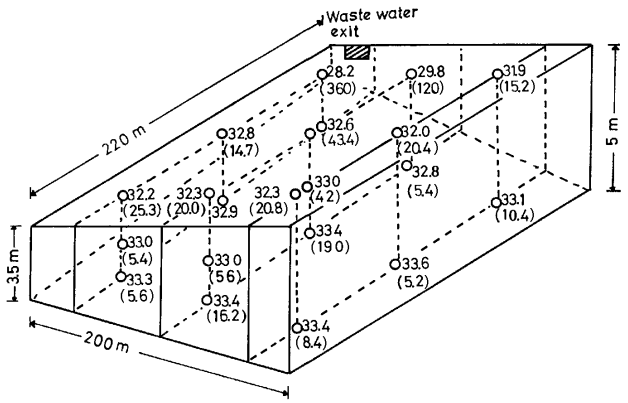

Fig. 4. Salinity, ‰ and the amount of suspended matter (mg dm^{-3}).

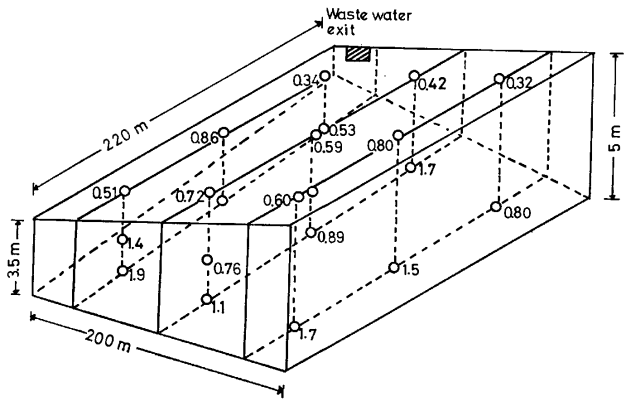

Fig. 5. The amount of mercury in suspended matter.

The salinity and the amount of suspended matter, and the amount of mercury in the suspended matters are shown in Figs. 4 and 5, respectively, for the samples at different depths collected in the area shown in Fig. 1. In the area, waste water diffuses from east to south, as is seen in the salinity distribution (Fig. 4) around the waste water exit. However, the salinity near the bottom is scarcely affected by waste water, except for the area adjacent to the discharge. The same tendency is observed in the suspended matter distribution, though suspended matters settle downward. The mercury concentration in suspended matters is about 0.1 ppm level in samples near the surface, while the concentration occasionally approaches 1 ppm level with increasing depth. This suggests that suspended matters adsorb and remove mercury from the water. The concentrations of ionic mercury in seawater samples are below 2 ng dm^{-3} in all of the samples measured; such values are about half of the values in unpolluted sewater at Hakodate Bay. The present results suggest that most of mercury in highly polluted waters is associated with suspended matter. As mentioned above, the determination of mercury can be simplified by treating water samples with a nitric and sulfuric acid mixture. For samples with salinity higher than 30‰ and acidified to 0.2 ml dm^{-3} with sulfuric acid, no adsorption of mercury on the walls of the glass container was observed. But significant adsorption of mercury occurred for samples with salinity less than 30‰, even if they were acidified to more than 0.2 mol dm^{-3}. Generally coastal seawater has a salinity lower than 30‰. Therefore, sodium chloride preheated at 500 °C must be added to the sample solutions to bring its salinity up higher than 30‰, unless the samples are quickly processed after sampling. By these procedures, adsorption of mercury on the walls of the container was avoided.[1] For open seawater samples, acidification to 0.2 mol dm^{-3} with sulfuric acid for a month at room temperature was found to be sufficient for quantitative determination of mercury.[1] However, this treatment yielded only 40% of the total mercury for samples with suspended matters concentration higher than 30 mg dm^{-3}. For polluted seawater samples, the treatment with sulfuric and nitric acid mixture is necessary for quantitative determination of mercury.

The authors wish to thank Prof. M. Nishimura for his advice and the Ministry of Education for the financial support granted for this research.

References

1) K. Matsunaga, *Mizu Shori Gijitsu*, **16**, 631 (1975).
2) K. Matsunaga, *Nature*, **257**, 49 (1975).
3) K. Matsunaga, M. Nishimura, and S. Konishi, *Nature*, **258**, 224 (1975).
4) K, Matsunaga, *J. Oceanogr. Soc. Jpn.*, **32**, 48 (1976).
5) K. Matsunaga and T. Goto, *Geochem. J.*, **10**, 107 (1976).
6) K. Matsunaga, *Jpn. J. Limnol.*, **37**, 131 (1976).
7) R. A. Carr and P. E. Wilkniss, *Environ. Sci. Tech.*, **7**, 62 (1973).
8) M. Nishimura, K. Matsunaga, and S. Konishi, *Bunseki Kagaku*, **24**, 655 (1975).
9) K. Matsunaga, Y. Shiraki, and Y. Kobayashi, paper presented at the Annual Meeting of the Oceanographical Society of Japan, Tokyo, April 1975.

Nickel(II) Complexes of Schiff Bases Derived from Salicylaldehyde and Glycyl-aspartate or -glutamate. Application to a Selective Hydrolysis Reaction of Dimethyl Glycylaspartate and Glycylglutamate

Yasuo NAKAO*,† and Akitsugu NAKAHARA

Institute of Chemistry, College of General Education, Osaka University, Toyonaka, Osaka 560

(Received May 6, 1978)

Nickel(II) complexes of Schiff bases derived from salicylaldehyde and glycylaspartate or glycylglutamate were prepared and their structures were determined on the basis of electronic absorption and ^{1}H NMR spectra. The relationship between structure of the chelates and stability of fused-ring systems was discussed in some detail, and was applied to a selective hydrolysis reaction of dimethyl glycylaspartate and glycylglutamate. Nickel(II) complexes of Schiff bases derived from salicylaldehyde and β-methyl glycylaspartate or γ-methyl glycylglutamate were obtained by a reaction between dimethyl glycylaspartate or glycylglutamate and bis(salicylaldehydato)-nickel(II) in methanol containing sodium or potassium hydroxide.

In a previous paper,[1] we reported as the result of a comparative study on copper(II) and nickel(II) complexes (**1**, **2**) of Schiff bases derived from salicylaldehyde and glycylglycine or glycyl-β-alanine that the fused-ring system of **1** (6-5-5) is more stable than that of **2** (6-5-6).[2] In connection with such delicate difference in the stability of fused-ring systems, we have extended the study to the preparation and structural determination of nickel(II) complexes of Schiff bases composed of salicylaldehyde and glycyl-aspartate and -glutamate. As an application of the result concerning the structure-stability relationship, we have also attempted selective hydrolysis reactions of dimethyl glycylaspartate and glycylglutamate.

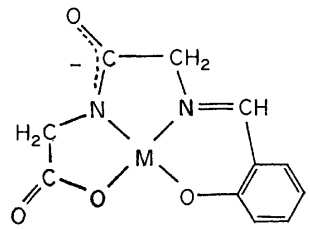

M = Cu(II), Ni(II)

1

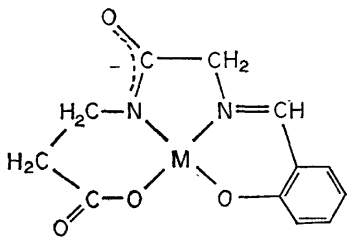

M = Cu(II), Ni(II)

2

† Present address: Chemical Laboratory, Faculty of Education, Okayama University, Okayama 700.

Experimental

Dibenzyl L-*Aspartate Hydrochloride* was prepared by the method of Miller *et al.*[3]

Glycyl-L-*aspartic Acid* was obtained by catalytic reduction of dibenzyl *N*-benzyloxycarbonylglycyl-L-aspartate, which had been prepared from *N*-benzyloxycarbonylglycine and dibenzyl L-aspartate hydrochloride according to the direction of Miller *et al.*[3]

Dibenzyl L- *and* DL-*Glutamate Benzenesulfonates* were prepared by a similar procedure to that for benzyl glycinate benzenesulfonate.[4] The L-compound was identified by comparing the melting point with that in literature.[5] Melting point and analytical data of dibenzyl DL-glutamate benzenesulfonate, which was recrystallized from ethanol are as follows: mp 118—119 °C. Found: C, 61.40; H, 5.63; N, 3.07%. Calcd for $C_{25}H_{27}O_7NS$: C, 61.83; H, 5.62; N, 2.89%.

Dibenzyl L- *and* DL-*Glutamate Hydrochlorides* were obtained from the corresponding benzenesulfonate described above.[6]

Dibenzyl N-*Benzyloxycarbonylglycyl*-L- *and* -DL-*glutamates* were prepared by the same method as that for the corresponding dibenzyl *N*-benzyloxycarbonylglycyl-L-aspartate, using dibenzyl L- and DL-glutamate hydrochlorides instead of dibenzyl L-aspartate hydrochloride.[3] These compounds were obtained as oily products, which were used for the subsequent reaction without further purification.

Glycyl-L- *and* -DL-*glutamic Acids.* These were obtained by the catalytic reduction of the corresponding dibenzyl *N*-benzyloxycarbonylglycyl-L- and -DL-glutamates by using palladium black as a catalyst. In all cases, methanol was used as solvent with a small amount of acetic acid. These peptides were recrystallized from water-ethanol. H·Gly·DL-Glu·OH: mp 184—187 °C (dec). Found: C, 40.78; H, 5.81; N, 13.71%. Calcd for $C_7H_{12}O_5N_2$: C, 41.17; H, 5.94; N, 13.72%.

Glycyl-L-glutamic Acid was identified from the melting point.[5]

Dimethyl DL-*Aspartate and* DL-*Glutamate Hydrochlorides* were prepared according to the ordinary method.[7]

Dimethyl N-*Benzyloxycarbonylglycyl*-DL-*aspartate.* This was prepared in a similar procedure as that reported by Winitz *et al.*[8] To a solution of 13.7 g of *N*-benzyloxycarbonylglycine, 13.0 g of dimethyl DL-aspartate hydrochloride and 9.2 cm^3 of triethylamine in 135 cm^3 of chloroform was added 14.1 g of dicyclohexylcarbodiimide. The reaction mixture was stirred at room temperature overnight. After removal of precipitated

N,N'-dicyclohexylurea, the filtrate was washed with water, 1 mol/dm³ HCl, saturated aqueous solution of $NaHCO_3$, and water. After the chloroform fraction had been dried over anhydrous magnesium sulfate, the filtrate was evaporated to dryness. The oily products obtained were recrystallized from ethyl acetate and petroleum benzine. Mp 93—95 °C. Found: C, 54.53; H, 5.75; N, 7.97%. Calcd for $C_{16}H_{20}O_7N_2$: C, 54.53; H, 5.75; N, 7.95%.

Dimethyl N-*Benzyloxycarbonylglycyl*-DL-*glutamate.* This was prepared from *N*-benzyloxycarbonylglycine and dimethyl DL-glutamate hydrochloride in the same way as described for dimethyl *N*-benzyloxycarbonylglycyl-DL-aspartate. Mp 64—65 °C. Found: C, 56.01; H, 6.18; N, 7.59%. Calcd for $C_{17}H_{22}O_7N_2$: C, 55.72; H, 6.06; N, 7.65%.

Hydrochlorides of Dimethyl Glycyl-DL-*aspartate and Glycyl*-DL-*glutamate.* These were obtained by catalytic reduction of dimethyl *N*-benzyloxycarbonylglycyl-DL-aspartate and -DL-*glu*tamate using palladium black catalyst. Methanol containing a small volume of concentrated hydrochloric acid was used as solvent. These compounds were obtained as oily products, which were recrystallized from methanol-ether. Gly·DL-Asp(OMe)$_2$·HCl: mp 146—148 °C. Found: C, 37.35; H, 5.88; N, 10.83%. Calcd for $C_8H_{15}O_5N_2Cl$: C, 37.72; H, 5.95; N, 11.00%. Gly·DL-Glu(OMe)$_2$·HCl: mp 139—141 °C. Found: C, 40.00; H, 6.38; N, 10.43%. Calcd for $C_9H_{17}O_5N_2Cl$: C, 40.22; H, 6.39; N, 10.43%.

Benzyl γ-Aminobutyrate p-*Toluenesulfonate* was prepared by the same method as that for the corresponding benzyl β-alaninate *p*-toluenesulfonate.[9] Recrystallization was carried out by using ethanol–ether. Mp 107—107.5 °C. Found: C, 59.29; H, 6.39; N, 3.91%. Calcd for $C_{18}H_{23}O_5NS$: C, 59.15; H, 6.36; N, 3.83%.

Benzyl N-*Benzyloxycarbonylglycyl-γ-aminobutyrate.* This was prepared in a similar method as that reported by Winitz *et al.*[8] To a solution of 14.6 g of *N*-benzyloxycarbonylglycine, 24.6 g of benzyl γ-aminobutyrate *p*-toluenesulfonate and 9.8 cm³ of triethylamine in 160 cm³ of chloroform was added 14.5 g of dicyclohexylcarbodiimide. The reaction mixture was stirred at 25 °C overnight. After removal of precipitated *N,N'*-dicyclohexylurea, the filtrate was washed with water, 1 mol/dm³ HCl, saturated aqueous solution of $NaHCO_3$, and water. After the chloroform fraction had been dried over anhydrous magnesium sulfate, the filtrate was evaporated to dryness. The crystalline materials obtained were recrystallized from ethyl acetate and petroleum benzine. Mp 83—84 °C. Found: C, 65.49; H, 6.39; N, 7.24%. Calcd for $C_{21}H_{24}O_5N_2$: C, 65.60; H, 6.30; N, 7.29%.

Glycyl-γ-aminobutyric Acid. This was obtained by catalytic reduction of benzyl *N*-benzyloxycarbonylglycyl-γ-aminobutyrate using palladium black catalyst. Methanol containing a small volume of glacial acetic acid was used as solvent. Recrystallization was carried out by using water and ethanol. Mp 198—202 °C (dec). Found: C, 44.50; H, 7.48; N, 17.09%. Calcd for $C_{13}H_{18}O_3N$: C, 44.98; H, 7.57; N, 17.49%.

Bis(salicylaldehydato)nickel(II) and Barium N-*Salicylideneglycyl-β-alaninatonickelate(II)*, **2** were prepared according to the direction described previously.[1]

Potassium N-*Salicylideneglycyl-γ-aminobutyratonickelate(II)*, **6**. Into 30 cm³ of a water: ethanol mixture (2: 1 by volume) were dissolved 0.8 g of glycyl-γ-aminobutyric acid and 1.5 g of bis(salicylaldehydato)nickel(II). The resulting mixture was adjusted to pH 9—10 with concentrated KOH solution and stirred at 40 °C for 3 h. After it had been filtered, the solution was evaporated to dryness *in vacuo* to give a yellowish green powder. The powder was recrystallized from hot ethanol. Found: C, 41.21; H, 4.59; N, 7.03%. Calcd for K[Ni($C_{13}H_{13}O_4N_2$)]·H_2O: C, 41.40; H, 4.02; N, 7.43%.

Dipotassium N-*Salicylideneglycyl*-L-*aspartatonickelate(II)*, **3a**. A mixture of 0.50 g of glycyl-L-aspartic acid and 0.79 g of bis(salicylaldehydato)nickel(II) was dissolved in 15 cm³ of water–ethanol (2: 1 by volume). The reaction mixture was adjusted to pH 9—10 by concentrated KOH solution and stirred at room temperature for 1 h. After it had been filtered, ethanol was added to the filtrate to give orange crystals, which were recrystallized from water–ethanol. Found: C, 35.36; H, 2.48; N, 6.33%. Calcd for K_2[Ni($C_{13}H_{10}O_6N_2$)]·H_2O: C, 35.07; H, 2.72; N, 6.29%.

Dipotassium N-*Salicylideneglycyl*-L- *and* -DL-*glutamatonickelates-(II)*, **4a** were prepared in the same way as for chelate **3a**. K_2[Ni(Sal=Gly·L-Glu)]·2.5H_2O: Found: C, 34.69; H, 4.04; N, 5.77%. Calcd for K_2[Ni($C_{14}H_{12}O_6N_2$)]·2.5H_2O: C, 34.58; H, 3.53; N, 5.76%. K_2[Ni(Sal=Gly·DL-Glu)]·3.5H_2O: Found: C, 33.33; H, 3.64; N, 5.67%. Calcd for K_2[Ni($C_{14}H_{12}O_6N_2$)]·3.5H_2O: C, 33.34; H, 3.81; N, 5.56%.

The Reaction between Dimethyl Glycyl-DL-*aspartate and Bis(salicylaldehydato)nickel(II) in Methanol.* To a mixture of 0.75 g (0.0025 mol) of bis(salicylaldehydato)nickel(II) and 0.64 g (0.0025 mol) of dimethyl glycyl-DL-aspartate hydrochloride in 10 cm³ of methanol was added a concentrated KOH methanol solution, until the color of the solution became completely orange. The reaction mixture was then stirred at room temperature for 2 h, being allowed to stand for a few more hours in a refrigerator; hereupon orange crystals were obtained in 70% yield. The products were filtered and recrystallized from methanol. Found: C, 41.35; H, 3.39; N, 6.88%. Calcd for K[Ni($C_{14}H_{13}O_6N_2$)], **7**: C, 41.71; H, 3.26; N, 6.95%.

The Reaction between Dimethyl Glycyl-DL-*glutamate and Bis(salicylaldehydato)nickel(II) in Methanol.* A mixture of 0.67 g (0.0025 mol) of dimethyl glycyl-DL-glutamate hydrochloride and 0.75 g (0.0025 mol) of bis(salicylaldehydato)nickel(II) was dissolved in 15 cm³ of methanol. To the solution was added 0.27 g of sodium hydroxide and 0.42 g of barium perchlorate. The mixture was stirred at room temperature for 2 h to give an orange crystalline material, yield 75%. This was filtered and washed several times by methanol. Found: C, 40.18; H, 3.79; N, 6.07%. Calcd for Ba/2[Ni($C_{15}H_{15}O_6N_2$)], **9**: C, 40.33; H, 3.39; N, 6.27%.

Measurements. Melting points were determined on a micro melting point apparatus and uncorrected. The PMR spectra were recorded by using a JEOL MH-100 spectrometer with sodium 2,2-dimethyl-2-silapentane-5-sulfonate as an internal standard and deuterium oxide was used as a solvent. The pD-adjustment was carried out by the addition of concentrated NaOD-heavy water solution. A Yanagimoto pH-66A pH meter equipped with a MGR-11A combined electrode was used after standardization with a Wako standard buffer solution (pH 6.86 and 9.18 at 25 °C). The visible and ultaviolet absorption spectra were obtained with a 323 Hitachi Recording Spectrophotometer. The IR spectra were recorded with a Hitachi EPI-2 Infrared Spectrophotometer. The measurements were carried out at room temperature using the pressed KBr disk technique in the wave number range 700—4000 cm^{-1} with a rock-salt prism.

Results and Discussion

Nickel(II) Complexes of Schiff Bases Derived from Salicylaldehyde and Glycylaspartate or Glycylglutamate. These nickel(II) complexes were prepared by reactions of each dipeptide with bis(salicylaldehydato)nickel(II) in the pH range 9—10. Since the complexes do not exhibit any absorption peak in the visible and near infrared region, they are expected to have such square-planar

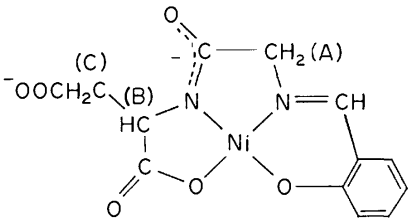

3a

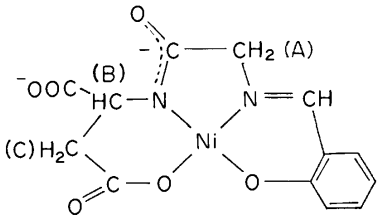

3b

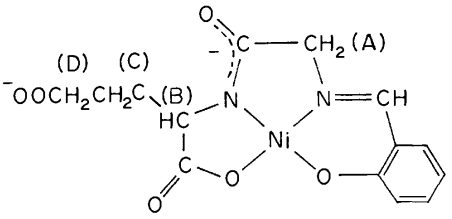

4a

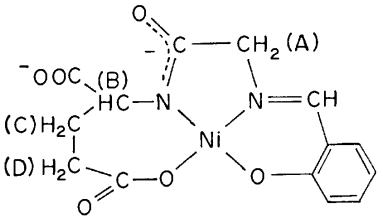

4b

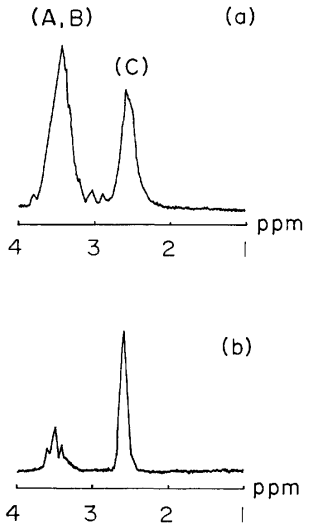

Fig. 1. PMR spectra of $[Ni(Sal{=}Gly\cdot L\text{-}Asp)]^{2-}$: (a) pD 7.8, room temp, after 2 h; (b) pD 13.1, 40 °C, after 8 days.

structures as **3**- and **4**-**a** or -**b**. In the structural formulas, the symbol (A) indicates the methylene group of glycinate residue, while (B), (C), and (D) indicate the methylene or methine groups of α-, β- and γ-position in the C-terminal amino acid residues. In order to confirm the structure of glycyl-L-aspartate-Schiff base complex, the PMR spectra were measured in D_2O under various conditions (Fig. 1). Inspection of the PMR spectrum represented in Fig. 1(a) reveals that signals for the methylene or methine protons of (A), (B), and (C) are not separated in three but two peaks, of which the ratio of absorption intensity at 3.56 and 2.60 ppm is 3:2. It was clealy observed that the peak at 3.56 ppm turned out triplet together with decrease in intensity after 8 days at pD 13.1, 40 °C, while the peak at 2.60 ppm remained unchanged (Fig. 1(b)). From the fact, the nickel(II) complex of Schiff base composed of salicylaldehyde and glycyl-L-aspartate may be reasonably accepted as the structure **3a** rather than as **3b**, since the deuteration of (A) methylene and (B) methine groups in **3a**, can be understood by taking into account the results obtained through the deuteration in *N*-salicylideneglycylglycinato- and -glycyl-L-α-alaninatonickelates(II).[10] In other words, (A) methylene protons of glycyl-L-aspartate residue in **3a** are entirely replaced by deuterons, whereas the (B) methine proton is not so entirely replaced as (A) under the same conditions. On the other hand, if *N*-salicylideneglycyl-L-aspartatonickelate(II) had the structural formula **3b**, only the

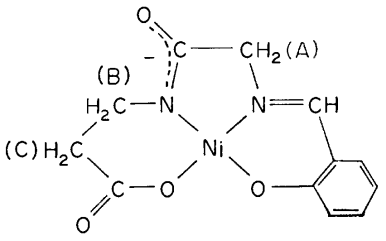

5

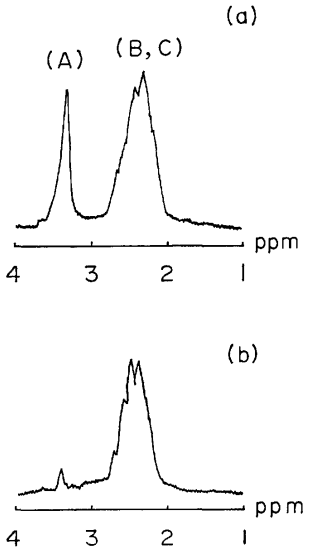

Fig. 2. PMR spectra of $[Ni(Sal{=}Gly\cdot\beta\text{-}Ala)]^{-}$: (a) pD 9.3, room temp, after 1 h; (b) pD 13.2, 40 °C, after 8 days.

deuteration of (A) methylene protons would take place. This is because of the fact that the deuteration of (A) methylene protons in *N*-salicylideneglycyl-β-alaninatonickelate(II), **5** occurs easily, whereas that of (B) and (C) methylene protons does not at all (Figs. 2(a) and (b)). Preferential formation of **3a** instead of **3b** suggests that the stability of fused-ring system decreases in the order 6-5-5>6-5-6, showing good agreement with the previous conclusion established for copper(II) and nickel(II) complexes, **1** and **2**.[1)]

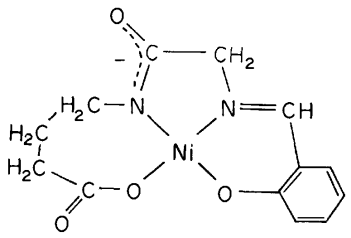

6

The *N*-salicylideneglycyl-L- or -DL-glutamatonickelate(II) is orange, while *N*-salicylideneglycylglycinato- and *N*-salicylideneglycyl-γ-aminobutyratonickelates(II) (**1** and **6**), are orange and brownish green, respectively. The d-d transition band of the complex, **6** was observed at 950 nm. On the basis of these facts, potassium *N*-salicylideneglycyl-γ-aminobutyratonickelate(II) is not supposed to be the square-planar type. This may be attributed to a rather weak ligand field of the *N*-salicylideneglycyl-γ-aminobutyrate, whose fused-ring structure involves a 7-membered ring. On the other hand, the square-planar structure of *N*-salicylideneglycylglycinato- and -glycylglutamato-nickelates(II) have been inferred from the absence of absorption peak in the visible and near infrared region. Thus, the nickel(II) complex of Schiff base

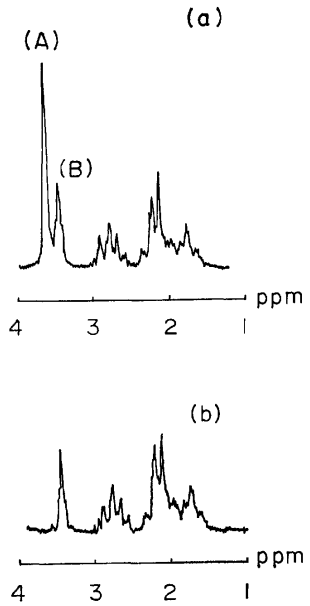

Fig. 3. PMR spectra of $[Ni(Sal{=}Gly\cdot L\text{-}Glu)]^{2-}$: (a) pD 9.6, room temp, after 1 h; (b) pD 13.8, 40 °C, after 9 days.

derived from salicylaldehyde and glycyl-L- or -DL-glutamate can be represented as the structure **4a**. The PMR spectrum shown in Fig. 3(a) also indicates that *N*-salicylideneglycyl-L-glutamatonickelate(II) is diamagnetic, and probably is planar. On the basis of the result of deuteration in *N*-salicylideneglycyl-L-aspartatonickelate(II), **3a**, it is expected that (A) methylene and (B) methine protons in **4a** are deuterated in D_2O solution. In fact, the peak at 3.64 ppm arising from the (A) methylene protons disappears on allowing the solution to stand at 40 °C, pD 13.8 for 9 days, as is clear from Figs. 3(a) and (b). On the other hand, the peak due to the (B) methine proton remains unchanged under the same conditions; the corresponding (B) methine proton of *N*-salicylideneglycyl-L-aspartatonickelate(II), **3a** was fairly deuterated under similar conditions. This may be correlated to the extent of the upfield shift of (B) methine peak in **3a** and **4a**. The (B) methine peak in **3a** and **4a** appeared at 3.58 and 3.47 ppm, respectively. We described previously that the methylene protons, of which the signal is observed at the lowest field in PMR spectra of a series of tripeptide-nickel(II) chelates, were most easily deuterated in D_2O solution.[11)] Therefore, the difficulty of deuteration of (B) methine in **4a** is thus understandable.

Selective Hydrolysis of Dimethyl Glycyl-DL-aspartate or Glycyl-DL-glutamate by Bis(salicylaldehydato)nickel(II) in Methanol. The reaction between dimethyl glycyl-DL-aspartate hydrochloride and bis(salicylaldehydato)-nickel(II) in methanol containing potassium hydroxide gave an orange nickel(II) complex. Inspection of the IR spectrum of the complex reveals the band characteristic of ester group at around 1720 cm^{-1}. The electronic spectrum in methanol-dimethyl sulfoxide solution resembles those observed for *N*-salicylideneglycyl-L-aspartato- and -glycyl-L-glutamato-nickelats(II) which are estimated to have the square planar structure. Thus, the structure of the nickel(II) complex obtained is considered as shown in formula **7** or **8**. The result of elemental analysis also supports the above presumption. Further, we are more in line with the structure **7**, since the 6-5-5-fused ring structure is supposed to be more

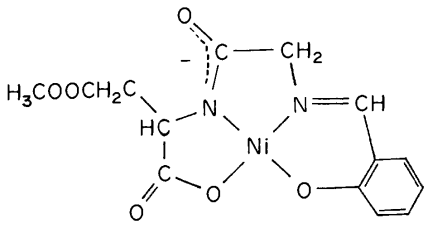

7

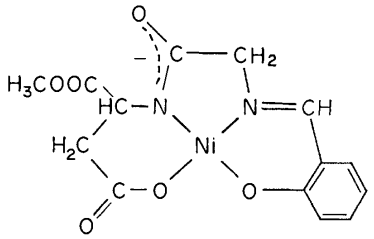

8

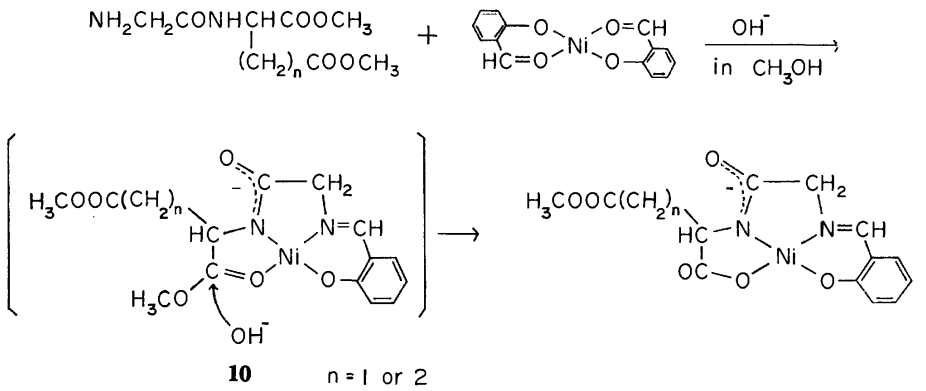

10 n = 1 or 2

Scheme 1.

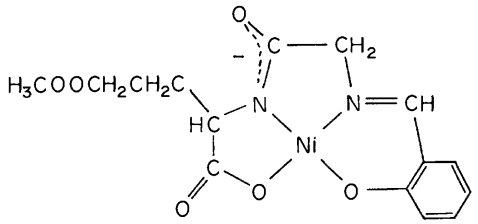

9

stable than the 6-5-6-fused ring structure. Accordingly, it can be concluded that the hydrolysis of ester groups occurred preferably at the α-position in the dimethyl glycyl-DL-aspartate. Likewise, the α-ester group in dimethyl glycyl-DL-glutamate is also selectively hydrolyzed under similar conditions. Since the isolation of potassium salt of γ-methyl *N*-salicylideneglycyl-DL-glutamatonickelate(II), **9** was a little more difficult, we obtained the same chelate as the barium salt. The selective hydrolysis of peptide ester of this kind can well be explained by a mechanism involving the intermediate **10** as illustrated in Scheme 1. In **10**, the carbon atom of the α-ester group would be readily attacked by hydroxide ion. Of course, there is a possibility for the ester group coming into coordination at the β- or γ-position as indicated in **11** or **12**. However, the coordination of the β- or γ-ester group is supposed to be much more difficult than that of the α-ester group. This is because of the foregoing argument that the 6-5-5-fused chelate ring is more stable than the 6-5-6 or 6-5-7 ring in the nickel(II) chelates of Schiff bases derived from salicylaldehyde and glycyl-aspartate or -glutamate.

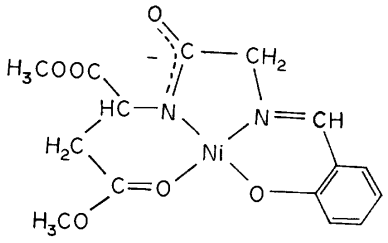

11

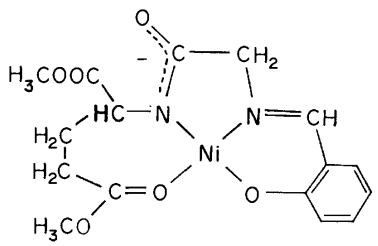

12

We thank Mr. Teruhisa Morishita for technical assistance. We are also indebted to Mr. Yoshio Terawaki of the Faculty of Engineering Science for PMR measurements and to Miss Teruko Kuroe for the elemental analyses. Expenses for this work were defrayed in part by a grant from the Ministry of Education.

References

1) Y. Nakao and A. Nakahara, *Bull. Chem. Soc. Jpn.*, **46**, 187 (1973).

2) The notations "6-5-5" *etc.* represent the skeletal structure of fused-chelate-rings in metal-multidentate chelates in view of the numbers of ring members, starting from the metal chelate ring containing the carbonyl compound moiety.

3) A. Miller, A. Neidle, and H. Waelsch, *Arch. Biochem. Biophys.*, **56**, 11 (1955).

4) J. D. Cipera and R. V. V. Nicholls, *Chem. Ind.*, **1955**, 16.

5) B. Helferich, P. Schellenberg, and J. Ulbrich, *Chem. Ber.*, **90**, 700 (1957).

6) H. K. Miller and H. Waelsch, *J. Am. Chem. Soc.*, **74**, 1092 (1952).

7) J. P. Greenstein and M. Winitz, Chemistry of the Amino Acid, Wiley, New York (1961), Vol. 2, p. 926.

8) M. Winitz, L. B. Frankenthal, N. Izumiya, S. M. Birnbaum, C. G. Baker, and J. P. Greenstein, *J. Am. Chem. Soc.*, **78**, 2423 (1956).

9) N. Izumiya and S. Makishima, *Nippon Kagaku Zasshi*, **78**, 1768 (1957).

10) O. Uyama, Y. Nakao, and A. Nakahara, *Bull. Chem. Soc. Jpn.*, **46**, 496 (1973).

11) Y. Nakao, O. Uyama, and A. Nakahara, *J. Inorg. Nucl. Chem.*, **36**, 685 (1974).

Reaction Process between Iron(II) Chloride and Oxygen

Yuzo Saeki,* Ryoko Matsuzaki, and Seiki Fujiwara

Research Laboratory of Resources Utilization, Tokyo Institute of Technology, 4259, Nagatsuta-cho, Midori-ku, Yokohama 227

(Received May 11, 1978)

The product formed by heating $FeCl_2$ in an oxygen stream has been examined in detail. The reaction processes of gaseous $FeCl_3$ and FeOCl, formed during the reaction between $FeCl_2$ and oxygen, with oxygen were also examined. The reaction process between $FeCl_2$ and oxygen can be represented as follows: $FeCl_2$ reacts with oxygen above about 250 °C to form FeOCl and gaseous $FeCl_3$, $2FeCl_2(s)+1/2O_2(g)\rightarrow FeOCl(s)+1/2Fe_2Cl_6(g)$. Subsequently, the resulting FeOCl reacts with oxygen to form α-Fe_2O_3 and chlorine, $2FeOCl(s)+1/2O_2(g)\rightarrow Fe_2O_3(s)+Cl_2(g)$. Above about 320 °C, the decomposition of the FeOCl to α-Fe_2O_3 and gaseous $FeCl_3$, $3FeOCl(s)\rightarrow Fe_2O_3(s)+1/2Fe_2Cl_6(g)$, also occurs. Above about 370 °C, the reaction between gaseous $FeCl_3$ formed and oxygen to form η-Fe_2O_3 and chlorine, $Fe_2Cl_6(g)+3/2O_2(g)\rightarrow Fe_2O_3(s)+3Cl_2(g)$, occurs in addition to the above reactions.

During the chlorination of ilmenite and many ores, iron(II) chloride($FeCl_2$) is usually formed in addition to the main products. This work was undertaken to obtain fundamental information on the chemical process for dechlorinating the $FeCl_2$ with oxygen(air) to produce a non-polluting iron oxide product and chlorine for recycle.

It has been reported in the early literature[1] that on heating $FeCl_2$ in a stream of air or oxygen, the reaction, $6FeCl_2+3/2O_2\rightarrow 2Fe_2Cl_6+Fe_2O_3$, occurs. Teterevkov *et al.*[2] have examined the relationship between the amount of chlorine evolved upon heating $FeCl_2$ in an oxygen stream and the heating time in the temperature range of 300—500 °C, and have conducted the experiment on the recovery of chlorine from $FeCl_2$. However, the reaction process between $FeCl_2$ and oxygen was not clarified.

In this paper, the product formed by heating $FeCl_2$ in an oxygen stream has been examined in detail. The reaction processes of gaseous iron(III) chloride($FeCl_3$) and iron chloride oxide(FeOCl), which were formed during the reaction between $FeCl_2$ and oxygen, with oxygen were also examined. From these experimental results, the reaction process between $FeCl_2$ and oxygen was revealed.

Experimental

The $FeCl_2$ used was prepared by the reaction between pure iron (Fe 99.98%) and HCl at 850 °C, and confirmed as $FeCl_2$ by X-ray analysis.[3] The chemical analysis gave Fe, 44.0; Cl, 55.9% (calcd for $FeCl_2$: Fe, 44.06; Cl, 55.94%). $FeCl_3$ was prepared by the reaction between pure iron and chlorine at 500 °C, and confirmed as $FeCl_3$ by X-ray analysis.[4] The chemical analysis gave Fe, 34.3; Cl, 65.5% (calcd for $FeCl_3$: Fe, 34.43; Cl, 65.57%). FeOCl was prepared from guaranteed reagent $FeCl_3\cdot 6H_2O$ and $FeCl_3$ by the method based on the report of Schäfer,[5] and confirmed as FeOCl by X-ray analysis.[6] The chemical analysis gave Fe, 52.0; Cl, 32.9% (calcd for FeOCl: Fe, 52.05; Cl, 33.04%). Oxygen was dried by passing it through conc. sulfuric acid and over phosphorus(V) oxide.

The Fe content of the sample was determined by chelatometric titration[7] after dissolving the sample in dilute hydrochloric acid followed by oxidation of Fe^{2+} ion to Fe^{3+} ion with aqueous H_2O_2 solution. The Cl content of the sample was gravimetrically determined as AgCl after dissolving the sample in dilute nitric acid. The chlorine evolved during the reaction was passed through KI solution and determined by iodometry.

X-ray analysis of the sample was performed with an X-ray powder diffractometer, equipped with a proportional counter, using Mn filtered Fe radiation. The sample chamber of the diffractometer was maintained under dry nitrogen atmosphere to prevent the contamination of the sample with moisture in the air during the irradiation.

Thermogravimetry (TG) was performed in an oxygen stream at 50 ml/min. The sensitivity of the quartz helix used was approximately 0.14 mg/0.01 mm. The heating rate was 2.5 °C/min.

Throughout this work, the chlorides and chloride oxide of iron were handled in an argon atmosphere to prevent any contamination with moisture in the air.

Results and Discussion

Reaction Products between $FeCl_2$ and Oxygen. The TG curves of $FeCl_2$ in an oxygen and an argon stream are shown in Fig. 1.

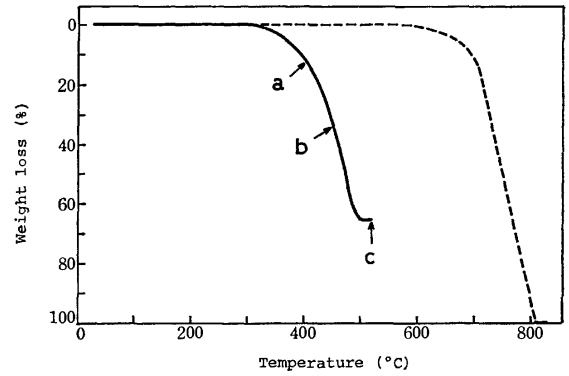

Fig. 1. TG curves of $FeCl_2$ in oxygen and argon streams. —— in O_2, ---- in Ar.

The results showed that $FeCl_2$ reacted with oxygen before vaporizing. The samples heated up to Points a(400 °C), b(450 °C), and c(520 °C) in Fig. 1 were found by X-ray analysis to be a mixture of $FeCl_2$ and FeOCl, a mixture of $FeCl_2$ and α-Fe_2O_3,[8] and α-Fe_2O_3, respectively. It was also observed that the weight loss was accompanied by the evolution of chlorine and gaseous $FeCl_3$.

To obtain more detailed information on the reaction between $FeCl_2$ and oxygen, $FeCl_2$ (4.0 g) in a quartz

Table 1. Reaction products between $FeCl_2$ and oxygen at various temperatures

Temp (°C)	Product: In the boat (%)	Product: Outside the heating zone (%)	Amount of Cl_2 formed (mg)	Unreacted $FeCl_2$ (%)
250	FeOCl (<0.1)	$FeCl_3$ (0.1)	0.1	99.8
280	FeOCl (0.8)	$FeCl_3$ (1.3)	0.9	97.8
300	FeOCl ≫ α-Fe_2O_3 (2.1)	$FeCl_3$ (3.0)	3.1	95.1
320	FeOCl ≫ α-Fe_2O_3 (4.1)	$FeCl_3$ (6.2)	6.6	90.1
350	FeOCl ≫ α-Fe_2O_3 (9.9)	$FeCl_3$ (15.8)	18	75.4
370	FeOCl > α-Fe_2O_3 (18.1)	$FeCl_3$ (30.2), η-Fe_2O_3 (<0.1)	29	53.9
400	FeOCl > α-Fe_2O_3 (27.8)	$FeCl_3$ (60.6), η-Fe_2O_3 (0.2)	80	15.5
420	α-Fe_2O_3 > FeOCl (21.5)	$FeCl_3$ (70.8), η-Fe_2O_3 ≫ FeOCl (1.0)	127	8.9
450	α-Fe_2O_3 (23.5)	$FeCl_3$ (77.6), η-Fe_2O_3 ≒ FeOCl (1.2)	190	0

boat (70 mm length, 15 mm width, 7 mm depth) was placed in a straight reaction tube (28 mm i.d., 1000 mm length). Oxygen was introduced into the reaction tube at a flow-rate of 100 ml/min. The sample part was then placed in the centre of an electric furnace (300 mm heating length) maintained at a specified temperature for 2 h. The temperature of the sample part was controlled to within ±2 °C. The temperature of the reaction tube outside the heating zone was below 50 °C.

At 230 °C, no reaction product was observed. The reaction products obtained at various temperatures above 250 °C are summarized in Table 1. The value in parentheses is the weight percentage of the product to the initial $FeCl_2$. The product obtained in the boat was identified by X-ray analysis after dissolving the unreacted $FeCl_2$ in ethyl alcohol. Small amounts of η-Fe_2O_3 and FeOCl formed outside the heating zone above 370 °C in addition to $FeCl_3$ were identified by X-ray analysis[9] after dissolving the $FeCl_3$ in ethyl alcohol.

At 250—280 °C, FeOCl, $FeCl_3$, and a small amount of chlorine were formed as shown in Table 1. Calculations showed that FeOCl and $FeCl_3$ were the main products and that the molar ratio of FeOCl: $FeCl_3$ was approximately 1 : 1. From this result, the formation of FeOCl and $FeCl_3$ was considered to be due to the reaction,

$$2FeCl_2(s) + 1/2O_2(g) \longrightarrow FeOCl(s) + 1/2Fe_2Cl_6(g). \quad (1)$$

It was assumed that the formation of chlorine was due to the reaction,

$$2FeOCl(s) + 1/2O_2(g) \longrightarrow Fe_2O_3(s) + Cl_2(g), \quad (2)$$

from the observation that the FeOCl obtained in the boat contained a small amount of insoluble product after dissolving the FeOCl in 1 M-H_2SO_4.[5,10]

The possible reactions which gave α-Fe_2O_3 in the boat were considered to be Reaction 2 and the thermal decomposition of FeOCl in oxygen,

$$3FeOCl(s) \longrightarrow Fe_2O_3(s) + 1/2Fe_2Cl_6(g).^{10} \quad (3)$$

Above 370 °C, a small amount of η-Fe_2O_3 was obtained outside the heating zone in addition to $FeCl_3$. It appeared that η-Fe_2O_3 was formed by the reaction,

$$Fe_2Cl_6(g) + 3/2O_2(g) \longrightarrow Fe_2O_3(s) + 3Cl_2(g).^{9} \quad (4)$$

Above 420 °C, a small amount of FeOCl was obtained outside the heating zone in addition to $FeCl_3$ and η-Fe_2O_3. The amount of chlorine evolved, shown in Table 1, indicated that Reaction 1 proceeded markedly above about 420 °C to form a large amount of gaseous $FeCl_3$. Consequently, the reaction between gaseous $FeCl_3$ and oxygen has been thought to proceed under a low ratio of oxygen to gaseous $FeCl_3$ to form FeOCl in addition to η-Fe_2O_3.

To clarify the possible reactions occurring between $FeCl_2$ and oxygen, experiments on the reaction processes of gaseous $FeCl_3$ and FeOCl with oxygen were carried out.

Reaction Process between Gaseous $FeCl_3$ and Oxygen. A transparent quartz reaction tube with an inner concentric tube was used. Gaseous $FeCl_3$ was formed by heating $FeCl_3$ placed in the inner tube at 250 °C and carried by a stream of argon (30 ml/min) to the reaction zone of 28 mm i.d. and 250 mm length, held at a specified temperature. The mean flow-rate of gaseous $FeCl_3$ was about 1.5 ml Fe_2Cl_6/min. Oxygen was simultaneously introduced through a separate tube into the reaction zone at a flow-rate of 100 ml/min. The reaction was allowed to proceed for 2 h.

The products were only obtained outside the heating zone and the experimental results are summarized in Table 2.

The vaporization of $FeCl_3$ is accompanied by the decomposition of $FeCl_3$ to $FeCl_2$ and chlorine.[11]

Table 2. Reaction products between gaseous $FeCl_3$ and oxygen at various temperatures

Temp (°C)	Product: Outside the heating zone (g)	Product: Amount of Cl_2 formed (mg)	Unreacted $FeCl_3$ (%)
350	Not detectable	40	100
370	η-Fe_2O_3 0.02	63	99.8
400	η-Fe_2O_3 0.04	99	96.5
450	η-Fe_2O_3 0.12	213	89.7
500	η-Fe_2O_3 0.21	330	82.8
550	η-Fe_2O_3 0.43	621	65.7
600	η-Fe_2O_3 0.83	1156	34.3
650	η-Fe_2O_3 1.11	1521	11.0
700	η-Fe_2O_3 > α-Fe_2O_3 1.25	1710	0

Consequently, the amount of chlorine evolved by heating $FeCl_3$ in the inner tube at 250 °C was examined in the same manner as described above, except that argon was introduced into the reaction zone instead of oxygen at the same flow-rate as that of oxygen. The amount of chlorine evolved was always approximately 40 mg.

The molar ratio of the amount of Fe_2O_3 to the amount of chlorine obtained by subtracting the amount of chlorine evolved by heating $FeCl_3$ in the inner tube from the total amount of chlorine was calculated to be approximately 1 : 3 above 370 °C.

From these results, the reaction between gaseous $FeCl_3$ and oxygen proceeds above about 370 °C according to Reaction 4. The Fe_2O_3 formed was η-Fe_2O_3 at 370—650 °C, and a mixture of η-Fe_2O_3 and α-Fe_2O_3 at 700 °C.

The effect of the molar ratio of $FeCl_3$: O_2 on the reaction product between gaseous $FeCl_3$ and oxygen was examined at 450 °C. The molar ratio was changed by raising the heating temperature of $FeCl_3$. The results are shown in Table 3.

Table 3. Effect of $FeCl_3$: O_2 molar ratio on reaction product between gaseous $FeCl_3$ and oxygen

$FeCl_3$: O_2 (molar ratio)	Product
1 : 33	η-Fe_2O_3
1 : 19	η-$Fe_2O_3 \gg$ FeOCl
1 : 11	η-$Fe_2O_3 >$ FeOCl
1 : 7	FeOCl $> \eta$-Fe_2O_3

This confirms the estimation on the formation of FeOCl obtained outside the heating zone by heating $FeCl_2$ in an oxygen stream above 420 °C, described in the preceding paragraph.

Reaction Process between FeOCl and Oxygen. The products obtained by heating FeOCl (2.0 g) at various temperatures in an oxygen stream were examined in the same manner as described in the previous paragraph.

At 230 °C, no reaction product was observed. The products obtained at various temperatures above 250 °C are shown in Table 4. The product in the boat was identified by X-ray analysis after dissolving the unreacted FeOCl in 1 M-H_2SO_4. Identification of the product in the boat below 300 °C was carried out using 20 g of FeOCl, because of the small amount of the product formed.

The results indicated that the reaction between FeOCl and oxygen proceeded according to Reaction 2 at 250—300 °C. Above 320 °C, $FeCl_3$ was obtained in addition to α-Fe_2O_3 and chlorine. The molar ratio of the amount of $FeCl_3$ to the amount of α-Fe_2O_3 obtained by subtracting the amount of α-Fe_2O_3 formed by Reaction 2 from the total amount of α-Fe_2O_3 was calculated to be approximately 1 : 1. This result indicated that Reaction 3 also occurred besides Reaction 2. It may be considered that the formation of a small amount of η-Fe_2O_3 obtained outside the heating zone in addition to $FeCl_3$ at 400 °C was due to the reaction between gaseous $FeCl_3$ formed by Reaction 3 and oxygen, Reaction 4, from the result described in the preceding paragraph.

From these results, FeOCl reacts with oxygen above about 250 °C according to Reaction 2. Above about 320 °C, Reaction 3 also occurs besides Reaction 2.

Reaction Process between $FeCl_2$ and Oxygen. From the experimental results, the reaction process between $FeCl_2$ and oxygen may be represented as follows: $FeCl_2$ reacts with oxygen above about 250 °C according to Reaction 1. Subsequently, the resulting FeOCl reacts with oxygen according to Reaction 2. Above about 320 °C, the decomposition of the FeOCl also occurs according to Reaction 3. Above about 370 °C, the reaction between gaseous $FeCl_3$, formed by Reactions 1 and 3, and oxygen occurs according to Reaction 4 (under a low ratio of O_2: $FeCl_3$, FeOCl is formed in addition to Fe_2O_3) in addition to the above reactions.

References

1) H. Schulze, *J. Prakt. Chem.*, **21**, 411 (1880).
2) A. I. Teterevkov, Ya. E. Vil'nyanskii, and M. V. Lapshina, *J. Appl. Chem. USSR*, **43**, 498 (1970).
3) ASTM X-Ray Powder Data File, 1-1106.
4) ASTM X-Ray Powder Data File, 1-1059.
5) H. Schäfer, *Z. Anorg. Allg. Chem.*, **260**, 286 (1949).
6) Joint Committee on Powder Diffraction Standards, Powder Diffraction File, 24-1005.
7) L. Erdey and G. Rady, *Z. Anal. Chem.*, **149**, 250 (1956).
8) Joint Committee on Powder Diffraction Standards, Powder Diffraction File, 24-72.
9) K. Funaki, Y. Saeki, and T. Nakai, *Denki Kagaku*, **40**, 72 (1972).
10) V. V. Pechkovskii and N. I. Vorob'ev, *Russian J. Inorg. Chem.*, **9**, 6 (1964).
11) L. E. Wilson and N. W. Gregory, *J. Phys. Chem.*, **62**, 433 (1958).

Table 4. Reaction products between FeOCl and oxygen at various temperatures

Temp (°C)	Product: In the boat (%)	Product: Outside the heating zone (%)	Amount of Cl_2 formed (mg)	Unreacted FeOCl(%)
250	α-Fe_2O_3 ($<$0.1)	Not detectable	0.2	99.9
280	α-Fe_2O_3 (0.1)	Not detectable	0.6	99.8
300	α-Fe_2O_3 (0.2)	Not detectable	2.1	99.7
320	α-Fe_2O_3 (1.0)	$FeCl_3$ (0.3)	6.5	98.5
350	α-Fe_2O_3 (12.4)	$FeCl_3$ (7.6)	47	78.1
400	α-Fe_2O_3 (53.8)	$FeCl_3$ (41.7), η-Fe_2O_3 (0.1)	112	0

Kinetics and Mechanism of the Oxidation Reaction of Bis(μ-dibutyldithiocarbamato-*S*,*S*′)-digold(I) by Halogens

Hidetoshi KITA, Kazuyuki ITOH, Koji TANAKA, and Toshio TANAKA*

Department of Applied Chemistry, Faculty of Engineering, Osaka University, Suita, Osaka 565

(Received June 2, 1978)

Kinetics of the reaction of bis(μ-dibutyldithiocarbamato-*S*,*S*′)-digold(I), [Au(*n*-Bu_2dtc)]$_2$, with I_2, IBr, and Br_2 in dichloromethane was studied by the stopped-flow technique. A 1 : 1 charge-transfer (CT) complex, [Au(*n*-Bu_2dtc)]$_2$·X_2 (X_2=I_2, IBr, and Br_2), formed in the initial process of reaction was identified spectrophotometrically at −50 °C. The rates of reaction were almost the same for I_2, IBr, and Br_2, and independent of the both [Au(*n*-Bu_2dtc)]$_2$ and halogen concentrations. The reaction has been interpreted to proceed *via* the charge-transfer complex, [Au(*n*-Bu_2dtc)]$_2$·X_2, which decomposes in a rate-determining step to give the final product, [Au^{III}(*n*-Bu_2dtc)$_2$][$Au^{I}X_2$]. The activation parameters for the reactions were determined: ΔH^*(kJ/mol)=43.7 (I_2), 26.0 (IBr), and 12.3 (Br_2); ΔS^*(J/(mol K))=−91.5 (I_2), −156 (IBr), and −201 (Br_2).

Reactions of dithiocarbamato metal complexes with halogens[1-4] are classified into two types; one of them is that the dithiocarbamato ligand is oxidized by halogen to give thiuram disulfide, and the other is the oxidation of the central metal by halogen. The authors previously reported the kinetic studies on the reactions of bis(diethyldithiocarbamato)dimethyltin(IV)[5] and bis(dibutyldithiocarbamato)zinc(II)[6] with iodine in cyclohexane, which belong to the former type of reaction. No kinetic study for the latter type of reaction, however, has been reported so far.

This paper describes a kinetic study on the oxidation reaction of bis(μ-dibutyldithiocarbamato-*S*,*S*′)-digold(I) by iodine, iodine bromide, and bromine in dichloromethane by the stopped-flow method. This reaction is known to give bis(dibutyldithiocarbamato)gold(III) dihalogenoaurate(I).[7,8]

Experimental

Materials. Bis(μ-dibutyldithiocarbamato-*S*,*S*′)-digold(I), [Au(*n*-Bu_2dtc)]$_2$ (*n*-Bu_2dtc=S_2CN(*n*-C_4H_9)$_2$), was prepared by the literature method[9] and recrystallized twice from 1,2-dichloroethane. Found: C, 26.70; H, 4.52; N, 3.29%. Calcd for $C_{18}H_{36}N_2S_4Au_2$: C, 26.93; H, 4.52; N, 3.49%.

Iodine and iodine bromide were purified by sublimation and bromine by distillation prior to use. A dichloroethane solution of Br_2 was standardized by 0.01 N $Na_2S_2O_3$ containing 0.1 M KI using starch as an indicator before use. Dichloromethane used as a solvent was purified in the usual method.[10]

Reactions of [Au(n-Bu_2dtc)]$_2$ with Halogens. A solution of X_2 (X_2=I_2, IBr, and Br_2) (0.5 mmol) in CH_2Cl_2(15 ml) was mixed with [Au(*n*-Bu_2dtc)]$_2$ (0.5 mmol) in CH_2Cl_2(15 ml) at room temperature to give a dark green (I_2 and IBr) or a red (Br_2) solution, followed by rapid decoloration. The solution was evaporated to dryness under reduced pressure. The resulting solid was recrystallized from acetonitrile to afford yellow needles of [Au^{III}(*n*-Bu_2dtc)$_2$][$Au^{I}X_2$] (95% based on the amount of gold). X_2=I_2: mp 135 °C (lit,[8] 135 °C). Found: C, 20.45; H, 3.44; N, 2.57%. Calcd for $C_{18}H_{36}N_2S_4I_2Au_2$: C, 20.46; H, 3.44; N, 2.65%. X_2=IBr: mp 139 °C. Found: C, 21.07; H, 3.49; N, 2.88%. Calcd for $C_{18}H_{36}N_2S_4BrIAu_2$: C, 21.41; H, 3.60; N, 2.78%. X_2=Br_2: mp 143 °C (lit,[8] 143—144 °C). Found: C, 22.31; H, 3.74; N, 2.91%. Calcd for $C_{18}H_{36}N_2S_4Br_2Au_2$: C, 22.46; H, 3.78; N, 2.91%.

The stoichiometry of reaction of [Au(*n*-Bu_2dtc)]$_2$ with halogens is, therefore, expressed as follows:

$$[Au(n\text{-}Bu_2dtc)]_2 + X_2 \longrightarrow [Au(n\text{-}Bu_2dtc)_2][AuX_2].$$

Spectra. Electronic spectra were recorded on a Hitachi 124 (at 25 °C) or a Hitachi 356 (at −50 °C) spectrophotometer, the latter of which was equipped with a glass Dewar. Rapid scanning spectra were measured with a Union RA-1300 stopped-flow rapid scan analyzer.

Kinetic Measurements. Kinetic runs were carried out under the conditions where equimolar amounts of the reactants were used and either one of those was used excessively relative to the other. The rate of reaction was followed by monitoring the absorbance at a fixed wavelength in the electronic spectra of the reaction mixture, using a Union RA-413 stopped-flow spectrophotometer equipped with a 0.2 cm quartz cell in a cell holder thermostated within ±0.2 °C. Absorbance-time data were accumulated at least five times on a Union System-71 data processor and average absorbance-time curves were recorded using a National VP-6421A X-Y recorder. Plots of $\ln|A_t-A_\infty|$ *vs.* time were found to be linear to at least 70% completion, where A_t and A_∞ are absorbances at a given wavelength at a time t and the end of the reaction, respectively. Observed first-order rate constants, k_{obsd}, were obtained by performing the least-squares analysis on the linear region of $\ln|A_t-A_\infty|$ *vs.* time plots.

Results and Discussion

Rapid Scanning Spectra and a Reaction Intermediate. Figure 1 shows a typical example of rapid scanning spectra for the [Au(*n*-Bu_2dtc)]$_2$–I_2 system. Four absorp-

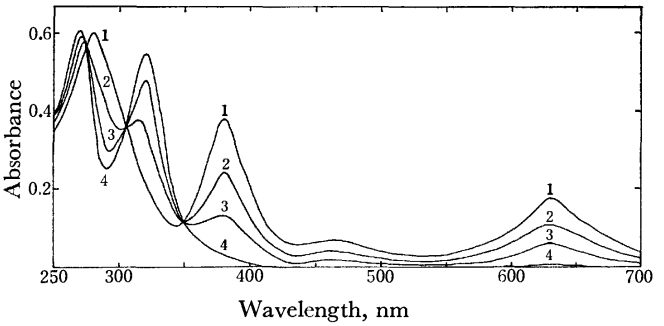

Fig. 1. Rapid scanning spectra of the reaction of [Au(*n*-Bu_2dtc)]$_2$ (2.11×10^{-4} M) with I_2 (2.08×10^{-4} M) in CH_2Cl_2 at 25 °C; scanning speed=150 nm/5 ms, cell length=0.2 cm.
1: 0.08 s, 2: 0.48 s, 3: 1.28 s, 4: the end of reaction.

tion peaks at 280, 380, 460, and 630 nm are observed immediately after mixing of the reactants. These bands are weakened with intensifying of the bands newly appeared at 270 and 320 nm, which are assigned to $[Au(n\text{-}Bu_2dtc)_2][AuI_2]$.[8] Then, isosbestic points are found at 275, 305, and 350 nm. This spectral change clearly indicates the occurrence of a transient species as a reaction intermediate. The transient species has been frozen at −50 °C; when a dichloromethane solution of $[Au(n\text{-}Bu_2dtc)]_2$ was mixed with iodine in the same solvent at −50 °C, the solution immediately displayed green color, which did not disappear over 10 h at this temperature, though a decoloration took place almost instantly above −15 °C. The absorption spectrum at −50 °C was quite similar to that immediately after mixing at 25 °C and the green color can be associated with the 630 nm band. It has been reported that $Au^{II}(Et_2dtc)_2$ exhibits an absorption near 600 nm.[11] No ESR signal has, however, been detected for the green solution obtained here, indicating that the transient species is not $Au^{II}(n\text{-}Bu_2dtc)_2$. By analogy with kinetic studies of the $Me_2Sn(Et_2dtc)_2$-I_2[5] and $Zn(n\text{-}Bu_2dtc)_2$-I_2[6] systems, the 380 nm band can be assigned to the charge-transfer (CT) transition from sulfur of the dithiocarbamato ligand to I_2 and the weak absorption at 460 nm to a blue-shifted band of the iodine moiety of the CT complex. The composition of the CT complex was determined by the mole ratio method in the visible spectrum at −50 °C. Figure 2 shows plots

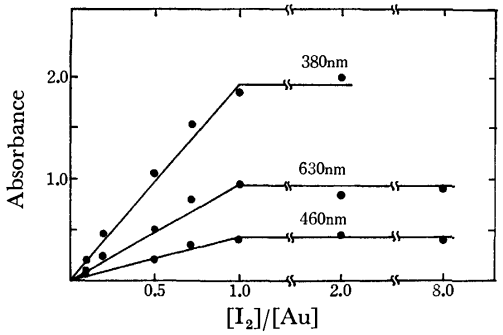

Fig. 2. Mole ratio study of $[Au(n\text{-}Bu_2dtc)]_2$-I_2 system in CH_2Cl_2 at −50 °C; $[Au(n\text{-}Bu_2dtc)]_2 = 5.0\times10^{-5}$ M.

of the absorbance at three different wavelengths against the mole ratio of I_2 to the gold(I) complex, indicating the composition of 1 : 1. It is to be noted that the band characteristic of $[Au(n\text{-}Bu_2dtc)]_2$ underwent only a little shift upon CT complexation (287→280 nm). This fact indicates that the CT complex may retain the parent dimeric structure of $[Au(n\text{-}Bu_2dtc)]_2$. The gold-gold distance in $[Au(n\text{-}Pr_2dtc)]_2$ was reported to be shorter than that in metallic gold,[12] however the valence state of Au(I), $5d^{10}$, predicts the presence of no metal-metal bondings. In spite of this, the fact that

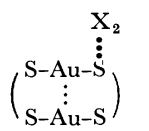

1: $\overset{\frown}{S\ \ S} = S_2CN(n\text{-}Bu)_2$.

$[Au(n\text{-}Bu_2dtc)]_2\cdot I_2$ exhibited the absorption band at 630 nm suggests the CT complex involving the skeleton with a gold-gold interaction shown in **1**. The Au(I)–Au(I) interaction would account for the absorption band at 630 nm observed in the CT complex.

The $[Au(n\text{-}Bu_2dtc)]_2$-IBr and $-Br_2$ systems also exhibited absorption maxima due to the CT transition at 380 nm. No blue-shifted band of halogens has, however, been observed in these systems (Table 1).

Table 1. Electronic spectra of $[Au(n\text{-}Bu_2dtc)]_2$, $[Au(n\text{-}Bu_2dtc)]_2\cdot X_2$, and $[Au(n\text{-}Bu_2dtc)_2]$-$[AuX_2]$ in CH_2Cl_2 at 25 °C

	λ_{max} / nm	ε[a] / $M^{-1}cm^{-1}$
$[Au(n\text{-}Bu_2dtc)]_2$	287	4.0×10^4
$[Au(n\text{-}Bu_2dtc)]_2\cdot X_2$		
$X_2=I_2$	280	b)
	380	(3.9×10^4)
	460	(8.3×10^3)[c]
	630	(1.8×10^4)
IBr	280	b)
	380	
	600	
Br_2	280	
	380	
	560	
$[Au(n\text{-}Bu_2dtc)_2][AuX_2]$		
$X_2=I_2$	270	4.0×10^4
	320	3.9×10^4
IBr	270	3.5×10^4
	320	3.0×10^4
Br_2	270	3.8×10^4
	320	3.1×10^4

a) Values in parentheses were calculated from the visible spectrum at −50 °C. b) Not measured. c) Uncorrected for the contribution from the overlap with the CT band.

This is probably due to the masking of it by the tail of the intense CT band at 380 nm, because of small molar extinction coefficients of IBr and Br_2 compared with that of I_2; $\varepsilon_{486nm}=3.7\times10^2$, $\varepsilon_{406nm}=2.6\times10^2$, and $\varepsilon_{505nm}=9.0\times10^2$ M^{-1} cm^{-1} for IBr, Br_2, and I_2 in CH_2Cl_2, respectively.

Molar extinction coefficients of the absorptions arising from the CT complex were determined from the visible spectra of dichloromethane solutions containing a fixed amount of the gold(I) complex and large excess I_2 or *vice versa* at −50 °C. The result is listed in Table 1 together with the ε values of absorptions due to $[Au(n\text{-}Bu_2dtc)]_2$ and $[Au(n\text{-}Bu_2dtc)_2][AuX_2]$. The ε value of the 380 nm band is very close to those of CT bands of the I_2 complexes with methyl dimethyldithiocarbamate ($\varepsilon_{347nm}=3.0\times10^4$ M^{-1} cm^{-1}) and tetraethylthiuram disulfide ($\varepsilon_{356nm}=3.8\times10^4$ M^{-1} cm^{-1}).[13] On the other hand, the value of the blue-shifted band of iodine (460 nm) is larger than those of other known iodine complexes ($\varepsilon_{max}=(2.7—4.2)\times10^3$ M^{-1} cm^{-1}).[13-17] This is due to an overlapping of this band with the tail of the CT band.

TABLE 2. OBSERVED RATE CONSTANTS FOR THE REACTION OF $[Au(n\text{-}Bu_2dtc)]_2$ WITH I_2 IN CH_2Cl_2 AT 25 °C

$\frac{I_2}{M}$	$\frac{[Au(n\text{-}Bu_2dtc)]_2}{M}$	$\frac{k_{obsd}}{s^{-1}}$			
		630 nm	460 nm	380 nm	320 nm
1.04×10^{-4}	1.06×10^{-4}	2.70		2.04	
1.04×10^{-3}		2.43		2.06	
2.08×10^{-3}		2.60		2.44	
2.08×10^{-4}	2.11×10^{-4}	2.51		2.23	2.90
4.93×10^{-4}	5.03×10^{-4}	2.65	2.65	2.11	2.87
3.91×10^{-3}		2.46			
9.46×10^{-5}	2.00×10^{-4}	2.50		2.68	
	2.00×10^{-5}	2.36		2.23	
1.02×10^{-4}	1.00×10^{-3}	2.35	2.00	2.05	
	2.04×10^{-3}	2.35	2.00	2.17	
	3.03×10^{-3}	2.40	2.28	2.38	
	3.96×10^{-3}	2.06	2.14	2.29	
	4.98×10^{-3}	2.39	2.25	2.10	
		Average = 2.35 ± 0.24[a]			

a) A standard deviation.

Kinetics and Mechanism. The rate of reaction was determined by following the decomposition of $[Au(n\text{-}Bu_2dtc)]_2\cdot X_2$ and the formation of $[Au(n\text{-}Bu_2dtc)_2][AuX_2]$. Observed first-order rate constants, k_{obsd}, obtained from the decay of three band maxima of the CT complex and the rise of a band maximum of the product for the reaction of $[Au(n\text{-}Bu_2dtc)]_2$ with I_2 in CH_2Cl_2 at 25 °C are listed in Table 2, which indicates that the k_{obsd} values obtained from the different wavelengths are consistent with one another within experimental error. They are also essentially the same in various concentrations and varying mole ratios of the reactants, indicating that the reaction is independent of both concentrations of $[Au(n\text{-}Bu_2dtc)]_2$ and I_2 in the measured range. Similar kinetic results were obtained in the $[Au(n\text{-}Bu_2dtc)]_2$–IBr and $-Br_2$ systems. It is therefore suggested that the reaction of $[Au(n\text{-}Bu_2dtc)]_2$ with halogens proceeds *via* a CT complex, which decomposes to give the final product as follows:

$$[Au(n\text{-}Bu_2dtc)]_2 + X_2 \xrightarrow{\text{fast}} [Au(n\text{-}Bu_2dtc)]_2\cdot X_2 \downarrow k \rightarrow [Au(n\text{-}Bu_2dtc)_2][AuX_2],$$

where k is equal to k_{obsd}. According to this scheme, the rate law can be written as

$$\frac{d[[Au(n\text{-}Bu_2dtc)_2][AuX_2]]}{dt} = -\frac{d[[Au(n\text{-}Bu_2dtc)]_2\cdot X_2]}{dt} = k[[Au(n\text{-}Bu_2dtc)]_2\cdot X_2].$$

Rate constants and activation parameters obtained from the Eyring plots of $\ln(k/T)$ against $1/T$ are summarized in Table 3.

Although there is no direct evidence for another transient species, at least two possible intermediates,

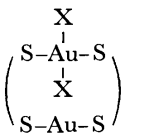

2

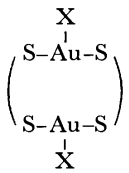

3

2 and **3**, can be envisaged in the decomposition pathway. Intermediate **2** which is a mixed valence gold(III)–gold(I) complex may be formed by the attack of iodine at a single gold atom. Alternatively, the simultaneous attack of iodine at both gold atoms will afford the gold(II) complex, **3**. The existence of both **2** and **3** may be supported from the fact that analogous gold complexes, **4** and **5**, were isolated in the oxidation

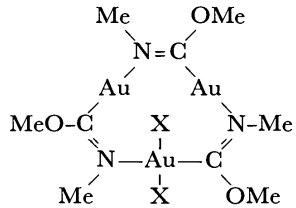

4

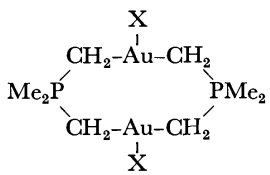

5

reactions of trimeric[18] and dimeric[19] gold(I) complexes with halogen, respectively. Of the two possible inter-

TABLE 3. RATE CONSTANTS AND ACTIVATION PARAMETERS FOR THE REACTION OF $[Au(n\text{-}Bu_2dtc)]_2$ WITH X_2 IN CH_2Cl_2[a]

X_2	$\frac{\text{Temp}}{°C}$	No. of runs	$\frac{k}{s^{-1}}$	$\frac{\Delta H^{\ddagger}_{298}}{kJ\ mol^{-1}}$	$\frac{\Delta S^{\ddagger}_{298}}{J\ mol^{-1}K^{-1}}$
I_2	10.1	15	0.89 ± 0.09	43.7 ± 8.4	-91.5 ± 28.9
	15.5	15	1.23 ± 0.10		
	20.2	34	1.75 ± 0.10		
	25.0	33	2.35 ± 0.24		
IBr	11.1	8	0.68 ± 0.13	26.0 ± 16.1	$-156\ \pm55$
	15.3	12	0.82 ± 0.21		
	20.8	5	1.08 ± 0.08		
	24.8	10	1.15 ± 0.09		
Br_2	10.5	8	0.97 ± 0.09	$12.3\pm\ 5.6$	$-201\ \pm19$
	15.4	8	1.11 ± 0.03		
	20.2	8	1.24 ± 0.07		
	25.4	9	1.31 ± 0.08		

a) Errors quoted are standard deviations.

mediates, however, **2** is more appealing since it requires a less reorganization of atoms, followed by reductive elimination at the gold(III) center to afford the final product, $[Au(n\text{-}Bu_2dtc)_2][AuX_2]$.

The authors are grateful to the Ministry of Education for support of this work through Grant-in-Aid for Scientific Research.

References

1) D. Coucouvanis, *Prog. Inorg. Chem.*, **11**, 233 (1970), and references cited therein.
2) J. Willemse, J. A. Cras, J. J. Steggerda, and C. P. Keijzers, *Structure and Bonding*, **28**, 83 (1976), and references cited therein.
3) E. A. Pasek and D. K. Straub, *Inorg. Chim. Acta*, **21**, 23 (1977).
4) B. M. Mattson and L. H. Pignolet, *Inorg. Chem.*, **16**, 488 (1977).
5) H. Kita, K. Tanaka, and T. Tanaka, *Bull. Chem. Soc. Jpn.*, **48**, 2816 (1975).
6) H. Kita, K. Tanaka, and T. Tanaka, *Inorg. Chim. Acta*, **21**, 229 (1977).
7) H. J. A. Blaauw, R. J. F. Nivard, and G. J. M. van der Kerk, *J. Organomet. Chem.*, **2**, 236 (1964).
8) P. T. Beurskens, H. J. A. Blaauw, J. A. Cras, and J. J. Steggerda, *Inorg. Chem.*, **7**, 805 (1968).
9) S. Åkerström, *Arkiv Kemi*, **14**, 387 (1959).
10) J. A. Riddick and E. E. Toops Jr., "Technique of Organic Chemistry," 2nd ed, ed by A. Weissberger, Interscience Publishers, New York (1955), Vol. 7, p. 409.
11) S. Åkerström, *Arkiv Kemi*, **14**, 403 (1959); and T. Vangard and S. Åkerström, *Nature*, **184**, 183 (1959).
12) R. Hesse and P. Jennische, *Acta Chem. Scand.*, **26**, 3855 (1972).
13) A. F. Grand and M. Tamres, *Inorg. Chem.*, **8**, 2459 (1969).
14) R. P. Lang, *J. Am. Chem. Soc.*, **84**, 1185 (1962).
15) K. R. Bhaskar, S. N. Bhat, A. S. N. Murthy, and C. N. R. Rao, *Trans. Faraday Soc.*, **62**, 788 (1966).
16) G. Reichenbach, S. Santini, and U. Mazzucato, *J. Chem. Soc., Faraday Trans. 1*, **69**, 143 (1973).
17) M. Tamres, "Molecular Complexes," ed by R. Foster, Paul Elek Ltd, London (1973), Vol. 1, p. 98.
18) A. L. Balch and D. J. Doonan, *J. Organomet. Chem.*, **131**, 137 (1977).
19) H. Schmidbaur and R. Franke, *Inorg. Chim. Acta*, **13**, 85 (1975); H. Schmidbaur, J. R. Mandl, A. Frank, and G. Huttner, *Chem. Ber.*, **109**, 466 (1976).

Crystal Structure and Absolute Configuration of (+)$_{546}$-*cis*(*O*)-Triammine(sarcosinate-*N*-propionato)cobalt(III) (+)$_{546}$-(Ethylenediaminetetraacetato)cobaltate(III) Monohydrate

Ken-ichi OKAMOTO,*,† Tomitake TSUKIHARA,** Jinsai HIDAKA,*** and Yoichi SHIMURA

Department of Chemistry, Faculty of Science, Osaka University, Toyonaka, Osaka 560
***Faculty of Engineering, Tottori University, Koyama-cho, Tottori 680*

(Received June 8, 1978)

The crystal structure of (+)$_{546}$-*cis*(*O*)-triammine(sarcosinate-*N*-propionato)cobalt(III) (+)$_{546}$-(ethylenediaminetetraacetato)cobaltate(III) monohydrate was solved by single crystal X-ray diffraction techniques. The crystal is orthorhombic, space group $P2_12_12_1$, with $a=10.792$, $b=26.816$, $c=8.203$ Å, and $Z=4$. The final R value was 0.054. The absolute configurations of two complex ions were determined by means of anomalous dispersion using Cu $K\alpha$ radiation. The coordinated asymmetric nitrogen atom of sarcosinate-*N*-propionate ligand takes an *R* configuration, and the (+)$_{546}$-(ethylenediaminetetraacetato)cobaltate(III) ion Δ one.

Sarcosinate-*N*-propionate ($sarmp^{2-}$) forms a five- and six-membered chelate ring by coordination of an α-amino carboxylate foot and an *N*-propionate one, respectively. *cis*(*O*)-Triammine(sarcosinate-*N*-propionato)cobalt(III) cation is a model complex, which contains only one asymmetrically coordinated nitrogen atom, and was optically resolved through its diastereomeric salt formation with (+)$_{546}$-(ethylenediaminetetraacetato)-cobaltate(III) anion, $[Co(edta)]^-$.[1] The absolute configuration of (+)$_{546}$-*cis*(*O*) isomer was presumed to be an *R* one from the consideration of its CD spectra, referring to the stereochemistry of several kinds of analogous complexes.[1-4]

This paper deals with the crystal structure of the diastereomeric salt, and the absolute configurations of (+)$_{546}$-*cis*(*O*)-$[Co(sarmp)(NH_3)_3]^+$ and (+)$_{546}$-$[Co(edta)]^-$ ions are established concurrently. A preliminary report has been presented.[5]

Experimental

Preparation of the Crystals. The diastereomer (+)$_{546}$-*cis*(*O*)-$[Co(sarmp)(NH_3)_3]\cdot$(+)$_{546}$-$[Co(edta)]\cdot H_2O$ was isolated first in the course of the study on the stereochemistry of cobalt(III) complexes with *O*,*N*,*O*-tridentate ligand.[1] Silver acetate (0.30 g) was added to a solution of 0.54 g of racemic $[Co(sarmp)(NH_3)_3]Cl$ in a small amount of water and the resulting silver chloride was filtered off. The filtrate was added to a solution of 0.375 g of (+)$_{546}$-$K[Co(edta)]\cdot 2H_2O$[6] in a minimum amount of water. After the mixed solution had been evaporated by a stream of air at room temperature, the concentrated solution was kept in a refrigerator. The violet needle crystals crystallized out as less soluble diastereomer were collected by filtration. The optically active chloride (+)$_{546}$-*cis*(*O*)-$[Co(sarmp)(NH_3)_3]Cl$ obtained from the diastereomer showed $\Delta\varepsilon_{346}=+0.35$.

Crystal Data. Preliminary Weissenberg and oscillation photographs established the fact that the crystals are orthorhombic with b axis along the needle axis. The systematic extinction restricts the space group to $P2_12_12_1$. The crystal data are listed in Table 1.

Data Collection. The intensity data were collected on a Rigaku Denki Computer-controlled four-circle diffractometer employing Mo $K\alpha$ radiation. A single crystal of size *ca.* 0.45 $\times$0.31$\times$0.41 mm was used for the intensity measurement of 2440 independent non-zero reflections. The ω-2θ scan technique was employed with a scan speed 2° min^{-1} by ω, and the background was measured for each 10.0 seconds at the start and end points of a scan range. A scan range of ω for each reflection was calculated by the formula $\Delta\omega=0.08°+0.35°\tan\theta$. Attenuators were automatically inserted when the maximum counting rate exceeded 9000 cps. The measurement of two reference reflections (0 0 2) and (0 10 0) was repeated every thirty reflections.

Table 1. Crystal data

$Co_2C_{16}H_{32}N_6O_{13}$	$M_r=634.33$	
Orthorhombic	$P2_12_12_1$	
$a=10.792(9)$Å	$b=26.816(4)$Å	$c=8.203(12)$Å
$\alpha=90.0°$	$\beta=90.0°$	$\gamma=90.0°$
$D_{calcd}=1.775$ g cm^{-3}		$Z=4$.
$D_{obsd}=1.766$ g cm^{-3} (by flotation)		

For the determination of absolute configurations of both complex ions, the intensities of pairs of reflections, *hkl* and $\bar{h}\bar{k}\bar{l}$, were measured by use of Cu $K\alpha$ radiation.

Structure Determination and Refinement. The structure was solved by the usual heavy-atom method. The positions of two cobalt atoms were determined by means of the Patterson synthesis, and all the non-hydrogen atoms were located by the subsequent Fourier synthesis. The trial structure was refined by a diagonal least-squares procedure with the positional and isotropic thermal parameters. The atomic scattering factors were taken from International Tables for X-ray Crystallography.[7] Further refinement was carried out by the least-squares method of a block-diagonal matrix approximation with the positional and anisotropic thermal parameters for all the non-hydrogen atoms (a program by Dr. T. Ashida was used). After several cycles of refinement, the R value ($R=\sum||F_o|-|F_c||/\sum|F_o|$) decreased to 0.054.

The final parameters of all atoms (except hydrogen atoms) are listed in Table 2. These positional parameters are normal within the estimated standard deviations: 0.0011 and 0.0015 Å for cobalts, 0.006—0.009 Å for oxygens, 0.008—0.010 Å for nitrogens, and 0.009—0.013 Å for carbons. Table 3 containing the observed and calculated structure factors is kept as Document No. 7841 at the Chemical Society of Japan.

Results and Discussion

Description of the Structure. The numbering schemes

† Present address: Shimadzu Seisakusho Ltd., 1 Nishinokyo Kuwabara-cho, Nakagyo-ku, Kyoto 604.
*** Present address: Department of Chemistry, The University of Tsukuba, Ibaraki 300-31.

Table 2a. Final atomic parameters

Atom	*X*	*Y*	*Z*	Atom	*X*	*Y*	*Z*
Co1	0.0249(1)	0.0427(1)	0.0764(1)	N5	−0.1175(9)	0.0856(8)	0.1341(9)
Co2	0.4913(1)	0.2489(1)	0.2807(1)	N6	−0.0115(9)	−0.0100(7)	0.2447(8)
O1	0.1594(7)	0.0018(7)	0.0113(7)	C1	0.1883(11)	−0.0345(10)	0.1068(11)
O2	0.5037(7)	0.3009(6)	0.1268(6)	C2	0.1085(11)	−0.0398(12)	0.2603(10)
O3	0.4682(7)	0.1968(6)	0.4340(7)	C3	0.3773(11)	0.1769(10)	0.1043(10)
O4	0.3518(7)	0.2205(7)	0.1623(7)	C4	0.6309(10)	0.3227(10)	0.4307(11)
O5	0.4137(6)	0.2982(7)	0.4215(7)	C5	0.5378(10)	0.2863(10)	−0.0192(10)
O6	−0.0807(8)	0.0153(7)	−0.0909(7)	C6	0.6409(10)	0.2386(10)	0.5557(9)
O7	0.2754(8)	−0.0630(8)	0.0871(9)	C7	0.7444(9)	0.2529(11)	0.2884(9)
O8	0.3011(8)	0.1494(8)	0.0403(8)	C8	0.5979(10)	0.2352(9)	−0.0267(9)
O9	0.5249(8)	0.3117(7)	−0.1398(6)	C9	0.7132(9)	0.2022(10)	0.2142(10)
O10	0.5426(9)	0.1677(7)	0.6678(7)	C10	0.4907(12)	0.3320(9)	0.4704(8)
O11	0.2735(9)	0.3568(9)	0.1535(9)	C11	0.5157(10)	0.1608(9)	0.1131(9)
O12	0.4581(8)	0.3702(7)	0.5381(7)	C12	−0.1159(11)	−0.0425(11)	0.1904(10)
O13	−0.1501(8)	−0.0449(9)	−0.2483(8)	C13	−0.1089(11)	−0.0300(11)	−0.1151(10)
N1	0.1346(9)	0.0795(9)	0.2256(10)	C14	−0.0458(12)	0.0087(11)	0.4133(11)
N2	0.0747(11)	0.0894(9)	−0.0998(10)	C15	0.5457(10)	0.1980(10)	0.5571(9)
N3	0.6391(7)	0.2677(7)	0.3959(8)	C16	−0.0988(14)	−0.0673(11)	0.0234(11)
N4	0.5879(8)	0.2075(7)	0.1362(8)				

Table 2b. Final atomic parameters

Atom	$B_{11}\times10^4$	$B_{22}\times10^4$	$B_{33}\times10^4$	$B_{12}\times10^4$	$B_{13}\times10^4$	$B_{23}\times10^4$
Co1	54(1)	5(0)	64(2)	−1(1)	20(3)	1(1)
Co2	35(1)	7(0)	43(1)	0(1)	1(2)	−2(1)
O1	77(7)	9(1)	74(11)	11(5)	55(16)	17(6)
O2	58(6)	7(1)	62(9)	5(4)	−14(15)	1(5)
O3	60(6)	8(1)	64(9)	−9(4)	16(16)	5(5)
O4	37(6)	10(1)	78(11)	−5(4)	−17(14)	0(6)
O5	47(6)	9(1)	67(10)	0(4)	26(15)	−11(6)
O6	103(8)	8(1)	70(11)	−5(5)	−36(18)	3(6)
O7	84(9)	15(1)	158(16)	29(6)	70(22)	21(9)
O8	72(8)	13(1)	135(15)	−30(5)	−7(18)	−22(7)
O9	93(8)	11(1)	49(9)	9(5)	−4(17)	17(5)
O10	140(11)	10(1)	47(10)	−10(6)	−4(18)	8(5)
O11	105(10)	16(1)	125(15)	24(7)	−10(21)	9(8)
O12	105(9)	8(1)	107(13)	10(5)	10(19)	−25(6)
O13	90(8)	18(2)	87(13)	−30(6)	−43(18)	−4(8)
N1	63(8)	11(1)	99(15)	−10(6)	8(21)	−11(8)
N2	122(12)	8(1)	95(15)	3(7)	60(24)	17(8)
N3	31(6)	7(1)	61(12)	−11(4)	−7(15)	6(6)
N4	46(7)	5(1)	55(11)	8(5)	−3(16)	2(6)
N5	68(9)	7(1)	109(15)	14(5)	19(20)	−4(7)
N6	57(7)	7(1)	67(11)	−5(5)	35(18)	3(6)
C1	56(9)	9(2)	106(18)	2(6)	25(22)	−3(9)
C2	60(9)	13(2)	70(15)	16(7)	9(21)	16(9)
C3	68(10)	9(1)	58(14)	−15(6)	−7(21)	10(8)
C4	47(9)	8(1)	111(17)	−8(6)	−20(24)	−10(9)
C5	39(8)	9(1)	73(14)	0(6)	−31(19)	−12(8)
C6	64(9)	10(2)	24(12)	−1(6)	−25(19)	10(7)
C7	36(7)	10(1)	54(13)	0(6)	19(17)	−2(9)
C8	66(9)	6(1)	40(13)	3(6)	−15(19)	8(6)
C9	32(8)	11(2)	71(15)	9(6)	−15(20)	−3(8)
C10	88(11)	7(1)	45(12)	5(7)	−29(23)	10(6)
C11	50(9)	6(1)	78(14)	−7(6)	9(21)	−10(7)
C12	74(10)	9(2)	77(16)	−18(7)	17(22)	14(9)
C13	58(10)	11(2)	86(17)	5(7)	4(22)	−8(8)
C14	96(12)	13(2)	55(15)	−7(8)	29(26)	−14(9)
C15	73(10)	8(1)	45(13)	4(6)	8(21)	−8(7)
C16	129(15)	8(2)	73(17)	−11(8)	−43(28)	−5(8)

Temperature factor $=\exp[-(B_{11}\times h^2+B_{22}\times k^2+B_{33}\times l^2+B_{12}\times hk+B_{13}\times hl+B_{23}\times kl)]$ or $\exp(-B(\sin\theta/\lambda)^2)$.
Estimated standard deviations are shown in parentheses.

are shown in Figs. 1 and 2. The packing mode of the complex cations, anions and the water molecules is illustrated in Fig. 3. The bond lengths and angles

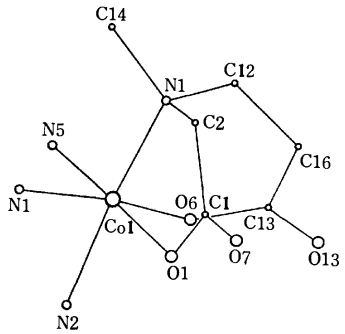

Fig. 1. Structure of *cis*(*O*)-[Co(sarmp)$(NH_3)_3$]$^+$ ion and the numbering scheme of atoms.

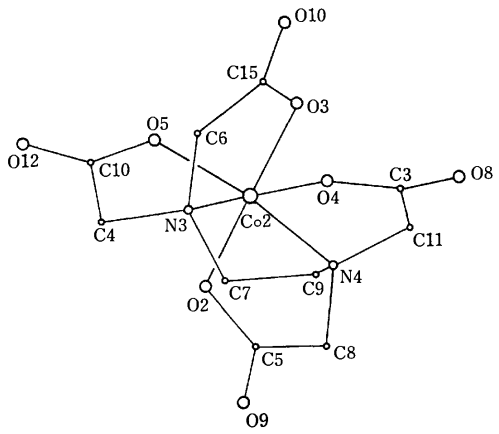

Fig. 2. Structure of [Co(edta)]$^-$ ion and the numbering scheme of atoms.

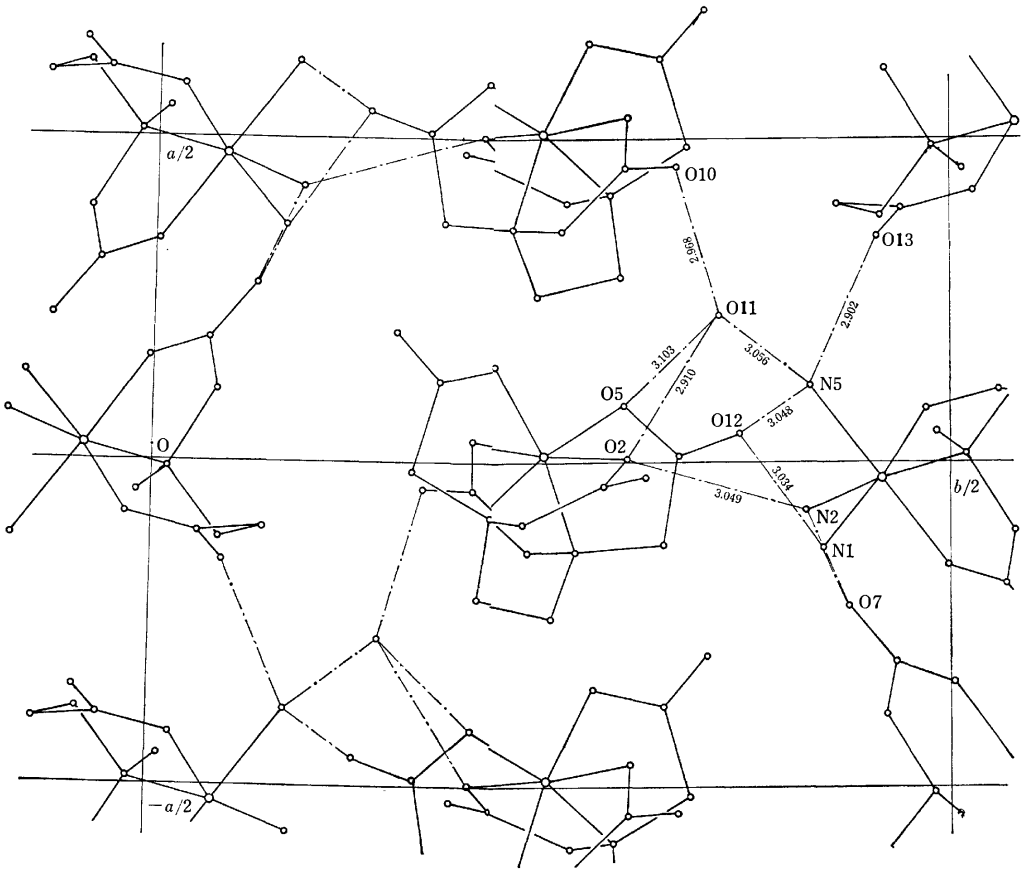

Fig. 3. A projection of the crystal packing viewed along c axis.

Table 4. Bond lengths in [Co(sarmp)$(NH_3)_3$]$^+$ ion

Bond	Length	e.s.d.	Bond	Length	e.s.d.
Co1–N1	1.968 Å	0.008 Å	O1–C1	1.288 Å	0.013 Å
Co1–N2	1.987	0.011	O6–C13	1.267	0.014
Co1–N5	1.978	0.009	O7–C1	1.222	0.014
Co1–N6	2.013	0.009	O13–C13	1.246	0.014
Co1–O1	1.896	0.008	N6–C2	1.526	0.014
Co1–O6	1.928	0.008	N6–C12	1.492	0.014
			N6–C14	1.516	0.015

Table 5. Angles in $[Co(sarmp)(NH_3)_3]^+$ ion

Angle	Degree	e.s.d.	Angle	Degree	e.s.d.
O1–Co1–O6	91.83°	0.34°	C2–N6–Cl4	107.66°	0.82°
O1–Co1–N1	90.27	0.36	C12–N6–C14	106.30	0.82
O1–Co1–N2	87.26	0.39	O1–C1–O7	125.38	1.05
O6–Co1–N2	83.21	0.40	O1–C1–C2	115.66	0.94
O6–Co1–N5	86.15	0.37	O7–C1–C2	118.90	1.01
N1–Co1–N2	88.46	0.42	N6–C2–C1	111.11	0.89
N1–Co1–N5	91.50	0.39	N6–C12–C16	115.43	0.95
N2–Co1–N5	90.98	0.42	O6–C13–C16	119.83	1.04
O6–Co1–N6	96.09	0.40	O13–C13–C16	118.01	1.05
Co1–O1–C1	116.81	0.69	C12–C16–C13	111.86	1.06
Co1–O6–C13	128.15	0.75	C2–N6–C12	111.12	0.82
Co1–N6–C12	110.57	0.60			

Table 6. Bond lengths in $[Co(edta)]^-$ ion

Bond	Length	e.s.d	Bond	Length	e.s.d
Co2–N3	1.921 Å	0.008 Å	O12–C10	1.216 Å	0.015 Å
Co2–N4	1.929	0.008	N3–C4	1.505	0.014
Co2–O2	1.887	0.007	N3–C6	1.526	0.013
Co2–O3	1.897	0.007	N3–C7	1.492	0.013
Co2–O4	1.946	0.007	N4–C8	1.532	0.013
Co2–O5	1.945	0.007	N4–C9	1.503	0.013
O2–C5	1.313	0.012	N4–C11	1.486	0.013
O3–C15	1.311	0.012	C3–C11	1.556	0.015
O4–C3	1.292	0.013	C4–C10	1.568	0.017
O5–C10	1.299	0.014	C5–C8	1.518	0.014
O8–C3	1.222	0.014	C6–C15	1.497	0.014
O9–C5	1.210	0.013	C7–C9	1.526	0.015
O10–C15	1.219	0.014			

Table 7. Angles in $[Co(edta)]^-$ ion

Angle	Degree	e.s.d.	Angle	Degree	e.s.d.
O2–Co2–O4	90.61°	0.30°	C4–N3–C7	114.69°	0.78°
O2–Co2–O5	85.72	0.30	C6–N3–C7	111.22	0.74
O2–Co2–N3	94.35	0.32	C8–N4–C9	110.68	0.74
O2–Co2–N4	88.64	0.32	C8–N4–C11	109.49	0.73
O3–Co2–O4	86.59	0.30	C9–N4–C11	116.56	0.75
O3–Co2–O5	92.89	0.29	O4–C3–O8	124.11	1.01
O3–Co2–N3	88.66	0.31	O4–C3–C11	115.93	0.89
O3–Co2–N4	93.10	0.31	O8–C3–C11	119.92	0.96
O4–Co2–O5	103.21	0.29	N3–C4–C10	104.57	0.86
O4–Co2–N4	83.47	0.31	O2–C5–O9	122.97	0.92
O5–Co2–N3	83.53	0.31	O2–C5–C8	115.30	0.84
N3–Co2–N4	90.28	0.33	O9–C5–C8	111.82	0.80
Co2–O2–C5	114.09	0.62	N3–C6–C15	111.70	0.80
Co2–O3–C15	114.08	0.62	N3–C7–C9	107.72	0.82
Co2–O4–C3	111.93	0.65	N4–C8–C5	111.82	0.80
Co2–O5–C10	112.52	0.68	N4–C9–C7	106.54	0.80
Co2–N3–C4	107.58	0.61	O5–C10–O12	123.07	1.08
Co2–N3–C6	107.39	0.57	O5–C10–C4	116.41	0.97
Co2–N3–C7	105.77	0.59	O12–C10–C4	120.46	1.04
Co2–N4–C8	107.18	0.58	N4–C11–C3	106.05	0.79
Co2–N4–C9	106.16	0.58	O6–C13–O13	122.09	1.05
Co2–N4–C11	116.56	0.75	O3–C15–O10	122.63	0.98
C4–N3–C6	109.80	0.75	O3–C15–C6	116.74	0.87
			O10–C15–C6	120.62	0.97

within the $[Co(sarmp)(NH_3)_3]^+$ ion are given in Tables 4 and 5. In the complex cation, the sarcosinate-*N*-propionate tridentate ligand coordinates facially giving a *cis*(*O*) configuration of the CoN_4O_2 octahedron. It is interesting that the bond length from cobalt to the coordinated nitrogen atom of this ligand, 2.013 Å, is the longest of all the Co–N bonds; the other three Co–NH_3 bonds are in the range 1.968—1.987 Å. Furthermore, this Co–N bond is significantly longer than that of an analogous *O*,*N*,*O*-tridentate ligand, iminodiacetate, which makes two five-membered chelate rings.[8] The bond lengths and angles in the six-membered chelate ring differ markedly from those in the five-membered chelate ring. This is in line with the tendency known for several α- and β-amino carboxylato complexes.[9–11] Though the bond lengths and angles of the five-membered chelate ring are similar to those of simple α-amino carboxylato or *O*,*N*,*O*-tridentato complexes, the bond angles of the six-membered chelate ring differ significantly from those

Table 8. Selected pairs of reflections demonstrating the absolute configuration of $(+)_{546}$-*cis*(*O*)-$[Co(sarmp)(NH_3)_3]\cdot(+)_{546}$-$[Co(edta)]\cdot H_2O$

h	*k*	*l*	$F_c(hkl)$	Obsd	$F_c(\bar{h}kl)$	*h*	*k*	*l*	$F_c(hkl)$	Obsd	$F_c(\bar{h}kl)$
1	11	1	25	>	1	3	3	4	89	>	74
1	15	1	15	<	31	3	11	4	35	>	23
1	1	2	63	>	46	4	6	2	78	>	65
1	9	2	35	<	54	4	14	3	21	>	10
1	20	2	12	<	26	5	5	1	73	<	88
2	3	1	79	<	96	5	9	1	30	<	45
2	6	1	18	>	4	5	12	2	36	>	30
2	13	1	49	<	61	5	16	2	30	>	17
2	2	2	43	>	24	5	3	3	33	<	52
2	4	2	58	>	45	5	10	3	64	>	45
2	1	3	38	>	21	5	11	4	28	<	45
2	15	3	23	>	8	6	2	1	26	<	38
2	18	3	30	<	44	6	1	2	53	>	40
3	1	1	69	>	53	6	2	2	82	>	62
3	4	1	57	>	42	6	4	2	49	>	34
3	1	2	43	<	58	6	3	3	38	>	24
3	6	2	39	<	53	6	2	4	4	<	25
3	17	3	34	<	45	8	2	2	43	>	30

Table 9. Displacements of atoms from the chelate ring plane

$(+)_{546}$-*cis*(*O*)-*R*-$[Co(sarmp)(NH_3)_3]^+$ ion

Plane 1. [Co1, O6, N6] (six-membered chelate ring)

$0.7642X-0.5469Y-0.3419Z+0.6349=0$

Co1	0.0000	O6	0.0000	N6	0.0000	O13	0.7519	C12	−0.2322	C13	0.4996
C16	0.7422										

Plane 2. [Co1, O1, N6] (five-membered chelate ring)

$-0.5951X-0.4712Y-0.6510Z+1.1066=0$

Co1	0.0000	O1	0.0000	N6	0.0000	O7	−0.3309	C1	−0.2365	C2	−0.4777

$(+)_{546}$-*Δ*-$[Co(edta)]^-$ ion

Plane 3. [Co2, N3, N4] (ethylenediamine chelate ring)

$-0.1218X-0.7756Y+0.6193Z+4.3964=0$

Co2	0.0000	N3	0.0000	N4	0.0000	C7	−0.3768	C9	0.3414		

Plane 4. [Co2, O3, N3] (out-of-plane)

$0.5368X-0.6151Y-0.5775Z+2.5890=0$

Co2	0.0000	O3	0.0000	N3	0.0000	C6	−0.2667	C15	−0.1552	O10	−0.1981

Plane 5. [Co2, O2, N4] (out-of-plane)

$-0.8396X-0.3179Y-0.4405Z+7.5876=0$

Co2	0.0000	O2	0.0000	N4	0.0000	C5	0.3443	C8	0.2614	O9	0.6800

Plane 6. [Co2, O4, N4] (in-plane)

$-0.0468X-0.7493Y+0.6606Z+3.7280=0$

Co2	0.0000	O4	0.0000	N4	0.0000	C3	0.5489	C11	0.8488	O8	0.7919

Plane 7. [Co2, O5, N3] (in-plane)

$-0.179X-0.7095Y+0.6814Z+4.1183=0$

Co2	0.0000	O5	0.0000	N3	0.0000	C4	−0.8364	C10	−0.5193	O12	−0.8041

The *X*, *Y*, and *Z* coordinates in Å are referred to the crystallographic axis.

of simple β-amino carboxylato complexes: *e.g.*, <O6–Co1–N6=96.1° (90° for $[Co^{II}(\beta\text{-alaninato})_2(H_2O)_2]$,[10] and 93.4° for *trans*-dinitro(β-alaninato)(1,3-propanediamine)cobalt(III),[11] <Co1–N6–C12=110.6° (115 and 116.2°, *vide ante*), and <N6–C12–C16=115.4° (111 and 113°, *vide ante*).

The bond lengths and angles within the $[Co(edta)]^-$ ion (Tables 6 and 7) agree well with the data for ammonium and rubidium salts.[12]

The oxygen atom O11 of the water molecule seems to have four nearest neighbor atoms, N5, O2, O5, and O10 (Fig. 3). Several hydrogen bonds are recognized between the complex ions; *e.g.*, N5–O13, N5–O12, N1–O12, and so on.

Absolute Configuration. The absolute configuration was determined by anomalous dispersion. The atomic scattering factors were taken from literature;[7] those of cobalt atoms were collected for real and imaginary parts of anomalous dispersion: $\Delta f' = -2.2$ and $\Delta f'' = 3.8$.

The intensities of the reflections, $|F_c(hkl)|$ and $|F_c(\bar{h}\bar{k}\bar{l})|$, were calculated by use of both sets of atomic parameter values given in Table 2, (X, Y, Z) and $(X, -Y, Z)$. The values calculated by $(X, -Y, Z)$ fit the observation satisfactorily (Table 8). Thus, it is confirmed that the nitrogen atom of the tridentate ligand takes *R* configuration in the $(+)_{546}$-*cis*(*O*)-[Co(sarmp)$(NH_3)_3$]$^+$ ion, which is in line with the assignment from its CD spectra.[1] This shows that the nitrogen atom has the same absolute configuration as the stereospecifically coordinated *R* nitrogen atom of *cis*(*O*)-*R*-triammine(L-prolinate-*N*-propionato)cobalt(III) ion. On the other hand, the absolute configuration of $(+)_{546}$-$[Co(edta)]^-$ ion can be designated as *Δ*. The complex ion has been assigned to this configuration from a comparison of its ORD[13] and CD[9] spectra with those of *Δ*-$(+)_{546}$-(*R*-propylenediaminetetraacetato)-cobaltate(III) formed stereospecifically.

Conformation of the Chelate Rings. In order to examine the conformation of chelate rings, the displacements of relevant atoms from the chelate ring plane, which is defined by the central cobalt atom and the two coordinating atoms in the chelate ring, were calculated. The results are given in Table 9. It is concluded that the six-membered chelate ring in the cation has an asymmetric skew-boat form with *δ* conformation taking C13 and C16 on the same side of the O6–Co–N6 plane. This type of conformation has been recognized in a few cobalt(III) complexes with β-alaninate.[11,14] The five-membered chelate ring in the present complex cation has an asymmetric envelope form with *λ* conformation.

The diamine chelate ring in the anion has an asymmetric gauche form with *λ* conformation. This is in line with the case of diamines such as ethylenediamine.[9] One of the two out-of-plane glycinate chelate rings has a strained asymmetric envelope form with *λ* conformation, and the other *δ* one. Both of the in-plane glycinate chelate rings have an asymmetric envelope form with *δ* conformation.

References

1) K. Okamoto, J. Hidaka, and Y. Shimura, *Bull. Chem. Soc. Jpn.*, **46**, 3134 (1973).
2) K. Okamoto, J. Hidaka, and Y. Shimura, *Bull. Chem. Soc. Jpn.*, **44**, 1601 (1971).
3) K. Okamoto, J. Hidaka, and Y. Shimura, *Bull. Chem. Soc. Jpn.*, **46**, 475 (1973).
4) K. Okamoto, J. Hidaka, and Y. Shimura, *Bull. Chem. Soc. Jpn.*, **48**, 2456 (1975).
5) K. Okamoto, T. Tsukihara, J. Hidaka, and Y. Shimura, *Chem. Lett.*, **1973**, 145.
6) F. P. Dwyer and F. L. Garvan, *Inorg. Syntheses*, **6**, 192 (1960).
7) "International Tables for X-Ray Crystallography," Kynoch Press, Birmingham (1962), Vol. III.
8) A. B. Corradi, C. G. Palmieri, M. Nardelli, M. A. Pellinghelli, and M. E. V. Tani, *J. Chem. Soc. Dalton Trans.*, **1973**, 655.
9) C. J. Hawkins, "Absolute Configuration of Metal Complexes," Interscience Publishers, Inc., New York (1971).
10) H. C. Freeman, *Adv. Protein Chem.*, **22**, 257 (1967).
11) R. M. Herak, M. B. Ćelap, and I. Krstanovič, *Acta Crystallogr., Sect. B*, **33**, 3368 (1977).
12) H. A. Weakliem and J. L. Hoard, *J. Am. Chem. Soc.*, **81**, 549 (1959).
13) T. E. MacDermott and A. M. Sargison, *Aust. J. Chem.*, **16**, 334 (1963).
14) B. Prelesmik, M. B. Ćelap, and R. Herak, *Inorg. Chim. Acta*, **7**, 569 (1973).

Resonance Energies of Nonbenzenoid Hydrocarbons†

Jun-ichi AIHARA
Department of Chemistry, Faculty of Science, Hokkaido University, Sapporo 060
(Received October 21, 1977)

Resonance energies of 30 conjugated hydrocarbons and their molecular ions have been calculated on the basis of the graph-theoretical theory of aromaticity. No difficulty was found in extending the aromaticity theory to ionic conjugated species. In general, the resonance energies obtained correlated well with typical chemical features of the compounds.

The chemistry of nonbenzenoid hydrocarbons has occupied the interest of many organic chemists to an increasing extent. The synthetic accessibility of a number of nonbenzenoid hydrocarbons has given rise to a new field of organic chemistry.[1,2] In parallel with this, a theoretical understanding of their electronic structures, centered on their aromaticity, has been attempted in a variety of sophisticated manners.[3]

The classical concept of aromaticity, based primarily upon the Hückel (4n+2) rule, has been adequately applied to benzenoid hydrocarbons.[4] However, it appears less effective in predicting aromaticities of nonbenzenoid hydrocarbons.[4] Recently, the classical concept of aromaticity has been replaced by a graph-theoretical theory of aromaticity.[5–8] This theory has proven quite suitable for describing aromaticities of nonbenzenoid hydrocarbons as well as those of the other kinds of conjugated compounds.[5] There has been a qualitative idea that aromatic compounds should be unusually stable.[9] In this paper, I would like to further examine the stabilities of typical nonbenzenoid hydrocarbons by means of the graph-theoretical theory of aromaticity.

Results and Discussion

Resonance energies of 30 conjugated hydrocarbons **1**—**30** and their molecular ions have been calculated. They are mostly non-alternant pyrene-like compounds of synthetic importance. For the other types of nonbenzenoid hydrocarbons, see Ref. 5. The method used for calculating resonance energies is the graph-theoretical one previously presented by the author.[5,8] The HMO theory used is the simplest one. Resonance energies obtained are all listed in Table 1. As shown in this table, a comparative study is made for the neutral and ionic species with an even number of π-electrons. Conjugated hydrocarbons with an even number of π-electrons have been of prime interest to synthetic organic chemists.[1,2] Free radicals are hence omitted from consideration. In fact, it is not easy to rationalize their stability in terms of an HMO model.

Pyrene-like tetracycles constitute the most attractive group of non-alternant hydrocarbons. It is interesting to see how these compounds are like or unlike the parent compound pyrene (**1**). Figure 1 shows the relative resonance energies of pyrene and its eight isomers (**2**—**9**) with the same formula of $C_{16}H_{10}$. First of all, pyrene (**1**) is quite a stable compound. Its resonance energy is almost twice as large as that of benzene (0.273β).[5] Most compounds cited in Fig. 1 have the largest resonance energy in the neutral 16-π-electronic state. They are Compounds **2**, **3**, **4**, **6**, **7**, and **8**. Stabilities of these compounds can roughly be justified by the fact that they have so far been synthesized.[10–15] One should here note that in general the easiness of synthesis is one of the most realistic measures of stability (or aromaticity) of a conjugated compound.[9,16]

Compound **5** has not been prepared yet. For this

Table 1. Resonance energies of nonbenzenoid hydrocarbons in units of β

Compound (M)	Resonance energy[a]				
	M^{2+}	M^{+}	M	M^{-}	M^{2-}
1	0.199	—	0.598(0.81)	—	0.199
2	−0.116	—	0.398(0.554)	—	−0.116
3	0.111	—	0.372(0.508)	—	−0.041
4	−0.057	—	0.376(0.522)	—	0.201
5	0.167	—	0.247(0.293)	—	0.255
6	−0.074	—	0.122(0.251)	—	−0.082
7	−0.270	—	0.217(0.353)	—	−0.104
8	−0.252	—	0.214(0.332)	—	−0.252
9	−0.084	—	−0.146	—	−0.084
10	−0.173	—	−0.016	—	−0.173
11	−0.376	—	0.222(0.246)	—	0.536
12	−0.289	—	0.106(0.254)	—	0.539
13	—	0.072	—	0.554	—
14	—	0.250	—	0.509	—
15	—	0.519	—	0.101	—
16	—	0.498	—	0.302	—
17	0.464	—	0.133(0.299)	—	−0.110
18	0.470	—	0.230(0.301)	—	−0.132
19	0.139	—	0.035(0.167)	—	−0.024
20	—	−0.179	—	0.267	—
21	−0.180	—	0.578(0.77)	—	0.316
22	—	−0.247	—	0.520	—
23	—	0.507	—	0.048	—
24	−0.248	—	0.303	—	0.679
25	−0.339	—	0.491	—	0.661
26	—	0.410	—	0.410	—
27	0.396	—	0.725(0.98)	—	0.398
28	0.230	—	0.506	—	0.125
29	0.407	—	0.508	—	0.037
30	−0.047	—	0.522	—	0.464

a) Values in parentheses are the resonance energies of Hess and Schaad.[9]

† Presented at the Symposium on Molecular Structures, Sapporo, Japan, August 1977.

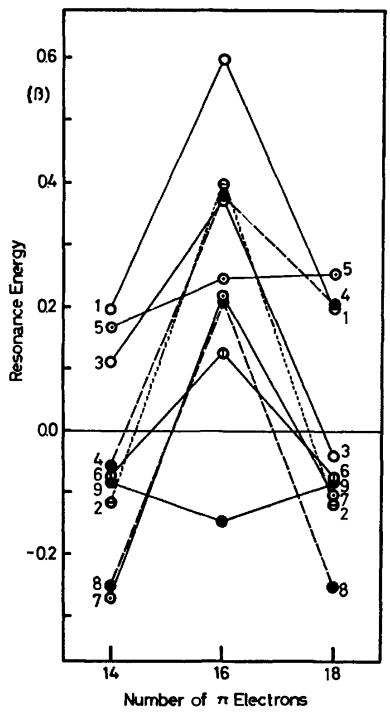

Fig. 1. Resonance energies of pyrene and its structural isomers.

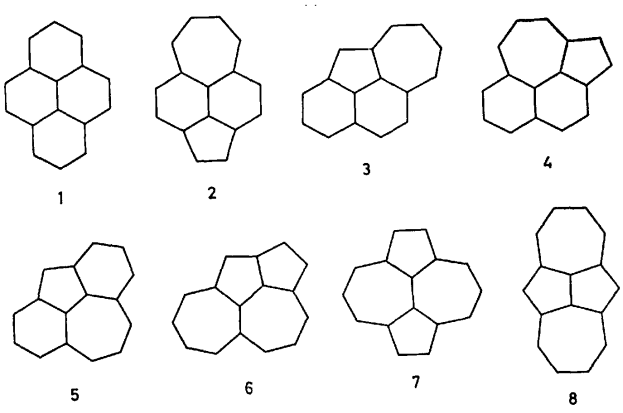

compound, the resonance energy of the neutral species is not so large and is comparable to that of the dianion. Such a situation may be less favorable to the exclusive existence of either species. Aromaticity of this compound may be depicted by means of a perimeter model,[17] since a central double bond in the canonical structure is fixed there. The resonance energy of Compound **6** is small even in the neutral state. This compound appears to gain additional stability by locally introducing bond alternation.[18] The resulting system is an azulene conjugated with a triene unit. The resonance energy is comparable to that of azulene (0.151 β).[5]

An alternant isomer of pyrene (**9**) is antiaromatic because of its negative resonance energy. This compound, however, has been synthesized by Wilcox *et al.*,[19] but the NMR spectrum shows it to be paratropic, in accord with the resonance energy. Compound **10** is essentially nonaromatic, since a conjugated system of Compound **9** is stabilized by the third benzene ring. It has also been synthesized by Wilcox *et al.*[20]

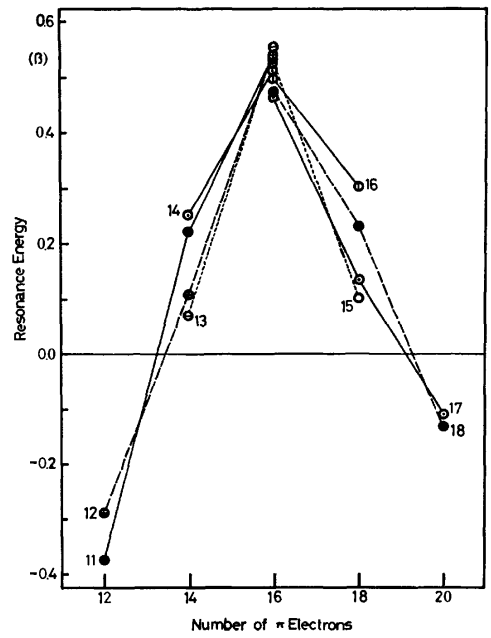

Fig. 2. Resonance energies of pyrene-like hydrocarbons.

Next, let us consider the aromaticities of eight conjugated hydrocarbons which are iso-π-electronic with pyrene (**1**); these are necessarily ionic species. The resonance energies are compared with each other in Fig. 2. One may notice at once that each of these compounds has the largest resonance energy when it has 16 π-electrons. Furthermore, it is noteworthy that the resonance energies of these 16-π-electronic species lie within a relatively narrow energy range of 0.46—0.56 β.

Compound **11** in its neutral state has not been prepared yet, although its dianion has been prepared by Trost *et al.*[21] This fact is quite consistent with the resonance energy of the dianion, which is twice as large as that of the neutral species. Compound **12** has also been prepared by Trost *et al.*[22] Its half-wave reduction potential is anomalously low, suggesting that this compound is not obviously aromatic. It readily reacts with butyllithium to form a dianion.[23] These aspects of the compound suggest reasons for the increased resonance energy of the dianion.

The anion of Compound **13** has been prepared by

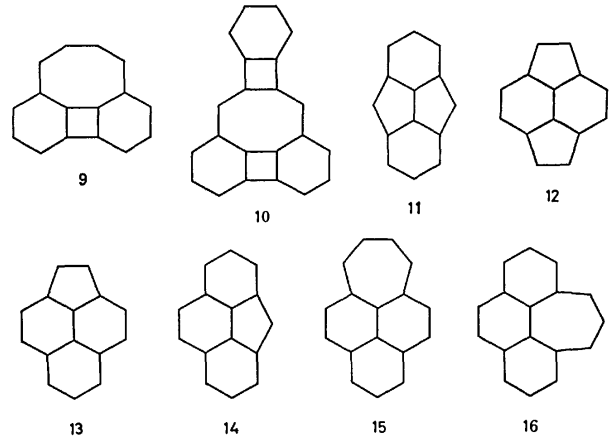

Murata *et al.*[24] The NMR spectrum indicates that the charge is delocalized over the entire conjugated system. This result is in marked contrast to the anion of Compound **14**, which has been prepared by Cox *et al.*,[25] in that the latter ion appears from an NMR viewpoint to be a phenanthrene derivative. The two anions likewise have resonance energies as large as pyrene (**1**). The cationic species of these compounds have not been prepared. Cationic species of Compounds **15** and **16** have so far been synthesized by Murata *et al.*[26,27] It should be stressed that the synthetic accessibility thus correlates very well with the large resonance energies. Two compounds (**17** and **18**) have not been prepared, nor have their ions.

The methyl derivative of Compound **19** has been prepared by Hafner *et al.*[28] It is thermally unstable, protonates easily, and has a relatively high-field proton. These facts evidently reflect the olefinic character shown by the small resonance energy. A mononegative anion of Compound **20** has been synthesized by Wilner and Ravinovitz.[29] The positive resonance energy is again in line with its synthesis.

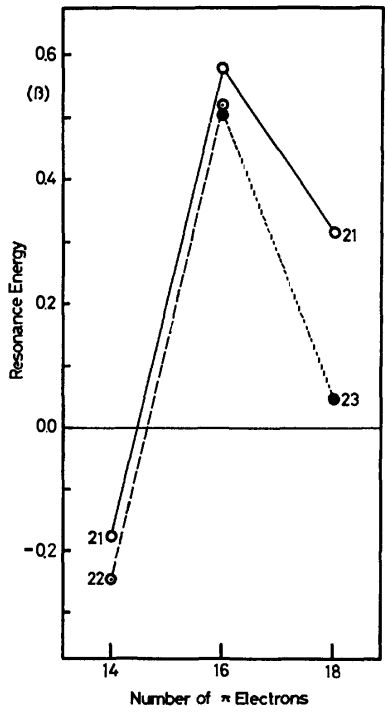

Fig. 3. Resonance energies of fluoranthene-like hydrocarbons.

Fluoranthene (**21**) is a structural isomer of pyrene (**1**). It is a stable nonbenzenoid hydrocarbon composed of two benzenoid units. The two iso-π-electronic species **22** and **23** have been synthesized by Murata and his coworkers.[30,31] In each of the 16-π-electronic ions, the charge is delocalized over the entire conjugated system. As shown in Fig. 3, these compounds likewise have the largest resonance energy in the 16-π-electronic state.

Derivatives of Compounds **24** and **25** have been prepared in their neutral state.[32,33] Every proton NMR signal of Compound **25** exhibits a downfield shift of 1—2 ppm compared with the corresponding signal of

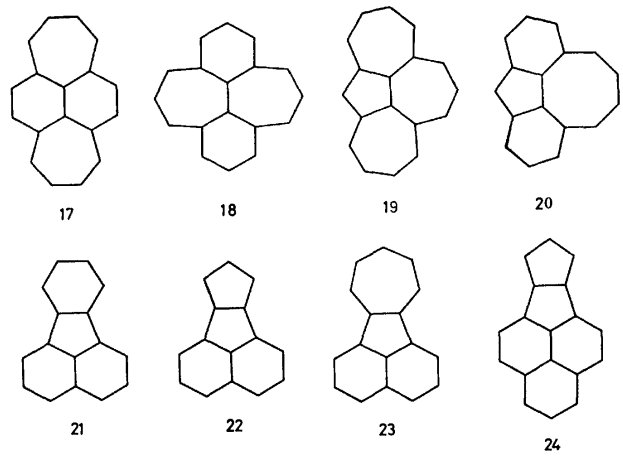

Compound **24**. This trend is in parallel with the order of magnitude of their resonance energies. In relation to these compounds, phenalene (**26**) is remakable in that it gives rise to a relatively stable anion and cation.[34] These mononegative and monopositive ions have the same resonance energies, which are seemingly large enough to justify the stability.

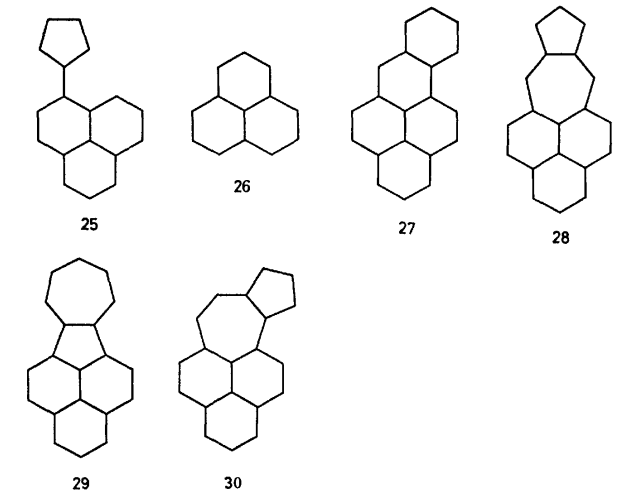

Compounds **28**—**30** are a set of benzo[*a*]pyrene isomers, benzo[*a*]pyrene (**27**) being famous for its carcinogenicity. Benzo[*a*]pyrene is stable in our chemical sense. All the isomers considered here have been prepared.[2,35,36] Our resonance energies predict these isomers to be fairly stable in the neutral state, in accord with their chemical properties.[2] Figure 4 shows this aspect of the benzo[*a*]pyrene isomers.

As has been seen above, our definition of resonance energy has proven very effective in predicting the stability of a non-alternant hydrocarbon with or without electric charges. This supports a view that the same approach can be used for designing novel conjugated systems. For example, appropriate attempts to prepare dications of Compounds **17** and **18** are quite promising because of their large resonance energies.

It goes without saying that some other effects must be considered at the same time when one attempts to design a new conjugated system. The strain of a molecular framework is of course a destabilizing factor. When

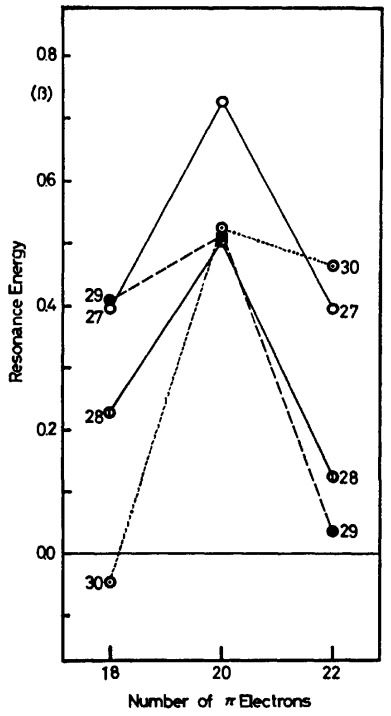

Fig. 4. Resonance energies of benzo[*a*]pyrene and its structural isomers.

a conjugated system is polycyclic, the resonance energy distribution is non-uniform in the system.[7] This may diversify the reactivity of the conjugated system. The least aromatic sites in the compound might be preferentially attacked by reagents even if the entire conjugated system has a large resonance energy.

The use of facilities of the Hokkaido University Computing Center is gratefully acknowledged. This work was motivated by a comprehensive review of Profs. I. Murata and K. Yamamoto on the condensed polycyclic conjugated systems (Ref. 2).

References

1) See, *e.g.*, P. J. Garratt, "Aromaticity," McGraw-Hill, London (1971); W. J. le Noble, "Highlights of Organic Chemistry," Marcel Dekker, New York, N. Y. (1974), Chap. 9.

2) I. Murata and K. Yamamoto, *Kagaku Sôsetsu*, **15**, 211 (1977).

3) See, *e.g.*, I. Murata, *Kagaku No Ryoiki*, **23**, 481, 589 (1969); H. Kuroda, *Yuki Gosei Kyokai Shi*, **28**, 414 (1970); J. Aihara, *Kagaku No Ryoiki*, **30**, 269 (1976).

4) W. C. Herndon, *J. Am. Chem. Soc.*, **95**, 2404 (1973); W. C. Herndon and M. L. Ellzey, Jr., *ibid.*, **96**, 6631 (1974); M. Randić, *Chem. Phys. Lett.*, **38**, 68 (1976); *J. Am. Chem. Soc.*, **99**, 444 (1977); *Tetrahedron*, **33**, 1905 (1977).

5) J. Aihara, *J. Am. Chem. Soc.*, **98**, 2750, 6840 (1976); *Kagaku No Ryoiki*, **30**, 379 (1976).

6) J. Aihara, *J. Org. Chem.*, **41**, 2488 (1976); *Bull. Chem. Soc. Jpn.*, **50**, 3057 (1977); *Kagaku No Ryoiki*, **30**, 812 (1976).

7) J. Aihara, *J. Am. Chem. Soc.*, **99**, 2048 (1977).

8) The definition of resonance energy presented in a recent paper [J. Aihara, *Bull. Chem. Soc. Jpn.*, **50**, 2010 (1977)] is not used here because the original definition proposed in Ref. 5 always appears most suitable for describing stability of a conjugated system. Note that the reference energy in Ref 5 defines the lowest energy of the reference structure. For all the conjugated hydrocarbons investigated here, however, both definitions of resonance energy give the same results. In such a case, the overrall resonance energy can be assigned to every occupied π-molecular orbital on the basis of the 1977 definition of resonance energy.

9) B. A. Hess, Jr., and L. J. Schaad, *J. Org. Chem.*, **36**, 3418 (1971); *J. Am. Chem. Soc.*, **93**, 305 (1971).

10) V. Boekelheide, W. E. Langeland, and C.-T. Liu, *J. Am. Chem. Soc.*, **73**, 2432 (1951).

11) D. H. Reid, W. H. Stafford, and J. P. Ward, *J. Chem. Soc.*, **1955**, 1193.

12) P. D. Gardner, C. E. Wulfman, and C. L. Osborn, *J. Am. Chem. Soc.*, **80**, 143 (1958).

13) K. Hafner, R. Fleischer, and K. Fritz, *Angew. Chem., Int. Ed. Engl.*, **4**, 69 (1965).

14) A. G. Anderson, Jr., A. A. MacDonald, and A. F. Montana, *J. Am. Chem. Soc.*, **90**, 2993 (1968).

15) H. Reel and E. Vogel, *Angew. Chem., Int. Ed. Engl.*, **11**, 1013 (1972).

16) L. J. Schaad and B. A. Hess, Jr., *J. Am. Chem. Soc.*, **94**, 3068 (1972); *J. Chem. Educ.*, **51**, 640 (1974).

17) J. R. Platt, *J. Chem. Phys.*, **17**, 484 (1949); *ibid.*, **22**, 1448 (1954).

18) H. J. Lindner, *Chem. Ber.*, **102**, 2456 (1969).

19) C. F. Wilcox, Jr., J. P. Uetrecht, and K. G. Grohman, *J. Am. Chem. Soc.*, **94**, 2532 (1972); C. F. Wilcox, Jr., J. P. Uetrecht, G. D. Grantham, and K. G. Grohman, *ibid.*, **97**, 1914 (1975).

20) C. F. Wilcox, Jr., and G. D. Grantham, *Tetrahedron*, **31**, 2889 (1975).

21) B. M. Trost and P. L. Kinson, *J. Am. Chem. Soc.*, **92**, 2591 (1970); *ibid.*, **97**, 2438 (1975).

22) B. M. Trost and G. M. Bright, *J. Am. Chem. Soc.*, **89**, 4244 (1967); B. M. Trost, G. M. Bright, C. Frihard, and D. Brittelli, *ibid.*, **93**, 737 (1971).

23) B. M. Trost, D. Buhner, and G. M. Bright, *Tetrahedron Lett.*, **1973**, 2787.

24) I. Murata, K. Yamamoto, M. Morioka, M. Tamura, and T. Hirotsu, *Tetrahedron Lett.*, **1975**, 2287.

25) R. H. Cox, E. G. Janzen, and J. L. Gerlock, *J. Am. Chem. Soc.*, **90**, 5906 (1968).

26) I. Murata, K. Yamamoto, and Y. Kayane, *Angew. Chem., Int. Ed. Engl.*, **13**, 808 (1974); K. Yamamoto, K. Kayane, and I. Murata, *Bull. Chem. Soc. Jpn.*, **50**, 1964 (1977).

27) I. Murata, K. Yamamoto, Y. Kayane, and H. Ori, *Tetrahedron Lett.*, **1975**, 131.

28) K. Hafner, G. Hafner-Schneider, and F. Bauer, *Angew. Chem., Int. Ed. Engl.*, **7**, 808 (1968).

29) I. Willner and M. Ravinovitz, *Tetrahedron Lett.*, **1976**, 1223.

30) K. Yamamoto, M. Morioka, and I. Murata, *Tetrahedron Lett.*, **1975**, 3009.

31) K. Yamamoto and I. Murata, *Angew. Chem., Int. Ed. Engl.*, **15**, 240 (1976).

32) I. Murata, T. Nakazawa, and M. Okazaki, *Tetrahedron Lett.*, **1970**, 3269; I. Murata, M. Okazaki, and T. Nakazawa, *Angew. Chem., Int. Ed. Engl.*, **10**, 576 (1971).

33) I. Murata, T. Nakazawa, and M. Okazaki, *Tetrahedron Lett.*, **1969**, 1921.

34) D. H. Reid, *Quart. Rev.*, **19**, 274 (1965).

35) C. Jutz and R. Kirchlechner, *Angew. Chem., Int. Ed. Engl.*, **5**, 516 (1966); C. Jutz, R. Kirchlechner, and H.-J. Seidel, *Chem. Ber.*, **102**, 2301 (1969).

36) I. Murata, K. Nakasuji, K. Yamamoto, T. Nakazawa, Y. Kayane, A. Kimura, and O. Hara, *Angew. Chem., Int. Ed. Engl.*, **14**, 170 (1975).

Coenzyme Models. XII. Kinetics and Mechanisms of 1,4-Dihydronicotinamide Reduction of Carbon-Carbon Double Bonds. Influence of Added Mg^{2+} Ion and Acetic Acid

Seiji SHINKAI,* Yumiko KUSANO, Toyoko IDE, Takaaki SONE, and Osamu MANABE

Department of Industrial Chemistry, Faculty of Engineering, Nagasaki University, Nagasaki 852

(Received December 17, 1978)

Nonenzymatic dihydronicotinamide reduction of carbon-carbon double bonds occurs with the aid of Mg^{2+} ion or acetic acid. The role of Mg^{2+} ion and acetic acid is discussed on the basis of spectral studies, kinetic measurements, and product analyses. The addition of Mg^{2+} ion caused the shift of the NMR peak of substrate α-proton to lower field, and the magnitude was parallel to the yield of reduced methylene derivatives. Kinetic studies suggested that the dihydronicotinamide reduction in the presence of Mg^{2+} ion is most reasonably understood by assuming a competitive complexation of dihydronicotinamide and substrate with Mg^{2+} ion. On the other hand, acetic acid aids the reduction by means of general acid catalysis, but an alternative mechanism is suggested for the reduction of benzylidenemalononitrile.

It has been established that the metal ion and the ortho hydroxyl group greatly assist the nonenzymatic dihydronicotinamide reduction of >C=O, >C=S, and >C=N double bonds.[1-3] The findings in nonenzymatic systems are considerably important in connection with the fact that most of NADH dependent enzymes employ metal ion (*e.g.*, Zn^{2+} ion) and/or Brönsted acid (*e.g.*, imidazolium ion) in the active sites.[4,5] From the mechanistic point of view, however, the reductions of these double bonds seem somewhat complicated because of (i) the possible interaction of substrates with the metal ion or the ortho hydroxyl group both in the initial state and in the transition state[6,7] and (ii) the equilibrium of substrate hydration which is catalyzed by acid and base.[8,9] In this respect, C=C double bonds are convenient substrates to assess the influence of added metal ions and Brönsted acids, since they are not subjected to hydration equilibria[10] and interact very weakly with added acids.[11]

We selected several styrene derivatives (Table 1) and performed the reduction by *N*-benzyl-1,4-dihydronicotinamide (BzlNicH) in a few solvents. The results are discussed on the bases of spectral studies, kinetic measurements, and product analyses.

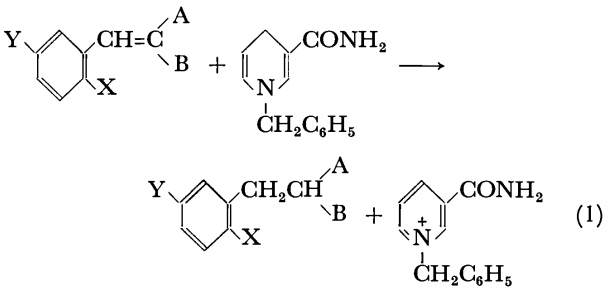

Experimental

Materials. The following styrene derivatives were prepared according to the literature and identified by spectroscopic (NMR and IR) methods and elemental analysis: benzylidenemalononitrile (**1**), mp 83—85 °C (lit,[12] 87 °C); β-nitrostyrene (**2**), mp 57—59 °C (lit,[13] 58—59 °C); diethyl benzylidenemalonate (**3**), bp 132—133 °C/2 mmHg (lit,[14] 160—163 °C/7 mmHg); isopropylidene benzylidenemalonate (**4**), mp 80—84 °C (lit,[15] 80—84 °C); 3,β-dinitrostyrene (**2NO$_2$**), mp 122—124 °C (lit,[16] 125 °C). 2-Hydroxy-β-nitrostyrene (**2OH**) was prepared from nitromethane and salicylaldehyde according to the method of Gairand and Lappin.[13] The product is a mixture of yellow solid and black oil. The mixture was heated to 60—70 °C on a steam bath, and the oily layer was decanted. Recrytallization of the residual yellow solid from methanol and water gave yellow needles, mp 130—133 °C. IR: ν_{OH} 3460 cm^{-1}, $\nu_{C=C}$ 1620 cm^{-1}, nitro group 1330 cm^{-1}. Found: C, 58.06; H, 4.31; N, 8.46%. Calcd for $C_8H_7NO_3$: C, 58.17; H, 4.28; N, 8.48%. The preparation of *N*-benzyl-1,4-dihydronicotinamide (BzlNicH) was described.[17]

Product Analyses. 1.0 mmol of a substrate and 1.2 mmol of BzlNicH were dissolved in 10 ml of dry solvent (acetonitrile or methanol), and the solution was gently refluxed in the dark for 2 h. The reaction was also carried out in the presence of acid (1.4 mmol $Mg(ClO_4)_2$ or 1.0 M acetic acid). In order to evaluate the relative reactivity of substrates, the reaction period was unified in 2 h. The solvent was evaporated at room temperature *in vacuo*, the residue being extracted with aqueous HCl (0.1 M) and chloroform. The chloroform layer was separated, dried over Na_2SO_4, and evaporated to dryness. The sample thus obtained was subjected to the NMR analysis (JEOL JNM-MH-100; solvent, Me_2SO-d_6 or $CDCl_3$). The reduced compounds provided doublet (for **1** and **3**) or triplet (**2**, **2OH**, and **2NO$_2$**) peaks at around 3.3 ppm which are characteristic of product α-methylenes. The yield of the reduced products was determined from integral intensity of the peaks with acetone oxime as internal standard. The reaction was repeated two to four times and the average value is recorded in Table 2. The solid product from **1** was recrystallized from ethanol, which gave benzylmalononitrile in 42% yield; mp 88—91 °C (lit,[18] 87 °C).

In the presence of acetic acid, the yield of the reduced product was not improved largely by elongation of the reaction period. For example, the reaction with **2** in methanol–acetic acid (1.0 M) for 24 h gave corresponding reduced product in 26% yield. This is probably due to the competing decomposition of BzlNicH.

The analysis of by-products was carried out mainly by the mass spectroscopic method. Black, viscous oil recovered from the reaction of BzlNicH and **2** in acetonitrile gave a M^+ peak at 306. If the dimer of **2**, $(C_6H_5C_2H_3NO_2)_2$, is formed, the M^+ peak is expected at 300. The reaction of BzlNicH and **4** in acetonitrile resulted in reddish-yellow solid, and the peak of the dimer (462 for $[C_6H_5C_2H_2(COO)_2C(CH_3)_2]_2$) could not be found in the mass spectrum. These results indicate that the dimer is not contained in the recovered solid. Since the

IR spectrum of the oily product from **2** showed strong absorptions due to nitro group, the nitro group of **2** is not reduced by BzlNicH under the present reaction conditions. Further investigation of the by-products is now continued in our laboratory.

Kinetics. The kinetic measurements were carried out at 30 °C in dry acetonitrile or ethanol. The progress of the reaction was followed spectrophotometrically by monitoring the decrease in the absorption of BzlNicH at 380 nm. Since excess substrate was used in all the cases, the pseudo first-order behavior was observed except in the presence of acetic acid. The rate of disappearance of BzlNicH(v_{obsd}) in the presence of acetic acid (AcOH) is described by

$$v_{obsd} = -\frac{[\text{BzlNicH}]}{dt} = v_r + k_d[\text{BzlNicH}][\text{AcOH}], \quad (2)$$

where k_d is the second-order rate constant for acid-catalyzed decomposition of BzlNicH and v_r is the disappearance rate of BzlNicH other than the acid-catalyzed decomposition. The k_d term was separately evaluated in the absence of substrate, and v_r was determined by substracting this value from v_{obsd}. The detail of the method has been described.[20]

Results and Discussion

Substituent Effect. The BzlNicH reduction of six styrene derivatives was carried out in acetonitrile or in methanol, and the yield of the reduced product was estimated by the NMR method (Table 2: for the detail of the method, see Experimental). The reaction rates were estimated from disappearance of the UV absorption band of BzlNicH at 30 °C, and the apparent second-order rate constants ($k_r = k_{obsd}$ (pseudo first-order rate constants)/[substrate]) are summarized in Table 3.

Table 1. Structure of substrates

Abbreviation	A	B	X	Y
1	CN	CN	H	H
2	NO_2	H	H	H
3	$COOC_2H_5$	$COOC_2H_5$	H	H
4[a]				
2OH	NO_2	H	OH	H
2NO$_2$	NO_2	H	H	NO_2

a) **4**, $C_6H_5CH{=}C(COO)(COO)C(CH_3)_2$.

Table 3. Apparent second-order rate constants ($k_r \times 10^2$, $M^{-1}s^{-1}$) for the BzlNicH reduction and third-order rate constants ($k_{AcOH} \times 10^2$, $M^{-2}s^{-1}$) for added acetic acid[a]

Substrate	CH_3CN		C_2H_5OH	
	k_r	k_{AcOH}	k_r	k_{AcOH}
1	3.8	0	6.3	0
2	0.5	22.3	0	6.3
2OH	16.7		23.3	
2NO$_2$	6.0	18.3	0.5	2.7

a) 30° C, pH 8.5, μ=0.02 with KCl, [BzlNicH]=1.00×10^{-4} M, [substrate]=5.00×10^{-3} M.

As shown in Table 2, the reduction of **1** in methanol gave the corresponding reduced products in 10% yield. On the other hand, **2** was not reduced by BzlNicH under the similar reaction conditions. Base on the σ° value,[21] the C=C double bond of **1** is presumed to be more electron-deficient than that of **2** ($2\sigma^\circ_{CN}=1.12$, $\sigma^\circ_{NO_2}=0.63$), and is more sensitive to BzlNicH reduction. The electron-withdrawing group on benzene ring (*e.g.*, **2NO$_2$**) also enhanced the yield. Evidently, the BzlNicH reduction without the aid of acids is limited to very electron-deficient C=C double bonds.

Interestingly, **1** is not reduced in acetonitrile (Table 2). The result may be rationalized based on the proposition by van Eikeren and Grier[22] that protic media greatly lower the free energy of activation for the dihydronicotinamide reduction of carbonyl compounds: in the present system, for example, solvent alcohol may provide a means of stabilizing the developing negative charge on the substrate β-carbon in the transition state through hydrogen bonding. However, **3** ($2\sigma^\circ_{COOEt}=0.60$), a less electron-deficient olefin is reduced in acetonitrile in 10% yield. Therefore, it is difficult to provide a consistent elucidation on the yield based on the proposition of van Eikeren and Grier.[22]

Here, it is worth mentioning that the disappearance rate of BzlNicH in the presence of **1** in acetonitrile is almost comparable with that in ethanol, despite the difference in the yield. Since the reduced product of **1** was not found in acetonitrile, the disappearance of BzlNicH should be attributed to the formation of some

Table 2. Product analyses of the BzlNicH reduction[a] and the influence of $Mg(ClO_4)_2$ on NMR chemical shift of α-proton of substrates[b]

Substrate	Yield of reduced products (%)					NMR shift to lower field (Hz)
	CH_3CN			CH_3OH		
	None	$Mg(ClO_4)_2$[c]	CH_3COOH[c]	None	CH_3COOH[c]	
1	0	62±7		10±4	71(42)[d]	7
2	0	22±4	8±3	0	16±6	3
3	10±2	96±6				10
4	0	0				2
2OH				0	5±3	
2NO$_2$				5±2	15±5	

a) 2 h reflux in the dark. b) [substrate]=1.0 M, [$Mg(ClO_4)_2$]=1.4 M, solvent: CD_3CN. c) [substrate]=0.10 M, [BzlNicH]=0.12 M, [$Mg(ClO_4)_2$]=0.14 M, [CH_3COOH]=1.0 M. d) Isolated yield for the 2 h reaction at room temperature in the dark.

by-products.

2OH is a suitable substrate to evaluate the effectiveness of the ortho hydroxyl group in the reduction of C=C double bonds. The NMR coupling constant between two olefinic protons (16 Hz) is compatible with *trans*-configuration, so that the steric hindrance between ortho hydroxyl group and β-nitro group would be almost disregarded. Table 3 indicates that the relatively fast disappearance of BzlNicH occurs on the addition of **2OH**, but the corresponding reduced product was neither detected by NMR nor isolated by extraction with chloroform. It would appear, therefore, that the fast disappearance of BzlNicH should be ascribed to the decomposition catalyzed by the ortho hydroxyl group.[19] In fact, the NMR spectrum of the reaction mixture showed that 20—40% of **2OH** were left unreacted. These results endorse that the ortho hydroxyl group is not effective in the reduction of the C=C double bond of **2OH** (and probably C=C double bonds in general). The finding provides a striking contrast to a number of precedents that the ortho hydroxyl group plays a crucial role in the dihydronicotinamide reduction of double bonds attached to aromatic rings.[23-26] The role of the ortho hydroxyl group has been ambiguous due to two undistinguishable effects: that is, the ortho hydroxyl group can activate the carbonyl (and its analogs) in the initial state through hydrogen bonding and, at the same time, it can stabilize the developed negative charge in the transition state by means of specific solvation (or intramolecular general acid catalysis).[20,22,26]

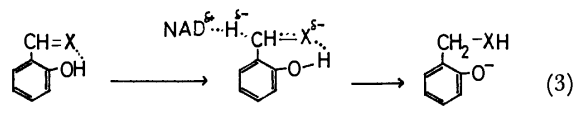

(3)

initial state transition state

We consider that the contribution of the ortho hydroxyl group in the initial state is less significant in the reduction of C=C double bonds, because it is well-known that C=C double bonds (as π bases) very weakly interact with the phenolic hydroxyl group.[11] On the other hand, the stabilization of the developing carbanion by the hydroxyl group in the transition state is still probable. The claim is supported by an example of the intermolecular reaction that BzlNicH reduction of **2** is general acid catalyzed by added acetic acid (*vide post*). Thus, the ineffectiveness of the ortho hydroxyl group suggests that, in the reduction of C=X (X: hetero atom) double bonds, hydrogen bonding with the ortho hydroxyl group in the initial state plays an indispensable role for the subsequent hydrogen transfer.

Influence of Added Mg^{2+} Ion. Prior to kinetic and product analyses, the possible interaction between substrates (**1**—**4**) and $Mg(ClO_4)_2$ (1.4 equivalents of substrate) was dissected. The UV spectrum of these four substrates (0.1 mM) in dry acetonitrile was hardly affected by added Mg^{2+} ion. The IR absorption band based on $\nu_{C=O}$ of **3** and **4** (solvent, acetonitrile) did not change appreciably in the presence of Mg^{2+} ion. On the other hand, added Mg^{2+} ion caused a significant change in the NMR chemical shifts of α-protons of **1** and **3** to lower field (Table 2), while those of **2** and **4** scarcely shifted. It is implicated, therefore, that the metal-substrate interaction does exist in **1** and **3** at least at the concentration used for the NMR measurements (*ca.* 1.0 M). On the contrary, the interaction with **2** and **4** is almost disregaded. It is expected that **3** would bahave as a bidentate ligand (*e.g.*, 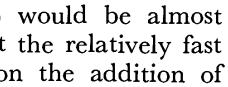), while the similar interaction between metal and **4** would be accompanied by condsiderable difficulty due to energetically-unfavorable conformational change (*e.g.*, chair form or other non-planar conformations between carbonyl and C=C double bond).

The reduction of **1**, **2**, and **3** was remarkably facilitated by added Mg^{2+} ion (Table 2). In particular, **3** was reduced quantitatively to the corresponding methylene compound within 2 h. It is interesting that the yield in the presence of Mg^{2+} ion shows a trend parallel to the NMR chemical shift. On the other hand, **4** which hardly interacts with Mg^{2+} ion was not subject to the Mg^{2+}-assisted reduction at all. Conceivably, the steric factor markedly suppresses the reactivity of **4**.

Ohno *et al.*[7,27] found that BzlNicH strongly interacts with Mg^{2+} ion. We also confirmed in the present study that the λ_{max} of BzlNicH in acetonitrile (345 nm) shifts to 352 nm on the addition of 2.0 equivalents of $Mg(ClO_4)_2$. The result substantiates, together with the absence of the spectral change of the substrates (*vide supra*), that BzlNicH preferentially interacts with Mg^{2+} ion. The parallel relation between the NMR shift and the yield suggests, however, that the interaction with the substrates is not necessarily meaningless: for example, the interaction could occur at least in the transition state. It is expected, of course, that, when the coordination ability of substrate is relatively superior,[6,28] the interaction with substrate occurs predominantly.

The kinetic measurements in the presence of Mg^{2+} ion were carried out at 30 °C in dry acetonitrile. Since **1** and **2** are not reduced by BzlNicH in the absence of Mg^{2+} ion, the decay of BzlNicH at $[Mg(ClO_4)_2]=0$ is attributed to the production of some by-products. The

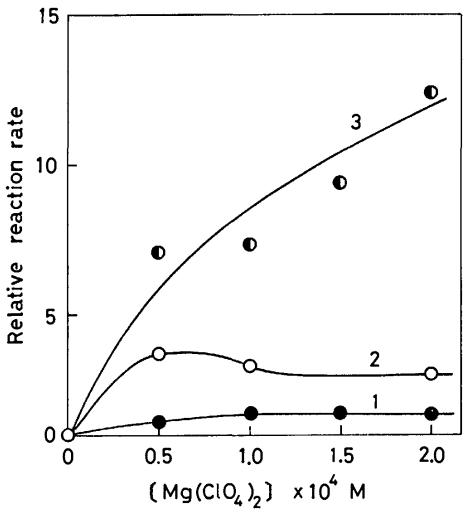

Fig. 1. $[Mg(ClO_4)_2]$ *vs.* relative reaction rate in acetonitrile.
[BzlNicH] = 1.00×10^{-4} M, [substrate] = 5.00×10^{-3} M.

reaction rates were determined by varying the concentration of Mg^{2+} ion while maintaining the concentration of BzlNicH constant. The relative reaction rates thus obtained were plotted as a function of the concentration of Mg^{2+} ion in Fig. 1. A small rate augmentation of 1.4—3.3 fold was observed for the reaction with **1** and **2**, and the reaction with **3** was further enhanced (7—12 fold). The largest rate increase in **3** is consistent with the expectation that **3** interacts with Mg^{2+} ion most strongly among three substrates employed. The reaction rates showed saturation tendencies with increasing Mg^{2+} concentration, but the clear rate maximum which was reported for the reaction with 2-benzoylpyridine[6] was not found.

Scheme 1 may be proposed for the reduction of **3**, where the k_3 term involves the reaction of Mg^{2+}-coordinated BzlNicH and substrate ($k_{Mg^{2+}-BzlNicH}$) and the reaction of BzlNicH and Mg^{2+}-coordinated substrate ($k_{Mg^{2+}-S}$). If a relation, $k_2 < k_{BzlNicH}, k_{Mg^{2+}-S}$, is assumed, the experimental results for **3** is explained consistently by Scheme 1.

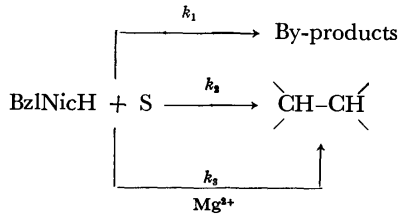

Scheme 1.

The reaction with **1** and **2** may be also rationalized by Scheme 1, but a question arises whether or not the drastic change in the yield (Table 2) can be explained by such small rate augmentations (for example, only 1.7 fold for **1**). It seems as if scheme 2 is more plausible for the reaction with **1** and **2** which features the rate-limiting formation of an intermediate followed by a Mg^{2+} dependent partition.

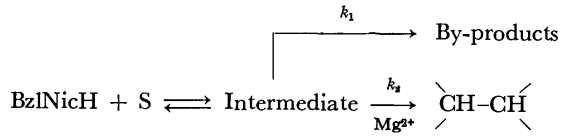

Scheme 2.

According to Scheme 2, the discrepancy between the slight rate enhancement and the dramatic improvement of the yield can be readily explained. It becomes difficult, however, to rationalize the saturation phenomena, for Mg^{2+} ion is not involved in the rate-limiting step in Scheme 2. Thus, both Schemes may be concurrent in the reduction of **1** and **2**.

Influence of Added Acetic Acid. The role of metal ion in dihydronicotinamide reduction is complicated because of its potential interaction with dihydronicotinamide and substrate both in the initial and transition states. In contrast, the role of Brösted acid is fairly simplified, since the interaction with dihydronicotinamide is offset as acid-catalyzed decomposition by the blank reaction in the absence of substrate. In addition, the interaction with substrate in the initial

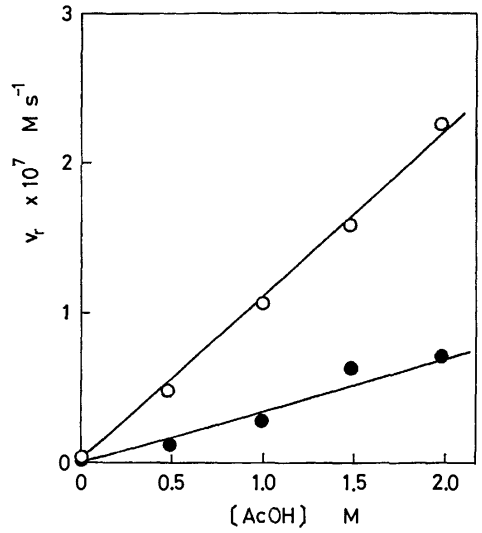

Fig. 2. v_r for the reaction of BzlNicH and **2** in acetonitrile (○) and in ethanol (●) plotted as a function of the concentration of acetic acid. [BzlNicH] = 1.00×10^{-4} M, [**2**] = 5.00×10^{-3} M.

state (*i.e.*, specific acid catalysis) is hardly conceivably. Thus, the interaction occurs only in the transition state.

As shown in Fig. 2, plots of v_r *vs.* [AcOH] gave good linear relations ($r > 0.98$), and Eq. 4 follows,

$$v_r = k_r[\text{BzlNicH}][\text{S}] + k_{\text{AcOH}}[\text{BzlNicH}][\text{S}][\text{AcOH}], \quad (4)$$

where k_{AcOH} is the third-order rate constant for acetic acid assisted rate acceleration which can be calculated from the slope in Fig. 2. The results are summarized in Table 3.

The reaction of BzlNicH and **2** is very slow without acetic acid, and the corresponding reduced product is not obtained. The addition of acetic acid brought forth the enhancement of the rate and the yield simultaneously. Evidently, acetic acid is involved in the rate-limiting step, and the role is reasonably designated as a general acid catalysis.[20,22] Thus, the reaction mechanism analogous to Scheme 1 is in effect for **2**.

The reduction of **1** is not the case, however. As shown in Tables 2 and 3, added acetic acid does not accelerate the disappearance of BzlNicH at all despite the fact that the yield is remarkably enhanced.[18] The discrepancy cannot be explained by Scheme 1 in which the improvement in the yield *must be* accompanied by the rate enhancement. Alternatively, Scheme 2 may be adopted as a possible mechanism for **1**. Although it is difficult to specify "intermediate" at present, the formation of some radical species is expected.[18,29,30]

Concluding Remark. The various kinds of electron-deficient C=C double bonds are reduced by the aid of metal ion or acetic acid, as has been reported by some groups.[18,31,32] However, the combination of kinetic studies with product analyses clarified that the role of added acids is not simple. We believe that the clear understanding of the behavior of metal ions and Brönsted acids would bear further application of nonenzymatic dihydronicotinamide reductions.

We thank Professor Toyoki Kunitake (Kyushu University) for helpful discussion.

References

1) T. C. Bruice and S. J. Benkovic, "Bioorganic Mechanisms," W. A. Benjamin, New York, N. Y. (1966), Vol. 2, Chap. 9.
2) A. Ohno and Y. Ohnishi, *Kagaku No Ryoiki Zokan*, **110**, 57 (1976).
3) S. Shinkai, *Kagaku*, **29**, 917 (1974).
4) M. J. Adams, M. Buehner, K. Chandrasekhar, G. C. Ford, M. L. Hackert, A. Liljas, M. G. Rossmann, I. E. Smiley, W. S. Allison, L. Everse, N. O. Kaplan, S. S. Taylor, *Proc. Nat. Acad. Sci. USA*, **70**, 1968 (1973).
5) D. Moras, K. W. Olsen, M. N. Sabesan, M. Buehner, G. C. Ford, and M. G. Rossmann, *J. Biol. Chem.*, **250**, 9137 (1975).
6) R. A. Gase, G. Boxhoorn, and U. K. Pandit, *Tetrahedron Lett.*, **1976**, 2889.
7) A. Ohno, H. Yamamoto, T. Kimura, and S. Oka, *Tetrahedron Lett.*, **1976**, 4585.
8) B. P. Bell and A. O. McDougall, *Trans. Faraday Soc.*, **56**, 1281 (1960).
9) Y. Pocker, J. E. Meary, and C. Zadorojny, *J. Phys. Chem.*, **75**, 792 (1971).
10) Y. Pocker and M. J. Hill, *J. Am. Chem. Soc.*, **91**, 7154 (1969).
11) H. Iwamura, *Kagaku Zokan*, **21**, 117 (1965).
12) R. Heuck, *Ber.*, **28**, 2253 (1895).
13) C. B. Gairand and G. R. Lappin, *J. Org. Chem.*, **18**, 3 (1953).
14) E. H. Kroeker and S. M. McElvain, *J. Am. Chem. Soc.*, **56**, 1172 (1934).
15) J. A. Hedge, C. W. Kruse, and H. R. Snyder, *J. Org. Chem.*, **26**, 3167 (1961).
16) K. H. Slatta and G. Szyszka, *Ber.*, **68**, 189 (1935).
17) S. Shinkai, R. Ando, and T. Kunitake, *Bull. Chem. Soc. Jpn.*, **48**, 1914 (1975).
18) K. Wallenfels, W. Ertel, and Friedrich, *Justus Liebigs Ann. Chem.*, **1973**, 1663.
19) C. C. Johnston, J. L. Gardner, C. H. Suelter, and D. E. Metzler, *Biochemistry*, **2**, 689 (1963).
20) S. Shinkai and T. Kunitake, *Chem. Lett.*, **1977**, 297.
21) R. W. Taft, Jr., and I. C. Lewis, *J. Am. Chem. Soc.*, **81**, 5343 (1959).
22) P. van Eikeren and D. L. Grier, *J. Am. Chem. Soc.*, **98**, 4655 (1976).
23) R. H. Abels, R. F. Hutton, and F. H. Westheimer, *J. Am. Chem. Soc.*, **79**, 712 (1957).
24) U. K. Pandit and F. R. Mas Cabre, *J. Chem. Soc., Chem. Commun.*, **1971**, 552.
25) S. Shinkai and T. C. Bruice, *Biochemistry*, **12**, 1750 (1973).
26) S. Shinkai, S. Shiraishi, and T. Kunitake, *Bull. Chem. Soc. Jpn.*, **49**, 3656 (1976).
27) A. Ohno, T. Kimura, H. Yamamoto, S. G. Kim, S. Oka, and Y. Ohnishi, *Bull. Chem. Soc. Jpn.*, **50**, 1535 (1977) and references cited therein.
28) U. K. Pandit, H. van Dam, and J. B. Steevens, *Tetrahedron Lett.*, **1977**, 913.
29) T. Okamoto, A. Ohno, and S. Oka, *J. Chem. Soc., Chem. Commun.*, **1977**, 181.
30) R. J. Kill and D. A. Widdoson, *J. Chem. Soc., Chem. Commun.*, **1976**, 755.
31) R. A. Gase and U. K. Pandit, *J. Chem. Soc., Chem. Commun.*, **1977**, 480.
32) Y. Ohnishi, M. Kagami, T. Numakunai, and A. Ohno, *Chem. Lett.*, **1976**, 915.

Reaction of Organic Tin(II) Compound with Phenyl Isothiocyanate and Carbon Disulfide

Ikuko WAKESHIMA,* Yoshihiro SAITOH, and Ichiro KIJIMA

Department of Industrial Chemistry, Faculty of Engineering, Science University of Tokyo, Kagurazaka, Shinjuku-ku, Tokyo 162

(Received December 22, 1977)

Reaction of organic tin(II) compounds, $Sn(OR)_2$[R=C_2H_5, $CH_2CH_2N(CH_3)_2$, C_6H_5, *o*-$CH_3C_6H_4$], with phenyl isothiocyanate and carbon disulfide have been investigated. The reaction of di(ethoxo)tin(II) with phenyl isothiocyanate in benzene at room temperature gave the corresponding addition product. The reaction at 80—81 °C however gave diethyl *N*-phenylcarbonimidate. Phenyl isothiocyanate reacted exothermically with bis[2-(dimethylamino)ethoxo]tin(II) to yield the 1:1 addition product. In the reaction with bis(2-methylphenoxo)-tin(II), a compound containing one molecule of phenyl isothiocyanate per two molecules of the tin(II) compound was isolated, but the reaction with di(phenoxo)tin(II) did not occur. Di(ethoxo)tin(II) reacted with carbon disulfide to give diethyl thiocarbonate, diethyl carbonate, and tetraethyl orthocarbonate. Bis(*o*-methylphenoxo)-tin(II) and di(phenoxo)tin(II) however did not react with carbon disulfide.

Since P. G. Harrison and J. J. Zuckerman reported the reaction between di(methoxo)tin(II) and multiple-bond compounds,[1] there have been many investigations concerning the reactivity of organic and organotin(II) compounds.[2-6] The reaction of alkylalkoxotin(IV) with phenyl isothiocyanate led to the corresponding *S*-stannyl derivatives[7-8] and di(methoxo)tin(II) reacted with phenyl isothiocyanate to give the corresponding *N*-stannyl derivative.[1] In the reaction of alkylalkoxotin-(IV) and di(ethoxo)tin(II) with carbon disulfide, S. Sakai and coworkers reported that alkylalkoxotin(IV) reacted with carbon disulfide to give the corresponding orthocarbonate, dithiocarbonate or carbonate. However di(ethoxo)tin(II) did not react.[9]

In this paper, the reaction of organic tin(II) compounds, $Sn(OR)_2$[R=C_2H_5, $CH_2CH_2N(CH_3)_2$, C_6H_5, *o*-$CH_3C_6H_4$], with phenyl isothiocyanate and carbon disulfide will be described.

Results and Discussion

Reaction of Organic Tin(II) Compound with Phenyl Isothiocyanate. The reaction of di(ethoxo)tin(II) (**1**), bis[2-(dimethylamino)ethoxo]tin(II) (**2**), bis(*o*-methyl-phenoxo)tin(II) (**3**), and di(phenoxo)tin(II) (**4**) with phenyl isothiocyanate (PhNCS) were conducted in

Table 1. Reactions of $Sn(OR)_2$ with PhNCS

$Sn(OR)_2$	Reaction conditions: [PhNCS]/[$Sn(OR)_2$]	Temp (°C)	Time(h)	Products[a]: Yield (%)	Mp(°C) (Dec)	Sn(%) (Calcd)	$\nu_{C=S}$ (cm^{-1})	Ref.	
1	1	48—50	10[b]	66	69	33.6[c] (34.6)	1225	$Sn(OC_2H_5)(NCSOC_2H_5)Ph$	(**5**)
1	2	30—32	3	96	53	24.9 (24.8)	1225	$Sn(NCSOC_2H_5)_2Ph$	(**6**)
2	1	17—19	3	92	110	27.1 (27.6)	1148	$Sn(OC_2H_4N(CH_3)_2)(NCSOC_2H_4N(CH_3)_2)Ph$	(**7**)
2	2	19—20	3	89	110	27.1 (27.6)	1148	(**7**)	
3	1	32—33	3	61	90	29.8 (29.8)	1150	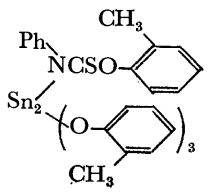	(**8**)[d]
3	2	30—34	15	23	90	29.8 (29.8)	1150	(**8**)	
4	1	30—31	3	85	171	38.1 (38.9)		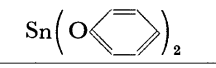	(**4**)

a) All compounds are white powders. b) In min. c) Although the existence of 1:2 addition product **6** is estimated, it was impossible to separate compound **6** from compound **5**. d) N (%); 1.74 (Calcd for $C_{35}H_{33}NO_4SSn_2$, 1.76%).

benzene and the results are summarized in Table 1.

Compound **1** reacted with two equivalents of PhNCS in benzene at 30—32 °C to give the 1 : 2 addition product (**6**) in good yield. However, in the case of 1 : 1 molar ratio, the reaction was sluggish and brought to completion by heating at 48—50 °C. The reaction between compound **2** and one or two equivalents of PhNCS was exothermic and proceeded smoothly below 20 °C to afford only the 1 : 1 addition product (**7**). In the case of compound **3** with PhNCS, the resulting product was found to be a compound containing one molecule of PhNCS per two molecules of compound **3**. Compound **4** did not react. All of the isolated products **5**—**8** were sensitive to atmospheric moisture, exhibiting a new characteristic absorption band assigned to $\nu_{C=S}$ at 1148—1225 cm^{-1}. These results suggest the formation of an Sn–N bond. In addition, the *N*-phenylthiocarbamate derivatives were isolated as the hydrolysis products of compounds **5**—**8**. On the basis of these results, the aryloxotin(II) compounds **3** and **4** may be considered less reactive than the alkoxotin(II) compounds **1** and **2**. This difference may be attributed to the decrease in nucleophilicity of oxygen by the R-effect of the aryl group on the Sn–O–Ar bond.

When compound **1** was treated with PhNCS under reflux in benzene, a transparent liquid and black-brown solid were formed. The liquid was assinged as diethyl *N*-phenylcarbonimidate (**9**) according to elemental analysis, IR and NMR spectra. The carbonimidate was also obtained by heating the addition product **5** in benzene at 80—81 °C. Therefore, it is thought that the intermediate **a** results from a rearrangement of the tin atom from nitrogen to sulfur which further reacts with $Sn(OC_2H_5)_2$ to give the elimination products as shown in Scheme 1.

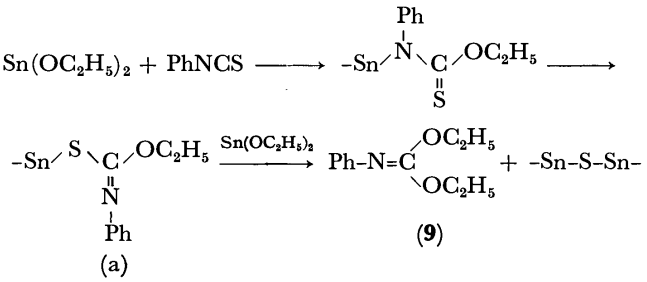

Scheme 1.

Reaction of Organic Tin(II) Compounds with Carbon Disulfide. The reaction of the compound **1** with carbon disulfide (CS_2) in benzene afforded diethyl thiocarbonate (**10**) ($\nu_{C=S}$ 1235 cm^{-1}), tetraethyl orthocarbonate (**11**) (ν_{C-O} 1185, 1115 cm^{-1}), and diethyl carbonate (**12**) ($\nu_{C=O}$ 1750 cm^{-1}). The yields depended on the reaction temperatures; the reaction at 69—71 °C for 20 h afforded compounds **10**, **11**, and **12** in 8, 16, and 48% yields, respectively, whereas the reaction at room temperature (below 22 °C) for one month lead to the formation of compound **10**, **11**, and **12** in 3, 42, and 4% yields, respectively. In each reaction, the NMR spectra of the benzene removed indicated the presence

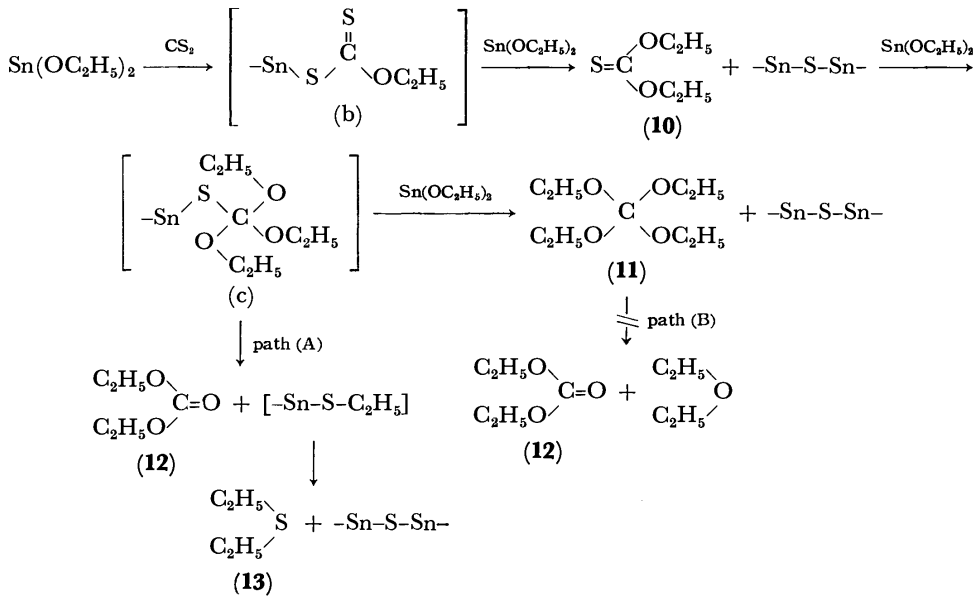

Scheme 2.

TABLE 2. REACTION OF $Sn(OR)_2$ WITH CS_2

$Sn(OR)_2$	Reaction conditions		Products and yields (%)[c]		
	Temp (°C),	Time (h)	Compound **10**,	Compound **11**,	Compound **12**
1	69—71[a]	20	8	16	46
	r.t.(<22°C)[a]	one month	3	42	4
3	68—71[a]	20		no reaction	
4	60—65[b]	8		no reaction	

a) Benzene solution. b) Hexane solution. c) Based on the proton ratio of NMR spectra.

of a slight amount of diethyl sulfide (**13**).

Scheme 2 suggests the following reaction route; first, the nucleophilic attack of compound **1** on carbon disulfide produces the intermediate **b**. Subsequently, the attack of compound **1** on the carbon atom of >C=S group on the intermediate **b** results in the formation of compound **10** and tin sulfide. Furthermore, the attack of $Sn(OC_2H_5)_2$ on compound **10** gives the intermediate **c** which may undergo either the nucleophilic attack of compound **1** with the formation of compound **11** or intramolecular elimination followed by the formation of compound **12** (path A). This path is supported from the proton NMR spectra data; CH_3 8.76 (t) and CH_2 7.50 (q) ppm.[10] Assuming path B is a possible route, then diethyl ether should be derived from compound **11** (path B). However, no direct evidence for the presence of diethyl ether has been obtained.

The reaction of compounds **3** and **4** with CS_2 at 69—71 °C in benzene, showed no appreciable change occured. These results are summarized in Table 2.

Experimental

Experiments were carried out in a nitrogen atmosphere dried with liquid nitrogen. The melting and boiling points are uncorrected. IR spectra were recorded with a Hitachi EPI-2S spectrometer and ^{1} NMR spectra on a Hitachi R-24 (60 MHz) using TMS as an internal standard. The elemental analysis were carried out with a Yanagimoto MT-2 CHN corder. Liquid chromatographic determinations were performed on a Nippon Bunseki LC-08, using a polystyrene–divinylbenzene copolymer GPC column.

PhNCS was dried with the azeotropic distillation method using benzene which was freshly distilled before use. Carbon disulfide was purified according to the method of Pestermer[11] and distilled after dehydration over P_2O_5.

Reaction of Compound 1 with PhNCS in a 1: 1 Molar Ratio. In a flask equipped with a mechanical stirrer, a condenser, and a dropping funnel, were placed compound **1** (11.6 g, 56 mmol) and benzene (28 ml). PhNCS (7.5 g, 55 mmol) was slowly added so that the temperature did not exceed 24—24.5 °C. After stirring at room temperature for 2 h, the flask was allowed to stand overnight, followed by heating at 48—50 °C for 10 min with stirring. During this time, the heterogeneous solution became almost clear together with a small amount of black solid. After suction filtration, the filtrate was concentrated *in vacuo* to about one-half of the volume, and hexane (30 ml) was added to the residue. The resulting white precipitates were collected by filtration, washed with benzene, and dried to give 12.8 g (66%) of product **5**. Analytical and physical data are summarized in Table 1.

Reaction of Compound 1 with PhNCS in a 1: 2 Molar Ratio. In a similar procedure, PhNCS (21.2 g, 157 mmol) was slowly added to the suspension of compound **1** (16.2 g, 78 mmol) in benzene and heated at 29—30 °C for 3 h. During this time, the heterogeneous solution became clear without any formation of the black solid. After concentration to one-half volume, hexane (30 ml) was added to the residue. The white powdery precipitates were isolated in a 96% yield (25.9 g).

Reaction between Compound 4 and PhNCS. After compound **4** was treated with PhNCS under the conditions described in Table 1, the unreacted compound **4** was recovered in a 85% yield.

Reaction of Compound 1 with PhNCS in Boiling Benzene. Compound **1** (12.5 g, 60 mmol) was refluxed in benzene for 5 h. After separation of the resultant black solid, ditillation of the filtrate under reduced pressure gave diethyl *N*-phenylcarbonimidate (**9**) in 50% yield (5.8 g): bp 117 °C at 8 mmHg (lit,[12] 122 °C at 12 mmHg); IR (liquid film), $\nu_{C=N}$ 1660cm^{-1}; NMR (CCl_4, τ), 8,85 (t, CH_3), 5.89 (q, CH_2), and 2.7—3.3 (m, C_6H_5) ppm; Found, C, 68.51; H, 7.91; N, 7.28%, Calcd for $C_{11}H_{15}NO_2$, C, 68.37; H, 7.82; N, 7.25%. The treatment of compound **9** with 2 M-HCl ethanolic solution lead to the formation of a compound having a characteristic band at 1745 cm^{-1}.

Reaction of Compound 1 with CS_2. CS_2 (10.2 g, 34 mmol) was added dropwise to a suspension of compound **1** (13.3 g, 63 mmol) in benzene (31 ml) with stirring, and the mixture refluxed for 20 h. The heterogeneous reaction mixture changed gradually from a semi-transparent mixture to yellowish transparent solution with the formation of a black suspension. After the insoluble solids were removed by filtration, the benzene solution was distilled to afford two fractions; bp 35—50 °C at 28 mmHg, bp 50—75 °C at 28 mmHg. Each fraction was subjected to liquid chromatography (eluant, $CHCl_3$): the former gave compound **12** and the latter a mixture of **10**, **11**, and **12**.

Compound **10**: IR (CCl_4 soln); 1235 cm^{-1} (C=S). NMR (τ); 8.57 (CH_3), 5.67 (CH_2) ppm.

Compound **11**: IR (liquid film); 1185, 1115 cm^{-1} (C–O), NMR (τ); 8.85 (CH_3), 6.48 (CH_2) ppm.

Compound **12**: IR (liquid film); 1750 cm^{-1} (C=O), 1260 cm^{-1} (C–O), NMR (τ); 8.75 (CH_3), 5.99 (CH_2) ppm.

Compound **3** and **4** were treated with CS_2 according to a similar procedure, and the unreacted tin(II) compounds were recovered in quantitative yields.

General Procedure of Hydrolysis. Compound **5**—**8** were hydrolyzed with a solution of water (5—6 ml) and acetone (100 ml) at room temperature. After separation of inorganic tin with a centrifugal separator, the organic layer was concentrated under reduced pressure and cooled with an ice bath. The resulting white crystals were filtered off and dried. Physical and analytical data were as follows:

$PhNHC(S)OC_2H_5$: Mp 68—70 °C (lit,[13] 71—72 °C), IR; 1205 cm^{-1} ($\nu_{C=S}$), Found, C, 59.4; H, 6.10; N, 7.60%. Calcd for $C_9H_{11}NOS$, C, 59.6; H, 6.12; N, 7.73%.

$PhNHC(S)OCH_2CH_2N(CH_3)_2$: A pale yellow viscous liquid, IR; 1115 cm^{-1} ($\nu_{C=S}$), Found, C, 58.1; H, 7.22; N, 12.2%. Calcd for $C_{11}H_{16}N_2OS$, C, 58.9; H, 7.14; N, 12.5%.

$PhNHC(S)O$-*o*-$CH_3C_6H_4$: Mp 146—148 °C, IR; 1150 cm^{-1} ($\nu_{C=S}$) Found, C, 69.2; H, 5.34; N, 5.86%, Calcd for $C_{14}H_{13}NOS$, C, 69.1; H, 5.35; N, 5.67%.

References

1) P. G. Harrison and J. J. Zuckerman, *Chem. Commun.*, **1969**, 321.

2) K. D. Bos, H. A. Budding, E. J. Bulten, and J. G. Noltes, *Inorg. Nucl. Chem. Lett.*, **9**, 963 (1973).

3) I. Wakeshima and I. Kijima, *Bull. Chem. Soc. Jpn.*, **48**, 953, 1069 (1975).

4) I. Wakeshima and I. Kijima, *J. Organomet. Chem.*, **76**, 37 (1974).

5) P. G. Harrison, *Chem. Commun.*, **1972**, 544.

6) A. B. Cornwell and P. G. Harrison, *J. Chem. Soc., Dalton Trans.*, **1975**, 1486, 2017.

7) A. G. Davies and P. G. Harrison, *J. Chem. Soc., C*, **1967**, 1313.

8) A. J. Bloodworth, A. G. Davies, and S. C. Vasishtha, *J. Chem. Soc., C*, **1967**, 1307.

9) S. Sakai, T. Fujinami, T. Yamada, and T. Furusawa,

Nippon Kagaku Kaishi, **1975**, 1789.
10) P. G. Harrison and S. H. Stobart, *Inorg. Chim. Acta*, **7**, 308 (1973).
11) M. Pestmer, *Angew. Chem.*, **63**, 121 (1951).
12) B. Prager, P. Jacobson, P. Schmidt, and D. Stern, "Beilsteins Handbuch der Organischen Chemie," (1929), Vol. 12, p. 446.
13) B. Prager, P. Jacobson, P. Schmidt, and D. Stern, "Beilsteins Handbuch der Organischen Chemie," (1929), Vol. 13, p. 386.

Chemical Transformation of Seldomycin 5 into 3′-Deoxyseldomycin 5 and Related Compounds[1)]

Hideo MATSUSHIMA,* Yasuki MORI, and Kozo KITAURA**

Tokyo Research Laboratory, Kyowa Hakko Kogyo Co., 3-6-6, Asahimachi, Machida, Tokyo 194

***Pharmaceuticals Research Laboratory, Kyowa Hakko Kogyo Co., Nagaizumimachi, Suntogun, Shizuoka 411*

(Received January 24, 1978)

3′-Deoxyseldomycin 5 (**2**), 2′-deamino-3′-epiamino-3′-deoxyseldomycin 5 (**14**), and 2′,3′-epimino-2′-deamino-3′-deoxyseldomycin 5 (**15**) were prepared from seldomycin 5 (**1**). Treatment of hexa-*N*-ethoxycarbonyl (ecb)-3′-*O*-tosylseldomycin 5 with sodium borohydride in DMSO gave the corresponding *N*-ecb-derivatives of **2**, **14**, and **15**. Removal of the ecb groups of these compounds with aq potassium hydroxide gave the free bases **2**, **14**, and **15**, respectively. Structure determination of the products was performed by means of MS, CMR, PMR, and chemical reactions. It was found that **2** exhibits a more potent and broader antibacterial activity than the parent compound **1**, and **14** shows unique antibacterial spectrum against resistant strains, whereas **15** has almost no activity.

Synthesis of 3′-deoxy derivatives of aminoglycoside antibiotics has been studied extensively, since it was disclosed by H. Umezawa and S. Umezawa that resistance of certain clinically isolated bacteria against kanamycin is due to enzymatic 3′-*O*-phosphorylation of the antibiotic, and that 3′-deoxykanamycin, designed rationally upon this mechanism of resistance, exhibits strongly recovered antibacterial activity against the resistant strains.[2)] Seldomycin 5 (SLD-5) (**1**), a new aminoglycoside antibiotic found in our institute, is inactivated, like other aminoglycoside antibiotics, by various resistant strains including those bacteria which produce aminoglycoside 3′-phosphotransferase.[3)] In a previous paper, we reported that the inactivation of SLD-5 by enzymatic 3′-*O*-phosphorylation is inhibited by the change of configuration of the 3′-hydroxyl group of **1**.[4)] In this paper, we describe the synthesis of 3′-deoxy-SLD-5 (**2**) and related compounds as a modification to enhance and broaden the antibacterial activity of **1**. We expected **2** to exhibit more potent activity than the parent compound since **2** has a pseudodisaccharide unit, 3′,4′-dideoxyneamine (**3**), which constructs the common partial structure of gentamicin C_{1a} (GM-C_{1a}) (**4**)[5)] and 3′,4′-dideoxykanamycin B (DKB) (**5**).[6)] The latter two compounds are well-known aminoglycoside antibiotics that have very strong intrinsic activity against various bacteria.

Results and Discussion

Synthesis and Identification of the Products. Attempts were made to convert hexa-*N*-ethoxycarbonyl(ecb)-3′-*O*-tosyl-SLD-5 (**6**)[4)] into 3′-iodo derivative by the usual procedure using sodium iodide, but TLC of the reaction mixture indicated that the reaction is complicated. S_N2 substitution reaction of a tosyloxy group by a nucleophile does not occur smoothly when an approaching nucleophile and a substituent at γ position are in 1,3-diaxial relationship. 1,2,4,6-Tetra-*O*-benzoyl-3-*O*-tosyl-α-D-glucopyranose is recovered on the nucleophilic displacement reaction with sodium benzoate.[7)] 1,2:5,6-Di-*O*-isopropylidene-3-*O*-tosyl-α-D-glucofuranose is recovered in a 90% yield on reaction with azide ion.[8)] Steric and polar factors affecting reactivity of a sulfonyloxy group of carbohydrate have been summarized[9)] and such steric hindrance has been reported in the field of steroid chemistry.[10)] The results suggest that the α-glycosidic linkage at the 1′ position of **6** blocks the approach of an iodide ion from side α to the 3′ position in our case also. However, penta-*N*-ecb-3′-*O*-tosylkanamycin B was successfully converted into 3′-iodo derivative in an exceptionally good yield.[11)] Successful iodination was attributed to the neighboring group participation of the 2′-ethoxycarbonylamino group.[11)] However, an alterna-

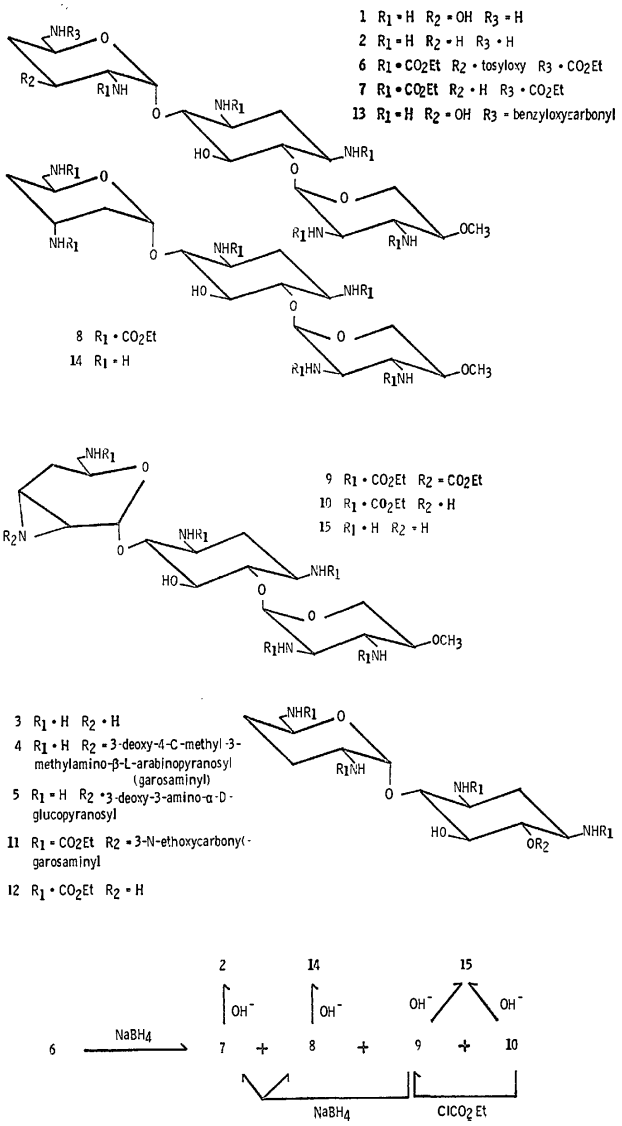

TABLE 1. CMR CHEMICAL SHIFTS OF COMPOUNDS **7**, **9**, **10**, AND **11**[a]

Compound	**7**		**11**[15),f)]	**9**		**10**	
Solvent	DMSO-d_6	pyr.-d_5[b)]	DMSO-d_6	DMSO-d_6	pyr.-d_5[b)]	DMSO-d_6	pyr.-d_5[b)]
C-1′	98.3	100.0	98.3	93.4	94.5	95.2	97.2[e)]
C-2′	50.7	51.5	50.2	36.5[c)]	37.2[d)]	27.7	28.3
C-3′	23.5	25.0	23.9	36.1[c)]	36.8[d)]	29.4	30.5
C-4′	27.2	28.1	27.5	26.9	27.4	27.7	28.3
C-5′	66.6	68.1	67.1	64.0	65.0	64.0	65.3
C-6′	44.6	45.5	45.0	44.0	44.9	44.2	45.2
C-1	50.7	51.9	50.8	50.7	51.8	50.7	52.0
C-2	35.0	36.0	34.7	35.1	35.8	35.1	36.0
C-3	49.9	51.1	50.2	49.2	50.3	49.6	50.7
C-4	82.1	83.0	82.4	80.1	80.6	79.5	81.1
C-5	74.8	76.3	74.9	74.7	75.7	74.5	75.7
C-6	79.6	81.8	81.8	79.4	80.0	79.0	79.9
C-1″	96.9	98.6	98.8	96.7	97.7	96.5	97.9[e)]
C-2″	54.4	55.5	64.5	54.4	55.2	54.4	55.4
C-3″	53.2	54.5	58.6	53.2	54.3	53.3	54.5
C-4″	76.2	78.5	73.1	76.4	78.0	76.4	78.5
C-5″	59.5	61.4	69.6	59.6	62.4	59.5	61.1
OCH_3	57.5	58.2	—	57.6	58.2	57.6	58.3
$CO_2CH_2\underline{CH_3}$	14.4	14.8	14.5	14.4	14.4	14.5	14.8
					14.8		
$CO_2\underline{CH_2}CH_3$	59.5	60.6	59.7	59.6	60.1	59.5	60.3
	60.0		60.5		60.3		
					61.0		
CO	155.7	156.8	155.7	155.9	156.5	155.6	156.6
	155.8	157.5	156.1	156.6	157.1	155.9	157.4
	156.5	157.7		162.5	157.3	156.5	157.5
		158.0			157.5		157.7
					163.2		

a) Reported in ppm from internal TMS. b) Pyridine-d_5 containing 10% DMSO-d_6 to increase solubility of the sample. c) d) e) Interconvertible. f) Data on N-CH_3 and C-CH_3 omitted.

tive explanation might be given by the present result.***

*** In the case of kanamycin B, the smooth displacement of the 3′-tosyloxyl group by iodide ion might occur with the aid of the neighboring 4′-hydroxyl group participation to form a 3′,4′-anhydro derivative as an intermediate, followed by dieq-uatorial opening of the epoxide ring [N. R. Williams, *Adv. Carbohydr. Chem. Biochem.*, **25**, 109 (1970)] due to the regio-specific attack of iodide ion at the 3′ position. The cause of regiospecifity can be explained as follows. The epoxide is considered to adopt one of the conformers (i) or (ii). If the epoxide exists as conformer (i), the attack of iodide ion at 4′ position might be hindered by the 1,3-diaxial electrostatic repulsion between the approaching iodide ion and the lone pair electrons of the pyranose-ring oxygen. If the epoxide

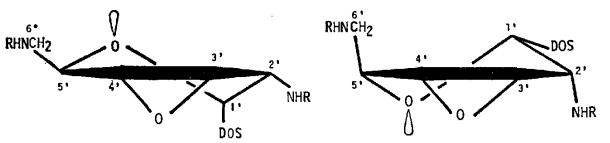

(i) (ii)

exists as conformer (ii), the attack of iodide ion at 4′ position might sterically be hindered by the adjacent *quasi*-axial 5′-ethoxycarbonylaminomethyl group, thus resulting in the regiospecific formation of the 3′-iodo derivative. In the case of compound **6**, no such epoxide intermediate can be formed since **6** has no 4′-hydroxyl group.

Bell *et al.* reported that treatment of several sulfonates with sodium borohydride in dimethyl sulfoxide (DMSO) or diglyme gives deoxygenated products.[12] Application of this method to carbohydrate derivatives has been reported.[13,14] We have adopted the reaction to reduce **6**.

Treatment of **6** with sodium borohydride in DMSO afforded the following four products after chromatographic separation; hexa-*N*-ecb-3′-deoxy-SLD-5 (**7**) (20.1%), hexa-*N*-ecb-2′-deamino-3′-epiamino-3′-deoxy-SLD-5 (**8**) (23.3%), 1,3,6′,2″,3″-penta-*N*-ecb-2′,3′-*N*-ecb-epimino-2′-deamino-3′-deoxy-SLD-5 (**9**) (21.8%), and 1,3,6′,2″,3″-penta-*N*-ecb-2′,3′-epimino-2′-deamino-3′-deoxy-SLD-5 (**10**) (14.8%). The structure of **7** was elucidated by comparison of its CMR spectrum with that of penta-*N*-ecb-GM-C_{1a}[15] (**11**) (Table 1). The chemical shifts for C-1′—C-6′ and C-1—C-5 of **7** correspond to those for the carbons of **11** which has a common disaccharide unit, 1,3,2′,6′-tetra-*N*-ecb-3′,4′-dideoxyneamine (**12**). The ecb groups of **7** were removed by aq methanolic potassium hydroxide to give 3′-deoxy-SLD-5 free base (**2**). Its structure was confirmed by MS, PMR, and CMR spectra.[1] Compound **2** consumed 1.00 mol/mol periodate (theoretical value: 1.00); **1** consumed 2.90 (theoretical value: 2.00) under carefully controlled conditions. Although we have tentatively attributed the excess uptake of periodate

Table 2. CMR chemical shifts of compounds **14** and **15**[a]

	14 (3′-epiamino-)			**15** (2′,3′-epimino-)		
	Free base	PD 1.5	*M*[b]	Free base	PD 1.7	*M*
C-1′	100.4	98.5	d	96.3	91.4	d
C-2′	36.6[c]	32.8	t	29.2[d]	36.1	d
C-3′	42.9	42.9	d	31.2[d]	36.1	d
C-4′	35.4[c]	29.2	t	27.3	21.9	t
C-5′	69.1	64.5	d	66.8	63.3	d
C-6′	44.9	43.6	t	45.3	43.3	t
C-1	51.3	50.9	d	51.4	50.9	d
C-2	36.9	28.9	t	36.4	28.8	t
C-3	50.0	48.7	d	49.8	49.1	d
C-4	88.0	80.8	d	83.7	78.0	d
C-5	75.1	73.9	d	75.6	74.7	d
C-6	86.9	81.2	d	87.1	81.4	d
C-1″	100.4	94.7	d	100.4	94.9	d
C-2″	56.2	50.7	d	56.1	50.6	d
C-3″	54.9	49.9	d	54.8	49.8	d
C-4″	80.3	73.9	d	80.2	73.9	d
C-5″	60.7	61.7	t	60.7	61.8	t
OCH_3	58.8	58.5	q	58.8	58.6	q

a) Measured in D_2O solution with dioxane as an internal reference and reported by ppm from TMS. b) Multiplicity by off-resonance. c), d) Interconvertible.

by **1** to non-Malapradian oxidation of vicinal amino and methoxyl groups,[16] the present result together with another result concerning periodate oxidation of 6′-*N*-benzyloxycarbonyl-SLD-5 (**13**)[17] (consumption: 1.52, theoretical value: 2.00), indicate that our previous speculation was incorrect. The over-oxidation seems to take place only when both the 3′-hydroxyl and 6′-amino groups exist in the molecule.

The structure of **8** was determined retrospectively on the basis of the following spectroscopic data for deethoxycarbonylated compound, 2′-deamino-3′-epi-amino-3′-deoxy-SLD-5 free base (**14**). i) High resolution mass spectrum indicates that the molecular weight of **14** is 434.2816, which is isomeric with **2**. The deoxygenated structure was supported by the appearance of a prominent peak at *m/e* 129.[18] ii) In PMR spectrum of **14**, the H-1′ signal appeared at τ 4.68 as a broad double doublet with J=*ca.* 5 and *ca.* 2 Hz, which indicates that the 2′ position has no substituent. iii) In CMR (Table 2), the signal of C-2′ appeared at 36.6 ppm as a triplet by off-resonance and that of C-3′ at 42.9 ppm as a doublet. Protonation-β-shift of the spectrum was in line with the structure. No evidence was obtained that 3′-amino group is axially oriented. However, its orientation was suggested from the reaction mechanism.

Compounds **9** and **10** gave the same product, 2′,3′-epimino-2′-deamino-3′-deoxy-SLD-5 free base (**15**), by alkaline hydrolysis to remove ecb groups. The structure of **15** was determined by the following data. i) Mass spectrum of **15** gives a (M+1) and M peak at *m/e* 433 and 432, respectively. ii) PMR spectrum of **15** shows no signal of an olefinic proton. iii) In CMR spectrum of **15** (Table 2), two signals attributable to C-2′ and C-3′ appear at 29.2 and 31.2 ppm (or *vice versa*) as doublets, respectively. These signals shifted *ca.* 5—7 ppm downfield by acidifying the media, C-1′ and C-4′ signals shifted *ca.* 5 ppm upfield.

Elemental analyses of **9** and **10** indicate that **9** has

Table 3. Minimum inhibitory concentrations of compounds **1**, **2**, **4**, **5**, **14**, and **15** against sensitive strains (mcg/ml)

Strain	**1**[a]	**2**	**14**	**15**	**4**[b]	**5**[c]
Staphylococcus aureus 209-P	0.78	1.56	3.12	100	0.4	0.2
Smith	0.4	0.4	0.78	50	0.1	0.2
Newman	1.56	0.78	1.56	100	0.4	0.4
Staphylococcus epidermidis	0.78	0.4	1.56	50	0.05	0.2
Batillus subtilis ATCC 6633	0.4	0.4	0.78	25	0.05	0.1
Escherichia coli NIHJC-2	3.12	1.56	12.5	100	0.78	1.56
GN2411-5	3.12	1.56	12.5	100	0.78	1.56
Juhl	3.12	3.12	12.5	100	0.78	1.56
3100	6.25	3.12	25	100	0.78	1.56
Klebsiella pneumoniae #8045	1.56	0.78	6.25	100	0.2	0.2
Salmonella enteritidis G-14	12.5	12.5	50	100	1.56	6.25
Salmonella typhimurium E-9	3.12	1.56	6.25	100	0.4	0.4
Shigella sonnei ATCC 9290	6.25	3.12	12.5	100	0.78	1.56
Pseudomonas aeruginosa BMH #1	6.25	1.56	6.25	100	0.4	0.4
BMH #10	3.12	0.78	1.56	100	0.2	0.2
E-2	25	6.25	25	100	0.78	0.78
Serratia marcescens T-55	6.25	6.25	12.5	100	0.78	3.12
T-26	12.5	12.5	25	100	1.56	12.5
176VA	12.5	12.5	25	100	0.78	6.25
Providencia KY-3947	12.5	12.5	12.5	100	0.78	3.12
Proteus vulgaris ATCC 6897	12.5	6.25	25	100	0.78	1.56
Proteus rettgeri KY-4288	6.25	1.56	12.5	100	0.4	1.56
Proteus morganii KY-4298	6.25	3.12	12.5	100	0.78	0.78

a) Seldomycin 5. b) Gentamicin C_{1a}. c) 3′,4′-Dideoxykanamycin B.

TABLE 4. MINIMUM INHIBITORY CONCENTRATIONS OF COMPOUNDS **1**, **2**, **4**, **5**, **14**, AND **15** AGAINST RESISTANT STRAINS (mcg/ml)

Strain	Inactivating enzyme[a]	**1**[b]	**2**	**14**	**15**	**4**[c]	**5**[d]
Escherichia coli R-5	APH(3′)-I	100	3.12	6.25	100	0.4	0.78
R-12	ANT(2″)	3.12	3.12	6.25	100	6.25	25
R-16	APH(3′)-I	100	0.78	1.56	50	0.2	0.4
R-18*	ANT(2″)	25	3.12	12.5	100	0.78	0.78
R-19	AAC(3)-I	50	100	6.25	100	12.5	0.4
R-20	APH(3′)-I	100	1.56	12.5	100	0.4	0.78
57R/W677	ANT(2″)	6.25	6.25	12.5	100	25	100
76-2*	ANT(2″)	50	3.12	25	100	12.5	25
Pseudomonas aeruginosa R-3	AAC(6′)	100	100	100	100	6.25	50
R-4	AAC(3)-I	100	100	25	100	12.5	0.78
R-5	APH(3′)-I,II	25	6.25	12.5	100	0.4	0.4
R-9	AAC(6′)	100	100	100	100	25	100
R-10	APH(3′)-I	100	3.12	12.5	100	0.4	0.4
R-12	AAC(3)-II	100	100	100	100	100	100
Serratia marcescens 1065	AAC(6′)	100	100	100	100	12.5	100
Providencia 164	AAC(2′)	100	100	25	100	25	50
Klebsiella pneumoniae Y-58*	ANT(2″)	25	1.56	6.25	100	6.25	12.5
Y-60*	ANT(2″)	25	3.12	12.5	100	12.5	50

a) Figure in parentheses indicates the position where the antibiotic is enzymatically modified. b) Seldomycin 5. c) Gentamicin C_{1a}. d) 3′,4′-Dideoxykanamycin B. * Strains which inactivate streptomycin.

six ecb groups whereas **10** has five. This is supported by the fact that **10** was converted into **9** by treatment with ethyl chloroformate. A comparison of the CMR spectra of both compounds (Table 1) reveals that the 2′,3′-aziridine ring of **10** bears no ecb group. The C-2′ and C-3′ signals of **9** appear at 36.5 and 36.1 ppm, those of **10** at 27.7 and 29.4 ppm accompanied by slight downfield shifts of C-1′ and C-4′. The peak appearing at 162.5 ppm in the spectrum of **9** is attributable to the carbonyl carbon of ecb group attached at the aziridine nitrogen. The fact that treatment of **9** with sodium borohydride in DMSO afforded **7** and **8** leads to the conclusion that, in the reaction of **6** with sodium borohydride, **9** was initially formed and then transformed into **7** and **8** by ring-opening of the aziridine due to an attack of hydride ion. It is not obvious whether **7** was formed, besides this mechanism, directly by the replacement of the 3′-tosyloxyl group with hydride. The course of formation of **10** remains unclarified. The formation might take place by hydrolysis of the ecb group attached to the aziridine nitrogen due to basic property of sodium borohydride. Recently, Okutani *et al.* reported that 2′,3′-epimino derivatives play the role of intermediate during the course of synthesis of 3′-deoxy and related compounds from butirosin 3′-phosphate *etc.*[19]

Antibacterial Activities of **2**, **14**, *and* **15**. The *in vitro* antibacterial activities of **2**, **14**, and **15** were measured and compared with those of SLD-5 (**1**), GM-C_{1a} (**4**), and DKB (**5**) (Tables 3 and 4). Compound **2** exhibits, as compared with **1**, both enhanced activity against gram-negative sensitive strains and strongly recovered potency against resistant strains which produce aminoglycoside 3′-phosphotransferase [APH(3′)]. Activity of **2**, however, is less potent than that of the two reference compounds, **4** and **5**, against both sensitive and resistant strains except aminoglycoside 2″-nucleotidyltransferase [ANT(2″)]-producing strains. The result

TABLE 5. ED_{50} VALUES OF COMPOUND **2** AGAINST EXPERIMENTAL INFECTIONS IN MICE (mg/kg)[a]

Organism	**1**	**2**	**5**
Escherichia coli Juhl	6.75	3.9	0.62
R-20	200	4.5	2.8
Pseudomonas aeruginosa BMH#1	265	150	18.8
R-5	180	52.5	—

a) Acute systemic infections in mice were produced by intraperitoneal inoculation. The dosage regimen for all infections was 1 or 2 h post-infection, all the compounds being administered subcutaneously.

of the test *in vivo* (Table 5) showed a similar tendency to that in the *in vitro* experiment. The difference in activity seems to arise from the structure of the monosaccharide attached to the 6 position of the deoxystreptamine core, since other portions of the molecules of these compounds are quite the same. We infer that, as compared with 2″-equatorial hydroxyl group, the 2″-equatorial amino group characteristically involved in the structures of **1** and **2** does not function to strengthen antibacterial activity.

It seems that **1** is inactive against four of the six ANT-producing resistant strains tested in spite of its lack of a 2″-hydroxyl group in the structure. The four strains which are moderately resistant to **1** inactivate streptomycin[20] (MIC: >100 mcg/ml, data not given in Table 4). The other two strains which are sensitive to **1** do not inactivate streptomycin (MIC: 3.12—12.5 mcg/ml). It should be noted that this inactivation of **1** was inhibited by deoxygenation or epimerization[4] at the 3′ position of **1**. The results suggest that in **1** the 3′-hydroxyl group might function as a substrate for the ANTs, or these four strains might produce, besides ANT, other enzymes which modify the 3′-hydroxyl group of **1**.

Compound **15** lacks antibacterial activity. It is

considered that construction of the aziridine ring deforms chair conformation of the 2,6-diaminohexose unit, causing the loss of activity.

The potency of **14** against sensitive strains is less strong than that of **1** except against *Pseudomonas*. However, the antibacterial spectrum of **14** against resistant strains was found to be interesting. Although less potent than **2**, it exhibits recovered activity against resistant strains which produce APH(3′)-I or aminoglycoside 2′-acetyltransferase [AAC(2′)]. This is understandable since the targets of these enzymes have been removed from the substrate. Compound **14** is active against AAC(3)-I-producing strains, indicating that 2′-deamino-3′-epiamino-3′-deoxygenation offers a new mode of modification to the established methods, such as 1-*N*-ω-amino-α-hydroxyalkanoylation,[21] 1-*N*-ethylation,[22] and 1-*N*-ω-amino-α-hydroxyalkylation,[23] for recovering activity of aminoglycoside antibiotics against AAC(3)-I-producing strains. Against the four ANT-producing strains, **14** shows improved activity than **1**. Compound **14** is an unique aminoglycoside antibiotic both in its structure and its width of antibacterial spectrum against resistant strains.

The LD_{50} value of **2** was estimated to be 300 mg/kg (mice, intraveneously).

Experimental

General. Melting points were determined with a Yanaco micro melting point apparatus and are uncorrected. Varian T-60, JEOL JNM-FX 100, or JEOL PS-100 was employed for NMR measurements with TMS or DSS as an internal reference. Samples of the free bases were decarbonated in the usual way[24] just before the NMR measurements. Thin layer chromatography (TLC) was carried out with Merck TLC plate and spots were located by iodine vapor and/or ninhydrin. Mass spectra were obtained with JEOL JMS-01SG-2 at 75 eV using direct insertion probe. Optical rotations were measured with a Hitachi-Perkin-Elmer 141 polarimeter at ambient temperature. Commercial DMSO and sodium borohydride were used without further purification. Quantitative determination of periodate uptake was made as reported.[16] No effort was made to crystallize the products. Antibacterial activity was determined by the agar dilution method at pH 7.2 specified by the Japan Society of Chemotherapy.

*Reaction of **6** with Sodium Borohydride.* To a solution of **6** (25.0 g) in DMSO (500 ml) was added sodium borohydride (12.5 g) in one portion and the solution was stirred at 65 °C for 17 h. DMSO was evaporated *in vacuo* and water (600 ml) was added to the residue. The mixture was extracted with chloroform (300 ml×10) and the organic layer was washed with water (50 ml×3), dried with anhydrous sodium sulfate and evaporated to give white powder. The residue was charged to a silica gel column (Merck, 2.2 kg, 8 cm×128 cm) and the column was washed with chloroform (7 liter), followed by elution with a mixture of chloroform–methanol (fraction *ca.* 200 ml each); eluent: Frs. 1—101, chloroform–methanol 30: 1; Frs. 102—199, 20: 1; Frs. 200—269, 10: 1. Fractions were monitored by TLC.

Frs. 56—72: hexa-*N*-ecb-3′-deoxy-SLD-5 (**7**), 4.20 g as white powder. Mp 278—279 °C, $[\alpha]_D^{25}$ +70.7 (*c* 0.382, DMF).

Found: C, 50.28; H, 7.41; N, 9.63; S, 0.00%. Calcd for $C_{36}H_{62}N_6O_{18}$: C, 49.87; H, 7.22; N, 9.70; S, 0.00%. Frs. 77—108: hexa-*N*-ecb-2′-deamino-3′-epiamino-3′-deoxy-SLD-5 (**8**), 4.85 g as white powder. Mp 237—241 °C, $[\alpha]_D^{22}$ +63.0 (*c* 0.437, DMF).

Found: C, 49.97; H, 7.44; N, 9.61; S, 0.00%. Calcd for $C_{36}H_{62}N_6O_{18}$: C, 49.87; H, 7.22; N, 9.70; S, 0.00%. Frs. 109—138: 1,3,6′,2″,3″-penta-*N*-ecb-2′,3′-*N*-ecb-epimino-2′-deamino-3′-deoxy-SLD-5 (**9**), 4.55 g as slightly yellow powder. Mp 235—238 °C, $[\alpha]_D^{20}$ +68.9 (*c* 0.409, DMF).

Found: C, 50.78; H, 7.40; N, 9.32; S, 0.00%. Calcd for $C_{36}H_{60}N_6O_{18}$: C, 49.98; H, 7.01; N, 9.72; S, 0.00%. Frs. 170—178: an unidentified product, 0.590 g as white powder. Frs. 195—231: 1,3,6′,2″,3″-penta-*N*-ecb-2′,3′-epimino-2′-deamino-3′-deoxy-SLD-5 (**10**), 3.10 g as white powder. Mp 272—273 °C, $[\alpha]_D^{23}$ +54.1 (*c* 0.455, DMF).

Found: C, 49.46; H, 7.29; N, 10.29; S, 0.00%. Calcd for $C_{33}H_{56}N_6O_{16}$: C, 49.98; H, 7.13; N, 10.60; S, 0.00%. Frs. 234—244: an unidentified product, 0.21 g as white powder.

*3′-Deoxy-SLD-5 Free Base (**2**).* Compound **7** (3.80 g) was dissolved in methanol (130 ml) and 10.2 M aq potassium hydroxide (130 ml) was added to the solution. The homogeneous solution was heated in a sealed vessel at 140 °C for *ca.* 6 h. After being cooled to room temperature, the solution was acidified to pH 4 by addition of concd hydrochloric acid under ice-cooling. The ppt formed was filtered off and the filtrate was charged to a column of Amberlite CG-50 (ammonium cycle, 500 ml). The column was washed with water (500 ml) and eluted with aq ammonia; eluent: Frs. 1—86, 0.1 M-ammonia; Frs. 87—160, 0.2 M-ammonia (fraction: 20 ml each). Frs. 102—110: compound **2** containing a small amount of impurities, 0.95 g. Frs. 111—126: pure **2**, 0.80 g as white powder. Mp 180—210 °C, $[\alpha]_D^{25}$ +105 (*c* 0.564, water); R_f value (relative to SLD-5 on silica gel TLC) 1.21 (1-butanol–ethanol–chloroform–conc ammonia 4: 5: 2: 5). PMR (D_2O): τ 4.93 (d, J=4 Hz, H-1′), 5.04 (d, J=3 Hz, H-1″), 7.9—9.0 (m, H-2_{eq}, H-2_{ax}, H-$3'_{eq}$, H-$3'_{ax}$, H-$4'_{eq}$, H-$4'_{ax}$); MS (*m/e*, relative intensity, possible assignment of fragment ion[25]): 435 (1, MH), 335 (8, A5), 307 (40, A7), 289 (37, A8), 274 (18, F2), 173 (12, A10), 163 (25, A11), 145 (100, Cl and A12), 129 (75, B1).

Found: C, 47.51; H, 8.43; N, 18.16%. Calcd for $C_{18}H_{38}N_6O_6 \cdot 1/2H_2CO_3$: C, 47.72; H, 8.46; N, 18.05%. Fractions 102—110 were rechromatographed on CG-50 to give 0.57 g of pure **2** and a trace amount of a compound supposed to be 6-*O*-(2,3-diamino-2,3-dideoxy-4-*O*-methyl-α-D-xylopyranosyl)-2-deoxystreptamine (DOS-seldamine). Mp 142—149 °C, $[\alpha]_D^{17}$ +59.9 (*c* 0.302, water). PMR (D_2O): τ 5.00 (d, J=3 Hz, H-1″), 6.53 (s, OCH_3); CMR (D_2O): C-1, 51.1; C-2, 36.8; C-3, 51.1; C-4, 78.8; C-5, 74.9; C-6, 87.4; C-1″, 100.1; C-2″, 56.2; C-3″, 54.7; C-4″, 80.2; C-5″, 60.8; OCH_3, 58.7. MS: 307 (1, MH), 306 (0.5, M), 289 (3, A8), 203 (37, unknown), 173 (7, A10), 163 (10, A11), 145 (100, Cl and A12). This compound is considered to be formed by hydrolysis of the glycosidic linkage under drastic conditions used for the removal of ecb groups. This compound exhibits no antibacterial activity.

*2′-Deamino-3′-epiamino-3′-deoxy-SLD-5 Free Base (**14**).* The ecb groups of **8** (2.50 g) was removed in a similar manner as described above and the product was purified by CG-50 to afford pure **14** (0.70 g), as slightly yellow powder. Mp 134—137 °C, $[\alpha]_D^{22}$ +106 (*c* 0.356, water).

Found: C, 44.75; H, 8.08; N, 16.55%. Calcd for $C_{18}H_{38}N_6O_6 \cdot H_2O \cdot H_2CO_3$: C, 44.34; H, 8.24; N, 16.33%.

PMR (D_2O): τ 4.68 (br dd, J=*ca.* 5, *ca.* 2 Hz, H-1′), 5.04 (d, J=3 Hz, H-1″); MS: 435 (1, MH), 307 (7, A7), 289 (5, A8), 274 (18, F2), 273 (29, A4), 258 (8, F1), 173 (13, A10), 163 (31, A11), 145 (100, Cl and A12), 129 (64, B1), 112 (25, F4).

*2′,3′-Epimino-2′-deamino-3′-deoxy-SLD-5 Free Base (**15**).* *From **9**:* Alkaline hydrolysis of **9** (2.00 g) and purification of

the crude product were carried out in a similar way to that mentioned above. Pure **15** was obtained as white powder, 0.54 g. Mp 120—149 °C, $[\alpha]_D^{23}$ +100 (*c* 0.667, water).

Found: C, 48.43; H, 8.80; N, 18.57%. Calcd for $C_{18}H_{36}N_6O_6 \cdot H_2O$: C, 47.97; H, 8.52; N, 18.65%.

PMR (D_2O): τ 4.42 (d, J=3 Hz, H-1′), 5.06 (d, J=3 Hz, H-1″), at pD 2: τ 3.83 (d, J=4 Hz, H-1′), 4.46 (d, J=*ca.* 0 Hz,[16] H-1″); MS: 433 (1, MH), 432 (0.5, M), 307 (20, A7), 289 (72, A8), 274 (4, F2), 163 (20, A11), 145 (100, Cl and A12), 127 (32, B1). Characteristics of the MS: no fragment peaks attributable to the species arising from the 4-*O*-glycosyl-2-deoxystreptamine were observed, peaks at *m/e* 347 (25) and 203 (10) appearing. These two fragments probably correspond to D9 and D10 fragments,[18] though hydrogen shift is needed in this case.

From ***10***: De-ethoxycarbonylation of **10** (0.45 g) and chromatography were carried out as described above. Compound **15** was obtained as white powder, 0.12 g. MS, PMR, and antibacterial activity of this material were identical with those obtained with a sample prepared from **9**. A small amount of DOS-seldamine (0.03 g) was also isolated.

Reaction of ***9*** *with Sodium Borohydride.* Sodium borohydride (13 mg) was added to a solution of **9** (25 mg) in DMSO (0.5 ml) and the solution was kept at 65 °C for 13 h. DMSO was evaporated *in vacuo* and the residue was extracted with chloroform (10 ml), washed with water (3 ml×2), and dried. The chloroform solution was then concentrated to *ca.* 1 ml. TLC (chloroform–methanol 10: 1) of the concentrate indicated that the starting material (R_f 0.61) had disappeared and the following products were formed; **7** (R_f 0.74), **8** (R_f 0.64), a trace of **10** (R_f 0.36), and an unidentified product (R_f 0.31).

Reaction of ***10*** *with Ethyl Chloroformate.* To a solution of **10** (50 mg) in DMF (2 ml) were added anhyd. sodium carbonate (16 mg) dissolved in water (0.5 ml) and ethyl chloroformate (17 mg). The solution was stirred overnight. Solvents were removed *in vacuo* and the residue was extracted with chloroform (10 ml), washed with water (2 ml), and dried with anhyd. sodium sulfate. TLC of the chloroform solution showed a single spot of **9**. Chloroform was evaporated to give white powder of **9** (55 mg); mixed mp with the material obtained above: 234—235 °C.

The authors wish to thank Mrs. Mayumi Yoshida and Mr. Noboru Kojima for the NMR measurements, Mrs. Kazuko Yamaguchi for the elemental analyses, and Miss Yuriko Adachi for obtaining the Mass spectra. The authors are also indebted to Sagami Chemical Research Center for the elemental analysis of sulfur.

References

1) A part of this work was presented at the 202nd Annual Meeting of Japan Antibiotics Research Association, Tokyo, September, 1977. A preliminary communication has been published: H. Matsushima, K. Kitaura, and Y. Mori, *J. Antibiot.*, **30**, 890 (1977).

2) H. Umezawa, *Adv. Carbohydr. Chem. Biochem.*, **30**, 183 (1974); S. Umezawa, *ibid.*, **30**, 164 (1974).

3) T. Nara, M. Yamamoto, S. Takasawa, S. Sato, T. Sato, I. Kawamoto, R. Okachi, I. Takahashi, and A. Morikawa, *J. Antibiot.*, **30**, 17 (1977).

4) H. Matsushima, K. Kitaura, and Y. Mori, *Bull. Chem. Soc. Jpn.*, **50**, 3039 (1977).

5) D. J. Copper, P. J. L. Daniels, M. D. Yudis, H. M. Marigliano, R. D. Guthrie, and S. T. K. Bukhari, *J. Chem. Soc., C*, **1971**, 3126.

6) S. Umezawa, H. Umezawa, Y. Okazaki, and T. Tsuchiya, *Bull. Chem. Soc. Jpn.*, **45**, 3624 (1972).

7) N. A. Hughes and P. R. H. Speakman, *J. Chem. Soc.*, **1965**, 2236.

8) M. L. Wolfrom, J. Bernsmann, and D. Horton, *J. Org. Chem.*, **27**, 4505 (1962).

9) A. C. Richardson, *Carbohydr. Res.*, **10**, 395 (1969).

10) U. Zehavi, *J. Org. Chem.*, **40**, 3870 (1975).

11) Y. Takagi, T. Miyake, T. Tsuchiya, S. Umezawa, and H. Umezawa, *Bull. Chem. Soc. Jpn.*, **49**, 3649 (1976).

12) H. M. Bell, C. W. Vanderslice, and A. Spehar, *J. Org. Chem.*, **34**, 3923 (1969).

13) H. Weidmann, N. Wolf, and W. Timpe, *Carbohydr. Res.*, **24**, 184 (1972).

14) H. Saeki, N. Takeda, Y. Shimada, and E. Ohki, *Chem. Pharm. Bull.*, **24**, 724 (1976).

15) Preparation and CMR measurement of this compound were carried out by Dr. McAlpine, Abbott Laboratories. The authors thank him for the information.

16) J. B. McAlpine, A. C. Sinclair, R. S. Egan, R. L. DeVault, R. S. Stanaszek, M. Cirovic, S. L. Mueller, P. C. Goodley, R. J. Mauritz, N. E. Wideburg, L. A. Mitscher, K. Shirahata, H. Matsushima, S. Sato, and T. Iida, *J. Antibiot.*, **30**, 39 (1977).

17) Prepared from seldomycin 5 and *N*-benzyloxycarbonyloxysuccinimide.

18) P. J. L. Daniels, A. K. Mallams, J. Weinstein, J. J. Wright, and G. W. A. Milne, *J. Chem. Soc., Perkin Trans. 1*, **1976**, 1078.

19) T. Okutani, T. Asako, K. Yoshioka, K. Hiraga, and M. Kida, *J. Am. Chem. Soc.*, **99**, 1278 (1977).

20) A. Schatz, E. Bugie, and S. A. Waksman, *Proc. Soc. Exp. Biol. Med.*, **55**, 66 (1944).

21) H. Kawaguchi, T. Naito, S. Nakagawa, and K. Fujisawa, *J. Antibiot.*, **25**, 695 (1972).

22) J. J. Wright, *J. Chem. Soc., Chem. Commun.*, **1976**, 206.

23) K. Richardson, S. Jevons, J. W. Moore, B. C. Ross, and J. R. Wright, *J. Antibiot.*, **30**, 843 (1977).

24) J. B. Morton, R. C. Long, P. J. L. Daniels, R. W. Tkach, and J. H. Goldstein, *J. Am. Chem. Soc.*, **95**, 7464 (1973).

25) For abbreviation of the fragment such as MH, A5, *etc.*, see Ref. 18.

Enantioface-Differentiating (Asymmetric) Hydrogenation of β-Ketoester with Modified Raney Nickel Catalyst (MRNi). XXXI. A Comparative Study of Reaction Rates and Optical Yields

Hiroshi OZAKI,* Akira TAI, Shinzo KOBATAKE, Hironobu WATANABE, and Yoshiharu IZUMI

Division of Organic Chemistry, Institute for Protein Research, Osaka University, Suita, Osaka 565

(Received February 3, 1978)

Enantioface-differentiating hydrogenations of methyl acetoacetate over (*S*)-alanine-, (*S*)-2-aminobutyric acid, (*S*)-valine-, (*S*)-leucine-, (*S*)-malic acid-, and (*R,R*)-tartaric acid-MRNi were carried out under atmospheric pressure of hydrogen and the effects of the modifying reagent on the rates of the formation of enantiomer, v_S and v_R, were investigated. The rates of hydrogenation, $v=v_S+v_R$, were the same for all the amino acid-MRNi and also for all the hydroxy dicarboxylic acid-MRNi. However, the v_R/v_S ratios were different. These results are explained in terms of the independence of the rate-determining and enantioface-differentiating steps in the reaction pathway of hydrogenation. The rate-determining step of hydrogenation was shown to be the hydrogen addition to the adsorbed substrate, while the enantioface-differentiating step was expected to occur prior to the rate-determining step.

Modified Raney nickel catalyst (MRNi) is the most intensively studied catalyst for the enantioface-differentiating hydrogenation of the C=O double bond.[1]

As reported in the preceding paper,[2] the features of the hydrogenation of methyl acetoacetate (MAA) to methyl 3-hydroxybutyrate (MHB) over MRNi have been summarized as follows. 1) The Arrhenius plots with respect to the initial rate of hydrogenation over various MRNi were parallel to one another and the resulting apparent activation energies were 10.5±0.5 kcal/mol in all cases. That is, the reaction mechanism of the rate-determining step was not influenced by the modifying reagent. 2) The rate of hydrogenation followed the equation: $v=k[\mathrm{MAA}]^{0.2-0.3}$. Taking the value of activation energy into consideration, the rate-determining step of hydrogenation was supposed to be the hydrogen addition to the adsorbed substrate (surface reaction). 3) The initial rate of hydrogenation linearly increased with the decrease in the amount of modifying reagent adsorbed on the catalyst, and the amounts of adsorption were found to be similar in so far as the structures of the modifying reagents were homologous. However, there was no systematic relation between the rate and the optical yield. Thus the roles of the modifying reagent were divided into two independent functions: one is to regulate the rate of reaction by occupying a part of the active sites of the catalyst and the other is to make the catalyst differentiate the enantioface of the substrate. We have pointed out[2] that these features of the enantio-differentiating reaction are not explained by the simple kinetic controlled enantio-differentiation usually claimed in the literature[3] and have proposed that the enantio-differentiation should take place elsewhere than in the rate-determining step. Recently, many experimental results favoring our proposal have been reported in the reaction with chiral homogeneous catalyst[4] and the proposal has gradually become general. In this report, the validity of our previous proposal in the reaction with MRNi will be verified on the basis of the detailed studies of the relations between the rate and the optical yield.

Results

Raney nickel catalyst suited for the kinetic studies was prepared by a newly developed method and was modified with α-amino acid or α-hydroxy acid under the conditions reported before.[5]

The resulting time courses of the hydrogenation and optical yields at 20% of conversion are shown in Fig. 1 (α-amino acid-MRNi) and Fig. 2 (α-hydroxy dicarboxylic acid).

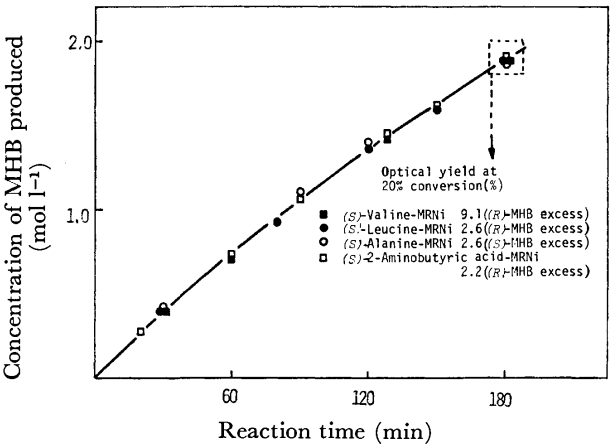

Fig. 1. Time courses of hydrogenation with α-amino acid MRNi.

All the plots in Fig. 1 overlapped one another, that is, all kinetic features of the hydrogenations with α-amino acid-MRNi appeared to be identical. On the other hand, the optical yields were intrinsic to each catalyst. As found in Fig. 2, similar results were obtained in the hydrogenations with α-hydroxy dicarboxylic acid-MRNi.

Figures 3 and 4 show the time courses of (*S*)- and (*R*)-MHB formations calculated from the optical yield of the product with α-amino acid-MRNi ((*S*)-valine and (*S*)-leucine) and α-hydroxy dicarboxylic acid-MRNi ((*S*)-malic acid and (*R,R*)-tartaric acid) respectively.

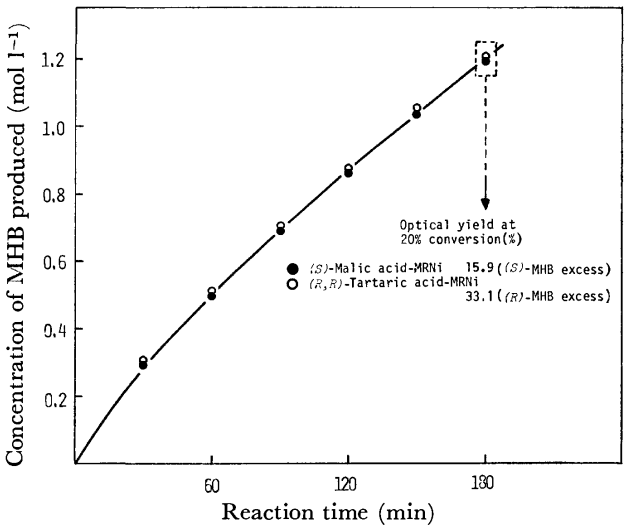

Fig. 2. Time courses of hydrogenation with α-hydroxy dicarboxylic acid-MRNi.

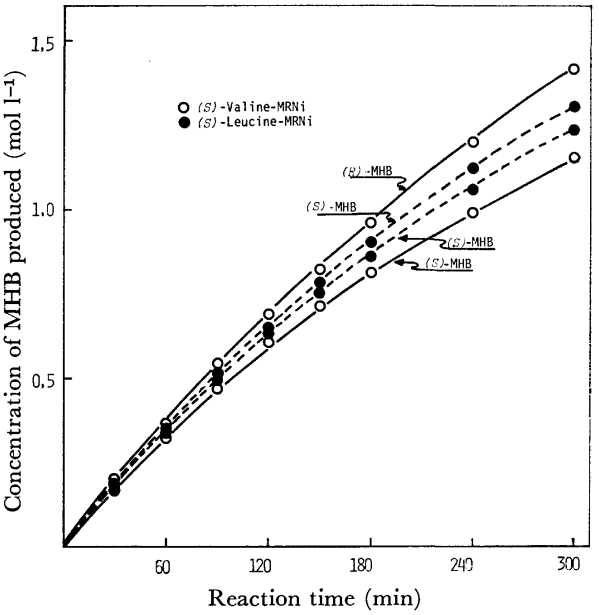

Fig. 3. Time courses of (*S*)- and (*R*)-MHB formation.

The rates of formations of *S*- and *R*-isomers, v_R and v_S, were determined graphically from the figures. The results are listed in Table 1.

From all these data, it became evident that the overall rates, $v=v_R+v_S$, at each reaction time were identical where the modifying reagents were of homologous structure, despite the difference in the rates of formation of each enantiomer, v_R and v_S, with respect to each catalyst.

The rate law of the hydrogenations with MRNi was determined in the usual manner. Initial rates, v_0, at different initial concentrations of MAA, [MAA], were determined by independent experiments. As shown in Fig. 5, plots of $1/v_0$ against 1/[MAA] gave straight lines and the plots corresponding to valine- and leucine-MRNi overlapped each other. Thus, the rates of the hydrogenations with α-amino acid-MRNi and α-hydroxy dicarboxylic acid-MRNi were found to follow the equation

$$v_0 = \beta^\circ[\mathrm{MAA}]/(1+\alpha^\circ[\mathrm{MAA}]) \quad (1)$$

and the following relations were expected to hold between valine- and leucine-MRNi:

$$\alpha^\circ_{(\mathrm{valine})} = \alpha^\circ_{(\mathrm{leucine})}, \quad \beta^\circ_{(\mathrm{valine})} = \beta^\circ_{(\mathrm{leucine})}. \quad (2)$$

The rates, v, determined in a single experiment (shown in Table 1), however, gradually deviated from the relations shown in Eq. 1 with increase of the conversion, owing to the decay of the catalyst.

Since all the α-amino acid-MRNi gave the same initial rates, as expected from Fig. 1, Eq. 2 was expected to hold among all the α-amino acid-MRNi examined.

The relations $\alpha^\circ_{(\mathrm{malic\ acid})}=\alpha^\circ_{(\mathrm{tartaric\ acid})}$ and $\beta^\circ_{(\mathrm{maric\ acid})}=\beta^\circ_{(\mathrm{tartaric\ acid})}$ were also expected to hold between malic acid- and tartaric acid-MRNi.

Table 1. The rates of the formations of (*S*)- and (*R*)-MHB

Catalyst (Reaction temp)		Reaction time (min) 30	60	90	120	150	180	240	300
(*S*)-Valine-MRNi (70 °C)	v_R (mol l^{-1} min^{-1}) × 10^3	6.15	5.90	5.32	4.81	4.51	4.33	3.73	3.62
	v_S	5.75	5.11	4.59	4.00	3.38	3.16	2.81	2.55
	v	11.90	11.01	9.91	8.81	7.89	7.49	6.54	6.17
	$(\lvert v_R-v_S\rvert/v)\times 10^2$	3.4	7.2	7.4	9.2	14.3	15.6	14.1	17.3
(*S*)-Leucine-MRNi (70 °C)	v_R (mol l^{-1} min^{-1}) × 10^3	6.01	5.37	5.10	4.55	4.24	4.00	3.42	3.21
	v_S	5.77	5.26	4.89	4.35	3.96	3.58	3.13	2.90
	v	11.78	10.63	9.90	8.90	8.20	7.58	6.55	6.11
	$(\lvert v_R-v_S\rvert/v)\times 10^2$	2.0	1.0	1.2	2.3	3.4	5.5	4.4	5.1
(*S*)-Malic acid-MRNi (60 °C)	v_R (mol l^{-1} min^{-1}) × 10^3	4.54	3.77	3.54	3.38	3.28	3.11	2.87	2.77
	v_S	3.98	2.99	2.54	2.51	2.38	2.27	1.94	1.63
	v	8.52	6.76	6.08	5.89	5.66	5.38	4.81	4.40
	$(\lvert v_R-v_S\rvert/v)\times 10^2$	6.6	11.5	16.4	14.8	15.9	15.6	19.3	25.9
(*R*,*R*)-Tartaric acid-MRNi (60 °C)	v_R (mol l^{-1} min^{-1}) × 10^3	5.16	4.52	4.18	4.01	3.94	3.63	3.47	3.32
	v_S	3.36	2.35	2.05	1.94	1.84	1.68	1.52	1.60
	v	8.52	6.87	6.23	5.95	5.78	5.31	4.99	4.93
	$(\lvert v_R-v_S\rvert/v)\times 10^2$	21.1	31.6	34.2	34.8	36.3	36.7	39.1	34.7

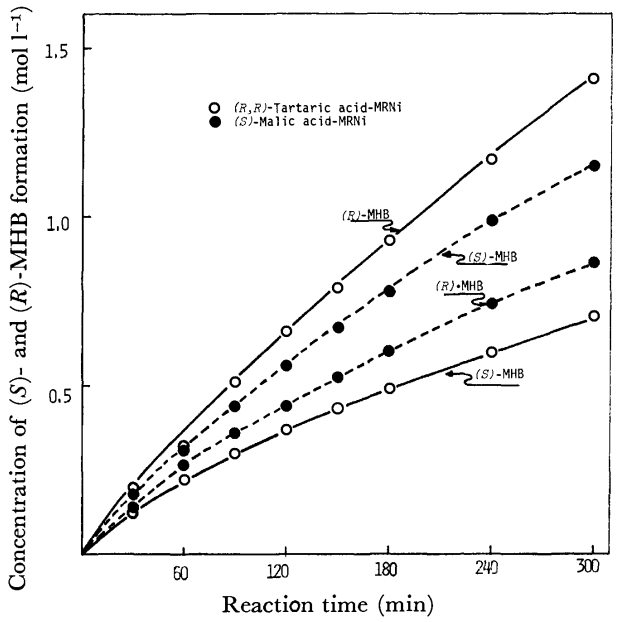

Fig. 4. Time courses of (*S*)- and (*R*)-MHB formation.

The relations mentioned above are also applicable to the values α and β at any reaction times, because the overlapping of the time courses shown in Figs. 1 and 2 indicated that all kinetic constants at each reaction time possess the same value within the same class of MRNi.

Discussions

The rate law shown in Eq. 1 can be derived from the following reaction Scheme, in which the adsorption of MAA to the modified and unmodified parts of catalyst is in competition and each adsorbed species is convertible with the others under the pre-equilibrium condition:

$$\begin{array}{ccccc} & \overset{K_S}{\longrightarrow} & (\mathrm{MAA}^*\cdot C)_S & \overset{H_2^*}{\underset{k_S}{\longrightarrow}} & (S)\text{-MHB} + C \\ \mathrm{MAA} + C & \overset{K_R}{\rightleftharpoons} & (\mathrm{MAA}^*\cdot C)_R & \overset{H_2^*}{\underset{k_R}{\longrightarrow}} & (R)\text{-MHB} + C \\ & \underset{K_O}{\longrightarrow} & (\mathrm{MAA}^*\cdot C)_O & \overset{H_2^*}{\underset{k_O}{\longrightarrow}} & \end{array} \qquad (3)$$

$$((S)\text{-MHB}+(R)\text{-MHB})/2 + C$$

C: Amount of adsorption site of MAA in given weight of catalyst.

K_S and K_R: Adsorption constants of MAA to be hydrogenated to (*S*)- and (*R*)-MHB under the influence of the modifying reagent.

K_O: Adsorption constant of MAA which did not interact with the modifying reagent.

k_S and k_R: Rate constants of the formations of (*S*)- and (*R*)-MHB from the $(\mathrm{MAA}^*\cdot C)$ interacted with the modifying reagent.

k_O: Rate constant of the formation of racemic MHB from the $(\mathrm{MAA}^*\cdot C)$ which did not interact with the modifying reagent.

Since the adsorption of hydrogen and MAA was not competitive[6] and all reactions were carried out under the same hydrogen pressure, the concentration of active hydrogen on the catalyst, $[H_2^*]$, would be constant under the experimental conditions.

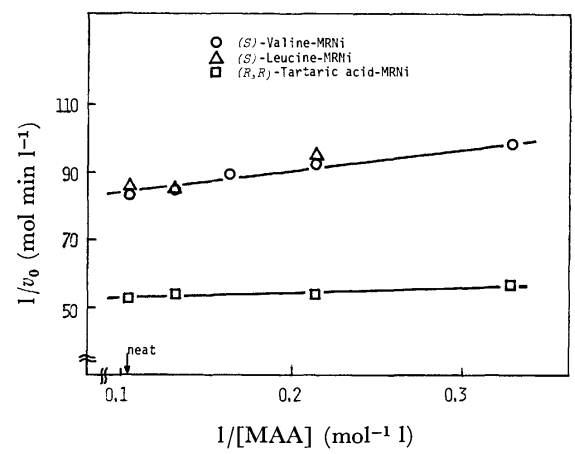

Fig. 5. Relation between initial rate (v_0) and initial concentration of substrate ([MHB]).

The rate of the reaction can be reduced to

$$v_R = \frac{(k_O K_O/2 + k_S K_S)[\mathrm{MAA}]C[\mathrm{H}^*]}{1+(K_O+K_S+K_R)[\mathrm{MAA}]}, \qquad (4)$$

$$v_S = \frac{(k_O K_O/2 + k_R K_R)[\mathrm{MAA}]C[\mathrm{H}^*]}{1+(K_O+K_S+K_R)[\mathrm{MAA}]}, \qquad (5)$$

$$v = \frac{(k_O K_O + k_S K_S + k_R K_R)[\mathrm{MAA}]C[\mathrm{H}^*]}{1+(K_O+K_S+K_R)[\mathrm{MAA}]}. \qquad (6)$$

When Eq. 6 was compared with Eq. 1, the following relations were deduced:

$$\alpha = K_R + K_S + K_O, \qquad (7)$$

$$\beta = (k_R K_R + k_S K_S + k_O K_O)\cdot C\cdot[\mathrm{H}^*]. \qquad (8)$$

If we simply assume that the enantio-differentiation takes place only at the rate-determining step of the hydrogenation and does not depend on the relative amounts of adsorption species, $[\mathrm{MAA}^*\cdot C]_R$, $[\mathrm{MAA}^*\cdot C]_S$, and $[\mathrm{MAA}^*\cdot C]_S$, the rates of formation of enantiomers, v_R and v_S should be proportional to $(k_S+k_O/2)$ and $(k_R+k_O/2)$. When the common adsorption constant of MAA is expressed by K, the relation $\beta=(k_O+k_R+k_S)\text{-}K\cdot C\cdot[\mathrm{H}^*]$ is expected to hold. In such a case, k_O is a common value for all the modified catalysts, while k_R and k_S should be independent values with respect to each catalyst. Therefore, the catalysts with different v_R and v_S values no longer give the same β value.

Thus this assumption would not be adequate to elucidate the present experimental results that the same class of MRNi gave the same β value but different v_R and v_S values.

The alternative assumption that the rates of formation of enantiomers are related to the amounts of $[\mathrm{MAA}^*\cdot C]_R$, $[\mathrm{MAA}^*\cdot C]_O$, and $[\mathrm{MAA}^*\cdot C]_S$ but not related to k_S, k_R, and k_O, leads to the equation

$$\beta = k(K_S+K_R+K_O)\cdot C\cdot[\mathrm{H}^*]. \qquad (9)$$

Here, k is the common rate constant of the all adsorption species $(k=k_R=k_S=k_O)$.

From the linear relation between the rate of hydrogenation and the amount of the adsorbed modifying reagent on the catalyst,[2] it is expected that the modifying reagent makes the adsorption site of MAA change by

occupying the adsorption site as a simple competitive adsorption species, but the exsistence of the modifying reagent on the catalyst does not affect the equilibrium constant between MAA and vacant adsorption sites. It has also been confirmed that the same class of modifying reagent was adsorbed on the catalyst in the same amount. Therefore, the same adsorption sites of MAA and C, and the same adsorption constants, K, are expected in the same class of MRNi. Hence the total amounts of the adsorbed MAA, that is $[MAA^*\cdot C]_S+[MAA^*\cdot C]_R+[MAA^*\cdot C]_O$, are the same for the same class of MRNi and only the molar fractions of the adsorption species, γ_S, γ_R, and γ_O, are determined by the chiral influence of the modifying reagent. Under these conditions, β can be reduced to

$$\beta = (K_O+K_R+K_S)\cdot C\cdot[H^*] = (\gamma_O+\gamma_R+\gamma_S)\cdot K\cdot C\cdot[H^*] = K\cdot C\cdot[H^*] = \alpha\cdot C\cdot[H^*],$$

where K is an adsorption constant of MAA and γ_O, γ_R, and γ_S are fraction coefficients of the adsorbed MAA. In this manner, the experimental result that the same class of MRNi gave the same β and α was justified.

Although the kinetic studies do not give any direct indications of the relations, $k_O=k_S=k_R=k$ and $K_O+K_R+K_S=(\gamma_O+\gamma_R+\gamma_S)K$, the present experimental results can only be rationalized without conflicting with the kinetic law under the assumption that the ratios of formation of enantiomers are determined by γ_O, γ_R, and γ_S. The function of the modifying reagent can be reduced to interacting with the substrate on the catalyst; such interaction results in the disproportionate formations of the diastereomeric adsorption species. The conclusion of the present studies is that the ratio of formation of enantiomers depends principally on the term, $(\gamma_O/2+\gamma_R)/(\gamma_O/2+\gamma_S)$, and that the enantioface-differentiating step occurs before the rate-determining step.

Another important finding of this study is that $|v_R-v_S|/v$ increased with the progress of the decay of the catalytic activity, as shown in Table 1. This may be caused by either the specific inactivation of the catalytic site at which the modifying reagent is absent and R- and S-isomers are produced at equal rates (decrease of γ_O), or the change of the adsorption mode of the modifying reagent with the change of the surface of the catalyst by the decay of the catalyst. Further detailed studies on this line are underway.

Experimental

Preparation of Modified Raney Nickel Catalyst. Into an alkaline solution (52 g of sodium hydroxide in 260 ml of water) whose temperature has been adjusted to 19 °C, 19.5 g of well-pulverized Raney alloy (Ni 42%, Al 58%, Kawaken Finechemical Co.) was added in portions at such a rate that the temperature of the mixture was maintained at 19±1 °C with vigorous shaking and cooling on an ice bath. It took 18 min to complete the addition of the alloy. The resulting suspension of Raney nickel was kept at 75—78 °C for 45 min, then allowed to stand at room temperature for 1.5—3 h. After the removal of the alkaline solution by decantation, the Raney nickel (RNi) was washed with eight 300 ml-portions of deionized water.

The modification of RNi was carried out in a 1% solution of modifying reagent. The pH of the modifying solution was adjusted to 5.1 for tartaric acid and malic acid with sodium hydroxide, and to an isoelectric point for each monoamino monocarboxylic acid.

Into 400 ml of the modifying solution, a 2.4 g-portion of the catalyst was immersed at 0 °C for 15 min. During that time, the solution was gently stirred for a few seconds every 5 min. After the removal of the solution, the catalyst was washed with a 40 ml-portion of water and three 200 ml-portions of methanol.

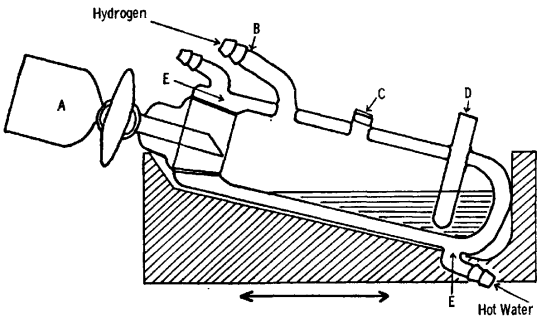

Fig. 6. Frask for hydrogenation.

Hydrogenation. The liquid-phase hydrogenation under atmospheric pressure was carried out with a specially designed 400 ml flask having a liquid inlet funnel (A), a gas inlet side-tube (B), a serum capped hole for sampling (C), a case for the thermometer (D), and a heating jacket with hot water (Fig. 6). Into the flask which had been filled with hydrogen and connected with a graduated hydrogen reservoir through the side-tube B, the modified catalyst suspended in 70 ml of

Table 2. The time course of the hydrogenation

Reaction time (min)	Hydrogen uptake (ml)					
	Reaction temp 70 °C				Reaction temp 60 °C	
	Ala-MRNi	But-MRNi[a)]	Val-MRNi	Leu-MRNi	Tar-MRNi[b)]	Mal-MRNi[c)]
0	0	0	0	0	0	0
30	710	684	649	674	529	507
60	1364	1240	1240	1250	898	860
90	1931	1855	1781	1790	1228	1187
120	2415	2380	2345	2345	1538	1493
150	2872	2866	2814	2804	1835	1785
180	3218	3315	3278	3236	2115	2066

a) 2-Aminobutyric acid. b) Tartaric acid. c) Malic acid.

MAA (or solution of MAA in MHB) was introduced. The flask was fixed to a reciprocating shaker and the jacket was connected with a hot water circulation system. The heating and shaking of the reaction mixture were started simultaneously. The hydrogen uptake was followed by measurement taken every 10 min. The hydrogen uptake of each catalyst is listed in Table 2; from this the concentration of MHB at each stage was calculated. The concentration of MHB thus calculated matched with that determined by GLPC. The plots of time against concentration of MHB in the reaction mixture are shown in the text (Figs. 1 and 2).

Determination of Optical Yield. The optical yield was determined from the optical purity of the MHB dissolved in MAA. After the removal of the catalyst from the reaction mixture by filtration, the filtrate was distilled under reduced pressure. The optical rotation and the ratio, MAA/MHB, in the distillate were determined by means of polarimetry (Perkin-Elmer Model 241 Polarimeter with a 1 dm cell) at 20 °C and GLPC (Shimadzu GC-3HA, 300×0.5 cm stainless-steel column packed with PEG 20 M (20%) on Chromosorb W) at 100 °C respectively. The optical purity of MHB was determined by means of a calibration chart prepared by the plotting of α_D against the concentrations of MHB of different optical purities in MAA.

Time Course of the Formations of (S)- and (R)-MHB. The hydrogenation was carried out in the apparatus described above. A 2 ml portion of the reaction mixture was taken out through the serum capped sampling hole, using an injection syringe, at the times shown in Figs. 3 and 4. The concentration of MAA and the optical rotation of each sample were determined by the procedures mentioned above.

The plots of time against concentrations of (*S*)-and (*R*)-MHB are shown in the text (Figs. 4 and 5).

Initial Rates of Hydrogenation. The hydrogenations of MAA diluted with DL-MHB ranging in concentration from 1.86 to 9.29 (neat) mol/l were carried out at 70 °C. The initial rates of each experiment was determined graphically from the plot of hydrogen uptake against reaction time.

The authors wishes to thank Professors S. Teranishi and T. Imanaka of Osaka University for advice on the kinetic problems. The authors are happy to acknowledge the support of a Scientific Research Grant from the Ministry of Education, Japan (110308), for part of this work.

References

1) Y. Izumi and A. Tai, "Stereo-Differentiating Reactions," Kodansha, Tokyo, and Academic Press, New York, (1971), Sec. 5.1.1. and references therein.

2) a) H. Ozaki, A. Tai, and Y. Izumi, *Chem. Lett.* **1974**, 935; b) T. Harada, Y. Hiraki, Y. Izumi, J. Muraoka, H. Ozaki, and A. Tai, *Proc. 6th Int. Congr. Catal., London*, 1976, pp. 1024—1033.

3) J. D. Morrison and H. S. Mosher, "Asymmetric Organic Reactions," Prentice-Hall, New Jersey (1971), pp. 28—30.

4) a) M. D. Fryzuk and B. Bosrich, *J. Am. Chem. Soc.*, **99**, 6262 (1977); b) B. D. Vineyard, W. S. Knowles, M. J Sabacky, G. L. Bachman, and D. J. Weinkauff, *J. Am. Chem. Soc.*, **99**, 5946 (1977); c) G. Consiglo and P. Pino, *Helv. Chim. Acta*, **59**, 642 (1976).

5) H. Ozaki, *Bull. Chem. Soc. Jpn.*, **51**, 257 (1978).

6) I. Yasumori, Y. Inoue, and K. Okabe, Int. Symp. on Relations between Heterogeneous and Homogeneous Catalytic Phenomena, 1974, p. 141.

Activation of Carbon Dioxide by Tetraphenylporphinatoaluminium Methoxide. Reaction with Epoxide

Norikazu TAKEDA and Shohei INOUE*

Department of Synthetic Chemistry, Faculty of Engineering, University of Tokyo, Bunkyo-ku, Tokyo 113

(Received March 27, 1978)

α,β,γ,δ-Tetraphenylporphinatoaluminium methoxide reacts reversibly with carbon dioxide in the presence of 1-methylimidazole, and this carbon dioxide is activated to react with propylene oxide to produce propylene carbonate under atmospheric pressure and at room temperature.

In the course of our studies on the reaction of carbon dioxide with organometallic compounds,[1-3] we have found that carbon dioxide reacts with tetraphenylporphinatoaluminium ethyl in the presence of 1-methylimidazole only in visible light, but not in the dark.[4] Further studies on the reaction of porphinatoaluminium complex with carbon dioxide have led to an interesting finding that tetraphenylporphinatoaluminium methoxide can be a carrier of carbon dioxide which is activated enough to easily react with propylene oxide.

Experimental

Materials. α,β,γ,δ-Tetraphenylporphine ($TPPH_2$) was synthesized from pyrrole and benzaldehyde in propionic acid.[5-6] Propylene oxide was purified by refluxing over potassium hydroxide, then fractional distillation. 1-Methylimidazole (Im) was purified by distillation over calcium hydride under reduced pressure. Dichloromethane was washed with sulfuric acid followed by water, dried over calcium chloride and then calcium hydride, and distilled over calcium hydride in a nitrogen atmosphere.

Carbon dioxide was purified by passing through a series of columns packed with copper(II) sulfate, potassium hydrogen carbonate, reduced copper, phosphorus pentaoxide and activated copper(II) oxide. Triethylaluminium was purified by distillation in a nitrogen atmosphere under reduced pressure (111 °C/24 mmHg).

Measurement. Infrared spectra were measured in a fixed cell (0.1—1.0 mm) using a Hitachi EPI-G3 spectrophotometer. Ultraviolet and visible spectra were measured in a quartz cell of length 0.1 cm using Shimadzu RSP-7B spectrophotometer. ^1H NMR spectra were measured using a JEOL 4H-A type spectrometer.

Gas chromatographic analysis was carried out using a Yanagimoto Model G80 gas chromatograph with the column of 1—1.5 m packed with silica gel with helium as the carrier gas. The composition of propylene oxide–carbon dioxide copolymer was determined by the ^1H NMR spectrum of its chloroform solution.[7]

Average molecular weight of the polymer was measured by using Toyo Soda HLC-802UR high speed liquid chromatograph.

Procedure. Formation of Tetraphenylporphinatoaluminium Methoxide (TPPAlOMe) by the Reaction of Tetraphenylporphinatoaluminium Ethyl (TPPAlEt) with Methanol: A 200 ml two-necked Pyrex flask containing tetraphenylporphine ($TPPH_2$; 3.07 g, 5.0 mmol) was purged with nitrogen, and dichloromethane (150 ml) was added to dissolve $TPPH_2$. Triethylaluminium (0.69 ml, 5.0 mmol) was added slowly to the solution in a nitrogen stream at room temperature to give a solution of TPPAlEt in a few minutes.[4] The solvent was removed under reduced pressure from this system, the purple residue was dissolved in methanol (100 ml), and the solution was refluxed for three hours in a nitrogen atmosphere. After removing most of methanol under reduced pressure, remaining trace of methanol was removed as benzene azetrope. The resulting product was dark reddish-purple powder (about 3.3 g). Found C, 80.18; H, 4.81; N, 8.15%. Calcd for $C_{45}H_{31}N_4OAl$: C, 80.58; H, 4.66; N, 8.35%.

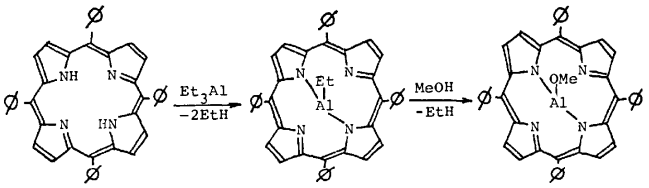

When dry hydrogen chloride was bubbled in the dichloromethane solution of the resulting product, the liberation of an equivalent amount of methanol to aluminium was detected in the solution by gas chromatography.

Reaction of Carbon Dioxide with TPPAlOMe: Reactions of tetraphenylporphinatoaluminium methoxide (TPPAlOMe) with carbon dioxide were carried out in a 20 ml quartz cell at 20 °C. The cell containing TPPAlOMe (0.168 g, 0.25 mmol), synthesized by the aforesaid method, was purged with nitrogen, and dichloromethane (20 ml) was added to dissolve TPPAlOMe. After the addition of 1-methylimidazole (0.033 g, 0.40 mmol), carbon dioxide was bubbled in the solution for one minute, and the reaction was followed by the infrared spectral measurement of the reaction mixture.

Reaction of Carbon Dioxide and Propylene Oxide with TPPAlOMe:

Reaction in Dichloromethane: Carbon dioxide was bubbled into the dichloromethane solution (20 ml) of TPPAlOMe (0.168 g, 0.25 mmol) with 1-methylimidazole (0.033 g, 0.40 mmol), and after two hours propylene oxide (0.35 ml, 5.0 mmol) was added to the solution in a carbon dioxide stream.

The solvent was removed from the solution after 45 h under reduced pressure at room temperature, followed by the addition of 5% hydrochloric acid (about 30 ml). After the insoluble materials were filtered off, sodium chloride (about 1 g) and diethyl ether (about 100 ml) were added to the aqueous filtrate, and the reaction product was extracted into the ether layer. After the evaporation of diethyl ether, the product was isolated by distillation under reduced pressure as a colorless oily liquid (0.2 g), which was identified as propylene carbonate by infrared spectral measurement and gas chromatography. The yield was directly determined by gas chromatography of the reaction mixture.

Reaction in Propylene Oxide in the Presence of 1-Methylimidazole:

The cell containing TPPAlOMe (0.168 g, 0.25 mmol) was purged with nitrogen and propylene oxide (8.3 g, 140 mmol) was added to dissolve TPPAlOMe. After the addition of 1-methylimidazole (0.033 g, 0.40 mmol), carbon dioxide was bubbled in the solution for one minute every 24 h.

After 96 h the reaction product was isolated by the same procedure as described above. In this case, about 1.2 g of propylene carbonate was obtained.

Reaction in Propylene Oxide in the Absence of 1-Methylimidazole: Carbon dioxide was bubbled in the propylene oxide solution (10 ml) of TPPAlOMe (0.12 or 0.25 mmol) for 1 min every 24 h. After 11 days, unreacted propylene oxide was removed from the reaction mixture under reduced pressure at room temperature. Diethyl ether was added to the residual viscous product, and the solvent was removed from the ether soluble part to obtain 9.3 g of propylene oxide–carbon dioxide copolymer.

Results and Discussion

Reaction of Carbon Dioxide with Tetraphenylporphinatoaluminium Methoxide (TPPAlOMe). When carbon dioxide was bubbled in a dichloromethane solution of TPPAlOMe in the presence of 1-methylimidazole (Im), a new carbonyl absorption band immediately appeared at 1697 cm^{-1} in the infrared spectrum of the reaction mixture (Fig. 1). If nitrogen gas was bubbled in this

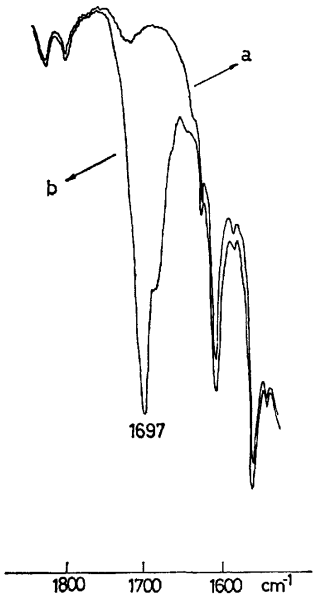

Fig. 1. Infrared spectra of the reaction mixture of tetraphenylporphinatoaluminium methoxide (TPPAlOMe) with carbon dioxide (CO_2) in the presence of 1-methylimidazole, TPPAlOMe; 0.25 mmol, 1-methylimidazole; 0.40 mmol, CH_2Cl_2; 20 ml, temp; 20 °C, a: before bubbling of CO_2, b: 20 min after bubbling of CO_2.

reaction mixture, this absorption band disappeared, and it appeared again by the introduction of carbon dioxide in the solution, indicating carbon dioxide reversibly reacted with TPPAlOMe in the presence of Im. In the absence of Im, no carbonyl absorption band was observed in the spectrum, in the reaction in 1 atm CO_2 at 20 °C for 120 h as well as in the reaction in 40 atm CO_2 at 60 °C for 20 h. No remarkable effect of irradiation of visible light was recognized in this reaction.

Figure 2 shows the visible spectra of TPPAlOMe and

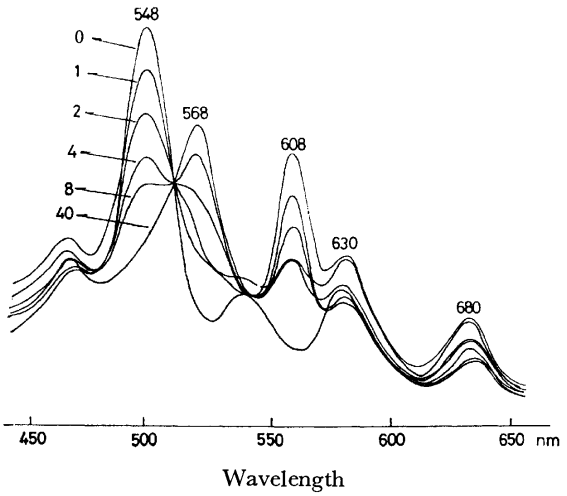

Fig. 2. Visible spectra of tetraphenylporphinatoaluminium methoxide (TPPAlOMe) and tetraphenylporphinatoaluminium methoxide–1-methylimidazole system in dichloromethane, TPPAlOMe; 7.0×10^{-3} mmol, CH_2Cl_2; 20 ml, 1-methylimidazole; 0, 7.0×10^{-3}, 1.4×10^{-2}, 2.8×10^{-2}, 5.6×10^{-2}, 2.8×10^{-1} mmol. The number in the figure represents the mole ratio of 1-methylimidazole to TPPAlOMe.

TPPAlOMe–Im (1 : 0.5—1 : 40) systems in dichloromethane at room temperature. The absorption maximum of the TPPAlOMe spectrum shifted from 548 to 568 nm in the presence of a sufficient amount of Im, and an isosbestic point was observed at 557 nm, which indicates the coordination of Im to TPPAlOMe probably as an axial ligand on the opposite side of methoxyl group with respect to the porphine ring.

As to the reactivity of other aluminium alkoxides with carbon dioxide, diethylaluminium ethoxide does not react with carbon dioxide even at 100 °C in the presence of several tertiary amines.[8] Thus, the reversible reaction with carbon dioxide at room temperature and under atmospheric pressure is very characteristic of the present system.

Reaction of Carbon Dioxide and Propylene Oxide with TPPAlOMe. Reaction in Dichloromethane in the Presence of 1-Methylimidazole: When the solution of TPPAlOMe with 1-methylimidazole (Im), saturated with carbon dioxide, was added by propylene oxide, the absorption at 1697 cm^{-1}, which was already observed in the TPPAlOMe–Im–CO_2 system, increased immediately (Fig. 3(A)). After three hours, a new carbonyl absorption band centered at 1805 cm^{-1} appeared, assigned to C=O stretching vibration of cyclic carbonate (propylene carbonate). And then after about 25 h other carbonyl absorption bands appeared at 1675 and 1750 cm^{-1}, which did not disappear by bubbling nitrogen gas or by removing the solvent. The band at 1750 cm^{-1} is considered due to linear carbonate as mentioned in the latter part of this paper, but the assignment of the band at 1675 cm^{-1} is not made at present.

The behavior of the absorption band at 1697 cm^{-1} is particularly interesting as shown in Fig. 3(B). As long as sufficient carbon dioxide existed in the solution as indicated by the absorption at 2340 cm^{-1}, the band at

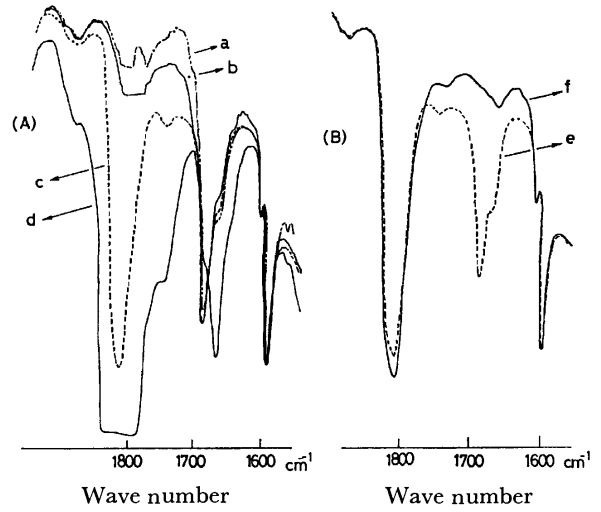

Fig. 3. Infrared spectra of the reaction mixture of tetraphenylporphinatoaluminium methoxide (TPPAlOMe), carbon dioxide (CO_2) and propylene oxide in the presence of 1-methylimidazole, TPPAlOMe; 0.25mmol, 1-methylimidazole; 0.40 mmol, PO; 5.0 mmol, CO_2; bubbling, (A); a: before addition of propylene oxide, b: 3 h after addition c: 25 h, d: 43 h, (B); e: when free CO_2 exists in the reaction mixture, f: when there remains no free CO_2 in the system.

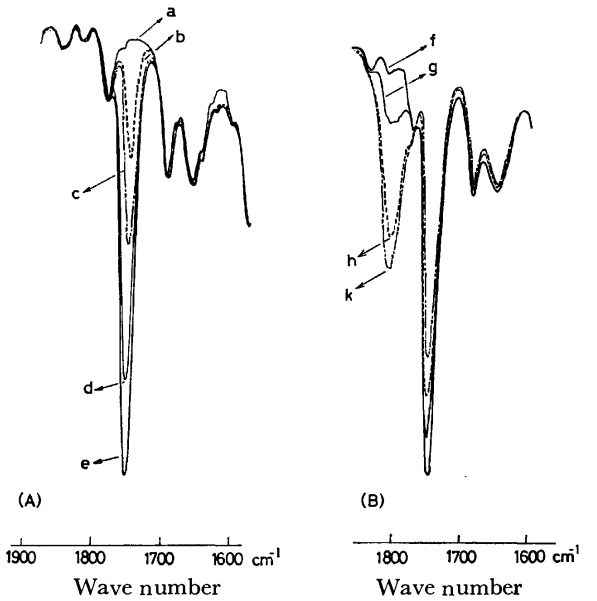

Fig. 4. Infrared spectra of the reaction mixture of tetraphenylporphinatoaluminium methoxide (TPPAlOMe), carbon dioxide (CO_2) and propylene oxide, (A); TPPAlOMe; 0.25 mmol, propylene oxide; 10 ml, CO_2; bubbling every 24 h, a: before bubbling of CO_2, b: 18 h after bubbling of CO_2, c: 44 h, d: 92 h, e: 167 h, (B) when there exists no free CO_2. Added 1-methylimidazole; 0.40 mmol, f: 20 min after addition of 1-methylimidazole, g: 2 h, h: 33 h, k: 49 h.

1697 cm^{-1} did not change its intensity. When the solution became deficient in carbon dioxide, it diminished rapidly, while the absorption band at 1805 cm^{-1} increased. Supply of carbon dioxide here in the solution made absorption band at 1697 cm^{-1} strong again. Thus, the absorption band at 1697 cm^{-1} is due to carbon dioxide activated by the TPPAlOMe–Im complex, which reacts immediately with propylene oxide to produce propylene carbonate at room temperature and under atmospheric pressure.

The formation of propylene carbonate proceeded catalytically with respect to TPPAlOMe: for example, 2.7 equivalent in dichloromethane and 4.0 equivalent in propylene oxide under 1 atm CO_2 at 20 °C, after 2.5 h, respectively.

As to other amines than Im, pyridine behaved similarly, showing a reversible absorption band at 1695 cm^{-1} in the infrared spectrum of the reaction system TPPAlOMe–pyridine–CO_2. In contrast, no new carbonyl absorption band was observed when carbon dioxide was bubbled in the TPPAlOMe–triethylamine system. However, when propylene oxide was added to the solution, a reversible absorption band appeared at 1697 cm^{-1}. Similar results were obtained in the case of *N,N*-dimethylbenzylamine or *N,N*-dimethylaniline. Nevertheless, propylene carbonate could be produced from propylene oxide and carbon dioxide under mild reaction conditions by using TPPAlOMe coupled with amine, such as 1-ethylimidazole, pyridine, picolines, *N,N*-dimethylbenzylamine, triethylamine, tributylamine, triethylenediamine and hexamethylenetetraamine.

However, under atmospheric pressure and at room temperature, a mixture of only carbon dioxide, propylene oxide and tertiary amine, without TPPAlOMe, could not produce propylene carbonate.

Reaction in Propylene Oxide in the Absence of 1-Methylimidazole: When TPPAlOMe, carbon dioxide and propylene oxide reacted in the absence of amine, the infrared spectra of the reaction mixture showed a carbonyl absorption band only at 1750 cm^{-1} (Fig. 4(A)) which was assigned to C=O stretching vibration of linear carbonate. In fact, from this reaction mixture was obtained 9.3 g of propylene oxide–carbon dioxide copolymer, which consisted of 15 mol % of oxycarbonyl and 85 mol % of oxy(2-methylethylene) units, and the average molecular weight was about 4000.[9]

By the removal of carbon dioxide perfectly from this

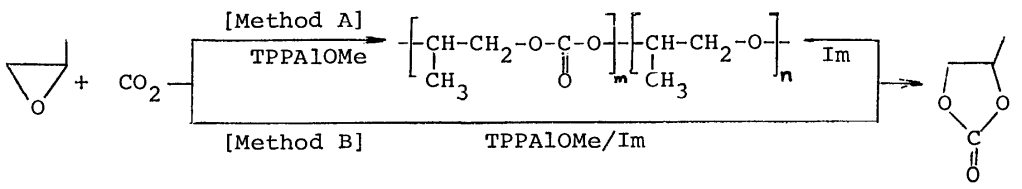

Scheme 1.

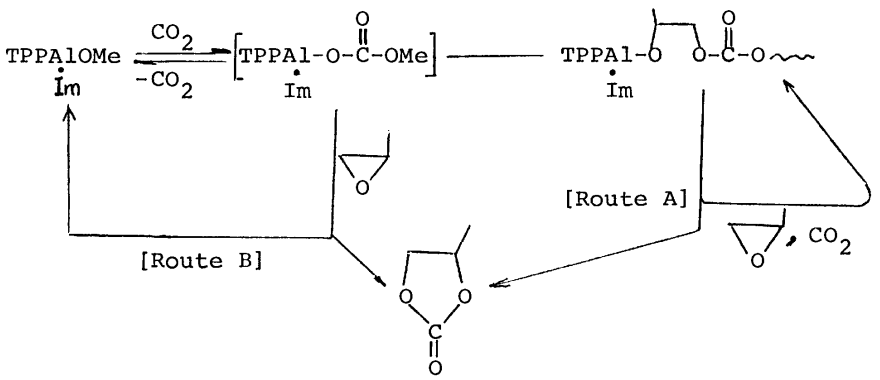

Scheme 2.

system, followed by the addition of Im or *N,N*-dimethylbenzylamine, the intensity of the absorption band at 1750 cm^{-1} decreased and an absorption at 1805 cm^{-1} appeared (Fig. 4(B)).

Therefore, propylene carbonate may be formed from the cyclization of carbon dioxide–propylene oxide copolymer (linear polyether–carbonate) by the effect of amine (Scheme 1).

However, as the formation reaction of propylene carbonate (PC) in the TPPAlOMe–Im–CO_2–propylene oxide system (Method B; 2.7 mol PC/mol TPPAlOMe/2.5 h) proceeds much faster than that *via* carbon dioxide–propylene oxide copolymer (Method A; 0.1 mol PC/mol TPPAlOMe/2.5 h), there seems to be another route than that *via* the copolymer, in which TPPAlOMe–Im–CO_2 complex reacts with propylene oxide to produce propylene carbonate directly.

Conclusion

Possible routes for the reaction in TPPAlOMe–Im–CO_2–propylene oxide system are shown in Scheme 2. In route A, carbon dioxide inserts between Al–OMe bond reversibly, propylene oxide reacts into the Al–carbonate bond thus formed, and the repeating reaction of propylene oxide and CO_2 results in the formation of copolymer. This copolymer may be gradually cyclized to propylene carbonate in the presence of amine, as actually confirmed. However, there still remains the possibility of the existence of another direct route, B, because of the difference in the rates of the formation of propylene carbonate in two methods of Scheme 1 (directly from TPPAlOMe–amine–CO_2–propylene oxide system, and *via* copolymer). Although TPPAlOMe–Im–CO_2 complex, having infrared absorption at 1697 cm^{-1}, would be an aluminium alkyl carbonate as shown in Scheme 2, the structure has not yet been confirmed, because of its highly reversible, unstable nature.

As the conclusion, TPPAlOMe–1-methylimidazole complex is a carrier of activated carbon dioxide which is able to react readily with propylene oxide to give propylene carbonate even under atmospheric pressure of carbon dioxide and at room temperature.

The authors wish to express their thanks to Professor Teiji Tsuruta for his valuable discussion, and to Mr. Hiroshi Yokoyama for his carrying out some of the preliminary experiments.

References

1) S. Inoue and Y. Yokoo, *J. Organomet. Chem.*, **39**, 11 (1972).
2) S. Inoue and Y. Yokoo, *Bull. Chem. Soc. Jpn.*, **45**, 3651, (1972).
3) S. Inoue, "Progress in Polymer Science Japan," Kodansha, Tokyo (1975), Vol. 8, p. 1.
4) S. Inoue and N. Takeda, *Bull. Chem. Soc. Jpn.*, **50**, 984 (1977).
5) A. D. Adler, F. R. Longo, J. D. Finarelli, J. Goldmacher, J. Assour, and L. Korsakoff, *J. Org. Chem.*, **32**, 476 (1967).
6) G. H. Barnett and M. F. Hudson, *J. Chem. Soc., Perkin Trans. 1*, **1975**, 1401.
7) S. Inoue, H. Koinuma, and T. Tsuruta, *Makromol. Chem.*, **130**, 210 (1969).
8) Y. Yokoo and S. Inoue, unpublished studies.
9) For further details on the copolymer, see: N. Takeda and S. Inoue, *Makromol. Chem.*, **179**, 1377 (1978).

The Chlorination of Norbornene and Cyclooctadienes with Sulfuryl Chloride and Phosphorus(V) Chloride. Ionic *vs.* Radical Chlorination with Each Reagent

Sakae UEMURA,* Hajime OKAZAKI, Akira ONOE, and Masaya OKANO

Institute for Chemical Research, Kyoto University, Uji, Kyoto 611

(Received March 31, 1978)

The chlorination of norbornene and cyclooctadienes with sulfuryl chloride and phosphorus(V) chloride has been investigated mainly in carbon tetrachloride under various conditions. From the studies of the product distributions and the effect of radical scavengers, the following facts have been revealed for the first time in olefin chlorination: chlorination with sulfuryl chloride proceeds through an ionic pathway at room temperature or in the presence of silica gel and that with phosphorus(V) chloride through a radical pathway at elevated temperature, and an ionic chlorination with phosphorus(V) chloride in nonpolar solvents does not seem to involve C–P bond formation through the reaction.

Sulfuryl chloride has generally been known to chlorinate olefin through a radical pathway,[1] while it is also known as the effective electrophile in nuclear chlorination of some aromatic compounds.[2] Phosphorus(V) chloride, on the other hand, can usually chlorinate olefin *via* an ionic mechanism,[3] while it also works as the effective catalyst[4] or the reagent[3] for the radical chlorination of alkanes. In order to know whether each chlorinating agent shows both an ionic and a radical nature in olefin chlorination, we have carried out the chlorination of norbornene and cyclooctadienes under various conditions; these olefins have already been shown to be good substrates to study the nature of chlorination because of clear-cut different distributions in the products between radical and ionic reactions.[5,6] We will describe the results and discuss the nature of both reagents.

Results and Discussion

Treatment of norbornene with sulfuryl chloride and phosphorus(V) chloride afforded four products: nortricyclenyl chloride (**1**) and *trans*-2,3- (**2**), *exo-cis*-2,3- (**3**), and *exo*-2-*syn*-7-dichloronorbornane (**4**); their distributions depended very much on reaction conditions. The results are summarized in Table 1, together with

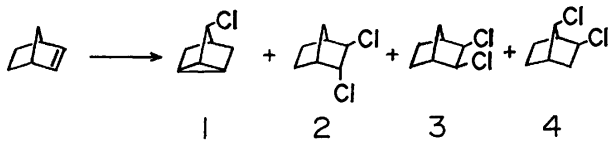

the data of typical ionic (Runs 13 and 15) and radical chlorination (Runs 14 and 16) by use of chlorine[7] and

Table 1. Chlorination of norbornene

Run	Norbornene (mmol)	Chlorinating agent (mmol)	Solvent (ml)	React. temp (°C)	React. time (h)	Additives *etc.* (mmol)	Products[a] Isomer distribution 1	2	3	4	Yield (%)
1	25	SO_2Cl_2 25	CCl_4 50	20	20	—	74	3	1	22	41
2	25	SO_2Cl_2 25	CCl_4 50	76	1	—	15	64	16	5	95
3	25	SO_2Cl_2 25	CCl_4 50	76	1	*m*-DNB[b] 5	61	17	7	15	25
4	25	SO_2Cl_2 25	CCl_4 50	25	2	*hν*	6	78	16	0	97
5	5	SO_2Cl_2 5	Benzene 25	80	2	—	7	74	16	3	97
6	25	SO_2Cl_2 25	CCl_4 50	76	1	SiO_2[c] 39	57	2	0	41	48
7	25	PCl_5 25	CCl_4 50	27	3	—	61	7	3	29	58
8	25	PCl_5 25	CCl_4 50	76	2	—	42	20	7	31	66
9	25	PCl_5 25	CCl_4 50	76	2	*m*-DNB[b] 5	57	5	3	35	72
10	25	PCl_5 25	CCl_4 50	25	3	*hν*	45	25	7	23	92
11	5	PCl_5 5	Benzene 25	80	3	—	45	5	4	46	58
12	5	PCl_5 5	$CHCl_3$ 25	65	2	—	97	trace	trace	3	43
13[d]	—	Cl_2 —	CCl_4 —	25	0.5	O_2	65	6	4	25	95
14[d]	—	Cl_2 —	CCl_4 —	25	0.5	N_2, *hν*	19	37	35	0	—
15[e]	—	$PhICl_2$ —	CCl_4 —	0	47	O_2	79	7	2	12	—
16[e]	—	$PhICl_2$ —	CCl_4 —	74	0.05	—	0	74	26	0	—

a) Determined by GLC. b) *m*-Dinitrobenzene. c) Silica gel, Wakogel C-300, 2.35 g, 100 wt % to norbornene. 2-Chloronorbornane (*ca.* 10%) and a small amount of unidentified compound were also formed. d) Ref. 7. The amounts of olefin and chlorine were not described. e) Ref. 8. Olefin (0.15—0.8 M) and $PhICl_2$ (0.13—0.2 M) were used. The yields of the products were not stated.

(dichloroiodo)benzene.[8] The chlorination with sulfuryl chloride in carbon tetrachloride gave a mixture of **1** and **4** or of **2** and **3** as the main products at room (Run 1) or reflux (Run 2) temperature, respectively. The comparison of the product distribution with that of Runs 13—16 reveals that the reaction has a radical nature at reflux temperature as expected, while it has an ionic nature at room temperature. In fact, when *m*-dinitrobenzene (*m*-DNB) was added as a radical scavenger in the reaction at reflux temperature (Run 3), the yields of the products decreased profoundly and the isomer distribution became similar to that in an ionic reaction, showing that the radical reaction was almost completely suppressed. A quite similar phenomenon was observed using phenol or *t*-butylcatechol instead of *m*-DNB. Under irradiation of UV light (Run 4) or in the presence of benzoyl peroxide, an almost complete radical reaction occurred even at room temperature. The reaction in benzene under reflux also showed a radical nature, as expected (Run 5). Since olefin chlorination with sulfuryl chloride has already been recognized as a radical reaction, as described above, the finding described here seems to be the first clear-cut example of ionic chlorination of olefins with sulfuryl chloride. The attempts of the chlorination in more polar solvents such as acetonitrile and nitromethane, in which the result of a more ionic reaction is expected, resulted in the low yield of products and/or the formation of various unidentified compounds. It has been found that electrophilic chlorination of aromatic compounds by sulfuryl chloride occurs if silica gel is added to the reaction system.[9] When we applied such a reaction to norbornene by using silica gel (Wakogel C-300, 300 mesh), the products whose distribution was clearly characteristic of an ionic reaction were obtained even in the reaction at refluxing temperature (Run 6).

The product distributions in the chlorination of norbornene by phosphorus(V) chloride in carbon tetrachloride, chloroform, and benzene suggest that all reactions proceeded mainly through an ionic pathway (Runs 7, 8, 11, and 12). Considering the results of Runs 8 and 10, however, it may be possible to say that the reaction has a slightly radical nature at refluxing temperature or under UV irradiation in carbon tetrachloride. In fact, the addition of *m*-DNB to a reaction system at refluxing temperature in carbon tetrachloride suppressed the formation of **2** and **3** (Run 9). These results revealed that both a homolytic and a heterolytic chlorination were operative at 76 °C (refluxing temperature of CCl_4) by use of phosphorus(V) chloride. Wyman *et al.*[3] have suggested the presence of a radical nature in the chlorination of *trans*-stilbene at more elevated temperatures (at 124 °C in chlorobenzene as solvent).

Treatment of 1,5-cyclooctadiene with sulfuryl chloride and phosphorus(V) chloride gave *trans*- (**5**) and *cis*-5,6-dichlorocyclooctene (**6**), together with a small amount (<1%) of an unidentified compound. Typical results are shown in Table 2. It has already been clarified

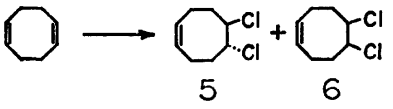

5 6

that an ionic reaction favored the formation of

Table 2. Chlorination of 1,5- and 1,3-cyclooctadienes

Run	Olefin (mmol)	Chlorinating agent (mmol)	Solvent (ml)	React. temp (°C)	React. time (h)	Additives *etc.* (mmol)	Products[a] Isomer distribution 5	6	7	8	9	10	Yield (%)
	1,5-COD[b]												
17	50	SO_2Cl_2 50	CCl_4 50	76	2	—	12	88					63
18	50	SO_2Cl_2 50	CCl_4 50	76	2	*m*-DNB[c] 10	75	25					38
19	50	SO_2Cl_2 50	CCl_4 50	25—35	2	SiO_2[d] 90	79	21					34
20	50	SO_2Cl_2 50	CCl_4 50	20	20	—	96	4					6
21	50	PCl_5 25	CCl_4 50	76	5	—	30	70					79
22	50	PCl_5 25	CCl_4 50	76	5	*m*-DNB[c] 5	80	20					54
23	50	PCl_5 25	CCl_4 50	20	5	—	48	52					20
24	50	PCl_5 25	$CHCl_3$ 50	65	2	—	98	2					65
25	50	PCl_5 25	CH_2Cl_2 50	40	6	—	99	1					88
26	50	PCl_5 25	Benzene 50	80	2	—	91	9					70
27	6[e]	$PhICl_2$ 5	CCl_4 25	76	1	N_2	20	80					47
28	50[f]	Cl_2 50	CH_2Cl_2 50	−50	0.5	—	93	7					18
	1,3-COD[g]												
29	100	SO_2Cl_2 100	CCl_4 100	76	2	—			19	2	58	21	62
30	50	PCl_5 50	CCl_4 50	76	5	—			17	9	49	25	63
31	25	PCl_5 25	CH_2Cl_2 50	40	5	—			40	7	18	35	56
32	10[e]	$PhICl_2$ 5	$CHCl_3$ 25	61	1	N_2			20	3	58	19	66
33	50[f]	Cl_2 50	CH_2Cl_2 100	−50	0.5	—			45	3	24	28	44

a) Determined by GLC. The yield is based on the chlorinating agent charged. b) 1,5-Cyclooctadiene. c) *m*-Dinitrobenzene. d) Silica gel, Wakogel C-300, 5.41 g, 100 wt % to 1,5-COD. Two unidentified compounds, probably HCl addition products, were also formed (*ca.* 5%). e) Ref. 6. Radical reaction. f) Ref. 6. Ionic reaction. g) 1,3-Cyclooctadiene.

5 (Run 28), while a radical reaction preferred that of **6** (Run 27).[6] The reaction with sulfuryl chloride at reflux temperature in carbon tetrachloride (Run 17) gave mainly **6**, as expected, while that at room temperature (Run 20) gave mainly **5**, although the yield was very low. The addition of silica gel promoted the ionic chlorination profoundly (Run 19), as in the case of norbornene. On the other hand, the reaction with phosphorus(V) chloride afforded mainly **5** in almost all cases (Runs 23—26), except in carbon tetrachloride in which the formation of **6** predominated (Runs 21 and 23). This result seems to be another and much clearer example of a homolytic olefin chlorination with phosphorus(V) chloride. In all cases where a radical reaction seems to prevail, the addition of *m*-DNB suppressed the yield of **6** markedly and increased that of **5** (Runs 18 and 22).

Although a detailed study was not carried out, the results of some reactions of 1,3-cyclooctadiene with both chlorinating agents were worth noting. The products were four dichlorocyclooctenes, **7**—**10**. Typical results are shown in Table 2, together with the results under

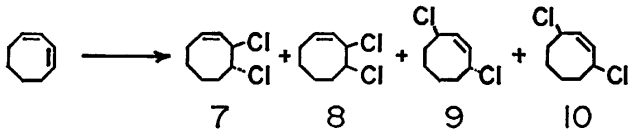

7 8 9 10

ionic (Run 33) and radical conditions (Run 32).[6] If we compare the isomer distributions in Runs 30 and 31 with those in Runs 32 and 33, it seems that chlorination with phosphorus(V) chloride has a radical nature in carbon tetrachloride at refluxing temperature, while it proceeds mainly through ionic pathway in dichloromethane.

Contrary to the case of radical chlorination with sulfuryl chloride, where it has already been clarified that sulfuryl chloride decomposed to chlorine atoms and chlorosulfonyl radicals, both acting as chain carriers,[1] there should be the polarization of sulfuryl chloride shown below in an ionic olefin chlorination. The

$$SO_2Cl_2 \longrightarrow SO_2\overset{\delta-}{Cl}\overset{\delta+}{Cl} \rightleftarrows SO_2Cl^- + Cl^+$$

addition of silica gel clearly enhances such polarization. On the other hand, in the radical chlorination of olefin with phosphorus(V) chloride the dissociation shown below seems to occur at elevated temperatures in carbon tetrachloride; such a dissociation was proposed by Olah *et al.*[4] in the phosphorus(V) chloride catalyzed radical chlorination of several alkanes.

$$PCl_5 \rightleftarrows PCl_4\cdot + Cl\cdot$$
$$PCl_5 \rightleftarrows PCl_3 + Cl_2$$
$$PCl_5 + Cl_2 \rightleftarrows PCl_4\cdot + Cl_3\cdot \quad (Cl\cdot + Cl_2)$$

For an ionic olefin chlorination with phosphorus(V) chloride, it has been proposed[3] that phosphorus(V) chloride (in the form of $PCl_4^+PCl_6^-$) added across the double bond to afford the β-chlorophosphorus(V) compound,[10] followed by the S_Ni attack of the chlorine of the PCl_4 moiety and the elimination of phosphorus(III) chloride. Although phosphorus(V) chloride is known to exist in two competing equilibria, (1) $2PCl_5 \rightleftarrows PCl_4^+ + PCl_6^-$ and (2) $PCl_5 \rightleftarrows PCl_4^+ + Cl^-$, in polar solvents, it exists as a monomer in nonpolar solvents such as benzene and carbon tetrachloride.[11] Therefore, a mechanism which does not involve C–P bond formation should also be conceivable in the ionic chlorination of olefins with phosphorus(V) chloride in nonpolar solvents. By comparing the product distribution in the case of phosphorus(V) chloride with that in an ionic chlorination with chlorine, one possible scheme may be the ionic attack of chlorine which may be formed by the equilibrium $PCl_5 \rightleftarrows PCl_3 + Cl_2$.[3,4]

The following two points were revealed. The chlorination with sulfuryl chloride proceeds through a radical pathway at elevated temperature, as has been reported, but also through an ionic pathway at lower temperature or in the presence of silica gel. The chlorination with phosphorus(V) chloride is mainly an ionic reaction, but it showed some radical nature in carbon tetrachloride at refluxing temperature.

Experimental

All organic materials and sulfuryl chloride were commercial products and distilled just before use. Commercial phosphorus(V) chloride was used without further purification. The reactions were carried out by mixing all the reagents at room temperature and then keeping the mixture at reaction temperature for appropriate times under the presence of atmospheric oxygen unless otherwise stated. After reaction the mixture was cooled and washed with water and then the organic layer was separated and dried over $MgSO_4$. The identifications of each product, **1**—**4**[5,12] and **5**—**10**[6] were described previously. The product mixtures were analyzed by GLC by the use of Shimadzu 4BMPF apparatus on EGSS-X (15%)-Chromosorb-W (1 or 3 m) column (carrier gas, N_2; ethyl benzoate as internal standard).

References

1) M. S. Kharasch and H. C. Brown, *J. Am. Chem. Soc.*, **61**, 2142 (1939); D. C. Nonhebel and J. C. Walton, "Free-radical Chemistry," Cambridge Univ. Press, Cambridge (1974), p. 189.
2) See for example, P. B. D. de la Mare, "Electrophilic halogenation," Cambridge Univ. Press, Cambridge (1976), p. 106.
3) D. P. Wyman, J. Y. C. Wang, and W. R. Freeman, *J. Org. Chem.*, **28**, 3173 (1963).
4) G. A. Olah, P. Schilling, R. Renner, and I. Kerekes, *J. Org. Chem.*, **39**, 3472 (1974).
5) S. Uemura, A. Onoe, and M. Okano, *Bull. Chem. Soc. Jpn.*, **48**, 3702 (1975).
6) S. Uemura, A. Onoe, H. Okazaki, M. Okano, and K. Ichikawa, *Bull. Chem. Soc. Jpn.*, **49**, 1437 (1976).
7) M. L. Poutsma, *J. Am. Chem. Soc.*, **87**, 4293 (1965).
8) D. D. Tanner and G. C. Gidley, *J. Org. Chem.*, **33**, 38 (1968).
9) M. Hojo and R. Masuda, *Synth. Commun.*, **5**, 169 (1975).
10) In some cases such intermediates have been formed and converted into the known derivatives: for example, W. H. Woodstock, U. S. Patent 2471471, *Chem. Abstr.*, **43**, 7499 (1949); G. M. Kosolapoff and J. F. McCullough, *J. Am. Chem. Soc.*, **73**, 855 (1951).
11) R. W. Suter, H. C. Knachel, V. P. Petro, J. H. Howatson, and S. G. Shore, *J. Am. Chem. Soc.*, **95**, 1474 (1973).
12) S. Uemura, A. Onoe, and M. Okano, *Bull. Chem. Soc. Jpn.*, **47**, 692, 3121 (1974).

Volatile Components of *Meratia praecox*

Yoko NAYA* and the late Munio KOTAKE
The Institute of Food Chemistry, Shimamoto-cho, Mishima-gun, Osaka 618
(Received April 10, 1978)

The major volatile constituents present in different parts of a deciduous tree, *Meratia praecox*, have been identified by combination of GC-MS and spectral analysis of the isolated compounds. From the results, some biogenetic implications were discussed.

The family Calycanthaceae consists of two genera, *Meratia* (Chinese origin) and *Calycanthus* (American origin). *Meratia praecox* Rehd. et Wils. (*Chimonanthus praecox*) is a small deciduous tree producing fragrant flowers during a period of two months in midwinter. Early works on the essential oils of Chimonanthus fragrance were reviewed by Louveau.[1] Among the compounds reported were benzyl alcohol, linalool, terpineol, farnesol, and indole. By means of recent techniques, we have made an exhaustive study of the oils isolated from the different parts of *M. praecox*, and determined the relative amounts of various components as a function of growing season. This paper presents the results of investigation and a discussion on biogenetic implications.

Experimental

Of many samples collected, the results for six characteristic specimens will be described. Samples were flower bud bursting flower, fresh flower, faded flower, leaf and fresh branch (Table 1). All the specimens were collected from the same tree. Each specimen was steam-distilled under atmospheric pressure. The distillates were saturated with sodium chloride and extracted with ether; the ether extract was dried over anhydrous sodium sulfate, and the ether was removed to give the essential oil. The yields of essential oils are also given in Table 1. Characterization of the components was carried out by a combination of GC-MS and spectral analysis after their isolation by adsorption chromatography (silica gel or silver nitrate-impregnated silica gel) and preparative gas chromatography (Carbowax-20M). The identity of the major constituents was confirmed by a comparison of their IR and NMR spectra with those of authentic samples.

TABLE 1. ANALYTICAL SAMPLES FROM THE DIFFERENT PARTS OF *M. praecox* AND THE CONTENTS OF VOLATILE COMPOUNDS

Sample No.	Plant part	Harvested date (1977)	Yield (%)
I	Flower bud	17/Jan.	0.082
II	Bursting flower	5/Feb.	0.087
III	Fresh flower	10/Feb.	0.19
IV	Faded flower	1/March	0.012
V	Leaf	7/June	0.04
VI	Fresh branch	1/March	0.02

Apparatus and Operating Conditions. Preparative GLC was carried out with a Varian Aerograph 920 fitted with a thermal conductivity detector, using a 10 ft.×3/8 in. aluminum column containing 20% Carbowax-20M on 60—80 mesh Diasolid-L. Helium was used as a carrier gas, the column temperature being set at 100—200 °C.

For quantitative analytical GLC, a Hitachi K-53 apparatus equipped with a flame ionization detector and a computer system was used. The capillary column used for the analysis was 45 m×0.25 mm, made of stainless steel and coated with HB 2000; the column temperature was 150 °C, isothermal. The inlet pressure for nitrogen carrier gas was set at 1.5 kg/cm^2.

The GC-MS spectra were measured by combination of GLC fitted with a Golay column (45 m×0.25 mm, HB 2000) and mass spectrometry using a Hitachi RMU-6 mass spectrometer with operating conditions: ionization energy, 70 eV; acceleration voltage, 2000 V. The column temperature was programmed non-linearly at 100—150 °C with a gas inlet pressure of 0.6 kg/cm^2.

The IR spectra were measured with a Hitachi EPI-G2 spectrometer. The PMR spectra were taken with a Hitachi R-20B spectrometer at 60 MHz in CCl_4 with TMS as internal standard.

Results and Discussion

The components identified in six specimens, together with their contents as determined with the GC/computer system are given in Table 2. The major compound common to the oils of the flower bud and the bursting flower was found to be elemol, corresponding to more than 80% of the volatile oils. However, hedycaryol, instead of elemol, was isolated from ether extracts obtained without steam distillation by preparative TLC on silica gel. Hedycaryol, identified by its NMR spectrum, was converted into elemol on being injected into a gas chromatograph. Elemol is known to be an artifact caused by thermal isomerization. Thus, its biosynthetic equivalent, hedycaryol, appears to be one of the basic products of sesquiterpene biosynthesis. The data for bursting flower oil indicate that benzyl alcohol is produced at an early stage in the flowering. In the fresh flower oil, bicyclogermacrene and related compounds, δ-, β-, γ-elemenes, and germacrene-B, were found to be the major components. Considerable amounts of benzyl alcohol, its acetate, and linalool (possibly responsible for the flowery odor) were detected. Because of the marked increase of volatiles in the fresh flower, the detection of elomol or its equivalent would be masked by the post-products. In the faded flower oil, elemol was found to be the main compound, the level of components predominant when the flower was in full bloom decreasing. The characteristic compounds of the flower odor might have evaporated into the air, only sesquiterpens remaining. The leaf oil was similar to the faded flower oil, but not to the woody branch oil. In the woody branch oil, major components were humulene, caryoph-

TABLE 2. IDENTIFIED COMPONENTS AND THEIR CONTENTS (%) IN SIX SPECIMENS

Compound	I	II	III	IV	V	VI
1-Pentanol					+	
cis-3-Hexen-1-ol					0.45	
trans-3-Hexen-1-ol						
Heptanal			0.38	0.31		
Nonanal	0.31		2.37	4.40		0.15
Furfural				+		+
Octane				+		
Tridecane			0.07	0.08		
Heptadecane			0.17	0.13		0.07
Nonadecane			0.50	0.39		
α-Pinene						4.17
Camphene						0.18
β-Pinene						7.10
Myrcene						0.44
α-Phellandrene						1.02
α-Terpinene						0.44
Limonene						1.22
β-Phellandrene						1.24
cis-β-Ocimene			0.27	0.23		
trans-β-Ocimene	4.83		0.87	8.44	0.17	
p-Cymene						2.58
Terpinolene						0.13
1,8-Cineol					+	+
trans-Linalool oxide (THF)			0.19			
cis-Linalool oxide (THF)			0.54			0.05
Linalool			6.92		0.66	0.44
Terpinen-4-ol						2.01
α-Terpineol						0.77
Borneol						0.61
trans-Linalool oxide (THP)			0.64			
Thymol						0.12
Benzaldehyde				0.04		
Benzyl acetate		0.93	2.39	0.48		
Benzyl alcohol		4.86	15.9	5.52		
Cinnamaldehyde				0.06		
Cinnamyl alcohol			+			
Cinnamic acid			+			
Indole			1.07			

Compound	I	II	III	IV	V	VI
α-Cubebene			0.43	+		0.02
δ-Elemene			1.79	0.47		
α-Copaene			0.76	0.10	0.11	1.02
β-Cubebene	+		0.59	0.10	0.37	0.54
α-Gurjunene						0.23
β-Elemene	0.69	1.38	8.87	0.78	3.60	2.14
Caryophyllene			2.17	1.26	4.30	18.6
γ-Elemene			2.72	1.85	4.60	0.06
β-Farnesene			0.32	0.16		0.11
α-Humulene	0.77		0.87	0.39	1.20	4.60
γ-Muurolene	+		0.30		0.28	0.49
Germacrene-D	1.01		4.56	0.26	0.54	0.30
Zingiberene			3.09	1.38	1.40	
α-Muurolene			+	0.12	1.30	0.94
Bicyclogermacrene	1.01		18.1	5.52	6.90	2.07
trans-α-Farnesene			2.16	0.45	0.50	0.19
δ-Cadinene	1.01	0.92	2.77		2.40	6.94
γ-Cadinene			+			1.98
1,4-Cadinadiene	+		0.16	0.07	0.60	0.34
α-Cadinene			0.10	0.08		0.09
Calamenene			+	+		0.29
Germacrene-B	1.01		1.93	2.90	4.00	0.51
α-Calacorene			0.13			0.28
Cadalene			+		0.40	0.25
Caryophyllene oxide			0.77	2.10	0.12	5.20
Humulene epoxide-II						0.67
Caryophyllene alcohol						0.01
Nerolidol	+		1.19	0.56	0.81	2.97
Elemol (hedycaryol)	81.0	84.9	1.84	45.5	43.3	1.14
epi-Cubenol			0.75	+	2.30	2.49
Spatulenol (tentative)			0.70	1.51	1.70	0.24
γ-Eudesmol	1.20	0.48	+	0.97	3.80	
T-Cadinol	+	0.31	1.66	0.69	0.90	9.52
δ-Cadinol						0.63
α-Eudesmol	3.00	1.52		2.38	1.90	
β-Eudesmol					1.60	
α-Cadinol			0.74	0.47	0.60	3.97
Total	95.84	95.30	91.62	90.15	90.81	91.57

Contents were calculated by means of the GC/computer system (HB 2000, 0.25 mm×45 m).

TABLE 3. CONTENTS (%) OF SOME DISTINCTIVE COMPONENTS FROM SIX SPECIMENS

Group of component	I	II	III	IV	V	VI
Linalools (linalool, its oxides)			**8.29**		0.66	0.49
Other monoterpenes	4.83		1.14	**8.67**	0.17	**22.03**
Aromatic comps.		5.79	**19.36**	6.10		
Germacrene-B type	**87.91**	**88.28**	**35.25**	**60.37**	**69.70**	5.92
(germacrene-B, elemenes)	1.70	1.38	**15.31**	6.00	**12.20**	2.71
(bicyclogermacrene)	1.01		**18.10**	5.52	6.90	2.07
(elemol, hedycaryol)	**81.0**	**84.9**	1.84	**45.5**	**43.3**	1.14
(eudesmols)	4.20	2.00		3.35	7.30	
Germacrene-D type	2.02	1.23	10.29	1.69	6.62	**25.20**
(germacrene-D, cadinenes, muurolenes)	2.02	0.92	7.89	0.53	5.12	**11.08**
(cadinols)		0.31	2.40	1.16	1.50	**14.12**
Humulene, caryophyllene type	0.77		3.81	3.75	5.62	**29.08**

yllene and its oxides (*t,t*-farnesyl-pp type), together with considerable amounts of compounds of *c,t*-farnesyl-pp type such as germacrene-D, cadinenes, and cadinols.

The contents (%) of some distinctive components are given in Table 3. Linalool, its oxides and aromatic compounds such as benzyl alcohol, its acetate and indole are distinctive components of the fresh flower oil, appearing to have been translocated or partly lost by evaporation in the faded flower. These compounds were formed before the leaf emerged, thus before the start of vigorous assimilation. Sesquiterpenes of the germacrene-B type, such as hedycaryol and related hydrocarbons, amounted to 35—88% of the flower oils (I—IV) and the leaf oil (V). The branch oils did not contain nearly as much, while germacrene-D and related hydrocarbons and oxygenated compounds, in addition to humulene and caryophyllene, were major components of the woody branch oils. All these components were absent or present in only small quantities in the oils of flowers and the leaf. The difference in biosynthetic pathways is thus distinct.

References

1) G. Louveau, *Rev. Marques Parfum. Savonn.*, **9**, 531, 573, 622 (1931); *cf. Chem. Abstr.*, **27**, 3776 (1933).

Vinyl Polymerization. 375.[1] Radical Polymerization of Vinyl Monomer in Water Initiated with Tin Mercaptides and Iron(III) Ion

Yoshiaki NAKAMURA, Tatsuro OUCHI, and Minoru IMOTO*

Department of Applied Chemistry, Faculty of Engineering, Kansai University, Suita-shi, Osaka 564

(Received April 12, 1978)

The polymerization of the vinyl monomer was carried out in water, using either dimethylbis(ethylthio)tin or triethyl(*p*-tolylthio)tin as an initiator. The polymerization required the coexistence of the iron(III) ion. The initiating species was concluded to be a thiyl radical. Macromolecular tin mercaptide was much more effective than monomeric tin mercaptide.

The present authors[2-4] have reported that dibutyltin dilaurate containing metal-oxygen bonds and tetrabutyltin or dimethylmercury bearing metal-carbon bonds are able to polymerize vinyl monomers in the presence of various metal chlorides. The present paper reports the polymerization in water, using either dimethylbis(ethylthio)tin (METT) or triethyl(*p*-tolylthio)tin (ETTT) as the organotin compound containing the metal-sulfur bond. Furthermore, in order to study the polymeric effects of organotin compounds, the polymerization of the monomer with macromolecular tin mercaptide has been conducted.

Tin mercaptides are used as stabilizers for poly(vinyl chloride) resins, and as catalysts for the ring-opening polymerization of epoxides and the reaction of isocyanate with alcohol. Ayrey *et al.*[5] conducted the radical polymerization of vinyl monomers initiated with α,α′-azobisisobutyronitrile in the presence of dibutylbis(ethylthio)tin. However, the radical polymerization of vinyl monomers initiated with tin mercaptide in the absence of the usual initiator has not been reported.

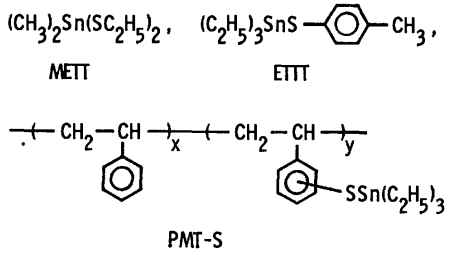

Experimental

Materials. METT, ETTT, and partially tin mercaptidated polystyrene (PMT-S) were prepared from dimethyltin dichloride (MTC) and ethanethiol, from triethyltin chloride (ETC) and *p*-toluenethiol, and from ETC and partial mercapto polystyrene, respectively, according to Abel *et al.*[6] Partially mercaptidated polystyrene was prepared by Ogawara's method[7] from polystyrene whose degree of polymerization was about 30. PMT-S was assumed to be wholly composed of units having para-substituted $SSnEt_3$, according to the IR spectrum and elemental analysis; δ_{C-H}: 1290, 1165, 1115, 1025, 815 cm^{-1}; Found: C, 49.51; H, 6.96%. Calcd for $(C_{14}H_{22}SSn)_n$: C, 49.30; H, 6.50%. ETC and 1,3,5-triphenylverdazyl (TPV) were synthesized by Grignard's[8] and Kuhn's methods,[9] respectively. *N,N′*-diphenylpicrylhydrazil (DPPH), metal chlorides and iron(III) compounds were of special grade, and used without further purification. Methyl methacrylate (MMA), styrene (St) and acrylonitrile (AN) were purified by the usual methods. The water was ion-exchanged and distilled.

Polymerization Procedure. The required amounts of monomer, tin mercaptide, metal compound and water were placed in a tube. The tube was cooled in a Dry Ice/methanol bath, thawed three times with nitrogen, and sealed under vacuum. The tube was shaken in a thermostat at 85 °C. After a specific interval, the contents were poured into a large amount of methanol to precipitate the polymer. The polymer was dried under vacuum until constant weight and the conversion determined from the polymer weight. In the case of PMT-S, the conversion was calculated by the following equation.

$$\text{Conversion (\%)} = \frac{\left(\begin{array}{c}\text{Weight of}\\ \text{precipitate (g)}\end{array}\right) - \left(\begin{array}{c}\text{Added weight}\\ \text{of PMT-S (g)}\end{array}\right)}{\text{Initial weight of monomer (g)}} \times 100$$

The number-average molecular weight ($\overline{M}_n$) of poly-MMA was calculated by the GPC method (Toyo Soda Co., Ltd., Model HLC-801A).

Results and Discussion

Polymerization of Vinyl Monomer Initiated with METT. Effect of Various Metal Chlorides: Table 1 shows the results of the polymerization of MMA in the presence of various metal chlorides. It was found that the polymerization of MMA was accelerated particularly with $FeCl_3$. As METT was immediately decomposed by the aqueous solution of $SnCl_4$, $HgCl_2$, $CuCl_2$, or CuCl, these chlorides were not applied to the polymerization system.

Table 1. Effect of various metal chlorides on the polymerization of MMA

(MMA 5 cm^3, METT 0.5 cm^3, H_2O 3 cm^3, metal chloride 5.32×10^{-4} mol; 85 °C, 6h.)

Metal chloride	Conversion (%)
None	1.5
$FeCl_3$	74.6
$FeCl_2$	3.3
$CdCl_2$	2.8
$MnCl_2$	1.8
$NiCl_2$	1.9
$CoCl_2$	1.6
$CeCl_3$	1.3

Selectivity of Vinyl Monomer: In order to observe the selectivity of METT for vinyl monomer, three kinds of vinyl monomer were used and the observed data are

Table 2. Polymerization of vinyl monomer initiated with METT in the presence of iron(III) chloride (Monomer 5 cm³, $FeCl_3$ 5.32×10^{-4} mol, H_2O 3 cm³; 85 °C, 6h.)

METT (cm³)	Conversion (%)		
	MMA	AN	St
0	1.8	2.3	4.8
0.5	74.6	7.8	12.7

shown in Table 2. The polymerizations of the three monomers were promoted by the chlorides.

Effect of Amount of Iron(III) Chloride on the Polymerization: The effect of added iron(III) chloride on the polymerization was studied, by keeping the amounts of water, monomer and METT constant and varying the amount of $FeCl_3$. The conversion of MMA and the molecular weight ($\bar{M}_n$) of poly-MMA were remarkably affected by the added amount of $FeCl_3$, as shown in Fig. 1. After exceeding a certain limit, $FeCl_3$ inhibited the polymerization of MMA through the following mechanism;[10]

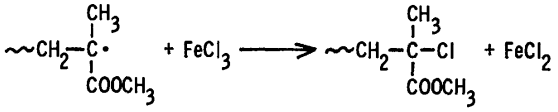

The inhibition was supported by the rapid decrease of $\bar{M}_n$ with the increase of added $FeCl_3$, as shown in Fig. 1.

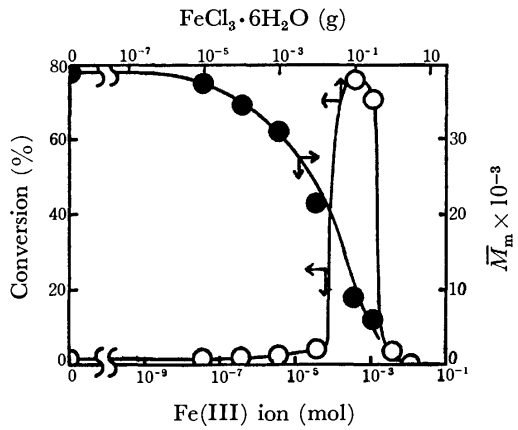

Fig. 1. Effect of the amount of iron(III) ion on the polymerization. MMA 5 cm³, METT 0.5 cm³, H_2O 3 cm³: 85 °C, 6 h.

Effect of the Kind of Anionic Part of the Iron(III) Compound: MMA 5 cm³ was polymerized with METT 0.5 cm³ and Fe(III) ion (5.32×10^{-4} mol) in water 3 cm³. The relationship between pK_a[11] of the protic acid (H_mX) of the anionic part (X^{m-}) and the conversion of MMA are shown in Table 3 and Fig. 2. It was found that the polymerization of MMA was promoted with iron(III) compounds, having the anion whose protic acid has a pK_a value less than 2 and the conversion was directly proportional to the pK_a. Iron(III) compounds having a pK_a value less than 2 were soluble, but those more than 2 were insoluble in water and ineffective in promoting the polymerization.

Table 3. Polymerization of MMA with iron(III) compound (MMA 5 cm³, METT 0.5 cm³, Fe(III) ion 5.32×10^{-4} mol, H_2O 3 cm³; 85 °C, 6h.)

Iron(III) compound	Anion part (X^{m-})	pK_a of H_mX[11]	Conversion (%)
None	—	—	1.5
$FeBr_3$	Br^-	−7.74	86.0
$FeCl_3$	Cl^-	−4.74	74.6
$Fe(NO_3)_3$	NO_3^-	−1.34	45.1
$Fe_2(SO_4)_3$	SO_4^{2-}	2.00[a]	11.6
$FePO_4$	PO_4^{3-}	—	1.5
FeF_3	F^-	3.16	1.0
$Fe(OH)_3$	OH^-	15.74	0.4
Fe_2O_3	O^{2-}	—	0

a) First equivalent point.

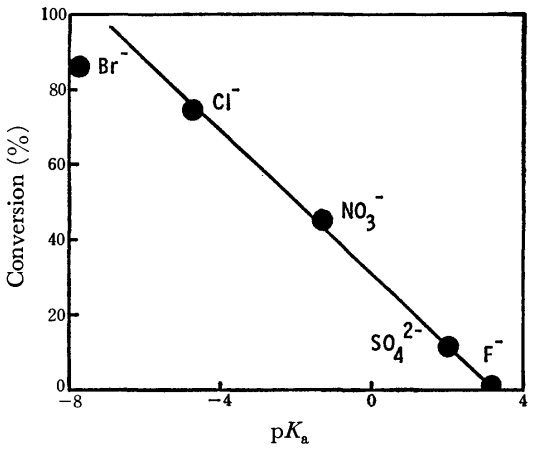

Fig. 2. Relationship between pK_a of H_mX and conversion of MMA.

Subsequent experiments were carried out, using iron(III) chloride.

Effect of Amount of Water on the Polymerization: Since it became clear that the dissociation of iron(III) ion was playing an important role in the polymerization, it was reasonable that the polymerization was required to be carried out in water. As shown in Fig. 3, the conversion of MMA increased with increasing amounts of water, and water was found to be indispensable for the polymerization.

Proof of Radical Mechanism: As shown in Table 1, the conversion of MMA amounted to 74.6%. Alternatively,

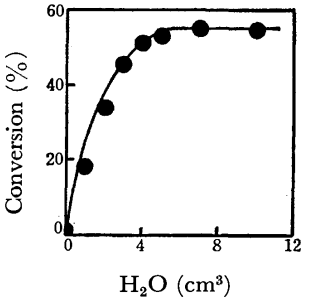

Fig. 3. Effect of the amount of water on the polymerization. MMA 5 cm³, METT 0.5 cm³, $FeCl_3$ 5.32×10^{-4} mol; 85 °C, 4 h.

0.1 g of DPPH or TPV, as radical scavenger, was added to the polymerization mixture. The polymerization was retarded with DPPH and inhibited with TPV, thus, it was concluded that the polymerization proceeded through a radical mechanism. Furthermore, the radical mechanism was verified by the method of copolymerization of MMA (M_1) with St (M_2) as shown in Fig. 4. By the Fineman-Ross method, r_1 and r_2 were estimated as 0.45 and 0.63, respectively (lit,[12] 0.46 and 0.57).

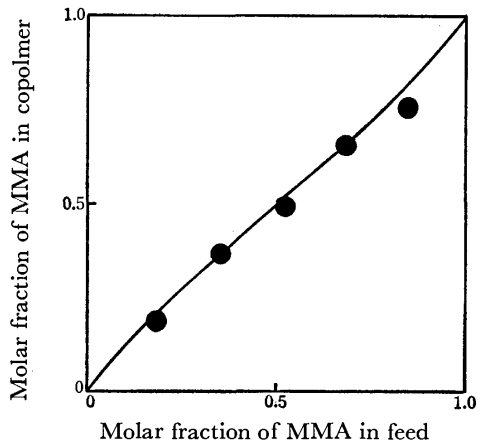

Fig. 4. Monomer-copolymer composition curve. (MMA+St) 6 cm³, METT 0.5 cm³, H_2O 3 cm³, $FeCl_3$ 5.32×10^{-4} mol, 85 °C, 6 h.

Polymerization of Vinyl Monomer Initiated with ETTT. In order to compare the activity of the aliphatic mercaptide with that of the aromatic one, the polymerization was carried out with triethyl(*p*-tolylthio)tin (ETTT).

MMA 5 cm³ was reacted with ETTT 0.1 cm³ and a varied amount of iron(III) chloride in water 3 cm³ at 85 °C for 6 h (Fig. 5). ETTT gave similar results to those obtained with METT. The molar quantity of $FeCl_3$ which gave maximum conversion was equal to the amount of ETTT applied and consequently, it was concluded that the reaction of ETTT and $FeCl_3$ took place by a 1: 1 molar ratio.

Maintaining the amounts of monomer, ETTT, $FeCl_3$, and water constant, the polymerizations of three kinds of vinyl monomer were carried out at 85 °C for 6 h.

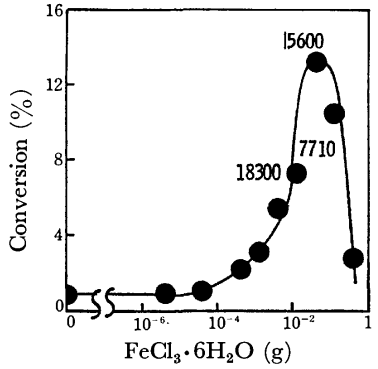

Fig. 5. Effect of the amount of iron(III) chloride on the polymerization of MMA. MMA 5 cm³, ETTT 0.1 cm³, H_2O 3 cm³; 85 °C, 6 h. (The numbers in the figure indicate mol wt of poly-MMA.)

Table 4. Polymerization of vinyl monomer initiated with ETTT
(Monomer 5 cm³, $FeCl_3\cdot6H_2O$ 0.06 g, H_2O 3 cm³; 85 °C, 6h.)

ETTT (cm³)	Conversion (%)		
	MMA	AN	St
0	0.6	0.7	0.6
0.1	13.2	43.5	7.2

By the present initiating system, all monomers could be polymerized as shown in Table 4.

As shown in Table 4, the conversion of MMA amounted to 13.2%. However, when 0.1 g of DPPH or TPV was added as a radical scavenger to this system, the polymerization did not proceed. Furthermore, the copolymerization of MMA (M_1) with St (M_2) was carried out. The composition curve obtained is shown in Fig. 6. By the Fineman-Ross method, r_1 and r_2 were estimated as 0.50 and 0.52, respectively (lit,[12] 0.46 and 0.57). From these results, it was concluded that the polymerization proceeded through a radical mechanism.

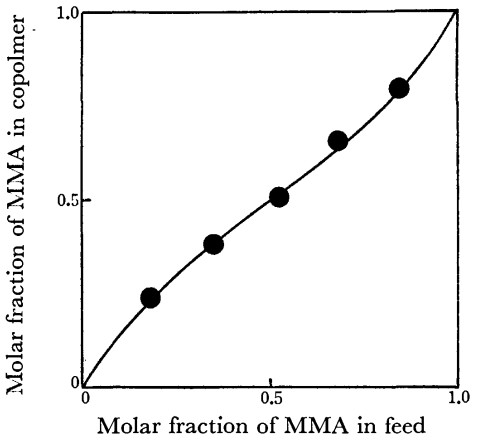

Fig. 6. Monomer-copolymer composition curve. (MMA +St) 6 cm³, ETTT 0.1 cm³, H_2O 3 cm³, $FeCl_3\cdot6H_2O$ 0.06 g; 85 °C, 6 h.

Determination of the Initiating Radical Species. The Reaction of METT with $FeCl_3$: In a tube, METT (1.06×10^{-2} mol), iron(III) chloride (2.13×10^{-2} mol) and water 8 cm³ were placed. The tube was evacuated and warmed at 85 °C for 8 h under shaking. The reaction mixture was fractionated into three portions by the procedure shown in Fig. 7.

Organic Layer I: The organic layer I gave a distillate having a boiling point of 41.5 °C/10 mmHg and a yield

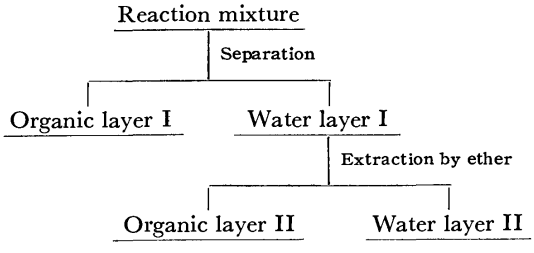

Fig. 7. Separation of the reaction mixture of METT with iron(III) chloride.

of 0.838 g. The IR spectrum and the gas chromatogram (GLC) of the distillate agreed completely with the reference diethyl disulfide (EDS) (bp 40 °C/10 mmHg[13]). Accordingly, the distillate was identified as EDS.

Organic Layer II: The ether extract was evaporated and a white solid residue was obtained. A white needle crystalline compound was obtained by the recrystallization from toluene (1.7 g). Mp and molar weight were 107—107.5 °C and 220.1 (by VPO-method in benzene at 37 °C), respectively. In the literature,[14] mp of dimethyltin dichloride (MTC) is 106 °C. The mixed mp of the crystals with the reference MTC was 107—108 °C. The organic layer II was identified as MTC; Found: C, 10.89; H, 2.74%. Calcd for $C_2H_6SnCl_2$: C, 10.93; H, 2.75%; mol wt 219.7.

Water Layer II: The water layer II was evaporated and the residue recrystallized from methanol to give blue-green powder-like crystals (3.85 g). The aqueous solution of the crystals gave a white precipitate of AgCl by adding a drop of $AgNO_3$ solution and a deep blue precipitate by potassium ferricyanide solution. Consequently, the crystalline compound from water layer II were concluded to be iron(II) chloride.

The Reaction of ETTT with $FeCl_3$: ETTT reacted with iron(III) chloride in a manner similar to METT. The reaction mixture was treated as shown in Fig. 8 and separated into the residue, the organic layer and the water layer.

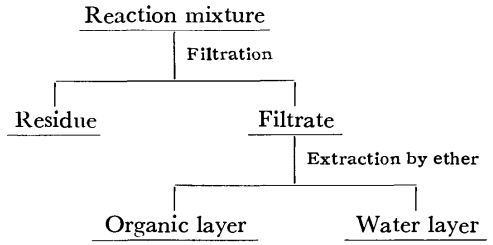

Fig. 8. Separation of the reaction mixture of ETTT with iron(III) chloride.

Residue: The residue was recrystallized from methanol and gave white needle-like crystals. Mp, mol wt and elemental analysis of the crystals were compared with those of di-*p*-tolyl disulfide (TDS), as shown in Table 5. Thus, the compound was identified as TDS.

Table 5. Crystals from the residue

	Found	Theor. values of TDS[15]
Mp (°C)	46.5—47	47—48
Mol wt	245.7	246.4
Elemental analysis (%)	C, 68.72	C, 68.25
	H, 5.69	H, 5.73

Organic Layer: The ether-extract was evaporated, distilled under reduced presure, and the middle fraction (bp 90—91 °C/10 mmHg) separated. From the IR spectrum, the GLC and elemental analysis of the distillate, the fraction was identified as triethyltin chloride (ETC). Found: C, 29.81; H, 6.27%. Calcd for $C_6H_{15}SnCl$: C, 29.86; H, 6.27%; bp of ETC was 91 °C/10 mmHg.[16]

Water Layer: The water layer was similarly treated as in the case of METT and $FeCl_2$ identified.

From these results, the reactions were concluded to proceed as follow:

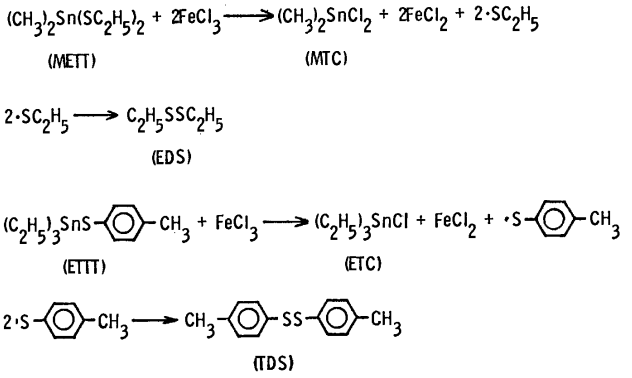

It was concluded that the initiating radical species for the polymerization were thiyl radicals, *i.e.*, $\cdot SC_2H_5$ or $\cdot S-C_6H_4-CH_3$, *i.e.*, the initiation reaction took place by a redox reaction; an electron transfered from tin to iron(III) ion. Fe(II), Cd(II), Co(II), Mn(II), Ni(II), and Ce(II) ions accept electrons with difficulty, so they were inactive to polymerization, as shown in Table 1.

Polymerization of Vinyl Monomer Initiated with PMT-S. In order to observe the polymer effect of the initiator, PMT-S was used. MMA 5 cm³ was polymerized in water 3 cm³ in the presence of PMT-S 0.1 g and various amounts of iron(II) chloride. The results are shown in Fig. 9. The polymerization proceeded in a similar fashion as in the cases of METT and ETTT.

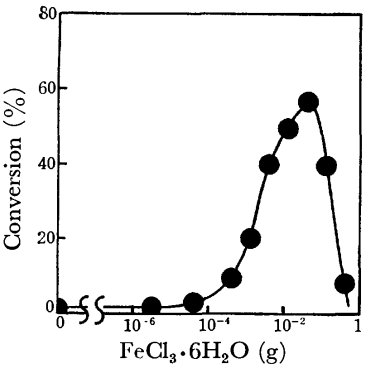

Fig. 9. Effect of the amount of iron(III) chloride on the polymerization of MMA. MMA 5 cm³, PMT-S 0.1 g, H_2O 3 cm³; 85 °C, 1 h.

Table 6. Polymerization of vinyl monomer initiated with PMT-S

(Monomer 5 cm³, $FeCl_3 \cdot 6H_2O$ 0.06 g, H_2O 3 cm³; 85 °C, 1h.)

PMT-S (g)	Conversion (%)		
	MMA	AN	St
0	0.3	0.3	0.5
0.1	56.3	30.7	13.7

Table 6 shows the results of the polymerizations of three kinds of vinyl monomers initiated with PMT-S in the presence of water and $FeCl_3$. The results were the same as in the above cases. From Tables 2, 4, and 6 and Figs. 1, 5, and 9, it may be seen that the rate of polymerization by PMT-S was larger than that by METT and ETTT. Thus the polymer effect of the initiator was clearly observed.

TABLE 7. EFFECT OF RADICAL SCAVENGER ON THE POLYMERIZATION OF MMA
(MMA 5 cm³, PMT-S 0.1 g, $FeCl_3 \cdot 6H_2O$ 0.06 g, H_2O 3 cm³, radical scavenger 0.1 g; 85 °C, 1h.)

Radical scavenger	Conversion (%)
None	56.3
DPPH	4.7
TPV	0

In order to confirm the radical mechanism, DPPH or TPV 0.1 g was added to the reaction system and the results are shown in Table 7. The polymerization was retarded with DPPH and inhibited with TPV. Thus, it was concluded that the polymerization proceeded through a radical mechanism.

It may be concluded that the polymerization with PMT-S was initiated through the same initiation mechanism as in the cases with METT and ETTT.

References

1) Part 374. M. Imoto, H. Suzuki, T. Yamada, and T. Ouchi, in preparation.
2) M. Imoto, Y. Nakamura, and T. Ouchi, *Nippon Kagaku Kaishi*, **1973**, 2244.
3) Y. Nakamura, T. Ouchi, and M. Imoto, *Kobunshi Ronbunshu*, **31**, 676 (1974).
4) M. Imoto, Y. Nakamura, and T. Ouchi, *Bull. Chem. Soc. Jpn.*, **48**, 1280 (1975).
5) G. Ayrey, B. C. Head, and C. Poller, *J. Polym. Sci., Polym. Chem. Ed.*, **13**, 69 (1975).
6) E. W. Abel and D. B. Brady, *J. Chem. Soc.*, **1965**, 1192.
7) S. Ogawara, Y. Onishi, and E. Imoto, *Kogyo Kagaku Zasshi*, **64**, 226 (1961).
8) G. J. M. Van Der Kerk, and J. G. A. Luijten, *Org. Synth.*, Coll. Vol. IV, 881 (1963).
9) R. Kuhn and H. Trishmann, *Monstsh. Chem.*, **95**, 457 (1964).
10) M. Imoto, K. Takemoto, and Y. Iikubo, *Bull. Chem. Soc. Jpn.*, **34**, 186 (1961).
11) F. Basolo and R. G. Pearson, "Mechanisms of Inorganic Reactions," John Wiley, New York (1965), p. 93.
12) T. Ito and T. Otsu, *J. Macromol. Sci., Chem.*, **3**, 197 (1969).
13) D. T. McAllan, T. V. Cullum, R. A. Dean, and F. A. Fidler, *J. Am. Chem. Soc.*, **73**, 3627 (1951).
14) R. Okawara, D. E. Webster, and E. G. Rechow, *J. Am. Chem. Soc.*, **82**, 3287 (1960).
15) "Handbook of Chemistry and Physics," 52 ed, Chemical Rubber Co. (1971—1972), p. C-274.
16) S. Matsuda and H. Matsuda, *Bull. Chem. Soc. Jpn.*, **35**, 208 (1962).

Synthesis of 6-Hydroxy-12-methyl-7,12-dihydrobenzo[6,7]-cyclohept[1,2-*b*]indol-7-one

Kunihide FUJIMORI and Kameji YAMANE*

Department of Chemistry, Faculty of Science, Shinshu University, Matsumoto 390

(Received April 26, 1978)

5,6,7,12-Tetrahydrobenzo[6,7]cyclohept[1,2-*b*]indol-7-ones were obtained by the oxidation of 5,6,7,12-tetrahydrobenzo[6,7]cyclohept[1,2-*b*]indoles with 2,3-dichloro-5,6-dicyano-*p*-benzoquinone (DDQ) in wet dioxane. The α,α-dibromo compound, obtained by bromination of 12-methyl-5,6,7,12-tetrahydrobenzo[6,7]cyclohept-[1,2-*b*]indol-7-one with phenyltrimethylammonium tribromide (PTAB), was hydrolyzed to give the diketone (**5**). By treatment with alkali, compound **5** was converted to 6-hydroxy-12-methyl-7,12-dihydrobenzo[6,7]cyclohept-[1,2-*b*]indol-7-one.

Many troponoid compounds which contain a tropone ring fused with a heterocyclic ring have been found. In a previous paper,[1,2] the preparation of fused tropones containing indole ring was reported. We now report the synthesis of 7,12-dihydrobenzo[6,7]cyclohept[1,2-*b*]-indol-7-ones.

Results and Discussion

5,6,7,12-Tetrahydrobenzo[6,7]cyclohept[1,2-*b*]indole (**1a**) and its 12-methyl derivative (**1b**) obtained from the reaction of benzosuberone (5*H*-6,7,8,9-tetrahydrobenzocyclohepten-5-one) with phenylhydrazine or *N*-methylphenylhydrazine underwent oxidation with 2,3-dichloro-5,6-dicyano-*p*-benzoquinone[3,4] (DDQ) in wet dioxane to give 5,6,7,12-tetrahydrobenzo[6,7]cyclohept-[1,2-*b*]indol-7-one (**2a**) and its 12-methyl derivative (**2b**) respectively. The IR and PMR spectra of compounds **2a** and **2b** supported the structure described above (Experimental section). Compound **2b** was also obtained by the treatment of **2a** with dimethyl sulfate.

Compounds **2a** and **2b** were brominated with phenyltrimethylammonium tribromide (PTAB) in dry tetrahydrofuran to give their 6,6-dibromo derivatives (**3a** and **3b**). Dichloro derivative (**3c**) was obtained by the treatment of **2b** with copper(I) chloride in 50% dioxane–water. The dehydrobromination of compounds **3a**—**c** with lithium chloride in boiling *N*,*N*-dimethylformamide (DMF) gave 6-halo-7,12-dihydrobenzo[6,7]cyclohept-[1,2-*b*]indol-7-ones (**4a**—**c**). Compound **3a** also gave **4a** when refluxed in ethanol with 2 M sodium hydroxide.

Compounds **3b** and **3c**, on the other hand, gave yellow prisms (mp 182—184 °C) upon being heated with dilute sodium hydroxide in ethanol. The analytical data revealed a composition with the formula $C_{18}H_{13}O_2N$. The mass spectrum showed a parent peak at *m/e* 275. On the basis of the spectral data (IR, PMR, and CMR: experimental section), the compound may be considered to have the structure of 12-methyl-5,6,7,12-tetrahydrobenzo[6,7]cyclohept[1,2-*b*]indole-6,7-dione (**5**).

Furthermore, compound **5**, when treated with 2 M sodium hydroxide and ethanol (1 : 2 vol%), was converted into yellow plates (mp 235—237 °C). The analytical data revealed a composition with the formula of $C_{18}H_{13}O_2N$, which is the same as that of **5**. The mass spectrum showed a parent peak at *m/e* 275. The IR and PMR spectral data support the assertion that the compound has the structure of 6-hydroxy-12-methyl-7,12-dihydrobenzo[6,7]cyclohept[1,2-*b*]indol-7-one (**6**). These spectral data are shown in the experimental section. Compound **5** was also converted into **6** in trifluoroacetic acid. Compound **6** produced a brown color with iron(III) chloride reagent and gave a complex by the treatment with copper(II) sulfate. The reaction of **6** with dimethyl sulfate gave the methyl ether of **6** as pale yellow plates.

The structure of **5** corresponds to a diketo form of **6**. But its enolization was not as easy as that described above. The unexpected stability of **5** is thought to be due to the steric interaction between the fused benzene and the indole ring, which are prevented from arranging in the same plane on enolization. However, no attempts to achieve the reverse change, from **6** to **5**, were successful. It has been reported[5] that the diketone type tautomer was isolated on monocyclic tropolone.

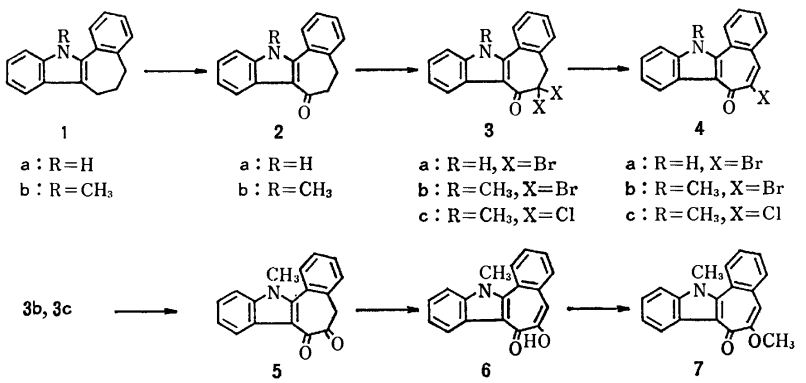

Experimental

All the melting points are uncorrected.

5,6,7,12-Tetrahydrobenzo[6,7]cyclohept[1,2-b]indol-7-one (2a). To a solution of 5,6,7,12-tetrahydrobenzo[6,7]cyclohept-[1,2-*b*]indole (2.0 g) obtained by the reaction of 5*H*-6,7,8,9-tetrahydrobenzocyclohepten-5-one with phenylhydrazine in dioxane (100 ml) and water (10 ml), we added 2,3-dichloro-5,6-dicyano-*p*-benzoquinone (DDQ) (3.88 g) at 5 °C. The mixture was stirred for 10 min, the resulting precipitate was filtered off, and the filtrate was concentrated. The residue was extracted with chloroform. The organic layer was washed with 2 M sodium hydroxide, dried on anhydrous sodium sulfate, and concentrated. The residue was recrystallized from benzene–ethanol to give colorless plates (1.5 g, 71%); mp 246—246.5 °C. IR(KBr): ν_{NH} 3210; $\nu_{C=O}$ 1610 cm^{-1}. Found: C, 82.44; H, 5.37; N, 5.29%. Calcd for $C_{17}H_{13}ON$: C, 82.57; H, 5.30; N, 5.66%.

12-Methyl-5,6,7,12-tetrahydrobenzo[6,7]cyclohept[1,2-b]indol-7-one (2b). *(a)*: Into a solution of **1b** (2.0 g) in dioxane (100 ml) and water (10 ml), we added DDQ (3.6 g). The reaction mixture was treated by a method similar to that used for the preparation of **2a**. Colorless plates (1.4 g, 66%); mp 214–216 °C. PMR (100 MHz, $CDCl_3$): δ 8.62 (1H, m, H-8), 7.3—7.6 (7H, m, benzenoid), 3.89 (3H, s, N–CH_3), and 2.7—3.2 (4H, m, 2×CH_2). The H-8 signal can be compared with that of **1b** (δ 7.73). IR(KBr): $\nu_{C=O}$ 1628 cm^{-1}. Found: C, 82.66; H, 5.61; N, 5.48%. Calcd for $C_{18}H_{15}ON$: C, 82.73; H, 5.79; N, 5.36%.

(b): A mixture of **2a** (3.0 g), dimethyl sulfate (5.0 g), and 2 M sodium hydroxide (25 ml) in acetone (150 ml) was refluxed for 2 h. The reaction mixture was concentrated and diluted with water, followed by extraction with chloroform. The extract was dried with anhydrous sodium sulfate and the solvent was removed. The residue was recrystallized from acetonitrile to give colorless plates (2.8 g, 89%); mp 214—216 °C. The IR spectrum was identical with that of the sample prepared by means of Method (a) and the mixed melting point with the sample was not depressed.

Dibromo Compound (3a) of 2a. To a solution of **2a** (1.43 g) in dry tetrahydrofuran (60 ml), we added phenyltrimethylammonium tribromide (PTAB) (4.35 g) at room temperature. The mixture was stirred for 4 h. The resulting precipitate was filtered off, the filtrate was evaporated, and the residue was recrystallized from methanol to give **3a** as yellowish green micro needles (1.87 g, 80%); mp 204—205 °C (dec). IR(KBr): ν_{NH} 3255, $\nu_{conjugated\ C=O}$ 1606 cm^{-1}. Found: C, 49.97; H, 2.90; N, 3.63; Br, 39.46%. Calcd for $C_{17}H_{11}ONBr_2$: C, 50.41; H, 2.74; N, 3.46; Br, 39.32%.

Dibromo Compound (3b) of 2b. To a solution of **2b** (1.28 g) in dry tetrahydrofuran (90 ml), we added PTAB (3.68 g). The mixture was then treated by a method similar to that used for the preparation of **3a**. Yellow micro needles (from methanol) (1.64 g, 80%); mp 183—184 °C. IR(KBr): $\nu_{C=O}$ 1649 cm^{-1}. Found: C, 51.29; H, 3.48; N, 3.77; Br, 38.34%. Calcd for $C_{18}H_{13}ONBr_2$: C, 51.58; H, 3.13; N, 3.34; Br, 38.14%.

Dichloro Compound (3c) of 2b. A mixture of **2b** (0.2 g) and copper(I) chloride dihydrate (2.61 g) in dioxane (35 ml) and water (35 ml) was refluxed for 24 h on the oil bath. The reaction mixture was concentrated and extracted with chloroform. The extract was dried with anhydrous sodium sulfate and the solvent was removed. The oily residue was recrystallized from cyclohexane to give pale yellow needles (0.15 g, 59%); mp 167—168 °C. IR(KBr): $\nu_{C=O}$ 1621 cm^{-1}. PMR (100 MHz, in $CDCl_3$): δ 8.40 (1H, m, H-8), 7.2—7.7 (7H, m, benzenoid), 3.97 (2H, s, methylene), and 3.90 (3H, s, N–CH_3). Found: C, 65.50; H, 3.91; N, 4.15; Cl, 21.31%. Calcd for $C_{18}H_{13}ONCl_2$: C, 65.47; H, 3.97; N, 4.24; Cl, 21.48%.

6-Bromo-7,12-dihydrobenzo[6,7]cyclohept[1,2-b]indol-7-one (4a). *(a)*: A mixture of dibromo compound (**3a**) (0.6 g) and lithium chloride (0.13 g) in *N,N*-dimethylformamide (20 ml) was refluxed under nitrogen for 4 h. The solvent was removed under reduced pressure, after which the residue was diluted with water. The resulting precipitate was collected, dried under reduced pressure, and chromatographed on a silica gel. The product obtained from the acetone effluent was recrystallized from acetone to give pale yellow micro needles (0.45 g; 94%); mp>290 °C. IR(KBr): $\nu_{conjugated\ C=O}$ 1597 cm^{-1}. Found: C, 62.80; H, 3.02; N, 4.32; Br, 24.70%. Calcd for $C_{17}H_{10}ONBr$: C, 62.97; H, 3.11; N, 4.32; Br, 24.65%.

(b): A mixture of **3a** (0.27 g) and 2 M sodium hydroxide (2 ml) in ethanol (10 ml) was refluxed for 30 min. The reaction mixture was concentrated and made slightly acid with 6 M sulfuric acid. The resulting precipitate was treated by a method similar to that used for Method (a). Pale yellow micro needles (0.2 g, 93%); mp>290 °C. The IR spectrum was identical with that of the sample prepared by means of Method (a).

6-Bromo-12-methyl-7,12-dihydrobenzo[6,7]cyclohept[1,2-b]indol-7-one (4b). A mixture of dibromo compound (**3a**) (0.6 g) and lithium chloride (0.12 g) in *N,N*-dimethylformamide (20 ml) was refluxed under nitrogen atmosphere for 4 h. The reaction mixture was treated by a method similar to that used for the preparation of **4a**. Yellow prisms (0.48 g, *ca.* 100%); mp 195—196 °C. IR(KBr): $\nu_{conjugated\ C=O}$ 1591 cm^{-1}. Found: C; 63.93; H, 3.52; N, 4.33%. Calcd for $C_{18}H_{21}ONBr$: C, 63.99; H, 3.58; N, 4.15%.

6-Chloro-12-methyl-7,12-dihydrobenzo[6,7]cyclohept[1,2-b]indol-7-one (4c). A mixture of dichloro compound (**3c**) (0.5 g) and lithium chloride (0.1 g) in *N,N*-dimethylformamide (20 ml) was refluxed under nitrogen atmosphere. The reaction mixture was treated by a method similar to that used for the preparation of **4a**. Yellow micro needles (0.38 g, 85%); mp 163—164 °C. IR(KBr): $\nu_{conjugated\ C=O}$ 1601 cm^{-1}. Found: C, 73.58; H, 4.01; N, 4.92; Cl, 12.07%. Calcd for $C_{18}H_{12}ONCl$: C, 73.59; H, 4.12; N, 4.77; Cl, 12.07%.

12-Methyl-5,6,7,12-tetrahydrobenzo[6,7]cyclohept[1,2-b]indole-6,7-dione (5). *(a)*: A mixture of dibromo compound (**3b**) (1.43 g) and 2 M sodium hydroxide (5 ml) in ethanol (50 ml) was refluxed for 30 min on the water bath. The mixture was concentrated, diluted with water, and made acid by adding 2 M sulfuric acid. The resulting precipitate was collected and dried under reduced pressure. It was chromatographed on silica gel. From the benzene effluent, **5** was obtained as pale yellow needles (0.55 g, 59%); mp 182—184 °C. IR(KBr): $\nu_{C=O}$ 1641 cm^{-1}. UV: λ_{max}^{MeOH} 244 (log ε=4.40), 250 (4.45), 269 (4.51), 291 (4.37), 363 (4.12), and 379 (4.18) nm. Found: C, 78.62; H, 4.63; N, 5.01%. Calcd for $C_{18}H_{13}O_2N$: C, 78.53; H, 4.76; N, 5.09%. MS: *m/e* 275 (M^+), 247 (M^+-CO), and 218 (M^+-2CO, base). PMR (100 MHz, in $CDCl_3$): δ 8.17 (1H, m, H-8), 7.2—7.8 (7H, m, benzenoid), 4.47 (1H, d, J=4.5 Hz, C_5-methylene Ha), 4.19 (1H, d, J=4.5 Hz, C_5-methylene Hb), and 3.96 (3H, s, N–CH_3). ^{13}C NMR (DMSO-d_6): δ 61.3 (N–$\underline{C}H_3$), 67.6 (C-5), 111.0, 119.9, 122.6, 123.9, 125.1, 127.1, 128.9, 131.4, 132.9, 138.5, and 192.1 (C=O). These signals at δ 67.6 and 61.3 were assigned to C-5 and N–$\underline{C}H_3$ respectively, using the off-resonance coherent proton spin-decoupling technique.

From the chloroform effluent, trace amounts of reddish brown micro needles was obtained; mp 278 °C (dec). The structure of this material has not been clarified yet. IR(KBr): 1634, 1592, and 1489 cm^{-1}.

(b): A mixture of dichloro compound (**3c**) (0.2 g) a 2 M sodium hydroxide (1 ml) in ethanol (20 ml) was refluxed for 1 h. The reaction mixture was treated by a method similar to that used for Method (a). Yellow needles (0.12 g, 72%); mp 182—184 °C. The IR spectrum was identical with that of a sample prepared by Method (a) and the mixed melting point was not depressed.

*6-Hydroxy-12-methyl-7,12-dihydrobenzo[6,7]cyclohept[1,2-*b*]indol-7-one (**6**).* *(a)*: A mixture of **5** (0.3 g) and 2 M sodium hydroxide (30 ml) in ethanol (60 ml) was refluxed for 1 h. The reaction mixture was concentrated and diluted with water. It was made slightly acid by adding 2 M sulfuric acid, and then extracted with chloroform. The solvent was removed and the residue was chromatographed on silica gel. From benzene effluent, **6** was obtained as yellow plates (0.14 g, 47%); mp 235—237 °C. IR(KBr): ν_{OH} 3272 and $\nu_{conjugated\ C=O}$ 1636 cm^{-1}. PMR (100 MHz, in DMSO) δ 7.3—9.1 (m) and 4.18 (s, N-CH_3). UV: λ_{max}^{MeOH} 233 (log ε=4.34); 312 (4.67); and 422 (3.86) nm. Found: C, 78.64; H, 4.70; N, 5.38%. Calcd for $C_{18}H_{13}O_2N$: C, 78.53; H, 4.76; N, 5.09%. MS: *m/e* 275 (M^+); 247 (M^+-CO, base), and 218 (M^+-2CO).

(b): Compound **5** was dissolved in trifluoroacetic acid, followed by dilution with water to give **6**.

*6-Methoxy-12-methyl-7,12-dihydrobenzo[6,7]cyclohept[1,2-*b*]indol-7-one (**7**).* A mixture of **6** (0.2 g); dimethyl sulfate (0.48 g); and 2 M sodium hydroxide (2.4 ml) in acetone (20 ml) was refluxed for 2 h. The reaction mixture was poured into water and extracted with chloroform. The extract was dried and the solvent was removed. The residue was chromatographed on silica gel. The product obtained from the benzene effluent was recrystallized from ethanol to give yellow needles (0.13 g, 62%); mp 211—213 °C. IR(KBr): 1593, 1581, and 1130 cm^{-1}. UV: λ_{max}^{MeOH} 244 (log ε=4.30); 266 (4.12), and 295 (4.72) nm. PMR (100 MHz, in $CDCl_3$): δ 8.74 (1H; m, H-8), 7.2—7.9 (7H, m, benzenoid), 6.80 (1H, s, H-5), 3.97 (3H, s, N-CH_3 or O-CH_3), and 3.93 (3H, s, C-CH_3 or O-CH_3). Found: C, 78.79; H, 5.19; N, 4.83%. Calcd for $C_{19}H_{15}O_2N$: C, 78.87; H, 5.23; N, 4.84%.

The authors wish to express their thanks to Dr. Masafumi Yasunami and Professor Kahei Takase of Tohoku University for their helpful suggestions and for obtaining the ^{13}C NMR spectrum. We also would like to thank Professor Yasuo Iwanami of Keio University and Dr. Takeshi Inagaki of Nitto Chemical Industry Co., Ltd, for measurements and analyses of the mass spectra. The authors are grateful to the Sankyo Co., Ltd., for doing a part of the elemental analyses.

References

1) K. Yamane and K. Fujimori, *Bull. Chem. Soc. Jpn.*, **45**, 269 (1972).

2) H. Yamane and K. Fujimori, *Bull. Chem. Soc. Jpn.*, **49**, 1101 (1976).

3) T. Amemiya, M. Yasunami, and K. Takase, *Chem. Lett.*, **1977**, 587.

4) a) 1,2,3,4-Tetrahydrocarbazol-4-one was obtained by the DDQ oxidation of 1,2,3,4-tetrahydrocarbazole in wet dioxane. K. Yamane and K. Fujimori, unpublished; b) We reported[2] that 5,6,7,8,9,10-hexahydrocyclohept[*b*]indoles were oxidized under similar conditions to afford the corresponding ketones; c) Y. Oikawa and O. Yonemitsu, *J. Org. Chem.*, **42**, 1213 (1977).

5) M. Yasunami, K. Takase, and T. Nozoe, *Tetrahedron Lett.*, **1970**, 4327.

Studies of the Azulenes. V.[1] Condensation Products of Guaiazulene and 4,6,8-Trimethylazulene with Active Methylene Compounds by Means of Selenium Dioxide. Molecular Asymmetry Induced by Chelate Ring and Its Anisotropy Effect†

Kazuko KOHARA

Konan Chemical Industry, Co., Ltd., 5-21, Nakagawa-cho, Takatsuki, Osaka 569

(Received May 1, 1978)

In the presence of selenium dioxide, guaiazulene and 4,6,8-trimethylazulene condensed with the active methylene compounds, ethyl acetoacetate and acetylacetone, to give ethyl α-(3-guaiazulenyl)acetoacetate (**3a**), α-(3-guaiazulenyl)acetylacetone, ethyl α-(4,6,8-trimethyl-1-azulenyl)acetoacetate (**5a**), and α-(4,6,8-trimethyl-1-azulenyl)acetylacetone. These α-substituted β-diketones exist exclusively in their corresponding enol forms, as evidenced by their NMR spectra. In the NMR spectra of **3a** and **5a**, the ethyl protons of the ester group show an ABX_3 pattern; the observed nonequivalence of the methylene protons is attributable to the restricted rotation between azulene and the substituent carbon atoms. From an inspection of the chemical shifts of the methyl group of metal chelate compounds of azulene derivatives, it is now reasonably concluded that there is no aromaticity associated with the chelate ring, providing further support for Musso's proposal.

It has previously been reported[2] that guaiazulene (**1**) condensed with active methyl compounds such as acetone and ethyl methyl ketone in the presence of selenium dioxide to give the di-3-guaiazulenylmethyl ketones. The experiments described in this paper deal with similar reactions of **1** and 4,6,8-trimethylazulene (**4**) with active methylene compounds (**2**) to give the corresponding α-(3-guaiazulenyl) and α-(4,6,8-trimethyl-1-azulenyl) derivatives. The condensation products (**3a**, **3b**, **5a**, and **5b**) involve an identical structural moiety, *e.g.*, a β-dicarbonyl substituent is located at peri-position to the methyl group attached to the seven-membered ring of the azulene skeleton.

In this paper we wish to report the molecular asymmetry of **3a** and **5a** induced by restricted rotation around the bond between the azulene skeleton and 3- and 1-substituted chelate ring. The anisotropy effect of the 6π chelate ring is also discussed.

Results and Discussion

We have recently found that guaiazulene (**1**) condensed with active methylene compounds (**2**) in the presence of selenium dioxide to give the corresponding α-guaiazulenyl derivatives (**3**).[3] Furthermore, 4,6,8-trimethylazulene (**4**) can also be condensed with the active methylene compounds (**2**) to produce similar products (**5**).

Although there are several possible mechanisms for the formation of **3a**, **3b**, **5a**, and **5b** from the reaction of guaiazulene and 4,6,8-trimethylazulene with active methylene compounds, the most likely one is *via* formation of the half ester (A) of selenious acid with the enol form of the active methylene compounds, followed by [2.3]sigmatropic shift to the intermediate (B).[4] A final nucleophilic attack of the azulene and elimination of the elements of hyposelenious acid (H_2SeO_2)[5] would account for the formation of the observed products.

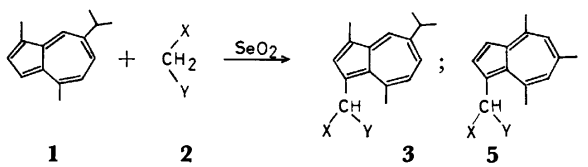

1 **2** **3** **5**

a: X=$COCH_3$, Y=$COOC_2H_5$ b: X=Y=$COCH_3$

Scheme 1.

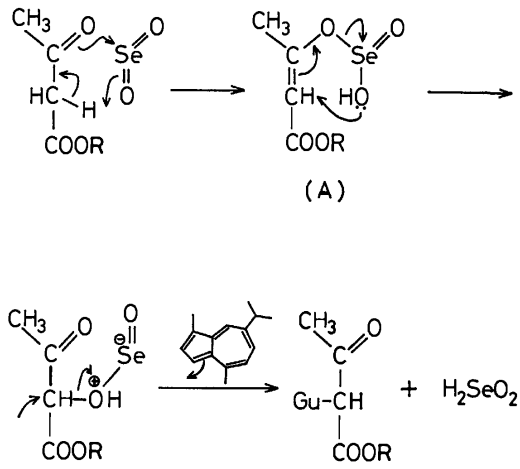

Scheme 2.

The structure of **3a** was established through its spectroscopic properties. Thus, in the NMR spectrum of **3a** (Fig. 1), the proton at C-2 of the azulene skeleton appears as a singlet at δ 7.34, indicating that it must be a 3-substituted guaiazulene. The singlet at δ 13.11 is assignable to a hydroxyl proton incorporated into a strong hydrogen bonding. This is also proved by its IR spectrum, which exhibits bands at 1608 cm^{-1} (C=C) and 1640 cm^{-1} (C=O) characteristic of a chelate ring. These findings accord well with the known linear relationship[6] between the chemical shift of the chelate hydroxyl proton and the stretching frequency of the carbonyl group associated with the hydrogen bonding.

† A preliminary report of this work was presented at the 7th International Congress of Essential Oils, Kyoto, Japan, October 1977.

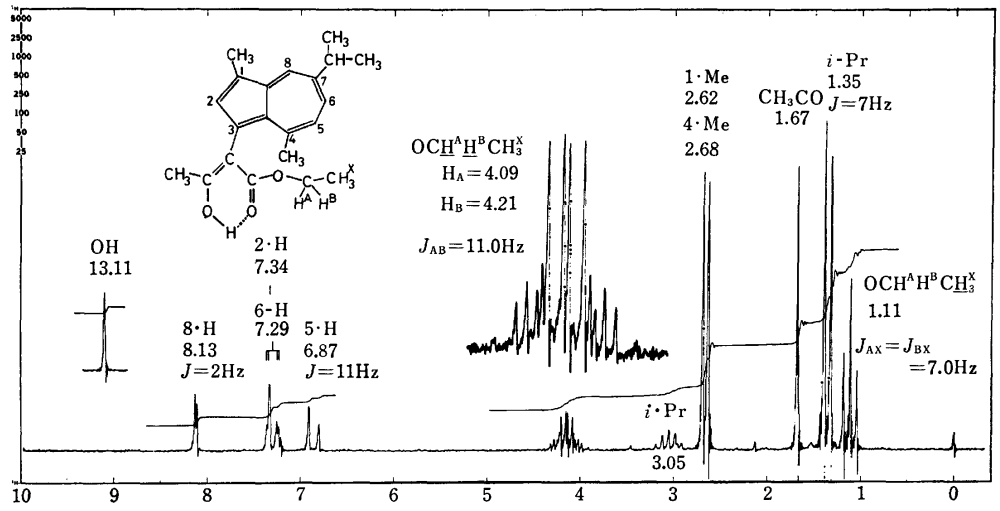

Fig. 1. 100 MHz NMR spectrum of **3a**.

The expanded spectrum of the methylene protons of **3a** is shown in Fig. 1; it could easily be analyzed as an AB-part of an ABX_3 spin system arising from the ethyl ester. The spectral parameters thus obtained are δ_A= 4.09, δ_B=4.21, δ_X=1.11 ppm, $J_{AX}=J_{BX}$=7.0, and J_{AB}=11.0 Hz. These assignments are fully confirmed by the comparison with the computer simulated spectrum, which agreed well with the experimental spectrum. Furthermore, irradiation at the site of the X-part signal at δ 1.11 assigned to the methyl protons changed the methylene protons multiplet to a broad AB-quartet, as illustrated in Fig. 2.

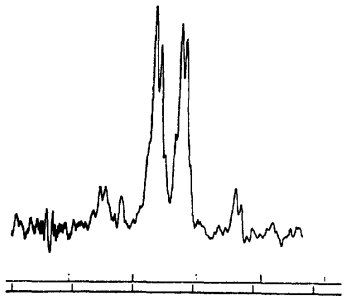

Fig. 2. Decoupled Spectrum of $-O-CH_2-$ region of **3a**.

Since the ethyl protons of the ester group of **3a** show an ABX_3 pattern, it is reasonable to assume that the nonequivalence of the methylene protons is attributable to the molecular asymmetry induced by restricted rotation about the bond between C-3 of the azulene nucleus and the substituent carbon atoms.[7-9] This is also the case for the corresponding derivative (**5a**) derived from 4,6,8-trimethylazulene (**4**). As can be seen from the NMR spectrum depicted in Fig. 3, the magnetic nonequivalence of the methylene protons is also observed.

The electronic spectrum of **3a** is illustrated in Fig. 4 and compared with that of guaiazulene (**1**). No appreciable differences between the spectra of **1** and **3a** could be discerned in intensities or in absorption maxima. These phenomena can reasonably be interpreted by the postulate that the six-membered chelate ring is oriented perpendicular to the plane of the azulene skeleton. This presumption is fully consistent with the afore-mentioned magnetic nonequivalence of the meth-

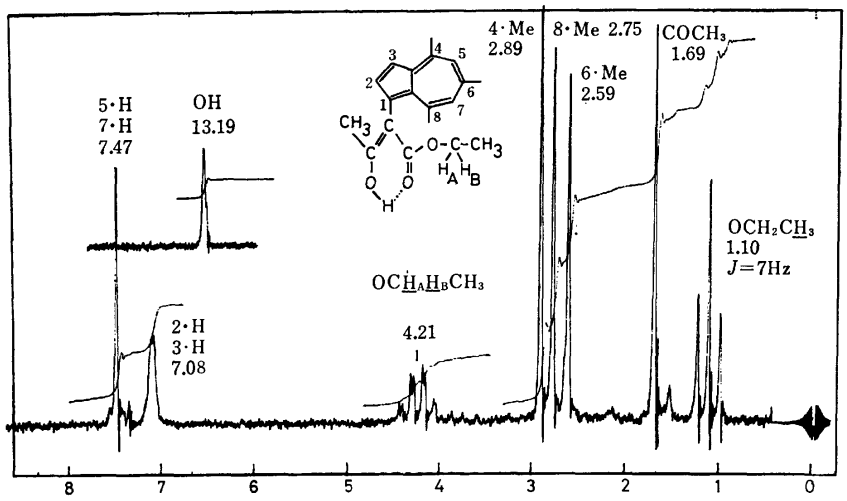

Fig. 3. 60 MHz NMR spectrum of **5a**.

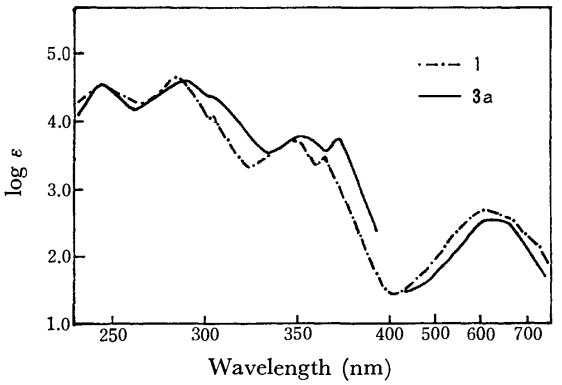

Fig. 4. Electronic spectra of **1** and **3a** in hexane.

ylene protons.

With these findings in mind, the series of compounds: **3a**, **3b**, **5a**, and **5b** provides a good model for the examination of the shielding effect of a chelate ring,[10] because one of the methyl groups attached to the azulene nucleus must be situated in a position just above the plane of the chelate ring, as shown schematically in Fig. 5.

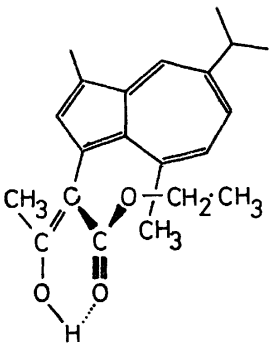

Fig. 5.

About a decade ago, Musso and coworkers[11] reported that in 9,9-bianthryl (**6**) the chemical shift of the 1- and 8-protons is more than 1 ppm higher than those at positions 4 and 5, while in the *C*-(9-anthryl)acetylacetonate salts (**7**) this difference is much smaller. Thus, these authors concluded that there is no ring current and no aromaticity in the chelate ring.

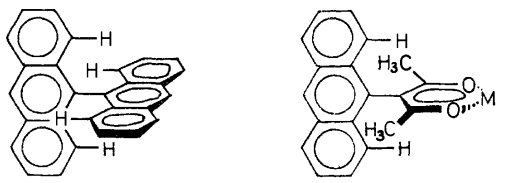

6 **7**

Fig. 6.

Our compounds (**3a**, **3b**, **5a**, and **5b**) possess several advantages over the model compounds reported by Musso *et al.*: *e.g.*, i) the methyl protons singlet in our compounds might more easily be recognized than the aromatic hydrogen multiplet in **7**; ii) the location of the methyl hydrogens of our compounds is above the plane of the chelate ring more precisely than that of the aromatic hydrogens of **7**.

TABLE 1. CHEMICAL SHIFTS OF 4-METHYL (GUAIAZULENE SERIES) AND 8-METHYL (TRIMETHYLAZULENE SERIES)

	R=H	R = 3a	3b	8	9
4-CH_3	2.76	2.68	2.67	2.72	2.80
$\Delta\delta$[a]		+0.08	+0.09	+0.04	−0.04
	R=H	R = 5a	5b	10	
8-CH_3	2.82	2.75	2.73	2.77	
$\Delta\delta$[a]		+0.07	+0.09	+0.05	

a) + and − denote upfield and downfield shifts, respectively.

In order to gain further evidence for the aromaticity of the chelate ring, we have examined the chemical shifts of the methyl groups being considered. These values are summarized in Table 1. Although the chemical shifts of the 4-methyl protons of **3a** and **3b** are shifted upfield compared with that of guaiazulene,[12] the difference (0.08—0.09 ppm) in chemical shifts cannot be regarded as significant. The same is true for compounds **5a** and **5b**. No appreciable upfield shift can be observed even in the palladium and beryllium salts of **3b** and the palladium salt of **5b**.

These results provide further confirmation of Musso's proposal.

Experimental

IR spectra were obtained on a Hitachi Model EPI-G2 spectrophotometer. NMR spectra were taken in $CDCl_3$ or CCl_4 solution with a Varian XL-100-15, A-60D, or T-60 spectrometer and are reported in δ-values with tetramethylsilane as the internal standard.

4,6,8-Trimethylazulene (**4**) was prepared according to the literature.[13]

Reaction of Azulenes with Ethyl Acetoacetate or Acetylacetone. General Procedure: To a solution of azulene (4 g) in 60 g of ethyl acetoacetate or acetylacetone was added a solution containing 2 g of selenium dioxide in 4 ml of water. The solution was stirred for 3 days at room temperature. Work-up was made in a similar manner with that of the literature.[2] All products, obtained in 15—20% yield, were recrystallized from methanol. These condensation products are sensitive to air and are converted gradually to unidentified, variously colored products.

*Ethyl α-(3-guaiazulenyl)acetoacetate (**3a**)*: Blue needles; mp 70—72 °C. IR (Nujol): 1608 (C=C), 1640 (C=O) cm^{-1}. UV (hexane): λ_{max} (log ε) 247 (4.51), 287 (4.61), 306[sh] (4.30), 354 (3.79), 372 (3.78), 612 (2.62), 666[sh] nm (2.51). NMR ($CDCl_3$, 100 MHz): δ 1.11 (3H, t, X_3-part of an ABX_3, $J_{AX}=J_{BX}=7.0$ Hz, $CH_2\underline{CH_3}$), 1.35 and 3.05 (6H, d, and 1H, septet, $J=7.0$ Hz, 7-*i*-Pr), 1.67 (3H, s, $COCH_3$), 2.62 (3H, s, 1-Me), 2.68 (3H, s, 4-Me), 4.15 (2H, m, AB-part of an ABX_3, $J_{AX}=J_{BX}=7.0$, $J_{AB}=11.0$ Hz; $\delta_A=4.09$, $\delta_B=4.21$, $C\underline{H_2}CH_3$), 6.87 (1H, d, $J=11.0$ Hz, 5-H), 7.29 (1H, dd, $J=11.0$, 2.0 Hz, 6-H), 7.34 (1H, s, 2-H), 8.13 (1H, d, $J=2.0$ Hz, 8-H), 13.11

ppm (1H, s, chelate OH). Found: C, 77.28; H, 7.96%. Calcd for $C_{21}H_{26}O_3$: C, 77.27; H, 8.03%.

*α-(3-Guaiazulenyl)acetylacetone (**3b**)*: Blue needles; mp 58 °C. IR (Nujol): 1600, br (C=O, C=C) cm^{-1}. UV (hexane): λ_{max} (log ε) 245 (4.42), 287 (4.65), 307^{sh} (4.34), 354 (3.82), 372 (3.76), 612 (2.69), 666^{sh} nm (2.60). NMR (CCl_4, 100 MHz): δ 1.39 and 3.05 (6H, d, and 1H, septet, J=7.0 Hz, 7-*i*-Pr), 1.75 (6H, s, $COCH_3$), 2.63 (3H, s, 1-Me), 2.67 (3H, s, 4-Me), 6.82 (1H, d, J=11.0 Hz, 5-H), 7.26 (1H, dd, J=11.0, 2.0 Hz, 6-H), 7.30 (1H, s, 2-H), 8.04 (1H, d, J=2.0 Hz, 8-H), 16.36 ppm (1H, s, chelate OH). Found: C, 80.80; H, 8.09%. Calcd for $C_{20}H_{24}O_2$: C, 81.04; H, 8.16%.

*Ethyl α-(4,6,8-Trimethyl-1-azulenyl)acetoacetate (**5a**)*: Purple needles; mp 86 °C. UV (cyclohexane): λ_{max} (log ε) 246 (4.54), 291 (4.64), 339 (3.70), 349^{sh} (3.74), 353.5 (3.76), 557 (2.70), 604^{sh} (2.60), 661 nm (2.13). NMR ($CDCl_3$, 60 MHz): δ 1.10 (3H, t, J=7 Hz, $CH_2C\underline{H}_3$), 1.69 (3H, s, $COCH_3$) 2.59 (3H, s, 6-Me), 2.75 (3H, s, 8-Me), 2.89 (3H, s, 4-Me), 4.21 (2H, m, $C\underline{H}_2CH_3$), 7.08 (2H, br s, 2- and 3-H), 7.47 (2H, s, 5- and 7-H), 13.19 ppm (1H, s, chelate OH). Found: C, 76.02; H, 7.30%. Calcd for $C_{19}H_{22}O_3$: C, 76.48; H, 7.43%.

*α-(4,6,8-Trimethyl-1-azulenyl)acetylacetone (**5b**)*: Purple needles; mp 106—108 °C. UV (cyclohexane): λ_{max} (log ε) 246.5 (4.48), 293 (4.70), 339 (3.78), 349^{sh} (3.76), 354 (3.73), 556 (2.72), 603^{sh} (2.63), 660 nm (2.14). NMR ($CDCl_3$, 60 MHz): δ 1.80 (6H, s, $COCH_3$), 2.61 (3H, s, 6-Me), 2.73 (3H, s, 8-Me), 2.89 (3H, s, 4-Me), 6.99 and 7.04 (each 1H, s, 2- and 3-H), 7.38 (1H, s, 5-H), 16.52 ppm (1H, s, chelate OH). Found: C, 80.13; H, 7.46%. Calcd for $C_{18}H_{20}O_2$: C, 80.56; H, 7.51%.

*Metal Chelates **8**, **9**, and **10***. Preparation of **8**, **9**, and **10** was carried out according to Musso's procedure[10b] at room temperature.

*α-(3-Guaiazulenyl)acetylacetonate Palladium(II) (**8**)*: Blue crystals; mp >280 °C. NMR ($CDCl_3$, 60 MHz): δ 1.37 and 3.08 (6H, d, and 1H, septet, J=7 Hz, 7-*i*-Pr), 1.77 (6H, s, $COCH_3$), 2.66 (3H, s, 1-Me), 2.72 (3H, s, 4-Me), 6.90 (1H, d, J=11 Hz, 5-H), 7.33 (1H, s, 2-H), 7.34 (1H, dd, J=11, 2 Hz, 6-H), 8.16 ppm (1H, d, J=2 Hz, 8-H).

*α-(3-Guaiazulenyl)acetylacetonate Beryllium(II) (**9**)*: Blue crystals; mp 213—214 °C. NMR ($CDCl_3$, 60 MHz): δ 1.37 and 3.08 (6H, d, and 1H, septet, J=7 Hz, 7-*i*-Pr), 1.85 (6H, s, $COCH_3$), 2.68 (3H, s, 1-Me), 2.80 (3H, s, 4-Me), 6.95 (1H, d, J=11 Hz, 5-H), 7.40 (1H, dd, J=11, 2 Hz, 6-H), 7.48 (1H, s, 2-H), 8.21 ppm (1H, d, J=2 Hz, 8-H).

*α-(4,6,8-Trimethyl-1-azulenyl)acetylacetonate Palladium (II) (**10**)*: Purple crystals; mp 269 °C. NMR ($CDCl_3$, 60 MHz): δ 1.77 (6H, s, $COCH_3$), 2.60 (3H, s, 6-Me), 2.77 (3H, s, 8-Me), 2.88 (3H, s, 4-Me), 7.05 (2H, br s, 2- and 3-H), 7.42 ppm (2H, s, 5- and 7-H).

The author wishes to express her thanks to Professor Shuichi Hayashi of Hiroshima University for valuable discussions.

References

1) Part. IV. K. Kohara, *Nippon Kagaku Kaishi*, **1978**, 1394.
2) K. Kohara, Y. Otani, and N. Sakota, *Nippon Kagaku Kaishi*, **1975**, 139.
3) K. Kohara and Y. Otani, Abstract of the 12th Symposium on the Chemistry of Terpenes, Essential Oils, and Aromatics, Hamamatsu, 1968, p. 90; K. Kohara, H. Tachibana, Y. Otani, and N. Sakota, Abstract of the 16th Symposium on the Chemistry of Terpenes, Essential Oils, and Aromatics, Hirosaki, 1972, p. 99.
4) J. P. Schaefer and E. J. Corey, *J. Org. Chem.*, **24**, 1825 (1959).
5) J. P. Schaefer, *J. Am. Chem. Soc.*, **84**, 713 (1962).
6) R. W. Hay and P. P. Williams, *J. Chem. Soc.*, **1964**, 2270.
7) M. Miyazaki, M. Hashi, and T. Ukita, *Chem. Pharm. Bull.*, **8**, 140 (1960).
8) M. Ōki and N. Nakamura, *Bull. Chem. Soc. Jpn.*, **44**, 1880 (1971).
9) *Cf.* L. M. Jackman and S. Sternhell, "Applications of Nuclear Magnetic Resonance Spectroscopy in Organic Chemistry," 2nd ed, Pergamon Press, Oxford (1969), p. 378.
10) R. C. Fay and N. Serpone, *J. Am. Chem. Soc.*, **90**, 5701 (1968).
11) a) M. Kuhr and H. Musso, *Angew. Chem., Int. Ed. Engl.*, **8**, 147 (1969); b) M. Kuhr, B. Bock, and H. Musso, *Chem. Ber.*, **109**, 1195 (1976).
12) D. Meuche, B. B. Molloy, D. H. Reid, and E. Heilbronner, *Helv. Chim. Acta*, **46**, 2483 (1963).
13) K. Hafner, *Angew. Chem.*, **69**, 393 (1957); German Patent Appl. Z 4770 IV b/12 o, 25 (1957).

Oxidation of 2,5-Dimethoxyacetophenone Derivatives with Thallium(III) Nitrate in Trimethyl Orthoformate-Methanol. I

Kazuhiro MARUYAMA* and Tadashi KOZUKA

Department of Chemistry, Faculty of Science, Kyoto University, Kyoto 606

(Received May 6, 1978)

Alkyl-substituted 2,5-dimethoxyacetophenones were oxidized with thallium(III) nitrate in methanol–trimethyl orthoformate (TMOF) to give methyl alkyl-substituted 2,5-dimethoxyphenylacetates in a good yield. A simple modification of separating method from the reacting mixture allowed us to obtain the corresponding methyl (alkyl-substituted 3,6-dioxo-1,4-cyclohexadienyl)acetates.

Oxidations of alkyl-substituted 2,5-dimethoxyacetophenones **1** with thallium(III) nitrate were investigated. Using an acidified methanol with perchloric acid as the solvent, we obtained methyl esters of alkyl-substituted-3,6-dioxo-1,4-cyclohexadienylacetic acids **4** by the oxidation in a high yield. By the oxidation we expected to have methyl esters of alkyl-substituted 2,5-dimethoxyphenylacetic acids **2**, but every effort to yield **2** ended without success. However, changing the solvent from MeOH–$HClO_4$ to absolute MeOH–trimethyl orthoformate (TMOF), we obtained **2** in excellent yields at last. In this paper the oxidation method will be described in detail.

Results and Discussion

Alkyl-substituted 2,5-dimethoxyacetophenones **1** dissolved in absolute MeOH–TMOF were oxidized with thallium(III) nitrate trihydrate at 0 °C. After approximately 10 min the oxidation was completed, and the resulting mixture was passed through a short column filled with basic alumina. Then, evaporation of the solvent gave us an excellent yield of methyl esters of alkyl-substituted 2,5-dimethoxyphenylacetic acids **2**. However, if we save the basic alumina treatment other products will be obtained; that is, **4**, oxidation product of **2**, instead of **2**. Recently, use of $Tl(NO_3)_3 \cdot 3H_2O$ in MeOH–TMOF, or anhydrous $Tl(NO_3)_3$ on solid support has been reported to allow a high conversion of acetophenones to the corresponding methyl esters of α-methoxyphenylacetic acids, $C_6H_5CH(OMe)CO_2Me$.[1,2]

On the contrast, the present work showed that oxidation of **1** with $Tl(NO_3)_3 \cdot 3H_2O$ in absolute MeOH–TMOF gave an excellent yield of **2** together with only a small amount of the corresponding α-methoxylated phenylacetates **3**. Thus, by our procedure **2** was obtained predominantly. If we saved the basic alumina treatment, **4** was the major product. The results of representative reactions are summarized in Table 1.

Oxidation of 2,5-dimethoxy-4-methylpropiophenone **6** with $Tl(NO_3)_3 \cdot 3H_2O$ in MeOH–TMOF gave a quantitative yield of methyl ester of 2-(2,5-dimethoxy-4-methylphenyl)propionic acid **7**, although the oxidation of **6** in MeOH–$HClO_4$ scarcely gave **7** or its oxidized product; methyl ester of 2-(4-methyl-3,6-dioxo-1,4-cyclohexadienyl)propionic acid **8**. Without the basic alumina treatment we obtained **8** as the single product (96%). 2,4,5-Trimethoxyacetophenone **1g** is also smoothly oxidized to yield methyl ester of 2,4,5-trimethoxyphenylacetic acid **2g**. Without basic alumina treatment we obtained a complex mixture composed of intractable substances.

Concerned to the oxidation of acetophenone in MeOH–TMOF, Taylor *et al.* have reported a smooth production of methyl ester of α-methoxyphenylacetic acid. However, they did not obtained any methyl ester of phenylacetic acid, and excluded the possible intermediacy of it in the oxidation. As the evidence they gave the fact that methyl phenylacetate was recovered unchanged in the oxidation with $Tl(NO_3)_3 \cdot 3H_2O$ in MeOH–TMOF. In spite of the Taylor's work, our investigation indicates a possible intermediacy of methyl ester of alkyl-substituted 2,5-dimethoxyphenylacetic acid **2**. Table 2 shows clearly the gradual change of **2b** to **3b** on standing the reacting mixture. The discrepancy between Taylor's work and ours might be due to the absence and presence of NO_3^-, HCO_2CH_3, and thallium(I) nitrate in the reacting mixture. As the oxidation proceeds, these three species can be produced in the reacting mixture. Taylor's blank test was performed in

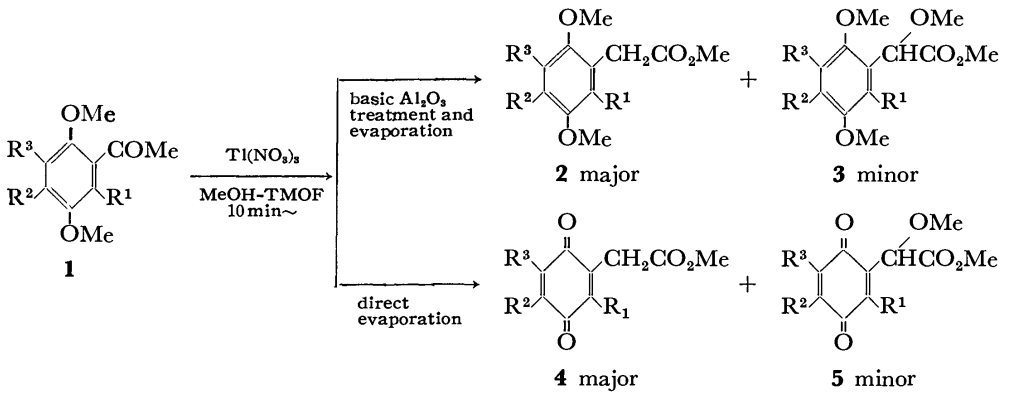

Table 1.

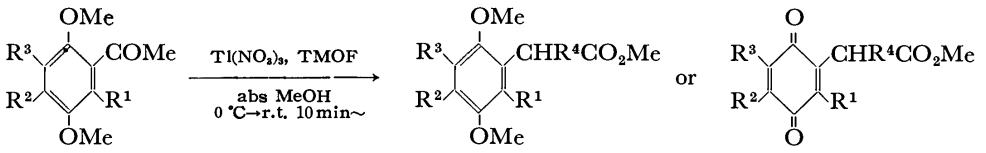

2 R^4=H **3** R^4=OMe **4** R^4=H **5** R^4=OMe

Compound	R^1	R^2	R^3	Yield[a] (%) of **2**+**3**	**2**: **3**[d]	Yield[b] (%) of **4**+**5**	**4**: **5**[d]
1a	H	H	H	84	85: 15	— (85)[c]	
1b	H	Me	H	90	90: 10	93	84: 16
1c	H	*t*-Bu	H	93	85: 15	95	88: 12
1d	H	Me	Me	96	80: 20	52	90: 10
1e	Me	Me	H	80	92: 8	47	70: 30
1f	H	CH=CH–CH=CH		84	81: 19	35	80: 20
1g	H	OMe	H	98	93: 7	—	—

a) Isolation of **2** and **3**: with Al_2O_3 treatment (work-up method A). b) Isolation of **4** and **5**: without Al_2O_3 treatment (work-up method B). c) No **4a** and **5a** were isolated, the yield of methyl 2,5-dimethoxy-4-nitrophenylacetate is given. d) The ratio of isomers (**2**/**3** and **4**/**5**) in both cases was determined by comparison of GLPC area ratios and/or integration of NMR signals.

Table 2. Oxidative rearrangement of **1b** to **2b**, **3b**

Reaction time (h)	**2b**/**3b**[a]	Isolated yield (%)	
		2b	**3b**
0.25[b]	90/10	81	9
1	85/15	—	—
3	83/17	—	—
24	13/87	9	61

a) The relative product ratio **2b**/**3b** were determined by GLPC analysis. b) At that time the oxidation was completed.

the absence of the above species in the reacting mixture.

Experimental

Melting points were taken on a Yanagimoto micro-melting apparatus and are uncorrected. ^{1}H NMR spectra were recorded in deuteriochloroform solutions with a JEOL PS-100 instrument using tetramethylsilane as an internal standard. IR spectra were measured with a JASCO IR-S spectrometer in KBr disk or liquid film techniques. Mass spectra were determined on a Hitachi M-52 mass spectrometer. Microanalyses were performed by the Microanalytical Laboratory of Kyoto University. GLPC analyses were performed using JEOL JGC-20K gas chromatographs equipped with a 2 m silicon SE-30 (5%) column. The analyses were reconfirmed with the use of another column; *i.e.*, 1 m silicon DC-550 (10%). Column chromatography was performed over basic alumina, silica gel (Wako Pure Chem. Ind.) and Florisil 100—200 mesh (Floridin Com., U.S.A). The ratio of isomeric products (**2**/**3** and **4**/**5**) was determined by integration of GLPC signals, and/or of the NMR signals (see Tables 1 and 2).

Starting Materials. All of the compounds **1a**—**g** were prepared by the Friedel-Crafts acylation of the corresponding hydroquinone dimethyl ethers with acetyl chloride in the presence of titanium tetrachloride in carbon disulfide. 2,5-Dimethoxy-4-methylpropiophenone **6** was prepared by the similar methods. All were purified by either distillation or recrystallization. 2,5-Dimethoxyacetophenone **1a**, bp 114—116 °C/5 mmHg (lit,[3] bp 156—158 °C/15 mmHg), 2,5-dimethoxy-4-methylacetophenone **1b**, mp 73—75 °C, 4-*t*-butyl-2,5-dimethoxyacetophenone **1c**, mp 64—65 °C, 2,5-dimethoxy-3,4-dimethylacetophenone **1d**, bp 123—130 °C/3 mmHg, 3,6-dimethoxy-2,4-dimethylacetophenone **1e**, bp 123—125 °C/3 mmHg, 2-acetyl-1,4-dimethoxynaphthalene **1f**, mp 59—60.5 °C, 2,4,5-trimethoxyacetophenone **1g**, mp 102 °C, 2,5-dimethoxy-4-methylpropiophenone **6**, mp 78 °C.

General Procedure for the Oxidation of 2,5-Dimethoxyacetophenones. To a solution of TMOF (1 ml) and $Tl(NO_3)_3 \cdot 3H_2O$ (1 g) in abs methanol (5 ml) 2,5-dimethoxyacetophenone **1** (2 mmol) was added at once with stirring at 0 °C, and then the resulting mixture was allowed to stand at room temperature for 5 min. The reaction was continued till the white precipitates of thallium(I) nitrate crystallized out. After filtration of thallium(I) nitrate the filtrate was worked up in the following two methods; A and B. Work-up method A: the filtrate was diluted with petroleum ether (50 ml), and passed through a short column of basic alumina (20 g) by eluting with dichloromethane (200 ml). Evaporation of dichloromethane gave a mixture of **2** and **3**. Work-up method B: the filtrate was concentrated directly *in vacuo* (<40 °C). The residure was passed through a short column of Florisil (20 g) using dichloromethane (200 ml) as an eluent. Evaporation of dichloromethane gave a mixture of **4** and **5**. The analytical samples **2** and **3** were separated by preparative GLPC. The pure product **4** was isolated by chromatography on silica gel using benzene or dichloromethane as an eluent.

Methyl 2,5-Dimethoxyphenylacetate ***2a*** *and Methyl α,2,5-Trimethoxyphenylacetate* ***3a***. Followed to the work-up method A oxidation of **1a** with $Tl(NO_3)_3$–TMOF–MeOH (reaction time: 15 min) gave a mixture of products **2a** and **3a** (**2a**: **3a**=85: 15) in 84% yield. Compound **2a**, mp 46—47 °C; MS, *m/e*, 210; IR(KBr) 1742 cm^{-1}; NMR($CDCl_3$) δ=3.59 (s, 2H, CH_2), 3.67 (s, 3H, CO_2CH_3), 3.73 (s, 3H, OCH_3), 3.75 (s, 3H, OCH_3), 6.75 (s, 3H, ArH); Found: C, 63.08; H, 6.75%. Calcd for $C_{11}H_{14}O_4$: C, 62.84, H, 6.71%. Compound **3a**, oil; MS, *m/e*, 240; IR(NaCl) 1752 cm^{-1}; NMR ($CDCl_3$) δ=3.40 (s, 3H, OCH_3), 3.71 (s, 3H, CO_2CH_3), 3.76 (s, 3H, OCH_3), 3.81 (s, 3H, OCH_3), 5.17 (s, 1H, CH), 6.82, 6.84, and 6.95 (m, 3H, ArH); Found: C, 59.73; H, 6.92%. Calcd for $C_{12}H_{16}O_5$: C, 59.99; H, 6.71%.

Methyl 2,5-Dimethoxy-4-methylphenylacetate ***2b*** *and Methyl α,2,5-Trimethoxy-4-methylphenylacetate* ***3b***. Oxidation of **1b** with $Tl(NO_3)_3$–TMOF–MeOH (reaction time: 15 min) applied

with the work-up method A gave a mixture of products **2b** and **3b** (**2b**: **3b**=90: 10) in 90% yield. Compound **2b**, mp 69—70 °C; MS; *m/e*, 224; IR(KBr) 1735 cm^{-1}; NMR($CDCl_3$) δ=2.26 (s, 3H, CH_3), 3.63 (s, 2H, CH_2), 3.72 (s, 3H, CO_2CH_3), 3.79 (s, 3H, OCH_3), 3.81 (s, 3H, OCH_3), 6.71 (s, 2H, ArH); Found: C, 64.32; H, 7.06%. Calcd for $C_{13}H_{18}O_5$: C, 64.27; H, 7.14%. Compound **3b**, mp 70—71 °C; MS, *m/e*, 254; IR(KBr) 1750 cm^{-1}; NMR($CDCl_3$) δ=2.23 (s, 3H, CH_3), 3.38 (s, 3H, OCH_3), 3.71 (s, 3H, CO_2CH_3), 3.78 (s, 3H, OCH_3), 3.80 (s, 3H, OCH_3), 5.20 (s, 1H, CH), 6.74 (s, 1H, ArH), 6.85 (s, 1H, ArH); Found: C, 61.29; H, 7.25%. Calcd for $C_{13}H_{18}O_5$: C, 61.40; H, 7.14%.

Methyl 4-t-Butyl-2,5-dimethoxyphenylacetate ***2c*** *and Methyl α,2,5-Trimethoxyphenylacetate* ***3c***. Oxidation of **1c** with $Tl(NO_3)_3$–TMOF–MeOH for 30 min resulted a reacting mixture. Immediate application of the work-up method A gave a mixture of products **2c** and **3c** (**2c**: **3c**=85: 15) in 93% yield. Compound **2c**, mp 52.5—54.5 °C; MS, *m/e*, 266; IR(KBr) 1741 cm^{-1}; NMR ($CDCl_3$) δ=1.36 (s, 9H, *t*-Bu), 3.57 (s, 2H, CH_2), 3.67 (s, 3H, CO_2CH_3), 3.76 (s, 6H,OCH_3), 6.70 (s, 1H, ArH), 6.81 (s, 1H, ArH); Found: C, 67.47; H, 8.37%. Calcd for $C_{15}H_{22}O_4$: C, 67.64; H, 8.33%. Compound **3c**, mp 46.5—47 °C, MS, *m/e*, 296; IR(KBr) 1760 cm^{-1}; NMR ($CDCl_3$) δ=1.36 (s, 9H, *t*-Bu), 3.38 (s, 3H, OCH_3), 3.71 (s, 3H, CO_2CH_3), 3.77 (s, 3H, OCH_3), 3.81 (s, 3H, OCH_3), 5.17 (s, 1H, CH), 6.84 (s, 1H, ArH); Found: C, 64.74; H, 8.29%. Calcd for $C_{16}H_{24}O_5$: C, 64.84; H, 8.16%.

Methyl 2,5-Dimethoxy-3,4-dimethylphenylacetate ***2d*** *and Methyl α,2,5-Trimethoxy-3,4-dimethylphenylacetate* ***3d***. Oxidation of **1d** with $Tl(NO_3)_3$–TMOF–MeOH for 30 min resulted a reacting mixture. Subsequent application of the work-up method A gave a mixture of products **2d** and **3d** (**2d**: **3d**= 80: 20) in 96% yield. Compound **2d**, oil; MS, *m/e*, 238; IR(NaCl) 1740 cm^{-1}; NMR ($CDCl_3$), δ=2.12 (s, 3H, CH_3), 2.20 (s, 3H, CH_3), 3.63 (s, 2H, CH_2), 3.65 (s, 3H, CO_2CH_3), 3.70 (s, 3H, OCH_3), 3.78 (s, 3H, OCH_3), 6.60 (s, 1H, ArH); Found: C, 65.33; H, 7.67%. Calcd for $C_{13}H_{18}O_4$: C, 65.53; H, 7.61%. Compound **3d**, oil; MS, *m/e*, 268; IR(NaCl) 1750 cm^{-1}; NMR ($CDCl_3$) δ=2.13 (s, 3H, CH_3), 2.22 (s, 3H, CH_3), 3.38 (s, 3H, OCH_3), 3.73 (s, 3H, CO_2CH_3), 3.73 (s, 3H, OCH_3), 3.78 (s, 3H, OCH_3), 5.15 (s, 1H, CH), 6.72 (s, 1H, ArH); Found: C, 62.66; H, 7.54%. Calcd for $C_{14}H_{20}O_5$: C, 62.67; H, 7.51%.

Methyl 3,6-Dimethoxy-2,4-dimethylphenylacetate ***2e*** *and Methyl α,3,6-Trimethoxy-2,4-dimethylphenylacetate* ***3e***. Oxidation of **1e** with $Tl(NO_3)_3$–TMOF–MeOH for 20 h application of the work-up method A gave a mixture of products **2e** and **3e** (**2e**: **3e**=92: 8) in 80% yield. Compound **2e**, mp 50—52 °C; MS, *m/e*, 238; IR(KBr) 1732 cm^{-1}; NMR ($CDCl_3$) δ=2.20 (s, 3H, CH_3), 2.28 (s, 3H, CH_3), 3.64 (s, 2H, CH_2), 3.67 (s, 3H, CO_2CH_3), 3.67 (s, 3H, OCH_3), 3.76 (s, 3H, CH_3), 6.56 (s, 1H, ArH); Found: C, 65.49; H, 7.57%. Calcd for $C_{13}H_{18}O_4$: C, 65.53; H, 7.61%. Compound **3e**, oil, MS, *m/e*, 268; IR(NaCl) 1745 cm^{-1}; NMR ($CDCl_3$) δ=2.25 (s, 3H, CH_3), 2.28 (s, 3H, CH_3), 3.39 (s, 3H, OCH_3), 3.65 (s, 3H, CO_2CH_3), 3.72 (s, 3H, OCH_3), 3.77 (s, 3H, OCH_3), 5.31 (s, 1H, CH), 6.59 (s, 1H, ArH); Found: C, 62.56; H, 7.59%. Calcd for $C_{14}H_{20}O_5$: C, 62.67; H, 7.51%.

Methyl (1,4-Dimethoxy-2-naphthyl)acetate ***2f*** *and Methyl α-Methoxy-α-(1,4-dimethoxy-2-naphthyl)acetate* ***3f***. Oxidation of **1f** with $Tl(NO_3)_3$–TMOF–MeOH for 5 h resulted a reacting mixture. Applying the work-up method A we obtained a mixture of products **2f** and **3f** (**2f**: **3f**=81: 19) in 84% yield. Compound **2f**, oil; MS, *m/e*, 260; IR(NaCl) 1730 cm^{-1}; NMR ($CDCl_3$) δ=3.71 (s, 3H, CO_2CH_3), 3.82 (s, 2H, CH_2), 3.88 (s. 3H, OCH_3), 3.96 (s, 3H, OCH_3), 6.65 (s, 1H, ArH), 7.47 (m, 2H, ArH), 8.00 (m, 1H, ArH), 8.19 (m, 1H, ArH); Found: C, 69.18; H, 6.35%. Calcd for $C_{15}H_{16}O_4$: C, 69.21; H, 6.20%. Compound **3f**, oil, MS, *m/e*, 290; IR(NaCl) 1750 cm^{-1}; NMR ($CDCl_3$) δ=3.41 (s, 3H, OCH_3), 3.73 (s, 3H, CO_2CH_3), 3.97 (s, 3H, OCH_3), 3.98 (s, 3H, OCH_3), 5.41 (s, 1H, CH), 6.77 (s, 1H, ArH), 7.51 (m, 2H, ArH), 8.04 (m, 1H, ArH), 8.21 (m, 1H, ArH); Found: C, 66.70; H, 6.14%. Calcd for $C_{16}H_{18}O_5$: C, 66.19; H, 6.25%.

Methyl 2,4,5-Trimethoxyphenylacetate ***2g*** *and Methyl α,2,4,5-Tetramethoxyphenylacetate* ***3g***. Oxidation of **1g** with $Tl(NO_3)_3$–TMOF–MeOH for 30 min gave a reacting mixture. After treating it with work-up method A a mixture of products **2g** and **3g** (**2g**: **3g**=93: 7) was obtained in 98% yield. Compound **2g**, mp 44—46 °C; MS, *m/e*, 240; IR(KBr) 1735 cm^{-1}; NMR ($CDCl_3$) δ=3.56 (s, 2H, CH_2), 3.67 (s, 3H, CO_2CH_3), 3.78 (s, 3H, OCH_3), 3.81 (s, 3H, OCH_3), 3.86 (s, 3H, OCH_3), 6.49 (s, 1H, ArH), 6.70 (s, 1H, ArH); Found: C, 59.99; H, 6.75%. Calcd for $C_{12}H_{16}O_5$: C, 59.99; H, 6.71%. Compound **3g**, mp 47—49 °C, MS, *m/e*, 270; IR(KBr) 1758 cm^{-1}; NMR ($CDCl_3$) δ=3.37 (s, 3H, OCH_3), 3.72 (s, 3H, CO_2CH_3), 3.84 (s, 6H, $OCH_3\times2$), 3.89 (s, 3H, OCH_3), 5.19 (s, 1H. CH). 6.52 (s, 1H, ArH), 6.91 (s, 1H, ArH); Found: C, 57.77; H, 6.77%. Calcd for $C_{13}H_{18}O_6$: C, 57.77; H, 6.71%.

Methyl 2,5-Dimethoxy-4-nitrophenylacetate. Treatment of **1a** with $Tl(NO_3)_3$–TMOF–MeOH for 15 min according to the general procedure, followed by work-up method B, gave the methyl 2,5-dimethoxy-4-nitrophenylacetate in 85% yield: mp 80—81 °C; MS, *m/e*, 255; IR(KBr) 1735 and 1519 cm^{-1}; NMR ($CDCl_3$) δ=3.66 (s, 2H, CH_2), 3.69 (s, 3H, CO_2CH_3), 3.83 (s, 3H, OCH_3), 3.91 (s, 3H, OCH_3), 6.94 (s, 1H, ArH), 7.35 (s, 1H, ArH); Found: C, 51.76; H, 5.17; N, 5.43%. Calcd for $C_{11}H_{13}O_6N$: C, 51.76; H, 5.13; N, 5.49%.

Methyl 4-Methyl-3,6-dioxo-1,4-cyclohexadienylacetate ***4b***. Oxidation of **1b** with $Tl(NO_3)_3$–TMOF–MeOH for 15 min according to the general procedure, followed by work-up method B, gave a mixture of products **4b** and **5b** (**4d**: **5b**= 84: 16) in 93% yield. Compound **4b**, mp 74—75 °C; MS, *m/e*, 194; IR(KBr) 1730 and 1675 cm^{-1}; NMR ($CDCl_3$) δ=2.03 (d, J=1.6 Hz, 3H, CH_3), 3.42 (d, J=1.2 Hz, 2H, CH_2), 3.69 (s, 3H, CO_2CH_3), 6.60 (q, J=1.6 Hz, 1H, =CH), 6.65 (t, J=1.2 Hz, 1H, =CH); Found: C, 61.60; H, 5.12%. Calcd for $C_{10}H_{10}O_4$: C, 61.85; H, 5.19%.

Methyl 4-t-Butyl-3,6-dioxo-1,4-cyclohexadienylacetate ***4c***. Oxidation of **1c** with $Tl(NO_3)_3$–TMOF–MeOH for 30 min according to the general procedure resulted a reacting mixture. Subsequent application of the work-up method B we obtained a mixture of products **4c** and **5c** (**4c**: **5c**=88: 12) in 95% yield. Isolation of the product **4c** was carried out as described above and gave oil; MS, *m/e*, 208; IR(NaCl) 1735 and 1670 cm^{-1}; NMR ($CDCl_3$) δ=2.02 (s, 6H, $CH_3\times2$), 3.45 (d, J=1.2 Hz, CH_2), 3.72 (s, 3H, CO_2CH_3), 6.67 (t, J=1.2 Hz, 1H, =CH); Found: C, 63.71; H, 5.99%. Calcd for $C_{11}H_{12}O_4$: C, 63.45; H, 5.81%.

Methyl 4,5-Dimethyl-3,6-dioxo-1,4-cyclohexadienylacetate ***4d***. Oxidation of **1d** with $Tl(NO_3)_3$–TMOF–MeOH for 30 min according to the general procedure, follwed by work-up method B, gave a mixture of products **4d** and **5d** (**4d**: **5d**= 90: 10) in 52% yield. Compound **4d**, oil; MS, *m/e*, 208; IR(NaCl) 1735 and 1670 cm^{-1}; NMR ($CDCl_3$) δ=2.02 (s, 6H, $CH_3\times2$), 3.45 (d, J=1.2 Hz, 2H, CH_2), 3.72 (s, 3H, CO_2CH_3), 6.67 (t, J=1.2 Hz, 1H, =CH); Found: C, 63.71; H, 5.99%. Calcd for $C_{11}H_{12}O_4$: C, 63.45; H, 5.81%.

Methyl 2,4-Dimethyl-3,6-dioxo-1,4-cyclohexadienylacetate ***4e***. Oxidation of **1e** with $Tl(NO_3)_3$–TMOF–MeOH for 20 h according to the general procedure resulted a reacting mixture. Applying the work-up method B we obtained a mixture of products **4e** and **5e** (**4e**: **5e**=70: 30) in 47% yield. Compound **4e**, oil; MS, *m/e*, 208; IR(NaCl) 1740 and 1652 cm^{-1}; NMR

($CDCl_3$) δ=2.05 (d, J=1.6 Hz, 3H, CH_3), 2.04 (s, 3H, CH_3), 3.54 (s, 2H, CH_2), 3.68 (s, 3H, CO_2CH_3), 6.56 (q, J=1.6 Hz, 1H, =CH), Found: C, 63.79; H, 6.02%. Calcd for $C_{11}H_{12}O_4$: C, 63.45; H, 5.81%.

Methyl 1,4-Dioxo-1,4-dihydro-2-naphthylacetate ***4f***. Oxidation of **1f** with $Tl(NO_3)_3$–TMOF–MeOH for 5 h according to the general procedure application of the work-up method B gave a mixture of products **4f** and **5f** (**4f**: **5f**=80: 20) in 35% yield. Compound **4f**, mp 123—125 °C; MS, *m/e*, 230; IR(KBr) 1735 and 1665 cm^{-1}; NMR ($CDCl_3$) δ=3.58 (d, J=1.5 Hz, 1H, CH_2), 3.72 (s, 3H, CO_2CH_3), 6.91 (t, J=1.5 Hz, 1H, =CH), 7.70 (m, 2H, ArH), 8.04 (m, 2H, ArH); Found: C, 67.55; H, 4.20%. Calcd for $C_{13}H_{10}O_4$: C, 67.82; H, 4.38%.

Methyl 2-(2,5-Dimethoxy-4-methylphenyl)propionate ***7***. Oxidation of **6** with $Tl(NO_3)_3$–TMOF–MeOH for 12 h gave a reacting mixture. Treatment of it with the work-up method A afforded a pure product **7** in 92% yield. Compound **7**, oil. MS, *m/e*, 238; IR(NaCl) 1735 cm^{-1}; NMR ($CDCl_3$) δ=1.42 (d, J=7 Hz, 3H, CH_3), 2.19 (s, 3H, CH_3), 3.64 (s, 3H, CO_2CH_3), 3.77 (s, 6H, $OCH_3\times2$), 4.03 (q, J=7 Hz, 1H, CH), 6.70 (s, 2H, ArH); Found: C, 65.39; H, 7.65%. Calcd for $C_{13}H_{18}O_4$: C, 65.53; H, 7.61%.

Methyl 2-(4-Methyl-3,6-dioxo-1,4-cyclohexadienyl)propionate ***8***. Treatment of **6** with $Tl(NO_3)_3$–TMOF–MeOH for 12 h according to the general procedure, followed by work-up method B, gave a pure product **8** in 96% yield. Compound **8**, mp 59—60 °C; MS, *m/e*, 208; IR(KBr) 1735 and 1655 cm^{-1}; NMR ($CDCl_3$) δ=1.41 (d, J=7.2 Hz, 3H, CH_3), 2.08 (d, J=1.6 Hz, 3H, CH_3), 3.70 (s, 3H, CO_2CH_3), 3.79 (dq, J=7.2 Hz, J=1.2 Hz, 1H, CH), 6.60 (m, 2H, $=CH\times2$); Found: C, 63.27; H, 6.11%. Calcd for $C_{11}H_{12}O_4$: C, 63.45; H, 5.81%.

References

1) E. C. Taylor, R. L. Robey, K-T. Liu, B. Favre, H. T. Bozino, R. D. Conley, C-S. Chiang, A. McKillop, and M. E. Ford, *J. Am. Chem. Soc.*, **98**, 3037 (1976).

2) E. C. Taylor, C-S. Chiang, A. McKillop, and J. F. White, *J. Am. Chem. Soc.*, **98**, 6750 (1976).

3) F. J. Villani and J. Lang, *J. Am. Chem. Soc.*, **72**, 2301 (1950).

A Synthesis of (±)-β-Vetivone and Its Related Spirovetivanes *via* the Base-catalyzed Spiroannelation of Phenolic Tosylates

Sigeru TORII,* Kenji UNEYAMA, and Kaoru OKAMOTO
Department of Industrial Chemistry, School of Engineering, Okayama University, Okayama 700
(Received May 10, 1978)

(±)-β-Vetivone was synthesized by the base-catalyzed spiroannelation of 2-[2-(4-hydroxy-2-methylphenyl)-ethyl]-3-methyl-3-butenyl *p*-toluenesulfonate followed by methylation and subsequent isomerization of the side chain double bond. The reactivities of the related tosylates, 4-(4-hydroxy-2-methylphenyl)-2-isopropylbutyl *p*-toluenesulfonate, 3-hydroxy-2-[2-(4-hydroxy-2-methylphenylethyl]-3-methylbutyl *p*-toluenesulfonate, and 2,3-epoxy-2-[2-(4-hydroxy-2-methylphenyl)ethyl]-3-methylbutyl *p*-toluenesulfonate have been discussed.

β-Vetivone (**1**),[1] a fragrance principle of vetiver oil, solavetivone (**2**),[2] hinesolone (**3**),[3] and the related alcohols **4** and **5**,[4] aroma substances from flue-cured Virginia tobacco, are spirovetivane-type sesquiterpenes bearing a 2-cyclohexenone group. Reported attempts to synthesize these sesquiterpenes[5] involve complex intermediates and many steps. Therefore, adequate use of promising intermediates for the synthesis of the desired terpenes would be important.

One of the attractive approaches to the spirovetivane may involve the preparation of 2-alkyl-6-methylspiro-[4.5]deca-6,9-dien-8-one *via* the base-catalyzed annelation of the corresponding phenols by the Winstein's method.[6] The spiroannelation has often been used for the synthesis of spiro[*n*.5]dienones,[7] but has not been employed yet for the spirovetivane synthesis.[8]

Phenolic tosylates **6a**—**c** and **7a** are considered to be promising precursors in obtaining **8** and **9**, which can be transformed to (±)-**1** and its related compounds **10a**—**c** by introducing methyl group at C-10. The isopropenyl group at C-2 of **8b** may be modified to isopropylidene, 1-(hydroxymethyl)vinyl, and 1,2-dihydroxy-1-methylethyl groups, leading to **1**, **4**, and **5**, respectively.

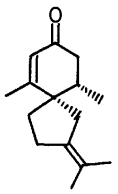

1

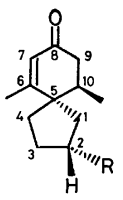

2 R; $C(CH_3)=CH_2$
3 $C(OH)(CH_3)_2$
4 $C(OH)(CH_2OH)CH_3$
5 $C(CH_2OH)=CH_2$

In this paper, we describe spiroannelation of 2-substituted butyl tosylates **6a**—**c** and **7a** leading to the corresponding spirodienones **8a**—**c** and **9** as well as a synthesis of (±)-β-vetivone (**1**).

Results and Discussion

*Preparation of Phenolic Tosylates **6a**—**c** and **7a**.*
The lactone **11**, prepared from 3-(4-methoxy-2-methylbenzoyl)propanoic acid[9] by reduction and following lactonization, was treated with lithium diisopropylamide (LDA) in THF at −78 °C followed by addition of acetone, affording a C-2 epimeric mixture of **12** in

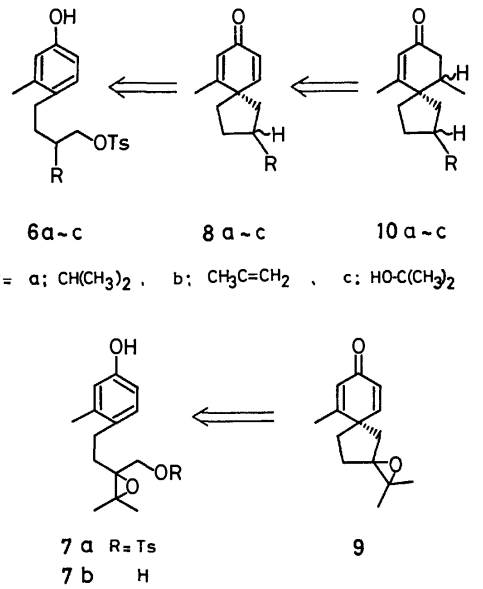

6a~c **8a~c** **10a~c**
R= a; $CH(CH_3)_2$, b; $CH_3C=CH_2$, c; $HO\text{-}C(CH_3)_2$

7a R=Ts
7b H
9

The arrow (⇐) indicates a reverse-synthesis.

quantitative yield. Dehydration of the alcohol **12** with thionyl chloride and subsequent hydrogenation of the resultant isopropylidene derivative **13** with Pt and then Pd on charcoal gave the carboxylic acid **14** in 98% yield. Treatment of **14** with boron tribromide in dichloromethane and next with diazomethane provided **15** in 87% yield. The desired **6a** was obtained by reduction of **15** with lithium aluminum hydride (LAH) followed by tosylation in 92% yield.

Similarly, methyl 4-(4-hydroxy-2-methylphenyl)-butanoate was converted into **16** in 86% yield. Dehydration of **16** with thionyl chloride afforded β,γ-unsaturated ester **17** as a sole product, which was then reduced with LAH to give **18**. Subsequent tosylation of **18** provided **6b** in 68% yield (from **16**).

On the other hand, the monotosylate **6c** was prepared by selective tosylation of the primary hydroxyl group of **19**, obtained by reduction of **16** with LAH in THF, on treatment with tosyl chloride in dry pyridine at −30 °C for 6 h in 86% yield.

The alcohol **20**, prepared by coupling reaction of methyl 4-(4-methoxy-2-methylphenyl)butanoate with acetone, was dehydrated with thionyl chloride to give **21** in 89% yield. The olefin **21** was isomerized to the α,β-unsaturated acid **22** using wet potassium *t*-butoxide in *t*-butylalcohol. Successful conversion of the acid **22**

into the phenolic ester **23** was carried out by demethylation with boron tribromide followed by esterification with diazomethane in 78% yield (from **21**). Thus, another tosylate **7a** was obtained in 82% yield by reduction of **23** with LAH followed by epoxidation of **24** with monoperoxyphthalic acid.

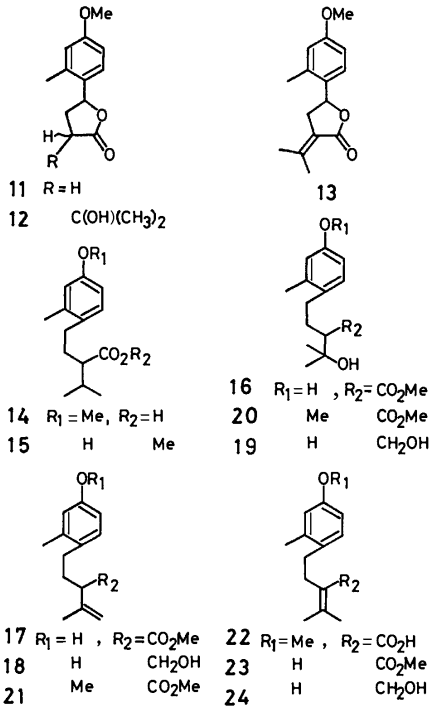

Spiroannelation of Phenolic Tosylates ***6a—c*** *and* ***7a***. The base-catalyzed spiroannelation of **6a** was performed by treatment with *t*-BuOK in refluxing *t*-butyl alcohol, providing C-2 epimers of **8a** in 83% yield after chromatography (SiO_2). Similarly, the tosylate **6b** gave **8b** in 74% yield.[10]

On the other hand, the hydroxy tosylate **6c** could lead to the corresponding spiro compound **8c** only in 17% yield, but it gave the oxetane **25** (67%) as a major product. Treatment of **6c** with sodium methoxide in methanol resulted in **8c** (7%) and **25** (74%). Other combinations of solvents and bases such as NaH–benzene, *t*-BuOK–DMSO, *t*-BuOK–THF, K_2CO_3–acetone, and BuLi–THF did not improve the yield of **8c**. The predominant formation of oxetane may be due to the faster intramolecular S_N2 reaction of the tertiary hydroxyl group toward the tosyloxyl group. The epoxy tosylate **7a** was similarly spiroannelated with *t*-BuOK in refluxing *t*-butyl alcohol, providing **9** in 45% yield. The low yield of **9** would arise from instability of the dienone in high temperature and strong base.

Conversion of ***8a—c*** *to (±)-β-Vetivone and Its Related Compounds.* The dienones **8a**, **8b**, and **8c** underwent methylation at the C-10 carbon with lithium dimethylcuprate(I). However, the epoxy dienone **9** did not afford the desired methylated compound, but it gave complex mixtures.[11] Thus, **8a** was allowed to react with lithiumdimethylcuprate(I) at −25 °C to give **10a** in 85% yield. Similarly, **8b** and **8c** provided **10b** and **10c** in 75 and 63% yield, respectively. The compound **10b** was subsequently converted into (±)-β-vetivone and (±)-10-epi-β-vetivone (1:1 by HPLC) in 80% yield by isomerization of the terminal double bond with rhodium trichloride[12] in ethanol at 110 °C. The pure (±)-**1** was separated by HPLC and identified by the spectroscopic comparison with the authentic data.[5f]

The compound **10c** as an epimeric mixture at C-2 and C-10 was converted into (±)-**1** and (±)-10-epi-**1** (1:1 by HPLC) in 72% yield by dehydration with thionyl chloride.[3,5a,5b,5j,5k] Similarly, the alcohol **8c** was transformed to the olefinic dienone **26** in 75% yield, which had been converted into (±)-**1** by Pesaro.[5h]

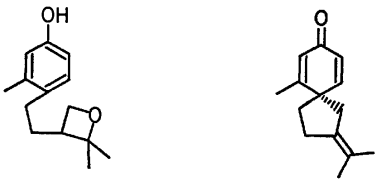

Experimental

Boiling points are indicated by an air-bath temperature and uncorrected. Melting points are taken on a Thomas-Hoover capillary melting point apparatus and uncorrected. IR spectra were obtained on a JASCO IRA-1 spectrometer. ^1H NMR spectra were measured at 60 MHz with a Hitachi R-24 or at 100 MHz with a JEOL FX-100. The chemical shift values are expressed in δ (ppm) downfield from Me_4Si as an internal standard.

*4-(4-Methoxy-2-methylphenyl)butanolide (**11**).* The mixture of 3-(4-methoxy-2-methylbenzoyl)propanoic acid (669 mg, 3 mmol) dissolved in 6.5 ml of 2% aq NaOH and $NaBH_4$ (65 mg, 1.7 mmol) was stirred at room temperature for 24 h, acidified with 10% H_2SO_4 under cooling with an ice bath, and then heated at 80 °C for 15 min. The organic phase was extracted with $CHCl_3$. The extract was washed with saturated $NaHCO_3$ and brine, dried (Na_2SO_4), and concentrated *in vacuo* to give a residue which was chromatographed (SiO_2, hexane:benzene=5:1) to provide **11** (608 mg, 98%) as colorless crystals: mp 52—54 °C (hexane–benzene); IR (neat) 1777 (C=O) cm^{-1}; ^1H NMR ($CDCl_3$) δ 2.27 (s, 3H, CH_3), 1.6—2.8 (m, 4H, CH_2), 3.72 (s, 3H, CH_3O), 5.4—5.8 (m, 1H, CH), 6.5—7.3 (m, 3H, ArH). Found: C, 69.87; H, 6.58%. Calcd for $C_{12}H_{14}O_3$: C, 69.89; H, 6.84%.

*2-(1-Hydroxy-1-methylethyl)-4-(methoxy-2-methylphenyl) butanolide (**12**).* The lactone **11** (722 mg, 3.5 mmol) was added dropwise to a THF solution of LDA, which was prepared by treatment of $NH(CHMe_2)_2$ (1 ml, 7 mmol) dissolved in 4.5 ml of THF with BuLi (5.3 mmol) at −78 °C under N_2. After stirring at −78 °C for 30 min, acetone (0.25 ml, 3.5 mmol) was added and stirred for 30 min. The mixture was quenched with 2 ml of saturated NH_4Cl and the organic phase was taken up in AcOEt. The extract was washed with saturated $NaHCO_3$ and water, dried (Na_2SO_4), and concentrated *in vacuo* to give a residue (970 mg), which was chromatographed (SiO_2, benzene:hexane:AcOEt=10:2:1), providing **12** (970 mg, quant) as a colorless liquid: bp 115—117 °C (0.01 mmHg); IR (neat) 3466 (OH), 1761 (C=O) cm^{-1}; ^1H NMR ($CDCl_3$) δ 1.32 (s, 6H, CH_3), 2.29 (s, 3H, CH_3), 1.8—3.0 (m, 3H, CH_2, CH) 3.41 (s, 1H, OH), 3.77 (s, 3H, CH_3O), 5.4—5.8 (m, 1H, CH), 6.5—7.3 (m, 3H, ArH). Found: C, 68.06; H, 7.53%. Calcd for $C_{15}H_{20}O_4$: C, 68.16; H, 7.63%.

*2-Isopropylidene-4-(4-methoxy-2-methylphenyl)butanolide (**13**).* Thionyl chloride (0.09 ml, 1.3 mmol) was added dropwise to a solution of **12** (300 mg, 1.1 mmol) dissolved in 0.5 ml of pyridine and 1.5 ml of CH_2Cl_2. The reaction mixture was stirred at 0 °C for 20 min and then at room temperature for 4 h. After addition of a few pieces of ice, the organic phase was extracted with ether. The extract was washed with 5% HCl and water, dried (Na_2SO_4), and concentrated under reduced pressure, providing 275 mg of the residue which was chromatographed (SiO_2, hexane: benzene: AcOEt=10: 4: 1) to give **13** (275 mg, 98%): bp 105—107 °C (0.003 mmHg); IR (neat) 1745 (C=O), 1668 (C=C) cm^{-1}; ^1H NMR ($CDCl_3$) δ 1.84 (s, 3H, CH_3), 2.29 (s, 6H, CH_3), 2.4—3.6 (m, 2H, CH_2), 3.75 (s, 3H, CH_3O), 5.51 (dd, $J_1=7$ Hz, $J_2=8$ Hz, 1H, CHO). 6.5—7.4 (m, 3H, ArH). Found: C, 73.19; H, 7.57%. Calcd for $C_{15}H_{18}O_3$: C, 73.15; H, 7.37%.

*2-Isopropyl-4-(4-methoxy-2-methylphenyl)butanoic Acid (**14**).* The lactone **13** (400 mg, 1.6 mmol) dissolved in 20 ml of MeOH was hydrogenated with PtO_2 (40 mg) at room temperature for 12 h and then Pd/C (40 mg) for 6 h to give **14** (388 mg, 96%): bp 111—113 °C (0.01 mmHg); IR (neat) 3500—2400 (CO_2H), 1702 (C=O) cm^{-1}; ^1H NMR ($CDCl_3$) δ 0.96 (d, $J=6$ Hz, 6H, CH_3), 1.4—2.9 (m, 6H, CH_2, CH) 2.26 (s, 3H, CH_3), 3.74 (s, 3H, CH_3O), 6.4—7.3 (m, 3H, ArH), 9.3—10.4 (br s, 1H, CO_2H). Found: C, 71.97; H, 9.03%. Calcd for $C_{15}H_{22}O_3$: C, 71.97; H, 8.86%.

*Methyl 4-(4-Hydroxy-2-methylphenyl)-2-isopropylbutanoate (**15**).* Boron tribromide (0.25 ml, 2.64 mmol) was added dropwise to a solution of **14** (335 mg, 1.32 mmol) dissolved in 3.5 ml of dry CH_2Cl_2 at −70 °C. The mixture was stirred for 1 h at −70 °C and 0 °C for 1 h, quenched with water, and extracted with AcOEt. The usual work-up gave yellow liquid, which was subsequently esterified with diazomethane and chromatographed (SiO_2, benzene: hexane: AcOEt=6: 2: 1) to afford **15** (283 mg, 86%) as an oil: bp 92—94 °C (0.005 mmHg); IR (neat) 3380 (OH), 1732, 1710 (C=O) cm^{-1}; ^1H NMR ($CDCl_3$) δ 0.88 (d, $J=6$ Hz, 6H, CH_3), 2.14 (s, 3H, CH_3), 1.4—2.6 (m, 6H, CH_2, CH), 3.63 (s, 3H, CH_3O), 6.3—6.9 (m, 4H, ArH, OH). Found: C, 71.99; H, 9.06%. Calcd for $C_{15}H_{22}O_3$: C, 71.97; H, 8.86%.

4-(4-Hydroxy-2-methylphenyl)-2-isopropylbutyl p-*Toluenesulfonate (**6a**).* A solution of sublimated *p*-TsCl (309 mg, 1.62 mmol) in 1.5 ml of dry pyridine was added dropwise to a solution of 4-(4-hydroxy-2-methylphenyl)-2-isopropyl-1-butanol (240 mg, 1.08 mmol) dissolved in 1.5 ml of dry pyridine at −30 °C. After stirring at −30 °C for 10 min and at 0 °C for 6 h, the mixture was quenched with water and then worked up to give an oil, which was chromatographed (SiO_2, benzene: AcOEt=2: 1) to yield **6a** (381 mg, 94%) as a pale yellow oil: IR (neat) 3470 (OH), 1354, 1175 (SO_2) cm^{-1}; ^1H NMR ($CDCl_3$) δ 0.82 (d, $J=7$ Hz, 6H, CH_3), 1.2—2.0 (m, 4H, CH_2, CH), 2.14 (s, 3H, CH_3), 2.41 (s, 3H, CH_3), 2.2—2.6 (m, 2H, CH_2), 4.04 (d, $J=4$ Hz, 2H, CH_2O), 5.11 (br s, 1H, OH), 6.4—7.0 (m, 3H, ArH), 7.28 (d, $J=8$ Hz, 2H, ArH), 7.77 (d, $J=8$ Hz, 2H, ArH). Found: C, 67.09; H, 7.58%. Calcd for $C_{21}H_{28}O_4S$: C, 66.99; H, 7.50%.

*Methyl 3-Hydroxy-2-[2-(4-hydroxy-2-methylphenyl)ethyl]-3-methylbutanoate (**16**).* The compound **16** was obtained as a colorless oil in 86% yield by alkylation of methyl 4-(4-hydroxy-2-methylphenyl)butanoate in the same reaction conditions as employed for **12** using a mixed solvent (HMPA: THF=1: 10); bp 123—126 °C (0.01 mmHg); IR (neat) 3320 (OH), 1707 (C=O) cm^{-1}; ^1H NMR ($CDCl_3$) δ 1.22 (s, 6H, CH_3), 2.19 (s, 3H, CH_3), 1.5—2.7 (m, 7H, CH_2, CH, OH), 3.73 (s, 3H, CH_3O), 6.4—7.1 (m, 3H, ArH). Found: C, 67.49; H, 8.08%. Calcd for $C_{15}H_{22}O_4$: C, 67.65; H, 8.33%.

*Methyl 2-[2-(4-Hydroxy-2-methylphenyl)ethyl]-3-methyl-3-butenoate (**17**):* Bp 123—125 °C (0.009 mmHg); IR (neat) 3440 (OH), 1733 (C=O), 1644 (C=C) cm^{-1}; NMR ($CDCl_3$) δ 1.75 (br s, 3H, CH_3), 2.29 (s, 3H, CH_3), 1.5—2.8 (m, 5H, CH_2, OH), 3.09 (t, $J=7$ Hz, 1H, CH), 3.68 (s, 3H, CH_3O), 4.8—5.0 (m, 2H, $CH_2=$), 6.8—7.2 (m, 3H, ArH). Found: C, 72.56; H, 8.25%. Calcd for $C_{15}H_{20}O_3$: C, 72.55; H, 8.12%.

*2-[2-(4-Hydroxy-2-methylphenyl)ethyl]-3-methyl-3-buten-1-ol(**18**).* Reduction of **17** with $LiAlH_4$ in dry THF provided **18** as an oil in 90% yield: bp 118—121 °C (0.015 mmHg); IR (neat) 3320 (OH), 1644 (C=C) cm^{-1}; NMR ($CDCl_3$) δ 1.69 (s, 3H, CH_3), 1.1—1.8 (m, 2H, CH_2), 2.16 (s, 3H, CH_3), 2.0—2.8 (m, 5H, CH_2, CH, OH), 3.54 (d, $J=7$ Hz, 2H, CH_2O), 4.8—5.1 (m, 2H, $CH_2=$), 6.4—7.1 (m, 3H, ArH). Found: C, 76.26; H, 9.00%. Calcd for $C_{14}H_{20}O_2$: C, 76.33; H, 9.15%.

2-[2-(4-Hydroxy-2-methylphenyl)ethyl]-3-methyl-3-butenyl p-*Toluenesulfonate (**6b**):* IR (neat) 3460 (OH), 1649 (C=C), 1358, 1178 (SO_2) cm^{-1}; NMR ($CDCl_3$) δ 1.58 (s, 3H, CH_3), 1.2—1.8 (m, 2H, CH_2), 2.12 (s, 3H, CH_3), 2.38 (s, 3H, CH_3), 2.0—2.7 (m, 3H, CH_2, CH), 3.96 (d, $J=7$ Hz, 2H, CH_2O), 4.7—5.0 (m, 2H, $CH_2=$), 5.67 (br s, 1H, OH), 6.4—7.0 (m, 3H, ArH), 7.23 (d, $J=8$ Hz, 2H, ArH), 7.70 (d, $J=8$ Hz, 2H, ArH). Found: C, 67.43; H, 7.07%. Calcd for $C_{21}H_{26}O_4S$: 67.35; H, 7.00%.

*2-[2-(4-Hydroxy-2-methylphenyl)ethyl]-3-methyl-1,3-butanediol (**19**):* Mp 111—113 °C (benzene: AcOEt=5: 1); IR (neat) 3320 (OH); NMR (acetone-d_6) δ 1.16 (s, 3H, CH_3), 1.21 (s, 3H, CH_3), 1.3—1.9 (m, 3H, CH_2, CH), 2.23 (s, 3H, CH_3), CH_3), 2.3—2.8 (m, 2H, CH_2), 2.88 (br. s, 1H, OH), 3.7—4.0 (m, 2H, CH_2O), 4.0—4.2 (m, 1H, OH), 6.4—7.1 (m, 3H, ArH), 7.89 (br s, 1H, OH). Found: C, 70.61; H, 9.53%. Calcd for $C_{14}H_{22}O_3$: C, 70.56; H, 9.30%.

3-Hydroxy-2-[2-(4-hydroxy-2-methylphenyl)ethyl]-3-methylbutyl p-*Toluenesulfonate (**6c**):* IR (neat) 3400 (OH), 1352, 1177 (SO_2) cm^{-1}; NMR ($CDCl_3$) δ 1.15 (s, 6H, CH_3), 1.3—2.0 (m, 3H, CH_2, CH), 2.12 (s, 3H, CH_3), 2.39 (s, 3H, CH_3), 2.2—2.8 (m, 2H, CH_2), 3.90 (br s, 2H, OH), 4.19 (d, $J=3$ Hz, 2H, CH_2O), 6.3—6.9 (m, 3H, ArH), 7.27 (d, $J=8$ Hz, 2H, ArH), 7.54 (d, $J=8$ Hz, 2H, ArH). Found: C, 64.13; H, 7.23%. Calcd for $C_{21}H_{28}O_5S$: C, 64.26; H, 7.19%.

*Methyl 3-Hydroxy-2-[2-(4-methoxy-2-methylphenyl)ethyl]-3-methylbutanoate (**20**):* Bp 103—105 °C (0.01 mmHg); IR (neat) 3460 (OH), 1728 (C=O) cm^{-1}; NMR ($CDCl_3$) δ 1.20 (s, 6H, CH_3), 1.5—2.1 (m, 2H, CH_2), 2.23 (s, 3H, CH_3), 2.2—2.7 (m, 3H, CH_2, CH), 2.78 (br s, 1H, OH), 3.69 (s, 3H, CH_3O), 3.71 (s, 3H, CH_3), 6.5—7.1 (m, 3H, ArH). Found: C, 68.48; H, 8.50%. Calcd for $C_{16}H_{24}O_4$: C, 68.55; H. 8.63%.

*Methyl 2-[2-(4-methoxy-2-methylphenyl)ethyl]-3-methyl-3-butenoate (**21**):* Bp 81—83 °C (0.003 mmHg); IR (neat) 1733 (C=O), 1646 (C=C) cm^{-1}; NMR ($CDCl_3$) δ 1.75 (br s, 3H, CH_3), 1.7—2.2 (m, 2H, CH_2), 2.26 (s, 3H, CH_3), 2.3—2.7 (m, 2H, CH_2), 3.07 (t, $J=7$ Hz, 1H, CH), 3.67 (s, 3H, CH_3O), 3.73 (s, 3H, CH_3O), 4.8—5.0 (m, 2H, $CH_2=$), 6.5—7.1 (m, 3H, ArH). Found: C, 73.29; H, 8.64%. Calcd for $C_{16}H_{22}O_3$: C, 73.25; H, 8.45%.

*2-[2-(4-Methoxy-2-methylphenyl)ethyl]-3-methyl-2-butenoic Acid (**22**).* The mixture of **21** (1.37 g, 5.22 mmol) and *t*-BuOK (2.59 g, 23.1 mmol) in 8 ml of dry *t*-BuOH and 18 ml of dry THF was refluxed for 30 h. After evaporation of the solvent *in vacuo*, the residue was mixed with 10 ml of water and then acidified with 5% HCl. The usual work-up gave 1.32 g of a solid, which was recrystallized from hexane/benzene (10/1) affording **22** (1.25 g, 96%) as colorless crystals: mp 108—110 °C; IR (nujol) 3400—2000 (CO_2H), 1687 (C=O), 1652 (C=C) cm^{-1}; ^1H NMR ($CDCl_3$) δ 1.77 (s, 3H, CH_3), 2.11 (s, 3H, CH_3), 2.31 (s, 3H, CH_3), 2.58 (br s, 4H, CH_2), 3.73 (s, 3H, CH_3O), 6.5—7.2 (m, 3H, ArH), 11.16 (br s, 1H, CO_2H).

Found: C, 72.55; H, 8.12%. Calcd for $C_{15}H_{20}O_3$: C, 72.55: H, 8.12%.

Methyl 2-[2-(4-Hydroxy-2-methylphenyl)ethyl]-3-methyl-2-butenoate (23): Mp 81—82 °C (hexane: benzene=15: 1); IR (Nujol) 3330 (OH), 1682 (C=O) cm^{-1}; ^1H NMR ($CDCl_3$) δ 1.74 (s, 3H, CH_3), 1.98 (s, 3H, CH_3), 2.24 (s, 3H, CH_3), 2.54 (br s, 4H, CH_2), 3.70 (s, 3H, CH_3O), 6.40 (br s, 1H, OH), 6.5—7.1 (m, 3H, ArH). Found: C, 72.56; H, 8.19%. Calcd for $C_{15}H_{20}O_3$: C, 72.55; H, 8.12%.

2-[2-(4-Hydroxy-2-methylphenyl)ethyl]-3-methyl-2-buten-1-ol (24): Mp 119—121 °C (CH_2Cl_2); IR (Nujol) 3340 (OH), 1653 (C=C) cm^{-1}; ^1H NMR ($CDCl_3$) δ 1.67 (s, 3H, CH_3), 1.75 (s, 3H, CH_3), 2.26 (s, 3H, CH_3), 1.9—2.9 (m, 6H, CH_2, OH), 4.13 (s, 2H, CH_2O), 6.4—7.1 (m, 3H, ArH). Found: C, 76.33; H, 9.20%. Calcd for $C_{14}H_{20}O_2$: C, 76.33; H, 9.15%.

2,3-Epoxy-2-[2-(4-hydroxy-2-methylphenyl)ethyl]-3-methyl-1-butanol (7b). An ethereal solution of monoperoxyphthalic acid (0.5 ml, *ca.* 0.5 mmol) was added to an ice-cooled solution of **24** (43 mg, 0.2 mmol) in 0.5 ml of ether with stirring. After stirring at 5 °C for 10 h, the reaction mixture was quenched with saturated $NaHCO_3$ and then extracted with ether. The extract was washed with brine, dried (Na_2SO_4), and concentrated *in vacuo* to give an oil, which was chromatographed (SiO_2, benzene: AcOEt=5: 1) affording **7b** (42 mg, 91%) as a colorless oil: bp 112—114 °C (0.009 mmHg); IR (neat) 3340 (OH) cm^{-1}; ^1H NMR ($CDCl_3$) δ 1.27 (s, 3H, CH_3), 1.34 (s, 3H, CH_3), 2.22 (s, 3H, CH_3), 1.5—2.9 (m, 6H, CH_2, OH), 3.78 (s, 2H, CH_2O), 6.4—7.1 (m, 3H, ArH). Found: C, 71.16; H, 8.31%. Calcd for $C_{14}H_{20}O_3$: C, 71.16; H, 8.53%.

2,3-Epoxy-2-[2-(4-hydroxy-2-methylphenyl)ethyl]-3-methylbutyl p-Toluenesulfonate (7a): Mp 79—81 °C (hexane: benzene=5: 1); IR (Nujol) 3250 (OH), 1365, 1168 (SO_2) cm^{-1}; ^1H NMR ($CDCl_3$) δ 1.27 (s, 6H, CH_3), 2.16 (s, 3H, CH_3), 2.40 (s, 3H, CH_3), 1.5—2.8 (m, 4H, CH_2), 4.15 (s, 2H, CH_2O), 6.00 (br s, 1H, OH), 6.4—7.1 (m, 3H, ArH), 7.30 (d, J=9 Hz, 2H, ArH), 7.79 (d, J=9 Hz, ArH). Found: C, 64.63; H, 6.60%. Calcd for $C_{21}H_{26}O_5S$: C, 64.59; H, 6.71%.

2-Isopropyl-6-methylspiro[4.5]deca-6,9-dien-8-one (8a). Sublimated *t*-BuOK (16 mg, 0.14 mmol) in 1.2 ml of dry BuOH was added dropwise to a solution of **6a** (45 mg, 0.12 mmol) in 0.8 ml of dry *t*-BuOH under N_2 and the mixture was refluxed for 12 h. After cooling to room temperature, the mixture was quenched with water and then worked up to afford a yellow oil, which was chromatographed (SiO_2, benzene: AcOEt=10: 1) to give **8a** (21 mg, 86%) as a pale yellow oil: bp 60—61 °C (0.01 mmHg); IR (neat) 1660 (C=O), 1625, 1604 (C=C) cm^{-1}; NMR ($CDCl_3$) δ 0.92 (d, J=6 Hz, 3H, CH_3), 0.96 (d, J=6 Hz, 3H, CH_3), 1.99, 2.01 (2s, 3H, CH_3), 1.1—2.3 (m, 8H, CH_2, CH), 5.9—6.2 (m, 2H, CH=), 6.87 (d, J=10 Hz, 1H, CH=). Found: C, 82.24; H, 9.92%. Calcd for $C_{14}H_{20}O$: C, 82.30; H, 9.87%.

2-Isopropenyl-6-methylspiro[4.5]deca-6,9-dien-8-one (8b): Bp 65—68 °C (0.007 mmHg); IR (neat) 1659 (C=O), 1624, 1602 (C=C) cm^{-1}; NMR ($CDCl_3$) δ 1.77 (br s, 3H, CH_3), 2.02, 2.04 (2s, 3H, CH_3), 1.5—2.3 (m, 6H, CH_2), 2.4—3.2 (m, 1H, CH), 4.7—4.9 (m, 2H, CH_2=), 5.9—6.2 (m, 2H, CH=), 6.91 (d, J=10 Hz, CH=). Found: C, 83.15; H, 9.12%. Calcd for $C_{14}H_{18}O$: C, 83.12; H, 8.97%.

2-(1-Hydroxy-1-methylethyl)-6-methylspiro[4.5]deca-6,9-dien-8-one (8c): IR (neat) 3380 (OH), 1650 (C=O), 1614 (C=C) cm^{-1}; NMR ($CDCl_3$) δ 1.25 (s, 3H, CH_3), 1.27 (s, 3H, CH_3), 2.00, 2.02 (2s, 3H, CH_3), 1.4—2.4 (m, 7H, CH_2, CH), 2.73 (br s, 1H, OH), 5.9—6.2 (m, 2H, CH=), 6.99 (d, J=10 Hz, 1H, CH=). Found: C, 76.21; H, 8.97%. Calcd for $C_{14}H_{20}O_2$: C, 76.33; H, 9.15%.

3-[2-(4-Hydroxy-2-methylphenyl)ethyl]-2,2-dimethyloxetane (25): Mp 78—80 °C (hexane: benzene=15: 1); IR (neat) 3280 (OH) cm^{-1}; NMR ($CDCl_3$) δ 1.34 (s, 3H, CH_3), 1.43 (s, 3H, CH_3), 1.6—2.0 (m, 2H, CH_2), 2.20 (s, 3H, CH_3), 2.1—3.0 (m, 3H, CH_2, CH), 4.09 (dd, J_1=6 Hz, J_2=7 Hz, 1H, CH_2O), 4.51 (dd, J_1=7 Hz, J_2=8 Hz, 1H, CH_2O), 6.4—7.0 (m, 3H, ArH), 7.60 (br s, 1H, OH). Found: C, 76.34; H, 9.17%. Calcd for $C_{14}H_{20}O_2$: C, 76.33; H, 9.15%.

2,2,6-Trimethyl-1-oxadispiro[2.1.5.2]dodeca-6,9-dien-8-one (9): Bp 75—77 °C (0.008 mmHg); IR 1662 (C=O), 1624, 1603 (C=C) cm^{-1}; ^1H NMR ($CDCl_3$) δ 1.32 (s, 3H, CH_3), 1.38 (s, 3H, CH_3), 2.01, 2.04 (2s, 3H, CH_3), 1.5—2.9 (m, 6H, CH_2), 6.0—6.3 (m, 2H, CH=), 6.90 (d, J=11 Hz, 1H, CH=). Found: C, 77.02; H, 8.37%. Calcd for $C_{14}H_{18}O_2$: C, 77.03; H, 8.13%.

2-Isopropyl-6,10-dimethylspiro[4.5]dec-6-en-8-one (10a). An ethereal solution of lithium dimethylcuprate (I) (1.0 mmol) was added to a solution of **8a** (70 mg, 0.34 mmol) in 1.5 ml of dry ethre over 20 min period under N_2 at −20——25 °C. The mixture was stirred for 1.5 h and quenched with water and 5% HCl. The usual work-up gave an oil, which was chromatographed (SiO_2, benzene: AcOEt=10: 1) providing **10a** (61 mg, 81%) as a slightly yellow oil: bp 56—57 °C (0.01 mmHg); IR (neat) 1669 (C=O), 1614 (C=C) cm^{-1}; ^1H NMR ($CDCl_3$) δ 0.92 (d, J=7 Hz, 6H, CH_3), 0.96—1.03 (m, 3H, CH_3), 1.93, 1.95, 1.96, 1.97 (4s, 3H, CH_3), 1.1—2.8 (m, 11H, CH_2, CH), 5.70 (br s, 1H, CH=). Found: C, 81.84; H, 10.98%. Calcd for $C_{15}H_{24}O$: C, 81.76; H, 10.98%.

2-Isopropenyl-6,10-dimethylspiro[4.5]dec-6-en-8-one (10b): Bp 65—67 °C (0.008 mmHg); IR (neat) 1667 (C=O), 1612 (C=C) cm^{-1}; ^1H NMR ($CDCl_3$) δ 1.00, 1.04 (2d, J=7 Hz, 3H, CH_3), 1.78 (br s, 3H, CH_3), 1.99, 2.00, 2.01, 2.02 (4s, 3H, CH_3), 1.30—2.80 (m, 10H, CH_2, CH), 4.75 (br s, 2H, CH_2=), 5.75 (br s, 1H, CH=). Found: C, 82.49; H, 10.35%. Calcd for $C_{15}H_{22}O$: C, 82.52; H, 10.16%.

2-(1-Hydroxy-1-methylethyl)-6,10-dimethylspiro[4.5]dec-6-en-8-one (10c): IR (neat) 3420 (OH), 1654 (C=O), 1612 (C=C) cm^{-1}; ^1H NMR ($CDCl_3$) δ 0.90—1.07 (m, 3H, CH_3), 1.25 (s, 6H, CH_3), 1.92—2.00 (m, 3H, CH_3), 1.30—2.62 (m, 11H, CH_2, CH, OH), 5.73 (br s, 1H, CH=). Found: C, 76.19; H, 10.24%. Calcd for $C_{15}H_{24}O_2$: C, 76.23; H, 10.24%.

2-Isopropylidene-6,10-dimethylspiro[4.5]dec-6-en-8-one (dl-β-Vetivone) (1) and Its C-10 Epimer. A mixture of **10b** (14 mg, 0.064 mmol) and $RhCl_3 \cdot 2H_2O$ (1.3 mg, 0.05 mmol) in 0.05 ml of dry EtOH was heated in a glass tube at 110 °C for 8 h. The mixture was filtered and the precipitate was rinsed several times with ether. The combined filtrates were concentrated *in vacuo* and the residue was chromatographed (SiO_2, benzene: AcOEt=10: 1) to give (±)-**1** and its C-10 epimer (11 mg, 80%). HPLC separation of the epimeric mixture (μ-Porasil, 4φ-30 cm, ether: hexane=1: 10, flow rate 2 ml/min, 1000 psi) and further purification through a short silica gel column to remove a paraffin provided (±)-**1** (3 mg, retention time 10.8 min) as an oil and 10-epi-(±)-**1** (3 mg, retention time 12.7 min); (±)-**1**: IR (CCl_4) 1670, 1658 (shoulder), 1612 cm^{-1}; ^1H NMR ($CDCl_3$) δ 0.96 (d, J=7 Hz, 3H, CH_3), 1.73—1.51 (m, 6H, CH_3), 1.89 (d, J=1.5 Hz, 3H, CH_3), 2.2—1.8 (m, 3H, CH, CH_2), 2.6—2.2 (m, 5H, CH_2), 2.63 (dd, J_1=17 Hz, J_2=5 Hz, 1H, CH_2CO), 5.78 (br s, 1H, CH=). 10-epi-(±)-**1**: IR (CCl_4) 1670, 1657 (shoulder), 1612 cm^{-1}; ^1H NMR ($CDCl_3$) δ 0.97 (d, J=7 Hz, 3H, CH_3), 1.62 (br s, 6H, CH_3), 1.90 (d, J=1.5 Hz, 3H, CH_3), 2.0—1.7 (m, 3H, CH, CH_2), 2.6—2.0 (m, 5H, CH_2), 2.59 (dd, J_1=17 Hz, J_2=6 Hz, 1H, CH_2CO), 5.78 (br s, 1H, CH=).

2-Isopropylidene-6-methylspiro[4.5]deca-6,9-dien-8-one (26). Thionyl chloride (0.014 ml, 0.19 mmol) was added to an ice-cooled solution of **8c** (35 mg, 0.16 mmol) in 0.15 ml of dry pyridine and 0.3 ml of dry CH_2Cl_2 under N_2. After 10 min stirring, the reaction mixture was warmed to room temperature for 3.5 h. The mixture was quenched with a few pieces

of ice and the organic substances were worked up to give an oil, which was chromatographed (SiO_2, benzene: AcOEt=5: 1) providing **26** (24 mg, 75%) as colorless crystals: mp 80—82 °C (pentane) (lit. 82—83 °C)[5h]; IR (neat) 1662 (C=O), 1627, 1605 (C=C) cm^{-1}; ^1H NMR ($CDCl_3$) δ 1.67 (br. s, 6H, CH_3), 2.00, 2.02 (2s, 3H, CH_3), 1.5—2.8 (m, 6H, CH_2), 5.9—6.3 (m, 2H, CH=), 6.92 (d, J=10 Hz, 1H, CH=).

We wish to thank Dr. M. Ueda and Mr. I. Akuta, Central Research Lab., Kuraray Co., Ltd., for their support of HPLC analysis.

References

1) S. Sebatien and T. Lucien, *Bull. Soc. Chim. Fr.*, **6**, 740 (1939); A. S. Pfau and P. A. Plattner, *Helv. Chim. Acta*, **22**, 640 (1939).

2) D. T. Coxon, K. R. Price, B. Howard, S. F. Osman, E. B. Kalan, and R. M. Zacharius, *Tetrahedron Lett.*, **1974**, 2921.

3) I. Yoshida and T. Kimura, *Chem. Pharm. Bull.*, **13**, 1430 (1965).

4) R. C. Anderson and D. M. Gunn, *J. Chem. Soc., Chem. Commun.*, **1977**, 27.

5) (a) J. A. Marshall and P. C. Johnson, *Chem. Commun.*, **1968**, 391; (b) J. A. Marshall and P. C. Johnson, *J. Org. Chem.*, **35**, 192 (1970); (c) K. Yamada, H. Nagase, Y. Hayakawa, K. Aoki, and Y. Hirata, *Tetrahedron Lett.*, **1973**, 4963; (d) P. M. McCurry, Jr., and R. K. Singh, *ibid.*, **1973**, 3325; (e) G. Stork, R. L. Danheiser, and B. Ganem, *J. Am. Chem. Soc.*, **95**, 3414 (1973); (f) P. M. McCurry, Jr., R. K. Singh, and S. Link, *Tetrahedron Lett.*, **1973**, 1155; (g) D. Caine and C-Y. Chu, *ibid.*, **1974**, 703; (h) G. Bozzato, J-P. Bachmann, and M. Pesaro, *J. Chem. Soc., Chem. Commun.*, **1974**, 1005; (i) W. G. Dauben and D. J. Hart, *J. Am. Chem. Soc.*, **97**, 1622 (1975); **99**, 7303 (1977); (j) M. Deighton, C. R. Hughes, and R. Ramage, *J. Chem. Soc., Chem. Commun.*, **1975**, 662; (k) G. Buchi, D. Berther, R. Decorzant, A. Grieder, and A. Hauser, *J. Org. Chem.*, **41**, 3208 (1976); (l) K. Yamada, S. Goto, H. Nagase, and Y. Hirata, *J. Chem. Soc., Chem. Commun.*, **1977**, 554; (m) E. Wenkert, B. L. Buckwalter, A. A. Craveiro, E. L. Sanchez, and S. S. Sathe, *J. Am. Chem. Soc.*, **100**, 1267 (1978).

6) S. Winstein and R. Baird, *J. Am. Chem. Soc.*, **79**, 756 (1957); S. Winstein, R. Heck, S. Lapponte, and R. Baird, *Experientia*, **12**, 138 (1956); R. Baird and S. Winstein, *J. Am. Chem. Soc.*, **84**, 138 (1962).

7) (a) A. S. Dreiding, *Helv. Chim. Acta*, **40**, 1812 (1957); (b) R. Barner, A. S. Dreiding, and H. Schmid, *Chem. Ind.*, **1958**, 1437; (c) S. Masamune, *J. Am. Chem. Soc.*, **83**, 1009 (1961); (d) S. Dorling and J. Harley-Mason, *Chem. Ind.*, **1959**, 1551; (e) S. Masamune, *J. Am. Chem. Soc.*, **86**, 288 (1964); (f) T. G. Grandall and R. G. Lawton, *ibid.*, **91**, 2127 (1969); (g) E. J. Corey, N. N. Girotra, and G. T. Mathew, *ibid.*, **91**, 1557 (1969); (h) A. Ogiso, M. Kurabayashi, H. Nagabori, and Mishima, *Chem. Pharm. Bull.* **18**, 1283 (1970).

8) K. Uneyama, K. Okamoto, and S. Torii, *Chem. Lett.*, **1977**, 493.

9) R. D. Desai and M. A. Wali, *Proc. Indian Acad. Sci., Sect. A*, **6**, 144 (1937).

10) A. P. Krapcho, *Synthesis*, **1976**, 425.

11) R. W. Herr, D. M. Weiland, and C. R. Johnson, *J. Am. Chem. Soc.*, **92**, 3813 (1970).

12) J. F. Harrod and A. J. Chalk, *J. Am. Chem. Soc.*, **86**, 1776 (1964).

Synthetic Studies on Pyridomycin. III.[1] Chiral Synthesis of (2*R*,2*S*)-(−)-2,3-Dihydroxy-3-methylpentanoic Acid from Sugar Derivative

Mitsuhiro KINOSHITA,* Hiroshi HAMAZAKI, and Masaki AWAMURA

Department of Applied Chemistry, Faculty of Engineering, Keio University, Hiyoshi, Kohoku-ku, Yokohama 223

(Received May 10, 1978)

The Grignard reaction of 3-*O*-benzyl-6-deoxy-1,2-*O*-isopropylidene-α-D-*xylo*-hexofuranos-5-ulose (**5**) with ethylmagnesium bromide yielded 3-*O*-benzyl-6-deoxy-5-*C*-ethyl-1,2-*O*-isopropylidene-α-D-glucofuranose (**6**) as a major product in 91% stereoselectivity. Hydrolysis of **6** followed by successive periodate oxidation and lithium aluminium hydride reduction gave 2-*O*-benzyl-5-deoxy-4-*C*-ethyl-D-arabinitol. Selective benzoylation of **9** followed by successive 3,4-*O*-isopropylidenation, debenzoylation, hydrogenolysis, and two-stage oxidation with periodate-hypoiodite afforded (4*R*,5*S*)-(+)-5-ethyl-2,2,5-trimethyl-1,3-dioxolane-4-carboxylic acid (**15**) in 24.6% overall yield from **5**. Hydrolysis of **15** gave (2*R*,3*S*)-(−)-2,3-dihydroxy-3-methylpentanoic acid. The acetonide **15** is usefull as a synthon for pyridomycin synthesis.

The structure of pyridomycin (**1**) contains (*Z*)-2-acyloxy-3-methyl-2-pentenoic ester (unit **A**) which corresponds to the unique exocyclic *s*-butylidene side chain moiety in the twelve-membered ring system.[2] For the total synthesis of pyridomycin, it was desirable for the precursor of **1** to contain an appropriate 2-*O*-acylated dihydroxy ester (unit **2**) derived from *threo*-2,3-dihydroxy-3-methylpentanoic acid such as structure **3**, since dehydration of unit **2** is expected to afford predominantly unit **A** in **1** by *trans*-elimination.[3]

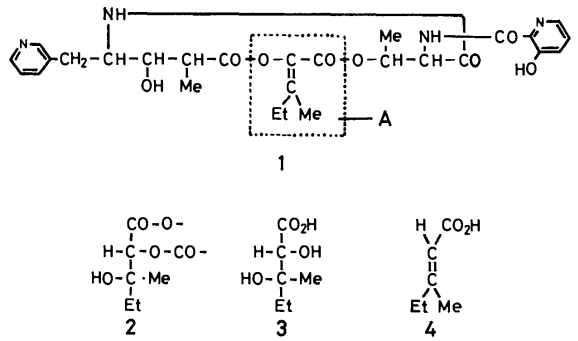

Fig. 1.

The (±)- and (−)-*threo*-2,3-dihydroxy-3-methylpentanoic acids have been prepared from (*E*)-3-methyl-2-pentenoic acid (**4**) by *cis*-hydroxylation[4,5] and by optical resolution of the (±)-*threo*-acid,[5] respectively. This synthetic method seems less promising since the isomerically pure key substance **4** can not be easily prepared on a large scale. On the other hand, a mixture of the *threo*- and *erythro*-dihydroxy acids has easily been prepared from ethyl 3-methyl-2,3-epoxypentanoate.[6,7] However, attempts to isolate the *threo*-isomer from the isomeric mixture have not yet been successful.

This paper presents a chiral synthesis of (2*R*,3*S*)-2,3-dihydroxy-3-methylpentanoic acid (**3**)[8] *via* its acetonide (2,3-*O*-isopropylidene derivative) **15** from 3-*O*-benzyl-6-deoxy-1,2-*O*-isopropylidene-α-D-*xylo*-hexofuranos-5-ulose (**5**)[9,10] through the route shown in Fig. 2. In the first step, the desired product **6** in which the configuration of the C-5 carbon is identical with that of the C-3 carbon in the target compound **3**, was obtained in high stereoselectivity by the asymmetric Grignard reaction.[11–13] The isomerically pure acetonide **15** derived from **6** substantially contributed to the configurational assignment of **6**. The acetonide **15** is useful not only as a precursor for **3** but also as a synthon for synthesis of a precursor of **1**. This synthesis is advantageous for all the optically active diastereo- and enantio-isomers of **3**. the (3*R*)-epimer **3'** (Fig. 2), which has been established[5–8] to be an intermediate in the biosynthesis of isoleucine, will be synthesized *via* **6'** by the use of the ulose **5'** as a starting material instead of **5**. The enantiomer of **5** will be converted into the optical antipode of **3** which is also useful in the pyridomycin synthesis.

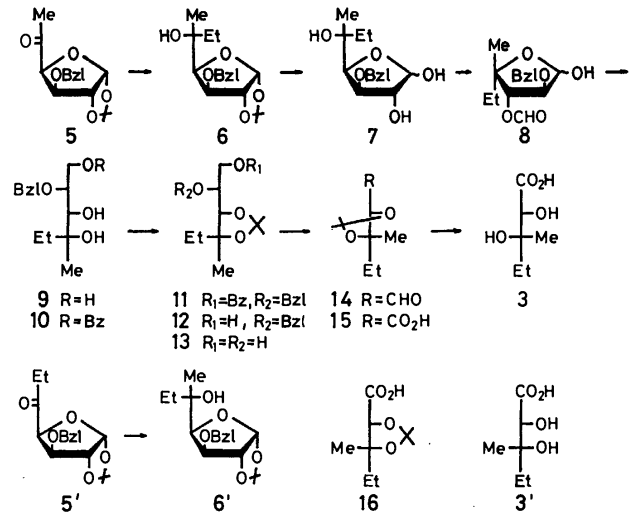

Fig. 2.

Results and Discussion

The Grignard reaction of **5** with an eight-fold excess of ethylmagnesium bromide in ether afforded a crystalline condensation product in 80.1% yield after recrystallization from pentane. A thorough examination of this product by PMR spectroscopy revealed that it is a *ca.* 91 : 9 mixture of the desired 3-*O*-benzyl-6-deoxy-5-*C*-ethyl-1,2-*O*-isopropylidene-α-D-glucofuranose (**6**) and its 5-epimer **6'**. Further purification of the product by recrystallization gave no isomerically pure major isomer **6**. For the PMR analysis a pure sample of **6** was isolated

from the product by silica gel column chromatography in a poor yield. A pure sample of the minor isomer **6'** was obtained by column chromatography of a product containing mainly **6'** (91%) prepared by the Grignard reaction of 3-*O*-benzyl-6,7-dideoxy-1,2-*O*-isopropylidene-α-D-*xylo*-heptofuranos-5-ulos (**5'**)[10] and methylmagnesium iodide. The PMR spectra of **6** and **6'** showed a characteristic singlet at δ 1.15 and 1.26 ascribed to the methyl protons of each isomer, respectively. The assignment of the (5*S*)-configuration for **6** was rationalized on the basis of the results of asymmetric Grignard reactions of free carbonyl sugar derivatives reported by Wolfrom and Hanessian,[11] Inch,[12] and Inch *et al.*[13] The assumed configuration was verified by PMR study of the acetonide **15** derived from **6** (see below). Hydrolysis of **6** (the aforesaid isomeric mixture) in a boiling 50% aqueous acetic acid afforded free sugar in 92% yield, to which the furanose structure **7** was given, because it could be smoothly converted into the subsequent product **8**. Periodate oxidation of **7** gave 2-*O*-benzyl-5-deoxy-4-*C*-ethyl-3-*O*-formyl-D-arabinofuranose (**8**) in 87.6% yield after treatment by silica gel chromatography. The PMR spectrum of **8** showed signals in line with the furanose structure. Lithium aluminium hydride reduction of **8** in THF afforded 2-*O*-benzyl-5-deoxy-4-*C*-ethyl-D-arabinitol (**9**) as colorless prisms in 98.3% yield. This sample appeared to be isomerically homogeneous as judged from its PMR spectrum. Selective benzoylation of **9** with benzoyl chloride in pyridine gave the 1-*O*-benzoate **10** in 86.3% yield after being subjected to silica gel chromatography. Treatment of **10** with 2,2-dimethoxypropane containing a small amount of *p*-toluenesulfonic acid yielded 3,4-acetonide **11** in 96.6% yield. Debenzoylation of **11** with sodium methoxide afforded 2-*O*-benzyl-5-deoxy-4-*C*-ethyl-3,4-*O*-isopropylidene-D-arabinitol (**12**) in 81.7% yield after being subjected to chromatography. Hydrogenolysis of **12** followed by periodate oxidation of the resulting diol **13** gave the crude aldehyde **14** in 71.9% yield. The aldehyde was then oxidized with potassium hypoiodite[14] to afford the crystalline acetonide **15** in 79.2% yield (24.6% overall yield from **5**). The sample of **15** was shown to be isomerically homogeneous by its PMR spectrum.

Hill and Yan[7] reported on the acetonide **16** corresponding to (2*R*,3*R*)-(—)-2,3-dihydroxy-3-methylpentanoic acid (**3'**).[5,7] A comparison of the PMR data of **15** with those of **16** shows significant differences between the chemical shifts of the corresponding 5-methyl and 5-ethyl protons on the 1,3-dioxolane ring of each acetonide (see Table). Thus acetonide **15** was proved to be the (5*S*)-epimer of **16**, the (5*S*)-configuration of **6** being verified.

Treatment of **15** with 50% trifluoroacetic acid yielded the title compound **3** as a syrup in quantitative yield. The PMR spectrum showed signals in line with the structure. The hydroxy acid **3** exhibited a weak positive CD Cotton effect at 235 nm in addition to the strong negative Cotton effect at 205 nm in water. The result is also consistent with the (2*R*)-configuration of **3**.[5,15]

Experimental

Melting points were determined on a micro hot-stage and are uncorrected. PMR spectra were taken on a Varian A-60D spectrometer using TMS and DSS as internal standards. Specific rotations were determined with a Zeiss Photoelectric Polarimeter. TLC and column chromatography were performed in Wakogel B-5 and C-200, respectively. Concentration was carried out under reduced pressure below 40 °C.

3-O-Benzyl-6-deoxy-5-C-ethyl-1,2-O-isopropylidene-α-D-glucofuranose (6). The starting material, 3-*O*-benzyl-6-deoxy-1,2-*O*-isopropylidene-α-D-*xylo*-hexofuranos-5-ulose (**5**)[9,10] was prepared in 91% yield by Jones oxidation[10] of 3-*O*-benzyl 6-deoxy-1,2-*O*-isopropylidene-α-D-glucofuranose[9,10,12] which was derived *via* 5,6-anhydro-3-*O*-benzyl-1,2-*O*-isopropylidene-α-D-glucofuranose[16] from 3-*O*-benzyl-1,2:5,6-di-*O*-isopropylidene-α-D-glucofuranose[17] in 83% overall yield. A solution of **5** (30 g, 0.1026 mol) in dry ether (900 ml) was added dropwise under stirring to an ether solution of ethylmagnesium bromide prepared from magnesium turnings (20.0 g, 0.8235 mol) and ethyl bromide (61.8 ml, 0.8227 mol) in dry ether (900 ml). The mixture which was stirred at room temperature for 3 h was treated with a cold saturated aqueous NH_4Cl solution (800 ml) under cooling. The aqueous layer was extracted with ether, and the combined ether layer were washed with saturated aqueous NaCl solution, dried and evaporated to afford a pale yellow crystalline solid (32.7 g, mp 51—60 °C). The solid was recrystallized from pentane to give needles of the condensation product (26.8 g, 80.1%, mp 64—64.5 °C) which was shown by PMR analysis to be a 91:9 mixture of the title compound **6** and its 5-epimer **6'**. The product (1 g) was recrystallized from pentane to afford colorless needles (0.79 g); mp 64—65 °C, $[\alpha]_D^{20}$ −68° (*c* 2.06, $CHCl_3$). The PMR spectrum showed no appreciable change in the proportion of **6** to **6'**. The product (1.00 g) was chromatographed on silica gel (180 g) with benzene–ethyl acetate (6:1). By PMR inspection, the effluent containing the pure isomer **6** was collected in the fore-run, giving a pure sample (82 mg, 8.2%) of **6**: colorless needles, mp 64.3—65 °C; $[\alpha]_D^{20}$ −72° (*c* 0.6, $CHCl_3$); δ ($CDCl_3$) 0.92 (t, 3H, 5-$CH_2\underline{CH_3}$, J=7 Hz, 1.15 (s, 3H, H-6), 1.34 and 1.50 [each s, 3H, C-$(CH_3)_2$], 1.72 (m, 2H, 5-$C\underline{H_2}CH_3$), 3.71 (s, 1H, OH), 4.01

Table 1. Comparison of 60 MHz PMR data (δ, $CDCl_3$) of **15** with the published PMR data (60 MHz, δ, $CDCl_3$)[7] of (4*R*,5*R*)-5-ethyl-2,2,5-trimethyl-1,3-dioxolane-4-carboxylic acid (**16**)

Substance	5-$CH_2\underline{CH_3}$ (t, 3H)	5-CH_3 (s,3H)	CH_3–C–CH_3 (each s, 3H)		5-$C\underline{H_2}CH_3$ (m,2H)	H-4 (s, 1H)	COOH (s, 1H)
15	1.02 (J=7 Hz)	1.23	1.41	1.57	1.80	4.42	9.18
16	0.94 (J=6 Hz)	1.44	1.41	1.52	1.68	4 41	9.91

and 4.18 (each d, H-3, H-4, $J_{3,4}=3$ Hz),** 4.69 (d, 1H, H-2, $J_{1,2}=4$ Hz), 4.57 and 4.78 (each d, each 1H, O-C$\underline{H}_2$Ph, $J_{gem}=12$ Hz),** 6.11 (d, 1H, H-1), and 7.44 (s, Ph).

Found: C, 67.05; H, 8.20%. Calcd for $C_{18}H_{26}O_5$: C, 67.06; H, 8.13%.

3-O-Benzyl-6-deoxy-5-C-ethyl-1,2-O-isopropylidene-α-D-idofuranose (6′). 3-*O*-Benzyl-6,7-dideoxy-1,2-*O*-isopropylidene-α-D-*xylo*-heptofuranos-5-ulose (**5′**)[10] (475 mg) was allowed to react with an eight-fold excess of methylmagnesium iodide in ether (29 ml) at room temperature for 3 h. Work-up as in the preparation of **6** followed by purification of the crude product through a silica gel column (27 g) with benzene–ethyl acetate (6: 1) afforded a syrup of the condensation product (471 mg, 94.1%) which was shown by PMR analysis to be a 91: 9 mixture of **6′** and **6**. The sample (422 mg) was again chromatographed on silica gel (76 g) with the same solvent system to give a pure sample (90 mg, 21.4%) of **6′** as colorless syrup: $[\alpha]_D^{19}$ −58° (*c* 1.0, $CHCl_3$); δ ($CDCl_3$) 0.92 (t, 3H, 5-$CH_2C\underline{H}_3$, $J=7$ Hz), 1.26 (s, 3H, H-6), 1.33 and 1.49 [each s, 3H, $C(CH_3)_3$], *ca.* 1.5 (m, 2H, 5-C$\underline{H}_2CH_3$), 3.40 (s, 1H, OH), 4.00 and 4.18 (each d, H-3, H-4, $J_{3,4}=3$ Hz),** 6.69 (d, 1H, H-2, $J_{1,2}=4$ Hz), 4.57 and 4.78 (each d,OC$\underline{H}_2$Ph, $J_{gem}=11.5$ Hz),** 6.11 (d, 1H, H-1), and 7.44 (s, 5H, Ph).

Found: C, 66.76; H, 8.13%. Calcd for $C_{18}H_{26}O_5$: C, 67.06; H, 7.91%.

2-O-Benzyl-5-deoxy-4-C-ethyl-D-arabinitol (9). Treatment of the Grignard reaction product (10.0 g) containing *ca.* 91% of **6** with 50% aqueous acetic acid (60 ml) at 115 °C for 6 h, followed by evaporation afforded a brown syrup, which was dissolved in ethyl acetate (200 ml). The solution was washed successively with saturated $NaHCO_3$ and saturated NaCl solutions, dried and evaporated. The residual pale brown syrup (10.5 g) was chromatographed on silica gel (300 g) with benzene–ethyl acetate (1: 1) to give 3-*O*-benzyl-6-deoxy-5-*C*-ethyl-D-glucofuranose (**7**) (8.06 g, 92%). A sample of the free sugar **7** (7.96 g) was dissolved in acetone (240 ml) and treated with a solution of sodium metaperiodate (12.06 g) in water (120 ml) at room temperature for 3 h. A solution of the periodate (6.03 g) in water (60 ml) was added to the reaction mixture, which was stirred at room temperature overnight and filtered. Acetone was removed from the filtrate by evaporation and the aqueous residue was extracted with ethyl acetate. The extract was washed with saturated NaCl solution, dried and evaporated. The residual syrup (7.64 g) was chromatographed on silica gel (300 g) with benzene–ethyl acetate (6: 1) to afford a colorless syrup of 2-*O*-benzyl-5-deoxy-4-*C*-ethyl-3-*O*-formyl-D-arabinofuranose (**8**) as an anomeric mixture, yield 6.92 g (87.6%); δ ($CDCl_3$) 0.96 (dt, 3H, 4-$CH_2C\underline{H}_3$), 1.36 and 1.45 (each s, 3H, H-5), 1.76 (m, 2H, 4-C$\underline{H}_2CH_3$), 3.8—4.2 (br, 2H, H-2 and OH), 4.78 (d, 2H, OC$\underline{H}_2$Ph), 5.3—5.6 (m, 2H, H-1 and H-3), 7.48 (s, 5H, Ph), and 8.25 (s, 1H, OC$\underline{H}$O). A sample of **8** (5.56 g, 19.84 mmol) was dissolved in dry THF (209 ml) and cooled in an ice-bath. Powdered $LiAlH_4$ (1.50 g, 39.67 mmol) was added slowly to the stirred solution and then refluxed for 6 h. Ethyl acetate (150 ml) and water (5 ml) were added to the cooled reaction mixture and stirred at room temperature overnight. The mixture was filtered and the filter cake was washed with ethyl acetate. The filtrate and washings were combined and washed with saturated NaCl solution, dried and evaporated to give **9** as colorless needles (4.96 g, 98.3%). Recrystallization from ether–petroleum ether afforded an analytical sample: prisms, mp 58—59 °C; $[\alpha]_D^{23}$ −60° (*c* 1.00, $CHCl_3$); δ ($CDCl_3$) 0.96 (t, 3H, 4-$CH_2C\underline{H}_3$), 1.13 (s, 3H, 5-H), 1.56 (q, 2H, 4-C$\underline{H}_2$-CH_3), 2.86 (s, 3H, OH), 3.51 (d, 1H, H-3, $J_{2,3}=2$ Hz), 3.6—4.2 (m, 3H, H-1,1′ and H-2), 4.48 and 4.75 (each d, 2H, OC$\underline{H}_2$Ph, $J_{gem}=11$ Hz),** and 7.30 (s, 5H, Ph).

Found: C, 66.25; H, 8.63%. Calcd for $C_{14}H_{22}O_4$: C, 66.11; H, 8.72%.

1-O-Benzoyl-2-O-benzyl-5-deoxy-4-C-ethyl-D-arabinitol (10). Benzoyl chloride (6.17 ml, 53.0 mmol) was added to a solution of **9** (12.26 g, 48.19 mmol) in dry pyridine (245 ml) cooled at −10 °C. The mixture was allowed to stand at 4 °C for 24 h and then poured into cold water (200 ml) and extracted with chloroform (300 ml × 3). The concentrated extract was diluted with chloroform (300 ml); this was washed with 50% aqueous $KHSO_4$ solution, saturated $NaHCO_3$ and saturated NaCl solutions successively, dried and evaporated to yield a syrup (18.73 g), which was chromatographed on silica gel (360 g) with benzene–ethyl acetate (6: 1) to afford a colorless syrup of **10** (14.9 g, 86.3%): $[\alpha]_D^{20}$ −19° (*c* 1.04, $CHCl_3$); IR $(CCl_4)_{max}$ 3500 (OH) and 1710 cm^{-1} (ester); δ ($CDCl_3$) 0.92 (t, 3H, 4-$CH_2C\underline{H}_3$, $J=7$ Hz), 1.16 (s, 3H, H-5), 1.66 (m, 2H, 4-C$\underline{H}_2$-CH_3), 3.30 (s, 2H, OH), 3.62 (d, 1H, H-3, $J_{2,3}=2$ Hz), 4.22 (dt, 1H, H-2, $J_{1,2}=5.5$ Hz), 4.79 (d, 2H, H-1), 4.74 and 5.00 (each d, 2H, OC$\underline{H}_2$Ph),** 7.48 (s, 5H, $OCH_2\underline{Ph}$), 7.60 (m, 3H, benzoyl), and 8.26 (m, 2H, benzoyl).

Found: C, 70.49; H, 7.20%. Calcd for $C_{21}H_{26}O_5$: C, 70.37; H, 7.31%.

1-O-Benzoyl-2-O-benzyl-5-deoxy-4-C-ethyl-3,4-O-isopropylidene-D-arabinitol (11). A solution of **10** (14.90 g, 41.57 mmol) and *p*-toluenesulfonic acid (515 mg) in 2,2-dimethoxypropane (204 ml) was kept at room temperature for 2 h and then diluted with ether (500 ml). The mixture was washed with saturated $NaHCO_3$ and saturated NaCl solutions, dried and evaporated to afford the crude acetonide **11** (16.00 g, 96.6%). Analytical sample of **11** was obtained by chromatograpy of the crude **11** through a silica gel column with benzene–ethyl acetate (12: 1): $[\alpha]_D^{21}$ +29° (*c* 1.03, $CHCl_3$); IR $(CCl_4)_{max}$ 1710 cm^{-1} (ester); δ ($CDCl_3$) 0.98 (t, 3H, 4-$CH_2C\underline{H}_3$, $J=7$ Hz), 1.24 (s, 3H, H-5), 1.40 and 1.51 [each s, 3H, $C(CH_3)_3$], 1.66 (m, 2H, 4-C$\underline{H}_2$-CH_3), 3.8—4.8 (m, 4H, H-3, H-2, and H-1), 4.91 (s, 2H, OC$\underline{H}_2$Ph), 7.46 (d, 5H, OCH_2Ph), 7.64 (m, 3H, benzoyl), and 8.22 (m, 2H, benzoyl).

Found: C, 72.10; H, 7.61%. Calcd for $C_{24}H_{30}O_5$: C, 72.33; H, 7.59%.

2-O-Benzyl-5-deoxy-4-C-ethyl-3,4-O-isopropylidene-D-arabinitol (12). The crude acetonide **11** (16.00 g) was dissolved in dry methanol (320 ml). A solution of 2.5 M sodium methoxide in methanol was added under ice-cooling and kept at room temperature for 1 h. The resulting mixture was poured into ice–water (230 ml) and extracted with chloroform (200 ml × 3). The extract was washed with saturated NaCl solution, dried and evaporated. The residual syrup (16.38 g) was chromatographed on silica gel (500 g) with benzene–ethyl acetate (6: 1) to afford a colorless syrup of **12** (9.66 g, 81.7%): $[\alpha]_D^{22}$ +35° (*c* 1.14, $CHCl_3$); δ ($CDCl_3$) 1.00 (t, 3H, 4-CH_2-$C\underline{H}_3$, $J=7$ Hz), 1.26 (s, 3H, 5-H), 1.38 and 1.51 [each s, 3H, $C(CH_3)_2$], 1.60 (m, 2H, 4-C$\underline{H}_2CH_3$), 3.4—4.2 (m, 4H, H-3, H-2, and H-1), 4.77 and 5.10 (each d, 2H, OC$\underline{H}_2$Ph, $J_{gem}=12$ Hz),** and 7.50 (s, 5H, Ph).

Found: C, 69.09; H, 8.74%. Calcd for $C_{17}H_{26}O_4$: C, 69.36; H, 8.90%.

(4R,5S)-(+)-5-Ethyl-2,2,5-trimehyl-1,3-dioxolane-4-carboxylic Acid (15). A solution of **12** (2.30 g) in methanol (70 ml) was stirred with palladium black for 1 h under bubbling with hydrogen gas. The filtered solution was evaporated to a colorless syrup of 5-deoxy-4-*C*-ethyl-3,4-*O*-isopropylidene-D-arabinitol (**13**) (1.60 g, 100%) which appeared to be homogeneous on TLC with benzene–ethyl acetate (1: 1). A sample of **13** (6.70 g, 32.8 mmol) was dissolved in acetone (200 ml)

** The chemical shifts for the protons of system AB were calculated.

and treated with a solution of sodium metaperiodate (14.04 g, 65.6 mmol) in water (140 ml). After being stirred in a dark place at room temperature for 1 h, the reaction mixture was filtered and the acetone was removed by concentration of the filtrate. The resulting aqueous residue was extracted with chloroform (100 ml×2). The extracts were washed with saturated NaCl solution, dried and evaporated to give (4*R*, 5*S*)-5-ethyl-2,2,5-trimethyl-1,3-dioxolane-4-carbaldehyde (**14**) (4.07 g, 71.9%) as a colorless liquid; δ($CDCl_3$) 1.02 (t, 3H, 5-$CH_2C\underline{H}_3$, J=7 Hz), 1.20 (s, 3H, 5-CH_3), 1.42 and 1.58 [each s, 3H, $C(CH_3)_2$], 1.74 (m, 2H, 5-$C\underline{H}_2CH_3$), 4.22 (d, 1H, H-4, $J_{5,CHO}$=2 Hz), and 9.98 (d, 1H, CHO). The aldehyde **14** (4.06 g, 23.6 mmol) was dissolved in dioxane (100 ml). The solution was diluted with water (37 ml), and a solution of K_2CO_3 (20.55 g, 148.7 mmol) and $KHCO_3$ (14.89 g, 148.7 mmol) in water (160 ml) was added. A solution of iodine (17.62 g, 69.4 mmol) and KI (23.04 g, 138.8 mmol) in water (20 ml) was added, and the mixture was stirred at room temperature for 2 h. The cooled mixture was reduced by the addition of solid sodium thiosulfate. The resulting colorless solution was washed with ether to remove the unchanged aldehyde and impurities. The aqueous solution was made acid (pH 2—3) with 10% sulfuric acid under ice-cooling, and immediately extracted with chloroform (100 ml×3). The extracts were washed with saturated NaCl solution, dried and evaporated to yield colorless crystals of **15** (3.52 g, 79.2%), whose PMR spectrum showed no signals indicating the presence of the (4*R*)-epimer **16**. The crude crystals (20 mg) were subjected to sublimation at 49 °C (bath temp) under reduced pressure (1 Torr) to afford a pure sample (18.8 mg) as hygroscopic colorless needles: mp 46.5—49 °C (subl); $[\alpha]_D^{20}$ +26° (*c* 0.84, $CHCl_3$).

Found: C, 57.58; H, 8.44%. Calcd for $C_9H_{16}O_4$: C, 57.43; H, 8.57%.

(2R3,S)-(−)-2,3-Dihydroxy-3-methylpentanoic Acid (3). A sample of **15** (200 mg) was dissolved in 50% aqueous trifluoroacetic acid (2 ml). After being kept at room temperature for 4 h, the solution was evaporated to afford **3** as a pale yellow syrup. The crude acid (217 mg) was purified by silica gel chromatography with chloroform–methanol–acetic acid (80: 10: 1) and the resulting colorless syrup was again chromatographed with chloroform–ethyl acetate (1: 1) to give a pure sample of **3** (155 mg, 98.2%): $[\alpha]_D$ −28°, $[\alpha]_{436}$ −63°, $[\alpha]_{365}$ −106° (*c* 1.48, $CHCl_3$, at 20°); $[\alpha]_D$ −16°, $[\alpha]_{436}$ −34°, $[\alpha]_{365}$ −55° (*c* 1.32, H_2O, at 20°); CD, $[\theta]_{235}$ +290 and $[\theta]_{205}$ −5460 (*c* 0.115, H_2O); δ (D_2O, DSS) 0.90 (t, 3H, H-5, J=7 Hz), 1.21 (s, 3H, 3-CH_3), *ca.* 1.6 (m, 2H, H-4), 4.10 (s, 1H, H-2), and 4.62 (s, DOH); δ ($CDCl_3$) 0.94 (t, 3H, H-5, J=7 Hz), 1.27 (s, 3H, 3-CH_3), *ca.* 1.6 (m, 2H, H-4), 4.07 (s, 1H, H-2), and 5.82 (s, 3H, CO_2H, OH).

Found: C, 48.47; H, 8.35%. Calcd for $C_6H_{12}O_4$: C, 48.64; H, 8.16%.

We thank Mr. Saburo Nakada for carrying out the microanalyses and Dr. Shimpei Aburaki for the CD spectral measurement.

References

1) Part II: M. Kinoshita and M. Awamura, *Bull. Chem. Soc. Jpn.*, **51**, 869 (1978).
2) G. Koyama, Y. Iitaka, K. Maeda, and H. Umezawa, *Tetrahedron Lett.*, **1967**, 3587.
3) An analogous example has been reported: A. Rosenthal and K. Shudo, *J. Org. Chem.*, **37**, 4391 (1972).
4) R. K. Hill and P. J. Foley, Jr., *Biochem. Biophys. Res. Commun.*, **33**, 480 (1968).
5) D. H. Crout and D. Whitehouse, *J. Chem. Soc., Chem. Commun.*, **1972**, 398.
6) J. Sjolander, K. Folkers, E. A. Adelberg, and E. Tatum, *J. Am. Chem. Soc.*, **76**, 1085 (1954).
7) R. K. Hill and S. Yan, *Bioorg. Chem.*, **1**, 446 (1971).
8) F. B. Armstrong, *J. Chem. Soc., Chem. Commun.*, **1974**, 351.
9) M. C. Wolfrom and S. Hanessian, *J. Org. Chem.*, **27**, 2107 (1962).
10) D. E. Kiely, H. Walls, and R. L. Black, *Carbohydr. Res.*, **31**, 387 (1973).
11) M. C. Wolfrom and S. Hanessian, *J. Org. Chem.*, **27**, 1800 (1962).
12) T. D. Inch, *Carbohydr. Res.*, **5**, 45 (1967).
13) T. D. Inch, R. V. Ley, and P. Rich., *J. Chem. Soc., C*, **1968**, 1683.
14) E. Zissis, R. K. Ness, and H. G. Fletcher, Jr., *Carbohydr. Res.*, **20**, 9 (1971).
15) I. P. Dirkx and F. J. L. Sixma, *Rec. Trav. Chim.*, **83**, 522 (1964); J. C. Craig and S. K. Roy, *Tetrahedron*, **21**, 1847 (1965); W. Bachelor and G. A. Mina, *Can. J. Chem.*, **47**, 4089 (1969); G. Barth, W. Voelter, E. Bunnenberg, and C. Djerassi, *Chem. Commun.*, **1969**, 355.
16) A. S. Meyer and T. Reichstein, *Helv. Chim. Acta*, **29**, 152 (1946).
17) R. E. Gramera, R. M. Bruce, S. Hirose, and R. L. Whistler, *J. Org. Chem.*, **28**, 140 (1963).

Thermal Curtius Rearrangement of *N*-Acyl-*S*,*S*-diphenylsulfilimine

Naomichi FURUKAWA,* Mitsuo FUKUMURA, Takehiko NISHIO, and Shigeru OAE
Department of Chemistry, University of Tsukuba, Sakura-mura, Niihari-gun, Ibaraki 300-31
(Received May 13, 1978)

Several *N*-acyl-*S*,*S*-arylphenylsulfilimines were prepared and subjected to thermal decomposition. They decomposed readily at 130—190 °C to give isocyanates together with diphenyl sulfide, quantitatively. However, *N*-tosyl-*S*,*S*-diphenylsulfilimine did not decompose even upon heating at 200 °C for 24 h. A kinetic study revealed that the rates of pyrolysis of *N*-aroyl-*S*,*S*-arylphenylsulfilimines (*p*-Y-C_6H_4(Ph)S→$NCOC_6H_4$-X-*p*) are nicely correlated with the Hammett σ-values, $\rho_X=-1.2$ and $\rho_Y=+0.92$, respectively, being obtained. The activation enthalpies and entropies were $\Delta H^{\neq}=38.7$ kcal/mol and $\Delta S^{\neq}=6.0$ e.u. for Ph_2S→NCOPh and $\Delta H^{\neq}=32.3$ kcal/mol and $\Delta S^{\neq}=5.5$ e.u. for Ph_2S→NCO- 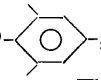 -, respectively. The rearrangement was accelerated considerably by *o*-methyl substituent in the aryl group. The effect of solvent on the rate of pyrolysis was small. The results indicate that the pyrolysis of sulfilimine proceeds *via* a concerted migration of the R group from carbonyl carbon to imino nitrogen similar to the Curtius type rearrangement of acid azide.

N-Tosylsulfilimines each having at least one β-hydrogen atom undergo facile intramolecular elimination (Ei) to afford olefin stereoselectively in high yields.[1] Meanwhile, *N*-tosylsulfilimines having no β-hydrogen atom, such as *N*-tosyl-*S*,*S*-dimethyl and *N*-tosyl-*S*,*S*-methylphenylsulfilimines are stable under the usual Ei conditions (benzene reflux) but decompose upon heating in DMSO or DMF at *ca.* 200 °C to afford interesting products as shown below.[2] In contrast, *N*-tosyl-*S*,*S*-diphenylsulfilimine is quite stable even upon heating at 200 °C and recovered almost quantitatively.[3]

Yoshida *et al.*[4] found that *N*-thiocarbonyl-*S*,*S*-diphenylsulfilimines undergo pyrolysis at 70 °C to afford the corresponding nitriles, diphenyl sulfide and sulfur. They proposed that the pyrolysis proceeds *via* the initial migration of the thione sulfur to the imino nitrogen to form incipiently the nitrile sulfide which decomposes rapidly to afford the nitrile and sulfur. Thermally stable *N*-acyl-*S*,*S*-diphenylsulfilimines were found to undergo facile photolysis, resulting in the photochemical Curtius rearrangement *via* an incipient formation of the corresponding nitrene.[5] Synthetic utilization of the thermolysis of sulfilimines has recently been shown by Gilchrist *et al.*[6] and Tamura *et al.*[7]

In the course of a preliminary study on the sulfilimines, we found that *N*-benzoyl-*S*,*S*-diphenylsulfilimine decomposes quite readily when heated at 200 °C *in situ* and also in such solvents as DMF, tetralin and even EtOH in a sealed tube.[3] The products obtained in high yields by the pyrolysis were found to be diphenyl sulfide, phenyl isocyanate and *N*,*N*′-diphenylurea. The facile thermal decomposition of *N*-benzoyl-*S*,*S*-diphenylsulfilimine prompted us to investigate the thermolysis of various *N*-acyl-*S*,*S*-diarylsulfilimines, all of which have been found to afford the corresponding isocyanates and diaryl sulfides almost quantitatively. Thus, we carried out a kinetic study on the pyrolysis of *N*-acyl-*S*,*S*-diarylsulfilimines and found that these rearrangements proceed through the Curtius type rearrangement as in the ordinary thermal Curtius rearrangement in the thermolysis of *N*-acyl azides.

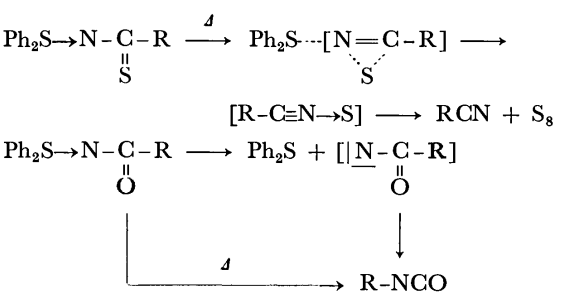

Scheme 2.

This paper describes detailed analysis of products, results of kinetic experiments on the Curtius type rearrangement of *N*-acyl-*S*,*S*-arylphenylsulfilimines and a plausible mechanism of the reaction in comparison with those of other reactions involving alkyl or aryl group migration from carbonyl group to electron deficient nitrogen or oxygen terminus.

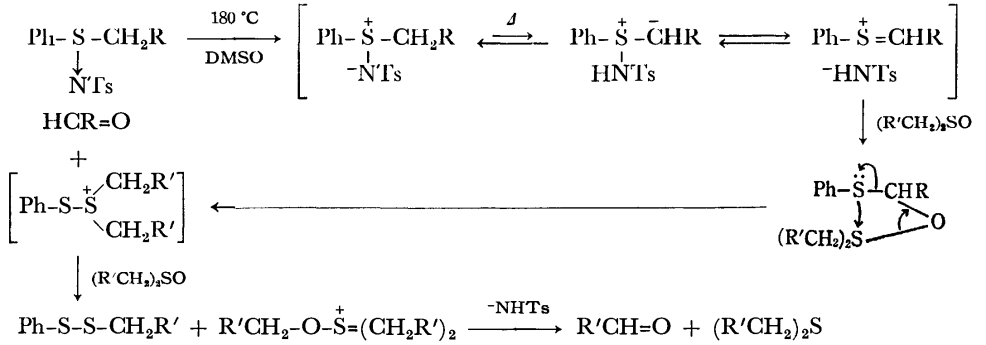

Scheme 1.

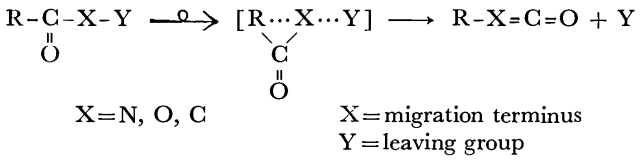

Scheme 3.

Results and Discussion

Preparation of N-*Acyl*-S,S-*diphenylsulfilimine.* *N*-Acyl-*S,S*-diphenylsulfilimines were prepared by acylating unsubstituted diphenylsulfilimine with appropriate acylating agents.[7] The yields and mp(°C) of sulfilimines thus prepared are summarized in Table 1 together with spectral data.

Pyrolyses of N-*Acyl*-S,S-*diphenylsulfilimines.* The pyrolysis of *N*-acyl-*S,S*-diphenylsulfilimines (Ia—f) was carried out by heating *in situ* or in such solvents as tetralin, DMF, toluene and EtOH. After the pyrolysis,

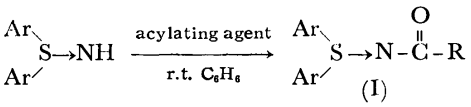

Scheme 4.

the products were separated by column chromatography or preparative GLC and identified by spectroscopic analysis by comparing their spectra with those of the authentic samples. The products thus obtained are summarized in Table 2. We see that the pyrolysis proceeds cleanly to afford the corresponding isocyanate-(II) and diphenyl sulfide nearly quantitatively except in the case of the *N*-benzoyl (R=Ph) derivative which gives a small amount of the isocyanate and a substantial portion of the dimerized product which is similarly obtained by photolysis; thus the total yield of phenyl isocyanate incipiently formed by the thermolysis of Ia is also quantitative.

Kinetic Studies. A kinetic study of the pyrolysis of

TABLE 1. YIELDS AND SPECTRAL DATA OF Ar, Ar′ S→NCOR (I)

	Sulfilimine (I) Ar	Ar′	R	Yield (%)	Mp (°C)	IR (cm^{-1})	NMR (δ, ppm, $CDCl_3$)	Elemental analysis (%)
a	Ph	Ph	-Ph	77.0	124—124.5	3050, 1595 1550, 1330 805	8.30—7.50 (m, 15H)	Found (Calcd for $C_{19}H_{15}NOS$) C H N 74.75 5.00 4.5 (74.7) (4.95) (4.6)
b	Ph	Ph	$-CH_2Ph$	59.8	120—121	3050, 1590 1570, 1445 1315, 1135	7.80—7.19 (m, 15H) 3.77 (s, 2H)	Found (Calcd for $C_{20}H_{17}NOS$) C H N 75.27 5.36 4.12 (75.21) (5.37) (4.39)
c	Ph	Ph	$-CHC_2H_5$ Ph	58.0	93.5—94.5	3050, 2950 1590, 1570 1475, 1440 1220	7.80—7.10 (m, 15H) 3.73 (t, 1H) 2.43—1.57 (m, 2H) 0.93 (t, 3H)	Found (Calcd for $C_{22}H_{21}NOS$) C H N 76.17 6.09 4.25 (76.04) (6.09) (4.03)
d	Ph	Ph		68.5	116—117	3050, 2900 1580, 1440 1275, 1250 1080	7.91—7.23 (m, 10H) 2.22—1.65 (m, 15H)	Found (Calcd for $C_{23}H_{25}NOS$) C H N 75.93 6.93 3.84 (75.99) (6.93) (3.85)
e	Ph	Ph	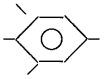	52.0	143—144	3050, 1610 1580, 1560 1480, 1445 1320, 1175 1100	7.92—7.67 (m, 4H) 7.57—7.33 (m, 6H) 6.77 (s, 2H) 2.33 (s, 6H) 2.22 (s, 3H)	Found (Calcd for $C_{22}H_{21}NOS$) C H N 76.00 5.00 3.99 (76.00) (6.09) (4.03)
f	Ph	Ph		62.9	96—97	3050, 1600 1580, 1560 1325, 1090	8.00—6.80 (m, 14H) 2.57 (s, 3H)	Found (Calcd for $C_{20}H_{17}NOS$) C H N 75.04 5.28 4.48 (75.20) (5.36) (4.38)
g	Ph	Ph	$-CH_3$[7]	95.0	87—88	3050, 1579 1560, 1475 1440, 1365 1310		Found (Calcd for $C_{14}H_{13}NOS$) C H N 69.1 5.40 5.70 (69.1) (5.40) (5.80)

	Sulfilimine (I)			Yield (%)	Mp (°C)	IR (cm^{-1})	NMR (δ, ppm, $CDCl_3$)	Elemental analysis (%)
	Ar	Ar′	R					
h	Ph	Ph	$-C_2H_5$	74.3	56—57	3040, 2960 1585, 1570 1360, 1235	7.72—7.17 (m, 10H) 2.50 (q, 2H) 1.22 (t, 3H)	Found (Calcd for $C_{15}H_{15}NOS$) C H N 69.83 5.80 5.56 (70.00) (5.87) (5.44)
i	Ph	Ph	$-CH(CH_3)_2$	81.5	60—61	3050, 2950 1580, 1570 1240	7.90—7.20 (m, 10H) 3.00—2.27 (m, 1H) 1.27 (d, 6H)	Found (Calcd for $C_{16}H_{17}NOS$) C H N 70.80 6.28 5.08 (70.81) (6.31) (5.16)
j	Ph	Ph	$-C(CH_3)_3$	70.5	64—65	3050, 2950 1580, 1560 1318, 1200	7.77—7.20 (m, 10H) 1.33 (s, 9H)	Found (Calcd for $C_{17}H_{19}NOS$) C H N 71.22 6.38 4.95 (71.54) (6.71) (4.90)
k	Ph	Ph	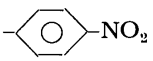	63.1	113—114	3050, 1560 1320	8.50—7.18 (m, 14H)	Found (Calcd for $C_{19}H_{14}N_2O_3S$) C H N 65.45 4.00 8.01 (65.12) (4.02) (7.99)
l	Ph	Ph	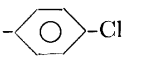	59.1	122—123	3040, 1585 1540, 1320 1300	8.07—7.13 (m, 14H)	Found (Calcd for $C_{19}H_{14}NOSCl$) C H N 67.15 4.04 4.12 (67.15) (4.15) (4.12)
m	Ph	Ph	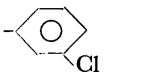	70.7	154—155.5	3050, 1590 1550, 1320 900, 745	8.20—7.13 (m, 14H)	Found (Calcd for $C_{19}H_{14}NOSCl$) C H N 67.45 3.99 4.14 (67.15) (4.15) (4.12)
n	Ph	Ph	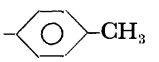	69.8	119—120	3050, 1590 1545, 1330	8.28—7.14 (m, 14H) 2.32 (s, 3H)	Found (Calcd for $C_{20}H_{17}NOS$) C H N 75.2 5.4 4.4 (74.6) (5.3) (4.3)
o	Ph	Ph	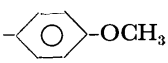	57.0	124.5—125.5	3050, 1600 1580, 1550 1320	8.23—6.73 (m, 14H) 3.77 (s, 3H)	Found (Calcd for $C_{20}H_{17}NO_2S$) C H N 71.89 5.13 4.24 (71.61) (5.10) (4.17)
p	Ph	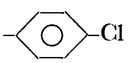	Ph	83.2	84—85	3050, 1595 1555, 1480 1330, 1295	8.28—7.17 (m, 14H)	Found (Calcd for $C_{19}H_{14}NOSCl$) C H N 66.99 3.90 4.20 (67.15) (4.15) (4.12)
q	Ph	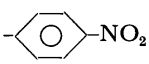	Ph	77.1	130—131	3050, 1595 1560, 1525 1350	8.30—7.13 (m, 14H)	Found (Calcd for $C_{19}H_{14}N_2O_3S$) C H N 65.40 3.90 7.96 (65.12) (4.02) (7.99)
r	Ph	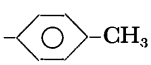	Ph	76.3	125.5—126.5	3050, 1590 1550, 1325 1295	8.40—7.07 (m, 14H) 2.35 (s, 3H)	Found (Calcd for $C_{20}H_{17}NOS$) C H N 75.32 5.33 4.45 (75.20) (5.36) (4.38)

TABLE 2. YIELD OF PRODUCTS IN THE THERMAL DECOMPOSITION OF I

$Ph_2S{\rightarrow}N{-}C{-}R$ (I, O) $\xrightarrow[190\,^\circ C]{\Delta}$ R–NCO (II) + Ph_2S

	R	Bp (mp) (°C)	Yield (%)		IR (cm^{-1})	NMR (δ, $CDCl_3$)
a	Ph	58—59/18 mmHg	34.7[a]	85.7	2270	7.6—6.9 (m, 5H)
b	CH_2Ph	118/200 mmHg	90.4	96.8	2270	7.37 (s, 5H) 4.50 (s, 2H)
c	CHC_2H_5 | Ph		98.8	98.0	2270	7.27 (s, 5H) 4.50 (t, 1H) 2.07—1.50 (m, 2H) 0.97 (t, 3H)
d	Adamantyl	135—136	97.6	98.0	2270	2.30—1.50 (m, 15H)
e	Mesityl	(45—46)	95.5	95.6	2270	6.77 (s, 2H) 2.23 (s, 9H)
f	CH_3	37—38	67.5	91.0	2270	3.03 (s, 3H)

a) Dimerized product of phenyl isocyanate was obtained.

TABLE 3. KINETIC DATA OF R′–S–(C6H4)–N(–CO–R) IN DMF

	Sulfilimine		$k \times s^{-1}$	Rel. rate
a	R=Ph	R′=Ph	$1.22\pm0.07\times10^{-4}$ [a]	1.0
b	R=CH_2Ph	R′=Ph	$1.25\pm0.12\times10^{-4}$ [b]	7.4
c	R=CHC_2H_5 | Ph	R′=Ph	$1.37\pm0.34\times10^{-3}$ [b]	81.6
d	R=Adamantyl	R′=Ph	$4.91\pm0.32\times10^{-4}$ [b]	29.2
e	R=–C6H4–	R′=Ph	$4.12\pm0.11\times10^{-4}$ [c]	2200
f	R=–C6H4–	R′=Ph	$1.17+0.09\times10^{-3}$ [b]	69.6
g	R=CH_3	R′=Ph	$4.87\pm0.13\times10^{-5}$ [d]	1.1
h	R=C_2H_5	R′=Ph	$2.39\pm0.05\times10^{-4}$ [d]	5.3
i	R=$CH(CH_3)_2$	R′=Ph	$9.46\pm0.05\times10^{-4}$ [d]	20.9
j	R=$C(CH_3)_3$	R′=Ph	$7.56\pm0.32\times10^{-4}$ [d]	16.7
k	R=–C6H4–NO_2	R′=Ph	$4.22\pm0.26\times10^{-5}$ [a]	0.35
l	R=–C6H4–Cl	R′=Ph	$6.10\pm0.31\times10^{-5}$ [a]	0.50
m	R=–C6H4–Cl (o)	R′=Ph	$4.31\pm0.17\times10^{-5}$ [a]	0.35
n	R=–C6H4–CH_3	R′=Ph	$1.94\pm0.09\times10^{-4}$ [a]	1.6
o	R=–C6H4–OCH_3	R′=Ph	$2.36\pm0.05\times10^{-4}$ [a]	1.9
p	R=Ph	R′=–C6H4–Cl	$2.06\pm0.18\times10^{-4}$ [a]	1.7
q	R=Ph	R′=–C6H4–NO_2	—	
r	R=Ph	R′=–C6H4–CH_3	$0.95\pm0.20\times10^{-4}$ [a]	0.78

a) At 190.8±0.06 °C. b) At 170.3±0.06 °C. c) At 129.2±0.06 °C. d) At 180.25±0.06 °C.

N-acyl-*S*,*S*-arylphenylsulfilimines (Ia—r) was carried out in DMF at around 130—190 °C. The rate of the pyrolysis followed the first order kinetic equation. The dependence of rate on concentration shows that the reaction is of the first order in sulfilimine. The rate constants of the pyrolysis of *N*-acyl-*S*,*S*-arylphenylsulfilimines are summarized in Table 3, together with the relative rates, assuming the rate of the *N*-benzoyl-*S*,*S*-diphenylsulfilimine at 190 °C as the standard. The rate constants can be correlated nicely with the Hammett σ-values, ρ-values of −1.20 (X-substituents) and +0.92 (Y-substituents) being obtained (except *p*-nitro group), (Fig. 1). Pyrolysis of the *p*-nitro derivatives also gave the corresponding isocyanates in low yields and some uncharacterized products. The effect of temperature on the rate is given in Table 4. The activation enthalpies and entropies of both sulfilimines (Ia, e) are calculated to be $\Delta H^{\neq}=38.7$ kcal/mol, $\Delta S^{\neq}=6.0$ e.u. ($E_a=39.5$

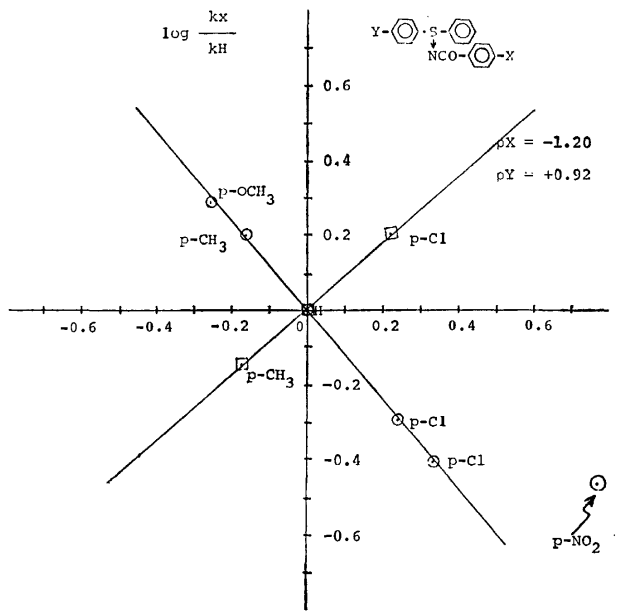

Fig. 1. Hammett plots of *p*- or *m*-substituted sulfilimine.

kcal/mol) for Ia, $\Delta H^{*}=32.3$ kcal/mol, $\Delta S^{*}=5.5$ e.u. ($E_a=33.0$ kcal/mol) for Ie. The effect of solvent on the rate of pyrolysis was examined with *N*-2,4,6-trimethylbenzoyl-*S*,*S*-diphenylsulfilimine in benzene, DMF and ethanol. The results are given in Table 4. The rate increases in a nonpolar aprotic solvent such as benzene but decreases in a polar protic solvent such as EtOH. However, difference in the rate is not large unlike the reaction in which the transition state is more polarized than the ground state.

In contrast to the thermal stability of *N*-tosyl-*S*,*S*-diphenylsulfilimine, *N*-acyl derivatives decompose readily giving the corresponding isocyanates in high yields as shown in Table 2. The facile thermolysis of *N*-acyl-*S*,*S*-diphenylsulfilimines reflects on their IR S–N stretching band which appears at *ca.* 800 cm^{-1} (*e.g.*, *N*-benzoyl-*S*,*S*-diphenylsulfilimine 805 cm^{-1}) and also on that of the carbonyl band of the *N*-acyl group which appears at 1500—1600 cm^{-1} (*e.g.*, *N*-benzoyl-*S*,*S*-diphenylsulfilimine 1595—1535 cm^{-1}). The IR absorptions are in sharp contrast to those of the *N*-tosyl derivatives in which the S–N stretching band appears at 930—970 cm^{-1} (*e.g.*, *N*-tosyl-*S*,*S*-diphenyl, 960 cm^{-1}). A comparison of the S–N bond of the *N*-benzoyl with that of the *N*-tosyl group indicates that the S–N bond of the former can be cleaved more readily. The low frequency shift of the absorption due to the carbonyl group of the *N*-acyl derivatives as compared to the corresponding amide group suggests that the carbonyl bond in the *N*-acylsulfilimines is markedly stretched and the contribution of structure B is greater than that of structure A in the resonance hybrid.

$$Ph_2\overset{+}{S}-\overset{-}{N}-\underset{\underset{O}{\|}}{C}-R \longleftrightarrow Ph_2\overset{+}{S}-N=\underset{\underset{O^-}{|}}{C}-R$$

(A) (B)

X-Ray crystallographic analysis of the *N*-acylsulfilimine indicates structure B to be more favored than structure A (*N*-dichloroacetylsulfilimine)[8] while the S–N–C–O atoms in the molecule are arranged nearly in a coplanar geometry, Ph_2S group and the R group being at the anti arrangement. This molecular

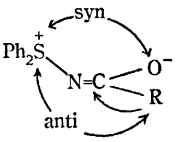

geometry suggests that in *N*-acylsulfilimine, the R group can readily migrate to the imino nitrogen from the back of the leaving group, *i.e.*, diphenyl sulfide, in keeping with the stereochemistry of the Curtius,[9] the Hoffman[10,11] the Lossen,[12] and the Schmidt[13] rearrangements.

The rearrangement of the *N*-acyl-*S*,*S*-arylphenylsulfilimines proceeds *via* simultaneous migration of the R group and cleavage of the S–N bond, since the effect of substituents on the phenyl ring of the migrating group shows a negative ρ-value ($\rho=-1.2$) against Hammett σ-values, while that of the leaving group shows a positive ρ-value ($\rho=+0.92$). The Hammett ρ-values

Table 4. Effect of temperature and solvent on pyrolysis of Ph_2S NCOR (I)

	Sulfilimine (I)	Temp (°C)	$k\times s^{-1}$	γ	ΔH^{*}(kcal/mol)	ΔS^{*}(e.u.)
a	R=⟨⟩ (DMF)	170.3	$1.68\pm0.09\times10^{-5}$	0.999	38.7	6.0
		180.25	$4.52\pm0.14\times10^{-5}$		(E_a=39.5 kcal/mol)	
		190.8	$1.22\pm0.07\times10^{-4}$			
e	R=⟨⟩- (DMF)	110.3	$5.32\pm0.48\times10^{-5}$	0.994	32.3	5.5
		120.25	$1.32\pm0.05\times10^{-5}$		(E_a=33.0 kcal/mol)	
		129.2	$4.12\pm0.11\times10^{-4}$			
e	R=⟨⟩- (C_6H_6)	102.9	$7.40\pm0.30\times10^{-5}$			
		110.55	$2.01\pm0.15\times10^{-4}$		(E_a=32.9 kcal/mol)	
		121.2	$5.71\pm0.06\times10^{-4}$	0.999	32.1	7.6
e	R=⟨⟩- (EtOH)	121.2	$1.44\pm0.09\times10^{-4}$			
		129.2	$3.31\pm0.30\times10^{-4}$		(E_a=29.72 kcal/mol)	
		139.8	$7.96\pm0.08\times10^{-4}$	0.998	28.9	−3.3

strongly suggest the concerted nature of C–N bond formation and S–N bond breaking in the transition state.

In the [1,2]-shift of the aryl group from carbon to an electron deficient hetero atoms such as nitrogen and oxygen, the Hammett plot with σ^+-values sometimes gives a better correlation than with σ-values.[10,14] However, in the pyrolysis of *N*-acyl-*S,S*-arylphenylsulfilimines the Hammett plot can be correlated better with σ-values than σ^+-values except in the NO_2 derivatives. This suggests that the charge separation in the transition state is rather small. This seems to be supported by the fact that the rate of reaction does not increase markedly in polar solvent; the rate of Ie varies from 3.2 in benzene to 1.0 in DMF and to 0.80 in EtOH.

In the pyrolysis of *N*-acyl-*S,S*-arylphenylsulfilimines, the migratory aptitude of the alkyl group lies in the order, *tert*$\simeq$*sec*>*prim*>Me. As compared to this the phenyl group does not accelerate the rate of rearrangement. This effect on the migratory aptitude is in contrast to other similar rearrangements such as Schmidt,[13] Lossen[12] or Bayer-Villiger[16] reactions. As seen from the data in Table 1, the ortho methyl group accelerates the rate of rearrangement enormously; one *o*-methyl group accelerates 70 times and two *o*-methyl groups increase the rate 2200 times. This is probably due to the steric inhibition of resonance between the phenyl group and N–C or carbonyl group, which prevents the planar conformation of the –NCOR group.[8,17,18] In the *N*-benzoylsulfilimine, the acylamide group would be in the same plane as the phenyl ring, a strong conjugation between the phenyl group and C=O and N=C group retarding the cleavage of the C–Ar bond. Two ortho methyl groups in *N*-2,4,6-trimethylbenzoyl derivative would prevent the conjugation between the phenyl ring and the N–CO– group, facilitating migration of the 2,4,6-trimethylbenzoyl group to the nitrogen atom. The same effect of *o*-substituent was observed in other Curtius type rearrangements.[9]

The activation parameters in the rearrangements are of interest. Despite the large rate difference in the pyrolysis of benzoyl and 2,4,6-trimethylbenzoyl derivatives, the values of activation entropies are similar. Thus, the large rate difference is due solely to that of the enthalpy values. The activation parameters in DMF and benzene are also similar. Similar values of both enthalpies and entropies of activation suggest that the transition states of the rearrangements in both solvents are nearly identical.

All these observations indicate that pyrolysis of the *N*-acyl-*S,S*-diphenylsulfilimine proceeds *via* a similar mechanistic path to that of the Curtius rearrangement

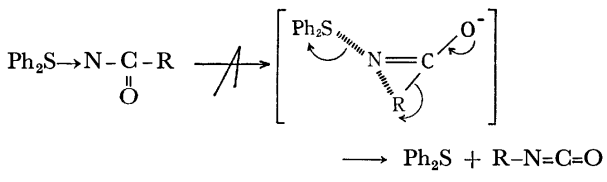

Scheme 5.

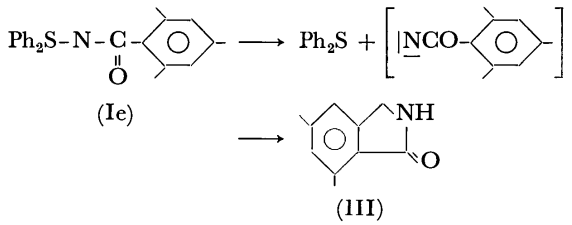

Scheme 6.

of acid azides involving the rate determining migration of alkyl or aryl group and the concomitant departure of the diaryl sulfide group eventually affording diphenyl sulfide and the isocyanate as shown below.

A similar rearrangement was observed in the photolysis of *N*-acylsulfilimine. The photolysis of *N*-2,4,6-trimethylbenzoyl-*S,S*-diphenylsulfilimine affords not only the rearrangement product but also a C–H insertion product which arises *via* the initial formation of a singlet nitrene as shown above. Singlet multiplicity of the nitrene thus generated has also been confirmed by other trapping experiments with an olefin. In the pyrolysis of the sulfilimine, the possibility of the formation of nitrene as intermediate should also be considered. However, no aziridine derivative was detected when pyrolysis of the *N*-benzoyl-*S,S*-diphenylsulfilimine in the presence of a large excess of diphenylacetylene was carried out. Furthermore, pyrolysis of *N*-2,4,6-trimethylbenzoylsulfilimine gave neither a trace amount of the inserted product such as 4,6-dimethyl-1-isoindolinone-(III) nor H-abstraction product such as 2,4,6-trimethylbenzoyl amide. Thus the pyrolysis of *N*-acyl-*S,S*-diphenylsulfilimines does not seem to involve the initial formation of a nitrene from which alkyl or aryl group migrates subsequently to afford the isocyanates but is considered to be a concerted process. The yields of both the isocyanate and diaryl sulfide are much higher in the pyrolysis than the photolysis of the same *N*-acyl-*S,S*-diarylsulfilimine. Thus, pyrolysis is a convenient method for preparation of isocyanates.

Experimental

Preparation of N-*Acyl*-S,S-*arylphenylsulfilimine.* *N*-Acyl-*S,S*-arylphenylsulfilimines were prepared according to the known method starting from free *S,S*-arylphenylsulfilimines and appropriate acylating agents. A typical example is shown below.

N-*2,4,6-Trimethylbenzoylsulfilimine.* Free *S,S*-diphenylsulfilimine (1.0 g, 4.98 mmol) was dissolved in 5 ml benzene. To this was added 1.1 g (5.99 mmol) of 2,4,6-trimethylbenzoyl chloride in 5 ml benzene at room temperature. Benzene was removed *in vacuo* and the residual solid was recrystallized from benzene–hexane. *N*-2,4,6-Trimethylbenzoyl-*S,S*-diphenylsulfilimine 0.9 g was obtained in 52.0% yield, mp 143—144 °C. Other *N*-acyl-*S,S*-arylphenylsulfilimines were similarly prepared. Their yields, spectral data and elemental analyses are given in Table 1.

Pyrolysis of N-*Acyl*-S,S-*arylphenylsulfilimine.* The pyrolysis of *N*-acyl-*S,S*-arylphenylsulfilimine was carried out *in situ* or such solvents as DMF, benzene, tetralin at *ca.* 120—200 °C for 0.3—3 h. A typical experiment is shown below.

Pyrolysis of N-*2,4,6-Trimethylbenzoyl*-S,S-*diphenylsulfilimine.* The sulfilimine, 60 mg, was heated in a sealed tube *in situ* at 190 °C for 20 min. After the usual work-up, diphenyl sulfide

and 2,4,6-trimethylbenzoyl isocyanate were obtained quantitatively by gas chromatography. 2,4,6-Trimethylbenzoyl isocyanate was isolated by GLC (TCD column SE-30, 2 m×2 mm, column temp 130 °C, He 1.6 kg/cm²) in 95.5% yield. All the isocyanates thus obtained are summarized in Table 2 together with their spectral data.

Kinetics of N-*Acyl*-S,S-*arylphenylsulfilimine*. A typical kinetic procedure is as follows; to a 0.1 mol/l solution of *N*-acyl-*S*,*S*-arylphenylsulfilimine in DMF, benzene and ethanol (10 ml) was added 170 mg of benzyl phenyl sulfide (0.085 mol/l) as an internal standard at room temperature. The solution (0.2 ml was taken in a 1 ml ampoule by a 1 ml syringe. Several ampoules were then immersed in an oil-bath maintained at the desired temperature. Ampoules were taken out at various time intervals. The solution was quenched immediately with 0.5 ml of water in an ampoule. After addition of 0.2 ml of hexane, it was shaken vigorously for a while. The hexane layer was then separated and 2 μl of the hexane solution was injected directly into a gas chromatography column. Gas chromatography was carried out under the following conditions; column SE-30, 1 m×2 mm, column temp 140 °C, He 0.7 kg/cm². The rate constants of the reaction were calculated by the first order kinetic equation, where a concentration change of diphenyl sulfide is calculated from the relative peak-height of benzyl phenyl sulfide (internal standard) each time. The activation parameters were calculated as usual and the Hammett plots were made against σ-values. The data obtained are summarized in Tables 3 and 4 and Fig. 1.

References

1) S. Oae, K. Tsujihara, and N. Furukawa, *Tetrahedron Lett.*, **1970**, 2663; K. Tsujihara, K. Harada, N. Furukawa, and S. Oae, *Tetrahedron*, **27**, 4921, (1971); N. Furukawa, T. Hatanaka, K. Harada, and S. Oae, *Bull. Chem. Soc. Jpn.*, **46**, 3482 (1972); **49**, 2337 (1976).

2) K. Tsujihara, T. Aida, N. Furukawa, and S. Oae, *Tetrahedron Lett.*, **1970**, 3415.

3) N. Furukawa T. Nishio, M. Fukumura, and S. Oae, *Chem. Lett.*, **1978**, 209.

4) H. Yoshida, H. Taketani, T. Ogata, and S. Inokawa, *Bull. Chem. Soc. Jpn.*, **49**, 3124 (1976).

5) Y. Hayashi and D. Swern, *J. Am. Chem. Soc.*, **95**, 5205 (1973); N. Furukawa, M. Fukumura, T. Nishio, and S. Oae, *J. Chem. Soc., Perkin Trans. 1*, **1976**, 96.

6) T. L. Gilchrist, C. G. Moody, and C. W. Rees, *J. Chem. Soc. Perkin Trans. 1*, **1975**, 1964; T. L. Gilchrist and C. J. Moody, *Chem. Rev.*, **77**, 409 (1977).

7) Y. Tamura, K. Sumoto, H. Matsusima, H. Taniguchi, and M. Ikeda, *J. Org. Chem.*, **38**, 4324 (1973).

8) A. Kucsman, F. Ruff, I. Kapovits, and J. G. Fischer, *Tetrahedron*, **22**, 1843 (1966).

9) Y. Yukawa and Y. Tsuno, *J. Am. Chem. Soc.*, **79**, 5530 (1957); **80**, 6346, (1958); **81**, 2007 (1959).

10) K. Swaminathan and N. Venkatasubramanian, *J. Chem. Soc., Perkin Trans. 2*, **1975**, 1161.

11) T. Imamoto, Y. Tsuno, and Y. Yukawa, *Bull. Chem. Soc. Jpn.*, **44**, 1632, 1639, 1644 (1971); **44**, 2776 (1971).

12) R. D. Bright and C. R. Hauser, *J. Am. Chem. Soc.*, **61**, 618 (1939); **72**, 4284 (1950).

13) R. F. Tietz and W. E. McEwen, *J. Am. Chem. Soc.*, **77**, 4007 (1955); P. A. S. Smith, *J. Am. Chem. Soc.*, **70**, 317 (1945); L. H. Briggs and J. W. Lyttleton, *J. Chem. Soc.*, **1943**, 421.

14) F. H. Seubold and W. E. Vaughan, *J. Am. Chem. Soc.*, **75**, 3790 (1953); *Rec. Trav. Chim.*, **79**, 413 (1960).

15) H. Hock and H. Knoph, *Chem. Ber.*, **88**, 1544 (1955); H. Kwart and R. T. Keen, *J. Am. Chem. Soc.*, **81**, 943 (1959).

16) M. F. Hawthorne, W. D. Emmons, and K. S. McCallum, *J. Am. Chem. Soc.*, **80**, 6393 (1958); M. F. Hawthorne and W. D. Emmons, *J. Am. Chem. Soc.*, **81**, 6398 (1959); S. L. Friess, *J. Am. Chem. Soc.*, **71**, 2571 (1949); **72**, 5518, (1950); **73**, 3968 (1951); **74**, 1302, 2679 (1952).

17) C. H. Gudmundsen and W. E. McEwen, *J. Am. Chem. Soc.*, **79**, 329 (1957); W. H. Saunders and J. C. Ware, *J. Am. Chem. Soc.*, **80**, 3328 (1958).

18) B. J. Gregory, R. B. Moodie, and K. Schofield, *J. Chem. Soc., B*, **1970**, 338; R. Huisgen, J. Witte, H. Walz, and W. Jira, *Ann.*, **604**, 191 (1957).

Study on Zinc *O,O*-Diisobutyl Dithiophosphate as Antioxidant

Yasukazu OHKATSU,* Kazumi KIKKAWA, and Tetsuo OSA
Department of Synthetic Chemistry, Faculty of Engineering, The University of Tokyo, Hongo, Bunkyo-ku, Tokyo 113
(Received May 15, 1978)

Cumyl hydroperoxide has been decomposed using zinc *O,O*-diisobutyl dithiophosphate. The decomposition reaction consisted of three stages including the first homolytic decomposition and the last heterolytic decomposition. These decomposition modes depended considerably on the relative concentration of the complex to the hydroperoxide and the total concentration. From these results and on the basis of decomposition reaction in the presence of both zinc *O,O*-diisobutyl dithiophosphate and bis(*O,O*-diisobutoxyphosphonothioyl) disulfide, it has been shown that the formation of sulfuric acid was most important for heterolytic decomposition.

The zinc *O,O*-diisoalkyl dithiophosphates are widely used as antioxidants, especially as hydroperoxide-decomposers. However it is not easy in practice to determine the kind and effective amount of such antioxidants, because the activities of decomposition of the hydroperoxides are very complicated, and considerably affected by the circumstances. Elucidation of the complicated action mechanism of such decomposes would clarify the mechanisms.

Burn *et al.*[1] found that the decomposition reaction of cumyl hydroperoxide with zinc *O,O*-diisopropyl dithiophosphate consisted of three stages: 1) a first homolytic decomposition, 2) an induction period, and 3) a fast heterolytic decomposition. However, they did not satisfactorily explain what kind of species induced the third stage which was the most important action expected of the complex. Other investigators[2-4] have proposed such species.

The decomposition reaction of cumyl hydroperoxide with bis(*O,O*-diisobutoxyphosphonothioyl) disulfide[5] (referred to as "the disulfide"), which is reported[1,6] to be formed during the decomposition reaction of a hydroperoxide with zinc *O,O*-diisoalkyl dithiophosphate. It was also found[5] that sulfuric acid from the disulfide was most effective for heterolytic decomposition. In this paper, the action mechanism of zinc *O,O*-diisobutyl dithiophosphate and the role of the disulfide in the decomposition of cumyl hydroperoxide are discussed.

Experimental

Materials. Zinc *O,O*-diisobutyl dithiophosphate (Zn–Bu^i_2–DTP),[6] and copper and nickel *O,O*-[3-(3,5-di-*t*-butyl-4-hydroxyphenyl)-propyl] phosphorodithioate (Cu and Ni–P–C_3–DTP)[7] were synthesized according to known procedures. Bis(*O,O*-diisobutoxyphosphonothioyl) disulfide was also prepared by a known method.[5]

Cumyl hydroperoxide and chlorobenzene were purified by convertional methods.

Procedure. Decomposition of cumyl hydroperoxide (CHP) was carried out using a reaction flask fitted with stirrer and sampling neck. For hydroperoxide analyses, an iodometric method was used.[1]

Decomposition products of cumyl hydroperoxide were analyzed by a GLC method (10% Silicone rubber on Diasolid S). ESR measurements were conducted on a JEOL Model JES-PE-1X spectrometer.

Results and Discussion

Decomposition of Cumyl Hydroperoxide. Cumyl hydroperoxide (0.1 M) was decomposed by Zn–Bu^i_2–DTP in chlorobenzene under a nitrogen or oxygen atmosphere at 70 °C. The results are shown in Figs. 1 and 2. The decomposition reactions, regardless of the kind of atmosphere, proceeded as reported by Burn *et al.*,[1] and consisted of three stages,** an initial fast homolytic decomposition, a slow reaction (induction period), and a last fast heterolytic decomposition. With decresing concentration of Zn–Bu^i_2–DTP, the induction period decreased. The presence of oxygen in the reaction system shortened the induction period and accelerated the final decomposition.

The formation of the cumylperoxyl radical during the initial stage of the decomposition of cumyl hydroperoxide with *O,O*-dialkyl dithiophosphates, such as Zn, Cu, and Ni *O,O*-[3-(3,5-di-*t*-butyl-4-hydroxyphenyl)-propyl]-phosphorodithioates (Me–P–C_3–DTP) was indirectly observed; the signal of the phenoxy radical derived from the secondary reaction of the phenolic moiety of

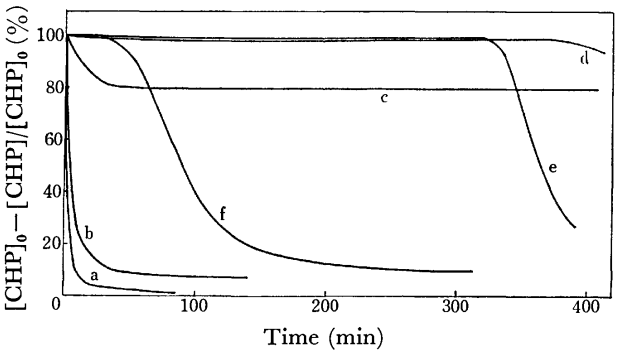

Fig. 1. Decomposition of cumyl hydroperoxide (0.1 M) with Zn–Bu^i_2–DTP in chlorobenzene under nitrogen atmosphere at 70 °C.
[Zn–Bu^i_2–DTP]: a, 10^{-1} M; b, 5×10^{-2} M; c, 10^{-2} M; d, 10^{-3} M; e, 5×10^{-4} M; f, 10^{-4} M.

** In Fig. 1, for example, curves a and b show only the initial decomposition, curve c shows the initial decomposition and induction period, and curve f shows the initial decomposition (not observed clearly due to a little amount of cumyl hydroperoxide decomposed at this stage, corresponding to a lower concentration of Zn–Bu^i_2–DTP), induction period and last decomposition.

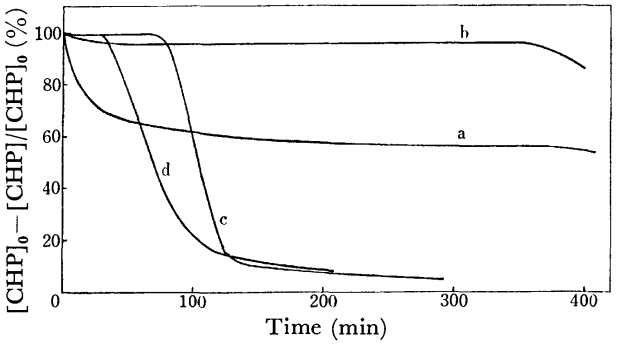

Fig. 2. Decomposition of cumyl hydroperoxide (0.1 M) with Zn-Bu$_2^i$-DTP in chlorobenzene under oxygen atmosphere at 70 °C.
[Zn-Bu$_2^i$-DTP]: a, 10^{-2} M; b, 10^{-3} M; c, 5×10^{-4} M; d, 10^{-4} M.

Me-P-C_3-DTP with cumylperoxyl radical, which is formed by the decomposition reaction of cumyl hydroperoxide with Me-P-C_3-DTP, being observed.[7] Figures 3 and 4 show the peak heights of the ESR signal of the phenoxy radical observed in the decomposition reactions of cumyl hydroperoxide with Ni-P-C_3-DTP and Cu(II)-P-C_3-DTP, respectively. The figures also include the

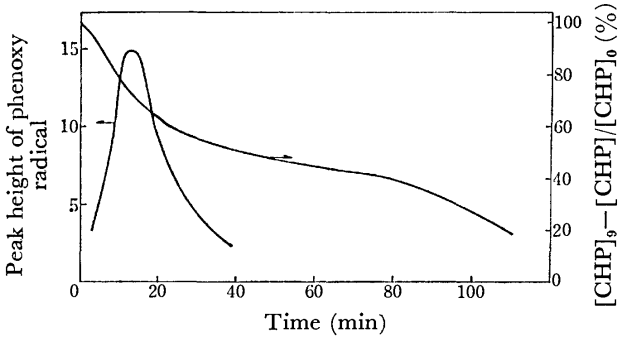

Fig. 3. Decomposition of cumyl hydroperoxide with Ni(II)-P-C_3-DTP in chlorobenzene at 70 °C.
Conditions: $[CHP]_0=1.25\times10^{-2}$ M, [Ni(II)-P-C_3-DTP]$=2.5\times10^{-3}$ M.

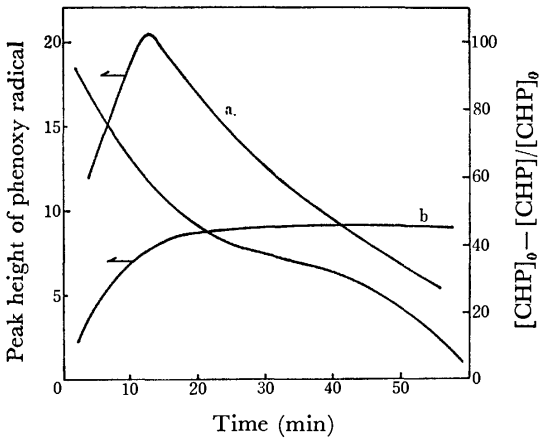

Fig. 4. Decomposition of cumyl hydroperoxide with Cu(II)-P-C_3-DTP in chlorobenzene at 70 °C.
Conditions: $[CHP]_0=1.25\times10^{-2}$ M, [Cu(II)-P-C_3-DTP]$=6.25\times10^{-3}$ M.

titration curves of cumyl hydroperoxide against time in decomposition reactions. When the titration curves are compared with the corresponding curves for the phenoxy radical, it is clearly seen that homolytic decomposition occurs in the initial stage as proposed by Burn *et al.*[1] Furthermore, cupric sulfate begins to form at the same time as the homolytic decomposition (Fig. 4). These results indicate that an acid, probably sulfuric acid, forms cupric sulfate by reacting with Cu-P-C_3-DTP during homolytic decomposition. The results with respect to Me-P-C_3-DTP may be employed to determine the decomposition activity of Zn-Bu$_2^i$-DTP, since the effect of the phenolic moieties of Me-P-C_3-DTP on the decomposition activity of cumyl hydroperoxide is negligible.[7]

The initial rates were found to be first order dependent on both Zn-Bu$_2^i$-DTP and cumyl hydroperoxide (CHP) (Table 1):

$$-d[CHP]/dt = k_D[Zn\text{-}Bu_2^i\text{-}DPT][CHP].$$

The rate constant, k_D, has been calculated to be 2.07×10^{-2} M^{-1} s^{-1} at 70 °C. This value seems somewhat

Table 1. Initial reactions betweenzinc O,O-diisobutyl dithiophosphate and cumyl hydroperoxide in chlorobenzene at 70 °C

Zinc O,O-diisobutyl dithiophopahte ($\times10^2$ M)	Cumyl hydroperoxide ($\times10$ M)	k_D [cumyl hydroperoxide] ($\times10^3$ s^{-1})	k_D ($\times10^2$ M^{-1} s^{-1})
1.0	1.0	1.87	1.87
1.0	5.0	10.7	2.14
1.0	10	20.6	2.06
2.5	1.0	1.73	1.73
2.5	5.0	10.8	2.15
5.0	5.0	10.6	2.13
5.0	10	24.2	2.42
			Av. 2.07
5.0	1.0	0.644	0.644[a]
5.0	1.0	0.119	0.199[b]

a) Zn-Pr^i-X. b) Zn-Bu_2-DTC. *Cf.* $k_{D,\,70°C}$ for zinc O,O-diisopropyl dithiophosphate$=1.55\times10^{-2}$ M^{-1} s^{-1} from Ref. 1.

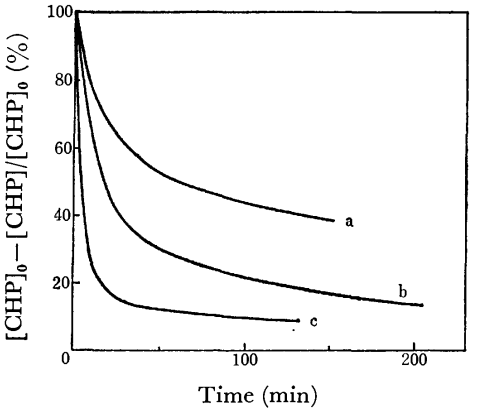

Fig. 5. Decomposition of cumyl hydroxide (0.1 M) with a complex (5×10^{-2} M) in chlorobenzene at 70 °C.
a: zinc N,N-dibutyl dithiocarbamate, b: zinc isopropyldithiocarbonate, c: zinc O,O-diisobutyl dithiophosphorate.

Table 2. Products of complete decomposition of cumyl hydroperoxide (1M) with zinc *O,O*-diisobutyl dithiophosphate in chlorobenzene at 70 °C

Zn–Bu^i_2–DTP (M)	Products (mol %)				
	Acetone	Phenol	α-Methyl styrene	α,α-Dimethyl benzylalcohol	Aceto-phenone
1.0	1	1	24	71	4
1.0×10^{-1}	1	1	25	72	3
1.0×10^{-2}	62	75	19	8	1
1.0×10^{-3}	62	78	16	5	1
1.0×10^{-4}	79	79	13	6	2
1.0×10^{-4} a)	—	—	9	87	5
2 vol %b)	94	100	—	—	—

a) Co(II) octanoate. b) H_2SO_4.

Table 3. Products of complete decomposition of cumyl hydroperoxide with zinc *O,O*-diisobutyl dithiophosphate in chlorobenzene at 70 °C

Zn–Bu^i_2–DTP (M)	Cumyl hydroperoxide (M)	Products (mol %)				
		Acetone	Phenol	α-Methyl styrene	α,α-Dimethyl benzylalcohol	Aceto-phenone
1.0	1.0	1	1	24	71	4
1.0×10^{-1}	1.0×10^{-1}	12	13	32	53	2
1.0×10^{-1} a)	1.0×10^{-1}	8	8	29	61	2
1.0×10^{-1} b)	1.0×10^{-1}	5	5	26	68	1
1.0×10^{-2}	1.0×10^{-2}	66	65	19	14	2
1.0×10^{-3}	1.0×10^{-3}	86	87	12	1	1

a) In the presence of 2,6-di-*t*-butyl-4-methoxyphenol: 2×10^{-3}M. b) In the presence of 2,6-di-*t*-butyl-4-methoxyphenol: 2×10^{-2}M.

higher than that for zinc *O,O*-diisopropyl dithiophosphate[1] and considerably higher than that for zinc *N,N*-diisobutyl dithiocarbamate (Zn–Bu^i_2–DTC) and isopropyl dithiocabonate (Zn–Pr^i–X) studied for comparison (Table 1 and Fig. 5).

Products Derived from Decomposition of Cumyl Hydroperoxide with Zinc O,O-*Diisobutyl Dithiophosphate.* When cumyl hydroperoxide (1 M) was completely decomposed with Zn–Bu^i_2–DTP ($1—1\times10^{-4}$ M) in chlorobenzene at 70 °C, several decomposition products were obtained (Table 2). The results shown in Table 2 suggest† the heterolytic decomposition of cumyl hydroperoxide in the presence of Zn–Bu^i_2–DTP above 1.0×10^{-1} M. When the ratio of cumyl hydroperoxide to Zn–Bu^i_2–DTP exceeded 100, cumyl hydroperoxide decomposed heterolytically. This suggests that one mole of Zn–Bu^i_2–DTP is able to decompose at least 10 mol of cumyl hydroperoxide homolytically.†† Cosequently, it appears that the decomposition modes (homolytic or heterolytic) are drastically dependent on the relative ratio of cumyl hydroperoxide to Zn–Bu^i_2–DTP.

It was found, however, that the decomposition modes were also affected by the total concentration of Zn–Bu^i_2–DTP and cumyl hydroperoxide, even though they coexist in the relative ratio of unity (Table 3). A total concentration above 2×10^{-1} M was preferable for homolytic decomposition; this was also supported by the increase in amount of α,α-dimethylbenzyl alcohol formed in the presence of 2,6-di-*t*-butyl-4-methoxyphenol. The total concentration below 2×10^{-2} M, on the other hand, was preferable for heterolytic decomposition.

In the decomposition reactions mentioned above, Zn–Bu^i_2–DTP itself was also decomposed into compounds, such as zinc sulfate, bis(*O,O*-diisobutoxyphosphonothioyl) disulfide and sulfuric acid, depending on the concentrations of Zn–Bu^i_2–DTP and the hydroperoxide. Zinc sulfate and bis(*O,O*-diisobutoxyphosphonothioyl) disulfide were separated from the reaction solution after the homolytic decomposition (for example, cumyl hydroperoxide, 1.0 M and Zn–Bu^i_2–DTP, 1×10^{-1} M), while sulfuric acid was obtained from the decomposition reaction (for example, cumyl hydroperoxide, 1×10^{-2} M and Zn–Bu^i_2–DTP, 1×10^{-2} M). These results support the formation of the disulfide, as reported by Burn *et al.*,[1] as follows:

$$(Bu^iO)_2P(S)(S)Zn(S)(S)P(OBu^i)_2 \xrightarrow{PhCMe_2OOH}$$

$$(BuO^i)_2P(S^{\ddagger})(S)P(OBu^i)_2 + PhCMe_2O + {}^-OH,$$

$$(Bu^iO)_2P(S^{\ddagger})(S)P(OBu^i)_2 \xrightarrow{PhCMe_2O\cdot}$$

$$(Bu^iO)_2P(S-S)P(OBu^i)_2 + Zn(OH)(OCMe_2Ph).$$

the disulfide

† It is well documented that the homolytic decomposition of cumyl hydroperoxide gives α,α-dimethylbenzyl alcohol, acetophenone and α-methylstyrene, while the heterolytic decomposition gives phenol and acetone.

†† J. A. Howard reported[8] that nickel diisopropyl dithiophosphate decomposed about 25 times of cumyl hydroperoxide homolytically.

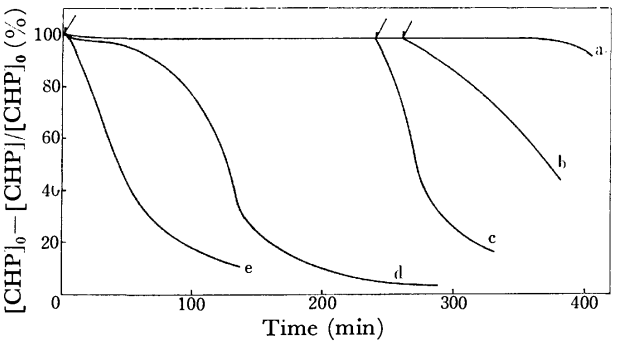

Fig. 6. Decomposition of cumyl hydroperoxide (0.1 M) with Zn-Bu^i_2-DTP and/or bis(*O,O*-diisobutylphosphonothioyl)disulfide in chlorobenzene at 70 °C.

	a	b	c
Zn-DTP	1×10^{-3} M	1×10^{-3} M	1×10^{-3} M
Disulfide	0	1×10^{-2} M	3×10^{-2} M
	d	e	
Zn-DTP	1×10^{-3} M	0	
Disulfide	1×10^{-2} M	1×10^{-2} M	

The resulting disulfide will react rapidly with the hydroperoxide and/or a free radical to form the sulfate ion,[5] which may be converted into zinc sulfate and free sulfuric acid.

Decomposition of Cumyl Hydroperoxide Using Zinc O,O-*Diisobutyl Dithiophosphate with Bis(*O,O-*diisobutoxyphosphonothioyl) Disulfide.* Cumyl hydroperoxide was decomposed in the presence of Zn-Bu^i_2-DTP and the disulfide. The result is shown in Fig. 6, in which the decompositions by either Zn-Bu^i_2-DTP or the disulfide are also shown for comparison. Only the Zn-Bu^i_2-DTP decomposed a little of the hydroperoxide after the start of decomposition (Curve a), while only the disulfide did considerably without any induction period (Curve e). When both decomposers co-existed in the same concentration (1×10^{-3} M) of Zn-Bu^i_2-DTP (Curve a) and in the same concentration (1×10^{-2} M) of the disulfide (Curve e), however, the curve of decomposition (Curve d) was not unexpectedly comparable to Curve e. This may be interpreted assuming that sulfuric acid, which is most effective for ionic decomposition and is derived from the decomposition of cumyl hydroperoxide with the disulfide,[5] is rapidly trapped by Zn-Bu^i_2-DTP present to form zinc sulfate as seen in Fig. 4 for Cu(II)-P-C_3-DTP. Sulfuric acid formed, therefore, is not an effective catalyst till all of the Zn-Bu^i_2-DTP is consumed as zinc sulfate, resulting in the induction period as shown by Curve d.

The assumption made may be supported by the result of Curves b and c. When the disulfide was added during decomposition started with the same concentration of Zn-Bu^i_2-DTP as in Curve a, no induction periods were observed (Curves b and c). This indicates that the addition of the disulfide, at the time of which almost all of the Zn-Bu^i_2-DTP is presumably converted into zinc sulfate, decomposes cumyl hydroperoxide immediately, as if only the disulfide were added at the beginning of decomposition reaction, for example, as shown in Curve e.

Conclusion

The present study has clarified the effects of the relative concentration of the complex to cumyl hydroperoxide (Table 2) and the total concentration of the complex and cumyl hydroperoxide (Table 3) on the decomposition activity of the complex.

It was also found that zinc *O,O*-dialkyl dithiophosphate was not an effective decomposer for the heterolytic decomposition till free sulfuric acid was formed. These results must contribute to select an useful amount of the zinc complex.

The authors would like to express their to Prof. Teiji Tsuruta for his fruitful discussion on this study.

References

1) A. J. Burn, R. Cecil, and V. O. Young, *J. Inst. Petr.*, **57**, 319 (1971).
2) G. W. Kennerly and W. L. Patterson, *Ind. Eng. Chem.*, **48**, 1917 (1956).
3) J. D. Holdworth, G. Scott, and D. Williams, *J. Chem. Soc.*, **1964**, 4692.
4) D. Shopov and S. K. Ivanov. *Neftekhimiya*, **5**, 410 (1965).
5) Y. Ohkatsu, H. Ueda, K. Kikkawa, and T. Osa, *Yukagaku*, **26**, 295 (1977).
6) A. J. Burn, *Tetrahedron*, **22**, 2153 (1966).
7) Y. Ohkatsu, K. Kikkawa, and T. Osa, *Yukagaku*, **27**, 277 (1978).
8) J. A. Howard and J. H. B. Chenier, *Can. J. Chem.*, **54**, 395 (1976).

Synthesis of (±)-Tetrahydroanhydroaucubigenone and (±)-Tetrahydroanhydroaucubigenin[1)]

Heitaro OBARA,* Hiroshi KIMURA, Masanobu SUZUKI, and Jun-ichi ONODERA
Department of Applied Chemistry, Faculty of Engineering, Yamagata University, Yonezawa 992
(Received May 15, 1978)

The racemate of tetrahydroanhydroaucubigenone (**3**), one of the related compounds of aucubin, was synthesized by the photoirradiation of 6-[2-(nitrosooxy)ethyl]-3-oxabicyclo[3.3.0]octan-7-one. (±)-Tetrahydroanhydroaucubigenin was also obtained by reduction of (±)-**3** with sodium in moist ether.

Tetrahydroanhydroaucubigenin (**2**), mp 85 °C, $[\alpha]_D^{19.6}$ +51.5° (ethanol), and its oxidation product, tetrahydroanhydroaucubigenone (**3**), mp 77—78 °C, $[\alpha]_D^{17}$ −41.3° (ethanol), have been known to be the key compounds for the determination of aucubin (**1**).[2)] These compounds have been already obtained by Karrer[3)] and Fujise[4)] in 1946 and 1953, independently, and the correct structures were established by Fujise *et al.*[5)] in 1960. However, the synthesis of **2** and **3** have not been accomplished yet. In this paper, we wish to report the synthesis of the racemates of **2** and **3** by the following scheme.

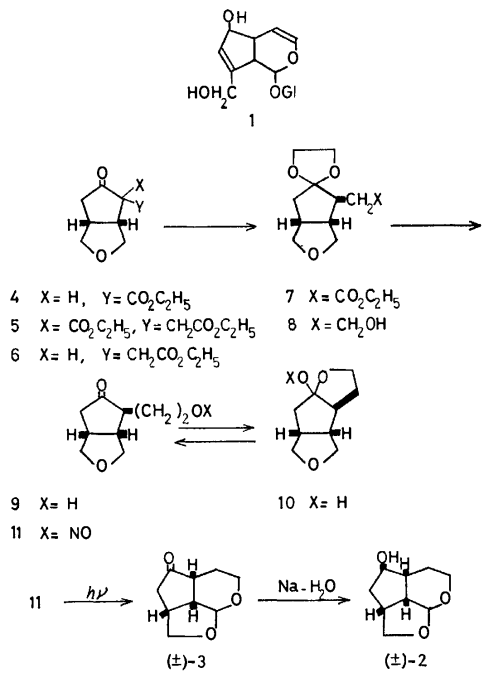

Scheme 1

6-Ethoxycarbonyl-6-ethoxycarbonylmethyl-3-oxabicyclo[3.3.0]octan-7-one (**5**) was obtained with a small amount of *O*-alkylated compound by alkylation of the sodio derivative of *cis*-6-ethoxycarbonyl-3-oxabicyclo[3.3.0]octan-7-one (**4**) with ethyl bromoacetate in toluene. Hydrolysis and decarboxylation of **5** with 6 M hydrochloric acid, followed by esterification, afforded 6-ethoxycarbonylmethyl-3-oxabicyclo[3.3.0]octan-7-one (**6**) in a 50% yield. This compound does not change by treatment with sodium ethoxide, so it is assumed that it has a more stereochemically favorable *cis-trans* (1,5- and 5,6-position) configuration. After acetalization of **6** with ethylene glycol, the acetal (**7**) was reduced into the alcohol (**8**) with lithium aluminium hydride in tetrahydrofuran in a 89% yield. Deacetalization of **8** by treatment with dilute hydrochloric acid or *p*-toluenesulfonic acid in acetone afforded a mixture of 6-(2-hydroxyethyl)-3-oxabicyclo[3.3.0]octan-7-one (**9**) and its intramolecular hemiacetal (**10**) in a 76% yield. The hemiacetal (**10**) is easily converted into the keto alcohol (**9**) by treatment with dilute hydrochloric acid. 6-[2-(Nitrosooxy)ethyl]-3-oxabicyclo[3.3.0]octan-7-one (**11**), a pale green unstable viscous oil, was obtained by the nitrosation of **9** with a mixture of sodium nitrite and dilute sulfuric acid in a 30% yield.

The irradiation of **11** was carried out in a benzene solution under a nitrogen atmosphere at 0 °C using a high-pressure 500 W mercury arc. After irradiation, the benzene was removed *in vacuo* and the residue was chromatographed on silica gel to give (±)-tetrahydroanhydroaucubigenone ((±)-**3**), colorless prisms, mp 57—57.5 °C. The IR spectrum of this compound in carbon tetrachloride was identical with that of the natural sample. Since the *cis-cis* configuration of the ring junction of **3** is already confirmed,[6)] it can be assumed that the photoisomerization at 6-position occurred simultaneously with the photochemical ring closure of **11**. The reduction of (±)-**3** was carried out by considering the configuration of the hydroxyl group of **2**. Fujise *et al.*[7)] previously reported that the epimer of **2** was obtained as an oil by reduction of **3** with lithium aluminium hydride in ether, and they have referred to the mechanism of its stereospecific reduction. We achieved the synthesis of ((±)-**2**), mp 74.5—75 °C, in a 46% yield by reduction of (±)-**3** with sodium in moist ether instead of lithium aluminium hydride. The IR spectrum was identical with that of the natural sample.

Experimental

All the boiling and melting points are uncorrected.

6-Ethoxycarbonyl-6-ethoxycarbonylmethyl-3-oxabicyclo[3.3.0]octan-7-one (5). To a suspension of 11.5 g of sodium metal in 240 ml of dry toluene was added 92.5 g of *cis*-6-ethoxycarbonyl-3-oxabicyclo[3.3.0]octan-7-one (**4**)[8)] dropwise with efficient stirring. The stirred mixture was heated on an oil bath until all the sodium was consumed. Then 83.5 g of ethyl bromoacetate was added to the solution at room temperature, and the mixture was refluxed for 4 h. Upon cooling, the mixture was poured into 150 ml of aqueous 10% acetic acid and the toluene layer was washed with aqueous $NaHCO_3$ and water, dried over Na_2SO_4, and freed from toluene to give a viscous liquid. Distillation of the residue under reduced pressure afforded 113.8 g (85%) of **5** containing a small amount of

O-alkylated by-product, bp 163—169 °C/6 mmHg, MS *m/e* 284 (M^+); IR (neat) 1755 and 1730 cm^{-1} (C=O). The additional absorption bands at 1635 and 1685 cm^{-1} can be attributed to an *O*-alkylated by-product. Found: C, 58.72; H, 7.08%. Calcd for $C_{14}H_{20}O_6$: C, 59.14; H, 7.09%.

6-Ethoxycarbonylmethyl-3-oxabicyclo[3.3.0]octan-7-one (6). The keto ester (**5**) (50 g), containing a small amount of the *O*-alkylated product, was hydrolyzed in 150 ml of aqueous 6 M HCl under boiling for 5 h. After removal of most of the HCl and water under reduced pressure, a mixture of 100 ml of ethanol, 50 ml of toluene, and 0.1 ml of concd H_2SO_4 was added to the oily residue, and the mixture was distilled slowly at atmosphere pressure. The esterification was completed by the redistillation with 100 ml of ethanol and 50 ml of toluene. After the solvent was removed *in vacuo*, the oily residue was extracted with ether, and the ether layer was washed with aqueous $NaHCO_3$ and water, dried over Na_2SO_4, and freed from ether to give a viscous oil. Distillation of the residue in reduced pressure afforded **6**, bp 140—144 °C/4 mmHg, in a 75% yield. MS *m/e* 212 (M^+); IR (neat) 1730 cm^{-1} (C=O). Found: C, 61.89; H, 7.44%. Calcd for $C_{11}H_{16}O_4$: C, 62.25; H, 7.60%. 3-Oxabicyclo[3.3.0]octan-7-one (0.5 g), bp 107—109 °C/14 mmHg (lit,[8] bp 118—119 °C/17 mmHg), 2,4-dinitrophenylhydrazone, mp 144—145 °C (lit,[8] mp 144—145 °C), was obtained as a minor fraction, which was derived from the *O*-alkylated product.

6-(2-Hydroxyethyl)-3-oxabicyclo[3.3.0]octan-7-one (9). A mixture of 30 g of 6-ethoxycarbonylmethyl-3-oxabicyclo[3.3.0]-octan-7-one (**6**), 9.7 g of ethylene glycol, 160 ml of dry benzene, and 60 mg of *p*-toluenesulfonic acid was refluxed on an oil bath for 3 h. Then, most of the water was removed azeotropically at atmospheric pressure. After removal of the solvent, the residue was taken up in ether and worked up in the usual manner to afford 28.1 g (78%) of ethylene acetal (**7**), bp 150—153 °C/3 mmHg, MS *m/e* 256 (M^+). To a mixture of 80 ml of dry THF and 2.5 g of $LiAlH_4$ was added 28.1 g of the ethylene acetal (**7**) over a period of 1 h with stirring on an ice bath and warmed at 40—50 °C for 2 h. Then, 20 ml of water was added cautiously to decompose the unreacted $LiAlH_4$. The THF layer was separated by decantation and freed from THF to give an oily residue. Distillation of the residue in diminished pressure afforded 6-(2-hydroxyethyl)-3-oxabicyclo[3.3.0]octan-7-one ethylene acetal (**8**) (18.9 g, 80%), bp 146—151 °C/2 mmHg, MS *m/e* 214 (M^+). A mixture of 18.2 g of **8** and 60 ml of aqueous 0.2 M HCl was warmed at 50—60 °C for 2 h. After neutralization with solid $NaHCO_3$, it was concentrated to about one-fifth of its original volume and extracted with ether. The ether layer was worked up by the usual manner and distilled to give 10.8 g (75%) of 6-(2-hydroxyethyl)-3-oxabicyclo[3.3.0]octan-7-one (**9**), bp 145—146 °C/3 mmHg, MS *m/e* 170 (M^+), IR (neat) 3450 cm^{-1} (OH) and 1736 cm^{-1} (C=O). Found: C, 62.72; H, 8.40%. Calcd for $C_9H_{14}O_3$: C, 63.51; H, 8.29%. 2,4-Dinitrophenylhydrazone, mp 151—152 °C. Found: C, 51.26; H, 5.21; N, 15.72%. Calcd for $C_{15}H_{17}O_6N_4$: C, 51.57; H, 4.91; N, 16.04%.

6-[2-(Nitrosooxy)ethyl]-3-oxabicyclo[3.3.0]octan-7-one (11). To a mixture of 2.0 g of **9**, 7.5 g of $NaNO_2$, and 10 ml of water, was added a mixed solution of 2.5 ml of concd H_2SO_4 and 1 ml of water dropwise with efficient stirring in an ice–salt bath over a period of 1 h. The reaction mixture was then extracted with ether and the ether layer was worked up in the usual manner. Distillation of the residue in reduced pressure afforded 0.7 g (30%) of **11**, bp 100—102 °C/2 mmHg, IR (neat) 1735 cm^{-1} (C=O), 1640, 1600, and 790 cm^{-1} (N=O and N–O). This green unstable oil was used immediately in the subsequent photoirradiation.

(±)-Tetrahydroanhydroaucubigenone ((±)-3). A solution of 0.4 g of **11** in 110 ml of dry benzene was irradiated with stirring for 15 h under a nitrogen atmosphere at 0 °C by a high-pressure 500 W mercury arc using a CS-054 filter (corning glass works). After irradiation, the solvent was removed *in vacuo*, and the residue was chromatographed on a column of silica gel. Elution with CCl_4–ethyl acetate gave crude (±)-**3** (36 mg) as an oil. Recrystallization from benzene–petroleum ether afforded (±)-**3** (21 mg, 5.7%), mp 57.5 °C. MS, *m/e* 168 (M^+), 139, 110, 83, 69 (base), 55, and 41; IR (CCl_4), ν_{max} 2970, 2900, 1748 (strong), 1175, 1148, 1100, 1065, 1040, 980, and 945 cm^{-1}. The IR spectrum of this compound in CCl_4 was identical with that of the natural sample.

(±)-Tetrahydroanhydroaucubigenin ((±)-2). To a mixture of 12.2 mg of (±)-**3**, 0.02 ml of water, and 3 ml of ether, was added slowly 20 mg of sodium metal in limited amounts over a period of 15 min at 0 °C. The subsequent alternate addition of 0.02 ml of water and 20 mg of sodium metal was continued until the disappearance of the spot of (±)-**3** has been confirmed by TLC. Then water was cautiously added to the reaction mixture and the ether layer was thoroughly washed with saturated brine, dried, and evaporated to leave a crystalline residue, which on recrystallization from petroleum ether–benzene yielded (±)-**2** (5.6 mg, 46%) as colorless prisms, mp 74.5—75 °C. IR (CCl_4), ν_{max} 3600, 3450, 1403, 1153, 1138, 1077, 1060, 1040, 1004, and 972 cm^{-1}. The IR spectrum of this compound in CCl_4 was identical with that of the natural sample.

One of the authors (H. O) is grateful to the late Professor Emeritus Shin-ichiro Fujise of Tohoku University for his encouragement during his lifetime.

References

1) The work relating to the synthesis of (±)-tetrahydroanhydroaucubigenone was reported in a preliminary form: H. Obara, H. Kimura, J. Onodera, and M. Suzuki, *Chem. Lett.*, **1975**, 221.

2) J. M. Bobbitt and K. P. Segebarth, in "Cyclopentanoid Terpene Derivatives," ed by W. I. Taylor and A. R. Battersby, Marcel Dekker, Inc., New York (1969), p. 25.

3) P. Karrer and H. Schmid, *Helv. Chim. Acta*, **29**, 525 (1946).

4) S. Fujise, *Nippon Kagaku Zasshi*, **74**, 725 (1953).

5) S. Fujise, H. Obara, and H. Uda, *Chem. Ind.*, **1960**, 289.

6) S. Fujise, M. Maruyama, and H. Uda, *Nippon Kagaku Zasshi*, **82**, 367 (1961).

7) H. Uda, M. Maruyama, K. Kabuki, and S. Fujise, *Nippon Kagaku Zasshi*, **85**, 279 (1964).

8) H. Obara, S. Kumazawa, J. Onodera, and H. Kimura, *Nippon Kagaku Zasshi*, **1974**, 2380.

Synthesis of 4-Cinnamylidene-2,5-cyclohexadien-1-ones

Kazu KUROSAWA,* Atsuko HASHIBA, and Hirobumi TAKAHASHI
Department of Chemistry, Faculty of Science, Kumamoto University, Kurokami, Kumamoto 860
(Received May 24, 1978)

Lithium aluminium hydride (LAH) reduction of 4′-hydroxychalcones, followed by dehydration, yielded 4-cinnamylidene-2,5-cyclohexadien-1-ones in 19—42% yields. The LAH reduction of 4′-acetoxychalcones also gave the same products in improved yields.

It has been reported that the oxidations of 2- and 4-alkylphenols with manganese dioxide,[1] lead dioxide,[2] silver oxide,[3] potassium hexacyanoferrate(III),[4] and 2,3-dichloro-5,6-dicyano-*p*-benzoquinone[5] (DDQ) gave 2-alkylidene-3,5-cyclohexadien-1-ones and 4-alkylidene-2,5-cyclohexadien-1-ones. Dehydrochlorination of *p*-(chloromethyl)phenol[6] and the elimination reaction of *p*-(methoxymethyl)phenols also yielded 4-methylene-2,5-cyclohexadien-1-ones, but have a limited value.[7] The lithium aluminium hydride (LAH) reduction of 2′-hydroxychalcones has been reported to give 2-phenyl-2*H*-1-benzopyrans,[8] and 2-cinnamylidene-3,5-cyclohexadien-1-one was postulated as a reaction intermediate. This was proved by obtaining pure 2-cinnamylidene-3,5-cyclohexadien-1-one and by converting the latter to 2-phenyl-2*H*-1-benzopyran[3b] (Fig. 1). We have investigated the synthesis of 4-cinnamylidene-2,5-cyclohexadien-1-ones by dehydration of 1-(*p*-hydroxyphenyl)-3-phenyl-2-propen-1-ols (III), which can be obtained by the LAH reduction of 4′-hydroxychalcones (Ia—i), and found that these reactions indeed yielded the desired compounds (IVc—i) in 19—42% yields (Fig. 1 and Table 1).

4′-Hydroxychalcones (Ia—i) were obtained by the condensation of *p*-hydroxyacetophenones and benzaldehydes with aqueous alkali. The structures of these new chalcones were determined by examining their IR and NMR spectra and by elemental analyses. All chalcones have a *trans*-double bond; this was shown by the large coupling constant (J=15—17 Hz) of the ethylenic hydrogens in their NMR spectra.

When 4′-hydroxy-3′,5′-dimethylchalcone (Ic) was treated with LAH in tetrahydrofuran, followed by the treatment with 1 M sulfuric acid, an orange-red crystalline product was separated by column chromatography on alumina. The NMR spectrum (CCl_4) of this compound indicates the presence of two methyl groups {δ=1.98 (3H, broad singlet) and δ=2.04 (3H, doublet, J=1.0 Hz)}, vinylic protons {δ=6.60 (1H, d, J=11.0 Hz), δ=6.78 (1H, multiplet), and δ=6.98 (1H, d, J=11.0 Hz)}, and seven protons {δ=7.1—7.5 (m)}. The multiplet at δ=6.78 becomes a doublet with a small coupling constant, J=2.5 Hz, when irradiated at the methyl signals. The IR spectrum showed multiple absorptions at 1570, 1592, 1612, and 1625 cm.$^{-1}$ These spectroscopic results are consistent with the structure of 4-cinnamylidene-2,5-cyclohexadien-1-one (IVc). A *cis*-configuration of the ethylenic double bond in the cinnamyl group in IVc is suggested by the coupling constant, J=11.0 Hz, of the ethylenic protons. However, the chalcone has a *trans*-configuration, as already mentioned, and isomerization from *trans* to *cis* is not likely to occur during the reaction. Further study would be neccessary to clarify the matter.

Phenolic products (V, VI, and VII) were separated from the ethyl acetate fraction of the chromatography (Fig. 3). Based on the NMR spectrum, the structure of the product V is 4-*trans*-cinnamyl-2,6-dimethylphenol; this was confirmed by a synthesis. The spectral properties of VI suggest that the structure of this compound

TABLE 1. SYNTHESIS OF 4-*trans*-CINNAMYLIDENE-2,5-CYCLOHEXADIEN-1-ONES (IV)

Entry	Chalcone	Reaction conditions				IV (% yield)
		Molar ratio of I: $LiAlH_4$	Solvent	Time (h)	Temp (°C)	
1	Ia[10]	1:3	ether	4.5	0	—
2	Ia	1:2	THF	2.5	20	—
3	Ib[11]	1:2	THF	2.0	20	—
4	Ic[12]	1:2	THF	2.0	20	IVc (27)
5	Ic	1:2	ether	1.0	0	IVc (22)
6	Id	1:2	THF	2.0	20	IVd (33)
7	Ie	1:2	THF	2.0	20	IVe (21)
8	If	1:2	THF	2.0	20	IVf (19)
9	Ig	1:2	THF	1.0	20	IVg (30)
10	Ih	1:2	THF	2.0	20	IVh (26)
11	Ii	1:2	THF	0.5	20	IVi (42)
12	Ij	1:2	THF	1.0	20	IVg (42)
13	IIc	1:2	THF	2.0	20	IVc (46)
14	IId	1:2	THF	2.0	20	IVd (58)
15	IIe	1:2	THF	2.0	20	IVe (28)

is 1-(3,5-dimethyl-4-hydroxyphenyl)-3-phenyl-1-propanone (VI). The structure of VII was determined to be 1-(3,5-dimethyl-4-hydroxyphenyl)-3-phenyl-1-propanol (VII).

The LAH reduction of Ic in ether gave IVc in a slightly decreased yield (22%, entry 5). Five other chalcones (Id—h) gave the corresponding 4-cinnamylidene-2,5-cyclohexadien-1-ones (IVd—h) (entries 6, 7, 8, 9, and 10), but no effort was made to isolate the phenolic products in these cases.

The methyl ether of Obtsusaquinone,[9] which is the first naturally occurring 4-cinnamylidene-2-hydroxy-5-methoxy-2,5-cyclohexadien-1-one, was also synthesized by the reaction of Ii (entry 11) and found to be identical

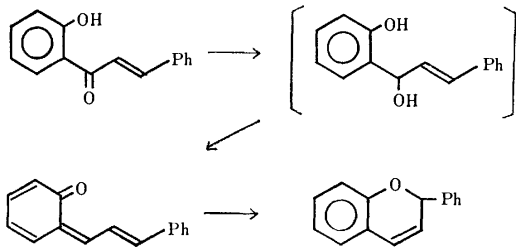

Fig. 1.

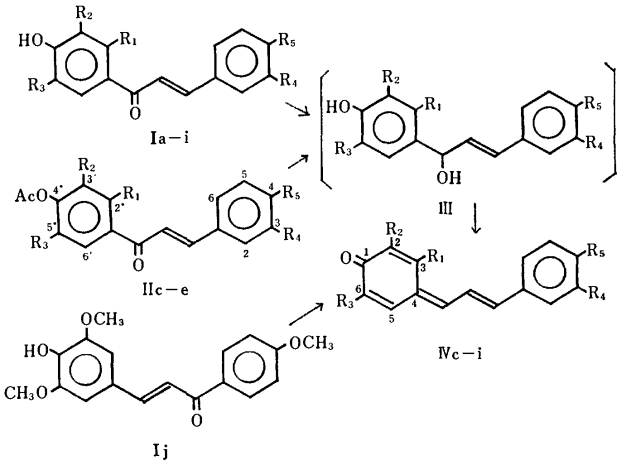

Ia–i IIc–e III IVc–i Ij

Fig. 2. a: $R_1=R_2=R_3=R_4=R_5=H$, b: $R_1=R_4=R_5=H$, $R_2=R_3=Br$, c: $R_1=R_4=R_5=H$, $R_2=R_3=CH_3$ d: $R_1=R_4=H$, $R_2=R_3=CH_3$, $R_5=OCH_3$, e: $R_1=H$, $R_2=R_3=CH_3$, $R_4=R_5=OCH_3$, f: $R_1=R_4=R_5=H$, $R_2=R_3=OCH_3$, g: $R_1=R_4=H$, $R_2=R_3=R_5=OCH_3$, h: $R_1=H$, $R_2=R_3=R_4=R_5=OCH_3$, i: $R_2=R_4=R_5=H$, $R_1=R_3=OCH_3$.

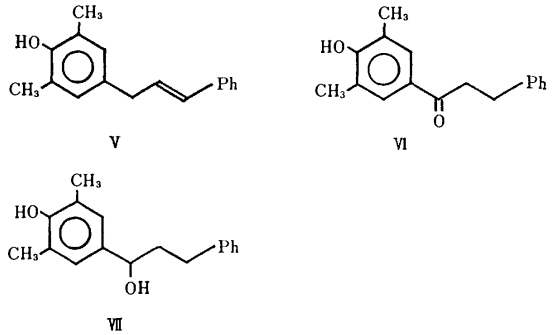

V VI VII

Fig. 3.

with the methyl ether by comparison of their spectral properties (the configuration of the styryl group in IVi could be reversed in Fig. 2).

The LAH reductions of 4'-hydroxychalcone (Ia) and 4'-hydroxy-3',5'-dibromochalcone (Ib) were also carried out, but pure compounds were not isolated due to the decomposition during chromatography. When 4'-acetoxychalcones (IIc—e) were reduced with LAH in tetrahydrofuran, followed by the treatment with 1 M sulfuric acid, IVc, IVd, and IVe were obtained in improved yields (46% (entry 13), 58% (entry 14), and 28% (entry 15)).

It seemed reasonable to assume that a chalcone having a hydroxyl group at the position 4 would also give a 4-cinnamylidene-2,5-cyclohexadien-1-one by the LAH reduction and the dehydration. This proved to be the case. The LAH reduction of 4-hydroxy-3,4',5-trimethoxychalcone (Ij) yielded IVg, identical with that obtained from Ig, but in a better yield (entry 12).

It is thus concluded that the LAH reductions of 4- and 4'-hydroxy-, and 4'-acetoxychalcones can be utilized as a convenient method for the synthesis of 4-cinnamylidene-2,5-cyclohexadien-1-ones.

Experimental

All ^1H NMR spectra were recorded with a Hitachi R 24 NMR spectrometer with TMS as an internal standard. The IR spectra were recoreded with a JASCO IRA-1 IR spectrometer, while the UV spectra were recorded with a Hitachi EPS-3T spectrophotometer. Melting points were determined on a Yanagimoto hot-stage and are uncorrected.

Preparations of Acetophenones. 4-Hydroxy-3,5-dimethoxyacetophenone was synthesized by partial demethylation of 3,4,5-trimethoxyacetophenone with aluminium chloride. 3,4,5-Trimethoxyacetophenone[13] (2.1 g) was dissolved in hot benzene (300 ml) containing anhydrous aluminium chloride (2.66 g) and heated under reflux for 2 h. 2 M hydrochloric acid (100 ml) was added to the solution and the benzene layer was separated. After removal of the benzene, the resulting solid was recrystallized from ether, giving colorless prisms (1.19 g, 61%), mp 119—120 °C (lit,[14] mp 120—121 °C).

4-Hydroxy-3,5-dimethylacetophenone was prepared by the modified Nencki reaction. 2,6-Dimethylphenol (1.22 g) was heated with boron trifluoride–acetic acid complex (5 ml) at 100 °C for 2 h. The reaction mixture was poured into 2 M hydrochloric acid (50 ml) and the precipitates were collected. The crude product was recrystallized from benzene to give colorless plates (623 mg, 38%), mp 150—151 °C(lit,[15] mp 150.5—151.2 °C).

4-Hydroxy-2,5-dimethoxyacetophenone was prepared similarly in 91% yield (mp 128—129 °C (lit,[16] mp 117—118 °C)).

Preparations of 4'-Hydroxy- and 4-Hydroxychalcones (Id—j). A typical preparation of 4'- and 4-hydroxychalcones was as follows. A mixture of an aldehyde (10 mmol) and an acetophenone (10 mmol) in ethanol (20 ml) was treated with 20—40% aqueous potassium hydroxide at an appropriate temperature overnight. The reaction mixture was poured into iced hydrochloric acid (10 ml), and the precipitates were collected and recrystallized.

4'-Hydroxy-3',5'-dimethyl-4-methoxychalcone (Id): Mp 146—147 °C (EtOH), 34% yield; IR ($CHCl_3$) 1656, 1670, and 3440 cm^{-1}. NMR ($CDCl_3$) $\delta=2.30$ (6H, s, $2\times CH_3$), 3.82 (3H, s, OCH_3), 5.7 (1H, broad s, OH), 6.90 (2H, m, $H_{(3)}$ and $H_{(5)}$), 7.41 (1H, d, $J=15.0$ Hz, H_a), 7.57 (2H, m, $H_{(2)}$ and

$H_{(6)}$), 7.73 (1H, d, J=15.0 Hz, H_β), and 7.71 (2H, s, $H_{(2')}$ and $H_{(6')}$). Found: C, 76.02; H, 6.63%. Calcd for $C_{18}H_{18}O_3 \cdot 1/10\ H_2O$: C, 76.08; H, 6.46%.

4'-Hydroxy-3,4-dimethoxy-3',5'-dimethylchalcone (Ie): Mp 184—186 °C (EtOH); 26% yield; IR ($CHCl_3$) 1668, 1675, and 3590 cm.$^{-1}$ NMR ($CDCl_3$) δ=2.33 (6H, s, 2×CH_3), 3.89 (3H, s, OCH_3), 3.91 (3H, s, OCH_3), 5.7 (1H, broad s, OH), 6.75—7.3 (3H, m, $H_{(2)}$, $H_{(5)}$, and $H_{(6)}$), 7.36 (1H, d, J=15.0 Hz, H_α), 7.67 (1H, d, J=15.0 Hz, H_β), and 7.67 (2H, s, $H_{(2')}$ and $H_{(6')}$). Found: C, 72.78; H, 6.55%. Calcd for $C_{19}H_{20}O_4$: 73.06; H, 6.45%.

4'-Hydroxy-3',5'-dimethoxychalcone (If): Mp 106—107 °C (aq EtOH); 55% yield; IR ($CHCl_3$) 1650 and 3500 cm^{-1}. NMR ($CDCl_3$) δ=3.98 (6H, s, 2×OCH_3), 6.0 (1H, s, OH), 7.30 (2H, s, $H_{(2')}$. and $H_{(6')}$), 7.48 (1H, d, J=16.0 Hz, H_α), 7.78 (1H, d, J=16.0 Hz, H_β), 7.3—7.7 (5H, m, Ph). Found: C, 71.64; H, 5.74%. Calcd for $C_{17}H_{16}O_4$: C, 71.82; H, 5.67%.

4'-Hydroxy-3',4,5'-trimethoxychalcone (Ig): Mp 79 °C (EtOH); 29% yield; IR ($CHCl_3$) 1650 and 3530 cm^{-1}. NMR ($CDCl_3$) δ=3.83 (3H, s, OCH_3), 3.95 (6H, s, 2×OCH_3), 6.0 (1H, broad s, OH), 6.95 (2H, m, $H_{(3)}$ and $H_{(5)}$), 7.35 (2H, s, $H_{(2')}$. and $H_{(6')}$), 7.43 (1H, d, J=16.0 Hz, H_α), 7.61 (2H, m, $H_{(2)}$ and $H_{(6)}$), and 7.78 1H, d, J=16.0 Hz, H_β). Found: C, 67.96; H, 5.85%. Calcd for $C_{18}H_{18}O_5 \cdot 1/5H_2O$: C, 68.00; H, 5.83%.

4'-Hydroxy-3,3',4,5'-tetramethoxychalcone (Ih): Mp 90 °C (EtOH); 49% yield; IR ($CHCl_3$) 1650 and 3520 cm^{-1}. NMR ($CDCl_3$) δ=3.90 (3H, s, OCH_3), 3.91 (3H, s, OCH_3), 3.95 (6H, s, 2×OCH_3), 6.1 (1H, s, OH), 6.89 (1H, m, $H_{(5)}$), 7.17 (2H, m, $H_{(2)}$ and $H_{(6)}$), 7.30 (2H, s, $H_{(2')}$ and $H_{(6')}$), 7.33 (1H, d, J=17.0 Hz, H_α), and 7.67 (1H, d, J=17.0 Hz, H_β). Found: C, 65.80; H, 5.92%. Calcd for $C_{19}H_{20}O_6 \cdot 1/10H_2O$: C, 65.92; H, 5.88%.

4'-Hydroxy-2',5'-dimethoxychalcone (Ii): Mp 162—163 °C (EtOH); 56% yield; IR ($CHCl_3$) 1630, 1660, and 3530 cm^{-1}. NMR ($CDCl_3$) δ=3.88 (3H, s, OCH_3), 3.89 (3H, s, OCH_3), 6.25 (1H, s, $H_{(3')}$), 6.62 (1H, s, $H_{(6')}$), 7.3—7.8 (6H, m, Ph and OH), and 7.69 (2H, s, H_α and H_β). Found: C, 71.23; H, 5.79%. Calcd for $C_{17}H_{16}O_4 \cdot 1/10H_2O$: 71.31; H, 5.71%.

4-Hydroxy-3,4',5-trimethoxychalcone (Ij): Mp 132 °C (EtOH); 28% yield; IR ($CHCl_3$) 1672 and 3540 cm^{-1}. NMR ($CDCl_3$) δ=3.88 (3H, s, OCH_3), 3.94 (6H, s, 2×OCH_3), 5.8 (1H, broad s, OH), 6.87 (2H, s, $H_{(2)}$ and $H_{(6)}$), 6.97 (2H, m, $H_{(3')}$ and $H_{(5')}$), 7.38 (1H, d, J=15 Hz, H_α), 7.70 (1H, d, J=15.0 Hz, H_β), and 8.00 (2H, m, $H_{(2')}$ and $H_{(6')}$). Found: C, 62.85; H, 5.40%. Calcd for $C_{18}H_{18}O_5 \cdot 4/5\ H_2O$: 62.71; H, 5.73%.

Preparation of 4'-Acetoxychalcones (IIc—e). A typical procedure for the preparation of 4'-acetoxychalcone was as follows. A 4'-hydroxychalcone (4 mmol) was treated with a mixture of acetic anhydride (1 ml), acetic acid (1 ml), and pyridine (6 ml) at room temperature overnight. The reaction mixture was poured into iced water and the precipitates were collected.

4'-Acetoxy-3',5'-dimethylchalcone (IIc): Mp 102 °C (EtOH); 92% yield; IR ($CHCl_3$) 1680 (C=O) and 1765 cm^{-1} (OAc). NMR ($CDCl_3$) δ=2.22 (6H, s, 2×CH_3), 2.33 (3H, s, OAc), 7.2—7.8 (5H, m, Ph), 7.43 (1H, d, J=15.0 Hz, H_α), 7.72 (2H, s, $H_{(2')}$ and $H_{(6')}$), and 7.75 (1H, d, J=15.0 Hz, H_β). Found: C, 77.32; H, 6.23%. Calcd for $C_{19}H_{18}O_3$: C, 77.53; H, 6.16%.

4'-Acetoxy-3',5'-dimethyl-4-methoxychalcone (IId): Mp 125—126 °C (EtOH); 65% yield; IR ($CHCl_3$) 1670 (C=O) and 1765 cm^{-1} (OAc). NMR ($CDCl_3$) δ=2.22 (6H, s, 2×CH_3), 2.35 (3H, s, OAc), 3.84 (3H, s, OCH_3), 6.91 (2H, m, $H_{(3)}$ and $H_{(5)}$), 7.36 (1H, d, J=15.0 Hz, H_α). 7.60 (2H, m, $H_{(2)}$ and $H_{(6)}$), 7.72 (2H, s, $H_{(2')}$ and $H_{(6')}$), and 7.80 (1H, d, J=15.0 Hz, H_β). Found: C, 73.75; H, 6.36%. Calcd for $C_{20}H_{20}O_4$: C, 74.05; H, 6.22%.

4'-Acetoxy-3,4-dimethoxy-3',5'-dimethylchalcone (IIe): Mp 135—136 °C (EtOH); 58% yield; IR ($CHCl_3$) 1680 (C=O) and 1770 cm^{-1} (OAc). NMR ($CDCl_3$) δ=2.23 (6H, s, 2×CH_3), 2.35 (3H, s, OAc), 3.92 (3H, s, OCH_3), 3.94 (3H, s, OCH_3), 6.8—7.3 (3H, m, $H_{(2)}$, $H_{(5)}$ and $H_{(6)}$), 7.30 (1H, d, J=16.0 Hz, H_α), 7.69 (1H, d, J=16.0 Hz, H_β), and 7.69 (2H, s, $H_{(2')}$ and $H_{(6')}$). Found: C, 70.92; H, 6.36%. Calcd for $C_{21}H_{22}O_5$: C, 71.17; H, 6.26%.

Lithium Aluminium Hydride Reduction of 4- and 4'-Hydroxychalcones (Ia—j) and 4'-Acetoxychalcones (IIc—e). A typical procedure of the LAH reduction of chalcones was as follows. To a stirred THF solution of LAH (2 mmol), a chalcone (1 mmol) was added and stirred for the time shown in the table. The color of the chalcones disappeared within 5—10 min. After the removal of the THF *in vacuo*, 1 M sulfuric acid (20 ml) was added to the residue and the mixture was extracted with chloroform. The chloroform solution was concentrated to a small volume and then passed through an alumina column (5—10 g) by eluting with chloroform. The chloroform was removed and the resulting orange-red colored substance was allowed to crystallize. In the case of Ic, the reaction mixture was extracted with benzene and passed through a silicagel column by eluting with chloroform and ethyl acetate successively. The chloroform fraction was again passed through an alumina column by eluting with benzene to give IVc. The ethyl acetate fraction was further purified by TLC effected with chloroform, yielding V, VI, and VII. The LAH reduction in ether was carried out similarly. Yields were based on the amount of chalcones used.

Ic gave IVc, mp 115—116 °C (cyclohexane); 27% yield THF and 22% yield (ether); IR ($CHCl_3$) 1570, 1592, 1612, and 1625 cm^{-1}; UV (MeOH) λ_{max} (ε) 260 (10800) and 406 nm (4530) (Found: C, 86.34; H, 6.88%. Calcd for $C_{17}H_{16}O$: C, 86.40, H, 6.83%); V: mp 56—57 °C (light petroleum); 1% yield; IR ($CHCl_3$) 3600 cm^{-1} (OH); UV (MeOH) λ_{max} (ε) 258 nm (20300); NMR ($CDCl_3$) δ=2.11 (6H, s, 2×CH_3), 3.25 (2H, m, $-CH_2-$), 4.4 (1H, broad s, OH), 5.85—6.5 (2H, m, $-CH=CH-$), 6.65 (2H, s, aromatic), and 7.15 (5H, m, Ph) (Found: C, 85.71; H, 7.77%. Calcd for $C_{17}H_{18}O$: C, 85.67; H, 7.61%); VI: liquid; 8% yield; IR ($CHCl_3$) 1690 (C=O) and 3580 cm^{-1} (OH); NMR ($CDCl_3$) δ=2.25 (6H, s, 2×CH_3), 2.7—3.4 (4H, m, $-CH_2-CH_2-$), 5.8 (1H, s, OH), 7.21 (5H, s, Ph), and 7.60 (2H, s, aromatic); and VII: liquid; 4% yield; IR ($CHCl_3$) 3400 (OH) and 3580 cm^{-1} (OH); NMR ($CDCl_3$) δ=2.21 (6H, 2×CH_3), 1.6—3.0 (5H, m, $-CH_2-CH_2-$, OH), 4.52 (1H, t, J=6.0 Hz, $-CHOH$), 4.65 (1H, broad s, OH), 6.92 (2H, s, aromatic), and 7.18 (5H, s, Ph). IIc gave IVc in a 46% yield.

2,6-Dimethyl-4-(4-methoxycinnamylidene)-2,5-cyclohexadien-1-one (IVd): Mp 141—142 °C (ethyl acetate); 33% yield; IR ($CHCl_3$) 1560, 1586, 1615, and 1650 cm^{-1}; UV (MeOH) λ_{max} (ε) 273 (15700) and 442 nm (20800); NMR ($CDCl_3$) δ=2.03 (3H, s, CH_3), 2.10 (3H, s, CH_3), 3.79 (3H, s, OCH_3), 6.6—7.6 (9H, m). Found: C, 81.18; H, 6.78%. Calcd for $C_{18}H_{18}O_2$: C, 81.17; H, 6.81%. IId yielded IVd in a 58% yield.

4-(3,4-Dimethoxycinnamylidene)-2,6-dimethyl-2,5-cyclohexadien-1-one (IVe): Mp 142—143 °C (benzene); 21% yield; IR ($CHCl_3$) 1575, 1595, 1615, and 1650 cm^{-1}; UV (MeOH) λ_{max} (ε) 275 (12700) and 450 nm (41400); NMR ($CDCl_3$) δ=2.05 (3H, s, CH_3), 2.11 (3H, s, CH_3), 3.89 (3H, s, OCH_3), 3.92 (3H, s, OCH_3), 6.7—7.5 (7H, m), and 7.55 (1H, m). Found: C, 76.80; H, 6.87%. Calcd for $C_{19}H_{20}O_3$: C, 77.00; H, 6.80%. IIe gave IVe in a 28% yield

4-Cinnamylidene-2,6-dimethoxy-2,5-cyclohexadien-1-one (IVf): Mp 113—114 °C (benzene); 19% yield; IR ($CHCl_3$) 1570,

1590, 1600, and 1635 cm^{-1}; UV (MeOH) λ_{max} (ε) 275 (shoulder) (4440) and 424 nm (3410) (the ε values could not be accurate as they decreased rapidly); NMR ($CDCl_3$) δ=3.75 (3H, s, OCH_3), 3.82 (3H, s, OCH_3) 6.23 (1H, d, J=2.0 Hz), 6.75 (1H, broad s), 6.74 (1H, d, J=12.7 Hz), 7.07 (1H, d, J=12.7 Hz), and 7.2—7.7 (6H, m). Found: C, 77.12; H, 6.05%. Calcd for $C_{17}H_{16}O_3 \cdot 1/5\ C_6H_6$: C, 76.99; H, 6.11%.

2,6-Dimethoxy-4-(4-methoxycinnamylidene)-2,5-cyclohexadien-1-one (IVg): Mp 142 °C (benzene); 30% yield (from Ig) and 42% yield (from Ij); IR ($CHCl_3$) 1572, 1588, and 1632 cm^{-1}; UV (MeOH) λ_{max} (ε) 245 (10300), 280 (shoulder) (6240), 300 (6240), and 456 nm (41900); NMR ($CDCl_3$) δ=3.77 (3H, s, OCH_3), 3.81 (3H, s, OCH_3), 3.96 (3H, s, OCH_3), 6.31 (1H, m), 6.5—7.2 (5H, m), 7.33 (1H, s), and 7.48 (2H, m). Found: C, 73.92; H, 6.15%. Calcd for $C_{18}H_{18}O_4 \cdot 1/4\ C_6H_6$: C, 73.68; H, 6.18%.

2,6-Dimethoxy-4-(3,4-dimethoxycinnamylidene)-2,5-cyclohexadien-1-one (IVh): Mp 149—151 °C (ethyl acetate); 26% yield; IR ($CHCl_3$) 1570, 1590, and 1632 cm^{-1}; UV (MeOH) λ_{max} (ε) 235 (shoulder) (13100), 280 (8450), 300 (shoulder) (5830), and 466 nm (40800); NMR ($CDCl_3$) δ=3.80 (3H, s, OCH_3), 3.88 (3H, s, OCH_3), 3.91 (3H, s, OCH_3), 3.93 (3H, s, OCH_3), 6.32 (1H, d, J=2.0 Hz), 6.6—7.5 (7H, m). Found: C, 69.30; H, 6.18%. Calcd for $C_{19}H_{20}O_5$: C, 69.50; H, 6.14%.

4-Cinnamylidene-3,6-dimethoxy-2,5-cyclohexadien-1-one (IVi): Mp 165 °C (primarily softening at 130—140 °C, lit,[9] mp 169 °C), 42% yield.

Preparation of 4-trans-Cinnamyl-2,6-dimethylphenol. trans-Cinnamyl 2,6-Dimethylphenyl Ether: A mixture of 2,6-dimethylphenol (15 g), *trans*-cinnamyl chloride (15 g), anhydrous potassium carbonate (15 g), and acetone (100 ml) was heated under reflux for 4 days. After the removal of the acetone, water was added to the residue. The mixture was extracted with benzene and the benzene layer was washed with 1 M sodium hydroxide. Evaporation of the benzene gave *trans*-cinnamyl 2,6-dimethylphenyl ether (21.5 g, 91%) as an oil, bp 180 °C (bath temp)/0.03 mmHg. UV (MeOH) λ_{max} (ε) 257 nm (19400); NMR ($CDCl_3$) δ=2.23 (6H, s, 2×CH_3), 4.34 (2H, d, J=4.5 Hz), 6.30 (1H, d t, J=16.0, 4.5 Hz), 6.66 (1H, d, J=16.0 Hz), 6.83 (3H, m, aromatic), and 7.20 (5H, m, Ph). Found: C, 85.72; H, 7.76%. Calcd for $C_{17}H_{18}O$: C, 85.67; H, 7.61%.

4-trans-Cinnamyl-2,6-dimethylphenol: *trans*-Cinnamyl 2,6-dimethylphenyl ether (5.0 g) was heated in *N,N*-dimethylaniline (20 ml) for 2 h at 200 °C under nitrogen atmosphere. The reaction mixture was dissolved into 2 M hydrochloric acid (100 ml) and then extracted with benzene. After the removal of the benzene, the resulting mixture was chromatographed through an alumina column (100 g) by eluting with benzene, giving colorless needles (2.95 g, 59%), mp 56—57 °C (light petroleum) identical with those obtained by the LAH reduction of Ic.

References

1) C. M. Orlando, Jr., *J. Org. Chem.*, **35**, 3714 (1970).
2) M Gregson, W. D. Ollis, R. T. Redman, I. O. Sutherland, and H. H. Dietrichs, *Chem. Commun.*, **1968**, 1395.
3) (a) L. K. Dyall and S. Winstein, *J. Am. Chem. Soc.*, **94**, 2196 (1972); (b) L. Jurd, *Tetrahedron*, **33**, 163 (1977).
4) (a) C. D. Cook and B. E. Norcross, *J. Am. Chem. Soc.*, **78**, 3797 (1956); (b) G. Leary and W. Thomas, *Tetrahedron Lett.*, **1975**, 3631
5) M. Cornia and L. Merlini, *J. Chem. Soc., Chem. Commun.*, **1975**, 428.
6) L. J. Filar and S. Winstein, *Tetrahedron Lett.*, **1960**, 9.
7) S. B. Cavitt, H. Sarrafizadeh R., and P. D. Gardner, *J. Org. Chem.*, **27**, 1211 (1962).
8 T. Hase, *Acta Chem. Scand.*, **22**, 2845 (1968).
9) L Jurd, K. Stevens, and G. Manners, *Phytochem.*, **11**, 3287 (1972).
10) St. v. Kostanecki and J. Tambor, *Ber.*, **32**, 1924 (1899).
11) H. R. Trivedi and M. N. Vakharia, *J. Univ. Bombay*, **30**, 83 (1961—1962); *Chem. Abstr.*, **60**, 5382 h (1964).
12) H. Wittmann and H. Uragg, *Monatsh Chem.*, **97**, 896 (1966).
13) J. Koo, *J. Am. Chem. Soc.*, **75**, 720 (1953)
14) J. M. Pepper and H. Hibbert, *J. Am. Chem. Soc.*, **70**, 67 (1948).
15) Z. Yoshida, N. Ishibe, and K. Shobatake, *Kogyo Kagaku Zasshi*, **68**, 809 (1965).
16) A. Ballio and L. Almirante, *Ricerca Sci.*, **20**, 829 (1950); *Chem. Abstr.*, **48**, 1999 b (1954).

5,9-Dihydroxy-4,8,11,11-tetramethyltricyclo[6.3.0.0^{2,4}]undecane. Acid-catalyzed Cyclization Product of 6,7-Epoxyhumula-2,9-diene[1]

Misuzu NAMIKAWA, Tatsushi MURAE, and Takeyoshi TAKAHASHI*

Department of Chemistry, Faculty of Science, The University of Tokyo, Bunkyo-ku, Tokyo 113

(Received June 8, 1978)

6,7-Epoxyhumula-2,9-diene (**2**) was treated with 1.8 M sulfuric acid–acetone (1 : 1) to yield a new tricyclic diol, 5,9-dihydroxy-4,8,11,11-tetramethyltricyclo[6.3.0.0^{2,4}]undecane (**9**; diol B), together with tricyclohumuladiol (**3**; diol A), humulenol-II (**4**), a diol C (**5b**), a diol D (**5a**), and an acetonide (**8a**). The same reaction at 0° gave only **3**. Tricyclohumuladiol (**3**) was shown to be a key intermediate in the reaction of **2** to form **4**, **5a**, **5b**, **8a**, and **9**.

Cyclization of humulene (**1**) and its derivatives has been the subject of a number of studies in connection with the biogenesis of sesquiterpenes.[2] Treatment of 6,7-epoxyhumula-2,9-diene[3] (**2**; 1,2-humulene epoxide;[4] humulene epoxide-II[5]) with 20% sulfuric acid in acetone at room temperature has been reported[4] to give a complex mixture of products containing tricyclohumuladiol (**3**),[6-9] humulenol-II (**4**),[5,6b] and an unsaturated diol (**5**).[4] In this reaction, **4** was suggested to be formed directly from **2** or by acid-catalyzed decyclization of **3**.[4] It has also been reported[7] that tricyclohumuladiol (**3**) affords humulenol-II (**4**), an alcohol (**6**), humuladienone (**7**),[9] and an acetonide (**8**) on treatment with sulfuric acid in acetone at room temperature. In the present paper, the formation of a diol (**9**) with a new skeletal structure of 4,8,11,11-tetramethyltricyclo[6.3.0.0^{2,4}]undecane in the cyclization of **2** is described.

Treatment of 6,7-epoxyhumula-2,9-diene (**2**)[3-5,11] with 1.8 M sulfuric acid and acetone (1 : 1) at 0 °C for 30 min gave tricyclohumuladiol (**3**;[6-9,11] diol A) as a sole product (yield: >95%). Further continuation of the reaction at room temperature for 7 h resulted in the formation of a mixture of at least seven products, which was subjected to separation by crystallization, column chromatography, and/or preparative gas chromatography to give the acetonide (**8**;[7,11] y: 10%), humulenol-II (**4**;[5,6b,11] y: 9%), tricyclohumuladiol (**3**; y: 4%), a diol B (**9**;[11] y: 25%), a diol C (**5b**;[11] y: *ca.* 4%), a diol D (**5a**;[11] y: 7%), and a diol E (y: *ca.* 4%). The same mixture of products was formed when tricyclohumuladiol (**3**) was treated with 1.8 M sulfuric acid in acetone (1 : 1) (at room temperature, 7 h).

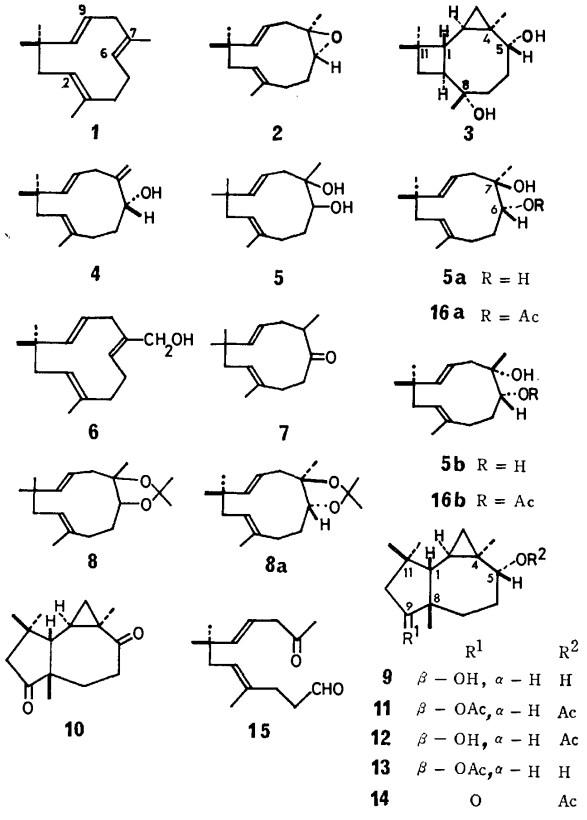

The elementary analysis of the diol B (**9**; mp 171.5—172 °C) fitted best for the molecular formula $C_{15}H_{26}O_2$ (M^+ at *m/e* 238.1861). The PMR and IR spectra showed the presence of four tertiary methyl groups, a trisubstituted cyclopropane ring, and hydroxyl group(s). A diol nature with two secondary hydroxyl groups was shown for **9** by oxidation with chromium trioxide–pyridine complex in dichloromethane (Ratcliffe's procedure[12]) to yield a diketone (**10**). The IR (1740 and 1680 cm^{-1}; no hydroxyl absorption) and UV (λ_{max} 212 nm, ε 2200) spectra of **10** suggested the presence of a five-membered ring ketone and a six- or larger-membered ring ketone conjugated with the cyclopropane ring.[6] Acetylation of **9** with acetic anhydride in pyridine at room temperature gave a diacetate (**11**) and two monoacetates (**12** and **13**). One (**12**) of the monoacetates was treated with chromium trioxide in pyridine to yield a keto acetate (**14**), whose IR spectrum (1742 cm^{-1}) indicated the presence of a five-membered ring ketone. The hydroxyl and acetoxyl groups of the monoacetate (**12**) must be located on a five-membered ring and on a carbon adjacent to the cyclopropane ring, respectively. Lanthanide induced shift (LIS) technique using Eu(fod)$_3$-d_{27} as a shift reagent coupled with double irradiation was applied for PMR measurements of **12** to show the presence of the partial structures **A**, **B**, and **C** (*cf.* Table 1). It was suggested from the large LIS value observed for the proton (H_h) that the hydroxyl group in **A** and the proton (H_h) in **C** are located closely to each other. The results described above

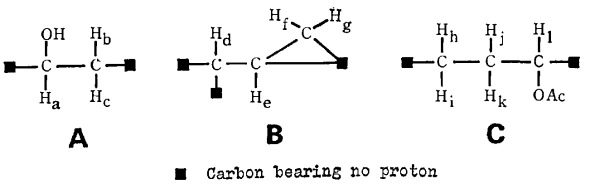

Table 1. Lanthanide induced shift values and coupling constants for the protons of the diol B monoacetate (**12**)

Protons	a	b	c	d	e	f	g	h	i	j	k	l
S[a]	24.7	19	13.7	6.3	5	3	3	15.5	8	8	5	6.3
Coupling constants (Hz)	$J_{a,b}=11$ $J_{a,c}=8$ $J_{b,c}=13$			$J_{d,e}=10$ $J_{e,f}=J_{e,g}=9$ $J_{f,g}=6$				$J_{h,i}$ or $J_{h,j}=10$ $J_{k,l}$ and/or $J_{k,j}=12$ $J_{h,k}=0$; $J_{j,l}=7$ $J_{k,l}=10$				
Methyls	$C_{(4)}$–CH_3		$C_{(8)}$–CH_3	$C_{(11)}$–CH_3		$C_{(11)}$–CH_3		$C_{(5)}$–$OCOCH_3$				
S[a]	2.0		12.5	4.3		3.2		2.7				

a) S: the slopes of shift values plotted against the molar ratio of [Eu(fod)$_3$-d_{27}]/**12** for a *ca.* 2%w/v soln of **12** in $CDCl_3$.

along with the evidence that the diol B was formed by acid-catalyzed rearrangement of tricyclohumuladiol (**3**) led to the structure of 5,9-dihydroxy-4,8,11,11-tetramethyltricyclo[6.3.0.0^{2,4}]undecane for the diol B (**9**). The large LIS value observed for the methyl group at C-8 of **12** showed that the C-9 hydroxyl group and the C-8 methyl group are in *cis* relationship for **9** and **12**.

The molecular formula of $C_{15}H_{26}O_2$ was given for both the diol C (**5b**; mp 182—183 °C) and the diol D (**5a**; a colorless oil). The diol D was treated with acetone in the presence of cupric sulfate to yield the known acetonide (**8**).[7] Acid hydrolysis of **8** gave the diol D. The diol D was also obtained on treatment of humulene [**1**; (2*E*,6*E*,9*E*)-3,7,11,11-tetramethylcycloundeca-2,6,9-triene)][3,13] with osmium tetroxide.[14] When the diol D as well as the diol C was oxidized with periodate, the same keto aldehyde (**15**) was formed. Therefore, the structure of (2*E*,9*E*)-6,7-dihydroxyhumula-2,9-diene[3] was confirmed for both the diols C (**5b**) and D (**5a**), which must be the diastereomers at C-7.

The presence of four preferred conformational isomers (**D**—**G**) could be suggested for each of the diols (**5a** and **5b**) based on an examination by the Dreiding model. The Newman projection about the bond axis $C_{(6)}$–$C_{(7)}$ for **D** and **F** is shown as in **DF**, and that for **E** and **G** as in **EG**. The presence of an intramolecular O–H···π hydrogen-bonding[15] could be expected for **D** and **F** for both the *trans*-diol (R^1=CH_3, R^2=OH) and the *cis*-diol (R^1=OH, R^2=CH_3). An intramolecular O–H···O hydrogen-bonding could be formed in **E** and **G** for the *trans*-diol; no formation of this hydrogen-bonding is expected for **D**—**G** for the *cis*-diol. The IR spectrum of the diol C (2.6 mM soln in carbon tetrachloride) showed the absorptions at 3640, 3625, and 3605 cm^{-1} due to a free secondary hydroxyl, a free tertiary hydroxyl, and an intramolecular O–H···π hydrogen-bonded hydroxyl group,[15] respectively, while the spectrum of the diol D (2.6 mM soln in carbon tetrachloride) indicated an absorption at 3588 cm^{-1} due to an intramolecular O–H···O hydrogen-bonded hydroxyl group in addition to the bands at 3642, 3627, and 3603 cm^{-1} (Fig. 1). The *trans*-diol (**5a**) and the *cis*-diol (**5b**) structures are suggested for the diol D and the diol C, respectively. The structure (**8a**) follows for the acetonide (**8**) of the diol D.

These results received support from the following observations. (i) The rate of the periodate cleavage of the *trans*-diol (**5a**) was found to be greater than that of the *cis*-diol (**5b**). This could be interpreted by the proximity of the two hydroxyl groups for **5a** shown as in **E-a**, **G-a**, and **EG-a**; the two hydroxyl groups are rather alienated to each other in **D**—**G** for **5b**. (ii) The formation of the acetonide (**8a**) from the *trans*-diol (**5a**) can be explained on the basis of the conformations **E-a** and **G-a**, while the corresponding acetonide could not be obtained from the *cis*-diol (**5b**). (iii) The R_f value on TLC for **5a** was observed higher than that for **5b**; this could be due to the formation of an intramolecular hydrogen-bonding in **5a**. (iv) In the IR spectrum of the monoacetate (**16a**) prepared from **5a**, the carbonyl absorption due to the acetoxyl group appears at the lower wave-number (1710 cm^{-1}). The presence of an intramolecular hydrogen-bonding between the C-7 hydroxyl group and the acetoxyl group at C-6 is suggested for **16a** which could adopt the conformations **E-a** and **G-a** (OAc in place of $C_{(6)}$–OH). (v) A *cis*-addition of osmium tetroxide to the (6*E*)-olefinic linkage of humulene (**1**) would lead to the *trans*-diol (**5a**).

In the mass spectra of the diol B (**9**) and its related compounds (**11**—**14**), the peaks due to cleavages **a**, **b**,

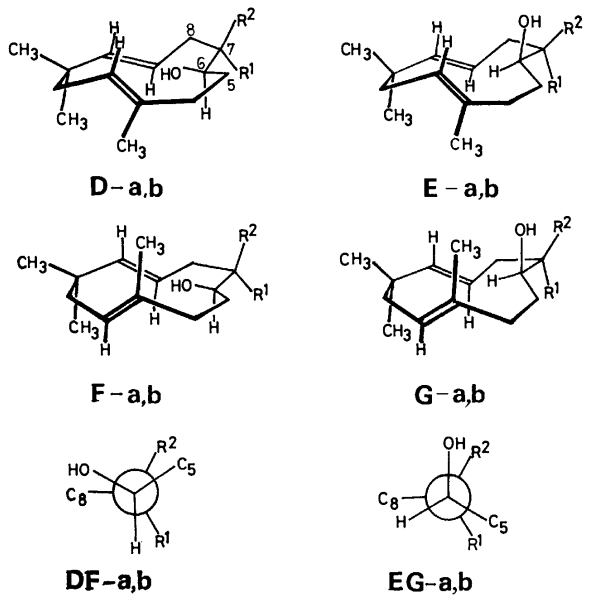

a R^1= CH_3, R^2= OH (**5a**: *trans*-diol)
b R^1= OH, R^2= CH_3 (**5b**: *cis*-diol)

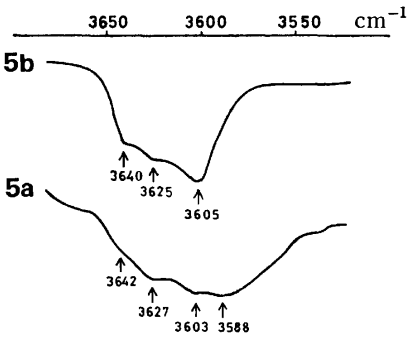

Fig. 1. IR Spectra of the diol D (**5a**) and the diol C (**5b**) in CCl_4 (2.6 mM soln for both compounds).

and **c** were observed (*cf.* **H**). The fragment ions due to fissions **d**, **e**, **e'**, and **f** were observed for the diols C (**5b**), D (**5a**), and their derivatives (**16a**, **b**) (*cf.* **I**).

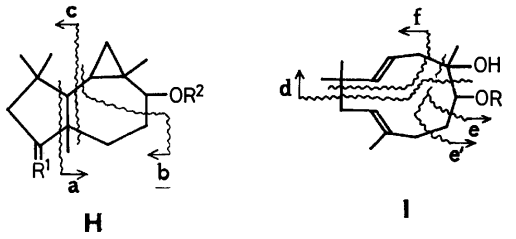

Finally, both the reaction of the epoxide (**2**) (Fig. 2) and the rearrangement of tricyclohumuladiol (**3**) (Fig. 3) were examined by a time-dependent product analysis (GLC). An initial formation of **3** and the subsequent

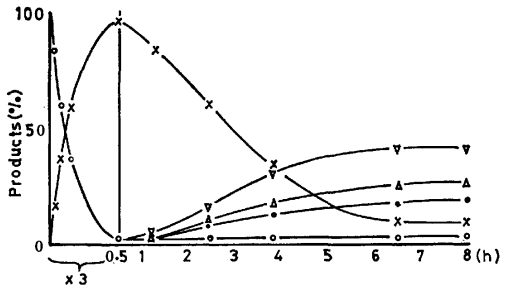

Fig. 2.

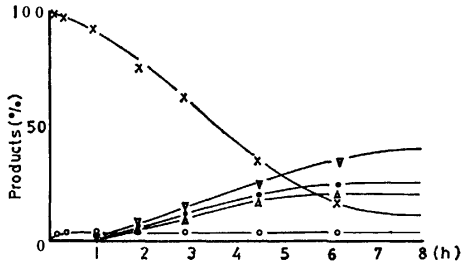

Fig. 3.

Figs. 2 and 3. Time-dependent product analysis for the reaction of the epoxide (**2**) (Fig. 2) and the rearrangement of tricyclohumuladiol (**3**) (Fig. 3): **2** (-○-), **3** (-×-), **4** (-△-), **8a** (-▽-), and **9** (-●-). The formation of the diol C (**5b**) was detected. However, this could not be registered in Figs. 2 and 3 due to a small quantity of **5b** formed. The diol D (**5a**) could not be detected due to decomposition of this compound under the conditions employed [column: SP-1000 (10%); 180—220 °C].

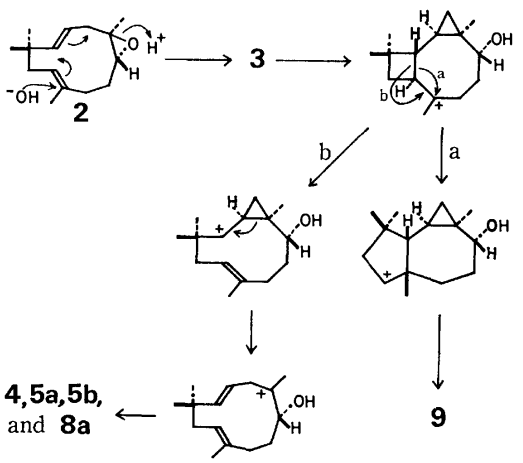

Scheme 1.

formation of a series of products (**4**, **5b**, **8a**, and **9**) in consumption of **3** were shown (Fig. 2). These results and the product isolation experiments (*vide supra*) indicate that tricyclohumuladiol (**3**) is a key intermediate in the reaction of **2** to form **4**, **5a**, **5b**, **8a**, and **9**. The sequence of the acid-catalyzed cyclization and the subsequent rearrangement of 6,7-epoxyhumula-2,9-diene (**2**) could be interpreted as in Scheme 1.[16]

Experimental

All mps were measured on a Mel-temp capillary melting point apparatus (Laboratory Devices) and uncorrected. IR spectra were measured on Hitachi EPI-G2, JASCO IRA-2, JASCO DS-402G spectrometers, and UV spectrum on a Hitachi EPS-2 spectrometer. Mass (MS) spectra were run on a Hitachi RMU-6-Tokugata mass spectrometer and high resolution mass spectra on a Hitachi RMH-2 mass spectrometer operating at 70 eV. The relative intensity observed in low resolution mass spectra was expressed in % in the parentheses. PMR spectra were taken using a Hitachi R-20B (60 MHz), or a JEOL FX-60 spectrometer, using TMS as an internal standard. Gas chromatography (GLC) was carried out using Shimadzu GC-6A equipped with a hydrogen flame ionization detector. Analytical TLC was carried out on Kieselgel GF_{254} (Merck) in 0.25 mm thickness and preparative TLC on Kieselgel PF_{254} (Merck) in 0.5 mm thickness. Wakogel C-200 (Wako) was used for column chromatography.

6,7-Epoxyhumula-2,9-diene (2). 6,7-Epoxyhumula-2,9-diene (**2**)[11] was prepared from humulene (**1**) by treatment with pervanadic acid (H_2O_2–V_2O_5)[17] in acetone according to the procedure described by Damodaran *et al.*[5]

Treatment of 6,7-Epoxyhumula-2,9-diene (2) with Sulfuric Acid in Acetone. To a solution of the epoxide (**2**; 100 mg) in acetone (10 ml) cooled to 0 °C was added 1.8 M sulfuric acid (10 ml) with stirring. The solution was stirred at 0 °C for 1 h and then at room temperature for 7 h. The reaction mixture was neutralized with aqueous sodium hydroxide solution and extracted thrice with ether after acetone was removed. The combined ethereal solutions were washed with brine, dried over sodium sulfate, and evaporated. Crystals (17 mg; **9**; *diol B*) separated from the residual oil (98 mg) were filtered and washed with a small amount of ether. The filtrate gave another crop of crystals [6 mg; a mixture of diols B, C, and E], which was collected by filtration. Evaporation of the filtrate gave a residue (75 mg), which was dissolved in hexane–ether (4: 1), passed through a column of silica gel (7 g), and

eluted with the following solvents (each fraction, 5 ml). Hexane–ether (7: 3), frs 1—4; hexane–ether (1: 1), frs 5—14; ether, frs 15—50. On evaporation, fractions 9—14 gave a *diol D* (**5a**; 4 mg), fractions 17—23 a mixture of diols B, C, and E (12.5 mg), fractions 24—30 a *diol C* (**5b**; 1 mg), fractions 31—36 a mixture (*ca.* 1: 1) of diols C and A (2 mg), fractions 37—43 a *diol A* (**3**; *tricyclohumuladiol*;[6-9] 2 mg), and fractions 44—47 a mixture (*ca.* 1: 1) of diol A and an unidentified product (2 mg). Fractions 3—8 were combined and the solvents were distilled off. The residue (44 mg) was dissolved in hexane and further chromatographed on a column of silica gel (8 g) using the following solvents as eluent (each fraction, 8 ml). Hexane, frs 1—6; hexane–ether (19: 1), frs 7—14; hexane–ether (9: 1), frs 15—31; ether, frs 32—36. On removal of the solvents, fractions 10—12 afforded an *acetonide* (**8a**; 14 mg; yield 10%), fractions 13—15 the starting material (**2**; 1 mg), fractions 25—28 *humulenol-II* (**4**;[5,6,11] 9 mg; y: 9%), and fraction 34 a mixture (*ca.* 1: 1) of diol D and another unidentified product (6 mg). From the mixture containing diols B, C, and E mentioned above, the diol C (R_t 15 min) and the *diol E* (R_t 10.3 min) were separated by means of preparative GLC [column, SP-1000 (10%), 4 (mm)×2 (m); 220 °C; N_2 flow rate, 50 ml/min]. The total yields for each of the diols A—E were estimated to be 4, 25, 4, 7, and 4%, respectively.

When the reaction (at 0 °C) was interrupted after 30 min, the diol A (**3**) was obtained as a sole product (y: >95%); a part of the starting material (**2**; <5%) left unchanged.

Characterization of the diols B, C, D, and E and the acetonide are as follows. *5,9-Dihydroxy-4,8,11,11-tetramethyltricyclo[6.3.0.0^{2,4}]undecane (**9**; Diol B).* The diol B (**9**) crystallized from benzene as colorless needles, mp 171.5—172 °C; IR (Nujol) 3280, 3050, 1380, 1365, 1350, 1260, 1055, 1045, 1035, 925, 910, and 880 cm^{-1}; PMR ($CDCl_3$) δ 0.16—0.63 (3H, m), 0.90, 1.03, 1.05, 1.12 (each 3H, s), 3.4 and 3.8 (each 1H, m); Found: C, 75.31; H, 11.02%. Calcd for $C_{15}H_{26}O_2$: C, 75.58; H, 10.99%; MS *m/e* 238.1861 (9%; M^+; calcd for $C_{15}H_{26}O_2$: 238.1931), 223.1684 [11%; $(M-CH_3)^+$], 220.1795 [13%; $(M-H_2O)^+$], 205.1585 [20%; $(M-H_2O-CH_3)^+$], 202.1658 [9%; $(M-2\times H_2O)^+$], 152.1229 [22%; **a** and/or (**b**−2H); $C_{10}H_{16}O$], 150.1083 [38%; (**a**−2H); $C_{10}H_{14}O$], 138.0976 (84%; $C_9H_{14}O$), 125.0963 [71%; (**c**−H); $C_8H_{13}O$], 121.1014 (73%; C_9H_{13}), 109.0886 (100%; C_8H_{13}), and 107.0833 (91%; C_8H_{11}).

*Diol C (**5b**).* The diol C (**5b**) crystallized from ethyl acetate as colorless needles, mp 182—183 °C; IR (Nujol) 3380, 1150, 980, and 860 cm^{-1}; PMR (CD_3OD) δ 1.04, 1.09, 1.31, and 1.66 (each 3H, s); MS *m/e* 238.2004 (3%; M^+; calcd for $C_{15}H_{26}O_2$: 238.1931), 220.1765 [3%; $(M-H_2O)^+$], 205.1450 [2%; $(M-H_2O-CH_3)^+$], 138.1037 (53%; $C_9H_{14}O$), 125.0959 [35%; (**d**−H); $C_8H_{13}O$], 109.0951 (57%; C_8H_{13}), 95.0853 (53%; C_7H_{11}), 87.0419 [23%; (**e′**−H); $C_4H_7O_2$], and 83.0831 [100%; (**f**+H); C_6H_{11}].

*Diol D (**5a**).* The diol D (**5a**) is a colorless oil, IR (liquid) 3400, 1040, 980, 910, 875, and 860 cm^{-1}; PMR ($CDCl_3$) δ 1.05 (3H, s), 1.11 (6H, s), 1.60 (3H, s), 3.68 (1H, *t*-like, *J*=*ca.* 4.5 Hz), and 4.8—5.6 (3H); MS *m/e* 238.2026 (4%; M^+; calcd for $C_{15}H_{26}O_2$: 238.1931), 220.1813 [6%; $(M-H_2O)^+$], 205.1552 [5%; $(M-H_2O-CH_3)^+$], 138.1053 (35%; $C_9H_{14}O$), 125.0946 [36%; (**d**−H); $C_8H_{13}O$], 109.1018 (74%; C_8H_{13}), 95.0853 (87%; C_7H_{11}), 87.0421 [19%; (**e′**−H); $C_4H_7O_2$], 83.0848 [100%; (**f**+H); C_6H_{11}], and 74.0359 [46%; **e**; $C_3H_6O_2$].

Diol E. The diol E is a crystalline compound, mp 131.5—132 °C; IR (Nujol) 3320, 1380, 1362, 1110, 1080, 928, and 868 cm^{-1}; PMR ($CDCl_3$) δ 0.82, 0.97, 1.11, 1.15 (each 3H, s), and 3.77 (1H, m); MS M^+ at *m/e* 238. The structure of the diol E remains undetermined due to paucity of this compound.

*Acetonide (**8a**).* The acetonide (**8a**) was obtained as a colorless oil, IR (liquid) 1250, 1095, 1085, 1050, 995, 970, and 860 cm^{-1}; PMR (CCl_4) δ 1.03, 1.06, 1.10, 1.28, 1.33 (each 3H, s), 1.63 (3H, br s), 3.88 (1H, dd, *J*=2, *J*=7 Hz), and 4.8—5.5 (3H) [lit,[7] 1.04 (6H, s), 1.08 (3H, s), 1.28, 1.34 (each 3H, s), 1.60 (3H, d, *J*=1 Hz), 3.92 (1H, m), and 5.10 (3H, m)], PMR ($CDCl_3$) δ 1.07 (3H, s), 1.11 (6H, s), 1.37, 1.44 (each 3H, s), 1.64 (3H, d, *J*=1 Hz), 4.01 (1H, dd, *J*=2, *J*=7 Hz), and 4.8—5.5 (3H); MS[7] (indirect) M^+ at *m/e* 278 ($C_{18}H_{30}O_2$).

*Time-dependent Product Analysis of the Reaction of 6,7-Epoxyhumula-2,9-diene (**2**) with Sulfuric Acid in Acetone by Means of GLC.* Sulfuric acid (8 ml; 1.8 M soln) was added to a solution of the epoxide (**2**: 60 mg) in acetone (8 ml) at 0 °C, and the reaction was allowed to proceed at 0 °C for 30 min and then at room temperature for 7.5 h. Product analysis was carried out as follows. A part of the solution (0.5 ml) was separated from the reaction mixture. To this solution was added a 10% aqueous sodium hydroxide solution (0.4 ml) and the resulting mixture was extracted four times with dichloromethane (total 5 ml). The dichloromethane solution was washed with brine, dried over magnesium sulfate, and evaporated to give a residue, which was dissolved in acetone (1.5 ml) and subjected to an examination by GLC [column, SP-1000 (10%), 4 (mm)×2 (m); 180—220 °C (temperature elevated at the rate of 5 °C/min); N_2 flow rate, 55 ml/min] (Fig. 2). The retention times under these conditions for **2**, **3**, **4**, **5b**, **8a**, and **9** were 5.6, 15.2, 8.2, 17.4, 4.8, and 24.6 min, respectively.

*Product Analysis of the Reaction of Tricyclohumuladiol (**3**) with Sulfuric Acid in Acetone by Means of GLC.* To a solution of tricyclohumuladiol (**3**: diol A; 71 mg) in acetone (9 ml) was added 1.8 M sulfuric acid (9 ml) with stirring at 0 °C. The reaction was allowed to proceed at room temperature for 8 h. Product analysis was effected as mentioned above. The result is shown as in Fig. 3.

*Oxidation of the Diol B (**9**).* Chromium trioxide (52 mg) was added to a mixture of pyridine (75 mg) and dichloromethane (1.3 ml) with stirring for 15 min. To the solution, the diol B (20 mg) in dichloromethane (2 ml) was added. The reaction mixture was stirred at room temperature for 40 min. The organic solution was separated by decantation and the residue was washed thoroughly with ether. The combined solution was evaporated *in vacuo* and the residue was extracted with ether. The ethereal layer was washed with 1% aqueous sodium hydroxide solution, brine, and dried over sodium sulfate. Evaporation of the solvent gave a residue which was dissolved in hexane, passed through a column of silica gel (5 g), and eluted with hexane–ether (2: 3) (each fraction, 3 ml). Fractions 5 and 6 gave a dione and fractions 8—13 a crude mixture of monoketones and the dione. This mixture was further subjected to separation by preparative TLC to afford the dione and a mixture of monoketones. *5,9-Dioxo-4,8,11,11-tetramethyltricyclo[6.3.0.0^{2,4}]undecane* (10; total 7.5 mg), a colorless oil; IR (CCl_4) 1740, 1710, 1680, 1380, and 1345 cm^{-1}; IR (liquid) 1735, 1700, 1670, 1380, 1345, 1275, 1230, and 895 cm^{-1}; UV (EtOH) λ_{max} 212 nm (ε 2200); PMR ($CDCl_3$) δ 1.11, 1.20, 1.22, 1.34 (each 3H, s), 2.30 (2H, d, *J*=*ca.* 1 Hz), and 2.56 (2H, dd, *J*=5, *J*=7 Hz); MS *m/e* 234.1612 (35%; M^+; calcd for $C_{15}H_{22}O_2$: 234.1618), 219.1394 [9%; $(M-CH_3)^+$], 151.1130 [94%; (**a**+H) and/or (**b**−H); $C_{10}H_{15}O$], 123.0805 [31%; (**c**−H); $C_8H_{11}O$], 109.1031 (100%; C_8H_{13}), and 69.0335 (66%; C_4H_5O); GLC R_t=10.8 min [column, SP-1000 (10%); 220 °C; N_2 flow rate 90 ml/min], R_t=4.0 min [column, Dexsil-300GC (5%); 170 °C; N_2 flow rate, 50 ml/min].

*Acetylation of the Diol B (**9**).* A solution of the diol B (**9**; 33 mg) in pyridine was treated with acetic anhydride at room temperature for 30 min. Methanol was added to decompose an excess of acetic anhydride. The solvents were evaporated under reduced pressure to give an oily residue, which was dissolved in hexane–ether. Crystals (7 mg; diol B) separated from the solution were removed by filtration and the filtrate was passed through a column of silica gel (5 g). Elution with hexane–ether (3: 2; each fraction, 5 ml) gave a *diacetate* (**11**; 8 mg; from frs 1—4), mp 88.5—90.5 °C (crystallized from hexane), IR (Nujol) 3050, 1735, 1245, 1040, and 980 cm^{-1}; PMR ($CDCl_3$) δ 0.35—0.63 (3H), 1.02, 1.04, 1.10, 1.16, 2.02, 2.05 (each 3H, s), 4.50 (1H, dd, J=7.5, J=10 Hz; H–C–OAc), and 4.82 (1H, dd, J=7.5, J=11 Hz; H–C–OAc); MS *m/e* 322.2155 (1%; M^+; calcd for $C_{19}H_{30}O_4$: 322.2142), 280.2031 [5%; $(M-CH_3CO+H)^+$], 263.2007 [17%; $(M-AcOH+H)^+$], 262.1904 [5%; $(M-AcOH)^+$], 220.1824 [17%; $(M-AcOH-CH_3CO+H)^+$], 205.1581 [18%; $(M-AcOH-CH_3CO-CH_3+H)^+$], 203.1774 [23%; $(M-2\times AcOH+H)^+$], 202.1709 [46%; $(M-2\times AcOH)^+$], 187.1482 [46%; $(M-2\times AcOH-CH_3)^+$], 162.1407 (100%, $C_{12}H_{19}$), 135.1164 [49%; (**a**−AcOH+H) and/or (**b**−AcOH−H); $C_{10}H_{15}$], 133.1015 [51%; (**a**−AcOH−H); $C_{10}H_{13}$], 109.1020 (66%; C_8H_{13}), and 107.0861 [80%; (**c**−AcOH−H); C_8H_{11}]. Fractions 5 and 6 yielded a *monoacetate* (**12**; 5 mg), a colorless oil, IR (liquid) 3420, 3050, 1735, 1720 (sh), 1380, 1365, 1250, and 1030 cm^{-1}; PMR ($CDCl_3$) δ *ca.* 0.4 (2H, m), 0.62 (1H, br s), 1.00 (3H, s), 1.06 (6H, s), 1.15, 2.05 (each 3H, s), 3.88 (1H, dd, J=8, J=11 Hz; H–C–OH), and 4.53 (1H, dd, J=7, J=10 Hz; H–C–OAc); MS *m/e* 280.2032 (3%; M^+; calcd for $C_{17}H_{28}O_3$: 280.2036), 265.1812 [2%; $(M-CH_3)^+$], 262.1926 [2%; $(M-H_2O)^+$], 238.1912 [7%; $(M-CH_3CO+H)^+$], 220.1818 [22%; $(M-AcOH)^+$], 205.1585 [33%; $(M-AcOH-CH_3)^+$], 202.1696 [23%; $(M-AcOH-H_2O)^+$], 180.1513 (54%; $C_{12}H_{20}O$), 162.1414 (60%; $C_{12}H_{18}$), 135.1109 [75%; (**a**−AcOH+H) and/or (**b**−H_2O−H); $C_{10}H_{15}$], 133.1002 [43%; (**a**−AcOH−H); $C_{10}H_{13}$], 125.0967 [75%; (**c**−H); $C_8H_{13}O$], 121.0984 (83%; C_9H_{13}), 109.1017 (83%; C_8H_{13}), and 107.0859 [100%; (**c**−H_2O−H); C_8H_{11}]. Fractions 7—11 were combined and the solvents were evaporated to give a residue, which was subjected to separation by silica gel dry column chromatography [9 g; elution with hexane–ether (1: 1); each fraction 2.3 ml]. Fractions 16—18 gave **12** (5 mg) and fractions 22—30 afforded another *monoacetate* (**13**; 3.8 mg), an amorphous solid, IR (Nujol) 3300, 1730, 1245, and 1030 cm^{-1}; PMR ($CDCl_3$) δ 0.2—0.7 (3H), 0.97, 1.02, 1.10, 1.15, 2.04 (each 3H, s), 3.38 (1H,m), and 4.82 (1H, dd, J=8, J=11 Hz); MS *m/e* 280.2120 (0.2%; M^+; calcd for $C_{17}H_{28}O_3$; 280.2036), 262.1938 [1%; $(M-H_2O)^+$], 220.1823 [5%; $(M-AcOH)^+$], 205.1591 [5%; $(M-AcOH-CH_3)^+$], 202.1722 [5%; $(M-AcOH-H_2O)^+$], 187.1482 (8%; $C_{14}H_{19}$), 135.1128 [16%; (**a**−H_2O+H) and/or (**b**−AcOH+H); $C_{10}H_{15}$], 133.1013 [16%; (**a**−H_2O−H); $C_{10}H_{13}$], 109.1027 (26%; C_8H_{13}), and 107.0866 [30%; (**c**−AcOH−H); C_8H_{11}], and 55.0563 (100%; C_4H_7).

*Oxidation of the Monoacetate (**12**).* The monoacetate (**12**; 4.7 mg) in dichloromethane (*ca.* 0.1 ml) was added to a solution prepared from chromium trioxide (11.1 mg), pyridine (18.5 mg), and dichloromethane (0.25 ml). The mixture was stirred at room temperature for 1 h. The reaction mixture was worked up as before to give a keto acetate (**14**; 2.1 mg), a colorless oil; IR (liquid) 3050, 1742, 1736, 1380, 1370, and 1250 cm^{-1}; MS *m/e* 278.1859 (15%; M^+; calcd for $C_{17}H_{26}O_3$: 278.1879), 236.1759 [8%; $(M-CH_3CO+H)^+$], 221.1534 [19%; $(M-CH_3CO-CH_3+H)^+$], 218.1654 [20%; $(M-AcOH)^+$], 203.1439 [22%; $(M-AcOH-CH_3)^+$], 152.1211 (43%; **b**; $C_{10}H_{16}O$), 134.1094 [99%; (**a**−AcOH); $C_{10}H_{14}$], 123.0855 [47%; (**c**−H), $C_8H_{11}O$], 119.0861 [87%; (**a**−AcOH−CH_3); C_9H_{11}], 109.1013 (79%; C_8H_{13}), and 94.0782 (100%; C_7H_{10}).

*Acetonization of the Diol D (**5a**).* To a solution of the diol D (**5a**; 19.5 mg) in acetone (0.5 ml) containing a trace of sulfuric acid, was added anhydrous cupric sulfate (40 mg) and the mixture was stirred vigorously at room temperature for 18 h. Cupric sulfate was separated by filtration and washed with acetone. The combined acetone solution was neutralized with powdered calcium hydroxide. After filtration, the solvent was removed to give a residue, which was chromatographed on a column of silica gel (5 g). Elution with hexane–ether (17: 3; each fraction, 2.5 ml) gave an acetonide (8.7 mg; from frs 4—7), whose spectral data were identical with those of the acetonide (**8a**).

*Acid Hydrolysis of the Acetonide (**8a**).* A mixture of the acetonide (**8a**; 52 mg), methanol (3 ml), and 0.5 M hydrochloric acid (1.5 ml) was stirred at room temperature for 7 h. The reaction mixture was neutralized with aqueous sodium hydroxide solution and extracted with ether after methanol was removed. The ethereal solution was washed with brine, dried over sodium sulfate, and evaporated to give a residue (37 mg), which was chromatographed on a column of silica gel (5 g; elution with hexane–ether (1: 2); each fraction, 5 ml). Fractions 13—21 yielded the diol D (**5a**; 26 mg).

*Treatment of Humulene (**1**) with Osmium Tetroxide.* To a solution of humulene (**1**; 54 mg) in dry ether (5 ml) was added osmium tetroxide (67 mg) in dry ether (1.5 ml) under nitrogen atomosphere and the reaction mixture was left for 14 h at room temperature in the dark. A solution of sodium sulfite (470 mg) in water (5 ml) and ethanol (2.5 ml) was added to the reaction mixture and refluxed for 4 h under nitrogen atmosphere in the dark. The precipitate was removed by filtration and washed with hot ethanol. The combined solution was concentrated under reduced pressure, and extracted with ether. The ethereal solution was washed with brine, dried over sodium sulfate, and the solvent was evaporated to give a residue (40 mg), which was chromatographed on a column of silica gel (5 g; elution with hexane–ether (1: 2); each fraction 2.5 ml). Fractions 7—11 gave a diol (27.3 mg) which was identified to be the diol D (**5a**).

*Periodate Oxidation of the Diol C (**5b**).* A solution of the diol C (**5b**; 5.3 mg) in methanol (5 ml) was treated with 22.6 mM aqueous potassium periodate solution (2 ml) at room temperature for 28 h. Aqueous sodium arsenite solution (5 ml; 26.3 mM soln) and 20% aqueous potassium iodide solution (1 ml) were added and the resulting mixture was titrated with iodine solution; it was shown that *ca.* 0.65 equivalent mole of periodate was consumed. After the titration was effected, the mixture was extracted with dichloromethane. The organic layer was washed with brine, dried over sodium sulfate, and the solvent was evaporated. Crystals (2.6 mg; **5b**; diol C) separated from the residual oil were filtered. The residue was then passed through a column of silica gel (1 g) and eluted with hexane–ether (1: 1) to give a *keto aldehyde* (**15**; 0.4 mg), a colorless oil, IR (liquid) 2720, 1720, 1380, 1360, 1160, and 975 cm^{-1}; PMR ($CDCl_3$) δ 0.99 (6H, s), 1.62 (3H, br s), 1.98 (2H, d, J=7 Hz), 2.14 (3H, s), 2.43 (4H), 3.11 (2H, d, J=6 Hz), 5.18 (1H, t, J=7 Hz), 5.49 (2H, d, J=2 Hz), and 9.75 (1H, br s); MS *m/e* 218 [0.3%; $(M-H_2O)^+$], 207 [0.3%; $(M-CHO)^+$], 193 [0.6%; $(M-CH_3CO)^+$], 178 (15%), 125 (45%), and 43 (100%); GLC R_t=6.2 min [column, SP-1000 (10%); 220 °C; N_2 flow rate, 55 ml/min], R_t=7.7 min [column, Dexsil-300GC (5%); 200 °C; N_2 flow rate, 53 ml/min].

*Periodate Oxidation of the Diol D (**5a**).* A solution of the diol D (**5a**; 6.5 mg) in methanol (3 ml) was treated with

24.2 mM aqueous potassium periodate solution (2 ml) at room temperature for 24 h; *ca.* 1.1 equivalent mole of periodate was consumed. Treatment of the reaction mixture as described above afforded a keto aldehyde (**15**; 5 mg), whose spectral data and chromatographic (TLC and GLC) properties were identical with those of the keto aldehyde obtained from the diol C (**5b**).

Acetylation of the Diol C (5b). A solution of the diol C (**5b**; 11.7 mg) in pyridine was acetylated with acetic anhydride at room temperature for 2 days. Treatment as usual gave an oily product, which was passed through a silica gel dry column [5 g; elution with hexane–ether (2: 3)] to yield a *monoacetate* (**16b**; 7.4 mg), an amorphous solid, IR (liquid) 3450, 1730, 1710 (sh), 1380, 1373, 1260 (sh), 1245, 1025, 980, 875, and 800 cm^{-1}; PMR ($CDCl_3$) δ 1.07, 1.16, 1.23, 1.64, 2.10 (each 3H, s), and 4.9—5.5 (4H); MS *m/e* 280 (1%; M^+; $C_{17}H_{28}O_3$), 262 [1%; $(M-H_2O)^+$], 220 [5.5%; $(M-AcOH)^+$], 202 [4%; $(M-AcOH-H_2O)^+$], 138 (18%), 129 [1.5%; (**e**′−H)], 125 [100 %; (**d**–H)], 116 (40%; **e**), 109 (36%), 95 (73%), 83 [50%; (**f**+H)], 74 (30%), and 68 (70%). Further purification was not effected due to paucity of the material.

Acetylation of the Diol D (5a). The diol (**5a**; 15.5 mg) in pyridine was acetylated with acetic anhydride at room temperature for 16 h. The usual treatment gave a product which was passed through a silica gel dry column (5 g) and eluted with hexane–ether (2: 3) to afford a *monoacetate* (**16a**; 6.2 mg), mp 132.5—133.0 °C (crystallized from hexane); IR (Nujol) 3450, 1740 (sh), 1710, 1260, 1240 (sh), 1035, 990, 965, and 880 cm^{-1}; PMR ($CDCl_3$) δ 1.07, 1.14, 1.18, 1.63, 2.11 (each 3H, s), and 4.7—5.7 (4H); MS *m/e* 280 (1%; M^+; $C_{17}H_{28}O_3$), 262 [2%; $(M-H_2O)^+$], 220 [5%; $(M-AcOH)^+$], 205 [2%; $(M-AcOH-CH_3)^+$], 202 [5%; $(M-AcOH-H_2O)^+$], 138 (32%), 129 [16%; (**e**′−H)], 125 [65%; (**d**−H)], 116 (71 %; **e**), 109 (45%), 95 (100%), 83 [59%; (**f**+H)], and 68 (96%).

The authors wish to thank Dr. Nobuo Nakamura, the University of Tokyo, for decoupling experiment by FT-NMR.

References

1) Preliminary accounts of this paper: M. Namikawa, T. Murae, and T. Takahashi, 21th Symposium on the Chemistry of Perfumes, Terpenes, and Essential Oils, Tokushima, November 1977, Abstr. No. B36; M. Namikawa, T. Murae, and T. Takahashi, *Chem. Lett.*, **1978**, 391.

2) *e.g.* A. A. Newman, "Chemistry of Terpenes and Terpenoids," Academic Press, London (1972), pp. 111, 118, 361; D. Baines, J. Forrester, and W. Parker, *J. Chem. Soc., Perkin Trans. 1*, **1974**, 1958. And references cited therein.

3) Nomenclature following biogenetic considerations is applied for humulene derivatives.

4) M. A. McKervey and J. R. Wright, *Chem. Commun.*, **1970**, 117.

5) N. P. Damodaran and Sukh Dev, *Tetrahedron*, **24**, 4113, 4123, 4133 (1968).

6) a) J. M. Greenwood, J. K. Sutherland, and A. Torre, *Chem. Commun.*, **1965**, 410; b) J. M. Greenwood, M. D. Solomon, J. K. Sutherland, and A. Torre, *J. Chem. Soc., C*, **1968**, 3004.

7) Y. Naya and M. Kotake, *Nihon Kagaku Zasshi*, **91**, 275 (1970).

8) Y. Naya and M. Kotake, *Bull. Chem. Soc. Jpn.*, **42**, 2405 (1969).

9) Y. Naya and M. Kotake, *Bull. Chem. Soc. Jpn.*, **42**, 2088 (1969).

10) Formation of **3** on treatment of **2** with mercuric nitrate, *t*-butyl alcohol, and water was reported: T. Ohtsuka, S. Misumi, Y. Ohfune, H. Shirahama, and T. Matsumoto, 36th National Meeting of the Chemical Society of Japan, April 1977, Abstr. No. 1U23.

11) Compounds (**2—5**, **8—14**, and **15**) described in the present paper refer to racemic modifications.

12) R. Ratcliffe and R. Rodehorst, *J. Org. Chem.*, **35**, 4000 (1970).

13) A. T. McPhail, R. I. Reed, and G. A. Sim, *Chem. Ind. (London)*, **1964**, 976; J. A. Hartsuck and I. C. Paul, *ibid.*, **1964**, 977; A. T. McPhail and G. A. Sim, *J. Chem. Soc., B*, **1966**, 112.

14) Formation of the diol (**5**) on treatment of 9,10-epoxyhumula-2,6-diene with BF_3–AcOH, and the oxidation of humulene (**1**) with OsO_4 followed by treatment with Ag^+ to give **15** were recently reported: S. Misumi, Y. Kanemoto, T. Ohtsuka, Y. Ohfune, H. Shirahama, and T. Matsumoto, 37th National Meeting of the Chemical Society of Japan, April 1978, Abstr. No. 1R40.

15) M. Ōki and H. Iwamura, *Bull. Chem. Soc. Jpn.*, **32**, 306 (1959); P. R. Schleyer, D. S. Trifan, and R. Backskai, *J. Am. Chem. Soc.*, **80**, 6691 (1958).

16) Concerted mechanism could also be applicable.

17) W. Treibes, *Ber., B*, **72**, 7 (1939); **80**, 56 (1947).

Preparation of Alkylthio- and Phenylthio(triphenylphosphine)copper(I) Complexes and Their Catalytic Activity for Transesterification of *S*-Alkyl Ethanethioates and Thiols

Minoru KUBOTA and Akio YAMAMOTO*

Research Laboratory of Resources Utilization, Tokyo Institute of Technology, Nagatsuta, Midori-ku, Yokohama, 227

(Received June 9, 1978)

Alkylcopper complexes, $RCu(PPh_3)_2$ (R=methyl, ethyl, propyl, isobutyl)reacted with sulfur smoothly at low temperatures to produce dialkyl disulfides. This indicates the insertion of sulfur to alkyl-Cu bond taking place followed by coupling of the two alkylthio-Cu bonds. Methylcopper complex, $CH_3Cu(PPh_3)_2 \cdot 0.5Et_2O$ reacted with thiols to produce alkylthio- and phenylthiocopper complexes having one or two triphenylphosphine ligands. The reactions of these alkylthiocopper complexes with acyl halides and acid anhydrides produced *S*-alkyl ethanethioates in high yields, whereas the reactions of alkylthiocopper complexes with alkyl halides produced dialkyl sulfides. Alkylthio- and phenylthiocopper complexes were found to catalyze the transesterification reactions between *S*-alkyl ethanethioates and thiols. The exchange reactions also take place between the alkylthiocopper complex and benzenethiol producing phenylthiocopper complex with liberation of alkanethiol.

As part of the project for studying the chemistry of organic copper complexes we have been investigating the properties of alkylcopper and alkoxocopper complexes containing tertiary phosphine ligands.[1-9] Natural extension of our study of alkoxocopper complexes[8,9] has led us to investigation of the chemistry of copper complexes containing organic sulfur moiety. Survey of the literature revealed that the chemistry of organic sulfur-copper complexes has been scarcely explored. Copper(I) alkanethiolates have been prepared by the reaction of copper(II) sulfate and thiols,[10] from copper(II) acetoacetate and sulfocyanate,[11] and from copper(II) acetate and thiols.[12] Phenylthiocopper complex also has been prepared from $ClCu(PPh_3)_3$ and NaSPh.[13] The copper(I) alkane- and benzenethiolates thus obtained are insoluble except for copper(I) alkanethiolates of higher secondary thiols in organic solvents, but their characterization is far from satisfactory.

Some reactions of the copper(I) alkane- and benzenethiolates have been examined sporadically, including the reactions of the complexes with carbon disulfide,[12] alkenyl halides,[14] phenyl acetylene,[15] sulfur dioxide.[16] Since most of the works concerning the copper(I) alkanethiolates have been done in rather old days and in none of the works the well defined copper(I) alkanethiolates have been prepared and their behavior examined, we consider it worthwhile to prepare a series of alkylthiocopper and phenylthiocopper complexes and examine their properties as chemical reagents which might be used for organic syntheses, particularly for catalytic reactions.

Our previous work on alkylcopper and alkoxocopper complexes having tertiary phosphine ligands[1-9] revealed the remarkable stabilizing effects of the tertiary phosphine ligands and employment of the tertiary phosphine ligands led to isolation of various well-characterized organic copper complexes. This paper deals with the preparation of new alkylthio- and phenylthiocopper complexes starting from the methylcopper complex having triphenylphosphine ligands and their properties including catalytic transesterification reactions of *S*-alkyl ethanethioate with thiols.

Results and Discussion

Preparation of Alkylthio- and Phenylthiocopper Complexes with Triphenylphosphine Ligands. As our previous studies on the properties of alkylcopper complexes having tertiary phosphine show, they have some similarities to Grignard reagents. Grignard reagents are known to react with sulfur giving magnesium alkanethiolates which on hydrolysis yield thiols.[17] Therefore we first attempted to prepare the alkylthiocopper complexes by reactions of sulfur with alkylcopper complexes having triphenylphosphine ligands in tetrahydrofuran below −10 °C. The reaction did not give isolable alkylthiocopper complexes but yielded dialkyl disulfides accompanied by small amounts of dialkyl sulfides as shown in Table 1. As our later study showed the alkylthiocopper complex once formed can be readily converted into dialkyl disulfide in high yields on reaction with sulfur. The small amount of dialkyl sulfide may have been produced by the reaction of alkylthiocopper

TABLE 1. REACTION OF ALKYLCOPPER COMPLEXES WITH SULFUR[a]

$$RCu(PPh_3)_2 \xrightarrow[\text{in THF}]{\text{Sulfur}} R\text{–}S\text{–}S\text{–}R + R\text{–}S\text{–}R$$

Alkylcopper complex (mmol)	Sulfur (g)	Products (yield %)[b] RSSR	RSR
$CH_3Cu(PPh_3)_2 \cdot 0.5Et_2O$ (1.00)	2.00	43	1
$CH_3CH_2Cu(PPh_3)_2$ (0.45)	1.50	30	7
$CH_3CH_2CH_2Cu(PPh_3)_2$ (0.89)	2.00	31	3
$(CH_3)_2CHCH_2Cu(PPh_3)_2$ (3.02)	2.50	48	2

a) The reactions were carried out in tetrahydrofuran for 5 h at −40 to −10 °C in a vacuum or under N_2 atmosphere. b) Yields were calculated based on alkyl group in alkylcopper complexes. Alkanes were also evolved in these reactions.

Table 2. Characterization data of alkylthio- and phenylthiocopper complex

Complex	Yield (%)	Mp[b] (°C)	Molecular weight (Calcd)	Elemental analyses Found (Calcd) (%) C	H	S	^{1}H-NMR (r.t., C_6D_6)
$CH_3CH_2SCu(PPh_3)_2$ **1**	78	139 (dec)	—[a]	70.4 (70.4)	5.3 (5.4)	5.1 (4.9)	δ 1.2 (t, 3H), δ 2.8 (q, 2H) δ 7.1 (m, 18H, *m,p*-phenyl) δ 7.5 (m, 12H, *o*-phenyl)
$CH_3CH_2CH_2SCuPPh_3$ **2**	84	57—58 (dec)	455±10 (400.5)	63.0 (62.9)	5.0 (5.5)	8.3 (8.0)	δ 0.75 (t, 3H), δ 1.7 (m, 2H) δ 2.8 (t, 2H), δ 7.1 (m, 9H, *m,p*-phenyl) δ 7.6 (m, 6H, *o*-phenyl)
$(CH_3)_2CHSCuPPh_3$ **3**	86	135—136 (dec)	448±10 (400.5)	63.0 (62.9)	5.2 (5.5)	7.7 (8.0)	δ 1.46 (d, 6H), δ 3.4 (m, 2H) δ 7.1 (m, 9H, *m,p*-phenyl) δ 7.6 (m, 6H, *o*-phenyl)
$(CH_3)_2CHCH_2SCu(PPh_3)_2$ **4**	81	75 (dec)	603±10 (676.5)	71.2 (71.0)	5.7 (5.8)	4.7 (4.7)	δ 1.0 (d, 6H), δ 1.8 (m, 1H) δ 2.7 (d, 2H), δ 7.1 (m, 18H, *m,p*-phenyl) δ 7.6 (m, 12H, *o*-phenyl)
$PhSCu(PPh_3)_2$ **5**	92	148—149 (dec)	620±10 (696.5)	72.0 (72.3)	4.8 (5.0)	4.5 (4.6)	δ 6.7 (m, 5H) δ 7.0 (m, 18H, *m,p*-phenyl) δ 7.5 (m, 12H, *o*-phenyl)

a) Complex **1** is not satisfactorily soluble in benzene to allow the molecular weight measurement.
b) Measured in vacuum-sealed capillaries.

complexes with remaining alkylcopper complexes or by the reaction of the dialkyl disulfide with triphenylphosphine which was present in the reaction mixture by dissociation from the copper complex.

Upon failure of our attempts to prepare an alkylthiocopper complex using sulfur powder we have tried reactions of thiols with a methylcopper complex having triphenylphosphine ligands and found that the reactions at 0 °C in diethyl ether gave a series of alkylthiocopper complexes and phenylthiocopper complex in considerably high yields evolving one mole of methane per mol of the copper complex.

$$CH_3Cu(PPh_3)_2\cdot 0.5Et_2O + RSH \xrightarrow[Et_2O]{0\,^\circ C} RSCu(PPh_3)_n + CH_4$$

$n=1$ for R=*n*-Pr (**2**), *i*-Pr (**3**)
$n=2$ for R=Et (**1**), *i*-Bu (**4**), Ph (**5**)

The phenylthiocopper complex could be also prepared by the reaction of PhSH with Cu_2O in the presence of PPh_3 in a high yield (92%) as well as from the methylcopper complex with PhSH. The alkylthio- and phenylthiocopper complexes were characterized by elemental analysis, molecular weight determination (cryoscopic in benzene), chemical reactions, and IR and NMR spectroscopy. Table 2 shows relevant data for characterization together with yields and melting points with decomposition of alkylthio- and phenylthiocopper complexes. Infrared spectra of the alkylthiocopper complexes (shown in Experimental section) showed a band in the range of 1220 to 1260 cm^{-1} which may be related to alkylthio group, in addition to other bands due to triphenylphosphine. The molecular weights of the alkylthiocopper complexes having one triphenylphosphine ligand (complexes **2** and **3**) were found to be slightly higher than the theoretical values, whereas those of complexes having two triphenylphosphine ligands were slightly lower. The possible explanation for the former cases is the association of the alkylthiocopper complexes whereas in the latter the partial dissociation of the triphenylphosphine ligands might be taking place as have been observed in other alkylcopper complexes.[1-2,6] The melting points (with decomposition) of the isolated alkylthiocopper complexes showed a considerable variance and no reasonable explanation for this was found. Although the complexes have relatively high thermal stabilities and are relatively insensitive to air when heated rapidly, they are gradually decomposed at room temperature even under nitrogen.

Reactions of Alkylthiocopper Complexes. Pyrolysis of the ethylthiocopper complex at 150 °C liberated diethyl sulfide (54%), diethyl disulfide (31%) and a

Table 3. Reactions of alkylthiocopper complexes with various reagents[a]

Alkylthiocopper complex (mmol)	Reagent (quantity)	Product (yield % per Cu)
$CH_3CH_2CH_2SCuPPh_3$ **2** (0.72)	$CH_3CH_2CH_2Br$ (2 ml)	$CH_3CH_2CH_2SCH_2CH_2CH_3$ (39)
$CH_3CH_2CH_2SCuPPh_3$ **2** (0.38)	CH_3COCl (1.15 mmol)	$CH_3COSCH_2CH_2CH_3$ (92)
$CH_3CH_2SCu(PPh_3)_2$ **1** (0.20)	$(CH_3CO)_2O$ (0.5 ml)	$CH_3COSCH_2CH_3$ (95) $CH_3COOCu(PPh_3)_2$ (90)
$(CH_3)_2CHSCuPPh_3$ **3** (0.36)	$CH_3COOCH=CH_2$ (2 ml)	polyvinylacetate
$CH_3CH_2CH_2SCuPPh_3$ **2**	PhSH (1 ml)	$PhSCuPPh_3$ (88)

a) For reaction conditions see Experimental section.

TABLE 4. TRANSESTERIFICATION REACTIONS OF *S*-ALKYL ETHANETHIOATES WITH THIOLS USING ALKYLTHIOCOPPER COMPLEXES[a)]

Starting ester (mmol)	Thiol (quantity)	Catalyst (mmol)	Product (yield % starting ester)
$CH_3COSCH_2CH_3$ (4.86)	$CH_3CH_2CH_2SH$ (11 mmol)	**2** (0.25)	$CH_3COSCH_2CH_2CH_3$ (64)
$CH_3COSCH_2CH_2CH_3$ (1.19)	$(CH_3)_2CHSH$ (2.5 mmol)	**3** (0.25)	$CH_3COSCH(CH_3)_2$ (40)
$CH_3COSCH(CH_3)_2$[b)] (8.06)	CH_3CH_2SH (5 ml)	**1** (0.25)	$CH_3COSCH_2CH_3$ (11)
$CH_3COSCH_2CH(CH_3)_2$ (10.7)	$CH_3CH_2CH_2SH$ (5 ml)	**2** (0.50)	$CH_3COSCH_2CH_2CH_3$ (66)
CH_3COSPh (5.51)	$(CH_3)_2CHSH$ (5 ml)	**3** (0.25)	$CH_3COSCH(CH_3)_2$ (22)
$CH_3COSCH_2CH_3$[c)] (4.86)	$CH_3CH_2CH_2SH$ (22 mmol)	**5** (0.25)	$CH_3COSCH_2CH_2CH_3$ (41)

a) These reactions were carried out at room temperature for 12 h. b) At 32 °C for 2 h.
c) In 2 ml of THF.

small amount of ethane (7%) and a trace of ethylene, the yields being based on the ethyl group. Pyrolysis of the phenylthiocopper complex at 150 °C similarly gave diphenyl sulfide (43%), diphenyl disulfide (52%), and benzene (2%). The formation of disulfides may be accounted for by assuming the homolytic splitting of the RS–Cu bond yielding RS radicals which are known to give the disulfide on recombination. On the other hand, the sulfide may have been formed either from the disulfide on reaction with triphenylphosphine which is known to convert the disulfide into sulfide with concomitant conversion of the triphenylphosphine to triphenyl phosphine sulfide,[18,19)] or by the recombination of R radical and RS radical produced on pyrolysis of these complexes. The small amount of RH (ethane and benzene) seems to be produced by the abstraction of *o*-hydrogen of the PPh_3 ligand by the R radical. A part of the ethyl radical seems to participate into the disproportionation to afford ethylene. For further characterizing the alkylthiocopper complexes and for getting information of their chemical properties the alkylthiocopper complexes were subjected to various chemical reactions. The main features of the chemical properties of the alkylthiocopper complexes parallel with those of the alkoxocopper complexes as shown in Table 3. They afford *S*-alkyl ethanethioate on reaction with acetic anhydride and acetyl chloride, dialkyl sulfide on treatment with alkyl halide under mild conditions, whereas vinyl acetate was polymerized with the alkylthiocopper complex. Propylthiocopper complex **2** reacts with benzenethiol at 0 °C to produce the more thermally stable phenylthiocopper complex **6** in a high yield.

Catalytic Transesterification Reactions Promoted by the Alkylthiocopper Complexes. Our previous study on the alkoxocopper complexes revealed their excellent catalytic activities for transesterification of carboxylic esters with alcohols under mild conditions. In the light of the importance of the thiol esters such as exemplified by coenzyme A in biosynthesis, the catalytic transesterification reactions of *S*-alkyl ethanethioates with thiols promoted by the alkylthiocopper complexes under mild conditions were examined. As Table 4 shows, the alkylthiocopper complexes were found to serve as the transesterification catalyst in a similar manner to the alkoxocopper complexes which catalyzed the transesterification of carboxylic esters with alcohols.[9)] In view of the reluctane for the exchange of the alkylthio group bound to copper with that in the other alkanethiol, a stepwise mechanism involving the exchange of RSCu entity with R'SH is not likely and attack of an ester carbonyl group, which is polarized on coordination to copper, by thiol in a nucleophilic manner as shown below seems to provide a reasonable explanation for the transesterification catalyzed by the copper complexes:

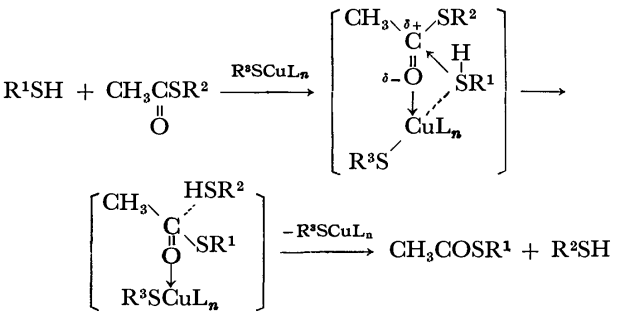

A similar S_N2 type mechanism has been proposed for the transesterification of carboxylic esters with alcohols catalyzed by alkoxocopper and phenoxocopper complexes.[9)]

Whereas the transesterification between the *S*-alkyl ethanethioates and thiols were catalyzed by the alkylthiocopper complexes, attempted transesterification of carboxylic esters with thiols has been so far unsuccessful. On the other hand transesterification of *S*-*t*-butyl ethanethioate with ethanol was found to be catalyzed by the ethoxocopper complex, $EtOCu(PPh_3)_2$. A related activation of thiol esters by copper, silver, and mercury compounds have been examined by Masamune and utilyzed for organic synthesis.[20,21)]

Experimental

General. All preparations and reactions of copper complexes were carried out in Schlenk type flasks under deoxygenated nitrogen, argon or in a vacuum. Solvents were dried by usual procedures, distilled, and stored under argon or nitrogen. IR spectra were recorded on a Hitachi Model

295 using KBr discs under nitrogen. ^{1}H-NMR spectra were recorded with a Japan Electron Optics Lab. JNM-PS-100 spectrometer. Evolved gas was analyzed with a Hitachi RMU 5B mass-spectrometer and a Shimadzu GC 5B gas chromatograph, and its volume was measured with a Toepler pump. The microanalysis of carbon, hydrogen, and nitrogen was performed by Mr. T. Saito of our labolatory with a Yanagimoto CHN Autocorder Type MT-2.

Reactions of Alkylcopper Complexes with Sulfur. Sulfur (2.0 g) was added into a Schlenk-type flask containing methylcopper complex, $CH_3Cu(PPh_3)_2 \cdot 0.5Et_2O$ (1 mmol) in THF (5 ml) and the yellow emulsion was stirred at -40 °C to -10 °C for 5 h to give a red solution. Analysis of the products in the solution by means of gas chromatography showed that dimethyl disulfide (yield 43%) and dimethyl sulfide (yield 1%) were produced (yields are based on the methyl group of the methylcopper complex). The other reactions between alkylcopper complexes and sulfur were carried in a similar way to the above reaction.

Preparation of Ethylthiobis(triphenylphosphine)copper (1). Ethanethiol (0.28 ml, 3.62 mmol) was added to a yellow suspension of $CH_3Cu(PPh_3)_2 \cdot 0.5Et_2O$ (1.932 g, 3.02 mmol) in 5 ml of Et_2O at -10 °C, and the mixture was stirred at -10 °C for about 10 min until the yellow emulsion turns to white. A quantative amount of methane (yield 98% on the basis of Cu) was evolved. The white complex produced was separated and recrystallized from toluene to give white crystals of $CH_3CH_2SCu(PPh_3)_2$ (**1**) (1.535 g, yield 78%). IR(KBr): 2950 w, 2900 w, 2840 w, 1235 w, 1235 m and other absorption bands due to PPh_3.

Preparation of Propylthiotriphenylphosphinecopper (2). The reaction of $CH_3Cu(PPh_3)_2 \cdot 0.5Et_2O$ (2.085 g, 3.26 mmol) with propanethiol (3.26 mmol) in 10 ml of Et_2O at -10 °C to 0 °C for 1 h produced a light yellow precipitate and methane (0.99 mol per Cu). The yellow precipitate was recrystallized from a mixture of Et_2O and toluene. Light yellow crystals of **2** (1.095 g, yield 84%) were obtained. IR(KBr): 2950 w, 2900 w, 2860 w, 1200 m cm^{-1} and other absorption bands due to PPh_3.

Preparation of Isopropylthiotriphenylphosphinecopper (3). The reaction of $CH_3Cu(PPh_3)_2 \cdot 0.5Et_2O$ (1.475 g, 2.3 mmol) with 1-methyl-ethanethiol (2.76 mmol) in 5 ml of Et_2O at -10 °C to 0 °C for 1 h produced a white precipitate from the yellow emulsion. Methane (0.94 mol per Cu) was evolved. The white precipitate was recrystallized from a mixture of Et_2O and toluene to give white crystals of **3** (0.795 g, yield 86%). IR(KBr): 2930 w, 2900 w, 2840 w, 1220 w, 1140 w cm^{-1} and other absorption bands due to PPh_3.

Preparation of Isobutylthiobis(triphenylphosphine)copper (4). To a yellow suspension of the methylcopper complex (1.832 g, 2.86 mmol) in Et_2O (5 ml) at -20 °C 2-methylpropanethiol (3.44 mmol) was added. After stirring the mixture at -20 to 0 °C for 3 h a yellow solution was produced. On concentrating the solution, a white complex precipitated and it was recrystallized from a mixture of Et_2O and hexane to give white crystals of **4** (1.572 g, yield 81%). IR(KBr): 2950w, 2920w, 2900w, 2860w, 1370w, 1350w, 1225w cm^{-1} and other absorption bands due to PPh_3.

Preparation of Phenylthiobis(triphenylphosphine)copper (5). The reaction of the methylcopper complex (0.941 g, 1.31 mmol) with benzenethiol (1.57 mmol) in diethyl ether (5 ml) at -10 °C for 10 min produced a white precipitate from a yellow heterogeneous system. The precipitate was recrystallized from a mixture of diethyl ether and toluene and was dried in a vacuum to give crystals of **5** (0.835 g, yield 92%). IR(KBr): 1570s, 1260w, 1075m cm^{-1} and absorption bands due to PPh_3.

Thermal Decomposition of Complex 1 and 5. Complex **1** (0.5 mmol) was decomposed by heating at 150 °C under nitrogen atmosphere and diethyl ether (2 ml) was added to the cooled thermolysis residue. After stirring the solution the amount of products formed on thermolysis was measured by means of gas chromatography.

Reactions of Alkylthiocopper Complexes with Alkyl Halide, Acyl Halide, Acid Anhydride, Vinyl Acetate, and Benezenethiol. Propyl bromide (2 ml) was introduced into a Schlenk type flask containing **3** (0.722 mmol) by a trap-to-trap distillation in a vacuum. After stirring the white emulsion at room temperature for 1 h a yellow solution was produced and finally a colorless supernatant and a white precipitate of bromocopper(I) complex were produced with further stirring the solution for 11 h. The mixture was filtered and the filtrate was introduced into another flask by distillation to remove copper compounds. The distillate was analyzed by means of gas chromatography to confirm the formation of dipropyl sulfide (yield 39% on the basis of Cu). Other products in the reactions of alkylthiocopper complexes with reagents were analyzed similarly.

Acetyl chloride (1.15 mmol) was added to a white emulsion of **3** (0.382 mmol) in diethyl ether (2 ml) and the mixture was stirred at room temperature overnight under nitrogen atmosphere to give *S*-propyl ethanethioate (yield 92% on the basis of Cu).

Acetic anhydride (0.5 ml) was added to a white emulsion of **2** (0.204 mmol) in diethyl ether (2 ml) and the mixture was stirred at room temperature overnight to produce *S*-propyl ethanethioate (yield 95% on the basis of Cu) and a white precipitate of $CH_3CO_2Cu(PPh_3)_2$ (yield 90%).

Vinyl acetate (2 ml) was introduced into a Schlenk type flask containing **4** (0.355 mmol) by a trap-to-trap distillation in a vacuum. The yellow solution was stirred at -10 to 0 °C for a day to give polyvinylacetate.

One ml of benzenethiol was added to complex **2** (0.20 g, 0.5 mmol) in diethyl ether (3 ml) and the mixture was stirred at 10 min to give a yellow solution. Further stirring it for 20 min gave a white precipitate. The precipitate was crystallized from toluene to give white crystals identified as PhSCu-PPh_3 (**6**) (191 mg, yield 88%). Complex **6**, mp 115—117 °C (dec.). Found: C, 67.0; H, 4.91; S, 7.27%. Calcd for $C_{24}H_{20}PSCu$: C, 66.3; H, 4.60; S, 7.36%. IR(KBr): 1570s, 1260w, 1075s cm^{-1} and absorption bands due to PPh_3. ^{1}H-NMR (C_6D_6): δ 6.7 (m, 5H, phenyl); δ 7.0 (m, 9H, *m,p*-phenyl of PPh_3); δ 7.5 (m, 6H, *o*-phenyl of PPh_3).

Transesterification Reactions between S-Alkyl Ethanethioates and Thiols with Alkylthiocopper Catalysts. *S*-Ethyl ethanethioate (4.86 mmol) was added into a flask containing propanethiol (11 mmol) and **2** (0.25 mmol). The yellow solution was stirred at room temperature overnight and the mixture was passed through a column of Wakogel C-200 (5 g) with diethyl ether to remove copper compounds. The solution was condensed under reduced pressure and the condensate was analyzed by means of gas chromatography to confirm the formation of *S*-propyl ethanethioate (yield 64% on the basis of starting *S*-ethyl ethanethioate) and thiol. The other transesterification reactions were carried in a similar way.

Reaction between S-Alkyl Ethanethioate and Alcohol with Alkoxocopper Catalyst. *S-t*-Butyl ethanethioate (10 mmol) was added to a solution containing ethanol (40 mmol) and EtOCu-$(PPh_3)_2$ (0.3 mmol). The mixture was stirred at room temperature overnight to produce ethyl acetate (yield 14% on the basis of thiol ester) and 1,1-dimethylethanethiol (yield 13%).

References

1) A. Miyashita and A. Yamamoto, *Bull. Chem. Soc. Jpn.*, **50**, 1102 (1977).
2) A. Miyashita, T. Yamamoto, and A. Yamamoto, *Bull. Chem. Soc. Jpn.*, **50**, 1109 (1977).
3) T. Ikariya and A. Yamamoto, *J. Organomet. Chem.*, **72**, 145 (1975).
4) A. Miyashita and A. Yamamoto, *J. Organomet. Chem.*, **113**, 187 (1976).
5) A. Yamamoto, A. Miyashita, T. Yamamoto, and S. Ikeda, *Bull. Chem. Soc. Jpn.*, **45**, 1583 (1972).
6) M. Kubota, A. Miyashita, S. Komiya, and A. Yamamoto, *J. Organomet. Chem.*, **139**, 111 (1977).
7) T. Yamamoto, M. Kubota, A. Miyashita, and A. Yamamoto, *Bull. Chem. Soc. Jpn.*, **51**, 1835 (1978).
8) M. Kubota and A. Yamamoto, *Bull. Chem. Soc. Jpn.*, **51**, 2909 (1978).
9) M. Kubota, T. Yamamoto, and A. Yamamoto, submitted to *Bull. Chem. Soc. Jpn.*
10) P. Klason, *Ber.*, **20**, 3412 (1887).
11) E. Kohler, *Am. Chem. J.*, **22**, 72 (1899).
12) W. E. Duncan, E. Ott, and E. E. Reid, *Ind. Eng. Chem.*, **23**, 381 (1931).
13) W. T. Reichle, *Inorg. Chim. Acta*, **5**, 325 (1971).
14) A. Commercon, J. Normant, and J. Villieras, *J. Organomet. Chem.*, **93**, 415 (1975).
15) W. T. Reichle, *Inorg. Nucl. Chem. Lett.*, **1969**, 981.
16) P. G. Eller and G. J. Kubas, *J. Am. Chem. Soc.*, **99**, 4346 (1977).
17) N. Rabjohn, Editor-in-Chief, "Organic Syntheses" collective Vol. 4, page 667.
18) M. B. Evans, G. M. C. Higgins, C. G. Moore, M. Porter, S. Savile, J. F. Smith, B. R. Trego, and A. A. Watson, *Chem. & Ind.*, **1960**, 88.
19) "Chemistry of Organosulfur Compounds," ed by S. Oae, Kagakudojin, Kyoto (1968), p. 80.
20) S. Masamune, Y. Hayase, W. Schilling, W. K. Chan, and G. S. Bates, *J. Am. Chem. Soc.*, **99**, 6756 (1977).
21) S. Masamune, S. Kamata, and W. Schilling, *J. Am. Chem. Soc.*, **97**, 3515 (1975).

Synthesis of 2′,3′,4,4′,6′-Pentahydroxychalcone, an Aglycone of Carthamin, and Its Isomerization into 4′,5,6,7- and 4′,5,7,8-Tetrahydroxyflavanone, Carthamidin and Isocarthamidin[1)]

Heitaro OBARA,* Jun-ichi ONODERA, Yuji KURIHARA, and Fumitada YAMAMOTO
Department of Applied Chemistry, Faculty of Engineering, Yamagata University, Yonezawa 992
(Received June 10, 1978)

2′,3′,4,4′,6′-Pentahydroxychalcone (**4**), an aglycone of carthamin, was synthesized by the demethoxymethylation of 2′,3′,4,4′,6′-pentakis(methoxymethoxy)chalcone prepared by the condensation of 2,3,4,6-tetrakis(methoxymethoxy)acetophenone with *p*-methoxymethoxybenzaldehyde. **4** was converted into 4′,5,6,7- and 4′,5,7,8-tetrahydroxyflavanone (**5** and **6**) by boiling with methanolic hydrochloric acid. On the basis of the comparisons of the properties of **5** and **6** with those of carthamidin (**A**) and isocarthamidin (**B**) derived from natural product, the structures originally assigned for **A** and **B** should be reversed.

In 1930, Kuroda[2)] obtained two flavanones, carthamidin (**A**) and isocarthamidin (**B**), by the hydrolysis of carthamin, the red coloring matter of the flowers of Safflower (*Carthamus tinctorius* L.) and proposed the structures of 4′,5,7,8- and 4′,5,6,7-tetrahydroxyflavanone (**6** and **5**) for **A** and **B**, respectively. However, the identification of **A** and **B** has not yet been accomplished synthetically. In 1949, Seshadri *et al.*[3)] reported the synthesis of **5** and **6** by the demethylation of the corresponding tetramethoxyflavanones in the presence

TABLE 1. CHEMICAL SHIFTS (δ) AND COUPLING CONSTANTS OF 4′,5,6,7- AND 4′,5,7,8-TETRAHYDROXYFLAVANONE (**5** AND **6**), 4′,5,6,7- AND 4′,5,7,8-TETRAACETOXYFLAVANONE (**7** AND **8**), AND 4′,5,6,7- AND 4′,5,7,8-TETRAMETHOXYFLAVANONE (**9** AND **10**)

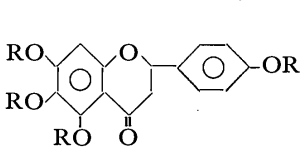

5 R=H, **7** R=Ac, **9** R=Me

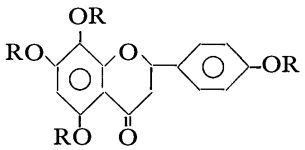

6 R=H, **8** R=Ac, **10** R=Me

	5[a)]	**6**[a)]
C_3–H	2.72 (1H, q, J=16.9 and 3.3 Hz)	2.64 (1H, q, J=17.2 and 3.3 Hz)
	3.21 (1H, q, J=16.9 and 11.9 Hz)	3.13 (1H, q, J=17.2 and 12.3 Hz)
C_2–H	5.43 (1H, q, J=11.9 and 3.3 Hz)	5.38 (1H, q, J=12.3 and 3.3 Hz)
C_6–H		5.84 (1H, s)
C_8–H	5.94 (1H, s)	
$C_{3',5'}$–H	6.80 (2H, d, J=8.5 Hz)	6.68 (2H, d, J=8.5 Hz)
$C_{2',6'}$–H	7.36 (2H, d, J=8.5 Hz)	7.25 (2H, d, J=8.5 Hz)
OH	8.01, 9.52, 10.36, and 11.72 (4H, s)	7.88, 9.46, 10.82, and 11.62 (4H, s)
	7[b)]	**8**[b)]
OAc	2.21, 2.23, 2.24, and 2.34 (12H, s)	2.21, 2.27, 2.28, and 2.34 (12H, s)
C_3–H	2.74 (1H, q, J=17.0 and 2.7 Hz)	2.78 (1H, q, J=16.9 and 2.8 Hz)
	2.99 (1H, q, J=17.0 and 13.7 Hz)	3.01 (1H, q, J=16.9 and 13.4 Hz)
C_2–H	5.46 (1H, q, J=13.7 and 2.7 Hz)	5.49 (1H, q, J=13.4 and 2.8 Hz)
C_6–H		6.22 (1H, s)
C_8–H	6.87 (1H, s)	
$C_{3',5'}$–H	7.10 (2H, d, J=8.5 Hz)	7.10 (2H, d, J=8.5 Hz)
$C_{2',6'}$–H	7.40 (2H, d, J=8.5 Hz)	7.40 (2H, d, J=8.5 Hz)
	9[b)]	**10**[b)]
OMe	3.82, 3.86, and 3.97 (12H, s)	3.78, 3.81, 3.91, and 3.93 (12H, s)
C_3–H	2.75 (1H, q, J=16.8 and 2.2 Hz)	2.83 (1H, q, J=16.7 and 3.7 Hz)
	3.01 (1H, q, J=16.8 and 14.0 Hz)	3.00 (1H, q, J=16.7 and 11.5 Hz)
C_2–H	5.36 (1H, q, J=14.0 and 2.2 Hz)	5.41 (1H, q, J=11.5 and 3.7 Hz)
C_6–H		6.10 (1H, s)
C_8–H	6.35 (1H, s)	
$C_{3',5'}$–H	6.95 (2H, d, J=8.5 Hz)	6.90 (2H, d, J=8.5 Hz)
$C_{2',6'}$–H	7.50 (2H, d, J=8.5 Hz)	7.50 (2H, d, J=8.5 Hz)

a) In DMSO-d_6. b) In $CDCl_3$.

of anhydrous aluminium chloride in benzene solution, but the direct comparisons with the natural products were not undertaken.

In this paper, we wish to report the synthesis of 2′,3′,4,4′,6′-pentahydroxychalcone (**4**) and its isomerization into 4′,5,6,7- and 4′,5,7,8-tetrahydroxyflavanone (**5** and **6**) and, furthermore, the new fact that the structures originally assigned for **A** and **B** should be reversed from the comparisons of the properties of **5** and **6** with those of **A** and **B** derived from the natural product.

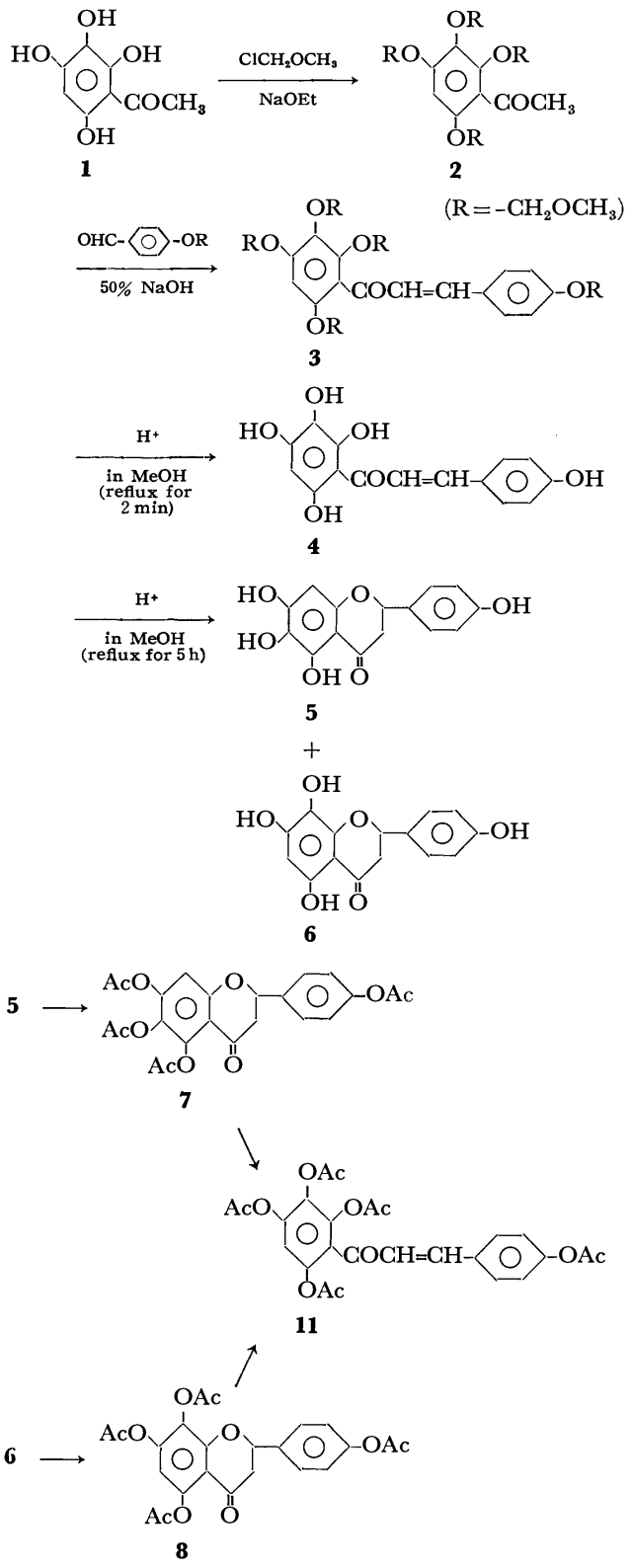

Scheme 1.

The alkaline condensation of 2,3,4,6-tetrakis(methoxymethoxy)acetophenone (**2**) prepared by the methoxymethylation of 2,3,4,6-tetrahydroxyacetophenone (**1**) with *p*-methoxymethoxybenzaldehyde afforded 2′,3′,4,-4′,6′-pentakis(methoxymethoxy)chalcone (**3**) as a pale yellow viscous oil. The subsequent demethoxymethylation of **3** with dilute hydrochloric acid in methanol gave 2′,3′,4,4′,6′-pentahydroxychalcone (**4**). The structure of this chalcone was identified by its conversion into 2′,3′,4,4′,6′-pentamethoxychalcone, which was identified by a comparison of the melting point, UV, and IR spectrum with those of an authentic sample.[2]

A mixture of 4′,5,6,7- and 4′,5,7,8-tetrahydroxyflavanone (**5** and **6**) was obtained by boiling **4** with dilute hydrochloric acid in methanol; it was chromatographed on a column of silica gel to give **5** and **6**, both in 25% yields. 4′,5,6,7- and 4′,5,7,8-Tetraacetoxyflavanone (**7** and **8**) were obtained by acetylation of **5** and **6** with acetic anhydride–sulfuric acid and both **7** and **8** afforded 2′,3′,4,4′,6′-pentaacetoxychalcone (**11**) by heating with a mixture of acetic anhydride and sodium acetate.

The structure of **5** and **6** were confirmed by the elemental analyses, by the studies of their UV, IR, and PMR spectra, and by the comparison of their tetramethyl ethers with the authentic samples of 4′,5,6,7-[4] and 4′,5,7,8-tetramethoxyflavanone[5] (**9** and **10**), prepared in a manner similar to that in the literature. The PMR spectral data of **5**, **6**, **7**, **8**, **9**, and **10** are shown in Table 1.

While Kuroda[2] proposed the structures **6** and **5** for carthamidin (**A**), mp 220 °C, and isocarthamidin (**B**), mp 240 °C, on the basis of the color phenomena of their hydroxyl groups, the IR spectra of **A** and **B** obtained from carthamin according to Kuroda's method[2] were identical with those of the synthetic **5** and **6**, respectively. Accordingly, it was proved that the old structures assigned for carthamidin (**A**) and isocarthamidin (**B**) should be reversed, as mentioned above. Finally, the comparison of the melting points of the synthetic **5**, **6**, **7**, **8**, and **11** with those of the derivatives of carthamin reported by Kuroda[2] are shown in Table 2.

Table 2. The melting points of the synthetic and reported **5**, **6**, **7**, **8**, and **11**

Compound	Synthesized (°C)	Reported (°C)
4′,5,6,7-Tetrahydroxyflavanone (**5**)	218	240
4′,5,7,8-Tetrahydroxyflavanone (**6**)	248	220
4′,5,6,7-Tetraacetoxyflavanone (**7**)	160	180
4′,5,7,8-Tetraacetoxyflavanone (**8**)	178	158
2′,3′,4,4′,6′-Pentaacetoxychalcone (**11**)	142	142

Experimental

All the melting points were uncorrected. The UV and IR spectra were recorded with a Hitachi 135 spectrophotom-

eter and Hitachi EPI-S2 spectrophotometer, respectively. The PMR spectra were measured with a Hitachi R-22 spectrometer (90 MHz), using tetramethylsilane as an internal standard. The mass spectra were obtained on a Hitachi RMU-6M mass spectrometer.

2,3,4,6-Tetrahydroxyacetophenone (1). Into a mixture of 20 g of 1,2,3,5-benzenetetrol,[6] 10 g of acetonitrile, and 7 g of anhydrous zinc chloride in 200 ml of dry ether, dry hydrogen chloride gas was passed for 3 h under cooling with ice water, and the reaction mixture was left to stand overnight at 0 °C. After the solvent was removed by decantation, the residue was refluxed with 600 ml of water for 3 h. The reaction mixture was decolored with charcoal and filtered. After cooling, **1** was obtained from the filtrate as light yellow needles (16.8 g, 65%), mp 236—238 °C (lit,[7] 206—208 °C); MS *m/e* 184 (M^+); IR (KBr) 1630 cm^{-1} (C=O); PMR (DMSO-d_6) δ 2.60 (3H, s, -OAc), 6.02 (1H, s, C_5-H), 9.98, 11.18, and 12.18 (4H, -OH). Found: C, 52.39; H, 4.63%. Calcd for $C_8H_8O_5$: C, 52.18; H, 4.38%. Tetramethyl ether, mp 55—56 °C (lit,[2] 54 °C). Found: C, 60.33; H, 6.95%. Calcd for $C_{12}H_{16}O_5$: C, 59.99; H, 6.71%. Tetraacetate, mp 110—111 °C. Found: C, 54.61; H, 4.70%. Calcd for $C_{16}H_{16}O_9$: C, 54.55; H, 4.58%.

2,3,4,6-Tetrakis(methoxymethoxy)acetophenone (2). Into a solution of **1** (5 g) in 100 ml of absolute ethanol was added one fifth volume of a solution of sodium (8.8 g) in 140 ml of absolute ethanol with stirring at 15—20 °C. After 30 s, one fifth volume of chloromethyl ether (31 g) was added to the above solution over a 5 min interval with stirring at 15—20 °C, this operation was repeated four times under the same conditions. After the addition was completed, the reaction mixture was stirred for 10 min at 40 °C. The solvent was removed *in vacuo* and 100 ml of water was added to the residue and extracted with ether. The ether was evaporated to give an oily residue, which was chromatographed over silica gel. Elution with benzene–ethyl acetate (4: 1) afforded **2** as a light yellow oil (2.9 g, 30%). IR ($CHCl_3$) 1963 cm^{-1} (C=O); PMR ($CDCl_3$) δ 2.53 (3H, s, -OAc), 3.49, 3.51, 3.53, and 3.62 (8H, s, $-CH_2-\times 4$), 5.12, 5.16, 5.17, and 5.24 (12H, s, $-CH_3\times 4$), 6.86 (1H, s, C_5-H). Found: C, 52.99; H, 6.61%. Calcd for $C_{16}H_{24}O_9$: C, 53.33; H, 6.71%.

2′,3′,4,4′,6′-Pentakis(methoxymethoxy)chalcone (3). To a mixed solution of **2** (600 mg) and *p*-methoxymethoxybenzaldehyde (510 mg) in 12 ml of methanol was added 6 ml of 50% aqueous sodium hydroxide solution with stirring at room temperature. After standing overnight, the reaction mixture was poured into cold water and extracted with ether. The evaporation of the solvent gave an oily residue, which was chromatographed over silica gel. Elution with benzene–ethyl acetate (4: 1) afforded **3** as a viscous light yellow oil (830 mg, 98%). IR ($CHCl_3$) 1640 cm^{-1} (C=O); PMR ($CDCl_3$) δ 3.34, 3.36, 3.42, 3.49, and 3.57 (15H, s, $-CH_3\times 5$), 5.05, 5.07, and 5.18 (6H, s, $-CH_2-\times 3$), 5.13 (4H, s, $-CH_2-\times 2$), 6.78 (1H, s, $C_{5'}$-H), 6.99 (2H, d, J=8.5 Hz, $C_{3,5}$-H), 7.43 (2H, d, J=8.5 Hz, $C_{2,6}$-H), 6.85 (1H, d, J=16.0 Hz, C_α-H), 7.32 (1H, d, J=16.0 Hz, C_β-H). Found: C, 59.44; H, 6.65%. Calcd for $C_{25}H_{32}O_{11}$: C, 59.05; H, 6.34%.

2′,3′,4,4′,6′-Pentahydroxychalcone (4). A mixture of **3** (400 mg) and 6 M hydrochloric acid (6 ml) in 16 ml of methanol was refluxed for 2 min. After cooling, the reaction mixture was poured into 30 ml of cold brine and extracted with ether. The ether layer was dried over anhydrous sodium sulfate and concentrated to about 10 ml *in vacuo*. A small quantity of petroleum ether was added to the concentrated solution to give **4** as yellow crystals (170 mg, 74%), mp 181 °C. UV (EtOH) max: 375 nm (log ε=4.47); IR (KBr) 1625 cm^{-1} (C=O); PMR (acetone-d_6) δ 6.07 (1H, s $C_{5'}$-H), 6.96 (2H, d, J=8.5 Hz, $C_{3,5}$-H), 6.73 (2H, d, J=8.5 Hz, $C_{2,6}$-H), 7.83 (1H, d, J=16.0 Hz, C_α-H), 8.24 (1H, d, J=16.0 Hz, C_β-H), 8.95, 11.36, and 11.54 (4H, s, OH). Found: C, 62.15; H, 4.54%. Calcd for $C_{15}H_{12}O_6$: C, 62.50; H, 4.20%.

Methylation of 4. A mixture of **4** (100 mg), potassium carbonate (2 g), and dimethyl sulfate (0.3 ml) in 20 ml of acetone was refluxed for 8 h. The reaction mixture was worked up in the usual manner and the crude product was chromatographed on a column of silica gel with benzene–ethyl acetate (4: 1) to give the methyl ether of **4** (50 mg, 40%), mp 92—93 °C. UV (EtOH) max: 326 nm (log ε=4.47); IR (KBr) 1640 cm^{-1} (C=O); PMR (acetone-d_6) δ 3.70 (6H, s, $-OMe\times 2$), 3.74, 3.77, and 3.87 (9H, s, $-OMe\times 3$), 6.52 (1H, s, $C_{5'}$-H), 6.77 (1H, d, J=16.0 Hz, C_α-H), 7.22 (1H, d, J=16.0 Hz, C_β-H), 6.90 (2H, d, J=8.5 Hz, $C_{3,5}$-H), 7.53 (2H, d, J=8.5 Hz, $C_{2,6}$-H). Found: C, 66.82; H, 6.31%. Calcd for $C_{20}H_{22}O_6$: C, 67.01; H, 6.19%. The UV, IR, and PMR spectra of this methyl ether were completely identical with those of 2′,3′,4,4′,6′-pentamethoxychalcone, mp 92—93 °C (lit,[2] 112 °C), which was prepared by the condensation of 2,3,4,6-tetramethoxyacetophenone with *p*-anisaldehyde.

Isomerization of 4 into 4′,5,6,7- and 4′,5,7,8-Tetrahydroxyflavanone (5 and 6). A mixture of **4** (500 mg) and 6 M hydrochloric acid (5 ml) in 40 ml of methanol was refluxed for 5 h. The reaction mixture was evaporated *in vacuo* and the resulting residue was extracted with ethyl acetate. The ethyl acetate solution was dried over anhydrous sodium sulfate, the solvent was removed *in vacuo*,and the residue was chromatographed on a column of silica gel. Elution with ether–petroleum ether–formic acid (24: 16: 1) afforded a mixture of **5** and **6**. The subsequent silica gel column chromatography with carbon tetrachloride–ether–acetic acid (8: 1: 1) afforded **5** (100 mg, 20%) and **6** (100 mg, 20%), respectively.

4′,5,6,7-Tetrahydroxyflavanone (5): Mp 218 °C (from chloroform); UV (EtOH) max: 300 nm (log ε=4.13) and 368 nm (log ε=3.18); IR (KBr) 1643 cm^{-1} (C=O). Found: C, 62.31; H, 4.40%. Calcd for $C_{15}H_{12}O_6$: C, 62.50; H, 4.20%.

Tetraacetate (7): Mp 158 °C; UV (EtOH) max: 313 nm (log ε=4.04) and 327 nm (log ε=3.63); IR (KBr) 1685 and 1775 cm^{-1} (C=O). Found: C, 60.22; H, 4.36%. Calcd for $C_{23}H_{20}O_{10}$: C, 60.52; H, 4.42%.

4′,5,7,8-Tetrahydroxyflavanone (6): Mp 248 °C; UV (EtOH) max: 299 nm (log ε=4.17) and 370 nm (log ε=3.52); IR (KBr) 1642 cm^{-1} (C=O). Found: C, 62.22; H, 4.68%. Calcd for $C_{15}H_{12}O_6$: C, 62.50; H, 4.20%.

Tetraacetate (8): Mp 178 °C; UV (EtOH) max: 264 nm (log ε=4.03) and 322 nm (log ε=3.52); IR (KBr) 1684 and 1770 cm^{-1} (C=O). Found: C, 60.22; H, 4.35%. Calcd for $C_{23}H_{20}O_{10}$: C, 60.52; H, 4.42%.

Methylation of 5. A mixture of **5** (50 mg), potassium carbonate (3 g), and dimethyl sulfate (2 ml) in 15 ml of dry acetone was refluxed for 1 h. The reaction mixture was worked up in the usual manner and the crude product was chromatographed on a column of silica gel with ether–petroleum ether (3: 1) to afford light yellow crystals. Recrystallization from methanol gave tetramethyl ether of **5** (27 mg, 46%), mp 120—121 °C; UV (EtOH) max: 280 nm (log ε=4.22) and 330 nm (log ε=3.68); IR (KBr) 1670 cm^{-1} (C=O). Found: C, 66.27; H, 5.85%. Calcd for $C_{19}H_{20}O_6$: C, 66.27; H, 5.85%. The IR spectrum of this compound was completely identical with that of the authentic sample of 4′,5,6,7-tetramethoxyflavanone (**9**) (mp 121 °C, lit,[4] 119.5—120.6 °C) prepared by the literature method.[4]

Methylation of 6. Tetramethyl ether of **6**, mp 114—116 °C (37%), was obtained in a similar manner to that

described above. UV (EtOH) max: 286 nm (log ε=4.23) and 332 nm (log ε=3.66); IR (KBr) 1673 cm^{-1} (C=O). Found: C, 66.09; H, 5.93%. Calcd for $C_{19}H_{20}O_6$: C, 66.27; H, 5.85%.

The IR spectrum of this compound was completely identical with that of the authentic sample of 4',5,7,8-tetramethoxyflavanone (**10**) (mp 114—115 °C, lit,[5] 138—140 °C) prepared by the literature method.[5]

*2',3',4,4',6'-Pentaacetoxychalcone (**11**).* This pentaacetate, mp 142 °C (lit,[2] mp 142 °C), was obtained by acetylation of **7** and **8** in a manner similar to that described by Kuroda.[2] UV (EtOH) max: 313 nm (log ε=4.47); IR (KBr) 1640 and 1770 cm^{-1} (C=O); PMR ($CDCl_3$) δ 2.09, 2.11, and 2.27 (9H, s, -OAc×3), 2.22 (6H, s, -OAc×2), 7.12 (1H, s, $C_{5'}$-H), 6.83 (1H, d, J=16.0 Hz, C_α-H), 7.43 (1H, d, J=16.0 Hz, C_β-H), 7.11 (2H, d, J=8.5 Hz, $C_{3,5}$-H), 7.54 (2H, d, J=8.5 Hz, $C_{2,6}$-H).

*Carthamidin (**A**) and Isocarthamidin (**B**).* Both **A**, mp 218 °C (lit,[2] 220 °C), and **B**, mp 248 °C (lit,[2] mp 240 °C), were obtained by hydrolysis of carthamin according to Kuroda's method.[2] The IR spectra of **A** and **B** were identical with those of **5** and **6**, respectively.

The present work was partly supported by a Grant-in Aid for Scientific Research from the Ministry of Education.

References

1) Preliminary communications: H. Obara, J. Onodera, and Y. Kurihara, *Bull. Chem. Soc. Jpn.*, **44**, 289 (1971); H. Obara, J. Onodera, and F. Yamamoto, *Chem. Lett.*, **1973**, 915.
2) C. Kuroda, *Nippon Kagaku Zasshi*, **51**, 237 (1930).
3) N. Narasimhachari, V. D. Nageswara, and T. R. Seshadri, *Proc. Indian Acad. Sci., Sect. A*, **29**, 404 (1949).
4) M. G. Stout, H. Reich, and M. N. Huffman, *J. Pharmaceutical Sciences*, **53**, 192 (1964).
5) G. Bargellini and S. M. Zoras, *Gazz. Chim. Ital.*, **64**, 202 (1934); *Chem. Abstr.*, **28**, 5054 (1934).
6) J. Onodera and H. Obara, *Nippon Kagaku Zasshi*, **1973**, 1808.
7) M. Nierenstein, *J. Chem. Soc.*, **1917**, 6.

The Hydrocracking of Alkyl-substituted Polynuclear Aromatic Hydrocarbons over $ZnCl_2$/CuCl Molten Salt Catalyst[1)]

Yohji NAKATSUJI,* Yasuhiko IKKAKU, Masakatsu NOMURA, and Shōichi KIKKAWA

Department of Applied Chemistry, Faculty of Engineering, Osaka University, Yamadakami, Suita, Osaka 565

(Received April 13, 1978)

The hydrocracking of alkyl derivatives of polynuclear aromatic hydrocarbons (naphthalene, anthracene, dihydroanthracene, phenanthrene, and dihydrophenanthrene) over $ZnCl_2$/CuCl molten salt was examined at 400 °C for 3 h in a batch autoclave system. The kinds of alkyl groups, the positions of the alkyl groups, and the types of condensed rings were changed in order to clarify the decomposition process of the polynuclear aromatic hydrocarbons. On the basis of the detailed product distribution obtained by using GC-MS, the behavior of the alkyl group attached to the condensed ring under these reaction conditions was found to be different. Generally, in this investigation, the alkyl group was not completely dealkylated in the initial stage and remained in the products as monocyclic aromatics; the extent of dealkylation was found to be dependent upon the type of starting materials. In the hydrocracking of 9,10-dihydroanthracene, dehydrogenation occurred in preference to the opening of the central ring.

Hydrocracking is one of the important methods of obtaining liquid fuels from coal. In order to obtain the fundamental data with regard to the hydrocracking of coal, we have already employed the following model substances: 1) A pure substance:[2)] The properties of the starting material are known and the reaction process will be easily deduced. 2) A heavy anthracene oil:[3)] The NMR analyses can be applied, and the main components can be determined by using analytical methods (ex. GC-MS). 3) Solvent refined coal (SRC):[4)] This is considered to be representative of the structure of coal. The NMR analyses can be applied, but the constituents cannot be determined.

Previously,[2)] we used polynuclear aromatic hydrocarbons (anthracene, phenanthrene, pyrene, chrysene, and fluoranthene), which were supposed to be structural units of bituminous coal, as the model substances. The detailed product distributions and the differences of the catalytic activities among some molten salts were presented and discussed. The $ZnCl_2$/CuCl molten salt was found to be one of the superior hydrocracking catalysts for polynuclear aromatic hydrocarbons.

In the study of structural units of coal, one of the major problems is to understand the behavior of the substituents which attach to the condensed aromatic rings in the hydrocracking reaction. From this standpoint, we will apply the findings reported in the previous paper[2)] to interprete the results obtained in the hydrocracking of alkyl-substituted polynuclear aromatic hydrocarbons, in order to clarify the effect of the alkyl substituents on the product distributions. The characteristic behavior of the alkyl groups on the starting material and the decomposition process will be described in this paper.

Experimental

General Procedure. A stainless steel vessel containing 8 g of feed (in the case of the unsubstituted aromatic hydrocarbon) and an equimolar amount of the catalyst ($ZnCl_2$: CuCl=60 mol %: 40 mol %) was placed in a stainless steel (SUS 32) autoclave with a capacity of 200 ml. In the hydrocracking of an alkyl-substituted or dihydro aromatic hydrocarbon, the quantity of feed used was equimolar with the unsubstituted derivative containing the same condensed ring. Hydrogen was introduced into the autoclave to achieve a pressure of 100 kg/cm^2; then the autoclave was heated up to the desired temperature. This took from 60 to 70 min. The reaction system was shaken in a horizontal direction (68 strokes/min) and maintained at 400 °C for 3 h. No attempts were made to maintain the hydrogen pressure at a constant level during the reaction. The identification and the determination of the products were carried out according to the methods described previously.[2)]

Materials. The naphthalene (Ia), 2,6-dimethylnaphthalene (Id), and fluorene (VII) were obtained from Wako Pure Chemical Industries, Ltd. The 1-methylnaphthalene (Ib), 2-methylnaphthalene (Ic), anthracene (IIa), and 9,10-dihydroanthracene (Va) were obtained from Nakarai Chemicals, Ltd. The phenanthrene (IIIa) and chrysene (IV) were obtained from the Tokyo Kasei Kogyo Co., Ltd. 9-Methylanthracene (IIb) and 9-propylanthracene (IIc) were prepared by the reaction of anthrone with methylmagnesium iodide and propylmagnesium bromide respectively.[5)] 2-Methylanthracene (IId) was prepared by the reduction of 2-methylanthraquinone with zinc dust in NaOH aqueous solution and toluene.[6)] 9,10-Dihydro-9-methylanthracene (Vb) was prepared from Va and methyl iodide by using BuLi.[7)] Similarly, 9,10-dihydro-9,10-dimethylanthracene (Vc) was synthesized by using Vb as the starting material. 9-Methylphenanthrene (IIIb) was prepared from 9-bromophenanthrene and methyl iodide in the presence of BuLi.[8)] 9-Bromophenanthrene was prepared by the addition of bromine to IIIa, followed by thermal elimination of hydrogen bromide. 9,10-Dihydro-9-methylphenanthrene (VI) was prepared by the reduction of IIIb by using Li in liquid NH_3 in the presence of iron(III) chloride.[8)] All the purities of these compounds, determined by GC, were more than 95%. The zinc chloride and copper(I) chloride were obtained from Nakarai Chemicals, Ltd. The mixture of $ZnCl_2$ and CuCl was dried before use at 400 °C for 1 h in nitrogen.

Classification of Products. In order to clarify the reactivity of the starting material over the molten salt, it is necessary to know the product distribution. The products were classified for convenience into seven groups as follows: **1**, C_1-C_4 gases; **2**, C_5-C_7 alkanes; **3**, cycloalkanes; **4**, monocyclic aromatics; **5**, indans, tetralins, and bicyclic aromatics; **6**, dihydrobenzindenes, tricyclic aromatics, and their hydrogenated compounds; **7**, coke.

Results and Discussion

Table 1 shows the product distributions according to the classification described in the experimental section. The reaction conditions were decided by considering the extent of the progress of the hydrocracking, because a high conversion is required in order to discuss the reaction process of hydrocracking based on the product distribution.

Influence of the Number of Rings in the Condensed Aromatic Hydrocarbon. Table 1 shows that the yield of cycloalkanes(**3**) increases with increasing number of rings, from the comparison of the results of naphthalene (Run 1), phenanthrene(Run 9), and chrysene(Run 11). Here, the yield of **3** in the hydrocracking of naphthalene is much lower than that in the hydrocracking of anthracene, phenanthrene, and chrysene. This finding strongly indicates that the cleavage of the C–C bonds of the central rings in highly hydrogenated polynuclear aromatic hydrocarbons containing more than three rings (ex. *unsym*-octahydroanthracene, *unsym*-octahydrophenanthrene, and so on) is one of the main decomposition pathways. Actually, the decomposition of *unsym*-octahydrophenanthrene to 1-cyclohexyl-2-phenylethane in the hydrocracking of phenanthrene and a similar cleavage in the hydrocracking of chrysene were found and reported in the previous paper.[2] This finding also demonstrates that the contribution of the pathway *via* decalin to the decomposition process of naphthalene is minor,[9] and that this type of catalyst is relatively inactive for the hydrogenation and hydrocracking of monocyclic aromatics. The latter seems to be desirable for obtaining a high yield of gasoline.[10]

Influence of Kinds of Alkyl Groups in the Hydrocracking of Anthracenes. Tables 2 and 3 describe the compositions of gases(**1**) and monocyclic aromatics(**4**) respectively. The behavior of the alkyl group can be deduced by using these results, because the difference in the composition of **1** or **4** between the alkyl polynuclear aromatic hydrocarbon and the corresponding unsubstituted compound is apparent. First we will discuss the results for anthracene derivatives and compare the reactivity of IIb with that of IIc. Two experiments(Runs 6 and 7) were carried out to investigate the difference of the composition of the products in accordance with the change in the alkyl group. The relative content of methane in Run 6 is higher than that in Run 5. Similarly the relative content of propane in Run 7 is quite a bit higher than that in Run 5. These findings show that the alkyl group is eliminated in the course of hydrocracking. In the case of methyl-substituted polynuclear aromatics, the ratio of benzene to toluene(R) is supposed to indicate the extent of demethylation, because the

TABLE 1. DISTRIBUTION OF HYDROCRACKED PRODUCTS

Reaction conditions: $ZnCl_2$: CuCl=60: 40 (mol: mol); Feed/Catalyst=1.0 (mol/mol); initial hydrogen pressure, 100 kg/cm²; reaction time, 3 h; reaction temperature, 400 °C.

		Run No. 1	2	3	4	5	6	7	8
	Feed	Ia	Ib	Ic	Id	IIa	IIb	IIc	IId
Products (wt %)	**1**	45.7	33.4	39.3	40.7	38.1	42.3	25.7	28.8
	2	3.7	6.6	6.6	7.2	7.9	7.9	10.3	10.7
	3	1.5	2.0	1.8	1.6	10.8	7.6	8.5	10.3
	4	46.4	47.7	45.3	44.8	27.7	24.3	27.6	24.6
	5	2.2	9.8	6.4	5.5	8.9	10.5	15.2	15.2
	6	—	—	—	—	2.5	5.0	11.3	10.3
	7	0.5	0.5	0.6	0.2	4.1	2.4	1.4	0.1

		Run No. 9	10	11	12	13	14	15	16
	Feed	IIIa	IIIb	IV	Va	Vb	Vc	VI	VII
Products (wt %)	**1**	27.7	41.4	28.2	42.0	35.9	55.6	41.7	30.6
	2	7.2	7.7	10.7	7.2	8.5	7.8	6.7	4.2
	3	7.0	6.4	17.6	8.6	8.8	3.9	6.4	6.5
	4	33.2	34.0	25.2	29.5	24.5	28.0	30.1	25.0
	5	14.6	6.0	11.0	9.1	14.5	3.0	10.0	14.3[b]
	6	5.7	3.3	4.5[a]	2.4	7.2	1.3	5.0	17.5
	7	4.6	1.2	2.7	1.2	0.6	0.4	0.1	1.9

a) Containing tetracyclic compounds (1.1%). b) Containing biphenyls (10.5%).

Table 2. Relative distribution of gases (mol %)

	Run No.															
	1	2	3	4	5	6	7	8	9	10	11	12	13	14	15	16
Feed	Ia	Ib	Ic	Id	IIa	IIb	IIc	IId	IIIa	IIIb	IV	Va	Vb	Vc	VI	VII
C1[a]	33.5	22.8	23.8	22.8	20.8	29.5	20.3	26.1	20.9	21.4	21.0	17.7	40.3	50.4	34.1	23.4
C2[b]	12.8	9.9	11.4	11.5	12.2	8.9	9.3	8.4	10.5	7.8	8.5	10.8	7.8	6.9	9.0	12.7
C3[c]	25.6	30.8	31.4	28.6	29.3	27.6	45.7	22.0	31.9	34.6	26.8	32.2	22.3	19.6	26.8	33.9
C4[d]	28.1	36.5	33.4	37.1	37.7	34.0	24.7	43.5	36.7	36.2	43.7	39.2	29.6	23.1	30.1	30.1

a) Methane. b) Ethane. c) Propane. d) Butanes and butenes.

Table 3. Relative distribution of monocyclic aromatics (mol %)

	Run No.															
	1	2	3	4	5	6	7	8	9	10	11	12	13	14	15	16
Feed	Ia	Ib	Ic	Id	IIa	IIb	IIc	IId	IIIa	IIIb	IV	Va	Vb	Vc	VI	VII
A[a]	68.9	25.7	25.9	7.9	41.7	27.9	41.4	19.9	38.4	23.0	39.1	39.1	26.3	19.0	22.1	47.9
B[b]	16.5	34.4	35.8	33.7	26.9	27.8	28.8	31.8	23.4	31.0	26.3	24.4	27.1	25.1	29.2	26.8
C[c]	11.3	28.3	27.9	31.3	17.5	24.0	16.3	22.6	23.3	28.6	22.5	24.7	29.9	32.5	29.5	19.3
D[d]	1.9	9.0	8.5	20.0	7.7	13.7	8.7	13.7	8.2	11.2	7.3	7.0	10.8	17.5	13.9	4.8
E[e]	1.4	2.6	1.9	7.1	6.2	6.6	4.8	12.0	6.7	6.2	4.8	4.8	6.0	5.9	5.3	1.1
R[f]	4.18	0.75	0.72	0.23	1.55	1.00	1.44	0.63	1.64	0.74	1.49	1.60	0.97	0.76	0.76	1.79

a) Benzene. b) Toluene. c) Ethylbenzene and xylenes (C_2 alkylbenzenes). d) C_3 alkylbenzenes. e) Alkylbenzenes containing more than C_4. f) R=benzene/toluene (mol/mol).

value may increase with increasing demethylation according to the main reaction scheme, as shown later (*cf.* Fig. 1), and we used this ratio as a convenient measure of demethylation. The comparison of R in Run 6 with R in Run 5 shows that the methyl group of IIb is conserved in monocyclic aromatics in the course of hydrocracking. The ratio of the yield of unsubstituted tricyclic compounds to that of alkylated tricyclic compounds was 8.9 in the case of IIc and 2.3 in the case of IIb. In addition, the composition of monocyclic aromatics in Run 7 was very similar to that in Run 5. All of these findings indicate that the propyl group is dealkylated more easily than the methyl group. Similar phenomena were observed in the hydrocracking of alkylbenzenes in the presence of acidic catalysts.[11] These findings may be explained by considering that propylanthracene possesses the possibility of isomerization to isopropylanthracene and that the secondary alkyl group can be dealkylated in preference to the primary alkyl group.[11,12] The similarity between IIa and IIc in the composition of monocyclic aromatics would demonstrate that the propyl group of IIc is mainly dealkylated in the initial decomposition stage. On the other hand, the decomposition process of the marginal hydrogenated rings prior to dealkylation is also considered to be of importance in the case of IIb.

Influence of Positions of Alkyl Groups and Types of Condensed Rings. Since the presence of methyl group remarkably influenced the decomposition of the polynuclear aromatics, the methyl derivatives were used for the following experiments. The experiments of IIb and IId were carried out to clarify the effect of the position of methyl group attached to the anthracene skeleton on the composition of the decomposed products. The value of R in IId is lower than that in IIb; this finding suggests that the methyl group of IId is well conserved in monocyclic aromatics in comparison with that of IIb. This result is interpreted by the idea that the demethylation prior to the hydrocracking of the condensed ring has a minor contribution to the reaction process in the hydrocracking of IId, that is, the methyl group of IIb is eliminated more easily than that of IId. The experiments of IIb and IIIb were carried out to clarify the difference of the type of condensed rings. The ease of demethylation in the initial decomposition process differs in these two cases. The methyl group of IIIb is conserved in monocyclic aromatics much more frequently than that of IIb. It is noteworthy that the composition of monocyclic aromatics of IV is fairly similar to that of IIIa. The effect of the presence of the methyl group on the composition of monocyclic aromatics (Run 10) is observed more dramatically than that of the increase of the number of the aromatic rings(Run 11).

Hydrocracking of Naphthalenes. It is noteworthy that a remarkable difference in the R values was observed

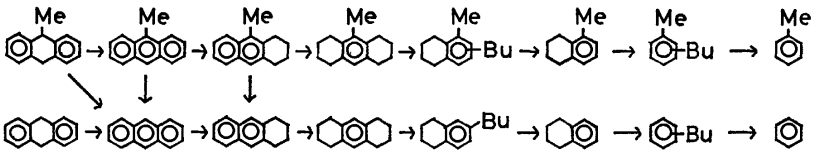

Fig. 1. Main reaction scheme of dihydroanthracene derivatives.

in the hydrocracking of naphthalene derivatives(Runs 1—3). This finding suggests that the unsubstituted ring is more easily hydrogenated than the methylated ring. This fact is the basis for asserting that the alkyl groups on the polynuclear aromatic hydrocarbons influence the composition of monocyclic aromatics in this hydrocracking. The effect of the position of the methyl group on the composition of monocyclic aromatics was hardly observed in the case of Ib and Ic(Runs 2 and 3). The experiment of Id (Run 4) seems to be most suitable for investigating the demethylation. If Id never undergoes the demethylation, the yield of benzene should become zero. The presence of a little quantity of benzene demonstrates the occurence of demethylation; however, the contribution of the demethylation in the initial stage to the composition of monocyclic aromatics seems rather insignificant.

Hydrocracking of Dihydro Tricyclic Aromatics. The hydrocracking of Va is of importance for clarifying the decomposition process of IIa.[13–15] If the central methylene bridge of Va is ruptured, the yield of monocyclic aromatics should increase remarkably compared with IIa. However, the product distributions of these two hydrocracking reactions are similar: Va seems to undergo dehydrogenation, followed by the decomposition process, in a way similar to IIa. The experiments of Vb and Vc were carried out in anticipation of the specific reaction caused by introducing the methyl group(s) to the central carbon atom(s) of 9,10-dihydroanthracene. The product distribution of Vb(Run 13) is successfully explained by considering that the dehydrogenation and demethylation occurred in the initial stage; that is, Vb was mainly decomposed *via* IIa or IIb. Vc is also considered to be decomposed in a manner similar to Vb, and so the opening of the central ring of this type of compound is considered to be small in this hydrocracking reaction. Fig. 1 shows the main decomposition scheme of 9,10-dihydroanthracene derivatives. The ease of dealkylation of the butyl group compared with the methyl group is considered to govern this decomposition process. If the C_{8a}–C_9 bond of VI is fairly well cleaved, the yield of biphenyl derivatives in the hydrocracking of VI should be higher than that in the hydrocracking of IIIb. However, no such increase of the yield of biphenyl derivatives could be observed, and so VI seems to undergo demethylation and dehydrogenation in the initial decomposition process. On the other hand, the pathway to the biphenyl derivatives becomes very important in the case of VII, because VII has no pathway of dehydrogenation to the stable aromatic compounds. In this case, the lowering of the reactivity was observed.

Conclusion

The hydrocracking of alkyl-substituted polynuclear aromatic hydrocarbons was carried out to clarify the decomposition scheme and the behavior of the alkyl group. The findings are outlined as follows: 1) The decomposition route *via* highly hydrogenated compounds becomes important with increasing numbers of rings of the polynuclear aromatics. 2) The alkyl group substituted on the polynuclear aromatic hydrocarbon is not completely dealkylated in the initial stage and remains in the products as monocyclic aromatics. The extent of dealkylation depends on the properties (that is, kinds and positions of alkyl groups, and types of condensed rings) of the starting materials. 3) In the hydrocracking of 9,10-dihydroanthracene, the dehydrogenation occurs in preference to the opening of the central ring; in the hydrocracking of the methylated 9,10-dihydroanthracenes and 9,10-dihydrophenanthrene, the dehydrogenation and demethylation take place in preference to the opening of the central ring; but in the hydrocracking of fluorene, the pathway to the biphenyls becomes important. These findings are expected to be useful for understanding the hydrocracked mechanism and the composition of the resulting products of coal.

References

1) Organic Reaction in Fused Salts. Part XIV, Part XIII: Y. Nakatsuji, T. Kubo, M. Nomura, and S. Kikkawa, *Bull. Chem. Soc. Jpn.*, **51**, 618 (1978); a part of this work was presented at the 38th National Meeting of the Chemical Society of Japan, Kanagawa, April 1978.
2) Y. Nakatsuji, T. Kubo, M. Nomura, and S. Kikkawa, *Bull. Chem. Soc. Jpn.*, **51**, 618 (1978).
3) Y. Nakatsuji, S. Fujioka, M. Nomura, and S. Kikkawa, *Bull. Chem. Soc. Jpn.*, **50**, 3406 (1977).
4) Unpublished data.
5) A. Sieglitz and R. Marx, *Chem. Ber.*, **56**, 1619 (1923).
6) E. L. Martin, *J. Am. Chem. Soc.*, **58**, 1438 (1936).
7) R. G. Harvey and H. Cho, *J. Am. Chem. Soc.*, **96**, 2434 (1974).
8) P. W. Rabideau and R. G. Harvey, *J. Org. Chem.*, **35**, 25 (1970).
9) S. Yamadaya, M. Oba, and Y. Miki, *Bull. Chem. Soc. Jpn.*, **50**, 79 (1977). They described the reaction process of the bicyclic compounds in detail on the basis of the hydrocracking of tetralin on supported Ni–W catalysts.
10) C. W. Zielke, R. T. Struck, J. M. Evans, C. P. Costanza, and E. Gorin, *Ind. Eng. Chem., Process Des. Dev.*, **5**, 158 (1966).
11) R. Covini and H. Pines, *J. Catal.*, **4**, 454 (1965).
12) K. Itoh, R. Kurashige, S. Hamanaka, and M. Ogawa, *Kogyo Kagaku Zasshi*, **70**, 918 (1967).
13) J. M. L. Penninger and H. W. Slotboom, *Erdöl Kohle*, **26**, 445 (1972).
14) P. W. E. Blom, J. Dekker, L. Fourie, J. A. Kruger, and H. G. J. Potigieter, *J. S. Afr. Chem. Inst.*, **28**, 130 (1975).
15) S. Kikkawa, M. Nomura, and K. Murase, *Sekiyu Gakkaishi*, **19**, 863 (1976).

NOTES

BULLETIN OF THE CHEMICAL SOCIETY OF JAPAN, VOL. 51 (12), 3635—3636 (1978)

Optical Spectra of the Picrate Ion in Micellar and Polymer Micellar Systems. Comment on the Solvation of Anions

Seiji SHINKAI,* Toyoko IDE, and Osamu MANABE
Department of Industrial Chemistry, Faculty of Engineering, Nagasaki University, Nagasaki 852
(Received January 27, 1978)

Synopsis. The optical spectra of the picrate ion in a micellar solution indicate that slightly below the CMC of CTAB surfactant the anion is relatively free and exists as an ion pair above the CMC. The hydrophobic aggregate of TMAC invariably gives free ion. The polymer micelle of quaternized poly(4-vinylpyridine) results in a tight ion pair.

Anionic nucleophiles are activated to a great extent in cationic hydrophobic aggregates such as micelles and polymer micelles.[1] The unusual activation is mainly attributed to the formation of hydrophobic ion pairs which are relatively "desolvated" in the hydrophobic domain.[2-6] Thus, it would be valuable to estimate the degree of solvation as a function of surfactant concentrations. According to Bourgoin *et al.*,[7] bathochromic shifts observed in the optical spectra of alkali picrates can be rationalized in terms of the formation of the free ion, and the apolar environment is characterized by a shoulder at around 400 nm. The spectrum of the picrate ion would thus be most useful for confirmation. We have measured the optical spectra of the picrate ion in the presence of hexadecyltrimethylammonium bromide (CTAB), sodium dodecyl sulfate (SDS), Brij-35, trioctylmethylammonium chloride (TMAC), and the following quaternized poly(4-vinylpyridine) polymers (4VP-D-0 and 4VP-D-22).[6] Typical results are summarized in Table 1.

4VP-D-0: —CH_2CH——CH_2CH—

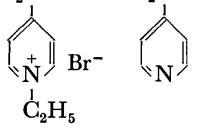

85 mol % 15 mol %

4VP-D-22: —CH_2CH——CH_2CH——CH_2CH—

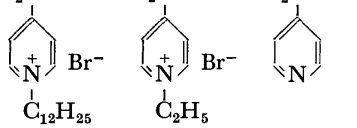

22 mol % 42 mol % 36 mol %

The λ_{max} of the picrate ion in an aqueous solution appeared at 355 nm. Addition of CTAB caused marked bathochromic shifts, the largest shift to 380 nm being observed at [CTAB]$=1.0\times10^{-4}$ M. This is comparable with the λ_{max} value of triethylammonium picrate in dimethyl sulfoxide (377 nm)[8] or of potassium picrate in tetrahydrofuran containing excess crown ether (380 nm).[7] Since the critical micelle concentration (CMC) of CTAB (determined by use of 2,6-dichlorophenolindophenol) is 4.0×10^{-4} M, the picrate ion is relatively free slightly below this. Further increase in CTAB concentration caused hypsochromic shifts to 350 nm with a new absorption maximum at 422 nm. The final spectrum at [CTAB]$=2.0\times10^{-3}$ M (λ_{max}, 350 and 412 nm) was similar to that in tetrahydrofuran (357 and 420 nm for the K^+ ion pair[7]) and 354 and 432 nm for the $HNEt_3^+$ ion pair). The results indicate that the nature of the picrate ion changes with increase in CATB concentration: hydrated (with hydrogen-bond)→dehydrated (without hydrogen-bond) and free→dehydrated and ion-paired.

Table 1. Absorption maxima and shoulders of picrate ions in the presence of surfactants[a]

Surfactant	Concentration mM	λ_{max} nm	(log ε_{max})	$\lambda_{shoulder}$[b] nm	(log ε_{max})
Water		355	(4.29)	—	
CTAB	0.02	355	(4.28)	—	
	0.05	360	(4.26)	—	
	0.10	380	(4.32)	+	
	0.20	360	(4.33)	422	(4.16)
	0.40	350	(4.26)	412	(4.07)
	0.80	350	(4.26)	412	(4.07)
4VP-D-0[c]	5.0	355	(4.29)	—	
4VP-D-22[c]	0.46	360	(4.28)	+	
	0.93	360	(4.27)	+	
	3.68	360	(4.27)	+	
SDS	15.0	355	(4.29)	—	
Brij-35	1.6	355	(4.29)	—	
TMAC	0.02	365	(4.28)	—	
	0.04	375	(4.35)	+	
	0.06	377	(4.38)	+	
	0.08	374	(4.38)	+	
	0.10	374	(4.37)	+	

a) 30 °C, pH 7.1 with 0.02 M phosphate (KH_2PO_4–K_2HPO_4) buffer, [picrate ion (added as picric acid)]$=3.90\times10^{-5}$M. b) "+" indicates that distinct shoulder appears but the absorption maximum cannot be determined clearly. c) The polymer concentration stands for the total concentration of monomeric units.

No appreciable shift was observed in the presence of SDS and Brij-35 above their CMC's (Table 1).

TMAC, a typical phase transfer catalyst, forms aggregates at very low concentrations (10^{-5}—10^{-4} M). They seem to be much smaller than the conventional globular micelles and enhance the nucleophilicity of the bound anions more than the conventional cationic micelles.[9] The λ_{max} values at [TMAC]$=0.04$—0.1 mM always appear in the range 374—377 nm (Table 1), indicating that the TMAC aggregate provides a relative-

ly free picrate ion. The result indicates that the nucleophilic reactivity of the anion bound to the TMAC aggregate is enhanced due to the desolvation to a greater extent than that bound to the conventional cationic micelle.[9]

It has been established on the basis of absorption and emission spectra of dye molecules that 4VP-D-0 is classified as a simple polyelectrolyte and 4VP-D-22 as a polymer micelle which possesses the hydrophobic domain.[6,10,11] The spectrum of the picrate ion was scarcely affected by 4VP-D-0, while addition of 4VP-D-22 caused appreciable bathochromic shifts to 360 nm accompanied by the appearance of a shoulder at around 400 nm. Further increase in the concentration of 4VP-D-22 did not change the spectrum. This indicates that the picrate ion pair formed in the polymer micelle is relatively tight.

Free, dehydrated picrate ion is formed at slightly below the CMC of CTAB. On the other hand, once the micelle formation takes place, the ion pair becomes relatively tight probably due to the apolar environment. It is suggested that the local hydrophobic domain is preferred to the globular hydrophobic domain of the micelle to produce the free ion. The TMAC aggregate may be the case.

Although the multi-phase dependence of the bimolecular reaction rate in the micellar catalysis has been rationalized in terms of concentration and dilution of reactants by micelles,[12–14] the present study indicates that the reactivity of the anion may be also dependent on surfactant concentrations.

References

1) T. Kunitake, S. Shinkai, and Y. Okahata, *Bull. Chem. Soc. Jpn.*, **49**, 540 (1976) and references cited therein.
2) W. Tagaki, T. Amada, Y. Yamashita, and Y. Yano, *J. Chem. Soc., Chem. Commun.*, **1972**, 1131.
3) R. A. Moss, R. C. Nahas, S. Ramaswami, and W. J. Sanders, *Tetrahedron Lett.*, **1975**, 3379.
4) I. Tabushi, Y. Kuroda, and S. Kita, *Tetrahedron Lett.*, **1974**, 643.
5) S. Shinkai and T. Kunitake, *J. Chem. Soc., Perkin Trans. 2*, **1976**, 980.
6) T. Kunitake, S. Shinkai, and S. Hirotsu, *J. Org. Chem.* **42**, 306 (1977).
7) H. Bourgoin, K. H. Wong, J. Y. Hui, and J. Smid, *J. Am. Chem. Soc.*, **97**, 3462 (1975).
8) S. Shinkai, T. Ide, and O. Manabe, *Rept. Fac. Eng., Nagasaki University*, **11**, 115 (1978).
9) Y. Okahata, R. Ando, and T. Kunitake, *J. Am. Chem. Soc. Jpn.*, **99**, 3067 (1977).
10) S. Shinkai and T. Kunitake, *Makromol. Chem.*, **178**, 1613 (1977).
11) T. Kunitake, S. Shinkai, and S. Hirotsu, *Biopolymers*, **15**, 1143 (1976).
12) E. H. Cordes and C. Gitler, *Progr. Bioorg. Chem.*, **2**, 1 (1973).
13) D. Piszkiewicz, *J. Am. Chem. Soc.*, **99**, 1550 (1977).
14) D. Piszkiewicz, *J. Am. Chem. Soc.*, **99**, 7695 (1977)

BULLETIN OF THE CHEMICAL SOCIETY OF JAPAN, VOL. 51 (12), 3637—3638 (1978)

Optical and Magnetic Properties of Crystalline Phenothiazine Cation Radical Salts

Yôichi IIDA

Department of Chemistry, Faculty of Science, Hokkaido University, Sapporo 060

(Received March 10, 1978)

Synopsis. Crystalline phenothiazine cation radical salts show charge-transfer transition between cation radicals in the low-energy region. These salts have antiferromagnetic exchange interaction between cation radicals. Their optical and magnetic properties were discussed in terms of one-dimensional Hubbard model.

The prominent magnetic, electrical and optical properties of a number of crystalline ion radical salts have been the subject of many theoretical and experimental investigations over the past fifteen years.[1-8] In such ion radical salts, the ion radical molecules are known to form, in themselves, a segregated stacking into infinite one-dimensional columns so as to make a large overlap between their half-occupied molecular orbitals.[1-8] In this case, since any individual radical molecule interacts through charge-transfer most strongly with two other neighboring radicals, the electronic spectrum of the solid salt differs distinctly from the monomer spectrum of the radical ion in solution but shows a charge-transfer transition between ion radicals in the low-energy region.[1-4] In a previous paper,[6] we applied one-dimensional Hubbard model to the columns of ion radical molecules, and investigated the optical properties of solid ion radical salts. In the present paper, we examined the optical and magnetic properties of several crystalline phenothiazine cation radical salts on the basis of such a model.

Phenothiazine (PT) is a strong electron donating molecule and forms chemically stable cation radical salts with various counter anions. Several years ago,[2] we prepared such cation radical salts as $PT^{+\cdot}Br^-$, $PT^{+\cdot}HSO_4^-\cdot H_2O$, and $PT^{+\cdot}C_6H_2(NO_2)_3O^-$ (picrate). Moreover, Sato *et al.* synthesized the salts with antimony pentachloride anions.[3] The absorption spectrum of the phenothiazine cation radical monomer dissolved in dilute hydrochloric acid has a weak band around 13500 cm^{-1} composed of several vibrational structures at 15000, 13500, and 12200 cm^{-1}, a strong band at 19300 cm^{-1} with a shoulder at 19900 cm^{-1} and a band at 22800 cm^{-1}.[2] On the other hand, the solid-state spectra of $PT^{+\cdot}Br^-$, $PT^{+\cdot}HSO_4^-\cdot H_2O$, and $PT^{+\cdot}C_6H_2(NO_2)_3O^-$ differ markedly from the monomer spectrum of the cation radical.[2] For example, the solid-state spectrum of $PT^{+\cdot}HSO_4^-\cdot H_2O$ is reproduced in Fig. 1, together with the absorption spectrum of the cation radical monomer. The solid-state spectrum shows a strong low-energy band at 12000 cm^{-1}, high-energy bands at 21100 and 23300 cm^{-1}, and a shoulder around 28000 cm^{-1}. The low-energy band at 12000 cm^{-1} has been assigned to the charge-transfer transition between the phenothiazine cation radicals in their segregated stacks, while the high-energy bands at 21100 and 23300 cm^{-1}, to the shifted bands of the cation radical monomer

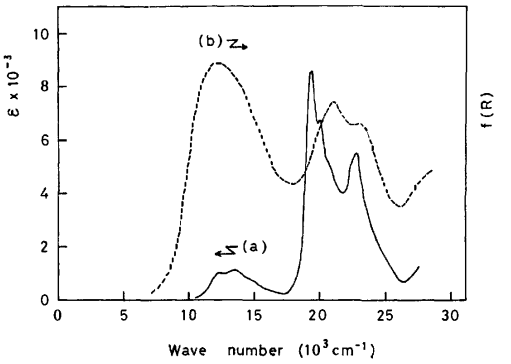

Fig. 1. (a) The absorption spectrum of the cation radical salt of phenothiazine hydrogen-sulfate monohydrate dissolved in hydrochloric acid and (b) the solid-state spectrum of the same salt. The solid-state spectrum was obtained by plotting the diffuse reflection spectrum using the Kubelka-Munk function, $f(R)=(1-R)^2/2R$, where R is the reflectance. See Ref. 2.

at 19300 and 22800 cm^{-1}, respectively.[2] The line shape of the charge-transfer absorption is almost symmetrical with respect to the axis of peak energy. The solid-state spectra of the bromide and the picrate are found to be very similar to that of the hydrogen-sulfate monohydrate salt. The charge-transfer absorptions of the bromide and picrate salts are located at 12900 and 12800 cm^{-1}, respectively.[2] On the other hand, according to Sato *et al.*,[3] the solid-state spectra of $PT^{+\cdot}SbCl_4^-$ and $PT^{+\cdot}SbCl_5^-$ salts are rather similar to the absorption spectrum of the phenothiazine cation radical monomer. The charge-transfer absorptions of these solid salts appear at 9350 and 10000 cm^{-1}, respectively. However, these absorptions have weak intensity and appear as a shoulder in the monomer spectrum of the cation radical.

In a previous paper,[6] we presented the theoretical line shape of the charge-transfer absorption on the basis of non-alternant one-dimensional Hubbard model. The shape of the absorption spectrum is given by

$$\sigma(\omega) \propto \frac{e^2}{4}\frac{I^2}{\omega^2\sqrt{\omega^2-I^2}}\sqrt{4T^2-\omega^2+I^2}. \quad (1)$$

Here, a δ-function was assumed for each elementary transition in which the spin and the wave vector of an electron are conserved; I is the intra-site Coulomb repulsion energy, and $T(<0)$ the transfer matrix element between nearest neighbor ion radicals in one-dimensional column of the phenothiazine cation radicals. A schematic representation of the absorption line shape of Eq. 1 has been given in Fig. 1 of Ref. 6. The theoretical charge-transfer absorption has a sharp divergent peak at $\omega=I$. The spectrum has no absorption in the region $\omega<I$, but has a distinct shoulder in the region $I<\omega<\sqrt{I^2+4T^2}$. Actually, however, the

elementary absorption is not a δ-function but involves a finite width, and the spectrum will become more smoothed,[6,7] so that the observed charge-transfer absorption has an intensity even in the energy region lower than the peak position. Then, the absorption peak of the observed charge-transfer band corresponds to $\omega=I$, and its band width comes partly from the width due to the elementary absorptions but partly from the width due to non-zero transfer matrix element, $\sqrt{I^2+4T^2}-I$. We divide the two contributions of the widths in a way similar to the previous work,[7] where the width, $\sqrt{I^2+4T^2}-I$, could be estimated by subtracting with respect to $\omega=I$, the lower-energy side from the higher-energy side of the observed charge-transfer absorption. For example, in the case of the $PT^{+\cdot}\cdot HSO_4^-\cdot H_2O$ salt (see Fig. 1, (b)), the observed peak energy of the charge-transfer absorption, 12000 cm^{-1}, thus corresponds to $I=12000$ cm^{-1}. From the observed line shape of the absorption, the width due to the transfer matrix element, $\sqrt{I^2+4T^2}-I$, is estimated to be of the order of 1500 cm^{-1}. This relation, together with $I=12000$ cm^{-1}, leads to the magnitude of the transfer matrix element, $|T|$, of the order of 3000 cm^{-1} or less in the hydrogen-sulfate monohydrate salt. In a similar way, from the observed solid-state spectra, the magnitudes of I for the bromide and the picrate are estimated to be 12900 and 12800 cm^{-1}, respectively. In both salts, the values of the transfer matrix element, $|T|$, again seem to be smaller than 3000 cm^{-1}. As for the $PT^{+\cdot}\,SbCl_4^-$ and $PT^{+\cdot}\,SbCl_5^-$ salts, from the observed charge-transfer absorptions, the I values are estimated to be 9350 and 10000 cm^{-1}, respectively, and the magnitudes of $|T|$ seem to be of the order of 1000 cm^{-1} or less. However, since those charge-transfer absorptions appear as a shoulder in the monomer spectrum of the phenothiazine cation radical, the estimated values of I and $|T|$ should be taken only as an indication.

In order to obtain more exact information on the magnitudes of the transfer matrix elements, we further examined the magnetic properties of solid phenothiazine cation radical salts. In a region of small $|T|$ limit, the Hubbard model leads to a stabilization of the antiferromagnetic state between ion radical molecules. For a pair of nearest neighbor ion radicals, if the small direct exchange is neglected, the energy gap between the parallel and antiparallel spin states is given by $2J=4T^2/I$. Therefore, we can well consider our solid phenothiazine cation radical salts as one-dimensional antiferromagnet with an exchange interaction, J.[8] By measuring the static magnetic susceptibility and its temperature dependence, Sato *et al.* reported the J values for $PT^{+\cdot}\,SbCl_5^-$, $PT^{+\cdot}\,SbCl_4^-$, and $PT^{+\cdot}\,Br^-$ to be 34, 270, and $\approx$970 cm^{-1}, respectively.[3] We also measured the magnetic susceptibility of the hydrogen-sulfate monohydrate.[2] It was found to be almost diamagnetic, indicating the J value of $\approx$800 cm^{-1}. Therefore, by using the relation $J=2T^2/I$, together with the I values determined previously, the $|T|$ values for $PT^{+\cdot}\,SbCl_5^-$, $PT^{+\cdot}\,SbCl_4^-$, and $PT^{+\cdot}\,Br^-$ are estimated to be 410, 1120, and $\approx$2500 cm^{-1}, respectively, while that for the hydrogen-sulfate monohydrate, to be of the order of 2200 cm^{-1}. Although the $|T|$ values estimated previously from the line shape of the charge-transfer absorptions include some uncertainties, for each of the salts the magnitude of the $|T|$ value obtained from the $|T|=\sqrt{J\,I/2}$ relation is found to agree with that estimated only from the spectroscopic data.

Turning back to the optical properties of those phenothiazine cation radical salts, we discuss how the intensity of the charge-transfer absorption is related to the $|T|$ value. According to our preliminary work,[9] the intensity of the charge-transfer absorption is roughly proportional to $|T|^2$. In this respect, the intensities of the charge-transfer absorptions of the bromide and the hydrogen-sulfate monohydrate should be the greatest, that of $PT^{+\cdot}\,SbCl_4^-$ should be intermediate, and that of $PT^{+\cdot}\,SbCl_5^-$, the weakest. In accordance with this prediction, the solid-state spectra observed with the former two compounds differ markedly from the phenothiazine cation radical monomer spectrum and show strong charge-transfer absorptions,[2] while the latter two compounds show only weak charge-transfer absorptions.[3] In particular, the solid-state spectrum of $PT^{+\cdot}\,SbCl_5^-$ is very similar to the monomer spectrum of the phenothiazine cation radical in solution.

On the basis of these considerations, we conclude that the phenothiazine cation radicals in the solid salts of the bromide, the hydrogen-sulfate monohydrate and the picrate stack, in themselves, very closely, while the intermolecular interaction between the phenothiazine cation radicals is weak in the solid $PT^{+\cdot}\,SbCl_4^-$ and $PT^{+\cdot}\,SbCl_5^-$ salts.

References

1) Y. Iida, *Bull. Chem. Soc. Jpn.*, **42**, 71, 637 (1969); **43**, 2772 (1970); **44**, 1777 (1971); **45**, 105, 624 (1972), and the references cited therein.

2) Y. Iida, *Bull. Chem. Soc. Jpn.*, **44**, 663 (1971).

3) Y. Sato, M. Kinoshita, M. Sano, and H. Akamatu, *Bull. Chem. Soc. Jpn.*, **42**, 548 (1969).

4) J. Tanaka, M. Tanaka, T. Kawai, T. Takabe, and O. Maki, *Bull. Chem. Soc. Jpn.*, **49**, 2358 (1976), and the references cited therein.

5) H. Kobayashi, Y. Ohashi, F. Marumo, and Y. Saito, *Acta Crystallogr., Sect. B*, **26**, 459 (1970), and the references cited therein.

6) Y. Iida, *Bull. Chem. Soc. Jpn.*, **50**, 1445 (1977).

7) Y. Iida, *Bull. Chem. Soc. Jpn.*, **50**, 2481 (1977).

8) Z. G. Soos and D. J. Klein, *J. Chem. Phys.*, **55**, 3284 (1971); M. Takahashi, *Progr. Theoret. Phys. (Kyoto)*, **42**, 1098 (1969).

9) Y. Iida, *Bull. Chem. Soc. Jpn.*, to be published.

BULLETIN OF THE CHEMICAL SOCIETY OF JAPAN, VOL. 51 (12), 3639—3640 (1978)

ESR Studies on 2,3,5-Triphenyltetrazolyl and 2,3-(2,2′-Biphenylylene)-5-phenyltetrazolyl Radicals

Yasuo DEGUCHI,* Yoshiko KAWAMURA, Yutaka TAKAGI,** and Saburo KAKO

Department of Chemistry, School of Liberal Arts and Sciences, Kyoto University, Sakyō-ku, Kyoto 606

***Department of Home Sciences, Osaka Kyoiku University, 3 Jōnan, Ikeda 563*

(Received March 20, 1978)

Synopsis. 2,3-(2,2′-Biphenylylene)-5-phenyltetrazolium chloride has been prepared. The ESR spectra of 2,3,5-triphenyltetrazolyl and 2,3-(2,2′-biphenylylene)-5-phenyltetrazolyl have been measured and their ESR coupling constants determined.

Since Deguchi and Takagi reported that 2,3,5-triphenyltetrazolium chloride with silver amalgam in 1,2-dimethoxyethane (DME) shows an ESR spectrum consisting of nine broad lines due to the hyperfine coupling of four equivalent N^{14} nuclei,[1] a few papers have been published concerning radicals of this type.[2]

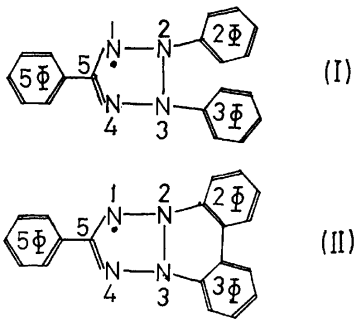

Fig. 1. Moleculer structure of 2,3,5-triphenyltetrazolyl radical (I) and 2,3-(2,2′-biphenylylene)-5-phenyltetrazolyl radical (II).

In this paper we will report the more detailed analyses of ESR spectra of radicals produced by alkali metal reduction from 2,3,5-triphenyltetrazolium chloride (TTC) and its photo-illuminated derivative; 2,3-(2,2′-biphenylylene)-5-phenyltetrazolium chloride (Photo-TTC).

Experimental

Commercial TTC was recrystallized from absolute ethanol by addition of dried ether. Photo-TTC was synthesized from the purified TTC following the photo-illumination method of Kuhn *et al.*[3] and the elementary analyses of carbon, hydrogen, nitrogen, and chlorine agreed with the values of the literature.

Found: H, 3.79; C, 68.38; N, 16.59; Cl, 10.56%. Calcd for $C_{19}H_{13}N_4Cl$: H, 3.91; C, 68.57; N, 16.84; Cl, 10.67%.

Each free radical was prepared *in vacuo* by contact reduction with alkali metal at −30——40 °C, the contact time being 1—2 s.

ESR spectra were observed using a X-band ESR apparatus equipped with 100 kHz field modulation.

Results and Discussion

2,3,5-Triphenyltetrazolyl (I). The ESR spectrum of 2,3,5-triphenyltetrazolyl obtained by reduction with potassium in DME is shown in Fig. 2a. In this spectrum the third line from the center is slightly flat and broader than the others. Thus the spectrum is satisfactorily analyzed if we assume the presence of two unequivalent pairs of N^{14} nuclei summarized in Table 1 from which the simulated spectrum (Fig. 2b) was calculated.

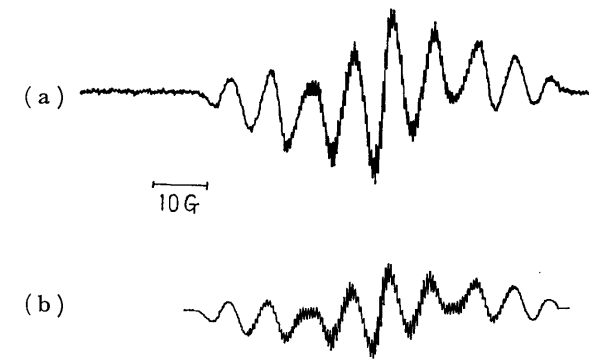

Fig. 2. ESR spectrum of radical (I) (2a) and its simulation (2b).

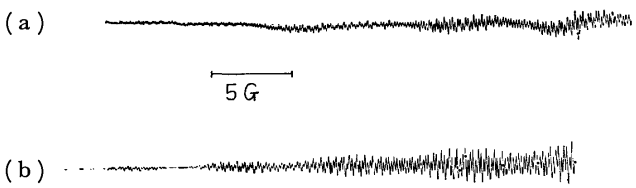

Fig. 3. Slightly more than one-half of ESR spectrum of radical (I) (better resolved than Fig. 2a) (3a) and its simulation (3b).

The better resolved spectrum is shown in Fig. 3a, and the simulated one using the coupling constant in the Table in Fig. 3b.

When the solution is kept in contact with alkali metal further, the color turns red and the ESR signal disappears. This suggests the formation of formazane in the solution, since formazane treated with alkali metal in the etheric solvent such as DME gives no ESR signal.

2,3-(2,2′-Biphenylylene)-5-phenyltetrazolyl (II). This radical was obtained by the same procedure as that for radical (I). The ESR spectrum of radical (II) (Fig. 4a) consists of twenty nine absorption lines were observed. Figure 4b shows the better resolved spectrum of radical (II) and Fig. 4c its simulated one calculated by the data in Table 1. The result reveals that *o,o′*-bridging between the two phenyl rings attached to the nitrogens at 2- and 3-positions of tetrazolium ring causes more conjugation of the two phenyl rings than in the case of TTC. The unpaired electron is, however,

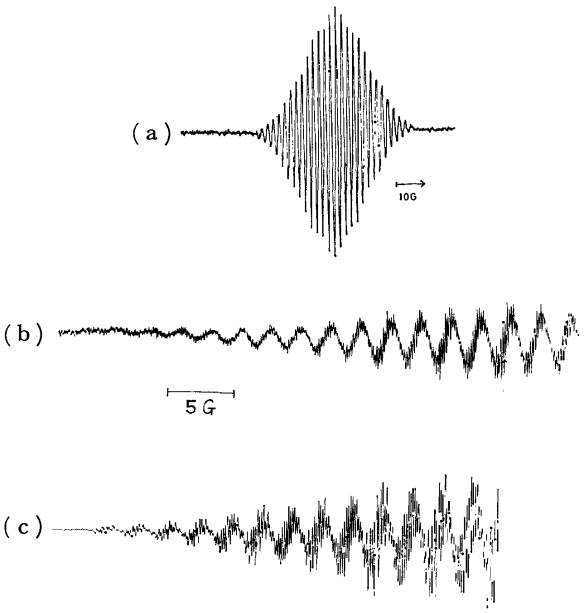

Fig. 4. ESR spectrum of radical (II) (4a), slightly more than one-half of ESR spectrum of radical (II) (better resolved than Fig. 4a) (4b), and its simulation (4c).

distributed to a greater extent to the tetrazolium ring rather than to the biphenylene ring. Both the results of Neugebauer[4] and the present MO calculation show that the distribution of the unpaired electron on the nitrogens does not differ remarkably between radicals (I) and (II).

Long contact of the solution with alkali metal, however, gives rise to the spectrum of benzo[*c*]cinnoline radical anion, the overall-width of which is about a half of that of radical (II). This result offers another evidence for the moleculer structure of Photo-TTC.[5]

The spectra of both radicals (I) and (II) do not change from 20 to —50 °C during observation. The same is true for those produced by sodium metal. Both experimental and calculated (by McLachlan method) data for radicals (I) and (II) are summarized in Table 1.

Table 1. Hyperfine splitting constants of radical (I) and radical (II)

	Radical (I)		Radical (II)	
	Found[a]	Calcd[b]	Found[a]	Calcd[b]
a_1^N	5.25G	4.61G	4.03G	4.00G
a_2^N	7.35	7.97	7.80	7.94
$a_{2\phi.o}^H$	0.90	1.63	1.95	1.74
$a_{2\phi.p}^H$	0.90	1.58	1.95	1.46
$a_{2\phi\ m}^H$	0.45	(−)0.63	0.39	(−)0.38
$a_{5\phi.o}^H$	0.30	(−)0.12	0.26	(−)0.11
$a_{5\phi.p}^H$	0.30	(−)0.10	0.26	(−)0.09
$a_{5\phi.m}^H$	—	0.0043	—	0.004

a) The values were determined by the analyses of the observed spectra referring to the simulated spectra. b) The values were estimated with the relations: $a_N=32.0\cdot|\rho_N^\pi|$ and $a_H=22.5|\rho_C^\pi|$. c) Parameters used in MO calculations are $h_{N1}=1.20$, $h_{N2}=1.50$, $k_{CN}=1.20$ and $k_{NN}=1.0$.

The authors appreciate the helpful discussions of Professors K. Ishizu and K. Mukai. Thanks are also due to Hideo Fujita for his help.

References

1) Y. Deguchi and Y. Takagi, *Tetrahedron Lett.*, **1967**, 3179.

2) F. A. Neugebauer and G. A. Russel, *J. Org. Chem.*, **33**, 2744 (1968); O. W. Maender and G. A. Russel, *J. Org. Chem.*, **31**, 442 (1966).

3) I. Hausser, D. Jerchel, and R. Kuhn, *Ber.*, **82**, 195 (1948); R. Kuhn and D. Jerchel, *Ann.*, **578**, 1 (1952).

4) F. A. Neugebauer, *Tetrahedron Lett.*, **1968**, 2129.

5) E. T. Storm, G. A. Russel, and R. Konaka, *J. Chem. Phys.*, **42**, 2033 (1965).

BULLETIN OF THE CHEMICAL SOCIETY OF JAPAN, VOL. 51 (12), 3641—3642 (1978)

Hydrogenation and Dehydrogenation of 4-Isopropenyl-1-methylcyclohexene Catalyzed by MgO, CaO, La_2O_3, ThO_2, and ZrO_2

Yasutaka TANAKA, Hideshi HATTORI,* and Kozo TANABE*

Department of Chemistry, Faculty of Science, Hokkaido University, Sapporo 060

(Received May 20, 1978)

Synopsis. 4-Isopropenyl-1-methylcyclohexene undergoes hydrogenation over ZrO_2 and ThO_2 to 4-isopropyl-1-methylcyclohexene, while it undergoes mainly dehydrogenation over MgO, CaO, and La_2O_3 to 1-isopropyl-4-methylbenzene. The activity variation of catalysts with pretreatment temperature and the reaction of 4-isopropyl-1-methyl-1,3-cyclohexadiene suggest that selectivity is determined by relative activity for hydrogenation to that for double bond isomerization.

In hydrogenation of diolefins, certain metal oxide catalysts exhibit characteristic selectivity which distinguishes the metal oxides from metallic hydrogenation catalysts. One characteristic of a metal oxide catalyst is partial hydrogenation to produce monoolefins selectively. Another is the 1,4-addition of hydrogen atoms to conjugated diolefins such as 1,3-butadiene and 2-methyl-1,3-butadiene. MgO,[1] ThO_2,[2] and ZrO_2[3] have been found to be active for hydrogenation as well as double bond isomerization of olefins. We have studied the hydrogenation of 4-isopropenyl-1-methylcyclohexene having two kinds of double bonds in a molecule over MgO, CaO, La_2O_3, ThO_2, and ZrO_2 in order to examine the selectivity-determining factor of each catalyst.

Experimental

Magnesium oxide and CaO were obtained by heating *in situ* $Mg(OH)_2$ and $Ca(OH)_2$, respectively. Lanthanum sesquioxide was obtained by heating *in situ* $La(OH)_3$ prepared by the hydrolysis of $La(NO)_3$. Zirconium oxide was obtained by calcination of $Zr(OH)_4$ in air. The $Zr(OH)_4$ was prepared by hydrolysis of $ZrOCl_2$. Thorium oxide was prepared by pyrolysis of $Th(NO_3)_4$ in air. 4-Isopropenyl-1-methylcyclohexene and 4-isopropyl-1-methyl-1,4-cyclohexadiene were supplied by Takasago Perfumery Co., Ltd.

For the reaction, a microcatalytic pulse reactor directly combined with a gas chromatographic column was employed. The oxides or hydroxides were heated at desired temperatures under a helium stream (flow rate, 80 ml/min) for 2 h. Eight μl of a reactant was injected into a hydrogen stream ahead of the catalyst. The reaction was carried out at room temperature, the flow rate of hydrogen stream being 60 ml/min. The reaction products were trapped in liquid nitrogen and then flash evaporated into a gas chromatographic column. A column (5 m, 6 mm o.d.) was packed with PEG 20 M on Celite 545, which was operated at 100 °C with a flow rate of 60 ml/min.

Results and Discussion

The reaction products of 4-isopropenyl-1-methylcyclohexene (**1**) were 4-isopropyl-1-methyl-1,3-cyclohexadiene (**2**), 4-isopropyl-1-methyl-1,4-cyclohexadiene (**3**), 4-isopropylidene-1-methylcyclohexene (**4**), 1-isopropenyl-4-methylcyclohexane (**5**), 1-isopropyl-4-methylcyclohexene (**6**), 3-isopropyl-6-methylcyclohexene (**7**), 4-isopropyl-1-methylcyclohexene (**8**) and 1-isopropyl-4-methylbenzene (**9**).

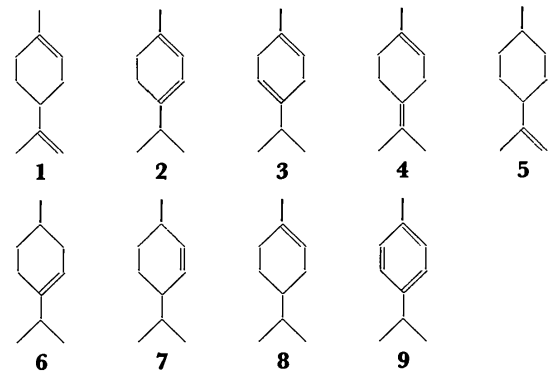

The composition of products over each catalyst is given in Table 1. In the reaction of **1** over CaO, dehydrogenation occurred producing **9** exclusively. Hydrogenated products **7** and **8** were formed over MgO in addition to the main product **9**. Formation of **4** increased with decrease in the conversion of the reactant. Over La_2O_3, product distribution was similar to that for MgO except that **6** was formed instead of **7**. In the reactions of **1** over ThO_2 and ZrO_2, the main product was **8** formed by the selective hydrogenation of the double bond in

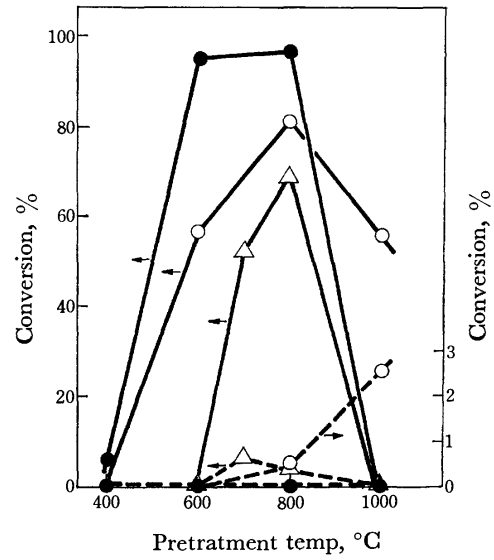

Fig. 1. Variations in conversions to 4-isopropyl-1-methylcyclohexene **8** and 1-isopropyl-4-methylbenzene **9** at the second pulse with pretreatment temperature of catalysts.
○, MgO (0.050 g); ●, CaO (0.050 g); △, La_2O_3 (0.050 g). Broken line, for **8**; solid line, for **9**.

Table 1. Composition of product in reactions of 4-isopropenyl-1-methylcyclohexene **1** and 4-isopropyl-1-methyl-1,3-cyclohexadiene **2** in hydrogen stream at room temperature

Catalyst	Weight g	Pretreatment temp °C	Pulse No.	Reactant	Mol % each product								
					1	**2**	**3**	**4**	**5**	**6**	**7**	**8**	**9**
MgO	0.050	1000	2	**1**	30	<1	0	29	0	0	2	3	36
			3	**1**	54	<1	<1	46	0	0	<1	<1	1
MgO	0.10	1000	3	**1**	0	0	0	0	0	0	7	13	80
			4	**2**	0	0	0	0	0	0	7	12	81
CaO	0.050	800	2	**1**	2	0	0	0	0	0	0	0	98
			4	**1**	8	0	0	0	0	0	0	0	92
La_2O_3	0.10	700	1	**1**	0	0	0	0	0	15	0	8	77
			3	**2**	0	2	3	0	0	18	0	8	69
ThO_2	0.20	650	3	**1**	34	0	0	0	<1	4	0	59	3
			5	**2**	0	19	<1	0	<1	19	0	21	41
ZrO_2	0.20	700	2	**1**	81	0	0	0	0	0	0	15	4
			4	**2**	0	80	1	0	0	0	0	<1	19

the isopropenyl group of the reactant.

In the reaction of **2**, MgO and La_2O_3 gave almost the same product composition as in the reaction of **1**. Over ZrO_2 and ThO_2, however, the product compositions differed from those in the reaction of **1**. Zirconium oxide gave mainly **9** and ThO_2 gave **6** and **8** in addition to **9**.

In Figs. 1 and 2, the conversion into **8** and **9** in the reaction of **1** is plotted against pretreatment temperature of catalysts. Magnesium oxide exhibited maximum activity for dehydrogenation at pretreatment temperature, 800 °C, while for hydrogenation, the activity increased with a rise in pretreatment temperature up to 1000 °C. Calcium oxide showed only dehydrogenation activity over the whole range of pretreatment temperature and maximum activity at pretreatment temperatures 600—800 °C. Over La_2O_3, dehydrogenation and hydrogenation changed nearly parallel with pretreatment temperature, the maximum activities being observed at pretreatment temperatures 700—800 °C. Over ThO_2 and ZrO_2, hydrogenation was predominant over the entire pretreatment temperature range, the maximum activities being obtained at pretreatment temperature 700 °C.

The reaction scheme might be as follows.

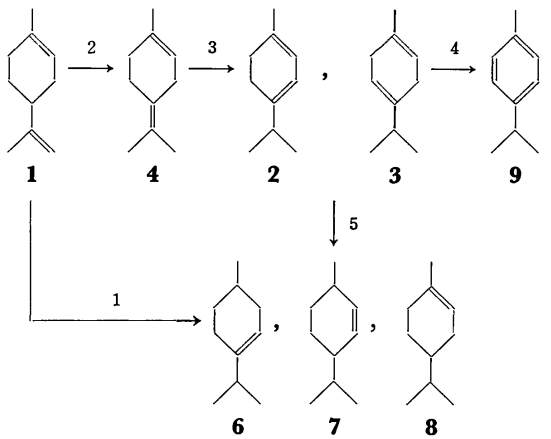

The catalytic feature of each catalyst could be explained as follows.

Over ZrO_2 and ThO_2, **1** undergoes hydrogenation by step 1 before it undergoes double bond migration by steps 2 and 3 to form **2** which would easily be converted into **9**. Step 5 is negligible with ZrO_2 but fast with ThO_2.

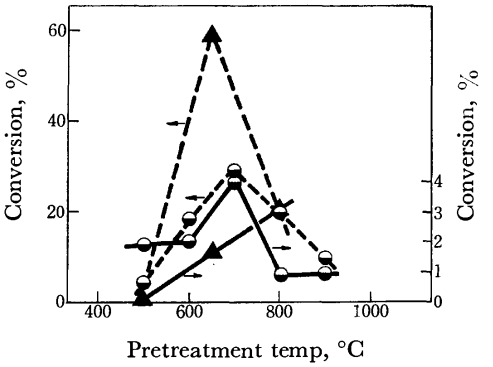

Fig. 2. Variations in conversions to 4-isopropyl-1-methylcyclohexene **8** and 1-isopropyl-4-methylbenzene **9** at the second pulse with pretreatment temperature of catalysts. ◒, ZrO_2 (0.20 g); ▲, ThO_2 (0.20 g). Broken line, for **8**; solid line, for **9**.

Over MgO, CaO, and La_2O_3, hydrogenation step 1 should be slower than steps 2, 3, and 4. Double bond isomerization by steps 2 and 3 quickly occurs to produce **2** or **3** which undergoes fast dehydrogenation to **9**. Since the product distribution of **6**, **7**, and **8** from **1** was practically the same as from **2**, step 5 is much faster than step 1.

Variations in the activities of MgO and CaO were reported for the isomerization of butenes and hydrogenation of olefins as a function of pretreatment temperature.[4–6] The activity of MgO for isomerization exhibited a maximum at 600 °C, while that for hydrogenation did not appear at 600 °C and reached a maximum around 1100 °C. The activity for dehydrogenation of **1** to **9** correlates better with that for isomerization of butenes.

Since the hydrogenation step in the reaction of **1** to **9** is considered to proceed on the hydrogenation sites, a correlation of dehydrogenation activity to **9** with isomerization activity suggests that dehydrogenation to **9** involves an isomerization step which is slower than the dehydrogenation step. This is in line with the proposed reaction scheme.

High selectivity of ThO_2 and ZrO_2 for hydrogenation is considered to be due to a relatively high activity for hydrogenation as compared with that for double bond isomerization, as actually observed in hydrogenation and isomerization of butenes.[2,3]

References

1) H. Hattori, Y. Tanaka, and K. Tanabe, *J. Am. Chem. Soc.*, **98**, 4652 (1976).

2) Y. Imizu, H. Hattori, and K. Tanabe, *Shokubai*, **19**, 64 (1977).

3) T. Yamaguchi and J. W. Hightower, *J. Am. Chem. Soc.*, **99**, 4201 (1977).

4) H. Hattori, N. Yoshii, and K. Tanabe, *Proc. 5th Intern. Congr. Catalysis*, Miami Beach, 1972, **10**, 233 (1973).

5) H. Hattori, Y. Tanaka, and K. Tanabe, *Chem. Lett.*, **1975**, 659.

6) Y. Tanaka, H. Hattori, and K. Tanabe, *Chem. Lett.*, **1976**, 37.

7) T. Yamaguchi and J. W. Hightower, *Shokubai*, **19**, 257 (1977).

BULLETIN OF THE CHEMICAL SOCIETY OF JAPAN, VOL. 51 (12), 3643—3644 (1978)

Intramolecular Dimer and Excimer Phosphorescence of Poly(2-vinylnaphthalene) and Copolymers of 2-Vinylnaphthalene and Phenyl Vinyl Ketone

Masayuki AIKAWA, Takeshi TAKEMURA,* Hiroaki BABA, Masahiro IRIE,** and Koichiro HAYASHI**

Division of Chemistry, Research Institute of Applied Electricity, Hokkaido University, Sapporo 060

***Institute of Scientific and Industrial Research, Osake University, Suita, Osake 565*

(Received July 25, 1978)

Synopsis. Phosphorescence spectra and lifetimes of poly(2-vinylnaphthalene) and copolymers of 2-vinylnaphthalene and phenyl vinyl ketone have been measured as a function of the composition ratio between the constituent benzoyl and naphthyl groups in both rigid and fluid solutions.

In a previous paper[1] it was shown that poly(vinylnaphthalene)s exhibit fluorescence emissions ascribable to the monomer, dimer, and excimer of the constituent naphthyl groups. The purpose of the present study is to examine whether such a polymer emits the intramolecular dimer and excimer phosphorescence. Copolymers of 2-vinylnaphthalene and phenyl vinyl ketone have been employed in addition to poly(2-vinylnaphthlene). Since the formation of the intramolecular dimer or excimer is expected to depend on the naphthyl group content of copolymer, the ratio between the components of the copolymer was varied to a considerable extent. The phosphorescence spectra of these compounds were measured in both rigid and fluid solutions.

Poly(2-vinylnaphthalene) (PVN) and copolymers of 2-vinylnaphthlene and phenyl vinyl ketone (VN–PVK) were synthesized in benzene with use of azobisisobutyronitrile. The compositions of copolymer I, II, III, and IV are 9/91, 16/84, 35/65, and 75/25, respectively, in mole fraction of 2-vinylnaphthalene-phenyl vinyl ketone. Spectro-grade THF and reagent-grade MTHF were passed through an activated alumina column and distilled repeatedly (4 or 5 times) over lithium aluminium hydride or phosphorus pentaoxide.

The concentrations of the copolymer solutions were so adjusted that the absorbance at the $n\rightarrow\pi^*$ transition band was less than 0.1. The sample solutions were carefully degassed by freeze-thaw cycles. The apparatus and techniques for measuring emission spectra and monitoring the time-dependent behavior of the emissions were the same as those reported.[2,3]

Results and Discussion

Phosphorescence Spectra in Rigid Glass. Figure 1 shows the phosphorescence spectra of VN–PVK copolymers in MTHF at 77 K. Excitation was carried out at 350 nm, where there is only the $n\rightarrow\pi^*$ absorption band of the constituent benzoyl group. The spectrum of copolymer I consists of two phosphorescence emissions. One located in the region of 400—460 nm is similar to the phosphorescence spectrum of acetophenone and ascribed to the triplet state of the benzoyl group; the other located in the region of 470—600 nm has an origin at 468 nm and is very similar to the phosphorescence spectrum of naphthalene, and is assigned to the naphthyl group. The appearance of the phosphorescence

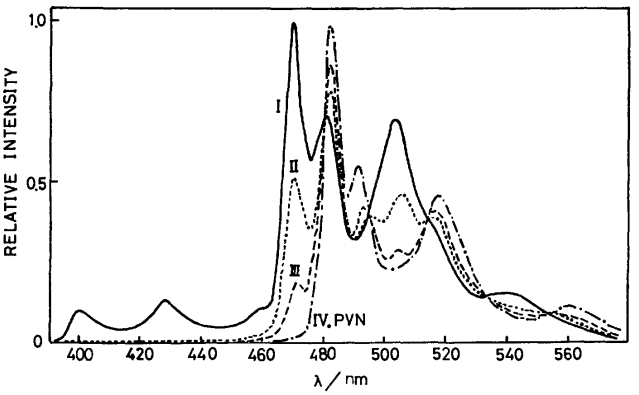

Fig. 1. The phosphorescence spectra (uncorrected) of VN–PVK copolymer I, II, III, and IV and of PVN in MTHF at 77 K obtained by exciting at 350 nm. The spectra of copolymer-IV and PVN were almost the same.

of the naphthyl group by excitation at 350 nm indicates that intramolecular triplet-triplet (T-T) energy transfer from the benzoyl group to the naphthyl group occurs effectively in the copolymer. This is supported by the fact that the emission due to the benzoyl group disappears with increase in content of the naphthyl group, which acts as an acceptor in the T-T energy transfer.

With increase in content of the naphthyl group in the copolymer the intensity of the 0-0 band at 468 nm in the phosphorescence spectrum decreases, while a new band grows at 482 nm. The intensity of the band at 482 nm is comparable to that at 468 nm for copolymer II, dominating over the latter intensity for copolymer III. On the other hand, copolymer IV and PVN give predominantly phosphorescence spectra with an origin at 482 nm which are very similar to the spectrum of the naphthalene dimer with a 0-0 band at 485 nm reported by Chandross and Dempster.[4] From the composition dependence of the phosphorescence spectra of the copolymer and PVN, the phosphorescence spectrum with the 0-0 band at 482 nm for the copolymers and PVN can be assigned to the dimer formed between the naphthyl groups in the ground state. This leads to the conclusion that the phosphorescence spectrum of PVN in rigid glass consists almost of the dimer phosphorescence in disagreement with a previous assignment of the monomer.[5]

The decay of the phosphorescence observed at 480 nm of copolymer I in MTHF at 77 K gives a single exponential curve with a lifetime 2.7 s. However, two exponential decays are observed in each of the copolymers II—IV. A relatively fast decaying component

appears in addition to the slowly decaying component corresponding to the component of copolymer I. The contribution of the fast decaying component increases with increase in content of the naphthyl group. Since copolymer I shows mainly the monomer phosphorescence and the intensity ratio of the dimer to monomer phosphorescence in copolymers II—IV increases with the content of the naphthyl group, it is obvious that the fast and slow components correspond to the dimer and monomer phosphorescence of the naphthyl groups, respectively. The lifetimes of the triplet monomer and dimer are 2.1 and 0.6 s for copolymer II, 2.3 and 0.5 s for copolymer III, and 2.0 and 0.5 s for copolymer IV.

With the change of copolymer from I to IV, the lifetime of the monomer decreases from 2.7 to 2.0 s, while that of the triplet dimer remains 0.5 s. The decrease in lifetime of the monomer phosphorescence can be explained in terms of the quenching of the monomer emission by the dimer species through T-T energy transfer.

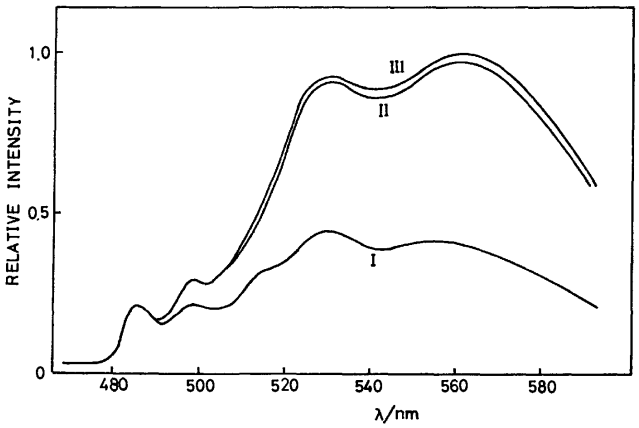

Fig. 2. The phosphorescence spectra (corrected) of VN-PVK copolymer I, II, and III in fluid THF solution at 187 K obtained by exciting at 350 nm.

Phosphorescence Spectra of the Copolymers in Fluid Solution. Figure 2 shows corrected phosphorescence spectra of the copolymers in fluid THF solution at 187 K. Each of these spectra consists of a structured spectrum with a 0-0 band at 485 nm and a broad, structureless spectrum with intensity maximum at *ca.* 550 nm. The former phosphorescence spectrum is attributable to the emission of the dimer of the naphthyl groups in the polymer since it is similar in position to the spectrum of the dimer of the naphthalene nuclei in rigid glass,[4] and in general $\pi \leftarrow \pi^*$ phosphorescence spectra of compounds such as naphthalene, phenanthrene, and quinoxaline remain almost unchanged in the position of the 0-0 band when the sample is changed from rigid glass solution to fluid.[2,3,6]

The broad emission spectra are attributed to the phosphorescence from the excimer of the naphthyl group in the polymers. This assignment is in line with the following experimental results: (1) The broad emission spectra of the copolymers correspond to the excimer phosphorescence spectra of naphthalene and its derivatives,[2,3] and 1,3-di(1-naphthyl)propane[7,8] in fluid solution. (2) The excitation spectra obtained by monitoring the emission at 560 nm of the copolymers agree with the absorption spectra. (3) No broad emission spectra are observed in rigid glass at 77 K. (4) The lifetimes of the emissions are of the order of 10^{-4} s.

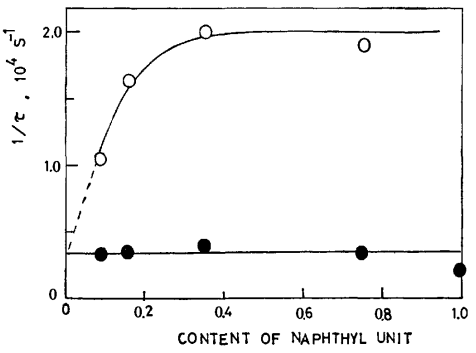

Fig. 3. The reciprocal lifetimes of the phosphorescence of VN-PVK copolymers as a function of VN-PVK composition. The measurements were carried out in fluid THF solution at 187 K. ○ corresponds to the reciprocal lifetime of the excimer and ● that of the dimer.

In the fluid solution at 187 K, the decay curves of the phosphorescence emissions of all the copolymers obtained by monitoring at 500 nm consist also of two exponentiallg decaying components. The results are shown in Fig. 3 where the reciprocal lifetimes of the two decaying components are plotted as a function of the composition of the copolymer. The monitoring wavelength dependence and VN-PVK composition dependence of the contribution of the two components indicate that the two components, fast and slow, are attributable to excimer and dimer phosphorescence, respectively. The lifetime of the dimer phosphorescence with a relatively slow decay, 3×10^{-4} s, is independent of the composition of the copolymer, while that of the excimer phosphorescence decreases rapidly, reaching a constant value of 5×10^{-5} s as the content of the naphthyl group increases.

References

1) M. Irie, T. Kamijo, M. Aikawa, T. Takemura, K. Hayashi, and H. Baba, *J. Phys. Chem.*, **81**, 1571 (1977).

2) T. Takemura, H. Baba, and Y. Shindo, *Chem. Lett.*, **1974**, 1091; T. Takemura, M. Aikawa, H. Baba, and Y. Shindo, *J. Am. Chem. Soc.*, **98**, 2205 (1976); T. Takemura, M. Aikawa, and H. Baba, *J. Lumin.*, **12/13**, 819 (1976).

3) M. Aikawa, T. Takemura, and H. Baba, *Bull. Chem. Soc. Jpn.*, **49**, 473 (1976).

4) E. A. Chandross and C. J. Dempster, *J. Am. Chem. Soc.*, **92**, 704 (1970).

5) M. T. Vala, Jr., J. Haebig, and S. A. Rice, *J. Chem. Phys.*, **43**, 886 (1965).

6) K. Yamamoto, T. Takemura, and H. Baba, *Bull. Chem. Soc. Jpn.*, **51**, 729 (1978).

7) P. C. Subudhi and E. C. Lim, *J. Chem. Phys.*, **63**, 5491 (1975).

8) S. Okajima, P. C. Subudhi, and E. C. Lim, *J. Chem. Phys.*, **67**, 4611 (1977).

BULLETIN OF THE CHEMICAL SOCIETY OF JAPAN, VOL. 51 (12), 3645—3646 (1978)

Syntheses of Rare Earth Orthophosphates

Yasuo HIKICHI,* Ken-iti HUKUO, and Jiro SHIOKAWA**

Materials Research Laboratory, Nagoya Institute of Technology, Gokiso-cho, Showa-ku, Nagoya 466

***Department of Applied Chemistry, Faculty of Engineering, Osaka University, Yamadakami, Suita 565*

(Received January 9, 1978)

Synopsis. Rare Earth orthophosphates have been synthesized and examined by X-ray diffraction, DTA and TGA. Six types have been found: a) the monazite type RPO_4, b) the xenotime type RPO_4, c) the hexagonal form $RPO_4 \cdot 0.5H_2O$, d) the weinschenkite type $RPO_4 \cdot 2H_2O$, e) the orthorhombic form $DyPO_4 \cdot 1.5H_2O$ and f) the amorphous phosphate.

In preceding papers,[1-4] the synthesized monazite type $CePO_4$, the hexagonal form $CePO_4 \cdot 0.5H_2O$, the xenotime type YPO_4, and the weinschenkite type $YPO_4 \cdot 2H_2O$ have been reported. The present study reports the syntheses and thermal stability of various rare earth orthophosphates RPO_4 (R=La, Ce, Pr, Nd, Sm, Gd, Y, Dy, Er, or Yb).

Experimental

Starting Materials. RCl_3 of 99.9% purity (R=La, Ce, Pr, Nd, Sm, Gd, Y, Dy, Er, or Yb) and H_3PO_4, $(NH_4)H_2PO_4$, $(NH_4)_2HPO_4$, $(NH_4)_3PO_4 \cdot 3H_2O$ or $NaPO_3$ were used as starting materials.

Synthesis by Solid State Reactions. Mixtures of RCl_3 and $NaPO_3$ with a mole ratio (P/R) of 2.5 were heated in the temperature range 200—1000 °C for 5 h in an electric furnace using a platinum crucible. After heating, the hot crucible was removed from the furnance and quenched to room temperature. The products were taken out from the crucible and washed successively with (1+10)HNO_3 solution, distilled water and acetone.

Synthesis by Precipitation. A solution of RCl_3 (0.05 mol/l) was rapidly added to dilute H_3PO_4 or phosphate solution and magnetically stirred. After one hour, the pH of the mixed solution was measured by a pH meter and the solution transfered to a conical flask, which was tightly stoppered. The mixed solutions were maintained at 20, 50, and 90 °C for 1 to 900 days in an air bath. The pH of the mixed solution was adjusted to a constant value with H_3PO_4 or phosphate solution. The solution was suction-filtered with a filter paper and washed five times with distilled water and finally with acetone. The precipitate was kept in a desiccator (drying agent: H_2SO_4) at room temperature.

Results and Discussion

Phases Obtained by Solid State Reaction. Feigelson[5] synthesized anhydrous RPO_4 by the fusion of rare earth oxides with excess $Pb_2P_2O_7$ at 1300 °C in a refractory (mullite) crucible in an electric furnace.

In the present investigation, the anhydrous phosphates of monazite type RPO_4 (R=La, Ce, Pr, Nd, Sm, or Gd) and xenotime type RPO_4 (R=Y, Dy, Er, or Yb) were first synthesized by the solid state reactions in air of RCl_3 with $NaPO_3$ at temperatures as low as 200 °C. No hydrated phosphates were detected in the heated samples. The intensity of the X-ray diffraction powder lines of the anhydrous phosphates increased with increasing preparation temperature.

Phases Obtained by Precipitation. Anthony[6] synthesized the monazite type $CePO_4$ by the hydrothermal treatment of mixtures of cerium hydroxide gel, H_3PO_4 and water at *ca.* 300 °C. Hydrated phosphates were not observed in the products.

In the present investigation, various types of phosphates were synthesized below 90 °C in solution. The crystalline phases obtained by precipitation from mixed solutions in the temperature range 20—90 °C for 1 to 900 days were the hexagonal form $RPO_4 \cdot 0.5H_2O$ (R=La, Ce, Pr, Nd, Sm, or Gd), the weinschenkite type $RPO_4 \cdot 2H_2O$ (R=Y, Dy, Er, or Yb), the orthorhombic form $DyPO_4 \cdot 1.5H_2O$, the monazite type RPO_4 (R=La, Ce, Pr, Nd, Sm, or Gd) and the xenotime type RPO_4 (R=Y, Dy, Er, or Yb). Table 1 illustrates the phases obtained by X-ray diffraction analysis under various experimental conditions.

The hexagonal form $RPO_4 \cdot 0.5H_2O$ was synthesized in the pH range 1—3 at 20 °C and was stable in the mother liquor for 900 days. Above 50 °C, however, the hexagonal form gradually changed into the monazite type RPO_4 in the solution. The rate of transformation from the hexagonal form to the monazite type by ageing in solution increased with decreasing pH and increasing preparation temperature. The weinschenkite type $RPO_4 \cdot 2H_2O$ was synthesized in the pH range 1—3 at 20 °C and was stable in solution for 900 days. When aged above 50 °C the weinschenkite type gradually changed to the xenotime type RPO_4. Amorphous phosphate was detected in the precipitate from the mixed solution above pH 3 at 20 °C. After ageing in solution above 50 °C, the amorphous phosphate became the crystalline hydrated or anhydrous phosphates of the hexagonal form, weinschenkite type, orthorhombic form, monazite type or xenotime type, depending on the kind of rare earth.

Thermal Stability. It has been established that monazite and xenotime are stable in air at high temperatures. Ueda and Korekawa,[7] and Ueda[8] found that the cone of natural monazite from Nogisawa-mura, Fukushima Pref. did not melt when fired at 1950 °C, and that natural xenotime from Ishikawa-cho, Fukushima Pref. did not decompose at 1800 °C. The thermal stability of the hydrated rare earth orthophosphates has been reported only for $CePO_4 \cdot 0.5H_2O$[9] and $YPO_4 \cdot 2H_2O$.[3]

The DTA curves of the hexagonal form $RPO_4 \cdot 0.5H_2O$ showed two endothermic peaks and the TGA curves showed a weight loss corresponding to $0.5H_2O$ at 204—234 °C. This weight loss appeares to correspond to the first endothermic DTA peak (204—234 °C).

Table 1. Synthetic runs and phases detected

R	Aging time (day)	Detected phases: 20 °C (pH) 0.5	1	3	5	50 °C (pH) 0.5	1	3	5	90 °C (pH) 0.5	1	3	5
La	3	—	H	H	A	—	H	H	A	M+H	H	H	A
	14	—	H	H	A	M+H	H	H	A	M+H	H	H	A
	28	—	H	H	A	M+H	H	H	A	M	H	H	A
	900	—	H	H	A	M	M	M	M	M	M	M	M
Gd	3	—	H	H	A	—	H	H	A	M+H	H	H	H
	14	—	H	H	A	H	H	H	H	M+H	H	H	H
	28	—	H	H	A	M+H	H	H	H	M	H	H	H
	900	—	H	H	A	M	M	M	M	M	M	M	M
Dy	3	—	W	A	A	—	W	O	A	—	O	O	O
	14	—	W	W	A	—	W	O	A	O	O	O	O
	28	—	W	W	A	W	W	O	A	O	O	O	O
	900	—	W	W	A	X	X	X	X	X	X	X	X
Y	3	—	W	A	A	—	W	W	A	—	W	W+X	X
	14	—	W	W	A	—	W	W	A	X	X	X	X
	28	—	W	W	A	—	W	W	X	X	X	X	X
	900	—	W	W	A	—	X	X	X	X	X	X	X
Yb	3	—	W	A	A	—	W	A	A	X	X	X	A
	14	—	W	W	A	X+W	X+W	X	A	X	X	X	X
	28	—	W	W	A	X	X	X	A	X	X	X	X
	900	—	W	W	A	X	X	X	X	X	X	X	X

—: No precipitate, H: hexagonal form $RPO_4 \cdot 0.5\ H_2O$, M: monazite type RPO_4, W: weinschenkite type $RPO_4 \cdot 2H_2O$, A: amorphous phosphate, X: xenotime type RPO_4, O: orthorhombic $DyPO_4 \cdot 1.5H_2O$.

Dehydrated RPO_4 had a hexagonal form and was easily rehydrated to form $RPO_4 \cdot 0.5H_2O$ when kept at ordinary humidity. Therefore this water corresponding to $0.5H_2O$ was concluded to be zeolitic water. The anhydrous hexagonal form RPO_4 gradually transformed into the monazite type at 500—600 °C. The DTA curves of the synthesized weinschenkite type $RPO_4 \cdot 2H_2O$ showed one endothermic peak and the TGA curves showed a weight loss corresponding to $2H_2O$ at 273—276 °C. This weight loss appeares to correspond to the endothermic DTA peak (273—276 °C). Anhydrous RPO_4 was xenotime type. The weinschenkite type $RPO_4 \cdot 2H_2O$ appeared to convert to the xenotime type in air in the temperature range 273—276 °C. The orthorhombic form $DyPO_4 \cdot 1.5H_2O$ converted to the xenotime type $DyPO_4$ at 270 °C in air.

References

1) Y. Hikichi and K. Hukuo, *Nippon Kagaku Kaishi*, **1975**, 1311.
2) K. Hukuo and Y. Hikichi, *Nippon Kagaku Kaishi*, **1975**, 622.
3) Y. Hikichi, K. Hukuo, and J. Shiokawa, *Nippon Kagaku Kaishi*, **1977**, 1634.
4) Y. Hikichi, K. Hukuo, and J. Shiokawa, *Nippon Kagaku Kaishi*, **1978**, 186.
5) R. S. Feigelson, *J. Am. Ceram. Soc.*, **47**, 257 (1964).
6) J.W. Anthony, *Am. Mineral.*, **42**, 904 (1957).
7) T. Ueda and M. Korekawa, *Mem. Coll. Sci. Univ. Kyoto, Ser. B*, **22**, 165 (1955).
8) T. Ueda, *Mem. Coll. Sci. Univ. Kyoto, Ser. B*, **24**, 81 (1957).
9) K. Hukuo, Y. Hikichi, and N. Ose, *Yogyo Kyokai Shi*, **82**, 284 (1974).

BULLETIN OF THE CHEMICAL SOCIETY OF JAPAN, VOL. 51 (12), 3647—3648 (1978)

Nitric Acid Oxidation of 3,5,7,7,10,12,14,14-Octamethyl-1,4,8,11-tetraazacyclotetradeca-4,11-dienenickel(II) Perchlorate

Tasuku Ito†

Department of Chemistry, Faculty of Science, Hokkaido University, Sapporo 060

(Received June 21, 1978)

Synopsis. Oxidative dehydrogenation of three kinds of the title compounds, *meso*[1*R*(*S*), 3*S*(*R*), 8*S*(*R*), 10*R*(*S*)]-, *rac*[1*S*(*R*), 3*R*(*S*), 8*S*(*R*), 10*R*(*S*)]-, and optically active[1*S*, 3*R*, 8*S*, 10*R*]-forms produced the complexes with four isolated imine groups. Some spectroscopic data of the tetraimine complexes are presented.

It has been found that some nickel(II) complexes of cyclic ligand containing secondary amine donors are chemically oxidized to forms containing a higher unsaturation in the ligand.[1-4] The *meso*-, *rac*-, and optically active-forms of the title complex **1**[5] underwent oxidative dehydrogenation of the ligand in concentrated nitric acid to give the respective tetraimine complexes **2**. The elemental analyses of each oxidation product indicated the presence of two additional sites of unsaturation. The IR spectra of the oxidation products showed no absorption for N–H stretching modes ($\approx$3200 cm^{-1}). These two results lead to the isolated tetraimine structure **2**.

The proton noise decoupling ^{13}C NMR spectra of the *meso*- and *rac*-complexes show nine resonance lines, respectively, indicating that each carbon atom within each isomer is pairwise equivalent. The *meso*- and *rac*-complexes have C_i and C_2 symmetry, respectively. The off-resonance spectrum of each isomer consists of four quartets, one triplet, two doublets, and two singlets. This spectral pattern is as expected from the structure **2**. The resonance lines were assigned in the way similar to that for the complex **1**.[6] The ^{1}H NMR spectra of the products also support the structure. The ^{1}H and ^{13}C NMR spectral data are listed in Tables 1 and 2, respectively.

Table 1. ^{1}H NMR spectral data for tetraimine complexes[a]

Assignments[b]	Signal shape[c]	Rel. intens.	Chem. shift, ppm *vs.* TMS	
			rac-isomer	*meso*-isomer
CH_3(a)[d]	s	3	1.38	1.40
CH_3(b)[e]	s	3	1.16	1.20
CH_3(c)	s	(3)	(2.33)	(2.32)
CH_3(d)	d	3	1.53	1.56
H_a, H_b	AB-q	(2)	(2.93)	(2.94)
H_c	q of d	1	5.02	4.98
H_d	d	1	7.98	7.88

a) Data for the perchlorate salts in DMSO-d_6 solutions. The signals, whose chemical shifts are given in parentheses, disappear upon d_{10}-deuteration. b) See the structure **2** for numbering. c) The abbreviations, s, d, AB-q, and q of d, denote singlet, doublet, AB-quartet, and quartet of doublet, respectively. d) Axial. e) Equatorial.

Table 2. ^{13}C NMR spectral data for the *rac*- and *meso*-tetraimine complexes[a]

Assignments[b]	Chemical shift, ppm *vs.* TMS	
	rac-isomer	*meso*-isomer
C_1[c]	24.7 q	24.5 q
C_2[d]	25.7 q	25.5 q
C_3	(23.6) q	(23.8) q
C_4	15.9 q	16.3 q
C_5	56.9 s	57.2 s
C_6	(50.9) t	(50.1) t
C_7	185.1 s	185.2 s
C_8	69.1 d	69.2 d
C_9	177.4 d	175.6 d

a) Data for the perchlorate salts in DMSO-d_6. The signals, whose chemical shifts are given in parentheses, disappear substantially upon d_{10}-deuteration. The abbreviations, q, t, d, and s, denote quartet, triplet, doublet, and singlet, respectively, which are signal shape upon off-resonance decoupling. b) See the structure **2** for numbering. c) Axial. d) Equatorial.

The perchlorate salts of the tetraimine complexes are square planar and diamagnetic in most solvents (H_2O, MeOH, DMSO, CH_3CN, Py) as revealed by the ligand field spectra. The optically active isomer in H_2O has a d-d electronic absorption band at 23000 cm^{-1} with an ε_{max} of 86 and an absorption at 34100 cm^{-1} (ε_{max}= 5580) associated with the isolated imine functions. The corresponding CD peaks appear at 20800 ($\Delta\varepsilon$= −0.29) and 24300 ($\Delta\varepsilon$=+2.62), and 33800 cm^{-1} ($\Delta\varepsilon$=−5.75). The *meso*-isomer shows a similar electronic spectrum; $\tilde{\nu}_{max}(\varepsilon_{max})$=23400 (58), 34400 cm^{-1} (5860).[7] These features of the electronic spectra and the circular dichroism spectrum demonstrate a square planar structure for these complexes in water.[1]

The tetraimine complexes are stable in neutral or acidic solutions but decompose in basic solutions.

It is well known for analogous marcrocyclic nickel(II) complexes that the protons α to the imine carbon atom can be exchanged for deuterium atoms in basic D_2O solution.[3-5,8] Recrystallization of **1** from basic D_2O deuterates selectively the methylene protons of the six-membered chelate rings and the protons of the imine methyl groups (CH_3(c)), giving the d_{12}-derivative **4**.[5] Oxidation of the d_{12}-derivatives **4** of the *rac*- and the *meso*-diene complexes with nitric acid produced the d_{10}-derivative of their respective tetraimine complexes **5**. The ^{1}H and ^{13}C NMR spectra of the deuterated,

† Present address: Institute for Molecular Science Okazaki 444.

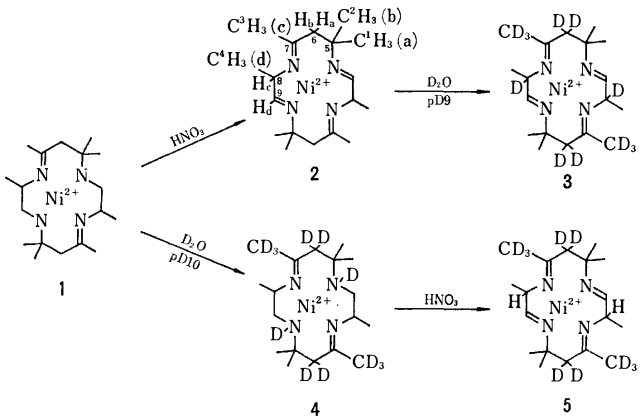

oxidized species indicate the deuterated sites remain intact upon oxidation.

Attempts to prepare d_{12}-derivatives **3** by recrystallization of **2** from basic D_2O solution were partly successful. The ^1H and ^{13}C NMR spectra of the *meso*-tetraimine complex recrystallized from weakly basic D_2O solution indicated that the desired deuteration accomplished. However, the resonance lines of the ^1H and ^{13}C NMR spectra were broad, indicating the presence of the paramagnetic species. All attempts to prepare the d_{12}-derivative **3** of the *rac*-tetraimine complexes in the same way were unsuccessful. As was mentioned before, the tetraimine complexes are unstable in basic solutions as compared with the parent diene complexes.

Experimental

Materials. meso[*1*R(S),*3*S(R),*8*S(R),*10*R(S)]-, rac-[*1*S(R),*3*R(S),*8*S(R),*10*R(S)]-, *and Optically Active*[*1*S,*3*R,*8*S,*10*R]-*form of 3,5,7,7,10,12,14,14-Octamethyl-1,4,8,11-tetraazacyclotetradeca-4,11-dienenickel(II) Perchlorates* (**1**): These complexes were prepared as reported in the previous papers.[5,6]

Oxidation of **1**: Ten grams of the *meso*-diene complex was dissolved in 30 ml of concentrated nitric acid. Dissolution was immediate and a deep orange solution was produced. This solution was heated on a water bath (80 °C) for 2 h. After cooling, 150 ml of cold acetone was added. A yellow product precipitated. This material was removed by filtration and recrystallized from hot water; yield 6.4 g. This was identified as the *meso*-isomer of **2** (see text). The *rac*- and optically active tetraimine complexes were prepared in a similar way. However, since these isomers were more soluble than the *meso*-isomer, an acetone–diethyl ether mixture (1:2 (v/v)) was used instead of acetone to obtain the precipitates. Found for the *meso*-isomer: C, 38.44; H, 5.70; N, 10.03%. Found for the *rac*-isomer: C, 38.77; H, 5.64; N, 10.17%. Found for the optically active isomer: C, 38.41; H, 5.98; N, 10.21%. Calcd for $NiC_{18}H_{32}N_4Cl_2O_8$: C, 38.46; H, 5.74; N, 9.97%.

The d_{10}*-Derivatives* **5**: The d_{12}-derivatives **4** of the *meso*-, *rac*-, and optically active dienes[5,6] were used as strating materials and oxidized with concentrated nitric acid in the same way.

Measurements. Instruments used for the spectral measurements were as follows: ^{13}C NMR spectra, a JEOL NMR Spectrometer, Model JNM-PFT-60, operating at 15.09 MHz; ^1H NMR spectra, a JEOL NMR Spectrometer, Model PS-100; Electronic spectra, a Hitachi EPS-3T Recording Spectrophotometer; Circular dichroism spectra, a JASCO ORD/UV-5 Spectrometer with CD attachment; Infrared spectra, a JASCO IR-G Spectrophotometer.

References

1) N. F. Curtis, *Coord. Chem. Rev.*, **3**, 3 (1968).
2) N. F. Curtis, *Chem. Commun.*, **1966**, 881.
3) E. K. Barefield and D. H. Busch, *Inorg. Chem.*, **10**, 108 (1971).
4) V. L. Goedken and D. H. Busch, *Inorg. Chem.*, **10**, 2679 (1971).
5) T. Ito and D. H. Busch, *Inorg. Chem.*, **13**, 1770 (1974).
6) T. Ito, K. Soma, and M. Watanabe, *Chem. Lett.*, **1976**, 421.
7) Because of the low solubility, the electronic absorption spectra for the *meso*-isomer were measured in 0.1 M HNO_3 for UV region and in *ca.* 2 M HNO_3 for visible region.
8) L. G. Warner, N. J. Rose and D. H. Busch, *J. Am. Chem. Soc.*, **90**, 6938 (1968).

BULLETIN OF THE CHEMICAL SOCIETY OF JAPAN, VOL. 51 (12), 3649—3650 (1978)

Preparation of Shark Powder and Shark Paste as Biological Standard Reference Materials

Yukiko DOKIYA, Satoru KUROSAWA, Shozo TODA,* and Keiichiro FUWA**

Department of Agricultural Chemistry, Faculty of Agriculture, The University of Tokyo, Yayoi, Bunkyo-ku, Tokyo 113

***Department of Chemistry, Faculty of Science, The University of Tokyo, Hongo, Bunkyo-ku, Tokyo 113*

(Received July 4, 1978)

Synopsis. As a possible biological standard reference material for metal analysis, shark powder has been prepared from the muscle of sharks (*Squalus mitsukurii*) and compared with shark paste which was prepared from the same raw material adopting the procedure of Japanese fish paste production. With respect to the homogeneity of metal contents and to the stability during storage, both samples were found to be similar.

As a possible biological standard reference for metal analysis the authors have suggested the preparation of powdered Japanese tea leaves.[1] Since there has been no fish reference material available, a search for a suitable fish reference material was commenced. A wet fish reference material, shark paste, has been proposed by the present authors as a possible candidate for a new biological reference material.[2] In this report, a comparison is made between the wet fish reference material and the dry powder, shark powder, prepared from the same raw material, from the standpoint of practical utilization.

Experimental

Preparation of Shark Powder. The procedure for preparation of shark powder in comparison with shark paste, is outlined in Fig. 1. Two equal amounts of the white muscle was dissected from eight sharks (*squalus mitsukurii*) and one was used for shark powder and the other was used for shark paste. The freeze-dried muscle was pulverized with an agate ball mill (Fritsch Co., Ltd.) followed by sieving with a polyvinylidene chloride fiber sieve (50 mesh). The powder obtained was bottled in polystyrene bottles of 20 ml and kept in a desiccator containing silica gel.

Other Reference Material. Tuna powder was obtained from NBS. This material is packed in a polyethylene pouch which is sealed in an aluminium can and it is necessary to use immediately after opening the can. The metal contents are not certified yet for this material.

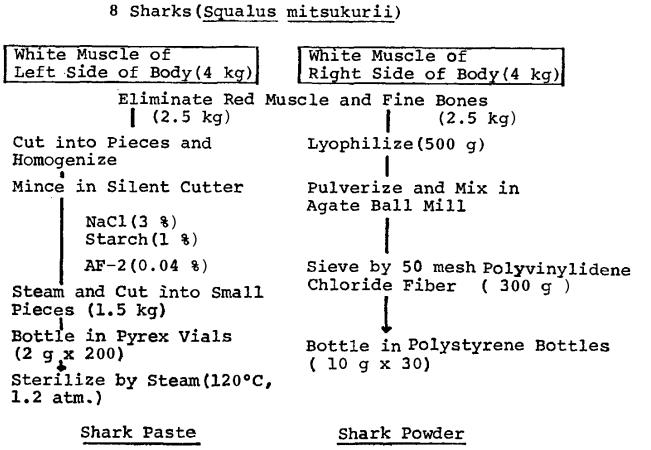

Fig. 1. Procedure for the preparation of shark paste and shark powder.

Determination of Water and Metal Content. Five lots of 0.1—0.5 g were taken from the bottles and dried at 90 °C in dry oven for 24 h to determine the water content. The powder was then used for the determination of metals by atomic absorption and flame emission spectrometry.

For mercury determination, 5 additional portions were taken and digested with HNO_3 and H_2O_2 in the same manner as previously reported.[3]

Results and Discussion

Homogeneity of Shark Powder. The content of metals in the shark powder and NBS-tuna is shown in Table 1. The homogeneity with respect to K, Na, Mg, and Hg is similar for both samples. However, with respect to Ca, the results for shark powder indicated a better homogeneity compared to NBS-tuna. According to Rook,[4] the comparatively poor homogeneity of Tuna with respect to Ca might be attributed to the bone meals in tuna meat. In this study, the raw materials, shark meat, which contains less bones than tuna meat was utilized. In addition, sieving with the polyvinylidene chloride fiber would eliminate the comparatively heterogeneous part which was considered to be mainly the fisca containing a higher amount of Ca than the muscle part.

According to Barnes,[5] the variation in calcium determinations for NBS-tuna can be controlled to within

Table 1. Metal content in shark powder and tuna powder (μg/g-dry)

	Shark powder	NBS-tuna[a]		Shark powder	NBS-tuna[a]
K	17300	12300	Ca	185	253
	17100	12000		208	385
	17400	12000		210	331
	17100	12700		200	493
	17300	12000		199	338
Na	4000	1240	Hg	7.68	0.59
	4080	1280		7.72	0.60
	4090	1310		7.88	0.57
	4080	1290		8.29	0.57
	4070	1270		7.75	0.50
Mg	1090	1080			
	1080	1080			
	1090	1060			
	1070	1100			
	1100	1110			

a) Determined by present authors.

5% relative standard deviation. Since the calcium determination by flame spectrometry tends to be subjected to chemical interferences, these values obtained in this study might be improved by adopting a more accurate method such as isotope dilution mass spectrometry. In any case it is considered that homogeneity of the prepared shark powder is higher with respect to calcium compared to that for NBS-tuna.

Preservation of Shark Powder. Preservation is one of the most important problems when a biological material is handled. With respect to shark powder and more particularly shark paste, changes of organic constituents by both chemical and biological activities during the preservation period should be considered. ^{60}Co irradiation which is often adopted in plant materials, however, is not suitable for this material, since chemical changes of some trace organic compounds are suspected during the irradiation.

As an index of preservation, the chang of weight was measured in a three month period during summer. The powders were kept in the same polystyrene bottles in a desiccator containing silica gel. The water and ash contents of both samples are shown in Table 2.

Table 2. Change of water and ash contents during storage

	June, 1977		September, 1977	
	Water	Ash	Water	Ash
Shark powder	7.34%	5.46%	5.27%	5.35%
NBS-tuna	1.04	4.28	1.64	4.04

Shark powder lost a little moisture during storage whereas NBS-tuna powder gained a little moisture. In plant samples, less change of weight was observed as previously reported.[1] This fact indicates that care should be taken in the preservation of these powders. With respect to the ash content in dry matter, little weight change was observed for shark powder and tuna powder. In addition, no change in flavor was observed with shark powder, which indicated that oxidation of oily materials did not take place during the storage. These observations suggest that NBS-tuna powder should be preserved in a can until it is used as stated by NBS. Shark powder, however, could be preserved in a desiccator for at least 3 months without any significant change of chemical components, provided the dry weight is measured prior to utilization.

Table 3. Metal contents in shark paste and shark powder

	Shark paste		Shark powder
	μg/g-wet	μg/g-dry	μg/g-dry
K	3650±100	11600±300	17200±200
Na	13700±450	43400±3000	4060±40
Mg	220±6	890±13	1080±10
Ca	59±3	187±13	200±10
Fe	26±5	83±15	12±1
Zn	3.1±0.6	10±2	15±1
Hg	1.96±0.05	6.22±0.16	7.88±0.22

average±s.d.

Comparison of Shark Powder and Shark Paste. In Table 3, the metal contents of shark powder and shark paste are shown. The values of shark paste are shown for a wet weight as well as a dry weight basis (dry weight are calculated from the values on the wet weight basis using the water content of 68.5%).

The Na content is ten times higher in shark paste than in shark powder, due to the addition of NaCl in the preparation process of shark paste. The contents of K and Mg are about 30% smaller in shark paste which might be caused by the addition of starch and by the loss during the steaming process. The high content of Fe in shark paste might be due to contamination from the material of the silent cutter.

Fundamentally, shark powder which was less processed in the preparation step, must be subjected to less contamination and loss of elements. Thus, its elementary composition represents that of the natural shark meat. Shark paste, a manufactured product is somewhat different from the natural fish meat, but the difference in metal contents is sufficiently small for Hg, K, Ca, and Mg (within 30%) to enable to be used as a standard reference material for the metal analysis of fish, because the metal contents are the same order as the natural ones.

With respect to the homogeneity of elements, both samples provided similar result, when 0.5 g, dry lots (*ca.* 2 g wet lots in shark paste) were analyzed.

The preservation test indicated that both samples can be preserved for at least 3 months at room temperature. Longer preservation is now under investigation, and it is thought that they will be preserved for one year or longer.

As a conclusion, both shark powder and shark paste are good candidates for new standard reference materials. Since most of the actual field determinations of metals in fish are performed with "wet" or "fresh" samples, shark paste might be a more suitable standard reference material, for example, in the determination of Hg in fish meat by the combustion-gold trap atomic absorption technique. On the other hand, when metal analysis is performed by X-ray fluorescence spectrometry, shark powder would be more suitable than shark paste. Therefore, these two samples can be utilized according to the fields and requirements of analysis.

This work is supported partially by Japan-U.S.A. Co-operative Project between JSPS and NSF No. 6R023.

References

1) K. Fuwa, K. Nozu, K. Tsunoda, H. Kato, Y. Yamamoto, K. Okamoto, Y. Dokiya, and S. Toda, *Bull. Chem. Soc. Jpn.*, **51**, 1078 (1978).

2) Y. Dokiya, M. Taguchi, S. Toda, and K. Fuwa, *Anal. Chem.*, **50**, 533 (1978).

3) M. Taguchi, K. Yasuda, Y. Dokiya, M. Shimizu, and S. Toda, *Bunseki Kagaku*, **26**, 438 (1977).

4) H. L. Rook, Anal. Div., NBS-USA, personal communication (1976).

5) B. L. Barnes, Anal. Div., NBS-USA, personal communication (1977).

BULLETIN OF THE CHEMICAL SOCIETY OF JAPAN, VOL. 51 (12), 3651—3652 (1978)

Preparation and Properties of Cobalt(III) Complexes Containing *meso*-1,2-Diphenyl-1,2-ethanediamine

Masaaki KOJIMA, Momoyo ISHIGURO, and Junnosuke FUJITA*

Department of Chemistry, Faculty of Science, Nagoya University, Chikusa, Nagoya 464

(Received July 20, 1978)

Synopsis. Two new complexes, $[Co(meso\text{-dpen})_3]^{3+}$ and $[Co(NH_3)_4(meso\text{-dpen})]^{3+}$ have been obtained, where *meso*-dpen denotes *meso*(*R*,*S*)-1,2-diphenyl-1,2-ethanediamine. The former is stable in the solid state, but decomposes slowly in solution at room temperature, while the latter is stable in solution.

Williams and Bailar[1] reported that *meso*(*R*,*S*)-1,2-diphenyl-1,2-ethanediamine (dpen) did not form a tris-chelate complex with a cobalt(III) ion, although the corresponding optically active (*R*,*R* or *S*,*S*) dpen complex was easily obtained. A *meso*-dpen chelate ring in the gauche conformation has one axially disposed phenyl group. Such an axial group may cause steric interactions with other ligands in an octahedral complex, and hence the tris-*meso*-dpen complex will be unstable compared with the tris-(*R*,*R* or *S*,*S*)-dpen complex in which both phenyl groups of the ligand can take the equatorial disposition. This note reports the preparation of $[Co(meso\text{-dpen})_3]^{3+}$ together with *trans*-$[CoCl_2(meso\text{-dpen})_2]^+$ and $[Co(NH_3)_4(meso\text{-dpen})]^{3+}$ and compares their properties with those of the corresponding *S*,*S*-dpen complexes.

Experimental

Ligand. *meso*-1,2-Diphenyl-1,2-ethanediamine (*meso*-dpen) was prepared by the method of Irving and Parkins.[2]

trans-$[CoCl_2(meso\text{-}dpen)_2]Cl\cdot 3H_2O$. To a solution of $CoCl_2\cdot 6H_2O$ (0.29 g, 1.2 mmol) in methanol (10 cm^3) was added a solution of *meso*-dpen (0.51 g, 2.4 mmol) in methanol (15 cm^3). The solution was aerated for 4 h at room temperature and then mixed with concd hydrochloric acid (1 cm^3) to yield green crystals. After standing the mixture overnight in a refrigerator, the crystals were filtered and recrystallized from methanol. Yield: 45%. Found: C, 51.81; H, 6.17; N, 8.90%. Calcd for $CoC_{28}H_{38}N_4Cl_3O_3$=*trans*-$[CoCl_2(meso\text{-dpen})_2]Cl\cdot 3H_2O$: C, 52.22; H, 5.95; N, 8.70%.

$[Co(meso\text{-}dpen)_3]Cl_3\cdot 6H_2O$. To a solution of *trans*-$[CoCl_2(meso\text{-dpen})_2]Cl\cdot 3H_2O$ (0.25 g, 0.39 mmol) in methanol (10 cm^3) was added a solution of *meso*-dpen (0.10 g, 0.47 mmol) in methanol (20 cm^3). Orange crystals which formed on standing the resulting solution for 2 days at room temperature were filtered and washed with methanol. Recrystallization was not carried out because of decomposition of the complex. Yield: 31%. Found: C, 55.92; H, 6.15; N, 9.45%. Calcd for $CoC_{42}H_{60}N_6Cl_3O_6$=$[Co(meso\text{-dpen})_3]Cl_3\cdot 6H_2O$: C, 55.97; H, 6.71; N, 9.32%.

$[Co(NH_3)_4(meso\text{-}dpen)]Cl_3\cdot 2.5H_2O$. This complex was prepared from $[Co(NH_3)_5(H_2O)](ClO_4)_3$ and *meso*-dpen in dimethyl sulfoxide (DMSO) by a method similar to that for the corresponding (*R*,*R*)-2,4-pentanediamine complex.[3] Yield: 30%. Found: C, 34.34; H, 6.81; N, 17.05%. Calcd for $CoC_{14}H_{33}N_6Cl_3O_{2.5}$=$[Co(NH_3)_4(meso\text{-dpen})]Cl_3\cdot 2.5H_2O$: C, 34.26; H, 6.78; N, 17.13%.

Measurements. Absorption spectra were recorded on a Hitachi 323 spectrophotometer. FT ^{13}C-NMR spectra were obtained in DMSO at 15.04 MHz on a JEOL FX-60 spectrometer using dioxane as an external reference, the chemical shift of which is at 67.6 ppm downfield from TMS sealed in an external capillary.

Results and Discussion

Williams and Bailar[1] prepared *trans*-$[CoCl_2(dpen)_2]^+$ by oxidizing a mixture of the diamine and $CoCl_2\cdot 6H_2O$ (molar ratio of 2:1) in ethanol with H_2O_2. They found that the *S*,*S*-dpen complex was prepared easily in good yield (62%), while the *meso*-dpen one was formed in very poor yield (*ca.* 1%). They also attempted to prepare $[Co(dpen)_3]^{3+}$ from the diamine and $CoCl_2\cdot 6H_2O$ (molar ratio of 4:1) by a similar method. The $[Co(S,S\text{-dpen})_3]^{3+}$ complex was obtained in good yield (81%), but the products from the *meso*-dpen were *trans*-$[CoCl_2(meso\text{-dpen})_2]^+$ and *trans*-$[CoCl(H_2O)(meso\text{-dpen})_2]^{2+}$. As stated previously, one of the phenyl groups of the *meso*-dpen ligand is forced to take the axial position upon coordination, regardless of the conformation assumed by the chelate ring, δ- or λ-gauche, while the *S*,*S*-dpen ligand should adopt the δ-gauche conformation with both phenyl groups in the equatorial disposition. The axial phenyl group may cause steric interactions with other ligands in a complex, and hence the *meso*-dpen complexes will be less stable than the *S*,*S*-dpen ones.

In the present study, we have obtained *trans*-$[CoCl_2(meso\text{-dpen})_2]^+$ in fairly good yield (45%) by oxidizing the cobalt(II) ions in methanol with air in place of ethanol and H_2O_2, respectively. By the reaction between this complex and *meso*-dpen in methanol, we have succeeded in preparing $[Co(meso\text{-dpen})_3]^{3+}$ in 31% yield. It is known that a reaction of a *trans*-dichloro-bis(diamine) complex with a diamine in organic solvents is very useful for obtaining an unstable tris(diamine) complex.[4] The $[Co(meso\text{-dpen})_3]Cl_3\cdot 6H_2O$ complex isolated is highly soluble in *N*,*N*-dimethylformamide (DMF) and DMSO, but hardly soluble in water, methanol, and ethanol. In the former solvents, the complex decomposes gradually to give unknown brown precipitate.

The $[Co(NH_3)_4(meso\text{-dpen})]^{3+}$ complex was prepared by the reaction between $[Co(NH_3)_5(H_2O)]^{3+}$ and *meso*-dpen in DMSO. Such a reaction is also known to be very useful for obtaining tetraammine complexes containing a diamine.[3] The complex is stable in water, methanol, ethanol, DMF, and DMSO.

Yano *et al.*[5] suggested by PMR study of $[Pt(en)(meso\text{-dpen})]Cl_2$ (en=ethylenediamine) that the *meso*-dpen chelate ring changes its conformation ($\delta \rightleftharpoons \lambda$-gauche) rapidly on the NMR time scale in solution at room

Table. Data of the first absorption bands

Complex	$\tilde{\nu}$/cm^{-1} (log ε)	Solvent	Reference
trans-[$CoCl_2$(*meso*-dpen)$_2$]$^+$	16180 (1.67)	b	This work
	21690 (1.68)		
trans-[$CoCl_2$(*S,S*-dpen)$_2$]$^+$	16500 (1.70)	b	7)
	22980 (1.78)		
[$Co(NH_3)_4$(*meso*-dpen)]$^{3+}$	21100 (1.87)	a	This work
[$Co(NH_3)_4$(*S,S*-dpen)]$^{3+}$	21280 (1.92)	a	8)
[Co(*meso*-dpen)$_3$]$^{3+}$	20900 (2.20)	c	This work
Λ(*lel*$_3$)-[Co(*S,S*-dpen)$_3$]$^{3+}$	21300 (2.13) [a]	b	9)
trans-[$CoCl_2$(*meso*-2,3-bn)$_2$]$^+$	16180 (1.60)	b	6)
	21900 (1.49)		
trans-[$CoCl_2$(*S,S*-2,3-bn)$_2$]$^+$	16370 (1.62)	b	6)
	22520 (1.52)		
[$Co(NH_3)_4$(*meso*-2,3-bn)]$^{3+}$	21100 (1.86)	a	6)
[$Co(NH_3)_4$(*S,S*-2,3-bn)]$^{3+}$	21230 (1.84)	a	6)
fac-[Co(*meso*-2,3-bn)$_3$]$^{3+}$	21100 (2.03)	a	10)
Λ(*lel*$_3$)-[Co(*S,S*-2,3-bn)$_3$]$^{3+}$	21500 (2.00)	a	6)

a) Taken from the figure in the text. Solvent, a: water, b: methanol c: DMSO.

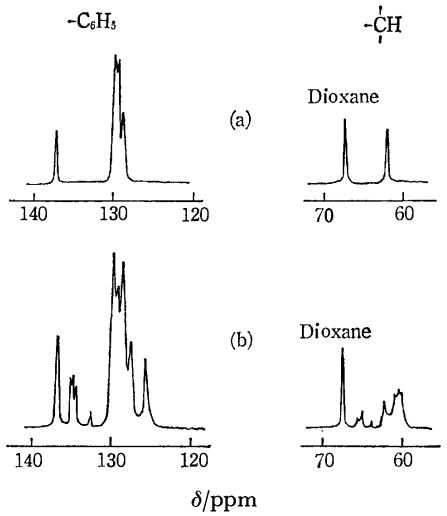

Fig. Proton-decoupled ^{13}C-NMR(15.04 MHz) spectra of (a) [$Co(NH_3)_4$(*meso*-dpen)]$Cl_3\cdot 2.5H_2O$ and (b) [Co-*meso*-dpen)$_3$]$Cl_3\cdot 6H_2O$ in DMSO.

temperature. In the present study, we have utilized ^{13}C-NMR spectroscopy. The spectrum of [$Co(NH_3)_4$-(*meso*-dpen)]$Cl_3\cdot 2.5H_2O$ gives one and four resonances for the methine and the phenyl carbons, respectively, indicating rapid inversion of the chelate ring (Fig. a).

The [Co(*meso*-dpen)$_3$]$^{3+}$ complex ion can give two geometric isomers, *mer* and *fac*, by the alignment of asymmetric carbons (*R* and *S*). If the conformational change were also rapid in this complex, the *mer*(C_1 symmetry) isomer would show six and twenty-four signals for the methine and the phenyl carbons, respectively, while the *fac*(C_3 symmetry) isomer two and eight signals for the corresponding carbons, respectively. The appearance of the multiplet due to the methine carbons indicates the presence of the *mer* isomer (Fig. b). Although the presence of the *fac* isomer is not clear, the complex seems to be a mixture of the *mer* and *fac* isomers, since the less crowded *fac* isomer should be formed to a greater extent than the more crowded *mer* one. Attempts to separate the geometric isomers by column chromatography were unsuccessful because of decomposition of the complex.

The absorption spectral data for the dpen complexes are listed in the Table. The first absorption maxima of the *meso*-dpen complexes shift to longer wavelengths compared with those of the corresponding *S,S*-dpen complexes. The shift may be caused by the crowded and strained structure due to the axial phenyl group of the *meso*-dpen ligand. A similar shift is observed for the 2,3-butanediamine (2,3-bn) complexes, as shown in the Table. The *meso*- and *S,S*-2,3-bn chelate rings have similar structures to those of the *meso*- and *S,S*-dpen ligands, respectively. The differences in the first absorption maxima between the *meso*- and *S,S*-dpen complexes are larger than those between the corresponding 2,3-bn complexes. This result may be correlated with larger steric interactions caused by the more bulky phenyl group than the methyl one.

The authors wish to thank the Ministry of Education for Scientific Research Grant-in-Aid No. 243013.

References

1) O. F. Williams and J. C. Bailar, Jr., *J. Am. Chem. Soc.*, **81**, 4464 (1959).
2) M. N. H. Irving and R. M. Parkins, *J. Inorg. Nucl. Chem.*, **27**, 270 (1965).
3) M. Kojima, M. Fujita, and J. Fujita, *Bull. Chem. Soc. Jpn.*, **50**, 898 (1977).
4) H. Ogino and J. Fujita, *Chem. Lett.*, **1973**, 517.
5) S. Yano, H. Ito, Y. Koike, J. Fujita, and K. Saito, *J. Chem. Soc., Chem. Commun.*, **1969**, 460.
6) M. Kojima and J. Fujita, unpublished data.
7) S. Yano, M. Saburi, S. Yoshikawa, and J. Fujita, *Bull. Chem. Soc. Jpn.*, **49**, 101 (1976).
8) S. Arakawa, K. Kashiwabara, J. Fujita, and K. Saito, *Bull. Chem. Soc. Jpn.*, **50**, 2108 (1977).
9) B. Bosnich and J. MacB. Harrowfield, *J. Am. Chem. Soc.*, **94**, 3425 (1972).
10) M. Kojima, H. Funaki, Y. Yoshikawa, and K. Yamasaki, *Bull. Chem. Soc. Jpn.*, **48**, 2801 (1975).

BULLETIN OF THE CHEMICAL SOCIETY OF JAPAN, VOL. 51 (12), 3653—3654 (1978)

The Reaction of Thio-substituted Cyclopropenium Ions with Iminopyridinium and Sulfonium Ylides

Shinichi INOUE,* Gorou YASUDA, and Takuya HORI

Department of Applied Chemistry, Aichi Institute of Technology, Yagusa-cho, Toyoda-shi, Aichi 470-03

(Received October 31, 1977)

Synopsis. The reaction of several thio-substituted cyclopropenium ions with iminopyridinium and sulfonium ylides in organic solvents at reflux and room temperature under N_2 gave *N,N'*-dicyclopropenylidene urea derivatives, together with some unidentified compounds.

Amino-substituted cyclopropenium ions react with iminopyridinium ylides to give only cyclopropenimine derivatives.[1] It would be of interest to investigate what reaction takes place between heteroatom-substituted cyclopropenium ions[2] and ylides. As regards the reactions of cyclopropenium ions substituted with heteroatom, Yoshida *et al.* reported that tris(alkylthio)-cyclopropenium ion reacts with trialkylphosphite to afford phosphonic acid esters and with hexamethylphosphorous triamide to give phosphonium salts and pyrrole derivatives, and with alkali to produce cyclopropenone and allene derivatives.[3]

Results and Discussion

When tris(ethylthio)cyclopropenium perchlorate (**1a**) was heated with three molar amount of *N*-benzoyliminopyridinium ylide (**2a**) in DMSO at 80 °C for 8 h under nitrogen atmosphere, *N,N'*-bis[bis(ethylthio)-cyclopropenylidene]urea (**4a**) was formed in 60% yield; 7% of **1a** was recovered. The reaction of **1a** with *N*-(ethoxycarbonyl)iminopyridinium ylide (**2b**) under the same conditions gave **4a** in 39% yield.

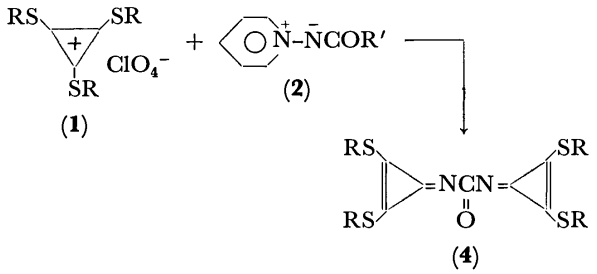

R : Et for **1a** and **4a**, *t*-Bu for **1b** and **4b**, *p*-*t*-BuC_6H_4 for **1c** and **4c**
R′: Ph for **2a**, EtO for **2b**

Reactions of tris(*t*-butylthio)cyclopropenium perchlorate (**1b**) with **2a** and **2b** under the same reaction conditions afforded *N,N'*-bis[bis(*t*-butylthio)cyclopropenylidene]urea (**4b**) in 75 and 31% yields, respectively.

The reactions of tris(*p*-*t*-butylphenylthio)cyclopropenium perchlorate (**1c**) with **2a** in DMSO and **2b** in THF gave *N,N'*-bis[bis(*p*-*t*-butylphenylthio)cyclopropenylidene]urea (**4c**) in 87 and 89% yields, respectively.

The structures of **4a**, **4b**, and **4c** were confirmed by elemental analyses and spectroscopy.

When **1c** was reacted with *S,S*-dimethyl-*N*-acetylsulfimide (**3a**) in chloroform at room temperature for 8 h under nitrogen atmosphere with stirring, **4c** was formed in 89% yield.

$$\mathbf{1a}\text{—}\mathbf{c} + (CH_3)_2\overset{+}{S}\text{–}\overset{-}{N}COR'' \longrightarrow \mathbf{4a}\text{—}\mathbf{c}$$

(**3**)

R″: **3a**=Me, **3b**=EtO

However, reactions of **1a** and **1b** with **3a** under the same conditions did not give the corresponding ureas **4a** and **4b**, **1a** and **1b** being recovered quantitatively.

Reactions of **1a**, **1b**, and **1c** with *S,S*-dimethyl-*N*-(ethoxycarbonyl)sulfimide (**3b**) under the same conditions gave **4a**, **4b**, and **4c** in 42, 43, and 73% yields, respectively.

Experimental

All the melting points were uncorrected. IR spectra were determined with a Hitachi Model 215 spectrophotometer, UV spectra with a Hitachi Model EPS-3T spectrophotometer, and NMR spectra with a JEOL Model JNM-C-60H spectrometer with use of tetramethylsilane as an internal standard. Mass spectra were determined with a Hitachi RMU-6E spectrometer.

Materials. Tris(*p*-*t*-butylphenylthio)cyclopropenium perchlorate (**1c**) was prepared by a modification of the method of Yoshida and Tawara.[4] **1c**, mp 180 °C (from ether); UV max (CH_3CN) 232 (ε 32300) and 290 nm (19900); IR (KBr) 3010, 2970, 1242, and 824 cm^{-1}; NMR (acetone-d_6) δ 7.85 (m, 6H), 7.65 (m, 6H), and 1.75 (s, 36H, *t*-Bu); MS *m/e* 534 (M^+). Found: C, 62.66; H, 6.17%. Calcd for $C_{33}H_{39}S_3O_4Cl$: C, 62.78; H, 6.24%. The ylides were synthesized according to the reported procedures[5] and identified by elemental analyses as well as by comparison of IR and melting points. The solvents were purified before use.[6]

*Reactions of Tris(ethylthio)-(**1a**), Tris(t-butylthio)-(**1b**), and Tris(p-t-butylphenylthio)cyclopropenium Perchlorate (**1c**) with N-Benzoyliminopyridinium Ylide (**2a**).* A mixture of **1a** (7 mmol) and **2a** (5.1 mmol) in freshly distilled DMSO (30 ml) was stirred at 80 °C for 8 h under nitrogen atmosphere. After the reaction mixture had been allowed to stand overnight, the solvent was removed under reduced pressure. Urea (**4a**), dark brown oil, was obtained in 60% yield by column chromatography (silica gel) of the residue. The reactions of **1b** and **1c** with **2a** under the same conditions afforded the corresponding ureas (**4b**), pale yellow powder, and (**4c**), pale yellow needles, in 75 and 89% yields, respectively.

*Urea (**4a**).* IR (neat) 2930, 1795, 1635 (N–CO–N), and 790 cm^{-1}. UV max (EtOH) 319.5 nm (ε 22400). NMR (CCl_4) δ 1.50 (t, 12H, J=7.4 Hz) and 3.12 (q, 8H, J=7.4 Hz). MS *m/e* 372 (M^+). Found: C, 48.15; H, 5.82; N, 7.57%. Calcd for $C_{15}H_{20}N_2OS_4$: C, 48.35; H, 5.42; N, 7.52%.

*Urea (**4b**).* Mp 113—114.5 °C (from MeOH–H_2O). IR (KBr) 2960, 1800, 1630 (N–CO–N), 1360, 1090, and 770 cm^{-1}. UV max (EtOH) 327 nm (ε 34100). NMR (CCl_4) δ 1.50 (s, 36H, *t*-Bu). MS *m/e* 484 (M^+). Found: C, 56.74;

H, 7.77; N, 5.54%. Calcd for $C_{23}H_{36}N_2OS_4$: C, 56.97; H, 7.50; N, 5.78%.

Urea (4c). Mp 120—121 °C (from chloroform–ether). IR (KBr) 2900, 1805, 1640 (N–CO–N), 1470, 820, and 760 cm^{-1}. UV max (CH_3CN) 247 (ε 18600) and 238 nm (10200). NMR (CD_3CN) δ 1.31 (s, 36H, *t*-Bu) and 7.26—7.35 (m, 16H). MS *m/e* 788 (M^+). Found: C, 71.86; H, 6.43; N, 3.87%. Calcd for $C_{47}H_{52}N_2OS_4$: C, 71.52; H, 6.65; N, 3.55%.

Reactions of **1a**, **1b**, *and* **1c** *with* N-*(Ethoxycarbonyl)iminopyridinium Ylide (2b).* By application of the same procedure as that for urea (**4a**), **1c** (2 mmol) was treated with **2b** (6 mmol) in dry THF (30 ml). The reaction mixture was worked up to give a crude oil, which was extracted with benzene. The solvent was then removed. The residue was extracted with ether to give **4c** in 89% yield. The reactions of **1a** and **1b** with **2b** were carried out by a similar procedure to give **4a** and **4b** in 39 and 31% yields, respectively.

Reactions of **1a**, **1b**, *and* **1c** *with* S,S-*Dimethyl*-N-*(ethoxycarbonyl)sulfimide (3b).* By a procedure similar to that described above, **1b** (2 mmol) was treated with **3b** (8 mmol) in dry THF (30 ml) at room temperature for 8 h under nitrogen atmosphere. The reaction mixture was worked up to give a hygroscopic residue. The residue was crystallized from MeOH–H_2O to give **4b** in 43% yield. The reactions of **1a** and **1c** with **3b** were carried out in the same manner to give **4a** and **4c** in 42 and 73% yields, respectively.

Reactions of **1a**, **1b**, *and* **1c** *with* S,S-*Dimethyl*-N-*acetylsulfimide (3a).* A mixture of **1c** (2.8 mmol) and **3a** (8.4 mmol) in chloroform (30 ml) was kept at room temperature for 8 h under nitrogen atmosphere with stirring. The reaction mixture was allowed to stand overnight and then the solvent was removed. The residual materials were dissolved in acetonitrile and the solution was extracted with petroleum ether. After removal of petroleum ether, the residue was recrystallized from chloroform–ether to afford **4c** in 84% yield. However, **1a** and **1b** did not react with **3a** and were recovered quantitatively.

References

1) S. Inoue, G. Yasuda, and T. Hori, *Chem. Lett.*, **1976**, 1215.

2) Z. Yoshida, *Topics Current Chem.*, **40**, 47 (1973).

3) Z. Yoshida, S. Yoneda, T. Miyamoto, and S. Miki, *Tetrahedron Lett.*, **1974**, 813; S. Yoneda, H. Hirai, and Z. Yoshida, *Chem. Lett.*, **1976**, 1051; Z. Yoshida, H. Konishi, and H. Ogushi, *Heterocycles*, **5**, 401 (1976).

4) Z. Yoshida and T. Tawara, *J. Am. Chem. Soc.*, **93**, 2573 (1971).

5) A. Balasubramanian, J. M. McIntosh, and V. Sieckus, *J. Org. Chem.*, **35**, 433 (1970); T. Okamoto, M. Hirobe, C. Mizushima, and A. Ohsawa, *Yakugaku Zasshi*, **83**, 308 (1963); G. F. Whitfield, H. S. Beilan, D. Saika, and D. Swern, *J. Org. Chem.*, **39**, 2148 (1974).

6) "Kagaku Zitken-hoh," ed by K. Hata, N. Sugiyama, T. Kobayashi, M. Ohta, and M. Ohki, Tokyo Kagaku Dohzin, Tokyo (1964), pp. 1—56.

BULLETIN OF THE CHEMICAL SOCIETY OF JAPAN, VOL. 51 (12), 3655—3656 (1978)

Coenzyme Models. XIII. Micellar Catalysis of 1,4-Dihydronicotinamide Reduction of Isoalloxazines and Acridinium Ion

Seiji SHINKAI,* Toyoko IDE, and Osamu MANABE
Department of Industrial Chemistry, Faculty of Engineering, Nagasaki University, Nagasaki 825
(Received December 17, 1977)

Synopsis. The 1,4-dihydronicotinamide reduction of isoalloxazines and acridinium ion was examined in cationic (CTAB, CPyB), anionic (SDS), and nonionic (POOA, Brij-35) micelles. The micellar effect is accounted for by micellar stabilization (or destabilization) of the micelle-bound species.

Micellar catalysis provides suitable model systems of enzymatic catalysis, since micelles can influence rates and equilibria of biologically important reactions.[1-4] Very recently, Hadju and Sigman[5,6] reported that *N*-(2-carboxybenzyl)-1,4-dihydronicotinamide and *N*-(*cis*-2-carboxycyclopentyl)-1,4-dihydronicotinamide where the carboxylate moiety is closely fixed near the nicotinamide moiety nonenzymatically reduce *N*-methylacridinium ion in acetonitrile 150—300 times faster than corresponding dihydronicotinamides, but the significant difference cannot be found in an aqueous solution. The result prompted us to investigate the NADH (and model) dependent reactions in micellar systems, since micelles can provide charged environment on the surface and apolar environment in the core. This paper deals with micellar catalysis of 1,4-dihydronicotinamide reduction of isoalloxazines and acridinium ion (Eqs. 1 and 2). We found that the reactions are subject to micellar catalysis, especially to micellar rate inhibition.

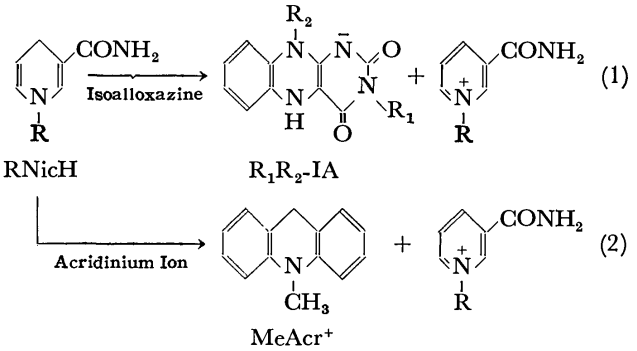

Figure 1 shows the second-order rate constants (k_2) for the reaction of BzlNicH ($R=CH_2C_6H_5$) and MeEt-IA ($R_1=CH_3$, $R_2=C_2H_5$) plotted against surfactant concentrations. The plots for three ionic surfactants (CATB, CPyB, and SDS)** gave sigmoidal curves followed by gradual rate suppression. Since the surfactant concentration where a considerable rate enhancement occurs is almost equal to the CMC for each surfactant (4×10^{-4} M for CTAB, 3×10^{-4} M for CPyB, and 3×10^{-3} M for SDS), the rate enhancement observed is attributable to the micelle formation. It is seen from Fig. 1 that the rate enhancement is transient and the magnitude is of 1.4—2.3 fold at optimal surfactant concentrations. On the other hand, the reaction rate

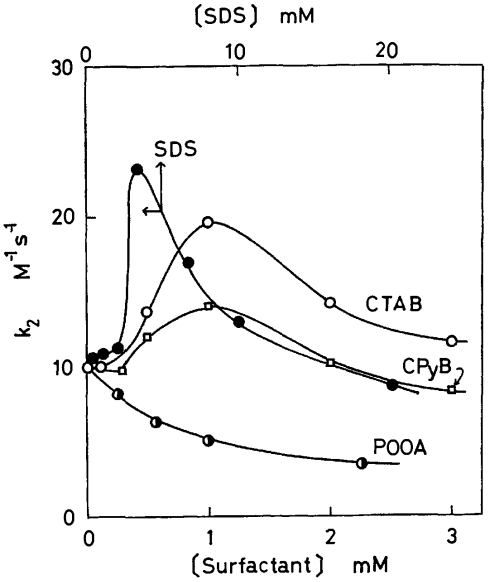

Fig. 1. Second-order rate constants for the reaction of BzlNicH and MeEt-IA plotted as a function of surfactant concentrations. pH 8.5 with 0.02 M phosphate, $\mu=0.02$ with KCl.

was simply retarded with increasing POOA** concentration. The contrasting influence observed between the ionic micelles and the nonionic micelle implies that the ionic environments (both cationic and anionic) are favorable to the reaction.

The micellar catalysis is substantiated more clearly by the reactions involving HxdecBu-IA ($R_1=C_{16}H_{33}$, $R_2=C_4H_9$) and DodNicH ($R=C_{12}H_{25}$), for these

Table 1. Second-order rate constants ($M^{-1}s^{-1}$) for the reaction of 1,4-dihydronicotinamides with isoalloxazines[a]

Surfactant	BzlNicH+ MeEt-IA	BzlNicH+ HxdecBu-IA	DodNicH+ MeEt-IA
None	10.0	10.0[b]	48.2[c]
CTAB	20—11	9.92 (3 mM)	4.00 (3 mM)
CPyB	14—8	14.1 (3 mM)	2.86 (3 mM)
SDS	23—9	1.16 (10 mM)	99.5 (10 mM)
POOA	10—3	7.36 (3.3 mM)	18.6 (3.3 mM)

a) 30 °C, $\mu=0.02$, pH 8.5 with 0.02 M phosphate, 3 vol% ethanol, [dihydronicotinamide] = $(2.2-5.0)\times10^{-4}$ M, [isoalloxazine] = $(2.1-4.0)\times10^{-5}$ M. The numbers in parentheses indicate surfactant concentrations. b) MeEt-IA was used instead of HxdecBu-IA. c) PrNicH was used instead of DodNicH.

** CATB: cetyltrimethylammonium bromide, CPyB: cetylpyridinium bromide, SDS: sodium dodecylsulfate, POOA: polyoxyethylene ($n=10$) oleyl alcohol.

compounds are bound to the micellar phase as shown by their spectral changes.[7,8] The second-order rate constants determined at a given surfactant concentration above the CMC are listed in Table 1. The reaction of BzlNicH with HxdecBu-IA (hydrophobic isoalloxazine) was markedly retarded on the addition of 10 mM SDS, while the addition of other surfactants was less significant. On the contrary, the reaction of DodNicH (hydrophobic dihydronicotinamide) with MeEt-IA was suppressed by the cationic micelles, and the SDS micelle accelerated the reaction by a factor of *ca.* 2. Evidently, the micellar effect in these systems reflects the electrostatic influence on the micelle-bound reactant. The examination of Table 1 also reveals that micelles result in the profound inhibitory effect on the dihydronicotinamide reduction, while the accelerative effect is rather small.

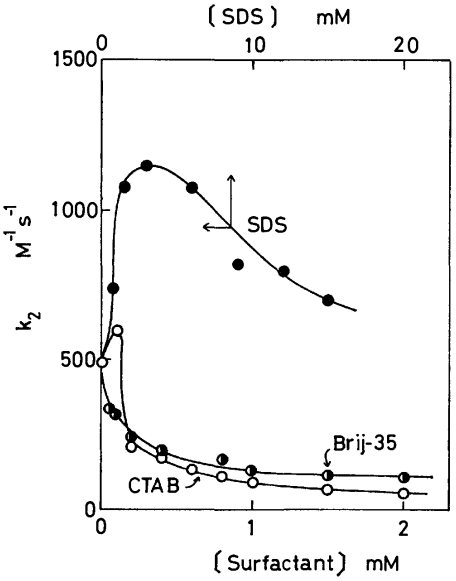

Fig. 2. Second-order rate constants for the reaction of Cl_2BzlNicH and MeAcr$^+$ plotted as a function of surfactant concentrations. pH 7.1 with 0.02 M phosphate, μ=0.02 with KCl.

Figure 2 shows the second-order rate constants for the reaction of Cl_2BzlNicH (R=2,4-dichlorobenzyl) and *N*-methylacridinium ion plotted against surfactant concentration. Plots of k_2 against the concentration of SDS gave the accelerative dependence upon the surfactant concentration, giving rise to the largest rate augmentation of 2.7 fold at the optimal SDS concentration (3 mM). In contrast, k_2 in CTAB and Brij-35 simply descended with increasing surfactant concentrations. The greatest rate suppression caused by the CTAB micelle was 8.7 fold.

The foregoing results establish that the micellar effect in the present system is attributable to the stabilization (or destabilization) of developed charge in the micellar phase. This suggests that NADH dependent reactions which involve the change in the transition state can be controlled by the ionic microenvironments.

Experimental

Materials. *N*-(2,4-Dichlorobenzyl)-1,4-dihydronicotinamide was prepared from *N*-(2,4-dichlorobenzyl)-nicotinamide according to the method of Kim and Chaykin;[9] mp 125—128 °C. Found: C, 54.87; H, 4.24; N, 9.91%. Calcd for $C_{13}H_{12}N_2OCl_2$: C, 55.12; H, 4.24 N, 9.89%. Preparations of other compounds were previously described.[7,8]

Kinetics. All the kinetic measurements were carried out at 30±0.1 °C at a calculated ionic strength (μ=0.02 with KCl) unless otherwise stated. The kinetic runs involving isoalloxazines were performed under strictly anaerobic(N_2) conditions in order to avoid air reoxidation of the reduced products. The progress of the reaction was followed spectrophotometrically by monitoring the disappearance of isoalloxazines (433 nm for MeEt-IA and 440 nm for HxdecBu-IA) and MeAcr$^+$ (420 nm). The reactions were first-order both in dihydronicotinamides and in oxidizing agents.

References

1) J. H. Fendler and E. J. Fendler, "Catalysis in Micellar and Macromolecular Systems," Academic Press, New York, N. Y. (1975).
2) E. H. Cordes and C. Gitler, *Progr. Bioorg. Chem.*, **2**, 1 (1973).
3) A. Ochoa-Solano, G. Romero, and C. Gitler, *Science*, **156**, 1234 (1967).
4) I. Tabushi, Y. Kuroda, and S. Kita, *Tetrahedron Lett.*, **1974**, 643.
5) J. Hadju and D. S. Sigman, *J. Am. Chem. Soc.*, **97**, 3524 (1975)
6) J. Hadju and D. S. Sigman, *Biochemistry*, **16**, 2841 (1977).
7) S. Shinkai, R. Ando, and T. Kunitake, *Bull. Chem. Soc. Jpn.*, **48**, 1614 (1975); **49**, 3652 (1976).
8) S. Shinkai, Y. Sakuma, and F. Yoneda, *J. Chem. Soc., Chem. Commun.*, **1976**, 986.
9) C. S. Y. Kim and S. Chaykin, *Biochemistry*, **7**, 2339 (1968).

BULLETIN OF THE CHEMICAL SOCIETY OF JAPAN, VOL. 51 (12), 3657—3658 (1978)

Photochemical Ethoxycarbonylmethylation of Alkylbenzenes with Ethyl Chloroacetate. MO Calculation for Prediction of Orientation[1)]

Yoshiro OGATA,* Eizi HAYASHI, and Hiroshi KATO†

Department of Applied Chemistry, Faculty of Engineering, Nagoya University, Chikusa-ku, Nagoya 464

†*Department of Chemistry, College of General Education, Nagoya University, Chikusa-ku, Nagoya 464*

(Received February 6, 1978)

Synopsis. Photoreaction of ethyl chloroacetate with cumene gives ethyl cumenylacetates (17.5%) in the ratio *o*: *m*: *p*=17: 46: 37. The same reaction with *t*-butylbenzene gives ethyl *t*-butylphenylacetate (23%) in the ratio *o*: *m*: *p*= trace: 65: 35. Addition of BF_3 increases the total yield of the substitution products. Orientations together with those for toluene and anisole in ethoxycarbonylmethylation were discussed in terms of INDO-type MO calculation of the lowest singlet excitation energies.

Reports were given on the ethoxycarbonylmethylation of aromatic compounds with haloacetate.[2-4)] Irradiation of a 0.3 M ethyl chloroacetate solution in toluene gave ethyl tolylacetate with isomer distribution: ortho, 33%; meta, 61%; and para, 6%; total yields 16%.[4)] Irradiation of a 0.1 M ethyl chloroacetate solution in anisole gave ethyl methoxyphenylacetates with isomer distribution: ortho, 59%; meta, 28%; and para, 13%; total yields 17%.[5)] The mechanism may involve an attack of radical species $\cdot CH_2COOEt$ on the aromatic ring in view of the by-products of dimerized $\cdot CH_2COOEt$, *i.e.*, diethyl succinate, but the yields of meta isomer are higher than those of para isomer. This is abnormal on the basis of the ground state π-electron densities.[6,7)]

We wish to report on the product distribution in the photo-reaction of ethyl chloroacetate and cumene or *t*-butylbenzene, where the yield of meta-substituted product is higher than that of para-substituted one as observed with toluene and anisole. The results including previous ones will be rationalized by the molecular orbital consideration.

Results and Discussion

Irradiation of 0.1 M ethyl chloroacetate in cumene for 60 h gave an isomeric mixture of ethyl cumylacetates. The isomer distribution of produced ethyl cumylacetates was as follows: ortho (Ia), 17%; meta (IIa), 46%; and para (IIIa), 37%, in a total yield of 54% based on the consumed ethyl chloroacetate. Ethyl 2-methyl-2-phenylpropionate (IVa) (7.5%) and dimeric cumene (V) were obtained, no β-ethoxycarbonylmethylation taking place. Addition of $BF_3 \cdot Et_2O$ (a Lewis acid) (0.1 M) to the same mixture gave higher yields with an analogous distribution of ethyl cumylacetates: ortho (Ia), 21%; meta (IIa), 45%; para (IIIa), 34%, in a total yield of 65% based on the consumed ethyl chloroacetate along with (IVa) (8.0%). In addition, isomeric bicumenyls were obtained.

Similar irradiation of a 0.1 M ethyl chloroacetate solution in *t*-butylbenzene for 60 h gave ethyl *t*-butylphenylacetates: ortho (Ib), trace; meta (IIb), 65%; and para (IIIb), 35%, in a total yield of 82% based on the consumed ethyl chloroacetate. In this case, the yield of dimeric *t*-butylbenzene was low. Addition of $BF_3 \cdot Et_2O$ (0.1 M) to the same mixture gave higher yields of ethyl *t*-butylphenylacetates composed of ortho (Ib), 5%; meta (IIb), 50%; and para (IIIb), 45%, in a total yield of 89% based on the consumed ethyl chloroacetate.

$$R\text{-}C_6H_5 + ClCH_2COOEt \xrightarrow{h\nu}$$

$$\begin{cases} o\text{-}R\text{-}C_6H_4\text{-}CH_2COOEt & (I) \\ m\text{-}R\text{-}C_6H_4\text{-}CH_2COOEt & (II) \\ p\text{-}R\text{-}C_6H_4\text{-}CH_2COOEt & (III) \\ C_6H_5\text{-}C(CH_3)_2COOEt & (IVa) \\ C_6H_5\text{-}C(CH_3)_2\text{-}C(CH_3)_2\text{-}C_6H_5 & (V) \end{cases}$$

a: $R=CH(CH_3)_2$ b: $R=C(CH_3)_3$

As apparent from the above data, isopropyl- and *t*-butylbenzenes afford lower yields of ortho isomers than toluene and anisole because of steric hindrance.

The yields of meta isomers, (IIa) and (IIb), are higher than those of the corresponding para isomers, (IIIa) and (IIIb), which are similar to the yield reported for toluene. Since the attacking species $\cdot CH_2COOEt$ would be cationic by the electron-withdrawing effect of carbonyl, it is difficult to explain the results in terms of ground state electron density. In the reactions of proton (H–D exchange), the π-π^* singlet excited aromatics react with the electrophile, giving ortho and meta orientation with toluene and anisole.[7,8)] A similar phenomenon, observed with solvolysis of methoxybenzylacetates is called "meta-transmission".[9)]

Calculations were made on the electronic structures of these alkylbenzenes by the INDO-type method.[10)] The calculated lowest singlet excitation energies and their transition moments are summarized in Table 1 together with the experimental ones. The calculated

Table 1. Excitation energy and transition moment of alkylbenzenes and anisole

R	Calcd by CI method		Obsd	
	Excitation energy (mm)	Transition moment[a)]	λ_{max} (mm)	$\log_{max}$
CH_3	224	−0.011	261	2.25[b)]
OCH_3	226	0.229	277	3.15[c)]
$CH(CH_3)_2$	223	0.037	261	2.31[b)]
$C(CH_3)_3$	224	−0.076	258	2.36[b)]

a) All transition moments are in the direction of short axis. b) A.P.I. Research Project, No. 44, I (1945). c) A.B. Raway and J.T. Chanberlain, *J. Chem. Soc.*, **1952**, 2310.

energy values are somewhat larger than the observed ones, the parallelism between the calculated and the observed values of excitation energy and their moments being fairly good.

Since the lowest excited states of alkylbenzenes are constructed by two important configurations, the frontier electron density of rth position is given by

$$f_r^R = C_1^2[(C_{ir})^2+(C_{kr})^2] + C_2^2[(C_{jr})^2+(C_{lr})^2],$$

where indices i and j denote the occupied MO's, k and l the vacant MO's in the ground state of alkylbenzene, and C_1 and C_2 are the CI coefficients of the i→k and j→l excited states, respectively.

Table 2. The frontier electron densities of aromatic compounds calculated by CI method and observed composition of products in the photoreaction of aromatic compounds with ethyl chloroacetate

R	Lowest excited state frontier electron density				Ethoxycarbonyl-methylation products composition		
	1	2(*o*)	3(*m*)	4(*p*)	2(*o*)	3(*m*)	4(*p*)
CH_3	0.309	0.340	0.321	0.309	33	61	6
OCH_3	0.238	0.350	0.314	0.267	59	28	13
$CH(CH_3)_2$	0.289	0.335	0.311	0.287	17	46	37
$C(CH_3)_3$	0.260	0.327	0.295	0.258	trace	65	35

In all cases, the frontier electron densities of lowest excited states decrease in the order: ortho>meta>para (Table 2). The difference in the calculated frontier electron densities can be used for an examination of the difference in relative reactivities for electrophilic attack. For example, in the case of toluene, the ground state π-electron densities calculated by a similar INDO-type MO calculation are: ortho, 1.012; meta, 1.000; and para, 1.016,[11] and those by the Hückel MO calculation are: ortho, 1.0044; meta, 0.9999; and para, 1.0037,[6] whereas the orientation in the nitration of toluene is: ortho 58; meta 4; para 38. The similar small difference in the ground-state π-electron densities of anisole (*o*, 1.056; *m*, 0.982; *p*, 1.020) gives rise to the observed large difference in *o*, *m*, and *p*-orientations.[11]

The calculated frontier electron densities in the lowest excited states coincide with the observation with anisole but not ground state electron densities. The yields of meta isomers in alkylbenzenes, however, are higher than the yields of ortho isomers. The lower yields of ortho isomers can be ascribed to the steric requirement, since the yields of ortho isomer decrease in the order: toluene>cumene>*t*-butylbenzene in spite of the small difference in the calculated frontier electron densities. As shown in Table 2 the reactivity of para position is higher than that expected from calculation. This might reflect the electrophilic nature of $\cdot CH_2COOEt$ radical which is increased by the presence of BF_3. The isomeric ratio in toluene, at least, (meta: para=10: 1) cannot be explained by statistical attack (2: 1) of neutral molecules on the ground state toluene. In the case of the other aromatic compounds, the isomeric distribution can be explained by the statistical ratio (meta: para=2: 1). However, on the basis of electrophilic nature of $\cdot CH_2COOEt$ the para attack should be preferred to the meta attack, if the attack were to occur on ground states.

Since the lowest energy for excitation of alkyl chloroacetate (4.56 eV) is lower than that of alkylbenzens (5.5—5.6 eV), the dissociation of C–Cl bond would be preferred to the excitation of alkylbenzenes. However, the very low concentration of chloroacetates would result in the simultaneous excitation of both reactants.

The attempted reaction of 0.1 M ethyl chloroacetate with chlorobenzene gave self-condensation products (biphenyl and diethyl succinate) together with ethyl phenylacetate (23%) but no ethoxycarbonylmethylation product. Nitrobenzene did not react with ethyl chloroacetate on irradiation. The results show the electrophilic nature of $\cdot CH_2COOEt$ radical.

Experimental

Materials. Isopropylbenzene (bp 152—153 °C) and *t*-butylbenzene (bp 167—169 °C) of guaranteed grade were used after washing with H_2SO_4 and distillation. Ethyl chloroacetate (bp 51—52 °C/20 Torr) was distilled before use.

A Typical Procedure. A Halos high-pressure 300 W Hg lamp was used as a light source. The sample solution was placed in a cylindrical quartz vessel (25×200 mm). The vessel and the lamp were immersed in a water bath (20 °C) at a distance of 5 cm. The sample solution was irradiated for 60 h.

Identification of the products was carried out by means of GLC using a column (1.2 m×4 mm) packed with Silicone OV-17 (5 wt %) on Shimalite W of 80—100 mesh and a column (1.2 m×4 mm) packed with PEG 20 M (10 wt %) on Chromosorb WAN of 60—80 mesh in comparison with the authentic specimen. The yields of products were determined also by means of GLC using a column (1.2 m×4 mm) packed with Silicone OV-17 (5 wt %) on Shimalite W of 80—100 mesh using N_2 as a carrier gas (20 cm³/min) at 80—270 °C (8 °C/min) using naphthalene as an internal standard.

UV Spectra. Following UV spectra peaks (λ_{max}) were observed for reactants: Ia, 262 nm; IIa, 259 nm, ethyl chloroacetate, 236 nm; Ia–BF_3, and IIa–BF_3 mixtures had the same peaks as those of Ia and IIa, respectively. Systems Ia–$ClCH_2CO_2Et$ and IIa–$ClCH_2CO_2Et$ showed no extra peak besides those of the component materials.

References

1) Contribution No. 242.

2) Y. Ogata, T. Itoh, and Y. Izawa, *Bull. Chem. Soc. Jpn.*, **42**, 794 (1969).

3) Y. Izawa, T. Ichihara, and Y. Ogata, *Tetrahedron*, **28** 211 (1972).

4) Y. Ogata and E. Hayashi, *Bull. Chem. Soc. Jpn.*, **50**, 323 (1977).

5) Y. Izawa, M. Kutsuna, and Y. Toyama, National Meeting of the Chemical Society of Japan, Tokyo, April 1975, Abstr. p. 1203.

6) C. A. Coulson and U. A. Crawford, *J. Chem. Soc.*, **1953**, 2052.

7) D. A. de Bie and E. Havinga, *Tetrahedron*, **21**, 2359 (1965).

8) J. P. Colpa, C. Mclean, and E. L. Macker, *Tetrahedron*, **19**, Suppl. 2, 65 (1963).

9) H. E. Zimmerman and V. R. Sandel, *J. Am. Chem. Soc.*, **85**, 915 (1963).

10) H. Kato, M. Konishi, and T. Yonezawa, *Bull. Chem. Soc. Jpn.*, **41**, 1031 (1968).

11) G. R. Howe, *J. Chem. Soc., B*, **1971**, 984.

BULLETIN OF THE CHEMICAL SOCIETY OF JAPAN, VOL. 51 (12), 3659—3660 (1978)

^{13}C NMR Spectra of 4,6-*O*-Benzylidenehexopyranosides and Their 2,3-Di-*O*-sulfonate Derivatives

Hiroshi SUGIYAMA,* Tatsumi YAMAZAKI,** Yasuhisa SENDA,*** Jun-ichi ISHIYAMA,*** Kazuo MATSUDA,** and Shuichi SETO

Chemical Research Institue of Non-Aqueous Solutions, Tohoku University, Katahira, Sendai 980
***Department of Agricultural Chemistry, Tohoku University, Tsutsumidori-amamiya, Sendai 980*
****Department of Applied Science, Tohoku University, Aoba, Sendai 980*

(Received May 17, 1978)

Synopsis. ^{13}C NMR spectra of the title compounds were measured. The relationship between their chemical shifts and reactivity is discussed.

In the course of studies on the 2,3-unsaturation of 4,6-*O*-benzylidene-2,3-di-*O*-sulfonylhexopyranosides[1] and of 4′,6′-*O*-benzylidene-2,2′-anhydro-3′-*O*-sulfonylhexopyranosyl nucleosides,[2] it was found that the configuration and conformation of a sugar ring mainly control unsaturation. This led us to study the C-13 NMR spectra of these compounds, since the C-13 chemical shift is highly susceptible to configurational and conformational changes.[3] The C-13 NMR spectra of some compounds in the present study were studied by Conway *et al.*,[4] and we have compared our results with theirs.

All methyl 4,6-*O*-benzylidenehexopyranosides (**1**—**10**) and 4′,6′-*O*-benzylidenehexopyranosyl nucleosides (**11**—**18**) showed almost the same phenyl carbon signals of benzylidene moiety, 126, 127.8, 128.6 (para), and 137.8 ppm (quarternary). Signals at 100.7 ± 0.6 ppm in these spectra should be assigned to C-7 of benzylidene moiety because of the same environment throughout the series of compounds. The shift values of methyl 4,6-*O*-benzylidene-α-D-glucopyranoside (**1**), its β-anomer (**2**), and methyl 4,6-*O*-benzylidene-α-D-mannopyranoside (**3**) are the results of the study of Conway *et al.*[4]

The anomeric signal of methyl 4,6-*O*-benzylidene-β-D-mannopyranoside (**4**) can be assigned to 101.9 ppm, since the anomeric signal of methyl β-mannoside shows a slightly lower chemical shift than that of the α-anomer;[5] those of 2,3-di-*O*-tolylsulfonyl derivatives (**9** and **10**) show the same tendency (Table 1). The signals at 78.4, 66.6, and 67.8 ppm of **4** can be assigned to C-4, -5, and -6, respectively, by comparison with those of **1**, **2**, and **3**. The signals at 70.8 and 69.8 ppm should be attributed to C-2 and -3, respectively, since 4,6-*O*-benzylidenation makes 3.0—4.2 ppm upfield shift on C-3 and 0.1—1.1 ppm upfield shift on C-2 of **1**, **2**, and **3**.[4,5]

The assignment of methyl 4,6-*O*-benzylidene-2,3-di-*O*-*p*-tolylsulfonyl-α-D-glucopyranoside (**5**) and its 2,3-di-*O*-methylsulfonyl substituent (**7**) is the same as the assignment by Conway *et al.*[4] However, there are slight differences due to the difference in solvent. In the cases of methyl 4,6-*O*-benzylidene-2,3-di-*O*-*p*-tolylsulfonyl-β-D-glucopyranoside (**6**) and its 2,3-di-*O*-methylsulfonyl substituent (**8**), the chemical shifts of *O*-methyl, C-5 and -6 can be assigned by a comparison with those of **2**, since sulfonation causes no noticeable effect on these carbons. Disulfonation makes 4.0—4.8 ppm downfield shift on C-2 and 5.2—5.5 ppm downfield shift on C-3 of **5** and **7**. The signals at 79.0 and 79.5 ppm of **6** can thus be assigned to C-2 and -3, respectively. Sulfonation effect on C-1 and -4 of **5** and **7** shows 0.6—3.7 ppm upfield shift, C-1 and -4 chemical shifts

Table 1. ^{13}C chemical shifts of 4,6-*O*-benzylidene derivatives of hexopyranosides

	C-1′	C-2′	C-3′	C-4′	C-5′	C-6′	C-7′	C-2	C-4	C-5	C-6	Me
1[a]	99.9	72.4	70.5	80.8	62.0	68.5	101.5					54.9
2[a]	104.2	74.2	72.9	80.3	65.9	68.3	101.5					56.8
3[a]	101.7	70.6	68.0	78.5	62.9	68.4	101.7					54.4
4	101.9	70.8	69.8	78.4	66.6	67.8	100.8					56.1
5	97.4	76.4	75.7	77.1	62.3	67.3	100.5					55.1
6	100.5	79.5	79.0	77.3	64.7	67.4	100.9					56.4
7	98.5	77.2	76.0	78.1	62.8	68.1	101.1					55.7
8	100.2	78.6	78.5	77.4	64.8	67.3	100.8					56.7
9	98.5	74.0	74.0	67.9	63.6	66.9	100.4					54.8
10	98.6	75.5	74.4	78.6	65.9	67.0	100.2					56.2
11	83.1	73.2	71.5	80.1	68.6	67.7	100.8	150.8	163.5	109.7	137.8	11.8
12	80.5	76.9	75.7	79.5	67.2	67.2	100.7	150.2	162.7	102.7	140.8	
13	80.0	76.9	75.6	78.9	67.1	67.0	100.5	150.2	163.3	110.5	136.6	11.8
14	81.2	68.5	74.4	78.3	68.3	67.2	100.7	149.7	162.8	100.4	141.8	
15	80.3	75.0	74.3	77.0	68.7	66.9	100.6	149.6	162.7	101.6	139.8	
16	80.7	75.8	75.0	78.1	69.5	67.7	101.3	150.3	163.3	109.9	137.7	12.6
17	83.4	73.8	74.4	78.8	65.0	66.7	100.2	159.9	170.4	108.9	136.8	
18	83.7	73.8	74.5	78.4	64.9	66.7	100.1	159.7	171.1	117.1	132.4	13.1

a) Data from Conway *et al.*[4]

being assigned as in Table 1. A similar procedure was used for the assignment of methyl 4,6-*O*-benzylidene-2,3-di-*O*-*p*-tolylsulfonyl-α-D-mannopyranoside (**9**) and its β-anomer (**10**).

In the cases of nucleosides 1-(4′,6′-*O*-benzylidene-β-D-glucopyranosyl)thymine (**11**), its 2′,3′-di-*O*-methylsulfonyl derivative (**13**), 1-(4′,6′-*O*-benzylidene-2′,3′-di-*O*-methylsulfonyl-β-D-glucopyranosyl)uracil (**12**), 1-(4′,6′-*O*-benzylidene-3′-*O*-methylsulfonyl-β-D-mannopyranosyl)uracil (**14**), its 2′,3′-di-*O*-methanesulfonate (**15**), 1-(4′,6′-*O*-benzylidene-2′,3′-di-*O*-methylsulfonyl-β-D-mannopyranosyl)thymine (**16**), 2,2′-anhydro-1-(4′,6′-*O*-benzylidene-3′-*O*-methylsulfonyl-β-D-mannopyranosyl)uracil (**17**), and 2,2′-anhydro-1-(4′,6′-*O*-benzylidene-3′-*O*-methylsulfonyl-β-D-mannopyranosyl)thymine (**18**), it is easy to assign the chemical shift of a sugar moiety, since the displacement of methyl by nucleoside base on C-1′ gives no serious effect on the chemical shifts of a sugar moiety except that of C-1′. It is easy to assign those of a sugar moiety of cyclic nucleosides **17** and **18**. The assignment of a base moiety is as the same as in previous reports.[6]

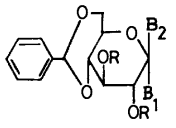

I, II, V, VI, VII, VIII, XI, XII, XIII

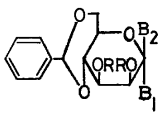

III, IV, IX, X, XIV, XV, XVI

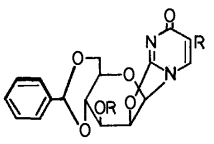

XVII, XVIII

Table 2. Chemical shift differences due to sulfonylation

Δ	C-1	C-2	C-3	C-4	C-5	Sum of $\lvert\Delta-\Delta'\rvert$
5−**1**	−2.5	4.0	5.2	−3.7	0.3	
$\lvert\Delta-\Delta'\rvert$	0.4	5.2	4.0	1.6	1.1	12.3
6−**2**	−3.7	5.3	6.1	−3.0	−1.2	
$\lvert\Delta-\Delta'\rvert$	1.6	3.9	3.1	0.9	0.4	9.9
7−**1**	−1.4	4.8	5.5	−2.7	0.8	
$\lvert\Delta-\Delta'\rvert$	0.7	4.4	3.7	0.6	1.6	11.0
8−**2**	−4.0	4.4	5.6	−2.9	−1.1	
$\lvert\Delta-\Delta'\rvert$	1.9	4.8	3.6	0.8	0.3	11.4
Predicted Δ' [a] (glucoside)	−2.1	9.2	9.2	−2.1	−0.8	
9−**3**	−3.2	3.4	6.0	−1.6	0.7	
$\lvert\Delta-\Delta'\rvert$	1.1	5.8	3.2	0.4	2.0	12.3
10−**4**	−3.3	4.7	4.6	0.2	−0.7	
$\lvert\Delta-\Delta'\rvert$	1.2	4.5	4.6	2.0	0.6	12.9
Predicted Δ' [a] (mannoside)	−2.1	9.2	9.2	−1.8	−1.3	

a) Predicted from Duddeck's results.[7] Negative sign represents upfield difference.

Duddeck has shown with adamantane derivatives that the effect of substitution hydroxyl group for sulfonyloxyl one is 10.9 ppm downfield shift on α-carbon, 1.7 ppm upfield shift on β-carbon, and less than 1 ppm upfield shift on γ- and δ-carbons.[7] Usually the substitution effect on carbon chemical shift is additive and predictable.[8] However, our results can hardly be predicted by Duddeck's results. This discrepancy can be attributed mainly to steric effect.[8,9] The sum of absolute values of these differences ($\Delta-\Delta'$) (Table 2) suggests the dgree of the steric compression due to sulfonylation. The order of reactivity of unsaturation of 2,3-disulfonates is **6**>**10**>**5**>**9**.[1] As seen in Table 2, there is no relationship between the sum of $\lvert\Delta-\Delta'\rvert$ and reactivity. Thus, the steric interaction of the starting static state is not important and the steric and electrostatic effects of the dynamic intermediates are important as regards unsaturation.[1]

Experimental

NMR Spectra. The spectra were obtained at 25.15 MHz on a JEOL JNM-MH-100 instrument with JNM-MFT-100 Fourier transform accessory and a JEC-6 computer. Saturated solution was used as a sample in $(CD_3)_2SO$. The deuterium signal provided a field frequency lock, the carbon signal being used as an internal standard (39.5 ppm downfield from Me_4Si). Measurement conditions were as follow: pulse width, 27.5 μs (*ca.* 45°); repetition time, 4 s; spectral width, 6.25 KHz; data points, 8192; acquisition time 0.655 s; noise modulated proton decoupling power, 20 W. All the chemical shifts are expressed in ppm downfield from Me_4Si.

Materials. Compounds **3**—**10**,[1] thymine nucleosides (**11**), (**13**), (**16**), and (**18**)[2] and uracil nucleosides (**12**), (**14**), (**15**), and (**17**)[10] were prepared according to the methods reported.

The authors thank Drs. T. Imanari and N. Esumi, JEOL, Tokyo, for measuring the spectrum of compound **18** with a JEOL FX-60 instrument at 15 MHz.

References

1) T. Yamazaki, H. Sugiyama, N. Yamaoka, K. Matsuda, and S. Seto, *J. Chem. Soc., Perkin Trans. 1*, **1977**, 1981.

2) T. Yamazaki, K. Matsuda, H. Sugiyama, S. Seto, and N. Yamaoka, *J. Chem. Soc., Perkin Trans. 1*, **1977**, 1654.

3) (a) J. B. Stothers, "Carbon-13 NMR Spectroscopy," Academic Press, New York (1972); (b) G. C. Levy and G. L. Nelson, "Carbon-13 Nuclear Magnetic Resonance for Organic Chemists," Wiley Interscience, New York (1972).

4) E. Conway, R. D. Guthrie, S. D. Gero, G. Lukacs, and A.-M. Sepulchre, *J. Chem. Soc., Perkin Trans. 2*, **1974**, 542.

5) Ref. 3a, p. 461.

6) Ref. 3a, pp. 469—471.

7) H. Duddeck, *Org. Magn. Reson.*, **7**, 151 (1975).

8) Ref. 3b, p. 24.

9) T. Sato, T. Takemura, and M. Kainosho, *J. Chem. Soc., Chem. Commun.*, **1974**, 97.

10) T. Yamazaki, H. Sugiyama, K. Matsuda, and S. Seto, *Bull. Chem. Soc. Jpn.*, **50**, 3423 (1977).

BULLETIN OF THE CHEMICAL SOCIETY OF JAPAN, VOL. 51 (12), 3661—3662 (1978)

Reactions of Benzyl 2-Benzyloxycarbonylamino-2-deoxy-3-*O*-mesyl-α-D-gluco- and -α-D-allopyranoside Derivative with Iodide

Hiroshi SANO, Seiji IIMURA, Tsutomu TSUCHIYA,* and Sumio UMEZAWA
Institute of Bioorganic Chemistry, 1614 Ida, Nakahara-ku, Kawasaki 211

(Received June 5, 1978)

Synopsis. The reactions of benzyl 4,6-*O*-benzylidene-2-benzyloxycarbonylamino-2-deoxy-3-*O*-mesyl-α-D-glucopyranoside (**1**), its *N*-methyl derivative (**4**) and 3-epimer (**8**) with sodium iodide in DMF were studied. Compound **1** gave several products including 2,3-alloepimine, **4** an oxazolidinone and **8** a 3-iodo derivative.

A number of synthetic C-3′ and C-3″ deoxy derivatives of aminoglycoside antibiotics were found to be active against resistant bacteria.[1-3] As reported,[4] 3-iodination of a kanamycin B derivative having 2,6-dideoxy-2,6-bis(ethoxycarbonylamino)-3-*O*-tosyl-α-D-glucopyranosyl moiety was successfully performed in the synthesis of tobramysin in spite of the presence of syn-diaxial interaction[5] between axial anomeric oxygen and a nucleophile approaching axially to C-3. We are interested in a similar iodination of sulfonyloxy derivatives of related aminosugars. We have studied the displacement reaction at C-3 of benzyl 4,6-*O*-benzylidene-2-benzyloxycarbonylamino-2-deoxy-3-*O*-mesyl-α-D-glucopyranoside[6] (**1**) and related compounds with iodide ion.

Treatment of **1** with 50% (W/V) sodium iodide in *N*,*N*-dimethylformamide (DMF) at 100 °C for 48 h gave three products. The major product (14% yield) was not the corresponding 3-iodo derivative but *N*-benzyl-2,3-epimino-α-D-allopyranoside (**2**). Its structure was evidenced by identity with the compound prepared by benzylation of benzyl 4,6-*O*-benzylidene-2,3-epimino-α-D-allopyranoside. Since the starting material was recovered by a similar treatment of **1** without sodium iodide, it is apparent that iodide ion plays an important role in this reaction though the mechanism of this reaction remains equivocal. One of the other two minor products was found to be an iodo derivative (2-amino-3-iodo derivative) on the basis of IR and NMR spectra and microanalysis of its acetylated product (**3**).

In order to examine the effect of *N*-methyl group on the above reaction, the *N*-methyl derivative (**4**) was prepared by methylation of **1** and treated with sodium iodide in DMF in a similar manner to that described for **1**. In this case, an oxazolidinone (**5**) was the sole product isolated (71% yield), identical with the specimen obtained by alkaline treatment[7] of **4**.

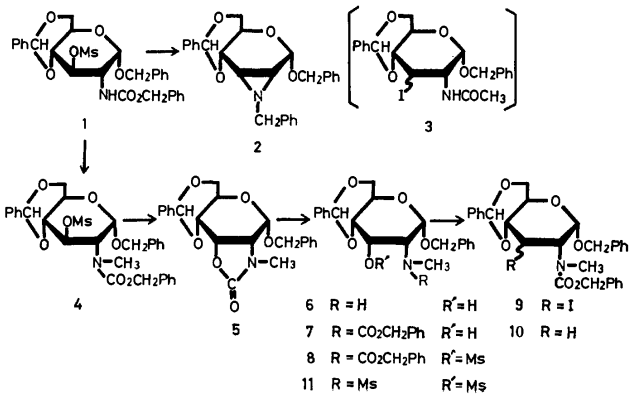

In order to examine the configurational effect at C-3, 3-epimer of **4**, *i.e.* 3-*O*-mesyl-α-D-allopyranoside derivative (**8**) was prepared from **5**. Basic hydrolysis of **5** gave the allo-aminol (**6**), which was *N*-benzyloxycarbonylated to give **7**. Mesylation of **7** gave **8**. Treatment of **8** with sodium iodide in DMF afforded the 3-iodo derivative (**9**) in 33% yield. Its structure was characterized by reduction with Raney nickel, giving 3-deoxy compound (**10**).

Since the direct iodination at C-3 is more or less restricted by syn-diaxial interaction in both reactions of epimeric 3-mesylates (**4** and **8**), it is suggested that the neighboring 2-*N*-benzyloxycarbonyl group plays an important role in the reaction of iodide ion,[8] participating in the elimination of the mesyloxy group. For the sake of confirmation, we have prepared a 2-*N*-mesyl derivative (**11**), which is assumed to take no such participation. By treatment of **11** with sodium iodide the starting material was mainly recovered along with some minor products containing no iodine.

Experimental

*Reaction of **1** with Sodium Iodide in DMF.* Dry sodium iodide (3.0 g) was added to a solution of **1** (300 mg) in dry DMF (4.5 ml) and the mixture was heated at 100 °C for 48 h. The chloroform extracts of the reaction mixture were concentrated by addition of toluene. The solution of the residue in chloroform was washed with 5% sodium thiosulfate solution and water, dried (Na_2SO_4), and concentrated. The thick syrup (287 mg) was chromatographed with silica gel (Wakogel C-200) with benzene–ethyl acetate (30: 1→1: 1, gradual change). From the earlier fractions, a solid (74 mg; TLC, R_f 0.75 with benzene–ethyl acetate 9: 1) was obtained, which was further purified by chromatography with hexane–benzene (1: 5→1: 10). Recrystallization from ethanol gave needles of **2**, 32 mg (14%), mp 165—166 °C, $[\alpha]_D^{25}$ + 120° (*c* 0.2, chloroform). Found: C, 75.53; H, 6.70; N, 2.98%. Calcd for $C_{27}H_{47}NO_4$: C, 75.50; H, 6.34; N, 3.26%.

1 (27 mg, R_f 0.5) was recovered from the middle fractions described above; a solid (24 mg; TLC, R_f 0.13) from the latest fractions. Acetylation of the solid gave a solid (13 mg) [IR (KBr): 1740, 1700, 1650, 1540 cm^{-1}] and another solid (**3**, 14 mg), IR (KBr): 1660, 1560 cm^{-1}; PMR (pyridine-d_5): δ 2.15 (3H s, Ac). Found: C, 52.18; H, 4.85; N, 2.76; I, 24.42%. Calcd for $C_{22}H_{24}NO_5I$: C, 51.88; H, 4.75; N, 2.75; I, 24.91%.

*Benzyl N-Benzyl-4,6-O-benzylidene-2,3-dideoxy-2,3-epimino-α-D-allopyranoside (**2**).* Sodium (10.3 mg) dissolved in 2-propanol (0.45 ml) was added to a solution of **1** (103 mg) in dry dioxane (1.4 ml), and the mixture was treated in a similar

way to that reported by Rhoads and Gross.[9] To a solution of the crude epimine (51 mg) in DMF (1.0 ml) were added benzyl bromide (0.06 ml) and silver oxide (70 mg) and the mixture was stirred at room temperature for 14 h. Usual purification gave a solid. Recrystallization from ethanol gave needles, 49 mg (32%), mp 165—166 °C, $[\alpha]_D^{25}+120°$ (*c* 0.2, chloroform). PMR ($CDCl_3$): 2H unresolved q centered at δ 2.18 (H-2,3) (J=6 Hz), which sharpened on irradiation at δ 5.05. Found: C, 75.24; H, 6.51; N, 2.97%. Calcd for $C_{27}H_{27}NO_4$: C, 75.50; H, 6.34; N, 3.26%.

Benzyl 4,6-O-Benzylidene-2-benzyloxycarbonylamino-2-deoxy-3-O-mesyl-2-N-methyl-α-D-glucopyranoside (4). Methyl iodide (0.22 ml) and silver oxide (408 mg) were added to a solution of **1** (503 mg) in dry DMF (10 ml) and the mixture was stirred vigorously at room temperature for 15 h. Work-up in the usual manner gave a solid. Recrystallization from ethyl acetate–hexane gave rods (496 mg, 97%), mp 160—162 °C, $[\alpha]_D^{21}+67°$ (*c* 2, chloroform). IR (KBr): 1690 cm^{-1} (amide I); the peak at 1540 cm^{-1} (amide II) was not observed. PMR ($CDCl_3$): δ 2.91 and 3.12 (each 3H s, SO_2CH_3 and NCH_3). Found: C, 61.88; H, 5.80; N, 2.46; S, 5.21%. Calcd for $C_{30}H_{33}NO_9S$: C, 61.74; H, 5.70; N, 2.40; S, 5.49%.

Benzyl 4,6-O-Benzylidene-2-N:3-O-carbonyl-2-deoxy-2-methylamino-α-D-allopyranoside (5). By Use of Sodium Iodide in DMF: Dry sodium iodide (0.83 g) was added to a solution of **4** (83 mg) in dry DMF (1.2 ml) and the mixture was heated at 100 °C for 48 h. Work-up in the usual manner gave a solid. Recrystallization from ethyl acetate gave rods, 40 mg (71%), mp 229—230 °C, $[\alpha]_D^{21}+190°$ (*c* 2, chloroform). IR (KBr): 1775 cm^{-1} (cyclic carbamate). PMR ($CDCl_3$): δ 2.82 (3H s, NCH_3), 5.06 (1H d, J=5 Hz, H-1), 5.64 (1H s, C_6H_5CH=). Found C, 66.69; H, 5.98; N, 3.54%. Calcd for $C_{22}H_{23}NO_6$: C, 66.49; H, 5.83; N, 3.52%.

By Use of Sodium Acetate: Sodium acetate trihydrate (431 mg) was added to a solution of **4** (431 mg) in 2-methoxyethanol (8.6 ml), and the mixture was refluxed for 45 h. Work-up in the usual manner gave a solid. Recrystallization from ethyl acetate gave rods, 256 mg (85%), mp 229—230 °C.

Benzyl 4,6-O-Benzylidene-2-deoxy-2-methylamino-α-D-allopyranoside (6). A solution of **5** (232 mg) in ethanolic 0.5 M potassium hydroxide (6.9 ml) was refluxed for 24 h. Work-up in the usual manner gave a solid. Recrystallization from ethyl acetate gave needles, 181 mg (85%), mp 210—211 °C, $[\alpha]_D^{31}+99°$ (*c* 1, chloroform). PMR ($CDCl_3$): δ 2.28 (1H m, H-2) which collapsed to a triplet (J=3.5 Hz) on deuteration; 2.48 (3H s, NCH_3), 5.08 (1H d, J=3.5 Hz, H-1). Found: C, 67.80; H, 6.80; N, 3.71%. Calcd for $C_{21}H_{25}NO_5$: C, 67.91; H, 6.78; N, 3.77%.

Benzyl 4,6-O-Benzylidene-2-N-benzyloxycarbonyl-2-deoxy-2-methylamino-α-D-allopyranoside (7). Work-up in the usual manner gave a thick syrup (86%), $[\alpha]_D^{26}+79°$ (*c* 2, chloroform). PMR ($CDCl_3$): δ 3.32 (3H s, NCH_3). Found: C, 68.90; H, 6.22; N, 2.73%. Calcd for $C_{29}H_{31}NO_7$: C, 68.91; H, 6.18; N, 2.77%.

Benzyl 4,6-O-Benzylidene-2-N-benzyloxycarbonyl-2-deoxy-3-O-mesyl-2-methylamino-α-D-allopyranoside (8) was prepared from **7** in the usual manner; a thick syrup (97%), $[\alpha]_D^{30}+88°$ (*c* 2, chloroform). PMR ($CDCl_3$): δ 2.97 (3H s, SO_2CH_3), 3.32 (3H s, NCH_3), 5.07 (1H d, J=3.5 Hz, H-1), 5.45 (1H t, J=2.5 Hz, H-3). Found: C, 61.90; H, 5.80; N, 2.47; S, 5.41%. Calcd for $C_{30}H_{33}NO_9S$: C, 61.73; H, 5.70; N, 2.40; S, 5.49%.

Benzyl 4,6-O-Benzylidene-2-N-benzyloxycarbonyl-2-deoxy-3-iodo-2-methylamino-α-D-gluco or allopyranoside (9). Dry sodium iodide (1.32 g) was added to a solution of **8** (132 mg) in dry DMF (2.6 ml) and the mixture was heated at 100 °C for 48 h. The solution contained at least 6 components (TLC, R_f 0, 0.1, 0.4, 0.45 (weak, **8**), 0.55 and 0.6 (major, **9**), with benzene–ethyl acetate=15:1). Separation of the products in a similar manner to that for the reaction of **1** with NaI gave a thick syrup of **9**, which crystallized on standing; 46 mg (33%). Recrystallization from benzene–hexane gave needles, mp 180—183 °C, $[\alpha]_D^{29}+28°$ (*c* 2, chloroform). PMR ($CDCl_3$): δ 3.02 and 3.04 (each s, 3H in total, NCH_3). Found: C, 56.55; H, 4.83; N, 2.20; I, 20.25%. Calcd for $C_{29}H_{30}NO_6I$: C, 56.59; H, 4.91; N, 2.28; I, 20.62%.

Benzyl 4,6-O-Benzylidene-2-N-benzyloxycarbonyl-2,3-dideoxy-2-methylamino-α-D-ribohexopyranoside (10). Hydrogenation of **9** (11.4 mg) in dioxane (0.2 ml) with Raney nickel (0.2 ml) and triethylamine (trace) gave a syrup, 5.6 mg (62%), $[\alpha]_D^{25}+132°$ (*c* 1, chloroform); PMR ($CDCl_3$): δ 1.8—2.5 (2H m, H-3, 3′), 3.01 (3H s, NCH_3). Found: C, 71.40; H, 6.49; N, 2.96%. Calcd for $C_{29}H_{31}NO_6$: C, 71.14; H, 6.38; N, 2.86%.

Benzyl 4,6-O-Benzylidene-2-deoxy-3-O-mesyl-2-methylsulfonylamino-2-N-methyl-α-D-allopyranoside (11). Hydrogenation of **8** (40 mg) in dioxane (1.5 ml) with palladium black gave a syrup (29 mg, 96%); PMR ($CDCl_3$): δ 2.49 (3H s, NCH_3), 2.29 (3H s, SO_2CH_3). Mesylation of the syrup in the usual manner gave a syrup, 17 mg (97%), $[\alpha]_D^{24}+58°$ (*c* 1, chloroform); PMR ($CDCl_3$): δ 2.87 and 2.93 (each 3H s, NSO_2CH_3 and NCH_3), 3.25 (3H s, SO_2CH_3). Found: C, 52.85; H, 5.65; N, 2.45%. Calcd for $C_{23}H_{29}NO_9S_2$: C, 52.36; H, 5.54; N, 2.65%.

References

1) S. Umezawa, *Adv. Carbohydr. Chem. Biochem.*, **30**, 111—182 (1974); H. Umezawa, *ibid.*, **30**, 183—225 (1974).

2) H. Sano, T. Tsuchiya, S. Kobayashi, M. Hamada, S. Umezawa, and H. Umezawa, *J. Antibiot.*, **29**, 978 (1976).

3) D. Ikeda, F. Nagaki, S. Umezawa, T. Tsuchiya, and H. Umezawa, *J. Antibiot.*, **28**, 616 (1975).

4) Y. Takagi, T. Miyake, T. Tsuchiya, S. Umezawa, and H. Umezawa, *J. Antibiot.*, **26**, 403 (1973); *Bull. Chem. Soc. Jpn.*, **49**, 3649 (1976).

5) A. C. Richardson, *Carbohydr. Res.*, **10**, 395 (1969).

6) P. H. Gross and H. K. Zimmerman, Jr., *Liebigs Ann. Chem.*, **674**, 211 (1964).

7) For example see: L. Goodman, *Adv. Carbohydr. Chem.*, **22**, 109—175 (1967).

8) For the cooperation of iodide ion and the neighboring group, we assume the following mechanisms (I) and (II) for the reactions of **8** and **4**, respectively. Though in the reaction of **8**, there is syn-diaxial interaction between the leaving mesyloxy anion and the axial anomeric oxygen in the transition state, iodination can be facilitated by the presence of the benzyloxycarbonyl group as depicted in I.

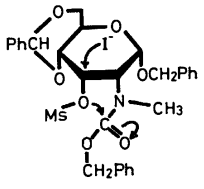

I

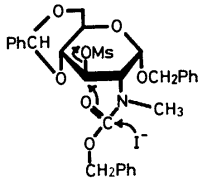

II

9) W. D. Rhoads and P. H. Gross, *Carbohydr. Res.*, **11**, 561 (1969).

BULLETIN OF THE CHEMICAL SOCIETY OF JAPAN, VOL. 51 (12), 3663—3664 (1978)

Oxidation of Thujopsene with Metal Acetate in Acetic Acid

Haruo SEKIZAKI,* Masaaki ITO, and Shoji INOUE**

Chemistry Laboratory, Department of General Education, Higashi Nippon Gakuen University, Onbetsu-cho, Hokkaido 088-01

***Faculty of Pharmacy, Meijo University, Tenpaku-ku, Nagoya 468*

(Received June 23, 1978)

Synopsis. Thujopsene has been oxidized with lead tetraacetate, cobalt triacetate and manganese triacetate, to different kinds of products being 4β-acetyl-6β,10,10-trimethyltricyclo[4.4.0.0^{1,3}]decane (**3**) and its diacetate; 2β-acetoxymethyl-2α,4aβ,8,8-tetramethyl-2,3,4,4a,5,6,7,8-octahydronaphthalene (**7**) and widdryl acetate; **3**, **7**, and widdrol, respectively.

In the oxidation of thujopsene (**1**) with metal acetates[1-3] much attention has been focused on the acetate of Pb(IV), Co(III), and Mn(III). The reactions with metal acetates are summarized in Table 1.

Results and Discussion

*Oxidation of **1** with Lead Tetraacetate.* Thujopsene (**1**) was oxidized with lead tetraacetate in acetic acid at 30 °C for 3 h. Workup and purification gave a stereospecifically ring-contracted ketone (**3**) in 60—65% yield, and the diacetate (**6**) in 16—20% yield. The structure of **3** was identical with that already reported by

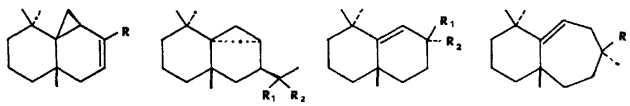

1: R=CH_3 **3**: R_1=R_2=O **5**: R_1=CH_3, **8**: R=OAc
2: R=CH_2OAc **6**: R_1=R_2=OAc R_2=CH_2OAc **9**: R=OH
4: R=CHO **7**: R_1=CH_2OAc, R_2=CH_3
10: R_1=CH_2OH, R_2=CH_3

Nagahama *et al.*[3] The configuration of the acetyl group of **3**[2] was determined and the structure of **6** deduced from the spectral data. The IR absorptions of **6** at 1753 cm^{-1} show the presence of an acetyl group and the presence of a methyl and two acetyl groups is indicated by the NMR signals at 1.91 and 2.06. Hydrolysis of **6** gave **3** in quantitative yield. Thus the minor product (**6**) on this reaction was identified as the stereospecifically ring-contracted diacetate.

*Oxidation of **1** with Cobalt Triacetate.* Onopchenko *et al.*[4] have reported that the preparation of cobalt triacetate and oxidation of cyclohexene with cobalt triacetate gave the 3-cyclohexenyl acetate in high yield. However, a similar reaction with **1** shows different results. After stirring the acetic acid solution of **1** and cobalt triacetate for 45 h, the usual workup yielded no oxidation product and gave the acid-catalyzed isomerization-acetoxylation products **7** and **8** in poor yields. Compound **7** was purified by column chromatography and the structure of **7** confirmed by comparing the IR and NMR spectra of an authentic sample.[5] The configuration of the acetoxymethyl group in **7** was the reverse of the acetate (**5**) prepared by the mercury diacetate oxidation.[1] The structure of the product **8** was determined from following chemical evidence. Hydrolysis of a mixture of **7** and **8** with ethanolic KOH at room temperature for 1 h afforded alcohols **9** and **10**, the spectral data of which were identical with authentic specimens.[6,7] These results indicate that product **8** is widdryl acetate.

*Oxidation of **1** with Manganese Triacetate.* The acetic acid solution of **1** and manganese triacetate was stirred at 80 °C for 54 h. The usual workup and purification gave the acetate (**7**), widdrol (**9**) and the ring-contracted ketone (**3**) in 13.8, 10.3, and 4.3% yields, respectively. The same reaction on general olefins (*e.g.* α-methylstyrene, octene-1 *etc.*) affords the corresponding γ-lactone.[8]

Experimental

The melting points were determined on a Yanagimoto micro melting point apparatus and are uncorrected. The NMR spectra were recorded on a JEOL PMX-60 spectrometer at 60 MHz, using Me_4Si as an internal standard. The IR spectra were determined on a Shimadzu IR-400 spectrometer.

*Oxidation of Thujopsene (**1**) with Lead Tetraacetate.* To the stirred solution of **1** (5.1 g, 25 mmol) in acetic acid (20 ml), kept at 5 °C, was added solid lead tetraacetate (9.0 g, 20 mmol) in portions for 30 min. The mixture was stirred for 3 h at 30 °C, then poured into ice-water and extracted with

TABLE 1. OXIDATION PRODUCTS OF THUJOPSENE WITH METAL ACETATES IN ACETIC ACID

Reagent	Reaction temp (°C)	Product No.							
		2	**3**	**4**	**5**	**6**	**7**	**8**	**9**
$Pb(OAc)_4$	30	—	60—65	—	—	16—20	—	—	—
$Hg(OAc)_2$[1]	70	14.4	—	11.1	5.4	—	—	—	—
$Tl(OAc)_3$[2]	room	76	10	—	—	—	—	—	—
	50	8	72	—	—	—	—	—	—
$Co(OAc)_3$	80	—	—	—	—	—	7.9	2.4	—
$Mn(OAc)_3$	80	—	4.3	—	—	—	14	—	10

ether. The ether solution was washed with aqueous $NaHCO_3$ solution, water, dried (Na_2SO_4), and evaporated to give an oily residue (7.3 g). The products were separated by column chromatography using silica gel. Elution with benzene gave **3** (3.6 g) as a colorless liquid and **6** (914 mg) as colorless crystals. The pure sample of **3** was obtained by distillation under reduced pressure. **3**: Bp 117—119 °C/5 mmHg. NMR ($CDCl_3$) δ 0.75 (s, 3, CH_3), 1.05 (s, 3, CH_3), 1.10 (s, 3, CH_3), 2.20 (s, 3, Ac), and 3.07 (t, 1, J=10.0 and 4.0 Hz); 2,4-dinitrophenylhydrazone: mp 168—169 °C (lit,[3] mp 170—170.5 °C). The pure sample of **6** was obtained by recrystallization from hexane. **6**: Mp 67—71 °C. IR (KBr) 3075, 3045 (cyclopropyl) and 1753 cm^{-1} (OAc); NMR ($CDCl_3$) δ 0.57 (s, 3, CH_3), 1.00 (s, 3, CH_3), 1.03 (s, 3, CH_3), 1.90 (s, 3, CH_3), 2.03 (s, 6, OAc), 3.17 (t, 1, J=10.0 and 4.0 Hz).

Hydrolysis of ***6***. The compound (**6**) (322 mg, 1 mmol) was hydrolyzed in ethanol (3 ml) with 5% HCl (1 ml) for 1 h at 50 °C. After the usual workup a crude product (**3**) (217 mg) was obtained.

*Oxidation of Thujopsene (****1****) with Cobalt Triacetate.* A mixed solution of cobalt triacetate[4] (prepared from $Co(OAc)_2 \cdot 4H_2O$ (25 g)) and **1** (20.4 g, 0.1 mol) was heated to 80 °C. Reaction was continued for 45 h, then the solution was poured into ice–water and extracted with benzene. The benzene solution was washed with aqueous $NaHCO_3$ solution, water, dried (Na_2SO_4) and evaporated to give an oily residue (22.7 g). The products were separated by column chromatography using silica gel. Elution with benzene gave **7** (1.25 g) as a colorless liquid and a mixture of **7** and **8** (1.45 g). **7**: IR (neat) 1743 cm^{-1} (OAc); NMR ($CDCl_3$) δ 0.93 (s, 3, CH_3), 1.05 (s, 6, $2CH_3$), 1.17 (s, 3, CH_3), 2.03 (s, 3, OAc), 3.81 (m, 2, $-\underline{CH_2}OAc$), and 5.10 (s, 1, olefinic). Accordingly, compound (**8**) could not be isolated by repeated column chromatography, a mixture of **7** and **8** was used for the following reaction.

Hydrolysis of Mixture of ***7*** *and* ***8***. To the stirred solution of the mixture of **7** and **8** (1.45 g) in ethanol (15 ml), kept at 10 °C, powdered KOH (56 mg, 10 mmol) was added. The solution was stirred for 1 h at room temperature, then the the solvent was evaporated under reduced pressure and the residue diluted by water and extracted with ether. The ether solution was washed with water, dried (Na_2SO_4), and evaporated to give an oily residue (1.17 g). The products were separated by column chromatography using silica gel. Elution with benzene and ether (5: 1) gave **10** (532 mg), colorless crystals. **10**: mp 70—72 °C (lit,[6] 71—72 °C); IR (KBr) 3230 cm^{-1} (–OH); NMR ($CDCl_3$) δ 0.92 (s, 3, CH_3), 1.07 (s, 3, CH_3), 1.10 (s, 3, CH_3), 3.27 (s, 2, $-\underline{CH_2}OAc$), 5.05 (s, 1, olefinic), and **9** (528 mg), colorless crystals. **9**: mp 83—85 °C (lit,[7] 86—87 °C); IR (KBr) 3255 cm^{-1} (–OH); NMR ($CDCl_3$) δ 1.10 (s, 6, $2CH_3$), 1.23 (s, 6, $2CH_3$), 5.52 (dd, 1, J=9.0 and 6.0 Hz, olefinic).

*Oxidation of Thujopsene (****1****) with Manganese Triacetate.* To a stirred solution of **1** (5.10 g, 25 mmol) in acetic acid (50 ml) was added solid manganase triacetate (13.6 g, 30 mmol) in portions for 10 min. The mixture was stirred for 54 h at 80 °C, then poured into ice–water and extracted with ether. The extract was washed with aqueous $NaHCO_3$ solution, water, dried (Na_2SO_4), and evaporated to give an oily residue (6.5 g). The products were separated by column chromatography using silica gel. Elution with benzene gave **7** (903 mg), **9** (549 mg), and **3** (344 mg).

The authors are grateful to Takasago Perfumery Co., Ltd. for providing the crude sample of thujopsene.

References

1) M. Ito, K. Abe, and H. Takeshita, *Bull. Chem. Soc. Jpn.*, **45**, 1913 (1972).
2) H. Sekizaki, M. Ito, and S. Inoue, *Bull. Chem. Soc. Jpn.*, **51**, 2439 (1978).
3) S. Nagahama, H. Kobayashi, and S. Akiyoshi, *Bull. Chem. Soc. Jpn.*, **32**, 366 (1959).
4) A. Onopchenko and J. G. D. Schuly, *J. Org. Chem.*, **40**, 3338 (1975).
5) K. Abe and M. Ito, *Bull. Chem. Soc. Jpn.*, **51**, 319 (1978).
6) W. G. Dauben and L. E. Friedrich, *Tetrahedron Lett.*, **1967**, 1735.
7) W. G. Dauben and L. E. Friedrich, *Tetrahedron Lett.*, **1964**, 2675.
8) E. I. Heiba, R. M. Dessan, and W. J. Koehl, *J. Am. Chem. Soc.*, **90**, 5905 (1968).

BULLETIN OF THE CHEMICAL SOCIETY OF JAPAN, VOL. 51 (12), 3665—3666 (1978)

Synthesis of *cyclo*(-L-Leucyl-L-lysyl-glycyl-)$_2$ and Its Hydrolysis by Trypsin

Nobuo Kosui, Tetsuo Kato, and Nobuo Izumiya*

Laboratory of Biochemistry, Faculty of Science, Kyushu University 33, Higashi-ku, Fukuoka 812

(Received July 10, 1978)

Synopsis. A protected cyclic hexapeptide, *cyclo*-(-L-Leu-L-Lys(ε-benzyloxycarbonyl)-Gly-)$_2$ (**6**), was synthesized by doubling cyclization of the corresponding tripeptide azide. Compound **6** was converted by hydrogenolysis into a cyclic hexapeptide, *cyclo*(-L-Leu-L-Lys-Gly-)$_2$, which was hydrolyzed by trypsin to a tripeptide, H-Gly-L-Leu-L-Lys-OH.

A few studies have been carried out on the enzymatic hydrolysis of cyclic peptides. Three cyclic hexapeptides, *cyclo*(-Gly$_5$-L-Lys-),[1] *cyclo*(-Gly$_2$-L-Lys-)$_2$,[2] and *cyclo*-(-Gly$_2$-L-Phe$_2$-Gly-L-Lys-),[3] all of which contain the -Gly-L-Lys-Gly- sequence, were hydrolyzed by trypsin at the L-Lys-Gly bond. Izumiya *et al.*[4] observed that the rate of tryptic hydrolysis of H-L-Leu-L-Lys-NH_2 is higher than that of H-Gly-L-Lys-NH_2. It thus seemed of interest to synthesize *cyclo*(-L-Leu-L-Lys-Gly-)$_2$ (**7**) and see if it is hydrolyzed by trypsin faster than *cyclo*-(-Gly$_2$-L-Lys-)$_2$.

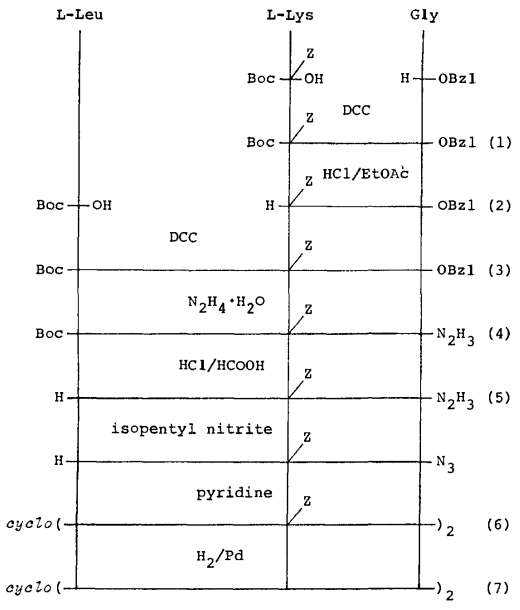

Fig. 1. Synthesis of cyclic hexapeptides, **6** and **7**.

The synthetic route[5] is shown in Fig. 1. A key intermediate, *cyclo*(-L-Leu-L-Lys(Z)-Gly-)$_2$ (**6**) was obtained in 30% yield by the cyclization of the tripeptide azide in pyridine (concentration, 5×10^{-3} M) at 0 °C. Compound **6** was hydrogenolyzed to give the final product **7** as crystalline dihydrochloride. The dimeric nature of **7** was confirmed by FD-mass spectrometry; M^+ 597 was observed, the calculated molecular weight corresponding to the cyclic hexapeptide being 596.7. The homogeneity of **7** was confirmed by TLC and paper chromatography.

Compound **7** was hydrolyzed by trypsin, giving a peptide (R_f^3 0.48) in Tris buffer at pH 7.8. No other spot except for the peptide with R_f^3 0.48 could be observed on a paper chromatogram during the course of incubation of **7**. The peptide with R_f^3 0.48 was assigned to a tripeptide, H-Gly-L-Leu-L-Lys-OH (**11**), by comparison with an authentic **11**, which was synthesized by the hydrogenation of Z-Gly-L-Leu-L-Lys-(Z)-OBzl (**10**). Compound **10** was prepared from Z-Gly-OH and H-L-Leu-L-Lys(Z)-OBzl (**9**) which was derived from Boc-L-Leu-L-Lys(Z)-OBzl (**8**). The result of tryptic digestion is similar to that obtained for *cyclo*-(-Gly$_2$-L-Lys-)$_2$.[2] This indicates that the rate-determining step is the conversion of **7** into a linear hexapeptide H-Gly-L-Leu-L-Lys-Gly-L-Leu-L-Lys-OH, which is cleaved to **11** immediately. It was observed, however, that tryptic hydrolysis of **7** proceeds slowly as compared to *cyclo*(-Gly$_2$-L-Lys-)$_2$. Steric effect of the bulky side chain in leucyl residues in the rigid backbone of **7** seems to hinder tryptic digestion.

Experimental

TLC was carried out on Merck silica gel G with the following systems: R_f^1, $CHCl_3$–MeOH (5: 1); R_f^2, *n*-BuOH–AcOH–pyridine–H_2O (4: 1: 1: 2). The ratio in parentheses is given in terms of vol. Paper chromatography was performed on Toyo Roshi No. 52 paper with the solvent system: R_f^3, the same solvent as used for R_f^2. Mass spectrum was taken on a Hitachi mass spectrometer Model JMS-01SG 2 equipped with combined sources: the sample was charged by emitter dipping technique; anode heating current, 18 mA. Crystalline trypsin (Nutritional Biochemicals, Cleveland, U.S.A.) was used without further purification.

Boc-L-Lys(Z)-Gly-OBzl (1). DCC (2.06 g, 10 mmol) was added to a solution of dicyclohexylamine salt[2] (5.62 g, 10 mmol) of Boc-L-Lys(Z)-OH and H-Gly-OBzl·TosOH (3.37 g, 10 mmol) in CH_2Cl_2 (20 ml) at 0 °C. The reaction mixture was stirred at 0 °C for 1 h and at room temperature overnight. After removal of *N,N'*-dicyclohexylurea, the filtrate was evaporated and the residue was diluted with EtOAc. The solution was successively washed with 0.5 M citric acid, 0.5 M $NaHCO_3$, and water, and then dried (Na_2SO_4). After evaporation under reduced pressure, the residue was solidified by the addition of ether. It was recrystallized from EtOAc–ether–petroleum ether; yield, 4.48 g (85%); R_f^1 0.86. Physical constants and results of elemental analyses of all crystalline compounds are given in Table 1.

H-L-Lys(Z)-Gly-OBzl·HCl (2·HCl). Compound **1** (1.32 g, 2.5 mmol) was dissolved in 2.57 M HCl in EtOAc (19.4 ml, 50 mmol), and the solution was left to stand at room temperature for 1 h and then evaporated. The resulting crystals were collected with the aid of ether; yield, 1.13 g (96%); R_f^1 0.50.

Boc-L-Leu-L-Lys(Z)-Gly-OBzl (3). This was prepared from Boc-L-Leu-OH and **2**·HCl as described for **1**;

Table 1. Analytical data of synthetic peptides

Compound	Mp (°C)	$[\alpha]_D^{20}$	Formula	Found (%)			Calcd (%)		
				C	H	N	C	H	N
1	72—74	−13.5° a)	$C_{28}H_{37}O_7N_3$	63.51	7.00	8.08	63.74	7.07	7.97
2·HCl	142—146		$C_{23}H_{30}O_5N_3Cl\cdot 1/2H_2O$	58.17	6.55	9.14	58.40	6.61	8.88
3	115—119	−29.0° a)	$C_{34}H_{48}O_8N_4$	63.54	7.48	8.80	63.73	7.55	8.74
4	78—84	−21.4° a)	$C_{27}H_{44}O_7N_6$	57.29	7.95	14.53	57.43	7.85	14.88
6	247—248(dec)	−101° b)	$C_{44}H_{64}O_{14}N_8$	60.89	7.47	12.60	61.09	7.46	12.96
7·2HCl	195—197(dec)	−120° b)	$C_{28}H_{54}O_6N_8Cl_2\cdot 3/2H_2O$	48.09	8.11	15.73	48.23	8.24	16.08
8	110—111	−29.5° a)	$C_{32}H_{45}O_7N_3$	65.36	7.78	7.29	65.84	7.77	7.20
10	96—98	−35.8° a)	$C_{37}H_{46}O_8N_4$	65.59	6.90	8.25	65.86	6.87	8.30

a) MeOH (*c* 2) used. b) AcOH (*c* 0.2) used.

yield, 82%; R_f^1 0.72.

*Boc-L-Leu-L-Lys(Z)-Gly-N_2H_3 (**4**).* A solution of **3** (640 mg, 1 mmol) and $N_2H_4\cdot H_2O$ (0.95 ml, 20 mmol) in DMF (10 ml) was left to stand for 3 days at 38 °C, and then evaporated. The residue was dissolved in $CHCl_3$ (50 ml), washed with water, and dried (Na_2SO_4). After removal of the solvent, the residue was solidified by the addition of ether. Recrystallization from MeOH–ether–petroleum ether yielded 468 mg (83%); R_f^1 0.60.

*H-L-Leu-L-Lys(Z)-Gly-N_2H_3·2HCl (**5**·2HCl).* This was prepared from **4** by use of a mixture of 0.0925 M HCl (2.2 eq) in HCOOH and CH_2Cl_2 (1: 1) in place of HCl in EtOAc as described for **2**·HCl; yield, 92%; R_f^1 0.10.

cyclo(*-L-Leu-L-Lys(Z)-Gly-*)$_2$ (**6**). Compound **5**·2HCl (860 mg, 1.6 mmol) was dissolved in DMF (20 ml) containing a few drops of glacial AcOH, and the solution was cooled to −50 °C. To the solution were added 2.7 M HCl in EtOAc (1.78 ml, 4.8 mmol) and isopentyl nitrite (0.237 ml, 1.76 mmol). The solution was stirred for 20 min at −30 °C, and then added dropwise to pyridine (300 ml) at 0 °C. The reaction mixture was stirred for 3 days at 0 °C, and then evaporated. The residue was dissolved in a mixture of MeOH (6 ml) and water (1 ml), and passed successively through columns (each 10.5×1.8 cm) of Dowex 50 (H^+ form) and Dowex 1 (OH^- form). The columns were washed with the same solvent, and the combined effluent (*ca.* 200 ml) was evaporated to dryness. The residue was collected with water. Recrystallization from MeOH-ether yielded 210 mg (30%); R_f^1 0.72, R_f^2 0.87.

cyclo(*-L-Leu-L-Lys-Gly-*)$_2$·2HCl (**7**·2HCl). Compound **6** (86.5 mg, 0.1 mmol) was suspended in a mixture of MeOH (1.5 ml) and AcOH (1.5 ml), and hydrogenated in the presence of palladium black. The suspension turned clear with the progress of reaction. In the course of the reaction, the solution showed 3 spots on TLC with R_f^2 values of 0.87 (A), 0.73 (B), and 0.55 (C). Spot A was of the starting material **6**, while spot C was of the final product **7**. Spot B was assumed to be a cyclic hexapeptide in which one of the Z group had been cleaved and another remained. When hydrogenation completed after 4 h, only one spot C was observed on TLC. To this solution was added 2.7 M HCl in EtOAc (0.081 ml, 0.22 mmol) and the filtrate from the catalyst was evaporated to dryness. It was recrystallized from MeOH–EtOAc; yield, 52 mg (75%); R_f^2 0.55, R_f^3 0.66. Found: M^+, 597. Calcd for $C_{28}H_{52}O_6N_8$ (**7**): M, 597.

*Boc-L-Leu-L-Lys(Z)-OBzl (**8**).* Isobutyl chloroformate (0.13 ml, 1 mmol) was added at −10 °C to a chilled solution of Boc-L-Leu-OH (231 mg, 1 mmol) and Et_3N (0.14 ml, 1 mmol) in tetrahydrofuran (2 ml). After 5 min, a chilled mixture of H-L-Lys(Z)-OBzl·TosOH[2] (543 mg, 1 mmol) and Et_3N (0.14 ml, 1 mmol) in $CHCl_3$ (2 ml) was added. The reaction mixture was stirred for 1 h at 0 °C and overnight at room temperature, and then evaporated. The residual oil was then dissolved in EtOAc, washed successively with 0.5 M citric acid, 0.5 M $NaHCO_3$, and water, and dried (Na_2SO_4). After evaporation, the residue was solidified by the addition of ether. It was recrystallized from EtOAc–ether–petroleum ether; yield, 425 mg (73%); R_f^1 0.85.

*H-L-Leu-L-Lys(Z)-OBzl·HCl (**9**·HCl).* This was prepared from **8** as described for **2**·HCl; yield, 93%; R_f^2 0.75.

*Z-Gly-L-Leu-L-Lys(Z)-OBzl (**10**).* This was prepared from Z-Gly-OH and **9**·HCl as described for **8**; yield, 89%; R_f^1 0.90.

*H-Gly-L-Leu-L-Lys-OH·2HCl (**11**·2HCl).* This was prepared from **10** as described for **7**; yield of hygroscopic crystals, 100%; R_f^2 0.43, R_f^3 0.48.

*Action of Trypsin on **7**.* Tryptic hydrolysis on the substrate **7** was carried out at pH 7.8 and at 30 °C. A solution of **7**·2HCl (6.7 mg, 0.01 mmol) in dimethyl sulfoxide (0.05 ml) was diluted with 0.2 M Tris buffer (0.50 ml) and with water to a total volume of 1 ml and incubated upon addition of trypsin (2 mg). The progress of the reaction was followed by paper chromatography in the course of time. A spot of **11** appeared after 10 min and the spot of **7** diasppeared after 24 h. In a similar experiment, *cyclo*(-Gly$_2$-L-Lys-)$_2$ was completely hydrolyzed within 4 h.

The authors wish to express their thanks to Mr. Akio Hashimoto, Kitakyushu Municipal Institute of Environmental Health Science, for his help in the measurement of mass spectroscopy.

References

1) M. Ohno and N. Izumiya, *Bull. Chem. Soc. Jpn.*, **38**, 1831 (1965).

2) O. Abe, H. Takiguchi, M. Ohno, S. Makisumi, and N. Izumiya, *Bull. Chem. Soc. Jpn.*, **40**, 1945 (1967).

3) S. Terada, T. Kato, and N. Izumiya, *Eur. J. Biochem.*, **52**, 273 (1975).

4) N. Izumiya, T. Yamashita, H. Uchio, and K. Kitagawa, *Arch. Biochem. Biophys.*, **90**, 170 (1960).

5) Abbreviations given by the IUPAC-IUB Commission (*J. Biol. Chem.*, **247**, 977 (1972)) have been used. Additional abbreviations: DCC, dicyclohexylcarbodiimide; DMF, *N,N*-dimethylformamide.

BULLETIN OF THE CHEMICAL SOCIETY OF JAPAN, VOL. 51 (12), 3667—3668 (1978)

Liquid-phase Oxidation of Anthracene in Acetic Acid by Copper(II) Chloro Complexes

Jinya KOSHITANI,* Masayoshi HIRAMATSU, Yoshio UENO, and Takatoshi YOSHIDA

Department of Industrial Chemistry, Nagoya Institute of Technology, Gokiso-cho, Showa-ku, Nagoya 466

(Received September 5, 1977)

Synopsis. Copper(II) chloro complexes contribute to the liquid-phase oxidation of anthracene in acetic acid. Products of the oxidation were anthrone, anthraquinone, 9-acetoxyanthracene, and 9-chloroanthracene.

It is known that the copper(II) chloro complexes[1-4] are formed by the reactions of copper(II) salts with alkali chlorides both in aqueous and nonaqueous solutions. Although the catalytic activities of copper(II) salts in liquid-phase oxidation are generally low, it was observed that the addition of lithium chloride highly improved the activity of copper(II) acetate in liquid-phase oxidation. No chain reaction in liquid-phase oxidation of a polynuclear aromatic hydrocarbon had been reported before the work[5] of Mahoney. There appears to be general agreement that a polynuclear aromatic hydrocarbon is not readily oxidized in liquid-phase oxidation. In this paper, the activities of copper-(II) chloro complexes and the reaction products in the liquid-phase oxidation of anthracene are reported.

Experimental

Materials. Acetic acid was distilled after refluxing with $KMnO_4$. The water content in the distllate was determined by the Karl-Fischer method and the water removed with the equivalent amount of acetic anhydride. Copper(II) acetate (reagent grade) and lithium chloride (reagent grade) were dried at 115 and 120 °C in vacuum respectively. Lithium acetate (reagent grade) was used without further purification. Commercial oxygen was purified by passing through 30% aqueous potassium hydroxide solution and concd sulfuric acid. Anthracene was dissolved in xylene, the solution poured into methanol and the precipitated anthracene dried in vacuum.

Oxidation Procedure. Oxidation was performed in a closed system using an apparatus equipped with a gas burette and oxygen absorption was followed by a manually controlled gas burette filled with mercury. The reaction was performed under the partial pressure of oxygen by which the rate of the oxidation was not affected.

Measurements. UV and visible absorption spectra were recorded with a Hitachi spectrophotometer model 124. The water content in acetic acid was determined with a Karl-Fischer apparatus, Kyoto Electronic Industry Ltd. MK-SS.

Analyses of Reaction Products. The reaction mixture was diluted with water and extracted with benzene which was removed in vacuum. The extracts were analyzed with a Yanagimoto model 550-TF gas chromatograph using a 2.25 m column of 30% Apieason grease L on Celite 545 at 190 °C and a 2 m column of 10% Silicone OV-17 on Chromosorb WAW at 230 °C. Gas-mass spectral analysis was performed with a JEOL model JMSD100-JGC20K spectrometer equipped with a 2 m column of 10% Silicone OV-17 on Chromosorb WAW.

Results and Discussion

Effect of Copper(II) Chloro Complexes. The following equilibrium exists in a mixture of acetic acid and lithium chloride.

$$AcOH + LiCl \rightleftarrows LiOAc + HCl \quad (1)$$

In a mixture of copper(II) acetate and hydrogen chloride, the following equilibria[4] have been proposed.

$$Cu_2(OAc)_4 + 2HCl \rightleftarrows 2CuCl(OAc) + 2AcOH \quad (2)$$

$$Cu_2(OAc)_4 + 4HCl \rightleftarrows 2CuCl_2 + 4AcOH \quad (3)$$

Further, the following equilibria[4] in a mixture of lithium chloride and copper(II) chloride in acetic acid have also been reported.

$$CuCl_2 + LiCl \rightleftarrows LiCuCl_3 \quad (4)$$

$$LiCuCl_3 + LiCl \rightleftarrows Li_2CuCl_4 \quad (5)$$

It is also known that copper(II) acetate exists mainly as the dimer[6] in acetic acid. In these experiments, the absorption maximums at 685 and 365 nm which were observed when copper(II) acetate was dissolved in acetic acid decreased and disappeared upon addition of lithium chloride respectively. This suggests that a part of the dimer of copper(II) acetate is converted into the monomer by the addition of lithium chloride and that copper(II) chloro complexes are formed. No oxygen absorption was detected when the oxidation of anthracene without any additive was performed at 90 °C in acetic acid. The rate of oxygen absorption in the oxidation of anthracene with copper(II) acetate was low but improved on addition of lithium chloride. However, without copper(II) acetate in the oxidation of anthracene, no oxygen absorption was observed either on adding lithium chloride or lithium acetate. A part of these results is shown in Table 1. Accordingly lithium chloride, lithium acetate and hydrogen chloride formed by the reaction of lithium chloride with acetic acid were not effective in the oxidation of anthracene directly. Moreover, the rate of oxygen absorption in the oxidation

Table 1. Effects of copper(II) acetate and lithium chloride addition on the oxidation of anthracene at 90 °C

Anthracene mol/l	Copper(II) acetate $Cu_2(OAc)_4$ mol/l	Lithium chloride mol/l	Initial rate of oxygen absorption mol/l·s
0.05	—	0.01	0 (reaction time 240 min)
0.05	0.01	—	1.3×10^{-7}
0.05	0.005	0.01	2.9×10^{-6}
0.05	0.01	0.01	4.2×10^{-6}

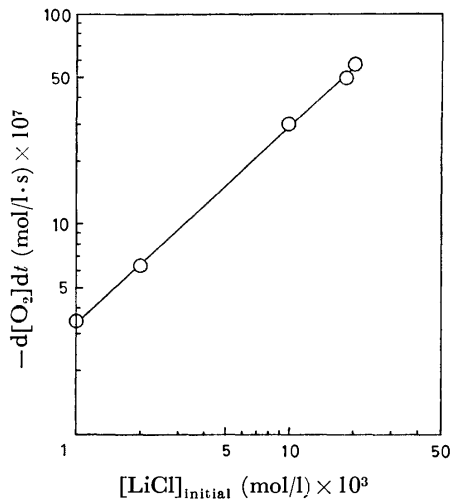

Fig. 1. Effect of $[LiCl]_{initial}$ at 90 °C under conditions, $[LiCl]_{initial}=2\times[Cu_2(OAc)_4]_{initial}$.
$[LiCl]_{initial}$: initial concentration of added lithium chloride.
$[Cu_2(OAc)_4]_{initial}$: initial concentration of added copper (II) acetate dimer.

of anthracene with copper(II) acetate and lithium acetate was low. Thus the increase of oxygen absorption rate is presumed to be related to the formation of copper(II) chloro complexes.

Effect of Added Amount of Copper(II) Acetate and Lithium Chloride on Oxygen Absorption Rate. When the molar ratio of copper(II) acetate dimer to lithium chloride is 0.5, the effect of various amounts of added copper(II) acetate and lithium chloride is shown in Fig. 1. Initial rates of oxygen absorption increase as concentrations of added copper(II) acetate and lithium chloride increase. That is, some copper(II) chloro complexes formed from copper(II) acetate and lithium chloride effectively work for the liquid-phase oxidation. The rates of oxygen absorption are approximately proportional to the added amounts of copper(II) acetate and lithium chloride under the experimental conditions.

Reaction Products. Anthraquinone, anthrone, 9-acetoxyanthracene, and 9-chloroanthracene were identified as reaction products by gas chromatography and gas-mass spectrometry. Formation of 10,10′-bianthrone was not observed. No generation of carbon dioxide from the reaction solution was detected. Typical

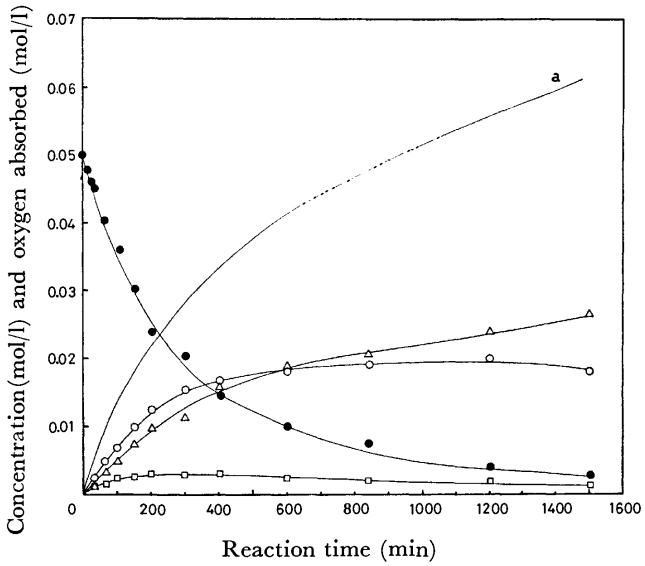

Fig. 2. Time course of oxidation of anthracene at 90 °C.
anthracene : 0.05 mol/l
copper(II) acetate $Cu_2(OAc)_4$: 0.005 mol/l
lithium chloride : 0.01 mol/l
●: Anthracene, □: 9-acetoxyanthracene, ○: anthrone, △: anthraquinone, a: oxygen absorbed.

patterns of production of anthraquinone, anthrone, and 9-acetoxyanthracene, decrease of anthracene, and oxygen absorption are shown in Fig. 2. 9-Chloroanthracene was detected in trace amounts. At the initial stage of oxidation, anthrone was a main product. 9-Acetoxyanthracene was produced at the initial stage of oxidation and then remained nearly constant in the reaction solution.

References

1) C. A. Angell and D. M. Gruen, *J. Am. Chem. Soc.*, **69**, 1038 (1947).
2) M. Baaz, V. Gurmann, G. Hampel, and J. R. Masaguer, *Monatsh. Chem.*, **93**, 1416 (1962).
3) C. Furlani and G. Morpurgo, *Theor. Chim. Acta*, **1**, 102 (1963).
4) K. Sawada, H. Ohtaki, and M. Tanaka, *J. Inorg. Nucl. Chem.*, **34**, 3455 (1972).
5) L. R. Mahoney, *J. Am. Chem. Soc.*, **86**, 444 (1964).
6) M. Kato, H. B. Jonassen, and J. C. Tanning, *Chem. Rev.*, **64**, 99 (1964).